ISSN 1070-4272, Russian Journal of Applied Chemistry, 2007, Vol. 80, No. 1, pp. 1–6. © Pleiades Publishing, Ltd., 2007.
Original Russian Text © N.A. Potolokov, A.V. Serov, V.N. Potolokov, A.V. Zhuravlev, V.P. Kolganov, E.G. Zhukov, V.A. Fedorov, V.I. Kholstov, 2007, published in Zhurnal Prikladnoi Khimii, 2007, Vol. 80, No. 1, pp. 3–8.

INORGANIC SYNTHESIS AND INDUSTRIAL INORGANIC CHEMISTRY

Reduction of Arsenic Trichloride with Hydrogen

N. A. Potolokov, A. V. Serov, V. N. Potolokov, A. V. Zhuravlev, V. P. Kolganov, E. G. Zhukov, V. A. Fedorov, and V. I. Kholstov

Research Institute of Electronics Materials, Open Joint-Stock Company, Kaluga, Russia
Kurnakov Institute of General and Inorganic Chemistry, Russian Academy of Sciences, Moscow, Russia
Kaluga Branch, Timiryazev Moscow Agricultural Academy, Kaluga, Russia
Federal Industry Agency, Moscow, Russia

Received March 3, 2006

Abstract—The composition of an equilibrium vapor–gas mixture in the range 700–1100 K was estimated for the reaction of arsenic trichloride with hydrogen taken in excess of a = 1.0–2.5 as compared to the stoichiometry. The temperatures of the onset of arsenic condensation (dew point) were found. Kinetic parameters of the chemical reaction were determined. Optimal conditions for the reduction of arsenic trichloride with hydrogen were refined and conditions for the condensation of arsenic with the minimum fraction of the amorphous modification were found.

DOI: 10.1134/S1070427207010016

The reaction of gaseous arsenic trichloride with hydrogen is one of the most important stages of the preparation of high-purity elemental arsenic [1–4]. Systematic study of $AsCl_3$ reduction with hydrogen is required for the development of physical and chemical principles for producing high-purity arsenic from an unconventional raw material, products of the detoxication (utilization) of chemical weapons (lewisite). The feasibility of organizing industrial production of high-purity arsenic-containing compounds on the basis of lewisite has been substantiated in [5–7].

It was found by studying thermodynamic and kinetic features of the $AsCl_3$ reduction with hydrogen [8–10] that the degree of conversion of arsenic trichloride is sufficiently high even at temperatures above 600 K and small hydrogen excesses against a stoichiometry. The chemical equilibria for real reaction conditions were simulated in [11].

This paper deals with an experimental study of the reduction of $AsCl_3$ with hydrogen. Appreciable attention is given to the process kinetics, and also to the optimization of conditions for the production of high-purity arsenic from unconventional raw materials, products of lewisite detoxication and wastes from nonferrous metallurgy.

EXPERIMENTAL

First we made a thermodynamic estimation of the arsenic trichloride reduction with hydrogen:

$$AsCl_{3g} + 1.5H_{2g} \rightleftarrows 0.25As_{4g} + 3HCl_g, \quad (1)$$

$$K_{eq} = \exp(-\Delta G_T^0/RT). \quad (2)$$

Such representation of the $AsCl_3$ transformation to arsenic is admissible, as it was shown previously [5, 7] that As_4 is the main arsenic species in the vapor phase at temperatures below 1100 K in the presence of a hydrogen excess $\alpha < 5$ against the stoichiometry. Equilibrium constants (2) of reaction (1) were calculated for the range 700–1100 K and an excess (α = 1–2.5) of hydrogen against the stoichiometry by two known methods:

$$\Delta G_T^0 = \Delta H_{298}^0 - T\Delta S_{298}^0 + \sum [n_i(H_T^0 - H_{298}^T)_i] - T\sum [n_i(S_T^0 - S_{298}^T)_i], \quad (3)$$

$$\Delta G_T^0 = \Delta H_{298}^0 - T\Delta\Phi_T^{**}, \quad (4)$$

where $\Delta\Phi_T^{**}$ is the reduced thermodynamic potential.

Both methods give similar K_{eq} values varying from 3.4×10^4 to 6.0×10^4 atm$^{0.75}$ for ΔG_T^0 varied from 60 to 100 kJ mol^{-1}. From the resulting K_{eq} values, we estimated the composition of the equilibrium vapor–gas mixture for a total pressure of 1 atm in the reaction zone. The calculated data are given in Fig. 1, which shows that the calculated partial pressures P_{eq} of arsenic vapor are practically independent of the process temperature and decrease by a factor of 1.7 with increasing α from 1 to 2.5. The partial pressure

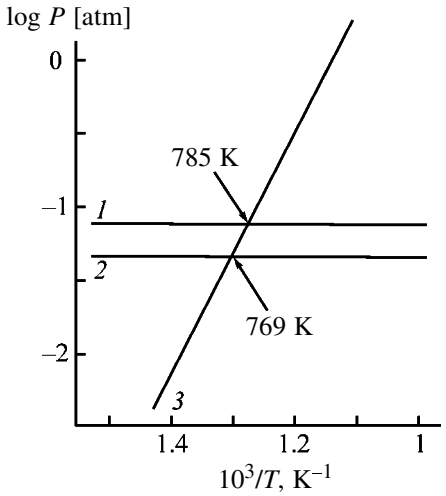

Fig. 1. Temperature dependence of arsenic pressure P under equilibrium conditions. α: (*1*) 1.0 and (*2*) 2.5; (*3*) saturated vapor pressure of arsenic.

of hydrogen decreases by a factor of 1.26 with increasing temperature from 700 to 1100 K at $\alpha = 1$, but at $\alpha > 1.5$ it becomes practically temperature-independent. The equilibrium concentration of $AsCl_3$ remains insignificant at all α values and decreases as α increases, confirming a high degree of $AsCl_3$ conversion to arsenic (Table 1).

The temperature dependence (5) of the saturated vapor pressure of arsenic over solid arsenic [8] is also shown in Fig. 1.

$$\log P\,[\text{atm}] = -8140/T + 9.244. \quad (5)$$

It is seen that the straight line crosses the horizontal lines of P_{As} in points corresponding to 785 and 769 K for $\alpha = 1$ and 2.5, respectively. These are the temperatures that are "dew points" for the initial proportions of the reactants and correspond to the conditions of the onset of arsenic condensation and to the lower temperature boundary of correct thermodynamic calculations for reaction (1). At lower temperatures, reaction (6) occurs, and the homogeneous process becomes heterogeneous.

$$AsCl_{3g} + 1.5H_{2g} \rightleftarrows As_s + 3HCl_g. \quad (6)$$

Thus, we can expect that $AsCl_3$ will be reduced by reactions (1) and (6) simultaneously below the dew point. In this case, the contribution of reaction (6) increases as the temperature decreases and can be estimated from expression (7).

$$D = (P_{eq} - P)/P_{eq}, \quad (7)$$

where P_{eq} is the equilibrium pressure of arsenic vapor for reaction (1). The process can be considered as passing homogeneously (1) in the gas phase with the subsequent condensation of arsenic vapor:

$$As_{4g} \rightleftarrows 4As_s. \quad (8)$$

The kinetics of $AsCl_3$ reduction with hydrogen was studied on an installation schematically shown in Fig. 2. The main element of the installation is a quartz reactor consisting of two sections. A high-temperature zone is constructed as a system of three coaxial cylinders ensuring a preset residence time of the reaction mixture ($AsCl_3 + H_2$) at a certain temperature.

A water-cooled condenser ensuring the deposition of arsenic in the form of a compact coarsely crystalline ingot is arranged in the low-temperature zone of the reactor. The reactor is placed inside a multizonal resistance heating unit where the required temperature of the reaction and arsenic condensation zones is created.

We used two methods for the determination of the degree of arsenic trichloride conversion to elemental arsenic: (1) direct monitoring of the $AsCl_3$ content in gaseous reaction products by sampling and subsequent analysis of the samples and (2) determination of the amount of the resulting elemental arsenic from the loss of a certain amount of the starting $AsCl_3$.

The first method makes it possible to reduce the experiment duration and to make several parallel analyses with a single portion of $AsCl_3$. The second method is more labor-consuming; however, it provides an integral characteristic of the process kinetics in the H_2–$AsCl_3$ system where the effect of fluctuations of process conditions will be leveled off. In this case, however, an essential complication is permanent formation of finely dispersed amorphous modification of arsenic, which is partially carried away from the condenser by a gas stream. Therefore, it is necessary to take into account the amount of elemental arsenic precipitated in the absorbing system.

We used a combined technique in the experiments,

Table 1. Degree of arsenic trichloride conversion to arsenic η as a function of temperature and hydrogen excess

α	η, %, at indicated temperature, K				
	700	800	900	1000	1100
1	97.32	97.55	97.74	97.78	97.86
1.5	99.97	99.97	99.98	99.98	99.98
2.0	99.99	99.99	99.99	99.99	99.99
2.5	99.99	99.99	99.99	99.99	99.99

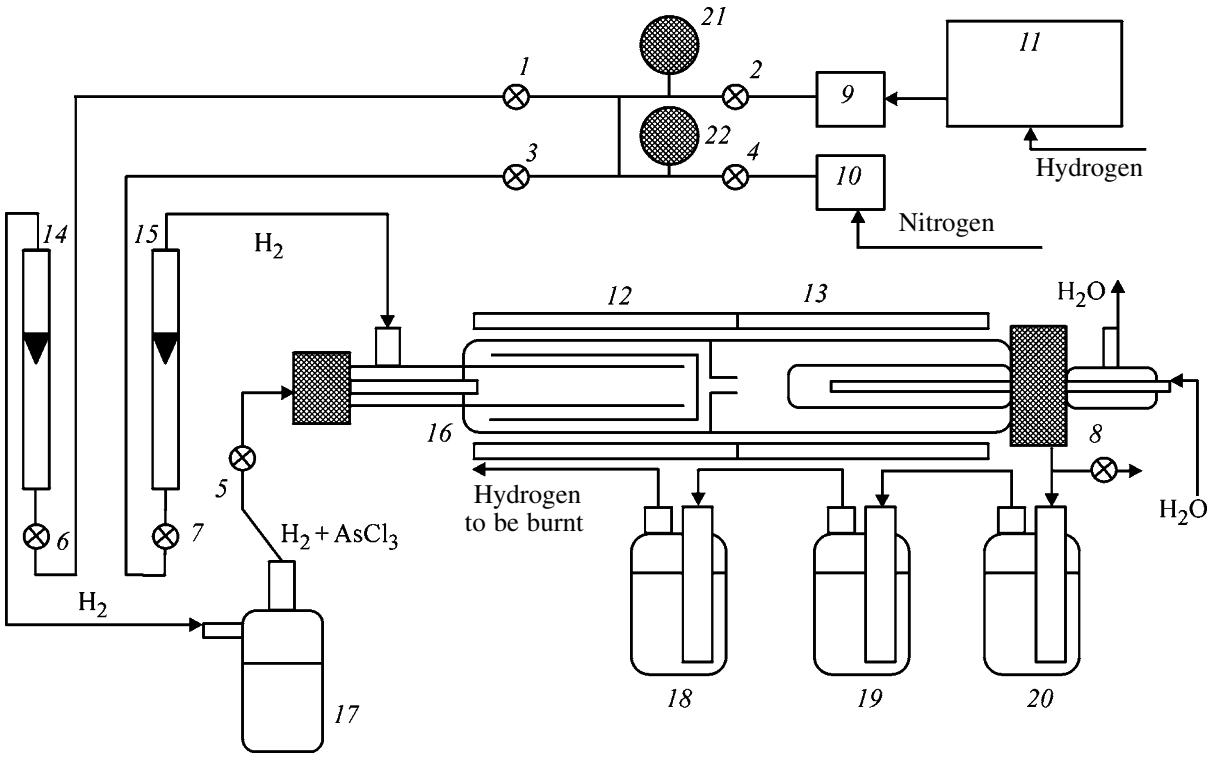

Fig. 2. Scheme of a pilot installation for studying kinetics of $AsCl_3$ reduction with hydrogen: (*1–8*) control stopcocks, (*9, 10*) gas pressure regulators for pressure adjustment, (*11*) installation for diffusion purification of hydrogen, (*12, 13*) heaters of high-temperature and low-temperature zones, (*14, 15*) flow meters, (*16*) reactor for arsenic trichloride reduction with hydrogen, (*17*) vessel with $AsCl_3$, (*18–20*) vessels for absorption of hydrogen chloride and residual arsenic trichloride, and (*21, 22*) manometers.

determining the total amount of unchanged $AsCl_3$ for the entire experiment duration with a sufficiently large amount of the starting substance (about 200 g). As a result, the advantages of the second method were realized and the error originating from incomplete collection of elemental arsenic formed was decreased. To check the correctness of the results obtained, we measured in addition the total amount of chlorine in the system for absorption of gaseous reaction products.

To describe the kinetics of the arsenic trichloride reduction, we used the approach developed in [8, 12, 13]. The rate of reaction (1) is determined by equation (9).

$$r = \mathrm{d}c/\mathrm{d}t = kc^X c_\mathrm{H}^Y, \quad (9)$$

where r is the reaction rate (mol l^{-1} s^{-1}); k, the reaction rate constant; c and c_H, concentrations of arsenic trichloride and hydrogen in the vapor–gas mixture (M); X and Y, partial reaction orders with respect to arsenic trichloride and hydrogen.

The reaction rate constant in a series of experiments can be calculated from the $AsCl_3$ residual concentration at a fixed residence time of the reaction mixture in the reaction zone. We found the residence time (chemical reaction duration) from expression (10)

$$t_\mathrm{r} = V_\mathrm{a}T_0/(Q_1 + Q_2)T_\mathrm{r}, \quad (10)$$

where t_r is the reaction duration (s); V_a, volume of the reaction zone (l); T_0, absolute temperature (K); Q_1 and Q_2, flow rates of vaporous $AsCl_3$ and gaseous hydrogen, respectively, reduced to the normal conditions (l s^{-1}); and T_r, reaction temperature (K). Generally the average value of T_r was determined by the graphical integration of the temperature variation along the reaction zone.

The concentrations of components in the starting vapor–gas mixture were calculated by formulas (11) and (12).

$$c_0 = T_0/V_0(1 + 1.5\alpha)T_\mathrm{r}, \quad (11)$$

$$c_{\mathrm{H}(0)} = 1.5\alpha T_0/V_0(1 + 1.5\alpha)T_\mathrm{r}, \quad (12)$$

where α is the ratio of the amount of hydrogen fed (mol) to its stoichiometric amount; V_0, volume of 22.4 l, which is occupied by 1 mol of ideal gas under normal conditions.

To determine the partial reaction orders and the reaction rate constant, it is necessary to solve rate

Table 2. Experimental and calculated parameters of the reduction of arsenic trichloride with hydrogen

T_r, K	α	t, s	$\eta_{exp} = 1 - f_{exp}$	$\eta_{calc} = 1 - f_{calc}$	$\Delta = (\eta_{exp} - \eta_{calc})/\eta_{exp}$
			%		
1072	1.03	16.1	88.4	90.6	–2.5
1072	1.29	17.5	96.9	97.8	–0.9
1072	1.88	19.7	99.8	99.7	0.1
1072	2.60	21.2	99.8	99.9	–0.1
1026	1.67	25.0	99.3	99.4	–0.1
932	1.97	25.4	99.0	98.9	0.1
886	1.91	25.2	97.9	97.7	0.2
980	1.98	20.0	99.5	99.3	0.2
980	1.79	14.6	99.0	98.7	0.3
980	1.96	9.9	98.8	98.5	0.3
980	2.36	10.4	99.0	99.1	–0.1
980	4.03	11.4	99.4	99.6	–0.2
980	2.01	8.0	97.2	98.3	–1.1
1072	1.58	11.6	99.1	99.0	0.1
1072	1.68	10.0	99.2	99.1	0.1

equation (9). Let us introduce a dimensionless variable f, the fraction of unchanged $AsCl_3$, defined by expression (13):

$$f = c/c_0. \quad (13)$$

Then, taking into account expression (14), we can write down the rate equation of the chemical reaction in form (15):

$$c_H = 1.5\alpha c, \quad (14)$$

$$df/[f^X(f + \beta)^Y] = -1.5^Y k c_0^{(X+Y-1)} dt, \quad (15)$$

where $\beta = \alpha - 1$. In view of the fact that at $t_r = 0$ $f = 1$, the integral form of the rate equation is

$$\int_f^1 df/[f^X(f + \beta)^Y] = 1.5^Y k c_0^{(X+Y-1)} t_r. \quad (16)$$

The integration of the left-hand side of Eq. (16) represents a certain problem, as the form of the integral depends on X and Y values, and only when X and Y are equal to integer and(or) half-integer numbers the integral can be expressed in elementary functions. In this connection, the problem was solved in such a way as to obtain an array of experimental concentrations of unchanged $AsCl_3$ by varying independent variables and to determine the partial reaction orders and the temperature dependence of the reaction rate constant on this basis.

The ranges of variation of the independent parameters were as follows: temperature of the reaction zone T_r = 886–1071 K, reaction duration τ = 5–28 s, and excess of hydrogen against the stoichiometric amount α = 1.02–4.03. The ranges of variation of these variables were chosen on the basis of the examination of real process modes and the data of [8, 10].

Typical experimental and calculated data are given in Table 2. To determine partial reaction orders, we used the method of finding a minimum of the dependence of the standard deviation of the reaction rate constant (and also of its logarithm) on X and Y calculated by Eq. (16) for each series of the experiments satisfying the requirement T_r = const. The application of such a procedure gave the following reaction orders with respect to arsenic trichloride and hydrogen: X = 1.86 and Y = 2.78. The order of reaction (1) in the system $AsCl_3$–H_2 is 4.6, suggesting its complicated mechanism.

Using the X and Y values obtained, we solved Eq. (16), calculated the reaction rate constant for the whole array of the experimental data, and determined its temperature dependence (17).

$$\ln k = B - A/T, \quad (17)$$

where A = 15287 and B = 36.509.

The apparent activation energy E is approximately 127 kJ mol^{-1}. The frequency factor K_0, determined in the collision theory from the relationship $\ln K_0 = B$, is 7.17×10^{15} (mol l^{-1})$^{-4.6}$ s^{-1}. We note that the reaction rate constant at 800 K exceeds 3.6×10^7 and increases to approximately 1.7×10^9 (mol l^{-1})$^{-4.6}$ s^{-1} at 1000 K. The degree of arsenic trichloride conversion under these conditions exceeds 99% at the residence time of

the mixture in the reaction zone longer than 15 s and at a hydrogen excess $\alpha > 1.5$.

The data obtained allowed us to calculate the degree of arsenic trichloride conversion η (%). The results of this calculation satisfactorily agree with the experiment (Table 2). The relative difference between the calculated and experimental data does not exceed 40% when estimating the fraction of unchanged $AsCl_3$ and 4% when determining the degree of its conversion. The rate constants of $AsCl_3$ reduction with hydrogen were used to optimize operation conditions for the production of high-purity arsenic on a pilot installation.

The calculation results are plotted in Fig. 3. It is seen that the maximal capacity of about 3 g min^{-1} of arsenic at the preset 99.9% conversion and temperature of 1100 K is reached at $\alpha = 3.4$. When choosing the reaction temperature, the possibility of contamination of the desired arsenic by apparatus impurities should be taken into account. In particular, at temperatures exceeding 1100 K the resulting arsenic contains an increased amount of silicon. The decrease in temperature below 900 K results in an appreciable decrease in the reaction rate. The increase in the hydrogen excess over 3.4 reduces the output capacity. In practice, the reduction of arsenic trichloride with hydrogen is carried out with a hydrogen excess of 1.5–2, as at $\alpha > 2$ the fraction of amorphous arsenic appreciably increases because of higher rates of the gas mixture at the reactor outlet and, as a consequence, greater breakthrough of arsenic vapor into the cold part of the reactor where arsenic condenses in the amorphous state.

We determined the optimal temperature of the condensation zone from the viewpoint of minimizing the amount of amorphous arsenic. We performed a series of experiments in which the temperature in the zone of the maximal thickness of the product layer was varied and the fraction of amorphous arsenic was determined. The results are given in Fig. 4, which shows that, at temperatures higher than 700 K, the amorphous arsenic fraction increases considerably (from 7.2 to 22% at $T > 730$ K). In the range 700–670 K, this fraction varies only slightly. Thus, the optimal temperature range where the residual pressure of arsenic is lower than 5×10^{-3} atm is 670–705 K.

To decrease arsenic removal in the form of aerosols from the reactor, it is necessary to use a trapping system. In our case, we used a special unit in which the direction of the gas stream changes and residual amorphous arsenic is trapped by a system of bubble absorbers. The amount of arsenic removed from the

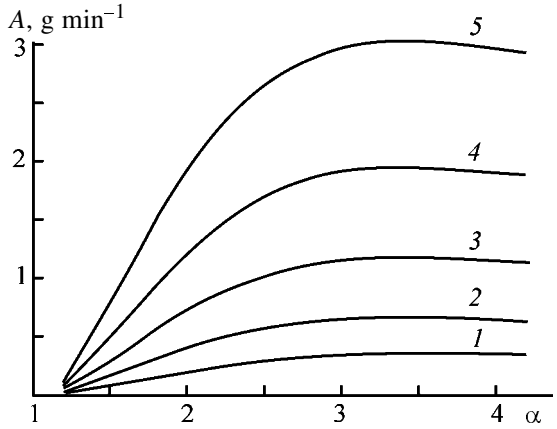

Fig. 3. Dependence of the pilot installation capacity for $AsCl_3$ reduction with hydrogen A on hydrogen excess α for various temperatures and 99.9% conversion. Temperature, K: (*1*) 900, (*2*) 950, (*3*) 1000, (*4*) 1050, and (*5*) 1100.

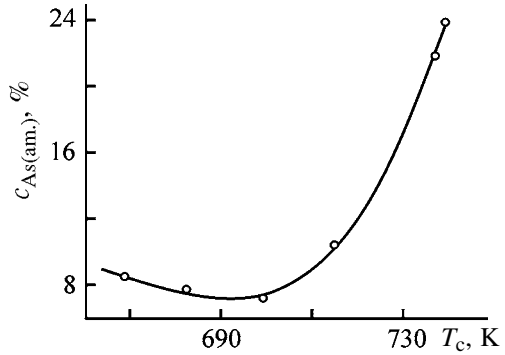

Fig. 4. Dependence of the amorphous arsenic content $c_{As(am.)}$ on the temperature T_c of the condensation zone.

condensation zone does not exceed 1.5%.

The found conditions for the reduction of arsenic compounds with hydrogen were used as the basis for constructing a pilot installation for the production of high-purity arsenic from such unconventional raw materials as products of the detoxication of chemical weapons (lewisite) and waste from nonferrous metallurgy.

The content of impurities in samples of high-purity arsenic prepared from lewisite is shown in Table 3. The impurity contents were monitored by spectral analysis with excitation of the spectrum in a dc arc and by atomic-emission spectroscopy with excitation of the spectrum in an inductively coupled plasma discharge. The high detection limit of impurities (up to 10^{-8} wt %) was reached by applying extraction preconcentration of impurities in the sample preparation stage.

It should be noted that the purity of amorphous and crystalline arsenic modifications is practically the same. Nevertheless, from the viewpoint of conveni-

Table 3. Content of impurities (A) in samples of high-purity arsenic

Impurity	$A \times 10^6$, wt %		
	crystalline arsenic	amorphous arsenic	detection limit
Al	<1.0	<1.0	1.0
Zn	0.1	0.1	0.03
Te	2.0	2.0	0.6
Si	0.5–0.1	2–0.5	0.06
S	4.0	2.0	1.0
Fe	0.7	2.0	0.1
Mn	<0.5	<0.5	0.01
Mg	<0.1	<0.1	0.01
Cu	<0.1	<0.1	0.07
Na	<0.1	<0.1	0.1
Cr	<0.5	<0.5	0.1
Pb	<5.0	<5.0	1.0

ence in the technology of semiconductor materials, amorphous arsenic is further sublimed to convert it to the crystalline form. The arsenic thus obtained is of 99.9999 wt % purity (6N grade) and is highly competitive with products of leading companies from the United States (Johnson Matthey) and Japan (Furukawa) produced from the traditional raw material, arsenic ores.

The use of high-purity arsenic obtained from unconventional raw materials ensures high and reproducible parameters for commercially produced single crystals of gallium arsenide and for epitaxial structures based on it.

CONCLUSIONS

(1) The composition of an equilibrium vapor–gas mixture was estimated for the reaction of $AsCl_3$ with hydrogen in the range 700–1100 K. The degree of $AsCl_3$ conversion varies from 97.3 up to 97.9% at the amount of hydrogen relative to the stoichiometry α = 1 and approaches 100% as α exceeds 1.5.

(2) The reaction order (X = 1.86, Y = 2.78), rate constant ($\ln k = 36.509–15287/T$), and apparent activation energy (E = 127 kJ mol^{-1}) were determined.

(3) The optimal conditions of the arsenic trichloride reduction with hydrogen were determined experimentally: temperature in the reaction zone 1050–1100 K, temperature in the condensation zone 670–705 K, residence time of vapor–gas mixture in the reaction zone 20–25 s, and hydrogen excess α = 1.5–2.0.

(4) The degree of $AsCl_3$ conversion to arsenic was shown to be no less than 99.99%, and the minimal amount of amorphous As, 7.2 %.

ACKNOWLEDGMENTS

This study was performed within the framework of the Program of Presidium of the Russian Academy of Sciences "Support of Innovations" and was financially supported by the Leading Scientific Schools grant of the Russian Foundation for Basic Research (grant no. NSh-4895.2006.3).

REFERENCES

1. Rtskhiladze, V.G., *Mysh'yak* (Arsenic), Moscow: Metallurgiya, 1969.
2. Nisel'son, L.A., Yaroshevskii, A.G., Gasanov, A.A., et al., *Vysokochist. Veshch.*, 1993, no. 4, pp. 62–64.
3. Fedorov, V.A., Pashinkin, A.S., Efremov, A.A., and Grinberg, E.E., *Vysokochist. Veshch.*, 1991, no. 5, pp. 7–30.
4. Fedorov, V.A., *Sovremennye problemy obshchei i neorganicheskoi khimii. Sbornik k 70-letiyu Inst. obshchei i neorganisheskoi khimii im. N.S. Kurnakova Ross. Akad. Nauk* (Modern Problems of General and Inorganic Chemistry. Coll. of Works Dedicated to 70th Anniversary of Kurnakov Institute of General and Inorganic Chemistry, Russian Acad. Sci.), Moscow: Nauka, 2004, pp. 464–472.
5. Fedorov, V.A., Efremov, A.A., Grinberg, E.E., et al., *Ross. Khim. Zh.*, 1994, vol. 38, no. 2, pp. 25–33.
6. Fedorov, V.A., Efremov, A.A., Zhukov, E.G., et. al., *Ros. Khim. Zh.*, 1995, vol. 39, no. 4, pp. 46–57.
7. Fedorov, V.A., *Russ. J. Inorg. Chem.*, 2001, vol. 46, suppl. 2, pp. 87–112.
8. Krapukhin, V.V., Sokolov, I.A., and Kostyuchenko, M.N., *Izv. Vyssh. Uchebn. Zaved., Tsvetn. Metall.*, 1967, no. 4, pp. 95–103.
9. Milovanova, M.V. and Krenev, V.A., *Zh. Neorg. Khim.*, 1997, vol. 32, no. 6, pp. 1699–1700.
10. Krenev, V.A. and Evdokimov, V.I., *O vosstanovlenii trikhlorida mysh'yaka vodorodom* (On the Reduction of Arsenic Trichloride with Hydrogen), Available from VINITI, 1972, no. 4049.
11. Potolokov, V.N., Efremov, V.A., Zhukov, E.G., et al., *Neorg. Mater.*, 2003, vol. 39, pp. 20–26.
12. Rusin, A.D., Agamirova, L.N., and Zhukov, E.G., *Vestn. Mosk. Gos. Univ., Khimiya*, 1982, vol. 23, no. 2, pp. 104–107.
13. Denisov, E.T., *Kinetika gomogennykh khimicheskikh reaktsii* (Kinetics of Homogeneous Chemical Reactions), Moscow: Vysshaya Shkola, 1978.

ISSN 1070-4272, Russian Journal of Applied Chemistry, 2007, Vol. 80, No. 1, pp. 7–12. © Pleiades Publishing, Ltd., 2007.
Original Russian Text © A.F. Dresvyannikov, M.E. Kolpakov, O.A. Lapina, 2007, published in Zhurnal Prikladnoi Khimii, 2007, Vol. 80, No. 1, pp. 9–14.

INORGANIC SYNTHESIS AND INDUSTRIAL INORGANIC CHEMISTRY

Preparation of Iron–Aluminum Powders from Aqueous Solutions and Their Physicochemical Properties

A. F. Dresvyannikov, M. E. Kolpakov, and O. A. Lapina

Kazan State Technological University, Kazan, Tatarstan, Russia

Received March 30, 2006

Abstract—Iron and iron–aluminum powders were obtained by the reduction of Fe(III) to α-Fe, occurring on a dispersed aluminum support. Their physical and mechanical properties were studied, and the possibility of obtaining compact samples with a lower bulk density as compared to known analogs, an elevated strength, and a high porosity was examined.

DOI: 10.1134/S1070427207010028

Increasing researchers' activity is focused on a search for procedures for preparing new nano- and microdimensional materials with unique physical and physicochemical properties. One of approaches consists in the precipitation of a metal layer from solutions of its compounds on microparticles of another metal. Such processes can be of interest also for recovery of metals from liquid and solid industrial media, their utilization, and production of metal-clad and alloyed metal powders with special properties [1].

One of urgent problems is the preparation of alloys and composites based on a binary iron–aluminum system exhibiting elevated strength and corrosion resistance. It was suggested previously to obtain this system from an aqueous solution by depositing iron on aluminum microparticles. It was found that iron(0) is deposited from such solutions in two steps: Fe(III) → Fe(II) → Fe(0), with simultaneous dissolution of aluminum support and formation of an α-iron layer on its surface [2]. As a result, dendrite spherical particles with large internal cavities and pores are formed, which determines low bulk density of the powder. The amount of residual aluminum is readily controlled by treating the precipitate with an alkali solution and can be made as low as tenth fractions of percent.

The surface of the precipitated particles is covered by spherulites of various sizes, which, in turn, bear nanodimensional spherical nuclei. Various sparingly soluble oxo and hydroxo compounds can be formed on the aluminum surface in the process; therefore, it is of interest to estimate the phase composition and structure of the deposits. Furthermore, it is important to reveal regular trends in the behavior of these objects under mechanical (pressing) and thermal (sintering) actions.

EXPERIMENTAL

The synthesis of iron–aluminum powders is based on the electrochemical reduction of iron(III) ions on an aluminum support suspended in solution. The resulting precipitate was separated from the mother liquor by magnetic separation, washed with double-distilled water to neutral reaction, and dried in a vacuum at 60°C.

The chemical and phase compositions of the samples were determined with a DRON-2 X-ray diffractometer. To decrease the noise from scattering of the primary X-ray beam in air, we used FeK_α long-wave radiation with a β-filter. The X-ray patterns were recorded under the following conditions: a voltage of 30 kV, a current of 15 mA, goniometer slits of 1–1–1×8 mm^2, and range of recording angles 2θ from 20° to 160°. Compact samples were pulverized prior to measurements.

The X-ray patterns were treated using the MAUD 1.999 multifunction software [3, 4]. Annealed copper foil was used as a reference for comparing line profiles (determination of coherent scattering areas and microstresses).

The analysis and microphotographing of particles of the starting aluminum and resulting precipitates were carried out on a Philips SM XL-30 TMP electron scanning microscope in the following mode: scale ΔE = 10 keV (0–500), collection time 100 s,

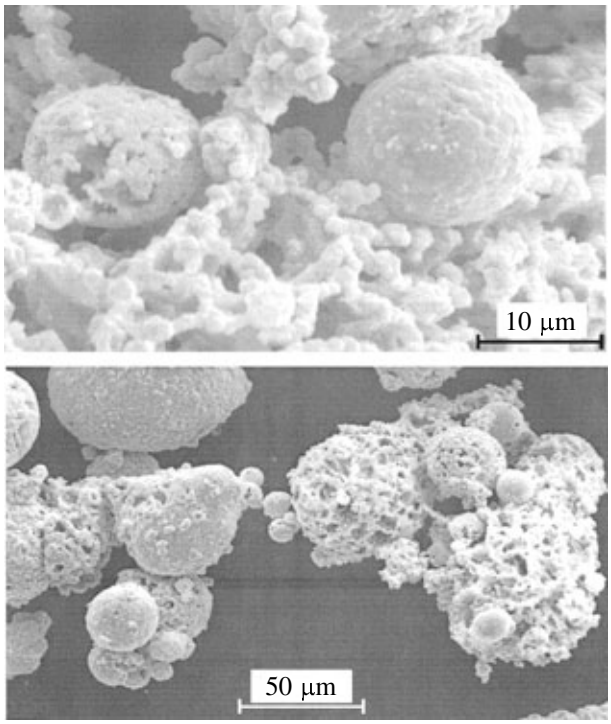

Fig. 1. Photomicrographs of particles of deposited iron.

and $E_{el.probe}$ = 30 keV. The microprobe area was varied from 20×30 to 50×75 μm^2.

The specific porosity of preliminarily evacuated (0.01 mm Hg) samples was determined by mercury porosimetry on a Milestone-200 instrument under pressures from 0.7 to 199 MPa.

The fractal dimension D was determined by processing the mercury porometry data using Neimark's equation [5]

$$D = 2 + d(\log \int_0^V P dV)/d\log P = 2 + d[\log f(P)]/d\log P, \quad (1)$$

where $f(P) = \int_0^V P dV$, V is the mercury intrusion, and P is the applied voltage.

Physicochemical characteristics of powders and compact samples made of them were estimated according to Russian and international standards currently in force [6].

It was found previously that the iron(III) reduction in aqueous solutions on a dispersed aluminum matrix occurs in two steps: Fe(III) → Fe(II) → Fe(0) [7]. As two products, iron (II) ions and iron(0), are formed in the course of the iron(III) reduction, we used the relative selectivity method [8] to elucidate the reaction mechanism. On the basis of thus obtained experimental data we suggest the following scheme of transformations of iron redox species in the course of reaction of iron(III) with aluminum [9]:

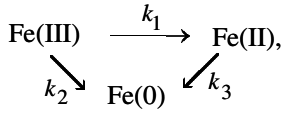

where k_1, k_2, and k_3 are the rate constants of the corresponding steps (s^{-1}).

In this case, the total process is described by the following system of rate equations [10]:

$$[Fe(III)] = [Fe(III)]_0 \exp[-(k_1 + k_2)t], \quad (2)$$

$$[Fe(0)] = [Fe(III)]_0 \{k_2(k_1 + k_2)^{-1} \{1 - \exp[-(k_1 + k_2)t]\} + [1 - k_3(k_3 - k_1)^{-1} \exp(-k_1 t) + k_1(k_3 - k_1)^{-1} \exp(-k_3 t)]\}, \quad (3)$$

$$[Fe(II)] = [Fe(III)]_0 - [Fe(III)] - [Fe(0)]$$

or

$$[Fe(II)] = [Fe(III)]_0 \{1 - \exp[-(k_1 + k_2)t] - k_2(k_1 + k_2)^{-1} \{1 - \exp[-(k_1 + k_2)t]\} - [1 - k_3(k_3 - k_1)^{-1} \exp(-k_1 t) + k_1(k_3 - k_1)^{-1} \exp(-k_3 t)]\}, \quad (4)$$

$$\alpha = m[Fe(0)]/m_0[Fe(III)] = \{k_2(k_1 + k_2)^{-1} \{1 - \exp[-(k_1 + k_2)t]\} + [1 - k_3(k_3 - k_1)^{-1} \exp(-k_1 t) + k_1(k_3 - k_1)^{-1} \exp(-k_3 t)]\}. \quad (5)$$

The iron(0) precipitate is formed on the surface of aluminum particles with the preservation of the shape and geometric sizes of a source matrix, i.e., aluminum is dissolved, and simultaneously spherical nuclei of metallic iron are formed. The main amount of aluminum is dissolved in the course of time, and the forming particles represent practically hollow spheres with a large number of spherical subindividuals on the surface, pores, and nuclei inside them (Fig. 1). This is also indirectly proved by the abnormally low bulk density of the resulting powders (1.25 ± 0.01 g cm^{-3}). Iron is precipitated nonuniformly on aluminum particles, i.e., particles completely covered by the deposit and particles that have not entered into the reaction coexist in any reaction step.

As in this case self-similarity of iron–aluminum particles predetermines a complicated contour of the

Table 1. Results of X-ray phase analysis

Sample no.	Unit cell parameter, nm	Size of coherent scattering area, nm	Microstress	Phase composition	Content of phases, wt %
1	0.28656 ± 0.00001	34.7	0.0034	α-Fe	100.00
				Al	0.00
2	0.28665 ± 0.00001	50.3	0.0029	α-Fe	99.10
				Al	0.90
3	0.28665 ± 0.00001	404.6	0.0000	α-Fe	80.74
				α-Al_2O_3	1.54
				Fe_3C	14.38
				Fe_2O_3	0.77
				θ-Al_2O_3	2.57
4	0.28662 ± 0.00001	40.0	0.0032	α-Fe	96.35
				Al	3.65
5	0.28654 ± 0.00001	38.1	0.0034	α-Fe	96.54
				Al	3.46
6	0.28669 ± 0.00001	402.5	0.0007	α-Fe	69.21
				α-Al_2O_3	11.50
				Fe_3C	14.19
				Fe_2O_3	1.26
				θ-Al_2O_3	3.84

* Nos. 1 and 4: iron and iron–aluminum powders; nos. 2 and 5: pressed samples of iron and iron–aluminum powders; nos. 3 and 6: sintered samples of iron and iron–aluminum powders.

surface, we determined the fractal dimension of particles by mercury porosimetry [5]. Figure 2 shows curves of mercury intrusion obtained by the above-mentioned method for three objects: dispersed aluminum, the synthesized composite iron–aluminum powder, and then iron powder obtained by etching the latter with an alkali. According to these curves, particles of dispersed aluminum exhibit a low porosity, the main part of pores being large. This is caused by the history of the aluminum powder (prepared from a melt), which determines predominantly smooth shape of the particles. We can note that the total volume of pores in iron–aluminum particles is larger by a factor of approximately three than that of aluminum particles; however, the pore sizes are smoothed out in this case. When residual aluminum is removed by etching the precipitate in NaOH solution (3.0 M), the total porosity slightly increases. Figure 2 shows that this change is connected mainly with increasing volume of large pores, whereas the total volume of small pores changes to a considerably lesser extent.

The examination of mercury intrusion curves using Neimark's equation [5] shows that the fractal dimension of aluminum microparticles is 2.04 ± 0.002 (a smooth surface). The fractal dimension of iron–aluminum particles is 2.87 ± 0.02, which is characteristic of rough objects. The latter result is caused by specific features of corrosive dissolution of aluminum in a chloride-containing medium and by features of the conjugate process of iron isolation. The greatest value corresponds to iron particles obtained by an additional treatment of iron–aluminum composite powders with an alkali; for them, D is 3.00 ± 0.02, which is a theoretical limit for a surface dimension. It is characteristic for samples with the maximal porosity and roughness of the external and internal surfaces.

Table 1 shows that powdered sample no. 1, which was prepared according to the suggested technique,

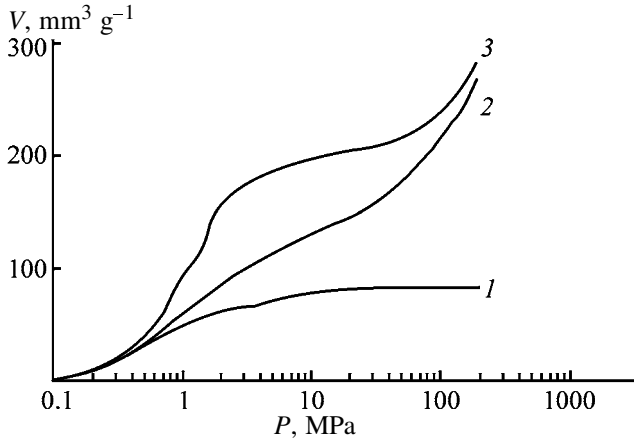

Fig. 2. Experimental curves of mercury intrusion for microparticles of (*1*) aluminum, (*2*) iron–aluminum samples, and (*3*) iron. (*V*) Pore volume and (*P*) pressure.

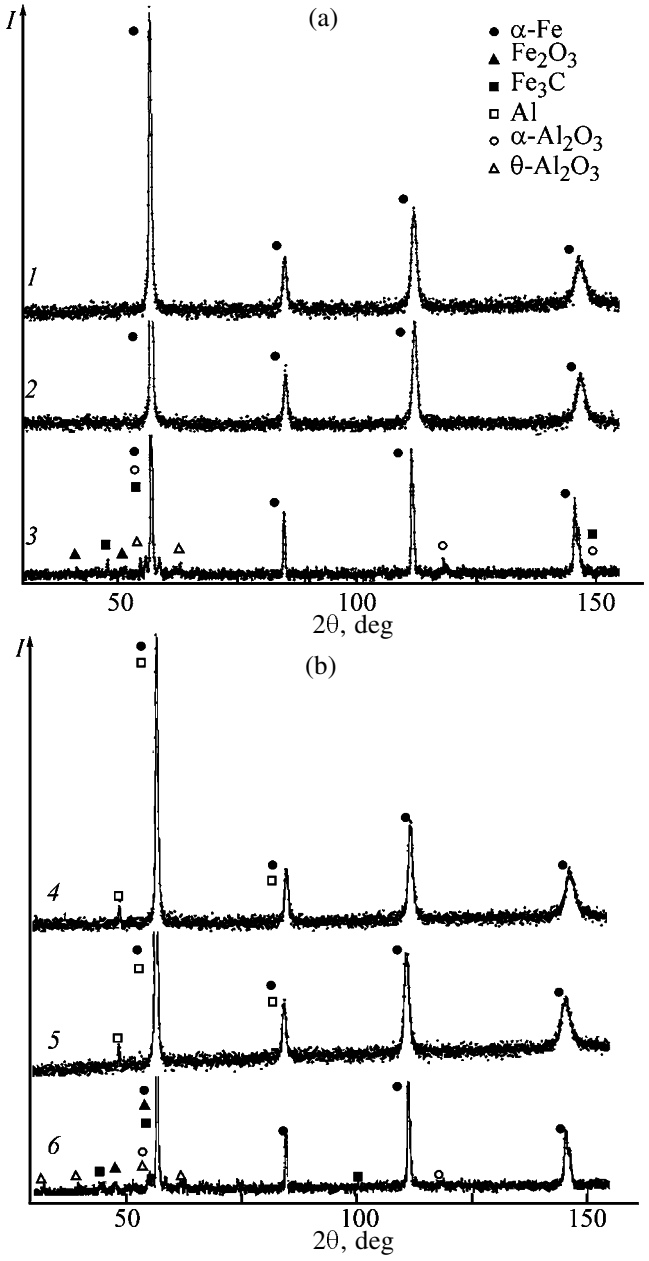

Fig. 3. X-ray patterns of (a) dispersed iron and (b) iron–aluminum composite. (*I*) Intensity and (2θ) Bragg angle. (*1–6*) Sample nos. in Table 1.

contains only one phase of α-Fe. After pressing aluminum "appears" in sample no. 2, apparently forming a thin layer on the internal surface of hollow particles of iron powder and outcropping on the external surface upon a strong deformation. In the X-ray patterns (Fig. 3, curve *2*), separate peaks of aluminum are very weak. It is interesting that iron crystallites become larger as a result of the mechanical action accompanied by aluminum outcrop.

When samples are sintered, aluminum transforms into various modifications of its oxide (Table 1, sample no. 3). X-ray phase analysis reveals the presence of two phases, θ-Al_2O_3 and α-Al_2O_3 (corundum). Apparently, the character of thermomechanical treatment strongly affects the structure, composition, and physicochemical properties of the object under study. The presence of moisture in pores of a source powder, most likely, leads to the reaction of water with metallic aluminum yielding α- and θ-Al_2O_3 on heating.

The presence of organic binding agents (sodium stearate), introduced before pressing and filling the pores of the initial sample, results in the formation of a Fe_3C phase. The presence of atmospheric oxygen in combination with moisture on the surface and in internal pores of the sample promotes partial transformation of iron into Fe_2O_3 (hematite).

The above-described processes significantly affect the fine structure of the samples under study. As iron is deposited, a significant amount of gas separates out and enters into the deposit together with iron [9]; therefore, hydrogen absorption along with polarization is the main cause of defects forming in the structure of the deposited iron and determining its stressed state [11]. It is seen that the sizes of α-iron crystallites somewhat increase after pressing (Table 1, sample no. 2), though their shape remains unchanged, and microstresses decrease, most likely, due to rearrangement of the internal load. After sintering in an ammonia atmosphere, the sizes of α-iron crystallites considerably increase and microstresses decrease. Apparently, in this case the grain size grows and the amount of lattice defects decreases.

Similar results were obtained on testing sample nos. 4 and 5 containing residual aluminum. Unlike sample nos. 1 and 2, after pressing the sizes of crystallites and their shape remain practically unchanged, and microstresses change only slightly. The crystallite sizes in these samples considerably decrease after sintering (Table 1, sample no. 6), and microstresses are relieved; however, in contrast to sample no. 3, they still remain relatively high.

According to the quantitative analysis, sample nos. 4 and 5 contain almost equal amounts of aluminum, i.e., pressing causes almost no changes. Sintering (Table 1, sample no. 6) gives a result close to that for sample no. 3, but differing from it by a larger amount of α-Al_2O_3.

It should be emphasized that microparticles formed by iron deposition from solution on an aluminum support are practically always spherical, and their size only slightly differs from that of the starting sample.

Table 2. Physicomechanical properties of dispersed and compact samples

Property	Composite powder Fe–Al	Dispersed iron	Industrial iron powder PZhRV 2
Outward appearance	Highly dispersed gray powder without foreign inclusions and clots		
Moisture content, %, GOST (State Standard) 9849–86	0.40 ± 0.02	0.19 ± 0.02	0.25
Bulk density, g cm^{-3}, GOST 19440–94	1.26 ± 0.02	1.20 ± 0.02	2.50–2.70
Compactibility, g cm^{-3}, GOST 25280–90	4.8 ± 0.1	5.6 ± 0.2	7.1
Strength of nonsintered pressed material, MPa, GOST 25282–93	16.3 ± 2.2 (ρ = 5.0 g cm^{-3})	77.0 ± 2.2 (ρ = 5.1 g cm^{-3})	20 (ρ = 6.5 g cm^{-3})
Porosity, %, GOST 18898–89	36.7 ± 0.7	35.4 ± 0.7	10.1
Strength of pressed material after sintering, MPa	194.6 ± 4.9 (ρ = 4.78 g cm^{-3})	122.4 ± 1.4 (ρ = 4.56 g cm^{-3})	No data

The granulometric study of iron powders obtained by the synthesis that was performed with a close-cut fraction of dispersed aluminum (85 ± 15 μm) shows that the narrow particle-size distribution is preserved [10].

Samples prepared by cold pressing of the resulting iron–aluminum powdered composite are characterized by a low mechanical strength. First of all, this is attributable to a difference in parameters of the components of the object under study and to its highly defective crystal lattice, which is indirectly indicated by a zero line rise in the X-ray pattern (Fig. 3, curve *5*).

The study of rheological characteristics of the objects under study has shown that the density of both the bulk powder and pressed briquettes is essentially lower than that prescribed by the standard [6] (Table 2), which is apparently caused by the formation of framework structures as a result of accretion of separate particles during the synthesis. The formation of such structures for iron powders and, as a consequence, a low density of the objects under study after pressing are responsible for the high porosity of the sintered samples.

This factor is very important; it determines the properties of composites prepared from such materials [12]. For example, the application of porous antifriction materials allows the service life of friction units to be considerably prolonged owing to their capacity to keep liquid lubricant in pores for a long time, which makes the parts self-lubricated.

The strength of the pressed samples results both from mechanical engagement and a weave of surface protrusions and imperfections of powder particles and from the action of interatomic adhesive forces, the degree of their action increasing as the contact area increases. Table 2 shows that the strength of the pressed sample of "pure" iron powder is considerably higher than that of the sample made of iron–aluminum powder. This is attributable to a more developed system of internal pores in powder particles, which are formed on leaching. Under the external loading, hollow particles are deformed in an unusual way, the ratio of the surface area of a particle to its volume increases, and surface films of adsorbed impurities are broken off. Flattened-out metal particles contact each other with freshly formed surfaces to give blocks of a complicated shape tightly engaged with each other. The strength of the blocks increases on sintering of these samples; however, it appears a little lower than that for analogs obtained from industrially produced iron powders [6]. This is attributable to the presence of hydrogen in the deposit, which is absorbed during the formation and growth of nuclei of α-iron and increases its brittleness [11].

At high pressure (>600 MPa) and temperature (>1000°C), aluminum reacts with chemically bound and adsorbed water in the medium of gaseous ammonia to form an iron matrix structured by aluminum oxides (α- and θ-Al_2O_3) and having no strong internal stresses. The presence of a significant amount of aluminum oxides in sample no. 6 (Table 1) seems to promote the formation of a strengthened dispersed structure due to a fairly uniform distribution of the oxides in the iron matrix reached during caking. It defines an increase in the mechanical strength of materials prepared by sintering.

CONCLUSIONS

(1) Particles of an iron–aluminum composite prepared by iron deposition from an aqueous solution on a dispersed aluminum support represent practically

hollow spheres with a large number of spherical subindividuals on the surface, pores, and nuclei inside them, which gives rise to unique physical properties of the dispersed metal.

(2) The resulting objects have a dendritic structure; the fractal dimension of the surface of the synthesized binary iron–aluminum systems was calculated from the data of mercury porosimetry.

(3) The powders have characteristics that make it possible to obtain pressed samples having, compared to the existing analogs, lower bulk density (by approximately 30%), higher strength (by a factor of 2–3), and high porosity and corrosion resistance.

(4) The heat treatment (sintering) of the samples synthesized in solution and containing iron and aluminum promotes the formation of new phases of α- and θ-Al_2O_3 as a result of dehydroxylation of aluminum hydroxo compounds formed in the reactions of aluminum with capillary and adsorbed water.

REFERENCES

1. Murashova, I.B. and Pomosov, A.V., *Itogi Nauki, Ser.: Elektrokhimiya*, 1989, vol. 30, pp. 55–145.
2. Dresvyannikov, A.F., and Kolpakov, M.E., *Mater. Res. Bull.*, 2002, vol. 37, no. 2, pp. 291–296.
3. Matthies, S., Lutterotti, L., and Wenk, H.-R., *J. Appl. Crystallogr.*, 1997, vol. 30, no. 1, pp. 31–42.
4. *The Rietveld Method*, Young, R.A., Ed., New York: Oxford Univ. Press, 1993.
5. Neimark, A.V., *Pis'ma Zh. Eksp. Teor. Fiz.*, 1990, vol. 51, no. 10, pp. 535–538.
6. Fomina, O.N., Suvorova, S.N., and Turetskii, Ya.M., *Poroshkovaya metallurgiya: Entsiklopediya mezhdunarodnykh standartov* (Powder Metallurgy: Encyclopedia of International Standards), Moscow: Izd. Standartov, 1999.
7. Dresvyannikov, A.F. and Kolpakov, M.E., *Zh. Prikl. Khim.*, 2002, vol. 75, no. 10, pp. 1602–1607.
8. Rozovskii, A.Ya., *Geterogennye khimicheskie reaktsii (kinetika i makrokinetika)* (Heterogeneous Chemical Reactions (Kinetics and Macrokinetics)), Moscow: Nauka, 1980.
9. Dresvyannikov, A.F. and Kolpakov, M.E., *Zh. Obshch. Khim.*, 2005, vol. 75, no. 2, pp. 177–183.
10. Dresvyannikov, A.F. and Kolpakov, M.E., *Zh. Fiz. Khim.*, 2003, vol. 77, no. 5, pp. 807–812.
11. Petrov, Yu.N., Gur'yanov, G.V., Bobanova, Zh.I., et al., *Elektroliticheskoe osazhdenie zheleza* (Electrolytic Deposition of Iron), Zaidman, G.N., Ed., Chisinau: Shtiintsa, 1990.
12. *Aluminum: Properties and Physical Metallurgy*, Hatch, J.E., Ed., Metals Park, Ohio: Am. Soc. for Metals, 1984.

ISSN 1070-4272, Russian Journal of Applied Chemistry, 2007, Vol. 80, No. 1, pp. 13–18. © Pleiades Publishing, Ltd., 2007.
Original Russian Text © A.M. Bessarabov, A.N. Ponomarenko, M.Ya. Ivanov, A.M. Yaroshenko, G.E. Zaikov, 2007, published in Zhurnal Prikladnoi Khimii, 2007, Vol. 80, No. 1, pp. 15–19.

INORGANIC SYNTHESIS AND INDUSTRIAL INORGANIC CHEMISTRY

CALS Information Technologies (ISO-10 303 STEP) in Development of Plasmochemical Processes for Synthesis of Ultrapure Ultradispersed Oxides

A. M. Bessarabov, A. N. Ponomarenko, M. Ya. Ivanov, A. M. Yaroshenko, and G. E. Zaikov

State Research Institute of Chemical Reagents and Ultrapure Chemical Substances, Federal State Unitary Enterprise, Moscow, Russia
Institute of Biochemical Physics, Russian Academy of Sciences, Moscow, Russia

Received March 16, 2006

Abstract—Information model of plasmochemical processes for synthesis of nano- and ultradispersed oxide materials was developed on the basis of the CALS concept (Continuous Acquisition and Life cycle Support) for the example of ultrapure tin oxides.

DOI: 10.1134/S107042720701003X

Modern CALS technologies [1] were used to develop an information model of the plasmochemical process for synthesis of ultrapure nano- and ultradispersed oxides. The process was thermodynamically modeled in a wide range of temperatures, pressures, and component ratios. A system for computerized quality management (CQM system) [2] was used for analytical monitoring of the target oxide materials.[1]

Ultrapure oxide materials are widely used in the most promising and science-intensive fields of Russia's economy [3]. In manufacture of ultrapure oxides, it is exceedingly important that a by-product of synthesis should not contaminate the target products or interact with process equipment, thereby taking up an additional amount of impurities. A promising way to tackle with this problem is application of low-temperature plasma, which makes it possible to create a set of modern apparatus with the minimum microimpurity background [4]. One more advantage of this technique is that it can yield ultra- and even nanodispersed powders, which is virtually impossible with other methods.

Low-temperature plasma enables studies and process operations at temperatures of 2×10^3–2×10^4 K, various pressures, and residence times of 10^{-5}–10^{-3} s. Low-temperature plasma can be successfully employed in those cases when the equilibrium is shifted to high temperatures; a high yield is achieved under strongly nonequilibrium conditions; the reaction rates markedly grow with temperature.

In the course of plasmochemical synthesis, the aggregative state of any starting substance, as well as its physical and chemical properties, are changed. The following reaction scheme has found wide application in plasmochemical synthesis: A → B + C, where A is a starting substance, B is an ultrapure product, and C is by-product of synthesis. It is important in this case that by-product C should not contaminate the ultrapure substance and should not interact with the process equipment to preclude additional contamination.

Numerous researchers have used chlorides and organoelement compounds as starting substances. The advantage of chlorides consists in their more convenient introduction into the plasma flare, compared with heterogeneous systems. However, synthesis with chlorides yields the following by-products: HCl, ClO, $MeCl_{n-1}$, where n = 2–4 [4]. These products strongly impair the purity of the finished product. With organoelement compounds as starting substances, one of the most undesirable by-products of synthesis is carbon [5].

The plasmochemical technology includes a number of units and process operations. A study of the be-

[1] The system was developed at Institute of Chemical Reagents, Federal State Unitary Enterprise on the basis of the CALS technology.

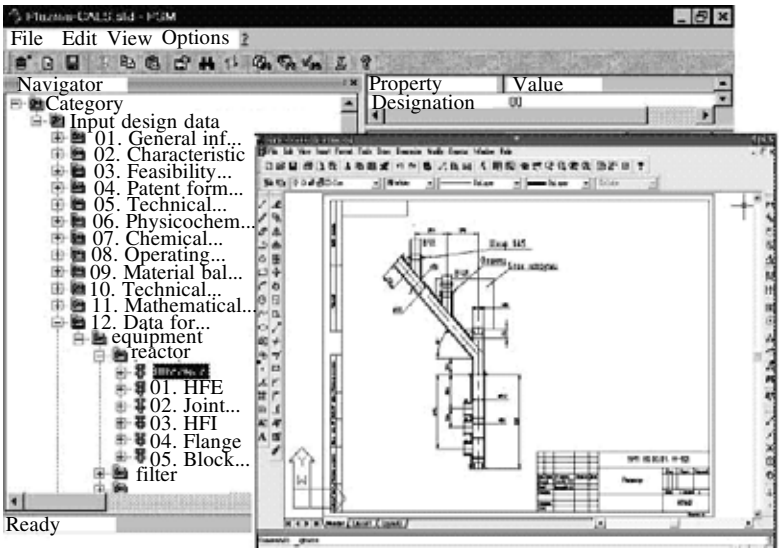

Fig. 1. Element of the CALS project: plasmochemical reactor for synthesis of ultrapure tin oxide.

havior of microimpurities in plasmochemical synthesis of ultrapure substances (oxides) furnished data on the influence exerted by limiting apparatus-related and process factors on the purity of the finished product [3]. Analysis of these data shows that the finished product is contaminated to the greatest extent in stages of trapping, discharge, and packaging.

In one of the first studies in this field, nano- and ultradispersed tin oxide was obtained [6]. Ultrapure tin oxide is a widely demanded chemical product used in manufacture of special kinds of glass and ceramics. A large number of enamels contain tin oxide, without which manufacture of acid- and fire-resistant chemical apparatus would be impossible. It is clear in this context that tin oxide should possess a certain granulometric composition and specific surface area and should contain less than 0.01% microimpurities. Modern ceramic technology has started to consume nanopowders. Naturally, the existing multistage industrial technology developed at the end of 1930s could not yield nanosized tin oxide. In addition, this multistage technology consumes large volumes of hydrochloric acid and requires neutralization and many days' stage-by-stage calcination [6].

A single-stage technology producing a nanosize (30–100 nm) tin oxide powder was developed. This could be only done with the use of plasmochemistry, one of the most promising tools of modern chemical technology.

The plasmochemical process was developed in the framework of the most modern and promising computer-support system, CALS technology (Continuous Acquisition and Life cycle Support) [1]. The CALS concept is based on a set of unified information models and on standardization of access ways to information and its adequate interpretation in conformity with international standards (ISO-10303 STEP). This provides unified methods for control over processes and enables interaction between all those involved in the development process. According to prognoses of foreign specialists, soon after 2005 it will be impossible to sell at the foreign market any high-tech products without electronic documentation conforming to international CALS standards (ISO-10303 STEP) [1]. Thus, use of CALS technologies is a must for promising domestic projects. With account of this circumstance, a number of promising processes have been reconsidered in terms of the CALS concept: syntheses of biologically active additives [7] and ultrapure materials [8].

In the development of a plasmochemical process for synthesis of ultrapure tin oxide, a type scheme (application protocol) "Input design data" was created in the framework of the CALS project (Fig. 1).

In conformity with the chemical industry's standard, the structure of the input data includes 17 necessary sections [8]. All these sections are incorporated in the CALS project. In the screen form (Fig. 1), additional subitems are only displayed in section no. 12 (data for calculation and choice of the process equipment). However, additional, specific to chemical industry, information is actually input into the CALS project for all the sections.

A designer's electronic description conforming to the STEP standard (Fig. 1) contains the structure and

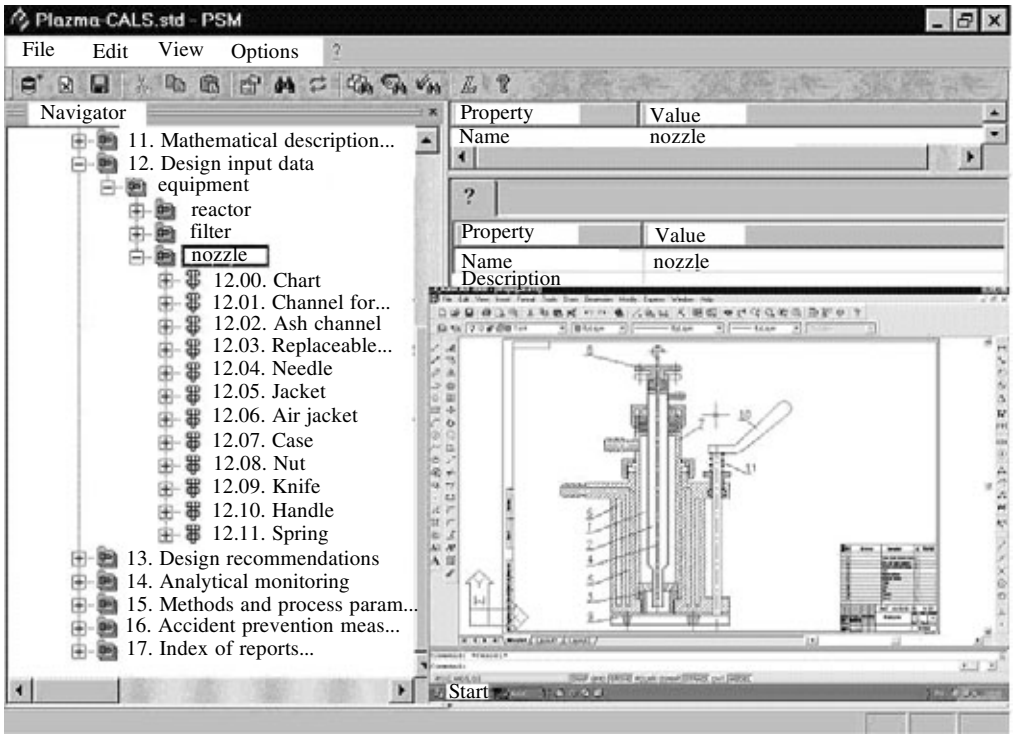

Fig. 2. Element of the CALS project, pneumatic nozzle for feeding of liquid-phase starting reagents into the reactor.

alternative configurations of an article, geometric models and drawings, properties and characteristics of the constituent parts. The STEP standard can be applied in several ways.

(1) Data can be stored as an exchangeable text file. In this form, the data can be conveniently transferred among automated systems having an appropriate converter for STEP files.

(2) Data structures can be created in a finished PDM system by its appropriate adjustment and by development of necessary visual applications. The already available solutions can be employed. Information is processed using PDM STEP suite 2.5 software developed at the Research Center for CALS technologies [9]. The use of the international CALS standard for defining the data structure and programmed access interfaces enables parallel work with information from different fields of technology and allows integration with information systems of any kind. This development potentiality is not presently observed for any other PDM system [9].

The versatile plasmochemical installation being developed can feed into the reactor (Fig. 1) not only the starting solid product via a powder feeder, but also liquid-phase reagents (chlorides and alkoxides) via a special jet (Fig. 2).

The versatility of the installation makes it possible to obtain ultradispersed oxides of Group II and III light and transition metals (aluminum, beryllium, cadmium, magnesium, scandium, yttrium, and zirconium). These products belong to a promising scientific area "Ceramic glassy materials and superhard materials."

Section no. 11 (mathematical description of the process) of the CALS project (Fig. 1) presents the results obtained in simulating the plasmochemical synthesis of ultrapure tin oxide. Analysis of chemical and heat-and-mass exchange processes at elevated temperatures leads to severe difficulties already in the stage of formulation of the simulation problem. It is appropriate to use thermodynamic simulation methods as a first approximation [6]. These methods presume that, in the processes under consideration, the working body forms a conditionally closed, isolated system in which a local thermodynamic equilibrium (LTE) is attained. In this approximation, the state of the system is only determined by the content of chemical elements in the system and by values of two parameters of state. The use of the thermodynamic equilibrium approximation is justified by the high concentration of energy in the volumes under consideration and by the resulting high rates of conversion processes, which instantaneously bring the system in the LTE state.

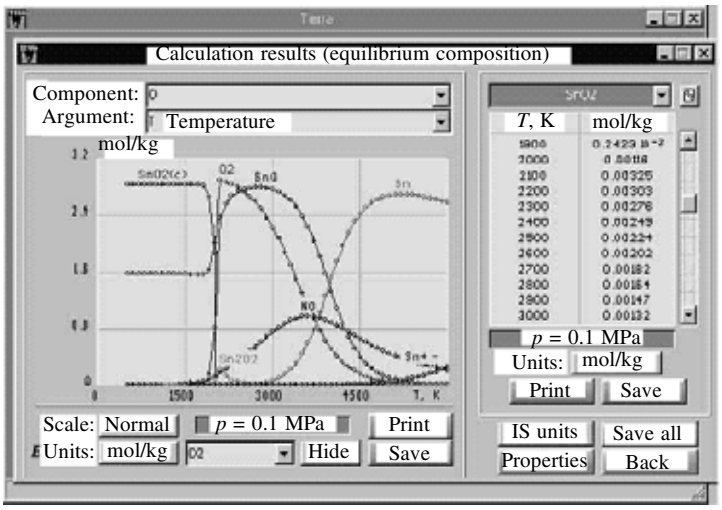

Fig. 3. Screen form of the results of thermodynamic simulation of the plasmochemical synthesis of ultrapure tin oxide.

A calculation of equilibrium for isolated multicomponent thermodynamic systems can be reduced to a problem of determination of a state with the minimum entropy. Therefore, to compose the sought-for system of equations, it is necessary to find an analytical relationship between the entropy of a unit mass of the working body and the thermodynamic parameters determining its composition, properties, and existence conditions.

In the general case, a gaseous system is constituted by neutral and electrically charged (ionized) components of the gas phase and separate condensed phases. The equation of state for an ideal gas is valid for the gas phase as a whole and for each of its components. The condensed phase will be considered single-component and immiscible. The content of the components of the gas phase (i = 1, 2, ..., k) and of separate condensed phases (l = 1, 2, .., L) in the system will be expressed in moles per unit mass, n_i and n_l. The entropy of such a system is given by

$$S = \sum_{i=1}^{k} S_i^{(p_i)} n_i + \sum_{l=1}^{L} S_l n_l = \sum_{i=1}^{k} [S_i^0 - R_0 \ln (R_0 T n_i/\nu)] n_i + \sum_{l=1}^{L} S_l^0 n_l,$$

where $S_i^{(p_i)}$ is the entropy of ith component of the gas phase at a partial pressure $p_i = R_0 T n_i/\nu$ at which it will be in the equilibrium state; S_l, entropy of lth condensed phase, dependent only on temperature; ν, specific volume of the whole system; S_i^0, standard entropy of ith component of the gas phase at temperature T and pressure equal to 1 physical atmosphere.

Determination of the parameters of the equilibrium state consists in finding all the dependent variables, including the number of moles of the components and the number of phases at which S reaches a maximum. This problem of a search for the extremum of the entropy of the system with account of constriction equations was solved using Astra-4 software developed at Bauman Higher Technical School in Moscow [10].

A thermodynamic calculation of the equilibrium states of the system is performed in a wide range of basic parameters of the plasmochemical process: starting component ratios, temperatures, and pressures (Fig. 3). A thermodynamic simulation makes it possible to choose the synthesis conditions, analyze the environmental safety of the production process, and assess the mechanism of thermal dissociation of the starting compounds.

The CALS technology and thermodynamic simulation were used to develop a pilot installation for single-stage synthesis of tin oxide. Powdered metallic tin is continuously fed into a plasmochemical reactor. In the reactor, the powder comes into an oxygen-containing plasma jet with a mass-average temperature of 4500 K. Depending on the feeding rate of the starting tin powder, flow rate of the plasma-forming gas, and input power, nanodispersed (0.03–0.1 μm) and ultradispersed tin oxide powders (0.1–0.3, 0.3–0.7, 0.7–1.2, 1.2–3, 3–7, 7–15, and 15–40 μm) can be obtained.

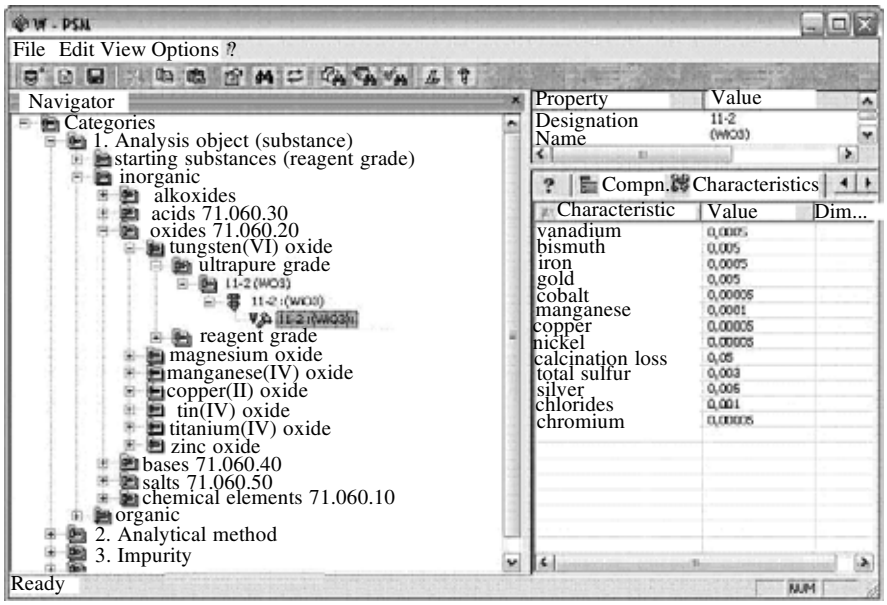

Fig. 4. Element of the CALS project of a CQM system for the example of ultrapure tungsten oxide of the 11-2 brand.

Industrial use of this project will make it possible to completely eliminate the inefficient, environmentally unsafe, and health-hazardous technology for manufacture of tin oxide at Russian chemical plants. The new technology is totally free of any harmful discharges. However, the most important factor is that it yields a fundamentally different product with high consumer's properties, which can well compete in the world market of ultrapure materials.

Recently, the requirements to the substance purity have become markedly more stringent and the number of parameters characterizing the quality of a product (ultrapure products) has increased. Simultaneously, the requirements to methods for analytical control of ultrapure substances have become more stringent. These problems can be only solved on the basis of a modern CQM system.

The CQM system developed has a hierarchic database structure (Fig. 4). Three main information categories are distinguished: (i) substance being analyzed, (ii) analytical methods and technical means of analysis and sample preparation, and (iii) output and standardizing documentation. Each category includes several subcategories for systematization of data in accordance with criteria appropriate for each category. Thus, the category substance includes the following groups: organic–inorganic, acids–salts–oxides (Fig. 4), and other classes of chemical compounds and simple substances.

CONCLUSION

Implementation of CALS technologies and modern computerized quality management systems in development of science-intensive plasmochemical processes raises the productivity and diminishes the expenditure of time and material resources. This is achieved by simplified access to information, reorganization of the working activities (without change of the tasks to be accomplished), computerization of the working environment, and significant improvement of relationships between partner designers.

ACKNOWLEDGMENTS

The study was supported in part by a European grant ECOPHOS no. 013359 (INCO).

REFERENCES

1. Bessarabov, A.M., Avseev, A.V., Avseev, V.V., and Kutepov, A.M., *Teor. Osn. Khim. Tekhnol.*, 2004, vol. 38, no. 2, pp. 229–233.
2. Bessarabov, A.M. and Zhdanovich, O.A., *Neorg. Mater.*, 2005, vol. 41, no. 11, pp. 1397–1404.
3. Bessarabov, A.M., *Reaktivy i osobo chistye veshchestva* (Reagents and Ultrapure Substances), Moscow: NIITEKhIM, 1988.
4. Ryabenko, E.A., Ivanov, M.Ya., and Parkhomenko, V.D., *Zh. Vses. Khim. O–va. im. D.I. Mendeleeva*, 1984, no. 6, pp. 646–650.

5. Ivanov, M.Ya., Bessarabov, A.M., Kupryashkina, T.N., and Tsybina, O.V., *Khim. Prom–st*., 1985, no. 1, pp. 34–35.
6. Bessarabov, A.M., Ivanov, M.Ya., Zhdanovich, O.A., and Ponomarenko, A.N., *Khim. Prom–st. Segodnya*, 2005, no. 12, pp. 33–37.
7. Bessarabov, A.M., Malyshev, R.M., and Dem'yanyuk, A.Yu., *Teor. Osn. Khim. Tekhnol*., 2004, vol. 38, no. 3, pp. 343–348.
8. Bessarabov, A.M. and Afanas'ev, A.N., *Khim. Tekhnol*., 2002, no. 3, pp. 26–30.
9. Davydov, A.N., Barabanov, V.V., and Sudov, E.V., *Stand. Kachestvo*, 2002, no. 7, pp. 12–18.
10. Sinyarev, G.B., Vatolin, N.A., Trusov, B.G., and Moiseev, G.K., *Primenenie EVM dlya termodinamicheskikh raschetov metallurgicheskikh protsessov* (Use of Computers for Thermodynamic Calculations of Metallurgical Processes), Moscow: Nauka, 1982.

ISSN 1070-4272, Russian Journal of Applied Chemistry, 2007, Vol. 80, No. 1, pp. 19–23. © Pleiades Publishing, Ltd., 2007.
Original Russian Text © S.V. Antipov, M.T. Sokolov, 2007, published in Zhurnal Prikladnoi Khimii, 2007, Vol. 80, No. 1, pp. 20–24.

INORGANIC SYNTHESIS AND INDUSTRIAL INORGANIC CHEMISTRY

Mechanochemical Activation in Manufacture of Defluorinated Forage Phosphate

S. V. Antipov and M. T. Sokolov

Belarussian State Technological University, Minsk, Belarus

Received May 4, 2006

Abstract—The effect of preliminary mechanochemical activation of phosphate rock on the temperature of hydrothermal calcination and degree of defluorination in manufacture of defluorinated forage phosphates conforming to GOST (State Standard) 23999–80 was studied. A mechanism of mechanochemical activation of phosphate raw materials, associated with changes in thermodynamic properties of the activated system, was suggested.

DOI: 10.1134/S1070427207010041

Phosphorus is a structural element of a living body. Its deficiency in rations weakens the resistance ability of the living mass, impairs the milk productivity, and disrupts the reproductive capacity. Phosphorus is second to protein in importance for animal feeding.

At present, the overwhelming majority of methods for processing of phosphorus-containing raw materials are either energy-intensive (thermal), or require use of inorganic (mostly sulfuric) acids, which leads to formation of a difficultly utilizable waste, phosphogypsum [2]. A topical problem is that of development of a simple power-saving technology for manufacture of this product. A possible way to obtain forage phosphates could be a method based on acid-thermal processing of natural phosphates [3]. This method consists in that, prior to hydrothermal defluorination, natural phosphate is treated with phosphoric acid. Such a treatment leads both to an increase in the content of the valuable component (P_2O_5) and to a deeper defluorination. A significant disadvantage of this method is, in the authors' opinion, the rather high defluorination temperature (1200–1350°C).

Of particular recent practical and theoretical interest is activation of chemical processes by mechanochemical activation [4–6]. The mechanochemical activation consists in initiation and acceleration of chemical transformations of reactants under a mechanical impact leading to deformation of the structure of solid reagents [4]. The plastic deformation of a solid commonly not only changes its shape, but also leads to accumulation of defects in the solid, which changes its physicochemical properties, including reactivity [5, 6].

The aim of our study was to examine the influence exerted by mechanochemical activation of phosphate raw materials on parameters of hydrothermal defluorination in manufacture of defluorinated forage phosphates.

EXPERIMENTAL

An analysis of the market of phosphate raw materials from the standpoint of a Belarussian manufacturer demonstrated that it is the most feasible either to use phosphate rock from CIS countries (Kingisepp, Polpino, Verkhnekamsk, Egor'evsk deposits) or to develop deposits in Belarus (Mstislavl, Lobkovichi, Orekhovskoe, and Prigranichnoe deposits). The chemical composition of primary concentrates from some of these deposits is listed in Table 1.

In the experiments, phosphate rocks from Polpino and Kingisepp deposits were used as phosphorus-containing raw materials. As activators served apparatus of various types: dismembrator and vibrational, planetary, and drum ball mills. The best results were obtained with activators of planetary and drum types. A ground phosphate rock was activated in a planetary or drum mill for 5–60 min. The activated mixture was treated with boiled-down (or not boiled-down) wet-process phosphoric acid (WPA, nWPA) to a molar ratio $CaO/P_2O_5 = 2.5$. The resulting plastic paste was granulated by extrusion through dies with various die aperture diameters. Weighed portions of humid grains were subjected to hydrothermal calcination at 900–1200°C. The results obtained in our study are listed in Tables 2 and 3.

Table 1. Chemical composition of phosphate rock

Phosphate rock	Content, wt %						
	CaO	P_2O_5	SiO_2	Al_2O_3	Fe_2O_3	F	calcination loss
Verkhnekamsk	37.50	21.83	14.23	4.60	3.90	2.10	15.84
Egor'evsk	31.52	19.90	22.20	5.80	5.00	1.77	13.81
Polpino	29.40	18.55	33.60	1.61	2.29	2.5	12.05
Mstislavl (flotation concentrate)	45.67	28.04	5.30	1.12	1.51	3.41	14.95
Kingisepp	41.42	27.71	11.39	1.16	1.84	2.21	14.27

Table 2. Results of the experimental study

Run no.	Type of phosphate rock and stages of its treatment	Activation time, min	Ball load	Activator type	Hydrothermal calcination temperature, °C	Hydrothermal calcination time, min	Residual fluorine content, wt %
1	Polpino ground phosphate rock → activation + WPA → hydrothermal calcination	5	3 : 1	Planetary mill	1200	20 40 60	0.246 0.161 0.051
2	Polpino ground phosphate rock + WPA → hydrothermal calcination	–	–	–	1200	20 40 60	1.191 0.513 0.18
3	Polpino ground phosphate rock → activation + WPA → hydrothermal calcination	5	3 : 1	Planetary mill	1100	20 40 60	0.022 0.021 0.019
4	Polpino ground phosphate rock + WPA → hydrothermal calcination	–	–	–	1100	20 40 60	1.134 0.765 0.439
5	Polpino ground phosphate rock → activation + WPA → hydrothermal calcination	5	3 : 1	Planetary mill	1000	20 40 60	0.058 0.031 0.016
6	Polpino ground phosphate rock + WPA → hydrothermal calcination	–	–	–	1000	20 40 60	1.241 0.975 0.734
7	Polpino ground phosphate rock → activation + WPA → hydrothermal calcination	5	3 : 1	Planetary mill	900	20 40 60	0.302 0.164 0.108
8	Polpino ground phosphate rock + WPA → hydrothermal calcination	–	–	–	900	20 40 60	1.283 1.054 0.987
9	Polpino ground phosphate rock → activation + WPA → hydrothermal calcination	5	3 : 1	Planetary mill	900	20 40 60	0.293 0.183 0.111
10	Polpino ground phosphate rock + WPA → activation → hydrothermal calcination	5	3 : 1	Planetary mill	900	20 40 60	0.234 0.053 0.028
11	Polpino ground phosphate rock + WPA → hydrothermal calcination	5	3 : 1	Planetary mill	900	20 40 60	1.247 1.103 1.081
12	Kingisepp ground phosphate rock + WPA → activation → hydrothermal calcination	5	3 : 1	Planetary mill	900	20 40 60	0.096 0.034 0.028

Table 2. (Contd.)

Run no.	Type of phosphate rock and stages of its treatment	Activation time, min	Ball load	Activator type	Hydrothermal calcination temperature, °C	Hydrothermal calcination time, min	Residual fluorine content, wt %
13	Kingisepp ground phosphate rock → activation + WPA → hydrothermal calcination	5	3 : 1	Planetary	900	20 40 60	0.065 0.058 0.051
14	Kingisepp ground phosphate rock + WPA → hydrothermal calcination	5	3 : 1	Planetary	900	20 40 60	0.452 0.387 0.321
15	Kingisepp ground phosphate rock + WPA → calcination (without blowing)	5	3 : 1	Planetary	900	20 40 60	1.261 1.062 0.921
16	Kingisepp ground phosphate rock + nWPA → activation → hydrothermal calcination	30	4 : 1	Drum mill	900	0 20 40 60	0.032 0.249 0.112 0.051
17	Kingisepp ground phosphate rock → activation + nWPA → hydrothermal calcination	30	4 : 1	Drum mill	900	0 20 40 60	2.048 0.422 0.287 0.165
18	Polpino ground phosphate rock + nWPA → activation → hydrothermal calcination	30	4 : 1	Drum mill	900	0 20 40 60	2.155 0.076 0.022 0.020
19	Polpino ground phosphate rock → activation + nWPA → hydrothermal calcination	30	4 : 1	Drum mill	900	0 20 40 60	1.874 0.432 0.131 0.122

Table 3. Content of phosphorus soluble in 0.4% HCl relative to its total content

Type of phosphate rock and stages of its treatment	Content, %, at indicated thermal treatment time, min		
	20	40	60
Polpino ground phosphate rock + WPA → activation → hydrothermal calcination at 900°C	91.4	93.0	92.1
Polpino ground phosphate rock + hydrothermal calcination at 900°C	95.5	97.8	94.8

It follows from Tables 2 and 3 that the defluorination yielding a product conforming to GOST (State Standard), i.e., that with $c_F \le 0.2$ wt %, without preliminary activation occurs at 1200°C and higher. The time of hydrothermal calcination is 60 min. The results of run nos. 3–8 (Table 2) show that defluorination performed without activation of the phosphorus-containing mixture is less intensive and the residual content of fluorine exceeds the value conforming to GOST. Use of a preliminary mechanochemical activation makes it possible to perform hydrothermal calcination at temperatures of about 900°C, with the calcination time equal to 20–40 min, depending on temperature. At present it is difficult to answer the question as to what is preferable in practice, calcination at 900°C for about 40 min or at 1000°C for 20 min. An answer

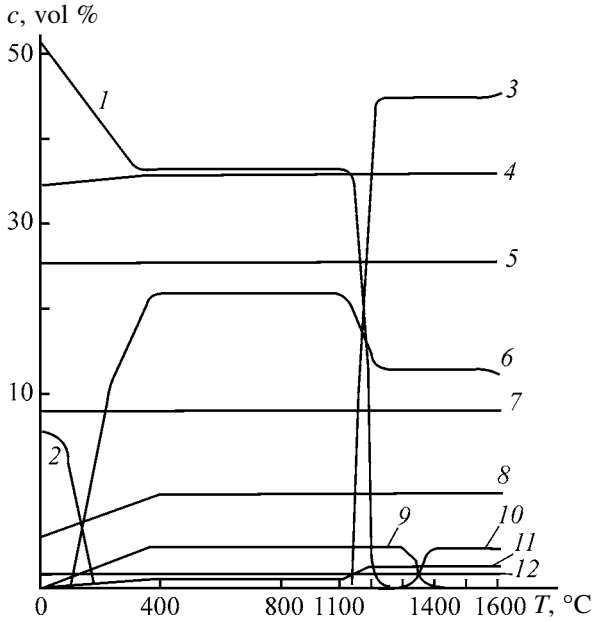

Fig. 1. Results of a thermodynamic analysis of the system constituted by phosphate rock, WPA, and H_2O. (*c*) Content and (*T*) temperature. (*1*) $Ca_{10}F_2(PO_4)_6$, (*2*) H_3PO_4, (*3*) $Ca_3P_2O_8$, (*4*) SiO_2, (*5*) H_2O, (*6*) $Ca_2P_2O_7$, (*7*) CO_2, (*8*) $AlPO_4$, (*9*) Fe_2O_3, (*10*) Fe_3O_4, (*11*) HF, and (*12*) O_2.

can be provided by an additional study aimed to find the minimum energy expenditure with account of the specific output capacity of the apparatus.

The defluorinated forage phosphate has the form of light porous grains. The content of P_2O_5 soluble in 0.4% HCl is higher than 33%, with the relative content of assimilable P_2O_5 exceeding 96%. The degree of defluorination is 90–95%, and the residual content of fluorine in the samples is less than 0.2%, which completely conforms to GOST 23999–80.

To elucidate how mechanochemical activation affects properties of phosphate rock, we thermodynamically analyzed the defluorination process by a calculation method. The analysis was performed using Astra-4 software package [7] for the system constituted by phosphorite rock, wet-process phosphoric acid, and water. The calculation demonstrated that defluorination is thermodynamically probable at temperatures of about 1200°C (Fig. 1).

As already noted, about the same defluorination temperatures (1200°C) were observed in a study of nonactivated phosphate rock on an experimental laboratory installation (Tables 2, 3). Thus, the preliminary mechanochemical activation of phosphate rock, performed prior to its thermal treatment, made it possible, all other conditions being the same, to lower the defluorination temperature from 1200 to 900°C.

In the study, the heat effect of dissolution of activated and nonactivated phosphate rock was calorimetrically determined in a calorimeter with an isothermal sheath. A 5% solution of hydrochloric acid served as a solvent. The calorimeter constant was found by the electric method.

The following processes occur upon introduction of a solid into the solvent: the crystal lattice of the substance disintegrates ($\Delta H_{disint} > 0$), ions pass into solution, are hydrated ($\Delta H_{hydr} < 0$), and interact with HCl. Depending on the relative values of ΔH_{disint}, ΔH_{hydr}, and ΔH of interaction with HCl, the substance dissolution may be either endothermic ($\Delta H > 0$) or exothermic ($\Delta H < 0$).

The experimental data we obtained show that dissolution of both activated and nonactivated phosphate rock is accompanied by heat release ($\Delta H < 0$), with the amount of heat released in dissolution of phosphate rock in hydrochloric acid exceeding by approximately 12–19% that in dissolution of a nonactivated sample (at equal sample weights).

The values of ΔH_{hydr} and ΔH of interaction between ions and HCl are the same for both phosphate rock samples, and, therefore, the difference between the heats of solution is due to that between changes in the enthalpy of crystal lattice disintegration, ΔH_{disint}. The value of ΔH_{disint} for the crystal lattice of activated phosphate rock exceeds that for nonactivated phosphate rock. This is quite understandable, because, in the course of mechanical activation, a solid undergoes first elastic, and then plastic and breaking deformation. As a result, ΔH_{disint} decreases.

Because the internal energy of a solid increases in the course of mechanical activation, it was assumed that thermodynamic characteristics of an activated substance differ from those of a nonactivated sample; the specific heat of the activated phosphate rock is somewhat lower that of the nonactivated substance.

Under real conditions, an activated system comes into equilibrium with the environment ($T_{amb} = T_{a.s}$) via relaxation (dissipation) processes, but a part of the energy received in the course of activation remains and leads to changes in thermodynamic properties.

As an example, we performed a thermodynamic analysis of the following reaction:

$$Ca_{10}F_2(PO_4)_6 + SiO_2 + H_2O = 3Ca_3(PO_4)_2 + CaSiO_3 + 2HF. \quad (1)$$

Taking into account the above assumption and the fact the amount of heat released in dissolution of

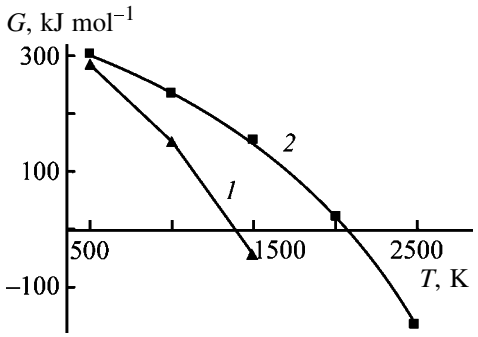

Fig. 2. Changes in the Gibbs energy, ΔG, vs. temperature T for (*1*) activated and (*2*) nonactivated systems.

activated phosphate rock in hydrochloric acid exceeds by approximately 12–19% that released in dissolution of a nonactivated substance, we lowered the value of the coefficient in formula (2) for activated phosphate rock [for SiO_2 and $Ca_{10}F_2(PO_4)_6$] by 15%:

$$c_p = a + bT = cT^{-2}. \quad (2)$$

For $Ca_{10}F_2(PO_4)_6$, $c_p = 946.38 + 120.91 \times 10^{-3}T - 204.4 \times 10^5 T^{-2}$; for SiO_2 (α-quartz), $c_p = 46.98 + 34.33 \times 10^{-3}T - 11.3 \times 10^5 T$.

The Gibbs energies of the processes involving the activated and nonactivated systems are plotted in Fig. 2. These quantities were calculated by the formula

$$\Delta G_T^0 = \Delta H_{298}^0 - T\Delta S_{298}^0 - T(M_0\Delta a + M_1\Delta b + M_{-2}\Delta c). \quad (3)$$

Figure 2 shows that a decrease in the specific heat leads to a pronounced change in the occurrence conditions of reaction (1) and that the temperature (at ΔG_T^0) is substantially lower than that for the reaction involving the starting raw material. A similar behavior was observed in experiments with activated phosphate rock.

CONCLUSIONS

(1) The experimental and calculated results of the study suggest that mechanochemical activation of the phosphate component of phosphate rock may become an efficient method for improving the conventional techniques for processing of phosphate raw materials.

(2) Preliminary mechanochemical activation in manufacture of defluorinated forage phosphates makes it possible, in particular, to lower the temperature of hydrothermal calcination by 300°C.

(3) The mechanochemical activation in the process studied affects the thermodynamic properties of the starting raw material.

REFERENCES

1. Karmyshov, V.F., Sobolev, B.P., and Nosov, V.N., *Proizvodstvo i primenenie kormovykh fosfatov* (Manufacture and Use of Forage Phosphates), Moscow: Khimiya, 1987.
2. *Tekhnologiya fosfornykh i kompleksnykh udobrenii* (Technology of Phosphate and Integrated Fertilizers), Evenchik, S.D. and Brodskii, A.A., Eds., Moscow: Khimiya, 1987.
3. Antipov, S.V. and Sokolov, M.T., *Tr. Bel. Gos. Tekh. Univ., Khim. Tekhnol. Neorg. Veshch.*, 2004, no. 12, pp. 56–60.
4. Boldyrev, V.V. and Avvakumov, E.G., *Usp. Khim.*, 1971, vol. 40, no. 10, pp. 835–856.
5. Avvakumov, V.G., *Mekhanokhimicheskie metody aktivatsii khimicheskikh protsessov* (Mechanochemical Methods for Activation of Chemical Processes), Novosibirsk: Nauka, 1979.
6. Molchanov, V.I., Selezneva, O.G., and Zhirnov, E.N., *Aktivatsiya mineralov pri izmel'chenii* (Activation of Minerals in Grinding), Moscow: Nedra, 1988.
7. Parkhomenko, V.D., Polak, L.S., Soroka, P.I., et al., *Protsessy i apparaty plazmokhimicheskoi tekhnologii* (Processes and Apparatus of Chemical Technology), Kiev: Vysshaya Shkola, 1979.

ISSN 1070-4272, Russian Journal of Applied Chemistry, 2007, Vol. 80, No. 1, pp. 24–30. © Pleiades Publishing, Ltd., 2006.
Original Russian Text © N.I. Golovina, G.N. Nechiporenko, G.G. Nemtsev, G.P. Dolganova, V.P. Roshchupkin, D.B. Lempert, G.B. Manelis, 2007, published in Zhurnal Prikladnoi Khimii, 2007, Vol. 80, No. 1, pp. 25–31.

PHYSICOCHEMICAL STUDIES OF SYSTEMS AND PROCESSES

Phase State Stabilization of Ammonium Nitrate for Creating an Oxidizing Agent for Smokeless Gas-Generating Formulations Yielding no Toxic Combustion Products

N. I. Golovina, G. N. Nechiporenko, G. G. Nemtsev, G. P. Dolganova, V. P. Roshchupkin, D. B. Lempert, and G. B. Manelis

Institute for Problems of Chemical Physics, Russian Academy of Sciences, Chernogolovka, Moscow oblast, Russia

Received June 19, 2006

Abstract—Methods for phase stabilization of ammonium nitrate were sought for in order to considerably expand the application area of this oxidizing agent in various-purpose self-combustible formulations, including that in a new generation of gas-generating formulations for automobile air bags. New methods for stabilization of ammonium nitrate were studied and, in particular, a search was made for organic compounds that can stabilize ammonium nitrate even at their low content. The mechanism of phase state stabilization of ammonium nitrate by compounds of this kind was examined.

DOI: 10.1134/S1070427207010053

The existence of five polymorphic modifications of ammonium nitrate (AN) and, accordingly, four phase transitions (°C): –17 (V $\rightleftarrows$ IV), +32.3 (IV $\rightleftarrows$ III), 84.2 (III $\rightleftarrows$ II), and 125.2 (II $\rightleftarrows$ I) strongly hinders use of AN in energetic formulations. This is due to the fact that the composite structure disintegrates in prolonged storage at varying temperature because of the occurrence of phase transitions with a change in volume and, as a result, articles undergo mechanical disintegration with uncontrollable changes in the combustion pattern. It is natural to find and introduce into the AN structure a minor additive that preserves AN in one of the modifications in the working temperature range, from –50 to +100°C for gas-generating formulations used in automobile air bags (AAB). Stabilizers of this kind have been found for some application areas of AN. These are potassium nitrate, ammonium sulfate, and ammonium phosphates [1, 2]. However, these stabilizers cannot be used in AAB because of the formation of condensed (which results in that a formulation ceases to be smokeless) or toxic (compounds of sulfur or halogens) combustion products. Phase state stabilizers for AN to be used in AAB should not contain any elements other than C, H, N, and O. In most cases, arbitrarily chosen additives penetrate into interblock spaces of crystallites and virtually do not affect the course of phase transitions. The only exception are minor additives of salts in which either the cation or the anion is close in volume to those in ammonium nitrate. In this case, isomorphic substitution of ions occurs in the AN lattice in cocrystallization or in fusion of salts, i.e., a substitution solid solution is formed [3]. If potassium nitrate is used as stabilizer, it should be introduced in an amount of no less than 8% [4] for reliable phase stabilization of AN at temperatures in the range from –50 to +100°C. However, the formulation ceases to be smokeless upon introduction of the potassium salt.

There are indications that AN can be stabilized with a number of organic pigments, most of which are either sulfonic acids or salts of sulfonic acids with metal cations [5]. Many of the compounds suggested contain chlorine or bromine. Only few of diazo or triphenylmethane dyes satisfy the requirements to the elemental composition, but all of these compounds were found to be inefficient in a thorough experimental analysis.

To develop a new generation of smokeless environmentally safe gas-generating formulations for AAB, we conducted a search for phase-state stabilizers for AN, based on organic compounds that contain no elements other than C, H, N, and O.

It seems attractive to stabilize AN by isomorphic introduction of an anion into the lattice. However,

the choice of anions comparable in size with the nitrate anion is extremely narrow. The anions NO_2^- and CO_3^{2-} are unacceptable because of the low stability of ammonium carbonate and nitrite. The azide, cyanate, and oxalate anions could not be introduced into the AN lattice by fusion or cocrystallization from solution, which is presumably due to the strong difference in the configurations of the anions. Only the formate anion could form isomorphous solutions in the AN lattice both in joint crystallization and in fusion [6]. An X-ray study of single crystals of a solid solution of salts demonstrated that the sample was close in composition to $2NH_4NO_3 \cdot NH_4HCO_2$. Unfortunately, the effect of introduction of the formate ion into the lattice was found to be considerably weaker than that upon substitution of the ammonium cation with potassium. The temperature of the IV $\rightarrow$ III phase transition could only be shifted by 20–30°C, which is apparently insufficient for working with composites.

An additional important way to stabilize the phase state of AN is its cocrystallization with salts or organic compounds in order to create mixed crystals or cocrystallizates. These crystals are new chemical compounds with a new lattice other than those of the starting pair of compounds and with different properties. They may exhibit no phase transitions inherent in the starting compounds or may show quite different phase transitions with widely different transition temperatures and volume changes. We found that AN does tend to form cocrystallizates, but cocrystallizates with positive oxygen balance could not be formed. In addition, all the cocrystallizates obtained have very low melting points. For example, a 1 : 1 cocrystallizate with aminotetrazole melts at 40°C. The best of all was a mixed crystal with ammonium formate of the composition $5NH_4NO_3 \cdot 3NH_4CHO_2$ [6], but it passes into the plastic state at higher temperatures. In addition, the oxygen balance of this compound is negative [this quantity is considered positive if O/(2C + 0.5H) > 1, and negative if this parameter is smaller than unity]. A search of AN cocrystallizates with organic compounds is a rather complicated task because of the necessity for obtaining a mixed crystal with a positive oxygen balance, i.e., the mass content of AN in the binary system constituted by AN and an organic compound should be commonly (depending on the oxygen balance of the latter) not smaller than 50–80%.

In this study, we examined the possibility of phase stabilization of AN by another method, with modifier substances that affect phase transformations by a mechanism different from those in the two techniques described above. In what follows we deliberately use two rather close terms "modifier" and "stabilizer." Substances of the first type affect to a certain extent the structure of AN and its phase transitions, whereas substances of the second type exert just stabilizing influence, which consists in that AN is in a smaller number of phase states in the temperature range under study. The experience gained when studying the effect of organic dyes and arenesulfonates on the phase state of AN and that acquired in a search for cocrystallizates made it possible to formulate the following principles governing the choice of substances that expectedly affect the phase state of AN, be it the true phase stabilization or only hindrance to a phase transition (i.e., transformation to the metastable state).

(1) The structure of a modifier should be close to that of AN in crystal-chemical parameters: interplanar spacings of the modifier should coincide to the maximum possible extent with those in AN itself. This should be manifested in the experiment in a nearly complete coincidence of X-ray diffraction patterns of the composite alloy and starting AN, whereas the modifier itself should be virtually not seen in the X-ray diffraction pattern at all.

(2) Additional interactions of the orbital and(or) electrostatic type, or additional hydrogen bonds except those already existing in the starting products, should appear between the atomic planes of the modifier and those of AN. Also possible is formation of a complex, with charge transfer in the solid phase. Introduction of atomic planes of the modifier into the initial lattice of AN and the additional intermolecular interaction between the ions of the starting material and modifier molecules (monitored by UV and IR spectra) distort the electrostatic field of AN and change the total energy of the structure, which leads to a significant change in the course of phase transitions in the composite material.

Thus, we had to select stabilizers by a search for molecular structures similar to that of AN. This, naturally, could be done by introducing some functional groups into certain original molecular skeletons. The choice of these latter could be rather wide, but we had to take into account the fact that the potential stabilizer should also be a combustible in a formulation for AAB, and the most acceptable compounds for accomplishing the task in hand are those with high thermal stability, comparatively low content of hydrogen, and comparatively high content of nitrogen. Therefore, we studied as starting skeletons nitrogen-containing heterorings, and especially derivatives of purine and pyrimidine bases, which well satisfy the above requirements. In the study, we oriented to com-

Table 1. Interplanar spacings d and relative intensities I_{rel} of peaks in X-ray diffraction patterns, which correspond to polycrystals of AN and modifier compounds

AN, phase IV		UA		Guanine		Barbituric acid		Isatin		Melamine cyanurate	
d, Å	I_{rel}	d, Å	I_{rel}	d, Å	I_{rel}	d, Å	I_{rel}	d, Å	I_{rel}	d, Å	I_{rel}
4.906	12.5	4.896	12.6	5.028	8.2	4.885	20.0	4.750	6.8		
3.941	28.8	3.850	12.6	3.636	8.4	3.897	8.6	3.863	5.6	4.040	47.7
3.091	69.6	3.091	13.1	3.026	8.1	3.004	100			3.171	100
2.868	7.5	2.863	5.6	2.901	7.9	2.923	19.2	2.859	10.6	2.870	3.4
2.713	100	2.795	4.6	2.788	7.8	2.666	5.5	2.727	3.0	2.692	31.4
2.480	5.9	2.422	6.3			2.429	5.9	2.458	7.0	2.471	12.7
3.377	10.0			2.306	5.9	2.308	3.5	2.368	5.1	3.369	3.9
2.256	24.0							2.268	3.9	2.291	6.8
2.243	17.6	2.244	5.8			2.242	3.4			2.238	4.1
2.088	3.1	2.096	2.5			2.046	3.1	2.070	4.4	2.069	5.4

pounds with a suitable set of functional groups; for most of the compounds we studied (>50), no evidence about their crystal-chemical parameters was available. Particular attention was given to compounds containing carbonyl, imino, amido, and amino groups, and especially the first two of these, in which both orbital interactions of the carbonyl group with the nitrate ion and formation of hydrogen bonds would be expected. We assumed that the electron density of the nitrate anion, concentrated on lone electron pairs, which are not involved in chemical bonding and occupy a higher energy position, can be donated to a vacant, lying lower in energy, orbital of the carbonyl group of the stabilizer molecule. In this case, the interacting orbitals have the same symmetry. The unique capacity of the carbonyl group as electron acceptor in molecules was reported in [7]. The natural additional conditions were at least partial solubility of a modifier in AN and absence of chemical interaction up to 160–170°C.

EXPERIMENTAL

Minor additives of substances were mostly introduced into AN by fusion at a temperature close to the melting point of AN. This method is the most efficient because the solubility of modifier substances in molten AN, as a rule, exceeds that in organic solvents and, what is more, polar solvents can compete with ammonium nitrate in formation of hydrogen bonds. The following experimental techniques were used: X-ray phase analysis (computer-controlled DRON-2 diffractometer, phase identification in transitions in the temperature range from –50 to +100°C by analysis of X-ray diffraction patterns with preliminary calculation of theoretical X-ray diffraction patterns of polycrystals of all the phases from atomic coordinates obtained in an X-ray diffraction study of single crystals), DTA (MOM derivatograph, Hungary, heating rate 0.6 deg min^{-1}), and, in some cases, studies of UV spectra on a Specord M40 spectrophotometer in the spectral range 200–900 nm and IR spectra on a Specord IR75 spectrophotometer at 4000–700 cm^{-1}.

X-ray phase studies and differential thermal analysis. As regards the influence exerted on the phase state, three groups of stabilizer substances can be distinguished: (a) the X-ray diffraction pattern of an alloy is identical to that of a mechanical mixture; (b) X-ray diffraction pattern of the alloy retains lines characteristic of each of the components being fused, but there are slight changes in the positions or relative intensities of the peaks; and (c) X-ray diffraction pattern of the alloy shows significant changes manifested in that the modifier peaks disappear or a set of entirely new peaks appears, which corresponds to the formation of a new mixed crystal. Situation (a) commonly (with rare exceptions) does not lead to changes of phase states and most frequently means that the substances are either not mixed in fusion or stratify upon cooling. Situation (b) most frequently indicates that new hydrogen bonds are formed, which undoubtedly affects the phase state of AN. However, this influence is not strong and requires introduction of considerable amounts of a modifier. Situation (c) indicates that a strong interaction occurs between the nitrate anion and modifier molecule, in addition to formation of hydrogen bonds. This is the case when the crystal-chemical parameters of the substances being fused are close and additional intermolecular interactions arise between the atomic planes of the partners. Even a new mixed crystal can be formed.

Table 1 compares the interplanar spacings in the crystal lattices of AN and most effective stabilizers

Table 2. Interplanar spacings d and relative intensities I_{rel} of peaks in X-ray diffraction patterns for AN alloys with a certain amount of UA, compared with the interplanar spacings in individual AN and UA

UA		AN, phase IV		AN + UA alloy at indicated UA content, wt %									
				10		18.9		34		42.5		85	
d, Å	I_{rel}	d, Å	I_{rel}	d, Å	I_{rel}	d, Å	I_{rel}	d, Å	I_{rel}	d, Å	I_{rel}	d, Å	I_{rel}
6.511	100					6.511	6.6	6.482	10.2	6.501	14.1	6.501	18.4
5.602	5.6							5.581	7.1	5.588	7.5	5.602	9.2
4.896	12.6	4.906	12.5	4.906	28.8	4.901	27.4	4.890	32.3	4.890	30.9	4.896	35.0
		3.941	28.8	3.945	41.1	3.938	38.7	3.931	47.0	3.938	46.0	3.934	37.2
3.850	12.6					3.844	9.6	3.837	5.9	3.848	19.0	3.847	26.9
3.581	4.1												
3.271	66.1					3.271	5.9	3.264	8.1	3.267	10.0	3.269	14.2
3.175	7.3					3.173	8.8	3.171	14.7	3.173	17.2	3.175	26.7
3.091	13.1	3.091	69.6	3.081	94.3	3.073	100	3.075	100	3.075	100	3.081	100
2.996	4.6												
2.863	5.6	2.868	7.5	2.874	12.7	2.868	12.2	2.865	16.4	2.867	17.6	2.867	22.5
2.795	4.6							2.790	7.1	2.787	7.1	2.792	10.0
		2.713	100	2.716	100	2.709	75.8	2.711	78.3	2.711	81.3	2.711	66.1
2.566	4.1					2.568	5.1	2.565	7.0	2.562	8.1	2.564	11.7
2.422	6.3	2.480	5.9	2.485	10	2.480	9.3	2.477	10	2.479	11.2	2.480	9.7
		2.377	10	2.377	14.3	2.374	10.8	2.375	10	2.375	11.1	2.375	9.6
		2.256	24	2.258	41	2.255	42.1	2.253	35	2.254	32.8	2.254	37.1
2.244	5.8	2.243	17.4	2.249	33	2.242	32	2.243	30	2.240	37.9	2.242	32.8
2.184	29.0							2.181	4.8			2.184	7.7
2.096	2.5	2.088	3.1	2.091	4.6	2.089	4.8	2.089	5.5	2.089	5.4	2.089	5.2
		1.974	3.5	1.975	5.0	1.973	5.1	1.972	5.3	1.974	6.0	1.974	5.2
		1.833	2.7										

(only those interplanar spacings in the stabilizer which coincide with the interplanar spacings in AN are given). The best coincidence of the interplanar spacings is observed for trihydroxypurine (uric acid, UA). Complete coincidence is impossible for the natural reason of differences between lattices of different compounds, but the best coincidence is necessary for obtaining a doped product. Widely known is the nearly complete coincidence of the interplanar spacings of γ-iron (high-temperature phase of iron) and iron carbide Fe_3C (cementite), whose fusion yields martensite with carbon content of less than 6.67% [8]. The nature of doping of the alloys is presumably the same for different types of substances: an additive does not form its own phase until its certain amount is introduced into the main substance. Only a minor amount of an additive can be introduced into the alloy before its presence starts to be seen in the X-ray diffraction pattern. The substance introduced into the alloy is distributed in the form of very small clusters among those crystalline blocks of AN which show coincidence of their interplanar spaces with those between similar atomic planes in the additive. Table 2 lists the interplanar spacings of alloys with varied UA content and, for comparison, full data for UA and AN crystals. The maximum amount of UA, which can be dissolved in AN without any visible indications of its presence, is about 13–15 wt %. The composition of an alloy containing 18.9 wt % UA (stoichiometry for complete burning of the composite to CO_2 and H_2O) shows presence of a minor amount of the intrinsic UA phase (Table 2). The atomic planes with coinciding interplanar spacings of the crystalline blocks of the alloy and of the constituent components show different interplanar spacings and peak intensities, compared with the starting components.

Having different mechanisms of influence on the phase states, all these compounds produce the same result. As shown by DTA measurements for AN fused with barbituric acid, melamine cyanurate, trihydroxypurine, guanine, and isatin, the V → IV transition is shifted to temperatures below –50°C, whereas in pure AN it occurs at –17°C. The IV → III transition is not

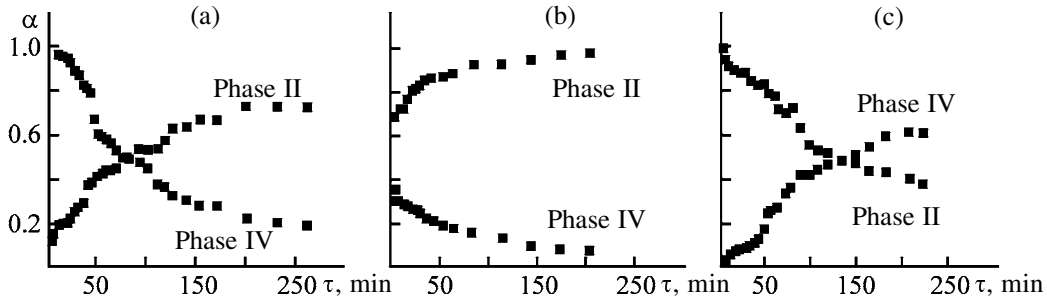

Fig. 1. Kinetics of phase transitions in an alloy of composition 90 wt % AN + 10 wt % UA. (α) Degree of conversion and (τ) time. (a) Direct transition IV → II at 53°C, (b) direct transition IV → II at 54°C, and (c) reverse transition II → IV at 46°C.

observed, phase IV directly transforms into phase II in the temperature range 45–55°C, and phase II remains stable up to 117–120°C, whereas in pure UA phase III transforms into phase II at 84.2°C. The method of quantitative X-ray phase analysis of polycrystals was used to examine the kinetics of direct and reverse IV → II transitions in an alloy containing 10 wt % UA and 90 wt % AN. The study was performed in a specially designed temperature chamber for DRON-2 diffractometer, which makes it possible to record variation of the phase ratio with time at a constant temperature. We measured the integral intensities of peaks corresponding to certain phase and then performed normalization to an internal reference. The normalized values of integral intensity, obtained at different prescribed instants of time, were related to the integral intensity at the initial instant of time. Further, we plotted kinetic curves describing the time dependence of the degree of conversion in direct and reverse transitions. To plot the kinetic curves, we followed the variation of three or four reflections in the starting and final phases. The direct transition (IV–II) was studied at two temperatures, 53 and 54°C, in the isothermal mode (Figs. 1a, 1b). At 53°C, the transition does not come to an end in 4 h. At 54°C, the transition occurs at higher rates and is complete in 3.5 h. It was shown that the conversion of phase IV into phase II occurs directly from a crystal to crystal, rather than via an intermediate state, because the sum of the initial and final phases is close to unity at any degree of conversion. The reverse transition was performed at 46°C, it occurred with a significant delay in time and temperature, and here, as also in the case of the direct transition, the sum of the initial and final phases is close to unity (Fig. 1c). Such a behavior of stabilized AN samples differs from that of pure AN, for which the transition of the initial phase to the new phase (transition IV → III and back) occurs via a certain intermediate (X-ray amorphous) state, which then forms the new phase [4]. In individual AN, a transition directly from phase IV to phase II can also be observed, and this occurs in the nearly total absence of moisture [9]. It was shown in [10, 11] that the phase transformation of a single crystal of one phase (IV) into a single crystal of another phase (II) and back is possible in the same single crystal without its disintegration. In this case, the structural transformation of phase IV into phase II reduces to a rotation of the NH_4^+ cation about the twofold axis by an angle of 90° and to an increase in the lattice constants, with the system of initial hydrogen bonds rearranged to give a new system.

When studying the stabilization of the phase state of AN, we found that the structure of, and differences between the functional groups present in the modifier molecule affect the stabilization efficiency. The strongest effect was observed in the presence of a carbonyl group and an imino group in the ring. We also observed the influence exerted by the position of the imino and carbonyl groups in the molecule. For example, AN is stabilized by isatin with neighboring carbonyl groups in the five-membered ring, whereas phthalimide, which is isomeric to isatin, but has carbonyl groups separated by an imino group, has no effect on the phase state of AN. Introduction of the electronegative nitro group enhances the effect of a substance on the phase state of AN. Below, we present, for clarity, structures of nine different substances tested as possible phase-state stabilizers for AN. In each of the six pairs of possible modifiers, the structures are closely similar, but the left-hand substance is a stabilizer, and the right-hand one is not:

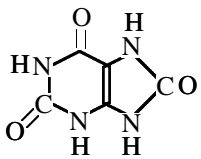

UA

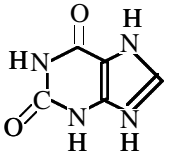

Dihydroxypurine

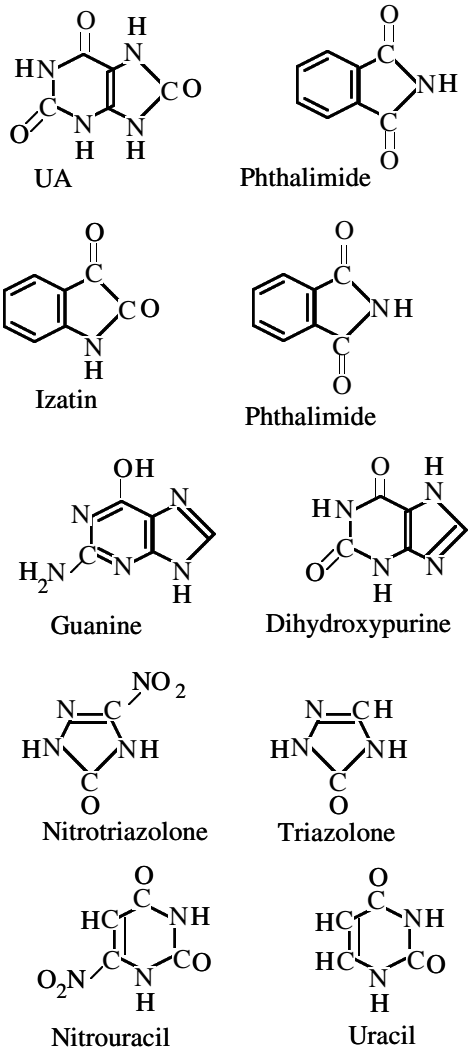

Spectral studies (UV and IR). Trihydroxypurine (UA) was found to be one of the best phase-state stabilizers for AN, and, therefore, we made an attempt to elucidate the mechanism of intermolecular interaction stabilizing this system by spectroscopic methods.

Samples for UV spectral measurements were prepared in the form of an emulsion in Vaseline oil, deposited as a thin layer on quartz plates. Samples for IR measurements were prepared as emulsions in Vaseline oil and hexachlorobutadiene (an important advantage of the latter is the absence of absorption bands in the range of vibrations of N–H bonds in the compounds under study). The emulsion was deposited as a thin layer on NaCl plates (with KBr plates, an interaction of AN with the material of the plates was observed).

The UV spectrum of AN contains a strong band peaked at ~200 nm and a weak shoulder at 222 nm, which corresponds to the $\pi \rightarrow \pi^*$ transition in the anion. The spectrum of UA exhibits three bands: the strongest band peaked at ~200 nm, the weakest broad band at 227 nm, and two overlapping medium-intensity bands at 290 and 305 nm. The UV spectrum of the alloy retains bands at ~200 and 227 nm. The bands at 290 and 305 nm, which may be associated with the $n \rightarrow \pi^*$ transition in the carbonyl groups of UA, are substantially weakened. It should be noted that a new weak band peaked at ~550 nm appears in the spectrum of the AN + UA alloy. This band can be attributed to a charge-transfer complex formed in interaction of frontier orbitals of the nitrate anion and UA molecule. The bands in the UV spectrum of the alloy, assigned to the $n \rightarrow \pi^*$ transition in the carbonyl groups, are markedly weakened, which can be attributed to donation of electron density from the highest occupied orbital of the nitrate anion to the lowest unoccupied orbital of the carbonyl group. This is possible if the orbitals are close in energy and have the same symmetry. The IR spectra of AN and UA have rather close vibration frequencies in the range of vibrations of N–H bonds, and the spectrum of the alloy has the form close to a simple sum of the spectra of the components. This means that the energetics of the systems of hydrogen bonds in AN and UA are close and remain virtually unchanged on passing to an alloy.

An unambiguous interpretation of the stabilizing action of intermolecular interaction as resulting from the appearance of charge-transfer complexes for the case of IV $\rightarrow$ II transitions in the alloy is not always possible. Presumably, the phase stabilization of alloys may result from appearance of other types of interaction between the nitrate anion and stabilizer molecule. We examined intermolecular interactions in an alloy of AN with barbituric acid (BA). Comparative analysis of the IR spectra of the starting components and the alloy reveals the disappearance of the bands at 3175 and 3080 cm^{-1}, associated with stretching vibrations of N–H bonds in barbituric acid, on passing to the alloy, which suggests that BA molecules form in the alloy a new system of hydrogen bonds. A new band at 3000 cm^{-1}, absent in the spectra of the starting components, appears in the spectrum of the alloy. The strong depression of the frequency of N–H vibrations suggests that BA molecules form in the alloy a more stable network of hydrogen bonds than the N–H···O=C network in the starting BA. At the same time, the vibration frequencies of the ammonium ion, 3125 and 3030 cm^{-1}, remain virtually unchanged on passing to the alloy. This suggests that BA molecules in the alloy mostly interact with nitrate ions. The assumption is confirmed by UV spectral data. The UV

spectrum of barbituric acid contains three broad absorption bands peaked at ~200, 220, and 256 nm. Four bands are observed in the spectrum of the alloy. The bands at ~204 and 220 nm are formed by superposition of the corresponding bands of the components. The band at 263 nm is associated with the $n \rightarrow \pi^*$ transition in the carbonyl groups of barbituric acid. Its shift to longer wavelengths (from 256 to 263 nm) is probably due to disruption of the system of hydrogen bonds N–H···O=C in the alloy. It should be noted that a new broad low-intensity absorption band appears in the UV spectrum of the alloy at 312–385 nm. This band can be attributed to a charge-transfer complex formed by the BA molecule and the nitrate ion. It should be noted, however, that bands of this kind commonly lie at longer wavelengths.

An important question is whether or not this action leads to a thermodynamically stable phase state of An or to a sufficiently stable in the course of time, but metastable state. The IV $\rightleftarrows$ II phase transition for the AN–UA system is reproduced in multiple transformations without any noticeable hysteresis. This, however, does not confirm the thermodynamic stability of the system. Upon exposure at 110°C for 400 h (standard test for thermal stability of the given class of formulations), followed by storage for a year under hermetically sealed conditions, the AN–UA alloys retain their properties. However, such a statement cannot be made for all of the systems studied. For example, AN modified with barbituric acid ceases to be phase-stabilized after the same test (400 h at 110°C).

As for AN samples stabilized with UA, cracks start to appear in compacted pellets subjected to multiple cyclic changes in temperature in a wide range only after several tens of such cycles, whereas the same pellets of a nonstabilized preparation totally disintegrate into powder after one to three cycles.

CONCLUSIONS

(1) A study of ammonium nitrate alloys with minor additions of organic substances demonstrated that compounds close to NH_4NO_3 in crystal-chemical parameters affect the phase state of ammonium nitrate.

(2) It was shown that a substance exerts a stabilizing influence on the phase state of ammonium nitrate if it contains functional groups that are involved in intermolecular interactions of orbital and electrostatic types and form new hydrogen bonds.

(3) It was determined that the most effective groups of this kind are carbonyl, amino, and imino groups, and especially those of carbimino and carbamino types. A high stabilization efficiency was observed for derivatives of purine and pyrimidine bases and similar nitrogen-containing heterocyclic compounds.

(4) Substances (trihydroxypurine, isatin, guanine, barbituric acid, etc.) that provide at a content of 2–5 wt % partial phase stabilization of ammonium nitrate were found. With these stabilizers, it exists in the temperature range from –50 to +100°C in only two phases, with a single phase transition at about 50°C, which leads to a manyfold increase in the stability of compacted samples to multiple cyclic changes in temperature.

REFERENCES

1. Campbell, A.N. and Campbell, J.R., *Can. J. Res., Sect. B*, 1946, vol. 24, pp. 93–108.
2. *Tekhnologiya ammiachnoi selitry* (Technology of Ammonium Nitrate), Moscow: Khimiya, 1978, pp. 9–20.
3. US Patent 6073438.
4. Manelis, G.B., Golovina, N.I., Lempert, D.B., et al., in *7th Int. Airbag-2004*, Karlsruhe (Germany), 2004, pp. 431–435.
5. US Patent 5723812.
6. Lempert, D.B., Nechiporenko, G.N., Golovina, N.I., et al., in *7th Int. Airbag-2004*, Karlsruhe (Germany), 2004, pp. 441–444.
7. Grier, D.L. and Streitwieser, A., *J. Am. Chem. Soc.*, 1982, vol. 104, pp. 3556–3564.
8. *Kratkaya khimicheskaya entsiklopediya* (Concise Chemical Encyclopedia), Moscow, 1963, vol. 2, p. 21.
9. Heintz, T., Reinhard, W., Hermann, M., and Teipel, U., in *6th Int. Airbag-2002*, Karlsruhe (Germany), 2002, pp. 261–2610.
10. Lucas, B.W., Ahtee, M., and Hewat, A.W., *Acta Crystallogr., Sect. B*, 1979, vol. 35, pp. 1038–1041.
11. Lucas, B.W., Ahtee, M., and Hewat, A.W., *Acta Crystallogr., Sect. B*, 1980, vol. 36, pp. 2005–2008.

ISSN 1070-4272, Russian Journal of Applied Chemistry, 2007, Vol. 80, No. 1, pp. 31–37. © Pleiades Publishing, Ltd., 2006.
Original Russian Text © M.V. Savos'kin, L.M. Kapkan, G.E. Vaiman, A.N. Vdovichenko, O.A. Gorkunenko, A.P. Yaroshenko, A.F. Popov, A.N. Mashchenko, V.A. Tkachev, M.L. Voloshin, Yu.F. Potapov, 2007, published in Zhurnal Prikladnoi Khimii, 2007, Vol. 80, No. 1, pp. 32–38.

PHYSICOCHEMICAL STUDIES OF SYSTEMS AND PROCESSES

New Approaches to the Development of High-Performance Hydrocarbon Propellants

M. V. Savos'kin, L. M. Kapkan, G. E. Vaiman, A. N. Vdovichenko, O. A. Gorkunenko, A. P. Yaroshenko, A. F. Popov, A. N. Mashchenko, V. A. Tkachev, M. L. Voloshin, and Yu. F. Potapov

Litvinenko Institute of Physical Organic and Coal Fuel Chemistry, National Academy of Sciences of Ukraine, Donetsk, Ukraine

Yangel' Yuzhnoe State Design Office, National Space Agency of Ukraine, Dnepropetrovsk, Ukraine

Received August 4, 2006

Abstract—An approach to express screening of promising hydrocarbon propellants, based on the calculation of the specific impulse of an engine from the results of quantum-chemical calculation of their heats of combustion, was suggested. The approach ensures high accuracy irrespective of the composition and structure of the compounds under consideration. Polycyclic and framework hydrocarbons with small rings were suggested as promising propellants.

DOI: 10.1134/S1070427207010065

The development of new hydrocarbon propellants for environmentally clean rockets is a priority research field, because the use of energetic propellants increases the pay load of carrier rockets and makes their launch more cost-efficient.

One of approaches to enhancing the performance of hydrocarbon propellants is increasing their density by using cyclic and framework compounds [1–7]. Such propellants are usually prepared by hydrogenation of dicyclopentadiene followed by catalytic rearrangement of the product from the *endo* to *exo* form, which is required for decreasing the melting point. Such propellants as, e.g., JP-10, RJ-4, and RJ-41 with a density of 0.94 g cm^{-3} were prepared by this procedure. With norbornane taken as starting compound, a propellant (RJ-5) with a still higher density, 1.08 g cm^{-3}, was prepared. Another way to increase the density is the condensation of dicyclopentadiene with adamantane derivatives; however, this leads to a significant increase in the melting point.

To enhance the performance of hydrocarbon propellants, their heat of combustion is increased, in particular, by using structurally strained hydrocarbons containing three- and four-membered rings [8]. These compounds contain fragments with strongly distorted C–C bond angles, which leads to appreciably larger heats of formation and hence higher heats of combustion. The suggested propellants based on 1-methyl-1,2-dicyclopropylcyclopropane [9] and dicyclobutyl [10–13] are characterized by record-breaking heats of combustion.

We believe that the use of polycyclic and framework hydrocarbons with small rings as propellants can further enhance the energy characteristics of rockets owing to high density and increased heat of combustion of such propellants.

Studies on synthesis and determination of the characteristics of new fuels require considerable expenses; therefore, it is appropriate to start searching for compounds having the required properties with the calculation of the relevant physicochemical characteristics. With the modern computers, the existing quantum-chemical methods allow quick screening of the potentially promising compounds with incommensurably lower time and money expenses compared to experimental studies. This approach also allows calculation of the characteristics of difficultly available and even hypothetical substances.

Various empirical additive schemes for calculating the heat of combustion require the knowledge of such molecular parameters as the bond energies or force constants. Additive schemes give particularly inaccu-

rate results when applied to compounds of different types, e.g., in going from normal hydrocarbons to cyclic hydrocarbons, especially those with small rings. Therefore, such calculations do not ensure the level of versatility and accuracy required for comparing the parameters of compounds with diverse chemical structures. Molecular mechanics methods suffer from the same drawback.

Since the heat of combustion of the compounds of interest varies in a relatively narrow range (10% at maximum and 2–3% in most cases), the only method giving the reliable and comparable data is direct ab initio calculation of the heat of combustion.

The overall reaction equation for the combustion of hydrocarbon propellants in oxygen at a stoichiometric component ratio,

$$C_nH_m + (n + m/4)O_2 = m/2H_2O + nCO_2, \quad (1)$$

corresponds to the real calorimetric experiment. Although the error in calculating the heat of combustion, as will be shown below, is 4–8 kJ mol^{-1} and somewhat exceeds the error of experimental determinations, the calculation accuracy attained is quite sufficient for comparing the power intensity of various hydrocarbons.

The calculations reported in this paper were performed ab initio using the GAMESS program package [14] which allows, in particular, calculation of the total energies of molecules and of the correlation and thermodynamic corrections to them. The molecular geometries were fully optimized within the framework of the restricted Hartree–Fock (RHF) method in the TZV(*d*,*p*) basis set [15] with the polarization *d* functions on the C atoms and *p* functions on the H atoms. To determine the thermochemical correction at 25°C, the harmonic vibration problem [16] was solved in the same approximation. For the molecular geometry corresponding to the total energy minimum in the TZV(*d*,*p*) basis set, the electron correlation was taken into account according to the Møller–Plesset perturbation theory (MP2) [17, 18] in a wider basis set, TZV(2*df*,2*p*). Several test calculations of small molecules showed that the geometry optimization in this basis set did not lead to appreciable decrease in the total energy. The oxygen molecule in the ground triplet state was calculated by the restricted open-shell Hartree–Fock (ROHF) method, and the MP2 electron correlation correction for this molecule was determined according to [19]. The required total energies with the MP2 correction, calculated in the TZV(2*df*,*p*) basis set (in atomic energy units) are as follows: H_2O –76.3204, CO_2 –188.3156, and O_2 –150.1218. The thermochemical corrections to their enthalpies at 25°C are 70.43, 42.80, and 20.64 kJ mol^{-1}, respectively.

The calculated heats of combustion in oxygen of saturated hydrocarbons of different chemical structures and several unsaturated hydrocarbons in the gas phase are listed in the table.

To evaluate the accuracy of calculating the heat of combustion within the framework of the above-described scheme, we calculated the total energies of aliphatic hydrocarbons for which these quantities are well-known. As follows from the table, the relative errors of the calculated heats of combustion of the homologous series of hydrocarbons (from methane to octane) are within 0.12–0.37%. Appreciably higher accuracy is attained for molecules containing small rings. In this case, the error does not exceed 0.1% and in most cases is within 0.03–0.04%. The experimental heats of combustion presented in the table refer to the gas phase.

Note that, when comparing the power intensity of various compounds, the heat of combustion is usually referred to 1 g of the combustible but not of the fuel (combustible + oxidant), which can lead to wrong conclusions when choosing the most efficient fuel. Indeed, assume that combustion of fuel of mass m results in evolution of Q J of heat. Then, neglecting the thermal dissociation of combustion products, we can determine the velocity of their outflow v from the law of energy preservation:

$$mv^2/2 = \eta Q, \quad (2)$$

where η is the engine efficiency factor.

Hence,

$$v = (2\eta H)^{1/2} \quad (3)$$

(Glushko's formula), where

$$H = Q/m \quad (4)$$

is the heat of combustion per unit mass of the fuel (J kg^{-1}), which, as seen from formula (3), is the major factor determining the outflow rate and hence the engine thrust.

Let us illustrate these reasonings by a simple example. Judging from the specific heat of combustion per kilogram of combustible h, methane is the most efficient (see table); however, its H value is relatively low, determining its moderate power characteristics as propellant. In the combustion of methane,

$$CH_4 + 2O_2 = CO_2 + 2H_2O, \quad (5)$$

Calculated heats of combustion of hydrocarbons and specific engine impulses

Compound no.	Hydrocarbon	Formula	Heat of combustion, kJ mol^{-1}		Specific heat of combustion, kJ kg^{-1}		Specific impulses,** s
			caculation	experiment*	of combustible, *h*	of fuel, *H*	
1	Methane	CH_4	797	794 [20]	49 657	9953	339.1
2	Ethane	C_2H_6	1423	1419 [21]	47 312	10 014	340.2
3	Propane	C_3H_8	2037	2040 [21]	46 184	9978	339.6
4	Butane	C_4H_{10}	2650	2658 [22]	45 595	9959	339.2
5	Octane	C_8H_{18}	5106	5112 [20]	44 696	9929	338.7
6	Dicyclobutyl		4911	4909	44 561	10 269	344.5
7	*exo*-Tetrahydrodicyclopentadiene (JP-10)		5780	5770 [5]	42 421	9893	338.1
8	Tetracyclo-[3.3.1.0^{2,4}0^{6,8}]nonane		5195	5193 [23]	43 225	10 305	345.1
9	ω-Pinene		5893	5891 [24]	43 253	10 086	341.4
10	β-Pinene		5905	5899 [24]	43 343	10 108	341.8
11	Pinane		6024		43 571	10 003	340.0
12	Tricyclo[5.2.0.0^{2,5}]-nonane I***		5347		43 754	10 240	344.0
13	Tricyclo[5.2.0.0^{2,5}]-nonane II***		5332		43 631	10 211	343.5
14	Tricyclo[5.2.0.0^{2,5}]-nonane III***		5544		45 366	10 617	350.3
15	Tricyclo[4.1.0.0^{2,4}]-heptane I***		4113	4113 [25]	43 682	10 330	345.5
16	Tricyclo[4.1.0.0^{2,4}]-heptane II***		4139		43 957	10 395	346.6
17	Tricyclo[4.1.0.0^{2,4}]-heptane III***		4623		49 096	11 610	366.3
18	Tricyclo[3.2.0.0^{2,4}]-heptane I***		4199		44 595	10 546	349.1
19	Tricyclo[3.2.0.0^{2,4}]-heptane II		4239		45 020	10 647	350.7
20	4,7,7-Trimethyltricyclo[4.1.1.0^{2,4}]octane****		6558		43 644	10 148	342.4
21	1,4,4-Trimethyltricyclo[5.1.1.0^{3,5}]octane****		6556		43 629	10 145	342.4
22	2,6-Dimethyl2ricyclo-[3.1.1.0^{3,6}]heptane		5384		44 057	10 311	345.2
23	Tricyclo[3.3.1.0]nonane		5239		42 870	10 033	340.5
24	Tricyclo[3.3.2.0]decane		5834		42 825	9987	339.7

Table. (Contd.)

Compound no.	Hydrocarbon	Formula	Heat of combustion, kJ mol^{-1}		Specific heat of combustion, kJ kg^{-1}		Specific impulses,** s
			caculation	experiment*	of combustible, h	of fuel, H	
25	Bicyclo[1.1.0]butane		2520		46592	10954	355.8
26	Tricyclo[2.1.0.0^{2,5}]-pentane		3087		46699	11262	360.7
27	Bicyclo[2.1.0]pentane		3089		45342	10574	349.5
28	Tricyclo[3.1.0.0^{2,4}]hexane		3595		44864	10696	351.6
29	Prismane		3646		46678	11462	363.9
30	Tricyclo[3.1.0.0^{2,6}]hexane		3550		44301	10561	349.3
31	Quadricyclane		4050		43956	10655	350.9
32	Cubane		4733		45439	11158	363.9
33	Spiropentane		3115		45731	10664	351.0
34	Norbornane		4139		43040	9947	339.0
35	Norbornene		4043		42936	10154	342.5
36	Norbornadiene		3968		43065	10439	347.3
37	Nortricyclene		4023		42731	10105	341.7
38	Adamantane		5720		41986	9791	336.4

* For the gas phase.
** Calculation by Glushko's formula (8) at $\eta = 0.556$.
*** Bold dots denote hydrogen atoms located over the molecular plane.
**** Because of the large molecular size, the calculations were performed in a somewhat less accurate basis set TZV(*df*,2*p*), which leads to ~1-s underestimation of the specific impulse.

the oxygen consumption is 3.9891 mass units per mass uinit of methane. Therefore, for complete combustion of methane in oxygen, we have

$$H = h/(1 + 3.9891) = 49657/4.9891 = 9953 \text{ kJ kg}^{-1}.$$

Similarly, in combustion of, e.g., dicyclobutane,

$$C_8H_{14} + 11.5O_2 = 8CO_2 + 7H_2O \quad (6)$$

the oxygen consumption is as low as 3.339 mass units per mass unit of the combustible; hence,

$$H \approx h/(1 + 3.339) = 44561/4.339 = 10269 \text{ kJ kg}^{-1}.$$

Thus, although the heat of combustion per kilogram of combustible (h) of methane, 49.657 kJ kg^{-1}, appreciably exceeds that of dicyclobutyl, 44.561 kJ kg^{-1}, methane is less efficient because of the lower heat of

combustion per kilogram of fuel (H): 9953 kJ kg^{-1} against 10 269 kJ kg^{-1} for dicyclobutyl. Note that the reasonings given here and below refer exclusively to the stoichiometric ratio of the fuel components, combustible and oxidant. Actually, to attain the maximal performance of a specific type of propellant, the optimal amounts of the oxidant are determined experimentally, and they are usually appreciably lower than the stoichiometric amount. In this case, our approach to assessing the performance of propellants can be used as a preliminary estimate.

To convert the specific heat of combustion of a hydrocarbon h to the specific heat of combustion of a fuel H, it is convenient to use a formula following from Eq. (1):

$$H = h(11.91 + x)/(43.66 + 8.936x), \quad (7)$$

where $x = m/n$ is the H/C atomic ratio in the given hydrocarbon C_nH_m.

An important conclusion follows from Eq. (7): With a decrease in the H/C ratio x in a hydrocarbon, the conversion factor from h to H increases. Thus, a propellant with a low hydrogen content can exhibit a higher specific impulse, even despite lower power intensity h per kilogram of the hydrocarbon.

By multiplying the outflow velocity of gaseous products v from formula (3) by the fuel consumption rate (kg s^{-1}), we obtain the tractive force in newtons. In the literature on rocket engines, the specific impulse p_{sp}, measured in kilogram-force (kgf) units and equal to the tractive force at a fuel consumption rate of 1 kg s^{-1}, is commonly used. Conversion of formula (3) to p_{sp} gives

$$p_{sp} = (2\eta H)^{1/2}/g, \quad (8)$$

i.e., the dimension of p_{sp} is kgf kg^{-1} s or simply s after the "cancellation" of kgf and kg, which is a common practice. The results of calculation by formula (8) are given in the table. The efficiency factor η was taken equal to 0.556 to bring the calculated and experimental [10–12] specific impulses of dicyclobutyl to coincidence; this value of η was also applied to calculate the specific impulses of all the other compounds listed in the table. Thus, the parameter η plays the role of a calibration factor taking into account, to a first approximation, the nonstoichiometric ratio of the combustible and oxidant, partial dissociation of combustion products, etc. It is assumed that these factors affect the specific impulse of the examined substances to approximately the same extent as that of dicyclobutyl.

The specific impulses given in the table range from 336.4 for adamantane to 366.3 for stereoisomer III of tricyclo[4.1.0.0^{2,4}]heptane (no. 17). Note that the specific impulses of adamantane and JP-10 propellant are close to that of kerosene, 337.9 s [10–12]. The natural terpenes α- and β-pinene present in turpentine exhibit higher specific impulse, 341.4–341.8 s. Still higher values, 345–350 s, are attained, e.g., with 2,6-dimethyltricyclo[3.1.1.0^{3,6}]heptane (no. 22), norbornadiene (no. 36), tricyclo[3.1.0.0^{2,6}]hexane (no. 30), and bicyclo[2.1.0]pentane (no. 27). Note that tetracyclo[3.3.1.-0^{2,4}0^{6,8}]nonane (no. 8) suggested in [23] as a promising aviation fuel, according to our calculations, has a specific impulse of 345.1 s, only slightly exceeding that of dicyclobutyl (344.5 s).

The highest values of the specific impulse (exceeding 350 s) are characteristic of such strained framework hydrocarbons as quadricyclane (no. 31), spiropentane (no. 33), bicyclobutane (no. 25), cubane (no. 32), tricyclo[2.1.0.0^{2,5}]pentane (no. 26), and prismane (no. 29). Many of these compounds are hypothetical and have not been synthesized up to now. The synthesis of the other compounds of this group is extremely difficult and labor-consuming, and it can hardly be realized on the commercial scale in the near future. Furthermore, such compounds have high molecular symmetry and hence should have high melting point at relatively low boiling point, which is hardly acceptable for propellants.

The three series of stereoisomers of tricyclo-[3.2.0.0^{2,4}]heptane (nos. 18, 19), tricyclo[5.2.0.0^{2,5}]-nonane (nos. 12–14), and tricyclo[4.1.0.0^{2,4}]heptane (nos. 15–17) deserve particular consideration. As seen from the table, in going from the "transoid" chair-like to "cisoid" boat-like molecular configuration, the specific impulse increases by only 0.5–1.6 s. However, a striking result was obtained with the "skewed" isomers: the specific impulse increased by 6.8 s for tricyclo[5.2.0.0^{2,5}]nonane III (no. 14) and even by 20.8 s fir tricyclo[4.1.0.0^{2,4}]heptane III (no. 17) (relative to the coresponding transoid structures). Compound no. 17 even exceeds prismane (no. 29) in the specific impulse, being a "champion" among the structures chosen.

Analysis of data in the table, taking into account the set of requirements to propellants (melting and boiling points, density, viscosity, stability, etc.) shows that the most promising for further experimental studies are terpene derivatives (nos. 20, 21) and tricycloheptanes (nos. 15–17), the more so as the raw materials for their synthesis (turpnetine oil and cyclopentadiene) are cheap and readily available.

For primary estimation of properties of potentially promising propellants, we synthesized laboratory samples of some of them. Tricyclo[4.1.0.0^{2,4}]heptane was prepared by the Simmons–Smith reaction [26] used for obtaining three-membered hydrocarbon rings. Cyclopentadiene prepared by thermal depolymerization of dicyclopentadiene was treated with methylene iodide in the presence of silver-plated zinc dust; in the process, it was smoothly converted to tricyclo[4.1.0.0^{2,4}]heptane:

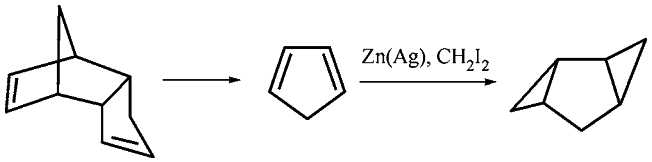

The product was identified by ^{1}H NMR spectroscopy as transoid stereoisomer I of tricyclo[4.1.0.0^{2,4}]-heptane (no. 15); its calculated specific impulse is 345.5 s. The compound synthesized has a density of 0.908 g cm^{-3} (0.8912 according to [25]); its freezing point is below –103°C, and the boiling point is 104°C (103°C [25]). Unfortunately, the other stereoisomers (nos. 16, 17) were not detected in the product.

Apparently, the purposeful synthesis of highly strained stereoisomers like nos. 14 and 17 requires a higher level of preparative organic chemistry. Such a synthesis may involve the use of coordinating matrices or catalysts ensuring formation and preservation of the required strained steric configuration.

For chemical modification of natural terpenes, it appeared feasible to use a two-step synthesis scheme involving addition of dichlorocarbene to the double bond of the substrate under phase-transfer conditions (with triethylbutylammonium chloride, TEBAC, as phase-transfer catalyst), followed by reductive dehalogenation of the intermediate product with sodium in liquid ammonia. This scheme is preferable over the Simmons–Smith reaction because of the availability of the reagents and solvents and high yield and purity of the products.

With α-pinene used as precursor, this scheme leads to 4,7,7-trimethyltricyclo[4.1.1.0^{2,4}]octane (no. 20) whose calculated specific impulse is 342.4 s:

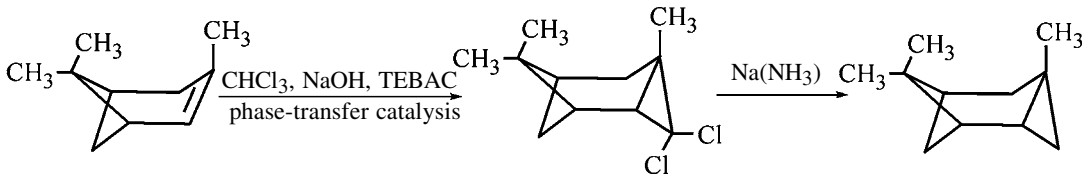

and from carene, 1,4,4-trimethyltricyclo[5.1.0.0^{3,5}]octane (no. 21) having the same specific impulse is obtained:

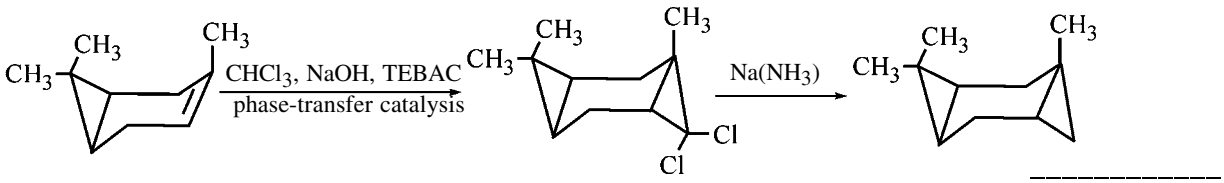

Since the above-described two-step synthesis with individual turpentine components occurs very smoothly and with high product yields, we made an attempt to use as starting reagent turpentine oil, a multicomponent mixture of natural terpenes. By so doing, we obtained a propellant with a density of 0.882 g cm^{-3}, freezing point below –90°C, and boiling onset point of 186°C. The expected specific impulse should be 342–343 s.

CONCLUSIONS

(1) Evaluation of the specific impulse of a rocket engine, based on quantum-chemical calculation of the heat of combustion of hydrocarbon propellants, is an efficient approach to their express screening. This approach ensures high accuracy when applied to hydrocarbons of diverse compositions and structures.

(2) The use of polycyclic and framework hydrocarbons with small rings as propellants can ensure further enhancement of the power characteristics of rocket engines due to high densities and high heats of combustion of such compounds.

(3) The power characteristics of strained polycyclic hydrocarbons essentially depend on their steric configuration. For example, the stereoisomers of tricyclo[4.1.0.0^{2,4}]heptane differ in the specific impulse by more than 20 s.

(4) Strained polycyclic and framework hydrocarbons selected according to the calculation results were synthesized by addition of carbenes to double bonds of natural terpenes and cyclopentadiene. The products obtained exhibit increased specific umpulse and density; they also meet other requirements to propellants.

REFERENCES

1. Burdette, G.W., *AIAA Pap.*, 1978, no. 267, pp. 1–6.
2. Burdette, G.W., Landert, H.R., and McCoy, J.R., *J. Energy*, 1978, vol. 5, no. 2, pp. 289–292.
3. Burdette, G.W., Landert, H.R., and McCoy, J.R., *Raketn. Tekh. Kosmonavt.*, 1978, vol. 16, no. 11, pp. 157–161.
4. Winter, F.H. and James, G.S., *Acta Astronaut.*, 1995, vol. 35, no. 9–11, pp. 677–698.
5. Bratkov, A.A., Seregin, E.P., Gorenkov, A.F., et al., *Khimmotologiya raketnykh i reaktivnykh topliv* (Chemistry and Power Characteristics of Propellants and Jet Fuels), Moscow: Khimiya, 1987.
6. Bol'shakov, G.F., *Khimiya i tekhnologiya komponentov zhidkogo raketnogo topliva* (Chemistry and Technology of Components of Liquid Propellants), Leningrad: Khimiya, 1983.
7. Chung, H.S., Chen, C.H.S., Kremer, R.A., et al., *Energy Fuels*, 1999, vol. 13, no. 3, pp. 641–649.
8. Grigor'ev, A.A., Flid, V.R., and Belov, A.P., *Katal. Neftekhim.*, 2001, no. 8, pp. 26–35.
9. RF Patent 2233385.
10. RF Patent 2146334.
11. WO Patent Appl. 00/06883.
12. US Patent 6415596.
13. RF Patent 2175212.
14. Schmidt, M.W., Baldridge, K.K., Boatz, J.A., et al., *J. Comput. Chem.*, 1993, vol. 14, no. 5, pp. 1347–1365.
15. Dunning, T.H., *J. Chem. Phys.*, 1971, vol. 55, no. 2, pp. 716–723.
16. Boatz, J.A. and Gordon, M.S., *J. Phys. Chem.*, 1989, vol. 93, no. 5, pp. 1819–1826.
17. Møller, C. and Plesset, M.S., *Phys. Rev.*, 1934, vol. 46, no. 7, pp. 618–622.
18. Pople, J.A., Binkley, J.S., and Seeger, R., *Int. J. Quantum Chem. Symp.*, 1976, vol. 10, pp. 1–19.
19. Lee, T.J. and Jayatilaka, D., *Chem. Phys. Lett.*, 1993, vol. 201, nos. 1–4, pp. 1–10.
20. *Khimicheskaya entsiklopediya* (Chemical Encyclopedia), Knunyants, I.L., Ed., Moscow: Bol'shaya Ross. Entsiklopediya, 1992, vol. 3.
21. *Spravochnik khimika* (Chemist's Handbook), vol. 1: *Obshchie svedeniya: Stroenie veshchestv. Svoistva vazhneishikh veshchestv. Laboratornaya tekhnika* (General Information: Structure of Substances. Properties of the Most Important Substances. Laboratory Techniques), Moscow: Khimiya, 1962.
22. *Khimicheskaya entsiklopediya* (Chemical Encyclopedia), Knunyants, I.L., Ed., Moscow: Bol'shaya Ross. Entsiklopediya, 1988, vol. 1.
23. Bol'shakov, G.F., *Vopr. Aviats. Khimmotol.* (Kiev), 1980, pp. 59–61.
24. Hawkins, J.E. and Eriksen, W.T., *J. Am. Chem. Soc.*, 1954, vol. 76, no. 10, pp. 2669–2671.
25. Pimenova, S.M., Vogel, L., Kozina, M.P., et al., *Zh. Obshch. Khim.*, 1974, vol. 44, no. 6, pp. 1383–1385.
26. Wittig, G. and Winberg, F., *Chem. Ber.*, 1964, vol. 97, no. 8, pp. 2146–2164.

ISSN 1070-4272, Russian Journal of Applied Chemistry, 2007, Vol. 80, No. 1, pp. 38–41. © Pleiades Publishing, Ltd., 2006.
Original Russian Text © K.N. Semenov, O.V. Arapov, A.K. Pyartman, V.A. Keskinov, V.V. Lishchuk, N.A. Charykov, N.I. Alekseev, 2007, published in Zhurnal Prikladnoi Khimii, 2007, Vol. 80, No. 1, pp. 39–42.

PHYSICOCHEMICAL STUDIES OF SYSTEMS AND PROCESSES

Polythermal Solubility of Fullerenes in Higher Isomeric Carboxylic Acids

K. N. Semenov, O. V. Arapov, A. K. Pyartman, V. A. Keskinov, V. V. Lishchuk, N. A. Charykov, and N. I. Alekseev

St. Petersburg State University, St. Petersburg, Russia
Innovations of Leningrad Institutes and Enterprises Closed Joint-Stock Company, St. Petersburg, Russia
St. Petersburg State Technological Institute (Technical University), St. Petersburg, Russia

Received July, 25, 2006

Abstract—The solubility of individual fullerenes C_{60} and C_{70} and a fullerene mixture enriched in higher fullerenes (C_{60} 38.8, C_{70} 33.0, $C_{76–78}$ 5.6, C_{84} 8.6, C_{90} 2.6, and C_{96} 3.3%) in higher isomeric carboxylic acids was studied within the 20–80°C temperature range; the corresponding solubility polytherms are presented.

DOI: 10.1134/S1070427207010077

This paper continues our previous studies [1] and deals with the solubility polytherms of individual fullerenes (C_{60} and C_{70}) and a mixture enriched in higher fullerenes (C_{60} 38.8, C_{70} 33.0, $C_{76–78}$ 5.6, C_{84} 8.6, C_{90} 2.6, and C_{96} 3.3%) in higher isomeric carboxylic acids (HICA). Such information is of interest for developing efficient methods of fullerene separation and enrichment.

The development of a process for the extraction separation and purification of fullerenes (mainly C_{60} and C_{70}) [2] based on the difference in their solubility in aromatic solvents becomes important for prechromatographic enrichment. Experimental data on solubility polytherms, quite necessary for this purpose, are very limited [3–9] for binary systems C_{60} or C_{70}–solvent (aromatic as benzene, toluene, *o*-xylene, 1,2-dichlorobenzene and nonaromatic as CCl_4, hexane, etc.) and are virtually lacking for more complex systems, e.g., two fullerenes in one solvent, or one fullerene in a binary solvent, etc. In particular, there are no data on the solubility polytherms for the most important ternary systems C_{60}–C_{70}–solvent. The solubility diagrams of the C_{60}–C_{70}–toluene system at 25°C and C_{60}–C_{70}–*o*-xylene system at 80°C, that we reported in [1], are the only exception.

Analysis of data on solubility of individual fullerenes (C_{60}, C_{70}) in organic solvents revealed the following features [4, 7, 8, 10–13]:

(1) Solubilities of C_{60} and C_{70} are of one order, but can be several times different. Exactly the difference in the solubilities can underlie the most efficient method of fullerene separation.

(2) Fullerenes are practically insoluble in polar solvents and poorly soluble in acyclic saturated hydrocarbons (they are the more soluble, the greater the number of carbon atoms in solvent molecule); this indicates insufficient role of the solvation mechanism of dissolution.

(3) The maximal solubility of fullerene is observed in solvents whose specific enthalpy of solution related to the volume of solvent molecule is close to the corresponding value of the fullerene molecule. Aromatic hydrocarbons and their derivatives can be examples of such solvents.

The influence of external parameters (e.g., temperature) on the solubility is manifested differently for individual fullerenes. This can be illustrated by the corresponding polytherms [4, 8, 13]. In contrast to C_{70}, for C_{60} the temperature dependence of the solubility in a series of solvents (CS_2, *o*-xylene, toluene, etc.) is nonmonotonic with its descending branch being due to the thermal decomposition of associates (C_{60} solvates) accompanied by an increase in the energy of fullerene interaction with solvent molecules and, correspondingly, by the shift of the phase equilibrium in direction to the solid phase. In [14], an anomalous effect of a sharp increase in the solubility of C_{60} with increasing pressure at 298.2 K was observed, although the solubility usually decreases for molecular crystals. Such a substantial difference in

dependences of the solubilities on the external conditions demonstrates complex character of solubility of fullerenes as a phenomenon and, in particular, the existence of various competitive mechanisms of their dissolution.

In this study, we used a mixture of α,α'-branched higher isomeric carboxylic acids with C_9–C_{11} carbon chains (HICA) as a fullerene solvent. It should be noted that the dissolving power of HICA only weakly depends on the size of the hydrocarbon substituent in the acid molecule. Therefore, in practice, in particular, in separation of rare-earth metals, mixtures of organic acids rather than individual acids are usually used [15].

EXPERIMENTAL

The following reagents were used in the study: fullerenes C_{60} and C_{70} of 99.9 and 99 wt % purity, respectively, with the content of the main determinable impurities (C_{70} in C_{60} and C_{60} in C_{70}) of about 0.1 wt %; a fullerene mixture enriched in higher fullerenes (C_{60} 38.8, C_{70} 33.0, $C_{76–78}$ 5.6, C_{84} 8.6, C_{90} 2.6, and C_{96} 3.3%) produced by ILIP Closed Joint-Stock Company (St. Peresburg, Russia); analytically pure grade *o*-xylene; and a technical mixture of higher isomeric carboxylic acids HICA.

HICA was purified by repeated washing with hydrochloric acid to remove metals. *o*-Xylene purity was monitored spectrophotometrically and refractometrically (with an IKR-20 refractometer; $n^{20} = 1.5054$).

The solubility was measured within the 20–80°C temperature range by an isothermal saturation method. Initially, solutions of C_{60}, C_{70}, and fullerene mixture in HICA were prepared (substantial excess of fullerene was taken in all cases). Then solutions were subjected to saturation in a temperature-controlled shaker (thermostating error ±0.05°C) for 8–10 h at each temperature. Preliminary experiments showed that this time was sufficient to attain the phase equilibrium in the HICA–fullerene system. The solution was separated from the precipitate by filtration through a Schott filter with a porosity of 16.

The C_{60} and C_{70} concentrations after each step of saturation were determined spectrophotometrically on a Specord-32 spectrophotometer at λ 335.5 and 472.0 nm. Aliquots of C_{60}, C_{70}, and fullerene mixture in HICA were taken and then diluted with *o*-xylene. Pure HICA diluted with *o*-xylene to the same degree as for fullerene solution in HICA was used as a reference solution. This procedure is dictated by substantial difficulties in recovery of fullerenes from HICA for subsequent analysis, in particular, due to high HICA boiling point of about 250°C. The fullerene concentrations were calculated using empirical equations for solutions in *o*-xylene [16]:

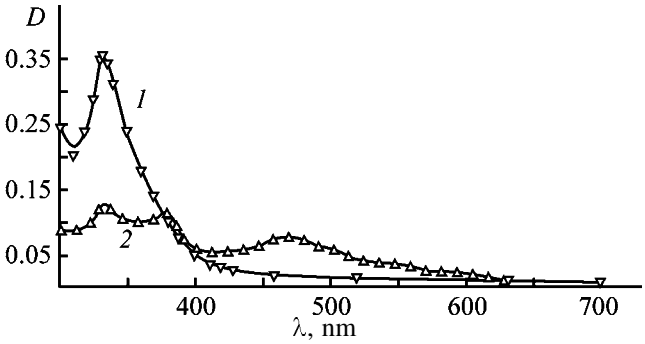

Fig. 1. Optical spectra in HICA of individual fullerenes (*1*) C_{60} and (*2*) C_{70}. Concentration of C_{60} 0.083 g l^{-1}, dilution with *o*-xylene 1 : 21; concentration of C_{70} 0.16 g l^{-1}, dilution with *o*-xylene 1 : 15; reference solution: HICA in *o*-xylene with the same dilution. (*D*) Optical density and (λ) wavelength; the same for Fig. 2.

$$c(C_{60}) = 13.10(D_{335} - 1.808D_{472}), \quad (1)$$

$$c(C_{70}) = 42.51(D_{472} - 0.0081D_{335}), \quad (2)$$

where D_{335} and D_{472} are optical densities of solutions referred to a solution thickness of 1 cm, and $c(C_{60})$ and $c(C_{70})$ are the concentrations of the corresponding fullerenes (mg l^{-1}).

The concentration of the fullerene mixture enriched in higher fullerenes after each step of saturation was performed by HPLC on a LYuMAKhROM liquid chromatograph (LUMEX, St. Petersburg, Russia) with detection through light absorption at λ 254 nm [17].

The electronic absorption spectra of solutions of individual fullerenes and enriched fullerene mixture in HICA are shown in Figs. 1, 2. In these spectra, solvatochromic effects (sharp change in the optical spectrum at moderate change in the solution concentration or solvent composition) characteristic of two-component mixtures (acetonitrile–toluene, benzene–methanol, benzene–hexane, etc.) and suggesting tendency toward formation of fillerene clusters [18] do not appear. Thus, fullerene solutions in HICA are similar to solutions in aromatic solvents (*o*-xylene, benzene, toluene, *o*-dichlorobenzene). This justifies the use of empirical equations (1) and (2) in this case. Such insensitivity of the absorption spectrum of fullerenes at λ = 335 nm to the solvent is observed only for dilute solutions, whereas for λ = 472 nm it is also observed in substantially more concentrated solutions.

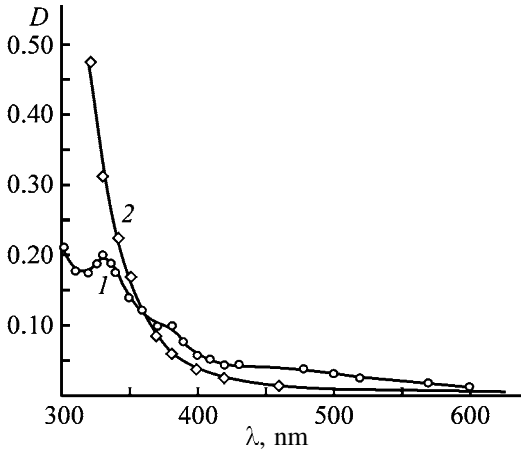

Fig. 2. Optical spectra of (*1*) the mixture enriched in higher fullerenes (C_{60} 38.8, C_{70} 33.0, $C_{76–78}$ 5.6, C_{84} 8.6, C_{90} 2.6, and C_{96} 3.3%) in HICA and (*2*) HICA. Fullerene concentration 0.168 g l^{-1}, dilution with *o*-xylene 1 : 51, reference solution: HICA in *o*-xylene with the same dilution. HICA in *o*-xylene (dilution with *o*-xylene 1 : 21, comparison solution is *o*-xylene).

The measured polytherms of fullerene solubility in HICA are shown in Figs. 3a–3c.

The curve of C_{60} solubility in HICA (Fig. 3a) is characterized by the initial sharp increase in the solubility followed by gradual saturation. Such type of the solubility polytherm shows that in this case nonsolvated fullerene C_{60} is the equilibrium solid phase [8].

The curve shape in Fig. 3b is characteristic for C_{70} (monotonic increase in the solubility) and is in good agreement with reference data [8] on solubility polytherms in solutions in *o*-xylene, toluene, and CS_2.

An attention is paid to lower solubility of C_{60} as compared to C_{70} (by a factor 3) in HICA, which is caused by higher polarizability of the latter due to lower symmetry of the molecular structure. Let us consider the character of intermolecular interactions in the HICA–C_{70} system. In this case, only induction and dispersion components contribute to the intermolecular interactions (polar molecular–nonpolar molecule) [19]: $U(r) = U_{ind} + U_{disp}$. The dispersion forces appear due to fast fluctuations of the electron density in the molecule, inducing an electric moment in the neighbouring molecule; this results in interaction between atoms. Induction forces are caused by polarization of C_{70} molecule in the electric field of the HICA molecule having a permanent dipole moment. As a result, the method for the prechromatographic separation of fullerenes, based on the above-found difference in the solubility of the individual fullerenes, can be suggested.

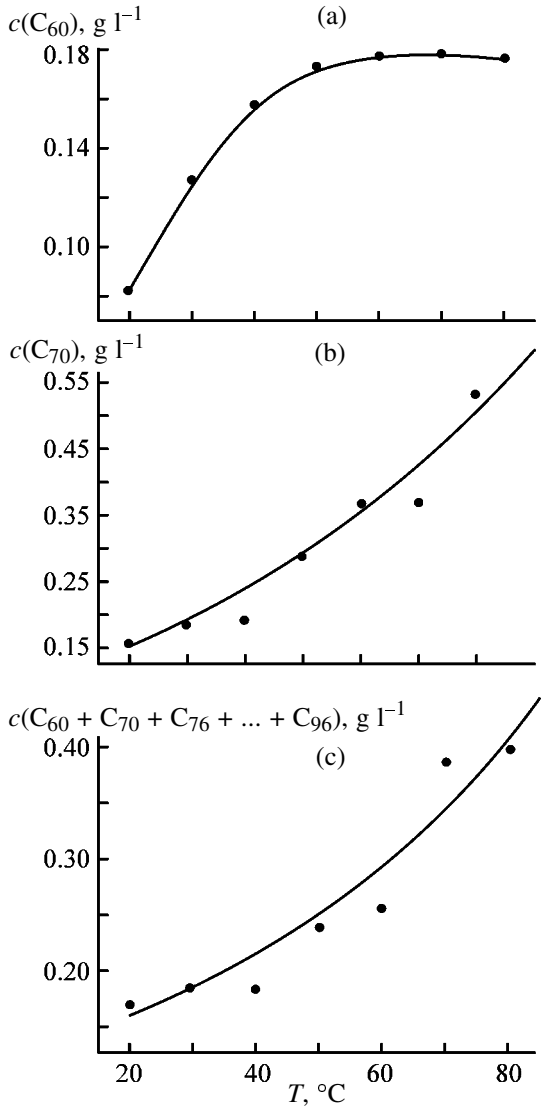

Fig. 3. Polytherm of solubility in HICA of (a) C_{60}, (b) C_{70}, and (c) C_{60} 38.8, C_{70} 33.0, $C_{76–78}$ 5.6, C_{84} 8.6, C_{90} 2.6, and C_{96} 3.3%. (*c*) Fullerene concentration and (*T*) temperature.

CONCLUSIONS

(1) Solubility polytherms of fullerenes C_{60} and C_{70} and of the mixture containing C_{60} 38.8, C_{70} 33.0, $C_{76–78}$ 5.6, C_{84} 8.6, C_{90} 2.6, and C_{96} 3.3% in a mixture of higher isomeric carboxylic acids were measured and characterized within the 20–80°C temperature range.

(2) Comparatively high solubility of light fullerenes in higher isomeric carboxylic acids was found. It monotonically increases with temperature to ~0.5 g per liter of acid at 80°C.

(3) Suitability of higher isomeric carboxylic acids

as solvents in prechromatigraphic separation of light fullerenes was demonstrated.

ACKNOWLEDGMENTS

The study was financially supported by the Federal Target Scientific and Technical Program "Research and Development in Priority Directions of Science and Engineering during the Years 2002–2006" (State Contract 02.467.11.7005, May 23, 2005).

REFERENCES

1. Arapov, O.V., Aksel'rod, B.M., Pronkin, A.A., et al., *Zh. Prikl. Khim.*, 2003, vol. 76, no. 1, pp. 35–38.
2. Arapov, O.V., Charykov, N.A., Semenov, K.N., et al., *Russ. J. Appl. Chem.*, 2006, vol. 79, pp. 201–205.
3. Ruoff, R.S., Tse, D.S., Malhorta, R., et al., *Nature*, 1993, vol. 362, no. 6416, pp. 140–141.
4. Ruoff, R.S., Malhorta, R., Huestis, D.L., et al., *J. Phys. Chem.*, 1993, vol. 97, pp. 3379–3383.
5. Xu, Z.D., Chen, W.X., Wu, J., et al., *Chin. Sci. Bull.*, 1994, vol. 39, no. 16, pp. 1347–1350.
6. Chen, W.X. and Xu, Z.D., *Fullerene Sci. Technol.*, 1998, vol. 6, no. 4, part 1, pp. 695–705.
7. Heyman, D., *Carbon*, 1996, vol. 34, no. 5, 627–631.
8. Bezmel'nitsyn, V.N., Eletskii, A.V., and Okun', M.V., *Usp. Fiz. Nauk*, 1998, vol. 168, no. 11, pp. 1195–1218.
9. Bezmel'nitsyn, V.N., Eletskii, A.V., and Stepanov, B.V., *Zh. Fiz. Khim.*, 1995, vol. 69, no. 4, pp. 735–738.
10. Ajie, H., Alvazer, M.M., Anz, S.J., et al., *J. Phys. Chem.*, 1990, vol. 94, pp. 8630–8633.
11. Sivarman, N., Dhamodaran, R., Kallippan, I., et al., *J. Org. Chem.*, 1992, vol. 57, pp. 6077–6079.
12. Meier, M.S. and Selegue, J.P., *J. Org. Chem.*, 1992, vol. 57, pp. 1924–1926.
13. Jan-Chan Huang, *Fluid Phase Equil.*, 2005, vol. 237, pp. 186–192.
14. Sawamura, S. and Nobuyuki, F., *Chem. Phys. Lett.*, 1999, vol. 299, no. 2, pp. 177–179.
15. Korpusov, G.V., Korpusova, R.D., Vaks, G.L., and Patrusheva, E.N., *Zh. Neorg. Khim.*, 1969, vol. 14, pp. 1912–1916.
16. Ponomarev, N., Yudovich, M.E., Charykov, N.A., et al., *Opt. Spectrosc.*, 2000, vol. 88, no. 2, pp. 195–197.
17. *GOST* (State Standard) *MVI-0128–2004: Method of Measurement of Weight Concentration of Fullerenes C_{60}, C_{70}, and Superheavy Fullerenes by High-Performance Liquid Chromatography*, St. Petersburg: VNII Metrologii im. D.I. Mendeleeva, 2004.
18. Ghosh, H.N., Sapre, A.V., and Mittal, J.P., *J. Phys. Chem.*, 1996, vol. 100, pp. 9439–9443.
19. Prigogine, I. and Defay, R., *Chemical Thermodynamics*, London: Longmans, 1954.

ISSN 1070-4272, Russian Journal of Applied Chemistry, 2007, Vol. 80, No. 1, pp. 42–47. © Pleiades Publishing, Ltd., 2006.
Original Russian Text © O.V. Surov, M.I. Voronova, A.G. Zakharov, 2007, published in Zhurnal Prikladnoi Khimii, 2007, Vol. 80, No. 1, pp. 43–48.

PHYSICOCHEMICAL STUDIES OF SYSTEMS AND PROCESSES

Application of the Effusion Technique to Water Sorption on Cellulose

O. V. Surov, M. I. Voronova, and A. G. Zakharov

Institute of Chemistry of Solutions, Russian Academy of Sciences, Ivanovo, Russia

Received April 26, 2006

Abstract—Equilibrium vapor pressure of water over mechanically and chemically treated cellulose is determined by the effusion method at 298, 303, and 308 K. Thermodynamic characteristics of water desorption from cellulose are determined.

DOI: 10.1134/S1070427207010089

Currently a great body of experimental data has been gained on the interaction of cellulose with water [1–5]. It is commonly accepted that only amorphous domains in the cellulose structure are involved in this interaction. Furthermore, the thermodynamic state of sorbed water differs from that in the bulk of the liquid, which is reflected in, e.g., decrease in the diffusion coefficient, spin–spin relaxation time, and freezing temperature [6]. This difference was also confirmed by the model calculations of the structure and properties of water in thin layers and small volumes [7]. It was demonstrated that the change in the characteristics of water in limited volumes is caused primarily by rearrangement of the hydrogen bonds. In small pores and capillaries (<50 Å in diameter), water cannot take the structure typical of bulk liquid water. The computer simulation data [7] show that, in thin films with a thickness well comparable with the diameter of the water molecules, disjoining pressure oscillations occur, playing the role of a hydration pump.

Cellulose-bound water may considerably influence the properties of cellulose-based materials, e.g., medical products. Therefore, it is important to know how various methods of mechanical treatment (crushing) influence the sorption properties of cellulose, what amount of water is sorbed or desorbed at various relative humidities and temperatures, and, at last, what is the thermodynamic state of cellulose-bound water in relation to the moisture content.

The goal of this study is to develop an accurate and time-saving method for determination of the equilibrium water vapor pressure over cellulose.

EXPERIMENTAL

Desorption of water from mechanically and chemically treated cellulose was studied using the effusion technique. Sulfite cellulose [TU (Technical Specifications) 5411-003-0025-3497–94] was mechanically treated on an extruder or shock-reset machine. The chemical treatment involved hydrolysis of cellulose for 2 h at 365 K in 10% HNO_3. As known, using the effusion technique, desorption isotherms of solvents can be obtained over the entire range of the relative vapor pressure at low time consumption. In this study, this technique was used to examine water desorption from cellulose materials.

Determination of the vapor pressure by the Knudsen's effusion technique is based on measuring the vapor effusion rate from a cell to a vacuum through an orifice in the membrane [8]. A great diversity in design characteristics of the existing effusion installations originates from a wide spectrum of research objectives. In our case, the design criteria were maximal simplicity and availability of equipment in combination with high precision and reproducibility of results. The experimental effusion installation was designed on the platform of a VOU-1A vacuum unit providing the residual pressure in the system no higher than 1×10^{-4} mm Hg. A cylindrical effusion cell (4 cm^3 in volume) was placed in an electric furnace. The temperature of the cell was controlled to within 0.1 K using a thermocouple assembly and a TRM-34 double-circuit thermoregulator. Additionally, the effusion cell was equipped with an electromagnetic valve hermetically closing the effusion hole until the desired temperature was attained. A cellulose sample (~100 mg), vacuum-dried at 338–343 K to constant weight, was wetted in a glass ampule with a small portion of distilled water (on the basis of 500 mg of water per gram of cellulose) and placed in the effusion cell. The cell was hermetically sealed, weighed, and allowed to stand in an air bath oven at the temperature of the

planned effusion experiment for at least 24 h. The cell was placed in a furnace heated to the desired temperature; the system was evacuated and allowed to stand at the preset temperature for at least 120 min. Then the orifice was opened, and the effusion experiment started. After completion of the experiment, the orifice was closed; the system was filled with air, and the ampule with the sample was weighed again. From the weight loss, effusion time, and temperature, we estimated the vapor pressure by the Knudsen equation:

$$P_k = (\Delta m/\alpha\beta S_h\tau)(2\pi RT/M)^{1/2}, \quad (1)$$

where Δm is the weight loss through effusion; α, condensation coefficient; S_h, orifice area; β, Clausing coefficient characterizing the resistance to mass transfer; τ, effusion time; R, gas constant; T, temperature; and M, molecular weight of the substance.

Following [9, 10], we used naphthalene and benzoic acid as reference compounds. The requirements to reference compounds for calorimetry of vaporization (availability, usability, high purity, and safety) essentially coincide with those to reference compounds for calorimetry of other processes such as combustion and dissolution. However, in calorimetric study of vaporization, it is needed to have quite a set of such compounds with the vapor pressures ranging over a broad interval, insofar as the fact that the method provides accurate results in a certain temperature range by no means guarantees the same accuracy over another temperature range. Many researchers prefer naphthalene, because, like other aromatic compounds, it can be quite easily purified using such methods as recrystallization, sublimation, zone melting, directional crystallization, and chromatography. Using these methods allows reduction of foreign impurities, e.g., anthracene, by several orders of magnitude. Benzoic acid is also often used as a reference. It was recommended by IUPAC, as having well-defined and reproducible melting and evaporation points.

In this study, benzoic acid (mp 395.5 K) and naphthalene (calorimetrically pure grade, mp 353.43 K) were further purified using fractional sublimation in a high vacuum. The middle fraction was used for making calibrations. Calibration with naphthalene was carried out over the temperature range from 298 to 318 K at an effective orifice area ($S_{eff} = \beta S_h$) of 2.21×10^{-7} and 2.7×10^{-8} m^2; and by benzoic acid, from 323 to 348 K at S_{eff} 8.48×10^{-7} and 2.21×10^{-7} m^2. We used a specially designed tool, which allowed making regularly round-shaped effusion holes up to 0.01 mm in diameter in 0.1-mm Al foil. The orifice areas were measured microscopically at a magnification of 200. The Clausing coefficient β was estimated as recommended in [8]. The experimental heats of sublimation of naphthalene and benzoic acid (72.4 ± 0.6 and 89.8 ± 0.7 kJ mol^{-1}, respectively) were well consistent with the recommended values [9, 10].

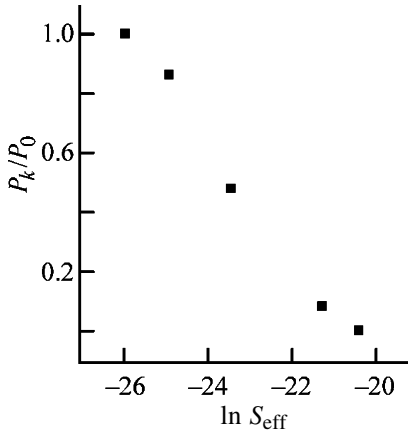

Fig. 1. Water vapor pressure in the Knudsen cell as a function of the effective area of the effusion hole ($S_{eff} = \beta S_h$) at 298 K. (P_k) Vapor pressure estimated by the Knudsen equation (1) and (P_0) saturated vapor pressure at 298 K.

Despite the advantage of the effusion technique, as a time-saving method, over, e.g., the isopiestic method, it has some limitations. It is well known that the applicability of the effusion method is limited to a pressure of 10 Pa and an effusion hole radius of 1 mm. This is caused by the fact that the condition of molecular flow is met if the free path of the molecules in the effusion cell significantly exceeds the hole diameter. However, there are examples in the literature for the application of the effusion technique to measuring pressures considerably exceeding 10 Pa. In these cases, various corrections should be introduced to take into account the deviation from the molecular flow mode. Furthermore, it was demonstrated in [8, 9] that, at a sufficiently small diameter of the effusion hole, all the limitations of the method, originating from the effusion mode deviation from the molecular flow, are eliminated; the condensation coefficient α becomes equal to unity, and the measured vapor pressure no longer depends on the effusion hole area and can be accepted equal to the true saturated vapor pressure.

Figure 1 shows the water vapor pressure estimated by the Knudsen equation (1), as influenced by the effusion hole size (at $\alpha = 1$). As seen, with decreasing orifice area, the estimated vapor pressure approaches the true value. Therefore, for the effusion cell used in this study, the estimated water vapor pressure corre-

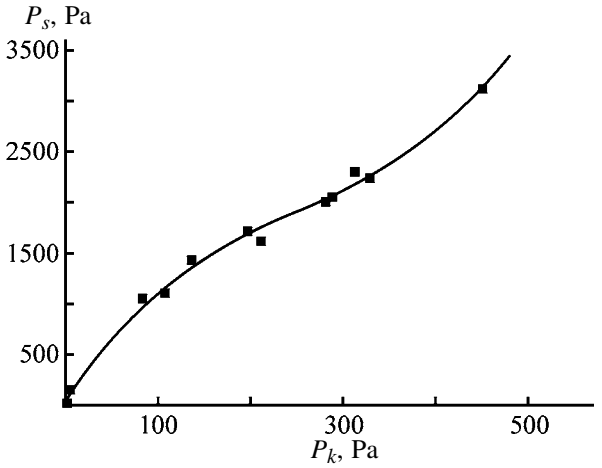

Fig. 2. Calibration curve for determination of the true water vapor pressure P_s from the experimental P_k values obtained using the effusion technique at 298 K.

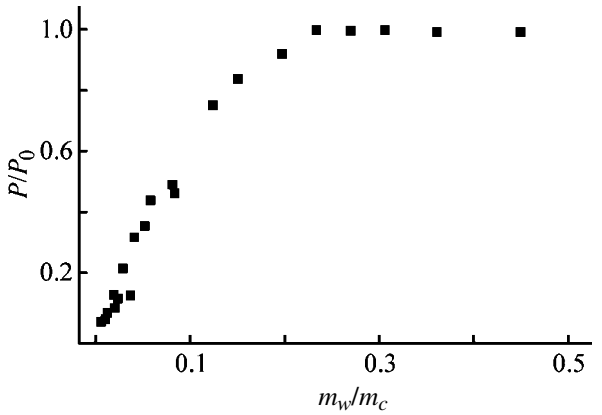

Fig. 3. Primary data obtained in the effusion experiment on desorption of water from cellulose sample I at 298 K. (m_w/m_c) Water content in cellulose and (P/P_0) relative vapor pressure of water.

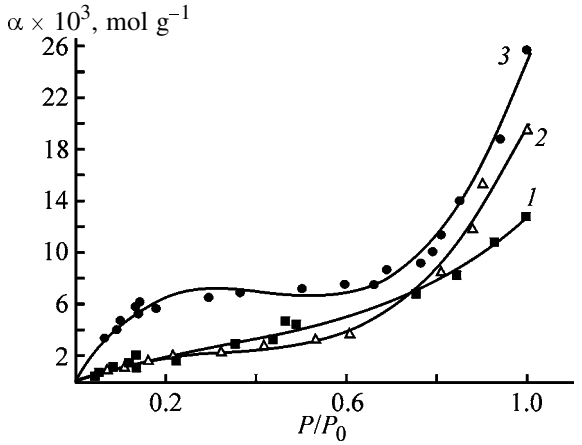

Fig. 4. Water desorption isotherms from cellulose samples (*1*) I, (*2*) II, and (*3*) III at 298 K. (a) Equilibrium sorption of water on cellulose and (P/P_0) relative vapor pressure of water; the same for Fig. 5.

sponds to the true value at a hole diameter of about several hundredth parts of millimeter and smaller. At such a small size of the effusion hole, the sensitivity of the method, and, therefore, its accuracy, decrease.

Therefore, there are certain difficulties in using the effusion method for studying water desorption over a wide pressure range. First, the correction factors used to take into account the deviation from the molecular flow mode are empirical, being dependent on the investigated system and the design of the effusion cell. Second, decrease in the orifice area results in deterioration in the sensitivity and accuracy of the method. Third, as will be demonstrated below, in the system in hand, the condensation coefficient α is pressure-dependent, so that its application becomes questionable in our case. To obviate complications inherent in the effusion method in the range of high relative water pressures, employing all the advantages of the method in measuring low pressures, we acted as follows. We prepared aqueous solutions of sulfuric acid of various concentrations and measured the water vapor pressures over these solutions using the effusion method (effective orifice area 8.206×10^{-10} m^2). The results were used to construct calibration curves coupling the vapor pressure obtained by the Knudsen method P_k with the true water vapor pressure P_s corresponding to a given concentration of sulfuric acid [11]. An example of such a calibration curve, obtained at 298 K, is presented in Fig. 2. As seen, this is not a straight line, but a curve which can be extrapolated by a third-order polynomial with a correlation factor of 0.995. The calibration curves obtained at 303 and 308 K are similar. Even at low pressures, the curve deviates from linearity, and, as the pressure increases, the function P_s vs. P_k becomes much more complex, which can be attributed to alteration in the vapor flow mode from the effusion hole.

Using the above procedure, we obtained desorption isotherms of water from the cellulose samples at 298, 303, and 308 K. The water vapor pressure was determined to within 10%. Figure 3 shows the primary data obtained in the effusion experiment and then used for construction of the desorption isotherms. In the experiment, we determined the water vapor pressure over a cellulose sample wetted with water. The moisture content in cellulose, at which the equilibrium vapor pressure P started to deviate from the saturated vapor pressure P_0 at a given temperature (in other words, when P/P_0 started to deviate from 1), corresponded to the maximal sorption of water on cellulose.

Figure 4 shows the water desorption isotherms from cellulose treated mechanically using an extruder

(sample I) or shock-reset machine (II), or chemically with dilute HNO_3 (III). For comparison, Fig. 5 shows the water desorption isotherms from sample I, obtained at 298 K using both the effusion and isopiestic (sample is kept in a desiccator at a fixed humidity) methods. The isopiestic experiments were carried out over the relative vapor pressure range P/P_0 = 1–0.0003. A cellulose sample of about 100 mg, vacuum-dried at 338–343 K to constant weight, was brought into the isopiestic equilibrium with aqueous sulfuric acid of a fixed concentration, for which the water vapor pressure over the solution is known [11]. The experiment was carried out in an air bath oven. The temperature was controlled to within 0.1 K. The equilibration time was from 7 to 21 days. The amount of sorbed water was determined gravimetrically. The same method was used to control the equilibrium conditions in the system.

The results obtained by both methods are in satisfactory agreement, even though the isopiestic method gives slightly overestimated values for water sorption, particularly, in the range of low relative pressures, which is probably due to longer time required for establishment of the sorption equilibrium in the isopiestic experiments. Previously we studied the equilibrium in the system water–cellulose using an MI-1201 mass spectrometer modified for performing effusion experiments [12]. Data on the H_2O^+ intensity in the mass spectrum suggested that, in the effusion experiment, the time required for establishment of the equilibrium is 90–120 min, depending on the moisture content and temperature of cellulose samples.

The dependence of the relative water vapor pressure at a given sorption value on the reciprocal temperature was then used to estimate the thermodynamic parameters of water desorption by the Clapeyron–Clausius equation (2)

$$[\ln(P/P_0)]_a = -A/T + B, \qquad (2)$$

where P/P_0 is the relative water vapor pressure corresponding to the given sorption of water a at the temperature T; $A = \Delta H_{des}/R$ and $B = \Delta S_{des}/R$ (ΔH_{des} and ΔS_{des} are the enthalpy and entropy of desorption); and R, gas constant.

The enthalpies and entropies of desorption of water from the cellulose samples are presented in Figs. 6a and 6b. The heat effects of water desorption from cellulose samples II and III at low sorption values are about 10–20 kJ mol^{-1}, decreasing to zero with increasing sorption, which is typical of the cellulose–water system. In this case, the entropy of the system is practically independent of the amount of sorbed water, differing only slightly from zero, suggesting that the interaction in the system is accompanied by ordering of the water molecules and disordering of the cellulose segments. Sample I stands out against a background of the other samples. For sample I, the enthalpy of water desorption at low sorption is about

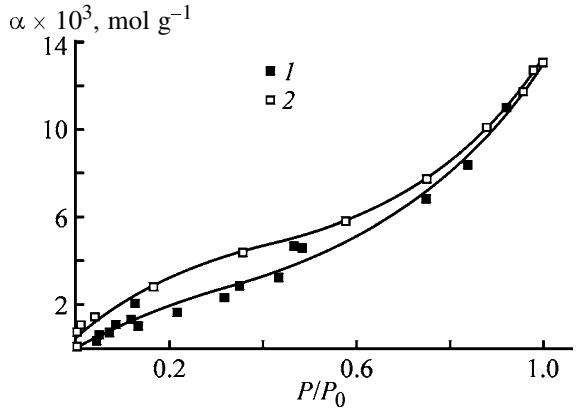

Fig. 5. Water desorption isotherms from cellulose sample I, obtained by (*1*) effusion and (*2*) isopiestic methods.

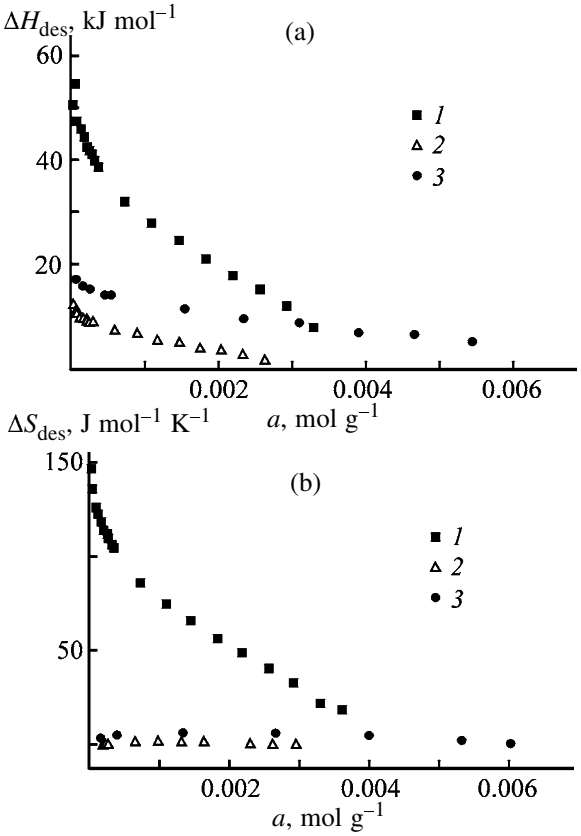

Fig. 6. (a) Enthalpy and (b) entropy of water desorption from cellulose samples (*1*) I, (*2*) II, and (*3*) III. (ΔH_{des}) Enthalpy and (ΔS_{des}) entropy of water desorption from cellulose, and (*a*) equilibrium sorption of water on cellulose.

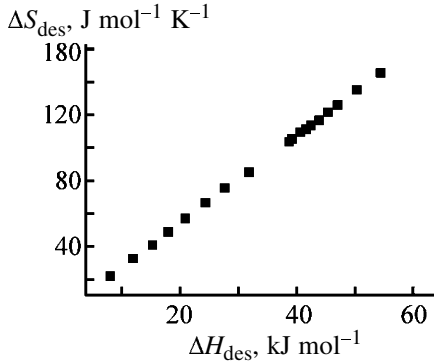

Fig. 7. Thermodynamic compensation effect in water desorption from cellulose sample I. (ΔH_{des}) Enthalpy and (ΔS_{des}) entropy of water desorption from cellulose.

55 kJ mol^{-1}, and the entropy of desorption changes in parallel to the enthalpy, i.e., the thermodynamic compensation effect takes place here (Fig. 7).

The compensation or isokinetic theory is widely used in physicochemical research. According to this theory, the enthalpy–entropy compensation originates from changing nature of the solute–solvent interaction due to a specific reaction, the relationship between the enthalpy and entropy being linear. Aguerre [13] applied this approach to the study of sorption of water on foodstuffs. He derived an equation relating the equilibrium sorption of water to its activity and the temperature, and demonstrated a linear correlation to occur between the enthalpy and entropy for a series of foodstuffs. It was demonstrated also that the penetration of water across the grape peel is a rate-controlling stage of drying, i.e., the resistance to water loss is provided primarily by the cell membrane [14]. The water loss can be decelerated through optimization of the storage conditions (temperature and humidity).

It may be suggested from the observed abnormally high heat effects of water desorption from sample I in combination with the thermodynamic compensation effect that the interaction of water with this sample differs from that with other samples. Among the reasons could be chemical interaction of water with some impurities introduced into cellulose during pretreatment, changing number of hydration centers and characteristics of the micropores; transformation of the crystalline domains, etc. By now we cannot fix the key factor. Nevertheless, the study of the conditions and factors controlling water desorption from cellulose is of crucial importance. In studying the water sorption on cellulose materials, it is necessary to take into account the history of the sample. There is no doubt that data on the equilibrium sorption of water are significant for optimization of drying and storage of foodstuffs and medical products. In this context, the effusion technique shows promise as an express method for characterization of desorption of water as well as other solvents.

CONCLUSIONS

(1) With precision calibration systems, the effusion method can be used for determination of the equilibrium water vapor pressure over cellulose.

(2) The experimental isotherms of water desorption from cellulose, obtained by the effusion method, are well consistent with those obtained using the isopiestic technique.

(3) Determination of the equilibrium water vapor pressure at various temperatures using the effusion method allows estimation of the thermodynamic characteristics of water desorption from cellulose.

REFERENCES

1. Klenkova, N.I., *Struktura i reaktsionnaya sposobnost' tsellyulozy* (Structure and Reactivity of Cellulose), Leningrad: Nauka, 1976.
2. Papkov, S.P. and Fainberg, E.Z., *Vzaimodeistvie tsellyulozy i tsellyuloznykh materialov s vodoi* (Interaction of Cellulose and Cellulose Materials with Water), Moscow: Khimiya, 1976.
3. Reizin'sh, R.E., *Strukturoobrazovanie v suspenziyakh tsellyuloznykh volokon* (Structurization in Suspensions of Cellulose Fibers), Riga: Zinatne, 1987.
4. Budtov, V.P., *Fiziko-khimiya rastvorov polimerov* (Physical Chemistry of Polymer Solutions), Moscow: Khimiya, 1992.
5. Bochek, A.M., in *Cellulose and Cellulose Derivatives: Physicochemical Aspects and Industrial Applications*, Kennedy, J.F., Phillips, G.O., Williams, P.O., and Picculel, L., Eds., Cambridge: Woodhead, 1995, pp. 131–137.
6. Syrnikov, Yu.P., *Khim. Drev.*, 1988, no. 4, pp. 3–9.
7. Antonchenko, V.Ya., *Fizika vody* (Water Physics), Kiev: Naukova Dumka, 1986.
8. Sidorov, L.N., Korobov, M.V., and Zhuravleva, L.V., *Mass-spektral'nye termodinamicheskie issledovaniya* (Mass Spectroscopic Thermodynamic Studies), Moscow: Mosk. Gos. Univ., 1985.
9. Lebedev, Yu.A. and Miroshnichenko, E.A., *Termo-*

khimiya paroobrazovaniya organicheskikh veshchestv: Teploty ispareniya, sublimatsii i davlenie nasyshchennogo para (Thermochemistry of Vaporization of Organic Substances: Heats of Vaporization and Sublimation and Saturation Vapor Pressure), Moscow: Nauka, 1981.

10. Chickos, J.S. and Acree, W.E. Jr., *J. Phys. Chem. Ref. Data*, 2002, vol. 31, no. 2, pp. 537–698.
11. *Kratkii spravochnik khimika* (A Concise Chemist's Handbook), Nikol'skii, B.P., Ed., Moscow: Khimiya, 1964.
12. Zakharov, A.G., Prusov, A.N., Voronova, M.I., et al., *J. Mol. Liq*., 2003, nos. 103–104, pp. 161–167.
13. Aguerre, R.J., Suarez, C., and Viollaz, P.E., *J. Food Sci*., 1986, vol. 51, no. 6, pp. 1547–1549.
14. Telis, V.R.N., Gabas, A.L., Menegalli, F.C., and Telis-Romero, J., *Thermochim. Acta*, 2000, vol. 343, pp. 49–56.

ISSN 1070-4272, Russian Journal of Applied Chemistry, 2007, Vol. 80, No. 1, pp. 48–52. © Pleiades Publishing, Ltd., 2006.
Original Russian Text © S.S. Stavitskaya, V.M. Vikarchuk, N.N. Tsyba, N.T. Kartel', O.N. Bakalinskaya, 2007, published in Zhurnal Prikladnoi Khimii, 2007, Vol. 80, No. 1, pp. 49–53.

PHYSICOCHEMICAL STUDIES OF SYSTEMS AND PROCESSES

Sorption of Organic Dyes of Various Molecular Weights on Mineral Sorbents and on Sea and Lake Bottom Sediments

S. S. Stavitskaya, V. M. Vikarchuk, N. N. Tsyba, N. T. Kartel', and O. N. Bakalinskaya

Institute of Sorption and Problems of Endoecology, National Academy of Sciences of Ukraine, Kiev, Ukraine

Received March 30, 2006

Abstract—The sorption of organic dyes of various molecular weights (from 100 to 700 amu) from aqueous solutions on minerals and on sea and lake bottom sediments was studied.

DOI: 10.1134/S1070427207010090

In the modern stage of development of human society, various aspects of human health are closely associated with the environmental problems. There is no doubt that the environmental pollution and deterioration of food and drinking water negatively affect the human health. Therefore, an urgent problem is the development of techniques allowing the elimination of these detrimental effects. One of approaches to solution of this problem is based on detoxication of human body by introducing specific sorbents ensuring its inner ecological purity (endoecological purity).

One of promising directions in the modern environmental science is the development of techniques for sanitation of human body by introduction of specific sorbents recovering toxic, ballast, and potentially detrimental compounds of endogenic and exogenic kinds. High-performance biocompatible sorbents based on polymeric materials are successfully used today for medical treatment of human body [1–3]. These medical sorbents include various carbon materials [1–9]. Activated carbons are used as application materials stabilizing the growth of tumor cells [8] and accelerating the healing of infected wounds, burns, and chilblains [2, 8, 10].

Recently the market of medical and cosmetic application materials was replenished owing to appearance of new biologically active dispersed minerals and other compounds taken from bottom sediments of the Black and Azov seas. These materials were found to contain the specific natural curative organomineral complex. The preparation of new domestic medical compositions based on these raw materials and development of effective techniques for their production is an urgent problem.

In this study we examined the sorption of organic dyes simulating the exo- and endogenic organic pollutants on clay minerals and bottom sediments collected from the Black Sea at different depths (200–2100 m) and also from limans and lakes located in the southern Ukraine.

The sorption power and selectivity of sorbents for organic pollutants are mainly determined by the size ratio of sorbent pores and organic pollutant molecules whose size, in turn, correlates with their molecular weight [10, 11].

It is known that the molecular weight of toxic organic compounds varies within a broad interval from several hundreds to tens thousands atomic units [12]. Therefore, purposeful choice of the optimal enterosorbent for removing particular organic pollutant from a living body requires understanding of correlation between the sorption power of the sorbent and the pollutant molecular weight.

EXPERIMENTAL

Since enterosorption is usually applied for detoxication of human body poisoned with organic compounds with the molecular weight below 1000, in our experiments we tested as simulating compounds organic dyes with the molecular weight (*MW*) from 100 to 700.

The sorption of organic dyes (Methylene Blue, *MW* = 320; Methyl Orange, *MW* = 324; Methyl Violet, *MW* = 410; Orange-Yellow, *MW* = 450; Bromocresol Purple, *MW* = 540; Bromphenol Blue, *MW* = 670; Congo Red, *MW* = 700; and creatinine,

Structural and sorption characteristics of bottom sediments of various origins

Sample no.	Sampling site	Sorption of nitrogen, $cm^3\ g^{-1}$	S_{sp} by N_2 sorption, $m^2\ g^{-1}$	Pore radius, Å	S_{mi}, $m^2\ g^{-1}$	V_{mi}, $cm^3\ g^{-1}$
1	Kuyal'nitskii liman, Odessa	36	36	20; 30	22	0.08
2	Lake Velikoe, Berdyansk	32	11	20	11	0.01
3	Station 5795, Black Sea bottom	14	20; 35	11	11	0.02

MW = 113) from aqueous solutions was studied under static conditions. The dye concentration in the solutions ranged from 0.1 to 1.5 $g\ l^{-1}$. The ratio of solid and liquid phases was 1 : 150. The initial and equilibrium dye concentrations were determined on a KFK-3 photocolorimeter. The creatinine content was determined on an SF-16 spectrophotometer.

The natural materials used as enterosorbents were as follows: minerals palygorskite and vermiculite and three samples of bottom sediments with different specific surface areas S_{sp} taken from the Black Sea, Kuyal'nitskii liman, and Lake Velikoe (see table).

The pore structure of the bottom sediments under consideration was studied with a NOVA 2000 E high-performance gas analyzer. In these experiments, the low-temperature sorption and desorption isotherms of nitrogen were obtained at 77 K and the pore size distribution was calculated. The specific surface area, micropore surface area S_{mi}, micropore volume V_{mi}, and pore radius r (Å) were calculated by the BET technique (MULTI POINT, BET, BJH etc.) with the correlation factor of 0.999.

Figure 1a shows the sorption and desorption isotherms of nitrogen plotted as A (specific sorption) vs. P/P_s (relative vapor pressure). The integral distribution of the pore volume with respect to pore radii for the sample of liman bottom sediments is shown in Fig. 1b. Our results listed in the table indicate that the tested samples of the liman, sea, and lake bottom sediments are microporous materials. Their pores have the size of about 20 Å, the specific volume of micropores of 0.01–0.08 $cm^3\ g^{-1}$, and the micropore surface area S_{mi} of 11–36 $m^2\ g^{-1}$. The sorption of dyes of higher molecular weight (Congo Red and Methyl Violet) was studied on palygorskite and vermiculite having more developed surface structure [13]. The sorption isotherms of organic dyes on palygorskite and vermiculite are shown in Figs. 2a and 2b. Figures 3a and 3b show the sorption of organic dyes on bottom sediments. It is seen that sorption of dyes on clay minerals (Figs. 2a and 2b) significantly depends on their molecular weight. This effect is apparently caused by the fact that the accessibility of the sorbent pore volume for dye molecules depends on their size. This hypothesis is consistent with the sorption isotherms of Methylene Blue on bottom sediments

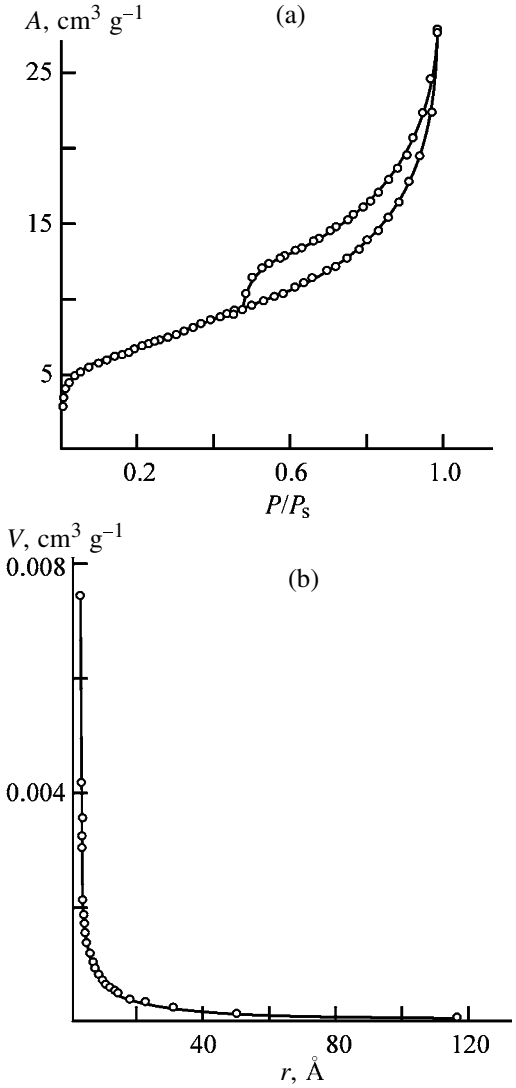

Fig. 1. (a) Sorption and desorption isotherms of nitrogen on sample no. 1 at 77 K and (b) the integral distribution of the pore volume V with respect to the pore radii for sample no. 1. (P/P_s) Ratio of the equilibrium pressures of sorbed and liquid nitrogen at 77 K. (A) Specific sorption of nitrogen.

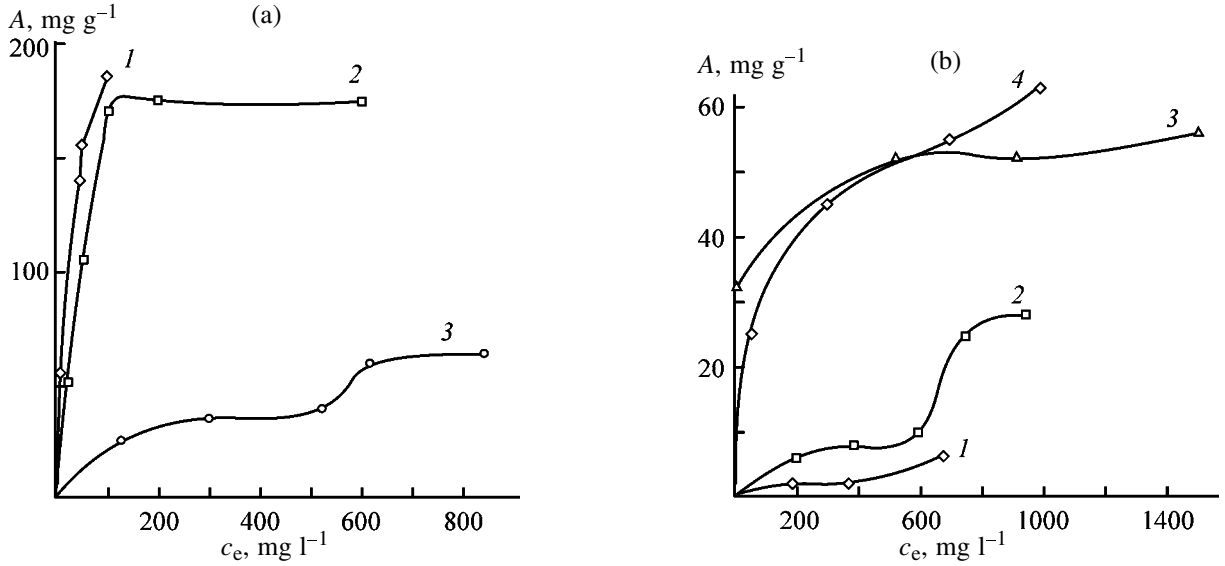

Fig. 2. Sorption isotherms of organic dyes from aqueous solutions on (a) palygorskite and (b) vermiculite. (*A*) Dye concentration in the sorbent; (c_e) equilibrium dye concentration in the aqueous phase; the same for Fig. 3. Dyes: (a) (*1*) Methylene Blue, (*2*) Methyl Violet, and (*3*) Congo Red; (b) (*1*) Bromophenol Blue, (*2*) Congo Red, (*3*) Methyl Violet, and (*4*) Methylene Blue.

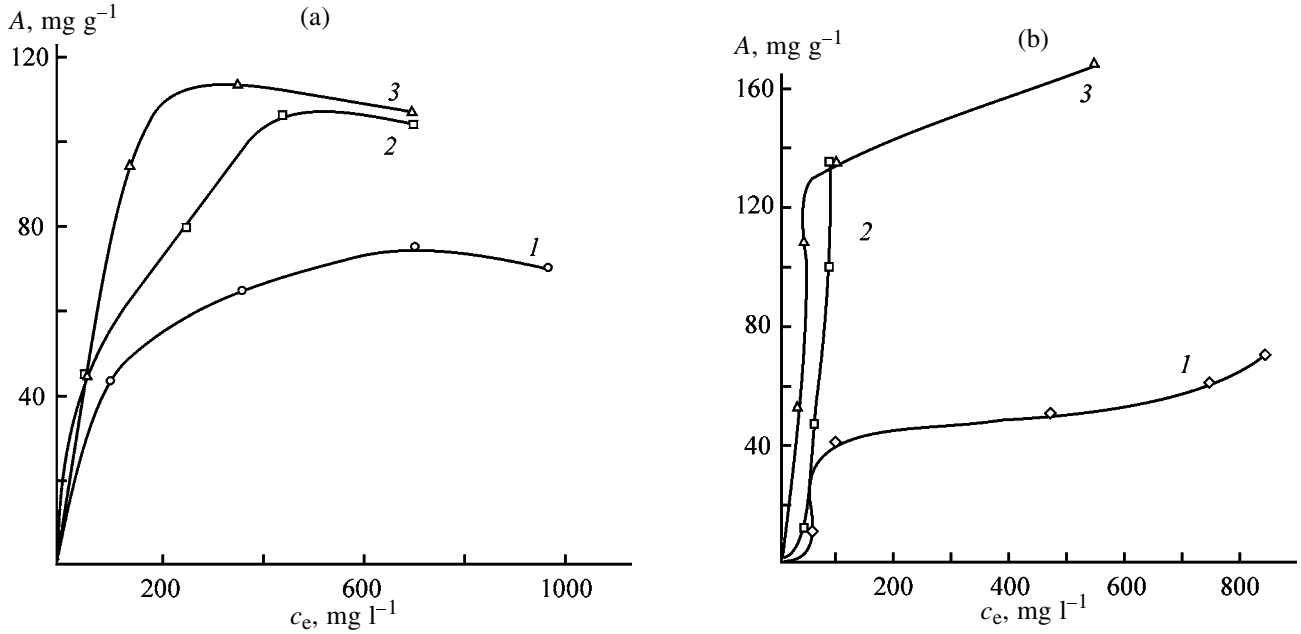

Fig. 3. Sorption isotherms of (a) Methylene Blue and (b) Methyl Orange from aqueous solutions on bottom sediments. Bottom sediments (see table): (*1*) no. 3, (*2*) no. 2, and (*3*) no. 1.

(Fig. 3): in going from liman bottom sediments (sample no. 1, S_{sp} = 36 $m^2 g^{-1}$) to sea bottom sediments (sample no. 3, S_{sp} =14 $m^2 g^{-1}$), the sorption of Methylene Blue decreases by a factor of approximately two. The pattern of sorption of creatinine was similar.

The sorption isotherms show that the specific sorption of dye *A* on bottom sediments decreases with decreasing its concentration in the aqueous phase. However, even at low concentrations of the dye in the aqueous solution, comparable with the content of an organic toxicant in a poisoned organism, the bottom sediments ensure sufficiently effective sorption of dyes.

The experimental values of sorption *A* allow calculation of the distribution factor K_d (ml g^{-1}) of dye between the sorbent and aqueous solution, which is determined as the ratio of the dye concentration in the sorbent to its equilibrium concentration in the aqueous

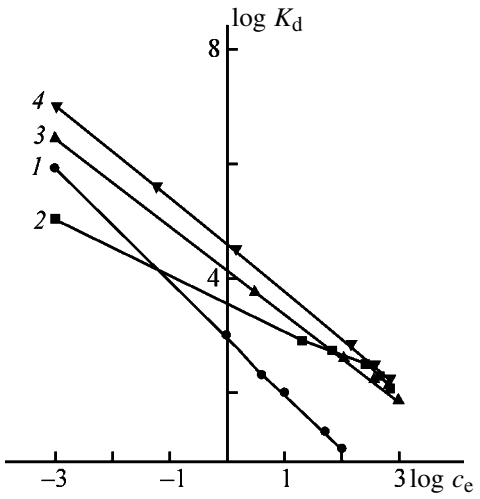

Fig. 4. The log–log plot of the distribution factors K_d of organic dyes between the sorbent and aqueous solutions vs. the equilibrium concentration of dyes in the aqueous solution. Sorbents: (*1*) palygorskite, (*2*) sample no. 3, (*3*) sample no. 2, and (*4*) sample no. 1 (see table).

phase. In other words, the distribution factor is equal to the equilibrium sorbate volume that contains the sorbate (dye) in the amount equal to its content in 1 g of the sorbent at equilibrium.

Figure 4 shows the plots of $\log K_d$ vs. $\log c_e$ in sorption of the dyes on palygorskite and bottom sediments under consideration. Taking into account that the maximal permissible concentration of stable organic pollutants in a human body is approximately 10^{-3} mg l^{-1} ($\log c_e = -3$), the mutual arrangement of straight lines in Fig. 4 allows us to expect that the detoxication efficiency of the sorbents under consideration for organic pollutants will increase in the order sample no. 3 < palygorskite < sample no. 2 < sample no. 1. The distribution factors of dyes between aqueous solution and sorbents are as large as several hundred thousands, i.e., these sorbents can be used as antidotic and neutralizing components of medicinial preparations and food additives.

The mechanism of sorption of dyes is sensitive to the sorbent kind. For example, palygorskite sorbs dyes owing to the large surface area of colloid clay particles (100 m^2 g^{-1}). In sorption on bottom sediments, the dye molecules are accommodated in pores whose size changes in the course of sorption due to swelling [14] and increase in the interplanar spacings [13].

The considered mechanisms of fixation of dyes ensure strong immobilization of organic pollutants on the sorbents concerned. Therefore, these natural materials can be used as enterosorbents suitable for treating human body to remove organic pollutants.

The sorption power of the sorbents under consideration is dependent on the organic pollutant concentration in the aqueous solution. For example, activated carbon better sorbs organic pollutants from their concentrated solutions (1–100 mg l^{-1}) [15, 16]. On the contrary, the clay mineral palygorskite and bottom sediments better sorb organic pollutants at their low (<1 mg l^{-1}) and ultralow (<10^{-2} mg l^{-1}) concentrations. In these systems, the distribution factor of Methylene Blue reaches 100 000 ml g^{-1}. These results suggest that activated carbons in combination with bottom sediments can be used as a food additive accelerating the removal of organic toxins from living body subjected to poisoning due to prolonged nega- tive environmental impacts and technogenic disasters.

CONCLUSIONS

(1) The sorption of organic dyes on sea and lake bottom sediments and also on minerals palygorskite and vermiculite was studied in relation to the organic dye molecular weight.

(2) The decrease in sorption of organic dyes with an increase in their molecular weight is caused by microporous structure of sorbents.

(3) At low and ultralow concentrations of dyes in aqueous solutions (1–10^{-2} mg l^{-1}), they are sorbed by mineral sorbents and bottom sediments most efficiently.

(4) The clay minerals sorb organic dyes with the distribution factors reaching several hundred thousands and therefore show much curative promise.

REFERENCES

1. Mukhin, V.M., Tarasov, A.V., and Klushin, V.N., *Aktivnye ugli Rossii* (Russian Actvated Carbon), Moscow: Metallurgiya, 2000.
2. *Enterosorbtsiya* (Enterosorption), Belyakov, N.A., Ed., Leningrad: TsST, 1991.
3. Andreichin, M.A. and Gnatyuk, M.S., *Enterosorbenty yak zasib ochishchennya organizmu* (Enterosorbents as Remedies for Cleaning Organism), Kiev: Znannya Ukraini, 1992.
4. Stavitskaya, S.S., Kartel', N.T., Bakalinskaya, O.N., et al., *Efferentn. Terap.*, 2004, vol. 10, no. 4, pp. 66–69.
5. Stavitskaya, S.S., Kartel', N.T., Vikarchuk, V.M.,

et al., *Efferentn. Terap*., 2001, vol. 7, no. 1, pp. 60–63.

6. Stavitskaya, S.S., *Ukr. Khim. Zh*., 1997, vol. 63, no. 8, pp. 96–102.
7. Kartel', N.T., Stavitskaya, S.S., Kupchik, L.A., et al., Abstracts of Papers, *Ist World Conf. on Carbon "Eurocarbon 2000,"* Berlin, July 9–13, 2000, vol. 2, pp. 603–604.
8. Dedenko, I.K., Starikov, A.V., and Strelko, V.V., *Efferentnye metody lecheniya luchevykh porazhenii* (Efferentive Methods for Treating Radiation Damages), Kiev: Nora, 1996.
9. Nikolaev, V.G. and Strelko, V.V., *Gemosorbtsiya na aktivirovannykh uglyakh* (Hemosorption on Activated Carbons), Kiev: Naukova Dumka, 1979.
10. Strelko, V.V. and Kartel', M.T., in *Naukovi osnovi razrobki likars'kikh preparativ* (Scientific Basis for Developing Drugs), Kharkov: Osnova, 1998, pp. 490–516.
11. Strelko, V.V., Sorochenko, G.K., and Il'yazov, R.G., Abstracts of Papers, *Nauchno-prakticheskaya konferentsiya "Sorbtsionnye sredstva i metody ekologicheskoi zashchity cheloveka i zhivotnykh"* (Scientific and Practical Conference "Sorption Materials and Methods for Biological Protection of Human Beings and Animals"), Gomel, 1999, pp. 12–14.
12. *Khimicheskaya entsiklopediya* (Chemical Encyclopedia), Knunyants, I.L. Ed., Moscow: Sov. Entsiklopediya, 1967, vol. 5.
13. Tarasevich, Yu.I. and Ovcharenko, F.D., *Adsorbtsiya na glinistykh mineralakh* (Adsorption on Clay Minerals), Kiev: Naukova Dumka, 1975.
14. Pakhovchishin, S.V., Prokopenko, V.A., Grishchenko, V.F. et al., Abstracts of Papers, *Konferentsya "Nanorozmirni sistemi. Elektronna, atomna budova i vlastivosti" (NANSIS-2004)* (Nanodimensional Systems. Electronic, Atomic Structure and Properties (NANSIS-2004)), Kiev, 2004, p. 244.
15. Kartel', N.T., Strelko, V.V., Stavitskaya, S.S., et al. in *Nauchno-prakticheskii seminar "Poiski i razrabotka serdechno-sosudistykh sredstv"* (Scientific and Practical Seminar "Search and Development of Cardiovascular Remedies"), Alushta, 2001, pp. 17–21.
16. Kupchik, L.A. and Kartel', M.T., in *Naukovo-praktichnii seminar "Planeta bez stiikikh organichnikh zabrudnyuvachiv"* (Scientific and Practical Seminar "Planet without Stable Organic Pollutants"), Kiev: Obrii, 2005, pp. 78–82.

ISSN 1070-4272, Russian Journal of Applied Chemistry, 2007, Vol. 80, No. 1, pp. 53–57. © Pleiades Publishing, Ltd., 2006.
Original Russian Text © T.I. Denisova, D.I. Shvets, T.G. Shramkova, M.F. Kovtun, 2007, published in Zhurnal Prikladnoi Khimii, 2007, Vol. 80, No. 1, pp. 54–58.

PHYSICOCHEMICAL STUDIES OF SYSTEMS AND PROCESSES

Recovery of Heavy Metal Ions from Aqueous Solutions Using Modified Organosilicas

T. I. Denisova, D. I. Shvets, T. G. Shramkova, and M. F. Kovtun

Institute of Sorption and Endoecology Problems, National Academy of Sciences of Ukraine, Kiev, Ukraine

Received June 20, 2006

Abstract—Sorption of Cu(II), Pb(II), Cd(II), and Zn(II) from aqueous solutions on two-component organosilicas was studied as influenced by sorbent composition, contact time, ratio of solid and liquid phases, solution pH, nature and concentration of heavy metal ions, and content of modifying agent. The degrees of sorption of these metal ions from aqueous solutions using organosilicas modified with aluminum(III) added into the siloxane matrix or with copper(II) grafted to the sorbent surface layer were compared.

DOI: 10.1134/S1070427207010107

Deterioration of the environment in both East and West Europe owing to anthropogenic factors and ecological accidents and disasters puts forward a requirement of treatment of aquatic media to remove inorganic ecological toxic agents (heavy metals). Among heavy metals, ions of copper(II), lead(II), cadmium(II), and zinc(II) whose toxicity increases in the order Cu(II) < Zn(II) < Pb(II) < Cd(II) [1] are of particular importance. It is known that silica-containing natural sorbents (clays, zeolites, aluminosilicates [2–5]) and synthetic sorbents (silica gel and its modified forms [6]) are used in water treatment to remove heavy metal ions. However, certain drawbacks are typical for these materials: nonselective sorption, insufficient efficiency of sorption of various heavy metal ions in the wide pH range, and, hence, relatively narrow range of their operation. Low maximum permissible concentrations (MPCs) of heavy metals and their ability to form complexes with organic compounds put forward certain requirements to the disperse sorption materials for treatment of aqueous and aqueous salt solutions to remove heavy metals. These requirements are as follows: selectivity of sorption by modification with metal ions, which increases the number of active ion-exchange and complexing centers on the sorbent surface, nontoxicity of sorption materials, their stability in a wide pH range, presence of various functional organic groups that interact with heavy metal ions, etc.

As compared to modern silica-containing sorbents used in water treatment to remove heavy metals, two-component organosilica sorbents (silicopolymethylsiloxanes) have certain advantages such as rigidity of the polymeric skeleton, insolubility in water and organic solvents, and chemical stability in aqueous and aqueous salt solutions at pH changing from 1 to 9. The surface silanol ≡Si–OH and methylsilyl ≡Si–CH_3 groups in two-component organosilica sorbents act as centers of specific adsorption of both molecular and ionic compounds [7]. It should be noted that the data on recovery of heavy metals from solutions using organosilica sorbents are scarce and nonsystematic. Voronkov et al. [8] showed that complexing sulfonic silicopolymethylsiloxanes are fairly efficient in treatment of potable and waste waters to remove heavy metal ions at pH 1–3. Chen et al. [9] estimated the sorption capacity for Sb(III), Bi(III), and Ag(I) of ion exchangers with organosiloxane structure, which are hydrolytically stable in the acidic medium.

In this work we studied the degree of recovery of heavy metal ions from aqueous solutions as influenced by various metal ions added to modify the structure of silicopolymethylsiloxanes.

As organosilica sorbents (OSs) we used silicopolymethylsiloxanes with various ratios of the silanol and methylsilyl groups (wt %), namely, 30 : 70 (OS-30), 50 : 50 (OS-50), and 70 : 30 (OS-70), and also their forms modified with metal ions: OS-30(Al), OS-30(Al,Cu), OS-50(Cu), OS-70(Cu), with the content of copper and aluminum differing by a factor of 2 (1.6 and 3.2 g g^{-1}, respectively). Various methods were used to introduce metal ions into the organosilica structure. For example, aluminum was incorporated in

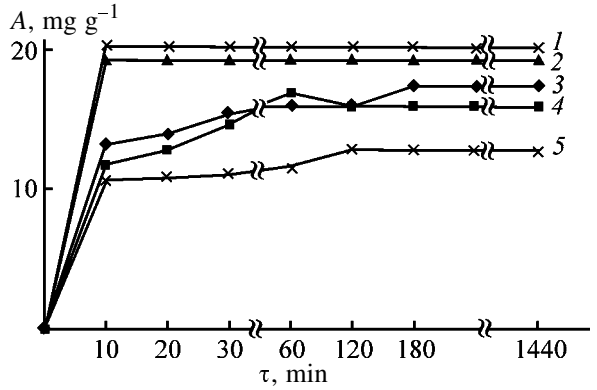

Fig. 1. Kinetic curves of sorption *A* of heavy metal ions on (*1–4*) OS-30(Al) and (*5*) OS-50 sorbents from aqueous solutions; c_{in} = 200 mg l^{-1} and s : l = 1 : 100; (τ) contact time. (*1, 5*) Pb(II), (*2*) Cd(II), (*3*) Cu(II), and (*4*) Zn(II).

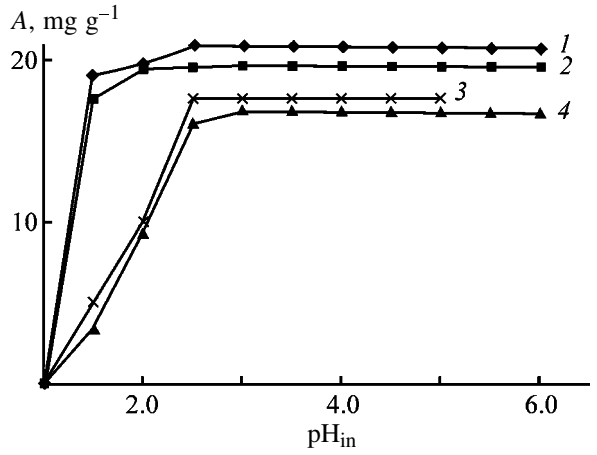

Fig. 2. Sorption *A* of heavy metal ions on OS-30(Al) sorbent as influenced by pH_{in} of the aqueous solutions; c_{in} = 200 mg l^{-1}, s : l = 1 : 100, τ = 3.5 h. (*1*) Pb(II), (*2*) Cd(II), (*3*) Cu(II), and (*4*) Zn(II).

the siloxane chain in the stage of coprecipitation of the initial sodium silicate and methylsiliconate in the course of organosilica synthesis [10]. The silica surface was modified with copper(II) by its contact with a solution of copper ammoniate using the procedure given elsewhere [11]. The structural and sorption characteristics of the resulting complexes (specific surface area and sorption pore volume for benzene and water) were determined using a Nova-2200E device (Guantachrom Corp.) and by a gravimetric procedure. The solution acidity and suspension pH were recorded with a 150M pH-meter, and pH of the surface zero charge was measured by the published procedure [12]. The content of the heavy metal ions in aqueous solutions before and after sorption was determined by atomic-absorption analysis on a C-115MT spectrophotometer using the supplied PC software. The sorption of heavy metal ions was studied under the static conditions in the concentration range from 50 to 1000 mg l^{-1} and ratio of the solid and liquid (s : l) phases from 1 : 100 to 1 : 300. The sorption of heavy metal ions and degree of their recovery were calculated in mg g^{-1} and %, respectively.

Solutions of heavy metal ions were prepared by dissolution of weighed portions of $CuSO_4 \cdot 5H_2O$, $Pb(CH_3COO)_2 \cdot 2H_2O$, and $Cd(NO_3)_2 \cdot 4H_2O$ in water. The kinetics of the metal ion sorption was studied at s : l = 1 : 100 and at initial concentrations exceeding many times MPC for potable water.

The IR spectra of the organosilica sorbents and their forms modified with aluminum(III) were recorded on a Specord-M80 spectrophotometer in the 4000 – 400 cm^{-1} range.

The resulting kinetic curves of sorption of heavy metal ions from aqueous solutions using the initial and modified organosilicas show that modification of OS-30 sorbent with aluminum(III) decreases the time of equilibrium attainment from 120 to 10 min and increases the sorption of lead(II) by a factor of 1.7 as compared to the initial sorbent (Fig. 1, curves *1–5*). The time of equilibrium attainment correlates with the sorption of heavy metal ions on OS-30(Al) sorbent [Pb(II) > Cd(II) > Cu(II) > Zn(II) (Fig. 1)] and agrees with the previous experimental data on the sorption kinetics of copper(II) and zink(II) ammoniates on OS-30(Al) [13]. In contrast to Cd(II) and Pb(II), for copper(II) and Zn(II), along with a fast section of the kinetic curve when 70–75% of heavy metal ions are recovered from the aqueous solutions in several minutes, we also observe a section of slow sorption with the time of equilibrium attainment of 2–3 h (Fig. 1, curves *3, 4*). The data obtained previously in [14] showed that, at high s : l ratios (>1 : 20), the sorption in silicopolymethylsiloxane is predominantly diffusion-controlled. Hence, this fact suggests that, at given s : l ratio from 1 : 100 to 1 : 300, the rate of recovery of heavy metal ions by organosilica sorbents would be determined by chemical kinetics. In this case, not only ion exchange but also specific interactions of complexing metal ions, such as Cu(II) and Zn(II), with the active centers on the sorbent surface [15] should be taken into account.

The pH dependences of the sorption of the heavy metal ions on OS-30(Al) sorbent show that sorption of lead(II) and cadmium(II) sharply increases at pH 1–2 (Fig. 2). Already at pH > 2, the sorption is maximal and remains constant with increasing pH to 7. At the same time, for copper(II) and zinc(II) the sorption increases to a maximum in the pH range from 1 to 3;

Degree of recovery of the heavy metal ions from aqueous solutions as influenced by modification of organosilica sorbents with Al(III) and Cu(II). Initial concentration of the heavy metal ions 200–250 mg l^{-1}, pH 4.8–5.2, contact time 3.5 h

Sorbent	S_{sp}, m^2 g^{-1}	Pore volume, cm^3 g^{-1}		pH of the surface zero charge	s : l	Degree of recovery, %			
		C_6H_6	H_2O			Pb(II)	Cd(II)	Cu(II)	Zn(II)
OS-30	358	0.98	0.19	4.5	1 : 100	38.7	27.8	15.8	65.7
					1 : 300	5.4	–	11.2	15.7
OS-30(Al)	408	0.59	0.24	5.9	1 : 100	100.0	88.0	85.0	67.4
					1 : 300	98.0	30.7	57.9	45.8
OS-30(Al, Cu)*	410	0.56	0.23	6.0	1 : 100	100.0	99.0	93.6	23.7
					1 : 300	99.8	97.2	75.2	34.6
OS-30(Al)	472	0.51	0.22	6.0	1 : 100	100.0	99.8	99.5	98.3
					1 : 300	75.6	70.3	31.2	40.7
OS-30(Al, Cu)*	480	0.48	0.21	6.2	1 : 100	99.5	98.4	93.2	76.4
					1 : 300	90.0	56.7	57.4	38.4
OS-50	560	1.10	0.21	5.5	1 : 300	4.5	–	12.4	16.8
OS-50(Cu)**	550	1.15	0.20	5.8	1 : 300	14.5	–	1.9	4.0
OS-50	610	0.92	0.22	6.5	1 : 300	13.2	–	9.2	9.0
OS-70	500	1.25	0.28	6.0	1 : 300	15.5	–	0.4	14.7
OS-70(Cu)*	470	1.26	0.26	6.5	1 : 300	22.0	–	8.7	18.4

* Cu 3.2 mg g^{-1}.
** Cu 1.6 mg g^{-1}.

it also remains constant with increasing pH to 7 (Fig. 2). In this case, in contrast to silica and natural aluminosilicates, sorption of the heavy metal ions on OS-30(Al) is accompanied not by acidification of solutions after their contact with the sorbent, but by increase in the solution pH by 0.2–0.9 unit depending on the metal ion [16, 17]. Changes in solution pH after sorption using the sorbent modified with Al(III) amount to 1, 0.5, 0.4, and 0.3 for Pb(II), Cd(II), Cu(II), and Zn(II), respectively, and correlate with variations in the degree of recovery of the heavy metal ions.

The sorption curves of the heavy metal ions on OS-30(Al) are similar to the sorption curves of these metals on silica gel with chelating groups grafted to the silica surface [18]. Two sections in the kinetic curves of Cu(II) and Zn(II) sorption indicate that their recovery on OS-30(Al) can occur not only through the ion exchange but also through the specific interaction with negatively charged ≡SiO groups on the sorbent surface (Fig. 1, curves *3, 4*). Addition of aluminum(III) and copper(II) coordinated with the surface silanol groups in the organosilica structure increases the sorbent selectivity. As seen from the table, the degree of recovery of the heavy metal ions correspondingly increases. As seen, irrespective of the modifying metal, the series of the degree of recovery of heavy metal ions on OS-30(Al), OS-30 (Al, Cu), and OS-70(Cu) are similar and correlate with the ionic radii of the sorbates [19]: Pb(II) 1.32 > Cd(II) 0.97 > Cu(II) 0.96 > Zn(II) 0.83 Å. For OS-30, OS-50, and OS-50(Cu), these series are different, which may be due to certain features of the surface chemistry of these sorbents owing to different amounts of active hydroxy groups in their composition.

The effect of the nature of heavy metal ions on their sorption is confirmed by a change in the shape of the sorption isotherms of Cu(II) and Zn(II) belonging to the classical Langmuir type L2 with a saturation section (plateau) in accordance with the Giles classification as compared to the H2 isotherms typical for sorption of Pb(II) and Cd(II) on OS-30(Al) and OS-30(Al, Cu) (Fig. 3). The H2 type of isotherms suggests that sorption is fairly high even at low equilibrium metal concentrations; with increasing concentration, the surface adsorption layer with new active centers for interaction with heavy metal ions is formed.

Our experimental data on the effect exerted by modification of two-component organosilica sorbent with Al(III) on the degree of recovery of heavy metal ions allow the following conclusions. Aluminum(III),

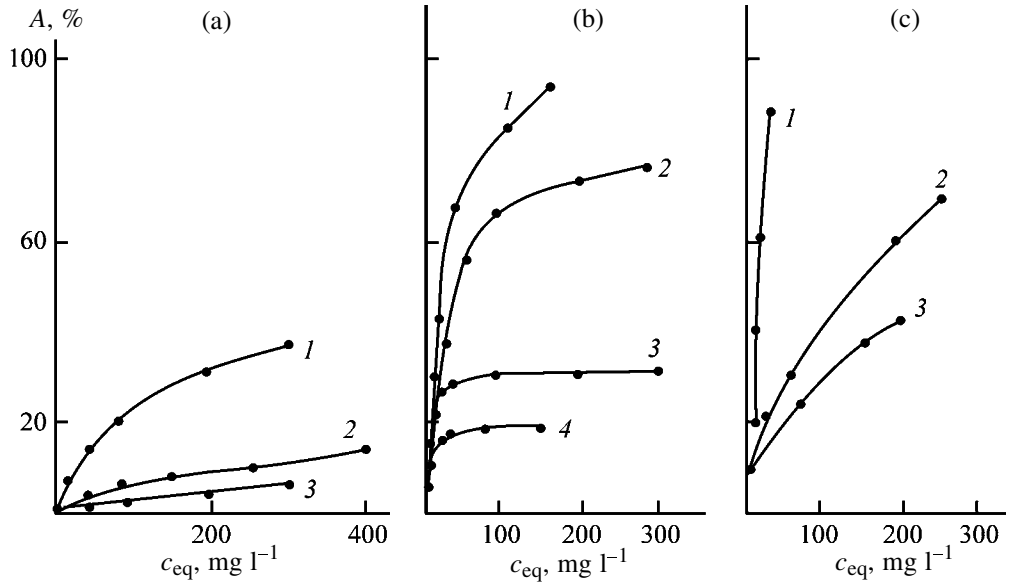

Fig. 3. Isotherms of sorption A of heavy metal ions on organosilica sorbents from aqueous solutions; s : l = 1 : 100, pH 4.8–5.2. (c_{eq}) Equilibrium concentration of the heavy metal ions in solutions. (a) OS-30, (b) OS-30(Al), and (c) OS-30(Al, Cu). (*1*) Pb(II), (*2*) Cd(II), (*3*) Cu(II), and (*4*) Zn(II).

when incorporated in the sorbent structure, probably polarizes the silanol groups [20], provides appearance of the negative charge, and increases its acidic and complexing properties and thus, its ion-exchange power. The selectivity of sorption of the heavy metal ions on the organosilica sorbents modified with Al(III) ions of acceptor type or with copper(II) ions containing *d* electrons is probably due to the increase in the amount of acid groups on the sorbent surface containing mobile protons, similarly to silica gel modified with Al(III) [21]. Introduction of aluminum(III) in the siloxane chain and formation of the ≡Si–O–Al–O–Si≡ bond are confirmed by the elemental analysis showing that the content of silicon decreases in the order OS-30 (42.4) > OS-30(Al) (37.0) > OS-30(Al, Cu) (36.1%). This suggests isomorphic substitution of aluminum for silicon, which is confirmed by the IR spectroscopic data for OS-30 modified with Al(III). For example, with a twofold increase in the aluminum content, the intensity of the bending vibrations of the OH groups at 1640 cm^{-1} increases, whereas the intensity of the strong stretching vibrations of the ≡Si–O–S≡ group in the 1100–1000 cm^{-1} range decreases and shifts toward lower frequencies. The frequency of the bending vibrations of the ≡Si–O bond at 400–500 cm^{-1} and its intensity slightly decrease. It is known that the absorption band of the hydroxy group in the aluminosilicate system is observed at 3610 cm^{-1} [22], and the observed shift of the vibration band of the OH groups from 3610 to 3500 cm^{-1} on passing from OS-30 to OS-30(Al) corresponds to an increase in the concentration of the hydroxy groups with increased proton mobility. This confirms our assumption that the modification of organosilica enhances its ion-exchange properties with respect to heavy metal ions in aqueous solutions.

CONCLUSIONS

(1) Kinetic characteristics of organosilica sorbents and degree of Pb(II), Cd(II), Cu(II), and Zn(II) recovery from aqueous solutions are improved with introduction of aluminum(III) or copper(II) ions into the siloxane matrix or sorbent surface layer, respectively.

(2) Depending on the nature of the modifying agent and ratio of the solid and liquid phases, for lead(II) and cadmium(II) the maximal recovery of 98–100 and 88–100%, respectively, is observed at pH 2–7, and for copper(II) and zinc(II) the highest recovery of 75.2–99.5 and 65.7–98.3%, respectively, is attained at pH 3–7.

(3) As seen from the IR spectroscopic data, the content of hydroxy groups with elevated proton mobility increases upon modification of two-component organosilica with acceptor aluminum(III) ions and, as a result, these sorbents effectively recover heavy metal ions from aqueous solutions.

REFERENCES

1. Vladimirov, A.M., Lyakhin, Yu.I., Matveev, L.T., and Orlov, V.G., *Okhrana okruzhayushchei sredy* (Preservation of the Environment), Leningrad: Gidrometeoizdat, 1991.
2. Tarasevich, Yu.I., *Prirodnye sorbenty dlya ochistki vody* (Natural Sorbents for Water Treatment), Kiev: Naukova Dumka, 1981.
3. Obal, M., Rosman, S., Jager, R., et al., *Kov. Zvit. Technol.*, 1991, vol. 26, nos. 1–2, pp. 234–239.
4. Vasylechko, V.O., Lebedunets, L.O., Kuz'ma, Yu.B., et al., *Adsorption. Sci. Technol.*, 1996, vol. 14, no. 3, pp. 267–273.
5. Guifen, Yu., Xin, J., Hongtao, W., et al., *Chin. J. Environ. Sci.*, 2002, vol. 23, no. 5, pp. 109–112.
6. Semenova, N.V., Morosanova, E.I., Zolotov, Yu.A., and Pletnev, I.V., *Vestn. Mosk. Univ., Ser. 2: Khimiya*, 1983, no. 34, pp. 394–399.
7. Slinyakova, I.B. and Denisova, T.I., *Kremniiorganicheskie sorbenty: Poluchenie, svoistva, primenenie* (Organosilicon Sorbents: Preparation, Properties, and Use), Kiev: Naukova Dumka, 1988.
8. Voronkov, M.G., Vlasova, N.N., and Pozhidaev, Yu.N., *Zh. Prikl. Khim.*, 1996, vol. 69, no. 5, pp. 705–717.
9. Chen, F.M., Cote, G., and Bauer, D., Abstracts of Papers, *Int. Solvent Extraction Conf. ISEC-90*, Kyoto (Japan), July 16–21, 1990, p. 72.
10. Ukrainian Patent 23325.
11. Ukrainian Patent 35287.
12. Nechaev, E.A. and Smirnova, L.M., *Kolloidn. Zh.*, 1981, vol. 43, no. 3, pp. 494–499.
13. Shvets, D.I., Denisova, T.I., and Strelko, V.V., *Centr. Eur. J. Chem.*, 2003, no. 2, pp. 178–191.
14. Karamushka, V.I., Denisova, T.I., Sklyarov, A.G., et al., *Zh. Prikl. Khim.*, 1989, vol. 62, no. 5, pp. 609–613.
15. Iler, R.K., *The Chemistry of Silica*, New York: Wiley–Interscience, 1979.
16. Denisova, T.I., Shramkova, T.G., Shvets, D.I., et al., *Extended Abstracts, VII Polish-Ukrainian Symp. "Theoretical and Experimental Studies of Interfacial Phenomena and Their Technological Applications,"* Lublin (Poland), September 15–18, 2003, pp. 42–44.
17. Pilipenko, A.T., Matsibura, G.S., Ryabushko, V.O., and Prishchepa, N.N., *Khim. Tekhnol. Vody*, 1992, vol. 14, no. 11, pp. 813–818.
18. Ayukaev, R.I., Venetsianov, E.V., Kotanova, E.A., and Tikhonov, N.A., *Khim. Tekhnol. Vody*, 1997, vol. 19, no. 2, pp. 115–121.
19. *Kratkii spravochnik po khimii* (Concise Handbook on Chemistry), Kiev: Akad. Nauk Ukr. SSR, 1962.
20. Voronkov, M.G., Mileshkevich, V.P., and Yuzhelevskii, Yu.A., *Siloksanovaya svyaz'* (Siloxane Bond), Novosibirsk: Nauka, 1976.
21. Strelko, V.V., Belyakov, V.N., Rubanik, S.K., and Strazhesko, D.N., *Adsorb. Adsorb.*, 1975, no. 3, pp. 64–69.
22. Andrianov, K.A., *Metody elementoorganicheskoi khimii* (Methods of Organometallic Chemistry), Moscow: Nauka, 1968.

ISSN 1070-4272, Russian Journal of Applied Chemistry, 2007, Vol. 80, No. 1, pp. 58–61. © Pleiades Publishing, Ltd., 2006.
Original Russian Text © V.M. Sedelkin, T.O. Ryabukhova, N.A. Okisheva, M.G. Pozdeeva, 2007, published in Zhurnal Prikladnoi Khimii, 2007, Vol. 80, No. 1, pp. 59–62.

PHYSICOCHEMICAL STUDIES OF SYSTEMS AND PROCESSES

Adsorption of Albumin on Charcoal-Filled Cellulose Diacetate Membranes

V. M. Sedelkin, T. O. Ryabukhova, N. A. Okisheva, and M. G. Pozdeeva

Engels Technological Institute, Branch of Saratov State Technical University, Engels, Saratov oblast, Russia

Received February 14, 2004

Abstract—Cellulose diacetate ultrafiltration membranes for separation of protein–carbohydrate raw materials are fabricated, and their performance characteristics (porosity, permeability, and selectivity) are examined.

DOI: 10.1134/S1070427207010119

Among the common methods for increasing the food and biological values of dairy products is introduction of additional amounts of protein and deficient amino acids, e.g., lysine and threonine. For this purpose, components derived from the secondary dairy material, whey, are widely used.

Whey is a natural by-product from manufacture of cheese, cottage cheese, and dairy-proteinic concentrates; it is classed with secondary dairy products. Data on the composition of whey are given in the table.

Whey contains fat and protein particles (suspended), and also lactose and minerals.

Ultrafiltration is widely used in processing dairy products [1]. In ultrafiltration, retention is caused primarily by the screening effect. However, adsorption of particles on the membrane surface also contributes significantly. Commercial membranes UAM-500 used for ultrafiltration of whey are not mechanically strong and exhibit practically no adsorption properties. Furthermore, their formulation includes such plasticizers and additives as formamide and magnesium perchlorate, whose contact with foodstuffs is undesirable.

In this study we examined the adsorption of proteins on ultrafiltration membranes based on cellulose diacetate (CDA) or, in any case, on cellulose acetate with the degree of substitution $\gamma \leq 240$, modified with charcoal (it was introduced to increase the adsorption capacity and improve the mechanical characteristics of the membranes).

In fabricating CDA ultrafiltration membranes by the dry-wet formation procedure, we used two fractions of charcoal: fine (85 μm) and coarse (160 μm), which were obtained by screening through Capron sieves. The mean degree of polymerization of CDA was 220–250.

Polymer macromolecules used for fabricating membranes should be sufficiently rigid or be capable of forming supramolecular structures. This is necessary, first, to obtain a loose matrix in formation of asymmetric membranes, and, second, to eliminate glass transition in the polymer during exploitation of the membranes, thus preventing their deformation under pressure. Cellulose esters meet these requirements in full measure. Furthermore, an important criterion is the inertness of a polymer against the components to be separated.

Thus, it appears quite reasonable to use cellulose acetate as a material for ultrafiltration membranes.

The membranes were produced from 5, 7, and 10% CDA solutions in acetone. A fixed amount of charcoal was added to the acetone solution, and the mixture was thoroughly stirred. To study the protein adsorption on the membranes, we used a blood substitute (10% albumin stabilized with NaCl). The adsorption was studied interferometrically [2]. The experimental isotherm of the excess adsorption of albumin on the charcoal-filled membranes is shown in Fig. 1.

Composition of whey

Whey	Content, %				
	ash	fat	protein	lactose	minerals
Sweet	6.5	0.20	0.70	4.50	0.50
Acid	6.0	0.20	0.80	4.20	0.60

Previously we reported on the adsorption of albumin on $NaHCO_3$-modified membranes [3] (Fig. 1, curve *1*). In the case of charcoal-filled membrane (Fig. 1, curve *2*), the adsorbate–adsorbate interaction is stronger as compared to the adsorbate–adsorbent interaction, as demonstrated by the convex shape of the isotherm against the concentration axis.

The experimental data were analyzed using the excess Gibbs functions [4]: we constructed the dependences of the chemical potential of the sorbent $\Delta\Phi$ and Gibbs energy ΔG on the albumin concentration (Fig. 2).

Our results show that the adsorption capacity for albumin of the charcoal-filled membranes is higher by a factor of 100 than that of the $NaHCO_3$-filled membranes. Therefore, the charcoal-filled membranes can be recommended for separating protein mixtures.

The membranes were also characterized by their porosity (pore size distribution was not examined) and performance characteristics (permeability and selectivity) as influenced by the porosity. The porosity was determined by electron microscopy on a Hitachi HU-12A microscope (resolution 50 Å).

The porosity of the membranes is plotted in Fig. 3 as a function of the filler content for two fractions of charcoal (85 and 160 μm). Various amounts of charcoal (0.25, 0.5, 0.75, and 1 g) were added into variously concentrated polymer solutions in acetone, and the charcoal content c was expressed in wt %.

Figure 3 shows that the porosity depends on the concentration of the initial polymer solution. The membranes obtained from a 5% solution demonstrate higher porosity: 18.42 and 15.35% in the membranes filled with the coarse and fine fractions of charcoal, respectively. The porosity depends also on the filler content (the higher content, the higher the porosity) and on the filler particle size (the coarser the particles, the higher the porosity).

The ultrafiltration was carried out on a laboratory unit at a pressure of 0.3–0.5 MPa. Figures 4a–4c show the permeability of the membranes as a function of the porosity.

The membranes fabricated from 7% CDA with fine charcoal particles and from 10% CDA with both fine and coarse charcoal particles demonstrated zero permeability for both water and whey.

Our results show (Fig. 4) that the permeability depends on the porosity (it increases with increasing porosity). Therefore, we obtained membranes with a large number of through pores. The permeability depends also on the CDA concentration in the initial acetone solution (the highest permeability was observed in the membranes prepared from a 5% solution). Finally, the permeability for water is higher than that for the whey.

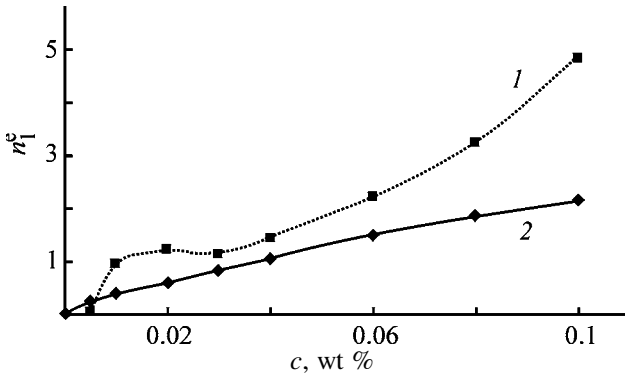

Fig. 1. Isotherms of albumin adsorption on membranes modified with (*1*) $NaHCO_3$ ($n_1^e \times 10^{-5}$) and (*2*) charcoal ($n_1^e \times 10^{-3}$). (n_1^e) Excess adsorption and (c) initial albumin concentration.

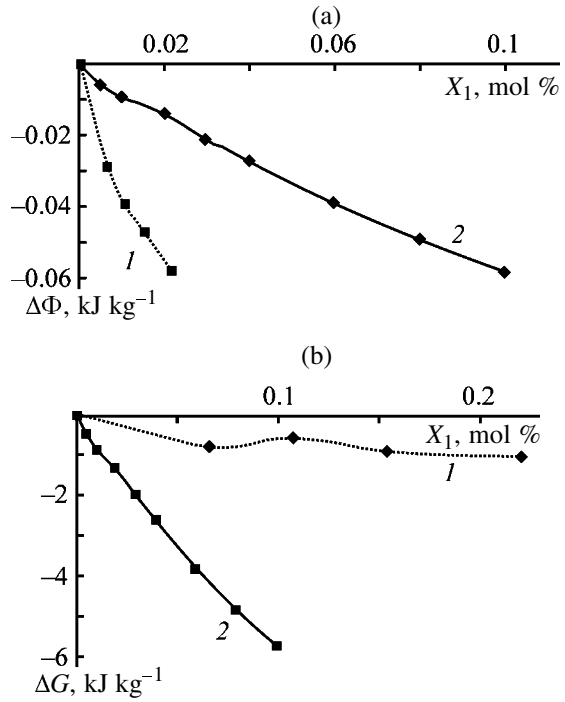

Fig. 2. (a) Chemical potential of the sorbent $\Delta\Phi$ and (b) Gibbs energy ΔG vs. the albumin concentration X_1 for membranes modified with (a) (*1*) $NaHCO_3$ ($X_1 \times 10^{-2}$%) and (*2*) charcoal, and (b) (*1*) $NaHCO_3$ ($X_1 \times 10^{-3}$%, $\Delta G \times 10$) and (*2*) charcoal.

The membrane selectivity with respect to albumin was determined by the Kjeldahl method [5]. The results were plotted as selectivity vs. filler content

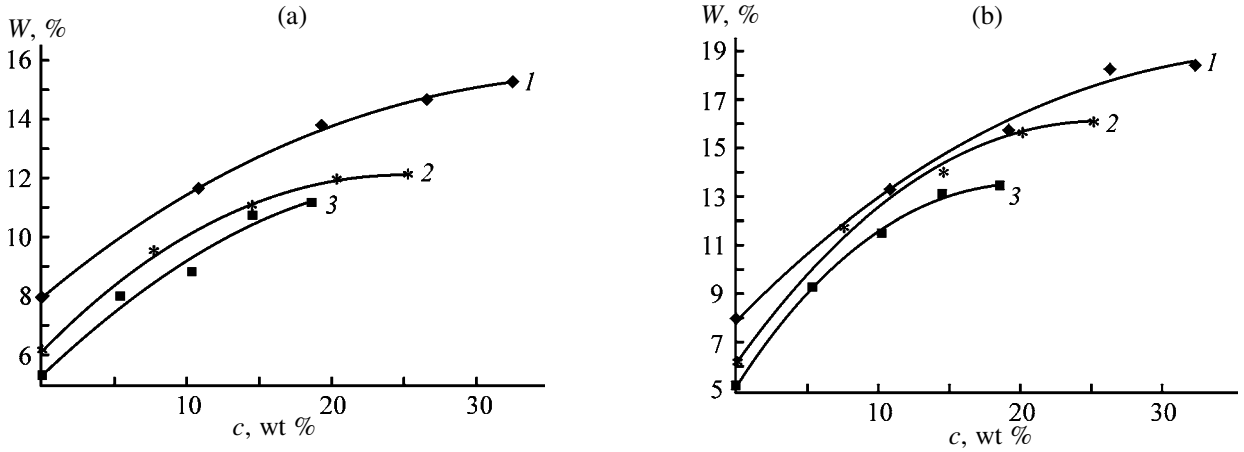

Fig. 3. Porosity W as a function of the filler content c in membranes modified with (a) fine (85 μm) and (b) coarse (160 μm) fractions of charcoal. CDA concentration in the initial acetone solution (%): (*1*) 5, (*2*) 7, and (*3*) 10.

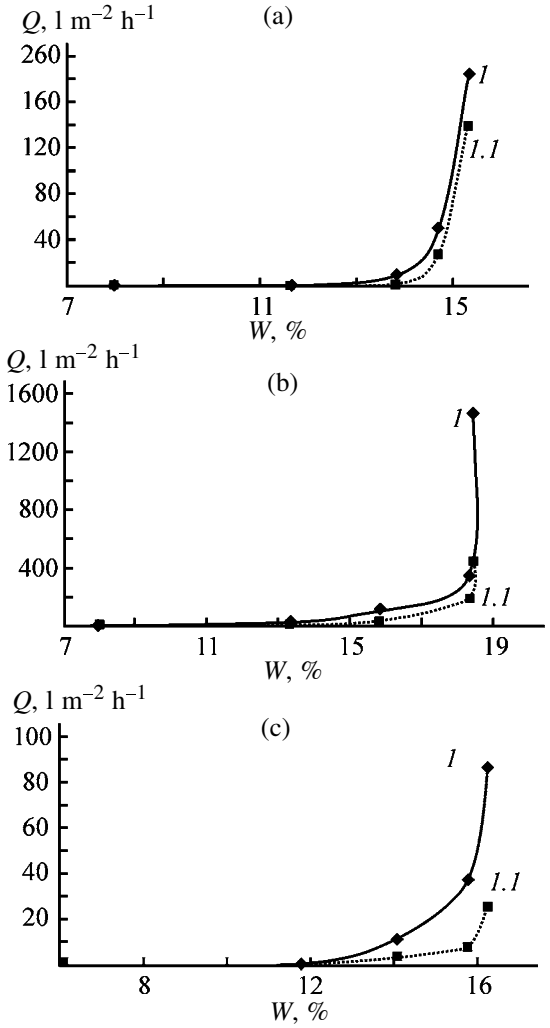

Fig. 4. Permeability Q as a function of the porosity W in membranes fabricated from (a, b) 5% and (c) 7% CDA in acetone. Filler: (a) fine (85 μm) and (b, c) coarse (160 μm). Permeability: (*1*) water and (*1.1*) whey.

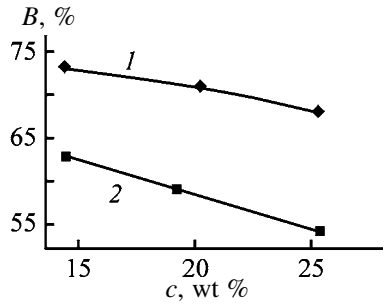

Fig. 5. Selectivity B as a function of the filler (coarse fraction 160 μm) concentration c. CDA concentration in acetone (%): (*1*) 5 and (*2*) 7.

(Fig. 5). The selectivity decreases with increasing permeability. The highest selectivity was observed in the membranes prepared from 5% CDA solutions with coarse charcoal filler (15 wt %) and porosity of 15%. However, the selectivity decreases with increasing CDA concentration in the initial solution. Our results show that the membranes prepared from 5% CDA solution are optimal by all the characteristics (porosity, permeability, and selectivity).

The permeability of the investigated membranes for water and the whey ranged from 0.17 to 24.45 and from 0.07 to 7.2 l m^{-2} min^{-1}, respectively. For commercial UAM-500 membranes, the permeability for water and the whey is 21.3 and 0.32 l m^{-2} min^{-1}, respectively. The selectivity of the membranes studied ranged from 50 to 75%, whereas that for UAM-500 membranes is 62%.

CONCLUSIONS

(1) Modification of cellulose acetate membranes with charcoal allows considerable improvement of the adsorption properties of the membranes for albumin:

sorption capacity increases by a factor of 100 against the $NaHCO_3$-modified membranes.

(2) Introduction of charcoal particles promotes the formation of through pores in the membrane structure, thus increasing its permeability; the total porosity of the membranes studied ranged from 13 to 18%. As a result, the permeability of the membranes for water and the whey increases by 3 and 7 $l\,m^{-2}\,min^{-1}$, respectively, as compared to commercial membranes.

REFERENCES

1. Fetisov, E.A. and Chagrovskii, A.P., *Membrannye molekulyarno-sitovye metody pererabotki moloka* (Membrane Molecular-Sieve Methods for Milk Processing), Moscow: Agropromizdat, 1991.
2. Kiselev, A.V. and Shikalova, I.V., *Zh. Fiz. Khim.*, 1956, vol. 30, no. 1, pp. 94–108.
3. Sedelkin, V.M., Surkova, A.N., Denisova, G.P., and Ramazaeva, L.F., *Zh. Prikl. Khim.*, 2005, vol. 78, no. 8, pp. 1292–1295.
4. Gibbs, J.W., *The Collected Works of J. Willard Gibbs*, New Haven: Yale Univ., 1948.
5. Korenman, Ya.I., *Praktikum po analiticheskoi khimii* (Practical Course of Analytical Chemistry), Voronezh: Voronezh. Gos. Univ., 1992, 2nd ed.

ISSN 1070-4272, Russian Journal of Applied Chemistry, 2007, Vol. 80, No. 1, pp. 62–65. © Pleiades Publishing, Ltd., 2007.
Original Russian Text © T.V. Goreva, Yu.P. Khranilov, 2007, published in Zhurnal Prikladnoi Khimii, 2007, Vol. 80, No. 1, pp. 63–66.

APPLIED ELECTROCHEMISTRY AND CORROSION PROTECTION OF METALS

Theoretical Foundations and Technology of Electrochemical Production of Lead Chrome Pigment from Electroplating Waste

T. V. Goreva and Yu. P. Khranilov

Vyatka State University, Kirov, Russia

Received September 4, 2006

Abstract—An electrochemical method was developed for production of lead chrome pigment from Cr(VI)-containing spent solutions of electroplating shops and lead battery scrap.

DOI: 10.1134/S1070427207010120

Electroplating shops are one of the main sources of environment pollution with compounds of toxic nonferrous metals, including chromium. There exist tens of various processes using chromium(VI) compounds. These are passivation of zinc coatings, anodizing, chromium-plating, etching of copper, chemical and electrochemical polishing, chemical oxidizing, enameling, etc. [1]. As impurities (Cr^{3+} cations and cations of a metal being treated and a coating metal) are accumulated, solutions cease to be usable, which requires their treatment (regeneration) or discharge to sewage works. In this context, collection of spent solutions and recovery of chromium compounds from these solutions are economically and environmentally important.

The most efficient method is that of full regeneration of spent solutions via removal of the impurities being accumulated and recycling of regenerated solutions into the electroplating process. However, integrated treatment to remove all impurities requires, because of their wide diversity, a gross material and energy expenditure and is frequently economically unfeasible.

There exist methods for recuperation of spent chromium-containing solutions (SCCS) with a minimum regenerating processing for their secondary industrial use in other, less demanding technologies. In [1], recommendations were given as to how SCCS should be use to prepare working process solutions containing Cr(VI) compounds. However, this method requires that plants should possess a set of processes employing Cr(VI) compounds and well developed techniques for analysis of SCCS and newly prepared working solutions.

Here we suggest an alternative procedure of SCCS utilization. It consists in processing of these solutions into lead chromate (main component of lead chrome pigment used as a pigment in paint-and-varnish industry) [2]. It is suggested to use starter battery scrap as source of lead. On disassembly of the batteries, the active paste of negative electrodes is utilized to a sufficient extent. Crushing of the paste and its successive dissolution in NaOH and CH_3COOH solutions yields a lead acetate solution for chemical synthesis of lead chrome pigment by interaction with purified SCCS. The metallic component of the battery scrap (plate-connection buses, terminals, element connectors, fragments of negative-plate grids) is remelted into anodes for electrochemical synthesis of lead chrome pigment, based on anodic dissolution of lead in Cr(VI)-containing solutions:

$$2Pb + Cr_2O_7^{2-} + H_2O \rightarrow 2PbCrO_4 + 2H^+ + 4e.$$

Previous studies [3–5] of the electrochemical synthesis of lead chrome pigment have been carried out with a flowing-through electrolyte of constant composition, prepared from pure salts, and a pure lead anode. The technique being developed employs an electrolyte prepared from SCCS. It is recommended to use an anode fabricated from a lead–antimony alloy produced in remelting of the metallic parts of battery scrap, rather than from pure lead.

EXPERIMENTAL

When developing the technique, we examined the following issues: method and mode of SCCS treatment to remove cationic contaminations; type and concentration of the agent activating the anodic dis-

solution of lead, introduced into the electrolyte composition; admissible Cr(IV) concentrations in SCCS; electrolysis mode; verification of the resulting recommendations on real SCCS, with an anode made of a lead–antimony alloy.

The most dangerous among cationic contaminants of SCCS are Cr^{3+} and Fe^{3+} ions, which is due to their interaction in electrolysis with the alkali formed at the cathode. The simplest and most economical is the method of alkaline treatment of SCCS. The residual concentrations of Cr(III) and Fe(III) (both as hydrated cations and as hydroxo complexes), as well as those of Cu(II), Al(III), and Zn(II), which can be contained in SCCS, were calculated by the equation [6]

$$[M] = [M^{n+}] + \Sigma M(OH)_m^{n-m} = [M^{n+}](1 + \Sigma K_m[OH^-]^m),$$

were $[M^{n+}]$ is found from the solubility product of the corresponding hydroxides [7], and K_m are stability constants of the corresponding complexes [7].

The results of the calculation are shown in Fig. 1.

These data show that, as the pH of spent solutions is brought to 7, the concentrations of all kinds of ions, except Zn^{2+}, decrease to values lower than 10^{-5} M. This provides a high degree of purification. However, the expenditure of chemicals for alkalization can be diminished by bringing the pH of SCCS to 5. At this pH value, a high degree of purification to remove Fe^{3+} and Al^{3+} can be achieved, and Cr^{3+}, Cu^{2+}, and Zn^{2+} ions will precipitate as poorly soluble chromates.

In electrochemical synthesis of lead chrome pigment, lead ions are delivered to a solution from the dissolving lead anode. Preliminarily, we studied the anodic behavior of lead in chromium-containing solutions by galvanostatic and potentiodynamic methods. As objects of study served potassium dichromate (PD) and chromium(VI) oxide (ChO) solutions of varied concentrations. A P5848 potentiostat was used; chronovoltammetric (CVA) curves were measured at a potential sweep rate of 2 mV s^{-1}.

As shown by galvanostatic measurements, the electrode is rapidly passivated in pure dichromate solutions (0.025–0.1 M) even at i = 0.01–0.05 A dm^{-2}. The maximum current densities in voltammograms linearly increase as the chromium(VI) concentration in solution decreases and do not exceed 0.06 A dm^{-2}. The calculated thickness of the passive $PbCrO_4$ film on reaching the peak current in the CVA curves is 0.07–0.13 μm. Thus, lead chrome pigment cannot be synthesized in pure potassium dichromate and chromium(VI) oxide solutions at an industrially acceptable

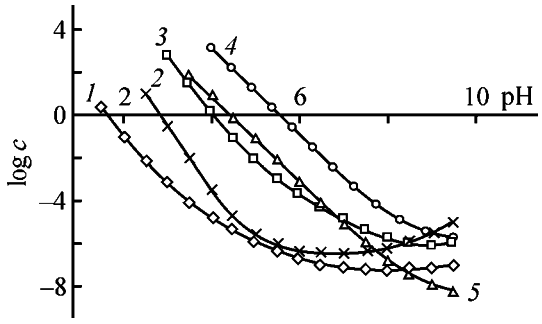

Fig. 1. Calculated pH dependence of the impurity concentration c in the solution: (*1*) Fe(III), (*2*) Al(III), (*3*) Cr(III), (*4*) Zn(II), and (*5*) Cu(II).

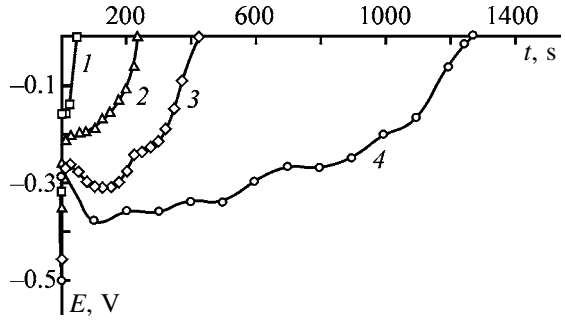

Fig. 2. Galvanostatic curves measured in a potassium dichromate solution. (*t*) Time and (*E*) potential. Sodium acetate concentration (M): (*1*) 0.1, (*2*) 0.2, (*3*) 0.4 (i = 0.1 A dm^{-2}), and (*4*) 0.6 (i = 1 A dm^{-2})

rate, which indicates that an additive that would favor dissolution of the lead anode should be introduced into the solution. As additives of this kind can serve chemical compounds whose anion gives a soluble salt with lead (NO_3^-, BF_4^-, CH_3COO^-). In [4], the behavior of a lead anode in solutions of sodium nitrate, acetate, and diphosphate, and in those simultaneously containing precipitating salts (potassium dichromates) and a depassivating additive, was studied and sodium nitrate was recommended as an agent activating the anodic process. In our case, sodium acetate is recommended as an activator. This is due to its buffer properties, which stabilizes the pH value during electrolysis. In addition, our preliminary experiments demonstrated that nitric acid formed in electrolysis of solutions containing sodium nitrate leads to spalling of the lead anode and contamination of the product.

The galvanostatic (Fig. 2) and CVA (Fig. 3) curves measured in model solutions with a sodium acetate additive demonstrated that, as the activator concentration is raised to 0.6 M and more, the operation of the lead anode at sufficiently high, for industrial purposes, current densities becomes possible. This is indicated in galvanostatic measurements by a steep rise in the transient time upon an increase in the sodium acetate

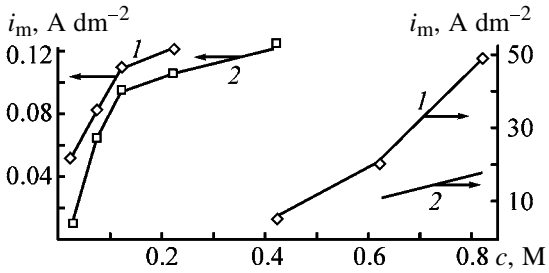

Fig. 3. Peak current density i_m vs. the sodium acetate concentration c in (*1*) 0.1 M solution of chromium(VI) oxide and (*2*) 0.05 M potassium dichromate solution.

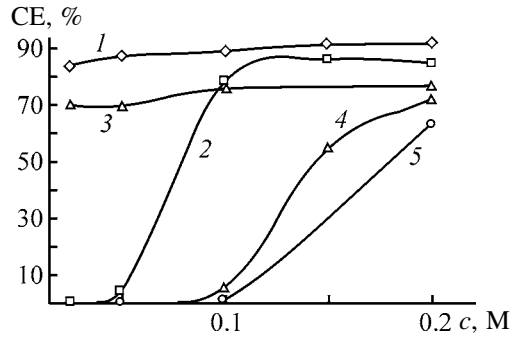

Fig. 4. Variation of the current efficiency CE by oxygen with increasing passivator concentration c in solutions. Q = 2 A h dm^{-2}, sodium acetate concentration 0.6 M. Solution: (*1*) potassium dichromate without sodium acetate, (*2*) potassium dichromate with sodium acetate, (*3*) chromium oxide without sodium acetate, (*4*) chromium oxide with SA, and (*5*) real SCCS based on chromium oxide with sodium acetate.

concentration from 0.1 to 0.6 M. It can be seen from the CVA curves that introduction of sodium acetate makes faster the anodic dissolution of lead, first only slightly, and then, at activator concentrations of 0.6 M and more, by more than two order of magnitude. Thus, the experiments we carried out make it possible to recommend a sodium acetate concentration of 0.6–0.8 M for performing the electrolysis.

The lower peak currents in solutions based on potassium dichromate (Fig. 3) point to a stronger passivation of the lead anode in these solutions. This is accounted for by the higher pH value of dichromate solutions, compared to solutions based on chromium(VI) oxide. It follows from the ionic equilibria of the type

$$Cr_2O_7^{2-} + 2OH^- \rightleftarrows 2CrO_4^{2-} + H_2O$$

that, as pH increases, the fraction of chromate ions, which directly cause precipitation of lead chromate, in solution grows.

Oxygen is evolved at the anode simultaneously with lead chromate formation. To obtain information about the role of oxygen in the anodic process, we measured potential–time curves in the galvanostatic mode at i = 4 A dm^{-2} and electrolysis time of 30 min and simultaneously determined the volume of the evolved oxygen with a gas-collecting buret. The current efficiency was found from the volume of evolved oxygen, reduced to normal conditions. To prevent transfer of oxygen to the solution, it was preliminarily air-saturated before a run. As shown by the study, the potential is shifted in the initial period of active anodic dissolution of lead in the E–t curves in the positive direction and reaches the oxygen evolution potential. After the maximum value is attained, the potential starts to decrease, which is accompanied by its fluctuations resulting from the knocking-off of the viscous near-anode film of lead chromate by gas bubbles.

The revealed fact of a weaker passivation of lead in chromium(VI) oxide solutions, compared with potassium dichromate solutions, is in agreement with the results obtained in a study of the oxygen evolution (Fig. 4, curves *1* and *3, 2* and *4*). The sodium acetate additive depassivates the anode and thereby suppresses oxygen evolution at low Cr(VI) concentrations (curves *2, 4*). At chromium(VI) oxide concentrations exceeding 0.1 M and chromium(VI) concentrations higher than 0.05 M, the oxygen evolution rate steeply increases, so that exceeding these concentrations in industrial electrolysis is not recommended. Measurements of the volume of oxygen evolved from a real spent solution based on chromium(VI) oxide, diluted to different concentrations in terms of chromium(VI), yielded results consistent with those obtained in experiments with model solutions (Fig. 4, curves *5* and *4*).

Experiments on prolonged electrolysis of solutions with various Cr(VI) concentrations and addition of 0.6 M of sodium acetate made it possible to determine the range of working current densities (2.5–12.5 A dm^{-2}) at which the process can be performed with high efficiency and confirmed the recommended limiting Cr(VI) concentration (≤0.1 M) for solutions to be used in electrochemical synthesis of chrome pigment.

It is known [2] that, depending of the solution pH, chrome pigments of different modifications (predetermining the color of the product) are obtained. Experiments in which the pH value was determined in the course of electrolysis made it possible to recommend to carry out the process until the solution is 80–90% depleted of Cr(VI). Under these conditions, the pH value does not exceed 8–9, which corresponds to for-

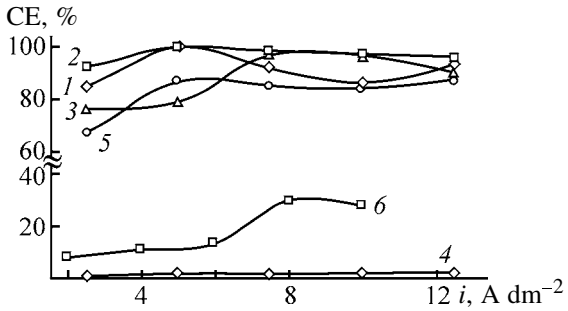

Fig. 5. Effect of the current density i on the CE by lead chromate in solutions of chromium(VI) oxide and potassium dichromate. Sodium acetate concentration 0.6 M, 100% depletion of Cr(VI). Concentration (M): chromium(VI) oxide: (*1*) 0.05, (*2*) 0.1, (*3*) 0.15, and (*4*) 0.2; potassium dichromate: (*5*) 0.05 and (*6*) 0.1.

mation of a neutral lead chromate of the monoclinic modification [2].

The assumption that an alloy of lead and antimony can be used as the anode was confirmed by polarization curves measured on lead and the alloy under comparable conditions. The presence in the alloy of a eutectic phase, which is more weakly passivated in dichromate solutions, predetermines the shift of the zero-current potential of the alloy in the negative direction, relative to the potential of lead. On applying an anodic polarization, the lead chromate film formed on the alloy is less compact than that on lead, which leads to an increase in the peak current and, consequently, to a higher anode dissolution rate. In the case of industrial electrolysis, it is recommended to place an alloy anode in a sheath in order to preclude contamination of the product with antimony.

The recommendations we made were confirmed by experiments on prolonged electrolysis in a solution prepared from an SCCS of the following composition (g l^{-1}): CrO_3 201, H_2SO_4 33.7, and HNO_3 98.3, and made it possible to obtain a high-quality deposit of lead chromate with high current efficiency.

The technology we developed includes the following stages: collection and accumulation of SCCS, with composition homogenization; treatment of SCCS, with pH brought to 5–7; preparation of the filtrate for electrolysis [dilution to a Cr(VI) concentration of 0.1 M and addition of sodium acetate]; electrolysis to 80–90% depletion of Cr(VI); filtration of the electrolyte; and drying of chrome pigment. After the electrolysis, the electrolyte is subjected to partial evaporation (which can be done in a natural way if the process is performed in the batch mode), after which the solution volume is brought to its initial value by introduction of purified SCCS. With the process organized in this way, sodium acetate can be recycled.

CONCLUSIONS

The following technological recommendations for performing an electrochemical synthesis of lead chrome pigment from spent chromium-containing solutions were experimentally substantiated: treatment to remove cationic contaminations with a NaOH solution, with pH brought to 5–7; Cr(VI) concentration in the electrolyte not exceeding 0.1 M; sodium acetate concentration in the electrolyte 0.6–0.8 M; current density range 2.5–12.5 A dm^{-2}; 80–90% depletion of the electrolyte of Cr(VI). The recommendations were confirmed by synthesis of chrome pigment from a real spent chromium-containing solution.

REFERENCES

1. Vinogradov, S.S., *Ekologicheski bezopasnoe gal'vanicheskoe proizvodstvo* (Environmentally Safe Electroplating Shop), Moscow: Globus, 1998.
2. Ermilov, P.I., Indeikin, E.A., and Tolmachev, I.A., *Pigmenty i pigmentirovannye lakokrasochnye materialy: uchebnoe posobie dlya vuzov* (Pigments and Pigmented Paint-and-Varnish Materials: Textbook for Higher Schools), Leningrad: Khimiya, 1987.
3. USSR Inventor's Certificate no. 558 067.
4. Shutov, A.A., Krivtsova, E.V., and Kuvaev, K.G., *Izv. Vyssh. Uchebn. Zaved., Khim. Khim. Tekhnol.*, 1981, vol. 25, no. 6, pp. 721–723.
5. Shutov, A.A. and Burmykina, E.I., *Izv. Vyssh. Uchebn. Zaved., Khim. Khim. Tekhnol.*, 1981, vol. 25, no. 6, pp. 77–80.
6. Butler, J.N., *Ionic Equilibrium (a Mathematical Approach)*, Reading, Massachusetts: Addison–Wesley, 1964.
7. Lur'e, Yu.Yu., *Spravochnik po analiticheskoi khimii* (Handbook of Analytical Chemistry), Moscow: Khimiya, 1989, 6th ed.

ISSN 1070-4272, Russian Journal of Applied Chemistry, 2007, Vol. 80, No. 1, pp. 66–70. © Pleiades Publishing, Ltd., 2007.
Original Russian Text © M.B. Dergacheva, V.N. Statsyuk, L.A. Fogel', 2007, published in Zhurnal Prikladnoi Khimii, 2007, Vol. 80, No. 1, pp. 67–71.

APPLIED ELECTROCHEMISTRY AND CORROSION PROTECTION OF METALS

Electrochemical Preparation of Semiconducting CdTe Films from Ammonia–Chloride Solutions Containing 2,2'-Bipyridine

M. B. Dergacheva, V. N. Statsyuk, and L. A. Fogel'

Sokol'skii Institute of Organic Catalysis and Electrochemistry, National Academy of Sciences of the Republic of Kazakhstan, Almaty, Kazakhstan

Received June 14, 2006

Abstract—An ammonia–chloride electrolyte containing 2,2'-bipyridine for preparing CdTe deposits on a glassy carbon electrode with a particle size of 3–5 nm was developed. The joint electroreduction of Cd(II) and Te(IV) ions was studied by voltammetry.

DOI: 10.1134/S1070427207010132

The existing methods for preparing semiconductor compounds with a particle size of 2.5–25 nm are labor-consuming and involve large number of operations. To such methods belong pyrolysis of organic reagents, dispersion sputtering on heated substrates, and chemical deposition from colloids with intense agitation and subsequent utilization of a stabilizer [1–6]. The disadvantages of these methods consist in complexity of a process, difficulty in obtaining a narrow size distribution of particles, and necessity of additional operations to prevent subsequent aggregation.

Here we suggest an electrochemical method of preparation of a CdTe semiconductor compound with a grain size of 3–5 nm. The advantages of the electrochemical method are that it allows control of synthesis parameters through change in electrochemical parameters, uses simple equipment, and involves complex formation with heterocyclic amines for stabilizing ultradispersed aggregates, which allows preparation of stable metal colloid systems.

Acid electrolytes (pH 0–2) are widely used for electrochemical deposition of CdTe films [7–10]. However, previous studies [11–13] demonstrated the possibility of using ammonia–chloride buffer electrolytes. This made it possible to improve properties of the formed films by decreasing the amount of elemental tellurium codeposited with CdTe, to increase the electrodeposition rate, and to prevent corrosion.

This study is concerned with electrodeposition of the CdTe films from ammonia–chloride buffer electrolytes containing 2,2'-bipyridine. The effect of the grain size of films on the volt–ampere characteristics of CdTe semiconductor under illumination was studied.

EXPERIMENTAL

The electrochemical processes occurring on a glassy carbon electrode upon deposition of CdTe were studied by voltammetry. The composition and properties of the deposits obtained were investigated by physical methods. These involved XPA, electron microscopy, and electron probe analysis. Also, the optical volt–ampere characteristics taken on a Z-curve tracer upon scattered illumination were analyzed. As electrolyte we used ammonia–chloride buffer solutions with pH 8.4 and 9.2, ionic strength $\mu = 2$, and high buffer capacity $\pi = 0.4$, which virtually eliminated variations of pH in a near-electrode layer in the case of discharge of both molecular oxygen and Te(IV) anions (TeO_3^{2-} and $HTeO_3^-$). The volt–ampere curves were measured in a three-electrode Pyrex glass cell with separated cathode and anode compartments. As working electrode we used a glassy carbon electrode with an apparent surface area of 0.07 cm^2. As auxiliary electrode served a platinum electrode with an apparent surface area of 1.5 cm^2. The potentials were measured relative to a silver chloride reference electrode in a saturated potassium chloride solution. The voltammetric studies were performed using a PI-50.1.1 potentiostat, with *I–E* curves recorded with a PDA-1 *XY* recorder.

The cathodic volt–ampere curve obtained in a solution containing 3.8×10^{-4} M Te(IV) (Fig. 1a) shows a region of limiting current, which is due to the reduc-

tion of Te(IV) to Te^0 by reactions (1) and (2),

$$HTeO_3^- + 2H_2O + 4e \rightarrow Te^0 + 5OH^-, \quad (1)$$

$$TeO_3^{2-} + 2H_2O + 4e \rightarrow Te^0 + 4OH^-, \quad (2)$$

with a current peak at the potential $E_m = -0.6$ V and a cathodic current peak at $E_p = -0.9$ V, which is due to the further reduction of elemental tellurium to telluride by reaction (3):

$$Te^0 + 2e \rightarrow Te^{2-}. \quad (3)$$

The ammonium ions, NH_4^+, along with water molecules, can serve as proton-donating molecules. When the direction of the potential sweep is changed in the anodic region, elemental tellurium is oxidized to Te(IV) ($E_p = 0.09$ V).

On introduction of Cd(II) ions into the electrolyte studied, the electroreduction potential of Te(IV) ions is strongly shifted to negative potentials ($\Delta E \geq 300$ mV, Fig. 1b), which corresponds to electroreduction of TeO_3^{2-} and $HTeO_3^-$ anions by the reactions

$$TeO_3^{2-} + 3H_2O + 6e \rightarrow Te^{2-} + 6OH^-, \quad (4)$$

$$HTeO_3^- + 3H_2O + 6e \rightarrow HTe^- + 6OH^-. \quad (5)$$

The effect observed is associated with a decrease in proton-donating ability of a near-electrode layer caused by adsorption of ammonia complexes of cadmium $Cd(NH_3)_4^{2+}$, which, unlike NH_4^+ cations, exhibit no proton-donating ability. This impedes the electrochemical reactions involving TeO_3^{2-} anions, which proceed solely in the presence of proton-donating ions near the electrode.

The complex cations of cadmium react with telluride ions:

$$Cd(NH_3)_4^{2+} + Te^{2-} \rightarrow CdTe + 4NH_3, \quad (6)$$

which results in the formation of CdTe in the near-electrode layer.

We found that CdTe obtained by the electrolysis is the electrochemically active compound and undergoes stepwise oxidation. The anodic volt–ampere curves at reverse sweep of the potential contain two anodic current peaks, at –0.1 and +0.13 V (Fig. 1b). To the anodic peak at $E_1 = -0.1$ V corresponds the reaction

$$CdTe + 4NH_3 - 2e \rightarrow Cd(NH_3)_4^{2+} + Te^0, \quad (7)$$

and to that at $E_2 = +0.13$ V, the reaction

$$Te^0 - 4e \rightarrow Te(IV). \quad (8)$$

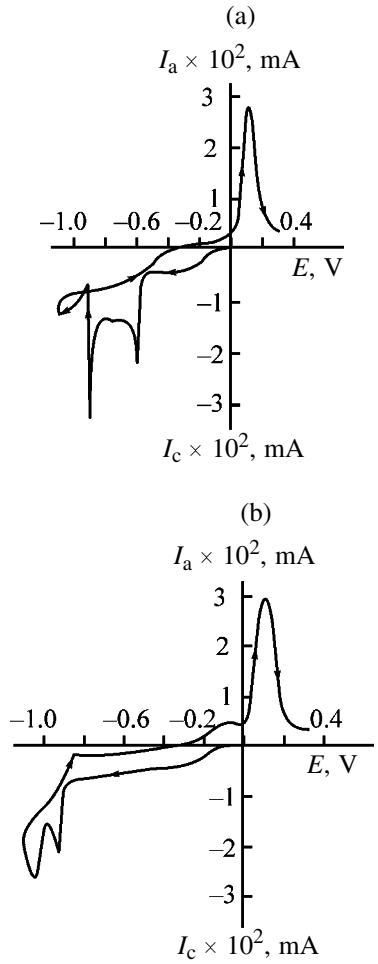

Fig. 1. Cathodic and anodic volt–ampere curves obtained on a glassy carbon electrode in an ammonia–chloride buffer electrolyte (pH 8.4, $\pi = 0.4$, and $\mu = 2$). (a) $c_{Te(IV)} = 3.8 \times 10^{-4}$ M and (b) $c_{Te(IV)} = c_{Cd(II)} = 3.8 \times 10^{-4}$ M. (*I*) Current and (*E*) potential; the same for Fig. 2.

We analyzed how variation of the ratios of the anodic peak currents, which are determined by contributions of CdTe and Te(0) formed on the electrode surface on changing concentration of cadmium ions in the electrolyte, affects the possibility of occurrence of the reaction

$$Te(IV) + 2Te^{2-} \rightarrow 3Te^0. \quad (9)$$

The potentiodynamic curves in oxidation of the CdTe films electroplated from ammonia–chloride buffer electrolytes as functions of the concentrations of the components were analyzed, and the data obtained were used to choose the optimal conditions for electrodeposition of this compound.

To stabilize the size of the CdTe crystals and create conditions for formation of colloid solutions in a near-

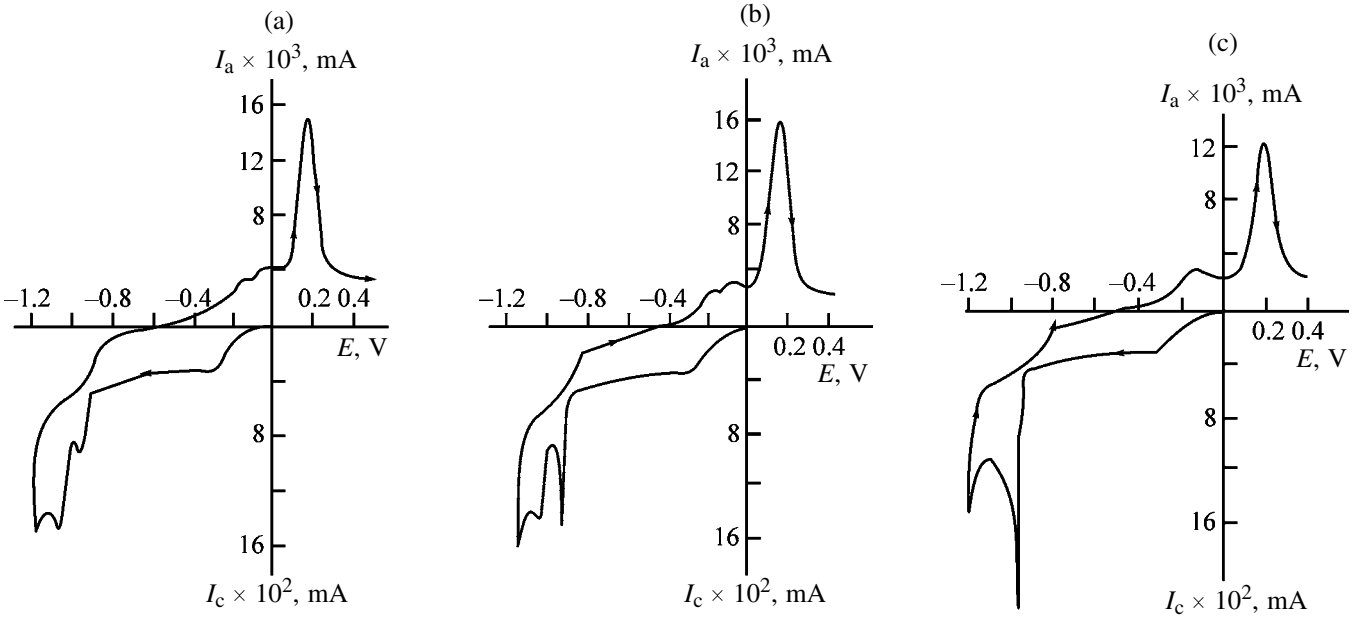

Fig. 2. Volt–ampere curves in joint discharge–ionization of Te(IV) and Cd(II) ions on a glassy carbon electrode in an ammonia–chloride buffer electrolyte with pH 9.2 at varied concentration of 2,2'-bipyridine. $c_{Cd(II)} = c_{Te(IV)} = 3.8 \times 10^{-4}$ M. c_{bipy}, M: (a) 1.8×10^{-4}, (b) 3.6×10^{-4}, and (c) 1×10^{-3}.

electrode space, we used in the study the electrolyte containing 2,2'-bipyridine, which exhibits high adsorption power and forms thermodynamically stable complexes differing in the compositions of the inner and outer coordination spheres. The effect of 2,2'-bipyridine on the electroreduction of Te(IV) and Cd(II) ions on a glassy carbon electrode was established at varied pH values. The above effect on the deposition of CdTe from an ammonia–chloride buffer electrolyte at pH 9.2 is demonstrated in Fig. 2.

The addition of 2,2'-bipyridine to an ammonia–chloride buffer electrolyte shifts the reduction wave related to reaction (1) and the peak at the limiting current of this wave associated with reaction (2) toward negative potentials (Fig. 2). In this case, 2,2'-bipyridine acts as organic surfactant displacing water molecules from the surface. As a result, the amount of the proton-donating ions at the electrode surface decreases. The Te(IV) ions do not form complexes with 2,2'-bipyridine.

At the same time, 2,2'-bipyridine, as the ligand incorporated into the inner coordination sphere, affects the electroreduction of Cd(II). The $[Cd(dipy)_3]TeO_3$ complexes with tellurite in the outer coordination sphere are formed as the 2,2'-bipyridine concentration increases. The electroreduction of Te(IV) anions from these complexes on a glassy carbon electrode is accelerated owing to a decrease in negative charge of the anion. This makes the electroreduction potentials of Te(IV) anions and Cd(II) ions closer. It should be taken into account that the concentration of the Cd^{2+} and Te(IV) ions increases owing to adsorption of the outer-sphere complexes, which allows the current to be increased. Thus, for obtaining CdTe with prescribed qualitative and quantitative characteristics, it is possible to create conditions at which the concentrations of Te(IV) and Cd(II) in the near-electrode space and on the electrode surface can be controlled by varying the 2,2'-bipyridine concentration in joint electroreduction of Te(IV) and Cd(II).

The optimal concentrations of 2,2'-bipyridine in an ammonia–chloride buffer solution with pH 8.4 were determined, ensuring the best conditions for the formation of CdTe deposits on a glassy carbon electrode, at which the electrodeposited CdTe virtually does not contain inclusions of elemental tellurium. The X-ray diffraction patterns of the films plated from these solutions contain solely reflections associated with CdTe, whose crystals have regular cubic structure (Fig. 3).

The effect of the pH of the buffer electrolyte within the pH range 8.4–10.0 at a constant buffer capacity ($\pi = 0.4$) and $\mu = 2.0$ was examined. In an ammonia–chloride solution with pH 9.2, CdTe is not electrodeposited at $E = -1.1$ V. At the same time, on addition of 2,2'-bipyridine, an X-ray amorphous CdTe film

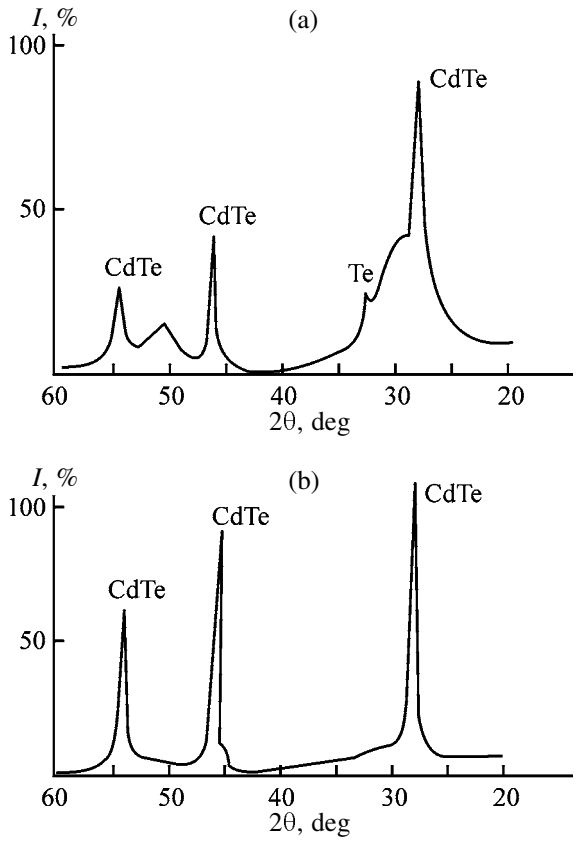

Fig. 3. X-ray diffraction patterns of the CdTe films obtained from an ammonia–chloride buffer electrolyte with pH 8.4 on a glassy carbon electrode. (*I*) Intensity and (2θ) Bragg angle. 2,2'-Bipyridine concentration, M: (a) 0 and (b) 2.9×10^{-4}.

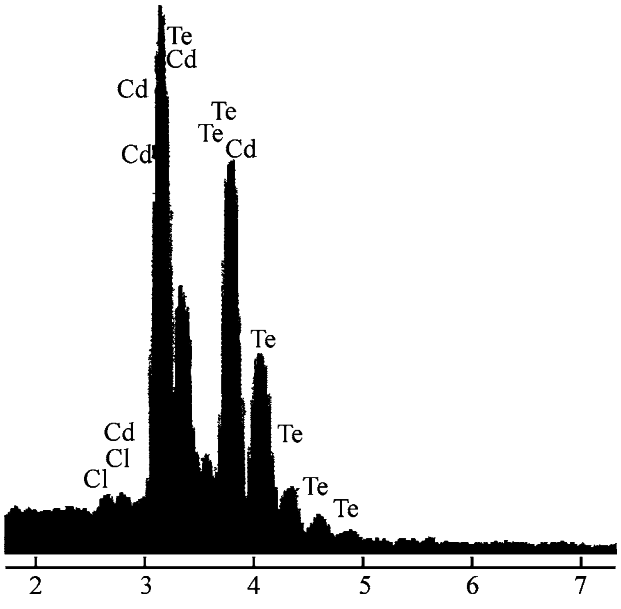

Fig. 4. Energy spectrum of the CdTe film.

Volt–ampere characteristics under illumination of the deposits plated from ammonia–chloride electrolytes at various pH values

pH	c_{dipyr}, M	Grain size, nm	Short-circuit current, μA
8.4	2.9×10^{-4}	5–10	4
	4.4×10^{-4}		5
	5.4×10^{-4}		20
	1×10^{-3}		40
9.2	2.9×10^{-4}	3–8	140
	1×10^{-3}	3–5	700

is formed. Its stoichiometric composition was confirmed by electron probe analysis; it was free of Te(0) impurities (Fig. 4).

The film has strong adhesion to the substrate. The grain size of the nonannealed samples, as determined with an electron microscope, was 5–10 nm for films obtained from an ammonia–chloride electrolyte with pH 8.4, and 3–5 nm for those obtained from an electrolyte with pH 9.2. The CdTe films with an area of 1 cm^2, annealed at 450°C for 10 min, were checked for the sensitivity to visible radiation (see table).

All the deposits give the typical volt–ampere characteristics, indicative of absorption and conversion of light. The samples plated from ammonia–chloride buffer electrolyte with pH 9.2 in the presence of 1×10^{-3} M 2,2'-bipyridine have the best characteristics. The filling coefficient of the loading characteristics was 75%.

CONCLUSIONS

(1) A decrease in the limiting current and the shift of the potential of reduction of Te(IV) ions on a glassy carbon electrode in the buffer solutions studied at low concentrations of Cd(II) ions are due to the occurrence of the surface reactions at the electrode–electrolyte interface, which depend on the concentration of the NH_4^+ proton-donating ions near the charged surface of the electrode.

(2) CdTe obtained by the electrolysis exhibits electrochemical activity and is oxidized in two steps to tellurium(IV) ions, giving two peaks of the anodic current at −0.1 and +0.13 V.

(3) The origin of the peaks in the anodic volt–ampere curves was determined. The possibility of identification of the products of electrochemical reactions obtained by joint electrodeposition of Te(IV) and Cd(II) was demonstrated.

(4) Raising pH of the solutions studied decreases the size of the CdTe grains. The buffer solutions with pH 9.2, $\pi = 0.4$, and $\mu = 2.0$ are optimal for obtaining films with a grain size of 3–5 nm. The formation of the stochiometric CdTe crystals containing no foreign impurities and Te^0 was established.

(5) The effect of the grain size on volt–ampere characteristics under illumination was demonstrated. Decreasing the grain size to 3–5 nm increases the short-circuit current to 700 μA.

REFERENCES

1. Murray, C.B., Norris, D.F., and Bawendi, M.G., *J. Am. Chem. Soc*., 1993, vol. 115, no. 19, pp. 8706–8715.
2. Brus, L., *J. Phys. Chem*., 1986, vol. 90, pp. 2555–2560.
3. Selvan, S.T., Li, C., Ando, N., and Murase, N., *Chem. Lett*., 2004, vol. 33, pp. 434–435.
4. Pehnt, M., Schulz, D.L., Curtis, C.J., et al., *Appl. Phys. Lett*., 1995, vol. 67, no. 15, pp. 2176–2178.
5. Mastai, Y., and Hodes, G., *J. Phys. Chem*., 1997, vol. 101, pp. 2685–2690.
6. Von Vindheim, J., and Cocivera, M.M., *J. Electrochem. Soc., Solid-State Sci. Technol*., 1987, vol. 134, no. 2, pp. 440–443.
7. Panicker, M.P.R., Knaster, M., and Kroger, F.A., *J. Electrochem. Soc*., 1978, vol. 125, no. 4, pp. 566–572.
8. Sella, K., Boncorps, P., and Vedel, J., *J. Electrochem. Soc*., 1986, vol. 133, no. 12, pp. 2043–2047.
9. Engelken, R.D. and Van Doren, T.P., *J. Electrochem. Soc*., 1985, vol. 132, no. 12, pp. 2910–2919.
10. Dergacheva, M.B., Statsyuk, V.N., Fogel', L.A., and Pen'kova, N.V., *Zh. Prikl. Khim*., 2003, vol. 76, no. 6, pp. 947–952.
11. Dergacheva, M.B., Statsyuk V.N., and Fogel, L.A., Abstracts of Papers, *54th ISE Meet*., San Pedro (Brazil), 2003.
12. Dergacheva, M.B., Statsyuk, V.N., and Fogel', L.A., *Zh. Prikl. Khim*., 2004, vol. 77, no. 2, pp. 230–234.
13. Dergacheva, M.B., Statsyuk, V.N., and Fogel, L.A., Abstracts of Papers, *VIII Int. Frumkin Symp. "Kinetics of Electrode Processes,"* Moscow, 2005, p. 264.

ISSN 1070-4272, Russian Journal of Applied Chemistry, 2007, Vol. 80, No. 1, pp. 71–73. © Pleiades Publishing, Ltd., 2007.
Original Russian Text © V.M. Nagirnyi, R.D. Apostolova, E.M. Shembel', 2007, published in Zhurnal Prikladnoi Khimii, 2007, Vol. 80, No. 1, pp. 72–74.

APPLIED ELECTROCHEMISTRY AND CORROSION PROTECTION OF METALS

Anodic Processes Occurring upon V_2O_5 Electrodeposition

V. M. Nagirnyi, R. D. Apostolova, and E. M. Shembel'

Ukrainian State University of Chemical Engineering, Dnepropetrovsk, Ukraine

Received May 12, 2006

Abstract—Kinetics of the anodic processes occurring upon V_2O_5 electrodeposition from $VOSO_4$ solutions containing Na^+ ions was studied by the method of polarization curves. The mechanism of their formation was suggested, based on the analysis of the morphology of the deposit surface.

DOI: 10.1134/S1070427207010144

The conditions of preparation of electrolytic V_2O_5 (e-V_2O_5) by the anodic deposition from aqueous solutions of $VOSO_4$, including those containing Na^+ ions, were considered in [1, 2]. Electrolytic V_2O_5 is a promising cathode material for lithium batteries [3, 4]. Owing to the formation of a compound of the type of $Na_xV_2O_5$, exhibiting higher electrochemical activity and high stable reversible capacity on repeated cycling, e-V_2O_5 plated in the presence of Na^+ ions is of particular interest [5, 6]. In the above studies, inadequate attention was given to the possible mechanisms of the electrolytic formation of oxide molecules and to the associated processes of phase transformations and formation of a molecular crystalline deposit. This was the subject of our study.

The study was performed by the method presented in [2]. The partial polarization curves of the V_2O_5 deposition were constructed on the basis of the current efficiencies at constant I_a. The morphology of the surface of the anodic deposits was studied by the atomic-force microscopy with a nanoscope.

The total and partial polarization curves recorded in anodic deposition of V_2O_5 in the coordinates I_a–E_a and E_a–$\log I_a$, respectively, are shown in Figs. 1a and 1b. In both cases, the total curves consist of lower and higher ascending branches separated by a certain plateau. The lower branches are arranged in order of increasing anode potential to fit the increase in the concentration of Na^+ ions in the solution. The decreasing order of the limiting currents I_a at the inflection points is the same. The higher branches are shifted relative to lower segments in the inverse order along the potential axis. Evidently, the lower portions of the curves mainly reflect the character of variations of the rate of the V_2O_5 deposition at weakly competing reaction of oxygen discharge. With feeding rate of the VO^{2+} ions in a near-electrode layer decreased, the anodic polarization increases, and the lower portions of the curves give way to transition plateaus and then to the higher ascending portions. In the process, the rate of the O_2 evolution becomes dominating and is the higher, the higher the concentration of the Na^+ ions in the solution (Figs. 1a, 1b, curves *2, 3*). The fact that the higher portoins of the curves are arranged in the inverse order with respect to their lower portions is associated with a decrease in oxygen overvoltage corresponding to a decrease in the rate of the V_2O_5 formation and hence to the weaker shielding of the anode surface by the deposit. The above conclusion is also confirmed by the fact that the slope of the total E_a–$\log I_a$ dependences decreases with increasing Na^+ concentration in the solution (Fig. 1b, curves *1–3*). At 0.4 M concentration of the Na^+ ions, the higher portions of the total and partial curves of the O_2 evolution virtually merge together (Fig. 1b, dashed), which shows that the rate of the V_2O_5 deposition under the corresponding conditions approaches zero.

The fact that the total and partial E_a–$\log I_a$ curves of the V_2O_5 deposition are strictly linear (Fig. 1b) allows the processes studied to be considered in terms of the electrochemical kinetics [7]. The slopes of the partial curves of the V_2O_5 deposition (Fig. 1b, curves *1'–3'*, lower portions) increase only slightly with increasing concentration of the Na^+ ions in the solution. Their abnormally high values (0.48, 0.52, and 0.54 V) are likely due to the considerable concentration polarization accompanying electrode processes under the conditions considered [8]. Probably, in the given case, the change in the $dE_a/d\log I_a$ value is also due to the filling of the anode surface by adsorbed oxygen, oxide molecules, and by the mutual influence of the simultaneously occurring anodic processes [7]. Also, it should be taken into account that the outer surface of the double layer, consisting mainly of VO^+ ions, is rather diffuse because of the lack of the elec-

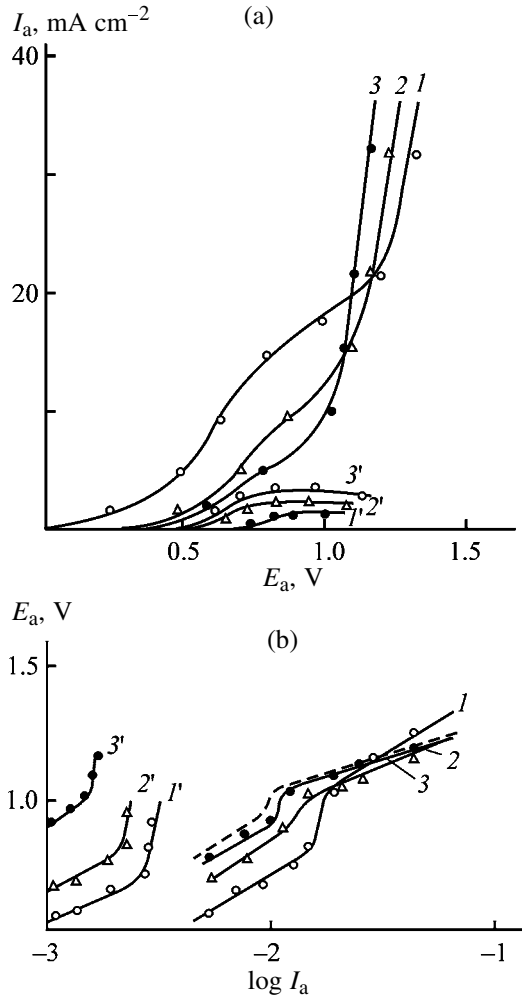

Fig. 1. (*1*–*3*) Total and (*1*'–*3*') partial dependences of the anode potential E_a on (a) anodic current density I_a and (b) $\log I_a$ in V_2O_5 deposition from a 0.25 M solution of $VOSO_4$ in the presence of Na_2SO_4. 80°C, pH 1.8–2.0. Na_2SO_4 concentration, M: (*1*, *1*') 0, (*2*, *2*') 0.2, and (*3*, *3*') 0.4.

trostatic interaction and of the influence of surface phenomena caused by adsorption and evolution of oxygen. Hence, it is probable that the transfer coefficient $\beta \ll 0.5$, which, correspondingly, results in the increased slope.

Thus, the factor largely determining the character of the V_2O_5 deposition is oxygen evolution. In terms of the latest theoretical concepts, oxygen is evolved on the anode through chemisorbed layer of its atoms [9]:

$$2[M + H_2O - 2e \rightarrow (M\text{–}O) + 2H^+] \quad (1)$$

$$(M\text{–}O) + (M\text{–}O) \rightarrow 2M + O_2 \quad (2)$$

$$2H_2O - 4e \rightarrow O_2 + 4H^+ \quad (3)$$

If reactions (1) and (2) actually occur, then the V_2O_5 deposition from a pure $VOSO_4$ solution can be presented by the following reaction equations:

$$M + H_2O - 2e \rightarrow (M\text{–}O) + 2H^+ \quad (4)$$

$$VO^{2+} + (M\text{–}O) - e \rightarrow VO_2^+ + M \quad (5)$$

$$VO_2^+ + VO_2^+ + H_2O \rightarrow V_2O_5 + 2H^+ \quad (6)$$

$$2VO^{2+} + 3H_2O - 2e \rightarrow V_2O_5 + 6H^+ \quad (7)$$

From the energy standpoint, such a mechanism seems quite correct, because adsorbed oxygen atoms may serve as an electron-transferring bridge. In this case, the exact value of the overvoltage in discharge of VO^{2+} ions cannot be determined because of superposition of side factors. At the same time, the standard potential of the V_2O_5 formation [Eq. (7)] and the potential of the start of its deposition on the anode are close, showing that the above value is comparatively low.

The presence of Na^+ ions may promote formation of OH^- ions in the near-electrode layer upon the discharge of water molecules. The OH^- ions can impede partial acidification of the latter layer by accumulation of SO_4^{2-} ions in it. In all probability, this may occur at a low concentration of Na_2SO_4 (0.05 M). Apparently, this effect is responsible for a certain increase in the rate of the V_2O_5 formation [2]. At a high concentration of Na_2SO_4 (0.2–0.4 M), acidification of the near-electrode layer becomes substantial, and the probability of the influence of OH^- ions on the anodic process is virtually reduced to zero. In this case, the anode potential considerably increases, which causes the rates of the V_2O_5 deposition and O_2 evolution to change in favor of the latter process.

The effect of Na^+ ions is clearly revealed in the character of the formation of V_2O_5 phases. Comparison of the morphology of the surface of anodic deposits formed from a pure $VOSO_4$ solution and from that containing Na_2SO_4 (Figs. 2a and 2b, respectively) shows that their structures differ considerably. The former deposits have the amorphous-crystalline structure with a developed surface relief formed by comb-shaped V_2O_5 deposites. The latter deposits have a pronounced crystalline structure characterized by compact and ordered arrangement of crystal growth steps. The mechanism of normal stacking of two-dimensional molecular-crystalline aggregates is assumed for probable nucleation and growth of crystals constituting the latter structure. Energetically, this may be facilitated by the three-dimensional structure of V_2O_5 molecules. Evidently, Na^+ ions suppress the sorption activity of V_2O_5 molecules and restrict the

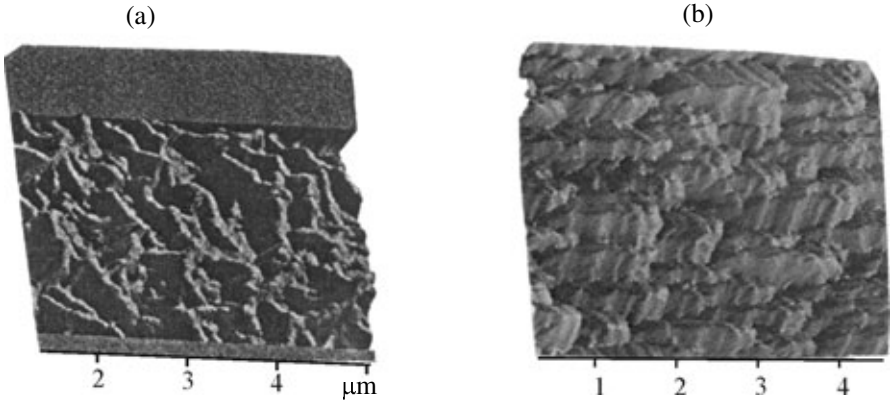

Fig. 2. Morphology of the surface of V_2O_5 electroplated (a) from pure $VOSO_4$ solution and (b) from a $VOSO_4$ solution containing 0.4 M Na_2SO_4; the electrolysis parameters are the same as in Fig. 1.

effect of H_2O molecules on the crystal nucleation and growth in this case.

The nucleation of V_2O_5 crystals starts at a certain potential, which exceeds its steady-state value under the electrolysis conditions. This is, in particular, confirmed by the fact that the anode potential, while switching on current, sharply increases and then gradually decreases to a constant value, which is determined by filling of the anode surface by a V_2O_5 layer. Evidently, this overpotential, along with the inevitable influence of concurrent factors, adsorption of oxygen and H_2O, can be assigned to the additional energy loss resulting from the change in the free surface energy upon appearance of a new phase.

According to X-ray structural and spectral analyses, Na^+ ions and V_2O_5 form a compound of the type of $Na_xV_2O_5$ (x = 0.23–0.28), which is classed with vanadium bronzes [5]. The additional energy consumption for the formation of a new phase is compensated by the heat liberated during the reaction and by the heat of phase transition. As a result, the phase overvoltage in the total energy balance of the electrode process is virtually reduced to zero.

Thus, the anodic deposition of V_2O_5 upon electrolysis from a $VOSO_4$ solution containing Na^+ ions undergoes marked qualitative changes, which are revealed in a decrease of the rate of the oxide deposition and in an increase of the anodic polarization. Simultaneously, the character of the V_2O_5 electrocrystallization changes, i.e., the amorphous-crystalline structure of the anodic deposit transforms into the pronounced crystalline structure.

CONCLUSIONS

(1) The possible mechanisms of the anodic deposition of V_2O_5 from a $VOSO_4$ solution with and without Na^+ ions were considered on the basis of analysis of the I_a–E_a and E_a–$\log I_a$ dependences. The competing evolution of O_2 exerts a decisive effect on the mechanism of the formation of the anodic deposit.

(2) In the presence of Na^+ ions, the rate of the O_2 evolution increases, thus changing the ratio of the formation rates of V_2O_5 and O_2.

(3) According to X-ray structural analysis, Na^+ ions and V_2O_5 form on the anode a compound of the type of $Na_xV_2O_5$. In the presence of Na^+ ions, V_2O_5 with pronounced crystalline structure is deposited on the anode.

REFERENCES

1. Shembel', E.M., Nagirnyi, V.M., Apostolova, R.D., et al., *Zh. Prikl. Khim.*, 2000, vol. 73, no. 3, pp. 409–412.
2. Nagirnyi, V.M., Apostolova, R.D., and Shembel', E.M., *Zh. Prikl. Khim.*, 2001, vol. 74, no. 9, pp. 1429–1432.
3. Andrukaitis, E., Jacobs, P.W.M., and Lorimer, J.W., *Solid State Ionics*, 1999, vol. 37, no. 2, pp. 157–169.
4. Sato, Y., Nomera, T., and Tanaka, H., *J. Electrochem. Soc.*, 1991, vol. 138, no. 9, pp. L37–L39.
5. Apostolova, R.D., Shembel', E.M., and Nagirnyi, V.M., *Elektrokhimiya*, 2001, vol. 37, no. 10, pp. 1205–1213.
6. Shembel, E., Apostolova, R., Nagirny, V., et al., *Power Sources*, 2001, vol. 96, pp. 266–271.
7. Frumkin, A.N., Bagotskii, V.S., Iofa, Z.A., and Kabanov, B.N., *Kinetika elektrodnykh protsessov* (Kinetics of Electrode Processes), Moscow: Mosk. Gos. Univ., 1952.
8. Skorcheletti, V.V., *Teoreticheskaya elektrokhimiya* (Theoretical Electrochemistry), Moscow: Goskhimizdat, 1959.
9. Vetter, K.J., *Elektrochemische Kinetik*, Frankfurt: Springer, 1961.

ISSN 1070-4272, Russian Journal of Applied Chemistry, 2007, Vol. 80, No. 1, pp. 74–77. © Pleiades Publishing, Ltd., 2007.
Original Russian Text © E.A. Belyanovskaya, D.A. Golovko, F.I. Danilov, 2007, published in Zhurnal Prikladnoi Khimii, 2007, Vol. 80, No. 1, pp. 75–78.

APPLIED ELECTROCHEMISTRY AND CORROSION PROTECTION OF METALS

Anodic Treatment of Tin in Alkaline Electrolytes

E. A. Belyanovskaya, D. A. Golovko, and F. I. Danilov

Ukrainian State University of Chemical Engineering, Dnepropetrovsk, Ukraine

Received March 24, 2006

Abstract—Processes of the formation of anodic films on the surface of tin in sodium hydroxide solutions were studied. The optimal conditions of the high-speed anodization, at which conversion coatings with high corrosion resistance can be formed, were determined.

DOI: 10.1134/S1070427207010156

The standard processes for tinplate production involve the step of surface finishing, which is performed in solutions of chromic acid or sodium dichromate [1, 2]. These compounds are highly toxic and hence environmentally hazardous. Active search for the ways to decrease toxicity of the solutions used is stimulated by the environmental standards becoming more and more stringent in many countries. Unfortunately, the developed electrolytes have a complex composition, and surface finishing in them is, as a rule, power-consuming and inefficient [3–5], making their use in the tinplate technology unfeasible. Alternative to traditional chromate coatings may be films formed by anodic treatment of tin in alkaline electrolytes [6–12]. To implement the anodization process in practice, it is necessary to know factors affecting formation of stable films.

Therefore, this study is concerned with the formation of anodic films on tin and with their functional properties.

EXPERIMENTAL

The processes occurring during anodic polarization of Sn were studied by voltammetry with linear potential sweeping. The potential sweep rate was 0.01 V s^{-1}. The electrochemical measurements were performed in solutions of sodium hydroxide (ultrapure grade). The voltammograms were recorded with a PI-50-1.1 potentiostat [13]. Prior to the measurements, the surface of the working electrode was treated by the method suggested in [9].

To determine the corrosion resistance of the anodic films, we recorded the spontaneous activation curves [9–11] in solutions containing 3 wt % NaCl, 0.5 M NaOH, and 0.5 M H_2SO_4, with acetic and citric acids used as buffer solutions. As a criterion of protective ability we used the activation time τ_a during which the film is destroyed in a corrosion-active medium, which results in the shift of the potential to a steady-state value corresponding to the nonoxidized surface. The traditional method [14] of testing the film stability in boiling sulfide-containing solutions of acetic acid was also applied. Testing was performed in a solution containing 0.52 M CH_3COOH + 0.01 M Na_2S (I) and under more rigorous conditions, in a solution containing 2.08 M CH_3COOH + 0.01 M Na_2S (II). The protective properties of the conversion coatings were judged by the appearance of dark brown tin sulfide compounds.

All potentials of the working electrodes were measured in a saturated solution of potassium chloride and are given relative to a silver chloride reference electrode (EVL1-M3.1). The electrolyte temperature was maintained constant with a U-4 ultrathermostat.

The polarization curves in the cathode direction, taken on a tin electrode preanodized at different potentials, are presented in Fig. 1. As seen, the anodic current peaks and a cathodic peak at $E \approx -1.1$ V are present in the voltammograms after the anodizing in the range of potentials from -0.92 to -0.52 V (Figs. 1a–1c). After the treatment at the more positive potentials, from -0.32 to -0.08 V (Figs. 1d–1f), the peak corresponding to the formation of Sn(IV) compounds was not recorded; the peaks of both the anodic dissolution and cathodic reduction were not found after the anodization at $E \geq -0.08$ V. The similar dependences are observed in the cyclic votammograms of the Sn–NaOH system.

Evidently, the revealed trends can be accounted for

by the fact that oxidation of tin to Sn(IV) yields tin hydroxide as intermediate [15–18], which is reduced at $E \approx -1.1$ V. It follows from the results obtained in studying the surface of a tin electrode by X-ray photoelectron spectroscopy [19] that the anodic film consisting of Sn(II) and Sn(IV) is dehydrated at more positive potentials ($E > -0.5$ V). Apparently, the oxides forming in the process are electrochemically stable and are not cathodically reduced in the range of potentials from –1.1 to –0.5 V.

It can be suggested that the increase in the concentration of Sn(IV) oxide, which is more stable than Sn(II) compounds, in the surface film should increase its corrosion resistance and that films obtained by tin anodization can be used as protective coatings. Apparently, industrial anodization of tin coatings should be performed under the conditions precluding formation of hydrated tin(II) oxides. To control the process of the anodic treatment and to optimize its conditions, it is necessary to reveal factors facilitating formation of corrosion-resistant coatings. The region of intense dissolution, wherein the anodic current peaks and the amount of electricity corresponding to them increase, is made broader with increasing concentration of hydroxide ions or the electrolyte temperature. To decrease the dissolution rate of the passive films, the anodization was performed in the electrolytes with a low concentration of hydroxide ions and at lower temperature.

The functional properties of the conversion films on tin are improved upon introduction of film-forming inorganic substances into the electrolyte [20, 21]. In this connection, we studied the effect of additions of sodium carbonate, tungstate, silicate, and phosphate on the anodic voltammograms of a tin electrode.

In the presence of sodium carbonate, the anodic current peaks and the associated amount of electricity Q do not noticeably change in comparison with the case when a 0.5 M NaOH solution is used. On the contrary, on addition of sodium tungstate, silicate, or phosphate, the current density peaks and Q decrease. In this case, for the reactions occurring in the region of oxygen evolution, in the presence of tungsten, silicate, or phosphate ions the overvoltage increases in comparison with that in a NaOH solution.

Nonetheless, the effects revealed are weak and do not allow unambiguous conclusion about the protective properties of the films. Therefore, the other methods allowing control of the film properties are required for the optimization of the processes of tin anodization in alkaline electrolytes. Evidently, it is

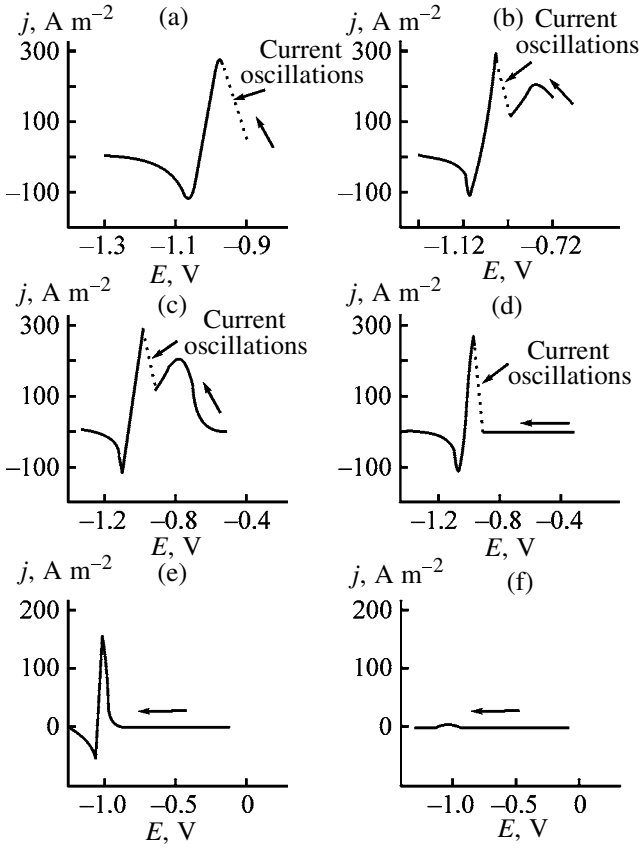

Fig. 1. Voltammograms taken in a 0.5 M NaOH solution at 298 K on a tin electrode anodized for 10 s at various potentials. (j) Current density and (E) potential. E, V: (a) –0.92, (b) –0.72, (c) –0.52, (d) –0.32, (e) –0.12, and (f) –0.08.

reasonable to use the corrosion resistance of the films as the optimization criterion. The times of activation in a 0.5 M NaOH solution of tin electrodes anodized at E = 3.0 V for 2 s in a 0.5 M NaOH solution containing 0.5 M of different additives are given below:

Additive	–	CO_3^{2-}	WO_4^{2-}	SiO_3^{2-}	PO_4^{3-}
τ_a, s	64	64	160	735	105

Our results show that the addition of sodium carbonate does not noticeably change the activation time τ_a in comparison with the pure electrolyte. In the presence of sodium tungstate or phosphate, the activation time of the anodized tin electrode somewhat increases. Nonetheless, the conversion coatings formed by high-speed anodization in a solution containing 0.5 M NaOH + 0.5 M Na_2WO_4, in that containing 0.5 M NaOH + 0.5 M Na_3PO_4, 0.5 M NaOH, or in that containing 0.5 M NaOH + 0.5 M Na_2CO_3 do not inhibit the formation of tin sulfide compounds under the standard conditions of the testing. Evidently, the corrosion resistance of the anodic films obtained from

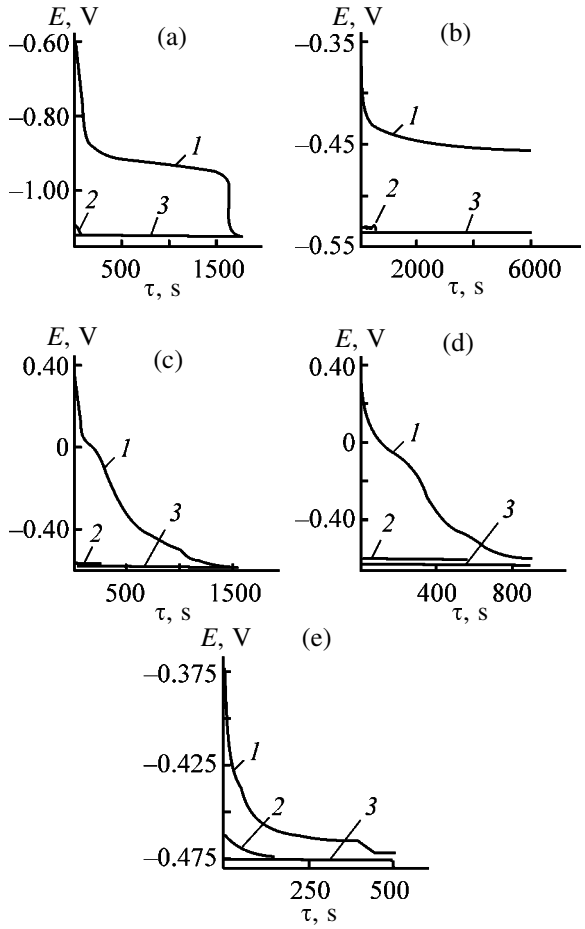

Fig. 2. Curves of spontaneous activation of a tin electrode in solutions containing (a) 0.5 M NaOH, (b) 3% NaCl, (c) 0.5 M CH_3COOH + 0.5 M CH_3COOK, (d) 0.5 M $C_6H_5O_7H_3$ + 0.5 M $C_6H_5O_7Na_3$, and (e) 0.5 M H_2SO_4 after the preliminary treatment by different methods. (*E*) Potential and (τ) time. Treatment method: (*1*) anodization in silicate-containing alkaline electrolyte for 2 s [11], (*2*) cathodic chromation for 2 s [2], and (*3*) no treatment.

the above electrolytes does not meet the existing requirements.

The activation time τ_a of a tin electrode anodized in a solution containing 0.5 M NaOH + 0.5 M Na_2SiO_3 exceeds by about an order of magnitude the activation time of this electrode anodized in a pure electrolyte. The films formed by high-speed anodization in silicate-containing alkaline electrolytes inhibit formation of tin sulfide compounds not only under the traditional (mild) conditions but under the more severe conditions as well.

Significant improvement of the corrosion resistance of the anodic films formed in silicate-containing electrolytes is accounted for by incorporation of silicon inclusions into the coating being formed, which is confirmed by the results of qualitative analysis. Probably, tin silicates are formed on a tin electrode [22].

Organic compounds can also be used to control the properties of oxide–hydroxide coatings. For example, when polyethylene glycol, which is selectively adsorbed on the oxidized surface of tin, is added to the anodizing electrolyte, the activation time can increase by a factor of approximately 2. Probably, the presence of polymer flocculants favorably changes the colloid-chemical conditions of formation of the oxide–hydroxide film and causes the activation time to increase.

Based on the trends revealed, for high-speed anodization of tin coatings we developed an electrolyte containing (M) NaOH 0.25–0.50 and Na_2SiO_3 0.25–1.0, to which 1–2 g l^{-1} of polyethylene glycol can be added [11]. The composition (M) 0.25–0.5 NaOH and 0.75–1.0 Na_2SiO_3 is optimal. The corrosion-resistant conversion coatings are formed in this electrolyte at current densities of 500–1000 A m^{-2} and temperatures not exceeding 298 K.

The comparative tests of the protective properties of the films obtained by the anodic treatment in silicate-containing electrolytes and of those obtained by the traditional method of the cathodic chrome plating [2] showed that the activation time of chrome-plated electrode is considerably shorter than that of the anodized electrode (Fig. 2). In this case, the potentials of the electrodes anodically treated in silicate-containing alkaline solutions are more positive in comparison with the potentials of chromated samples (Fig. 2, curves *1, 2*). The closeness of the potentials of the chromated and unmodified electrodes shows that films forming upon this treatment are porous (Fig. 2, curves *2, 3*). Moreover, the stability of the suggested anodic films in sodium chloride solutions is considerably improved on storage of the anodized samples [24].

The tests performed in a traditional solution containing 0.52 M CH_3COOH + 0.01 M Na_2S, recommended in [14], showed that both the samples oxidized in chromate media and those anodized in silicate-containing alkaline electrolytes contain no tin sulfides, which indicates that the films formed are continuous. Evidently, with increasing acetic acid concentration to 2.08 M, the dissolution rate of the oxide–hydroxide coatings increases. The samples subjected to preliminary chemical treatment or to the cathodic chrome plating, tested in a solution containing 2.08 M CH_3COOH + 0.01 M Na_2S, are coated with SnS. The films obtained by the high-speed treatment (τ_a = 2 s) in the solutions containing silicate ions and polyethylene glycol impede the formation of sulfide com-

pounds on the surface of anodized samples, which confirms the high protective properties of the coatings obtained.

Thus, the corrosion resistance of the conversion coatings formed on tin by the high-speed anodic treatment not only satisfies to the current regulations but also surpasses well that of the traditional chromate coatings.

CONCLUSIONS

(1) Films highly stable in aggressive media owing to the formation of a conversion coating containing the oxide SnO_2 as major component can be obtained by the anodic treatment of tin in alkaline electrolytes.

(2) The corrosion resistance of the conversion coatings formed by the high-speed anodic treatment can be improved by addition into an anodizing electrolyte of alkali metal silicate, tungstate, or phosphate and (or) an organic compound that is selectively adsorbed on hydrated tin oxides. Improvement of the protective properties of anodic films in the presence of Na_2SiO_3, Na_3PO_4, and Na_2WO_4 is associated with the incorporation of SiO_3^{2-}, PO_4^{3-}, and WO_4^{2-} into the forming coating. Among the compounds used, the most effective additive is sodium silicate.

(3) The recommendations to preparation of a high-speed anodizing electrolyte were developed. The optimal composition of the electrolyte and the conditions of the anodic treatment were determined.

(4) The protective properties of the films formed by the suggested process conform to the existing standards and not only compare well with the traditional chromate coatings but even considerably surpass them.

REFERENCES

1. Chernyakhovskaya, I.A., Vilkul, S.V., Cherkasskii, R.I., and Kushnarev, A.V., *Proizv. Prokata*, 2000, no. 5, pp. 19–21.
2. Kantser, I.M., Ilalova, R.Kh., Gulyaeva, G.S., et al., *Stal'*, 1984, no. 11, pp. 73–75.
3. Paramonov, V.A., and Filatova, N.G., *Zashch. Met.*, 2004, vol. 40, no. 3, pp. 295–298.
4. EP Patent 1 445 352.
5. US Patent 5 498 300.
6. Levin, A.I., Prostakov, M.E., and Kochergin, V.P., *Zh. Fiz. Khim.*, 1960, vol. 34, no. 5, pp. 1117–1120.
7. Levin, A.I., Prostakov, M.E., and Kochergin, V.P., *Zh. Prikl. Khim.*, 1960, vol. 33, no. 9, pp. 2102–2108.
8. Levin, A.I. and Prostakov, M.E., *Zh. Vses. Khim. O–va. im. D.I. Mendeleeva*, 1963, vol. 8, no. 5, pp. 524–529.
9. Golovko, D.A., and Belyanovskaya, E.A., *Vopr. Khim. Khim. Tekhnol.*, 1999, no. 1, pp. 84–87.
10. Golovko, D.A., Belyanovskaya, E.A., and Danilov, F.I., *Fiz.-Khim. Mekh. Mater.*, 2000, no. 1, pp. 307–310.
11. Ukrainian Patent 49 220.
12. Golovko, D.A., and Belyanovskaya, E.A., *Vopr. Khim. Khim. Tekhnol.*, 1999, no. 1, pp. 83–84.
13. Golovko, D.A., Belyanovskaya, E.A., Krivoruchko, V.M., and Danilov, F.I., *Materialy IV Mezhdunarodnoi konferentsii "Problemy korrozii i protivokorrozionnoi zashchity materialov (Korroziya 98)"* (Proc. IV Int. Conf. "Corrosion and Corrosion Protection of Materials (Corrosion 98)"), Lviv, 1998, pp. 448–450.
14. Vitkin, A.I., *Proizvodstvo elektroliticheski luzhenoi zhesti* (Tinplate Production), Moscow: Metallurgizdat, 1959.
15. Nguen Dyk, K., and Sukhotin, A.M., *Zh. Prikl. Khim.*, 1990, vol. 63, no. 8, pp. 1818–1821.
16. Nguen Dyk, K., and Sukhotin, A.M., *Zh. Prikl. Khim.*, 1990, vol. 63, no. 8, pp. 1737–1743.
17. Reingeverts, M.D. and Sergeeva, N.A., *Zh. Prikl. Khim.*, 1996, vol. 69, no. 11, pp. 1862–1868.
18. Huang, B.X., Tornatore, P., and Li, Y.-S., *Electrochim. Acta*, 2000, vol. 46, no. 5, pp. 671–679.
19. Ansell, R.O., Dickinson, T., Povey, A.F., and Sherwood, P.M.A., *J. Electrochem. Soc.*, 1977, vol. 124, no. 9, pp. 1360–1364.
20. Chernenko, V.I., Snezhko, L.A., and Papanova, I.I., *Poluchenie pokrytii anodno-iskrovym elektrolizom* (Formation of Coatings by Anodic Spark Electrolysis), Leningrad: Khimiya, 1991.
21. *Spravochnik po elektrokhimii* (Handbook on Electrochemistry), Sukhotin, A.M., Ed., Leningrad: Khimiya, 1981.
22. Golovko, D.A., Belyanovskaya, E.A., and Danilov, F.I., *Visn. Dnipropetrovs'k. Univ.*, 2000, no. 5, pp. 50–56.
23. Nechaev, E.A., *Khemosorbtsiya organicheskikh veshchestv na oksidakh i metallakh* (Chemisorption of Organic Substances on Metals and Oxides), Kharkov: Vyshcha Shkola, 1989.
24. Golovko, D.A., Belyanovskaya, E.A., and Danilov, F.I., *Vopr. Khim. Khim. Tekhnol.*, 2000, no. 1, pp. 124–127.

ISSN 1070-4272, Russian Journal of Applied Chemistry, 2007, Vol. 80, No. 1, pp. 78–82. © Pleiades Publishing, Ltd., 2007.
Original Russian Text © I.N. Ganiev, M.T. Norova, F.U. Obidov, 2007, published in Zhurnal Prikladnoi Khimii, 2007, Vol. 80, No. 1, pp. 79–83.

APPLIED ELECTROCHEMISTRY AND CORROSION PROTECTION OF METALS

Effect of Strontium Additions on the Corrosion-Electrochemical Behavior and High-Temperature Oxidation of Al + 6% Li Alloy

I. N. Ganiev, M. T. Norova, and F. U. Obidov

Nikitin Institute of Chemistry, Academy of Sciences of the Republic of Tajikistan, Dushanbe, Tajikistan

Received April 13, 2006

Abstract—Effect of strontium on the corrosion-electrochemical behavior of the Al + 6% Li alloy was studied.

DOI: 10.1134/S1070427207010168

One of the most important present-day goals in manufacture of structural materials is the necessity for improving their strength and anticorrosion characteristics. Aluminum and its alloys are used in various areas of modern technology, and, in this context, the problem of corrosion control to prolong the service life of equipment becomes increasingly important.

A study of the electrochemical behavior of aluminum in neutral and alkaline–salt solutions is of indubitable importance, because it can reveal specific features of how the metal is activated on the background of comparatively high rates of the anodic process [1].

Studies of this kind are also of theoretical interest, because, despite the available publications on the electrochemistry of aluminum, many processes occurring on aluminum in solutions of varied nature have no unambiguous theoretical interpretation based on reliable experimental results. Experimental data on the effect of the solution pH in a wide range of concentration on the anodic behavior of aluminum are scarce. The mechanisms of corrosion and anodic dissolution of aluminum in neutral electrolytes are insufficiently understood [2].

Alloying of aluminum alloys with lithium leads to a significant decrease in the density of an alloy and raises its strength, heat resistance, and elastic modulus. In this case, depending on the nature of a third alloying component, the density of Al–Li alloys decreases by approximately 11% and the elastic modulus, by 4%, compared to D16 alloy. Alloys of the Al–Li system have been used to develop industrial alloys VAD-23, 1420, 1430, 1450, etc., which exceed D16T alloy in corrosion resistance and approach AMg6M alloy in this regard. These alloys are used to fabricate half-finished presswork and rolled products. To improve the corrosion resistance of aluminum alloys with lithium, they are additionally alloyed with manganese, cadmium, or zirconium [3].

Based on the concept of improvement, by alloying with anodic microadditives, of the corrosion resistance of alloys that can be passivated, we examined in this study the effect of strontium additives on the electrochemical behavior of an aluminum–lithium alloy containing 6% Li [4, 5]. As is known, the standard potential of the Sr/Sr^{2+} system is –2.89 V [6]. Thus, strontium is an anode with respect to the Al + 6% Li alloy whose stationary potential is –1.020 V.

EXPERIMENTAL

We prepared alloys from A995 aluminum, LE1 lithium, and StM1 metallic strontium. The alloys were obtained in corundum crucibles in a resistance furnace at 750°C under a layer of a flux of the composition (wt %): NaCl 32.5, KCl 32.5, and LiCl 35. Taking into account the anodic properties of strontium and its solubility in the aluminum–lithium alloy, we chose the following relative concentrations of the alloying component (wt %): 0.01, 0.05, 0.10, and 0.50. The study was performed using a PI-50-1 potentiostat with an LKD-4 self-recorder in a 3, 0.3, or 0.03% NaCl

Table 1. Corrosion potential of the Al + 6% Li alloy modified with strontium in relation to the NaCl electrolyte concentration

c_{Sr}, wt %	$-E_{cor}$, V, at indicated NaCl content, wt %		
	0.03	0.3	3.0
–	0.980	1.000	1.080
0.01	0.980	1.000	1.050
0.05	0.950	0.950	1.000
0.10	0.900	0.940	0.950
0.50	0.860	0.920	0.920

Table 2. Corrosion rate of the Al + 6% Li alloy in a NaCl electrolyte at varied content of strontium

c_{Sr}, wt %	NaCl content, wt %					
	0.03		0.3		3.0	
	i_{cor}, A m^{-2}	$K \times 10^{-3}$, g m^{-2} h^{-1}	i_{cor}, A m^{-2}	$K \times 10^{-3}$, g m^{-2} h^{-1}	i_{cor}, A m^{-2}	$K \times 10^{-3}$, g m^{-2} h^{-1}
–	0.035	11.7	0.060	20.01	0.080	26.8
0.01	0.029	9.72	0.024	8.04	0.024	8.04
0.05	0.015	5.03	0.019	6.37	0.020	6.70
0.10	0.022	7.38	0.025	8.38	0.028	9.38
0.50	0.024	8.04	0.030	10.05	0.038	12.73

solution at a potential sweep rate of 2 mV s^{-1} by the procedure described in [7]. A silver chloride electrode served as reference. All the potentials are given relative to this electrode. The results obtained are listed in Tables 1–3.

As is known, the corrosion behavior of metals and alloys can be judged from various electrochemical characteristics. The steady-state value of the free-corrosion potential and the type of its dependence on the test time can give important evidence concerning the behavior of a metal in a corrosion medium. As a rule, a large shift of the corrosion potential in the positive direction indicates that the rate of the anodic reaction may decrease due to passivation. Thereby, it can be tentatively predicted that a system of this kind will be more corrosion-resistant under natural working conditions [8]. The time dependence of the free-corrosion potential of the starting Al + 6% Li alloy and alloys with varied content of strontium (Fig. 1) indicates that a sharp shift of the potential to more positive values is observed during the first minutes after an alloy is submerged in the electrolyte solution. In this case, the free-corrosion potential stabilizes in 40 min for the unmodified alloy and in 20–30 min for modified alloys, which points to their rather strong passivation under the action of strontium additives. For example, the corrosion potential of the unmodified alloy kept in a 3% NaCl solution for 1 h is –1.020 V, whereas for the alloy containing 0.50% Sr, it is –0.840 V. A similar tendency is observed in all the three media we studied. However, the variation of

Table 3. Pitting potential E_p of alloys of the Al–Li–Sr system in relation to the NaCl content

c_{Sr}, wt %	$-E_p$, V, at indicated NaCl content, wt %		
	0.03	0.3	3.0
–	0.620	0.680	0.680
0.01	0.620	0.640	0.680
0.05	0.580	0.630	0.680
0.10	0.480	0.620	0.680
0.50	0.460	0.620	0.670

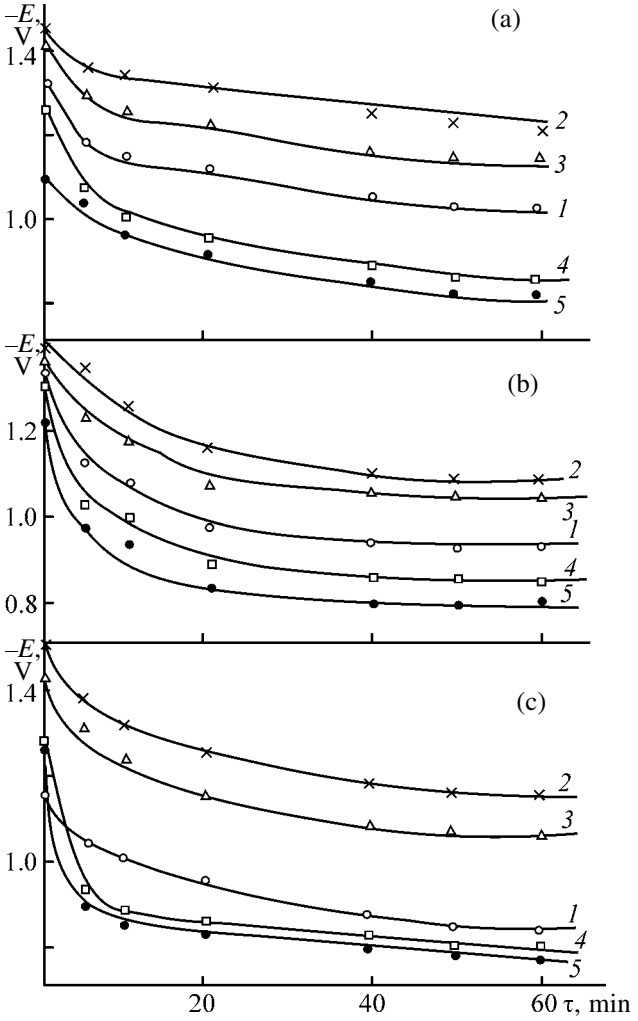

Fig. 1. Variation with time τ of the free-corrosion potential $-E$ of (*1*) Al + 6% Li alloy and (*2*–*5*) that containing strontium. Electrolyte: NaCl solution; NaCl concentration, wt %: (a) 3.0, (b) 0.3, and (c) 0.03. Sr content, wt %: (*2*) 0.01, (*3*) 0.05, (*4*) 0.10, and (*5*) 0.50; the same for Fig. 2.

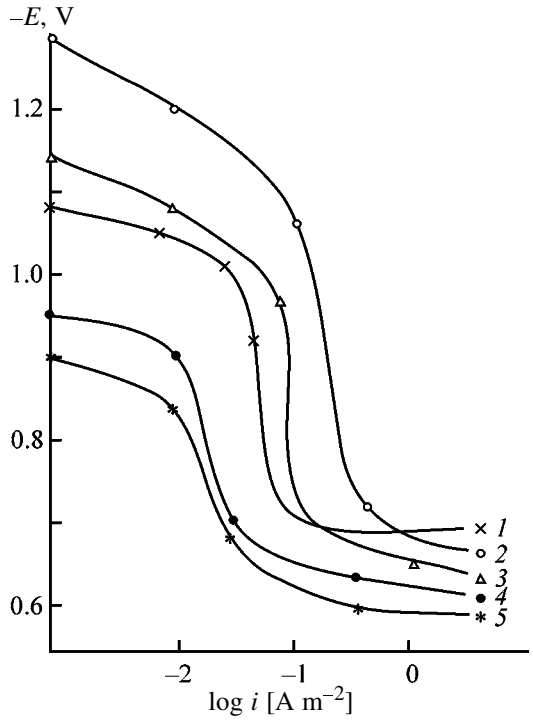

Fig. 2. Potentiodynamic anodic polarization curves (potential sweep rate 2 mV s^{-1}) of (*1*) Al + 6% Li alloy and (*2*–*5*) that containing strontium. Electrolyte: 3% NaCl solution; 298 K. (*E*) Potential and (*i*) current density.

the free-corrosion potential depends on the strontium content in a different way. At 0.05 wt % strontium in the alloy, the free-corrosion potential is more negative that that of the starting alloy. Further increase in the concentration of strontium makes the free-corrosion potential more positive, compared with that of the starting alloy.

Addition of the alloying component in amounts of 0.01–0.05 wt % shifts the corrosion potential of the starting alloy in the positive direction. As the concentration of chloride ions increases, the corrosion potential shifts in the negative direction, which indicates that the corrosion resistance of alloys decreases as the medium becomes more corrosive (Table 1). This is confirmed by a calculation of the corrosion rate of the alloys from the cathodic branch of potentiodynamic curves. The results of this calculation are listed in Table 3.

It can be seen that addition of the alloying components in an amount of up to 0.05 wt % decreases the corrosion rate of the alloys by a factor of approximately 3–3.5 in media with 0.3 and 3% NaCl and by a factor of 2 in a medium with 0.03% NaCl.

Table 3 lists the pitting potentials of the alloys in relation to the concentrations of the NaCl electrolyte and the alloying additive. As the concentration of chloride ions increases, the pitting potential shifts, similarly to the corrosion potential of the alloys, in the negative direction. In an electrolyte with 0.03% NaCl, addition of strontium leads to an increase in the pitting potential of the alloys, thereby making them more pitting-resistant. In the rest of the media studied, such a behavior is not observed.

Figure 2 shows anodic polarization curves of the alloys of the Al–Li–Sr system, measured in 3% NaCl solution after a preliminary cathodic treatment. Thus, any influence of an oxide film was ruled out. As can be seen in Fig. 2, the polarization curves of the alloys containing 0.01–0.05 wt % strontium lie to the right of the curve for the starting alloy, and the curves of the alloys with 0.1–0.5 wt % Sr lie below the curves of the unmodified alloy.

Analysis of the anodic curves of the alloys, measured in other media, shows that, as the NaCl solution is diluted (the effect of the chloride ions of the medium becomes weaker), the width of the passive region, ΔE_{pas}, increases from 300 (in a 3% NaCl solution) to 700 mV (in 0.03 and 0.3% NaCl solutions). Consequently, the alloy samples under study are more passive in the solution with the lowest content of chloride ions, i.e., more resistant to corrosion-induced degradation. This is also evidenced by the fact that E_p shifts in the positive direction as the solution is diluted.

In view of the fact that various-purpose articles are cast under industrial conditions from liquid aluminum alloys containing 3–8% lithium, it was of interest to study oxidation of binary aluminum–lithium alloys that serve as a basis in the development of more complex formulations. A study of the oxidation of binary alloys containing 5–6% lithium demonstrated that alloys of more complex composition can be developed using these alloys. The effect of strontium on the oxidizability of the alloys was examined for the example of an alloy containing 6% lithium.

To study the kinetics of oxidation of alloys of the systems Al–Li and Al–Li–Sr under isothermal conditions, we used the thermogravimetric method based on continuous weighing of the molten metal [9]. The change in the mass was judged from the extension of a spring, with a KM-8 cathetometer. The true oxidation rate was calculated from tangents drawn from the origin of coordinates to the alloy oxidation curves by the formula $K = g/s\Delta\tau$. The apparent activation energy of oxidation was calculated from the slope of the straight line describing the dependence $\log K$–$1/T$.

Table 4. Kinetic parameters of oxidation of liquid alloys in the aluminum–lithium system with atmospheric oxygen

Content in alloy, at %		Oxidation temperature, K	True oxidation rate $K \times 10^4$, kg m^{-2} s^{-1}	Apparent activation energy, kJ mol^{-1}
Al	Li			
100	–	973	20.0	74.48
		1023	34.48	
99.9	0.1	973	24.06	60.03
		1023	35.29	
99.0	1.0	973	26.33	42.48
		1023	40.00	
95.0	5.0	973	36.42	15.60
		1023	42.30	
90.0	10.0	973	48.40	14.58
		1023	55.09	

Table 5. Effect of strontium on kinetic and energy parameters of oxidation of the solid Al + 6% Li alloy

Sr content of Al + 6% Li alloy, wt %	Oxidation temperature, K	True oxidation rate $K \times 10^4$, kg m^{-2} s^{-1}	Apparent activation energy, kJ mol^{-1}
0.0	723	6.02	15.92
	793	7.58	
0.01	723	4.33	33.44
	793	7.09	
0.05	723	5.50	31.85
	793	8.70	
0.1	723	9.75	25.48
	793	14.17	

We studied the kinetics of oxidation of liquid alloys of the aluminum–lithium system in the temperature range 973–1023 K. The compositions of the alloys we studied are listed in Table 4.

As the temperature becomes higher, the specific mass of a sample, g/s, increases with time. The oxidation of liquid aluminum is intensive during the first 20 min and the oxidation curves are linear. Further, the oxidation process becomes hindered and the curves become parabolic because of the formation of a protective oxide layer mostly composed of γ-Al_2O_3. The oxidation rate of aluminum at temperatures of 973–1023 K is in the range from 20.0×10^{-4} to 34.38×10^{-4} kg m^{-2} s^{-1}. The apparent activation energy of oxidation is 74.48 kJ mol^{-1}.

The oxidation of liquid Al–Li alloys containing 0.1, 1.0, 5.0, and 10.0 at. % Li was studied at 973 and 1023 K. The process follows the linear law and then, as a dense oxide film is formed, the curves become parabolic. As the temperature increases and the lithium content grows, the oxidation rate increases. The true oxidation rate becomes higher, which is, in turn, accompanied by a decrease in the apparent activation energy of oxidation (Table 4).

The kinetic and energy parameters of oxidation of Al + 6% Li alloys containing 0.01, 0.05, and 0.1 wt % strontium are listed in Table 5. The oxidation of the alloy with 0.01 wt % strontium was studied at 723 and 793 K. During the first 10 min, we observed a steep increase in the oxidation rate of the sample, which reached a value of 46 mg cm^{-2}, and then a slight increase in the specific mass of the sample, which is presumably due to the protecting capacity of the oxide film. However, at a large thickness of this film, the maximum value of $\Delta g/s$ was 55 mg cm^{-2}, and the apparent activation energy was as high as 33.44 kJ mol^{-1}.

The kinetic oxidation curves of the Al + 6% Li alloy containing 0.05 wt % strontium demonstrate that the oxidation of the alloy follows the parabolic

law with diffusion hindrance, and the process is complete by the 15th–20th minute. The true oxidation rate changes from 5.59 to 8.70 kg m^{-2} s^{-1}, and the apparent oxidation energy reaches a value of 31.85 kJ mol^{-1}.

The alloy with 0.1 wt % strontium was subjected to oxidation at 723 and 793 K. The kinetic curves of this alloy are described by the parabolic law. The oxidation process is complete by 25th minute of interaction between the metal and atmospheric oxygen. The true oxidation rate is 9.75×10^{-4} and 14.17×10^{-4} at 723 and 793 K, respectively, and the apparent activation energy is 25.48 kJ mol^{-1}.

CONCLUSIONS

(1) The corrosion-electrochemical behavior of alloys of the Al–Li–Sr system in a NaCl electrolyte was studied by the potentiometric method. It was shown that alloying with strontium makes the corrosion rate of the alloys 2–3 times lower, depending on the concentration of the NaCl electrolyte.

(2) The effect of chloride ions on electrochemical characteristics of aluminum–lithium alloys modified with strontium was examined by the potentiodynamic method. It was shown that a 10- or 100-fold decrease in the concentration of chloride ions makes the corrosion rate of the alloys lower and shifts the electrode potentials in the positive direction.

(3) A study of the anodic behavior of aluminum–lithium alloys modified with strontium demonstrated that the pitting resistance of the alloys increases with the strontium concentration, which is evidenced by a shift of the pitting potential in the positive direction for the alloys with 0.1 wt % strontium. The highest pitting resistance is observed for the alloys in a medium with NaCl content of 0.03 and 0.3%.

(4) The kinetics of oxidation of aluminum–lithium alloys modified with strontium was studied by the method of thermogravimetry, and it was found that the oxidation process follows the parabolic law. Addition of up to 0.05 wt % strontium to the Al + 6% Li alloy enhances its oxidation resistance. Further increase in the strontium concentration leads to a rise in the oxidation rate of the basic alloy.

REFERENCES

1. Izotova, S.G., Sysoeva, V.V., and Artyugina, E.D., *Zh. Prikl. Khim.*, 1985, vol. 58, no. 9, pp. 2115–2118.
2. Artyugina, E.D. and Sysoeva, V.V., *Zh. Prikl. Khim.*, 1985, vol. 58, no. 4, pp. 921–924.
3. Fridlyander, I.N., *Alyuminievye deformiruemye konstruktsionnye splavy* (Deformable Aluminum Structural Alloys), Moscow: Metallurgiya, 1979.
4. Vyazovikina, N.V., *Zashch. Met.*, 1999, vol. 35, no. 5, pp. 493– 499.
5. Vyazovikina, N.V. and Ponomarev, S.S., Abstracts of Papers, *The 1997 Joint Int. Meet.*, Paris, 1997, vol. 97-2, no. 350, p. 428.
6. Akhmetov, N.S., *Obshchaya i neorganicheskaya khimiya* (General and Inorganic Chemistry), Moscow: Vysshaya Shkola, 1988.
7. Norova, M.T. and Ganiev, I.N., *Zh. Prikl. Khim.*, 2002, vol. 75, no. 4, pp. 567–569.
8. Sinyavskii, V.S., Volkov, V.D., and Kalinin, V.D., *Korroziya i zashchita alyuminievykh splavov* (Corrosion and Protection of Aluminum Alloys), Moscow: Metallurgiya, 1986.
9. Lepinskikh, B.M. and Kiselev, V.M., *Izv. Akad. Nauk SSSR*, *Metally*, 1974, no. 5, pp. 51–54.

ISSN 1070-4272, Russian Journal of Applied Chemistry, 2007, Vol. 80, No. 1, pp. 83–86. © Pleiades Publishing, Ltd., 2007.
Original Russian Text © D.Yu. Turaev, 2007, published in Zhurnal Prikladnoi Khimii, 2007, Vol. 80, No. 1, pp. 84–87.

APPLIED ELECTROCHEMISTRY AND CORROSION PROTECTION OF METALS

Use of Membrane Electrolysis for Recovery of Heavy Metal Ions

D. Yu. Turaev

Mendeleev Russian University of Chemical Engineering, Moscow, Russia

Received March 30, 2006

Abstract—Use of membrane electrolysis for recovery of heavy metal ions from cyanide electrolytes at a zinc- and cadmium-plating shop, with subsequent processing of zinc- or cadmium-plated articles in solutions containing Cr(VI) compounds, was studied.

DOI: 10.1134/S107042720701017X

The method of membrane electrolysis makes it possible to regenerate solutions for cadmium and zinc passivation and to diminish discharge of cadmium ions, Cr(VI) compounds, and cyanide ions into wastewater of electroplating shops.

The maximum permissible concentrations (MPC) for fishery basins of cadmium, Cr(VI), and cyanide ions are 0.005, 0.02, and 0.05 mg l^{-1}, respectively [1].

To diminish the discharge of heavy metal ions into wastewater of electroplating shops, it has been suggested to prolong the working life of the solution for zinc and cadmium passivation via its regeneration by membrane electrolysis. The regeneration precludes one-time or batch discharges of this solution. Recovery of ions of heavy metals, cadmium and Cr(VI), and cyanide ions from catching baths (baths for batch washing) maintains their low concentration and diminishes their discharge into wastewater [2, 3].

EXPERIMENTAL

We chose as objects of study industrial solutions and electrolytes whose composition is presented in the table. Our study was performed on installations using the membrane electrolysis and having the form of two-chamber electrolyzers in which the cathode space (catholyte) is separated from the anode space (anolyte) by an ion-exchange membrane.

The regeneration of the solution for passivation of zinc or cadmium coatings (see table, solution no. 1) consists in that zinc and cadmium ions are recovered and Cr(III) and Cr(VI) are oxidized when electric current is passed. To preclude reduction of Cr(VI) at the cathode to Cr(III) by the reactions

$$Cr_2O_7^{2-} + 14H^+ + 6e = 2Cr^{3+} + 7H_2O, \quad (1)$$

$$CrO_4^{2-} + 8H^+ + 3e = Cr^{3+} + 4H_2O, \quad (2)$$

it is necessary to separate the cathode space with a 1.0 N sulfuric acid solution (catholyte) from the anode space, bath with the solution being regenerated (anolyte), with a cation-exchange membrane, e.g., of the MK-40 type. The virtually total absence of nitrate and chloride ions in the solution being regenerated allows use of anodes with high overvoltage of oxygen evolution, fabricated from lead coated with a lead dioxide layer or from platinum-plated titanium. When electric current is passed, ions of hydrogen, zinc, cadmium, and Cr(III), present in the solution being regenerated, migrate into the cathode space, in which the main cathodic reaction is the multistage process of reduction of hydroxonium ions to hydrogen gas:

$$2H_3O^+ + 2e = H_2 + 2H_2O. \quad (3)$$

As the pH value of the catholyte, cathode current density, and concentration of cadmium and zinc ions increase, deposition of these ions at the cathode in

Nominal composition of solutions

Component	Concentration, g l^{-1}, in solution				
	no. 1	no. 2	no. 3	no. 4	no. 5
CrO_3		100–150			300
H_2SO_4	8–10	8–10		20	15
$Na_2Cr_2O_7$	100–150			100	
CdO			35–45		
NaOH			20–30		
NaCN			90–130		
HNO_3		50–70			140

the form of a metal becomes possible:

$$Cd^{2+} + 2e = Cd, \quad (4)$$

$$Zn^{2+} + 2e = Zn. \quad (5)$$

The zinc and cadmium deposited onto the cathode are etched-off from the cathode in an H_2SO_4 solution in a separate vessel.

In the course of regeneration, Cr(III) ions are accumulated in the catholyte because electrolysis is performed under the conditions that preclude recovery of chromium at the cathode in the form of a metal. An increase in the concentration of Na^+ ions leads to a gradual rise in the solution pH in the cathode space. At a solution pH exceeding 5, the deposition of zinc and cadmium at the cathode is virtually completely terminated because of the formation of zinc and cadmium hydroxides and their precipitation in the cathode space. Addition of H_2SO_4 to the catholyte to dissolve zinc and cadmium hydroxides favors deposition of zinc and cadmium at the cathode in the form of metals.

The main anodic reaction is oxidation of water molecules to oxygen gas:

$$2H_2O = 4H^+ + O_2 + 4e. \quad (6)$$

Cr(III) ions formed in the working bath in the course of passivation are oxidized in the aqueous solution at an anode fabricated from platinum-plated titanium or from lead dioxide to dichromate ions, which enter into the composition of the passivating solution, with hydrogen ions formed:

$$2Cr^{3+} + 7H_2O = Cr_2O_7^{2-} + 14H^+ + 6e. \quad (7)$$

The migration of zinc, cadmium, and Cr(III) ions from the solution being regenerated maintains, together with reactions (6) and (7), the necessary concentration of hydrogen ions in the passivation solution.

The method of membrane electrolysis was introduced into industrial practice for regeneration of solutions for passivation of zinc and cadmium coatings (solution no. 1 containing 113 g l^{-1} of $Na_2Cr_2O_7$ and 9.8 g l^{-1} of H_2SO_4). On passing 427.1 A h of electricity, 4.7 g of zinc and 2.0 g of cadmium was recovered into the catholyte (1.0 N H_2SO_4 solution) in the form of ions, with the electric power consumption equal to 4.09 kW h. At a current strength of 5 to 10 A, the voltage across the installation varied from 7 to 16 V. The calculated transport numbers for zinc and cadmium ions were found to be small, 0.009 and 0.0022, respectively, which can be attributed both to migration of competing hydrogen and sodium ions and to the low initial concentration of zinc and cadmium cations, equal to 1.2 and 0.19 g l^{-1}, respectively. Despite the comparatively high electric power consumption, 870 and 2045 kW h kg^{-1} for zinc and cadmium ions, respectively, the recovery of these ions from the passivation solution precludes their discharge into wastewater.

The membrane electrolysis was used to recover cadmium and cyanide ions from a catching bath for article washing after cadmium plating in a cyanide electrolyte (solution no. 3). In this case, we used two cathodes fabricated from steel and connected in parallel. The first cathode and its cathode space were separated from the catching bath by an MK-40 cation-exchange membrane. The second cathode is mounted, together with the anode, directly in the catching bath, with the anode fabricated from graphite (or platinum-plated titanium) and placed between the two cathodes.

Only the reduction of water occurs at the cathode separated from the solution by the cation-exchange membrane:

$$2H_2O + 2e = 2OH^- + H_2. \quad (8)$$

Simultaneously with reaction (8), a sodium hydroxide solution is accumulated in the cathode space. As the sodium hydroxide concentration reaches approximately 50% of its concentration in the cadmium-plating bath, it is used to adjust the bath.

At the cathode directly introduced into the catching bath, there occurs, together with reaction (8), reduction of cadmium(II) from its complex cyanide compound:

$$Cd(CN)_4^{2-} + 2e = Cd + 4CN^-, \quad (9)$$

The metallic cadmium formed at the cathode as a loose deposit can be reused in cyanide cadmium plating in two ways: (i) as a soluble anode fabricated by remelting the cadmium powder and (ii) for adjustment of the electrolyte for cyanide cadmium plating with cadmium oxide produced by calcination of the cadmium powder with free access of air.

In the course of electrolysis, cyanide and hydroxide ions are oxidized at the anode:

$$CN^- + 2OH^- = CNO^- + H_2O + 2e, \quad (10)$$

$$2CNO^- + 8OH^- = 2CO_3^{2-} + N_2 + 4H_2O + 6e, \quad (11)$$

$$4OH^- = 2H_2O + O_2 + 4e. \quad (12)$$

When a graphite anode is used, it is gradually oxidized:

$$C + 6OH^- - 4e = CO_3^{2-} + 3H_2O. \quad (13)$$

It can be seen from Eqs. (10) and (11) that the oxidation of cyanide ions is accompanied by consumption of hydroxide ions, which leads to a decrease in the concentration of free alkali. At a too low concentration of the alkali, cyanide ions undergo hydrolysis to give free hydrocyanic acid:

$$CN^- + H_2O \rightarrow HCN + OH^-. \quad (14)$$

To suppress hydrolysis, it is necessary to monitor the pH value in the catching bath and to add NaOH when necessary.

With the apparatus employing the method of membrane electrolysis and installed in the catching bath (bath for batch washing), we obtained from the catholyte, after cadmium plating in a cyanide electrolyte [solution no. 3, containing (g l^{-1}): CdO 36, NaCN 108, and NaOH 23], 15 l of a NaOH solution of concentration 9.7 g l^{-1} (at the initial concentration of 0.58 g l^{-1}), and 24.0 g of powdered cadmium was deposited on the cathode mounted directly in the catching bath. In this case, the expenditure of electric power for both processes, formation of the NaOH solution and deposition of metallic cadmium, was 3.76 kW h. The low concentration of NaOH in the working bath, equal to 20–30 g l^{-1}, makes it possible to use the resulting alkali solution for adjustment of the working bath in terms of sodium hydroxide, and the metallic cadmium powder deposited at the steel cathode can be recycled in cyanide cadmium plating. Owing to use of membrane electrolysis, the cadmium(II) concentration in the catching bath is maintained at 0.4 g l^{-1}, and that of cyanide ions (in terms of sodium cyanide), at 0.3 g l^{-1}. This diminishes the loss of cadmium(II) into washing water by a factor of approximately 80, and that of sodium cyanide, by a factor of 360, compared with a catching bath from which cadmium and cyanide ions are not recovered.

To recover Cr(VI) ions from the catching bath, in order to obtain a solution containing chromic acid, after passivation and brightening, it is necessary to separate the cathode space, catching bath, from the anode space by a specially treated MA-40 anion-exchange membrane. An untreated MA-40 membrane cannot be used because it is blocked in the course of electrolysis as a result of the reaction of Cr(VI) compounds with the anion-exchange resin, with the current rapidly decreasing virtually to zero. A treatment (modification) of the MA-40 membrane in a solution with peroxydisulfate ions makes it possible to perform electrolysis at a current density through the membrane of about 1–2 A dm^{-2} and voltage across the electrodes not exceeding 16 V [4]. Stainless steel is used as a cathode, and platinum-plated niobium, as anode.

When electric current is passed, chromate, dichromate, sulfate, and nitrate ions migrate from the cathode space into the anode space. Hydrogen ions move in the opposite direction because of the nonideal selectivity of the anion-exchange membrane.

The main cathodic process is reduction of Cr(VI) compounds in the form of chromate and dichromate ions to Cr(III) ions by reactions (1) and (2), which leads, together with reaction (3), to a considerable consumption of hydrogen cations. As a result, the pH value of the catholyte increases and formation of a mixture of zinc, cadmium, and Cr(III) chromates and hydroxides and its precipitation become possible.

The main anodic process is oxidation of water to oxygen gas, reaction (6). If a solution from the catching bath is used when first putting the installation in operation to impart electrical conductivity to the solution in the anode space, then reaction (7) will occur at the anode, together with reaction (6). The solution accumulated in the anode space contains chromic, sulfuric, and nitric acids and is used only for adjusting the brightening bath.

This method has been introduced into industrial practice in the form of an apparatus that employs the method of membrane electrolysis and is installed in the catching bath (catholyte) for recovery of metal ions after brightening of zinc and cadmium coatings [in solution no. 2 containing (g l^{-1}): CrO_3 105, H_2SO_4 9.5, HNO_3 54]. In the course of electrolysis, Cr(VI) compounds (with a concentration of 8–12 g l^{-1} in terms of CrO_3) are recovered from the catching bath, which diminishes their discharge into wastewater. A solution containing 14.7 g l^{-1} of CrO_3 (against the initial concentration of 10.4 g l^{-1}) is obtained in the anolyte. The apparent transport number, determined for chromate ions, is 0.0735, and the electric power expenditure, 54.8 kW h kg^{-1} CrO_3. These values are characteristic of dilute solutions.

In a similar way are recovered chromium(VI) compounds from the washing water of the catching bath in which articles are washed after brightening in solution no. 5 and passivation in solution no. 4. This method has been introduced into industrial practice. It can give a solution containing chromic acid, which can be used to adjust the brightening bath. The results ob-

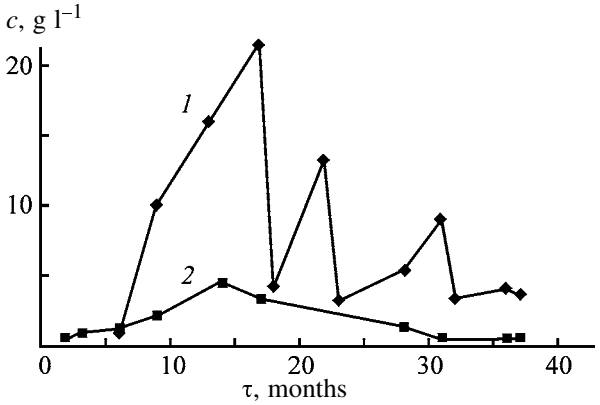

Recovery of chromium(VI) compounds from the washing water of a catching bath. (*c*) Cr(VI) concentration and (τ) time. Chromium(VI) concentration: (*1*) in anolyte and (*2*) in the catching bath.

tained are shown in the figure. It can be seen (curve *2*) that the maximum concentration of chromium(VI) in the catching bath did not exceed 5 g l^{-1}, and the minimum concentration is about 0.5 g l^{-1} and is maintained at this level for a long time. Accordingly, the loss of toxic chromium(VI) compounds into the next washing bath with running water decreased by a factor of approximately 80–300, compared with the bath having no installation based on membrane electrolysis. The decrease in the concentration of chromium(VI) in the anolyte (see figure, curve *1*) is due to discharge of a part of the solution containing the accumulated chromic acid in a concentration of approximately 18 to 42 g l^{-1} in terms of CrO_3 from the anolyte and filling of the free volume with tap water. The right-hand part of the figure is characterized by a more intensive, compared with that in the right-hand part, operation mode, i.e., longer working periods of the installation and more frequent discharging of a part of the anolyte and its use for adjusting the zinc and cadmium brightening bath in CrO_3. As a result, the chromium(VI) concentration in the washing water in the catching bath steadily decreases. Further considerable decrease in the chromium(VI) concentration in wastewater can be achieved by mixing the washing waster from an electroplating shop with household sewage.

CONCLUSIONS

(1) Membrane electrolysis can be used to recover cadmium ions from low-concentration solutions.

(2) Methods for recycling of an alkali solution and cadmium powder recovered from the catching bath after cadmium-plating in a cyanide electrolyte by membrane electrolysis were suggested.

(3) A method for modification of the MA-40 anion-exchange membrane was suggested. This method enables use of this membrane for recovery of chromium(VI) compounds from catching baths by membrane electrolysis, with their subsequent recycling in the form of a solution containing chromic acid.

(4) It was demonstrated that application of membrane electrolysis in an electroplating shop enables a closed cycle for toxic components, with these components recycled and discharge of heavy metal ions and poisonous compounds, such as cadmium, chromium(VI), and cyanide ions, into wastewater of an electroplating shop substantially diminished.

REFERENCES

1. Vinogradov, S.S., *Ekologicheski bezopasnoe gal'vanicheskoe proizvodstvo* (Environmentally Safe Electroplating), Moscow: Globus, 2002.
2. Turaev, D.Yu., Sirotkin, V.I., Zobkova, I.E., and Kruglikov, S.S., Abstracts of Papers, *Uspekhi v khimii i khimicheskoi tekhnologii* (Advances in Chemistry and Chemical Technology), Moscow: Ross. Khim.-Tekhnol. Univ. im. D.I. Mendeleeva, 2000, vol. 14, no. 5, p. 37.
3. Turaev, D.Yu. and Kruglikov, S.S., Abstracts of Papers, *Ezhegodnaya Vserossiiskaya nauchno-prakticheskaya konferentsiya i vystavka "Gal'vanotekhnika, obrabotka poverkhnosti i ekologiya v 21 veke"* (Annual All-Russia Scientific and Practical Conf. "Electroplating, Surface Treatment, and Ecology in the XXI Century"), Moscow: Ross. Khim.-Tekhnol. Univ. im. D.I. Mendeleeva, 2003, p. 135.
4. Turaev, D.Yu., Valge, I.E., and Kruglikov, S.S., Abstracts of Papers, *Uspekhi v khimii i khimicheskoi tekhnologii* (Advances in Chemistry and Chemical Technology), Moscow: Ross. Khim.-Tekhnol. Univ. im. D.I. Mendeleeva, 1999, vol. 13, no. 4.

ISSN 1070-4272, Russian Journal of Applied Chemistry, 2007, Vol. 80, No. 1, pp. 87–92. © Pleiades Publishing, Ltd., 2007.
Original Russian Text © N.B. Danilenko, G.G. Savel'ev, N.A. Yavorovskii, T.A. Yurmazova, 2007, published in Zhurnal Prikladnoi Khimii, 2007, Vol. 80, No. 1, pp. 88–93.

APPLIED ELECTROCHEMISTRY AND CORROSION PROTECTION OF METALS

Chemical Reactions in Treatment with Pulsed Electric Discharges of an Active Metallic Charge in a Solution of a Chromium(VI) Salt

N. B. Danilenko, G. G. Savel'ev, N. A. Yavorovskii, and T. A. Yurmazova

Research Institute of High Voltages, Tomsk, Russia
Tomsk Polytechnic University, Tomsk, Russia

Received May 4, 2006

Abstract—Effect of pulsed electric discharges on aqueous solutions of chromium(VI) in a reactor with an aluminum or iron charge was studied. A mechanism of the occurring processes was suggested. Changes in the pH values of the aqueous solutions of chromium(VI) and the composition and yield of the products formed were determined. The possibility of water treatment to remove chromium by this method was demonstrated.

DOI: 10.1134/S1070427207010181

Recently, publications have appeared devoted to the electric-discharge method for water treatment in reactors with a metallic charge in the form of grains or shavings [1–10]. The experimental conditions used in these studies differed in the reactor design, in the position, shape, and composition of electrodes, and in the composition and concentration of solutions. All these factors affect the composition of dispersion products and efficiency of impurity removal, and, therefore, no adequate model of the occurring processes has been developed. The scientific interest in this issue is due to the particular conditions of occurrence of chemical reactions in a pulsed electric discharge (PED), their kinetics and mechanism. It is apparent, in particular, that different kinds of impurities are involved in different types of reactions: redox, acid–base, ion-exchange, chemisorption, coprecipitation, etc. At the same time, the type and parameters of discharges predetermine both the reaction conditions and the kind of reactants. For example, the electrode material can be involved in the reaction in the case of a zero-barrier discharge, and the fraction of PED energy expended for electric erosion (EE) of the electrode and heating, evaporation, and ionization of the medium may vary as the electrical parameters change.

Previously, we studied the removal of As(V) impurity from water [2] and demonstrated that the results obtained can be understood in terms of a mechanism including stages of oxidation of the eroded metal with water and oxygen, with sorption of arsenate ions by the forming iron hydroxide.

This study is a continuation of [1, 2] and is devoted to analysis of chemical reactions and of the dependence of the yields of the products formed in these reactions on pH and Cr(VI) concentration in the case of PED treatment of metallic charges in aqueous solutions.

EXPERIMENTAL

The study was performed on the experimental installation described in [1]. The electrical parameters used were as follows: voltage pulse width τ_p = 10 μs; pulse repetition frequency f = 300 Hz; voltage U = 500 V for iron charge and U = 1000 V; maximum current I = 250–400 A; pulse energy E = 0.5 J.

The solution was treated in a reactor of 10×10 cm^2 area and 20 cm height. The reactor was filled with a charge to a height of 2.5–3 cm. Model $K_2Cr_2O_7$ solutions of various concentrations (10 to 400 mg l^{-1}) in distilled water were used in the study. The suspension produced upon the PED treatment of the solution was analyzed for the total content of dispersed iron, Fe_{tot}, and in particular for Fe(II) and Fe(III) by dissolving an aliquot in hydrochloric acid [11]. The content of Fe(0) in the suspension was determined by volumometry, and the concentration of Cr(VI) in the filtrate was found after separating the solid precipitate [11]. The composition of the solid precipitate was determined by X-ray phase analysis (XPA). The XPA data were interpreted using the JCPDS (International Centre for Diffraction Data) database.

Table 1. Content of iron in various forms in the suspension produced in EE of shavings in water and Cr(VI) solution. Initial chromium(VI) concentration in model solutions, $c_{Cr(VI)}$ = 50 mg l^{-1}; PED treatment time 60 s

System	pH	Content, wt %		
		Fe(0)	Fe(II)	Fe(III)
Fe + water	2.5	44	3	53
	5.5	87	3.7	9.3
Fe + Cr(VI) solution	2.5	32	28	40
	5.5	51	35.5	13.5

Table 1 lists data on the content of Fe(0), Fe(II), and Fe(III) in the suspension. It can be seen that the presence and involvement of Cr(VI) leads to oxidation of a large amount of iron. As the pH value decreases, the fraction of oxidized iron in the suspension grows. The extent of iron oxidation by chromium(VI) to Fe(II) exceeds that to Fe(III). The PED treatment of an iron charge in distilled water gives a black solid precipitate. A study of the precipitate by XPA demonstrated that it contains Fe(0) and Fe(II) and Fe(III) oxides.

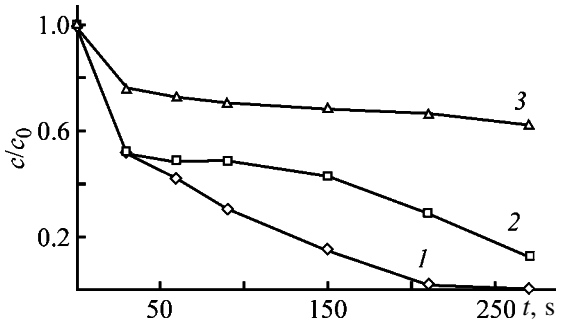

Fig. 1. Degree of Cr(VI) extraction from water vs. time t of PED treatment of various charges at c_0 = 25 mg l^{-1}. (c_0, c) Initial and running Cr(VI) concentrations. Charge: (*1*) iron shavings, (*2*) iron grains, and (*3*) aluminum shavings.

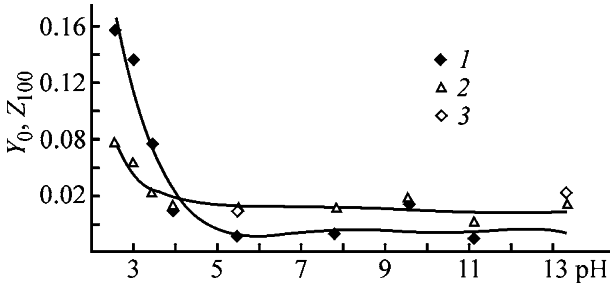

Fig. 2. Fraction of reduced Cr(VI) vs. the solution pH. (Y_0) Fraction of chromium(VI) that reacted before PED treatment and (Z_{100}) relative yield of chromium(VI) reduced during the PED treatment for t = 100 s and c_0 = 50 mg l^{-1}. (*1*) Y_0, extrapolation of the equation $Y(t) = Y_0 + \beta t$; (*2*) Z_{100}, after PED treatment for 100 s; and (*3*) Y_0, experiment (without PED).

Figure 1 shows curves describing the decrease in the Cr(VI) concentration in solution under PED treatment for different charges: Al and Fe shavings and Fe grains. The process is the most efficient with Fe shavings. The reduction yield per unit mass of eroded metal is the same for iron shavings and grains. In contrast to the case of spherical grains, use of shavings leads to enhanced erosion, which, in turn, accelerates chemical reactions of Cr(VI) reduction. Although aluminum is more thermodynamically active than iron, it is less efficient in the reaction with the solution.

There exists an initial region of fast Cr(VI) reduction by the metal (Fig. 1), which occurs via a reaction without any discharge. After the initial interaction, the reaction stops. The extent of this region can be found both in experiments without RED and from curves measured under EE conditions. In doing so, the following circumstance can be used for taking into account the oxidation before the PED treatment: after the initial interaction, the chromium(VI) concentration in solution varies virtually linearly, so that the fraction of reacted chromium(VI) is given by

$$Y = 1 - c_{Cr(VI)}/c_{0Cr(VI)} = Y_0 + \beta t. \quad (1)$$

Figure 2 (curve *1*) shows the dependence of the fraction of chromium(VI), Y_0, reduced by iron without PED on the pH value. The fraction of chromium(VI) reacted before the PED treatment is independent of pH in the range 4–13.5. At pH values lower than 4, this fraction sharply increases. The points obtained directly in the experiment are close to those found by extrapolation.

Measurements of $c_{Cr(VI)}$ on switching off PED also demonstrated that further reduction of Cr(VI) is terminated, i.e., the iron surface formed upon erosion is rapidly passivated.

Because it is assumed that reactions involving H^+ and OH^- ions occur in the course of iron erosion in water (Table 2), changes in the pH value were measured in the course of the experiment (Table 3). It can be seen that, in the case of iron erosion in water, pH increases to approximately 9.0 (Table 3). It follows from Table 3 that the pH value increases upon PED treatment of acid and neutral solutions of Cr(VI) salts, and this effect becomes insignificant in the case of PED treatment of alkaline solutions (pH ≥ 11).

Table 2. Chemical reactions in EE of an iron charge in water and Cr(VI) solution

Reaction		$\Delta\varphi^0$,* V
pH > 3.5		
$Fe + 2H_2O = Fe(OH)_2 + H_2$	(1)	+0.9
$2Fe + 6H_2O = 2Fe(OH)_3 + 3H_2$	(2)	+0.8
$2Fe + 2H_2O + O_2 = 2Fe(OH)_2$	(3)	+1.2
$4Fe + 6H_2O + 3O_2 = 4Fe(OH)_3$	(4)	+0.85
$2CrO_4^{2-} + 3Fe + 8H_2O = 2Cr(OH)_3 + 3Fe(OH)_2 + 4OH^-$	(5)	+0.81
$CrO_4^{2-} + Fe + 4H_2O = Cr(OH)_3 + Fe(OH)_3 + 2OH^-$	(6)	+0.70
pH < 3.5		
$Fe + 2H^+ = Fe^{2+} + H_2$	(7)	+0.44
$2Fe + 6H^+ = 2Fe^{3+} + 3H_2$	(8)	+0.06
$4Fe + 4H^+ + O_2 = 4Fe^{2+} + 2H_2O$	(9)	+1.67
$4Fe + 12H^+ + 3O_2 = 4Fe^{3+} + 6H_2O$	(10)	+1.3
$Cr_2O_7^{2-} + 14H^+ + 3Fe = 2Cr^{3+} + 3Fe^{2+} + 7H_2O$	(11)	+2.23
$Cr_2O_7^{2-} + 14H^+ + 2Fe = 2Cr^{3+}\ 2Fe^{3+} + 7H_2O$	(12)	+2.12
$Cr_2O_7^{2-} + 14H^+ + 6Fe^{2+} = 2Cr^{3+} + 6Fe^{3+} + 7H_2O$	(13)	+0.61

* $\Delta\varphi^0$, standard change in the potential.

Table 3. Changes in the pH value in extraction of Cr(VI) from model solutions by PED with an iron charge. Initial chromium(VI) concentration $c_{Cr(VI)}$ = 50 mg l^{-1}, time of PED treatment 110 s

Solution	Solution pH							
	K_2CrO_4			$K_2Cr_2O_7$				H_2O
Before PED treatment	7.84	9.6	11.15	2.55	3	3.47	3.95	5.5
After PED treatment:								
suspension	11.5	11.26	11.25	4.43	5.1	6.94	8.5	9.13
filtrate	11.1	10.82	11	5.48	5.8	6.95	8.2	8.95

The effect of pH on the erosion of iron and reduction of chromium(VI) under a PED treatment is illustrated by Figs. 3 and 4.

In accordance with the previously obtained results [1], the mass of eroded iron is proportional to $t^{0.72}$ (Fig. 3). The linearization was made using the equation $m = k_2 t^{0.72}$ [1]. The pH dependence of the effective erosion constant k_2 is shown in Fig. 4.

The yield of Fe erosion as a function of pH passes through a maximum at pH ~7. This circumstance was taken into account when studying the effect of pH on the reaction of Cr(VI) with eroded iron: for comparison we took masses of reacted chromium(VI) per unit mass of eroded iron. Figure 5 shows examples of how the pH value affects the kinetics of interaction between Cr(VI) and iron. It can be seen that the relative yield of chromium(VI) reduction, $Z_t = (m_0 - m)_{Cr}/m_{Fe} =$

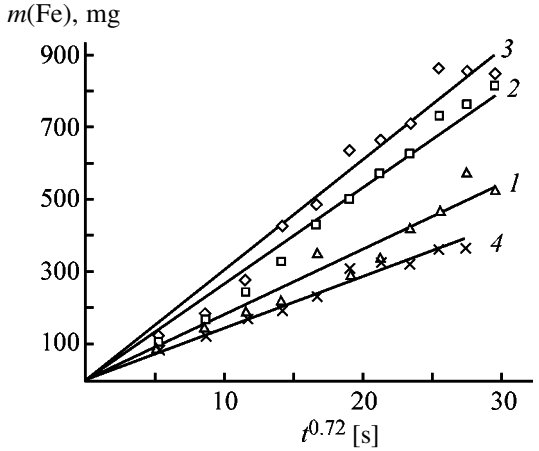

Fig. 3. Amount of eroded Fe, m(Fe), vs. treatment time $t^{0.72}$ under PED at different pH values. pH: (*1*) 3.95, (*2*) 5.5, (*3*) 7.84, and (*4*) 13.33.

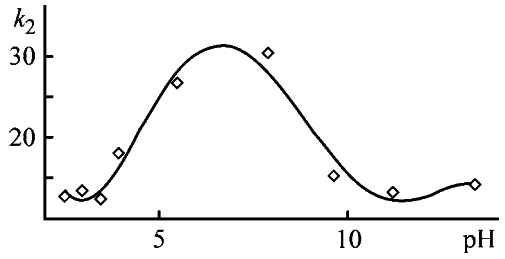

Fig. 4. Specific erosion constant of iron shavings, k_2, vs. pH.

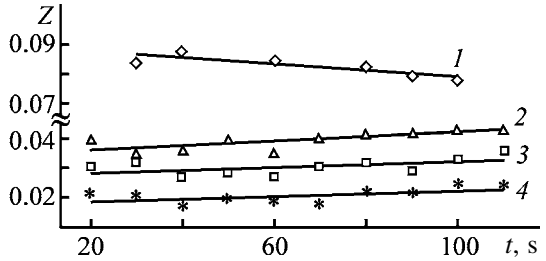

Fig. 5. Relative yield of the reaction, $Z = (m_0 - m)_{Cr}/m_{Fe} = Z_0 + \alpha t$, vs. the PED treatment time t at different pH values. Initial chromium(VI) concentration c_0 = 50 mg l^{-1}. pH: (*1*) 2.55, (*2*) 3.47, (*3*) 7.84, and (*4*) 11.15.

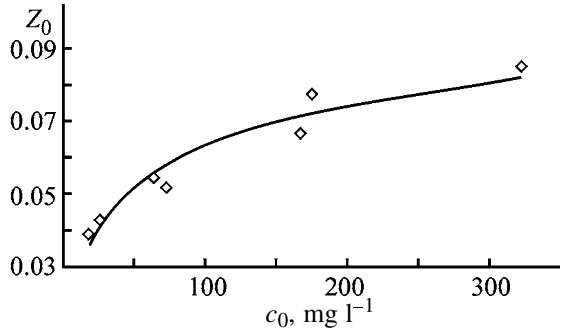

Fig. 6. Relative initial yield of Cr(VI) reduction, Z_0, vs. the initial chromium(VI) concentration c_0 in solution.

$Z_0 + \alpha t$, weakly and nearly linearly varies as the time of PED treatment increases (the coefficient α at t is small).

The pH dependences of the relative yield Z_t at different treatment times are qualitatively the same and similar to that of the yield Y_0 before the PED treatment (Fig. 2). In Fig. 5, a dependence of this kind is shown for t = 100 s. It can be seen that the yield Z_{100} is weakly dependent on pH in the range 3.5–13.5 and steeply increases at pH < 3.5.

Figure 6 shows how the initial relative yield Z_0 depends on the starting concentration of the Cr(VI) solution at pH 5.5. In the absence of PED, the surface of iron and aluminum is covered with oxohydroxide films. In the case of Al, the films are thinner and denser. In the presence of oxidizing ions, $Cr_2O_7^{2-}$ and CrO_4^{2-}, the film may become thicker and denser via formation of oxohydroxides and other Cr(III) compounds. This hinders and terminates the reaction, i.e., additional passivation of the metal may occur. For Al this effect is more pronounced, which can be seen in Fig. 1. At pH 5.5, the initial yield of Cr(VI) reduction is approximately 0.06 mol of Cr per mole of Fe in the case of iron and 0.05 for aluminum. Outside the range of the initial steep rise, this difference is considerably stronger: the yields are 0.02 and 0.005, respectively. These differences are apparently due to the thickness and density of passivating films and to the fact that the film is formed faster in the case of Al. It can also be seen that the fraction of a utilized metal is small because of the passivation. If it is assumed that the specific surface area of the eroded metal is about 10.0 $m^2\ g^{-1}$, which is characteristic of electric-explosion-produced powders, about 0.1% of atoms will lie on the particle surface and, consequently, several tens of iron monolayers and several aluminum monolayers will react with chromium(VI). Thus, two processes noticeably contribute to the formation of a passivating film: interaction of surface metal atoms with Cr(VI) and water.

In a PED treatment of metallic charges in water or aqueous solutions, the metal is heated at places of discharges to a high temperature and its micro- and nanoparticles are ejected into the liquid. The particles are rapidly cooled and, in the process, react with neighboring molecules and ions. Also reacts the metal situated at places of particle detachment. As a result, the reaction surface of the metal strongly increases, compared with its initial value (by a factor of $\geq 10^4$), and just this circumstance leads to an increase in the fraction of reacted impurity, compared with the case of a reaction without discharges. Because of the change in the configuration of discharge gaps, the amount of eroded iron varies with time in proportion to $t^{0.72}$, rather than linearly. For the aluminum charge, this dependence is linear [1], which was taken into account in experimental data processing (Figs. 3, 4). In this case, the fraction of the eroded metal that enters into the reaction is determined by the thickness and density of the passivating film, both intrinsic, formed in interaction with water and oxygen dissolved in the liquid, and that constituted by products of impurity reduction. Upon a PED treatment of an iron charge in distilled water, the pH value increases to approximately 9. It should be noted that pH 9.0 is the equilibrium value for a $Fe(OH)_2$ solution in water, saturated at 298 K [12]. Although iron(II) and (III) hydroxides are formed in erosion according to the data

presented, the concentration of dissolved iron is determined by the more soluble component, $Fe(OH)_2$.

Thus, the experimental data obtained indicate that reactions (1)–(4) occur simultaneously in EE in distilled water (Table 2). In accordance with the potential presented, iron is predominantly oxidized to $Fe(OH)_2$ in the experiment. Upon acidification of water, the advantageousness of iron oxidation to Fe(II) becomes even more pronounced, which is due to a decrease in the potential of reaction (8). The high pH-independent potential of the Fe^{3+}/Fe^{2+} couple (φ^0 = 0.77 V) precludes additional oxidation of Fe^{2+} with such oxidizing agents as H^+ and H_2O. As a result, there occurs gradual oxidation with O_2 as it is dissolved in water from the atmosphere. It can be seen that, as pH varies (Figs. 3, 4), the yield of Fe erosion passes through a maximum at about pH 7. The erosion is a physical process related to conductivity of intergrain spaces, and, therefore, such a behavior of the erosion yield can be attributed to the apparent change in the solution conductivity, which must pass through a minimum at pH 7. Apparently, the fraction of PED energy released into the solution will increase with the solution conductivity, whereas the energy expenditure for heating and dispersion of the metal will decrease.

The degree of iron oxidation in the reaction products and their composition are determined by both thermodynamic and kinetic factors. The former can be evaluated by the standard electrode potentials φ^0 [13] for electrodes in an alkaline medium (V): $Fe(OH)_2/Fe$ = –0.896, $Fe(OH)_3/Fe$ = –0.79, $Fe(OH)_3/Fe(OH)_2$ = –0.58, and $CrO_4^{2-}/Cr(OH)_3$ = –0.086. Here, the potential for a freshly precipitated chromium(VI) hydroxide is used. These values point to a somewhat higher thermodynamic probability of iron oxidation to Fe(II) by Eq. (5). At a chromium(VI) concentration in solution of 50 mg l^{-1}, the potentials of reactions (5) and (6) decrease by 0.22 V at pH 7 and remain virtually unchanged at pH 13, so that both reactions are thermodynamically probable for freshly formed precipitates. And even a decrease in the chromium(VI) concentration by additional three orders of magnitude does not change the sign of the difference of these potentials, which indicates that deep purification of water is possible. The oxidation to Fe(II) is also kinetically advantageous, because transfer of a smaller number of electrons is necessary in this case. The existence of this pathway is also evidenced by the above pH value of 9, established after the PED treatment.

In the acid medium, the φ^0 values for the electrodes are important (V): Fe^{2+}/Fe = –0.44, Fe^{3+}/Fe = –0.062, and $Cr_2O_7^{2-}/Cr^{3+}$ = +1.33. These data indicate that two alternative pathways of interaction are possible: reactions (11) and (12). As in the alkaline medium, oxidation to Fe(II) is kinetically advantageous. However, reaction (11) can be followed by additional oxidation of Fe(II) by reaction (13). This liquid-phase reaction is kinetically more probable than oxidation of $Fe(OH)_2$ to $Fe(OH)_3$ by reaction (5) in an alkaline medium, because the latter occurs in the solid phase. It was experimentally demonstrated (Table 1) that the contribution from these reactions depends on pH of the starting solution: as pH becomes lower, the yield of Fe(III) increases from 13.5 to 40%, whereas that of Fe(II), contrariwise, decreases from 35 to 28% because of the occurrence of reaction (13).

It can also be seen that the yield of oxidation of eroded iron in the presence of Cr(VI) exceeds that in the case of erosion in pure water. This indicates that reactions (5), (6), and (10)–(13) occur, with reactions (5), (6), and (11) predominant. Measurements of the solution pH in PED (Table 3) demonstrated that, in accordance with reactions (5), (6), and (10)–(13), pH increases upon discharge treatment of Cr(VI)-containing solutions. The yield of the reduction of Cr(VI), based on metal unit mass, under PED for 100 s (Fig. 2, curve *2*; Fig. 5) is virtually independent of pH in the range 3.5–13.5. The steep rise in the yield at pH < 3.5 is due to a change of the reaction mechanism from that described by Eqs. (5) and (6) to that by (11). The independence of the yield from pH in the range 3.5–13.5 indicates that reaction (5) is irreversible under the experimental conditions. Some information about iron passivation in PED in a solution of a chromium(VI) salt was obtained by determining the dependence of the relative yield of the reaction on the initial concentration of the salt (Fig. 6). This dependence is weak, described by a flattening-out curve, which confirms that a passivating film is formed, because a linear or superlinear dependence would be expected in its absence. At the same time, the yield somewhat increases as the concentration becomes higher, which points to a low, but still noticeable permeability of the passivating film and to involvement of chromium(VI) compounds in its formation.

In conclusion, the energy expenditure for treatment of wastewater to remove the chromium(VI) impurity will be calculated. Let the energy expenditure for iron erosion be 0.067 kW h mol^{-1} [1], and the yield of chromium(VI) removal, 0.02 mol Cr per mole of Fe, as shown above. Then, 0.4 kW h of electric energy will be necessary for removal of 300 mg l^{-1} of chro-

mium(VI) from 1 m^3 of wastewater at pH > 3.5. This value is tens of times lower than that consumed in treatment of a grained iron charge with high-voltage (3–15 kV) electric discharges [3, 4]: 90 MJ m^{-3} at c = 100 mg l^{-1}. This difference is possibly due to expenditure of the PED energy both for metal erosion and for evaporation and ionization of the solution in intergrain spaces. In this case, in accordance with the mechanism suggested, the expenditure for erosion purifies water by removing impurities and that for evaporation and ionization either does not lead to purification, or purification occurs by a less efficient mechanism.

CONCLUSIONS

(1) In treatment of Cr(VI) solutions with pulsed electric discharges in a reactor with an aluminum or iron charge, the eroded metal directly interacts with the impurity via dispersion of a metal, disintegration of the passivating film, and oxidation of the metal to the corresponding hydroxides.

(2) The efficiency of the interaction with Cr(VI) depends on the rate of formation of the passivating film, pH value, and initial concentration of the solution: it is 0.02–0.03 mol Cr(VI) per mole of eroded Fe.

(3) The yield of chromium(VI) reduction is virtually independent of pH in the range 3.5–13.5 and sharply increases at pH < 3.5. This is due to a change of the reaction mechanism: from oxidation of iron to give solid hydroxides to its oxidation to simple ions, Fe(II) and Fe(III), in solution.

(4) The possible energy expenditure for wastewater treatment to remove Cr(VI) ions at c = 300 mg l^{-1} is about 1.5 MJ m^{-3}, which makes this method promising for practical use.

REFERENCES

1. Danilenko, N.B., Savel'ev, G.G., Yavorovskii, N.A., et al., *Zh. Prikl. Khim.*, 2005, vol. 78, no. 9, pp. 1463–1468.
2. Danilenko, N.B., Savel'ev, G.G., Yavorovskii, N.A., et al., *Zh. Prikl. Khim.*, 2005, vol. 78, no. 10, pp. 1659–1663.
3. Khainatskii, S.A., Zubenko, A.A., Petrichenko, L.A., et al., *Elektronn. Obrab. Mater.*, 2005, no. 6, pp. 47–52.
4. Khainatskii, S.A., Zubenko, A.A., Smal'ko, A.A., et al., *Elektronn. Obrab. Mater.*, 2005, no. 6, pp. 53–58.
5. RF Patent 2220110.
6. RF Patent 2049733.
7. RF Patent 1353743.
8. Kul'skii, L.A., Grebenyuk, V.D., and Savchuk, O.S., *Elektrokhimiya v protsessakh ochistki vody* (Electrochemistry in Water Treatment), Kiev: Tekhnika, 1987.
9. Fominskii, L.P., *Elektronn. Obrab. Mater.*, 1980, no. 1, pp. 46–49.
10. Bairamov, R.K., Vedernikova, N.R., and Ermakov, A.I., *Zh. Prikl. Khim.*, 2001, vol. 74, no. 10, pp. 1703–1705.
11. *Unifitsirovannye metody analiza vod* (Unified Methods for Water Analysis), Lur'e, Yu.Yu., Ed., Moscow: Khimiya, 1973.
12. Shkol'nikov, E.V., *Zh. Prikl. Khim.*, 2005, vol. 78, no. 11, pp. 1819–1823.
13. *Kratkii spravochnik fiziko-khimicheskikh velichin* (Concise Handbook of Physicochemical Quantities), Ravdel', A.A. and Ponomareva, A.M., Eds., Leningrad: Khimiya, 1983.

ISSN 1070-4272, Russian Journal of Applied Chemistry, 2007, Vol. 80, No. 1, pp. 93–101. © Pleiades Publishing, Ltd., 2007.
Original Russian Text © V.N. Pavlyuchenko, O.V. Sorochinskaya, S.Ya. Khaikin, S.P. Fedorov, E.A. Sosnov, S.S. Pesetskii, S.S. Ivanchev, 2007, published in Zhurnal Prikladnoi Khimii, 2007, Vol. 80, No. 1, pp. 94–102.

MACROMOLECULAR CHEMISTRY AND POLYMERIC MATERIALS

Organic–Inorganic Cross-Linked Structures Prepared from Reactive *n*-Butyl Methacrylate–3-(Trimethoxysilyl)propyl Methacrylate Copolymers

V. N. Pavlyuchenko, O. V. Sorochinskaya, S. Ya. Khaikin, S. P. Fedorov, E. A. Sosnov, S. S. Pesetskii, and S. S. Ivanchev

St. Petersburg Branch, Boreskov Institute of Catalysis, Siberian Division, Russian Academy of Sciences, St. Petersburg, Russia

St. Petersburg State Technological Institute (Technical University), St. Petersburg, Russia

Belyi Institute of Mechanics of Metal–Polymer Systems, National Academy of Sciences of Belarus, Gomel, Belarus

Received November 22, 2006

Abstract—The features of formation of organic–inorganic cross-linked structures prepared by copolymerization of *n*-butyl methacrylate with 3-(trimethoxysilyl)propyl methacrylate, followed by hydrolysis of the trimethoxysilane groups of the copolymers and condensation of the resulting silanol groups, were studied. The quantitative composition of the functional groups of the cross-linked copolymers was determined. The physicomechnaical and mechanical properties of the copolymers were studied in relation to the copolymer composition and conditions of hydrolytic condensation.

DOI: 10.1134/S1070427207010193

Cross-linking polymer systems containing reactive oligomers and polymers are conventionally used for preparing films, coatings, and polymer articles by so-called reaction molding. The advantage of this process is that cross-linking of the polymer and molding of the article are combined in one step, with the three-dimensional cross-linked structure of the polymer improving the mechanical, thermal, and other properties of the article.

This approach was widely used mainly in thermosetting systems prepared by the polycondensation mechanism. At the present time, copolymers with different functional groups (hydroxy, carboxy, epoxy, etc.) are used for preparing cross-linked systems. Usually low-molecular-weight cross-linking additives are introduced into these systems, i.e., these systems are "double-packed composites" since the cross-linking agent can be introduced into the reaction mixture only prior to its use, which is inconvenient for industrial processes. Systems cross-linked without cross-linking additives, or more precisely, by cross-linking agents contained in the environment, are more promising. For examples, reactive copolymers with isocyanate functional groups are cross-linked under the action of atmospheric moisture. The disadvantage of isocyanate systems is their high toxicity. More attractive in this respect are copolymers with alkoxysilane functional groups cross-linked by the following reactions:

$$\equiv SiOR + HOH \rightarrow \equiv SiOH + ROH,$$

$$\equiv SiOH + \equiv SiOH \rightarrow \equiv SiOSi\equiv + HOH,$$

$$\equiv SiOH + \equiv SiOR \rightarrow \equiv SiOSi\equiv + ROH,$$

to form organic and inorganic (≡SiOSi≡) cross-links. These copolymers are used for preparing organic–inorganic cross-linked structures from epoxy resins [1], polyurethanes [2], and polycarbonates [3]. Condensation cross-linking of polymers involves at least three steps: polycondensation of the monomer to obtain the oligomer; addition of alkoxysilane fragment to the terminal groups of the oligomer using functionalized trialkoxysilanes; and cross-linking of the system by hydrolytic condensation.

Hybrid cross-linking polymerization is simpler from the technological point of view, since preparation and functionalization of the polymer are com-

bined in one step. Preparation of organic–inorganic cross-linked polymers from acryl copolymers containing 3-(trimethoxysilyl)propyl methacrylate (TMPM) chains $CH_2=C(CH_3)C(O)OCH_2CH_2CH_2Si(OCH_3)_3$ was studied in [4–6].

It was noted [5, 7] that not all functional groups are involved in hydrolytic condensation, i.e., the system contains the methoxy and silanol groups, and the siloxane bonds as the condensation product. It is clear that the properties of a copolymer and its possible application fields will depend on its functional composition. However, no quantitative data on the content of functional groups in similar systems were reported. To predict the polymer properties, it should be taken into account that the cross-linked structure in the examined systems is formed not only by cross-linking of silanol groups but also by formation of hydrogen bonds between the silanol groups and electron-donor fragments of macromolecules [4, 8]. It should also be noted that inorganic micro- or nanofragments with polysiloxane structure can be formed under definite conditions in the polymer matrix by condensation of the ≡SiOH groups. However, this process can be almost completely suppressed under definite copolymerization conditions. Chan and Chu [4] showed that the polymerization system became heterogeneous only at more than 40 mol % content of TMPM in the initial monomer mixture. Similarly, the inorganic phase in a mixture of polymethyl methacrylate and tetraethoxysilane (TEOS) is formed only when the content of TEOS in the system exceeds 20 wt % [8].

The aim of this study was to examine formation of organic–inorganic cross-links in the course of copolymerization of *n*-butyl methacrylate (BMA) with TMPM in relation to the content of TMPM units in the copolymer and conditions of hydrolytic condensation. We also determined the quantitative composition of functional groups in the intermediate and final products and studied their properties.

EXPERIMENTAL

We used BMA [Russia, GOST (State Standard) 16756–71] and TMPM (Fluka) containing 99% main compound. The monomers were distilled in a vacuum prior to use. The solvents were benzene (analytically pure grade, GOST 5955–75) dried over calcium hydride and chloroform [chemically pure grade, TU (Technical Specifications) 2631-066-444493/79-01] used as received.

Polymerization was initiated by benzoyl peroxide recrystallized from ethanol.

Hydrolytic condensation was catalyzed by 0.1 N H_2SO_4 (titration standard), *p*-toluenesulfonic acid (TSA) (Merck), and dibutyltin dilaurate (DBTDL) (Sigma–Aldrich).

Copolymerization of BMA with TMPM was performed in a benzene solution at the monomer : solvent ratio of 1 : 5, initiator concentration of 1% relative to the copolymer weight, and 70°C in sealed glass ampules under nitrogen atmosphere for 48 h.

The copolymerization kinetics was studied by gas-chromatographic analysis on a Tsvet-800 chromatograph with a flame ionization detector. A 2-m column 4 mm in diameter was packed with Inerton-Super (grain size 0.125–0.160 mm) containing 5% Carbowax 20M. The flow rates of the carrier gas (helium) and hydrogen and air used for detection were 20, 20, and 200 ml min^{-1}, respectively. The column programmed temperature was in the range from 80 to 140°C. The content of components in the reaction mixture was determined using toluene as an internal reference.

The morphology of the copolymers prepared by hydrolytic condensation was studied by atomic force microscopy (AFM) on a Solver P47 Pro scanning probe microscope (NT-MDT, Russia) in the tapping mode in air. The samples were scanned in the topographical survey and phase contrast modes. The difference in the surface composition was determined from the change in the phase shift of the amplitude–frequency parameter of the cantilever caused by adhesion interactions [9].

The films were prepared at 25°C and 50–60% air humidity on a Teflon support or, to accelerate hydrolysis of $\equiv SiOCH_3$ groups, on the water surface.

Hydrolytic condensation was studied by FTIR spectroscopy. For this purpose, the changes in the intensity of the IR bands at 820, 1000–1200, and 3500 cm^{-1} were monitored. The content of the silanol groups ≡SiOH was determined from the integral intensities of their stretching vibrations at 3500 cm^{-1}, measured after subtraction of the spectrum of the freshly prepared initial sample. The content of the $\equiv SiOCH_3$ groups was determined from the integral intensity of the band at 820 cm^{-1}, measured after subtraction of the spectrum of completely hydrolyzed samples with the similar composition. The initial and completely hydrolyzed samples were used as references for calculation of the absorption coefficients. Since the siloxane bands overlap with other bands, the concentration of siloxane groups was calculated form the difference in the initial and current concen-

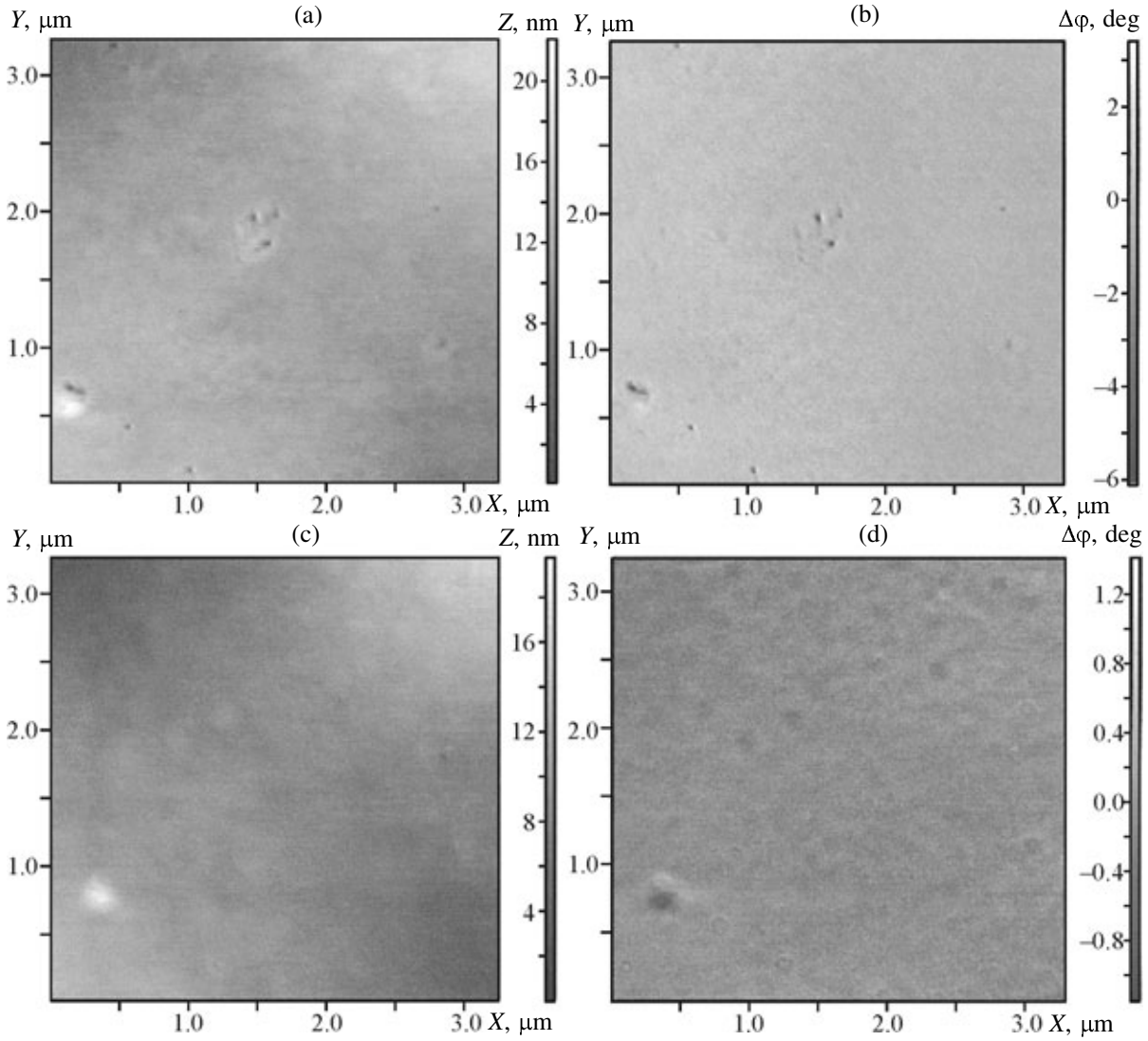

Fig. 1. AFM pattern of the films of BMA–TMPM copolymer (72.4 : 27.6 mol %) after hydrolytic condensation on heating from 25 to 120°C in the presence of DBTDL (0.539×10^{-2} mmol g^{-1} of the copolymer). (*X, Y*) Scanning range, (*Z*) height, and (Δφ) phase shift of the amplitude–frequency parameter of the cantilever. (a, b) film surface and (c, d) transverse section; (a, c) topography and (b, d) phase contracts mode.

tration of the ≡$SiOCH_3$ groups and the concentration of the silanol groups.

The chemical composition of the polymer films was determined by FTIR spectroscopy using a multiple attenuated total internal reflection (MATIR) attachment.

The degree of swelling of the films in chloroform at 25°C was determined gravimetrically.

The glass-transition point of the polymers T_g was measured by differential scanning calorimetry on a DSC-60 calorimeter (Shimadzu) at a heating rate of 10 deg min^{-1} in the range 50–100°C.

The mechanical properties of the films were measured by the conventional procedures (GOST 12589–78) on an RTM-1T universal tensile-testing machine (Orientec, Japan).

To prevent formation of inorganic polysiloxane inclusions in the polymer matrix, copolymerization was performed at the content of TMPM in the monomer mixture lower than 30 mol %. The results of AFM examination of the film surface (Figs. 1a and 1b) shows that the copolymer structure is homogeneous even at the maximal content of the TMPM units in the copolymer (27.6 mol %). We obtained the AFM patterns of the copolymer films prepared by hydrolytic condensation in the course of gradual heating from 25 to 120°C. As shown below, under these conditions

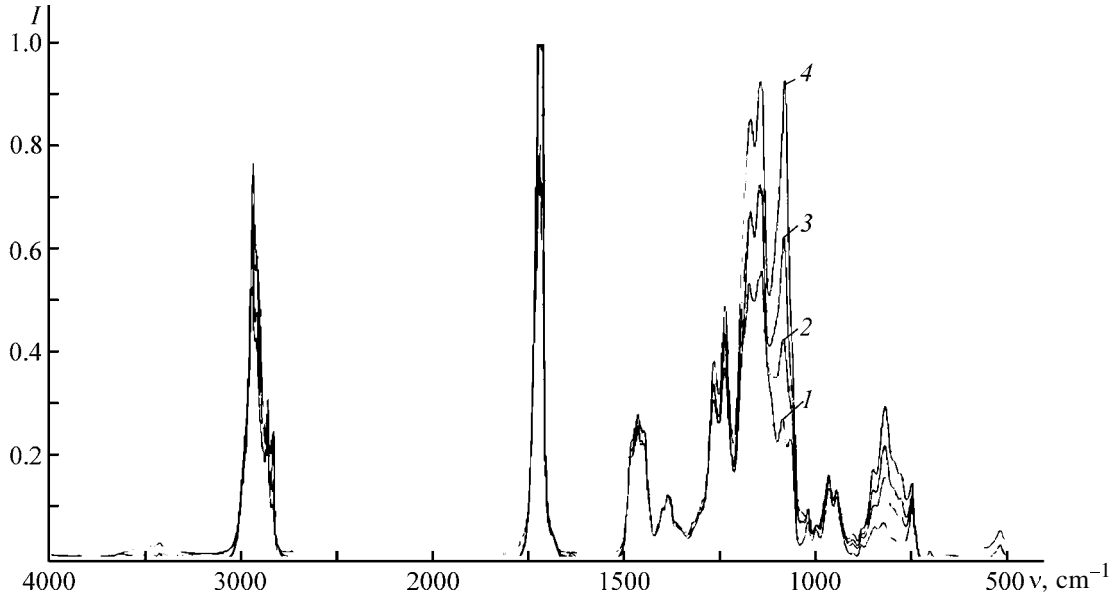

Fig. 2. IR spectra of BMA–TMPM copolymer containing (*1*) 6.0, (*2*) 12.5, (*3*) 19.7, and (*4*) 27.6 mol % of the TMPM units. (*I*) Intensity and (ν) wavenumber; the same for Figs. 4 and 5.

the degree of condensation of the silanol groups is maximal. No areas of the films having different adhesion to the cantilever were observed in the pattern measured in the phase contrast mode, which suggests the homogeneous structure of the film.

The AFM pattern of the film section (Figs. 1c and 1d) also shows that the bulk chemical composition of the copolymer is uniform. In addition, as determined by scanning of the section in the phase contrast mode (Fig. 1d), the copolymer consists of spherical globules grown together. The globule size is approximately 300 nm.

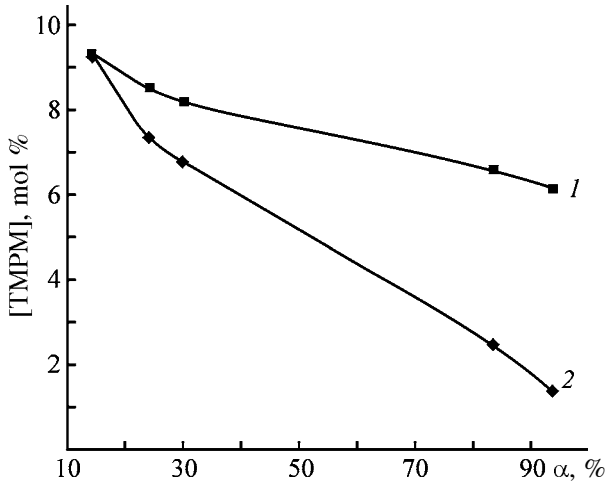

Fig. 3. (*1*) Total and (*2*) current content of TMPM units in BMA–TMPM copolymer as a function of the total conversion of a BMA + TMPM monomer mixture α. TMPM content in the initial monomer mixture 6.0 mol %.

In what follows, the copolymer properties will be discussed from the standpoint of formation of the three dimensional cross-linked structure of the copolymer containing inorganic cross-links.

The IR spectra of the copolymers with different content of the TMPM units are shown in Fig. 2. The samples were prepared on a Teflon support in the absence of catalysts and without heat treatment. The intensity of the bands at 820–1085 cm^{-1} assigned to the stretching vibration of the $-OCH_3$ groups of the TMPM units increases with an increase in the content on these units in the copolymer. In addition, a small silanol band at 3500 cm^{-1} suggests hydrolysis of the $\equiv SiOCH_3$ groups during formation of the films in air.

We recorded the IR spectra of the copolymers prepared at almost complete monomer conversion. The change in the copolymer composition in the course of copolymerization is shown in Fig. 3. In all copolymerization steps, the copolymer is enriched in the TMPM units as compared to the composition of the initial monomer mixture. The dependence of the total copolymer composition on the monomer conversion supports this conclusion. Calculation of the current copolymer composition shows that the content of the TMPM units in the copolymer at low monomer conversions is higher by a factor of 1.5 than the content of this monomer in the initial monomer mixture, whereas the copolymer formed in the final copolymerization steps contains less than 1.5 mol % TMPM. These data suggest nonuniform copolymer composi-

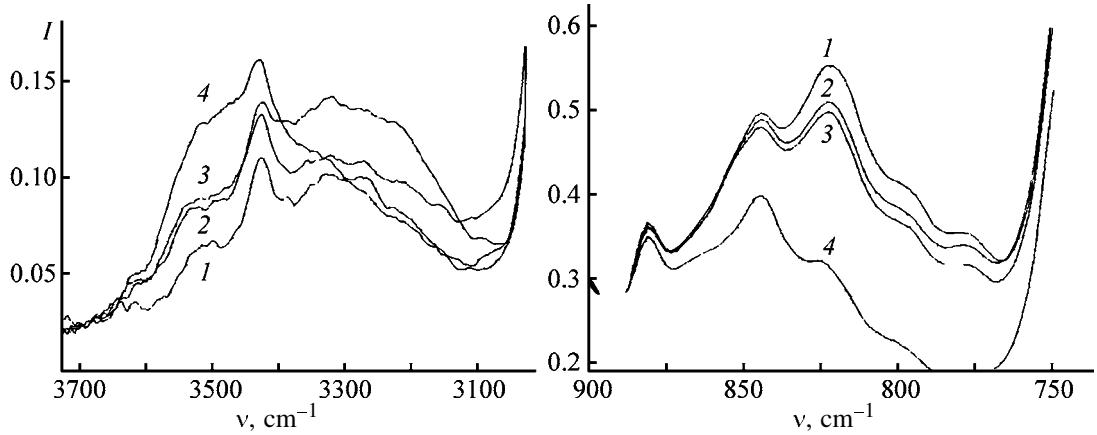

Fig. 4. IR MATIR spectra of BMA–TMPM copolymer (94.0 : 6.0 mol %) films (copolymer–support interface) formed on (*1*) Teflon and (*2–4*) water supports (*1, 2*) in the absence of catalyst and in the presence of (*3*) H_2SO_4 and (*4*) TSA.

tion, which can result in its nonuniform cross-linked structure.

The copolymers prepared at all the examined ratios of the monomers are soluble, despite consumption of the $\equiv SiOCH_3$ groups in the course of film formation. It should be noted that the IR spectra of copolymers formed on Teflon and water surfaces are similar even when the aqueous phase contains an inorganic acid catalyzing hydrolytic condensation.

To understand this phenomenon, let us consider the MATIR IR spectra of the samples (Fig. 4). The intensity of the band at 3500 cm^{-1} in the spectra of the films prepared on the water surface is substantially higher than that of the films prepared on the Teflon support. The opposite pattern was observed for the band at 820 cm^{-1}. It should be noted that the intensity of the band at 3500 cm^{-1} in the IR MATIR spectra appreciably increases when the polymer films is formed on the surface of the aqueous phase containing a strong organic acid (TSA). Thus, the $\equiv SiOCH_3$ groups of the films are hydrolyzed mainly at the copolymer–support interface. Propagation of this process in the bulk of the film is controlled by diffusion, since the surface copolymer layer structured by hydrogen bonds prevents diffusion of water in the bulk of the film. The number of covalent siloxane cross-links formed in this step is negligible since the copolymer remains soluble. This assumption is confirmed by an increase in the content of silanol groups in the bulk of the film with a decrease in its thickness.

The IR spectra of the samples were recorded immediately after their preparation. When the films are kept in an acid aqueous solution (pH 2.2), the conversion of the $\equiv SiOCH_3$ groups into the $\equiv SiOH$ groups increases. In this case, the intensity of the band of the silanol group at 3500 cm^{-1} increases with time. The mechanical strength of the films formed from soluble copolymers is low. When the content of TMPM units in the copolymer increases from 6.0 to 19.7 mol %, the ultimate tensile strength decreases from 7.1 to 4.2 MPa and the relative elongation increases from 200 to 275%.

To obtain polymers with the best performances, the conversion of the functional groups should be increased. For this purpose, we increased the reaction temperature and used an effective catalyst. At elevated temperatures the water diffusion in the bulk of the film increases owing to both an increase in the free volume in the copolymer and the rupture of the network of hydrogen bonds. To catalyze the hydrolytic condensation, compounds having increased affinity for the polymeric matrix are preferable. This assumption is confirmed by the fact that the hydrolytic condensation catalyzed by TSA is faster that that catalyzed by sulfuric acid having lower affinity for the copolymer. In the subsequent experiments, we used oil-soluble DBTDL as a catalyst of hydrolytic condensation.

The influence of the temperature and time of heat treatment of the copolymers on their properties and the processes occurring in the reaction mixture in the absence of the catalyst is shown in Table 1. It is seen that cross-linking of the copolymer by condensation of silanol groups in ineffective in the absence of the catalyst. Even under the most rigid conditions, no more that 10% of silanol groups formed by complete hydrolysis of $\equiv SiOCH_3$ groups are converted into the siloxane bonds. It should be noted that the dependences of all the examined properties on the temperature and time of heat treatment are abnormal. The cross-link density naturally increases after the heat

Table 1. Properties of BMA–TMPM copolymers (94.0 : 6.0 mol %) prepared under different heat treatment conditions

Heat treatment conditions*	Content of functional groups, mmol g^{-1}		Degree of swelling in chloroform, wt %	T_g, °C	σ_t, MPa	ε, %
	≡SiOCH$_3$	≡SiOH				
0	1.15	0.06	Soluble	33	7.1	207
1a	0.63	0.58	〃			
1	0.52		186		15.8	69
2	0.40	0.68	143	47		
3		1.09	176	30	8.8	160

* (0) No treatment; (1a) heating to 50°C for 1 h; (1) heating to 70°C for 5 h; (2) 1+ heating to 120°C for 1 h; (3) 1+ heating at 120°C for 3 h.

Table 2. Physicomechanical properties of copolymer films with different compositions, prepared under different heat treatment conditions

Copolymer composition, mol %		Heat treatment mode	σ_t, MPa	ε, %
BMA	TMPM			
94.0	6.0	1	15.8	69
87.5	12.5	3	8.9	194
80.3	19.7	2	6.1	177
72.4	27.6	2	4.7	148

treatment in modes 1 and 2. This is indicated by an increase in the content of silanol groups, T_g, and film strength and by a decrease in the degree of swelling and specific elongation of the film. All these transformations suggest restriction of the segmental mobility of the macromolecules, mainly owing to formation of a large number of hydrogen bonds between the ≡SiOH hydroxy groups and probably carbonyl groups of BMA or TMPM [8]. In the final heat treatment step (conditions 3), all the examined parameters change in the opposite direction despite additional formation of ≡SiOSi≡ cross-links.

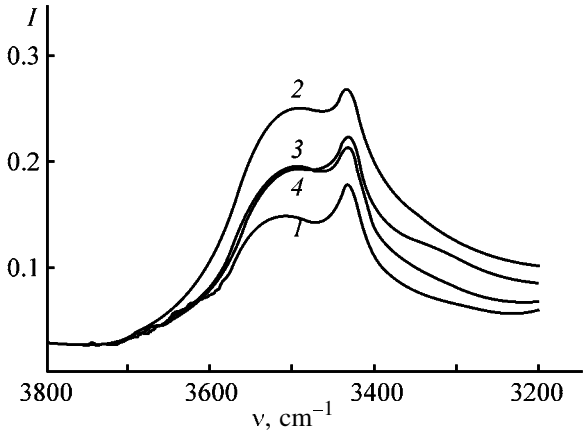

Fig. 5. IR spectra of the films of BMA–TMPM copolymers (94.0 : 6.0 mol %) subjected to hydrolytic condensation at room temperature in the presence of (*1*) 0.539×10^{-2}, (*2*) 0.792×10^{-2}, (*3*) 1.585×10^{-2}, and (*4*) 3.169×10^{-2} mM DBTDL.

We are not able to give unambiguous explanation of these effects. It is possible that microzones with an increased content of hydrolyzed TMPM units can be formed in the copolymers owing to their nouniform composition. The presence of these zones can prevent macromolecules from taking the equilibrium conformation and can change the free volume of the polymer system, thus affecting the physicochemical and mechanical properties of the copolymers. It is known [8] that introduction of silica in polymethyl methacrylate by the sol–gel procedure (hydrolytic condensation of TEOS) decreases T_g by 10–15°C. The decrease in the mechanical strength of cross-linked films win increasing content of the TMPM units in the copolymer confirms this assumption (Table 2). The siloxane cross-links formed in this step are not numerous and enhance the mechanical strength insignificantly. Our calculation shows that more than 100 carbon atoms are located, on the average, between two ≡SiOSi≡ cross-links. It is significantly higher than the size of the statistical segment in methacrylate polymers [10]. Thus, a small number of the covalent cross-links insignificantly affects T_g.

Introduction of DBTDL in the reaction system catalyzes hydrolytic condensation. As seem from the IR spectra (Fig. 5), the reaction performed at room temperature in the presence of DBTDL is relatively fast. The insoluble copolymer is formed at the catalyst concentration of 0.0079 mmol g^{-1}. At this concentration, the ≡SiOCH$_3$ groups are completely consumed and the intensity of the absorption band at 3500 cm^{-1} becomes maximal. At higher DBTDL concentration, the silanol groups are involved in condensation processes to a greater extent and their content in the copolymer decreases.

Table 3. Degree of swelling in chloroform of BMA–TMPM copolymers (94.0 : 6.0 mol %) prepared at different concentration of the catalyst and in different heat treatment modes

$[DBTDL] \times 10^2$, mmol g^{-1}	Degree of swelling, wt % of the copolymers prepared in the indicated heat treatment mode		
	0	1	2
0.792	250	128	198
1.585	235	140	258
6.339	290	264	363

The heat treatment in the presence of the catalyst additionally accelerates the polycondensation. It is seen from the degree of swelling of the films prepared under these conditions (Table 3). As in the absence of the catalyst, the dependence of the degree of swelling on the heat treatment temperature passes through a minimum under relatively mild conditions (heat treatment conditions 1). This can be due to the fact that the appropriate ratio between hydrogen and covalent bonds is attained in the earlier steps of the process. It should be noted that the degree of swelling of the copolymer prepared in all the heat treatment modes increases with increasing the DBTDL concentration. We cannot explain this fact using the above-considered arguments. As seen from Table 4, the content of the silanol groups and hence the probability of hydrogen bond formation in the samples prepared in all the heat treatment modes increase with increasing the catalyst concentration. This phenomenon deserves a separate consideration. We can only suggest that chloroform used as the solvent can compete for hydrogen bond formation with other components of the reaction system.

Table 4 shows that the role of inorganic cross-links increases under more rigid conditions of hydrolytic condensation. However, since the concentration of the ≡SiOH groups is high in the course of the overall process, formation of hydrogen bonds between macromolecules is possible in all the condensation steps. Thus, the organic–inorganic network of the copolymer consists of both inorganic cross-links and hydrogen bonds. However, the relative contributions of processes leading to these intra- and intermolecular cross-links remains unclear.

The mechanical properties of the copolymers are summarized in Table 5. It should be noted that some of cross-linked copolymers withstand substantial deformation before failure. Since these experiments were performed at temperatures below T_g of the copolymers, high deformations are caused by the state of induced elasticity. Hence, to understand the copolymer properties, the possibility of formation of this state in relation to the copolymer composition and

Table 4. Content of functional groups in BMA–TMPM copolymers (94.0 : 6.0 mol %) prepared in different heat treatment modes

Heat treatment modes	$[DBTDL] \times 10^2$	$[\equiv SiOCH_3] \times 10^2$	$[\equiv SiOH] \times 10^2$	$[\equiv SiOSi\equiv]^* \times 10^2$
	mmol g^{-1}			
0	0.206	0.810	0.399	0.000
1		0.617	0.499	0.047
2		0.508	0.556	0.072
0	0.539	0.810	0.387	0.006
1		0.544	0.605	0.030
3		0.327	0.532	0.175
0	3.169	0.411	0.762	0.018
1		0.194	0.738	0.138
2		0.169	0.629	0.205
3		0.145	0.653	0.206
0	6.339	0.302	0.847	0.030
1		0.000	0.847	0.181
2		0.000	0.750	0.230
3		0.000	0.665	0.272

* $[\equiv SiOSi\equiv] = 0.5([\equiv SiOCH_3]_0 - [\equiv SiOCH_3] - [\equiv SiOH])$, where $[\equiv SiOCH_3]_0$ is the initial concentration of $\equiv SiOCH_3$ groups in the copolymer (1.209 mmol g^{-1}).

Table 5. Mechanical properties of films of BMA–TMPM copolymers (94.0 : 6.0 mol %) prepared in different heat treatment modes

Copolymer composition, mol %		[DBTDL] × 10^2, mmol g^{-1}	Heat treatment modes	σ_t, MPa	ε, %
BMA	TMPM				
94.0	6.0	0	0	7.1	207
		0	1	15.8	69
		0.206	1	21.3	36
		0.206	2	21.7	47
		0.539	0	18.4	92
87.5	12.5	0	0	3.3	313
		0	3	8.9	194
		0.206	1	23.9	15
		0.206	2	26.4	12
		0.206	3	6.4	8
		0.539	1	31.2	8
		0.539	2	12.5	6
		0.539	3	0.9	4
80.3	19.7	0	0	4.2	275
		0	2	6.1	177
		0.206	1	18.5	11
		0.206	2	21.3	10
		0.206	3	25.9	14
		0.539	1	22.9	9
72.4	27.6	0	0	2.4	230
		0	2	4.7	148
		0.206	1	25.6	8
		0.206	3	9.4	4

conditions of hydrolytic condensation should be considered.

When the degree of hydrolysis and condensation of all copolymers increase, the strength of the products increases and their elasticity decreases. This is quite natural, since presence of small number of cross-links restricts the segmental mobility of the macromolecules. However, displacement of some macromolecular fragments under a load (induced elasticity) results in partial ordering of macromolecules and strengthening of the material. At high concentration of cross-links in the sample, the segmental mobility is impossible and the films readily undergo brittle failure. In this case, not only the specific elongation but also the strength of the samples decrease, since all parts of the macromolecules are fixed and their additional ordering is impossible. Probably this is the case for the examined systems also. The strong induced deformation decreases with increasing TMPM content in the copolymer. The higher the content of the units of this monomer in the copolymer, the lower the temperature and the catalyst concentration corresponding to sharp deterioration of the elastic and mechanical properties. It should be taken into account that randomly distributed heterogeneous regions resulting in intermolecular interaction of the functional groups can be formed in the copolymer. This concerns formation of both covalent cross-links and hydrogen bonds. This effect should be the most pronounced in the copolymers with a high content of the TMPM units. The AFM pattern of the material with the globular structure (Fig. 1) confirms this assumption. The heterogeneous regions can concentrate the stress, which results in brittle failure of the material.

The properties of the copolymers with the minimal (6.0 mol %) TMPM content differ. Previously we discussed interesting effects appearing in these systems. When the organic–inorganic cross-linked structure of these copolymers is formed at a low catalyst concentrations and moderate temperatures, the strength of the samples can be substantially increased with preservation of their high elasticity.

As noted above, the cross-linked copolymers contain a large amount of free silanol groups. This is a known phenomenon. Similar systems cured by a sol–gel procedure also contain residual silanol groups

[5, 7]. On the one hand, the presence of the residual SiOH groups in a copolymer allows preparation of polymer coatings with a high adhesion to particular supports. For this purpose, high-strength copolymers with poor elastic properties (e.g., copolymers containing 12.5 mol % TMPM) can be used. Coatings formed by these copolymers on a glass cannot be separated without failure from the support. On the other hand, the properties of materials containing residual silanol groups can be changed in the course of their prolonged operation. On prolonged storage, the elasticity of some films decreases without changing their strength. Hence, these copolymers are unsuitable for film preparation and can be used for preparing coatings and bulk articles.

CONCLUSIONS

(1) Hydrolysis of $\equiv SiOCH_3$ groups in the course of preparation of organic–inorganic cross-linked copolymers of *n*-butyl methacrylate and 3-(trimethoxysilyl)propyl methacrylate is substantially faster than condensation of the ≡SiOH groups. Conversion of ≡SiOH groups into the siloxane bonds is incomplete even at high temperatures.

(2) Cross-linking of the copolymers containing large number of the residual silanol groups involves simultaneous formation of covalent inorganic cross-links and hydrogen bonds between the macromolecules.

(3) The dependences of physicochemical and mechanical properties of the copolymers cross-linked by the covalent and hydrogen bonds on the heat treatment temperature passes through extrema with gradual accumulation of the siloxane cross-links in the polymeric matrix.

(4) Copolymers with a high content of the ≡SiOH groups can be used for preparing coatings cross-linked in the course of their formation on surfaces reactive with respect to the silnaol groups.

REFERENCES

1. Bauer, B.J., Liu, D.-W., Jackson, C.L., and Barnes, J.D., *Polym. Adv. Technol.*, 1999, vol. 7, no. 4, pp. 333–339.
2. Recondo, A., Fernandez-Berridi, M.J., and Irusta, L., *Eur. Polym. J.*, 2000, vol. 42, no. 9, pp. 2069–2080.
3. Arakawa, M., Surata, K., Shimada, M., and Agari, I., *J. Appl. Polym. Sci.*, 2006, vol. 100, no. 6, pp. 4273–4279.
4. Chan, C.-K. and Chu, I-M., *Polymer*, 2001, vol. 42, pp. 6823–6831.
5. Yu, Y.-Y., Chen, C.-Y., and Chen, W.-C., *Polymer*, 2003, vol. 44, pp. 593–601.
6. Castelvetro, V. and Vita, C.D., *Adv. Colloid Interface Sci.*, 2004, vols. 108–109, May, pp. 167–185.
7. Saegusa, T., *J. Macromol. Sci., Chem. A*, 1991, vol. 28, no. 9, pp. 817–829.
8. Chan, C.-K., Peng, S.L., Chu, I.-M., and Ni, S.-C., *Polymer*, 2001, vol. 42, pp. 4189–4196.
9. Magonov, S.N., Elings, V., and Whangbo, M.-H., *Surf. Sci.*, 1997, vol. 375, no. 24, pp. L385–L391.
10. *Entsiklopediya polimerov* (Encyclopedia of Polymers), Moscow: Sov. Entsiklopediya, 1972, vol. 1, p. 618.

ISSN 1070-4272, Russian Journal of Applied Chemistry, 2007, Vol. 80, No. 1, pp. 102–105. © Pleiades Publishing, Ltd., 2007.
Original Russian Text © G.M. Pavlov, 2007, published in Zhurnal Prikladnoi Khimii, 2007, Vol. 80, No. 1, pp. 103–105.

MACROMOLECULAR CHEMISTRY AND POLYMERIC MATERIALS

Orientational Ordering of Polymer Chains near the Surface and Asymmetry of the Statistical Segment of Macromolecules

G. M. Pavlov

Fock Research Institute of Physics, St. Petersburg State University, St. Petersburg, Russia

Received September 13, 2006

Abstract—The parameter of the orientational order of polymer chain fragments near the substrate (film) surface in relation to the degree of asymmetry of the statistical segment of the macromolecule was discussed in terms of the model of adsorption of rigid cylinders on the substrate surface. The theoretical parameters of the orientational order were analyzed and compared with the experimental data for films of polysaccharides, sulfated phenyl-containing polymers, and polytrimethylsilylpropynes.

DOI: 10.1134/S107042720701020X

The properties of polymer films and polymers at interfaces have been the subject of numerous studies [1–4]. Spontaneous ordering of the macromolecules near the surface in films prepared by free evaporation of the solvent from solutions is examined by the polarized-beam technique at oblique incidence [5, 6]. The theory of Cherkasov–Vitovskaya–Bushin [5] provides a quantitative interpretation to the birefringence observed in films and estimates the parameter of the orientational order of the polymer chain fragments near the surface as

$$S_0 = (3\langle\cos^2\theta\rangle - 1)/2, \quad (1)$$

where θ is the angle between the normal to the film (substrate) surface and the long axis of the statistical segment of the macromolecule.

We found that the orientational order parameter S_0 is unambiguously dependent on the length of the statistical segment characterizing the equilibrium rigidity of the macromolecular chains forming the polymer film [7–10].

Published data [1, 2, 11–13] suggest that formation of the surface layers of polymer films from solutions under solvent evaporation involves adsorption of the macromolecules on the substrate surface and that the contact of the polymer with the substrate surface is energetically favorable. In this case, the molecule and its constituting segments tend to be arranged in a way ensuring the largest area of contact with the surface. Then the arrangement of the chain segments with respect to the substrate surface is dependent on their geometric shape/asymmetry, rather than equiprobable. The polymer chain in solution will be modeled in this study as a cloud of identical statistically independent segments (cylinders); each of them will have a length A and will be characterized by the axial ratio $p = A/d$ ($d = 2r$ is the diameter of the cylinder, and r, its radius). The energy of adsorption (adhesion) E_a of the polymer segment on the flat surface of the substrate will be taken proportional to the area s of the contact of the segment with the surface: $E_a = \alpha_a s$, where α_a is the surface density of the adsorption (adhesion) energy. We will assume that α_a is identical for the end faces and lateral surface of the cylinder, as well as in the series of homologous polymers. Then, the probability of the orthogonal arrangement of the cylinder simulating the statistical segment of the polymer chain will be proportional to the area of its base. The probability of the parallel arrangement of the cylinder will be proportional to the area of contact between the lateral surface of the segment and the substrate surface, which will be calculated as $s = A l_c$, where l_c is the effective cross-sectional dimension of the contact (a priori unknown). In this case, the parameter $\langle\cos^2\theta\rangle$ can be calculated as

$$\langle\cos^2\theta\rangle = (\pi r^2\cos^2\theta + Al_c\cos^2\pi/2)/(\pi r^2 + Al_c)$$
$$= \pi r^2/(\pi r^2 + Al_c) = [1 + (2l_c p/\pi r)]^{-1}, \quad (2)$$

which yields

$$S_0 = (3\langle\cos^2\theta\rangle - 1)/2 = [1 - p/\pi(r/l_c)]/[1 + 2p/\pi(r/l_c)] \quad (3)$$

for the orientational order parameter S_0.

Length of the statistical segment A, cross-sectional diameter of the macromolecules d, asymmetry of the segment p for selected sulfated phenyl-containing polymers (nos. 1–3) and polysaccharides (nos. 4–10), and the orientational order parameter of the polymer chain fragments near the surface S_0, determined by the polarized-beam technique with oblique incidence in the films of the corresponding polymers

Compound no.*	Polymer	A, nm	d nm	$p = A/d$	S_0**
1	$PSTSO_3Na$	4 ± 0.6	0.9 ± 0.2	4.3 ± 1	–(0.14–0.085)
2	PASA-*meta*	9 ± 1	0.5 ± 0.1	18 ± 4	–0.19
3	PASA-*para*	70 ± 10	0.5 ± 0.1	140 ± 30	–0.50
4	Dextran	1.3 ± 0.2	0.6 ± 0.2	2.2 ± 0.8	–0.007
5	Pullulan	2.1 ± 0.4	0.6 ± 0.2	3.5 ± 1	–0.032
6	Mannan	5 ± 0.9	0.5 ± 0.2	10 ± 4	–0.16
7	Hydroxypropyl methyl cellulose	17 ± 2	0.6 ± 0.1	28 ± 6	–0.29
8	Methyl cellulose	15.5 ± 2.5	0.6 ± 0.2	26 ± 10	–0.44
9	Chitosan	24 ± 3	0.5 ± 0.1	48 ± 10	–0.46
10	Xanthane	240 ± 40	2.4 ± 0.3	100 ± 20	–(0.43–0.50)

* no. 1, sodium polystyrene sulfonate; no. 2, sulfated polyamide with the benzene ring in the *meta* position; and no. 3, sulfated polyamide with the benzene ring in the *para* position.

** The parameter S_0 was estimated accurately to within 10%.

The condition for the predominantly planar ordering of the segments on the surface, when $S_0 < 0$, is $Al_c > \pi r^2$, i.e., the area of contact of the lateral surface of the cylinder with the substrate surface should exceed the area of its end face. In this case, at high degrees of asymmetry of the statistical segment, when $p \to \infty$, the parameter S_0 tends to a limiting value: $S_0 \to -0.5$, corresponding to the ideal planar packing of the segments near the surface. In the case when $\pi r^2 > Al_c$, $S_0 > 0$, and the segments near the surface exhibit orthogonal ordering (the directrix of the cylinder makes an angle $\theta < 57°$ with the normal to the substrate surface).

When $\pi r^2 \gg Al_c$, the order parameter tends to another limit, $S_0 \to 1$, corresponding to the ideal orthogonal packing of the segments near the surface. Thus, expression (3) describes both types of the possible orientation ordering of the segments with respect to the surface (planar and orthogonal) in relation to the r/l_c ratio. Virtually all linear polymers exhibit planar ordering of the chains near the surface, i.e., $\pi r^2 > Al_c$.

The parameter S_0 is governed both by the asymmetry of the statistical segment p and the dimensionless ratio r/l_c. The plot of the module of S_0 vs. p in the log–log coordinates breaks down into a number of curves shifting to the right along the p axis with increasing r/l_c (see figure). The smaller the surface area of contact of the segment with the surface, the greater the degree of asymmetry of the segment corresponding to the same degree of the orientational order in the surface layer of the polymer film.

Testing the calculated dependences $S_0 = f(p, r/l_c)$ is best conducted via comparison with the experimental data for films formed under identical conditions, which excludes possible uncontrollable impact of additional factors (substrate, solvent) on the properties of the near-surface layers. Let us consider the birefringence of the films formed on glass from solutions of water-soluble polysaccharides and water-soluble sulfated phenyl-containing polymers (see table). The

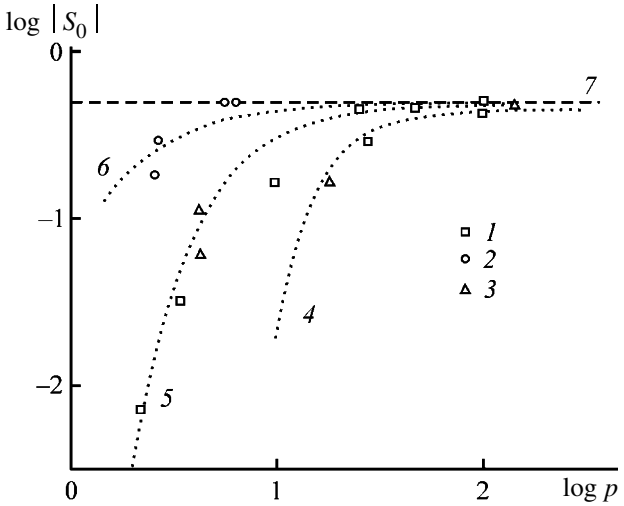

Module of the orientational order parameter $|S_0|$ in relation to the asymmetry of the statistical segment p in the log–log coordinates. (*1, 2, 3*) Points: data for (*1*) linear water-soluble polysaccharides, (*2*) polytrimethylsilylpropynes, and (*3*) water-soluble sulfated phenyl-containing polymers. (*4–6*) Theoretical curves [Eq. (3)], corresponding to r/l_c of (*4*) 3, (*5*) 1, and (*6*) π^{-1}. Straight line *7* corresponds to the limiting value of the orientational order parameter $S_0 = -0.5$ for the planar ordering.

table presents the parameters A, d, and p and their corresponding errors, as well as the parameter S_0. For references to original works, in which the lengths of the statistical segment A and the molecular diameter d were determined, see [7–10, 14]. It should be noted that the polysaccharide series holds a record on the scope of possible lengths of the statistical segment of linear chains (see table) and, hence, its asymmetry.

The figure compares the theoretical dependences $S_0 = f(p, r/l_c)$ calculated by relationship (3) with the experimentally estimated parameters S_0 and p. Also, the figure presents the data from studies [15, 16] concerned with the surface birefringence of the films of polytrimethylsilylpropynes prepared on cellophane substrates under evaporation of their solutions in toluene or CCl_4.

The experimental points obtained for the films formed from water-soluble sulfated aromatic polymers and polysaccharides are intermediate between the curves corresponding to the dimensionless parameter $1 \le r/l_c \le 3$. For polytrimethylsilylpropyne chains, the best agreement between the experiment and the theory is observed in the case when the contact area of the polymer chain segment with the substrate satisfies the condition $l_c \approx \pi r$. This means that the polytrimethylsilylpropyne chains are relatively better oriented at interfaces, which, in turn, can provide an explanation to the unique gas-separation properties of membranes thereof [17].

It should be noted that comparison of our experimental results with the relationship (3) allows estimating the contact surface area $s = Al_c$ of the polymer segment with the rigid flat surface of the substrate. For the water-soluble polymer/substrate systems examined, the surface area of contact of the statistical segment varies within 0.4–300 nm^2, depending on the thermodynamic rigidity of the polymer chains. The contact surface area for the statistical segments of the chains of polytrimethylsilylpropynes is relatively larger: $s \approx \pi Ar$. We will note that a larger or a smaller cross-sectional dimension of the contact l_c can mean that some polymer/solvent/substrate systems have a higher or a lower adsorption (adhesion) energy compared to other systems. In other words, the cross-sectional dimension of the contact is an effective parameter which needs to be reduced to the corresponding surface density of the adhesion energy in comparison of various polymer/solvent/substrate systems. The resulting structure of the macromolecules near the surface is dictated by the competition of the entropy factor, to a first approximation depending on the asymmetry p, and the energy factor governed by l_c.

Naumova and Grishchenko [18] assumed that the orientational ordering of rigid impenetrable cylinders near the surface is governed by purely steric factors and obtained for the order parameter

$$S_0 = (1 - p)/(1 + 2p). \quad (4)$$

Evidently, relationship (4) is a special case of relationship (3) at $l_c = \pi r$.

CONCLUSION

The relationship $S_0 = [1 - (pl_c/\pi p)]/[1 + (2pl_c/\pi p)]$ was obtained, which, along with the degree of asymmetry of the statistical segment of the macromolecules p, contains the ratio of the cross-sectional dimension of the contact between the segment of the macromolecule and the substrate surface l_c to the segment radius r.

REFERENCES

1. Silberberg, A., *J. Macromol. Sci. Phys.*, 1980, vol. B18, no. 4, pp. 677–684.
2. Eisenriegler, E., *Polymer Near Surfaces*, Singapore: World Scientific, 1993.
3. Mischler, C., Baschwagel, J., Dasputa, S., and Binder, K., *Polymer*, 2002, vol. 43, no. 2, pp. 467–476.
4. Chen, N., Maeda, N., Tirrell, M., and Israelachvili, J., *Macromolecules*, 2005, vol. 38, no. 8, pp. 3491–3503.
5. Cherkasov, A.N., Vitovskaya, M.G., and Bushin, S.V., *Vysokomol. Soedin., Ser. A*, 1976, vol. 18, no. 7, pp. 1628–1634.
6. Grishchenko, A.E. and Cherkasov, A.N., *Usp. Fiz. Nauk*, 1997, vol. 167, no. 3, pp. 269–285.
7. Pavlov, G.M. and Grishchenko, A.E., *Biotechnol. Genetic Eng. Rev.*, 1999, vol. 16, pp. 347–359.
8. Pavlov, G.M. and Grishchenko, A.E., *Vysokomol. Soedin., Ser. B*, 2005, vol. 47, no. 10, pp. 1882–1886.
9. Pavlov, G.M., Gubarev, A.S., Zaitseva, I.I., and Fedotov, Yu.A., Abstracts of Papers, *Eur. Polymer Congr.*, Moscow (Russia), June 27–July 1, 2005, p. 222.
10. Pavlov, G.M., Gubarev, A.S., Zaitseva, I.I., and Fedotov, Yu.A., *Vysokomol. Soedin., Ser. A*, 2006, vol. 48, no. 12, pp. 2001–2006.
11. Gennes, P.-G. de, *Rep. Prog. Phys.*, 1969, vol. 32, no. 1, pp. 187–205.

12. Malinskii, Yu.M., *Usp. Khim.*, 1970, vol. 39, pp. 1311–1326.
13. Ten Bosch, A., *Phys. Rev. E.*, 2001, vol. 63, no. 061 818.
14. Pavlov, G.M., Molecular Hydrodynamics and Optics of Natural and Synthetic Polysaccharides, *Doctoral Dissertation*, St. Petersburg, 2004.
15. Grishchenko, A.E., Mikhailova, N.A., Khotimskii, V.S., et al., *Opt. Zh.*, 2003, vol. 70, no. 10, pp. 30–34.
16. Grishchenko, A.E., Khotimskii, V.S, Mikhailova, N.A., et al., *Zh. Prikl. Khim.*, 2003, vol. 76, no. 8, pp. 1325–1328.
17. Nagai, K., Masuda, T., Nakagawa, T., et al., *Prog. Polym. Sci.*, 2001, vol. 26, pp. 721–798.
18. Naumova, L.V. and Grishchenko, A.E., *Vysokomol. Soedin., Ser. B*, 2005, vol. 47, no. 11, pp. 2056–2059.

ISSN 1070-4272, Russian Journal of Applied Chemistry, 2007, Vol. 80, No. 1, pp. 106–109. © Pleiades Publishing, Ltd., 2007.
Original Russian Text © O.Yu. Golubeva, V.E. Yudin, A.L. Didenko, V.M. Svetlichnyi, V.V. Gusarov, 2007, published in Zhurnal Prikladnoi Khimii, 2007, Vol. 80, No. 1, pp. 106–110.

MACROMOLECULAR CHEMISTRY AND POLYMERIC MATERIALS

Nanocomposites Based on Polyimide Thermoplastics and Magnesium Silicate Nanoparticles with Montmorillonite Structure

O. Yu. Golubeva, V. E. Yudin, A. L. Didenko, V. M. Svetlichnyi, and V. V. Gusarov

Grebenshchikov Institute of Silicate Chemistry, Russian Academy of Sciences, St. Petersburg, Russia
Institute of Macromolecular Compounds, Russian Academy of Sciences, St. Petersburg, Russia

Received August 4, 2006

Abstract—Nanocomposites based on a thermoplastic polyimide, poly{1,3-bis(3',4-dicarboxyphenoxy)benzene [4,4'-bis(4"-*N*-phenoxy)diphenyl sulfone]imide}, and synthetic magnesium silicate nanoparticles with montmorillonite structure were prepared from melts. Efficient modification of the surface of the initial nanoparticles with (aminoethylaminomethyl)phenethyltrimethoxysilane was performed.

DOI: 10.1134/S1070427207010211

At present one of the most efficient approaches to the development of new polymeric materials is the preparation of hybrid nanocomposites of polymers with inorganic nanoparticles, i.e., with inorganic particles of size no more than 100 nm. It should be noted that the polymeric materials formed on both molecular and supramolecular levels from organic (polymer) and inorganic (nanoparticles) components are absolutely new polymeric systems and not a simple "sum" of these components. This fact is confirmed in a series of experimental studies [1, 2]. It is known [3–8] that lamellar silicates, when added as fillers, strongly enhance characteristics of the resulting polymeric materials, e.g., they improve the strength, crack resistance, softening point, and heat resistance of polymers and decrease their coefficient of linear thermal expansion, gas permeability, etc.

Polyimides (PIs) are highly thermally stable polymers widely used in various branches of industry, such as electrical engineering and electronics. Polymer–inorganic nanocomposites based on PI thermoplastics and natural lamellar silicate montmorillonite were prepared and studied in [9–12]. For example, PI nanocomposites prepared from natural montmorillonite modified with various organic compounds [11, 12] exhibit elevated barrier and mechanical properties as compared to unfilled PIs. At the same time, composites with natural montmorillonite filler have certain drawbacks associated with heterogeneity of the chemical, phase, and disperse composition of the filler [13–15]. The use of synthetic nanoparticles eliminates these drawbacks.

Lamellar silicates are capable of isomorphic substitution of atoms in their structure, allowing direct synthesis of nanoparticles of given composition. The choice of the composition and size of nanoparticles is dictated by the destination of the resulting composites. Thus, synthetic nanoparticles with given characteristics provide preparation of polymeric composites with required properties.

In this study we prepared nanocomposites based on polyimide thermoplastics and synthetic magnesium silicate montmorillonite (MMT-Mg) synthesized under the hydrothermal conditions [13] and examined the mechanical characteristics of these materials.

EXPERIMENTAL

Synthetic magnesium silicate montmorillonite was used as a filler to prepare composites based on polyimide matrices. Montmorillonite was prepared under the hydrothermal conditions given elsewhere [13]. The size of the resulting particles was about 50 nm, and the composition of the resulting magnesium silicate montmorillonite (analog of natural saponite) was $Mg_3Si_4O_{10}(OH)_2 \cdot nH_2O$.

The hydrophobicity and affinity for polymeric materials of the MMT-Mg nanoparticles were improved by modification of their surface with (aminoethyl-

aminomethyl)phenethyltrimethoxysilane (hereinafter, silane). A weighed portion (1 g) of MMT-Mg nanoparticles was preliminarily dispersed in ethanol (50 ml) using an ultrasonic bath (20 kHz) for 1 h. Then, the resulting dispersion was mixed with silane (0.2 ml) und ultrasonic treatment was performed for an additional 10 min. The resulting dispersion in the ethanolic solution of silane was centrifuged, the precipitate was additionally washed with ethanol for 30 min to remove excess silane not consumed in the reaction with MMT-Mg nanoparticles, and the mixture was centrifuged. The resulting MMT-Mg nanoparticles treated with silane were dried to remove ethanol in a vacuum at 60°C for 5 h.

The efficiency of the nanoparticle surface treatment with silane was monitored by X-ray diffraction (XRD) analysis on a MiroMax007 device (Rigaku Denki Co. Ltd, Japan). The increase in the distance between the silica layers in MMT-Mg after its treatment with silane was determined from the shift of the (001) reflection toward smaller angles θ, and the corresponding interlayer spacing d was calculated using the Bragg equation:

$$D = \lambda/2\sin\theta,$$

where λ = 1.54 Å (wavelength of CuK_α radiation).

The thermogravimetric analysis (TGA) of the MMT-Mg samples before and after treatment with silane was performed on a Perkin–Elmer 7 device under nitrogen atmosphere; the sample weight was 5–10 mg, and the heating rate, 10 deg min^{-1}.

As a polymeric matrix we used, poly{1,3-bis(3',4-dicarboxyphenoxy)benzene [4,4'-bis(4"-*N*-phenoxy)-diphenyl sulfone]imide} (PI P-SOD) [13] of the following structure:

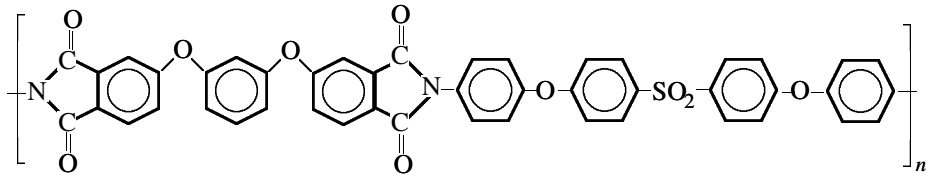

The P-SOD + 10 wt % MMT-Mg/silane mixture was prepared on a Haake Minilab microblender, which allows combining a small amount (5 g) of the molten polymer with MMT-Mg/silane powder (0.5 g). Blending was performed at 340°C for 20 min at a screw rotation rate of 100 rpm.

The block samples for mechanical tests were prepared from both unfilled of PI P-SOD and P-SOD + 10 wt % MMT-Mg/silane composite using a microinjector (DACA Instruments); the melt temperature was 360°C, the mold temperature, 90°C, and injection pressure, 100 atm.

The mechanical properties (bending strength σ, bending elastic modulus E, and ultimate bending strain ε) of block samples P-SOD polyimide and nanocomposites based on it were determined on a 1958U-10-1 tensile-testing machine (Russia). For mechanical tests, the samples of polyimide and composite were prepared as $1 \times 5 \times 20$ mm plates. The bending properties were studied at room temperature under the mode of active loading at a rate of 10^{-3} m min^{-1}. The shear Young's modulus G' of the block samples was determined with an MK-002 torsional balance wheel (Institute of Macromolecular Compounds) in the mode of freely damping torsional oscillations (oscillation frequency ~0.5 Hz) at room temperature.

Modification of the surface of lamellar silicates is an important stage of the preparation of nanocomposites based on them. Treatment of silicates with organic compounds makes their surface more hydrophobic, improves the compatibility of nanoparticles with the polymer, and increases the interlayer spacing to simplify exfoliation of the silicate filler in the polymer matrix [1, 2]. Since the main process occurring at interaction of the polymers with lamellar silicates is the exchange adsorption, the behavior of the exchanging cations (Na^+, K^+, Ca^{2+}) localized between the silica layers is of particular importance. High cation-exchange capacities determine the simplicity and completeness of modification of the clay materials. In turn, the cation-exchange capacity is determined by the composition and structure of the lamellar material. Isomorphic substitution of aluminum atoms for silicon and of magnesium, iron, and some other elements for aluminum in tetrahedral and octahedral positions of the structure provides formation of the surface negative charge and improves the cation-exchange capacity of the lamellar silicate.

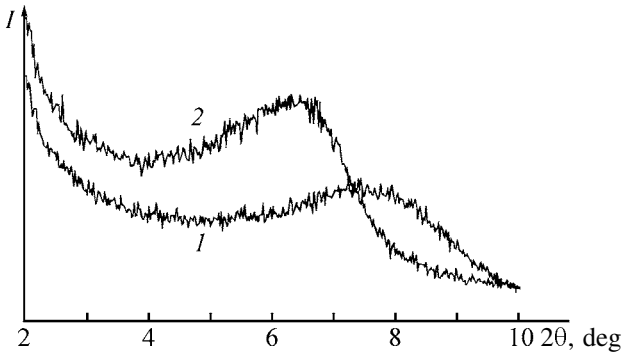

Fig. 1. XRD patterns of (*1*) initial MMT-Mg and (*2*) MMT-Mg modified with silane. (*I*) Intensity and (2θ) Bragg angle.

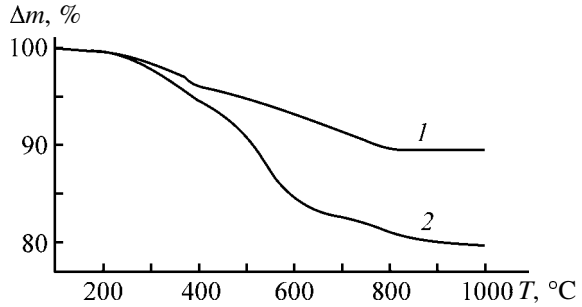

Fig. 2. TGA curves of (*1*) initial MMT-Mg and (*2*) MMT-Mg modified with silane. (Δ*m*) Weight loss and (*T*) temperature.

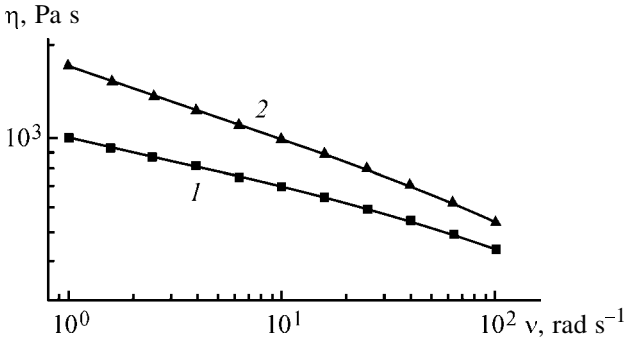

Fig. 3. Viscosity η of melts: (*1*) PI P-SOD and (*2*) nanocomposite PI P-SOD + 10 wt % MMT-Mg/silane as a function of frequency ν; temperature 360°C, deformation amplitude 1%.

In the absence of isomorphic substitution, as in the case of MMT-Mg studied in this work, the crystallochemical charge of the particle surface should be neutral and the cation-exchange capacity should be close to zero. From this viewpoint, the composition of montmorillonite is not optimal. At the same time, synthetic montmorillonite exhibits adsorption capacity allowing efficient modification of its surface with organic compounds. This is due to the fact that the surface of lamellar silicates, along with exchanging cations, contains wide assortment of active adsorption centers of various nature [16, 17]. Along with exchanging cations and coordination-unsaturated magnesium and aluminum ions, they can include single and geminal OH groups at the silicon atoms at the edges of tetrahedral and octahedral layers, uncompensated bonds at the crack surfaces, etc. [17].

The XRD patterns of the initial MMT-Mg and of MMT-Mg treated with silane are shown in Fig. 1. As seen, the reflection at 2θ = 7.55° (d_{001} 11.7 Å) characterizing the basal distance between the silicon–oxygen layers in the initial montmorillonite shifts toward smaller angles after treatment with silane. The reflection at 2θ = 6.31° corresponds to an increase in the interlayer spacing to 13.8 Å. Thus, treatment of the initial sample with silane increases the interlayer spacing, which confirms formation of a hybrid organic–inorganic material.

As seen from the TGA data (Fig. 2), the MMT-Mg samples treated with silane exhibit relatively high heat resistance; intensive weight loss is observed in the 230–250°C range, which allows their use for modification of heat-resistant polyimide matrices. It should be noted that low stability of aliphatic amines often used in modification of the lamellar silicate surface [3–8] is the main drawback hindering their use for preparing nanocomposites based on polyimides.

Compounding of silane-MMt-Mg nanoparticles modified with PI P-SOD in a microblender only insignificantly increases the polyimide viscosity at 360°C (Fig. 3). For example, filling of PI P-SOD with MMT-Mg/silane (10 wt %) increases the viscosity of the polyimide matrix by a factor of 1.5, which allows preparation of high-quality nanocomposite samples using the DACA microinjector without increasing temperature of the melt or press mold. Small increase in the melt viscosity can be probably explained by a small size (50 nm) of the MMT-Mg nanoparticles. In contrast, coarser natural montmorillonite with the particle size more than 100 nm, when added to the polymeric matrix, strongly increases the viscosity of the polymer melt [4, 5]. Increased viscosity of the resulting composites complicates their molding.

The mechanical characteristics of samples of polyimide thermoplastics and nanocomposites based on P-SOD and filled with MMT-Mg nanoparticles modified with silane are listed in the table. Addition of MMT-Mg/silane (10 wt %) into the PI P-SOD matrix increases the bending strength σ_f of the composite from 170 to 195 MPa and, especially, its bending elastic modulus E_f and shear elastic modulus G' from 2.3 to 3.2 GPa and from 1.3 to 1.8 GPa, respectively. This increase in the strength and hardness of the poly-

Mechanical properties of polyimide thermoplastics and nanocomposites prepared from PI P-SOD and nanoparticles of synthetic MMT-Mg modified with silane*

Sample	σ_f, MPa	E_f, GPa	ε_f, %	G', GPa
ULTEM-1000	180 ± 3	2.7	>10	1.4
P-SOD	170 ± 4	2.3	>10	1.3
P-SOD + 10wt % MMT-Mg/silane	195 ± 7	3.2	5	1.8

* (ε_f) Bending strength, (E_f) bending elastic modulus, (χ_f) ultimate bending strain, (G') shear elastic modulus.

imide composite confirms the reinforcing effect of MMT-Mg nanoparticles owing to anisotropic platelike shape of the nanoparticles and their strong binding with the P-SOD matrix. For comparison, the properties of thermoplastic ULTEM-1000 polyamide (GE, the United States), whose test samples were prepared by a similar procedure using a DACA microinjector, are also listed in the table. As seen, the strength and elastic characteristics of commercial ULTEM-1000 composite are slightly higher than those of PI P-SOD thermoplastics, but they are lower than those of P-SOD + 10 wt % MMT-Mg/silane nanocomposite. Slight decrease in the ultimate bending strain ε_f of the nanocomposite is probably due to insufficiently uniform distribution of the MMT-Mg nanoparticles in the PI P-SOD matrix and formation of submicron particle aggregates, which can initiate formation of critical microcracks in the composite bulk.

CONCLUSIONS

(1) The surface of magnesium silicate nanoparticles with montmorillonite structure was modified using (aminoethylaminomethyl)phenethyltrimethoxysilane. As a result, the basal spacing between the silicon-oxygen layers increased from 11.7 to 13.8 Å, which confirms the efficiency of the surface modification.

(2) Nanocomposites based on thermoplastic polyimide poly{1,3-bis(3',4-dicarboxyphenoxy)benzene [4,4'bis(4"-*N*-phenoxy)diphenyl sulfone]imide} and magnesium silicate nanoparticles modified with silane were prepared.

(3) Filling of the polyimide matrix with magnesium silicate nanoparticles modified with silane (10 wt %) increases the nanocomposite strength by 15% and its bending elastic modulus and shear elastic modulus by a factor of 1.4.

ACKNOWLEDGMENTS

The study was financially supported by the Russian Foundation for Basic Research (project nos. 06-08-00202a and 04-03-81005-Bel2004a), by the Grant for Young Candidates of Sciences of St. Petersburg (project no. PD-6-1.3-26), and by the Grant of St. Petersburg Scientific Center of the Russian Academy of Sciences.

REFERENCES

1. Zeng, Q.H., Yu, A.B., Lu, G.Q., et al., *J. Nanosci. Nanotechnol.*, 2005, vol. 5, pp. 1574–1592.
2. Ray, S.S. and Okamoto, M., *Prog. Polym. Sci.*, 2003, vol. 28, pp. 1539–1641.
3. Abdalla, M.O., Dean, D.D., and Campbell, S., *Polymer*, 2002, vol. 43, pp. 5887–5893.
4. Wang, Z.M., Chung, T.C., Gilman, J.W., et al., *J. Polym. Sci.*, 2002, vol. 41, pp. 3173–3187.
5. Manias, E., Touny, L., Strawhecker, K., et al., *Chem. Mater.*, 2001, vol. 13, pp. 3516–3523.
6. Strawhecker, K.E. and Manias, E., *Chem. Mater.*, 2000, vol. 12, pp. 2943–2949.
7. Huang, J., Zhu, Z., Yin, J., et al., *Polymer*, 2001, vol. 43, pp. 873–877.
8. Brune, D. and Bicerano, J., *Polymer*, 2002, vol. 43, pp. 369–387.
9. Tyan, H., Wu, C., and Wei, K., *J. Appl. Polym. Sci.*, 2001, vol. 81, pp. 1742–1747.
10. Delozier, D.M., Orwoll, R.A., Cahoon, J.F., et al., *Polymer*, 2002, vol. 43. pp. 813–822.
11. Tyan, H., Leu, C., and Wei, K., *Chem. Mater.*, 2001, vol. 13, pp. 222–226.
12. Tyan, H., Wei, K., and Hsieh, T., *J. Polym. Sci.*, 2000, vol. 38, pp. 2873–2878.
13. Golubeva, O.Yu., Korytkova, E.N., and Gusarov, V.V., *Zh. Prikl. Khim.*, 2005, vol. 78, no. 1, pp. 26–33.
14. Corrado, K. A., *Appl. Clay Sci.*, 2000, vol. 17, pp. 1–23.
15. Yudin, V.E., Divoux, G.M., Otaigbe, J.U., et al., *Polymer*, 2005, vol. 46, pp. 10866–10872.
16. Aripov, E.A. and Agzamkhodzhaev, A.A., *Aktivnye tsentry montmorillonita i khemosorbtsiya* (Active Centers of Montmorillonite and Chemisorption), Tashkent: Fan, 1983.
17. Komarov, V.S., *Adsorbtsionno-strukturnye, fiziko-khimicheskie i kataliticheskie svoistva glin Belorussii* (Adsorption-Structural, Physicochemical, and Catalytic Properties of Belarussian Clays), Minsk: Nauka i Tekhnika, 1970.

ISSN 1070-4272, Russian Journal of Applied Chemistry, 2007, Vol. 80, No. 1, pp. 110–114. © Pleiades Publishing, Ltd., 2007.
Original Russian Text © Z.T. Dmitrieva, N.A. Khomchenko, 2007, published in Zhurnal Prikladnoi Khimii, 2007, Vol. 80, No. 1, pp. 111–115.

MACROMOLECULAR CHEMISTRY AND POLYMERIC MATERIALS

A Thermogravimetric Study of Lithium Tetraalkoxyborates

Z. T. Dmitrieva and N. A. Khomchenko

Institute of Petroleum Chemistry, Siberian Division, Russian Academy of Sciences, Tomsk, Russia

Received March 16, 2006

Abstract—Properties of lithium tetraalkoxyborates Li[*t*-$C_4H_9OB(OR)_3$] (R = *n*-C_4H_9 to *n*-C_8H_{17}, *n*-$C_{12}H_{25}$) were studied by differential thermogravimetry. The kinetic parameters and heat effects of thermal decomposition of lithium tetraalkoxyborates in air and inert gas atmosphere as functions of the carbon chain length were determined.

DOI: 10.1134/S1070427207010223

Our previous studies [1–5] by mass spectrometry, rheometry, NMR spectroscopy, and small-angle X-ray scattering showed that lithium tetraalkoxyborates Li[$B(OR)_4$] (R = C_4H_9–$C_{16}H_{33}$) in the solid state and in hydrocarbon liquids are polyassociated through Li···O bonds and van der Waals bondings between alkyl groups R···R with the formation of three-dimensional chelate structures. In liquids with low permittivity, compounds swell similarly to polymers with the formation of thermodynamically stable structured systems [6–8]. After mechanical breakdown under the action of shear stress in various deformation modes, the supramolecular structure of solutions and gels is restored without changes in rheological properties [3, 4, 8, 9].

Due to thixotropic properties, hydrocarbon gels of compounds are used, for instance, in the technology of hydraulic fracturing of low-permeability gas- and oil-bearing strata in order to increase their filter-output. The thermodynamic parameters of thermal desorption show high affinity of lithium tetraalkoxyborates for hydrocarbons [10].

In this study, to obtain additional information on the stability of associative intermolecular interactions and of Li[*t*-$C_4H_9OB(OR)_3$], e.g., under conditions of stratal temperature, we examined these compounds by differential thermogravimetry.

EXPERIMENTAL

Thermal decomposition (pyrolysis) and thermal oxidative decomposition of Li[*t*-$C_4H_9OB(OR)_3$] (R = *n*-C_4H_9 to *n*-C_8H_{17}, *n*-$C_{12}H_{25}$) were performed in a platinum crucible in an argon flow (10 l h^{-1}) and in air, respectively, at a heating rate 5 deg min^{-1} on a MOM derivatograph (Hungary). Lithium tetraalkoxyborates were synthesized in a flow of dry inert gas by the reaction of boron trialcoholates with lithium *t*-butylate in dry pentane and without diluent. The purity of compounds obtained was checked by elemental microanalysis and IR and ^1H NMR spectroscopy.

The parameters of the formal kinetics of the thermal transformation were obtained with appropriate computer software under the assumption that the thermal transformation obeys the Arrhenius law

$$K = A\exp(-E/RT)$$

and involves the pyrolysis reaction only [11]. With regard to the kinetics of decomposition of polymeric materials [12], we assumed that the pyrolysis of lithium *t*-butoxytrialkoxyborates is also described by the

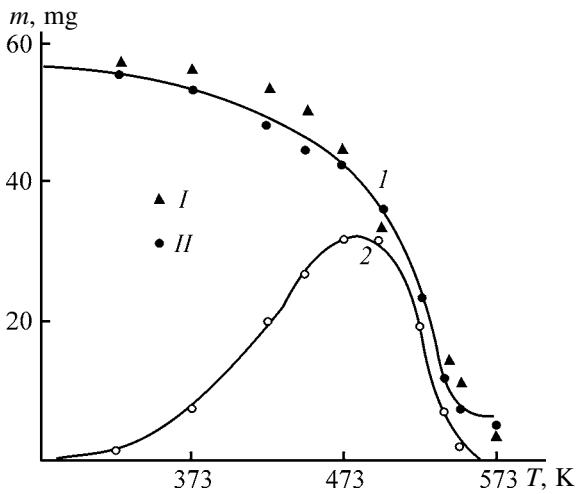

Fig. 1. Change in weight *m* (TG) in the course of Li[*t*-$C_4H_9OB(OC_7H_{15})_3$] pyrolysis. (*T*) Temperature. (*1*) Experimental TG of pyrolysis: (*I*) by one-stage scheme and (*II*) by two-stage scheme; (*2*) accumulation of an intermediate, calculated by the two-stage scheme.

Table 1. Kinetic characteristics of Li[*t*-$C_4H_9OB(OR)_3$] pyrolysis

R	First stage			Second stage		
	ΔE_a, kJ mol^{-1}	T, K	k_1, s^{-1}	ΔE_a, kJ mol^{-1}	T, K (T_{max})	k_2, s^{-1} (k_{2max})
C_4H_9	22.6	348–473	1.78×10^{-4}–1.4×10^{-3}	121.7	473–530 (517)	2.6×10^{-4}–7.3×10^{-3} (3.6×10^{-3})
C_5H_{11}	19.7	398–448	7.8×10^{-4}–1.5×10^{-3}	123.5	448–548 (521)	5.9×10^{-4}–2.5×10^{-3} (6.2×10^{-2})
C_6H_{13}	23.2	348–423	1.5×10^{-4}–6.4×10^{-4}	121.6	423–547 (535)	1.2×10^{-5}–1.5×10^{-2} (8.0×10^{-3})
C_7H_{15}	26.8	373–453	3.5×10^{-4}–1.6×10^{-4}	127.5	453–553 (539)	3.8×10^{-5}–1.7×10^{-2} (8.4×10^{-3})
C_8H_{17}	34.8	373–448	9.8×10^{-5}–6.4×10^{-4}	125.1	448–573 (548)	1.5×10^{-5}–2.4×10^{-2} (7.1×10^{-3})
$C_{12}H_{25}$	76.9	423–498	3.1×10^{-5}–8.3×10^{-4}	158.0	498–573 (533)	2.5×10^{-7}–3.7×10^{-5} (3.0×10^{-6})

first-order equation. The calculated dependences of the compound weight loss with temperature (TG curves) well coincide with experimental thermograms of the compound pyrolysis (Fig. 1). The pyrolysis parameters were calculated using a two-stage scheme (Table 1). The DTA curves recorded in an inert atmosphere are characterized by a large endothermic effect with two ill-resolved maxima within the 403–423 and 473–498 K ranges, whose position depends on the R length (Figs. 2a, 2b). The first of them is accompanied by uniform weight loss (the TG curve descends at a constant rate). The second endotheric effect is characterized by an extremum in the DTG curve at 518–548 K corresponding to the maximal reaction rate. The pyrolysis is completed by the exothermic effects within the 480–673 K range for Li[*t*-$C_4H_9OB\cdot(OC_7H_{15})_3$] (Fig. 2a, Fig. 3, curve *1*) and within the 528–688 K range for Li[*t*-$C_4H_9OB(OC_{12}H_{25})_3$] (Fig. 2b, Fig. 3, curve *2*) without weight change, which can be assigned to rearrangement of the unit cell of the inorganic residue after the compound thermal decomposition. With lengthening of R, both the maximum of this effect and the maximum of heat absorption shift to higher temperatures.

In the first stage of the thermal decomposition, lengthening of R reduces the weight loss rate (Table 1). The slower pyrolysis of bulkier compounds is probably caused by an equilibrium between the elimination of alkyl radicals and their recombination with both decomposed compound and with each other with the formation of the condensed phase because of

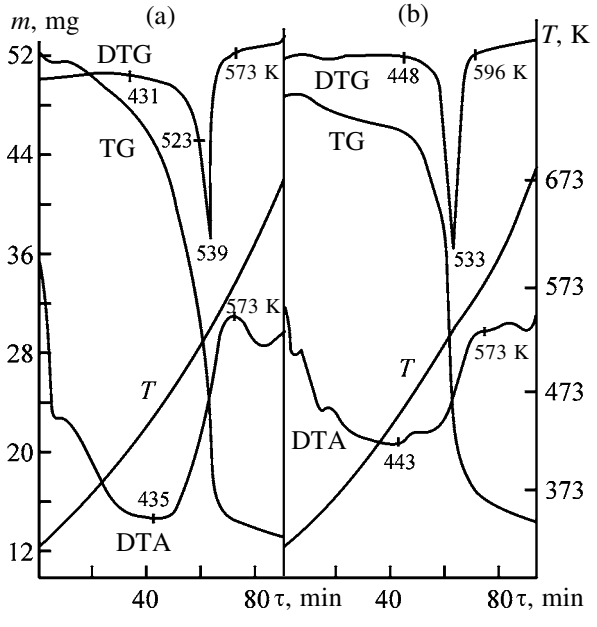

Fig. 2. Thermograms of (a) Li[*t*-$C_4H_9OB(OC_7H_{15})_3$] and (b) Li[*t*-$C_4H_9OB(OC_{12}H_{25})_3$] in an argon atmosphere. DTA 1/5, DTG 1/10, TG 50, m = 49 mg, v_h = 5 deg min^{-1}. (m) Weight, (T) temperature, and (τ) time; the same for Fig. 4.

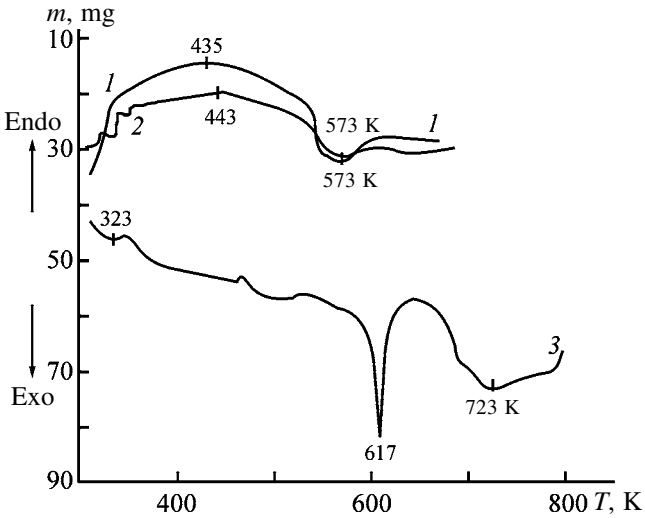

Fig. 3. DTA curves of (*1*) Li[*t*-$C_4H_9OB(OC_7H_{15})_3$] and (*2*) Li[*t*-$C_4H_9OB(OC_{12}H_{25})_3$] in an argon atmosphere and (*3*) Li[*t*-$C_4H_9OB(OC_7H_{15})_3$] in air. (m) Weight and (T) temperature.

Table 2. Dependence of the weight loss in two-stage pyrolysis of Li[*t*-$C_4H_9OB(OR)_3$] compounds on the size of R

First stage			Second stage		
T, K	R	Δ*m*, %	*T*, K	R	Δ*m*, %
348–473	C_4H_9	31.5	473–530	C_4H_9	48.5
398–448	C_5H_{11}	29.2	448–548	C_5H_{11}	46.9
348–423	C_6H_{13}	24.5	423–547	C_6H_{13}	67.3
373–453	C_7H_{15}	20.2	453–553	C_7H_{15}	72.1
373–448	C_8H_{17}	13.8	448–573	C_8H_{17}	79.2
423–498	$C_{12}H_{25}$	5.1	498–573	$C_{12}H_{25}$	81.6

insufficiently high temperature (348–498 K). Under these conditions, the equilibrium dissociation–association of Li···O coordination bonds can still occur. This process itself does not change the shape of the weight loss curve, but affects the thermal stability of the peripheral part of the associate by means of the orientation effect. The distribution of the weight losses in the first and second stages of the compound pyrolysis depending on R size is listed in Table 2. The first stage of the pyrolysis presumably involves elimination of hydrocarbon fragments through which alkyl substituents interact in the intermolecular associate:

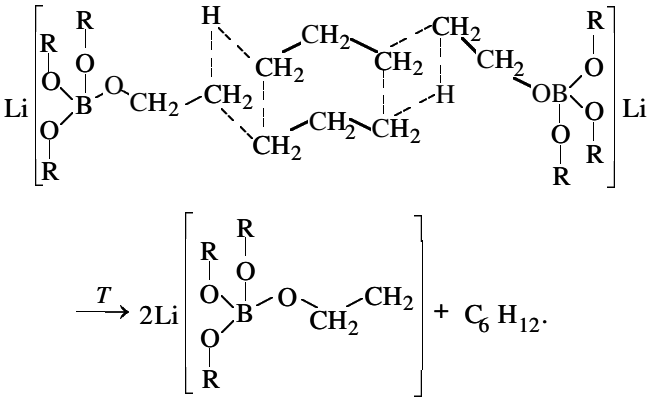

The longer R, the larger set of associates through the alkyl substituents is formed and the stronger is the R···R intermolecular interaction [1, 10]. In this case, the pyrolysis should be accompanied by a set of parallel and consequtive reactions of cleavage of C–C and C–H bonds with the formation of different hydrocarbons and active intermediates. This assumption does not contradict the kinetic parameters of the pyrolysis of lithium *t*-butoxytrialkoxyborates. The rate constant of weight loss decreases, and the activation energy of thermal decomposition increases with lengthening of R. In the series from C_4H_9 to $C_{12}H_{25}$, ΔE_a of the pyrolysis changes more sharply in the first stage than in the second stage (Table 1). In associated hydrocarbon chains, the energy of C···C bonds and the number of such bonds should increase in proportion to the R length because of intermolecular R···R interactions. Correspondingly, ΔE_a increases with increasing the length of R. The trend in variation of the activation entropy of decomposition at 423 K in going from Li[*t*-$C_4H_9OB(OC_4H_9)_3$] to Li[*t*-$C_4H_9OB(OC_{12}H_{25})_3$] ($\Delta S_a$ = –0.26 ans –0.16 kJ mol^{-1} K^{-1}, respectively) shows that the size of R largely governs the number of degrees of freedom of the system.

The second stage of the pyrolysis has an explosive character with the maximal rate of weight loss within a narrow temperature range (Figs. 2a, 2b, DTG curves). The activation energy increases by a factor of 2–6 as compared to the first stage and slightly changes with the length of R (Table 1). Under these conditions, there is no dissociation–association equilibrium, and fragments with short R are accumulated. At a definite temperature, they simultaneously decompose with the rupture of nonassociated C–C, C–O, and partially B–O bonds. The total weight loss of compounds is 80–90%, which corresponds to the composition LiBO + $LiBO_4$. Both stages formally proceed with the same overall reaction rate. The leveling of the kinetic parameters of thermogravimetry is probably caused by superposition of many independent reactions with different periods of maximal rates. This is especially characteristic for the first stage of the process.

In air, compounds undergo oxidative thermal decomposition also in two stages with the total weight loss of 85–94% within the 558–575 and 607–689 K ranges corresponding to maximal reaction rates (Fig. 4). In the first stage, the weight loss amounts to 38–40%. As follows from the analysis of the heat absorption (DTA curves) and weight loss (DTG and TG) curves, the thermal stability of lithium *t*-butoxytrialkoxyborates in air is higher than that in an inert gas (Figs. 2, 4). Thermal oxidative decomposition even in the first stage of the process occurs at higher temperature than thermal decomposition in an inert atmosphere. The thermograms show that in air noticeable weight loss begins at higher temperature than in an inert gas (Ar). This can be due to the fact that in the first stage of thermal oxidation the loss of air sorbed on the crystal surface is compensated by addition of oxygen and carbon monoxide to the compound molecule. Obviously, oxygen and carbon monoxide primarily interact with coordination-unsaturated lithium cation with the formation of new compounds. Therefore, the thermal stability of the complexes

Table 3. Kinetic and thermodynamic characteristics of thermal oxidative decomposition of Li[*t*-$C_4H_9OB(OR)_3$]

R	First stage			Second stage			ΔH	Q
	ΔE_a, kJ mol^{-1}	T_{max}, K	$k_1 \times 10^{-4}$, s^{-1}	ΔE_a, kJ mol^{-1}	T_{max}, K	k_2, s^{-1}	kJ mol^{-1}	
C_3H_7	25.3	531	7.0	24.7	597	–	7578.5	7930.4
C_4H_9	24.9	557	9.0	80.7	607	4.7×10^{-3}	10811.0	9257.1
C_7H_{15}	84.4	449	1.5	133.2	613	4.5×10^{-2}	12682.5	15003.4
$C_{12}H_{25}$	80.2	575	1.3	173.4	689	3.1×10^{-3}	–	25120.7

increases, whereas their heat absorption ability substantially decreases.

During thermal oxidative decomposition, the heat absorption ability of compounds is compensated by the heat release due to formation of new bonds because of oxidation. The comparison of the pronounced endothermic maximum in the DTA curves in an inert atmosphere (Fig. 1, curves *1, 2*) with the exothermic effect in curve *3* recorded in air shows that a large amount of heat is released during oxidation of lithium tetraalkoxyborate. Thus, the absorbed heat is almost completely compensated by the released heat. This results in the fact that the temperature corresponding to the maximum of the exothermic effect (617 K) of the complete decomposition of the oxidized compounds coincides with the temperature (613 K) of maximal rate of the weight loss (Fig. 4), whereas in the case of pyrolysis these processes do not coincide (Fig. 2): the exothermic effect (573 K) appears after the intense weight loss at 530–540 K. In the thermograms of the thermal oxidative decomposition of compounds, similarly to pyrolysis, the exothermic maximum appears at a constant weight (Fig. 3). Due to coordination unsaturation of the lithium cation, the structure of lithium *t*-butoxytrialkoxyborates contains a stored energy, which is manifested as additional heat release in the course of thermal oxidation.

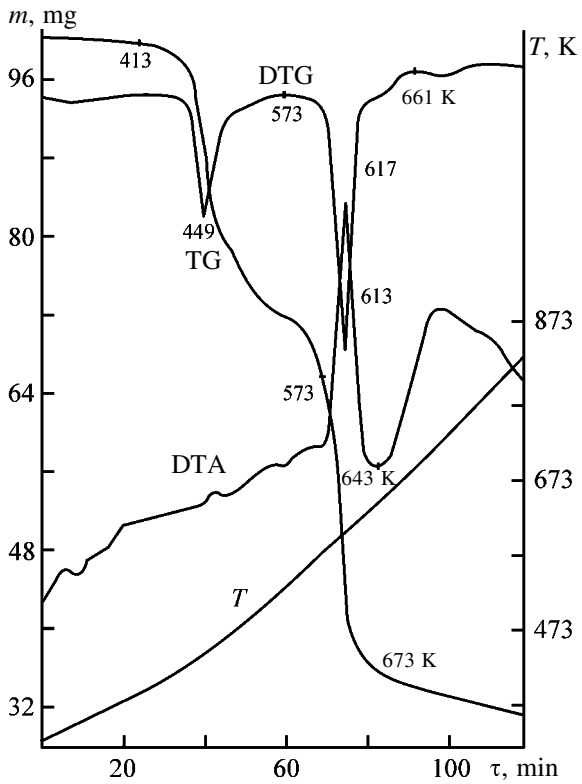

Fig. 4. Thermograms of Li[*t*-$C_4H_9OB(OC_7H_{15})_3$] in air. DTA 1/3, DTG 1/10, TG 100, m = 97 mg, v_h 5 deg min^{-1}.

The thermal effects ($-\Delta H$) of the oxidative decomposition of compounds in air, calculated from the DTA curves relative to a reference (*D*-glucose), are close to the heats of combustion Q found by calorimetry (Table 3). Increase in the heat effect with lengthening of R is proportional to the number of new bonds formed during oxidation. The positive heat of melting, increasing with decrease in the length of R, makes a certain correction to correlation of the heat effect with the length of R. The dependence of the kinetic parameters of the Li[*t*-$C_4H_9OB(OR)_3$] oxidative thermal decomposition on the length of R (Table 3) is similar to that observed for the pyrolysis (Table 1).

CONCLUSIONS

(1) Kinetic and thermodynamic parameters of the pyrolysis and thermal oxidative decomposition of lithium *t*-butoxyltrialkoxyborates were determined; the dependences of these parameters on the length of alkyl substituents were determined.

(2) The activation energy of lithium *t*-butoxytrialkoxyborate thermal decomposition increases with lengthening of R, which suggest strengthening of cooperative intermolecular R···R dispersion interactions.

(3) In contrast to activation energy, the rate constants of the pyrolysis and thermal oxidative decomposition are only slightly sensitive to the compound size.

(4) Thermal analysis of lithium *t*-butoxytrialkoxyborates in an inert gas and in air showed that the compound stability is higher under the conditions of thermal-oxidative decomposition.

REFERENCES

1. Dmitrieva, Z.T., Kadychagov, P.B., Turov, Yu.P., and Mezhibor, N.G., *Koord. Khim.*, 1986, vol. 12, no. 7, pp. 878–881.
2. Dmitrieva, Z.T. and Tailashev, A.S., *Izv. Akad Nauk SSSR, Ser. Khim.*, 1987, no. 12, pp. 2756–2760.
3. Dmitrieva, Z.T. and Tikhonova, L.D., *Makromol. Chem.*, 1990, vol. 39, pp. 197–202.
4. Dmitrieva, Z.T., *Mol. Cryst. Liq. Cryst. Incl. Nonlin. Opt.*, 1988, vol. 161, pp. 529–542.
5. Dmitrieva, Z.T., *Izv. Ross. Akad Nauk, Ser. Khim.*, 2005, no. 4, pp. 1035–1036.
6. Dmitrieva, Z.T., Bol'shakov, G.F., and Levus, Yu.I., *Dokl. Akad. Nauk SSSR*, 1985, vol. 281, pp. 883–887.
7. Dmitrieva, Z.T. and Ryzhikova, I.G., *Kolloidn. Zh.*, 1990, vol. 52, no. 1, pp. 123–127.
8. Dmitrieva, Z.T., Levus, Yu.I., and Tikhonova, L.D., *Kolloidn. Zh.*, 1986, vol. 48, no. 3, pp. 549–552.
9. Dmitrieva, Z.T., *Materialy 2-i nauchno-prakticheskoi konferentsii "Dobycha, podgotovka, transport nefti i gaza"* (Proc. 2nd Scientific and Practical Conf. "Oil and Gas Production, Conditioning, and Transport"), Tomsk, September 24–27, 2001, pp. 54–57.
10. Dmitrieva, Z.T., Tikhonova, L.D., Mezhibor, N.G., and Erofeev, V.I., *Neftekhimiya*, 1997, vol. 37, no. 1, pp. 62–67.
11. Grishin, A.M. and Sinitsin, S.P., *Fiz. Goren. Vzryva*, 1984, no. 6, pp. 67–79.
12. Venger, A.E. and Fraiman, Yu.E., *Inzh.-Fiz. Zh.*, 1981, vol. 40, no. 2, pp. 278–287.

ISSN 1070-4272, Russian Journal of Applied Chemistry, 2007, Vol. 80, No. 1, pp. 115–117. © Pleiades Publishing, Ltd., 2007.
Original Russian Text © A.M. Magerramov, M.R. Bairamov, M.G. Allakhverdieva, M.A. Agaeva, I.G. Mamedov, M.A. Dzhavadov, 2007, published in Zhurnal Prikladnoi Khimii, 2007, Vol. 80, No. 1, pp. 116–118.

MACROMOLECULAR CHEMISTRY AND POLYMERIC MATERIALS

Di(4-isopropenylphenoxy)alkanes as Cross-Linking Comonomers in Three-Dimensional Copolymerization with Styrene

A. M. Magerramov, M. R. Bairamov, M. G. Allakhverdieva, M. A. Agaeva, I. G. Mamedov, and M. A. Dzhavadov

Baku State University, Baku, Azerbaijan

Received May 19, 2006

Abstract—Di(4-isopropenylphenoxy)alkanes were synthesized by condensation of 4-isopropenylphenol with symmetrical dihaloalkanes in the presence of KI promoter. Three-dimensional polymeric structures were prepared by compolymerization of these monomers with styrene.

DOI: 10.1134/S1070427207010235

Copolymerization of various monomers with polyfunctional comonomers is a way to construct polymer networks and impart to them imporant service characteristics [1]. Many modern high-tech processes for preparing polymeric sorbents, photoresists for microelectronics and laser engineering, specialty composites, supported coordination catalysts, etc. [2–6] are based on this procedure.

Both thickly and thinly cross-linked polymers are required depending on destination [7]. In most cases, the required functional properties are imparted by polymer-analogous transformations. In particular, a cross-linked three-dimensional framework of the styrene–divinylbenzene copolymer is modified by introducing ionic groups (e.g., SO_3H groups by sulfonation). It should be noted, however, that the preparation of such cross-linked copolymers often involves problems associated with the high reactivity of the cross-linking comonomer (divinylbenzene), heat release in the process, and impossibility of controlling the network density in the products. This negatively affects the physicochemical properties and compositional homogeneity of the product.

Previously [8] we demonstrated that di(4-isopropenylphenoxy)alkanes are efficient as cross-linking comonomers in the copolymerization with styrene. These monomers are prepared by condensation of 4-isopropenylphenol with symmetrical dihaloalkanes in isopropanol in the presence of a base catalyst:

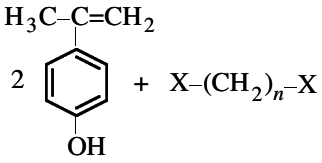

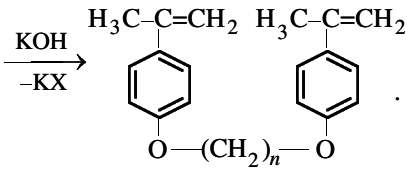

where n = 1–4; X = Cl, Br, I.

The starting compound, 4-isopropenylphenol, was prepared by cracking of 4,4'-isopropylidenediphenol in the presence of a base catalyst according to [9]; reagent grade dihaloalkanes were freshly distilled before use.

The condensation readily occurs at 80°C in the presence of KI promoter at the molar ratio 4-isopropenylphenol : dihaloalkane = (2–3) : 1. The yield of the desired compounds (white solids) ranged from 42.5 to 91.0% depending on particular dihaloalkane.

The structures of the di(4-isopropenylphenoxy)alkanes obtained were proved by spectral data. The ^1H NMR spectra were recorded on a Bruker spectrometer (300 MHz), and the IR spectra, on a Specord 75-IR spectrometer.

In this study we examined the behavior of these compounds in radical three-dimensional copolymerization with styrene depending on various factors (temperature, monomer ratio, reaction time) and determined some functional properties of the cross-linked copolymers obtained.

EXPERIMENTAL

To find conditions for preparing three-dimensional copolymers with preset physicochemical properties,

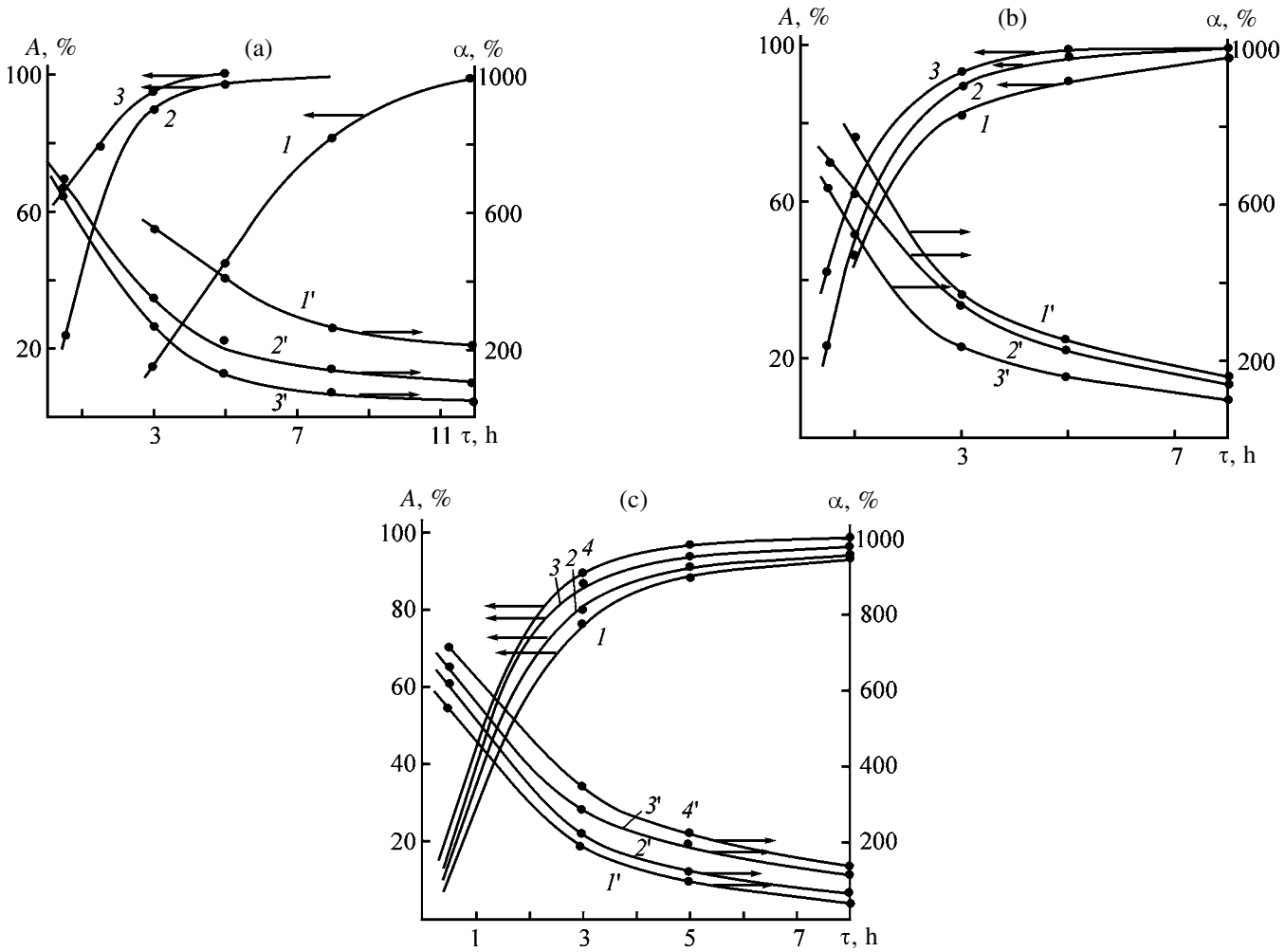

Fig. 1. Influence of (a) temperature, (b) amount of 1,4-di(4-isopropenylphenoxy)butane, and (c) kind of di(4-isopropenylphenoxy)alkane on the gel fraction yield *A* and degree of swelling of the cross-linked copolymer α. (τ) Time. 1,4-Di(4-isopropenylphenoxy)butane concentration, mol %: (a) 1; (b) (*1*, *1*') 0.5, (*2*, *2*') 1, and (*3*, *3*') 2. Temperature, °C: (a) (*1*, *1*') 80, (*2*, *2*') 100, and (*3*, *3*') 140; (b, c) 100. (c) (*1*, *1*') di(4-isopropenylphenoxy)methane, (*2*, *2*') 1,2-di(4-isopropenylphenoxy)ethane, (*3*, *3*') 1,3-Di(4-isopropenylphenoxy)propane, and (*4*, *4*') 1,4-di(4-isopropenylphenoxy)butane.

we chose the copolymerization of styrene with 1,4-di-(4-isopropenylphenoxy)butane as example and examined the effect of various factors on the copolymerization course, gel fraction yield, and degree of swelling of the cured three-dimensional copolymers. The aim of these studies was not only to replace divinylbenzene in the copolymerization with styrene, but also to obtain polymeric matrices of a different structure. Major attention is given today to the development of new ion exchangers with improved physicochemical properties, especially of ion exchangers in which the ionic groups are accessible to large organic ions and metal ions.

The copolymerization was performed in sealed glass ampules in the bulk. The reaction rate was judged from the gel fraction yield and degree of swelling of the cross-linked copolymer in benzene. The gel fraction yield was determined by extraction of the sol fraction with refluxing benzene in a Soxhlet apparatus.

Figures 1a–1c illustrate the influence of temperature and of the amount and kind of the cross-linking monomer on the yield of the cross-linked copolymers and degree of their swelling. As seen from Fig. 1a (curves *1*–*3*), with an increase in temperature from 80 to 140°C the reaction rate grows; at 100°C, the gel fraction yield in 5 h is about 97%. However, further increase in temperature from 100 to 140°C exerts a less significant effect. Curves *1*'–*3*' show that the degree of swelling of the copolymers regularly decreases with an increase in temperature to 140°C. On the contrary, the cross-linked copolymers prepared at relatively low temperatures show larger swellability.

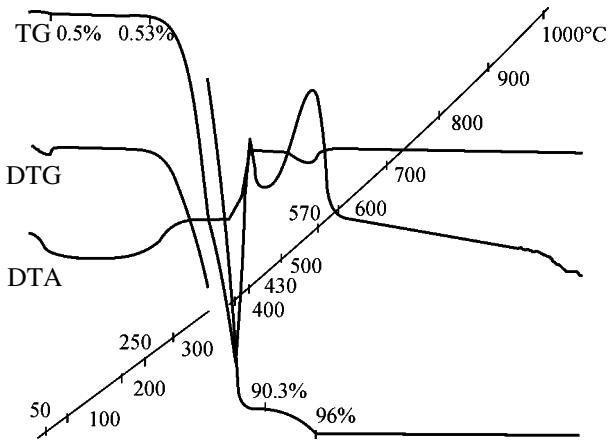

Fig. 2. Derivatogram of a sample of cross-linked 1,4-di(4-isopropenylphenoxy)butane–styrene copolymer.

Thus, the temperature strongly affects the formation of cross-linked structures with a controllable network density, i.e., relatively thickly cross-linked structures are formed at relatively high temperatures, and thinly cross-linked structures, at lower temperatures.

At the temperature that appeared to be optimal (100°C), we examined the effect of the amount of the cross-linking comonomer, 1,4-di(4-isopropenylphenoxy)butane, on the gel fraction yield and degree of swelling (Fig. 1b). With an increase in the content of this monomer from 0.5 to 1 and 2 mol %, the reaction rate noticeably increased; the gel fraction yield in 3 h was 81.8, 90.3, and 93.5%, respectively. At the reaction time increased to 8 h, the yield of the cross-linked copolymers reached 98–99%. An increase in the content of the cross-linking monomer from 1 to 2 mol % leads to a certain decrease in the copolymer swellability (curves *1'–3'*).

The structure of the cross-linking monomer strongly affects the gel fraction yield and swellability of the copolymers (Fig. 1c). Curves *1–3* show that the copolymerization rate noticeably grows with an increase in the number of methylene groups in the cross-linking monomer from 1 to 4. The swellability of the cross-linked copolymers, as expected, increases in the same order (curves *1'–3'*), i.e., the structure of the resulting three-dimensional copolymer (and hence the properties of sulfonic cation exchangers derived from it) can be controlled by choosing appropriate cross-linking monomer.

The heat resistance of the cross-linked copolymers was evaluated by thermal analysis (reference Al_2O_3, heating rate 5 deg min^{-1}). The results of the thermogravimetric and differential thermal analyses show that all the cross-linked copolymers prepared, irrespective of the structure of the cross-linking comonomer, undergo major transformations in a relatively narrow temperature range, 320–430°C. The mass loss at 430°C is about 90%, and the thermal oxidative degradation is complete at 430–600°C (Fig. 2).

The cross-linked copolymers synthesized were used as framework matrices for preparing sulfonic cation exchangers. Sulfo groups were introduced by treatment with 5% oleum at 90°C for 3 h, following the standard protocol [10]. The exchange capacity of these sulfonic cation exchangers was 5.2–5.4 mg-equiv g^{-1}, which is suitable for practical applications.

CONCLUSION

The di(4-isopropenylphenoxy)alkanes synthesized can act as cross-linking monomers in the copolymerization with styrene. The process yields three-dimensional copolymers with a controllable network density, showing promise as matrices for preparing sulfonic cation exchangers for various applications.

REFERENCES

1. Roshchupkin, V.P. and Kurmaz, S.V., *Usp. Khim.*, 2004, vol. 73, no. 3, pp. 247–274.
2. US Patent 6566036.
3. US Patent 6365321.
4. US Patent 6432608.
5. US Patent 6433118.
6. Askadskii, A.A., *Usp. Khim.*, 1998, vol. 67, no. 8, pp. 755–787.
7. Shatalov, V.M., *Khim. Prom–st.*, 1992, no. 7, pp. 411–413.
8. Bairamov, M.R., Magerramov, A.M., and Allakhverdieva, M.G., *Khim. Khim. Tekhnol.* (Ivanovo), 2005, vol. 48, no. 9, pp. 138–139.
9. Magerramov, A.M. and Bairamov, M.R., *Khimiya alkenilfenolov* (Chemistry of Alkenylphenols), Baku: Bakinsk. Gos. Univ., 2002.
10. Toroptseva, A.M., Belogorodskaya, K.V., and Bondarenko, V.M., *Laboratornyi praktikum po khimii i tekhnologii vysokomolekulyarnykh soedinenii* (Laboratory Manual on Chemistry and Technology of Macromolecular Compounds), Leningrad: Khimiya, 1972.

ISSN 1070-4272, Russian Journal of Applied Chemistry, 2007, Vol. 80, No. 1, pp. 118–121. © Pleiades Publishing, Ltd., 2007.
Original Russian Text © E.V. Udoratina, V.A. Demin, 2007, published in Zhurnal Prikladnoi Khimii, 2007, Vol. 80, No. 1, pp. 119–122.

MACROMOLECULAR CHEMISTRY AND POLYMERIC MATERIALS

Preparation of a Lignocellulose Material from Wastes

E. V. Udoratina and V. A. Demin

Institute of Chemistry, Komi Scientific Center, Ural Division, Russian Academy of Sciences, Syktyvkar, Komi Republic, Russia

Received September 4, 2006

Abstract—A powder lignocellulose material was prepared from waste paper and characterized. Waste paper is partially hydrolyzed with peroxomonosulfuric acid. Physicochemical characteristics, functional composition, and the IR spectra of the resulting samples were studied. The parameters of supramolecular structure were estimated from the evidence of the IR spectra.

DOI: 10.1134/S1070427207010247

Interest in the use of fibrous secondary material (waste paper) for production of various types of paper products grows steadily. Reprocessing of waste paper into paper and cardboard reduces water consumption, release of detrimental gases into the environment, and saves many hectares of forests. A search for new applications of waste paper is an urgent problem.

The chemical and physical structure of secondary fibers undergoes irreversible transformations during reprocessing (milling and drying). The majority of pores and capillaries are destroyed, and the fiber surface contracts and is keratinized, which prevents swelling of the fiber [1]. The mechanical characteristics of the paper from wastes are deteriorated. Along with this, waste paper fiber is of interest as a raw material for production of powder materials (PMs).

In recent years, powder celluloses find increasing application in various branches of industry. They are used as fillers, stabilizers, binding and filtering materials, and chromatographic media. Powder materials can be prepared from various raw materials, including unbleached cellulose and wood pulps, containing lignin and lignocarbohydrate complex, by treatment with hydrolyzing and oxidizing agents causing partial degradation of cellulose to limiting values of the degree of polymerization.

Unbleached cellulose fiber containing lignin is used for production of various types of cardboard and can be incorporated into the composition of newsprint. Therefore, spent cardboard package and newspapers can be considered as the secondary raw materials for production of powder lignocellulose material.

The aim of this study was to examine the possibility of utilization of package cardboard and newsprint as cellulose raw materials for production of powder forms of cellulose and powder lignocellulose sorbents.

EXPERIMENTAL

The milled initial material was hydrolyzed with peroxomonosulfuric acid (PMA), prepared by mixing of concentrated H_2O_2 solution and concentrated sulfuric acid, in a solution containing 10% H_2SO_4 and 1% H_2O_2. The treatment temperature was 100°C, duration, 3–4 h, and solid-to-liquid ratio, 1 : 30. The resulting material was washed to neutral reaction, included with a 1 : 1 acetone : ethanol mixture, and dried in air. The dried samples were milled to obtain homogeneous samples [2].

The resulting powder lignocellulose materials were characterized by functional analysis performed by the common procedures of wood chemistry. The content of carboxy groups was determined by the chemisorption method based on the exchange reaction of COOH groups with an 0.2 M solution of calcium acetate [3]. To a weighed portion of raw material after decationation (treatment with 0.1 M HCl for 1 h at room temperature and washing with distilled water) and drying to absolutely dry state we added a solution of calcium acetate (solid-to-liquid ratio 1 : 100) and kept for 2 h and room temperature. Potentiometric titration of the sample solution was performed with an 0.05 M NaOH solution to pH 7.8 (pH of the initial 0.2 M solution of calcium acetate) after separation of the material on a Schott filter.

The content of carbonyl groups was determined by the reaction of the sample with hydroxylamine hydrochloride to form oximes; the released equivalent

Table 1. Physicochemical characteristics of lignocellulose powders

Sample	Content of groups, %		DP	$-q_{max} \times 10^{-3}$, C g^{-1}
	COOH	CHO		
LCP:				
from cardboard	0.80	0.25	150	26.40
from newsprint	1.81	0.39	145	40.51
from deciduous unbleached cellulose	0.23	0.11	140	5.62
from coniferous unbleached cellulose	0.28	0.10	220	–
from TWP	1.42	0.57	120	37.59
MCC	0.14	0.04	250	–

amount of hydrochloric acid was determined by the potentiometric titration with sodium hydroxide solution [4]. The decationated weighed portion of absolutely dry sample was kept for 2 h at room temperature in a freshly prepared 0.3 M ethanol solution of hydroxylamine hydrochloride, filtered, and titrated with 0.05 M NaOH to pH of the initial $NH_2OH \cdot HCl$ solution 3.25–3.30.

The content of carboxy and carbonyl groups (%) was calculated by the formula

$$X = \frac{VNM \times 100}{g},$$

where V is the volume of the titrant solution spent for titration of the sample (ml), N is the normality of the titrant solution (g-equv l^{-1}), M is the molecular weight of carboxy and carbonyl groups, respectively (g mol^{-1}), and g is the weighed portion of absolutely dry material (mg).

The error of determination was approximately 3%. The degree of polymerization (DP) of the powder materials was evaluated from their intrinsic viscosity in Cadoxen solutions using the equation $[\eta] = DP^{0.94} \times 7.1 \times 10^{-3}$ [5].

To evaluate the accessibility of functional groups of powder lignocellulose materials we studied their electrical surface characteristics. The total surface charge of lignocellulose powders (LCPs) q_{max} was measured by the potentiometric back-titration and calculated by the published procedure [6]. To a 2% suspension of the powder in an electrolyte solution (1×10^{-3} M NaCl), 1 ml of 0.1 M HCl was added, and the mixture was titrated with 5×10^{-2} M NaOH.

The supramolecular structure of the resulting powder materials was characterized by IR spectroscopy (MIR 8000 Fourier spectrometer). The samples were pelletized with KBr. The spectra were processed by the method of baselines and normalized using the internal reference, the band at 2900 cm^{-1} (C–H stretching vibrations of methyl and methylene groups) [7]. The standard error in evaluation of the relative optical density for each absorption band was ±5%.

Some physicochemical characteristics of LCPs prepared from various types of raw materials, involving waste paper (newspaper and cardboard), are presented in Table 1. The yield of target products from secondary raw materials was 63–66%. For comparison, the characteristics of commercial microcrystalline cellulose from cotton raw materials (Biisk) are presented.

The minimal content of functional groups, carbonyl and carboxy, is observed in the sample of microcrystalline cellulose (MCC), which is thus the most inert (with respect to ionogenic groups) material. Lignocellulose powders from thermochemical wood pulp (TWP) and from newsprint (waste paper) contain the maximum amount of carboxy and carbonyl groups (1.4–1.8% COOH and 0.4–0.6% CHO groups). The amount of functional groups is significant in the LCP from waste cardboard (0.80% COOH and 0.25% CHO groups) and is low, close to that in ordinary unbleached cellulose, in LCP from coniferous and deciduous unbleached celluloses. It seems likely that the higher the amount of lignin-containing intermediate products in the initial raw materials, i.e., wood pulp in which the lignin content can reach 30–33%, the higher the content of functional groups in the sample. The treatment used results in breakdown of the fibrous structure of the initial raw materials and degradation of cellulose, as suggested by the low degrees of polymerization of the resulting products (200 and less).

The higher the content of carboxy groups in the powder material, the higher the total surface charge of its particles $-q_{max}$. The sample from unbleached

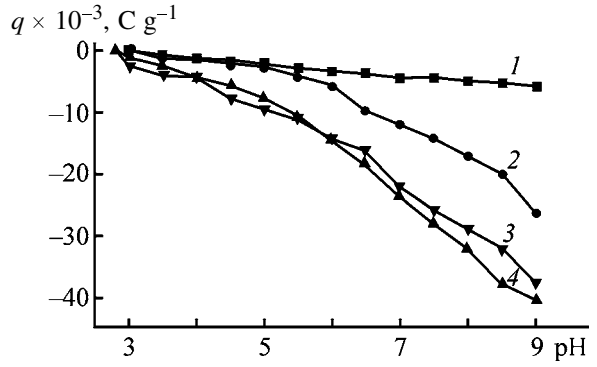

Fig. 1. Total surface charge q as a function of the type of LCP and pH value of aqueous suspension. LCP: (*1*) from unbleached deciduous kraft cellulose, (*2*) from cardboard, (*3*) from thermomechanical pulp, and (*4*) from newsprint.

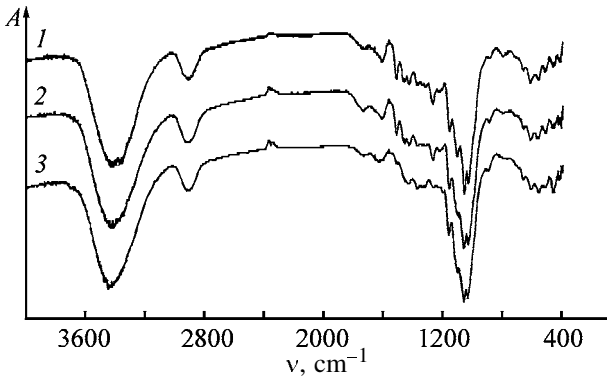

Fig. 2. IR spectra of powder lignocellulose materials. (*A*) Transmission and (ν) wavenumber. (*1*) TWP; waste paper: (*2*) newsprint and (*3*) cardboard.

deciduous kraft cellulose has the minimum charge of the surface throughout the entire pH range of aqueous suspension: $-q_{max}$ is approximately 5620 C g^{-1} (at pH 9). The negative surface charge of LCP prepared from cardboard is higher by a factor of approximately 4.5 and at the same pH, $-q_{max}$ = 26400 C g^{-1}. The negative surface charge of LCP from TWP and newsprint is higher than the above value by a factor of 1.4–1.5 ($-q_{max}$ 37 590 and 40507 C g^{-1}, respectively). The dependence of the negative surface charge on the type of LCP and pH of the aqueous suspension is shown in Fig. 1.

The IR spectra of lignocellulose powders from (1) thermomechanical wood pulp and waste paper raw materials, (2) newsprint, and (3) cardboard, are presented in Fig. 2. The IR spectra contain the characteristic bands of celluloses. In the range of stretching vibrations of OH groups there is a broad band with a maximum at approximately 3400 cm^{-1}. The band at approximately 2900 cm^{-1} is also strong. In the range 900–1500 cm^{-1}, there are absorption bands forming a complex pattern with several maxima.

The resulting samples contain residual lignin and hemicelluloses. The presence of these components is suggested by the corresponding absorption bands. Hemicelluloses can be revealed from the band at 1730 cm^{-1} (stretching vibrations of the C=O groups in ester fragments) [7] and lignin, from the bands at 1595–1500 cm^{-1} corresponding to the skeleton vibrations of the benzene ring and characteristic band at 1460 cm^{-1} (bending modes of the CH groups) [8].

The IR spectra show that in the resulting samples almost all hydroxyls are involved in hydrogen bonds, which is suggested by the shape of the absorption band in the range 3000–3700 cm^{-1} (ν_{OH}). This absorption band can be characterized by the position of the maximum ν_{OH}(max), values of the symmetry index a/b (the ratio of the widths of the high- and low-frequency wings of the absorption band at half-maximum), and the ratio of the optical densities at 3570 and 3330 cm^{-1} D_{3570}/D_{3330} [9].

The characteristics of the state of hydroxy groups and the relative optical densities of some analytical absorption bands are also presented in Table 2. For comparison, data for unbleached deciduous cellulose and MCC are presented.

The maximum of the absorption band of stretching modes of OH groups in the spectra is practically unchanged. The newsprint sample has the lowest symmetry index a/b (ν_{OH}) 0.60, which suggests formation of a dense network of strong hydrogen bonds; the TWP sample has the highest symmetry index, i.e., the sample is characterized by a fairly loose network of hydrogen bonds.

The ordering index (analog of the crystallinity index in X-ray diffractometry) is determined from the ratio of optical densities at 1375 (bending modes of CH groups) and 2900 cm^{-1}. For powder materials it is higher than that for unbleached cellulose. This means that in hydrolysis the fraction of the amorphous part decreases and the fraction of crystalline part increases. For LCP from cardboard, this effect is observed to a greater extent.

The content of crystalline and amorphous parts in the sample can also be judged from the ratio of the intensities of the band at 1430 cm^{-1} (bending modes of CH_2 groups), related to the crystalline areas, and the band at 900 cm^{-1}, related to amorphous areas (C–O stretching modes in amorphous area). This ratio increases from 1.27 for the initial cellulose to 2.08 for "classic" MCC (Table 2), which suggests an increase in the fraction of the crystalline phase, i.e., formation of a more ordered structure of MCC. In the samples of

Table 2. Variation of frequencies and intensities of the absorption bands in the IR spectra of powder celluloses from various types of raw materials

LCP type	Characteristic of the state of hydroxy groups			Relative optical densities of analytical absorption bands	
	ν_{OH}(max), cm^{-1}	a/b (ν_{OH})	D_{3570}/D_{3330}	D_{1375}/D_{2900}	D_{1430}/D_{900}
Unbleached cellulose	3432	0.83	0.76	1.39	1.27
MCC	3430	0.69	0.48	1.41	2.08
TWP	3430	0.70	0.33	1.52	2.69
Newsprint	3434	0.60	0.44	1.46	3.30
Cardboard	3449	0.64	0.59	2.02	2.65

LPC from waste paper, the crystallinity index is higher than that for MCC (2.65–3.30).

CONCLUSIONS

(1) Powder lignocellulose materials prepared from waste paper of different origins have different physicochemical characteristics.

(2) It was shown by chemical analysis that the resulting samples are characterized by a high content of carboxy and carbonyl groups, 0.80–1.81 and 0.25–0.57%, respectively. They have significantly higher ion-exchange activity of surface functional groups (primarily, COOH) than the powders from cellulose.

(3) The IR spectra of lignin-containing powder materials suggest that the hydrolysis of the initial waste paper and thermomechanical wood pulp results in formation of a more reactive microcrystalline structure than that of microcrystalline cellulose from cotton raw materials.

REFERENCES

1. Dul'kin, D.A., Yuzhaninova, L.A., Mironova, V.G., and Spiridonov, V.A., *Lesn. Zh.*, 2005, nos. 1–2, pp. 104–122.
2. Demin, V.A., Filatov, B.N., German, E.V., and Pavlova, I.N., *Khim. Drev. Lesokhim.: Tr. Komi Nauchn. Tsentra Ural. Otd. Ross. Akad. Nauk*, 1993, no. 129, pp. 40–46.
3. Obolenskaya, A.V., El'tsinskaya, Z.P., and Leonovich, A.A., *Laboratornye raboty po khimii drevesiny i tsellyulozy* (Laboratory Manual on Chemistry of Wood and Cellulose), Moscow: Ekologiya, 1991.
4. Klimova, V.A., *Osnovnye mikrometody analiza organicheskikh soedinenii* (Main Methods of Microanalysis of Organic Compounds), Moscow: Khimiya, 1975.
5. Bolotnikova, L.S., Danilova, S.N., and Samsonova, T.I., *Zh. Prikl. Khim.*, 1966, vol. 39, no. 1, p. 176.
6. Chernoberezhskii, Yu.M., Kizim, A.I., Kashipova, I.V., et al., *Kolloidn. Zh.*, 1991, vol. 53, no. 2, pp. 404–405.
7. Bazarova, N.G., Karpova, E.V., Batrakov, I.B., et al., *Metody issledovaniya drevesiny i ee proizvodnykh: Uchebnoe posobie* (Methods of Studying Wood and Its Derivatives: Textbook), Barnaul: Altai Gos. Univ., 2002.
8. Mironov, V.A. and Yankovskii, S.A., *Spektroskopiya v organicheskoi khimii* (Spectroscopy in Organic Chemistry), Moscow: Khimiya, 1985.
9. Petropavlovskii, G.A., *Gidrofil'nye chastichno zameshchennye efiry tsellyulozy i ikh modifikatsiya putem khimicheskogo sshivaniya* (Hydrophilic Partially Substituted Cellulose Ethers and Esters and Their Modification by Chemical Cross-Linking), Leningrad: Nauka, 1988.

ISSN 1070-4272, Russian Journal of Applied Chemistry, 2007, Vol. 80, No. 1, pp. 122–130. © Pleiades Publishing, Ltd., 2007.
Original Russian Text © D.F. Grishin, E.V. Kolyakina, V.V. Polyanskova, I.D. Grishin, 2007, published in Zhurnal Prikladnoi Khimii, 2007, Vol. 80, No. 1, pp. 123–131.

MACROMOLECULAR CHEMISTRY AND POLYMERIC MATERIALS

Radical Copolymerization of *N*-Vinylpyrrolidone with Methyl Methacrylate and Styrene in the Presence of *C*-Phenyl-*N*-*tert*-butylnitrone

D. F. Grishin, E. V. Kolyakina, V. V. Polyanskova, and I. D. Grishin

Lobachevsky Research Institute of Chemistry, Nizhni Novgorod State University, Nizhni Novgorod, Russia

Received May 25, 2006

Abstract—The effect of *C*-phenyl-*N*-*tert*-butylnitrone on the features of radical copolymerization of *N*-vinylpyrrolidone with methyl methacrylate and styrene was examined. Nitrone exerts virtually no effect on the relative activities of the comonomers. At the same time, *C*-phenyl-*N*-*tert*-butylnitrone as a potential source of nitroxyl radical makes it possible to prepare copolymers of *N*-vinylpyrrolidone with methyl methacrylate and styrene to high conversions without gel effect, to control the molecular-weight characteristics of the copolymers, and to prepare block copolymers.

DOI: 10.1134/S1070427207010259

Polyvinylpyrrolidone (PVP) and its copolymers find diverse applications: from blood plasma substitutes to propellant additives [1, 2].

The requirements to copolymers for medicobiological purposes are more stringent than those to general-purpose polymers. First, these copolymers should be nontoxic in amounts ensuring the therapeutic effect. Second, medicinal preparations should have a definite molecular mass M and a narrow molecular-mass distribution (MMD), because the pharmacological effect essentially depends on these parameters. In particular, the molecular mass should not be too large to provide spontaneous excretion. Finally, environmentally clean methods for efficient commercial production of such preparations should be developed.

Therefore, a search for efficient ways to control the copolymerization of *N*-vinylpyrrolidone (VP) with vinyl monomers is a key problem of *N*-vinylpyrrolidone chemistry.

The goal of this study was the development of procedures for preparing gradient copolymers of VP with methyl methacrylate (MMA) and styrene (ST), and also block copolymers derived from them with controllable composition and molecular-mass characteristics in the presence of *C*-phenyl-*N*-*tert*-butylnitrone (PBN) as one of effective chain-terminating agents under the conditions of radical initiation, maximally similar to the industrial conditions [3–5].

EXPERIMENTAL

C-Phenyl-*N*-*tert*-butylnitrone was prepared by the procedure described in [6]. The solvents, initiator [azobis(isobutyronitrile), AIBN], and monomers (VP, ST, MMA) were purified by standard procedures [7–9]; VP met the requirements of TU (Technical Specifications) 6-09-2991–78. The physicochemical constants of all the compounds were in agreement with published data. The (co)polymers were prepared from the freshly distilled monomers. The samples were prepared as follows: The monomer was placed in glass ampules, degassed by threefold freezing–pumping–thawing, and polymerized at a residual pressure of 1.3 Pa. The polymerization progress was monitored gravimetrically, dilatometrically [10], and thermographically [11].

When plotting the kinetic curves of the copolymerization from thermographic data, we used the running heats of copolymerization, calculated from the published heats of homopolymerization of VP (64.3 ± 1.9 kJ mol^{-1}) [12], MMA (55.6 ± 1.1 kJ mol^{-1}) [13], and ST (69.4 ± 0.8 kJ mol^{-1}) [13], taking into account the running compositions of the copolymers.

The copolymers obtained were purified to remove residual initiator and monomers by twofold reprecipitation from chloroform into hexane. The VP homopolymer was washed out with distilled water.

The intrinsic viscosity of VP–MMA and VP–ST copolymers was determined in chloroform at 25°C [14]. The molecular-mass characteristics of the copolymers were examined by GPC on a chromatograph equipped with five Styrogel columns with pore diameters of 1×10^5, 3×10^4, 1×10^4, 1×10^3, and 250 Å (Waters, the United States). An R-403 differential refractometer (Waters) was used as detector, and THF was the eluent. Close-cut polystyrene (PS) references were used for calibration. For VP–ST copolymers, M was calculated using the constants K and α for PS. Conversion of the mean M values from the polystyrene references to the examined VP–MMA copolymers was done using standard formulas for poly(methyl methacrylate) (PMMA) [15].

The composition of the copolymers was determined by IR spectroscopy with an Infralum FT-80 spectrophotometer. The spectra were measured in the range 5500–550 cm^{-1} with an accuracy of ± 0.05 cm^{-1}. Stretching vibration bands of the carbonyl groups of VP (1675 cm^{-1}) and MMA (1725 cm^{-1}) were chosen as analytical bands, because of transparence of the solvent ($CHCl_3$) in this range and good resolution of these bands. As calibration plots we used the concentration dependences of the optical density of PVP and PMMA solutions in chloroform, plotted using solutions of exactly known concentration. The absorption intensity was determined using the baseline method [16]. The spectra of the copolymers were recorded similarly to those of the homopolymers. The content of carbonyl fragments in VP–MMA copolymers was determined from calibration plots, and that in VP–ST copolymers, from the calibration plot for PVP.

The effective relative activity constants in the VP–MMA and VP–ST copolymerization were determined by the Kelen–Tudös [17] and "fitted curve" [18] methods.

Block copolymerization was performed in a solution of PS macroinitiator in VP at 70°C and in solution of PVP macroinitiator and ST in dioxane at 80°C. The mixture was evacuated by the same procedure as in the common copolymerization. The product of the polymerization involving the macroinitiator was separated into three fractions (homo-PS, homo-PVP, and block copolymer) by sequential dissolution of the polymer in cyclohexane and water. The separation completeness was checked by IR spectroscopy.

N-Vinylpyrrolidone readily polymerizes by the radical polymerization mechanism, and its polymers have valuable properties. It should be noted, however, that published data on the VP activity in copolymerization even with such common monomers as MMA and ST are rather contradictory [19–21]. Therefore, we considered it necessary to estimate the relative activity constants for the comonomer systems VP–MMA and VP–ST, and also to examine the effect of PBN on these parameters. The copolymerization was performed in a wide range of compositions of the monomer mixtures, from 5 to 95 mol % VP.

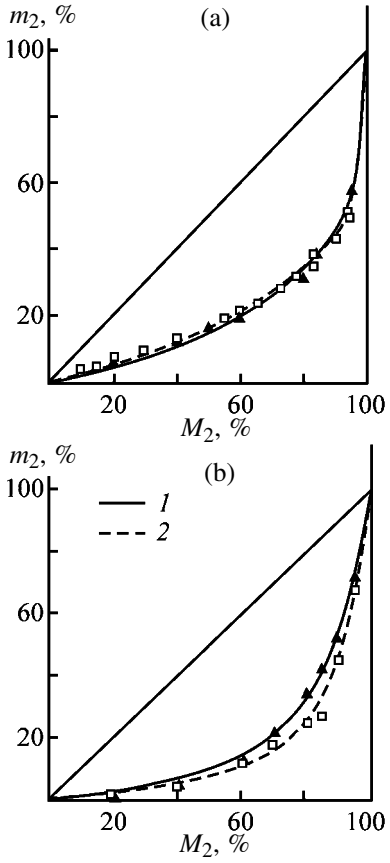

Fig. 1. Composition curves for (a) MMA–VP and (b) ST–VP copolymers prepared at (a) 60 and (b) 80°C. (M_2) *N*-Vinylpyrrolidone content in the monomer mixture and (m_2) its content in the copolymer. Initiator AIBN (0.8 mol %); the same for Figs. 2 and 3. PBN concentration, mol %: (*1*) 0 and (*2*) 0.1.

An IR spectroscopic analysis of the copolymer compositions showed that, irrespective of the monomer ratio in the starting mixture, the copolymer is always enriched in the more active monomer, either MMA or ST. Such a pattern is observed for samples prepared both in the presence of PBN and without it. The dependences of the copolymer composition on that of the monomer mixture are shown in Fig. 1.

These data show that addition of PBN exerts no effect on the composition of VP–MMA copolymers. The composition curves obtained in the presence of

Table 1. Copolymerization constants in the VP–MMA (60°C) and VP–ST (80°C) systems (initiator AIBN, 0.8 mol %)

Determination method	PBN content, mol %			
	0.0		0.1	
	r_1	r_2	r_1	r_2
VP (1)–MMA (2)				
Kelen–Tudös	0.001 ± 0.01	4.32 ± 0.43	0.001 ± 0.01	4.34 ± 0.48
Fitted curve	0.04 ± 0.02	4.60 ± 0.45	0.02 ± 0.02	4.14 ± 0.40
VP (1)–ST (2)				
Kelen–Tudös	0.08 ± 0.03	12.3 ± 1.3	0.07 ± 0.02	16.7 ± 1.7
Fitted curve	0.17 ± 0.05	10.2 ± 1.2	0.13 ± 0.04	14.2 ± 1.4

PBN and without it virtually coincide (Fig. 1a). Thus, in this case the coordination interaction of propagating radicals with nitroxyls does not noticeably affect the copolymer composition. The enrichment in MMA units is due to the higher activity of this monomer.

In contrast to the VP–MMA system, in the VP–ST system the composition curves obtained in the presence of PBN and without it are somewhat different (Fig. 1b). In the presence of PBN, the enrichment of the copolymer with styrene is still more pronounced.

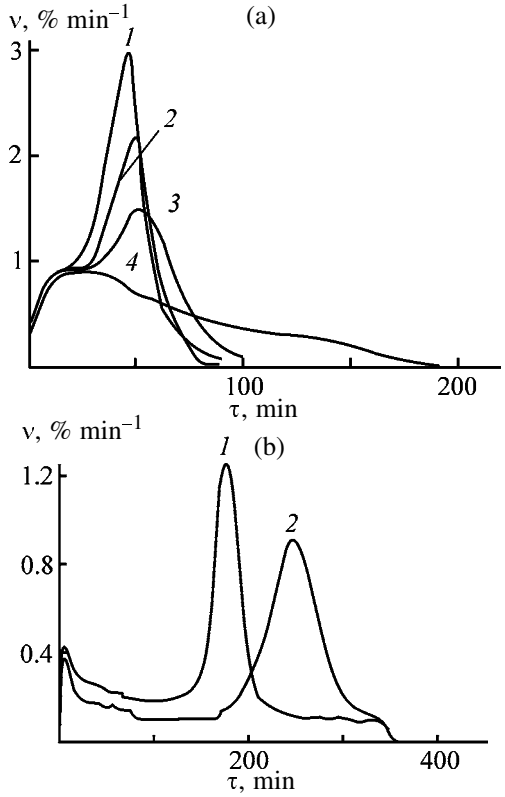

Fig. 2. Differential kinetic curves of the copolymerization of VP with (a) MMA and (b) ST in the presence of PBN at (a) 60 and (b) 80°C. (ν) Polymerization rate and (τ) polymerization time. PBN concentration, mol %: (a) (*1*) 0, (*2*) 0.01, (*3*) 0.05, and (*4*) 0.10; (b) (*1*) 0 and (*2*) 0.05.

The results of determining the relative activities of the monomers by the above methods are given in Table 1. It is seen that the relative activities determined by the two procedures show good agreement with each other and with published data [20, 21]. Certain differences in the results obtained by the two methods can be attributed to the fact that the Kelen–Tudös method takes into account variation of the monomer mixture composition with increasing conversion, and the copolymer composition is averaged over the conversion range from zero to the final value, whereas in the fitted curve method the copolymer is considered as obtained exclusively at the initial monomer concentrations.

The relative activities of the monomers and the dependences of the copolymer composition on that of the monomer mixture indicate that addition of PBN does not affect the activity of the monomers in the VP–MMA copolymerization and slightly enhances the activity of styrene in the VP–ST copolymerization.

The effect of PBN on the kinetic features of copolymerization of VP with MMA and ST and on the molecular-mass characteristics of the copolymers was examined at monomer molar ratios of 50 : 50 and 80 : 20, respectively.

We found that PBN affected the kinetics of AIBN-initiated copolymerization of VP with MMA and ST in the bulk at 60 and 80°C, respectively. Figure 2 shows the differential kinetic curves of the copolymerization in the presence of PBN at these temperatures. It is seen that addition of PBN in an amount comparable with that of the initiator appreciably decreases the

Table 2. Initial rate of homo- and copolymerization of VP with MMA and ST in the presence of PBN (initiator AIBN, 0.8 mol %)

Run no.	T, °C	Monomer	[PBN], mol %	Induction period, min	$V \times 10^4$, mol l^{-1} s^{-1}
1	60	VP	–	–	28.0
2			0.05	–	1.0
3			0.20	~25	0.2
4	50	MMA*	–	–	1.2
5			0.10	–	1.1
6			0.80	~6–9	0.8
7	60	ST	–	–	1.6
8			0.08	–	1.5
9			0.80	~20	0.6
10	60	VP–MMA	–	–	11.0
11			0.10	–	10.0
12			0.20	–	9.9
13	60	VP–ST	–	–	0.7
14			0.10	–	0.6
15			0.20	–	0.6

* AIBN concentration 0.1 mol %.

gel effect (Fig. 2). At the same time, as follows from the integral kinetic curves shown in Fig. 3, addition of nitrone in various concentrations also considerably decreases the overall polymerization rate and limiting conversion.

For example, in the copolymerization of VP with MMA and ST without PBN additions, the dependence of the conversion on time is S-shaped, which is characteristic of the polymerization with a gel effect, whereas in the presence of PBN the conversion increases in time more uniformly, without rate splashes and pronounced self-acceleration (Fig. 3).

To estimate additionally the kinetic parameters of the polymerization at small conversions, we analyzed dilatometrically the initial portions of the kinetic curves. We found that PBN does not noticeably affect the initial rate of MMA–ST homopolymerization, but in its presence the VP homopolymerization rate decreases considerably (by two orders of magnitude) relative to the process performed with the traditional initiator without additives (Table 2, run nos. 1–9). The kinetic data derived from the initial portions of the VP–MMA and VP–ST copolymerization curves indicate that addition of PBN in various concentrations to the polymerizing system does not noticeably affect the copolymerization rate compared to the process initiated by AIBN only (Table 2, run nos. 10–15), as in the case of the homopolymerization of MMA and ST. The essential difference in the effect of PBN on the homopolymerization of the VP, MMA, and ST and on the copolymerization of VP with MMA and

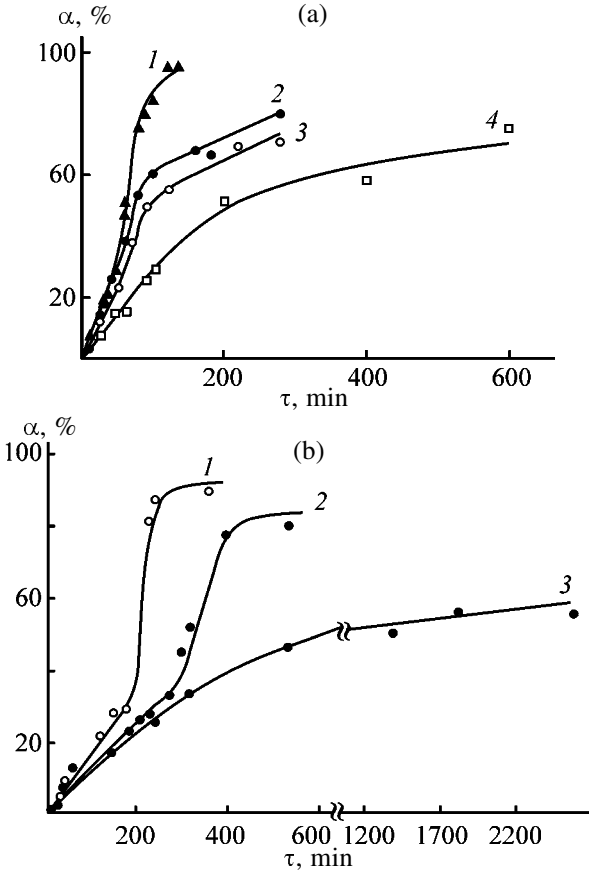

Fig. 3. Integral kinetic curves of the copolymerization of VP with (a) MMA and (b) ST in the presence of PBN at (a) 60 and (b) 80°C. (α) Conversion and (τ) polymerization time. PBN concentration, mol %: (a) (*1*) 0, (*2*) 0.1, (*3*) 0.2, and (*4*) 1.0; (b) (*1*) 0, (*2*) 0.05, and (*3*) 0.10.

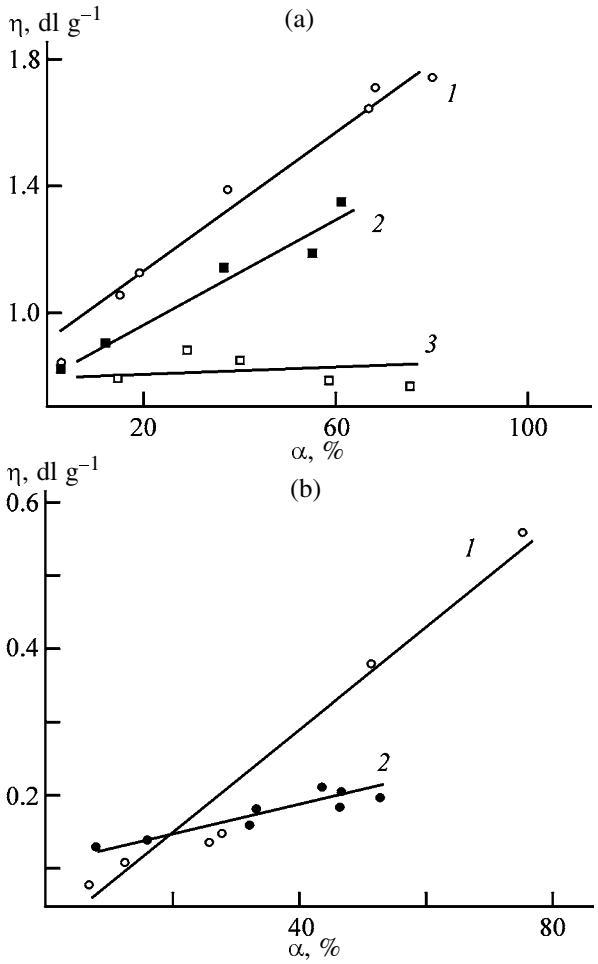

Fig. 4. Intrinsic viscosity η of copolymers of VP with (a) MMA and (b) ST as a function of conversion α. Initiator AIBN, 0.8 mol %; samples prepared at (a) 60 and (b) 80°C. PBN concentration, mol %: (a) (*1*) 0.1, (*2*) 0.2, and (*3*) 1.0; (b) (*1*) 0.05 and (*2*) 0.10.

ST may be due to large difference in the monomer activities and in the accepting power of PBN relative to the arising secondary (VP or ST terminal unit) and tertiary (MMA terminal unit) propagating radicals [22]. Since, as determined above, the relative activities of components of the VP–MMA and VP–ST pairs differ by several orders of magnitude, the first step of the copolymerization yields macroradicals enriched in the more active monomer, MMA or ST. Correspondingly, as in the case of the homopolymerization of MMA and ST, addition of PBN does not strongly affect the initial copolymerization rate.

We found that PBN as a potential source of stable radicals can efficiently control not only the kinetic parameters of the copolymerization of VP with MMA and ST, but also the molecular-mass characteristics of the (co)polymers.

In contrast to the copolymers prepared by common (noncontrolled) radical polymerization, for which the dependence of M on conversion shows a pronounced jump corresponding to an increase in the intrinsic viscosity at the instant of the gel effect, addition of PBN to the polymerizing system results in linear growth of the intrinsic viscosity of the VP–MMA and VP–ST copolymers with the conversion (Fig. 4). In the case of the VP and MMA copolymers prepared in the presence of excess PBN (1.0 mol %), the intrinsic viscosity does not noticeably change with the conversion and remains constant throughout the process (Fig. 4a, curve *3*).

The GPC studies of the copolymers show that the MMD cuurves of the samples prepared in the presence of PBN are unimodal, in contrast to the copolymers prepared in the presence of AIBN without PBN (Figs. 5a, 5b); with an increase in the polymerization time, the MMD maxima regularly shift toward higher MM. These data indicate that the copolymerization is accompanied by a continuous increase in M_n of the copolymer with the conversion. The polydispersity coefficients of the copolymers somewhat increase with the conversion, but remain considerably lower than those of the copolymers prepared in the presence of AIBN without PBN additions (Table 3).

Since the monomers in the pairs chosen essentially differ in the activity, at the end of the copolymerization, with the exhaustion of the active monomers (MMA and ST), VP homopolymer can accumulate in the system, which can lead to MMD broadning and to the growth of the polydispersity coefficient at high conversions.

To quantitatively determine the PVP content in the copolymers, we separated PVP with distilled water and determined the molecular-mass parameters of the washed copolymers (Table 4). We found that the samples synthesized in the presence of the traditional initiator AIBN to high conversions contained appreciable amounts of PVP. This fact accounts for the appearance of the second mode in the copolymers at high conversions (Figs. 5a, 5b), which is not observed in the washed samples. The copolymers prepared in the presence of PBN contain virtually no PVP. Thus, addition of PBN allows preparation of copolymers free of impurities of VP homopolymer.

The composition of the copolymers obtained at different conversions was studied by IR spectroscopy (Table 5). At the initial monomer molar ratio VP : MMA = 50 : 50, the copolymer composition varies with the conversion.

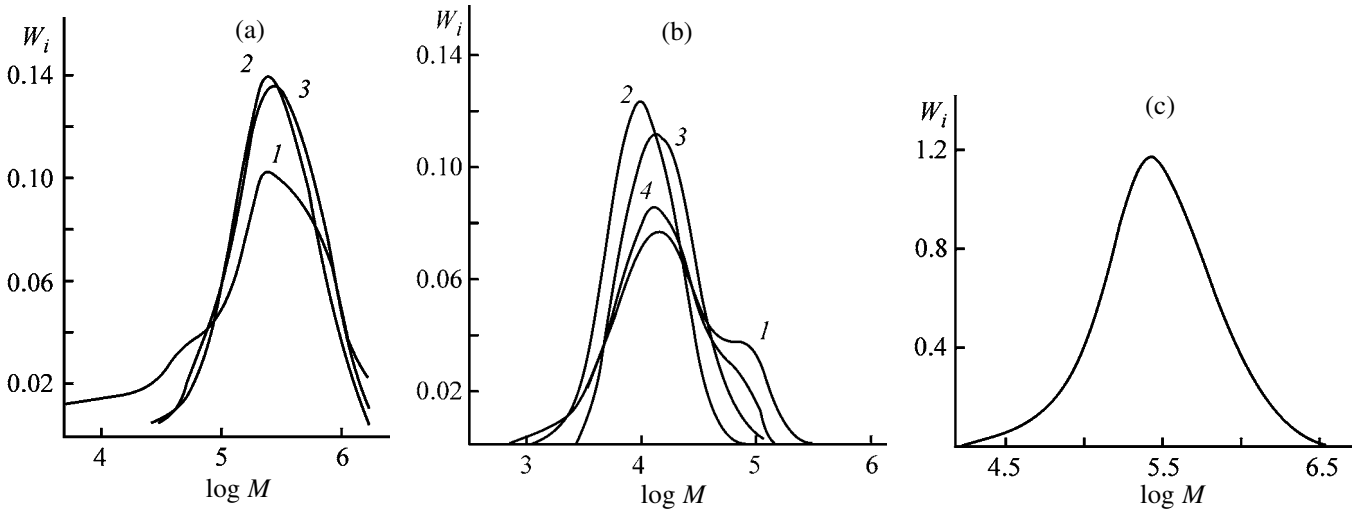

Fig. 5. MMD curves of copolymer samples (a) VP–MMA and (b) VP–ST prepared in the presence of PBN to various conversions; (c) MMD curve of PVP-σ-PST block copolymer. (a, b) Initiator AIBN, 0.8 mol %. Synthesis temperature, °C: (a) 60 and (b, c) 80. (W_i) relative content of the fraction (by mass) and (log M) logarithm of molecular mass. (a) PBN concentration, mol %: (*1*) 0 and (*2*, *3*) 0.1; conversion, %: (*1*) 95, (*2*) 3, and (*3*) 80. (b) PBN concentration, mol %: (*1*) 0 amd (*2*–*4*) 0.05; conversion, %: (*1*) 91, (*2*) 7, (*3*) 52, and (*4*) 76. (c) Conversion 22%.

Table 3. Molecular-mass characteristics of VP–MMA* and VP–ST** copolymers prepared at 60 and 80°C, respectively

PBN concentration, mol %	Conversion α, %	$M_n \times 10^{-3}$	$M_w \times 10^{-3}$	M_w/M_n
	VP–MMA			
–	80	138	597	4.3
0.1	3	134	236	1.8
	25	148	252	1.7
	80	193	353	1.8
0.2	3	92	168	1.8
	74	149	301	2.0
1	7	70	119	1.7
	75	72	145	2.0
	VP–ST			
–	91	10	29	2.9
0.05	7	7	11	1.6
	33	8	15	1.9
	52	9	16	1.8
	76	10	21	2.1
0.1	8	5	8	1.6
	17	5	9	1.8
	33	6	10	1.7
	47	7	12	1.7

* The molecular masses were calculated using the constants K and α for PMMA.

** The molecular masses were calculated using the constants K and α for PST.

The data obtained (Table 5) show that the polymer formed in the initial steps of the process is enriched in MMA units relative to the starting monomer mixture. However, the average composition of the copolymer varies with the conversion, and the relative content of VP units increases. This trend is observed with the copolymers prepared both in the presence of PBN and without it.

Table 4. Molecular-mass characteristics of VP–MMA and VP–ST copolymers prepared at 60 and 80°C, respectively, before and after separation of PVP by washing

PBN concentration, mol %	Conversion α, %	Fraction of washed-out PVP, wt %	$M_n \times 10^{-3}$	M_w/M_n
	VP–MMA			
–	80	36	138	4.3
			184*	3.1*
0.2	69	5	151	2.0
			102*	1.8*
	VP–ST			
–	68	48	–	–
	91	50	10	2.9
			7*	2.2*
0.05	76	49	10	2.1
			8*	1.9*
0.1	47	Absent	7	1.7
			7*	1.7*

* Characteristics of washed copolymers.

Table 5. Composition of VP–MMA* and VP–ST** copolymers at various conversions

PBN concentration, mol %	Conversion, %	VP content, mol %	Content of second monomer, mol %
		VP–MMA	
0	4	15±2	85±9
	19	18±2	82±8
	28	18±2	82±8
	51	21±2	79±8
	96	44±4	56±6
0.1	3	16±2	84±8
	14	16±2	84±8
	25	16±2	84±8
	51	20±2	80±8
	80	25±3	75±8
1	15	17±2	83±8
	33	19±2	81±8
	41	18±2	82±8
	64	23±2	77±8
		VP–ST	
0	9	30±3	70±7
	29	48±5	52±5
	42	66±7	34±3
	90	83±8	17±2
0.05	7	23±2	77±8
	33	53±5	47±5
	52	75±7	25±3
	76	84±8	16±2
0.1	8	23±2	77±8
	17	26±3	74±7
	26	40±4	60±6
	33	46±5	54±5
	47	63±6	37±4

* Monomer molar ratio in the starting mixture 50 : 50, 60°C.
** Monomer molar ratio in the starting mixture 80 : 20, 80°C.

A similar trend is observed in the copolymerization of VP with styrene (Table 5).

It is known [3–5] that PBN is an effective agent for controlled polymerization of ST and some other monomers. To prove the realization of the pseudoliving mechanism in the copolymerization of VP with MMA and ST in the presence of PBN, we prepared block copolymers PVP-σ-PS and PS-σ-PVP. As macroinitiators of the block copolymerization we used PVP prepared by controlled polymerization in the presence of 0.2 mol % PBN and 0.8 mol % AIBN at 60°C and PS prepared at 70°C in the presence of 0.8 mol % PBN and 0.8 mol % AIBN. To determine the relative content of the homopolymers, we fractionated the copolymers by sequential selective extraction; the results are given in Table 6. The GPC data show that the MMD of the PVP-σ-PS block copolymer is unimodal (Fig. 5c).

Our results suggest that, as in the case of other vinyl monomers [3–5], a decrease in the gel effect is due to formation in the system of stable nitroxyl radicals X$^{\bullet}$ [Eq. (1)] and their subsequent participation in the chain propagation:

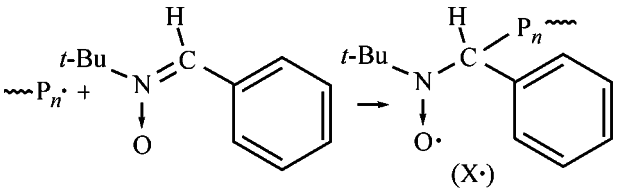

(1)

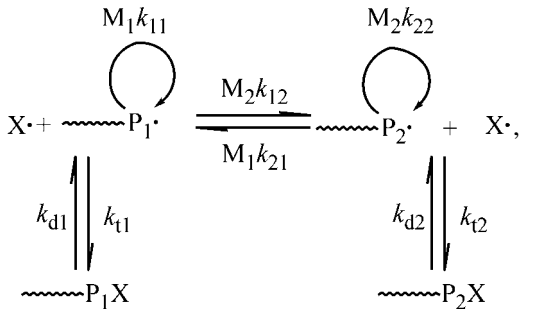

(2)

where M_1 and M_2 are the molecules of the respective monomers; X$^{\bullet}$, nitroxyl radical; P$^{\bullet}$, propagating radical; k_{d1} and k_{d2}, dissociation rate constants of adducts P_1X and P_2X, respectively; k_{t1} and k_{t2}, rate constants of the recombination of the nitroxyl radical X$^{\bullet}$ with the macroradicals $P_1^{\bullet}$ and $P_2^{\bullet}$, respectively; and k_{11}, k_{22}, k_{12}, and k_{21}, rate constants of chain propagation (addition of macroradical to the corresponding monomer).

The reinitiation by equilibrium reaction (2) leads to the realization of the reversible inhibition mechanism. The occurrence of reinitiation is also suggested by data on the synthesis of VP–ST block copolymers in the presence of AIBN and PBN.

Our results show that the chosen monomer pairs VP–MMA and especially VP–ST are examples of systems prone to damped copolymerization in the presence of nitroxyls. More difficultly dissociating adducts P_2–X containing a VP unit at the terminus of the polymeric macroradical are inevitably accumulated in the course of the process. Macroradicals with MMA or ST terminal units, prone to reversible recombination–dissociation, remain active in the polymerization. Addition of active monomers does not reduce the activity, but addition of a VP molecule increases the

Table 6. Postpolymerization in the systems ST + PVP (80°C) and VP + PST (70°C)

Macro-initiator	τ, h	*T*, °C	Conversion, %	Content in polymerization product, %			Characteristics of block copolymer	
				PST	PVP	block copolymer	$M_n \times 10^{-3}$	M_w/M_n
PVP	25	80	22	26	45	29	221	2.1
PST	68	70	13	32	Absent	68	–	–

probability of transition of the chain to the dormant state, which inhibits its propagation. Thus, chains with MMA or ST terminal units propagate faster. This leads to an increase in the content of active monomers in the copolymer and allows preparation of gradient copolymers in which the composition varies from one end of the macromolecule to the other.

It is not improbable that stable nitroxyl radicals formed in the system can react with propagating macroradicals not only through recombination, but, in the case of MMA, also through disproportionation:

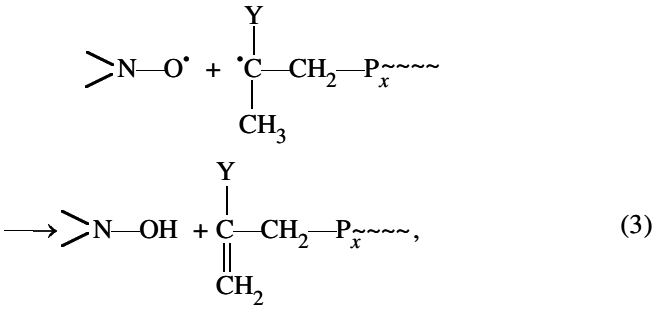

(3)

where Y is a functional group.

Reaction (3) allows control of the kinetic parameters of the copolymerization. In this case, however, a "dead" polymer is formed in the system, which results in deviations from the ideal pseudoliving polymerization mechanism and, in particular, in increased polydispersity.

CONCLUSIONS

(1) *C*-Phenyl-*N*-*tert*-butylnitrone as a potential source of stable radicals directly participates in the chain propagation in the copolymerization of *N*-vinylpyrrolidone with methyl methacrylate and styrene, actively affecting both the initial rate and the overall reaction kinetics, inhibiting the autoacceleration step.

(2) Additions of *C*-phenyl-*N*-*tert*-butylnitrone control the molecular-mass characteristics of macromolecules and allow the synthesis under mild conditions (60–80°C) of low-molecular-weight copolymers derived from *N*-vinylpyrrolidone, which are the most demanded by parmaceutical industry.

(3) *C*-Phenyl-*N*-*tert*-butylnitrone does not affect the composition of copolymers of *N*-vinylpyrrolidone with methyl methacrylate and styrene under the examined conditions.

ACKNOWLEDGMENTS

The study was financially supported by the Russian Foundation for Basic Research (project no. 05-03-32688) and Federal Target Scientific and Technical Program "Research and Development in Priority Fields of Engineering" (project no. 02.442.11.7285).

REFERENCES

1. Sidel'kovskaya, F.P., *Khimiya N-vinilpirrolidona i ego polimerov* (Chemistry of *N*-Vinylpyrrolidone and Its Polymers), Moscow: Nauka, 1970.
2. Kirsh, Yu.E., *Poli-N-vinilpirrolidon i drugie poli-N-vinilamidy* (Poly-*N*-vinylpyrrolidone and Other Poly-*N*-vinylamides), Moscow: Nauka, 1998.
3. Grishin, D.F., Semenycheva, L.L., and Kolyakina, E.V., *Dokl. Ross. Akad. Nauk*, 1998, vol. 362, no. 5, pp. 634–638.
4. Detrembleur, C., Sciannamea, V., Koulic, C., et al., *Macromolecules*, 2002, vol. 35, no. 19, pp. 7214–7233.
5. Zaremskii, M.Yu., Orlova, A.P., Garina, E.S., et al., *Vysokomol. Soedin., Ser. A*, 2003, vol. 45, no. 6, pp. 871–882.
6. Emmons, W.D., *J. Am. Chem. Soc.*, 1957, vol. 79, no. 21, pp. 5739–5754.
7. *Organic Syntheses*, Blatt, A.H., Ed., New York: Wiley, 1944. Translated under the title *Sintezy organicheskikh preparatov*, Moscow: Inostrannaya Literatura, 1953, vol. 4.
8. Weissberger, A. and Proskauer, E.S., *Organic Solvents. Physical Properties and Methods of Purification*, Riddick, J.A. and Toops, E.E., Eds., New York: Interscience, 1955.

9. *Entsiklopediya polimerov* (Polymer Encyclopedia), Kargin, V.A., Ed., Moscow: Sov. Entsiklopediya, 1972, vol. 1, p. 932.
10. Emel'yanov, D.N., Panova, G.D., and Ryabov, A.V., *Praktikum po metodam issledovaniya vysokomolekulyarnykh soedinenii* (Manual on Methods for Studying Macromolecular Compounds), Gor'kii: Gor'k. Gos. Univ., 1963.
11. Arulin, V.I. and Efimov, L.I., *Tr. Khim. Khim. Tekhnol.* (Gor'kii), 1970, issue 2, pp. 74–77.
12. Kulagina, T.G. and Lebedev, B.V., *Zh. Fiz. Khim.*, 1999, vol. 73, no. 5, pp. 800–805.
13. Smirnova, N.N., Chemical Thermodynamics of Hydrocarbon Polymers, *Doctoral Dissertation*, Nizhni Novgorod, 2002.
14. Rafikov, S.R., Pavlov, S.A., and Tverdokhlebova, I.I., *Metody opredeleniya molekulyarnykh vesov i polidispersnosti vysokomolekulyarnykh soedinenii* (Methods for Determining the Molecular Masses and Polydispersity of Macromolecular Compounds), Moscow: Khimiya, 1963)
15. Belen'kii, B.G. and Vilenchik, L.Z., *Khromatografiya polimerov* (Chromatography of Polymers), Moscow: Khimiya, 1978.
16. Nakanishi, K., *Infrared Absorption Spectroscopy*, San Francisco: Holden-Day, 1962.
17. Kelen, T. and Tudös, F., *J. Polym. Sci.*, 1977, vol. 15, pp. 3047–3074.
18. Begantsova, Yu.E., Malyshev, A.S., Zaitsev, S.D., and Semchikov, Yu.D., *Vysokomol. Soedin., Ser. A*, 2002, vol. 44, no. 4, pp. 560–566.
19. Shostakovskii, M.F., Khomutov, A.M., and Sidel'kovskaya, F.P., *Izv. Akad. Nauk SSSR, Otd. Khim. Nauk*, 1961, pp. 2222–2225.
20. Bork, J.F. and Coleman, L.E., *J. Polym. Sci.*, 1960, vol. 43, pp. 418–421.
21. *Copolymerization*, Ham, G.E., Ed., New York: Interscience, 1964.
22. Zubarev, V.E., *Metod spinovykh lovushek* (Method of Spin Traps), Moscow: Mosk. Gos. Univ., 1984.

ISSN 1070-4272, Russian Journal of Applied Chemistry, 2007, Vol. 80, No. 1, pp. 131–138. © Pleiades Publishing, Ltd., 2007.
Original Russian Text © V.V. Platonov, A.A. Khadartsev, A.Yu. Shvykin, D.V. Prokopchenkov, V.A. Proskuryakov, T.V. Chestnova, 2007, published in Zhurnal Prikladnoi Khimii, 2007, Vol. 80, No. 1, pp. 132–139.

MACROMOLECULAR CHEMISTRY AND POLYMERIC MATERIALS

Chemical Composition of Oxidative Degradation Products of the Organic Matter of Shungite Rock from the Zazhogino Deposit (Karelia, Trans-Onega Region)

V. V. Platonov, A. A. Khadartsev, A. Yu. Shvykin, D. V. Prokopchenkov, V. A. Proskuryakov, and T. V. Chestnova

Leo Tolstoy State Pedagogical University, Tula, Russia
Tula State University, Tula, Russia
St. Petersburg State Technological Institute (Technical University), St. Petersburg, Russia

Received April 25, 2006

Abstract—Oxidative degradation of the organic matter of shungite rock from the Zazhogino deposit (Karelia, trans-Onega region) with various reagents was performed. The composition of the products obtained was studied by IR Fourier spectroscopy and gas chromatography–mass spectrometry. The set of the compounds identified reflects the structure and origin of the macromolecular network and mobile phase of shungite.

DOI: 10.1134/S1070427207010260

Oxidative degradation is relatively widely used for determining the features of chemical composition and structural organization of macromolecules of various caustobioliths [1–9]. In this study we examined the chemical composition of the organic matter (OM) of shungite rock (SR) from the Zazhogino deposit (Karelia, trans-Onega region) by oxidative degradation with various reagents.

EXPERIMENTAL

The starting shungite rock ground in a ball mill to a particle size of 70–90 μm was charged into a Teflon vessel and thoroughly stirred for 6 h at 20°C with 40% HF. The resulting slurry was allowed to settle, and the solid phase was repeatedly washed with water to pH ~7 by decanting, vacuum-filtered on a Büchner funnel, and dried to constant weight at 100°C, after which the OM content in SR was determined by thermal gravimetric analysis of the resulting OM-enriched product. According to the elemental analysis, treatment of the initial SR with aqueous HF increased the OM content from 30.21 to 82.00 wt %. The elemental composition of SR OM (wt % daf) is as follows: C 95.45, H 0.30, N 0.60, and O + S 3.65.

Oxidation of SR OM with an alkaline solution of ammonium peroxodisulfate was performed as follows. A 100-ml three-necked flask with a power-driven stirrer and a thermometer was charged with 10 g of the enriched SR and 50 ml of 16 wt % aqueous NaOH. The resulting suspension was heated to 60°C with vigorous stirring, after which 5 g of dry $(NH_4)_2S_2O_8$ was added in small portions through the third neck. In so doing, intense foaming was observed because of the release of ammonia and oxygen. After 1 h, the temperature was raised to 90°C, an additional 5 g of $(NH_4)_2S_2O_8$ was added, and the mixture was stirred at 90°C for 2 h, after which the third portion (5 g) of $(NH_4)_2S_2O_8$ was added. Then the mixture was stirred at 90°C for 3 h more, cooled to room temperature, and vacuum-filtered through a glass frit no. 4; the residue of the enriched SR was washed with distilled water to neutral reaction, dried in a vacuum oven to constant weight, and weighed. The weight of the solid obtained was 8.50 g.

The brown filtrate was combined with wash waters and extracted in a separating funnel with CH_2Cl_2 (4 × 50 ml). The combined extracts were dried over anhydrous $MgSO_4$, and the solvent was distilled off on a water bath. The residue was dissolved in a small amount of chloroform, the solution was quantitatively transferred into a weighed bottle, and the solvent was evaporated in an oven at 70°C. The resulting extract was dried in a vacuum oven to constant weight. The yield of the CH_2Cl_2 extract was 0.04 wt % relative to SR OM.

The remaining red-brown filtrate was acidified with 34.6 wt % HCl to pH 2–3. In so doing, vigorous evolution of CO_2 was observed, and the solution became light brown. It was evaporated to dryness on a water bath, and the residue was thoroughly triturated in an agate mortar with acetone and kept in a stoppered weighing bottle for 3 h. The dark orange acetone extract was separated by decanting, and the solid residue was additionally extracted with two portions of refluxing acetone. The acetone extracts were combined, and the solvent was distilled off. The resulting brown residue was triturated in a weighing bottle with a 1 : 1 (by volume) mixture of CH_2Cl_2 and Et_2O. In so doing, the solid partially dissolved. The solution was separated by decanting, quantitatively transferred into a weighed bottle, and evaporated to constant weight. The yield of the light yellow CH_2Cl_2–Et_2O extract from the acetone extract was 1.07 wt % based on SR OM. The brown residue of the acetone extract, insoluble in CH_2Cl_2–Et_2O, was dried in a vacuum oven to constant weight. Its yield based on SR OM was 7.77 wt %. For the analysis by gas chromatography–mass spectrometry (GC–MS), the CH_2Cl_2–Et_2O extract from the acetone extract and the residual amount of the acetone extract were methylated with diazomethane in ether.

All the products obtained were studied by IR Fourier spectroscopy and GC–MS [10–14].

In the experiments on SR OM oxidation with HNO_3, a 50-ml three-necked flask equipped with a power-driven stirrer, a thermometer, and a dropping funnel was charged with 10 g of enriched SR, and 23 ml of a 50 wt % HNO_3 solution was gradually added with careful stirring through the dropping funnel. After adding HNO_3, the mixture was slowly heated with vigorous stirring to 60°C and kept at this temperature for 3 h. In so doing, slight foaming and evolution of nitrogen oxides were observed. After 3 h, the mixture was cooled to room temperature and filtered through a glass frit no. 4. The residue of the enriched SR was repeatedly washed with distilled water to pH ~7 and dried to constant weight; its weight was 8.25 g.

The filtrate was evaporated to dryness on a water bath to obtain an orange-brown solid. It was thoroughly triturated with chloroform in an agate mortar, and the mixture was quantitatively transferred into a weighing bottle with a ground-glass stopper and allowed to stand at room temperature for 3 days. Then the yellow chloroform solution was separated by decanting from the undissolved solid residue, and the residue was washed twice with chloroform by decanting; the chloroform extracts were combined, and the solvent was distilled off on a water bath. The extract was finally dried in a vacuum oven to constant weight. The yield of the chloroform extract was 0.16 wt % based on SR OM. For GC–MS analysis, the extract was methylated with diazomethane in ether; characteristic odor of carboxylic acid esters was noted. The methylation products were dissolved in CH_2Cl_2, and the solution was evaporated; yellow needle-like crystals were obtained, which were analyzed by IR Fourier spectroscopy and GC–MS [10–14].

In the experiments on SR OM oxidation with potassium permanganate in alkali solution, a 50-ml three-necked flask equipped with a power-driven stirrer, a reflux condenser, and a thermometer was charged with 12 g of enriched SR, 12 g of $KMnO_4$, and 50 ml of 6 M aqueous NaOH. The mixture was heated to 90°C with moderate stirring and stirred at this temperature for 3 h. After that, the mixture was cooled to room temperature and vacuum-filtered through a glass frit no. 4; the residue of the enriched SR was washed with distilled water to neutral reaction and dried in a vacuum oven to constant weight. The weight of the residue was 11.52 g. The dark orange filtrate was neutralized with 3 M HCl to pH ~7. The solution became yellow, and a yellow precipitate formed. The solution and precipitate were extracted without their separation with chloroform (4 × 50 ml) in a dropping funnel. The combined chloroform extracts were dried over anhydrous $MgSO_4$, after which the solvent was distilled off on a water bath. The resulting extract was finally dried in a vacuum oven in a weighing bottle to constant weight. The yield of the chloroform extract was 0.10 wt % based on SR OM. Its chemical composition was characterized by IR Fourier spectroscopy [10–13].

In the IR Fourier spectrum (Fig. 1) of the CH_2Cl_2 extract of the alkali fraction from peroxodisulfate oxidation of SR OM, we identified the absorption bands of the following structural fragments (ν, cm^{-1}):

alkanes: ν_{CH_3} (2960.0, 2876.0), ν_{CH_2} (2921.9, 2848.6), ν_{CH} (tertiary, 2896.9), δ_{-CH_2-} (1465.7), δ_{C-CH_3} (antisymmetric, 1450.0), $\delta_{-C(CH_3)_2-}$ (1386.6–1380.0, 1370–1365.0), ρ_{CH_2} (750.0–713.5);

alkenes: $\nu_{CH=CH-}$ (3047.2–3010.0), $\delta_{-CH=CH-}$ (out-of-plane, 970.0–960.0), $\delta_{-CH=CH-}$ (in-plane, 1310.0–1290.0), $\delta_{C=C}$ (nonconjugated, 1680.0–1620.0), $\delta_{C=C}$ (conjugated with benzene rings, 1620.0);

aromatic rings: $\nu_{=C-H}$ (3030.0, 3047.2); $\nu_{C=C}$ (in-plane skeleton vibrations, 1580.0, 1550.6, 1530.0, 1510.0, 1600.0); conjugated rings (1580.0, 1450.0,

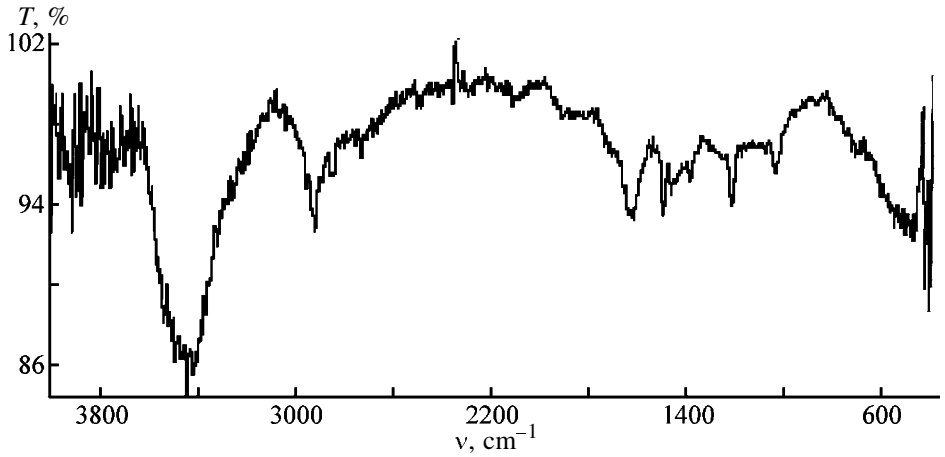

Fig. 1. IR Fourier spectrum of the CH_2Cl_2 extract of the alkali fraction from oxidative degradation of SR OM with ammonium peroxodisulfate. (*T*) Transmission and (ν) wavenumber; the same for Figs. 3, 4, 6, 8 and 9.

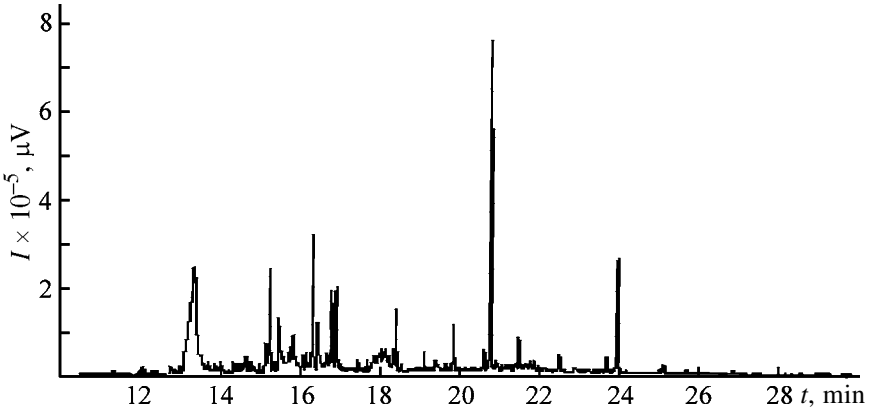

Fig. 2. Chromatogram of a CH_2Cl_2 extract of the alkali fraction from oxidative degradation of SR OM with ammonium peroxodidulfate. (*I*) Intensity and (*t*) time; the same for Figs. 5 and 7.

1465.7); aromatic rings, mainly fused (1620.0, 1680.0, 1580.0–1550.6, 1550.6–1465.7);

cyclic carboxylic acid anhydrides (1822.5, 1784.0); ν_{O-H} (phenols, alcohols, 3656.7–3595.0); ν_{O-H} (phenols, 1216.9, 1410.0–1310.0); δ_{O-H} (primary alcohols, 1039.5, 1050.0, 1350.0–1260.0); δ_{O-H} (in-plane, 1386.6); δ_{O-H} (out-of-plane, 690.3, 650.0); carboxylic acids (3000.0–2500.0, 1620.0, 1465.7, 1386.6, 1300.0–1200.0); acid amides (3000.0–3251.7, 3265.2, 1620.0, 3411.8, 3442.6, 3465.8, 1216.9, 1280.0); ketones (1730.0, 1720.0); aliphatic ethers (1125.0); aromatic and alkyl aromatic ethers (1083.8–1039.4);

pyrrole, indole, pyridine, piperidine, quinoline heterorings (3319.2–3384.7, 3367.4, 3490.8, 1465.7, 1498.5, 1216.9, 1280.0, 713.5, 750.0).

In this extract, we identified by GC–MS (Fig. 2) alkanes (heptadecane, octadecane, eicosane, tricosane, tetracosane, hexacosane heptacosane) and an alkene, 2,6,10,15,19,23-hexamethyltetracosa-2,6,10,14,18,22-hexaene.

In the IR Fourier spectrum of the residue of the acetone extract of the acid fraction from oxidative degradation of SR OM with ammonium peroxodisulfate (Fig. 3), we identified the absorption bands of the following fragments (ν, cm^{-1}):

alkanes: ν_{CH_3} (2958.5, 2873.6), ν_{CH_2} (2925.7, 2854.4), δ_{-CH_2-} (1465.0), $\delta(C-CH_3)$ (symmetric, 1380.0–1370.0), $\rho_{-(CH_2)_4-}$ (rocking, 750.0–720.0);

alkenes: $\nu_{CH=CH-}$ (3031.8–3006.7), $\delta_{CH=CH-}$ (out-of plane, 979.7–960.4), $\nu_{CH=CH_2}$ (vinyl, 3093.5–3078.1, 3031.8–3006.7), $\rho_{-CH=CH_2}$ (conjugated with benzene ring, 1633.5);

phenols, alcohols, ν_{O-H} (free –OH group, 3650.0–3590.0); intramolecular hydrogen bond (3579.5–3444.5); chelate compounds (3203.5–2500.0); δ_{O-H} and ν_{C-O} (primary alcohols, 1050.0, 1350–1260.0,

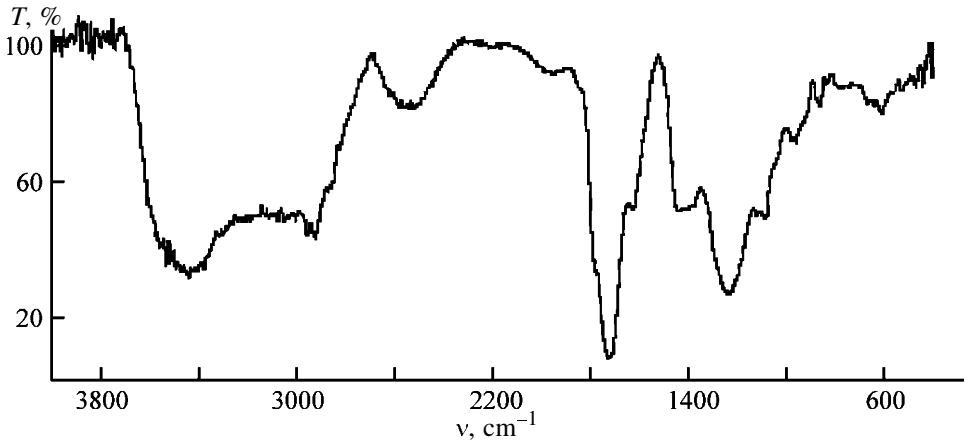

Fig. 3. IR Fourier spectrum of the residue of the acetone extract of the acid fraction from oxidative degradation of SR OM with ammonium peroxodisulfate.

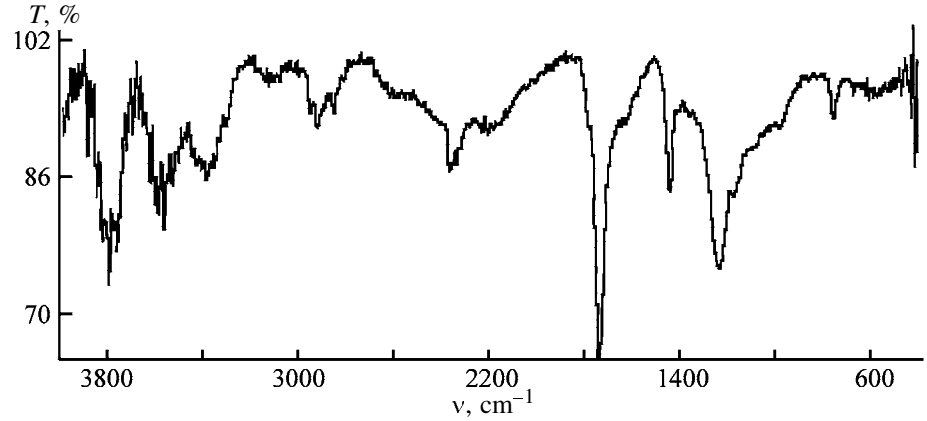

Fig. 4. IR Fourier spectrum of the methylated residue of the acetone extract of the acid fraction from oxidative degradation of SR OM with ammonium peroxodisulfate.

1236.2); phenols, δ_{O-H} (1236.2, 1410.0–1310.0); aromatic and other ethers with =C–O– group (1270.0–1236.2); open-chain saturated ketones (–CH_2–CO–CH_2–, 1728.0–1700.0); diketones (1633.5–1540.0); quinones (1655.0–1633.5); carboxylic acids ($\nu_{C=O}$): unsaturated aliphatic (1728.0–1700.0), aromatic (1700.0–1728.0), unsaturated (1728.0–1717.0); acetates (1250.0–1236.2);

pyrrole, indole, pyridine, piperidine, quinoline heterorings (3303.7–3384.7, 3323.0, 3475.4, 3498.5, 3006.7, 3031.8, 1633.5, 3054.9–3006.7, 1000.0–960.4, 1438.7, 1236.2, 744.4, 767.5); amides (ν_{N-H}): primary amides, free –NH_2 group (3498.5, 3409.8); bound NH_2 group (3172.6, 3350.0); secondary amides (3444.5–3409.8, 3323.0–3265.2, 3172.6–3134.0); sulfur-containing groups –S–H (2622.9–2541.9), –S–S– (406.8–524.5), –SO_2–OH (1085.7).

In the IR Fourier spectrum of the methylated residue of the acetone extract of the acid fraction from oxidative degradation of SR OM with ammonium peroxodisulfate (Fig. 4), we identified the absorption bands of the following structural fragments (ν, cm^{-1}):

alkanes: ν_{CH_3} (2952.7, 2873.7), ν_{CH_2} (2923.8, 2850.5), δ_{CH_2} (1440.0), δ_{C-CH_3} (antisymmetric; 1450.0), $\delta_{-C(CH_3)_2-}$ (1359.6, 1380.0, 1370–1365.0), ρ_{CH_2} (rocking, 752.0–720.0);

alkenes: $\nu_{-CH=CH-}$ (3049.2–3010.0), $\delta_{-CH=CH-}$ (out-of-plane, 983.5–960.0), $\delta_{-CH=CH-}$ (in-plane, 1325.0–1290.0), $\delta_{C=C}$ (nonconjugated, 1680.0–1630.0, 1645.1), $\delta_{C=C}$ (conjugated with benzene rings, 1630.0);

aromatic rings, $\nu_{=C-H}$ (3022.2, 3049.2, 3064.6, 3080.0), mainly fused (1630.0, 1645.1, 1580.0–1560.0, 1440.6), substituted with alkyl chains (1230.4, 1178.3, 1020.0, 1050.0); $\nu_{C=C}$ (in-plane skeleton vibrations, 1580.0, 1560.0, 1440.6); δ_{C-H} (out-of-plane; 725.1–720.0, 856.2–800.0, 900.0–856.2);

alcohols, phenols, ν_{O-H} (free –OH, 3647.1–3591.1); intramolecular hydrogen bond (3568.0–3448.4); chelates (3195.7–2500.0); δ_{O-H} (phenols, 1230.4, 1410.0–1310.0); δ_{O-H} and ν_{C-O} (primary alcohols,

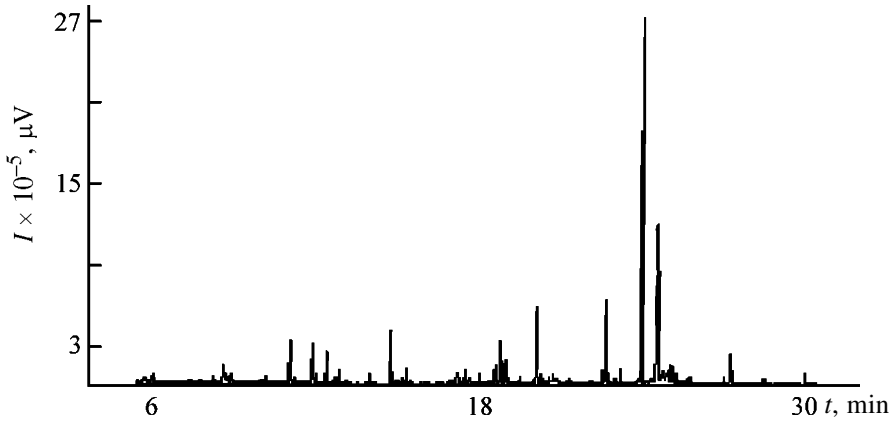

Fig. 5. Chromatogram of the methylated residue of the acetone extract of the acid fraction from oxidative degradation of SR OM with ammonium peroxodisulfate.

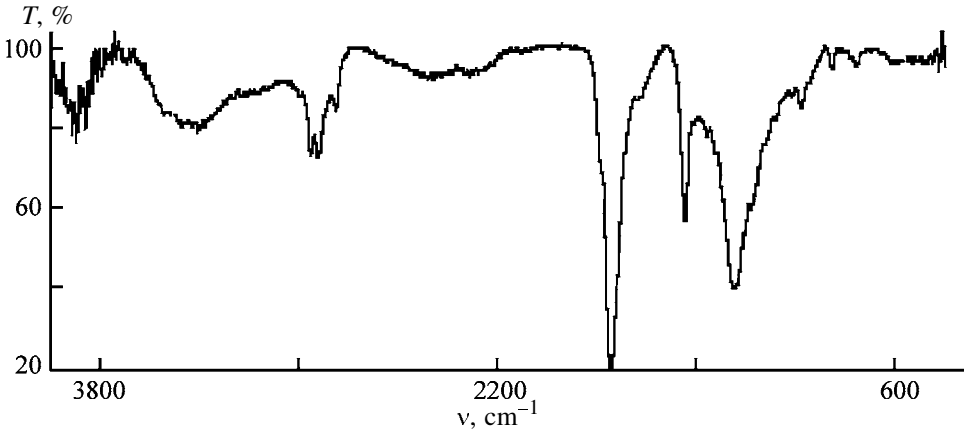

Fig. 6. IR Fourier spectrum of the CH_2Cl_2–Et_2O extract from the acetone extract of the acid fraction from oxidative degradation of SR OM with ammonium peroxodisulfate.

1050.0, 1359.6–1230.4, 1260.0); open-chain unsaturated ketones (–CH_2–CO–CH_2–, 1280.0–1230.4); diketones (1630.0–1540.0); quinones (1645.1–1630.0); carboxylic acids ($\nu_{C=O}$): saturated aliphatic (1737.6–1700.0), aromatic (1700.0–1680.0); esters ($\nu_{C=O}$): normal saturated (1750.0–1737.6), unsaturated (1737.6–1720.0), acetates (1260.0–1230.4);

pyrrole, indole, pyridine, piperidine, quinoline, thiophene heterorings (3022.2, 3064.6–3000.9, 3000.9–3049.2, 1645.1, 3307.6–3394.4, 3352.0, 3473.5, 3409.8, 1440.6, 1230.4, 752.1); primary amines (3195.7, 3352.0, 3487.0, 3409.8); secondary amines (3448.4–3409.8, 3320.0–3270.0, 3195.7–3126.3); sulfur-containing groups: –S–H (2621.0–2530.3), –S–S– (410.7–528.3).

In the methylated residue of the acetone extract of the acid fraction from oxidative degradation of SR OM with ammonium peroxodisulfate, we identified by GC–MS (Fig. 5) the following compounds: alkanes (dodecane, tetradecane, pentadecane, hexadecane, octadecane, eicosane, docosane, tetracosane, heptacosane, octacosane); alkenes (1-tetradecene, 1-hexadecene, 1-octadecene, 1-nonadecene, 2,6,10,15,19,23-hexamethyltetracosa-2,6,10,14,18,22-hexaene); cycloalkane (cyclodecane); esters of saturated, unsaturated, and polybasic carboxylic acids (hexadecanoic, 14-methylpentadecanoic, octadec-7-enoic, octadec-9-enoic; tetramethyl benzenetetracarboxylate; hexamethyl benzenehexacarboxylate).

In the IR Fourier spectrum of the methylated CH_2Cl_2–Et_2O extract form the acetone extract of the acid fraction from oxidative degradation of SR OM with ammonium peroxodisulfate (Fig. 6), we identified the following absorption bands (ν, cm^{-1}):

alkenes: $\nu_{-CH=CH-}$ (3045.3–3001.0), $\delta_{-CH=CH-}$ (out-of-plane, 983.5–960.0); $\delta_{-CH=CH-}$ (in-plane, 1320.0–1290.0);

aromatic ($\nu_{=C-H}$, 3031.8), mainly fused (3031.8–3080.0, 1643.1, 1442.5, 1178.3–1100.0, 720.0–757.9), naphthenic (2925.7, 2954.6, 1442.5, 983.5) and aromatic rings (720.0–825.4, ill-resolved triplet);

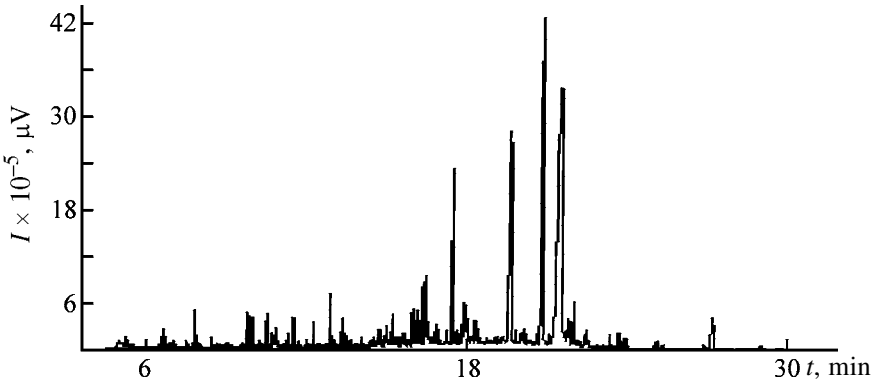

Fig. 7. Chromatogram of the methylated CH_2Cl_2–Et_2O extract from the acetone extract of the acid fraction from oxidative degradation of SR OM with ammonium peroxodisulfate.

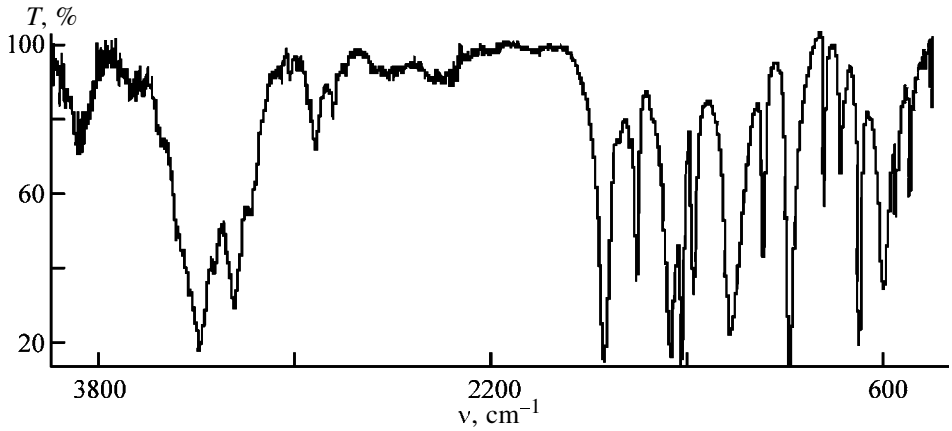

Fig. 8. IR Fourier spectrum of the methylated chloroform extract from oxidative degradation of SR OM with nitric acid.

phenols, alcohols (3633.6–3580.0, 3211.2–3250.0, 1410.0–1310.0, 1242.0–1178.3); quinoid groups (1643.1, 1660.0, 1680.0); ketones (1720.0–1739.6, 1178.3); carboxy groups of aliphatic and aromatic acids (1705.0–1739.6, 3580.0–3500.0, 3519.8, 3546.8, 1800.0–1739.6, 1359.6–1242.0, 1080.0–1178.3);

pyrrole, indole, pyridine, quinoline, furan heterorings (3170.0–3134.0, 1560.0, 1410.0–1310.0, 1178.3–1242.0, 720.0, 757.9, 825.4, 3300.0–3355.8, 3431.0, 3473.5, 1411.7); conjugated pyrrole rings of porphyrins and chlorophylls (3519.8, 3487.0, 3134.0, 3045.3, 1560.0, 1018.2, 700.0–757.9); sulfides and disulfides (1411.7, 1359.6, 588.1, 472.4, 451.2, 428.0).

In the methylated CH_2Cl_2–Et_2O extract from the acetone extract of the acid fraction from oxidative degradation of SR OM with $(NH_4)_2S_2O_8$, we identified by GC–MS (Fig. 7) the following compounds: alkanes (dodecane, tetradecane, hexadecane, octadecane, eicosane, tetracosane, heptacosane, nonacosane); complete methyl esters of mono-, di-, and polycarboxylic acids (tetradecanoic, hexadecanoic, propanedioic, butanedioic, thiophenetetracarboxylic, benzenehexacarboxylic).

In the IR Fourier spectrum of the methylated chloroform extract of products of SR OM oxidation with 50% HNO_3 (Fig. 8), we identified the absorption bands of the following structural fragments (ν, cm^{-1}):

alkanes: ν_{CH_3} (2948.9, 2889.1), ν_{CH_2} (2920.0, 2848.6), δ_{CH_2} (1459.9), $\rho_{(CH_2)_n}$ (775.2);

alkenes: $\nu_{-CH=CH-}$ (3060.7–2995.9), $\delta_{-CH=CH-}$ (out-of-plane, 979.7), $\delta_{-CH=CH-}$ (in-plane, 1310.0–1290.0), $\delta_{C=C}$ (nonconjugated, 1680.0–1606.5, 1637.3);

aromatic rings ($\nu_{=C-H}$), mainly fused (3000.0, 3060.7, 3024.1); δ_{C-H} (out-of-plane, 775.2, 842.7); naphthenic (2920.0, 2948.9, 1459.9, 979.7) and hydroaromatic rings (775.2, 842.7, 979.7);

phenols, alcohols (3635.5–3583.4, 3247.8–3203.5, 1410.0–1310, 1220.7–1089.6), δ_{O-H} (alcohols, 1419.4–1371.2, 1089.6); quinones (1637.3, 1680.0); ketones (1735.7, 1180.0); aliphatic and aromatic acids (1735.7–1700.0, 3583.4–3500.0, 3514.0, 3521.7,

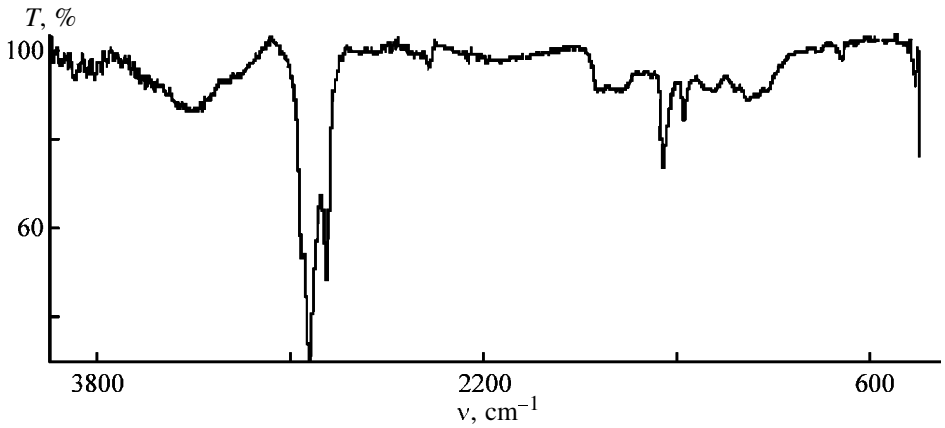

Fig. 9. IR Fourier spectrum of the chloroform extract from oxidative degradation of SR OM with potassium permanganate in alkali solution.

3529.4, 3566.0, 3583.4, 1800–1735.7, 1371.2–1220.7, 1220.7–1089.6);

esters ($\nu_{C=O-O-}$) with acetate group conjugated with benzene ring (1750.0–1735.7); ethers, ν_{C-O-C} (symmetric, 1089.6; antisymmetric, 1220.7);

pyrrole, indole, quinoline, furan heterorings (3180.0–3105.1, 1580.0, 1410.0–1310.0, 1220.7–1089.6, 3379.0–3307.6, 3431.0, 3425.3, 3465.8, 3485.0, 1419.4, 1459.9); conjugated pyrrole rings of porphyrins and chlorophylls (3514.0, 3521.7, 3485.0, 3105.1, 3060.7, 3024.1, 1560.0, 1220.7, 700.0–775.2); sulfides and disulfides (1419.4, 1459.9, 1371.2, 593.9, 696.1, 491.7, 441.5, 426.1).

In this extract from products of SR OM oxidation with 50% nitric acid, we identified by GC–MS eicosane, pentacosane, octacosane, methyl hexadecanoate, 2-methyl-7-phenylindole, 1,1-dicyano-2-methyl-3-(*p*-cyanophenyl)propene.

In the IR Fourier spectrum of the chloroform extract from products of SR OM oxidation with an alkaline solution of potassium permanganate (Fig. 9), we identified the absorption bands of the following structural fragments (ν, cm^{-1}):

alkanes: $\nu^{as}_{CH_3}$ (2960.0), $\nu^{s}_{CH_2}$ (2865.0), $\delta^{as}_{CH_3}$ (1461.8), $\delta^{s}_{CH_2}$ (1377.0), $\nu^{as}_{CH_2}$ (2921.9), $\nu^{s}_{CH_2}$ (2850.5), CH_2 (scissor, 1461.8), $\rho_{-(CH_2)_n}$ (rocking, 728.9, 719.3);

aromatic rings (3030.0, 3060.0, 3097.4, 1540.9, 1506.2, 1558.3, 1654.7);

alcohols, phenols (3583.4–3515.9); ν_{C-O} (phenolic, 1220.0, 1261.2); ν_{O-H} (alcohol, 1040.0); δ_{O-H} (1261.2); quinones (1654.7–1680); diketones (1710.6); carboxylic acids (3010.0–2500.0, 1710.6, 1461.8, 1300.0–1200.0);

pyrrole, indole, pyridine, quinoline heterorings (3328.8–3369.3, 3413.7, 3433.0, 3467.7, 1461.8, 1377.0, 1377.0–1261.2, 719.3, 728.9).

CONCLUSIONS

(1) Each of the oxidants tested gives rise to a complex set of products among which carboxylic acids, alcohols, phenols, ketones, and quinones prevail. *n*-Alkanes, alkenes, and cycloalkanes were also identified.

(2) Hydrocarbons, especially alkanes and alkenes, and also aliphatic saturated and unsaturated carboxylic acids, identified by gas chromatography–mass spectrometry in methylated extracts, are presumably coextracted from the network matrix of shungite macromolecules, i.e., are components of the mobile phase reflecting the lipid composition of ancient unicellular algae. The detection of benzenetetra- and benzenehexacarboxylic acids shows that the organic matter of shungite rock has a highly fused structure; in the course of oxidative degradation, these acids could form from pyrene, coronene, and fullerene fragments of its macromolecular network.

(3) According to the results obtained, separate highly condensed aromatic fragments are presumably linked with each other by polymethylene, cycloalkane, indole, furan, thiophene, and other bridges.

REFERENCES

1. *Preparativnaya organicheskaya khimiya* (Preparative Organic Chemistry), Vul'fson, N.S., Ed., Moscow: GNTIKhL, 1959.
2. Hayatsu, R., Winans, R., Scott, R.G., et al., *Fuel*, 1978, vol. 57, no. 9, pp. 541–548.

3. Studier, M.H., Hayatsu, R., and Winans, R., *Anal. Meth. Coal Coal Prod.*, 1978, vol. 2, pp. 43–75.
4. Hayatsu, R., Winans, R., Scott, R.G., et al., *Fuel*, 1981, vol. 60, no. 1, pp. 77–82.
5. Mayo, F.R., *Fuel*, 1975, vol. 54, no. 10, pp. 273–275.
6. Heard, J. and Senftle, F.E., *Fuel*, 1984, vol. 63, no. 2, pp. 221–226.
7. Shishkov, V.F., Randin, O.I., and Tuturina, V.V., *Khim. Tverd. Topl.*, 1987, no. 3, pp. 44 – 48.
8. Olson, E.S., Diehl, J.W., and Frochlich, M.L., *Fuel*, 1987, vol. 66, no. 7, pp. 968–972.
9. Hayatsu, R., Scott, R.G., and Botto, R.E., *Fuel*, 1986, vol. 65, no. 7, pp. 901–908.
10. Mironov, V.A. and Yankovskii, S.A., *Spektroskopiya v organicheskoi khimii* (Spectroscopy in Organic Chemistry), Moscow: Khimiya, 1985.
11. Nakanishi, K., *Infrared Absorption Spectroscopy*, San Francisco: Holden-Day, 1962.
12. Silverstein, R.M., Bassler, G.C., and Morrill, T.C., *Spectrometric Identification of Organic Compounds*, New York: Wiley, 1974.
13. Kazitsyna, L.A. and Kupletskaya, N.B., *Primenenie UF, IK, YaMR i mass-spektroskopii v organicheskoi khimii* (Applications of UV, IR, NMR, and Mass Spectroscopy to Organic Chemistry), Moscow: Mosk. Gos. Univ., 1979.
14. Chapman, J.R., *Practical Organic Mass Spectrometry*, New York: Wiley, 1983.

ISSN 1070-4272, Russian Journal of Applied Chemistry, 2007, Vol. 80, No. 1, pp. 139–146. © Pleiades Publishing, Ltd., 2007.
Original Russian Text © N.I. Alekseev, D.V. Afanas'ev, B.O. Bodyagin, A.K. Sirotkin, N.A. Charykov, O.V. Arapov, 2007, published in Zhurnal Prikladnoi Khimii, 2007, Vol. 80, No. 1, pp. 140–147.

MACROMOLECULAR CHEMISTRY AND POLYMERIC MATERIALS

A Possible Mechanism of Formation of Fullerene Nanoparticles in Shungites

N. I. Alekseev, D. V. Afanas'ev, B. O. Bodyagin, A. K. Sirotkin, N. A. Charykov, and O. V. Arapov

Ioffe Physicotechnical Institute, Russian Academy of Sciences, St. Petersburg, Russia
Innovations of Leningrad Institutes and Enterprises, Closed Joint-Stock Company, St. Petersburg, Russia
Institute of Flu, Russian Academy of Medical Sciences, St. Petersburg, Russia

Received April 27, 2006

Abstract—A mechanism of formation of fulleroid nanoparticles in shungites, adequate to the principal structural features of these particles (a cavity filled with nothing but water traces, the absence of the catalyst nanoclusters, and some other) was suggested.

DOI: 10.1134/S1070427207010272

Natural mineral shungite is extremely promising from the viewpoint of nanocarbon science and applications. Some of these applications, e.g., water treatment, are known for at least 300 years, while others, e.g., coke substitution or addition to building materials, are now under development [1, 2] or research [3].

Fullerene and carbon nanotube (CNT) science treats shungite as an important natural material unique in containing fulleroid particles such as multilayer fullerenes and, probably, true fullerenes. Data on the presence of true fullerenes are contradictory. The first encouraging results obtained in mass-spectrometric experiments [4] were disproved by the results of extraction with conventional organic solvents, but those studies were underlain by the views on the molecular character of the bond for fullerenes in shungites. Covalent and donor–acceptor compounds of fullerenes, yielded by their reactions with nucleophilic molecules, are being actively studied today. It is believed that specifically the chemical character of the bonding of fullerenes in shungites complicates their detection [5].

By contrast to fullerenes, the existence of fulleroid particles as multilayer globules, nanotubes, nanobarrels, and onion-like nanocarbons with an internal cavity is beyond question, and they were repeatedly observed [6, 7]. Like carbon in shungites on the whole, fulleroid structures are rigidly connected to the aluminosilicate matrix [7]: Both phases are uniformly distributed even in particles prepared by micrometer grinding. Along with noncrystalline carbon and aluminosilicates, shungite contains a small amount of a bituminous organic material.

The richest in carbon (up to 90 %) is shungite-I [8]; however, it is fairly expensive, and its deposits are extremely limited. Evidently, more promising is shungite-III containing 30–40% carbon [8, 9] (with the remaining 60–70% accounted for primarily by aluminosilicates). The total resources of the shungite rocks of the Onega basin exceed 1 bln tons, and the explored reserves of the largest Zazhoginskoe deposit are estimated at ca. 150 mln tons.

Typical electron micrographs of the nanostructures of shungite-III were obtained after chemical recovery of the carbon component (the resulting material was named MNS, modified nanoshungite). The sequence of the operations in removal of the mineral components was described in [10]. The samples were analyzed on a JEM-100S (JEOL, Japan) transmitting electron microscope at a magnification of 10^4–10^5. Figure 1 shows one of compact accumulations of the nanoparticles, irregularly distributed over the bulk of the material. The micrograph shows a closed-end multilayer CNT with a cavity, comprising numerous layers, with the channel diameter of ca. 3 nm, outside diameter of 20 nm, and length of ca. 0.2 μm, as well as nanobarrels with a cavity and onion-like nanocarbons without cavity. All the nanostructures are clearly separated from the silicate matrix.

The morphology of the carbon filling the inter-

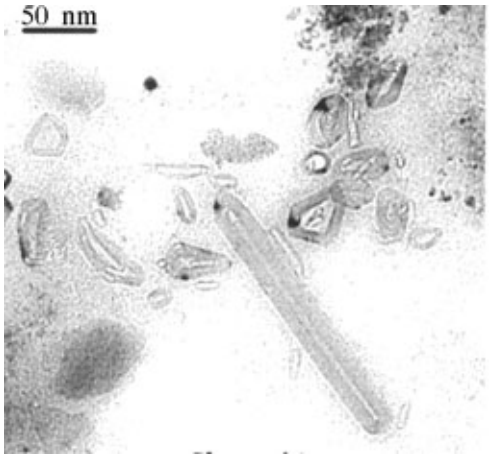

Fig. 1. Tunneling electron micrograph (TEM) of the chemically modified shungite-III.

globular space in nonsplit shungite still remains to be examined. Published data characterize it as a carbon material resistant to graphitization up to very high temperatures [7, 8].

The task of developing a model of formation of fulleroid particles (FPs) in shungites is clearly not as broad as the global geological problem of formation of shungite rocks. The model we propose here, rather, provides an alternative treatment of the mechanism of formation of FPs (or globules), that is, not underlain by the concept of the organic nature of the initial carbon.

Up to now, two hypotheses of formation of shungites, biogenic and abiogenic, were proposed [8, 9]. They fundamentally differ but are similar in treating the globular structure of the matter, characteristic of shungites, as due to the presence in the prehistoric carbon substance of long polymeric molecules with flexible linear segments. Under the action of intramolecular forces, these molecules can roll themselves into balls which subsequently turn into globules. This rolling is driven by the tendency of the molecules to minimize the free surface energy caused by the "projecting" active groups [11, 12]. Basically, the only difference between the biogenic and abiogenic hypotheses consists in how they treat the nature of carbon which in both cases is assumed to be organic. Various versions of the biogenic hypothesis consider as organic substance Cyanophyceae, naphthoids, or bitumen–resin substances. The abiogenic hypothesis also considers various types of hydrocarbons in organosilicate complexes. A common feature is that these complexes gradually replace the previously formed silicate and aluminosilicate rocks. A special place is occupied by the model of formation of FPs by a mechanism similar to that in formation of carbon black particles in the flame synthesis of fullerenes by oxidation of methane [13].

Formation of globules from carbonization of some organic substances was unambiguously established long before arising of science of nanotubes. The globules were observed, e.g., in glassy carbons [11], where polyvinyl alcohols or phenol–formaldehyde resins can act as the initial products. Later, carbonization of specially selected organic substances was applied in synthesis of CNTs as well [14]. Importantly, such carbon materials are synthesized, however, under specific conditions in the absence of aluminosilicates. Therefore, in the absence of real simulation experiments with a substance close to shungite, only those versions of arising of fulleroid particles have a right to exist that do not at all appeal to the assumed organic nature of the initial carbon.

It is essential that the hypothetical mechanism of formation of the shungite FPs takes into account a number of the morphological features distinguishing these particles of shungites from the nanoparticles obtained by the chemical and arc syntheses.

(1) The particles have a cavity filled with nothing but, probably, water or its traces.

(2) There are no clear metal nanoclusters encapsulated inside the fulleroid layers.

(3) The fulleroid layers around the nanoparticles can have topological breaks, i.e., the surface typically does not have a fullerene nature in the strict sense of the word.

(4) The fullerene particles exist both in shungite-III containing ca. 60% aluminosilicates and in shungite-I, where the content of aluminosilicates can be no higher than several per cent.

General geological views on magma [15] and a typical chemical composition of shungite suggest that our considerations can start from a combination of the main components, carbon–aluminosilicate–water, if we will consider the following sequence of events. Carbon, molten in the aluminosilicate rock, rises from the interior of the Earth and is cooled. The melt also contains certain amount of water completely dissolved in it. Gradual decrease of pressure and lowering of temperature to a certain value T_{boil} result in supersaturation of the melt with the water separated out in the bulk of this melt as bubbles (the aggregation state at temperatures close to 1000°C can be only steam, since the critical point of water corresponds to a pressure of ca. 200 atm and temperature close to

300°C). As temperatures promising for synthesis of the nanostructures markedly exceed 300°C, water can be considered as steam throughout the synthesis of the nanostructures, even if this steam will be able of condensation upon further cooling.

A larger decrease in temperature results in separation of the melt components, since the solubility of carbon in SiO_2 attains the limiting value. This leads to supersaturation of the melt with carbon, which precipitates at the separation temperature T_{separ}. The bubble boundary becomes a natural site for precipitation of carbon from the melt as a solid phase. The shape of the nucleus during precipitation of carbon is similar to the fulleroid surface island on the surface of the catalytic particle (CP) (or nanodrop) [16, 17] (Fig. 2a). We showed in [17] that, in the case of a nanodrop, precipitation of the island (Fig. 2a, surface *1*) does not necessarily result in appearance of a nanotube. At high energies A of the van der Waals interaction of the catalyst atom with the fulleroid surface, encapsulation of the CP inside this surface (Fig. 2a, surface *3*) is more favorable than formation of a nanotube nucleus (Fig. 2a, surface *2*). A special place occupied by the iron group (or palladium group) elements is due specifically to the fact that they have a minimal A (Fig. 3), and the fulleroid island can fairly easily be detached from the catalyst surface and turn into CNT. Moreover, these elements are characterized by an optimal combination of A with the energy difference of the carbon–carbon chemical bond E_{CC} in graphite and carbon–melt(metal) atom bond $E_{M–C}$. This difference is specifically responsible for separation of the carbon atom from the melt and its incorporation into the fulleroid surface. For other elements (e.g., silicon), the parameter A is much higher (Fig. 3), but this does not hinder nucleation of the island, if we do not consider further detachment of such an island from the melt. Also, if $E_{M–C}$ somewhat exceeds E_{CC}, the growth of the perimeter and the spread of the island are energetically favorable. For silicon, the energy $E_{M–C} \equiv E_{Si–C}$ was estimated by the PM3 semiempirical quantum-chemical method at $E_{Si–C} \approx 12$ eV, while E_{CC}, at ≈ 6.5 eV.

Realization of the above-described sequence of events requires the following prerequisites. The solid carbon–melt phase segregation should occur before solidification of the melt as a whole, i.e., the condition $T_{boil} > T_{separ} > T_{solid}$ (where T_{solid} is the solidification temperature) should be satisfied. Also, the carbon content in the melt should decrease along the line of separation of the solid carbon phase rather than of sublimation of the excess carbon in the form of CO.

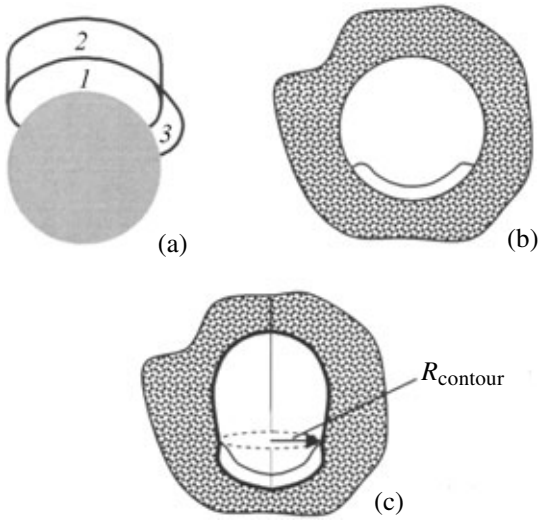

Fig. 2. (a) (*1*) CNT nucleus on the catalytic nanodrop surface, (*2*) CNT nucleus generated by the primary CNT nucleus, and (*3*) further spread of the island over the surface; (b) a fulleroid island on the internal surface of the nanobubble under assumption of a nondeformable surface; and (c) fulleroid island on the internal surface of the nanobubble (of the liquid surface of the melt).

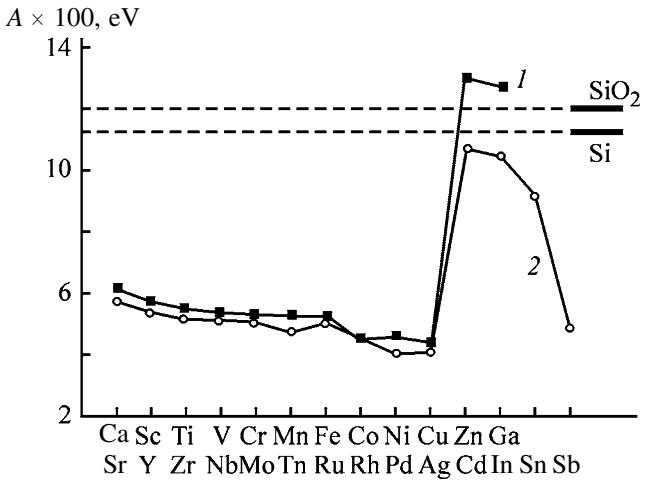

Fig. 3. Van der Waals interaction energy A of period III and IV atoms with the graphene plane. Period: (*1*) III and (*2*) IV. Dashed lines: energies of interaction of silicon and silicon dioxide SiO_2 with the graphene plane.

The phase diagram of the water–SiO_2 system was discussed in [18]; it is shown in Fig. 4 for the pressure of 1 atm. It is seen that, at the water content $c \geq$ (6–7) wt % and temperature $T \geq 1200$°C, the steam bubbles begin to evolve from the melt, and this pattern is preserved to at least 2000°C. The crystal phase, in which SiO_2 is transformed under cooling to 1200–1000°C (depending on the pressure), can have various modifications, e.g., quartz, tridymite, and cristobalite.

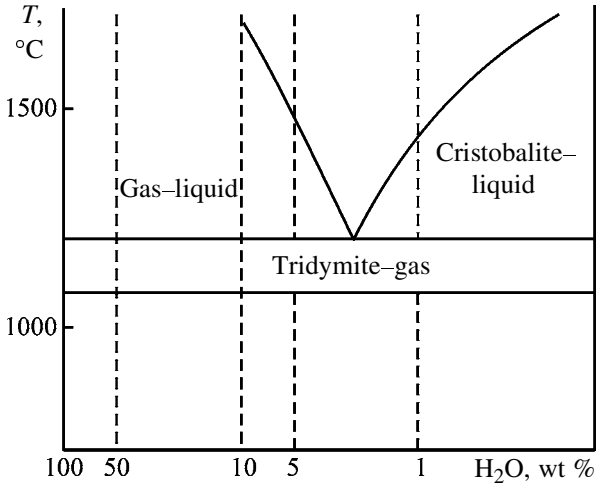

Fig. 4. Phase diagram of the water–SiO_2 melt system [18] at a pressure of 1 atm.

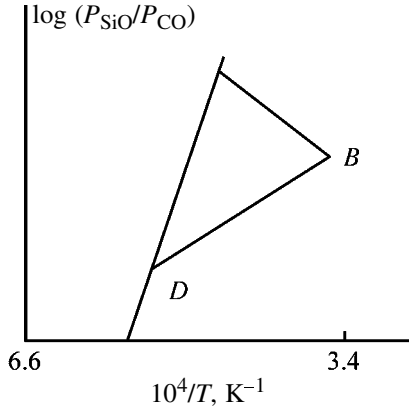

Fig. 5. A characteristic shape of equilibrium phase diagrams of the Si–C–O system [19]. (T) Temperature.

At pressures above 2 atm, the melt solidifies only as quartz; however, the pressure does not markedly affect the behavior at high temperatures.

The range of the conditions corresponding to specifically SiO_2 and C as condensed phases was identified in [19]. The schematic phase diagrams of the Si–O–C system are plotted in the $\log(P_{SiO}/P_{CO})$ vs. T coordinates, where the oxides SiO and CO are the components that are constantly present in the gas phase. A characteristic diagram is shown in Fig. 5; this pattern depends on the total pressure. To the left from the point D, the condensed phases are really SiO_2 and C, and to the right (along the DB line), a carbide phase SiC appears in the system. Taking into account the diagrams presented in [19] for pressures of 0.1, 1.0, and 10 atm, the $\log(P_{SiO}/P_{CO})$ vs. P, atm, and T, K, dependence to the left from the point D can be represented as

$$\log(P_{SiO}/P_{CO}) = -3.08 \times 10^4 T^{-1} + 14.864 - 1.702 \log P, \quad (1)$$

and the temperature at the point D, as

$$T = \frac{10^4}{5.4 - 0.621 \log P}. \quad (2)$$

Since no carbide traces were revealed in shungites, the evolution of the melt actually proceeds to the left from point D. Equation (1) suggests that the temperature corresponding to the onset of an appreciable decrease in the solubility of carbon is no less than 1700 K. Below this temperature, the gas phase should become virtually purely carbonic, and this could be due to faster evaporation of carbon compared to silicon (in the form of SiO), which is accompanied by the escape of "excess" carbon from the melt. In fact, relationship (1) suggests a gas phase, not limited by the total volume of the bubbles, and the absence of water. The steam occurring inside the bubble hinders the escape of carbon, and it should be condensed in a solid phase.

Thus, water plays a dual role. The steam pressure favors precipitation of the solid phase of carbon. At the same time, water as a component of a fluid–silicate melt causes the solidification temperature to decrease [15]. For example, it is known that, in the absence of volatile components, fluids, the solidification temperature of aluminosilicate slags is near 1500°C. At a significant content of water, the solidification temperature decreases to 1100–1200°C, and the condition $T_{boil} > T_{separ} > T_{solid}$ can be well satisfied.

Unfortunately, it is a difficult task to compare with a fairly high accuracy the activation energies of reduction of silicon dioxide with carbon and of precipitation of the fulleroid island. In the latter case, the free energy of the island–bubble–melt system can be estimated as [17]:

$$\Delta G_g = m(\beta + 6\Delta E_{SiO_2\text{–}C}) - g(wT + A), \quad (3)$$

where m and $g = 6m(m + 2)$ are the numbers of the rings of pentagonal cells (pentagons) and hexagonal cells (hexagons) (if the shape of the island boundary is taken close to a circumference and its size, equal to the number of the rings of the polygons around the central hexagon) and of atoms in the island, respectively; the term βm takes into account the spheroidal segments of the CNT surface and distortion of the bond angles when the island is bent to the nanodrop surface; $\beta = \alpha_{NT}\pi\Psi/3$, $\alpha_{NT} \approx 1$ eV, is the distortion energy per hexagon row in the tubular part of the nanotube; and, Ψ, ratio of the width of the ring of the hexagons to the length of the C–C bond, $a \approx 1.5$ Å.

At $\Omega = \beta - 12(wT + A) + 6\Delta E_{SiO_2-C} < 0$, the ΔG_g function monotonically decreases at any size of the island. Clearly, this does not suggest barrier-free formation of the islands. Equations of type (3) correspond to a smoothened curve ΔG_g, when the local maxima associated with the onset of filling of the next ring of the hexagons are neglected (Fig. 6). Since the growth of a projection begins with the cleavage of the radical–metal bond having the energy E_{SiO_2-C} (the run of the ΔG_g curve is shown qualitatively in Fig. 6), such local maxima can be taken into account by adding the term γE_{SiO_2-C} to the expression for the global maximum $(\Delta G_g)_{max}$ of the ΔG_g curve ($0 < \gamma < 1$ is a free parameter). At $\Omega < 0$, this maximum is of the order of

$$(\Delta G_g)_{max} = \gamma E_{M-C}. \quad (4)$$

Clearly, at $\Omega < 0$, the nucleation of the smallest island (e.g., one of the hexagons) should be analyzed; in this case, expression (3) is inapplicable. As to the activation barrier in nucleation of such an island, we will only mention that it is of the order of γE_{SiO_2-C}. It hardly exceeds considerably the activation energy of a reaction such as $SiO_2 + C_{(sol)} = SiO + CO$.

Consideration of the mechanism of nucleation of fulleroid islands on the internal surface of a nanobubble should take into account the fact that the island can effectively expand over the surface in the absence of catalytic atoms as well. Then the situation with the CNT nucleation is partly similar to the growth of the CNT of the cathodic deposit, observed in arc synthesis of fullerenes [20]. Fullerene molecules can serve as a CNT nucleus. These molecules can be partially broken down when deposited onto the lateral surface of the cathode (with a temperature close to 1300 K). The preserved part of the fullerene can easily become a CNT nucleus, since there is no need in detachment of its central part from the cathode surface, associated with overcoming at least van der Waals forces. A close mechanism, even not connected with fullerenes, can also be realized in uncatalyzed electrochemical growth of CNTs [21].

An insignificant influence of the metal catalyst on formation of FPs in shungite is suggested by the absence of the catalyst macroparticles in the electron micrographs. The role of the metal as a catalyst of the CNT growth at the atomic level was analyzed so far only hypothetically [22–24] and was not confirmed experimentally. Therefore, it is extremely difficult to suggest a true form of the metal capable of catalyzing formation of the FPs.

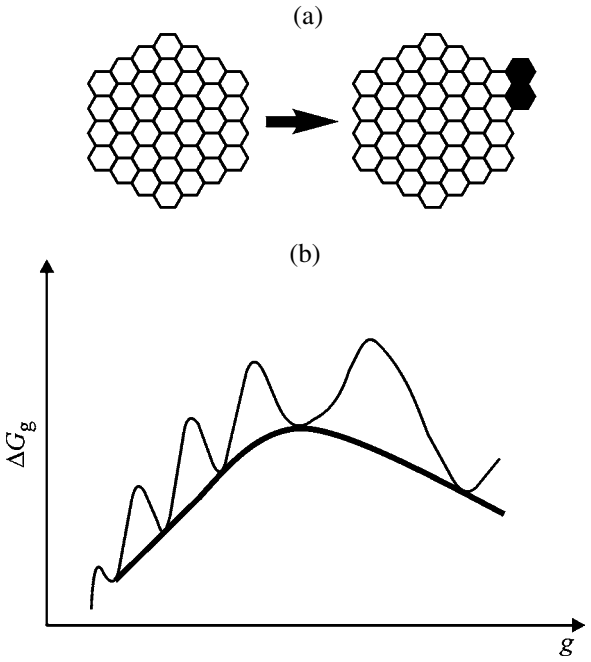

Fig. 6. (a) Initial stage of formation of the next ring of hexagons in the island and (b) oscillating pattern of the true curve of the Gibbs energy ΔG_g as a function of the number of atoms in the island g.

Another prerequisite to precipitation of the solid carbon phase as an island is the presence of atomic carbon in the melt. At $\Delta \log f_{O_2}$ from approximately –2 to –3 (f is the fugacity), carbon is dissolved specifically in the atomic form, although the melt contains only insignificant amounts of both carbonate ions and "silicide" carbon linked by the Si bonds, Si–C [25]. Under identical conditions, the inevitably occurring hydrogen also exists mainly as water. At $\Delta \log f_{O_2}$ from approximately –4 to –6, the situation changes radically (the dissolved carbon forms in the melt a C–H bond, typical for alkanes, e.g., CH_4). The model discussed is applicable specifically to the former case.

Thus, the model of nucleation of the fulleroid island on the internal surface of the bubble seems to be consistent. The following relationships in nucleation and growth of such an island can be assumed.

(1) The arising fulleroid surfaces can have diverse shapes. The reason is that, under expansion of the island, the total surface energy is determined by at least two factors: the surface energy of the bubble and the stress of bending of the island to the melt surface. The latter factor arises because the bending area is represented mainly by hexagonal cells with strongly distorted bond angles. The number of pentagonal cells, capable of lowering the stress, can be only such that, upon subsequent incorporation of the pen-

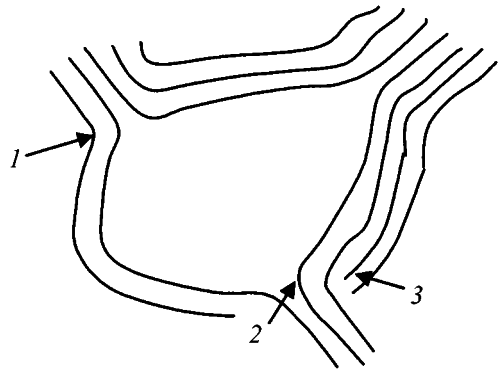

Fig. 7. Topological breaks of the fulleroid surface being formed and nucleation of the stack structures.

tagon into the surface, the total curvature corresponds to that of the melt surface. The tendency of the island to minimize the stress of bending to the melt surface can be responsible for gradual deformation of the bubble into an irregular dumbbell or, further, into a nanotube, nanocone, or flattened nanoparticle. In the general case, a functional of the type

$$\oint dS' \sigma = (\alpha_{NT}/6a)2\pi R_{contour}$$

should be minimized. Here, the integral is taken over the surface free from the island; $R_{contour}$ is the radius of the line of bending of the island to the melt surface (Fig. 2c), and σ, surface tension on the melt–steam interface. The integral is of the order of $\pi\sigma R^2$, and the second term, of $2\pi(\alpha_{NT}/6a)R$. Thus, at $R \leq \alpha_{NT}/3a\sigma$, the total surface energy is weakly sensitive to the shape of the bubble, and the morphology of the FPs is determined by the condition of the minimal stress of bending of the island. At $\sigma \sim 200$ erg cm^{-2}, this yields $R \sim 5$ nm, which is somewhat less than the nanoparticle size. However, it is clear that this condition implies a series of possible morphologies of the island–melt boundary system, slightly differing in the energy and entropy, which, moreover, tend both to the spherical and edged shapes. Indeed, as mentioned above, it is convenient to represent the expansion of the island along the surface of the boundary with the melt as an increase in the number of the rings of the polygons (mainly, hexagons), formed in sequence around the initial nucleation area, rather than in the number of polygons. If the frequency of the occurrence of pentagonal distortions in the external rings corresponds to the curvature of the nanobubble, the shape of the first fullerene surface should approximately correspond to that of the fullerene with the characteristic size identical to that of this nanobubble. Such a fullerene should be very large: The number of atoms in the fullerene is related to its diameter D_{ful} approximately as $N \sim 20 + 2(\pi/6 \times 3^{1/2})(D_{ful}/a)^2$; hence, at the bubble diameter close to 15 nm, $N \sim 40\,000$. It is known that, with growing size, the fullerene tends from the spherical to the edged shape. Therefore, even under assumption of the perfect fulleroid surface in shungite, its shape should be edged, rather than spherical.

(2) In fact, the fulleroid surface of shungite is imperfect and has topological breaks [7, 8]. The model considered here treats this as due to the fact that, in the problem of the cavity, geometrically "inverted" with respect to the problem of the nanodrop, local precipitation of carbon at some point of the cavity does not decrease the supersaturation with carbon on the opposite side of the cavity. Some islands can start to grow simultaneously, and, strictly speaking, their contact with one another does not necessarily involve cross-linking, especially at low temperatures.

(3) The fullerene particles growing around the bubbles should have a multilayer structure. The subsequent layers are formed from the side of the areas more distant from the nanobubble. Clearly, graphitization initiated by a small amount of local sources (bubbles) results in formation of ever more defective fulleroid layers. With increasing distance from the initial globule, the fulleroid layers change their structure ever more profoundly and resemble a "stack." The model considered here attributes this to the fact that simultaneous and independent growth of several islands results in formation of fulleroid surfaces sharply turned to one another (e.g., areas *1* and *2* in Fig. 7). For each subsequent layer growing on such a break, the breakage of the plane can be thermodynamically as favorable as its bending (Fig. 7, area *3*). Formation of one break of this kind apparently suggests the growth of subsequent layers, whereby a stack structure is formed.

The assumption that the stacks begin to dominate over the fulleroid layers with increasing distance from the globule can be verified by the results of experiments on vibrocavitational treatment of shungite [3], when chemically treated shungite is placed into a field of a standing sound wave of a very small power (ca. 60 W per bath volume of ca. 0.5 l) in water. The field was created by plates oscillating with a sound frequency in antiphase with one another. The total treatment time was 2.5 h. The resulting suspension was left to stand, whereupon both fractions were analyzed, namely, that deposited to the bottom of the vessel with the suspension and the floating, emerged onto

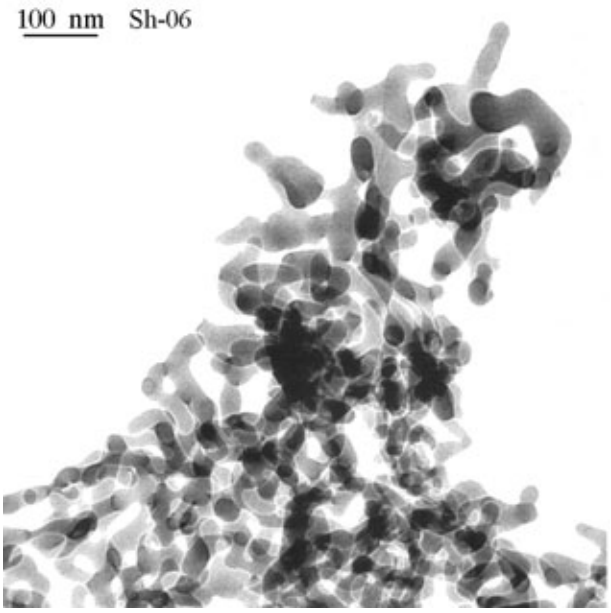

Fig. 8. TEM images of the material yielded by vibrocavitational treatment of the chemically pretreated shungite-III.

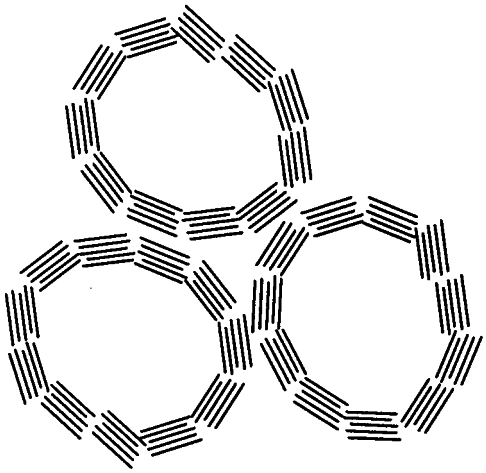

Fig. 9. Aggregation of the stack structures destroyed by vibrocavitational treatment into a new nanoporous structure.

the surface. Vibrocavitational treatment yields two types of macroparticles: with the same morphology as the initial material and a specific nanoporous carbon with numerous globules, absolutely different from the initial material. Figure 8 shows typical electron micrographs of such nanoporous carbon having one of the two slightly different morphologies. The structure consists of numerous nanopores 5–20 nm in size and short appendices 30–100 nm in size.

Such structures can be formed by the following mechanism. In the course of vibrocavitational treatment, a part of the graphitized stacks not fixed by the aluminosilicate matrix (the result of chemical etching of aluminosilicates) is "thrown out" into a water dispersion. Such stack behaves as a specific "quadrupole" towards another analogous stack: During coagulation, the energy of interaction, associated with the torn-off edges of the graphite stacks, tends to decrease, if the stacks are arranged in the edge-to-edge fashion (Fig. 9). The newly formed structure tends to reduce the surface energy, thereby yielding a globule.

CONCLUSIONS

(1) Formation of fulleroid particles in shungites can be interpreted in terms of a model absolutely analogous to that interpreting the formation of fulleroid structures on the surface of the nanoparticles of a metal catalyst, supersaturated with carbon.

(2) In terms of the model, the fulleroid particles arise from precipitation of carbon from the aluminosilicate melt, supersaturated with carbon during cooling.

(3) The natural surface of precipitation of the islands of the fulleroid surface is the internal surface of the bubbles of steam evolving from the same melt at a higher temperature (1500–1800°C).

(4) The natural structural motif arising from precipitation of carbon from the melt is represented by graphitized stacks with torn-off graphene layers. These stacks can release during chemical degradation of the aluminosilicate matrix and the subsequent vibrocavitational treatment with water.

(5) A water dispersion of such graphitized stacks is an effective medium for nucleation of a nanoporous carbon material.

ACKNOWLEDGMENTS

This study was financially supported by the International Science and Technology Centre (project no. 2769) and the "Research and Development on the Priority Lines of Development of Science and Technology in 2002–2006" Federal Target Scientific and Technical Program (State Contract no. 02.467.11. 7005, May 23, 2005).

REFERENCES

1. Rozhkova N.N., *Perspectives of Fullerene Technology*, Osawa, E., Ed., Kluwer Academic, 2002, pp. 231–237.
2. Grigorieva, I.N. and Rozhkova, N.N., *Russ. J. Appl. Chem.*, 2000, vol. 73, no. 4, pp. 600–606.

3. Alekseev, N.I., Bodyagin, B.O., Kudenko, V.V., et al., *Zh. Prikl. Khim*., 2006, vol. 79, no. 9, pp. 1439–1443.
4. Hettich, R.L. and Buseck, P.R., *Carbon*, 1996, vol. 34, no. 5, pp. 685–687.
5. Rozhkova, N.N., Program and Abstracts, *Carbon-2002 Int. Conf*., Beijing (China), September 15–19, 2002, report no. 81 (CD).
6. Zaidenberg, A.Z., Rozhkova, N.N., and Kovalevsky, V.V., *Mol. Mater*., 1996, vol. 8, pp. 107–110.
7. Kovalevskii, V.V., *Neorg. Mater*., 1994, vol. 39, pp. 28–32.
8. Sokolov, V.A., Kalinin, Yu.K., and Dyukkiev, E.F., *Shungity – novoe uglerodnoe syr'e* (Shungites: A New Carbonic Raw Material), Petrozavodsk: Karel. Filial Akad. Nauk SSSR, 1984.
9. Mikhailov, V.P., *Uglerodsoderzhashchie formatsii v geologicheskoi istorii* (Carbon-Containing Formations in the Geological History), Petrozavodsk: Karel. Filial Akad. Nauk SSSR, 1998.
10. Charykov, N.A., Alekseev, N.I., Arapov, O.V., et al., *Zh. Prikl. Khim*., 2005, vol. 78, no. 6, pp. 865–870.
11. Virgil'ev, Yu.S. and Kurolenkin, E.I., in *Sb. Nauchn. Tr. Nauchno-Issled. Inst. Grafita* (Coll. of Scientific Works of Research Inst. of Graphite), Moscow, 1991, pp. 60–66.
12. Fedorov, V.B., Shorshorov, M.Kh., and Khakimova, D.K., *Uglerod i ego vzaimodeistvie s metallami* (Carbon and Its Interaction with Metals), Moscow: Metallurgiya, 1978.
13. Berezkin, I.I., *Geokhimiya*, 2003, no. 3. pp. 253–260.
14. Hulicova, D., Sato, F., Okabe, K., et al., *Carbon*, 2001, vol. 39, no. 9, pp. 1438–1442.
15. Koronovskii, N.V. and Yakushova, A.F., *Osnovy geologii* (Fundamentals of Geology), Moscow: Mosk. Gos. Univ., 2004.
16. Butenko, Yu.V, Kuznetsov, V.L., and Usol'tseva, A.L., *Kinet. Katal*., 2003, vol. 44, no. 5, pp. 791–800.
17. Alekseev, N.I., *Zh. Tekh. Fiz*., 2004, vol. 74, no. 9, pp. 63–71.
18. Toropov, I.A., Borzakovskii, V.P., and Lapin, V.V., *Diagrammy sostoyaniya silikatnykh sistem: Spravochnik* (Phase Diagrams of Silicate Systems: Reference Book), vol. 3: *Troinye sistemy* (Ternary Systems), Leningrad: Nauka, 1972.
19. Ryabchikov, I.V., *Izv. Akad. Nauk SSSR, Met*., 1966, no. 2, pp. 14–19.
20. Harris, P.J.E., Tsang, S.C., Claridge, J.B., and Green, M.L., *J. Chem. Soc., Faraday Trans*., 1994, vol. 90, pp. 2799–2803.
21. Alekseev, N.I., Polovtsev, S.V., and Charykov, N.A., *Zh. Tekh. Fiz*., 2006, vol. 76, no. 3, pp. 57–63.
22. Kiang, C.H. and Goddard, W., *Phys. Rev. Lett*., 1996, vol. 76, no. 14, pp. 2515–2520.
23. Lee, Y.H., Kim, S.G., and Tomanek, D., *Phys. Rev. Lett*., 1997, vol. 78, pp. 536–541.
24. Alekseev, N.I. and Dyuzhev, G.A., *Zh. Tekh. Fiz*., vol. 75, no. 11, pp. 112–119.
25. Kadik, A.A., Litvin, Yu.A., Koltashev, V.V, et al., *Geokhimiya*, 2006, no. 1, pp. 38–53.

ISSN 1070-4272, Russian Journal of Applied Chemistry, 2007, Vol. 80, No. 1, pp. 147–151. © Pleiades Publishing, Ltd., 2007.
Original Russian Text © S.M. Kuz'min, V.V. Kuznetsov, A.M. Kolker, 2007, published in Zhurnal Prikladnoi Khimii, 2007, Vol. 80, No. 1, pp. 148–151.

MACROMOLECULAR CHEMISTRY AND POLYMERIC MATERIALS

Formation of the Diamond-Like Phase in Electric-Arc Synthesis of Fullerenes

S. M. Kuz'min, V. V. Kuznetsov, and A. M. Kolker

Institute of Chemistry of Solutions, Russian Academy of Sciences, Ivanovo, Russia

Received April 26, 2006

Abstract—Formation of transparent crystallites embedded in the deposited substrate obtained in a reactor for arc synthesis of fullerenes was studied. An X-ray diffraction analysis of the substrate was made.

DOI: 10.1134/S1070427207010284

The interest in mono- and polycrystalline diamond-like materials is due to their unique properties. The materials are synthesized both by chemical vapor deposition onto a hot (800–1200 K) support and by structural transformation of carbon under conditions of high temperature and pressure. Fullerene molecules can be used as a starting carbon material in both the first and second approaches to synthesis of diamond-like structures [1, 2].

The aim of our study was to examine processes in which various kinds of carbon are formed in arc sputtering of a graphite rod and to find the conditions necessary for a diamond-like structure to be produced.

EXPERIMENTAL

An uncooled metallic support *1* was mounted in a reactor for electric-arc synthesis of fullerenes (Fig. 1) at a distance of 1–10 cm from the arc. We used as electrodes rectangular graphite rods of length 10 cm and 2×4 to 4×6 mm in cross section. The electrodes were annealed by passing dc current of 50–70 A through short-circuited electrodes for 8–10 h at a residual pressure in the reactor on the order of 10^{-2} Pa or in a helium atmosphere. The working pressure of 2×10^4 Pa provides the maximum yield of fullerenes for the given reactor. In the curse of sputtering, the arc current was 100–150 A at a voltage across the discharge gap equal to 20–25 V. The completion of the sputtering process was judged by visual inspection.

The substrate deposited on the support was examined by X-ray diffraction analysis and microphotography. The X-ray diffraction analysis was made on a DRON-UM1 X-ray diffractometer (MoK_α radiation monochromated with a Zr filter) modified for work with substances in condensed and polycrystalline states, with the possibility of obtaining X-ray diffraction patterns at diffraction angles θ of 1°–50° by the Debye–Scherrer scheme.

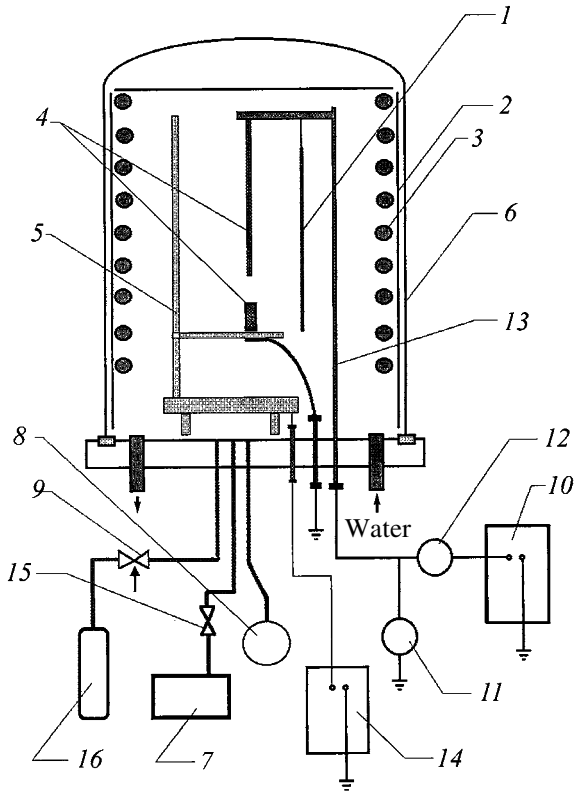

Fig. 1. Schematic of the experimental setup: (*1*) support, (*2*) reflector, (*3*) cooling circuit, (*4*) graphite rods, (*5*) microlift, (*6*) vacuum bell, (*7*) vacuum pump unit, (*8*) vacuum gage, (*9*) leak, (*10*) discharge power supply, (*11*) voltmeter, (*12*) ammeter, (*13*) current-lead rod, (*14*) microlift power supply, (*15*) vacuum cock, and (*16*) cylinder with helium.

Table 1. Effect of the support material and of the distance from the graphite evaporation zone to the support on the possibility of crystallite formation

Support material	Arc-to-support distance, cm	Crystallites in the substrate
Copper	1	None
	3	None
	10	None
Aluminum (foil)	1	None*
	5	Present
	10	None
Zinc-plated iron	1	None**
	3	Present
	10	None

* The support melted.
** No substrate formed.

Data in Table 1 suggest that the formation of crystallites (Fig. 2) is governed both by the support material and by the distance from the graphite evaporation zone to the support. The possible critical parameters of the process are the following: (a) composition of the carbon vapor near the support, (b) support temperature, (c) existence of zones of a melted metal on the support surface, and (d) chemical nature of the interaction between carbon and the support material.

The composition of the carbon vapor formed near the support is governed by the following factors. Graphite evaporated by the arc method forms a flow of a carbon vapor in which carbon clusters condense. The vapor composition is determined by the following processes [3]: first stage, $C_i + C_j \rightarrow C_k$, where *i, j* are integers in the range from 2 to *k*/2; second stage, $C_{k1} + C_{k2} \rightarrow C_{60}$.

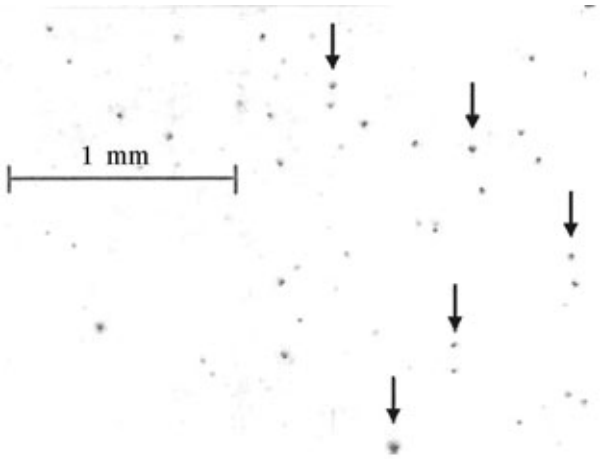

Fig. 2. Micrograph (negative) of a typical substrate obtained after the synthesis is complete. Arrows point to crystallites.

The reverse process, disintegration of vibrationally excited clusters, is suppressed via collision transfer of excitation to inert gas atoms.

Afanas'ev et al. [4] estimated the size of the zone in which C_{60} is formed at approximately 2.5 cm, and the time in which clusters are formed, at ~2.5×10^{-4} s at a vapor flow velocity of about 10^4 cm s^{-1}. In accordance with this estimate, the distances from the graphite evaporation zone to the support were chosen in such a way that the compositions of the carbon vapor near the support were strongly different. In particular, the vapor was represented by species with markedly different properties: small carbon fragments (1 cm from the evaporation zone), "hot" fullerene and nonfullerene clusters (3 cm from the evaporation zone), and "cold" clusters (10 cm from the evaporation zone).

In our opinion, the absence of crystallites at a relatively large distance from the support indicates that they are formed on the support, rather than in the gas phase. This circumstance makes the process under study similar to the CVD technique. Obraztsov et al. [5] noted that various structures were formed, depending on the gas composition and support temperature, and reported the ranges of support temperatures (800–1000°C) and hydrocarbon concentrations (≤5%) in which diamonds were effectively formed. It may be assumed that, placing a support at a distance of 3 cm from the arc, we should obtain process parameters that are in agreement with [5]. It can be stated, in particular, that the support temperature markedly exceeds the melting point of zinc in the experiment with zinc-plated iron as the support material at distances from the graphite evaporation zone of 1 and 3 cm.

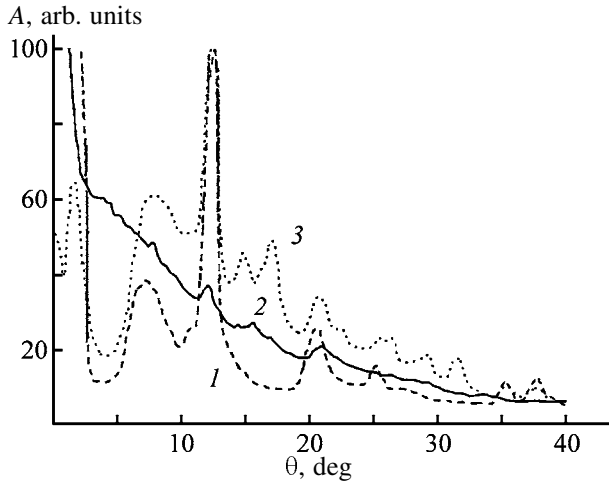

Fig. 3. X-ray diffraction patterns demonstrating that the nature of the carbon material changes in the course of the experiment. (*A*) Intensity and (θ) diffraction angle. (*1*) Starting graphite, (*2*) substrate collected from an uncooled zinc-plated support, and (*3*) annealed substrate.

Table 2. Interplanar spacings and intensities of diffraction lines of carbon materials

Sample	θ, deg	*D*, nm	*A*, rel. units	*hkl*
1 (starting graphite)	12.2	0.336	90	002 graphite
	20.5	0.2027	15	101 graphite
	25.1	0.1674	6	004 graphite
	35.5	0.1223	6	110 graphite
	37.8	0.1158	6	112 graphite
2 (sputtered substrate)	3.3–5.7	0.715–1.233	–	–
	12.2	0.336	5	002 graphite
	20.5	0.2027	4	101 graphite + 111 diamond
3 (annealed substrate)	12.2	0.336	62	002 graphite
	14.9	0.276	9	–
	17	0.243	23	–
	20.5	0.2027	12	101 graphite + 111 diamond
	22.5	0.185	4?	–
	25.3	0.166	4	004 graphite?
	26.5	0.159	6	–
	29.4	0.145	5.5	–
	31.5	0.136	8	–
	35.5	0.1223	3	110 graphite
	37.8	0.1158	3	112 graphite
Graphite (ASTM file 23-65)		0.336	100	002
		0.203	50	101
		0.1678	80	004
		0.1232	30	110
		0.1158	50	112
		0.0994	40	114 + 106
		0.0829	40	116
Diamond (ASTM file 6-0675)		0.206	100	111
		0.1261	27	220
		0.10754	16	311
		0.08182	15	331
Chaoite (ASTM file 22-1069)		0.447	100	110
		0.426	100	111
		0.412	80	103
		0.371	40	201
		0.322	40	104
		0.303	60	203
		0.294	20	210
		0.255	60	310
		0.246	40	213
		0.228	60	205
		0.224	40	220
		0.21	40	304
		0.1985	20	306
		0.191	20	401
		0.1496	20	227
		0.137	20	416 + 228
		0.1289	20	600 + 506
		0.126	20	336
		0.1197	40	337 + 523
		0.1184	40	427

The existence of nucleation centers on the support used is an important factor for formation of diamond crystallites. The corresponding carbide (e.g., SiC formed on a silicon support [6]) most frequently acts as a center of this kind. In the case under study, the chemical properties of the supports are strongly different. For aluminum [7], formation of both a composite material Al/C_{60} and aluminum carbide Al_4C_3

would be expected. Zinc rather easily forms a carbide, ZnC_2. By contrast, copper difficultly reacts with carbon [9–11]. This is presumably one of the reasons why crystallites are not formed on the copper support.

The X-ray diffraction patterns in Fig. 3 characterize changes in the structure of the carbon material in the course of the experiment. The experimentally obtained diffraction patterns are compared with published data in Table 2. It can be readily seen that the starting carbon material (pattern *1*) corresponds to graphite, for which the strongest reflection is that from the (002) plane (interplanar spacing 0.336 nm, θ 12.2°). X-ray diffraction pattern *2* corresponds to the substrate sputtered under the experimental conditions and collected from an uncooled zinc-plated support. Apparently the substrate is composed of a mixture of various kinds of carbon. In agreement with published data [12], pattern *2* contains a broad halo of amorphous carbon, on whose background low-intensity diffraction peaks can be seen. The peak at 12.2° can be attributed to recrystallized graphite present in the substrate. It is noteworthy that the relative intensities of the reflections at 12.2° and 20.5° for dispersed substrate markedly differ from those for the starting graphite. The noticeable increase in the relative intensity of the reflection at 20.5° [interplanar spacings of 0.203 nm for the (101) plane of graphite and 0.206 nm for the (111) plane of diamond] may indicate that a diamond-like phase appears in the substrate obtained. The presence of the fullerene fraction in the substrate has been demonstrated previously by spectroscopy, HPLC, and mass spectrometry [13–16]. Disordered fullerenes present in the substrate appear as a shoulder in X-ray diffraction pattern *2* at 3.3°–5.7° (d = 0.715–1.233 nm) [7, 16]. The fact that peaks appear on annealing the substrate in air at 500°C is due to partial removal (via oxidation and structural rearrangements) of the amorphous carbon fraction. In addition, as can be seen from the X-ray diffraction pattern *3* of the sample, the annealing is accompanied by a decrease in the relative amount of the fullerene fraction in the sample. By contrast, the relative amount of graphitized carbon markedly increases. The graphitization of various kinds of carbon is presumably the most frequent result obtained in annealing of carbon materials [17]. The set of reflections of the annealed substrate partly belongs to various kinds of crystalline carbon (Table 2). Despite the exceedingly wide variety of different forms of carbon, some peaks at 14°–18° and 26°–32° can be attributed to zinc oxide ZnO (hexagonal lattice, a = 0.325 nm, c = 0.52 nm, according to [18, 19] and JCPDS file 36-1451). The formation of this product, which is the known white pigment, changes the color of the annealed sample and indirectly confirms the above considerations concerning the involvement of zinc in the nucleation of crystallites.

An analysis of the X-ray diffraction patterns suggests, with a sufficient certainty, that the crystallites we observed in the sputtered substrate belong to a diamond-like fraction of carbon. This conclusion can be indirectly confirmed by the high refractive index and high hardness of the crystallites obtained. The average size of the crystallites, measured using a set of photographs, is about 0.05 mm. Taking into account the fact that the duration of the arc sputtering of the starting graphite rod is about 10 min, we can estimate the growth rate of the crystallites to be approximately 0.3 mm h^{-1}. Such a crystal growth rate is abnormally high, because the growth rate commonly does not exceed 10 μm h^{-1} for a diamond-like structure [20]. In our case, the higher rate of formation of the diamond-like phase is possibly due to presence of fullerenes in the carbon vapor being deposited onto the support.

CONCLUSIONS

It was shown that conversion of carbon to a diamond-like phase may accompany electric-arc synthesis of fullerenes. The formation of crystallites (average crystallite growth rate 0.3 mm h^{-1}) depends on the support material and on the distance between the support and the graphite evaporation zone. According to qualitative estimates, crystallites with an average size of about 0.05 mm have high hardness and high refractive index.

REFERENCES

1. Erdevir, A., Bindal, C., Fenske, G.R., et al., *Diamond Relat. Mater.*, 1996, vol. 5, pp. 923–931.
2. Homae, T., Wakabayashi, K., Nakamura, K.G., and Kondo, K., *J. Mater. Sci. Lett.*, 2001, vol. 20, pp. 1107–1108.
3. Churilov, G.N., Fedorov, A.S., and Novikov, P.V., *Carbon*, 2003, vol. 41, pp. 173–178.
4. Afanas'ev, D.I., Dyuzhev, G.A., and Kruglikov, A.A., *Zh. Tekh. Fiz.*, 2001, vol. 71, no. 7, pp. 137–139.
5. Obraztsov, A.N., Zolotukhin, A.A., Ustinov, A.O., et al., *Carbon*, 2003, vol. 41, pp. 837–839.
6. Stockel, R., Janischwsky, K., Stammer, M., et al., *Diamond Relat. Mater.*, 1998, vol. 7, pp. 7147–7151.
7. Khalid, F.A., Beffort, O., Klotz, U.E., et al., *Acta Mater.*, 2003, vol. 51, pp. 4575–4582.

8. Shulzhenko, A.A., Ignatyeva, I.Yu., Osipov, A.S., and Smirnova, T.I., *Diamond Relat. Mater.*, 2000, vol. 9, pp. 129–133.
9. Berner, A., Fuks, D., Ellis, D.E., et al., *Appl. Surf. Sci.*, 1999, vol. 144–145, pp. 677–681.
10. Pauleau, Y. and Thiery, F., *Mater. Lett.*, 2002, vol. 56, pp. 1053–1058.
11. Sinnghal, S.K. and Kanda, H., *J. Cryst. Growth*, 1995, vol. 154, pp. 297–302.
12. Ginzburg, B.M., Tuichiev, Sh., Tabarov, S.Kh., et al., *Zh. Tekh. Fiz.*, 2005, vol. 75, no. 11, pp. 65–68.
13. Kuz'min, S.M. and Pelipets, O.V., Abstracts of Papers, *VII Mezhdunarodnaya konferentsiya "Problemy sol'vatatsii i kompleksoobrazovaniya v rastvorakh"* (VII Int. Conf. "Problems of Solvation and Complexation in Solutions"), Ivanovo, October 8–11, 2001, p. 184.
14. Kuz'min, S.M., Kozlov, A.V., and Leonov, A.A., Abstracts of Papers, *VII Mezhdunarodnaya konferentsiya "Problemy sol'vatatsii i kompleksoobrazovaniya v rastvorakh"* (VII Int. Conf. "Problems of Solvation and Complexation in Solutions"), Ivanovo, October 8–11, 2001, p. 185.
15. Kuz'min, S.M., Borovkov, M.Yu., Kolker, A.M., and Brazhyunas, V.L., *Zh. Prikl. Khim.*, 2005, vol. 78, no. 4, pp. 566–571.
16. Nikitina, E.A., http://plasma.karelia.ru, Petrozavodsk: NOTs Plazma, 2003.
17. Tomita, S., Burian, A., Dore, J.C., et al., *Carbon*, 2002, vol. 40, pp. 1469–1474.
18. Ormont, B.F., *Struktury neorganicheskikh veshchestv* (Structure of Inorganic Substances), Moscow: GITTL, 1950.
19. Xu, C., Xu, G., Liu, Y., and Wang, G., *Solid State Commun.*, 2002, vol. 122, pp. 175–179.
20. Samokhvalov, N.V., Opalev, O.A., Volkov, Yu.Ya., et al., *Diamond Relat. Mater.*, 1998, vol. 7, pp. 1433–1436.

ISSN 1070-4272, Russian Journal of Applied Chemistry, 2007, Vol. 80, No. 1, pp. 152–154. © Pleiades Publishing, Ltd., 2006.
Original Russian Text © V.G. Maiorov, A.I. Nikolaev, B.Ya. Zilberman, 2007, published in Zhurnal Prikladnoi Khimii, 2007, Vol. 80, No. 1, pp. 152–154.

BRIEF COMMUNICATIONS

Preparation of Thorium Concentrate from Concentrated Calcium Chloride Solutions

V. G. Maiorov, A. I. Nikolaev, and B. Ya. Zilberman

Tananaev Institute of Chemistry and Technology of Rare Elements and Mineral Raw Materials, Kola Scientific Center, Russian Academy of Sciences, Apatity, Murmansk oblast, Russia
Khlopin Radium Institute, St. Petersburg, Russia

Received May 29, 2006

Abstract—Extraction, washing, back extraction, and precipitation of Th(IV) from the backwash in the hydrochloric acid processing of perovskite are studied. Process conditions are optimized to obtain a concentrate with a ThO_2 content of about 85 wt %.

DOI: 10.1134/S1070427207010296

Integrated hydrochloric acid technologies for processing rare-metal raw materials are being developed at the Institute of Chemistry, Kola Scientific Center, Russian Academy of Sciences [1–5]. The presence of Th(IV), U(VI), and Ra(II) in rare-earth metal titanoniobates (loparite, perovskite) makes it necessary to treat the chloride process solutions to remove these radionuclides. In processing perovskite containing up to 40 wt % CaO, this task is complicated by the fact that high concentration of $CaCl_2$ present in the process solutions strongly influences both recovery of target components and treatment of waste solutions. At the same time, there is steadily growing interest in the use of Th(IV) as a fuel component for the future nuclear power engineering [6]. Kosynkin et al. [6] recommended to recover Th(IV) as a coproduct, the more so as the treatment to remove radionuclides is a necessary element of any technology for processing radionuclide-containing raw materials.

This paper concerns preparation of Th(IV) concentrate from perovskite containing 0.07–0.14 wt % ThO_2. After hydrochloric acid breakdown of perovskite (see [4] for its composition), hydrolytic precipitation of Ti(IV), Nb(V), and Ta(V), and concentration by evaporation, the composition of the resulting process solution was as follows (g l^{-1}): HCl 70–90, $CaCl_2$ 430–470, ThO_2 0.54–1.38, Ln_2O_3 25–30 (here and hereinafter Ln_2O_3 refers to the sum of REE oxides), Fe_2O_3 27–32 [Fe(II) + Fe(III) recalculated to Fe_2O_3], TiO_2 1–5, ZnO 0.5–1.5, Al_2O_3 2–6, and V_2O_5 0.1–0.4. Previously we have optimized the conditions for removal of Fe(III) by extraction with octanol; we also tested various extractants for Th(IV), and the best results were obtained with tributyl phosphate (TBP) [4, 7].

Table 1 summarizes data on TBP extraction of Th(IV) from solutions of the above-specified composition. From the starting solution (100–300 ml), Fe(III) was first extracted with octanol at $V_o : V_w$ = 1 : 1, and then Th(IV) was extracted in single stage with TBP (pure grade) at $V_o : V_w$ = 1 : 1. The degree of Th(IV) recovery in this stage was 92–94%. The extract was washed with water, and Th(IV) was backwashed from the organic phase with water or 10 g l^{-1} HCl. The backwash was neutralized to the desired pH with aqueous NaOH. Further details of the experimental procedure, including analytical control, were reported elsewhere [4].

In the experiments we varied the factors controlling separation of Th(IV) from Ln(III) and other associated components (Table 1). In run no. 4 we obtained a concentrate with a ThO_2 content of about 60 wt %. In run no. 3, the Th(IV) recovery in the extraction, washing, back extraction, and precipitation steps was 93.2, 95.0, 93.2, and 75.5%, respectively; the total degree of recovery from the starting solution to the concentrate was 62.3%.

However, our attempts to increase the ThO_2 content of the concentrate above 60 wt % failed, which was caused by the instability of the parameters characterizing both the recovery of Th(IV) and the composition of the concentrate. The reason was the high $CaCl_2$ concentration in the starting solutions. In fact, the back extraction and washing were carried out not

Table 1. Effect of process conditions on characteristics of Th concentrate

Run no.	$V_o : V_w$ in washing	Content of aqueos phase after washing, g l^{-1}		Degree of removal with washings, %		$V_o : V_w$ in back extraction	pH of precipitation	Content of concentrate, wt %	
		ThO_2	Ln_2O_3	Th(IV)	Ln(III)			ThO_2	Ln_2O_3
1	50 : 1	0.022	22	<1	25	1 : 0.2	~6.5	2.7	72.1
2	15 : 1	0.056	23	1.1	–	1 : 3	6.2	11.2	45.4
3	10 : 1	0.25	19	~5	~70	1 : 3	6.9	19.6	18.7
4	10 : 1	–	–	–	–	1 : 1.5	5.9	60.0	23.1

with water, but with aqueous $CaCl_2$, which was caused by Ca(II) transfer from the extract to the corresponding aqueous phases. For example, the $CaCl_2$ concentration in the aqueous phase after washing was 311–362 g l^{-1} and higher. At the same time, changing $CaCl_2$ concentration in the system strongly influences the component distribution between the phases. It should be pointed out that this effect becomes clearly pronounced only above a sufficiently high $CaCl_2$ concentration, which is accompanied by abrupt increase in the component recovery. Above this critical concentration, even slight change in the $CaCl_2$ concentration strongly affects the extraction efficiency, causing the above-mentioned instability in the composition of both intermediate solutions and concentrate.

According to our and published data [8], at a $CaCl_2$ concentration in the starting solution up to 200–250 g l^{-1}, the Ca(II) recovery to TBP is insignificant (<2%). With increasing the $CaCl_2$ concentration to above 500 g l^{-1}, the degree of Ca(II) extraction rapidly increases to 12% and higher. Similar data on the effect of the $CaCl_2$ concentration were obtained also for other components of the investigated system. We demonstrated that the Th(IV) recovery is insignificant at $[CaCl_2]$ < 300 g l^{-1}. With increasing $[CaCl_2]$, the degree of Th(IV) extraction rapidly increases to 80% and higher at $[CaCl_2]$ = 450 g l^{-1}. According to [8], at $[CaCl_2] \le 220–330$ g l^{-1}, the Mn(II) and Co(II) distribution coefficients are low, but they rapidly increase to 20 and 140, respectively, with increasing $[CaCl_2]$ to 540–610 g l^{-1}. It is clearly seen from all the above data that the minimal concentration at which $CaCl_2$ starts to strongly influence the recovery of components is 200–300 g l^{-1}. Since in washing and back extraction Ca(II) readily passes into the aqueous phase, in these stages (particularly in washing) also the Ca(II) concentration has a considerable effect on the extraction behavior of the components. In this respect, it would be interesting to study in more detail the reasons for such an abrupt change in the nature of the effect of $CaCl_2$ concentration on the extraction properties of the system, particularly, in comparison with chlorides of metals in an oxidation state other than +2.

During this study, we also observed a significant effect of $[CaCl_2]$ on pH values of Th(IV) and Ln(III) precipitation. For example, with increasing $[CaCl_2]$ from 35 to 442 g l^{-1}, pH of the onset of precipitation of Th(IV) and Ln(III) decreased from 3.9 and 6.1 to 2 and 5, respectively.

We performed additional experiments with the aim to increase the Th(IV) content of the concentrate. Table 2 shows that, with a decrease in $V_o : V_w$ by half, the recovery of major foreign elements, Ln(III) and Ca(II), becomes several times lower.

In this case, the extraction of Th(IV) also decreased to 78%. However, this extraction efficiency is sufficient to practically completely remove Th to the organic phase using a 4–5-step cascade operating in the continuous countercurrent mode. The low degree of Ln(III) and Ca(II) extraction allows elimination of the washing stage, i.e., the operation responsible for deterioration of the stability of the process parameters. Using back extraction at $V_o : V_w$ = 1 : 1, followed by neutralization of the backwash to pH ~5, we obtained a concentrate with the following content (wt %) (ac-

Table 2. Effect of $V_o : V_w$ on extraction of Th(IV) and major impurities*

$V_o : V_w$	Degree of recovery, %		
	Th(IV)	Ln(III)	Ca(II)
1 : 1**	92–94	9–13	10–14
0.5 : 1	78	2.6	~5

* See text for the composition of the initial solution.

** Degree of recovery obtained in the experiments described in Table 1.

cording to X-ray spectrum analysis): ThO_2 84.8, CuO 6.2, CaO 0.2, Al_2O_3 3.6, CeO_2 1.1, SiO_2 0.7, TiO_2 0.4, Nb_2O_5 0.6, MnO_2 0.9, and Fe_2O_3 1.4 [presence of Cu(II) originates from an occasional contamination of perovskite with copper–nickel concentrate]. The Th(IV) recovery from the starting solution to the concentrate is about 76%, and that from the backwash to the precipitate, ~97%.

It is easy to increase the Th(IV) content of the concentrate to >95 wt %, e.g., by treating with dilute HCl to remove Cu(II), Ca(II), Al(III), and Fe(III). The quality of the concentrate can be further improved to above 98 wt % of the Th content by introducing the stage of precipitation of Al(III), Ce(IV), Ti(IV), Nb(V), and other elements from the backwash at pH 2–3 prior to precipitation of Th(IV).

Also we tested TBP in dodecane (as analog of kerosene) as an extractant. Introduction of 25 vol % of dodecane into the extractant remarkably improves the phase separation. In this case, the extraction of Th(IV) decreases by only several percents. Octanol and benzene can also be used as diluents, but from the safety measures standpoint, it is preferable to use dodecane.

CONCLUSIONS

(1) To obtain a Th-rich concentrate, the necessary condition in extraction is to decrease $V_o : V_w$ to (0.5–0.6) : 1. In this mode, the coextraction of Ln(III) and Ca(II) strongly decreases, allowing recovery of a product with a ThO_2 content of about 85 wt %.

(2) It is advisable to perform back extraction of Th(IV) from the organic phase at $V_o : V_w = 1 : (1–1.5)$, and its precipitation from the backwash, at pH ~5.

REFERENCES

1. Nikolaev, A.I., *Pererabotka netraditsionnogo titanovogo syr'ya Kol'skogo poluostrova* (Processing of Unconventional Titanium Raw Materials from the Kola Peninsula), Apatity: Kol'skii Nauchn. Tsentr, Ross. Akad. Nauk, 1991.
2. Kalinnikov, V.T., Nikolaev, A.I., and Zakharov, V.I., *Gidrometallurgicheskaya kompleksnaya pererabotka netraditsionnogo titano-redkometal'nogo i alyumosilikatnogo syr'ya* (Integrated Hydrometallurgical Processing of Unconventional Titanium–Rare Earth and Aluminosilicate Raw Materials), Apatity: Kol'skii Nauchn. Tsentr, Ross. Akad. Nauk, 1999.
3. Nikolaev, A.I., Gerasimova, L.G., Maiorov, V.G., et al., Abstracts of Papers, *XVII Mendeleevskii s"ezd po obshchei i priklandoi khimii* (XVII Mendeleev Congr. on General and Applied Chemistry), vol. 3: *Materialy i nanotekhnologii* (Materials and Nanotechnologies), Kazan, 2003, p. 313.
4. Maiorov, V.G., Nikolaev, A.I., Kopkov, V.K., et al., *Zh. Prikl. Khim.*, 2004, vol. 77, no. 5, pp. 715–719.
5. Skiba, G.S., Voskoboinikov, N.B., Solov'ev, A.V., et al., *Zh. Prikl. Khim.*, 2003, vol. 76, no. 10, pp. 1738–1739.
6. Kosynkin, V.V., Kotova, V.M., and Shatalov, V.V., *Khim. Tekhnol.*, 2004, no. 3, pp. 30–35.
7. Maiorov, V.G., Nikolaev, A.I., Kopkov, V.K., and Safonova, L.A., *Tsvetn. Metall.*, 2004, no. 2, pp. 15–20.
8. Jezowska-Trzebiatowska, B. and Kopacz, S., *Radiokhimiya*, 1966, vol. 8, no. 2, pp. 145–153.

ISSN 1070-4272, Russian Journal of Applied Chemistry, 2007, Vol. 80, No. 1, pp. 155–156. © Pleiades Publishing, Ltd., 2006.
Original Russian Text © I.B. Sladkov, N.A. Semenov, 2007, published in Zhurnal Prikladnoi Khimii, 2007, Vol. 80, No. 1, pp. 155–156.

BRIEF COMMUNICATIONS

A Simple Procedure for Evaluation of the Critical Pressure of Molecular Inorganic Compounds

I. B. Sladkov and N. A. Semenov

St. Petersburg State Polytechnic University, St. Petersburg, Russia

Received December 19, 2006

Abstract—A procedure was suggested for evaluation of the critical pressure of molecular inorganic compounds from a single experimental characteristic of a substance, its boiling point.

DOI: 10.1134/S1070427207010302

The critical pressure is a fundamental constant of a substance and is used as the initial parameter for evaluation of many physicochemical characteristics (saturated vapor pressure, heat of vaporization, surface tension of liquid, calculations by the equations of the state of real gases, etc.) [1]. The experimental data on the critical pressure are very limited; therefore, estimation of the critical pressure by calculations becomes an important problem. Here we present a method allowing estimation of the critical pressure from the minimum number of readily available initial data.

From the expression for the critical factor of compressibility

$$z_c = P_c V_c / RT_c$$

it follows that the critical pressure is

$$P_c = z_c RT_c / V_c. \quad (1)$$

When the critical temperature T_c is expressed in K, critical volume V_c is expressed in $cm^3\ mol^{-1}$, and the universal gas constant R is taken equal to 8.314 $J\ mol^{-1}\ K^{-1}$, an evaluation gives the critical pressure P_c expressed in MPa. However, Eq. (1) cannot be used in practice since all the initial parameters are difficult to determine.

For practical use of Eq. (1) it should be considered that the critical factor of compressibility lies in fairly narrow limits: for the majority substances it lies in the limits of 0.25–0.30. The analysis of a large body of experimental data on the critical factor of compressibility (50 substances, whose characteristics are taken from [2]) shows that its average can be taken equal to 0.280. This allows one variable in Eq. (1) to be excluded:

$$P_c = 0.28\,RT_c / V_c. \quad (2)$$

In addition, we can pass from the difficult-to-determine values of critical temperature and volume to the readily available parameters of the boiling point. We can do this using the relations given in [3]:

$$T_c = T_b/(0.667 - 0.055f^{0.5}), \quad (3)$$

$$V_c = V_b(0.05f + 2.69), \quad (4)$$

$$V_b = (-6.2f + 31.2)\prod^{0.54}, \quad (5)$$

where f is the deciding factor of thermodynamic similarity,

$$f = \ln T_b - 1.1 \ln \prod - 4,$$

T_b is the standard boiling point (K), V_b is the molar volume of liquid in the boiling point ($cm^3\ mol^{-1}$), and $\prod$ is the parachor ($J^{1/4}\ cm^{5/2}\ mol^{-1}$).

The parachor $\prod$ is evaluated by the additive method based on stoichiometric formula of the compound [2].

Eqs. (2)–(5) allows evaluation of the critical pressure from the only one experimental characteristic of a substance, its boiling point, instead of difficult-to-determine values of critical temperature and critical volume.

The suggested procedure for evaluation of the critical pressure was checked on the body of data for 50 molecular compounds [2]. Among them are sub-

Error of evaluation of the critical pressure by Eqs. (2)–(4) for some substances

Substance	Calculation	Published data	Discrepancy, %
MoF_6	5.17	4.94	3.8
$SiCl_4$	3.66	3.73	–1.9
$GeBr_4$	4.24	4.20	0.9
BI_3	4.99	5.00	–0.2
$CBrF_3$	3.93	3.97	–1.2
$SiHBr_3$	4.40	4.36	0.9
PBr_3O	5.36	5.39	–0.6
$SeOF_2$	10.89	10.84	0.4
VCl_3O	5.14	5.17	–0.6
OsO_4	8.18	8.61	–4.9

stances of various chemical classes and various polarities: hydrides (B_2H_6, N_2H_4), fluorides (PF_3, MoF_6, PtF_6, UF_6, ReF_6), chlorides (CCl_4, $SiCl_4$, $GeCl_4$, $SnCl_4$, $TiCl_4$, BCl_3, PCl_3, $AsCl_3$, $SbCl_3$, S_2Cl_2, $HgCl_2$, HCl), bromides (BBr_3, $SnBr_4$, $GeBr_4$, PBr_3, $TiBr_4$), iodides (BI_3, SiI_4, SnI_4), mixed halides (CCl_3F, CCl_2F_2, $CClF_3$, CBr_2F_2, $SiBrCl_3$, $SiBr_2Cl_2$, $PFCl_2$, PCl_2F, $PBrF_2$, PBr_2F), hydrohalides ($CHClF_2$, $SiHBr_3$), oxohalides (PCl_3O, PBr_3O, SCl_2O, $SeOF_2$, WCl_4O, VCl_3O, ClO_3F), and oxides (SO_2, OsO_4).

The results of calculations by Eqs. (2)–(5) for various substances are presented in the table. For 50 substances, the average absolute error of evaluation of the critical pressure by the suggested procedure was 2.4% (the maximum error did not exceed 10%). When the evaluation for these substances is performed by Eq. (2) using the experimental values of T_c and V_c, the error is 1.9%.

Thus, substitution of boiling point for critical parameters decreases the accuracy of estimating the critical pressure by only 0.5%. When the experimental values of molar volume of liquid in the boiling point V_b are known, Eq. (5) can be excluded from the calculation scheme; in this case, the accuracy does not decrease at all (1.9%).

It should be borne in mind that, among 50 substances used, there were no associated liquids (NH_3, H_2O), for which the evaluation error significantly increases.

CONCLUSION

A new calculation procedure allowing reliable estimation of the critical pressure from the minimum number of available initial data is suggested.

REFERENCES

1. Reid, R.C., Prausnitz, J.M., and Sherwood, T.K., *The Properties of Gases and Liquids*, New York: McGraw-Hill, 1977.
2. Morachevskii, A.G. and Sladkov, I.B., *Fiziko-khimicheskie svoistva molekulyarnykh neorganicheskikh soedinenii* (Physicochemical Properties of Molecular Inorganic Compounds), St. Petersburg: Khimiya, 1996.
3. Sladkov, I.B., *Zh. Prikl. Khim.*, 2003, vol. 76, no. 12, pp. 1961–1965.

ISSN 1070-4272, Russian Journal of Applied Chemistry, 2007, Vol. 80, No. 1, pp. 157–158. © Pleiades Publishing, Ltd., 2006.
Original Russian Text © V.N. Pavlechko, 2007, published in Zhurnal Prikladnoi Khimii, 2007, Vol. 80, No. 1, pp. 157–158.

BRIEF COMMUNICATIONS

Determination of the Number of Transport Units from Data on Equilibria in Binary Mixtures

V. N. Pavlechko

Belarussian State Technological University, Minsk, Belarus

Received January 18, 2006

Abstract—Relations for analytical determination of the number of transport units are suggested. These relations contain coefficients found from experimental data on equilibria in binary mixtures. Examples for four binary mixtures are considered.

DOI: 10.1134/S1070427207010314

The number of transport units (NTU) is an important characteristic of mass transfer. These numbers can be used as an independent quantity that reflects the driving force of the mass-transfer process, with its kinetics expressed in terms of the height of transport units [1], or as an auxiliary quantity in determining the efficiency of a mass-transfer stage [2].

Expressions used to determine NTU depend on the adopted mass-transfer model and on properties of a mixture being separated. Their applicability is limited to the range in which the parameters being analyzed were studied [3]. Frequently, the known methods for NTU calculation yield strongly different results, poorly consistent with experimental data, for the same mixtures [4], which necessitates development of new models that are valid in a somewhat different range of properties or mode parameters [5].

The numbers of transport units can be analytically determined if the equilibrium line is straight for the range under consideration. This assumption is valid for a limited portion of the equilibrium line or for strongly dilute solutions. Values of NTU can also be determined by numerical methods in the case when expressions for equilibrium curves are known. Occasionally, NTUs are found graphically, because the known equation

$$N = \int_{y_{in}}^{y_{fin}} dy/(y^* - y), \quad (1)$$

(y is the mole fraction of the readily volatile component in the vapor phase) cannot be solved analytically because the integrand is unknown. The minimum labor intensity and acceptable accuracy can be only provided by analytical techniques.

The equilibrium dependence of the content of the readily volatile component in the vapor and liquid phases can be represented as the equation

$$y^* = \frac{Ax + B}{Cx + D}x, \quad (2)$$

where x is the mole fraction of the readily volatile component in the liquid; coefficients A, B, C, and D are found from experimental data.

This enables generalization of the factual material and makes it possible to obtain equilibrium relations for a wide variety of mixtures being separated. In particular, the coefficients of Eq. (2) have been found for some solutions, with the content of the readily volatile component expressed in mole fractions: $A = 0.24$, $B = -2$, $C = 1$, and $D = 0.03$ for water and furfural [6]; $A = 1.35$, $B = -0.1$, $C = 0.58$, and $D = 0.67$ for toluene and benzene [7]; $A = 1$, $B = 1.5$, $C = 1.8$, and $D = 0.7$ for acetic acid and water; and $A = 3$, $B = 8$, $C = 10$, and $D = 1$ for water and methanol. These values of the coefficients provide an acceptable accuracy in the whole range of concentration, with the exception of the water–furfural mixture, for which they are valid in the range from zero to the azeotropic point ($x = 4$ mol %).

Relations (1) and (2) and the working-line equations

$$x = x_{fin} + V/L(y - y_{in}), \quad (3)$$

where L and V are the molar flow rates of the liquid

and vapor, respectively, give Eq. (4) (with V/L denoted for brevity as k, $x_{fin}L/V - y_{in}$, as E, and $x_{fin}V/L - y_{in}$, as E'):

$$N = \int_{y_{in}}^{y_{fin}} dy/(y - y) = C[2(Ak - C)]^{-1} \ln \left| y_2 + [(C - 2Ak^{-1})E' + Dk - B]y(C - Ak)^{-1} - (AkE^2 + BE)(C - 2Ak)^{-1} \right|_{y_{in}}^{y_{fin}}$$
$$+ (Ak - C)^{-1}[C^2E + D(Ck^{-1} - A)/2 + (BC - AD)/2] [(CE + B - Dk)^2 + 4D(C - A)E]^{-1/2} \ln \left| \{2y(C - Ak^{-1}) + (C - 2Ak^{-1})E - B + Dk^{-1} - [(B - Dk^{-1} + CE)^2 + 4D(C - A)E]^{1/2}\} \right.$$
$$\left. \times \{2y(C - Ak^{-1}) + (C - 2Ak^{-1})E - B + Dk^{-1} + [(B - Dk^{-1} + CE)^2 + 4D(C - A)E]^{1/2}\}^{-1} \right|_{y_{in}}^{y_{fin}}. \quad (4)$$

For the stripping part of the column, at low x_{in} and y_{fin}, the term E can be neglected. Then expression (4) can be simplified:

$$N = \int_{y_{in}}^{y_{fin}} dy/(y - y) = (Ak/C - 1)^{-1} \ln \left| y_2 - (B - Dk^{-1}) \times (C - Ak)^{-1} \right|_{y_{in}}^{y_{fin}} + (Bk/D - 1)^{-1} \ln \left| 1 - (B - Dk^{-1}) \times [y(C - Ak)]^{-1} \right|_{y_{in}}^{y_{fin}}. \quad (5)$$

Formula (4) provides high calculation accuracy for both low and high component concentrations. Calculations by the simplified formula (5) provide an acceptable accuracy only for low concentrations, with the calculation accuracy largely determined by the ratio of the flow rates of the liquid and vapor. The upper limit of component concentrations in the vapor and liquid phases at which the simplified expression can be used depends on the ratio of the compositions and molar flow rates of the vapor and liquid. As the difference $(x_{fin}L/V - y_{in})$ approaches zero, the applicability range of dependence (5) becomes wider. At higher component concentrations, this formula leads to gross errors and its application is unfeasible in this case.

CONCLUSIONS

(1) The numbers of transport units can be calculated for binary mixtures by the formula derived at known analytical equilibrium dependences containing four coefficients determined from experimental data.

(2) Use of a simplified formula to determine NTU is justified only at low concentrations of the readily volatile component. The applicability range of the simplified relation depends on the ratios of the compositions and molar flow rates of the vapor and liquid phases.

REFERENCES

1. Kafarov, V.V., *Osnovy massoperedachi* (Fundamentals of Mass Transfer), Moscow: Vysshaya Shkola, 1972, p. 217.
2. Chen Guang, X. and Chung Karl, T., *Ind. Eng. Chem. Res.*, 1993, vol. 32, no. 4, pp. 701–708.
3. Klemona Kimmo, T. and Ilme Jarno, K., *Ind. Eng. Chem. Res.*, 1996, vol. 35, no. 12, pp. 4579–4586.
4. Chen Guang, X. and Chung Karl, T., *Ind. Eng. Chem. Res.*, 1994, vol. 33, no. 4, pp. 907–913.
5. Klemona Kimmo, T., *Acta Polytechn. Scand., Chem. Technol. Ser.*, 1997, no. 250, pp. 1–95.
6. Pavlechko, V.N., *Gidrolizn. Lesokhim. Prom–st.*, 1987, no. 8, pp. 2–3.
7. Pavlechko, V.N., *Inzh.-Fiz. Zh.*, 2003, vol. 76, no. 2, pp. 111–115.

ISSN 1070-4272, Russian Journal of Applied Chemistry, 2007, Vol. 80, No. 1, pp. 159–161. © Pleiades Publishing, Ltd., 2006.
Original Russian Text © K.Yu. Murinov, T.V. Romanko, A.R. Kuramshina, N.N. Kabal'nova, Yu.I. Murinov, 2007, published in Zhurnal Prikladnoi Khimii, 2007, Vol. 80, No. 1, pp. 159–161.

BRIEF COMMUNICATIONS

Oxidative Degradation of Chitosan under the Action of Hydrogen Peroxide

K. Yu. Murinov, T. V. Romanko, A. R. Kuramshina, N. N. Kabal'nova, and Yu. I. Murinov

Institute of Organic Chemistry, Ufa Scientific Center, Russian Academy of Sciences, Ufa, Bashkortostan, Russia

Received May 25, 2006

Abstract—The reaction of chitosan with hydrogen peroxide in homogeneous medium and the influence of iron(II) sulfate, copper(II) chloride, and disodium ethylenediaminetetraacetate on oxidative degradation of chitosan were studied by the rheology method.

DOI: 10.1134/S1070427207010326

Materials based on chitosan (CS) with various molecular weights are widely used in medicine [1, 2]. For production of chitosan oligomers, hydrogen peroxide can be used, [3] and the oxidation is accompanied by visible chemiluminescence [4].

Here we studied the influence of variable-valence metal ions on oxidative degradation of chitosan under the action of hydrogen peroxide by the rheology method.

EXPERIMENTAL

In the experiments we used chitosan of Far-Eastern crab {poly[(1→4)-2-amino-2-deoxy-β-*D*-glucose], RIG Production Association, TU (Technical Specifications) 6-09-05-397–75}. Milled CS (particle size less than 0.6 mm) was treated with 1 N HCl four times for 3 h at room temperature until the supernatant became colorless. The precipitate was filtered off and kept for 1.5 h in 2 N NaOH. Then, the precipitate was washed with distilled water to neutral reaction and ash free CS was dried at room temperature to constant weight. The molecular weight (*MW*) of CS was (1.5–2.0) × 10^5; moisture content, 11%; and degree of deacetylation, 74.5% [5]. Elemental composition (%): C 44.0, H 7.5, N 7.9, O 42.6, and ash traces.

The rheological characteristics of hydrochloric acid solutions of CS were studied in the temperature range 273–333 K at pH 4.5 on a modified Rheotest-2.1 viscometer equipped with a special accessory with a cylinder–cylinder working unit. The thermodynamic characteristics of the solutions were evaluated from the viscosity determined at a shear rate $D = 1200\ s^{-1}$. The experimental error was 3%.

The dependence of the viscosity of CS solutions on the shear rate is shown in Fig. 1. As seen, at [CS] = 5.8×10^{-2} M (recalculated to elementary unit), its aqueous solutions acidified to pH 4.5 behave as non-Newtonian fluids, for which a decrease in the viscosity is observed throughout the studied range of the shear rate. On addition of hydrogen peroxide to a CS solution in the temperature range 273–333 K, the viscosity decreases (Fig. 2), which is caused by oxidative degradation of CS. We did not observe noticeable changes in the IR spectrum of the product in comparison with the initial CS. It is likely that, similarly to published data [6], treatment with hydrogen peroxide induces oxidative degradation with the rupture of glycoside bonds in the CS molecule.

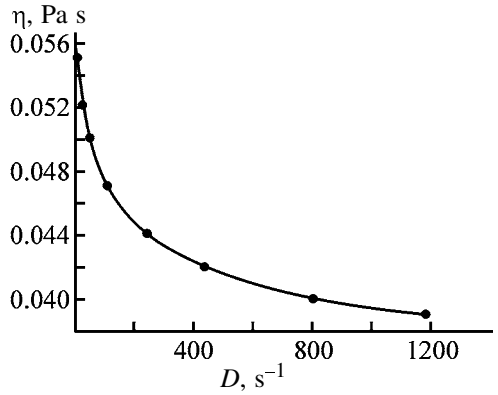

Fig. 1. Viscosity of CS solutions η as a function of shear rate *D*. pH 4.5 and [CS] = 5.8×10^{-2} M.

Activation parameters of viscous flow of chitosan solutions in the presence of iron(II) sulfate, copper(II) chloride, and hydrogen peroxide

Parameter	[CS]	[CS] + [$CuCl_2$]	[CS] + [Fe^{2+}]	[CS] + [H_2O_2]	[CS] + [$CuCl_2$] + [H_2O_2]	[CS] + [Fe^{2+}] + [H_2O_2]
ΔG, kJ mol^{-1} at T, K						
273	–6.4	–7.3	–8.2	–9.4	–10.6	–13.4
283	–7.8	–8.6	–9.5	–10.8	–12.3	–14.8
293	–9.2	–10.0	–10.8	–12.2	–13.9	–16.1
303	–10.6	–11.4	–12.2	–13.6	–15.5	–17.5
313	–12.0	–12.8	–13.5	–15.0	–17.2	–18.8
ΔH, kJ mol^{-1}, 273–313 K	31.9	30.4	28.0	28.5	33.9	23.3
ΔS, J (mol^{-1} K^{-1}), 273–313 K	0.14	0.14	0.13	0.14	0.16	0.13

It is well known that variable-valence metals catalyze decomposition of hydrogen peroxide [7]:

$$Fe^{2+} + H_2O_2 \rightarrow Fe^{3+} + OH^- + OH^\bullet.$$

Therefore, we studied the influence of Fe^{2+} and Cu^{2+} ions on the oxidative degradation of CS under the action of H_2O_2. Addition of variable-valence metal salts into CS solutions causes the viscosity of the solutions to decrease by a factor of 1.5–2 (Fig. 2, curves *2, 3*). The decrease in the viscosity of the CS solutions in the presence of metal salts can be caused by variation of the ionic strength of the chitosan solutions. Upon subsequent addition of hydrogen peroxide into the reaction medium, the viscosity of the solutions decreases significantly, suggesting oxidative degradation (Fig. 2, curves *5, 6*). As seen from the table, variation of the activation parameters of viscous flow of CS solutions is insignificant. However, after oxidative degradation the Gibbs energy of viscous flow of the CS solutions decreases in the order CS+ H_2O_2, CS + Cu^{2+} + H_2O_2, CS + Fe^{2+} + H_2O_2. Variation of the enthalpies of viscous flow of CS solutions are significantly larger for the system CS + Cu^{2+} + H_2O_2, which is apparently caused by higher complexing power of copper(II) ions compared to iron(II) ions [8]. The decrease in the enthalpy of viscous flow of chitosan solution in the presence of iron(II) ions and hydrogen peroxide is caused by significant influence of iron ions on the oxidative degradation of chitosan.

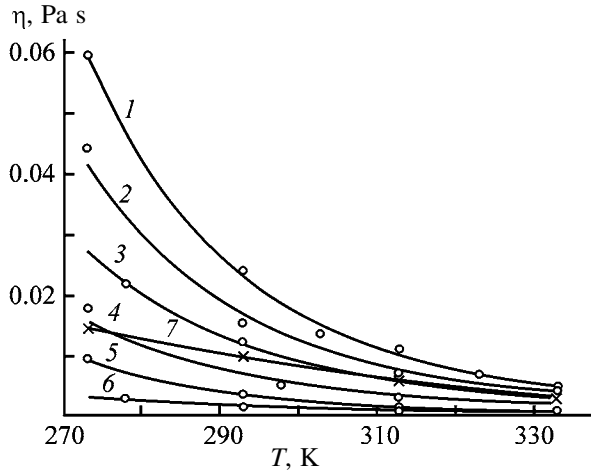

Fig. 2. Viscosity of CS solutions η as a function of temperature T in the reaction with hydrogen peroxide in the presence of variable-valence metal ions. [CS] = 5.84×10^{-2} M. (*1*) Solution without additives; concentration (M): (*2*) [Cu^{2+}] = 5×10^{-3}; (*3*) [Fe^{2+}] = 5×10^{-3}; (*4*) [H_2O_2] = 2.94×10^{-1}; (*5*) [Cu^{2+} = 5×10^{-3}, [H_2O_2] = 2.94×10^{-1}; (*6*) [Fe^{2+}] = 5×10^{-3}, [H_2O_2] = 2.94×10^{-1}; and (*7*) [Fe^{2+}] = 5×10^{-3}, [Na_2EDTA] = 5×10^{-3}.

It is well known [4] that salts of ethylenediaminetetraacetic acid form complexes with metal ions; therefore, addition of sodium ethylenediaminetetraace-

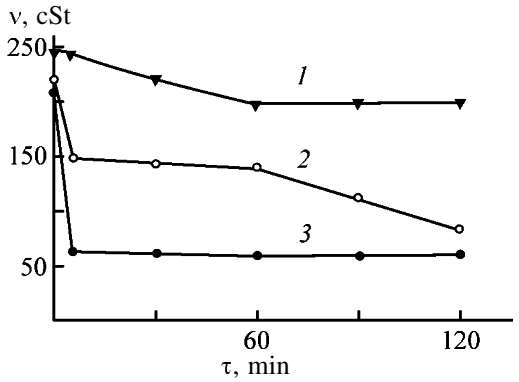

Fig. 3. Influence of variable-valence metal salts on oxidative degradation of chitosan under the action of hydrogen peroxide. T = 25°C, [CS] = 5.84×10^{-2} M. (ν) Intrinsic viscosity and (τ) time. (*1*) [CS] : [H_2O_2] = 1 : 10, (*2*) [CS] : [Cu^{2+}] : [H_2O_2] = 1 : 0.1 : 10, and (*3*) [CS] : [Fe^{2+}] : [H_2O_2] = 1 : 0.1 : 10.

tate (Na_2EDTA) into the reaction mixture decreased the influence of Fe^{2+} ions on oxidative degradation of CS under the action of H_2O_2 (Fig. 2, curve *7*).

Variation of the intrinsic viscosity in the course of oxidative degradation of CS under the action of hydrogen peroxide in the presence of variable-valence metal ions is shown in Fig. 3. As seen, the time of oxidative degradation and average molecular weight of oligomers in the presence of iron(II) are significantly lower than those in the presence of copper(II). This is caused by higher efficiency of generation of OH radicals in decomposition of hydrogen peroxide in the presence of iron(II) ions [7].

CONCLUSIONS

(1) Oxidative degradation is the main process in the reaction of hydrochloric acid solutions of chitosan in the range 273–333 K.

(2) Addition of variable-valence metal ions makes shorter the reaction time and allows preparation of chitosan oligomers with a lower molecular weight.

REFERENCES

1. Muzzarelli, R.A.A., *Chitin*, Oxford: Pergamon, 1970.
2. *Chitin in Nature and Technology*, Muzzarelli, R., Ed., New York: Plenum, 1985.
3. Muzzarelli, R.A.A., Tanfani, F., and Emanuelli, M., *J. Membr. Sci*., 1983, vol. 16, pp. 295–308.
4. Murinov, K.Yu., Voloshin, A.I., Krasnogorskaya, N.N., et al., *Izv. Ross. Akad. Nauk, Ser. Khim*., 2002, no. 1, pp. 52–55.
5. Domard, A. and Rinaudo, M., *Int. J. Biol. Macromol*., 1983, vol. 5, no. 1, pp. 49–51.
6. Murinov, K.Yu., Kabal'nova, N.N., Mullagalriev, I.R., and Monakov, Yu.B., *Nature Polysaccharides: Oxidative Reactions of Chitosan*, Zaikov, G.E., Ed., 2005.
7. Sychev, A.Ya. and Issak, V.G., *Usp. Khim*., 1995, vol. 64, pp. 1183–1209.
8. Shlick, S., *Macromolecules*, 1986, vol. 19, no. 1, pp. 192–195.

ISSN 1070-4272, Russian Journal of Applied Chemistry, 2007, Vol. 80, No. 1, pp. 162–163. © Pleiades Publishing, Ltd., 2006.
Original Russian Text © A.V. Arkhipova, K.V. Malkova, T.N. Sokolova, V.R. Kartashov, 2007, published in Zhurnal Prikladnoi Khimii, 2007, Vol. 80, No. 1, pp. 162–163.

BRIEF COMMUNICATIONS

Synthesis of a New Thiocarbamate by the Reaction of Benzyl Thiocyanate with Camphene, Catalyzed by Heteropoly Acids

A. V. Arkhipova, K. V. Malkova, T. N. Sokolova, and V. R. Kartashov

Nizhni Novgorod State Technical University, Nizhni Novgorod, Russia

Received May 30, 2006

Abstract—The reaction of benzyl thiocyanate with camphene in the presence of heteropoly acids, 12-phosphotungstic and 12-silicotungstic, at 65°C was studied. *S*-Benzyl (1,7,7-trimethylnorbornyl)thiocarbamate was prepared in 66% yield.

DOI: 10.1134/S1070427207010338

Previously [1] we reported on the reactions of a series of thiocyanates with a natural terpene, camphene, in the presence of concentrated sulfuric acid, yielding the coresponding N-substituted thiocarbamates. We examined the possibility of using heteropoly acids (HPAs) for catalyzing this reaction. It is of fundamental importance for catalysis that HPAs have high Brønsted acidity, considerably exceeding that of common mineral acids and traditional acid catalysts [2].

By the reaction of benzyl thiocyanate with camphene in the presence of the most typical tungstic heteropolyacids, $H_3PW_{12}O_{40}$ and $H_4SiW_{12}O_{40}$, we prepared a new camphene derivatives, *S*-benzyl (1,7,7-trimethylnorbornyl)thiocarbamate:

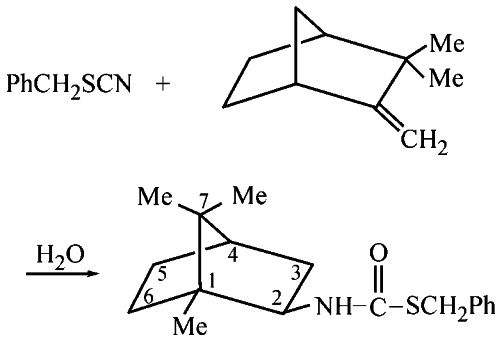

It should be noted that benzyl thiocyanate does not react with camphene in the presence of sulfuric acid as catalyst [1].

The reaction was performed in acetic acid, taking into account published data on related syntheses of N-substituted thiocarbamates [1]. Heteropoly acids of the Keggin structure in acetic acid are relatively weak electrolytes dissociating by the first step only [3], but in the acidity they exceed by 2–5 pK units the traditional acid catalyst, sulfuric acid [4].

The initial camphene : thiocyanate molar ratio was 1 : 1.48. The reaction was performed with water additions, because without water the HPA precipitates. It should also be noted that small amounts of water allow the reaction to be performed at a relatively low temperature.

It is known [5] that camphene can isomerize in acid-catalyzed reactions; as a result, several compounds are usually formed. Comparison of the ^{13}C NMR spectrum of the purified product with those of various camphene derivatives [5] allowed identification of the compound obtained.

Analysis of the mother liquor revealed formation of small amounts of isobornyl acetate and isoborneol along with the major product, benzyl (1,7,7-trimethylnorbornyl)thiocabamate. These by-products were identified by GLC using authentic samples.

We optimized the concentrations of the acids used, reaction temperature, and reactant weight ratio. We found that the reaction mixture, when heated above 65°C, undergoes tarring (as judged from its color and amount of the bottoms), which considerably decreases the yield of the target product.

The heteropoly acid $H_4SiW_{12}O_{40}$ also actively catalyzes the reaction in question. On the whole, however, it does not surpass in performance $H_3PW_{12}O_{40}$. This fact is consistent with close strength of these acids. It is known that the strength of heteropolytungstic acids depends on the nature of the central atom insignificantly [2].

EXPERIMENTAL

The synthesis was performed for 2–8 h at various temperatures in a temperature-controlled glass reactor equipped with a reflux condenser. After the reaction completion, the mixture was extracted with diethyl ether in an amount equal to a half of the volume of the aqueous phase. The organic phase was washed with 10% NaOH and then with water to neutral reaction of the wash waters, after which it was dried for 24 h over Na_2SO_4. The organic layer was analyzed by GLC. To obtain pure samples of the product, the solvent was removed at reduced pressure. The crystalline residue was repeatedly recrystallized from *n*-hexane until the melting point became constant.

The heteropoly acids of the 12th series $H_3PW_{12}O_{40}$ and $H_4SiW_{12}O_{40}$ (pure grade commercial products) were used without additional purification. The starting optically active camphene {$[\alpha]_{580}^{22}$ +12.5° (*c* 11.6, $CHCl_3$)}, which initially contained 10% tricyclene (GLC data), was brought to 99% purity by recrystallization from EtOH, mp 50°C (published data [6]: mp 50°C). Acetic acid was purified by distillation of the ultrapure grade acid on a 0.3-m distillation column. Commercial chemically pure grade (97% purity) benzyl thiocyanate was used without additional purification. Technical-grade isoborneol was brought to 96% purity (GLC data) by fractional recrystallization from ethanol. Diethyl ether, ethanol, and *n*-hexane (chemically pure grade) were purified by standard procedures [7]. Isobornyl acetate was prepared by the procedure described in [8].

The purity of the starting substances was checked and the reaction products analyzed by GLC on a Chrom 5 chromatograph equipped with a flame ionization detector and a 30000 × 10-mm column; stationary phase polyphenylmethylsiloxane-4 (15%) on Chromaton N-AW-DMSC (0.20–0.25 mm), column temperature 180–190°C, carrier gas (nitrogen) pressure 2.5 atm. As internal reference we used *N*-(1,7,7-trimethylnorbornyl)propionamide.

The ^{13}C NMR spectra (32 MHz) were recorded on a Bruker AC-200 spectrometer using the solvent ($CDCl_3$) signal as internal reference (δ 7.24, δ_C 76.90 ppm).

The elemental composition of the compound obtained was determined from the high-resolution mass spectrum taken with a Finnigan MATINCOS 50 mass spectrometer. For recording the IR spectra, samples were prepared as KBr pellets or mulls in mineral oil.

A solution of 0.2 g (1.34 mmol) of benzyl thiocyanate and 0.12 g (0.88 mmol) of camphene in 3 ml of acetic acid was added to 1.34 g (0.46 mol) of $H_3PW_{12}O_{40}$ wetted with water (0.2 ml, 11.11 mmol). The mixture was heated for 4 h at 65°C. White crystals of benzyl (1,7,7-trimethylnorbornyl)thiocarbamate were obtained; yield 0.18 g (66% based on the initial amount of camphene), mp 87°C.

Found, %: C 71.9, H 8.5, N 4.3.
$C_{18}H_{25}NOS$.
Calculated, %: C 71.3, H 8.3, N 4.6.

Mass spectrum (electron impact, 70 eV), *m*/*z* (I_{rel}, %): 303 $[M]^+$ (20), 212 (11), 180 (14), 137 (16), 124 (98), 109 (10), 91 (100), 81 (36), 55 (8), 41(12). ^{13}C NMR spectrum ($CDCl_3$, δ, ppm): 49.3 C(1); 57.3 C(2); 36.2 C(3); 44.5 C(4); 26.1 C(5); 35.4 C(6); 46.2 C(7); 19.8, 20.3 [$2CH_3$, CH_3C(7)]; 11.5 [CH_3C(1)]; 127.2, 127.5, 130.0 (C_o, C_p, C_m); 136.4 (C_{ipso}); 28.8 (CH_2, COSCH_2Ph); 166.8 (CO, COSCH_2Ph).

CONCLUSIONS

(1) Benzyl (1,7,7-trimethylnorbornyl)thiocarbamate was prepared in 66% yield by the reaction of benzyl thiocyanate with camphene in the presence of heteropoly acids. With sulfuric acid as catalyst, this compound is not formed at all.

(2) Isoborneol and isobornyl acetate are formed in this reaction as by-products.

REFERENCES

1. Riemschneider, R., *J. Am. Chem. Soc.*, 1956, vol. 78, pp. 844–847.
2. Kozhevnikov, I.V., *Usp. Khim.*, 1987, vol. 56, pp. 1417–1443.
3. Timofeeva, M.N., Matrosova, M.M., Maksimov, G.M., and Likholobov, V.A., *Kinet. Katal.*, 2001, vol. 42, no. 6, pp. 863–867.
4. Kulikov, S.M. and Kozhevnikov, I.V., *Izv. Akad. Nauk SSSR, Ser. Khim.*, 1981, no. 3, pp. 498–504.
5. Fomenko, V.V., Korchagina, D.V., Yarovaya, O.I., et al., *Zh. Org. Khim.*, 1999, vol. 35, no. 7, pp. 1031–1041.
6. *Spravochnik khimika* (Chemist's Handbook), Nikol'skii, B.P., Ed., Moscow: Khimiya, 1963, vol. 2.
7. Becker, H., Berger, W., Domschke, G., et al., *Organikum. Organisch-chemisches Grundpraktikum*, Berlin: Wissenschaften, 1976, vol. 2.
8. Weygand–Hilgetag, *Organisch-chemische Experimentierkunst*, Leipzig: Barth, 1964, 3rd ed.

ISSN 1070-4272, Russian Journal of Applied Chemistry, 2007, Vol. 80, No. 1, pp. 164–165. © Pleiades Publishing, Ltd., 2006.
Original Russian Text © T.A. Aslanov, U.M. Mamedli, A.M. Guliev, A.A. Efendiev, 2007, published in Zhurnal Prikladnoi Khimii, 2007, Vol. 80, No. 1, pp. 164–166.

BRIEF COMMUNICATIONS

Synthesis of Diester Disulfimides Derived from 4- and 5-Methoxycarbonyl-2-sulfobenzoic Acid Imides

T. A. Aslanov, U. M. Mamedli, A. M. Guliev, and A. A. Efendiev

Institute of Polymeric Materials, National Academy of Sciences of Azerbaijan, Sumgaiyt, Azerbaijan

Received May 19, 2006

Abstract—Ester interchange of 4- and 5-methoxycarbonyl-2-sulfobenzoic acid imides with glycols was studied.

DOI: 10.1134/S107042720701034X

Trimellitic acid esters are used as monomers for heat-resistant polymers, poly(ester imides) [1]. Babe et al. [2] reported on diester diimides prepared by ester interchange of trimellitimide methyl ester with glycols. Recently we reported on diester disulfimides derived from saccharinmonocarboxylic acids and aromatic diols [3].

Here we report on imides of 4- and 5-methoxycarbonyl-2-sulfobenzoic acids (**Ia**, **Ib**) and on a series of diester disulfimides **IIa**–**VIIIa** and **IIb**–**VIIIb** derived from these imides. Compounds **IIa**–**VIIIa** and **IIb**–**VIIIb** are of interest as potential monomers for preparing poly(ester sulfimides).

Imides **Ia** and **Ib** were prepared from imides of 2-sulfo-1,4- and 2-sulfo-1,5-benzenedicarboxylic acids, respectively, and anhydrous methanol in the presence of sulfuric acid as catalyst [4]. Yield 76%, mp 164–165°C. The IR spectra of **Ia** and **Ib** contained characteristic absorption bands of the saccharin ring at 1720 (>C=O), 1300–1250 (>SO_2), and 1120–1100 cm^{-1} (>NH).

Diester disulfimides **IIa**–**VIIIa** and **IIb**–**VIIIb** were prepared by ester interchange of **Ia** and **Ib** with various aliphatic glycols:

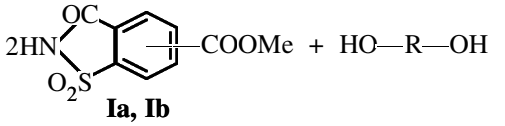

Ia, Ib

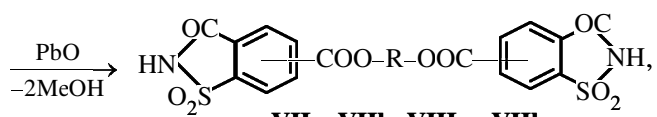

VIIa–**VIIb, VIIIa** –**VIIb**

where R = $(CH_2)_2$ (**IIa**, **IIb**), $(CH_2)_3$ (**IIIa**, **IIIb**), $CH(Me)CH_2$ (**IVa**, **IVb**), $(CH_2)_4$ (**Va**, **Vb**), $(CH_2)_6$ (**VIa**, **VIb**), $(CH_2)_2O(CH_2)_2O(CH_2)_2$ (**VIIa**, **VIIb**), $CH_2CH(OH)CH_2$ (**VIIIa**, **VIIIb**).

Diester disulfimides **IIa**–**VIIIa** and **IIb**–**VIIIb** were synthesized in excess glycol; the ratio of imide **Ia** or **Ib** to glycol was 1 : 3. Lead(II) oxide was used as catalyst; the mixture was gradually heated in the temperature range 80–170°C. The reaction time was 3–4 h. The reactions with glycols containing a longer hydrocarbon chain between hydroxy groups occurred at lower temperatures.

The compositions of diester disulfimides **IIa**–**VIIIa** and **IIb**–**VIIIb** were determined by elemental analysis (see table), and their structure was confirmed by IR spectroscopy. The IR spectra contained characteristic absorption bands at 1760–1720 (C=O of saccharin ring), 1370–1300 and 1200–1180 (SO_2), 1300–1250 and 1120–1100 (C–O–C of ester group), and 3350–3310 cm^{-1} (N–H) [5].

EXPERIMENTAL

The IR spectra were recorded on a Specord M-80 spectrophotometer from liquid films in the range 3700–700 cm^{-1} using KBr prisms. The boiling points of glycols and solvents agreed with reference data [6].

Ethylene glycol bis(2-sulfo-1,4-benzenedicarboxylic acid imide) ester IIa. A mixture of 24.1 g (0.1 mol) of methyl ester of imide **Ia** and 1.2 g of PbO in 31 g (0.5 mol) of 1,2-ethanediol was heated with stirring to 170–175°C over a period of 3–4 h. The resulting mixture was dissolved in acetone, and the product was precipitated with distilled water. The grayish-white crystalline product was dried at room

Characteristics of diester disulfimides **IIa**–**VIIIa** and **IIb**–**VIIIb**

Compound	Yield, %	mp, °C	Empirical formula	Found, %/Calculated, %				*M*
				C	H	N	S	
IIa	85	208–210	$C_{18}H_{12}O_{10}N_2S_2$	44.40/45.04	2.45/2.50	5.73/5.83	12.95/13.36	475
IIb	83	190–192	$C_{18}H_{12}O_{10}N_2S_2$	44.38/45.05	2.46/2.50	5.71/5.83	12.92/13.36	475
IIIa	84	195–196	$C_{19}H_{14}O_{10}N_2S_2$	45.51/46.15	2.88/2.83	5.58/5.66	13.03/12.95	491
IIIb	83	179–181	$C_{19}H_{14}O_{10}N_2S_2$	45.52/46.15	2.88/2.83	5.59/5.66	13.04/12.95	491
IVa	82	180–182	$C_{19}H_{14}O_{10}N_2S_2$	44.45/46.15	2.89/2.83	5.71/5.66	12.05/12.95	489
IVb	81	164–166	$C_{19}H_{14}O_{10}N_2S_2$	44.43/46.15	2.90/2.83	5.73/5.66	12.03/12.95	489
Va	84	188–190	$C_{20}H_{16}O_{10}N_2S_2$	45.80/47.30	3.03/3.15	5.15/5.51	13.31/12.62	506
Vb	82	175–177	$C_{20}H_{16}O_{10}N_2S_2$	45.75/47.305	3.02/3.15	5.13/5.51	13.32/12.62	506
VIa	86	178–180	$C_{22}H_{16}O_{10}N_2S_2$	48.11/49.30	3.66/3.73	5.16/5.33	11.98/12.96	539
VIb	83	161–163	$C_{22}H_{16}O_{10}N_2S_2$	48.12/49.30	3.65/3.73	5.15/5.22	12.99/11.96	539
VIIa	85	165–167	$C_{20}H_{16}O_{10}N_2S_2$	44.50/45.84	2.95/3.05	5.10/5.34	11.15/12.24	526
VIIb	84	149–151	$C_{20}H_{16}O_{10}N_2S_2$	44.48/45.84	2.94/3.05	5.11/5.34	11.13/12.24	526
VIIIa	88	158–160	$C_{19}H_{14}O_{10}N_2S_2$	43.80/44.74	2.50/2.74	5.16/5.34	12.05/12.57	508
VIIb	84	149–151	$C_{19}H_{14}O_{10}N_2S_2$	43.81/44.74	2.50/2.74	5.15/5.49	12.06/12.57	508

temperature and vacuum-dried to constant weight; mp 208–210°C.

Compounds **IIIa**–**VIIIa** and **IIb**–**VIIIb** were prepared similarly.

CONCLUSION

Diester disulfimides derived from 4- and 5-methoxycarbonyl-2-sulfobenzoic acid imides, showing promise as monomers for preparing polyester imides, were synthesized in a high yield (76–88%).

REFERENCES

1. Suvorov, B.V., Zhubanov, B.A., and Mashkevich, S.A., *Trimellitovaya kislota i polimery na ee osnove* (Trimellitic Acid and Polymers Derived from It), Alma-Ata: Nauka, 1975.
2. Babe, S.G., Abajo, J. de, and Fontan, J., *Angew. Makromol. Chem.*, 1972, vol. 21, pp. 65–77.
3. Aslanov, T.A., Mamedli, U.M., and Guliev, A.M., *Zh. Prikl. Khim.*, 2005, vol. 78, no. 3, pp. 444–446.
4. Tagiev, B.A. and Aslanov, T.A., *Azerb. Khim. Zh.*, 1997, nos. 1–4, pp. 62–66.
5. Kazitsyna, L.A. and Kupletskaya, N.B., *Primenenie UF-, IK-, YaMR- i mass-spektroskopii v organicheskoi khimii* (Applications of UV, IR, NMR, and Mass Spectroscopy to Organic Chemistry), Moscow: Mosk. Gos. Univ., 1979.
6. Gordon, A.J. and Ford, R.A., *The Chemist's Companion. A Handbook of Practical Data, Techniques, and References*, New York: Wiley, 1972.

ISSN 1070-4272, Russian Journal of Applied Chemistry, 2007, Vol. 80, No. 1, pp. 166–171. © Pleiades Publishing, Ltd., 2007.
Original Russian Text © A.G. Morachevskii, 2007, published in Zhurnal Prikladnoi Khimii, 2007, Vol. 80, No. 1, pp. 167–172.

HISTORY OF CHEMISTRY AND CHEMICAL TECHNOLOGY

Nikolai Aleksandrovich Menshutkin (to 100th Anniversary of His Death)

DOI: 10.1134/S1070427207010351

N.A. Menshutkin is, together with his closest associates from St. Petersburg University, A.M. Butlerov (1828–1886) and D.I. Mendeleev (1834–1907), among the most prominent Russian chemists of the second half of the XIX century. N.A. Menshutkin's research in chemical kinetics actually initiated application of physicochemical techniques in organic chemistry. The textbook *Analiticheskaya khimiya* (Analytical Chemistry), written by N.A. Menshutkin, presented a novel approach to a study of this discipline, ran into 16 editions, was the main manual of analytical chemistry during many years, and was translated into German and English. The scientist made a major contribution to the organization of laboratories at St. Petersburg University and Polytechnic Institute and development of chemical education in Russia.

Nikolai Aleksandrovich Menshutkin was born on October 12 (24), 1842, in St. Petersburg into a rather wealthy trader's family. His father, hereditary honorary citizen, paid a considerable attention to education of his children. The scientist-to-be received his initial education at one of the best St. Petersburg boarding schools, where he studied from the age of six. Beginning at the age of ten, he was also educated in St. Petersburg, at the technical department of the St. Peter principal German school. Already during this period, N.A. Menshutkin's abilities and high sense of responsibility manifested themselves. In December 1857, he successfully, the first among the graduates, finished the school and, in the next year, being under 16, he entered, having passed an examination, the natural department of the physicomathematical faculty of St. Petersburg University. In those years, lectures on inorganic and analytical chemistry were delivered by A.A. Voskresenskii (1809–1880, corresponding member of St. Petersburg Academy of Sciences since 1864), professor of a number of higher school institutions of St. Petersburg and a prominent scientist in the field of organic chemistry. Lectures on organic chemistry were delivered by Prof. N.N. Sokolov (1826–1877), a talented pedagogue and scientist, one of founders of Russia's first chemical journal [1]. Sokolov paid a considerable attention to students

Nikolai Aleksandrovich Menshutkin (1906).

and was held in deserved high respect by students. N.A. Menshutkin left very warm reminiscences about his teacher [2]. Under Sokolov's influence, N.A. Menshutkin exhibited a particular interest in chemistry from the first years of education at the University. Being a second-year student, he established a chemical laboratory at his home.

In the spring of 1862, N.A. Menshutkin successfully finished the University with a candidate degree from the physicomathematical faculty and a solid intention to be engaged in research and pedagogical activities in the field of chemistry. In those years, Russia's universities, including St. Petersburg University (founded in 1819), provided a fundamental training in general theory, but possessed a very limited number of laboratories. In order to primarily improve his experimental abilities, N.A. Menshutkin went, after the example of his numerous colleagues, abroad, to Germany, having chosen the University of

Tübingen, one of the oldest in Europe (founded in 1477). For more than a year, the Russian scientist was trained on methods for qualitative and quantitative analysis at the laboratory of Prof. A. Strecker (1812–1871), a known organic chemist mostly interested in natural compounds. At the same laboratory, N.A. Menshutkin carried out his first scientific study, published in France in 1864.

At the end of March 1864, N.A. Menshutkin moved to Paris, to the laboratory a known chemist, Prof. A. Wurtz (1817–1884, member of Paris Academy of Sciences since 1867, president of this academy in 1881–1884, foreign corresponding member of St. Petersburg Academy of Sciences since 1873), at Ecole de Medicine and spent there a year. Scientists from many countries, including Russia, worked at different times at Wurtz's laboratory. Among the known Russian scientists, those who improved their skills at this laboratory included P.P. Alekseev (1840–1891), F.F. Beilstein (1838–1906), A.M. Butlerov, G.G. Gustavson (1843–1908) A.M. Zaitsev (1845–1904), A.L. Potylitsyn (1845–1905), and others [3, 4].

N.A. Menshutkin commenced, on his own initiative, studies of phosphorous acid and its derivatives. The results obtained were published in French chemical journals and formed the basis of his master's dissertation. In the spring of 1865, the young scientist left Paris and again went to Germany, to Marburg University (founded in 1527), to Prof. A.W.H. Kolbe (1818–1884), a prominent German organic chemist. At Kolbe's laboratory, N.A. Menshutkin completed the experimental part of his dissertation work and published one more article in the same area: on the action of anhydrous ethanol on phosphorus trichloride. In August of the same year, the scientist returned to homeland with a finished dissertation.

In the spring of 1865, N.A. Menshutkin successfully passed examinations at St. Petersburg University for master's degree in chemistry, and at the very beginning of 1866, submitted dissertation "On Hydrogen of Phosphorous Acid that is Incapable of Substitution with Metals under Conditions Ordinary for Acids." In conformity with the existing regulations, the complete text of the dissertation was published as a separate brochure (St. Petersburg, 1866). Based on a vast body of experimental data, N.A. Menshutkin was the first to establish that only two out of the three hydrogen atoms contained in phosphorous acid H_3PO_3 can be substituted with a metal. He noted that "this hydrogen is involved only in those reactions which are successful with alcohols." This study was of particular methodological and general scientific interest and was distinguished by a new formulation of the problem. In March 1866, N.A. Menshutkin defended his dissertation, with Mendeleev and Voskresenskii as opponents. After master's degree was conferred on N.A. Menshutkin and he delivered trial lectures, he became a privatdocent at St. Petersburg University.

In the 1866/67 academic year, N.A. Menshutkin commenced his pedagogical activities at the University and was soon elected a permanent docent at the chair of chemistry. Among his duties was teaching of analytical chemistry and management of the analytical department of the chemical laboratory. In addition to a course of lectures on analytical chemistry, N.A. Menshutkin also delivered a special course of organic chemistry (alcohols). Simultaneously, the scientist commenced work on his doctoral dissertation. Already at the beginning of 1869, he published as a separate edition (St. Petersburg, 1869) and submitted his doctoral (chemistry) dissertation "Synthesis and Properties of Ureides." The dissertation was defended in April 1869, and the opponents, Mendeleev and Butlerov, noted the high scientific level and the experimental skills of the defendant. On defending the dissertation, N.A. Menshutkin was elected an extraordinary professor and continued teaching of the same disciplines. In 1876, he was appointed ordinary professor. In 1871, the young scientists occupied for three years the position of the secretary of the faculty; in 1874, he was elected to this position for a second term. In 1879, N.A. Menshutkin was elected dean of the physicomathematical faculty (till 1887). During all these years, he was intensively engaged in all the faculty's activities.

In 1885, N.A. Menshutkin abandoned teaching of analytical chemistry and headed the department of organic chemistry, teaching exclusively this discipline. In 1891, the degree of honored professor was conferred on the scientist. In 1893, in view of his prolonged service, N.A. Menshutkin occupied the position of a supernumerary professor of the University.

A major N.A. Menshutkin's achievement was the organization, beginning in 1867, of systematic practical studies in qualitative and quantitative chemical analysis, which were obligatory for all students of the natural department of the physicomathematical faculty. To simplify mastering of chemical analysis, N.A. Menshutkin published an original textbook *Analiticheskaya khimiya* (Analytical Chemistry) in 1871. As noted [5] by M.I. Usanovich (1894–1981), a known historian of chemistry, *Osnovy khimii* (Fundamentals of Chemistry) (1st edition in 1868–1871) by Mendeleev and *Analiticheskaya khimiya* (Analytic-

Chemical laboratory of St. Petersburg University (1894).

al Chemistry) by N.A. Menshutkin, published nearly simultaneously, laid the foundation of the chemical education in Russia and were many times republished during the authors' life and posthumously. In 1877, *Analiticheskaya khimiya* was translated into German and published in Leipzig; its third German edition was published in 1892. In 1895, the book was published in English in London and New York.

Beginning with the 10th edition in Russia (1908), *Analiticheskaya khimiya* was remade and supplemented by the author's son, B.N. Menshutkin (1874–1938), a chemist and science historian, a professor of St. Petersburg Polytechnic Institute (in 1902–1938). An N.A. Menshutkin's disciple, Prof. D.N. Monastyrskii (1875–1959), was actively involved [6, 7] in preparing the last, 16th edition of the book for publication.

Having passed to teaching of organic chemistry, N.A. Menshutkin prepared for publication *Lektsii po organicheskoi khimiii* (Lectures on Organic Chemistry). All the four editions of these lectures (1884, 1891, 1896, 1901) strongly differ, which reflects the development of science and the evolution of authors' views. In 1878, N.A. Menshutkin delivered for the first time at St. Petersburg University a course of lectures on the history of science. Based on these lectures, he later published *Ocherk razvitiya khimicheskikh vozzrenii* (Essay on the Evolution of Chemical Concepts) (St. Petersburg, 1888), the first original work of the Russian scientist in the field of the history of chemistry. The essay begins from deeply ancient past and covers a period of time extending to the 1880s. It, in particular, analyzes publications devoted to kinetic patterns and chemical affinity, which appeared by that time. The essay only disregards the theory of electrolytic dissociation by S.A. Arrhenius (1859–1927, foreign corresponding member of St. Petersburg Academy of Sciences since 1903, honorary member of the Academy of Sciences of the USSR since 1926, 1903 Nobel Prize Laureate in Chemistry), which was only in the initial stage of its development by that time. It is known, however, that, in contrast to Mendeleev and D.P. Konovalov (1856–1929, academician of the Academy of Sciences of the USSR since 1923), a professor of St. Petersburg University, N.A. Menshutkin' attitude toward the concepts put forward by Arrhenius was positive and he presented these ideas in third edition of *Analiticheskaya khimiya* (St. Petersburg, 1893) [8].

N.A. Menshutkin have done great services to St. Petersburg University in the construction of a chemical laboratory. The new University's statutes and regulations adopted in 1884 envisaged a significant expansion of laboratory studies in teaching of natural sciences. In this context, Mendeleev, Butlerov, and N.A. Menshutkin substantiated, in a special memorandum, the necessity for creating an absolutely new chemical laboratory at the University. In 1890, the Ministry of Finance suggested to St. Petersburg University to make up an estimate of expenditure for construction of the new laboratory. N.A. Menshutkin was appointed head of a commission organized at the

physicomathematical faculty and intended to prepare the estimate and a working design of the chemical laboratory. In the summer of 1891, N.A. Menshutkin and A.F. Krasovskii, an academician of architecture involved in the construction, were sent to a business trip abroad, where they visited laboratories of quite a number of higher-school institutions in Germany, Austria–Hungary, and Switzerland. Already in the autumn of 1891, the work on the design and estimate of the new chemical laboratory was complete; the construction of the new building was commenced in the spring of 1892 and was finished by the autumn of 1894. N.A. Menshutkin was a member of the construction commission; on October 16, 1894, he delivered a brilliant speech at the opening ceremony of the laboratory [9]. Assessing the extent of development of chemical science in Russia in the XIX century, N.A. Menshutkin noted that "the success of chemistry in the last quarter century is largely due to works of Russian scientists."

At the turn of the XX century, after a decision was made to organize a polytechnic institute in St. Petersburg, N.A. Menshutkin and other known chemists, Mendeleev, P.I. Walden (1863–1957, professor of Riga Polytechnic Institute, academician of St. Petersburg Academy of Sciences since 1910), and N.S. Kurnakov (1860–1941, professor of the Mining Institute, academician of St. Petersburg Academy of Sciences since 1913) took part, by invitation of the Ministry of Finance, in the work of a commission for making up curricula for the metallurgical department and the electrochemical subdepartment of the institute being organized. The commission was head by the Finance Minister of Russia, S.Yu. Vitte (1849–1915). In July 1901, Walden was appointed dean of the metallurgical department of the Polytechnic Institute. It was presumed that he would also occupy the position of the professor of general chemistry [1, 10]. However, already in October of the same year, Walden reported that he could not accept this appointment in view of circumstances and recommended N.A. Menshutkin as a dean. At the beginning of 1902, Walden was elected director of Riga Polytechnic Institute.

On November 1, 1901, N.A. Menshutkin was appointed, and later elected, dean of the metallurgical department and also headed the chair of analytical and organic chemistry. A major N.A. Menshutkin's achievement as dean of the metallurgical department was that he invited most prominent, worldwide-known specialists to teach basic disciplines. Kurnakov was invited as professor of general chemistry. A graduate from the Mining Institute, Kurnakov occupied there the position of a professor of inorganic chemistry already beginning in 1893. The well-equipped laboratories of the Polytechnic Institute enabled Kurnakov to commence extensive experimental studies in the field of physicochemical analysis of metallic and salt systems and to develop a prominent research area. On Kurnakov's initiative, supported by other professors of chemistry, students of the metallurgical department were entitled, for the first time in the practice of Russia's technical higher school institutions, to defend either the design of a plant or the results of an experimental study performed at the final stage of their education.

V.A. Kistyakovskii (1865–1952, academician of the Academy of Sciences of the USSR since 1929) was to deliver lectures on physical chemistry and theoretical electrochemistry. The author of quite a number of well-known studies in the theory of electrolyte solutions, he, having graduated from St. Petersburg University, worked in Germany and was a follower of concepts put forward by Arrhenius and J.H. van't Hoff (1852–1911, foreign corresponding member of St. Petersburg Academy of Sciences since 1895, 1901 Nobel Prize Laureate in chemistry). In 1903–1904, Kistyakovskii equipped at the Polytechnic Institute the first Russia's laboratory of physical chemistry, which not only provided the teaching process, but also made it possible to commence various experimental studies in the field of electrochemistry, corrosion of metals, and nature of the liquid state. The position of an ordinary professor of geology and mineralogy was occupied, by N.A. Menshutkin's invitation, by F.Yu. Levinson-Lessing (1861–1939, academician of the Academy of Sciences of the USSR since 1925). He was a professor at Yur'ev (now Tartu, Estonia) University and headed the chemical direction in petrography in Russia. Technical electrochemistry and mineral technology were to be taught in 1902 by P.P. Fedot'ev (1864–1934, corresponding member of the Academy of Sciences of the USSR since 1933), an experienced technologist-engineer, the author of a number of monographs in technical chemistry. The studies at the St. Petersburg Polytechnic Institute commenced on October 2, 1902. As a member of the construction commission and dean of the metallurgical department, N.A. Menshutkin paid a considerable attention to completion of the construction of the chemical building and equipment of laboratories.

N.A. Menshutkin's scientific activities have been described in detail [10–14]. The central place is occupied by studies in chemical kinetics, commenced in 1877. The first series of works was devoted to the

Chemical building of St. Petersburg Polytechnic Institute (1902).

relationship between the structure of organic compounds and the esterification rate. The scientist accumulated a large body of factual data and demonstrated for the first time that the esterification rate can give information about the structure of organic compounds. For example, methanol shows the highest reaction rate when involved in reactions to give esters. Any other alcohol with a higher molecular weight shows a lower esterification rate. The reaction rate decreases in a similar way when the molecular weight of an acid involved in the esterification increases. For studies of the effect of isomerism of alcohols and acids on formation of esters, N.A. Menshutkin was awarded the N.N. Sokolov Prize by the Russian Physicochemical Society in 1878.

In the second series of kinetic studies, commenced in 1887, N.A. Menshutkin systematically analyzed for the first time the effect of indifferent solvents on the rate of chemical reactions. All textbooks on chemical kinetics give as example N.A. Menshutkin's evidence that the rate of the reaction between triethylamine and ethyl iodide is 742 times faster in benzyl alcohol, compared with hexane. The final series of N.A. Menshutkin's studies in kinetics of chemical reactions was devoted to the effect of side chains and cyclic structure on the rate of reactions between organic compounds.

N.A. Menshutkin devoted about 30 years of his life to kinetic research, with the last studies carried out at the Polytechnic Institute [10, 16]. In 1904, N.A. Menshutkin received the highest award of St. Petersburg Academy of Sciences, Lomonosov Prize, for his research in the field of chemical kinetics. The scientist's achievements were recognized by the whole world's chemical community. The list of N.A. Menshutkin's publications as of 1895, composed by him, is contained in the biographic dictionary of St. Petersburg University's professors and teachers [15]. The full list of the scientist's publications is included in B.N. Menshutkin's book about his father [10].

Together with carrying out intensive pedagogical and scientific work, N.A. Menshutkin was permanently engaged in various kinds of social activities. In 1868, he was, together with Mendeleev, N.N. Beketov (1827–1911), V.V. Markovnikov (1837–1904), and other known chemists, among those who founded the Russian Chemical society. N.A. Menshutkin composed the statutes of the Society, was permanent editor of the Transactions of the Society, and made 82 reports at its meetings. Having a perfect knowledge of main European languages, N.A. Menshutkin annually published in *Zhurnal Rossiiskogo fiziko-khimicheskogo obshchestva* (Journal of the Russian Physicochemical Society) tens of summaries of the most interesting foreign studies. N.A. Menshutkin repeatedly occupied various elected positions at the Russian Physicochemical Society and was president of the Society in 1906.

N.A. Menshutkin was a permanent participant of congresses of Russian natural scientists and physicians, the first of which was held in St. Petersburg at the end of 1867, was member of the Organizing Committees of a number of congresses, and chairman of the XI congress (1901).

In 1892, N.A. Menshutkin was actively involved in the activities of zemstvo (local self-government) institutions in Luga uezd of St. Petersburg guberniya and

Zemstvo of St. Petersburg guberniya, where he represented Luga uezd. Beginning in 1894 and till the end of his life, N.A. Menshutkin was a member of the Nobiliary assembly of St. Petersburg guberniya, and represented Luga uezd.

Unsatisfied by programs of political parties that appeared in Russia after the Manifesto of October 17, 1905, N.A. Menshutkin and a group of professors from the Polytechnic Institute organized, with the participation of a number of prominent public figures of St. Petersburg, a new political party, party of democratic reforms. Its program was close to that of the constitutional-democratic party (kadets). The principal points of the program of the party of democratic reforms were presented in [10]. In the political orientation of the program, this party can be characterized as a left-center party.

Nikolai Aleksandrovich Menshutkin died on January 22 (February 5), 1907, of cerebral hemorrhage. An outstanding Russian chemist, public figure, broadly educated and talented person, he was among the most advanced professors of St. Petersburg and Russia.

REFERENCES

1. Morachevskii, A.G., *Ocherki ob uchenykh-khimikakh Sankt-Peterburga. XIX vek i pervaya polovina XX veka* (Essays about Scientists-Chemists of St. Petersburg: XIX Century and First Half of the XX Century), St. Petersburg: Politekh. Inst., 2004.
2. Menshutkin, N.A., *Zh. Ross. Fiz.-Khim. O–va.*, 1878, vol. 10, no. 1, pp. 8–15.
3. Musabekov, Yu.S., *Uch. Zap. Yaroslav. Tekhnol. Inst.*, 1960, vol. 5, pp. 191–197.
4. Musabekov, Yu.S., *Sharl' Adol'f Vyurtts. 1817–1884* (Charle Adolf Wurtz. 1817–1884), Moscow: Akad. Nauk SSSR, 1963.
5. Usanovich, M.I., *Iz istorii khimii. Ocherki iz zhizni i deyatel'nosti vydayushchikhsya uchenykh* (Excerpts from the History of Chemistry: Essays about Life and Activities of Outstanding Scientists), Almaty: Kazakh. Univ., 2004.
6. Smolegovskii, A.M. and Solov'ev, Yu.I., *Boris Nikolaevich Menshutkin. Khimik i istorik nauki* (Boris Nikolaevich Menshutkin: Chemist and Historian of Science), Moscow: Nauka, 1983.
7. Morachevskii, A.G., *Ocherki ob uchenykh-khimikakh Sankt-Peterburgskogo politekhnicheskogo institute* (Essays about Scientists-Chemists of St. Petersburg Polytechnic Institute), St. Petersburg: Sankt-Peterb. Gos. Politekh. Univ., 2002.
8. *Akademik Vladimir Aleksandrovich Kistyakovskii. Sbornik materialov* (Academician Vladimir Aleksandrovich Kistyakovskii: Coll. of Materials), Morachevskii, A.G. and Demidov, A.I., Compilers, St. Petersburg: Politekh. Inst., 2005.
9. Menshutkin, N.A., *Zh. Ross. Fiz.-Khim. O–va.*, 1894, vol. 26, no. 8, pp. 404–411.
10. Menshutkin, B.N., *Zhizn' i deyatel'nost' Nikolaya Aleksandrovicha Menshutkina* (Life and Activities of Nikolai Aleksandrovich Menshutkin), St. Petersburg, 1908.
11. Starosel'skii, P.I. and Solov'ev, Yu.I., *Nikolai Aleksandrovich Menshutkin. 1842–1907*, Moscow: Nauka, 1969.
12. Solov'ev, Yu.I., *Istoriya khimii. Razvitie khimii s drevneishikh vremen do kontsa XIX veka* (History of Chemistry. Development of Chemistry from Very Ancient Times till the End of the XIX Century), Moscow: Prosveshchenie, 1983.
13. Solov'ev, Yu.I., *Istoriya khimii v Rossii. Nauchnye tsentry i osnovnye napravleniya issledovanii* (History of Chemistry in Russia: Scientific Centers and Main Areas of Research), Moscow: Nauka, 1985.
14. Rodnyi, N.I., in *Ocherki po istorii khimii* (Essays on the History of Chemistry), Moscow: Akad. Nauk SSSR, 1963, pp. 99–167.
15. *Biograficheskii slovar' professorov i prepodavatelei Imperatorskogo Sankt-Peterburgskogo universiteta za istekshuyu tret'yu chetvert' veka ego sushchestvovaniya. 1869–1894* (Biographic Dictionary of Professors and Teachers from Imperial St. Petersburg University for the Elapsed Third Quarter Century of Its Existence, 1869–1894), St. Petersburg, 1898, vol. 2.
16. Monastyrskii, D.N., *Zh. Obshch. Khim.*, 1957, vol. 27, no. 12, pp. 3181–3182.

A. G. Morachevskii

ISSN 1070-4272, Russian Journal of Applied Chemistry, 2007, Vol. 80, No. 1, p. 172. © Pleiades Publishing, Ltd., 2007.
Original Russian Text © A.G. Morachevskii, 2007, published in Zhurnal Prikladnoi Khimii, 2007, Vol. 80, No. 1, p. 173.

BOOK REVIEWS

Gamburg, Yu.D., *Gal'vanicheskie pokrytiya. Spravochnik po primeneniyu* (Application Reference Book of Electroplated Coatings)

Moscow: Tekhnosfera, 2006, 216 pp.

DOI: 10.1134/S1070427207010363

Deposition of various kinds of electroplated coatings and the electroplating technology constitute the most rapidly developing part of applied electrochemistry. The new reference book for this area, written by one of the leading Russian electrochemists, is of indubitable interest. The book is intended for a wide audience of users and is, simultaneously, a reference book and a textbook. The latter is favored by the manner of presentation.

The book comprises a preface, four chapters, brief list of recommended literature, and list of principal designations. In the preface (pp. 14, 15), the author emphasizes that the technology of deposition of metal and alloy coatings has not changed fundamentally during the 150 years of its history, but has substantially developed owing to the success and advances of the electrochemical science. As a result, the application area of electroplating in a wide variety of modern technologies has strongly expanded.

Chapter 1 (pp. 16–28) considers the application areas of electrochemical coatings and their purpose and choice. Coatings are classed, the electrochemical processes occurring in their deposition are described in a popular manner, and principles that underlie the choice of a coating material, coating thickness, and deposition technique are noted. The whole body of evidence is of a most general nature. Chapter 2 (pp. 29–99) presents the electrochemical foundations of coating deposition processes. The author managed to combine modern scientific approaches to complex electrochemical processes with the simplicity and understandability of presentation. All the mathematical relations used are commented to a sufficient extent. Stages of electrochemical processes, current distribution over the electrode surface, metal deposition modes, and specific features of the electrodeposition of alloys are described in detail. A special section is devoted to analysis of the most frequently occurring disruptions of coating deposition processes.

Chapter 3 (pp. 100–160), which occupies the central position in the reference book, summarizes evidence concerning the technology of deposition of metal and alloy coatings. On describing procedures used to prepare the base surface for coating deposition (degreasing, etching, etc.), it considers deposition of coatings composed of copper, silver, gold, zinc, tin, nickel, chromium, iron, low-melting metals, platinum metals, and a large number of alloys. A small section is devoted to use of the electroless reduction of metals in coating deposition.

Chapter 4 of the reference book is devoted to methods for analysis of coating properties: mechanical: plasticity, hardness, internal stresses, and adhesion to the base surface; electrical: resistivity and contact resistance; and quite a number of other important parameters: porosity, thickness, corrosion resistance, solderability, hydrogenation, etc. The techniques employed to study the coating properties are described in the reference book by Yu.D. Gamburg in more detail and more thoroughly, compared with previous publications by other authors. The list of recommended literature (p. 214) contains three reference books, six monographs, five reviews, and two textbooks.

The book by Gamburg produces quite a favorable impression. It can be of use both for technologists and engineers working with electroplated coatings and for students specialized in technology of electrochemical industries.

A. G. Morachevskii

ISSN 1070-4272, Russian Journal of Applied Chemistry, 2007, Vol. 80, No. 1, p. 173. © Pleiades Publishing, Ltd., 2007.
Original Russian Text © A.G. Morachevskii, M.S. Kokhatskaya, 2007, published in Zhurnal Prikladnoi Khimii, 2007, Vol. 80, No. 1, p. 174.

BOOK REVIEWS

Medvedev, A.S., *Vyshchelachivanie i sposoby ego intensifikatsii* (Leaching and Methods for Intensification of This Process)

Moscow: Mosk. Gos. Inst. Stali i Splavov, 2005, 240 pp.

DOI: 10.1134/S1070427207010375

Hydrometallurgical processes presently occupy an important place in manufacture of a large number of nonferrous metals, including aluminum, zinc, uranium and thorium, tungsten and molybdenum, tantalum and niobium, zirconium and hafnium, rare-earth metals, gold and silver, platinum-group metals, indium, thallium, rhenium, and others. In some countries, hydrometallurgical processes are employed to manufacture a considerable amount of copper, nickel, cobalt, and zinc. The main procedure predetermining the extent of metal recovery from ores and secondary raw materials in their hydrometallurgical processing is leaching, i.e., selective dissolution of one or several components of a raw material with an aqueous solvent (water or solutions of acids, alkalis, and salts).

The monograph by A.S. Medvedev, totally devoted to leaching and methods for intensification of this process, comprises a preface, three chapters, conclusion, and bibliographic list containing 304 references. The preface (pp. 4–6) describes specific features of the leaching process. Chapter 1 (pp. 7–74) is devoted to theoretical foundations of leaching processes. The author describes the thermodynamics and kinetics of leaching and presents a number of examples illustrating kinetic features of the processes. Chapter 2 (pp. 75–178) describes quite a number of preparatory procedures that intensify leaching. To these belong thermal, mechanical, ultrasonic, and radiation treatments. Despite the specific nature of each kind of treatment, their common feature is that they give rise to structural defects in solids and disrupt the structure of liquids. The presentation is accompanied by a large number of examples. Particular attention is given to description of the influence exerted by mechanical treatment of minerals on their structure and reactivity. Chapter 3 (pp. 179–218) discusses methods for mechanical, ultrasonic, and radiation treatment of pulp in the course of leaching. The brief conclusion (pp. 219–221) summarizes the main results obtained in analyzing the methods for intensification of leaching.

The monograph by Medvedev is provided with an extensive bibliography (pp. 222–239), but, unfortunately, most of references are to publications older than 30 years. The number of references to studies published later than 1995 does not exceed 10 (out of 304).

The book summarizes and analyzes a vast body of experimental data on leaching of widely diverse materials. It seems, however, that the author's desire to make scientific to the maximum possible extent the presentation of purely technological information is not always successful. It is hardly necessary to invoke Einstein's or Landau's concepts for explaining the effect of additives on leaching of scheelite, tungstite, or uranium ore or to calculate the "probability of a fluctuation changing the entropy of an equilibrium system" (p. 71).

The book by Medvedev has been published in the series "Metallurgy and Materials Science in the XXI Century," devoted to the 75th anniversary of the foundation of Moscow Institute of Steel and Alloys (Technological University). The book is primarily intended for technologists-engineers and research workers of metallurgical and chemical industries. It may also be of use for teachers, postgraduate students, undergraduates of metallurgical and chemical-technological higher-school institutions.

A. G. Morachevskii and M. S. Kokhatskaya

ISSN 1070-4272, Russian Journal of Applied Chemistry, 2007, Vol. 80, No. 2, pp. 175–180. © Pleiades Publishing, Ltd., 2007.
Original Russian Text © D.V. Makarov, A.T. Belyaevskii, Yu.P. Men'shikov, D.P. Nesterov, M.F. Yusupova, 2007, published in Zhurnal Prikladnoi Khimii, 2007, Vol. 80, No. 2, pp. 177–182.

INORGANIC SYNTHESIS AND INDUSTRIAL INORGANIC CHEMISTRY

A Study of the Mechanism and Kinetics of Interaction between Nepheline Powder and Ammonium Hydrofluoride

D. V. Makarov, A. T. Belyaevskii, Yu. P. Men'shikov, D. P. Nesterov, and M. F. Yusupova

Tananaev Institute of Chemistry and Technology of Rare Elements and Mineral Resources, Kola Scientific Center, Russian Academy of Sciences, Apatity, Murmansk oblast, Russia

Received September 4, 2006

Abstract—Behavior of a skeleton silicate, nepheline, in the reaction of fluorination with ammonium hydrofluoride was studied by means of differential-thermal, X-ray phase, and chemical analyses, IR spectroscopy, and scanning electron microscopy.

DOI: 10.1134/S1070427207020012

As shown by numerous studies [1–8], use of fluoride metallurgy may favor a more intensive development of a closed technology for processing of mineral raw materials and a transition to conditioning of waste or its components into products compatible with ecologically safe technologies.

However, practical development of hydrofluoride methods for processing of various ores and concentrates requires more detailed and specific evidence about mechanisms and kinetics of interaction of both ores and rock-forming minerals with NH_4HF_2. It has been found, in particular, that many ore minerals are fluorinated under more severe conditions, compared with silicates [1, 7]. This offers an opportunity to perform desilicification of concentrates, e.g., at lower temperatures (below the melting point of ammonium hydrofluoride), without evolution of NH_4F into the gas phase in the first stage.

It was shown in [4] that decomposition of island silicates is the most difficult process. Complete fluorination of such minerals with NH_4HF_2 is achieved in Teflon autoclaves at 200°C. At the same time, it has been found [8] that the structure of magnesium silicates has no noticeable effect on the fluorination process.

It is, therefore, of indubitable interest to study specific features of interaction between a set of silicate minerals of varied structure with ammonium hydrofluoride.

In this study, the behavior of powdered nepheline in the reaction of fluorination was examined. Nepheline (simplified formula $Na_3K[AlSiO_4]_4$) is a mineral with aluminosilicate tetrahedra (skeleton silicate), which belongs to the hexagonal crystal system. The structure of minerals that belong to the nepheline group is based on a tetrahedral skeleton of the type of high-temperature tridymite, in which half of Si atoms are substituted by Al and lattice voids are filled with alkali metal cations neutralizing the negative charge of the skeleton [9].

A nepheline concentrate containing (wt %): SiO_2 44.28, Al_2O_3 29.48, and Na_2O 13.28, and the monomineral fraction of nepheline from a rock sample from the Khibiny massif were used in the study. As the fluorinating agent served twice recrystallized ammonium hydrofluoride NH_4HF_2 of analytically pure grade.

The thermogravimetric analysis was carried out on a Q-1500D derivatograph (Hungary) in air in the dynamic and quasi-isothermal modes. The X-ray phase analysis (XPA) of the reaction products was made on a DRON-2 diffractometer with Cu_{K_α} radiation. The IR spectral study was performed on a UR-20 instrument.

The surface of particles of nepheline powder and reaction products was analyzed by means of digital scanning electron microscopy (SEM) on a computerized LEO-420 electron microscope (Germany) [10].

To study the degree of decomposition of the mineral after leaching, the solid residue was spectro-

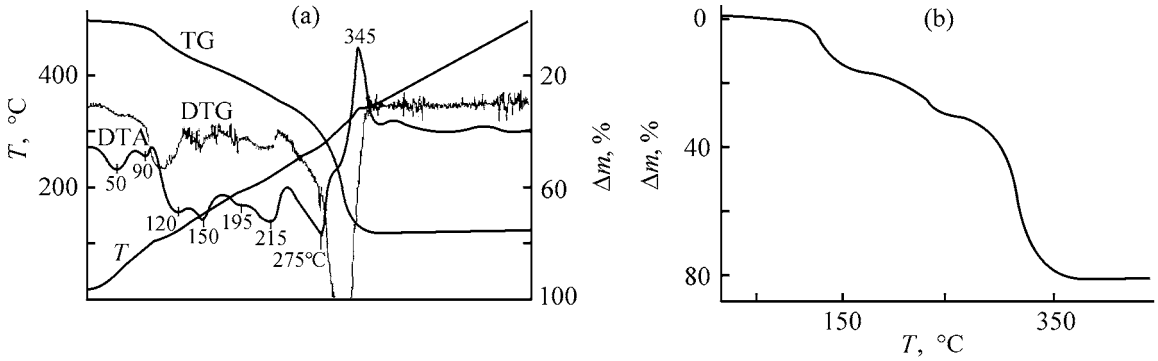

Fig. 1. (a) Derivatogram of a mixture of nepheline and ammonium hydrofluoride and (b) thermogravigram measured in the quasi-isothermal mode. Molar ratio 1 : 7. (*T*) Temperature and (Δ*m*) mass loss.

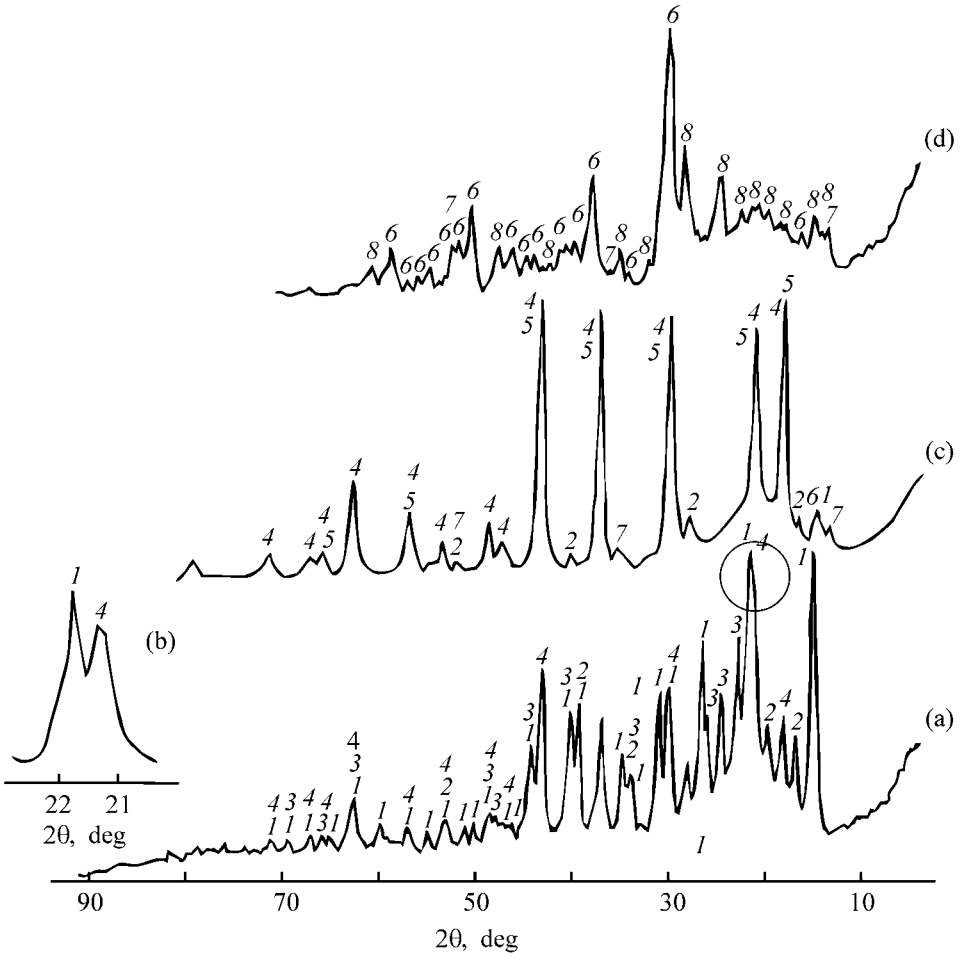

Fig. 2. X-ray diffraction patterns of products formed in the reaction of nepheline with ammonium hydrofluoride upon isothermal keeping at different temperatures. (2θ) Bragg angle; the same for Fig. 5. Keeping temperature (°C): (a, b) 150, (c) 275, and (d) 345. Reflection: (*1*) $(NH_4)_3SiF_7$, (*2*) $(NH_4)_3AlF_6$, (*3*) NH_4F, (*4*) $(NH_4)_2NaAlF_6$, (*5*) $(NH_4)_2SiF_6$, (*6*) $Na_5Al_3F_{14}$, (*7*) NH_4AlF_4, and (*8*) $NaAlF_4$. The measurement at Bragg angles 2θ = 20°–23° with a step of 0.02° made it possible to resolve reflections belonging to $(NH_4)_3SiF_7$ and $(NH_4)_2NaAlF_6$ (b).

photometrically analyzed for the content of silicon (SF-46) by determining the blue complex with Mohr's salt.

Figure 1a shows a derivatogram of the mixture of nepheline and NH_4HF_2, taken in the 1 : 7 molar ratio. The DTA curves exhibit a number of endo- and exo-

thermic effects. The fluorination process starts at temperatures exceeding 40°C and becomes considerably more intensive upon the melting of ammonium hydrofluoride (endothermic effect with a minimum at 120°C). The interaction accompanied by loss of mass ends in a strong exothermic effect peaked at 345°C. Further, no loss of mass occurs in the temperature range 350–500°C.

The thermogravigram obtained in the quasi-isothermal mode shows a set of plateaus (Fig. 1b). To determine the composition of intermediate reaction products, experiments with slow heating (at about 1 deg min^{-1}) and isothermal keeping for 1.5 h at 150, 275, and 345°C were performed.

In the X-ray diffraction pattern of the mixture kept at 150°C, the compounds $(NH_4)_2SiF_6$ and $(NH_4)_3AlF_6$ were identified and reflections were observed that can be attributed to $(NH_4)_2NaAlF_6$ [11] (Figs. 2a, 2b). According to [11], the last compound decomposes at 240–360°C by the scheme

$$5(NH_4)_2NaAlF_6 = Na_5Al_3F_{14} + 2NH_4AlF_4 + 8HF\uparrow + 8NH_3\uparrow,$$

$$NH_4AlF_4 = AlF_3 + HF\uparrow + NH_3\uparrow. \quad (1)$$

At 275°C, the compounds $(NH_4)_2SiF_6$ and $(NH_4)_3AlF_6$ and a minor amount of NH_4AlF_4 were found. Trace amounts of chiolite $Na_5Al_3F_{14}$, formed in thermal decomposition of $(NH_4)_2NaAlF_6$, which begins under these conditions (Fig. 2c), were observed. At 345°C, $Na_5Al_3F_{14}$, $NaAlF_4$, and NH_4AlF_4 are identified (Fig. 2d).

Figure 3a shows the IR spectrum of a nepheline sample. The absorption bands at 472, 513, 700, 1000, and 1090 cm^{-1} correspond to vibrations of the crystal lattice of the mineral [12]. Figure 3b shows the spectrum of a mixture of nepheline and ammonium hydrofluoride kept at 150°C for 2 h. The spectrum contains bands at 1230 and 1440 cm^{-1}, which are associated with deformation vibrations of $[NH_4]^+$ and HF_2^- ions [13]. The bands at 3040 and 3145 cm^{-1} correspond to stretching vibrations of the $[NH_4]^+$ ion. The bands at 480 and 730 cm^{-1} are associated with vibrations of the $[SiF_6]^{2-}$ octahedron in the compound $(NH_4)_3SiF_7$. The bands at 410 and 580–590 cm^{-1} correspond to vibrations of the $[AlF_6]^{3-}$ octahedron. No bands related to nepheline or other silicates are observed in the spectrum, and, consequently, silicon is completely bound into silicon heptafluorosilicate.

Thus, the stages of fluorination of the nepheline powder and subsequent decomposition of intermediate products can be represented by the equations

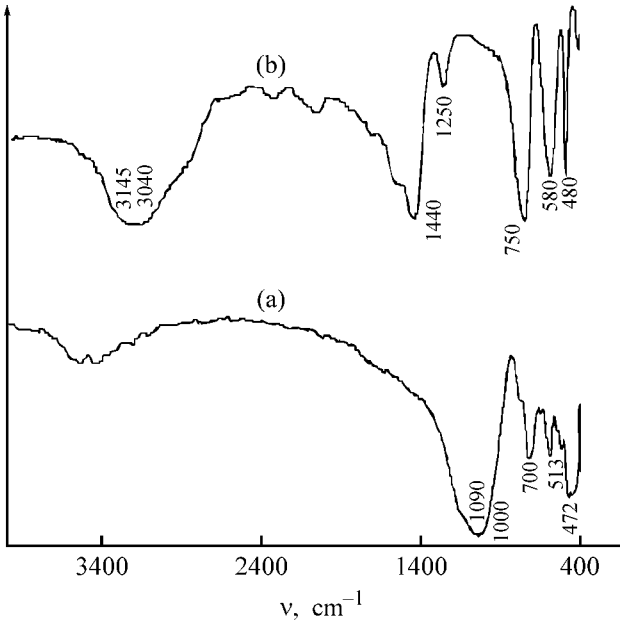

Fig. 3. IR spectra of (a) nepheline and (b) a mixture of nepheline and NH_4HF_2 at 150°C. (ν) Wave number.

$$(1 + n)NaAlSiO_4 + 6.5(1 + n)NH_4HF_2 = n(NH_4)_3AlF_6 + (1 + n)(NH_4)_3SiF_7 + (NH_4)_{2-n}Na_{1+n}AlF_6 + 1.5(1 + n)NH_3 + 4(1 + n)H_2O, \quad (2)$$

$$(NH_4)_3SiF_7 = (NH_4)_2SiF_6 + NH_3\uparrow + HF\uparrow, \quad (3)$$

$$(NH_4)_2SiF_6 = SiF_4\uparrow + 2NH_3\uparrow + 2HF\uparrow, \quad (4)$$

$$(NH_4)_{2-n}Na_{1+n}AlF_6 = (1 + n)Na_5Al_3F_{14} + (1 + n)NaAlF_4 + (2 - 4n)NH_4AlF_4 + (10 - 2n)NH_3\uparrow + (10 - 2n)HF\uparrow, \quad (5)$$

$$(NH_4)_2AlF_6 = NH_4AlF_4 + 2NH_3\uparrow + 2HF\uparrow. \quad (6)$$

The scheme presumes that sodium is in a certain excess with respect to aluminum in the compound $(NH_4)_{n-2}Na_{1+n}AlF_6$.

To elucidate the mechanism of the first stage, a mixture of nepheline particles with ammonium hydrofluoride, taken in a molar ratio of 1 : 0.5 and kept at 150°C for 1.5 h, was subjected to SEM analysis (Fig. 4). The deficiency of ammonium hydrofluoride with respect to the stoichiometry of reaction (2) enables a more detailed examination of changes in the surface morphology of particles of the mineral and reaction products. It can be seen that nepheline grains are covered by reaction products, with the characteristic cracking of the newly formed phases. The depth

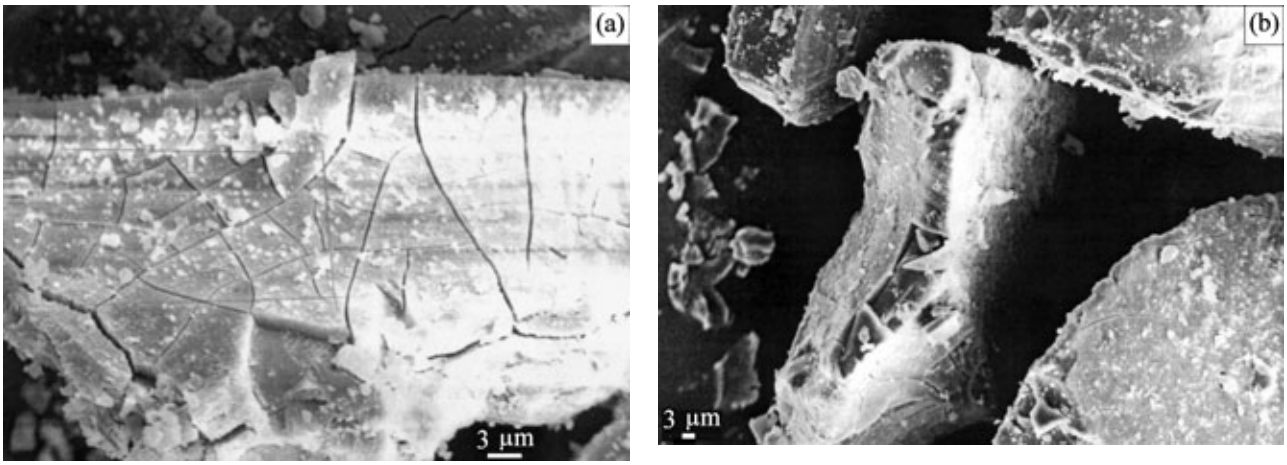

Fig. 4. SEM micrographs of particles of a mixture of nepheline and reaction products on keeping the mixture at 150°C. (a) Cracking of the reaction products on the nepheline surface and (b) depth of interaction.

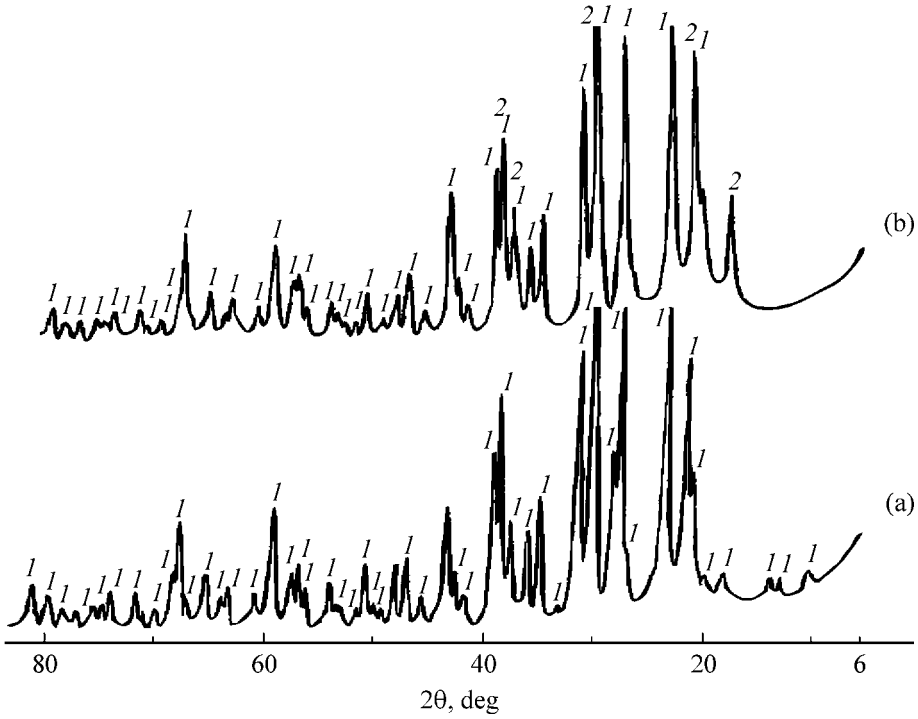

Fig. 5. X-ray diffraction pattern of (a) nepheline and (b) 1 : 0.5 mixture of nepheline and NH_4HF_2, kept at 150°C. Reflection: (*1*) nepheline and (*2*) a phase isostructural with $(NH_4)_2NaAlF_6$.

of interaction can be traced (Fig. 4). Thus, it may be assumed that the fluorination process is limited by diffusion within the layer of a solid product. XPA was used to determine the composition of the reaction products. It was found that, in addition to the nepheline reflections, a compound isostructural with $(NH_4)_2NaAlF_6$ is identified (Fig. 5). It is noteworthy that reflections associated with $(NH_4)_3SiF_7$ are not observed in the diffraction pattern. Thus, it may be assumed that the fluorination of nepheline begins with disintegration of aluminum-oxygen tetrahedra, with Na^+ contained in the structural voids entering into the composition of the hexafluoroaluminate being formed.

The kinetics of nepheline fluorination was studied in the temperature range 130–170°C. The specific surface area of nepheline was 0.21–0.26 $m^2\ g^{-1}$. Kinetic curves were plotted by measuring the loss of mass. The conversion was calculated by the equation

$$\alpha = \Delta m/m_{theor}. \quad (7)$$

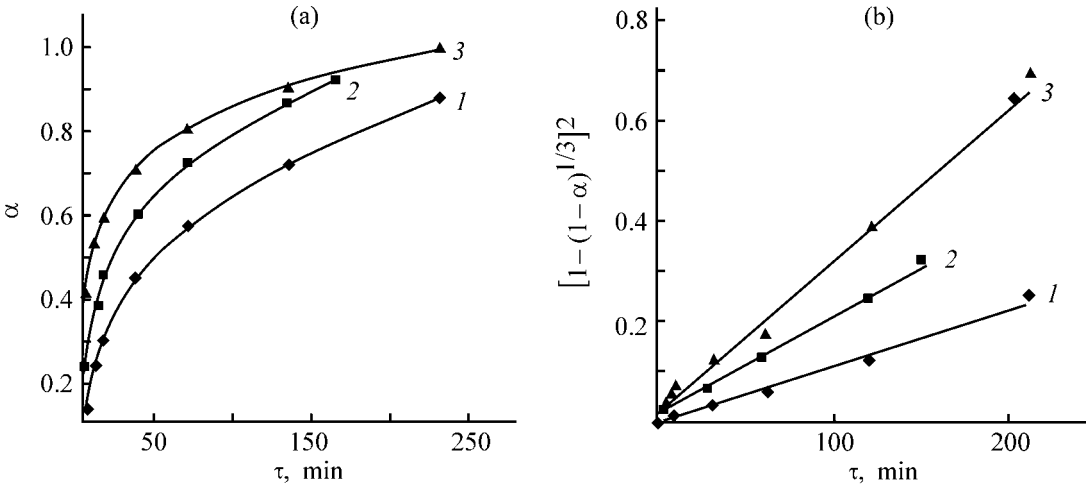

Fig. 6. (a) Degree of nepheline decomposition, α, vs. time τ and (b) kinetic curves of fluorination, plotted in the coordinates $[(1 - (1 - \alpha)^{1/3})^2]$–τ. Temperature (°C): (*1*) 130, (*2*) 150, and (*3*) 170.

The variable Δm was found as the difference of masses, initial and obtained as a result of a reaction in the stock; m_{theor} was calculated using the reaction equation corresponding to the initial stage of fluorination. Control runs, in which the residual amount of nepheline in the mixture was determined by chemical analysis, yielded closely similar results. The run of the curves indicates that, for all the temperatures studied, the duration of the autocatalytic process and its contribution to the overall balance of the process, are negligibly small (Fig. 6a). This, in particular, may take place at a sufficiently high probability of nucleation of a new phase on the surface of a crystalline body. All the transformations occur during the averaged front (The reaction rate decreases because the front motion toward the particle center is accompanied by a decrease in the area of the phase boundary.). The fraction of nepheline fluorinated at 130°C in 210 min, in melting of ammonium hydrofluoride, is 87%; at a temperature raised by 20°C, the conversion of nepheline is 92%; and at 170°C, nepheline is virtually completely transformed into a mixture of fluorides.

With account of the results of SEM diagnostics, the kinetic data were processed using the parabolic equation of a shrinking sphere

$$[1 - (1 - \alpha)^{1/3}]^2 = k\tau,$$

which is used in kinetics to describe topochemical reactions occurring simultaneously over the entire surface (Fig. 6b) [14]. The slope of the curves was used to find the apparent rate constants of fluorination; the apparent activation energy E_a^* was calculated by the Arrhenius equation, with the initial values of the pre-exponential factor found by the least-squares procedure for the linearized form of this equation. The calculated kinetic parameters of the nepheline fluorination process are given below:

$$E_a^* = 35.922 \text{ kJ mol}^{-1}$$

Temperature, °C	130	150	170
Rate constant, min^{-1}	0.0697	0.1218	0.1832

The process occurs under the ionic-diffusion control. Thus, an increase in the degree of cracking of the mineral and in the number of defects in the crystal lattice makes the reaction rate faster.

CONCLUSIONS

(1) The process of nepheline fluorination was studied using a set of physicochemical methods. It was found that, initially, aluminum-oxygen tetrahedra disintegrate, with Na^+ contained in voids of the structure entering into the composition of the hexafluoroaluminate $(NH_4)_{2-n}Na_{1+n}AlF_6$ being formed.

(2) Intermediate reaction products were identified and the temperatures of their formation and thermal decomposition were determined.

(3) Kinetic studies of nepheline fluorination demonstrated that, in the temperature range 130–170°C, transformations occur in the averaged-front mode. It was found that the process occurs under the ionic-diffusion control. The apparent activation energy is 35.9 kJ mol^{-1}.

REFERENCES

1. Rakov, E.G., *Ftoridy ammoniya* (Ammonium Fluorides), Moscow: VINITI, 1988.
2. Rakov, E.G., *Tsvet. Met.*, 1985, no. 11, pp. 55–58.
3. Mel'nichenko, E.I., *Ftoridnaya pererabotka redkometall'nykh rud Dal'nego Vostoka* (Fluoride Processing of Rare-Metal Ores of the Far East), Vladivostok: Dal'nauka, 2002.
4. Kurilenko, L.N., Interaction of Silicon-containing Minerals with Ammonium Hydrofluoride, *Cand. Sci. Dissertation*, Vladivostok, 2003.
5. Rimkevich, V.S., Malovitskii, Yu.N., Dem'yanova, L.P., et al., *Kompleksnaya pererabotka netraditsionnogo titano-redkometall'nogo i alyumosilikatnogo syr'ya* (Integrated Processing of Unconventional Titanium–Rare-Metal and Aluminosilicate Raw Materials), Apatiy: Kola Nauchn. Tsentr Ross. Akad. Nauk, 2006, pp. 214–220.
6. Solov'ev, A.I., Malyutina, V.M., Rikhvanov, L.P., et al., *Gorn. Zh., Tsv. Met.: Special issue*, 2006, no. 4, pp. 52–56.
7. Nesterov, D.P., Prokhorova, N.I., and Makarov, D.V., *Mineralogiya vo vsem prostranstve sego slova: Trudy II Fersmanovskoi nauchnoi sessii Kol'skogo otdeleniya Rossiiskogo Mineralogicheskogo Obshchestva* (Mineralogy in the Full Meaning of This Word: Pro. Fersman Sci. Meeting of Kola Division of the Russian Mineralogical Society), Apatity: K & M, 2005, pp. 167–169.
8. Nesterov, D.P., Makarov, D.V., and Kalinnikov, V.T., *Zh. Neorg. Khim.*, 2006, vol. 51, no. 5, pp. 780–784.
9. *Mineraly: Spravochnik* (Minerals: Reference Book), Moscow: Nauka, 2003, vol. 5, issue 2.
10. Belyaevskii, A.T., *Elektronometriya morfologii chastits poroshkovykh materialov* (Electronometry of the Particle Morphology of Powdered Materials), St. Petersburg: RA–AVIKA OOO, 2004.
11. Morozov, V.G., Popova, R.A., Shchegoleva, R.I., et al., *Fiziko-khimicheskie issledovaniya soedinenii, metallov i ikh splavov* (Physicochemical Studies of Compounds, Metals, and Metal Alloys), Apatity: Kola Filial Akad. Nauk SSSR, 1981, pp. 123–130.
12. Farmer, V.C., *The Infra-Red Spectra of Minerals, Mineralogical Society*, 1974.
13. Nakamoto, K., *Infrared Spectra of Inorganic and Coordination Compounds*, New York: John Wiley & Sons, 1963.
14. Rakov, E.G. and Teslenko, V.V., *Pirogidroliz neorganicheskikh ftoridov* (Pyrohydrolysis of Inorganic Fluorides), Moscow: Energoatomizdat, 1988.

ISSN 1070-4272, Russian Journal of Applied Chemistry, 2007, Vol. 80, No. 2, pp. 181–184. © Pleiades Publishing, Ltd., 2007.
Original Russian Text © V.A. Matveev, 2007, published in Zhurnal Prikladnoi Khimii, 2007, Vol. 80, No. 2, pp. 183–186.

INORGANIC SYNTHESIS AND INDUSTRIAL INORGANIC CHEMISTRY

Hydrolysis of Aluminum Sulfates in the Presence of Ammonium Sulfite

V. A. Matveev

Tananaev Institute of Chemistry and Technology of Rare Elements and Mineral Raw Materials, Kola Scientific Center, Russian Academy of Sciences, Apatity, Murmansk oblast, Russia

Received September 4, 2006

Abstract—Hydrolysis of aluminum sulfate and potash alum in the presence of an ammonium sulfite additive in the temperature range T_{boil}–200°C was studied. A possible reaction mechanism was suggested. The composition and structure of the precipitates formed were determined and certain differences in their morphology were noted. Recommendations for practical implementation of the method of hydrolytic recovery of aluminum from solutions of its sulfate salts were given.

DOI: 10.1134/S1070427207020024

Hydrolysis of aluminum sulfates is the most widespread method for recovery of aluminum(III) from solutions in sulfuric acid processing of aluminum-containing raw materials into alumina [1–5]. It has been found that aluminum sulfates can be arranged in order of increasing susceptibility to hydrolysis as follows: aluminum sulfate < ammonium alum < sodium alum < potash alum [6].

The effect of additions of ammonium, sodium, and potassium sulfates on the hydrolysis of aluminum sulfate has been studied [7, 8]. It was shown that the cations can be arranged in order of increasing effect on the degree of hydrolysis as follows: $H^+ < NH_4^+ < Na^+ < K^+$. It was noted that the ionic radii increase in the same order, which suggests that the solubility of basic aluminum salts decreases as the ionic radius of cations becomes larger.

The effect of temperature has been studied in detail. It was found that a noticeable precipitation of the basic aluminum sulfate is observed only at $T >$ 200°C. For example, according to [6], the degree of hydrolysis of potash alum $KAl(SO_4)_2$, which is the most susceptible to hydrolysis, does not exceed 84% at 240°C. The process is hindered by accumulation of sulfuric acid in solution.

High-temperature hydrolysis involves a large power expenditure and requires an intricate equipment (autoclaves working under a pressure $P > 30$ atm). This is one of the principal reasons why the hydrolytic recovery of basic aluminum salts from sulfate solutions has not been implemented in practice so far. Therefore, it is a topical task to develop procedures that would increase the degree of aluminum(III) extraction into a precipitate of a basic salt, with a simultaneous pronounced decrease in the hydrolysis temperature.

In this study, the hydrolysis of aluminum sulfate (AS) and potash alum (PA) in the presence of ammonium sulfite was examined.

Ammonium sulfite was obtained by bubbling sulfur dioxide through a concentrated solution of ammonium hydrate. As the solution was saturated, ammonium sulfite monohydrate $(NH_4)_2SO_3 \cdot H_2O$ precipitated, which was confirmed by chemical, X-ray phase, and IR spectroscopic analyses. According to [9], ammonium sulfite obtained by various methods contains up to 9–9.4% ammonium sulfate. Therefore, it was taken that the content of the main substance in the resulting salt is 95 wt %. The solution containing 10 wt % ammonium sulfite had pH = 8.2–8.4.

For the experiments, we prepared AS and PA (analytical grade) solutions containing 80 g l^{-1} of Al_2O_3, which is characteristic of solutions obtained by processing aluminosilicate raw materials. The expenditure of ammonium sulfite varied from 0.5 to 2 mol per mole of Al_2O_3. The experimental temperature range was from T_{boil} to 200°C (the boiling points of AS and PA solutions were 103 and 105°C, respectively). The duration of the process at the boiling points of the solutions was 4 h. Hydrolysis at 125, 150, 175, and

Parameters of hydrolysis of aluminum sulfate and potash alum

T, °C	Expenditure of ammonium sulfite, mol mol^{-1} Al_2O_3	Degree of salt hydrolysis, %	
		AS	PA
T_{boil}	–	–	–
	0.5	15.5	46.7
	1.0	42.7	74.9
	1.5	54.9	84.5
	2.0	61.9	88.3
125	–	–	39.5
	0.5	17.2	78.4
	1.0	44.9	86.3
	1.5	58.0	90.7
	2.0	67.9	94.1
150	–	–	58.3
	0.5	22.9	87.5
	1.0	57.1	97.4
	1.5	79.8	98.1
	2.0	85.9	98.8
175	–	–	70.7
	0.5	37.7	92.4
	1.0	61.2	98.2
	1.5	83.6	99.0
	2.0	90.8	99.2
200	–	–	76.9
	0.5	43.7	93.9
	1.0	72.8	99.1
	1.5	87.7	99.3
	2.0	93.0	100.0

200°C was carried out in autoclave bombs, into which 40 ml of a solution was charged and a necessary amount of ammonium sulfite was added. Then the bombs were kept at a prescribed temperature for 1.5 h. The solutions were agitated by tumbling rotation of the bombs. After the process was complete, the autoclave was cooled and the precipitate formed was filtered off, thoroughly washed, and dried to constant weight at 105°C. The precipitates and solutions were analyzed for the content of Al_2O_3. The experimental data listed in the table clearly demonstrate that ammonium sulfite most strongly affects the hydrolysis of aluminum sulfates. No basic aluminum sulfate was precipitated on heating an aluminum sulfate solution up to 200°C.

The addition of ammonium sulfite results in a sharp shift of the reaction equilibrium toward hydrolysis. At the minimum expenditure of the sulfite (0.5 mol per mole of Al_2O_3), a precipitate is formed even at the boiling point of the solutions. At the same temperature, an increase in the expenditure of ammonium sulfite from 0.5 to 2.0 mol per mole of Al_2O_3 results in that the degree of hydrolysis grows by a factor of 2.1–4. At the boiling point (103°C) and an expenditure of ammonium sulfite equal to 1.0 mol per mole of Al_2O_3, a higher degree of hydrolysis (42.7%) is reached, compared with the case of hydrolysis of aluminum sulfate at 230°C, but in the absence of ammonium sulfite (23.2%) [7]. The fullest and technologically acceptable recovery of aluminum(III) into a precipitate of the basic sulfate salt (90.8–93.0%) occurs at an expenditure of ammonium sulfite equal to 2.0 mol per mole of Al_2O_3 and 175–200°C. It is apparent that a virtually complete hydrolysis of aluminum sulfate can be achieved by further raising the temperature.

It is seen from the data obtained that the effect of ammonium sulfite on the PA hydrolysis is more clearly pronounced than that in hydrolysis of aluminum sulfate. At the boiling point (expenditure of ammonium sulfite equal to 1–2 mol per mole of Al_2O_3), the recovery of aluminum(III) into a precipitate of the basic salt reaches 75–88%; the degree of hydrolysis is 86–94% at 125°C and a virtually complete recovery of aluminum(III) into a precipitate of the basic salt is reached at 150°C and higher temperatures.

The role of ammonium sulfite in the hydrolysis of aluminum sulfates is as follows. In an aqueous solution, aluminum sulfate and potash alum are hydrolyzed in accordance with the equation

$$Al_2(SO_4)_3 + 2nH_2O \rightleftarrows Al_2(OH)_{2n}(SO_4)_{3-n} + nH_2SO_4, \quad (1)$$

where $0 < n \leq 3$.

The forming sulfuric acid reacts with ammonium sulfite introduced into a solution in accordance with the equation

$$nH_2SO_4 + n(NH_4)_2SO_3 \rightarrow n(NH_4)_2SO_4 + nH_2O + nSO_2\uparrow, \quad (2)$$

with the weaker sulfurous acid displaced and ammonium sulfate formed. Being unstable, sulfurous acid readily decomposes into H_2O and SO_2. A part of SO_2, which corresponds to its solubility at a given temperature, remains in the solution, whereas its main part is discharged into the gas phase. As a result, the acid is not accumulated in the solution, and the equilibrium of reaction (1) is shifted toward hydrolysis of aluminum salts.

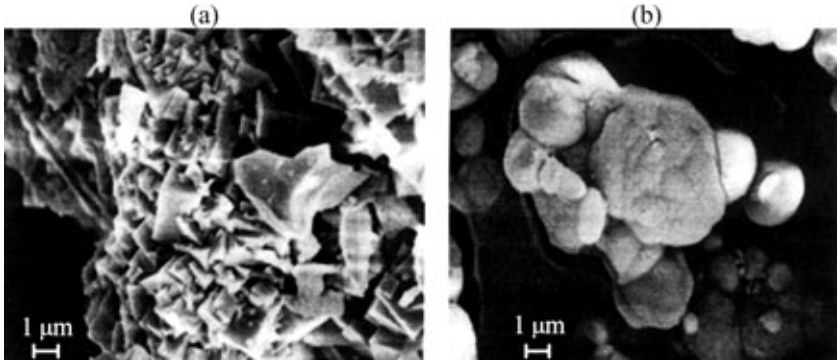

Fig 1. Micrographs (×10000) of basic aluminum sulfates obtained in hydrolysis of potash alum; (a) in the absence of ammonium sulfite and (b) in the presence of ammonium sulfite.

Summing up the left- and right-hand parts of Eqs. (1) and (2), we obtain the following equation of the hydrolysis reaction.

$$\begin{aligned} &Al_2(SO_4)_3 + n(NH_4)_2SO_3 + nH_2O \\ &\rightarrow Al_2(OH)_{2n}(SO_4)_{3-n} + n(NH_4)_2SO_4 \\ &\quad + nH_2SO_3,\ (nH_2O + nSO_3), \end{aligned} \tag{3}$$

where $0 < n \leq 2$.

In this scheme, one of the conditions for a shift of the equilibrium toward hydrolysis is satisfied: the forming sulfuric acid is continuously bound into a neutral compound.

When there is no free sulfuric acid, ammonium sulfite enters into an exchange reaction directly with aluminum sulfate or potash alum in accordance with the equation (for the example of aluminum sulfate)

$$\begin{aligned} &Al_2(SO_4)_3 + n(NH_4)_2SO_3 \\ &\rightarrow Al_2(SO_4)_{3-n}(SO_3)_n + n(NH_4)_2SO_4 \end{aligned} \tag{4}$$

($0 < n \leq 2$) to form aluminum sulfate-sulfite, which is hydrolyzed by the reaction

$$\begin{aligned} &Al_2(SO_4)_{3-n}(SO_3)_n + 2nH_2O \\ &\rightarrow Al_2(OH)_{2n}(SO_4)_{3-n} + nH_2O + nSO_2\uparrow. \end{aligned} \tag{5}$$

The overall reaction equation is similar to Eq. (3):

$$\begin{aligned} &Al_2(SO_4)_3 + n(NH_4)_2SO_3 + nH_2O \\ &\rightarrow Al_2(OH)_{2n}(SO_4)_{3-n} + n(NH_4)_2SO_4 \\ &\quad + nH_2SO_3,\ (nH_2O + nSO_2\uparrow), \end{aligned} \tag{6}$$

where $0 < n \leq 2$.

According to this scheme, the process goes through a stage of formation of an intermediate salt that is more susceptible to hydrolysis than the starting aluminum sulfate or PA.

As the reactions of ammonium sulfite with sulfuric acid and aluminum sulfate or potash alum occur simultaneously and yield the same products, it is impossible to determine the priority of a particular reaction pathway.

The composition of the basic salts formed in hydrolysis of aluminum sulfate and potash alum in the presence of ammonium sulfite is close to the formula $(H_2O, NH_3, R_2O) \cdot 3Al_2O_3 \cdot 5SO_3 \cdot 9H_2O$, where R is Na or K. According to the X-ray phase analysis, all the basic sulfates formed have a similar structure analogous to that of natural rock alum. The basic salt produced in hydrolysis of aluminum sulfate is an isomorphous mixture of ammonium and hydrogen rock alums, and that formed in hydrolysis of potash alum is potassium rock alum with a minor admixture of ammonium rock alum.

The electron micrographs of basic aluminum sulfates formed in hydrolysis of potash alum in the absence (Fig. 1a) and presence (Fig. 1b) of ammonium sulfite show different shapes of the resulting particles. According to the crystal-optical analysis, the particles obtained in the first case are polycrystalline formations with a refractive index $N = 1.575$. A slight tendency for individual grains to have a rounded oval shape is seen. In the second case, the overwhelming part of particles are isometric (rounded) grains with $N = 1.510$.

The study performed is of technological importance. It is shown for the first time that aluminum sulfates can be hydrolyzed with virtually complete precipitation of aluminum(III) basic salts at compara-

tively low temperatures (150°C), which allows the process to be carried out in standard chemical apparatus working at pressures of up to 6 atm. The suggested method of hydrolysis also furnishes a real opportunity for preparation of basic aluminum sulfates with a decreased content of iron. Furthermore, there are prerequisites for regeneration of ammonium sulfite and its recycling.

CONCLUSIONS

(1) A study of the effect of ammonium sulfite on the hydrolysis of aluminum sulfate and potash alum in the temperature range from T_{boil} to 200°C demonstrated that the role of ammonium sulfite consists in that it reacts both with the forming sulfuric acid and directly with aluminum sulfate or potash alum. In the first case, sulfuric acid is bound, whereas in the second, intermediate compounds more susceptible to hydrolysis, compared with the starting salts, are formed. As a result the reaction equilibrium is shifted toward a fuller hydrolysis.

(2) Parameters of the hydrolysis process were determined: at an expenditure of ammonium sulfite equal to 1–2 mol per mole of Al_2O_3 at 150°C, potash alum is almost completely hydrolyzed. In hydrolysis of aluminum sulfate under similar conditions, the recovery of aluminum(III) into a precipitate of a basic sulfate reaches almost 86%.

(3) It was found that all the basic aluminum salts formed are similar in composition and structure to the natural mineral rock alum.

(4) The comparatively low hydrolysis temperature and the possibility of using the standard equipment create real prerequisites for implementation of the method in sulfuric acid processing of alumina-containing raw materials.

ACKNOWLEDGMENTS

This study was financially supported by the "Leading Scientific Schools" Program (project no. NSh-4383.2006.3) and by the regional Collective Use Center "Materials Science and Diagnostics in High Technologies."

REFERENCES

1. Bretsznajder, St. and Kawecki, W. *Rocz. Chem.*, 1955, no. 29, pp. 287–299.
2. Scott, T.R., *J. Metals*, 1962, vol. 14, no. 2, pp. 9–13.
3. Kawecki, W., *Przem. Chem.*, 1965, vol. 44, no. 11.
4. USSR Inventor's Certificate, no. 941291.
5. Zapol'skii, A.K., *Sernokislotnaya pererabotka vysokokremnistogo alyuminievogo syr'ya* (Sulfuric Acid Processing of High-Silica Aluminum Raw Materials), Kiev: Naukova Dumka, 1981.
6. Eremin, N.I., *Tsvet. Met.*, 1968, no. 12, pp. 52–56.
7. Sazhin, V.S., Zapol'skii, A.K., and Zakharova, N.N., *Zh. Prikl. Khim.*, 1968, vol. 41, no. 7, pp. 1420–1423.
8. Kryzhanovskii, M.M. and Eremin, N.I., *Zh. Prikl. Khim.*, 1975, vol. 48, no. 12, pp. 2593–2595.
9. Averbukh, T.D., Telepneva A.E., Blyakher, I.G., and Gofman, M.S., *Tekhnologiya sul'fitov* (Technology of Sulfites), Moscow: Khimiya, 1984.

ISSN 1070-4272, Russian Journal of Applied Chemistry, 2007, Vol. 80, No. 2, pp. 185–188. © Pleiades Publishing, Ltd., 2007.
Original Russian Text © D.E. Chirkst, T.E. Litvinova, V.S. Starshinova, G.S. Roshchin, 2007, published in Zhurnal Prikladnoi Khimii, 2007, Vol. 80, No. 2, pp. 187–190.

INORGANIC SYNTHESIS AND INDUSTRIAL INORGANIC CHEMISTRY

Cerium(III) Extraction with Oleic Acid from Nitrate Solutions

D. E. Chirkst, T. E. Litvinova, V. S. Starshinova, and G. S. Roshchin

St. Petersburg Mining Institute, St. Petersburg, Russia

Received October 10, 2005; in final form, October 2006

Abstract—Cerium(III) extraction with oleic acid in *o*-xylene from nitrate solutions was studied. The extraction mechanism and the dependence of the distribution ratio on pH and composition of the organic and aqueous phases were examined. The thermodynamic characteristics of extraction were calculated.

DOI: 10.1134/S1070427207020036

The best studied among extractants used for recovery of REEs from nitrate solutions are organophosphorus compounds, mainly tributyl phosphate. However, with sulfuric [1] and hydrochloric [2–4] acids are more effective in leaching of lean ores and technologically produced raw materials and TBP is inefficient with these media [5].

REEs are present in acid solutions in the form of anionic complexes $[M(An)_x]^{3-zx}$, where An is anion, and x is the anionic charge equal to 1 or 2 [6]. Therefore, REEs are commonly recovered from acid solutions with anion-exchange extractants, mainly with carboxylic acids [7].

In this study, the characteristics of cerium(III) extraction with oleic acid from nitrate solutions were determined and compared with those of tributyl phosphate and trialkylbenzylammonium nitrate.

In our experiments, cerium(III) was extracted from aqueous nitrate solutions of Ce(III) with a concentration of 0.01 mol kg^{-1}, which is close to the REEs concentration in process solutions formed in extractive recovery of REE from depleted and technogenic raw materials. An 0.5 M solution of oleic acid in *o*-xylene was used as extractant. The dissociation constant of oleic acid is 1.25×10^{-6} [8]. The required pH was adjusted by adding sodium hydroxide or nitric acid. The REE concentration in the initial and equilibrium solutions was determined photometrically with Arsenazo III [9].

The cerium(III) concentration in the organic phase was determined from the difference between its concentrations in the initial solution and equilibrium aqueous phase with account of the difference between the volumes (weights) of the organic and aqueous phases

$$c_{org} = (c_0 - c_{aq})\frac{m_{aq}}{m_{org}} = (c_0 - c_{aq})\frac{V_{aq}}{V_{org}\rho_{org}}, \qquad (1)$$

where c_{org} and c_{aq} are the equilibrium concentrations (mol kg^{-1}) of metals in the organic and aqueous phases, respectively; c_0, REE concentration in the initial aqueous solution (mol kg^{-1}); V_{aq}/V_{org}, volume ratio of the aqueous and organic phases equal to 50 : 5; and the organic phase density $\rho_{orq} = 0.86 \pm 0.1$ g cm^{-3}.

The distribution ratio was calculated by the equation

$$D = c_{org}/c_{aq}. \qquad (2)$$

The data on cerium(III) extraction with 0.5 M oleic acid in *o*-xylene from nitrate solutions within the pH range 3–3.5 are listed in Table 1.

Table 1. Distribution ratios of Ce(III) D_{Ce} at various pH (initial Ce(III) concentration 0.014 mol kg^{-1}, pH 5)

pH	$c_{aq} \times 10^3$	$c_{org} \times 10^2$	D_{Ce}
	mol kg^{-1}		
3.0	13.1	0.9	0.65
3.5	9.6	4.4	4.52
4.0	8.9	5.1	5.81
4.4	6.4	7.6	11.78
4.5	4.7	9.3	19.70
4.8	1.7	12.3	71.67
5.0	1.3	12.7	98.89
5.5	0.6	13.4	235.00

Table 2. Distribution ratio of cerium(III) as a function of oleic acid concentration c_{ol} in the organic phase (initial Ce(III) concentration 0.014 mol kg^{-1}, pH 5)

c_{ol}, M	$c_{aq} \times 10^3$	$c_{org} \times 10^2$	D_{Ce}
	mol kg^{-1}		
0.1	4.7	2.2	4.60
0.2	3.1	4.9	15.69
0.3	2.7	8.0	29.10
0.4	1.8	11.4	63.21
0.5	1.4	14.6	103.28

The distribution ratios of Ce(III) were studied at constant pH 5.0 ± 0.1 in relation to the oleic acid concentration in the organic phase at the molar ratio of oleic acid and the metal equal to 4. The oleic acid concentration in the organic phase was varied by its dilution with *o*-xylene. The distribution ratios of Ce(III) at various oleic acid concentrations in the organic phase are listed in Table 2.

In special experiments, we found that the distribution ratio of cerium is not influenced by the nitrate concentration in the aqueous phase. This means that the cerium-containing extractable complex contains no nitrate anions. Oleic acid poorly dissociates in the organic phase. Therefore, extraction of Ce(III) can be regarded as consisting of the following steps: oleic acid first passes into aqueous phase where it dissociates to form cerium(III) oleate insoluble in water (pL = 12 [8]), but is readily soluble in the organic phase. Therefore, the extraction of cerium with oleic acid can be described by the equation of the following heterogeneous reaction:

$$M^{3+} + zH_2O + (3 - z)R^- \rightleftarrows M(OH)_zR_{3-z(org)} + zH^+. \quad (3)$$

The extraction constant is determined by the following equation

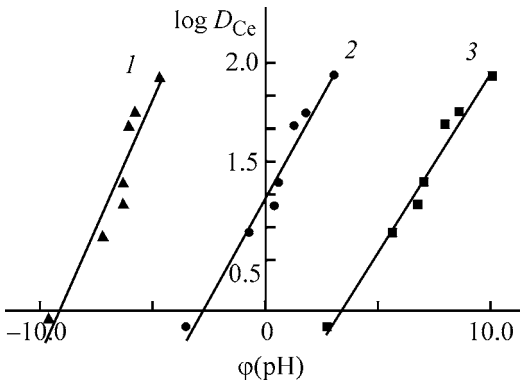

Fig. 1. Plot of the logarithm of the Ce ($\log D_{Ce}$) distribution ratio vs. φ(pH) [Eq. 10)] at z (*1*) 0, (*2*) 1, and (*3*) 2.

$$K = \frac{c_{org} a_{H^+}^z}{c_{aq} \gamma_{\pm} [R^-]^{3-z}} = \frac{D a_{H^+}^z}{\gamma_{\pm} [R^-]^{3-z}}, \quad (4)$$

where $\gamma_{\pm}$ is the mean ionic activity coefficient of REE nitrate in the equilibrium aqueous phase, and $[R^-]$ is the oleate anion concentration dependent on pH [8]:

$$[R^-] = \frac{[HR]_{org} K_d}{a_{H^+}}, \quad (5)$$

where K_d is the dissociation constant of oleic acid.

The concentration of the nondissociated oleic acid species in the organic phase $[HR]_{org}$ is determined by the equation

$$[HR]_{org} = c_{extr} - (3 - z)c_{org} - [R^-]_{org}, \quad (6)$$

where c_{extr} is the total extractant concentration in the organic phase; c_{org}, REE concentration in the organic phase; and $(3 - z)c_{org}$, concentration of the oleate anion bound in the extractable complex.

The equilibrium concentration of free oleate anions is determined by the equation obtained by joint solution of Eqs. (5) and (6):

$$[R^-]_{org} = \frac{c_{extr} - (3 - z)c_{org}}{\left(1 + \frac{a_{H_{aq}^+}}{K_d}\right)}. \quad (7)$$

On substitution of Eq. (7) in Eq. (4), the following equation is obtained:

$$K = \frac{D a_{H_{aq}^+}^z \left(1 + \frac{a_{H_{aq}^+}}{K_d}\right)^{3-z}}{\gamma_{\pm} [c_{extr} - (3 - z)c_{org}]^{3-z}}. \quad (8)$$

On taking the logarithm, Eq. (8) is converted to the form

$$\log D = \log K + z\,\mathrm{pH} - (3 - z)\log\left(1 + \frac{a_{H_{aq}^+}}{K_d}\right) + (3 - z)\log [c_{extr} - (3 - z)c_{org}] + \log \gamma_{\pm}. \quad (9)$$

Then, using the experimental D values listed in Table 1, we plotted the dependences of $\log D_{Ce}$ on

$$\varphi(\mathrm{pH}) = z\,\mathrm{pH} + (3 - z)\log [c_{extr} - (3 - z)c_{org}] - (3 - z)\log\left(1 + \frac{a_{H_{aq}^+}}{K_d}\right), \quad (10)$$

for z = 0, 1, and 2 (Fig. 1).

In accordance with Eq. (9), these dependences are linear at $z = 0$, 1 and 2 and are described by the following equations with $R^2 = 0.93$

$$\log D = 0.52\varphi(\mathrm{pH}) + 4.72 \quad (z = 0), \qquad (11)$$

$$\log D = 0.41\varphi(\mathrm{pH}) + 1.11 \quad (z = 1), \qquad (12)$$

$$\log D = 0.37\varphi(\mathrm{pH}) - 1.29 \quad (z = 2). \qquad (13)$$

We calculated from the absolute term in Eqs. (11)–(13), taking into account (9), the extraction constant and the Gibbs free energy of cerium(III) extraction with oleic acid at a certain z. The mean ionic activity coefficients of cerium(III) nitrate in the equilibrium aqueous phase, $\gamma_{\pm}$, used in the calculations, were estimated in the framework of the Debye–Hückel theory from the ionic strength of the solution. The ionic strength of the equilibrium aqueous phase was determined taking into account the cerium(III) nitrate concentration and also HNO_3 and NaOH amounts added to adjust the required pH. The calculated thermodynamic characteristics of cerium(III) extraction with oleic acid are as follows:

$\log K = 4.72$ ($z = 0$), $K = 5.2 \times 10^4$, $\Delta_r G = -26.9$ kJ mol^{-1},

$\log K = 1.11$ ($z = 1$), $K = 12.9$, $\Delta_r G = -6.3$ kJ mol^{-1},

$\log K = -1.29$, ($z = 2$), $K = 0.05$; $\Delta_r G = 7.4$ kJ mol^{-1}.

These results show that the extraction constant of Ce(III) with oleic acid, calculated at $z = 2$, is much less than the experimental value. Therefore, the assumption that $z = 2$ was rejected.

The thermodynamic characteristics of cerium(III) extraction with oleic acid can also be determined from the plots of $\log D_{Ce}$ vs. the following function of the extractant concentration $\varphi(c_{ol}) = (3 - z)\log[c_{extr} - (3 - z)c_{org}]$. These plots at $z = 0$ and 1 are shown in Fig. 2.

It was found that, at $z = 1$, $\log D_{Ce}$ is a linear function of $\varphi(c_{ol})$ with $R^2 = 0.97$:

$$\log D = 1.2\varphi(c_{ol}) + 3.59. \qquad (14)$$

The slope in Eq. (14) shows that the solvate number of the extractable complex is 2. The extraction constant and the Gibbs free energy of cerium(III) extraction were calculated from the absolute term of (14), taking into account Eq. (9). These values were as follows: $\log K = 0.51$, $K = 3.2$, and $\Delta_r G = -2.9$ kJ mol^{-1}.

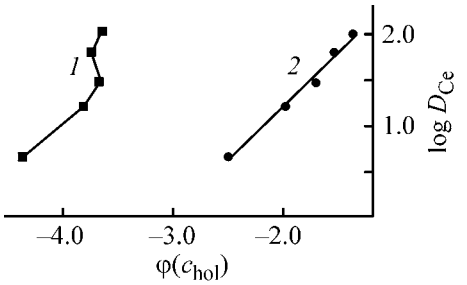

Fig. 2. Logarithm of the distribution ratios of cerium(III) ($\log D_{Ce}$) vs. $\varphi(c_{ol})$ at z (*1*) 0 and (*2*) 1.

Thus, both the approaches used for mathematical processing of experimental data on cerium(III) extraction with oleic acid resulted in consistent thermodynamic characteristics. The average extraction constant and Gibbs free energy of Ce(III) extraction were found to be: $K_{extr} = 8 \pm 4$ and $\Delta_{extr} G = -4.6 \pm 1.7$ kJ mol^{-1}. The solvate number of Ce(III) in the extractable complex, determined by both methods, is 2.

The Ce(III) extraction with oleic acid can be described by the equation of a chemical reaction

$$(CeOH)^{2+}_{aq} + 2R^-_{org} = CeOHR_{2(org)}, \qquad (15)$$

where the $(CeOH)^{2+}$ cation is formed by hydrolysis:

$$Ce^{3+} + H_2O = [CeOH]^{2+} + H^+. \qquad (16)$$

The Gibbs free energy of this reaction, $\Delta_h G$, calculated from reference data, is 53.98 kJ mol^{-1}.

The Gibbs free energy of the solvation reaction [Eq. (15)] was calculated from the difference between the Gibbs free energies of extraction of Ce(III) and its hydrolysis: $\Delta_{solv} G = \Delta_{extr} G - \Delta_h G = -58.6 \pm 1.7$ kJ mol^{-1}.

The characteristics of cerium(III) extraction with 20% TBP in *o*-xylene, 0.5 M trialkylbenzylammonium nitrate (TABAN) in *o*-xylene, and 0.5 M oleic acid in *o*-xylene are listed in Table 3.

Table 3 shows that, in cerium(III) extraction from nitrate solutions at pH 5, the highest extractive power

Table 3. Characteristics of extraction of cerium(III) nitrate with various extractants

Extractant	pH	D	$-\Delta_r G^0_{298}$, kJ mol^{-1}	Solvate number
TBP [10]	5	9.0 ± 0.4	5.92 ± 0.03	2
TABAN [5]	3	35 ± 4	8.9 ± 0.3	2
Oleic acid	5	100 ± 3	58.6 ± 1.7	2

is exhibited by oleic acid. This fact confirms the assumption that cerium(III) in the aqueous phase forms positively charged hydroxocomplexes at pH 5. In more acidic media (pH 3), cerium(III) forms anionic complexes and, therefore, its extraction with a salt of a quaternary ammonium base is more efficient.

CONCLUSIONS

(1) At pH 5, Ce(III) occurs in aqueous nitrate solutions in the form of hydroxo complexes $Ce(OH)^{2+}$.

(2) In extraction of Ce(III) with oleic acid at pH 5, the solvate number in the extractable complex is 2, i.e., cerium(III) is extracted in the form of hydroxo complexes $Ce(OH)^{2+}$ coordinated with two oleate anions.

(3) The thermodynamic characteristics of extraction of cerium(III) from aqueous nitrate solutions with oleic acid are calculated.

(4) In extraction of cerium(III) from nitrate solutions at pH 5, the extractive power of oleic acid exceeds that of tributyl phosphate and trialkylbenzylammonium nitrare.

ACKNOWLEDGMENTS

This study was carried out within the framework of Departmental Scientific and Technical Program of the Ministry of Education and Science of the Russian Federation "Development of the Scientific Potential of Higher School."

REFERENCES

1. Dibrov, I.A., Chirkst, D.E., and Litvinova, T.E., *Zh. Prikl. Khim.*, 1996, vol. 69, no. 5, pp. 727–730.
2. Zakharov, V.I., Voskoboinikov, N.B., Skiba, G.S., et al., *Zap. Gorn. Inst.*, 2005, vol. 164, pp. 102–105.
3. Lebedev, V.N. and Masloboev, V.A., *Khim. Tekhnol.*, 2003, no. 3, pp. 26–30.
4. Lebedev, V.N. and Rudenko, A.V., *Khim. Tekhnol.*, 2003, no. 1, pp. 26–29.
5. Dibrov, I.A., Chirkst, D.E., and Litvinova, T.E., *Zh. Prikl. Khim.*, 2002, vol. 75, no. 2, pp. 197–201.
6. Dibrov, I.A., Chirkst, D.E., and Litvinova, T.E., *Z. Tsvetn. Met.*, 2003, no. 7, pp. 112–115.
7. Voropanova, L.A. and Yakovleva, V.N., *Zap. Gorn. Inst.*, 2005, vol. 164, pp. 63–65.
8. Khan, I.V. and Gabrielova. Yu.A., *Khimiya flotatsionnykh reagentov* (Chemistry of Flotation Reagents), Moscow: Nauka, 1981.
9. Savvin, S.B., *Arsenazo III* (Arsenazo III), Moscow: Atomizdat, 1966.
10. Chirkst, D.A., Litvinova, T.E., Chistyakov, A.A., and Ionova, M.Yu., *Zh. Prikl. Khim.*, 2004, vol. 77, no. 9, pp. 1430–1434.

ISSN 1070-4272, Russian Journal of Applied Chemistry, 2007, Vol. 80, No. 2, pp. 189–192. © Pleiades Publishing, Ltd., 2007.
Original Russian Text © O.I. Kuntyi, G.I. Zozulya, O.G. Kurilets, 2007, published in Zhurnal Prikladnoi Khimii, 2007, Vol. 80, No. 2, pp. 191–194.

INORGANIC SYNTHESIS AND INDUSTRIAL INORGANIC CHEMISTRY

Silver Cementation with Magnesium in Cyanide Solutions

O. I. Kuntyi, G. I. Zozulya, and O. G. Kurilets

Lvivska Politekhnika National University, Lviv, Ukraine

Received July 29, 2006

Abstract—Contact precipitation of silver with a magnesium powder from 0.0025–0.01 M solutions of the system $[Ag(CN)_2]^-$–CN^- in the hydrodynamic mode was studied. The dependence of the silver cementation rate in the initial stage on the concentration of the $[Ag(CN)_2]^-$ complex and on the surface area of the cementing agent was examined, and the relationship of the temperature factor with the depolarization of silver reduction on microcathodes and acceleration of magnesium dissolution on microanodes was analyzed.

DOI: 10.1134/S1070427207020048

A number of techniques for recovery of gold and silver from ores and secondary raw materials are based on hydrometallurgical processes [1–3]. Analysis of publications devoted to this issue [3] shows that the cyanide method is the most widespread in the world practice of leaching-out of these metals. Further, metallic gold and silver (M) are precipitated from the resulting solutions by cementation with zinc [1, 2] by the reaction

$$2[M(CN)_2]^- + Zn \rightarrow 2M + [Zn(CN)_4]^{2-}. \quad (1)$$

The formation of the cyanide complex $[Zn(CN)_4]^{2-}$ by the main reaction results in binding of free cyanide ions CN^-. Side reactions (2) and (3), whose share exceeds that of the main reaction, also lead to binding of CN^- anions:

$$Zn + 4CN^- + 2H_2O \rightarrow [Zn(CN)_4]^{2-} + H_2 + 2OH^-, \quad (2)$$

$$2Zn + 8CN^- + O_2 + 2H_2O \rightarrow 2[Zn(CN)_4]^{2-} + 4OH^-. \quad (3)$$

In view of the fact that the actual consumption of zinc is tens of times that theoretically calculated for cementation [2], its use as a cementing metal makes difficult the technological cycle of leaching, cementation, leaching, etc. Furthermore, it is necessary to recover zinc from spent solutions after the reduced metals are isolated and CN^- ions are neutralized. Because the concentration of zinc is low, this process is not economically feasible.

Similar complications arise if zinc is used as a cementing metal in noncyanide leaching solutions, with thiosulfate or thiocarbamide. Therefore, cementation with metals whose ions do not form complexes with ligands, the main components of leaching solutions, aluminum [4–6] and magnesium [7–9], have become more intensive in the last decade.

The aim of this study was to examine the possibility of using magnesium for contact precipitation of silver from cyanide solutions that model solutions for leaching of ores, scrap metal, and spent electrolytes and washing water formed in silver plating. This study proceeds with systematic examination of the recovery of nonferrous and precious metals from solutions by cementation with magnesium [7–9].

EXPERIMENTAL

Contact precipitation of silver was carried out in the system $[Ag(CN)_2]^-$–CN^-. Solutions for cyanide leaching of ores and secondary raw materials were modeled and kinetic and electrochemical features of the process, as well as the morphology of the reduced metal, were analyzed. Solutions containing equimolar amounts of $[Ag(CN)_2]^-$ complexes and free cyanide ions CN^- were prepared from $AgNO_3$ and NaCN. The cementation was carried out in a thermostated glass container with a solution volume of 0.1 l in the atmosphere nitrogen at 20–40°C, with vigorous mechanical stirring. A magnesium powder with average particle size of $0.42 \times 0.15 \times 0.04$ mm, scrap metal of the 1.0–1.1-mm fraction, and a magnesium disk 30 mm in diameter were used for the experiments. Before each experiment, the disc was trimmed with a fine emery paper, degreased with alcohol, and its

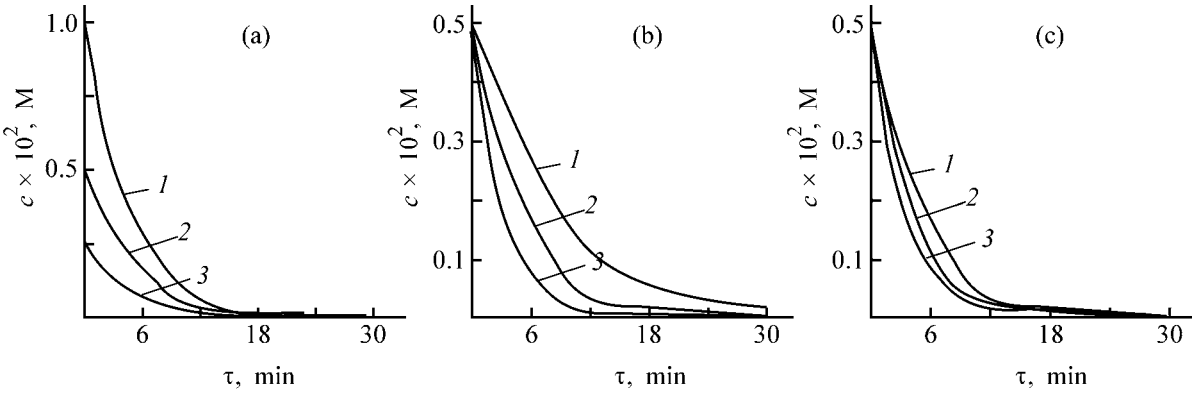

Fig. 1. Variation of the silver concentration c with time τ in cementation with a magnesium powder in solutions of the system $[Ag(CN)_2]^-$–CN^- in relation to (a) initial content of silver cyanide complex c_0(Ag), (b) magnesium powder weight m(Mg), and (c) temperature. (a) T = 20°C, m(Mg) = 0.10 g. c_0(Ag) (M): (*1*) 0.01, (*2*) 0.005, (*3*) 0.0025. (b) T = 20°C, c_0(Ag) = 0.005 M. m(Mg) (g): (*1*) 0.05, (*2*) 0.10, (*3*) 0.15. (c) c_0(Ag) = 0.005 M, m(Mg) = 0.10 g. T (°C): (*1*) 20, (*2*) 30, (3) 40.

lateral surface was insulated with a Teflon tape. During the cementation, samples of a solution were periodically taken and analyzed for the silver content by atomic-adsorption spectroscopy (AAS-IN atomic-absorption spectrophotometer in an air–propane–butane flame at a wavelength of 328.1 nm).

After the cementation was complete, the powders, scrap metal, and disc were washed with water and acetone, dried in air at 80°C, weighed, and examined with an optical microscope equipped with a digital camera. On separating the precipitate, the content of magnesium ions in solution was determined by titration with Trilon B.

It was found that the rate of cementation with powdered magnesium in solutions of the system $[Ag(CN)_2]^-$–CN^- is directly proportional to the content of the complex. For example, the cementation rate in 0.0025, 0.005, and 0.01 M solutions of the $[Ag(CN)_2]^-$ complex at 20°C is 0.00044, 0.00077, and 0.00186 mol min^{-1}, respectively, during the initial 2 min, when a virtually linear time dependence of the silver concentration is observed (Fig. 1a). Thus, the contact precipitation of silver with magnesium in cyanide solutions can be considered a first-order pseudoreaction ?(pseudo-first-order reaction)? in the initial stage.

The cementation rate is also virtually directly-proportional to the surface area of the magnesium powder in the initial stage (Fig. 1b). For example, the cementation rate in a 0.005 M $[Ag(CN)_2]^-$ solution is, during the first 2 min, 0.00040, 0.00077 and 0.00121 mol min^{-1}, respectively, for a magnesium powder weight of 0.05, 0.10, and 0.15 g. This agrees with the general dependence of the contact precipitation rate of a metal on the surface area of a cementing agent in contact with a solution [10].

The temperature factor is of no importance for acceleration of the silver cementation (Fig. 1c). For example, the cementation rate increases by about 15% in the initial stage for 0.005 M solutions in the range 20–30°C and by about 25% in the range 30–40°C. This behavior can be accounted for by acceleration of electrode processes associated with depolarization of process (4) at microcathodes [11], and also by acceleration of reaction (5) at microanodes; in addition, heating promotes diffusion:

$$[Ag(CN)_2]^- + e \rightarrow Ag + 2CN^-, \quad (4)$$

$$Mg \rightarrow Mg^{2+} + 2e. \quad (5)$$

In a wide range of concentrations of the cyanide complex $[Ag(CN)_2]^-$, silver films (Figs. 2a–2d) or compact metal formations (Figs. 2e–2i) appear on the smooth magnesium surface. This is primarily attributable to a strong cathodic polarization of silver in cyanide electrolytes [11]. Silver films are not homogeneous, which is caused by the electrochemical nonuniformity of the magnesium surface. For example, outgrowths, which are known to have an increased energy [12], are formed in prolonged cementation at crystallite boundaries on smooth magnesium samples (discs) (Figs. 2a, 2b). The heterogeneity of the silver precipitate is considerably more pronounced on the surface of magnesium scrap (Figs. 2c, 2d) and especially on powder particles (Figs. 2e, 2f). In the last case, the corrugated surface and internal stresses are reasons for the increased electrochemical (energy-related) heterogeneity, which leads to a high current density on microcathode and microanode parts and,

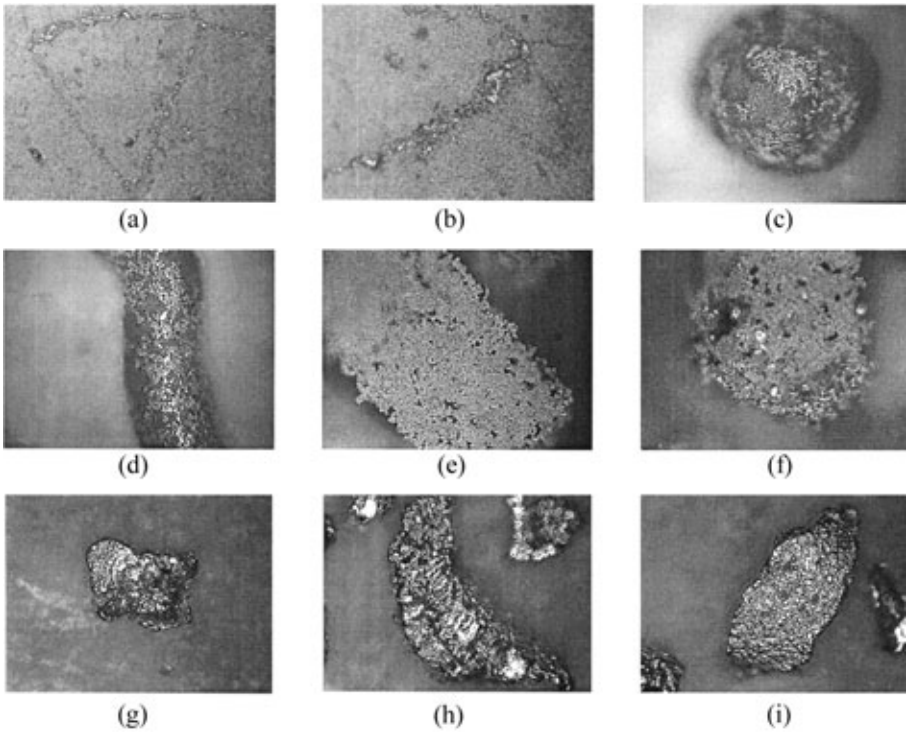

Fig. 2. Micrographs of the surface of (a, b) magnesium discs, (c, d) scrap, (e, f) powder, and (g–i) silver formations upon contact precipitation at 20°C from a 0.005 M $[Ag(CN)_2]^-$ + 0.005 M CN^- solution. Magnification: (a, g–i) 100; (b, e, f) 200; (c, d) 50.

accordingly, to a high cementation rate. Furthermore, the corrugated surface of magnesium powder particles precludes formation of solid silver films, which is characteristic of the contact precipitation from solutions of complex salts [10] and is observed on the magnesium disc (Figs. 2a, 2b). Therefore, the microanode parts are not blocked by a bulk silver precipitate reduced on microcathodes. These latter are formed as outgrowths during cementation (Fig. 2f), which are agglomerated in anodic dissolution of magnesium. After the cementing agent is completely consumed, the silver particles formed reproduce particles of magnesium powder or their fragments (Fig. 2g–2i).

Thus, the contact precipitation of silver with a magnesium powder from cyanide solutions enables complete utilization of magnesium as a cementing metal. The specific expenditure of magnesium is only determined by microcathod?ic reactions of silver reduction (4) and side reaction (6), because reactions similar to (2) and (3) do not occur:

$$2H_2O + 2e \rightarrow H_2 + 2OH^-. \quad (6)$$

As demonstrated by the experimental results, the practical expenditure of magnesium on reaching a 99% extraction of silver is 150–300% of the theoretical value, i.e., 0.17–0.34 g per gram of reduced silver.

No precipitation of magnesium hydroxide was observed during the cementation and a long time after its completion, which is due to the low concentration of Mg^{2+} formed by microanod?ic reaction (5) and to a comparatively low alkalinity of the medium. The precipitation of $Mg(OH)_2$ from a 0.01 M solution begins at pH 10.4 and is complete at pH 12.4 [13]. In the model solutions under study, this value does not exceed 10.5. Thus, the precipitation of silver from cyanide solutions with a magnesium powder makes it possible to obtain a pure reduced metal, with cyanide ions not bound by ions of the cementing agent.

CONCLUSIONS

(1) Compact silver films are deposited from solutions of the system $[Ag(CN)_2]^-$–CN^- on a smooth magnesium surface, and monolithic silver particles are formed on a corrugated surface.

(2) The rate of silver cementation with a magnesium powder is directly proportional to the concentration of the complex $[Ag(CN)_2]^-$ and to the surface area of the cementing agent in the initial stage of the process. The temperature factor is associated with

the depolarization of silver reduction on microcathodes and with the acceleration of magnesium dissolution on microanodes.

3. The specific expenditure of magnesium for a 99% extraction of silver is 0.17–0.34 g per gram of reduced silver, which corresponds to a 150–300% dissolution of the cementing agent relative to the theoretical value. No magnesium hydroxide is formed during the cementation and a long time after its completion, which makes it possible to obtain pure silver precipitates.

REFERENCES

1. Zelikman, A.N. and Korshunov, B.G., *Metallurgiya redkikh metallov* (Metallurgy of Rare Metals), Moscow: Metallurgiya, 1991.
2. Maslenitskii, I.N., Chugaev, L.V., Borbat, V.F., et al., *Metallurgiya blagorodnykh metallov* (Metallurgy of Noble Metals), Moscow: Metallurgiya, 1987.
3. Pivovarov, A.A., Sytnik, S.V., Pololii, N.M., and Burya, A.I., *Tsianidnoe izvlechenie blagorodnykh metallov iz promyshlennykh otkhodov i rudnyakh kontsentratov* (Cyanide Recovery of Noble Metals from Industrial Wastes and Ore Concentrates), Dnepropetrovsk: Nauka i Obrazovanie, 1999.
4. Dresvyannikov, A.F., Petukhova, L.V., and Sopin, V.F., *Zh. Prikl. Khim.*, 1998, vol. 71, no. 10, pp. 1656–1659.
5. Dresvyannikov, A.F., Ivshin, Ya.V., and Grigor'eva, I.O., *Elektrokhimiya*, 2001, vol. 37, no. 7, pp. 892–896.
6. Tatarinov, A.P., Byval'tsev, V.Ya., Dement'ev, V.Ya., and Emel'yanov, Yu.E., *Tsvet. Met.*, 1999, no. 3, pp. 28–30.
7. Kuntyi, O.I., Masyk, O.B., Khoma, M.S., and Kaminskii, R.M., *Voprosy Khim. Khim. Tekhnol.*, 2003, no. 4, pp. 116–119.
8. Kuntyi, O.I., Znak, Z.O., and Gnatishin, N.M., *Khim. Prom. Ukraini*, 2003, no. 5, pp. 34–37.
9. Kuntyi, O.I., Khoma, M.S., and Koltun, O.M., *Ekotekhnol. Resursosberezhenie*, 2004, no. 5, pp. 39–42.
10. Rotinyan, A.L. and Kheifets, V.L., *Teoreticheskie osnovy kontaktnogo vytesneniya metallov* (Theoretical Foundations of Contact Displacement of Metals), Leningrad: Len. Tekhnol. Inst. im. Lensoveta, 1979.
11. *Prikladnaya elektrokhimiya* (Applied Electrochemistry), Tomilov, A.P., Ed., Moscow: Khimiya, 1984.
12. Orlov, A.N., Perevezentsev, V.N., and Rybin, V.V., *Granitsy zeren v metallakh* (Grain Boundaries in Metals), Moscow: Metallurgiya, 1980.
13. Lur'e, Yu.Yu., *Spravochnik po analiticheskoi khimii* (Handbook of Analytical Chemistry), Moscow: Khimiya, 1979.

ISSN 1070-4272, Russian Journal of Applied Chemistry, 2007, Vol. 80, No. 2, pp. 193–200. © Pleiades Publishing, Ltd., 2007.
Original Russian Text © S.V. Volkov, L.B. Khar'kova, Z.A. Fokina, O.G. Yanko, P.E. Strizhak, G.R. Kosmambetova, V.I. Gritsenko, A.M. Korduban, 2007, published in Zhurnal Prikladnoi Khimii, 2007, Vol. 80, No. 2, pp. 195–201.

INORGANIC SYNTHESIS AND INDUSTRIAL INORGANIC CHEMISTRY

New Cluster-Type Rhodium Selenochlorides in Oxidative Carbonylation of Methane

S. V. Volkov, L. B. Khar'kova, Z. A. Fokina, O. G. Yanko, P. E. Strizhak, G. R. Kosmambetova, V. I. Gritsenko, and A. M. Korduban

Vernadskii Institute of General and Inorganic Chemistry, National Academy of Sciences of Ukraine, Kiev, Ukraine

Pisarzhevskii Institute of Physical Chemistry, National Academy of Sciences of Ukraine, Kiev, Ukraine

Kurdyumov Institute of Metal-Physics, National Academy of Sciences of Ukraine, Kiev, Ukraine

Received March 30, 2006; in final form, October 2006

Abstract—New rhodium selenochlorides $Rh_4Se_{16}Cl_{10}$ and $Rh_4Se_{18}Cl_{10}$ whose structure is based on the cluster "cubane" $[Rh_4(\mu_3\text{-}Se)_4]$ and products of their thermal transformations were obtained. The catalytic properties of the compounds on various carbon and silica supports in oxidative carbonylation of methane in the gas phase and their dependence on the catalyst preparation technique, type of support, and size of its nanopores were analyzed.

DOI: 10.1134/S107042720702005X

The ability to coordinate in the inner coordination sphere both organic and inorganic ligands creates a wide variety of complex compounds of rhodium, with the resulting opportunity to use these systems to develop catalytic systems with controllable functional properties. Possibly promising objects as catalysts for organic synthesis are chalcogenide and chalcohalide compounds of rhodium, synthesized in nonaqueous organic media without use of expensive templates [1, 2], and products of thermal destruction of these compounds. In systems of this kind, activation and conversion of reagents may occur not only at the central metal atoms, but also at chalcogenide sites. As a result, rhodium chalcohalides may be of particular interest for direct synthesis of complex substances from simple molecules. Single-stage synthesis of alcohols, aldehydes, acids, and esters from methane, carbon monoxide, and oxygen is a possible alternative to the multistage and energy-intensive processing of natural gas, which includes stages of steam reforming of methane into a mixture of H_2 and CO (3 : 1), high-temperature conversion of a mixture of H_2 and CO (2 : 1) into methanol, and subsequent synthesis of aromatic oxygen-containing compounds from methanol [3].

The reaction of oxidative carbonylation of methane to give acetic acid was first performed in the liquid phase under elevated pressure [4], but carrying out the reaction in a heterogeneous catalytic system under atmospheric pressure is a simpler and more attractive method [5–8]. In this case, no aggressive and toxic solvents are used and liquid reaction products are easily removed from the reaction mixture.

In this study, catalysts prepared by deposition of new cluster-type rhodium selenochlorides onto silica and porous carbon materials in the reaction of oxidative carbonylation of methane to give oxygen-containing compounds were examined.

EXPERIMENTAL

Rhodium selenochlorides were synthesized in the medium of Se_2Cl_2, with rhodium(III) chloride $RhCl_3 \cdot 4H_2O$ used as a reaction form. In this medium, selenium can be present in various states and oxidation levels: as neutral molecules Se_2Cl_2, anions, Se^{2-}, chain anions Se_n^{2-} or molecules Se_n^0, selenium dioxide SeO_2, and selenyl dichloride $SeOCl_2$. For this reason, the first stage of synthesis was performed at 80–90°C in the course of 120 h ($RhCl_3 \cdot 4H_2O$: Se_2Cl_2 = 1 : 10) in an open reactor to enable release of the gaseous products, H_2Se and HCl. In the second stage, the reactor was sealed and the heating was continued at 100°C in two different temperature modes:

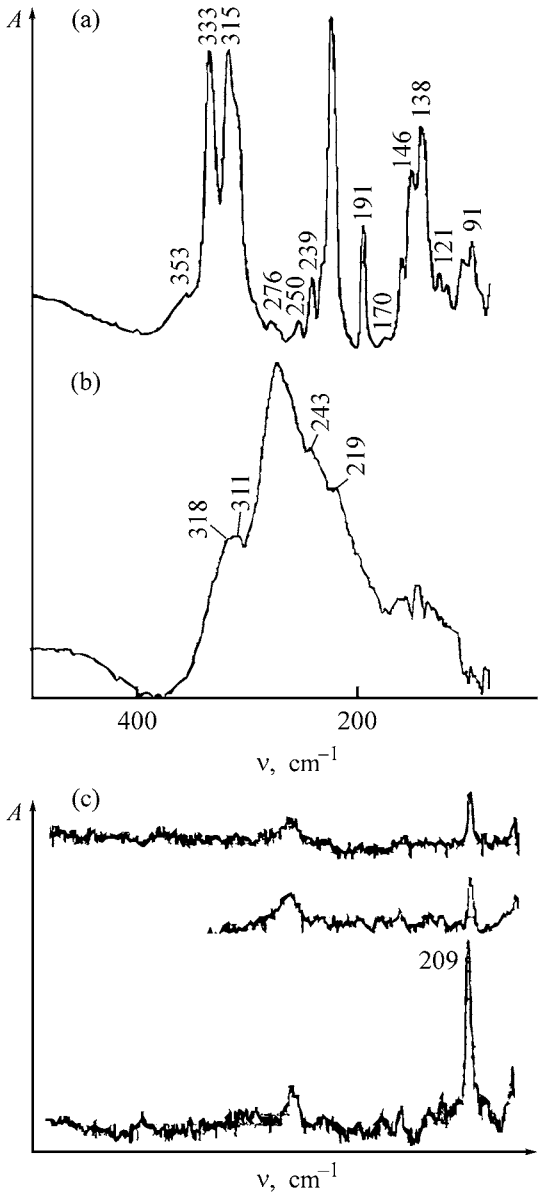

Fig. 1. IR spectra: (a) $Rh_4Se_{16}Cl_{10}$, $Rh_4Se_{18}Cl_{10}$ and (b) Rh_3Se_3Cl, Rh_3Se_5Cl; (c) variation of the relative intensities of lines of the Raman spectrum of $Rh_4Se_{18}Cl_{10}$ in the course of 2 h. (*A*) Absorption and (ν) wave number.

with cyclic heating–cooling (60–80 h) and with continuous heating (180 h). The forming solid products, $Rh_4Se_{16}Cl_{10}$ (**1**) and $Rh_4Se_{18}Cl_{10}$ (**2**), were yielded by the following reactions

$$4RhCl_3 \cdot 4H_2O + 12H_2O + 15Se_2Cl_2 = Rh_4Se_{16}Cl_{10} + 32HCl + 6Se + 8SeO_2,$$

$$4RhCl_3 \cdot 4H_2O + 12H_2O + 23Se_2Cl_2 = Rh_4Se_{18}Cl_{10} + 32HCl + 16Se + 8SeOCl_2 + 4SeO_2.$$

The thermal decomposition products, Rh_3Se_3Cl and Rh_3Se_5Cl, were obtained in 40 h at 345 and 320°C in accordance with the reactions

$$3Rh_4Se_{16}Cl_{10} \xrightarrow{345^\circ C} 4Rh_3Se_3Cl + 13Se_2Cl_2 + 10Se,$$

$$3Rh_4Se_{18}Cl_{10} \xrightarrow{320^\circ C} 4Rh_3Se_5Cl + 13Se_2Cl_2 + 8Se.$$

Rhodium selenochlorides were studied using a set of mutually complementary physicochemical techniques: vibrational and X-ray photoelectron (XPS) spectroscopies; X-ray phase, thermal, and elemental chemical analyses. It was found that the complexes contain the structural fragments μ-Se^{2-}, μ-Se_2^{2-}, μ_3-Se^{2-}, Cl^-_{term}, and Cl^-_{bridge}, as well as coordinated Se_2Cl_2 molecules.

A thermographic study was performed on an MOM Q-1500 instrument (Hungary) in the temperature range 20–1000°C (sample heating rate 5 deg min^{-1}, sensitivity 250 μV, sample weight 0.5–1 g) in special cuvettes under a constant lowered pressure, with gaseous decomposition products condensed in liquid nitrogen. To isolate solid thermolysis products, the starting compounds were kept at the temperatures of the effects recorded in the thermograms (345 and 320°C) for 40 h to constant weight of the solid residue.

For all the compounds formed both by direct synthesis and by thermal destruction, a chemical elemental analysis was made. The content of the metal was determined gravimetrically upon reduction of weighed portions of the compounds in a flow of hydrogen at 20–1000°C; that of chlorine, by argentometry in alkaline solutions through which gases evolved in reduction by hydrogen were passed; and that of selenium, from the difference.

IR spectra of the compounds suspended in Nujol were recorded on Nicolet Magna-IR 750 and Specord M-80 spectrometers,[1] and Raman spectra, on a DFS-24 spectrometer with a He–Ne laser excitation source (632.8 nm).

XPS spectra were measured with a modified ES-2402 electron spectrometer. An X-ray gun with a magnetic anode ($E_{Mg\,K_\alpha}$ = 1253.6 eV, P = 300 W) served as excitation source.

The catalytic properties of the samples were studied by passing a gas mixture with component ratio

[1] The authors are grateful to B.V. Lokshin and Z.S. Klemenkova, staff members of INESS (Moscow), for assistance in IR spectral measurements.

$CH_4 : CO : O_2 = 10 : 4 : 1$ through a quartz reactor with an inner diameter of 10 mm. The catalyst volume was 1.0 cm^3. The experiments were performed under atmospheric pressure in the temperature range 400–600°C at a volumetric flow rate of 6000 h^{-1}. The specific surface area of the samples, S_{BET}, was found by the method of thermal desorption of nitrogen. The starting substances and gaseous reaction products (CH_4, CO, O_2, CO_2) were analyzed with an LKhM-80 gas chromatograph equipped with a heat-conductivity detector. Liquid reaction products were frozen-out in a trap at a temperature of –70°C and then analyzed on a Khrom-5 chromatograph with a flame-ionization detector and a column packed with Separon-BD sorbent.

The vibrational spectra of $Rh_4Se_{16}Cl_{10}$ and $Rh_4Se_{18}Cl_{10}$ are identical. The spectra contain a complex set of frequencies repeated in the IR and Raman spectra (Figs. 1a, 1c). The broad band at 360–350 cm^{-1} (IR), and the strong band at 350 cm^{-1} (Raman) are associated with stretching vibrations of the Se–Cl bond in the Se_2Cl_2 molecule. The frequencies 334, 315, 307 cm^{-1} (IR) and 331, 319, 310 cm^{-1} (Raman) can be attributed to stretching vibrations of the Rh–Cl and Rh–μ_3–Se^{2-} bonds. The weak bands at 274, 251, and 239 cm^{-1} (IR) and the lines at 269, 255, and 240 cm^{-1} (Raman) lie in the range of vibrations of the Se–Se bond in chain and annular Se_n molecules. From the whole set of frequencies of deformation vibrations, which lie below 200 cm^{-1}, the following frequencies can be distinguished: 146, 138 cm^{-1} (IR) and 149, 138 cm^{-1} (Raman). These frequencies correspond to deformation vibrations of the SeSeCl bonds in the individual Se_2Cl_2 molecule (149 and 135 cm^{-1}). Particular attention is attracted by the strong band at 215 cm^{-1} (IR) and the line at 209 cm^{-1} (Raman). The intensity of this line in the Raman spectrum sharply decreases under the action of laser light, whereas the intensities of the other lines remain unchanged (Fig. 1c). This frequency can be attributed to vibrations of the $(Se–Se)^0$ group coordinatively bound to rhodium. This group lies as a kind of dumbbell over faces of the cubane core. Relatively weakly bound μ-Se_2 fragments can be split-off under the action of laser light, with the cubane structure preserved.

The IR spectra of the products of thermal decomposition, Rh_3Se_3Cl and Rh_3Se_5Cl, are identical (Fig. 1b), but strongly differ from the IR spectra of the starting rhodium selenochlorides, $Rh_4Se_{16}Cl_{10}$ and $Rh_4Se_{18}Cl_{10}$, which points to profound changes in the original molecular structure. The doublet at 318 and 311 cm^{-1} corresponds to vibrations of Rh–Cl and Rh–μ_3-Se^{2-}. The broad absorption band peaked at 270 cm^{-1} is associated with vibrations of the Rh–Se^{2-} and Se–Se bonds, which indicates that selenide bridges μ-Se^{2-} and "perselenide" fragments μ-Se_2^{2-} appear in the structure.

Table 1. Rh3$d_{5/2}$ XPS spectra of rhodium selenochlorides

Se3d FWHM = 1.5 eV	I of component a	I of component b	I of component c
	at E_b, eV		
	306.4	308.3	309.6
$Rh_4Se_{16}Cl_{10}$ $Rh_4Se_{18}Cl_{10}$	–	–	1.0
Rh_3Se_3Cl Rh_3Se_5Cl	–	1.0	–
Rh_3Se_5Cl/F1	0.2	0.8	–

The Rh3$d_{5/2}$ XPS spectra of the compounds $Rh_4Se_{16}Cl_{10}$ and $Rh_4Se_{18}Cl_{10}$, Rh_3Se_3Cl and Rh_3Se_5Cl, and of Rh_3Se_5Cl on a carbon support are presented in Table 1 and Fig. 2. The spectra were analyzed by decomposition into components by the Gauss–Newton method. The Rh3$d_{5/2}$ XPS spectra of the compounds $Rh_4Se_{16}Cl_{10}$ and $Rh_4Se_{18}Cl_{10}$ (Fig. 2a) have a single component (c) with Rh3$d_{5/2}$ E_b = 309.6 eV, which indicates that rhodium is present in the oxidation state +3. The spectra of the thermal decomposition products Rh_3Se_3Cl and Rh_3Se_5Cl (Fig. 2b) contain a single component (b) with Rh3$d_{5/2}$

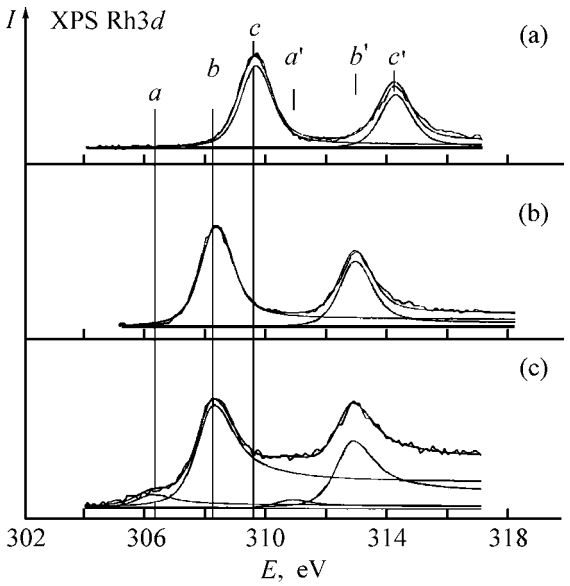

Fig. 2. Rh3$d_{5/2}$ XPS spectra of rhodium selenochlorides: (a) $Rh_4Se_{16}Cl_{10}$, $Rh_4Se_{18}Cl_{10}$; (b) Rh_3Se_3Cl, Rh_3Se_5Cl; and (c) Rh_3Se_5Cl on a carbon support (fullerene black F1). (I) Intensity and (E) energy.

Table 2. Cl $2p_{3/2}$ XPS spectra of rhodium selenochlorides

Cl $2p_{3/2}$ FWHM = 1.2 eV	I of a component at E_b, eV		
$Rh_4Se_{16}Cl_{10}$	0.64/197.8	0.36/198.1	
$Rh_4Se_{18}Cl_{10}$			
Rh_3Se_3Cl	0.42/197.2	0.53/198.0	0.05/200.5
Rh_3Se_5Cl			

Table 3. Se3*d* XPS spectra of rhodium selenochlorides

Se3*d* FWHM = 1.5 eV	I of a component at E_b, eV			
$Rh_4Se_{16}Cl_{10}$		0.24/55.9	0.53/56.5	0.23/57.0
$Rh_4Se_{18}Cl_{10}$				
Rh_3Se_3Cl	0.38/54.6	0.62/55.3		
Rh_3Se_5Cl				

E_b = 308.3 eV, which may be due both to a significant decrease in the number of chlorine atoms substituted by selenium and to a lowering of the oxidation state of rhodium.

The Cl$2p_{3/2}$ spectra of the starting rhodium selenochlorides (Table 2) contain two components with Cl$2p_{3/2}$ E_b 197 and 198 eV, which can be attributed, according to published data [9], to a bridging chloride atom in the polymeric structure of rhodium selenochlorides. The Se3*d* spectra of rhodium selenochlorides (Table 3) have three components, which points to three different energy states of selenium in these molecules. To the μ_3-Se^{2-} group is attributed the peak at Se3*d* E_b = 55.9 eV. This energy somewhat exceeds the corresponding value for selenides MSe with Se3*d* E_b = 53.3–54.5 eV [9] and is caused by a decrease in the amount of negative charge on the selenium atom bonded to three, rather than one, metal atoms. The component Se3*d* E_b = 56.5 eV is attributed to –Se–Se– chain fragments with zero charge and is larger than that in elementary selenium, in which Se3*d* E_b = 55.5 eV because of the complexation. The higher-lying line Se3*d* E_b = 57.0 eV must be associated with the Se_2Cl_2 molecule, in which the strong "electrophile," chlorine, makes greater the positive charge on selenium atoms, with the complexation acting in the same direction.

Selenium derivatives are characterized by formation of multinuclear complexes whose structure is based on a cubane-like core [$Rh_4(\mu_3$-Se$)_4$] [10]. The "cubane" structure [$Rh_4(\mu_3$-Se$)_4$] is due to a specific electronic structure of the selenium atom, which has free, comparatively low-lying *d*-orbitals capable of additional bonding [11]. Therefore, analysis of the vibrational and XPS spectra suggests that the structure of the compounds obtained is $Rh_4(\mu_3$-Se$)_4(\mu$-$Se_2)_3Cl_4(Se_2Cl_2)_3$ and $Rh_4(\mu_3$-Se$)_4(\mu$-$Se_2)_4Cl_4(Se_2Cl_2)_3$. The intensity ratio of the lines in the Se3*d* spectrum, 0.23 : 0.53 : 0.24, approximately corresponds to the selenium distribution among the fragments.

The Se3*d* spectra of the thermal decomposition products, Rh_3Se_3Cl and Rh_3Se_5Cl, have two components with Se3*d* E_b = 54.6 and 55.3 eV. The binding energy of 54.6 eV is typical of metal selenides. This means that the charge on selenium is close to –2e and confirms the conclusion furnished by vibrational spectroscopy, according to which the molecules of the starting selenochlorides undergo a deep transformation in thermal decomposition to give "selenide" fragments μ-Se^{2-} and μ-Se_2^{2-}. The value of 55.3 eV can be attributed to the μ_3-Se^{2-} fragment.

On heating rhodium selenochlorides, Se_2Cl_2 molecules and Se_2 "dumbbells" are eliminated and the remaining molecular structure is constituted by the μ_3-Se fragment linking three rhodium atoms, between which the fragments μ-Se and μ-Se_2 are situated. The structure of the compounds can be represented as $Rh_3(\mu_3$-Se$)(\mu$-$Se)_2Cl$ and $Rh_3(\mu_3$-Se$)(\mu$-$Se)_2(\mu$-$Se_2)Cl$.

The compositions of these compounds might indicate that rhodium is in the oxidation state +1 and μ-SE and μ-Se_2 fragments have zero charges. However, the IR and XPS spectra more likely correspond to selenide fragments μ-Se^{2-} and μ-Se_2^{2-}. In this case, rhodium retains the oxidation state +3.

A decomposition of the Rh$3d_{5/2}$ XPS spectrum of a sample synthesized in Se_2Cl_2 in the presence of a carbon support gave two lines indicating that there exist two different states of rhodium (Fig. 2c, Table 1). Presumably, the line Rh$3d_{5/2}$ E_b = 308.3 eV with the highest intensity (b) belongs to rhodium which is possibly in the oxidation state Rh^{2+} in a ligand environment of selenium and chlorine, and the low-lying weak line Rh$3d_{5/2}$ E_b = 306.4 eV is associated with Rh^0 (a), i.e., with metallic rhodium. The second line lies at somewhat lower energies, compared with Rh$3d_{5/2}$ E_b = 307.2 eV for pure metallic rhodium, which may be due to interaction of adsorbed rhodium with the carbon of the substrate. The presence of three lines in the spectrum indicates that the thermal decomposition of $Rh_4Se_{18}Cl_{10}$ in the presence of carbon

Table 4. Catalytic properties of rhodium selenochlorides on carbon supports in oxidative carbonylation of methane [reaction mixture (MPa): CH_4 0.066, CO 0.027, O_2 0.007; volumetric flow rate of the process 6000 h^{-1}]

Type of support	Preparation method	T, °C	Output capacity, μmol g_{cat}^{-1} h^{-1}			
			CH_3OH	C_2H_5OH	CH_3COOH	C_2H_5COOH
S1	II	400	–	–	–	–
		450	–	–	–	–
		500	–	0.0412	0.026	–
		550	–	0.018	0.009	–
S1	III	400	–	–	–	–
		450	–	0.077	–	–
		500	–	0.006	–	–
		550	–	–	–	–
S1	IV	400	–	–	0.047	–
		450	–	–	0.971	–
		500	–	0.103	0.090	–
		550	–	–	0.125	–
S2	IV	400	–	–	–	–
		450	0.040	1.391	0.050	0.04
		500	–	–	–	–
		550	0.04	0.001	0.015	0.04
F1	IV	400	–	–	–	–
		450	–	0.022	0.014	–
		500	–	0.08	–	–
		550	–	–	–	–
F2	IV	400	–	0.038	0.028	–
		450	0.031	–	0.056	–
		500	0.019	–	–	–
		550	–	–	–	–

supports yields three potentially possible catalytically active centers.

Tests with various catalyst supports (SiO_2, Al_2O_3, ZrO_2, TiO_2, MgO) in synthesis of rhodium selenochlorides demonstrated that only carbon materials are stable in Se_2Cl_2.

Catalysts containing rhodium compounds on carbon supports (SKT-1 carbon: S1, S_{sp} = 700 $m^2 g^{-1}$; spherical enterosorbent: S2, S_{sp} = 1400 $m^2 g^{-1}$; and two fractions of fullerene black: F1, S_{sp} = 20 $m^2 g^{-1}$ and F2, 65 $m^2 g^{-1}$, produced by pyrolysis of styrene and a copolymer of divinylbenzene) were prepared by the following four methods. The first included impregnation of carbon supports with an aqueous solution of $RhCl_3$ and subsequent thermal decomposition at 120°C for 5 h and 320°C for 40 h (method I). The second was based on thermal decomposition of a mechanical mixture of a preliminarily synthesized $Rh_4Se_{18}Cl_{10}$ and carbon supports (method II). In the third technique, rhodium selenochloride $Rh_4Se_{18}Cl_{10}$ was synthesized on the surface of carbon supports and then subjected to thermal destruction (method III). Finally, the fourth procedure included mechanical mixing of the thermal decomposition product Rh_3Se_5Cl with carbon supports (method IV).

The thermal decomposition of samples prepared using methods II and III was carried out at 320°C for 40 h.

The data on the catalytic activity of the samples are listed in Table 4. The first set of catalysts was prepared by ordinary impregnation of carbon supports with an aqueous solution of rhodium chloride (method I). Tests of impregnated samples in oxidative carbonylation of methane revealed that CO_2 is the only reaction product.

It was found in a study of catalysts containing rhodium selenochlorides that methanol and acetic and propionic acids are formed in addition to the main reaction product, CO_2 (Table 4). A comparison of the data in Table 4 demonstrated that the activity and

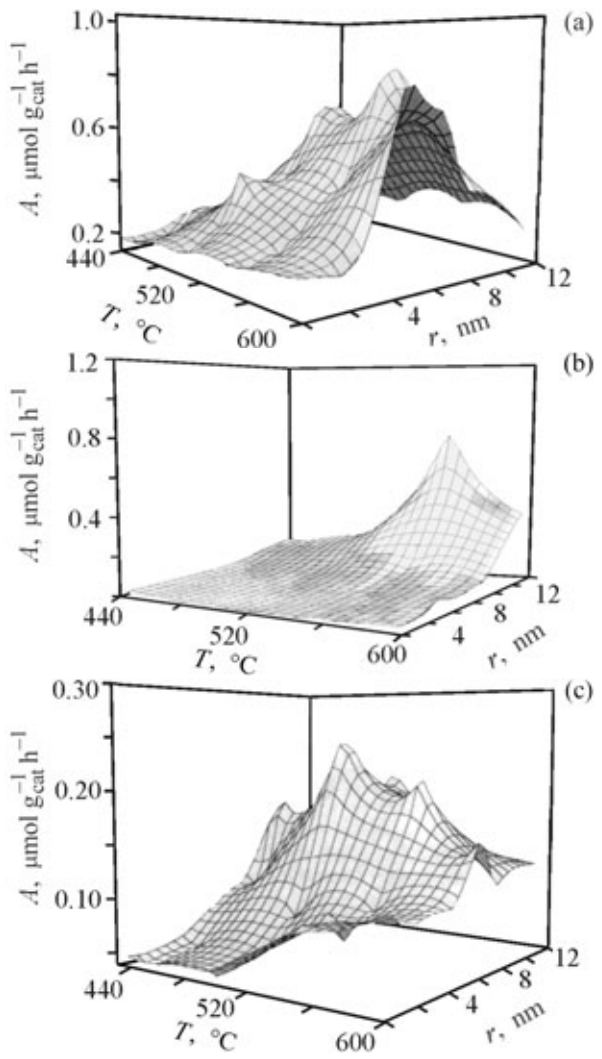

Fig. 3. Output capacity of Rh_3Se_3Cl/SiO_2 catalysts for (a) methanol, (b) ethanol, and (c) acetic acid in relation to the process temperature *T* and support pore size. (*A*) Output capacity and (*r*) pore radius.

selectivity of rhodium selenochlorides on carbon supports largely depends on the catalyst preparation technique. This result can be illustrated by the example of a catalyst deposited on an S1 support by three different methods. It can be seen from Table 4 that C_2-oxygenates are formed on the samples synthesized by methods II and IV, but the quantitative composition of the products depends on the catalyst preparation method. A higher output capacity for acetic acid (0.971 μmol $g_{cat}^{-1} h^{-1}$) is observed in the case when the support is mixed with the thermal destruction product (method IV), compared with the starting selenochloride (method II). Only ethanol is found in liquid reaction products formed on a sample synthesized by introducing a support into the starting reaction mixture $RhCl_3 \cdot 4H_2O : Se_2Cl_2 = 1 : 10$ (method III). A test in the reaction of samples prepared by method IV on other carbon supports demonstrated that acetic acid and alcohols are formed on all the catalysts, but the output capacity of the process depends on the nature of a carbon support.

Table 5. Texture characteristics of silica supports

Support	*S*, $m^2 g^{-1}$	Pore volume, $cm^3 g^{-1}$	Pore diameter, nm
KSK	270	0.76–0.93	12–15
KSS-3	520	0.920	7
KSS-4	650	0.76	5
KSS-5	500	0.71	3
ShSM	720	0.40	1.1–1.2

The data obtained show that the widest variety of reaction products (methanol, ethanol, acetic and propionic acids) is observed when the catalyst is prepared by mechanical mixing of the thermal destruction product Rh_3Se_5Cl with carbon support S2, spherical enterosorbent.

The next series of experiments was devoted to catalytic properties of rhodium selenochlorides on silica supports, synthesized by their mechanical mixing with Rh_3Se_3Cl, which is a product of thermal destruction of a cluster selenochloride $Rh_4Se_{16}Cl_{10}$, and of samples prepared by impregnation of the KSS-5 support with rhodium trichloride and its mixture with ammonium metavanadate. As supports for rhodium selenochlorides served the following silicas: KSS-5, KSS-4, KSS-3, ShSM, and KSK, which differ in specific surface area, volume, and average pore size (Table 5).

It has been shown previously that pure silica supports are inactive in oxidative carbonylation of methane carbonylation and insignificant amounts of methyl acetate (0.05–0.5 μmol $g_{cat}^{-1} h^{-1}$) are formed on samples prepared by introduction of ammonium metavanadate in template synthesis of MCM-41 mesoporous silica [8]. Only gaseous products, carbon oxides, were formed on catalysts prepared by impregnation of the supports KSS-5, KSS-4, KSS-3, ShSM, and KSK supports with a rhodium trichloride solution. Trace amounts of acetic acid (0.02 μmol $g_{cat}^{-1} h^{-1}$) were found on a catalyst synthesized by joint deposition of rhodium trichloride and ammonium metavanadate onto a KSS-5 silica, with the catalyst strongly carbonized in the course of the reaction. Methanol, ethanol, and acetic acid were formed in oxidative carbonylation of methane on samples prepared by mixing Rh_3Se_3Cl with silicas. Figure 3

shows how the output capacity of the catalysts for methanol, ethanol, and acetic acid depends on the process temperature and support pore size. As can be seen in Fig. 3a, the highest output capacity for methanol (1.5 μmol $g_{cat}^{-1} h^{-1}$) is observed on the Rh_3Se_3Cl/KSS-3 sample with a support pore size of 3 nm. Acetic acid is mostly formed on Rh_3Se_3Cl/KSS-4 and Rh_3Se_3Cl/KSS-5 samples with a pore size of 7–8 nm. As the support pore size increases to 12 nm, ethanol becomes the main liquid product of the process.

It was shown in [12] that single-stage synthesis from methane and carbon monoxide yields methanol in the presence of nitrogen(II) oxide as oxidizing agent and iron(III) phosphate as catalyst, and methyl acetate upon addition of highly dispersed Rh_2O_3 to the catalyst. A conclusion was made on the basis of these data that presence of a single active center ($FePO_4$) on the catalyst surface leads to activation of methane to give a methyl radical and, subsequently, C_1-oxygenate. Presence of a second closely lying active center (Rh_2O_3) enables carbonylation and makes it possible to obtain longer-chain C_2–C_3-oxygenates.

It was experimentally demonstrated that oxygen-containing products are formed in oxidative carbonylation of methane either on a rhodium selenochloride or in the joint presence of rhodium and vanadium oxides. The formation of acetic acid on the rhodium-vanadium catalyst can be attributed, by analogy with [12], to presence of two active centers responsible for activation of methane and its subsequent carbonylation into acetic acid. Use of rhodium selenochloride instead of rhodium and vanadium oxides can improve the output capacity for acetic acid by more than an order of magnitude. In addition, the reaction of oxidative carbonylation of methane yields ethanol and ethanol.

A detailed study of the structure of active centers of the reaction of oxidative carbonylation of methane on rhodium selenochlorides is beyond the scope of this study. The suggested structure of both the starting rhodium selenochlorides, $Rh_4(\mu_3\text{-}Se)_4(\mu\text{-}Se_2)_3Cl_4(Se_2Cl_2)_3$ and $Rh_4(\mu_3\text{-}Se)_4(\mu\text{-}Se_2)_4Cl_4(Se_2Cl_2)_3$, and products of their thermal transformations, $Rh_3(\mu_3\text{-}Se)(\mu\text{-}Se)_2Cl$ and $Rh_3(\mu_3\text{-}Se)(\mu\text{-}Se)_2(\mu\text{-}Se_2)Cl$, leads to a conclusion that the starting reagents are activated not only on rhodium atoms, but on selenium as well. The subsequent transformations of the activated complex and the qualitative composition of the reaction products strongly depend both on the nature of a support and on its texture characteristics. This makes it possible to regard nanovoids in porous silicas and carbon materials as nanoreactors whose size affects the selectivity of oxidative carbonylation of methane on rhodium selenochlorides [13]. It should be noted that none of the catalyst samples containing rhodium seleno-chlorides was carbonized in the tests, in contrast to the catalyst prepared by impregnation with rhodium trichloride and ammonium metavanadate.

CONCLUSIONS

(1) New cluster-type cubane-like rhodium selenochlorides $Rh_4Se_{16}Cl_{10}$ and $Rh_4Se_{18}Cl_{10}$ were synthesized and products of their thermal transformations, Rh_3Se_3Cl and Rh_3Se_5Cl, were obtained. An analysis of the vibrational (IR, Raman) and Rh3$d_{5/2}$, Se3d, and Cl2$p_{3/2}$ XPS spectra of these compounds suggested the following structure of the rhodium selenochlorides obtained: $Rh_4(\mu_3\text{-}Se)_4(\mu\text{-}Se_2)_3Cl_4(Se_2Cl_2)_3$ and $Rh_4(\mu_3\text{-}Se)_4(\mu\text{-}Se_2)_4Cl_4(Se_2Cl_2)_3$, based on the "cubane" core $[Rh_4(\mu_3\text{-}Se)_4]$.

(2) The catalytic properties of $Rh_4Se_{18}Cl_{10}$ and a product of its thermal destruction, Rh_3Se_5Cl, deposited on various carbon supports were studied in the reaction of oxidative carbonylation of methane. It was shown that, in contrast to samples prepared by impregnation of supports with rhodium trichloride, rhodium selenochlorides exhibit catalytic activity in carbonylation of methane. The output capacity of the process for methanol, ethanol, and acetic acid depends on the method of catalyst preparation and type of a carbon support.

(3) A study of the catalytic properties of a mechanical mixture of rhodium selenochloride Rh_3Se_3Cl and silicas with various texture characteristics demonstrated that support nanopores can be regarded as nanoreactors whose size affects the output capacity and selectivity of oxidative carbonylation of methane.

REFERENCES

1. Kosmambetova, G.R., Gritsenko, V.I., Strizhak, P.E., et al. *The Eur. Catalysis Forum "EuropaCat-VI", 31.08–4.09, 2003*, Austria, Innsbruck, CD: Abstracts, 2003, Poster 1546.
2. Kosmambetova, G.R., Gritsenko, V.I., Strizhak, P.E., et al., *Ukr. Khim. Zh.*, 2004, vol. 70, no. 2, pp. 75–80.
3. Sheldon, R.A., *Chemicals from Synthesis Gas: Catalytic Reactions of CO and H_2*, Dordrecht: Reidel, 1983.

4. Lin, M. and Sen, F., *Nature*, 1994, vol. 368, pp. 613–615.
5. Wilcox, E.M., Roberts, G.W., and Sprivey, J.J., *Catal. Today*, 2003, vol. 88, pp. 83–90.
6. Wang, Y., Katagiri, M., and Otsuka, K., *Chem. Commun.*, 1997, pp. 1187–1188.
7. Otsuka, K. and Wang, Y., *Appl. Catal., Ser. A*, 2001, vol. 222, pp. 145–161.
8. Pavlenko, N.V., Kosmambetova, G.R., Gritsenko, V.I., et al., *Ukr. Khim. Zh.*, 2003, vol. 69, no. 11, pp. 27–32.
9. Nefedov, V.I., *Rentgenoelektronnaya spektroskopiya khimicheskikh soedinenii* (X-ray Photoelectron Spectroscopy of Chemical Compounds), Moscow: Khimiya, 1984.
10. Pekhn'o, V.I., Stepanenko, I.N., Fokina, Z.A., et al., *Zh. Neorg. Khim.*, 2004, vol. 49, no. 5, pp. 813–816.
11. Schulz, S., Andruh, M., and Pape, T., *Organometallics*, 1994, vol. 13, pp. 4005–4007.
12. Yuan, Q., Zhang, Q., and Wang, Y., *J. Catal.*, 2005, vol. 233, pp. 221–233.
13. Buchachenko, A.L., *Usp. Khim.*, 2003, vol. 72, no. 5, pp. 420–437.

ISSN 1070-4272, Russian Journal of Applied Chemistry, 2007, Vol. 80, No. 2, pp. 201–205. © Pleiades Publishing, Ltd., 2007.
Original Russian Text © I.G. Chudotvortsev, O.B. Yatsenko, 2007, published in Zhurnal Prikladnoi Khimii, 2007, Vol. 80, No. 2, pp. 202–205.

PHYSICOCHEMICAL STUDIES OF SYSTEMS AND PROCESSES

Concentration and Temperature of Eutectic Points in Glucose–Water and Saccharose–Water Systems, Determined by the Method of Fractional Melting of Ice

I. G. Chudotvortsev and O. B. Yatsenko

Voronezh State University, Voronezh, Russia

Received September 26, 2006

Abstract—Method based on fractional melting of ice was used to determine the concentration and temperature of eutectic points in aqueous systems with glucose and saccharose.

DOI: 10.1134/S1070427207020061

Presently, aqueous systems are studied at low temperatures by specialists from many fields of science and technology, with particular attention given to aqueous solutions of electrolytes. A number of models have been constructed for describing solutions of this kind. For example, changes in the solution structure near 0°C are commonly described in terms of hydration. The negative hydration of many ions is replaced by positive hydration, and the structuring effect of these ions on water becomes stronger at lower temperatures [1]. Below 0°C, a number of effects difficultly described in terms of the classical concepts of solutions are observed near eutectics. In particular, there is evidence that solutions are transformed into microheterogeneous systems under these conditions [2].

Aqueous solutions of nonelectrolytes at low temperatures have been studied to a considerably lesser extent. No general theory satisfactorily describing the structure of aqueous solutions of nonelectrolytes has been developed so far, especially for temperatures below 0°C.

Information about phase diagrams of aqueous systems of nonelectrolytes also remains incomplete. Most of data represented in reference and scientific publications refer to solutions of electrolytes, such as metal chlorides and sulfates. The published evidence concerning aqueous solutions of nonelectrolytes at temperatures below 0°C is extremely scarce.

Meanwhile, the behavior of solutions of this kind in phase transitions gives deeper insight into the structure of water at low temperatures, which is a topical scientific problem, which has not been completely resolved until now. Knowledge of phase diagrams is, in addition, necessary for solving a number of technological problems, e.g., those associated with separation and purification of components.

Determining the concentration of eutectics of complex aqueous-organic systems, such as water–glucose, by direct methods, i.e., by gradual cooling of a solution of prescribed concentration, is hindered for a number of reasons. First, solutions of organic substances are susceptible to supercooling. Second, many of these solutions show a gradually sloping run of the liquidus line with a shallow eutectic, which hinders accurate determination of the eutectic concentration.

The method of fractional melting of ice has already been applied to determine eutectics in complex aqueous systems. It has been used to determine eutectics in systems constituted by water and glycine, triglycine sulfate, thiourea, lysine, and lysine hydrochloride [3–5].

An advantage of this method is that it is based on melting of ice ingots, rather than on cooling of a solution. Consequently, this makes it possible to eliminate errors associated with the supercooling characteristic of systems with such components.

EXPERIMENTAL

The experiments were carried out with a solution of a substance under study, with a certain concentration and volume of 10 to 40 cm^3. Further, the solution in a cylindrical plastic vessel was cooled in a freezer

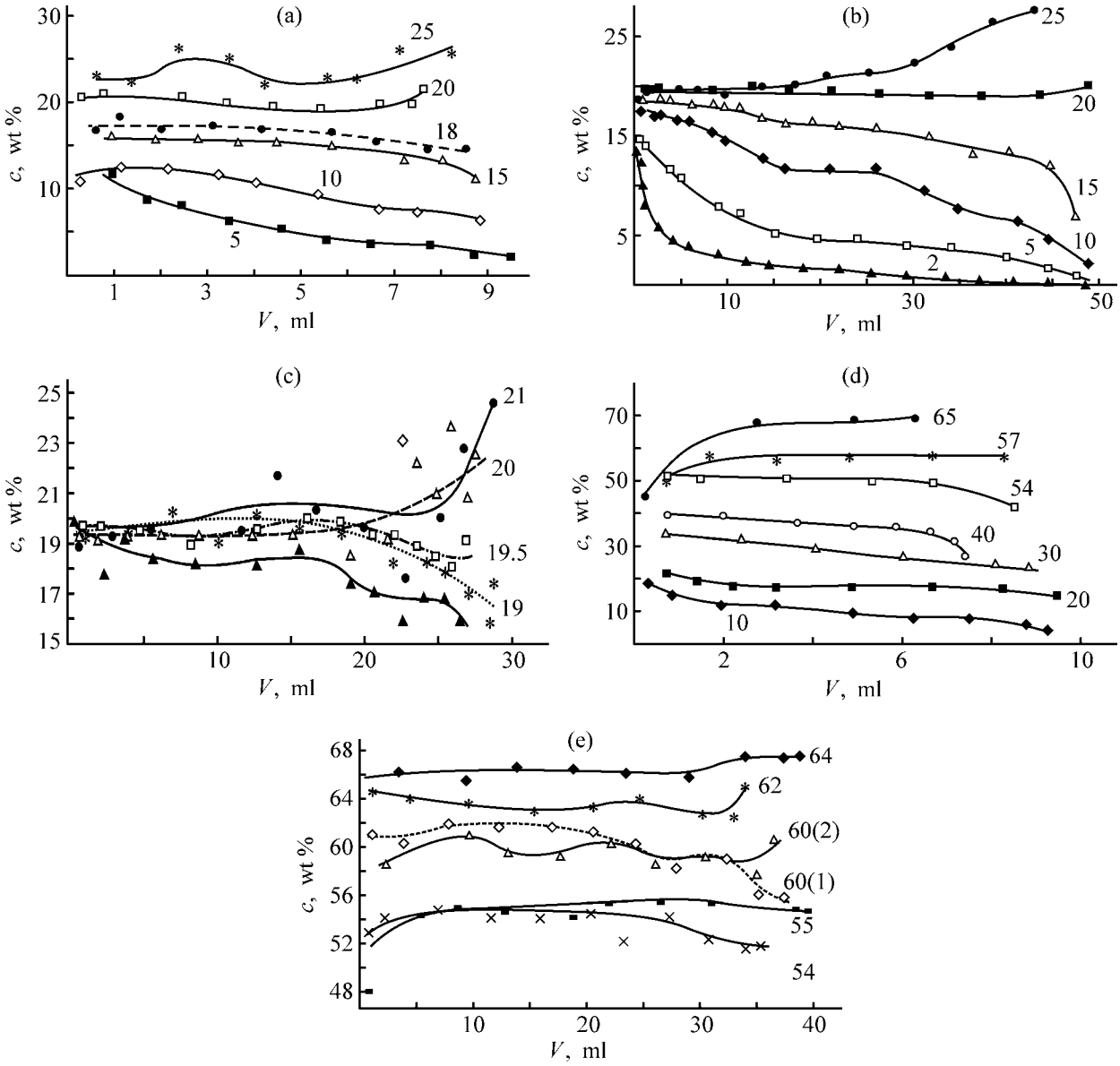

Fig. 1. Concentration c vs. melt volume V in the systems (a) glucose–water, (b) H_2O–NH_4Cl (eutectic concentration 19.6 wt %), (c) glucose–water with the volume of the starting solution equal to 30 ml, (d) saccharose–water (10 ml), and (e) saccharose–water (40 ml). Samples with concentrations of 56 and 58 wt % behave similarly to the composition with 60 wt % and, therefore, are not represented in Fig. 1e. *Digits at curves* are the concentrations (wt %) of the starting solutions from which ice was crystallized.

to –30°C and kept at this temperature for 24 h. After that, the resulting ice ingot was extracted from the freezer and melted at room temperature. As a melt was formed, it was sampled with a micropipette. The solute concentration was determined by refractometry in each of the melt fractions. The data obtained were used to plot the dependence of the substance concentration in the melt on its total volume. The volume of the fractions was varied in different experiments from 0.5 to 5.0 ml, depending on a particular task.

The greatest body of information can be obtained from the type of component distribution among melt fractions (Figs. 1a–1e). These plots show how the solute concentration varies in the course of melting of the ice crystallized from a solution of prescribed concentration.

In fractional melting of ice ingots (Fig. 1a) crystallized from solutions with a concentration of 5 wt %, the first fractions of the melt are enriched in glucose (with respect to the initial concentration). The glucose concentration in the subsequent fractions decreases. In melts formed from ingots with a higher initial concentration (10, 15, and 18 wt %), no noticeable enrichment is observed in the initial stage, with the concentration gradually decreasing. Contrariwise, the melting curve of the ingot crystallized from a solution with a concentration of 20 wt % goes up in the last fractions. The curve for a melt with a concentration of 25 % shows steps and the glucose concentration in the last fractions steeply increases. Simultaneously, growth of glucose crystals is observed, which is characteristic of supereutectic concentrations.

The general type of the component distribution in this system remains the same as that for water–salt systems (Fig. 1b).

In both cases, the most important specific feature is that the run of the dependences is not the same for super- and subeutectic concentrations. The eutectic concentration in the water–NH_4Cl system is 19.6 wt % [6]. It can be seen that, for the melting curves of ingots with concentrations of 15 wt % and lower, the content of the solute in the last fractions of the melt steeply falls. By contrast, the last fractions are enriched in the solute at a concentration of the starting solution equal to 25 wt %. The curve for 20 wt % shows a minor rise in the very last fraction. Thus, the type of the component distribution changes at the eutectic concentration. Owing to this effect, the method of fractional melting of ice can be used to determine the compositions of eutectics.

The data obtained (Figs. 1a, 1b) confirm that the processes occurring in fractional melting of ice have the same nature for electrolyte and nonelectrolyte solutions.

Analysis of the curves (Fig. 1a) suggests that concentrations of up to 18 wt % are subeutectic for the glucose–water system. The eutectic point lies within the range 18–20 wt %.

To find more precisely the position of the eutectic, an experiment with a larger melt volume (30 ml) was carried out. The results obtained are shown in Fig. 1c. It can be seen that no noticeable change in concentration is observed at the beginning of fractional melting for most of samples. For ingots crystallized from the solutions with 18 and 19 wt %, the concentration markedly decreases as the volume of melted ice becomes larger. By contrast, a pronounced rise is observed in last fractions for samples with 20 and 21 wt %. The curve for the composition with 21 wt % shows wide scatter of points, which is due to strong fluctuations of the melt composition, which are accompanied by growth of glucose crystals.

The distribution at 19.5 wt % is the closest to the eutectic distribution: the decrease in the substance content of the last fractions is less noticeable than that for 19 wt % and gives way to a rise in the last fraction.

It should be noted that the initial portions of all the curves are horizontal and lie in the range 19 and 20 wt %.

Thus, the eutectic concentration in the water–glucose system is 19.5 ± 0.5 wt %.

The results of similar experiments for the saccharose–water system are presented in Fig. 1d. As also in the case of glucose, first fractions of the melt formed in melting of ice ingots crystallized from low-concentration solutions (10 to 40 %) are enriched in the solute; as the concentration of the starting solution increases, the enrichment becomes less pronounced. By contrast, last fractions show a noticeable increase in concentration. At the same time, the concentration grows along the entire plot for the saccharose solution with an initial concentration of 65 wt %. Consequently, the eutectic point lies in the concentration range 54–65 wt %. Characteristically, the solution with 57 wt % behaves as the closest to the eutectic. Therefore, the interval between 54 and 65 wt % was chosen for further experiments with a solution volume of 40 ml.

The general pattern of component distribution for the saccharose–water system in the region close to the eutectic (Fig. 1e) is markedly different from that for the same distribution in the glucose–water system (Fig. 1c). On the one hand, solutions with concentrations of 54 wt % and (to a lesser extent) 55 wt % show a decrease in concentration in the course of melting, and the content of the substance increases in last fractions for solutions with concentrations of 62 and 64 wt %, which gives reason to identify these compositions as sub- and supereutectic, respectively.

On the other hand, all the solutions behave in approximately the same way in the range 55–62 wt %. A nonmonotonic dependence of the concentrations on the melt volume is observed, with characteristic minima and maxima.

Statistical processing of the results smoothes the run of the curves, but does not change the pattern as a whole. Both an increase and a decrease in concentration in last fractions are observed for the same con-

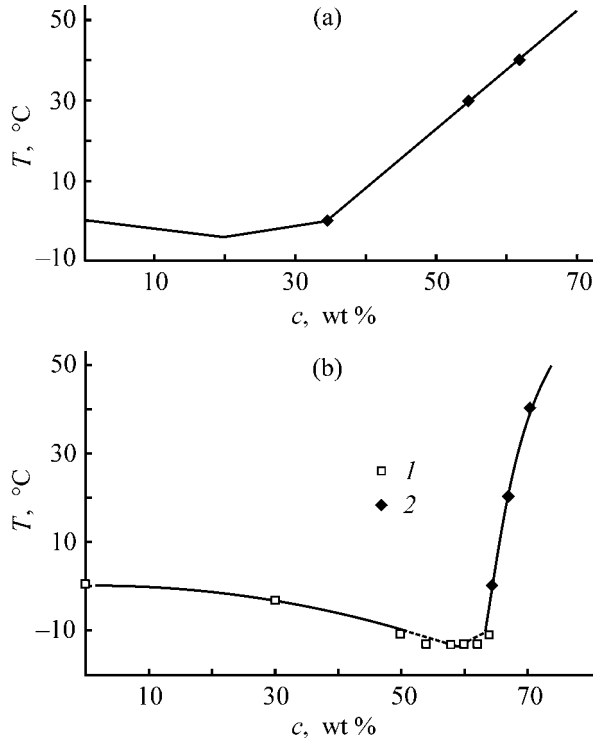

Fig. 2. Phase diagrams of the systems (a) glucose–water and (b) saccharose–water. (a) T_{eu} = –4.5°C, c_{eu} = 19.5 wt %; (b) T_{eu} = –13°C, $c_{eu} \approx$ 58.5 wt %. (*1*) Points obtained by solution cooling and (*2*) published data; the eutectic concentration was found by the fractional melting method. (*T*) Temperature and (*c*) concentration.

centrations (e.g., 60 wt %) (Fig. 1e). Thus, the lower and upper boundaries of the eutectic region could be determined: 55 and 62 wt %. The point at 58.5 wt % corresponds to the middle of this interval.

The unusual behavior of this system is also confirmed by the initial portions of the curves in Fig. 1e. For the glucose–water system (Fig. 1c), all the curves originate from a narrow interval of less than 1%, whereas for the saccharose–water system, this is not observed. The curves do not originate from any definite point, being distributed over the entire range under study. This behavior distinguishes saccharose not only from glucose, but also from other substances previously studied by the authors [3–5].

The anomalous behavior in the saccharose–water system is also confirmed by direct experiments aimed to determine the temperature of the eutectic point. In these experiments, the eutectic temperature was found by cooling a solution of prescribed concentration until the onset of its crystallization.

The composition with a concentration of 19.5 wt % was studied in this way in the glucose–water system. The eutectic temperature was found to be –4.5°C.

The saccharose–water system was examined not only at a concentration of 58.5 wt %, determined to be eutectic, but over the entire range under study. It was found that crystallization in the range 54–62 wt % onsets at the same temperature (–13°C). This certainly may be due to the susceptibility of this system to supercooling. At the same time, the fact that the results obtained in determining the concentration distribution in the melt in fractional melting (Fig. 1e) and in experiments aimed to find the eutectic temperature coincide may indicate that there is an "anomalous" region in the phase diagram of the saccharose–water system, e.g., a nearly horizontal fragment of the liquidus line near the eutectic.

It should also be mentioned in this context that, according to some data [7], aqueous saccharose solutions tend to pass to the glassy state at high concentrations.

The phase diagrams of the systems glucose–water and saccharose–water are shown in Figs. 2a, 2b. The solubilities of the substances in the supereutectic region were taken from the literature [6], and the eutectic points were found in the experiments described above. For the saccharose–water system, the portion near the eutectic is plotted as a dashed line, because the run of the equilibrium liquidus line in the vicinity of the eutectic point is ambiguous.

CONCLUSIONS

(1) It was shown that the processes occurring in crystallization and melting of ice have a common nature for aqueous solutions of electrolytes and nonelectrolytes.

The method of fractional melting of ice was used to determine the temperatures and concentrations of eutectics in the systems under study: glucose–water (c_{eu} = 19.5 wt %, T_{eu} = –4.5°C) and saccharose–water (c_{eu} = 58.5 wt %, T_{eu} = –13°C).

(2) An anomalous behavior near the eutectic point was observed in the saccharose–water system: solutions with concentrations of 55–62% behave identically both in fractional melting of ice and in cooling of a solution until the onset of crystallization. At the same time, the component distribution in the saccharose–water system at other concentrations is similar to that for the rest of the systems studied.

(3) It was demonstrated that the advantage of the method of fractional melting of ice consists in

that it can avoid errors associated with solution supercooling.

REFERENCES

1. Krestov, G.A. and Abrosimov, V.K., *Zh. Strukt. Khim.*, 1967, no. 8, pp. 822–826.
2. Zalkin, V.M., *Zh. Fiz. Khim.*, 1995, vol. 62, no. 2, pp. 373–382.
3. Yatsenko, O.B., Chudotvortsev, I.G., Fedorets, A.A., et al., *Neorg. Mater.*, 2001, vol. 37, no. 5, pp. 617–621.
4. Yatsenko, O.B. and Chudotvortsev, I.G., *Neorg. Mater.*, 2002, vol. 38, no. 9, pp. 1079–1086.
5. Chudotvortsev, I.G., Crystallization of Components of Aqueous Solutions of Metal Chlorides and Sulfates, Urea, Thiourea, and Triglycine Sulfate at Temperatures lower than 0°C, *Cand. Sci. Dissertation*, Voronezh, 2003.
6. *Spravochnik khimika* (Chemist's Handbook), Nikol'skii, B.P., Ed., Moscow: Khimiya, 1973.
7. Krebs, H., *Grundzüge der anorganischen Kristallchemie*, Stuttgart: Enke, 1968.

ISSN 1070-4272, Russian Journal of Applied Chemistry, 2007, Vol. 80, No. 2, pp. 206–208. © Pleiades Publishing, Ltd., 2007.
Original Russian Text © V.A. Keskinov, A.K. Pyartman, N.A. Charykov, O.V. Arapov, A.A. Pronkin, V.V. Lishchuk, V.V. Leonov, 2007, published in Zhurnal Prikladnoi Khimii, 2007, Vol. 80, No. 2, pp. 206–208.

PHYSICOCHEMICAL STUDIES OF SYSTEMS AND PROCESSES

Phase Equilibria in the System Fullerene C_{60}–Hexane–*o*-Xylene–Dimethylformamide

V. A. Keskinov, A. K. Pyartman, N. A. Charykov, O. V. Arapov, A. A. Pronkin, V. V. Lishchuk, and V. V. Leonov

St. Petersburg State Technological Institute, St. Petersburg, Russia

Innovations of Leningrad Institutions and Enterprises, Joint-Stock Company, St. Petersburg, Russia

Received September 28, 2006

Abstract—Phase diagrams in ternary liquid systems hexane–*o*-xylene–DMF were studied at 298.15–333.15 K. Critical points in these systems were determined. The fullerene C_{60} distribution in the ternary liquid systems with constant and variable compositions of two organic phases was studied at variable fullerene concentration.

DOI: 10.1134/S1070427207020073

Extraction separation and purification of fullerenes (primarily C_{60} and C_{70}) prior to their chromatographic isolation is a topical problem [1–5].

Experimental data on the fullerene distribution in liquid–liquid systems with phase separation are very limited and often contradictory. Generally, data are available only for binary systems constituted by fullerene (C_{60} or C_{70}) and a solvent [aromatic (benzene, toluene, *o*-xylene, 1,2-dichlorobenzene) or nonaromatic (CCl_4, hexane)] [6–13], but not on the mutual solubility of two different fullerenes in one solvent or of an individual fullerene in a mixed solvent, except for data reported in [1–5]. Some of the systems investigated contained water as a component of the system, with complicates the extraction because of the long time of phase separation or limitations on the solubility of fullerenes in liquid phases [1–5].

Data on the phase diagrams in the ternary liquid system hexane–*o*-xylene–DMF at various temperatures as well as on the fullerene distribution between two liquid phases of different compositions are lacking in the literature. Since these data are practically significant, we examined in this study the extraction of fullerenes in multicomponent liquid systems with phase separation.

EXPERIMENTAL

In the experiments, we used solvents of analytically pure grade: hexane ($\rho_{298.15}$ = 0.6548 g cm^{-3}), *o*-xylene ($\rho_{298.15}$ = 0.8760 g cm^{-3}), and DMF ($\rho_{298.15}$ = 0.9440 g cm^{-3}). The binodal curves for the ternary systems were constructed using Alekseev's visual polythermal method [14]. The component concentrations in the coexisting phases were determined with gas chromatographs Model 3700 (Khromatograph, Moscow) and LKhM-8MD (carrier gas N_2, Chromaton N-AW-DMCS, stationary phase PEG-6000).

The compositions of the coexisting phases in volume percent were converted to weight fractions, taking into account the solution densities. The binodal curves were approximated by third- or fourth-order polynomials. The phase diagrams of the ternary liquid system were constructed using the second-type Roseboom triangle (Figs. 1 and 2). The orthogonal coordinates represent the weight fractions of two components of the ternary system (for the third component, $\omega_3 = 1 - \omega_1 - \omega_2$). The weight fractions of the components were determined to within 0.001–0.002, and the temperature, to within 0.2 K.

We used fullerene C_{60} of 99.8% purity. The content of fullerene in the coexisting phases was determined spectrophotometrically on an SF-16 instrument with 1-cm quartz cells [15]. To study the fullerene distribution between two organic phases, a 1–2 g l^{-1} stock fullerene solution in *o*-xylene was introduced into the hexane–DMF binary solvent at various component ratios. The total time of mixing, phase separation, and thermostating was 15–30 min, the time of phase separation being within 3 min. In separate experiments,

homogeneous fullerene solutions in *o*-xylene–DMF mixtures of various compositions were obtained and then contacted with various volumes of hexane.

The hexane–*o*-xylene and DMF–*o*-xylene binary mixtures form homogeneous solutions, while the hexane–DMF binary mixtures form a liquid two-phase system over the entire experimental temperature range from 298.15 to 333.15 K (Fig. 1). At $T < 340.9$ K (bp of hexane), we failed to determine the upper critical temperature of mixing for the DMF–hexane binary system. Further increase in temperature results in evaporation of hexane from the liquid phase, rather then in homogenization in the binary system.

The hexane–*o*-xylene–DMF ternary system has a region of homogeneous liquid solutions (*B*) and a two-phase region (*A*) bounded by a binodal curve at a given temperature (Fig. 1). The area of region *A* is minimal at 298.15 K. Analysis of the nodes in the ternary liquid systems at various temperatures, e.g., at 298.15 K (Fig. 2) shows that, in region A, one of the coexisting phases is enriched in DMF at fairly close concentrations of *o*-xylene and hexane (phase I), and the other is enriched in hexane at fairly close concentrations of DMF and *o*-xylene (phase II). At the critical points, the DMF and *o*-xylene concentrations are also close, being, however, considerably lower than the hexane concentration. For example, at 298.15 K, the composition of the system corresponding to the critical point is as follows (weight fractions): DMF 0.19, *o*-xylene 0.22, and hexane 0.59.

Figure 3 shows the isotherm of the C_{60} distribution between phases I and II at the following compositions (weight fractions): phase I (Fig. 2, node 5): DMF 0.276, *o*-xylene 0.266, and hexane 0.542.; phase II: DMF 0.076, *o*-xylene 0.070, and hexane 0.886. The extraction isotherm was obtained at a constant volume ratio of the three liquid components at various fullerene concentrations in the starting *o*-xylene solution. The extraction isotherm is virtually linear (Fig. 3). The distribution coefficient is independent of the fullerene concentration in both phases, being equal to 0.88 ± 0.02. Figure 3 shows also the distribution of C_{60} between phases I and II along different nodes (see Fig. 2, nodes *2*–*5*). The fullerene concentrations in these phases were determined by treating the solutions of C_{60} in *o*-xylene–DMF mixtures with various volumes of hexane. The resulting values are fairly close to those obtained in studying the fullerene distribution at a constant phase composition. The mean distribution coefficient was estimated to be 0.97 ± 0.11. Therefore, regardless of the composition of the coexisting phases, the mean distribution coefficient of

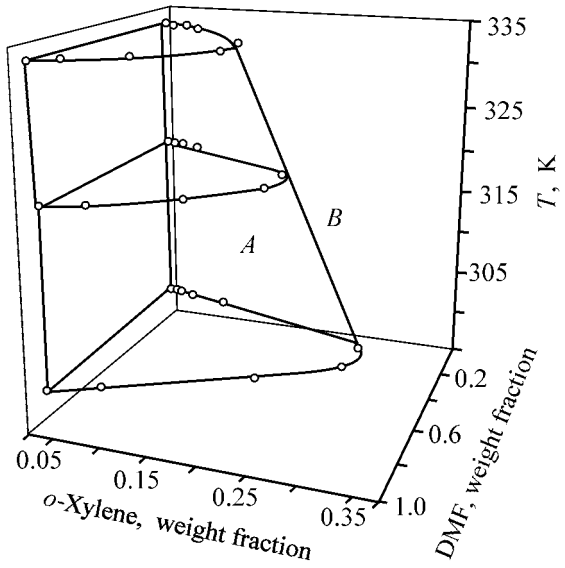

Fig. 1. Phase diagram of the ternary system hexane–DMF–*o*-xylene at various temperatures. (*T*) Temperature, (*A*) region of heterogeneity and (*B*) region of homogeneity; the same for Fig. 2.

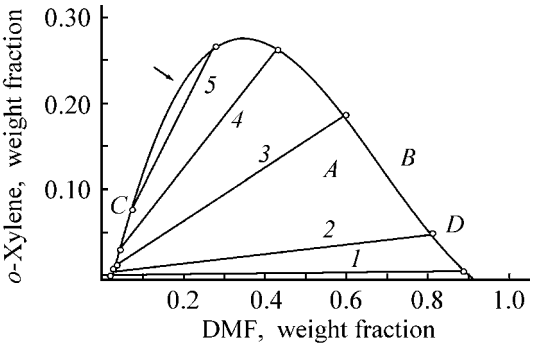

Fig. 2. Section of the phase diagram at 298.15 K. (*1*–*5*) Nodes and (*CD*) binodal curve; the arrow indicates the critical point.

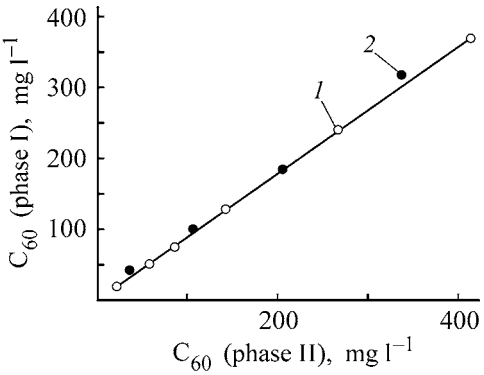

Fig. 3. Fullerene C_{60} distribution between phases I and II. Phases I and II are enriched in DMF and hexane, respectively. Composition of the coexisting phases: (*1*) corresponds to node *5* in Fig. 2 and (*2*) variable; corresponds to nodes *2*–*5* in Fig. 2.

C_{60} is about 0.92, which is close to the statistical distribution. The extraction system investigated makes it possible to work with fullerene concentration in both phases of up to 500 mg l^{-1}.

CONCLUSIONS

(1) The hexane–dimethylformamide binary system has limitations on the mutual solubility of the components. An increase in temperature from 298.15 to 333.15 K has no significant effect on the mutual solubility.

(2) The phase diagram of the ternary liquid system hexane–dimethylformamide–*o*-xylene consists of the region of homogeneous solutions and the region of two-phase liquid systems (systems with phase separation). One of the coexisting phases (I) is enriched in dimethylformamide at fairly close concentrations of *o*-xylene and hexane, and the other (II), in hexane at fairly close concentrations of dimethylformamide and *o*-xylene. The two-phase region is minimal at 298.15 K. The critical points of the system are determined.

(3) The distribution of fullerene C_{60} is considered at its various concentrations in the ternary liquid system, using the section with constant composition of the coexisting phases and sections with variable phase composition. The extraction isotherm of fullerene C_{60} is virtually linear under the experimental conditions, and the mean distribution coefficient of C_{60} between the two liquid phases is about 0.92.

ACKNOWLEDGMENTS

The study was financially supported by the Target Federal Scientific Program "Research and Developments in Priority Areas of Science and Engineering in 2002–2006" (State Contract no. 02.467.11.7005, May 23, 2005).

REFERENCES

1. Arapov, O.V., Aksel'rod, B.M., Pronkin, A.A., et al., *Zh. Prikl. Khim.*, 2003, vol. 76, no. 1, pp. 35–38.
2. Arapov, O.V., Charykov, N.A., Semenov, K.N., et al., *Russ. J. Appl. Chem.*, 2006, vol. 79, no. 2, pp. 201–205.
3. Arapov, O.V., Charykov, N.A., Seregin, V.I., et al., Pis'ma Zh. Tekh. Fiz., 2003, vol. 29, no. 2, pp. 74–81.
4. Arapov, O.V., Pronkin, A.A., Charykov, N.A., et al., *Zh. Prikl. Khim.*, 2003, vol. 76, no. 1, pp. 39–45.
5. Arapov, O.V., Abovskii, N.D., Charykov, N.A., et al., *Russ. J. Appl. Chem.*, 2006, vol. 79, no. 1, pp. 166–168.
6. Ruoff, R.S., Malhorta, R., Huestis, D.L., et al., *Nature*, 1993, vol. 362, no. 6416, pp. 140–141.
7. Ruoff, R.S., Tse, D.S., Malhorta, R., et al., *J. Phys. Chem.*, 1993, vol. 97, pp. 3379–3383.
8. Xu, Z.D., Chen, W.X., Wu, J., et al., *Chin. Sci. Bull.*, 1994, vol. 39, no. 16, pp. 1347–1350.
9. Chen, W. and Xu, Z., *Fullerene Sci. Technol.*, 1998, vol. 6, no. 4, part 1, pp. 695–705.
10. Heyman, D., *Carbon*, 1996, vol. 34, no. 5, pp. 627–631.
11. Bezmel'nitsyn, V.N., Eletskii, A.V., and Okun', M.V., *Usp. Fiz. Nauk*, 1998, vol. 168, no. 11, pp. 1195–1218.
12. Bezmel'nitsyn, V.N., Eletskii, A.V., and Stepanov, V., *Zh. Fiz. Khim.*, 1995, vol. 69, no. 4, pp. 735–738.
13. Marcus, Y., *J. Phys. Chem., Ser. B*, 1997, vol. 101, pp. 8617–8623.
14. Treybal, R.E., *Liquid Extraction*, New York: McGraw-Hill, 1963.
15. Ponomarev, A.N., Yudovich, M.E., Charykov, N.A., et al., *Opt. Spectrosc.*, 2000, vol. 88, no. 2, pp. 195–197.

ISSN 1070-4272, Russian Journal of Applied Chemistry, 2007, Vol. 80, No. 2, pp. 209–212. © Pleiades Publishing, Ltd., 2007.
Original Russian Text © A.N. Marinichev, 2007, published in Zhurnal Prikladnoi Khimii, 2007, Vol. 80, No. 2, pp. 209–212.

PHYSICOCHEMICAL STUDIES OF SYSTEMS AND PROCESSES

Concentration Dependence of the Boiling Point of Binary Equidistant Solutions

A. N. Marinichev

St. Petersburg State University, St. Petersburg, Russia

Received December 26, 2006

Abstract—A concentration dependence of the boiling point of binary equidistant mixtures in isobaric conditions was revealed. The dependence is a solution to a second-order inhomogeneous difference equation describing the autoregression properties of solutions.

DOI: 10.1134/S1070427207020085

Binary solutions of volatile organic substances whose concentrations (e.g., in mole fractions of one of their components) are arranged in increasing order, with the same constant increment, form the so-called equidistant series. For example, a series of this kind is constituted by a set of concentrations of eleven mole fractions of a component x of the mixture: 0, 0.1, 0.2, 0.3, 0.4, 0.5, 0.6, 0.7, 0.8, 0.9, and 1. If values of an experimentally measured property (e.g., boiling point T, composition of the vapor phase, density, refractive index) are known for each concentration, ordered data of this kind can be named equidistant. A similar situation occurs in analysis of, e.g., boiling points of substances that form homologous series (alkanes, alkenes-1, alkyl arenes, etc.). It was shown in [1] that the boiling points of such series are well described by a first-order difference equation

$$T(n + 1) = aT(n) + b. \quad (1)$$

Here a and b are constants whose values are found by processing an array of equidistant data by the least-squares method; n are numbers of homologues in an equidistant series or the number of carbon atoms, or the number of some structural fragments, which varies along the series.

A large body of ebulliometric equidistant binary data can be found in the literature devoted to phase equilibria: the reference book [2] contains such experimental data for more than 60 systems. The reference book [3] presents in the equidistant form for a number of systems verified data obtained in processing of experimental information by finding parameters of the concentration dependence of the activity coefficients on the basis of an appropriate interpolation equation (mostly these are one-, two-, or three-parameter Redlich–Kister equations), with or without account of the nonideality of the vapor phase. If equidistant data on boiling points are available, the possibility of their description by various-order difference equations can be analyzed. It should be noted here that equations of type (1) cannot, as a rule, be used to derive satisfactory concentration dependences, because deviations of calculated values from those found experimentally markedly exceed the errors in determining the boiling points.

Below, we discuss equidistant isobaric data on boiling points of binary systems, presented on the centigrade scale with an accuracy, as a rule, as good as tenths of a degree, both with a monotonic run of the boiling points and with azeotropes corresponding to the minimum and(or) minimum of the boiling point. As the basic relation we take the following second-order difference equation

$$T(n + 2) = aT(n) + bT(n + 1) + c, \quad (2)$$

where $n = 10x + 1$; a, b, and c constants found by the least-squares method.

Relation (2) is known in the literature [4] as the Yule–Walker equation; it was used for the first time in spectral analysis. At the same time, this equation apparently characterizes an autoregression in which each term of the equidistant series (beginning from the third term), figuratively speaking, possesses "memory" about two nearest preceding terms, with the contributions of these latter determined by "weighting" coefficients a and b.

We illustrate finding the coefficients of Eq. (2) by equidistant data for the methanol–*N*,*N*-dimethyloxyethylamine system [2] with a monotonic variation of the boiling point: 134.2, 112.9, 102.2, 94.9, 88.8, 83.3, 78.4, 74.4, 70.7, 67, 64.6. Let us construct an array of nine sets, each containing three nearest values $\{T_i, T_{i+1}, T_{i+2}\}$, i = 1, ..., 9. The values of the autoregression coefficients and their standard deviations calculated by the least-squares method are found to be: $a = -0.20 \pm 0.06$, $b = 1.11 \pm 0.06$, and $c = 4.0 \pm 1.1$. It is noteworthy that, in this case, the coefficient of determination (designated as $r2$ in Excel electronic tables, and just these tables were used in the calculations) was found to be rather large: $r2$ = 0.9995, which points that the data are very well correlated by Eq. (2).. Further, we find the roots Z_1 and Z_2 of the quadratic equation $Z^2 = a + bZ$ (Z_1 = 0.8811 and Z_2 = 0.2275), calculate the so-called basis functions of the type Z_j^n (j = 1 and 2), and write the solution to Eq. (2) as

$$T_{\text{calc}}(n) = C_0 + C_1 Z_1^n + C_2 Z_2^n. \quad (3)$$

To find the parameters C_0, C_1, and C_2 (as least-squares estimates relative to the values of the basis functions), we used the entire array of boiling temperatures (for n 1, 2, 3, 4, 5, 6, 7, 8, 9, 10, 11). This equation can also be represented as a linear combination of two exponential functions of the molar fraction x of methanol, with a free term C_0:

$$T_{\text{calc}}(x) = C_0 + C_1 \exp(-k_1 x) + C_2 \exp(-k_2 x),$$

where $k_1 = -(1/10)\ln Z_1$, $k_2 = -(1/10)\ln Z_2$ are parameters in the exponents.

It should be noted that the calculated boiling points of pure components can be found from the last equation at x = 0 and x = 1 to be, respectively, $C_0 + C_1 + C_2$ and $C_0 + C_1 \exp(-k_1) + C_2 \exp(-k_2)$. At the same time, the free term C_0 is related to the autoregression parameters a, b, and c by the expression $C_0 = c/(1 - a - b)$. If, thus, the boiling points of the pure components are known, we have three linear equations with three unknowns C_0, C_1, and C_2, which makes an alternative way of their calculation. In addition, the calculated values of the parameters can be used to find the azeotrope composition x_{az} by the formula

$$x_{\text{az}} = \frac{\ln\left(-\dfrac{k_2 C_2}{k_1 C_1}\right)}{k_2 - k_1}. \quad (4)$$

Finally, we obtain, after simple rearrangements, the equation

$$T_{\text{calc}}(x) = 43.42 + 74.88 \exp(-1.266x) + 15.9 \exp(-14.8x). \quad (5)$$

The free term C_0 was calculated from the autoregression parameters to be 43.76, which is quite acceptable with account of the temperature determination error (±0.5°C) in the system under study. The expression under the logarithm sign in Eq. (4) is negative, which confirms the absence of an azeotrope in the system under discussion.

For the azeotropic case (with a minimum of the boiling point), we consider data on boiling points for the system constituted by methanoic acid and butyl methanoate [2]: 107, 105.85, 104.7, 103.6, 102.55, 101.5, 100.55, 99.7, 99.1, 99.1, 100.8. For these data, the coefficient $r2$ found with Eq. (2) is 0.9993. After similar calculations, the final result is represented by the following equation:

$$T_{\text{calc}}(x) = 66.31 + 40.692 \exp(-0.2905x) + 0.000144 \exp(10.25x). \quad (6)$$

The boiling point and the azeotrope composition can be readily found from Eqs. (4) and (6) to be 98.97°C and 0.853 (mole fraction of the acid). For solutions with molar fractions of the acid equal to 0.05 and 0.95, the calculated boiling points of 106.41 and 99.62°C are very close to those found experimentally: 106.4 and 99.55°C, respectively.

Let us consider the binary system constituted by methanol and 2-methyl butadiene-1,3 [2], which also shows a minimum of the boiling point: 34.1, 31.6, 30.6, 30.5, 30.6, 31, 31.7, 34.1, 37.6, 44.7, 64.7. It was found, when determining the autoregression coefficients, that $r2$ = 0.990. On performing calculations similar to those described above, we have

$$T_{\text{calc}}(x) = 30.73 + 0.0059 \exp(8.658x) + 13.342 \exp(-13.83x). \quad (7)$$

The boiling point and the azeotrope composition calculated by Eqs. (4) and (7) are 30.86°C and 0.303 (mole fraction of methanol). It can be readily seen that the calculated boiling point of the azeotrope is not equal to the minimum boiling point, but coincides with it within the determination error.

The system constituted by propenic acid and methyl-3-methyloxypropanoate [2] has an azeotrope with a maximum of the boiling point. Data on boiling points of pure components (with x = 0 and x = 1) are unavailable. Let us use data on the boiling points:

Calculated values of $T_{calc} - T$ for each solution composition (x, mole fraction of the first component) and the average value $|\overline{T_{calc} - T}|$, found by Eqs. (5)–(12)

n	x	$T_{calc} - T$ (°C) found by indicated equation						
		(5)	(6)	(7)	(8)	(9)	(10)	(12)
1	0	0	0.002	–0.03	–	–0.002	–	–0.06
2	0.1	0.12	–0.013	–0.02	–0.01	–0.002	–0.005	–0.09
3	0.2	0.17	0.006	0.37	0	0.002	–0.005	0.01
4	0.3	–0.07	0.009	0.36	0.05	0.013	0.003	0.05
5	0.4	–0.21	–0.003	0.33	0	0.015	0.005	0.04
6	0.5	–0.11	0.025	0.18	–0.09	0.006	0.001	–0.02
7	0.6	0.06	0.011	0.09	0.05	–0.006	–0.007	–0.06
8	0.7	–0.11	–0.011	–0.84	0.01	–0.011	–0.006	–0.04
9	0.8	–0.08	–0.002	–0.85	–0.02	–0.004	0.004	0.05
10	0.9	0.38	–0.012	0.35	0	0.008	0.008	0.11
11	1	–0.07	0.016	0.06	–	0.0013	–	0.02
$\lvert\overline{T_{calc} - T}\rvert$		0.13	0.009	0.32	0.03	0.007	0.005	0.05

144.6, 146, 146.9, 147.5, 147.8, 147.5, 147, 146, 144.3 for the following nine solutions: 0.1, 0.2, 0.3, 0.4, 0.5, 0.6, 0.7, 0.8, 0.9. It was found, when determining the autoregression parameters, that $r2 = 0.985$, and the following equation was obtained for the calculated boiling point:

$$T_{calc}(x) = 150.82 - 0.2105\exp(3.721x) - 8.028\exp(-3.033x). \quad (8)$$

According to Eq. (8), the azeotrope corresponding to the maximum temperature boils at 147.7°C and has a molar fraction of the acid equal to 0.535 [with Eq. (5), this value is 0.509 and corresponds to a boiling point of 149.2°C]. Such a strong difference between the azeotrope compositions and the corresponding boiling points is probably due to errors in the experimental data. The boiling points of pure components, calculated by Eq. (8) for $x = 0$ and $x = 1$, are 142.6 and 141.7°C, respectively.

Let us consider the extent to which availability or lack of data on the boiling points of pure components affects the accuracy of prediction of the boiling points (K) and azeotropic properties. This will be done for the example of verified equidistant data on boiling points (K): 354.03, 352.46, 351.36, 350.61, 350.15, 349.94, 349.96, 350.22, 350.77, 351.72, 353.25, in the azeotropic system constituted by benzene and 2,2,3-trimethyl butane [3]. For this system, the boiling points are known to within hundredths of a degree. The dependence of type (2) for the data set including the boiling points of the pure substances has $r2 = 0.99992$. The final equation, which is a solution to the corresponding difference equation, can be represented as

$$T_{calc}(x) = 348.21 + 0.083\exp(4.066x) + 5.735\exp(-3.299x). \quad (9)$$

If we disregard the boiling points of the pure substances, the equation of type (2) is characterized by a value $r2 = 0.9998$ and the concentration dependence is described by an equation similar to (8):

$$T_{calc}(x) = 348.10 + 0.098\exp(3.913x) + 5.828\exp(-3.253x). \quad (10)$$

The exclusion of the information about pure components from the data set being processed somewhat improves the agreement between the calculation and the experiment: the boiling point found for benzene by Eq. (4) is 353.22 K (experimental value 353.25 K), and that for 2,2,3-trimethyl butane, 354.03 K (354.03 K). For the binary azeotrope, the calculated boiling point and mole fraction of pyridine are 349.921 K and 0.547 for Eq. (9) and 349.917 K and 0.545 for Eq. (10). Apparently, it is difficult to give preference to one of these equations for data with so small error in temperatures (hundredths of a degree).

The results obtained in calculating the boiling points for the systems under discussion by Eqs. (5)–(10) are presented in the form of the differences $T_{calc} - T$ for each solution composition x (see table). The average absolute values of these differences demonstrate

a good agreement between the experimental and calculated data. Equations (4)–(10) can also be used for interpolation purposes, i.e., for calculation of boiling points at any intermediate value of x and for prediction of azeotropes.

In processing of equidistant data by the method under discussion, the value of $r2$ is important in calculation of the autoregression parameters. If $r2 < 0.9$ for some set of data (with a complex concentration dependence of the boiling point in the presence of, e.g., several azeotropes), it can be stated that an equation of type (2) should not be used for these data. In this case, it may be appropriate to use a third-order difference equation. In the examples presented above, the roots of the quadratic equation were real and positive. If, however, one of the real roots is negative, the corresponding term in the dependence $T_{calc}(x)$ will contain a factor $(-1)^x$, and the calculated values may be complex. If the roots of the quadratic equation are complex-conjugate, i.e., $Z_{1,2} = u \pm vI$ (I is imaginary unity), then Eq. (3) can be written as follows [5]:

$$T_{calc}(n) = C_0 + \rho^n[C_1 \cos(\varphi n) + C_2 \sin(\varphi n)], \quad (11)$$

where $\rho^2 = (u^2 + v^2)$ is squared modulus, and $\varphi = \arccos(u/\rho)$, argument of the complex root. Then the basis functions for making least-square estimates of the parameters C_0, C_1, and C_2 are products of the exponential function ρ^n by the appropriate trigonometric function. This actually exhausts all the possible variants of solutions to the second-order difference equation of type (2), because the case of multiple roots seems to be exceedingly improbable in practice.

Let us consider as an example of application of Eq. (11) equidistant data on boiling points (°C) in the benzene–perfluorobenzene system, selected from an array corresponding to normal pressure [2]: 79.06, 80.34, 80.46, 80.4, 80.21, 79.95, 79.7, 79.51, 79.44, 79.54, 79.94. This system has two azeotropes: with a minimum and a maximum of the boiling point. In determining the autoregression coefficients, it was found that $r2 = 0.977$. As expected, the roots of the quadratic equation were complex-conjugated, and, therefore, the calculation equation (11) took, on making appropriate rearrangements, the following form:

$$T_{calc}(x) = 79.993 - \exp(-0.2842x) \times [0.030\cos(6.39x) - 0.590\sin(6.39x)]. \quad (12)$$

Both the azeotropes found using (12) had the following compositions (in mole fractions of benzene) and the corresponding boiling points: 0.247 and 80.48°C, and 0.738 and 79.45°C. The experimental values for these azeotropes were as follows: 0.240 and 80.45°C, 0.8168 and 79.35°C. The results of the calculations are listed, and compared with the experiment, in the table.

REFERENCES

1. Zenkevich, I.G., *Zh. Obshch. Khim.*, 2006, vol. 42, no. 1, pp. 9–20.
2. Lyudmirskaya, G.S., Barsukova, T.A., and Bogomol'nyi, A.M., *Ravnovesie zhidkost'–par: Spravochnoe izdanie* (Liquid–Vapor Equilibrium: Reference Book), Leningrad: Khimiya, 1987.
3. Maczyński, A., *Verified Vapor–Liquid Equilibrium Data, vol. 1, Binary Hydrocarbon Systems*, Warsaw: PWN, 1976.
4. Marple, S.L., Jr., *Digital Spectral Analysis with Applications*, Engelwood Cliffs, New Jersey: Prentice-Hall, 1987.
5. Selivanov, D., *Kurs ischisleniya konechnykh raznostei* (A Course of Calculation of Finite Differences), St. Petersburg: Tipogr. Imper. Akad. Nauk, 1908.

ISSN 1070-4272, Russian Journal of Applied Chemistry, 2007, Vol. 80, No. 2, pp. 213–220. © Pleiades Publishing, Ltd., 2007.
Original Russian Text © G.G. Aseev, I.M. Ryshchenko, A.S. Savenkov, 2007, published in Zhurnal Prikladnoi Khimii, 2007, Vol. 80, No. 2, pp. 213–220.

PHYSICOCHEMICAL STUDIES OF SYSTEMS AND PROCESSES

Equations and Determination of Physicochemical Properties of Ammonium Sulfate-Nitrate Solutions

G. G. Aseev, I. M. Ryshchenko, and A. S. Savenkov

Khar'kovskii Politekhnicheskii Institut National Technical University, Kharkov, Ukraine

Received July 6, 2005; in final form, June 2006

Abstract—Theoretical and correlation equations for calculation of multicomponent systems were considered in terms of a previously developed theory of ion–ion interactions in steady- and nonsteady-state processes for the example of ammonium sulfate-nitrate solutions formed from effluent gases of thermal power plants.

DOI: 10.1134/S1070427207020097

Effluent gases of thermal power plants contain a significant amount of sulfur dioxide (~7 g m^{-3}) and nitrogen oxides (~1.5 g m^{-3}), which are discharged into the atmosphere and contaminate air, soil, and water basins. Previously a new technology for manufacture of ammonium sulfate–nitrate (ASN) fertilizers from these contaminants has been developed [1–3]. The technology includes introduction of gaseous ammonia, electron-beam processing of dusty effluent gases, absorption of the forming SO_3 and NO_2 by water, concentration of ASN solutions, evaporation, and granulation.

Development of new technologies and choice of the optimal ways of utilization of industrial waste require that thermodynamics, kinetics, and various physicochemical parameters should be known. The technology suggested requires particularly reliable and authentic data on physicochemical properties of concentrated solutions of inorganic substances.

The theory of interparticle interactions in steady-state processes in concentrated electrolyte solutions [4] and some implications of this theory [5] were used to suggest methods for determination of physicochemical parameters of multicomponent systems. The following properties of the solutions were analyzed: density, specific heat, thermal conductivity, water vapor pressure over solution, activity of water, surface tension, dynamic viscosity coefficient, electrical conductivity, and boiling and freezing points.

The present study is devoted to analysis of the physicochemical properties of solutions of multicomponent systems based on $(NH_4)_2SO_4$ and NH_4NO_3, with minor additions of NH_4HSO_3, NH_4HSO_4, $(NH_4)_2SO_3$, and NH_4NO_2. The concentrations of the components in solutions was varied from 10 to 70 wt % at an $(NH_4)_2SO_4/NH_4NO_3$ ratio equal to 4 and temperatures of 25–80°C.

The density of a multicomponent solution was calculated by the formula

$$\rho = \rho_0 + \sum_{i=1}^{h} c_i (A_{1i} + A_{2i} t + A_{3i} c_i), \qquad (1)$$

where ρ is the solution density (kg m^{-3}); ρ_0, water density (kg m^{-3}); h, number of solution components; c, electrolyte concentration (wt %); t, temperature (°C); and A_{ij}, coefficients found by processing by methods of regression analysis of the authors' own data and those published in the literature for a large number of electrolytes [5]. The values of these coefficients for the components of the ASN solution are listed in Table 1.

Table 1. Coefficients of Eq. (1)

Electrolyte	A_{1i}	A_{2i}	A_{3i}	c, wt %	t, °C	S_ρ,* kg m^{-3}	Δ,* %
NH_4NO_3	4.1148	–0.0101	0.0165	0–70	0–100	4.15	0.26
$(NH_4)_2SO_4$	5.8719	–0.0012	–0.0020	0–70	0–100	1.89	0.13

* S_ρ is the root-mean-square error, and Δ, average relative error of calculation.

Table 2. Density ρ of ASN solutions

c, wt %	ρ, kg m^{-3}, at indicated temperature, °C						
	25	30	40	50	60	70	80
10	1052.4	1050.9	1047.5	1043.2	1038.3	1032.8	1026.8
20	1107.5	1106.1	1102.6	1098.4	1093.5	1088.0	1082.0
30	1162.6	1161.2	1157.8	1153.6	1148.6	1143.1	1137.1
40	1217.8	1216.4	1212.9	1208.6	1203.7	1198.2	1192.2
50	1272.5	1271.4	1268.0	1263.7	1258.8	1253.3	1247.3
60	1327.9	1326.5	1323.0	1318.8	1313.9	1308.3	1302.3
70	1383.0	1381.6	1378.1	1373.8	1368.9	1363.4	1357.3

Table 3. Coefficients of Eq. (3)

Electrolyte	B_{1i}	$B_{2i} \times 10^2$	$B_{3i} \times 10^2$	$B_{4i} \times 10^3$	c, wt %	t, °C	S_{C_p}, J kg^{-1} K^{-1}	Δ, %
NH_4NO_3	–39.21	31.0495	–19.0210	–2.0051	4–16	20–10	13.76	0.25
$(NH_4)_2SO_4$	–55.40	5.3285	96.0142	0.3568	0–15	10–10	10.20	0.1
	–43.30	4.3392	21.5319	0.0312	15–60	10–10	11.46	0.29

The density of water (kg m^{-3}) on the saturation line at 0–150°C was calculated with a relative error of 4.8×10^{-3}% by the formula

$$\rho_0 = 999.810745 + R_1 t^* + R_2 t_*^{1.5} + R_3 t_*^2 + R_4 t_*^{2.5} + R_5 t_*^3 + R_6 t_*^{3.5} + R_7 t_*^4 + R_8 t_*^{4.5}, \quad (2)$$

where $t^* = 0.01t$, $R_1 = 15.910174$, $R_2 = -73.840671$, $R_3 = 141.693443$, $R_4 = -297.162815$, $R_5 = 160.758796$, $1R_6 = 146.727674$, $R_7 = -194.580793$, $R_8 = 58.847919$.

The results obtained in calculating the density of the ASN solution are listed in Table 2.

The specific heat of the multicomponent solution, C_p (J kg^{-1} K^{-1}) can be calculated by the formula

$$C_p = C_{p0} + \sum_{i=1}^{k} (B_{1i} + B_{2i} c_i + B_{3i} t + B_{4i} t^2) c_i. \quad (3)$$

Here, C_{p0} is the specific heat of water (J kg^{-1} K^{-1}); $\tilde{c}_i$, concentration of ith component in a binary isopiestic solution (wt %); t, temperature (°C); c_i, concentration of ith component in the multicomponent solution (wt %); k, number of the solution components; and B_{ni}, coefficients found by processing by methods of regression analysis of the authors' own data and those published in the literature for a large number of electrolytes [6, 7]. The values of these coefficients for the components of the ASN solution are listed in Table 3.

The specific heat of water (J kg^{-1} K^{-1}) on the saturation line at 0°C ≤ t < 40°C was calculated with a root-mean-square and average relative calculation errors of 3.95 J kg^{-1} K^{-1} and 0.035%, respectively, by the formula

$$C_{p0} = 4.21703 - 0.068372 t_*^{0.5} - 0.193808 t_*^{1.5} + 0.340252 t_*^2, \quad (4)$$

where $t_* = 0.01t$.

In the temperature range 40°C ≤ t < 250°C, the specific heat of water was found by the formula

$$C_{p0} = 4.178232 - 0.200822 t_*^{2.5} + 0.551896 t_*^{1.3} - 0.435824 t_*^{3.5} + 0.123167 t_*^4. \quad (5)$$

The value of $\tilde{c}_i$ was calculated as

$$\tilde{c}_i = E_i^{-1} \sum_{j=1}^{k} E_j c_i. \quad (6)$$

Here E_i is a coefficient characterizing the vapor pressure over solution, which can be found from the dependence [5, 7]:

$$E_i = (1 - a_w^s) c_i^s, \quad (7)$$

where a_w^s and c_i^s are, respectively, the activity of water and the mass fraction of a saturated solution of a separate component of the system under consideration at a given temperature.

Table 4. Specific heat of ASN solutions, C_p

c, wt %	C_p, J kg^{-1} K^{-1} at indicated temperature, °C						
	25	30	40	50	60	70	80
10	4175.1	4173.3	4173.3	4174.9	4178.0	4182.6	4189.0
20	4170.2	4168.3	4167.8	4168.9	4171.5	4175.5	4181.3
30	4165.4	4163.2	4162.3	4163.0	4164.9	4168.5	4173.6
40	4160.6	4158.2	4156.8	4157.0	4158.4	4161.4	4165.9
50	4155.7	4153.1	4151.3	4151.0	4151.9	4154.3	4158.2
60	4150.9	4148.1	4145.8	4145.0	4145.4	4147.2	4150.5

Table 5. Coefficients of Eq. (8)

Electrolyte	$-\beta \times 10^3$	c, wt %	t, °C	$S_\lambda \times 10^3$, W m^{-1} K^{-1}	Δ, %	Electrolyte	$-\beta \times 10^3$	c, wt %	t, °C	$S_\lambda \times 10^3$, W m^{-1} K^{-1}	Δ, %
NH_4NO_3	1.1598	0–50	10–100	5.97	0.79	$(NH_4)_2SO_4$	2.3668	0–30	10–90	9.69	1.22

Table 6. Thermal conductivity λ of ASN solutions

c, wt %	λ, W m^{-1} K^{-1} at indicated temperature, °C						
	25	30	40	50	60	70	80
10	0.594	0.602	0.617	0.630	0.640	0.649	0.656
20	0.581	0.589	0.604	0.616	0.626	0.635	0.641
30	0.569	0.576	0.590	0.602	0.613	0.621	0.627

The results obtained in calculating the specific heat of the ASN solution are listed in Table 4.

The thermal conductivity of multicomponent electrolyte solutions was calculated by the formula

$$\lambda = \lambda_0\left(1 + \sum_{i=1}^{k}\beta_i c_i\right). \quad (8)$$

Here, λ is the thermal conductivity of the solution (W m^{-1} K^{-1}); λ_0, thermal conductivity of water (W m^{-1} K^{-1}); c_i, concentration of ith component in the multicomponent solution (wt %); k, number of solution components; and β_i, coefficients found by processing by methods of regression analysis the authors' own data and those published in the literature for a large number of electrolytes [8]. The values of these coefficients for the components of the ASN solution are listed in Table 5.

The thermal conductivity of water on the saturation line at temperatures of 0 to 135°C was approximated with a root-mean-square calculation error S_λ = 0.29 W m^{-1} K^{-1} and average relative calculation error Δ = 0.03% with the polynomial

$$\lambda_0 = 10^{-3}(L_0 + L_1T^* + L_2T_*^{1.5} + L_3T_*^{2.5} + L_4T_*^3), \quad (9)$$

where L_0 = 560.971778, L_1 = 178.153112, L_2 = 59.731618, L_3 = –245.008302, L_4 = 124.973313, T^* = 0.01t, and t is temperature (°C).

The results of calculation of the thermal conductivity of an ASN solution are listed in Table 6.

The water vapor pressure (Pa) over a multicomponent electrolyte solution was calculated by the equation

$$P = P_0\exp\left(2.3026\sum_{i=1}^{k} m_i P_i^*\right), \quad (10)$$

where P_0 is the water vapor pressure over pure water (Pa); m_i, mass concentration of the electrolyte in

Table 7. Coefficients of Eq. (15)

Coefficient	c, wt %	t, °C	Δ, %	Coefficient	c, wt %	t, °C	Δ, %
NH_4NO_3 electrolyte				$(NH_4)_2SO_4$ electrolyte			
$W_{0i} = -9.0900 \times 10^{-3}$ $W_{1i} = 6.2000 \times 10^{-5}$ $W_{2i} = 7.5700 \times 10^{-5}$ $W_{3i} = -9.0000 \times 10^{-7}$ $W_{4i} = -7.6000 \times 10^{-6}$ $W_{5i} = 0.1000 \times 10^{-6}$	2–50	0–100	0.46	$W_{0i} = -1.6377 \times 10^{-2}$ $W_{1i} = 9.9500 \times 10^{-5}$ $W_{2i} = -2.3900 \times 10^{-5}$ $W_{3i} = -8.0000 \times 10^{-7}$ $W_{4i} = -2.0900 \times 10^{-5}$ $W_{5i} = 2.0000 \times 10^{-7}$	2–50	0–100	0.17

Table 8. Water vapor pressure P over an ASN solution

c, wt %	P, Pa, at indicated temperature, °C						
	25	30	40	50	60	70	80
10	3079	4127	7179	12010	19394	30329	46065
20	2970	3982	6931	11597	18727	29279	44445
30	2829	3794	6606	11057	17856	27914	42366
40	2643	3543	6168	10325	16678	26083	39611
50	2385	3194	5554	9294	15022	23530	35823
60	2014	2689	4655	7778	12590	19809	30382

the solution (mol kg^{-1}); k, number of solution components; and P_i^*, correction for the decrease in the water vapor pressure over the multicomponent electrolyte solution.

The water vapor pressure over pure water on the saturation line is calculated with root-mean-square and average relative errors of 39.54 Pa and 0.006% by the formula

$$P_0 = P_c \exp B. \quad (11)$$

Here, P_c is the critical pressure equal to 2.2064×10^7 Pa and B is given by

$$B = T_c A/T, \quad (12)$$

where T_c is the critical temperature equal to 647.14; T, temperature (K); and A is found from the following dependence at temperature of 0 to 100°C:

$$A = A_0 + A_1 T_*^{1.5} + A_2 T_*^3 + A_3 T_*^{3.5}, \quad (13)$$

$A_0 = -0.595684$, $A_1 = -11.039345$, $A_2 = 17.449275$, $A_3 = -16.028445$,

$$T^* = 1 - T/T_c. \quad (14)$$

The value of P_i^* in Eq. (10) was found using the formula

$$P_i^* = W_{0i} + W_{1i} t_i + W_{2i} m_i + W_{3i} t_i^2 + W_{4i} t_i m_i + W_{5i} t_i^2 m_i, \quad (15)$$

where the coefficients W_{ji} are found by processing by methods of regression analysis of the authors' own data and those published in the literature for a large number of electrolytes [5]. The values of these coefficients for the components of the ASN solution are listed in Table 7.

The results obtained by calculating the water vapor pressure over an ASN solution are listed in Table 8.

The activity of water can be calculated by theoretical and semiempirical equations reported in [4, 5], where various calculation examples were demonstrated. In view of the limited volume of the present communication, the following formula can be recommended in the given case

$$a_w = \exp(2.3026 \sum_{i=1}^{k} m_i P_i^*). \quad (16)$$

Table 9. Activity a_w of water over an ASN solution

c, wt %	a_w at indicated temperature, °C						
	25	30	40	50	60	70	80
10	0.9725	0.9729	0.9735	0.9737	0.9737	0.9733	0.9727
20	0.9379	0.9387	0.9397	0.9403	0.9402	0.9396	0.9385
30	0.8935	0.8944	0.8957	0.8964	0.8964	0.8958	0.8946
40	0.8345	0.8352	0.8364	0.8371	0.8373	0.8371	0.8364
50	0.7531	0.7530	0.7531	0.7535	0.7542	0.7551	0.7564
60	0.6360	0.6339	0.6312	0.6306	0.6321	0.6357	0.6416

Table 10. Surface tension σ of ASN solutions

c, wt %	σ, N m^{-1}, at indicated temperature, °C						
	25	30	40	50	60	70	80
10	0.073	0.072	0.071	0.069	0.067	0.066	0.064
20	0.075	0.074	0.073	0.071	0.069	0.067	0.066
30	0.077	0.076	0.075	0.073	0.071	0.070	0.068
40	0.080	0.079	0.078	0.076	0.074	0.072	0.071
50	0.084	0.083	0.082	0.080	0.078	0.076	0.075
60	0.090	0.089	0.088	0.086	0.084	0.082	0.080

Table 11. Coefficients of Eq. (19)

Electrolyte	$A_0 \times 10^3$	$A_1 \times 10^4$	$A_2 \times 10^5$	$A_3 \times 10^6$	c, wt %	t, °C	$S_\eta \times 10^2$	Δ, %
NH_4NO_3	–13.765	3.956	13.88	–2.1	5–40	25–95	1.50	1.32
$(NH_4)_2SO_4$	15.434	0.744	12.29	0.0	0–50	20–90	3.54	1.72

The results obtained by calculating the activity of water over the ASN solution are listed in Table 9.

The surface tension of a multicomponent solution can be calculated by the formula [8]:

$$\sigma = \sigma_0 + 0.049(1 - a_w), \quad (17)$$

where σ is the surface tension of the multicomponent electrolyte solution (N m^{-1}); σ_0, surface tension of water (N m^{-1}); and a_w, activity of water in the multicomponent solution.

The surface tension was calculated with high accuracy for the entire range of existence of water from the data of [9]:

$$\sigma_0 = B\left(\frac{T_0 - T}{T_0}\right)^m \left[1 + b\left(\frac{T_0 - T}{T_0}\right)\right], \quad (18)$$

where $B = 235.6 \times 10^{-3}$, $T_0 = 647.15$, $m = 1.256$ $b = -0.625$.

The results of calculation of the surface tension of ASN solutions are listed in Table 10.

The dynamic viscosity coefficient η (Pa s) of a multicomponent solution was calculated by the formula

$$\eta = \eta_0 \exp V, \quad (19)$$

$$V = \sum_{i=1}^{k} c_i(A_{0i} + A_{1i}t + A_{2i}c_i + A_{3i}t^2),$$

where η_0 is the dynamic viscosity coefficient of water (Pa s); k, number of electrolyte components in the solution; c_i, mass fraction of ith component in the multicomponent solution (%); t, temperature (°C); and A_{ij}, found by processing by methods of regression analysis of the authors' own data and those published in the literature for a large number of electrolytes [10, 11]. The values of these coefficients for the components of the ASN solution are listed in Table 11.

The viscosity of water, η_0 (Pa s), on the saturation line in the temperature range 0–350°C was calcu-

Table 12. Dynamic viscosity coefficient η of ASN solutions

c, wt %	$\eta \times 10^{-3}$, Pa s, at indicated temperature, °C						
	25	30	40	50	60	70	80
10	1.018	0.919	0.762	0.645	0.555	0.483	0.426
20	1.187	1.077	0.904	0.773	0.670	0.589	0.523
30	1.407	1.284	1.089	0.941	0.824	0.730	0.654
40	1.696	1.557	1.335	1.165	1.030	0.920	0.830
50	2.080	1.920	1.665	1.467	1.309	1.179	1.072
60	2.593	2.408	2.110	1.879	1.691	1.537	1.408

lated with root-mean-square and average relative calculation errors of, respectively, 1.19 (Pa s) and 0.07% in the temperature interval 0–200°C by the formula

$$\eta_0 = S_0 + S_1 t + S_2/t + S_3 \exp(-0.1t) + S_4/t^2 + S_5\sqrt{t} + S_6 \ln t, \quad (20)$$

where S_0 = 4496.839782, S_1 = –4.644252, S_2 = –7025.494506, S_3 = –159.419139, S_4 = 4104.442382, S_5 = 316.705387, and S_6 = –1486.934219.

The results of a calculation of the dynamic viscosity coefficient of ASN solutions are listed in Table 12.

The electrical conductivity Λ (S cm^2 mol^{-1}) of a multicomponent electrolyte solution can be calculated using the following theoretical equation [4–6]:

$$\Lambda = \frac{1}{c_{kg}} \sum_{i=1}^{k} \nu_i c_{ki} [\Lambda_i (1 - L_i) + K_{1i} c_{ki}^2]. \quad (21)$$

Here, c_{kg} is the total molar concentration of the equivalent of the solution components (g-equiv dm^{-3}); k, number of electrolyte components in the solution; ν_i, number of like charges of the electrolyte molecule; c_{ki}, molar concentration of each electrolyte component (mol dm^{-3}); Λ_i^0, limiting molar electrical conductivity of each component of the multicomponent solution in water (S cm^2 mol^{-1}); L_i, parameter of ith component in the solution; and K_{1i}, correction factor for ith component of the solution [4, 5].

In turn, Λ_i^0 was found using the formula

$$\Lambda_i^0 = \lambda_i^0 + \lambda_j^0, \quad (22)$$

where λ_i^0 and λ_j^0 are the limiting electrical conductivities of cations and anions in water (S cm^2 mol^{-1}).

The limiting molar electrical conductivities of cations and anions in water were calculated using expressions reported in [5].

The parameter L_i was found using the equation

$$L_i = V_{0i} + V_{1i} t + V_{2i} c_{ki} + V_{3i} t c_{ki} + V_{4i} (t c_{ki})^2 + V_{5i} c_{ki}^{0.7} + V_{6i} c_{ki}^{0.7} + V_{7i} (t c_{ki})^{0.5}, \quad (23)$$

where t is temperature (°C), and V_{ij} are coefficients found by processing by methods of regression analysis of the authors' own data and those published in the literature for a large number of electrolytes [5].

The correction factor K_{1i} was determined by the formula [5]:

$$K_1 = -3.161 \times 10^{17} \frac{(\nu_k z_i)^2 \alpha_a}{\eta_0 \varepsilon (\varepsilon T)^3 (6 - \alpha_a^2)}, \quad (24)$$

where ν_k is the number of ions in the electrolyte molecule; z_i, cation charge; α_a, theoretical parameter [4, 6]; η_0, viscosity of water (Pa s); ε, dielectric constant; and T, temperature (K).

The value of α_a was found using the expression derived in [4]:

$$\alpha_a = \sinh(\beta/a), \quad (25)$$

where β is calculated by the formula

$$\beta = \frac{1.6718 \times 10^{-3} |z_i z_j|}{\varepsilon T}. \quad (26)$$

The value of ε can be calculated with a standard deviation of 0.33 in ε units by the equation [12]:

$$\varepsilon = 1 + (a_1/T^*)\rho + (a_2/T^* + a_3 + a_4 T^*)\rho_*^2 + (a_5/T^* + a_6 T^* + a_7 T_*^2)\rho_*^3 + (a_8/T_*^2 + a_9/T^* + a_{10})\rho_*^4, \quad (27)$$

where

$$T^* = T/298.15, \ \rho^* = \rho_0/1000, \quad (28)$$

and ρ_0 is the density of water (kg m^{-3}).

Table 13. Electrical conductivity Λ of ASN solutions

c, wt %	Λ, S cm^2 mol^{-1}, at indicated temperature, °C						
	25	30	40	50	60	70	80
10	32.81	35.92	42.14	48.47	54.98	61.74	68.78
20	31.13	33.96	39.59	45.27	51.10	57.12	63.38
30	29.36	31.93	37.04	42.17	47.43	52.87	58.52
40	27.69	30.04	34.70	39.39	44.20	49.18	54.37
50	26.15	28.31	32.59	36.91	41.36	45.99	50.82
60	24.74	26.74	30.70	34.72	38.88	43.21	47.75

The coefficients a_i have the following values: a_1 = 7.62571, a_2 = 244.003, a_3 = –140.569, a_4 = 27.7841, a_5 = –96.2805, a_6 = 41.7909, a_7 = –10.2099, a_8 = –45.2059, a_9 = 84.6395, a_{10} = –35.8644.

Equation (27) is applicable under the following conditions: temperature 273.15–823.15 K, density 0–1150 kg m^{-3}, pressure 0–500 MPa. The value of a in Eq. (25) is found by the formula

$$a = \chi_f(a_i + a_j), \quad (29)$$

where χ_f = 1 for electrolytes of the symmetric type and χ_f = 2 for those of the asymmetric type, and distances from the ion center to the oxygen of water for ions in solution and the effective radii of polyatomic ions a_i and a_j (nm) can be found in [5].

The results of calculation of the electrical conductivity of ASN solutions are listed in Table 13.

The boiling point T_b (K) of a multicomponent solution can be calculated with an accuracy acceptable for practical purposes by the modified formula [5]:

$$T_b = 500.2238/[(24.6536 + \ln a_w)^{1/2} - 3.6249], \quad (30)$$

$$0 < t < 215°C, \; S_{T_b} = 0.6 \text{ K},$$

where S_{T_b} is the root-mean-square calculation error (K).

Equation (30) is solved by the method of iterations. First a_w (0.99) is set and T_b is calculated. This value of T_b is used to find a_w, using formulas (10)–(16) or some others. Then, T_b is again calculated [calculation of the vapor pressure over solution with the use of coefficients in formulas (13) and (15) allows a slight extrapolation beyond 100°C]. The number of iterations is 2. Making this number larger impairs the calculation accuracy. Instead of calculating a_w, it is possible to use its experimental values reported in [13] at temperatures below 100°C for many tens of electrolytes, with the activity of water at T_b found by means of a linear approximation. The results of calculation of the boiling points of ASN solutions are presented below (°C):

c, wt %	10	20	30	40	50	60
T_b, °C	100.86	101.97	103.28	105.16	107.97	112.42

The freezing temperature of a multicomponent solution, T_f (K) is commonly found in the entire range of activities of water, using the equation [5]:

$$T_f = \frac{555.316}{2.76375 - \sqrt{\ln a_w^{(25)} + 0.53398}}, \quad (31)$$

where $\ln a_w^{(25)}$ is the activity of water over solution at 25°C.

The applicability of formula (31) is limited by the lower bound of the interval $|\ln a_w^{(25)}| < 0.53398$, because the expression within the square root should be positive.

The results of calculation of the freezing point of ASN solutions are presented below (°C):

c, wt %	10	20	30	40	50
T_f, °C	–2.58	–5.95	–10.54	–17.19	–27.79

The whole set of the physicochemical studies performed enabled optimal consideration of heat-and-mass exchange processes in the technology for manufacture of a complex integrated fertilizer based on ammonium sulfate and nitrate with microelements from effluent gases discharged by thermal power plants.

CONCLUSIONS

(1) The previously developed theory of ion–ion interactions in steady- and nonsteady-state processes in concentrated electrolyte solutions was used to derive new equations for calculation of physicochemical properties of multicomponent systems of electrolyte

solutions: density, specific heat, thermal conductivity, water vapor pressure over solution, activity of water, surface tension, dynamic viscosity coefficient, boiling and freezing points, and electrical conductivity.

(2) New correlation equations were suggested for determining the density of water, specific heat, thermal conductivity, water vapor pressure over solution, dynamic viscosity of water on the saturation line in a wide range of temperatures and pressures. These equations provide the minimum calculation errors.

(3) The physicochemical properties of ammonium sulfate-nitrate solutions were calculated for a mass fraction of the components equal to 10–70% in the temperature range 25–80°C. This made it possible to recommend the equations under consideration for determining these properties for other multicomponent systems of electrolytes as well.

(4) The set of the physicochemical studies performed enabled optimal consideration of heat-and-mass exchange processes that occur in manufacture of a complex integrated fertilizer based on ammonium sulfate and nitrate with addition of microelements from effluent gases of thermal power plants.

REFERENCES

1. Savenkov, A.S., Ryshchenko, I.M., and Ushakova, N.M., *Vestn. Kharkov. Gos. Politekhn. Univ.*, Kharkov: Kharkov. Gos. Politekhn. Univ., 2000, issue 105, pp. 39–41.
2. Savenkov, A.S., Ryshchenko, I.M., and Ushakova, N.M., *Khimiya i tekhnologiya proizvodstva osnovnoi khimicheskoi produktsii: Trudy NIOKhIM* (Chemistry and Technology of Manufacture of Basic Chemical Products: Trans. NIOKhIM), Kharkov, 2001, vol. 72, pp. 199–203.
3. Savenkov, A.S. and Fanshtein, A.L., *Sbornik nauchnykh trudov "Ekologiya-98"* (Coll. of Sci. Works: "Ecology-98"), Severodonetsk, 1998, pp. 71–72.
4. Aseyev, G.G., *Electrolytes: Interparticle Interactions: Theory, Calculation Methods and Experimental Data.*, New York: Begell House, 1998.
5. Aseev, G.G., Ryshchenko, I.M., and Savenkov, A.S., *Elektrolity: Fiziko-khimicheskie parametry kontsentrirovannykh mnogokomponentnykh sistem: Monografiya* (Electrolytes: Physicochemical Parameters of Concentrated Multicomponent Systems: Monograph), Kharkov: KhPI NTU, 2005.
6. Aseev, G.G., Ryshchenko, I.M., and Savenkov, A.S., *Vopr. Khim. Khim. Tekhnol.*, 2004, no. 4, pp. 61–66.
7. Aseev, G.G., Ryshchenko, I.M., and Savenkov, A.S., *Vestnnik Natsional'nogo tekhnicheskogo universiteta "KhPI": Sbornik nauchykh trudov, Tematicheskii vypusk "Khimiya, khimicheskaya tekhnologiya i ekologiya"* (Journal of KhPI National Technical University, Col. of Sci. Works: Subject Issue "Chemistry, Chemcal Technology, and Ecology)", Kharkov: KhPI NTU, 2001, no. 23, vol. 2, pp. 104–107.
8. Aseyev, G.G., *Electrolytes: Properties of Solutions Methods for Calculation of Multicomponent Systems and Experimental data on Thermal Conductivity and Surface Tension*, New York: Begell House, 1999.
9. Rivkin C.L. and Aleksandrov, A.A., *Teplofizicheskie svoistva vody i vodyanogo para* (Thermal Properties of Water and Water Vapor), Moscow: Energiya, 1980.
10. Aseyev, G.G., *Electrolytes: Transport Phenomena: Methods for Calculation of Multicomponent Solutions and Experimental data on Viscosities and Diffusion Coefficients*, New York: Begell House, 1998.
11. Ryshchenko, I.M., Aseev, G.G., and Savenkov, A.S., *Zbirn. nauk. prats' mizhnar. nauk.-prakt. konf. "Kompleksne vikoristannya sirovini, energo- ta resursozberigayuchi tekhnologii u virobnitstvi neorganichnikh rechovin", 27–29 travnya 2004 r.* (Proc. Int. Sci.-Pract. Conf. "Integrated Use of Raw Materials and Energy- and Resource-Saving Technologies in Manufacture of Inorganic Substances," May 27–29, 2004), Cherkasi: Vertikal', 2004, pp. 126–127.
12. Uematsu, M. and Franck, E.U., *J. Phys. Ref. Data*, 1980, vol. 9, no. 4, pp. 1291–1305.
13. Aseyev, G.G., *Electrolytes, Equilibria in Solutions and Phase Equilibria: Calculation of Multicomponent Systems and Experimental Data on the Activities of Water, Pressure Vapor and Osmotic Coefficients*, New York: Begell House, 1998.

ISSN 1070-4272, Russian Journal of Applied Chemistry, 2007, Vol. 80, No. 2, pp. 221–225. © Pleiades Publishing, Ltd., 2007.
Original Russian Text © V.N. Pak, E.S. Stromova, 2007, published in Zhurnal Prikladnoi Khimii, 2007, Vol. 80, No. 2, pp. 221–225.

PHYSICOCHEMICAL STUDIES OF SYSTEMS AND PROCESSES

Temperature Dependence of the Diffusion Coefficient of Copper(II) Chloride in Porous-Glass Membranes

V. N. Pak and E. S. Stromova

Hertzen Russian State Pedagogical University, St. Petersburg, Russia

Received October 23, 2006

Abstract—Diffusion transport of a 0.5 M aqueous solution of $CuCl_2$ was studied in a set of porous-glass membranes with predominant pore radii of 4.5 to 70 nm in the temperature range 25–70°C. Raising the temperature causes a rise in diffusion coefficients and their gradual equalization, which eliminates their dimension dependence on the radius of membrane channels.

DOI: 10.1134/S1070427207020103

It is well known that the diffusion coefficients D of many substances, which characterize transport of their aqueous solutions across finely porous hydrophilic membranes, are lower than the values for free solutions [1, 2]. The hindrance to diffusion mobility, created by the effect of the surface, must be the stronger, the narrower the cross-section of transport channels. A quantitative verification of this concept is possible, but requires experiments with a number of membranes of the same chemical nature, with structural parameters that are variable and can be rather precisely set. This is possible in the case of porous glasses produced by acid etching of liquated glasses of the sodium–borosilicate system, followed by alkaline etching [3–5]. It has been found previously [6–10] that, in a number of cases, the dimension dependence of the diffusion coefficient on the pore radius in porous-glass membranes has the form

$$D = D_\infty \exp(-K_w r^{-1}), \quad (1)$$

where D_∞ corresponds to a free solution (at $r \to \infty$), and K_w characterizes the effective thickness of the near-wall structured solution layer with a limited diffusion.

If relation (1) is steadily satisfied, prospects arise for use of the dimension parameter K_w as a characteristic of the structuring effect of the silica surface on boundary layers of aqueous solutions of a wide variety of compounds. In addition, determining the temperature dependence of the parameter K_w can give a rather reliable notion of the thermal stability of the structure of thin water layers modified by the silica surface [6]. However, information on diffusion in porous glasses [11–14], and especially on its dimension and temperature dependences, is available only for a limited number of systems [6–10]. To supplement and refine this information, we studied the effect of temperature on the diffusion mobility of $CuCl_2$ in a number of porous glasses with effective pore radii in the range 4.5–70 nm. The possibility of direct photometric determination of Cu^{2+} cations in aqueous solutions and the negligible amount of their sorption by the silica surface in an acid medium [15] markedly facilitate the formulation and solution of the problem and make it possible to distinguish the membrane pore radius and temperature as the principal factors responsible for the value of the diffusion coefficient.

EXPERIMENTAL

Porous-glass membranes were prepared in the form of thin (1 mm) discs of diameter 25 mm. The pore radii r_p and the porosity δ of porous glasses were set by preliminary thermal treatment and by the conditions of the subsequent acid-alkaline etching of a DV-1M sodium-borosilicate glass [3–5]:

r_p, nm	4.5	6.5	10	19	25	30	38	45	70
δ, $cm^3\ cm^{-3}$	0.313	0.345	0.436	0.389	0.512	0.480	0.429	0.313	0.569

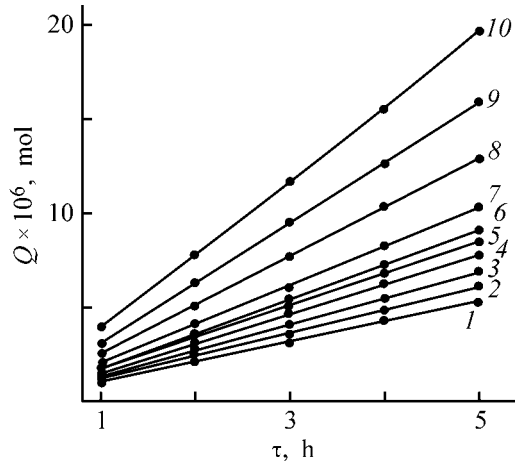

Fig. 1. Amount Q of $CuCl_2$ transferred across a membrane with a pore radius of 38 nm vs. time τ. Experimental temperature T (°C): (*1*) 25, (*2*) 30, (*3*) 35, (*4*) 40, (*5*) 45, (*6*) 50, (*7*) 55, (*8*) 60, (*9*) 65, and (*10*) 70; the same for Fig. 4.

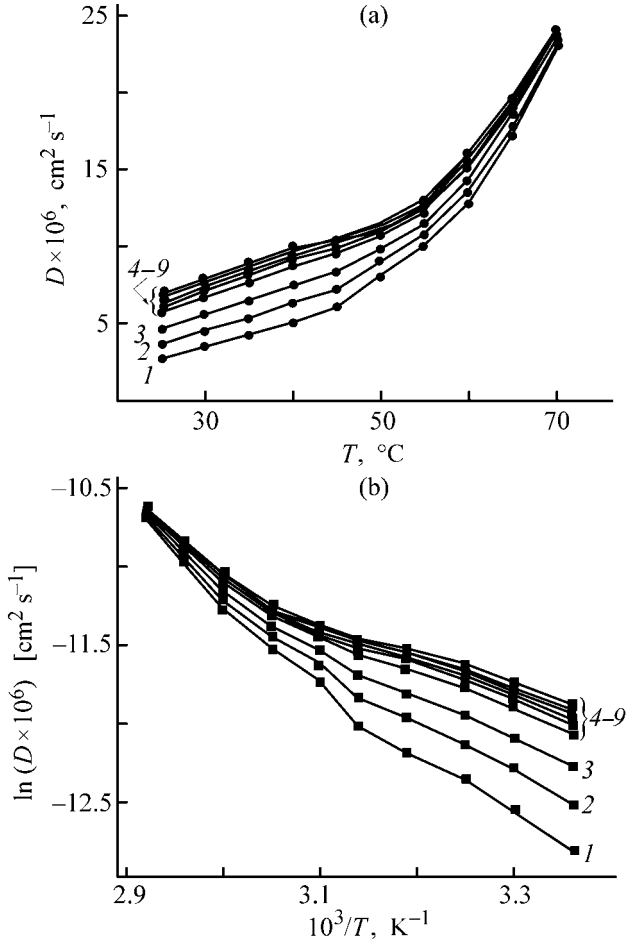

Fig. 2. (a) Dependence of the diffusion coefficient D of $CuCl_2$ in porous-glass membranes on temperature T and (b) the same dependence plotted in the Arrhenius coordinates. Membrane channel radius r_p (nm): (*1*) 4.5, (*2*) 6.5, (*3*) 10, (*4*) 19, (*5*) 25, (*6*) 30, (*7*) 38, (*8*) 45, and (*9*) 70.

As in our previous studies [6–10], we examined the diffusion by fixing membranes between two cells, one of which (receiver) was filled with twice-distilled water, and the other (feeder), with a 0.5 M aqueous solution of $CuCl_2$. The dynamics of the diffusion transport was judged from the results of a direct photometric determination of aqua complexes of Cu^{2+} (λ_{max} = 800 nm, ε = 11.32 mol cm^{-1} l^{-1}). The experiments were carried out with permanent agitation of the system and thermostating of the system in the temperature range 25–70°C. The time in which a steady diffusion flow across the membranes was attained depended on temperature and pore structure parameters of porous glasses. However, a linear time dependence of the amount of the salt, Q, that passed across the membranes was recorded in all cases after 1 h. In calculations of the diffusion coefficient D, the concentration gradient was taken to be

$$\Delta c/h = (c_{in} - c_{out})/h - c_{in}/h, \quad (2)$$

where h = 1 mm is the membrane thickness, and c_{in} = 0.5 M is the concentration of the $CuCl_2$ solution before the membrane, which markedly exceeds, in all cases, the running concentration c_{out} of the solution in the receiving cell.

In the case of a steady-state process, we considered justified application of the first Fick law, according to which the diffusion flux was represented as

$$dQ/d\tau = DS\delta c_{in}/h, \quad (3)$$

with the free cross-section of the membrane taken equal to its geometric area S, with a correction for the porosity δ.

Selected experimental results demonstrating the steady state of the process and the general, on the whole, type and extent of the influence exerted by temperature on the rate of the diffusion transport of $CuCl_2$ are shown in Fig. 1 for a porous glass with a pore radius r_p = 38 nm. The temperature dependences of the diffusion coefficient in a set of membranes, calculated using these and similar data, are shown in Fig. 2a. The most pronounced decrease in the salt mobility, which characterizes the hindrance to diffusion in the near-boundary layer of the pore solution [6–10], is observed in pores with small radius $r_p \le 20$ nm and is reliably recorded at moderate experimental temperatures. The "rigidity" of the network of hydrogen bonds in the near-wall water, imposed by the silica surface, diminishes, on the whole, the mobilities of pore solution components by hindering the diffusion transport of the salt. We believe that,

in the given case, we can reliably conclude that the structural constituent of forces, specifically, hydrogen bonds exerts a dominating influence on the rate of the membrane transport. As for the increase in the diffusion coefficients with temperature, it is accompanied by their progressive convergence to become virtually coinciding, with $D = (2.35 \pm 0.05) \times 10^{-5}$ cm^2 s^{-1} at 70°C.

The dependences obtained (Fig. 2a) characterize the activation of the thermal mobility of the pore solution, which overcomes the structuring effect of the membrane channel walls. The disintegration of the boundary layers of the solution is, thus, complete as a temperature of approximately 70°C is reached. This agrees with the known concept [1, 16, 17] that, near this temperature, the properties of water in narrow pores of silica cease to be different from those of the bulk liquid.

It should be noted that the D–T dependences are not linearized in the Arrhenius equation coordinates (Fig. 2b). This is a reflection of the pronounced structural and energetic inhomogeneity of the pore solution, preserved up to a temperature of 70°C, at which the properties of the solution in the membranes are completely equalized, irrespective of the size of transport channels. Nevertheless, the run of the $\ln D$–T^{-1} dependences clearly demonstrates that the energy expenditure substantially increases in the course of a gradual thermal disintegration of the near-wall layers of the solution. This can be additionally confirmed by estimating the conditional activation energies E^* of diffusion, with the gently and steeply sloping portions of the $\ln D$–T^{-1} dependences approximated by straight lines. The results presented in Fig. 3 clearly demonstrate both a significant rise in E^* in the range of disintegration of the near-wall layers of the solution and a general enhancement of the hindrance to diffusion in small-radius pores.

The dependences of the diffusion coefficient of $CuCl_2$ on the pore radius of porous-glass membranes are shown in the explicit form in Fig. 4a. The fact that the experimental data are described by Eq. (1) suggested in this study is confirmed by the clearly pronounced linearity of their plots in the $\ln D$–$1/r_p$ coordinates in the entire temperature range 25–70°C (Fig. 4b). The thus revealed "dimensional" behavior of D on the whole corresponds to the generally exponential type of the dependence of the structural forces on the boundary layer thickness [1, 16, 17].

The asymptotics of Eq. (1) reflects the physically justified conditions: $D \to D_\infty$ at $r_p \to \infty$ and $D \to 0$ at $r_p \to 0$ and shows that the rule $D = 0.368D_\infty$

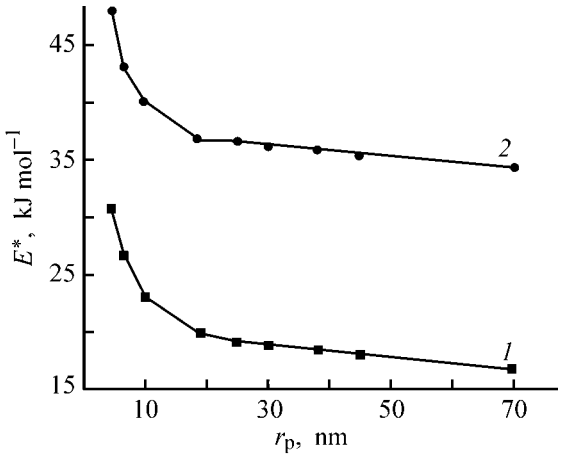

Fig. 3. Activation energy E^* of diffusion vs. the membrane channel radius r_p on (*1*) gently and (*2*) steeply sloping portions of the $\ln D$–T^{-1} dependence.

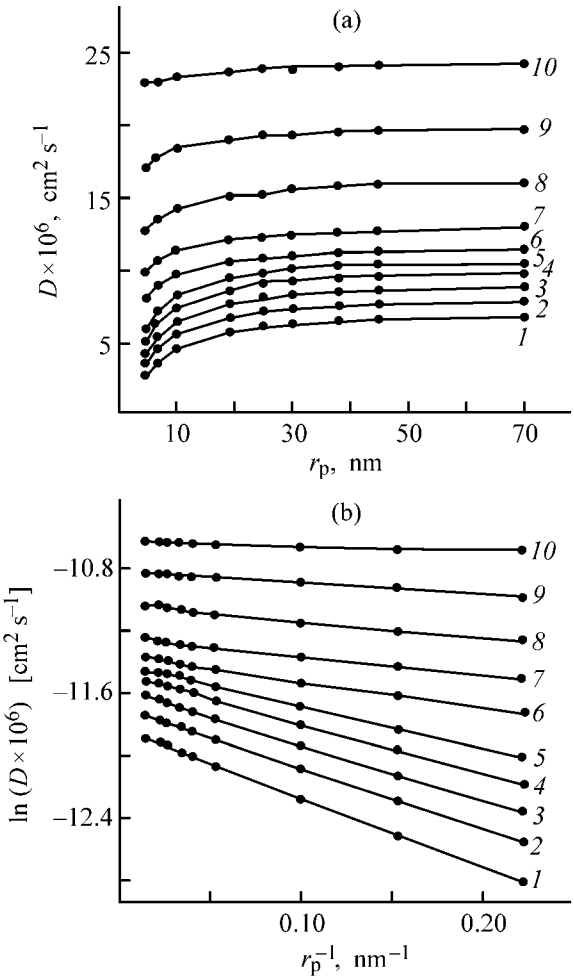

Fig. 4. Dependence of the diffusion coefficient D of $CuCl_2$ in porous-glass membranes on the transport channel radius r_p and (b) its linearization in the coordinates of Eq. (1).

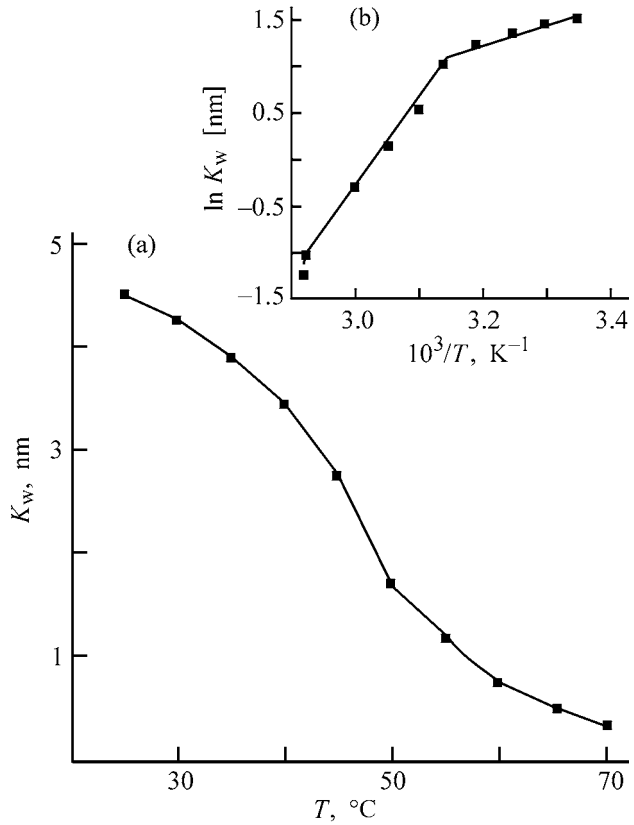

Fig. 5. (a) Dependence of the dimension parameter K_w on temperature T and (b) linearization of its two portions.

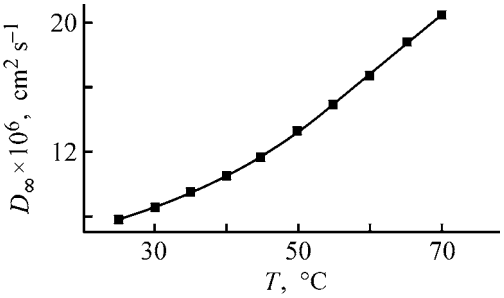

Fig. 6. Limiting diffusion coefficient D_∞ vs. temperature T.

is satisfied at $r_p = K_w$, i.e., the "long-range-action" parameter of the surface is numerically equal to the pore radius of the glass membrane in which the diffusion coefficient of the solute is approximately 2.7 times smaller than its value in a free solution. Processing of the isotherms obtained (Fig. 4b) gives values of K_w and D_∞. The temperature dependence of K_w (Fig. 5) in fact characterizes the rate of thermal disintegration of the boundary layer of the pore solution. As in the D–T case, two portions can be distinguished in the K_w–T curve, and these portions are satisfactorily linearized in the coordinates of the Arrhenius equation. The relative values of the calculated activation energies $E_1^* = 19.6$ kJ mol^{-1} and $E_2^* = 77.0$ kJ mol^{-1} indicate that thermal disordering of the peripheral region of the pore solution, subject to a weak influence of the silica surface, proceeds easily, whereas disintegration of its part adjacent to the membrane channel walls is strongly hindered.

The values of D_∞ estimated by extrapolation are, as a rule, close to the diffusion coefficients in free solutions [6–10]. Thus, the results obtained when measuring the rate of membrane transport in a set of porous glasses give a knowledge of both the diffusion coefficient D of $CuCl_2$ in water, which cannot be found in the literature, and its temperature dependence (Fig. 6). An estimate of the activation energy of diffusion, based on the data of Fig. 6, gives a value $E^* = 19.2$ kJ mol^{-1}, which virtually coincides with that found for the peripheral part of the pore solution in a porous glass with $r_p = 70$ nm. This is in an agreement with the fact that the room-temperature diffusion coefficients are close: the value $D = 6.9 \times 10^{-6}$ cm^2 s^{-1} is 91% of $D_\infty = 7.6 \times 10^{-6}$ cm^2 s^{-1} for a membrane with as channel radius of 70 nm. Thus, there is reason to believe that the structuring of an aqueous solution of $CuCl_2$ in a porous glass exponentially decays away from the surface and its influence extends to boundary layers of thickness of about 70 nm.

CONCLUSIONS

(1) A reduction in the channel radius of porous glasses from 70 to 4.5 nm is accompanied by a substantial decrease in the diffusion coefficient of copper(II) chloride in its membrane transport. The general run of the D–r_p dependences is consistent with the concept that there exists a near-wall layer of the pore solution, with a limited diffusion mobility.

(2) The activation of the thermal mobility of a $CuCl_2$ solution in silica membranes on raising the temperature of the experiment to 70°C leads to total disintegration of the boundary layer, with the structuring effect of the surface on the diffusion transport of the salt eliminated.

REFERENCES

1. Churaev, N.V., *Fizikokhimiya protsessov massoperenosa v poristykh sredakh* (Physical Chemistry of Mass Transfer in Porous Media), Moscow: Khimiya, 1990.
2. Nikolaev, N.I., *Diffuziya v membranakh* (Diffusion in Membranes), Moscow: Khimiya, 1980.
3. Mazurin, O.V., Roskova, G.P., Aver'yanov, V.N., and Antropova, T.V., *Dvukhfaznye stekla: struktura, svoistva, primenenie* (Two-Phase Glasses: Structure, Properties, and Application), Leningrad: Nauka, 1991.

4. Roskova, G.P. and Tsekhomskaya, T.S., *Fiz. Khim. Stekla*, 1981, vol. 7, no. 5, pp. 513–534.
5. Burkat, T.M. and Dobychin, D.P., *Fiz. Khim. Stekla*, 1981, vol. 18, no. 5, pp. 129–140.
6. Pak, V.N., Nepomnyashchii, A.B., Burkat, T.M., and Kun, Sh.R., *Zh. Fiz. Khim.*, 2005, vol. 79, no. 9, pp. 1411–1414.
7. Pak, V.N., Stromova, E.S., Lobov, B.I., and Levkin, A.N., *Zh. Prikl. Khim.*, 2006, vol. 79, no. 3, pp. 363–366.
8. Pak, V.N., Nepomnyashchii, A.B., and Burkat, T.M., *Zh. Fiz. Khim.*, 2003, vol. 77, no. 11, pp. 1979–1982.
9. Pak, V.N., Nepomnyashchii, A.B., Burkat, T.M., and Mal'kova, S.V., *Zh. Prikl. Khim.*, 2002, vol. 75, no. 12, pp. 1959–1962.
10. Voloshina, O.S., Burkat, T.M., and Pak, V.N., *Zh. Fiz. Khim.*, 2000, vol. 74, no. 6, pp. 1099–1102.
11. Takahashi, R., Sodesava, T., and Nishida, H., *Phys. Chem. Chem. Phys.*, 2002, vol. 4, no. 12, pp. 3800–3805.
12. Takahashi, R., Sato, S., Sodesava, T., and Katotae, Y., *Phys. Chem. Chem. Phys.*, 2000, vol. 2, no. 4, pp. 1199–1204.
13. Antropova, T.V., Tsyganova, T.A., and Krylova, N.L., *Fiz. Khim. Stekla*, 1990, vol. 16, no. 5, pp. 732–737.
14. Mazurin, O.V. and Antropova, T.V., *Fiz. Khim. Stekla*, 1986, vol. 12, no. 4, pp. 507–510.
15. Pak, V.N., Tikhomirova, I.Yu., Burkat, T.M., and Lobov, B.I., *Zh. Fiz. Khim.*, 1999, vol. 93, no. 11, pp. 2024–2028.
16. Chyraev, N.V., *Adv. Coll. Interface Sci.*, 2003, vol. 104, no. 1, pp. 15–21.
17. Derjaguin, B.V. and Churaev, N.V., *Langmuir*, 1987, vol. 3, no. 2, pp. 607–612.

ISSN 1070-4272, Russian Journal of Applied Chemistry, 2007, Vol. 80, No. 2, pp. 226–229. © Pleiades Publishing, Ltd., 2007.
Original Russian Text © E.N. Brazhnikova, V.N. Pak, 2007, published in Zhurnal Prikladnoi Khimii, 2007, Vol. 80, No. 2, pp. 226–229.

PHYSICOCHEMICAL STUDIES OF SYSTEMS AND PROCESSES

Optical Properties of a Perfluorosulfonic Membrane Modified with Co^{2+} Cations

E. N. Brazhnikova and V. N. Pak

Hertzen Russian State Pedagogical University, St. Petersburg, Russia

Received December 8, 2006

Abstract—A perfluorosulfonic membrane was modified with Co^{2+} cations. A comparative study of the thermal stabilities of the starting (hydrogen) and cobalt(II)-containing forms of the membrane was carried out. Optical electronic spectroscopy was used to characterize color transformations accompanying sorption–desorption of water by the modified membrane.

DOI: 10.1134/S1070427207020115

Perfluorosulfomic membranes (PFSM) belong to a special type of porous fluorocarbon polymers containing grafted sulfo groups. In accordance with the existing concepts [1–3], a continuous system of spherical voids about 4 nm in diameter, connected by narrow channels with a diameter of approximately 1 nm, is formed in the PFSM skeleton constituted by fluorocarbon and ether chains. In turn, the functional sulfo groups with protons (or cations) neutralizing their charge are situated on void walls and provide the hydrophilicity of the membranes. The high transparency, accessibility of the pore space, and clearly pronounced cation-exchange capacity predetermine the possibility of directed modification of PFSM to impart necessary optical properties to these membranes. For example, studies have been carried out of luminescent and spectral properties of a number of complex compounds of transition and rare-earth metals [4–6], uranyl ion [7], and dyes [8] fixed in PFS membranes by the ion-exchange mechanism. Proceeding with these investigations, we tested whether a system for visual monitoring of humidity can be created on the basis of a PFSM modified with Co^{2+} ions.

EXPERIMENTAL

MF-4SK membranes of domestic manufacture, with a thickness of 0.25 mm and linear dimensions of 1×3 cm, were cleaned by boiling in concentrated nitric acid for 2–3 h, with the subsequent thorough washing with distilled water to zero reaction to NO_3^- ions. The content of accessible sulfo groups was determined as follows [6]: membranes of known mass were submerged in an aqueous NaOH solution for 24 h to provide complete substitution of protons of the sulfo groups by sodium cations, and then the alkali was titrated with hydrochloric acid and $[-SO_3H]$ was found from the difference of its concentrations before and after contact with PFSM. The membranes were modified at a fixed s : 1 ratio by keeping samples with a mass of about 0.1 g in 10 ml of aqueous $Co(NO_3)_2$ solutions with a concentration of 0.1 to 3.5 M for 24 h, with the subsequent thorough washing with distilled water. The content of irreversibly sorbed Co^{2+} cations was determined gravimetrically on drying the starting and modified PFSM to constant weight at 120°C. It is important to note that incomplete removal of the weakly retained form of Co^{2+} and, the more so, of residual amounts of the impregnating solution from the pore space led to formation of cobalt oxide particles in heating of the membranes, which diminished or completely eliminated the characteristic optical properties. The adsorption of water by pure and modified membranes was controlled at relative vapor pressures in the range $p/p_0 = 0.1–0.8$ by the desiccator method with the use of sulfuric acid solutions. The optical absorption of the membranes in the visible spectral range was recorded on an SF-56 spectrometer.

The content of sulfo groups in the membrane was, according to the results of titration, $[-SO_3H] = 0.84$ mmol g^{-1}. The ion-exchange modification of PFSM samples with Co^{2+} cations under the conditions specified above occurred on the background of their considerable molar excess (12- to 420-fold) over sulfo groups of the membranes. It is all the more characteristic that the content of irreversibly sorbed cobalt

was found to be independent of the solution concentration and was $[Co^{2+}] = 0.22 \pm 0.04$ mmol g^{-1} in all cases. This result suggests that the electrically neutral sorbed form $(–SO_3)_2Co$, in whose formation is involved approximately 0.44 mmol g^{-1} of sulfo groups of the membrane, i.e., about 52% of their total content, is firmly fixed and water-stable. In this case, the remaining 48% of functional groups are "single" because of the nonuniformity of their distribution in the support voids, and the salt-type exchange form $(–SO_3)Co(NO_3)$, produced with their participation is hydrolytically unstable and is removed in membrane washing.

The replacement of protons in a considerable part of sulfo groups in PFSM with Co^{2+} cations leads to a noticeable suppression of water adsorption in the whole range of pressures (Fig. 1). Thus, hydration of fixed cations to give $=Co(H_2O)_n$ aqua complexes can compensate to an only insignificant extent for the loss of the adsorption activity, caused by substitution of sulfo groups in the membrane. In addition, the modification of PFSM results in a substantial decrease in the pore volume V_p from 0.20 to 0.15 cm^3 g^{-1}. Relating the quantity ΔV_p to the content of cobalt in the membrane makes it possible to estimate the effective volume occupied by a hydrated cation by $\Delta V_p/[Co^{2+}]N_A = 0.38$ nm^3 (N_A is the Avogadro number), which gives in the spherical model approximation a reasonable value of the cation radius $r = 0.45$ nm.

It is important to note that, despite the contraction of the internal space, modification of the membrane strongly improves its thermal stability. For example, it has been found [6] that, in the case of a hydrogen form of PFSM, irreversible changes of the pore structure begin even at a temperature of 100–105°C. Figure 2 shows as an example the results demonstrating the decrease dynamics of V_p to a residual value of 0.1 cm^3 g^{-1} in the course of heating of a pure membrane in air at 120°C. It is not improbable that, in this case, there occurs irreversible condensation of sulfo groups, the most probable at places of narrowing of the hydrophilic voids of PFSM:

$$2(–SO_3H) \rightarrow –\overset{\overset{O}{\|}}{\underset{\underset{O}{\|}}{S}}–O–\overset{\overset{O}{\|}}{\underset{\underset{O}{\|}}{S}}– + H_2O. \qquad (1)$$

In the case of a membrane modified with Co^{2+} cations, the contraction of the pore volume occurs at temperatures higher than 200°C and is observed only upon a prolonged thermal treatment (Fig. 3); for example, short (for 10–15 min) treatments even at 250°C are not accompanied by any recordable change in the pore space. The most probable reasons for the improvement of the thermal stability of the porous structure are the firm fixation and valence saturation of cobalt(II) in the grafted aqua complexes, which

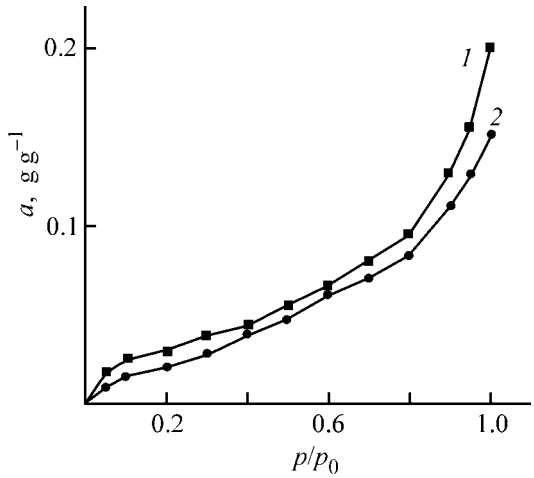

Fig. 1. Isotherms of water adsorption by (*1*) initial and (*2*) modified membranes. (*a*) Adsorption and (p/p_0) relative water vapor pressure.

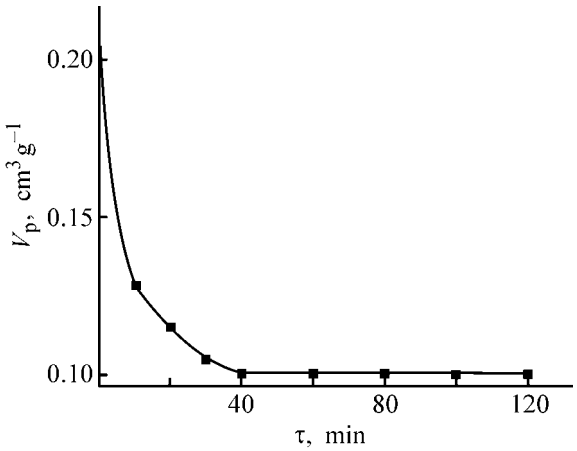

Fig. 2. Pore volume V_p of a pure PFS membrane vs. time τ of its heating in air at 120°C.

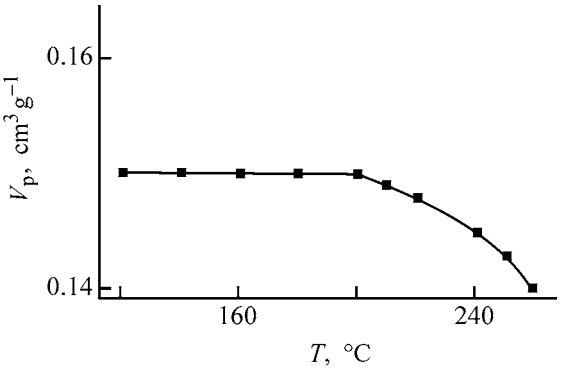

Fig. 3. Pore volume V_p of a cobalt(II)-containing membrane vs. temperature T at a heating duration at each point of 1 h.

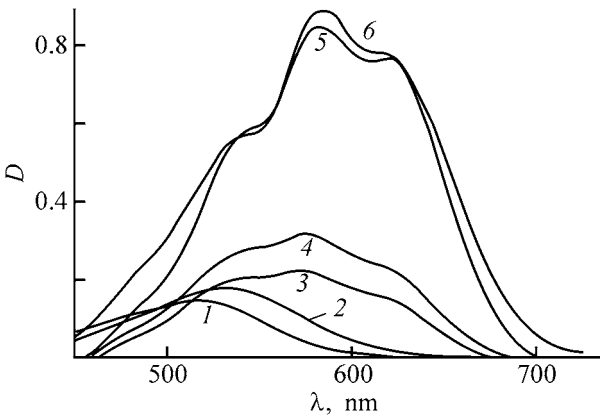

Fig. 4. Spectra of a modified membrane (*1*) in the hydrated state and (*2–6*) upon heating at various temperatures. (*D*) Optical density and (λ) wavelength. *T* (°C): (*2*) 120, (*3*) 150, (*4*) 200, (*5*) 230, and (*6*) 250.

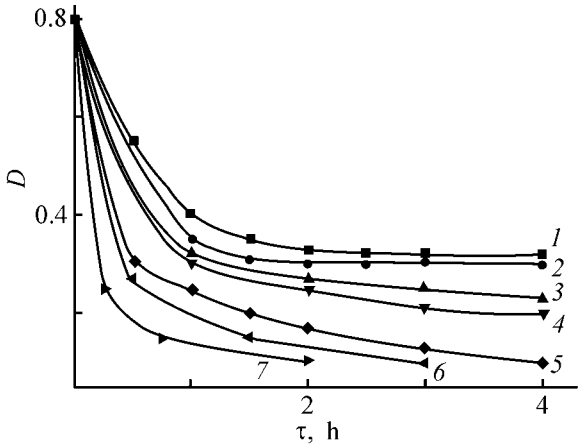

Fig. 5. Optical density *D* at a wavelength of 580 nm vs. the keeping time τ of a dehydrated modified membrane in the atmosphere with varied relative humidity. Relative humidity: (*1*) 0.1, (*2*) 0.2, (*3*) 0.3, (*4*) 0.4, (*5*) 0.5, (*6*) 0.75, and (*7*) 0.95.

rule out any possibility of their "cross-linking" to form Co–O–Co bonds.

The spectrum of a modified membrane saturated with moisture contains a broad band peaked at about 517 nm (Fig. 4), whose position and profile are closely similar to those of the well-known spectrum of a pink octahedral complex $Co(H_2O)_6^{2+}$ and correspond to the main single-electron transition $^4T_{1g} \rightarrow {}^4T_{1g}(P)$ [9, 10]. Heating of a sample at 100–120°C is accompanied by a weak long-wavelength shift (λ_{max} = 530 nm) and an insignificant increase in the intensity of the absorption band. These minor spectral changes are, nevertheless, manifested in the appearance of a clearly pronounced violet coloration of the membrane. Further increase in temperature gives rise to a more complex spectrum with a peak at 570 nm and two shoulders at 540 and 610 nm (Fig. 4), preserved in the temperature range 150–200°C. As a result, the membrane becomes light blue. And finally, at temperatures exceeding 200°C, we observe an additional shift and sharp enhancement of the intensity of the spectrum having a clearly pronounced three-component structure (peaks at 545, 580, and 620 nm), which makes the sample bright blue.

The transformations we observed undoubtedly reflect the generation of several structural forms, which appear as the starting hexacoordinated state $=Co(H_2O)_4$. In this case, the transition from pink to violet coloration, caused by an insignificant change of the spectrum at 100–120°C, is in all probability due to a slight distortion of the configuration of grafted $=Co(H_2O)_4$ complexes upon removal of water molecules (outer sphere) adsorbed on these complexes. In turn, it is reasonable to believe that the strong changes of the membrane spectrum with further rise in temperature are due to successive desorption of coordinatively bound water molecules

$$=Co(H_2O)_4 \rightarrow =Co(H_2O)_3 + H_2O,\ T = 150\text{–}200^\circ C, \quad (2)$$

$$=Co(H_2O)_3 \rightarrow =Co(H_2O)_2 + H_2O,\ T > 200^\circ C, \quad (3)$$

which results in that the membrane color changes to light and intense blue, respectively. The long-wavelength shifts of the spectral bands in Fig. 4, observed in the course of dehydration, correspond, on the whole, to a decrease in the coordination number of the Co^{2+} cations and to the resulting weakening of the splitting effect of ligands on its 3*d*-states.

Despite the similar types of coloration, we observed noticeable differences between the spectra of a dehydrated Co(II) : PFS membrane and a dehydrated blue form of a cobalt(II)-containing silica gel (widely used humidity indicator). For the latter, the doublet band peaked at 620 and 670 nm has been attributed to the $[CoO_4]$ tetrahedron; however, it was not specified whether or not the T_d symmetry is observed in this case [11, 12]. It should be noted, in this context, that not only reliable interpretation of spectra (assignment of peaks to electronic transitions), but even their comparative analysis are hindered in the case in question because it is very difficult to take into account the strong influence exerted by the type and extent of distortion of the structure of Co(II) complexes on the splitting of terms of excited states [9, 10].

On bringing a dehydrated membrane in contact with water vapor, we observed reverse transitions of coloration, whose completeness and occurrence duration depend on the relative humidity p/p_0. Figure 5

shows a set of kinetic dependences obtained by recording the optical density D at λ_{max} = 580 nm for a sample heated to 250°C and kept in an atmosphere with p/p_0 = 0.1–0.95. The transition of the indicator membrane color from blue ($D_{580} \approx 0.85$) to pink ($D_{580} \approx 0.15$) is complete at p/p_0 of 0.95, 0.75, and 0.5 in 1, 2, and 3 h, respectively. At moderate and low humidities p/p_0 = 0.4–0.1, only a transition from blue to light blue can be observed, with complete restoration of the pink coloration taking days under these conditions. The results we obtained point to an enhanced stability of the intermediate form of the grafted complex $=Co(H_2O)_3$, which is clearly manifested in the process of both sorption and removal of coordinatively bound water. At the same time, the noticeable slowness of the optical "response" is primarily due to the diffusion hindrance of water molecules in the nanosize channels of PFSM. Nevertheless, under certain conditions and with account of the dynamics of color variation, a Co(II)-containing PFS membrane may be of use as a compact means of qualitative visual determination of the humidity of gaseous media.

CONCLUSIONS

(1) Ion-exchange modification of a perfluorosulfonic membrane in aqueous $Co(NO_3)_2$ solutions is accompanied by firm sorption of Co^{2+} cations in an amount of 0.22 ± 0.04 mmol g^{-1}.

(2) Modification of the membrane significantly improves of the thermal stability of its pore structure, with the stability threshold increasing from 100 to 200°C.

(3) Four reliably visually distinguishable forms of hydrated Co^{2+} cations (pink, violet, light blue, and blue) in the membrane occur in sorption–desorption of water, which creates prerequisites for use of the membrane for determining the humidity of gaseous media.

REFERENCES

1. Heiter-Wirguin, C., *J. Membr. Sci.*, 1996, vol. 120, no. 1, pp. 1–33.
2. Gierke, T.D., Munn, G.E., and Wilson, F.C., *J. Polym. Sci.*, 1981, vol. 19, no. 11, pp. 1687–1704.
3. Yeager, H.L. and Steck, A., *Anal. Chem.*, 1979, vol. 51, no. 7, pp. 862–865.
4. Finlayson, M.F., Park, K.H., Kakuta, N., et. al., *J. Lumin.*, 1988, vol. 39, no. 4, pp. 205–214.
5. Li, X.-H., Wu, L.-Z., Zhang, L.-P., et al., *Chem. Comm.*, 2001, vol. 21, pp. 2280–2281.
6. Petushkov, A.A., Shilov, S.M., and Pak, V.N., *J. Lumin.*, 2006, vol. 116, nos. 1–2, pp. 127–131.
7. Lopez, M. and Birch, D.J.S., *J. Lumin.*, 1997, vol. 71, no. 3, pp. 221–228.
8. Zinger, B. and Shier, P., *Sensors Actuators, Ser. B*, 1999, vol. 56, no. 3, pp. 206–214.
9. Ballhausen, C.J., *Introduction to Ligand Field Theory*, New York: McGraw-Hill, 1962.
10. Lever, A.B.P., *Inorganic Electronic Spectroscopy*, Amsterdam: Elsevier, 1984.
11. Belotserkovskaya, N.G., Dobychin, D.P., Pak, V.N., et al., *Zh. Prikl. Khim.*, 1985, vol. 58, no. 9, pp. 2136–2139.
12. Tsvetkov, V.K., Pak, V.N., and Aleskovskii, V.B., *Zh. Prikl. Khim.*, 1976, vol. 49, no. 5, pp. 984–987.

ISSN 1070-4272, Russian Journal of Applied Chemistry, 2007, Vol. 80, No. 2, pp. 230–235. © Pleiades Publishing, Ltd., 2007.
Original Russian Text © Yu.E. Zevatskii, D.V. Samoilov, 2007, published in Zhurnal Prikladnoi Khimii, 2007, Vol. 80, No. 2, pp. 230–235.

PHYSICOCHEMICAL STUDIES OF SYSTEMS AND PROCESSES

Empirical Method for Calculation of Thermodynamic Potentials of Organic Substances

Yu. E. Zevatskii and D. V. Samoilov

St. Petersburg State Technological Institute, St. Petersburg, Russia

Received June 4, 2006; in final form, December 2006

Abstract—A method for establishing relationships between various physicochemical properties of organic substances is developed. The method is based on the concept of linear deviations of physicochemical parameters calculated by additive techniques from experimentally determined values for some broad groups covering various classes of organic substances. The deviations from linearity are analyzed for the example of thermodynamic potentials of 1055 organic substances.

DOI: 10.1134/S1070427207020127

The relationship between the structure of organic substances and their reactivity is one of the most fundamental problems of modern chemistry. At present, the reactivity of organic compounds is evaluated by reactivity indices (RI) based on local electronic (hardness, softness, electronegativity, polarizability, delocalization) and pseudothermodynamic (chemical potential, entropy, electronic temperature) properties of a molecule [1, 2]. These local parameters are determined by formal equations in quantum-chemical calculations in terms of the electron density functional (EDF) theory.

The main advantage of this approach is its presumed versatility, i.e., applicability to any group of reagents or reaction series. The main commonly accepted disadvantages are as follows: use of the isolated-molecule approximation (which, e.g., gives no way of taking into account the effect of medium), not quite clear physical meaning of these local properties, and a pronounced dependence of the calculation accuracy on the choice of initial conditions.

There also exists an empirical method of correlation analysis (CA), suggested long ago by Hammett [3]. This method is based on the chemical similarity and linear free energy (LFE) principles and on application of the mathematical formalism of polylinearity [4], which remains an effective way to evaluate the reactivity of substances and their physicochemical properties.

This is indicated by publications of the last 10 years, which are devoted to evaluation of the inductive effect of substituents [5], development of criteria for a quantitative description of free-radical reactions [6], thermodynamic substantiation of the experimentally observed nonlinearity of the Brønsted equation for CH-acids by CA and of the hard soft acid base (HSAB) principle [8, 9], and by a review of correlation methods of analysis and prognostication of reactions of nucleophilic substitution [10]. The correlation analysis and the LFE principle have been successfully used in a number of studies concerned with the effect of substituents, including those of the organoelement type, on the ionization potentials of amines [11], sulfides [12], and phosphines and other organophosphorus compounds [13].

The key issue is that thermodynamic potentials of reactions are to be known for applying the CA technique. This is because this method is based on the commonly known simple relationship of the equilibrium constants K and rate k of a reaction with, respectively, the enthalpy H and activation energy E_a of the reaction (Vant-Hoff and Arrhenius equations) and on models that relate these kinetic parameters with thermodynamic characteristics. These relationships make it possible to express, using the CA method, the effect of substituents on the reaction center and physicochemical properties on a universal energy scale. Therefore, improvement of methods for calculation of thermodynamic parameters of compounds for prognostication of their reactivity is a topical task for physical organic chemistry.

Thermodynamic potentials have been recently used not only in theoretical and physical organic chemistry,

but also in neighboring research areas: geochemistry [14], biological docking [15, 16], colloid chemistry [17], and chemical industry [18]. Particular importance has been acquired by development of reliable and efficient techniques for prognostication of the heat of evaporation [19–22], mostly for the purpose of finding new effective and ecologically safe cooling agents [20–22]. For these reasons, techniques for calculation of various thermodynamic parameters continue to be improved.

A comparative analysis of the most important additive methods for calculation of the enthalpy of formation and other molecular parameters has been made earlier [23]. As a result, a conclusion was made that each of the methods considered has a number of advantages and disadvantages over other techniques; however, all of them give deviations from experimental data. The discrepancies are small, but exceed the measurement errors of the corresponding quantities. In this context, it has been suggested that the existing gap between the values calculated by additive schemes and those found experimentally (nonlinear effect or defect) is of not only quantitative, but also qualitative nature, which has its own physical meaning. This circumstance was mentioned long ago in the classical monograph by Pal'm [4]. Following this suggestion, dependences of deviations from linearity (defects) of one parameter on another parameter were analyzed with account of the results of [24] in order to improve the accuracy of additive methods. It was found that defects of different quantities also linearly depend on each other, and do so with a considerably larger correlation coefficient. As a result, the correlation coefficients were improved for the dependences of polarizability, enthalpy of atomization, and ionization potential on the defect of the volume.

However, an analysis of the input data used in [23, 24] demonstrated that the correlation coefficient is only seemingly improved on passing from additive schemes for molecular parameters themselves to additive schemes for their defects. This is mainly due to the purely mathematical effect of "smoothing" of deviations in subtraction of sums of atomic parameters, which frequently exceed the quantities themselves by more than an order of magnitude. Apparently, the dependences of the sum of atomic values of one parameter on another parameter are represented by an ideal straight line for homologous series and a degenerate point for isomers with the same empirical formula. Therefore, the correlations of defects, calculated for series of this kind, will certainly have a larger coefficient than the initial correlations of molecular parameters.

Taking into account the urgent need for improvement of methods for calculation of thermodynamic parameters, we carried out, similarly to [23], a comparative analysis of mutual correlations of the values and defects of linearity of the standard enthalpy (ΔH_f, kJ mol^{-1}), entropy (ΔS_f, J mol^{-1} K^{-1}), Gibbs energy of formation (ΔG_f, kJ mol^{-1}), and isobaric specific heats (C_p, J mol^{-1} K^{-1}) for 1055 organic compounds, with the above thermodynamic quantities regarded as independent parameters. We chose among these compounds, with account of the above comments, series of compounds that are certainly not homologues or isomers, but have similar chemical properties (which are characteristic of functional groups) or the same structural fragment (nucleus).

We took as input data the table of standard thermodynamic constants [25], in which all values of the parameters listed above were not available for all the compounds represented in the table. The phase for which a thermodynamic parameter was determined was denoted by superscripts s, l, and g for the solid, liquid, and gaseous states, respectively.

Preliminarily, we found the sum of the atomic constituents of a thermodynamic quantity under consideration for all the molecules:

$$\Sigma g_i X_i. \quad (1)$$

Here, g_i is the stoichiometric coefficient of ith atom in the molecular formula, and X_i is the experimentally determined value of the corresponding thermodynamic parameter of the atom in the gas phase [26].

We introduced the value of the defect of a molecular parameter as the difference between the experimentally found values δX [25] and the sum of atomic constituents

$$\delta X = X - A\Sigma g_i X_i. \quad (2)$$

Initially, the dimensionless coefficient A was taken to be unity.

Further, we considered correlations of the experimental values of the molecular parameters under study with each other in all the possible combinations (66 pairs). We excluded from consideration the dependences of the same thermodynamic quantity in different phases (12 pairs). This is so for it is apparent that the sums (1) of atomic values, used for calculations, were the same because they belong to the gas phase by definition. For the remaining 54 combinations, we compared the correlation coefficients between the experimental values [25], atomic sums (1), and defects of these thermodynamic quantities by Eq. (2).

Table 1. Parameters of the correlations and the optimized coefficients A_X

Group	Substance	Pair of quantities Y–X	Experiment r_{ex}	Correlation of deviations (2)			Sums (1) r_{at}	Number of points	A_X
				a	b	r			
1	Alkyl derivatives of benzene	C_p^l–ΔH^l	–0.9489	0.105	36.68	0.99752	1.0000	12	0.27
		C_p^l–ΔH^g	–0.9289	0.144	24.90	0.99752	1.0000	11	0.19
2	Halo, hydroxy, and alkyl derivatives of benzene	ΔS^l–ΔH^l	–0.9350	0.379	172.5	0.9914	0.54243	6	0.78
3	All derivatives of benzene	ΔS^c–ΔH^c	0.1283	0.167	–116.0	0.98832	0.98173	14	1.61
		ΔS^l–ΔH^l	–0.6680	0.369	104.6	0.99811	0.94892	15	0.77
		ΔS^g–ΔG^g	0.3583	0.022	370.9	0.9999	0.9996	5	15
4	Carboxylic acids and their derivatives (amides, nitriles, esters)	ΔS^s–ΔH^s	–0.3746	0.358	165.7	0.9976	0.9963	8	0.86
		ΔS^g–ΔH^g	–0.7872	0.339	63.80	0.9946	0.9404	7	0.79
		ΔS^l–ΔH^l	–0.3369	0.500	50.37	0.9949	0.9331	10	0.56
5	Six-membered heterorings with one and two nitrogen atoms	ΔS^l–ΔH^l	–0.1589	1.532	–145.8	0.9917	0.8661	10	0.17
		ΔS^l–ΔH^g	–0.1349	1.408	–158.8	0.9908	0.8661	10	0.19
6	Noncyclic monoatomic alcohols, thiols, esters, sulfides	ΔS^l–ΔG^l	0.73014	0.156	–55.55	0.9878	0.97632	5	2.1
		ΔS^g–ΔG^g	0.43003	0.033	26.82	0.99099	0.97736	6	10
7	Cyclic esters, sulfides	ΔS^g–ΔH^g	0.16402	0.307	204.3	0.96701	0.94200	7	1.07
		C_p^g–ΔH^g	0.23371	0.097	8.81	0.98495	0.93405	7	0.39
8	All alcohols, esters, thiols, sulfides	C^g–ΔG^g	0.69302	0.070	–8.77	0.99349	0.98082	11	0.54
		ΔS^g–ΔH^l	0.09366	0.387	50.34	0.98356	0.97805	24	0.76
		C_p^g–ΔH^l	–0.27918	0.037	–11.89	0.99008	0.97842	18	0.89
		ΔS^g–ΔH^g	0.15213	0.382	48.14	0.98341	0.97922	27	0.78
		C_p^g–ΔH^g	–0.18640	0.038	–12.85	0.99079	0.97935	21	0.87
9	Monoatomic alcohols, ethers, aldehydes, ketones of the C_1–C_8 group	S_p^g–ΔH^l	–0.48094	0.625	152.9	0.99371	0.99287	12	0.46
		S^g–ΔH^g	–0.70739	0.795	159.7	0.99555	0.99420	14	0.36

To find series of substances and pairs of quantities for which the correlation can be really achieved on passing from experimental values to defects, we used the following scheme for each of the groups we chose.

(1) We considered correlations of the molecular parameters under study with each other in the combinations specified above. In most cases, the correlation coefficient did not exceed 0.8.

(2) Of all the possible pairs of thermodynamic parameters, we chose those whose dependence on each other was constituted for the given group of substances by more than five points.

(3) We analyzed the types of dependences of the sums of atomic parameters on each other for different series of compounds. In those cases when the correlation coefficient was unity (straight line in the plot), the series were excluded as being "unsuccessful."

(4) We chose those combinations in which the correlation coefficient for the dependence of the defects of the given pair of quantities δY and δX by Eq. (2) exceeded that for their atomic sums (1). This definitely indicated that there is a real relationship between the defects for the chosen pair of thermodynamic quantities. For the chosen dependences of δY on δX, we optimized coefficient A in Eq. (2) for δX. We considered optimal that value of A_X at which the correlation coefficient was improve to the maximum possible extent, compared with that for the atomic sums. The values of A_X were within the range 0.17–15 for all the cases we analyzed (Table 1).

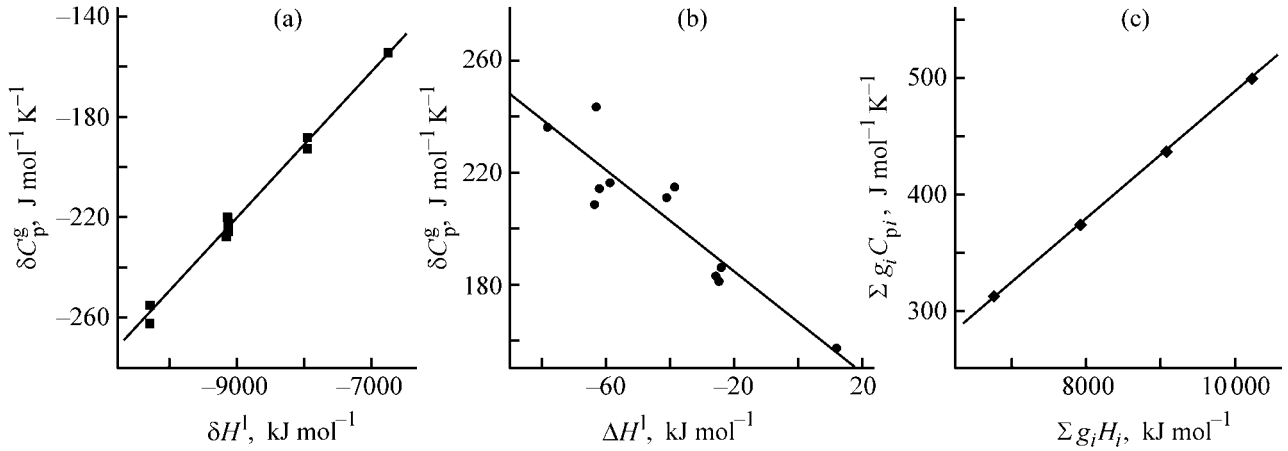

Fig. 1. Dependences for group 1. Dependence: (a) of the defect of the isobaric specific heat in the gaseous state, δC_p^g on the defect of the standard enthalpy of formation in the liquid state, δH^l; (b) of the isobaric specific heat in the gaseous state, C_p^g on the standard enthalpy of formation in the liquid state, H^l; and (c) of the specific heat $\Sigma g_i C_{pi}$ on the standard enthalpy of formation, $\Sigma g_i H_i$; the dependences were calculated by the additive formula (1); the same for Fig. 3.

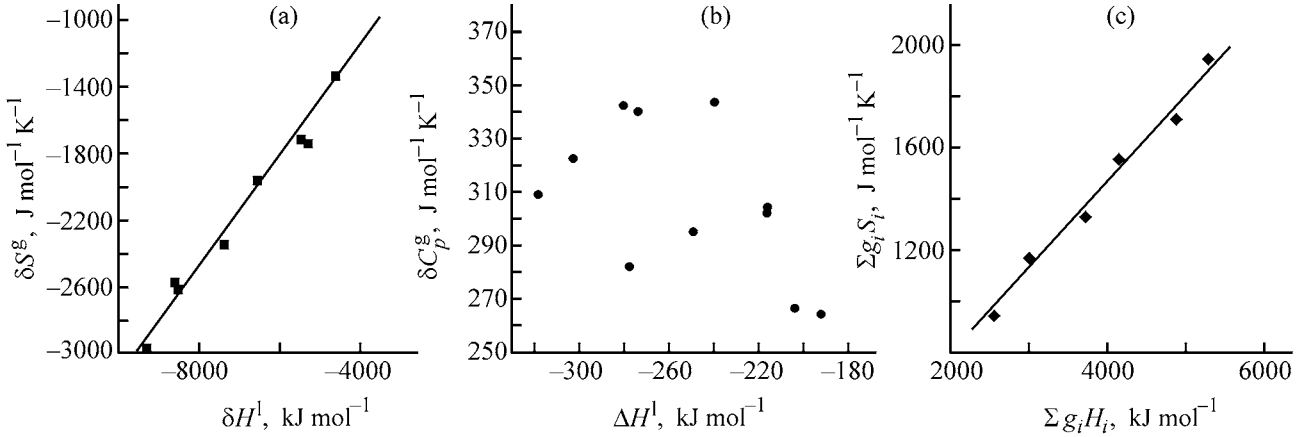

Fig. 2. Dependences for group 9. Dependence: Dependence: (a) of the defect of the entropy of formation in the gaseous state, δS^g on the defect of the standard enthalpy of formation in the liquid state, δH^l; (b) of the entropy of formation in the gaseous state, ΔS^g on the standard enthalpy of formation in the liquid state, H^l; and (c) of the entropy of formation, $\Sigma g_i S_i$, on the standard enthalpy of formation, $\Sigma g_i H_i$; the dependences were calculated by the additive formula (1).

Using the procedure described above, we found strong correlations between the defects of thermodynamic parameters for the following groups of substances: (1) alkyl derivatives of benzene; (2) halo, hydroxy, and alkyl derivatives of benzene; (3) all derivatives of benzene; (4) carboxylic acids and their derivatives (amides, nitriles, esters); (5) six-membered heterorings with one and two nitrogen atoms; (6) noncyclic monoatomic alcohols, thiols, esters, sulfides; (7) cyclic esters, sulfides; (8) all alcohols, esters, thiols, sulfides; and (9) monoatomic alcohols, ethers, aldehydes, ketones of the C_1–C_8 group.

As regards the applicability of the method under consideration, these groups can be accepted as series. Groups 1 and 9 are of particular interest in that they are, on the one hand, combinations of exclusively partial functional homologous series, and on the other hand, combinations of exclusively partial series of isomers. For these groups, the dependence of the sums of atomic parameters on each other is a straight line formed by several degenerate points (Fig. 1c) or two straight lines (Fig. 2c).

Consequently, despite that each of the partial series constituting the groups is unsuccessful, we markedly improved the correlation by considering these series together. In most cases, the remaining groups also included such combinations of unsuccessful series, but, in addition, contained a considerable number

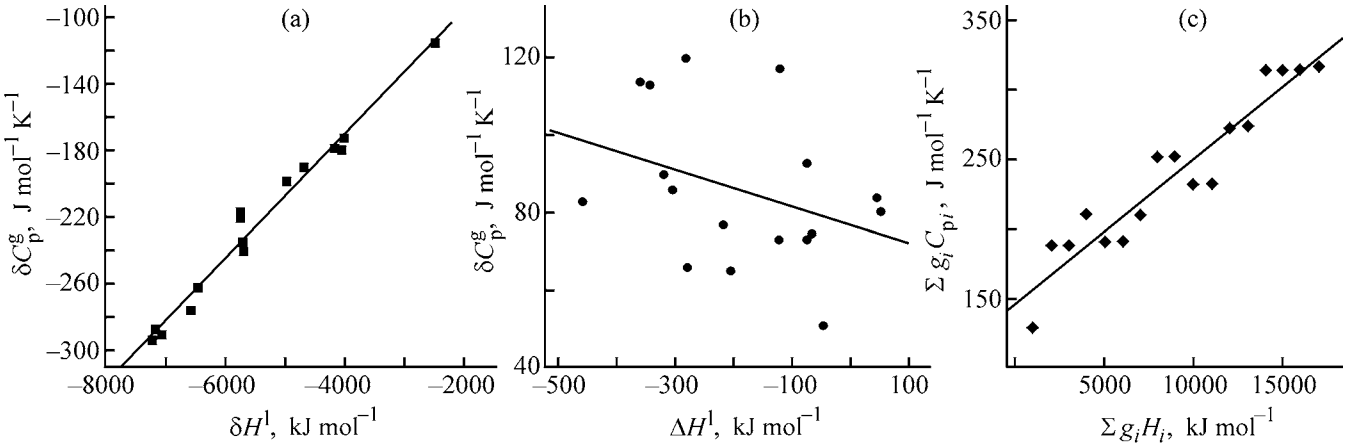

Fig. 3. Example of dependences for group 8.

of compounds not entering into any of these series (Fig. 3).

The parameters of the correlations and the optimized coefficients A_X for all the dependences of parameters in the selected groups of substances, processed using the procedure described above, are listed in Table 1. The correlation coefficients of the experimental X and Y in the dependence

$$Y = d_{ex}X + b_{ex} \quad (3)$$

are designated as r_{ex}; the correlation coefficients of the sums of the atomic values in the dependences

$$\Sigma g_i Y_i = a_{at}\Sigma g_i Y_i + b_{at} \quad (4)$$

are denoted by r_{at}; a and b are the coefficients in the equations

$$\delta Y = a\delta X + b, \quad (5)$$

where δY and δX are the defects of the corresponding quantities, given by Eq. (2); and r is the correlation coefficient.

The unknown values of one of the thermodynamic parameters, Y, was calculated within the chosen series and the improvement of correlations for the known values in this series, at a known value of the other parameter X, was verified using the equation

$$Y = \Sigma g_i Y_i + a(X - A_X\Sigma g_i X_i) + b. \quad (6)$$

The table containing 1010 calculated values of thermodynamic potentials for 365 organic compounds can be found on the Internet [27].

Table 2 lists the results of calculation of the standard entropies of formation in the gas phase, ΔS^g,

Table 2. Standard entropies of formation in the gas phase, ΔS^g, calculated from experimental values of the standard enthalpies of formation in the gas phase, ΔH^g

Substance	CAS no.	Experiment ΔH^g, kJ mol^{-1}	ΔS^g, J mol^{-1} K^{-1}	
			group 7	group 8
1,3-Dioxolane	646-06-0	–298	385	316
1,3,5-Trioxane	110-88-3	–465.9	418	344
Diketene	647-82-8	–190.3	260	207
2-Methyl-1,3-dioxolane	497-26-7	–352	402	361
4-Methyl-1,3-dioxolane	1072-47-5	–376.9	428	418
Paraldehyde	123-63-7	–631.7	469	478
Oxetane	503-30-0	–80.5	366	307
2-Oxetanone	57-57-8	–282.9	293	214
1,3-Dioxane	505-22-6	–340.6	406	366
1,4-Dioxane	123-91-1	–315.3	413	375
Tetrahydro-2H-pyrane-2-one	542-28-9	–379.6	332	309
Tetrahydropyrane	142-68-7	–223.4	390	384
3,3-Dimethyloxetane	6921-35-3	–148.2	414	413

which cannot be found in [25], from experimental values of ΔH^g for the compounds that are contained simultaneously in groups 7 and 8.

CONCLUSIONS

(1) A method was suggested, which is a variety of correlation analysis, modified by taking into account sums of contributions of atomic parameters to the molecular parameter. This is particularly important in practical regard in those cases when significant deviations from the principle of linearity of free energies are observed when studying the reactivity of series of compounds.

(2) It was demonstrated that the method makes it possible to calculate, within the series of substances that were specified in the study, an unknown thermodynamic potential from another, known, one by the relations established.

(3) Nine series exhibiting strong correlations of deviations for certain thermodynamic quantities were found. The coefficients obtained were used to calculate 1010 values for 365 organic substances for which no experimental data could be found in the literature.

REFERENCES

1. Perez, P., Parra-Mouchet, J., and Contreras, R.R., *J. Chil. Chem. Soc.*, 2004, vol. 49, no. 1, pp. 30–56.
2. Eshermann, B., Martin, B., Horn, A.H.C., and Clark, T., *J. Mol. Model.*, 2003, vol. 9, pp. 342–347.
3. Hammett, L.R., *Physical Organic Chemistry. Reaction, Rates, Equilibria and Mechanisms*, Second Edition, New York: McGraw–Hill, 1970.
4. Pal'm, V.A., *Osnovy kolichestvennoi teorii khimicheskikh reaktsii* (Fundamentals of the Quantitative Theory of Chemical Reactions), Leningrad: Khimiya, 1977.
5. Cherkasov, A.R., Galkin, V.I., and Cherkasov, R.A., *Usp. Khim.*, 1996, vol. 65, no. 8, pp. 695–711.
6. Cherkasov, A.R., Ionsson, M., Galkin, V.I., and Cherkasov, R.A., *Usp. Khim.*, 2001, vol. 70, no. 1, pp. 3–27.
7. Tupitsyn, I.F., *Zh. Obshch. Khim.*, 2004, vol. 74, no. 1, pp. 25–38.
8. Tupitsyn, I.F., *Zh. Obshch. Khim.*, 2004, vol. 74, no. 2, pp. 202–213.
9. Tupitsyn, I.F., *Zh. Obshch. Khim.*, 2004, vol. 74, no. 7, pp. 1105–1118.
10. Trushkov, L.E., Chuvylkin, N.D., Koz'min, A.S., and Zefirov, N.S., *Russ. Chem. Bull.*, 1995, vol. 44, no. 5, pp. 777–800.
11. Egorochkin, A.N., Voronkov, M.G., Zderenova, O.V., and Skobeleva, S.E., *Izv. Akad. Nauk, Ser. Khim.*, 2000, vol. 1, pp. 253–260.
12. Egorochkin, A.N., Voronkov, M.G., Zderenova, O.V., and Skobeleva, S.E., *Izv. Akad. Nauk, Ser. Khim.*, 2001, no. 1, pp. 41–47.
13. Egorochkin, A.N., Voronkov, M.G., Skobeleva, S.E., and Zderenova, O.V., *Izv. Akad. Nauk, Ser. Khim.*, 2001, no. 1, pp. 34–40.
14. Amend, J.P. and Hegelson, H.C., *Geochim. Cosmochim. Acta*, 1997, vol. 61, no. 1, pp. 11–46.
15. Ladbury, J.E. and Chowdhry, B.Z., *Chem. Biol.*, 1996, vol. 3, no. 10, pp. 791–801.
16. Hinz, H.J. and Schwarz, F.P., *Pure Appl. Chem.*, 2001, vol. 73, no. 4, pp. 745–759.
17. Eads, C.D., *J. Phys. Chem., Ser. B*, 1999, vol. 103, no. 28, pp. 5869–5880.
18. Horak, J., *Chem. Listy*, 1999, vol. 93, no. 10, pp. 616–622.
19. Smith, D.W., *J. Chem. Soc., Faraday Trans.*, 1998, vol. 94, pp. 3087–3901.
20. Mutelet, F. and Rogalski, M., *Phys. Chem. Chem. Phys.*, 2001, vol. 3, pp. 432–436.
21. Scalabrin, G., Grigiante, M., Cristofoli, G., and Piazza, L., *Int. J. Refrigeration*, 2003, vol. 26, no. 1, pp. 35–50.
22. Chouai, A., Laugier, S., and Richon, D., *Fluid Phase Equilibr.*, 2002, vol. 199, nos. 1–2, pp. 53–62
23. Zevatskii, Yu.E. and Lysova, S.S., *Zh. Prikl. Khim.*, 2006, vol. 79, no. 6, pp. 978–985.
24. de Visser, S.P., *Phys. Chem. Chem. Phys.*, 1999, vol. 1, pp. 749–753.
25. Standard Thermodynamic Properties of Chemical Substances, http://www.update.uu.se/~jolkkonen/pdf/CRC_TD.pdf.
26. Cox, J.D., Wagman, D.D., and Medvedev, V.A., *CODATA Key Values for Thermodynamics*, New York: Hemisphere, 1989. p. 1.
27. http://upiterburg.newchem.ru/technic/tables.rtf.

ISSN 1070-4272, Russian Journal of Applied Chemistry, 2007, Vol. 80, No. 2, pp. 236–240. © Pleiades Publishing, Ltd., 2007.
Original Russian Text © T.E. Nikiforova, V.A. Kozlov, N.A. Bagrovskaya, M.V. Rodionova, 2007, published in Zhurnal Prikladnoi Khimii, 2007, Vol. 80, No. 2, pp. 236–241.

SORPTION AND ION-EXCHANGE PROCESSES

Sorption Properties of Enzymatically Modified Flax Fiber

T. E. Nikiforova, V. A. Kozlov, N. A. Bagrovskaya, and M. V. Rodionova

Ivanovo State University of Chemical Engineering, State Educational Establishment, Ivanovo, Russia
Institute of Solution Chemistry, Russian Academy of Sciences, Ivanovo, Russia

Received July 3, 2006; in final form, November 2006

Abstract—The influence of enzymatic modification on the sorption properties of a short flax fiber with respect to the Cu(II) ions was examined. The optimal parameters were determined for treatment of natural cellulose-containing sorbent with various enzymatic preparations, $B_{1\,mix}$, NCE, and protease, which affords the maximal sorption capacity of the sorbent and the shortest time required for establishment of equilibrium. IR spectroscopy was applied to examine changes in the structure of the substrate via rupture of inter- and intramolecular bonds in its constituent biopolymers under the action of the enzymes.

DOI: 10.1134/S1070427207020139

In the context of development of resource-saving processes, of particular interest is development of sorption methods for removal of heavy metal ions from aqueous solutions of varied nature, including food media. The easy accessibility and low cost of the waste from agroindustrial and wood-processing sectors make them promising sorbents for this purpose [1–3].

Such sorbents, however, typically exhibit poor kinetic characteristics and a comparatively low sorption capacity. This makes the search for a procedure for treatment of cellulose-based polymers to increase their sorption capacity and decrease the sorption time an important avenue in the development of new sorbents. Various methods [4–9] have been suggested for treatment of cellulose-containing sorbents, including mechanical, physical, chemical, and physicochemical methods (wet grinding, freezing, plasma activation, treatment with sodium polysulfides, coloration with active dyes, grafting of amino acid residues, etc.). In our opinion, enzymes and enzymatic preparations (EPs) are promising for treatment of sorbents.

Today, wide application of biotechnological methods in solving specific practical problems is limited by the lack of a databank covering the specific features of the influence exerted by both individual enzymes and EPs on various substrates. This makes examination of the impact of enzymes and their formulations on biopolymers an important step in this direction. Shibashova et al. [10] and Cheshkova et al. [11] reported on biochemical modification of cellulose and flax materials for textile industry.

We examined here the sorption properties with respect to the copper(II) ions of natural cellulose-containing material, short flax fiber, in relation to the conditions of the enzymatic treatment.

EXPERIMENTAL

We examined a short flax fiber, a secondary processing product of flax industry, with the composition, wt %: cellulose, 75–78; hemicellulose, 9.4–11.9; lignin, 3.8; pectins, 2.9–3.2; waxy substances, 2.7; nitrogen-containing substances calculated for proteins, 1.9–2.1; and mineral substances, 1.3–2.8 [12].

We also used enzymatic preparations[1] $B_{1\,mix}$ and NCE, as well as the alkaline protease manufactured in Russia. The enzymatic complex NCE comprises cellulases, pectinases, and esterases, and $B_{1\,mix}$, cellulases, pectinases, esterases, and hemicellulases. Both EPs are beige powders with a specific odor. The alkaline protease is produced in the form of 0.2–1.0-mm light gray or light beige granules. The proteolytic activity of the preparation is 50000 units g^{-1}, in accordance with TU (Technical Specifications) 64-13-19–89 (bacteria, fungi). Solutions containing Cu(II) were prepared by dissolving $CuSO_4 \cdot 5H_2O$ of chemically pure grade.

[1] Developed by gene engineering at the Chair of Enzymology, Moscow State University.

The short flax fiber was modified in aqueous solutions of EPs at the solution/sorbent ratio of 5–50 and enzyme concentration of 1–10% of the sorbent mass for 1–3 h at 25–40°C, whereupon the sorbent was filtered off, washed with distilled water, and dried.

The copper ion sorption was examined under static conditions from aqueous solutions of copper sulfate.

The sorption kinetics was studied by the method of a limited volume of solution. To a series of test tubes containing weighed portions of the polymer m = 0.1 g we added V = 0.01 l of the reference solution with the initial concentration $c_0 = 1.5 \times 10^{-4}$ M and kept for 0.5–3 h with stirring at a constant temperature (293 K). The solutions were intermittently filtered; in the filtrate, we determined the residual concentration of the metal ions and, under the equilibrium conditions, the equilibrium concentration of the metal ions in solutions c_{eq}, by the atomic absorption spectroscopy on a Saturn instrument.

The sorption power of the polymer was evaluated by the sorption capacity A

$$A = (c_0 - c_{eq})V/m.$$

The IR spectra of samples of the natural and treated flax fiber were measured by the reflection technique. The spectra were recorded on an Avatar 360 FT-IR E.S.P. spectrometer in the range 400–4000 cm^{-1}.

Important characteristics of polymeric sorbents are the sorption capacity and the time required for attainment of the sorption equilibrium [13]. Our kinetic examinations showed that, in sorption of the Cu(II) ions with a short flax fiber, the equilibrium is established within 40 min. The sorption capacity of the natural polymer is 10.1×10^{-3} mol kg^{-1} (Fig. 1). Thus, similarly to other cellulose-based materials, the flax fiber is a sorbent with poor sorption and kinetic characteristics.

Hydrophobic components present in this fiber and, in particular, lignin and waxy substances, hinder adsorption of aqueous solutions of the reactants (copper ions) and decelerate their penetration deep inside the fiber. Hence, improving the sorption characteristics of the short flax fiber requires removing hydrophobic substances. Therefore, we examined the equilibrium and kinetic characteristics of the polymer in relation to the procedure of treating short flax fiber by enzymatic preparations of varied nature.

The impurity components that are the most difficult to remove from natural plant fibers are waxy substances. They contain a natural mixture of esters,

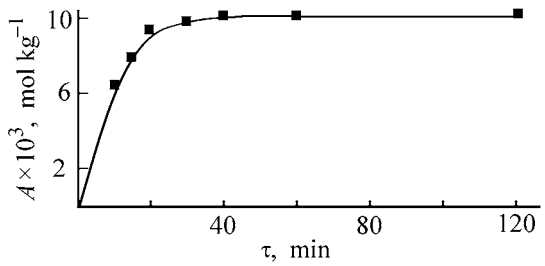

Fig. 1. Kinetics of sorption of Cu(II) ions by native flax fiber. (A) Sorption capacity and (τ) process time.

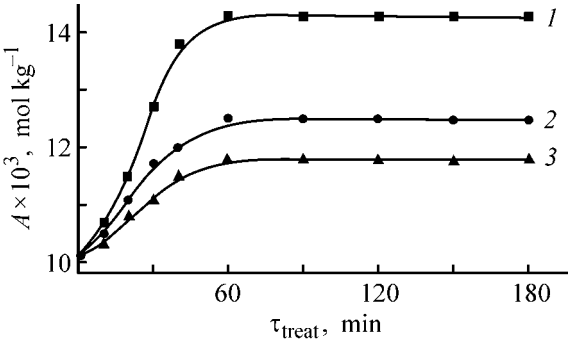

Fig. 2. Sorption capacity A vs. the time of treatment of a short flax fiber, τ_{treat}, with (*1*) $B_{1\,mix}$, (*2*) NCE, and (*3*) protease solutions. EP solution concentration 2% of the sorbent mass; temperature of the EP solutions 25°C, EP solution/sorbent ratio 50.

free saturated and unsaturated fatty acids, various high-molecular-weight alcohols, and some hydrocarbons. These substances prevent wetting of the fibers with aqueous solutions, thereby making them water-resistant. The esterase enzymes used in this study hydrolyze ester bonds and thus can destruct waxy substances.

Modification of the flax fiber with an enzymatic formulation containing pectinases, hemicellulases, and cellulases disturbs the stable system of cellulose–lignin–polysaccharides intermolecular bonds via hydrolytic degradation of the components of the carbohydrate complex (pectins, hemocelluloses) and partial degradation of cellulose, which is responsible for the removal of lignin from the fiber [11].

To determine the best conditions for treatment of the sorbent with EPs, we varied the following parameters: time of treatment of the sorbent with the EP solutions, EP solution concentration, EP solution/sorbent ratio, and EP solution temperature.

Figures 2–5 show how the sorption properties of the natural sorbent are influenced by treatment of the short flax fiber with EPs. The time of sorption of copper(II) ions by the short flax fiber treated

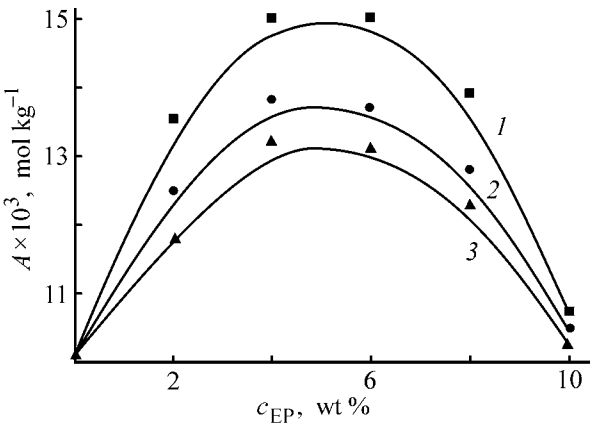

Fig. 3. Sorption capacity A of the short flax fiber vs. the content c_{EP} of (*1*) $B_{1\,mix}$, (*2*) NCE, and (*3*) protease in the solution used for treatment. Temperature of the EP solutions 25°C; EP solution/sorbent ratio 50; treatment time 60 min.

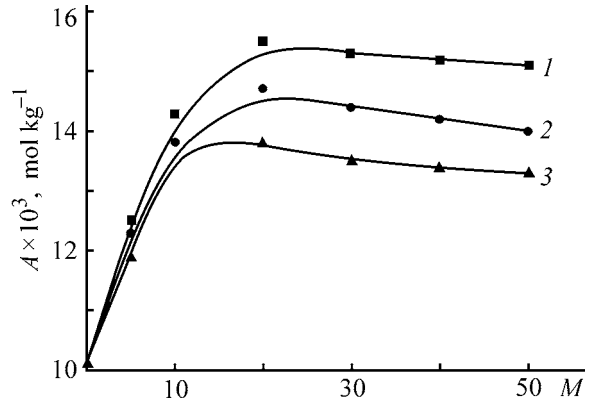

Fig. 4. Sorption capacity A of the short flax fiber vs. the EP solution/sorbent ratio M in treatment with solutions of (*1*) $B_{1\,mix}$, (*2*) NCE, and (*3*) protease. Treatment time 60 min; EP solution concentration 5% relative to the sorbent mass; temperature of EP solutions 25°C.

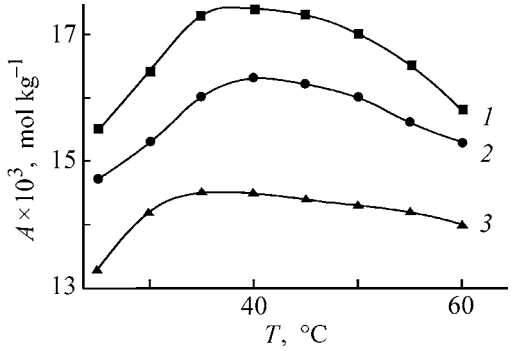

Fig. 5. Sorption capacity A of the short flax fiber vs. temperature T of the solutions of enzymes (*1*) $B_{1\,mix}$, (*2*) NCE, and (*3*) protease during treatment. Treatment time 60 min; EP solution/sorbent ratio 20 for $B_{1\,mix}$ and NCE, and 10 for protease. EP solution concentration 5% relative to the sorbent mass.

with the EP solutions decreases by half relative to that for the untreated sorbent. Therefore, the sorption time in all the experiments with the treated sorbent was not longer than 20 min.

The plots of the sorption capacity of the short flax fiber as a function of the time of enzymatic treatment (Fig. 2) suggest that the optimal time of treatment of the substrate is 60 min for all the EPs examined.

The enzyme concentration is known to substantially affect the rate of the enzymatic reaction, which is at maximum at the saturating concentration of the substrate. Under an excess of the substrate, the initial rate of the enzymatic reaction will vary with the enzyme concentration. Therefore, the concentration of the EP solutions for treating the short flax fiber was varied within 1–10% of the sorbent mass.

Figure 3 shows plots of the sorption capacity of the short flax fiber vs. the concentration of the EP solutions during sorbent treatment, which exhibit a weakly pronounced maximum at concentrations of 2–7% relative to the sorbent mass.

Figure 4 shows plots of the sorption capacity of the short flax fiber vs. the EP solution/sorbent ratio M for $B_{1\,mix}$, NCE, and protease. It is seen that the sorption capacity of the treated short flax fiber for copper(II) ions insignificantly changes at M = 5–50. The best results for enzymatic preparations $B_{1\,mix}$ and NCE were obtained at the EP solution/sorbent ratio of 20. In the case of protease, the maximal sorption capacity for the copper(II) ions is observed at the ratio of 10.

The optimal temperature affording the maximal activity for most of enzymes lies within 37–50°C, but some enzymes have a temperature optimum beyond this range. Temperature typically exerts a complex influence on the enzyme activity, depending on numerous factors: affinity of the enzyme for the substrate, ionization of the reaction components, rate of cleavage of the enzyme–substrate complex, formation of enzyme–activator or enzyme–inhibitor complex, and denaturation of the enzymatic protein [14].

Figure 5 shows plots of the sorption capacity of the short flax fiber vs. the temperature of the enzyme solution during treatment. Heat treatment of flax with the enzyme solutions at 20–60°C noticeably affects the sorption capacity of the short flax fiber. There is a broad maximum at 30–55°C. Our results are consistent with the published data on the optimal temperature limits of the activity of the enzymes.

Thus, our experiments showed that the imfluence exerted by the EPs examined on the sorption capacity

Optimal parameters of treatment of the short flax fiber with EP

EP	τ_{treat}, min	EP solution concentration, % relative to the sorbent mass	EP solution/sorbent ratio	T_{treat}, °C	$A \times 10^3$, mol kg^{-1}
No treatment	–	–	–	–	10.1
$B_{1\,mix}$	60	2	20	35	17.4
NCE	60	2	20	35	16.3
Protease	60	4	10	35	14.5

of the short flax fiber varies as follows: protease < NCE < $B_{1\,mix}$.

The optimal parameters of treatment of the short flax fiber with the EP solutions are listed in the table.

Treatment of the sorbent under the optimal modification conditions increases its sorption capacity for copper ions by 43–72% and decreases the sorption time by half relative to the natural samples. The maximal effect is achieved in the case when the short flax fiber is treated with a complex enzymatic preparation $B_{1\,mix}$, comprising cellulases, hemicellulases, pectinases, and esterases. Treatment with protease increases the sorption capacity of the sorbent to the smallest extent.

The observed decrease in the time required for attainment of the sorption equilibrium in the heterogeneous system constituted by the short flax fiber and a copper(II) sulfate solution and the increase in the sorption capacity of the modified sorbent can be accounted for by the simultaneous changes in the carbohydrate, protein, and lipid complexes of flax during its treatment with the enzymatic preparation. This leads to an increase in its porosity and hydrophilicity, as well as in the number and accessibility of the functional groups that can bind heavy metal ions.

These changes are also reflected in the IR spectra of samples of the short flax fiber. The natural flax is a mixture of polymers containing various functional groups with donating properties: carboxy, ether/ester, and hydroxy groups. The IR spectrum of the initial flax fiber exhibits a characteristic set of absorption bands of cellulose enriched in lignin. The spectrum contains intense absorption bands associated with stretching vibrations of the C=O, C–O–C, and OH bonds [15].

Comparison of the IR spectra of the initial and modified samples of the flax fiber (Fig. 6) demonstrates a certain decrease in intensity and resolution of the bands of the flax fiber treated with the enzyme. The observed decrease in the intensity of the broad absorption band at 3100–3600 cm^{-1}, associated with stretching vibrations of the hydrogen-bonded hydroxy groups, can be attributed to a decrease in the intensity of the intermolecular interaction via hydrogen bonds of cellulose and incrusting substances due to removal of pectins and hemicelluloses [16].

In the spectra of the flax treated with enzymes with different substrate activities, the absorption bands at 2917 and 2852 cm^{-1} decrease in intensity relative to the initial flax This can be due to changes in the structure of the substrate. These changes are observed near the characteristic absorption bands of mono- and polyphenols, i.e., lignin and tanning substances. For example, at 3000–2800 cm^{-1} there are absorption bands associated with stretching vibrations of the C–H bonds in the alkyl groups.

In the range 1800–1600 cm^{-1}, the IR spectra of the initial flax contain prominent absorption bands at 1740, 1664, and 1646 cm^{-1} due to the presence of carboxy groups of substrates of varied nature.

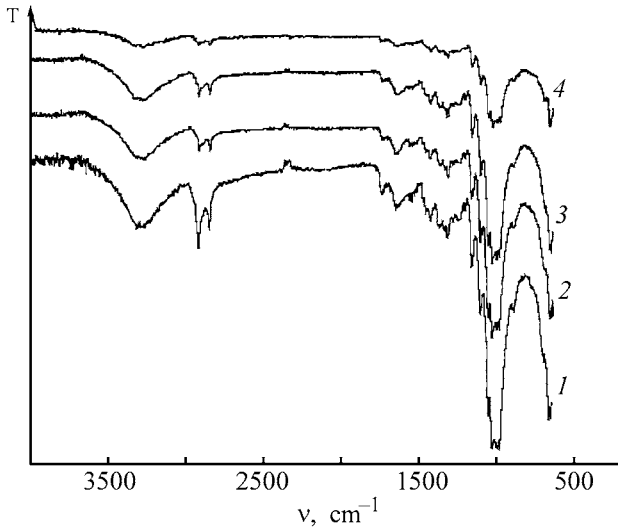

Fig. 6. IR spectra of (*1*) initial flax fiber and (*2*, *3*, *4*) flax fiber treated with (*2*) protease and (*3*, *4*) enzymatic preparations (*3*) NCE and (*4*) $B_{1\,mix}$. (T) Transmission and (ν) wavenumber.

In the spectra of the samples of the flax modified with the enzymatic formulation, the band at 1740 cm^{-1} decreases in intensity. Decreases in the intensity and diffuseness of absorption for the samples of the treated flax in this spectral region can be due to removal of the pectins from the fiber.

The bands at 1600–1510 cm^{-1} are associated with the absorption due to skeleton vibrations of the aromatic structures; the spectrum of the native flax exhibits closely lying bands at 1568 and 1560 cm^{-1} and a band at 1520 cm^{-1}. In the spectra of the fiber treated with the enzymes, this configuration of the bands is less prominent.

In the region 1210–830 cm^{-1} in the spectra of the sample of the flax treated with the enzymatic formulation, the intensity of the absorption bands associated with vibrations of the CC and CO bonds decreases relative to the native substrate.

It should be noted that the most pronounced changes in the spectra of the samples of the modified flax are observed for the flax treated with $B_{1\,mix}$, and the least prominent changes, for the flax treated with protease. These data are consistent with the trends in variation of the sorption capacity of the modified sorbents.

CONCLUSIONS

(1) Modification of the short flax fiber with an enzymatic formulation increases its sorption capacity by 43–72%. The maximal effect is achieved with the complex enzymatic preparation $B_{1\,mix}$.

(2) The time required for attainment of the sorption equilibrium in the aqueous solution of the system copper(II) sulfate–short flax fiber modified with various enzymes is 20 min, which is half that for the untreated polymer.

(3) The improvement of the equilibrium and kinetic characteristics of the natural polymer can be accounted for by the change in its structure due to degradation of inter- and intramolecular bonds of the biopolymers of the flax under the action of the complex of enzymes, as well as to an increased accessibility of cellulose and loosening of its structure. This is confirmed by the IR spectra of a sample of the natural flax fiber and fibers treated with various enzymes.

ACKNOWLEDGMENTS

This study was financially supported by the Russian Foundation for Basic Research (project no. 06-03-96346).

REFERENCES

1. Bagrovskaya, N.A., Nikiforova, T.E., Kozlov, V.A., and Lilin, S.A., *Izv. Vyssh. Uchebn. Zaved., Khim. Khim. Tekhnol.*, 2002, vol. 45, no. 4, pp. 131–133.
2. Michado, R., Carvalho, J.R., and Correia, M.J.N., *J. Chem. Technol. Biotechnol.*, 2002, vol. 77, no. 12, pp. 1340–1348.
3. Chamarthy, S., Seo, C.W., and Marshall, W.E., *J. Chem. Technol. Biotechnol.*, 2001, vol. 76, no. 6, pp. 593–597.
4. USSR Inventor's Certificate no. 1 696 399.
5. Shukla, S.R. and Sakhardande, V.D., *J. Appl. Polym. Sci.*, 1990, vol. 41, nos. 11–12, pp. 2655–2663.
6. Toshihiko, S., Kazuhiro, K., Hiromi, K., and Yasuo, O., *J. Soc. Fiber Sci. Technol.*, 1983, vol. 39, no. 12, pp. 519–524.
7. RF Patent 2 217 231.
8. RF Patent 2 217 389.
9. RF Patent 2 258 560.
10. Shibashova, S.Yu., Cheshkova, A.V., and Kuz'min, A.P., *Izv. Vyssh. Uchebn. Zaved., Tekhnol. Tekstil. Prom–sti.*, 2003, issue 4, pp. 50–52.
11. Cheshkova, A.V., Kuz'min, A.P., and Telegin, F.Yu., in *Vserossiiskaya nauchno-tekhnicheskaya konferentsiya "Kataliz i sorbtsiya v biotekhnologii, khimii, khimicheskikh tekhnologiyakh i ekologii"* (All-Russia Conf. "Catalysis and Sorption in Biotechnology, Chemistry, Chemical Technologies, and Ecology"), Tver, September 11–13, 2003, issue 5, pp. 11–14.
12. Krichevskii, G.E., Korchagin, M.V., and Senakhov, A.V., *Khimicheskaya tekhnologiya tekstil'nykh materialov* (Chemical Technology of Textile Materials), Moscow, 1985.
13. Ashirov, A., *Ionoobmennaya ochistka stochnykh vod, rastvorov i gazov* (Ion-Exchange Treatment of Wastewater, Solutions, and Gases), Leningrad: Khimiya, 1983.
14. Nikolaev, A.N., *Fermenty* (Enzymes), Moscow: Khimiya, 1981.
15. Zbinden, R., *Infrared Spectroscopy of High Polymers*, New York: Academic, 1964.
16. Cheshkova, A.V., Nadtoka, I.B., Mel'nikov, B.N., and Murav'ev, O.M., *Izv. Vyssh. Uchebn. Zaved., Khim. Khim. Tekhnol.*, 1999, vol. 42, no. 6, pp. 95–98.

ISSN 1070-4272, Russian Journal of Applied Chemistry, 2007, Vol. 80, No. 2, pp. 241–247. © Pleiades Publishing, Ltd., 2007.
Original Russian Text © V.I. Varentsova, V.K. Varentsov, 2007, published in Zhurnal Prikladnoi Khimii, 2007, Vol. 80, No. 2, pp. 242–248.

APPLIED ELECTROCHEMISTRY AND CORROSION PROTECTION OF METALS

Recovery of Cadmium and Change in Properties of a Fibrous Carbon Electrode in Electrolytic Processing of Ammonia Washing Solutions Formed in Cadmium Plating

V. I. Varentsova and V. K. Varentsov

Institute of Solid-State Chemistry and Mechanochemistry, Siberian Division, Russian Academy of Sciences, Novosibirsk, Russia

Novosibirsk State Technical University, Novosibirsk, Russia

Received May 29, 2006

Abstract—The possibility of recovering cadmium deposited on fibrous carbon electrodes from ammonium washing solutions formed in cadmium plating via operation of a short-circuited electrochemical system or anodic dissolution was examined. A polarization study of electrode processes that occur on a renewable graphite microelectrode in ammonium solutions of varied composition was carried out. The change in the properties of fibrous carbon electrodes in their cyclic use in electrodeposition–recovery of cadmium and the possibility of their repeated use were analyzed.

DOI: 10.1134/S1070427207020140

Owing to their specific properties, cadmium coatings are used for protection of articles in aggressive media (high humidity or tropic conditions) [1–3]. Cadmium(II) is to be removed from washing solutions formed in cadmium plating for detoxication of these solutions and recycling of cadmium into the electroplating process. Electrolysis is a way to simultaneously solve these two problems. With account of the low concentration of cadmium(II) in washing solutions, it is preferable to use electrolysis with 3*D* flow-through electrodes and, in particular, with electrodes made of fibrous carbon materials (FCM) [4].

In the recent decades, electrolysis with fibrous carbon electrodes (FCE) has been successfully used to recover noble and nonferrous metals in hydrometallurgy and electroplating [4, 5]. The use of FCM for electrolytic recovery of nonferrous metals from washing solutions formed in electroplating is due to the necessity for regeneration of carbon electrodes and recycling of the recovered metal into main process. An important issue is that of changes in the FCM properties during their cyclic use in electrodeposition–recovery and of the influence exerted by these changes on the parameters of both the processes. No systematic studies have been performed in this area. The results of previous studies [6–9] suggest that use of FCM in cyclic processes will strongly affect their properties. However, no unambiguous conclusion can be made about whether these changes exert positive or negative influence on the main process of metal electrodeposition because of the scarcity of the available data.

This study was undertaken in order to examine experimentally the possibility of recovery of cadmium deposited on FCE, changes in the FCE properties in an electrodeposition–regeneration cycle, and influence exerted by these changes on the main process for the example of electrolytic processing of washing ammonium solutions formed in cadmium plating.

EXPERIMENTAL

Industrial cadmium-plating ammonium electrolytes of two compositions were chosen for study. Solution no. 1 contained (g l^{-1}): $CdSO_4$ 50, $(NH_4)_2SO_4$ 150, H_3BO_3 25 (pH 5); and solution no. 2: $CdSO_4$ 50, $(NH_4)_2SO_4$ 250, urotropin 20, NF dispersant 75 ml l^{-1} (pH 6) [2, 3]. Supporting electrolytes contained all the components listed above except cadmium. The electrode polarization was carried out using a TES-14 dc power supply in the galvanostatic mode, with the solution circulated by a pmp-304 peristaltic pump through the FCE volume and an intermediate tank at a rate of 0.2 ml cm^{-2} s^{-1} [9]. The solution was delivered to

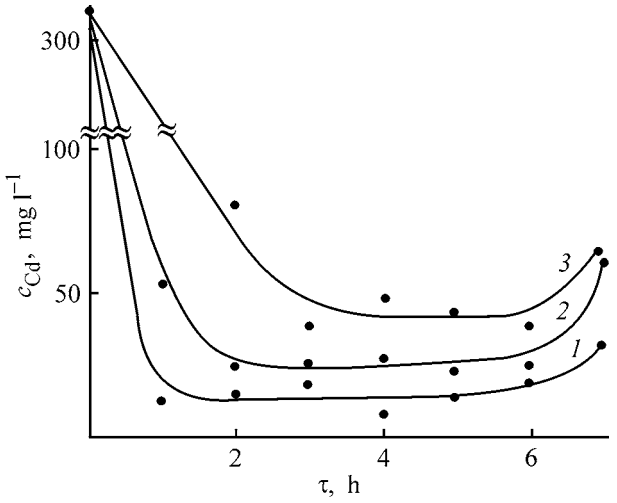

Fig. 1. Kinetic curves of electrolytic recovery of cadmium(II) from electrolyte no. 1 in modeling of the electrolytic recovery of cadmium(II) from a catching bath. Initial cadmium(II) concentration 330 mg l^{-1}, dilution factor n = 20, interval between washings 15 min. (c) Cd(II) concentration, and (τ), time. Rise in the cadmium(II) concentration upon a single washing (mg l^{-1}): (*1*) 27, (*2*) 54, and (*3*) 81.

an electrode with a back current lead from the back side with respect to the counter electrode. The FCE was made of NT-1 carbonized carbon graphite material, its geometric area was 2 cm^2. A perforated titanium or platinum plate served as a current lead, and a platinum wire, as a counter electrode. To measure changes in the mass and electrical conductivity of the FCE electrode, it was washed with distilled water and dried at 80–100°C. The steady-state electrode potential of a cadmium plate and FCE in the electrolytes were measured relative to a saturated silver chloride reference electrode and recalculated to the hydrogen scale, without drying of the FCE.

The electrical conductivity of FCE was measured with a VM-509 ac bridge and the steady-state electrode potential, with an OR-265/1 pH-meter, using the procedure and setup described in [4]. Polarization curves were measured in the potentiodynamic mode with an RA-2 polarograph on a graphite microelectrode 2 mm in diameter with a surface freshened in the electrolyte solution [10], with a potential sweep rate of 50 mV s^{-1}.

The efficiency of electrolytic recovery of cadmium was evaluated by the degree of recovery, $\alpha = (c_0 - c_\tau)/c_0$; current efficiency by cadmium, $C_E = [(c_0 - c_\tau)VF]/I\tau M_{eqiv}$; and electric power consumption $W = IU\tau/(c_0 - c_\tau)V$. Here c_0 and c_τ are the initial and final cadmium concentrations in solution (g l^{-1}); V, solution volume (l); F, Faraday constant (26.8 A h mol^{-1}); I, current (A); U, cell voltage (V); τ, experiment duration (h); and M_{equiv}, molar mass of the metal equivalent. The cadmium(II) concentration in solution was determined by the atomic-absorption method.

Figure 1 demonstrates the results of experiments on modeling of the electrolytic recovery of cadmium(II) from a catching bath for an automated cadmium-plating line. A portion of the cadmium-plating electrolyte was introduced at regular intervals of time (15 min) into a solution circulated between the electrolyzer and the intermediate tank, which models a catching bath. The Cd(II) concentration in the solution modeling a single washing of articles changed by 27 to 81 mg l^{-1}. The electrolytic recovery of cadmium(II) was carried out at a current density of 750 A m^{-2}. The kinetic curves presented in Fig. 1 reflect the change in the cadmium(II) concentration in a solution before introduction of a portion of the cadmium-plating electrolyte. It can be seen that the time in which a constant cadmium(II) concentration in solution is attained and the level of this constant concentration increase with the amount of the electrolyte introduced in a single washing. The fact that a constant cadmium(II) concentration in solution is reached shows that, under the chosen electrolysis conditions, the whole amount of cadmium(II) introduced in article washing is recovered by electrolysis between two successive washings. Depending on the introduced amount of electrolyte modeling washing of articles with different surface areas, this concentration is 10–35 mg l^{-1} before deposition of a certain amount of cadmium onto FCE. After that the efficiency of cadmium electrodeposition decreases, which is characterized by an increase in its concentration in solution. Evidently, the main reason for the decrease in the process efficiency is that the reaction surface area and the rate of electrolyte circulation decrease because of the plugging of the pore space in FCE by the deposited metal.

The amount of cadmium deposited per 1 g of FCE varies with the electrolyte composition and is determined by the deposit structure and by the localization of cadmium within the FCE volume, which are governed by specific features of cadmium electrodeposition from the electrolytes under consideration. In the case of metal electrodeposition onto FCM cathodes, the overvoltages of hydrogen evolution on FCM and on a metal being deposited are important for the metal distribution throughout the electrode volume [4]. The overvoltage of hydrogen evolution on cadmium is 1.1 V, and that on graphite, 0.8 V [1, 11]. Therefore, the overgrowth of the electrode with cadmium predominantly occurs on the metal deposited during

the initial stage of electrolysis. No less important is the solution pH, which is responsible for the stability of ammine complexes of cadmium; at pH > 5, $Cd(NH_3)_2^{2+}$ complexes predominate in the solution ($K_n = 1.8 \times 10^{-5}$) [2, 12]. In addition, electrolyte no. 2 contains cadmium(II) complexes with urotropin and a surfactant additive, and, therefore, the electrodeposition of cadmium from this electrolyte should be characterized by a higher polarizability [2, 3]. Thus, the varied content of components of the supporting electrolyte, inherent to washing solutions, should affect the polarization characteristics of the cathodic process in cadmium-plating electrolytes.

The polarization curves characterizing cadmium(II) discharge on a graphite microelectrode at different dilutions of the supporting electrolyte and a constant cadmium(II) concentration in the solution (300 mg l^{-1}) are shown in Fig. 2. The polarization curves have four characteristic portions. The first of these (portion *II*) ranges from the steady-state potential to a sharp rise in current, which is associated with cadmium(II) reduction. This portion apparently corresponds to oxygen reduction, and the fourth portion, to intense hydrogen evolution. For both the electrolytes, the reduction of cadmium(II) is determined by a clearly pronounced plateau of the limiting current (third portion), whose length is about 500 mV for electrolyte no. 1 and 300 to 500 mV for electrolyte no. 2 and increases with the dilution of the solution. For both the electrolytes, the height of the plateau of the limiting current is proportional to the cadmium(II) concentration in a solution.

For electrolyte no. 1, the run of the polarization curve is little affected by dilution of the supporting electrolyte, with the potential of the onset of cadmium deposition only somewhat shifted in the positive direction. For electrolyte no. 2, a strong effect is observed. In this case, the potential of the onset of cadmium deposition is shifted in the positive direction, the length of the plateau characterizing cadmium deposition at the limiting current becomes longer, and the limiting current itself also increases. In addition, electrolyte no. 2 possesses a higher electrical conductivity (0.21 Cm cm^{-1}), which is approximately 1.5–1.7 times that of electrolyte no. 1. Therefore, electrodeposition of cadmium from electrolyte no. 2 is characterized by a higher polarizability, which is clearly seen in curve *1* in Fig. 2b.

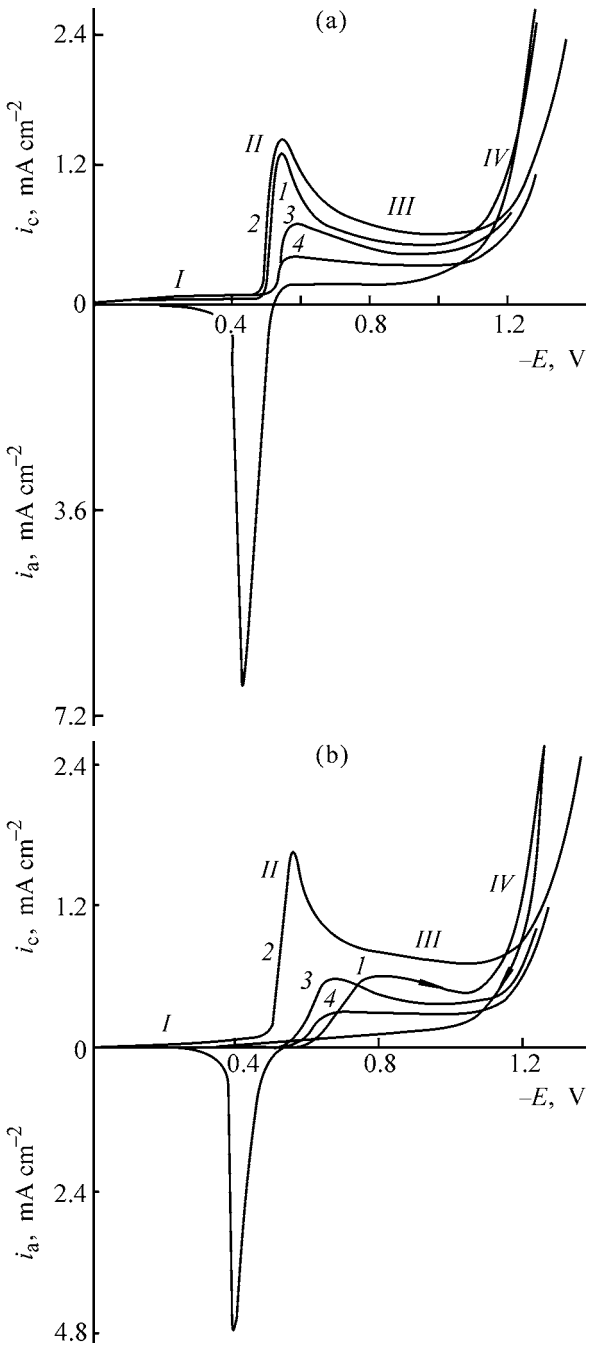

Fig. 2. Polarization curves characterizing the electrode processes on graphite microelectrode in electrolyte nos. (a) 1 and (b) 2. (*i*) Current density, (*E*) potential; the same for Fig. 6. Cadmium(II) concentration (mg l^{-1}): (*1*, *2*) 300, (*3*) 150, and (*4*) 50. Supporting electrolyte dilution factor (times): (a) (*1*) 0, (*2*) 50, (*3*, *4*) 20; (b) (*1*) 0, (*2*) 50, and (*3*, *4*) 5. (*I*, *II*, *III*, *IV*) For explanation see text.

It was shown experimentally that, in the case of electrolytic recovery of cadmium(II) from electrolyte no. 1, cadmium is deposited on FCE on the front (closer to the counter electrode, anode) side of the electrode, whereas in the case of recovery from electrolyte no. 2, it is localized on the back (closer to the current lead) side of the electrode. The electrolytic deposits of cadmium also differ in structure. In

Table 1. Degree of anodic dissolution, α, of cadmium deposited onto FCE in a supporting ammonium solution; current efficiency by cadmium, C_E; dissolution rate v; and energy expenditure W for dissolution of 1 g of cadmium at varied anode current density i (dissolution time 0.5 h, solution volume 100 ml, geometric surface area of the anode 2 cm^2)

i, A m^{-2}	α	C_E	v, g m^{-2} h^{-1}	W, W h g^{-1}
	%			
Electrolyte no. 1				
50	79.2	385	400 (105)*	0.28 (1.00)
100	96.0	230	480 (210)	0.50 (1.43)
150	89.6	140	445 (315)	1.27 (1.80)
200	99.5	120	500 (410)	1.60 (1.95)
Electrolyte no. 2				
50	87.7	450	465 (105)	0.2 (0.86)
100	90.8	215	450 (210)	0.60 (1.38)
150	92.8	145	460 (315)	1.21 (1.80)
200	99.9	120	500 (410)	1.60 (1.95)

* Values of the parameters at C_E = 100%.

the case of electrodeposition from electrolyte no. 1, the deposit is porous, its adhesion to the surface of carbon fibers is weak, and deposit scales off. The cadmium deposit formed from electrolyte no. 2 is less porous and covers each fiber of the FCE. The amount of cadmium deposited on FCE from electrolyte no. 1 does not exceed 4.5 g per 1 g of FCE, the deposit grows on fibers in the direction of the electrolyte bulk and falls-off into the solution. In the case of cadmium(II) electrodeposition from electrolyte no. 2, cadmium is deposited on the back side of the electrode and then grows into the electrode, with the amount of deposited cadmium equal to 6.0–6.5 g per 1 g of FCE.

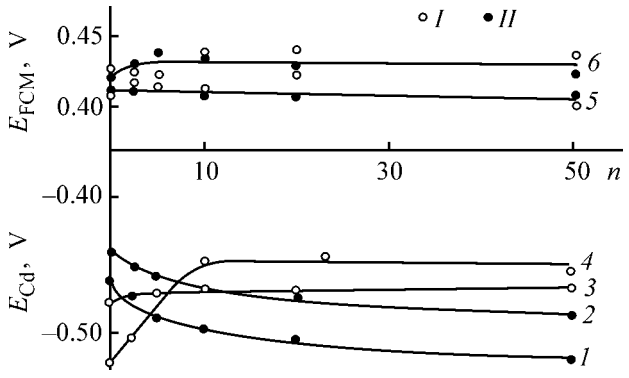

Fig. 3. Steady-state electrode potential (V) of (*1–4*) cadmium electrode (E_{Cd}) and (*5*, *6*) FCM electrode (E_{FCM}) vs. the dilution factor n of the electrolyte for the supporting solution and cadmium(II). Composition of supporting solutions (g l^{-1}): electrolyte no. 1 $(NH_4)_2SO_4$ 150 and H_3BO_3 25; electrolyte no. 2 $(NH_4)_2SO_4$ 250, urotropin 20, and NF dispersant 75 ml l^{-1}. Electrolyte dilution (*I*) by supporting solution, cadmium(II) concentration 100 mg l^{-1}, and (*II*) by cadmium(II). Electrolyte: (*2*, *3*, *5*) no. 1 and (*1*, *4*, *6*) no. 2.

Cadmium deposited on FCE should be regenerated and recycled into the electroplating process. A promising way to achieve this objective is anodic dissolution.

The anodic polarization curves reflecting cadmium dissolution show that cadmium dissolves without any difficulties in both the electrolytes and the potentials corresponding to a steep rise in the anodic current are close (Fig. 2). The results obtained in studying the anodic dissolution of the cadmium deposit on FCE in the supporting solutions of electrolyte nos. 1 and 2 at different anode current densities are listed in Table 1. It can be seen that cadmium well dissolves in both the solutions and the degree of dissolution increases with the current density.

If anodic polarization of an FCE by a metal is performed without separation of the electrode spaces, dissolved cadmium is deposited on the cathode to give an electrolytic powder of cadmium.

If the electrode spaces are separated with an ion-exchange membrane and the anodic dissolution is performed in the supporting solution of the corresponding electrolyte, a solution of the cadmium-plating electrolyte can be obtained. Such a procedure for recycling of cadmium deposited on the FCE can be performed in the same electrolyzer that is used for electrolytic recovery of cadmium. It follows from the data of Table 1 that, depending on the anode current density, the current efficiency by cadmium exceeds 100% by a factor of 1.2–4.5 for both the electrolytes. The rate of anodic dissolution depends on the current density only slightly. If, however, the rate of the anodic dissolution of cadmium is calculated for a 100% current efficiency the rate is 4–4.5 times lower at low current densities and increases as the current density becomes higher. The electric energy expenditure for dissolution of 1 g of cadmium is low; its values differ by a factor of 5–8 for current densities of 50 and 200 A m^{-2}. If the energy expenditure for dissolution of 1 g of cadmium is calculated for a current efficiency of 100%, the difference tends to zero. The aforesaid shows that there occurs a concurrent reaction accompanied by dissolution of cadmium. Such a reaction may be cadmium dissolution through operation of a short-circuited electrochemical system (SES) constituted by FCE, cadmium, and electrolyte solution.

Measurements of the steady-state electrode potentials of cadmium (E_{Cd}) and FCE (E_{FCE}) in solutions of electrolyte nos. 1 and 2 demonstrated (Fig. 3) that E_{FCE} is independent of the electrolyte dilution, whereas E_{Cd} depends on the electrolyte dilution for cadmium and components of a supporting solution. For electrolyte no. 2, this dependence is more pronounced (curves *1*, *4*). The difference between the steady-state potentials of cadmium and FCE for both the electrolytes remains considerable (850–950 mV). Therefore, cadmium deposited on FCE must dissolve in the supporting ammonium electrolyte via SES operation.

The process of cadmium dissolution via SES operation can be independently used for cadmium regeneration, because it is a simpler cadmium regeneration technique, which has been effectively used previously for regeneration of zinc and palladium deposited on FCE [13]. The studies performed demonstrated that cadmium deposited on FCE dissolves in the supporting solution of the corresponding electrolyte at a considerable rate (Fig. 4). Solutions containing 35–40 g l^{-1} $CdSO_4$ were obtained as a result of the cadmium dissolution through SES operation. These solutions can be used for preparation of cadmium-plating electrolytes.

In the course of cadmium regeneration, FCE undergoes cyclic cathodic and anodic polarizations. It has been shown previously [6–9] that the FCE properties can be considerably changed in the process. Therefore, it was necessary to study how the properties of fibrous carbon electrodes change after several cycles of cadmium electrodeposition–regeneration. The results obtained in measuring the mass and the electrical conductivity of FCE after several cycles of cadmium electrodeposition–dissolution are listed in Table 2.

It follows from the data of Table 2 that, when cadmium is dissolved in a cycle through operation of a short-circuited electrochemical system, the mass of FCE and its electrical conductivity decrease. This is due to electrode processes occurring in the cathodic and anodic periods of the polarization. The decrease in the FCE mass may also be due to mechanical disintegration of carbon fibers. The electrical conductivity decreases by a factor of 1.7–2. More significant changes in the FCE properties are observed after cadmium is regenerated via anodic dissolution. The FCE mass increases, whereas the electrical conductivity decreases by a factor of 6–12, depending on the electrolyte composition. This is due to the formation of oxide groups on the surface of carbon fibers during the anodic cycle and also to the possible interaction of the electrolyte components with the FCM fibers [6, 7]. The less pronounced changes in the electrical conductivity and FCM mass in electrolyte no. 2 may be due to adsorption of the electrolyte components (urotropin and NF dispersant) on the FCE surface.

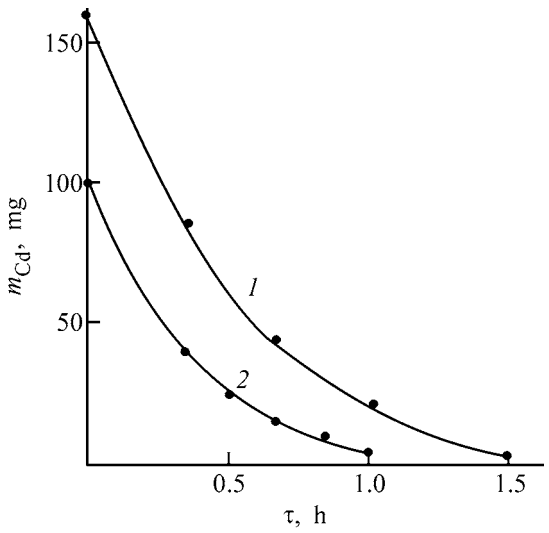

Fig. 4. Kinetic curves of dissolution of cadmium deposited onto FCE through SES operation in the supporting solutions of electrolyte nos. (*1*) 2 and (*2*) 1. Solution volume 100 ml. m_{Cd} Mass of soluble Cd, τ time.

The change in the FCE properties can affect the process of cadmium electrodeposition. Figure 5 shows the results obtained in studying the cadmium electrodeposition on FCE samples on performing five cycles of cadmium electrodeposition–dissolution. It can be seen that the parameters of the electrolytic recovery of cadmium on fibrous carbon electrodes on their cycling in electrolyte no. 1 are not deteriorated significantly, with only a 10–15% decrease in α_{Cd} observed during cadmium recovery via anodic dissolu-

Table 2. Change in mass, Δ*m*, and electrical conductivity χ of FCE after five cycles of cadmium electrodeposition–dissolution

Cycle	Electrolyte no.	Δ*m*, %	χ, Cm cm^{-1}
Initial FCE			0.024
Electrodeposition–dissolution via SES operation	1	–6.2	0.012
	2	–3.0	0.014
Electrodeposition–anodic dissolution	1	+8.2	0.002
	2	+7.0	0.004

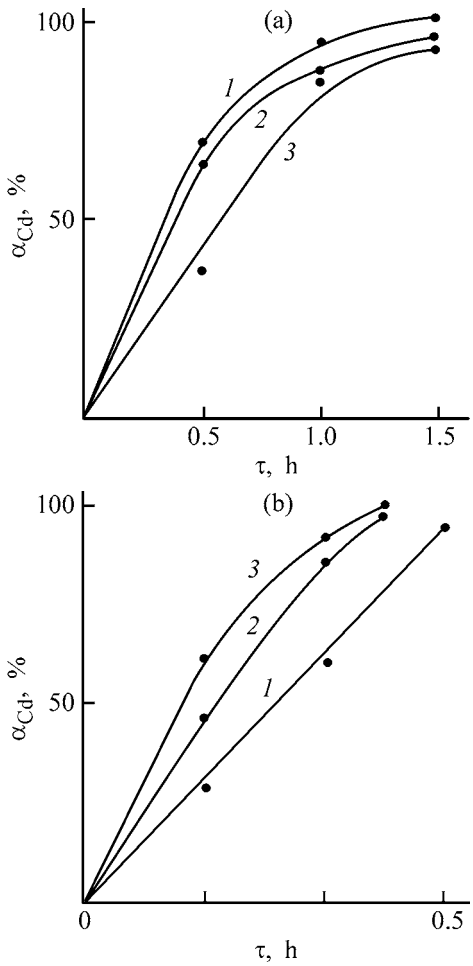

Fig. 5. Kinetic curves of electrolytic recovery of cadmium(II) during electrolysis on initial and regenerated FCE from electrolyte nos. (a) 1 and (b) 2. (a) Initial cadmium concentration 300 mg l^{-1}, $n = 20$, current density 500 A m^{-2}; (b) Initial cadmium concentration 250 mg l^{-1}, $n = 5$, current density 750 A m^{-2}. (α) Degree of Cd(II) recovery, (τ) time. (*1*) Initial FCM; FCM after five cycles of cadmium electrodeposition–dissolution (*2*) through SES operation, and (*3*) via anodic dissolution.

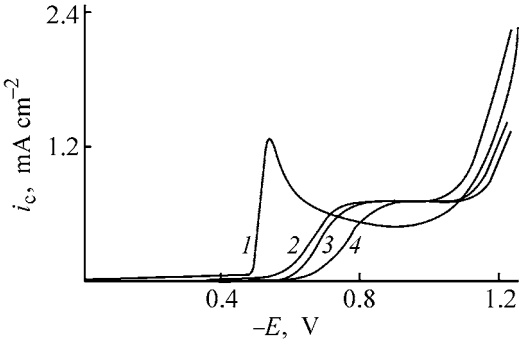

Fig. 6. Polarization curves of cadmium(II) recovery in cyclic cathodic–anodic polarization of a graphite microelectrode in electrolyte nos. (*1*) 1, cycles 1–5; and 2: (*2*) 1st cycle, (*3*) 2nd cycle, and (*4*) 3rd–5th cycles.

tion (Fig. 5a). The mass of cadmium deposited per unit FCE mass changed only slightly, compared with that of the starting material.

As for the results obtained in electrolyte no. 2, the parameters of cadmium electrodeposition on the electrodes used in five cadmium electrodeposition–dissolution cycles are improved (Fig. 5b). The adhesion of deposited cadmium to the surface of carbon fibers becomes considerably better, the deposit is more uniformly distributed across the electrode thickness, and the amount of cadmium deposited per 1 g of FCE increases to 7–7.5 g.

It is known that the efficiency of the electrochemical process in 3*D* flow-through electrodes is characterized by a distribution of the potential, polarization, and local current densities across the electrode thickness. The change in the distribution of the electrochemical process across the thickness of the FCM electrode, which is responsible for the change in the efficiency of cadmium electrodeposition in the cyclic deposition–dissolution, may be due to presence of such components as urotropin and NF dispersant in electrolyte no. 2. Presumably, the positive effect of urotropin and NF dispersant on the electrolytic recovery of cadmium from ammonium electrolytes is accounted for by the interaction of these components with the surface of carbon fibers of the electrode during its cyclic polarization. To verify this suggestion, special polarization studies were carried out. A graphite electrode was preliminarily subjected to up to five cycles of cathodic–anodic polarization in electrolyte nos. 1 and 2 containing 300 mg l^{-1} of cadmium(II).

It follows from Fig. 6 that cyclic treatment of FCE in a solution containing no urotropin and NF dispersant (electrolyte no. 1) has virtually no effect on the run of the polarization curve (Fig. 6, curve *1*). In a solution containing urotropin, the polarization curve is shifted toward electronegative potentials already after the first cycle, the slope of the second portion of the polarization curve markedly increases (Fig. 6, curve *3*), and, consequently, the polarizability is enhanced, too. Renewal of the electrode surface by cutting in a solution "returns" the polarization curve to the initial state, i.e., makes the run of the polarization curve similar to that measured in the initial solution without any cyclic treatment (curve *2*). The most significant changes in the cathodic portion of the curve are observed during the first three cycles of polarization (curves *3*, *4*), which is probably due to adsorption of urotropin and NF dispersant on the surface of carbon fibers. Further increase in the number of po-

larization cycles has no effect on the cathodic polarization curve.

CONCLUSIONS

(1) It was demonstrated that cadmium(II) can be electrolytically recovered from ammonium solutions formed in catching baths on a fibrous carbon electrode. The structure of the electrolytic deposit of cadmium and its distribution across the electrode thickness depend on the solution composition. The amount of cadmium deposited per 1 g of the fibrous carbon material is 4.5–6.5 g.

(2) The polarization study showed that the current of cadmium(II) reduction depends on the composition and dilution of the solution; presence of organic substances (urotropin, NF dispersant) shifts the potential of the onset of cathodic reduction of cadmium in the negative direction and leads to a decrease in the limiting current of reduction of cadmium(II) ions and in the length of the plateau of the limiting current. The anodic process proceeds without any hindrance.

(3) The possibility of regeneration of cadmium deposited on a fibrous carbon electrode through operation of a short-circuited electrochemical cell or via anodic dissolution was demonstrated. Solutions containing 35–40 g l^{-1} $CdSO_4$ were obtained. In the case of cadmium regeneration via anodic dissolution, an electrolytic powder of cadmium can also be obtained.

(4) A change in the mass and electrical conductivity of fibrous carbon electrodes in their cycling in electrodeposition–dissolution of cadmium was found. The most pronounced changes were observed in cadmium recovery via anodic dissolution: the mass of the electrode subjected to five cycles increased by 7–8%, whereas its electrical conductivity decreased by a factor of 6–12, depending on the solution composition.

(5) It was found that the characteristics of cadmium(II) electroreduction on fibrous carbon electrodes are not deteriorated upon their cycling. The degree of electrolytic recovery of cadmium from solutions containing organic components is 20–30% higher, the structure of the deposit and its distribution across the electrode thickness of the electrode are better, with up to 7.5 g of cadmium deposited per 1 g of electrode.

REFERENCES

1. Kudryavtsev, N.T., *Elektroliticheskie pokrytiya metallami* (Electroplated Metal Coatings), Moscow: Khimiya, 1979.
2. Il'in, V.A., *Tsinkovanie, kadmirovanie, luzhenie i svintsevanie* (Zinc, Cadmium, Tin, and Lead Plating), Leningrad: Mashinostroenie, 1977.
3. Azhogin, F.F., Belen'kii, M.A., Gal', I.E., et al., *Gal'vanotekhnika: Spravochnik* (Electroplating: Reference Book), Moscow: Metallurgiya, 1987.
4. Varentsov, V.K., Electrochemical Processes and Apparatus with Porous Flow-Through Electrodes for Recovery of Metals from Dilute Solutions, *Doctoral Dissertation*, Sverdlovsk, 1990.
5. Varentsov, V.K., *Zh. Prikl. Khim.*, 2003, vol. 76, no. 10, pp. 1635–1638.
6. Varentsov, V.K. and Varentsova, V.I., *Elektrokhimiya*, 2001, vol. 37, no. 7, pp. 811–820.
7. Zonova, E.B., Bratskaya, S.Yu., Artem'yanov, A.P., et al., *Izv. Vyssh. Uchebn. Zaved., Khim. Khim. Tekhnol.*, 2004, vol. 47, issue 2, pp. 7–11.
8. Varentsova, V.I. and Varentsov, V.K., *Zh. Prikl. Khim.*, 2005, vol. 78, no. 3, pp. 433–437.
9. Varentsov, V.K. and Varentsova, V.I., *Zh. Prikl. Khim.*, 1999, vol. 72, no. 4, pp. 605–609.
10. Kletenik, Yu.B., Bek, R.Yu., Polyakin, L.Yu., and Zamyatin, A.P., *Izv. Sib. Otd. Akad. Nauk SSSR, Ser. Khim. Nauk*, 1985, issue 1, no. 2, pp. 93–97.
11. Varypaev, V.N. and Krasikov, V.L., *Zh. Prikl. Khim.*, 1980, vol. 53, no. 3, pp. 586–590.
12. Yatsimirskii, K.B. and Vasil'ev, V.P., *Konstanty nestoikosti kompleksnykh soedinenii* (Instability Constants of Complex Compounds), Moscow: Akad. Nauk SSSR, 1959.
13. Varentsova, V.I. and Varentsov, V.K., *Zh. Prikl. Khim.*, 2003, vol. 76, no. 11, pp. 1788–1793.

ISSN 1070-4272, Russian Journal of Applied Chemistry, 2007, Vol. 80, No. 2, pp. 248–251. © Pleiades Publishing, Ltd., 2007.
Original Russian Text © E.P. Grishina, L.M. Ramenskaya, T.V. Vladimirova, A.M. Pimenova, 2007, published in Zhurnal Prikladnoi Khimii, 2007, Vol. 80, No. 2, pp. 249–252.

APPLIED ELECTROCHEMISTRY AND CORROSION PROTECTION OF METALS

Kinetics of Anodic Oxidation of Copper in an Ionic Liquid Composed of 1-Butyl-3-Methyl Imidazolium Bromide Monohydrate

E. P. Grishina, L. M. Ramenskaya, T. V. Vladimirova, and A. M. Pimenova

Institute of Solution Chemistry, Russian Academy of Sciences, Ivanovo, Russia

Received August 4, 2006; in final form, November 2006

Abstract—Cyclic voltammetry, chronopotentiometry, and gravimetry were used to study the electrochemical oxidation of copper in an ionic liquid, 1-butyl-3-methyl imidazolium bromide monohydrate.

DOI: 10.1134/S1070427207020152

Ionic liquids, room-temperature molten salts (RTMS) composed of dialkyl imidazolium cations (R,R'-Im-) and complex metal-containing anions, e.g., chloroaluminate ionic liquids R,R'-ImAlCl_4, are regarded as promising media for carrying out various catalytic reactions of organic synthesis, electrodeposition of metals, etc. [1–4]. Considerable attention is given to synthesis and study of compounds that belong to this group of ionic liquids. Ionic liquids containing $[InCl_4]^-$, $[NiCl_4]^{2-}$, $[CuCl_2]^-$, and $[ZnCl_3]^-$ anions are known and have been characterized [5–7]. Commonly, salts of this kind are prepared by simple mixing of appropriate halide salts of a metal and dialkyl imidazolium to give a considerable number of metal-containing anions of various compositions dependent on the molar ratio of the starting components. For example, mixing of $ZnCl_2$ and 1-ethyl-3-methyl imidazolium chloride can give complex anions $[ZnCl_3]^-$ and $[ZnCl_4]^{2-}$, as well as polynuclear complex anions $[Zn_2Cl_5]^-$ and $[Zn_3Cl_7]^-$ [7]. The presence of $[CuCl_2]^-$, $[Cu_2Cl_3]^-$, and $[Cu_3Cl_4]^-$ anions has been revealed in chlorocuprate ionic liquids [6].

The applicability of metal salt solutions in ionic liquids in electrochemical deposition of thin films of various metals has been studied [8–10]. Particular researchers' attention has been given to the electrodeposition kinetics and quality of metal deposits, with the anodic processes accompanied by dissolution of the corresponding metal electrodes virtually not understood at all. A study of the anodic behavior of metals in RTMS is of interest because these processes largely determine the operation stability of a galvanic cell and the corrosion resistance of materials. It is known that various processes are possible in anodic oxidation of metals, including dissolution and formation of passivating films.

The aim of this study was to examine the kinetics of anodic oxidation of copper in a halide ionic liquid, 1-butyl-3-methylimidazolium bromide monohydrate.

EXPERIMENTAL

The ionic liquid [BMIm]Br was synthesized by the procedure described in [11] from *N*-methyl imidazole (Acros organics, 99%) and freshly distilled bromobutane (pure grade). This liquid has the form of brown crystals with a melting point of 65°C and decomposition temperature of 275°C (thermographic data, 1000 D derivatograph), in agreement with published data [12]. Its monohydrate (molar ratio [BMIm]Br : H_2O = 1 : 1) is in the liquid state at room temperature (concentration of bromide ions 5.49 M and water content 6.5%, as determined by the Fisher method). The composition was confirmed by elemental analysis (CPNS) (Flash EA 1112 instrument).

Found (%): C 39.97, H 7.65, N 12.19.

$C_8H_{17}N_2BrO$.

Calculated (%): C 40.51, H 7.17, N 11.81.

Copper of M0b (oxygen-free) brand served as a metal under study. The electrode was fabricated in the form of a 0.2-cm^2 plate with insulated nonworking surface. Platinum was used as auxiliary elec-

trode. A platinum electrode served as reference in the [BMIm]Br · H_2O melt. In the case of RMTS, this electrode is regarded as a reference quasi-electrode and is widely used in polarization studies in electrolyte media of this kind [13].

The following electrochemical research methods were used in the study: cyclic voltammetry, chronoammetry (PI-50.1 potentiostat), and gravimetric analysis (Sartorius ME215S analytical balance with a weighing accuracy of 1×10^{-5} g) for determining the current efficiency by the metal. The study was carried out at a temperature of 18 ± 0.2°C.

Experimental details are described in figure captions.

The electrochemical window of a naturally aerated melt of 1-butyl-3-methyl imidazolium bromide monohydrate was measured on a platinum electrode (Fig. 1, curve *1*). This window is presumably limited by oxidation of bromide ions at anodic potentials and by reduction of the cation at cathodic potentials and is approximately equal to 1.9 V. It was noted in [1] that presence of water in hydrophilic RTMS leads to a significant narrowing of the electrochemical window to values comparable with those obtained in the present study.

It can be seen in Fig. 1, curves *2*, that the electrode processes involving the copper electrode and products of its oxidation occur at potentials of electrochemical stability of components of the BMImBr salt, and the electrochemical response of H_2O is negligible, compared with the reduction currents of the products of the anodic reaction. Therefore, it was assumed that presence of water has no significant effect on the mechanism of anodic oxidation of copper in the electrolyte under study.

The steady-state potential E_{st} of the copper electrode relative to the platinum electrode is $-(0.70 \pm 0.03)$ V. The cyclic voltammograms of the copper electrode, measured in [BMIm]Br · H_2O are shown in Fig. 1 (curves *2*). It can be seen that, in anodic polarization, the current steadily grows and the forward and return portions of the polarization curve coincide at positive potentials (as far as the anodic boundary of the electrochemical window). As the potential sweep direction is changed and the polarization curve enters the region of negative potentials, it can show one or two cathodic current peaks. Their number depends on the limiting anodic polarization potential. The processes characterized by the first and second cathodic waves C_1 and C_2 reflect the reduction of the anodic product formed at more positive anodic potentials

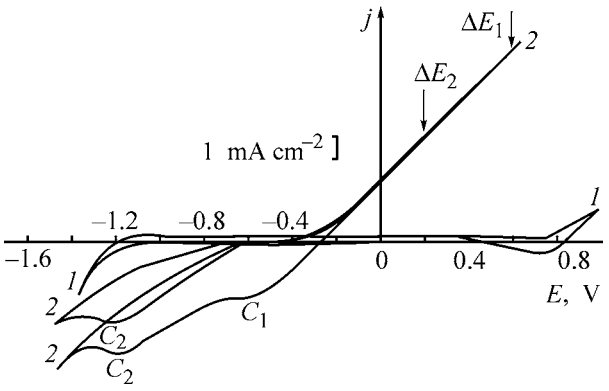

Fig. 1. Cyclic voltammograms measured on (*1*) platinum and (*2*) copper electrodes in [BMIm]Br · H_2O. Potential sweep rate 5 mB s^{-1}. (*E*) Potential and (*j*) current density.

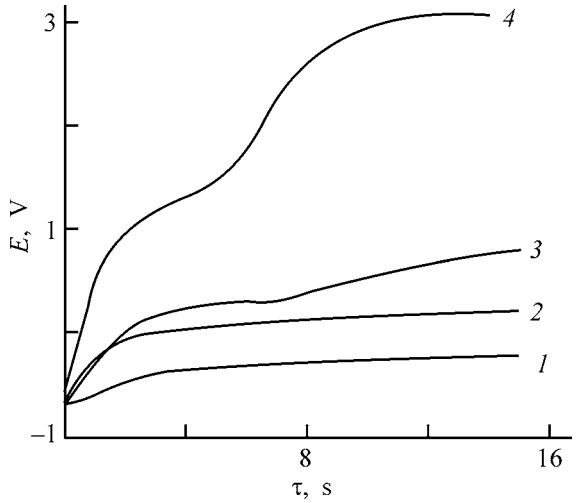

Fig. 2. Chronopotentiogram of a copper electrode in [BMIm]Br · H_2O. (*E*) Potential and (τ) time. Current density (mA cm^{-2}): (*1*) 0.99, (*2*) 2.05, (*3*) 5.31, and (*4*) 9.58.

ΔE_1 and at smaller anodic polarization ΔE_2, respectively. Thus, it follows from Fig. 1 and from the theory of chronovoltammetry [14] that two irreversible processes of electrochemical oxidation of copper may occur in the potential range studied.

Both the electrode processes are recorded under the conditions of a galvanostatic anodic polarization of the copper electrode (Fig. 2). As the current density *j* increases, the second wave appears in the chronopotentiogram, which is due to a decrease in the transient time in which the potential of the electrode process occurring at more positive potentials is reached. The slopes of the *E*–τ curves ($\Delta E/\Delta\tau$, where τ is time) for the first and second waves are close (0.010–0.011 V min^{-1}), which is due to the formation of anodic products that do not passivate the electrode.

The following results were obtained by determining the anodic current efficiency and visually examin-

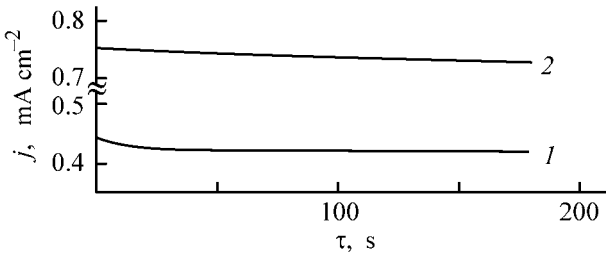

Fig. 3. Chronoammograms of a copper electrode in [BMIm]Br · H_2O under polarization. (*j*) Current density and (τ) time. Polarization ΔE (V): (*1*) 0.43 and (*2*) 0.56.

ing the state of the electrode surface upon the galvanostatic polarization. At the potentials of the first wave (current density of up to 5 mA cm^{-2}), the anodic current efficiency by Cu(I) is at the 100% level. The slope of the Tafel curve is 0.126 V, which points to an irreversible transfer of an electron in the ionization of copper. It should be noted that no phase film of a poorly soluble compound CuBr is formed on the surface of copper in the course of anodic polarization and bromide ions form stable complex compounds with Cu(I) cations [15]. With account of this circumstance, the following electrode reaction characterizing the anodic dissolution of copper is the most probable:

$$Cu + 2[BMIm]^+Br^- \rightarrow [BMIm]^+[CuBr_2]^- + [BMIm]^+ + e. \quad (1)$$

In this range of potentials, the electrode surface is corroded, but a thin white CuBr film is present on the surface [16]. Presumably, the film is formed by the dissolution-deposition mechanism, because it is easily removed from the metal surface. In this case, CuBr may be formed in decomposition of a complex compound on the active surface of the electrode by the reaction

$$[BMIm]^+[CuBr_2]^- \rightleftarrows [BMIm]^+Br^- + CuBr\downarrow. \quad (2)$$

Presumably, reversible formation of polynuclear complex compounds [3] may occur, under the conditions of supersaturation of the near-electrode space by the substance $[BMIm]^+$ $[CuBr_2]^-$, e.g.,

$$2[BMIm]^+[CuBr_2]^- \rightleftarrows [BMIm]^+[Cu_2Br_3]^- + [BMIm]^+Br, \quad (3)$$

followed by their decomposition

$$[BMIm]^+[Cu_2Br_3]^- \rightleftarrows [BMIm]^+[CuBr_2]^- + CuBr\downarrow. \quad (4)$$

The exchange current j_0 was determined by chronopotentiometry for the irreversible process occurring at anodic potentials ranging from E_{st} to $\Delta E \approx 0.9$ V (cathodic current wave C_2). The current–time curves in Fig. 3 were transformed to $j(\tau^{1/2})$ plots. The portions *j*, intercepted on the current axis by these plots, are related to j_0 by [17]:

$$j = \frac{j_0 z F (E - E_{st})}{RT},$$

where *z* is the number of electrons; *F*, Faraday number; *E*, preset potential; *R*, universal gas constant; and *T*, temperature.

The value of j_0 was found to be 3×10^{-5} A cm^{-2}, which also points to the irreversibility of the electrochemical process under study.

The second wave in the *E*–τ curve is associated with the appearance of a black substance $CuBr_2$ [16] in the near-electrode zone. This substance does not block the reaction surface of the electrode and its gradual dissolution in [BMIm]Br results in that the coloration changes from yellow-brown (color of molten [BMIm]Br) to green. An experiment demonstrated that $CuBr_2$ solutions in [BMIm]Br are green in the presence of a minor amount of water, as also is a solution of products formed in anodic oxidation of copper in this liquid, which may be due to formation of a partly hydrated compound $[BMIm]^+[CuBr_3]^-$.

As the current density increases and the potentials corresponding to the second wave are reached (Fig. 2), the current efficiency by Cu(I) decreases to 50–70% and less, which is probably due to oxidation of Cu(I) to Cu(II). Therefore, the second process occurring on the copper electrode in the potential range under study can be represented by the reactions

$$[BMIm]^+[CuBr_2]^- + Br^- \rightarrow CuBr_2 + [BMIm]^+Br^- + e, \quad (5)$$

$$CuBr + Br^- \rightarrow CuBr_2 + e. \quad (6)$$

It should also be noted that the ionic liquid containing products of electrochemical dissolution of copper at the potentials of the first wave does not change its coloration in the initial stage. However, its color changes to green upon its prolonged contact with air, and the electronic absorption spectrum becomes similar to that obtained after anodic dissolution of copper, which is presumably also due to the reaction Cu(I) → Cu(II). It should be noted that reactions (2) and (4) are written as possible, because a semitransparent CuBr film is manifested in the *E*–τ curve (Fig. 2).

CONCLUSIONS

(1) The study demonstrated that two irreversible electrode processes occur in the potential range under study on a copper electrode in $[BMIm]Br \cdot H_2O$. These processes are accompanied by formation of a well-soluble compound $[BMIm]^+[CuBr_2]^-$, which is rather stable under the experimental conditions and is oxidized to $CuBr_2$ at more positive potentials and upon interaction with the atmospheric oxygen.

(2) Electrochemical oxidation of metals in ionic liquids can be regarded as a possible way to obtain ionic liquids with complex metal-containing anions.

ACKNOWLEDGMENTS

The study was carried out in the framework of the Program of basic research no. 9 (OKhMN, Russian Academy of Sciences) "New Approaches to Improvement of the Corrosion Resistance and Radiation Hardness of Materials and Radioecological Safety," (2006, project no. 1).

REFERENCES

1. Wassersheid, P. and Welton, T., *Ionic Liquids in Synthesis*, New York: Wiley, 2003.
2. Artem'ev, A.V. and Yarosh, E.V., *Kataliz Prom–sti*, 2004, no. 4, pp. 24–40.
3. Olivier-Bourbigou, H. and Magna, L., *J. Mol. Catal. Ser. A., Chemical*, 2002, vol. 182–183, pp. 419–437.
4. Huddleston, J.G., Visser, A.E., Reichert, W.M., et al., *Green Chem.*, 2001, vol. 3, pp. 156–164.
5. Yang, J.-Z., Tian, P., He, L.-L., et al., *Fluid Phase Equilibria*, 2003, vol. 204, pp. 295–302.
6. Dyson, P.J., *Trans. Metal. Chem.*, 2002, vol. 27, pp. 353–355.
7. Hsiu, S.-I., Huang, J.-F., Sun, I.-W., et al., *Electrochim. Acta*, 2002, vol. 47, pp. 4367–4372.
8. Endres, F., *Electrochem. Solid-State Lett.*, 2002, vol. 5, no. 3, pp. 38–40.
9. Endres, F., *Phys. Chem. Phys.*, 2001, vol. 3, no. 15, pp. 2165–3174.
10. Huang. J.-F. and Sun, I.-W., *J. Electrochem. Soc.*, 2002, vol. 149, no. 9, pp. 348–355.
11. Bonhôte, P., A.-Dias, P., Papageorgion, N., et al., *Inorg. Chem.*, 1996, vol. 35, pp. 1168.
12. Vygodskii, Ya.S., Lozinskaya, E.I., and Shaplov, A.S., *Dokl. Akad. Nauk*, 2001, vol. 381, pp. 634.
13. Nagiwara, R. and Ito, Y., *J. Fluor. Chem.*, 2000, vol. 105, pp. 221.
14. Galus, Zb., *Teoretyczue Podstawy Elektroanalisy Chemicznej*, Warszawa: Panstwowe Wydawnictwo Naukowe, 1971.
15. Lur'e, Yu.Yu., *Spravochnik po analiticheskoi khimii* (Handbook of Analytical Chemistry), Moscow: Khimiya, 1971.
16. Rabinovich, V.A. and Khavin, Z.Ya., *Kratkii khimicheskii spravochnik* (Concise Chemical Reference Book), Leningrad: Khimiya, 1991.
17. Damaskin, B.B., *Printsipy sovremennykh metodov izucheniya elektrokhimicheskikh reaktsii* (Principles of Modern Methods for Study of Electrochemical Reactions), Moscow: Mosk. Gos. Univ., 1965.

ISSN 1070-4272, Russian Journal of Applied Chemistry, 2007, Vol. 80, No. 2, pp. 252–256. © Pleiades Publishing, Ltd., 2007.
Original Russian Text © G. Myagmarsuren, V.S. Tkach, D.S. Suslov, F.K. Shmidt, 2007, published in Zhurnal Prikladnoi Khimii, 2007, Vol. 80, No. 2, pp. 253–257.

CATALYSIS

High-Efficiency Catalysts for Norbornene Polymerization, Based on Palladium Carboxylates and Boron Trifluoride

G. Myagmarsuren, V. S. Tkach, D. S. Suslov, and F. K. Shmidt

Irkutsk State University, Irkutsk, Russia
Mongolian National University, Ulan-Bator, Mongolia

Received September 26, 2006

Abstract—Catalytic systems based on palladium carboxylates and boron trifluoride etherate were studied in the reaction of additive polymerization of nonbornene. The system $Pd(OAc)_2$ + $25BF_3OEt_2$ exhibits a high activity, up to 154 100 kg of nonbornene per mole of Pd per hour.

DOI: 10.1134/S1070427207020164

Polymerization of cyclic olefins under the action of metal-complex catalysts has been arousing a considerable interest recently. Nonbornene (bicyclo-[2.2.1]heptene-2) can polymerize via metathesis or by radical, cationic, and additive mechanisms (Scheme 1). Additive polymerization occurs with cleavage of the double bond and yields polymers containing unchanged cyclic structures in the backbone chain. Polymers of this kind show good thermal and chemical stability, are amorphous, exhibit high transparency in the IR, visible, and UV spectral ranges, and have low refractive index, narrow range of decomposition temperatures, and small dielectric constant. These factors make them promising for deposition of coatings in electronics, manufacture of telecommunication materials, optical lenses, substrates for plastic displays, photoresistors for chips and displays, and insulators for semiconductors [1, 2].

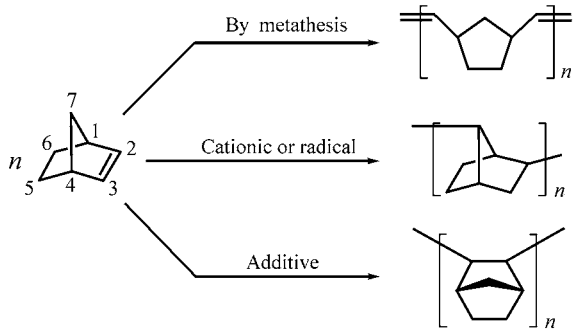

Scheme 1. Variants of nonbornene polymerization.

Data on additive polymerization, published by the year of 2000, were reviewed by Makovetskii [1] and Janiak [2]. In the last six years, a vast body of new information on metal-complex catalysts for this process has appeared in the literature. All the known catalysts can be conventionally divided into two groups: individual complexes of transition metals, mostly of the cationic type, and commonly neutral complexes used in combination with cocatalysts, mostly with methylaluminoxane (MAO) or tris(pentafluorophenyl) borate $B(C_6F_5)_3$ and with triethylaluminum (TEA) or without this compound. However, the production cost of organoaluminum or organoboron cocatalysts is high. Moreover, MAO is named a "black hole" because of its indeterminate structure. Therefore, development of less expensive and structurally simpler cocatalysts is an important task for chemical industry.

It has been shown previously [3–10] that systems based on bis(acetylacetonato)palladium Pd(acac) and boron trifluoride etherate BF_3OEt_2 are active catalysts for di- and oligomerization of ethylene and propylene [3–5], selective dimerization of styrene [6], telomerization of diene hydrocarbons with secondary amines [7], positional isomerization of hexene-1 [8], and additive polymerization of nonbornene and alkyl nonbornenes [9, 10]. The present communication reports on a study of the additive polymerization of nonbornene under the action of new catalytic systems based on palladium carboxylates of general formula $Pd(RCOO)_2$, combined with BF_3OEt_2.

EXPERIMENTAL

Nonbornene was polymerized in 10-ml glass reactor with a magnetic rabble in the atmosphere of

nitrogen. A solution of nonbornene and a Pd(II) complex in toluene was allowed to stand at a required temperature for 15 min; polymerization was initiated by introduction of BF_3OEt_2. After the reaction was complete, the polymers formed were precipitated with ethanol acidified with hydrochloric acid, separated by filtration, and dried in a vacuum (6 h at 80°C).

NMR spectra of solutions in $CDCl_3$ were recorded on a Bruker AMX-500 instrument with working frequencies of 500 MHz for ^1H and 125 MHz for ^{13}C. IR spectra were recorded on a Nicolet FT-IR spectrometer. The viscosity was measured at 25°C with an Ubellohde viscometer. Gel-permeation chromatography (GPC) was performed on a WATERS 150 HPLC instrument with 300 × 7.5-mm columns packed with 10-μm MIXED-B (135°C polystyrene standards); 1,2,4-trichlorobenzene served as a solvent. Thermal analyses were made on a DSC Q100 instrument at 10–800°C and a heating rate of 10 deg min^{-1}.

Toluene (Sigma-Aldrich, 99.8%) was used as a solvent without additional purification. Pd(II) carboxylates were synthesized by a procedure described in [11] and recrystallized from benzene.

In standard experiments, the amount of Pd was 1.0×10^{-6} mol, with the mol/mol ratios B : Pd = 25 and nonbornene : Pd = 5.104 (4.71 g); reaction time 30 min; temperature 25°C; solvent toluene; total volume of the reaction mixture, 7 ml.

In the study of how the amount of the cocatalyst in the system $Pd(OAc)_2$ + nBF_3OEt_2 on the process of nonbornene polymerization, the atomic ratio B : Pd was varied from 5 to 60 at 25°C at a constant concentration of Pd(II). The results obtained are listed in Table 1. As the B : Pd ratio is raised from 5 to 20, both the polymer yield and the intrinsic viscosity (and, accordingly, the molecular weight) steeply increase. The maximum conversion of the substrate into target products is reached at B : Pd = 25. The highest intrinsic viscosity [η] of the polymer is obtained at B : Pd = 40. Further increase in the B : Pd ratio to 60 leads to a slight decrease in conversion and intrinsic viscosity. This decrease may be due to partial destruction of active centers.

Such a dependence of the activity on the ratio between a cocatalyst and a transition metal rather widely occurs in metal-complex catalysis and is frequently accounted for by formation of an active complex from an inactive precursor and cocatalyst under equilibrium conditions, when the number of active centers grows with the B : Pd ratio [12]. In the present study, the mechanism of interaction between $Pd(OAc)_2$ and BF_3OEt_2 in the presence of nonbornene was not analyzed in detail. Therefore, the equilibrium between the inactive and active complexes can be represented in the general form as

$$Pd(OAc)_2 + BF_3OEt_2 \rightleftarrows \text{Active complex}.$$

The formation of α-alkylpalladium complexes via incorporation of coordinated alkenes at the Pd–OAc bond and further β-elimination to form a Pd–H bond have been described in detail in the literature [13]. Therefore, it can be assumed that catalytically active Pd hydrides are also formed in the $Pd(OAc)_2$ + BF_3OEt_2 system in the presence of nonbornene. The effect of the nature of carboxylate ligands at Pd on the nonbornene polymerization is illustrated by Table 2.

As can be seen from Table 2, the nature of carboxylate ligands at Pd(II) has no effect, within experimental error, on the nonbornene conversion into

Table 1. Effect of the B:Pd ratio on the nonbornene polymerization in the presence of the system $Pd(OAc)_2$ + nBF_3OEt_2 (25°C, 30 min, 4.71 g of nonbornene, solvent toluene, total volume 7 ml, nonbornene : Pd = 5×10^4, catalyst content 1×10^{-6} mol)

B : Pd	Yield, g	Conversion, %	Activity, $\frac{\text{kg nonbornene}}{\text{(mol Pd h)}}$	[η], dl g^{-1}
5	0.20	4.2	400	0.43
10	0.58	12.3	1160	0.68
15	1.28	27.2	2560	1.18
20	1.50	31.8	3000	1.24
25	1.59	33.8	3180	1.29
40	1.56	33.1	3120	1.40
60	1.53	32.5	3060	1.34

Table 2. Effect of the nature of a carboxylate ligand on the nonbornene polymerization in the presence of the system $Pd(OAc)_2$ + $25BF_3OEt_2$ (25°C, 30 min, 4.71 g of nonbornene, solvent toluene, total volume 7 ml, nonbornene : Pd = 5×10^4, catalyst content 1×10^{-6} mol)

Ligand, C_n	Acidity,* pK_a	Yield, g	Conversion, %	[η], dl g^{-1}
Benzoate, C_7	4.20	1.49	31.6	1.09
Acetate, C_2	4.76	1.59	33.8	1.29
Propionate, C_3	4.87	1.52	32.3	1.32
Heptanoate, C_7	4.89	1.63	34.6	1.36
Stearate, C_{18}	10.15	1.61	34.2	1.68

* pK_a values taken from [14, 15].

Table 3. Effect of the amount of the catalytic precursor on the nonbornene polymerization in the presence of the system $Pd(OAc)_2$ + $25BF_3OEt_2$ 25°C, 30 min, 4.71 g of nonbornene, solvent toluene, total volume 7 ml

$c_{Pd} \times 10^6$, mol	nonbornene : Pd	Yield, g	τ, min	Activity, kg nonbornene/(mol Pd h)	[η], dl g^{-1}
0.5	100000	30	1.11	4440	1.36
1.0	50000	30	1.59	3180	1.29
2.0	25000	30	2.47	2470	1.23
3.0	16700	30	4.70	3140	0.69
5.0	10000	1	3.11	37320	1.1
10.0	5000	<10 s	4.28	>154100	0.56

polymers. These data may indicate that the active complexes formed in these systems are of a homogeneous nature. A nearly linear dependence of the intrinsic viscosity of the polymers on the acidity of the carboxylate ligand is observed in this case. The nature of this dependence is the subject of a separate study.

Raising the temperature to 65°C for the $Pd(OAc)_2$ + $25BF_3OEt_2$ system leads to a significant decrease in the nonbornene conversion to 17.4% and in the polymer viscosity to 0.19 dl g^{-1}. The decrease in conversion on raising the temperature points to the low thermal stability of the system. The decrease in the intrinsic viscosity of the polymers at higher temperatures can be attributed to a faster rise with temperature in the rate constant of chain termination, compared with the rate constant of chain growth.

To study the effect of the amount of monomer on the nonbornene polymerization, several experiments were carried out with nonbornene : Pd molar ratios of 25000 to 100000 at a constant Pd(II) concentration. It was shown that the nonbornene : Pd ratio has no effect on the nonbornene conversion into polymers. This indicates that the reaction is zeroth-order with respect to the monomer. The intrinsic viscosity decreases from 1.45 to 1.18 dl g^{-1} as the nonbornene : Pd ratio is raised from 25000 to 100000. The possible reason is that the diffusion of the monomer toward an active center is hindered at high monomer concentrations by the poor solubility of the growing polymer chain. In this case, the termination of a chain and initiation of a new one become preferable.

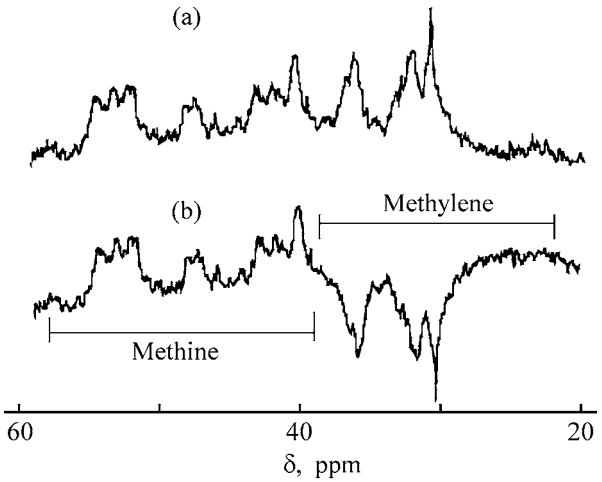

^{13}C NMR spectra of polynonbornene: (a) full spectrum and (b) DEPT 135° spectrum. (δ) Chemical shift.

The effect of the Pd(II) concentration on the nonbornene polymerization in the presence of the $Pd(OAc)_2$ + $25BF_3OEt_2$ system at a constant monomer concentration is illustrated by Table 3. An increase in the amount of Pd(II) is accompanied by a rise in the nonbornene conversion and a decrease in the intrinsic viscosity of polymers. At an amount of Pd(II) equal to 1.0×10^{-5} mol, the catalytic activity is as high as 154100 kg of nonbornene per mole of Pd per hour. This activity is comparable with the best published data [16–19] and exceeds by approximately a factor of 7 that achieved for the $Pd(acac)_2$ + $25BF_3OEt_2$ system [9]. It should be noted that an exothermic effect starts to be observed beginning with an amount of Pg(II) equal to 3.0×10^{-6} mol. At a Pd(II) content of 1.0×10^{-5} mol, the reaction is strongly exothermic and the reaction mixture instantaneously becomes a solid white mass.

The structure of the resulting nonbornene was studied by NMR and IR spectroscopies. The data obtained demonstrated that the structure corresponds to that of the additive polymer. The ^1H NMR spectrum contains no resonances associated with C=C bonds. The IR spectrum does not contain, either, bands at 1620–1680 cm^{-1}, associated with double bonds, but there are strong absorption bands at 1452–1474 cm^{-1}, associated with δ_{H-C-H} deformation vibrations of the bridging CH_2 groups of the nonbornene ring [20]. The ^{13}C NMR spectra of polynonbornene are shown in the figure. The NMR signals were assigned in ac-

Table 4. GPC data and results of thermal analyses of polymer samples obtained in the presence of the $Pd(OAc)_2$ + $25BF_3OEt_2$ system (30 min, 4.71 g of nonbornene, solvent toluene, total volume 7 ml)

[η], dl g^{-1}	T, °C	Catalyst, $c \times 10^6$, mol	τ, min	M_w, g mol^{-1}	$Q = M_w/M_n$	T_d	T_g
						°C	
1.40*	25	1.0	30	293; 800	2.27	324	262
1.29	25	1.0	30	179 100	2.14	324	258
1.10	25	5.0	1	141 900	2.72	319	252
0.56	25	10.0	<10 s	192 900	3.02	317	235
1.19	45	1.0	30	174 900	3.10	313	250
0.19	65	1.0	30	77 700	3.51	313	240

* B/Pd = 40.

cordance with the following numbering of carbon atoms:

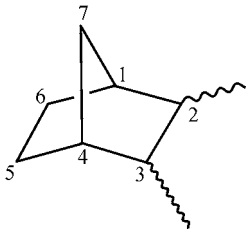

The resonance peaks at 28–34 ppm are related to nonbridging CH_2 groups (C_5 and C_6). The bridging CH_2 groups (C_7) show signals at 34–38 ppm. The nodal CH groups (C_1 and C_4) appear as signals at 38–45 ppm. The signals at 45–55 ppm belong to the CH groups (C_2 and C_3) of the backbone chain of the polymer. The absence of resonances at 20–24 ppm indicates that the polymer chain has the exo configuration [21].

The signal from the C_7 atom appears as a group of strong resonances at 34–38 ppm. This indicates that the microstructure of the polymer is a combination of *rr* and *mr* triads with low diisotacticity [22]. The absence of *mm* triads is confirmed by the fact that there is no resonance signal at 39 ppm [21].

The data obtained in analyses by derivatography, differential-scanning calorimetry (DSC), and GPC for selected samples are listed in Table 4. The molecular-weight distribution (MWD) $Q = M_w/M_n$ in polymerization under the standard conditions is close to 2, which is the theoretical value of the Flory–Schultz distribution for the ideal polymerization with chain termination. This value shows that the active complexes are of the single-center, highly homogeneous nature. The deviation of MWD to larger values at high palladium(II) concentrations and high temperatures may be due both to destruction of active centers and to an increase in the rate of chain termination. The thermal decomposition temperature T_d of the polymers varies from 313 to 324°C, and the glass-transition temperature T_g, from 240 to 262°C.

CONCLUSIONS

(1) The catalytic system $Pd(OAc)_2$ + $25BF_3OEt_2$ shows high activity in additive polymerization of nonbornene, up to 154 100 kg of nonbornene per mole of Pd(II) per hour.

(2) The results of ^{13}C NMR studies demonstrate that the microstructure of the polymers formed is a combination of *rr* and *mr* triads with low diisotacticity.

(3) The value of the molecular-weight distribution of polymers obtained under the standard conditions indicates that the active complexes are of the single-center, highly homogeneous nature.

REFERENCES

1. Makovetskii, K.L., *Vysokomol. Soedin., Ser. B*, 1999, vol. 41, no. 9, pp. 1525–1543.
2. Janiak, C. and Lassahn, P.G., *Macromol. Rapid Commun.*, 2001, vol. 22, no. 1, pp. 479–492.
3. USSR Inventor's Certificate, no. 991 193.
4. USSR Inventor's Certificate, no. 1 160 631.
5. Myagmarsuren, G., Tkach, V.S., Suslov, D.S., and Shmidt, F.K., *React. Kinet. Catal. Lett.*, 2005, vol. 85, no. 1, pp. 197–203.
6. Myagmarsuren, G., Tkach, V.S., Shmidt, F.K., et al., *J. Mol. Catal. A*, 2005, vol. 235, nos. 1–2, pp. 154–160.
7. Chernyshev, M.L., Tkach, V.S., Dmitrieva, T.V., et al., *Kinet. Kataliz*, 1997, vol. 38, no. 4, pp. 575.

8. Tkach, V.S., Suslov, D.S., Myagmarsuren, G., et al., *Zh. Prikl. Khim.*, 2006, vol. 79, no. 1, pp. 88–91.
9. Myagmarsuren, G., Lee, K.-S., Jeong, O.-Y., and Ihm, S.-K., *Polymer*, 2004, vol. 45, no. 10, pp. 3227–3232.
10. Myagmarsuren, G., Lee, K.-S., Jeong, O.-Y., and Ihm, S.-K., *Polymer*, 2005, vol. 46, no. 11, pp. 3685–3692.
11. Stephenson, T.A., Morehouse, S.M., Powell, A.R., et al., *J. Chem. Soc.*, 1965, vol. 3, no. 5, pp. 3632–3640.
12. Mathew, J.P., Reinmuth, A., Melia, J., et al., *Macromolecules*, 1996, vol. 29, no. 8, pp. 2755–2763.
13. Gusevskaya, E.V., *Quim. Nova*, 2003, no. 26, pp. 242–248.
14. Namazian, M., Halvani, S., and Iranian, J., *Chem. Soc.*, 2005, vol. 2, pp. 65–70.
15. Kanicky, J.R., Shah, D.O., and Coll, J., *Interface Sci.*, 2002, vol. 256, pp. 201–207.
16. Mast, C., Krieger, M., Dehnicke, K., and Greiner, A., *Macromol. Rapid. Commun.*, 1999, vol. 20, no. 4, pp. 232–235.
17. Zhang, D., Jin, G.-X., Weng, L.-H., and Wang, F., *Organometallics*, 2004, vol. 23, no. 13, pp. 3270–3275.
18. Lassahn, P.G., Janiak, C., and Oh, J.-S., *Macromol. Rapid. Commun.*, 2002, vol. 23, no. 12, pp. 16–20.
19. Hennis, A.D., Polley, J.D., Long, G.S., et al., *Organometallics*, 2001, vol. 20, no. 13, pp. 2802–2812.
20. Bondarenko, G.N., Gorbacheva, L.I., Golenko, T.G., et al., *Vysokomol. Soedin., Ser. A*, 1996, vol. 38, no. 3, pp. 469–472.
21. Arndt, M., Engehausen, R., Kaminsky, W., and Zoumis, K., *J. Mol. Catal. A*, 1995, vol. 101, no. 3, pp. 171–178.
22. Barnes, D.A., Benedikt, G.M., Goodall, B.L., et al., *Macromolecules*, 2003, vol. 36, no. 8, pp. 2623–2632.

ISSN 1070-4272, Russian Journal of Applied Chemistry, 2007, Vol. 80, No. 2, pp. 257–262. © Pleiades Publishing, Ltd., 2007.
Original Russian Text © A.A. Ostroushko, M.Yu. Sennikov, M.O. Tonkushina, 2007, published in Zhurnal Prikladnoi Khimii, 2007, Vol. 80, No. 2, pp. 258–263.

CATALYSIS

Simulation of Oxidation of Carbon Particles at the Surface of Mixed Oxide Catalysts

A. A. Ostroushko, M. Yu. Sennikov, and M. O. Tonkushina

Research Institute of Physics and Applied Mathematics, Gor'ky Ural State University, Yekaterinburg, Russia

Received August 3, 2006

Abstract—A model of catalytic oxidation of a cylindrical carbon particle was suggested. The model considers the rate of layer-by-layer burning of the particle, variation of its geometry, and remote action of the catalyst. A software for calculations was developed; the data obtained correlate well with the experimental data for catalysts based on lanthanum cesium vanadate. The kinetics of carbon oxidation on catalysts of varied nature was compared.

DOI: 10.1134/S1070427207020176

The reactions of catalytic oxidation of carbon [1] are of practical significance for, in particular, treatment of exhaust gases in industry and transport. One of the main aspects providing a successful development of thermal catalytic devices is the knowledge of the kinetics and mechanism of the above reactions. It is important to understand, for example, how the oxidation of carbon particles on the whole, proceeds on the filter-catalyst [2, 3]. At the same time, for optimization of the oxidation conditions, there is need to have a notion of the behavior of individual particles. Here, we report on theoretical simulation and experimental modeling of their behavior.

Carbon particles of two shapes, cylindrical and spherical, can be selected as model. Here we consider the oxidation of individual particles with the shape close to cylindrical by atmospheric oxygen at the catalyst surface. This corresponds to the optimal mode of the device operation at which the burning rate of particles is comparable with the rate of their deposition, i.e., no layer covering the catalyst surface and deteriorating its performance is accumulated. These conditions can be more easily created when using reverse gas flows through the catalytic device of a batch operation cycle. We assume that individual particles are relatively small, so that the catalyst surface can be considered to be flat. Cylinder-shaped particles contact with the catalyst through the base of cylinder. We assume that the oxidation of small particles proceeds mainly at the catalyst surface.

For experimental modeling of the behavior of carbon particles we used compact samples of the corresponding shape prepared from carbon-graphite mixture used, for example, for production of electrodes for manganese–zinc power cells. We performed pyrolytic synthesis of mixed oxide catalysts of the composition $Cz_{0.3}La_{0.7}VO_{4\pm y}$ [1] and $La_{0.75}Ag_{0.25}MnO_{3\pm y}$ [4]. The catalysts were prepared in the form of pellets and sintered for 6 h at 650 and 900°C, respectively. The pelletized carbon samples were pressed against the catalyst pellets with a springing attachment and annealed isothermally in air. After annealing, the weight change was monitored. To take into account the possible contribution of removal of volatile products and noncatalytic oxidation to the weight loss of carbon, we performed concurrent blank experiments without a catalyst.

In oxidation of particles, an important parameter is variation of their shape with time. The configuration of the area of carbon oxidation was studied by the microscopic method. In particular, variation in the sample shape is fairly conveniently recorded by photographing the sample from one side or in cross section. In this case, we can model a spherical particle by considering variation of the cross-section of a round rod contacting with the catalyst through the generatrix of the cylindrical surface.

Let us consider a model of oxidation of a cylindrical particle. As assumed previously [1, 2, 5, 6], a catalyst accelerates the burning process both when in direct contact with carbon and at a certain distance from it. To verify this assumption, we performed the following experiment. For contact annealing, we took a catalyst pellet with a smaller diameter than that of the carbon pellet. This case simulates a situation when a particle or carbonaceous agglomerate with a fairly large diameter contacts with a peak on

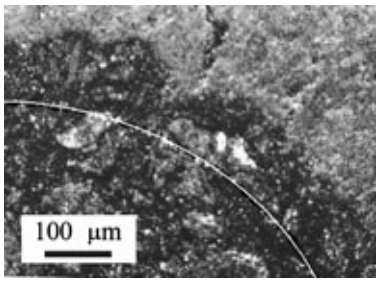

Fig. 1. Micrograph of a carbon sample oxidized at 550°C for 1 h in contact with the catalyst $Cs_{0.3}La_{0.7}VO_{4 \pm y}$. (*Line*) Boundary of the catalyst pellet.

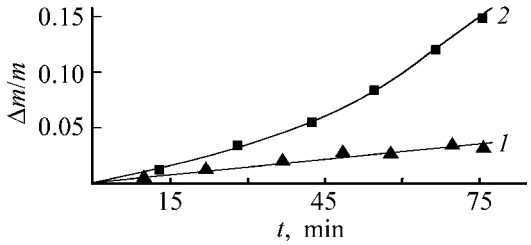

Fig. 2. Relative weight loss $\Delta m/m_0$ vs. oxidation time t of carbon samples in contact with the catalyst $Cs_{0.3}La_{0.7}VO_{4 \pm y}$. Temperature, °C: (*1*) 380 and (*2*) 470.

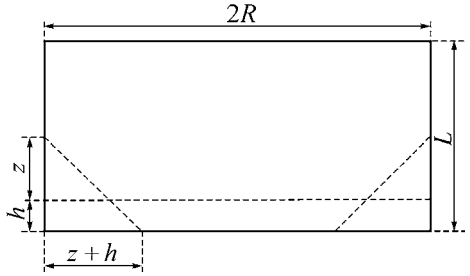

Fig. 3. Scheme for evaluation of particle burning. For explanation, see text.

the rough catalyst surface. This is quite possible in using mixed oxide catalysts applied onto foamed materials [4, 7–10]. The experiment showed that the oxidation area of carbon extends in fact around the catalyst pellet to a noticeable distance (Fig. 1), in our case, on the average, to 170–180 μm. To describe the process of particle burning, consideration must be given, on the one hand, to the decrease in its thickness due to the contact action and, on the other hand, to the variation of the shape and sizes due to the remote action of the catalyst.

In consideration of the carbon oxidation, we proceeded from the presence of two main stages of chemical conversion: initial formation of carbon monoxide CO and its conversion into carbon dioxide CO_2. In this case, the contact action on carbon oxidation is apparently caused by accelerated formation of CO in the contact area, which is due in part to the formation of unstable carbonate complexes [1, 11]. The remote action can be assigned to the existence of the outer area of exothermic oxidation of CO, which raises the effective temperature in the vicinity of the carbon surface and thereby accelerates the first stage of carbon oxidation. In the dependences of the weight loss of the samples on time with heating, this remote action is manifested in changes in the run of the curves describing the overall oxidation rate (Fig. 2). In the case of the remote action, the surface area of the particle subjected to oxidation increases with time due to the appearance of an additional area of oxidation on the side surface of the sample (particle). At even higher temperatures, the as yet disregarded noncatalytic oxidation has a pronounced effect on oxidation of carbon materials.

A mathematical model of the process can be developed in a general form. For example, in the cross section of a carbon pellet, the angle between its surface adjacent to the catalyst and tangent to the surface formed as a result of the remote action can be arbitrary and varying with time, which should complicate the model. An experimental observation of the variation of the shape of a sample being oxidized allows us to simplify the model and make it more adequate to actual processes. In particular, it was found that the surface of the remote action can be regarded with a good accuracy as the generatrix of a truncated cone. In this case, in the cross section of the pellet the angle between the generatrix and the pellet, base remains constant and close to 45°. In such a situation, it is reasonable to assume that the rate of motion of this generatrix into the particle is constant. Naturally, the surface area accessible for the remote action increases with time until the expanded generatrix of the cone reaches the upper base of the initial cylinder. One more important fact is that the area of the remote action can spread to a distance larger than the particle thickness. It seems likely that the unburnt part can shield the backside of carbon particles from the remote action of the catalyst. The condition occurence of both mechanisms of catalytic action is that the rate of motion of the carbon oxidation front due to the contact action is lower than that due to the remote action; otherwise the generatrix of a truncated cone should not be observed. It is believed that at higher temperatures, when both processes occur, the boundary of contact burning moves also linearly. These are the boundary conditions for construction of a model of oxidation of a cylindrical particle.

With the aim to perform model calculations of burning of carbon particles contacting with the catalyst surface in the Maple 9 environment, we developed a software in which, according to the scheme (Fig. 3), the following designations were made: *C*, rate con-

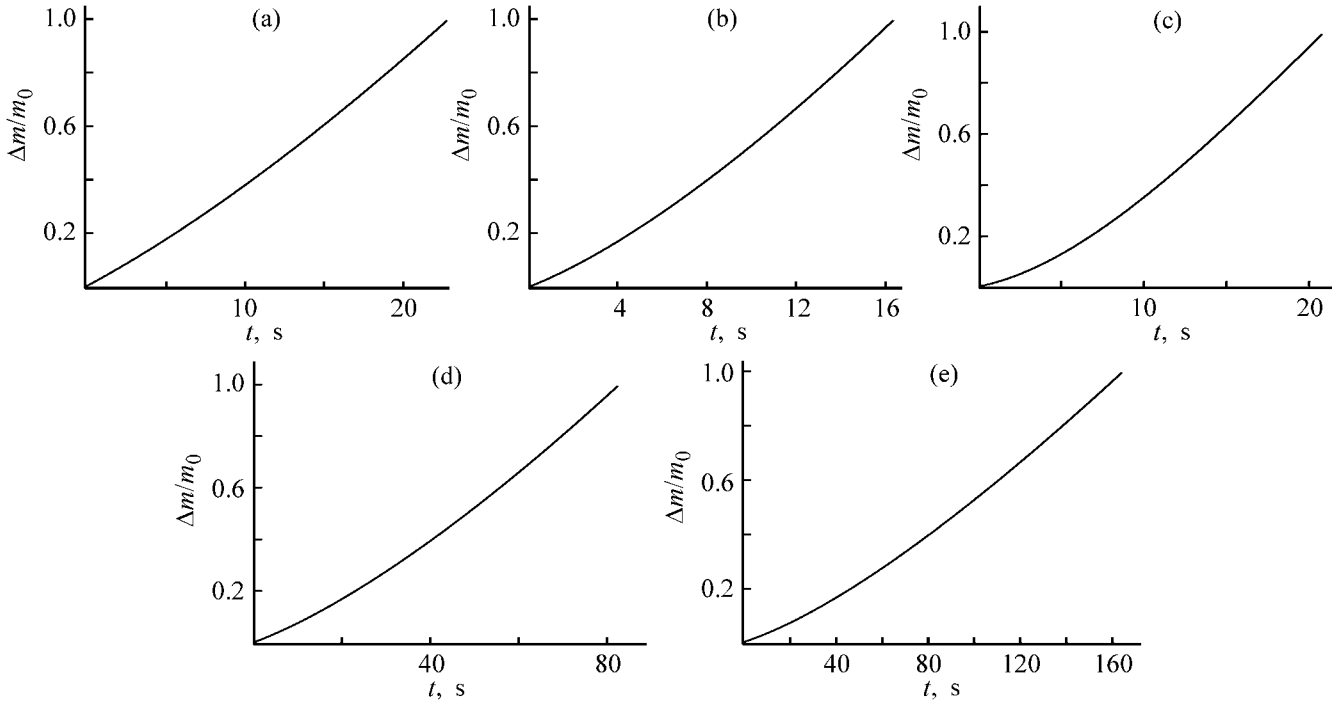

Fig. 4. Calculated curves of the relative weight loss $\Delta m/m_0$ in catalytic oxidation of quasicylindrical carbon particles at the catalyst surface. (t) Time. Radius and height of particles, μm: (a–c) 1, (d) 5, and (e) 10. Rate constants H and C, respectively, μm s^{-1}: (a) 0.33, 0.017; (b, d, e) 0.033, 0.033; and (c) 0.017, 0.033.

stant of remote oxidation at given temperature, μm s^{-1}; H, rate constant of contact oxidation at the same temperature, μm s^{-1}; R, particle radius, μm; L, initial height of the particle, μm; h, thickness of the layer burnt due to contact action in a time t; and c, thickness of the layer burnt due to the remote action in a time t,

$$h = Ht, \quad (1)$$

$$c = Ct \quad (2)$$

at a linear dependence of the thickness of the burnt layer due to each processes.

In the calculations, we considered V_0 (initial particle volume, μm^3) and V_t (particle volume after a some time when a part of the material was burnt), based on the model configuration

$$V_t = \Pi[R^2(1 - z - h) + zR^2 - Rz^2 + z^3/3] \quad (3)$$

(z is shown in Fig. 3), and also V_b (volume of the burnt part of the material):

$$V_b = \Pi[R^2h + Rz^2 - z^3/3]. \quad (4)$$

Variation of the volume is in direct proportion to the weight loss by the particle (sample).

The results of calculation for various ratios of the burning rates of particles by each mechanism are presented in Fig. 4 and Table 1. The ratio of the burning rates of a particle by the mechanism of contact and remote actions can vary with temperature, since these processes have different activation energies. It is believed that the contact action predominates at relatively low temperatures and the remote action, with heating. A comparison of the shapes of the experimental dependences for the weight loss by the pellet in the contact and remote actions of the catalyst (Fig. 2) with the calculated curves gave a good correlation, which suggests that the model suggested is valid. The experiments confirmed that at relatively low temperatures virtually only contact oxidation at

Table 1. Time of complete burning (τ_{cb}) of quasicylindrical particles, calculated in terms of the model suggested

H, μm s^{-1}	C, μm s^{-1}	τ_{cb}, s, at indicated R, L^*, μm		
		1	5	10
0.033	0.017	22.9	114.2	228.5
0.033	0.033	16.5	82.6	165.8
0.017	0.033	20.9	104.5	228.5
0.033	0	30	150	300
0	0.033	28.6	142.9	285.8

* For calculations, the radius and height of particles were taken equal.

Table 2. Exponents x in Eq. (5)

T, °C	x for indicated catalyst	
	$La_{0.75}Ag_{0.25}MnO_{3 \pm y}$	$Cs_{0.3}La_{0.7}VO_{4 \pm y}$
350		1.3
400	2.76	1
430		~0.5
450	0.80	
500	0.63	

a constant rate occurs on vanadate catalysts, which is accompanied by the linear weight loss and is satisfactorily described by the equation with x values close to 1:

$$m^x = Kt, \quad (5)$$

where m is the total weight loss of the sample in a time t and K is the effective rate constant.

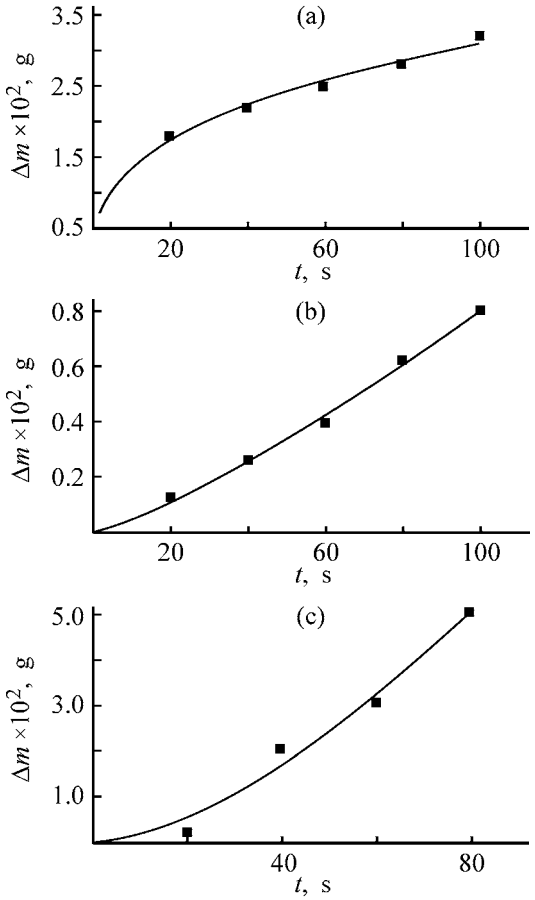

Fig. 5. Kinetic curves for weight loss Δm by carbon samples in the presence of the catalyst $La_{0.75}Ag_{0.25}MnO_{3 \pm y}$ at (a) 400, (b) 450, and (c) 500°C.

The exponent x in these equations is governed by the oxidation mechanism [1]. With heating, a component corresponding to the remote action of the catalyst appears and the formal value of x decreases.

The developed software allows calculation of the oxidation of particles with an arbitrary height-to-diameter ratio even in the case when the oxidation of particles due to the contact and remote action is not described by a linear law. In this case, the experimentally determined actual dependences $h = f(t)$ and $c = f_1(t)$ can be used. In a similar manner, we can describe the oxidation of spherical particles that take, due to the remote action, an egg-like shape with a cut-off bottom end, which is caused by the contact oxidation. This was confirmed experimentally. Observation of the oxidation of a cylindrical sample, initially brought in contact with the catalyst through the generatrix of the cylinder, can be conveniently used for calculating the configuration of spherical particles. In the course of burning, the round cross-section of the sample changes, which is recorded photographically.

Based on the fact that the catalysts of varied nature can accelerate each stage of carbon oxidation to different extents, we performed comparative experiments. Along with the oxidation on the vanadate catalyst with a monazite structure, we performed experiments with catalysts in the system Ag–La–Mn–O. Typically, these catalysts contain perovskite phases doped with silver [12–15] and also a certain amount of metallic silver and manganese oxides. Such compositions are very active in deep oxidation of gaseous products (organic substances of various classes, carbon monoxide, etc.).

A comparison of the kinetics of carbon oxidation at 400–500°C on the catalysts of the $Cs_xLa_{1-x}VO_{4 \pm y}$ and $La_{0.75}Ag_{0.25}MnO_{3 \pm y}$ types confirmed that the catalyst nature is an extremely important factor in this case. The experimental data obtained for the total weight loss were described satisfactorily by power dependences of type (5), irrespective of the mechanism of the catalyst action.

As mentioned above, the oxidation mechanism for vanadate catalyst changes with heating. At relatively low temperatures, the contact action predominates, and with heating the remote action is manifested. The system Ag–La–Mn–O at relatively low temperatures (400°C) is presumably characterized by a stronger hindrance associated with the substance transfer in the gas phase (Table 2, Fig. 5), compared to the vanadate catalyst. In this case, virtually no area of remote burning of the pellets was observed, as in the case of vanadate catalysts at low temperatures.

The differences in the influence of the catalysts can be caused by the fact that the system Ag–La–Mn–O is less able to exert the contact action manifested in the first stage of carbon oxidation to CO and, at the same time, significantly accelerates oxidation of CO to CO_2. As in the preceding case, the oxidation mechanism changes as the temperature of the experiments increases, which is suggested by the changed shapes of the dependences of pellet weight loss on time. It is likely that the appearance of a sufficient amount of CO results in local heating and initiation of the "remote" mechanism manifested in the formation of an additional burning front at an angle of 45° to the catalyst surface. The overall oxidation abruptly accelerates with time.

The activity of catalysts based on cesium vanadate promoted with cesium sulfate and without promoter [1] in CO oxidation was determined using a Katakon 1.1 flow-circulating reactor and a Testo-350 XL electronic gas analyzer. The content of CO in the gas–air mixture was 0.2 vol %, and the feeding rate, 6.3 l h^{-1}; in this case, the specific load on the catalyst was 1500 h^{-1}. For dosing of the mixture, we used a gas cylinder with 20.3 vol % CO in nitrogen. As a result, we found that the vanadate phases actually have poorer catalytic characteristics with respect to CO (Fig. 6) in comparison with doped perovskites [4, 5, 15]. It is likely that the presence of cesium sulfate as a promoter results in a decrease in the effective surface area of the catalyst with heating due to the possible appearance of a local eutectic melt [1], which results in decrease in the degree of CO conversion. The specific surface area of promoted and unpromoted samples was 0.25 and 0.52 $m^2 g^{-1}$, respectively (Tristar-3000 equipment was used), while perovskite catalysts have a surface area of approximately 20 $m^2 g^{-1}$.

In addition, the difference in the type of behavior of the catalytic systems studied may be due to the possible contact reduction of silver, initially originally contained in the perovskite structure, by carbon, which was found experimentally as a silver film covering the catalyst pellet after contact annealing. This can hinder transfer of gaseous products to the contact area. In this case, the previous assumptions on the advisability of using combined blocks containing catalysts of different compositions [1–3] are confirmed. In particular, vanadate catalysts can remove carbonic products from exhaust gases, with further, more efficient, purification on perovskites.

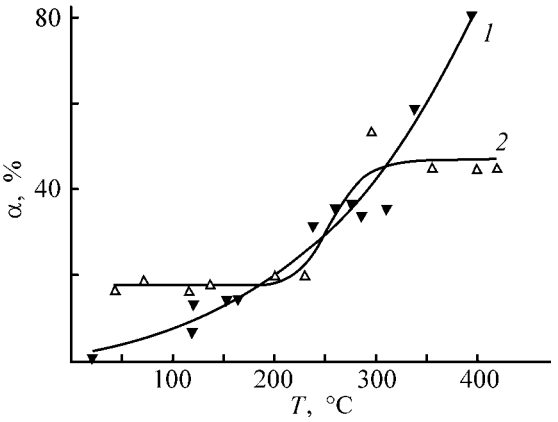

Fig. 6. Degree of CO conversion α vs. temperature *T*. Catalyst: (*1*) $Cs_{0.1}La_{0.9}VO_4$ (R^2 = 0.9653) and (*2*) $Cs_{0.1}La_{0.9}VO_4$ + 10% Cs_2SO_4 (R^2 = 0.9445).

ACKNOWLEDGMENTS

The authors are grateful to the Government of Sverdlovsk oblast for financial support, to V.I. Minyaev, Yu.V. Mokin, and E.A. Suslov for participation in the experiments on measurement of catalytic activity, and to A.P. Safronov for measurements of the specific surface area of the samples.

REFERENCES

1. Ostroushko, A.A., Makarov, A.M., and Minyaev, V.I., *Zh. Prikl. Khim.*, 2004, vol. 77, no. 7, pp. 1136–1143.
2. Ostroushko, A.A., Sennikov, M.Yu., Minjaev, V.I., et al., Abstracts of Papers, *4th Int. Conf. "Automobile and Technosphere" (ICATS'05)*, Kazan, June 14–16, 2005, Sect. B, ref. no. 585.
3. Ostroushko, A.A., Minyaev, V.I., and Makarov, A.M., Abstracts of Papers, *3d Int. Conf. "Automobile and Technosphere" (ICATS'03)*, Kazan, June 17–20, 2003, Sect. B, ref. no. 370.
4. Ostroushko, A.A., Schubert, E., Minyaev, V.I., et al., *Zh. Prikl. Khim.*, 2003, vol. 76, no. 8, pp. 1292–1297.
5. Ostroushko, A.A., Schubert, E., Minyaev, V.I., et al., *Materialy Vserossiiskoi konferentsii "Ekologicheskie problemy promyshlennykh regionov* (Proc. Russian Conf. "Environmental Problems of Industrial Regions"), Yekaterinburg, March 10–12, 2004, pp. 240–242.
6. Minyaev, V.I., Mokina, Yu.V., and Ostroushko, A.A., Abstracts of Papers, *Vserossiiskaya konferentsiya "Khimiya tverdogo tela i funktsional'nye materialy 2004" i seminar Sib. Otd. Ross. Akad. Nauk–Ural. Otd. Ross. Akad. Nauk "Termodinamika i materialovedenie"* (Russian Conf. "Chemistry of Solids and Functional Materials 2004" and Seminar of Russian Academy of Sciences, Ural and Siberian Divisions,

"Thermodynamics and Materials Technology"), Yekaterinburg, October 25–28, 2004, Yekaterinburg: Ural. Otd. Ross. Akad. Nauk, 2004, p. 268.

7. Antsiferov, V.N. and Porozova, S.E., *Vysokoporistye pronitsaemye materialy na osnove alyumosilikatov* (High-Porous Permeable Materials Based on Aluminosilicates), Perm: Perm. Gos. Tekh. Univ., 1996.
8. Antsiferov, V.N., Kalashnikov, M.Yu., Makarov, A.M., and Filimonova, I.V., *Zh. Prikl. Khim.*, 1997, vol. 70, no. 1, pp. 105–110.
9. Antsiferov, V.N., Kalashnikov, M.Yu., Makarov, A.M., et al., *Zh. Prikl. Khim.*, 1997, vol. 70, no. 1, pp. 111–114.
10. Antsiferov, V.N., Makarov, A.M., and Ostroushko, A.A., Abstracts of Papers, *I Vserossiiskaya konferentsiya "Khimiya dlya avtomobil'nogo transporta"* (I Russian Conf. "Chemistry for Motor Transport"), Novosibirsk, October 27–30, 2004, Novosibirsk: Inst. Kataliza Sib. Otd. Ross. Akad. Nauk, 2004, pp. 44–47.
11. Ostashkova, I.V. and Kosinets, N.I., *Zh. Vses. Khim. O–va im. D.I. Mendeleeva*, 1984, vol. 29, no. 4, pp. 434–436.
12. Udilov, A.E. and Ostroushko, A.A., Abstracts of Papers, *Vserossiiskaya konferentsiya "Khimiya tverdogo tela i funktsional'nye materialy 2004" i seminar Sib. Otd. Ross. Akad. Nauk–Ural. Otd. Ross. Akad. Nauk "Termodinamika i materialovedenie"* (Russian Conf. "Chemistry of Solids and Functional Materials 2004" and Seminar of Russian Academy of Sciences, Ural and Siberian Divisions, "Thermodynamics and Materials Technology"), Yekaterinburg, October 25–28, Yekaterinburg: Ural. Otd. Ross. Akad. Nauk, 2004, p. 416.
13. Udilov, A.E., Ostroushko, A.A., and Schubert, E., Abstract of Papers, *V Vserossiiskaya konferentsiya "Keramika i kompozitsionnye materialy"* (V Russian Conf. "Ceramics and Composite Materials"), Syktyvkar, June 20–27, 2004, Syktyvkar: Komi Nauchn. Tsentr Ross. Akad. Nauk, 2004, pp. 127–128.
14. Udilov, A.E. and Ostroushko, A.A., Abstracts of Papers, *7 Vserossiiiskoe soveshchanie "Vysokotemperaturnaya khimiya silikatov i oksidov"* (7th Russian Meet. "High-Temperature Chemistry of Silicates and Oxides"), St. Petersburg, November 19–21, 2002, St. Petersburg: Yanus, 2002, p. 175.
15. Ostroushko, A.A., Schubert, E., Zhuravleva, L.I., et al., *Zh. Prikl. Khim.*, 2000, vol. 73, no. 8, pp. 1311–1320.

ISSN 1070-4272, Russian Journal of Applied Chemistry, 2007, Vol. 80, No. 2, pp. 263–267. © Pleiades Publishing, Ltd., 2007.
Original Russian Text © L.D. Asnin, A.A. Fedorov, Yu.S. Chekryshkin, 2007, published in Zhurnal Prikladnoi Khimii, 2007, Vol. 80, No. 2, pp. 264–268.

CATALYSIS

Adsorption of Chlorobenzene on V_2O_5/Al_2O_3 Catalyst under Dynamic Conditions

L. D. Asnin, A. A. Fedorov, and Yu. S. Chekryshkin

Institute of Technical Chemistry, Ural Division, Russian Academy of Sciences, Perm, Russia

Received June 6, 2006

Abstract—Frontal chromatography was used to study the adsorption dynamics and adsorption equilibrium of chlorobenzene on a 5% V_2O_5/Al_2O_3 catalyst at temperatures of 50 and 100°C. The mixed-diffusion model was employed to describe the elution curve and evaluate the effective coefficients of external mass exchange and diffusion within transport pores.

DOI: 10.1134/S1070427207020188

Vanadium oxide catalysts exhibit high activity in reactions of deep oxidation of chloroaromatic compounds [1–4], which makes them attractive for development of systems for detoxication of gas discharges containing compounds of this kind. Oxides of aluminum, titanium, and zirconium and various double oxides have been studied as supports for vanadium oxide [1–6], with mostly titanium oxide used in recent years [1, 3, 5, 7, 8]. Comparative studies of V_2O_5/Al_2O_3 and V_2O_5/TiO_2 catalysts have shown that the latter is more active in oxidation of 1,2-dichlorobenzene [1] and benzene [6]. At the same time, vanadium(V) oxide supported by Al_2O_3 shows a no less activity in oxidation of chloroethylene than catalysts on other supports [4]. The data of [9–11] suggest that vanadium-aluminum oxide catalysts provide a conversion of chloroaromatic compounds that is sufficient for industrial purposes. An advantage of aluminum oxide over titanium oxide is the larger specific surface area of the former. This circumstance becomes particularly important in the case of the adsorption-catalytic method for elimination of toxic contaminants, in which the catalytic stage proper is preceded by the stage of substance concentration on the surface of an adsorbent-catalyst. Thus, catalysts with a more developed surface will provide a higher specific capacity of the reactor-adsorber. Another important factor that predetermined the choice of a support was the existence of a well-developed domestic industry for manufacture of aluminum oxide for catalytic purposes [12].

The mechanism of oxidation of chlorobenzenes on the surface of the V_2O_5/Al_2O_3 catalyst has been studied at elevated temperatures by means of IR spectroscopy and thermal desorption method [2, 11, 13]. In [14], data on the adsorption equilibrium and adsorption thermodynamics in the system constituted by chlorobenzene and 5% V_2O_5/γ-Al_2O_3 at partial pressures of the adsorbate of up to 18 Pa in the temperature range 190–240°C were reported. No studies have been carried out in the practically important temperature range below 100°C. Data on dynamic characteristics of adsorption and catalyst capacity in concentrated gas media, necessary for development of adsorption-catalytic processes, are not available in the literature. The present study was aimed to close this gap.

EXPERIMENTAL

The measurements were made by means of frontal chromatography on a Tsvet-530 chromatograph with a flame-ionization detector, connected to a Power-Graph 2.0 computerized data acquisition unit via E24 analog-to-digital converter (L-card, Moscow). Nitrogen additionally dried with aluminum oxide and CaA zeolite was used as carrier gas. Prior to use, chlorobenzene (analytically pure grade) was dried over a freshly calcined NaA zeolite. A gas–vapor mixture was obtained by passing the carrier gas through a glass saturator thermostated at 0°C. The mass flow rate of chlorobenzene, Q, was found from the loss of mass by the saturator. If Q and the volumetric flow rate of the carrier gas, φ, are known, the chlorobenzene concentration in the gas flow can be calculated by

$$c_0 = Q/\omega.$$

A 1.975-g portion of the catalyst (0.63–0.80-mm fraction) was charged into an absorbing cartridge having the form of a brass tube of length L = 5 cm and inner diameter of 0.9 cm. Before carrying out the ex-

Table 1. Porous structure parameters of the support and catalyst*

Sample	S_{sp}, $m^2\ g^{-1}$	V_{ma}	V_{me}	V_{tot}	Sample	S_{sp}, $m^2\ g^{-1}$	V_{ma}	V_{me}	V_{tot}
		$cm^3\ g^{-1}$					$cm^3\ g^{-1}$		
Al_2O_3	215	0.02	0.63	0.65	V_2O_5/Al_2O_3	213	0.01	0.61	0.62

* S_{sp}, specific surface area; V_{ma}, V_{me}, V_{tot}, specific volumes of macropores, mesopores, and total porosity, respectively; no micropores wee found in the samples studied.

Table 2. Adsorption capacity parameters of the catalyst

T, °C	Volumetric flow rate of the carrier gas, $cm^3\ min^{-1}$	Chlorobenzene concentration in the flow, $g\ dm^{-3}$	a^*_{br}	a_{eq}	θ**
100	31.0	0.0149	0.0164	0.0180	0.21
100	61.1	0.0078	0.0117	0.0137	0.16
100	60.5	0.0151	0.0160	0.0183	0.21
100	93.7	0.0047	0.0082	0.0098	0.11
100	94.0	0.0098	0.0124	0.0148	0.17
50	60.3	0.0149	0.0483	0.0539	0.63
50	92.2	0.0098	0.0410	0.0470	0.55

* Relative standard deviation in measurements of a_{br} and a_{eq} did not exceed 5.5%.

** Surface coverage calculated for a molecular landing area of chlorobenzene equal to 0.465 nm^2 [18].

periments, a sample was conditioned in a flow of the carrier gas at 140°C for 5 h. The catalyst was prepared by deposition of V_2O_5 in an amount of 5% relative to the support mass from an aqueous solution of NH_4VO_3 of pure grade, drying at 100°C, and subsequent calcination in air at 450°C for 5 h. Technical-grade aluminum oxide was used as a support. The parameters of the support and the catalyst, measured by the method of low-temperature adsorption of nitrogen on a Micromeritics ASAP 2400 installation, are presented in Table 1 and Fig. 1.

As a measure of the adsorption activity of a catalyst were used the breakthrough (a_{br}) and equilibrium (a_{eq}) adsorption capacities. The value of a_{br} was calculated from the time at which chlorobenzene appears at the outlet of the absorbing cartridge. The equilibrium capacity was found as the area of the figure delimited by the elution curve plotted in the c–V coordinates and the horizontal line $c = c_0$, where c is the chlorobenzene concentration at the outlet of the absorbing cartridge; c_0, chlorobenzene concentration in the flow; and V, volume of the gas–vapor mixture passed through the absorbing cartridge (c_0 and V at room temperature and normal pressure). In both cases, a correction was made for the dead volume, determined with methane. Each measurement was repeated no less than two times.

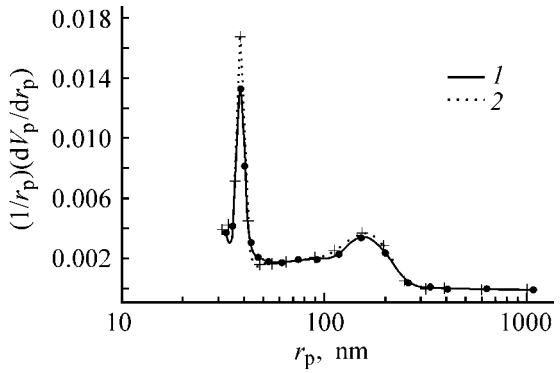

Fig. 1. Pore size distribution for samples of (*1*) catalyst and (*2*) support. (r_p) Pore radius and (V_p) pore volume.

In the adsorption isotherm, the equilibrium concentration c_{eq} reduced to the temperature and average pressure in the absorbing cartridge corresponds to a_{eq}.

As shows comparison of the structural parameters of the support and catalyst, deposition of 5% vanadium oxide does not change the type of the porous structure (the catalyst remains mostly mesoporous), but leads to a slight decrease in the pore volume, with the deposition of vanadium oxide occurring in both macro- and mesopores. According to [15–17], vanadium(V) oxide is deposited on the surface of metal oxide supports in the form of a monolayer.

Table 2 lists the data obtained in measurements of the breakthrough and equilibrium adsorption capaci-

ties. It can be seen that a_{br} is virtually independent of the gas flow rate, but strongly depends on the adsorbate concentration in the gas phase. The equilibrium adsorption capacity exceeds the breakthrough capacity by approximately a factor of 1.15, and this ratio is independent of experimental conditions. Thus, about 13% of the sorbent capacity remains unused in the dynamic mode. On raising the temperature from 50 to 100°C, the sample capacity becomes three times lower, all other conditions being the same.

As follows from Table 2, the reached filling of the catalyst surface is far from the range of monolayer filling, but does not correspond, either, to the linear portion of the adsorption isotherm (Fig. 2).

The data obtained are well linearized in the coordinates of the Langmuir equation. At the same time, it cannot be suggested that the conditions of the Langmuir model (adsorption on a uniform surface) are, indeed, satisfied. This is so because, as demonstrated previously [14], the chlorobenzene adsorption on the V_2O_5/γ-Al_2O_3 catalyst is described at small degrees of filling by the Freundlich adsorption isotherm. Two explanations of this contradiction are possible. The first of these consists in that deviations from the Langmuir model are not noticeable in a narrow range of the data obtained, which covers θ values of 0.11 to 0.21. At the same time, it has been noted [19] that the fraction of highly active adsorption centers on the surface of V_2O_5/γ-Al_2O_3 is small, on the order of 10^{-2}%. After a certain degree of filling is reached, the thermodynamic adsorption parameters start to decrease, as the amount of adsorption increases, at a considerably lower rate. The same conclusion can be based on the results of studies concerned with the adsorption of chlorobenzene and benzene on aluminum oxide and vanadium oxide catalyst [14, 20]. Hence, it seems reasonable to suggest that, after "particularly active" adsorption centers are filled, the surface becomes quasi-uniform and the adsorption equilibrium on such a surface is described by the Langmuir isotherm. It was reported in the review [21] that a phenomenon of this kind is observed in various adsorption systems containing chlorobenzenes and a polar adsorbate (water or pyridine). Pyridine acts as a catalytic poison that blocks strong-adsorption centers, upon which the surface of a solid becomes quasi-uniform and the interaction of the target adsorbate with the adsorbent is described in terms of the Langmuir model.

Lukin and Novosel'skii [22] derived, based on the model of a mixed-diffusion adsorption dynamics, suggested by Akulov and co-authors [23], an expression describing the elution curve in the case of the Langmuir isotherm. This expression has the form of the Shilov equation:

Table 3. Dynamic adsorption parameters at T = 100°C

v,* cm min^{-1}	c,* g dm^{-3}	$K = \Gamma/v$, min^{-1}	K[Eq. (1)], min^{-1}	β_e, s^{-1}	$D \times 10^2$, cm^2 s^{-1}
59	0.0124	15.5	15.5	293	0.30
115	0.0065	11.5	11.4	97	0.29
113	0.0127	8.0	7.9	274	0.40
173	0.0040	8.9	9.0	33	0.36
174	0.0083	6.4	6.4	326	0.37

* Reduced to the temperature and pressure in the absorbing cartridge.

$$t = KL - t_0, \quad (1)$$

where

$$t_0 = K_1 z_1 + K_2 z_2,$$

$$z_1 = \ln(1/y) - 1 + h\ln[(1 - y)/y],$$

$$z_2 = 1.5(1 - y)^{1/3} + y - 1.4 + h\left\{1.5\ln[1 + (1 - y)^{1/3} + (1 - y)^{2/3}] - \sqrt{3}\arctan\{[2(1 - y)^{1/3} + 1)]/\sqrt{3}\} - 0.5 + 3.464\pi\right\},$$

$y = c/c_{eq}$, and h is the parameter of the Langmuir equation written in the dimensionless form:

$$a/a_{eq} = [(1 + h)y]/(h + y).$$

The coefficient K has the same meaning as that in the ordinary Shilov equation and characterizes the mo-

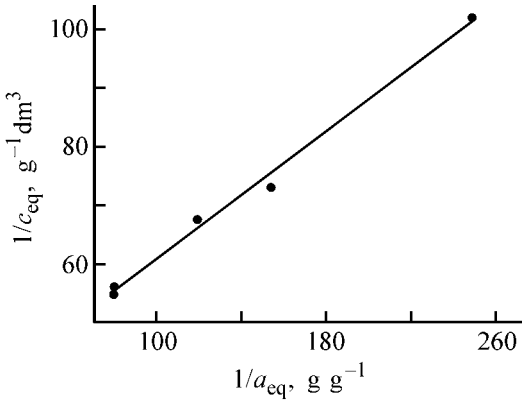

Fig. 2. Isotherm of chlorobenzene adsorption a_{eq} on the V_2O_5/Al_2O_3 catalyst at 100°C. (c_{eq}) Equilibrium adsorbate concentration in the gas phase.

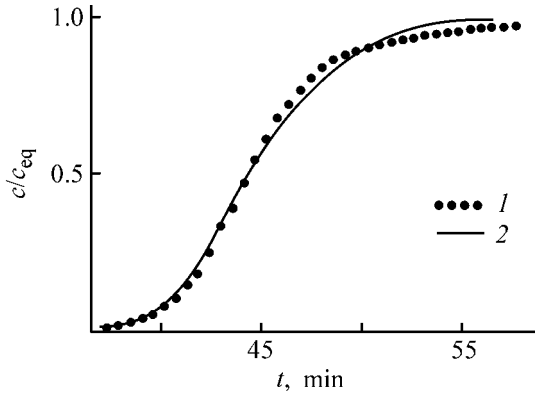

Fig. 3. (*1*) Experimental elution curve and (*2*) that calculated by Eq. (1). T = 100°C, v = 173 cm min^{-1}, c_{eq} = 0.0047 g dm^{-3}. (*c*) Chlorobenzene concentration at the outlet of the absorbing cartridge and (*t*) time.

tion velocity of the adsorption front along the layer. The parameters K_1 and K_2 are related to the external-mass-exchange coefficient β_{ex} and diffusion coefficient D in transport pores and to the catalyst grain radius R by the following expressions

$$K_1 = \Gamma/\beta_e, \quad K_2 = \Gamma R^2/3D.$$

The adsorption coefficient $\Gamma = a'_{eq}/c_{eq}$ is expressed in terms of the adsorption calculated per unit cartridge volume.

Because the dependence of t on variables z_1 and z_2 is linear, the parameters of Eq. (1) can be found by the least-squares procedure and, consequently, the dynamic coefficients can be calculated (Table 3). Figure 3 shows an example of approximation of the experimental data with the theoretical elution curve. The applicability of the model employed is also indicated by the fact that the protective-action coefficients K obtained by regression analysis coincide with their theoretical values $K = \Gamma/v$, where v is the linear flow velocity calculated per full cross-section of the tube.

The coefficient β_e varies within an order of magnitude, commonly has smaller values at lower adsorbate concentrations, and, presumably, is independent of the flow velocity. Close values of the external-mass-exchange coefficient (about 100 s^{-1}) were observed in the case of benzene adsorption on AU-1 and AU-2 carbons under similar experimental conditions [24].

The effective inner-sphere-diffusion coefficient randomly fluctuates around a certain average value, which suggests that concentration-dependent effects, e.g., the surface diffusion [22], exert no influence on the transport within pores. The value of D is approximately two orders of magnitude smaller than that of the "normal" diffusion coefficient of chlorobenzene in nitrogen (D_0 = 0.12 cm^2 s^{-1} as calculated by the Fuller–Schettler–Gidding equation [25]). It was noted in [24] that the D/D_0 ratio approximately gives the specific volume of transport pores, being equal to 3% in the case in question. The so small fraction of transport pores can be understood on the assumption that transport pores are macropores, whereas mesopores have a closed structure. The presence of two peaks in the pore size distribution curve in Fig. 1 does not contradict this assumption.

CONCLUSIONS

(1) The 5% V_2O_5/Al_2O_3 catalyst prepared on an industrial support has high adsorption parameters and can be recommended for adsorption-catalytic purification of gas discharges. The excess of the equilibrium adsorption capacity over the breakthrough capacity is independent, within the range studied, on experimental conditions and is about 13% for the given granulometric composition of the catalyst.

(2) The mixed-diffusion model was successfully used to describe the dynamics of chlorobenzene adsorption, which made it possible to evaluate the coefficients of external mass transfer and transport diffusion. The order of magnitude of the first coefficient is consistent with the known published data on the range of variation of this quantity. The low ratio between the effective diffusion coefficient in transport pores and the normal diffusion coefficient indicates that the volume fraction of transport pores in the samples is small.

ACKNOWLEDGMENTS

The study was supported by the Russian Foundation for Basic Research (grant r-ofi no. 04-03-97502). L.D. Asnin also thanks the Foundation for Support of National Science.

REFERENCES

1. Bertinchamps, F., Gregoire, C., and Gaigneaux, E.M., *Appl. Catal. B*, 2006, vol. 66, pp. 10–22.
2. Krishnamoorthy, S. and Amiridis, M.D., *Catal. Today*, 1999, vol. 51, pp. 203–214.
3. Krishnamoorthy, S., Baker, J., and Amiridis, M.D., *Catal. Today*, 1998, vol. 40, pp. 39–46.
4. Jones, J. and Ross, J.R.H., *Catal. Today*, 1997, vol. 35, pp. 97–105.

5. Krishnamoorthy, S., Rivas, J.A., and Amiridis, M.D., *J. Catal.*, 2000, vol. 193, pp. 264–272.
6. Mori, K. and Inomata, M., *J. Chem. Soc., Faraday Trans. 1*, 1984, vol. 80, pp. 2655–2668.
7. Everaert, K. and Baeyens, J., *J. Hazard. Materials*, 2004, vol. B109, pp. 113–139.
8. Larrubia, M.A. and Busca, G., *Appl. Catal. B*, 2002, vol. 39, pp. 343–352.
9. Jin, L. and Abraham, M.A., *Ind. Eng. Chem. Res.*, 1991, vol. 30, pp. 89–95.
10. Davidenko, I.V., Belokopytov, Yu.V., and Pyatnitskii, Yu.I., *Ukr. Khim. Zh.*, 1991, vol. 57, pp. 18–22.
11. Davidenko, I.V., Davydov, A.A., Pyatnitskii, Yu.I., et al., *Teor. Eksper. Khim.*, 1990, vol. 26, no. 4, pp. 468–473.
12. Ismagilov, Z.R, Shkrabina, R.A., and Koryabkina, N.A., *Alyumooksidnye nositeli: proizvodstvo, svoistva i primenenie v kataliticheskikh protsessakh zashchity okruzhayushchei sredy: Analiticheskii obzor* (Alumina Supports: Manufacture, Properties, and Use in Catalytic Processes for Environment Protection: Analytical Review), Novosibirsk: Inst. Kataliza, Sib. Otd. Ross. Akad. Nauk, 1998.
13. Davidenko, I.V., Davydov, A.A., Pyatnitskii, Yu.I., et al., *Zh. Fiz. Khim.*, 1991, vol. 65, no. 1, pp. 164–169.
14. Asnin, L.D., Fedorov, A.A., Chekryshkin, Yu.S., and Yakushev, R.M., *Zh. Prikl. Khim.*, 2001, vol. 74, no. 9, pp. 1417–1419.
15. *Vanadievye katalizatory okisleniya geterotsiklicheskikh soedinenii* (Vanadium Catalysts for Oxidation of Heterocyclic Compounds), Shimanskaya, M.V., Ed., Riga: Zinatne, 1990.
16. Wachs, I.E., Deo, G., Weckhuysen, B.M., et al., *J. Catal.*, 1996, vol. 161, pp. 211–221.
17. Wachs, I.E. and Weckhuysen, B.M., *Appl. Catal. A*, 1997, vol. 157, pp. 67–90.
18. Nagao, M. and Matsuoka, K., *J. Chem. Soc., Faraday Trans. 1*, 1988, vol. 84, no. 4, pp. 1277–1285.
19. Asnin, L.D., Fedorov, A.A., and Chekryshkin, Yu.S., *Izv. Akad. Nauk, Ser. Khim.*, 2003, no. 4, pp. 845–847.
20. Asnin, L.D. and Fedorov, A.A., *Zh. Prikl. Khim.*, 2003, vol. 76, no. 5, pp. 747–750.
21. Asnin, L.D., Fedorov, A.A., and Chekryshkin, Yu.S., *Khim. Prom–st.*, 2005, vol. 82, no. 11, pp. 529.
22. Lukin, V.D. and Novosel'skii, A.V., *Tsiklicheskie adsorbtsionnye protsessy* (Cyclic Adsorption Processes), Leningrad: Khimiya, 1989.
23. Akulov, A.K., Grebennikov, S.F., and Pakhomov, Yu.I., *Zh. Prikl. Khim.*, 1986, vol. 59, no. 6, pp. 1236–1240.
24. Ustinov, E.A., Polyakov, N.S., Nikolaev, K.M., and Dubinin, M.M., *Izv. Akad. Nauk, Ser. Khim.*, 1981, no. 1, pp. 56–62.
25. Reid, R.G. and Sherwood, T.K., *The Properties of Gases and Liquids*, New York: McGraw–Hill, 1966.

ISSN 1070-4272, Russian Journal of Applied Chemistry, 2007, Vol. 80, No. 2, pp. 268–271. © Pleiades Publishing, Ltd., 2007.
Original Russian Text © D.B. Tagiev, R.V. Starikov, A.A. Imanova, M.I. Rustamov, 2007, published in Zhurnal Prikladnoi Khimii, 2007, Vol. 80, No. 2, pp. 269–272.

CATALYSIS

Isomerization of *n*-Butane on Dealuminated Mordenite Promoted with Zirconium Dioxide

D. B. Tagiev, R. V. Starikov, A. A. Imanova, and M. I. Rustamov

Mamedaliev Institute of Petrochemical Processes, National Academy of Sciences of Azerbaijan, Baku, Azerbaijan

Received June 21, 2006

Abstract—Zirconiun dioxide promotes the catalytic activity of a dealuminated mordenite in *n*-butane isomerization. A method is suggested for preparing, without any solvents, a sulfated mordenite-zirconium catalyst active at relatively low temperatures.

DOI: 10.1134/S107042720702019X

Isomerization of *n*-butane is one of the most important processes of petrochemical industry in production of alkylates and other valuable products [1, 2]. To perform this reaction, different heterogeneous catalysts have been suggested. Among them the chlorinated platinum-alumina catalysts, metallozeolites, and sulfated zirconium dioxide are of particular interest [1–8]. Each of these catalysts has advantages and disadvantages. For instance, chlorinated platinum-alumina catalyst require a thorough pretreatment of the raw material and are environmetally unfavorable. Isomerization with metallozeolites is performed at high temperatures; they are favorable in isomerization of C_5 and C_5–C_6 paraffins. Sulfated zirconium dioxide is active at relatively low temperatures. However, additional studies are required to improve the stability and reproducibility of its catalytic properties.

Due to cellular structure and possibility of purposeful modification of the physicochemical properties, zeolites are promising catalysts for *n*-butane isomerization. It was shown in [9, 10] that dealumination of H-mordenite enchances its isomerization activity. The activity of dealuminated H-mordenite can be further raised by choosing appropriate promoters [11, 12].

In this study, we examined the catalytic properties of binary mordenite-zirconium and ternary sulfated mordenite-zirconium catalysts to find the probable synergism of such systems and to develop on their base low-temperature catalysts of *n*-butane isomerization.

EXPERIMENTAL

The catalysts were prepared from dealuminated H-mordenite with the SiO_2/Al_2O_3 ratio of 17 (sample HM_{17}). To promote HM_{17} with zirconium dioxide, we used impregnation and mechanical mixing of the zeolite with $ZrO(NO_3)_2$ or $ZrO(OH)_2$, with subsequent decomposition of the mixture at 823–873 K [the samples were denoted as $a\,ZrO_2/HM_{17}$ (impregnation) and HM_{17}–$a\,ZrO_2$ (mixing), where a is the ZrO_2 content, wt %]. The samples obtained were sulfated by their treatment with 2 M solution of $(NH_4)_2SO_4$. Catalysts were molded with aluminum hydroxide as a binding agent, dried at 383–393 K, and calcined at 823–873 K.

The conversion of *n*-butane was studied in a flow-type apparatus at atmospheric pressure within the 433–523 K range. A 2 cm^3 portion of cylindrical catalyst granules 1–3 mm in size was charged into a quartz reactor and activated in an air flow at 773 K for 3 h. After the experiments, the catalyst was regenerated under the same conditions. After activation or regeneration, catalysts were cooled in an N_2 flow to the reaction temperature, and *n*-butane was started to be delivered at a flow rate of 300 ml h^{-1}. No carrier gas was used.

The induction period of the reaction was 20–30 min, depending on the experimental conditions. During this time, the isobutane yield reached the maximum and then decreased to a constant value. The data reported in this paper are related to 20th minute of the reaction run. The reaction products were monitored chromatographically, and catalysts, by powder X-ray

diffraction (DRON-3M X-ray diffractometer) and thermal analysis (Q-1500D derivatograph).

Zirconium dioxide synthesized by decomposition of $ZrO(NO_3)_2 \cdot 2H_2O$ and calcination of $ZrO(OH)_2$ hydrogel precipitated with NH_4OH solution shows low activity in *n*-butane isomerization. Sulfation of ZrO_2 preliminarily calcined at 823–873 K does not raise the isobutane yield. The active catalyst is formed after treatment with an $(NH_4)_2SO_4$ solution of $ZrO(OH)_2$ dried at room temperature. In this case, the *n*-butane conversion is 22.0% at 493 K; the yield of isobutane reaches 16.9% (the residue consists of propane and *n*- and isopentanes).

Impregnation of dealuminated mordenite HM_{17} with $ZrO(NO_3)_2$ aqueous solution, with further calcinations at 823 K, substantially improves the catalyst activity, which appears in a rise in the isobutane and isopentane yield and in a decrease in the optimal temperature of the reaction. That is, ZrO_2 has a promoting effect on the activity of dealuminated mordenite.

It should be noted that, in contrast to HM_{17}, whose sulfation does not substantially affect its isomerization activity, $a ZrO_2/HM_{17}$ samples (a = 2.5–10.0 wt %) show after sulfation a higher activity in *n*-butane isomerization at relatively low temperatures. These data show that, in contrast to ZrO_2, which directly promotes HM_{17}, sulfate ions raise the activity of dealuminated mordenite only when the latter contains zirconium dioxide. The data obtained are listed in Table 1.

Depending on the ZrO_2 content in mordenite-zirconium and sulfated mordenite-zirconium catalysts, the *n*-butane conversion and the total yield of isoparaffins (isobutane and isopentane) pass through maxima. As can be seen from the figure, the maximal activity of the catalysts prepared by impregnation is observed for samples containing 5.0–7.5 wt % ZrO_2.

The same extremal dependences are observed for catalysts prepared more simply by mechanical mixing of HM_{17} and $ZrO(NO_3)_2 \cdot 2H_2O$ without any solvent, followed by molding with a binding agent, drying, and calcination. A comparison of samples containing from 5 to 20 wt % ZrO_2 showed that the HM_{17}–10 wt % ZrO_2 catalyst has the highest activity in *n*-butane isomerization. The corresponding data are listed in Table 2.

It should be noted that such an extremal dependence of the activity on the ZrO_2 content is observed for the catalysts prepared by mechanical mixing of HM_{17} with a $ZrO(OH)_2$ hydrogel synthesized by precipitation from $ZrOCl_2 \cdot 8H_2O$ solution with aqueous

Table 1. Isomerization of *n*-butane on mordenite-containing catalysts prepared by impregnation

Catalyst	T, K	*n*-Butane conversion, %	Yield, wt %	
			isobutene	isopentane
HM_{17}	523	28.0	16.1	2.5
$4\% SO_4^{2-}/HM_{17}$	523	28.2	15.4	3.7
$27\% SO_4^{2-}/ZrO_2$	493	22.0	16.9	2.4
$5\% ZrO_2/HM_{17}$	493	30.0	18.5	3.0
$4\% SO_4^{2-}/5\% ZrO_2/HM_{17}$	463	34.5	21.3	4.0

Table 2. Isomerization of *n*-butane on mordenite-zirconium catalysts prepared by mechanical mixing of HM_{17} and $ZrO(NO_3)_2 \cdot 2H_2O$

Sample no.	Catalyst	T, K	*n*-Butane conversion, %	Yield, wt %	
				isobutene	isopentane
1	HM_{17}	493	24.5	12.0	0.6
2	HM_{17}–5% ZrO_2	493	48.2	25.9	3.1
3	HM_{17}–10% ZrO_2	463	12.7	9.1	1.6
		493	54.5	28.5	5.3
4	HM_{17}–15% ZrO_2	463	3.0	2.6	–
		493	52.7	25.5	3.4
5	HM_{17}–20% ZrO_2	493	33.5	19.9	4.6
6	HM_{17}–$ZrO(OH)_2$ (as calculated for 10% ZrO_2)	463	5.8	4.5	0.6
		493	31.8	20.2	2.9
7	ZrO_2	493	0.9	0.5	–

NH_4OH. However, at the same ZrO_2 content, the activity of catalysts prepared using a zirconium salt (Table 2, sample 3) is higher than the activity of

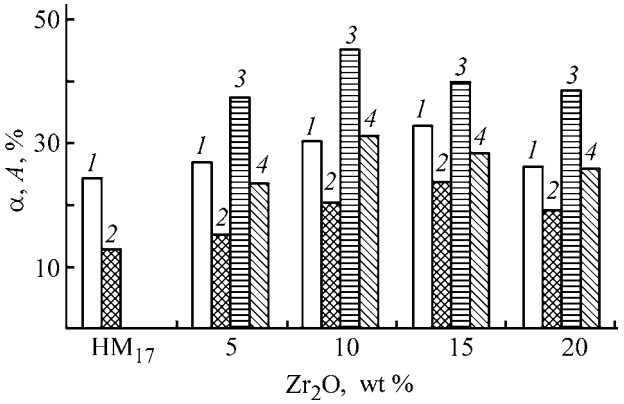

(*1*, *3*) conversion α of *n*-butane and (*2*, *4*) total yield of isoparaffins A vs. the ZrO_2 content in (*1*, *2*) $a ZrO_2/HM_{17}$ and (*3*, *4*) $4\% SO_4^{2-}/a ZrO_2/HM_{17}$ catalysts.

Table 3. *n*-Butane conversion in an apparatus with two series-connected reactors (catalyst HM_{17}–10% ZrO_2–4% SO_4^{2-})

Temperature, K		*n*-Butane conversion, %	Yiels, %	
reactor 1	reactor 2		isobutene	isopentane
448	–	8.9	7.4	0.2
463	–	36.3	19.2	2.3
493	–	51.6	26.0	4.9
448	463	37.2	25.3	3.4
463	463	43.9	28.9	4.1

the sample prepared from ZrO(OH) hydrogel (Table 2, sample 6).

The difference in the properties of mordenite-zirconium catalysts prepared by impregnation or mechanical mixing is also manifested in that sulfation of impregnated catalysts $a ZrO_2/HM_{17}$ calcined at 823 K raised their activity, while sulfation of the HM_{17}–$a ZrO_2$ (mixed catalysts) samples calcined at the same temperature does not substantially affect the activity.

The three-component catalyst HM_{17}–10% ZrO_2–4% SO_4^{2-} prepared by simultaneous mixing of HM_{17}, $ZrO(NO_3)_2 \cdot 2H_2O$, and $(NH_4)_2SO_4$ followed by thermal treatment under the above standard conditions has a higher isomerization activity. At 463–493 K, the yield of isobutane and isopentane on this catalyst was 19.2–26.0 and 2.3–4.9%, respectively, at an *n*-butane conversion of 36.3–51.6%. The yield of the main by-product of the reaction, propane, decreases substantially faster as compared to the isobutane yield, and the selectivity of the reaction correspondingly increases.

Taking into account the data obtained, we studied the conversion of *n*-butane on a catalytic apparatus with two series-connected reactors. In this case, a higher yield of isoparaffins and selectivity can be reached at lower temperatures. The data on *n*-butane conversion and the yield of isoparaffins after the first and second reactors at various temperatures are listed in Table 3. As seen, the yield of isobutane in the two-reactor system at 448–463 K increases to 25.3–28.9% at a small decrease in the isopentane yield. The reaction selectivity with respect to isoparaffins increases to 75% due to a substantial decrease in the propane yield. These results are of certain interest because the catalyst used contained no precious metals (Pt, Pd) and was prepared by a simple and convenient method at atmospheric pressure and without any carrier gas. Such catalysts can be used as a basis for preparation of more active catalysts for isomerization of *n*-paraffins.

The high catalytic activity of sulfated ZrO_2 promoted with various metals (Mn, Fe, Ga, Pt, etc.) was discussed in a number papers [6–8, 13–17]. In this study, we showed that zirconium compounds promote the activity of dealuminated mordenite, whereas sulfation does not affect isomerization activity of mordenite itself, but substantially improves that of the mordenite-zirconium catalysts. This fact suggests that the promoting effect of sulfate ions is caused by the presence of ZrO_2 in the catalysts. At the same time, it should be noted that dealuminated mordenite is not only a support for ZrO_2 and SO_4^{2-}, but is the dominating component of the mordenite-zirconium catalysts, as indicated by the attainment of the maximal catalytic activity at small concentrations of ZrO_2 and SO_4^{2-} and by the preservation of the same features of the reaction before and after promotion of HM_{17}. The parallel variation of the yields of propane, isobutane, and isopentane with time can be caused by the bimolecular mechanism of the reaction. However, this matter requires a further study.

The thermal analysis of the systems HM_{17}, 5% ZrO_2/HM_{17} and 4% SO_4^{2-}/5% ZrO_2/HM_{17} and of samples prepared by mechanical mixing (HM_{17}–10% ZrO_2 and HM_{17}–10% ZrO_2–6% SO_4^{2-}) does not show any substantial difference in their thermal behavior. Only one endothermic peak at 388 K, caused by elimination of adsorbed water, exists in the DTA curve of HM_{17}. After impregnation of HM_{17} with $ZrO(NO_3)_2$, this peak shifts to 398 K and a weak endothermic peak appears at 628 K.

These facts are probably caused by dehydration and decomposition of the zirconium salts. The high-temperature peaks of sulfate decomposition were not found, probably, because of the small amounts of sulfate groups in the samples examined.

The X-ray diffraction patterns show that the crystal structure of H-mordenite is preserved after dealumination and promotion with zirconium dioxide. In the diffraction patterns of a powder with the composition 7.5% ZrO_2/HM_{17} and ZrO_2, prepared by decomposition of $ZrO(NO_3)_2 \cdot 2H_2O$ at 873 K, reflections characteristic of tetragonal ZrO_2 at $2\theta = 30^\circ$ were observed [18]. Based on the data obtained, we can suggest that impregnation of HM_{17} with a $ZrO(NO_3)_2$ aqueous solution, followed by thermal treatment at 823–873 K, yields a mixed mordenite-zirconium system with a higher isomerization activity at relatively low temperatures because of the interaction between the decomposing zirconium salt and HM_{17}. This process affects the specific texture and acid–base properties of the catalytic mixture.

CONCLUSIONS

(1) The promoting effect of ZrO_2 on the catalytic activity of dealuminated mordenite in isomerization of *n*-butane was found.

(2) It was shown that the sulfated mordenite-zirconium catalyst prepared by a simple and convenient method shows high activity in *n*-butane isomerization at atmospheric pressure and relatively low temperatures.

REFERENCES

1. Egizarov, Yu.G., Savchits, M.F., and Ustilovskaya, E.Ya., *Geterogenno-kataliticheskaya isomerizatsiya uglevodorodov* (Heterogeneous Catalytic Isomerization of Hydrocarbons), Moscow: Nauka i Tekhnika, 1989.
2. Yadav, G.D. and Nair, J.J., *Microporous Mesi Mater.*, 1999, vol. 3, no. 1, pp. 1–11.
3. Tran, M.-T., Gnep, N.S., Szabop, G., and Guisnet, M., *Appl. Catal. A.*, 1998, vol. 170, no. 1, pp. 49–58.
4. Gembicki, S.A., *Stud. Surf. Sci. Catal.*, 2000, vol. 130, pp. 147–154.
5. Willegas, J.I., Kumar, N., Smeiskova, A., et al., *Appl. Catal. A.*, 2005, vol. 284, nos. 1–2, pp. 223–230.
6. Sony, X. and Sayari, A., *Catal. Rev. Sci. Eng.*, 1996, vol. 38, p. 239–412.
7. De Rossi, S., Ferraris, G., Valigi, M., and Gazroli, D., *Appl. Catal. A*, 2002, vol. 231, nos. 1–2, pp. 173–184.
8. Li, X., Nagoaka, N., Simon, L.J., et al., *J. Catal.*, 2005, vol. 232, no. 2, pp. 456–466.
9. Ganizares, P., de Lukas, A., and Dorado, F., *Appl. Catal. A*, 200, vol. 196, no. 2, pp. 225–231.
10. Tagiev, D.B., Starikov, R.V., Imanova, A.A., et al., *Protsessy Neftekhim. Neftepererab.*, 2004, no. 2, pp. 103–107.
11. Tagiyev, D.B., Starikov, R.V., and Imanova, A.A., Abstracts of Papers. *3rd FEZA Conf.*, Prague, 2005, p. 166.
12. Tagiev, D.B., Starikov, R.V., Imanova, A.A., et al., *Protsessy Neftekhim. Neftepererab.*, 2004, no. 3, pp. 75–80.
13. Keiich, N., Akihoro, O., and Kaoru, F., *Appl. Catal. A*, 2000, vol. 195, pp. 383–393.
14. Moreno, J.A.and Poncelet, D., *Appl. Catal. A*, 2001, vol. 210, nos. 1–2, pp. 151–164.
15. Hua, W. and Sommer, J., *Appl. Catal. A*, 2002, vol. 227, nos. 1–2, pp. 279–286.
16. Wong, S.-T., Li, T., Cheng, S., et al., *Appl. Catal. A*, 2005, vol. 296, no. 1, pp. 90–99.
17. Li, X., Nagaoka, K., Simon, L.J., et al., *J. Catal.*, 2005, vol. 232, no. 2, pp. 456–466.
18. Morterra, C., Cerrato, G., Pinna, F., and Signoretto, M., *J. Catal.*, 1995, vol. 157, no. 1, pp. 109–123.

ISSN 1070-4272, Russian Journal of Applied Chemistry, 2007, Vol. 80, No. 2, pp. 272–274. © Pleiades Publishing, Ltd., 2007.
Original Russian Text © I.S. Faizrakhmanov, L.F. Zainullina, R.F. Talipov, A.Kh. Sharipov, 2007, published in Zhurnal Prikladnoi Khimii, 2007, Vol. 80, No. 2, pp. 273–275.

CATALYSIS

Oxidation of Organic Sulfides with Atmospheric Oxygen in the Presence of Phthalocyanine Complexes as Catalysts

I. S. Faizrakhmanov, L. F. Zainullina, R. F. Talipov, and A. Kh. Sharipov

Bashkir State University, Ufa, Bashkortostan, Russia

Institute of Petrochemistry and Catalysis, Ufa Research Center, Russian Academy of Sciences, Bashkortostan, Russia

Received March 29, 2006; in final form, September 2006

Abstract—Catalytic oxidation of a mixture of low-molecular-weight sulfides with atmospheric oxygen was studied. The catalytic activity of poly(cobalt phthalocyanine) in this process is higher than that of monomeric cobalt phthalocyanine.

DOI: 10.1134/S1070427207020206

The use of the gas condensate of the Karachagansk deposit in natural gas processing increased the sulfur content in the isopentane and pentane fractions to 0.02 and 0.2 wt %, respectively [1]. The total sulfur content of the isopentane and pentane fractions used in production of synthetic rubbers should not exceed 0.003 and 0.01 wt %, respectively [2].

An analysis of pentanes for sulfur-containing compounds showed the presence of mercaptans and sulfides [1]. The mercaptan fraction consists mainly of ethyl isopropyl, and butyl mercaptans. The sulfide fraction contains dimethyl sulfide as the major component and a minor amount of methyl ethyl sulfide.

One of the procedures for removing sulfur-containing compounds is their catalytic oxidation with atmospheric oxygen [2]. Therefore, a search for effective catalysts for this reaction is a topical problem.

EXPERIMENTAL

The amount of sulfide sulfur in the pentane–isopentane fractions ranges from 35 to 50 wt % relative to the total sulfur content [3]. The efficiency of desulfurization by alkali treatment and demercaptanization in the presence of cobalt disulfophathalocyanine decreases when both sulfides and mercaptan are present in the substrate [4]. We studied comparatively the oxidation of a mixture of sulfur-containing compounds in the presence of cobalt(II) phthalocyanine [PhCo(II)] and its polymer [PPcCo(II)] as catalysts. For this purpose, we used isooctane solutions of a mixture of sulfides with a sulfide sulfur content of 0.052–0.059 wt % and of a sulfide-mercaptan mixture with a mercaptan sulfur content of up to 0.055 wt %. The phthalocyanine complexes were used in the form of a suspension or a solution in aqueous sodium hydroxide. The PPcCo(II) and PcCo(II) concentration in the alkaline solution was 0.025 and 0.033 wt %, respectively. A suspension or a solution (50 ml) of the phthalocyanine complex and a solution of sulfur-containing compounds in isooctane (100 ml) were placed in a 250-ml conical flask. Air was bubbled through a glass tube. The mixture was vigorously stirred for 30 min at 40°C and then the sulfide sulfur content in isooctane was determined.

Sulfur-containing compounds were analyzed by gas chromatography–mass spectrometry on a Finnigan 4021 spectrometer. The total sulfur content of the pentane–isopentane fraction was determined in accordance with GOSTs (State Standards) 22986–78 and 13380–81. The experimental results are presented in Table 1. It is seen that PPcCo(II) is a more efficient catalyst for oxidation of low-molecular-weight sulfides that PcCo(II). At the same time, the catalytic activity of poly(metal phthalocyanines) (PPcM) in oxidation may be lower, higher, or equal to that of the monomers (PcM) [5]. The reasons for this phenomenon were not understood. However, the catalytic activity of PPcM was believed to be due to structural features of the intermediates and to the influence of the reaction medium.

Because the PcM–S bond formed by σ electrons of the sulfur atom and donation of d_π-electrons of the metal ion to the unoccupied σ-orbital of the sul-

Table 1. Oxidation of sulfides and sulfide–mercaptan mixtures in the presence of cobalt(II) phthalocyanines

Sulfide	Initial S^{2-} content, wt %	PcCo(II)		PPcCo(II)	
		S^{2-} content after oxidation, wt %	conversion of S^{2-}, %	S^{2-} content after oxidation, wt %	conversion of S^{2-}, %
Sulfide					
Dimethyl sulfide	0.0592	0.0370	37.5	0.0105	82.2
Methyl ethyl sulfide	0.0584	0.0382	34.5	0.0126	78.4
Diethyl sulfide	0.0575	0.0387	32.7	0.0132	77.0
Sulfide–mercaptan					
Dimethyl sulfide	0.0592	0.0299	49.5	0.0017	97.1
Methyl ethyl sulfide	0.0584	0.0312	46.5	0.0028	95.2
Diethyl sulfide	0.0575	0.0356	38.0	0.0027	95.3

fur atom is strong [6, 7], the PcM–$S(CH_3)_2$ complex should be stable. In the presence of molecular oxygen a PcM–$S(CH_3)_2$–O_2 complex can be formed. Decomposition of this complex yields the initial catalyst and dimethyl sulfoxide.

The high catalytic activity of PPcCo(II) in oxidation of sulfides by atmospheric oxygen can be due to an undistorted planar structure of the phthalocanine rings in the polymeric chain and, hence to a higher stability of intermolecular complexes of PPcCo(II) as compared to those of PcCo(II) [5]. It should be noted that the degree of sulfide oxidation catalyzed by both PPcCo(II) and PcCo(II) increases in the presence of mercaptans, which can be probably due to involvement of mercaptans and their derivatives in the formation of the intermolecular complexes [7–9].

Based on the experimental results, we developed an industrial installation for removal of sulfur-containing compounds from the pentane–isopentane fraction in the presence of PPcCo(II) (see figure). Raw material, stabilized sulfurous naphtha (C_5–C_6 fraction), is fed by a pump *2* from receiver *1* to a preliminary washing column *3*. The column is washed with 6% NaOH solution to remove traces of hydrogen sulfide. The prewashed petrol (100 volumes) is mixed with 6–10% NaOH solution (12–15 volumes). The mixture is bubbled with air using a compressor *4* and then is fed into a mixer *6* equipped with nine flow-measuring diaphragms. The turbulence produced in the course of passage of the naphtha, alkali, and air through the diaphragm holes provides a good contact between these components. Mercaptan passes into the alkaline solution and is oxidized to the disulfide [1, 2] which is extracted into the hydrocarbon phase. Sulfides are oxidized mainly to the corresponding sulfoxides. Since low-molecular-weight sulfoxides are readily soluble in water, the major portion of these compounds formed in the system passes into the alkaline solution. The residence time of the system in the mixer is sufficient for the reaction completion. The reaction mixture is fed from the mixer to a settler *7* where the sodium hydroxide solution is separated and recycled with a pump *8* to mixer *6*. The NaOH

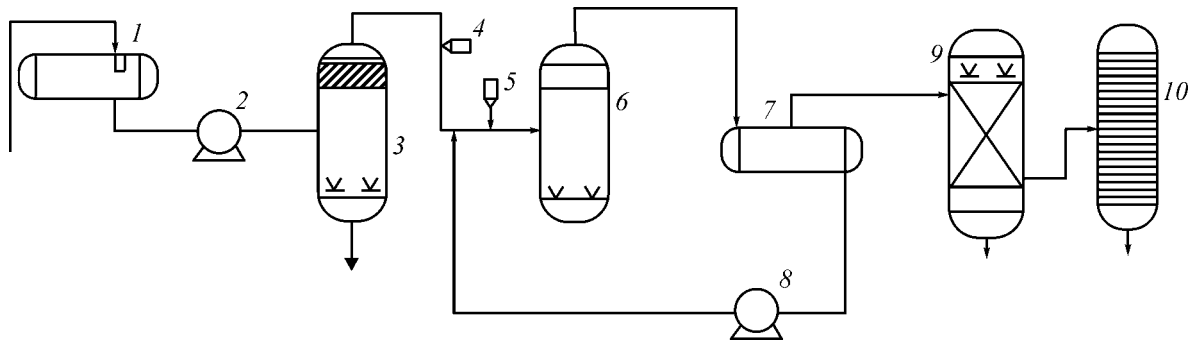

Scheme of an installation for catalytic oxidation of sulfur-containing compounds of the pentane–isopentane fractions with atmospheric oxygen: (*1*) receiver for raw material, (*2*, *8*) pump, (*3*) column for preliminary alkali washing, (*4*) compressed air, (*5*) vessel with catalyst, (*6*) mixer, (*7*) settler for alkali, (*9*) sand filter, and (*10*) distillation column.

Table 2. Distributiion of DMSO between hydrocarbon and aqueous phases (initial aqueous phase: 10% NaOH solution)

DMSO concentration in initial solution, wt %	Hydrocarbon : aqueous solution weight ratio	Hydrocarbon	Total sulfur content of the hydrocarbon phase, wt %
1	1 : 3	*n*-Hexane	0.0012
25	1 : 3	″	0.0029
50	1 : 3	″	0.0082
5	1.4 : 1	Isopentane	0.0007
9	1.3 : 1	″	0.0016
20	1.2 : 1	″	0.0024
33	1 : 1	″	0.0020
19	1.1 : 1	″	0.0025

solution circulating through the mixer contains 0.01–0.005 wt % PPcCo(II). This complex is added from a vessel *5* at regular intervals.

To remove traces of the alkali emulsion, the hydrocarbon fraction is passed through filter *9*. Then the hydrocarbon fraction containing oxidized sulfur compounds is fed into a distillation column *10* (15 TP, reflux ratio 3). Pentane and isopentane fractions are taken from the top of the column. The total sulfur content in these fraction meets the requirements of TU (Technical Specifications) 38.101 790–79.

The boiling points of the oxidation products, disulfides and sulfoxides, are higher than those of the initial mercaptans and sulfides and, hence, these products can be separated by distillation. Low-boiling sulfoxides (C_5–C_6) are readily soluble in water and are removed by washing.

The main sulfur-containing compound present in the pentane fraction examined, dimethyl sulfide, is oxidized to dimethyl sulfoxide. Dimethyl sulfoxide can be distributed between the aqueous alkali and the hydroxarbon fraction. Dimethyl sulfoxide (DMSO) can be accumulated in the aqueous phase in the course of multiple circulation of the oxidizing agent. Hence, its content in the hydrocarbon fraction should also increase. To determine the maximal DMSO content of the aqueous phase, we studied phase equilibria in the hydrocarbon–DMSO–NaOH solution system. Hydrocarbons were isopentane and *n*-hexane. The DMSO distribution was estimated from the total sulfur content in the hydrocarbon fraction.

The experimental results listed in Table 2 show that, even at a very high concentration of DMSO in the aqueous phase, the total sulfur content of the hydrocarbon fraction is not higher than hundredth of a persent. The distribution coefficient of DMSO between the aqueous and hydrocarbon fractions is 100. Thus, isopentane meeting the TU can be obtained at the DMSO content in the aqueous phase lower than 10%.

CONCLUSIONS

(1) It was shown that the catalytic activity of poly(cobalt(II)phthalocyanine) in oxidation of a sulfide mixture by atmospheric oxygen is higher than that of monomeric cobalt(II) phthalocyanine. The conversion of a sulfide mixture increases in the presence of mercaptans.

(2) A flow sheet was developed for removal of sulfur-containing compounds from pentane–isopentane fractions by oxidation with atmospheric oxygen in the presence of poly(cobalt(II) phthalocyanine).

REFERENCES

1. Sharipov, A.Kh., Kolychev, V.M., Faizrakhmanov, I.S., Abstracts of Papers, *18-ya Vserossiskaya konferentsiya po khimii i tekhnologii organicheskikh soedinenii sery* (18th All-Russian Conf. on Chemistry and Technology of Organosulfur Compounds), Kazan: VNIIUS, 1992, part 4, p. 236.
2. Mazgarov, A.M., Akhmadullina, A.G., Tukov, V.G., et al., *Neftepererab. Neftekhim.*, 1975, no. 5, p. 28.
3. Faizrakhmanov, I.S., Oxidation of Sulfides in Oil and Gas Condenstae, *Cand. Sci. Dissertation*, Ufa, 1992.
4. Sharipov, A.Kh., Kolychev, V.M., Faizrakhmanov, I.S., Abstracts of Papers, *18-ya Vserossiskaya konferentsiya po khimii i tekhnologii organicheskikh soedinenii sery* (18th All-Russian Conf. on Chemistry and Technology of Organosulfur Compounds), Kazan: VNIIUS, 1992, p. 290.
5. Berezin, B.D., *Koordinatsionnye soedineniya porfirinov i ftalotsianina* (Coordination compounds of Porphyrins and Phthalocyanins), Moscow: Nauka, 1978.
6. Galderazzo, F., Pampaloni, G., Vitali, D., et al., *J. Chem. Soc., Dalton Trans.*, 1980, no. 10, pp. 1965–1969.
7. Borisenkova, S.A., *Neftekhimiya*, 1991, vol. 31, no. 3, pp. 391–408.
8. Akhmadullina, A.G., Orlova, L.N., Khrushcheva, I.K., et al., *Zh. Prikl. Khim.*, 1989, vol. 62, no. 1, pp. 53–57.
9. Ovsyannikova, L.V., Digurov, N.G., Mazgarov, A.M., et al., *Zh. Prikl. Khim.*, 1986, vol. 59, no. 4, pp. 830–834.

ISSN 1070-4272, Russian Journal of Applied Chemistry, 2007, Vol. 80, No. 2, pp. 275–278. © Pleiades Publishing, Ltd., 2007.
Original Russian Text © A.A. Solov'ev, M.A. Pashina, O.E. Lebedeva, 2007, published in Zhurnal Prikladnoi Khimii, 2007, Vol. 80, No. 2, pp. 276–279.

ORGANIC SYNTHESIS AND INDUSTRIAL ORGANIC CHEMISTRY

Oxidative Destruction of Dinitrophenols by Fenton's Reagent in the Presence of Inorganic Salts

A. A. Solov'ev, M. A. Pashina, and O. E. Lebedeva

Belgorod State University, Belgorod, Russia

Received August 3, 2006

Abstract—The influence of inorganic salts on the kinetics of oxidation of 2,4- and 2,6-dinitrophenols by Fenton's reagent, hydrogen peroxide, in the presence of iron(II) ions was studied.

DOI: 10.1134/S1070427207020218

Nitro derivatives of phenol are basic chemicals in production of some dyes and explosives and are widely used in agriculture as compounds having a multipurpose pesticide effect. However, by their toxicity for warm-blooded animals, compounds of the nitrophenol series are offensive and highly toxic substances with a cumulative effect. Water treatment to remove nitro derivatives of phenol is an important environmental problem.

Complete oxidation of organic contaminants (so-called mineralization) is considered to be the most reliable procedure of their inactivation. Oxygen, ozone, and hydrogen peroxide can serve as oxidants [1]. Hydrogen peroxide is an environmentally safe oxidant convenient in use. However, its oxidizing potential is insufficient to oxidize many persistent contaminants. More effective are oxidizing systems in which radical species are generated from H_2O_2. The best known system is Fenton's reagent: hydrogen peroxide in combination with iron(II) ions. Hydroxy radicals are formed by the scheme [2]

$$Fe^{2+} + H_2O_2 \rightarrow Fe^{3+} + OH^{\cdot} + OH^{-}.$$

Along with organic contaminants, inorganic salts, such as chlorides, sulfates, nitrates, and phosphates, are present in natural and waste water. However, only several studies have been devoted to the influence of these salts on the Fenton process, and only low concentrations of salts have been examined. For example, phenol, 2-chlorophenol, and 2-nitrophenol were oxidized with Fenton's reagent in solutions of sodium chloride and sulfate; the concentrations of salts did not exceed 20 mM [3]. The influence of inorganic ions on the oxidation of phenol was studied in [4]; the concentration of anions was 100 mg l^{-1}.

Here we studied mineralization of 2,4- and 2,6-dinitrophenols with Fenton's reagent in the presence of high concentrations of inorganic salts.

EXPERIMENTAL

We used 2,4- and 2,6-dinitrophenols of analytically pure grade without additional purification.

In all experiments, we studied the oxidation of 2,4- and 2,6-dinitrophenols at 23°C in an aqueous solution with a volume of 25 ml. The substrate concentration was constant and equal to 0.25 mM. Calculated amounts of H_2O_2 and $FeSO_4$ solutions were added to the test solution. The H_2O_2 concentration was varied from 4 to 16 mM, and the $FeSO_4$ concentration, from 0.125 to 0.5 mM. The experiment was carried out during for 60 min. The course of the process was monitored by measuring the optical density of the solution on a KFK-3-01 photometer at a wavelength of 345 nm. The pH was measured with a Mettler Toledo pH meter. In all runs, the pH value was kept equal to 3.0.

The initial pH value is one of the key parameters in the optimization of processes in the system H_2O_2–Fe^{2+}–substrate. Oxidation of most of organic compounds, among them such stable as chlorophenols, under the action of Fenton's reagent proceeds more efficiently at the initial pH 2.7–3.5 [5–9]. The dependence observed is caused by the influence of acidity on the rate of H_2O_2 decomposition and on the state of iron(II) ions in the solution and, hence, on their catalytic characteristics.

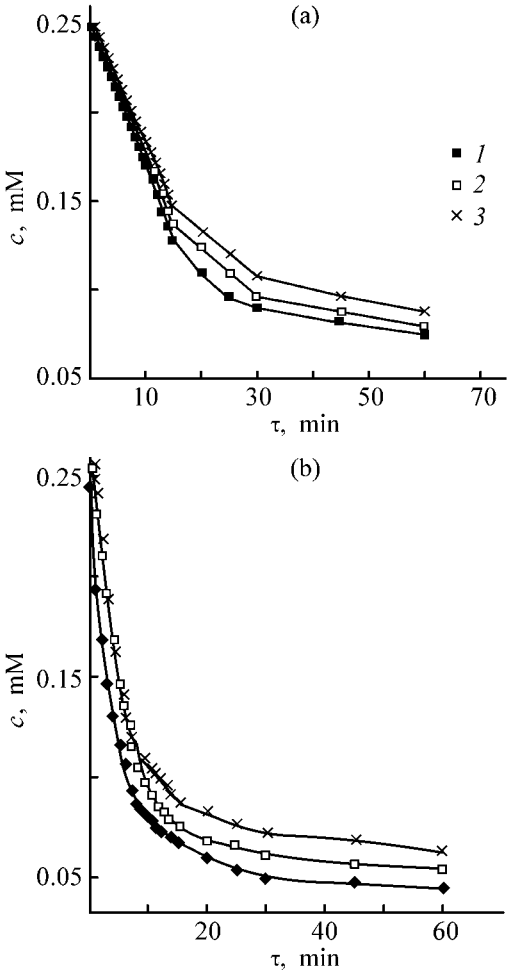

Fig. 1. Variation of the concentration c of (a) 2,4-dinitrophenol and (b) 2,6-dinitrophenol in the course of oxidation by Fenton's reagent in aqueous solutions of sodium nitrate. (τ) Time; the same for Fig. 2. Concentration of $NaNO_3$, mM: (*1*) 0, (*2*) 0.1, and (*3*) 1.0.

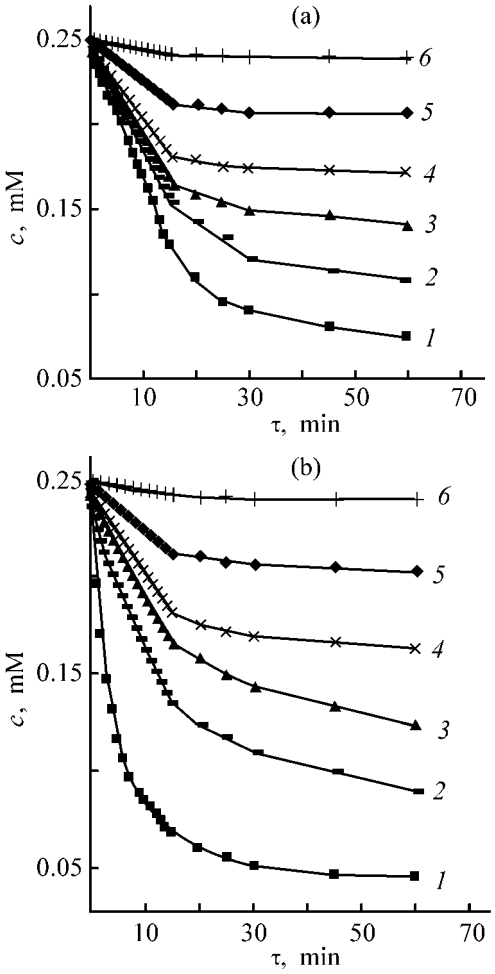

Fig. 2. Variation of the concentration c of (a) 2,4-dinitrophenol and (b) 2,6-dinitrophenol in the course of oxidation by Fenton's reagent in aqueous solutions of sodium chloride. Concentration of NaCl, mM: (*1*) 0, (*2*) 0.1, (*3*) 0.3, (*4*) 0.5, (*5*) 0.7, and (*6*) 1.0.

In the first series of experiments, we determined the optimal conditions of decomposition of dinitrophenols and the concentrations of H_2O_2 and iron(II) ions, because the oxidation mechanism depends on the $H_2O_2 : Fe^{2+}$: substrate ratio [10]. The experimental results showed that the optimal concentration of H_2O_2 for decomposition of dinitrophenols is 8 mM at a Fe^{2+} concentration of 0.25 mM. These conditions were maintained in all the subsequent experiments when studying the influence of inorganic salts on the decomposition of dinitrophenols.

It should be noted that the assortment of salts that can be used in the study is rather narrow, since organic anions are excluded due to ease of their oxidation by Fenton's reagent and fluorides, phosphates, and other anions of weak inorganic acids or acids of medium strength shift the solution pH to the alkaline region, making Fenton's reagent inefficient. In this context we used salts of strong acids.

The kinetic curves of oxidation of dinitrophenols by Fenton's reagent in 0.1 and 1 M $NaNO_3$ aqueous solutions are shown in Figs. 1a and 1b. The curves obtained do not significantly depart from the curves of oxidation of the corresponding substrates in distilled water. Ammonium nitrate does not affect the oxidation of dinitrophenols either. The kinetic parameters typical for the process in distilled water are kept in the presence of 0.1–1.0 M NH_4NO_3.

A different situation arises with addition of chloride ions into the solution. As can be seen from Figs. 2a and 2b, the rate of oxidation of dinitrophe-

nols in the presence of NaCl significantly decreases, whereas in an 1 M NaCl solution, the substrates are not oxidized: the concentrations of dinitrophenols do not noticeably vary.

Figures 2a and 2b show that, as the NaCl concentration increases, the kinetics parameters of the process regularly vary. The initial rate of the process and the final degree of conversion depend linearly on the NaCl concentration, with the linear dependence observed for both dinitrophenols (Figs. 3a, 3b).

It can be assumed that chloride ions, rather than sodium ions, are the main inhibiting species, because $NaNO_3$ does not exhibit this effect. Substitution of Cs^+ ions for Na^+ ions does not essentially alter the influence of the salt on the course of the process. The curves obtained in the presence of CsCl are similar to those obtained with of NaCl. Data for CsCl are described by the same linear dependence as that in the case of NaCl.

To explain the results obtained, it necessary, first and foremost, to check whether H_2O_2 is consumed in side processes, including those involving trace contaminants. The experiment showed that the H_2O_2 concentration in NaCl solutions without dinitrophenols and iron(II) ions remains constant for a long time.

According to published data, one of the reasons why anions affect the oxidation by Fenton's reagent is that iron complexes are formed. It was appropriate to study one more anion able to form complexes. The next series of experiments was performed in solutions of sodium sulfate. We revealed no noticeable inhibiting effect of sodium sulfate similar to that of chloride ions. The resulting kinetic curves do not significantly depart from the curve of oxidation of the corresponding substrate by Fenton's reagent in distilled water.

A more probable assumption is that chloride ions are oxidized by Fenton's reagent in the systems studied in parallel with oxidation of dinitrophenol. It has been noted that Fenton's reagent has a high redox potential (2.8 V [11]).

It should be noted that Bali and Catalkaya [4] studied only low concentrations of anions (1–3 mM) and reported only the inhibiting effect of phosphate ions, byt no noticeable influence of chloride or sulfate ions on phenol oxidation by Fenton's reagent was not revealed.

The nature of the cation of an inorganic salt does not affect the oxidation of dinitrophenols. It is likely that, in these studies, ammonium cations are not oxidized or are extremely weakly oxidized by Fenton's reagent, even though ammonium is a possible reducing agent similarly to chloride ions. In any case, the presence of NH_4NO_3 in the system does not affect the course of oxidation of dinitrophenols.

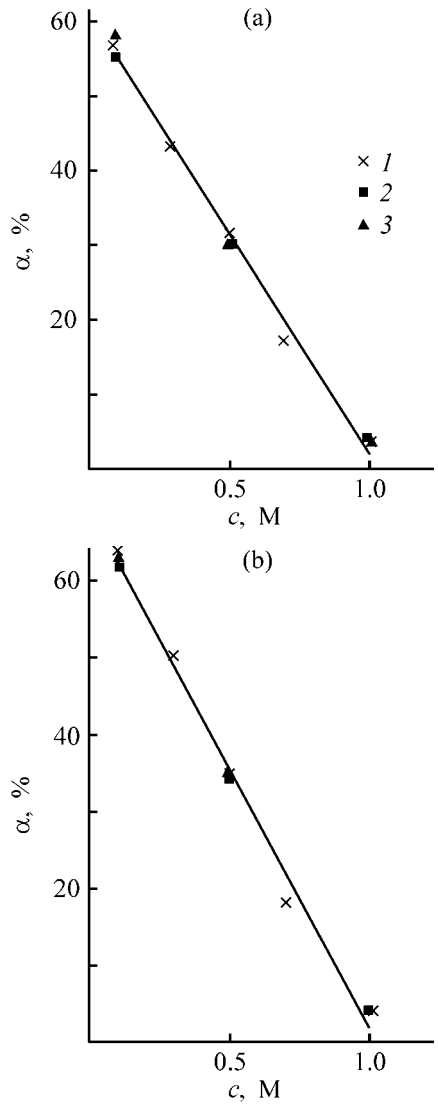

Fig. 3. Degree of conversion α of (a) 2,4-dinitrophenol and (b) 2,6-dinitrophenol in oxidation by Fenton's reagent for 60 min vs. salt concentration *c*. Salt: (*1*) NaCl, (*2*) NH_4Cl, and (*3*) CsCl.

The reducing power of ammonium ions is not manifested when they are added to the system in the form of ammonium chloride. Oxidation of dinitrophenols is inhibited at the same concentrations as in the case of sodium and cesium chlorides, i.e., inhibition is caused by the presence of chloride ions. Data for NH_4Cl are described by the same dependence as data obtained for sodium and cesium chlorides.

CONCLUSIONS

(1) 2.4- and 2,6-Dinitrophenols are oxidized by Fenton's reagent in the presence of inorganic salts under comparable conditions. Sodium, cesium, and ammonium cations, as well as nitrate and sulfate anions, do not noticeably affect the oxidation of dinitrophenols.

(2) The presence of impurities of fluoride, phosphate, and other anions of weak acids or acids of medium strength in water shifts the solution pH to the range in which Fenton's reagent is ineffective.

(3) The presence of chloride ions in water inhibits the oxidation of dinitrophenol by Fenton's reagent, probably due to a competing oxidation of chloride ions.

REFERENCES

1. Dolgoplosk, B.A. and Tinyakova, E.I., *Generirovanie svobodnykh radikalov i ikh reaktsii* (Generation of Free Radicals and Their Reactions), Moscow: Nauka, 1982.
2. Sychev, A.Ya. and Isak, V.G., *Gomogennyi kataliz soedineniyami zheleza* (Homogeneous Catalysis with Iron Compounds), Chisinau: Shtiintsa, 1988.
3. Siedlecka, E.M. and Stepnowski, P., *Pol. J. Environ. Stud.*, 2005, vol. 14, no. 16, pp. 823–828.
4. Bali, U. and Catalkaya, E.C., *J. Environ. Sci. Health*, 2003, vol. 38, no. 10, pp. 2259–2275.
5. Mordechai, L.K., *J. Phys. Chem.*, 2003, vol. 107, pp. 1734–1741.
6. Sedlak, D.L. and Andren, A.W., *Environ. Sci. Technol.*, 1991, vol. 25, no. 4, pp. 777–782.
7. Pignatello, J.J., *Environ. Sci. Technol.*, 1992, vol. 26, no. 5, pp. 944–951.
8. Lin, S.H. and Lo, C.C., *Water Res.*, 1997, vol. 31, no. 8, pp. 2050–2056.
9. Kang, W.K. and Hwang, K.-Y., *Water Res.*, 2000, vol. 34, no. 10, pp. 2786–2790.
10. Weiss, J., *Advances in Catalysis and Related Subjects*, Frankenburg, W.G. and Komarewsky, V.I., Eds., New York: Academic, 1954, vol. IV, pp. 343–365.
11. Baxendale, J., *Advances in Catalysis and Related Subjects*, Frankenburg, W.G. and Komarewsky, V.I., Eds., New York: Academic, 1954, vol. IV, pp. 31–86.

ISSN 1070-4272, Russian Journal of Applied Chemistry, 2007, Vol. 80, No. 2, pp. 279–284. © Pleiades Publishing, Ltd., 2007.
Original Russian Text © S.O. Bondareva, Yu.I. Murinov, V.V. Lisitskii, 2007, published in Zhurnal Prikladnoi Khimii, 2007, Vol. 80, No. 2, pp. 280–285.

ORGANIC SYNTHESIS AND INDUSTRIAL ORGANIC CHEMISTRY

Bisacylated Diethylenetriamines as Extractants for Nonferrous Metals from Hydrochloric Acid Solutions

S. O. Bondareva, Yu. I. Murinov, and V. V. Lisitskii

Institute of Organic Chemistry, Ufa Scientific Center, Russian Academy of Sciences, Ufa, Bashkortostan, Russia

Bashkir State University, Ufa, Bashkortostan, Russia

Received June 27, 2006

Abstract—A series of bisacylated polyethylenepolyamines with linear and α- and α,α'-branched substituents were synthesized. The effects of the number of the nitrogen atoms in the polyethylenepolyamine fragment of the reagent and of the length and branching of its alkyl radicals on the extractant distribution between the organic and aqueous phases was studied. The performance characteristics of the extractants, such as the loss with the aqueous phase, hydrolytic stability, back extraction conditions for nonferrous metals, and $\beta_{Zn(II)/Fe(III)}$ and $\beta_{Zn(II)/Cu(II)}$ partition coefficients, were examined.

DOI: 10.1134/S107042720702022X

Previously we have reported the extraction characteristics of certain bisacylated polyethylenepolyamines (PEPAs) with respect to some nonferrous and noble metals [1–3]. The goal of this study is to optimize the number of nitrogen atoms and the structure of the alkyl substituents in bisacylated polyethylenepolyamines for extraction of nonferrous metals and also to determine the performance characteristics of the most efficient extractants from this series.

EXPERIMENTAL

The PEPAs and other organic reagents used were distilled prior to use: ethylenediamine (bp 117–118°C), diethylenetriamine (59–60°C/2 mm Hg), triethylenetetramine (142°C/8 mm Hg), tetraethylenepentamine (167–170°C/8 mm Hg), caprylic acid (105–107°C/5 mm Hg), 2-ethylhexanoic acid (89–90°C/5 mm Hg), and narrow fractions of α,α'-branched fatty carboxylic acids: ~C_9 (116–120°C/4 mm Hg) and $C_{13,15}$ (205–210°C/8 mm Hg). The fraction of higher isomeric acids VIK-1 (propionic acid telomeres), narrow fractions of synthetic α,α'-branched fatty carboxylic acids ~C_9 and ~$C_{12,14,16}$ (Kaustik Production Association, Sterlitamak), and lauric acid (pure grade) were used without additional purification. Bisacylated PEPAs (BAPs) were synthesized by the following scheme [1]:

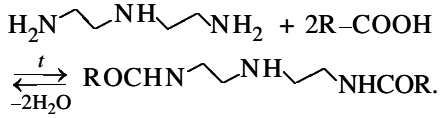

The reagents synthesized are listed in Table 1. The reagents with linear and α-branched substituents are paraffin-like compounds, and those with α,α'-branched substituents, viscous liquids. All the reagents are readily soluble in alcohols, aromatic hydrocarbons, and chloroform (0.1–0.5 M) and moderately soluble in saturated hydrocarbons (<0.1 M). The BAPs obtained were identified by the strong amide **I** and amide **II** bands in the IR spectra and by the low-field peaks of the sp^2-hybridized atoms of the amide groups in the ^{13}C NMR spectra (Table 2). The lack of imidazoline derivatives, the most probable by-products in the synthesis of BAPs, was confirmed by the UV and IR spectra [4].

The electronic spectra were recorded on a Specord M40 spectrophotometer over the range 50000–11000 cm^{-1}; the IR spectra of the films, on a Specord M80 instrument, and the ^{13}C NMR spectra, on a Bruker AM-300 instrument ($CDCl_3$, TMS).

As diluents we used toluene and *n*-octanol (analytically pure grade) without additional purification. Addition of *n*-octanol (15 vol %) eliminates the formation of interfacial films.

Table 1. Formulas, number, full names, and molecular weights of reagents

Reagent	Formula of acylating acid	BAP	Moleculat weight
	ROCHN⌒⌒NHCOR		
I	$CH_3C(CH_2)_3COOH$ (CH₃ and C₂H₅ on C)	Bis(*N*-methyl-2-methyl-2-ethylhexanamide)	~326
II	$CH_3(CH_2)_6COOH$	Aminobis(*N*-ethyloctanamide)	355.4
III	$CH_3CH(CH_2)_3COOH$ (C₂H₅ on C)	Aminobis(*N*-ethyl-2-ethylhexanamide)	355.4
IV	$CH_3C(CH_2)_3COOH$ (CH₃ and C₂H₅ on C)	Aminobis(*N*-ethyl-2-methyl-2-ethylhexanamide)	~369
V	$CH_3C(CH_2)_{7,9}COOH$ (CH₃ and C₂H₅ on C)	–	~460
VI	CH_3C-CH_2-COOH (CH₃ and CH₃ on C)	Aminobis(*N*-ethyl-2,2-dimethylbutanamide)	~300
VII	$CH_3C-(CH_2)_{7,9,11}-COOH$ (CH₃ and CH₃ on C)	–	~500
VIII	VIK-I fraction = $CH_3C(CH_2)_{3-9}COOH + CH_3C(CH_2)_{2-8}COOH$ (CH₃ and C₂H₅ on C)	–	~440
IX	$CH_3(CH_2)_{10}COOH$	Aminobis(*N*-ethyldodecanamide)	467.8
	ROCHN⌒⌒NH⌒⌒NH⌒⌒NHCOR		
X	$CH_3C(CH_2)_3COOH$ (CH₃ and C₂H₅ on C)	Bis(*N*-(3-azabutyl)-2-methyl-2-ethylhexanamide)	~412
	ROCHN⌒⌒NH⌒⌒NH⌒⌒NH⌒⌒NHCOR		
XI	$CH_3C(CH_2)_3COOH$ (CH₃ and C₂H₅ on C)	Aminobis(*N*-(3-azapentyl)-2-methyl-2-ethylhexanamide)	~455

Table 2. IR and ^{13}C NMR spectra of selected BAPs

Reagent	ν, cm^{-1}	Chemical shift, ppm
II	1645, ν(C=O), amide I band; 1560, δ(NH) amide II band	176.55
III	1648, ν(C=O); 1560, δ(NH)	176.32
IV	1644, ν(C=O); 1552, δ(NH)	176.82
V	1632, ν(C=O); 1520, δ(NH)	177.26
VI	1648, ν(C=O); 1560, δ(NH)	–
VII	1628, ν(C=O); 1516, δ(NH)	178.26
VIII	1640, ν(C=O); 1532, δ(NH)	176.5–177.3 (group of signals)

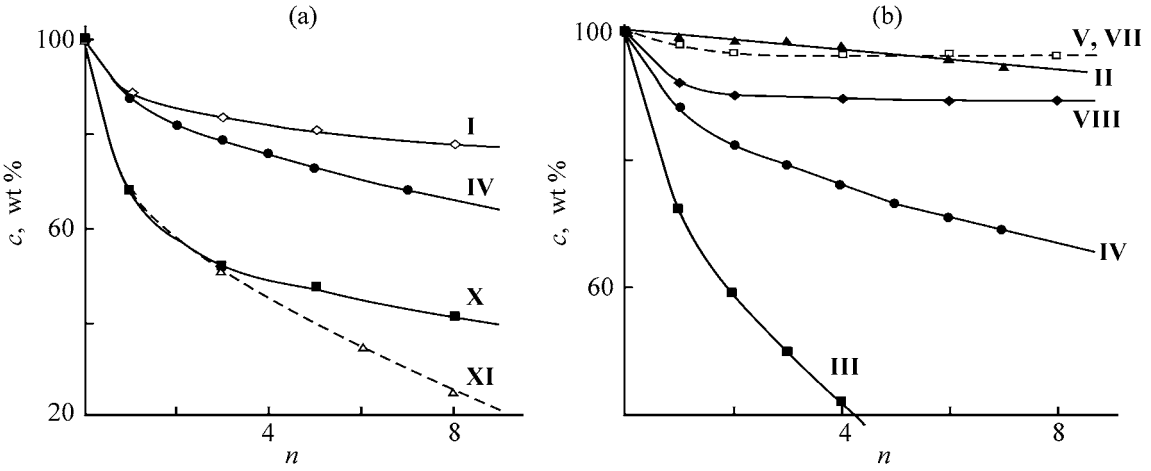

Fig. 1. Distribution of reagents between the organic phase and 1 M HCl. Initial concentration of the reagent in the organic phase 0.1 M (corresponds to 100%), diluent 15% octanol in toluene (30% octanol in toluene for **XI**). (*c*) Concentration of the reagent in the organic phase and (*n*) number of washing runs.

To remove the unchanged starting acids, the solutions of reagents were washed with three portions of equivalently concentrated NaOH, and then with 0.1 M HCl, to remove residual PEPA (until disappearance of the blue coloration upon adding 0.1 M copper chloride). Finally, the extractant was washed with 1 M NaCl.

Iron(III) in the raffinate and backwash was determined chelatometrically with Na_2EDTA in the presence of sulfosalicylic acid, and Zn(II), Cu(II), Mn(II), Co(II), and Ni(II), with Murexide in the presence of ammonia buffer.

Initially, the BAP concentration was monitored pH-metrically using an OP-211/1 pH meter with a combined glass electrode in 90% isopropanol (0.5 M $NaClO_4$). Then we found that, with all the BAPs that are capable of extracting Zn, the Zn(II) : ligand ratio at saturation was 1 : 2, which allowed determination of the reagent concentration using the simpler and less time consuming extraction method.

Equal volumes (5–10 ml) of the organic and aqueous phases were brought contact in temperature-controlled separating funnels at 20.0 ± 1.0°C. The extractant concentration was 0.1 M, and the working concentration of a metal, about 3×10^{-2} M (in the concentrated Zn solution, 0.2 M). The HCl concentration was varied from 0.05 to 9.0 M. The extraction equilibrium in the system was attained in 45–60 s. Therefore, the contacting time of the phases was chosen to be 5 min. The phase separation was observed immediately after the termination of the mixing.

The extractant distribution between the organic and aqueous phases was studied using the above extraction procedure. In this case, a fixed volume of the extractant solution of a known concentration (~0.1 M) was contacted with the equal volume of 0.1 M HCl. The aqueous phase was separated, and a part of the organic phase was used for extraction of Zn ($[Zn^{2+}]$ = 0.2 M, [HCl] = 5 M). Finally, the reagent concentration in the organic phase was determined. Then the cycle was repeated.

In the hydrolytic tests, an extractant (10 ml of 0.1 M solution) was stirred with a magnetic stirrer for a fixed time at 60.0 ± 0.2°C with 10 ml of 1.75 M sulfuric acid. Then the mixture was placed in a separating funnel and washed with 1 M NaCl. The organic phase was separated, and its volume was adjusted to 10 ml at 20°C by adding the diluent. The extractant concentration was determined by the extraction method.

The extraction–back extraction experiments were carried out as follows. Equal volumes of 0.1 M solution of an extractant and 3×10^{-2} M solution of the Zn(II) salt in 1.8 M HCl were shaken for 5 min. The raffinate was separated and analyzed for residual Zn(II). Back extraction was carried out with three portions of 1.75 M sulfuric acid at o : w = 2 : 1 by shaking for 2 min. Finally, the organic phase was washed with 1 M NaCl.

With increasing acidity of the aqueous phase, BAPs undergo protonation, and the solubility in water of all the previously synthesized BAPs increases [1]. To optimize the performance characteristics of the extractants of this series, we varied the number of nitrogen atoms in the PEPA fragment and also the length and branching of the alkyl radicals (Table 1). Then the extractants were tested for the distribution between the organic phase and 1 M HCl (Fig. 1).

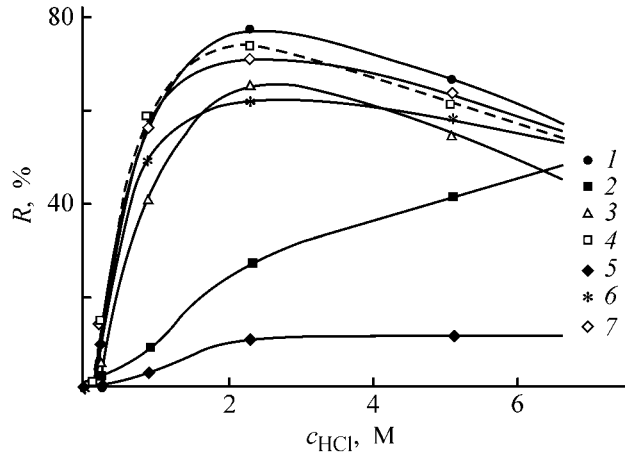

Fig. 2. Extraction power of the extractants *R* vs. the length and branching of their hydrocarbon radical in extraction of Zn(II) (0.032 M). Initial concentration of the extractants 0.1 M; diluent 15% octanol in Nefras (commercial solvent based on butylbenzene). (c_{HCl}) HCl concentration. Extractant: (*1*) **II**, (*2*) **III**, (*3*) **IV**, (*4*) **V**, (*5*) **VI**, (*6*) **VII**, and (*7*) **VIII**.

Figure 1a presents data for the extractants differing in the PEPA fragment only. As expected, bisacylated ethylenediamine **I** containing no amino groups does not extract nonferrous metals (NFMs) over the HCl concentration range 0.5–0.6 M. Therefore, despite the lowest solubility in water, BAP with the ethylenediamine fragment was not further examined in this study. Protonated reagent **XI**, when contacted with 1 M HCl, practically totally separated into a third phase, which vanished only when the fraction of octanol in the diluent was raised to 30%.

Figure 1 shows that, as the number of the nitrogen atoms in the PEPA fragment of BAPs becomes larger, the solubility of their protonated forms does increase. The lowest solubility in water can be expected for diethylenetriamine derivatives. The effect of the length and branching of the hydrocarbon radical on the solubility of bisacylated diethylenetriamines (BADs) is shown in Fig. 1b. Unfortunately, we failed to obtain a narrow fraction of the α,α'-branched acid C_8. Therefore, the results for individual isomers **II** and **III**, obtained on the basis of the linear and α-branched acids, respectively, were compared with those for **IV** synthesized from a very narrow fraction of α,α'-branched acids (primarily C_9). Here the lowest solubility was observed for **II**, i.e., for the reagent with linear substituents. An increase in the length of the linear alkyl radical (**IX**) results in a higher emulsifying power of the reagent: in the systems with **IX**, the phases were not separated even in 24 h. We were able to extract Zn(II) from saturated solutions with **IX**, since the phase separation is facilitated near the limit of the extractant capacity, but we faced difficulties in separating the phases in back extraction and washing with 1 M HCl. For these reasons, the curve for **IX** is lacking in Fig. 1.

Table 3. Characteristics of the hydrolytic stability of the extractants in 1.75 M sulfuric acid at 60°C

Heating time, h	Extractant concentration after heating, % of the initial value			
	II	**III**	**IV**	**VIII**
0.5	98	–	–	–
1.0	94	95	98.5	100
2.0	90	93.5	99	100
3.0	86.5	94	98	100
4.0	83	93	99	100

An increase in the length of the branched alkyl radical [**V**, **VII**, **VIII**] significantly suppesses the transfer of BADs to the aqueous phase. The initial part in the curves can be attributed to the presence of small amounts of more soluble monoacylated diethylenetriamines, and, in the case of **VIII**, of lower-molecular-weight homologues, e.g., **IV**. After three washings, the concentrations of **V**, **VII**, and **VIII** remained unchanged: no transfer of BADs to the aqueous phase was observed.

The extraction properties of BADs are illustrated in Fig. 2 by an example of extraction of Zn(II) from HCl. The lowest extraction power is shown by the most water-soluble BADs (**III** and **VI**).[1] Generally, variation of the alkyl radical only slightly influenced the extraction characteristics of the reagents.

Since BADs were suggested to be used for extraction of NFMs from HCl solutions, followed by back extraction with dilute sulfuric acid, we studied the resistance of these reagents to acid hydrolysis. To be able to compare the results with published data [5], we carried out hydrolysis at 60°C (Table 3). Previously, we have shown [6] that, in base hydrolysis of imidazolines, introduction of a branched substituent into the α-position relative to the reactive center hampers addition of the hydroxide ion, thus decelerating the hydrolysis. The results of this study are well consistent: the highest hydrolytic stability is observed for the reagents with α,α'-branched substituents, and the lowest stability, for those with linear substituents.

[1] Reagent **VI** is readily soluble in water and HCl (~0.2 M). For this reason, the curve for this reagent is lacking in Fig. 1.

Table 4. Selectivity characteristics of the reagents

Extraction conditions (M)	V		VII		VIII	
	$\beta_{Zn/Fe}$	$\beta_{Zn/Cu}$	$\beta_{Zn/Fe}$	$\beta_{Zn/Cu}$	$\beta_{Zn/Fe}$	$\beta_{Zn/Cu}$
o : w = 1 : 1, [HCl] = 1, $[Cu^{2+}] = [Fe^{3+}] = 0.2$, $[Zn^{2+}] = 0.021$	–	–	145	650	55	440
o : w = 1 : 1, [HCl] = 1, $[Cu^{2+}] = [Fe^{3+}] = 0.2$, $[Zn^{2+}] = 0.0021$	–	–	240	1700	130	1000
o : w = 1 : 5, [HCl] = 1.8, $[Cu^{2+}] = [Fe^{3+}] = 0.2$, $[Zn^{2+}] = 0.021$	30	330	55	635	19	370

Table 5. Performance characteristics of the reagents in HCl

Reagent	Phase separation time in extraction (back extraction), min	Extraction capacity for Zn (5% solution), g l^{-1}	Conditions of back extraction
V	30–40 (3–5)	3.1–3.5	1.8 M H_2SO_4, two steps: (I) 85–90% and (II) 10–15%; washing time 2 min
VII	40–90 (2–5)	2.7–3.2	
VIII	~1(2–5)	3.3–3.7	100% back extraction in a single step, washing time 2 min

Table 6. Evolution of the reagent concentration in the organic phase in the extraction–back extraction cycles (% of the initial)

Extraction cycle no.	Concentration, %			Extraction cycle no.	Concentration, %		
	V	**VII**	**VIII**		**V**	**VII**	**VIII**
1	100	100	100	4	–	–	99
2	–	–	100	5	100	100	99
3	100	100	100	6	–	–	98
				7	100	100	98

A decrease in the HCl concentration in the aqueous phase to 0.5 M deteriorates the phase separation, and a third phase is formed. As the HCl concentration is raised to 9 M, reagents **VII** and **VIII** are totally separated into the third phase. Therefore, it is practical to use BADs for extraction of NFMs at HCl concentrations from 0.8–1.0 to 8.5 M. In this range, for reagents **VII**, **VIII**, and **X**, the extraction of NFMs decreases in the order Zn(II) > Fe(III) > Cu(II) > Co(II) > Mn(II) > Ni(II)[2] (Fig. 3).

At an HCl concentration of about 2 M and lower, all the BADs are selective for Zn(II) (Table 4). Nonferrous metals are totally backwashed with dilute sulfuric acid (0.2–2 M) in 1–2 steps.

In the case of **VIII**, back extraction with water is quite efficient (Table 5), while reagents **V** and **VII** form poorly settled emulsions with water.

Since the best results in extraction of NFMs from HCl were obtained with reagents **V**, **VII**, and **VIII**, they were tested in extraction–back extraction cycles. With **V** and **VII**, the reagent concentration in the organic phase remained unchanged in at least seven cycles. In the case of **VIII**, the recovery of Zn(II) regularly decreased as a result of the loss of the extractant (Table 6). Taking into account some un-

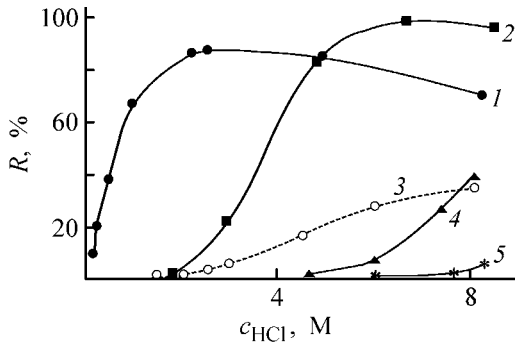

Fig. 3. Recovery of nonferrous metals R with 0.11 M solution of **VIII** in toluene vs. the HCl concentration c_{HCl}. Initial metal concentration ~0.03 M.

[2] Reagent **VIII** does not extract Ni(II).

certainties, the loss factor for a 0.1 M solution of **VIII** was estimated at 0.12–0.13 g l^{-1} per cycle, which can be attributed to the presence of some lower-molecular-weight homologues. However, the loss can be considerably reduced by changing sulfuric acid for water in back extraction of NFMs. The advantages of the systems with **VIII** are the more rapid phase separation (Table 5) and the fact that, even in the absence of octanol, this reagent does not form a third phase.

CONCLUSIONS

(1) Diethylenetriamines bisacylated with α,α'-branched acids ~C_{11}–C_{14} show promise as extractants for nonferrous metals from hydrochloric acid solutions.

(2) These reagents are virtually insoluble in the aqueous phase, demonstrate no tendency toward formation of emulsions, are stable against sulfuric acid hydrolysis, and extraction systems with them relatively rapidly settle. Nonferrous metals can be quantitatively backwashed with dilute sulfuric acid.

(3) At HCl concentrations ≥0.5 M and total chloride concentrations in the aqueous phase $c \leq 2$ M, these extractants are selective for Zn(II).

REFERENCES

1. Bondareva, S.O., Murinov, Yu.I., and Lisitskii, V.V., *Zh. Neorg. Khim.*, 2004, vol. 49, no. 10, p. 1746.
2. Afzaletdinova, N.G., Murinov, Yu.I., Bibikova, M.Yu., et al., *Zh. Neorg. Khim.*, 2004, vol. 49, no. 6, p. 1044.
3. Khisamutdinov, R.A., Bondareva, S.O., and Murinov, Yu.I., Abstracts of Papers, *XIII Rossiiskaya konferentsiya po ekstraktsii* (XIII Russian Conf. on Extraction), Moscow, 2004, p. 188.
4. Bondareva, S.O., Chelating and Extraction Properties of 1,2-Disubstituted Imidazolines and Certain Acylated Polyethylenepolyamines with Respect to *d* Metals, *Cand. Sci. Dissertation*, Ufa, 2003.
5. Radushev, A.V., Gusev, V.Yu., Bogomazova, G.S., et al., *Zh. Prikl. Khim.*, 1996, vol. 69, no. 8, p. 1287.
6. Bondareva, S.O., Lisitskii, V.V., Yakovtseva, N.I., and Murinov, Yu.I., *Izv. Ross. Akad. Nauk, Ser. Khim.*, 2004, no. 4, p. 767.

ISSN 1070-4272, Russian Journal of Applied Chemistry, 2007, Vol. 80, No. 2, pp. 285–289. © Pleiades Publishing, Ltd., 2007.
Original Russian Text © I.A. Bashmakov, V.A. Dorosinets, V.K. Ksenevich, A.A. Mel'nikov, F.N. Kaputskii, 2007, published in Zhurnal Prikladnoi Khimii, 2007, Vol. 80, No. 2, pp. 286–290.

Formation of Thin Carbon Films Containing Metal Nanoparticles by Thermolysis of a Polymer Precursor

I. A. Bashmakov, V. A. Dorosinets, V. K. Ksenevich, A. A. Mel'nikov, and F. N. Kaputskii

Research Institute of Physicochemical Problems, Belarussian State University, Minsk, Belarus

Belarussaian State University, Minsk, Belarus

Received June 29, 2006

Abstract—A new procedure was developed for preparing carbon films with magnetic metal nanoparticles by thermolysis of a polymer precursor. The conditions for preparing carbon films with required surface concentration of the metal nanoparticles and hence with dielectric or metallic properties were determined.

DOI: 10.1134/S1070427207020231

The unabated interest in nanoheterogeneous structures consisting of a matrix and metal nanoparticles as a filler is caused by their unusual dielectric, magnetic, chemical, and biological properties [1, 2], which, in turn, are due to the size effects. The properties of these composites can be changed by using an insulating or conducting matrix with different concentrations of metal nanoparticles.

Nanoheterogeneous systems are characterized by interesting mechanisms of charge transport, in particular, quantum corrections to the conductivity [3, 4] and tunnel effects and giant magnetoresistance [5, 6]. The materials can be used in practice for production of gas sensors, magnetic field transducers, magnetic memory units with superhigh packing density of the components, etc. [7, 8]. Metal nanoparticles are widely used as catalysts not only for conventional reactions but also for growth of carbon nanotubes [9, 10] and onion-like structures [11].

Films and, especially, thin films occupy a prominent place among composites containing metal nanoparticles. The properties of these films are determined mainly by the properties and transformations of their surface. Carbon films containing metal nanoparticles are promising materials for micro- and nanoelectronics.

One of the procedures for preparing carbon films containing metal nanoparticles is thermolysis of metal-containing polymer precursors [12, 13]. The conductivity of films prepared by this method can be varied in a wide range (from dielectric to metal) by changing the thermolysis temperature. However, it is difficult to prepare monodisperse metal particles by this method (especially at high annealing temperatures) and to control the content of metal nanoparticles in the carbon matrix.

The aim of this study was to prepare dielectric and conducting thin carbon films with a required content of magnetic metal nanoparticles from a polymer precursor.

EXPERIMENTAL

The procedure for preparing carbon films with required content of metal nanoparticles consists of three steps.

The fist step involves preparation of thin polymer films, introduction of an appropriate transition metal ion (e.g., Co^{2+}, Ni^{2+}, Cu^{2+}, etc.) into the film, and thermolysis of the polymer precursor. The second step is treatment of the metal-carbon film with an aqueous solution of palladium chloride. The third (final) step is treatment of the film containing palladium nanoparticles with a nickel-plating solution.

The first step can be conventionally subdivided in three steps: (I–1) preparation of thin polymer films, (I–2) introduction of inorganic cations into the films, and (I–3) thermolysis of metal salts of the polymer in a vacuum.

We used starch as an initial polymer. Starch macromolecules were modified with nitro ester and carboxy groups [14]. The modified starch is soluble in ethers, esters, and alcohol-ether mixtures. Because the coefficient of spreading of a polymer solution over the water surface is positive [14] ($S > 0$ is the neces-

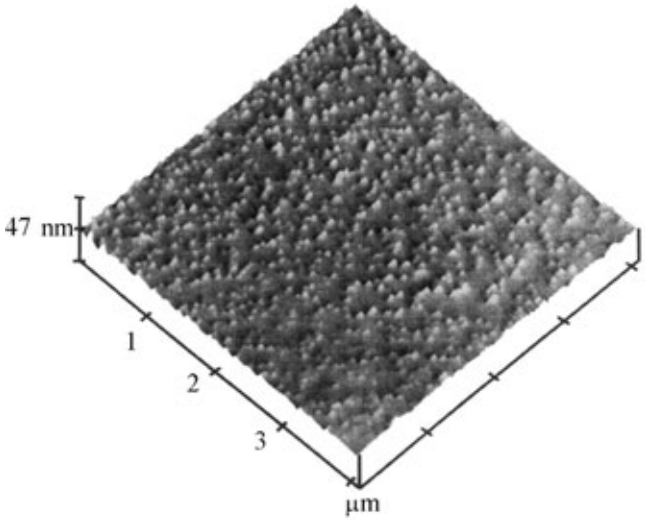

Fig. 1 AFM image of a surface of the carbon film containing Co nanoparticles. The cobalt salt of CNS was heated at 350°C.

sary thermodynamic conditions for complete spreading of a solution), the polymer solution is spread over a water surface.

Metal cations were introduced into a polysaccharide molecule by ion exchange of protons of its –COOH groups with the appropriate metal cation by the procedure described in our previous paper [14].

Thin films of carboxylated nitrostach (CNS) were prepared by dropping a polymer solution in isoamyl acetate on the water surface. A drop was completely spread to form a thin film solidified after removal of the solvent. The resulting film was put on a solid support made of polycor or sapphire. The film thickness calculated from the drop volume (0.02 ml), solution concentration (10 g/100 ml), film diameter (9 cm), and CNS density (1.58 g cm^{-1}) was 200 nm.

Sorption of metal cations and, in particular, cobalt(II) was performed by immersion of a supported CNS film in a 0.125 M aqueous solution of cobalt(II) acetate for 2 h at 20 ± 0.2°C.

The polymer films modified with cobalt(II) cations were isothermally heated at 350–700°C in a vacuum for 30 min. The heating rate was 10 deg min^{-1}. Under these conditions, the polymer degrades to form a carbon matrix containing cobalt nanoparticles produced by thermolysis of the cobalt carboxylate groups with simultaneous cobalt reduction

$$Co^{2+} \rightarrow Co. \quad (1)$$

The cobalt atoms are agglomerated into clusters which grow to form larger metal nanoparticles. Since the content of the –COOH groups in CNS was 16.0 wt %, the metal content of the carbon matrix was approximately 6.5 mol %. After the thermolysis, the film thickness decreased by approximately a factor of 5, whereas the parameters of the film in the plane did not noticeably change.

Clusters with an average size of 10–50 nm are formed in the carbon film in the course of low-temperature thermolysis (350–500°C). Their distribution in the carbon matrix was analyzed by atomic-force microscopy (AFM) (Fig. 1). As can be seen from Fig. 1, the nonuniformity of the surface of the carbon film does not exceed 1–2 nm. However, the profile of the cobalt-containing carbon films is nanogranular: the height difference along the film surface reaches 15–20 nm. Clearly, this is due to the formation of cobalt nanoparticles.

As can be seen from Fig. 1, the distance between cobalt clusters substantially exceeds the cluster size (a micrograph of a carbon film containing 6.5 mol %) cobalt is shown in Fig.1; the limited exchange capacity of the polymer matrix does not allow preparation of carbon films with a higher cobalt content).

The cluster size increases after heat treatment at temperatures of 700°C and higher. The conductivity of the carbon and metal-containing carbon films annealed at these temperatures substantially increases [15] and is determined mainly by the properties of the carbon matrix. The indirect influence of metal nanoparticles on the conductivity of the carbon matrix can consist only in their catalytic effect on the formation of the carbon structure. Previously, we have observed similar effect for carbon fibers containing cobalt particles [16].

Thus, although cobalt nanoparticles are formed by low-temperature thermolysis of a cobalt salt of CSN, the cobalt content in the thus obtained films is limited.

The carbon matrix is structured after a high-temperature treatment. However, in this case, the size of the metal particles substantially increases and their distribution in the carbon film becomes random. In other words, carbon films with close packing of cobalt nanoparticles cannot be prepared by thermolysis of the cobalt salt of CNS. To raise the metal content, the second step is used. This step involves treatment of a carbon film prepared by low- and/or high-temperature thermolysis with a 10^{-3} M aqueous solution of palladium(II) chloride for 15 min. Under these con-

ditions, almost all cobalt particles present in the carbon matrix react with palladium chloride in accordance with the equation

$$Co + PdCl_2 = CoCl_2 + Pd. \quad (2)$$

Cobalt chloride is washed out with distilled water from the carbon film, whereas palladium particles formed by reaction (2) are retained in the matrix. This is confirmed by an X-ray fluorescence microanalysis: the cobalt peaks disappear and palladium peaks appear after this treatment.

It is known [17] that palladium particles actively catalyze almost all reactions of electroless deposition of metals from aqueous solutions. Palladium nuclei (5 nm) exhibit the highest catalytic activity. When the particle size increases over 5 nm, the catalytic activity decreases. The catalytic activity of 15-nm Pd particles is very low [18]. Palladium particles formed in the film by reaction (2) actively catalyze nickel deposition from a nickel–plating solution, which suggests their small size. The third step is treatment of the palladium–containing film with a nickel–plating solution.

Carbon films containing palladium particles can be also prepared by direct thermolysis of palladium salt of CNS, which would eliminate the second step. However, as shown by Ermolenko et al. [19], the carbon matrix is not structured in this case and palladium particles are subject to autocoalescence (especially at temperatures of 700°C and above), which affects their catalytic activity.

Thus, the second step consists in introduction into the carbon matrix of palladium nanoparticles catalyzing electroless nickel deposition from a nickel-plating solution. The composition of the nickel-plating solution (solution a: $NiCl_2 \cdot 6H_2O$ 30 g l^{-1}; solution b: $NaH_2PO_2 \cdot H_2O$ 10 g l^{-1}, $Na_3C_6H_5O_7$ 88 g l^{-1}, NH_4Cl 50 g l^{-1}, and 25% NH_4OH 25 ml) was taken from [20]. When the palladium-modified carbon film is treated with a mixture of solutions a and b taken in a 1 : 4 ratio, nickel is reduced on catalytically active palladium nanoparticles by the reaction

$$2Ni^{2+} + H_2PO_2^- + 6OH^- \rightarrow 2Ni + PO_4^{3-} + 4H_2O. \quad (3)$$

The film was nickel-plated at 35°C for 5–15 min. As determined by scanning electron microscopy, the nickel content of the film increases with the plaiting time.

As can be seen from Fig. 2, treatment of the palladium-modified carbon film with the nickel-plating solution for 15 is sufficient for a dense layer of nickel nanoparticles to be formed. The morphology and composition of the particles were determined by scanning electron microscopy and X-ray fluorescence microanalysis.

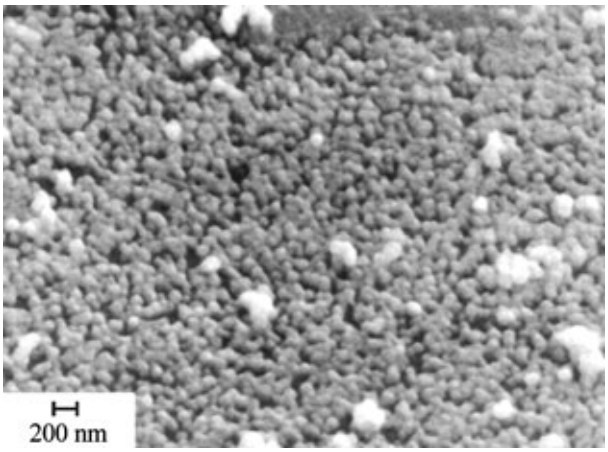

Fig. 2. Scanning electron micrograph of nickel nanoparticles on the surface of carbon film. Treatment with the nickel plating solution for 15 min; the same for Fig. 4.

In addition, the temperature dependences of a 2*D* film of nickel nanoparticles formed in the carbon matrix in different preparation steps were measured in the range 4.2–300 K. Changes in the temperature dependences of the film conductivity prepared by gradual increase in the time of treatment with the nickel-plating solution were also analyzed. To perform the electrical measurements, Al contacts were applied onto the film surface by thermal evaporation through metallic templates. The temperature dependence of the film resistance was measured by the conventional four-probe procedure.

The room-temperature resistance of the cobalt-containing carbon film prepared in the first step and of the films containing palladium particles prepared by treatment with a palladium chloride solution is approximately several tens of megaohms. The resistance substantially increases at temperatures below 100 K. The $R(T)$ dependences for both samples can be described by the Mott law typical of the variable-range hopping conductivity [21]:

$$R(T) = BT^{-1/2}\exp(T_0/T)^{1/4}, \quad (4)$$

where B is a constant independent of temperature, and T_0 is a parameter proportional to the density of states in the vicinity of the Fermi level.

The fact that the $R(T)$ dependences for the films containing cobalt and palladium nanoparticles are similar suggests that the conductivity of these films

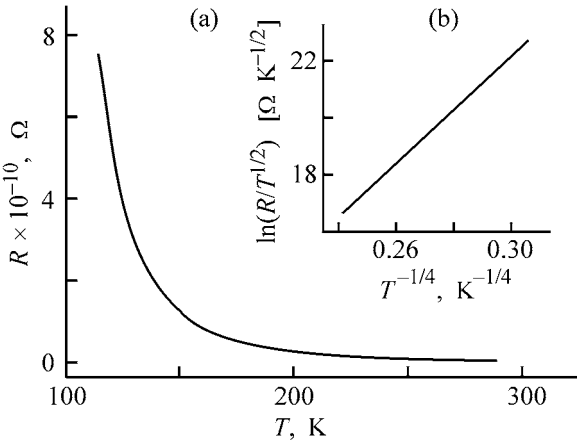

Fig. 3. (a) Resistance R of a nickel-carbon film vs. temperature T and (b) temperature dependence of the resistance plotted in the Mott coordinates. Time of nickel plating 5 min.

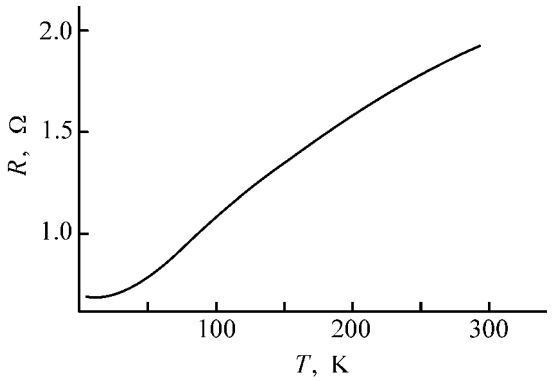

Fig. 4. Resistance R of a carbon film containing nickel nanoparticles vs. temperature T.

is due to the carbon matrix and replacement of cobalt nanoparticles with palladium nanoparticles by reaction (2) has no effect on the structural properties of the matrix and on the formation of percolation conductivity pathways.

The palladium-containing films treated with the nickel-plating solution for a short time (up to 5 min) also have a high room-temperature resistance, and the temperature dependence of their resistance is described by the Mott law. When the treatment time is increased to 10 min, the film resistance decreases. However, the temperature coefficient of resistance remains negative, i.e., the nickel-palladium-carbon films prepared under these conditions behave as insulators. An increase in the time of treatment with the nickel-plating solution to 15 min not only decreases the film conductivity to several ohms but also changes the sign of the temperature coefficient to positive. In other words, an insulator–metal transition caused by an increase in the surface concentration of nickel naonoparticles to form a granular nickel film is observed.

The temperature dependence of the resistance of a carbon film containing nickel nanoparticles in the range 290–115 K is shown in Fig. 3a as an example. This film was prepared under the following conditions: thermolysis temperature of the cobalt-containing film 700°C and time of the treatment with nickel-plating solution 5 min. As can be seen from Fig. 3b, this dependence is linear in the $\ln(R/T^{1/2})$–$T^{1/2}$ coordinates, which suggests prevalence of the variable-range hopping conductivity described by Eq. (4).

The $R(T)$ dependence for the carbon film containing nickel nanoparticles prepared by the same procedure, but at a nickel plating time of 15 min, is shown in Fig. 4. The $R(T)$ dependence is characterized by the positive temperature coefficient of resistance and a residual conductivity at low temperatures, which is typical of metals.

CONCLUSIONS

(1) The procedure for preparing thin carbon films containing surface nickel nanoparticles involves the following steps: (1) thermolysis of the solid polymer precursor (salt of carboxylated nitrostarch) in a vacuum; (2) reduction of palladium ions with nickel nanoparticles by treatment of the nickel-containing carbon film with an aqueous solution of palladium chloride; (3) deposition of magnetic nickel nanoparticles on catalytically active palladium particles present in the carbon film.

(2) The possibility of preparing carbon films with required surface density of nickel nanoparticles and the conductivity ranging from dielectric to metal was demonstrated. The surface concentration of nickel nanoparticles was controlled by the time of treatment with the nickel-plaiting solution.

ACKNOWLEDGMENTS

The authors are grateful to Prof. A.D. Wieck (Bochum University, Germany) for measuring the low-temperature resistance.

REFERENCES

1. Fendler, J.H., *Chem. Mater.*, 2001, vol. 13, no. 10, pp. 3196–3210.
2. Philipp, G., Muller-Schwanneke, C., Burghard, M.,

et al., *J. Appl. Phys.*, 1999, vol. 85, no. 6, pp. 3374–3377.

3. Carl, A., Dumpich, G., and Wassermann, E.F., *Phys. Rev.*, 1994, vol. B50, no. 7, pp. 4802–4809.
4. Carl, A., Dumpich, G., and Hallfarth, D., *Phys. Rev.*, 1989, vol. B39, no. 2, pp. 915–922.
5. Fettar, F., Maurice, J.-L., Petroff, F., et al., *Thin Solid Films*, 1998, vol. 319, pp. 120–123.
6. Yoe, D.-F., Banerjee, G., Meller, A.E., et al., *Superlattices Microstruct.*, 1996, vol. 19, no. 3, pp. 191–195.
7. Todorovic, M. and Schultz, S., *Appl. Phys. Lett.*, 1999, vol. 74, no. 17, pp. 2516–2618.
8. Yu, M., Liu, Y., and Sellmyer, D.J., *J. Appl. Phys.*, 2000, vol. 87, no. 9, pp. 6959–6961.
9. Seraphin, S. and Zhou, D., *Appl. Phys. Lett.*, 1994, vol. 64, no. 16, pp. 2087–2089.
10. Hafner, J.H., Bronuikowski, M.J., Azamian, B.R., et al., *Chem. Phys. Lett.*, 1998, vol. 296, nos. 1–2, pp. 195–202.
11. Saito, Y., Yoshikawa, T., Okuda, M., et al., *Chem. Phys. Lett.*, 1993, vol. 209, nos. 1–2, pp. 72–76.
12. Hishijama, Y., Yoshida, A., and Kaburagi, Y., *Carbon*, 1993, vol. 31, no. 8, pp. 1265–1272.
13. Nikolaeva, O.A., Kodolov, V.I., Makarova, L.G., et al., *Fiz. Tverd. Tela*, 2002, vol. 41, no. 3, pp. 502–503.
14. Bashmakov, I.A., Dorosinets, V.A., Ksenevich, V.K., and Kaputskii, F.N., *Vestn. Bel. Gos. Univ., Ser. 2*, 2005, no. 4, pp. 3–9.
15. Ksenevich, V.K., Bashmakov, I.A., Melnikov, A.A., and Wieck, A.D., *Acta Phys. Polon. A*, 2005, vol. 107, no. 2, pp. 356–360.
16. Bashmakov, I.A., Dorosinets, V.A., Lukashevich, M.G., et al., *Fiz. Tverd. Tela*, 2002, vol. 44, no. 9, pp. 1614–1621.
17. Stepanova, L.I., *Izbr. Nauchn. Tr. Bel. Gos. Univ.*, 2001, vol. 5, pp. 196–215.
18. Ermolenko, I.N., Savastenko, G.N., Komar', V.V., et al., *Svetochuvstvitel'nye materialy na osnove polimerov s kislotnymi gruppami* (Photosensitive Materials Prepared from Polymers with Acid Groups), Minsk: Nauka i Tekhnika, 1988.
19. Ermolenko, I.N., Lyubliner, I.P., and Gul'ko, I.V., *Elementosoderzhashchie ugol'nye voloknistye materialy* (Element-Containing Fibrous Carbon Materials), Minsk, Nauka i Tekhnika, 1982.
20. Lutskina, T.V. and Sviridov, V.V., *Izv. Akad. Nauk BSSR, Ser. Khim. Nauk*, 1973, no. 3, pp. 45–49
21. Mott, N.F. and Davis, E.A., *Electron Processes in Non-Crystalline Materials*, Oxford: Clarendon, 1979.

ISSN 1070-4272, Russian Journal of Applied Chemistry, 2007, Vol. 80, No. 2, pp. 290–294. © Pleiades Publishing, Ltd., 2007.
Original Russian Text © V.F. Kurenkov, S.S. Grigor'eva, A.V. Kurenkov, F.I. Lobanov, 2007, published in Zhurnal Prikladnoi Khimii, 2007, Vol. 80, No. 2, pp. 291–295.

MACROMOLECULAR CHEMISTRY AND POLYMERIC MATERIALS

Copolymerization of Acrylamide with Ammonium Acrylate in Concentrated Aqueous Solutions

V. F. Kurenkov, S. S. Grigor'eva, A. V. Kurenkov, and F. I. Lobanov

Kazan State Technological University, Kazan, Tatarstan, Russia
Ashlend Eurasia Joint-Stock Company, Moscow, Russia

Received October 24, 2006

Abstract—The kinetics of formation of water-soluble copolymers of acrylamide and ammonium acrylate with various molecular properties by copolymerization in concentrated aqueous solutions at 60°C in the presence of potassium persulfate initiator was studied by dilatometry.

DOI: 10.1134/S1070427207020243

Owing to their valuable properties, water-soluble polymers are widely used in various branches of industry. Moreover, their production and application exclude toxic, inflammable, and explosive solvents, strongly decrease the volume of noxious substances discharged into the environment, and improve the hygienic working conditions [1]. These water-soluble polymers include polyacrylamide, its derivatives, and copolymers of acrylamide (AA), which are effectively used in water treatment, papermaking, mining operations, and petroleum production [1, 2]. Copolymers of AA with acrylic acid and its salts are frequently prepared by copolymerization of monomers [2, 3] or by partial hydrolysis of polyacrylamide [4]. It is advisable to use concentrated aqueous solutions. Previously, we have studied polymerization of acrylic acid in the presence of sodium hydroxide [5] and copolymerization of AA with sodium acrylate in concentrated aqueous solutions [6].

In this study we examined copolymerization of AA with ammonium acrylate (AmA) in concentrated aqueous solutions at 60°C in the presence of potassium persulfate initiator (PP).

EXPERIMENTAL

In our study, we used an 18% aqueous solution of AmA and a 42.8% aqueous solution of AA, prepared by the biocatalytic method at the Moscow–Stockhausen–Perm Joint-Stock Company; PP twice recrystallized from water, sodium hydroxide and acetone of analytically pure grade, and ultrapure helium. All the working solutions were prepared using distilled water.

Copolymerization was performed in 12-ml glass dilatometers (low conversion) and in 50-ml sealed weighing bottles (deep conversion). First, aqueous solutions of AA and AmA were mixed in a flask, the required solution pH was adjusted using an aqueous solution of sodium hydroxide, and the required volume of distilled water was added to attain the required concentration. Then, using a Schott filter, helium was bubbled through the reaction mixture to remove oxygen acting as a polymerization inhibitor. An aqueous solution of PP was added and the reaction mixture was transferred with a syringe into a dilatometer and weighing bottle, which were then placed in a thermostat and kept at 60°C. At low conversion, copolymerization was monitored by the shift of the meniscus of the reaction mixture in a dilatometer capillary, using a KM-8 cathetometer, and copolymerization to deep conversion was performed for 1 h. Then the resulting copolymers were precipitated with a large excess of acetone and dried in a vacuum at 50°C to constant weight.

The process kinetics was monitored dilatometrically. From the dilatometric data, we obtained the kinetic dependences, which in all the cases were linear, and then calculated the initial rates of polymerization v_0 from their slopes at low conversions ($X < 2\%$). The conversion X (%) was calculated from the following expression:

$$X = \Delta V/(VK) \times 100,$$

where V and ΔV are the initial volume of the reaction mixture in the dilatometer and its change with time, respectively; and K is the contraction factor of copolymerization, $K = K_1\omega + K_2(100 - \omega)$. Here K_1 and K_2 are the contraction factors for AA and AmA, respectively; and ω is the content of AA in the initial monomer mixture.

The factors K_1 and K_2 were determined using the equation

$$K_1,\ K_2 = (\rho_p - \rho_m)/\rho_p,$$

where ρ_p and ρ_m are the densities of the polymer and monomer, respectively.

The conversion was calculated using the correction factor:

$$K' = K[1 + \alpha_m(T_1 - T_2)],$$

where α_m is the cubic expansion coefficient of the monomer solution, and T_1 and T_2 are, respectively, the temperatures at which the experiment was performed and the dilatometer was filled.

The values of α_m were calculated as follows:

$$\alpha_m = (1/V)(dV/dT),$$

where dV is the change in the volume of the reaction mixture; V, initial volume; and dT, temperature range corresponding to the volume change dV.

The content of the ionic units was determined by a potentiometric procedure [7] using a pH-121 pH-millivoltmeter equipped with an ESL-63-07 working glass electrode and an EVL-1M3 silver chloride reference electrode.

The viscometric measurements were carried out in a 0.5 M NaCl solution at 30°C, using an Ubbelohde viscometer (d_c = 0.56 mm). The intrinsic viscosities [η] were evaluated from the experimental dependences of the reduced viscosity η_{sp}/c_p on the copolymer concentration c_p; $[\eta] = \lim(\eta_{sp}/c_p)$ at $c_p \to 0$. Then, from the [η] values and the content of the ionic groups in AA–AmA copolymer, we calculated the viscosity-average molecular weight of copolymers ($\overline{M}_\eta$) by the Mark–Houwink–Kuhn equation:

$$[\eta] = K''M^{\alpha},$$

where K'' and α [8] were varied depending on the content of AmA ionic units in the copolymer.

Copolymerization of AA (M_1) with AmA (M_2) was carried out in 18% aqueous solutions at 60°C in the presence of PP initiator ($c = 7.4 \times 10^{-4}$ M). In the experiments, copolymerization proceeded under the homogeneous conditions at any conversions and no spontaneous copolymerization was observed.

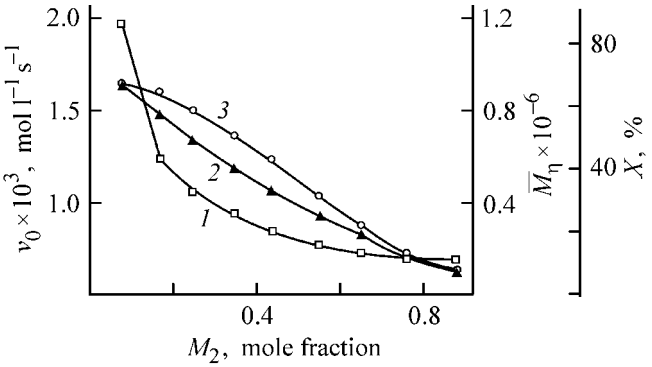

Fig. 1. (*1*) Viscosity-average molecular weight, (*2*) initial copolymerization rate v_0, and (*3*) yield of copolymer X vs. the AmA mole fraction in the initial monomer mixture M_2.

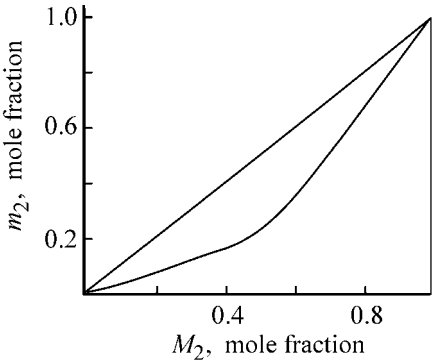

Fig. 2. Mole fraction of the ionic AmA units in the AA–AmA copolymer m_2 at low conversion ($X < 3$) vs. the mole fraction of AmA in the initial monomer mixture M_2.

First, we examined the effect of the composition of the initial monomer mixture on the copolymerization of AA with AmA. Figure 1 shows the dependences of v_0, $\overline{M}_\eta$, and copolymer yield on the content of the ionic monomer M_2 in the initial monomer mixture. It is seen that v_0, $\overline{M}_\eta$, and the copolymer yield decrease as M_2 increases. The data on v_0 indicate that, under the given experimental conditions, the reactivity of AA in the course of copolymerization is higher than that of AmA. In accordance with $\overline{M}_\eta$, the higher-molecular-weight compounds were obtained in the mixtures enriched with AA. The highest yield of the copolymer is also observed in the monomer mixtures enriched with AA.

The dependence of the current composition of the copolymer prepared by copolymerization of AA and AmA at low conversion ($X < 2\%$) on the composition of the initial monomer mixture is shown in Fig. 2. As seen, copolymers enriched in AA are

Table 1. Relative activities of AA (r_A) and AmA (r_B) in copolymerization in aqueous solutions

Equation	$[M_1 + M_2]$, %	r_A	r_B
Fineman–Ross	18	2.25 ± 0.03	0.15 ± 0.03
Kelen–Tudo	18	2.2 ± 0.03	0.1 ± 0.03

Table 2. Properties of the resulting copolymers as influenced by the total monomer concentration in the reaction mixture

$[M_1 + M]_2$, %	m_2, mol %	[η], $cm^3\ g^{-1}$	$\overline{M}_\eta \times 10^{-6}$	Yield, %
30.4	46.0	300	0.38	99.3
22.8	35.6	220	0.30	63.3
15.2	31.2	200	0.27	36.7

formed in a wide range of compositions of the initial monomer mixture, which is due to higher reactivity of AA in the course of copolymerization as compared to AmA. The relative monomer activities were determined from Fig. 2 as the quantitative parameters of the monomer reactivity in copolymerization:

$$r_A = k_{AA}/k_{AB} \text{ (for AA) and } r_B = k_{BB}/k_{BA} \text{ (for AmA).}$$

The values of r_A and r_B, determined using various procedures, are listed in Table 1. As seen, these values well agree with each other and, in all the cases, $r_A > r_B$, which confirms the higher reactivity of AA in copolymerization as compared to AmA.

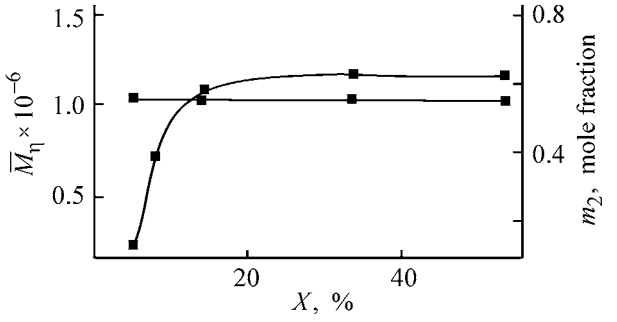

Fig. 3. (*1*) $\overline{M}_\eta$ and (*2*) mole fraction of the AmA ionic units in the AA–AmA copolymer m_2 vs. the conversion X in copolymerization of AA and AmA.

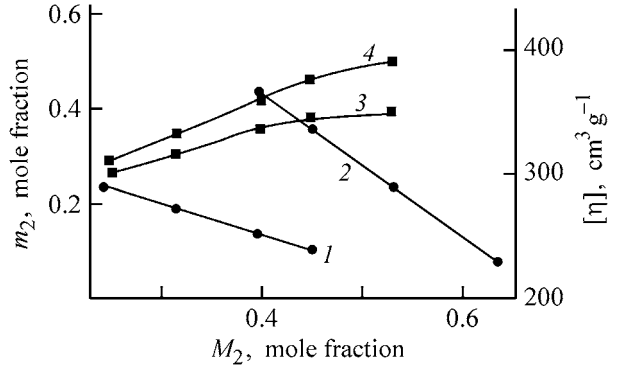

Fig. 4. (*1*, *2*) Intrinsic viscosity [η] and (*3*, *4*) mole fraction m_2 of the AmA units in copolymer vs. the AmA mole fraction in the initial monomer mixture M_2 at pH (*2*, *3*) 10 and (*1*, *4*) 12.

The dependence of the AA copolymerization with AmA on the conversion under given experimental conditions is shown in Fig. 3. As seen, the copolymer composition remains unchanged in the course of copolymerization; a similar phenomenon has been observed previously for other systems (e.g., in copolymerization of AA with dimethylaminoethyl methacrylate [9]). This fact can be attributed to formation of aggregates (micelles) with external hydrophilic and internal hydrophobic groups in concentrated aqueous solutions of the copolymer. Owing to the electrostatic repulsion between like-charged AmA monomer and its units on the micelle surface, penetration of the AmA species inside the micelle to react with a macroradical is hindered. With increasing conversion, the decrease in the AA content in copolymerization is compensated for by the preferential penetration of the AA molecules inside the micelles; as a result, the composition of the monomer mixture near macroradicals in the course of the reaction and, thus, the copolymer composition remain constant.

As seen, $\overline{M}_\eta$ increases with the conversion (Fig. 3, curve *1*). This is obviously due to the increasing viscosity of the reaction mixture in copolymerization, which decreases the probability of the chain termination.

The effect of the total monomer concentration in the initial mixture on the running composition of copolymers was evaluated at a mole fraction $[M_2]$ = 0.25, other experimental conditions being equal. As can be seen from Table 2, with the total monomer concentration the AmA content in the reaction solution increases; the resulting increase in the ionic strength of the solution weakens the electrostatic repulsion between the AmA monomer and macroradical, and the forming copolymer becomes enriched in AmA units. It also follows from the data in Table 2 that the yield of copolymer also increases with the total monomer concentration in the initial mixture.

The effect of the reaction mixture pH on the copolymerization was evaluated at different compositions of the initial monomer mixture, other experimental conditions being equal (Fig. 4). As seen,

as the AmA content in the initial mixture increases at pH 10 and 12, m_2 increases (Fig. 4, curves 3 and 4) and [η] decreases (Fig. 4, curves *1* and *2*) owing to a decrease in the copolymer molecular weight, which well agrees with the experimental data in Fig. 1 (pH 8). Comparison of the experimental data at M_2 = const shows that, on going from pH 10 to pH 12, [η] decreases (Fig. 4, curves *1* and *2*) and m_2 increases (Fig. 4, curves *3* and *4*). The observed increase in m_2 is due to a rise in ionic strength of the solution upon addition of NaOH.

To determine the overall rate equation of copolymerization in the system in question, experiments were carried out at various concentrations of the monomers and initiator, other conditions being equal. The results obtained are shown in Fig. 5. As seen, v_0 increases with [AA], [AmA], and [PP]. The reaction orders with respect to monomers and initiator were determined from the slopes of the curves (Fig. 5). As a result, we determined the empirical equation of the overall rate of copolymerization of AA and AmA in aqueous solution:

$$V = K_c[\mathrm{AA}]^{1.5}[\mathrm{AmA}]^{1.4}[\mathrm{PP}]^{1.0},$$

where K_c is the rate constant of copolymerization.

The reaction orders with respect to the monomers exceeding unity are probably due to the increasing viscosity of the initial solutions, which agrees with published data [2]. The reaction order with respect to the initiator suggests monomolecular termination of the kinetic chains in copolymerization in concentrated aqueous solutions, which is due to the increasing viscosity of the reaction mixture.

The effect of temperature on the copolymerization of AA and AmA was studied at 40 and 60°C, other conditions being equal. Figure 6 illustrates the dependences of the content of AmA units in copolymer m_2 (curves *1* and *2*) on the content of AmA monomer in the initial monomer mixture at various temperatures. As seen, at the temperatures examined [η] decreases with increasing M_2 (curve *3* and *4*) owing to a decrease in the copolymer molecular weight, whereas m_2 increases (curves *1* and *2*). This increase in m_2 with temperature in probably due to a decreasing ionization of the ionic groups of AmA monomer and its units in macromolecules [3], which decreases electrostatic repulsion between AmA and macroradical, i.e., promotes enrichment of the copolymer with ionic units (passing from curve *1* to curve *2*, Fig. 6). Comparison of the experimental data at M_2 = const shows that, at smaller content of the AA units in copolymers

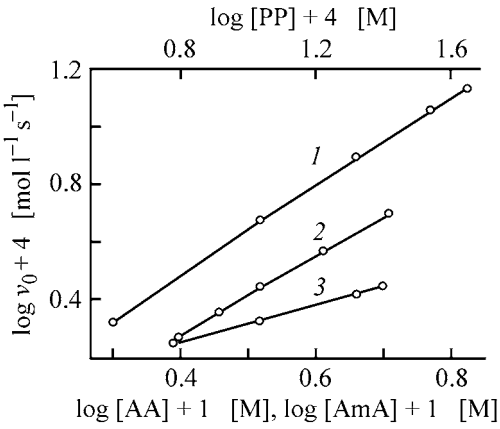

Fig. 5. Initial rate of copolymerization of AA and AmA v_0 vs. concentration of (*1*) AA, (*2*) AmA, and (*3*) PP (log–log plots). Concentration, M: (*1*) [AmA] 2.01 and [PP] 7.4×10^{-4}; (*2*) [AA] 6.03 and [PP] 7.4×10^{-4}; and (*3*) [AA] = [AmA] = 2.01.

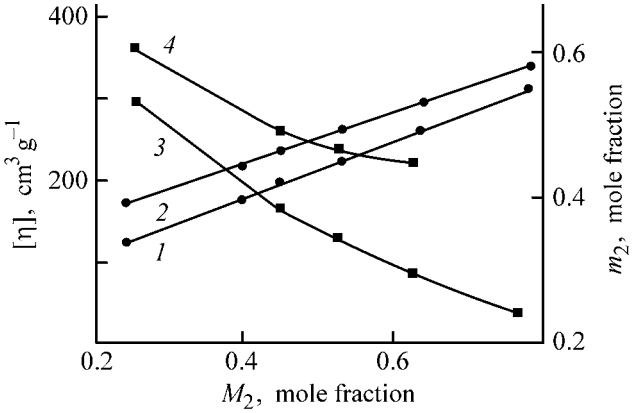

Fig. 6. (*1*, *2*) Mole fraction of AmA units in copolymer m_2 and (*3*, *4*) intrinsic viscosity of solutions [η] vs. the AmA mole fraction in the initial monomer mixture M_2 in copolymerization of AA and AmA at (*1*, *4*) 40 and (*2*, *3*) 60°C.

prepared at 60°C, smaller [η] and lower molecular weight are observed (Fig. 6, passing from curve *3* to curve *4*).

CONCLUSIONS

(1) Macromolecular copolymers were prepared from acrylamide and ammonium acrylate with a mole fraction of the ionic units of 0.01 to 0.55, viscosity-average molecular weight of $(0.03–1.15) \times 10^6$, and intrinsic viscosity of 40–360 cm^3 g^{-1} by copolymerization in concentrated aqueous solutions at 60°C in the presence of potassium persulfate initiator.

(2) The initial copolymerization rate increases with the concentrations of acrylamide, ammonium

acrylate, potassium persulfate, and monomer mixture ($M_1 + M_2$).

(3) The molecular weight of the copolymer increases as the concentration of acrylamide, monomer mixture, and conversion increase, and as the concentration of initiator and the solution pH decrease (from 12 to 10) and as the temperature is lowered from 60 to 40°C.

(4) The content of the ionic units in the copolymer increases with an increase in the concentrations of ammonium acrylate and monomer mixture and in pH (from 10 to 12) and with a decrease in temperature from 60 to 40°C and is almost independent of conversion.

(5) The copolymer yield grows as the concentrations of acrylamide and monomer mixture increase and pH decreases from 12 to 10.

REFERENCES

1. Nikolaev, A.F. and Okhrimenko, G.I., *Vodorastvorimye polimery* (Water-Soluble Polymers), Leningrad: Khimiya, 1975.
2. Abramova, L.I., Baiburdov, T.A., Grigoryan, E.P., et al., *Poliakrilamid* (Polyacrylamide), Kurenkov, V.F., Ed., Moscow: Khimiya, 1992.
3. Kabanov, V.A. and Topchiev, D.A., *Polimerizatsiya ionizuyushchikhsya monomerov* (Polymerization of Ionizable Monomers), Moscow: Nauka, 1975.
4. Kurenkov, V.F., Hartan, H.-G., and Lobanov, F.I., *Zh. Prikl. Khim.*, 2001, vol. 74, no. 4, pp. 529–540.
5. Kurenkov, V.F., Kabal'nova, N.V., and Aleeva, Yu.V., *Zh. Prikl. Khim.*, 1993, vol. 66, no. 7, pp. 1603–1608.
6. Kurenkov, V.F., Bulgakova, G.I., Filippova, A.N., and Aleeva, Yu.V., *Zh. Prikl. Khim.*, 1994, vol. 67, no. 7, pp. 1157–1161.
7. Kurenkov, V.F., Baiburdov, T.A., and Stupen'kova, L.L., in *Fiziko-khimicheskie osnovy sinteza i pererabotki polimerov* (Physicochemical Bases of Synthesis and Processing of Polymers), Gor'kii: Gor'k. Gos. Univ., 1985, pp. 79–86.
8. Klein, J. and Conrad, K.-D., *Macromol. Chem.*, 1980, vol. 181, no. 1, pp. 227–229.
9. Gromov, V.F., Bogachev, Yu.S., Bune, E.V., et al., *Vysokomol. Soedin.*, 1993, vol. 35, no. 1, pp. 7–12.

ISSN 1070-4272, Russian Journal of Applied Chemistry, 2007, Vol. 80, No. 2, pp. 295–299. © Pleiades Publishing, Ltd., 2007.
Original Russian Text © V.P. Lesnyak, D.I. Shiman, L.V. Gaponik, F.N. Kaputskii, A.I. Lamotkin, Zh.V. Bondarenko, 2007, published in Zhurnal Prikladnoi Khimii, 2007, Vol. 80, No. 2, pp. 296–300.

MACROMOLECULAR CHEMISTRY AND POLYMERIC MATERIALS

Copolymers of the C_9 Hydrocarbon Fraction of Liquid Pyrolysis Products with Maleic Anhydride and Their Esterification Products as Additives to Paper Pulp

V. P. Lesnyak, D. I. Shiman, L. V. Gaponik, F. N. Kaputskii, A. I. Lamotkin, and Zh. V. Bondarenko

Institute of Physicochemical Problems, Belarussian State University, Minsk, Belarus
Belarussian State Technological University, Minsk, Belarus

Received October 23, 2006

Abstract—The influence exerted by copolymers of the C_9 fraction of liquid pyrolysis products of petroleum raw materials with maleic anhydride and by their esterification products, added to paper pulp, on the main paper properties was examined.

DOI: 10.1134/S1070427207020255

Sizing of paper pulp is one of important steps in production of sized kinds of paper; it allows control over the hydrophobic properties of the product. Presently sizing is performed in an acidic medium by adding a sizing emulsion (or dispersion) and a coagulant solution to the paper pulp, after which the paper sheet is formed on the frame of the paper-making machine [1].

The most commonly used sizing materials are rosin and products of its modification. However, active efforts are made today to develop synthetic sizing materials that would not only allow the characteristics of sized paper to be varied in a wider range, but also impart to the paper some specific properties that cannot be imparted by rosin sizing. In particular, polymeric adhesives enhance the mechanical strength of paper [2] and the resistance of its surface to picking, inhibit its aging [3], enhance its acid and alkali resistance [4], and improve its printing properties [5]. Furthermore, polymeric adhesives do not absorb UV radiation in the range 350–370 nm and thus do not decrease the efficiency of optical brighteners [6].

The copolymer of maleic anhydride (MA) with styrene (Styromal) and products of its esterification have been fairly well studied and tested as synthetic additives in paper production. Along with styrene–MA copolymers, polymers containing units of acrylic acid, its esters, or acrylonitrile are also used for preparing synthetic adhesives. Copolymers of styrene with MA are classed with nonreactive anionic synthetic sizing materials, despite that they exhibit no sizing effect when taken alone and can be used only in a mixture with a rosin adhesive [1]. Therefore, it would be more adequate to consider such products as modifying additives.

As an analog of Styromal, we tested as an additive to paper pulp the copolymer of MA with C_9 hydrocarbon fraction of liquid pyrolysis products (CPM) whose main polymerizable components are styrene, its derivatives, and dicyclopentadiene.

The goal of this study was to examine the effect of additions of CPMs and their ester derivatives on the hydrophobic, strength, and special properties of paper.

It is known that nonreactive synthetic sizing materials and, in particular, polymeric adhesives, do not form strong chemical bonds with cellulose fibers [2]. The effect of paper sizing is based on the mechanism of fixation of coagulated particles on the fiber surface via adsorption-electrostatic interactions, similar to the mechanism of sizing with rosin products [1]. Therefore, we compared the properties of paper with CPM additions to those of the unsized paper and paper sized with ZhM rosin adhesive (adhesive paste from modified oleoresin rosin) in acidic medium (pH 4.8–5.2). Because direct interaction of copoly-

Table 1. Properties of paper prepared from sulfite pulp with ZhM and CPM additions

Additive, % of a.d.f.*	Content		Breaking length, m	Breaking strength, kgf		Wet strength, %
	$Al_2(SO_4)_3$, % of a.d.f.	MA in CPM, wt %		dry	wet	
–	–	–	3810	4.3	0.2	4.6
ZhM, 1.5	4.5	–	4030	4.5	0.6	13.5
CPM **1**:						
0.5	1	29	4800	5.3	0.2	3.8
1.5	4.5		4490	5.8	0.2	3.5
CPM **2**:						
0.5	1	26	5085	5.6	0.2	3.6
1.5	4.5		4415	5.0	0.2	4.0

* (a.d.f.) Absolutely dry fiber.

mer particles bearing a negative charge with cellulose fibers, also charged negatively, is impossible, it is necessary to add a coagulant (most commonly aluminum sulfate) to the paper pulp to attain the hydrophobizing effect.

Copolymers of the C_9 fraction and MA in the form of ammonium salts were introduced into sulfite pulp before casting the paper sheet. We found that the copolymers under consideration, like Styromal, show no sizing properties but enhance the mechanical strength of paper sheet. Table 1 shows that even at 0.5% concentration of the copolymer in the system the strength of the paper sheet (dry breaking strength and breaking length) are 20–30% higher than those of the paper without additives and paper sized with ZhM rosin adhesive. The wet strength of paper remains similar to that of the unsized paper. It is of interest that the strength does not grow as the amounts of the additive and coagulant [$Al_2(SO_4)_3$] increase.

A turbidimetric analysis demonstrated that aqueous solutions of copolymers **1** and **2** (Table 1) contain particles with mean diameters of 186 and 104 nm, respectively. The rosin emulsion of ZhM contains dispersed phase particles of smaller size, 93 nm. The electrolytic coagulation of copolymer solutions with $Al_2(SO_4)_3$ occurs more slowly than that of the ZhM rosin emulsion. A 2 : 1 weight ratio of the coagulant to the additive is preferable; at a higher content of $Al_2(SO_4)_3$ (3 : 1, 4 : 1), the coagulation decelerates. A higher strength was obtained with copolymer **2** (0.5% of a.d.f., Table 1), which, compared to copolymer **1**, was characterized by lower MA content and smaller size of dispersed phase particles.

To make CPMs more hydrophobic, we studied their esterification with 1-tetradecanol (myristyl alcohol) and alcohol fractions $C_{12}H_{25}OH$–$C_{16}H_{33}OH$ and $C_{16}H_{33}OH$–$C_{21}H_{43}OH$. To vary the hydrophilic–hydrophobic balance of macromolecules, the MA : alcohol molar ratio in the esterification was varied from 1 : 1 to 1 : 4. The esterified copolymers were converted to the salt form by treatment with aqueous ammonia:

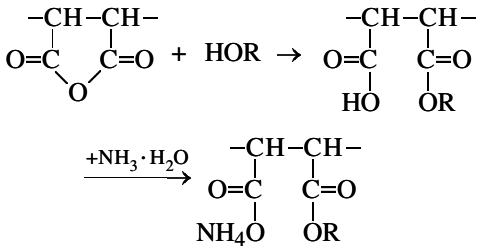

An IR study of the esterified CPMs showed that the anhydride groups are virtually completely converted in the course of esterification. The neutralization of the esterified copolymer is accompanied by partial base hydrolysis of the ester. The yield of the reaction product is virtually quantitative. The products obtained were tested as additives to paper pulp prepared from sulfate pulp [GOST (State Standard) 7269–86], sulfite pulp (GOST 3914–74), and MS-1 waste paper. The quality of paper specimens was evaluated by their hydrophobicity (extent of sizing determined by the stroke method and absorbency in one-sided wetting), strength (dry and wet breaking strength, breaking length, energy absorption and elongation at break), and special properties (wet strength).

Studies of CPMs showed that the maximal yields of the copolymers were attained at an equimolar ratio of MA to monomers of the C_9 fraction in the starting mixture. The MA content in such copolymers was about 30 wt %. Therefore, we chose these substrates to be tested in esterification first. We found that the esterification performed at the molar ratio of MA in copolymer to tetradecanol from 3 : 1 to 2 : 1, followed by neutralization, yielded water-soluble prod-

Table 2. Properties of CPMs esterified with tetradecanol (solvent cyclohexanone, 150°C, 3 h, MA content in the starting copolymer 30 wt %)

Initial molar ratio MA : alcohol	Acid number, (mg KOH) g^{-1}	Solubility in water
Nonesterified	349	Soluble
3 : 1*	267	
2 : 1**	205	
1 : 1	105	Insoluble

* Hereinafter, CPM **3**. ** Hereinafter, CPM **4**.

Table 3. Properties of paper prepared from sulfite pulp with additions of CPMs esterified with tetradecanol

Additive	Additive : $Al_2(SO_4)_3$ ratio, % of a.d.f.	Breaking length, m	Breaking strength, kgf		Breaking elongation, %	Wet strength,%
			dry	wet		
–	–	6570	4.3	0.2	1.85	4.6
ZhM	1.5 : 4.5	5300	4.5	0.6	1.78	13.5
CPM **3**	0.5 : 1	5910	5.5	0.24	1.95	4.4
	1.5 : 4.5	5300	4.6	0.34	1.85	7.4
CPM **4**	0.5 : 1	5460	4.6	0.38	1.75	8.3
	1.5 : 4.5	5550	5.2	0.38	1.87	7.3

Table 4. Properties of paper prepared from various fibrous materials with addition of CPM esterified with tetradecanol (content of ZhM rosin adhesive 1.5% of a.d.f., ZhM : $Al_2(SO_4)_3$ = 1 : 3, CPM **5** content 0.5% of a.d.f., CPM **5** : $Al_2(SO_4)_3$ = 1 : 2)

Fibrous material	Additive	Breaking length, m	Breaking strength, kgf		Breaking elongation, %	Wet strength, %
			dry	wet		
Sulfate pulp	–	7940	8.3	0.2	1.94	2.4
	ZhM	8300	7.5	0.54	1.78	7.2
	CPM **5***	9740	10.7	0.62	1.73	5.8
Sulfite pulp	–	9320	4.3	0.2	1.58	4.6
	ZhM	8300	7.5	0.54	1.78	7.2
	CPM **5**	10490	10.2	0.56	1.99	5.5
Waste paper	–	6150	5.0	0.16	1.41	3.2
	ZhM	5890	4.6	0.24	1.34	5.2
	CPM **5**	5980	4.8	0.38	1.72	7.9

* MA content of the starting copolymer 21 wt %, molar ratio of MA in CPM to alcohol in esterification 4 : 1.

ucts (Table 2). At the equimolar ratio, the products obtained did not dissolve in water even on boiling.

Our studies showed that, like unmodified CPMs, the esterified CPM derivatives exhibit no sizing effect. Table 3 shows that, with the copolymers containing 30 wt % MA and esterified with tetradecanol, the wet breaking strength and wet strength of the paper sheet are considerably lower (by a factor of 1.5–3.0) than those of the paper specimen sized with a rosin adhesive. The dry breaking strength and the elongation and energy absorption at break for the paper specimens containing the synthesized additives are similar to those of the unsized paper and paper sized with ZhM adhesive. We found that it is preferable to use as an additive to paper pulp the esterified copolymer with a lower acid number (CPM **4**) at its 0.5% content in the system and additive : coagulant ratio of 1 : 2.

We found that addition of the esterified copolymer with a lower MA content (21 wt %, molar ratio MA : alcohol = 4 : 1) to the paper pulp in an amount of 1.5 wt % of a.d.f. imparts to the paper a wet strength comparable with that of the paper impregnated with rosin adhesive. Furthermore, the dry strength of the thus obtained paper sheet, even at the additive content as low as 0.5%, is higher than that of the paper sized with rosin adhesive and unsized paper. This additive is fairly versatile, as it improves the properties of paper prepared both from sulfate and sulfite pulps and from waste paper (Table 4).

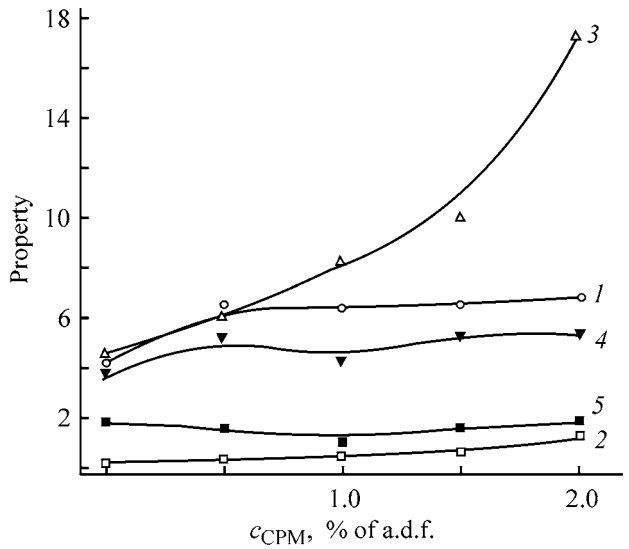

Properties of a paper sheet based on sulfite pulp vs. the concentration (c_{CPM}) of the esterified copolymer (CPM **6**, MA content in the starting copolymet 32 wt %, molar ratio MA : alcohol in esterification 1.5 : 1) in the paper pulp. CPM **6** : $Al_2(SO_4)_3$ ratio 1 : 2. Property: (*1*) dry breaking strength, kgf; (*2*) wet breaking strength, kgf; (*3*) wet strength, %; (*4*) breaking length, mm; and (*5*) breaking elongation, %.

Similar results were obtained upon addition to the paper pulp of copolymers with a higher MA content (30 wt %), esterified with tetradecanol at the molar ratio MA : alcohol = 1.5 : 1. Using the copolymers with an MA content of about 20 wt %, esterified with tetradecanol at the molar ratio MA : alcohol = (1.5–2) : 1, we obtained paper specimens whose wet strength exceeded that of the paper sized with the ZhM rosin adhesive [ZhM content 1.5%, ratio ZhM : $Al_2(SO_4)_3$ = 1 : 3]. As in the preceding cases, the optimal concentration of the copolymer was 0.5 wt % of absolutely dry fiber, and the additive : coagulant ratio was 1 : 2.

An examination of paper specimens prepared using copolymers esterified with different alcohols ($C_{14}H_{29}OH$, alcohol fractions $C_{12}H_{25}OH$– $C_{16}H_{33}OH$ and $C_{16}H_{33}OH$–$C_{21}H_{43}OH$) showed that the paper sheet characteristics were virtually independent of the hydrocarbon chain length in the alcohol molecule in the interval from $C_{12}H_{25}$ to $C_{21}H_{43}$. Replacement of ammonium salts of the esterified copolymers with their sodium salts had no appreciable effect on the paper properties, either. It should be noted that an increase in the concentration of the additive in the system, as a rule, does not lead to proportional changes in the properties of the paper sheet obtained (see figure).

EXPERIMENTAL

CPM ammonium salts were prepared by adding to 3 g of the copolymer 6 ml of 10% aqueous ammonia (molar ratio NH_3 : MA = 4 : 1). The mixture was refluxed until the copolymer fully dissolved. Excess ammonia and water were distilled off on a rotary evaporator at 60–70°C (15–20 mm Hg). The resulting product was dried at 90–100°C in a vacuum (2 mm Hg) to constant weight.

Esterification of the copolymers was performed in the bulk or in a cyclohexanone solution. A glass vessel equipped with a power-driven stirrer, a thermometer, and a reflux condenser was charged with 3 g of the copolymer (MA content 30 wt %), 15 ml of cyclohexanone (if the reaction was performed in solution), and 1 g of tetradecanol (molar ratio MA : alcohol = 2 : 1). In some experiments, pyridine was used as esterification catalyst. The mixture was heated to 140–150°C with vigorous stirring for 3 h, after which cyclohexanone was distilled off in a vacuum (90–100°C, 2 mm Hg). The product was washed with several portions of diethyl ether to remove the unchanged tetradecanol. The washed copolymer was vacuum-dried (90–100°C, 2 mm Hg) to constant weight. The yield of the esterified copolymer was up to 98 wt %.

The acid number of the esterified copolymers was determined by direct titration with phenolphthalein as indicator; a 0.1–0.2-g sample was dissolved in 10 ml of acetone, 10 ml of water was added, and the mixture was titrated with 0.1 N KOH.

The mean particle diameter and kinetic features of the electrolytic coagulation of the copolymers and rosin emulsion were determined by turbidimetric examination of 0.04% aqueous solutions with a KFK-2 photoelectric colorimeter.

Paper specimens (70 g m^{-2}) were prepared on a Rapid–Ketten paper-casting apparatus. Fibrous pulp was first unraveled in a BM-3 disintegrator and then milled in a laboratory roll by a standard procedure to the Schopper–Riegler freeness of 40° (concentration of milled fibrous suspension 1%). To prepare paper specimens, a 2% aqueous solution of the salt form of the MA–C_9 fraction copolymer and then a 0.5% solution of aluminum sulfate were added to 220 cm^3 of the fibrous suspension containing 2.2 g of a.d.f. The copolymer content was varied from 0.5 to 2.0 wt % of a.d.f., and the $Al_2(SO_4)_3$ content, from 1 to 6% of a.d.f.; the additive : coagulant weight ratios were 1 : 2, 1 : 3, and 1 : 4.

The hydrophobic properties of paper specimens were evaluated by the degree of sizing (stroke method,

GOST 8049–91) and by absorbency in one-sided wetting (GOST 12605–82). The strength and special properties of paper specimens were evaluated by the dry and wet breaking strength (GOST 135225.1–79) and wet strength (GOST 8049–62). The breaking length, breaking elongation, wet strength, and dry and wet bending strength were determined with Lorentzen a. Wetter devices.

CONCLUSIONS

(1) The influence exerted by additions of esterified and nonesterified copolymers of C_9 fraction and MA to paper pulp on the properties of paper sheets was examined. Addition of the unmodified copolymers enhances the paper strength, and addition of esterified copolymer enhances both the strength properties and wet strength. Some strength characteristics considerably exceed those of the paper with additions of the ZhM rosin adhesive. The modified and unmodified copolymers exhibit no sizing effect. The optimal concentration of the additives is 0.5 wt % of absolutely dry fiber, and the optimal additive : coagulant weight ratio is 1 : 2.

(2) Paper with the best properties is obtained when esterified copolymers with a lower MA content (about 20 wt %) and copolymers with the molar ratio MA : alcohol = (1.5–2) : 1, which are more hydrophobic, are used as additives. The hydrophobicity of the products can be increased both in the copolymerization step (synthesis of copolymers with a low MA content) and by esterification with long-chain alcohols.

REFERENCES

1. Chernaya, N.V. and Lamotkin, A.I., *Prokleika bumagi i kartona v kisloi i neitral'noi sredakh* (Sizing of Paper and Cardboard in Acidic and Neutral Media), Minsk: Bel. Gos. Tekh. Univ., 2003.
2. Sokolova, O.K., Rishes, N.M., Shneider, K.S., et al., *Zameniteli kanifoli dlya prokleiki bumagi i drugikh tselei: Obzornaya informatsiya: Lesokhimiya i podsochka* (Rosin Substitutes for Paper Sizing and Other Purposes: Review: Wood Chemistry and Boxing), Moscow: VNIPIEIlesprom, 1983.
3. Ivanov, G.A. and Flyate, D.M., *Starenie bumagi* (Paper Aging), Moscow: VNIPIEIlesprom, 1971.
4. Poluiko, E.G., Afanas'eva, V.V., and Volkov, V.A., *Gidrolizn. Lesokhim. Prom–st.*, 1975, no. 8, pp. 6–7.
5. Pshenichnikov, V.S., Volkov, V.A., Tatiev, D.A., et al., *Poligrafiya*, 1977, no. 1, pp. 23–31.
6. Afanas'eva, V.V., Poluiko, E.G., Lapin, V.V., and Volkov, V.A., *Sinteticheskie materialy dlya prokleiki bumagi* (Synthetic Materials for Paper Sizing), Moscow: Lesn. Prom–st., 1983.

ISSN 1070-4272, Russian Journal of Applied Chemistry, 2007, Vol. 80, No. 2, pp. 300–304. © Pleiades Publishing, Ltd., 2007.
Original Russian Text © N.M. Zabivalova, A.M. Bochek, E.N. Vlasova, B.Z. Volchek, 2007, published in Zhurnal Prikladnoi Khimii, 2007, Vol. 80, No. 2, pp. 301–305.

MACROMOLECULAR CHEMISTRY AND POLYMERIC MATERIALS

Preparation of Mixed Cellulose Ethers by the Reaction of Short Flax Fibers and Cotton Linter with Monochloroacetamide

N. M. Zabivalova, A. M. Bochek, E. N. Vlasova, and B. Z. Volchek

Institute of Macromolecular Compounds, Russian Academy of Sciences, St. Petersburg, Russia

Received July 3, 2006; in final form, October 2006

Abstract—The conditions of preparation of mixed cellulose ethers containing carboxy and amino groups by the reaction of samples of short flax fiber and cotton linter with monochloroacetamide were examined. The influence of the amino groups of the mixed cellulose ethers on the rheological properties of their aqueous solutions was elucidated.

DOI: 10.1134/S1070427207020267

An increased interest is presently attracted by self-associated polymer systems based on biodegradable and environmentally safe natural polymers. These systems include water-soluble compounds of cellulose and, in particular, its ethers: carboxymethyl cellulose in the form of a sodium salt (NaCMC), methyl cellulose (MC), hydroxyethyl cellulose (HEC), methoxypropyl cellulose, etc. Most of the above-mentioned ethers possess a set of valuable properties: water solubility, lack of toxicity, and good thickening power. They find wide application in food industry, perfumery, oil extraction, and medicine [1]. The principal raw materials for preparation of the ethers are wood and cotton varieties of cellulose. Large-capacity waste from flax production, short flax fibers and the hardwood part of the flax stem (flax boon) can serve as an alternative source of cellulose for preparation of its various ethers.

Among ionic compounds of cellulose, the most extensively used is carboxymethyl cellulose; it serves as a thickening and structuring agent in production of adhesives, lacquers, paints, detergents, and toothpastes. Chemical modification of CMC is one of the ways to modify the properties of this widespread ether. Introduction of new functional groups (in this case, amide) into CMC macromolecules implies changing the physicochemical properties of a new cellulose compound.

The physicochemical properties of the resulting ether are influenced by the nature of the initial polymer, namely, the molecular weight, chemical composition, presence of associated substances, structural uniformity, and fiber morphology.

Here, we examined the conditions of synthesis of cellulose ethers by the reaction of cotton and flax cellulose with monochloroacetamide (MCAA). It can be assumed that new cellulose compounds containing carboxy and amide groups exhibit ion-exchanging properties.

Carboxymethyl cellulose amides (CMCAs) can be prepared by the reaction of CMC acid chlorides with amines [2–4] and by the reaction of CMC in the acid form (HCMC) with amines [5]. By contrast to the above-mentioned methods of preparation of CMCAs, we studied here the conditions of synthesis without employing high temperatures and such reagents as dimethylformamide, $SOCl_2$, benzene, and xylene. The synthesis conditions and the apparatus in our experiments were identical to those in preparation of NaCMC.

EXPERIMENTAL

As initial materials served cotton linter with a degree of polymerization DP_η = 1500 and pretreated short flax fibers with DP_η = 3700. The flax fibers were treated by boiling for 3 h in the cooking solution of composition NaOH : $Na_2S_2O_3$: H_2O (at a fiber : NaOH : $Na_2S_2O_3$ ratio of 1 : 1.2 : 0.7) in a nitrogen medium [6]. Such a treatment removes most of associated substances (hemicelluloses, lignin, pectins)

from the flax fibers, with a minor decrease in the DP of cellulose.

The cellulose compounds were synthesized by the reaction

$$Cell(OH)_3 + NaOH + ClCH_2{-}\overset{\overset{O}{\|}}{C}{-}NH_2$$

$$\xrightarrow{T = 60^\circ C,\ i\text{-PrOH}} Cell(OH)_{(3-x)}(OCH_2{-}\overset{\overset{O}{\|}}{C}{-}NH_2)_x + NaCl.$$

The initial samples were stirred in isopropyl alcohol, whereupon 30% aqueous NaOH was introduced, and the resulting mixture was stirred at room temperature for another 1 h. Next, MCAA was introduced, and the reaction was run at T = 55°C. Upon completion of the reaction, the liquid was decanted, 70% methanol was added, and the resulting mixture was stirred, whereupon the liquid was decanted and the product was washed with 70% aqueous ethanol to neutral pH [6, 7]. The removal of NaOH was monitored by phenolphthalein coloration, and the removal of Cl^- ions, by the reaction with an $AgNO_3$ solution. The washed samples were dried to constant weight in a vacuum desiccator at T = 60°C. The nitrogen content was determined by the Kjeldahl method [8]. The degree of substitution, DS, with respect to the carboxy groups was calculated as

$$DS_{Na} = \frac{Na\% \times 162}{2300 - Na\% \times 80},$$

where Na is the sodium content of the polymer, wt %.

The amount of Na was determined by conductometric back-titration of the CMCA samples. The solubility of CMCA was calculated by the formula

$$S = \left(100 - \frac{g_2 - g_3}{g_1}\right) \times 100,$$

where g_1 is the mass of the polymer sample, g; g_2, mass of the precipitate with the filter, g; and g_3, mass of the filter, g.

A weighed portion of the polymer (with due account of its moisture content) was placed in distilled water (in an amount corresponding to 1% solution), and the mixture was stirred for several hours at room temperature. The resulting solution was filtered through a weighed (dried to constant weight at T = 105°C) Schott filter no. 2. The precipitate was washed with water and dried to constant weight.

The table lists the conditions of synthesis of mixed cellulose ethers and selected characteristics of the products. It is seen that, for all the resulting cellulose ethers, the number of carboxy groups substantially exceeds that of amide groups. Hence, a number of side chemical reactions proceed during synthesis.

Conditions of synthesis of mixed cellulose ethers and their solubility in water (washing of the samples with EtOH)

Reaction time, h	Content, %		Degree of substitution with respect to Na	Solubility in water, %
	N	Na		
Short flax fibers				
2.0	0.60	4.87	0.41	77.0
3.5	0.55	5.13	0.43	73.0
5.0	0.50	4.64	0.40	77.0
Cotton linter				
2.0	1.30	4.84	0.41	83.0
3.5	1.60	5.32	0.53	93.0
5.0	0.69	5.60	0.50	82.0

(1) Hydrolysis of the initial MCAA, yielding sodium monochloroacetate, which reacts with cellulose, to give NaCMC and NaCl [1]:

$$ClCH_2{-}\overset{\overset{O}{\|}}{C}{-}NH_2 \xrightarrow{NaOH,\ H_2O} ClCH_2{-}\overset{\overset{O}{\|}}{C}{-}ONa + NH_3,$$

$$Cell(OH)_3 + NaOH + ClCH_2{-}\overset{\overset{O}{\|}}{C}{-}ONa$$

$$\xrightarrow[NaOH]{T = 60^\circ C,\ i\text{-PrOH},} Cell(OH)_{(3-x)}(OCH_2{-}\overset{\overset{O}{\|}}{C}{-}ONa)_x + NaCl.$$

(2) Hydrolysis (saponification) of the resulting CMC amide (more precisely, of the mixed cellulose ether), to give NaCMC:

$$Cell(OH)_{(3-x)}(OCH_2{-}\overset{\overset{O}{\|}}{C}{-}NH_2)_x$$

$$\xrightarrow{NaOH} Cell(OH)_{(3-x)}(OCH_2{-}\overset{\overset{O}{\|}}{C}{-}ONa)_x + NH_3.$$

The side reactions decrease the yield of the main product. The sodium content in the samples is no higher than 5.32% (DS_{Na} = 0.53), and the maximal content of nitrogen is 1.6%.

The chemical analysis data (content of nitrogen and carboxy groups) were confirmed by the IR Fourier spectra of the mixed cellulose ethers, measured on an FS-88 Bruker IR Fourier spectrometer (KBr pellets).

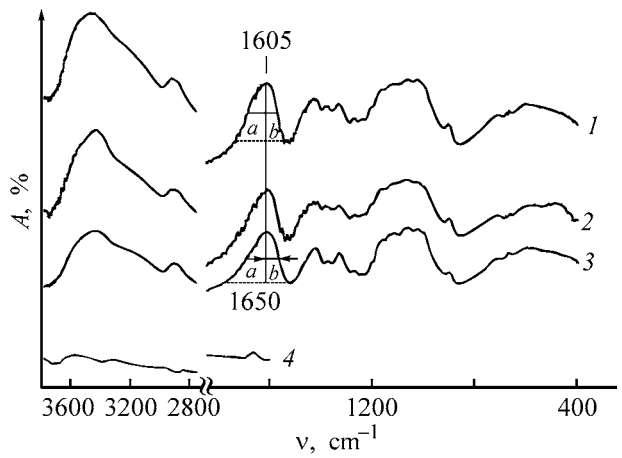

Fig. 1. (*1*, *2*) IR Fourier spectra of the mixed cellulose ethers prepared from (*1*) flax fibers and (*2*) cotton linter, (*3*) IR spectrum of refined commercial NaCMC, and (*4*) difference spectrum obtained by subtracting the spectrum of NaCMC from spectrum *2*. (*A*) Absorption and (ν) wavenumber.

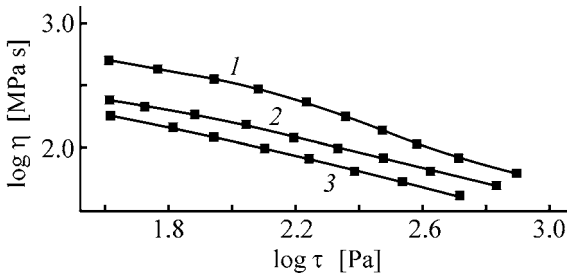

Fig. 2. Flow curves of 1.0% aqueous solutions of the mixed ethers of cellulose based on cotton at (*1*) 20, (*2*) 30, and (*3*) 40°C. Reaction time 2 h. (η) Viscosity and (τ) shear stress; the same for Fig. 3.

Figure 1 shows as an example the IR spectra of the mixed cellulose ethers prepared from cotton linter and flax fibers at 55°C and a reaction time of 3.5 h. Also, Figure 1 presents for comparison the IR spectrum of commercial refined NaCMC. The IR spectra of all the cellulose ethers synthesized in this study are similar to spectra *1* and *2*.

Spectral features characteristic of refined cotton cellulose include a broad absorption band at 3000–3700 cm^{-1}, associated with OH groups of the polymer, both free and linked by intra- and intermolecular hydrogen bonds, and absorption at 2900 cm^{-1}, associated with the CH_2 and CH groups of the polymers. The band at 2900 cm^{-1} in the spectrum of refined cellulose is nearly symmetrical [9]. The IR spectrum of NaCMC contains a band at 1597–1605 cm^{-1}, associated with antisymmetrical vibrations of the ionized carboxy groups COO^- [1]. Upon convertion of NaCMC to the H form, an absorption band at 1740 cm^{-1}, associated with the COOH groups, appears along with a shoulder at 1647 cm^{-1} [5]. For the CO groups of amide, an absorption band at 1650 cm^{-1} is characteristic (amide **I**), as well as a band at 1515–1570 cm^{-1}, associated with the bending vibrations of the NH groups (amide **II**) [10].

The content of the amide groups in the samples synthesized is not high (see table) compared to that of the COONa groups, whose absorption bands occur in close proximity. Therefore, we analyzed the IR spectra to reveal the amide groups in the products by two procedures. The first procedure consisted in analyzing the change in the ratio of the left-to-right parts of the half-width of the band at 1605 cm^{-1} by the technique suggested for analyzing changes in the system of hydrogen bonds in cellulose ethers [1]. It is believed that the total absorption band is composed of the contributions made by the COONa group (1605 cm^{-1}) and the CO groups of amide I (1650 cm^{-1}). For refined NaCMC, the *a*/*b* ratio of the band half-widths was estimated at 2.0, while that for all the samples of the mixed cellulose ethers, at 2.3–2.8. The broadening of the left part of the absorption band suggests the presence of the CO groups of amide.

The second procedure consisted in obtaining the difference (subtraction) spectra by subtracting the IR spectrum of NaCMC from that of the mixed cellulose ethers synthesized. Figure 1 shows as an example the difference spectrum obtained by subtracting spectrum *3* from spectrum *2* (curve *4*). Near 1650 cm^{-1}, there is a characteristic absorption band of amide **I**. It should be noted that the absorption band at 1515–1570 cm^{-1} (amide **II**) is 2–3 times less intense than that at 1650 cm^{-1} [10]. Thus, the absence of the absorption band associated with amide **II** can be attributed to the small number of amide groups in the samples synthesized.

Thus, our IR Fourier spectroscopic examination confirmed the presence in the samples of carboxy and amide groups, revealed by the chemical and physicochemical methods of analysis of the mixed cellulose ethers synthesized.

Since CMC is widely used in the form of aqueous solutions, we carried out a comparative examination of the rheological properties of moderately concentrated (1.0 wt %) aqueous solutions of the mixed ethers synthesized from flax and cotton cellulose. Figure 2 shows as an example the flow curves of 1% aqueous solution of mixed ether of cotton cellulose. For all the remaining samples we obtained similar flow curves; these are partial flow curves of non-New-

tonian fluids. Based on the temperature dependences of the viscosity, we calculated the heats E_a of activation of viscous flow of the solutions. These parameters were calculated for temperatures within 20–40°C. For solutions of the ethers based on cotton, E_a varies within 32.0–40.0 kJ mol^{-1}, and for the samples based on flax fibers, within 40.0–55.0 kJ mol^{-1}. For NaCMC solutions, E_a was estimated at 20.0 kJ mol^{-1}.

Figure 3 shows the flow curves of equiconcentrated solutions of CMCAs synthesized from cotton and flax fiber cellulose. For comparison, Fig. 3 shows the flow curve of an aqueous solution of commercial NaCMC obtained by the reaction of cotton linter with monochloroacetic acid. The conditions of synthesis for NaCMC (in isopropanol at 55°C) are identical to those for CMCAs.

The difference in the viscosity of the solutions is due to that in the molecular weights of the initial polymers, as well as to the presence in the mixed cellulose ethers of amide groups contributing to formation of a hydrogen bond system in concentrated solutions of polymers. It should be noted that commercial NaCMC has a higher DS_{Na}, which, in turn, increases the water solubility of the ether [1].

To elucidate how the time of synthesis of the cellulose ethers influences the viscosity of their aqueous solutions, we plotted the viscosity of the solutions of the mixed ethers vs. the reaction time at identical shear stresses ($\log \tau = 2.2$). Figure 4 shows that the viscosity of the mixed ethers of both flax and cotton cellulose we examined tends to decrease with increasing reaction time. The decrease in viscosity is presumably due to oxidative degradation of the glycoside bonds in the cellulose macromolecules (in an alkaline medium in the presence of atmospheric oxygen [1]) and to the change in the ratio of the numbers of carboxy to amide groups (see table).

CONCLUSIONS

(1) Mixed cellulose ethers were synthesized by the reaction of cellulose with monochloroacetamide.

(2) Chemical, physicochemical, and IR Fourier spectroscopic examinations confirmed the presence of carboxy and amide groups in the resulting cellulose compounds. The number of the functional groups and their ratio depend on the reaction time.

(3) Rheological properties of 1 wt% aqueous solutions of the mixed cellulose ethers were examined.

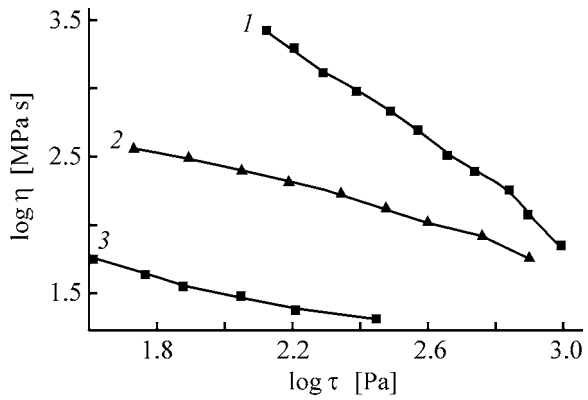

Fig. 3. Flow curves of 1.0 wt % aqueous solutions of the mixed ethers of cellulose based on (*1*) flax (DS_{Na} = 0.43), (*2*) cotton (DS_{Na} = 0.53), and (*3*) commercial NaCMC (DS_{Na} = 0.58). Temperature 20°C.

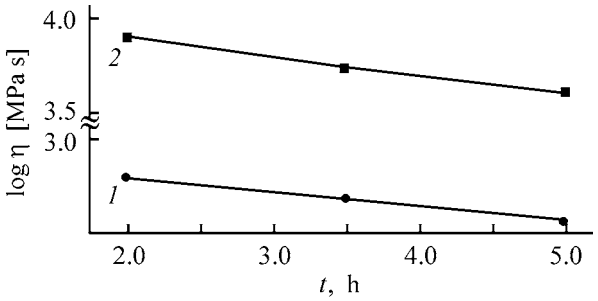

Fig. 4. Viscosity η of 1.0 wt % aqueous solutions of mixed ethers of cellulose based on (*1*) cotton linter and (*2*) short flax fibers (at 20°C $\log \tau = 2.2$) vs. the synthesis time *t*.

Aqueous solutions of the mixed ethers have a higher viscosity than the commercially produced carboxymethyl cellulose. This difference is due to that in the molecular weights of the ethers synthesized and commercial carboxymethyl cellulose, as well as to the presence in the mixed cellulose ethers of amide groups contributing to formation of the hydrogen bond system in concentrated solutions of the polymers.

REFERENCES

1. Petropavlovskii, G.A., *Gidrofil'nye chastichno zameshchennye efiry tsellyulozy i ikh modifikatsiya putem khimicheskogo sshivaniya* (Hydrophilic Partial ly Substituted Cellulose Ethers and Their Modification by Chemical Cross-Linking), Leningrad: Nauka, 1989.
2. Sun-Tun, Derevitskaya, V.A., and Rogovin, Z.A., *Vysokomol. Soedin.*, 1959, vol. 1, no. 8, pp. 1178–1183.
3. Kinstler, O.B. and Porsham, M.L., *Izv. Akad. Nauk Latv. SSR., Ser. Khim.*, 1977, no. 6, pp. 730–742.
4. Klem, D., Scnaberrauch, M., and Geschwend, G.,

Wiss. Z., Friedrich Schiller Univ., Jena Naturwiss. R., 1985, nos. 5–6, pp. 34–39.

5. Zabivalova, N.M., Bochek, A.M., Kalyuzhnaya, L.M., et al., *Zh. Prikl. Khim.*, 2003, vol. 76, no. 12, pp. 2048–2052.
6. *Spravochnik po khimicheskoi tekhnologii obrabotki l'nyanykh tkanei* (A Reference Book on Chemical Technology of Processing of Flax Fabrics), Fridlyand, G.I., Ed., Moscow: Legkaya Industriya, 1973.
7. Obolenskaya, A.V., Shchegolev, V.P., Akim, G.A., et al., *Prakticheskie raboty po khimii drevesiny i tsellyulozy* (Practical Works on Wood and Cellulose Chemistry), Moscow: Lesnaya Prom–st., 1965.
8. Klimova, V.A., *Osnovnye mikrometody analiza organicheskikh soedinenii* (Basic Micromethods of Analysis of Organic Compounds), Moscow: Khimiya, 1965.
9. Zhbankov, R.G., *Infrakrasnye spektry tsellyulozy i ee proizvodnykh* (Infrared Spectra of Cellulose and Its Compounds), Minsk: Nauka i Tekhnika, 1964.
10. Bellamy, L.J., *The Infra-Red Spectra of Complex Molecules*, London: Methuen, 1954.

ISSN 1070-4272, Russian Journal of Applied Chemistry, 2007, Vol. 80, No. 2, pp. 305–310. © Pleiades Publishing, Ltd., 2007.
Original Russian Text © S.S. Nikulin, O.N. Filimonova, N.S. Nikulina, 2007, published in Zhurnal Prikladnoi Khimii, 2007, Vol. 80, No. 2, pp. 306–311.

MACROMOLECULAR CHEMISTRY AND POLYMERIC MATERIALS

Modification with Maleic Acid of the Copolymer from By-Products of Polybutadiene Production and Use of the Modified Copolymer for Protective Treatment of Wood Fiberboards

S. S. Nikulin, O. N. Filimonova, and N. S. Nikulina

Voronezh State Academy of Forestry Engineering, Voronezh, Russia

Received May 6, 2006

Abstract—Modification with maleic acid of a styrene-containing polymeric material prepared from by-products of polybutadiene production was studied.

DOI: 10.1134/S1070427207020279

Many wastes from petrochemical enterprises, including synthetic rubber plants, contain numerous reactive compounds.

It is known that butadiene dimers and trimers, on the one hand, are by-products in some petrochemical processes involving butadiene and, on the other hand, can be valuable raw materials for various organic and petrochemical syntheses and for production of polymeric materials [1, 2]. A process for production of styrene-containing low-molecular-weight polymeric materials from these by-products has been commercially implemented [3, 4]. However, the polymeric materials thus obtained contain no functional groups, which restricts their possible applications.

The problems of chemical modification of synthetic polymers, rubber stocks, and vulcanizates are given much attention today from both scientific and practical viewpoints. Introducing functional groups into the copolymers and finding new fields of their applications are important problems.

In this study, we examined the possibility of using for impregnation of wood materials a low-molecular-weight copolymer prepared from unsaturated compounds of recycled toluene distillation bottoms (TDB) from polybutadiene production, modified with maleic acid (MA). The interest in maleic acid as a modifying agent is based on the fact that maleic acid is a by-product in the production of phthalic and maleic anhydrides. Therefore, this process not only allows modification of polymeric materials prepared from by-products of polybutadiene production, with new properties imparted to the resulting compounds, but also provides utilization of production waste.

Maleic (*cis*-butenedioic) acid can be dehydrated to obtain maleic anhydride. Maleic acid and its esters readily isomerize into fumaric acid and its derivatives under the action of heat, light, and catalysts. Maleic acid is widely used for preparing various surfactants. Certain amount of MA is used in food industry for preparing tartaric acid [5].

EXPERIMENTAL

We examined how the MA content of the reaction mixture, temperature, and process duration affect the properties of the styrene-containing polymeric material based on unsaturated TDB (bound styrene content 75–80 wt %).

The modification was performed as follows. A reactor was charged with 100 g of 70% toluene solution of a low-molecular-weight styrene-containing polymeric material based on unsaturated TDB, and MA was added in various ratios to the starting polymer. The best modification conditions were determined by using the method of experiment design. We examined the effects of such factors as MA content, temperature, and process duration using the 4×4 Latin square plan [6]. For each factor, we took four levels of variation: factor A (MA dosage), 0, 3.0, 6.0, and 9.0 wt %; factor B (process temperature), 120, 150, 180, and 210°C; and factor C (process duration), 8, 16, 24, and 32 h. The reaction progress was monitored by analytical methods from the variation of the mean molecular

Table 1. Plan and results of the experiment*

A, wt %	B, °C			
	b_1 = 120	b_2 = 150	b_3 = 180	b_4 = 210
a_1 = 0	c_1 = 8 h y_1 = 1540 y_1' = 18.4 y_1'' = 1.2	c_2 = 16 h y_2 = 1570 y_2' = 17.8 y_2'' = 2.9	c_3 = 24 h y_3 = 1890 y_3' = 17.0 y_3'' = 2.4	c_4 = 32 h y_4 = 1580 y_4' = 16.2 y_4'' = 1.7
a_2 = 3	c_2 = 16 h y_5 = 1700 y_5' = 17.8 y_5'' = 8.1	c_3 = 24 h y_6 = 1920 y_6' = 16.9 y_6'' = 15.3	c_4 = 32 h y_7 = 1570 y_7' = 16.0 y_7'' = 11.4	c_1 = 8 h y_8 = 1820 y_8' = 15.1 y_8'' = 7.5
a_3 = 6	c_3 = 24 h y_9 = 1650 y_9' = 16.1 y_9'' = 8.8	c_4 = 32 h y_{10} = 2190 y_{10}' = 15.7 y_{10}'' = 5.6	c_1 = 8 h y_{11} = 1400 y_{11}' = 15.5 y_{11}'' = 13.1	c_2 = 16 h y_{12} = 2010 y_{12}' = 14.9 y_{12}'' = 9.7
a_4 = 9	c_4 = 32 h y_{13} = 1840 y_{13}' = 14.7 y_{13}'' = 13.4	c_1 = 8 h y_{14} = 2380 y_{14}' = 15.3 y_{14}'' = 6.7	c_2 = 16 h y_{15} = 2320 y_{15}' = 14.0 y_{15}'' = 11.3	c_3 = 24 h y_{16} = 2830 y_{16}' = 13.7 y_{16}'' = 15.5

* (y_i) Molecular weight; (y_i'), bromine number, (g Br_2) (100 g)$^{-1}$; and (y_i'') acid number, (mg KOH) g^{-1}.

weight $\overline{M}_v$ and of the acid and bromine numbers, which were determined in reaction mixture samples taken at regular intervals. The matrix of the Latin square plan is shown in Table 1.

Based on the experimental results, we plotted (Fig. 1) the dependences of the modification results on the above factors and obtained the regression equations. The equations of the dependences of the mean

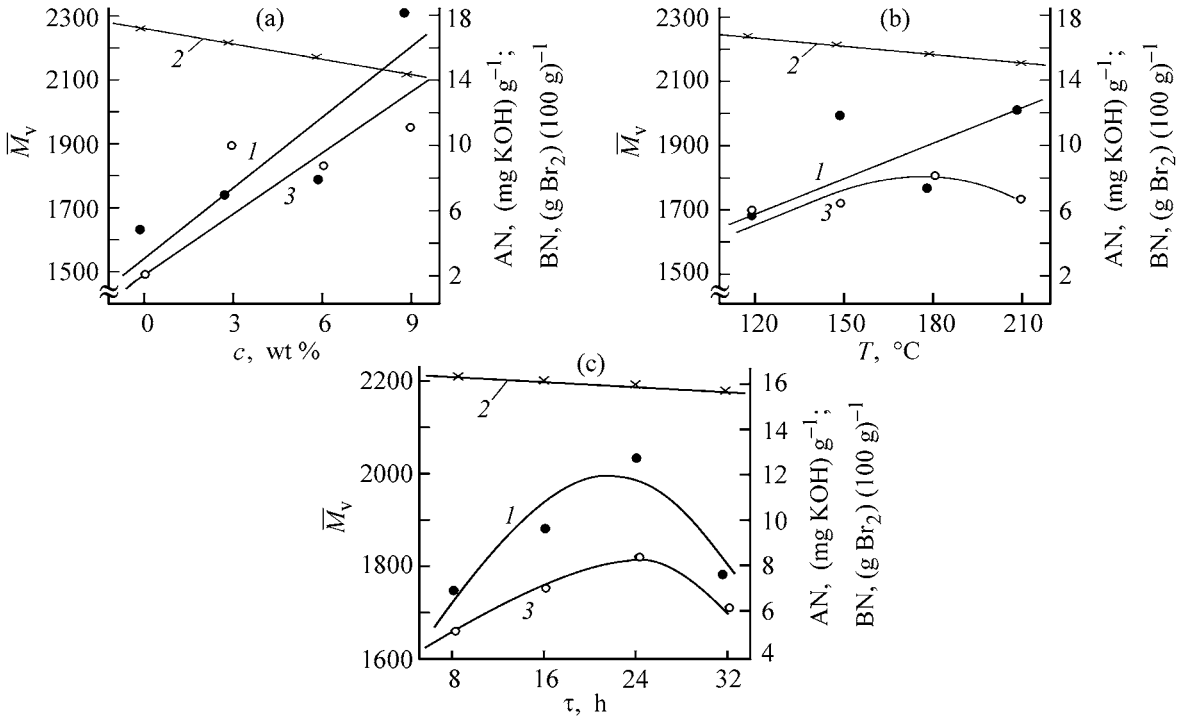

Fig. 1. Influence of (a) MA content c (0, 3.0, 6.0, 9.0 wt %, factor A), (b) process temperature T (120, 150, 180, 210°C, facotr B), and (c) process duration τ (8, 16, 24, 32 h, factor C) on (*1*) mean molecular weight $\overline{M}_v$, (*2*) bromine number BN, and (*3*) acid number AN.

Table 2. Plan and results of the experiment*

A, s	B, °C			
	$b_1 = 25$	$b_2 = 50$	$b_3 = 75$	$b_4 = 100$
$a_1 = 30$	$c_1 = 1$ h	$c_2 = 3$ h	$c_3 = 5$ h	$c_4 = 7$ h
	$d_1 = 120$°C	$d_2 = 140$°C	$d_3 = 160$°C	$d_4 = 180$°C
	$y_1 = 32.7$	$y_2 = 36.6$	$y_3 = 40.7$	$y_4 = 49.8$
	$y_1' = 20.6$	$y_2' = 19.1$	$y_3' = 17.8$	$y_4' = 16.9$
	$y_1'' = 14.5$	$y_2'' = 13.9$	$y_3'' = 13.8$	$y_4'' = 11.3$
$a_2 = 60$	$c_2 = 3$ h	$c_1 = 1$ h	$c_4 = 7$ h	$c_3 = 5$ h
	$d_3 = 160$°C	$d_4 = 180$°C	$d_1 = 120$°C	$d_2 = 140$°C
	$y_5 = 35.1$	$y_6 = 37.9$	$y_7 = 32.0$	$y_8 = 41.2$
	$y_5' = 18.9$	$y_6' = 18.1$	$y_7' = 18.6$	$y_8' = 17.2$
	$y_5'' = 13.4$	$y_6'' = 14.2$	$y_7'' = 14.5$	$y_8'' = 12.7$
$a_3 = 90$	$c_3 = 5$ h	$c_4 = 7$ h	$c_1 = 1$ h	$c_2 = 3$ h
	$d_4 = 180$°C	$d_3 = 160$°C	$d_2 = 140$°C	$d_1 = 120$°C
	$y_9 = 53.1$	$y_{10} = 48.9$	$y_{11} = 39.3$	$y_{12} = 34.6$
	$y_9' = 18.0$	$y_{10}' = 17.9$	$y_{11}' = 17.0$	$y_{12}' = 17.0$
	$y_9'' = 11.6$	$y_{10}'' = 12.4$	$y_{11}'' = 13.1$	$y_{12}'' = 12.9$
$a_4 = 120$	$c_4 = 7$ h	$c_3 = 5$ h	$c_2 = 3$ h	$c_1 = 1$ h
	$d_2 = 140$°C	$d_1 = 120$°C	$d_4 = 180$°C	$d_3 = 160$°C
	$y_{13} = 45.3$	$y_{14} = 39.5$	$y_{15} = 44.8$	$y_{16} = 40.2$
	$y_{13}' = 17.5$	$y_{14}' = 17.2$	$y_{15}' = 16.9$	$y_{16}' = 16.5$
	$y_{13}'' = 12.1$	$y_{14}'' = 11.7$	$y_{15}'' = 11.2$	$y_{16}'' = 10.9$

* (y_i) Bending strength, MPa; (y_i') water absorption in 24 h, %; (y_i'') swelling in thickness in 24 h, %.

molecular weight and of the bromine and acid numbers on the above factors are as follows:

for the molecular weight $\overline{M}_v$,

$$Y = 2.92 \times 10^{-7} \times (1562 + 69a)(1439 + 2.6b)(1322 + 63c - 1.5c^2);$$

for the bromine number, (g Br_2) (100 g)$^{-1}$,

$$Y' = 3.96 \times 10^{-3}(17.34 - 0.32a) \times (19.31 - 2.07 \times 10^{-2}b)(16.22 - 1.625 \times 10^{-2}c);$$

and for the acid number, (mg KOH) g^{-1},

$$Y'' = 2.32 \times 10^{-2}(4.07 + 0.884a) \times (-9.48 + 0.19b - 5.367 \times 10^{-4}b^2) \times (0.708 + 0.682c - 1.58 \times 10^{-2}c^2).$$

Thus, an increase in the MA content and temperature leads to a rise in the mean molecular weight of the product, described by first-order equations. This fact can be attributed to the cross-linking in the system through Diels–Alder addition of MA to the macromolecules [7] and addition of MA to sites of double bond cleavage in the polymeric chains. It is important that MA can behave at high temperatures as a cationic catalyst and can accelerate the cross-linking. The influence of the reaction duration on the modification can be described by a second-order equation with a maximum, indicating that degradation processes become prevalent after approximately 20 h.

The acid number steadily grows with an increase in the MA content of the reaction mixture. However, the influence of the temperature and process duration on the acid number is described by second-order equations with maxima. This may be due to partial dehydration of MA and its transformation into maleic anhydride. The extent of this process increases with temperature. It is known that active dehydration of MA starts at ≥130°C, and at 150°C an equilibrium with 50% conversion is attained in 0.3 h [5, 8].

Thus, by varying the MA content, process duration, and temperature, it is possible to control the properties of the resulting products so as to meet consumer's requirements.

Functionalization of the styrene-containing polymeric material prepared from by-products formed in polybutadiene production opens new prospects for its application, such as production of rubber by emulsion (co)polymerization and protective treatment of wood materials with the aim to enhance their resistance to water and moisture and their mechanical strength.

We examined the application of the MA-modified product to treatment of wood fiberboards (WFBs). In so doing, we used the fourth-order 4×4 Greco-Latin square plan [6]. As the major factors exerting the strongest effect on the WFB properties we chose the impregnation duration (factor A; 30, 60, 90, 120 s), impregnating formulation temperature (factor B; 25, 50, 75, 100°C), heat treatment temperature (factor C; 120, 140, 160, 180°C), and heat treatment time (factor D; 1, 3, 5, 7 h). The following WFB parameters were monitored: bending strength, water absorption, and swelling in thickness. The matrix of the Greco-Latin square plan is given in Table 2.

The WFB treatment was performed as follows. Dried and weighed specimens were placed in an impregnation bath containing a polymeric material modified with MA, with addition of ~10 wt % drier, and kept for a prescribed time at a prescribed temperature according to the experimental plan. For impregnation we took the polymeric material modified with 6.0 wt % MA for 24 h. The impregnated WFB specimens were withdrawn from the bath, predried, and subjected to a heat treatment, after which they were cooled to room temperature and weighed. The copolymer content of the specimens was determined gravimetrically from the weight gain.

Addition of a drier accelerates both formation and decomposition of hydroperoxides. The reactions involving atmospheric oxygen actively occur in the surface layers. The oxygen access into the bulk of the formulation is limited, which leads to decreased contribution of oxidative processes and increased contribution of high-temperature polymerization. The last process is activated by various radicals present in the system ($R^{\cdot}$, $RO^{\cdot}$, $ROO^{\cdot}$, see scheme).

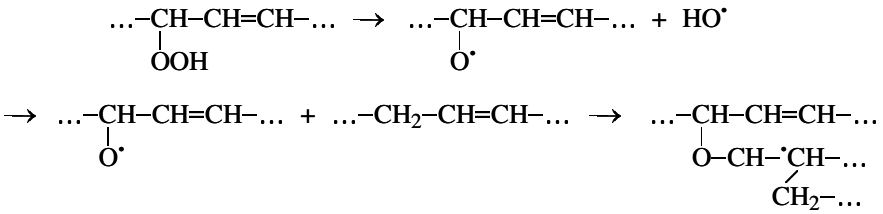

The film formation is inevitably accompanied by oxidative degradation yielding compounds that contain carbonyl, carboxy, and hydroxy groups. This leads to a further increase in the content of functional groups capable of reacting with active groups of lignin and cellulose. The probability of occurrence of such reactions is particularly high in surface layers under the conditions of film formation with a better efficient access of atmospheric oxygen.

By computer processing of the experimental results we obtained regression equations describing the effect of the main process parameters on the properties of the WFB specimens:

for the bending strength, MPa,

$$Y = 1.53 \times 10^{-5}(36.5 + 0.052a) \times (40.5 - 0.0028b)(35.7 + 1.17c)(14.5 + 0.174d);$$

for the water absorption in 24 h, %,

$$Y' = 1.77 \times 10^{-4}(19.1 - 0.0173a) \times (19.3 - 0.0236b)(18.0 - 0.065c)(19.6 - 0.0117d);$$

and for the swelling in thickness in 24 h, %,

$$Y'' = 4.87 \times 10^{-4}(14.4 - 0.022a) \times (13.45 - 0.0116b)(13.14 - 0.11c)(15.85 - 0.021d).$$

These dependences are plotted in Fig. 2. They show that the following conditions ensure the best characteristics of the modified fiberboards: impregnation duration of 30 s, impregnating–formulation temperature of 100°C, heat treatment temperature of 180°C, and heat treatment duration of 7 h. However, the effect of the impregnation duration in the examined interval on the WFB properties is insignificant. This is caused by the fact that WFBs have low density, and the MA-modified copolymeric material readily penetrates into the WFB structure within a short

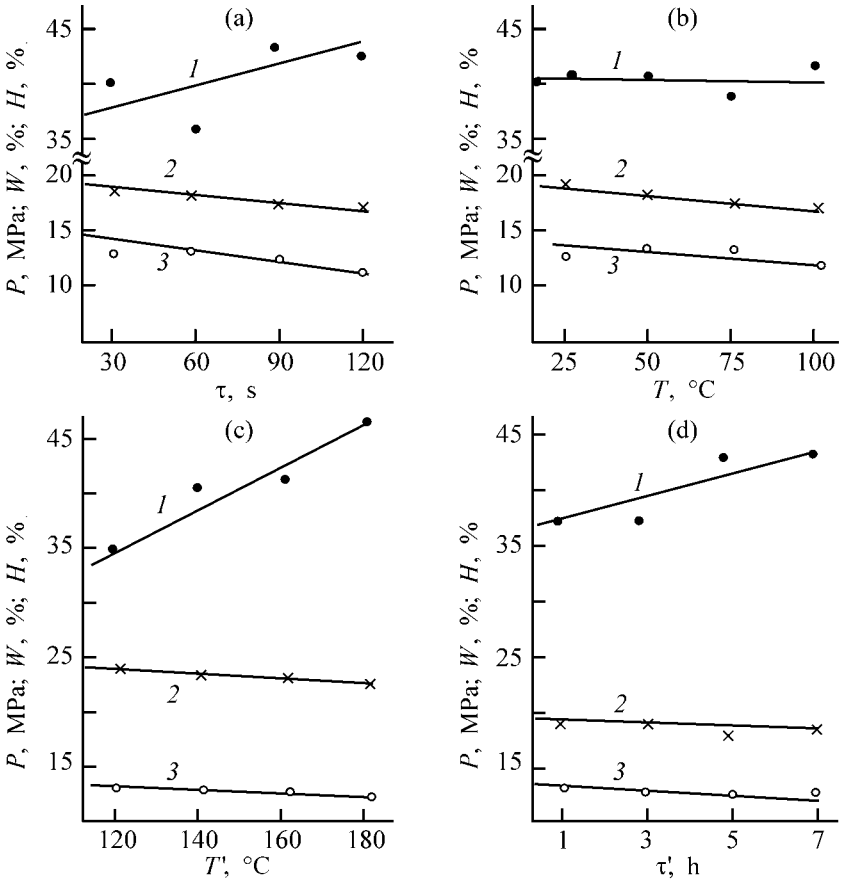

Fig. 2. Influence of (a) impregnation duration τ (30, 60, 90, 120 s; factor A), (b) impregnating formulation temperature T (25, 50, 75, 100°C; factor B), (c) heat treatment temperature T (120, 140, 160, 180°C; factor C), and (d) heat treatment duration τ (1, 3, 5, 7 h; factor D) on the parameters of WFB treated with the MA-modified polymeric material. (*1*) Water absorption W, (*2*) swelling in thickness H, and (*3*) bending strength P.

time. The effect of the impregnating–formulation temperature is also insignificant. To save power, it is advisable to perform the impregnation without heating. The strongest influence is exerted by the duration and especially by the heat treatment temperature, because cross-linking processes faster at elevated temperatures. Furthermore, at elevated temperatures maleic acid can undergo dehydration to maleic anhydride, and both can react with the wood components. Thus, elevated temperature and longer time of the heat treatment make possible the occurrence of a number of consecutive, parallel, and consecutive-parallel processes. The resulting 3*D* cross-linked copolymeric framework and its chemical bonding with the wood fiber impart to WFB not only increased hydrophobicity but also enhanced strength.

The content of the modified copolymeric material in the WFBs, influenced by the conditions of the impregnation and subsequent heat treatment, varied in a relatively narrow range, in most cases from 12 to 14.5% relative to the WFB weight.

Comparison of the experimental values with those calculated by the above-given regression equations for the corresponding conditions (Table 3) shows their good agreement.

The experimental results and the general physicomechanical and physicochemical concepts suggest the existence of an intimate correlation with a positive effect between the water absorption and swelling in thickness and between the water absorption and bending strength. These quantities are plotted in

Table 3. Experimental characteristics of WFB specimens treated with the MA-modified polymeric material

Parameter	Experiment	Calculation
Bending strength, MPa	44.8	47.1
Water absorption, %	15.9	17.1
Swelling in thickness, %	11.6	12.3

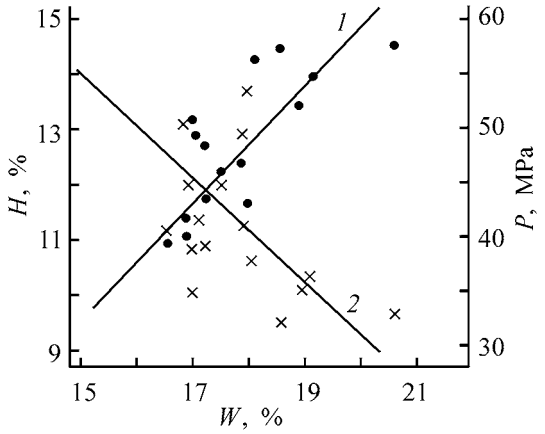

Fig. 3. (*1*) Swelling in thickness *H* and (*2*) bending strength *P* of WFB specimens as functions of the water absorption *W*.

Fig. 3; indeed, there is a positive correlation of the swelling in thickness and bending strength with the water absorption.

Visual examination of cuts of WFBs impregnated with the MA-modified copolymeric material shows that this material is uniformly distributed in the bulk of the fiberboard, filling the production defects and micro- and macropores. The resulting copolymeric framework of the MA-modified copolymeric material and products of its reaction with wood components reduces the release of formaldehyde from articles in which phenol– or urea–formaldehyde resins were used as binders.

The use of copolymeric materials prepared from petrochemical production wastes and by-products can not only improve of the properties of items but also solve environmental problems.

CONCLUSIONS

(1) Modification with maleic acid of a low-molecular-weight styrene-containing copolymer from by-product formed in polybutadiene production allows preparation of a material with an increased content of oxygen-containing functional groups.

(2) The copolymers modified with maleic acid can be used for protective treatment of wood materials with the aim to impart to them increased hydrophobicity and mechanical strength.

REFERENCES

1. Nikulin, S.S., Shein, V.S., Zlotskii, S.S., et al., *Otkhody i pobochnye produkty neftekhimicheskikh proizvodstv – syr'e dlya organicheskogo sinteza* (Petrochemical Production Wastes and By-Products as Raw Materials for Organic Synthesis), Moscow: Khimiya, 1989.
2. Krol', V.A., Rivin, E.M., and Shcherban', G.T., *Svoistva i primenenie dienovykh oligomerov* (Properties and Applications of Diene Oligomers), Moscow: TsNIITEneftekhim, 1984.
3. Nikulin, S.S., Filimonova, O.N., Sergeev, Yu.A., et al., *Proizv. Ispol'z. Elastom.*, 2000, no. 1, pp. 10–14.
4. Sidorov, S.L., Shapovalova, N.N., Molodyka, A.V., et al., *Proizv. Ispol'z. Elastom.*, 1993, no. 4, pp. 7–12.
5. Moldavskii, B.L. and Kernos, Yu.D., *Maleinovyi angidrid i maleinovaya kislota* (Maleic Anhydride and Maleic Acid), Leningrad: Khimiya, 1976.
6. Akhnazarova, S.A. and Kafarov, V.V., *Optimizatsiya eksperimenta v khimii i khimicheskoi tekhnologii: Uchebnoe posobie dlya khimiko-tekhnologicheskikh vuzov* (Optimization of Experiment in Chemistry and Chemical Technology: Textbook for Higher Schools of Chemistry and Technology), Moscow: Vysshaya Shkola, 1978.
7. Wassermann, A., *Diels–Alder Reactions. Organic Background and Physico-Chemical Aspects*, Amsterdam: Elsevier, 1965.
8. Filimonova, O.N. and Nikulin, S.S., *Zh. Prikl. Khim.*, 2002, vol. 75, no. 8, pp. 1315–1319.

ISSN 1070-4272, Russian Journal of Applied Chemistry, 2007, Vol. 80, No. 2, pp. 311–315. © Pleiades Publishing, Ltd., 2007.
Original Russian Text © V.A. Solodov, L.K. Khvatova, B.R. Fakhrutdinov, O.A. Varnavskaya, N.A. Lebedev, I.N. Diyarov, 2007, published in Zhurnal Prikladnoi Khimii, 2007, Vol. 80, No. 2, pp. 312–316.

MACROMOLECULAR CHEMISTRY AND POLYMERIC MATERIALS

Pentaerythritol-Based Demulsifying Agents and Their Surfactant Properties

V. A. Solodov, L. K. Khvatova, B. R. Fakhrutdinov, O. A. Varnavskaya, N. A. Lebedev, and I. N. Diyarov

NIInefteprom khim Joint-Stock Company, Kazan, Tatarstan, Russia

Kazan State Technological University, Kazan, Tatarstan, Russia

Received September 12, 2006

Abstract—Pentaerythritol-based block copolymers of ethylene and propylene oxides were synthesized and characterized as surfactants and demulsifiers.

DOI: 10.1134/S1070427207020280

The wide diversity of oil production and treatment processes, and the large number of properties of the produced oil makes a search for new high-performance demulsifiers a topical task [1]. Presently, the most efficient demulsifiers are nonionic surfactants such as alkylene oxide block copolymers [1–4]. Nonionic surfactants are mostly synthesized from glycols, amines, synthetic fatty acids, and phenols.

Alkylene oxide block copolymers based on polyhydric alcohols have not been adequately explored as demulsifying surfactants [1–4].

Therefore, we prepared in this study polyoxyalkylated derivatives of pentaerythritol and characterized their surfactant and demulsifying properties.

EXPERIMENTAL

Oxyalkylated pentaerythritols were synthesized using the conventional anionic polymerization route [5]. First, we synthesized a prepolymer by adding four moles of propylene oxide (PO) to the starting reagent. Then PO and ethylene oxide (EO) were successively added. Hydroxyalkylation was carried out at 135–150°C and 1.0–1.6 atm in the presence of a base catalyst.

As a result, we prepared a series of block copolymers with various hydrophobic to hydrophilic group ratios (Table 1). Sample nos. 1–7 have hydroxyethyl terminal groups, and sample nos. 8–14, hydroxypropyl groups.

Table 1. Characteristics of samples (MW 7000)

Sample no.	PO : EO, wt %	Cloud point, °C	Hydroxyl number, mg KOH/g		Mean demulsifying efficiency, %	
			experiment	theory	1*	2*
1	20 : 80	72	34	32	13	12
2	30 : 70	63	34	32	40	31
3	40 : 60	51	33	32	60	53
4	50 : 50	33	33	32	67	70
5	60 : 40	17	33	32	67	75
6	70 : 30	12	32	32	80	88
7	80 : 20	10	32	32	75	80
8	80 : 20	19	32	32	78	85
9	70 : 30	26	33	32	73	83
10	60 : 40	36	33	32	33	61
11	50 : 50	44	34	32	20	53
12	40 : 60	61	34	32	3	23
13	30 : 70	68	34	32	0	17
14	20 : 80	79	34	32	0	10

* Oil field: (1) Novo-Suksinskoe and (2) Peschanoe.

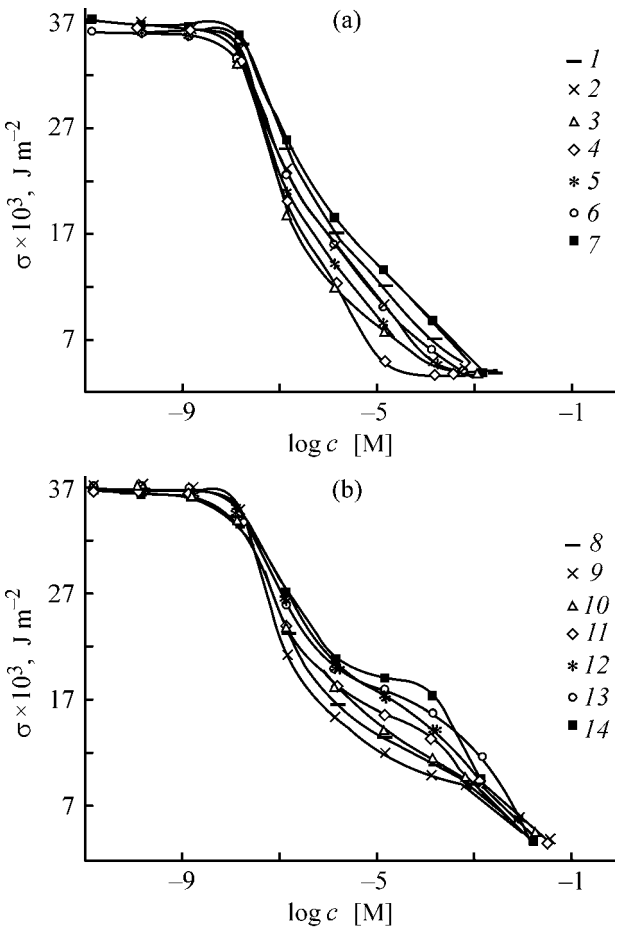

Fig. 1. Isotherms of surface tension at toluene/water interface for the samples with (a) EO and (b) PO terminal groups. (σ) Surface tension and (*c*) concentration. The *curve numbers* correspond to the numbering in Table 1.

The characteristic of the block copolymers that reflects the addition of ethylene oxide is the cloud point of their aqueous solutions. When dissolved in water, nonionic substances form hydrates through hydrogen bonding between water molecules and ether oxygen atoms of the polyethylene glycol residue [5]. Heating ruptures the hydrogen bonds, and the solution becomes turbid (solute separates out as suspended droplets). Cooling makes the solution clear again [4, 5]. The cloud points of the samples are listed in Table 1. Since the cloud point of several samples was above 100°C, 1% solutions of the block investigated copolymers were prepared in 10% NaCl [4].

Table 1 shows that the cloud point increases with the number of the hydroxyethyl units, i.e., the number of hydrogen bonds between the EO units and water molecules grows.

To determine the molecular weight of the samples, we measured the hydroxyl number by the procedure involving esterification of the hydroxy groups with acid chlorides or anhydrides. The theoretical and experimental hydroxyl numbers are also listed in Table 1.

The difference between the experimental and theoretical hydroxyl numbers can be attributed to the formation of polyethylene glycols and to the resulting the broad molecular-weight distribution in the products obtained. As the number of the hydroxyethyl groups added increases, the main reactions are accompanied by side reactions. This makes more pronounced the difference between the experimental and theoretical data.

Among the significant characteristics of surfactants is their ability to reduce the surface tension at the interface between the solution and a gas or another liquid. The interfacial tension of the nonionic surfactant solutions at the toluene/water interface was measured by the ring detachment (Du Nouy) method using a LAUDA tensiometer. In this method, the force acting on an immersed body is measured electronically. Figure 1 shows the surface tension isotherms of the toluene solutions of the nonionic surfactants at the toluene/water interface.

As we pass from infinitesimal concentrations to the critical micelle concentrations (CMC) two portions are observed in the surface tension isotherms, These portions differ in the extent to which the surface tention varies with the nonionic surfactant concentration in the solution.

It is known that, in mixtures of ethers with different numbers of glycol residues, compounds with shorter polyglycol chains form micelles at a lower concentration, compared to longer-chain compounds [4, 6, 7]. Therefore, the surface tension isotherms level out smoothly in our case, and the critical micelle concentration range is extended. For sample nos. 8–14 (Fig. 1b), the increase in the EO content in the molecule is reflected in the occurrence of an additional nearly horizontal portion suggesting the presence in the sample of an admixture of nonionic surfactants with a lower molecular weight, formed in the final oxypropylation stage. Sample nos. 1–7 (Fig. 1a) do not contain such admixtures, because ethylene oxide added in the final stage "landed" on the target block copolymer, forming polyethylene glycol side products to a lesser extent. The resulting polyethylene glycols are composed of the starting compound (pentaerythritol) and various amounts of ethylene oxide. These compounds demonstrate a weak surface activity.

From the surface tension isotherms we estimated the adsorption Γ, limiting adsorption Γ_m, work of

Table 2. Adsorption parameters of samples with EO and PO terminal groups

Sample no.	CMC × 10^3, M	$\Gamma_m \times 10^7$, g-mol m^{-2}	$S_m \times 10^{18}$, m^2	W_a, kJ mol^{-1}	$\sigma \times 10^3$, J m^{-2}	Sample no.	CMC × 10^3, M	$\Gamma_m \times 10^7$, g-mol m^{-2}	$S_m \times 10^{18}$, m^2	W_a, kJ mol^{-1}	$\sigma \times 10^3$, J m^{-2}
Compounds with EO terminal groups						Compounds with PO terminal groups					
1	1.259	5.942	2.794	43.668	3.8	8	0.020	7.751	2.142	54.033	3.6
2	0.251	9.168	1.811	47.444	4.1	9	0.016	9.677	1.715	50.327	3.6
3	0.200	1.188	1.397	47.674	3.9	10	0.016	10.102	1.643	47.830	3.9
4	0.018	13.205	1.257	48.229	3.6	11	0.016	10.300	1.612	46.397	3.7
5	0.063	11.884	1.397	48.818	3.6	12	0.020	9.359	1.774	45.985	3.6
6	0.501	6.932	2.395	51.303	3.6	13	0.016	12.835	1.293	45.851	3.8
7	1.585	5.348	3.104	46.591	3.7	14	0.016	10.696	1.552	45.541	3.8

adsorption W_a, landing area of the molecule S_m, and CMC [8–10].

The adsorption Γ (g-mol m^{-2}) was determined from the slope of the tangent to the initial portion of the isotherm. The slope $d\sigma/d\log c$ was then substituted in the Gibbs equation [9]:

$$\Gamma = -(1/2.3RT)(d\sigma/d\log c).$$

The limiting adsorption Γ_m (g-mol m^{-2}) was found from the slope of the second linear portion of the isotherm, in which the limiting adsorption is attained. Again the slope $d\sigma/d\log c$ was substituted in the Gibbs equation [9]:

$$\Gamma_m = -(1/2.3RT)(d\sigma/d\log c).$$

The landing area of the molecule, S_m (m^2), was estimated from the limiting adsorption [9]:

$$S_m = 1/(\Gamma_m N),$$

where N is the Avogadro number (6.022057×10^{23} mol^{-1}).

The work of adsorption, W_a (kJ mol^{-1}), is among the most significant characteristics of surfactants. This parameter represents the energy gain in the transfer of a mole of a surfactant from the bulk to the interface [9]:

$$W_a = RT\ln(\Gamma/\delta c),$$

where δ is the adsorption layer thickness determined taking into account the range of intermolecular forces at the interface and equal to 12×10^{-10} m for the toluene/water interface [8, 11].

The maximal work of adsorption of the surfactants under study was estimated at the maximum dilution by extrapolation to zero concentration, i.e., for the case of ideal solution. The CMC values were also determined from the surface tension isotherms ploted in the coordinates σ–$\log c$ (Table 2).

Using data of Table 2, we plotted the dependences of CMC, landing area of the molecule, S_m, and work of adsorption W_a on the degree of oxyethylation (Figs. 2, 3). The resulting dependences are well consistent with the data from [5, 8, 9, 12]. The surface tension at the water/toluene interface only slightly depends on the degree of oxyethylation (Table 2), because the molecular weight of the resulting samples is

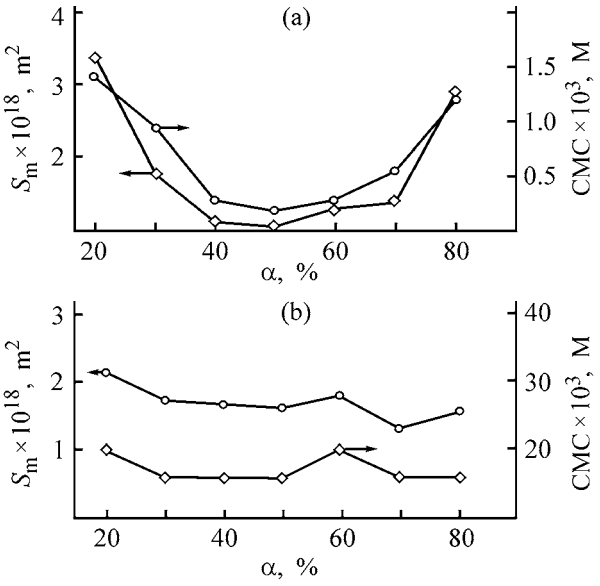

Fig. 2. Landing area of the molecule, S_m, and CMC vs. the degree of oxyethylation, α, in sample nos. 1–14. α is taken from Table 1; the same for Fig. 3.

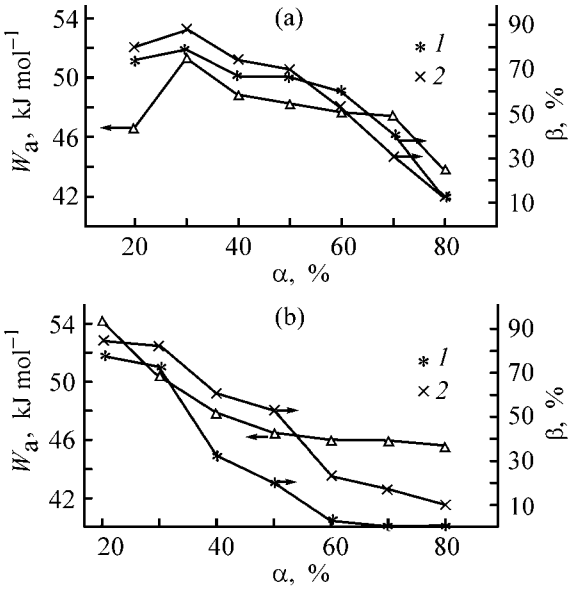

Fig. 3. Work of adsorption W_a vs. the degree of oxyethylation α in sample nos. 1–14. Oil field: (*1*) Novo-Suksinskoe and (*2*) Peschanoe.

constant, and the PO : OE ratio only changes. The different solubilities in toluene and water of nonionic surfactants of the same molecular weight only slightly affect the surface tension. It has been demonstrated previously [13] that the surface tension is significantly affected by an increase in the molecular weight of a nonionic surfactant and changes in the EO : PO ratio in the molecule.

Figure 2 shows that there is a minimum in the CMC–α dependence, which is due to different solubilities of the samples in toluene and water. The occurrence of the maximum in the most hydrophobic sample nos. 7 and 8 suggests that they have the highest solubility in toluene. Among the most hydrophilic anionic surfactants, the maximum is shown by sample nos. 1 and 12. Sample nos. 13 and 14 are even more hydrophilic, but their CMC is lower, which can be attributed to a larger amount of lower-molecular-weight anionic surfactants in their composition, formed by side reactions.

The landing area of the molecule at the toluene/water interface also shows a minimum coincident with that in the CMC dependence. The arrangement of the molecule at the interface depends on its solubility in each phase. The most hydrophobic molecule is entirely distributed in the toluene phase, as well as a part of the hydrophilic block. In this case, both the landing area and CMC are at a maximum. Minima in the dependences are observed for sample no. 4 with equal amounts of the PO and EO blocks. In this case, the landing area is at a minimum, since the molecule of the indicated block copolymer is equally soluble in both phases, and no retraction of the hydrophobic and hydrophilic blocks occurs. The landing area of the compounds with the PO terminal groups also shows a minimum corresponding to the sample having equal amounts of the PO and EO blocks. However, sample nos. 13 and 14 have low landing areas because they contain large amounts of side products.

The dependences of the demulsifying efficiency of surfactants on the landing area of the molecule and CMC have been analyzed previously in [5, 10–12] for the compounds in which the hydrophobic blocks were represented by long alkyl radicals. For these compounds, correlations were found. In our case, nonionic surfactants are block copolymers, and no correlations were found between their demulsifying efficiency and landing area and CMC.

It was interesting to study the effect of the work of adsorption on the demulsifying efficiency.

The demulsifying efficiency was studied using the conventional bottle sampling method with artificial and natural emulsions. The artificial emulsion with 30% watering was prepared from anhydrous coal-bearing oils from the Novo-Suksinskoe oil field (oil well no. 1090, Tatneft' Joint-Stock Company) using a simulated stratal water. The natural emulsion was taken from the Peschanoe oil field (Archneftegeologiya Joint-Stock Company). The data obtained in testing the samples for the demulsifying efficiency are listed in Table 1. These data were plotted in Fig. 3 against the work of adsorption taken from Table 2.

Figure 3 shows that the most efficient demulsifiers are the samples with an EO group content from 32 to 40% in the series with EO terminal groups and from 20 to 30% in the series with PO terminal groups. The decrease in the demulsifying efficiency directly correlates with the decreasing work of adsorption.

CONCLUSIONS

(1) Pentaerythritol-based block copolymers of ethylene and propylene oxides with various hydrophobic to hydrophilic part ratios demonstrate a surface and demulsifying activity.

(2) The critical micelle concentration, landing area of the molecule, work of adsorption, and demulsifying efficiency were determined as functions of the degree of oxyethylation of the samples. The highest demulsifying efficiency was observed for the compounds with a content of the hydroxyalkyl groups of 32–40 and 20–30 wt % in the series with hydroxyethyl and hydroxypropyl terminal groups, respectively.

REFERENCES

1. Levchenko, D.N., Bergshtein, N.V., Khudyakova, A.D., and Nikolaeva, N.M., *Emul'sii nefti s vodoi i metody ikh razrusheniya* (Oil/Water Emulsions and Methods for Their Breaking), Moscow: Khimiya, 1967.
2. Tronov, V.P., *Promyslovaya podgotovka nefti* (Oil Treating), Kazan: Fen, 2000.
3. Volkov, Yu.M., Ranneva, E.A., Abdullina, L.L., and Bashukhina, I.N., in *Novoe v tekhnologii i primenenii PAV: Sbornik nauchnykh trudov* (Advances in Technology and Application of Surfactants: Collection of Scientific Works), Moscow: TsNIITEneftekhim, 1982, pp. 26–34.
4. *Poverkhnostno-aktivnye veshchestva i kompozitsii: Spravochnik* (Surfactants and Composite Surfactants: A Handbook), Pletnev, M.Yu., Ed., Moscow: Klavel', 2002.
5. Schönfeld, N., *Grenzflachenaktive–Athylenoxid-Addukte*, Stuttgart: Wissenschaftliche, 1976.
6. Petrov, A.A., Pozdnyshev, G.N., and Smirnov, Yu.S., in *Sbor, transport, podgotovka nefti i avtomatizatsiya nefte promyslov: Sbornik nauchnykh trudov* (Oil Gathering, Transportation, and Treating, and Oil-Field Automation), Moscow: Gostoptekhizdat, 1963, issue 6, pp. 12–21.
7. Lange, K.R., *Poverkhnostno-aktivnye veshchestva: Sintez, svoistva, analiz, primenenie* (Surfactants: Synthesis, Properties, Analysis, and Applications), St. Petersburg: Professiya, 2004.
8. Abramzon, A.A., *Poverkhnostno-aktivnye veshchestva: svoistva i primenenie* (Surfactants: Properties and Applications), Leningrad: Khimiya, 1981.
9. Abramzon, A.A., Zaichenko, L.P., Faingol'd, S.I., et al., *Poverkhnostno-aktivnye veshchestva. Sintez, analiz, svoistva, primenenie* (Surfactants: Synthesis, Analysis, Properties, and Applications), Leningrad: Khimiya, 1988.
10. Abramzon, A.A., Zaichenko, L.P., and Petukhova, L.A., *Metodicheskie ukazaniya k raschetnym zanyatiyam po svoistvam i primeneniyu PAV* (Guideline to Theoretical Studies in Properties and Applications of Surfactants), Leningrad: Khimiya, 1980.
11. Abramzon, A.A. and Pankratov, V.A., *Zh. Prikl. Khim.*, 1984, vol. 57, no. 2, pp. 293–297.
12. Pozdnyshev, G.N., *Stabilizatsiya i razrushenie neftyanykh emulsii* (Oil Emulsion Stabilization and Breaking), Moscow: Nedra, 1982.
13. Solodov, V.A., Varnavskaya, O.A., Khvatova, L.K., et al., *Zh. Prikl. Khim.*, 2005, vol. 78, no. 6, pp. 966–971.

ISSN 1070-4272, Russian Journal of Applied Chemistry, 2007, Vol. 80, No. 2, pp. 316–321. © Pleiades Publishing, Ltd., 2007.
Original Russian Text © A.V. Kashevskii, M.A. Mamalyga, T.L. Petrova, A.Yu. Safronov, V.N. Kizhnyaev, 2007, published in Zhurnal Prikladnoi Khimii, 2007, Vol. 80, No. 2, pp. 317–322.

MACROMOLECULAR CHEMISTRY AND POLYMERIC MATERIALS

Synthesis and Electrochemical Applications of Fluorinated Vinylazole Copolymers for Monitoring NO in Model and Biological Systems

A. V. Kashevskii, M. A. Mamalyga, T. L. Petrova, A. Yu. Safronov, and V. N. Kizhnyaev

Irkutsk State University, Irkutsk, Russia

Received April 7, 2006; in final form, September 2006

Abstract—Copolymers of 1-vinyl-1,2,4-triazole and 5-vinyltetrazole with 1,1,5-trihydrooctafluoropentyl methacrylate and 1,1,7-trihydrododecafluoroheptyl methacrylate were prepared under the conditions of radical initiation. These copolymers were used for modification of the surface of a glassy carbon electrode, and the effect of the modification on the electrochemical behavior of the electrode in anodic oxidation of dopamine and NO was studied. The possibility of enhancing the selectivity of the electrochemical sensor for monitoring NO in biological media was demonstrated.

DOI: 10.1134/S1070427207020292

Nitrogen(II) oxide exhibits a broad spectrum of biological effects [1], and the NO functions in mammal bodies critically depend on its concentration [2]. Numerous methods have been developed for determining NO in biological systems [3], but the electrochemical method allowing on-line determination of the NO concentration is justly considered to be particularly efficient. Electrochemical redox reactions of NO can be performed in model buffer solutions on smooth unmodified metal or glassy carbon electrodes [4], but the development of an electrochemical sensor for measuring the NO concentration in biological media requires enhancing the selectivity of the working electrode. Among interfering species are both anions (NO_2^-, NO_3^-) and cations (e.g., dopamine).

The common procedure for eliminating the effect of anions is modification of the working electrode surface with a Nafion polymeric cation-exchange membrane [5, 6]; however, higher electrode selectivity can be attained by applying multilayer electrode coatings based on polyfunctional polymeric materials. Polymers combining in their structure azole rings and fluorinated fragments can be one of the components of such selective membranes. Synthesis of copolymers of 1-vinyl-1,2,4-triazole with fluorinated alkyl methacrylates [7] and preparation of materials for medicine based on these copolymers [8] have been reported. 1,2,4-Triazole rings impart to the copolymers hydrophilicity, chemical and hydrolytic stability, and complexing ability, whereas fluorinated fragments should enhance the mechanical strength of the copolymer film coatings and their adhesion to other fluorinated polymers and, in particular, to Nafion, which is very important in preparation of high-selectivity multilayer coatings for an amperometric sensor.

In this study, we prepared copolymers of 1-vinyl-1,2,4-triazole (VTr) and 5-vinyltetrazole (VT) with 1,1,5-trihydrooctafluoropentyl methacrylate (8-FAMA) and 1,1,7-trihydrododecafluoroheptyl methacrylate (12-FAMA), and examined the influence exerted on the electrochemical behavior of NO by film coatings based on these copolymers, applied onto the electrode surface.

EXPERIMENTAL

The starting monomers were prepared and purified by published procedures: VTr [9], bp 41–42°C/10 Pa, n = 1.5100; 8-FAMA [10], bp 71°C/1.73 kPa, n = 1.3570; 12-FAMA [10], bp 100°C/1.73 kPa, n = 1.3490. VT was recrystallized from chloroform, mp 126°C. The polymerization initiator [azobis(isobutyronitrile, AIBN] and solvents (DMF, acetone, diethyl

ether) were purified by standard procedures. The copolymerization of monomer mixtures was performed to maximal conversion in ampules under argon at 60°C in DMF solution containing AIBN. The copolymers were isolated by precipitation into water, reprecipitated, and vacuum-dried to constant weight. The composition and structure of the copolymers were determined by elemental analysis and IR spectroscopy. The viscosity of the copolymers in DMF was determined with an Ubbelohde viscometer at 20°C. The degree of swelling of the copolymers in water was determined gravimetrically using films prepared by evaporation of 1–3% solutions of the copolymers in acetone or dimethylformamide, cast on a glass surface. To make the films based on VT copolymers hydrophilic, they were additionally kept for 3–5 min in 0.1 M NaOH, with the subsequent drying in a vacuum. The degree of swelling (%) was calculated by the formula

$$K_{sw} = [(M_h - M_0)/M_0] \times 100,$$

where M_h is the weight of the swollen hydrogel, and M_0, that of the dry polymer.

The IR spectra of the copolymers were recorded on a Specord M-60 spectrometer; samples were taken as mulls in mineral oil and thin films.

The main voltammetric measurements were performed as described in [11, 12]. In addition, we used for voltammetric analyses an installation based on an EP20A potentiostat and a PR-8 programmer. Measurements were performed in a three-electrode glass cell with a working volume of 15 ml. The reference electrode was a BAS RE-1B silver chloride electrode, and the auxiliary electrode was a platinum grid. The surface area of the working glassy carbon (GC) electrode was 7.1 mm^2.

In the study, we used $FeSO_4 \cdot 7H_2O$ (chemically pure grade), KNO_2 (chemically pure grade), KH_2PO_4 (ultrapure grade, recrystallized), NaOH (chemically pure grade), HCl (analytically pure grade), 5% aqueous–alcoholic solution of Nafion (Aldrich), and 0.5% solution of dopamine (Ferane). As supporting electrolytes we used 0.1 M phosphate and phosphate–alkaline buffer solutions [11]; their pH was varied from 2.0 to 9.0. The majority of electrochemical measurements were performed at pH 7.4.

Nitrogen(II) oxide prepared according to [13] was introduced into the system as described in [11, 12]; the concentration of the saturated NO solution was 2 mM [14].

Before each experiment, the GC electrode was pretreated by polishing the working surface with alumina powder, after which the electrode was kept in an ultrasonic bath for 7 min to remove solid particles from the surface and washed with double-distilled water. The glassy carbon electrodes were modified with Nafion and/or synthesized copolymers of VTr with 8-FAMA and 12-FAMA at various ratios of monomeric units. The surface of the working GC electrode with Nafion was modified as described in [11, 12]. A similar procedure was used for modifying the GC electrode with the azole-containing copolymers synthesized. A 10-μl portion of a 5% solution of a copolymer in acetone was applied onto the electrode surface. The coating was dried for 40 min at room temperature and then for 40 min at 60°C. To prepare multicomponent coatings, the electrode was first coated with Nafion, after which it was dried and the modifying copolymer layer was applied over the Nafion film.

The cell and other glassware were treated with a hot mixture of concentrated sulfuric acid with 30% hydrogen peroxide solution, which was followed by washing with hot tap water and then with double-distilled water. To provide an inert atmosphere, the solution in the electrochemical cell was bubbled with argon for 10 min.

The potential sweeping rate in various potentiodynamic experiments was varied from 0.002 to 0.500 $V\ s^{-1}$. The potentials are given vs. the silver chloride electrode. The measurements were performed at room temperature.

The elemental and spectral analyses and turbidimetric titration show that joint polymerization of vinylazoles with fluorinated methacrylates under the conditions of radical initation yields copolymers. The IR spectra of copolymers of VTr with 8- and 12-FAMA are identical to those given in the literature [7]: The absorption bands of the vinyl groups of the comonomers at 1650 and 964 cm^{-1} are lacking, but there are bands characteristic of the 1,2,4-triazole moiety (1508, 1450, 1100 cm^{-1}), carbonyl group (1740 cm^{-1}), and CF_2 groups (420–970 cm^{-1}). The IR spectra of the copolymers of VT with 8- and 12-FAMA contain, along with the above-noted bands of the fluorinated monomers, also the bands characteristic of the N–H-unsubstituted tetrazole ring [15] at 2200–3500, 1560, and 1250 cm^{-1}.

The results of the copolymerization and analysis of the products are given in the table. The copolymerization of VTr with 8- and 12-FAMA, as noted

Copolymerization of vinylazoles (M_1) with fluorinated alkyl methacrylates (M_2) ([AIBN] = 5×10^{-3} M, $[M_1] + [M_2]$ = 2 M, DMF, 60°C, 8 h)

System	Initial $M_1 : M_2$ molar ratio	Copolymer yield, wt %	Nitrogen content of copolymer, wt %	$m_1 : m_2$ molar ratio in copolymer	$[\eta]$, dl g^{-1}, in DMF at 20°C	K_{sw}, %, in water at 20°C
VTr–8-FAMA	0.30 : 0.70	72	4.6	0.27 : 0.73	0.24	30
	0.40 : 0.60	68	6.0	0.33 : 0.67	0.25	–
	0.55 : 0.45	65	8.7	0.44 : 0.56	0.32	85
	0.75 : 0.25	51	22.1	0.74 : 0.26	0.38	150
VTr–12-FAMA	0.15 : 0.85	63	0.3	0.03 : 0.97	–	–
	0.25 : 0.75	60	0.7	0.06 : 0.94	0.42	–
	0.40 : 0.60	48	1.6	0.14 : 0.86	0.47	18
	0.70 : 0.30	45	13.4	0.65 : 0.35	–	95
VT–8-FAMA	0.30 : 0.70	88	9.3	0.37 : 0.63	–	–
	0.70 : 0.30	79	26.6	0.72 : 0.28	–	–
VT–12-FAMA	0.20 : 0.80	67	3.7	0.22 : 0.78	–	70
	0.30 : 0.70	39	6.1	0.33 : 0.67	–	135
	0.50 : 0.50	37	12.7	0.54 : 0.46	–	270
	0.70 : 0.30	70	25.4	0.63 : 0.37	–	350

previously [7], is characterized by a decrease in the yield of the polymeric product with an increase in the VTr content of the starting mixture and by enrichment of the copolymers with the units of the fluorinated monomer, which indicates that the vinylazole is less reactive. The viscosity of the copolymers grows with an increase in the content of VTr units. For the copolymerization systems with VT, there is no apparent correlation between the yield of the reaction product and the composition of the starting mixture. The ratio of the comonomer units in the polymeric product differs insignificantly from that in the starting mixture, i.e., the copolymerization of VT with fluorinated methacrylate is approximately azeotropic.

The copolymers prepared are colorless powders whose solubility strongly depends on the structure of units of the vinylazole comonomer and on their content. For example, copolymers of VTr with 8- and 12-FAMA, with the mole fraction of vinylazole units less than 0.5, are soluble in DMF, acetonitrile, and acetone, whereas the copolymers with a higher VTr content are soluble only in DMF. DMF is the common solvent for the copolymers of VT with 8- and 12-FAMA, irrespective of their composition. The 1,2,4-triazole ring shows very weak base properties; therefore, the polymeric products containing the triazole ring exhibit no polyelectrolytic behavior, despite the capability to swell in water. The degree of swelling of the films prepared from the VTr copolymers grows with an increase in the content of vinylazole units and varies within 18–150%. The N–H-unsubstituted tetrazole ring is a typical acid; therefore, the copolymers containing VT units behave as polymeric acids. This is manifested in the formation of polymeric salts in the reactions of the copolymers with alkalis. The water affinity of the copolymers considerably increases upon ionization. The water absorption by samples of VT–12-FAMA copolymer films treated with NaOH ranges from 70 to 350%. The hydrated films preserve a fairly high mechanical strength. The compatibility with water of the films based on the synthesized copolymers of vinylazoles with fluorinated methacrylates makes them promising as an electrode coating for determining the NO concentration in aqueous solutions.

When preparing model solutions, we added to the buffer solution typical anionic and cationic substances that could interfere with the determination of NO: solutions of KNO_2 and dopamine, respectively, taking into account that their oxidation can mask the oxidation of NO. It is known that, even without a modifier, the redox response of dopamine is influenced by the electrode material, mechanical and/or electrochemical pretreatment of the surface, composition and ionic strength of the supporting electrolyte [16], and other factors associated with the conditions of electrochemical measurements [17, 18]. Therefore, to obtain the initial data, we studied the electrochemical behavior of dopamine (35 μM) on the unmodified

GC electrode (Fig. 1). An anodic current peak corresponding to the oxidation of dopamine under these conditions is observed at E = +0.15 V. To this peak corresponds a reduction current peak in the cathodic branch, suggesting reversibility of the electrochemical oxidation of dopamine. This is confirmed by the fact that, at potential sweeping rates as low as 0.002–0.010 V s^{-1}, the difference between the maximum potentials of the anodic and cathodic peaks (ΔE) is about 30 mV, and the anodic and cathodic currents in these peaks increase in proportion with the square root of the potential sweeping rate ($V^{0.5}$). The latter dependence holds through the entire range of sweeping rates examined, from 0.002 to 0.500 V s^{-1}, which is clearly seen in Fig. 2. The above-noted features allow us to characterize the redox transformations of dopamine as a quasireversible two-electron process typical of biologically active substances of the quinone nature [19].

The voltammograms of dopamine on the unmodified GC electrode were recorded in supporting electrolytes with different pH values. We found that ΔE of the redox peaks of dopamine remained constant in the pH range 3.0–9.0, with both cathodic and anodic peaks shifting toward less positive potentials with increasing pH. This trend suggests that protons are involved in electrochemical transformations of dopamine. In the pH range 3.0–8.0, the dependences for both peaks are linear, with a slope of 60 mV per pH unit. This slope suggests that the ratio of the number of protons involved in the redox process to the number of electrons transferred is 1 : 1 [19]. Taking into account the above assumptions that two electrons are transferred in the redox reaction of dopamine, the overall reaction equation can be written as

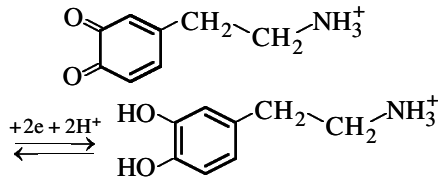

Figure 3 shows that, at high pH values (>8), the slopes of the E–pH dependences decrease. According to [20], such a decrease in the slope is observed in oxidation of dibasic acids at pH values close to pK_1. Indeed, for dopamine, pK_a is 8.9 [21]. Then at pH > 8 the contribution of the partially deprotonated reduced form of dopamine becomes significant:

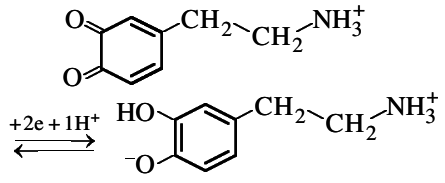

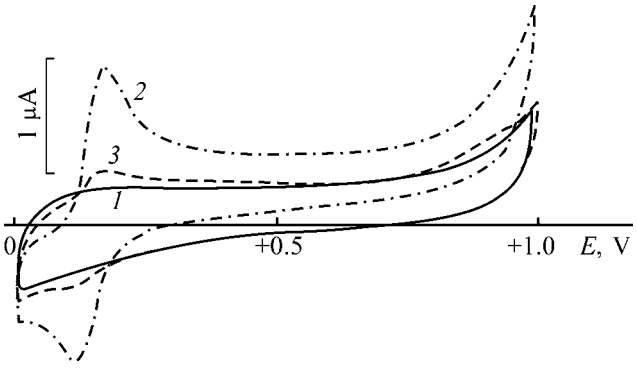

Fig. 1. Voltammograms measured on an unmodified GC electrode in a 0.1 M phosphate buffer solution (pH 7.4) at a sweeping rate of 20 mV s^{-1}. (*E*) Potential (vs. silver chloride electrode); the same for Figs. 3–5. (*1*) Straight supporting electrolyte; (*2*) 35 μM dopamine, first cycle; and (*3*) 35 μM dopamine, after cycling.

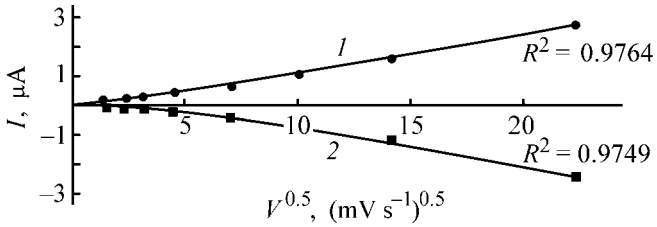

Fig. 2. Currents I of (*1*) anodic and (*2*) cathodic peaks vs. the potential sweeping rates V for voltammograms measured on an unmodified GC electrode in a solution containing 35 μM dopamine. Supporting electrolyte: 0.1 M phosphate buffer, pH 7.4.

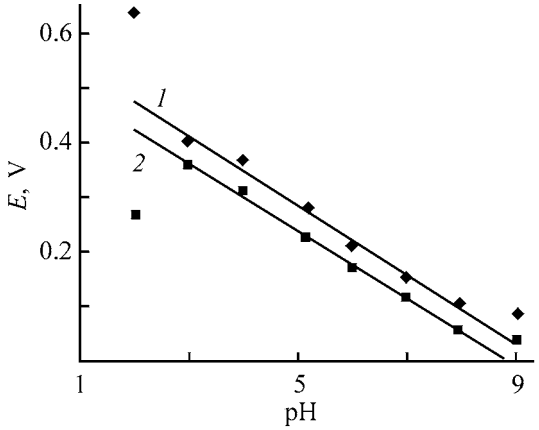

Fig. 3. Potentials of (*1*) anodic and (*2*) cathodic peaks of the voltammograms measured on the unmodified GC electrode vs. pH of a 0.1 M phosphate supporting electrolytes containing 35 μM dopamine (V = 20 mV s^{-1}). E_a^p = –0.0628pH + 0.5966, R^2 = 0.9878; E_c^p = 30.0612pH + 0.5415, R^2 = 0.9973.

At pH < 3, ΔE no longer meets the conditions of a quasireversible electron transfer and increases to several hundreds of millivolts. This fact suggests that the mechanism of electrochemical transformations

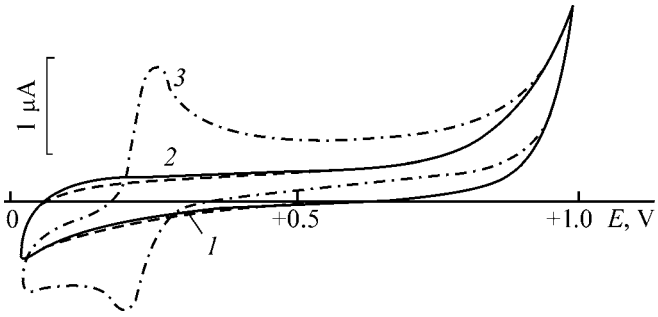

Fig. 4. Voltammograms measured at V = 20 mV s^{-1} on a GC electrode modified with 1-VTr–8-FAMA (*1*) before and (*2*) after adding dopamine (35 μm) to 0.1 M phosphate buffer solution (pH 7.4). Copolymer composition (molar ratio) 0.44 : 0.56. Curve *3* was measured under conditions similar to curve *2* but after removing the modifier from the electrode surface.

of dopamine on glassy carbon changes in in going to strongly acidic solutions. Similar phenomena were noted previously [22].

One more feature of the electrochemical behavior of the system under consideration is manifested after multiply repeated potential cycling. The redox responses of dopamine in the first cycle (curve *2*) and after prolonged potential cycling (curve *3*) are compared in Fig. 1. In the latter curve, the anodic and cathodic current peaks corresponding to the reversible electrochemical transformations of dopamine become considerably less pronounced than those in the first cycle. Furthermore, one more anodic current wave appears in curve *3* at potentials of +0.8 to +1.0 V. This anodic process is apparently irreversible, because no corresponding current peaks or waves are observed in the cathodic branch of the curve. These phenomena can be attributed to further transformations of products formed in the first (reversible) step of oxidation of the pyrocatechol fragment of the dopamine molecule. It is known [23] that such products, can not only be electrochemically reduced to the initial form, but also can be involved in side chemical processes, including reaction with water (hydroxylation) or with the initial reduced form (coupling).

The above features of the electrochemical behavior of dopamine show that the unmodified GC sensor electrode is unsuitable for determining the NO content in the presence of dopamine. Since dopamine is oxidized at considerably less positive potentials than those of NO oxidation (from +0.7 to +0.9 V [11, 12]), the presence of dopamine in solution will cause a considerable increase in the background current of the sensor operating in the amperometric mode. Furthermore, appearance, accumulation, and side reactions of dopamine oxidation products lead to formation of substances that are oxidized in the range of potentials overlapping with that of NO oxidation. Moreover, these side processes will apparently lead to an appreciable degradation of the electrode surface. In the context of searching for ways to improve the stability and selectivity of a sensor for NO determination, dopamine seems to be a good model simulating the presence in solution of cations interfering with the electrochemical determination of NO in biological systems.

To eliminate the interfering effect of dopamine in the determination of NO, the surface of the working GC electrode was modified with copolymers of VTr with 8-FAMA and 12-FAMA. We tested eight samples of the copolymers with different ratios of the monomeric units.

After the modification, the electrode was kept for 24 h in a 0.1 M phosphate buffer solution (pH 7.4) and transferred into an electrochemical cell filled with the same buffer solution, to measure cyclic voltammograms. After obtaining the background curve, dopamine was added to a concentration of 35 μM, and the measurement was repeated. Then the voltammogram was measured in the same solution but on the unmodified electrode, after removing the polymeric coating from the working surface (Fig. 4). The voltammograms recorded similarly for all the eight samples (Fig. 4) clealry show that coating the GC electrode surface with the copolymers considerably decreases the currents corresponding to reversible redox transformations of dopamine under the conditions examined, as compared to the unmodified electrode. An increase in the content of hydrophilic VTr units in the copolymer decreases the sensitivity of the working electrode to dopamine, which is protonated at physiological pH values. However, when the content of hydrophilic groups becomes higher than a certain critical value (specific to each type of copolymers), the polymer films swell too strongly (see table), which impairs the mechanical properties of the modified coatings.

We also modified the GC electrode by successive application onto its working surface of films of Nafion and the copolymers synthesized. Such multilayer multicomponent coating is necessary for preparing a sensor electrode suitable for NO determination in real systems containing both anionic and cationic interfering components. We measured cyclic voltammograms in the buffer solution and after adding dopamine to its maximal concentration of 35 μM. Under the same conditions, we recorded the curves after adding KNO_2 (7 mM) and

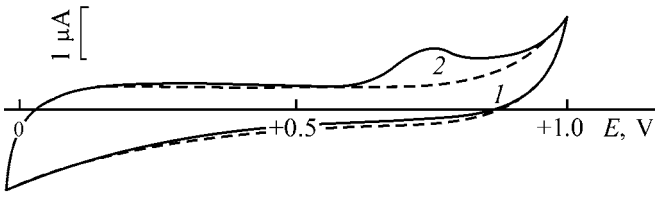

Fig. 5. Voltammograms measured at $V = 20$ mV s^{-1} on a GC electrode modified successively with Nafion and 1-VTr– 8-FAMA (*1*) before and (*2*) after saturating the solution with NO. Solution composition: 0.1 M phosphate buffer solution (pH 7.4), KNO_2 (7 mM), and dopamine (35 μM); copolymer composition (molar ratio) 0.33 : 0.67.

after saturating the solution with NO by its bubbling for 10 min. The voltammograms obtained (Fig. 5) show that the bilayer modifying coatings used do not interfere with the anodic oxidation of NO. The background curve does not change after adding KNO_2 and dopamine in the above-indicated concentrations.

CONCLUSIONS

(1) VTr–8-FAMA copolymers with the mole fraction of vinylazole units of 0.33–0.44 are effective modifiers of the electrode surface, which fully suppress the interfering effect of dopamine and, probably, of other cationic species. The modified electrode remains active in the electrochemical oxidation of NO.

(2) Good adhesion of copolymers with fluorinated and azole-containing units to a Nafion film allows preparation of multilayer coatings promising for the development of a selective electrochemical sensor for measuring the NO concentration in biological media.

REFERENCES

1. Men'shchikova, E.B., Zenkov, N.K., and Reutov, V.P., *Biokhimiya*, 2000, vol. 65, pp. 485–503.
2. Hofseth, L.J., Hussain, S.P., Wogan, G.N., and Harris, C.C., *Free Radical Biol. Med.*, 2003, vol. 34, pp. 955–968.
3. Archer, S., *FASEB J.*, 1993, vol. 7, pp. 349–360.
4. Pallini, M., Curulli, A., Amine, A., and Palleschi, G., *Electroanalysis*, 1998, vol. 10, pp. 1010–1016.
5. Malinski, T. and Taha, Z., *Nature*, 1992, vol. 358, pp. 676–678.
6. Shibuki, K. and Okada, D., *Nature*, 1991, vol. 349, pp. 326–328.
7. Kuznetsova, N.P., Kanitskaya, L.V., Fedorov, S.V., and Ermakova, T.G., *Vysokomol. Soedin., Ser. B*, 2001, vol. 43, no. 9, pp. 1565–1569.
8. Ermakova, T.G., Kuznetsova, N.P., and Annenkov, V.V., *Zh. Prikl. Khim.*, 1999, vol. 72, no. 6, pp. 1004–1009.
9. Kizhnyaev, V.N., Pokatilov, F.A., Tsypina, N.A., et al., *Zh. Org. Khim.*, 2002, vol. 38, no. 7, pp. 1099–1104.
10. Gol'din, G.S., Averbakh, K.O., Nekrasova, L.A., et al., *Zh. Prikl. Khim.*, 1985, vol. 58, no. 6, pp. 1349–1356.
11. Kashevskii, A.V., Safronov, A.Y., and Ikeda, O., *J. Electroanal. Chem.*, 2001, vol. 530, pp. 86–95.
12. Kashevskii, A.V., Lei, J., Safronov, A.Y., and Ikeda, O., *J. Electroanal. Chem.*, 2002, vol. 531, pp. 71–79.
13. Karyakin, Yu.V. and Angelov, I.I., *Chistye khimicheskie veshchestva* (Pure Chemicals), Moscow: Khimiya, 1974.
14. Zhang, M., Cardosa, V., Broderick, M., et al., *Electroanalysis*, 2000, vol. 12, pp. 1113–1117.
15. Kizhnyaev, V.N. and Vereshchagin, L.I., *Usp. Khim.*, 2003, vol. 72, no. 3, pp. 159–182.
16. Gmucova, K., Orlicky, J., and Pavlasek, J., *Coll. Czech. Chem. Commun.*, 2004, vol. 69, pp. 419–425.
17. Heien, M.L.A.V., Khan, A.S., Ariansen, J.L., et al., *PNAS*, 2005, vol. 102, pp. 10023–10028.
18. Venton, B.J. and Wightman, R.M., *Anal. Chem.*, 2003, vol. 75 (19), pp. 414A–421A.
19. Ksenzhek, O.S. and Petrova, S.A., *Elektrokhimicheskie svoistva obratimykh biologicheskikh redoks-sistem* (Electrochemical Properties of Reversible Biological Redox Systems), Moscow: Nauka, 1986.
20. Dawes, E.A., *Quantitative Problems in Biochemistry*, London: Longman, 1979, 6th ed.
21. Tukerman, M.M., Mayer, J.R., and Nachod, F.C., *J. Am. Chem. Soc.*, 1959, vol. 81, pp. 92–94.
22. Danilewicz, J.C., *Am. J. Enol. Vitic.*, 2003, vol. 54, pp. 73–85.
23. *Organic Electrochemistry. An Introduction and a Guide*, Baizer, M.M. and Lund, H., Eds., New York: Dekker, 1983.

ISSN 1070-4272, Russian Journal of Applied Chemistry, 2007, Vol. 80, No. 2, pp. 322–329. © Pleiades Publishing, Ltd., 2007.
Original Russian Text © N.E. Kotel'nikova, S.A. Mikhailova, E.N. Vlasova, 2007, published in Zhurnal Prikladnoi Khimii, 2007, Vol. 80, No. 2, pp. 323–330.

MACROMOLECULAR CHEMISTRY AND POLYMERIC MATERIALS

Immobilization of Proteolytic Enzymes Trypsin and α-Chymotrypsin to Cellulose Matrix

N. E. Kotel'nikova, S. A. Mikhailova, and E. N. Vlasova

Institute of Macromolecular Compounds, Russian Academy of Sciences, St. Petersburg, Russia

Received June 5, 2006; in final form, November 2006

Abstract—Trypsin and α-chymotrypsin were immobilized on a microcrystalline cellulose matrix by adsorption interaction with cellulose. The adsorption of enzymes was determined as a function of their concentration and the pH of solutions. Mechanisms of enzyme binding to functional groups of cellulose were suggested.

DOI: 10.1134/S1070427207020309

The adsorption of proteins and, in particular, enzymes on solid interfaces and interactions between surfactants and enzymes at liquid | solid interfaces are processes of significance in our daily life and in such fields as medicine, food processing, biotechnology, etc. Adsorption acquires particular importance in biological systems because enzymes in them are mostly in the immobilized state on surfaces of cell membranes and subcellular structures. In fact, the conjugates of proteins and interfaces are heterogeneous systems and, taking into account their biological activity, they are heterogeneous biocatalysts [1]. Polymer fibers and films, including polysaccharides, are widely used as carriers of such biocatalysts. The immobilization of physiologically active compounds of protein nature is a convenient method for developing biomedical preparations that can be inserted into the injured zone and can stay in it for an indefinite period. They continuously emit an active preparation into the environment to achieve its high local concentration. The most widespread immobilization method is attachment of an enzyme to a polymer support by covalent, ionic, or adsorption bonds.

Cellulose, due to its unique properties, is of particular interest among other polysaccharides and is widely applied for various purposes. In this study, microcrystalline cellulose (MCC) was used as matrix for immobilization of enzymes. It exhibits specific properties, and its powder morphology makes it possible to use it in processes for which fiber celluloses are unsuitable [2]. There is a positive experience in applying this cellulose as a matrix to prepare conjugates with drugs, with synthetic polymers (for instance, with PVP and its complexes [3, 4]), and also for immobilization of human serum albumin (HSA) [5].

Proteolytic enzymes trypsin and α-chymotrypsin have the key position in the system of digestive enzymes. There is poor information in the literature about preparation of heterogeneous biocatalysts based on cellulose and these enzymes [6, 7]. Modified, e.g., oxidized, cellulose has been mainly used [8]. In this study, adsorption interaction between enzymes and cellulose matrix was performed to immobilize enzymes on MCC. Enzyme adsorption mostly depends on the surface properties of adsorbent, such as its chemical structure, hydrophilicity or hydrophobicity, charge, and porosity. Adsorption is also determined by the chemical composition, structure, and other properties of enzymes themselves. All these factors determine the properties of their conjugates with the matrix and, primarily, the activity of enzymes or their tendency to inactivation.

The goal of this study was to examine immobilization of trypsin and α-chymotrypsin on MCC by their adsorption interaction and the properties of the resulting adsorption complexes MCC–enzymes (ACs). Their preparation is not only of practical interest. From the scientific viewpoint, formation of the complexes with retention of the enzymatic activity may serve as a model for preparation of a peculiar kind of "glycoproteins," in which polysaccharides (cellu-

lose) molecules are bound to polypeptide chains of protein.

EXPERIMENTAL

The powdered microcrystalline cellulose used as a matrix for immobilization of enzymes contained no more than 2.0 wt % water. Its particle size was <0.05 mm. The viscosity-average degree of polymerization DPv of MCC was 190. The volume of pores, their radius, and specific surface area determined by water vapor sorption were 2.16 $cm^3\ g^{-1}$, 20 μm, and 230 $m^2\ g^{-1}$, respectively. The content of aldehyde end groups in cellulose chains was 3.2×10^{-5} mol g^{-1}, and that of carboxy groups on the surface of cellulose macromolecules, 5.8×10^{-6} mol g^{-1} [9].

Crystalline bovine trypsin was taken from SPOFA (Czech Republic), and crystalline bovine α-chymotrypsin, from Samson-Med Ltd. (Russia). The main characteristics of enzymes are listed in Table 1.

The enzymatic activity of trypsin was determined by the Erlanger method [12] from the hydrolysis rate of a low-molecular-weight substrate, *p*-nitroanilide of *N*,α-benzoyl-*D*,*L*-arginine (BAPNA). The enzymatic activity of α-chymotrypsin was determined with respect to a low-molecular-weight substrate, ethyl ether of *N*-benzoyl-*L*-tyrosine (BTEE) (both enzymes from Sigma, the United States). The rate of enzymatic hydrolysis was determined with the aid of a Specord UV VIS 20 spectrometer (Carl Zeiss, Germany). The relative activity of immobilized enzymes in ACs and in solutions after desorption was calculated with respect to the enzymatic activity of the pristine enzymes.

Trypsin and α-chymotrypsin were immobilized from solutions by adsorption onto the cellulose matrix under isothermal conditions at 15°C with continuous stirring. Cellulose feeds (m) were 0.1 g in 30 ml of enzyme solution. Solutions were separated from ACs by filtration through a Schott filter with a porosity of 16. The resulting ACs were vacuum-dried at 40°C. The initial (c_0) and equilibrium (c_{eq}) concentrations of the enzymes in solutions were determined by the Lowry method [13] and by direct measurement of the optical density of solutions on a Specord UV VIS 20 spectrometer at a wavelength λ = 280 nm. The content of the adsorbed enzyme (adsorption value *A*, mg g^{-1}) was calculated from the equation

$$A = (c_0V_0 - c_{eq}V_{eq})/m,$$

where V_0 and V_{eq} are the volumes of the filtrates before and after adsorption.

Table 1. Main characteristics of trypsin and α-chymotrypsin [10, 11]

Constants	Bovine trypsin	Bovine α-chymotrypsin
Molecular mass, kDa	23.8	25
pH of optimum activity	7–8	8
Isoelectric point p*I*	10.6	8.1
pH range of stability	Acid	Acid
Relative activity, %	76	84
K_{bound} $(Ca^{2+}) \times 10^{-4}$, 1 mol^{-1}	11.0	0.92

To obtain the dependence of the content of the adsorbed trypsin on pH of its solution (in the pH range from 4.8 to 12.0), we used its 2.3 and 4.0 mg ml^{-1} solutions in a buffer. For α-chymotrypsin adsorption, we used its 1.1 and 2.6 mg ml^{-1} solutions. To obtain the kinetic dependences, we used trypsin and α-chymotrypsin solutions of the same concentrations at pH 8.2 (in case of trypsin) and at pH 8.0 (in case of α-chymotrypsin). To obtain the adsorption isotherms, we used trypsin solutions in the concentration range from 0.5 to 7.2 mg ml^{-1} and those of α-chymotrypsin in the concentration range from 0.5 to 4.5 mg ml^{-1} at the same pH values. Buffer solutions with pH 4.0–6.3 were prepared by titration of a 0.1 M solution of trisubstituted sodium citrate $Na_3C_6H_5O_7$ with a 0.5 M solution of HCl. Buffer solutions with pH 7.0–10.3 were prepared by titration of 0.05 M solution of tris(hydroxymethyl)aminomethane $[(HOCH_2)_3CNH_2]$ with 1 M HCl. Buffer solutions with pH 11.0–12.0 were prepared by the method described in [14]. All the buffer solutions were filtered before use through a Schott filter with a porosity of 16.

The enzymes were desorbed from ACs containing various amounts of adsorbed enzymes at buffer solution pH 2.0 and 8.2. The desorption conditions and procedures for treatment of feeds after desorption, sample drying, and determination of enzyme concentration were similar to those used in the adsorption study. The desorption (*D*) was calculated in percent of the enzyme adsorption. The content of enzyme strongly bound to MCC was designated as the residual adsorption (Ar, mg g^{-1}).

To study the chemical composition of ACs and enzymes by IR Fourier spectroscopy, samples were prepared in KBr pellets. Transmission spectra were recorded on a Bruker IFS 88 IR Fourier spectrometer (Bruker, Germany) with a 4 cm^{-1} resolution. Differential spectra of enzymes in ACs were obtained by subtraction of the MCC spectrum from the AC spectra.

Wide-angle X-ray scattering was applied to study the supramolecular structure of ACs. X-ray diffraction patterns were obtained with a DRON-48 diffractome-

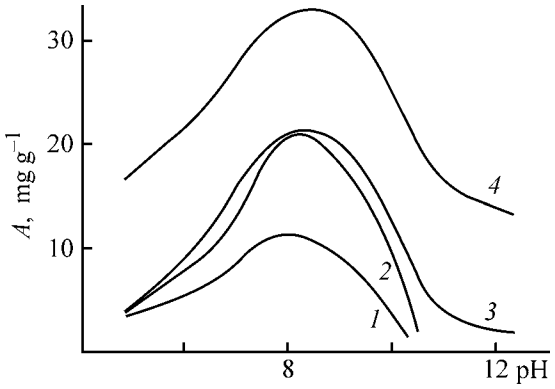

Fig. 1. pH dependence of the maximum adsorption A of (*1*, *2*) α-chymotrypsin and (*3*, *4*) trypsin on MCC. c_0, mg ml^{-1}: (*1*) 1.1, (*2*) 2.6, (*3*) 2.3, and (*4*) 4.0; the same for Fig. 2.

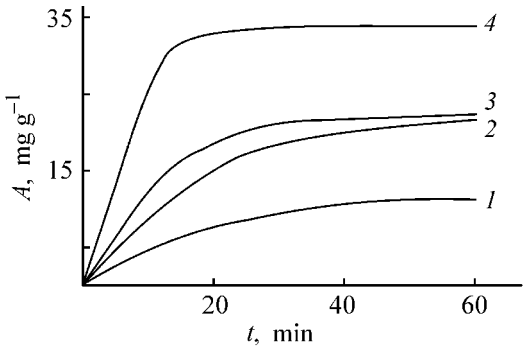

Fig. 2. Adsorption kinetics of (*1*, *2*) α-chymotrypsin and (*3*, *4*) trypsin. (*t*) Time.

ter (Burevestnik NPO, USSR) with a Geiger counter for recording the intensity of reflected beams at any 2θ angle. The samples were prepared as isotropic discs 10 mm in diameter by compacting powder samples at a pressure of 100 kg cm^{-2}. The diffraction patterns were recorded under the following conditions: Cu_{K_α} radiation monochromatized with a Ni filter, voltage 3.5 kV, current 8 mA, goniometer rate 2 deg min^{-1}, and time constant 3.5. The crystallinity indices of ACs were calculated by the Segal method [15], and the size of cellulose crystallites, by the Scherrer method [16].

Table 2. Rate constants (k_1, k_2) of adsorption of trypsin and α-chymotrypsin from solutions onto MCC

Enzymes	c_0, mg ml^{-1}	A, mg g^{-1}	$k_1 \times 10^3$	$k_2 \times 10^3$
			min^{-1}	
Trypsin	2.4	21	7.5	–
	4.0	33	8.5	–
α-Chymo-	1.1	11	12.6	3.5
trypsin	2.6	21	15.3	2.4

Changes in the morphological structure of MCC during adsorption were studied by scanning electron microscopy (SEM) with a Jeol JCM-35 CF (Jeol, the United Kingdom) scanning electron microscope. To obtain micrographs, samples of pristine cellulose and ACs were preliminarily placed on an aluminum support coated with a carbon layer in a special chamber and were sprayed using a gold target in an inert gas atmosphere. The electron micrographs were obtained at a magnification of 40 to 2000 at a 15 kV voltage.

The pH of solutions of enzymes profoundly affects their adsorption. Figure 1 shows the dependence of the maximum adsorption values for trypsin and α-chymotrypsin on the pH of the medium. The maximum A for trypsin (21 and 33 mg g^{-1} at the initial concentration C0 of solutions 2.3 and 4.0 mg ml^{-1}, respectively) is reached at pH 8.0–8.5, and that for α-chymotrypsin (11 and 21 mg g^{-1} at the initial concentration of solutions 1.1 and 2.6 mg ml^{-1}, respectively), at pH 7.9–8.2. These results are in agreement with the data on adsorption of these enzymes onto other polymer adsorbents [8, 17, 18]. MCC has a negative surface charge in the pH range 3.5–11.0 due to dissociation of its surface carboxy groups [9]. The isoelectric point for trypsin is 10.6 [10]. Consequently, trypsin molecules are positively charged in the pH range 8.0–8.5. In this case, the electrostatic factor contrib- utes to the adsorption interaction in the pH range <10.6. The isoelectric point of α-chymotrypsin is 8.1 [11]. Hence, α-chymotrypsin molecules are not charged in the pH range 7.9–8.2. In contrast to trypsin, the contribution of electrostatic factor to the adsorption interaction with MCC should be lower in the case of α-chymotrypsin.

Kinetic dependences of the adsorption of trypsin and α-chymotrypsin onto cellulose at different initial enzyme concentrations are shown in Fig. 2. The dependences have a shape typical of adsorption from solutions on porous surfaces. The adsorption is a two-stage process. The first stage proceeds at a high rate, and in the second stage the rate becomes much lower. The equilibrium trypsin adsorption is attained in 30 min, with the rate of the second stage close to zero. The equilibrium α-chymotrypsin adsorption is attained in 50 min, with the adsorption terminated in the second stage. The rate constants of enzyme adsorption onto cellulose were calculated from the semilog kinetic plots, according to the pseudo-first-order rate equation (Table 2). It should be noted that the rate constants of trypsin adsorption onto cellulose are comparable with those of adsorption of a synthetic polymer, PVP, onto MCC [3] and

three-four times lower than those of HSA adsorption onto MCC [5]. The rate constants of α-chymotrypsin adsorption onto cellulose are higher than those of PVP and are comparable with those of HSA.

Adsorption isotherms of trypsin and α-chymotrypsin are shown in Fig. 3. The S-shaped dependences can be referred to type IV and can be satisfactorily described by Freundlich equations [19]. This is in agreement with the results of immobilization of enzymes on other matrices described in [8, 18, 20]. An analysis of Freundlich constants calculated from the isotherms plotted in log-log coordinates showed that the capacity of MCC to adsorb those enzymes is 8–10 times that to adsorb serum albumin [5] and comparable with its capacity to adsorb PVP [3]. The S-shape is known to be characteristic of adsorption that combines physical sorption and chemisorption of enzymes [19]. The occurrence of enzyme chemisorption was confirmed by IR spectroscopy (see below).

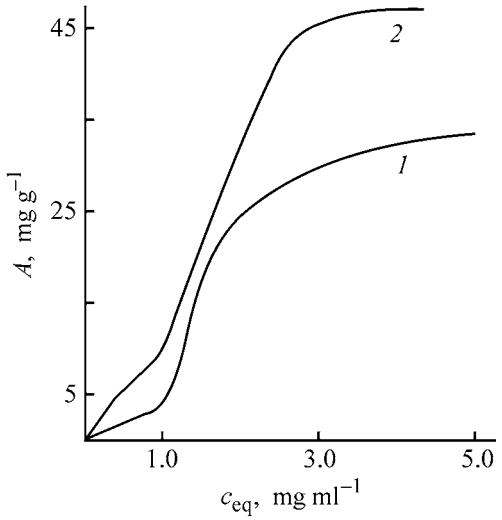

Fig. 3. Adsorption isotherms of (*1*) trypsin and (*2*) α-chymotrypsin to MCC. (*A*) adsorption and (c_{eq}) equilibrium enzyme concentration.

A study of desorption of both enzymes from the ACs demonstrated that the desorption *D* only slightly depends on the pH of the medium (Table 3). In the case of trypsin, *D* increases proportionally to the content of the enzyme adsorbed. However, in the case of α-chymotrypsin, *D* depends on the content of the adsorbed enzyme to a lesser extent. It is important that both enzymes are not completely released from the cellulose matrix. The maximum value of *D* for trypsin is 69 wt %, which is in agreement with the data reported in [8]. The amount of trypsin retained in the matrix is constant (~10 mg g^{-1}), i.e., ~1% of the AC mass. In contrast to trypsin, α-chymotrypsin is retained in the cellulose matrix to a greater extent. The maximum value of *D* is 18 wt %, and the amount of retained α-chymotrypsin is as high as 41 mg g^{-1}. Consequently, the results of enzyme desorption from the AC indicate that a part of immobilized enzymes is strongly bound to the cellulose matrix.

The relative enzymatic activities of the enzymes in AC and in solutions after desorption, calculated relative to the enzymatic activity of pristine enzymes, are also listed in Table 3. The enzymatic activity of trypsin solutions after the desorption (carried out at pH 2.0 and 8.2) is low (lower than that of pristine trypsin) and depends on the amount of desorbed trypsin only in the case of desorption at pH 8.2. This is probably caused by autolysis of trypsin, which can take place both in solutions and on the cellulose matrix directly during the adsorption.

The relative enzymatic activity of α-chymotrypsin desorbed from AC at pH 2.0 and 8.2 is 70%. It is much higher than that of adsorbed trypsin. In this case,

Table 3. Desorption of enzymes from ACs and their relative activity *A*

A, mg g^{-1}	pH of desorption	*D*, %	Content of enzymes in matrix after desorption, mg g^{-1}	Concentration of enzymes in solution after desorption, mg ml^{-1}	Relative activity, %
			Trypsin		
20	2.0	51	10	0.34	16
33	2.0	69	10	0.76	8
17	8.2	52	9	0.30	18
33	8.2	69	10	0.70	18
			α-Chymotrypsin		
10	2.0	10	9	–	–
34	2.0	12	30	0.14	70
34	8.2	13	29	–	–
49	8.2	18	41	0.29	71

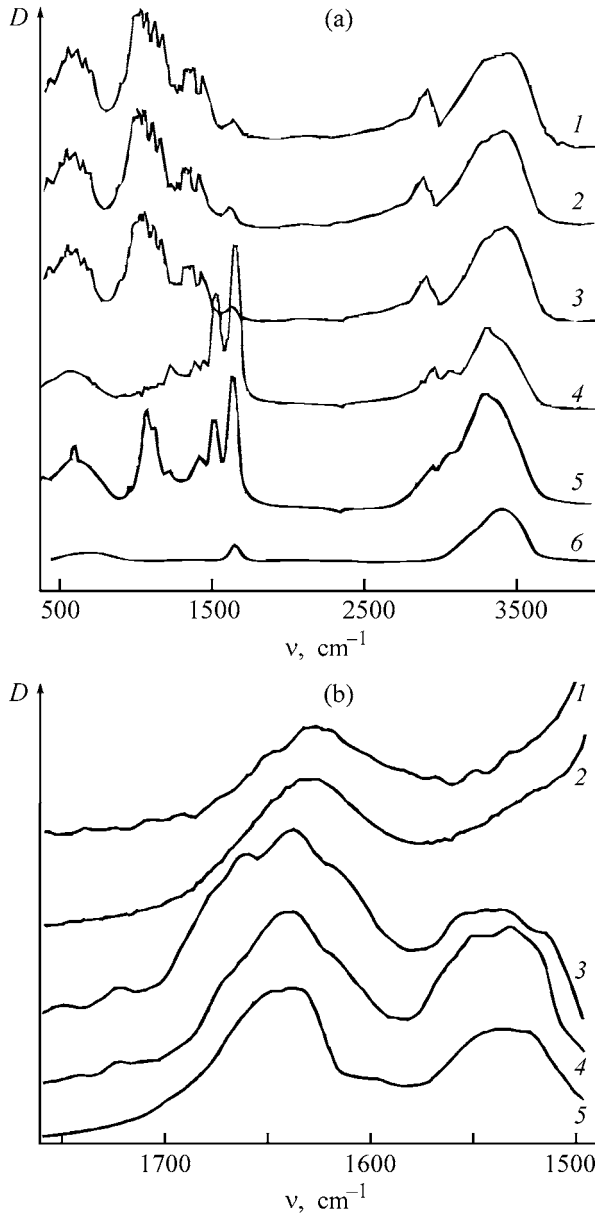

Fig. 4. IR Fourier spectra. (*D*) Absorption and (ν) wavenumber. (a) wavelength range 400–3700 cm^{-1}; (*1*) MCC, (*2*) AC MCC–trypsin (A = 21 mg g^{-1}), (*3*) the same AC after desorption of trypsin (A_r = 10 mg g^{-1}), (*4*) α-chymotrypsin, (*5*) trypsin, and (*6*) water; (b) wavelength range 1500–1775 cm^{-1}; (*1*) MCC and (*2*) AC MCC-trypsin (A = 21 mg g^{-1}); differential spectra of (*3*) trypsin and (*4*) α-chymotrypsin; (*5*) pristine trypsin.

the enzymatic activity is independent of the content of enzyme in AC.

Thus, the resulting data on the isolation of both trypsin and α-chymotrypsin from ACs, carried out under conditions simulating the physiological pH range in gastrointestinal tract, show that ACs MCC–trypsin and MCC–α-chymotrypsin can be applied to control the functions of gastrointestinal tract, both in stomach (pH 2.0) and in the upper part of the intestines (pH 8.2). Their enzymatic properties will be manifested most strongly in the latter case.

It is known that, in protein adsorption on solid surfaces under heterogeneous conditions, the surface influences protein binding and its structure as well as proteins influence the adsorption matrix. For instance, in the case of adsorption of HSA onto MCC, conformational changes of protein molecules occur, but also the morphological structure of cellulose greatly changes [5]. An X-ray diffraction study of cellulose–enzyme ACs has shown that MCC keeps the structure of cellulose I. The crystallinity index is 0.80 both in the pristine MCC and in the AC. It is known that the shape and intensity of the 040 reflection can serve as criteria of crystallite order [21]. The decrease by half in the intensity of the 040 reflection in ACs suggests that the shape of cellulose crystallites in AC changes and their packing becomes more defective. This fact confirms that the enzyme adsorption affects the supramolecular structure of the cellulose matrix.

The IR spectra of trypsin and α-chymotrypsin (Figs. 4a, 4b) contain characteristic absorption bands peaked at about 1640–1645 (amide I), 1532 (amide II), 1142–1087 (in the spectrum of trypsin) and 1236 (in the spectrum of α-chymotrypsin) (amide III), 590 cm^{-1} (amide V), as well as bands peaked at about 2900 (C–H stretching vibrations) and 3300 cm^{-1} (N–H stretching vibrations) [22]. The spectra show that the chemical composition of the pristine cellulose in the ACs does not change. The differential spectra of enzymes, obtained by subtracting MCC spectra from those of the ACs (in the ranges 1500–1750 cm–1, Fig. 4b and 3000–3600 cm^{-1}), indicate that immobilized enzymes remain in the ACs. This confirms the conclusion that a part of enzymes is strongly bound to the matrix. The position and shape of the amide I and amide II absorption bands in differential spectra of trypsin and α-chymotrypsin are sensitive to changes in the conformation of enzymes. Their analysis shows that the absorption band peaked at 1532 cm^{-1} changes only slightly as compared to that of pristine enzymes. The change in the shape of the absorption band in the range 1620–1680 cm^{-1}, specifically, its splitting into three bands, in the differential spectra of both enzymes is more noticeable (Fig. 4b). These changes are probably due to interaction between enzymes and cellulose. However, the overlapping of some absorption bands in the range 3000–3600 cm^{-1}, for instance, the amide I band in the spectra of enzymes and

the HOH bending band of adsorbed water in cellulose, the broad absorption band of OH groups of cellulose, peaked at 3410 cm^{-1}, and that of NH groups of enzymes, peaked at 3250 cm^{-1}, do not allow any unambiguous conclusion on the mechanism of component interaction. The revealed presence of a considerable amount of unremovable water bound both to the enzyme and to the cellulose matrix is in agreement with data obtained by other authors, according to which water can form stable cluster systems when strongly bound to enzymes and cellulose [23–25].

Thus, the results of an IR study indicate that immobilized trypsin and α-chymotrypsin are strongly bound to the cellulose matrix and interact with cellulose. This is in agreement with the conclusions based on the adsorption isotherms.

Changes in the morphological structure of cellulose also occur during enzyme immobilization on cellulose fibers. According to the results obtained by scanning electron microscopy (Figs. 5a–5d), the pristine cellulose fibers (Fig. 5a) become swollen and partly destroyed. The fibrillar order on the fiber surface is disturbed; the fibers are destroyed in transverse and longitudinal directions (Fig. 5b). This is especially noticeable after partial desorption of adsorbed enzymes (Figs. 5c, 5d).

Thus, immobilization of enzymes on a cellulose matrix is accompanied by mutual effect of enzymes on the supramolecular and morphological structure of cellulose and of cellulose on some properties of enzymes, for instance, their solubility.

To elucidate the mechanism of enzyme binding to the cellulose matrix, the content of enzymes immobilized on cellulose and retained after desorption was correlated to the amount of cellulose chains and, correspondingly, to that of the main reactive (carboxy and aldehyde) groups of cellulose (Table 4).

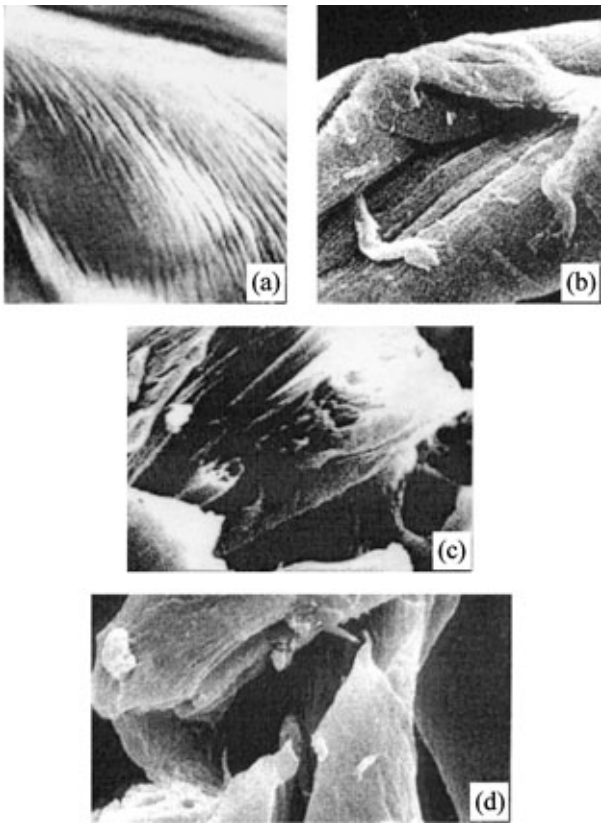

Fig. 5. Electron micrographs of (a) MCC fiber, (b, c) AC of MCC containing immobilized (b) trypsin or (c) α-chymotrypsin, and (d) MCC fiber after desorption of trypsin from AC MCC–trypsin.

Table 4. Molar ratio of enzymes and functional groups of cellulose in ACs MCC–trypsin or MCC–α-chymotrypsin with varied content of immobilized enzymes

Sample no.*	A, mg g^{-1}	Amount of cellulose chains and functional groups of cellulose capable to be bound with 1 mol of enzyme			Sample no.*	A, mg g^{-1}	Amount of cellulose chains and functional groups of cellulose capable to be bound with 1 mol of enzyme		
		cellulose chains	–HC=O groups	–COOH groups			cellulose chains	–HC=O groups	–COOH groups
Trypsin					α-Chymotrypsin				
1	3.0	256	191	45	6	7.0	116	116	21
2	13.0	59	59	11	7	18.0	45	45	8
3	21.0	36	36	7	8	49.0	17	17	3
4	33.0	23	23	4	9	38.0	21	21	4
5	9.9	77	77	14					

* Samples 1–4 and 6–8 are ACs MCC–trypsin and MCC–α-chymotrypsin, respectively; samples 5 and 9 are the same ACs after desorption of enzymes from samples 4 and 8, respectively.

Table 4 confirms the conclusion that α-chymotrypsin is retained in the cellulose matrix to a greater extent than trypsin. The macromolecule of immobilized α-chymotrypsin is strongly bound by a smaller amount of cellulose chains than that of trypsin (compare samples 5 and 9), i.e., α-chymotrypsin is more labile with respect to cellulose.

According to these results, three possible ways of formation of cellulose-enzyme complexes can be suggested. Stable bonds between cellulose and enzymes are formed owing to the interaction of amino groups of enzymes with aldehyde end groups of cellulose and surface carboxy groups, as well as due to binding of amino groups to hydroxy groups of the cellulose surface (schemes 1–3).

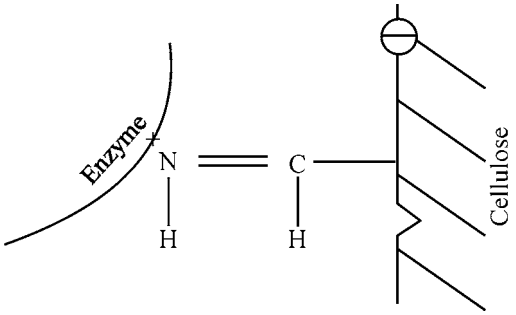

Scheme 1.

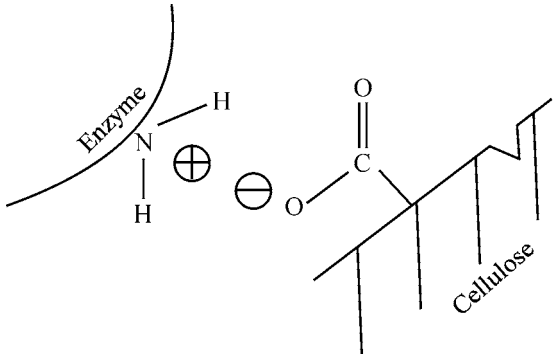

Scheme 2.

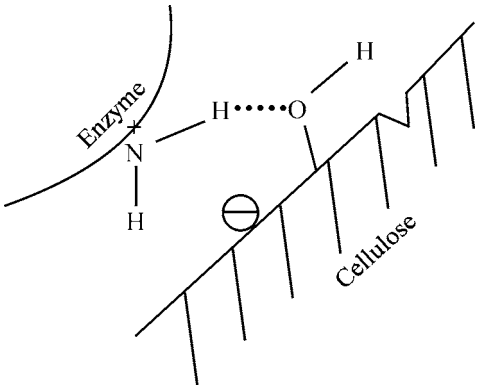

Scheme 3.

The surface of MCC is very hydrophilic because it is enriched in hydroxy groups. This favors multipoint interaction between the amino groups of enzymes and the hydroxy groups of cellulose (scheme 3). This process does not exclude binding of both cellulose macromolecules and enzymes to water molecules, as described in [23–25].

CONCLUSIONS

(1) Adsorption isotherms are described by the Freundlich equation.

(2) Adsorption of enzymes is partly reversible. The content of immobilized trypsin strongly bound to cellulose is 10 mg g^{-1} and that of α-chymotrypsin attains 41 mg g^{-1}.

(3) It is shown by wide-angle X-ray scattering and scanning electron microscopy that enzyme adsorption promotes changes in the supramolecular and morphological structure of the cellulose matrix.

ACKNOWLEDGMENTS

The authors are grateful to V.K. Lavrent'ev [Institute of Macromolecular Compounds, Russian Academy of Sciences (IVS)] for recording X-ray diffraction patterns of the samples, to N.N. Saprykina (Prikladnaya Khimiya State Unitary Enterprise) for performing scanning electron microscopy, to B.Z. Volchek (IVS) for discussing IR data, to T.B. Tennikova (IVS) for submitting samples of substrates, and to E.F. Panarin and G.P. Vlasov (both IVS) for discussing the results and making valuable comments.

REFERENCES

1. Beresin, I. V., *Biotekhnologiya*, 1985, vol. 1, no. 2, pp. 113–116.
2. Petropavlovskii, G.A. and Kotelnikova, N.E., *Khim. Drev.*, 1979, no. 6, pp. 3–21.
3. Kotelnikova, N.E., Panarin, E.F., and Kudina, N.P., *Zh. Obshch. Khim.*, 1997, vol. 67, no. 2, pp. 335–340.
4. Panarin, E.F., Kotelnikova, N.E., Jie Song, et al., *Zh. Prikl. Khim.*, 1995, vol. 68, no. 11, pp. 1883–1889.
5. Kotelnikova, N.E., Lashkevich, O.V., and Panarin, E. F., *Macromol. Symp.*, 2001, no. 166, pp. 73–76.
6. Virnik, A.D., Kildeeva, N.P., Krasovskaya, S.B., et al., *Biotekhnologiya*, 1988, vol. 4, no. 1, pp. 91–96.
7. Virnik, A.D., Kildeeva, N.P., Krasovskaya, S.B., et al., *Biotekhnologiya*, 1987, vol. 3, no. 5, pp. 602–611.
8. Van Leemputten, E. and Horisberger, M., *Biotechnol. Bioeng.*, 1974, vol. 16, no. 7, pp. 997–1003.
9. Sidorova, M.P., Ermakova, L.E., Kotelnikova, N.E., et al., *Kolloidn. Zh.*, 2001, vol. 63, no. 1, pp. 106–113.
10. Bresler, S.E., *Vvedenie v molekulyarnuyu biologiyu* (Introduction to Molecular Biology), Moscow: Akad. Nauk SSSR, 1963.
11. Dixon, M. and Webb,. E.C., *Enzymes*, London: Longman, 1958, 1964, 1979.
12. Erlanger, B.F., Korowsky, N., and Cohen, W., *Arch. Biochem. Biophys.*, 1961, no. 95, pp. 271–276.
13. Lowry, O.H., Rosebrough, N.J., Farr, A.L., and Randall, R.J., *J. Biol. Chem.*, 1951, vol. 16, no. 193, pp. 265–275.
14. Lur'e, Yu.Yu., *Spravochnik po analiticheskoi khimii* (Handbook of Analytical Chemistry), Moscow: Khimiya, 1967, pp. 223–230.
15. Segal, L., Creely, I., and Martin, A.E., *Textile Res. J.*, 1959, no. 29, pp. 783–786.
16. Scherrer, P., *Kolloid-Chemie, Zsigmondy, R.*, Ed., Berlin: Max Hueber, 1933, 3rd ed.
17. Okubo, V., Mori, K., Kamei, Sh., and Matsumoto, T., *Kobunshi Ronbunshu*, 1983, vol. 40, no. 12, pp. 809–816.
18. Rudenskaya, G.N., Isaev, V.A.,. Kalebina, T.S., et al., *Bioorg. Khim.*, 1998, vol. 24, no. 2, pp. 112–118.
19. Gregg, S.J. and Sing, K.S.W., *Adsorption, Surface Area and Porosity*, London: Academic, 1982. Translated under the title *Adsorbtsiya, udel'naya poverkhnost', poristost'*, Moscow: Mir, 1970, pp. 142–151.
20. Sevast'anov, V.I., Volkov, A.V., Rodin, O.N., et al., *Dokl. Akad. Nauk SSSR*, 1981, vol. 260, no. 2, pp. 383–386.
21. Kotelnikova, N.E., Adrosption-Chemical Modification of Cellulose with Biologically Active Substances, *Doctoral Dissertation*, St. Petersburg, 2002.
22. Bellamy, L.J., *The Infra-Red Spectra of Complex Molecules*, London: Methuen, 1954.
23. Grdadolnik, J. and Marechal, Y., *Biopolymers (Biospectroscopy)*, 2001, no. 62, pp. 40–53.
24. Grdadolnik, J. and Marechal, Y., *Biopolymers (Biospectroscopy)*, 2001, no. 62, pp. 54–67.
25. Howard, W.S., Jr., *Macromolecules*, 1975, vol. 8, no. 4, pp. 476–479.

ISSN 1070-4272, Russian Journal of Applied Chemistry, 2007, Vol. 80, No. 2, pp. 330–334. © Pleiades Publishing, Ltd., 2007.
Original Russian Text © R.P. Pogorilyi, E.Yu. Siletskaya, V.P. Goncharik, L.I. Kozhara, Yu.L. Zub, 2007, published in Zhurnal Prikladnoi Khimii, 2007, Vol. 80, No. 2, pp. 331–335.

MACROMOLECULAR CHEMISTRY AND POLYMERIC MATERIALS

Immobilization of Urease on the Silica Gel Surface by Sol–Gel Method

R. P. Pogorilyi, E. Yu. Siletskaya, V. P. Goncharik, L. I. Kozhara, and Yu. L. Zub

Institute of Surface Chemistry, Ukrainian National Academy of Sciences, Kiev, Ukraine

Received February 14, 2006; in final form, June 2006

Abstract—The possibility of "double immobilization" of urease on silica gel, involving enzyme incorporation into the polysiloxane polymer prepared by sol-gel procedure on the surface of an inorganic support was studied. The optimal composition and thickness of the polysiloxane film, providing relatively high activity of urease, were determined.

DOI: 10.1134/S1070427207020310

One of the main problems of biotechnology is development of new simple and practically feasible methods for immobilization of enzymes to prepare stable and highly active heterogeneous biocatalysts for commercial use [1]. Among modern procedures of enzyme immobilization, the sol–gel method and, especially, the procedure based on hydrolytic polycondensation of alkoxysilanes [2] seems promising. In this mode, an enzyme can be immobilized both by sorption on preliminarily prepared polysiloxane supports and by incorporation into polysiloxane matrices in the course of the above reaction [3, 4]. In the first case, we frequently obtained porous materials with fairly developed surface and pores of certain diameter. The parameters of the pore structure of these matrices directly affect the degree of enzyme binding and the preservation of its activity [5, 6]. In the second case, a certain (frequently large) fraction of the enzyme is completely incorporated into the siloxane support and, thus, becomes inaccessible for the substrate [7]. To eliminate this disadvantage, the procedure of so-called double immobilization of enzymes on the surface of porous silica gel by the sol–gel procedure was suggested [8, 9]. This approach for preparing biocatalysts is based on the uniform distribution of a solution containing alkoxysilanes and enzyme on the surface of the inorganic support. Subsequent hydrolytic polycondensation in the supported solution leads to the formation of polysiloxane layer (PL) containing an enzyme on the silica gel surface.

This method is rather simple and does not require expensive supports and reagents. In this study, which continues our systematic investigations, we attempted to develop a procedure for double immobilization of urease on the silica gel surface and to study the activity and stability of the immobilized enzyme as influenced by the nature of alkoxysilanes and the component ratio.

EXPERIMENTAL

The experiments were performed using the hydrolase class enzyme, specifically, soybean urease (Jack beans, EC 3.5.1.5) with an activity of 46.2 units mg^{-1} at pH 7 (Fluka). The sol–gel procedures were carried out using tetraethoxysilane $Si(OC_2H_5)$ (TEOS, 98%), 3-mercaptopropyltrimethoxysilane $(CH_3O)_3Si–(CH_2)_3SH$ (MPTMS, 99%), methyltriethoxysilane $(C_2H_5O)_3SiCH_3$ (MTES, 995), and dimethyldiethoxysilane $(C_2H_5O)_2Si(CH_3)_2$ (DMDES, 99%); all the chemicals were purchased from Aldrich (United States). Porous Davesil silica gel (Aldrich, S_{sp} 300 $m^2 g^{-1}$, d 0.015 μm) was used as a support. We also used a 0.06 M phosphate buffer (pH 7), 0.05 M solution of sodium ethylenediaminetetraacetate (analytically pure grade Na_2EDTA), 2 M solution of chemically pure grade urea, 4% aqueous solution of polyvinyl alcohol (PVA), and 0.01 M solution of NH_4F as a catalyst for hydrolytic polycondensation.

Urease was immobilized by hydrolytic polycondensation on the silica gel surface of alkoxysilanes

preliminarily mixed in the required ratios in the presence of a catalyst (fluoride ions), PVA, and urease:

Hydrolysis of alkoxysilanes

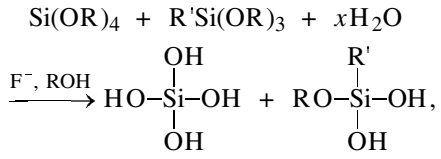

where R = CH_3, C_2H_5; R' = functional group;

Condensation

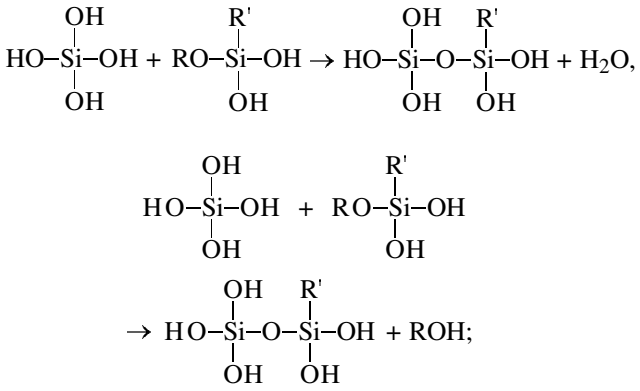

Polycondensation

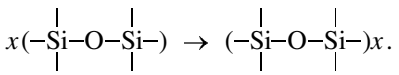

The volume ratio of the initial solution and silica gel was selected so as to eliminate formation of a supernatant liquid fraction. The suspension was thoroughly mixed and placed in a refrigerator (4°C) for subsequent hydrolysis of alkoxysilyl groups and condensation of the resulting silanol groups, (silanol groups on the silica gel surface are also involved in this process). The activity of the immobilized urease was measured at regular intervals. For example, the component ratio in the preparation of a sample was as follows: TEOS 0.15 cm^3, MTES 0.05 cm^3, DMDES 0.05 cm^3, PVA solution 0.05 cm^3, NH_4F 0.01 cm^3, urease solution (20 mg of urease in a phosphate buffer at pH 7) 0.25 cm^3, and silica gel 1.5 g.

For comparison, urease was directly immobilized in the initial silica gel by equilibrium adsorption from a phosphate buffer solution (pH 7) or by its wetting with the urease solution in the phosphate buffer, with subsequent drying of the sample in a refrigerator and washing with water. The washing water

Table 1. Activity of urease immobilized on silica gel by adsorption from a buffer solution

Method of urease immobilization	Urease added, mg g^{-1}	Urease immobilized		A_{im}, units g^{-1}	A_{pr}, %
		mg g^{-1}	%		
Adsorption:					
equilib-	34.4	9.5	26.3	0.1	0.3
rium	40.1	8.1	20.2	0.1	0.2
	80.0	8.8	11.0	0.4	0.9
nonequi-	36.4	36.3	99.8	3.0	6.5
librium	41.2	37.4	90.7	3.0	6.8

after urease immobilization on the silica gel surface was analyzed for the content of urease, and the degree of urease immobilization was determined from the difference between the initial content of urease and its concentration in the wash water. The content of urease in the wash water was evaluated from its enzymatic activity, taking into account that the specific activity of urease in the wash water was similar to that in the native sample (46.2 units g^{-1}).

The enzymatic activity of urease in the wash water and of immobilized urease A_{im} was determined by the kinetic method from the rate of urea hydrolysis catalyzed by urease. The rate of the urea hydrolysis was evaluated from the amount of ammonia formed during a certain period of time. The concentration of the ammonium cations was determined colorimetrically with the Nessler reagent [10]. Conversion of 1 μmol of urea per minute of the enzymatic reaction was taken as a unit activity of the urease. In all the cases, the activity was determined as the average of three parallel runs; the measurement error of the urease activity did not exceed 10%.

The retention of the immobilized urease was evaluated using the following expression:

$$A_{pr} = A_{im} \times 100/46.2m,$$

where A_{pr} is the preserved urease activity (%); A_{im}, activity of immobilized urease units g^{-1}); and m, weight of the native urease contained in 1 g of the sample (mg).

The data on the activity of urease immobilized on the Devisil silica gel surface by equilibrium and nonequilibrium adsorption from the buffer solution are listed in Table 1. As seen, the evaporation of the urease solution provides irreversible immobilization (90–

Table 2. Activity of urease immobilized on silica gel by the sol–gel method as influenced by the composition of the initial reaction mixtures

Initial components of the polysiloxane layer	Alkoxysilanes added, $cm^3\ g^{-1}$	Urease added, $mg\ g^{-1}$	A_{im}, units g^{-1}	A_{pr}, %
TEOS : PVA = 2.5 : 1	1.0	38.0	0.2	0.6
TEOS : MPTMS : PVA = 2,5 : 0.1 : 1	1.0	41.0	0.2	0.6
TEOS : MTES : PVA = 4 : 1 : 1	1.0	36.0	1.4	4.0
TEOS : MTES : DMDES : PVA = 3 : 1 : 1 : 1	1.0	48.0	3.2	9.0
	0.5	22.0	5.7	16.0
TEOS : MTES : DMDES = 3 : 1 : 1	0.5	20.0	3.5	10.0

100%) of the enzyme in the silica gel. At the same time, only a small fraction of the enzyme (10–26%) is irreversibly retained on the silica gel surface in the case of equilibrium adsorption. However, the enzymatic activity of immobilized urease is very low in both cases.

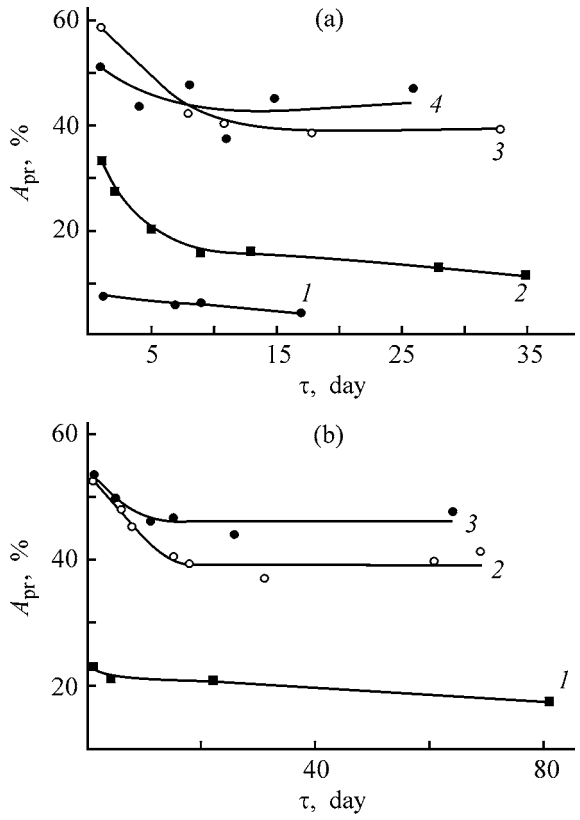

Fig. 1. Preserved activity A_{pr} of urease immobilized in polysiloxane layer on silica gel vs. time τ for (a) three-component TEOS : MTES : DMDES and (b) two-component TEOS : MTES systems. Alkoxysilanes added ($cm^3\ g^{-1}$): (a) (*1*) 1.0, (*2*) 0.5, (*3*) 0.25, and (*4*) 0.16; (b) (*1*) 0.4, (*2*) 0.3, and (*3*) 0.13.

The data on the urease activity in the samples prepared by double immobilization with various systems are listed in Table 2. As seen, the activity and the preservation of the activity of immobilized urease increase upon introduction of the hydrophobic groups (methylsilyl or dimethylsilyl) into the polysiloxane layer. These groups at the silicon atom in alkoxysilanes, especially $=Si(CH_3)_2$, hinder formation of a 3*D* matrix network, because they cannot be involved in condensation. These groups also cannot form hydrogen bonds with amino residues of urease. As a result, the enzyme binding should be weaker [11]. Hence, the effect of the polysiloxane matrix on the structure of immobilized urease will be smaller. The effect of PVA is probably the same: on mixing with alkoxysilanes, it prevents formation of the 3*D* network of the polysiloxane matrix [6]. As a result, the activity of urease in the films prepared on the silica gel surface in the presence of PVA is higher by a factor of 1.5 as compared to the samples prepared without PVA.

The data listed in Table 2 suggest that the preservation of the activity of immobilized urease also depends on the ratio of the volume of alkoxysilanes and weight of the support. The effect of this factor was studied in detail for the example of two-component TEOS : MTES and three-component TEOS : MTES : DMDES systems. The results are shown in Figs. 1 and 2. As can be seen from Figs. 1a and 1b, the activity of immobilized urease slightly decreases in the initial period of the samples storage (about 10 days) in both systems in most cases. In this time, the polysiloxane layer probably undergoes further structuring in which a certain fraction of urease either loses its enzymatic activity or gets encapsulated and becomes inaccessible. Moreover, as the ratio of the liquid and solid phases decreases, i.e., as the polysiloxane layer becomes thinner, the activity of immobilized enzyme increases.

It has been found previously that the activity of urease immobilized in polysiloxane xerogels by adsorption is determined by the pore structure of the matrix and, in particular, by the pore diameter [7]. However, the structural and adsorption properties of silica gel (Table 3), determined from the isotherms of nitrogen adsorption, show that formation of PL on the sorbent surface does not significantly affect the parameters of the pore structure of the resulting samples as compared to the initial silica gel. Thus, the variation of the activity of urease immobilized in PL on the silica gel surface with the ratio of the volume of alkoxysilanes and weight of silica gel is governed by some other factor.

Obviously, the smaller the volume of alkoxysilanes per gram of silica gel, the thinner the resulting polysiloxane layer. Assuming that the reaction solution of alkoxysilanes is uniformly distributed over the silica gel surface, we can calculate from its volume and specific surface area the thickness of the resulting layer. The ratio of the solid and liquid phases used in this study provides formation of the polysiloxane layers with a thickness from 0.4 to 3.3 nm. On drying, the layer thickness will decrease. At the same time, the resulting PL may be discontinuous (islet-like), rather than uniform. In this case, the layer (islet) will be thicker. Taking into account the diameter of the urease molecule (about 5 nm) [12] we can assume that a greater fraction of the enzyme is accessible for the substrate in a thin polysiloxane layer. With increasing layer thickness, the probability of urease encapsulation grows, which decreases its activity to values typical of xerogels (Table 4).

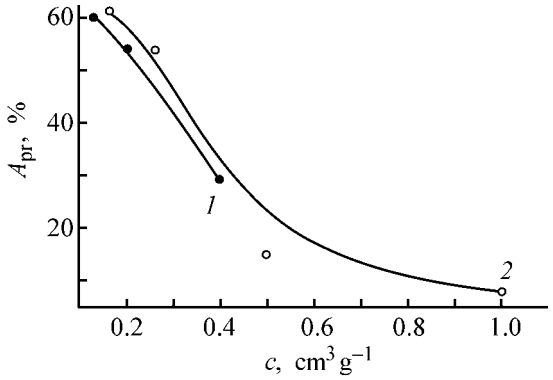

Fig. 2. Preserved activity A_{pr} of immobilized urease for (*1*) TEOS : MTES and (*2*) TEOS : MTES : DMDES systems vs. the content c of alkoxysilanes used for preparing PL on the silica gel surface; samples stored for 20 days at 4°C.

In conclusion, we can compare the activity of urease immobilized in the polysiloxane layer on the silica gel surface with the activity of urease incorporated into the polysiloxane xerogel in the course of its preparation by the sol–gel method [7] (Table 4). As can be seen from Table 4, the activity of immobilized

Table 3. Structural and adsorption properties of silica gel samples with a polysiloxane layer and immobilized urease

Sample	Ratio of liquid components	Alkoxysilanes added cm^3 g^{-1}	S_{sp}, m^2 g^{-1}	V_s, m^3 g^{-1}	d_{ef}, nm
Silica gel	–	–	277	1.12	12.2
Silica gel + TEOS : MTES : PVA	3 : 1 : 1	0.45	262	0.95	12.0
	3 : 1 : 1	0.13	273	1.08	14.4
Silica gel + TEOS : MTES : DMDES : PVA	3 : 1 : 1 : 1	1	251	0.96	12.0
	3 : 1 : 1 : 1	0.5	249	0.85	12.0
	3 : 1 : 1 : 1	0.17	260	1.05	14.4

Table 4. Activity of urease immobilized in xerogels and in a polysiloxane layer deposited on silica gel (initial ratio TEOS : MTES : MDMES : PVA = 3 : 1 : 1 : 1)

Sample	Alkoxysilanes added, cm^3 g^{-1}	A_{pr}, %	Sample	Alkoxysilanes added, cm^3 g^{-1}	A_{pr}, %
Silica gel + PL	0.16	61	Silica gel + PL	0.5	16
	0.25	53		1.0	5.5
			Xerogel*	–	5.7

* Urease was immobilized in the course of xerogel preparation by the sol–gel method.

urease strongly decreases on passing from film-forming samples to samples of polysiloxane xerogels with immobilized urease. The decrease in the urease activity on passing form film-forming samples to xerogels with incorporated enzyme can be accounted for by the fact that the enzyme is almost completely incorporated in the matrix in the latter case; as a result, the enzyme not only loses its activity but becomes inaccessible to the substrate [7]. At double immobilization, significantly smaller amounts of alkoxysilanes are used for the enzyme binding, and it occurs in the fine polysiloxane layers and, in most cases, is accessible to the substrate. Moreover, introduction of hydrophobic groups into these layers decreases the number of hydrogen bonds between the enzyme molecule and matrix surface. As a result, the effect of the rigid polysiloxane matrix on the enzyme being immobilized decreases, which should improve the preservation of the urease activity. The decrease in the activity of urease immobilized in xerogels, compared to the samples of urease immobilized in a thin polysiloxane layer, was predictable, whereas the relatively low activity of urease adsorbed on silica gel (Table 1) was unexpected. In sorption of urease on the silica gel surface, the interaction of the enzyme with the surface silanol groups is probably of the type many-point [13, 14], which causes its rigid linking and hence deactivation. As a result, only an insignificant fraction of the adsorbed urease retains its activity in enzymatic reactions. A similar pattern has been observed for similarly immobilized alcohol dehydrogenases and glucose oxidases [9].

CONCLUSION

An efficient sol–gel method was developed for immobilization of urease in polysiloxane layer on the silica gel surface. The activity of urease immobilized by this procedure is determined by the composition and thickness of the film; it increases upon addition of the hydrophobic (methyl) groups and polyvinyl alcohol and with decreasing thickness of the polysiloxane layer.

REFERENCES

1. *Immobilizovannye fermenty* (Immobilized Enzymes), Berezin, I.V., Ed., Moscow: Nauka, 1976.
2. Brinker, C.J. and Scherer, G.W., *Sol–Gel Science: the Physics and Chemistry of Sol–Gel Processing*, San Diego: Academic, 1990.
3. Gill, I., *Encyclopedia of Nanoscience and Nanotechnology*, Nalwa, H.S., Ed., Am. Sci., 2003, vol. 10, pp. 1–24.
4. Collinson, M.M., *Trend Anal. Chem.*, 2002, vol. 21, no. 1, pp. 30–38.
5. Davydenko, T.I., Sevast'yanova, O.V., Yuodval'kite, D.Yu., et al., *Dopov. Akad. Nauk Ukr. RSR, Ser. B*, 1984, no. 2, pp. 64–66.
6. Tertykh, V.A. and Yanishpol'skii, V.V., *Meditsinskaya khimiya i klinicheskoe primenenie dioksida kremniya* (Medical Chemistry and Clinical Use of Silica), Chuiko, A.A., Ed., Kiev: Naukova Dumka, 2003, pp. 43–58.
7. Pogorilyi, R.P., Goncharik, V.P., Kozhara, L.I., et al., *Ukr. Biokhim. Zh.*, 2006, vol. 78, no. 1, pp. 94–101.
8. Reetz, M.T., *Adv. Mater.*, 1997, vol. 9, no. 12, pp. 943–947.
9. Kovalenko, G.A. and Sokolovskii, V.D., *Biotekhnologiya*, 1987, vol. 3, no. 5, pp. 612–617.
10. Lur'e, Yu.Yu., *Analiticheskaya khimiya promyshlennykh stochnykh vod* (Analytic Chemistry of Industrial Wastewaters), Moscow; Khimiya, 1984.
11. Reetz, M.T., Zonta, A., Vijayakrishnan, V., and Schmossek, K., *J. Mol. Catal. Chem.*, 1998, vol. 134, pp. 251–258.
12. Krishna, M.R., Kallury, Lee, W.E., and Thompson, M., *Anal Chem.*, 1992, vol. 64, pp. 1062–1088.
13. Kazakova, O.A., Gun'ko, V.M., Voronin, E.F., et al., *Kolloidn. Zh.*, 1998, vol. 60, no. 5, pp. 613–617.
14. Pogorilyi, R.P., Goncharik, V.P., Kozhara, L.I., et al., *Vopr. Khim. Khim. Tekhnol.*, 2005, no. 6, pp. 103–107.

ISSN 1070-4272, Russian Journal of Applied Chemistry, 2007, Vol. 80, No. 2, pp. 335–337. © Pleiades Publishing, Ltd., 2007.
Original Russian Text © G.V. Kiseleva, S.V. Smirnov, B.P. Sereda, 2007, published in Zhurnal Prikladnoi Khimii, 2007, Vol. 80, No. 2, pp. 336–338.

BRIEF COMMUNICATIONS

Specific Feature of Synthesis and Technological Scheme for Manufacture of Nonstoichiometric Hydroxo Chromium(III) Formates

G. V. Kiseleva, S. V. Smirnov, and B. P. Sereda

Ural State Forestry University, Yekaterinburg, Russia

Received March 1, 2006; in final form, July 2006

Abstract—Specific features of the hydrothermal interaction between chromium(VI) oxide and formic acid to give water-soluble nonstoichiometric hydroxo chromium(III) formates with compositions from the range $Cr(OH)_{0.66}(HCOO)_{2.34}$–$Cr(OH)_{1.55}(HCOO)_{1.45}$ were studied. These compounds can be used in formulations for chromium-plating electrolytes and tanning agents.

DOI: 10.1134/S1070427207020322

Chromium(III) sulfate is the most accessible and least expensive among water-soluble chromium(III) compounds applied in chemical technology. Use of chromium(III) sulfate leads to a substantial contamination of wastewater, because methods for removal and utilization of chromium(III) are mostly based on its binding into poorly soluble compounds, with further separation from the aqueous phase, whereas sulfate ions remain in solutions and are accumulated to concentrations exceeding those established by regulations. It has been shown previously that reduction of chromium(VI) compounds in formic acid can give hydroxo chromium(III) formates having rather high solubility and exhibiting properties that enable their effective use, instead of chromium(III) sulfate, in formulations for chromium-plating electrolytes and tanning agents. [1, 2]. Chromium can be rather simply bound into poorly soluble compounds in wastewater purification by pyrolysis, because formate ions decompose at high temperatures to give carbon(IV) oxide and water [3].

This study is concerned with specific features of synthesis of nonstoichiometric hydroxo chromium(III) formates from chromium(VI) oxide and formic acid. The compounds were synthesized by the known procedure [4]. The course of the reactions was monitored, which the initial concentrations, reactant ratios, temperature, and mixing rate of substances varied. The results of the laboratory studies were used to develop a technological scheme tested under real industrial conditions.

EXPERIMENTAL

The choice of chromium(III) oxide as a raw material is due to the fact that this compound is the main product formed in processing of natural chromium compounds [5]. Formic acid simultaneously acts as an agent that reduces chromium(VI) and an anion in the formation of basic formate salts. Hydroxo chromium(III) formate is formed by the reaction

$$2CrO_3 + 7HCOOH = 2CrOH(HCOO)_2 + 3CO_2\uparrow + 4H_2O. \quad (1)$$

The reaction was performed in an aqueous solution at temperatures of 313–368 K, initial chromium(VI) oxide concentrations of 0.85 to 1.65 mol dm^{-3}, and CrO_3/HCOOH ratios of 0.16–0.34. The mixing rates of the reactants and the duration of separate studies of synthesis were chosen empirically by visual inspection and on the basis of data furnished by chemical analysis of intermediate phases and synthesis products. The cationic complexes of chromium(III), formed in reduction, undergo hydrolysis dependent on the concentration, pH value, and temperature of the solution. As result, the forming hydroxo chromium(III) formates contain different amounts of hydroxo groups per mole of chromium(III). With account of the acid-neutralizing capacity h, Eq. (1) can be transformed to

$$CrO_3 + (4.5 - 3h)HCOOH = Cr(OH)_{3h}(HCOO)_{3-3h} + 1.5CO_2 + (3 - 3h)H_2O, \quad (2)$$

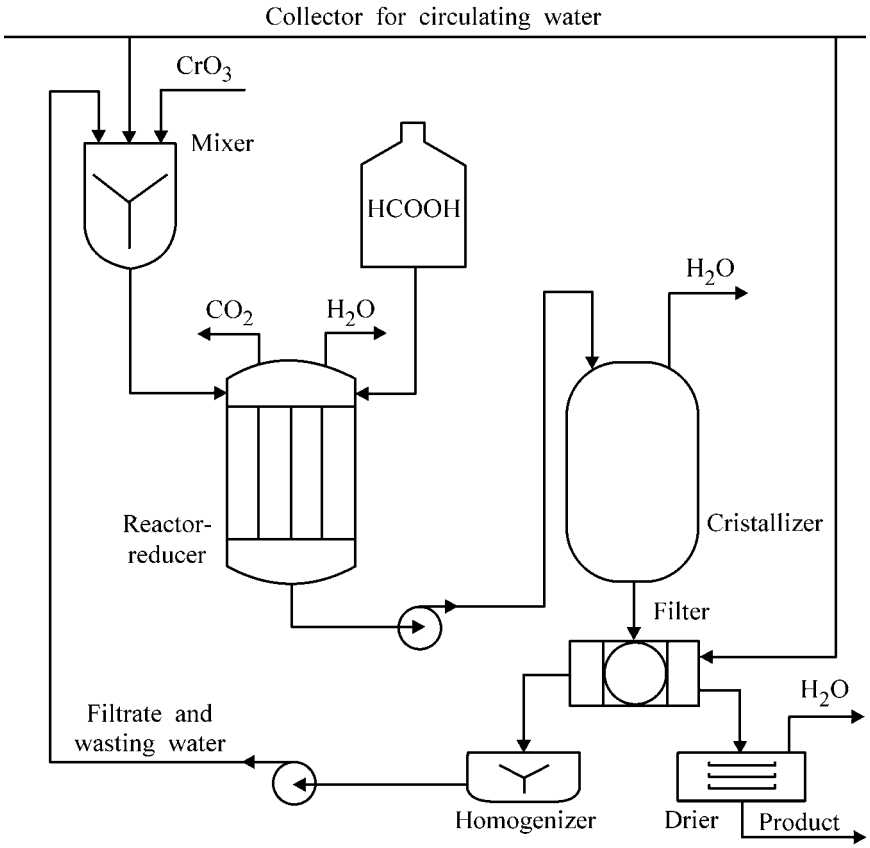

Technological scheme of synthesis of hydroxo chromium(III) formates.

where h can theoretically take values ranging from zero for the neutral salt to unity for chromium(III) hydroxide.

It was found that water-soluble hydroxo chromium(III) formates, which can be used in technologies involving preparation of aqueous solutions, formed at h in the range 0.22–0.50 and correspond to the end compositions $Cr(OH)_{0.66}(HCOO)_{2.34}$ and $Cr(OH)_{1.55}(HCOO)_{1.45}$. A statistical processing of the experimental data produced regression equations relating the product yield η and the acid-neutralizing capacity h to the initial mass concentration c_1 of chromium(VI) oxide (g dm^{-3}) and the mass fraction c_2 of the initial HCOOH [percent relative to stoichiometry (1)]:

$$\eta = 0.60c_1 + 0.64c_2 - 0.004_4c_1c_2, \quad (3)$$

$$h = 0.45c_1 + 0.31c_2 - 0.004c_1c_2. \quad (4)$$

An optimization of Eqs. (3) and (4) with respect to the yield of the product and its solubility in water demonstrated that the best initial parameters are the concentration of 120–160 g dm^{-3} CrO_3 and the amount of HCOOH equal to 150% relative to the stoichiometry.

It was found in calorimetric studies that reaction (1) is exothermic and 155.6 kJ of heat per 1 dm^3 of a solution is released in interaction of 1 mol of CrO_3 with the stoichiometric amount of HCOOH [1]. To preclude boiling-up and spraying of the reaction mass, a limiting mixing rate of reactants was set and the temperature of the reaction mass was lowered by heat removal from the reactor walls. Lowering the temperature to below 350 K at sufficiently high mixing rates of the reactants results in thickening of the reaction mixture and hinders its agitation.

Synthesis of the target process by reaction (2) with a prescribed acid-neutralizing capacity comprises two processes: reduction of chromium(VI) oxide by formic acid upon mixing of the reactants and formation of formate salts of hydroxo chromium(III) in hydrothermal treatment of the reaction mass. At 363–370 K, the duration of the reduction stage is 180–210 min. At synthesis temperatures below 340 K, reaction fails to provide complete reduction of chromium(VI) in 8 h, which results in an increase, in particular, in the duration of sample fil-

tration. A rather complex, extremal dependence of the acidity index of the samples on the temperature of the stage of thermal treatment. At 300–315 K, compounds with average h fluctuating within the range from 0.4 to 0.5. Below 300 K, the acidity index decreases because of the weakening of hydrolysis and enhancement of the competing effect of formate ions, and above 315 K, because of the decreasing stability of hydroxo complexes. At 313 and 370 K, the average values of h are 0.25–0.27. Thus, hydroxo chromium(III) formates with a prescribed acidity factor can be obtained by varying the solution treatment temperature. The duration of the complex formation stage depends on temperature and is 30–420 min.

The final stage of synthesis of the target product involves crystallization of the samples by cooling the reaction mass formed upon the thermal treatment and by keeping it under constant agitation at temperatures of 293–303 K for 360–7200 min. Hydroxo chromium(III) formates are produced in the form of a polydisperse precipitate with irregular elongated crystals. The average transverse size and length of the most representative fraction are 45 and 700 μm, respectively.

The conditions of synthesis of hydroxo chromium(III) formates, found in this study, were tested at a chromium industry plant. The synthesis of the target product (see scheme) included the following main stages.

(1) Dissolution of chromium(VI) oxide in water mixed with the filtrate produced at a subsequent stage and washing water formed at the stage of recovery of formate compounds of hydroxo chromium(III) from a suspension.

(2) Reduction of chromium(VI) with formic acid at 363–370 K and controlled rate of reactant mixing.

(3) Treatment of the reaction mass at a prescribed temperature of 300 to 370 K in order to form formate salts of hydroxo chromium(III).

(4) Crystallization of the target product by cooling the reaction mixture and keeping the suspension formed at 293–303 K.

(5) Separation of the suspension into the liquid and crystalline phases, with the washing water and the filtrate delivered to the initial stage, at which an aqueous solution of chromium(VI) oxide is prepared.

(6) Drying and packaging of the product.

A reactor-reducer with enameled walls of the reaction zone served as the technological apparatus under plant conditions. The reactor was equipped with electric heater, stirrer, Nutsch filter, and shelf drier.

Results of industrial tests of the procedure for synthesis of hydroxo chromium(III) formates

Starting reagents		Composition of hydroxo chromium(III) formates		η, %
CrO_3 c_1, g dm^{-3}	HCOOH c_2, mass fraction, %	h	$HCOO^-$ index $(1 - h)$	
100	150	0.18	0.51	62.0
120	150	0.22	0.55	88.7
120	200	0.20	0.56	87.3
140	150	0.20	0.55	67.9
160	150	0.18	0.55	95.8

The results obtained in a set of experiments performed under industrial conditions are listed in the table. The plant tests confirmed the results of the laboratory experiments. Minor changes in the composition of the products have virtually no effect on their service characteristics, which is confirmed by tests of the samples synthesized in formulations for chromium-plating electrolytes.

CONCLUSIONS

(1) The optimal conditions of chromium(VI) oxide reduction by formic acid and synthesis of water-soluble hydroxo chromium(III) formates with prescribed acidity index were determined. The composition of formate salts of hydroxo chromium(III) is determined by the temperature of hydrothermal treatment of the reaction mass and corresponds to $Cr(OH)_{0.66}(HCOO)_{2.34}$–$Cr(OH)_{1.55}(HCOO)_{1.45}$.

(2) It was found that crystallization of samples near room temperature gives a polydisperse precipitate with elongated crystals, whose transverse size and length are 45 and 700 μm, respectively.

(3) A procedure for synthesis of hydroxo chromium(III) formates under industrial conditions was suggested.

REFERENCES

1. Kiseleva, G.V., Smirnov, S.V., and Sereda, B.P., *Zh. Prikl. Khim.*, 1993, vol. 66, no. 9, pp. 2111–2114.
2. Smirnov, S.V., Kiseleva, G.V., and Sereda, B.P., *Zh. Prikl. Khim.*, 1995, vol. 68, no. 9, pp. 1445–1448.
3. Smirnov, S.V. and Kiseleva, G.V., *Zh. Prikl. Khim.*, 1995, vol. 68, no. 3, pp. 518–519.
4. USSR Inventor's Certificate, no. 1420888.
5. Averbukh, T.D. and Pavlov, P.G., *Tekhnologiya soedinenii khroma* (Technology of Chromium Compounds), Leningrad: Khimiya, 1973.

ISSN 1070-4272, Russian Journal of Applied Chemistry, 2007, Vol. 80, No. 2, p. 338. © Pleiades Publishing, Ltd., 2007.
Original Russian Text © M.G. Voronkov, R.G. Mirskov, S.N. Adamovich, 2007, published in Zhurnal Prikladnoi Khimii, 2007, Vol. 80, No. 2, p. 339.

BRIEF COMMUNICATIONS

Synthesis of High-Purity Trialkylgermanethiols

M. G. Voronkov, R. G. Mirskov, and S. N. Adamovich

Favorksii Irkutsk Institute of Chemistry, Siberian Division, Russian Academy of Sciences, Irkutsk, Russia

Received December 26, 2006

Abstract—A procedure was developed for preparing high-purity trialkylgermanethiols by the reaction of hexaalkyldigermoxanes with hydrogen sulfide.

DOI: 10.1134/S1070427207020334

Trialkylgermanethiols R_3GeSH (**I**) (R = Alk) are promising chemicals for fine organometallic synthesis and precursors for plasmochemical deposition of thin dielectric layers containing germanium and sulfur atoms.

Henry and Davidson [1] prepared triarylgermanethiols by reacting triarylhalogermanes with hydrogen sulfide in the presence of pyridine. However, this procedure appeared to be unsuitable for preparing the related alkyl compounds **I**.

Vyazankin et al. [2] prepared previously unknown trialkylgermanethiols **I** in 49.5% yield by heating trialkylgermanes with sulfur at 140°C for 4 h in an inert atmosphere. The drawbacks of their procedure are the relatively low yield of **I**, difficult synthesis of the starting trialkylgermanes, and use of high temperatures and inert gases.

For applications in microelectronics, compounds **I** of ultrahigh purity should be prepared. To this end, we developed a procedure for preparing high-purity trialkylgermanethiols in high yield by the reactions of hexaalkyldigermoxanes (which are readily prepared by hydrolysis of trialkylhalogermanes) with hydrogen sulfide at room temperature:

$$R_3GeOGeR_3 + 2H_2S \rightarrow 2R_3GeSH + H_2O,$$

where R = C_2H_5 or C_4H_9.

Triethylgermanethiol. Hydrogen sulfide was bubbled for 2 h at 20°C through a flask containing 16.8 g (0.05 mol) of hexaethyldigermoxane, until the mixture became turbid. After a 1-h pause, hydrogen sulfide was bubbled for an additional 0.5 h. In the process, the mixture spontaneously warmed up to 50°C and then cooled to room temperature. By vacuum distillation we isolated 15.4 g (80%) of triethylgermanethiol, bp 47–48°C (6 mm Hg), d_{20}^4 = 1.1249, n_D^{20} = 1.4900. Published data [2]: bp 86°C (35 mm Hg), d_{20}^4 = 1.1270, n_D^{20} = 1.4852.

Found, %: C 37.44, H 8.45, Ge 37.57, S 16.52.
$C_6H_{16}GeS$.
Calculated, %: C 37.40, H 8.40, Ge 37.60, S 16.60.

^{1}H NMR ($CDCl_3$, HMDS), δ, ppm: 1.81 (CH_3), 2.02 (CH_2), 3.6 (SH); IR, ν, cm^{-1}: 2555 (ν_{S-H}), 408 (ν_{Ge-S}).

Tributylgermanethiol was prepared similarly from 10 g (0.02 mol) of hexabutyldigermoxane; yield 7.2 g (65%), bp 104–106°C (3 mm Hg), d_{20}^4 = 1.0219, n_D^{20} = 1.4810.

Found, %: S 11.37.
$C_{12}H_{28}GeS$.
Calculated, %: S 11.57.

According to GLC analysis, the products purified by vacuum distillation on a quartz column contained no traces of organic impurities. The content of metals (Na, K, Ca, Fe, Ni, Co, etc.), according to atomic absorption analysis, did not exceed 10^{-5}–10^{-6} wt % for each metal.

CONCLUSION

A procedure was developed for preparing high-purity trialkylgermanethiols for micro- and optoelectronics technology in 65–80% yields by reactions of accessible hexaalkylgermoxanes with hydrogen sulfide for 3 h at room temperature, followed by isolation of the products by fractional distillation in a vacuum.

ACKNOWLEDGMENTS

The study was supported by the Grant Council of the President of the Russian Federation (NSh-4575.2006.3).

REFERENCES

1. Henry, M.C. and Davidson, W.E., *Can. J. Chem.*, 1963, vol. 41, p. 1276.
2. Vyazankin, N.S., Bochkarev, M.N., and Sanina, L.P., *Zh. Obshch. Khim.*, 1966, vol. 36, p. 1154.

ISSN 1070-4272, Russian Journal of Applied Chemistry, 2007, Vol. 80, No. 2, pp. 339–340. © Pleiades Publishing, Ltd., 2007.
Original Russian Text © Yu.S. Kononov, G.L. Pashkov, V.V. Patrushev, A.G. Kholmogorov, V.P. Plekhanov, 2007, published in Zhurnal Prikladnoi Khimii, 2007, Vol. 80, No. 2, pp. 339–340.

BRIEF COMMUNICATIONS

Synthesis of Electrolytic Manganese Dioxide on a Heated Anode

Yu. S. Kononov, G. L. Pashkov, V. V. Patrushev, A. G. Kholmogorov, and V. P. Plekhanov

Institute of Chemistry and Chemical Technology, Siberian Division, Russian Academy of Sciences, Krasnoyarsk, Russia

Received September 26, 2006

Abstract—Synthesis of electrolytic manganese dioxide on a heated anode was studied. The specific energy of chemical power cells fabricated using this dioxide in the Zn–Mn system is as high as 100 W h kg^{-1}.

DOI: 10.1134/S1070427207020346

The research aimed to improve the galvanic cell with a cathode paste composed of manganese dioxide (MD) is concentrated on making higher the operation speed and energy density of the cells [1]. As regards mass production, raising the specific energy of chemical power cells (CPC) is, naturally, of primary importance.

This communication describes a method for synthesis of electrolytic MD of improved quality and presents the results of tests of CPC fabricated from the electrolytic manganese dioxide (EMD) synthesized by anodic oxidation of manganese(II) ions from an electrolyte heated to 90–95°C. A significant disadvantage of this technique is that the resulting EMD contains, in addition to the γ-modification of MnO_2, its other modifications, which are inactive in the Zn–Mn system of CPC [2].

The novelty of the previously developed technique [3] consists in that EMD is synthesized at a heated anode. This makes it possible to heat to a higher temperature the electrosynthesis zone, in which an anodic deposit of MnO_2 of mostly γ-modification crystallizes. The higher temperature of EMD synthesis favorably affects the quantitative yield of the necessary γ-modification of manganese dioxide at the expense of other modifications (β-, α-, ...).

EXPERIMENTAL

The electrolytic synthesis of MD was carried out on an anode made of platinum-plated VT1-0 titanium. The anode comprising 10 titanium plates (25 mm wide and 300 mm long) welded in series to form a labyrinth was heated with 80–200-A ac current. The heating was controlled by varying the applied voltage, commonly 3–5 V at currents of up to 100 A. The anode temperature was measured with a thermometer introduced into a tube welded in the anode. VT1-0 titanium plates served as cathodes.

The electrolyte was of the commonly used composition (100–200 g l^{-1} of manganese sulfate) [4]. It was not specially heated; its temperature varied, depending on the circulation rate ?between leaching and electrolysis procedures, from 30 to 95°C.

When determining the specific energy of CPC, discharge curves were recorded with a self-recorder connected to an unconventional electrolytic cell with a zinc anode 25 mm in diameter and 2.5 g of EMD with addition of 20% carbon black. A solution of $ZnCl_2$ and NH_4Cl served as electrolyte. The cell load was 10 or 56 Ω. The CPC discharge was continued until the cell voltage decreased to 700–750 mV.

The chemical power cell fabricated from this kind of EMD has a specific energy (in the Zn–Mn system) of 100 W h kg^{-1}, which markedly exceeds that of commercial CPC of the same type (see table).

Phase composition of electrolytic manganese dioxide and specific energy of CPC based on this manganese dioxide in the Zn–Mn system

EMD	Anode temperature in synthesis, °C	Phase composition of EMD	Specific energy in the Zn–Mn system, W h kg^{-1}
Comparison sample	80–90	γ-,α-,β-	45–60 [5]
	No data	No data	80 [6]
Trial sample:			
1	90	γ-,α-,β-	60
2	105	γ-,α-,β-	70
3	110	γ-	100

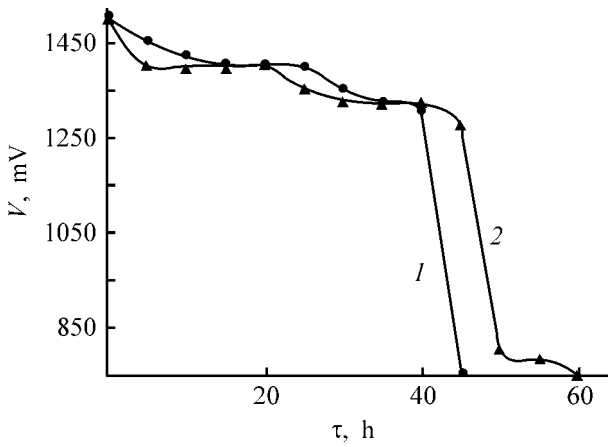

Discharge curves of CPC. (V) Voltage and (τ) time. (*1*) Standard Varta R6P AA · UM.3 · 1.5 V and (*2*) trial sample Uran-1 R6 (316) 1.5 V.

A trial batch of EMD was produced on a pilot installation with an electrolysis bath holding about 40 l of electrolyte and platelike platinum-plated titanium anodes of the labyrinth type (10 series-connected 300-mm-long and 25-mm-wide plates) at a current density of 100–300 A m^{-2}. Titanium plates served as cathodes. The electrolyte (100–200 g l^{-1} $MnSO_4$, 10 g l^{-1} H_2SO_4) was purified to remove admixtures of nonferrous metals and iron by successive hydrolytic precipitation of iron and ion-exchange precipitation of nonferrous metal ions on an An-35 chelate ion-exchange resin at pH 3–4 to a level of 1–2 mg l^{-1}. The platelike labyrinth anode was heated with an ac current of mains frequency, with a voltage not exceeding 10 V. The heating level was controlled by varying the current in the range from 80 to 200 A. About 900 g of manganese dioxide was obtained in three batches differing in the extent of anode heating. It was found that the maximum heating (with a current of about 200 A) leads to partial conversion of the dioxide into Mn_2O_3, which is undesirable. The best results were obtained in the case of heating with a current of 80–100 A. The quality of the resulting manganese dioxide was judged from its phase composition and capacity of CPC in discharge to 750 mV. The previously obtained EMD samples [3] are virtually totally composed of the γ-modification of manganese dioxide and have capacities in the range from 90 to 116 A h kg^{-1} (cf 65 A h kg^{-1} for a cell with Japanese EMD) at a discharge current density of 20 A m^{-2}.

The EMD obtained was used to fabricate a trial batch of chemical power cells at Svirskie promyshlennye seti (Svirsk Industrial Power Supply) plant.[1] The discharge characteristics of these CPC [Uran-1 R6 (316) 1.5 V trial sample] (see figure) show that the electric energy produced on a load of 56 Ω is 1.1 A h per cell, which corresponds to the output capacity of commercial CPC of the same design (Standard Varta R6P AA · UM.3 · 1.5 V) under comparable conditions.

CONCLUSIONS

It was demonstrated that raising the anode temperature in synthesis results in that mostly the γ-modification of electrolytic manganese dioxide is formed. As a result, the specific energy of a chemical power cell increases.

REFERENCES

1. Andersen, T.N., *Modern Aspects Electrochem.*, 1996, no. 30, pp. 313–413.
2. *Prikladnaya elektrokhimiya* (Applied Electrochemistry), Kudryavtsev, N.T., Ed., Moscow: Khimiya, 1975.
3. RF Patent 2115769.
4. Kononov, Yu.S., Zhizhaev, A.M., and Kulebakin, V.G., *Zh. Prikl. Khim.*, 1998, vol. 71, no. 4, pp. 396–398.
5. Bagotskii, V.S., *Khimicheskie istochniki toka* (Chemical Power Cells), Moscow: Energoizdat, 1987.
6. Crompton, T.R., *Primary Cells*, London: Basingstoke, 1982.

[1] Svirsk, Irkutsk oblast, Russia).

ISSN 1070-4272, Russian Journal of Applied Chemistry, 2007, Vol. 80, No. 2, pp. 341–343. © Pleiades Publishing, Ltd., 2007.
Original Russian Text © O.V. Sibikina, E.V. Novikova, A.A. Iozep, L.I. Iozep, N.G. Tikhomirova, L.S. Kozhevnikova, 2007, published in Zhurnal Prikladnoi Khimii, 2007, Vol. 80, No. 2, pp. 342–344.

BRIEF COMMUNICATIONS

Reaction between Dextran Polyaldehyde and Iron(III)

O. V. Sibikina, E. V. Novikova, A. A. Iozep, L. I. Iozep, N. G. Tikhomirova, and L. S. Kozhevnikova

St. Petersburg State Academy of Pharmaceutical Chemistry, St. Petersburg, Russia

Received June 27, 2006

Abstract—The reaction of dextran polyaldehyde with iron(III) chloride was studied. The dependences of the Fe^{3+} content in the resulting complex on the number of aldehyde groups in polysaccharide and pH of the solution were found.

DOI: 10.1134/S1070427207020356

Metal complexes with polysaccharides and their derivatives are of growing importance in medicine and pharmacy. For instance, polypher is well known as a blood substitute [1]. New blood substitutes with hemostimulating and antianemic function, Rondferrin, Spaceferron, Neorondex, and Microdez, which are complexes of dextran with Fe^{2+}, Fe^{3+}, Co^{2+}, and Cu^{2+}, respectively [2, 3], differ from the existing analogues in good bio- and hemocompatibility and more pronounced and prolonged action. Magnetic complexes based on polysaccharide derivatives with Fe, Ca, Zn, Co, Ni, and Cu oxides are used in roentgenologic studies [4]. These complexes are very stable during prolonged storage and are not toxic, when introduced in blood as X-ray contrast substances. In this context, we studied reactions of dextran polyaldehyde (DPA) with iron(III).

Dextran polyaldehyde was prepared by oxidation of dextran with sodium meta-periodate, separated, and analyzed as in [5]. Samples containing 0.55–0.84 mol of aldehyde groups per mole of the monomeric fragment (C_{sa}) were used.

The reaction of DPA with iron(III) chloride was performed in water at 18–23°C; 1.2–3.6 mol of salt was taken per mole of aldehyde groups: 0.2 g DPA was dissolved in 3 ml of 0.04 – 0.48 M NaOH within 30 min, and then 2 ml of a 5–15 wt % $FeCl_3$ solution in 0.1 M HCl was added. On doing so, the reaction mixture immediately became reddish-brown. The reaction product was precipitated with acetone, filtered, washed with acetone (to remove iron chloride) and ethyl ether, and dried in a vacuum at a residual pressure of 20–25 mm Hg at 61°C.

The compound synthesized is beige amorphous powder soluble in water and insoluble in ethanol, acetone, and ethyl ether. The complex is fairly stable; it does not decompose during reprecipitation from aqueous solution or dialysis for 24 h at pH < 7.

The IR spectra of DPA and of iron(III) complex with DPA strongly differ in the intensity of absorption bands. In the spectrum of the complex, bands at 1370–1420 and 1620 cm^{-1} are substantially stronger than those in the DPA spectrum, suggesting a considerably larger amount of the aldoenol form in the first case. In addition, there is no band at 1270 cm^{-1} belonging to hydrated aldehyde group in the spectrum of the complex.

A peak at 321 nm is observed in the UV spectrum of the complex in 0.1 M HCl, in contrast to the initial substances which do not absorb light in this spectral range. Similar absorption at 310 nm in the spectra of DPA alkaline solutions is attributed to aldoenol fragments.

The spectrum of the DPA complex with iron(III) compared to that of the Fe(III) salt solution of the same concentration, exhibits a new peak at 510–520 nm. In the spectrum of the initial DPA, this peak is absent. The reaction product was characterized by the degree of substitution, C_{sFe} (number of iron ions per monosaccharide unit), which was calculated from the results of determination of the iron content by potentiometric titration with ascorbic acid [6] and spectrophotometrically with sulfosalicylic acid in ammonia solution [7]. The values of C_{sFe} obtained by these two methods differ by no more than 2%. The degree of substitution varied from 0.11 to 0.32.

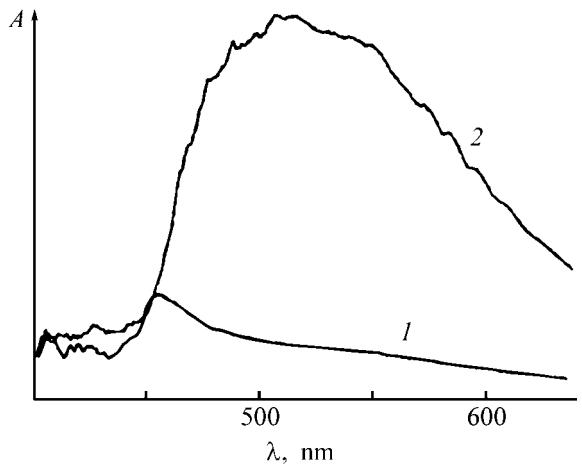

Electronic spectra of the reaction mixture after addition of $FeCl_3$ solution to a DPA solution (*1*) with preliminary neutralization of DPA alkaline solution and (*2*) without neutralization. (*A*) Absorption and (λ) wavelength.

We also found that $C_{s\,Fe}$ strongly depends on the pH of the initial DPA solution. Complexes characterized by the 510–520 nm band are formed only when iron(III) chloride is mixed with DPA in alkaline solutions. At pH < 7, only substances with a weak band at 455 nm (but not at 510–520 nm) are formed. The same substances are also formed when an alkaline solution of DPA is neutralized before addition of the Fe(III) salt solution (see figure).

Table 1. Influence of the alkali concentration c_{NaOH} on the number of enol groups per monosaccharide unit of dextran polyaldehyde (C_{sa} = 0.55)

c_{NaOH}, M	Number of enol groups per monosaccharide unit	Number of aldehyde groups converted into enols, %
0.0034	0.029	4.60
0.0051	0.040	6.79
0.0068	0.070	11.43
0.0092	0.085	13.41
0.0136	0.100	16.15

Table 2. Influence of the alkali concentration c_{NaOH} in the initial DPA solution on the content of iron reacted

c_{NaOH}, M	C_{sa}, mol mol^{-1}	Number of aldehyde groups reacted, %
0.040	0.11	17.3
0.079	0.13	20.6
0.119	0.14	22.2
0.159	0.17	27.0
0.318	0.21	33.2
0.477	0.27	42.9

It is known that DPA aldehyde groups can exist in different forms in aqueous solutions; at pH < 4, DPA has the aldehyde structure, whereas at pH > 5.2 the aldoenol structure appears. At pH 4.0–5.2, hydrated or hemiacetal structures are probably stable [8–10].

Neishlos et al. [11] showed that individual (dry) DPA also contains an aldoenol form, whose content increases with the pH of the solution in which dextran is oxidized with periodate.

Taking this fact into account, we suggested, similarly to [9], that just the aldoenol forms of DPA, which appear in the course of polyaldehyde dissolution in aqueous alkali, form coordination bonds with the metal ion.

To determine the conditions of iron(III) introduction into the polymer, we studied the effect of alkali concentration in the solution on the content of enol groups in DPA. A solution containing 0.2 g of DPA and $(2.38–9.52) \times 10^{-4}$ M NaOH was conductometrically titrated with 0.1 M HCl. The titration curve has two inflections corresponding to equivalence points. The calculated number of the equilibrium enol groups per each monomeric unit and the percentage of aldehyde groups converted into enols are listed in Table 1.

As expected, the degree of conversion of aldehyde groups into enol groups increases with the alkali concentration (Table 1), which makes higher the ligand reactivity. Indeed, the more concentrated alkaline solution is used, the larger amount of iron(III) reacts with DPA (Table 2), which confirms the reaction of iron(III) ions with the DPA aldoenol form. The dependence of the number of iron moles per mole of the DPA monomeric fragment on the alkali concentration is linear: $y = 0.354x + 0.1$ ($R^2 = 0.988$, $n = 6$).

However, other types of iron bonding with the polysacchride are possible in the substances obtained. For instance, products of Fe(III) reaction with DPA aqueous solutions (pH ≤ 7) are characterized by a peak at 455 nm and contain up to 0.05 mol of iron per monosaccharide fragment.

To determine the influence of DPA and excess complexing agent on the yield of the target product, we studied the dependence of the iron(III) content in the complex on the number of aldehyde groups in

Table 3. Influence of the number of aldehyde groups in the polysaccharide on the iron(III) content in the reaction product (0.2 g of DPA in 2 ml of 0.48 M NaOH and 2 ml of 10% $FeCl_3$ solution in 0.1 M HCl)

Number of aldehyde groups per monomeric unit of DPA	Fe^{3+} content (mol) per monomeric unit of reaction product
0.52	0.23
0.63	0.26
0.75	0.28
0.84	0.32

Table 4. Influence of the $FeCl_3$ excess on the iron(III) content in the reaction product (0.2 g of DPA in 2 ml of 0.48 M NaOH, C_{sa} = 0.55)

c_{FeCl_3}, %	$FeCl_3$ excess, mol per mol of aldehyde groups	Fe^{3+} content per monomeric unit of reaction product
5	1.2	0.25
7.5	1.8	0.27
10	2.4	0.27
15	3.6	0.26

the polysaccharide and on the concentration of iron(III) chloride (Tables 3, 4).

As expected, the iron content of the reaction product linearly increases with the number of aldehyde groups in the polymer ($y = 0.27x + 0.09$, $n = 4$, $R^2 = 0.97$), being independent of the concentration of the complexing agent.

CONCLUSIONS

(1) Dextran polyaldehyde reacts with iron(III) in aqueous alkaline solutions to form stable complexes.

(2) The content of iron(III) in the complex linearly depends on the alkali concentration and on the number of aldehyde groups in the polysaccharide.

REFERENCES

1. Mashkovskii, M.D., *Lekarstvennye sredstva* (Drugs), Kharkov: Torsing, 1998 vol. 1, p. 140.
2. Klimovich, O.M., Gapanovich, V.N., Petrov, P.T., et al., Abstracts of papers, *V Rossiiskii natsional'nyi kongress "Chelovek i lekarstvo"* (V Russian National Congr. "Human and Drug"), Moscow, 1998, p. 493.
3. Gapanovich, V.N., Petrov, P.T., Melnova, N.I., et al., Abstracts of papers, *V Rossiiskii natsional'nyi kongress "Chelovek i lekarstvo"* (V Russian National Congr. "Human and Drug"), Moscow, 1998, pp. 480, 489.
4. US Patent 5 204 457.
5. Novikova, E.V., Tishchenko, E.V., Iozep, A.A., and Passet, B.V., *Zh. Prikl. Khim.*, 2002, vol. 75, no. 6, pp. 1003–1006.
6. Iozep, A.A., Suvorova, O.B., Iozep, L.I., and Passet, B.V., *Zh. Prikl. Khim.*, 1998, vol. 71, no. 7, pp. 1202–1205.
7. Vasil'ev, V.P., Morozova, R.P., and Kochergina, L.A., *Praktikum po analiticheskoi khimii* (Practical Works on Analytical Chemistry), Moscow: Khimiya, 2000, p. 157.
8. Drobchenko, S.N., Isaeva-Ivanova, L.S., Grachev, S.A., and Bondarev, G.N., *Vysokomol. Soedin., Ser. B*, 1990, vol. 32, no. 4, pp. 254–258.
9. Drobchenko, S.N., Isaeva-Ivanova, L.S., Kleiner, A.R., et al., *Vysokomol. Soedin., Ser. B*, 1991, vol. 33, no. 3, pp. 220–224.
10. Bondarev, G.N., Drobchenko, S.N., and Isaeva-Ivanova, L.S., *Vysokomol. Soedin., Ser. A*, 1994, vol. 36, no. 7, pp. 1109–1112.
11. Neishlos, A.L., Novikova, E.V., Passet, B.V., and Moskvin, A.V., *Zh. Prikl. Khim.*, 2004, vol. 77, no. 1, pp. 132–134.

ISSN 1070-4272, Russian Journal of Applied Chemistry, 2007, Vol. 80, No. 2, pp. 344–345. © Pleiades Publishing, Ltd., 2007.
Original Russian Text © A.V. Kurzin, A.N. Evdokimov, O.S. Pavlova, V.B. Antipin, 2007, published in Zhurnal Prikladnoi Khimii, 2007, Vol. 80, No. 2, pp. 345–346.

BRIEF COMMUNICATIONS

Esters of Sucrose and Tall Oil Fatty Acids

A. V. Kurzin, A. N. Evdokimov, O. S. Pavlova, and V. B. Antipina

St. Petersburg State Technological University of Plant Polymers, St. Peterbsurg, Russia

Received July 18, 2006

Abstract—The possibility of preparing monoesters derived from sucrose and tall oil fatty acids was examined.

DOI: 10.1134/S107042720702036X

Esters derived from carbohydrates and higher fatty acids (so-called fat–sugars) are promising nonionic surfactants used in various branches of industry and in medicine [1–3]. A wide variety of different procedures for their preparation have been reported. Some procedures involve esterification of carbohydrates (in particular, sucrose) with acid chlorides and anhydrides [1], which are difficultly available. More promising are chemical and biochemical methods based on ester interchange of methyl or ethyl esters of higher fatty acids with carbohydrates or their acetates [1, 4–6]. The search for the best conditions for performing this reaction is still continued [2, 3].

As ester interchange catalysts are used alkali metals or their alloys, hydroxides, carbonates, and alkoxides [1, 2]. The most frequently used solvents are dimethylformamide, dimethyl sulfoxide, dimethylacetamide, *o*-xylene, etc. [1, 2]. The reaction is performed at temperatures ranging from 60 to 190°C at atmospheric or reduced pressure, or in an inert gas atmosphere. The isolation and purification methods depend on the structure and degree of substitution of the resulting esters [1].

Methyl and ethyl esters of higher fatty acids can be prepared by esterification of fats and oils with the corresponding alcohol. A promising source of fatty acids is tall oil, a by-product of kraft pulp production. The main components of tall oil fatty acids (TOFAs) are unsaturated acids: oleic, linoleic, and linolenic [7].

The goal of this study is preparation of fat–sugars by ester interchange of TOFA methyl esters with sucrose, catalyzed by a suspension of potassium carbonate in methanol.

It is known that the most reactive in acylation of carbohydrates are primary OH groups, and in the case of sucrose, mainly those in the 6-position of the glucoside moiety [4]. An effective base catalyst of ester interchange is potassium methoxide generated in the system K_2CO_3–CH_3OH [8].

The choice of solvents and of the sequence of their use for synthesis and purification depends on the structure of a desired ester. As it is difficult to find a specific solvent for the esters to be obtained, it was suggested to successively remove the impurities and starting compounds by different solvents. The procedure suggested allowed isolation of only monoesters of sucrose and TOFAs. The product is a noncrystallizing light yellow greasy substance.

EXPERIMENTAL

The ^1H NMR spectrum of the sucrose monoester obtained was recorded on a Bruker AC-200 spectrometer (200 MHz) from a 5% solution in $CDCl_3$; the chemical shifts were determined relative to internal TMS.

To monitor the reaction progress and assess the purity of the products, we used TLC on Silufol UV 254 plates {eluent 1: *n*-butanol–acetic acid–diethyl ether–water, 9 : 6 : 3 : 1 [9]; eluent 2: petroleum ether (40–70°C)–diethyl ether–acetic acid, 75 : 25 : 1 [5]}.

TOFAs (from Segezha Pulp and Paper Combine) were additionally purified by vacuum distillation; the fraction boiling in the range 170–205°C (1 mm Hg) was collected. Methyl esters of TOFAs were prepared by refluxing the acids with a threefold excess of methanol in the presence of *p*-toluenesulfonic acid [10]. The suspension of K_2CO_3 in CH_3OH was prepared according to [8].

Monoesters of sucrose and TOFAs. To a solution of 0.15 mol of sucrose in 250 ml of DMF, we added

0.05 mol of TOFA methyl esters and a suspension of 1.0 g of K_2CO_3 in 20 ml of CH_3OH. The mixture was stirred for 20 h at 95°C under a pressure of 160 mm Hg, after which it was cooled to room temperature. Analysis of the reaction mixture revealed the presence of the major component, monoester, and a small impurity of esters with a higher degree of substitution, and also of the unchanged TOFA methyl esters. The mixture was washed with three portions of petroleum ether to remove the unchanged TOFA methyl esters, and the solvents were distilled off in a vacuum. The residue was dissolved in a two-phase mixture of 220 ml of chloroform and 50 ml of water; the aqueous phase was separated and extracted with two portions of chloroform. All the chloroform extracts were combined and dried over $MgSO_4$; the solvent was distilled off on a rotary evaporator. The residue was extracted with methanol (3×150 ml); in so doing, only the monoesters of sucrose and fatty acids dissolved. The solvent was distilled off, and the product was dried in a vacuum; yield of esters 72%. The TLC analysis showed the absence of impurities of the starting TOFA esters and of esters with a higher degree of substitution. ^{1}H NMR spectrum, δ, ppm: 0.89 t (3H, CH_3), 1.20–2.75 m (2H, CH_2), 5.34 m (CH=CH), 3.60 m (1H, O–CH–C/O–CH_2–O), 5.30 m (1H, O–CH–O), 4.50 s (4H, OH), 4.05 d (2H, C–CH_2–O–CO).

CONCLUSION

A procedure was developed for preparing monoesters of sucrose and TOFAs in 72% yield, using the K_2CO_3–CH_3OH catalytic system.

REFERENCES

1. Zhoglo, F.A., *Zhirosakhara (Poluchenie, svoistva, primenenie)* [Fat–Sugars (Synthesis, Properties, Applications)], Moscow: Meditsina, 1975.
2. Watanabe, T., *Foods Food Ingr. J. Jpn.*, 1999, vol. 180, no. 1, pp. 18–25.
3. Polat, T. and Linhardt, R.J., *J. Surf. Deterg.*, 2001, vol. 4, no. 2, pp. 415–421.
4. Osipow, L., Snell, F.D., York, W.C., and Finchler, A., *Ind. Eng. Chem.*, 1956, vol. 48, no. 9, pp. 1459–1462.
5. Akoh, C.C. and Swanson, B.G., *J. Food Sci.*, 1990, vol. 55, no. 1, pp. 236–243.
6. Ferrer, M., Cruces, M.A., Bernabe, M., et al., *Biotechnol. Bioeng.*, 1999, vol. 65, no. 1, pp. 10–16.
7. Fengel D., Vegener G. *Drevesina: Khimiya, ul'trastruktura, reaktsii.*, M.: Lesnaya Prom–st., 1988. 512 s.?
8. RF Patent 2178402.
9. Komori, S., Okahra, M., and Okamoto, K., *J. Am. Oil Chem. Soc.*, 1960, vol. 37, no. 4, pp. 468–473.
10. Soboleva, L.M., Solov'ev, V.V., Chernova, I.K., et al., *Vestn. Yaroslavl. Gos. Tekh. Univ.*, 1999, no. 2, pp. 80–83.

ISSN 1070-4272, Russian Journal of Applied Chemistry, 2007, Vol. 80, No. 2, pp. 346–347. © Pleiades Publishing, Ltd., 2007.
Original Russian Text © A.I. Akhmedov, D.Sh. Gamidova, 2007, published in Zhurnal Prikladnoi Khimii, 2007, Vol. 80, No. 2, pp. 347–348.

BRIEF COMMUNICATIONS

Polyfunctional Additives to Oils, Based on Sulfonated Oligomers

A. I. Akhmedov and D. Sh. Gamidova

Kuliev Institute of Chemistry of Additives, National Academy of Sciences of Azerbaijan, Baku, Azerbaijan

Received October 16, 2006

Abstract—Studies in the field of development of polymeric oligoalkenesulfonate additives derived from sulfonated oligomers and exhibiting multifunctional effect when added to petroleum oils are summarized.

DOI: 10.1134/S1070427207020371

Among the first additives used in motor oils are various sulfonates prepared by sulfonation of petroleum oils, followed by reactions of the resulting sulfo acids with various oxides or hydroxides of Group II metals [1]. These sulfonates are used as detergent and dispersing additives to motor oils.

The functional properties of sulfonate additives depend on the chemical nature of a petroleum oil being sulfonated, i.e., on the content of aromatic hydrocarbons; such additives do not improve other performance characteristics of petroleum oils. Therefore, it would be appropriate to replace petroleum oils as sulfonation substrates with oligomers or cooligomers of various vinyl monomers. These oligomers, owing to the nonvolatility, chemical affinity for petroleum products, and mutual miscibility with them, and also to the possibility of widely varying their chemical nature, allow purposeful synthesis of polymeric additives with prescribed performance characteristics and are indispensable in functionalization reactions.

The polymeric additives prepared by such procedure not only preserve the main functional characteristics of sulfonates but also improve the viscosity–temperature properties of petroleum oils, making larger their viscosity index. This is a pressing problem for Baku oils whose viscosity index is low.

This paper summarizes the results of studies performed at the Institute of Chemistry of Additives, National Academy of Sciences of Azerbaijan, in the field of development of polymeric additives based on sulfonated oligomers. The sulfonation was performed both with oleum and with chlorosulfonic acid. The products were neutralized with various amines, and also with magnesium or calcium oxide or hydroxide [2, 3].

As starting compounds were used cooligomers of α-olefins (isobutylene, 1-hexene, 4-methyl-1-pentene) with styrene, α-methylstyrene, dicyclopentadiene, or indene, and also cooligomers of vinyl butyl ether with styrene. Introduction of cyclic fragments into cooligomers creates an additional reaction center for the sulfonation and makes the products resistant to oxidation.

Copolymerization of α-olefins and vinyl *n*-butyl ether with styrene and of α-olefins with the other comonomers was performed in the presence of $AlCl_3$ at 5–20°C; the content of the comonomer units was 10–20 wt %; the molecular weight of the binary cooligomers obtained was 1000–2000.

The sulfonation of the cooligomers was performed by the standard procedure. Depending on particular requirements, the sulfonation products were neutralized so as to obtain ash-free and ash additives.

The compositions and structures of the compounds obtained were studied by IR and ^{1}H NMR spectroscopy and by elemental analysis. The presence of aromatic fragments was confirmed by the IR absorption band at 1610 cm^{-1}. The content of aromatic units in the cooligomers was determined by ^{1}H NMR spectroscopy from the integral intensity of signals of the aromatic ring protons (δ 6.6 ppm).

As the studies showed, a decrease in the molecular weight impairs viscosity–temperature properties of petroleum oils and leads to an increased consumption of the cooligomer for thickening, which is not economically profitable. At the same time, additives with molecular weight exceeding 2000 are less stable thermally.

When present in an amount less than 10%, the comonomer units in the cooligomer affect the performance characteristics of the additives insignificantly. At the same time, at the content of comonomer units

exceeding 30%, the solubility of the additives in petroleum oils decreases.

We found that the main function of the cooligomers is to act as ligands, which makes it possible to impart to them solubility in petroleum oils. Therefore, the specific chemical nature of the cooligomers is not essential in the synthesis of sulfonates and sulfonamides. The choice of particular oligomer is governed by the availability of the raw materials for its synthesis and by the amount of its production in Azerbaijan. Preference is given to cooligomers of C_6 α-olefins with styrene as low-cost and readily available compound; introduction of such additives into oils increases their viscosity index to an extent exceeding by 5–7 points that attained with the other additives. In the preparation of sulfonates, $Ca(OH)_2$ is used as a neutralizing agent.

The resulting calcium oligoalkenesulfonates contain 1.2–1.8% Ca and 1.5–2.0% S; the alkali number of the additive is 40–60 (mg KOH) g^{-1}.

Laboratory tests of the sulfonate additives in petroleum oils gave the following results: detergent properties 0–0.5 point; anticorrosion properties 3–5 g cm^{-2}; decrease in viscosity 1.5–2% upon thermal degradation. The viscosity index of the initial oil increases by 10–15 points.

The synthesis of oligoalkenesulfonates and sulfamides can be described by the reactions

$$\text{R–H} \xrightarrow{SO_3} \text{R–SO}_2\text{OH},$$
$$\text{R–H} \xrightarrow{HOSO_2Cl} \text{R–SO}_2\text{Cl},$$
$$\text{R–SO}_2\text{OH} \xrightarrow{Me(OH)_2} (\text{R–SO}_3)_2\text{Me},$$
$$\text{R–SO}_2\text{OH} \xrightarrow{R'\text{–NH}_2} \text{R–SO}_2\text{NH–R}',$$
$$\text{R–SO}_2\text{Cl} + \text{NH}_3 \rightarrow \text{R–SO}_2\text{NH–R}',$$

where R is a cooligomer radical, and R', radical in amines.

Thus, oligoalkenesulfonates acting as multifunctional additives to petroleum oils were prepared from cooligomers of α-olefins and vinyl butyl ether with vinylaromatic and carbocyclic monomers. The nature of the starting comonomer and the synthesis conditions are chosen on the basis of particular requirements to the quality of the sulfonates.

The use of the synthesized oligoalkenesulfonates as additives to petroleum oils allows development of lubricating formulations meeting the modern requirements to motor oils with respect to the viscosity–temperature and other performance characteristics.

CONCLUSIONS

(1) Sulfonation with oleum or chlorosulfonic acid of cooligomers of α-olefins (isobutylene, 1-hexene, 4-methyl-1-pentene) with styrene, α-methylstyrene, dicyclopentadiene, or indene, and of cooligomers of vinyl n-butyl ether with styrene, followed by neutralization with various amines and with magnesium or calcium oxide or hydroxide, was studied, and multifunctional polymeric additives were obtained.

(2) The major function of the cooligomers is to act as ligands, which makes it possible to impart to them solubility in petroleum oils. The chemical nature of the starting cooligomers in the synthesis of sulfonates and sulfamides is insignificant. Their choice is based on specific requirements to the quality of the sulfonates.

REFERENCES

1. Kuliev, A.M., *Khimiya i tekhnologiya prisadok i toplivam* (Chemistry and Technology of Fuel Additives), Leningrad: Khimiya, 1985.
2. Akhmedov, A.I., Farzaliev, V.M., and Aliguliev, R.M., *Polimernye prisadki i masla* (Polymeric Additives and Oils), Baku: Elm, 2000.
3. Akhmedov, A.I., *Azerb. Neft. Khoz.*, 2003, no. 2, pp. 44–47.

ISSN 1070-4272, Russian Journal of Applied Chemistry, 2007, Vol. 80, No. 2, pp. 348–349. © Pleiades Publishing, Ltd., 2007.
Original Russian Text © A.G. Morachevskii, 2007, published in Zhurnal Prikladnoi Khimii, 2007, Vol. 80, No. 2, pp. 349–350.

BOOK REVIEWS

Kulifeev, V.K., Miklushevskii, V.V., and Vatulin, I.I., *Litii* (Lithium),

Moscow: Mosk. Inst. Stali Splavov, 2006, 240 pp.

DOI: 10.1134/S1070427207020383

Lithium is among the most important metals whose role in modern technology steadily grows. The monograph by V.K. Kulifeev and co-authors notes that the world's production of lithium and its compounds (in terms of the metal) was 17 100 tons in 2004. The annual-average rise in world's consumption of lithium and its compounds was 7–8% in the last 10 years. Lithium is virtually irreplaceable in nuclear technology, manufacture of ultralight alloys, and modern chemical power cells.

The book by Kulifeev and co-authors comprises an introduction, nine chapters, and reference list for the entire monograph. The brief introduction (pp. 3, 4) describes the important and steadily growing role of lithium in modern technology and notes that domestic monographs devoted to chemistry and technology of lithium [Ostroushko, Yu.I. et al., *Litii, ego khimiya i tekhnologiya* (Lithium: Chemistry and Technology), Moscow: Atomizdat, 1960, 200 pp.; Plyushchev, V.E. and Stepin, B.D., *Khimiya i tekhnologiya soedinenii litiya, rubidiya i tseziya* (Chemistry and Technology of Compounds of Lithium, Rubidium, and Cesium), Moscow: Khimiya, 1970, 358 pp.) have become largely outdated and fail to reflect the modern development level of lithium industry. A small first chapter (pp. 5–16) considers the world's production and main application fields of lithium and its compounds. In 1990, our country was second in manufacture of lithium and its compounds only to the United States. Later, the internal demand for lithium diminished and the manufacture of lithium decreased fivefold, with the lithium products obtained mostly exported. By now, the manufacture of lithium in Russia from domestic raw materials has been terminated and all the acting plants work with imported raw materials. The second chapter (pp. 17–54) considers the physical and chemical properties of lithium and its compounds and alloys. The third chapter (pp. 55–77) describes minerals containing lithium compounds. The fourth chapter (pp. 78–101) discusses the state of mineral resources of lithium in foreign countries, Russia, and CIS countries. The fifth chapter (pp. 102–123) contains evidence about dressing of lithium ores of industrial importance. The sixth chapter (pp. 124–171), which seems to occupy the central place in the monograph, describes methods for processing of lithium ores and concentrates and for manufacture of such compounds as lithium hydroxide and chloride.

The seventh chapter (pp. 172–205) describes techniques for manufacture of metallic lithium. The authors do not specify present places and scale of lithium is production by carbothermic and metallothermic reduction. It is unclear whether there are prospects for application of these methods in the XXI century. At the same time, the electrolytic method is described very superficially. No data are presented on refining of electrolytic lithium. Primary attention is given to production of lithium by aluminothermic reduction of lithium aluminates. Such an exotic method is not considered in the foreign literature among the possible alternative thermal methods for manufacture of lithium [see, e.g., a review of new technologies for manufacture of lithium in J. of Metals (JOM), 1998, May, pp. 24–26].

The eighth chapter (pp. 206–228) is devoted to secondary metallurgy of lithium. No data on the scale of manufacture of secondary lithium are presented by the authors. In the discussion of the possible utilization of lithium power cells, nothing is said about whether collection of these cells is really feasible. A very brief ninth chapter (pp. 229–233) gives notion of basic safety rules to be observed when working with lithium. The bibliographic list (pp. 234–237) contains references to 63 Russian and 17 foreign publications, which seems to be apparently insufficient.

The book is published in the series Metallurgy and Materials Science of the XXI Century, timed with the 75th foundation anniversary of Moscow State Institute (Technological University) of Steel and Alloys. The polygraphy of the book deserves the highest appraisal, but, as regards the content of the book, there is no escape from making a number of critical remarks. Not all sections of the book create favorable impression, the structure of the monograph seems to be questionable as regards its title, and the directly

relevant literature is far from being represented in full measure.

The impression created by the second chapter is impaired by quite a number of annoying inaccuracies in the description of thermodynamic quantities. The section "Lithium Compounds with Silicon" (pp. 50–54) is very poorly written; the diagrams of state of the systems Li–Pb, Li–Al, Li–Ge, and Li–Cu, presented in this section, are not commented at all. The diagram of state of the system Li–Si, shown in Fig. 2.12, is not consistent with the text. Technologically important alloys of lithium with potassium and magnesium are not mentioned. The highly detailed description of lithium-containing minerals is hardly appropriate (ch. 3). This evidence can be found in full measure in specialized publications. A question arises whether it is worthwhile to describe in such detail dressing and processing of ores from Russia's deposits, when none of them is presently in service, and whether use of these deposits in the XXI century is economically feasible.

It seems that the metal itself, its compounds and methods for their production, and modern and promising application areas should occupy the central place in a monograph having the "Lithium" title. The monograph fails to pay due attention to lithium alloys and their specific features, production of the metal by electrolysis, electrochemistry and thermodynamics of this process, and interaction of lithium with an electrolyte. Metallothermic reduction methods for production of lithium are described very one-sidedly, nothing is said about the scale of manufacture of lithium power cells in Russia, there is not even mention of lithium-ion batteries, intercalation phenomena, application areas of the Li–Pb alloy, and methods for changing the isotope composition.

Naturally, it is impossible to cover in a comparatively small book such a wide variety of issues, but the information value of the monograph could have been made considerably higher by extending the bibliographic list. A large number of monographs, reviews directly devoted to lithium, and its rather promising application areas remained out of the authors' sight. For example, no mention is made of the following publications: Shpil'rain, E.E. and Yakimovich, K.A., *Gidrid litiya* (Lithium Hydride), Moscow: Izd. Standartov, 1972, 108 pp.; Bystrov, P.I. et al., *Zhidkometallicheskie teplonositeli teplovykh trub i energeticheskikh ustanovok* (Liquid-Metal Heat Carriers for Heat Tubes and Power Installations), Moscow: Nauka, 1988, 263 pp.; Kedrinskii, I.A. et al., *Litievye istochniki toka* (Lithium Power Cells), Moscow: Energoatomizdat, 1992, 240 pp.; Kedrinskii, I.A. and Yakovlev, V.G., *Li-ionnye akkumulyatory* (Li-Ion Batteries), Krasnoyarsk: Platina IPK, 2002, 268 pp.; Borgstedt, H.U. and Mathews, Ch.K., *Applied Chemistry of the Alkali Metals*, New York: Plenum, 1987, 282 pp.; and reviews: *Zh. Fiz. Khim.*, 1983, no. 9, pp. 529–546; *Zh. Prikl. Khim.*, 1994, no. 12, pp. 1937–1950; *Zh. Prikl. Khim.*, 1996, no. 4, pp. 529–546.

The on the whole useful monograph by Kulifeev and coauthors should have been titled *Litii: Mineral'nosyr'evye resursy i ikh pererabotka* (Lithium: Mineral Resources and Their Processing). This title would be consistent both with the structure of the book and with the contents of its main chapters.

A. G. Morachevskii

ISSN 1070-4272, Russian Journal of Applied Chemistry, 2007, Vol. 80, No. 3, p. 351. © Pleiades Publishing, Ltd., 2007.
Original Russian Text © Editorial Board, 2007, published in Zhurnal Prikladnoi Khimii, 2007, Vol. 80, No. 3, inset.

Vladimir Stepanovich Shpak (to His 98th Birthday)

DOI: 10.1134/S1070427207030019

On February 20, 2007, was celebrated 98th birthday of Vladimir Stepanovich Shpak, Academician of the Russian Academy of Sciences, advisor of the Director General of Prikladnaya Khimiya Russian Scientific Center, Editor-in-Chief of *Zhurnal Prikladnoi Khimii* (Russian Journal of Applied Chemistry), and member of the Editorial Board of *Zhurnal Prikladnoi Khimii*. Hero of Socialist Labor, Honored Scientist and Technologist of the Russian Soviet Federative Socialist Republic, and Honored Chemist, V.S. Shpak has made an outstanding contribution to the creation of quite a number of chemical industries, strengthening of the defense potential of the country, and development of the rocket-and-space technology. Among the large number of congratulations received by Shpak is that from the Chairman of the Federation Council of the Federal Assembly of the Russian Federation, S.M. Mironov.

Editorial Board and Editorial Staff of *Zhurnal Prikladnoi Khimii* and numerous colleagues heartily congratulate dear Vladimir Stepanovich Shpak on his birthday and wish him cheerfulness and health.

GOVERNMENTAL TELEGRAM

Highest governmental. Notification by telegraph. To Academician V.S. Shpak, Editorial Office of *Zhurnal Prikladnoi Khimii*, Mendeleevskaya liniya 1, St. Petersburg.

"Dear Vladimir Stepanovich, please accept my congratulations on your birthday. You have worked a long way up in science. Your whole life is a remarkable example of devotion to the chosen profession and persistence and aspiration in goal achievement. Your contribution to the development of domestic science and advanced technologies has been deservedly appreciated by the State. I wish you, Vladimir Stepanovich, sound health, active longevity, and well-being.

Chairman of the Federation Council of the Federal Assembly of the Russian Federation and Chairman of *Spravedlivaya Rossia (Rodina/Pensionery/Zhizn')* [Just Russia (Motherland/Pensioners/Life)] party,

S. M. Mironov."

Editorial Board and Editorial Staff of *Zhurnal Prikladnoi Khimii*

ISSN 1070-4272, Russian Journal of Applied Chemistry, 2007, Vol. 80, No. 3, pp. 352–357. © Pleiades Publishing, Ltd., 2007.
Original Russian Text © R. Paleckiene, A. Sviklas, R. Šlinkšiene, 2007, published in Zhurnal Prikladnoi Khimii, 2007, Vol. 80, No. 3, pp. 353–359.

INORGANIC SYNTHESIS AND INDUSTRIAL INORGANIC CHEMISTRY

Physicochemical Properties of a Microelement Fertilizer with Amino Acids

R. Paleckiene, A. Sviklas, and R. Šlinkšiene

Kaunas Technological University, Kaunas, Lithuania

Received June 19, 2006

Abstract—The physicochemical properties of the initial components and products were studied with the aim of production of a microelement fertilizer with an amino acid concentrate. The physicochemical properties of the amino acid concentrate and its influence on the stability and sorption properties of fertilizers enriched in microelements were studied.

DOI: 10.1134/S1070427207030020

Intensification of agriculture requires using not only effective mineral fertilizers containing macro- and microelements [1, 2], but also physiologically active substances, growth stimulants. In the past years, much attention was given to testing as growth stimulants various synthetic and natural physiologically active substances: citric acid, humates, amino acids, etc. [3–6].

The use of amino acids is most often recommended under critical conditions of plant growth: after transplantation, in the flowering period, and also at climatic stresses (night frosts, drought) or plant diseases. Amino acids are particularly effective in fertilizers when used in combination with microelements [7–12].

In this study we examined the physicochemical properties of the amino acid concentrate (AAC) and its effect on the stability and sorption properties of fertilizers enriched in microelements.

As AAC we used Naturamin-WSP product (DAYMSA, Spain), and as fertilizer, ARVI-micro product (ARVI and Co., Lithuania) containing ammonium sulfate and microelements.

The compositions of substances were determined by chemical and physicochemical methods of analysis. The nitrogen concentration was determined by standard methods [13, 14]. The solid substances were examined by IR spectroscopy, thermal analysis, and X-ray phase analysis [15–18]. The IR spectra were recorded on a Spectrum GX FTIR spectrometer (Perkin–Elmer); samples were prepared as KBr pellets. Thermal analysis was performed by differential scanning calorimetry (DSC) with a Du Pont Instruments 990 Thermal Analyzer at a heating rate of 10 deg min^{-1}. X-ray phase analysis was performed with a DRON-6 diffractometer (Ni-filtered Cu radiation, range of diffraction angles 0°–166.5°, relative error ≤0.5%).

Naturamin-WSP amino acid concentrate was prepared by chemical hydrolysis of proteins, collagen, and keratin. The chemical formula of the product depends on the ratio of free amino acids and oligopeptides. Naturamin-WSP product is a concentrate of water-soluble amino acids containing 80% free amino acids and 12.8% nitrogen; the total weight fraction of organic matter is 90%.

Naturamin-WSP concentrate is a homogeneous mixture of microgranules; it contains 17 amino acids in amounts shown in Fig. 1.

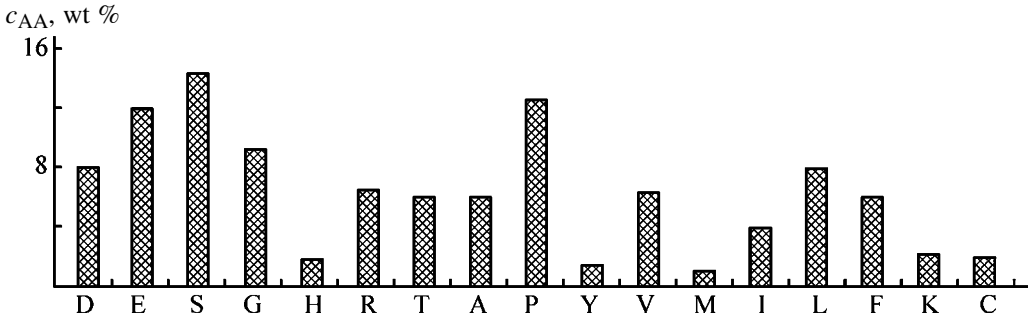

Fig. 1. Content of amino acids c_{AA} in Naturamin-WSP: (D) aspartic acid, (E) glutamic acid, (S) serine, (G) glycine, (H) histidine, (R) arginine, (T) threonine, (A) alanine, (P) proline, (Y) tyrosine, (V) valine, (M) methionine, (I) isoleucine, (L) leucine, (F) phenylalanine, (K) lysine, and (C) cysteine.

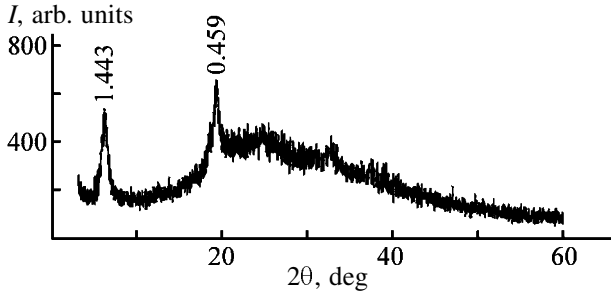

Fig. 2. X-ray diffraction pattern of Naturamin-WSP amino acid concentrate: (*I*) intensity and (2θ) Bragg angle; the same for Fig. 6.

The X-ray diffraction pattern of Naturamin-WSP is shown in Fig. 2; the TG and DSC curves, in Fig. 3; and the IR spectrum, in Fig. 4.

The X-ray diffraction pattern of ACC amino acids (Fig. 2) is typical of amorphous compounds. Only the reflections at 1.443 and 0.449 nm of similar intensity are pronounced; other reflections cannot be identified.

The DSC and TG curves of ACC (Fig. 3) show that, starting from 70°C, Naturamin-WSP loses moisture (TG curve) and remains virtually stable up to ~210°C. At 214.1°C, a pronounced endothermic effect is observed, followed by weight loss. Further heating causes decomposition of the substance (DSC curve exhibits exothermic peaks at 339.0 and 350.0°C, and endothermic peaks at 293.5 and 305.4°C). In the crystalline state, amino acids exist in the form of bipolar ions; their IR spectra (Fig. 4) are similar irrespective of the position of carboxy and amino groups and of the functional substituent. The NH_2 bands are observed at 3500–3000 cm^{-1}; a characteristic C=O band, at 1590–1650 cm^{-1}; and bands of CH, NH_2, and COO^- groups, in the range 1520–450 cm^{-1}.

We studied gravimetrically [13] the sorption of water on AAC under ambient conditions (20–22°C, humidity 25–37%) and in a desiccator over water (~21°C, humidity ~98%). The dynamic curves of water sorption by AAC are shown in Fig. 5.

Under ambient conditions (Fig. 5, curve *1*), AAC takes up a small amount of water (up to 5% in 69 days). Small oscillations of the dynamic curves arise from fluctuations of the ambient temperature and humidity. In a desiccator over water, AAC concentrate absorbs water more actively. Point *a* in curve *2* corresponds to the limiting content of water after which AAC starts to dissolve. Point *b* corresponds to the appearance of mold. Thus, AAC is a hydrophilic substance, and the water absorption depends on the humidity of the medium. This property should be evaluated when using amino acids in production of mineral fertilizers.

For agrochemical and economic reasons, we prepared fertilizers based on ARVI microfertilizer and Naturamin-WSP AAC. ARVI microfertilizer containing 14% nitrogen consists of ammonium sulfate and microcomplex (Mg, S, Mn, Cu, Zn, B, Mo). To this substance we added 1, 3, and 4% AAC and mechanically mixed the components. Therefore, it was necessary to study possible interactions between the components and the stability of the composition. The separate components, ARVI microfertilizers, and ARVI microfertilizers with various additions of AAC were subjected to X-ray diffraction, thermal, and IR analyses (Figs. 6–8).

In the X-ray diffraction pattern of ammonium sulfate (Fig. 6, pattern *1*), we identified its characteristic reflections at 0.519, 0.433, 0.389, 0.314, 0.305,

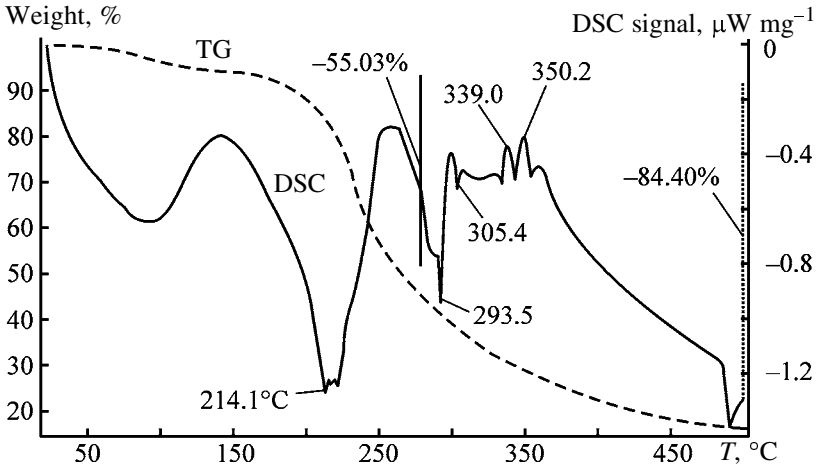

Fig. 3. DSC and TG curves of Naturamin-WSP AAC; (*T*) temperature; the same for Fig. 7.

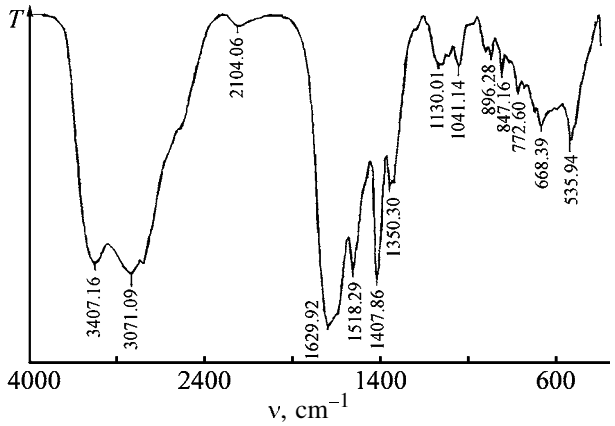

Fig. 4. IR spectrum of Naturamin-WSP AAC: (*T*) transmission and (ν) wavenumber; the same for Fig. 8.

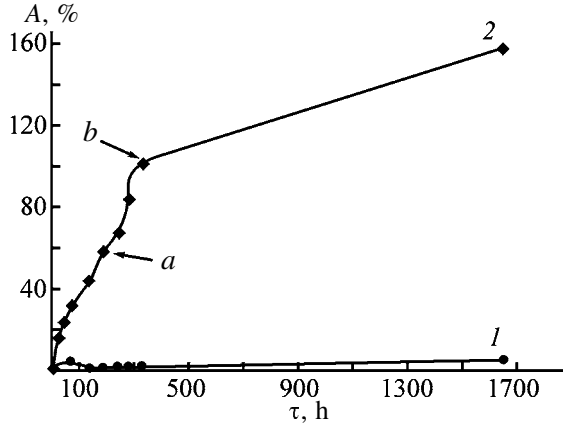

Fig. 5. Dynamic curve of water sorption *A* by AAC (*1*) under ambient conditions and (*2*) in a desiccator over water. (τ) Time; the same for Figs. 9 and 10.

0.299, 0.266, 0.252, 0.232, 0.217, 0.194, 0.177, and 0.164 nm. The microcomplex consists of sulfates of microelements and their crystal hydrates, and also of boric acid; therefore, its diffraction pattern (Fig. 6, pattern *2*) contains reflections of magnesium, manganese, copper, and zinc sulfates and of boric acid at 0.754, 0.598, 0.534, 0.470, 0.447, 0.421, 0.378, 0.341, 0.317, 0.299, 0.287, 0.267, 0.225, 0.220, 0.209, 0.195, and 0.179 nm. The diffraction pattern of ARVI microfertilizer (Fig. 6, pattern *3*) contains reflections of ammonium sulfate and the microcomplex. The diffraction patterns of ARVI microfertilizer with addition of 1, 3, and 4% AAC (Fig. 6, patterns *4*–*6*) exhibit reflections of ammonium sulfate, sulfates of microelements, and AAC. No new reflections are observed, which indicates that the mixture is stable and no chemical reactions occur between the fertilizer components.

The results of thermal analysis are given in Fig. 7. The DSC curve of ammonium sulfate (Fig. 7a) dem-

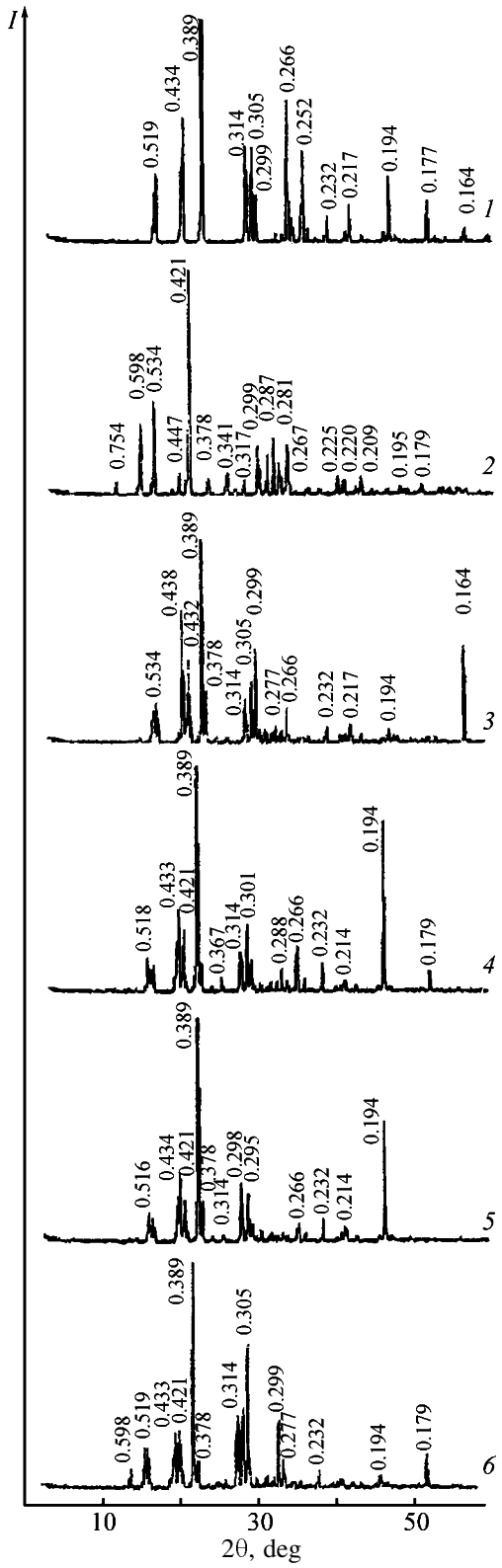

Fig. 6. X-ray diffraction patterns of (*1*) ammonium sulfate, (*2*) microcomplex, (*3*) ARVI microfertilizer, and (*4*–*6*) the same + 1, 3, and 4% AAC, respectively.

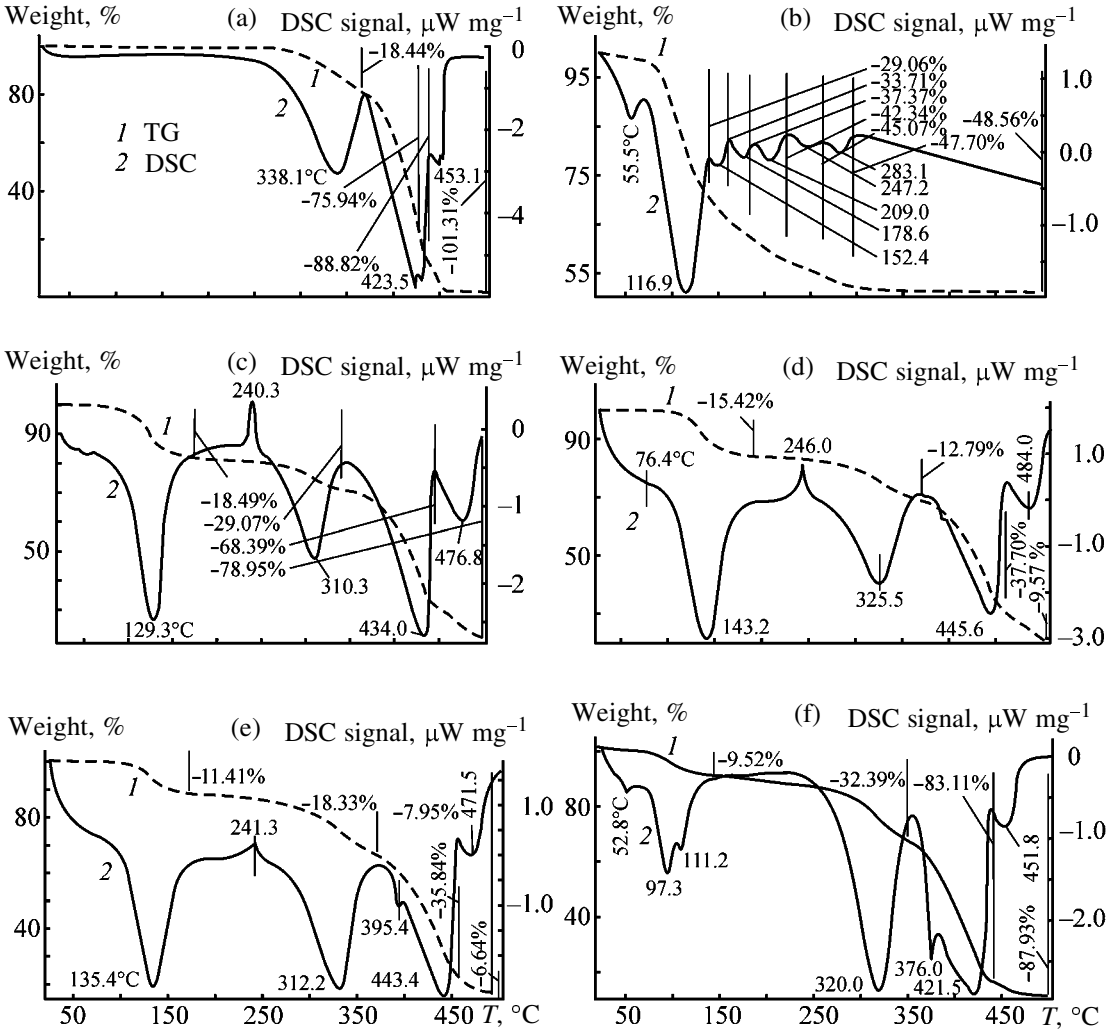

Fig. 7. (*1*) TG and (2) DSC curves of (a) ammonium sulfate, (b) microcomplex, (c) ARVI microfertilizer, and (d–f) the same + 1, 3, and 4% AAC, respectively.

onstrates endothermic decomposition of the compound into gaseous ammonia and an acidic salt, NH_4HSO_4. The decomposition starts at about 300 and is complete at 455°C. The weight loss observed in the TG curve is consistent with the elimination of ammonia.

The DSC curve of the microcomplex (Fig. 7b) exhibits an endothermic peak at 55.5°C indicative of the dehydration of boric acid to metaboric acid HBO_2 followed by further dehydration to boron oxide B_2O_3. A pronounced endothermic effect at 116.9°C corresponds to the onset of dehydration of magnesium, manganese, copper, and zinc sulfate crystal hydrates. The effect is complete at 283.1°C. The anhydrous salts remain stable up to 600°C. A continuous weight loss starting about 100°C corresponds to the dehydration.

Thermal analysis of ARVI microfertilizer (Fig. 7c) reveals a total endothermic effect (DSC curve) in combination with weight loss (TG curve) from the initial components, ammonium sulfate and the microcomplex. The DSC and TG curves of ARVI microfertilizer with 1, 3, and 4% AAC (Figs. 7d–7f) exhibit the same peaks as in the curves for the separate components. Some changes in the peak intensities and positions (some of peaks overlap) are natural and insignificant; thus, mixing of the components involves no chemical reactions, and no new chemical compounds are formed.

The IR spectra of the initial substances, ARVI microfertilizer, and ARVI microfertilizer with additions of AAC are shown in Fig. 8. In the IR spectrum of ammonium sulfate (Fig. 8, curve *1*) there are characteristic absorption bands of the NH_4^+ ion at 3000, 2000, and 1400 cm^{-1} and of the SO_4^{2-} ion at 1150–450 cm^{-1}. Since the microcomplex contains a number

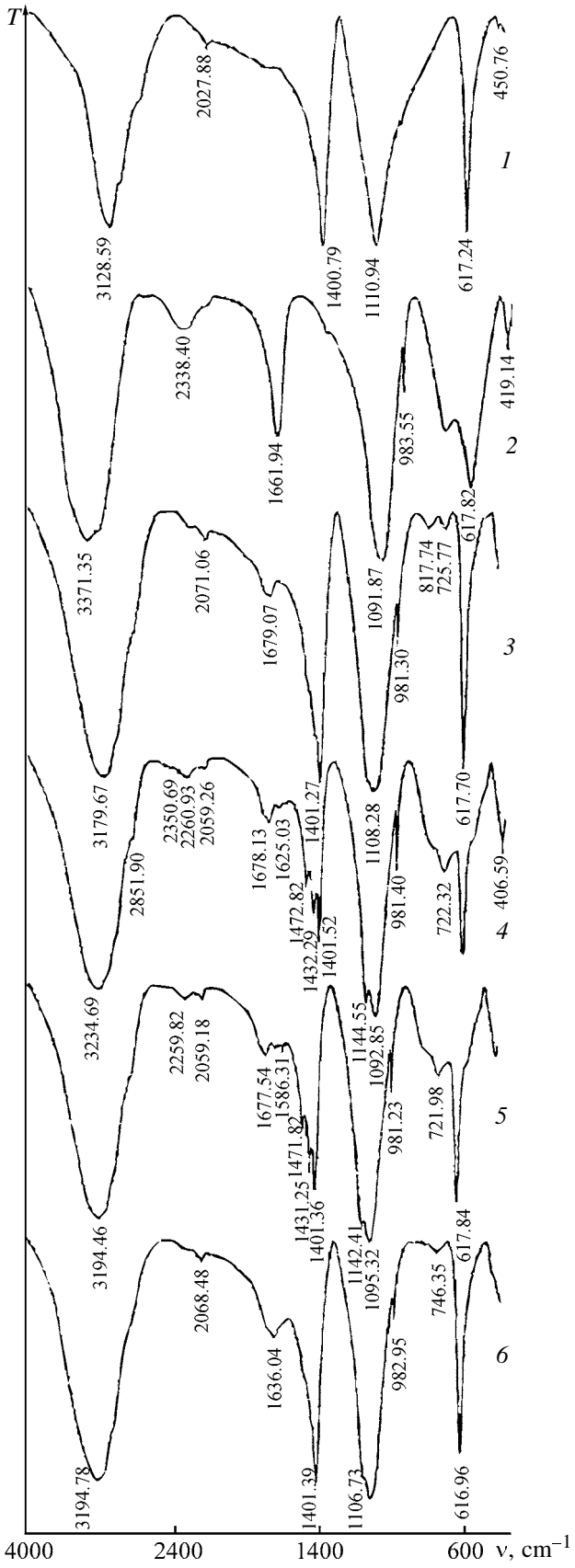

Fig. 8. IR spectra of (*1*) ammonium sulfate, (*2*) microcomplex, (*3*) ARVI microfertilizer, and (*4–6*) the same + 1, 3, and 4% AAC, respectively.

of sulfates, in its IR spectrum there are strong absorption bands of SO_4^{2-} at 1150–450 cm^{-1}. Also present are bands of boric acid at 1490–1428 cm^{-1} and a weak band at 2400–3000 cm^{-1} assignable to the bridging BH group.

The IR spectrum of ARVI microfertilizer (Fig. 8, spectrum *3*) exhibits characteristic absorption bands of both ammonium sulfate and the microcomplex.

The IR spectra of ARVI microfertilizer with AAC additions are shown in Fig. 8, curves *4–6*. The spectra exhibit characteristic absorption bands of ammonium sulfate, microcomplex, and AAC. In the frequency range 3500–3000 cm^{-1} there are absorption bands of the NH_2 group, and a band at 1590–1650 cm^{-1} corresponds to the C=O bond. Bands at 1520–450 cm^{-1} are characteristic of the NH_2, CH_2, and COO^- groups. All the absorption bands in spectra *4–6* are observed at the same (or slightly shifted) positions as in the spectra of the separate components (ammonium sulfate, microcomplex, AAC); therefore, we can conclude that no chemical reactions occur in ARVI microfertilizers.

To evaluate the sorption properties, we examined the hygroscopicity of the separate components, ARVI microfertilizers, and ARVI microfertilizers with AAC additions under the same conditions as in the above-described AAC tests. The dynamic sorption curves are shown in Figs. 9 and 10.

Experiments on the water absorption under ambient conditions (Fig. 9; 20–22°C, 25–37% humidity) show that only ammonium sulfate (Fig. 9, curve *6*) slightly absorbs water, whereas the other components and fertilizers with AAC (curve *2–5*), especially the microcomplex (curve *1*), even lose moisture.

In a desiccator over water (~21°C, ~98% humidity), all the samples show a linear dependence of the water absorption on time (Fig. 10). In 192 h, the samples start to dissolve, and on samples with AAC a mold appears in 336 h. The lowest water absorption is shown by the microcomplex (curve *1*). All the other substances (ammonium sulfate, ARVI microfertilizers, ARVI microfertilizers with 1, 3, and 4% AAC) take up considerably larger amount of water. The dynamic sorption curves of the fertilizers with AAC resemble that of ammonium sulfate (Fig. 10, curve *2*), which is the major component of the fertilizers.

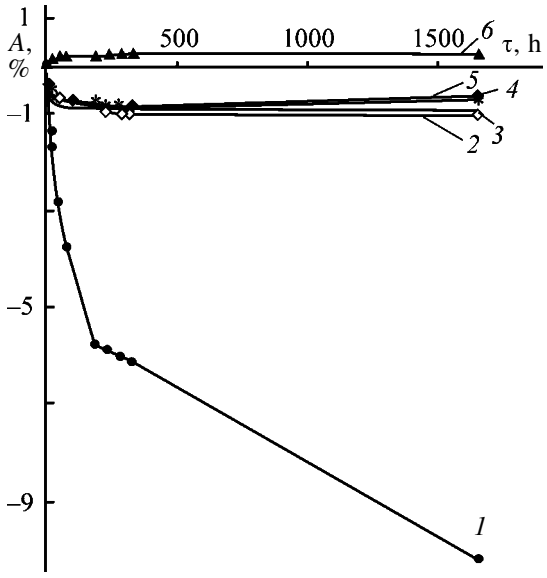

Fig. 9. Dynamic curves of water absorption *A* under ambient conditions by (*1*) microcomplex; (*2*) ARVI microfertilizer; (*3*–*5*) the same + 1, 3, and 4% AAC, respectively; and (*6*) ammonium sulfate.

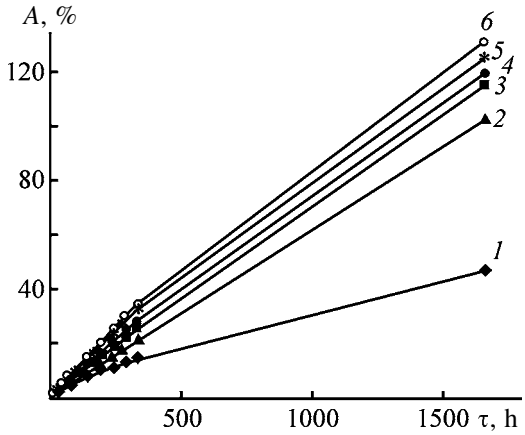

Fig. 10. Dynamic curves of water absorption *A* in a desiccator over water by (*1*) microcomplex, (*2*) ammonium sulfate, (*3*) ARVI microfertilizer, and (*4*–*6*) the same + 1, 3, and 4% AAC, respectively.

CONCLUSIONS

(1) Data obtained by instrumental methods show that no chemical reactions between the components occur in ARVI microfertilizer with additions of amino acid concentrate. The amino acid concentrate decreases the thermal stability of the fertilizers. Traditional conditions of granulation, drying, and storage are quite suitable for the fertilizers in question.

(2) Studies of water absorption under various conditions show that microelement fertilizers based on ammonium sulfate and containing amino acid concentrate do not change their physical properties.

REFERENCES

1. Sviklas, A., *Russ. J. Appl. Chem.*, 2003, vol. 76, no. 12, pp. 1885–1890.
2. Sviklas, A. and Paletskene, R., *Russ. J. Appl. Chem.*, 2004, vol. 77, no. 4, pp. 521–526.
3. Paleckiene, R., Sviklas, A., and Šlinkšiene, R., *Russ. J. Appl. Chem.*, 2005, vol. 78, no. 10, pp. 1651–1655.
4. Lithuanian Patent 5297.
5. Lithuanian Patent 5298.
6. Lithuanian Patent 2005-066.
7. Laurinavičius, V., *Organine ir bioorganine chemija*, Vilnius: Ziburio leidykla, 2002.
8. Ashmead, H.D., Ashmead, H.H., Miller, G.W., et al., *Foliar Feeding of Plants with Amino Acid Chelates*, Park Ridge, NJ: Noyes, 1986.
9. Koren'kov, D.A., *Produktivnoe ispol'zovanie mineral'nykh udobrenii* (Productive Use of Mineral Fertilizers), Moscow, 1985.
10. Araki, K. and Ozeki, T., Amino Acids (Survey), *Kirk–Othmer Encyclopedia of Chemical Technology*, 4th ed., pp. 504–571.
11. *Association of American Plant Food Control Officials, Official Publication*, Raleigh, NC: AAPFCO, 1998.
12. *Naturamin®-WSP*, DAYMSA, 2005–05–24, www.daymsa.com.
13. Regulation (EC) no. 2003/2003 of the European Parliament and of the Council of 13 October 2003 Relating to Fertilisers, *Off. J. L*, 2003-11-21, no. 304-1.
14. Pokhodenko, L.A., *Metody opredeleniya razlichnykh form azota v mineral'nykh azotnykh udobreniyakh: Instruktsiya* (Manual on Methods for Determination of Various Nitrogen Forms in Mineral Nitrogen Fertilizers), Lvov: L'vovsk. Politekh. Inst., 1986.
15. Mickevičius, D., *Chemines analizes metodai*, Kaunas: VDU, 2000, 3rd ed., p. 179.
16. Ewing, G.W., *Instrumental Methods of Chemical Analysis*, New York: McGraw-Hill, 1985.
17. *Rukovodstvo po rentgenovskomu issledovaniyu mineralov* (Manual on X-ray Diffraction Study of Minerals), Frank-Kamenetskii, V.A., Ed., Leningrad: Nedra, 1975.
18. McMurdie, H., Morris, M., Evans, E., et al., *Powder Diffract.*, 1986, no. 1, p. 345.

ISSN 1070-4272, Russian Journal of Applied Chemistry, 2007, Vol. 80, No. 3, pp. 358–363. © Pleiades Publishing, Ltd., 2007.
Original Russian Text © N.N. Khimich, A.V. Zdravkov, M.A. Aleksashkina, L.F. Chepik, 2007, published in Zhurnal Prikladnoi Khimii, 2007, Vol. 80, No. 3, pp. 360–365.

INORGANIC SYNTHESIS AND INDUSTRIAL INORGANIC CHEMISTRY

Organic–Inorganic Hybrids in the System Ruthenium Tris(diimine) Complexes–Silica

N. N. Khimich, A. V. Zdravkov, M. A. Aleksashkina, and L. F. Chepik

Grebenshchikov Institute of Silicate Chemistry, Russian Academy of Sciences, St. Petersburg, Russia
St. Petersburg State University, St. Petersburg, Russia

Received October 9, 2006

Abstract—Organic–inorganic composites in which ruthenium(II) complexes are covalently bound to the silicate matrix were prepared by the sol–gel method. The physicomechanical and optical properties of the monolithic samples obtained were studied.

DOI: 10.1134/S1070427207030032

The majority of transition metals form stable complexes with 2,2'-bipyridine, 1,10-phenanthroline, their derivatives, and related compounds [1]. The diversity of electronic transitions in these compounds, due to accessibility of the *d* and *f* electronic sublevels of transition metals in combination with conjugated π-electron systems of ligands, gives rise to interesting photophysical, photochemical, and electrochemical properties [2–6]. Complexes of the type $[RuL_3]^{2+}$ exhibit a unique combination of these properties with high thermal and chemical stability [7]. Large interest in these compounds is caused by prospects for their use in the fields of photochemistry, photophysics, electrochemistry, chemiluminescence, and electroluminescence (especially after the discovery in 1976 of the catalytic effect of ruthenium complexes on decomposition of water into elements under the action of visible light [7]).

The practical use of photophysical and electrochemical properties of such structures involves their incorporation into an organic or inorganic matrix. Various organic polymers (polymethacrylates, polyurethanes, polyamides, polyimides, polybenzimidazoles, etc.) can be used as matrix [8–13]. The stability and uniformity of films, coatings, fibers, and other materials thus obtained are mainly determined by the possibility of chemical bonding between the system components, i.e., of formation of a covalent bond between the matrix and ligands of the complex (or at least one of them) [14, 15]. There are several synthetic strategies for preparing a ruthenium complex chemically bound with a polymer chain. The majority of researchers believe that, from the viewpoint of attaining chemical stability and high deformation and strength characteristics, the best choice is synthesis of a polymer chain containing 2,2'-bipyridine-type units, followed by complexation with Ru^{2+} derivatives. In so doing, however, some problems arise: The viscosity of polymer solutions considerably increases as a result of cross-linking of polymer chains upon formation of the Ru^{2+} complex, and the polymer becomes less soluble, which can lead to formation of a nonuniform material. Therefore, the metal concentration in the polymer–metal complex rarely exceeds 1%.

A good solution to this problem is replacement of a polymer matrix by an inorganic SiO_2 matrix prepared by the organic sol–gel method: hydrolysis of tetraalkoxysilanes followed by polycondensation of the hydrolysis products [16]. In so doing, the organic complex of ruthenium is added into the initial system, and the sol–gel process yields a hybrid material with intermolecular binding of the organic ($[RuL_3]^{2+}$) and inorganic (SiO_2) components of the system [17–19]. This intermolecular binding is due to van der Waals and hydrophobic–hydrophilic interactions of the components; naturally, it is relatively weak [20]. Therefore, the physicomechanical properties of the hybrids obtained in the $[RuL_3]^{2+}$–SiO_2 system are unsatisfactory. Furthermore, clusterization of the molecules of the organic component in the course of sol–gel synthesis will disturb the uniformity of the material. Apparently, the prospects of this strategy are associated with the synthesis of nanocomposites in which the organic and inorganic components of the system will be chemically bound with each other.

To prepare such nanohybrid structures, we used ruthenium complexes containing a trimethoxysilyl group in the side chain of one of the ligands (Scheme 1).

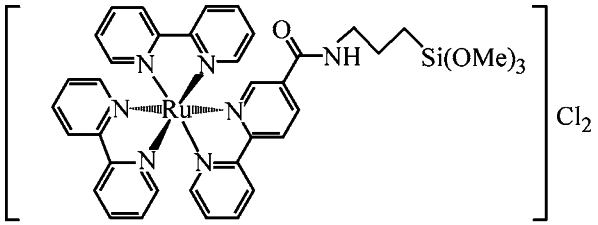

Ia

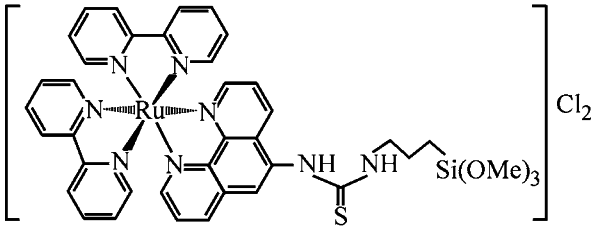

IIa

Scheme 1. Ruthenium complexes.

Our goals were to synthesize such complexes, to incorporate them into a silica matrix prepared by hydrolytic polycondensation of tetramethoxysilane, and to study the physicomechanical and optical properties of the materials obtained.

EXPERIMENTAL

The ^{1}H and ^{13}C NMR spectra were recorded on a Bruker DPX-300 device (operating frequencies 300.13 and 75.5 MHz, respectively; internal reference TMS). The UV spectra were measured on an SF-2000 spectrometer, and the luminescence spectra, on a Lyumeks device. Thermal analysis was performed with a Q-1500 D derivatograph. The reaction mixtures were analyzed and the product purity checked by TLC on Silica Gel 60 F254 and Armsorb TSKh-AN-UF 254 plates. Substances were separated by column chromatography on Silica Gel 60 (0.040–0.063 μm) and alumina L 40/350 (40–250 μm). In the syntheses we used $[Ru(bipy)_3]Cl_2$, 5% Pd/C, thiophosgene, and 3-aminopropyltrimethoxysilane (Aldrich). *cis*-[Bis-(2,2'-bipyridine)dichlororuthenium] [7], 5-nitro-1,10-phenanthroline [21], and ruthenium complexes **Ib**–**Id** [22, 23] were prepared by previously described procedures.

$[Ru(bipy)_2(phenNO_2)]Cl_2$ (IIb). A suspension of 600 mg of bis(2,2'-bipyridine)dichlororuthenium **III** and 1.1 equiv of 5-nitro-1,10-phenanthroline in 40 ml of water was refluxed for 1 h to complete conversion of **III** (TLC monitoring on alumina). The resulting solution was cooled and filtered; the filtrate was evaporated to dryness in a water-jet-pump vacuum, and the residue was dissolved in 1 ml of methanol and reprecipitated into 20 ml of absolute diethyl ether. Yield 90%.

^{1}H NMR spectrum [$(CD_3)_2SO$], δ, ppm: 9.50 s (1H), 9.10 m (2H), 8.35 d (2H), 8.30 d (2H), 8.25 t (2H), 8.15 t (2H), 8.05 m (2H), 7.80 d (2H), 7.65 m (4H), 7.40 t (2H).

$[Ru(bipy)_2(phenNH_2)]Cl_2$ (IIc). A solution of 0.5 g of **IIb** in 12 ml of water was hydrogenated at room temperature and atmospheric pressure with stirring in the presence of 170 mg of the palladium catalyst. After the uptake of the theoretical amount of hydrogen (24 h), the catalyst was filtered off, and the resulting yellow-orange solution was used in further synthesis without isolation of the amino derivative. To confirm the structure of **IIc**, a sample of **IIb** was hydrogenated in DMF-d_7. ^{1}H NMR spectrum [$(CD_3)_2NCDO$], δ, ppm: 8.95 m (6H, $H^{3,3'}$-bipy, $H^{4,7}$-phen), 8.30 m (3H, $H^{6,6'}$-bipy, H^8-phen), 8.17 t (2H, $H^{4,4'}$-bipy), 8.07 t (2H, $H^{4,4'}$-bipy), 7.95 d (1H, H^3-phen), 7.85 m (4H, $H^{6,6'}$-bipy, $H^{5,5'}$-bipy), 7.67 t (2H, $H^{5,5'}$-bipy), 7.62 s (1H, H^6-phen), 7.47 m (2H, $H^{2,9}$-phen). ^{13}C NMR spectrum [$(CD_3)_2NCDO$], δ, ppm: 124.9, 126.1, 127.5, 127.6, 132.3, 133.6, 137.9, 138.1, 146.7, 147.2, 151.8, 152.4, 152.8, 157.1.

$[Ru(bipy)_2(phenNCS)]Cl_2$ (IId). A solution of NaOAc in 5 ml of water was added to a solution of **IIc** in water, cooled to –5°C, after which a solution of thiophosgene in 2 ml of acetone was added dropwise with vigorous stirring over a period of 5 min. After 15 min (TLC monitoring), the solution was evaporated in a vacuum, and the residue was separated chromatographically on alumina, eluent methylene chloride–methanol, 10 : 1. Yield 50% based on the starting complex with nitrophenanthroline. ^{1}H NMR spectrum [$(CD_3)_2SO$], δ, ppm: 8.90 m (4H, $H^{3,3'}$-bipy), 8.75 d (1H, H^7-phen), 8.55 d (1H, H^4-phen), 8.12 m (6H, $H^{4,4'}$-bipy, $H^{3,8}$-phen), 7.78 m (5H, $H^{6,6'}$-bipy, H^6-phen), 7.58 m (4H, $H^{5,5'}$-bipy), 7.40 m (2H, $H^{2,9}$-phen). ^{13}C NMR spectrum [$(CD_3)_2SO$], δ, ppm: 125.4, 125.5, 126.2, 126.7, 128.7, 129.8, 132.1, 134.8, 136.3, 138.7, 138.9, 144.2, 148.1, 151.8, 152.2, 157.4, 157.7.

Ruthenium complexes **Ia** and **IIa** can be prepared by two routes. The first route involves condensation of $Ru(bipy)_2Cl_2$ with appropriate derivative of 2,2'-bipyridine (**IV**) or 1,10-phenanthroline (**V**) (Scheme 2).

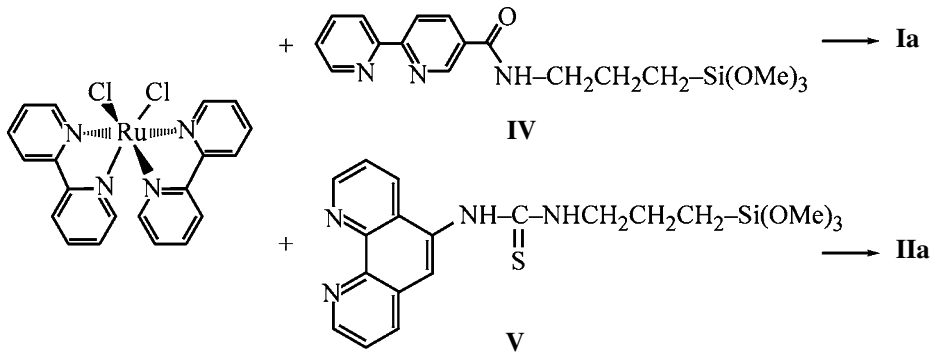

Scheme 2. Synthesis of ruthenium complexes

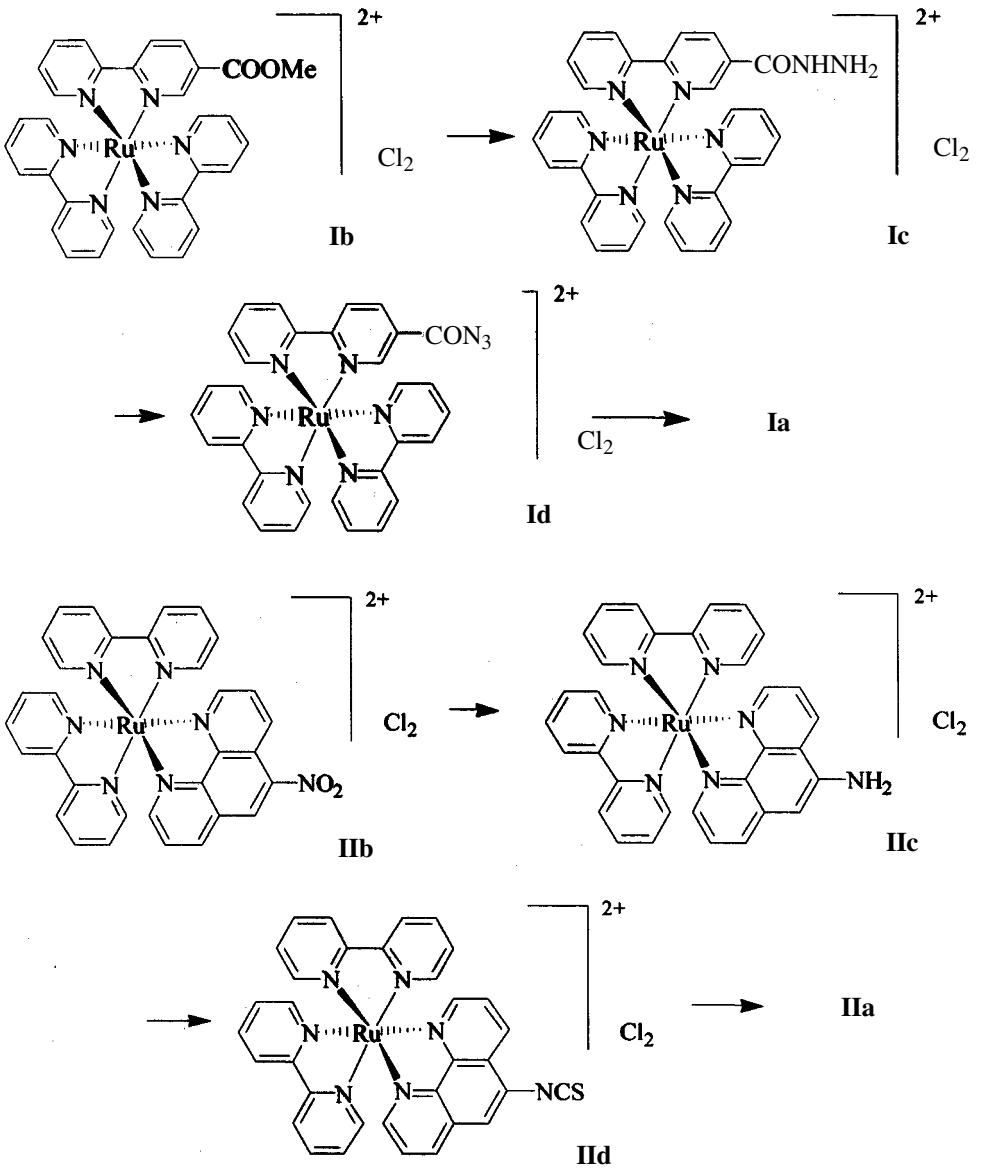

Scheme 3.

Synthesis of **IV** and **V** involves no serious problems and was described previously [23]. Unfortunately, in anhydrous medium (absolute methanol), required to prevent possible hydrolysis, the reactions of formation of **Ia** and **IIa** are slow and do not go to completion. We found that the reaction $Ru(bipy)_2Cl_2 + L \rightarrow [Ru(bipy)_2L]Cl_2$ occurs considerably faster and with a higher yield in the presence of water, even if the ligand L is insoluble in water.

It is extremely difficult to prepare pure compounds **Ia** and **IIa** by this route, because common methods of column chromatography are unsuitable for their purification.

The second pathway involves direct transformation of functional groups in the complexes $[Ru(bipy)_2 \cdot (bipy')]Cl_2$ and $[Ru(bipy)_2(phen')]Cl_2$ (Scheme 3).

This route allows preparation of the desired complexes **Ia** and **IIa** in a higher yield and by less labor-consuming procedures, because transformations of functional groups in ruthenium complexes require considerably milder conditions than formation of the complexes themselves.

Complexes **Id** [22] and **IIb**–**IId** were isolated and characterized in the course of the synthesis. Because of easy hydrolysis of trimethoxysilyl groups, compounds **Ia** and **IIa** were synthesized directly in the sol–gel system. Their structure was confirmed by NMR spectroscopy; for this purpose, the reactions of azide **Id** and isothiocyanate **IId** with 3-aminopropyltrimethoxysilane were performed in DMSO-d_6.

To perform sol–gel synthesis of nanohybrids, to a mixture of tetramethoxysilane (TMOS) (1 equiv), acetic acid (1 equiv), and water (4 equiv) we added a methanol solution of **Ia** or **IIa**, prepared by mixing **Id** or **IId** with 3-aminopropyltrimethoxysilane taken in an equivalent amount. Compound **IIa** is formed immediately; formation of **Ia** requires keeping the solution at room temperature in the absence of atmospheric moisture for 3 days.

The resulting solutions were placed in hermetically stoppered polypropylene test tubes and kept at 55°C for 2 days. Then the hermetic stoppers were replaced by stoppers with holes (hole diameter about 1 mm), and wet gels were dried for 2 h at 55, 2 h at 70, 2 h at 80, and 17 h at 90°C. The temperature was raised at a rate of 3 deg h^{-1}. After that, the gels were transferred into glass test tubes equipped with stoppers with holes and were heated to 90 (15 deg h^{-1}) and then to 120°C (3 deg h^{-1}); at 120°C, the samples were kept for 12 h.

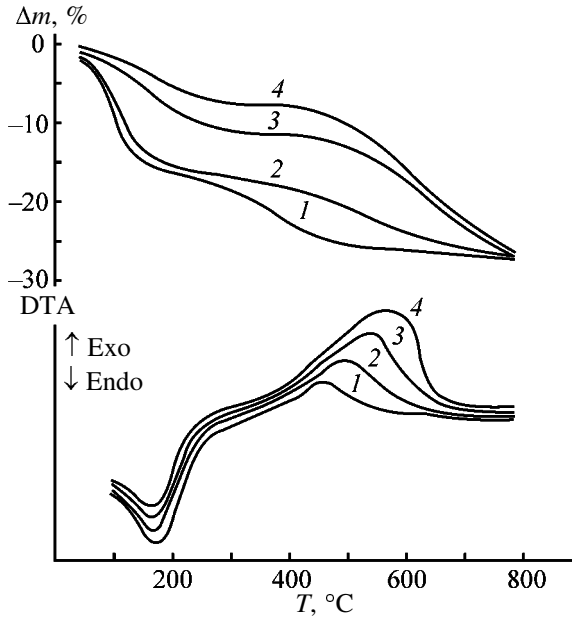

Fig. 1. Curves of thermal analysis of composites: (*1*) **1a**, (*2*) **1b**, (*3*) **1c**, and (*4*) **1d**. (Δm) Weight loss and (T) temperature.

With 1, 5, 10, and 20% complex **Ia**, we prepared composites **1a**–**1d**, respectively, and with the same amounts of **IIa**, composites **2a**–**2d**, respectively. Hybrids **3a**–**3d** containing the same amounts of commercial $[Ru(bipy)_3]Cl_2$ were prepared as references.

All the hybrids **1a**–**1d**, **2a**–**2d**, and **3a**–**3d** are monolithic transparent cylinders with the color gradually changing from yellow for **1a**–**3a** to red-brown for **1d**–**3d**. The composition and structure of the SiO_2 gel prepared by the organic sol–gel method under similar conditions are described in detail elsewhere [16]. Introduction of Ru(II) complexes into the SiO_2 matrix is accompanied by a gradual increase in the density from 1.38 for **1a** to 1.68 g cm^{-3} for **Id**, and in the microhardness from 100 to 165 kg mm^{-2}, respectively. Similar changes in the density and microhardness, though less pronounced, occur in formation of composites **2a**–**2d** and **3a**–**3d**. According to the results of thermal analysis of composites **1c**–**3c**, the formation of hybrids **1c** and **2c** in which the Ru(II) complexes are linked with the inorganic matrix by a chemical bond is accompanied by a considerable increase in their thermal stability compared to **3c**. It should be particularly emphasized that, in contrast to **3c**, the total content of volatile impurities in hybrids **1a**–**1d** and **2a**–**2d** remains constant, i.e., introduction of an organic component into the sol–gel system is accompanied by displacement of a part of water and methanol sorbed by the gel matrix (Fig. 1).

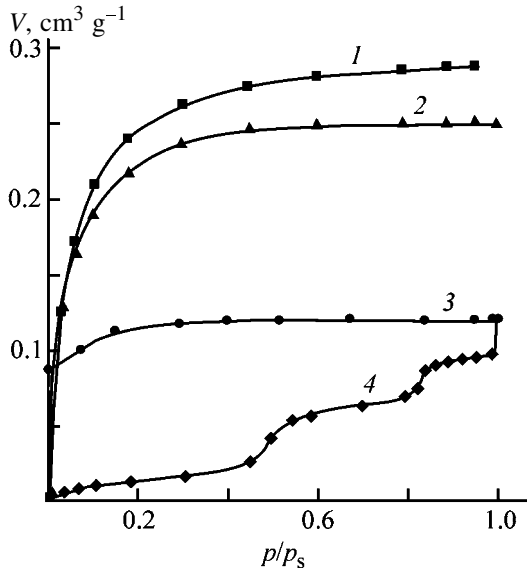

Fig. 2. Isotherms of ethanol adsorption–desorption at 18°C on composites (*1*) **1a**, (*2*) **1b**, and (*3*, *4*) **1d** (adsorption and desorption, respectively). (*V*) pore volume and (p/p_s) ratio of the ethanol vapor pressure to its saturated vapor pressure.

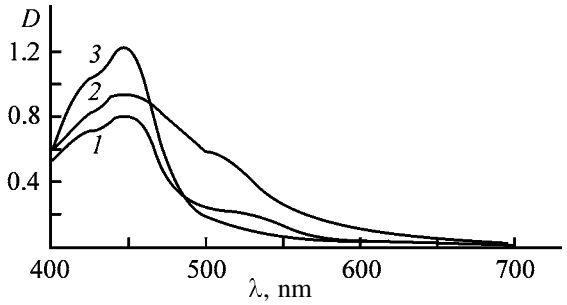

Fig. 3. Absorption spectra of composites (*1*) **1b**, (*2*) **2b**, and (*3*) **3b**. (*D*) Optical density and (λ) wavelength.

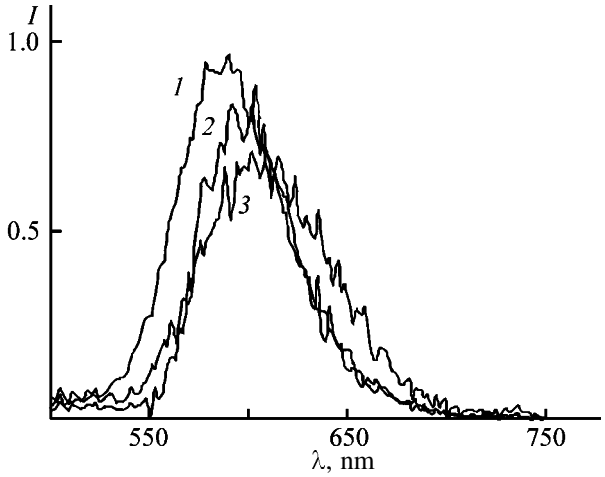

Fig. 4. Luminescence spectra of composites (*1*) **1b**, (*2*) **2b**, and (*3*) **3b**. (*I*) Normalized intensity (relative to I_{max}) and (λ) wavelength.

Figure 2 shows the isotherms of ethanol adsorption–desorption on composites **1a**, **1b**, and **1d**. From these curves, we can calculate the specific surface area of the composites and the mean pore size [24]:

Composite	**1a**	**1b**	**1d**
S, $m^2\ g^{-1}$	500	440	30
r, nm	0.8	0.7	–

The calculated specific surface areas of hybrids **2a**–**2d** are close to those of **1a**–**1d**.

Apparently, with an increase in the content of organic component in hybrids formed by chemical binding of system components with each other, the number and size of pores in the SiO_2 matrix decrease, and at a 15–20% concentration of the Ru complex the matrix becomes monolithic.

The absorption spectra of the composites (Fig. 3) are very similar, although their maxima are red-shifted by approximately 3–5 nm. All the complexes synthesized show a strong luminescence in the range 550–650 nm (excitation with a xenon lamp, λ = 450 nm) (Fig. 4).

It should be noted that in composites **1**–**3** the concentration quenching of the luminescence is not decisive, in contrast to the lanthanide complex–silica system in which even a minor increase in the Ln(III) concentration, leading to clusterization of the molecules of the complex (for hybrids formed without chemical bonding between the system components), is fatal.

CONCLUSIONS

(1) New metal–polymer Ru(II) complexes in the form of organic–inorganic hybrids, with the organic and inorganic components linked by a chemical bond, were synthesized.

(2) The use of an inorganic SiO_2 matrix as a polymeric base allows control of the content of the Ru(II) complex in the composite, significant improvement of the physicomechanical properties of the material, enhancement of its heat resistance, and simplification of the synthesis of the initial polymeric structures.

ACKNOWLEDGMENTS

The authors are grateful to the Russian Foundation for Basic Research for financial support (project no. 06-03-33 002-a).

REFERENCES

1. *Heterocyclic Compounds*, Elderfield, R.C., Ed., New York: Wiley, 1961, vol. 7.
2. Lo, K.K.-W., Chan-Ming, Ng D., and Chung, C.-K., *Organometallics*, 2001, vol. 20, pp. 4999–5002.
3. Tyson, D.S. and Castellano, F.N., *Inorg. Chem.*, 1999, vol. 38, pp. 4382–4386.
4. Lo, K.K.-W., Chung, C.-K., and Zhu, N., *Chem. Eur. J.*, 2003, vol. 9, pp. 475–480.
5. Yang, J., Gordon, K., Zidon, Y., and Shapira, Y., *J. Appl. Phys.*, 2003, vol. 94, no. 10, pp. 6391–6395.
6. Zemskii, V.I., Veresov, A.V., and Ershov, A.Yu., *Opt. Spektrosk.*, 1996, vol. 81, no. 2, pp. 251–257.
7. Seddon, A. and Seddon, K.R., *The Chemistry of Ruthenium*, Amsterdam: Elsevier, 1984.
8. Younathan, J.N., McClanahan, S.F., and Meyer, T.J., *Macromolecules*, 1989, vol. 22, pp. 1048–1052.
9. Rasmussen, S.C., Thompson, D.W., Singh, V.S., and Petersen, J.D., *Inorg. Chem.*, 1996, vol. 35, pp. 3449–3450.
10. Farah, A.A., Veirot, J.G.C., Najman, M., and Pietro, W.J., *Pure Appl. Chem.*, 2000, vol. A37, no. 11, pp. 1507–1529.
11. Ikeda, S. and Senna, M., *J. Mater. Chem.*, 2004, no. 14, pp. 1071–1074.
12. Tokura, S., Yasuda, T., Segawa, Y., and Kira, M., *Chem. Lett.*, 1997, no. 5, pp. 1163–1164.
13. Peng, Z. and Yu, L., *J. Am. Chem. Soc.*, 1996, vol. 118, pp. 3777–3778.
14. Shavaleev, N.M., Moorcraft, L.P., Pope, S.J.A., et al., *Chem. Eur. J.*, 2003, vol. 9, pp. 5283–5285.
15. Khimich, N.N., Semov, M.P., and Chepik, L.F., *Dokl. Ross. Akad. Nauk*, 2004, vol. 394, no. 5, pp. 636–638.
16. Khimich, N.N., Venzel', B.I., Drozdova, I.A., and Koptelova, L.A., *Zh. Prikl. Khim.*, 2002, vol. 75, no. 7, pp. 1125–1130.
17. Matsui, K. and Momose, F., *Chem. Mater.*, 1997, no. 9, pp. 2588–2591.
18. Castellano, F.N., Heimer, T.A., Tandhasetti, M.T., and Meyer, G.J., *Chem. Mater.*, 1994, no. 6, pp. 1041–1048.
19. Lin, J.M., Ma, C.C.M., Wang, F.Y., et al., *J. Polym. Sci., Part B: Polym. Phys.*, 2000, vol. 38, pp. 1699–1706.
20. *Sol–Gel Science and Technology*, vol. 1: *Processing Characterisation and Applications*, Sakka, S., Ed., New York: Kluwer Academic, 2005.
21. Smith, G.F. and Cagle, F.W., *J. Org. Chem.*, 1947, vol. 12, pp. 781–784.
22. Khimich, N.N., Zdravkov, A.V., and Aleksashkina, M.A., *Zh. Obshch. Khim.*, 2004, vol. 74, no. 7, pp. 1076–1079.
23. Khimich, N.N., Obrezkov, N.P., and Koptelova, L.A., *Zh. Org. Khim.*, 2006, vol. 42, no. 4, pp. 574–576.
24. *Eksperimental'nye metody v adsorbtsii i molekulyarnoi khromatografii* (Experimental Methods in Adsorption and Molecular Chromatography), Kiselev, A.V. and Drevint, V.P., Eds., Moscow: Mosk. Gos. Univ., 1973.

ISSN 1070-4272, Russian Journal of Applied Chemistry, 2007, Vol. 80, No. 3, pp. 364–367. © Pleiades Publishing, Ltd., 2007.
Original Russian Text © K.A. Gavronskaya, S.M. Shilov, V.N. Pak, 2007, published in Zhurnal Prikladnoi Khimii, 2007, Vol. 80, No. 3, pp. 366–369.

PHYSICOCHEMICAL STUDIES OF SYSTEMS AND PROCESSES

Luminescence of Terbium(III) Chloride in Porous Glass

K. A. Gavronskaya, S. M. Shilov, and V. N. Pak

Herzen Russian State Pedagogical University, St. Petersburg, Russia

Received November 12, 2006

Abstract—Terbium(III) chloride (1.5–150 μmol g^{-1}) was encapsulated in porous glass by impregnation of the support with aqueous solutions of various concentrations. The concentration dependences of the luminescence parameters and luminescence quenching in the course of water vapor adsorption in the salt intercalates were analyzed.

DOI: 10.1134/S1070427207030044

Porous glasses (PGs) with a pore size of 2–100 nm [1, 2] can be used as supports for preparing and stabilizing nanoparticles of various compounds [2–7]. Particular interest in the size-dependent optical properties of nanocomposites based on PGs is determined by their transparence in a wide wavelength range. Impregnation of PGs with solutions of optically active components of various concentrations with subsequent solvent removal is a simple and reliable procedure providing profound fragmentation and immobilization of small particles of various salts and complexes on the silica surface [4–7]. Owing to pronounced luminescence, microsecond lifetime of the excited states, and fixed positions of the excited levels, rare-earth elements (REEs) are interesting guest compounds. Porous glasses modified with REE compounds are systems with individual optical properties, which can be used as components of various photoluminescence, electroluminescence, light-converting, and sensor devices. Essentially, PGs act as nanoreactors determining the size specificity of the occurring processes and thus the properties of the resulting composites. Here we analyze the potentialities of this approach by the example of size features of luminescence of terbium(III) chloride encapsulated in PG.

EXPERIMENTAL

As a support we used finely dispersed glass with the particle size of 0.05–0.07 mm (predominant pore radius 4.5 nm, porosity 0.166 $cm^3\ g^{-1}$, and specific surface area 80 $m^2\ g^{-1}$). The PG modification was performed by impregnation with aqueous solutions of terbium chloride (0.01–1.0 M) and subsequent drying of the impregnated glasses at 120°C. The content of terbium in the support was determined photocolorimetrically with Arsenazo [8] using the solution prepared by boiling of the sample in water to transfer the terbium salt into the aqueous phase. The required concentration of $TbCl_3$ in PG can be attained at maximal and reproducible filling of the pore volume with the impregnation solution. The actually attainable molar content of salt Q introduced into PG is determined by the salt concentration c and pore volume ε:

$$Q = c\varepsilon\gamma, \quad (1)$$

where $\gamma < 1$ is a coefficient reflecting the deviation from the ideal filling of the pore volume.

The effective value was determined as the ratio of the salt content in PG to its highest content calculated at $\gamma = 1$. Our experimental data showed that the average value $\gamma = 0.9$ corresponds to the ratio of the through (open) and difficultly accessible (blind) pores, or to the fraction of the total PG pore volume in which the terbium chloride solution is distributed in the course of impregnation.

The spectra of the dry powder samples and those with adsorbed water were recorded using sealed quartz tubes 5 mm in diameter. The luminescence in the visible range and lifetimes of the excited state were recorded at room temperature using a device based on a KSVU-1 spectrometer interfaced with a computer and equipped with an FEU-100 photoelectron multiplier [9]. The luminescence was excited with an LGI21 pulse nitrogen laser ($\lambda = 337$ nm, $\tau = 10$ ns) and was recorded at the right angle to the laser beam. Samples with various content of adsorbed water on the initial and impregnated glasses in the range of relative humidity p/p_0 from 0.1 to 0.8 were prepared

by their keeping over solutions of sulfuric acid of the required concentrations.

The luminescence spectra of $TbCl_3$/PG samples with the content of terbium chloride Q = 1.5–150 μmol g^{-1}, recorded after drying at 120°C, are shown in Fig. 1. In all the cases, the band of the hypersensitive transition $^5D_4 \rightarrow {}^7F_4$ (λ_{ma}) dominates in the luminescence spectra of terbium(III) [10]. Additional weak bands at 590, 625, and 680 nm are also typical for $TbCl_3$ and correspond to the transitions from the lowest excited level $^5D_4$ to the $F_{1,3,4}$ levels of the Tb(III) cation [10]. It should be noted that even minimal concentrations of intercalate in the support (~0.04 wt %) provide reliably recordable green luminescence.

The nature of accumulation and distribution of the salt species on the through pore surface can be analyzed from the changes in the integral intensity I of the band of the main transition $^5D_4 \rightarrow {}^7F_4$ and lifetimes of the excited state τ* in the series of $TbCl_3$/PG samples (Fig. 2). With increasing intercalate content Q, I and τ* both increase and reach maximal values at Q = 120 μmol g^{-1}. Probably, the main portions of the dependences shown in Fig. 2 correspond to the monotonic increase in the amount of isolated luminescence centers uniformly distributed over the support surface. Their aggregation, causing concentration quenching of the luminescence, is essential only at relatively high intercalate concentrations and becomes a decisive factor only at Q = 120 μmol g^{-1}. The known specific surface area of 80 $m^2\,g^{-1}$ allows evaluation of the topographic density of $TbCl_3$ distribution over the silica surface:

$$n = QN_A/S, \quad (2)$$

where N_A is the Avogadro number. For example, at Q = 120 μmol g^{-1}, n is equal to one formula unit (molecule) of $TbCl_3$ per 1 nm^2, which well agrees with the concept of the monolayer coverage of the support surface with the intercalate. This fact suggests maximal (molecular) dispersion and predominantly tangential distribution of $TbCl_3$ at its accumulation in PGs. Strong interaction of the salt species with the glass surface due to the electron-acceptor power of amorphous silica [10] hinders aggregation of $TbCl_3$ molecules in three-dimensional networks of the cluster type, which, in turn, determines the monotonic increase in the luminescence intensity and lifetime of the excited state in the main sections of their dependences on the $TbCl_3$ content (Fig. 2). It should be noted that predominantly monolayer distribution of some metallic and oxide intercalates in PGs were found previously by electric resistivity measurements [4, 12, 13].

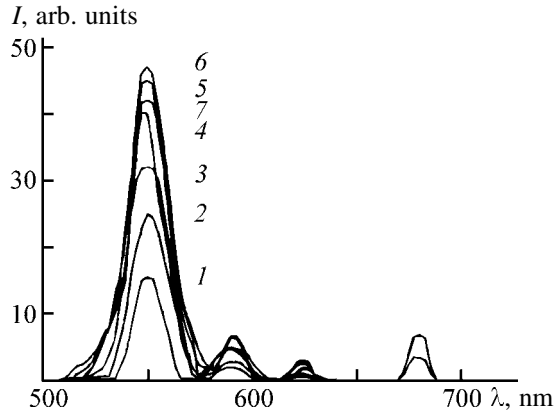

Fig. 1. Luminescence spectra of modified porous glasses with various content of $TbCl_3$. (*I*) Intensity and (λ) wavenumber. Content of $TbCl_3$, μmol g^{-1}: (*1*) 1.5, (*2*) 15, (*3*) 30, (*4*) 60, (*5*) 90, (*6*) 120, and (*7*) 150.

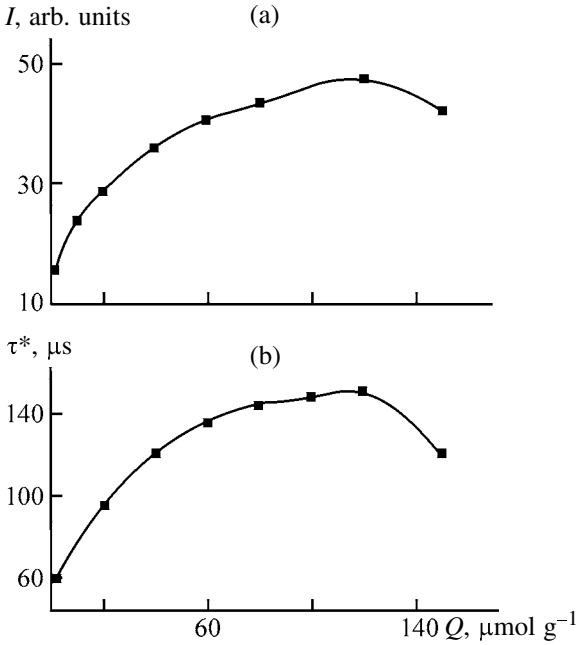

Fig. 2. (a) Intensity of the hypersensitive transition band I and (b) lifetime of the excited state τ* as functions of the $TbCl_3$ content Q in porous glass.

The features of luminescence quenching with water can give additional information on the state of salt species in porous glass. It should be noted that impregnation of PGs with $TbCl_3$ does not noticeaboly affect the water adsorption. The adsorption isotherms of the initial and impregnated samples with the $TbCl_3$ content changing from 1.5 to 150 μmol g^{-1} are so close (Fig. 3) that we failed to reveal any regular trends in their variation. We assume that $TbCl_3$

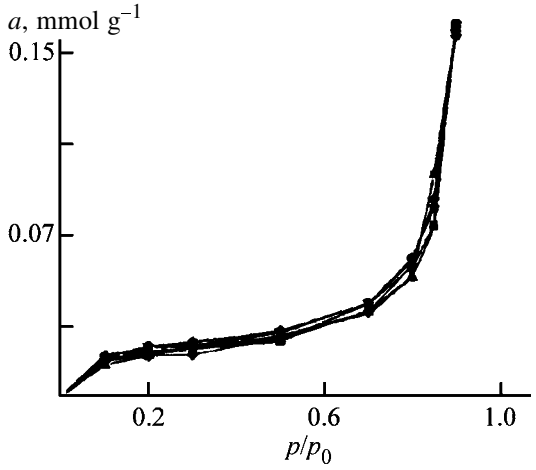

Fig. 3. Isotherms of water adsorption on the initial and modified porous glasses (for explanation, see text). (*a*) Adsorption and (p/p_0) relative humidity.

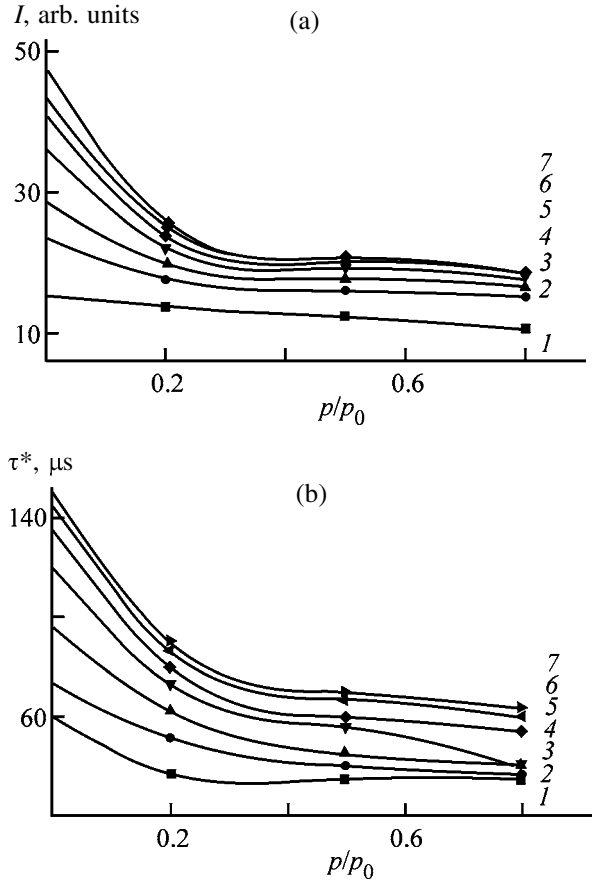

Fig. 4. (a) Luminescence intensity I and (b) lifetime of the excited state τ^* in a series of $TbCl_3$/PG samples as functions of the relative humidity p/p_0. Content of $TbCl_3$, μmol g^{-1}: (*1*) 1.5, (*2*) 10, (*3*) 20, (*4*) 40, (*5*) 60, (*6*) 90, and (*7*) 120.

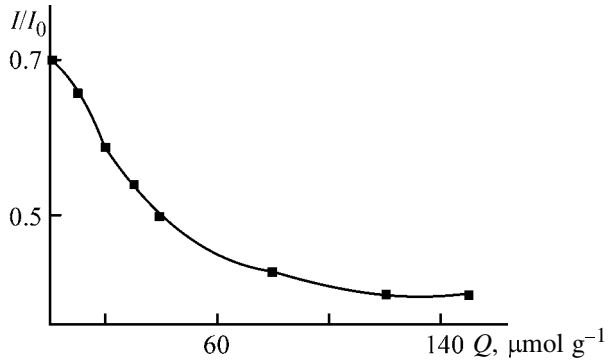

Fig. 5. Normalized intensity of the hypersensitive transition band I/I_0 at $p/p_0 = 0.8$ as a function of the $TbCl_3$ content Q in porous glass.

molecules with their affinity for water compensate the decrease in the adsorption activity of silanol groups on the glass surface, caused by their shielding.

The dependences of the intensity of the $^5D_4 \rightarrow {}^7F_4$ transition band and lifetime of the excited state on the relative humidity for a series of $TbCl_3$/PG samples are shown in Fig. 4. As seen, the main luminescence quenching is observed in the initial stage of adsorption. This fact suggests that water molecules are incorporated in the coordination sphere of Tb^{3+}, which determines the nonradiative loss of the energy of the excited state as a result of its interaction with high-frequency vibrations ν_{OH} [10]. Moreover, the most intense quenching is observed for samples with a high content of terbium(III) chloride. This feature is additionally illustrated by the dependence of normalized intensity I/I_0 (reflecting the extent to which the initial intensity decreases upon attainment of the relative humidity $p/p_0 = 0.8$) on the intercalate content (Fig. 5). Thus, the number of centers excluded from the luminescence process owing to water desorption decreases by 30% with a decrease in Q from 150 to 1.5 μmol g^{-1}. Such a behavior probably reflects the specificity of distribution of water molecules over the adsorption centers of silica and modifying agent. Therefore, small amounts of $TbCl_3$ in porous glass only slightly participate in the adsorption, which predominantly proceeds on the free surface OH groups. However, with increasing degree of the surface filling, intercalate molecules begin to dominate in water adsorption, which causes an increase in the quenching of their luminescence.

CONCLUSION

The maximal intensity of the luminescence of terbium(III) chloride in porous glass is attained at its

content of 120 μmol g^{-1}, which is close to that at monomolecular filling of the support surface. The concentration dependences of the luminescence and the features of its quenching in the presence of adsorbed water are consistent with the concept of molecular fragmentation and uniform distribution of the impregnated salt over the support surface.

REFERENCES

1. Roskova, G.P. and Tsekhomskaya, T.S., *Fiz. Khim. Stekla*, 1981, vol. 7, no. 5, pp. 513–534.
2. Enke, D., Janovski, F., and Schwieger, W., *Micropor. Mesopor. Mater.*, 2003, vol. 60, no. 1, pp. 19–30.
3. Sunil, D., Gafney, H.D., Rafailovich, M.H., et al., *J. Non-Cryst. Solids*, 2003, vol. 319, no. 1, pp. 154–162.
4. Verezhinskaya, R.L., Burkat, T.M., and Pak, V.N., *Fiz. Khim. Stekla*, 1999, vol. 25, no. 6, pp. 688–692.
5. Pak, V.N. and Sukhanov, S.V., *Zh. Prikl. Khim.*, 2003, vol. 76, no. 8, pp. 1241–1244.
6. Pak, V.N., Potkina, G.G., Sukhanov, S.V., and Shilov, S.M., *Zh. Prikl. Khim.*, 2004, vol. 77, no. 4, pp. 544–547.
7. Petushkov, A.A., Shilov, S.M., Puzyk, M.V., and Pak, V., *Pis'ma Zh. Tekh. Fiz.*, 2006, vol. 32, no. 9, pp. 65–70.
8. Charlot, G., *Les methods de la chimie analytique. Analyse quantitative minerale*, Paris: Masson, 1961, 4th ed.
9. Andreeva, D.A. and Puzyk, M.V., *Opt. Spektrosk.*, 2003, vol. 95, no. 5, pp. 764–765.
10. Poluektov, N.S., Kononenko, L.I., Efryushina, N.P., and Bel'tyukova, S.V., *Spektrofotometricheskie i lyuminestsentnye metody opredeleniya lantanoidov* (Spectrophotometric and Luminescence Methods of Lanthanide Determination), Kiev: Naukova Dumka, 1989.
11. Chuiko, V.N., *Teor. Eksp. Khim.*, 1987, vol. 23, no. 5, pp. 597–620.
12. Pak, V.N., Salomatina, O.Yu., Burkat, T.M., and Tikhomirova, I.Yu., *Zh. Prikl. Khim.*, 2004, vol. 77, no. 1, pp. 17–21.
13. Pak, V.N. and Salomatina, O.Yu., *Pis'ma Zh. Tekh. Fiz.*, 2004, vol. 30, no. 10, pp. 26–30.

ISSN 1070-4272, Russian Journal of Applied Chemistry, 2007, Vol. 80, No. 3, pp. 368–371. © Pleiades Publishing, Ltd., 2007.
Original Russian Text © A.V. Radushev, L.G. Chekanova, Yu.B. El'chishcheva, A.V. Ershova, 2007, published in Zhurnal Prikladnoi Khimii, 2007, Vol. 80, No. 3, pp. 370–373.

PHYSICOCHEMICAL STUDIES OF SYSTEMS AND PROCESSES

1,2-Dibenzoyl- and 1-Benzoyl-2-acetylhydrazines as Reagents for Recovering Cu(II) Ions from Alkaline Solutions

A. V. Radushev, L. G. Chekanova, Yu. B. El'chishcheva, and A. V. Ershova

Institute of Technical Chemistry, Ural Division, Russian Academy of Sciences, Perm, Russia
Perm State University, Perm, Russia

Received October 12, 2005; in final form, April 2006

Abstract—The conditions of complexation of 1,2-diacylhydrazines (H_2L) $C_6H_5C(O)NHNHC(O)R$, where R = C_6H_5 or CH_3, with Cu(II) ions in alkaline solutions were studied. The composition of the complexes formed by precipitation of Cu(II) from alkaline solutions, $(CuOH)_2L$ and CuL, was determined. The possibility of afterpurification of solutions with a low Cu(II) content by pneumatic flotation using H_2L was examined.

DOI: 10.1134/S1070427207030056

1,2-Diacylhydrazines $RC(O)NHNHC(O)R$ (H_2L) are tetradentate ligands and form stable flotation-active complexes ML with ions of Cu(II) and other nonferrous metals in ammonia or alkaline solutions [1, 2]. Replacement of alkyl radicals in symmetrical 1,2-diacylhydrazine molecules by phenyl radicals enhances the acid properties of the reagent, so that poorly soluble complexes of 1,2-dibenzoylhydrazine (DBzH) with Cu(II) are formed in ammonia solutions at pH 5–8 [3].

The goal of this study was to examine the conditions of complexation of 1,2-diacylhydrazines $C_6H_5 \cdot C(O)NHNHC(O)R$, where R = C_6H_5 or CH_3, with Cu(II) ions in alkaline solutions and the possibility of using these reagents for afterpurification of wastewater to remove Cu(II) after precipitation of the major amount of Cu(II) in the form of $Cu(OH)_2$.

EXPERIMENTAL

1,2-Dibenzoylhydrazine was prepared as described in [4], by thermal decomposition of $2C_6H_5COOH \cdot N_2H_4 \cdot H_2O$ [4]; 1-acetyl-2-benzoylhydrazine (BAH) was prepared similarly by the reaction of benzhydrazide with concentrated acetic acid. The main substance content in the reagent samples was 97% as determined by conductometric titration on an OK-102/1 conductometer (Hungary) with a bell-shaped OK-0902P electrode [5]. The optical density of solutions was measured on SF-26 and KFK-2 spectrophotometers, and pH, on an EV-74 pH meter with glass and silver chloride electrodes. The IR spectra were recorded in mineral oil on a Specord M 80 spectrophotometer. The derivatograms were taken on an MOM Q-1500D derivatograph (Hungary). The Cu(II) concentration in solution was determined by an extraction-photometric method with sodium diethyldithiocarbamate [6].

Complexation of reagents with Cu(II) ions was studied by the precipitation method, because the precipitates formed are insoluble in water and common solvents. Figure 1 (curve *4*) shows that the maximal

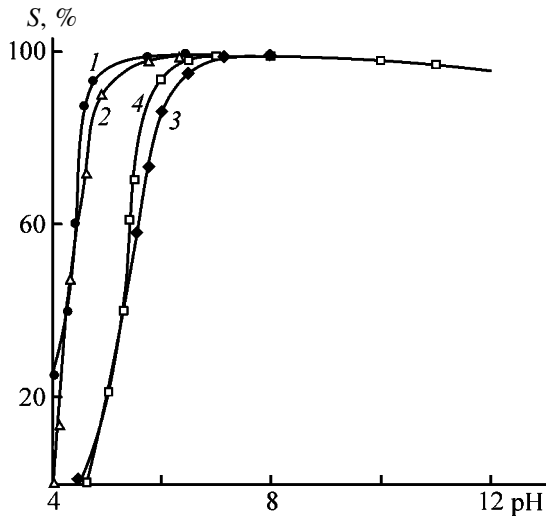

Fig. 1. pH dependences of the recovery *S* of Cu(II) ions with (*1*) DBzH, (*2*) BAH, and (*3*) DPH, and (*4*) in the form of $Cu(OH)_2$ without adding reagents. $c_{Cu(II)} = 63.5$ mg l^{-1}, $c_{H_2L} = 10^{-2}$ M in EtOH; [Cu(II)] : [H_2L] = 1 : 1, $\tau = 5$ min.

degree of precipitation of Cu(II) in the form of $Cu(OH)_2$ under the action of alkali is 99.8% in the pH range 7.0–10.0. The 99.9% precipitation of Cu(II) in the presence of DBzH was observed at pH 5.5 (curve *1*); in the presence of BAH, at pH 6.3 (curve *2*); and in the presence of dipropionylhydrazine (DPH), at pH 7 (curve *3*). These differences can be accounted for by considering the dissociation of 1,2-diacylhydrazines:

$$H_2L \xrightleftharpoons{pK_{a_1}} HL^- \xrightleftharpoons{pK_{a_2}} L^{2-}. \quad (1)$$

The acid properties of the reagents under consideration increase in the order DPH (pK_{a_1} 11.21 ± 0.04, pK_{a_2} 12.5 ± 0.3 [7]) < BAH (pK_{a_1} 9.37 ± 0.03, pK_{a_2} 10.9 ± 0.2) < DBzH (pK_{a_1} 9.22 ± 0.04, pK_{a_2} 10.8 ± 0.3 [3]). Therefore, the complexation of Cu(II) with DPH occurs in neutral and weakly alkaline solutions, whereas BAH and DBzH form complexes with Cu(II) even at pH 4.5–5.

We calculated the amount of H^+ (moles) released in complexation of DBzH and BAH with Cu(II) at varied pH_{eq} and constant concentration ratio Cu(II) : H_2L = 1 : 1 by slope analysis in the coordinates log ε–pH_{eq}, where ε is the sorption ratio [$\varepsilon = S_i/(1 - S_i)$]. Equations (2) and (3) wre obtained by the least-squares method for BAH and DBzH, respectively:

$$\log\varepsilon = 1.8 \pm 0.1 \quad (r = 0.9995,\ n = 4,\ P = 0.95), \quad (2)$$

$$\log\varepsilon = 1.7 \pm 0.1 \quad (r = 0.9995,\ n = 4,\ P = 0.95). \quad (3)$$

Hence, Cu(II) ions form with DBzH and BAH the complexes CuL in which the ligand is double-deprotonated.

The composition of the complexes was confirmed by potentiometric titration. For this purpose, a 100-ml beaker was charged with 5.0 ml of a 0.9×10^{-3} M solution of $CuSO_4$ and 60 ml of a 1 : 1 EtOH–H_2O mixture. The resulting solution was titrated with 1×10^{-3} M solutions of potassium salts of the reagents. The complexation with DBzH and BAH occurred in steps; the bends in the curve were observed at Cu(II) : H_2L concentration ratios of 2 : 1, 1 : 1, and 1 : 2 (Fig. 2).

Then we isolated complexes at the Cu(II) : H_2L concentration ratios of 1 : 1 and 2 : 1 in alkaline solutions. A 250-ml beaker was charged with 50 ml of a 1×10^{-2} or 2×10^{-2} M solution of $CuSO_4$, 1.6 ml of a 1×10^{-1} M KOH solution was added, and 50 ml of a 1×10^{-2} M solution of DBzH or BAH in ethanol

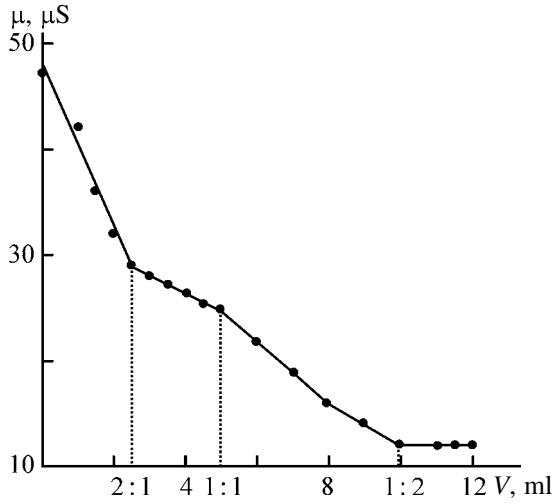

Fig. 2. Electrical conductivity μ of a $CuSO_4$ solution as a function of the precipitant (BAH) solution volume *V* (alkaline medium). $c_{Cu(II)} = 0.9 \times 10^{-3}$ M, $c_{BAH} = 10^{-3}$ M.

was added with stirring. The mixture was allowed to stand for 20 min. The precipitates were filtered off, washed on the filter with ethanol and hot water, and dried in air.

With DBzH and BAH at a Cu(II) : H_2L concentration ratio of 2 : 1 we obtained green precipitates, and at the 1 : 1 ratio, brown precipitates insoluble in water and common organic solvents, which is characteristic of polymeric compounds.

Analysis of the precipitates for Cu(II) gave the following results, wt %: [Cu(II)] : [DBzH] = 1 : 1, 20.75 and 2 : 1, 28.82; [Cu(II)] : [BAH] = 1 : 1, 25.9 and 2 : 1, 33.87. The composition of the complexes corresponds to the following formulas [calculated Cu(II), wt %]: $[Cu(C_6H_5OCNNCOC_6H_5)]$, 21.06; $[(CuOH)_2 \cdot (C_6H_5OCNNCOC_6H_5) \cdot 2H_2O]$, 29.20; $[Cu(C_6H_5O \cdot CNNCOCH_3)]$, 26.51; and $[(CuOH)_2(C_6H_5OCNN \cdot COCH_3) \cdot 2H_2O]$, 34.05.

To determine the structure of the complexes, we recorded their IR spectra. As compared to the starting DBzH and BAH, the IR spectra of the complexes do not contain stretching vibration bands of the C=O and N–H bonds, but contain bands at 1395–1404 cm^{-1} corresponding to stretching vibrations of C–O single bonds. The bands at 1520–1535 cm^{-1}, absent in the spectra of the starting diacylhydrazines, can be assigned to stretching vibrations of the C=N bonds [8]. Thus, the IR spectra confirm that Cu(II) ions form complexes with the reagent molecules in the double-deprotonated enol form. The spectra of the 2 : 1 complexes, in contrast to those of the 1 : 1 complexes,

Calculated solubility products SP and molar solubilities S of the complexes CuL with reagents $C_6H_5C(O)NHNHC(O)R$ in alkaline solutions

R	$c_{Cu} \times 10^4$, M	$c_{H_2L} \times 10^4$, M	S_i, %	$[Cu]^b_{eq} \times 10^6$, M	pH_{eq}	$c_{L^{2-}} \times 10^{12}$, M	$c_{Cu^{2+}} \times 10^6$, M	–log SP	$S \times 10^9$, M
CH_3	8.9	8.9	99.8	1.57	7.0	1.8	1.57	17.6	1.70
C_6H_5	10.0	10.0	99.9	1.26	6.5	0.1	1.26	18.9	0.35

also contain absorption bands in the range 3350–3520 cm^{-1} corresponding to stretching vibrations of hydroxy groups and water of crystallization. The presence of water of crystallization is also confirmed by thermal analysis of the complexes. The DTA curve exhibits endothermic peaks in the interval 170–210°C with maxima at 180°C for the Cu–BAH (2 : 1) complex and at 190°C for the Cu–DBzH (2 : 1) complex, assignable to the loss of water of crystallization.

On the basis of the above facts, the suggested structures of the 2 : 1 and 1 : 1 complexes can be presented by formulas (4) and (5), where R = CH_3 or C_6H_5.

The complexation of DBzH and BAH with Cu(II) ions in alkaline solution at a component ratio of 1 : 1 can be described by Eq. (6).

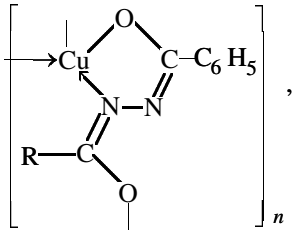

(4)

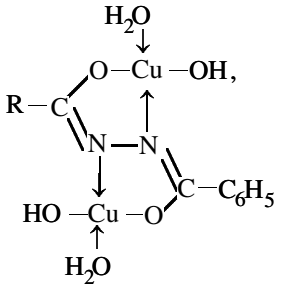

(5)

$$Cu^{2+} + H_2L + 2OH^- \rightleftarrows CuL\downarrow + 2H_2O. \quad (6)$$

To calculate the equilibrium concentrations of Cu^{2+} and L^{2-}, we used data from [9].

The solubility products SP and molar solubilities S of the complexes, calculated from data in Fig. 1, are given in the table. It is seen that the molar solubilities of the precipitates of the complexes are lower than that of $Cu(OH)_2$ (1.8×10^{-7} M [10]) by two orders of magnitude. Therefore, Cu(II) ions are recovered from alkaline solutions in the form of complexes with the ligands in question more completely than in the form of $Cu(OH)_2$.

We found that, at the initial Cu(II) concentration of 57 mg l^{-1}, precipitation of the complexes at the 1 : 1 component ratio reduces the residual Cu(II) concentration to 0.08 mg l^{-1} with DBzH and 0.1 mg l^{-1} with BAH. However, to precipitate Cu(II), large amounts of the reagent should be added [2.8 mg of BAH per milligram of Cu(II)], and the reagent is not regenerated. Therefore, it was interesting to examine the possibility of additional recovery of Cu(II) ions from solutions with their low content [after precipitation of Cu(II) in the form of $Cu(OH)_2$] by pneumatic flotation with BAH.

To a solution containing 3 mg l^{-1} of Cu(II) [after precipitation of $Cu(OH)_2$ with NaOH], we added BAH in 0.1 M KOH or in ethanol at the [Cu(II)] : [BAH] ratio of 1 : 1 or 1 : 2; the mixture was stirred for 1–2 min. The precipitates, Cu(II) complexes with the reagents, passed into the foam and were removed from the solution. The flotation installation and the experimental conditions were similar to those described in [11]. The experiments were performed at 20±2°C. The sample of the purified solution was taken through a sampler and analyzed for the residual Cu(II) content by the extraction-photometric method [6]. The degree of additional recovery of Cu(II) at pH 9 was 83.8 and 95%; the residual concentration of Cu(II) ions was 0.5 and 0.15 mg l^{-1}, respectively, which is below MPC for household water [12].

CONCLUSIONS

(1) Conditions for complexation of Cu(II) with 1,2-dibenzoyl- and 1-benzoyl-2-acetylhydrazines in the course of precipitation were optimized. The 1 : 1 and 2 : 1 complexes of Cu(II) with H_2L were isolated from alkaline solutions (pH ~9) and identified.

(2) Replacement of one phenyl radical in 1,2-dibenzoylhydrazine by the acetyl radical increases the solubility of the complex and decreases the degree of recovery of Cu(II) ions.

(3) 1-Acetyl-1-benzoylhydrazine is suitable for afterpurification of wastewater by pneumatic flotation after precipitation of Cu(II) with alkali in the form of $Cu(OH)_2$.

REFERENCES

1. Radushev, A.V., Zubareva, G.I., and Chekanova, L.G., *Izv. Vyssh. Uchebn. Zaved., Tsvetn. Metall.*, 1999, no. 1, pp. 3–6.
2. Chekanova, L.G., Radushev, A.V., and Shabalina, L.S., in *Khimiya i tekhnologiya ekstraktsii: Sbornik nauchnykh trudov* (Chemistry and Technology of Extraction: Coll. of Scientific Works), Moscow: Ross. Khimiko-Tekhnol. Univ. im. D.I. Mendeleeva, 2001, vol. 2, pp. 111–115.
3. Chekanova, L.G., Radushev, A.V., El'chishcheva, Yu.B., and Kazakova, Yu.V., *Zh. Prikl. Khim.*, 2004, vol. 77, no. 7, pp. 1090–1093.
4. Drozdetskii, A.G., Radushev, A.V., Turbin, A.S., et al., *Zh. Prikl. Khim.*, 1998, vol. 71, no. 2, pp. 288–293.
5. Radushev, A.V., Chekanova, L.G., Gusev, V.Yu., and Sazonova, E.A., *Zh. Anal. Khim.*, 2000, vol. 55, no. 5, pp. 496–499.
6. Podchainova, V.N. and Simonova, L.N., *Analiticheskaya khimiya elementov: Med'* (Analytical Chemistry of Elements: Copper), Moscow: Nauka, 1990.
7. Chekanova, L.G., Radushev, A.V., Lesnov, A.E., and Sazonova, E.A., *Zh. Obshch. Khim.*, 2002, vol. 72, no. 8, pp. 1315–1319.
8. Machkhoshvili, R.I., Coordination Compounds of Metals with Hydrazines, *Doctoral Dissertation*, Moscow, 1983.
9. Chekanova, L.G., Radushev, A.V., Shabalina, L.S., and Tiunova, T.G., *Izv. Vyssh. Uchebn. Zaved., Tsvetn. Metall.*, 2004, no. 5, pp. 23–26.
10. Lur'e, Yu.Yu., *Spravochnik po analiticheskoi khimii* (Handbook of Analytical Chemistry), Moscow: Khimiya, 1979.
11. Teterina, N.N., Adeev, S.M., Zubareva, G.I., and Radushev, A.V., *Izv. Vyssh. Uchebn. Zaved., Tsvetn. Metall.*, 1997, no. 3, pp. 6–9.
12. *Pravila okhrany poverkhnostnykh vod ot zagryazneniya stochnymi vodami* (Regulations on Protection of Surface Waters from Pollution by Wastewater), Moscow: Ministerstvo Melioratsii i Vodnogo Khozyaistva SSSR, 1975.

ISSN 1070-4272, Russian Journal of Applied Chemistry, 2007, Vol. 80, No. 3, pp. 372–375. © Pleiades Publishing, Ltd., 2007.
Original Russian Text © S.A. Tarasenko, V.F. Zinchenko, I.V. Stoyanova, I.P. Kovalevskaya, 2007, published in Zhurnal Prikladnoi Khimii, 2007, Vol. 80, No. 3, pp. 374–377.

SORPTION AND ION-EXCHANGE PROCESSES

Sorption of Lead and Copper Ions on Synthetic Apatite Samples Produced by Melt Thermal Process

S. A. Tarasenko, V. F. Zinchenko, I. V. Stoyanova, and I. P. Kovalevskaya

Bogatskii Physicochemical Institute, National Academy of Sciences of Ukraine, Odessa, Ukraine

Received March 30, 2006; in final form, November 2006

Abstract—The possibility of using calcium fluoro- and hydroxylapatites synthesized in a NaCl–KCl salt melt as sorbents of heavy metal ions from aqueous solutions was analyzed. The sorption products formed were identified by chemical and X-ray phase analyses and diffuse reflection spectroscopy.

DOI: 10.1134/S1070427207030068

To the class of apatites belong compounds of the composition $M_{10}(ZO_4)_6X_2$, where M most frequently stands for Ca, Sr, Ba, Eu, Pb, Cd, and other ions with a charge of +2; Z = P, V, and other ions with a formal charge of +5; and X = OH, F, Cl, Br, and other ions with a charge of –1. In recent years, a considerable success has been achieved in basic research and development of technologies for production of apatite materials with prescribed properties, which initiated efforts aimed at their large-scale industrial production [1, 2]. Calcium fluoroapatite (CaFAp) and, especially, calcium hydroxylapatite (CaHAp) are close in chemical composition and structure to the inorganic component of bones, and, therefore, are promising as artificial biologically compatible implants. They are capable of isovalent substitution of calcium ions in a wide range of compositions, which enables their use as supports for luminescent materials and hosts for disposal of radioactive wastes. At the same time, this property of apatite is negatively manifested as the ability of the bone tissue to accumulate toxic heavy metals (lead, cadmium, mercury, etc.) upon prolonged exposure of vertebrate organisms (including humans) to an environment containing increased concentrations of these toxicants.

In this study we examined the possibility of using apatites produced by melt thermal process (synthesis in a NaCl–KCl salt melt) as sorbents of certain heavy metals (lead, copper) from aqueous solutions.

EXPERIMENTAL

The previously developed melt thermal process, applied to synthesis of apatites, combines the main advantages of "dry" (short process duration) and "wet" (completeness of the reaction and sufficiently high dispersity of the products formed) techniques. Apatites were produced by the reaction of an intimate mixture (stock) of the starting compounds: CaF_2 (in the case of CaFAp) or $Ca(OH)_2$ (in the case of CaHAp), CaO, $CaCO_3$, and KPO_3 in a NaCl–KCl melt of equimolar composition at an approximately 1 : 1 mass ratio of the stock and the eutectic mixture in an Alundum crucible in open air at 700°C. The synthesis duration did not exceed 2 h. The product was formed as a cake having the shape of the crucible, which was readily detached from the latter. The cake was removed from the crucible, ground, and washed several times with distilled water to a weakly alkaline reaction (pH 7.58), after which it was dried in an oven at $T \approx 150$°C. The resulting material had the form of a white fluffy powder. The yield of the product was about 98%, and its mass, about 50 g. The phase composition of the apatites obtained was determined by X-ray phase analysis (XPA) on a DRON-3 installation by the standard technique. According to XPA data, all the samples obtained were highly crystalline and contained only the phase of the corresponding apatite. The specific surface area of the powders was estimated at approximately 10 $m^2\ g^{-1}$, which corresponds to an average particle size of about 0.1 μm. The particle size distribution was not studied in detail.

To study the sorption of Pb^{2+} ions, two 50-ml portions of 1 M solution of $Pb(NO_3)_2$ were prepared by dissolving weighed portions of anhydrous $Pb(NO_3)_2$ in distilled water in volumetric flasks of appropriate capacity. The concentration of the solutions was checked by titration. The content of Pb^{2+} ions in the

solutions was determined by direct chelatometric titration in a weakly acidic medium (pH ~5) in the presence of Xylenol Orange indicator. An acetate buffer solution was used to maintain constant pH. A standard (0.05 M) solution of Na_2EDTA served as a titrant. To an aliquot of the solution were added 5 ml of the buffer solution and 2 drops of a 0.1% solution of the indicator, and the mixture was titrated with a solution of Na_2EDTA until the coloration changed from pink to yellow. The analysis yielded a concentration of 0.1005 M, which is close to the preset value. The solution pH indicated a weakly acidic medium (4.55). The pH was measured with a pH-121 instrument with a glass working electrode and a silver chloride reference electrode.

To study the sorption, a 2.0000-g portion of the apatite obtained was placed in a beaker and the solution prepared was added. In order to prevent evaporation of water, the vessel was hermetically sealed with a polyethylene film. The sorption was studied under static conditions with intermittent (twice in 24 h) manual agitation at a temperature of about 20°C. It was noticed that the pH of the medium changed only slightly during sorption (to 4.99 for CaFAp and 5.15 for CaHAp by the end of the process). The concentration of Pb^{2+} ions in solutions brought in contact with the sorbents was determined in 24 and 72 h; the volume of the solution samples taken was 5.0 ml. According to chemical analysis data, the content of Pb^{2+} ions in solution after sorption on CaHAp is considerably lower than that after sorption on CaFAp (see table). The absolute value of sorption, Γ (mmol g^{-1}), was calculated by the formula

$$\Gamma = \frac{c_0V_0 - cV}{m_0},$$

where c_0 and c are the initial and running concentrations of Pb^{2+} ions in the solution (M); V_0 and V, initial and running volumes of the solution (ml); and m_0, initial mass of the sorbent (g).

These data were used to plot time dependences of the Pb^{2+} sorption on CaFAp and CaHAp (Fig. 1, curves *1a* and *1b*). It can be seen that the sorption equilibrium is not attained during the experiment.

To elucidate the mechanism of sorption of Pb^{2+} ions, the content of Ca^{2+} ions in the solutions under study was determined upon the completion of the process by a procedure similar to that for Pb^{2+}. This was done at pH > 10 after Pb^{2+} ions were precipitated with potassium iodide as PbI_2. An analysis demonstrated that a considerable amount of Ca^{2+} ions appeared in the solutions under study. This amount is not equivalent to the decrease in the content of Pb^{2+} ions in solution. For example, the concentration of Ca^{2+} ions is lower by a factor of 3.5 for CaFAp and by a factor of more than 5 for CaHAp, compared with the decrease in the concentration of Pb^{2+}. This fact indicates that the ion exchange plays an important, but not a key role in Pb^{2+} sorption from solution; it is inconsistent with the statement that the sorption process has an ion-exchange nature [5] and confirms the data obtained in [6]. The sorption products obtained were separated from the solutions by filtration and kept in an oven at 70°C to constant weight. A significant gain in the sorbent mass, Δm, due to sorption of Pb^{2+} is observed, with the value of Δm for CaHAp markedly exceeding that for CaFAp. A chemical analysis demonstrated that lead(II) is present in the sorption products, with its content being in satisfactory agreement with the mass gain of apatite samples and Γ values (see table).

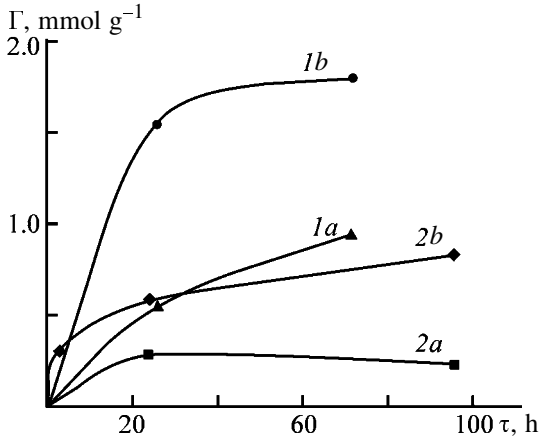

Fig. 1. Kinetic curves of sorption Γ of (*1*) Pb^{2+} and (*2*) Ca^{2+} ions on (*a*) CaFAp and (*b*) CaHAp. (τ) Time.

The products formed in sorption of Pb^{2+} ions by the apatites were studied, upon thorough drying, by XPA and diffuse reflection spectroscopy (DRS). The X-ray diffraction patterns of the starting sorbents significantly change after sorption (Figs. 2a, 2b). According to XPA data, the phases of the starting apatites undergo partial decomposition, with separate phases formed on the basis of PbFAp and PbHAp (see table). Presumably, this is due to the substantially larger radius of Pb^{2+} ions (0.126 nm), compared with Ca^{2+} ions (0.104 nm), which hinders incorporation of Pb^{2+} ions into the structure of the calcium apatite. In addition, strong absorption bands characteristic of Pb^{2+} compounds appear in the DRS spectra in the UV range (Fig. 3, curves *2a*, *2b*). It should be noted

Summary data on sorption of heavy metal ions on apatites

M^{2+}	Sorbent	$c_{M^{2+}}$ final	$c_{Ca^{2+}}$ in solution	Δm of sorbent, g (%)	Content of M^{2+} in sorbent, wt %	Phase composition of sorbent
		M				
Pb^{2+}	CaFAp	0.078	0.006	0.1384 (6.9)	9.0	$Ca_{10}(PO_4)_6F_2$, $Pb_{10}(PO_4)_6F_2$ (low)
	CaHAp	0.027	0.014	0.5358 (26.8)	26.4	$Ca_{10}(PO_4)_6(OH)_2$, $Pb_{10}(PO_4)_6(OH)_2$
Cu^{2+}	CaFAp	0.091	–	0.0382 (1.0)	0.9	$Cu_xCa_{10-x}(PO_4)_6F_2$*
	CaHAp	0.067	–	0.1067 (2.7)	4.4	$Cu_yCa_{10-y}(PO_4)_6(OH)_2$*

* $0 < x < 1$, $0 < y < 1$, $y > x$.

that the intensity of the absorption band for the product of Pb^{2+} sorption on CaHAp markedly exceeds that for the product of Pb^{2+} sorption on CaFAp, even though there is no complete correlation between the band intensities and Pb^{2+} contents of the sorption products.

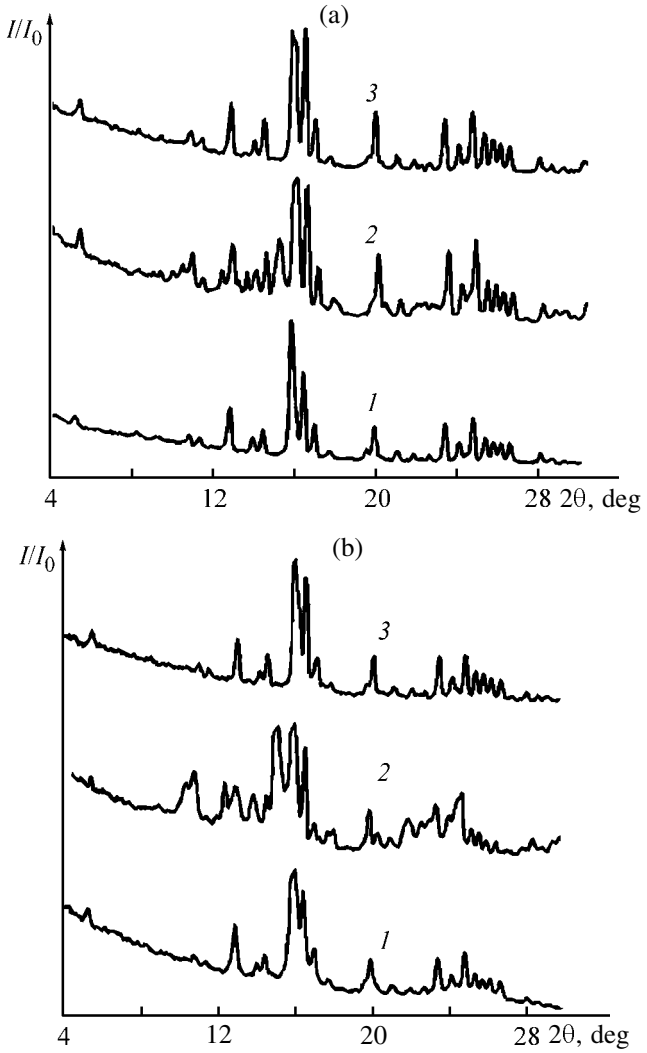

Fig. 2. X-ray diffraction patterns of (*1*) starting sorbent [(a) CaFAp and (b) CaHAp] and products of sorption of (*2*) Pb^{2+} and (*3*) Cu^{2+}. (I/I_0) Relative intensity and (2θ) Bragg angle.

Preliminary experiments demonstrated that Cu^{2+} ions are sorbed by the apatites to a lesser extent than Pb^{2+} ions. Therefore, 4.00-g portions of CaHAp and CaFAp powders were taken to study the sorption of Cu^{2+} ions. To the sorbents we added 100 ml of a 0.1 M $CuSO_4$ solution prepared by dissolving a weighed portion of $CuSO_4 \cdot 5H_2O$ in distilled water in a volumetric flask. The concentration of Cu^{2+} ions, $c_{Cu^{2+}}$, in the solutions was photometrically determined on an SF-26 spectrophotometer at a wavelength of 810 nm, which corresponds to the absorption maximum of $[Cu(H_2O)_4]^{2+}$ ions. According to chemical analysis data, the concentration of Cu^{2+} ions in a solution that was brought in contact with CaHAp is

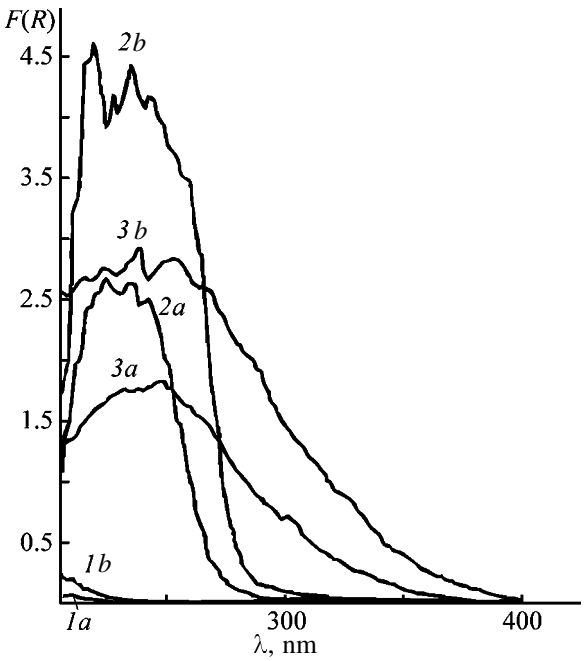

Fig. 3. Diffuse reflection spectra of (*1*) starting apatites and products of sorption of (*2*) Pb^{2+} and (*3*) Cu^{2+} ions on (*a*) CaFAp and (*b*) CaHAp in the UV range. [$F(R)$] Kubelka–Munk function and (λ) wavelength.

lower than $c_{Cu^{2+}}$ in a solution with CaFAp (see table). The concentrations of Cu^{2+} in solutions that were brought in contact with the sorbents were determined in 24 and 96 h.

The values of Cu^{2+} sorption were calculated by a formula similar to that presented above. Data on the sorption of Cu^{2+} ions from an aqueous solution on CaFAp and CaHAp are listed in the table, and the time dependences of Γ are shown in Fig. 1, curves *2a* and *2b*. This evidence indicates that the sorption on CaHAp is more effective, compared with that on CaFAp. On the whole, the sorption of Cu^{2+} on apatites is considerably weaker than that of Pb^{2+}. In addition, an interesting specific feature of Cu^{2+} sorption on CaFAp is that the saturation range is reached.

According to XPA, the sorption of Cu^{2+} ions does not change the phase composition of the starting apatites and only distorts their lattices. Figures 2a and 2b show that the X-ray diffraction pattern of the product of Cu^{2+} sorption on CaHAp is closely similar to that of the starting CaFAp and of the product of Cu^{2+} sorption on CaFAp. This fact can be explained as follows. The ionic radius of Cu^{2+} (0.080 nm) is markedly smaller than that of the Ca^{2+} ion (0.104 nm), and, therefore, partial substitution of Ca^{2+} by Cu^{2+} ions is possible in the structure of CaHAp. This should lead to contraction of its lattice, with its structure becoming more similar to that of CaFAp. Analogous distortions of the CaFAp structure upon sorption of Cu^{2+} ions must be less pronounced because of the considerably smaller value of sorption.

As in the case of Pb^{2+} sorption, strong but broadened absorption bands characteristic of Cu^{2+} compounds appear in the DRS curves of dried products of Cu^{2+} sorption on apatites in the UV range (Fig. 3, curves *3a* and *3b*). Their intensity qualitatively correlates with the content of Cu^{2+} in the products of sorption on the apatites, which is considerably (6–10 times) lower than that of Pb^{2+} (see table). The change in the mass of the sorbents upon sorption is also considerably smaller in the last case (see table). This is due, on the one hand, to the close atomic masses of Cu and Ca and, on the other hand, to the lower sorbability of Cu^{2+} ions, compared with Pb^{2+}. Presumably, the mechanism of Pb^{2+} sorption with disintegration of the structure of the starting sorbents is more effective than the mechanism of Cu^{2+} sorption via incorporation into the apatite structure. A similar conclusion was made in [7]. In addition, a certain role is presumably played by differences in the degrees of hydration of Pb^{2+} and Cu^{2+} ions. This parameter is considerably larger for Cu^{2+}, which also hinders sorption.

CONCLUSIONS

(1) It was found that sorption of Pb^{2+} ions on calcium fluoro- and hydroxylapatites leads to formation of separate phases based on lead apatites. In the case of sorption of Cu^{2+} ions on the apatites, the ions are incorporated into the structure of the apatites, with its subsequent distortion.

(2) It was demonstrated that the efficiency of sorption on the hydroxylapatite markedly exceeds that on the fluoroapatite. This makes it possible to recommend hydroxylapatite, including (and especially) that of natural origin, as a promising sorbent of ions of toxic heavy metals from aqueous media.

ACKNOWLEDGMENTS

The study was carried out in the framework of the Target Integrated Research Program of the National Academy of Sciences of Ukraine “Nanostructure Systems, Nanomaterials, Nanotechnologies.”

REFERENCES

1. *Inorganic Phosphate Materials*, Kanazawa, T., Ed., Tokyo: Kodansha, 1989.
2. Shpak, A.P., Karbovskii, V.L., and Trachevskii, V.V., *Apatity* (Apatites), Kiev: Akademperiodika, 2002.
3. Ukrainian Patent 69746A.
4. Ukrainian Patent 72729A.
5. McGrellis, S., Serafini, J.N., JeanJean, J., et al., *Sep. Purif. Technol.*, 2001, vol. 24, pp. 129–138.
6. Vysotskaya, E.V., Tarasevich, Yu.I., Klimova, G.M., and Kuz’menko, L.N., *Khim. Tekhnol. Vody*, 2002, vol. 24, no. 6, pp. 535–546.
7. Shashkova, I.L., Shul’ga, N.V., and Samuskevich, V.V., *Zh. Neorg. Khim.*, 1998, vol. 43, no. 1, pp. 52–57.

ISSN 1070-4272, Russian Journal of Applied Chemistry, 2007, Vol. 80, No. 3, pp. 376–378. © Pleiades Publishing, Ltd., 2007.
Original Russian Text © S.L. Alekseeva, S.N. Bolotin, T.G. Tsyupko, 2007, published in Zhurnal Prikladnoi Khimii, 2007, Vol. 80, No. 3, pp. 378–380.

SORPTION AND ION-EXCHANGE PROCESSES

Sorption of Chromium(VI) on Ion-Exchange Resins and Sorbents

S. L. Alekseeva, S. N. Bolotin, and T. G. Tsyupko

Kuban State University, Krasnodar, Russia

Received June 6, 2006; in final form, September 2006

Abstract—Sorption of Cr(VI) on AV-17 and EDE-10P anion exchangers, KU-2 and KB-4 cation exchangers, activated charcoal, and foamed graphite (STRG) is studied.

DOI: 10.1134/S107042720703007X

Transition metals are persistent cumulative pollutants of natural waters. Generally, they demonstrate a strong tendency to hydrolysis and complexation, forming products stable in water [1]. Among the most toxic pollutants are chromium compounds (natural Cr concentration in natural waters is relatively small, 0.1–0.6 $\mu g\ l^{-1}$) [1]. Technogenic Cr compounds can remain migrationally active in aquatic systems for a long time [2].

Treatment of natural and waste waters to remove Cr salts is complicated by its very complex redox chemistry and complexation with natural compounds [3]. It is often necessary to remove chromium in water pretreatment and also in analytical practice (in the stage of preconcentration of an analyte to eliminate the interfering effect of Cr). For these purposes, ion exchange is widely used. Therefore, optimization of ion-exchange procedure to remove Cr compounds, including decision on the ion-exchange resin and sorbent, is a topical problem.

Vishnevskaya et al. [4, 5] reported on the interaction of Cr(III) and Cr(VI) with the sites of various cation- and anion-exchange resins in the course of static sorption. It was concluded from the ESR spectra of the Cr-containing resins that, in these systems, the ion exchange is accompanied by redox reactions of Cr.

In this study we examined the mechanisms of ion exchange of Cr(III) and Cr(VI) on AV-17 and EDE-10P anion exchangers and KU-2 and KB-4 cation exchangers, and also of their sorption on activated charcoal and foamed graphite (STRG) in the dynamic mode (laminar flow mode).

In the experiments we used potassium dichromate solutions with Cr concentrations of 1.0, 1.5, and 2.0 $mg\ l^{-1}$ (pH 5.5 and 6.0). The experiments were conducted in the dynamic mode using the laminar flow mode. The solutions were passed through the columns at a velocity of 1 $cm\ min^{-1}$. The eluate was analyzed for Cr(III) and Cr(VI) photometrically using the standard procedure [2] based on the reaction of hexavalent chromium with diphenylcarbazide under acid conditions to form a red-violet compound containing Cr(III) and diphenylcarbazone. In this method, the Cr concentration should be within 0.01–1.0 $mg\ l^{-1}$, and dilution or preconcentration was used to adjust the Cr concentration to this range.

pH was measured on an EV-U4 ion meter with an ESL-63-07 glass electrode using an Ag/AgCl reference electrode.

The ESR spectra were recorded on a RADIOPAN SE/X 2543 instrument. The magnetic field was determined using a JTM-6 built-in NMR magnetometer. The samples after sorption were kept in air to constant weight.

Figure 1 shows the elution curves of Cr(VI) for anion exchangers AV-17 (Fig. 1a) and EDE-10P (Fig. 1b), and cation exchangers KU-2 (Fig. 1c) and KB-4 (Fig. 1d). In the former two cases, the shape of the curves is classical: initially the Cr(VI) concentration in the eluate is nearly zero, and then it increases to reach that in the starting solution.

AV-17 anion-exchange resin contains only one kind of sites (quarternary ammonium groups), whereas EDE-10P is a polyfunctional resin with the hydroxyl as a counterion. It may be suggested that, depending on pH, the dichromate is absorbed from the

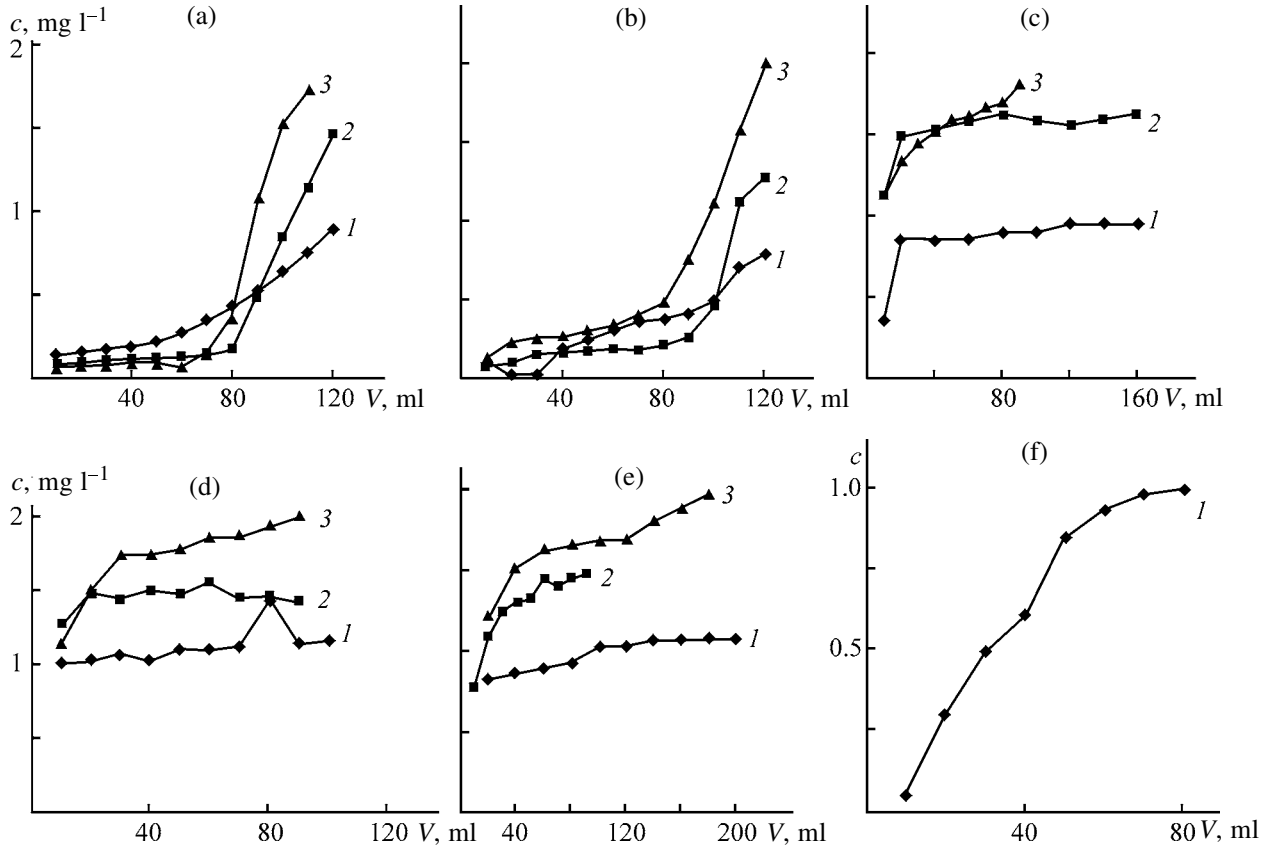

Fig. 1. Cr(VI) concentration c in the eluate. Initial $K_2Cr_2O_7$ concentration, mg l^{-1}: (*1*) 1.0, (*2*) 1.5, and (*3*) 2.0. Columns: (a) AV-17, (b) EDE-10P, (c) KU-2, (d) KB-4, (e) activated charcoal, and (f) STRG. (*V*) Eluate volume.

solution according to the following reactions:

$$2ROH + K_2Cr_2O_7 = R_2Cr_2O_7 + 2KOH,$$

$$4ROH + K_2Cr_2O_7 + H_2O = 2R_2CrO_4 + 2KOH.$$

This is supported by the fact that the dynamic exchange capacity is practically independent of the starting solution concentration.

At the same time, for these ion exchangers, we detected Cr(III) in the eluate, and its concentration increased with increasing concentration of the starting solutions. Evidently, in sorption of the dichromate ions from weakly acidic solutions, in the interfacial diffuse layer, Cr(VI) can be reduced to Cr(III) by the organic matter of the resin:

$$Cr_2O_7^{2-} + 14H^+ + 6e = 2Cr^{3+} + 7H_2O.$$

In studying the static sorption of potassium dichromate on an anion-exchange resin, Vishnevskaya et al. [4, 5] demonstrated the appearance of Cr(III) in the resin phase. Their thought is that the reduction of Cr(VI) can occur only in the resin phase. In this study we obtained similar results for the dynamic mode of sorption. The occurrence of Cr(III) in the eluate suggests that, after reduction of the adsorbed complex containing the dichromate ions, Cr(III) is partially eluted from the resin.

Figures 1c and 1d show that the sorption of the dichromate ions on the cation exchangers is not an ordinary process: After passing the potassium dichromate solution through the columns, we found Cr(III) in the eluate, which suggests that in this case Cr(VI) is reduced at the interface also.

Then chromium is sorbed on the cation exchanger in the form of Cr(III). As a result, the Cr(VI) concentration in the eluate decreases, and Cr(III) is detected in the eluate.

It is seen from the sorption curves of Cr(VI) on the anion exchangers that, after passing the starting solution, the Cr(VI) concentration abruptly decreases, suggesting absorption of Cr(VI). Then the Cr concentration in the eluate gradually increases to reach that in the initial solution, suggesting the ion-exchange mechanism of sorption.

To characterize the sorption mechanism, we studied the ESR spectra of the air-dry samples of KU-2, AV-17, activated charcoal, and STRG. The occurrence of the signal in the ESR spectrum of KU-2 suggests the presence of paramagnetic Cr(III), which confirms that, in this case, Cr(VI) is reduced to Cr(III) through Cr(V) intermediate.

In the cases of activated charcoal and STRG (Figs. 1e, 1f), Cr is absorbed without changing its oxidation state.

CONCLUSION

Chromium is absorbed on ion exchangers and sorbents by both the classical mechanism and a mechanism involving a redox reaction, which can occur in both the resin phase and solution.

REFERENCES

1. Linnik, N.P. and Nabivanets, G.N., *Formy migratsii metallov v presnykh poverkhnostnykh vodakh* (Mobile Forms of Metals in Fresh Surface Waters), Leningrad: Nauka, 1986.
2. Lavrukhina, A.K. and Yunina, L.V., *Analiticheskaya khimiya khroma, Ser. "Analiticheskaya khimiya elementov"* (Analytical Chemistry of Chromium, Ser.: Analytical Chemistry of Elements), Moscow: Nauka, 1979.
3. Gol'farb, A.S., *Udalenie metallov iz stochnykh vod* (Wastewater Treatment to Remove Metals), Moscow: Khimiya, 1980.
4. Vishnevskaya, G.P., Safin, R.I., and Frolova, E.N., *Zh. Fiz. Khim.*, 1996, vol. 70, no. 12, p. 2225.
5. Vishnevskaya, G.P., Safin, R.I., and Frolova, E.N., *Zh. Fiz. Khim.*, 1996, vol. 70, no. 12, p. 2203.

ISSN 1070-4272, Russian Journal of Applied Chemistry, 2007, Vol. 80, No. 3, pp. 379–385. © Pleiades Publishing, Ltd., 2007.
Original Russian Text © S.S. Stavitskaya, N.T. Kartel', N.N. Tsyba, M.F. Kovtun, T.P. Petrenko, 2007, published in Zhurnal Prikladnoi Khimii, 2007, Vol. 80, No. 3, pp. 381–387.

SORPTION AND ION-EXCHANGE PROCESSES

Mineral and Chemical Compositions and Structure–Sorption Properties of Bottom Sediments as the Basic Components of Enterosorbents and Application Materials

S. S. Stavitskaya, N. T. Kartel', N. N. Tsyba, M. F. Kovtun, and T. P. Petrenko

Institute of Sorption and Problems of Endoecology, National Academy of Sciences of Ukraine, Kiev, Ukraine

Received March 30, 2006; in final form, November 2006

Abstract—The mineral and chemical compositions, as well as some structure–sorption characteristics were determined for clay minerals selected for examination. The integrated coefficients of contamination of bottom sediments with each of the toxicant metals (Fe, Ni, Co, Cu, Zn, Pb, Mn) were calculated. The minerals examined presumably can be used in medicine as efficient application materials, cosmetic agents, and sorbents (enterosorbents).

DOI: 10.1134/S1070427207030081

The present environmental situation in many regions of Ukraine and other CIS countries is characterized by the occurrence of zones with enhanced contamination levels of toxic metals, in particular, radionuclides (RNs), which increases the number of environment-dependent diseases. Ever widening use in treatments and prevention of various diseases is found by sorption methods of detoxication [1–6], especially by the simplest method, enterosorption.

Enterosorbents are medical preparations of different structures, binding exo- and endogenic substances in the gastrointestinal tract (GIT) by adsorption, ion exchange, and complexing. The enterosorbents used either have a broad-action spectrum (combined enterosorbents) or exert selective action (selective enterosorbents), i.e., absorb toxicants, e.g., some RNs and heavy metals. In experts' opinion [6–14], combined enterosorbents are promising for solving the problem of body purification with simultaneous improvement of the basic biochemical parameters, i.e., normalization of the composition of the biological media.

Finding solutions to a wide range of problems of sorption therapy requires novel selective adsorption materials with polyfunctional ion-exchange sites. Such materials are prepared, e.g., from mechanical compositions made up of adsorbents principally differing in the nature, taken in strictly fixed proportions. For example, such compositions can include oxidized carbon [7, 8], a weakly acidic cation exchanger with a complexing function [15], and natural clay minerals exhibiting the properties of selective inorganic cation exchangers [9].

In our previous works [10, 11, 14] we showed that the properties of the initial components make a good combination in Ul'trasorb composite sorbent (earlier suggested for examination as a candidate medicinal substance of selective enterosorbents for treating diseases associated with accumulation of heavy metals and RNs in the body). This is evidenced by the corresponding distribution coefficients, which were estimated, e.g., at 30000 and over for radioactive cesium at the clay-to-carbon component ratio of 1 : 3.

Also, mention should be made of one of the developments of the Ukrainian sorption therapy, application sorbents, exhibiting unique properties in treatment of wounds and burns [6].

The underlying concept of this study is the use of mineral resources of the Black Sea (biologically active disperse minerals and other components of bottom sediments) as application materials, cosmetic agents, and enterosorbents for preparing medical formulations comprising a carbon component to treat GIT diseases and inflammatory processes in joints.

World practice of recent years suggests that the market of application medicinal materials, cosmetic agents, and enterosorbents based on natural biological complexes is steadily extending to include bottom sediments [16–20]. In this context, the use of raw materials of CIS countries for preparation of such

Table 1. Bottom sediments selected for examination

Sample no.	Material, source of sampling	Appearance
–	St. 24*	Aleurite silt with mussel biocenosis; light grey
–	St. 31	Grey clay; the color changes from light green to white on drying
–	St. 34	Low-limestone silt with a thin-layer structure
	Black Sea bottom:	
1	St. 5780, 2020 m	Homogeneous silt; quickly dries: dark grey
2	St. 5782, 2026 m	Homogeneous silt; quickly dries: dark grey
3	St. 5789, 2026 m	Homogeneous silt; quickly dries: dark grey
4	St. 5792, 2026 m	Homogeneous silt; quickly dries: dark grey
5	Bentonite B-B	Light-sand-colored
6	Bentonite B-G	Pink
7	Bentonite B-D	Light pink
8	Bentonite (Varvarovka)	Light brown
9	Bentonite B-3	Light pink
10	Bentonite 10-U	Dark brown
11	Salt-water liman, Dnepropetrovsk oblast	Dark grey silt; quickly dries at 100–120°C
12	Kuyal'nitskii liman, Odessa	Pastelike silt; slowly loses moisture on heating
13	Lake Velikoe, town of Berdyansk	Dark grey silt; quickly dries
	Black Sea bottom sediments:	
14	St. 4	Light-steel-colored silt
15	St. 20	Dark grey silt
16	St. 17	Dark grey silt
17	St. 18	Dark grey silt
18	St. 5795, 2026 m	Homogeneous silt; light grey; quickly dries; color gets lighter on drying

* St., sampling station; St. 24, St. 31, St. 34: Black Sea bottom sediments taken at different depths (~2000 m).

materials seems to be undoubtedly topical, promising, and environmentally attractive choice, as implementation of such a project can result in development of new, competitive, and efficient formulations based on inexpensive and readily available natural raw materials. This was the aim of our study.

The primary goal of the first stage was to select the objects for research and to examine the physicochemical, as well as the structure–sorption, properties of the preparations, making use of up-to-date methods of research.

The core material characterizing the bottom sediments from the northwest shelf of Crimea to the Caucasian shelf of Russia and Georgia was supplied by three expeditions organized in 2003–2005 with participation of staff members of the Research Institute of Geological Sciences, Ukraine. These samples were supplemented with those taken in different water bodies (lakes, limans of the Black Sea) and different regions of Ukraine. A total of 20 samples of silts of different origin and nature and bentonites taken at different depths, from 279 to 2026 m (Table 1), were examined. The bottom sediments from the Black Sea shelf are represented by clay–aleurite materials with quartz, feldspar, and other impurities. Out of eight samples of the core material, taken during the first expedition, we selected three samples: two samples of the Ukrainian origin, taken at station 24 from the Sevastopol beam and at station 31 from the town of Vilkovo beam, and, for comparison, a sample taken at station 34 from the Caucasian shelf (between Novorossiisk and Tuapse). Other materials were silts, bentonites differing in the appearance and color (pastelike, homogeneous, or having impurities, solid inclusions), differently behaving on drying as well: quickly or, on the contrary, slowly losing moisture at 100–120°C with a simultaneous change in color for some of the samples.

It is known that the pore structure characteristics allow predicting the performance of a sorbent under real conditions as part of a specific sorption technique. Therefore, we examined the structure–sorption characteristics of all the samples of the bottom sediments taken. Prior to measurements, the sorbents were dried in a desiccator at 100–120°C to constant weight and then thoroughly ground in an agate mortar. Based on the benzene vapor sorption, the sorption pore volume W_s, $cm^3\ g^{-1}$, was estimated by the desiccator method

Table 2. Results of examination of some physicochemical and adsorption characteristics of the bottom sediments*

Sample no.	B	Δ	Amount, %, of the sediment soluble in		A_{MB}, mg g^{-1}	$SiO_2 \cdot H_2O$ %	W_s, $cm^3\ g^{-1}$	S_{sp} for Ar, $m^2\ g^{-1}$	pH
	%		water	acid mixture					
St. 24	4.9	13.9	10.4	29.8	96	49.4	0.09	70	6.5
St. 31	2.5	12.0	16.3	34.2	95	61.4	0.08	68	7.2
St. 34	3.6	14.5	9.4	36.9	85	52.4	0.06	54	8.0
1	4.7	13.6	15.3	38.0	157	55.4	0.07	55	8.5
2	57.1	15.5	14.4	28.8	87	–	0.11	54	7.5
3	35.9	28.9	13.5	37.4	69	–	0.09	20	9.0
4	45.8	14.5	18.9	38.3	149	53.2	0.09	35	9.1
5	–	–	16.4	29.9	345	–	0.12	107	9.1
6	–	–	–	–	296	–	0.09	21	9.1
7	–	–	–	–	217	–	0.10	72	9.9
8	–	–	–	–	187	–	0.06	20	10.0
9	–	–	–	–	185	–	0.13	81	5.8
10	–	–	–	–	307	–	0.11	21	9.3
14	–	–	16.3	37.0	168	8.9	0.01	47	8.6
15	–	14.2	15.3	34.5	170	57.6	0.09	53	8.5
16	–	15.3	14.4	25.4	80	52.4	0.07	55	8.5
17	–	18.9	9.9	30.0	177	58.8	0.07	24	8.4

* B is the moisture content of the sample; Δ, mass loss on calcination; A_{Mb}, Methylene Blue adsorption; and pH, pH of the water extract.

[21]; based on adsorption of Methylene Blue (MB) with the molecular weight of 319 amu, the pores of the samples were qualitatively analyzed [22]. Gas-chromatographic method of thermal desorption of argon [22] was applied to tentatively estimate the specific surface area of the bottom sediments S_{sp}, $m^2\ g^{-1}$, for Ar.

Using a NOVA 2200 E high-speed gas sorption analyzer, the isotherms of low-temperature (77 K) nitrogen sorption–desorption by the samples were measured; the specific surface area was calculated by the BET method [22]; the curves of differential ($dV/d\log r$) and integrated (V) distribution of the micropore volume with respect to the pore radii were obtained; the micropore volumes were determined by various calculation methods (Multi Point, BET Plot, BJH, DFT) at the chosen correlation coefficient of 0.999.

The mass losses on drying and calcination [22, 23] were determined for the preparation; pH of a water extract was measured; substances soluble in water [23] and mixtures of acids, HCl (1 : 1) and concentrated HNO_3 and H_2SO_4, were determined. Also, for some samples the amount of silicic acid $SiO_2 \cdot nH_2O$ was determined by the method of fusing the samples with Na_2CO_3 in platinum crucibles in a muffle furnace at 900°C [21, 23].

Chemical analysis of the solutions upon boiling the bottom sediments in water and in an acid mixture and upon melting and extraction of silicate was carried out by the atomic-adsorption method on a KAS-120.1 instrument (Table 2).

Table 2 presents the moisture content of the bottom sediments examined, the calcination loss, the amount of the samples soluble in water and in an acid mixture, pH of the water extracts, Methylene Blue adsorption (A_{MB}), S_{sp} estimated for argon, and the amount of silicic acid in some of the preparations examined. The sample nos. in Table 1 are identical to those in the tables and figures that follow.

Tables 3 and 4 present the chemical analysis data for the bottom sediments upon boiling in water and treating with an acid mixture, and Table 5, the calculated integrated coefficients of contamination against the reference (for each element mentioned in the MPC standards [17]). Table 6 gives a classification of the grounds for the Azov–Black Sea basin within Ukraine and the Sea of Azov. According to these data, the sediments examined belong to class A (naturally clean ground, reference); sample no. 1 was assigned to class II (moderately contaminated ground) only because of the content of Pb^{2+}.

Bazelyan et al. [24] and Berlinskii et al. [25] summarized the data on the content of heavy metal toxicants in the bottom sediments from the objects of dredging works in the Azov–Black Sea basin and

Table 3. Chemical analysis data for the bottom sediments upon boiling in water

Sample no.	Amount of ions, mg g^{-1} (MPC, mg g^{-1})						
	Mn^{2+}	Fe^{3+}	Ni^{2+} (0.035)	Co^{2+} (0.02)	Cu^{2+} (0.03)	Zn^{2+} (0.06)	Pb^{2+} (0.01)
St. 24	0	0	0	0	0	0	–
St. 31	0	0	0	0	0	0	–
St. 34	0	0	0	0	0	0	–
1	0.36	Traces	0	0	0.01	0	0.19
2	–	″	0	0	Traces	0	0
3	0	0	0	0	0	0	–
4	–	Traces	Traces	0	0.004	0	0
11	–	″	0	0	0.026	0	0
12	–	″	Traces	0	0.006	0	0
13	–	″	″	0	0.007	0.0004	0

Table 4. Chemical analysis data for the bottom sediments upon boiling in an acid mixture

Sample no.	Amount of ions, mg g^{-1} (MPC, mg g^{-1})						
	Fe^{2+}	Ni^{2+} (0.035)	Co^{2+} (0.02)	Cu^{2+} (0.03)	Zn^{2+} (0.06)	Pb^{2+} (0.01)	Mn^{2+}
St. 24	35.2	0.07	0.0	0.0	0.12	–	0.29
St. 31	24.8	0.06	–	0.0	0.01	–	0.29
St. 34	31.4	0.07	0.0	0.0	0.1	–	0.28
1	5.52	0.080	0.060	0.080	0.290	0.45	0.36
2	3.21	0.110	0.021	0.023	0.104	0	–
3	2.48	0.060	0.040	0.000	0.240	–	0.20
4	2.85	0.092	0.027	0.032	0.062	0	–
5	2.65	0.110	0.000	0.025	0.160	Traces	–
6	7.20	0.160	0.000	0.020	0.190	″	–
7	7.55	0.150	0.000	0.020	0.190	″	–
8	5.60	0.080	0.000	0.000	0.260	″	–
9	5.87	0.170	0.000	0.040	0.180	″	–
10	7.80	Traces	0.000	0.040	0.230	″	–
11	2.87	0.057	0.020	0.029	0.070	0	–
12	2.99	0.068	0.017	0.013	0.057	0	–
13	2.78	0.083	0.030	0.430	0.220	0	–
14	11.30	0.320	0.000	0.060	0.220	0.05	–
15	9.62	0.220	0.000	0.070	0.230	0.04	–
16	10.42	0.300	0.000	0.020	0.190	0.03	–
17	9.40	0.350	0.000	0.040	0.260	Traces	–
18	3.01	0.071	0.021	0.032	0.045	0	–

determined the levels of contamination with various microelements for the waters of ports in the western part of the Black Sea (Ust'-Dunaisk, Il'ichevsk, Odessa, Yuzhnyi, etc.) and in other regions: Kerch, Novorossiisk, Batumi, Anapa, Tuapse, and Sea of Azov ports (Mariupol, Taganrog). Strakhov [26] characterized the general features of distribution of elements over the surface layer area of the Black Sea, taking into account the migration forms of the elements in the river basins and the hydrodynamic regime of the surface oxygen zone of the water mass (Fe, Mn, Ni, Co, Cu, As).

Based on the concept postulating the existence of toxic concentration of elements, rather than of toxic elements proper [27], we calculated the contamination coefficients K_c [24]. The highest toxic concentrations were revealed for lead, nickel, copper, zinc, and, in some cases, for mercury. The highest contamination levels [24] for the bottom sediments were detected in the ports of Odessa, Nikolaev, and Kerch. For exam-

ple, the K_c parameters varied from 0.01 to 10 for zinc, from 0 to 3.7 for nickel, from 0.4 to 10.0 for copper, and from 0.2 to 7.6 for cobalt [24].

In the samples examined (Table 5), the amount of the nickel ions is of the same order as that reported in [24], and for the remaining toxicant metals, 1.5–3 times lower.

Of primary importance for correctly choosing the adsorbent for a specific practical application are the data on its pore structure. Above all, it is necessary to know whether the pore radius distribution corresponds to the molecular sizes of the specific sorbates and whether such a distribution provides sufficient penetration of these substances inside the sorbent granules. Depending on the size, the sorbent pores are typically divided into macro-, meso-, and micropores [9, 15, 28]. Most often, researchers deal with adsorbents of mixed structural types. This applies to clay minerals. Vermiculite is assigned to finely porous sorbents whose pore size varies during adsorption due to increase in the interplanar spacings, e.g., in adsorption of polar substances (methanol, water) [9]. Palygorskite is distinguished by the presence of finely porous zeolite channels in its structure.

Complete analysis of the pore structure of sorbents typically includes examinations using a set of physical and physicochemical methods, optical and electron microscopy, X-ray diffraction analysis, adsorption methods, and mercury porosimetry [22].

The use of microporous sorbents is expedient for removal from biological liquids of products with a low molecular weight, e.g., creatinine, aliphatic hydroxy acids, amino acids, uric acid, etc. Fairly uniformly porous sorbents of this kind allow solving to some extent the problem of selectivity of sorption, as for large molecules (hormones, vitamins, polypeptides) micropores are inaccessible, which prevents their absorption in appreciable amounts. The main characteristic of the micropores is their volume V_{mi} (Table 7).

The most widely used for pore structure examination is the structure–sorption method [29] based on analyzing the relationships in adsorption from vapor (gas) phase, derived experimentally in the form of adsorption isotherms, i.e., the plots of the amount of the absorbed sorbates vs. their relative pressure P/P_0 at a constant temperature.

Table 7 and Figs. 1, 2a, and 2b present the results of examination of the structure–sorption properties of the bottom sediments on a high-speed gas sorption analyzer based on the nitrogen sorption at 77 K. Figure 1 shows the obtained isotherms of nitrogen adsorption–desorption A as plots of A vs. P/P_s, and Figs. 2a and 2b, the plots of the pore volume V, $cm^3\ g^{-1}$, vs. the pore radius in the differential ($dV/d\log r$) and integrated (V) forms, calculated by the Multi-Point BET Plot and BJH Desorption methods for one of the samples. Table 7 presents the nitrogen

Table 5. Integrated coefficients (ICs) of contamination against the reference

Sample no.	IC of contamination for indicated ions*				
	Ni^{2+}	Co^{2+}	Cu^{2+}	Zn^{2+}	Pb^{2+}
St. 24	2.0	0.0	0.0	2.00	–
St. 31	1.7	–	0.0	0.20	–
St. 34	2.0	0.0	0.0	1.67	–
1	1.5	3.60	3.30	–	–
2	3.1	1.05	0.77	1.70	0.0
3	1.7	0.00	–	–	–
4	2.6	1.35	1.00	1.00	0.0
5	3.1	0.83	0.83	2.70	0.0
6	4.6	0.66	0.66	3.20	0.0
7	4.3	0.66	0.66	3.20	0.0
8	2.3	0.00	0.00	4.30	0.0
9	4.8	1.33	1.30	3.00	0.0
10	Traces	1.33	1.30	3.83	0.0
11	1.6	1.00	0.97	1.30	0.0
12	1.9	0.85	0.43	0.95	0.0
13	2.4	1.15	1.40	2.00	0.0
14	9.1	2.00	2.00	3.83	5.0
15	6.3	2.33	2.33	3.80	4.0
16	8.6	0.66	0.66	3.20	3.0
17	10.0	1.33	1.30	4.00	0.0
18	2.0	1.05	1.00	0.75	0.0

* Contamination class A with respect to Cu^{2+}, Zn^{2+}, and Pb^{2+} (except sample no. 1: class II with respect to Pb^{2+}).

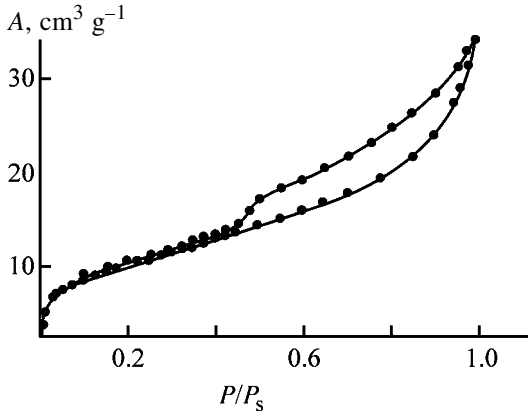

Fig. 1. Isotherms of nitrogen sorption–desorption A at 77 K for sample no. 11. (P/P_s) Ratio of the equilibrium to normal pressure of saturated gas.

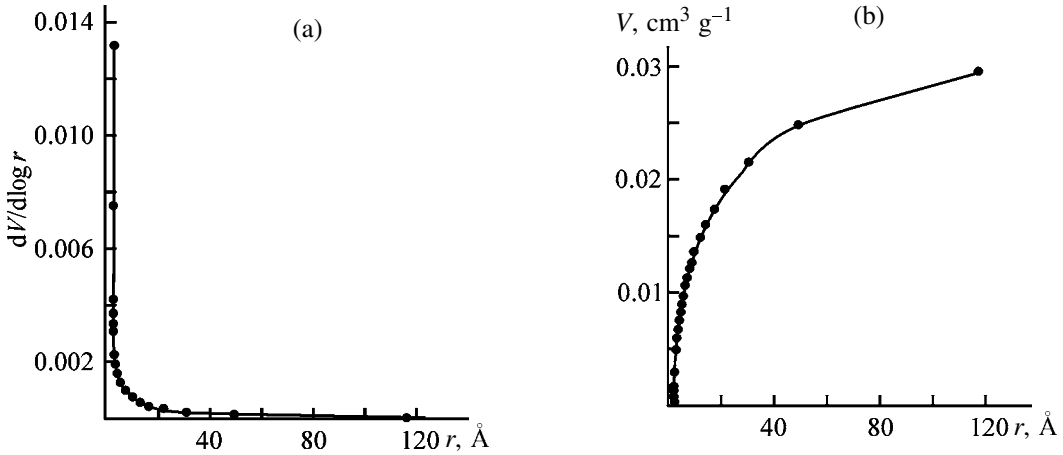

Fig. 2. Curves of (a) differential $dV/d\log r$ and (b) integrated distribution of the pore volume V over the pore radii r for sample no. 11.

Table 6. Classification of the grounds from objects of dredging works, depending on the contamination level*

Sample no.	Ingredient	Content, mg kg^{-1}, for indicated class**				
		A	I	II	III	IV
1	Cd^{2+}	<1.0	1–2	23	3–5	>5
2	Hg^{2+}	<0.1	0.1–0.2	0.2–0.3	0.3–0.5	>0.5
3	Pb^{2+}	<10	10–20	20–100	100–200	>200
4	Zn^{2+}	<60	60–80	80–150	150–400	>400
5	Cu^{2+}	<30	30–50	50–100	100–250	>250

* For the Azov–Black Sea basin within Ukraine.

** Ground, class: A, naturally clean; I, conditionally clean; II, moderately contaminated and contaminated; III, heavily contaminated; and IV, toxic.

Table 7. Structure–sorption characteristics of the bottom sediments examined

Sample no.	A,* cm^3 g^{-1}	S_{sp}, m^2 g^{-1}	V_{mi}, cm^3 g^{-1}	S_{mi}, m^2 g^{-1}	r, Å (BJH method)
St. 24	28	24	0.010	26.8	4; 6
St. 31	26	12.4	0.010	15.0	4; 6
St. 34	31	13.0	0.010	14.8	4; 7
1	48	47	0.012	28	4
2	42	44	0.003	38	20
3	26	12	0.001	12	4
4	64	7	0.001	6	4
11	60	53	0.002	49	18; 50
12	35	35	0.008	21	20
13	30	11	0.001	10	20; 70
14	37	37	0.005	27	20
15	52	43	0.005	34	20; 40
17	28	14	0.001	14	20

* A, nitrogen adsorption at 77 K.

adsorption at $P/P_s = 1$, obtained by these methods, as well as the specific surface area of the samples, the micropore surface area S_{mi}, the micropore volume V_{mi}, and the micropore radius r, determined from the pore radius distribution curves.

These data show that the samples chosen for examination are really microporous samples with a small pore radius varying from 4 to 70 Å, micropore volume of 1×10^{-3}–8×10^{-3} cm^3 g^{-1}, and the micropore surface area S_{mi} varying from 10 to 50 m^2 g^{-1}.

It should be noted that the medicinal effect of bottom sediments can be governed not only by their physicochemical parameters and chemical cleanliness but also by the complex effect exerted by all the components (biologically active components, minerals, and salts).

CONCLUSIONS

(1) Up-to-date methods were applied to examination of the physicochemical and structure–sorption

properties of bottom sediments of different origin. All the bottom sediments examined have a microporous structure with the pore radius varying from 4 to 70 Å and a specific surface area of 14–50 $m^2 g^{-1}$. Based on the contamination levels, the bottom sediments examined were assigned to class A (naturally clean ground).

(2) Analysis showed that the selected bottom sediments have the cleanliness required of enterosorbents.

REFERENCES

1. *Sorbents and Their Clinical Applications*, Giordano, C., Ed., New York: Academic, 1980.
2. *Enterosorbtsiya* (Enterosorption), Belyakov, N.V., Ed., Leningrad: TsST, 1991.
3. Dedenko, I.K., Starikov, A.V., and Strelko, V.V., *Efferentnye metody lecheniya luchevykh povrezhdenii* (Efferent Methods of Treatment of Radiation-Induced Damages), Kiev: Nora, 1996.
4. Andreichin, M.A. and Gnatyuk, M.S., *Enterosorbenty yak zasib ochyshchennya organizmu* (Enterosorbents as a Way to Clean a Body), Kiev: Znannya Ukrainy, 1992.
5. *Novye voloknistye sorbenty meditsinskogo naznacheniya* (New Fibrous Sorbents for Medical Applications), Ermolenko, I.N., Ed., Minsk: Nauka i Tekhnika, 1978.
6. Davydov, V.I., Stavitskaya, S.S., Strelko, V.V., and Kartel', N.T., Enterosorption: Current Status, Problems, and Application Prospects, *Preprint of the Inst. of Sorption and Problems of Endoecology*, Kiev: National Acad. Sci. of Urkraine, 1993, no. 93/03.
7. Stavitskaya, S.S., Petrenko, T.P., Gerasimenko, N.V., and Davydov, V.I., *Zh. Prikl. Khim.*, 1995, vol. 68, no. 11, pp. 1792–1797.
8. Stavitskaya S. and Davydov V., *Proc. 22nd Biennial Conf. on Carbon "Carbon-95,"* San Diego (the United States), 1995, pp. 536–537.
9. Tarasevich Yu.I. and Ovcharenko, F.D., *Adsorbtsiya na glinistykh mineralakh* (Adsorption on Clay Minerals), Kiev: Naukova Dumka, 1975.
10. Kartel', N.T., Stavitskaya, S.S., Vikarchuk, V.M., et al., *Teor. Eksp. Khim.*, 2000, vol. 36, no. 1, pp. 53–57.
11. Stavitskaya, S.S., Strelko, V.V., Vikarchuk, V.M., et al., *Efferentn. Terap.*, 2001, vol. 7, no. 1, pp. 60–63.
12. Strelko, V.V., Gerasimenko, N.V., Stavitskaya, S.S., et al., *Efferentn. Terap.*, 1999, vol. 5, no. 4, pp. 66–71.
13. Stavitskaya, S., Kartel, N., Vikarchuk, V., et al., *Proc. 24th Biennial Conf. on Carbon "Carbon-99,"* Charleston (the United States): Am. Chem. Soc., 1999, vol. 2, pp. 746–747.
14. Stavitskaya, S.S., Kartel', N.T., Kupchik, L.A., et al., *Efferentn. Terap.*, 2004, vol. 9, no. 4, pp. 66–69.
15. Tarkovskaya, I.A., *Okislennyi ugol'* (Oxidized Carbon), Kiev: Naukova Dumka, 1981.
16. Stelmach, S. and Sobolewski, A., *Inz. Ochr. Srod.*, 2002, vol. 5, no. 2, pp. 149–168.
17. Kondrasheva, A.N. and Bayanova, N.V., Abstracts of Papers, *2-ya Mezhdunarodnaya konferentsiya molodykh uchenykh Tomskogo politekhnicheskogo universiteta* (2nd Int. Conf. of Young Scientists of Tomsk Polytechnic Univ.), April 7–10, 1998, Tomsk: Izd. Nauhno-Tekh. Liter., 1998, part 2, pp. 145–146.
18. Ivanova, G.I. and Sverdlova, N.F., *Khim. Zhizn'*, 2000, no. 8, pp. 5–8.
19. Mel'nik, R.M., Lebovka, S.V., Pakhovchishin, S.V., and Ogenko, V.N., *Dopov. Nats. Akad. Nauk Ukr.*, 2003, no. 11, pp. 89–113.
20. Pakhovchishin, S.V., Prokopenko, V.A., Grishchenko, V.F., et al., Abstracts of Papers, *NANSIS 2004*, Kiev, October 12–14, 2004, p. 244.
21. *Analiz mineral'nogo syr'ya* (Analysis of Mineral Raw Materials), Knipovich, Yu.N. and Morachevskii, Yu.V., Eds., Leningrad: Goskhimizdat, 1959.
22. Kel'tsev, N.V., *Osnovy adsorbtsionnoi tekhniki* (Fundamentals of Adsorption Technique), Moscow: Khimiya, 1984.
23. *Derzhavna Farmakopeya Ukrainy* (State Pharmacopoeia of Ukraine), Kharkov, 2001.
24. Bazelyan, V.L., Kasilov, Yu.I., Kolomeichenko, G.Yu., and Ponomarev, L.P., in *Trudy konferentsii "Ekologichni problemy Chornogo morya"* (Proc. Conf. "Environmental Problems of the Black Sea"), Odessa: OTsNTEI, October 12–14, 2004, pp. 27–34.
25. Berlinskii, N.A., Bogatova, Yu.I., Bol'shakov, V.N., et al., in *Trudy konferentsii "Ekologichni problemy Chornogo morya"* (Proc. Conf. "Environmental Problems of the Black Sea"), Odessa, OTsNTEI, October 12–14, 2004, pp. 51–55.
26. Strakhov, N.M., *Geokhimicheskaya evolyutsiya Chernogo moray v golotsene: Litologiya i poleznye iskopaemye* (Geochemical Evolution of the Black Sea in the Holocene: Lithology and Mineral Resources), 1971, pp. 16–19.
27. Dobrovol'skii, V.V., *Geokhimiya mikroelementov: Global'nye rasseyaniya* (Geochemistry of Microelements: Global Dissipations), Moscow: Mysl', 1983.
28. Nikolaev, V.G. and Strelko, V.V., *Gemosorbtsiya na aktivirovannykh uglyakh* (Hemosorption on Activated Carbons), Kiev: Naukova Dumka, 1979.
29. Greg, S.J. and Sing K.S.W., *Adsorption, Surface Area, and Porosity*, London: Academic, 1982.

ISSN 1070-4272, Russian Journal of Applied Chemistry, 2007, Vol. 80, No. 3, pp. 386–388. © Pleiades Publishing, Ltd., 2007.
Original Russian Text © G.F. Myachina, E.N. Sukhomazova, S.A. Korzhova, I.V. Rodionova, E.N. Deryagina, 2007, published in Zhurnal Prikladnoi Khimii, 2007, Vol. 80, No. 3, pp. 388–390.

APPLIED ELECTROCHEMISTRY AND CORROSION PROTECTION OF METALS

Synthesis and Redox Activity of Sulfurized Poly(Methylene Polysulfides)

G. F. Myachina, E. N. Sukhomazova, S. A. Korzhova, I. V. Rodionova, and E. N. Deryagina

Favorskii Irkutsk Institute of Chemistry, Siberian Division, Russian Academy of Sciences, Irkutsk, Russia

Received September 13, 2006

Abstract—Redox-active sulfurized poly(methylene polysulfides) $-[CH_2S_y]_n-$ (y = 4–22) were prepared by deep sulfurization of poly(methylene di- and trisulfides) with elemental sulfur. The use of the substances obtained as an active cathode material of rechargeable lithium cells ensures their cycling with a specific discharge capacity of 418–550 mA h g^{-1}.

DOI: 10.1134/S1070427207030093

Sulfur-containing polymers exhibit high electrochemical activity and are promising materials for modern rechargeable chemical power sources [1–5]. Their electrochemical behavior is determined by the presence and number of redox-active S–S bonds in the structure of these polymers. It is well known that elemental sulfur can be inserted into S–S bonds of organic disulfides [6] and that this process is initiated by Lewis acids or bases.

Here we report on deep sulfurization of accessible poly(methylene di- and trisulfides) [7, 8] with elemental sulfur with the aim to prepare new redox-active sulfurized poly(methylene polysulfides).

EXPERIMENTAL

The starting poly(methylene di- and trisulfides) were prepared by procedures described previously [7, 8]. Their subsequent sulfurization was performed by heating with elemental sulfur at 125–135°C for 1.5 h. We examined the effect of a highly basic amine, diazabicyclooctane (dabco), of a cobalt salt, $CoCl_2 \cdot 6H_2O$, and of their combination on the sulfurization process and properties of the resulting poly(methylene polysulfides):

$$\left[-CH_2S_x-\right]_n \xrightarrow{S_8} \left[-CH_2S_y-\right]_n$$

x = 2, 3 nos. 1–8 y = 4–22

(y was determined by elemental analysis).

The polymers obtained (nos. 1–8) were washed with CS_2 to remove the soluble oligomers and unchanged sulfur and were vacuum-dried. The reaction conditions and characteristics of polymers are given in the table.

We found that, under the reaction conditions, elemental sulfur was actively inserted into the S–S bonds of the starting poly(methylene di- and trisulfides), which led to the formation of new polymers enriched in sulfur to 90–98%. The reaction performed without initiators yielded poly(methylene polysulfides) containing 92.10 and 95.48% S (nos. 1, 5). In the presence of dabco, the polymer yield increased by 2.9 (no. 2) and 4.3% (no. 6), and the sulfur content in the sample increased to 94.28 and 98.14%, respectively. Addition of the cobalt salt (both alone and in combination with dabco) led to a decrease in the sulfur content (sample nos. 3, 4, 7, 8; 90.06, 91.65, 94.04, and 93.34%, respectively).

The synthesized poly(methylene polysulfides) are insoluble light brown powders (nos. 1, 2, 4, 5, 6, 8) or viscous resins (nos. 3, 7). The wide melting interval of the samples is indicative of their wide molecular-mass distribution.

The IR spectra of the polymers (Specord IR-75 IFS 25 spectrometer, KBr pellets) contain absorption bands belonging to aliphatic CH_2 groups: 2922, 2855 (ν CH_2); 1511, 1457, 1361, 1176, 1027 cm^{-1} (δ CH_2); the band with a maximum at about 864 cm^{-1} is typical of the bending vibrations of aliphatic C–H groups [9], and the peaks at 776–705 cm^{-1} and narrow bands

Reaction conditions and characteristics of poly(methylene polysulfides). Reaction temperature 125–135°C, time 1.5 h

Polymer no.	$-[CH_2S_2]_n-$	$-[CH_2S_3]_n$	S	Additive, 0.02 g	Yield, %	Characteristics of poly(methylene polysulfide)	
	mol					mp, °C	S, %
1	0.013	None	0.1	None	42.4	75–90	92.10
2	0.013	None	0.1	dabco	45.3	72–87	94.28
3	0.013	None	0.1	$CoCl_2 \cdot 6H_2O$	29.2	52–60	90.06
4	0.013	None	0.1	dabco+ $CoCl_2 \cdot 6H_2O$	52.1	75–85	91.65
5	None	0.009	0.1	None	40.2	60–75	95.48
6	None	0.009	0.1	dabco	44.5	72–90	98.14
7	None	0.009	0.1	$CoCl_2 \cdot 6H_2O$	66.2	60–75	94.04
8	None	0.009	0.1	dabco+ $CoCl_2 \cdot 6H_2O$	43.3	75–85	93.34

at 466–490 cm^{-1} correspond to the stretching vibrations of the C–S and S–S bonds, respectively [9, 10].

When studying the redox activity of poly(methylene polysulfides), we used thin-layer two-electrode disk cells with a lithium anode and an aluminum cathode (1.5 cm^2) onto which a composition of a polymer, carbon, and poly(ethylene oxide) (50 : 35 : 15 wt %) was applied. Porous polypropylene was used as separator, and 1 M $(CF_3SO_2)_2NLi$ in 1,2-dimethoxyethane, as supporting electrolyte. Cyclic voltammograms were recorded at a potential sweeping rate of 1 mV s^{-1} in the potential range 1.25–3.00 V (vs. Li/Li^+) using a PI-50-1.1 potentiostat and a PDA-1 *XY*-recorder. The cell cycling was performed at a current density of 0.25 mA cm^{-2} in the voltage range 1.25–3.00 V on a testing and measuring bench for chemical power sources.

The cyclic voltammograms of the poly(methylene polysulfides) under consideration (a typical pattern is shown in Fig. 1) are indicative of a multistep redox process with maxima at 2.30, 2.10, and 1.96 V at cathodic polarization and at 2.46 and 2.54 V at anodic polarization; such a pattern is characteristic of elemental sulfur and polysulfides [11–13] and confirms the presence of S–S bonds in the polymers prepared.

The first step of the cathodic process at a potential of 2.30 V yields soluble lithium polysulfides; in the course of further potential sweeping, at 2.10 and 1.96 V, they are reduced to lithium methanepolythiolates and lithium sulfide, respectively:

$$[-CH_2S_y-] \xrightarrow[n\text{Partial reduction}]{(Li^0)} \underset{nx + nx' + mx'' = y_n}{n(LiS_xCH_2S_{x'}Li) + mLi_2S_{x''}}$$

$$\xrightarrow[\text{Complete reduction}]{(Li^0)} \underset{2n + m = y_n}{n(LiSCH_2SLi) + mLi_2S}.$$

However, the products formed are oxidized under anodic polarization (at 2.46 and 2.54 V) incompletely. A part of lithium methanepolythiolates and sulfide do not participate in further electrochemical reactions, which is manifested as a decrease in the amplitudes of the cathodic and anodic maxima in the cyclic voltammograms. Such redox behavior is characteristic of organic compounds containing polysulfide blocks [4, 5, 11–13] and is apparently caused by homooxidation of sulfide and polysulfide ions with the formation of poly(methylene polysulfide) of somewhat different structure and molecular weight, along with polymeric sulfur:

$$n(LiS_xCH_2S_{x'}Li) + mLi_2S_{x''} \xrightarrow{\text{Oxidation}} \underset{ny' + y'' = y_n}{[-CH_2S_{y'}-]_n + S_{y''}} + Li^0.$$

Cathodes based on the synthesized poly(methylene polysulfides) were cycled in lithium cells with a higher discharge capacity *Q* compared to the cathodes

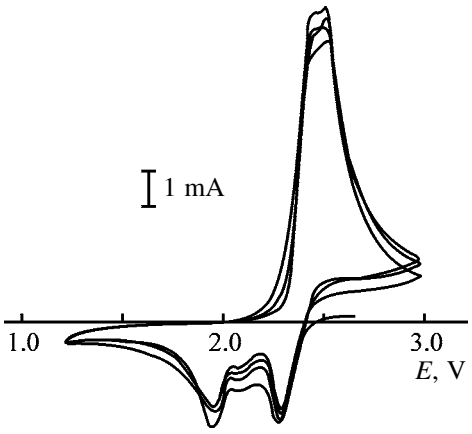

Fig. 1. Cyclic voltammogram of poly(methylene polysulfide) no. 6 (cycles 1–4). (*E*) Voltage (vs. Li/Li^+).

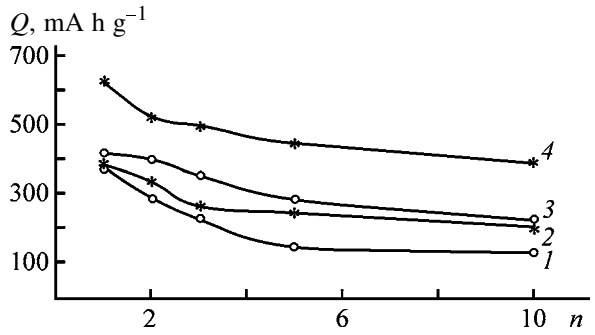

Fig. 2. Variation of the discharge capacity Q of cathodes based on (*1*) poly(methylene disulfide), (*2*) poly(methylene trisulfide), (*3*) poly(methylene polysulfide) no. 2, and (*4*) poly(methylene polysulfide) no. 6 in cycling in lithium cells. (n) Number of cycles.

based on the starting poly(methylene di- and trisulfides) (Fig. 2), which is indicative of a larger number of redox-active bonds in the structure of the polymers obtained. The specific discharge capacity correlates with the sulfur content in the samples.

CONCLUSION

High-sulfur poly(methylene polysulfides) (S content up to 98%) showing promise for the development of active cathode materials for modern lithium cells were prepared by deep sulfurization of poly(methylene di- and trisulfides).

REFERENCES

1. Novak, P., Miller, K., Santhanam, K.S.V., and Haas, O., *Chem. Rev.*, 1997, vol. 97, pp. 207–281.
2. Skotheim, T.A., Elsenbaumer, R.L., and Reynolds, J.R., *Handbook of Conducting Polymers*, New York: Dekker, 1998, p. 1097.
3. Fanghänel, E., Richter, A.M., and Kordts, B., *Proc. XIII Symp. on the Organic Chemistry of Sulfur*, Pedersen, C.D. and Becher, J., Eds., New York: Gordon and Breach, 1989, vol. 43, pp. 165–185.
4. Trofimov, B.A., Skotheim, T.A., Mal'kina, A.G., et al., *Izv. Ross. Akad. Nauk, Ser. Khim.*, 2000, no. 5, pp. 872–875.
5. Trofimov, B.A., Skotheim, T.A., Mal'kina, A.G., et al., *Izv. Ross. Akad. Nauk, Ser. Khim.*, 2001, no. 2, pp. 245–251.
6. *Organic Chemistry of Sulfur*, Oae, S., Ed., New York: Plenum, 1977.
7. Trofimov, B.A., Sukhomazova, E.N., Levanova, E.P., et al. *Sulfur Lett.*, 1999, vol. 23, pp. 99–109.
8. Deryagina, E.N., Russavskaya, N.V., Alekminskaya, O.V., et al., *Sulfur Lett.*, 1999, vol. 22, pp. 85–88.
9. Nakanishi, K., *Infrared Absorption Spectroscopy*, San Francisco: Holden-Day, 1962.
10. Bellamy, L.J., *The Infra-Red Spectra of Complex Molecules*, New York: Wiley, 1957.
11. Kolosnitsin, V.S., Karaseva, E.V., Amineva, N.A., and Batyrshina, G.A., *Elektrokhimiya*, 2002, vol. 38, no. 3, pp. 371–374.
12. Kolosnitsin, V.S., Karaseva, E.V., Shakirova, N.V., et al., *Elektrokhimiya*, 2002, vol. 38, no. 12, pp. 1501–1504.
13. Trofimov, B.A., Myachina, G.F., Korzhova, S.A., et al., *Elektrokhimiya*, 2002, vol. 38, no. 2, pp. 217–221.

ISSN 1070-4272, Russian Journal of Applied Chemistry, 2007, Vol. 80, No. 3, pp. 389–396. © Pleiades Publishing, Ltd., 2007.
Original Russian Text © V.V. Strelko, S.S. Stavitskaya, N.N. Tsyba, A.A. Lysenko, S.V. Zhuravskii, V.E. Goba, 2007, published in Zhurnal Prikladnoi Khimii, 2007, Vol. 80, No. 3, pp. 391–398.

CATALYSIS

Directed Modification of Carbons of Varied Origin and Chemical Nature of the Surface in Order to Control Their Catalytic Activity

V. V. Strelko, S. S. Stavitskaya, N. N. Tsyba, A. A. Lysenko, S. V. Zhuravskii, and V. E. Goba

Institute of Sorption and Endoecology Problems, National Academy of Sciences of Ukraine, Kiev, Ukraine

Received March 24, 2006; in final form, November 2006

Abstract—Simple methods were suggested and conditions were found under which modified carbon materials with varied chemical nature of the surface and controllable catalytic activity in the model reaction of hydrogen peroxide decomposition can be produced from various raw materials. The pore structure parameters of the carbons synthesized were determined, the kinetics of the reaction under study on these carbons was analyzed, and the possibility of synthesis of carbon catalysts with high catalytic activity exceeding that of the known active carbons was demonstrated.

DOI: 10.1134/S107042720703010X

The increasing role of adsorption (ion-exchange) and catalytic processes in various fields of technology and medicine predetermines the topicality of a search for new materials (e.g., based on carbon sorbents) with improved physicochemical and service characteristics and catalytic properties. Indeed, activated carbons widely used in medicine and technology [1–5] possess, as demonstrated by numerous studies [3–15], a broad spectrum of catalytic action and accelerate many redox and acid–base reactions. Recently, a number of reports have appeared [6–11] in which the knowledge of carbon materials as catalysts was substantially extended and the causes of their catalytic behavior were elucidated. A study of the influence exerted by a number of factors on particular catalytic processes has more than once been the subject of analysis by various scientists, including the authors of this study [7–9].

The following basic factors governing the catalytic properties of carbons should be named [9]: presence of surface functional groups (–COOH, –OH, $=NH_2$, $–SO_3H$, etc.) and their relative numbers, presence of heteroatoms in surface formations (N, P, S) and of metal ions substituting hydrogen ions in surface groups, structure of the carbon matrix, electrical conductivity of carbon materials, and structural-sorption characteristics of carbons.

The surface modification of carbons by introduction of heteroatoms, e.g., nitrogen, phosphorus, or sulfur, into their structure opens up new opportunities for synthesis and use of effective carbon-based catalysts.

It has been shown [3, 6–10] that nitrogen-containing carbons, such as synthetic carbons of the SKN brand, possess clearly pronounced catalytic properties owing to the high perfection and long extension of their graphite lattice containing nitrogen atoms [7, 12–15]. These factors diminish the electron work function of the lattice and raise the electron-donor power of the carbon, and, consequently, enhance its activity in catalytic reactions of the electronic type, e.g., in the model reaction of H_2O_2 decomposition and oxidation of cumene, *o*-xylene, H_2S, SO_2, creatinine, and amino acids [3, 7–15].

However, the knowledge of the properties of carbon materials (including those oxidized) suffers from considerable gaps and ambiguities, which should be eliminated for development of both scientific foundations of synthesis of a new class of cation-exchange resins and catalysts on carbon matrices and reproducible technologies for their manufacture and further rational use for practical purposes. For example, we are not aware of any systematic studies concerned with the influence exerted by the extent of oxidation of carbon materials and by relative amounts of various types of surface acid groups (SAGs) on the catalytic properties of carbons in redox reactions, as it has been done for numerous protolytic properties [3, 8]. Methods for directed control over the content of SAGs in

oxidized carbons in order to create catalysts with prescribed capacity for acceleration of numerous industrially important reactions of the electronic type have not been developed, either.

In this study, we attempted to reveal a general pattern of the influence exerted by the extent of oxidation of carbons on their catalytic activity and a relationship between the total static ion-exchange capacity (SEC), which characterizes the total amount of SAGs, and the catalytic activity in the model reaction of H_2O_2 decomposition, and also to elucidate what are these relationships, if they do exist, for carbons of varied nature and origin.

EXPERIMENTAL

We suggested an improved procedure for modification of the carbon surface with nitrogen atoms and used a method for control over the SAG content of carbon by high-temperature (~700°C) vacuum treatment of the carbon surface to remove, when necessary, surface acid compounds whose presence impairs the catalytic activity to some extent. It should be noted that vacuum treatment of activated carbons, with determining the composition of the gases being released in various temperature intervals, was studied as long ago as 1947 in [16]. At the same time, we carried out a systematic study and applied this technique to a set of samples of the same origin, varied surface nature, and different kinds of modification.

For this purpose, we chose natural carbons produced from KAU fruit kernels and synthetic carbons prepared from vinylpyridine (SKN) and phenol–formaldehyde resins (FF and FFK, with various extents of oxidation). The surface of the chosen carbons was oxidized to various extents in the liquid phase of 25% HNO_3, with boiling on a water bath for varied time [3]. The SAG content was evaluated in relation to the origin of a carbon and extent of its oxidation by the conventional method of SAG titration with a 0.1 N aqueous solution of NaOH [3].

The vacuum treatment was performed in a quartz reactor at 750°C for 1 h after the optimal temperature was attained; the heating rate of a weighed portion of a catalyst (commonly 10 cm^3) was 20 deg min^{-1}. After the vacuum treatment, the sample was cooled to room temperature and placed in a vessel with a ground-glass stopper in a desiccator. The residual pressure varied from 13 Pa at the beginning of the process to 133 Pa by the time when T = 750°C was attained and was maintained at this level for 1 h.

Carbons containing nitrogen chemically bound to the graphite-like lattice are commonly prepared by various methods: calcination of starting carbons in the presence of ammonia, dicyan, nitrogen oxides, and ammonium salts or carbonization of nitrogen-rich compounds, as in synthesis of SKN [2, 3, 14, 15, 17]. To prepare nitrogen-containing carbons, we developed and suggested our own improved procedure using melamine. The oxidized carbon was treated with melamine solutions with addition of acetic acid of a certain concentration, dried, and thermally treated in a flow of an inert gas at a high temperature. To obtain a nitrogen-containing sorbent with a varied amount of the modifying additive (commonly 3 to 5%), the concentration of the impregnating solution, treatment time, and melamine : carbon ratio were varied.

We studied the structural-sorption characteristics of the samples obtained [18]: total volume of sorption pores for benzene, W_s ($cm^3\ g^{-1}$); sorption activity with respect to Methylene Blue, A_{MB} (mg g^{-1}); anion-exchange capacity with respect to a 0.1 N aqueous solution of HCl. The method of low-temperature (77 K) adsorption of nitrogen on a Quantochrome NOVA 2200 E high-speed gas sorption analyzer was employed to determine the following parameters: total specific surface area of the carbons, S_{sp} ($m^2\ g^{-1}$); volume V_{mi} ($cm^3\ g^{-1}$) and surface area S_{mi} ($m^2\ g^{-1}$) of micropores; the pore radius distribution curves (Fig. 1) were used to find micropore radii r (Å). The parameters obtained are listed in Table 1.

The catalytic effect of the carbons synthesized was studied for the example of a model reaction of H_2O_2 decomposition. We used hydrogen peroxide of chemically pure grade; the concentration of H_2O_2 solutions was determined by permanganatometric titration [19]. Kinetic measurements (Figs. 2–5) were made in a temperature-controlled cell (T = 20°C) with agitation, which eliminated the outer-diffusion hindrance. The volume of the H_2O_2 solution was 25 ml in each experiment, and the weighed portion of a catalyst of the same granulometric composition (average grain size 0.25–0.5 mm) was 0.25 g. The concentration was found as a function of time by sampling at regular intervals.

Table 1 illustrates certain structural-sorption properties of the samples studied. It can be seen that, as the degree of oxidation increases, S_{sp} of the sorbents becomes smaller, with S_{mi}, V_{mi}, and A_{MB} simultaneously decreasing. The vacuum treatment of the samples leads to an increase in their specific surface area (compare, e.g., sample nos. 3 and 4, 6 and 7, 18 and

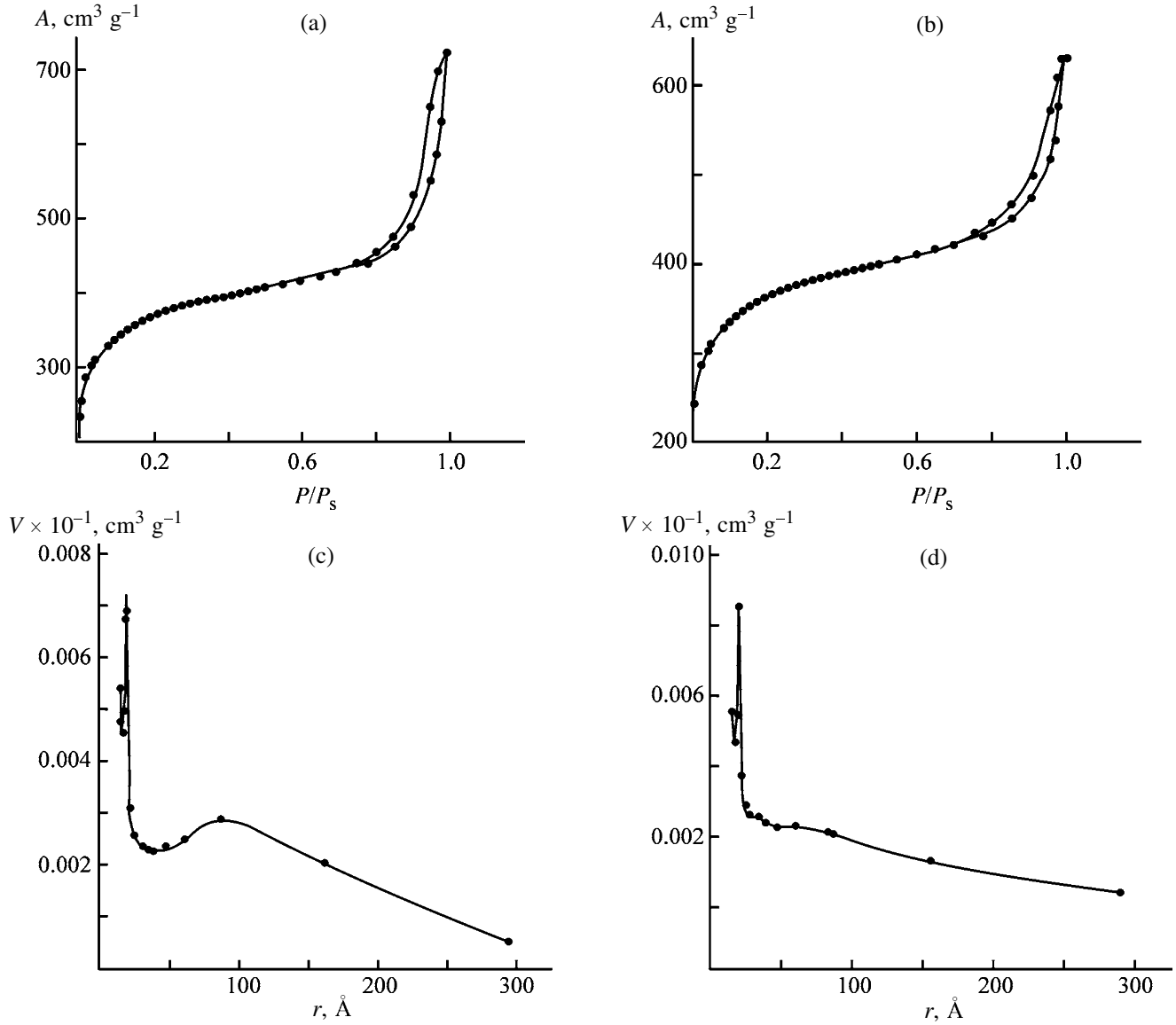

Fig. 1. (a, b) Isotherms of nitrogen sorption–desorption A and (c, d) curves of integral distribution of pore volume V with respect to pore radius r for various carbons. Carbon: (a, c) FF_{ox} (SEC = 1.72 mg-equiv g^{-1}), nitrogen-containing; (b, d) FF_{ox} (SEC = 1.72 mg-equiv g^{-1}), nitrogen-containing, vacuum-treated.

19). The sorption of N_2 from the gas phase is determined by V_{mi} and S_{sp}: 240–360 $cm^3\ g^{-1}$ for KAU carbons with smaller V_{mi} equal to 0.26–0.31 $cm^3\ g^{-1}$ and S_{sp} of 650–850 $m^2\ g^{-1}$ and a two- to threefold larger value (600–850 $cm^3\ g^{-1}$) for wider-porous carbons FF and SKN with V_{mi} of 0.49–0.63 $cm^3\ g^{-1}$ and S_{sp} of 1500–1690 $m^2\ g^{-1}$. These same carbons better sorbed Methylene Blue (260–300 mg g^{-1}; cf. A_{MB} of 80–118 mg g^{-1} for KAU carbon).

The study demonstrated that the catalytic activity of the samples synthesized is determined by the chemical nature of the carbon surface and, to a lesser extent, by the type of their pore structure (Figs. 2–5, Table 2), as, e.g., it was noted in [12, 20].

It has been found previously [3, 8, 12–15, 20–25] that the decomposition of H_2O_2 is substantially accelerated only in the presence of ordinary activated carbons positively charged in an aqueous solution. At the same time, oxidized carbons, which have a larger amount of SAGs on the surface and are negatively charged [3, 15], virtually do not catalyze this reaction.

The capacity for acceleration of the H_2O_2 decomposition increases with the number of basic groups (anion-exchange capacity), and H_2O_2 decomposes after exchange absorption of OOH^- ions, with OH^-

Table 1. Directed modification (oxidation to various extents, characterized by SEC; introduction of nitrogen atoms, vacuum treatment) of carbons of various origins

Sample no.	Sample, type of treatment	SEC, mg-equiv g^{-1}		W_s, $cm^3\ g^{-1}$	S_{sp}, $m^2\ g^{-1}$	S_{mi}, $m^2\ g^{-1}$	V_{mi}, $cm^3\ g^{-1}$	r, Å	Adsorption	
		for NaOH	for HCl						N_2, $cm^3\ g^{-1}$	MB, mg g^{-1}
1	KAU activated	–	0.5	–	1841	817	0.330	20		–
2	No. 1 + vacuum treatment	–	–	–						
3	KAU oxidized with HNO_3	0.60	0.2	0.40	809	710	0.299	20		118
4	No. 3 + vacuum treatment	0.00			850	750	0.300			
5	No. 3 + melamine				810	800	0.310			
6	KAU oxidized with HNO_3	1.60	0.1	0.40	781	626	0.260	20	280	85
7	No. 6 + vacuum treatment	0.20	–	–	997	770	0.314	20	360	
8	No. 6 + melamine								240	
9	No. 8 + vacuum treatment									
10	KAU oxidized with HNO_3	2.50	0.0		650	485	0.209		246	
11	No. 10 + vacuum treatment	0.10	–	–	672	579	0.239	20		81
12	FF activated, starting	0.12	0.7	0.85	1505	1196	0.488	20;150	840	309
13	FF + vacuum treatment				1511	1183	0.477	20;180	850	
14	FF oxidized with HNO_3	0.84	0.7	0.78	1470	1140	0.460			
15	No. 14 + vacuum treatment	0.00			1500	1190	0.485			
16	No. 14 + melamine				1490	1200	0.490			
17	No. 16 + vacuum treatment				1500	1200	0.490			
18	FF oxidized with HNO_3	1.72	0.5	0.79	1433	1069	0.429	20;180	740	218
19	No. 18 + vacuum treatment	0.10			1521	1128	0.455	20;100	680	
20	No. 18 + melamine				1368	1051	0.427	20;170	640	
21	No. 20 + vacuum treatment				1380	1011	0.408	20;170	720	
22	FF oxidized with HNO_3	3.00	0.4		1250	910	0.395			195
23	No. 22 + vacuum treatment	0.20			1300	950	0.401			141
24	No. 22 + melamine				1240	900	0.388			
25	No. 24 + vacuum treatment				1290	910	0.389			
26	SKN-M activated		1.0	0.91	1650	1466	0.633	20	640	
27	No. 26 + vacuum treatment				1690	1464	0.630			
28	SKN-M oxidized with HNO_3	0.80	0.8	0.89	1632	1464	0.633	20	600	
29	No. 28 + vacuum treatment				1650	1200	0.440			
30	No. 28 + melamine				1610	1190	0.485			
31	No. 30 + vacuum treatment				1640	1200	0.441			
32	SKN-M oxidized with HNO_3	1.40	0.7	0.78	1482	1290	0.566	20	560	
33	No. 32 + vacuum treatment	0.10			1460	1150	0.477			
34	No. 32 + melamine				1492	1170	0.470			
35	No. 34 + vacuum treatment				1430	1200	0.477			
36	FFK activated	0.20	0.60	0.48	–	–	–	–	–	–
37	FFK_{ox}-1	0.90	0.56	0.42	–	–	–	–	–	–
38	FFK_{ox}-2	1.50	0.56	0.46	–	–	–	–	–	–
39	FFK_{ox}-3	2.30	0.37	0.49	–	–	–	–	–	–

ions released into the solution [12, 20, 21]. The OOH^- anions in the surface layer have an increased oxidizing potential and can either undergo self-disintegration or oxidize a new H_2O_2 molecule to give oxygen and OH groups in the surface layer, with the result that the outer "plate" of the double layer of carbon takes on the original composition. The appearance of an excess of OH^- ions in the system is indicated [12, 20] by an increase in the pH value of the H_2O_2 solution in the course of H_2O_2 decomposition [12, 20], with the maximum pH shift observed on nitrogen-containing samples, and the minimum shift, on KAU carbon. In the course of several minutes, the H_2O_2 solution became alkaline (pH 8); on removing the carbon from

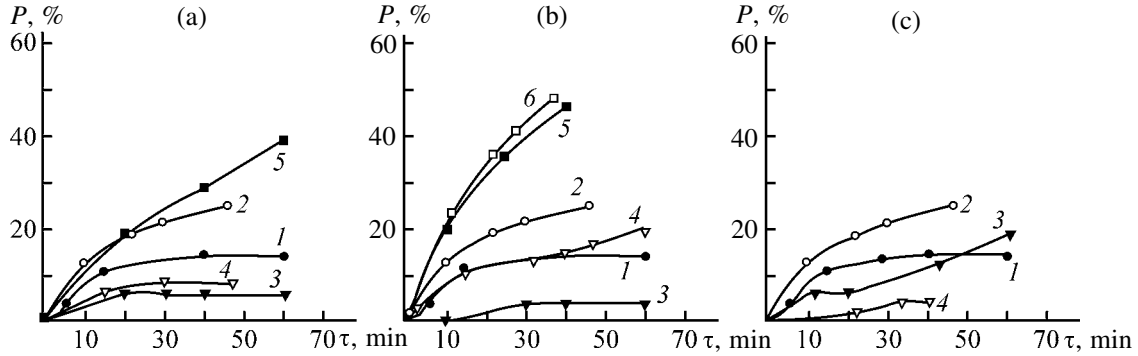

Fig. 2. Kinetics of decomposition of a 1% H_2O_2 solution on KAU carbons, (*1*) activated and (*2–6*) modified by various methods. (*P*) Degree of decomposition and (τ) time; the same for Figs. 3–5. Sample: (*2*) KAU, activated and vacuum-treated; (*3*) KAU_{ox}; (*4*) KAU_{ox}, vacuum-treated; (*5*) KAU_{ox}, melamine-treated; and (*6*) KAU_{ox}, melamine- and vacuum-treated. KAU_{ox}, SEC, mg-equiv g^{-1}: (a) 0.60, (b) 1.6, and (c) 2.5.

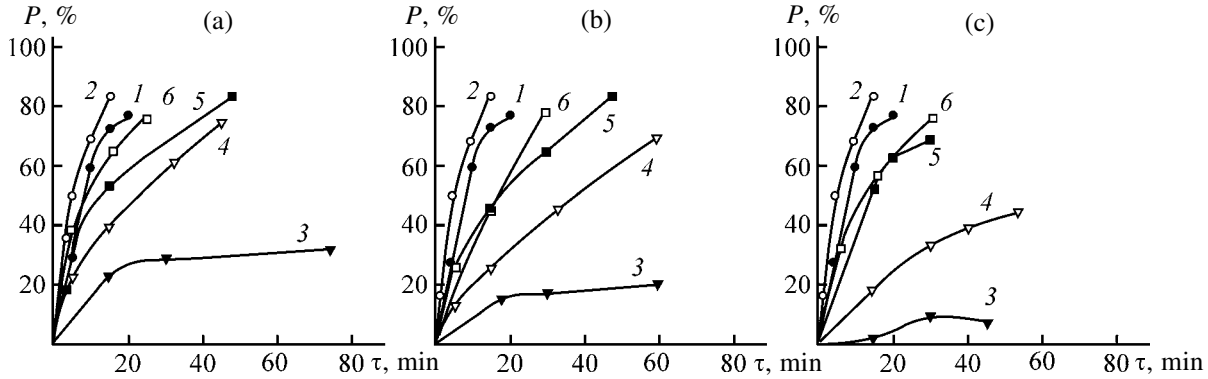

Fig. 3. Kinetics of decomposition of a 1% H_2O_2 solution on FF carbons, (*1*) activated and (*2–6*) modified by various methods. Sample: (*2*) FF, activated and vacuum-treated; (*3*) FF_{ox}; (*4*) FF_{ox}, vacuum-treated; (*5*) FF_{ox}, melamine-treated; and (*6*) FF_{ox}, melamine- and vacuum-treated. FF_{ox}, SEC, mg-equiv g^{-1}: (a) 0.84, (b) 1.72, and (c) 3.0.

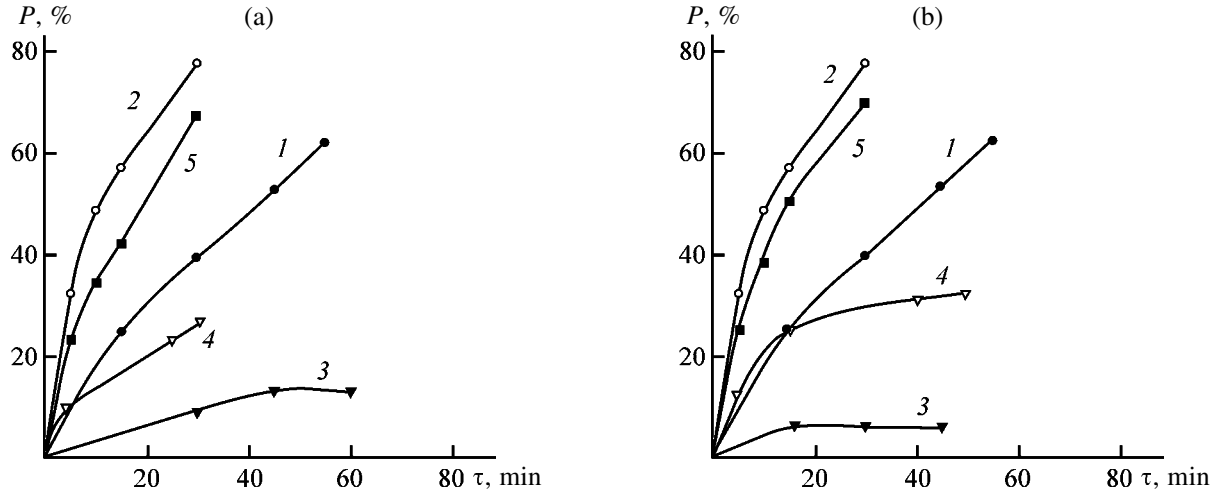

Fig. 4. Kinetics of decomposition of a 1% H_2O_2 solution on FFK carbons, (*1*) activated and (*2–5*) modified by various methods. Sample: (*2*) FFK, activated and vacuum-treated; (*3*) FFK_{ox}; (*4*) FFK_{ox}, vacuum-treated; and (*5*) FFK_{ox}, melamine-treated. FFK_{ox}, SEC, mg-equiv g^{-1}: (a) 0.88 and (b) 1.5.

the H_2O_2 solution, the pH value instantaneously became 3.5–4.0. By contrast, the presence of oxidized samples led to acidification of the solution being decomposed.

The presence of basic nitrogen atoms, which change the charge of carbons and raise the capacitance of the electrical double layer and the anion-exchange capacity, strongly affects the catalytic properties of

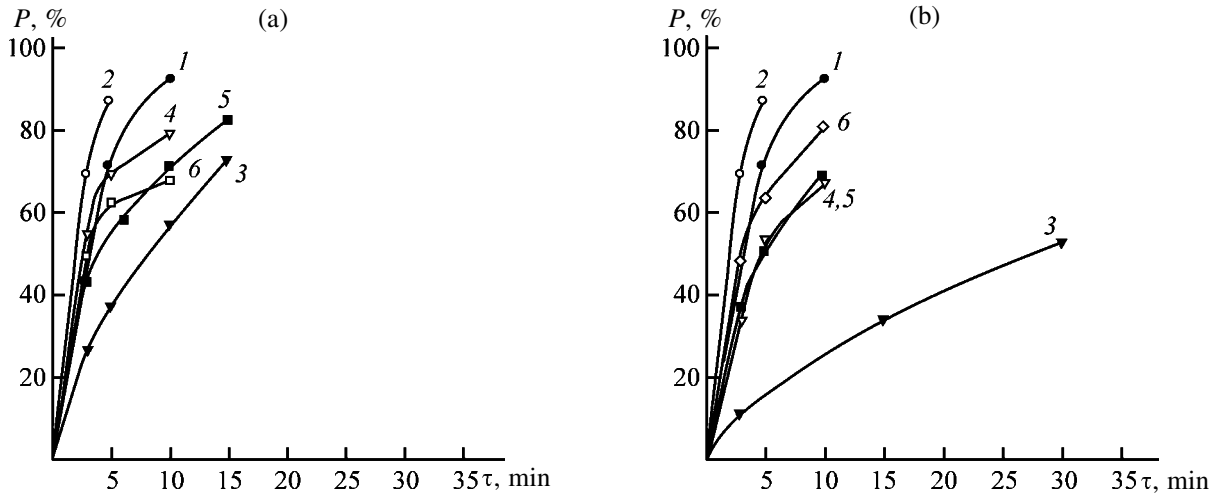

Fig. 5. Kinetics of decomposition of a 1% H_2O_2 solution on SKN-M carbons, (*1*) activated and (*2*–*6*) modified by various methods. Sample: (*2*) SKN-M, activated and vacuum-treated; (*3*) SKN-M_{ox}; (*4*) SKN-M_{ox}, vacuum-treated; (*5*) SKN-M_{ox}, melamine-treated; and (*6*) SKN-M_{ox}, melamine- and vacuum-treated. SKN-M_{ox}, SEC, mg-equiv g^{-1}: (a) 0.8 and (b) 1.4.

carbon materials. The catalytic activity of oxidized carbons is affected by their highly developed surface to a lesser extent. For example, KAU sample nos. 3 and 4 (Table 2) possess about the same sorption pore volumes (W_s = 0.3–0.4 $cm^3\ g^{-1}$) and S_{sp} = 800–900 $m^2\ g^{-1}$ as carbon nos. 24 and 25 (SKN). However, the former (KAU) decompose 6–8% of H_2O_2 in 40 min, whereas the degree of decomposition on nitrogen-containing SKN with similar pore structure parameters is 68–76% (Table 2).

As can be seen in Figs. 2–5, H_2O_2 decomposes slowly in the presence of oxidized KAU, FF, and FFK carbons. As the extent of oxidation (SEC) of the carbons increases, the degree of decomposition decreases. At the same time, activated samples of the same carbons exhibit a pronounced catalytic effect (compare Figs. 2–5, curves *1* and *3*). Vacuum treatment of oxidized samples leads to an increase in their catalytic activity. As follows from Table 1, this occurs because vacuum treatment of the carbon surface changes its chemical nature: for example, the capacity for 0.1 N NaOH decreases virtually to zero (sample nos. 4, 7, 11, 15, 20, 23, 29, 31), i.e., the number of acid functional groups decelerating the catalysis decreases dramatically, and the degree of H_2O_2 decomposition on such modified samples grows, compared to their oxidized modifications.

Introduction of nitrogen atoms leads to an even more effective decomposition of H_2O_2 (Figs. 2–5, curves *5*), with the nitrogen-containing SKN carbons decomposing H_2O_2 approximately four times more actively than do activated KAU carbons. For example, H_2O_2 decomposed to 90–95% in 5–10 min on an activated SKN sample (Fig. 5, curve *1*) and on the same, but vacuum-treated carbon (curve *2*).

It should be noted that the catalytic activity of the carbons formed from phenol–formaldehyde resin is high, compared to KAU carbons. The FFK sample activated at a lower temperature (Fig. 4) is somewhat worse than the activated carbon of the FF brand in decomposition of H_2O_2. Under identical conditions, the nitrogen-containing carbons of the SKN type exhibited a considerably higher catalytic activity, compared to the KAU and FF carbons.

The presence of nitrogen atoms in the surface layer also imparts catalytic activity to oxidized SKN carbons: in contrast to KAU_{ox} and FF_{ox}, a considerable, although less pronounced than that on SKN-M, decomposition of H_2O_2 is observed in the presence of SKN-M_{ox} (Fig. 5, curves *3*). The procedures used in the study to control the catalytic activity of carbons: directed vacuum treatment and treatment with a nitrogen-containing reagent (melamine) by the new method, favored synthesis of carbon catalysts whose catalytic activity approached, or even exceeded, that of the known catalysts with high catalytic properties, activated carbons (anion exchangers).

The knowledge of the causes of the catalytic action of carbon materials should favor proper choice of carbon sorbents with prescribed properties and enable control not only over their sorption properties, but over their catalytic transformations as well. Taking into account the basic factors that affect the course of catalytic processes involving carbons makes it poss-

Table 2. Catalytic activity of carbons of varied nature and origin (starting and modified by vacuum treatment, oxidation to various SEC values, and introduction of nitrogen atoms) in the decomposition of H_2O_2. m = 0.25 g, V = 25 ml, T = 20°C, average grain diameter 0.25–0.5 mm

Sample no.	Starting carbon	Treatment	H_2O_2 decomposition, %, in indicated time		SEC, mg-equiv g^{-1}, for 0.1 N NaOH
			10 min	40 min	
1	KAU activated			14.3	
2	KAU activated	Vacuum treatment		25.0	8
3	KAU oxidized with HNO_3	Oxidation		6.0	0.60
4	KAU oxidized with HNO_3	Vacuum treatment		8.3	
5	KAU oxidized with HNO_3	Melamine		29.2	
6	KAU oxidized with HNO_3	Oxidation		4.0	1.60
7	KAU oxidized with HNO_3	Vacuum treatment		14.6	
8	KAU oxidized with HNO_3	Melamine		33.3	
9	KAU oxidized with HNO_3	Melamine + vacuum treatment		48.2	
10	KAU oxidized with HNO_3	Oxidation		4.1	2.50
11	KAU oxidized with HNO_3	Vacuum treatment		12.5	
12	FF activated			78.0	
13	FF activated	Vacuum treatment	83.3		
14	FF activated	Oxidation		38.9	0.84
15	FF activated	Vacuum treatment		74.1	
16	FF activated	Melamine		83.0	
17	FF activated	Melamine + vacuum treatment		88.1	
18	FF activated	Oxidation		18.0	1.72
19	FF activated	Vacuum treatment		57.0	
20	FF activated	Melamine		71.3	
21	FF activated	Melamine + vacuum treatment		78.3	
22	FF oxidized	Oxidation		10.0	3.00
23	FF oxidized	Vacuum treatment		39.0	
24	FF oxidized	Melamine		68.5	
25	FF oxidized	Melamine + vacuum treatment		76.1	
26	FFK activated			50.0	0.20
27	FFK activated	Vacuum treatment		78.0	
28	FFK oxidized			13.2	0.88
29	FFK oxidized	Vacuum treatment		27.0	
30	FFK oxidized	Melamine		67.5	
31	FFK oxidized			5.8	1.50
32	FFK oxidized	Vacuum treatment		30.8	
33	FFK oxidized	Melamine		69.2	
34	FFK oxidized			6.9	2.32
35	FFK oxidized	Vacuum treatment		19.2	
36	SKN-M activated			92.4	
37	SKN-M activated	Vacuum treatment		97.0	
38	SKN-M oxidized	Oxidation		73.6	0.8
39	SKN-M oxidized	Vacuum treatment		79.2	
40	SKN-M oxidized	Melamine		83.0	
41	SKN-M oxidized	Melamine + vacuum treatment	90.0	92.0	
42	SKN-M oxidized	Oxidation	52.8		1.4
43	SKN-M oxidized	Vacuum treatment	67.9		
44	SKN-M oxidized	Melamine	69.8		
45	SKN-M oxidized	Melamine + vacuum treatment	81.1		

ible to modify these sorbents and thereby to determine the ways of varying and controlling the properties of carbon materials and obtaining technologically important materials with prescribed properties on the basis of these materials.

CONCLUSIONS

(1) Activated carbons of various origins, from synthetic and natural raw materials, were used to obtain their modifications oxidized to varied extent. The standard techniques were used to study some structural-sorption characteristics of the samples studied: specific surface area varying from 670 to 1800 $m^2 g^{-1}$, total volume of sorption pores, and size of micropores found in the carbon materials. The extent of oxidation varied from 0.2 to 3.0 mg-equiv g^{-1}.

(2) Simple methods were used to change the chemical nature of the surface of the samples synthesized: by raising or diminishing the number of surface acid groups via vacuum treatment of the surface and introduction of nitrogen atoms into the surface layer (3 to 5%).

(3) The possibility of controlling the catalytic activity of the carbon catalysts synthesized was shown for the example of the model reaction of the electronic type, decomposition of H_2O_2. The kinetic dependences obtained demonstrated that the catalytic effect of the carbons is not affected to any significant extent by pore structure parameters. At the same time, purposefully modified carbon materials can effectively decompose H_2O_2, with the degree of decomposition changing in a short time (5–10 min) from 6 to 95%.

REFERENCES

1. Mukhin, V.M., Tarasov, A.V., and Klushin, V.N., *Aktivnie ugli Rossii* (Activated Carbons of Russia), Tarasov, A.V., Ed., Moscow: Metallurgiya, 2000.
2. Nikolaev, V.G. and Strelko, V.V., *Gemosorbtsiya na aktivnykh uglyakh* (Hemosorption on Activated Carbons), Kiev: Naukova Dumka, 1979.
3. Tarkovskaya, I.A., *Okislennyi ugol'* (Oxidized Carbon), Kiev: Naukova Dumka, 1981.
4. Coughlin, R.W., *Ind. Eng. Chem. Prod. Res. Develop.*, 1969, vol. 8, no. 1, pp. 12–23.
5. Kalra, K.C., Katyal, P.J., and Sing, K.C., *J. Sci. Ind. Res.*, 1989, vol. 48, no. 4, pp. 186–192.
6. Strelko, V.V., Glukhovskii, P.V., and Kartel', N.T., *Ukr. Khim. Zh.*, 1994, vol. 60, no. 10, pp. 677–681.
7. Stavitskaya, S.S. and Strelko, V.V., *Teor. Eksp. Khim.*, 1995, vol. 31, no. 2, pp. 76–80.
8. Tarkovskaya, I.A. and Stavitskaya, S.S., *Ross. Khim. Zh.*, 1995, vol. 39, no. 6, pp. 44–51.
9. Stavitskaya, S.S., Tarkovskaya, I.A., and Petrenko, T.P., *Teor. Eksp. Khim.*, 1996, vol. 32, no. 6, pp. 336–344.
10. Stavitskaya, S.S., Tarkovskaya, I.A., Lukomskaya, A.Yu., and Luk'yanchuk, V.M., *Zh. Fiz. Khim.*, 1998, vol. 72, no. 10, pp. 1824–1829.
11. Tarkovskaya, I.A. and Stavitskaya, S.S., *Teor. Eksp. Khim.*, 1998, vol. 34, no. 1, pp. 47–52.
12. Strelko, V.V., Nemoshkalenko, V.V., Kartel', N.T., and Medvedev, S.L., *Adsorb. Adsorb.*, 1983, no. 11, pp. 76–80.
13. Shcherbitskii, A.B., Kartel', N.T., Mikhalovskii, S.V., et al., *Adsorb. Adsorb.*, 1983, no. 11, pp. 80–84.
14. Mikhalovskii, S.V., Butylin, Yu.P., and Strelko, V.V., *Teor. Eksp. Khim.*, 1989, vol. 25, no. 3, pp. 366–370.
15. Taranenko, E.N., Puzii, A.M., and Mikhalovskii, S.V., *Katal. Katal.*, 1990, no. 27, pp. 83–87.
16. Andersen, P.B. and Emmet, P.H., *Phys. Colloid Chem.*, 1947, vol. 51, no. 6, pp. 1308–1314.
17. Kuzin, I.A. and Loskutov, A.I., *Zh. Prikl. Khim.*, 1966, vol. 39, no. 1, pp. 100–104.
18. Kel'tsev, N.V., *Osnovy adsorbtsionnoi tekhniki* (Fundamentals of Adsorption Technology), Moscow: Khimiya, 1984.
19. Babko, A.K. and Pyatnitskii, I.V., *Kolichestvennyi analiz* (Quanitative Analysis), Moscow: Vysshaya Shkola, 1968.
20. Kartel', N.T., Carbon Hemosorbents Based on Synthetic Activated Carbons, *Doctoral Dissertation*, Kiev, 1988.
21. Schumb, W.C., Satterfield, Ch.N., and Wentworth, R.L., *Hydrogen Peroxide*, New York: Reinhold, 1955.
22. Shpota, G.P. and Tarkovskaya, I.A., *Katal. Katal.*, 1982, no. 20, pp. 69–72.
23. Strazhesko, D.N., *Adsorb. Adsorb.*, 1976, no. 4, pp. 3–14.
24. Tarkovskaya, I.A., Stavitskaya, S.S., and Petrenko, T.P., *Adsorb. Adsorb.*, 1979, no. 7, pp. 3–7.
25. Brinkmann, G., *Kolloid. Z.*, 1951, vol. 123, no. 2/3, pp. 116–129.

ISSN 1070-4272, Russian Journal of Applied Chemistry, 2007, Vol. 80, No. 3, pp. 397–404. © Pleiades Publishing, Ltd., 2007.
Original Russian Text © V.O. Yablonskii, 2007, published in Zhurnal Prikladnoi Khimii, 2007, Vol. 80, No. 3, pp. 399–404.

PROCESSES AND EQUIPMENT OF CHEMICAL INDUSTRY

Simulation of Suspension Separation by Two-Stage Pressure-Head Flotation in a Cylindrical Direct-Flow Hydrocyclone

V. O. Yablonskii

Volgograd State Technical University, Volgograd, Russia

Received February 13, 2006; in final form, August 2006

Abstract—A mathematical model of separation of suspensions with a non-Newtonian dispersion medium by two-stage pressure-head flotation in a cylindrical direct-flow hydrocyclone was developed. A system of differential equations describing convective diffusion and motion of a particle–bubble complex was solved numerically. The concentration field was modeled and integral separation parameters were determined.

DOI: 10.1134/S1070427207030111

Pressure-head flotation is used in chemical industry for separation and purification of inhomogeneous liquid systems in the field of centrifugal forces. The necessity for achieving a high recovery of the solid phase in a number of chemical technologies predetermines use of two-stage flotation with additional introduction of a dispersed gas for these purposes. The apparatus that ensures the highest efficiency of this process is direct-flow cylindrical hydrocyclone in which the separation occurs in the film mode and the condition of linkage between a particle and a gas bubble is provided [1].

In [1, 2], a procedure was suggested for calculating, by solving the equation describing the radial motion of the particle–bubble system, the separation parameters of a hydrocyclone-flotator and the diameter of the cylindrical part of the apparatus at which prescribed separation parameters and minimal investment and energy expenditure are provided. The condition for a stable floating-up of the particle–bubble system was derived and the diameter of solid phase particles that can be removed at given operation mode parameters of the hydrocyclone was determined.

It was noted in [3, 4] that the number of probable collisions of solid particles and gas bubbles depends on the centrifugal acceleration; it was shown that the centrifugal field is a factor that makes larger the number of collisions between particles and bubbles. It was found that the prevalent mechanism of formation of flotation complexes in pressure-head flotation is that by collisions of solid particles and gas bubbles. The efficiency of pressure-head flotation, dependent on the number of collisions, is governed by the distance traveled by a solid particle in the liquid dispersion medium.

Kutepov et al. [5] came to a conclusion that the best way is to deliver air into the feeding pipe of a hydrocyclone, instead of using pressure-head flotation methods. As a result, the particle–bubble interaction can start already at the inlet of the hydrocyclone and the apparatus design can be significantly simplified. However, they disregarded the fact that the kinetic constant of flotation increases because of the formation of gas bubbles directly on solid particles in the case of pressure-head flotation. Therefore, it seems appropriate, in order to improve the kinetic characteristics of the pressure-head flotation process and markedly raise the recovery of solid particles, to use two-stage flotation with supply of the secondary through porous walls of the hydrocyclone, which combines the advantages of both methods.

The two-stage flotation occurs as follows (Fig. 1): a preliminarily aerated suspension is delivered at an elevated pressure (up to 0.8 MPa) into a cylindrical direct-flow hydrocyclone, tangentially along the generatrix, via the inlet pipe *1* mounted in the upper part of the hydrocyclone case. The suspension fed into the hydrocyclone flows down, forming a spinning film, along its walls, and has the circumferential (V_φ), axial (V_h), and radial (V_r) velocity components. As the pressure is lowered to the atmospheric value, a supersaturation of the dissolved gas is created and the

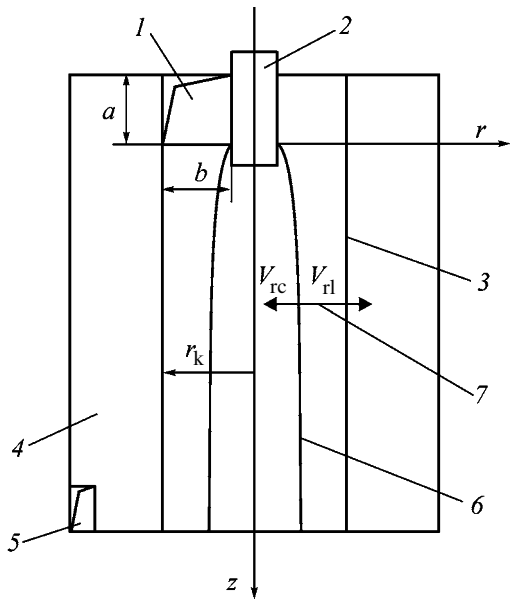

Fig. 1. Schematic of suspension separation by two-stage pressure-head flotation in a cylindrical hydrocyclone: (*1*) inlet pipe, (*2*) froth discharge pipe, (*3*) porous permeable wall of the hydrocyclone case, (*4*) gas supply collector, (*5*) pipe for gas delivery into the collector, (*6*) suspension film boundary, (*7*) particle–bubble complex.

suspension "boils up." Solid particles move under the action of the centrifugal force toward the wall of the hydrocyclone case, and gas bubbles driven by the buoyancy centripetal Archimedes force, in the opposite direction, toward the film surface. In the first stage of pressure-head flotation, flotation complexes are formed in collisions of solid particles with gas bubbles. These complexes carry the solid particles to the froth layer at the film surface, and this layer is removed via the froth discharge pipe *2*. Bubbles of the secondary gas are fed through the porous permeable wall *3* of the hydrocyclone case from the annular collector *4*. These bubbles, whose diameter exceeds by an order of magnitude that of gas bubbles formed in the suspension upon pressure drop, have a considerably higher velocity of floating-up to the film surface, compared with the complexes formed. In the second stage of flotation, secondary-gas bubbles collide with the floating-up complexes to form with them secondary complexes in which a particle is a bridge between gas bubbles [6]. These complexes rapidly move toward the film surface. The clarified suspension is removed from the apparatus via the bottom discharge pipe.

Owing to the high effective viscosity of non-Newtonian media, the flow in the cylindrical hydrocyclone occurs in the film mode [7], which provides a stable linkage in the particle–bubble complex because there is no steep increase in the circumferential velocity near the hydrocyclone axis. A mathematical model of the first stage of pressure-head flotation was considered in [8, 9].

The problem for the case of two-stage flotation is mathematically formulated under the following assumptions. Bubbles of the secondary gas delivered across the porous wall of the hydrocyclone case have a diameter an order of magnitude larger than that of gas bubbles formed in the first stage of pressure-head flotation. For this reason, the efficiency of collision of free solid particles with secondary-gas bubbles is low in accordance with the Sutherland formula [6] and can be neglected. In addition, the concentration of free solid particles rather rapidly decreases after the suspension enters the hydrocyclone. This occurs because of the formation of flotation complexes with gas bubbles formed in the first stage of flotation. Thus, it is reasonable to consider that secondary-gas bubbles, which float-up to the film surface at a higher velocity than complexes produced in the first stage, collide with the latter and remove them to the froth layer via formation of secondary complexes.

We assume that the solid phase of the suspension being separated, gas bubbles formed in the first stage of pressure-head flotation, particle–bubble complexes, and secondary-gas bubbles are all monodisperse. This will make it possible to achieve a prescribed recovery when simulating the separation by two-stage pressure-head flotation for the finest fraction of the solid phase.

For a film flow with a non-Newtonian dispersion medium having high effective viscosity, the flow mode is laminar and the mode of floating-up of gas bubbles and complexes is laminar, too [10].

The concentration field of solid particles bound into complexes in separation of suspensions with a non-Newtonian dispersion medium by two-stage pressure-head flotation in a cylindrical hydrocyclone is mathematically modeled using a differential equation describing convective diffusion in cylindrical coordinates. This equation can be written for solid particles and secondary-gas bubbles, with account of the inflow of particles, bound into complexes, via their formation in the first stage of pressure-head flotation and loss via formation of secondary complexes in the second stage, as follows:

$$\operatorname{div}(\bar{\mathbf{V}}_c c_{hc}) = j_{hc1} - j_{hc2},$$
$$\operatorname{div}(\bar{\mathbf{V}}_{g2} c_{g2}) = -j_{g2}, \quad (1)$$

where $\bar{\mathbf{V}}_c$ is the velocity vector of the complexes; $\bar{\mathbf{V}}_{g2}$,

velocity vector of secondary-gas bubbles; c_{hc}, volume fraction of solid particles bound into complexes ($m^3\ m^{-3}$); j_{hc1}, inflow of solid particles bound into complexes, formed in the first stage of flotation; j_{hc2}, loss of solid particles bound into complexes in the second stage of flotation; j_{g2}, loss of secondary-gas bubbles in the second stage of flotation.

The most widely occurring in the practice of hydrocyclone flotation is the case in which the volume fraction of secondary-gas bubbles in the suspension film markedly exceeds the volume fraction of solid particles bound into complexes, $c_{g2} > c_{hc}$, and it can be assumed that c_{g2} = const throughout the volume of the suspension film in the hydrocyclone. The volume fraction of gas bubbles formed in the suspension in the first stage of flotation also markedly exceeds the volume fraction of free solid particles, $c_{g1} > c_h$. In this case, the second equation in system (1) can be excluded and the system reduces to a single equation in which the loss of solid particles, bound into complexes, via flotation by secondary-gas bubbles, j_{hc2}, and their inflow from the first stage of flotation, j_{hc1}, have the form [6] similar to that in the kinetic equation of a first-order chemical reaction:

$$\bar{\mathbf{V}}_c \operatorname{grad} c_{hc} + c_{hc} \operatorname{div} \bar{\mathbf{V}}_c = A_1 c_h c_{g1} - A_2 c_{hc} c_{g2}, \quad (2)$$

where A_1 is the kinetic constant of the first stage of flotation (s^{-1}); A_2, kinetic constant of the second stage of flotation (s^{-1}); c_h, volume fraction of free solid particles ($m^3\ m^{-3}$); and c_{g1}, volume fraction of gas bubbles formed in the first stage of flotation ($m^3\ m^{-3}$).

We assume that complexes move in the axial direction without inertia, i.e., the axial velocities of the complexes and the dispersion medium are equal: $V_{zc} = V_{zl}$.

Because the radial velocities of the complexes and of the continuous flow of the dispersion medium are different, Eq. (2) takes, under the assumptions made, the following form:

$$V_{rc}(\partial c_{hc}/\partial r) + V_{zc}(\partial c_{hc}/\partial z) = -A_1 c_h c_g - c_{hc}\{A_2 c_{g2} + r^{-1}\partial[r(V_{rc} - V_{rl})]/\partial r\}, \quad (3)$$

where $V_{rc}(r, z)$ and $V_{zc}(r, z)$ are the radial and axial velocity components of a complex ($m\ s^{-1}$); $V_{rl}(r, z)$, radial velocity component of the dispersion medium ($m\ s^{-1}$); r and z, radial and axial coordinates (m).

Equation (3) was solved together with the motion equation of the particle–bubble complex.

We assume that the main mechanism by which secondary complexes are formed in the second stage of flotation, similarly to the case of single-stage pressure-head flotation, is collision of secondary-gas bubbles with complexes floating-up to the film surface. This mechanism is governed by dispersity characteristics and physical properties of phases.

Similarly to the assumptions made in [6], we believe that all collisions of secondary-gas bubbles with complexes are effective (produce secondary complexes) and the forming secondary complexes are not disintegrated in floating-up into the froth layer and do not fall down from this layer. With these assumptions, the stage of collision between secondary gas complexes and complexes predetermines the efficiency of two-stage pressure-head flotation under the conditions of a film flow of the suspension being separated in a cylindrical hydrocyclone. This is so because secondary-gas bubbles, which have an order of magnitude larger radius than bubbles formed in the first stage of pressure-head flotation, provide a considerably larger floating-up velocity of secondary complexes to the film surface. In the case of a single-stage pressure-head flotation, the rate-determining stage is that of transportation of complexes.

The kinetic constants of the first and second stages of flotation, A_1 and A_2, were found using a formula modified for the case of flotation in a field of centrifugal forces [11, 12]. This formula was derived on the basis of the fact that the probabilities of collision of solid particles with gas bubbles formed in the first stage of flotation and of secondary-gas bubbles with complexes are similar to the probabilities of molecule collisions in the molecular-kinetic theory of gases.

The inertia force acting on particle–bubble complexes and secondary-gas bubbles in the axial direction, gravity force, and buoyant Archimedes force were neglected by assuming that the axial velocities of the complexes and secondary-gas bubbles are equal to the axial velocity of the dispersion medium. This condition is well satisfied in practice because suspensions with a non-Newtonian dispersion medium having high effective viscosity are separated in hydrocyclones at large Froude numbers (separation factors). We assumed that complexes and secondary-gas bubbles move in the circumferential direction without inertia and their circumferential velocities are equal to the circumferential velocity of the dispersion medium.

When developing a model of the two-stage pressure-head flotation in a hydrocyclone, it is necessary to take into account the inertia forces acting on the particle–bubble complex in the radial direction. These

forces are important in the case of flotation of coarse particles in the field of centrifugal forces and at a significant difference in density between solid particles and the dispersion medium.

The radial velocity of the complex, V_{rc}, was found by solving a differential equation of motion, which has the following form, provided that the complex experiences the action of the centrifugal inertia force, buoyant centripetal Archimedes force, and resistance force in the radial direction:

$$V_{rc}(\partial V_{hc}/\partial r) + V_{zc}(\partial V_{rc}/\partial z) = V_{\varphi c}^2/r\left[1 - \frac{\rho(d_h^3/d_{g1}^2 + d_{g1})}{\rho_h d_h^3/d_{g1}^2 + \rho_g d_{g1}}\right] - \frac{3}{4}\frac{K_{fr}\rho(V_{rc} - V_{rl})\left|V_{rc} - V_{rl}\right|}{(\rho_h d_h^3/d_{g1}^2 + \rho_g d_{g1})\Phi(c_c)}, \quad (4)$$

where $V_{rc}(r, z)$ and $V_{zc}(r, z)$ are the radial and axial velocities of the particle–bubble complex (m s^{-1}); d_h, diameter of solid particles (m); d_{g1}, diameter of gas bubbles formed in the first stage of pressure-head flotation (m); K_{fr}, resistance coefficient for motion of the complex in the radial direction; and $\Phi(c_c)$, correction coefficient taking into account the hindrance to motion of complexes, found using the Brenner formula [2] in relation to the volume fraction c_c of complexes in the suspension.

Taking into account the orientation of the particle–bubble complex in its floating-up to the film surface, we took as the characteristic size d_c of the complex the diameter d_{g1} of gas bubbles formed in the suspension in the first stage of pressure-head flotation because d_{g1} markedly exceeds the diameter of solid particles. On making this assumption, the resistance force acting on a solid particle bound into a complex can be disregarded and the resistance coefficient K_{fr} in radial motion of a complex in the non-Newtonian liquid can be calculated for the characteristic size d_c of complex using an empirical formula from [13].

If the method of characteristics [14] is used, the system of partial differential equations (3), (4) reduces to an equivalent system of ordinary differential equations, which can be represented in the dimensionless form as

$$\begin{cases} dR/dZ = G_c/H_c, \\ dC_{hc}/dZ = -\dfrac{C_{hc}}{H_c}[d(G_c - G_l)/dR + (G_c - G_l)/R + F_{g2}] + C_h F_{gl}/H_c, \\ dG_c/dZ = \dfrac{\Theta_c^2}{H_c R}(1 - P) - \dfrac{3}{4}\dfrac{K_{fr}P(G_c - G_l)\left|G_c - C_l\right|}{(D_h^3/D_{g1}^2 + D_{g1})\Phi(c_c)}, \end{cases} \quad (5)$$

where $G_c(R,Z) = V_{rc}(r, z)/U_0$, $H_c(R,Z) = V_{zc}(r, z)/U_0$, $\Theta_c(R,Z) = V_{\varphi c}(r, z)/U_0$ are the dimensionless radial, axial, and circumferential velocities of the complex; $G_c(R,Z) = V_{rl}(r, z)/U_0$, dimensionless radial velocity of the dispersion medium; $F_{g1} = A_1 C_{g1} r_k/U_0$, dimensionless number characterizing the rate of the first stage of pressure-head flotation; $F_{g2} = A_2 C_{g2} r_k/U_0$, dimensionless number characterizing the rate of the second stage of pressure-head flotation; $C_h = c_h/c_{h0}$, dimensionless volume fraction of free solid particles; $C_{hc} = c_{hc}/c_{h0}$, dimensionless volume fraction of solid particles bound into complexes; $C_{g1} = c_{g1}/c_{h0}$, dimensionless fraction of gas bubbles formed in the suspension; $C_{g2} = c_{g2}/c_{h0}$, dimensionless volume fraction of bubbles of the gas fed through the porous wall of the hydrocyclone; $P = \rho(d_h^3/d_{g1}^2 + d_{g1})/[\rho_h(d_h^3/d_{g1}^2) + \rho_g d_{g1}]$, density parameter; $D_h = d_h/r_k$, dimensionless diameter of gas bubbles formed in the first stage of pressure-head flotation; $R = r/r_k$, $Z = z/r_k$, dimensionless radial and axial coordinates; r_k, radius of the hydrocyclone case (m); c_{h0}, initial volume fraction of free solid particles in the inlet pipe of the hydrocyclone (m^3 m^{-3}); $U_0 = q/(ab)$, average suspension velocity in the inlet pipe of the hydrocyclone (m s^{-1}); q, flow rate of the suspension (m^3 s^{-1}); and a, b, height and width of the inlet pipe of the hydrocyclone (m).

The boundary condition for the system of ordinary differential equations (5) has the form

$$Z = 0,\ 1 - B \le R \le 1,\ C_{hc0} = 0, \quad (6)$$

where $C_{hc0} = c_{hc0}/c_{h0}$ is the dimensionless volume fraction of solid particles bound into complexes in the inlet pipe of the hydrocyclone; c_{hc0}, volume fraction of solid particles bound into complexes in the pipe of the hydrocyclone (m^3 m^{-3}); and $B = b/r_k$, dimensionless width of the inlet pipe of the hydrocyclone.

The system of ordinary differential equations (5) with the boundary condition (6) was solved by the fourth-order Runge–Kutta method with fixed step. The simulation of the process of two-stage pressure-head flotation consisted in numerical solution of the system of differential equations (5) with the boundary condition (6), with approximation of the results obtained in modeling of the concentration field of free solid particles in the first stage of pressure-head flotation [8, 9] and of distributions of the velocities of the dispersion medium [15]. The simulation was performed for various values of the determining similarity criteria and for the rheological properties of the dispersion medium widely varying in the range corresponding to real rheological properties of media

separated in chemical industry and to operation modes of separating apparatus.

The flow of a non-Newtonian liquid in a hydrocyclone is characterized [7] by the centrifugal Froude number (separation factor) $\mathrm{Fr} = U_0^2/(g\,r_\mathrm{k})$, modified Reynolds number $\mathrm{Re}_n = (\rho_1 U_0^{2-n} r_k^n)/k$, and dimensionless flow rate $Q = q/(\pi r_\mathrm{k}^2 U_0) = (ab)/(\pi r_\mathrm{k}^2)$. The rheological properties of the liquid are described by the nonlinearity index n of the flow curve and the consistency factor k (Pa s^n).

To evaluate the influence exerted by the determining similarity numbers and rheological properties of the liquid on the efficiency of suspension separation by two-stage pressure-head flotation, it is necessary to use integral characteristics of the apparatus, the most important of which is the integral-average dimensionless volume fraction of solid particles that are bound into complexes and remain in the suspension in a given cross section of the film. This fraction is calculated by the formula

$$\bar{C} = \int_{1-\Delta(Z)}^{1} C_\mathrm{hc} H(R,Z)\,R\mathrm{d}R \Big/ \int_{1-B}^{1} C_{\mathrm{h}0} H_0(R,Z)\,\mathrm{d}R, \qquad (7)$$

where $\Delta(Z) = [\delta(z)]/r_\mathrm{k}$ is the dimensionless thickness of the suspension film and $\delta(z)$ is the suspension film thickness (m). To obtain operation characteristics of the hydrocyclone, the integral-average dimensionless volume fraction of solid particles bound into complexes was found in the outlet cross section of the apparatus. The results obtained in numerical simulation are presented in Figs. 2–5.

Figure 2 shows trajectories of complexes in the suspension film (Fug. 2a) and distributions of the dimensionless volume fraction of solid particles bound into complexes on the corresponding trajectories (Fig. 2b) for Fr = 73.4, $\mathrm{Re}_n = 4 \times 10^3$, $Q = 0.04$, and $n = 0.6$ in separation of a suspension with a pronounced anomaly of the non-Newtonian properties of the dispersion medium. Analysis of Fig. 2a shows that the trajectories originating at a certain distance from the wall emerge at the film surface under the action of the buoyant centripetal Archimedes wall, but trajectories 3 and 4 have portions in which a complex approaches the wall because of the radial velocity of the dispersion medium. The trajectories originating near the wall, where the centripetal Archimedes force is weak, come to the wall under the action of the radial velocity of the dispersion medium. Thus, instead of emerging to the froth layer, a part of solid

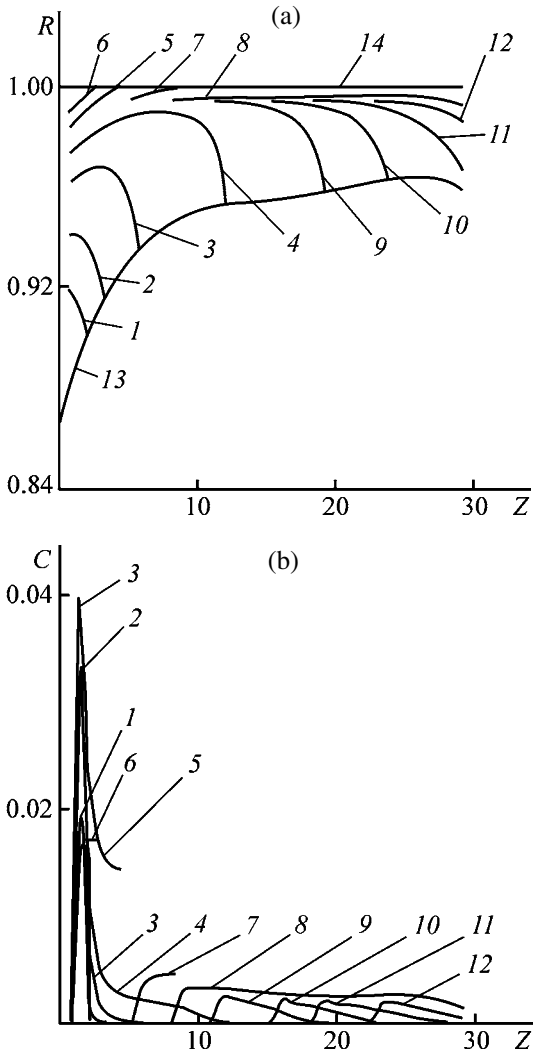

Fig. 2. (a) Trajectories of particle–bubble complexes and (b) distributions of the volume fraction of solid particles bound into complexes on the trajectories for Fr = 73.4, $\mathrm{Re}_n = 4 \times 10^3$, $Q = 0.04$, $n = 0.6$, $k = 0.02$ Pa s^n, $c_{\mathrm{h}0} = 0.05$ $\mathrm{m}^3\,\mathrm{m}^{-3}$, $c_{\mathrm{g}1} = 0.1$ $\mathrm{m}^3\,\mathrm{m}^{-3}$, $c_{\mathrm{g}2} = 0.01$ $\mathrm{m}^3\,\mathrm{m}^{-3}$, $d_\mathrm{h} = 2 \times 10^{-5}$ m, $d_{\mathrm{g}1} = 3 \times 10^{-5}$ m, $d_{\mathrm{g}2} = 3 \times 10^{-4}$ m, $r_\mathrm{k} = 0.2$ m, $a = 0.1$ m, $b = 0.05$ m, $\rho_\mathrm{h} = 1040$ kg m^{-3}, $\rho_\mathrm{l} = 1000$ kg m^{-3}, and $\rho_\mathrm{g} = 1.293$ kg m^{-3}. (*R, Z*) Dimensionless radial and axial coordinates of bubbles and (*C*) dimensionless volume fraction of solid particles; the same for Figs. 3–5. (*1–12*) (a) Trajectories of complexes and (b) distributions of the volume fraction of solid particles on the trajectories, (*13*) boundary of the suspension film, and (*14*) wall of the hydrocyclone case.

particles arrive at the wall of the hydrocyclone case, to form a deposit. Use of a two-stage flotation makes it possible to eliminate this undesirable phenomenon by reducing the volume fraction of solid particles bound into complexes on these trajectories to a negligible value and to accelerate the emergence of

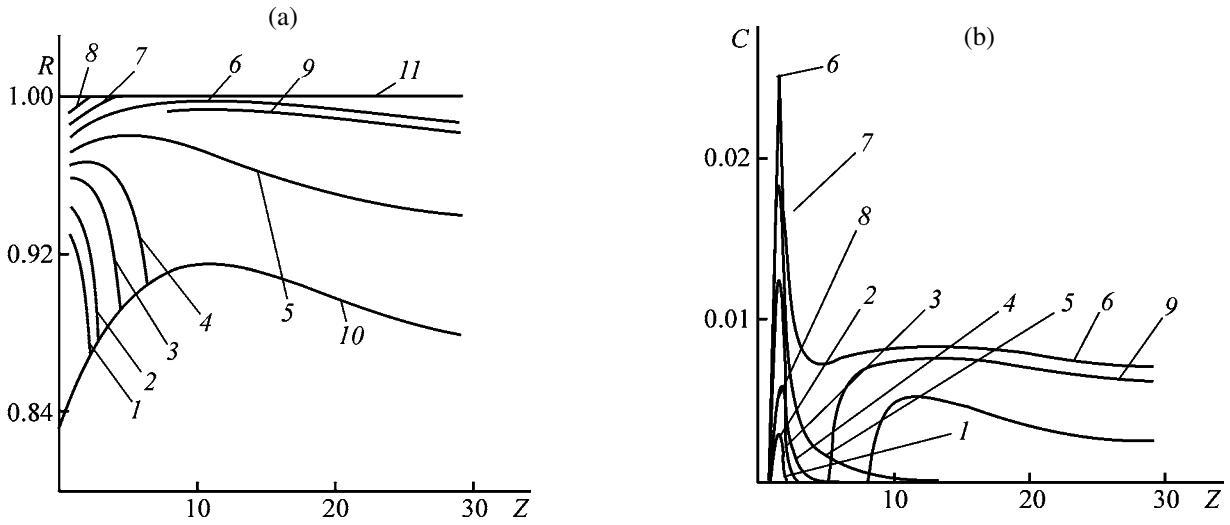

Fig. 3. (a) Trajectories of particle–bubble complexes and (b) distributions of the volume fraction of solid particles bound into complexes on the trajectories for Fr = 207 and the same values of the parameters as in Fig. 2. (*1*–*9*) (a) Trajectories of complexes and (b) distributions of the volume fraction of solid particles on the trajectories, (*10*) boundary of the suspension film, and (*11*) wall of the hydrocyclone case.

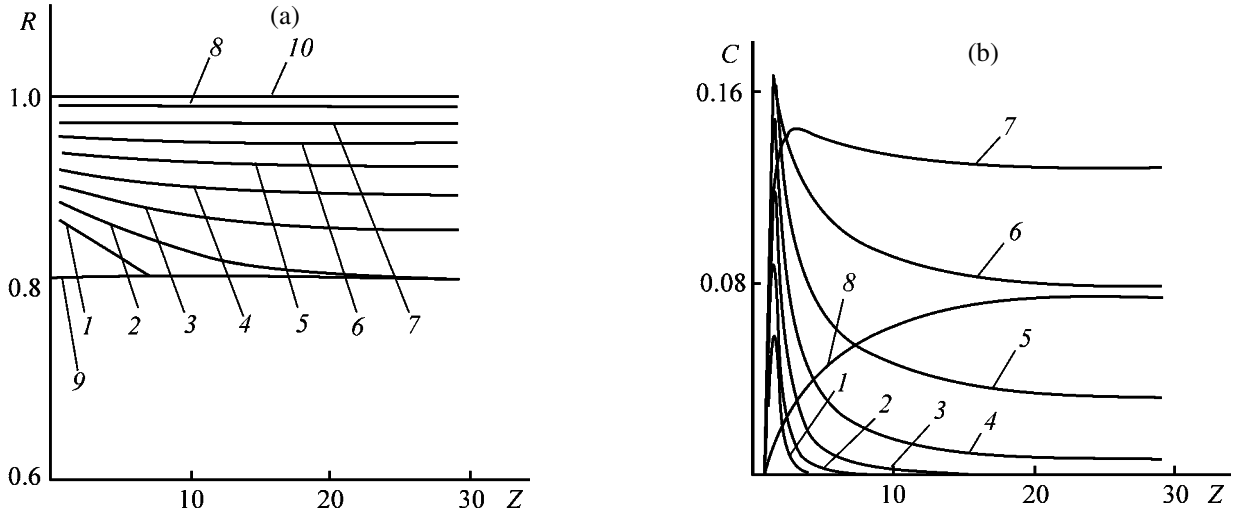

Fig. 4. (a) Trajectories of particle–bubble complexes and (b) distributions of the volume fraction of solid particles bound into complexes on the trajectories for $Re_n = 5 \times 10^2$ and the same values of the parameters as in Fig. 1. (*1*–*8*) (a) Trajectories of complexes and (b) distributions of the volume fraction of solid particles on the trajectories, (*9*) boundary of the suspension film, and (*10*) wall of the hydrocyclone case.

complexes being extracted by secondary-gas bubbles into the froth layer at the film surface.

As follows from Fig. 2b, the largest values of the volume fraction of solid particles bound into complexes are observed on trajectories located in the zone of high circumferential velocities of the dispersion medium, because of their considerable recovery in the first step of flotation [8, 9].

The volume fraction of solid particles bound into complexes on the trajectories first increases in the axial direction because of formation of complexes in the first stage of flotation and then decreases to negligible values owing to extraction of the complexes by secondary-gas bubbles. The integral-average residual dimensionless volume fraction of solid particles bound into complexes in the outlet cross section of the hydrocyclone at $Z = 30$ is $\bar{C} = 1.33 \times 10^{-4}$ for the given case. For the single-stage flotation at $C_{g2} = 0$, the same operation mode parameters of the hydrocyclone, and the same coordinate Z, $\bar{C}_0 = 6.52 \times 10^{-2}$.

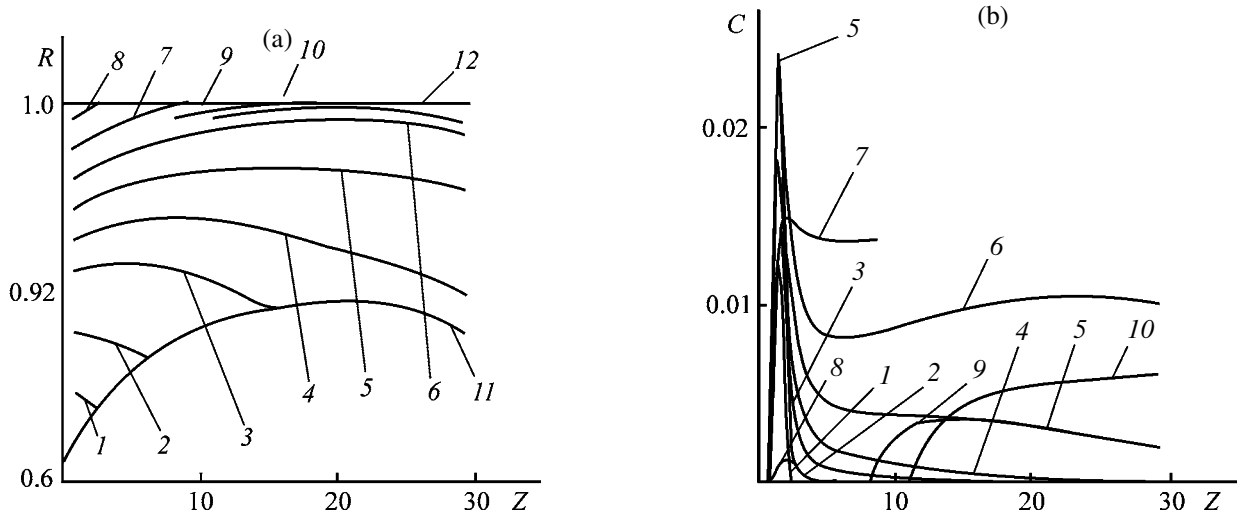

Fig. 5. (a) Trajectories of particle–bubble complexes and (b) distributions of the volume fraction of solid particles bound into complexes on the trajectories for $n = 1$ and the same values of the parameters as in Fig. 1. (*1–10*) (a) Trajectories of complexes and (b) distributions of the volume fraction of solid particles on the trajectories, (*11*) boundary of the suspension film, and (*12*) wall of the hydrocyclone case.

These values of C indicate that the two-stage pressure-head flotation is more efficient than the single-stage process.

Figure 3 shows trajectories of complexes (Fig. 3a) and distributions of the volume fraction of solid particles bound into complexes (Fig. 3b) for Fr = 207 and the same values of the parameters as in Fig. 2. Comparison of the data in Figs. 3 and 2 shows that the maximum values of the volume fraction of solid particles bound into complexes on the trajectories for Fr = 207 are considerably smaller than those for Fr = 73.4, whereas in the outlet cross section of the hydrocyclone, their volume fraction at Fr = 207 exceeds that at Fr = 73.4. This is due to the fact that the circumferential velocity of the dispersion medium, Θ_1, decreases in regions remote from the film surface because of a considerable increase in the suspension film thickness [7] and a decrease in the fullness of the radial distribution of the circumferential velocity of the dispersion medium at Fr = 207. Complexes are formed in the first stage of flotation at larger values of the axial coordinate Z and their extraction by secondary-gas bubbles decreases (kinetic constants of the first and second stages of flotation, A_1 and A_2, decrease). In addition, the decrease in the circumferential velocity of the dispersion medium, Θ_1, and the increase in the suspension film thickness result in that the emergence of complexes at the film surface becomes lower, which also leads to an increase in the residual volume fraction of solid particles bound into complexes in the outlet cross section of the film. In this case, $\bar{C} = 2.56 \times 10^{-4}$ and $\bar{C}_0 = 6.32 \times 10^{-1}$, in agreement with the results of the analysis we made.

Figure 4 shows trajectories of complexes (Fig. 4a) and distributions of the volume fraction of solid particles bound into complexes (Fig. 4b) for $\mathrm{Re}_n = 5 \times 10^2$ and the same values of the parameters as those in Fig. 2. Comparison of Figs. 4 and 2 shows that at $\mathrm{Re}_n = 5 \times 10^2$ the maximum volume fraction of solid particles bound into complexes on the trajectories decreases compared with the values at $\mathrm{Re}_n = 4 \times 10^3$, and their volume fraction in the outlet cross section of the hydrocyclone increases. This is due to a significant increase in the suspension film thickness [7], decrease in the fullness of the radial distribution of the circumferential velocity of the dispersion medium, and increase in the decay of the circumferential velocity of the dispersion medium, Θ_1, in the axial direction at $\mathrm{Re}_n = 5 \cdot 10^2$. The decrease in the circumferential velocity of the dispersion medium, Θ_1, results in that the kinetic constant of the first stage of pressure-head flotation, A_1, becomes smaller and complexes are formed at larger values of the axial component Z, the amount of complexes transferred to the froth layer on the film surface diminishes (see trajectories in Fig. 4a), and their extraction by secondary-gas bubbles falls down, which is due to a decrease in the kinetic constant of the second stage of flotation, A_2. $\bar{C} = 2.17 \times 10^{-3}$ and $\bar{C}_0 = 8.1 \times 10^{-1}$ at $Z = 30$, which points to a significant increase in the integral-average residual volume fraction of solid particles bound into complexes, compared with that at $\mathrm{Re}_n = 4 \times 10^3$.

Figure 5 shows trajectories of complexes (Fig. 4a)

and distributions of the volume fraction of solid particles bound into complexes (Fig. 4b) for $n = 1$ and the same values of the parameters as those in Fig. 2; this corresponds to separation in a hydrocyclone of a suspension with a Newtonian dispersion medium. Comparison of Figs. 5 and 2 shows that at $n = 1$ the maximum volume fraction of solid particles bound into complexes on the trajectories is significantly smaller than that at $n = 0.6$, whereas their volume fractions in the outlet cross section of the hydrocyclone considerably exceed the values at $n = 0.6$. This is due to a stronger decay of the circumferential velocity of the dispersion medium, Θ_1, in the axial direction at $n = 1$ [7], corresponding increase in the suspension film thickness, and decrease in the fullness of the radial distribution of the circumferential velocity of the dispersion medium, Θ_1. This results in that the kinetic constants of the first and second stages of pressure-head flotation decrease, complexes are formed at larger values of the axial coordinate Z, and the amounts of their extraction by secondary-gas bubbles and transfer to the froth layer on the film surface become smaller. In the case of separation of a suspension with a Newtonian dispersion medium ($n = 1$) at $Z = 30$, $\bar{C} = 1.97 \times 10^{-3}$ and $\bar{C}_0 = 6.33 \times 10^{-1}$. These values considerably exceed those for $n = 0.6$, which demonstrates that the separation of suspensions with a pronounced anomaly of the non-Newtonian properties of the dispersion medium by two-stage pressure-head flotation is markedly more efficient.

CONCLUSIONS

(1) A mathematical model of separation of suspensions with a non-Newtonian dispersion medium by two-stage pressure-head flotation in a cylindrical direct-flow hydrocyclone was developed. This model makes it possible to calculate the concentration field of solid particles and to find the average-integral residual volume fraction of solid particles in the suspension film.

(2) It was shown that the two-stage pressure-head flotation can markedly reduce the residual volume fraction of solid particles in the suspension film, compared with the single-stage process.

(3) The influence exerted by the determining similarity numbers and by the rheological properties of the dispersion medium on the separation parameters was analyzed and it was found that separation of suspensions with a pronounced anomaly of the non-Newtonian properties of the dispersion medium is more efficient and provides a smaller residual volume fraction of solid particles.

REFERENCES

1. Kutepov, A.M., Lagutkin, M.G., Mushtaev, V.I., and Bulychev, S.Yu., *Khim. Neftegaz. Mashinostr*., 2002, no. 7, pp. 14–18.
2. Khudobin, L.V. and Ryabov, G.K., *Almaznaya i abrazivnaya obrabotka detalei mashin i instrumenta: Mezhvuzovskii sbornik nauchnykh trudov* (Diamond and Abrasive Processing of Machine Parts and Tools: Intercollegiate Coll. of Scientific Works), Penza: Penz. Politekh. Inst., 1985, issue 13, pp. 41–45.
3. Orlov, S.L., *Razvitie metodov mehanicheskoi i biologicheskoi ochistki stochnykh vod: Trudy inst. "VODGEO"* (Development of Methods for Mechanical and Biological Purification of Wastewater: Trans. VODGEO Inst.), Moscow, 1982, pp. 131–136.
4. Sotskova, T.Z., Bazhenov, Yu.F., and Golik, G.A., *Khim. Tekhnol. Vody*, 1984, vol. 6, no. 1, pp. 17–22.
5. Kutepov, A.M., Lagutkin, M.G., Pavlovskii, G.V., and Mushtaev, V.I., *Teor. Osn. Khim. Tekhnol*., 1999, vol. 33, no. 5, pp. 571–577.
6. Deryagin, B.V., Dukhin, S.S., and Rulev, N.N., *Mikroflotatsiya: Vodoochistka, obogashchenie* (Microflotation: Water Treatment, Ore Dressing), Moscow: Khimiya, 1986.
7. Yablonskii, V.O., *Zh. Prikl. Khim*., 2000, vol. 73, no. 1, pp. 95–99.
8. Yablonskii, V.O. and Ryabchuk, G.V., *Zh. Prikl. Khim*., 2002, vol. 75, no. 10, pp. 1687–1693.
9. Yablonskii, V.O., *Khim. Neftegaz. Mashinostr*., 2003, no. 12, pp. 15–18.
10. Dyakowski, T., Hornung, G., and Williams, R.A., *Chem. Eng. Res. Des. A*, 1994, vol. 72, no. 4, pp. 513–520.
11. Tyabin, N.V., Dakhina, G.L., Golovanchikov, A.B., and Mamakov, A.A., *Teor. Osn. Khim. Tekhnol*., 1979, vol. 13, no. 6, pp. 880–884.
12. Tyabin, N.V., Golovanchikov, A.B., Dakhina, G.L., and Zelentsov, V.I., *Elektronnaya obrabotka materialov* (Electron Treatment of Materials), Chisinau: Shtiintsa, 1986, no. 5, pp. 65–67.
13. Acharya, A., Mashelkar, R.A., and Ulbrecht, J., *Rheol. Acta*, 1976, vol. 15, no. 9, pp. 454–463.
14. Matveev, N.M., *Differentsial'nye uravneniya* (Differential Equations), Minsk: Vysheisha Shkola, 1976.
15. Yablonskii, V.O., *Khim. Prom–st*., 2005, vol. 82, no. 1, pp. 40–48.

ISSN 1070-4272, Russian Journal of Applied Chemistry, 2007, Vol. 80, No. 3, pp. 405–418. © Pleiades Publishing, Ltd., 2007.
Original Russian Text © A.A. Il'in, A.N. Il'in, Yu.L. Bakhmutov, G.G. Furin, L.M. Pokrovskii, 2007, published in Zhurnal Prikladnoi Khimii, 2007, Vol. 80, No. 3, pp. 405–420.

ORGANIC SYNTHESIS AND INDUSTRIAL ORGANIC CHEMISTRY

Promising Prospects for Using Partially Fluorinated Alcohols as O-Nucleophilic Reagents in Organofluoric Synthesis

A. A. Il'in, A. N. Il'in, Yu. L. Bakhmutov, G. G. Furin, and L. M. Pokrovskii

Galogen Open Joint-Stock Company, Perm, Russia
Vorozhtsov Novosibirsk Institute of Organic Chemistry, Siberian Division, Russian Academy of Sciences, Novosibirsk, Russia

Received April 5, 2006

Abstract—Perfluoroolefins react with isopropyl alcohol under the conditions of radical initiation to form partially fluorinated aliphatic alcohols. The reactions of these alcohols with hexafluoropropylene and compounds containing labile halogen atoms (in particular, with allyl bromide and epichlorohydrin) were studied.

DOI: 10.1134/S1070427207030123

Partially fluorinated primary alcohols of the type $H(CF_2CF_2)_nCH_2OH$ (n = 1–6), produced by the reaction of tetrafluoroethylene with methanol at elevated temperature and pressure in the presence of a peroxy initiator decomposing above 100°C [1–3], are widely used in organofluoric synthesis [4]. In particular, they are intermediates for the production of many fluorinated substances whose functionalization, occurring at the $CH_2OH^{\bullet}$ and CHF_2 groups, yields primarily partially fluorinated carboxylic [5–9] and alkanesulfinic [4] acids, as well as fluorinated glycol ethers [4]. At the same time, in the presence of bases fluorinated alcohols behave as active O-nucleophiles allowing preparation of a large set of ethers and esters [10]. The interest in the development of processes for the production of a definite alcohol considerably increased recently, when these alcohols proved to be efficient as materials for information-displaying media with the reproducing layer capable of reading the information with a laser, and also in production of high-performance surfactants and developers for photography [11].

In the new patents, the procedure for preparing fluorinated alcohols is based on the main process, radical addition of methanol to tetrafluoroethylene, and the difference between the patents mainly consists in optimization of the process conditions with the aim to obtain the most demanded product, 2,2,3,3-tetrafluoropropyl alcohol [2]. The process proved to be more efficient in the presence of $CaCO_3$ [12–14]. When the reaction is performed at 60–65°C for 4 h, 2,2,3,3-tetrafluoropropyl alcohol is formed [13], whereas at 125°C and a pressure of 0.8 atm (6 h) the reaction gives a mixture of alcohols [13]. The best results were obtained at the tetrafluoroethylene : methanol ratio of 1 : 15 [14], when 2,2,3,3-tetrafluoropropyl alcohol was the only product. The possibilities of this method were somewhat extended by bringing into the reaction with methanol hexafluoropropylene and terminal perfluoroolefins $RCF{=}CF_2$ (R = C_1–C_4 perfluoroalkyl) in the presence of dialkyl peroxides [2, 11, 15]. A wider range of partially fluorinated alcohols thus became accessible. On the whole, there is growing interest in the development of processes for production of such alcohols; their accessibility will expand the prospects for their application.

Proceeding with studies on the synthesis of various partially fluorinated alcohols by reactions of available perfluoroolefins with aliphatic alcohols in the presence of peroxy initiators [16, 17], we examined in this work the possibility of performing this reaction with other perfluoroolefins and using the products obtained as O-nucleophilic agents in synthesis of promising intermediates.

Further development of the process suggested in [2] showed that the reactions of tetrafluoroethylene **I** and hexafluoropropylene **IV** with aliphatic alcohols in excess di-*tert*-butyl peroxide at 125°C and a pressure of 0.8 MPa smoothly yield partially fluorinated alcohols **II**, **III**, and **V**–**VII** by addition of aliphatic alcohols across the double bond (Scheme 1). We

showed previously [16] that alcohol **VI** occurs in the form of two stable diastereomers (in approximately 50 : 50 ratio) which can be separated on a capillary column; a GC–MS analysis gives two mass spectra. It is interesting that alcohol **VII** also occurs in two diastereomeric forms, but their ratio is 26.4 : 1. The target products should be isolated by direct distillation of the reaction mixtures:

Scheme 1.

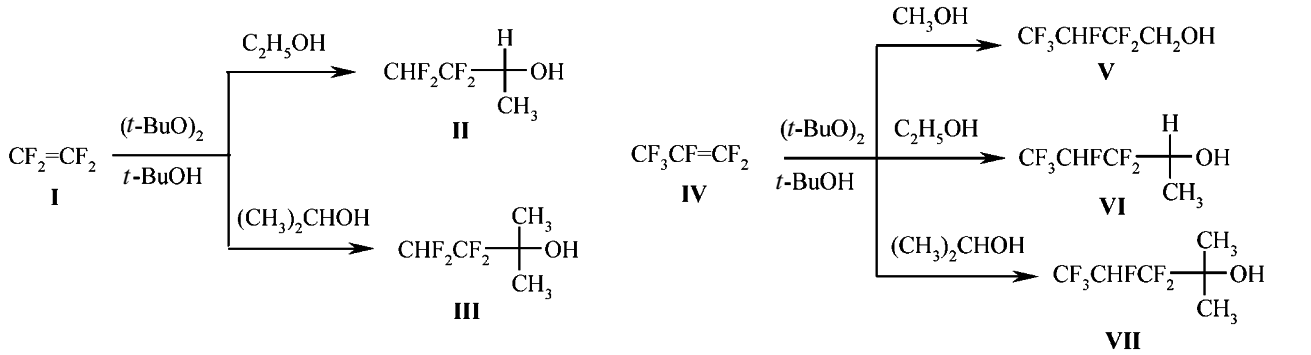

Presumably, these reactions in the presence of di-*tert*-butyl peroxide occur via intermediate radicals generated from the alcohol by abstraction of the α-H atom with the peroxide, followed by the reaction of the resulting radical with perfluoroolefin. Various aliphatic alcohols (methanol, ethanol, isopropanol) can be sources of alkyl radicals.

Experimental syntheses of polyfluorinated telomeric alcohols showed that, to attain the maximal yield of the target products, it is necessary to keep within strictly definite limits the reaction time, temperature, and pressure, with the optimal parameters being different for each polyfluorinated alcohol. For example, the optimal reaction time is directly related to the activity of the starting aliphatic alcohol in telomerization with perfluoroolefins, which can be illustrated by a comparative diagram shown in Fig. 1.

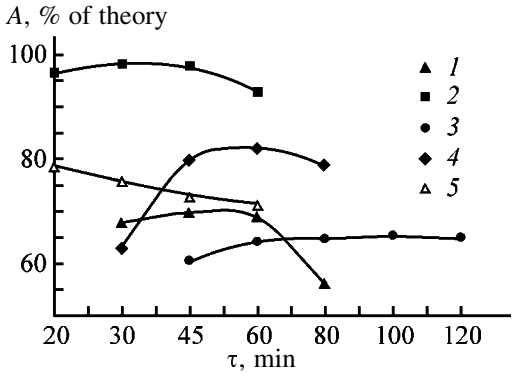

Fig. 1. Comparative diagram of the yields *A* of polyfluorinated telomeric alcohols vs. synthesis time τ: (*1*) 3,3,4,4-tetrafluorobutan-2-ol, (*2*) 3,3,4,4-tetrafluoro-2-methylbutan-2-ol, (*3*) 2,2,3,4,4,4-hexafluorobutan-1-ol, (*4*) 3,3,4,5,5,5-hexafluoropentan-2-ol, amd (*5*) 3,3,4,5,5,5-hexafluoro-2-methylpentan-2-ol; the same for Fig. 3.

This diagram shows that the optimal time of the synthesis of a polyfluorinated alcohol is the shorter, the higher the activity of the starting aliphatic alcohol (according to the radical telomerization theory, the activity of aliphatic alcohols decreases in the order isopropanol > ethanol > methanol) in telomerization with a perfluoroolefin. It should also be emphasized that the yield of a polyfluorinated alcohol derived from hexafluoropropylene is, as a rule (irrespective of the aliphatic alcohol used), lower (under the optimal conditions) than the yield of the corresponding telomer derived from tetrafluoroethylene. This may be due to the occurrence of side isomerization reactions in the course of the synthesis, in accordance with the above-described mechanism. At the same time, a decrease in the yield of the desired polyfluorinated alcohol with an increase in the synthesis time is due to the fact that the arising radical further reacts with tetrafluoroethylene (hexafluoropropylene forms exclusively monoaddition products), with the propagation of the polyfluorinated chain of the alkanol and formation of higher telomers. As a result, the reaction selectivity decreases and the amount of impurities increases. Simultaneously with the formation of higher telomers, decomposition of the initiator, di-*tert*-butyl peroxide, yields *tert*-butanol which actively reacts with the target polyfluorinated alcohol under the conditions existing at the end of the reaction (increased temperature and pressure, low pH), to form *tert*-butyl ether of the polyfluorinated alcohol. It should be noted, however, that too short reaction time also results in

increased content of impurities because of increased amount of unchanged aliphatic (starting) alcohol and initiator, especially at low temperatures and pressures of the synthesis. Thus, the amount of impurities formed in the synthesis depends on the conditions that are set or arise when the reaction time is made shorter or longer than the optimum, and also on the amount of the initiator participating in the synthesis. Figure 2 shows how the amount of impurities depends on the temperature and on the amount of the initiator taken for the synthesis.

Figure 2 shows that the optimal amount of the initiator participating in the process is 7–8 wt % relative to the starting aliphatic alcohol; in this case, the optimal temperature range is the broadest (135–150°C), and the yield of the desired polyfluorinated alcohol is reproducibly high provided that the synthesis time is wiithin the optimal range (Fig. 1). As the initiator amount is decreased below 7 wt %, the content of the desired perfluorinated alcohol in the reaction mixture decreases; this is due to an increase in the amount of unchanged aliphatic alcohols and di-*tert*-butyl peroxide, and if the temperature is increased to 145–150°C and the reaction time is made longer, the relative content of higher telomeric alcohols increases. When the initiator amount is higher (>9 wt %) than the optimal level, the increased content of impurities is due to decomposition of excess initiator and reaction of its decomposition products with polyfluorinated alcohols, and also to formation of higher telomers.

One more parameter significantly affecting the yield of polyfluorinated alcohols is the pressure produced by the perfluoroolefin in the reaction volume at optimal temperature and time of the synthesis. Within the framework of our method, with the aim to improve the synthesis safety and ensure control over the reaction rate, we fed the perfluoroolefin into the reaction volume in portions. As a fresh portion of perfluoroolefin is fed into the reactor, it starts to react with radicals of the aliphatic alcohol; as a result, the pressure in the reaction vessel decreases until the reaction is complete or until a new portion of the olefin is fed. Thus, pressure oscillations are always observed in the course of the synthesis (due to cyclic feeding of perfluoroolefin into the reaction mixture). The dependence of the yield of polyfluorinated alkanols on the mean synthesis pressure is shown in Fig. 3.

As seen from Fig. 3, the maximal yield of the desired polyfluorinated alcohols is attained in the range of mean working pressures from 9 to 11 atm, and for each polyfluorinated alcohol the optimal working pressure is specific for each combination of

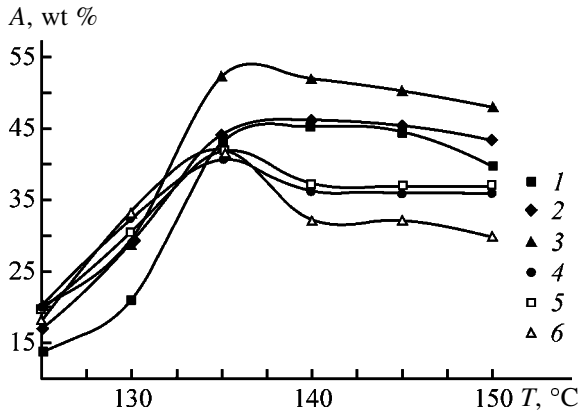

Fig. 2. Average statistical dependence of the content of polyfluorinated alcohols in the reaction mixture *A* on the synthesis temperature *T* and amount of initiator taken. Initiator amount, % relative to the starting alcohol: (*1*) 6, (*2*) 7, (*3*) 8, (*4*) 9, (*5*) 10, and (*6*) 12.

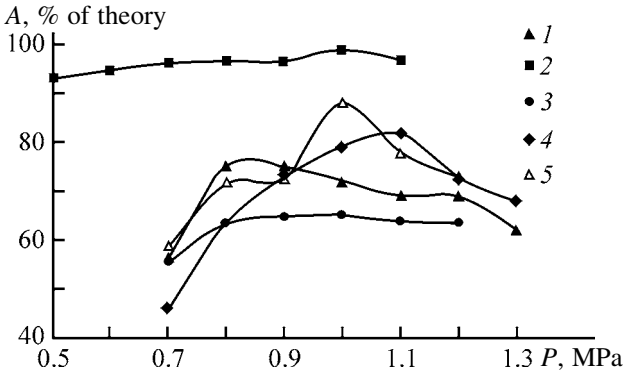

Fig. 3. Comparative diagram of the yield *A* of polyfluorinated alcohols vs. mean synthesis pressure *P*.

the starting aliphatic alcohol and perfluoroolefin, provided that the temperature and time of the synthesis and the amount of the peroxy initiator are within the optimal range. It should be noted that, if the working pressure exceeds the optimal level, the yield of polyfluorinated alcohols decreases as a result of formation of higher telomers (with tetrafluoroethylene) or of isomerization of the desired polyfluorinated alcohols under severe reaction conditions. This trend is due to an increase in the amount of perfluoroolefin dissolved in the liquid phase (i.e., occurring in the reaction zone) with an increase in the pressure. Excess perfluoroolefin will cause propagation (or branching) of the perfluorinated chain of the molecule (or radical) of polyfluorinated alcohol, especially at minimal saturation of the reaction mixture with free radicals of the peroxy initiator and starting aliphatic alcohol; just such conditions arise by the end of the reaction or at a long reaction time. At the same time, too low work-

Table 1. Optimal conditions of synthesis of polyfluorinated telomeric alcohols

Alcohol	*t*, h	*T*, °C	*P*, atm	Amount of $(t\text{-BuO})_2$, %	Yield, %
II	60	140	9	8	Up to 75
III	30	140	10	7	Up to 97
V	10 0	140	10	8	Up to 66
VI	60	140	11	8	Up to 83
VII	20	140	10	7	Up to 88

ing pressures are also undesirable, because the content of the perfluoroolefin in the reaction zone in this case decreases; as a result, the decomposition products of the peroxy initiator are formed more actively, and the concentration of impurities capabale to react with the desired polyfluorinated alcohol increases.

Thus, to attain the maximal yield of a specific polyfluorinated telomeric alcohol, it is necessary to strictly keep the working pressure, temperature and time of the synthesis, and initiator amount in the optimal ranges. The optimal values of these parameters for each of the polyfluorinated alcohols obtained and the corresponding values of the average yield and main substance content are given in Table 1.

By the example of the reaction of isopropyl alcohol with perfluoroolefins **IV** and **VIII**, and also with internal perfluoroolefin **IX**, in excess $(t\text{-BuO})_2$ at 125°C and a pressure of 0.8 MPa, we demonstrated the principal possibility of preparing other partially fluorinated alcohols, in particular, **VII**, **X**, and **XI**. According to GC–MS analysis, alcohol **X** exists in the form of two stable diastereomers in a 1.65 : 1 ratio (Scheme 2). From perfluoroolefin **IX**, along with alcohol **XIa**, alcohol **XIb** is formed in a yield of up to 10%, which can be accounted for by isomerization of the starting perfluoroolefin into perfluoro-2-methyl-2-pentene and its reaction with isopropyl alcohol.

Scheme 2.

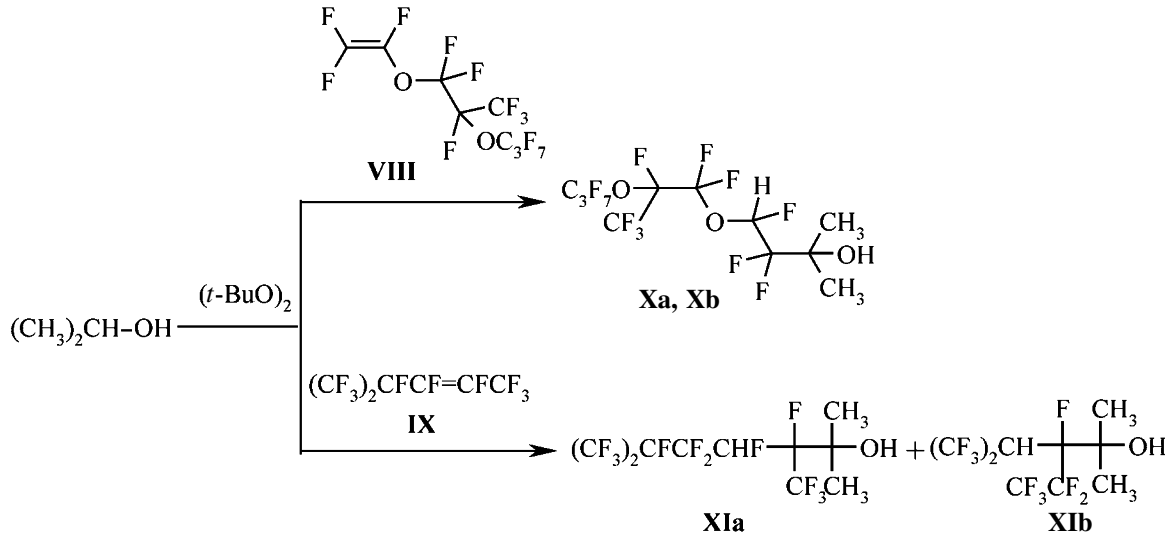

The structures of alcohols **VII**, **X**, and **XI** were confirmed by ^1H, ^{13}C, and ^{19}F NMR spectroscopy (Table 2), IR spectroscopy, and mass spectrometry. Despite the fact that all these alcohols contain the same $HCFCF_2$ fragment, the signals in the ^{19}F NMR spectrum show an *AB* pattern (Table 2). The position of the OH proton signal in the ^1H NMR spectrum depends on the solvent. For neat compound **VII**, the OH proton signal lies at 4.21 ppm, whereas for a 10% solution of **VII** in $CDCl_3$ it lies at 3.12 ppm. Similarly, for neat compound **XIa** the OH proton signal lies at 2.97 ppm, and for a 10% solution of **XIa** in $CDCl_3$, at 1.69 ppm. This is caused by differences in association of OH groups via intermolecular hydrogen bonds.

Introduction of fluorine atoms into the carbon chain of aliphatic alcohols decreases their nucleophilic activity. Nevertheless, telomeric alcohols $H(CF_2CF_2)_n \cdot CH_2OH$ [n = 1 (**XII**), 2 (**XIII**), 3 (**XIV**), 4 (**XV**)] in the presence of a catalytic amount of KOH react with hexafluoropropylene to form, though in a low yield,

Table 2. ^{1}H, ^{13}C, and ^{19}F NMR data for the new partially fluorinated compounds

^{1}H NMR spectrum, δ_H, ppm (J, Hz)	^{13}C NMR spectrum, δ_C, ppm (J_{CF}, Hz)	^{19}F NMR spectrum, δ_F, ppm (J, Hz)
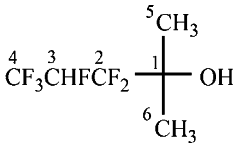		
5.22 (H^3) d (43.6); sextet (6.4); 4.21 (OH); 1.37 ($H^{5,6}$)	121.5 (C^4, $^1J_{CF}$ 282.0; $^2J_{CF}$ 26.1); 121.0 (C^1, $^1J_{CF}$ 249.9; $^2J_{CF}$ 21.8); 115.8 (C^2, $^1J_{CF}$ 249.9; $^2J_{CF}$ 21.8); 83.3 (C^3, $^1J_{CF}$ 195.4; $^2J_{CF}$ 24.5); 73.4 (C^1, $^2J_{CF}$ 25.6); 22.5 ($C^{5,6}$)	89.6 (F^4), 41.1 and 37.0 (F^2) *AB* system, J_{FF} 266.4; –43.4 (F^3) d (43.3), sextet (3.2)
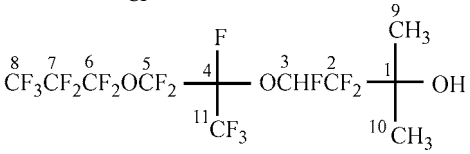		
6.25 (H^3) d (52.8); 4.35 (OH); 1.27 and 1.20 s ($H^{9,10}$)	118.1 (C^{11}, $^1J_{CF}$ 287.1; $^2J_{CF}$ 31.0); 117.5 (C^8, $^1J_{CF}$ 286.6; $^2J_{CF}$ 32.9); 116.9 (C^2, $^1J_{CF}$ 259.6; $^2J_{CF}$ 32.4); 116.2 (C^4, $^1J_{CF}$ 319.2; $^2J_{CF}$ 31.3); 111.8 (C^6, $^1J_{CF}$ 272.3; $^2J_{CF}$ 25.8); 106.8 (C^7, $^1J_{CF}$ 268.7; $^2J_{CF}$ 37.5); 103.2 (C^5, $^1J_{CF}$ 268.5; $^2J_{CF}$ 36.9); 99.7 (C^3, $^1J_{CF}$ 240.9; $^2J_{CF}$ 29.1); 72.9 (C^1, $^2J_{CF}$ 24.6); 23.0 ($C^{9,10}$)	83.4 (F^8); 81.9 (F^{11}); 79.9 and 78.5 (F^2) *AB* system, J_{FF} 147.8; 39.8 and 33.4 (F^4) *AB* system, J_{FF} 263; 32.6 ($F^{6,7}$); 23.6 (F^3); 18.8 (F^5)
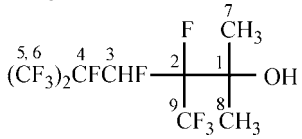		
5.84 (H^3) d.d (44.8; 20.6); 2.97 (OH); 1.43 ($H^{7,8}$) s	122.2 (C^9, $^1J_{CF}$ 286.9; $^2J_{CF}$ 27.9); 120.7 ($C^{5,6}$, $^1J_{CF}$ 287.4; $^2J_{CF}$ 22.6); 96.5 (C^4, $^1J_{CF}$ 234.9; $^2J_{CF}$ 24.8); 92.5 (C^2, $^1J_{CF}$ 235.0; $^2J_{CF}$ 31.8); 85.6 (C^3, $^1J_{CF}$ 196.9; $^2J_{CF}$ 21.8); 74.4 (C^1, $^2J_{CF}$ 21.9); 25.7 (C^7), 24.2 (C^8)	95.2 ($F^{6,5}$); 92.8 (F^9); –16.9 (F^4); –23.1 (F^2); –38.9 (F^3)
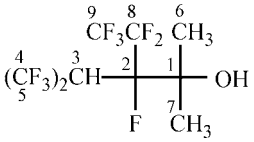		
3.97 (H3) d (6.0); 3.71 (OH); 1.15 ($H^{7,8}$)	*	88.7 and 91.4 ($F^{4,5}$); 85.8 (F^9); 40.6 and 37.1 (F^8) *AB* system, J_{FF} 263; –19.1 (F^2)
$CF_3^1CHF^2CF_2^3OCH_2^4CF_2^5CF_2^6CF_2^7CHF_2^8$		
5.95 (H^8) t.t (52.0, 5.2); 4.79 (H^2) d (38.4), sextet (5.0); 4.46 (H^4) t (12.8)	119.8 (C^1, $^1J_{CF}$ 281.0; $^2J_{CF}$ 25.1); 115.4 (C^3, $^1J_{CF}$ 272.0; $^2J_{CF}$ 21.7); 113.7 (C^5, $^1J_{CF}$ 257.5; $^2J_{CF}$ 31.4); 110.5 ($C^{6,7}$, $^1J_{CF}$ 238.1; $^2J_{CF}$ 26.3); 107.6 (C^8, $^1J_{CF}$ 253.8; $^2J_{CF}$ 31.4); 59.8 (C^4)	88.3 (F^1); 82.1 and 79.6 (F^3) *AB* system, J_{FF} 146.7; 43.9 (F^5); 39.2 (F^6); 34.2 (F^7); 26.6 (F^8) d (52)

Table 2. (Contd.)

^{1}H NMR spectrum, δ_H, ppm (J, Hz)	^{13}C NMR spectrum, δ_C, ppm (J_{CF}, Hz)	^{19}F NMR spectrum, δ_F, ppm (J, Hz)
$^{1}CF_3{}^{2}CHF{}^{3}CF_2O{}^{4}CH_2{}^{5}CF_2{}^{6}CF_2{}^{7}CF_2{}^{8}CF_2{}^{9}CF_2{}^{10}CHF_2$		
5.93 (H^{10}) t.t (52.0, 5.2); 4.75 (H^2) d (44.0), sextet (6.2); 4.28 (H^4) t (12.8)	120.5 (C^1, $^1J_{CF}$ 280.5; $^2J_{CF}$ 27.1); 119.0 (C^{10}, $^1J_{CF}$ 188.3; $^2J_{CF}$ 23.3); 111.7 (C^{6-8}, $^1J_{CF}$ 280.0; $^2J_{CF}$ 21.6); 114.6 (C^3, $^1J_{CF}$ 176.8; $^2J_{CF}$ 25.1); 108.4 (C^5, $^1J_{CF}$ 254.2; $^2J_{CF}$ 31.6); 85.2 (C^2, $^1J_{CF}$ 199.6; $^2J_{CF}$ 35.9); 61.7 (C^4, $^2J_{CF}$ 27.2; $^3J_{CF}$ 6.2)	88.3 (F^1); 81.9 and 79.6 (F^3) *AB* system, J_{FF} 139.6; 34.5 (F^5); 41.7 ($F^{6,7}$); 42.4 (F^8); 44.0 (F^9); 26.6 (F^{10}) d (52)
$^{1}CF_3{}^{2}CHF{}^{3}CF_2O{}^{4}CH_2{}^{5}CF_2{}^{6}CF_2{}^{7}CF_2{}^{8}CF_2{}^{9}CF_2{}^{10}CF_2{}^{11}CF_2{}^{12}CHF_2$		
5.87 (H^{12}) t.t (52.0, 4.8); 4.78 (H^2) d (44), sextet (5.6); 4.39 (H^4) t (12.6)	120.1 (C^1, $^1J_{CF}$ 280.9; $^2J_{CF}$ 27.2); 118.3 (C^3, $^1J_{CF}$ 271.3; $^2J_{CF}$ 22.7); 114.2 (C^{9-11}, $^1J_{CF}$ 259.5; $^2J_{CF}$ 31.7); 111.1 (C^{5-8}, $^1J_{CF}$ 295.0; $^2J_{CF}$ 35.1); 107.9 (C^{12}, $^1J_{CF}$ 254.7; $^2J_{CF}$ 31.6) 84.9 (C^2, $^1J_{CF}$ 202.0; $^2J_{CF}$ 35.3); 60.5 (C^4)	88.2 (F^1); 81.8 and 79.5 (F^3) *AB* system, J_{FF} 146.7; 44.0 (F^5); 42.7 (F^{6-8}); 41.2 ($F^{9,10}$); 34.6 (F^{11}); 26.6 (F^{12}) d (52.0); –48.3 (F^2) m
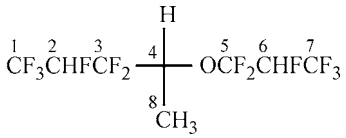		
5.20 (H^4) m; 4.92 ($H^{2,6}$) m; 1.50 (H^8) d (6.0)	120.9 ($C^{1,7}$, $^1J_{CF}$ 281.9; $^2J_{CF}$ 25.3); 116.5 ($C^{2,5}$, $^1J_{CF}$ 254.3; $^2J_{CF}$ 23.3); 84.0 (C^2, $^1J_{CF}$ 196.3; $^2J_{CF}$ 35.2); 69.9 (C^6, $^1J_{CF}$ 160.5; $^2J_{CF}$ 28.8); 15.2 (C^4); 12.7 (C^8)	89.7 ($F^{1,7}$); 40.8 and 37.9 ($F^{3,5}$) *AB* system, J_{FF} 267; –43.5 ($F^{2,6}$)
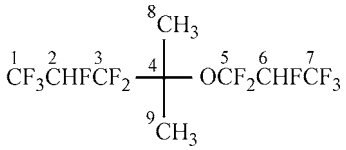		
5.25 ($H^{2,6}$) d.sextet (43.6; 18.4; 6.4); 1.33 (H^8); 1.36 (H^9)	121.5 ($C^{1,7}$, $^1J_{CF}$ 282.1; $^2J_{CF}$ 26.1); 120.9 ($C^{3,5}$, $^1J_{CF}$ 250.2; $^2J_{CF}$ 21.8); 115.7 ($C^{3,5}$, $^1J_{CF}$ 250.2; $^2J_{CF}$ 21.8); 83.4 ($C^{2,6}$, $^1J_{CF}$ 164.7; $^2J_{CF}$ 24.5); 73.3 (C^4, $^2J_{CF}$ 25.6); 22.4 ($C^{8,9}$)	89.7 ($F^{1,7}$); 40.9 and 37.3 ($F^{3,5}$) *AB* system, J_{FF} 275.2; –43.5 ($F^{2,6}$)
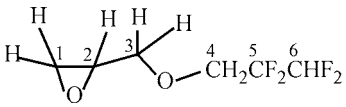		
6.00 (H^6) t.t (51.8, 5.2); 3.86 (H^4) t (11.8); 3.44 (H^3) d.d (11.8, 6.2); 4.02 t.d (13.8, 2.2); 3.10 (H^2) m; 2.53 ($H^{1'}$) m; 2.71 ($H^{1''}$) t (4.8)	114.8 (C^6, $^1J_{CF}$ 249.1; $^2J_{CF}$ 26.4); 109.0 (C^5, $^1J_{CF}$ 248.3; $^2J_{CF}$ 33.8); 72.5 (C^3); 67.5 (C^4, $^2J_{CF}$ 28.2); 49.7 (C^1); 42.6 (C^2)	37.8 (F^5); 23.8 ($F^{6'}$) t (3.8); 23.5 ($F^{6''}$) t (4.3)

Table 2. (Contd.)

^{1}H NMR spectrum, δ_H, ppm (J, Hz)	^{13}C NMR spectrum, δ_C, ppm (J_{CF}, Hz)	^{19}F NMR spectrum, δ_F, ppm (J, Hz)
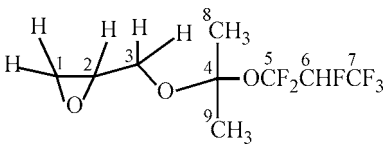		
5.30 (H^6) d.sextet (50, 5.2); 3.62 (H^3) d (9.8); 3.12 (H^2) m; 2.77 ($H^{1'}$) t (4.8); 2.12 ($H^{1''}$) m	121.2 (C^7, $^1J_{CF}$ 282.4; $^2J_{CF}$ 26.0); 118.1 (C^5, $^1J_{CF}$ 242.5; $^2J_{CF}$ 21.6); 82.8 (C^6, $^1J_{CF}$ 195.2; $^2J_{CF}$ 27.4); 72.7 (C^4, $^2J_{CF}$ 24.8); 51.5 (C^3); 46.6 (C^1); 44.5 (C^2); 26.2 ($C^{8,9}$)	95.2 (F^7); 39.8 and 36.3 (F^5) *AB* system, J_{FF} 275.2; –44.2 (F^6)
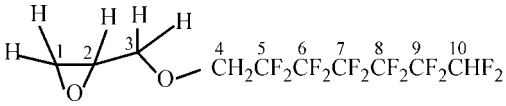		
6.13 (H^{10}) t.t (51.8); 3.95 (H^4) t (11.8); 3.44 (H^3) d.d (11.8, 6.2); 3.10 (H^2) m; 2.71 ($H^{1'}$) m; 2.53 ($H^{1''}$) t (4.8)	115.4 (C^{10}, $^1J_{CF}$ 257.6; $^2J_{CF}$ 30.6); 110.9 ($C^{6–9}$, $^1J_{CF}$ 268.3; $^2J_{CF}$ 35.5); 107.8 (C^5, $^1J_{CF}$ 253.9; $^2J_{CF}$ 31.4); 73.4 (C^3); 67.7 (C^4, $^2J_{CF}$ 25.2); 50.0 (C^2); 42.9 (C^1)	43.8 (F^5); 41.6 (F^6); 40.3 ($F^{7,8}$); 34.0 (F^9); 26.0 (F^{10}) d (51.0)
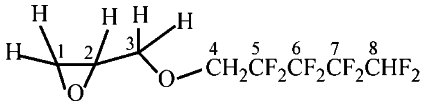		
6.09 (H^8) t.t (51.8, 5.4); 4.03 (H^4) t.t (14.8, 2.8); 3.44 (H^3) d.d (11.8, 6.2); 4.02 t.d (13.8, 2.2); 3.10 (H^2) m; 2.53 ($H^{1'}$) m; 2.71 ($H^{1''}$) t (4.8)	115.4 (C^8, $^1J_{CF}$ 256.1; $^2J_{CF}$ 30.6); 110.9 ($C^{6,7}$, $^1J_{CF}$ 233.5; $^2J_{CF}$ 30.7); 107.7 (C^5, $^1J_{CF}$ 253.0; $^2J_{CF}$ 30.7); 72.9 (C^3); 67.5 (C^4, $^2J_{CF}$ 25.5); 49.9 (C^2); 43.0 (C^1)	43.9 (F^5); 38.4 (F^6); 33.6 (F^7); 26.3 (F^8) d (54.9)
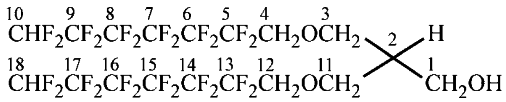		
6.09 ($H^{10,18}$) d (51.6); 4.04 ($H^{4,12}$) t.t (13.2, 5.6); 3.44 (H^2) t (4.4); 3.71 (H^1) d.d (12.8, 4.8); 3.11 (OH) s; 2.73 and 2.55 ($H^{3,11}$) d.d (11.6, 6.0)	115.6 ($C^{9,16}$, $^1J_{CF}$ 261.6; $^2J_{CF}$ 30.2); 107.7 ($C^{4,11}$, $^1J_{CF}$ 254.5); 110.7 ($C^{5–8,12–15}$, $^1J_{CF}$ 256.9; $^2J_{CF}$ 34.1; $^2J_{CF}$ 31.4); 73.3 (C^2); 69.3 (C^1); 68.2 ($C^{3,10}$, $^2J_{CF}$ 25.4)	44.3 ($F^{5,13}$) d (12.0); 42.1 ($F^{6,14}$); 40.8 ($F^{7,8,15,16}$); 34.4 ($F^{9,17}$); 26.5 ($F^{10,18}$) d (51.6)
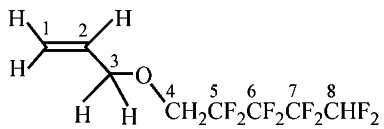		
5.90 (H^8) t.t (47.6, 5.4); 5.99 (H^2) t.d.d (4, 10, 20); 5.23 ($H^{1'}$) d (10.4); 4.09 (H^3) d (5); 3.90 (H^4) t (14.0)	132.9 (C^2), 118.4 (C^1); 115.3 ($C^{6,7}$, $^1J_{CF}$ 230.5; $^2J_{CF}$ 33.6); 108.0 ($C^{5,8}$, $^1J_{CF}$ 253.2; $^2J_{CF}$ 30.8); 73.5 (C^3); 66.3 (C^4, $^2J_{CF}$ 25.4)	44.0 (F^7); 38.2 (F^6); 33.4 (F^5, $^3J_{FH}$ 12; $^4J_{FH}$ 1.5); 26.0 (F^8, $^2J_{FH}$ 52.7; $^3J_{FH}$ 5.0)

Table 2. (Contd.)

^{1}H NMR spectrum, δ_H, ppm (J, Hz)	^{13}C NMR spectrum, δ_C, ppm (J_{CF}, Hz)	^{19}F NMR spectrum, δ_F, ppm (J, Hz)
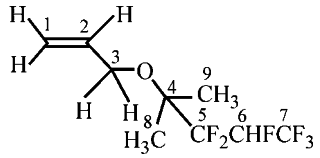		
5.82 (H^2) m; 5.45 (H^6) d.sextet (8); 5.28 ($H^{1'}$)d (17); 5.19 ($H^{1''}$) d (10); 4.00 (H^3) d (4.8); 1.33 ($H^{8,9}$)	122.1 (C^7, $^1J_{CF}$ 282.5; $^2J_{CF}$ 26.3); 118.9 (C^5, $^1J_{CF}$ 262.1; $^2J_{CF}$ 21.3); 83.9 (C^6, J_{CF} 95.5; $^2J_{CF}$ 33.9; $^2J_{CF}$ 13.6); 74.2 (C^3); 73.2 (C^4, $^2J_{CF}$ 24.7); 20.5 ($C^{8,9}$); 135.1 (C^2); 119.1 (C^1)	89.2 (F^7); 41.6 and 38.3 (F^5) *AB* system, J_{FF} 278.6; −43.8 d (F^6) (37.6)
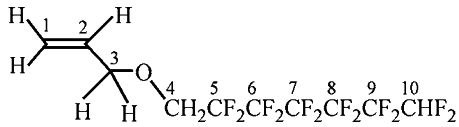		
6.13 (H^{10}) t.t (51.6, (5.2); 5.85 (H^2) t.t (5.6, 4.8); 5.30 ($H^{1'}$) d (17.2); 5.19 ($H^{1''}$) d (3.2); 4.08 (H^3) d (6.0); 3.90 (H^4) t (14.0)	133.0 (C^2); 117.7 (C^1); 116.4 (C^5, $^1J_{CF}$ 254.5; $^2J_{CF}$ 21.3); 110.8 (C^{6-9}, $^1J_{CF}$ 248.9; $^2J_{CF}$ 28.2); 107.7 (C^{10}, $^1J_{CF}$ 253.9; $^2J_{CF}$ 31.5); 73.1 (C^3); 66.5 (C^4, $^2J_{CF}$ 25.6)	44.4 (F^5) t (J_{FH} 13.6); 42.0 (F^6); 40.7 ($F^{7,8}$); 34.2 (F^9); 26.2 (F^{10}) d (51.6)
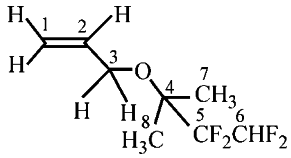		
6.16 (H^6) t.t (48.0, 4.8); 5.86 (H^2) m; 5.27 ($H^{1'}$) d.t (24, 2); 5.12 ($H^{1''}$) d.t (24, 2); 4.00 (H^3) d (4.8); 1.33 ($H^{7,8}$)	134.1 (C^2); 115.7 (C^1); 116.2 (C^6, $^1J_{CF}$ 255.9; $^2J_{CF}$ 23.2); 109.3 (C^5, $^1J_{CF}$ 249.9; $^2J_{CF}$ 32.2); 71.8 (C^4, $^2J_{CF}$ 27.2); 63.2 (C^3); 19.1 ($C^{7,8}$)	36.3 (F^6); 28.3 (F^5)
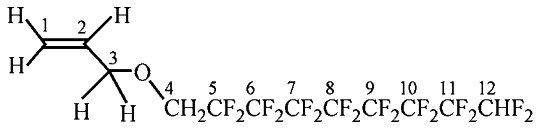		
5.84 (H^{12}) t.t (47.0; 7.0); 5.83 (H^2) m; 5.28 ($H^{1'}$) d (17.2); 5.19 ($H^{1''}$) d (10); 4.06 (H^4) t (14.0); 3.86 (H^3) d (5.6)	133.2 (C^2); 118.5 (C^1); 111.0 (C^{6-11}, $^1J_{CF}$ 241.3; $^2J_{CF}$ 32.8); 115.9 (C^5, $^2J_{CF}$ 30.5); 107.9 (C^{12}, $^2J_{CF}$ 31.5); 73.4 (C^3); 66.7 (C^4, $^2J_{CF}$ 25.7)	44.3 (F^5); 42.2 (F^{6-8}); 40.7 (F^9); 34.2 ($F^{10,11}$); 26.3 (F^{12}) d (50)

* The chemical shifts and coupling constants for this isomer (**XIb**) could not be determined because of its low content in the mixture.

partially fluorinated dialkyl ethers [18]. In the presence of equimolar amounts of bases, by-products are formed, apparently due to transformations of the starting hexafluoropropylene, occurring in this system.

To enhance the activity of O-nucleophiles, especially with a long carbon chain, it was suggested to use trimethylsilyl ethers of the corresponding telomeric alcohols, which are prepared from the alcohols by treatment with trimethylchlorosilane in the presence of an equimolar amount of triethylamine, or with bis(trimethylsilyl)amine [19, 20]. The subsequent reaction of these ethers with hexafluoropropylene, catalyzed by fluoride ion, yields the corresponding dialkyl ethers **XVI**–**XIX** (Scheme 3).

Scheme 3.

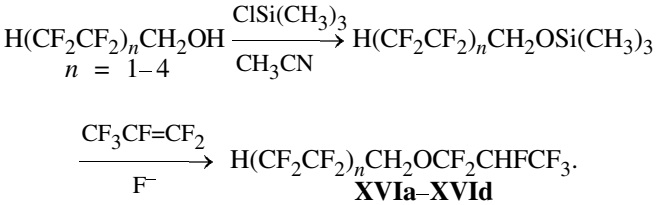

n = 1, **XVIa**; n = 2, **XVIb**; n = 3, **XVIc**; n = 4, **XVId**.

This route ensures appreciably higher yield of the target products because of lower contribution of degradation processes and controllable extent of polysubstitution.

An increase in the content of KOH relative to the telomeric alcohol leads to formation of high-molecular-weight by-products, apparently due to differences in the transformation pathways of intermediate carbanion **A**. The possible pathways of reaction of the alcohol $HCF_2CF_2CH_2OH$ with hexafluoropropylene are shown in Scheme 4.

Scheme 4.

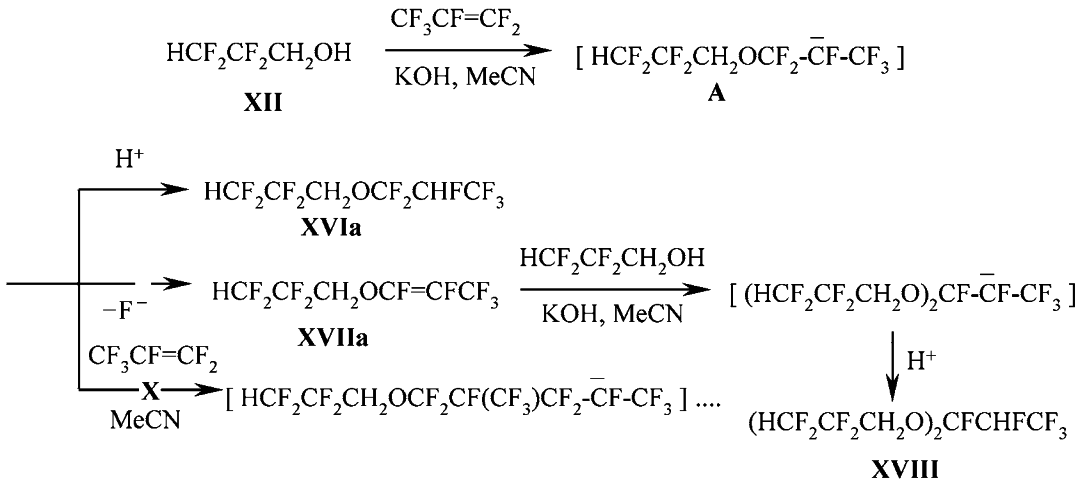

In one of these pathways, carbanion **A** reacts with a proton of the medium to give product **XVI**. Another pathway involves elimination of the fluoride ion with the formation of unsaturated ether **XVIIa**, which subsequently reacts with the O-nucleophilic agent to form by-product **XVIII**. Such compounds were not further studied, although they may be of practical interest as high-boiling liquids.

We found that ether **XVIa** under the action of solid KOH in acetonitrile undergoes cleavage to the starting alcohol **XII**, without formation of **XVIIa**. The pathway involving oligomerization with hexafluoropropylene under the action of fluoride ion is not realized under these conditions.

We believe that this approach has significant advantages and allows economically efficient preparation of diverse polyfluorinated dialkyl ethers. Indeed, the procedure for preparing partially fluorinated dialkyl ethers appeared to be fairly versatile (suitable not only for primary but also for secondary and tertiary alcohols). In particular, secondary alcohol **VI** and tertiary alcohols **VII** and **XI** react with hexafluoropropylene to form ethers **XIXa** and **XIXb** (Scheme 5).

Scheme 5.

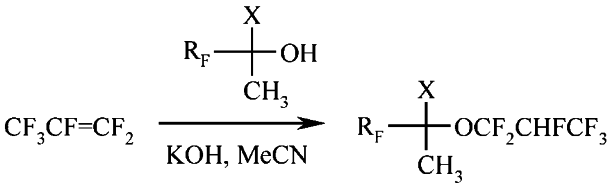

XIXa, XIXb

$R_F = CF_3CHFCF_2$, X = H (**XIXa**),
CF_3CHFCF_2, X = CH_3 (**XIXb**).

The partially fluorinated dialkyl ethers obtained can be of interest as intermediates for the synthesis of perfluorinated dialkyl ethers by direct additional fluorination with elemental fluorine and can be used as liquid

dielectrics for various purposes. Another area of their possible application can be preparation of partially fluorinated acrylates. It is known [16] that dialkyl ethers containing alkyl and CF_3CHFCF_2 groups at the oxygen atom readily transform into tetrafluoropropionic acid esters at room temperature in sulfuric acid solutions. On the contrary, ethers **XVIa**–**XVId** under these conditions are resistant to the action of concentrated H_2SO_4 and transform into propionic acid esters only upon prolonged heating [18]. Presumably, the limiting step of this reaction is the heterolysis of the C–F bond in the α-position relative to ether oxygen, with the generation of carbocation **B** whose subsequent reaction with the anion of the medium yields an intermediate transforming into propionic acid ester under the action of water (Scheme 6). Dehydrofluorination of the product formed can yield trifluoroacrylic acid ester.

Scheme 6.

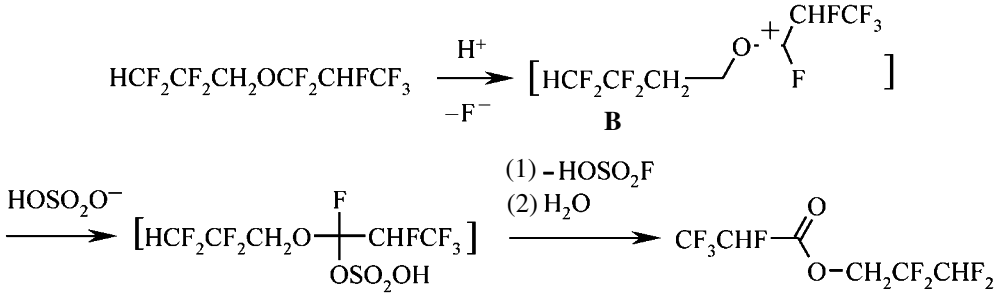

In the reaction of polyfluorinated telomeric alcohols with epichlorohydrin, opening of the epoxy ring could be expected, although an example of preservation of the epoxy ring has been reported. It was shown [19, 20] that 2-fluoro-2,2-dinitroethyl alcohol in the presence of NaOH transforms into the corresponding epoxide. We found that the reaction of epichlorohydrin with telomeric alcohols **XII**–**XIV** in the presence of K_2CO_3 in acetonitrile gave the coresponding epoxides **XXa**–**XXd** (Scheme 7). However, their yield was low. A similar pattern was observed with alochols **V**–**VII** under the same conditions. The use of NaOH or KOH instead of K_2CO_3 increases the yield of products of the epoxy ring opening.

Scheme 7.

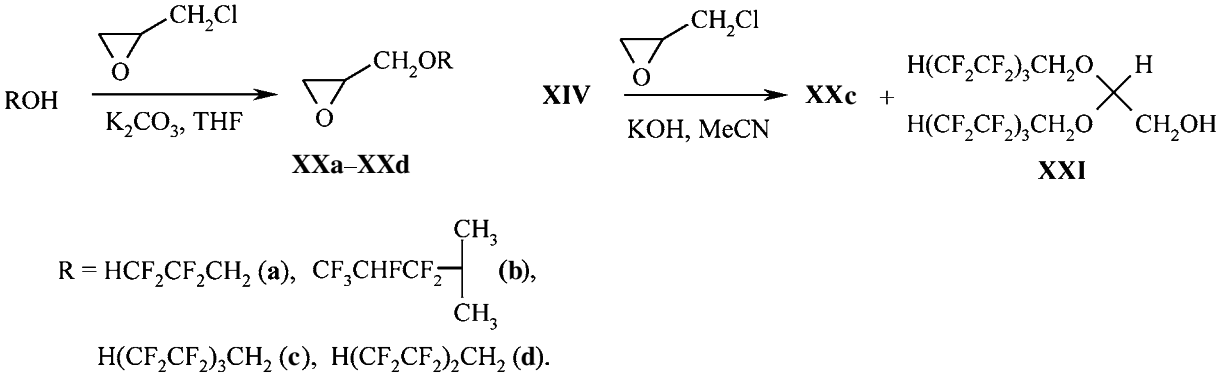

From the reaction of epichlorohydrin with alcohol **XIV**, we isolated the ring opening product **XXI** formed by attack of the O-anion $[H(CF_2CF_2)_3CH_2O^-]$ at the 2-position of the epoxy ring (Scheme 7).

Oxidation of perfluoroalkyl allyl ethers can be one of routes to polyfluorinated epoxides. It was shown previously [21] that telomeric alcohol **XII**, $HCF_2CF_2 \cdot CH_2OH$, reacts with allyl chloride in dimethylform-

amide in the presence of NaOH to form a partially fluorinated alkyl allyl ether. We further developed this approach and brought telomeric alcohols $H(CF_2CF_2)_n \cdot CH_2OH$ (n = 2–4) and the synthesized partially fluorinated alcohols into the reaction with allyl bromide in acetonitrile in the presence of KOH, to obtain polyfluoroalkyl allyl ethers **XXIIa**–**XXIIe** (Scheme 8).

Scheme 8.

$$ROH \xrightarrow[KOH,\ MeCN]{BrCH_2CH=CH_2} ROCH_2CH=CH_2,$$

XXIIa–**XXIIe**

R = $H(CF_2CF_2)_2CH_2$ (**a**), $CF_3CHFCF_2C(CH_3)_2$ (**b**), $H(CF_2CF_2)_3CH_2$ (**c**), $CHF_2CF_2C(CH_3)_2$ (**d**), $H(CF_2CF_2)_4CH_2$ (**e**).

The structure of the products obtained was confirmed by IR and ^1H, ^{13}C, and ^{19}F NMR spectroscopy (Table 2) and by mass spectrometry. The ^1H NMR spectra of the partially fluorinated compounds prepared contain proton signals of the $CH_2CH=CH_2$ and $CH_2=CHC(O)$ groups with the chemical shifts typical of such fragments. In the ^{19}F and ^{13}C NMR spectra, there are signals with the same chemical shifts and coupling constants from the F and C atoms of the CF_3CHFCF_2– and –$OCH_2CF_2CF_2$– groups; the CF_2 group in the CF_3CHFCF_2– fragment gives in the ^{19}F NMR spectrum an *AB* pattern with J_{FF} = 140–280 Hz. The fluorine signal of the CHF group (CF_3CHFCF_2–) is located in a higher field (from –40 to –49 ppm).

Thus, partially fluorinated aliphatic alcohols can be efficient O-nucleophilic reagents, which extends their possible applications for preparing various fluorinated materials.

EXPERIMENTAL

The ^1H, ^{13}C, and ^{19}F NMR spectra were recorded on a Bruker WP 400 SY spectrometer at operating frequencies of 400, 100, and 188 MHz, respectively [internal references HMDS, C_6F_6 (J_{CH} values were not measured), and $CDCl_3$]. The IR spectra (5% solutions in CCl_4) were recorded on a Specord M-80 spectrometer; GC–MS analysis was performed on a VG 707 OE device (ionizing electron energy 70 eV) and on a Hewlett–Packard G 1800 A GCD chromatograph with a mass-selective detector. In the latter case, we used a 30-m-long column 0.25 mm in diameter, coated with a 0.25-μm layer of HP-5 (5% diphenyl–95% dimethylsiloxane copolymer); carrier gas He, flow rate 1 ml min^{-1}, vaporizer temperature 280°C. The column temperature schedule was as follows: 50°C, 2 min; heating to 280°C, 10 deg min^{-1}; 280°C, 5 min. All the reactions were monitored by ^{19}F NMR. The reaction mixtures were analyzed with an LKhM 72 chromatograph (15% SE-30 on SKTF-803, QF-1, Chromosorb W, 4000 × 4-mm column). Compound **XVIa** was prepared as described in [20]. The NMR data are given in Table 2, and the analytical data and characteristics of the compounds, in Table 3.

The general procedure for preparing partially fluorinated alcohols was as follows. A reactor was charged with isopropyl alcohol and di-*tert*-butyl peroxide (3.5–15.4 wt % relative to the alcohol), sealed, and heated to 150°C in the presence of the polyfluorinated alcohol taken in an amount of 0.2–1.2 wt % relative to isopropyl alcohol, after which perfluoroolefin was fed at a pressure of 9–15 atm. The molar ratios were as follows: fluoroolefin : initiator (7.2–28.2) : 1, fluoroolefin : alcohol 1 : 15. The mixture was kept for 4 h, after which excess perfluoroolefin was removed and the mixture was distilled. After distillation of excess isopropyl alcohol, a base ($CaCO_3$) was added, and 99.9% pure partially fluorinated alcohol was distilled off. The characteristics of the alcohols obtained are given in Tables 2 and 3.

Reactions of hexafluoropropylene with partially fluorinated alcohols. To a suspension of 0.12 mol of KOH in 50 ml of acetonitrile, we added with stirring and cooling with cold water 0.1 mol of a partially fluorinated alcohol and then passed 0.1 mol of hexafluoropropylene with stirring and monitoring the reaction temperature. The solution volume increased. The mixture was poured into water, and the organic layer was separated, washed with water, dried over $MgSO_4$, and distilled. The results are given in Table 3.

Synthesis of α,α,β,ω-tetrahydroperfluoropropyl nonyl ether XVId. To a suspension of 7 g (0.12 mol) of KOH in 100 ml of acetonitrile at 20°C, we added dropwise with vigorous stirring 41.6 g (0.1 mol) of alcohol **XV**. The mixture was allowed to stand for 0.5 h, after which gaseous hexafluoropropylene (15 g, 0.1 mol) was passed at a rate allowing counting of separate bubbles. The reaction was exothermic; therefore, the mixture was cooled with ice-cold water. The gas was passed until the heat evolution ceased. The volume of the reaction mixture increased. After approximately 1.5 h, the mixture was poured into water, and the organic layer was separated, washed with water, dried over $MgSO_4$, and distilled; 40.2 g (69%) of **XVId** was obtained.

Table 3. Results of chemical and mass-spectrometric analyses and physical constants of the new partially fluorinated compounds

Compound	Yield, %	bp, °C (*P*, mm Hg)	Found, %			Formula	Calculated, %			*m/z*, found (calculated)	Formula
			C	H	F		C	H	F		
VII	89	125–126	34.27 34.53	3.93 4.14	53.43 53.68	$C_6H_5F_6O$	34.29	3.81	54.29	195.02371 (195.02445)	$C_5H_5F_6O$ $[M - CH_3]^+$
Xa, Xb	10	90–91 (20)	26.87 26.34	1.70 1.99	61.72 61.59	$C_{11}H_8F_{16}O_3$	26.83	1.63	61.79	476.99900 (476.99830)	$C_{10}H_5F_{16}0_3$ $[M - CH_3]^+$
XIa, XIb	64	77–80 (50)	29.83 29.54	3.04 2.80	63.62 63.33	$C_9H_8F_{12}O$	30.00	2.22	63.33	345.01486 345.01624	$C_8H_5F_{12}O$ $[M - CH_3]^+$
XVIb	89	73–74 (20)	25.86 25.88	1.22 0.99	70.11 70.35	$C_8H_4F_{14}O$	25.13	1.05	69.63	363.00710 (363.00544)	$C_8H_4F_{13}O$ $[M - F]^+$
XVIc	31.8	120–122 (6)	24.08 23.89	1.34 1.29	69.55 69.94	$C_{10}H_4F_{18}O$	24.90	0.83	70.95	462.99892 (462.99905)	$C_{10}H_4F_{17}O$ $[M - F]^+$
XVId	84	80–81(6)	24.63 24.64	0.63 0.89	71.69 71.29	$C_{12}H_4F_{22}O$	24.74	0.69	71.82	562.99680 (562.99266)	$C_{12}H_4F_{21}O$ $[M - F]^+$
XIXb	79	83–84 (20)	30.44 29.94	2.87 2.78	63.23 63.12	$C_9H_8F_{12}O$	30.00	2.22	63.33	345.01549 (345.01486)	$C_8H_5F_{12}O$ $[M - CH_3]^+$
XXa	84	110–111	38.50 38.48	3.91 4.01	40.32 40.03	$C_6H_8F_4O_2$	38.30	4.26	40.43	188.04640 (188.04603)	$C_6H_8F_4O_2$ $[M]^+$
XXc	89	88–89 (6)	31.07 30.78	2.12 2.15	58.73 59.01	$C_{10}H_8F_{12}O_2$	30.93	2.06	58.76	368.02400 (368.02702)	$C_{10}H_7F_{11}O_2$ $[M - H]^+$
XXd	69	60–62 (24)	32.22 32.53	3.05 2.75	52.82 52.76	$C_8H_8F_8O_2$	33.33	2.78	52.78	268.03719 (268.03342)	$C_8H_8F_7O_2$ $[M - F]^+$
XXI	12	125–127 (20)	27.47 27.60	1.96 2.24	64.26 64.39	$C_{16}H_{10}F_{24}O_3$	27·20	1.42	64.59	706	$C_{16}H_{10}F_{24}O_3$ $[M]^+$
XXIIa	95	126–127 (20)	35.61 35.96	2.91 2.10	55.36 55.08	$C_8H_8F_8O$	35.29	2.94	55.88	272.04478 (272.04473)	$C_8H_8F_8O$ $[M]^+$
XXIIb	65	62–63 (20)	46.29 46.59	4.98 4.29	41.55 41.25	$C_9H_{12}F_6O$	46.55	5.17	41.38	231	$C_8H_9F_6O$ $[M - CH_3]^+$
XXIIc	88	65–67 (6)	32.41 32.12	2.17 2.36	61.38 61.03	$C_{10}H_8F_{12}O$	32.26	2.15	61.29	372.03810 (372.03834)	$C_{10}H_8F_{12}O$ $[M]^+$
XXIId	78	55–56 (20)	48.01 47.76	5.69 5.51	37.87 37.97	$C_8H_{12}F_4O$	48.00	6.00	38.00	185.06261 (185.05894)	$C_7H_9F_4O$ $[M - CH_3]^+$
XXIIe	83	75–76 (6)	29.79 29.92	1.94 2.19	63.65 63.34	$C_{12}H_8F_{16}O$	30.51	1.69	64.41	472.03110 (472.3195)	$C_{12}H_8F_{16}O$ $[M]^+$

IR spectrum (CCl_4, 5%), ν, cm^{-1}: 2981 (C–H), 1399 and 1379 (C–O), 1289 (C–O), 1184 and 1149 (C–F). Mass spectrum, *m/z* (I_{rel}, %): 562 $[M - HF]^+$ (3.94), 543 $[M - HF - F]^+$ (2.58), 413 $[M - F - (CF_2)_3]^+$ (6.91), 393 $[M - HF - H(CF_2)_4O]^+$ (40.43), 281 $[CF_2CF_2CH_2OCF_2CHFCF_3]^+$ (1.56), 231 $[CF_2 \cdot CH_2OCF_2CHFCF_3]^+$ (9.34), 181 $[CH_2OCF_2CHF \cdot CF_3]^+$ (80.54), 163 $[CHF_2CF_2OCF_2CHF]^+$ (4.57), 151 $[CF_2CHFCF_3]^+$ (79.58), 131 $[CHF_2CH_2OCF_2]^+$ (41.14), 119 $[C_2F_5]^+$ (15.71), 101 $[CHFCF_3]^+$ (17.46), 100 $[CF_2CF_2]^+$ (9.95), 81 $[CF_2CF]^+$ (1.27), 69 $[CF_3]^+$ (90.92), 51 $[CHF_2]^+$ (100).

The reactions of hexafluoropropylene with the other fluorinated alcohols, yielding ethers **XVIa**–**XVIc** (Tables 2, 3), were performed similarly.

Reactions of partially fluorinated alcohols with epichlorohydrin. To a suspension of 6.7 g (0.12 mol)

of KOH in 50 ml of acetonitrile, we added dropwise with stirring and cooling with ice-cold water 23.2 g (0.1 mol) of alcohol **XIII** over a period of 20 min. The mixture was stirred for 6 h at 20°C, after which 9.2 g (0.1 mol) of epichlorohydrin was added. The resulting mixture was stirred at room temperature for 3 h and then at 50°C for 1 h, after which it was poured into water. The organic layer was separated, washed with water, dried over $MgSO_4$, and distilled. (2,2,3,3,4,4,5,5-Octafluoropentyloxymethyl)oxirane **XXd** was obtained; yield 22.5 g (78%). IR spectrum (CCl_4, 5%), ν, cm^{-1}: 3055, 3002, 2928 (C–H), 1401 and 1251 (epoxy group), 1226 (C–O), 1175 and 1134 (C–F), 906 (epoxy group). Mass spectrum, *m*/*z* (I_{rel}, %): 268 $[M - HF]^+$ (1.99), 245 $[M - CHCH_2O]^+$ (6.05), 145 $[CF_2CFCF_2CH_2)]^+$ (9.76), 100 $[CF_2CF_2]^+$ (1.36), 69 $[CF_3]^+$ (7.07), 57 $[CH_2CHCH_2O]^+$ (39.71), 51 $[CHF_2]^+$ (30.08).

(2,2,3,3,4,4,5,5,6,6,7,7-Dodecafluoroheptyloxymethyl)oxirane XXc. IR spectrum (CCl_4, 5%), ν, cm^{-1}: 3064, 3002, 2928 (C–H), 1441 and 1250 (epoxy group), 1201 (C–O), 1169 and 1143 (C–F), 998 and 906 (epoxy group). Mass spectrum, *m*/*z* (I_{rel}, %): 368 $[M - HF]^+$ (15.29), 358 $[M - CH_2O]^+$ (2.55), 345 $[M - CHCH_2O]^+$ (54.01), 338 $[M - CF_2]^+$ (4.23), 245 $[CF_2CF(CF_2)CH_2]^+$ (16.75), 181 $[CF_2CF(CF_2)_3CH_2]^+$ (2.52), 151 $[HCF_2CF_2CF_2]^+$ (3.01), 131 $[CF_2CFCF_2]^+$ (13.94), 101 $[HCF_2CF_2]^+$ (9.72), 100 $[CF_2CF_2]^+$ (5.78), 87 $[CH_2OCH_2CHCH_2O]^+$ (2.84), 69 $[CF_3]^+$ (19.79), 57 $[CH_2CHCH_2O]^+$ (100), 51 $[CHF_2]^+$ (32.05).

The reactions of epichlorohydrin with the other partially fluorinated alcohols, yielding the corresponding oxiranes **XIIa**–**XIIc** (Tables 2, 3), were performed similarly.

Reactions of partially fluorinated alcohols with allyl bromide. To a suspension of 6.7 g (0.1 mol) of KOH in 50 ml of acetonitrile, we added with stirring and cooling with ice-cold water 23.2 g (0.1 mol) of alcohol **XIII**; the mixture was allowed to stand for 1 h at room temperature. Then 12.1 g (0.1 mol) of allyl bromide was added; the mixture was heated at 45°C for 4 h with stirring, after which it was poured into water. The organic layer was separated, washed with water, dried over $MgSO_4$, and distilled. 1,1,5-Trihydrooctafluoropentyl allyl ether **XXIIa** was obtained; yield 25.8 g (95%), bp 126–127°C (20 mm Hg). IR spectrum (CCl_4, 5%), ν, cm^{-1}: 3088, 3001, 2943, 2865 (C–H), 1673 (C=C), 1461 and 1402 (C–O), 1174 and 1134 (C–F), 935 and 898 (C–O). Mass spectrum, *m*/*z* (I_{rel}, %): 272 $[M]^+$ (29.33), 182 $[HCF_2CF_2 \cdot CF_2CF]^+$ (1.74), 131 $[HCF_2CF_2CH_2O]^+$ (6.14), 100 $[CF_2CF_2]^+$ (3.39), 71 $[CH_2OCH_2CHCH_2]^+$ (44.97), 69 $[CF_3]^+$ (13.76), 57 $[CH_2CHCH_2O]^+$ (12.19), 51 $[CHF_2]^+$ (24.78), 41 $[CH_2CH{=}CH_2]^+$ (100), 31 $[CH_2OH]^+$ (24.08).

The reactions of allyl bromide with the other partially fluorinated alcohols, yielding the corresponding ethers **XXIIb**–**XXIIe** (Tables 2, 3), were performed similarly.

CONCLUSIONS

(1) Partially fluorinated alcohols were prepared by reactions of perfluoroolefins with ethanol and isopropanol in the presence of di-*tert*-butyl peroxide. The reactions yield mixtures of thermodynamically stable diastereomers.

(2) The reactions of partially fluorinated alcohols with epichlorohydrin and allyl bromide in the presence of a base (K_2CO_3, KOH) give products of halogen replacement. With KOH, the products of epoxy ring opening are also formed in a low yield.

(3) The reaction of hexafluoropropylene with partially fluorinated alcohols in the presence of KOH yields dialkyl ethers and polysubstituted ethers, whereas with trimethylsilyl ethers of these alcohols the dialkyl ethers are formed without a base as the only products.

REFERENCES

1. US Patent 6187969.
2. RF Patent 2150459.
3. FRG Patent 3915759.
4. Rakhimov, A.I., Vostrikova, O.A., and Ermakov, A.V., Abstracts of Papers, *5-ya mezhdunarodnaya konferentsiya "Naukoemkie khimicheskie tekhnologii"* (5th Int. Conf. "High Chemical Technologies"), Yaroslavl, May 19–21, 1998, vol. 1, pp. 141–142.
5. US Patent 5495034.
6. EPW Appl. 1085006.
7. Nguyen, T. and Wakselman, C., *Synth. Commun.*, 1990, vol. 20, no. 1, pp. 97–99.
8. RF Patent 2107751.
9. Szlavik, Z., Tarkanyi, G., Skribanek, Z., et al., *Org. Lett.*, 2001, vol. 3, no. 15, pp. 2365–2366.
10. *Fluorine Compounds. Modern Techonology and Application*, Ishikawa, N., Ed., Tokyo: CMC, 1987.

11. EPW Appl. 1 191 009.
12. EPW Appl. 1 179 521.
13. PCT Int. Appl. WO 02 28 807.
14. JPN Patent 2002 53 505.
15. PCT Int. Appl. WO 02 16 295.
16. Il'in, A.A., Bakhmutov, Yu.L., Ivanova, L.M., et al., *Zh. Prikl. Khim.*, 2004, vol. 77, no. 1, pp. 102–105.
17. Furin, G.G., Il'in, A.A., Bakhmutov, Yu.L., et al., *Nauka Proizv.*, 2004, no. 5, pp. 26–36.
18. Fokin, A.V., Komarov, V.A., Kolomnets, A.F., et al., *Izv. Akad. Nauk SSSR, Ser. Khim.*, 1977, no. 9, pp. 2141–2144.
19. Krolevits, A.A., *Itogi Nauki Tekh., Ser.: Org. Khim.*, 1985, vol. 6, pp. 40–46.
20. Boutevin, B., Hugon, J.-P., and Pietrasauta, J., *J. Fluorine Chem.*, 1981, vol. 17, no. 4, p. 357.
21. Boutevin, B., Youssef, D., Boileau, S., and Garnault, A.M., *J. Fluorine Chem.*, 1987, vol. 35, no. 2, pp. 399–410.

ISSN 1070-4272, Russian Journal of Applied Chemistry, 2007, Vol. 80, No. 3, pp. 419–423. © Pleiades Publishing, Ltd., 2007.
Original Russian Text © T.P. Ostrovskaya, I.G. Trukshin, 2007, published in Zhurnal Prikladnoi Khimii, 2007, Vol. 80, No. 3, pp. 421–425.

ORGANIC SYNTHESIS AND INDUSTRIAL ORGANIC CHEMISTRY

Reaction of Hexadecafluorobicyclo[4.4.0]dec-1(6)-ene with Diethylamine

T. P. Ostrovskaya and I. G. Trukshin

Polymer Plant, Kirovo-Chepetsk Chemical Combine, Limited Liability Company, Kirovo-Chepetsk, Kirov oblast, Russia
Prikladnaya Khimiya Russian Scientific Center, Federal State Unitary Enterprise, St. Petersburg, Russia

Received April 12, 2006; in final form, November 2006

Abstract—The spectral characteristics of products formed in the reaction of an incompletely fluorinated impurity in perfluorodecalin, hexadecafluorobicyclo[4.4.0]dec-1(6)-ene, with amines in various solvents were studied. The reaction rates in various solvents were compared, and the distribution of the reaction products between perfluorodecalin and solvents was examined.

DOI: 10.1134/S1070427207030135

In perfluoroorganic compounds, all hydrogen atoms are replaced by fluorine atoms. Generally these compounds consist of carbon and fluorine atoms; they also can include other atoms, e.g., N, O, and S. The C–F bond energy is higher than the energy of the C–H and C–C bonds, which provides high thermal and chemical stability of perfluoroorganic compounds. As hydrogen atoms are replaced by fluorine atoms, e.g., in methane, the C–F bond becomes shorter and its energy increases. One more factor accounting for the stability of fluorocarbons is favorable ratio between the length of the C–C bond and the size of the F atom. The van der Waals radius of F is shorter than the C–C bond length; therefore, accumulation of F atoms in perfluoroorganic compounds does not lead to extension and weakening of C–C bonds as in perchlorocarbons. The fluorine atoms build up a dense shell reliably protecting the carbon chain from external effects and making it chemically inert; due to weak van der Waals interactions, perfluorocarbons are more volatile than common hydrocarbons [1, 2].

Thanks to unique chemical and physical properties, perfluoroorganic compounds are used as dielectrics, heat carriers, and inert materials, and also in medicine as perfusion fluids and components of blood substitutes [3–5].

Preparation of perfluorinated products by fluorination of the corresponding hydrocarbons is accompanied by formation of a large set of partially or fully fluorinated impurities. Perfluorinated impurities are analogs of the target products and have similar electrochemical and thermal characteristics, differing from the target products only in the lower viscosity and lower boiling point. When present in an amount of up to 5 wt %, these impurities do not noticeably impair the service characteristics of the target perfluoroorganic product. At the same time, partially fluorinated compounds, i.e., hydrogen-containing and unsaturated polyfluorinated impurities, even in minor amounts (below 10^{-3} wt %) impair the chemical and service properties of the perfluoroorganic products, imparting to them toxicity and corrosion activity and making worse the dielectric properties of the compositions [6].

A typical perfluoroorganic compound is perfluorodecalin (PFD), used in industry as a heat carrier and a dielectric, and also in medicine as a component of an artificial blood substitute and perfusion fluid [4, 5]. Production of PFD by fluorination of naphthalene and tetralin involves formation of a series of hydrogen-containing and unsaturated impurities (Table 1) [7, 8].

Partially fluorinated impurities with a high degree of substitution with fluorine atoms only slightly differ in physical properties from the fully fluorinated products; therefore, their separation from the target product is difficult. The main distinction of partially fluorinated compounds is their chemical activity. A characteristic reaction of partially fluorinated compounds is that with nucleophilic agents [1, 2]. The reactions of fluoroolefins and hydrogen-containing polyfluorinated compounds with amines yield amino derivatives, which essentially differ in the physicochemical properties from the starting fluoroolefins and target perflu-

Table 1. Partially fluorinated compounds formed by fluorination of naphthalene [7, 8]

Structural formula	Name
	PFDC, hexadecafluorobicyclo[4.4.0]dec-1(6)-ene
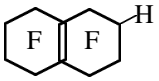	PFHDC, 3*H*-pentadecafluorobicyclo-[4.4.0]dec-1(6)-ene
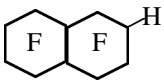	3*H*-Heptadecafluorobicyclo[4.4.0]decane

orinated products. Conversion of partially fluorinated impurities into amino derivatives facilitates their separation from the target products. At the same time, the reaction of partially fluorinated impurities with amines can be used for estimating the degree of fluorination of a perfluoroorganic product and revealing partially fluorinated impurities.

In this study we examined the reactions of PFDC and PFHDC with amines.

It is known that solutions of products formed by reaction of diethylamine (DEA) with insufficiently pure PFD samples are red-brown [9]; however, no data on spectral characteristics of these colored compounds have been reported.

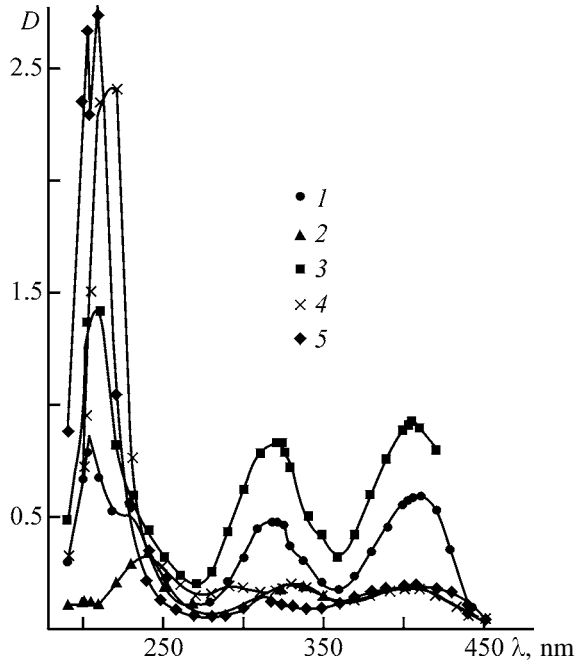

Fig. 1. Absorption spectra of products formed by reaction of PFDC (2.18×10^{-4} M) with DEA (2.19×10^{-3} M). (*D*) Optical density and (λ) wavelength; the same for Figs. 2 and 3. Solvent: (*1*) ethanol, (*2*) butanol, (*3*) acetonitrile, (*4*) 2-propanol, and (*5*) hexane.

EXPERIMENTAL

The UV/visible absorption spectra were recorded on an SF-46 spectrophotometer in the point-by-point mode with a step of 10 nm (near peaks, 2 nm) using 10-mm quartz cells. The ^{19}F NMR spectra were measured on a Bruker Spectrospin device (84.8 MHz, internal reference hexafluorobenzene).

Perfluorobicyclo[4.4.0]dec-1(6)-ene was isolated from crude PFD by two successive fractional distillations. The compound was chromatographically pure (stationary phase dibutyl phthalate). The ^{19}F NMR spectrum consisted of two singlets at 111.7 and 134.8 ppm, in agreement with published data [7].

3*H*-Heptadecafluorobicyclo[4.4.0]dec-1(6)-ene was isolated from crude PFD. According to the GLC analysis, the fraction in hand contained 39.8% 3*H*-heptadecafluorobicyclo[4.4.0]dec-1(6)-ene and 58.0% *trans*-perfluorodecalin. The ^{19}F NMR spectrum contained two characteristic high-field signals: a singlet at 187.7 ppm corresponding to the fluorine atom at the tertiary carbon atom in *trans*-perfluorodecalin and a broad signal at 214.2 ppm corresponding to the fluorine atom in the geminal position relative to the H atom. The ratio of the peak areas, 3 : 1, is equal to the ratio of the corresponding fluorine atoms, taking into account the relative content of both components.

The distribution ratios of the reaction products between PFD and the solvent were calculated as ratios of the optical densities of the solvent and PFD layers after performing the reaction for 30 min with continuous stirring and temperature control. The initial solutions were prepared by dissolution of PFDC and PFHDC in PFD and of DEA in appropriate organic solvent. The phase volume ratio was 1 : 1. As proved in [10], the optical densities of solutions are proportional to the concentrations of the reaction products. In calculations we took into account the hyperchromic effect observed in dissolution of reaction products in various solvents relative to hexane and PFD [11].

The spectra of products formed by the reaction of PFDC with diethylamine in various solvents have the following bands: λ_{max1} = 204–224, λ_{max2} = 310–322, and λ_{max3} = 401–408 nm (Fig. 1, Table 2).

The band at 204 nm is difficult to assign because of absorption of the starting compounds in this range. Amino derivatives prepared in different solvents have

Table 2. Characteristics of absorption bands of PFDC, DEA, and products of their reaction in different solvents

Solvent	Bands of starting compounds				Bands of reaction products		
	DEA		PFDC		λ_{max1}	λ_{max2}	λ_{max3}
	λ_{max}	ε_{max}*	λ_{max}	ε_{max}*			
Hexane	210	1170	200	360	210	310	406
2-Propanol	214		206		220	332	402–406
Butanol	224		206		226	330–336	406–410
Ethanol	204		206		204	322	408
Acetonitrile	200		200		210	322	408

* (ε_{max}) Molar extinction coefficient.

similar absorption bands with a small relative shift depending on particular solvent.

The products of reactions of PFDC with primary (ethylenediamine) and tertiary (triethylamine) amines give two appreciably overlapping absorption bands (Fig. 2).

The absorption spectra of products formed by reactions of PFHDC with amines are similar (Fig. 2); therefore, the products presumably have similar structures. The absorption intensity of the products formed from PFHDC is higher than that of the products formed from PFDC.

The relative reaction rates in various solvents and the solvent parameters [12] are given in Table 3.

For reactions of fluoroolefins with amines, a mechanism with formation of an intermediate zwitterion was suggested [13, 14]:

$$>C=CF_2 + R_2NH \rightleftarrows >\bar{C}-CF_2\overset{+}{N}HR_2 \xrightarrow{-HF} >C=CFNR_2. \quad (1)$$

In the reaction of PFDC with diethylamine in 2-propanol, the formation of the zwitterion is presumably preceded by the formation of a π complex as a result of interaction of the nitrogen lone electron pair with the antibonding π* orbital of PFDC (*n*–π* state). This hypothesis is supported by the calculated activation energy, 34.2 kJ mol^{-1} [15], which is appreciably lower than the energies of formation of excited singlet and triplet states of perfluoroolefins (18 kcal mol^{-1}, or 75 kJ mol^{-1} [16]) but is in the range typical of *n*–π* and charge-transfer states (21–42 kJ mol^{-1} [17]). It can also be assumed that formation of the π complex from the starting reagents is reversible, but its transformation into the zwitterion is irreversible. The rearrangement of the π complex into the zwitterion should be very sensitive to the medium and to nucleophilic agents.

The observed (Table 3) increase in the reaction rate with an increase in the solvent polarity is consistent with the suggested mechanism. The abnormal, at first glance, results for dioxane are associated with the fact that the dioxane molecule consists of polar fragments but is symmetrical, which results in zero dipole mo-

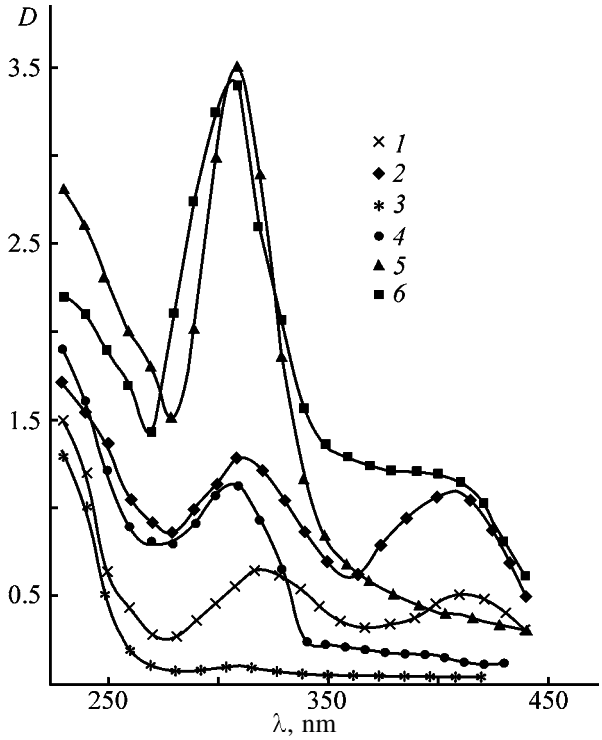

Fig. 2. Absorption spectra of products formed by reaction of PFDC and PFHDC with diethylamine (DEA), triethylamine (TEA), and ethylenediamine (EDA) (0.2 M solutions in ethanol): (*1*) PFDC + DEA, (*2*) PFHDC + DEA, (*3*) PFDC + TEA, (*4*) PFHDC + TEA, (*5*) PFDC + EDA, and (*6*) PFHDC + EDA.

Table 3. Solvent effect on the rate of product formation in the reaction of PFDC (0.002 M) with diethylamine (0.008 M) at room temperature

Solvent	Solvent parameters		Relative reaction rate* monitored at indicated λ_{max}, nm	
	μ, D	ε	310	406
Hexane	0.08	1.89	1	1
Chloroform	1.87	4.70	26	53
2-Propanol	1.66	18.3	34	55
Butanol	1.66	17.1	153	344
Dioxane	0	2.21	939	349
Ethanol	1.69	24.3	2160	4166
Acetonitrile	3.92	36.2	2500	4876

* Taking into account hyperchromic effect. The rate of reaction in hexane is taken as unity.

Table 4. Distribution ratios of PFDC + diethylamine reaction products between solvents of various polarities and PFD at 60°C

Solvent	Concentration of starting components		ε	K_{310}	K_{406}
	PFDC, M, $\times 10^4$	DEA, M			
Hexane	7.04	3.0	1.89	4±0.5	13±1
Dioxane	6.76	3.0	2.21	61±5	92±9
Butanol	6.60	3.0	17.1	78±8	140±12
2-Propanol	6.60	3.0	18.3	64±6	210±20
Ethanol	6.80	3.0	24.3	54±5	100±10

ment and low dielectric permittivity. However, in this case the macroscopic characteristics of the solvent do not reflect in full measure its physicochemical properties associated with separate fragments of molecules.

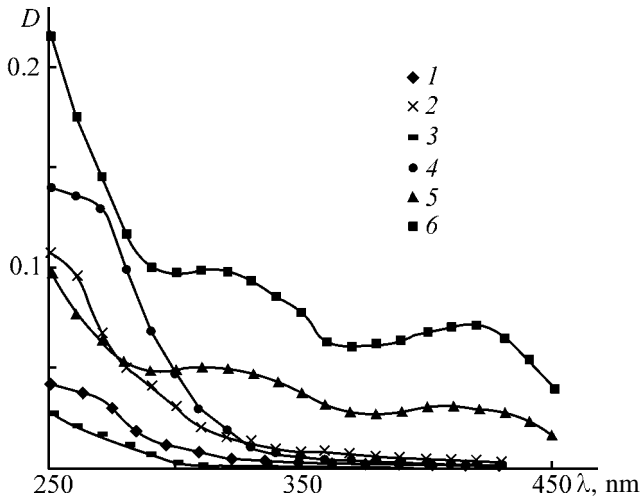

Fig. 3. Absorption spectra: (*1*, *2*) starting substances, (*3*, *4*) ethanol extracts, and (*5*, *6*) products of reaction of 0.2 M solution of diethylamine in ethanol with the samples. Crude PDF: (*1*, *3*) sample 1, (*2*, *4*) sample 2, (*5*) operation 42, and (*6*) operation 23.

The distribution ratios (ratios of equilibrium concentrations in the solvent and in the perfluoroorganic compound) of reaction products are important for assessing the suitability of the reaction for technological (purification to remove partially fluorinated compounds) and analytical purposes. The distribution ratios of the PFDC + diethylamine reaction products between various solvents and PFD are given in Table 4. These quantities were calculated from two absorption bands of the reaction products at 310 and 406 nm. Introduction of amino groups into the molecule of the initial polyfluorinated compound makes it more polar and thus enhances its affinity for polar solvents. At the same time, with an increase in the degree of substitution of fluorine atoms by amino groups, the proportion of hydrocarbon fragments in the molecule increases, and the compound becomes more soluble in less polar solvents. The combination of these two opposite trends gives a dependence with a maximum (point for 2-propanol).

Figure 3 shows the absorption spectra of ethanol extracts from treatment of process PFD samples with a diethylamine solution. These spectra are similar to those obtained for model compounds. This fact indi-

cates that the reactions of diethylamine with various partially fluorinated compounds (whose full identification is practically impossible) yields products structurally similar to those of the reaction of PFDC with diethylamine. This similarity opens prospects for the development, using this reaction, of procedures both for PFD purification and for integrated determination of partially fluorinated compounds in PFD in various steps of the production process.

CONCLUSION

The reaction of partially fluorinated hexadecafluorobicyclo[4.4.0]dec-1(16)-ene (an impurity in perfluorodecalin) with amines in various solvents is promising for purifying the target perfluoro compounds to remove partially fluorinated impurities and for evaluating the degree of fluorination of the target product.

REFERENCES

1. Ishikawa, N. and Kobayashi, Y., *Fluorine Compounds. Chemistry and Applications*, Kodansha, 1979.
2. Sheppard, W.A. and Sharts, C.M., *Organic Fluorine Chemistry*, New York: Benjamin, 1969.
3. *Fluorine Compounds. Modern Techonology and Applications*, Ishikawa, N., Ed., Tokyo: CMC, 1987.
4. Maksimov, B.N., Barabanov, V.G., et al., *Promyshlennye ftororganicheskie produkty: Spravochnoe izdanie* (Commercial Organofluoric Products: Handbook), St. Petersburg: Khimiya, 1996.
5. Ivanitskii, G.R., in *Perftororganicheskie soedineniya v biologii i meditsine* (Perfluoroorganic Compounds in Biology and Medicine), Pushchino: Perftoran, 2001, pp. 4–48.
6. Bispen, T.A., Mikhailova, T.V., Moldavskii, D.D., and Furin, G.G., *Zh. Prikl. Khim.*, 1995, vol. 68, no. 11, pp. 1867–1871.
7. Plevey, R.G., Sallomi, I.J., Thomas, D.F., and Tatlow, J.C., *J. Chem. Soc., Perkin Trans. 1*, 1976, pp. 2270–2272.
8. Coe, P.L., Habib, R.M., and Tatlow, J.C., *J. Fluorine Chem.*, 1982, vol. 20, no. 2, pp. 203–213.
9. Clark, L.C. and Moore, R.E., Abstracts of Papers, *IV Winter Fluorine Conf.*, Daytona Beach, Florida, January 20–February 2, 1979; *AIPS–Ftor*, 1980, no. 16, abstract no. 49181.
10. USSR Inventor's Certificate no. 1063187.
11. Ostrovskaya, T.P. and Ostrovskii, N.V., *UF spektry produktov aminirovaniya ftorolefinov* (UV Spectra of fluoroolefin Amination Products), Available from VIMI, 1990, no. 11, paper no. D08350, March 1, 1991.
12. Gordon, A.J. and Ford, R.A., *The Chemist's Companion. A Handbook of Practical Data, Techniques, and References*, New York: Wiley, 1972.
13. Robson, P. et al., *J. Chem. Soc.*, 1964, September, pp. 5748–5753.
14. Leffek, K.T. and Maciejewska, U., *Can. J. Chem.*, 1986, pp. 2274–2278.
15. Ostrovskaya, T.P., Ostrovskii, N.V., and Zozulya, A.P., *Kinetika vzaimodeistviya perftor[4.4.0]detsena-1(6) s dietilaminom* (Kinetics of the Reaction of Perfluoro-[4.4.0]dec-1(6)-ene with Diethylamine), Available from VIMI, 1991, no. 11, paper no. D08486.
16. Kalnin'sh, K.K. and Semenov, S.G., *Zh. Prikl. Khim.*, 2003, vol. 76, no. 10, pp. 1585–1600.
17. Kalnin'sh, K.K., *Zh. Prikl. Khim.*, 2002, vol. 75, no. 4, pp. 603–611.

ISSN 1070-4272, Russian Journal of Applied Chemistry, 2007, Vol. 80, No. 3, pp. 424–427. © Pleiades Publishing, Ltd., 2007.
Original Russian Text © N.V. Lebedev, G.A. Emel'yanov, F.A. Makhmutov, D.D. Moldavskii, V.V. Berenblit, 2007, published in Zhurnal Prikladnoi Khimii, 2007, Vol. 80, No. 3, pp. 426–429.

ORGANIC SYNTHESIS AND INDUSTRIAL ORGANIC CHEMISTRY

A ^{19}F NMR Study of Products of Hexafluorobutadiene Sulfotrioxidation

N. V. Lebedev, G. A. Emel'yanov, F. A. Makhmutov, D. D. Moldavskii, and V. V. Berenblit

Lebedev Research Institute of Synthetic Rubber, Federal State Unitary Enterprise, St. Petersburg, Russia
Prikladnaya Khimiya Russian Scientific Center, St. Petersburg, Russia
Medical and Environmental Chemistry Research Center, Tula, Russia

Received September 12, 2006

Abstract—The products of hexafluorobutadiene sulfotrioxidation were identified by ^{19}F NMR. The major products are hexafluoro-1-butene-3,4-β-sultone, hexafluoro-2-butene-1,4-sultone, hexafluoro-1-butene-3,4-pyrosultone, and hexafluoro-2-buten-1,4-diyl sulfate.

DOI: 10.1134/S1070427207030147

Hexafluorobutadiene, as fairly accessible perfluoro analog of divinyl, monomer of Lebedev's synthetic rubber, still attracts researchers' attention. However, it did not justify hopes in the field of fluoropolymer chemistry, since the fluorine electronegativity extended the conjugation of its double bonds, which precluded formation of *cis*-1,4 elastomer structures.

The variety of the reactions of fluoroolefins with sulfur trioxide resulting in formation of β-sultones in sulfotrioxidation or fluorosulfates in fluorosulfation attracted attention to the reaction of hexafluorobutadiene with sulfur trioxide.

From the evidence of ^{19}F NMR data (a Hitachi H60 spectrometer operating at 56.4 MHz), Knunyants et al. [1] assigned the structure of 4-(trifluorovinyl)-3,3,4-trifluoro-1-oxa-2-thiacyclobutane 2,2-dioxide (**I**), i.e., hexafluoro-1-butene-3,4-β-sultone, to the product:

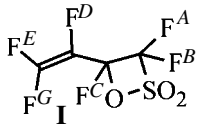

I

F^E: δ_F –88.7 ppm (d.d.d), J_{E-C} 5.6 Hz, J_{E-D} 38.6 Hz, J_{E-G} 49.5 Hz; F^D: δ_F –191.4 ppm (d.d.d.d), J_{D-B} 8.7 Hz, J_{D-C} 20.5 Hz, J_{D-E} 38.6 Hz, J_{D-G} 118.3 Hz; F^A: δ_F –94.5 ppm (d.d.d), J_{A-D} 1.8 Hz, J_{A-C} 7.8 Hz, J_{A-B} 163.5 Hz; F_G: δ_F –105.7 ppm (d.d.d.d), J_{G-D} 118.3 Hz, J_{G-E} 48.5 Hz, J_{G-C} 28.0 Hz, J_{G-B} 2.5 Hz; F^C: δ_F –123.5 ppm (d.d.d.d.d), J_{C-G} 28.0 Hz, J_{C-D} 20.5 Hz, J_{C-A} 7.8 Hz, J_{C-E} 5.6 Hz, J_{C-B} 3.1 Hz; F^B: δ_F –102.2 ppm (d.d.d.d), J_{B-A} 163.5 Hz, J_{B-D} 8.7 Hz, J_{B-C} 3.1 Hz, J_{B-G} 2.5 Hz.

However, actually the chemical shifts and spin–spin coupling constants disagree with the above structure. Signals of the F^A and F^B atoms of the CF_2 group neighboring to the SO_2 group have typically chemical shifts in the region of 115±5 ppm, while the F^C signal of the CF group neighboring to ester oxygen should lie at about 135 ppm. The geminal coupling constant in the four-membered ring commonly does not exceed 130 Hz, whereas the coupling constant equal to 163 Hz suggests that magnetically non-equivalent OCF_2 group is incorporated in the six-membered ring of pyrosultone.

In this study we examined the products formed in the reaction of hexafluorobutadiene with sulfur trioxide under various conditions and in various media. As the major sulfotrioxidation product (content in the mixture from 30 to 70 mol %) we identified hexafluoro-1-butadiene-β-sultone (**II**) from the following signals (^{19}F NMR spectra were recorded on a Bruker Spectrospin AM-500 spectrometer operating at 470.572 MHz against the background of hexafluorobenzene):

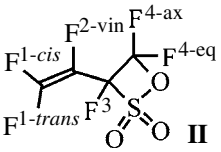

II

$F^{1\text{-}cis}$: δ_F –85.3±0.2 ppm (d.d.d), $J_{1\text{-}cis\text{-}3}$ 5.3±0.3 Hz,

$J_{1\text{-}cis\text{–}2\text{-vin}}$ 39.4 ± 0.6 Hz, $J_{1\text{-}cis\text{–}1\text{-}trans}$ 48.4 ± 0.4 Hz; $F^{2\text{-vin}}$: δ_F –188.5 ± 0.1 ppm (d.d.d), $J_{2\text{-vin}\text{–}3}$ 18.7 ± 0.3 Hz, $J_{2\text{-vin}\text{–}1\text{-}cis}$ 39.5 ± 0.3 Hz, $J_{2\text{-vin}\text{–}1\text{-}trans}$ 118.0 ± 0.2 Hz; $F^{4\text{-ax}}$: δ_F –76.3 ± 0.2 ppm (d.d.d), $J_{4\text{-ax}\text{–}3}$ 12.1 ± 0.4 Hz, $J_{4\text{-ax}\text{–}2\text{-vin}}$ 16.9 ± 0.5 Hz, $J_{4\text{-ax}\text{–}4\text{-eq}}$ 127.5 ± 0.5 Hz; $F^{1\text{-}trans}$: δ_F –102.5 ± 0.5 ppm (d.d.d.t), $J_{1\text{-}trans\text{–}2\text{-vin}}$ 118.0 ± 0.2 Hz, $J_{1\text{-}trans\text{–}1\text{-}cis}$ 48.4 ± 0.4 Hz, $J_{1\text{-}trans\text{–}3}$ 33.3 ± 0.3 Hz, $J_{1\text{-}trans\text{–}4\text{-eq}}$ 2.4 Hz; F^3: δ_F –115.0 ± 0.2 ppm (d.t.d.d), $J_{3\text{–}1\text{-}trans}$ 33.3 ± 0.3 Hz, $J_{3\text{–}2\text{-vin, }4\text{-ax}}$ 18.7 ± 0.3 Hz, $J_{3\text{–}1\text{-}trans}$ 10.3 ± 0.5 Hz, $J_{3\text{–}1\text{-}cis}$ 5.3 ± 0.3 Hz; $F^{4\text{-eq}}$: δ_F –88.5 ± 0.3 ppm (d.d.d), $J_{4\text{-eq}\text{–}4\text{-ax}}$ 127.5 ± 0.5 Hz, $J_{4\text{-eq}\text{–}4\text{-eq}}$ 10.7 ± 0.3 Hz, $J_{4\text{-eq}\text{–}1\text{-}trans}$ 2.5 Hz.

In the case of sulfotrioxidation of hexafluorobutadiene in the presence of an excess of sulfur trioxide, the structure of hexafluoro-1-butene-3,4-pyrosultone (**III**) was identified. This compound gives the following signals in the spectrum:

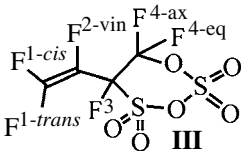

III

$F^{1\text{-}cis}$: δ_F –86.4 ppm (d.d.d), $J_{1\text{-}cis\text{–}3}$ 5.7 Hz, $J_{1\text{-}cis\text{–}2\text{-vin}}$ 40.0 Hz, $J_{1\text{-}cis\text{–}1\text{-}trans}$ 47.7 Hz: $F^{2\text{-vin}}$: δ_F –188.3 ± 0.1 ppm (d.d.d), $J_{2\text{-vin}\text{–}3}$ 19.1 Hz, $J_{2\text{-vin}\text{–}1\text{-}cis}$ 40.0 Hz, $J_{2\text{-vin}\text{–}1\text{-}trans}$ 118.0 Hz; $F^{4\text{-ax}}$: δ_F –92.9 ppm (d.d), $J_{4\text{-ax}\text{–}2\text{-vin}}$ 8.5 Hz, $J_{4\text{-ax}\text{–}4\text{-eq}}$ 163 Hz; $F^{1\text{-}trans}$: δ_F –103.6 ± 0.5 ppm (d.d.d), $J_{1\text{-}trans\text{–}1\text{-vin}}$ 118.2 Hz, $J_{1\text{-}trans\text{–}1\text{-}cis}$ 49.6 Hz, $J_{1\text{-}trans\text{–}3}$ 26.7 Hz; F^3: δ_F –120.7 ± 0.2 ppm (d.t.d), $J_{3\text{–}1\text{-}trans}$ 26.7 Hz, $J_{3\text{–}2\text{-vin, }4\text{-ax}}$ 21.0 Hz, $J_{3\text{–}1\text{-}cis}$ 3.8 Hz; $F^{4\text{-eq}}$: δ_F –103.3 ppm (d.d.d), $J_{4\text{-eq}\text{–}4\text{-ax}}$ 164 Hz, $J_{4\text{-eq}\text{–}3\text{-eq}}$ 28.6 Hz, $J_{4\text{-eq}\text{–}1\text{-}trans}$ 5.7 Hz.

It is evident that the signals in the ^{19}F NMR spectrum corresponding to this six-membered structure of pyrosultone do not noticeably differ from the signals of four-membered sultone **I** [1].

Among the reaction products we found a compound whose content varied from 15 to 25 mol % depending on the synthesis conditions. This compound was identified as a product of 1,4-addition of sulfur trioxide to hexafluorobutadiene with the formation of hexafluoro-2-butene-1,4-sultone (**IV**).

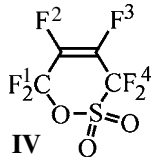

IV

F^1: δ_F –70.8 ppm (d.t), $J_{1\text{–}4}$ 9.6 Hz, $J_{1\text{–}2}$ 22.6 Hz; F^2: δ_F –143.6 ppm (t.m), $J_{2\text{–}3}$ 13.3 Hz, $J_{2\text{–}1}$ 22.6 Hz: F^3: δ_F –149.5 ppm (t.t), $J_{3\text{–}1}$ 9.6 Hz, $J_{3\text{–}4}$ 17.2 Hz; F^4: δ_F –104.6 ppm (t.t), $J_{4\text{–}3}$ 15.3 Hz, $J_{4\text{–}1}$ 9.6 Hz.

It should be emphasized that in [1] the chemical shifts were assigned incorrectly.

The ^{19}F NMR spectra always contained two signals at –68.0 and –140 ppm with the intensity ratio of 2 : 1 and the coupling constant corresponding to the $–OCF^1_2CF^2=$ fragment of structure **IV**. The content of this compound in the mixture varied from 1 to 15 mol %. These signals should be assigned to seven-membered hexafluoro-2-butene-1,4-diyl sulfate (**V**):

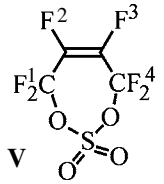

V

F^3: δ_F –140.2 ppm (t.t), $J_{3\text{–}4}$ 8.6 Hz, $J_{3\text{–}1}$ 22.6 Hz; F^4: δ_F –68.0 ppm (d.d), $J_{4\text{–}3}$ 8.6 Hz, $J_{4\text{–}2}$ 22.6 Hz.

Knunyants et al. [1] obtained this product by heating hexafluoro-2-butene-1,4-sultone. The mechanism of this conversion is not evident; on the other hand, this sulfate should be formed by elimination of sulfur dioxide with hexafluoro-2-butene-1,4-pyrosultone, which, contrary to sultone and 3,4-pyrosultone, has the same chemical shifts and coupling constants as hexafluoro-2-butene-1,4-sultone and cannot be distinguished by NMR.

Among the products in the mixture we identified up to 5 mol % of perfluoro-4-fluorosulfatobut-2-enoyl fluorides **VI** and **VII**, formed by ring opening in **V**, in the form of isomers different in the chemical shifts and coupling constants of fluorine nuclei in *cis* and *trans* positions. These constants agree well with published data [2] for α,β-unsaturated acyl fluorides.

The ratio of intensities of the corresponding signals shows that the concentration of the *trans* species was higher than that of the *cis* species.

The mixtures contained up to 15% of perfluorinated polymer products, which were manifested in the ^{19}F NMR spectra as broad signals in the regions of –70 and –104 ppm.

We found that four- and six-membered sultone rings formed by sulfotrioxidation of hexafluorobutadiene are extremely stable and undergo only partial opening even on heating to 150–170°C in the presence of potassium fluoride or potassium hydrofluoride. This thermal treatment of the mixtures results

also in desulfotrioxidation of fluorosulfate groups in perfluoro-4-fluorosulfatobut-2-enoyl fluorides. After thermal treatment, the following compounds were identified in the mixture: (1) perfluoro-2-fluorosulfo-2-vinylacetyl fluoride (**VIII**) formed by the ring opening in hexafluoro-1-butene-3,4-sultone (**II**); (2) perfluoro-4-fluorosulfo-2-buteneoyl fluoride (**IX**) formed by the ring opening in hexafluoro-2-butene-1,4-sultone (**IV**); (3) perfluoro-*trans*-crotonoyl fluoride (**X**) formed by elimination of sulfur trioxide from perfluoro-4-fluorosulfato-*trans*-but-2-enoyl fluoride (**VII**); and (4) perfluoro-*cis*-crotonoyl fluoride (**XI**) formed by elimination of sulfur trioxide from perfluoro-4-fluorosulfato-*cis*-but-2-enoyl fluoride (**VI**):

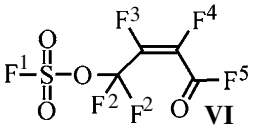

VI

F^1: δ_F 49.8 ppm (t), J_{1-2} 8.3 Hz; F^2: δ_F –68.1 ppm (q), $J_{2-1;3;4;5}$ 8.3 Hz; F^3: δ_F –134.9 ppm (d.d.t), $J_{3\text{-}cis-2}$ 9.5 Hz, $J_{3\text{-}cis-5}$ 14.3 Hz, $J_{3\text{-}cis-4\text{-}cis}$ 25.0 Hz; F^4: δ_F –122.7 ppm (d.t.d), J_{4-2} 8.3 Hz, $J_{4\text{-}cis-5}$ 14.3 Hz, $J_{4\text{-}cis-3\text{-}cis}$ 25.3 Hz; F^5: δ_F 27.5 ppm (d.q), $J_{4\text{-}cis-5}$ 14.3 Hz, $J_{5-2;3\text{-}cis;4\text{-}cis}$ 8.3 Hz.

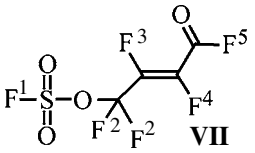

VII

F^1: δ_F 50.6 ppm (q), $J_{1-2;3}$ 8.3 Hz; F^2: δ_F –72.2 ppm (d.t), $J_{2-3\text{-}trans}$ 25.8 Hz, $J_{2-1;4\text{-}trans}$ 8.3 Hz; F^3: δ_F –150.6 ppm (d.t.d), $J_{3\text{-}trans-5}$ 21.3 Hz, $J_{3\text{-}trans-2}$ 25.8 Hz, $J_{3\text{-}trans-4\text{-}trans}$ 137.0 Hz; F^4: δ_F –141.3 ppm (d.d.t), $J_{4\text{-}trans-3\text{-}trans}$ 137.0 Hz, $J_{4\text{-}trans-5}$ 55.6 Hz, $J_{4\text{-}trans-2}$ 8.3 Hz; F^5: δ_F 27.9 ppm (d.d), $J_{5-3\text{-}trans}$ 21.3 Hz, $J_{5-4\text{-}trans}$ 55.3 Hz.

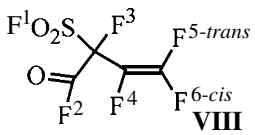

VIII

F^1: δ_F 51.2 ppm (t), $J_{1-2;3}$ 7.6 Hz; F^2: δ_F 29.0 ppm (d.d), J_{2-3} 25.4 Hz, J_{2-1} 7.6 Hz; F^3: δ_F –138.6 ppm (d.d), J_{3-1} 7.6 Hz, J_{3-2} 25.4 Hz; F^4: δ_F –147.1 ppm (d.t), $J_{4-5\text{-}trans}$ 138.0 Hz, $J_{4-6\text{-}trans;3}$ 20.5 Hz; F^5: δ_F –141.1 ppm (d.d.t), $J_{5\text{-}trans-1;2}$ 7.6 Hz, $J_{5\text{-}trans-6\text{-}cis}$ 46.0 Hz, $J_{5\text{-}trans-4}$ 138.0 Hz; F^6: δ_F –139.2 ppm (d.d), $J_{6\text{-}cis-5\text{-}trans}$ 22.9 Hz, $J_{6\text{-}cis-4}$ 21.0 Hz.

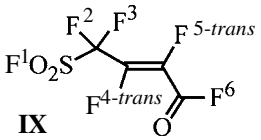

IX

F^1: δ_F 51.2 ppm (t), $J_{1-2;3}$ 7.6 Hz; F^2: δ_F –83.4 ppm (d.t), $J_{2-1;3}$ 7.6 Hz, J_{2-3} 140 Hz; F^3: δ_F –84.0 ppm (d.t), J_{3-1} 7.6 Hz, J_{3-2} 140 Hz; F^4: δ_F –150.7 ppm (d.d), $J_{4\text{-}trans-5}$ 138.0 Hz, $J_{4\text{-}trans-6}$ 22.9 Hz; F^5: δ_F –141.1 ppm (d.d.t), $J_{5\text{-}trans\text{-}3}$ 7.6 Hz, $J_{5\text{-}trans-6}$ 53.4 Hz, $J_{5\text{-}trans-4}$ 138.0 Hz; F^6: δ_F 29.0 ppm (d.d), $J_{6-5\text{-}trans}$ 56 Hz, $J_{6-4\text{-}trans}$ 22.9 Hz.

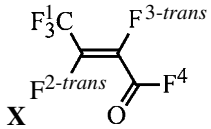

X

F^1: δ_F –71.5 ppm (t.d), J_{1-3} 7.6 Hz, $J_{1-2;4}$ 24.4 Hz; F^2: δ_F –150.7 ppm (d.q), $J_{2\text{-}trans-3}$ 138.0 Hz, J_{2-4} 22.9 Hz; F^3: δ_F –141.9 ppm (d.d.q), $J_{3\text{-}trans-1}$ 7.6 Hz, $J_{3\text{-}trans-2}$ 138.0 Hz, $J_{3\text{-}trans-4}$ 56.5 Hz; F^4: δ_F 28.2 ppm (d.q), $J_{4-3\text{-}trans}$ 56.0 Hz, J_{4-1} 22.9 Hz.

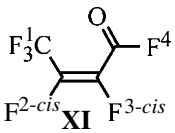

XI

F^1: δ_F –68.3 ppm (q), $J_{1-2;3;4}$ 10.2 Hz; F^2: δ_F –134.8 ppm (d.q), $J_{2\text{-}cis-4}$ 28.0 Hz, $J_{2\text{-}cis-1}$ 10.2 Hz; F^3: δ_F –123.7 ppm (q), $J_{3\text{-}cis-1;2;4}$ 12.7 Hz; F^4: δ_F 28.6 ppm (d.m), $J_{4-1;2;3}$ 10.2 Hz; $J_{4-2\text{-}cis}$ 25.4 Hz.

EXPERIMENTAL

The ^{19}F NMR spectra were recorded on a Bruker Spectrospin AM-500 spectrometer operating at 470.572 MHz in the pulse mode with the pulse delay of up to 5 s. Hexafluorobenzene as internal reference was added to the samples fuming in air. The samples were hermetically sealed and placed into the standard glass ampules 5 mm in diameter. Deuteroacetone whose signal was used for stabilization of the spectrometer was placed between ampule walls.

The composition of the mixtures was monitored by GLC using an LKhM-90 chromatograph equipped with a thermal conductivity detector on a column with d = 4 mm and l = 3 m (stationary phase 15 wt % SKTFT-50 on Silokhrom-2, 70°C, carrier gas helium).

In sulfotrioxidation of hexafluorobutadiene, 96 g of sulfur trioxide freshly distilled from oleum was charged into a 250-ml stainless-steel ampule, and

162 g of hexafluorodutadiene was fed into the ampule at room temperature. The ampule was hermetically sealed and heated at 80°C for 20 h. The resulting mixture contained virtually no sulfur trioxide, and the conversion of hexafluorobutadiene reached 90%. The raw material was distilled, and the resulting product contained approximately 70% of a fraction with bp 93–95°C. From the evidence of the ^{19}F NMR spectrum, this fraction contained three components: hexafluoro-1-butene-3,4-β-sultone, hexafluoro-2-butene-1,4-sultone, and hexafluoro-2-butene-1,4-diyl sulfate in 70 : 20 : 10 mol % ratio, respectively. The GLC analysis practically confirmed this result. The distillation bottoms amounted to 20% of the reaction mixture and were viscous polymeric tars. This product gave broad unresolved singlets in the NMR spectra, which did not allow its identification.

In the ^{19}F NMR spectrum of the reaction mixture we found the signals of fluorosulfate and carbonyl fluoride groups, whose intensities were proportional to those of difluoromethylene and fluoromethine groups in *cis* and *trans* structures of perfluoro-4-fluorosulfato-2-butenoyl fluorides whose content in the mixture reached 6%. The intensity of signals of the *trans* structure was approximately three times higher than that of the *cis* structure. The reaction mixture also contained polymeric products.

An attempt to reproduce the synthesis in the presence of sulfur dioxide, described in [1], led to a considerable decrease in the yield of the above sultones and sulfates. The ratio of these compounds in the mixture was 40 : 20 : 20 mol %, and the intensity of the polymer signals increased.

In sulfotrioxidation in the medium of 1,1,2-trifluorochloroethane, the conversion of hexafluorobutadiene did not exceed 65%; however, the yield of hexafluoro-2-butene-1,4-diyl sulfate noticeably decreased.

CONCLUSIONS

(1) In sulfotrioxidation of hexafluorobutadiene, the main process is 1,2-addition of sulfur trioxide yielding hexafluoro-1-butene-β-sultone and 3,4-pyrosultone.

(2) Sulfur trioxide also undergoes 1,4-addition yielding hexafluoro-2-butene-1,4-sultone. It is likely that elimination of sulfur dioxide from the related pyrosultone results in formation of hexafluoro-2-butene-1,4-diyl sulfate.

REFERENCES

1. Kazmina, N.B., Knunyants, I.L., Knunyants, G.M., et al., *Izv. Akad. Nauk SSSR. Ser. Khim.*, 1979, no. 1, p. 118.
2. Cherstkov, V.F., Sterlin, S.R., German, L.S., and Knunyants, I.L., *Izv. Akad. Nauk SSSR, Ser. Khim.*, 1983, no. 8, p. 1872.

ISSN 1070-4272, Russian Journal of Applied Chemistry, 2007, Vol. 80, No. 3, pp. 428–432. © Pleiades Publishing, Ltd., 2007.
Original Russian Text © M.G. Shcherban', T.Yu. Nasretdinova, N.A. Kladova, A.V. Radushev, E.V. Burdakova, 2007, published in Zhurnal Prikladnoi Khimii, 2007, Vol. 80, No. 3, pp. 430–434.

ORGANIC SYNTHESIS AND INDUSTRIAL ORGANIC CHEMISTRY

Surface-Active Properties of a Series of 1,1-Dimethyl-1-alkylhydrazinium Chlorides

M. G. Shcherban', T. Yu. Nasretdinova, N. A. Kladova, A. V. Radushev, and E. V. Burdakova

Perm State University, Perm, Russia
Institute of Technical Chemistry, Ural Division, Russian Academy of Sciences, Perm, Russia

Received August 3, 2006

Abstract—The surface-active properties of a series of 1,1-dimethyl-1-alkylhydrazinium chlorides with C_{10}–C_{18} in length were studied in comparison with Neonol AF 9-12 and Oksifos B surfactants. The limiting wetting angle, detergent and solubilization power, and foaming kinetics of these surfactants were studied in relation to the concentration of formation of monomolecular layer and type of the resulting micellar structures.

DOI: 10.1134/S1070427207030159

In contrast to highly toxic 1,1-dimethylhydrazine widely used as a component of liquid propellant, the use of its low-toxic 1-alkyl derivatives in various branches of industry seems promising [1–5].

1,1-Dimethyl-1-alkylhydrazinium chlorides (DMAHCs) are tertiary hydrazinium salts (THSs) and surfactants, which strongly decrease the surface tension at the water–air boundary [6]. However, the data on their surface-active properties are scarce and available only for a few compounds [6, 7]. In this study we examined the surface-active properties throughout the DMAHC homologous series.

EXPERIMENTAL

DMAHCs of the general formula $[R(CH_3)_2 \cdot NNH_2]Cl$ (where $R = C_nH_{2n+1}$; n = 10, 12, 14, 16, and 18 and mixture 12 + 14) were prepared by quaternization of 1,1-dimethylhydrazine with primary chloroalkanes using the known procedure [8] and purified by double or triple recrystallization from acetone. The content of the product in the samples, which was no less than 96%, was determined by the modified procedure given elsewhere [9].

The solubilization power was evaluated with respect to Sudan I oleophilic dye, which, being insoluble in water, is soluble in the hydrophobic part of micelles. The dye content was determined from the optical density of the solution recorded on an FEK-56M photocolorimeter (λ = 400 nm). Then, using the calibration curve, the content of the solubilized dye s in unit volume was calculated. The calibration curve was plotted using the solutions of Sudan I in benzene. The solubilization power of surfactants S was calculated as the ratio of s to the surfactant concentration:

$$S = s/c, \quad (1)$$

where c is the surfactant concentration in the solution (g l^{-1}) and s is the concentration of the solubilized dye (mg l^{-1}).

The detergent power with respect to M20 industrial oil and Tsiatim-221 lubricant was determined by the gravimetric method using St. 20 steel plates. A drop of the pollutant was deposited onto the plate, spread over its surface with a brush, and dried. Then, after drying, this procedure was repeated. After 1-day storage, the plates were weighed on an analytical balance with an accuracy of ±0.0002 g. The samples were immersed in the washing solution (40 ml) and stored in this solution with shaking for 3 and 30 min for the oil and lubricant, respectively. Then, the plates were carefully removed (holding at the edge), thoroughly washed with distilled water, and dried in air for a day. The dried plates were weighed. The detergent power (DP) (%) of the solutions in question was calculated from the following expression:

$$WP = (P_2 - P_3)/(P_2 - P_1) \times 100, \quad (2)$$

where P_1, P_2, and P_3 are the weights (g) of the plate before the experiment, with deposited model pollutant, and after treatment with the washing solution and distilled water, respectively.

The limiting wetting angle at the glass–DMAHC solution boundary and the kinetic stability of the foam were determined by the bubbling and shaking procedures, respectively [10].

The results given in this paper were averaged over three or four measurements, and the relative measurement error, as a rule, did not exceed 2–4%. The foam volume was normalized to 1 l of the disperse system. The experiments were performed at 20°C.

RESULTS AND DISCUSSION

The limiting wetting angles of DMAHC studied and of known surfactants of the other classes (anionic Oksifos B and nonionic Neonol AF 9-12) are listed in Table 1. All the compounds studied are the penetrating (wetting) agents, i.e., they hydrophilize the glass surface and decrease the limiting wetting angle at the glass–surfactant solution boundary (limiting wetting angle at the glass–water boundary 44°). As seen, Neonol AF 9-12 is the most active agent, except the concentration of 1 g l^{-1}, when the minimal wetting angle is observed for DMAHC with R = C_{12} and C_{14} (technical name ChGS-1214).

As seen from Table 1, the dependences of cos θ on the surfactant concentration are nonmonotonic for both individual compounds (DMAHC with R = C_{10}–C_{18}) and their mixtures (Neonol AF 9-12, Oksifos B, and DMAHC with C_{12} + C_{14}), which is probably due to the features of the surface layer structure and micelle formation with increasing surfactant concentration.

The isotherm of the limiting wetting angle of DMAHCs passes through a minimum at low surfactant concentrations (3–4 g l^{-1}). Similar minima for DMAHCs were found previously in the isotherms of the surface tension at concentrations smaller than the critical micellization concentration (CMC), which was attributed to the presence of impurities with higher surface activity as compared to DMAHCs [6]. The disappearance of this minimum with increasing surfactant concentration is probably due to the solubilization of the impurity with the micelles of the main surfactant, appearing upon attainment of CMC, which slightly increases the limiting wetting angle at high concentrations of the surfactant.

Study of foaming in the aqueous surfactant solutions showed that, for all the compounds studied, the kinetic dependences of changes in the foam volume are similar; first the foam volume sharply decreases and then it remains virtually constant (Fig. 1). As seen, the mixture of DMAHCs with C_{12} + C_{14} gives the highest foam column in the initial moment, but its stability is smaller as compared to Neonol AF 9-12 and Oksifos B.

Table 1. Limiting wetting angle θ at various concentrations of DMAHC $[R(CH_3)_2NNH_2]Cl$

R	θ, deg, at indicated concentration, g l^{-1}				
	1	2	3	4	5
$C_{10}H_{21}$	47	44	46	44	50
$C_{12}H_{25}$	41	43	45	41	36
$C_{16}H_{33}$	40	38	36	34	36
$C_{18}H_{37}$	38	41	36	39	38
C_{12-14}	33	34	39±2	44	40
Oksifos B	36	39	37	47	38
Neonol AF 9-12	36	32	35	37	28

In most cases, foams prepared at high surfactant concentration (c > 30 g l^{-1}) are unstable (Fig. 2). This is probably due to the fact that, with increasing concentration, the viscosity of the adsorption surfactant layers increases and they become heavier, which causes rapid foam degradation. The maximal lifetimes of the foam are listed in Table 2. The most stable foams are observed in the concentration range corresponding to the formation of the saturated adsorption layers [6].

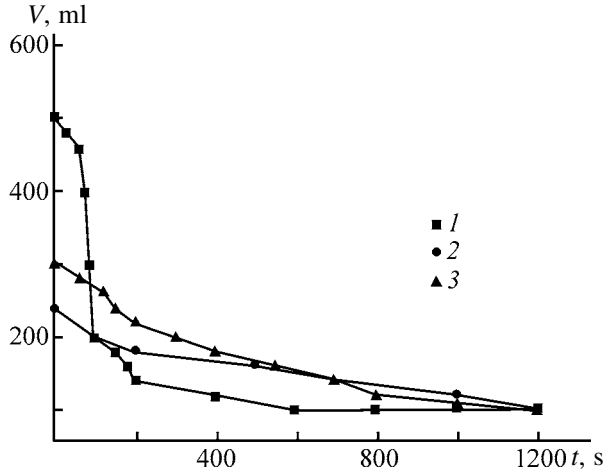

Fig. 1. Stability of foam obtained with different surfactants; surfactant concentration 5 g l^{-1}. (*V*) Foam volume and (*t*) time. (*1*) DMAHC with R = C_{12} + C_{14}, (*2*) Oksifos B, and (*3*) Neonol AF 9-12.

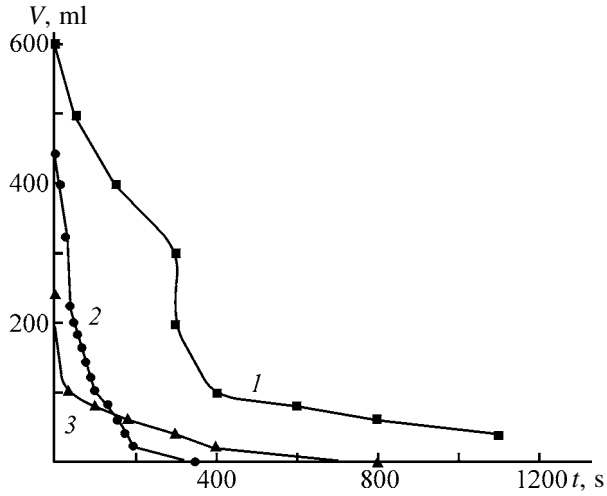

Fig. 2. Kinetics of changes in the foam volume V of an aqueous solution of DMAHC (R = $C_{12}H_{25}$) at various surfactant concentrations. (t) Time. Surfactant concentration, g l^{-1}: (*1*) 18, (*2*) 36, and (*3*) 9.

The data on the detergent power of the surfactant solutions with respect to industrial pollutants (Tsiatim-221 lubricant, M20 oil) are listed in Table 3. As seen, the detergent power of all the surfactants with respect to M20 oil is higher than that with respect to Tsiatim-221 lubricant, and the best results (98–99%) were obtained for DMAHCs with R = C_{18} (c = 0.12–0.25 g l^{-1}) and with R = C_{12} + C_{14} (c = 2 g l^{-1}, 92%). The detergent power of Neonol AF 9-12 and Oksifos B was lower and comprised 59 and 92%, respectively. As for Tsiatim-221 lubricant, the best result (94%) was obtained for DMAHC (R = C_{12} + C_{14}, c = 2 g l^{-1}), whereas Neonol AF 9-12 and Oksifos B were inefficient.

Table 2. Kinetic stability of the foam prepared from aqueous solution of DMAHC $[R(CH_3)_2NNH_2]Cl$

R	c_{sur} at maximal foam stability, g l^{-1}	Foam lifetime, s
$C_{10}H_{21}$	60	1600
	7.5	800
$C_{12}H_{25}$	18	1100
	9	800
$C_{14}H_{29}$	35	1100
	17	1100
$C_{18}H_{37}$	0.04	800
	2.5	1200
Gidrazeks	30	1300
	15	1300
Oksifos B	7.5	1000
	3.75	1200
Neonol AF 9-12	20	1000
	10	1100
	1.25	1500

Our experimental results correlate with the surface-active properties of DMAHCs at the water–air boundary, and they are primarily determined by the surface tension and micelle formation.

Analysis of the detergent power (Table 3) along with data on the kinetic stability of foams (Figs. 1, 2) shows that the highest detergent power of all the surfactants studied corresponds to the surfactant concentration at which the maximal foam stability is observed.

Solubilization power is one of the most important surfactant characteristics. The data on the solubilization power with respect to Sudan I oleophilic dye are shown in Table 4. In the DMAHC homologous series, the solubilization power increases with increasing length of the hydrocarbon chain, which is due to the increase in the surface activity in accordance with the Traube–Duclaux rule [11]. The maximal solubilization power corresponds to the surfactant concentra-

Table 3. Detergent power of the foam prepared from aqueous solution of DMAHC $[R(CH_3)_2NNH_2]Cl$ for St. 20 steel

R	c, g l^{-1}	Washing power, %	
		M20	Tsiatim-221
$C_{10}H_{21}$	12.5	91 ± 4	81 ± 3
	3.0	78 ± 3	19 ± 2
	1.5	67 ± 2	25 ± 2
C_{12}, C_{14}	2.0	92 ± 4	94 ± 4
	1.0	86 ± 3	51 ± 2
	0.5	85 ± 3	22 ± 2
	0.25	83 ± 3	35 ± 3
	0.125	81 ± 3	35 ± 3
$C_{18}H_{37}$	1.0	85 ± 2	8.0 ± 1
	0.5	96 ± 3	13 ± 2
	0.25	98 ± 2	26 ± 2
	0.125	99 ± 1	19 ± 2
Oksifos B	25.0	55 ± 2	1.0 ± 0.2
	12.5	41 ± 2	1.4 ± 0.3
	6.25	59 ± 3	4.5 ± 0.3
	1.56	66 ± 3	4.9 ± 0.5
Neonol AF 9-12	5.0	89 ± 3	9.8 ± 1.0
	2.5	86 ± 3	4.6 ± 0.5
	1.25	92 ± 2	7.2 ± 1.0
	0.625	89 ± 4	14.0 ± 1.0

Table 4. Solubilization power of an aqueous solution of DMAHC $[R(CH_3)_2NNH_2]Cl$ with respect to Sudan I dye as compared to known surfactants

R	c_{sur}, g l^{-1}	c_{dye}	S
		mg l^{-1}	
$C_{10}H_{21}$	10.0	5.0	0.5
	5.0	3.0	0.6
	0.5–2.0	0	0
$C_{12}H_{25}$	40.0	42.0	1.0
	20.0	8.0	0.4
	10.0	1.0	0.1
	5.0	1.0	0.2
	2.0	0.5	0.3
	1.0	0.2	0.2
$C_{14}H_{29}$	10.0	82.0	8.2
	5.0	50.0	10.0
	2.0	20.0	10.0
	0.2	0.4	2.0
$C_{16}H_{33}$	2.0	8.0	4.0
	1.0	3.0	3.0
	0.5	1.0	2.0
	0.25	0.5	2.0
C_{12}, C_{14}	10.0	70	7.0
	5.0	30	6.0
	2.0	9	4.5
	0.1	0.2	2.0
Oksifos B	20.0	55	2.8
	10.0	35	3.5
	5.0	18	3.6
	2.0	8	4.0
	1.0	4	4.0
	0.5	2	4.0
	0.2	0.5	2.5
Neonol AF 9-12	20.0	60	3.0
	2.0	13	6.5
	1.0	8	8.0
	0.5	1	2.0
	0.2	0.4	2.0

Note: Concentrations of solubilized dye are given.

tions close to CMC at which spherical micelles begin to transform into the micelles of more complex structure [6].

Colloidal electrolytes (including DMAHCs) are completely dissociated and do not aggregate up to concentrations close to CMC. In the narrow concentration range, the spherical particles are formed whose size and shape are constant at concentrations slightly higher than CMC. In this concentration range, solubilization only slightly affects the micelle size. In concentrated surfactant solutions ($c \gg$ CMC), spherical

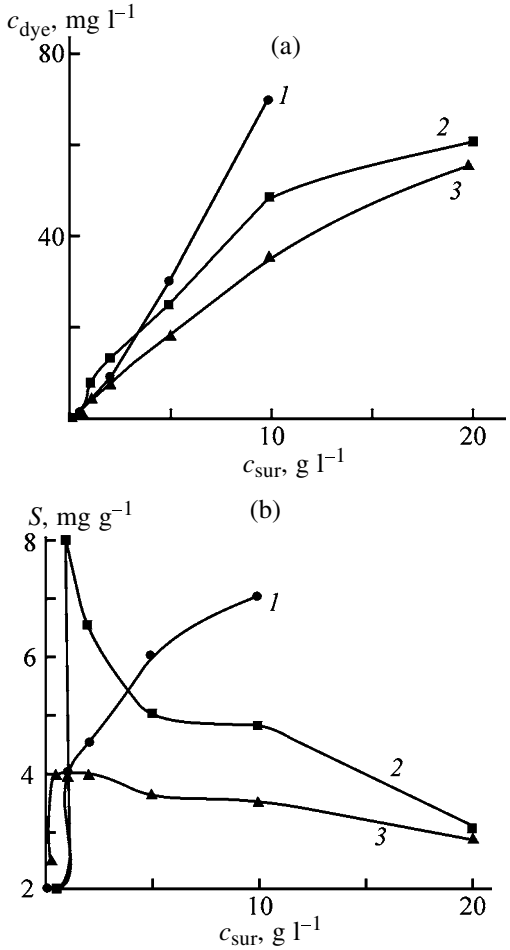

Fig. 3. (a) Concentration of solubilized dye c_{dye} and (b) solubilization power S as functions of the surfactant concentration c_{sur}. (*1*) DMAHC (R = C_{12} + C_{14}), (*2*) Neonol AF 9-12, and (*3*) Oksifos B.

micelles transform into thermodynamically more stable lamellar particles. This transformation increases the weight of the micellar nucleus, which increases the intramicellar solubility of the dye and the solubilization power of the surfactant solution. As a result, the colloidal structure of the solution sharply changes, which was confirmed visually.

The surfactant nature largely determines the solubilization mechanism. In the presence of ionic surfactants, an oleophilic dye containing polar groups penetrates into the surface layer of a micelle, where its molecules are arranged between the surfactant molecules (with parallel orientation) and their polar groups are turned to the aqueous phase. In this case, the dye molecules are dissolved either in the micelle core or in the hydrophilic micelle shell. In the case of nonionic surfactants, the localization of the dye is different: its molecules occur on the outer hydrophilic shell of the micelles.

These differences in the solubilization mechanism with surfactants of different nature give rise to certain features in the dependences of the solubilized dye concentration and solubilization power *S* on the surfactant concentration (Figs. 3a, 3b). For Neonol AF 9-12 and Oksifos B, the dependence of the concentration of the solubilized dye on the surfactant concentration tends to a constant value, whereas in the case of DMAHCs ($R = C_{12} + C_{14}$) this dependence is ascending. In the case of Neonol AF 9-12 and Oksifos, the concentration dependences of *S* on the surfactant concentration pass through the maxima, whereas for DMAHC ($R = C_{12} + C_{14}$) no peaks are observed.

Data on the aqueous solutions with 5–10 g l^{-1} concentrations of the surfactants studied show that the DMAHC with $R = C_{12} + C_{14}$ is the most effective solubilization agent, capable to dissolve the largest amounts of pollutants.

CONCLUSIONS

(1) The limiting wetting angle, detergent and solubilization power of a series of 1,1-dimethyl-1-alkylhydrazinium chlorides, Neonol AF 9-12, and Oksifos B surfactants, and their foaming kinetics are determined by the concentration of formation of monomolecular layer and type of the resulting micellar structures.

(2) The detergent and solubilization powers of a technical mixture of 1,1-dimethyl-1-alkylhydrazinium chlorides with $R = C_{12} + C_{14}$ are significantly higher than those of Neonol AF 9-12 and Oksifos B. Taking into account low toxicity of 1,1-dimethyl-1-alkylhydrazinium chlorides (hazard class 4), these surfactants can be used for preparing fireproof, low-concentrated, and environmentally mild aqueous-organic detergent formulations.

REFERENCES

1. Tul'bovich, B.I., Kazakova, L.B., Radushev, A.V., et al., *Neft. Khoz.*, 1995, no. 11, pp. 44–45.
2. RF Patent 2123893.
3. Lopyrev, V.A., Dolgushin, G.V., and Laskin, B.M., *Ross. Khim. Zh.*, 2001, vol. 45, nos. 5–6, pp. 22–24.
4. Aleksandrova, G.A., Prokhorova, G.A., Leonov, A.E., et al., *Khim.-Farm. Zh.*, 1995, vol. 29, no. 11, pp. 22–24.
5. RF Patent 2245244.
6. Shcherban', M.G., Radushev, A.V., Nasretdinova, T.Yu., et al., *Zh. Prikl. Khim.*, 2004, vol. 77, no. 11, pp. 1861–1864.
7. Katayama, E. and Minegishi, Y., *J. Chem. Soc. Jpn., Ind. Chem. Soc.*, 1968, vol. 71, no. 10, pp. 1671–1674.
8. RF Patent 2074174.
9. Siggia, S. and Hanna, J.G., *Quantitative Organic Analysis via Functional Groups*, New York: Wiley–Interscience, 1979.
10. Zhukov, I.I., *Kolloidnaya khimiya* (Colloid Chemistry), Leningrad: Leningr. Gos. Univ., 1949.
11. Shchukin, E.D., Amelina, E.A., and Pertsov, A.R., *Kolloidnaya khimiya* (Colloid Chemistry), Moscow: Mosk. Gos. Univ., 1982.

ISSN 1070-4272, Russian Journal of Applied Chemistry, 2007, Vol. 80, No. 3, pp. 433–437. © Pleiades Publishing, Ltd., 2007.
Original Russian Text © D.V. Batov, 2007, published in Zhurnal Prikladnoi Khimii, 2007, Vol. 80, No. 3, pp. 435–439.

ORGANIC SYNTHESIS AND INDUSTRIAL ORGANIC CHEMISTRY

Additive Scheme for Estimating Properties of Solutions of Organic Compounds: Limiting Partial Molar Volumes of Alkanols in Water

D. V. Batov

Institute of Solution Chemistry, Russian Academy of Sciences, Ivanovo, Russia

Received October 9, 2006

Abstract—An additive scheme based on determination of the partial contributions of structural fragments proved to be applicable to analysis and prediction of the bulk and other properties of aqueous solutions of alkanols.

DOI: 10.1134/S1070427207030160

The additive-group contribution approach has been most thoroughly developed for estimating thermodynamic parameters of formation of molecules in the gas phase [1] and enthalpies of phase transitions [2]. As for condensed systems, the use of this approach is complicated by the need in taking into account different kinds of intermolecular interaction. Nevertheless, studies in this direction are being intensively performed [3–7].

Additive models are used generally to gain some thermodynamic and other information about systems for which no experimental data are available. Kizin et al. [8] noted that the additive-group contribution method combines sufficient accuracy and relative simplicity. It should be pointed out also that this method proved to be applicable to analysis of correlations between the physicochemical and thermodynamic properties of solutions, on the one hand, and the molecular structures of a solute and a solvent, on the other hand. Until recently, in terms of the additive-group contribution approach, the limiting partial molar volumes of organic compounds in solutions $\bar{V}_2^\infty$ were approximated generally by Eq. (1) [9, 10]:

$$\bar{V}_2^\infty = a_v + b_v N_C, \quad (1)$$

where N_C is the number of the carbon atoms in the chain of the organic molecule, and coefficient b_v characterizes the contribution of the methylene group to $\bar{V}_2^\infty$.

Deviations of $\bar{V}_2^\infty$ from the value obtained using the simple additive scheme are considered as resulting from intergroup interactions in the molecule [11, 12].

The figure shows the increments of the limiting partial molar volume and enthalpy of hydration of *n*-alkanols, obtained using data taken from [13]. As seen, the properties of methanol and, in most cases, ethanol deviate significantly from the linear approximation [Eq. (1)] obtained for the homologs with $N_C \geq 3$.

To provide the energetic and geometrical equivalence of allocated structural fragments in the additive models, these fragments should be selected taking into account their nearest surrounding. If this condition is not met, the resulting additive expansion includes some terms (absolute terms) having no clear physical sense, and properties of the first members of a homol-

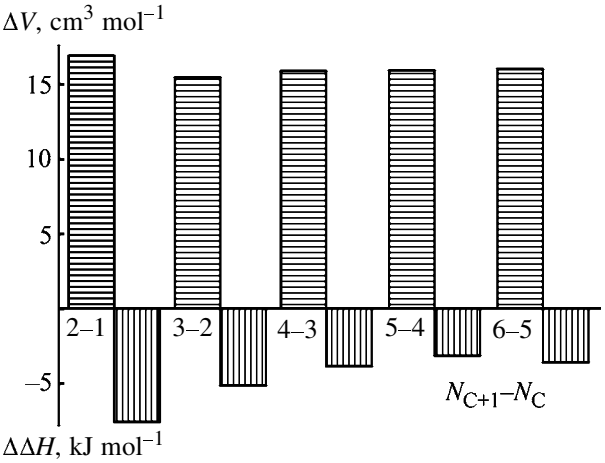

Differences in the limiting partial molar volumes $\Delta V = [\bar{V}_2^\infty(N_{C+1}) - \bar{V}_2^\infty(N_C)]$ and enthalpies of hydration $\Delta\Delta H^0 = [\Delta_1 H^0(N_{C+1}) - \Delta_1 H^0(N_C)]$ in a series of *n*-alkanols. (N_C) Number of the carbon atoms of the hydrocarbon radical of the molecule.

ogous series and isomers deviate from the additive model.

To quantitatively describe the bulk properties of solutions, we used in this study the additive scheme that we proposed previously for the enthalpy characteristics of solutions [14, 15]. In this scheme, a compound is divided into structural elements in which some nuclei of atoms can belong to two or more structural fragments [16]. We selected the CH bond as such a structural element of hydrocarbon radicals. There are two reasons for this decision. First, more detailed specification (allocation of bonds, instead of radicals) makes it possible to include more substances into consideration without changing the number of structural elements. Secondly, no fractional values are used for the contributions of radicals (in [18], the fragment CH is set to be equivalent to the half of the methylene group). The summation of the partial bond contributions gives the contributions of the corresponding hydrocarbon radicals. According to the recommendations formulated in [16], the allocation of structural fragments is specified taking into account their nearest (first) surrounding. The basic scheme of allocation of structural fragments in the alkanol molecules with saturated hydrocarbon radicals is illustrated below with an example of 4-ethyl-6,7,7'-trimethyl-4-octanol:

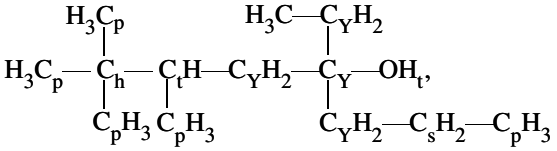

where C_YH refers to the CH bonds in the hydrocarbon radical from the nearest surrounding of the functional group.

Taking into account the specific features of the hydration of organic nonelectrolyte molecules, we set the first surrounding of the functional group so as to include the CH bonds formed by two carbon atoms nearest to the functional group. Here C_sH, C_tH, and C_pH refer to the CH bonds formed by the carbon atoms distant from the functional group by at least two carbon atoms; C_h is the quaternary carbon atom; and OH_t is the functional group bound to the tertiary carbon atom. Correspondingly, in the *n*- and isoalkanol molecules, OH_p and OH_s groups are allocated.

Analysis of published data shows that, for monohydric alcohols, there is one of the most extended databases covering the bulk characteristics of aqueous solutions. Table 1 summarizes the types and numbers of the structural fragments allocated according to the above scheme in a series of monohydric alcohols and their limiting partial molar volumes in aqueous solutions at 298.15 K [18–22]. The theoretical $\bar{V}_2^\infty$ values were obtained using multiparametric Eq. (2):

$$\bar{V}_2^\infty = \bar{V}_2^\infty(Y_p) + \delta\bar{V}_2^\infty(Y_s) + \bar{V}_2^\infty(Y_t) + y\bar{V}_2^\infty(CH_Y) + p\bar{V}_2^\infty(CH_p) + s\bar{V}_2^\infty(CH_s) + t\bar{V}_2^\infty(CH_t), \quad (2)$$

where $\bar{V}_2^\infty$ is the limiting partial molar volume of the solute; $\bar{V}_2^\infty(Y_p)$, contribution of the polar OH group bound to the primary carbon atom; and $\delta\bar{V}_2^\infty(Y_s)$ and $\delta\bar{V}_2^\infty(Y_t)$ are the corrections introduced to take into account the differences between the bulk characteristics of the functional groups bound to the secondary and tertiary carbon atoms and those of the functional group bound to the primary carbon atom.

The contribution of the functional group bound to the secondary or tertiary carbon atom can be estimated by summing $\bar{V}_2^\infty(Y_p)$ and the corresponding correction term $\delta\bar{V}_2^\infty(Y_s)$ of $\delta\bar{V}_2^\infty(Y_t)$. The y, p, s, t; and $\bar{V}_2^\infty(C_YH)$, $\bar{V}_2^\infty(C_pH)$, $\bar{V}_2^\infty(C_sH)$, and $\bar{V}_2^\infty(C_tH)$ are the numbers and contributions of the allocated hydrocarbon fragments. If experimental data are available for the compounds containing the quaternary carbon atoms, the term $h\bar{V}_2^\infty(C_h)$ should be introduced in Eq. (2).

The calculated contributions of the allocated structural fragments to the limiting partial molar volumes of alkanols in water and the regression parameters are presented in Table 1. The $\bar{V}_2^\infty(Y_p)$ is determined as an absolute term in Eq. (2). The results show that the experimental data are well reproduced in the framework of the model proposed. The allocation of the CH bonds in the radicals directly bound to the functional group and in those separated from it by a carbon atom as structural fragments of the nearest surrounding of the heteroatom allows fairly fine differentiation of the compounds by the molecular structure. Previously we demonstrated in studying the enthalpy characteristics [14, 15] that such an allocation of the structural fragments is particularly efficient in analysis of the properties of aqueous solutions. The equality of the group contributions reflects the energy equivalence of the groups, suggesting their nearly same geometric configuration [16], which, in turn, suggests similar solvation surrounding of the groups.

The approach used in this study makes it possible to take into account the specific features of the structure and hydration of the two first members of the homologous series (all their CH bonds are energetically equivalent). Table 1 shows that Pr^{i}OH and Bu^{t}OH are structurally similar to methanol and ethanol. Struc-

Table 1. Limiting partial molar volumes of alkanols in aqueous solutions at 298.15 K, kind and number of structural fragments allocated in the alkanol molecules, and group contributions of these fragments to the bulk properties

Compound no.	Alcohol	$\bar{V}_2^\infty$, cm^3 mol^{-1}		C_YH	C_sH	C_pH	C_tH	OH_s	OH_t	OH_p
		experiment	calculation							
1	MeOH	38.17		3	0	0	0	0	0	
2	EtOH	55.2		5	0	0	0	0	0	
3	Pe^{n}OH	102.6		4	4	3	0	0	0	
4	Bu^{i}OH	86.72		2	0	6	1	0	0	
5	Bu^{t}OH	87.8		9	0	0	0	0	1	
6	Pe^{2}OH	102.6		6	2	3	0	1	0	
7	Pe^{3}OH	101.2		5	0	6	0	1	0	
8	Pr^{n}OH	70.74	70.06	4	0	3	0	0	0	
9	Bu^{n}OH	86.67	86.30	4	2	3	0	0	0	
10	Hex^{n}OH	118.7	118.80	4	6	3	0	0	0	
11	Pr^{2}OH	71.93	71.45	7	0	0	0	1	0	
12	Bu^{2}OH	86.57	86.30	6	0	3	0	1	0	
13	Pe^{t}OH	101.9	102.66	8	0	3	0	0	1	
14	Hex^{2}OH	118.5	118.80	6	4	3	0	1	0	
15	Hex^{3}OH	117.1	117.41	5	2	6	0	1	0	
16	Hep^{2}OH	134.4	135.04	6	6	3	0	1	0	
17	Hep^{3}OH	133.3	133.65	5	4	6	0	1	0	
18	Hep^{4}OH	133.2	133.65	5	4	6	0	1	0	
	Contributions (base set)			8.51	8.12	7.79	10.3	–0.78	–1.46	12.6
	Contributions (se = 0.25, R = 0.9999)			8.8	8.01	7.84	10.3	–1.59	–3.46	11.8

Note: (MeOH) methanol, (EtOH) ethanol, (Pr^{n}OH) 1-propanol, (Pr^{2}OH) 2-propanol, (Bu^{n}OH) 1-butanol, (Bu^{i}OH) 2-methyl-1-propanol, (Bu^{2}OH) 2-butanol, (Bu^{t}OH) 2-methyl-2-propanol, (Pe^{n}OH) 1-pentanol, (Pe^{2}OH) 2-pentanol, (Pe^{3}OH) 3-pentanol, (Pe^{t}OH) 2-methyl-2-butanol, (Hex^{n}OH) 1-hexanol, (Hex^{2}OH) 2-hexanol, (Hex^{3}OH) 3-hexanol, (Hep^{2}OH) 2-heptanol, (Hep^{3}OH) 3-heptanol, (Hep^{4}OH) 4-heptanol; (se) standard error; and (R) correlation factor.

tural similarity of solutions of water in MeOH and EtOH was also suggested in [23] on the basis of the bulk characteristics of the indicated systems. The phenomenon of a negative partial dilatability of water was observed in methanol and *tert*-butanol [24]. In the series MeOH, EtOH, Pr^{i}OH, and Bu^{t}OH, there was observed a monotonic change of such physicochemical characteristics as the density [23] and donor and acceptor numbers [25]. All these findings can be interpreted in terms of our additive scheme. It follows from Table 1 that, in the series MeOH, EtOH, Pr^{i}OH, and Bu^{t}OH, the number of unitypical C_YH fragments increases. Abrosimov and Ivanov [23] consider the indicated alkanols as homologs of methanol formed from it by successive substitution of the methyl protons by the methyl radicals. With an example of $\bar{V}_2^\infty$, it may be suggested that the contributions from OH_p, OH_s, and OH_t only slightly differ.

The results show that our additive scheme is quite sensitive to geometric isomerism. Thus, Table 1 shows that the group compositions of 2-pentanol and 2-hexanol significantly differ from those of 3-pentanol and 3-hexanol, and that the limiting partial molar volumes of the corresponding 2- and 3-alkanols also differ remarkably. At the same time, according to our scheme, the group composition of 3-heptanol is similar to that of 4-heptanol. Correspondingly, the experimental and calculated bulk characteristics of these compounds are practically equal (Table 1).

Data on the bulk properties illustrate high predictive ability of the additive method used. Let us restrict ourselves to the minimal basic dataset for the seven first compounds from Table 1, to calculate the contributions from the structural fragments and then estimate $\bar{V}_2^\infty$ for the other eleven compounds. We obtain good agreement between the calculated and experimental results (arithmetic mean error is within 0.43 cm^3 mol^{-1}).

Finally, let us examine the applicability of our ad-

Table 2. Group contributions to the molar volumes V_m, limiting partial molar heat capacities $\bar{C}_{p2}^{\infty}$, limiting activity coefficients γ_2^{∞} in aqueous solutions, and entropy of solution in water of alkanols $\Delta_s S^0$ at 298.15 K

Characteristics	OH_p	CH_Y	CH_s	CH_p	CH_t	OH_s	OH_t	se	Compound*
V_m, $cm^3\ mol^{-1}$	13.61	9.03	8.28	8.60	7.89	–0.59	0.03	0.55	no. 1–5, 8–10, Pe^iOH, Oc^nOH
$\bar{C}_{p2}^{\infty}$ J mol^{-1} K^{-1}	–6.70	54.10	51.84	45.27	71.25	–2.72	–9.20	12.00	no. 1–5, 7–9, 11, 12, Pe^iOH, $Pe^{neo}OH$
$\Delta_s S^0$, J mol^{-1} K^{-1}	–9.87	–6.88	–5.06	–5.66		–2.51	–5.24	1.51	no. 1, 2, 5, 7–9, 11, 12, 15, 18
γ_2^{∞}	1.40	0.09	12.33	4.70	17.34	8.21	10.12	4.15	no. 1–5, 7–9, 11, 12, 15, 18

* Numbers of the compounds from Table 1, whose characteristics were used in regression analysis, are indicated; (Pe^iOH) 2-methyl-1-butanol, ($Pe^{neo}OH$) 2,2-dimethyl-1-propanol, and (Oc^nOH) 1-octanol; in all cases, the correlation factor was no less than 0.996.

ditive scheme to other thermodynamic characteristics of alkanols and their aqueous solutions. From the experimental data on the molar volumes [25], limiting partial molar heat capacities of alkanols in water [26–28], entropies of solution [26, 29], and limiting activity coefficients [26, 29, 30] at 298.15 K, we estimated the contributions of the allocated structural fragments to the indicated characteristics using Eq. (2) and data on the type and number of the structural elements of the alkanol molecules (Table 1). The results are summarized in Table 2. As seen, these thermodynamic characteristics can also be well approximated using our additive scheme. The approximation errors are well comparable with the experimental errors, which are as follows: V_m 0.1 $cm^3\ mol^{-1}$, $\bar{C}_{p2}^{\infty}$ 3–6 J mol^{-1} K^{-1}, and $\Delta_s S^0$ 1 J mol^{-1} K^{-1}.

CONCLUSIONS

(1) Analysis of the bulk and other properties of alkanols demonstrates the applicability of the additive scheme proposed. The contributions of structural fragments to the limiting partial molar volumes of alkanols in water at 298.15 K are estimated.

(2) The additive scheme allows taking into account specific features of the structure and hydration of the two first members of the homologous series, as well as the structural differences caused by the molecular isomerism. This scheme proved to be particularly efficient in describing properties of aqueous solutions of organic nonelectrolytes.

(3) The scheme of determination of the group contributions provides optimization of the experimental design aimed at further calculation of the corresponding characteristics in a homologous series or class of organic compounds.

REFERENCES

1. Benson, S.W., *Thermochemical Kinetics; Methods for the Estimation of Thermochemical Data and Rate Parameters*, New York: Wiley, 1968.
2. Lebedev, Yu.A. and Miroshnichenko, E.A., *Termokhimiya paroobrazovaniya organicheskikh veshchestv* (Thermochemistry of Vaporization of Organic Substances), Moscow: Nauka, 1981.
3. Kehiaian, H.V., *Fluid Phase Equil.*, 1983, vol. 13, pp. 243–252.
4. Smirnova, N.A. and Piotrovskaya, E.M., *Zh. Prikl. Khim.*, 1984, vol. 57, no. 8, pp. 1701–1705.
5. Kizin, A.N., Dvorkin, P.L., Ryzhova, G.L., and Lebedev, Yu.A., *Izv. Akad. Nauk SSSR, Ser. Khim.*, 1986, no. 2, pp. 372–375.
6. Dvorkin, P.L., Ryzhova, G.L., and Lebedev, Yu.A., *Izv. Akad. Nauk SSSR, Ser. Khim.*, 1983, no. 5, pp. 1101–1105.
7. Ribeiro da Silva, M.A.V., *Pure Appl. Chem.*, 1999, vol. 71, no. 7, pp. 1257–1265.
8. Kizin, A.N., Orlov, Yu.D., and Lebedev, Yu.A., in *Problemy khimii rastvorov i tekhnologii zhidkofaznykh materialov: Sbornik nauchnykh Trudov* (Problems of Chemistry of Solutions and Technology of Liquid-Phase Materials: Coll. of Sci. Works), Ivanovo, 2001, pp. 73–81.
9. Inglese, A., Mavelli, F., De List, R., and Milioto, S., *J. Solution Chem.*, 1997, vol. 27, no. 3, pp. 319–336.
10. Nishimura, N., Tanaka, T., and Motoyama, T., *Can. J. Chem.*, 1987, vol. 65, no. 9, pp. 2248–2253.
11. Edward, J.T., Farrell, P.G., and Shahidi, F., *J. Phys. Chem.*, 1978, vol. 82, no. 21, pp. 2310–2313.
12. Shahidi, F., Farrell, P.G., and Edward, J.T., *J. Phys. Chem.*, 1979, vol. 83, no. 3, pp. 419–422.
13. Belousov, V.P. and Panov, M.Yu., *Termodinamika vodnykh rastvorov neelektrolitov* (Thermodynamics of

Aqueous Nonelectrolyte Solutions), Leningrad: Khimiya, 1983.

14. Batov, D.V., Thermochemistry of Organic Nonelectrolyte Solutions in Mixed Solvents, *Doctoral Dissertation*, Ivanovo, 2002.
15. Batov, D.V. and Zaichikov, A.M., *Zh. Obshch. Khim.*, 2003, vol. 73, no. 4, pp. 545–552.
16. Tatevskii, V.M., *Teoriya fiziko-khimicheskikh svoistv molekul i veshchestv* (Theory of Physicochemical Properties of Molecules and Compounds), Moscow: Mosk. Gos. Univ., 1987.
17. Savage, J.J. and Wood, R.H., *J. Solution Chem.*, 1976, vol. 5, pp. 733–750.
18. Franks, F. and Smith, H.T., *J. Chem. Eng. Data*, 1968, vol. 13, pp. 538–547.
19. Holland, H., *J. Solution Chem.*, 1976, vol. 5, no. 11, pp. 773–780.
20. Nakajima, T., Komatsu, T., and Nakagawa, T., *Bull. Chem. Soc. Jpn.*, 1975, vol. 48, no. 3, pp. 783–787.
21. Marsh, K.N. and Richards, A.E., *Aust. J. Chem.*, 1980, vol. 33, no. 10, pp. 2121–2132.
22. Cabani, S., Conti, G., and Lepori, I., *J. Phys. Chem.*, 1974, vol. 78, no. 10, pp. 1030–1034.
23. Abrosimov, V.K. and Ivanov, E.V., *Voda: struktura, sostoyanie, sol'vatatsiya: Dostizheniya poslednikh let* (Water: Structure, State, and Solvation: Recent Advances), Kutepov, A.M., Ed., Moscow: Nauka, 2003, pp. 277–346.
24. Ivanov, E.V., Abrosimov, V.K., and Lebedeva, E.Yu., *Dokl. Ross. Akad. Nauk*, 2003, vol. 391, no. 1, pp. 58–61.
25. Marcus, Y., *Ion Solvation*, New York: Wiley, 1985.
26. Arnett, E.M., Kover, W.B., and Carter, J.V., *J. Am. Chem. Soc.*, 1969, vol. 91, no. 15, pp. 4028–4034.
27. Panov, M.Yu., Belousov, V.P., and Morachevskii, A.G., in *Khimiya i termodinamika rastvorov* (Solution Chemistry and Thermodynamics), Leningrad: Leningr. Gos. Univ., 1977, issue 4, pp. 158–213.
28. Jolicocur, C. and Lacroix, G., *Can. J. Chem.*, 1976, vol. 54, no. 4, pp. 624–631.
29. Cabani, S., Conti, G., Mollica, V., and Lepori, L., *J. Chem. Soc., Faraday Trans. I*, 1975, vol. 71, no. 10, pp. 1943–1952.
30. Larkin, J.A. and Pemberton, R.G., Abstracts of Papers, *3rd Int. Conf. on Chemical Thermodynamics*, Baden, September 3, 1973, vol. 3, p. 163.

ISSN 1070-4272, Russian Journal of Applied Chemistry, 2007, Vol. 80, No. 3, pp. 438–442. © Pleiades Publishing, Ltd., 2007.
Original Russian Text © A.Yu. Solov'ev, T.S. Potekhina, I.A. Chernova, B.Ya. Basin, 2007, published in Zhurnal Prikladnoi Khimii, 2007, Vol. 80, No. 3, pp. 440–444.

NANOTECHNOLOGIES AND NANOMATERIALS

Track Membrane with Immobilized Colloid Silver Particles

A. Yu. Solov'ev, T. S. Potekhina, I. A. Chernova, and B. Ya. Basin

Institute of Macromolecular Compounds, Russian Academy of Sciences, St. Petersburg, Russia
St. Petersburg State Chemical-Pharmaceutical Academy, St. Petersburg, Russia
Plazmofil'tr Private Company, St. Petersburg, Russia

Received November 21, 2006

Abstract—A method for modification of track membranes by immobilization of polymer complexes of colloid silver nanoparticles on the surface of microfiltration membranes was developed. The antimicrobial properties of track membranes modified with silver nanoparticles were tested on *E. coli*, *Ps. aeruginosa*, *St. aureus*, and *B. cereus*.

DOI: 10.1134/S1070427207030172

Microfiltration track membranes (TMs) are widely used in separation of virus-containing and colloid solutions and in final stages of drinking water treatment under household conditions [1–3]. When a membrane is brought in contact with an aqueous medium in the course of filtration, various components, with high and low molecular weight, are sorbed on its surface, as also do microbe cells to form a biological film [4–6]. This film is firmly fixed on the membrane surface, which leads to clogging of the filter and to contamination of drinking water with products formed by microorganisms.

Use of TM for drinking water treatment provides sterile working conditions. However, a currently topical issue is the improvement of the antiseptic properties of TM and cartridges based on these membranes in order to preclude overgrowth of the filtering surface of TM.

This study is devoted to immobilization of colloid silver on the surface of polyethylene terephthalate TMs.

EXPERIMENTAL

Polyethylene terephthalate (PET) TMs with a thickness of 10 nm, nominal pore size of 0.5 μm, and pore density of 5×10^7 cm^{-2} were used in the study, as well as PFM-800 membrane units manufactured by Plazmofil'tr Private Company (St. Petersburg). The following reagents were used: silver nitrate ($AgNO_3$), sodium thiocyanate (NaSCN), iron(III) perchlorate [$Fe(ClO_4)_3$], 96% ethanol manufactured by Vekton, and medicinal polyvinylpyrrolidone (PVP) with a molecular weight of 12600 [FS (Pharmacopoeia Item) 42-1194–98], manufactured by Novocherkassk Plant of Synthetic Products.

The track membranes were cleaned by the procedure described in [7]; the rest of the materials and reagents were used without any additional treatment.

A scanning electron microscopic (SEM) study of the surface of intact and modified TM samples was performed on a TESCAN Vega Plus TS 5135 MM (Czech Republic) electron microscope. For this purpose, a platinum layer of thickness 40–50 Å was preliminarily deposited on the TM samples by vacuum evaporation. The morphology of the membranes was studied by atomic-force microscopy (AFM) in the contact-force mode on a Digital Instruments Nanoscope-2 instrument (the United States).

The amount of silver immobilized on a track membrane was found using the modified Volhard method [8].

A silver-containing membrane sample was placed in a 50-ml glass vessel and poured over with a 10-ml portion of a 5% HNO_3 solution. The membrane was thermostated at 80°C on a water bath for 3–5 min, until the yellow coloration of the membrane disappeared. When the solution became transparent, the extraction was terminated and the hot extract was carefully discharged into a clean vessel. The hot extract was cooled in air to room temperature. A sample of volume V_s = 3 ml was taken for titration and 0.2 ml of an aqueous solution of $Fe(ClO_4)_3$, with a concen-

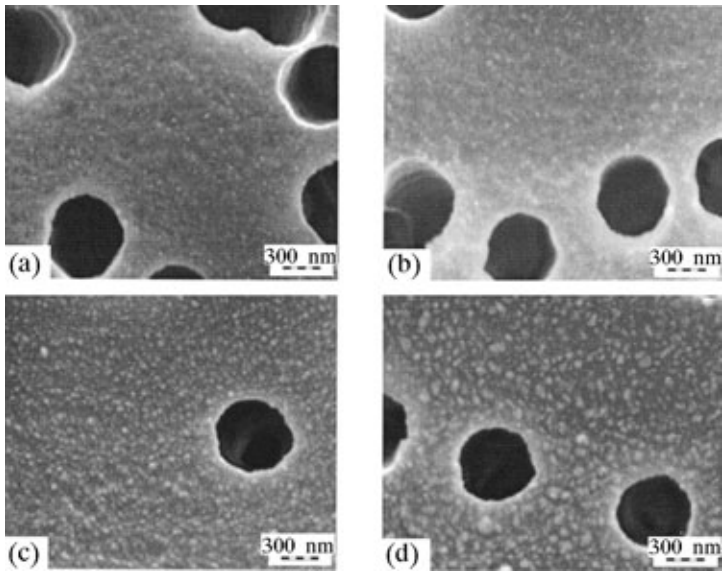

Fig. 1. SEM micrographs of the surface of track membranes with silver nanoparticles. Reaction time (min): (a) 15, (b) 60, (c) 120, and (d) 180.

tration of 0.56 M (0.2 mg ml^{-1}) (solution A), was added.

Solution A under study was gradually titrated with a NaSCN solution of concentration 8 mM (0.7 mg ml^{-1}) until the red coloration of $Fe(SCN)_3$ appeared, which indicates the end of titration. The volume of NaSCN, V_{NaSCN}, was measured and the amount of silver in the coating was calculated by the formula

$$m_{Ag} = \frac{V_{NaSCN} c_{NaSCN} V_{HNO_3}}{V_{sp}},$$

where V_{NaSCN} is the volume of the NaSCN solution consumed for sample titration (ml); c_{NaSCN}, concentration of the NaSCN solution (mg ml^{-1}); and V_{HNO_3}, volume of 5% nitric acid necessary for sample extraction (ml).

Highly dispersed colloid particles of silver were immobilized on the membrane surface by the chemical method of dispersion of this metal via reduction of silver ions to the molecular state in an aqueous–alcoholic medium in the presence of a water-soluble polymer (PVP), with subsequent deposition of silver nanoparticles onto the membrane surface [9, 10].

For this purpose, 0.15 g (0.9 mmol) of $AgNO_3$ and 29 g (2.3 mmol) of PVP were dissolved in a round-bottomed flask equipped with a reflux condenser and charged with 1 l of aqueous alcohol with an ethanol content of 70 wt %. After that, a membrane cut into fragments in the form of circles 4.5 cm in diameter was placed in the flask and the resulting solution was heated on a water bath with a reflux at 60–80°C. The process duration was set in the range from 10 to 120 min, depending on the amount of silver required for immobilization on the membrane. As the amount of silver on the membrane increased, its color changed from light yellow to dark brown. To find the optimal conditions of particle immobilization, the temperature and the relative and absolute concentrations of the reagents were varied. After silver immobilization on a membrane was complete, the sample was removed from the reaction mixture, successively washed with a 40% water–ethanol solution and distilled water, and dried between sheets of filter paper. The modified membranes were stored in a dry and dark place.

Figure 1 shows SEM micrographs of membranes with silver particles immobilized at a reaction mixture temperature of 80°C and varied process duration. The minimum size of clusters immobilized in 15 min (18 nm) is clearly seen in the micrographs.

Further course of the reaction leads to an increase in the particle size and number and to gradual saturation of the membrane surface with silver, as it is shown in Fig. 2. The saturation of the surface with silver is virtually complete in 120 min. Further, the mass of the already formed particles on the surface grows.

The AFM micrographs (Fig. 3) clearly demonstrate the regular spherical shape of colloid particles, whose average size is 70 nm. It should be noted that, under

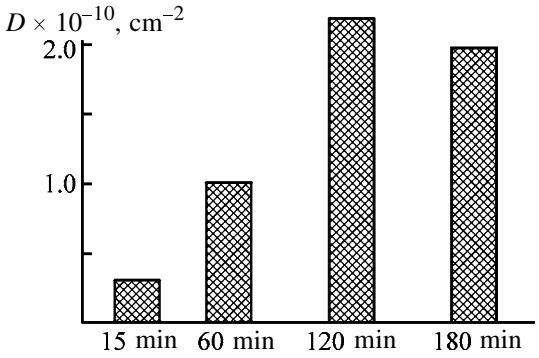

Fig. 2. Variation of the number density D of silver colloid particles per unit area of the track membrane with the duration of the immobilization process.

the optimal modification conditions (temperature and relative and absolute concentrations of the reagents), the shape and permeability of cylindrical pores of the membrane are preserved.

The rate of metal reduction in the presence of a water-soluble polymer is governed by numerous factors, the most important of which are the diffusion rate of ions of the metal and reducing agent into the polymer matrix, velocity of their motion within pores or polymer coils, rate of the chemical reduction itself, and, finally, the crystallization rate of the metal deposited. The size of the forming nanoparticles is also affected by the nature of the polymer [11].

To study the mechanism of formation and growth of colloid nanoparticles, temperature dependences of silver reduction in an aqueous–alcoholic solution in the presence of PVP was studied. Figure 4 shows curves that describe the kinetics of silver immobilization on a track membrane at 60, 70, and 80°C. It can be seen that the immobilization at 60 and 70°C is of about the same nature: the curves are S-shaped and consist of portions corresponding to the induction period I, acceleration period II, and deceleration period III.

The induction period is associated with the initial stages of the following concurrent processes: chemical reduction of silver in the solution bulk and sorption of metal cations on carboxy groups of the membrane, i.e., on hydrolyzed PET, with their subsequent reduction to metal and formation of stable particles of the new phase. Very small conversions correspond to this period.

The time in which nanoparticles are formed depends on numerous factors: relative and absolute concentrations of the reagents and presence of impurities.

At the end of the induction period, particle of size larger than 1 nm appear in the solution and on the membrane surface. These particles are formed via successive overgrowth of fine particles with metal atoms. After the completion of the induction period, metallic clusters-nuclei for the most part cease to form, i.e., further reduction occurs without any change in the number of particles, with their mass increasing.

At 80°C, the process is characterized by a smooth curve with a leveling-off portion, which has the form of the Langmuir isotherm. The rate of mass transfer at this temperature is an order of magnitude higher than that at 60°C. Presumably, the rate of particle formation in the bulk exceeds at this temperature that on the surface. Therefore, the induction period is weakly pronounced in the plot and the surface is rapidly saturated with the nanoparticles formed, i.e., particles that completed their growth are immobilized on the membrane surface. Data on the sorption rate in rela-

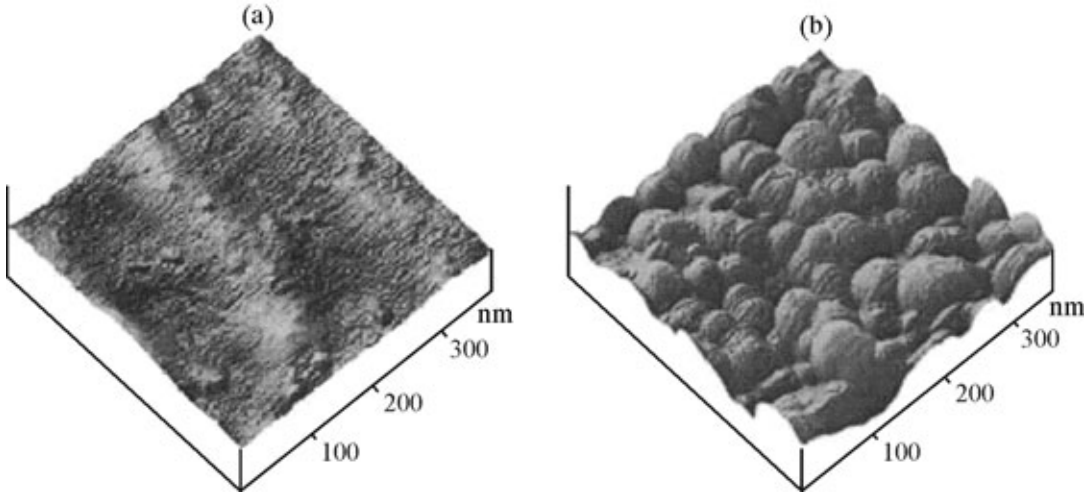

Fig. 3. AFM images of the membrane surface with immobilized silver. Membrane: (a) initial and (b) modified with silver.

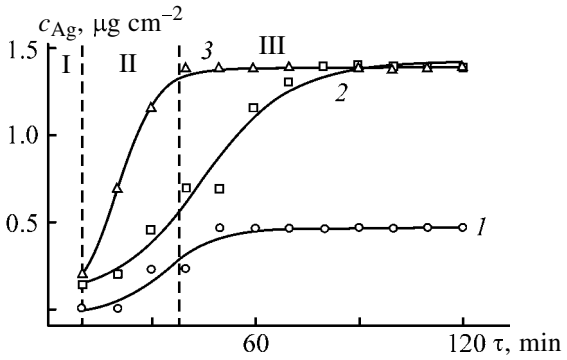

Fig. 4. Amount of silver immobilized on a track membrane, c_{Ag}, vs. time τ. Temperature, °C: (*1*) 60, (*2*) 70, and (*3*) 80.

tion to the temperature of the reaction mixture, which are calculated from the initial portion of the curve, are presented below:

Temperature, °C	60	70	80
Sorption rate, 10^2 μg cm^{-2} min^{-1}	0.4	1	4

Experiments on filtration of buffer solutions with modified membranes demonstrated that their hydrodynamic resistance remains virtually the same as that of control membranes. This indicates that the immobilization of nanoparticles does not change the effective diameter of pores in the membrane.

The bactericidal action of the membranes modified with silver nanoparticles was tested on model strains of microorganisms, recommended by the State Pharmacopoeia for tests of antimicrobial properties of medicinal preparations: *Escherichia coli*, *Pseudomonas aeruginosa*, *Staphylococcus aureus*, and *Bacillus cereus*.

The modified membranes were placed in Petri dishes, each containing 15 ml of a solidified MPA nutritional medium. Suspensions with a concentration of 5×10^3 cells ml^{-1} were prepared from populations of 18–24-h-old cultures. A 0.1-ml portion of a suspension was applied to the membrane surface and evenly distributed over the entire surface. The inoculated Petri dishes were incubated at 37°C for 24 h. The results were recorded as presence or absence of colonies on the membrane (see table).

The experiments demonstrated that the concentration of immobilized silver on a membrane governs the growth of microorganisms. Silver in a concentration of 0.5 μg cm^{-2} suppresses only *E. coli*, whereas a threefold increase in the concentration of immobilized silver on the membrane results in that no colonies of microorganisms grow for all of the cultures studied.

Figure 5 shows photographs of growth of microbial cultures on membranes with different silver concentra-

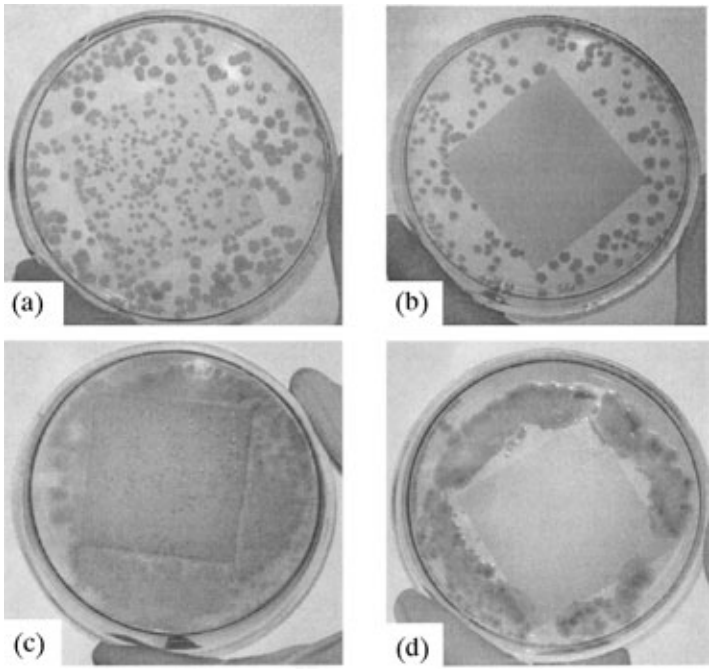

Fig. 5. Effect of the concentration of immobilized silver on the antimicrobial properties of modified track membranes. (a, b) Growth of a *St. aureus* culture on membranes with silver concentration of (a) 0.5 and (b) 1.4 μg cm^{-2}; (c, d) growth of *Ps. aeruginosa* culture on membranes with silver concentration of (c) 0.5 and (d) 1.4 μg cm^{-2}.

Antimicrobial effect of modified track membranes on test-strains of bacteria*

c_{Ag}, μg cm^{-2}	Microorganism culture			
	E. coli	*Ps. aeruginosa*	*St. aureus*	*B. cereus*
TM (control)	++	++	++	++
0.5	–	+	+	+
1.4	–	–	–	–

* (–) No growth of microorganism colonies. (+) Growth of microorganism colonies.

tions. The growth of staphylococcus and *B. cereus* colonies can be seen in the Petri dish with a membrane with a silver concentration equal to 0.5 μg cm^{-2}. It is also seen that staphylococcus colonies on the membrane are smaller than in the case of growth on agar, and colonies on the membrane with a higher silver concentration are absent.

Thus, imparting antimicrobial properties to a membrane makes wider the applicability of these materials in water treatment and in fine biotechnology of tissue cultures.

CONCLUSIONS

(1) A method for modification of track membranes by immobilization of colloid silver nanoparticles on the surface of microfiltration membranes was developed.

(2) The optimal conditions of immobilization of silver particles on the filtering surface of a membrane were determined.

(3) It was shown that track membranes modified with silver nanoparticles have an antimicrobial effect on *E. coli, Ps. aeruginosa, St. aureus*, and *B. cereus* microorganisms.

ACKNOWLEDGMENTS

The study was supported by the Foundation for Support of Domestic Science (grant no. K-407).

REFERENCES

1. Butylina, S., Shataeva, L., and Nyström, M., *Sep. Purif. Technol.*, 2007, vol. 53, no. 1, pp. 64–70.
2. Vrouwenveldera, H.S., Paassenb, J.A.M., Folmerc, H.C., et al., *Desalination, Conf. on Membranes in Drinking and Industrial Water Production*, 1998, vol. 118, no. 1–3, pp. 157–166.
3. Mchedlishvili, B.V., Bresler, S.E., Kolikov, V.M., et al., *Kolloidn. Zh.*, 1978, vol. 40, no. 1, pp. 59–63.
4. Lamminena, M.O., Walker, H.W., and Weaversa, L.K., *J. Membr. Sci.*, 2006, vol. 283, nos. 1–2, pp. 225–232.
5. Yebo, L., Shahbazia, A., and Kadzereb, Ch.T., *J. Food Eng.*, 2006, vol. 75, no. 4, pp. 574–580.
6. Ridgway, H., Ishida, K., Rodriguez, G., et al., *Meth. Enzymol.*, 1999, vol. 310, pp. 463–494.
7. Solov'ev, A.Yu., Brynda, E., Houska, M., et al., *Vysokomol. Soedin., Ser. A*, 2003, vol. 45, no. 9, pp. 1574–1579.
8. Alekseev, V.N., *Kolichestvennyi analiz* (Quantitative Analysis), Moscow: Khimiya, 1972.
9. Panarin, E.F., Pavlov, G.M., and Santuryan, Yu.G., *Khim.-Farm. Zh.*, 1991, no. 3, pp. 68–70.
10. Kopeikin, V.V., Santuryan, Yu.G., and Danilova, M.Ya., *Khim.-Farm. Zh.*, 1988, no. 10, pp. 1253–1256.
11. Pomogailo, A.D., Rozenberg, A.S., and Uflyand, I.E., *Nanochastitsy metallov v polimerakh* (Metal Nanoparticles in Polymers), Moscow: Khimiya, 2000.

ISSN 1070-4272, Russian Journal of Applied Chemistry, 2007, Vol. 80, No. 3, pp. 443–447. © Pleiades Publishing, Ltd., 2007.
Original Russian Text © Nguyen Chan Hung, I.V. Anoshkin, E.G. Rakov, 2007, published in Zhurnal Prikladnoi Khimii, 2007, Vol. 80, No. 3, pp. 445–449.

NANOTECHNOLOGIES AND NANOMATERIALS

Chemical Activation of Carbon Nanofibers and Nanotubes

Nguyen Chan Hung, I. V. Anoshkin, and E. G. Rakov

Mendeleev Russian University of Chemical Technology, Moscow, Russia

Received September 27, 2006

Abstract—Method of thermodynamic simulation was used to calculate the equilibrium parameters of reactions of graphite with anhydrous LiOH, NaOH, and KOH and with the alkalis in the presence of water vapor. The change in the specific surface area and mass loss were used to analyze the interaction of carbon nanofibers and multilayer carbon nanotubes produced by catalytic pyrolysis of CH_4 with the alkalis.

DOI: 10.1134/S1070427207030184

Threadlike carbon materials, nanofibers (NF) and nanotubes (NT), attract the attention of researchers and technologists owing to their dimensions and properties. They can serve as catalyst supports and electrocatalysts, electrodes of supercapacitors and lithium–ion power cells, and components of chemical sensors and composites [1, 2]. In many cases, the efficiency of use of such materials is determined by their specific surface area S_{sp}, which is comparatively small in the most readily available materials.

The value of S_{sp} of carbon materials can be raised (activation) in several ways: partial oxidation with air, water vapor, CO_2, molten alkalis, and some other reagents. Of these, alkalis are most frequently used to develop the surface and porosity. In particular, studies have been performed of the interaction with KOH of carbon NF [3–5] and multilayer carbon NT [6–9]. The S_{sp} of NF 50–500 nm in diameter has been raised from 13 to 212 $m^2 g^{-1}$ [3]. The action of KOH was the most effective (increase in S_{sp} from 24.5 to 360 $m^2 g^{-1}$) at a mass ratio KOH : NF = 7 : 1, but, simultaneously, the yield of activated NF decreased [5]. In the case of NT, a twofold increase in S_{sp} (to 1050 $m^2 g^{-1}$) was achieved at KOH : NT = 4 : 1, and even a 2.5-fold increase (to 1184 $m^2 g^{-1}$), at a 5 : 1 ratio [7]. Differences in the effect of KOH and NaOH on the NT morphology have been noted [8, 9].

However, the available published evidence is insufficient for determining the possibility and conditions of activation of materials produced by methods different from those used in the references cited, and, in particular, of carbon NT [10, 11] and multilayer carbon NT [12, 13]. Results of thermodynamic calculations have not been invoked previously when discussing the reaction mechanisms.

The aim of this study was to examine the activation of these materials.

EXPERIMENTAL

To activation were subjected three types of carbon NT and two samples of carbon NF. The NT-1 sample was an NT produced by pyrolysis of CH_4 in the presence of H_2 on a Co–Mo : MgO catalyst containing 6 mol % active components ($CoO : MoO_3$ = 1 : 5 mol/mol) at 970°C with recycling of the gas mixture. The product was washed with concentrated HCl to remove the catalyst support. Its ash content was $9.4 \pm 0.1\%$, and $S_{sp} = 221.7 \pm 2.4$ $m^2 g^{-1}$.

The NT-2 sample was produced by pyrolysis of CH_4 in the presence of hydrogen on a Co–Mo/MgO catalyst at 950°C by the procedure described in [12, 13]. It was also washed with concentrated HCl to remove the catalyst support and had the form of a mixture of thin multilayer carbon nanotubes 2 to 10 nm in diameter. The NT were annealed in air at 380°C for 30 min in order to remove admixtures of amorphous carbon. This was accompanied by an 8.15% mass loss. $S_{sp} = 358 \pm 2$ $m^2 g^{-1}$.

The NT-3 sample was produced by pyrolysis of CH_4 in the presence of hydrogen on a Co–Mo/MgO catalyst containing 3 mol % active components ($CoO : MoO_3 = 1 : 1$) at 900°C in a filtering bed. The sample was washed with concentrated HCl to remove the catalyst support. The ash content was 0.1%, and $S_{sp} = 694.8 \pm 4.0$ $m^2 g^{-1}$.

Table 1. Yield in terms of carbon of products formed in the reaction of graphite with KOH at 700°C

KOH : C ratio	$CH_4 \times 10^3$	C_c	$K_2CO_3 \times 10^2$
	fraction units		
1 : 1	6.85	0.9217	7.14
2 : 1	13.69	0.8435	14.28
3 : 1	20.53	0.7653	21.42
4 : 1	27.38	0.6869	28.57
5 : 1	34.22	0.6087	35.71
6 : 1	41.07	0.5305	42.85

Table 2. Yield in terms of carbon of products formed in the reaction of graphite with KOH at 1000°C

KOH : C ratio	$CH_4 \times 10^3$	C_c	$K_2CO_3 \times 10^2$	$CO \times 10^3$
	fraction units			
1 : 1	4.81	0.9100	6.18	2.766
2 : 1	9.62	0.8199	12.35	5.528
3 : 1	14.43	0.7303	18.53	8.298
4 : 1	19.25	0.6402	24.71	11.067
5 : 1	24.05	0.5503	30.89	13.853
6 : 1	28.10	0.4605	37.07	16.597

Both NF samples (NF-1 and NF-2) were produced by pyrolysis of CH_4 on a Ni/MgO catalyst [11]. Preliminary purification was done with a 10% HNO_3 solution. The NF diameter was 30–60 nm and length up to 2 μm. The NF-1 sample was preliminarily treated at 500°C in a flow of H_2 and had $S_{sp} = 82.8 \pm 0.4$ $m^2 g^{-1}$, and the NF-2 sample had $S_{sp} = 74.3 \pm 0.7$ $m^2 g^{-1}$. The loss of NF mass upon annealing in air at 410°C for 60 min was 6.6 wt %. According to the results of thermogravimetric measurements, the ash content of NF upon heating in air at 850°C for 30 min was 4.1 wt %.

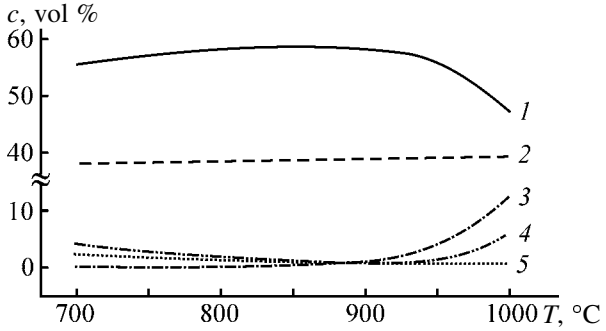

Fig. 1. Effect of temperature T on the equilibrium volume concentration c of gaseous components at a KOH : C mass ratio of 4 : 1. (*1*) H_2, (*2*) K (monatomic), (*3*) CO, (*4*) hydrocarbons, and (*5*) K (diatomic).

Carbon nanotubes and nanofibers were treated with molten KOH, NaOH, and NaOH–KOH mixtures at 800–850°C in a flow of dry Ar (flow rate 250 $cm^3 min^{-1}$) or in Ar saturated with H_2O vapor at 22°C (calculated flow rate about 100 $cm^3 min^{-1}$). Before being charged into the reactor, the starting NT and NF were ground in a mortar with a necessary amount of alkali until a paste of uniform gray color was formed. Part of NT and NF samples were subjected, prior to activation, to compaction at 280 MPa. The process was carried out in heated hermetic reactors of two types, vertical and horizontal, in which cylindrical nickel boats with, respectively, high and low rims were placed. The temperature was elevated at a rate of 10 or 20 deg min^{-1} to 850°C and maintained at this level for 60 or 90 min.

After performing the reaction, cooled products were treated with distilled water and 3 M HCl and filtered. The precipitate formed on the filter was three times washed with distilled water and dried at 110°C.

The specific surface area was determined with a Tristar 3000 instrument.

The reaction equilibria were calculated using the Astra software on the assumption that the thermodynamic parameters of carbon NF and NT coincide with those of graphite. It was presumed that this assumption does not strongly affect the results of calculations, even though it introduces a certain error. In addition, the database used for the calculations contains no evidence concerning characteristics of molten alkalis (melting points of LiOH, NaOH, and KOH are 473, 322, and 405°C, respectively), which affects the results obtained to a greater extent. However, disregarding the phase transitions in alkalis cannot strongly impair the calculation results, because their enthalpies of melting are low (4.8, 1.52, and 2.24 kcal mol^{-1}, respectively [14, 15]).

The calculations were performed in the temperature range 700–1000°C and alkali : carbon mass ratios of 1 : 1 to 6 : 1 at a total pressure of 101.3 kPa (1 atm). An example of the calculated results is presented in Tables 1 and 2.

It can be seen that the main solid products are graphite and K_2CO_3, with amount of graphite decreasing and that of the carbonate increasing as the KOH : C ratio grows. The yield of CO markedly increases at elevated temperatures.

The situation with other gaseous products is more complicated. As expected, the main gaseous components are hydrogen and potassium. Potassium is in the form of mono- and diatomic vapor, and hydrogen may

Table 3. Relationship between changes in mass and in S_{sp}

Material	S_{sp}, $m^2\ g^{-1}$		G	n	References
	initial	final			
NF (d = 50–200 nm)	13	212	0.58	5.12	[3]
NF	40	183	0.52	2.32	[3]
MNT, d, mn:					
15–25	430	1035	0.55	1.47	[6]
15–25	465	1184	0.55	1.56	[7]
12	220	885	0.80	6.24	[6]
12	222	877	0.77	5.30	[7]
15–20	194	510	0.85	5.95	[8]

be present not only as molecular H_2, but as CH_4 as well (at low temperatures). At the same time, the concentration of the main component is weakly dependent on temperature (Fig. 1) and varies nearly linearly as the KOH : C ratio becomes larger. In particular, the fraction α of reacted C at various temperatures is, at the KOH : C mass ratio of 4 : 1 under equilibrium conditions, as follows:

T, °C	α, fraction units
700	0.313
750	0.295
800	0.297
850	0.294
900	0.295
950	0.307
1000	0.360

Introduction of even minor amounts of water vapor markedly changes the distribution of the reaction products (Fig. 2) and leads to an increase in the fraction α. As the H_2O : C ratio increases, the concentration of H_2 becomes lower and that of K vapor decreases. It would be the best to maintain the ratio at 0.65, in which case the concentration of H_2 is the highest, that of K vapor is already low, and that of CO is as yet low. However, it is not known how such a ratio can be maintained in a flow of gases.

The KOH : C mass ratio of 4 : 1 corresponds to a molar ratio of 6 : 7. Replacement of KOH with NaOH at the same molar ratio does not change α significantly, whereas replacement with LiOH at 950°C makes α significantly larger:

Reagent	KOH	NaOH	LiOH
α, fraction units	0.307	0.306	0.424

The effect of LiOH is the most pronounced at a LiOH : C molar ratio of 1 : 1 at 950°C, when α becomes as large as 0.495.

The principal result of the calculations is that the gasification of carbon materials with alkalis can be performed in a humid atmosphere with the minimum evolution of K vapor and CO.

Relationship between changes in mass and in the specific surface area. S_{sp} of solid cylinders subjected to chemical etching, with their radius R_{out} decreasing in this treatment, can be calculated on the assumption that the etching occurs uniformly over the entire surface and the substance density ρ remains unchanged. In this case, $S_{sp} = 2/R_{out}\rho$. Because $R_{out} = [m/(\pi l \rho)]^{0.5}$ (m is the cylinder mass), the equalities $R_{out} = \text{const}_1 m^{0.5}$ and $S_{sp} = \text{const}_2 m^{-0.5}$ will be valid at invariable cylinder length l and ρ. If, consequently, the initial mass m_0 and S_{sp}^0 of a sample composed of cylindrical particles are known, the behavior of $S_{sp} = S_{sp}^0(m_0/m)^{0.5}$ can be judged from variation of the mass in the course of etching.

In the case of a nonuniform etching and formation of local reaction zones (caverns), changes in mass must lead to a more pronounced increase in S_{sp} in accordance with the equation $S_{sp} = S_{sp}^0(m_0/m)^n$, where

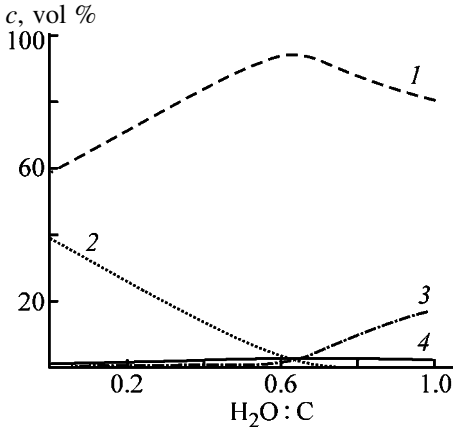

Fig. 2. Equilibrium volume concentration c of the main gaseous components as a function of the H_2O : C mass ratio at a KOH : C mass ratio of 4 : 1 and temperature of 850°C. (*1*) H_2, (*2*) K (monatomic), (*3*) CO, and (*4*) CH_4.

Table 4. Results of activation of NF and NT at 850°C in the course of 1 h

Sample	Reagents and mass ratio to NF	Reactor*	S_{sp}, $m^2 g^{-1}$	G	n
NF-1	KOH (1) + NaOH (3)	v	105	70.5	0.68
NF-1	KOH (1) + NaOH (3)	v	110	66.8	1.42
NF-1	KOH (4) + H_2O vapor	v	236	59.4	2.00
NF-2	KOH (4) + H_2O vapor	h	142	58.5	1.21
NF-2**	KOH (4) + H_2O vapor	h	268	63.0	2.77
NF-2	KOH (4) + H_2O vapor	h	267	55.2	2.15
NT-1	KOH (1) + NaOH (6)	v	325	41.4	0.43
NT-1	KOH (1) + NaOH (3)	v	290	62.4	0.57
NT-2	KOH (4) + H_2O vapor	v	520	51.4	0.56
NT-2**	KOH (4) + H_2O vapor	h	467	52.4	0.41
NT-3	KOH (4) + H_2O vapor	v	861	62.5	0.46

* Reactor type: (v) vertical and (h) horizontal.
** Compacted sample, activation duration 1.5 h.

$n > 0.5$. Published data can be used to find the experimentally observed value of n (Table 3). All the results refer to multilayer NT (MNT) with a number of layers not exceeding five.

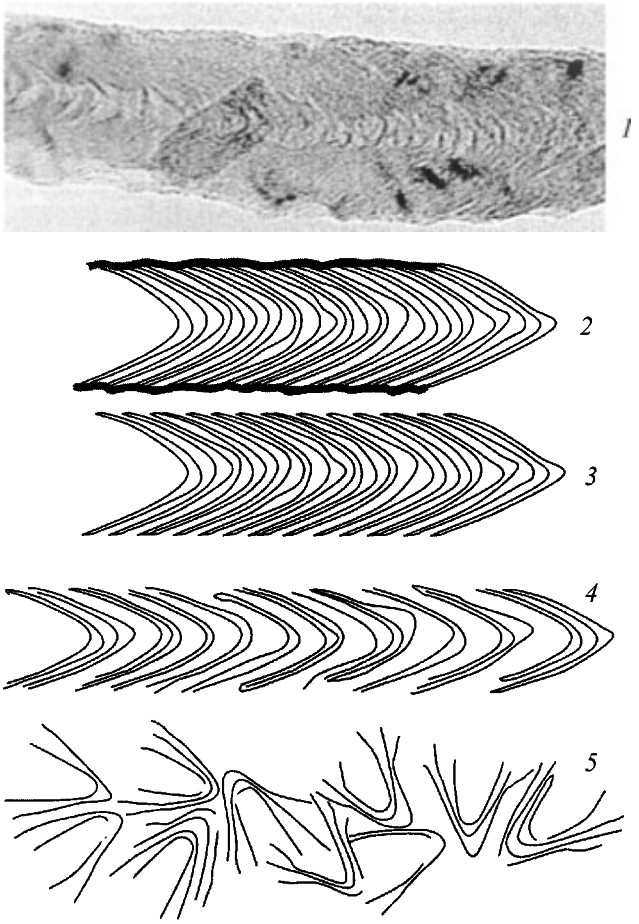

Fig. 3. Schematic of the successive surface development in interaction between carbon nanofibers. (*1*) Electron micrograph of a nanofiber and (*2–5*) successive stages of activation.

A certain pattern is observed: n markedly exceeds 0.5, i.e., the activation occurs with an increase in the contour surface area of particles. At a larger initial S_{sp}, the values of n are small.

The results obtained in the study are presented in Table 4. They, on the whole, agree with previously published data on the temperature and duration of activation and on the mass loss reached under closely similar conditions. As can be seen from the data presented, the behavior of NF and MNT in activation under similar conditions is not the same: the NF surface develops more intensively. For NF, n exceeds 0.5 in all cases and reaches values of 2.77. In the case of NT, all the three samples behave as if the gasification reaction involves only the outer layer of the tubes, because the value of n remains close to 0.5 even at a mass loss of about 50%.

The difference in behavior between NF and NT can be attributed to their different structures: in NF, graphene layers are arranged at angle to the axis (arborescent structure), which enables reagents to penetrate into the interlayer space, to make larger the reaction surface, and, presumably, in the end, to cut fibers into comparatively short fragments. The possibility of KOH intercalation into the interlayer space of NF was noted previously in [4]. The mechanism is schematically shown in Fig. 3.

At the same time, NT are characterized by a cylindrical arrangement of graphene layers and a considerably lower defect density, which predetermines localization of the reaction on the surface of the outer sheath. Here, the reaction occurs by another mechanism.

The difference between the data in Tables 3 and 4 may be due to the different diameters of NT used in

the present and earlier studies. If the way in which S_{sp} changes on removing one external layer is analyzed [16], it can be seen that, e.g., it changes by less than 100 $m^2 g^{-1}$ on passing from 20- to 10-layer NT and by 200–300 and 700–800 $m^2 g^{-1}$ on going from three-layer NT to two- and one-layer NT, respectively. The smaller the number of layers in NT, the faster should be the development of their surface in the course of activation. Another reason consists in the degree of ordering of NF and NT. This was clearly demonstrated in [9], where activation of NT with close initial S_{sp} (345, 330, and 326 $m^2 g^{-1}$), but different structures led to strongly different final S_{sp} (1670, 1220, and 868 $m^2 g^{-1}$).

Attempts to intensify the process by raising the mass ratio of alkalis to NT and by compaction of the samples studied failed, even though the same values of S_{sp} were obtained in the case of NF compaction at a somewhat higher yield. The addition of $AgNO_3$ in activation of NT-2 did not lead to any significant change in the mass loss. Changing the reactor configuration and boat shape did not produce any strongly different results, either. It seems that a more rational activation procedure is that using H_2O vapor in combination with alkalis. If the process is performed in dry Ar, noticeable amounts of metallic K are formed as a deposit on the inner wall of the gas-discharge pipe. Nothing of the kind occurred if water vapor was supplied.

The problem of efficiency of activation with mixtures of KOH with low-cost NaOH requires further analysis. The potassium vapor has a higher pressure, which favors its removal from the reaction zone. Sodium is less volatile than potassium, which may cause difficulties with removal of its vapor.

CONCLUSIONS

(1) The equilibrium yield of products formed in the reaction of alkalis with graphite was calculated. It was shown that the concentrations of the main gaseous components (H_2 and K) only slightly depend on temperature in the range 700–1000°C and linearly increase with the KOH : C ratio.

(2) It was demonstrated that introduction of H_2O vapor changes the equilibrium composition of the gaseous product, with the concentration of H_2 increasing and that of K vapor decreasing. At a H_2O : C mass ratio of 0.65, the concentrations of H_2 and K vapor reach the maximum and minimum values, respectively.

(3) The activation of two samples of carbon nanofibers and three samples of carbon nanotubes with KOH and its mixtures with NaOH in a flow of dry and humid Ar was studied on the basis of data on changes in mass and specific surface area. It was found that the specific surface area increases in activation of carbon nanofibers and nanotubes with alkalis in different ways: under identical conditions, nanofibers are activated more intensively. It was suggested that these dissimilarities are due to differences in the structure of nanofibers and nanotubes. Introduction of an $AgNO_3$ additive and compaction does not lead to any significant intensification of the process.

ACKNOWLEDGMENTS

The authors are grateful to S.N. Blinov and I.G. Ivanov for the carbon materials provided and assistance in experiments.

REFERENCES

1. Ajayan, P.M. and Zhou, O.Z., Carbon Nanotubes, *Top. Appl. Phys.*, 2001, vol. 80, pp. 391–425.
2. Rakov, E.G., *Usp. Khim.*, 2001, vol. 70, no. 11, pp. 934–973.
3. Merino, C., Soto, P., Vilaplana-Ortego, E., et al., *Carbon*, 2005, vol. 43, no. 3, pp. 551–557.
4. Yoon, S.-H., Lim, S., Song, Y., et al., *Carbon*, 2004, vol. 42, nos. 8–9, pp. 1723–1729.
5. Liu, Y.-F., Shen, Z.-M., Yokogawa, K., et al., *New Carbon Mater.*, 2004, vol. 19, no. 3, pp. 197–203.
6. Frakowiak, E., Delpeux, S., Jurewicz, K., et al., *Chem. Phys. Lett.*, 2002, vol. 361, nos. 1–2, pp. 35–41.
7. Raymundo-Pinero, E., Cazorla-Amoros, D., Linares-Solano, A., et al., *Carbon*, 2002, vol. 40, no. 9, pp. 1614–1617.
8. Jiang, Q., Qu, M.-Z., Zhang, B.-L., and Yu, Z.-L., *Carbon*, 2002, vol. 40, no. 14, pp. 2743–2745.
9. Raymundo-Pinero, E., Azais, P., Cacciaguerra, T., et al., *Carbon*, 2005, vol. 43, no. 4, pp. 786–795.
10. Rakov, E.G., *Khim. Tekhnol.*, 2003, no. 10, pp. 2–7.
11. Rakov, E.G., Blinov, S.N., Ivanov, I.G., et al., *Zh. Prikl. Khim.*, 2004, vol. 77, no. 2, pp. 193–196.
12. Rakov, E.G., Grishin, D.A., Gavrilov, Yu.V., et al., *Zh. Fiz. Khim.*, 2005, vol. 79, no. 12, pp. 2204–2209.
13. Grishin, D.A., Gavrilov, Yu.V., Nasibulin, A.G., et al., *Poverkhn.: Rentg., Sinkhrotronn. Neitronn. Issled.*, 2005, no. 12, pp. 52–58.
14. *Termicheskie konstanty veschestv* (Thermal Constants of Substances), Glushko, V.P., Ed., Moscow: VINITI, 1981, issue 10, part 1.
15. *Termicheskie konstanty veschestv* (Thermal Constants of Substances), Glushko, V.P., Ed., Moscow: VINITI, 1981, issue 10, part 2.
16. Peigney, A., Laurent, Ch., Flahaut, E., et al., *Carbon*, 2001, vol. 39, pp. 507–514.

ISSN 1070-4272, Russian Journal of Applied Chemistry, 2007, Vol. 80, No. 3, pp. 448–455. © Pleiades Publishing, Ltd., 2007.
Original Russian Text © Yu.S. Grushko, V.P. Sedov, V.A. Shilin, 2007, published in Zhurnal Prikladnoi Khimii, 2007, Vol. 80, No. 3, pp. 450–457.

NANOTECHNOLOGIES AND NANOMATERIALS

Technology for Manufacture of Pure Fullerenes C_{60}, C_{70} and a Concentrate of Higher Fullerenes

Yu. S. Grushko, V. P. Sedov, and V. A. Shilin

Konstantinov Institute of Nuclear Physics, Russian Academy of Sciences, Gatchina, Leningrad oblast, Russia

Received September 28, 2006; in final form, December 2006

Abstract—An integrated technology for manufacture of fullerenes was developed. It includes the following stages: synthesis of a fullerene black, extraction of a mixture of fullerenes from the black, preliminary separation of the mixture into concentrates enriched in C_{60} and C_{70} fullerenes, and production of C_{60} and C_{70} fullerenes of purity exceeding 99.5 and 98.0 wt %, respectively, from the concentrates.

DOI: 10.1134/S1070427207030196

The development of nanotechnologies is a priority of the XXI century and, beginning in 2000, has been attracting considerable investment in all the developed countries of the world. In 2007, the Federal Target Program "Development of the Infrastructure of Nanotechnologies in the Russian Federation in 2007–2010" is brought in force in Russia. According to estimates, no less than 25% of current nanotechnological designs are, and will be, associated with use of fullerenes. However, despite the considerable progress in studies of fullerenes and development of technologies for their production, a number of problems have not been resolved, which hinders wide application of fullerene nanostructures. The major problem is high cost of production, separation, and purification of fullerenes.

Several methods for synthesis of fullerenes are presently known [1–10]. The most preferable of these are the electric-arc technique [9] and method of incomplete combustion of hydrocarbons (benzene, toluene, etc.) [6]. Other methods have been poorly studied and can be only used on a limited scale.

In both methods, the main synthesis product is the so-called fullerene-containing carbon black (FB). In addition to fullerenes, the black contains amorphous carbon and, in the case of incomplete combustion of hydrocarbons, also impurities of polycondensed aromatic hydrocarbons.

A characteristic distinction of fullerenes from other structures composed of pure carbon is their ability to dissolve in organic solvents. This enables recovery of fullerenes from FB by extraction with organic solvents [11–14].

The integrated technology for manufacture of fullerenes, suggested in this paper, includes stages of FB synthesis, extraction of a mixture of fullerenes from the black, and subsequent separation and purification of the fullerenes (see scheme). This technology has been used for more than 10 years at the St. Petersburg Institute of Nuclear Physics for production of kilogram amounts of C_{60} of 99.5% purity (here and hereinafter, the composition of fullerenes is given in weight percents).

Manufacture of FB by electric-arc evaporation of graphite. The fullerene-containing carbon black produced by the electric-arc method, as a rule, contains a mixture of fullerenes with the following content of the main components (wt %): C_{60} 65–88, C_{70} 12–30, and $C_{n>70}$ 1–5. A specific feature of the electric-arc method is that it produces, together with a carbon black containing up to 20 wt % fullerenes, also so-called cathode deposits containing up to 40 wt % multilayer carbon nanotubes, which a valuable material for nanotechnologies.

The designs of electric-arc carbon-black generators (EACBGs), developed by now, provide, under certain conditions, a fullerene yield of up to 43 wt % [5]. However, the increase in the fullerene yield entails a decrease in the evaporation rate of graphite [15]. It has been noted [2] that, as the diameter of the electrodes being evaporated increases, the yield of fullerenes should necessarily decrease. This circumstance serves as a certain limitation in developments of a high-capacity EACBG design [5, 16–19].

Processing of FB with low content of fullerenes is unprofitable because of the increasing expenditure of

Integrated flowsheet for manufacture of fullerenes

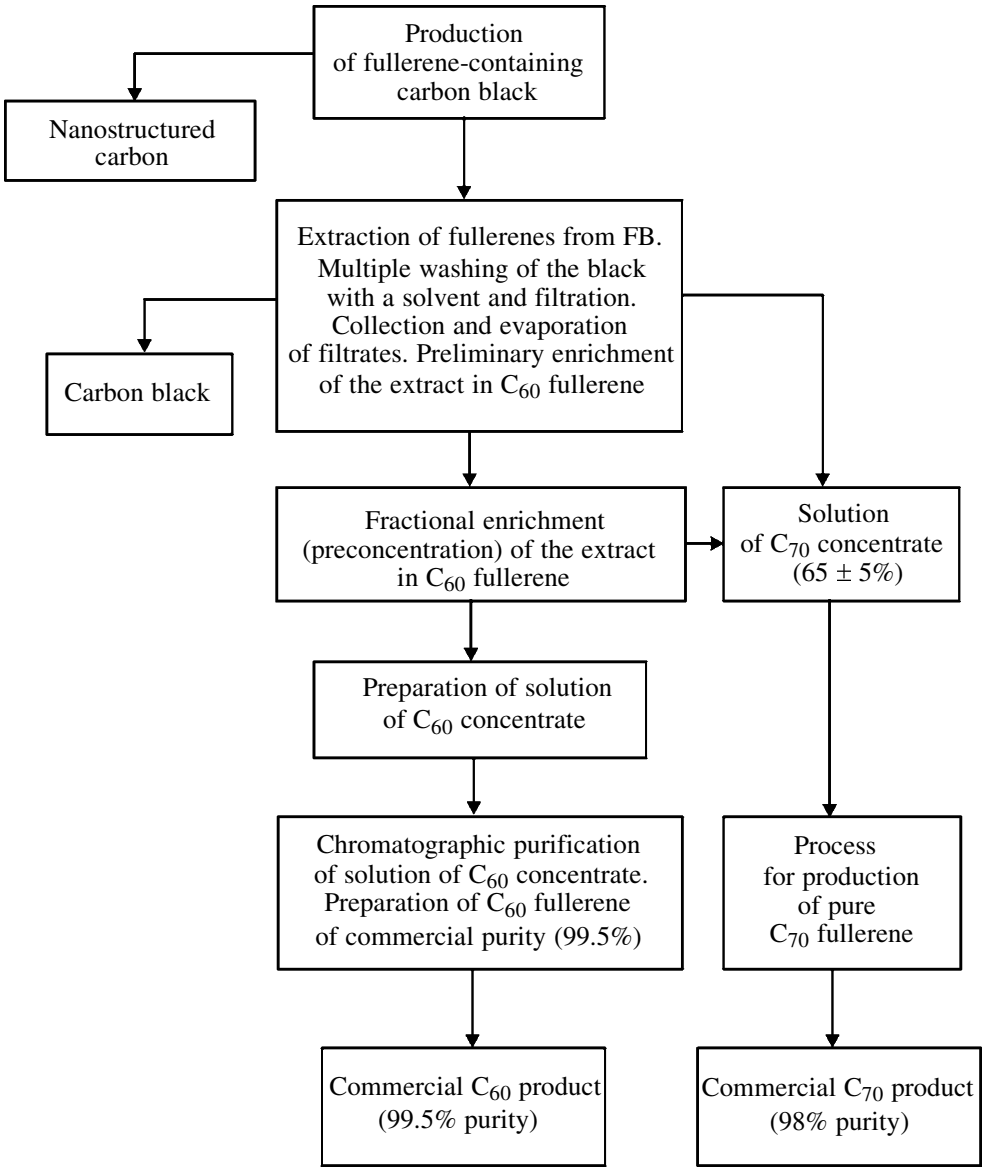

electric power, solvents, and labor per gram of the final product. The experience of EACBG exploitation made it possible to find a balance between the content of fullerenes in a black and the output capacity that would be optimal from the profitability standpoint. The optimal output characteristics are provided both by limiting the diameter of a graphite rod being evaporated (as a rule, to 6–15 mm) and by choosing the rate of its evaporation. The generator designs used show the best performance with rods (electrodes) 6–8 mm in diameter. In prolonged operation modes, the average yield of fullerenes varies within 6–10% of the mass of the fullerene-containing carbon black, which, in turn, constitutes 35–50% of the mass of the evaporated graphite (the rest is the cathode deposit). The yield of the carbon black can be raised by reversing the polarity of the electrodes for "back" evaporation of the cathode deposit. However, the evaporation of the cathode deposit is slow because of its high electrical resistivity, which makes the gain in the output capacity insignificant.

The fullerene yield is markedly raised if water-cooled screens, coils, and other devices that shield fullerenes from the detrimental action of hard UV radiation of the arc are present in the evaporation chamber [5, 18]. The yield of fullerenes also depends on the purity of the graphite material. The best results were obtained with domestic raw materials on MPG-6

Table 1. Parameters of an extraction installation for extraction of fullerenes from electric-arc FB

Parameter	Value
Maximum weight of FB charged into extractor, kg	3
Preferable mass of FB charge, kg	1.5–2.0
Extractant/FB ratio, liters of solution/kg of FB	10–12
Number of extraction cycles	3
Duration of agitation (extraction), h:	
first cycle	~1
second cycle	~3
third cycle	~6
Efficiency of extraction process (3 cycles), %	92–95
Residual content of fullerenes in carbon black (3 cycles), %	0.2–0.3
Irrecoverable loss of solvent, %	9.0
Duration of extraction process (3 cycles), h	15–17

spectroscopic graphite rods of ultrapure 7-2 and 7-3 grades [TU (Technical Specifications) 48-4802-14–88].

An EACBG of basic design was used to process 225 kg of graphite rods (6 mm in diameter, 200 mm long). The capacity of the generator in terms of evaporation of graphite rods was, on the average, 100 g per hour. The mean fullerene content of FB was 6–8 wt %.

It was found in a prolonged exploitation of a working prototype of an electric-arc generator that maintaining the fullerene yield at a level not lower than 6 wt % in continuous operation requires that the helium atmosphere in the evaporation chamber should be renewed at regular intervals of time. This is necessary because impurities released from the graphite being evaporated (trace amounts of sorbed moisture, atmospheric oxygen, etc.) accumulate and suppress generation of fullerenes. A promising technical solution concerning the removal of FB from the electric-arc zone with a directed flow of inert gas (helium) and its collection in special containers proved to be poorly efficient for the given case because the system for helium recycling is bulky and complicated in use. A more practically feasible procedure is that with periodic renewal of the helium atmosphere in the evaporation chamber, correlated with maintenance stops.

Thus, the presently used electric-arc FB generators have limited output capacity, mainly determined by the evaporation parameters of the graphite material. The problem of raising the FB yield can be partly resolved by incorporating the electric-arc unit into a computer-controlled multiunit system [10]. This will markedly diminish loss of time for unit recharging.

Extraction of fullerenes from FB. Several methods are known for recovery of fullerenes from FB [11, 12, 14]. Their principal disadvantage consists in long duration of extraction and filtration and low degree of fullerene recovery (≤70 wt %). The solvents used in the process of fullerene recovery from carbon black should satisfy the following requirements: high solubility of fullerenes, as low boiling point as possible, low fire and explosion hazard, low toxicity, and low cost. Published data (e.g., [20, 21]) on the solubility of fullerenes in various solvents can be used to compose a list of solvents best suitable for large-scale extraction: toluene, *o*-xylene, *o*-dichlorobenzene, 1,2,4-trichlorobenzene, and 1,2,4-trimethylbenzene. Of these, *o*-xylene was chosen as satisfying the above requirements to the fullest extent. C_{60} and C_{70} fullerenes have a comparatively high solubility in *o*-xylene at 25°C: 8–10 and 15 g l^{-1}, respectively. Use of *o*-xylene instead of toluene, which frequently serves as an agent for extraction of fullerenes from carbon black, makes it possible to considerably reduce the volumes of the solutions being processed and thereby to minimize the dimensions of the basic process apparatus. The extraction installation developed in this study includes a mechanical stirrer with a filter, collectors for solutions and solvent, and a vacuum evaporator. The following parameters were found when using this installation: optimal mass of carbon black charged into the extractor, solvent/carbon black ratio, duration and number of repetitions of the extraction procedure, loss of the solvent via its capture by the carbon black, extraction efficiency, and residual content of fullerenes in the carbon black. The values of these parameters are listed in Table 1.

To accelerate the extraction process, the filtration was carried out under a nitrogen pressure of up to 5 kg cm^{-2}. A suspension of carbon black in the solvent was mechanically agitated at 2–3 revolutions per second. The material remaining on the filter is composed of a solid phase (carbon black, ~40 wt %) and a captured solvent (60 wt %), and, therefore, solvent regeneration requires that an additional operation, vacuum evaporation of the solvent from carbon black, should be performed.

As can be seen from Table 1, the extraction process is long and labor-consuming and involves a considerable irrecoverable loss of the solvent. The previously developed sublimation technique [22, 23] is devoid of the above-mentioned disadvantages. This method con-

sists in the following: A bulk finely dispersed carbon black is mixed in a certain proportion with a noninflammable mixture of solvents and agitated until free-flowing and no-dust-forming grains are formed (compaction). Then the resulting product is charged into a sublimation apparatus and fullerenes are sublimed at a temperature of 500–800°C and residual pressure of 0.1–1.0 Pa and condensed on a water-cooled removable collector. The conditions under which the sublimation occurs with an 88–90 wt % yield in 1–1.5 h were experimentally found. Experiments performed on larger FB samples demonstrated that a large-scale sublimation installation can be, in principle, developed.

A prompt analysis was made using spectrophotometry or microcolumn high-performance liquid chromatography (HPLC) on the C_{18} phase with a 60 : 40 acetonitrile–toluene mixture as eluent. Chromatography on this phase enables reliable observation of C_{60}, C_{70}, and their oxides, but, in this case, the peaks of the higher fullerenes are strongly broadened and their analysis is difficult. For analysis of high-purity fullerenes and higher fullerenes, we used chromatographic columns specially developed by Nacalai Tesque Inc. (Japan) for analysis and separation of fullerenes and metallofullerenes: analytical/semipreparative Cosmosil BuckyPrep 4.6×250 column and preparative Cosmosil BuckyPrep 10×250 column. The stationary phase of both of these columns is pyrenylpropyl silica gel. Standard analyses and separations use as the mobile phase (eluent) pure toluene. The sample volume and the eluent flow rate were 20 μl and 1 ml min^{-1} for the analytical column, and 4 ml and 4.7 ml min^{-1} in preparative separations. The peaks were recorded by absorption at a wavelength of 330 nm. The ratio of the molar extinctions of C_{70} and C_{60} at this wavelength is 0.76.

A single-stage analysis on the analytical column is sufficient for analysis of C_{60} with a 99.5%+ purity. In analysis of ultrapure (99.9%+) C_{60}, a weighed portion of the substance to be analyzed is preliminarily enriched with impurities on the preparative column. In this case, a fraction that follows C_{60} is taken. This fraction is concentrated to a certain volume and its aliquot is taken for analysis on the analytical column. The main impurities in pure C_{60} are monoxide $C_{60}O$ and C_{70}. On these columns, the retention time of fullerene oxides exceeds that for the corresponding unoxidized fullerenes, in contrast to the case of the C_{18} phase (octadecyl silica gel), on which the oxides are eluted earlier than the corresponding fullerenes with a 60 : 40 acetonitrile–toluene mixture as eluent. Under the above-mentioned analytical conditions, the peaks of C_{60} and C_{70} are well-resolved (the distance between the peaks is 11 times the width of the C_{60} line at half-maximum) and the relative content of impurities can be easily determined.

Enrichment of the extract by fractional concentration. At present, numerous technical solutions that enable production of pure fullerenes C_{60}, C_{70} and $C_{n>70}$ are known [24–26, 28–34]. These solutions are mostly based on the chromatographic method, which produces, in some cases, very pure solutions of C_{60} and C_{70} fullerenes of purity exceeding 99.5 and 98%, respectively. A disadvantage of the chromatographic method is its low output capacity in terms of the target component.

The previously revealed property of the anomalous temperature dependence of the solubility of C_{60} fullerene [20, 21, 24–28] served as a basis for a method of fullerene purification by fractional concentration [28]. The method of fractional crystallization [26, 27] can produce C_{60} fullerene of 99.5% purity; however, the process involves numerous stages and the yield of the target product is very low, only several percents [27]. In [26], a mixed solvent composed of toluene and 1,3-diphenylacetone was used. Three stages of crystallization yielded C_{60} of 99.5% purity, according to HPLC analysis. With this method, the total yield of pure C_{60} fullerene was 69% relative to the mass of the starting extract (at initial C_{60} content of the extract equal to 84%). The main disadvantages of this technique are as follows: large solvent volumes are used because of the low solubility of fullerenes in this solvent, toluene should be completely removed from the solvent after performing the procedure, high temperature (110°C) is necessary, duration of each stage is long, a difficultly available solvent component is used (1,3-diphenylacetone), and the mixed solvent is to be regenerated. Therefore, this technique should also be considered labor-consuming and poorly efficient despite the high yield of pure C_{60}.

The technique we suggest here employs, to obtain pure C_{60}, a kind of liquid chromatography, flash chromatography or flash filtration. This separation method can be used in those cases when the retention time of the components being separated differs by a factor of more than several tens. This method is devoid of the principal disadvantage of the classical chromatography, low output capacity, because it does not require a fixed one-time charging of a limited amount of the starting material. However, the service life of the sorbent in this technique is limited by its capacity for impurities being sorbed. Therefore, in order to make longer the working time of a column

Table 2. Main parameters of the FC process

FC stage	Time, h	Solvent : crystals, ml g^{-1}	Fraction composition, wt %				Mass of deposit, wt % relative to starting extract, for each stage
			deposit		filtrate		
			C_{60}	C_{70}	C_{60}	C_{70}	
First	1.5	10	87.0	13.0	31.4	68.6	79.5
Second	2.0	19	92.0	8.0	75.4	24.6	66.3
Third	3.0	15	96.7	3.3	84.6	15.4	60.8

without replacement of the sorbent, the content of the component being purified in the raw material should be as high as possible.

To obtain a concentrate of this kind, with a C_{60} content of up to 96%, a procedure for enrichment of the starting raw material for flash chromatography, fractional concentration (FC), was developed. The FC process is for the most part performed in three stages, the yield of the enriched product remains high, and the content of C_{60} fullerene in the concentrate is as high as $96 \pm 2\%$. The procedure consists in the following. A fullerene extract with a C_{60} content of 72–85% is dissolved in a certain amount of *o*-xylene heated to 80–85°C until a saturated solution is formed, this solution is filtered on a vacuum filter heated to the same temperature, and the separated crystals are dried under reduced pressure to constant mass. As a result, the crystals are enriched with C_{60} fullerene, and the filtrate, with C_{70} fullerene. The composition and yield of the enriched concentrate of C_{60} depends on the composition of the starting extract of fullerenes and solvent/crystals ratio. A decrease in the enrichment was observed on making longer the time for which the saturated fullerene solution is heated. In the multistage enrichment scheme, the decrease in enrichment becomes noticeable already in the third stage, with no enrichment occurring at a larger number of stages. Presumably, this is due to cross oligomerization of C_{60} and C_{70} under the action of temperature. It was found that the total time of all thermal treatments, including the duration of agitation and hot filtration, should not exceed 7 h. With account of this limitation, a process scheme of FC was developed. This scheme enables effective enrichment of extracts of virtually any composition in C_{60} fullerene, with a considerable yield of the final product. Table 2 lists the results of FC of C_{60} fullerene at the initial C_{60}/C_{70} ratio of 75/25.

It follows from the results presented that three stages of FC give in a 60% yield a concentrate of the following composition (wt %): $C_{60}O$ 2.2, C_{60} 94.9, C_{70} 2.9. This concentrate is a good half-product for production of pure C_{60} by flash-chromatographic purification.

The fractional enrichment procedure enables the following: (1) production of a concentrate with a C_{60} content sufficiently high for practical use in further flash-chromatographic purification; (2) removal of C_{70} from the starting extract in a smaller number of stages; (3) choice of the FC mode in which a first-stage solution with high C_{60} content, suitable for subsequent preparation of this fullerene, is formed; (4) determination of the conditions in which filtrate solutions of second and third stages have a composition close to that of the starting extract and the extract formed in the first stage of FC, respectively, which enables their use in the subsequent cycles of enrichment; (5) reduction of the volume of fractions with a low content of expensive C_{70}.

In continuous processing of fullerene extracts, the yield of the C_{60} concentrate is optimized and the loss of C_{70} is reduced to a minimum.

Production of pure C_{60} fullerene. Several methods for preparation of a pure C_{60} fullerene are known: chromatographic [29–36], fractional crystallization [26, 27], selective extraction [37, 38], and chemical techniques that use complexing agents, such as, e.g., 1,8-diazabicyclo[5.4.0]undec-7-ene (DBU) [39] or calixarenes [40], or those based on functionalization of the fullerene molecule (bromination [41] etc.). As already noted, the most efficient method for production of pure C_{60} is flash chromatography. The best, as regards the output capacity, stationary phase in purification of C_{60} fullerene by this method are activated carbons with a large specific surface area, e.g., of Darco (Fluka) or DCL GDC (Waterlink Sutcliffe Carbons) brands [42] or sorbents based on these carbons. Solvents of aliphatic or aromatic nature or mixtures of these, *o*-xylene in the given case, are commonly used as the mobile phase.

The use of a granulated activated carbon as a sorbent enabled application of a simple version of gravitational liquid chromatography. The choice of *o*-xylene for preparing the starting solution is due to the fact that *o*-xylene has been used previously for extraction and fractional concentration. An additional advantage of *o*-xylene over toluene frequently used for this purpose [37] is that, in this case, solutions with high concentration of fullerenes can be prepared; as a result, solutions with considerably smaller working volumes can be used and the duration of the chromatographic process can be made markedly shorter.

A saturated solution of a mixture of fullerenes in *o*-xylene, with a C_{60} content of about 96%, is continuously fed into the column, and the eluate contains C_{60}, in which no C_{70} or higher fullerenes are detected. The process of chromatographic purification is monitored by the concentration of C_{70} fullerene in the eluate. To obtain, e.g., C_{60} of 99.5% purity, the process is terminated when C_{70} appears at the outlet in a concentration exceeding 0.1 %. After C_{70} appears at the outlet, the supply of the feeding solution is terminated and pure solvent is fed into the column. The washing is performed to a C_{60} concentration in the eluate equal to 0.1–0.2 g l^{-1}. Further washing is inadvisable for practical reasons.

The mobile phase is supplied at a velocity of 0.2–0.8 ml min^{-1} cm^{-2} (preferably 0.4–0.5 ml min^{-1} cm^{-2}). If the process is carried out at a lower rate, the purity of the product obtained is improved, but the output capacity of the process decreases. An increased flow rate of the mobile phase not only impairs the quality of C_{60} obtained, but also leads to a decrease in the amount of the pure product obtained in a single cycle of use of the sorbent.

The yield of pure C_{60} is 72–78% relative to the amount of the concentrate charged, with 15–18% being the loss for irreversible sorption and up to 10% representing a material in which the content of C_{70} fullerene exceeds 0.5% (raw material for further recycling). The solvent is removed from the solution collected at the column outlet and crystals of pure C_{60} fullerene. Analysis shows that crystals of C_{60} fullerene, as a rule, contain, in addition to an insignificant impurity of C_{70} fullerene, that of the oxide $C_{60}O$ in an amount of up to 1.5–2.0% in some cases. Activated carbon has low selectivity with respect to this impurity, whose fraction increases in the course of chromatographic purification. This impurity can be removed in several ways. The most efficient way is vacuum treatment of the crystals obtained. This method can reduce the content of the oxide $C_{60}O$ to 0.05–0.1%. An advantage of the technology developed consists in that first portions of the eluate contain high-purity C_{60} fullerene (better than 99.9%). At a flow rate of the liquid phase exceeding 0.2 ml min^{-1} cm^{-2}, the fraction of such a product in the total output can be markedly raised, which improves the profitability of the production process.

With this technology used on a working equipment at St. Petersburg Institute of Nuclear Physics, Russian Academy of Sciences, the average rate of 99.5% C_{60} manufacture with double-shift work was 1–2 g h^{-1} (or 500–600 g per month). The developed flowsheet can be used without any significant change for manufacture of C_{60} fullerene in an amount exceeding 10 kg per month.

Manufacture of pure C_{70} fullerene. Flash chromatography on activated carbon cannot be used to separate C_{70} from C_{60} because C_{70} is sorbed on the carbon considerably more firmly than C_{60}. Therefore, it is advisable to use a combination of several methods for large-scale manufacture of pure C_{70} fullerene [43]. The technology we suggest includes the following sequence of procedures: enrichment of a mixture of C_{60}/C_{70} fullerenes with C_{70} fullerene by fractional concentration to a level of 85–92%; flash chromatographic purification of the concentrate obtained to remove the admixture of higher fullerenes on activated carbon; separation of trace amounts of C_{60} by fractional purification to obtain pure (98%) C_{70} fullerene.

The fractional concentration from *o*-xylene, which is an efficient and high-output-capacity technique for enrichment of C_{60}, has also been successfully used for enrichment of C_{70} fullerene [44].

The stage of fractional concentration in C_{70} fullerene is continuation of the first stage of fractional enrichment with C_{70} fullerene. The concentrate obtained in this stage (20–22% relative to the weight of the starting mixture of fullerenes) is a supersaturated solution (up to 26 g l^{-1}), from which crystals containing 85–92% C_{70} precipitate upon cooling. The yield of the crystals depends on temperature and duration of crystallization, and can be as high as 80% relative to the material contained in the filtrate at –24°C. The mother liquor contains 2–3 g l^{-1} of fullerenes and is enriched in C_{60} fullerene, compared with crystals.

Depending on the composition of the starting extract, the crystals obtained may contain admixtures of higher fullerenes in an amount of up to 4–5%. Such a high content of higher fullerenes makes their recovery feasible. This procedure can be effectively performed with 1,2,4-trichlorobenzene by multistage frac-

tional concentration. It was found experimentally that the content of higher fullerenes in C_{70} crystals can be reduced from 4–5 to 0.7–0.8% at room temperature in three to four stages. In this case, concentrates are obtained in all stages, which contain up to 10% higher fullerenes. The crystalline concentrate of C_{70} fullerene is further dissolved in *o*-xylene and subjected to chromatographic purification on activated carbon. The impurity of higher fullerenes is completely removed in this stage.

The process we suggest allows production of pure C_{70} fullerene in considerable amounts. For example, the concentrate of C_{70} fullerene, obtained in the first stage of fractional concentration from the starting mixture of fullerenes, contains less than 2% higher fullerenes, whereas a single cycle of two-stage crystallization can give C_{70} fullerene with the purity better than 98%. The total yield of pure C_{70} exceeds 100 g in a cycle (48 h) per 1000 g of the starting mixture of fullerenes [composition (%): C_{60}/C_{70} 75/25]. Presence of higher fullerenes in the starting extract in an amount exceeding 2% diminishes nearly twofold the yield of pure fullerene and makes nearly twice longer the purification of the C_{70} concentrate to remove impurities. Therefore, additional one or two stages of crystallization are necessary for obtaining C_{70} fullerene of 98% purity if more than 2% higher fullerenes is contained in the starting C_{70} concentrate.

The scheme suggested can be used to obtain, without any significant modification of the available inexpensive equipment, to produce up to 1 kg of C_{70} of commercial purity in a month. Because this method for production of C_{70} is a part of a unified flowsheet for synthesis of C_{60} and C_{70}, its use makes it possible to improve the output capacity in terms of pure C_{70} and reduce its cost severalfold, compared with the technique suggested in [40].

In 2003, Frontier Carbon Corp. declared that its annual output capacity of fullerenes by incomplete combustion of hydrocarbon raw materials was 40 t [45]. A plant constructed by this company could satisfy the whole world's demand for fullerenes, and their price would decrease severalfold. However, the authors are unaware of any offers by this company on the fullerene market. It would be expected that the raw mixture of fullerenes, produced by this technique, will be contaminated with polycondensed aromatic hydrocarbons. Isolation of pure fullerenes from a raw material of this kind is presently possible only with low-output-capacity and rather expensive chromatographic methods, and, consequently, the production cost of these fullerenes will long exceed that of fullerenes produced by the electric-arc technique.

CONCLUSIONS

(1) A semicommercial technology for manufacture of pure C_{60} and C_{70} fullerenes was developed.

(2) An apparatus for production of up to 1 kg of a fullerene-containing carbon black in 24 h was designed and fabricated.

(3) An apparatus for recovery of a mixture of fullerenes from a fullerene-containing carbon black, with a monthly processing capacity of up to 40 kg of carbon black, was designed and fabricated.

(4) An installation for chromatographic purification of C_{60} (to 99.5 or 99.9%), with a monthly output capacity of up to 500 g of 99.5% C_{60}, was designed and fabricated.

(5) The flowsheet developed can be used to produce up to 100 g of C_{70} (98%) in a month on the already existing equipment, provided that the content of higher fullerenes in the starting C_{70} concentrate is less than 2%. An additional special procedure for removal of higher fullerenes was developed for obtaining C_{70} fullerene of 98% purity from a concentrate with increased content of higher fullerenes.

REFERENCES

1. Howard, J.B., McKinnon, J.T., Johnson, M.E., et al., *J. Phys. Chem.*, 1992, vol. 96, no. 16, pp. 6657–6662.
2. Taylor, R., Langley, G.J., Kroto, H.W., and Walton, D.R.M., *Nature*, 1993, vol. 366, no. 6457, pp. 728–731.
3. Fields, C.L., Pitts, J.R., Hale, M.J., et al., *J. Phys. Chem.*, 1993, vol. 97, pp. 8701–8702.
4. Laska, L., *Czech. J. Phys.*, 1993, vol. 43, no. 2, pp. 193–195.
5. Bubnov, V.P., Krainskii, I.S., Laukhina, E.E., and Yagubskii, E.B., *Izv. Ross. Akad. Nauk., Ser. Khim.*, 1994, no. 5, pp. 805–809.
6. RF Patent 2086503.
7. RF Patent 2139241.
8. RF Patent 2146647.
9. RF Patent 2234457.
10. RF Certificate for Useful Model no. 25317.
11. Parker, D.H., Wurz, P., Chatterjee, K., et al., *J. Am. Chem. Soc.*, 1991, vol. 113, pp. 7499–7503.
12. RF Patent 2107536.

13. Sedov, V.P. and Shilin, V.A., Extraction of Fullerenes with a Solvent from Electric-Arc Carbon Black on a Pilot Installation, *Preprint of St. Petersburg Inst. of Nuclear Physics*, *Russ. Acad. Sci.*, Gatchina, 2001, no. 2424.
14. Laukhina, E.E. and Bubnov, V.P., *Izv. Ross. Akad. Nauk, Ser. Khim.*, 1995, no. 5, pp. 1223–1225.
15. Belousov, V.P., Belousova, I.M., Budtov, V.P., et al., *Opt. Zh.*, 1997, vol. 64, no. 12, pp. 3–37.
16. Afanas'ev, D.V., Blinov, I.O., Bogdanov, A.A., et al., *Zh. Tekh. Fiz.*, 1994, vol. 64, no. 10, pp. 76–90.
17. Afanas'ev, D.V., Bogdanov, A.A., Dyuzhev, G.A., and Kruglikov, A.A., *Zh. Tekh. Fiz.*, 1997, vol. 67, no. 2, pp. 125–128.
18. Sedov, V.P. and Shilin, V.A., Experience in Manufacture of a Fullerene-Containing Carbon Black, *Preprint of St. Petersburg Inst. of Nuclear Physics, Russ. Acad. Sci.*, Gatchina, 2001, no. 2433.
19. Krestinin, A.V. and Moravskii, A.P., *Khim. Fiz.*, 1999, vol. 18, no. 3, pp. 58–66.
20. Bezmel'nitsyn, V.N., Eletskii, A.V., and Okun', M.V., *Usp. Fiz. Nauk*, 1998, vol. 168, no. 11, pp. 1195–1220.
21. Eletskii, A.V., *Teplofiz. Vys. Temp.*, 1996, vol. 34, no. 2, pp. 308–323.
22. RF Patent 2124473.
23. Moskalev, P.N., Sedov, V.P., and Grushko, Yu.S., Experience in Sublimation Recovery of Fullerenes from a Fullerene-Containing Carbon Black, *Preprint of St. Petersburg Inst. of Nuclear Physics, Russ. Acad. Sci.*, Gatchina, 2001, no. 2423.
24. Zhou, X., Lin, J., Jin, Z., et al., *Fullerene Sci. Technol.*, 1997, vol. 5, no. 1, pp. 285–290.
25. Beck, M.T. and Mandi, G., *Fullerene Sci. Technol.*, 1997, vol. 5, no. 2, pp. 291–310.
26. Doome, R.J., Fonseca, A., Richter, H., et al., *J. Phys. Chem. Solids*, 1997, vol. 58, no. 11, pp. 1839–1843.
27. Zhou, X., Gu, Z., Wu, Y., et al., *Chin. Sci. Bull.*, 1993, vol. 38, pp. 175–184.
28. Sedov, V.P., Pretreatment of a C_{60} Fullerene Concentrate by Fractional Concentration, *Preprint of St. Petersburg Inst. of Nuclear Physics, Russ. Acad. Sci.*, Gatchina, 2002, no. 2476.
29. Spitsyna N.G., Buravov, L.I., and Lobach, A.S., *Zh. Anal. Khim.*, 1995, vol. 50, no. 6, pp. 673–676.
30. Isaacs, L., Wehsig, A., and Diederich, F., *Helv. Chim. Acta*, 1993, vol. 76, pp. 1231–1250.
31. US Patent 5310532.
32. US Patent 5662876.
33. US Patent 5904852.
34. Meier, M.S. and Selegue, J.P., *J. Org. Chem.*, 1992, vol. 57, pp. 1924–1926.
35. RF Patent 2224714.
36. Grushko, Yu.S., Sedov, V.P., Alekseev, E.G., et al., Production of C_{60} Fullerene by Liquid Chromatography on Activated Carbon, *Preprint of St. Petersburg Inst. of Nuclear Physics, Russ. Acad. Sci.*, Gatchina, 2004, no. 2556.
37. Khemani, K.C., Prato, M., and Wudl, F., *J. Org. Chem.*, 1992, vol. 57, pp. 3254–3256.
38. Coustel, N., Bernier, P., Aznar, R., et al., *J. Chem. Soc., Chem. Commun.*, 1992, pp. 1402–1403.
39. Nagota, K., Dejima, E., Kikuchi, Y., and Hashiguchi, M., *Chem. Lett.*, 2005, vol. 34, pp. 178.
40. US Patent 5711927.
41. Troshin, P.A. and Lyubovskaya, R.N., Abstracts of Papers, *7th Biennial Int. Workshop "Fullerenes and Atomic Clusters,"* St. Petersburg (Russia), June 25–July 1, 2005, p. 114.
42. Moskalev, P.N., Sedov, V.P., and Shilin, V.A., A Study of Adsorption Properties of Activated Carbons for C_{60} and C_{70} Fullerenes, *Preprint of St. Petersburg Inst. of Nuclear Physics, Russ. Acad. Sci.*, Gatchina, 2006, no. 2695.
43. Grushko, Yu.S. and Sedov, V.P., Choice of a Technology for Production of Pure C_{70} Fullerene, *Preprint of St. Petersburg Inst. of Nuclear Physics, Russ. Acad. Sci.*, Gatchina, 2005, no. 2617.
44. Sedov, V.P., Use of the Crystallization Method for Production of Pure C_{60} and C_{70} Fullerenes, *Preprint of St. Petersburg Inst. of Nuclear Physics, Russ. Acad. Sci.*, Gatchina, 2005, no. 2417.
45. Murayama, H., Tomonoh, S., Alford, J.M., and Karpuk, M.E., Abstracts of Papers, *6th Biennial Int. Workshop "Fullerenes and Atomic Clusters,"* St. Petersburg (Russia), June 30–July 4, 2003, p. 35.

ISSN 1070-4272, Russian Journal of Applied Chemistry, 2007, Vol. 80, No. 3, pp. 456–460. © Pleiades Publishing, Ltd., 2007.
Original Russian Text © K.N. Semenov, N.A. Charykov, A.K. Pyartman, V.A. Keskinov, V.V. Lishchuk, O.V. Arapov, N.I. Alekseev, 2007, published in Zhurnal Prikladnoi Khimii, 2007, Vol. 80, No. 3, pp. 458–462.

NANOTECHNOLOGIES AND NANOMATERIALS

Solubility of Fullerenes in *n*-Alkanoic Acids C_2–C_9

K. N. Semenov, N. A. Charykov, A. K. Pyartman, V. A. Keskinov, V. V. Lishchuk, O. V. Arapov, and N. I. Alekseev

St. Petersburg State University, St. Petersburg, Russia
Innovations of Leningrad Institutes and Enterprises, Private Company, St. Petersburg, Russia
St. Petersburg State Institue of Technology (Technical University), St. Petersburg, Russia

Received September 28, 2006

Abstract—The solubility of fullerene C_{60} and a fullerene mixture [C_{60} (75%), C_{70} (24%), C_{76-80} (1%)] in linear alkanoic acids (C_2–C_9) was determined at 20°C. The solubilities of C_{60} and a fullerene mixture in carboxylic acids were examined in relation to the number of carbon atoms in the carboxylic acid.

DOI: 10.1134/S1070427207030202

Our preliminary study of the solubility of fullerenes were reported in [1]. In this study we examined the solubility of an individual fullerene C_{60} and a fullerene mixture [C_{60} (75%), C_{70} (24%), C_{76-80} (1%)] in linear carboxylic acids.

The development of techniques for efficient extractive separation and purification of fullerene mixtures to an extent suitable for their final chromatographic separation is an urgent problem [2, 3]. These processes are based on differences in the solubility of particular fullerenes (primarily C_{60} and C_{70}) in organic solvents.

However, published data on the solubility of fullerenes are scarce and contradictory. As a rule, these data refer to binary systems, for example, C_{60} or C_{70}–solvent. In these studies, aromatic (benzene, toluene, *o*-xylene, 1,2-dichlorobenzene) and nonaromatic (CCl_4, hexane) solvents were used [4–11]. Data on the solubility of binary fullerene mixtures in a certain solvent as well as on the solubility of a particular fullerene in solvent mixtures are lacking. The data on polythermal solubility of fullerenes in the ternary systems, such as C_{60}–C_{70}–solvent, which are necessary for choosing the optimal conditions for extractive separation of fullerenes, are also virtually lacking. An exception is a paper [2] in which the solubility diagrams of the ternary systems C_{60}–C_{70}–toluene at 25°C and C_{60}–C_{70}–*o*-xylene at 80°C were reported.

The only published paper on polythermal solubility of fullerenes in carboxylic acid homologs is [1]. In that study, the solubility of a multicomponent fullerene mixture enriched in C_{60} and C_{70} (C_{60} 38.8, C_{70} 33.0, C_{76-78} 5.6, C_{84} 8.6, C_{90} 2.6, and C_{96} 3.3%) and also the solubility of individual fullerenes C_{60} and C_{70} in higher isomerized carboxylic acids C_7–C_9 (HICAs) were studied within the temperature range 20–80°C. It was found that light fullerenes show relatively high solubility in HICAs, up to 0.5 g l^{-1}, and the solubility of C_{60} is lower than that of C_{70} by a factor of three. This difference in solubility allows preliminary separation of lighter fullerenes from the fullerene mixture before final chromatographic separation.

EXPERIMENTAL

In experiments we used fullerene C_{60} containing 99.9% main compound and about 0.1% C_{70} and a fullerene mixture [C_{70} 24, C_{60} 75, C_n (n > 70) 1%] produced by ILIP Private Company (St. Petersburg), *o*-xylene (analytically pure grade), and also *n*-alkanoic acids (C_2–C_9) (chemically pure grade).

The dependence of the solubility both the individual C_{60} and a fullerene mixture in carboxylic acids on the number of carbon atoms in them was studied by the isothermal saturation method at 20°C as follows. Large excess of fullerene was added to 10 ml of each carboxylic acid under consideration (homologous series from acetic acid to pelargonic acid), and the resulting suspension was shaken on a temperature-controlled shaker at 20 ± 0.05°C to attain the saturation. Dissolution of fullerenes in carboxylic acids is slow: the saturation is attained within 8–10 h. The saturated solutions were separated from the solid

phase by filtration through a Schott filter (porosity no. 16) and analyzed.

At each saturation step, an aliquot of a solution of C_{60} or the fullerene mixture in carboxylic acid was sampled, and after dilution with *o*-xylene, the optical densities at λ = 335.5 and 472.0 nm were measured on a Specord-32 spectrophotometer. The solutions of carboxylic acids in *o*-xylene of the same concentration were used as reference. This procedure was chosen because of problems with recovering fullerenes from high-boiling carboxylic acids.

The C_{60} and C_{70} concentrations in their *o*-xylene solutions were calculated by the following empirical equations reported in [12]:

$$c(C_{60}) = 13.10(D_{335} - 1.808D_{472}), \quad (1)$$

$$c(C_{70}) = 42.51(D_{472} - 0.0081D_{335}), \quad (2)$$

where D_{335} and D_{472} are the optical densities measured in a 1-cm cell; $c(C_{60})$ and $c(C_{70})$ are the fullerene concentrations (mg l^{-1}).

In these calculations, the presence of minor amounts of higher fullerenes (about 1 wt %) was neglected.

The electronic absorption spectra of solutions of C_{60} and the fullerene mixture in *n*-alkanoic acids (acetic to pelargonic) diluted with *o*-xylene (Fig. 1, 2) do not show solvatochromic effects typical of other binary solvents (acetonitrile–toluene, benzene–methanol, benzene–hexane, etc). The solvatochromic effect in fullerene spectra appears as a sharp change in the electronic spectra of fullerene due to its clusterization on minor variations in both the fullerene concentration and solvent composition [13–16]. Since solvatochromic effect is absent in solutions of fullerenes in the binary solvents carboxylic acid–aromatic solvent (*o*-xylene, benzene, toluene, *o*-dichlorobenzene, etc.), in these systems the concentration of particular fullerenes can be reliably determined spectrophotometrically by empirical equations (1) and (2).

Figure 3 shows the solubility of C_{60} and the fullerene mixture in carboxylic acids in relation to the number of carbon atoms in them. These dependences are nonmonotonic. With increasing number of carbon atoms, the solubility slightly increases from acetic to valeric acid, sharply increases to the maximum from valeric to enanthic acid, then sharply decreases from enanthic to caprylic acid, and finally sharply increases from caprylic to pelargonic acid.

Analysis of the published data on the solubility of

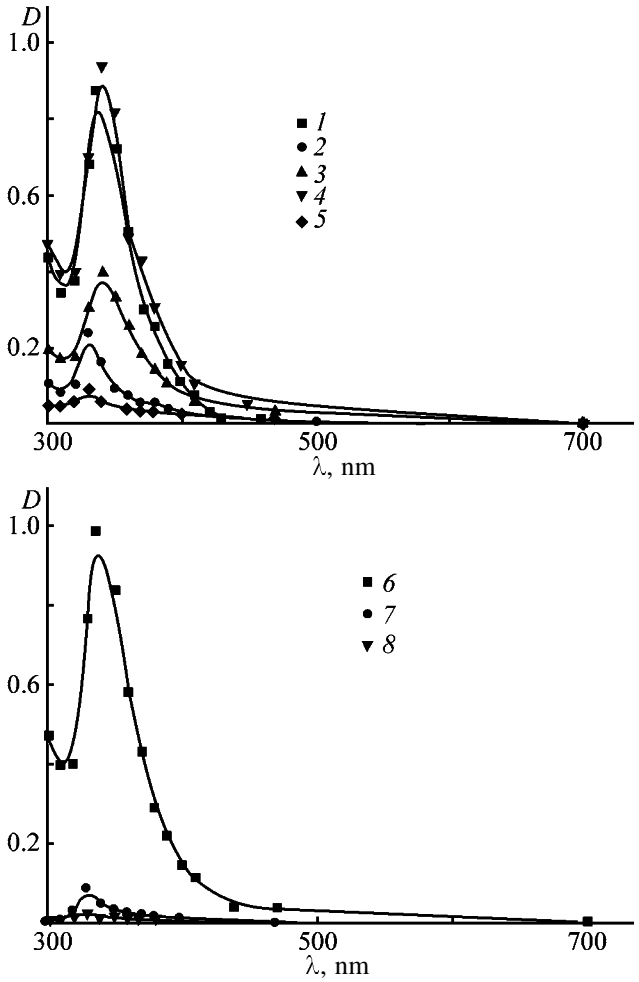

Fig. 1. Electronic spectra of solutions of C_{60} in carboxylic acid–*o*-xylene mixture. Test solution: solution of fullerene in carboxylic acid diluted with *o*-xylene in a volume ratio of 1 : 22. Reference solution: carboxylic acid diluted with *o*-xylene in the same ratio. (*D*) Optical density and (λ) wavelength (nm); the same for Fig. 2. Carboxylic acid, fullerene cocnentration, mg l^{-1}: (*1*) pelargonic, 177.9; (*2*) caprylic, 58.3; (*3*) valeric, 95.1; (*4*) caproic, 243.8; (*5*) propionic, 15.6, (*6*) enanthic, 256.7; (*7*) butyric, 21.4; and (*8*) acetic, 6.8.

fullerenes in organic solvents [11, 16–18] shows that this characteristic does not correlate with main physicochemical parameters of solvents (refractive index, permittivity, molar volume, etc). However, it was found that high solubility of fullerenes is typical of solvents with a certain combination of physicochemical parameters: high refractive index, permittivity of about 4, large molecular volume V_m, the Hildebrand solubility parameter approaching 20 $(J\ cm^{-3})^{1/2}$, and moderate nucleophilicity [16, 18].

The nonmonotonic dependence of the solubility of fullerenes on the number of carbon atoms in carboxyl-

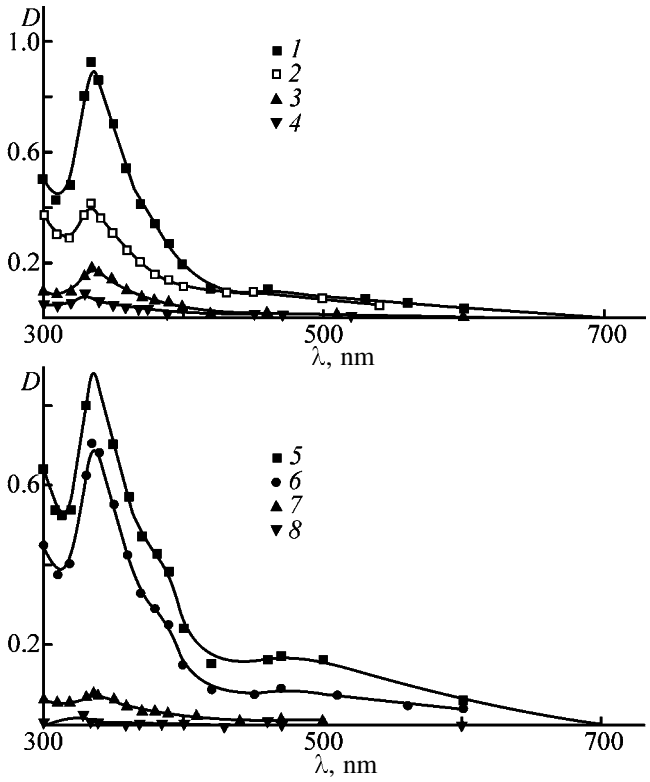

Fig. 2. Electronic spectra of solutions of a fullerene mixture (C_{70} 24%, C_{60} 75%, and C_{76-90} 1%) in carboxylic acid–*o*-xylene mixture. Test solution: solution of fullerene in carboxylic acid diluted with *o*-xylene in a volume ratio of 1 : 82. Reference solution: carboxylic acid diluted with *o*-xylene in the same ratio. Carboxylic acid, fullerene concentration, mg l^{-1}: (*1*) pelargonic, 1107.8; (*2*) caprylic, 537.7; (*3*) valeric, 204.9; (*4*) butyric, 108; (*5*) enanthic, 1207.5; (*6*) caproic, 870.5; (*7*) propionic, 95.5; and (*8*) acetic, 41.

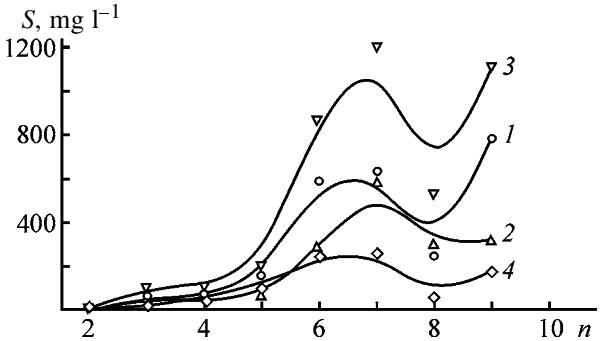

Fig. 3. Solubility of (*1–3*) fullerene mixture [(*1*) C_{60}, (*2*) C_{70}, (*3*) $C_{60} + C_{70}$] and (*4*) individual C_{60} in carboxylic acids vs. the number of carbon atoms in them. (*S*) Solubility and (*n*) number of carbon atoms in carboxylic acids $C_{n-1}H_{2n-1}COOH$.

ic acid can be analyzed in terms of the Hildebrand theory of regular solutions. In this theoretical approach, the solubility is controlled by the solubility parameters of both the solute and solvent. The solubility parameter is determined by the equation [19]

$$\delta = [(\Delta H_{vap} - RT)/V]^{1/2}, \quad (3)$$

where ΔH_{vap} is the enthalpy of vaporization, J mol^{-1}; *T*, temperature, K; *V*, molar volume, mol cm^{-3}; and *R*, gas constant, J mol^{-1} K^{-1}.

The solubility parameter characterizes the energy of pair intermolecular interactions between identical components of solution: solvent–solvent and solute–solute [19]. In the Hildebrand theory, the solubility parameter δ is related to liquid components. Therefore, in calculation of δ of fullerene, its hypothetical state in the form of a supercooled liquid is used as the standard state and the enthalpy of sublimation is used instead of the enthalpy of vaporization [16].

The solubility of fullerenes under consideration in homologous series of carboxylic acids and the Hildebrand solubility parameters of these acids are listed in the table. These data show that, as a rule, the solubility of fullerenes is the higher, the smaller is the difference between the solubility parameters of fullerene and solvent. The maximal solubility of fullerene is reached at equality of the solubility parameters of the fullerene and solvent. Under these conditions, the solvent cohesion parameter also reaches a maximum.

The table shows that, in going from acetic to pelargonic acid, the solubility parameter of caprylic acid exhibits the large positive deviation from the general trend. We believe that this is the reason for the appearance of a minimum in the plot of solubility of fullerenes in carboxylic acids vs. the number of carbon atoms in them. An increase in solubility of C_{60} in going from acetic to enanthic acid correlates with a decrease in the carboxylic acid permittivity. In accordance with Semenchenko's rule [22], this means that the solubility of fullerenes increases with weakening of the carboxylic acid molecular field caused by growing inductive effect of hydrocarbon radicals. However, in going from caprylic to pelargonic acid, this rule does not hold. In this case, the increase in the permittivity of carboxylic acid is accompanied by a sharp increase in the solubility of fullerenes, which correlates with a decrease in the solubility parameter. Another factor is that the molar volume of pelargonic acid, compared to that of the other carboxylic acids, is closer to that of fullerene (429 cm^3 mol^{-1}).

The comparison of the relative content of C_{60} in the initial fullerene mixture (upper horizontal line in Fig. 4) and that in its saturated solutions in carboxylic acids shows that in all the systems the liquid phase is enriched in C_{70}. Thus, in dissolution of fullerene

Solubility of fullerene mixture $C_{60} + C_{70}$ in *n*-alkanoic acids [20, 21]

Acid	ΔH^0_{vap}, kJ mol^{-1}	V_m, cm^3	ε	δ, (J cm^{-3})$^{0.5}$	Solubility, mg l^{-1}	
					C_{60}	fullerene mixture (C_{70} 24, C_{60} 75, C_{76-90} 1%)
Acetic	51.6	57.2	6.15	29.3	6.8	4.1
Propionic	55	74.6	3.44	26.5	15.6	95.5
Butyric	58	91.9	2.90	24.5	21.4	108
Valeric	62.4	108.8	2.67	23.9	95.1	204.9
Caproic	73.2	125.8	2.63	23.7	243.8	870.5
Enanthic	72	141.8	2.59	22.1	256.7	1207.5
Caprylic	82.9	158.6	2.45	22.6	58.3	537.7
Pelargonic	82.4	174.7	2.49	21.39	177.9	1107.8

mixture in carboxylic acids, the transfer of C_{70} into the liquid phase prevails. This phenomenon was previously found [1] in studies of the solubility of individual fullerenes and their mixtures enriched in higher fullerenes in a mixture of higher isomerized carboxylic acids HICAs.

The higher solubility of C_{70} as compared to C_{60} is caused by its less symmetrical structure and higher polarizability, equal to 8×10^{-23} and 6.4×10^{-23} cm^3 for C_{70} and C_{60}, respectively [22, 23]. The inductive and dispersion forces are mainly responsible for intermolecular interactions in the system carboxylic acid (polar molecules)–C_{70} (nonpolar molecules): $U(r) = U_{ind} + U_{disp}$. The dispersion forces arise from fast fluctuations of the electron density in molecules. These fluctuations induce the electrical moment in neighboring molecules and, as a result, cause molecular attraction. The appearance of inductive forces in contact of C_{70} with polar carboxylic acid molecules is caused by polarization of fullerene. From practical point of view, the most interesting is the fact that the difference in the solubility of particular fullerenes in carboxylic acids can be used for efficient separation of fullerene mixtures.

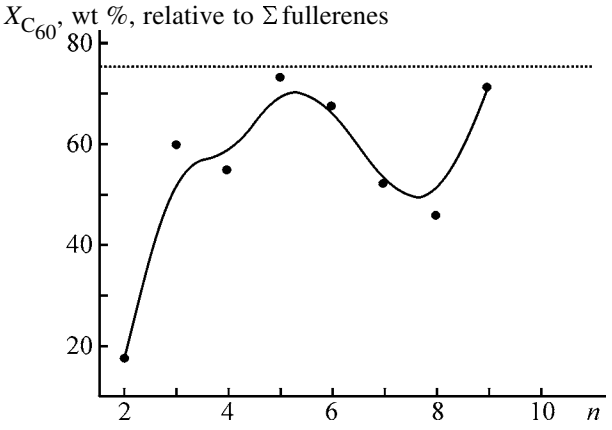

Fig. 4. Relative content of C_{60} in saturated solution of fullerene mixture in carboxylic acids as a function of the number of carbon atoms *n* in carboxylic acid.

CONCLUSIONS

(1) The variation in solubility of C_{60} and fullerene mixture (C_{60} 75, C_{70} 24, C_{76-90} 1%) in *n*-alkanoic acids (C_2–C_9) has a maximum for enanthic acid. In going from acetic to enanthic acid, the solubility increases from 6.8 to 256 mg l^{-1} for C_{60} and from 41 to 1207 mg l^{-1} for the fullerene mixture.

(2) In dissolution of fullerene mixture in carboxylic acids, the saturated solution is enriched in C_{70} as compared to the solid fullerene mixture, and this effect is maximal for acetic acid.

ACKNOWLEDGMENTS

This study was financially supported by the Target Federal Scientific Program "Research and Development in Priority Lines of Science and Engineering" in 2002–2006 (State Contract no. 02.467.11.7005, May 23, 2005).

REFERENCES

1. Semenov, K.N., Arapov, O.V., Pyartman, A.K., et al., *Zh. Prikl. Khim.*, 2007, vol. 80, no. 1, pp. 39–42.
2. Arapov, O.V., Aksel'rod, B.M., Pronkin, A.A., et al., *Zh. Prikl. Khim.*, 2003, vol. 76, no. 1, pp. 35–38.
3. Arapov, O.V., Charykov, N.A., Semenov, K.N., et al., *Russ. J. Appl. Chem.*, 2006, vol. 79, pp. 201–205.
4. Ruoff, R.S., Malhorta, R., Huestis, D.L., et al., *Nature*, 1993, vol. 362, no. 6416, pp. 140–141.
5. Ruoff, R.S., Tse, D.S., Malhorta, R., et al., *J. Phys. Chem.*, 1993, vol. 97, pp. 3379–3383.

6. Xu, Z.D., Chen, W.X., Wu, J., et al., *Chin. Sci. Bull.*, 1994, vol. 39, no. 16, pp. 1347–1350.
7. Chen, W.X. and Xu Z.D., *Fullerene Sci. Technol.*, 1998, vol. 6, no. 4, part 1, pp. 695–705.
8. Heyman, D., *Carbon*, 1996, vol. 34, no. 5, pp. 627–631.
9. Bezmel'nitsyn, V.N., Eletskii, A.V., and Okun', M.V., *Usp. Fiz. Nauk*, 1998, vol. 168, no. 11, pp. 1195–1218.
10. Bezmel'nitsyn, V.N., Eletskii, A.V., and Stepanov, V.A., *Zh. Fiz. Khim.*, 1995, vol. 69, no. 4, pp. 735–738.
11. Marcus, Y., *J. Phys. Chem. B*, 1997, vol. 101, pp. 8617–8623.
12. Ponomarev, N., Yudovich, M.E., Charykov, N.A., et al., *Opt. Spectrosc.*, 2000, vol. 88, no. 2, pp. 195–197.
13. Ghosh, H.N., Avinash, V., and Mittal, J.P., *J. Phys. Chem.*, 1996, vol. 100, pp. 9439–9443.
14. Sukhendu, N., Haridas, P., and Avinash, V., *Chem. Phys. Lett.*, 2000, vol. 327, pp. 143–148.
15. Sukhendu, N., Haridas, P., and Avinash, V., *Chem. Phys. Lett.*, 2002, vol. 360, pp. 422–428.
16. Ruoff, R.S., Tse, D., Malhorta, R., et al., *J. Phys. Chem.*, 1993, vol. 97, pp. 3379–3383.
17. Beck, M., *Pure Appl. Chem.*, 1998, vol. 70, no. 10, pp. 1881–1887.
18. Sivarman, N., Dhamodaran, R., Kallipan, I., et al., *J. Org. Chem.*, 1992, vol. 57, pp. 6077–6079.
19. Hildebrand, J.H. and Scott, R.L., *Regular Solutions*, New York: Prentice-Hall, 1962.
20. *Internet-resurs (termodinamicheskaya baza dannykh)* (Internet Resourse (Thermodynamic Database)), http://webbook.nist.gov./chemistry/.
21. Dean, J.A., *Lange's Handbook of Chemistry*, New York: McGraw-Hill, 1999, section 5.
22. Shakhparonov, M.I., *Vvedenie v molekulyarnuyu teoriyu rastvorov* (Introduction to Molecular Theory of Solutions), Moscow: Gos. Izd. Tekhniko-Teoreticheskoi Literatury, 1956.
23. Matsuzawa, N. and Dixon, D.A., *J. Phys. Chem.*, 1992, vol. 96, pp. 6241–6244.
24. Prigogine, I. and Defay, R., *Chemical Thermodynamics*, London: Longmans Green, 1954.

ISSN 1070-4272, Russian Journal of Applied Chemistry, 2007, Vol. 80, No. 3, pp. 461–465. © Pleiades Publishing, Ltd., 2007.
Original Russian Text © A.A. Rychkov, S.A. Trifonov, A.E. Kuznetsov, E.A. Sosnov, D.A. Rychkov, A.A. Malygin, 2007, published in Zhurnal Prikladnoi Khimii, 2007, Vol. 80, No. 3, pp. 463–467.

NANOTECHNOLOGIES AND NANOMATERIALS

Influence of Chemical Modification of the Surface of Low-Density Polyethylene on Its Electret Properties

A. A. Rychkov, S. A. Trifonov, A. E. Kuznetsov, E. A. Sosnov, D. A. Rychkov, and A. A. Malygin

St. Petersburg State Institute of Technology (Technical University), St. Petersburg, Russia
Herzen Russian State Pedagogical University, St. Petersburg, Russia

Received June 29, 2006; in final form, October 2006

Abstract—The electret properties of low-density polyethylene with phosphorus-containing surface nanostructures were examined.

DOI: 10.1134/S1070427207030214

As known [1], when irradiated with charged particle (ion, electron) fluxes, polymer dielectrics accumulate a charge on their surface to form an electret state. The charged state of such materials, which are termed electrets, can be preserved for a fairly long time (years). This finds wide application in modern high technologies, in particular, in the development of electroacoustic transformers and sensors, as well as of nonlinear-optics components [2]. Of great practical importance for such systems is the stability of the electret state.

In our previous studies [3, 4] we showed that the stability of the electret charge in polytetrafluoroethylene (PTFE) films is substantially enhanced by chemical modification of the surface with phosphorus trichloride vapor. Therefore, it is of interest to examine the electret properties of other modified polyolefins, in particular, such commercially significant material as low-density polyethylene (LDPE). In this connection, we examined here the electret properties of LDPE as influenced by chemical modification of its surface with phosphorus trichloride vapor.

This study was underlain by the following concepts.

(1) The electret state in nonpolar polymers is determined not only by the charge capture sites in the bulk but also, to a significant extent, by the localized states on the surface [5].

(2) Surface modification of nonpolar polymers enables directed formation in such materials of surface deep energy wells acting as charge capture sites able of efficiently retaining the electret charge [3–5].

(3) An efficient way of polymer surface modification is the chemical nanotechnology based on the molecular layer deposition principles [6]. This technology enables incorporation of element-containing nanostructures into surface macromolecules in a controllable manner, thereby controlling the physicochemical, in particular, electret, properties of polymers [3, 4].

EXPERIMENTAL

Polymer films, $40 \times 20 \times 0.14$ mm in size, were chemically modified in a flow reactor by successive treatment of the substrate with PCl_3 and H_2O vapors by molecular layer deposition. For conditions of synthesis of phosphorus-containing structures on the polymer matrix surface, see [7].

The samples for electret measurements were prepared in the form of planar metal–polymer structures, whose basis was a 95-μm-thick St.3 steel substrate. A polymeric layer of the LDPE film, unmodified or modified with phosphorus trichloride, was fixed on the substrate surface by the thermal fitting method [5]. We used extrusion films of 10 203-003 brand polyethylene manufactured in Russia in accordance with GOST (State Standard) 16 337–70. This polymer has acceptable dielectric characteristics for producing corona electrets, namely, low values of dielectric permittivity (2.2 at a frequency of 1 MHz), dielectric dispersion, and dielectric loss tangent (2.7×10^{-4} at a frequency of 1 MHz).

Thermal fitting was carried out at 170°C for 60 s; it was followed by cooling in air to room temperature

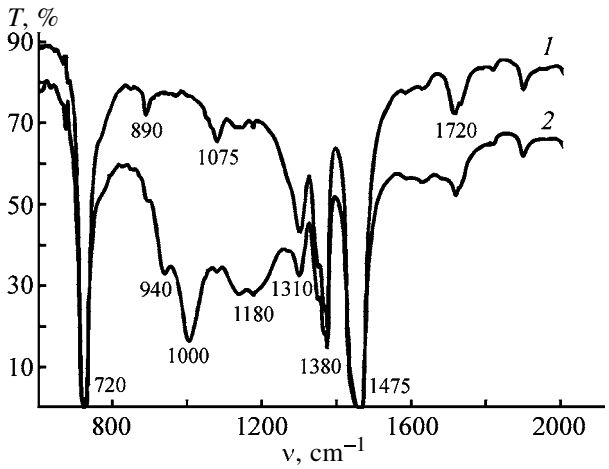

Fig. 1. IR spectra of low-density polyethylene films. (*T*) Transmission and (ν) wavenumber. Sample: (*1*) initial and (*2*) modified with PCl_3 vapor.

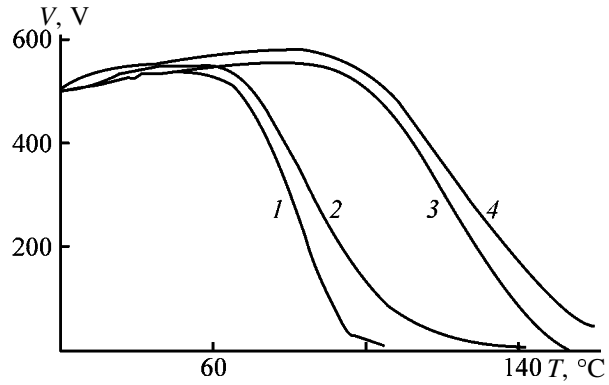

Fig. 2. Thermoinduced relaxation of the surface potential *V* of the (*1, 3*) positively and (*2, 4*) negatively charged electrets of LDPE. Sample: (*1, 2*) unmodified and (*3, 4*) modified; the same for Fig. 4.

over a period of about 2 min. The resulting samples exhibited fairly reliable adhesive contact between the polymer and the metal substrate. Because of shrinking, the average thickness of the polymeric layer of the LDPE–steel structures was 150 μm.

The electret state in LDPE–steel structures was formed by charging the samples in a corona discharge at room temperature for 30 s on a setup with control grid electrode [3]. The charging device allowed preparation of samples with identical preset initial surface potential V_0 of +500 and +1700 V for charging in a positive, and of –500 and –1700 V, for charging in a negative corona discharge. Thus, without taking into account the sign, the initial effective surface density of the homocharge of the electrets examined was 6.5×10^{-5} and 2.2×10^{-4} C m^{-2}, respectively.

The electret properties of the LDPE films were examined by the method of thermoinduced relaxation of the surface potential (TIRSP) [5] in the linear heating mode at a constant rate of 5.9 deg min^{-1}. The surface potential was measured by the contactless technique. To this end we used the method of dynamic capacitor in which the capacity between the measuring electrode and the charged surface of the electret was modulated using a rotating disk with holes [5].

The phosphorus concentration in the reaction products was determined by a standard technique [8]. The IR spectra[1] of the initial and modified samples were recorded on an FSM-1201 IR Fourier spectrometer (400–4000 cm^{-1} range, resolution 1 cm^{-1}, self-compensation interferometer). The IR examination and chemical analysis provided data on the composition and structure of the phosphorus-containing surface groups.

The examination of the films by atomic-force microscopy (AFM)[1] was carried out on a Solver P47 Pro (NT-MDT, Russia) scanning probe microscope in the tapping mode using a silicon cantilever in two scanning modes: topographic survey and phase contrast. The latter mode reveals the difference in the compositions of the sample surface sections from analysis of the changes in the phase shift of the amplitude–frequency characteristic (AFC) of the cantilever, due to adhesion interactions.

Chemical analysis of the samples showed that, under the actual conditions of synthesis, the total phosphorus concentration in the modified LDPE attains a maximum of ca. 0.4 wt %.

Figure 1 shows the IR transmission spectra of the films of the initial and modified polyethylene. The major changes of the spectral characteristics of the polymer upon treatment with PCl_3 vapor are observed within 400–2000 cm^{-1}. Introduction of phosphorus-containing structures into the material is responsible for appearance in the IR spectrum of absorption bands characteristic of phosphorus compounds at 1000 (stretching vibrations of the P–O bonds in the P–O–Alk groups) and 1140 and 1180 cm^{-1} (bending vibrations of the P=O bond) [9]. A decrease in the intensity of the bands at 890 and 1075 cm^{-1} (out-of-plane and in-plane bending vibrations of the C–H bonds in the –CH=CH_2 group, respectively) is due to replacement of the substituent in the polymer chain (appearance of phosphorus-containing groups) [10]. Vapor-phase hydrolysis of the modified films results in appearance of an absorption band near 940 cm^{-1}, associated with

[1] The physicochemical studies were carried out at Chemical Assembling of Nanomaterials, Center for Collective Use, St. Petersburg State Institute of Technology (Technical University).

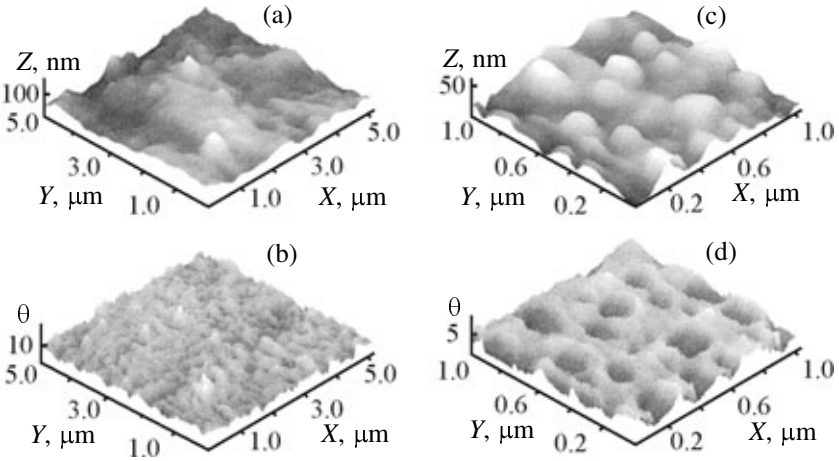

Fig. 3. AFM reconstruction of the surface of the (a, b) initial and (c, d) phosphorus-containing polyethylene. (θ) Phase of AFM probe vibrations. (a, c) Surface topography and (b, d) adhesive interaction pattern.

the out-of-plane bending vibrations of the OH groups in phosphorus compounds.

Chemical analysis and spectroscopic examination suggest chemical grafting of phosphorus-containing groups at reactive centers of the polymer matrix. These include the hydrogen atoms at the tertiary carbon atoms and those in the α-position with respect to the double bonds, as well as unsaturated groups [11].

Figure 2 shows the data on thermoinduced relaxation of the surface potential of the modified and unmodified LDPE film. Analysis of these dependences suggests that treatment of the polyethylene surface with phosphorus trichloride vapor significantly enhances the thermal stability of the electret state. It should be noted that the shift of the TIESP curves to higher temperatures is virtually identical for the positively and negatively charged electrets, about 40°C (Fig. 2, curves *3, 4*).

We showed previously [3] that chemical modification of the PTFE film surface also enhances the thermal stability of the potential of the electret structures. However, we found that the surface potential relaxation depends on the sign of the charge. Only for electrets pretreated with PCl_3 vapor and charged positively this electrophysical parameter exhibits a significant (~80°C) increase. The effect of modification of the LDPE film surface, increasing the thermal stability of the electret state, is manifested for both positive and negative charges. This is evidently due to the structural transformations of the surface layer, which favor formation of additional sites of capture of the electret charge, at chemical modification of polymers of different chemical nature. An explanation to this phenomenon can be provided by AFM examination of the surface morphology of the initial and phosphorus-containing samples of the polymer materials.

Examination of the surface layer of polyethylene shows that the initial film is fairly uniform (Fig. 3a). Individual polymeric structures (up to 0.5 μm in size), partially and mutually fused, can be distinguished on its surface. However, the surface roughness of the initial polymer is insignificant, 16–20 nm. There are no profound relief defects and foreign inclusions affecting the adhesion interactions of polyethylene with the AFM probe (Fig. 3b).

Chemical modification of polyethylene with PCl_3 vapor (Fig. 3c) yields on the LDPE surface round "islet" structures 80–200 nm in diameter, in amount of 20–25 μm^{-2}. Scanning in the phase contrast mode reveals a sharp change in the AFC (θ) of the cantilever when crossing the boundary of such an islet (Fig. 3d). This suggests a difference in the structural and chemical properties of these "islets" from those of the surrounding polyethylene matrix [12]. The IR examination (Fig. 1) and chemical analysis show that treatment of the LDPE surface with PCl_3 vapor results in chemical grafting of the phosphorus-containing groups, which, apparently, can form the basis for such "islets." In view of their high hydrophilicity [13], it can be presumed that, due to adsorption of the water vapor, a hydrate shell is formed on the surface around the grafted structures. These topographic changes suggest formation of a larger number of new sites of the electret charge capture on the LDPE surface compared to PTFE.

Evidently, the efficiency of the electret charge capture on these structural traps will be governed by the ratio of the surface density of the incorporated

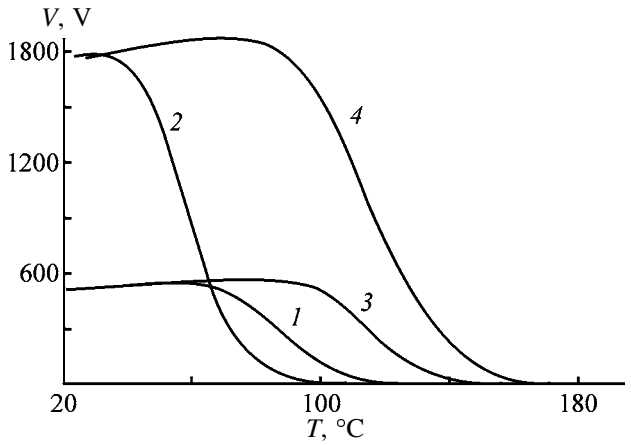

Fig. 4. Thermoinduced relaxation of the surface potential V of the electrets of LDPE, charged to the initial potential of (*1, 3*) 500 and (*2, 4*) 1700 V.

charge and the concentration of the nanostructures acting as electret charge capture sites. In our experiments, there are ca. 400 charges μm^{-2} at the charge density of 6.5×10^{-5} C m^{-2} (we believe that, at charging in a corona discharge, the charge carriers bear one elementary charge). Hence, one nanoformation retains no less than ten charge carriers. Presumably, the local electrostatic interaction of the electret charges in the vicinity of the nanoformation will substantially affect formation and relaxation of the electret state. For example, Coulomb repulsion decreases the probability of a charge capture by the trap belonging to the specific structure. Also, the local electric field of the captured charges decreases the energy depth of the corresponding traps [1, 2]. Therefore, it was of interest to examine the electret properties of LDPE at higher charge densities.

Figure 4 presents the data characterizing the electret properties of the modified (curves *3, 4*) and unmodified (curves *1, 2*) LDPE films charged in the corona discharge to the initial potential of 500 and 1700 V. In the case of the initial films, the "crossing" effect typical of electrets of polyethylene is observed [1, 2, 5]. This effect is manifested as a decrease in the stability of the electret state with increasing initial surface density of the electret charge. The curve of the potential drop of samples with a higher initial charge density during relaxation crosses the corresponding curve for samples with a lower initial charge density. This fact makes virtually impossible preparation of stable electrets from LDPE film with a high surface charge density.

A different situation is observed in the case of the LDPE films treated with phosphorus trichloride vapor. The plots in Fig. 4 (curves *3, 4*) show that there is no crossing effect and the samples charged to V_0 = 1700 V exhibit a high thermal stability of the charge. The shift of curve *4* to higher temperatures relative to curve *2* is about 55°C. Thus, chemical modification of the LDPE surface in phosphorus trichloride vapor significantly increases the electret charge and its stability. For example, in thermal stability of the charge the modified polyethylene surpasses such well-known electret materials as polyethylene terephthalate, polyvinyl chloride, and polyvinylidene fluoride [1, 2, 5].

CONCLUSIONS

(1) Chemical modification of low-density polyethylene with phosphorus trichloride vapor involves addition of phosphorus-containing groups to the reactive centers of the polymer via substitution reactions.

(2) Atomic-force microscopic and IR-spectroscopic examinations, as well as chemical analysis, revealed the differences in the morphology and chemical composition of the surface of the initial and modified polymers. The phosphorus-containing groups added to the reactive centers of polyethylene are responsible for formation on its surface of round nanoformations, 80–200 nm in diameter, whose surface concentration was estimated at 20–25 μm^{-2}.

(3) Chemical gas-phase modification substantially increases the electret charge and its stability in low-density polyethylene films. This effect is achieved via stabilization of the electret charge on the structural traps associated with the phosphorus-containing nanofomations arising on the polymer surface.

ACKNOWLEDGMENTS

This study was performed under State Contract no. 02.442.11.7531 and financially supported by Russian Foundation for Basic Research (project nos. 05-03-32056, 06-02-81034-Bel2006-a).

REFERENCES

1. *Electrets*, Sessler, G.M., Ed., Berlin: Springer, 1980.
2. *Electrets*, Gerhard, R., Ed., California: Multhaupt-Laplacian, 1999.
3. Rychkov, A.A., Malygin, A.A., Trifonov, S.A., and Rychkov, D.A., *Zh. Prikl. Khim.*, 2004, vol. 77, no. 2, pp. 280–284.
4. Rychkov, A.A., Gorokhovatskii, Yu.A., Rychkov, D.A., and Kuznetsov, A.E., *Mater. Tekhnol. Instr.*, 2005, vol. 10, no. 3, pp. 74–78.

5. Rychkov, A.A. and Boitsov V.G., *Elektretnyi effekt v strukturakh polimer–metall* (Electret Effect in Polymer–Metal Structures), St. Petersburg: Ross. Gos. Pedagog. Univ., 2000.
6. Malygin, A.A., *Zh. Prikl. Khim.*, 1996, vol. 69, no. 10, pp. 1585–1593.
7. Trifonov, S.A., Lapikov, V.A., and Malygin, A.A., *Vliyanie khimicheskogo modifitsirovaniya khloridom fosfora(III) poverkhnosti polietilena na ego termookislitel'nuyu stoikost'* (Influence of Chemical Modification with Phosphorus(III) Chloride of the Surface of Polyethylene on Its Thermooxidation Stability), 2000, Available from VINITI, Ross. Akad. Nauk, February 26, 2002, no. 374-V2002.
8. Balandina, V.A., Gurvich, D.B., and Kleshcheeva, M.S., *Analiz polimerizatsionnykh plastmass* (Analysis of Polymerization Plastics), Leningrad: Khimiya, 1967.
9. Kazitsyna, L.A. and Kupletskaya, N.B., *Primenenie UF, IK i YaMR spektroskopii v organicheskoi khimii: Uchebnoe posobie dlya vuzov* (Application of UV, IR, and NMR Spectroscopy to Organic Chemistry: Manual for Higher School), Moscow: Vysshaya Shkola, 1971.
10. Silverstein, R.M., Bassler, G.C., and Morrill, T.C., *Spectrometric Identification of Organic Compounds*, New York: Wiley, 1974.
11. Sirota, A.G., *Modifikatsiya struktury i svoistv poliolefinov* (Modification of the Structure and Properties of Polyolefins), Leningrad: Khimiya, 1984.
12. Magonov, S.N., Elings, V., and Whangbo, M.-H., *Surf. Sci.*, 1997, vol. 375, nos. 2–3, pp. L385–L391.
13. Van Wazer, I.R., *Phosphorus and Its Compounds*, New York: Wiley–Interscience, 1958, vol. 1.

ISSN 1070-4272, Russian Journal of Applied Chemistry, 2007, Vol. 80, No. 3, pp. 466–471. © Pleiades Publishing, Ltd., 2007.
Original Russian Text © E.S. Sashina, N.P. Novoselov, A.V. Vnuchkin, A.Yu. Golubikhin, 2007, published in Zhurnal Prikladnoi Khimii, 2007, Vol. 80, No. 3, pp. 468–472.

MACROMOLECULAR CHEMISTRY AND POLYMERIC MATERIALS

Preparation and Properties of Films of Fibroin–Polyvinyl Alcohol Blends from Solutions in Hexafluoroisopropanol

E. S. Sashina, N. P. Novoselov, A. V. Vnuchkin, and A. Yu. Golubikhin

St. Petersburg State University of Technology and Design, St. Petersburg, Russia

Received October 30, 2006

Abstract—The compatibility of fibroin with polyvinyl alcohol in blend films prepared from a common organic solvent, hexafluoroisopropanol, was studied by IR spectroscopy and DSC.

DOI: 10.1134/S1070427207030226

Moisture and oxygen permeability of fibroin membranes [1] and bacteriostatic properties of fibroin [2] make this polymer attractive for the development of biomedical materials, in particular, for contact lenses. However, films of fibroin regenerated from solutions are brittle. To improve the physicomechanical properties of films, fibroin should be modified by adding other polymers, e.g., in the step of dissolution. The following polymers are used today for producing contact lenses: polyacrylic acid derivatives, polyvinylpyrrolidone, and polyvinyl alcohol (PVA) [3, 4]; the latter is used as either a homopolymer [3, 5] or copolymer [6]. Polyvinyl alcohol has good film-forming properties; its films are elastic and strong. This fact, in combination with nontoxicity of polyvinyl alcohol, makes this polymer suitable for modification of fibroin in preparation of a material for contact lenses.

However, published data on the compatibility of fibroin with other polymers, both natural (cellulose [7, 8], chitosan [9, 10]) and synthetic (polyhydroxybutyrate [11], polyacrylamide [12]), show that micro- or macrophase segregation occurs in many blend films in a wide range of component ratios. The phase segregation makes the material nonuniform and complicates its use.

One of conditions for preparation of homogeneous polymer blends is the use of a common solvent for both components, which creates conditions for interaction of active groups of the macrochains in solution and then in the solid state. Silkworm fibroin is soluble in concentrated solutions of salts in water and nonaqueous solvents [13], in hexafluoroisopropanol [14], and in *N*-methylmorpholine *N*-oxide [15]; the choice of the solvent and conditions of dissolution and precipitation largely determine the supramolecular structure of the polymer [16, 17]. Fibroin/PVA blends prepared from 0.5–1.5% aqueous solutions of the components were studied in [18–21]. Tsukada et al. [18] used an aqueous solution of silk (so-called "liquid silk") directly from silkworm glands, and Tanaka, Suzuki, et al. [19– 21] used diluted aqueous solutions of fibroin in 9 M LiBr after dialysis. In both cases, the conformational state of fibroin in solutions and films was characterized as a random coil with a small content of macromolecules in the α-helical form. The phase segregation in the blends studied in [18–21] occurred in the entire range of component ratios. The IR and DSC data revealed no intermolecular interaction of components in the blends [18].

We studied the compatibility of fibroin with PVA and conditions for preparing their homogeneous blends from a common organic solvent, hexafluoroisopropanol (HFIP). Whereas dialyzed fibroin solutions are unstable (salt-free water is not a solvent for fibroin) and tend to gelation, HFIP allows preparation of solutions stable for a long time. In this solvent, fibroin has a structure of random coil and α-helix, with a certain fraction of macromolecules occurring in the β-folded form [16]. Polyvinyl alcohol is also soluble in HFIP [22]; thus, conditions are provided for preparing homogeneous blends stabilized by intermolecular interaction of the components. The regeneration is done by solvent evaporation; the films contain no traces of HFIP, and additional washing is unnecessary. As compared to aqueous solutions, commercial use of HFIP is less safe (LD_{50} 1040 mg kg^{-1}), and it becomes topical to develop a closed-loop process without emission of the solvent vapor into the environment.

EXPERIMENTAL

To prepare films, we used *Bombyx mori* silkworm fibroin in the form of short fibers, washed to remove impurities, PVA (molecular weight 31000–50000, degree of deacetylation 98–99%), and HFIP (1,1,1,-3,3,3-hexafluoro-2-propanol, Merck–Schuchardt, main substance content 99%, boiling point 58°C, density at 20°C 1.615–1.618 g cm^{-3}).

The dissolution of fibroin in HFIP was performed as described in [14]; PVA was dissolved in HFIP on heating to 30–40°C. The polymer concentrations in solutions were 4 wt %. The solutions were vacuum-filtered through a glass frit no. 1 and mixed in required proportions. The films were prepared by applying the solutions onto glass plates, with the subsequent solvent evaporation. The fibroin/PVA blend films prepared from HFIP solutions are optically transparent in the entire range of component ratios. The film thickness was 0.04–0.06 mm.

To compare the optical transparence, we also prepared fibroin/PVA blend films similarly to [19–21] from aqueous solutions with polymer concentrations of 4%. The films prepared from aqueous solutions are opaque; the most pronounced phase segregation, evaluated visually from the film turbidity, occurred at the polymer ratios from 70/30 to 30/70. The opacity of films prepared from aqueous solutions is associated with the thermodynamic instability of the dialyzed solution of fibroin, in which gelation starts within 2 days.

The IR absorption spectra were recorded on a Bruker IFS25 IR spectrometer. Thermal analysis of film samples was performed on a Mettler Toledo Star differential scanning calorimeter in the range from 25 to 500°C (heating rate 10 deg min^{-1}) in a nitrogen flow (flow rate 50 ml min^{-1}).

Figure 1 shows the DSC curves for films of fibroin, fibroin/PVA blends, and PVA, prepared from HFIP solutions. In the DSC curve of a fibroin film, there are endothermic effects caused by evaporation of bound water (maximum at 78°C) and devitrification of the amorphous part of the polymer (152°C), followed by a small exothermic effect due to transition to the β-crystalline modification [23–27]; a small endothermic peak at 246°C is associated with the molecular motion in α-crystals on heating [27]. The strong endothermic effect with a peak at 280°C is due to thermal degradation of the polymer. The DSC curve shows that fibroin exists in the films mainly in the amorphous form, with a certain amount of α-crystals. The DSC data give no evidence for the β-crystalline structure of fibroin in films.

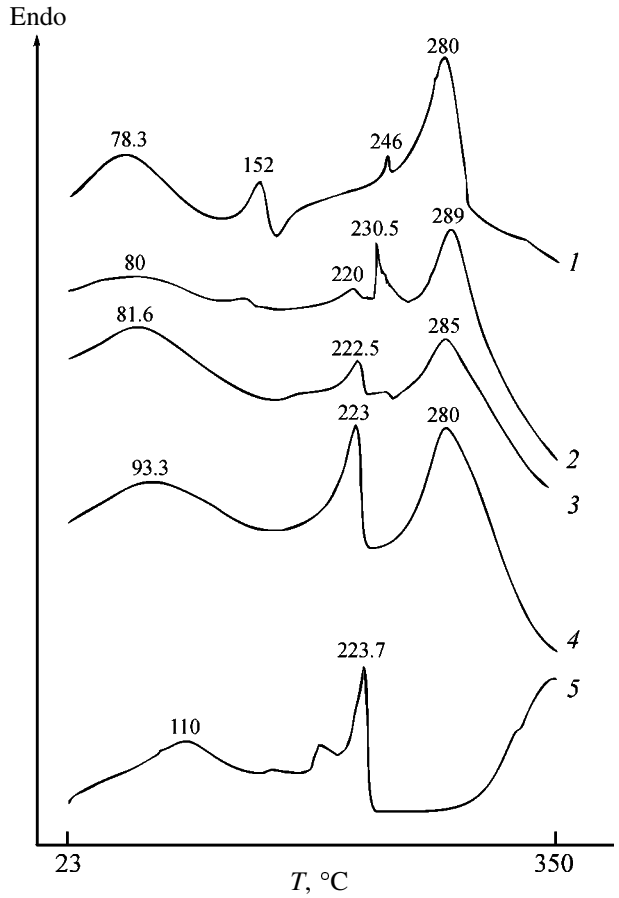

Fig. 1. DSC curves of fibroin/PVA blends prepared from solution in HFIP. Fibroin/PVA: (*1*) 100/0, (*2*) 80/20, (*3*) 60/40, (*4*) 20/80, and (*5*) 0/100. (*T*) Temperature.

In the DSC curve of polyvinyl alcohol, there are overlapping endothermic effects from evaporation of water and devitrification of the polymer, with a common peak at 110°C; melting of the crystalline parts starts at 223.7°C and is followed by gradual degradation of PVA [22].

Comparison of the phase transition temperatures in fibroin/PVA blend films with various component ratios reveals a gradual shift of the PVA melting point toward lower temperatures with an increase in the fibroin content. From the thermodynamic viewpoint, a decrease in the PVA melting point is due to exothermic interaction of the blend components [28–30].

Simultaneously, the enthalpy of melting ΔH_m per gram of PVA gradually decreases. Taking for ΔH_m^0 of fully crystalline PVA the value of 152 kJ g^{-1} [22], we estimated the degree of crystallinity of PVA in films as the ratio $(\Delta H_m/\Delta H_m^0) \times 100\%$. The experimental

Enthalpies of melting and degree of crystallinity of PVA in films of its blends with fibroin, prepared from HFIP solutions

Sample no.	Fibroin/PVA, wt %	ΔH_m of PVA, J g^{-1} PVA	Degree of crystallinity of PVA, %
1	100/0	–	–
2	80/20	16.5	10.8
3	60/40	50.8	33.4
4	40/60	52.8	34.7
5	0/100	61.0	40.1

values of ΔH_m of PVA and the calculated degrees of crystallinity are given in the table.

The state of fibroin also changes on blending with PVA. As a result of intermolecular interaction with the second component, the peak of fibroin degradation shifts toward higher temperatures. This trend is especially pronounced on adding 20% PVA: The peak of fibroin degradation shifted from 280 to 289°C (Fig. 1, curve *2*).

On adding 20% PVA, the endothermic peak of devitrification of the amorphous part of fibroin at about 152°C becomes considerably less pronounced (cf. curves *1* and *2*). This may be due to decreased content of the amorphous part of fibroin in the blend; the same conclusion follows from the IR spectra (see below). For the other blends (curves *3*, *4*), the devitrification peak merges with the peak of evaporation of bound water into a broad endothermic peak. On blending with PVA, the position of the endothermic peak of molecular motion in fibroin α-crystals changes, and its intensity increases. The shift toward lower temperatures (from 246 to 230.5°C) is caused by strong interaction with macromolecules of PVA occurring in the molten state at this temperature. An increase in the intensity is caused by an increase in the amount of fibroin macromolecules in this conformation (at 20% content of PVA in the blend). With a further increase in the PVA content, the peak becomes ill-defined (curve *3*) and then fully disappears (curve *4*).

The IR spectra of films of fibroin, PVA, and their blends are shown in Fig. 2. Structural studies of fibroin and other polypeptides show that the conformational state of a polypeptide can be judged from the positions in the spectra of the amide I (C=O), amide II (bound N–H, C–N), and amide III (C–N, bound N–H, CH_3–C) bands [23, 31, 32]. Since the amorphous coil and α-helix conformations are characterized by predominant formation of intramolecular hydrogen bonds, and the β-folded conformation, by an ordered system of intermolecular bonds, from the positions of the absorption bands we can reliably distinguish the β-structure of the polymer, for which the amide I and amide II frequencies are 20–40 cm^{-1} lower compared to the other conformations and the amide III frequency is, on the contrary, higher. However, IR spectroscopy does not allow the amorphous and α-helical structures to be unambiguously distinguished, and in this case the DSC data are additionally used.

The IR spectrum of a 100% fibroin film (curve *1*) suggests coexistence of different conformations of macromolecules in the film: a certain amount of β-crystals (weak shoulder of 1630 cm^{-1}, amide I; 1513 cm^{-1}, amide II; 1260 cm^{-1}, amide III) and the α-helical or random coil conformation (strong amide I, II, and III bands at 1650, 1536, and 1213 cm^{-1}, respectively).

The spectrum of a PVA film (curve *4*) in the frequency range shown in the figure has absorption bands at 1375, 1283, 1095, 892, and 839 cm^{-1}, characterizing the δ(CH–OH), ω(CH), γ(CO), γ(CH_2), and γ(C–C) vibrations, respectively [18]. The crystallization-sensitive band of PVA is observed at 1140 cm^{-1}. In the spectra of fibroin/PVA blends, the following changes in the position and intensity of absorption bands are observed. On adding 20% PVA to fibroin (curve *2*), the intensity of absorption bands at 1630 (a barely perceptible shoulder in curve *1* for 100% fibroin) and 1513 cm^{-1}, characteristic of the β-folded crystalline structure of fibroin, increases. This fact indicate that the presence of 20% flexible-chain PVA not only does not prevent but even favors β-folding of fibroin macrochians; due to strong macromolecular interactions of components, favorable steric conditions are provided for more ordered folding of fibroin macromolecules.

With a further increase in the PVA content in the blend, the absorption bands at 1630 and 1513 cm^{-1}, characteristic of the β-crystalline structure of fibroin, virtually disappear (curve *3*), i.e., at a high content of the second component the β-folded structure is absent from fibroin.

The crystallization-sensitive PVA band at 1140 cm^{-1} is barely visible at a PVA content in the blend of up to 20%, which confirms the conclusion made above from the DSC data that the degree of crystallinity of PVA decreases on blending with fibroin.

It can be concluded that, in HFIP solution, the conditions are favorable for the interaction between fibroin and PVA macromolecules, affecting the crys-

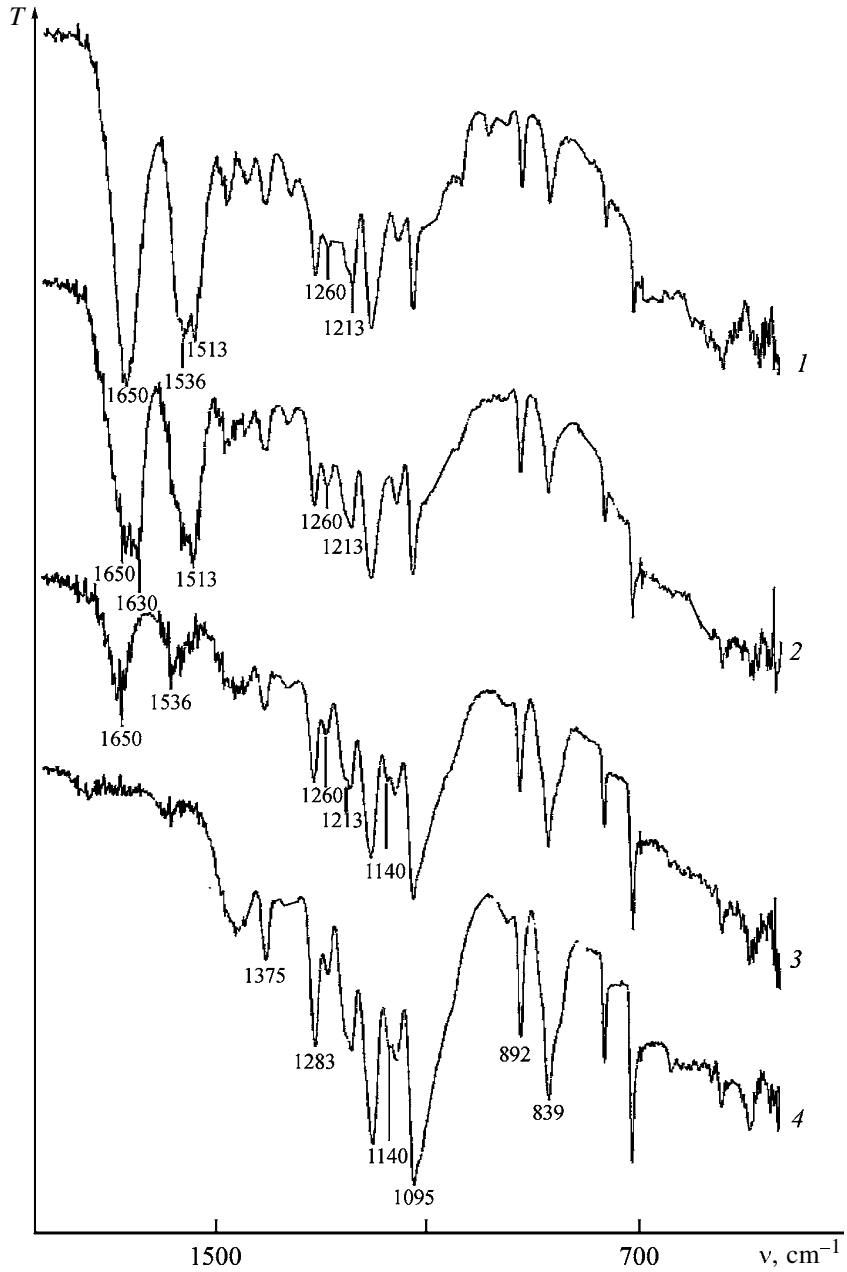

Fig. 2. IR absorption spectra of fibroin/PVA blend films prepared from HFIP solutions. (*T*) Transmission and (ν) wavenumber. Fibroin/PVA: (*1*) 100/0, (*2*) 80/20, (*3*) 20/80, and (*4*) 0/100.

tallization of the blend components; the most pronounced conformational changes are observed at 80/20 ratio of the components. In this blend, PVA is the least ordered, and fibroin is more ordered than in the 100% fibroin film. The content of both β-folded (according to IR spectra) and α-helical (according to DSC data) crystalline structures of fibroin increases. Apparently, the crystalline parts are stabilized by layers of flexible PVA chains owing to intermolecular interactions. Similarly, in natural silk a hydroxyl-containing polymer sericin interacts with fibroin, making silk fibers strong and elastic.

Microscopic examination of the blend films in a polarized light at ×200 magnification revealed that the fibroin/PVA 80/20 blend was homogeneous. Microscopic examination of the other films revealed phase segregation and formation of oval particles of size from 1–3 μm for the 20/80 blend to 4–7 μm for the 60/40–40/60 blends. In accordance with the character of phase segregation, more hydrophilic PVA tends to

form a continuous dispersion medium in which oval fibroin particles are distributed; the particle core is more crystalline, and the shell contacting with PVA is amorphous.

Addition of hydrophilic PVA to fibroin, on the one hand, allows the moisture content of the films to be increased from 8 to 11% in proportion with the PVA content, which is important for practical use. On the other hand, the PVA-containing films become more sensitive to water: They swell and, at a high PVA content, gradually become turbid; water competes with fibroin for the H-bonding with PVA, which can induce phase segregation. To enhance the resistance of intermolecular bonds in the blends to water without adding cross-linking agents, we examined the effect of heat treatment of the films at 70–80°C for 20 min. This treatment enhanced the moisture resistance of the films; the degree of swelling of the blends in water decreased by a factor of 1.5–3 depending on the PVA content. This effect is caused by the conformational transition of fibroin macromolecules upon heat treatment into the crystalline β-folded structure [10, 17], less accessible to the action of water.

CONCLUSIONS

(1) Films of fibroin/polyvinyl alcohol blends, prepared from solutions in hexafluoroisopropanol, are transparent in the entire range of component ratios, in contrast to the blend films prepared from aqueous solutions.

(2) In the films prepared from hexafluoroisopropanol, intermolecular interactions occur between fibroin and polyvinyl alcohol macromolecules, affecting the crystallinity and conformational state of the polymeric components.

(3) The strongest interaction between the components is observed at a fibroin/polyvinyl alcohol ratio of 80/20; in this case, the relative content of fibroin macromolecules in the crystalline modification is the highest.

ACKNOWLEDGMENTS

The study was supported by the Russian Foundation for Basic Research (project no. 06-08-00278a).

REFERENCES

1. Minoura, N., *Polymer*, 1990, vol. 31, no. 3, pp. 265–269.
2. Strobin, G., Struszkyk, H., Ciechanska, D., et al., in *Modification of Polymers*, Wroclaw: Technical Univ. of Wroclaw, 2005, pp. 68–73.
3. Lloyd, A.W., Faragher, R., and Denyer, S.P., *Biomaterials*, 2001, vol. 22, no. 8, pp. 769–785.
4. Nicolson, P.C. and Vogt, Y., *Biomaterials*, 2001, vol. 22, no. 24, pp. 3273–3283.
5. Kuriaki, M., Nakamura, K., and Mizutani, J., *Kobunshi Ronbunshu*, 1989, vol. 46, no. 11, pp. 739–743.
6. Chin-Hu Ho and Heady, V., *Biomaterials*, 1996, vol. 16, no. 6, pp. 479–482.
7. Yang, G., Zhang, L., and Liu, Y.J., *Membrane Sci.*, 2000, vol. 177, no. 2, pp. 153–161.
8. Sashina, E.S., Vnuchkin, A.V., and Novoselov, N.P., *Zh. Prikl. Khim.*, 2006, vol. 79, no. 5, pp. 816–820.
9. Kweon, H., Ha, H.C., Um, I.C., and Park, Y.H., *J. Appl. Polym. Sci.*, 2001, vol. 80, no. 7, pp. 928–934.
10. Sashina, E.S. and Novoselov, N.P., *Zh. Prikl. Khim.*, 2005, vol. 78, no. 3, pp. 493–498.
11. Sashina, E.S., Novoselov, N.P., and Heinemann, K., *Zh. Prikl. Khim.*, 2005, vol. 78, no. 1, pp. 155–160.
12. Freddi, G., Tsukada, M., and Beretta, S., *J. Appl. Polym. Sci.*, 1999, vol. 71, no. 10, pp. 1563–1571.
13. Finkel'shtein, A.V. and Ptitsyn, O.B., *Fizika belka* (Protein Physics), Moscow: Mosk. Gos. Univ., 2002.
14. WO Patent 93/15244.
15. RF Patent 2002 107622.
16. Sashina, E.S., Bochek, A.M., Novoselov, N.P., and Kirichenko, D.A., *Zh. Prikl. Khim.*, 2006, vol. 79, no. 6, pp. 881–888.
17. Sashina, E.S., Novoselov, N.P., Vorbach, D., and Meister, F., *Vysokomol. Soedin., Ser. A*, 2005, vol. 47, no. 10, pp. 1832–1840.
18. Tsukada, M., Freddi, G., and Crighton, J.S., *J. Polym. Sci., Part B: Polym. Phys.*, 1994, vol. 32, no. 2, pp. 243–248.
19. Tanaka, T., Suzuki, M., Kuranuki, T., et al., *Polym. Int.*, 1997, vol. 42, no. 1, pp. 107–111.
20. Tanaka, T., Tanigami, T., and Yamaura, K., *Polym. Int.*, 1998, vol. 45, no. 2, pp. 175–184.
21. Yamaura, K., Kuranuki, N., Suzuki, M., et al., *Polym. Sci.*, 1990, vol. 41, no. 18, pp. 2409–2425.
22. Azuma, Y., Yoshie, N., Sakura, M., et al., *Polymer*, 1992, vol. 33, no. 22, pp. 4763–4767.
23. Magoshi, J., Mizuide, M., and Magoshi, Y., *J. Polym. Sci., Polym. Phys. Ed.*, 1979, vol. 17, pp. 515–520.
24. Nam, J. and Park, Y.H., *J. Appl. Polym. Sci.*, 2001, vol. 81, pp. 3008–3021.
25. Motta, A., Fambri, L., and Migliaresi, C., *Macromol.*

Chem. Phys., 2002, vol. 203, pp. 1658–1665.

26. Kweon, H. and Park, Y.H., *J. Appl. Polym. Sci.*, 2001, vol. 82, pp. 750–758.
27. Kweon, H., Woo, S.O., and Park, Y.H., *J. Appl. Polym. Sci.*, 2001, vol. 81, pp. 2271–2276.
28. Harris, J.E., Goh, S.H., Paul, D.R., and Barlow, J.W., *J. Appl. Polym. Sci.*, 1982, vol. 27, no. 6, pp. 839–844.
29. Nishio, Y., Haratani, T., and Takahashi, T., *Macromolecules*, 1989, vol. 22, no. 19, pp. 2547–2549.
30. Nishio, Y., Hirose, N., and Takahashi, T., *Polym. J.*, 1989, vol. 21, no. 4, pp. 347–351.
31. Asai, M., Tsuboi, M., Shimanouchi, T., and Mizushima, S., *J. Phys. Chem.*, 1955, vol. 59, pp. 322–325.
32. Venyaminov, S.Yu. and Kalnin, N.N., *Biopolymers*, 1990, vol. 30, pp. 1259–1271.

ISSN 1070-4272, Russian Journal of Applied Chemistry, 2007, Vol. 80, No. 3, pp. 472–476. © Pleiades Publishing, Ltd., 2007.
Original Russian Text © E.E. Ergozhin, B.E. Begenova, T.K. Chalov, 2007, published in Zhurnal Prikladnoi Khimii, 2007, Vol. 80, No. 3, pp. 473–478.

MACROMOLECULAR CHEMISTRY AND POLYMERIC MATERIALS

Synthesis and Study of Physicochemical, Acid–Base, and Complexing Properties of Ion Exchangers Based on Glycidyl Derivatives of Aromatic Compounds and Polyamines

E. E. Ergozhin, B. E. Begenova, and T. K. Chalov

Bekturov Institute of Chemical Sciences, Ministry of Education and Science of Kazakhstan Republic, Almaty, Kazakhstan

Received September 7, 2006

Abstract—Data on the synthesis of thermally and chemically stable ion exchangers based on glycidyl ethers of aromatic compounds and their derivatives with high exchange capacity are summarized. Optimal conditions of the synthesis of ion exchangers, their composition, structure, main physicochemical characteristics, and acid–base properties are determined. The complexing ability of the new polyelectrolytes and stability constants of complexes with transition metal ions are determined potentiometrically.

DOI: 10.1134/S1070427207030238

Introduction of aromatic amines and *N*-heterocyclic and phenolic compounds into epoxy polymers is one of ways to improve their physicochemical characteristics. To obtain thermally and chemically stable anion exchangers with high sorption ability, we studied formation of anion-exchange polymers by condensation of polyethylenepolyamine (PEPA) and polyethylenimine (PEI) with diglycidyl compounds: diglycidylaniline (DGA), diglycidyl phenol–aniline–formaldehyde (DGPAF) oligomer, and diglycidyl toluene–phenol–formaldehyde (DGTPF) oligomer of the following structures [1]:

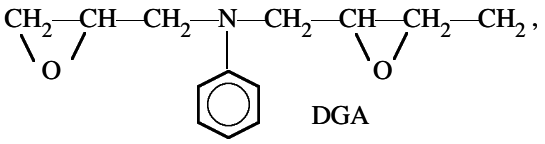

DGA

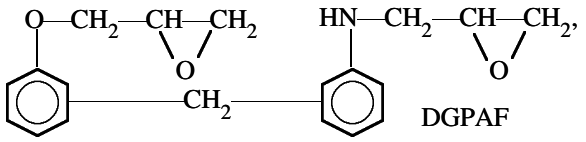

DGPAF

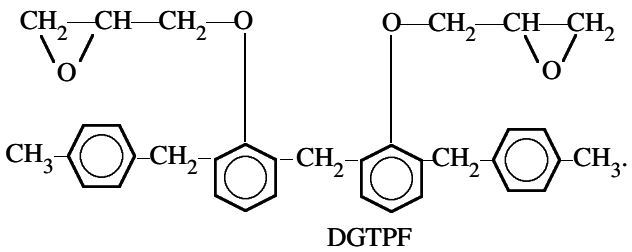

DGTPF

The diglycidyl compounds synthesized are very reactive due to strained epoxy rings. The uniformity of functional groups and the presence of repeating aromatic rings enhance the thermal and chemical stability and improve the macronetwork structure, making the three-dimensional structure of the ion exchangers more regular.

As shown in [2, 3], polymeric amines are more nucleophilic than their low-molecular-weight analogs. Therefore, to synthesize ion exchangers with elevated sorption ability, we used soluble polyamines: PEPA and PEI.

EXPERIMENTAL

The epoxy compounds were condensed with amines in dimethylformamide at 80°C for 0.5 h. The resulting gel was cured in an oven at 80–100°C for 5 h.

To find the optimal conditions of the synthesis of anion exchangers, we studied the influence of the reactant ratio, amine composition, temperature, and reaction time on the properties of the resulting polymers [4]. It was found that the static exchange capacity (SEC) of the ion exchanger substantially depends on the amine composition and reactant ratio (Table 1). As seen, PEI is the most efficient aminating agent, which is caused by its high molecular weight and by high content of active groups in it. The increase in the amine concentration in the initial mixture from 0.5 to 2.5 wt parts (Table 1) increases the exchange capacity

Table 1. Influence of amine structure and reactant ratio on SEC_{HCl} (mg-equiv g^{-1}) and V_{sp} (ml g^{-1}) of ion exchangers (100°C, 5 h)

Anion exchanger based on	Reactant weight ratio									
	1.0 : 0.5		1.0 : 0.75		1.0 : 1.0		1.0 : 2.0		1.0 : 2.5	
	SEC_{HCl}	V_{sp}	SEC_{HCl}	V_{sp}	SEC_{HCl}	V_{sp}	SEC_{HCl}	V_{sp}	SEC_{HCl}	V_{sp}
DGA : PEI	6.5	2.5	8.9	3.8	11.8	4.5	12.5	6.5	Dissolves	
DGA : PEPA	6.0	3.0	8.3	3.5	11.0	5.4	Strongly swells		Dissolves	
DGPAF : PEI	6.5	2.6	8.5	3.8	10.6	5.0	12.3	5.7	Dissolves	
DGPAF : PEPA	6.2	3.5	7.1	3.8	8.5	5.6	Strongly swells		Dissolves	
DGTPF : PEI (100°C, 20 h)	Dissolves		7.0	3.9	8.1	4.1	10.4	6.2	10.4	7.0
DGTPF : PEPA (100°C, 20 h)	Dissolves		6.5	4.9	6.9	5.6	7.0	7.0	Strongly swells	

of anion exchanger from 6.5 to 12.5 mg-equiv g^{-1} in the case of polycondensation of diglycidyl derivatives with PEI and from 6.0 to 11.0 mg-equiv g^{-1} in the case of polycondensation with PEPA, with simultaneous increase in their specific volume in the swollen state from 2.5 to 7.0 and from 3.0 to 7.0 ml g^{-1}, respectively. In practice, ion exchangers should have high exchange capacity and small swelling. For amination, the optimal reactant ratio for DGA, DGPAF, and DGTPF is 1.0 : 1.0 with PEPA and 1.0 : 2.0 with PEI. At a large excess of polyamine, insufficient amount of reactive epoxy groups hinders formation of network ion exchangers.

The IR spectra of the anion exchangers obtained contain no characteristic bands of epoxy groups (810–920, 1250, 3000–3010 cm^{-1}), which indicates that their chemical conversion was complete. At the same time, bands of N–H bending (1600–1670 cm^{-1}) and C–N stretching (1020–1220 cm^{-1}) vibrations of amino groups are observed (Fig. 1).

To outline the field of application of the new ion exchangers, we studied their acid–base properties, exchange capacity, selectivity of metal ion sorption, kinetic properties, swelling, and stability.

The sorption properties of the ion exchangers are determined by the concentration of functional groups in the polymer unit weight. The concentration of functional groups (SEC, mg-equiv g^{-1}) in the ion exchangers synthesized was determined chemically under static conditions and by potentiometric titration [5]. The potentiometric curves were recorded in concentrated solutions of a supporting electrolyte, because weakly and moderately basic anion exchangers contain only weakly dissociating functional groups.

The potentiometric titration curves are plotted in the pH–titrant amount (mg-equiv per gram of ion exchanger) coordinates (Fig. 2). Inflection in the titration curve corresponds to the concentration of functional groups in the ion exchanger. More precisely, the posi-

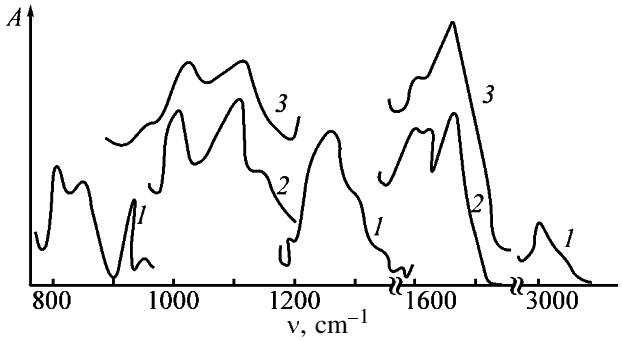

Fig. 1. IR spectra of (*1*) initial DGPAF and anion exchangers based on (*2*) DGPAF : PEPA and (*3*) DGPAF : PEI. (*A*) Absorption and (ν) wavenumber.

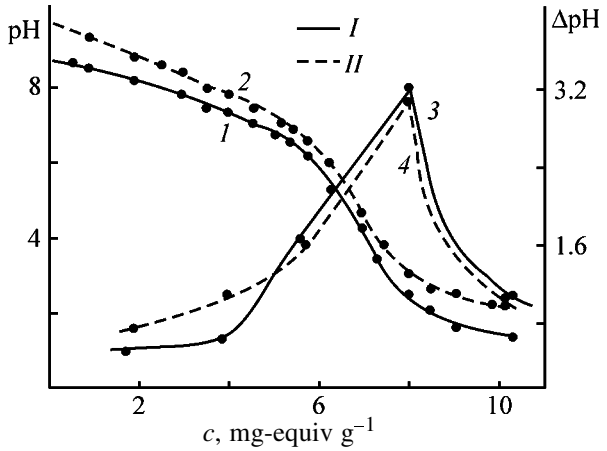

Fig. 2. (*1, 2*) Integral and (*3, 4*) differential potentiometric titration curves of anion exchangers based on (*I*) DGPAF : PEI and (*II*) DGA : PEPA. (*c*) HNO_3 titrant amount.

Table 2. Physicochemical characteristics of anion exchangers

Anion exchanger based on	SEC (potentiometric titration), mg-equiv g^{-1}	Specific volume, ml g^{-1}	pK_a	m
DGA : PEI = 1.0 : 1.0	8	3.6	7.8	2.0
DGPAF : PEI = 1.0 : 1.0	8	3.7	7.5	2.2
DGA : PEPA = 1.0 : 1.0	8	3.5	7.8	2.2
DGPAF : PEPA = 1.0 : 0.75	6	3.5	7.8	2.0

tion of the inflection is determined from the differential curve plotted in ΔpH–amount of working solution (mg-equiv per gram of ion exchanger) coordinates, where ΔpH is the pH change on addition of a definite amount (mg-equiv) of the working solution. The curve maximum corresponds to the equivalence point (Fig. 2).

To find the average constant of the acid–base dissociation of weakly basic groups of the anion exchanger, we used graphic solution of the Henderson–Hasselbach equation [5]

$$pH = pK_a + m\log[(1 - \alpha)/\alpha],$$

where pH is pH of the equilibrium solution; pK_a, negative logarithm of the acid–base dissociation constant of the polymer functional groups; m, empirical coefficient considering interunit interaction in the polymeric chain; and α, degree of protonation of the anion exchanger functional groups.

Typical straight lines of the graphic solution of this equation in the pH–log[(1 – α)/α] coordinates are shown in Fig. 3.

The coefficient m was determined as the slope of the above straight lines, and pK_a, as a segment cut off on the ordinate (Table 2).

Thus, our study confirms the polyfunctionality of the ion exchangers synthesized, determined by secondary and tertiary amine groups [6]. However, due to small difference in pK_a values of the functional groups, only one inflection is observed in the potentiometric titration curves. Therefore, only the total concentration of functional groups can be determined by potentiometric titration.

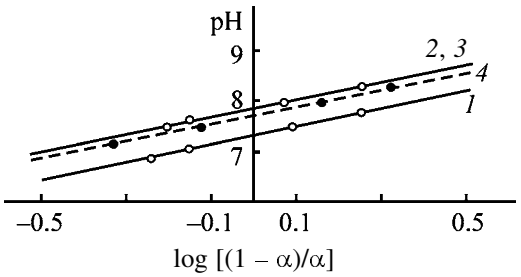

Fig. 3. pH of equilibrium solution as a function of log[(1 – α)/α] for anion exchangers (*1*) DGPAF : PEI, (*2*) DGA : PEI, (*3*) DGA : PEPA, and (*4*) DGPAF : PEPA.

The complex formation of the ion exchangers is characterized by the sorption of the metal ions on the polymer ligand groups due to donor–acceptor interaction, by the energy of the metal ion interaction with electron-donor atoms of the polymer ligand groups, and by the stability constant of the complex [5, 7, 8]. The role of nitrogen atoms of the ion exchanger, forming σ bonds with metal ion vacant orbitals, is determined by their lone electron pair on the sp^3 hybrid orbital.

To study the complexing properties of anion exchangers, we used solutions prepared from chemically pure grade copper, nickel and sodium nitrates. The composition and stability of the complexes formed were determined by potentiometric titration of anion exchangers in the absence and in the presence of the complexing metal ions by the method of separate weighed portions [5] at the ion exchanger content of 0.2 g per 50 ml of the solution (the ion exchanger was preliminarily dried to constant weight). To an ion exchanger sample we added a solution containing copper or nickel nitrate (0.025 M in 1 M $NaNO_3$, 10 ml), nitric acid (from 0 to 10 mg-equiv per gram of ion exchanger with the step of 0.5 mg-equiv g^{-1}), and 1 M sodium nitrate (added to the total volume of 50 ml). The ionic strength of the resulting solution was 1, and the experiment temperature, 20°C. After attaining the equilibrium (15 days), the pH of solutions was measured with a PB-11 pH meter (Sartorius), and the metal ion concentration was measured by atomic absorption spectroscopy.

In aqueous solutions, ionogenic groups of the nitrogen-containing anion exchangers exist in interdependent chemical forms:

$$\underset{\text{Free base}}{\geqslant N} + HOH \rightleftarrows \underset{\text{Hydrated form}}{\geqslant N\ldots HOH} \rightleftarrows \underset{\text{Protonated form}}{\geqslant NH^+} + OH^-,$$

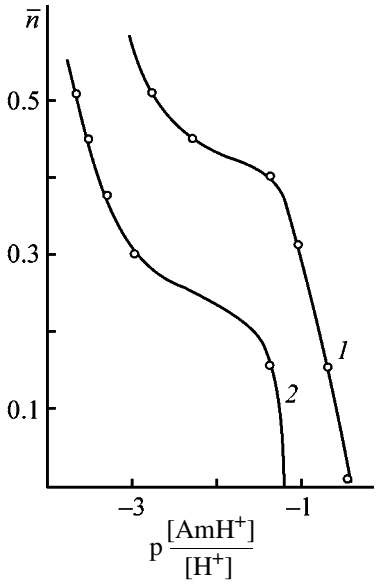

Fig. 4. Complexation of copper(II) with anion exchangers (*1*) DGPAFA : PEI and (*2*) DGA : PEI as a function of $p[AmH^+]/[H^+]$. ($\bar{n}$) Bjerrum formation function; the same for Fig. 5.

whose presence determines the possibility of ion exchange reactions

$$\geqslant NH^+OH^- + An^- \rightleftarrows \geqslant NH^+An^- + OH^- \qquad (1)$$

and complex formation with hydrated transition metal cations

$$n(\geqslant N\ldots HOH) + M(H_2O)_N \rightarrow M(\geqslant N)_n(H_2O)_{N-n} + 2nH_2O. \qquad (2)$$

Reactions (1) and (2) occur simultaneously and independently. The process direction as a whole is determined by the ratio of their equilibrium constants, experimental conditions, and first of all by the degree of protonation of anion exchanger amino groups.

In the presence of metal ions, the total concentration of the amino groups in the system [Σ Am] consists of amino groups bound in the complex [Am_c], protonated anino groups [AmH^+], and free amino groups [Am]:

$$[\Sigma\,Am] = [Am_c] + [AmH^+] + [Am].$$

The concentration of protonated amino groups was determined in each point of the potentiometric titration curve:

$$[AmH^+] = NV/V_{tot} = 0.1V_{HNO_3}/50 \text{ ml (mg-equiv ml}^{-1}).$$

Using the equation $pH = pK_a + m\log[Am]/[AmH^+]$,

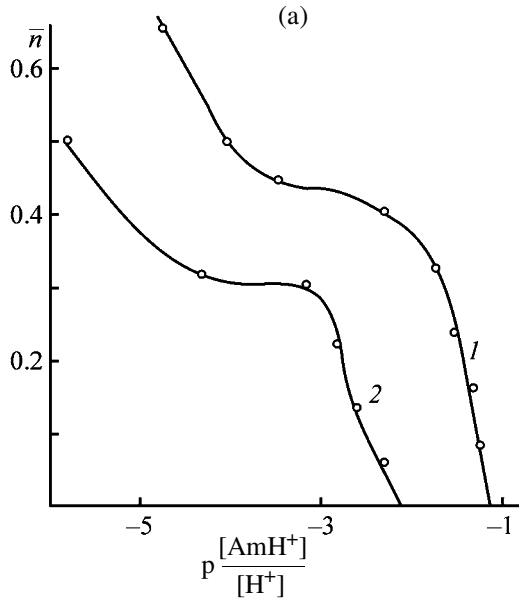

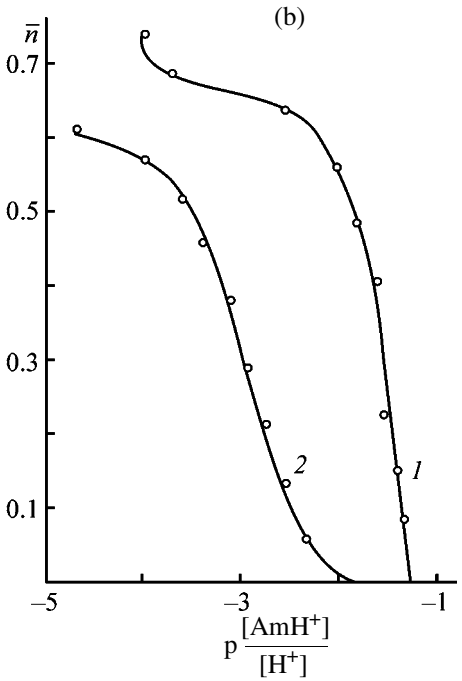

Fig. 5. Complexation of (*1*) copper(II) and (*2*) nickel (II) with anion exchangers (a) DGPAF : PEPA and (b) DGA : PEPA.

we calculated the concentration of free amino groups [Am] in the solution by the formula

$$p[Am] = (pK_a - pH)/m - \log[AmH^+].$$

The concentration of bound amino groups in the complex [Am_c] was determined as the difference between the total concentration of the amino groups in the system, SEC (mg-equiv ml^{-1}), and the sum

Table 3. Stability constants of copper(II) and nickel(II) complexes with anion exchangers

Complex, 0.025 M	$\log K_{st}$ with indicated anion exchangers			
	DGPAF : PEI = 1.0 : 1.0	DGA : PEI = 1.0 : 1.0	DGA : PEPA = 1.0 : 1.0	DGPAF : PEPA = 1.0 : 0.75
$Cu(NO_3)_2$	4.6	4.2	6.0	4.0
$Ni(NO_3)_2$	3.5	3.0	4.5	3.0

$[AmH^+]$ + [Am]:

$$[Am_c] = [\Sigma Am] - [AmH^+] - [Am].$$

The Bjerrum formation function (i.e., the amount of amino groups in the complex per metal ion) was calculated by the formula

$$\bar{n} = [Am_c]/c_M,$$

where c_M is the initial metal ion concentration in the solution (M).

The complex formation curves were plotted in $\bar{n}$ – $p[AmH^+]/[H^+]$ coordinates (Figs. 4, 5).

The shape of the curves of copper(II) and Ni(II) complex formation with anion exchangers at a cation concentration of 0.025 M corresponds to primary formation of 1.0 : 1.0 complexes, because $\bar{n}$ tends to 1. The composition of the complexes depends on the anion exchanger ionic composition and metal ion concentration in the solution [9–11]. The higher the concentration of hydrated coordination-active ionogenic groups and the lower the concentration of metal ions, the larger number of amino groups is coordinated to the metal ion.

The stability constants of copper(II) and Ni(II) complexes with the anion exchangers studied were determined by the Bjerrum–Gregor potentiometric method:

$$\log K_{st} = \log \beta_n + pK_a,$$

where β_n is the complexation step constant found from the complexation curves at half $\bar{n}$ values (in our case, $\bar{n} = 0.5$).

The most stable complexes are formed by the DGA : PEPA anion exchanger. The stability of the copper complex is higher than that of the nickel complex, which is probably caused by smaller ionic radius of copper. The stability of the complex with ionogenic groups of the same anion exchanger depends on particular metal, namely, on the charge and radius of the hydrated metal ion, its electronic state, and electronegativity.

CONCLUSIONS

(1) Polyfunctional ion exchangers were synthesized by condensation of glycidyl derivatives of aromatic compounds with polyamines. The influence of the type of the initial reagents and reaction conditions on formation of network polyelectrolytes was determined.

(2) The polymers synthesized are polyfunctional anion exchangers with pK_a 7.5–7.8 and high exchange capacity (up to 12.5 mg-equiv g^{-1}).

REFERENCES

1. Paquin, A.M., *Epoxydverbindungen und Epoxydharze*, Berlin: Springer, 1958.
2. Gembitskii, P.A., Zhuk, D.S., and Kargin, V.A., *Polietilenimin* (Polyethylenimine), Moscow: Nauka, 1971.
3. Chetverikova, A.T., Chetverikov, A.F., Vakulenko, V.A., et al., *Plast. Massy*, 1979, no. 5, pp. 6–8.
4. Chalov, T.K., *Izv. Minist. Obraz. Nauki Resp. Kaz., Nats. Akad. Nauk Resp. Kaz., Ser. Khim.*, 2002, no. 2, pp. 98–102.
5. Saldadze, K.M. and Kopylova-Valova, V.D., *Kompleksuyushchie ionity (kompleksity)* (Complexing Ion Exchangers), Moscow: Khimiya, 1980.
6. Chalov, T.K., *Doctoral Dissertation*, Almaty, 2005.
7. Basargin, N.N., Salikhov, V.D., Dorofeev, D.N., et al., *Izv. Vyssh. Uchebn. Zaved., Khim. Khim. Tekhnol.*, 2000, vol. 43, no. 1, pp. 63–67.
8. Kovalenko, Yu.A. and Gorshkov, V.I., *Sorbts. Khromatogr. Prots.*, 2001, vol. 1, no. 6, pp. 940–942.
9. Vishnevskaya, G.P. and Frolova, E.N., *Plast. Massy*, 1999, no. 1, pp. 39–40.
10. Neagu, V., Untea, I., Tudorache, E., and Orbeci, C., *J. Appl. Polym. Sci.*, 2004, vol. 93, no. 4, pp. 1957–1963.
11. Mutalov, Sh.A., Tursunov, T., and Nazirova, R.A., *Plast. Massy*, 2005, no. 5, pp. 37–38.

ISSN 1070-4272, Russian Journal of Applied Chemistry, 2007, Vol. 80, No. 3, pp. 477–481. © Pleiades Publishing, Ltd., 2007.
Original Russian Text © S.V. Zhil'tsova, V.M. Mikhal'chuk, E.M. Petrova, L.A. Savenkova, A.A. Perepelitsa, 2007, published in Zhurnal Prikladnoi Khimii, 2007, Vol. 80, No. 3, pp. 479–483.

MACROMOLECULAR CHEMISTRY AND POLYMERIC MATERIALS

Preparation of Epoxy–Silica Composites Cured with *iso*-Methyltetrahydrophthalic Anhydride

S. V. Zhil'tsova, V. M. Mikhal'chuk, E. M. Petrova, L. A. Savenkova, and A. A. Perepelitsa

Donetsk National University, Donetsk, Ukraine

Received August 22, 2006; in final form, December 2006

Abstract—The possibility of preparing epoxy–silica composites using *iso*-methyltetrahydrophthalic anhydride as curing agent was examined; the composition of the composites and conditions of their preparation were determined. The effect exerted by the concentration of precursors, tetraethoxysilane and epoxypropoxypropyltriethoxysilane, on the glass transition point, sol fraction yield, heat resistance, and adhesion properties of the hybrid materials obtained was studied.

DOI: 10.1134/S107042720703024X

The mechanical and thermal properties of polymeric materials are often improved by introducing an inorganic filler. The properties of such composites are determined by the properties of both physically mixed phases. In the past decades, numerous elastomers, thermoplastics, and linear or cross-linked polymers were modified with inorganic fillers formed in situ [1–4]. Such systems constitute a new class of composites, organic–inorganic hybrids. Inorganic particles in hybrid materials have usually nanometer size, so that the system is optically transparent. In such hybrids, the properties of inorganic and organic phases are combined, which allows preparation of materials with high levels of adhesion strength and resistance to heat, wear, scratching, and action of aggressive media; therefore, these materials are often used as protective and anticorrosion coatings.

The inorganic phase in hybrids is generated inside the forming polymer matrix using the sol–gel process: hydrolysis of alkoxy derivatives of Si, Ti, Al, and Zr followed by polycondensation of hydrolysis products and gelation of the system. The organic and inorganic components of the system can undergo polymerization (or polycondensation) both successively and simultaneously [5, 6]. The properties of the resulting composites largely depend on the interphase interaction determining their morphology; the compatibility of the organic and inorganic phases is often improved by adding compatibilizers: organic monomers or polymers modified with alkoxysilanol groups, e.g., 3-glycidyloxypropyltrimethoxysilane, aminopropyltrimethoxysilane, aminoethylaminopropyltriethoxysilane, etc. [7, 8]. In this case, hybrids with covalent bonding of the inorganic component with the polymer matrix can be prepared.

Epoxy–silica hybrids are among widely used organic–inorganic composites. The organic constituent of such systems is cured with polyamines, dicarboxylic acids, anhydrides, boron trifluoride, and tertiary amines. However, today the use of dicarboxylic acid anhydrides for preparing epoxy–silica nanocomposites is limited.

The goal of this study was to prepare epoxy–silica hybrid composites curable with *iso*-methyltetrahydrophthalic anhydride and to examine the effect of the silica component on the properties of the composites.

EXPERIMENTAL

To form the organic constituent of hybrid composites, we used a triepoxide based on 1,1-dimethylol-3-cyclohexene (UP-650T, MW = 360 g mol^{-1}, epoxy number EN = 37.4%), *iso*-methyltetrahydrophthalic anhydride (*iso*-MTHPA, acid number AN = 662 mg of KOH per gram), and a curing accelerator, 2,4,6-tris-(dimethylaminomethyl)phenol (UP-606/2). To obtain silicon oxide particles, we used tetraethoxysilane (TEOS, ρ = 0.9334 g cm^{-3}, n_D^{20} = 1.383) and epoxypropoxypropyltriethoxysilane (ES-1, ρ = 1.000 g cm^{-3}, n_D^{20} = 1.425).

Sol of colloidal particles of silicon oxide was pre-

Table 1. Influence of the composition of epoxy–silica composites on the gelation time and optical transmission coefficient

System	Content of epoxysilanes, wt %	Gelation time t_{gel} at 22±2°C, days	Optical transmission coefficient T_{540}, %
Uncured	0	23	97
	10	26	96
	20	35	95
	30	50	95
Cured	0	–	95
	10	–	93
	20	–	91
	30	–	90

pared by joint hydrolysis of TEOS and ES-1 (molar ratio 2 : 1) in the presence of 1 N aqueous HNO_3 and epoxy resin (molar ratio TEOS : H_2O = 1 : 2, ES-1 : H_2O = 1 : 2). The content of ethoxysilanes in the system was varied from 2 to 30 wt %. As solvent for performing the sol–gel process we used methyl ethyl ketone (35 vol % relative to the sol). After 24 h, water, solvent, and ehanol formed by hydrolysis of ethoxysilanes were removed in a vacuum at 25°C; then a stoichiometric amount of the curing agent (*iso*-MTHPA) and curing accelerator (UP-606/2, 0.3 wt % relative to the total amount of the anhydride and epoxy resin) were added. Film samples were prepared between glass plates coated with an antiadhesive (dimethyldichlorosilane). The film thickness was set with a 200-μm-thick fish line.

Photometric studies were performed with a KFK-3 photocolorimeter at λ = 540 nm. The DSC curves were taken on a DSM-2M device in the temperature range 70–240°C (heating rate 4 deg min^{-1}). The IR spectra of organic–inorganic composites were recorded on a Specord 75-IR spectrophotometer at room temperature using KBr windows. The wavelength range was 1400–400 cm^{-1}. The epoxy number of UP-650T resin was determined according to GOST (State Standard) 2087–92 by acid–base back-titration. The acid number of *iso*-MTHPA was determined by titration of a sample of the anhydride in acetone with 0.1 M NaOH [9].

The glass transition point of polymer samples was determined by a thermomechanical method with an automatic laboratory installation consisting of a TK-500 thermocryochamber, a BTP-78 programmable temperature regulator, an M-217 electronic measuring system, and an *XY* recording potentiometer. Measurements were performed with film samples (25 × 6 × 0.2 mm) at a constant tensile stress (2 MPa). The heating rate was 4 deg min^{-1}. The glass transition point was determined as the intersection point of the tangents to the flat and ascending portions of the curve.

The yield of the sol fraction of the polymers was determined from the weight loss of the film samples after extraction of low-molecular-weight products with methanol at 50°C for 3 days. To determine the adhesion strength, the compounds were applied onto aluminum foil and cured under the common conditions. The coating thickness was 20–30 μm. Adhesion to aluminum foil was evaluated by the lattice notch method in the five-point scale according to GOST 15 140–78 [10].

Thermogravimetric analysis was performed with an MOM Q-1500 D derivatograph (Hungary) in the dynamic mode in the temperature range 20–850°C. Finely divided film samples of the polymers (200 mg) were placed in ceramic crucibles. The heating rate was 10 deg min^{-1}. Aluminum oxide was used as reference. Measurements were performed in air. The device scale was 200 mg.

It is known that hydrolysis of ethoxysilanes at acid catalysis in the presence of UP-650T epoxy resin and an inert solvent is relatively fast [1] and is followed by polycondensation of the hydrolysis products. Under such conditions, nanosized silica particles with a defective structure are usually formed [12]. The preliminary tests showed that ethanol released in the course of hydrolysis of ethoxysilanes and HNO_3 present in the system do not cause opening of the epoxy ring to an appreciable extent. The epoxy number of UP-650T resin decreased by only 1.9% in 24 h after the start of the reaction. At the same time, the presence of ethanol causes unproductive consumption of the anhydride curing agent, namely, its transformation into the monoester. For a mixture of *iso*-MTHPA and ethanol in 1 : 1 molar ratio in methyl ethyl ketone, the degree of conversion (esterification) is 0.76 in 24 h. In the process, an S-shaped kinetic curve is observed, typical of autocatalytic reactions, which may be due to the catalytic effect of the carboxylic acid formed by opening of the anhydride ring [13].

The sols prepared by simultaneous mixing of all the components are stable in time, have uniform structure, and are optically transparent (Table 1). Table 1 shows that the gelation time is minimal for the composition containing no organosilicon precursors and increases with an increase in their content in the reaction mixture. This fact indicates that the sol–gel transition in the systems under consideration mainly oc-

curs via the reaction of epoxide with anhydride, which is slow at room temperature.

At a high concentration of ethoxysilanes in the starting mixture and hence high concentration of ethanol in the reaction zone, esterification can significantly distort the epoxide–anhydride stoichiometric ratio. Therefore, it becomes necessary to remove ethanol in a vacuum before adding anhydride. Water introduced into the system for the hydrolysis of ethoxysilanes is removed simultaneously, which prevents hydrolysis of the anhydride curing agent.

From the DSC data, we determined the temperature range of curing of the unfilled and filled compounds. The temperatures of the onset and end of the process and of the maximal rate of heat release are 75, 170, and 130°C, respectively, being essentially independent of the content of ethoxysilanes in the system. Based on these data, we chose the temperature and time conditions for preparing maximally cured epoxy polymers and epoxy–silica composites: 2 h at 130°C + 4 h at 160°C + 1 h at 180°C. Under these conditions, the limiting glass transition point of the film samples of the polymers is reached. Formation of the maximally cured polymers is also confirmed by the IR data, namely, by the disappearance of the absorption bands of the epoxy groups (910 and 840 cm^{-1}).

We studied how the concentration of ethoxysilanes added into the system affects the thermomechanical properties of the composites and found that the glass transition point decreased with an increase in the content of the silicon oxide constituent (Fig. 1). This results can be attributed to the fact that the condensation of hydrolyzed organosilicon precursors involves formation of –Si–O–Si– bonds with a low rotation barrier, which gives rise to a plasticization effect and causes a decrease in the glass transition point.

A decrease in the glass transition point can also be accounted for by formation of a structure with topological defects in the polymer matrix of the composite. Formation of topological defects is confirmed by the results of sol–gel analysis. We found that the content of low-molecular-weight compounds in the hybrid materials increases with an increase in the concentration of ethoxysilanes (Fig. 2). It is known that acid hydrolysis of ethoxysilanes in the presence of monosubstituted alkoxysilanes yields silica particles with a defective structure, containing organic substituents [12]. In the process, interpenetrating epoxy–silica polymer network can form, which can result in steric hindrance to formation of a three-dimensional epoxide structure; therefore, the glass transition point of the

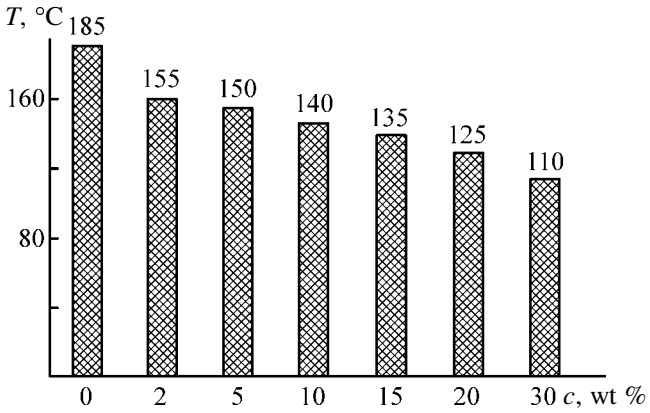

Fig. 1. Glass transition point T of epoxy polymers and epoxy–silica composites as a function of the content c of ethoxysilanes in the initial reaction mixture.

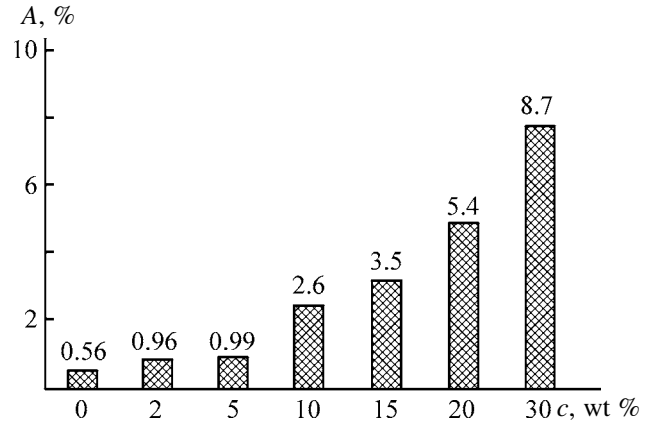

Fig. 2. Yield A of sol fraction from epoxy polymers and epoxy–silica composites as a function of the content c of ethoxysilanes in the initial reaction mixture.

composite should decrease. Similar phenomena are observed with classical interpenetrating polymer–polymer networks [14].

A decrease in the glass transition point is observed both when the anhydride is added after removing the volatiles in a vacuum and when all the components are mixed simultaneously (Fig. 3). In the latter case, as noted above, esterification of the anhydride with ethanol released from hydrolysis of ethoxysilanes occurs simultaneously with the formation of the sol. As a result, the overall stoichiometric ratio of the components is distorted, causing still stronger plasticization of the polymer matrix: the glass transition point decreases to 55°C. The esterification process in such a complex system is difficult to control, and attempts to reduce its effect on the thermomechanical properties of the polymers by introducing an additional amount of *iso*-MTHPA failed. Figure 3 shows that addition of the anhydride in amount fully compensat-

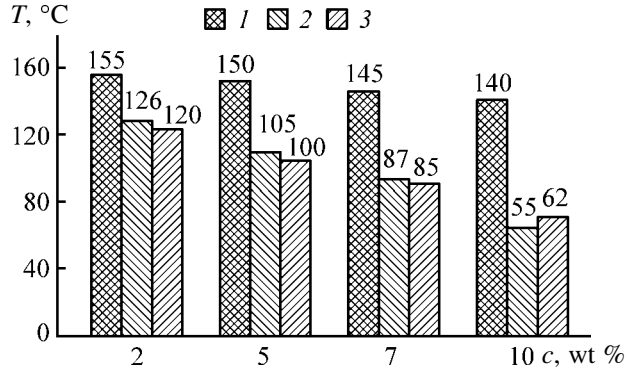

Fig. 3. Influence of conditions for preparation of epoxy–silica composites on their glass transition point T at various content c of ethoxysilanes in the initial reaction mixture: (*1*) vacuum treatment to remove volatiles, (*2*) no vacuum treatment, and (*3*) no vacuum treatment, with compensation of the anhydride loss in the reaction with alcohol.

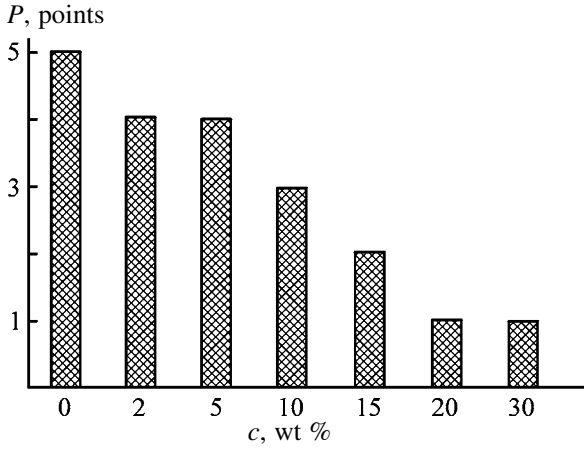

Fig. 4. Adhesion P of coatings based on epoxy–silica composites as a function of the concentration c of ethoxysilanes in the initial reaction mixture.

ing its theoretical loss in the reaction with the alcohol released by hydrolysis does not noticeably change the glass transition point of the product. In this case, the high plasticizing effect of ethoxysilanes is caused by formation of the monoester in the reaction of the anhydride with the alcohol (with a decrease in the density of the polymer network), in agreement with data of [15].

Unmodified thickly cross-linked epoxy polymers cured with anhydrides are very brittle and exhibit relatively low adhesion strength. Plasticization of the polymer matrix improves the adhesion characteristics of composite materials. Furthermore, it is known that epoxy–silica composites show increased affinity for aluminum surfaces compared to epoxy polymers because of interaction of hydroxy groups on the support surface with the inorganic constituent of the system [16, 17]. This interaction results in formation of the Si–O–Al bond on the coating | aluminum substrate interface. In the systems under consideration, with an increase in the content of the inorganic constituent, the capability to spread over the aluminum foil surface and the adhesion strength of the coatings increase (Fig. 4).

It is known that introduction of silica nanoparticles into epoxy polymers enhances their heat resistance [18]. For the systems under consideration, variation of the initial concentration of ethoxysilanes in the reaction mixture also strongly affects the heat resistance of the composites. As shown by thermogravimetric analysis (Fig. 5), the temperature of 5% weight loss of the epoxy–silica hybrids increases from 225 to 275°C with an increase in the content of TEOS and ES-1 from 0 to 10 wt %. The temperature of the maximal weight loss rate also increases (by 15°C). However, as the concentration of ethoxysilanes is increased further, the temperature of 5% weight loss decreases (to 175°C at 30 wt % content of TEOS and ES-1, Table 2). This significant decrease in the heat resistance may be due to the fact that, at high concentrations of ethoxysilanes in the initial reaction mixture, the three-dimensional network of the polymer matrix becomes looser and the content of low-molecular-weight compounds in the composites increases. This

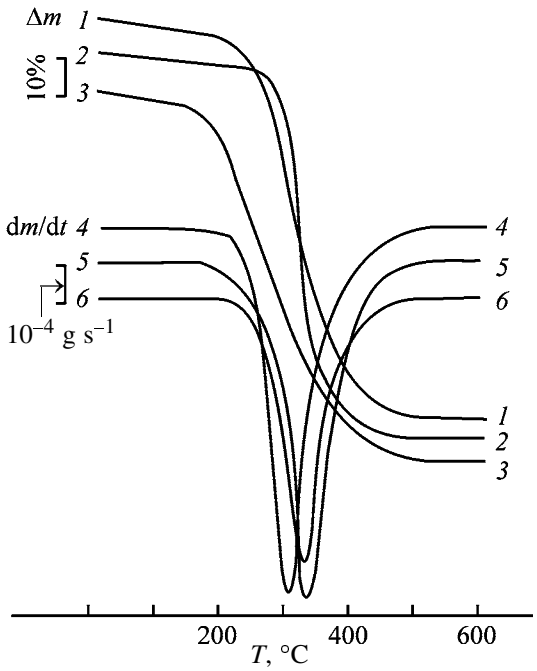

Fig. 5. (*1–3*) TG and (*4–6*) DTG curves of epoxy polymers and epoxy–silica composites. (Δm) Weight loss, (dm/dt) weight loss rate, and (T) temperature. Content of ethoxysilanes, wt %: (*1*, *4*) 0, (*2*, *5*) 10, and (*3*, *6*) 20.

Table 2. Parameters characeterizing the thermal degradation of epoxy–silica composites

Content of ethoxysilanes, wt %	Temperature, °C	
	of 5% weight loss	of maximal weight loss rate
0	225	305
5	235	320
10	275	320
15	230	330
20	180	320
30	175	320

explanation is well consistent with the above-given results of thermomechanical and sol–gel analysis.

CONCLUSIONS

(1) The use of *iso*-methyltetrahydrophthalic anhydride as a curing agent for UP-650T epoxy resin ensures preparation of uniform and transparent epoxy–silica composites (using sol–gel technology).

(2) As the concentrations of tetraethoxysilane and epoxypropoxypropyltriethoxysilane in the initial reaction mixture and, correspondingly, the content of the inorganic constituent in the composites are increased, the glass transition point of the composites decreases and their adhesion to aluminum substrates increases.

(3) Introduction into the system of up to 10 wt % tetraethoxysilane and epoxypropoxypropyltriethoxysilane appreciably enhances the heat resistance of the hybrid materials obtained. Further increase in the concentration of these ethoxysilanes to 30 wt % leads to a decrease in the heat resistance of the polymers.

REFERENCES

1. Pomogailo, A.D., *Usp. Khim.*, 2000, vol. 69, no. 1, pp. 60–89.
2. Tomoki Ogoshi and Yoshiki Chujo, *Composite Interfaces*, 2005, vol. 11, nos. 8–9, pp. 539–566.
3. Zhabrev, V.A., Moshnikov, V.A., Tairov, Yu.M., et al., *Zol'-gel' tekhnologiya: Uchebnoe posobie* (Sol–Gel Technology: Textbook), St. Petersburg: Sankt-Peterb. Gos. Elektrotekh. Univ., 2005.
4. Schubert, U., Husing, N., and Lorenz, A., *Chem. Mater.*, 1995, no. 7, pp. 2010–2027.
5. Matejka, L., Plestil, J., and Dusek, K., *J. Non-Cryst. Solids*, 1998, vol. 226, pp. 114–121.
6. Matejka, L., Dukh, O., and Kolarik, J., *Polymer*, 2000, vol. 41, pp. 1449–1459.
7. Brusatin, G., Innocenzi, P., Guglielmi, M., and Babonneau, F., *J. Sol–Gel Sci. Technol.*, 2003, vol. 26, pp. 303–306.
8. Davis, S.R., Brough, A.R., and Atkinson, A., *J. Non-Cryst. Solids*, 2003, vol. 315, pp. 197–205.
9. Bratichak, M., Bzhozovs'kii, Z., Bukovs'kii, A., et al., *Laboratornii praktikum z khimii ta tekhnologii polimeriv: Navchal'nii posibnik dlya vuziv* (Practical Laboratory Course of Chemistry and Technology of Polymers: Primary Textbook for Higher Schools), Slovikovs'ka, I., Ed., Warsaw: Varshavs'ka Politekhnika, 2002.
10. Karyakina, M.I., *Ispytanie lakokrasochnykh materialov i pokrytii* (Testing of Paint-and-Varnish Materials and Coatings), Moscow: Khimiya, 1988.
11. Volnyanskaya, R.I., Maneshina, L.A., and Mikhal'chuk, V.M., *Vopr. Khim. Khim. Tekhnol.*, 2005, no. 5, pp. 125–129.
12. Matejka, L., Dukh, O., Brus, J., et al., *J. Non-Cryst. Solids*, 2000, vol. 270, pp. 34–47.
13. Shologon, I.M., Klebanov, M.S., and Karat, L.D., *Ukr. Khim. Zh.*, 1986, vol. 52, no. 2, pp. 181–186.
14. Mikhal'chuk, V.M., *Zh. Prikl. Khim.*, 1998, vol. 71, no. 10, pp. 1699–1703.
15. Mascia, L. and Tang, T., *J. Sol–Gel Sci. Technol.*, 1998, vol. 13, pp. 405–408.
16. Yuan, J., Zhou, Sh., Gu, G., and Wu, L., *J. Mater. Sci.*, 2005, vol. 40, pp. 3927–3932.
17. Du, Y.J., Damron, M., Tang, G., et al., *Prog. Org. Coat.*, 2001, vol. 41, pp. 226–232.
18. Liu, Y.-L., Wei, W.-L., Hsu, K.-Y., et al., *Thermochim. Acta*, 2004, vol. 412, nos. 1–2, pp. 139–147.

ISSN 1070-4272, Russian Journal of Applied Chemistry, 2007, Vol. 80, No. 3, pp. 482–485. © Pleiades Publishing, Ltd., 2007.
Original Russian Text © O.V. Alekseeva, O.V. Eliseeva, A.V. Noskov, O.V. Rozhkova, 2007, published in Zhurnal Prikladnoi Khimii, 2007, Vol. 80, No. 3, pp. 484–487.

MACROMOLECULAR CHEMISTRY AND POLYMERIC MATERIALS

Hydrodynamic and Bulk Properties of Dextrans in Liquid Media

O. V. Alekseeva, O. V. Eliseeva, A. V. Noskov, and O. V. Rozhkova

Institute of Solution Chemistry, Russian Academy of Sciences, Ivanovo, Russia

Received June 29, 2006; in final form, November 2006

Abstract—Bulk and viscous properties of solutions of dextrans of different molecular weights in formamide, water, and dimethyl sulfoxide were studied. The fractal dimension of the biopolymer was estimated from the hydrodynamic data.

DOI: 10.1134/S1070427207030251

Biopolymers, natural physiologically active compounds, attract considerable interest today. Since these compounds are biodegradable, they are widely used in medicine, microbiology, and pharmacy. Among these compound are dextrans. The colloidal osmotic and viscous properties of solutions of these polysaccharides allow their use as antishock blood substitutes. In addition, irregular structure and random branching of the polymer chains are the major factors responsible for high sorption capacity of these polysaccharides.

In this study we examined the influence of the solvent on the structural features and physicochemical properties of solutions of dextrans with different molecular weights.

EXPERIMENTAL

We studied dextrans with molecular weight of $(40–50) \times 10^3$ (Fluka AG, Buchs, Switzerland). The dextrans were dried in a vacuum at 313 K for 24 h. Formamide (FA) and dimethyl sulfoxide (DMSO) purified and dried by the standard procedure [1] and double-distilled water were used as the solvents. The water content of the solvents, determined by amperometric Fischer titration, was within 0.002%. The polymer solutions were prepared by weighing on a VLR-200 balance with an accuracy of $\pm 5 \times 10^{-5}$ g.

The bulk properties were estimated from the experimental density of the solutions by the procedure described in [2]. The density of the solutions was measured with a vibratory densimeter with an accuracy of $\pm 2 \times 10^{-6}$ g cm^{-3}, which allowed reliable calculation of the bulk properties of dextran (± 0.02 cm^3 mol^{-1}). The temperature was maintained with an accuracy of ± 0.002 K.

To decrease the calculation error, the partial and apparent molar volumes were calculated directly from the experimental results by the equations

$$V_2 = \frac{M_2}{\rho} - \frac{(1000 + mM_2)}{\rho^2}\frac{\partial\rho}{\partial m}, \quad (1)$$

$$V_\varphi = \frac{1000(\rho_0 - \rho)}{m\rho\rho_0} + \frac{M_2}{\rho}, \quad (2)$$

where V_2 is the partial molar volume of the solute, V_φ is the apparent molar volume of the solute, M_2 is the molecular weight of the solute, ρ is the density of the solution, ρ_0 is the density of the pure solvent, and m is the molar concentration of the solution.

The viscosity of the solution with the polymer concentration of 3–16 kg m^{-3} was measured on an Ubbelohde viscometer at 293–308 K. The root-mean-square error of these measurements was $\pm 0.5\%$. The reduced viscosity of all the examined dilute dextran solutions η_{sp}/c was a linear function of the polymer concentration (correlation coefficient $r = 0.95–0.98$). The Huggins constant was calculated by the equation [4]

$$\eta_{sp}/c = [\eta] + K_H c[\eta]^2, \quad (3)$$

where K_H is the Huggins constant characterizing the interaction between the segments of the polymer macromolecules and the solvent, and $[\eta]$ is the intrinsic viscosity.

Table 1. Density and partial and apparent volumes of dextrans of different molecular weights M_2 in formamide at 298 K

c, wt %	$M_2 = 70 \times 10^3$			$M_2 = 110 \times 10^3$			$M_2 = 500 \times 10^3$		
	ρ, g cm^{-3}	V_2, cm^3 mol^{-1}	V_φ, cm^3 mol^{-1}	ρ, g cm^{-3}	V_2, cm^3 mol^{-1}	V_φ, cm^3 mol^{-1}	ρ, g cm^{-3}	V_2, cm^3 mol^{-1}	V_φ, cm^3 mol^{-1}
0	1.133191	39202.52		1.133191	58356.73		1.133191	319535.68	
0.2	1.134060	41673.58	40448.56	1.134005	64108.18	61344.88	1.133825	299343.16	308413.66
0.4	1.134590	44034.77	41660.88	1.134748	68531.06	63896.06	1.134676	291469.22	301361.32
0.6	1.135354	46269.06	42830.78	1.135375	71601.43	66002.63	1.135353	296258.30	298480.03
0.8	1.135816	48376.93	43958.42	1.135927	73287.63	67648.70	1.136099	313475.83	299809.68
1.0	1.136276	50372.01	45051.30	1.136495	73582.33	68838.41	1.136654	342248.96	305087.18

The root-mean-square distance between the chain ends in polymer macromolecules $\langle\eta^2\rangle^{1/2}$ was calculated by the equation

$$[\eta] = \Phi\frac{\langle\eta^2\rangle^{3/2}}{M_2}, \quad (4)$$

where Φ is the Flory coefficient characterizing the deviation of the actual volume of macromolecules from the sphere volume and partial penetrability of a macromolecule globule for the solvent.

The concentration dependences of the density and partial and apparent molar volumes of dextrans of different molecular weights in FA are presented in Table 1. It is seen that the density and the bulk properties of the polymers in the solution increase with an increase in their molecular weight.

To understand structure formation in dilute polysaccharide solutions, we studied the concentration dependences of the partial molar volumes of the polymer of $M_2 = 110 \times 10^3$ in different solvents (Fig. 1). The bulk properties of dextran solutions in water and DMSO are reported in [7]. As seen from Fig. 1, the partial molar volumes of the macromolecules in dilute solutions ($c < 0.4$ wt %) increase with an increase in the solvent polarity. Solvation and hydration probably substantially affect the structure of the dextran solutions. In aqueous solutions, the volume of a macromolecular coil increases owing to its swelling and hydration and then decreases owing to formation of denser structures. The behavior of dextrans in nonaqueous solutions is different. Solvation of the macromolecules in DMSO and FA enhances their volume parameters. Intersection of $V_2 = f(c)$ curves at the concentration of 0.4 wt % (Fig. 1) is probably due to resolvation in liquid systems [8].

It is known that thermodynamic parameters of a solvent can be indirectly estimated form the results of viscometric measurements. The intrinsic viscosity, Huggins constants, and root-mean-square distance between the chain ends of dextran macromolecules in formamide are summarized in Table 2. The viscosity of dextrans of different molecular weights in FA is low. An increase in K_H and decrease in [η] and hydrodynamic size of the macromolecules with a decrease in the molecular weight of the polymer from 500×10^3 to 40×10^3 suggest structure formation even in dilute dextran solutions.

Let us compare the molecular properties of dextran solutions in formamide (Table 2) with viscosity of solutions of these polysaccharides in DMSO and water [7]. It is seen that the intrinsic viscosity and root-mean-square distance between the chain ends are maximal in DMSO and minimal in water. Apparently, coils of dextran molecules substantially swell in DMSO, which promotes dissolution of the polymer. These differences in the hydrodynamic parameters are probably due to different mechanism of solvation of

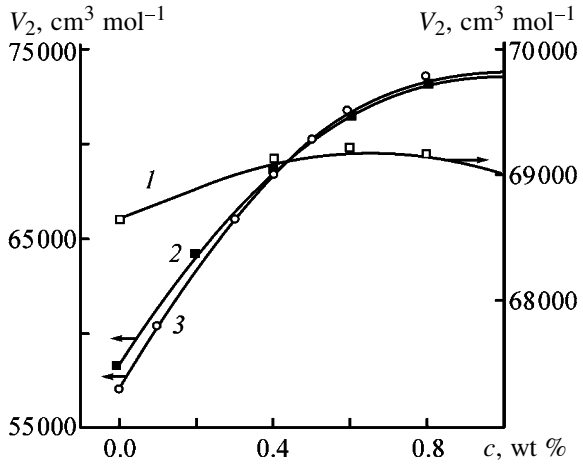

Fig. 1. Partial molar volume V_2 of dextran with $M_2 = 110 \times 10^3$ in (*1*) water, (*2*) formamide, and (*3*) dimethyl sulfoxide at 298.15 K as a function of the concentration c.

Table 2. Intrinsic viscosity [η], Huggins constants K_H, and root-mean-square distance between chain ends ($\langle\eta^2\rangle^{1/2}$) of dextrans of different molecular weights M_2 in formamide

M_2	T, K	[η], $m^3\ kg^{-1}$	K_H	$\langle\eta^2\rangle^{1/2}$, nm
500×10^3	293.15	0.0467	0.473	46.65
	298.15	0.0466	0.508	46.62
	303.15	0.0401	0.547	44.34
	308.15	0.0378	0.621	43.48
110×10^3	293.15	0.0331	0.840	25.11
	298.15	0.0301	0.890	24.33
	303.15	0.0288	0.950	23.97
	308.15	0.0231	0.980	22.27
70×10^3	293.15	0.0253	1.011	19.75
	298.15	0.0232	1.015	19.18
	303.15	0.0198	1.022	18.20
	308.15	0.0184	1.031	17.76
40×10^3	293.15	0.0165	1.053	14.21
	298.15	0.0153	1.448	13.86
	303.15	0.0147	1.651	13.67
	308.15	0.0135	2.350	13.29

polymer macromolecules in FA, water, and DMSO, which, in turn, is caused by structural features of both the solvent and the dissolved macromolecules. It is known that water and formamide molecules can be bound by hydrogen bonds or dipole–dipole interactions to form associates or clusters.

Dimethyl sulfoxide is associated in the liquid phase to form clusters [9]. Since the lone electron pair of the oxygen atom of a DMSO molecule can interact with both polar (ionic compounds) and nonpolar molecules, dextran molecules are readily incorporated into the DMSO structure (the energy required for this process is lower than that for water) to form stable complexes with DMSO clusters. In this case, the size of a macromolecular coil increases and a developed intermolecular hydrogen bond network is formed. The increase in the intrinsic viscosity and root-mean-square distance between the chain ends can be due both to a decrease in the thermodynamic flexibility of a macromolecular coil and to formation of its unfolded conformation owing to formation of new polymer–DMSO intermolecular bonds.

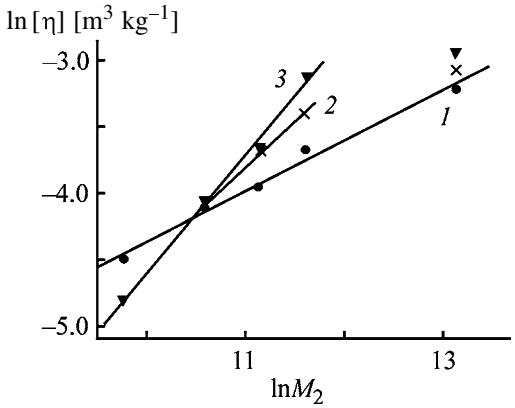

Fig. 2. Logarithm of the intrinsic viscosity [η] of dextran solutions in (*1*) water, (*2*) formamide, and (*3*) dimethyl sulfoxide at 298.15 K as a function of the logarithm of the molecular weight of dextrans M_2.

The fractal dimension [10] of the polymer in the examined solvents at different temperatures was estimated from the viscosity of solutions of dextrans with different molecular weights measured in [7] and in this study. Since the viscosity of polymer solutions is caused mainly by the factors determining the macromolecule volume in a solution, we constructed the $\ln[\eta]$–$\ln M_2$ dependences. These dependences for the dextran–water system are linear in the whole examined range of molecular weights (Fig. 2). In the case of the nonaqueous solvents, the dependence is linear at $M_2 < 110 \times 10^3$ and is not linear at higher molecular weights. The nonlinearity is probably caused by the influence of the solvent on the volume and shape of a dextran macromolecule in the solution.

The parameter α of the Mark–Kuhn–Houwink equation [5]

$$[\eta] = KM_2^{\alpha} \quad (5)$$

given in Table 3 characterizes the extent to which a macromolecule forms a coil. A decrease in parameter α for dextran macromolecules in going form aqueous to DMSO solutions suggests an increase in the penetrability of the macromolecular coil and hence higher solubility of the polymer in DMSO, which agrees well with the parameters of Flory–Huggins equation reported in [11].

It should be noted that, although dextran macromolecules are branched, they are characterized by internal order based on the scale invariance principle [10, 12] fundamental for polymer systems. This allows the scaling approach, including the concept of fractal objects, to be applied to dextrans.

The parameter α of the Mark–Kuhn–Houwink equation is related to the fractal dimension D_f by the equation [11]

$$D_f = \frac{3}{1 + \alpha}. \quad (6)$$

Hence, the fractal dimension can be determined

Table 3. Parameter α of Mark–Kuhn–Houwink equation and fractal dimension of dextrans in different solvents and at different temperatures

Solvent	T, K	α	D_f
DMSO	293.15	0.893	1.585
	298.15	0.970	1.523
	303.15	1.087	1.437
	308.15	1.223	1.350
FA	293.15	0.691	1.774
	298.15	0.672	1.794
	303.15	0.660	1.807
	308.15	0.532	1.958
H_2O	293.15	0.385	2.166
	298.15	0.392	2.156
	303.15	0.364	2.200
	308.15	0.363	2.201

from the slope of the experimental dependence $\ln[\eta] = f(\ln M_2)$ using Eq. (6). Fractal dimensions D_f of the dextrans in the examined solutions, given in Table 2, substantially differ from 3, which is typical for loose structures. It should be noted that fractal dimension D_f characterizes the structure of a polymer macromolecule in the solution rather than the initial polymer structure.

CONCLUSIONS

(1) The viscous and volume properties of solutions of dextrans with different molecular weights in different solvents were studied. The different behavior of dextrans is caused by different solvation mechanism of macromolecular chains.

(2) The fractal approach can be used to describe the dextran structure in the solutions.

ACKNOWLEDGMENTS

This study was financially supported by the Ministry of Education and Science of the Russian Federation (project no. RNP.2.2.1.1.7280) and the Russian Foundation for Basic Research (project no. 06-03-96346-r-center-a).

REFERENCES

1. Gordon, A.J. and Ford, R.A., *The Chemist's Companion. A Handbook of Practical Data, Techniques, and References*, New York: Wiley, 1972.
2. Korolev, V.V., *Zh. Fiz. Khim.*, 1989, vol. 64, no. 7, pp. 1701–1705.
3. Kolker, A.M. and Safonova, L.P., *Ionnaya sol'vatatsiya* (Ion Solvation), Krestov, G.A., Ed., Moscow: Nauka, 1987, pp. 199–226.
4. Rabek, J.F., *Experimental Methods in Polymer Chemistry. Physical Principles and Applications*, Chichester: Wiley, 1980.
5. *Cellulose and Cellulose Derivatives*, Bikales, N.M. and Segal, L., Eds., New York: Wiley, 1972, part 4. Translated under the title *Tsellyuloza i ee proizvodnye*, Moscow: Mir, 1974, vol. 1, pp. 361–382.
6. Pavlova, S.A., *Metody issledovanita tsellyulozy* (Methods for Studying Cellulose), Karlivan, V.P., Ed., Riga: Zinatne, 1981, pp. 161–191.
7. Alekseev, O.V., Rozhkova, O.V., Eliseeva, O.V., and Prusov, A.N., *Zh. Prikl. Khim.*, 2005, vol. 78, no. 6, pp. 993–996.
8. Abrosimov, V.K. and Chumakova, R.V., *Biologicheski aktivnye veshchestva v rastvorakh: struktura, termodinamika, reaktsionnaya sposobnost'* (Biologically Active Compounds in Solutions: Structure, Thermodynamics, and Reactivity), Kutepov, A.M., Ed., Moscow: Nauka, 2001, pp. 47–109.
9. Koga, Y., Kaasahara, Y., Yoshino, K., and Nishikawa, K., *J. Solution Chem.*, 2001, vol. 30, no. 10, pp. 885–893.
10. Karmanov, A.P. and Monakov, Yu.B., *Vysokomol. Soedin., Ser. B*, 1995, vol. 37, no. 2, pp. 328–331.
11. Basedov, A.M., Ebert, K.H., and Feigenbutz, W., *Macromol. Chem.*, 1980, vol. 181, no. 5, pp. 1071–1080.
12. Kozlov, G.V., Temiraev, K.B., and Mikitaev, A.K., *Izv. Vyssh. Uchebn. Zaved., Khim. Khim. Tekhnol.*, 2002, vol. 45, no. 2, pp. 30–33.

ISSN 1070-4272, Russian Journal of Applied Chemistry, 2007, Vol. 80, No. 3, pp. 486–491. © Pleiades Publishing, Ltd., 2007.
Original Russian Text © S.G. Agaev, N.S. Yakovlev, S.V. Gul'tyaev, 2007, published in Zhurnal Prikladnoi Khimii, 2007, Vol. 80, No. 3, pp. 488–495.

CHEMISTRY OF FOSSIL FUEL

Improvement of Low-Temperature Properties of Diesel Fuels

S. G. Agaev, N. S. Yakovlev, and S. V. Gul'tyaev

Tyumen State University of Oil and Gas, Tyumen, Russia

Received December 21, 2005; in final form, October 2006

Abstract—Ways to improve low-temperature properties of summer diesel fuels by introduction of depressant additives and partial dewaxing of fuels in an electrostatic field are examined. Synthesis of amidopolyformaldehyde depressant additives for diesel fuels is described, and optimal synthesis conditions are determined.

DOI: 10.1134/S1070427207030263

The demand for winter grades of diesel fuels (DFs) is met to no more than 40%. Therefore, it is necessary to expand their production [1]. One of ways to prepare winter diesel fuels is urea dewaxing of oil fractions or their dewaxing on zeolites. Dewaxing results in removal from diesel fuels of not only relatively high-melting but also (which is undesirable) of relatively low-melting *n*-paraffins. This leads to reduction of diesel fuel resources and to a noticeable decrease in their cetane numbers.

In this study we consider two ways to improve low-temperature properties of diesel fuels with complete or partial preservation of paraffin hydrocarbons: use of depressant additives and partial dewaxing in an electric field.

Various low-molecular-weight and polymeric organic compounds were suggested to decrease the congelation point of diesel fuels [2]. At the same time, production of the best depressant additives (DAs), ethylene–vinyl acetate copolymers, has not been set up in Russia because of sophisticated technology. Polycondensation depressant additives [3–5] show high performance and their production process is simpler, but the required raw materials are not produced in Russia.

In this study we examined the possibility of preparing polycondensation amidopolyformaldehyde additives from the raw materials available in Russia. The depressant additives were prepared in two steps. The first step involved condensation of stearic acid (SA) with polyethylenepolyamines (PEPAs) to prepare acid amides. These amides were then brought into condensation with formaldehyde (FA) at the reactant molar ratio SA : PEPA : FA = (2.3–3.0) : 1.0 : (0.5–25). The condensation of SA–PEPA amides with FA presumably ensures higher molecular weight and better hydrophilic–lipophilic balance of the additives, which should enhance the depressant effect at the same consumption of the additives or to decrease the amount of the additives required to attain the same depressing effect.

We used technical-grade SA, PEPA, and Formalin. Stearic acid of T-18 brand met the requirements of GOST (State Standard) 6484–96 and had the following characteristics: molecular weight 284, congelation point 64.2°C, acid number 192.7 mg KOH/g, saponification number 195.1 mg KOH/g, iodine number 11.9 g I_2/100 g, and weight fraction of unsaponifiable substances 0.48%. Formalin met the requirements of GOST 1625–89 and contained 36.6 wt % FA and 7 wt % methanol; the content of acids (counting on formic acid) was 0.01 wt %. Polyethylenepolyamines met the requirements of TU (Technical Specifications) 2413-357-00203447–99: molecular weight 144; total nitrogen, 31 wt %; tertiary amino groups, 6.6 wt %; bottoms boiling above 200°C, 69.6 wt %; fraction distilled below 75°C/1.3 kPa, traces; fraction distilled at 75–200°C/1.3 kPa, 28.9%. To prepare SA–PEPA amides in the first step, we used technical-grade diethylbenzene as an azeotropic solvent (main substance content ≥99.8 wt %; isomeric composition, %: *para* ~30, *ortho* ≤ 3.8, and *meta* the rest). Diethylbenzene met the requirements of TU 2414-040-00203772–96. The other products used for preparing depressant additives, benzene and zinc oxide, were of reagent grade; their physicochemical properties agreed with reference data.

In the first step, by condensation of SA with PEPA we prepared amides with various degrees of substitution, which were then subjected to formaldehyde condensation. SA–PEPA amides were prepared by con-

densation in a 50% diethylbenzene solution at its boiling point, 183°C. Stearic acid and PEPA form an ammonium salt soluble in diethylbenzene. Therefore, the synthesis is performed under homogeneous conditions without mechanical stirring. The first step of the synthesis is performed with a Dean–Stark trap filled with diethylbenzene, until the distillation of water released in the process is complete. Then the solvent is completely distilled off, and the condensation is continued at a temperature gradually raised from 183 to 235°C, to obtain amides with the required acid number in the melt. The synthesis of amides is performed in the presence of 0.5 wt % ZnO as catalyst (relative to the sum of the reactants without solvent). The total synthesis time is determined from the final acid number of the amides, which does not exceed 20 mg KOH/g. The synthesis of SA amides takes approximately 6–10 h.

In the second step, a calculated amount of FA in the form of 37% aqueous solution (Formalin) and 50 wt % benzene (relative to the sum of the reactants) are added to the SA amide. The formaldehyde condensation is performed at the boiling point of benzene (80°C); water released in the reaction and present in Formalin is distilled off with a Dean–Stark trap. To prevent distortions of the reactant concentrations, the trap is initially filled with benzene. The synthesis is heterogeneous. The phase contact is provided by refluxing of the reaction mixture. To avoid overheating and violent boiling of the reaction mixture in the second step, water at its boiling point is used as a heat carrier in the reactor bath. The reaction time is counted from the onset of boiling of the reaction mixture and start of the solvent circulation through the Dean–Stark trap. Water is collected in the Dean–Stark trap within 0.5 h, and the total reaction time is 2 h. After the reaction completion, the solvent is distilled off in a vacuum. The additive is obtained as a neat substance. The molar ratios of the reactants in the synthesis of the additives are given in Table 1.

The performance of the depressant additives prepared was checked with summer diesel fuel from the Achinsk oil refinery. The DA content was 0.005–1.0 wt %. The diesel fuel used had the following characteristics: congelation point –10°C, cloud point –5°C, density at 20°C 835 kg m^{-3}, viscosity at 20°C 5 $mm^2 s^{-1}$, temperature of 50% distillation 277°C, aniline point 67.5°C, and content of hydrocarbons that formed the complex with urea 6.6 wt %. The latter compounds (*n*-alkanes) consist of the following fractions (wt %): $C_{12–15}$ 45.9, $C_{16–21}$ 48.3, and C_{22} 5.8. The congelation point of DF was determined according to GOST 20287–91 on introduction of depressant additives. The results are listed in Table 1. The congelation point of the diesel fuel containing SA–PEPA amides is given in Table 1 for comparison.

Table 1 shows that amidopolyformaldehyde depressant additives are more effective than SA–PEPA amides. Thus, the additional step of formaldehyde condensation is quite useful. The maximal depression of the congelation point of the diesel fuel at 0.05 wt % content of SA–PEPA amides (run nos. 1, 13) is 6–7°C, and at the same content of amidopolyformaldehyde DAs it reaches 12–16°C (run nos. 16, 7). At 0.5–1.0 wt % content of SA–PEPA amides, the maximal depression of the congelation point is 14–17°C, and at the same content of the suggested additives it reaches 22–23°C. The positive effect at a content of amidopolyformaldehyde additives within 0.1–1.0 wt % is attained in the entire range of molar ratios tested, SA : PEPA : FA = (2.3–3.0) : 1.0 : (0.5–25) [weight ratio (4.5–6.0) : 1.0 : (0.1–4.5)]. At 0.05 wt % content of amidopolyformaldehyde additives, the depressing effect is attained in a narrower range of component ratios: molar ratio SA : PEPA : FA = (2.3–3.0) : 1.0 : (0.5–15) [weight ratio (4.5–6.0) : 1.0 : (0.1–3)]. Apparently, additional step of the formaldehyde condensation increases the molecular weight of depressant additives and improves their hydrophilic–lipophilic balance.

For a series of amidopolyformaldehyde DAs prepared at the molar ratio SA : PEPA = 2.27 : 1.0, we determined the performance with respect to the cloud point of the diesel fuel. The cloud point of DF was determined according to GOST 5066–91 at a content of depressant additives from 0.005 to 1.0 wt %. We found (Table 2) that, at a high content (0.5–1.0 wt %), the additives appreciably increase the could point of DF, and only at a content of 0.01–0.05 wt % they meet the requirements to the cloud point of winter diesel fuels. The whole set of data on the congelation and cloud points allows us to recommend for use in winter DFs the additives prepared in run nos. 4–7 at their content of 0.1 wt %. The additive from run no. 7 can also be recommended at its content of 0.05 wt %.

Like many other additives, amidopolyformaldehyde depressant additives efficiently decrease the congelation point of diesel fuels. However, the depressant additives have a significant drawback: They do not decrease the cloud point of diesel fuels.

Partial dewaxing of oils and intermediates from straw oil production in an electrostatic field of high intensity is free of this drawback. This treatment en-

Table 1. Congelation points of summer diesel fuel in the presence of amidopolyformaldehyde depressant additives

Run no.	Reactant ratio						DF congelation point, °C, at indicated DA content, wt %						
	molar			weight									
	SA	PEPA	FA	SA	PEPA	FA	0	0.005	0.01	0.05	0.1	0.5	1.0
1	2.3	1.0	–	4.5	1.0	–	–10	–16	–16	–16	–20	–24	–24
2	2.3	1.0	0.5	4.5	1.0	0.1	–10	–16	–16	–17	–25	–28	–30
3	2.3	1.0	1.0	4.5	1.0	0.2	–10	–16	–16	–17	–24	–27	–30
4	2.3	1.0	1.5	4.5	1.0	0.3	–10	–17	–17	–18	–26	–33	–32
5	2.3	1.0	2.5	4.5	1.0	0.5	–10	–18	–18	–18	–25	–29	–32
6	2.3	1.0	5	4.5	1.0	1.0	–10	–17	–17	–18	–26	–32	–33
7	2.3	1.0	7.5	4.5	1.0	1.5	–10	–17	–21	–26	–26	–30	–32
8	2.3	1.0	10	4.5	1.0	2	–10	–21	–21	–21	–21	–30	–29
9	2.3	1.0	12.5	4.5	1.0	2.5	–10	–20	–20	–20	–22	–33	–33
10	2.3	1.0	15	4.5	1.0	3	–10	–20	–20	–22	–22	–33	–32
11	2.3	1.0	20	4.5	1.0	4	–10	–15	–15	–16	–18	–28	30
12	2.3	1.0	25	4.5	1.0	4.5	–10	–14	–14	–16	–19	–27	–27
13	3.0	1.0	–	6.0	1.0	–	–10	–15	–15	–17	–21	–25	–27
14	3.0	1.0	0.5	6.0	1.0	0.1	–10	–17	–17	–19	–25	–32	–33
15	3.0	1.0	2.5	6.0	1.0	0.5	–10	–17	–17	–18	–25	–32	–33
16	3.0	1.0	5	6.0	1.0	1.0	–10	–20	–20	–22	–32	–28	–30
17	3.0	1.0	7.5	6.0	1.0	1.5	–10	–18	–21	–21	–22	–28	–29
18	3.0	1.0	10	6.0	1.0	2	–10	–15	–18	–23	–23	–28	–29

sures a decrease not only in the congelation point of petroleum products, but also in the cloud point [6–8], due to removal of the highest-melting fraction of solid hydrocarbons. Here we report the experimental data on partial dewaxing of summer diesel fuel from the Sibneft–Omsk Refinery Joint-Stock Company in an electrostatic field with the aim to prepare winter diesel fuel. The physicochemical parameters of the fuel used are given in Table 3.

Dewaxing of diesel fuel was performed in an electrostatic field in the presence of ester depressant additives; their characteristics are given in Table 4 [3–5, 9, 10]. Dewaxing of petroleum products is based on

Table 2. Cloud points of summer diesel fuel in the presence of amidopolyformaldehyde depressant additives

Run no.	DF clould point, °C, at indicated DA content, wt %					
	0	0.01	0.05	0.1	0.5	1.0
1	–5	–6	0	0	37	39
2	–5	–6	–5	2	37	38
3	–5	–5	–4	6	35	36
4	–5	–6	–4	–6	34	35
5	–5	–7	–6	–6	33	35
6	–5	–6	–6	–5	33	36
7	–5	–5	–6	–6	31	35
8	–5	–6	–6	–1	30	35
9	–5	–5	–6	–2	30	34
10	–5	–5	–4	1	30	37
11	–5	–6	–5	1	31	32
12	–5	–6	–5	2	23	28

Table 3. Physicochemical parameters of summer diesel fuel from Sibneft–Omsk Refinery Joint-Stock Company

Parameter	Value
Cloud point, °C:	–5
Congelation point, °C	–10
Density at 20°C, kg m^{-3}	838
Viscosity at 20°C, mm^2 s^{-1}	4.1
Aniline point, °C	63.8
Fractional composition, %:	
distilled at 265.5°C	50
distilled at 353.5°C	96
Content, wt %:	
n-paraffins that formed complex with urea	9.6
among them, *n*-alkanes:	
$C_{12–15}$	55.27
$C_{16–21}$	41.34
C_{22}	3.39

Table 4. Characteristics of depressant additives*

Additive**	Molar ratio of components	Percentage of active substance/ solvent	Acid number, mg KOH/g	Characteristics of 10% DA solutions in depressing oil		Melting point of active substance, °C
				viscosity at 70°C, $mm^2\ s^{-1}$	congelation point, °C	
DA-19/9PE, ester	HFA : PDA : EG = 2.0 : 1.0 : 2.0	100/0	6.9	11.1	–4	36
DA-65EPA, ester–polyamide	HFA : PDA : PEPA = 2.8 : 1.0 : 1.0	10/90	1.3	15.2	8	–
DA-20EPU, ester–polyurethane	HFA : PDA : EG : TDI = 2.0 : 1.0 : 2.0 : 1.0	50/50	12	11.4	12	–
DA-62, polyamide	SFA : PEPA = 2.1 : 1.0	100/0	8.3	15.5	45	87

* (HFA) Higher fatty alcohols of C_{10-18} fraction, (PDA) pyrromellitic dianhydride, (EG) ethylene glycol, (TDI) toluene diisocyanate, and (SFA) synthetic fatty acids of C_{21-25} fraction.
** DA-65EPA and DA-20EPU additives were prepared in the medium-viscosity oil component (420–490°C fraction).
*** Acid number for additives was determined without considering the solvent.

the effects of electrophoresis, double electrophoresis, dipolophoresis, and dielectrophoresis. The depressant additives were introduced into diesel fuel in amounts of 0.01–1.0 wt %. The mixture of the initial diesel oil and additive was heat-treated at 60–70°C until the additive completely dissolved.

Then the mixture was placed into a bronze cell for electrodewaxing. The cell was a system of coaxial electrodes. To prevent the electric breakdown, the cell bottom was made of a dielectric. The external diameter of the internal electrode was 15 mm, and the internal diameter of the external electrode, 30 mm; the height of both electrodes was 20 mm. The interelectrode spacing was 7.5 mm. The cell was placed in a temperature-controlled glass chamber equipped with a jacket through which kerosene was circulated as a cooling agent. The temperature-controlled cell had a glass lid. The glass chamber and lid had a hermetic grond-glass joint. Cold kerosene with a temperature no higher than –17 to –18°C was fed to the jacket from a Lauda E 100 low-temperature cryostat with a remote supply of the coolant. Double thermostating was used to prevent icing of the glass chamber. For this purpose, the glass chamber was placed into a Freon temperature-controlled air condenser with a temperature from –5 to –10°C. The cell with the petroleum product was cooled to a dewaxing temperature of –15°C. The required temperature inside the glass chamber was maintained with an accuracy of ±1°C and was monitored with a thermometer. The bronze cell was connected to a VS-20-10 rectifier. The additive imparted an electrokinetic potential to crystals of paraffin hydrocarbons formed at the dewaxing temperature. At an electric field intensity of 10000 V cm^{-1}, the paraffin hydrocarbons were separated from the petroleum products, forming a dense deposit on the electrodes, and the partially dewaxed diesel fuel remained in the interelectrode space. The electric treatment time was 60 min.

The efficiency of dewaxing of petroleum products was evaluated by the yield of the dewaxed diesel fuel, by a decrease in the congelation point of the dewaxed diesel fuel (congelation point depression) relative to that of the initial fuel without additive, and by a decrease in the cloud point of the dewaxed diesel fuel (cloud point depression) relative to that of the initial fuel without additive.

Data on the electrodewaxing of diesel fuel, given in Table 5, show that, in the presence of all depressant additives, the summer diesel fuel from the Sibneft–Omsk Refinery Joint-Stock Company is capable of dewaxing in an electric field. An exception is the DA-20EPU additive at its content in the initial DF of 0.5–1.0 wt %. The yield of dewaxed diesel fuel (DDF) as a function of the content of additives passes through a maximum. With an increase in the content of additives in DF, the DDF yield first increases and then, after reaching a maximum, starts to decrease. The latter trend is caused by adsorption saturation of the surface of paraffin crystals with the molecules of the additive and by passing of excess additive into the solution. In the process, the electrokinetic potential of paraffin particles decreases [11].

Table 5. Electrodewaxing of summer diesel fuel in the presence of depressant additives. Dewaxing temperature –15°C, mean electric field intensity 10 kV cm^{-1}, deposition time 1 h; time of cooling of the initial DF with the additive from room temperature to dewaxing temperature 60 min, time of electric treatment 60 min

DA	[DA], wt %	Yield, wt %			Deposit charge sign	Congelation point of DF, °C			Cloud point of DF, °C			ΔT,* °C
		DDF	paraffin	loss		initial	dewaxed	depression	initial	dewaxed	depression	
–	–	68.1	29.9	2.0	+ –**	–10	–20	10	–5	–10	5	–5
DA-19/9PE	0.01	82.3	11.1	6.6	+	–18	–23	13	–7	–15	10	0
	0.05	91.2	7.1	1.7	+	–23	–30	20	–10	–15	10	0
	0.1	85.2	4.0	10.8	+	–29	–30	20	–8	–13	8	–2
	0.5	86.5	7.7	5.8	+	–37	–36	26	–11	–15	10	0
	1.0	89.3	4.0	6.7	+	–15	–36	26	–11	–15	10	0
DA-65EPA	0.01	87.2	10.2	2.6	+	–12	–24	14	–6	–12	7	–3
	0.05	89.6	8.1	2.3	–	–21	–26	16	–8	–10	5	–5
	0.1	88.1	11.1	0.8	–	–24	–36	26	–9	–14	9	–1
	0.5	89.6	7.9	2.5	+ –	–43***	–40***	>30	–11	–11	6	–4
	1.0	94.5	4.0	1.5	+ –	–32	–42***	>32	–11	–11	6	–4
DA-20EPU	0.01	87.1	11.7	1.2	+ –	–22	–26	16	–7	–12	7	–3
	0.05	89.1	5.7	5.2	–	–26	–31	21	–8	–10	5	–5
	0.1	96.1	2.5	1.4	–	–27	–28	18	–8	–9	4	–6
	0.5	No phase separation****				–28	–	–	–12	–	–	–
	1.0	No phase separation****				–40***	–	–	–13	–	–	–
DA-62	0.01	59.8	38.1	2.0	+ –	–15	–18	8	–7	–13	8	–2
	0.05	85.8	12.8	1.4	+ –	–14	–22	12	–7	–14	9	–1
	0.1	89.7	6.4	3.9	+ –	–15	–22	12	–7	–15	10	0
	0.5	80.5	17.0	2.5	+ –	–12	–18	8	+8	–14	9	–1
	1.0	52.0	42.4	5.6	+	–13	–20	10	+8	–15	10	0

* Temperature effect of dewaxing.
** (+ –) Deposition of paraffin on both electrodes.
*** Congelation point below the indicated value (is not attained with the available equipment).
**** No deposition of paraffin.

Dewaxing of the initial diesel fuel also occurs without additives. However, deposition of paraffin hydrocarbons occus on both electrodes (double electrophoresis effect). The yield of dewaxed DF is as low as 68.1 wt %. On adding DA-19/9PE and DA-20EPU additives, the paraffin crystals acquire stable positive and negative electrokinetic potential, respectively. The DA-65EPA additive also imparts a negative electrokinetic potential to crystals of paraffin hydrocarbons, but this potential is unstable and is readily lost; at a higher content of the additive, the paraffin crystals pass into the isoelectric state (double electrophoresis).

The DA-62 additive at its high content also imparts a positive electrokinetic potential to paraffin crystals. Irrespective of the existence of any kind of electrokinetic potential of paraffin crystals, introduction of additives increases the yield of the dewaxed diesel fuel. This is apparently due to a decrease in the congelation point of the initial diesel fuel in the presence of additives, i.e., to a decrease in their structural viscosity. Less viscous fuels are more readily separated into the solid and liquid phases in the electric field. The dewaxing of diesel fuel is particularly efficient when a stable electrokinetic potential is combined with the relatively strong depression of the congelation point on introducing a depressant additive. Such a pattern is observed with DA-19/9PE, DA-65EPA, and DA-20EPU additives. A decrease in the cloud point of the diesel fuel on introducing a depressant additive is undesirable for the dewaxing in an electric field. This negative effect is observed with DA-20EPU additive at its content of 0.5–1.0 wt %. In this case, the cloud point of DF decreases virtually to the level of the dewaxing temperature, and the process becomes inefficient because of the absence of the solid phase in the system.

Apparently, to characterize the dewaxing of diesel fuels, by analogy with low-temperature dewaxing of oils in selective solvents, it is appropriate to introduce

the parameter TED (temperature effect of dewaxing), namely, the difference between the dewaxing temperature and the attained cloud point of the dewaxed diesel fuel. With respect to this parameter, dewaxing of the initial diesel fuel is the most efficient in the presence of DA-19/9PE and DA-62. In this case, TED is close to zero, i.e., overcooling of the raw material is not required to attain the preset cloud point. Negative TED values are observed with diesel fuels containing DA-65EPA and DA-20EPU additives, because of relatively low cloud point of DF in the presence of these additives and unstable electrokinetic potential.

Our results show that the dewaxed diesel fuel prepared in the presence of DA-19/9PE additive (Table 5) meets requirements to DZp winter diesel fuel (TU 38.101 889–00) with respect to two parameters: cloud point (required –5°C, actually –15°C) and congelation point (required –25°C, actually –30°C). The limiting filterability temperature for DZp fuel should not exceed –15°C, and, most probably, the dewaxed diesel fuel with a cloud point of –15°C will meet this requirement also. The properties of the dewaxed fuels prepared in the presence of DA-62 additive (Table 5) are also close to those prescribed by the above TU. Only the congelation point slightly exceeds the prescribed level, but it can be readily brought to this level by additional introduction into the dewaxed diesel fuel of any of three effective additives: DA-19/9PE, DA-65EPA, or DA-20EPU. With respect to the combination of DDF yield and quality parameters, it can be recommended to take in dewaxing the DA-19/9PE additive in an amount of 0.1–1.0 wt %, or the DA-62 additive in an amount of 0.05–1.0 wt % with the subsequent introduction of, e.g., DA-19/9PE additive.

CONCLUSIONS

(1) The possibility of dewaxing of diesel fuels in a high-intensity electric field in the presence of depressant additives DA-19/9PE and DA-62 was examined. Under the optimal conditions, it is possible to prepare DZp winter diesel fuel meeting the requirements of TU 38.101 889–00 from summer diesel fuel produced by Sibneft–Omsk Refinery Joint-Stock Company.

(2) Among the suggested procedures for improving low-temperature properties of diesel fuel, the best is dewaxing of diesel fuel in an electric field. The thus treated fuel meets the requirements of TU 38.101 889–00) with respect to both congelation point and cloud point, although the process requires more sophisticated equipment compared to simple introduction of an additive.

REFERENCES

1. Kaminskii, E.F. and Khavkin, V.A., *Glubokaya pererabotka nefti: tekhnologicheskii i ekologicheskii aspekty* (Deep Processing of Oil: Technological and Environmental Aspects), Moscow: Tekhnika, 2001.
2. Terteryan, R.A., *Depressornye prisadki k neftyam, toplivam i maslam* (Depressant Additives to Crude Oils, Fuels, and Oils), Moscow: Khimiya, 1990.
3. RF Patent 2 181 136.
4. RF Patent 2 183 657.
5. RF Patent 2 208 042.
6. Agaev, S.G. and Savchenkov, A.L., *Zh. Prikl. Khim.*, 1994, vol. 67, no. 7, pp. 1148–1151.
7. Agaev, S.G. and Khalin, A.N., *Khim. Tekhnol. Topl. Masel*, 2001, no. 3, pp. 38–42.
8. RF Patent 2 106 390.
9. Agaev, S.G. and Khalin, A.N., *Zh. Prikl. Khim.*, 1997, vol. 70, no. 11, pp. 1893–1896.
10. Agaev, S.G. and Glazunov, A.M., *Neftepererab. Neftekhim.*, 2001, no. 10, pp. 32–36.
11. Savchenkov, A.L. and Agaev, S.G., *Khim. Tekhnol. Topl. Masel*, 1991, no. 5, pp. 29–30.

ISSN 1070-4272, Russian Journal of Applied Chemistry, 2007, Vol. 80, No. 3, pp. 492–494. © Pleiades Publishing, Ltd., 2007.
Original Russian Text © T.N. Khamaganova, A.E. Sarapulova, K.N. Fedorov, 2007, published in Zhurnal Prikladnoi Khimii, 2007, Vol. 80, No. 3, pp. 496–498.

BRIEF COMMUNICATIONS

Synthesis and Electrical Properties of Double Borates $Ba_3R(BO_3)_3$, R = Ho, Yb, Sc

T. N. Khamaganova, A. E. Sarapulova, and K. N. Fedorov

Baikal Institute of Nature Management, Siberian Division, Russian Academy of Sciences, Ulan-Ude, Buryatia, Russia

Received December 26, 2006

Abstract—Polycrystalline samples of double barium borates of the composition $Ba_3R(BO_3)_3$, R = Ho, Yb, Sc, were synthesized by the method of solid-phase reactions. The temperature dependence of the electrical conductivity of the compounds obtained was studied at 200–500°C.

DOI: 10.1134/S1070427207030275

The development of modern fields of technology is impossible without directed synthesis and study of materials possessing a set of necessary physicochemical properties. To materials of this kind belong double borates of rare-earth elements of composition $Ba_3R(BO_3)_3$, whose specific structure results in that they show promise as nonlinear optical, ferroelectric, and pyroelectric materials. Crystals of barium ytterbium borate $Ba_3Yb(BO_3)_3$ have been grown and its crystal structure has been determined [1]. The compound crystallizes in the hexagonal crystal system (space group $P6_3cm$). The double borates $Ba_3R(BO_3)_3$, R = Ho, Yb, Sc, belong to the same structural type [2–4]. Their structure has the form of a 3D framework formed by networks of nine-vertex barium polyhedra that alternate in the (001) plane and are connected by six-vertex rare-earth polyhedra and BO_3 groups (Fig. 1).

A study of the temperature dependence of second optical harmonic generation (SHG) in the borates $Ba_3R(BO_3)_3$ for R = Y and Ho–Lu [5] demonstrated occurrence of reversible phase transitions to the state with axial symmetry. In the low-temperature phase,

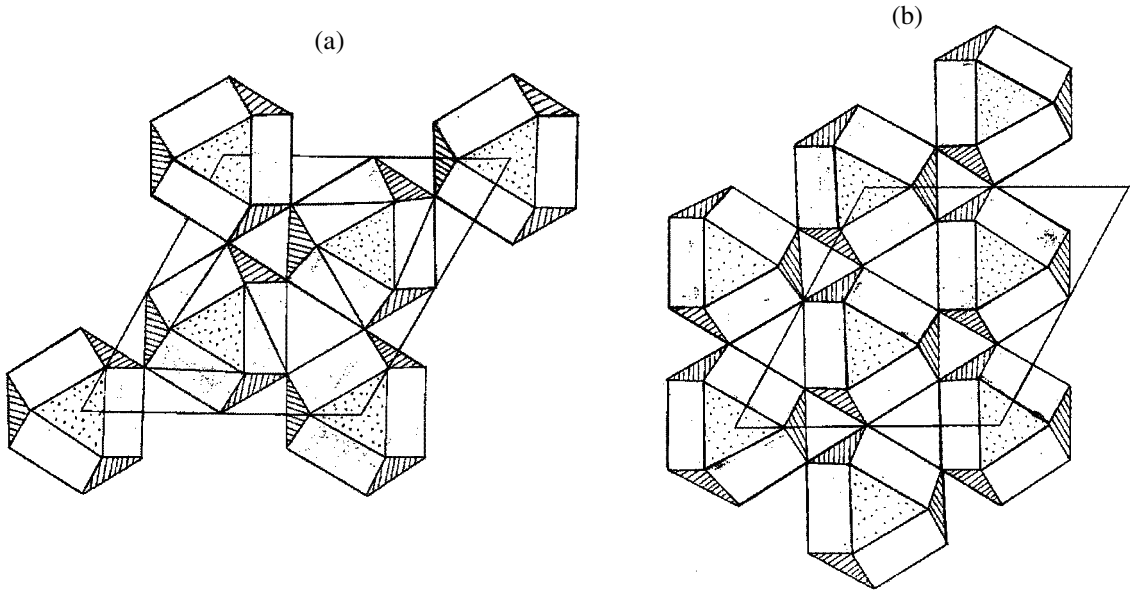

Fig. 1. Projection of the structure of $Ba_3Yb(BO_3)_4$ onto the (001) plane at a height of (a) 0.125 and (b) 0.250.

these compounds show optical nonlinearity, whose magnitude increases as the radius of a rare-earth element becomes smaller. A study by the SHG method makes it possible to relate the double borate $Ba_3Yb(BO_3)_3$ to new optical materials of B grade [6]. The pyroelectric coefficient measured on a single crystal of this compound [7], combined with the occurrence of a first-kind phase transition, indicates that it possesses ferroelectric properties.

The aim of this study was to synthesize and study the conductivity of the double borates $Ba_3R(BO_3)_3$, R = Ho, Yb, Sc.

The following compounds were used as starting reagents: barium carbonate of analytically pure grade; strontium carbonate of ultrapure grde; holmium, ytterbium, and scandium oxides with no less than 99.99% of the main component; and boric acid of chemically pure grade. Rare-earth oxides were preliminarily calcined at 850°C for 5–6 h, and the carbonates, at 400°C. Polycrystalline samples were synthesized by the method of solid-phase reactions in platinum crucibles in air at 600–1000°C. The attainment of equilibrium was monitored by measuring X-ray powder diffraction patterns on DRON-UM1 (CuK_α radiation) and Bruker D-8 Advance (CuK_α radiation, graphite monochromator, 2θ angles 10°–60°, 0.02° step mode) diffractometers.

The temperature dependences of the electrical conductivity σ, dielectric constant ε, and dielectric loss tanδ were studied by the polarization method of Vest and Tallan [8]. Dense ceramic samples in the form of pellets 10 mm in diameter and 1–1.5 mm thick were used for measurements. Electrodes were deposited by firing-in a platinum paste. The measurements were made with an E8-4 ac bridge at a frequency of 10^3 Hz, with an R-5025 capacitor box (determination accuracy ±5%). The dc current was recorded with an E6-13A teraohmmeter at a voltage set to 30–50 mV.

A phase analysis of samples annealed at 1000°C demonstrated that they do not contain the starting oxides of lanthanides and scandium, barium borates, and rare-earth borates. The X-ray diffraction patterns measured on a D-8 Advance diffractometer (Fig. 2) were identified using unit cell parameters of the $Ba_3Yb(BO_3)_3$ single crystal [1].

The temperature dependence of the electrical conductivity of $Ba_3R(BO_3)_3$ was studied in the range 200–500°C (Fig. 3). The experimental values of the activation energy of conductivity, E_a, and electrical conductivity σ for the double borates of this composition are listed in the table. An analysis of the electronic transport numbers t_e at various temperatures demonstrated that the samples have, in the temperature range under study, a mixed ionic-electronic conduction, with predominance of the electronic component. The result obtained is in agreement with the previously determined value of the electrical conductivity

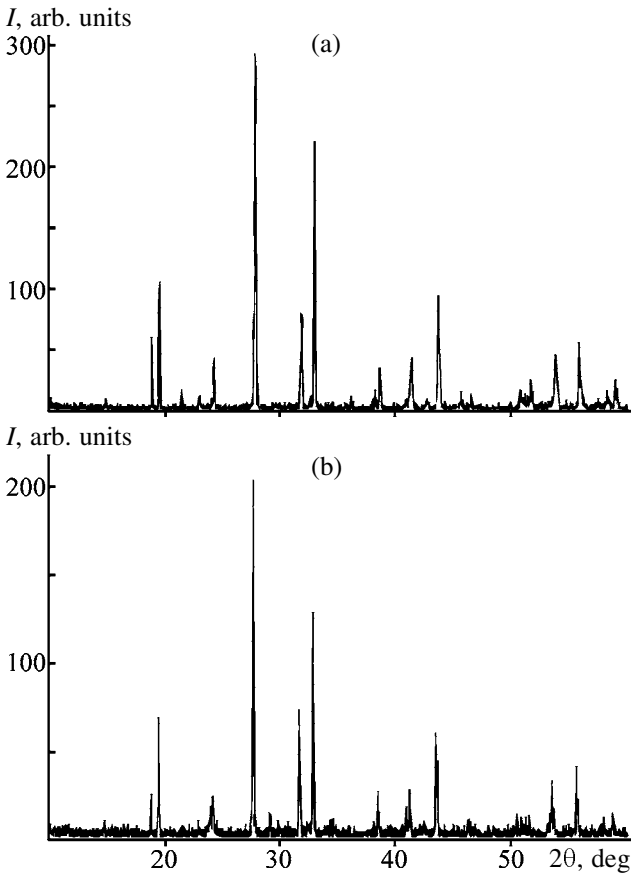

Fig. 2. X-ray diffraction patterns of double borates (a) $Ba_3Yb(BO_3)_3$ and (b) $Ba_3Ho(BO_3)_3$. (*I*) Intensity and (2θ) Bragg angle.

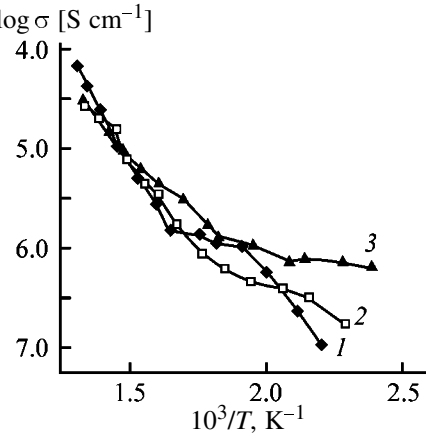

Fig. 3. Temperature dependence of the electrical conductivity σ of $Ba_3R(BO_3)_3$, where R = (*1*) Ho, (*2*) Sc, and (*3*) Yb.

Electrical conductivity σ and activation energy of conductivity of the double borates $Ba_3R(BO_3)_3$

R	σ, S cm^{-1}	E_a, eV
Ho	1.1×10^{-5}	0.2
Yb	6.5×10^{-6}	0.2
Sc	4.3×10^{-6}	0.3

of the $Ba_3Yb(BO_3)_3$ single crystal, 10^{-12} Ω mm^{-1}, measured with an R 4059 dc bridge [7].

CONCLUSIONS

(1) The method of solid-phase reactions was used to produce double borates $Ba_3R(BO_3)_3$, R = Ho, Yb, Sc from the starting oxides, barium carbonate, and boric acid.

(2) An X-ray phase analysis demonstrated that the compounds obtained are isostructural and crystallize in the hexagonal crystal system.

(3) A study of the temperature dependence of the electrical conductivity demonstrated that the double borates show a mixed ionic-electronic conduction, with predominance of the electronic component.

REFERENCES

1. Khamaganova, T.N., *Cand. Sci. Dissertation*, Moscow, 1990.
2. Khamaganova, T.N., Trunov, V.K., and Makarevich, L.G., *Zh. Neorg. Khim.*, 1993, vol. 38, no. 12, pp. 1792–1793.
3. Ilyukhin, A.B. and Dzhurinskii, B.F., *Zh. Neorg. Khim.*, 1993, vol. 38, no. 10, pp. 1625–1630.
4. Khamaganova, T.N. and Khrushcheva, N.M., *Zh. Prikl. Khim.*, 2005, vol. 78, no. 1, pp. 25–27.
5. Stefanovich, S.Yu. and Khamaganova, T.N., *Neorg. Mater.*, 2002, vol. 38, no. 1, pp. 78–80.
6. Kurtz, S.K. and Perry, T.T., *J. Appl. Phys.*, 1968, vol. 39, no. 8, pp. 3798–3813.
7. Khamaganova, T.N. and Trunov, V.K., *Zh. Neorg. Khim.*, 1997, vol. 42, no. 1, pp. 26–28.
8. Vest, R.W. and Tallan, N.M., *J. Appl. Phys.*, 1965, vol. 36, no. 2, pp. 547–552.

ISSN 1070-4272, Russian Journal of Applied Chemistry, 2007, Vol. 80, No. 3, pp. 495–497. © Pleiades Publishing, Ltd., 2007.
Original Russian Text © N.F. Fedorov, M.A. Andreev, 2007, published in Zhurnal Prikladnoi Khimii, 2007, Vol. 80, No. 3, pp. 499–501.

BRIEF COMMUNICATIONS

Specific Features of Thermal Dissociation of Magnesite in Calcination in Furnaces with a Solid Metallic Heat-Transfer Agent

N. F. Fedorov and M. A. Andreev

St. Petersburg State Institute of Technology (Technical University), St. Petersburg, Russia

Received April 4, 2006; in final form, September 2006

Abstract—The kinetics of thermal decomposition of magnesite in a furnace in which the gaseous heat-transfer agent is replaced with a solid metallic heat-transfer element was studied.

DOI: 10.1134/S1070427207030287

Decarbonation processes are the most energy-consuming stage of thermal treatment in manufacture of technical products, such as lime, portland cement, caustic magnesite, and caustic dolomite. In the conventional firing technology, raw materials are decomposed in rotary kilns by the energy of flue gases. It has been suggested [1–4] to intensify the thermal decomposition of the material by using a liquid metallic heat-transfer agent, which provides a thermal-shock action on a material being fired. However, this solution involves a number of negative factors, the main of which are the complicated choice and high cost of the liquid metallic heat-transfer agent, intricate apparatus and stringent requirement to this equipment, contamination with the heat-transfer agent of the material being treated, and loss of the heat-transfer agent with a porous material.

All these factors preclude wide industrial use of liquid heat-transfer agents and require that alternative modes of heat treatment by thermal shock should be sought for. A possible solution is replacement of a liquid metallic heat-transfer agent with a solid one. Even though the coefficient of heat transfer from a solid metal to a material being processed is inferior to that in transfer of thermal energy from a molten metal to a solid substance, the former is still sufficiently high and markedly exceeds that for a gaseous heat-transfer agent. This is the principal factor responsible for the acceleration of solid-phase transformations. In addition, the possibility of using induction heating, which is known to provide the highest efficiency in conversion of electric energy into heat, counts in favor of the solid metallic heat-transfer agent. Finally, it is necessary to take into account the fact that replacement of a liquid metallic heat-transfer agent with a solid one shows promise of a less intricate equipment of the firing device.

In view of the aforesaid, it seems appropriate to study thermal decomposition of inorganic substances under conditions of a thermal shock produced when a material to be thermally treated is brought in contact with a solid metal heated to a prescribed temperature.

We consider the process of magnesite decomposition by thermal-shock calcination to magnesium oxide, whose application area includes such branches of chemical industry as technology of building materials, refractories, binders, and materials for electronics and electrical engineering, medicine, and cosmetology [5, 6].

We used magnesite of composition (wt %) SiO_2 1.5, CaO 0.49, MgO 46.14, R_2O_3 1.27, and calcination loss 50.60, from the Savinskoe deposit. The dependence of the degree of decomposition of magnesite on its residence time in the furnace and on the calcination temperature was studied. The starting magnesite was placed, in the form of 3–5-mm lumps, to produce a monolayer on the metallic heat-transfer agent heated to the temperature of the experiment and was kept there for a prescribed time. The temperature range 700–900°C was studied. In parallel, we performed thermal treatment with a gaseous heat-transfer agent, for which purpose a sample was placed in a heated muffle surface. For the calcined material, we evaluated the degree of conversion by measuring the calcination loss (900°C, 1 h).

Figure 1a shows kinetic curves of thermal decomposition of magnesite at various temperatures on a

Kinetic parameters and apparent activation energy at different temperatures and magnesite decomposition conditions

Heat-transfer agent	700°C		800°C		900°C		E, kJ mol^{-1}
	$K \times 10^3$	n	$K \times 10^3$	n	$K \times 10^3$	n	
Solid metallic	25.81	1.89	78.23	2.33	96.93	1.95	22.4
Gaseous	4.28	1.48	6.60	1.58	10.35	1.69	47.1

solid heat-transfer agent, and Fig. 1b, those for calcination by the conventional scheme with a gaseous heat-transfer agent. It can be seen that the decomposition in air and that in the installation with a solid metallic heat-transfer agent show a pronounced difference, which consists in that there is no induction period on the metallic heat-transfer agent. The times in which nearly 100% degree of decomposition is reached are also different. This time was 10 and 2.5 min for, respectively, the gaseous and metallic heat-transfer agents at 700°C, and 5 and 1 min at 900°C.

To find the kinetic parameter of magnesite decarbonation, we processed the experimental data with the use of the Erofeev equation [7]:

$$\alpha = 1 - \exp(-kt^n),$$

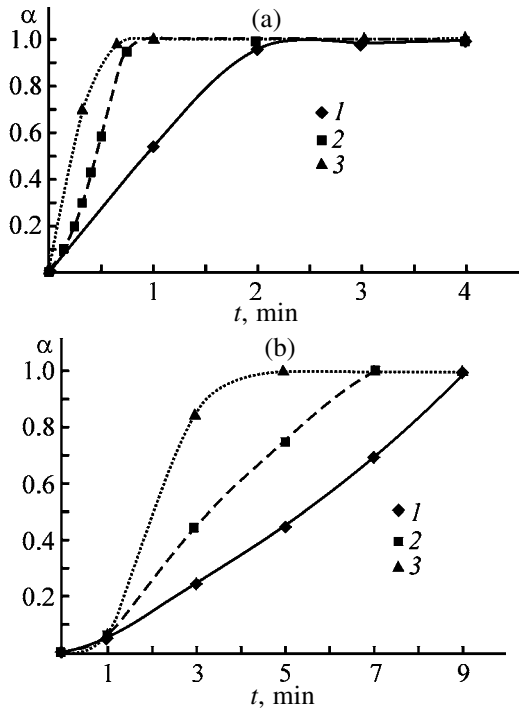

Fig. 1. Degree of magnesite decomposition, α, with (a) solid metallic heat-transfer agent and (b) gaseous heat-transfer agent vs. time t. Temperature, °C: (*1*) 700, (*2*) 800, and (*3*) 900.

where α is the degree of decomposition (fraction units); k, kinetic parameter of the reaction rate; n, parameter dependent on the reaction mechanism, nucleation rate, and nucleus configuration; and t, time elapsed from the beginning of the reaction (s).

Comparison of values of the kinetic parameter k for reactions carried out in different conditions is hindered by the necessity for taking into account the variation of both k and n. Sakovich [8] suggested to use the reduced reaction rate constant related to the constants k and n by $K = nk^{1/n}$, with K having the dimension of t^{-1}, which corresponds to the dimension of the rate constant of a monomolecular reaction. The table lists values of the kinetic parameter n, reduced rate constant K (s^{-1}), and apparent activation energy E found in terms of the Arrhenius equation.

The table shows that the reaction rate constant K is higher in calcination of magnesite with a solid metallic heat-transfer agent, compared with the conventional process. This is due to the acceleration of the heat supply to the material from the metallic heat-transfer agent. Simultaneously with an increase in K, we observe a rise in the parameter n, whose value provides information about nucleation processes [9, 10]. In the given case, we can assume that the rise in n is due to an increase in the nucleation rate because of the growing number of defects of the crystal structure, generated by abrupt heating (thermal shock).

Below are presented values of the specific surface area of magnesite calcined at 800°C with a solid metallic heat-transfer agent at different thermal treatment times:

Calcination time, s	15	40	90
Degree of $MgCO_3$ decomposition	0.15	0.70	1.00
Specific surface area, m^2 g^{-1}	10	30	95

The specific surface area increases with the exposure time, and thermal decomposition under thermal-shock conditions gives a product with a highly developed specific surface area, which is rather im-

portant for use of MgO as a component of binders and fillers.

The data obtained indicate that it is worthwhile to replace the gaseous heat-transfer agent with a solid metallic one and to develop furnace apparatus with a solid metallic heat-transfer agent for calcination of magnesite and other carbonates.

CONCLUSIONS

(1) It was found that the time of thermal decomposition of magnesite becomes considerably shorter (by a factor of 5–7) in the case of calcination in a furnace with a solid metallic heat-transfer agent, compared with thermal treatment in the gas phase.

(2) Kinetic parameters of $MgCO_3$ decomposition under the conditions studied were determined. It was found that the rate constant K varies from 25.8×10^{-3} to 96.9×10^{-3} s^{-1} and the activation energy is 22.4 kJ mol^{-1}.

(3) It was experimentally demonstrated that thermal decomposition of magnesite under thermal-shock conditions yields magnesium oxide with a highly developed specific surface area, up to 95 $m^2 g^{-1}$.

ACKNOWLEDGMENTS

The study was financially supported by Sibirskie Poroshki (Siberian Powders) Limited Liability Company.

REFERENCES

1. Fedorov, N.F., Gavrilov, A.P., and Kuzyak, V.A., in *Khimiya i tekhnologiya vyazhushchikh veshchestv, silikatnykh i neorganicheskikh materialov: Mezhvuzovskii sbornik* (Chemistry and Technology of Binders and Silicate and Inorganic Materials: Intercollegiate Coll. of Works), Leningrad, 1977, p. 33.
2. Gavrilov, A.P., Ivanov, N.I., and Stepovaya, N.M., in *Khimiya i tekhnologiya vyazhushchikh veshchestv, silikatnykh i neorganicheskikh materialov: Mezhvuzovskii sbornik* (Chemistry and Technology of Binders and Silicate and Inorganic Materials: Intercollegiate Coll. of Works), Leningrad, 1977, p. 77.
3. Ivanov, N.I., A Study of High-Temperature Synthesis of Clinker Materials in Metallic Melts and Development of Technological Principles of Calcination of Portland Cement and Other Oxide Materials in a Reactor with a Metallic Heat-Transfer Agent, *Cand. Sci. Dissertation*, Leningrad, 1981.
4. Fedorov, N.F. Gavrilov, A.P. Ivanov, N.I., et al., *Energet. Stroit.*, 1992, no. 5, pp. 15–18.
5. Kainarskii, I.S. and Degtyareva, E.V., *Osnovnye ogneupory* (Main Refractories), Moscow: Metallurgiya, 1974, p. 202.
6. Butt, Yu.M., Sychev, M.M., and Timashev, V.V., *Khimicheskaya tekhnologiya vyazhushchikh materialov: Uchebnik dlya vuzov* (Chemical Technology of Binders: Textbook for Higher School), Timashev, V.V., Ed., Moscow: Vysshaya Shkola, 1980.
7. Erofeev, B.E., *Dokl. Akad. Nauk SSSR*, 1946, vol. 52, no. 6, p. 515.
8. Sakovich, V.G., *Uchen. Zap. Tomsk. Gos. Univ., Khim.*, 1955, vol. 26, p. 103.
9. *Comprehensive Chemical Kinetics*, Bamford, C.H. and Tipper, C.F.H., Eds., vol. 22: Brown, M.E., Dollimore, D., and Galwey, A.K., *Reactions in the Solid State*, Amsterdam: Elsevier, 1980.
10. Chechetkin, A.V., *Vysokotemperaturnye teplonositeli* (High-Temperature Heat-Transfer Agents), Moscow: Gosenergoizdat, 1992.

ISSN 1070-4272, Russian Journal of Applied Chemistry, 2007, Vol. 80, No. 3, pp. 498–500. © Pleiades Publishing, Ltd., 2007.
Original Russian Text © V.A. Patrikeev, M.L. Pavlov, B.I. Kutepov, R.A. Makhamatkhanov, O.S. Travkina, A.L. Shestopal, U.M. Dzhemilev, 2007, published in Zhurnal Prikladnoi Khimii, 2007, Vol. 80, No. 3, pp. 502–504.

BRIEF COMMUNICATIONS

Crystallization of X-Type Zeolite from Concentrated Sodium Silicate and Aluminate Solutions

V. A. Patrikeev, M. L. Pavlov, B. I. Kutepov, R. A. Makhamatkhanov, O. S. Travkina, A. L. Shestopal, and U. M. Dzhemilev

Institute of Petrochemistry and Catalysis, Russian Academy of Sciences, Ufa, Bashkortostan, Russia

Received April 7, 2006; in final form, September 2006

Abstract—Crystallization of an X-type zeolite from concentrated solutions of sodium aluminate (Al_2O_3 90–330 g l^{-1}) and silicate (SiO_2 110–180 g l^{-1}) was studied.

DOI: 10.1134/S1070427207030299

Methods for synthesis of powdered X-type zeolites, used to prepare adsorbents for dehydration and purification of various media, have been described in detail [1–6]. In these studies, X-type zeolites were synthesized by mixing solutions of sodium aluminate and silicate, with the concentrations of Al_2O_3 and SiO_2 equal to 70–90 and 80–110 g l^{-1}, respectively. An X-ray-amorphous colloid seed is added to the resulting silica–alumina hydrogel, and the reaction mixture is crystallized at low temperatures (<100°C) in the course of 12–16 h.

It was noted in [1] that an increase in the concentration of crystal-forming solutions should make higher the crystallization rate and dispersity of the forming zeolite crystals and improve its yield per unit reaction volume. However, crystallization of X-type zeolites from sodium aluminate and silicate solutions with concentrations exceeding those mentioned above has not been described in the literature.

This paper concerns crystallization of X-type zeolite from concentrated sodium aluminate and silicate solutions.

EXPERIMENTAL

Silica–alumina hydrogels were prepared by mixing in varied order calculated amounts of solutions of sodium aluminate, silicate, and hydroxide. Sodium aluminate solutions with a concentration of 90–330 g l^{-1} in terms of aluminum oxide and $NaOH/Al_2O_3$ molar ratio of 1.5–2.0 were used as raw materials for preparing silica–alumina hydrogels that can crystallize to give a highly dispersed NaX zeolite. Sodium silicate solutions with a concentration of 110–180 g l^{-1} in terms of silicon oxide and SiO_2/Na_2O molar ratio of 2.6–3.0 served as the silicate component.

The reaction mixtures from which the highly dispersed NaX zeolite was crystallized were prepared using 2.5–3.5 vol % X-ray amorphous colloid seeds preliminarily precipitated and aged (keeping at T = 20–35°C for 4–18 h). The chemical composition of the seeds corresponded to the formula $12.7Na_2O \cdot Al_2O_3 \cdot 12.0SiO_2 \cdot 220H_2O$. The NaX zeolite was crystallized from reaction mixtures of composition $(2.8–3.5)Na_2O \cdot Al_2O_3 \cdot (3.0–5.1)SiO_2 \cdot (75–170)H_2O$.

When studying how the order in which gel-forming solutions and the colloid seed are mixed affects the dispersion composition of the zeolite, the seed was introduced after all the solutions were combined (Table 1, sample nos. 1, 3, 5, 7, 9) or preliminarily, into the sodium silicate solution (Table 1, sample nos. 2, 4, 6, 8, 10). To obtain a chemically homogeneous silica–alumina hydrogel, the gel-forming solutions were mixed under continuous agitation of the reaction mass. The agitation was continued for 10–30 min after the solutions were discharged. The mixtures were crystallized at 98°C in the course of various intervals of time until a phase-pure X-type zeolite was obtained.

The samples synthesized were washed to remove impurities, dried at 150°C for 3 h, and then calcined at 540°C in air for 4 h. The chemical composition of the liquid and solid phases was determined by methods described in [7]. The phase composition of powder samples was determined by X-ray diffraction analysis on a Philips PW-1800 automated diffractometer. The X-ray diffraction patterns were identified using the known diffraction data [1].

Table 1. Dispersion composition and yield of X-type zeolite in relation to the concentration and order of mixing of gel-forming solutions with X-ray amorphous colloid seed (3 vol %)*

Sample no.**	Concentration of the starting solution, g l^{-1}		Crystallization time, h, at 98°C	Yield of zeolite per unit volume, g l^{-1}	Content of crystals and their aggregations, wt %				
	SiO_2	Al_2O_3			<30 μm	<10 μm	<8 μm	<4 μm	<2 μm
1	90	70	12	90	86.2	34.6	25.0	10.0	2.7
2	90	70	10	90	94.7	58.4	37.9	25.1	13.6
3	90	200	8	125	100	94.2	80.6	31.2	10.0
4	90	200	7	125	100	96.8	83.8	48.6	22.1
5	110	250	6	160	100	97.2	85.0	35.6	14.2
6	110	250	5	160	100	98.2	91.0	55.6	28.2
7	140	250	3	185	100	98.0	86.4	36.8	16.0
8	140	250	2.5	185	100	99.0	92.4	56.8	30.0
9	140	300	2.0	200	100	100	92.7	44.1	21.0
10	140	300	1.5	200	100	100	100	62.9	34.1

* Composition of the silica–alumina hydrogel $3.0Na_2O \cdot Al_2O_3 \cdot 3.2SiO_2 \cdot N_{1-5}H_2O$; sample nos. 1 and 2, N_1 = 170; nos. 3 and 4, N_2 = 145; nos. 5 and 6, N_3 = 115; nos. 7 and 8, N_4 = 95; nos. 9 and 10, N_5 = 75.

** According to XPA data, the content of the X-type zeolite is close to 100% in all the samples.

The dispersion composition of the zeolites was determined by sedimentation analysis. The adsorption properties of the samples obtained were evaluated by the adsorption capacity for vapors of water and benzene [8].

Table 1 lists the results of syntheses, which show how the concentration of gel-forming solutions and the order of their mixing with the colloid seed affect the duration of crystallization, yield, and dispersion composition of the X-type zeolite.

The method of sedimentation analysis revealed that, irrespective of the way in which the seed is introduced into the reaction mixture, the size of separate crystals in the high-phase-purity X-type zeolites synthesized is 1–2 μm. At the same time, particles as large as 20–30 μm were found in some samples, which are presumably aggregations of crystals. The number and size of the aggregations formed on introducing the seed into the sodium silicate solution are considerably smaller (Table 1, sample nos. 2, 4, 6, 8, 10) than those obtained when the seed was introduced into the silica–alumina hydrogel formed on mixing the sodium aluminate and silicate solutions (Table 1, sample nos. 1, 3, 5, 7, 9). Presumably, if the seed is introduced in the second way, crystallization centers are uniformly distributed throughout the reaction mass and their aggregation is hindered.

It should be noted that, if concentrated sodium aluminate and silicate solutions (SiO_2 110–140 g l^{-1} and Al_2O_3 250–300 g l^{-1}) are used, the dilution leading to their possible partial decomposition can be eliminated. As a result, the prescribed chemical composition of the reaction mixture is preserved and appearance of foreign crystallization centers, coarsely dispersed particles of aluminum hydroxide, is ruled out. The yield of the crystalline phase of the X-type zeolite is close to 100%. The duration of crystallization is 2–10 h, depending on the concentration of crystal-forming components.

It was found that use of more concentrated solutions leads to inhomogeneity of the reaction mass because of the high viscosity of hydrogels. A mixture of zeolites, composed of faujasite, phillipsite, and hydrosodalite is formed in crystallization of reaction masses of this kind (Table 2).

It was found that, if the seed is introduced into the sodium silicate solution, the synthesis becomes shorter. Presumably, crystallization centers are uniformly distributed throughout the reaction mass, which favors rapid formation and growth of zeolite crystals. It should be noted that, under the synthesis conditions found in this study, the yield of zeolite is 1.6–2.1 times higher, and the duration of crystallization, 2–4 times shorter than those in synthesis with conventional solutions.

The figure presents experimental data on the influence exerted by dilution of a silica–alumina hydrogel of the same chemical composition and by the order of introduction of the X-ray amorphous colloid seed into reaction mixtures on the kinetics of crystallization of highly dispersed NaX zeolite. As the dilution increases, i.e., as the H_2O/Al_2O_3 molar ratio in

Table 2. Effect of the concentration of gel-forming solutions and crystallization conditions on the phase composition of the zeolite

Solution concentration, g l^{-1}		Crystallization time, h	Phase composition of the zeolite, wt %
sodium silicate, SiO_2	sodium aluminate, Al_2O_3		
110	250	6.0	100 NaX
140	300	1.5	100 NaX
225	250	2.0	60 NaX; 30 phillipsite, 10 hydrosodalite
150	320	1.5	80 NaX; 20 phillipsite
180	300	1.5	75 NaX; 15 phillipsite, 10 hydrosodalite

the reaction mixtures grows from 95 to 170, the synthesis duration of the zeolite increases from 2.5–3.0 to 10–12 h.

Introduction of a preliminarily prepared X-ray amorphous colloid seed of the composition $12.7Na_2O \cdot Al_2O_3 \cdot 12.0SiO_2 \cdot 220H_2O$ in an amount of 3.0 vol % into the sodium silicate solution prior to mixing of this solution with a sodium aluminate solution leads to rather strong acceleration of the zeolite crystallization (see figure, curves *1–4*). In parallel experiments with the conventional order of mixing of gel-forming solutions and seed introduction into the already formed silica–alumina hydrogel, synthesis of the X-type zeolite is complete 0.25–2.0 h later.

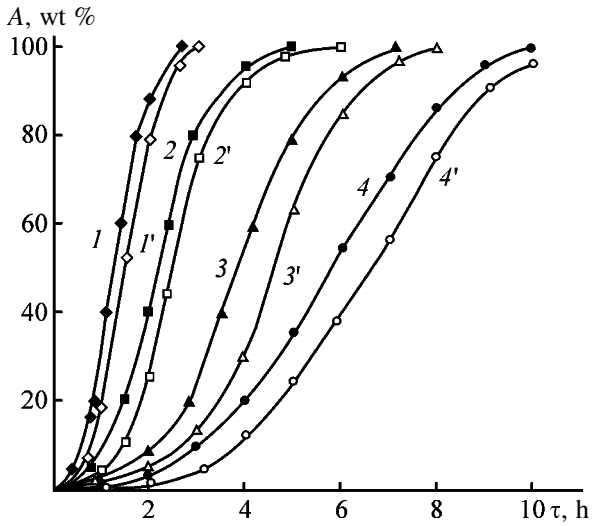

Effect of the concentration of silica-alumino hydrogel and order of seed introduction on the yield *A* of the crystalline phase of the X-type zeolite. Composition of the silica–alumina hydrogel $3.0Na_2O \cdot Al_2O_3 \cdot 3.2SiO_2 \cdot N_{1-4}H_2O$, where N_1 = 95, N_2 = 115, N_3 = 145, and N_4 = 170; T = 98°C. (τ) Crystallization duration. Seed introduction: (*1–4*) into sodium silicate solution; (*1'–4'*) into precipitated silica–alumina hydrogel.

CONCLUSIONS

(1) A method for synthesis of a high-phase-purity X-type zeolite was developed. This method is based on use of solutions of sodium aluminate, with concentrations of up to 300 g l^{-1} in terms of aluminum oxide, and sodium silicate, with concentrations of up to 140 g l^{-1} in terms of silicon oxide, and on introduction of an X-ray-amorphous seed of the composition $12.7Na_2O \cdot Al_2O_3 \cdot 12.0SiO_2 \cdot 220H_2O$ into the sodium silicate solution before its mixing with the sodium aluminate solution.

(2) Under the synthesis conditions found in the study, the dispersity of the zeolite and its yield per unit volume of the reaction mass increase by a factor of 1.6–2.1 and the crystallization time decreases by a factor of 2–4.

REFERENCES

1. Breck, D.W., *Zeolite Molecular Sieves*, New York: Wiley, 1974.
2. Flanigen, E.M., *Pure Appl. Chem.*, 1980, vol. 52, pp. 2191–2211.
3. *Zeolite Chemistry and Catalysis*, Rabo, J.A., Ed., Washington: Am. Chem. Soc., 1976.
4. Zhdanov, S.P., Khvoshchev, S.S., and Samulevich, N.N., *Sinteticheskie tseolity* (Synthetic Zeolites), Moscow: Khimiya, 1981.
5. Barrer, R.M., *Hydrothermal Chemistry of Zeolites*, London: Academic, 1982.
6. Clifton, R., *Natural and Synthetic Zeolites, Inf. Circ. U.S. Bur. Mines*, 1987, 1C 9140. p. 21.
7. Kreshkov, A.P. and Yaroslavets, A.A., *Kurs analiticheskoi khimii* (A Course of Analytical Chemistry), Moscow: Khimiya, 1975, vol. 1.
8. Kel'tsev, N.V., *Osnovy adsorbtsionnoi tehniki* (Fundamentals of Adsorption Technology), Moscow: Khimiya, 1984.

ISSN 1070-4272, Russian Journal of Applied Chemistry, 2007, Vol. 80, No. 3, pp. 501–503. © Pleiades Publishing, Ltd., 2007.
Original Russian Text © I.B. Sladkov, M.A. Shmakova, 2007, published in Zhurnal Prikladnoi Khimii, 2007, Vol. 80, No. 3, pp. 505–507.

BRIEF COMMUNICATIONS

Calculation of Coefficients of the Temperature Dependence of Density of Inorganic Molecular Liquids

I. B. Sladkov and M. A. Shmakova

St. Petersburg State Polytechnic University, St. Petersburg, Russia

Received December 19, 2006

Abstract—A procedure is developed for estimating the temperature dependence of the liquid density on the basis of a minimum set of input data.

DOI: 10.1134/S1070427207030305

The majority of molecular compounds under normal conditions exist in the liquid state. While a quite extensive information on the liquid density is available for organic compounds [1], such data for inorganic molecular liquids are rather limited, especially as far as the temperature dependence of the liquid density is concerned. Here we report a theoretical method combining such advantages as the minimal set of input data and high reliability of the prediction of the liquid density at various temperatures.

Within the temperature range limited by the melting and boiling points, the density of molecular liquids is sufficiently well described by interpolation polynomial (1) [2]:

$$\rho = a - bT. \quad (1)$$

Let us demonstrate that, with lacking published data, parameters a and b of Eq. (1) can be estimated using the Mathias equation for the temperatures below the boiling point [2]:

$$\rho = 2\rho_{cr}(2 - T/T_{cr}), \quad (2)$$

where ρ_{cr} and T_{cr} are the critical density and critical temperature, respectively.

Equation (2) can be rearranged to the form of Eq. (3):

$$\rho = 4\rho_{cr} - (2\rho_{cr}/T_{cr})T. \quad (3)$$

Comparison of Eqs. (1) and (3) yields

$$a = 4\rho_{cr}, \quad b = 2\rho_{cr}/T_{cr}. \quad (4)$$

In this study, the calculation of the coefficients of Eq. (1) taking into account relations (4), followed by the estimation of the density, was performed by using three calculation procedures differing in the input data.

Procedure no. 1. Input data: experimental critical point parameters, temperature T_{cr} and volume V_{cr} ($cm^3\ mol^{-1}$) related to the critical density ($g\ cm^{-3}$) as $V_{cr} = M/\rho_{cr}$. Since the critical point parameters are not readily available, it is advisable to replace them by more accessible boiling point parameters. As a result, we obtain two more calculation procedures.

Procedure no. 2. Input data: T_{cr} and V_{cr} calculated from the boiling point parameters by the relationships including the determining criterion of the thermodynamic similarity ψ [2]:

$$T_{cr} = T_b + 0.89T_b^{0.2\psi + 0.92}, \quad (5)$$

$$V_{cr} = T_b(1.067\psi + 2.69), \quad (6)$$

$$\psi = 0.1\ln T_b - 0.122\ln V_b + 0.006, \quad (7)$$

where T_b is the boiling point (K) and V_b is the molar volume of the liquid at its boiling point ($cm^3\ mol^{-1}$).

Procedure no. 3. Input data: T_{cr} and V_{cr} calculated taking into account the determining criterion of the thermodynamic similarity f [3]:

$$T_{cr} = T_b/(0.667 - 0.055f^{0.5}), \quad (8)$$

$$V_{cr} = V_b(0.05f + 2.69), \quad (9)$$

$$V_b = (-6.2f + 31.2)\prod^{0.94}, \quad (10)$$

$$f = \ln T_b - 1.1\ln\prod - 4, \quad (11)$$

where $\prod$ is the parachor ($J^{1/4}\ cm^{5/2}\ mol^{-1}$) determined using the additive method [2].

Table 1. Error in calculating liquid density of $TiCl_4$ at various temperatures

T, K	ρ_{exp}, g cm^{-3} [2]	Error x, %, at indicated a, g cm^{-3}, and b, g K cm^{-3}, for different calculation procedures					
		a	$b \times 10^3$	a	$b \times 10^3$	a	$b \times 10^3$
		2.258	1.77	2.249	1.76	2.265	1.71
249	1.796	1.2		0.8		1.7	
281	1.746	0.9		0.5		1.4	
313	1.694	0.6		0.3		1.2	
345	1.639	0.5		0.2		1.1	
377	1.583	0.5		0.2		1.2	
	Mean:	0.8		0.4		1.3	

As seen, for the set of equations (8)–(11), the only input parameter is the boiling point.

We performed calculations for 50 substances with input data taken from [2]. Among them are hydrides B_2H_6, NH_3, and N_2H_4; fluorides PF_3, MoF_6, UF_6, PtF_6, PuF_6, and ReF_6; chlorides CCl_4, $SiCl_4$, $GeCl_4$, $SnCl_4$, $TiCl_4$, BCl_3, PCl_3, $AsCl_3$, $BiCl_3$, $SbCl_3$, and HCl; bromides BBr_3, $SnBr_4$, $GeBr_4$, PBr_3, and $TiBr_4$; iodides BI_3, SiI_4, and SnI_4; mixed halides CCl_3F, CCl_2F_2, $CClF_3$, PCl_2F, $PClF_2$, $PBrF_2$, PBr_2F, $SiBr_2Cl_2$, and $SiBrCl_3$; hydrohalides $CHClF_2$, $SiHCl_3$, and $SiHBr_3$; oxyhalides PCl_3O, PBr_3O, SCl_2O, WCl_4O, VCl_3O, and ClO_3F; and oxides SO_2, RuO_4, and OsO_4. This set of substances includes variously polar compounds, among them such strongly polar compounds as SO_2, HCl, NH_3, etc.

Table 2. Error in calculating the liquid density from melting point to boiling point

Substance	Error Δ, %, with indicated calculation procedures		
	1	2	3
B_2H_6	0.9	2.0	3.2
NH_3	2.3	1.9	3.4
ReF_6	0.4	0.5	2.0
$TiCl_4$	0.8	0.4	1.3
$GeBr_4$	1.3	0.3	0.1
SiI_4	0.5	0.1	0.7
PCl_3O	0.7	0.3	2.5
WCl_4O	1.1	0.9	0.4
$SiBr_2Cl_2$	1.1	1.1	2.0
$SiHCl_3$	2.0	1.9	1.6
SO_2	0.1	0.7	0.6
RuO_4	0.3	0.8	1.7

For each compound, the density was estimated at five temperatures between melting and boiling points. For each temperature, the relative error of determination x (%) was determined as

$$\rho = 100\ (\rho^{calc} - \rho^{exp})/\rho^{exp}.$$

Then the relative error was averaged in the absolute values over the entire temperature range to obtain Δ (%). Data on x and δ are listed in Tables 1 and 2 for several compounds. The accuracy of different calculation procedures was characterized by the mean error σ:

$$\delta = \Sigma\Delta/N,$$

where N is the number of substances.

The resulting error σ, which is the average value over the whole set of 50 substances, is given in Table 3 for different calculation procedures.

Table 3 shows that, for any of the calculation procedures, the mean absolute error δ is within 2%. The lowest δ (0.8%) was obtained for calculation procedure no. 2, in which the critical parameters T_{cr} and V_{cr} were estimated by Eqs. (5)–(7). It should be pointed out that the accuracy of calculation procedure

Table 3. Comparison of different procedures for determination of the liquid density (accuracy and input data used)

Calculation procedure no.	Input data	Error δ, %
1	T_{cr}, V_{cr}	1.4
2	T_b, V_b	0.8
3	T_b	1.9

no. 2 appears to be even slightly better than that of procedure no. 1 employing the experimental critical parameters, which can be attributed to mutual compensation of the errors arising from estimating critical parameters from the boiling point parameters using the approximate relationships.

Calculation procedure no. 3, in which the critical parameters are estimated from the only experimental characteristic, the boiling point, also provides a quite satisfactory accuracy in predicting the liquid density (δ <2%). A significant advantage of this procedure is not only in that it employs the only input parameter, but also that it provides a prediction of the liquid density with absolutely lacking experimental data on the density of an investigated substance.

CONCLUSION

A method for estimating the temperature dependence of the liquid density of inorganic molecular compounds is developed, combining a satisfactory precision with the minimal set of easily accessible input data.

REFERENCES

1. Reid, R.C., Prausnitz, J.M., and Sherwood, T.K., *The Properties of Gases and Liquids*, New York: McGraw-Hill, 1977.
2. Morachevskii, A.G. and Sladkov, I.B., *Fiziko-khimicheskie svoistva molekulyarnykh neorganicheskikh soedinenii* (Physicochemical Properties of Inorganic Molecular Compounds), Leningrad: Khimiya, 1996.
3. Sladkov, I.B., *Zh. Prikl. Khim.*, 2003, vol. 76, no. 12, pp. 1961–1965.

ISSN 1070-4272, Russian Journal of Applied Chemistry, 2007, Vol. 80, No. 3, pp. 504–505. © Pleiades Publishing, Ltd., 2007.
Original Russian Text © B.F. Kukharev, V.K. Stankevich, G.R. Klimenko, O.N. Bel'kova, T.F. Lelyukh, V.A. Kukhareva, 2007, published in Zhurnal Prikladnoi Khimii, 2007, Vol. 80, No. 3, pp. 508–509.

BRIEF COMMUNICATIONS

Synthesis and Flotation Characteristics of Copolymers of Monoethanolamine Vinyl Ether with (*Z*)-4-[2-(Vinyloxy)ethyl]amino-3-penten-2-one

B. F. Kukharev, V. K. Stankevich, G. R. Klimenko, O. N. Bel'kova, T. F. Lelyukh, and V. A. Kukhareva

Favorskii Irkutsk Institute of Chemistry, Siberian Division, Russian Academy of Sciences, Irkutsk, Russia

Received September 13, 2006

Abstract—Polyvinyloxyalkylamines with the content of modified units from 25 to 75% were synthesized by condensation of poly(monoethanolamine vinyl ether). Their suitability as modifying agents in dressing of copper–zinc sulfide ores was examined.

DOI: 10.1134/S1070427207030317

It is well known that the homopolymer and copolymers of monoethanolamine vinyl ether are efficient reagents for flotation of polymetallic ores [1]. Various low-molecular-weight enaminones are modifying agents in flotation of Pb–Zn and Pb–Cr–Zn ores [2, 3].

We expected that introduction of units containing enaminone fragments into the chain of poly(monoethanolamine vinyl ether) would enhance its flotation characteristics.

The compounds were synthesized by condensation of poly(monoethanolamine vinyl ether) (**I**) with various amounts of acetylacetone. Copolymers **II**–**IV** of monoethanolamine vinyl ether with (*Z*)-4-[2-(vinyloxy)ethyl]amino-3-penten-2-one with the content of the latter of approximately 25, 50, and 75%, respectively, were prepared. The yield of **II**–**IV** was 92–94%.

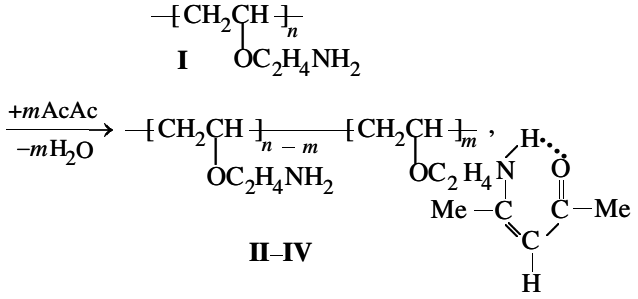

II–**IV**, n = 6–10; **II**, $m = 0.25n$; **III**, $m = 0.5n$; **IV**, $m = 0.75n$.

In the ^{1}H NMR spectrum of copolymer **III** (Bruker DPX-400 spectrometer operating at 400 MHz, solvent $CDCl_3$, 26°C, internal reference hexamethyldisiloxane), along with multiplets in the range 1.7–3.8 ppm belonging to the CH_2CH and NCH_2CH_2O groups, there are singlets with chemical shifts of 1.94, 1.98, 4.99, and 10.93 ppm assigned to protons of the enaminone fragment: $C{=}CCH_3$, $O{=}CCH_3$, C=CH, and NH, respectively. These signals (with the integral intensity corresponding to the theoretical intensity) suggest that the enaminone fragment exists in the form of only one of possible tautomers. A comparison of the chemical shifts of these protons with published data for the same protons in enaminones synthesized from acetylacetone and primary amines [4, 5] suggests that in the resulting compounds the enaminone fragment has the *cis,cis* configuration.

The flotation activity of **II**–**IV** was studied on the Cu–Zn ores of the Karabash pyrites deposit.

Under industrial conditions, the collective-selective scheme is used for the ore dressing. According to this scheme, first only copper and lead sulfides are recovered, with the depression of sphalerite and pyrite. Zinc sulfide is extracted from the tails. The resulting Cu–Pb concentrate is separated by flotation of copper minerals.

Copolymers **II**–**IV** were tested in a laboratory flotation machine of the mechanical type with a 1-l chamber.

An optimization of the conditions of flotation of

the copper–zinc–pyrite ore with copolymers **II**–**IV** showed that recovery of copper and zinc into the foamed product increases in comparison with the base run by 4.01 and 1.63%, respectively, for copolymer **II**; by 4.88 and 1.93%, respectively, for copolymer **III**; and by 4.19 and 1.72%, respectively, for copolymer **IV**. In all the cases, the expenditures of the copolymers were 4 g per ton of the ore. In addition, introduction of copolymers into the process allowed the expenditure of potassium butylxanthate to be decreased from 60 to 50 g per ton of the ore.

In selection of the collective copper–zinc concentrate, the recovery of copper and zinc by the base procedure was 57.78 and 27.40%, respectively. With the copolymers, the recovery of these minerals was 60.54 and 26.91 (copolymer **II**), 68.11 and 20.59 (copolymer **III**), and 69.65 and 17.15% (copolymer **IV**), respectively.

General procedure for synthesis of copolymers of monoethanolamine vinyl ether and (*Z*)-4-[2-vinyloxy)ethyl]amino-3-penten-2-one (II–IV). To a solution of poly(monoethanolamine vinyl ether) (**I**) (number-average molecular weight 710) in 100 ml of ethanol, acetylacetone was added at such a rate that the temperature of the reaction mixture did not exceed 30°C. After addition of the whole amount of acetylacetone, the reaction mixture was kept for 6 h at room temperature and poured into 900 ml of petroleum ether. The precipitated oil was separated and dried to constant weight at a pressure of 2 mm Hg and a temperature of 30°C.

Synthesis of copolymer II. From 69.7 g (0.8 mol) of poly(monoethanolamine vinyl ether) (**I**) and 20.0 g (0.2 mol) of acetylacetone, 81.1 g (94%) of copolymer **II** was obtained in the form of a light brown viscous resin.

Found (%): C 60.07, H 10.02, N 14.12.
$C_{42}H_{84}N_8O_{10}$.
Calculated (%): C 58.58, H 9.83, N 13.01.

IR spectrum (thin film), cm^{-1}: 1518, 1643 (N–C=C–C=O), 3000–3450 (NH, NH_2).

Synthesis of copolymer III. From 69.7 g (0.8 mol) of poly(monoethanolamine vinyl ether) (**I**) and 40.0 g (0.4 mol) of acetylacetone, 96.2 g (94%) of copolymer **III** was obtained in the form of a light brown viscous resin.

Found (%): C 61.87, H 9.96, N 11.31.
$C_{52}H_{96}N_8O_{12}$.
Calculated (%): C 61.91, H 9.44, N 10.93.

IR spectrum (thin film), cm^{-1}: 1527, 1645 (N–C=C–C=O), 3000–3450 (NH, NH_2).

Synthesis of copolymer IV. From 69.7 g (0.8 mol) of poly(monoethanolamine vinyl ether) (**I**) and 60.0 g (0.6 mol) of acetylacetone, 109.4 g (92%) of copolymer **IV** was obtained in the form of a light brown viscous resin.

Found (%): C 63.78, H 9.49, N 9.18.
$C_{62}H_{108}N_8O_{14}$.
Calculated (%): C 62.60, H 9.15, N 9.42.

IR spectrum (thin film), cm^{-1}: 1522, 1640 (N–C=C–C=O), 3000–3450 (NH, NH_2).

CONCLUSIONS

(1) Addition of a copolymer prepared by modification of poly(monoethanolamine vinyl ether) with acetylacetone in the stage of collective flotation of copper–zinc–pyrite ore in the amount of 4 g per ton of ore increases the recovery of copper and zinc into the foamed product in comparison with the base procedure by 4.01–4.88 and 1.63–1.93%, respectively.

(2) In selection of collective copper–zinc concentrate, the copolymers obtained increase the copper recovery in comparison with the base procedure by 2.76–11.87%.

REFERENCES

1. Bel'kova, O.N., Kukharev, B.F., and Stankevich, V.K., *Izv. Vyssh. Uchebn. Zaved., Gorn. Zh.*, 1996, no. 2, pp. 134–139.
2. Kukharev, B.F., Stankevich, V.K., Klimenko, G.R., et al., *Zh. Prikl. Khim.*, 1998, vol. 71, no. 9, pp. 1574–1576.
3. Kukharev, B.F., Stankevich, V.K., Bel'kova, O.N., et al., *Zh. Prikl. Khim.*, 1998, vol. 71, no. 4, pp. 639–641.
4. *The Chemistry of Enamines*, Rappoport, Z., Ed., Chichester: Wiley, 1994, part 1.
5. Freimanis, Ya.F., *Khimiya enaminoketonov, enaminoiminov, enaminotionov* (Chemistry of Enamino Ketones, Enamino Imines, and Enamino Thiones), Riga: Zinatne, 1974.

ISSN 1070-4272, Russian Journal of Applied Chemistry, 2007, Vol. 80, No. 3, pp. 506–508. © Pleiades Publishing, Ltd., 2007.
Original Russian Text © D.V. Bessonov, I.V. Kulakov, A.M. Gazaliev, O.A. Nurkenov, 2007, published in Zhurnal Prikladnoi Khimii, 2007, Vol. 80, No. 3, pp. 510–512.

BRIEF COMMUNICATIONS

Synthesis of Glycoconjugates of Physiologically Active Compounds

D. V. Bessonov, I. V. Kulakov, A. M. Gazaliev, and O. A. Nurkenov

Institute of Organic Synthesis and Coal Fuel Chemistry of Kazakhstan Republic, Limited Liability Company, Karaganda, Kazakhstan

Received August 3, 2006

Abstract—Synthesis of *N*-glycosylamines derived from *D*-glucose and *D*-galactose (glycoconjugates of aniline derivatives and of *d*-pseudoephedrine and cytisine alkaloids) was studied with the aim to develop new pharmaceuticals.

DOI: 10.1134/S1070427207030329

N-Glycosylamines find growing use for preparing natural glycopeptides, their analogs, and glycoconjugates used for various biological studies. *N*-Glycosylamines, the reaction products of carbohydrates with alkyl- and arylamines, attract attention of chemists, biochemists, and biologists. *N*-Glycosylamines can also be used for preparing new pharmaceuticals [2].

It is known than aniline is an antipyretic. However, it is too toxic to be used as a pharmaceutical. Introduction of various substituents into the benzene ring or the amino groups yields compounds with a wide range of pharmacological properties. Halogenation increases the lipophilicity of pharmaceuticals and facilitates their penetration through biomembranes [2]. For example, *p*-thiocyanatoaniline is a strong insecticide [3], and *p*-bromoaniline is a precursor for preparing Fenazepam, which is a tranquilizer with hypnotic and anticonvulsant effect [4].

N-Glycosylamines were prepared by condensation of *p*-substituted anilines and *D*-glucose (**1, 3, 5**) or *D*-galactose (**2, 4, 6**). Their biological activity was studied. The condensation was performed in an alcoholic solution on heating by the procedure described in [5]:

1–6

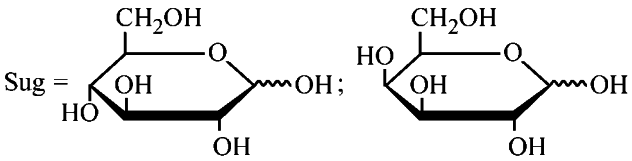

1, 3, 5 **2, 4, 6**

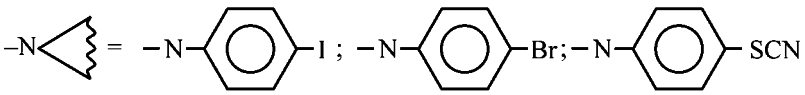

1, 2 **3, 4** **5, 6**

N-Glycosylamines **1**–**6** are white crystalline compounds readily soluble in water, ethanol, and DMF.

The presence of the band at 891 ± 7 cm^{-1} in the IR spectra of compounds **1**–**6** suggests the β-confor-

mation at the anomeric center. The bands in the range 1010–1090 cm^{-1} are assigned to the pyranose form of the glycoside residue. The bands in the range 2130–2160 cm^{-1} in the IR spectrum of compound **5** are due to the –S–C≡N group. The C–Hal and C–N stretching bands of compounds **1**–**4** are observed in the ranges 500–700 and 1280–1330 cm^{-1}, respectively.

New biologically active compounds can be prepared by functionalization of monosaccharide with phramacophore groups and physiologically active alkaloid fragments. In addition, it is known that introduction of carbohydrate residues into the structure of biologically active molecules increases their solubility in water, decreases their toxicity, and increases their target transport and penetrability into a cell.

To prepare biologically active compounds and to increase the solubility and decrease the toxicity of alkaloid derivatives, we used commercial *D*-galactose as a substituent at the nitrogen atom. Condensation of *D*-galactose with an alkaloid, *d*-pseudoephedrine or cytisine, in a small volume of ethanol containing catalytic amounts of acetic acid yields *N*-galactosylamines **7** and **8**:

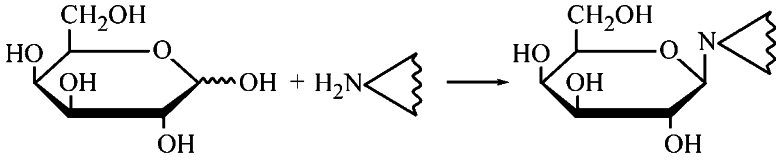

7, 8

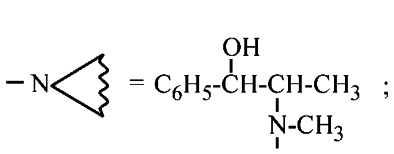

7

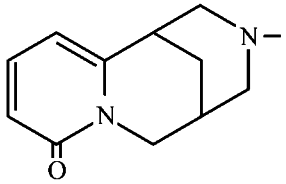

8

Galactosylamines **7** and **8** are white crystalline compounds; their composition and structure were confirmed by elemental analysis and by ^1H NMR and IR spectroscopy. The absence of the band at 844 ± 8 cm^{-1} in the IR spectra of these compounds suggests their β-conformation. According to data of [6], absorption in the range 1120–1170 cm^{-1} is typical for cyclic sugars, and open-chain sugars do not absorb in this range. The strong band of the amide group (N–C=O) of the alkaloid at 1640–1650 cm^{-1} is present, along with bands of the carbohydrate fragment, in the IR spectrum of compound **8**.

The properties of compounds **1**–**8** are presented in the table.

The IR spectra of all the compounds presented in the table are characterized by strong stretching bands of the OH and NH groups in the range 3250–3400 cm^{-1}.

The ^1H NMR spectrum of compound **7** contains the signals of the protons of the alkaloid and carbohydrates moieties. The doublet of the CH_3–C group is observed at 1.14 ppm (J = 5.75 Hz), and the intense singlet of the *N*-methyl group, at 2.53 ppm. The signal of the methine proton of the CH–N group appears in the form of complex multiplet at 2.64–2.85 ppm. The doublet at 4.55 ppm is assigned to the methine proton of the CHO group (J = 3.5 Hz). The doublet of the anomeric proton H(1) of the carbohydrate residue is observed at 4.48 ppm (J = 9.2 Hz), which confirms the β-conformation of the reaction product.

EXPERIMENTAL

The ^1H NMR spectra of solutions in DMF–d_7 were recorded on a Varian XL-100 spectrometer operating at 100 MHz. The IR spectra of the samples in KBr pellets were recorded on an Avatar-320 spectrometer. Melting points were determined on a Boetius apparatus. The reaction course was monitored and the purity of the condensation products was determined by thin-layer chromatography on Sorbfil plates using isopropanol : benzene : ammonia = 10 : 5 : 2 system

Physicochemical constants and elemental analyses of the compounds

Compound	Yield, %	mp, °C	Found, %			Empirical formula	Calculated, %		
			C	H	N		C	H	N
1	75.5	118–119	38.25	4.04	3.93	$C_{12}H_{16}INO_5$	37.81	4.21	3.67
2	65.2	181–182	38.19	4.01	3.99	$C_{12}H_{16}INO_5$	37.81	4.21	3.67
3	72.5	117–118	43.46	4.61	4.47	$C_{12}H_{16}BrNO_5$	43.13	4.83	4.19
4	64.9	119–120	43.50	4.56	4.42	$C_{12}H_{16}BrNO_5$	43.13	4.83	4.19
5	87.6	171–172	50.43	4.89	9.23	$C_{13}H_{16}N_2O_5S$	49.99	5.16	8.97
6	70.1	179–180	50.41	4.91	9.25	$C_{13}H_{16}N_2O_5S$	49.99	5.16	8.97
7	55.4	146–147	59.12	7.46	4.55	$C_{16}H_{25}NO_6$	58.70	7.70	4.28
8	71.6	188–189	58.41	6.59	8.29	$C_{17}H_{24}N_2O_6$	57.94	6.86	7.95

as the eluent. The chromatograms were developed with iodine vapor.

Glucosyl-*p*-iodoaniline (1). To a solution of glucose (0.02 mol) in ethanol (20 ml), *p*-iodoaniline (0.02 mol) was added. The mixture was stirred at 50–55°C for 4 h. Excess solvent was removed on a water bath. White crystals that precipitated on slight cooling were filtered off and washed with cold isopropanol. The product was recrystallized from an ethanol: isopropanol (5 : 1) mixture. Galactosyl-*p*-iodoaniline (**2**) was prepared similarly.

Glucosyl-*p*-bromoaniline (3). To a solution of glucose (0.02 mol) in ethanol (20 ml), *p*-bromoaniline (0.02 mol) was added with stirring. The mixture was stirred at 55–60°C for 5 h. Excess solvent was removed on a water bath. White crystals that precipitated on slight cooling were filtered off and washed with cold isopropanol. The product was recrystallized from ethanol. Galactosyl-*p*-bromoaniline was prepared similarly.

Glucosyl-*p*-thiocyanatoaniline (5). To a solution of glucose (0.01 mol) in ethanol (15 ml), *p*-thiocyanatoaniline (0.01 mol) was added. The mixture was stirred at 60–65°C for 6 h. Crystals that precipitated on cooling were filtered off and washed with cold isopropanol. The product was recrystallized from an ethanol : isopropanol (2 : 1) mixture. Galactosyl-*p*-thiocyanatoaniline (**6**) was prepared similarly.

Galactosyl-*d*-pseudoephedrine (7). To a solution of galactose (0.01 mol) in ethanol (15 ml), *d*-pseudoephedrine (0.01 mol) was added. The mixture was stirred at 55–60°C for 24 h in the presence of 1–2 drops of glacial acetic acid. White crystals that precipitated on cooling were washed with cold isopropanol and then with absolute ether. The product was recrystallized from isopropanol.

Galactosylcytisine (8). To a solution of galactose (0.01 mol) in ethanol (15 ml), cytisine (0.01 mol) was added. The mixture was stirred at 55–60°C for 24 h in the presence of 1–2 drops of glacial acetic acid. White crystals that precipitated on cooling were washed with absolute ether. The product was recrystallized from an isopropanol : benzene : ethanol (3 : 2 : 1) mixture.

CONCLUSIONS

(1) The carbohydrates were condensed with biologically active amines (*p*-iodoaniline, *p*-bromoaniline, and *p*-thiocyanatoaniline) and with alkaloids (*d*-pseudoephedrine and cytisine).

(2) The physicochemical constants, compositions, and structures of the condensation products were determined.

REFERENCES

1. Grogan, M.J., Pratt, M.R., and Marcaurelle, L.A., *Ann. Rev. Biochem.*, 2002, vol. 71, p. 593.
2. Soldatenkov, A.T., Kolyadina, N.M., and Shendrik, I.V., *Osnovy organicheskoi khimii lekarstvennykh veshchestv* (Foundations of the Organic Chemistry of Pharmaceuticals), Moscow: Khimiya, 2001.
3. Mel'nikov, N.N., *Pestitsidy: Khimiya, tekhnologiya i primenenie* (Pesticides: Chemistry, Technology, and Application), Moscow: Khimiya, 1987.
4. Granik, V.G., *Osnovy meditsinskoi khimii* (Foundations of Medical Chemistry), Moscow: Vuzovskaya Kniga, 2001.
5. Sorokin, W., *Ber*, 1887, vol. 20, p. 783.
6. Prima, A.M., Zhbanov, R.G., and Marunov, R., *Zh. Strukt. Khim.*, 1964, vol. 5, no. 6, pp. 845–850.

ISSN 1070-4272, Russian Journal of Applied Chemistry, 2007, Vol. 80, No. 3, pp. 509–510. © Pleiades Publishing, Ltd., 2007.
Original Russian Text © Editorial Board, 2007, published in Zhurnal Prikladnoi Khimii, 2007, Vol. 80, No. 3, pp. 513–514.

OBITUARIES

Konstantin Ivanovich Tikhonov (June 5, 1939–December 24, 2006)

DOI: 10.1134/S1070427207030330

On December 24, 2006, head of the Chair of Technology of Electrochemical Industries of St. Petersburg State Institute of Technology (Technical Univesity), doctor of chemical sciences, Professor Konstantin Ivanovich Tikhonov died of a severe illness at the age of 67. A prominent specialist in theoretical and applied electrochemistry, a man of great intellect and rare modesty untimely passed away.

Konstantin Ivanovich Tikhonov was born in Leningrad into a workers' family. His father worked at Elektrosila plant. The life of Konstantin Ivanovich is typical of children born before the Great Patriotic War (World War II). His father took part, in ranks of the Red Army, in bloody battles at Oranienbaum bridgehead, and his mother, together with a small son, was evacuated with the plant to the town of Baranchi in the Urals.

After the war, the family returned to the war-ravaged Leningrad. In 1956, Tikhonov finished school and started to work as a metal craftsman at Elektrosila plant.

In 1957, Tikhonov entered Leningrad industrial technical college. He graduated from the college as a specialist in technology of electrochemical industries and worked as a technologist at one of defense plants of Leningrad. When serving in the army, Tikhonov took part in the construction of Plesetsk space launching site.

In 1963, Tikhonov entered the Leningrad Institute of Technology. Having graduated with brilliant success from this institute (chair of technology of electrochemical industries) and having completed his postgraduate education under the supervision of professors N.P. Fedot'ev and A.L. Rotinyan, Konstantin Ivanovich moved up in the ranks from assistant to head of the chair, which was headed by him from 1986 till the end of his life.

Professor Tikhonov was a prominent electrochemist. The principal works by Tikhonov were devoted to problems of electrochemical kinetics and development of theoretical foundations of technically important processes of electrochemical technology. He was the

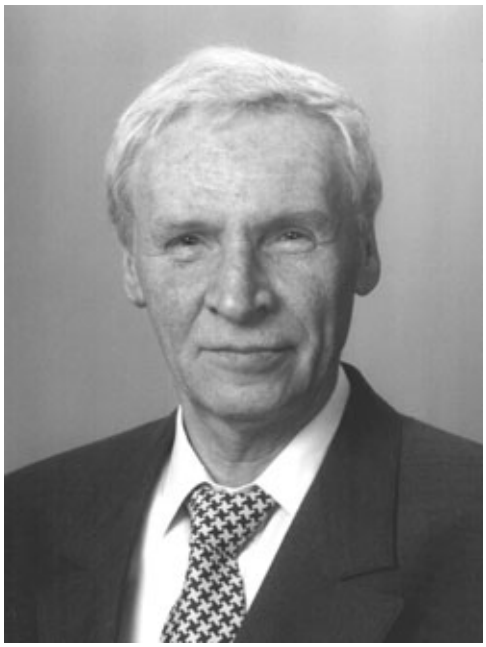

first in the country to commence fundamental studies of the kinetics of electrochemical processes of charging–discharge of metals and nonmetallic compounds in aprotic solvents. The results obtained were directly relevant to design of lithium–ion chemical power cells and development of technologies for electrodeposition of metals, including aluminum, from organic solvents. Of considerable importance are Tikhonov's studies of the thermodynamics and kinetics of electrochemical reactions of cathodic reduction and anodic oxidation of solid nonmetallic compounds and metals as applied to the electrochemical behavior of electrodes in chemical power cells with an aprotic solvent.

It is this series of Tikhonov's works that made it possible to substantiate scientifically ways of development of new systems for chemical power cells with a negative alkali metal electrode and an aprotic solvent and principles of choice of active substances and electrolytes for these power cells. He also exhibited scientific interest in environmental problems of applied electrochemistry. His works of recent years were

concerned with specific features of lithium–ion secondary power cells.

He was an excellent lecturer who delivered lectures on basic theoretical disciplines of electrochemistry during many years. Twenty-five persons successfully prepared and defended candidate dissertations under his supervision. Many Tikhonov's former students and postgraduate students are successfully working in the field of electrochemistry or electrochemical technology at plants in Russia and abroad.

Tikhonov was the author of a number of books and brochures on theoretical and applied electrochemistry, the most important of which are *Teoreticheskaya elektrokhimiya* (Theoretical Electrochemistry), Leningrad: Khimiya, 1981, in co-authorship with Rotinyan and I.A. Shoshina and *Elektrokhimicheskie i khimicheskie pokrytiya* (Electrodeposited and Electroless Coatings), Leningrad: Khimiya, 1990, in co-authorship with S.Ya. Grilikhes. He published more than 200 papers and abstracts of papers and received 14 inventor's certificates.

He was an active participant of numerous scientific conferences in various cities of the country and abroad, chairman of the specialized scientific council of St. Petersburg Institute of Technology and member of specialized councils of St. Petersburg State University and Istochnik Research Institute of Batteries, Joint-Stock Company.

Konstantin Ivanovish did much for his coworkers and postgraduate students and gave up a considerable emotional power to them. His lecture courses on theoretical electrochemistry and methods of electrochemical studies are remembered by numerous graduates from the chair of electrochemistry.

Professor Tikhonov lived a brilliant creative life and was far from exhausting his scientific potential of an electrochemist. He was distinguished by a high professional level, creative initiative, scientific principles, and devotion to work. The memory of a prominent scientist and charming and kind man will be forever preserved in the hearts of his colleagues and disciples.

Staff members of the Chair of Technology of Electrochemical Industries of St. Petersburg State Institute of Technology (Technical University)

Editorial board and editorial staff members of *Zhurnal Prikladnoi Khimii*

ISSN 1070-4272, Russian Journal of Applied Chemistry, 2007, Vol. 80, No. 3, pp. 511–512. © Pleiades Publishing, Ltd., 2007.
Original Russian Text © A.G. Morachevskii, 2007, published in Zhurnal Prikladnoi Khimii, 2007, Vol. 80, No. 3, pp. 515–516.

BOOK REVIEWS

Nemtsov, M.S., *Vospominaniya i razmyshleniya (zapiski khimika)* (Recollections and Reflection (Chemist's Memoirs))

St. Petersburg: GIPT, 2006, 96 pp.

DOI: 10.1134/S1070427207030342

One of the known Russian chemists of the XX century, Mark Semenovich Nemtsov (1900–1997), doctor of chemical sciences, professor, and Lenin Prize laureate (1967) wrote his recollections as far back as 1990. These memoirs, published only now on the initiative of a group of his co-workers from VNIIneftekhim Joint-Stock Company, are lively and interestingly written, have in full measure retained their topicality, and make a valuable contribution to the history of domestic chemical technology. The recollections of a scientist, who had lived a long life, reproduce the scientific, cultural, and political life of the country in the XX century. M.S. Nemtsov was actively involved in the development of four original processes successfully implemented in the industry. The author suffered from unsubstantiated repressions and worked for a number of years in detention, at a special laboratory of NKVD (Peoples' Commissariat of Internal Affairs). In his recollections, the coeval with the century pays a considerable attention to meetings with scientists and cultural workers, to presentation of the essence of scientific issues, and to moral and ethical problems encountered in scientific collectives.

The book comprises 28 brief essays, each containing scientist's recollections of events or meetings. In fact, the essays cover Nemtsov's life, from the time of his education at Petrograd commercial school till the end of perestroika in our country (1990). In 1917, the author graduated with a gold medal from the school and, after a break caused by the civil war, entered in 1921 the chemical faculty of the Petrograd Polytechnic Institute. It is noted that the curriculum at the institute was rather broad and based on profound study of the theoretical foundations of physics and chemistry. Among the lecturers were such known scientists as A.F. Ioffe, N.N. Semenov, N.S. Kurnakov, A.A. Baikov, and V.A. Kistyakovskii. Nemtsov very warmly recalls the consultant of his graduation work performed at the laboratory of Neftegaz plant, Prof. A.F. Dobryanskii, a talented scientist with broad interests.

Having successfully defended his graduation thesis in 1928, Nemtsov was assigned, with account of his inclination to research activities, to work at the laboratory of high pressures of the State Institute of Applied Chemistry, headed by Academician V.N. Ipat'ev (1867–1952). Already in 1929, the laboratory was transformed into the independent Institute of High Pressure, where Nemtsov worked till 1941. The author of the essays exceedingly highly appreciates V.N. Ipat'ev as a scientist and head of a large research team. Quite a number of later widely known young chemists worked at the Institute of High Pressure under Ipat'ev's supervision. These include A.A. Vvedenskii, B.N. Dolgov, V.V. Ipat'ev, B.L. Moldavskii, G.A. Razuvaev, and A.V. Frost.

At the beginning of July 1941, Nemtsov was arrested without any charges and sentenced to five years of imprisonment. Till March 1943 he was in prison at Andizhan, Uzbek SSR, and later was transferred to a special chemical laboratory of NKVD in Moscow. Till July 1946, the end of his imprisonment term, Nemtsov developed under laboratory conditions, together with P.G. Sergeev and R.Yu. Udris, disciples of Academician A.E. Chichibabin (1871–1945), a method for synthesis of phenol and acetone by acid decomposition of isopropylbenzene hydroperoxide (cumene method). All of these facts are described in sufficient detail in Nemtsov's recollections. In particular, a large essay is devoted to works and tragic fate of Udris (1899–1949), discoverer of the cumene method.

After being discharged, Nemtsov was sent to Leningrad, to the Lebedev Institute of Synthetic Rubber (VNIISK), to continue his studies of isoprene synthesis. Nemtsov and co-workers found the optimal conditions of isoprene synthesis from butylenes and formaldehyde via a stage of dimethyldioxane formation. This laid foundation of the industrial technology for manufacture of isoprene and isoprene rubber. For the development and industrial implementation of a method for synthesis of a rubber replacing natural caoutchouc, Nemtsov was awarded, in a group of

authors, a Lenin Prize. Nemtsov worked at VNIISK for nearly 17 years, till January 1963, when his laboratory was transferred to VNIIneftekhim institute.

A large essay presents Nemtsov's views concerning the state of the domestic science during the complete stagnation (zastoi) period. The author illustrates by quite a number of examples the degradation of the moral-ethical principles in scientific teams and among the supervising and administrative staff.

The supplement to *Vospominaniya i razmyshleniya* presents Nemtsov's letters to his wife, I.I. Nemtsova, exiled from Leningrad in March 1942 and an afterword written by T.M. Lesteva, one Nemtsov's coworkers, to 105th anniversary of the scientist's death.

The recollections and reflection by Mark Semenovich Nemtsov, a prominent scientist, are of interest for an exceedingly wide audience of readers and their publication is very timely.

A. G. Morachevskii

ISSN 1070-4272, Russian Journal of Applied Chemistry, 2007, Vol. 80, No. 3, p. 513. © Pleiades Publishing, Ltd., 2007.
Original Russian Text © A.G. Morachevskii, 2007, published in Zhurnal Prikladnoi Khimii, 2007, Vol. 80, No. 3, p. 516.

BOOK REVIEWS

Kazanbaev, L.A., Kozlov, P.A., Kubasov, V.L., and Kolesnikov, A.V., *Gidrometallurgiya tsinka (ochistka rastvorov i elektroliz)* (Hydrometallurgy of Zinc (Solution Purification and Electrolysis))

Moscow: Ruda i Metally, 2006, 176 pp.

DOI: 10.1134/S1070427207030354

The metallurgy of zinc has been developing in the last decade under conditions of degrading quality of the raw materials being processed, growing cost of fuel and electric power, and increasing stringency of environmental requirements. The resulting rise in the production cost requires cardinal improvement of the technologies employed in the zinc subindustry. The book by L.A. Kazanbaev and co-authors discusses two key issues of the hydrometallurgy of zinc: purification of solutions formed in leaching of zinc-containing raw materials (fired zinc concentrates and other kinds of oxidized raw materials) and the theory and practice of solution electrolysis to give commercial zinc and various zinc-based alloys.

The brief introduction (pp. 3–19) presents general evidence concerning the physicochemical and mechanical properties of zinc, fields of its application, and composition of zinc concentrates processed at domestic and foreign plants, and gives the most characteristic results of solution purification to remove impurities prior to electrolysis. A considerable proportion of zinc (30 to 50% of the whole amount of the metal consumed) is expended for zinc-plating of iron. The consumption of zinc steadily grows and its application fields become wider.

The first part of the book (pp. 20–101) analyzes preparation of zinc-containing solutions for electrolysis: purification of the solutions to remove metallic and nonmetallic impurities. The classical flowsheet of this process envisages a stage-by-stage purification by hydrolytic, chemical, and cementation methods. The main attention is given by the authors to the cementation method for solution purification to primarily remove impurities of copper, cadmium, nickel, and cobalt. Zinc serves as a cementing metal. The authors present the theoretical foundations of the cementation purification technique and discuss the kinetics of cementation, sequence of impurity removal, effect of various factors on the cementation, the technology of cementation, and the apparatus used in the process.

The second part of the book (pp. 102–169) contains evidence on electrolysis of sulfate zinc-containing solutions after their purification. It describes cathodic and anodic processes and the effect of impurities of metal ions, chloride and fluoride anions, and organic substances on electrolysis parameters and quality of metallic zinc. The technology of electrolysis, equipment employed, remelting of cathodic zinc, and manufacture of zinc alloys are discussed in detail. All the descriptions of the technological part are mostly based on the experience of operation of Chelyabinsk zinc plant.

The introduction and two other parts of the book are provided with bibliographic lists. In some cases, references to publications could be more specific, with indication of the original works, rather than monographs devoted to metallurgy of zinc. The book by Kazanbaev and co-authors has a production-technological orientation. The way in which theoretical sections explaining the cementation (pp. 28–49) and electrolysis (pp. 103–115) processes are included in the book invites some critical remarks concerning the terminology used. The whole amount of the necessary electrochemical evidence could be presented in a simpler manner in a production-oriented book.

Similarly to other books published by Ruda i Metally Publishing House, the book by Kazanbaev and co-authors is distinguished by high polygraphic level. A success is the inclusion of color photographs forming a photo album of Chelyabinsk zinc plant. It only remains to wish that the publishing house should more widely recruit external referees and scientific editors.

A. G. Morachevskii

ISSN 1070-4272, Russian Journal of Applied Chemistry, 2007, Vol. 80, No. 4, pp. 515–527. © Pleiades Publishing, Ltd., 2007.
Original Russian Text © Yu.A. Anufrikov, G.L. Kuranov, N.A. Smirnova, 2007, published in Zhurnal Prikladnoi Khimii, 2007, Vol. 80, No. 4, pp. 529–540.

REVIEWS

Solubility of CO_2 and H_2S in Alkanolamine-containing Aqueous Solutions

Yu. A. Anufrikov, G. L. Kuranov, and N. A. Smirnova

St. Petersburg State University, St. Petersburg, Russia

Received February 1, 2007

Abstract—Experimental studies of the solubility of carbon dioxide and hydrogen sulfide in aqueous solutions of alkanolamines, widely used industrial absorbents of acid gases, are reviewed. A comparative analysis of methods employed by various authors is made. The available published data on the solubility of CO_2 and H_2S in solutions of primary, secondary, and tertiary alkanolamines are analyzed. Fundamental aspects of the influence exerted by various additives on the phase behavior of systems constituted by an acid gas, alkanolamine, and water are considered.

DOI: 10.1134/S1070427207040015

Data on phase equilibria in aqueous systems containing alkanolamines and acid gases, such as hydrogen sulfide and carbon dioxide, are primarily required for solving problems associated with purification of industrial gas flows to remove the above-mentioned noxious components. These problems are topical for numerous technological processes. In particular, hydrogen sulfide frequently occurs as accompanying components in oil-and-gas fields. Carbon dioxide is formed as a by-product in many chemical industries. Absorption of these gases is important both economically and ecologically.

After the first patent [1] for use of an aqueous solution of triethanolamine as an absorbent was received, a large number of studies concerned with the solubility of acid gases in aqueous solutions of alkanolamines have been reported. These nitrogen-containing compounds are widely used for absorption of acid gases. Technological schemes of industrial installations for gas purification with alkanolamine solutions and specific features of their application were described in detail in a book by Kohl and Nielsen [2].

The effective absorption of acid gases by alkanolamine solutions is due to the capacity of amine molecules for protonation and chemical interaction with acid gases, which results in that molecular forms of gases are converted into the corresponding ionic forms. The conversion schemes are as follows form.

(1) Formation of hydrocarbonate and hydrosulfide ions:

$$CO_2 + H_2O + R^1R^2R^3N \rightleftarrows HCO_3^- + R^1R^2R^3NH^+,$$

$$H_2S + R^1R^2R^3N \rightleftarrows HS^- + R^1R^2R^3NH^+,$$

where at least one of the substituents R^1, R^2, R^3 is an alkanol radical ($-C_nH_{2n}OH$), whereas the others may be hydrogen atoms or methyl groups.

(2) Formation of carbamates (in the case of CO_2, also primary or secondary amines):

$$CO_2 + 2R^1R^2NH \rightleftarrows R^1R^2NCOO^- + R^1R^2NH_2^+.$$

To choose the optimal conditions of the absorption process, it is primarily necessary to have reliable experimental data on the solubility of acid gases in aqueous solutions of individual or mixed amines in a wide range of temperatures and pressures. Also required is information about the influence exerted on the solubility by various additives dealt with in purification of gas flows on industrial installations.

This review systematizes and analyzes the presently available relevant publications. The first to be considered in detail are experimental techniques used by various authors.

EXPERIMENTAL TECHNIQUES FOR STUDY OF THE SOLUBILITY OF ACID GASES

The list of experimentally determinable parameters providing full information about the liquid–vapor equilibrium in multicomponent systems includes the fol-

lowing: T and p, temperature and pressure, which are the same in both the coexisting phases in the thermodynamic equilibrium; x_i and y_i, mole fractions of the components in the liquid and vapor phases, respectively (i = 1, ..., k, where k is the number of components).

According to the rule of phases, only k variables can be independently varied. One of variables commonly fixed in experiments with the systems under study is temperature, whose constancy is provided by thermostating. What variables are additionally fixed depends on a particular experimental technique. This may be the empirical composition of the system (total amounts of component moles in both phases), composition of the liquid phase, and partial pressure of volatile components in the gas phase. Other parameters are determined in the course of an experiment after equilibrium between the liquid and vapor phases is attained. It is advisable to classify the methods by ways in which the parameters are set and equilibrium is attained.

The most widely employed techniques are the static and circulation methods, as well as the flow method.

Static method. Most of the available data on the solubility in the systems studied have been obtained by the static method [3–15]. The technique consists in that a thermostated system of a prescribed empirical composition is brought in thermodynamic equilibrium and the phase compositions and pressure are directly determined. The measurement procedure used in this method consists in the following. A known amount of an aqueous solution of an amine is placed in the cell, a required amount of carbon dioxide and (or) hydrogen sulfide is introduced, and the system is kept until equilibrium is established, after which values of the following thermodynamic parameters are recorded: equilibrium pressure and mole fractions of components in each of the coexisting phases.

Let us briefly describe specific features of various experimental installations, which make it possible to trace the development of the method from early publications to the present time.

In the study by Jones [3], a stainless steel cylinder placed in a thermostat served as a cell in which equilibrium was established. On one of its sides, the cylinder was equipped with a capillary with a valve for sampling the liquid phase. On its other side, it had a gage. A capillary for sampling the vapor phase was connected to the upper part of the cylinder. A similar cell design was used by Lawson and co-authors [5]. To agitate the contents of the cell, the installation was equipped with an attachment that rocked the cell during an experiment. In the later studies [7–9], the agitation was effected by a rabble placed within the cell and driven by a magnetic activator.

It should be noted that, in the case of H_2S, equilibrium is attained rather rapidly because an amine can be protonated without any solvent (water), with hydrogen sulfide molecules serving as a source of protons. At the same time, the amine cannot be protonated in the case of CO_2 without involvement of water and equilibrium is attained considerably more slowly in systems with CO_2. However, agitation is important in both cases, because it provides dissolution of fine gas bubbles, which could otherwise reside for a long time, e.g., at places where the capillaries are connected to the cell.

If a cell fully made of stainless steel is used, the data obtained in measurements at low pressures may be underestimated because of the adsorption of gases on metallic surfaces. The installation employed in [10] comprised a glass cylinder with stainless steel flanges. Use of this cell variety enables a convenient visual inspection of the state of a system under study and allows measurements at both elevated and low partial pressures of CO_2. Impeller rabbles served to agitate both the liquid and vapor phases, which favored a faster establishment of equilibrium.

In [11], a cell with a variable volume controlled with two pistons was used. The state of a system under study was observed through a sapphire window of the cell. The advantage of this design is in that the pressure within the cell can be varied by changing the cell volume, whereas in the designs described above, the pressure can be raised by introducing an additional amount of gas and lowering the pressure in the course of an experiment is impossible in principle.

The temperature was monitored in early experiments with mercury thermometers, with resistance thermometers widely used for this purpose in present-day studies. The pressure has been for the most part measured with electronic transducers having a rather high precision. In earlier studies, however, the pressure was measured with spring or mercury gages having poorer measurement accuracy.

Solvents are, as a rule, batched by the gravimetric method. In the automated static installation used in [12, 13], solvents were fed into a cell with calibrated piston batchers, which allowed accurate determination of the volume of a liquid placed in the cell. The recalculation in terms of mass is done using density data. The mass of the gas in the cell was found in

many studies by weighing the cylinder from which the gas was introduced, before and after an experiment. Some researchers use special-purpose batching devices of a known volume, with controlled pressure and temperature. The amount of a gas in the cell is calculated in this case using p–V–T data.

In many cases, the composition of the vapor phase was determined by gas chromatography [4, 8] or mass spectrometry [3, 5]. Occasionally, another method has been used to analyze the vapor for the content of H_2S: a vapor sample was absorbed with a 25% solution of methyldiethanolamine and the content of sulfide ions was found by potentiometric titration with a NH_4NO_3 solution with a salt concentration of 0.1 M. The concentration of H_2S in the liquid phase was determined in most cases by adding an excess amount of an acidified iodine solution, followed by back titration with a thiosulfate. In [11], small concentrations of H_2S in the vapor phase were determined using Methylene Blue. In this method, sulfide ions react with paraaminodimethylamine to give Methylene Blue and then the coloration intensity is quantitatively measured with a spectrophotometer calibrated against standard sulfide solutions.

Samples for determining the content of CO_2 in the liquid phase were commonly taken into a NaOH solution, with the gas thereby converted into nonvolatile ionic forms. Further, these forms were precipitated as barium carbonate, which was then titrated with a sulfuric acid solution. In [4], samples for analysis for the content of CO_2 were taken into a vessel containing a weighed amount of sulfuric acid. The CO_2 evolved was collected into a graduated burette for determining the volume of the gas. This method is rather simple in use, but fails to provide good accuracy. In [3], the concentration of CO_2 in the liquid was found by the Knorr method modified by Scott. The method consists in that a sample is acidified with sulfuric acid and then heated. The CO_2 evolved is washed out with nitrogen, dried, and passed through a tube packed with special Caroxite absorbent. The amount of the gas absorbed is found by weighing. If hydrogen sulfide is present, it is removed from the gas flow with an acidified solution of potassium permanganate. In [11], an $AgNO_3$ solution added in a minor excess was used to oxidize H_2S, instead of potassium permanganate. The content of the amine in solution was determined by titrating an aliquot of the liquid phase with sulfuric acid, with Methyl Red as indicator.

There exists an attractive variety of the static method, which does not require any analysis of equilibrium phases. This technique was used in [14, 15] in a study of methyldiethanolamine-containing aqueous solutions of CO_2 and H_2S in the pressure range 100–8000 kPa. These measurements were performed at Prof. Maurer's laboratory at the chair of technical thermodynamics of the University of Kaiserslautern. The initial state of the system in the measuring cell is an aqueous solution of an amine of prescribed composition. In the course of an experiment, a certain amount of a gas is introduced under pressure into the cell and additional portions of an aqueous amine solution are introduced until the system comes to a homogeneous state. After equilibrium is attained, the pressure in the cell is gradually lowered by taking small samples of the liquid until first bubbles of the gas phase appear. The pressure is recorded at this instant of time. In this case, the amount of the gas phase is very small, and, therefore, the composition of the saturated liquid coincides with the general composition of the mixture. The advantages of the method consist in that phase analysis can be avoided, the expenditure of reagents is small, and the measurement accuracy is high.

Circulation method. Another technique widely used for studying the solubility of gases is the circulation method [16–22]. In this method, the saturation of an amine solution with a gas is provided by a circulation pump serving to bubble the gas through the liquid phase. The experimental installation includes a measuring cell equipped with a system for vapor circulation, vapor tank, cell for gas batching, and pressure transducers [17]. A constant temperature is maintained with a thermostat. As in the static method, the amounts of each of the components of the system are fixed; the equilibrium pressure and phase compositions are determined in the course of an experiment. The difference is in that the vapor is circulated and an inert component, nitrogen, is present in the system. At the beginning of an experiment, a weighed amount of a solution of water and of an amine of prescribed composition are placed in the measuring cell. Nitrogen is introduced into the cell (for further control over CO_2 batching) and, after the temperature is equilibrated, the equilibrium pressure, constituted by water and amine vapor pressures and nitrogen pressure, is recorded. Then a portion of CO_2 is introduced into the cell by a special device. The amount of the gas introduced is determined from a change in the pressure in the batching vessel with the use of p–V–T data. The total pressure in the cell is measured and equilibrium is considered to be attained if the pressure remains constant during a long interval of time (say, 30 min). Commonly, this process takes 3–4 h. The equilibrium partial pressure of CO_2 is found as the difference of the total pressure and the equilibrium pressure recorded

before the introduction of CO_2. Further, a new portion of CO_2 is introduced into the cell. This experimental procedure is repeated several times for each solution until a sufficient body of data on the liquid–vapor equilibrium is obtained.

The specific feature of the circulation technique used in [18] is in that a constant gas concentration in the vapor phase serves as an indication that equilibrium is attained. To determine this concentration, small vapor samples were taken so that changes in the composition of the liquid were negligible. A vapor sample was cooled to 283 K in order to condense water and the amine, and the content of CO_2 was determined with an IR analyzer. After the system came to equilibrium (in 2–3 h), both liquid and vapor phases were sampled for analysis.

Flow method. In addition to the static and circulation methods, the flow method [23–26] is occasionally used to study the solubility of gases. The specificity of this technique is in that the partial pressure of the acid gas in the gas flow is set in the course of an experiment and the composition of the liquid solution through which the gas flow is passed changes until the solution comes to equilibrium with the gas. Thus, the quantities set in the experiment are temperature, number of moles of water and an amine in the solution, and partial pressure of the gas (for definiteness, this will be CO_2 in what follows). A typical description of an installation of this kind can be found in [25].

The installation comprised two stainless steel cylinders placed in the vertical position in a water thermostat. The first cylinder, a water saturator, served to feed a gas saturated with a water vapor into the cell. The second cylinder contained the alkanolamine solution under study. A stainless steel pipe was inserted into the upper part of each of the cylinders. A capillary via which a gas flow was passed through the solution ran from this pipe into the cylinder. The flow contained, in addition to an acid gas under study, an inert carrier-gas (helium), which was necessary for providing a sufficient rate of solution saturation and for controlling the concentration of CO_2 by varying the relative amounts of gaseous components delivered into the cell. An accurately calibrated flow regulator served to provide a stable flow of a gas mixture. In the course of an experiment, the content of CO_2 in the input gas flow could be gradually changed using the flow regulator. The gas flow at the cell outlet was cooled to 273 K to remove water, after which the concentration of CO_2 in the gas was determined with an IR analyzer. The analyzer was preliminarily calibrated against a CO_2–N_2 mixture of a known composition. The equality of compositions of the gas mixture at the cell input and output served as an indication that equilibrium was attained between the gas phase and the solution. After these compositions became equal, the partial pressure of CO_2 in the flow at the cell inlet was taken as the equilibrium partial pressure in the cell over the CO_2–amine–water solution. The content of CO_2 in the saturated solution was found analytically. In summary of the description of experimental methods used to study the solubility of gases, distinctive features of each of these methods should be noted. The static method is sufficiently accurate, but requires, in some variants, a considerable expenditure of reagents. The technique enables studies under widely varying conditions. However, it cannot always be used in measurements at low gas concentrations, which is due to a significant contribution from the adsorption of gases of the apparatus surface to the experimental error.

The flow method is simpler in use and involves a smaller expenditure of substances, but its applicability area is limited to low pressures, in contrast to the static method.

The circulation method enables measurements at low and medium pressures. In contrast to the flow method, it does not require a carrier-gas. Compared with the static method, the circulation technique is less accurate at elevated pressures. Nevertheless, each of the techniques has its own advantages in certain cases, and all of them find application in modern research.

EXPERIMENTAL DATA ON TE SOLUBILITY OF ACID GASES

In recent decades, a large body of experimental data on the solubility of acid gases in alkanolamine solutions has been accumulated. The most widely used in the industry are aqueous solutions containing individual amines: monoethanolamine (MEA), diethanolamine (DEA), methyldiethanolamine (MDEA), and "sterically hindered" amines, as well as amine solutions with various modifying additives.

Solutions of Individual Amines

Systems constituted by an acid gas, MEA, and H_2O. Aqueous solutions of monoethanolamine have long been the main absorption system for extraction of CO_2 and H_2S from natural gas. Nowadays, MEA solutions are replaced with more effective mixtures, but still remain preferable absorbents in the case when

gas flows with low content of acid gases are used and these gases are to be removed to the maximum possible extent.

The main advantages of MEA, which predetermine its still wide use, are the following: high reactivity, low cost, and low capacity for absorption of hydrocarbons.

The efficiency of this amine as an absorbent of acid gases is illustrated by Fig. 1, in which the solubility of CO_2 in an aqueous solution of monoethanolamine is compared with the solubility of the same gas in pure water. It can be seen that presence of the amine in the aqueous solution markedly changes the run of the solubility isotherm of the gas. In the case of pure water, the isotherm is a curve along which the pressure strongly increases as the CO_2 concentration grows, beginning at its zero concentration. In an aqueous solution of the amine, two portions can be distinguished in the solubility isotherms of acid gases. While the mole ratio of the gas and the amine remains markedly smaller than unity, the pressure increases only slightly with the gas concentration in the solution, because the amine is protonated and molecular forms of CO_2 are converted into ionic forms. As the equilibrium concentrations of the ionic forms in the solution are reached, the curve abruptly changes its run, because further increase in the gas concentration is not accompanied by chemical transformations. In this region, dissolution occurs via physical absorption.

As disadvantages of MEA should be mentioned the following: instability at elevated temperatures, which results in a corrosion activity with respect to the equipment, especially in the case of mixtures of CO_2 and H_2S; formation of stable carbamates, which leads to a gross energy expenditure in regeneration of the amine; high heat of the reaction with CO_2 and H_2S (30% higher, compared with DEA); comparatively high vapor pressure of MEA, which leads to a considerable loss of the amine via evaporation.

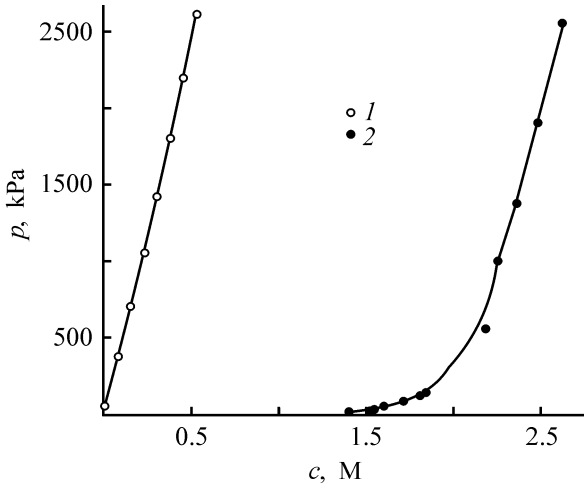

Fig. 1. Comparison of the solubilities of CO_2 in water and in an aqueous solution of MEA at T = 313 K. (c) CO_2 concentration and (p) pressure. (*1*) CO_2–H_2O [27] and (*2*) CO_2–MEA–H_2O [28] (c_{MEA} = 2.5 M).

Table 1 systematizes the available published data on the solubility of CO_2 and H_2S in aqueous solutions of MEA.

Systems constituted by an acid gas, DEA, and H_2O. Together with monoethanolamine, another representative of the same class of compounds, diethanolamine, is widely used in the industry. It retains all the advantages of MEA and, moreover, is thermally stable and, therefore, is not so aggressive with respect to the equipment. In addition, this secondary amine forms less stable carbamates. An additional important specific feature of DEA is its higher absorbing capacity, compared with monoethanolamine. As a disadvantage of DEA should be mentioned the need to use vacuum distillation in regeneration of spent solutions.

Table 1. Published data on the solubility of CO_2 and H_2S in aqueous solutions of MEA

Reference	Year of publication	MEA concentration	T, K	p, kPa	Reference	Year of publication	MEA concentration	T, K	p, kPa
Solubility of CO_2					Solubility of H_2S				
[3]	1959	3 mol kg^{-1} H_2O	313–413	0–931	[29]	1944	0.6–5 M	298–333	3–93
[5]	1976	3, 7 mol kg^{-1} H_2O	313–413	1–2786	[3]	1959	3 mol kg^{-1} H_2O	313–413	0–113
[28]	1992	7 mol kg^{-1} H_2O	313–373	1–1975	[5]	1976	3, 7 mol kg^{-1} H_2O	300–413	0–3853
[26]	2004	2.5 M	303–343	10–71	[23]	1980	2.5 M	373	0–1.5
[18]	2005	7 mol kg^{-1} H_2O	393	7–192	[21]	1991	2 M	313	1–2253

Table 2. Published data on the solubility of CO_2 and H_2S in aqueous solutions of DEA

Reference	Year of publication	DEA concentration	T, K	p, kPa
		Solubility of CO_2		
[30]	1931	9.5 mol kg^{-1} H_2O	298–328	1.3–101
[31]	1936	0.5–38 mol kg^{-1} H_2O	0–348	1.3–101
[32]	1941	3 mol kg^{-1} H_2O	373–413	241–1571
[33]	1962	0.5–6 mol kg^{-1} H_2O	293–373	1.3–400
[34]	1971	0.5–38 mol kg^{-1} H_2O	293–363	0–93
[4]	1972	0.5–8.0 M	298–413	1–5702
[5]	1976	3 mol kg^{-1} H_2O	311–394	0–3506
[35]	1984	0.5–2.5 M	298	68–2013
[6]	1984	1 mol kg^{-1} H_2O	373–478	2.0–41
[36]	1985	2.5 mol kg^{-1} H_2O	313, 373	0–101
[37]	1987	0.5, 6 mol kg^{-1} H_2O	298	7–2013
[38]	1989	0.5–9.5 mol kg^{-1} H_2O	300–389	0–64.9
[39]	1989	1–3 mol kg^{-1} H_2O	298	2–15
[40]	1994	7 mol kg^{-1} H_2O	373	0–101
[41]	1996	20.2 mol kg^{-1} H_2O	323	0–0.6
[42]	1996	4 mol kg^{-1} H_2O	313–353	5–357
		Solubility of H_2S		
[30]	1931	9.5 mol kg^{-1} H_2O	298–328	0–101
[43]	1950	1, 2.5 mol kg^{-1} H_2O	288–323	0–42
[44]	1957	1–9.5 mol kg^{-1} H_2O	300–333	0–90
[16]	1973	0.5–5 M	298–393	0–1711
[5]	1976	3 mol kg^{-1} H_2O	311–394	0–37
[36]	1985	2.4–14 mol kg^{-1} H_2O	313–373	0–3.2
[38]	1989	2.4–9.5 mol kg^{-1} H_2O	300–389	0–75
[45]	1991	2.5 mol kg^{-1} H_2O	298, 313	0–10
[46]	1999	2.5 mol kg^{-1} H_2O	313, 323	0–0.5

Published data on the solubility of acid gases in aqueous solutions of DEA are listed in Table 2.

Systems constituted by an acid gas, MDEA, and H_2O. Methyldiethanolamine found industrial use in the 1950s [47]. Despite the high coast, compared with MEA and DEA, and low rate of the reaction with CO_2, it has a number of specific features, which not only compensate for these disadvantages, but even make the process of gas treatment with MDEA economically more feasible than that with primary and secondary amines.

A most important specific feature of MDEA is its capacity for selective absorption of hydrogen sulfide from its mixture with carbon dioxide [48–50]. The selectivity of absorption is due in the given case to the kinetic factor, specifically, to the higher rate of the reaction of MDEA with H_2S. This is associated with specific features of the mechanism of chemical interaction, already mentioned above. It should be recalled that these two compounds can react directly, without involvement of solvent molecules. As for CO_2, its reaction with MDEA requires an aqueous medium as a source of protons for formation of hydrocarbonate ions.

Apart from the selectivity with respect to H_2S, MDEA has a number of additional advantages over MEA and DEA [48, 50]. This amine is a difficultly volatile compound, which makes it possible to avoid loss of the solvent via evaporation in processing of the gas flow. Use of this solvent is also economically justified in some cases for absorption of CO_2 [50], despite the unfavorable kinetic factor. The enthalpy of the reaction of acid gases with MDEA is sufficiently low [2], and, therefore the regeneration of the amine is considerably less energy-consuming than that in the case of MEA and DEA. The energy saving in re-

Table 3. Published data on the solubility of CO_2 and H_2S in aqueous solutions of MDEA

Reference	Year of publication	DEA concentration	T, K	p, kPa
		Solubility of CO_2		
[24]	1982	2, 4.28 M	298–393	0–6600
[35]	1984	1, 2 M	298, 323	10–4900
[35]	1984	2 mol kg^{-1} H_2O	311–389	20–5800
[51]	1987	1.69, 4.28 M	373–473	1–49
[25]	1991	2, 4.28 M	313	0–90
[52]	1991	2 M	313	0–3800
[28]	1992	3.6 mol kg^{-1} H_2O	313–373	0–2000
[53]	1993	2, 4.5 mol kg^{-1} H_2O	313, 373	0–240
[54]	1994	3.6 mol kg^{-1} H_2O	313, 393	200–19 000
[40]	1994	4.28 M	373, 393	160–3800
[14]	1996	2, 4 mol kg^{-1} H_2O	313–413	70–4100
[17]	1997	0.44–25 mol kg^{-1} H_2O	323–373	0–270
[15]	2001	8 mol kg^{-1} H_2O	313–393	2.3–7600
[12]	2004	2.9, 7.4 mol kg^{-1} H_2O	298–348	0–4600
		Solubility of H_2S		
[24]	1982	1–4.28 M	298–393	0–5900
[35]	1984	1.1 M	298	0–13
[37]	1987	2.1 mol kg^{-1} H_2O	311–389	0–16
[52]	1991	2 M	313	0–16
[53]	1993	4.5, 8.4 mol kg^{-1} H_2O	13, 373	0–300
[21]	1993	2.57 M	313–373	0–450
[14]	1996	2, 4 mol kg^{-1} H_2O	313–413	180–4 300
[15]	2001	8 mol kg^{-1} H_2O	313–393	150–2800
[13]	2004	7.4 mol kg^{-1} H_2O	313–373	0–1000

generation is also favored by the fact that the MDEA molecule has no hydrogen atoms directly bonded to nitrogen. Thus, the reaction with CO_2 yields no carbamates, whose decomposition requires additional energy expenditure in the case of primary and secondary amines. At the same time, the absorbing capacity of this amine exceeds that of MEA and DEA because of the very weak dissociation of the protonated form of MDEA.

Finally, the very high stability of the MDEA molecule should be noted. It does not decompose even upon strong heating, and, therefore, its corrosiveness with respect to the equipment is considerably lower than that of the other amines.

The available published experimental data on the solubility of acid gases in aqueous solutions of MDEA are summarized in Table 3.

These data were obtained in a wide range of temperatures and pressures. This is due to the practical demand for information about the phase behavior of the systems under consideration in various conditions. Gases are for the most part absorbed in industrial installations in the temperature range 313–333 K. Absorption at lower temperatures is unfeasible from the standpoint of the process kinetics. In addition, the chemical reaction of the gases with the amines is exothermic. Accordingly, there inevitably occurs heating by the heat of the reaction. The temperature range 373–413 K is also of interest for the industry. At these temperatures, amine solutions are regenerated via desorption. At higher temperatures the amines decompose, which leads to corrosion of the equipment. However, in the case of thermally stable amines, such as MDEA, desorption is also performed at temperatures higher than 413 K.

Of interest for development of various semiempirical models of industrial processes involving absorption–desorption of gases are data for other temperatures and, in particular, those for the temperature range 333–373 K. Therefore, there have been numerous reports on studies under these conditions.

Table 4. Published data on the solubility of acid gases in solutions of sterically hindered amines

Reference	Year of publication	System	Amine concentration	T, K	p, kPa
[22]	1997	CO_2–AMP–H_2O	2 M	313	30–160
		H_2S–AMP–H_2O	2 M	313	0–180
[8]	1998	CO_2–AMP–H_2O	2.43–6.24 mol kg^{-1} H_2O	313–353	0–2700
[9]	2002	CO_2–AEPD–H_2O	10, 30 wt %	313–333	0–2800
[20]	2003	CO_2–TIPA–H_2O	0.58, 2.24 mol kg^{-1} H_2O	313–333	0–2800
[26]	2004	CO_2–TIPA–H_2O	2 M	303–343	11–78

The greatest body of experimental data on the solubility of acid gases in aqueous solutions of alkanolamines has been obtained by the research group of Prof. Mather [4, 16, 23, 24, 36, 52–54]. The solubility of CO_2 and H_2S in solutions of mono- and diethanolamine has been studied in detail by Lawson et al. [5]. Systematic data on the solubility of CO_2 and H_2S in aqueous solutions of MDEA under widely different conditions have been obtained in the framework of a joint scientific project of the authors of this review with the research group of Prof. Maurer (University of Kaiserslautern, Germany) [14, 15]. A large body of experimental data was also reported in [3, 6, 29].

Systems containing sterically hindered amines. A number of studies have been concerned with the solubility of acid gases in aqueous solutions of the so-called sterically hindered amines and, in particular, 2-amino-2-ethyl-1,3-prop-anediol (AEPD), triisopropanolamine (TIPA), and 2-amno-2-methyl-1-propanol (AMP). The interest in objects of this kind is due both to their high boiling point and to a low corrosion activity with respect to the equipment. Published data on the solubility of acid gases in solutions of sterically hindered amines are summarized in Table 4.

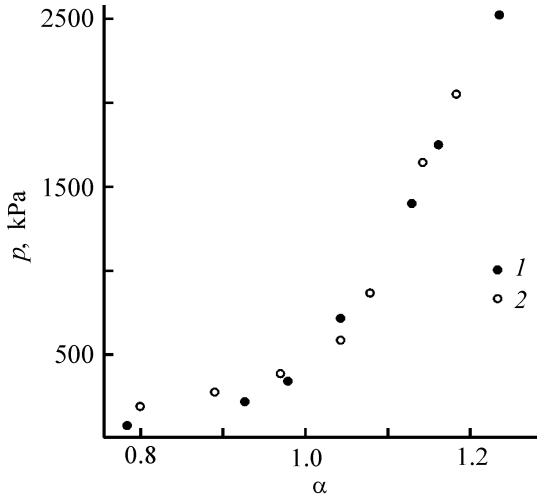

Fig. 2. Isotherms of CO_2 solubility in aqueous solutions of MDEA and TIPA at T = 313 K. (α) Ratio between the numbers of moles of the gas and the amine and (p) pressure; the same for Figs. 5, 6. (*1*) MDEA [14] (m = 2 mol kg^{-1} H_2O) and (*2*) TIPA [20] (m = 2.2 mol kg^{-1} H_2O).

The absorbing capacity of solutions of these amines is rather high. This is illustrated by Fig. 2, in which isotherms of CO_2 solubility in aqueous solutions of MDEA and TIPA are compared.

The data in Fig. 2 refer to a TIPA solution somewhat more concentrated than the MDEA solution. The coincidence of the isotherms under consideration means that the absorbing capacity of the TIPA solution is only slightly lower than that of the MDEA solution. A disadvantage of the sterically hindered amines is that carbamates are formed as in the case of extended primary and secondary amines. However, the carbamates formed with sterically hindered amines are considerably less stable than those formed by MEA and DEA and require a considerably smaller energy expenditure for their decomposition.

Use of Various Additives for Improving the Efficiency of Absorption of Acid Gases

A separate area of research is associated with analysis of the solubility of gases in aqueous solutions of amines in the presence of various compounds. These are the so-called modifying additives, whose role consists in minimizing the effect of factors unfavorable for absorption of gases. For example, it was already mentioned that, although MDEA has a number of advantages over other alkanolamines, its use for absorption of CO_2 is limited in some cases by the kinetic factor [28]. Therefore, it was suggested in 1985 to use aqueous solutions containing MDEA and a primary or secondary amine for treatment of gas flows [55]. The interaction of gases with MEA and DEA is faster than that with MDEA. At the same time, MDEA shows capacity for selective binding of H_2S and forms no stable carbamates (which is an important circumstance in regeneration of the amine). Thus, use of

a mixed solution makes it possible to simultaneously take advantage of the virtues of each of the amines. The solubility of CO_2 and H_2S in aqueous solutions of MDEA with MEA and DEA additives was studied in [56–58].

Addition of primary and secondary amines improves the interaction kinetics, but makes higher the corrosion activity of the solvent. Here, too, the choice of the solvent is aimed to raise the absorption rate without introduction of additional negative factors. Piperazine is frequently used as a modifying additive. A high efficiency of CO_2 absorption by the MDEA solution is achieved in the presence of piperazine. The effect of this compound is due, firstly, to its high capacity for protonation (one molecule of piperazine can add two protons). Secondly, piperazine can form three different carbamate ions with CO_2. Owing to this circumstance, its use in a mixture with MDEA for absorption of CO_2 is economically feasible. Addition of piperazine also has a positive effect in treatment of a mixture of carbon dioxide and hydrogen sulfide with an MDEA solution. In this case, piperazine improves the selectivity of hydrogen sulfide absorption.

The effect of piperazine on the solubility of CO_2 in aqueous solutions of MDEA was studied in [7, 59]. A systematic study of the solubility of the gas in the H_2S–MDEA–H_2O–piperazine system was carried out in [60].

One more way to improve the efficiency of absorption of acid gases is addition of "physical" solvents, i.e., compounds that do not react chemically with gas molecules, but can effectively absorb these molecules via physical absorption. The following positive factors are characteristic of absorbents of this kind: substantial increase in the solubility of the gases because of the larger contribution of the physical absorption and minimum energy expenditure for regeneration of the solvent.

One of the most widely used physical solvents is methanol. In [61], the effect of methanol on the solubility of CO_2 in an aqueous solution of MEA was studied. Henni and Mather [62] examined the effect of methanol on the solubility of CO_2 in an aqueous solution of MDEA and analyzed the solubility of the same gas in a nonaqueous solvent, MDEA–methanol, containing 50% of each of the components. A pronounced improvement of the solubility of CO_2 in the presence of methanol was observed.

Another widely used physical solvent is tetrahydrothiophene-1,1-dioxide (sulfolane). In [63], the solubility of carbon dioxide and hydrogen sulfide in a solution with a patented name Sulfinol, which contained 40 wt % diisopropanolamine (DIPA), 40 wt % sulfolane, and 20 wt % water, was studied. McGregor et al. [52] analyzed the effect of sulfolane on the solubility of CO_2 and H_2S in aqueous solutions of MDEA. In [64], the solubility of CO_2 in an aqueous solution of MDEA, simultaneously containing piperazine and sulfolane, was examined.

One more example of solutions of this kind is ethylene glycol. A study by Song [65] was devoted to analysis of the influence exerted by this additive on the solubility of CO_2 in an aqueous solution of monoethanolamine. It was found experimentally under what conditions addition of ethylene glycol improves the absorption capacity of the MEA solution to the greatest extent. The advantage of ethylene glycol also consists in that the selectivity of absorption of hydrogen sulfide from its mixture with carbon dioxide by an MDEA solution is improved. In this case, the selectivity is not due to the kinetic factor, as in to the case of the piperazine additive. Here, the positive property of ethylene glycol is manifested in that chemical binding of CO_2 by methyldiethanolamine is impossible without participation of water because of the lack of a sufficient number of protons. As for H_2S, it can react with MDEA even in a non-aqueous medium, because it is a source of protons by itself. A systematic study of the effect of ethylene glycol on the solubility of CO_2 and H_2S in aqueous solutions of MDEA was carried out in [66].

Compounds that Hinder Absorption of Acid Gases

The studies mentioned above were concerned with the effect of various compounds intentionally added to an absorbent solution to raise its absorption capacity on the solubility of gases. However, industrial processes include cases in which compounds are formed in an absorbent solution in treatment of gas flows.

An important particular case in which chemical compounds appear in the course of absorption of acid gases is formation of strong electrolytes. For example, the following process occurs in the aqueous solution of MDEA in the presence of sulfur trioxide in the gas flow:

$$SO_3 + H_2O + 2MDEA \rightarrow (MDEAH)_2SO_4$$

In the subsequent regeneration of the amine with an alkali, sodium sulfate is formed as a by-product:

$$(MDEAH)_2SO_4 + 2NaOH \rightarrow 2MDEA + 2H_2O + Na_2SO_4.$$

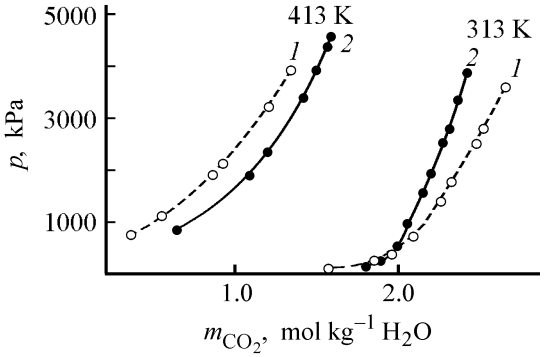

Fig. 3. Effect of sodium sulfate on the solubility of CO_2 in an aqueous solution of MDEA. (*m*) CO_2 concentration and (*p*) pressure. (*1*) CO_2–H_2O–MDEA [14] (m_{MDEA} = 2 mol kg^{-1} H_2O) and (*2*) CO_2–H_2O–MDEA–Na_2SO_4 [67] (m_{MDEA} = 2 mol kg^{-1} H_2O, m_{salt} = 1 mol kg^{-1} H_2O).

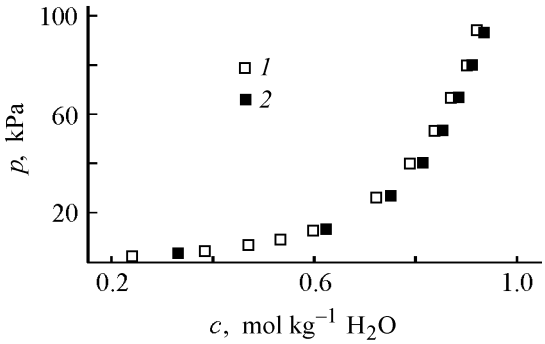

Fig. 4. Comparison of the data on the solubility of H_2S in an aqueous solution of MEA (c_{MEA} = 7 M) at T = 313 K, obtained by different authors. (*c*) H_2S concentration and (*p*) pressure. Data of: (*1*) [28] and (*2*) [29].

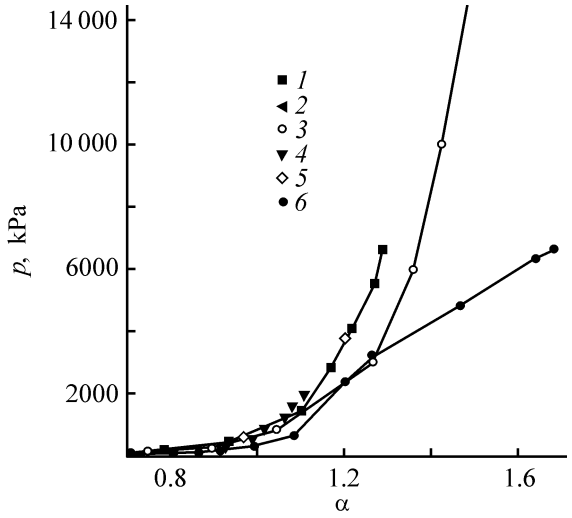

Fig. 5. Comparison of the data on the solubility of the gas in the CO_2–MDEA–H_2O system at T = 313 K, obtained by different authors. Data of: (*1*, *6*) [24], (*2*) [53], (*3*) [54], (*4*) [28], and (*5*) [52]. Amine concentration (mol kg^{-1} H_2O): (*1*) 8.02, (*2*) 4.50, (*3*, *4*) 3.60, and (*5*, *6*) 2.56.

Obtaining quantitative information about the effect of electrolytes on the solubility of gases in MDEA solutions is an important task, because these compounds strongly affect the solubility of acid gases in aqueous solutions of the amine. As demonstrated by the results of [67, 68], this influence is of a rather complicated nature, although electrolytes are not directly involved in chemical reactions. In some cases and, in particular, at elevated temperatures, it is impossible to predict a priori even qualitatively the effect of electrolytes on the solubility of gases in amine solutions.

For example, sodium sulfate commonly exerts a strong salting-out effect on gases, but at low CO_2 concentrations it, by contrast, improves the solubility of the gas (Fig. 3). This example of the seemingly unusual phase behavior of electrolyte-containing systems is not the only one.

A strong difference between the effects of sodium sulfate and methyldiethanolammonium on the solubility of CO_2 and H_2S in an aqueous solution of MDEA has been revealed [69]. The phenomena observed were interpreted with account of the ion sizes, different capacities for solvation, and ion association occurring in the solutions. Understanding of the effects observed furnishes an opportunity to prognosticate the phase behavior of the systems under study, which is important for optimization of industrial processes of absorption of CO_2 and H_2S.

RELIABILITY OF EXPERIMENTAL DATA ON THE SOLUBILITY OF ACID GASES

An important characteristic of any experimental data is their accuracy. For the systems under discussion, the experimental results obtained by different authors are well consistent in many cases. The reliability of data obtained even many decades ago is beyond any doubt and they are in a good agreement with the results of present-day studies. Figure 4 shows as an example the data of Shen [28] and Riegger [29] (obtained in 1992 and 1944, respectively) on the solubility of CO_2 in an aqueous solution of MEA.

The reliability of the data obtained is confirmed by use of modern precision techniques in the related measurements. For example, the solubility of gases in the systems CO_2–MEA–H_2O, CO_2/H_2S–DEA–H_2O, and CO_2/H_2S–MDEA–H_2O has been studied at a high experimental level [12–15, 60, 67, 68].

At the same time, quite a number of examples of strong discrepancies between data of different authors can be given. As can be seen in Fig. 5, a significant

difference is observed for the CO_2–MDEA–H_2O system between the data of Jou [24] and MacGregor [52] for the amine molality of 2.56. At the same time, isotherms reported by these authors and Shen [28] for solutions with different amine concentrations coincide. The solubility isotherm in plots of pressure against the ratio α between the numbers of moles of the gas and the amine should run the higher, the greater the content of the amine in a solution. However, the H_2S pressures obtained by Li and Shen [21] for a solution with a MDEA concentration of 3.56 mol kg^{-1} H_2O lie in Fig. 6 higher than the values obtained by Jou [24] for a MDEA concentration of 8.02 mol kg^{-1} H_2O.

To assess the reliability of published data on the solubility of gases in aqueous solutions of MDEA, it is necessary to subject these data to a thorough analysis. The assessment of the data quality is aided by comparison of results obtained by different authors. However, either there are no published data for comparison or the comparison is difficult because the data to be compared are obtained in different studies under dissimilar conditions.

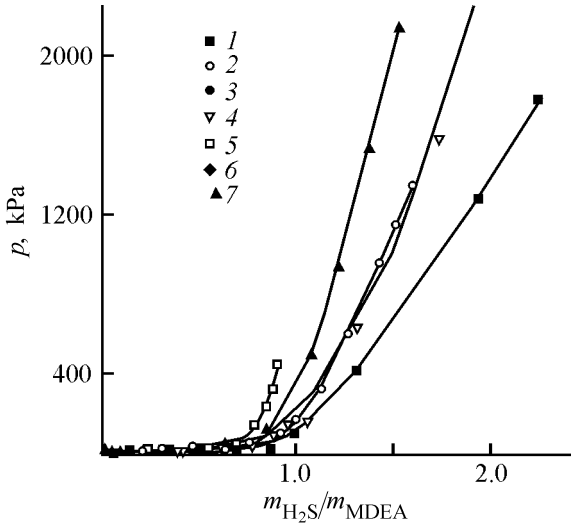

Fig. 6. Comparison of data on the solubility of the gas in the H_2S–MDEA–H_2O system at T = 313 K, obtained by different authors. Data of: (*1*, *3*, *7*) [24], (*2*) [37], (*4*) [52], (*5*) [21], and (*6*) [53]. Amine concentration (mol kg^{-1} H_2O): (*1*) 1.12, (*2*) 2.1 (T = 311 K), (*3*, *4*) 2.56, (*5*) 3.56, (*6*) 4.5, and (*7*) 8.02.

In addition, reports on studies of mixed amine solutions frequently present data that are rather detailed, but inconvenient for a thermodynamic analysis. For example, the solubility of CO_2 and H_2S in mixed solutions of AMP and DEA was studied in [22] at varied relative contents of the amines but constant total content of AMP and DEA, equal to 30 wt %. These data are undoubtedly useful for a particular industrial application, but it would be of real interest from the thermodynamic standpoint to have data obtained at a constant total number of moles of the amines in solution.

The verification of the accuracy of experimental data is well aided by thermodynamic models. However, the potentialities of these models are considerably higher. They enable correction of experimental data and prognostication of properties of systems under conditions for which there are no data. The important role of the models consists in that they relate the behavior of a system to molecular characteristics of its components and to contributions of physical and chemical interactions. The modeling of phase equilibria in aqueous systems containing alkanolamines and acid gases constitutes a separate research area in which a large number of studies have been carried out [70–73].

CONCLUSIONS

Effective and reliable methods for experimental studies of the solubility of acid gases have been developed. The choice of a particular technique is governed by specific conditions of a process being designed. There are sufficiently detailed published data on the solubility of gases in aqueous solutions of both individual amines and amines with additives improving the solubility. However, unreliable experimental results frequently occur, and attention should be given to the choice of a set of experimental data. As for the effect of additives that hinder the dissolution of acid gases, it has been studied in insufficient detail. For example, there are no data of the effect of additions of sodium sulfate and alkanolammonium in systems with primary, secondary, and sterically hindered amines. Information about the effect of other electrolytes cannot be found in the literature at all. Further studies are necessary in this area of research.

REFERENCES

1. US Patent 1 783 901.
2. Kohl, A.L. and Nielsen, R.B., *Gas Purification*, Houston, Texas: Gulf, 1997, 5th ed.
3. Jones, J.H., Froning, H.R., and Claytor, E.E., *J. Chem. Eng. Data*, 1959, vol. 4, no. 1, pp. 85–92.
4. Lee, J.I., Otto, F.D., and Mather, A.E., *J. Chem. Eng. Data,* 1972, vol. 17, no. 4, pp. 465–468.
5. Lawson, J.D. and Garst, A.W., *J. Chem. Eng. Data,* 1976, vol. 21, no. 1, pp. 20–30.
6. Kennard, M.L. and Meisen, A., *J. Chem. Eng. Data*, 1984, vol. 29, pp. 309–312.

7. Xu, G.-W., Zhang, C.-F., Qin, S.-J., et al., *Ind. Eng. Chem. Res.*, 1998, vol. 37, no. 4, pp. 1473–1477.
8. Silkenbaeumer, D., Rumpf, B., and Lichtenthaler, R.N., *Ind. Eng. Chem. Res.*, 1998, vol. 37, no. 8, pp. 3133–3141.
9. Park, M.K. and Sandall, O.C., *J. Chem. Eng. Data*, 2001, vol. 46, no. 1, pp. 166–168.
10. Lemoine, B., Li, Y.-G., Cadours, R., et al., *Fluid Phase Equilib.*, 2000, vol. 172, pp. 261–277.
11. Addicks, J. and Owren, G.A., *J. Chem. Eng. Data*, 2002, vol. 47, no. 4, pp. 855–860.
12. Sidi-Boumedine, R., Horstmann, S., Fisher, K., et al., *Fluid Phase Equilib.*, 2004, vol. 218, pp. 85–94.
13. Sidi-Boumedine, R., Horstmann, S., Fisher, K., et al., *Fluid Phase Equilib.*, 2004, vol. 218, pp. 149–155.
14. Kuranov, G., Rumpf, B., Smirnova, N.A., and Maurer, G., *Ind. Eng. Chem. Res.*, 1996, vol. 35, pp. 1959–1966.
15. Perez-Salado Kamps, A., Balaban, A., Jodecke, M., et al., *Ind. Eng. Chem. Res.*, 2001, vol. 40, pp. 696–706.
16. Lee, J.I., Otto, F.D., and Mather, A.E., *J. Chem. Eng. Data*, 1973, vol.18, no. 4, p. 420.
17. Rho, S.-W., Yoo, K.-P., Lee, J.S., et al., *J. Chem. Eng. Data*, 1997, vol. 42, no. 6, pp. 1161–1164.
18. Ma'mun, S., Nilsen, R., and Svendsen, H., *J. Chem. Eng. Data*, 2005, vol. 50, no. 2, pp. 630–634.
19. Park, J-Y., Yoon, S.J., Lee, H., et al., *Fluid Phase Equilib.*, 2002, vol. 202, pp. 359–366.
20. Chauhan, R.K., Yoon, S.J., Lee, H., et al., *Fluid Phase Equilib.*, 2003, vol. 208, pp. 239–245.
21. Li, M.-H. and Shen, K.-P., *J. Chem. Eng. Data*, 1993, vol. 38, no. 1, pp. 105–108.
22. Jane, I.-S. and Li, M.-H., *J. Chem. Eng. Data*, 1997, vol. 42, no. 1, pp. 98–105.
23. Isaacs, E.E., Otto, F.D., and Mather, A.E., *J. Chem. Eng. Data*, 1980, vol. 25, no. 1, pp. 118–120.
24. Jou, F.-J., Mather, A.E., and Otto, F.D., *Ind. Eng. Chem. Process Des. Dev.*, 1982, vol. 21, pp. 539–544.
25. Austgen, D.M. and Rochelle, G.T., *Ind. Eng. Chem. Res.*, 1991, vol. 30, no. 3, pp. 543–555.
26. Daneshvar, N., Zaafarani Moattar, M., Abedinzadegan Abdi, T.M., and Aber, S., *Sep. Purif. Technol.*, 2004, vol. 37, pp. 135–147.
27. Zawisza, A. and Malesinska, D., *J. Chem. Eng. Data*, 1981, vol. 26, pp. 388–391.
28. Shen, K.-P. and Li, M.-H., *J. Chem. Eng. Data*, 1992, vol. 37, no. 1, pp. 96–100.
29. Riegger, E., Tartar, H.V., and Lingafelter, E.C., *J. Am. Chem. Soc.*, 1944, vol. 66, pp. 2024–2027.
30. Bottoms, R.R., *Ind. Eng. Chem.*, 1931, vol. 25, pp. 501–504.
31. Mason, J.W. and Dodge, D.F., *Trans. Am. Inst. Chem. Eng.*, 1936, vol. 32, no. 1, pp. 27–48.
32. Reed, R.M. and Wood, W.R., *Trans. Am. Inst. Chem. Eng.*, 1941, vol. 37, pp. 363–384.
33. *Gas Conditioning Fact Book*, Midland, Michigan: The Dow Chemical Co., 1962.
34. Murzin, V.I. and Leits, I.L., *Zh. Fiz. Khim.*, 1971, vol. 45, pp. 417–420.
35. Bhairi, A.M., Experimental Equilibrium between Acid Gas and Ethanolamine Solutions, *Ph.D. Dissertation*, Stillwater, 1984.
36. Lal, D., Otto, F.D., and Mather, A.E., *Canad. J. Chem. Eng*. 1985, vol. 63 P, pp. 681–685.
37. Maddox, R.N., Bhairi, A.H., Diers, J.R., et al., *Gas Process Assn. Res. Rep.*, 1987, p. 104.
38. Maddox, R.N. and Elizondo, E.M., *Gas Process Assn. Res. Rep.*, 1989, p. 124.
39. Oyevaar, M.H., Fontein, H.J., and Westerterp, K.R., *J. Chem. Eng. Data*, 1989, vol. 34, pp. 405–408.
40. Dawodu, O.F. and Meisen, A., *J. Chem. Eng. Data*, 1994, vol. 39, pp. 548–552.
41. Rogers, W.J., Bullin, J.A., Davison, R.R., et al., *Am. Inst. Chem. Eng. J.*, 1997, vol. 43, pp. 3223–3231.
42. Seo, D.-J. and Hong, W.-H., *J. Chem. Eng. Data*, 1996, vol. 41, pp. 258–260.
43. Leibush, A.G. and Shneerson, A.L., *Zh. Prikl. Khim.*, 1950, vol. 23, no. 2, pp. 145–152.
44. Atwood, K., Arnold, M.R., and Kindrick, R.C., *Ind. Eng. Chem.*, 1957, vol. 49, no. 9, pp. 1439–1444.
45. Cheng, G.-X., Tang, W.-L., and Shen, F., *Fuel Sci. Technol. Int.*, 1991, vol. 9, no. 8, pp. 935–947.
46. Jagushte, M.V. and Mahajani, V.V., *Ind. J. Chem. Technol.*, 1999, vol. 6, pp. 125–133.
47. Frazer, H.H. and Kohl, A.L., *Ind. Eng. Chem.*, 1950, vol. 42, pp. 2288–2292.
48. Goar, B.G., *Oil Gas J.*, 1980, vol. 78, no. 18, pp. 239–242.
49. Yu, W.C. and Astarita, C., *Chem. Eng. Sci.*, 1987, vol. 42, no. 3, pp. 419–424.
50. Srinivasan, V. and Aiken, R.C., *Fuel Process. Technol.*, 1988, vol. 19, pp. 141–152.
51. Chakma, A. and Meisen, A., *Ind. Eng. Chem. Res.*, 1987, vol. 26, pp. 2461–2466.
52. MacGregor, R.J. and Mather, A.E., *Canad. J. Chem. Eng.*, 1991, vol. 69, pp. 1357–1366.
53. Jou, F.Y., Carroll, J.J., Mather, A.E., and Otto, F.D., *Canad. J. Chem. Eng.*, 1993 V. 71, pp. 264–268.
54. Jou, F.Y., Otto, F.D., and Mather, A.E., *Ind. Eng. Chem. Res.*, 1994, vol. 33, no. 8, pp. 2002–2005.
55. Chakravarty, T., Phukan, U.K., and Weiland, R.H., *Chem. Eng. Prog.*, 1985, vol. 81, p. 32.
56. Hagewieshe, D.P., Ashour, S.S., Al-Ghawas, H.A., and Sandall, O.C., *Chem. Eng. Sci.*, 1995, vol. 50, no. 7, pp. 1071–1079.
57. Murrieta-Guevara, F., Rebolledo-Libreros, Ma.E.,

Romero-Martinez, A., and Trejo, A., *Fluid Phase Equilib.*, 1998, vol. 150–151, pp. 721–729.

58. Rebolledo-Liberos, Ma.E. and Trejo, A., *Fluid Phase Equilib.*, 2004, vol. 218, pp. 261–267.
59. Liu, H.B., Zhang, C.-F., and Xu, G.-W., *Ind. Eng. Chem. Res.*, 1999, vol. 38, no. 10, pp. 4032–4036.
60. Xia, J., Perez-Salado-Kamps, A., and Maurer, G., *Fluid Phase Equilib.*, 2003, vol. 207, pp. 23–34.
61. Banasjak, J., *Gaz, Woda Tech. Sanit.*, 1981, vol. 55, pp. 196–199.
62. Henni, A. and Mather, A.E., *J. Chem. Eng. Data*, 1995, vol. 40, no. 2, pp. 493–495.
63. Isaacs, E.E., Otto, F.D., and Mather, A.E., *J. Chem. Eng. Data*, 1977, vol. 22, no. 3, pp. 317–319.
64. Jenab, M.H., Abdi, M.A., Najibi, S.H., and Matin, N.S., *J. Chem. Eng. Data*, 2005, vol. 50, no. 2, pp. 583–586.
65. Song, J.-H., *J. Chem. Eng. Data*, 1996, vol. 41, pp. 497–499.
66. Xu, H.-J., Zhang, C.-F., and Zheng, Z.-S., *Ind. Eng. Chem. Res.*, 2002, vol. 41, no. 24, pp. 6175–6180.
67. Anufrikov, Yu., Perez-Salado Kamps, A., Kuranov, G., et al., *Am. Inst. Chem. Eng. J.*, 2002, vol. 48, pp. 168–177.
68. Anufrikov, Yu., Perez-Salado Kamps, A., and Rumpf, B., *Ind. Eng. Chem. Res.*, 2002, vol. 40, no. 10, pp. 2571–2578.
69. Anufrikov, Yu.A., Phase Equilibria in Aqueous Systems Containing Alkanolamines, Acid Gases, and Strong Electrolytes, *Cand. Sci. Dissertation*, St. Petersburg, 2006.
70. Smirnova, N.A., Victorov, A.I., and Kuranov, G.L., *Fluid Phase Equilib.*, 1998, vol. 150–151, pp. 161–171.
71. Kuranov, G.L. and Smirnova, N.A., *Rus. J. Phys. Chem.*, 2001, vol. 75, Suppl. 1, pp. 5170–5180.
72. Kaewsichan, L., Al-Bofersen, O., Yesavage, V.F., and Selim, S., *Fluid Phase Equilib.*, 2001, vol. 183–184, pp. 159–171.
73. Vrachnos, A., Voutsas, E., Magoulas, K., and Lygeros, A., *Ind. Eng. Chem. Res.*, 2004, vol. 43, no. 11, pp. 2798–2804.

ISSN 1070-4272, Russian Journal of Applied Chemistry, 2007, Vol. 80, No. 4, pp. 528–535. © Pleiades Publishing, Ltd., 2007.
Original Russian Text © V.V. Gusarov, V.I. Al'myashev, V.B. Khabenskii, S.V. Beshta, V.S. Granovskii, 2007, published in Zhurnal Prikladnoi Khimii, 2007, Vol. 80, No. 4, pp. 541–548.

INORGANIC SYNTHESIS AND INDUSTRIAL INORGANIC CHEMISTRY

Interaction of a Material Based on Aluminum and Iron Oxides with a Metal Melt

V. V. Gusarov, V. I. Al'myashev, V. B. Khabenskii, S. V. Beshta, and V. S. Granovskii

Grebenshchikov Institute of Silicate Chemistry, Russian Academy of Sciences, St. Petersburg, Russia

Federal State Unitary Enterprise Aleksandrov Research Technological Institute, Sosnovyi Bor, Leningrad oblast, Russia

Received March 13, 2007

Abstract—Interaction of an oxide material with a melt of metals in the combustion mode was studied experimentally. The conditions in which processes of this kind can occur without any increase in the temperature of the environment are possible were analyzed.

DOI: 10.1134/S1070427207040027

Commonly, oxide materials brought in contact with liquid media, including molten metals, perform barrier functions and represent in this case a group of refractory materials [1–3]. Such an application of these materials imposes certain limitations on the nature of their interaction with liquids. Primarily, materials of this kind should, as a rule, provide an invariable chemical composition of the liquid in the course of their contact. In addition, the construction and functional characteristics of these materials should be preserved during an as long a period of time as possible. At the same time, the interest has increased in recent years in materials exhibiting a fundamentally different type of interaction with liquid media and, in particular, with high-temperature melts, which is due to their different functional purposes. Primarily, sacrificial materials should be distinguished in this regard.

The sacrificial materials are used in, e.g., production of inorganic nanotubes [4–7]. In this case, the primary goal of these materials is to create conditions for rolling of nanorolls after the sacrificial material is dissolved in the liquid phase.

Another example of sacrificial materials is constituted by materials for the passive safety system of nuclear reactors [8, 9]. The development of this class of functional materials was a consequence of the need to provide a significantly higher safety level for nuclear power engineering and the resulting design of new safety systems [10]. The sacrificial materials for the passive safety system of nuclear reactors should satisfy a large number of requirements, which are contradictory in some cases. It was shown in [11, 12] that a preferable mode of the interaction between a sacrificial material and a melt is the combustion of the material.

However, the combustion, as a rule, occurs with a strong exothermic effect [13, 14], which leads to a significant heating-up of the environment. In the case of interaction of a sacrificial material with a melt in the core of a nuclear reactor, this contradicts one of the basic fundamental requirements: the melt should be cooled in the course of its interaction with the material. Thus, combustion of a sacrificial material without heating of the melt with which it interacts would be preferable for providing the functionality of the material. Sacrificial materials with this type of interaction with a melt in the core of nuclear reactors have been developed [15–19]. At the same time, it should be noted that this type of combustion can find wider application than use only in safety systems in nuclear power engineering.

Of interest in accordance with the reasons mentioned above is a broader experimental study of processes of this kind, concerned with the interaction of oxide materials with melts of reducing agents having a composition different from that of the melt in the core of nuclear reactors.

EXPERIMENTAL

To study the interaction of an oxide material with a melt, a material based on aluminum and iron(III) oxides was synthesized. For this purpose, the starting components, alumina of G-OO brand [GOST (State Standard) 30558–98] containing no less than 99.5 wt % Al_2O_3 and iron(III) oxide [TU (Technical Specification) 14-15-228–90 with mod. 1] containing no less than 99.2 wt % Fe_2O_3, were mixed in a 40 : 60 wt % ratio, compacted under a pressure of 50 MPa, and calcined at a temperature of 1380°C for 2 h. The sintered material was crushed, ground to pass a sieve with a 0.063 mm mesh (GOST 6613–86), and again sintered at 1380°C. The resulting material had a total porosity of $23 \pm 2\%$.

The heat conductivity of the material, determined in conformity with GOST 12170–85, is approximated by the expression $\lambda(T) = (-16.12-2.119 \times 10^{-2}T)/(1-2.43 \times 10^{-2}T)$ W m^{-1} K^{-1} (interpolation range 500 K $\le T \le$ 1200 K).

The metal melt was prepared by induction melting in a cold crucible [20] on a Rasplav-3 installation. According to the results of an analysis, the melt contained (wt %): Fe 66.8, Cr 18.3, Ni 8.9, Zr 4.5, Ti 0.7, Mn 0.6, Cu 0.1, Mo 0.1, and impurities less than 0.1. It should be noted that the content of zirconium in the melt slightly varied in the course of the experiment because zirconium dioxide formed in oxidation of steel components by oxygen that passed into the melt with components of the oxide material interacting with the melt crystallized on cold members of the experimental setup.

Changes in the dimensions of samples upon their contact with the melt were determined in relation to the melt temperature and duration of contact between the material and the melt with an error not exceeding 0.1 mm.

The temperature was measured with a pyrometer both before the material was brought in contact with the melt and during the interaction, by a procedure described in [21]. Deviations from the average melt temperatures in the experiments varied between the runs, depending on the melt temperature and amount of aerosols released, which were the main sources of error in pyrometric measurements. However, these deviations did not exceed 100°C in all cases.

The microstructure and elemental composition in the interaction zone and separate phases in this region were studied by electron microscopy and microprobe analysis on an ABT-55 electron microscope (Japan) equipped with an Oxford Link AN10000/S85 X-ray fluorescence microanalyzer (Great Britain).

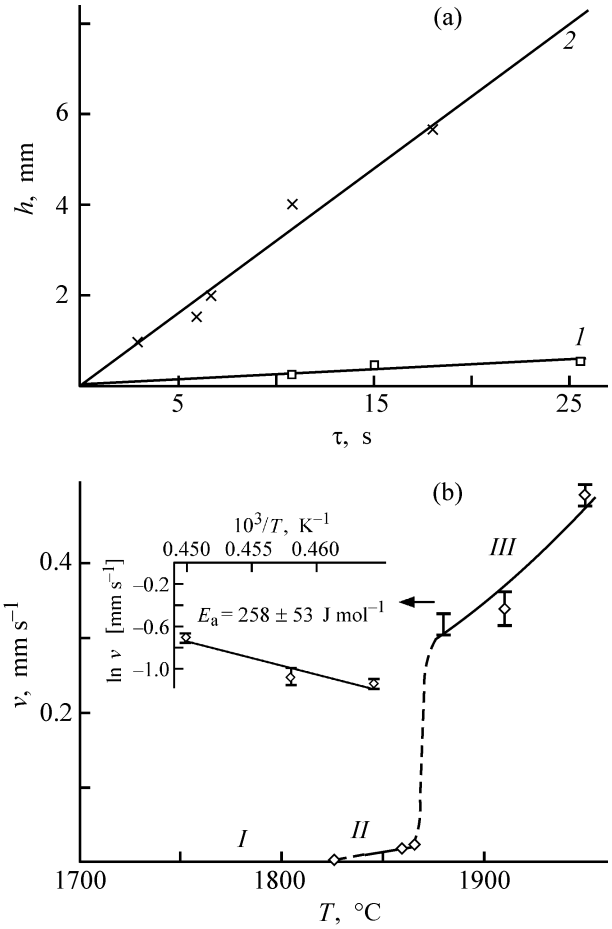

Fig. 1. (a) Distance h traveled by the front of interaction between the oxide material and the melt vs. the residence time τ of the material in the melt and (b) rate v of interaction of the oxide material vs. the melt temperature T. Melt temperature (°C): (*1*) 1865 and (*2*) 1880. (*I*, *II*, *III*) Temperature regions strongly differing in the rate of interaction between the melt and the material; the same for Figs. 2, 3.

Data on the motion of the front of interaction between the material based on aluminum and iron(III) oxides and the metal melt at different temperatures are presented in Fig. 1. The results obtained indicate that, in the entire temperature range studied, the motion velocity of the front is independent, within experimental error, of the time of interaction with the melt. Figure 1 shows as an example the corresponding kinetic data for two melt temperatures. Therefore, the results of the kinetic study can be represented in the case in question as a dependence of the rate of interaction between the metal melt and the oxide material on the melt temperature (Fig. 1b). The kinetic data in Fig. 1b make it possible to distinguish three temperature ranges differing in the nature of the process.

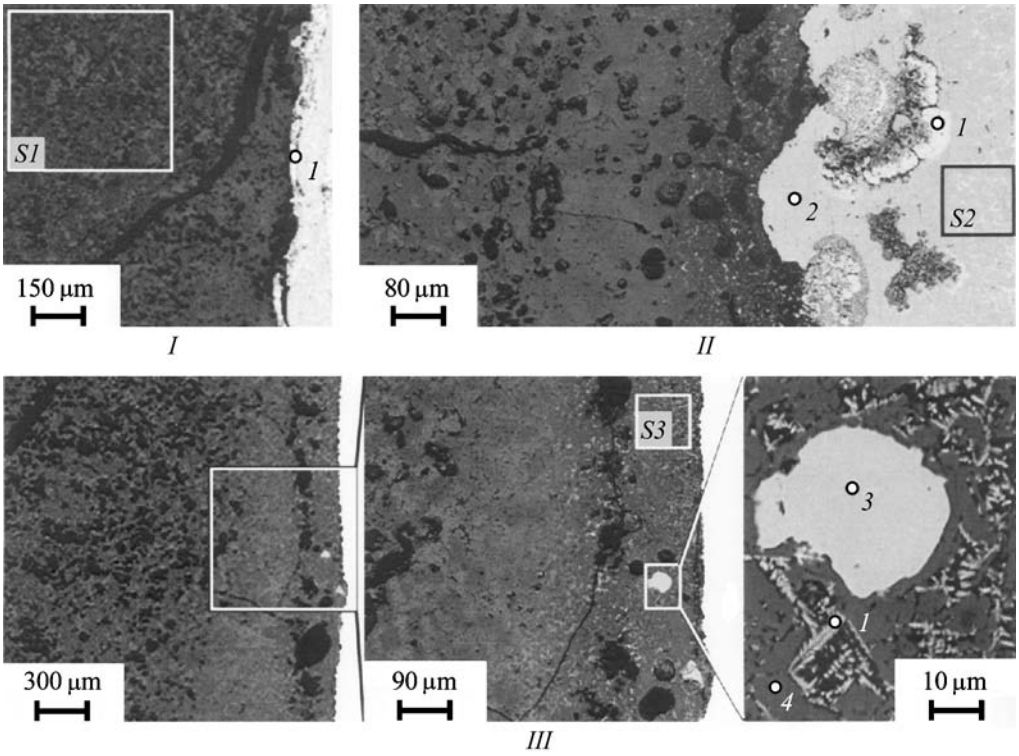

Fig. 2. Microstructure of the front of interaction between the oxide material and the metal melt (cooling from the interaction temperature in the quenching mode).

The first temperature region ($T < 1830$°C) is characterized by absence of any noticeable interaction between the material and the melt (Fig. 1b, region *I*). Presumably, this occurs because a ZrO_2 layer is formed at the interface between the oxide material and the melt, which is confirmed by electron microscopy and microanalysis (Fig. 2a, Table 1; region *I*). This layer is formed via oxidation of zirconium, the most active reducing agent contained in the metal melt, with a simultaneous full or partial reduction of the surface layer of iron(III) oxide and crystallization of the high-melting ZrO_2 at the interface between the sol-

Table 1. Chemical composition of the regions marked in Fig. 2

Region	Composition, wt %											
S1	Fe_2O_3* 61.5							Al_2O_3 38.5				
S2	Fe 67.7		Cr 17.1		Ni 10.3		Zr 4.4		Ti 0.3		Mn 0.2	
S3	Fe 20.0	Al 14.4		Cr 15.6		Zr 10.5		Ti 1.2		Mn 0.7		O** 37.6
1						ZrO_2 100						
2		Fe 74.2				Cr 17.5					Ni 8.2	
3		95.1				4.0					0.9	
4	Fe 17.8		Al 13.5		Cr 31.5		Ti 0.4		Mn 1.3			O** 35.6

* The content of the oxides is calculated using data on the cation ratio on the assumption that iron is in the oxidation state (+3).

** The content of oxygen is found from the mass balance.

id and liquid media. ZrO_2 forms rather high-temperature eutectics both with Al_2O_3 (1900°C) [22] and with Fe_3O_4 (1525°C) [23], the product of partial reduction of Fe_2O_3. Therefore, further interaction of the metal melt with the oxide material, which consists in transport of the oxidizing agent from the oxide material across the barrier layer of ZrO_2 and oxidation of melt components, limited during the time interval considered in the study (up to 27 s) solely by solid-phase processes, is rather slow [24], and just this is manifested in the kinetic curve (Fig. 1b, region *I*). This type of interaction between the material and the melt is confirmed by comparison of the microstructures of samples of the material after their interaction with the melt having temperatures of 1830°C, 1860°C, and more. In the first case, no zirconium dioxide is observed in the material beyond the zirconium dioxide layer formed at the interface between the solid and liquid media (Fig. 2a). At a higher temperature, a rather pronounced change in both the microstructure and composition can be observed at the interface between the sample and the melt (Figs. 2b, 2c; Table 1), which indicates that the liquid phase is present. At a temperature exceeding 1880°C, even metallic inclusions are observed in the material (Fig. 2c; Table 1, region *2*). According to the results of calculation by the software package GEMINI2 with the NUCLEA database of phase diagrams [25], there are no traces of the liquid phase beyond the ZrO_2 layer at a melt temperature of 1830°C exceeding the eutectic temperature in ZrO_2–Al_2O_3–Fe_3O_4(FeO) systems. This is presumably due to the low heat conductivity of both the porous ZrO_2 layer [26] and the material itself. What is more, the heat conductivity of the material decreases in the course of experiments because (i) microcracks are formed in the sample under the action of the temperature drop across the interface between the material and the melt (Fig. 2a) and (ii) the time of contact between the sample and the melt under the experimental conditions is short (27 s), which results in that the material has not enough time to be heated to the eutectic temperature.

In the temperature range 1830°C < T < 1880°C, a minor, but reliably recorded change in the size of a sample of the oxide material is observed upon its interaction with the metal melt (Fig. 1). The motion velocity of the interaction front is about 0.025 mm s^{-1} at a temperature of about 1879°C. A microstructure of the interaction interface, typical of this temperature interval, is shown in Fig. 2b. The type of microstructure of the sample suggests that, in interaction of the material with the metal melt, the boundary region of the oxide material melts and liquids flow into each other, with the process having exhibiting the behavior (Fig. 2b) typical of a slow flow of a less viscous liquid into a more viscous one (effect of "viscous fingers" [27]). Noteworthy is the configuration of the interface between melts based on oxides and those based on metals: drops of the liquids flowing into each other are separated from the main part by narrow necks, which hinders the transport of the reagents and removal of the reaction products and, consequently, restricts the motion velocity of the interaction front (Fig. 1, region *II*). That the existence of narrow necks at the contact between the drops and the main part of the liquid restricts the supply of reagents and the removal of the reaction products can be confirmed by comparison of the data on the composition of the drops and of the bulk of the liquid, connected to the drops via these necks. For example 4.4 wt % Zr is contained in the bulk of the metal melt (Fig. 2b, Table 1, region *S2*), whereas the content of zirconium in the drop itself is virtually zero (Fig. 2b; Table 1, region *2*). Conversely, the drop of molten oxides is enriched in the product of zirconium oxidation, zirconium dioxide (Fig. 2b; Table 1, region *1*), in contrast to the adjacent bulk of the oxides, in which white inclusions composed of zirconium dioxide are observed after crystallization.

It should be noted that, similarly to region *I*, the temperature region *II* under consideration is characterized by microcrack formation, but the microcracks are formed at a large distance from the contact boundary between the sample and the melt. In the case in question, the front of interaction between the material and the melt and the region in which cracks are formed, i.e., the region with a rather brittle behavior of the material, are separated by a zone whose microstructure indicates that the material is sintered on being placed in a high-temperature melt and by a zone in which, as follows from an analysis of its composition (Fig. 2b, Table 1), the solid and liquid phases coexist. The second zone contains oxidation products of certain components of the metal melt (primarily, ZrO_2 and a certain amount of Cr_2O_3).

The temperature region *III* (Fig. 1) is characterized by a constant and comparatively high motion velocity of the front of interaction between the oxide material and the metal melt, which is a distinctive feature of the combustion process [14, 28].

Analysis of the sample microstructure shows that the given case strongly differs from the interaction at lower temperatures, i.e., from the temperature regions *I* and *II* (Fig. 2). This is primarily manifested in that at the interaction front there are no barrier layers,

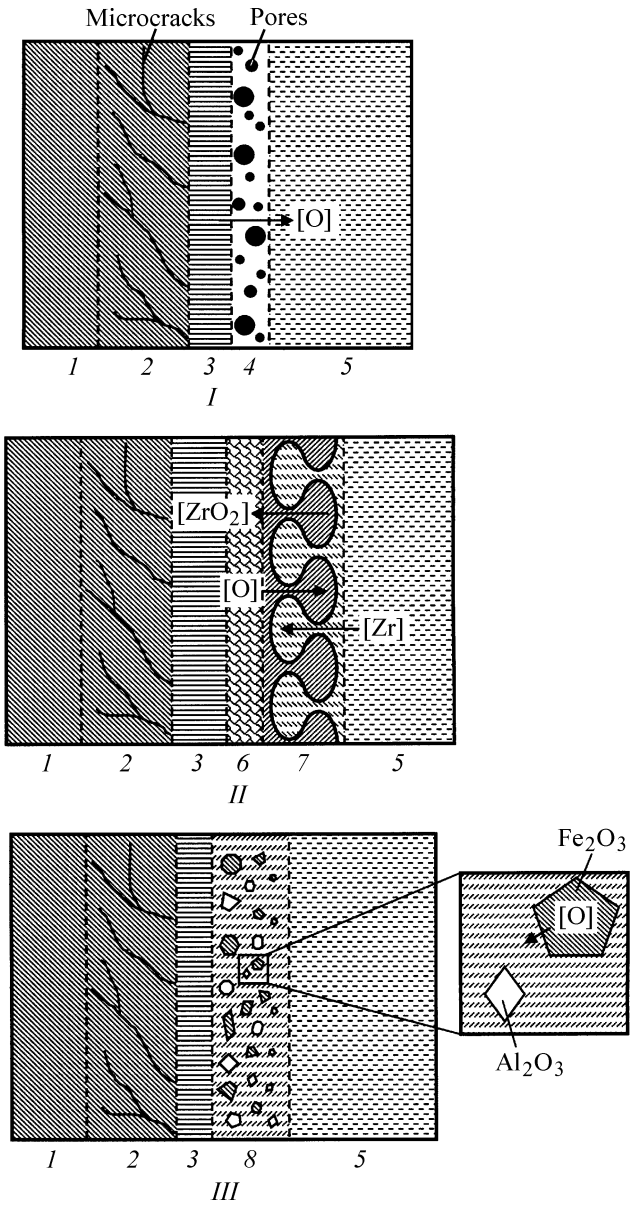

Fig. 3. Scheme of zones distinguished in the microstructure of the samples studied. (*1*) Oxide material without any indications of changes in the initial composition and microstructure; (*2*) zone of an oxide material with microcracks formed under the action of thermal stresses; (*3*) zone of sintering of the oxide material; (*4*) layer of porous ZrO_2; (*5*) metal melt; (*6*) layer of a material partly reacted with the melt components in the temperature range between the solidus and the liquidus of the system; (*7*) zone of mutual flowing-in of the melts of oxides and metals at the interaction front; and (*8*) reaction zone under the conditions of the liquid-phase combustion of the oxide material. The arrows show the motion direction of a component ([O], [ZrO_2], or [Zr]) that limits the interaction between the metal melt and the oxide material.

either solid, as in region *I* (Fig. 2a), or liquid-phase structures of the type of "viscous fingers" characteristic of the temperature region *II* (Fig. 2b). Another important difference is that a new zone appears in the sample near the contact boundary between the sample and the metal melt. This zone is separated from the rest of the material by a porous layer and contains inclusions of metal drops (Fig. 2c, Table 1). Analysis of the composition of this zone suggests that further reduction of Fe_2O_3 to give iron(II) oxide has occurred in this zone. This, in turn, made lower the eutectic temperature of the system [29] and led to a decrease in the viscosity of the oxide melt and, consequently, to an increase in the agitation rate of molten oxides and metals. Thus, there are virtually no significant kinetic hindrance to supply of reagents and removal of products from the interaction front via the liquid phase in the latter case. This, combined with the exothermic nature of the interaction between the melt and the material, creates conditions for the process to occur in the liquid-phase combustion mode [8, 11, 12]. A kinetic analysis of data on the temperature dependence of motion of the front of interaction between the material and the metal melt (Fig. 1b) demonstrated that the effective activation energy of the interaction process is $E_a = 258 \pm 53$ kJ mol^{-1}, i.e., is characteristic of most of the processes limited by diffusion in the solid phase [30]. In particular, the E_a value obtained coincides, within the experimental error, with $E_a = 259$ kJ mol^{-1}, the activation energy of oxygen diffusion in iron oxide [31]. Thus, in the case when there is virtually no diffusion hindrance to the supply of reagents and removal of reaction products in the liquid phase, the motion of the front of interaction between the metal melt and the oxide material is limited by the diffusion of the oxidizing agent (oxygen) in the solid phase (iron oxide) to the reaction zone.

The main processes occurring at the contact boundary between the material and the melt are shown schematically in Fig. 3 for the three temperature regions under consideration. Analysis of the results of the kinetic study, generalized in the form of the corresponding process schemes (Fig. 3), shows that, depending on the dynamic structure of the region of contact between the sample and the liquid phase, formed in the interaction between the material and the melt, widely diverse processes may restrict the motion velocity of the interaction front. This leads to the corresponding abrupt change in the interaction rate of the components.

The processes of oxidation of the main reducing agents, zirconium and chromium, in their interaction with iron oxide

$$2/3Fe_2O_3 + Zr = ZrO_2 + 4/3Fe, \quad (1)$$

$$1/2Fe_2O_3 + Cr = 1/2Cr_2O_3 + Fe, \quad (2)$$

are strongly exothermic with a change in enthalpy $\Delta H(1) = -520.99$ kJ mol^{-1} and $\Delta H(2) = -167.19$ kJ mol^{-1} (here and hereinafter the change in enthalpy is calculated using the IVTANTHERMO database of thermodynamic properties of substances [32]. In this context, it would be expected that the temperature in the system, including that in the melt, should considerably increase. However, the temperature of the metal melt near the oxide sample interacting with the melt remained, as shown by the experimental results, at the same level within the temperature measurement error. This can presumably be accounted for by compensation of the local rise in temperature in the zone of occurrence of redox reactions (1) and (2) by the endothermic effect associated with transfer of aluminum oxide into the melt and heating of the components of the material to the temperature of the metal melt. To analyze this possibility, calculations were carried out, whose results are listed in Table 2. For example, the change in the enthalpy of the system can be represented, with account of the redox reaction (ΔH_{redox}), heating of the components of the material (ΔH_h), and transfer of the components into the melt (ΔH_m), as

$$\Delta H = \Delta H_{redox} + \Delta H_h + \Delta H_m. \quad (3)$$

A calculation of the heat effects, carried out per mole of the metal melt interacting with the material on the assumption that the initial temperature of the material is 25°C and only zirconium contained in the melt is oxidized, gave a value $\Delta H(3) = 0.41$ kJ mol^{-1}. This means that, despite the large exothermic effect of reaction (1), a decrease in the melt temperature by 0.4% from the initial melt temperature would be expected in this case (Table 2). The experiment demonstrated that partial oxidation of chromium is observed together with the oxidation of zirconium (Fig. 2, Table 1). In this connection, the changes in the melt temperature because of the occurrence of oxidation reactions (1) and (2) were calculated. The calculation demonstrated that, although a rise in temperature would be expected because reaction (2) is exothermic, the total effect calculated by expression (3) with account of the heating of the material from 25°C must lead to a significant decrease in the melt temperature by 115.9°C (i.e., by about 6% relative to the initial temperature of the melt). Such a change in temperature is beyond the measurement error and it could be recorded experimentally. The fact that no changes in the melt temperature beyond the measurement error are observed in the experiment (Table 2) is presumably accounted for by only partial oxidation of chromium

Table 2. Change in the temperature of the metal melt in the liquid-phase combustion of oxide materials of various compositions

Composition of the material, wt %		Enthalpy of the reaction of zirconium oxidation by iron oxide, kJ mol^{-1}	Initial temperature of the material	Change in the melt temperature in the reaction zone		
				calculation with Al_2O_3 melting disregarded*	calculation based on expression (3)*	experiment
$AlO_{1.5}$	FeO_x		°C			
Material of the system $AlO_{1.5}$–$FeO_{1.5}$						
38.5	61.5	–520.99	25	95.1	–7.9	None**
36.9	63.1		25	98.1	0	–
79.7	20.3		1900	197.9		
Material of the system $AlO_{1.5}$–$FeO_{1.33}$						
31.6	68.4	–515.04	25	62.0	0	–
77.0	23.0		1900	198.9		
Material of the system $AlO_{1.5}$–FeO						
27.7	72.3	–511.90	25	51.9	0	–
74.7	25.3		1900	191.6		

* The initial temperature of the melt was taken to be 1900°C in the calculations.

** The temperature of the melt was measured near the sample of the material, interacting with the melt. No changes in the melt temperature beyond the limits of the measurement error were observed.

in the course of interaction between the melt of metals and the oxide material (Fig. 2, Table 1).

Comparison of the calculated and experimental data shows that, with account of the above remarks, they coincide within the experimental error, which makes it possible to expect that the reliability of prognostication of changes in the temperature of the metal melt in liquid-phase combustion of oxide materials of various compositions, listed in Table 2, should be high.

Thus, the experimental data and the results of calculations show that the material based on aluminum and iron oxides interacts with a Fe–Cr–Ni–Zr melt in a certain temperature range in such a way that the kinetics of this process can be described in terms of the combustion theory [28], similarly to the interaction of the sacrificial material with a melt in the core of a nuclear reactor [8, 11, 12]. A specific feature of the process under consideration is that, despite the rather large exothermic effect of the reaction of oxidation of the melt components in their interaction with separate components of the oxide material, which is characteristic of combustion, the total heat effect of the interaction between the melt and the material is such that it does not lead to any significant increase in the melt temperature, or even makes this temperature lower. Consequently, combustion of substances without any increase in the temperature of the environment can be achieved not only in the interaction of sacrificial materials with a melt in the core of nuclear reactors, but includes a wider variety of chemical processes and can have a broader application field.

CONCLUSIONS

(1) Analysis of kinetic data and a study of the mechanism by which a zirconium-containing metal melt with a material based on aluminum and iron oxides shows that, beginning at a temperature of about 1800°C, the process occurs in a mode that can be described in terms of the combustion theory.

(2) Under certain conditions, the interaction between the oxide material and the metal melt containing active reducing agents can occur by the following scheme. The interaction of a part of components of the material and the melt, which occurs with an exothermic effect in the combustion mode, initiates a conjugated endothermic process, with the result that the total heat effect in the reaction zone may be close to zero or even lead to heat absorption.

ACKNOWLEDGMENTS

The authors thank M.D. Tolkachev (Institute of Precambrian Geology and Geochronology, Russian Academy of Sciences) for assistance in electron-microscopic and microprobe studies.

The study was financially supported by the Russian Foundation for Basic Research (project no. 05-08–49971).

REFERENCES

1. Rotenberg, G.B., *Ogneupornye materially* (Refractory Materials), Moscow: Metallurgiya, 1980.
2. Strelov, K.K., *Teoreticheskie osnovy tekhnologii ogneupornykh materialov* (Theoretical Foundations of the Technology of Refractory Materials), Moscow: Metallurgiya, 1985.
3. Suvorov, S.A., *Nov. Ogneupory*, 2002, no. 3, pp. 38–45.
4. Prinz, V.Ya., Seleznev, V.A., Gutakovsky, A.K., et al., *Physica E*, 2000, vol. 6, nos. 1–4, pp. 828–831.
5. Schmidt, O.G. and Eberl, K., *Nature*, 2001, vol. 410, p. 168.
6. Prints, V.Ya., *Izv. Vyssh. Uchebn. Zaved., Fiz.*, 2003, vol. 46, no. 6, pp. 35–43.
7. Deneke, Ch. and Schmidt, O.G., *Appl. Phys. Lett.*, 2004, vol. 85, no. 14, pp. 2914–2916.
8. Gusarov, V.V., Al'myashev, V.I., Khabenskii, V.B., et al., *Fiz. Khim. Stekla*, 2005, vol. 31, no. 1, pp. 71–90.
9. Gusarov, V.V., Al'myashev, V.I., Khabenskii, V.B., et al., *Ross. Khim. Zh.*, 2005, vol. 49, no. 4, pp. 42–53.
10. RF Patent 2253914.
11. Gusarov, V.V., Beshta, S.V., Khabenskii, V.B., et al., *Trudy Vserossiiskoi konferentsii "Protsessy goreniya i vzryva v fizikokhimii i tekhnologii neorganicheskikh materialov"* (Proc. All-Russia Conf. "Processes of Combustion and Explosion in Physical Chemistry and Technology of Inorganic Materials"), Chernogolovka: ISMAN, 2002, pp. 99–103.
12. Al'myashev, V.I., Beshta, S.V., Vitol', S.A., et al., *Novye dostizheniya v khimii i tekhnologii materialov: Sbornik materialov konferentsii* (New Advances in Chemistry and Technology of Materials: Proc. Conf.), St. Petersburg, 2002, pp. 33–37.
13. Zel'dovich, Ya.B., *Zh. Fiz. Khim.*, 1948, vol. 22, no. 1, pp. 27–48.
14. Zel'dovich, Ya.B., Barenblat, G.I., Librovich, V.B., and Makhvelidze, G.M., *Matematicheskaya teoriya goreniya i vzryva* (Mathematical Theory of Combustion and Explosion), Moscow: Nauka, 1980.
15. RF Patent 2178924.
16. RF Patent 2191436.

17. RF Patent 2192053.
18. RF Patent 2212719.
19. RF Patent 2206930.
20. Petrov, Yu.B., *Induktsionnaya plavka okislov* (Induction Melting of Oxides), Leningrad: Energoatomizdat, 1983.
21. Bechta, S.V., Khabensky, V.B., Vitol, S.A., et al., *Nuclear Eng. Design*, 2001, vol. 210, nos. 1–3, pp. 193–224.
22. *Diagrammy sostoyaniya sistem tugoplavkikh oksidov: Spravochnik, Vyp. 5, Dvoinye sistemy, Ch. I* (State Diagrams of Systems Constituted by High-Melting Oxides: Reference Book, issue 5, Binary Systems, part 1), Galakhov, F.Ya., Ed., Grebenshchikov Institute of Silicate Chemistry, Leningrad: Nauka, 1985.
23. Toropov, N.A., Barzakovskii, V.P., Lapin, V.V., and Kurtseva, N.N., *Diagrammy sostoyaniya silikatnykh sistem: Spravochnik, Vyp. 1, Dvoinye sistemy* (State Diagrams of Systems: Reference Book, issue 1, Binary Systems), Toropov, N.A., Ed., Leningrad: Nauka, 1969, 2nd ed.
24. Gusarov, V.V., *Zh. Obshch. Khim.*, 1997, vol. 67, no. 12, pp. 1959–1964.
25. Chevalier, P.Y., Fischer, E., and Cheynet, B., *CALPHAD*, 2004, vol. 28, pp. 15–40.
26. Andrievskii, R.A. and Spivak, I.I., *Prochnost' tugoplavkikh soedinenii i materialov na ikh osnove: Spravochnik* (Strength of High-Melting Compounds and Materials Based on These Compounds: Reference Book), Chelyabinsk: Metallurgiya, 1989.
27. Feder, J., *Fractals*, New York: Plenum, 1988.
28. Williams, F. A., *Combustion Theory*, Reading (Massachusetts): Addison-Wesley, 1965. Translated under the titles *Teoriya goreniya*, Moscow: Nauka, 1971.
29. Beshta, S.V., Krushinov, E.V., Al'myashev, V.I., et al., *Zh. Neorg. Khim.*, 2006, vol. 51, no. 2, pp. 367–374.
30. Tret'yakov, Yu.D., *Tverdofaznye reaktsii* (Solid-Phase Reactions), Moscow: Khimiya, 1978.
31. Ryabukhin, A.G., Teplyakov, Yu.N., and Kozhaeva, A.A., *Izv. Chelyab. Nauchn. Tsentr., Fiz. Khim. Tekhnol. Neorg. Mater.*, 2001, no. 1, pp. 31–33.
32. Belov, G.V., Iorish, V.S., and Yungman, V.S., *CALPHAD*, 1999, vol. 23, no. 2, pp. 173–180.

ISSN 1070-4272, Russian Journal of Applied Chemistry, 2007, Vol. 80, No. 4, pp. 536–541. © Pleiades Publishing, Ltd., 2007.
Original Russian Text © E.S. Kshumaneva, A.G. Kasikov, 2007, published in Zhurnal Prikladnoi Khimii, 2007, Vol. 80, No. 4, pp. 549–554.

INORGANIC SYNTHESIS AND INDUSTRIAL INORGANIC CHEMISTRY

Leaching-out of Residues of Carbonyl Nickel Synthesis with Iron(III) Chloride Solutions

E. S. Kshumaneva and A. G. Kasikov

Tananaev Institute of Chemistry and Technology of Rare Elements and Mineral Resources, Kola Scientific Center, Russian Academy of Sciences, Apatity, Murmansk oblast, Russia

Received October 16, 2006

Abstract—Behavior of the phase components of residues of carbonyl nickel synthesis in leaching with an iron(III) chloride solution was studied.

DOI: 10.1134/S1070427207040039

The development of hydrometallurgical processes as an alternative to pyrometallurgical processing of sulfide materials has given rise to technologies based on use of iron(III) chloride as a leaching agent [1–3]. The use of this reagent is advantageous in that no sulfur(IV) oxide is released in the process and leaching of high-complex materials can be carried out under normal pressure.

These advantages have favored the development of new kinds of processing of such materials as scrap metal, copper-nickel mattes, and complex nickel and copper sulfide concentrates. A significant progress has been achieved in application of chloride processes in the metallurgy of nickel; these techniques are employed at three plants processing copper-nickel and nickel converter matte and nickel-cobalt sulfide concentrate: Kristiansand (Norway), Sanouville (France), and Niihama (Japan) [1].

Hydrochloride processes developed by the following companies are known in the metallurgy of copper: Cuprus Metallurgical (Cymet), Duval (CLEAR), Minemet Recherche, Henkel, and US Mining Bureau. Also known are processes developed by MINTEK, Cominco, Cuprex, and Great Central Mines, which have passed the stage of large-scale laboratory and industrial tests [2, 3].

In addition to processing of the raw materials mentioned above, the feasibility of application of hydrochloride leaching directly to nickel ores and slags has been considered [4, 5].

In these reports are represented, with varied extent of understanding, mechanisms and decomposition rates of copper and nickel phase components of materials involved in processing. There is virtually no published evidence concerning the behavior of cobalt sulfides in hydrochloride leaching. At the same time, a low, compared with nickel, recovery of cobalt has been mentioned in a number of reports devoted to hydrochloride leaching of copper-nickel sulfide minerals [5–7]. The explanations given were undetailed and had a probabilistic nature.

In the context of the available published data, the possibility and specific features of leaching, with the above-mentioned solutions, of residues of carbonyl nickel synthesis (RCS) were studied. These residues are a sulfide product whose phase composition is represented by a complex multicomponent phase M_9S_8 (M = Co, Ni, Fe, Cu) including the nickel $Ni_{3.18}Fe_{3.36}Cu_{2.25}Co_{0.21}S_8$, cobalt $Co_{4.74}Fe_{2.06}Cu_{1.32} \times Ni_{0.84}S_8$, and copper $Cu_{7.13}Fe_{1.07}Ni_{0.48}Co_{0.35}S_8$ components and chalcosine Cu_2S [8, 9].

EXPERIMENTAL

Experiments were performed with RCS,* which were decarbonylated by keeping under a vacuum at the boiling point of nickel carbonyl (~45°C) and had the following composition (wt %): Ni 3.8, Co 14.0, Cu 33.0, Fe 4.4, S 18.9, and total platinum metals ~0.2. The specific surface area of RCS was 7.5 $m^2 g^{-1}$, which made it possible to exclude fine grinding of the material, the basic procedure providing a satisfactory recovery of valuable components.

* Supplied by Severonikel' combine, Kola Mining-and Smelting Co.

Laboratory studies of the leaching procedure were carried out in a 0.25-l thermostated three-necked vessel equipped with an impeller rabble and reflux. After the required temperature was reached, the starting material was charged into a vessel with an iron(III) chloride solution. All the experiments were performed in the temperature range 298–353 K. After the process was complete, the sludge formed was filtered and the chemical composition of the solid and liquid phases was determined. The weighed portion of RCS was 50 g in all the experiments.

Iron(III) and copper(II) sulfide solutions were prepared from reagents $FeCl_3 \cdot 6H_2O$ and $CuCl_2 \cdot 2H_2O$ of chemically pure grade. The chloride background was created by dissolution of the reactive $CoCl_2 \cdot 6H_2O$ of chemically pure grade, with this procedure guided by the composition of the starting material, in which copper(II) and cobalt(II) predominate.

The content of nickel, copper, cobalt, and iron was found by flame atomic-absorption spectrometry on an AAS-30 instrument (Carl Zeiss, Germany). The content of sulfate ions in solution was determined by a gravimetric method based on precipitation of SO_4^{2-} ions with barium chloride. An X-ray phase analysis was carried out on a DRON-2 diffractometer (Cu_{K_α} radiation). The specific surface area was measured with a Flow Sorb 2300 II analyzer.

The results of experiments on RCS leaching with iron(III) chloride solutions of various concentrations, presented in Fig. 1, indicate that the recovery of all the metals being monitored gradually increases with the concentration of iron(III) ions in the concentration range under study. The maximum recovery is achieved at a $FeCl_3$ concentration of 3.8 M (%): Cu 99.6, Fe 99.5, Ni 83.4, Co 27.3. According to X-ray phase analysis data, the phase composition of the resulting leaching residue is represented by two phases: elementary sulfur and thiospinel M_3S_4 (Fig. 2). The residue has the following elemental composition (wt %): Co 30.2, Ni 2.4, Cu 2.8, Fe 1.5, and S_{tot} 54.9, including S_{elem} 17.0.

As follows from the data obtained, virtually total decomposition of chalcosine and considerable decomposition of pentlandite occur in the course of RCS leaching, with cobalt compounds for the most part remaining in the leaching residue.

The dissolution of chalcosine in $FeCl_3$ solutions was studied in [10–12]. It was found that this process occurs by the inner-diffusion mechanism via formation of covelline and its decomposition to give elementary sulfur, which hinders penetration of the solvent to the surface of the mineral. The activation energy of the process depends on time and temperature and increases, in leaching for 30 min in the temperature range 333–423 K, from 15.3 to 16.9 kJ mol^{-1}.

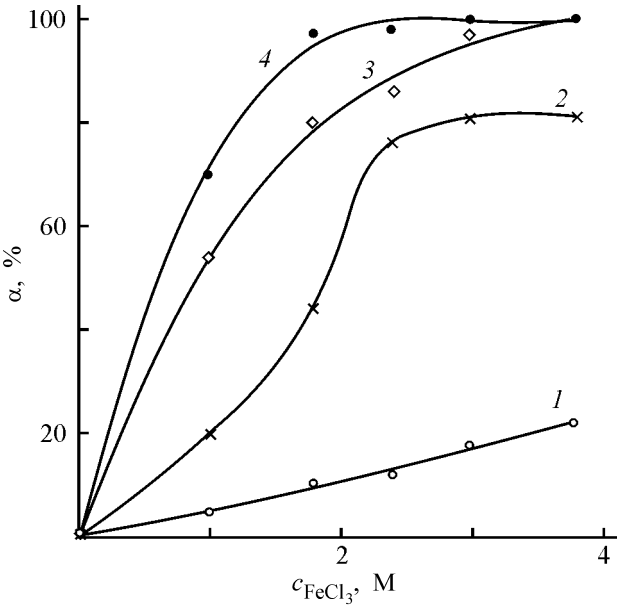

Fig. 1. Degree of recovery, α, of nonferrous metals and iron from RCS vs. $FeCl_3$ c_{FeCl_3}. T = 353 K, τ = 4 h, s : l = 1 : 5. Element being recovered: (*1*) cobalt, (*2*) nickel, (*3*) copper, and (*4*) iron; the same for Fig. 3.

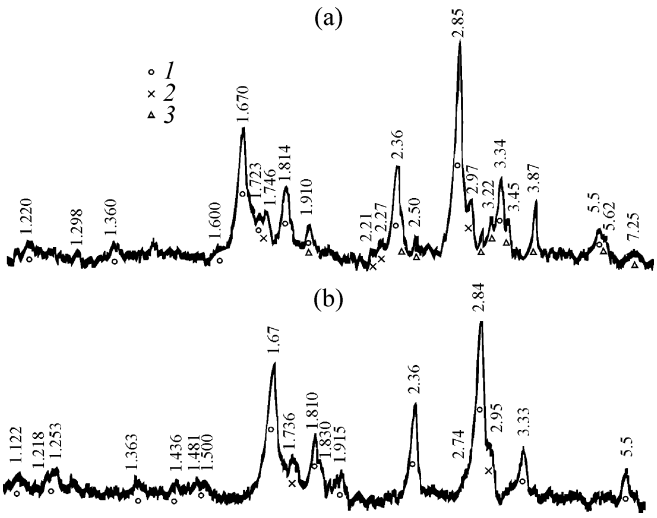

Fig. 2. X-ray diffraction pattern of an RCS leached with a 3.8 M solution of $FeCl_3$. (a) Without removal of sulfur and (b) after removal of sulfur. (*1*) M_3S_4, (*2*) M_9S_8, and (*3*) S.

Mineralogical and X-ray phase analyses revealed that, in leaching of chalcosine contained in RCS with a $FeCl_3$ solution, its complete recrystallization to give covelline CuS occurs in the first 10–15 min from

the beginning of leaching under optimal conditions and then CuS dissolves to give elementary sulfur in the course of 1 h. The high rate of chalcosine decomposition is apparently due to the large specific surface area of the starting material.

The interest manifested by the authors of [4, 5, 13–15] in a study of the decomposition of pentlandite $Ni_{4.5}Fe_{4.5}S_8$ with $FeCl_3$ solutions is associated with the question of whether or not it is advisable to apply hydrochloride leaching directly to nickel ores and complex nickel sulfide concentrates or slags, whose main nickel-containing mineral is pentlandite.

Mineralogical observations [16], data of X-ray photoelectron spectroscopy [13], and thermodynamic calculations [14] demonstrate that leaching-out of iron and nickel from pentlandite in an oxidizing medium yields intermediate compounds, such as violarite $FeNi_2S_4$ and bravoite $(Fe,Ni)S_2$, and phases containing sulfur in a higher oxidation state, e.g., orthorhombic sulfur or sulfate ions:

$$Fe_{4.5}Ni_{4.5}S_{8(s)} = FeNi_2S_{4(s)} + 3.5Fe^{2+}_{(aq)} + 2.5Ni^{2+}_{(aq)} + 4S. \quad (1)$$

However, a study of the decomposition of synthetic pentlandite in hydrochloric acid and $FeCl_3$ solutions [15] demonstrated that, under potentiostatic conditions in an acid medium close to that in leaching with iron(III) chloride (1 M HCl and 0.05 M $FeCl_3$) in the temperature range 293–353 K, pentlandite is oxidized directly to elementary sulfur without formation of any intermediate phases of metal sulfides:

$$Fe_{4.5}Ni_{4.5}S_{8(s)} = 4.5Fe^{2+}_{(aq)} + 4.5Ni^{2+}_{(aq)} + 8S_{(s)}. \quad (2)$$

The fact that no violarite is formed demonstrates that the system departs from equilibrium because of the slow solid-phase diffusion of metal atoms within the sulfur sublattice and the layer of forming sulfur is the factor limiting the reaction rate. The low rates of pentlandite dissolution in acid $FeCl_3$ solutions, obtained in the experiments, led the authors of this study to conclude that the most efficient way is the modern practice of pentlandite conversion into nickel matte, whose main phase is, as mentioned above, heazlewoodite Ni_3S_2. This is so because the dissolution of Ni_3S_2 in hydrochloric solutions of $CuCl_2$ and $FeCl_3$ occurs via formation of millerite NiS, which decomposes to give elementary sulfur at an acceptable rate and a low potential [17, 18].

The authors of [6, 19] found that the decomposition of pentlandite with a $FeCl_3$ solution (about 5 M Cl^-) can be accelerated by mechanical activation of the material, with the surface area of the material increased (to 7 $m^2\ g^{-1}$) and its reactivity enhanced by the deformation of its crystal lattice, caused by grinding. As a result, a 80% recovery of nickel is achieved and a conclusion is made that mechanical activation of the material may become an alternative to matte formation.

Thus, published data demonstrate that the decomposition of the nickel and cobalt components of the pentlandite-like phase of RCS can give a set of thiospinels: $FeNi_2S_4$, Ni_3S_4, $CoNi_2S_4$, $NiCo_2S_4$, Co_3S_4, whose individual identification by X-ray phase analysis is difficult in the case of their joint presence and varied content. Also, phases in leaching residues could not be identified on an MS-46 Cameca microprobe analyzer with a resolution of 0.2 μm because of the decrease in the size of grains of the starting material. The nature of dissolution of cobalt pentlandite under the conditions studied was unambiguously identified, specifically, the Co_3S_4 thiospinel was formed, and, therefore, it was necessary to explain the behavior of pentlandite. For this purpose, additional studies were carried out with natural pentlandite.

As a result, the nature of decomposition of natural pentlandite $Ni_{4.5}Fe_{4.5}S_8$ under conditions similar to those in RCS leaching with $FeCl_3$ solutions with a concentration of 3.8 M in the absence of hydrochloric acid and with 1 M HCl. In this case, an X-ray phase analysis of the residues formed in leaching of pentlandite (content of the main phase ~95%) identified two phases: starting pentlandite and elementary sulfur. The degree of decomposition of pentlandite was determined by the size of its particles. For example, the degree of decomposition of the –100…+50- and –50-mm fractions of the starting material in its leaching was 31.1 and 78.2%, respectively, in agreement with the results reported in [13]. An attempt of additional introduction of chalcosine (Cu_2S) in an amount corresponding to its content in RCS, or of $CuCl_2$ in an amount corresponding to its content in the solution formed in RCS leaching with a $FeCl_3$ solution led to similar results: no intermediate phases were formed. However, the rate and degree of decomposition of pentlandite markedly increases in this case. The synergetic effect of homogeneous catalysts based on halide salts of Cu(II) and Fe(III), whose occurrence is attributed by the authors to the formation of a heteronuclear complex $(CuClFe)Cl^{5-j}_{j-1} \cdot aq$, has been noted previously [20].

Analysis of the aforesaid suggests that leaching of pentlandite with $FeCl_3$ solutions under the condi-

tions studied occurs without formation of intermediate phases (in particular, violarite) and the reaction rate markedly increases as the surface area of the material increases and its crystal lattice is deformed.

The calculations performed demonstrated that the consumption of $FeCl_3$ at a concentration of 3.8 M and a s : l ratio of 1 : 4 in leaching of RCS of the composition specified corresponds to the stoichiometric consumption by the reactions

$$Cu_2S + 3FeCl_3 = CuCl + CuCl_2 + 3FeCl_2 + S, \quad (3)$$

$$M_9S_8 + 18FeCl_3 = 9MCl_2 + 18FeCl_2 + 8S, \quad (4)$$

$$M_9S_8 + 12FeCl_3 = M_3S_4 + 12FeCl_2 + 6MCl_2 + 4S, \quad (5)$$

where M = Ni, Co, Fe, Cu.

An analysis of published data [14, 15], results of additional experiments, and data furnished by chemical and X-ray phase analyses demonstrated that decomposition of the nickel component of the pentlandite-like phase occurs by reaction (4), and that of the cobalt component, by reaction (5).

Consequently, the composition of the phase formed in hydrochloric leaching under the optimal conditions corresponds to the formula Co_3S_4, with nickel, copper, and iron either present in the composition of undecomposed initial phases or contained in an insignificant amount in the thiospinel, isomorphically substituting cobalt.

The results obtained suggest that, in the case of hydrochloride processing of copper-nickel sulfide materials in whose composition cobalt is represented by its own sulfide compounds (e.g., cobalt pentlandite), cobalt remains in leaching products in the form of a Co_3S_4 compound, which is highly stable in chloride media [8].

It is known that presence of free hydrochloric acid in a $FeCl_3$ solution has a catalytic effect on the degree of decomposition of numerous materials [21]. Therefore, the behavior and degree of decomposition of the phase components of RCS at various concentrations of hydrochloric acid in the $FeCl_3$ solution was examined.

The results of these experiments (Fig. 3) demonstrated that, at an HCl concentration of 1–2 M and a $FeCl_3$ concentration lowered nearly twofold, the degree of copper and nickel recovery increases by 20 and 10%, respectively. In all probability, the process occurs with, first, the sulfides reacting with hydrochloric acid:

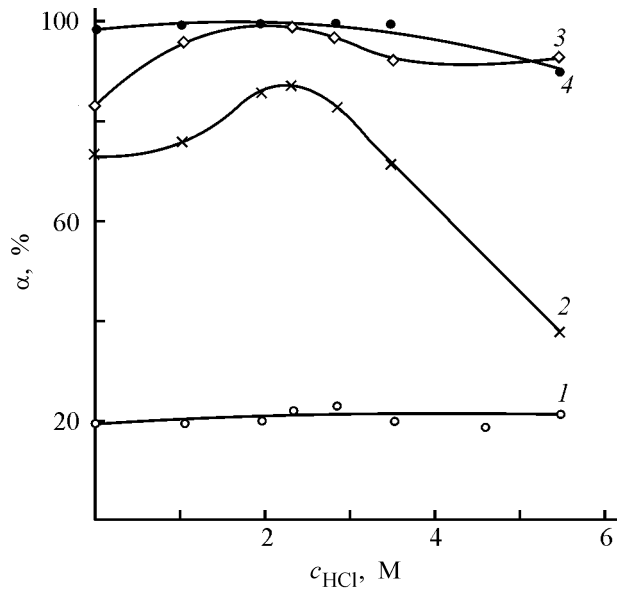

Fig. 3. Degree of recovery, α, of nonferrous metals and iron from RCS vs. the concentration of hydrochloric acid. c_{FeCl_3} = 2 M, T = 353 K, τ = 4 h, s : l = 1 : 5.

$$Cu_2S + 2HCl = 2CuCl + H_2S, \quad (6)$$

$$M_9S_8 + 18HCl = 9MCl_2 + 8H_2S + H_2, \quad (7)$$

$$M_9S_8 + 12HCl = 6MCl_2 + M_3S_4 + 4H_2S + 2H_2, \quad (8)$$

and then reaction with $FeCl_3$ proceeding in the solution bulk:

$$H_2S + 2FeCl_3 = 2FeCl_2 + S + 2HCl. \quad (9)$$

Reaction (9) proceeds to a rather full extent, because a chemical analysis demonstrated that the content of total sulfur in the reaction products is equal to its content in the starting material in the $FeCl_3$ and HCl concentration ranges studied.

Raising the HCl concentration to more than 2 M leads to a decrease in the degree of copper and nickel recovery into solution. This is apparently due to reverse precipitation of copper sulfide by the evolving hydrogen sulfide in the first case, and to formation of Ni_3S_4 and Co_3S_4 phases poorly soluble in chloride media, in the second case. This conclusion is confirmed by the X-ray diffraction pattern of the leaching residues obtained, which is identical to that shown in Fig. 2.

Thus, RCS leaching with a 2.0–2.3 M $FeCl_3$ solution in the presence of 1–2 M HCl at s : l = 1 : 4 and temperature of 80°C can provide in 4 h a degree of copper, nickel, and iron recovery into solution equal

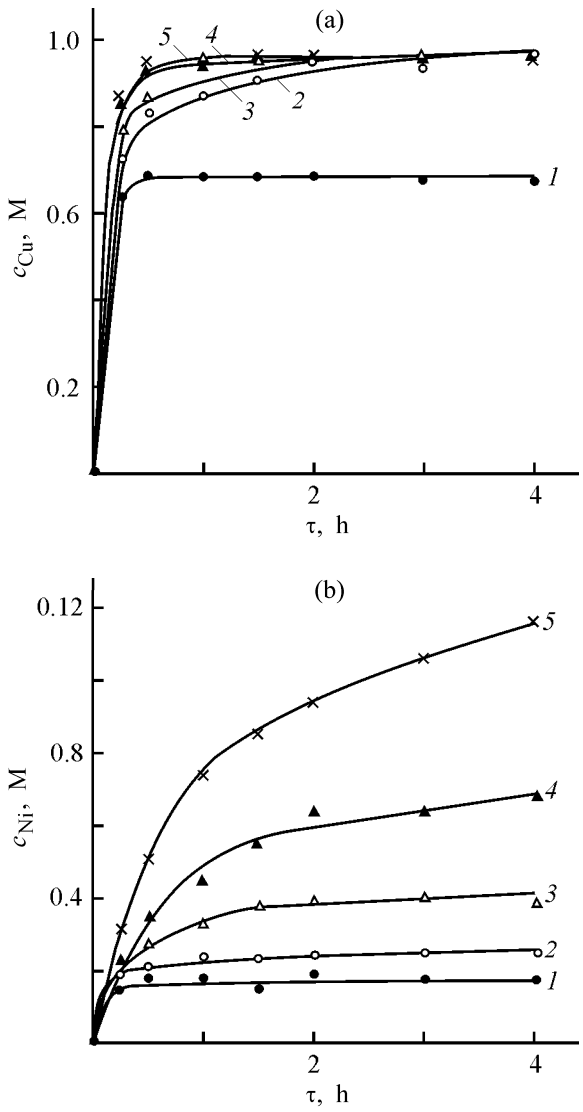

Fig. 4. Kinetic curves of (a) copper and (b) nickel leaching-out. c_{FeCl_3} = 2 M, c_{HCl} = 2 M, s : l = 1 : 5. (c_{Cu}, c_{Ni}) Concentration of an ion being leached-out and (τ) time. Temperature (K): (*1*) 298, (*2*) 323, (*3*) 333, (*4*) 343, and (*5*) 353.

to 99.6, 84.5, and 99.1%, respectively. Cobalt is concentrated in the solid phase in the form of Co_3S_4. As a result, solutions of the following composition are obtained (M): Cu 1.0, Ni 0.1, Fe 2.0, and Co 0.1.

The effect of temperature on the copper leaching in the temperature range 298–353 K at $FeCl_3$ and HCl concentrations of 2 M is illustrated by Fig. 4a. An increase in the degree of chalcosine dissolution is observed as the temperature is raised from 298 to 323 K. At above 323 K and copper concentration in solution of about 1 M, chalcosine virtually completely decomposes in 45–120 min.

An analysis of the experimental data demonstrated that, in the temperature range studied, the dependences obtained can be adequately described by the Erofeev–Kolmogorov equation, derived for describing the kinetics of topochemical processes:

$$\alpha = 1 - e^{-k\tau^n},$$

where α is the fraction of the reacted substance; τ, reaction time; and *k* and *n*, coefficients; coefficient *n* can serve as a criterion of departure of the leaching process from a first-order-reaction behavior.

The thus obtained value of coefficient *n* is 0.1–0.2 for chalcosine.

Raising the temperature in the range 298–353 at $FeCl_3$ and HCl concentrations of 2 M leads to an increase in the degree of pentlandite dissolution (Fig. 4b), with the value of *n*, obtained in analysis of the experimental data in terms of Erofeev–Kolmogorov equation, equal to 0.6.

Thus, it was found on the basis of the experimental data obtained that RCS can be leached with $FeCl_3$ solutions containing hydrochloric acid in two modes: the first, at a temperature of 60°C in the course of 1 h, with copper recovered into solution and the main part of nickel remaining in the solid residue; and the second, at a temperature of 80°C in the course of 4 h, with copper, nickel, and iron passing into solution in this case. Irrespective of the leaching conditions, 80% of nickel remains in the solid solution.

CONCLUSIONS

(1) It was found in a study of the behavior of phase components of residues of carbonyl nickel synthesis in leaching with $FeCl_3$ solutions that pentlandite decomposes without formation of intermediates, whereas cobalt pentlandite decomposes to give linnaeite Co_3S_4.

(2) It was shown that hydrochloric acid has a catalytic effect in the presence of $FeCl_3$ in decomposition of the phase components of the residues of carbonyl nickel synthesis.

(3) Conditions of selective leaching-out of copper, with nickel and cobalt remaining in the solid residue, were determined.

(4) It was found that the key influence on the degree of chalcosine decomposition is exerted by the concentration of the oxidizing agent, $FeCl_3$, whereas decomposition of pentlandite largely depends on temperature.

ACKNOWLEDGMENTS

The study was supported by the program "Leading Scientific Schools" project no. NSh-4383.2006.3.

REFERENCES

1. Reznik, I.D., Ermakov, G.P., and Shneerson, Ya.M., *Nikel'*, Moscow: Mashinostroenie, 1995, vol. 3
2. Dutrizac, J.E., *Hydrometallurgy*, 1992, vol. 29, pp. 1–45.
3. Habashi, F., *Hydrometallurgy*, 1995, vol. 38, pp. 219.
4. Fang, Z., *Eng. Chem. Metall.*, 1997, vol. 18, no. 3, pp. 202–206.
5. Lu, Z.Y., Jeffrey, M.I., Zhu, Y., and Lawson, F., *Hydrometallurgy*, 2000, vol. 56, pp. 63–74.
6. Amer, A.M., *Hydrometallurgy*, 1995, vol. 38, pp. 225–234.
7. Zatitskii, B.E., Volkov, L.V., and Shalygina, E.M., *Tsv. Met.*, 2004, no. 1, pp. 23–25.
8. Kasikov, A.G., Kshumaneva, E.S., and Neradovskii, Yu.N., *Mineralogiya vo vsem prostranstve sego slova: Sbornik trudov II Fersmanovskoi nauchnoi sessii Kol'skogo otdeleniya Rossiiskogo mineralogicheskogo obshchestva* (Mineralogy in Full Meaning of This Word: Proc. of Sci. Session of Kola division of Russian Mineralogical Society), Apatity, 2005, p. 155.
9. Kshumaneva, E.S., Kasikov, A.G., and Neradovskii, Yu.N., *Zh. Prikl. Khim.*, 2005, vol. 78, no. 2, pp. 185–190.
10. Tkachenko, O.B. and Tseft, A.L., *Sbornik nauchnykh trudov Instituta metallurgii i obogashcheniya Akademii nauk Kazakhskoi SSR* (Coll. of Sci. Works of the Institute of Metallurgy and Ore Dressing, Academy of Sciences, Kazakh SSR), Alma-Ata, 1969, vol. 30, pp. 15–23.
11. Buketov, E.A. and Ugorets, M.Z., *Gidrokhimicheskoe okislenie khal'kogenov i khal'kogenidov* (Hydrochemical Oxidation of Chalcogens and Chalcogenides), Alma-Ata: Nauka KazSSR, 1975, pp. 174–175.
12. Ospanov, Kh.K., Zhusupova, A.K., Sharipova, S.A., and Syzdykov, R.R., *Zh. Fiz. Khim.*, 1999, vol. 73, no. 5, pp. 940–942.
13. Vaughan, D.J. and Craig, J.R., *Mineral Chemistry of Metal Sulfides*, Cambridge: Cambridge Univ., 1978.
14. Legrand, D.L., Bancroft, G.M., and Nesbitt, H.W., *Int. J. Mineral Process.*, 1997, vol. 51, pp. 217–228.
15. Warner, T.E., Rice, N.M., and Taylor, N., *Hydrometallurgy*, 1996, vol. 41, pp. 107–118.
16. Warner, T.E., Rice, N.M., and Taylor, N., *Hydrometallurgy*, 1992, vol. 31, pp. 55–90.
17. Agievskii, D.A., Pavlova, L.I., and Kipnis, M.A., *Zh. Neorg. Khim.*, 1984, vol. 29, no. 7, pp. 1661–1663.
18. Hubli, R.C., Mukherjee, T.K., Venkatachalam, S., et al., *Hydrometallurgy*, 1995, vol. 38, pp. 149–174.
19. Maurice, D. and Hawk, J.A., *Hydrometallurgy*, 1999, vol. 52, pp. 289–312.
20. Khobotova, E.B., Nikolov, O.T., Kholin, Yu.V., and Gorobets, S.D., *Zh. Prikl. Khim.*, 1992, vol. 65, no. 3, pp. 552–556.
21. Rubtsov, Yu.I., *Emerdzhentnost' kak faktor optimizatsii v tekhnologiyakh blagorodnometal'nogo syr'ya* (Emergentness as an Optimization Factor in Technologies of Noble-metal Raw Materials), Chita, 2003.

ISSN 1070-4272, Russian Journal of Applied Chemistry, 2007, Vol. 80, No. 4, pp. 542–548. © Pleiades Publishing, Ltd., 2007.
Original Russian Text © I.V. Prikhod'ko, F. Tumakaka, G. Sadowski, 2007, published in Zhurnal Prikladnoi Khimii, 2007, Vol. 80, No. 4, pp. 555–561.

PHYSICOCHEMICAL STUDIES OF SYSTEMS AND PROCESSES

Application of the PC-SAFT Equation of State to Modeling of Solid–Liquid Equilibria in Systems with Organic Components Forming Chemical Compounds

I. V. Prikhod'ko, F. Tumakaka, and G. Sadowski

St. Petersburg State University, St. Petersburg, Russia
University of Dortmund, Dortmund, Germany

Received February 1, 2007

Abstract—Equilibrium diagrams of liquid and solid phases were calculated by the equation of state, based on the perturbed-chain statistical associating fluid theory (PC-SAFT) for binary and ternary systems constituted by associating substances (water, alcohols, amines, phenol, bisphenol A, acetamide). Phase diagrams were considered for systems in which congruently and incongruently melting intermolecular compounds are formed and for a system with limited mutual solubility of the components in the liquid state. The results of prognostication of phase equilibria were illustrated by the example of a ternary system constituted by bisphenol A, phenol, and water, in which an adduct of bisphenol A and phenol is formed.

DOI: 10.1134/S1070427207040040

Data on the equilibrium between solid and liquid phases are rather important for analysis of crystallization, which is a method for separation and purification of various substances. Types of solid–liquid equilibrium phase diagrams in binary systems are widely diverse and include, in particular, solid–melt diagrams with limited mutual solubility of the components in the solid (liquid) state and formation of chemical compounds melting with or without decomposition. In the case of diagrams of the latter type, intermolecular compounds, frequently named adducts and hydrates (in aqueous systems) or solvates (in nonaqueous systems), can be formed. In the case of compound formation, liquidus curves corresponding to crystallization of compounds appear in the fusibility diagrams, in addition to the lines of crystallization of pure components. The main experimental technique for obtaining the diagrams mentioned above is differential scanning calorimetry.

In this study, the equation of state, suggested by Gross and Sadowski [1] on the basis of the perturbed-chain statistical associating fluid theory (PC-SAFT), was used to model the solid–liquid phase equilibrium in systems involving chemical compounds. This equation of state is a modification of the known molecular-statistical model SAFT (Statistical Associating Fluid Theory), which has been popular in engineering calculations recently. It is based on the results of the perturbation theory and a numerical experiment for a fluid formed by chains of solid spheres. The molecular model underlying the PC-SAFT takes into account the formation of chains of solid spheres, dispersion interaction described in terms of the Barker–Henderson perturbation theory [2], and association. It is assumed that there are contact areas on the molecule surface, which are capable of specific interactions with contact areas of other molecules. The PC-SAFT model is being intensively developed; in particular, its variants that take into account multipole interactions in description of polar components have been developed [3–5].

The PC-SAFT model has been successfully tested on various systems, including nonpolar, polar, and associating substances, as well as polymers and copolymers, in a wide range of conditions [1, 3–10].[1] The results obtained are rather promising for further development of this model. However, the consideration has been limited to only fluid phases (liquid–vapor, liquid–liquid, liquid–liquid–vapor). It was of interest to apply this equation to modeling of an equi-

[1] For the software package for calculation of phase equilibria in terms of various models, including SAFT and PC-SAFT, see http://www.tu-harburg.de/vt2/pe2000/HomePage.html.

Table 1. Parameters of the PC-SAFT equation for pure associating components

Substance	M, g mol^{-1}	m	σ, Å	ε/k, K	$\varepsilon^{A_iB_i}$, K	$k^{A_iB_i}$
Water	18.015	1.0656	3.0007	366.51	2500.7	0.034868
Methanol	32.042	1.5255	3.2300	188.90	2899.5	0.035176
n-Octanol	130.23	4.3555	3.7145	262.74	2754.8	0.002197
Hexylamine	101.19	2.8724	4.0036	285.87	1229.0	0.020030
Octylamine	129.24	3.7717	3.9403	272.83	1375.6	0.020101
Phenol	94.113	2.6844	3.5660	250.37	2827.6	0.086578
Acetamide	59.07	2.0233	3.4995	333.91	3441.2	0.030047
Bisphenol A	228.29	9.8321	3.0307	238.92	2763.3	0.030044

librium between solid and liquid phases. The goals of the study were as follows: description of solid–liquid equilibria for a number of binary systems including associating components [water, alcohols, amines, phenol, bisphenol A (BPA), acetamide], which form stable and unstable chemical compounds of varied stoichiometry; description of liquid–liquid and solid–liquid equilibria for the water–phenol system; and prognostication of the fusibility diagram for the ternary mixture of BPA, phenol, and water, in which an adduct of BPA and phenol is formed. Systems in which the solid phase is a solid solution are beyond the scope of this study.

A detailed description of the PC-SAFT equation of state can be found in [1, 3, 6–8], and, therefore, only a brief consideration will be made here. According to the PC-SAFT model, the expression for the compressibility factor z can be written as

$$z = 1 + z^{hc} + z^{\text{disp}} + z^{\text{assoc}}, \quad (1)$$

where $z = PV/RT$; P, pressure; V, molar volume; R, universal gas constant; and T, temperature. The first term in the sum accounts for the contribution of the ideal gas ($z^{\text{id.gas}} = 1$), and the remaining three are related to contributions of chain formation, dispersion component, and association, respectively. Formulas for calculation of z^{hc} and z^{disp} were reported in [1], and the expression for z^{assoc} can be found in [11–13].

Description of ith pure associated substance requires five parameters: number m_i of segments forming the molecule-chain; segment diameter σ_i; segment interaction energy ε_i/k; effective association volume $k^{A_iB_i}$, and association energy $\varepsilon^{A_iB_i}/k$ (k is the Boltzmann constant). The last two parameters define the specific interaction between the contact areas A_i and B_i of ith component. When applying the model to mixtures, the Lorenz–Berthelot combination rules are used, with only a single fitting parameter of the binary interaction, k_{ij}, introduced to correct the dispersion component of interactions in the PC-SAFT equation:

$$\sigma_{ij} = \frac{1}{2}(\sigma_i + \sigma_j), \quad (2)$$

$$\varepsilon_{ij} = \sqrt{\varepsilon_i \varepsilon_j}(1 - k_{ij}). \quad (3)$$

To take into account the association between different-type molecules of ith and jth components, simple mixing rules suggested by Wolbach and Sandler [14] are introduced into the model without an additional fitting parameter:

$$\varepsilon^{A_iB_j} = \frac{1}{2}(\varepsilon^{A_iB_i} + \varepsilon^{A_jB_j}), \quad (4)$$

$$k^{A_iB_j} = \sqrt{k^{A_iB_i} k^{A_jB_j}} \left(\frac{\sqrt{\sigma_{ii}\sigma_{jj}}}{\frac{1}{2}(\sigma_{ii} + \sigma_{jj})} \right)^3. \quad (5)$$

Values of the parameters of the PC-SAFT equation of state for a number of pure associating components (water, alcohols) have been reported in the literature [6], and the lacking parameters for amines, phenol, BPA, and acetamide were determined in this study (Table 1). It was assumed that all molecules of associating components have two specific contact areas each.

Let us now pass to a thermodynamic description of the solid–liquid equilibrium for the case when the solid phase is a pure component, rather than a solid solution. The solubility of a solid in a solvent can be represented, in the case of low pressures and disregarded changes in specific heat, as the expression [15]:

$$x_i^{\text{L}} = \frac{\varphi_{0i}^{\text{L}}}{\varphi_i^{\text{L}}} \exp\left[-\frac{\Delta H_{0i}^{\text{m}}}{RT}\left(1 - \frac{T}{T_{0i}^{\text{m}}}\right)\right], \quad (6)$$

Table 2. Melting point and enthalpy of melting of pure substances

Substance	T_{0i}^{m}, K	ΔH_{0i}^{m}, J mol^{-1}
Water	273.15	6020
Methanol	175.25	3180
n-Octanol	258.03	23700
Hexylamine	252.15	25040
Octylamine	273.37	34740
Phenol	314.0	11510
Acetamide	353.5	15610
Bisphenol A	431.1	30100

where x_i^{L} is the mole fraction of *i*th component in the liquid phase (superscript L); ΔH_{0i}^{m} and T_{0i}^{m}, enthalpy of melting and melting point of pure *i*th component; and φ_{0i}^{L} and φ_i^{L}, fugacity coefficients of *i*th pure component and the same component in a mixture at prescribed temperature and pressure.

The values of the fugacity coefficients are calculated using the PC-SAFT equation of state [1]. Solving Eq. (6) for x_i^{L} at various temperatures, we finally obtain the crystallization line of the pure substance. The thermodynamic properties of the pure substances (H_{0i}^{m} and T_{0i}^{m}) considered in this study are listed in Table 2.

If a chemical compound $A_{\nu_A}B_{\nu_B}^{(S)}$ (S, superscript denoting the solid phase; ν_A and ν_B, stoichiometric coefficients) is formed in the system, then the crystallization curve of this compound can be calculated by considering the chemical reaction

$$\nu_A A^{(L)} + \nu_B B^{(L)} \rightleftarrows A_{\nu_A}B_{\nu_B}^{(S)}. \quad (7)$$

Taking the activity of the chemical compound in the solid phase to be unity, we can write for the equilibrium constant K_a

$$K_a = \Pi a_i^{\nu_i} = (x_A\gamma_A)^{-\nu_A}(x_B\gamma_B)^{-\nu_B}, \quad (8)$$

with the activity coefficients γ_i in the liquid phase expressed in terms of the ratio between the fugacity coefficients in solution and in *i*th pure liquid as

$$\gamma_i = \varphi_i/\varphi_{0i}. \quad (9)$$

We denote the enthalpy of melting and melting point of the compound by ΔH^{ref} and T^{ref}, respectively. If the compound fully dissociates in the liquid phase, the enthalpy of melting of the compound and the enthalpy of reaction (7) coincide. The temperature dependence of the constant of chemical equilibrium (8) is written as

$$\ln K_a = \ln K_a^{ref} + \frac{\Delta H^{ref}}{R}\left(\frac{1}{T^{ref}} - \frac{1}{T}\right). \quad (10)$$

Expression (10) is the integral form of the equation of the isobar of the chemical reaction. In a narrow temperature range, the enthalpy of reaction (7) can be considered constant and equal to ΔH^{ref}. The temperature T^{ref} may correspond to a congruent or an incongruent point in the fusibility diagram. Occasionally, there are no direct experimental data on values of ΔH^{ref}. Several methods for evaluating this quantity have been suggested in the literature.

(1) Method of weighted-average values of the entropies of melting of the starting compounds [16]; ΔH^{ref} is calculated by the formula

$$\Delta H^{ref} = T^{ref}\sum_i x_i \frac{\Delta H_{0i}^{m}}{T_{0i}^{m}}, \quad (11)$$

where x_i is the mole fraction of *i*th component in the compound.

(2) ΔH^{ref} and T^{ref} are found by extrapolation to the composition of the compound of the experimentally found concentration dependence of the heat (and temperature) of crystallization of the mixtures [17].

(3) The value of ΔH^{ref} is found by processing of experimental data (melting point–composition) on the assumption of an ideal mixture of monomers and the compound or with account of its nonideality; this value determines the temperature dependence of the association constant [18].

(4) The value of ΔH^{ref} serves as a fitting parameter in processing of experimental data on the crystallization of the compound; in this case, the activity coefficients are calculated using the equation of state [19].

(5) ΔH^{ref} is evaluated using the Schroder equation for ideal solutions [20].

The crystallization line of the chemical compound is calculated using Eqs. (8) and (10), which are solved by the iteration method for the mole fraction of the component in the range from the melting point of the compound (or incongruent point) to the eutectic point. The calculation procedure begins with finding K^{ref} at prescribed values of ΔH^{ref} and T^{ref} and molar composition of the chemical compound formed by reaction (7) [19]:

$$K_a^{ref} = \Pi a_i^{\nu_i} = [x_A\gamma_A(T^{ref}, x_A)]^{-\nu_A}[x_B\gamma_B(T^{ref}, x_B)]^{-\nu_B}. \quad (12)$$

Table 3. Melting points and enthalpies of melting of intermolecular compounds in the system under consideration

Compound and its stoichiometry	T^{ref}, K	ΔH^{ref}, J mol^{-1}
Water : methanol = 1 : 1	171.5	8700
Phenol : acetamide:		
1 : 1	307.15	11670
2 : 1	315.45	11770
Hexylamine : *n*-octanol = 1 : 1	255.03	24480
Octylamine : *n*-octanol = 1 : 1	267.19	25060
Phenol : bisphenol A:		
1 : 1	375.15	36870
1 : 1, in ternary system (30 mol % water)	359.0	36870
1 : 1, in ternary system (50 mol % water)	343.0	36870

Table 4. Binary interaction parameters evaluated for the systems under study

System	k_{ij}
Water–methanol	–0.18
Phenol–acetamide	–0.055
Hexylamine–*n*-octanol	–0.06
Octylamine–*n*-octanol	0.0
Phenol–bisphenol A	–0.01
Phenol–water	–0.018
Bisphenol A–water	–0.018

In a particular case in which an adduct of A and B of a stoichiometric composition is formed, $\nu_A = \nu_B = 1$ and $x_A = x_B = 0.5$. The activity coefficients $\gamma_A(T^{ref}, x_A)$ and $\gamma_B(T^{ref}, x_B)$ are calculated in terms of the PC-SAFT model. After finding K^{ref} from (12), Eqs. (8) and (10) are solved in the next stage of the calculation, at each running value of temperature, lower than T^{ref}, for the unknown quantity x_i^L. Repeating this procedure at other values of T, we can obtain the branch of the crystallization curve of the chemical compound, which intersects the lines corresponding to crystallization of pure components in the system. Table 3 lists the numerical values of T^{ref} and ΔH^{ref} for the chemical compounds formed in the systems under consideration. The optimal values of the binary-interaction parameter k_{ij}, used to describe the phase diagrams, are listed in Table 4.

Let us now discuss the results obtained. The results of modeling of the equilibrium between the solid phase and the liquid for the systems studied are illustrated by Figs. 1–6. Figure 1 shows the fusibility diagram for the methanol–water system in which alcohol monohydrate is formed (1 : 1 stoichiometry). This system shows noticeable negative deviations from the ideal behavior. We carefully checked the sensitivity of the calculation results to the chosen value of ΔH^{ref}, determined by various methods [16, 18, 19]. A testing of the PC-SAFT model demonstrated that the best agreement with the experimental data [18, 21] is provided by ΔH^{ref} equal to 8700 J mol^{-1}, found in [18] using the dimerization model for a nonideal water–methanol solution. The enthalpy of melting of the monohydrate, found using the method of average-weighted values of the entropies of melting of metha-

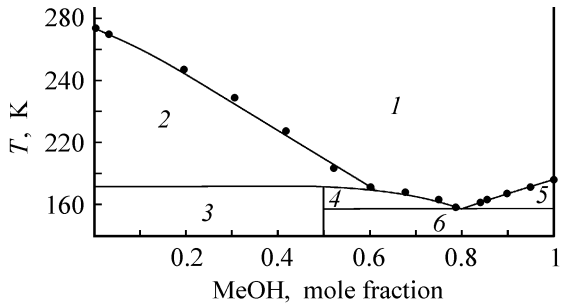

Fig. 1. Fusibility diagram for the system constituted by water and methanol (MeOH) with indication of two-phase region. (*T*) Temperature; the same for Figs. 3–6. (1 : 1) methanol monohydrate $MeOH \cdot H_2O$. (*1*) Liquid phase, (*2*) region of equilibrium between ice and the liquid phase, (*3*) region of coexistence of ice and crystals of methanol monohydrate, (*4*) region of equilibrium between $MeOH \cdot H_2O$ crystals and solution, (*5*) region of coexistence of solid methanol and solution, (*6*) region of coexistence of two crystalline phases: $MeOH \cdot H_2O$ and methanol. *Points*, experimental data [18, 21]; *lines*, calculation by the PC-SAFT equation.

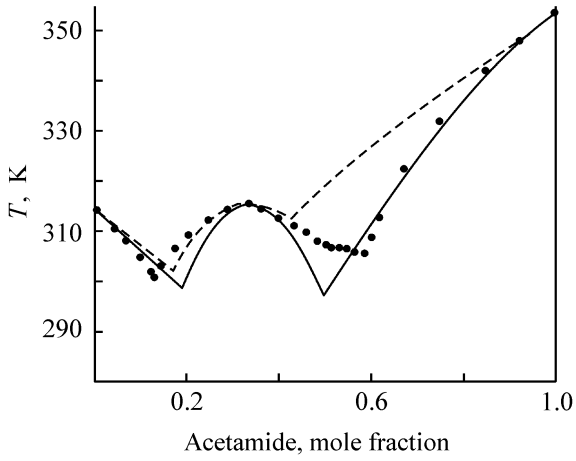

Fig. 2. Melting point vs. composition for the phenol–acetamide system in which two compounds are formed. *Points*, experimental data [16]; *lines*, calculation by the PC-SAFT equation at k_{ij} = –0.055 (*solid lines*) and k_{ij} = 0 (*dashed lines*).

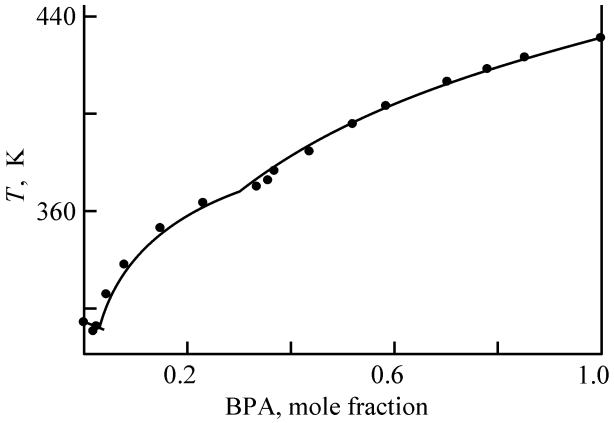

Fig. 3. Liquid–solid equilibrium for the phenol–BPA system. *Points*, experimental data [17]; *lines*, calculation by the PC-SAFT equation.

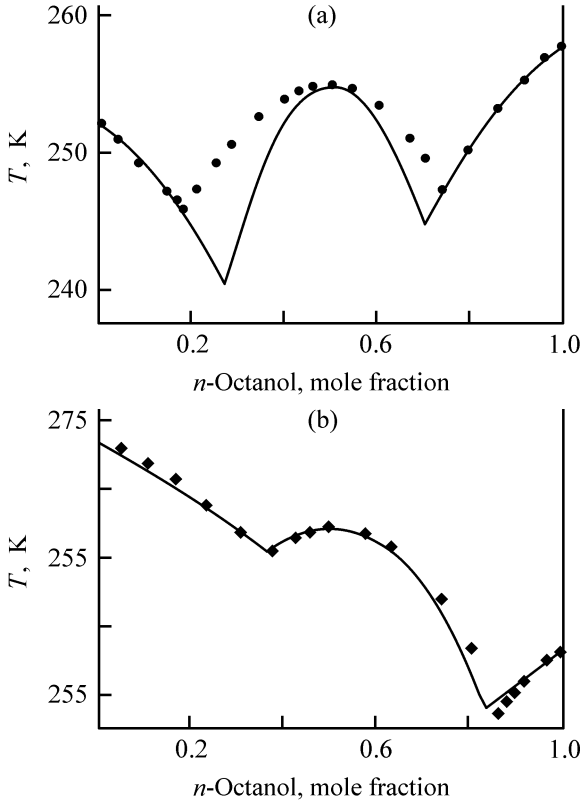

Fig. 4. Fusibility diagrams for the systems (a) hexylamine–*n*-octanol and (b) octylamine–*n*-octanol. *Points*, experimental data [22, 23]; *lines*, calculation by the PC-SAFT equation.

nol and water, is 3440 J mol^{-1}. At this value of ΔH^{ref} and in the case of a varied parameter k_{ij}, a satisfactory description of this system cannot be obtained. It is noteworthy that, at zero k_{ij}, the PC-SAFT equation of state predicts for the methanol–water mixture an incorrect type of the phase diagram (two crystallization branches of the pure components intersecting at the eutectic point). Figure 2 presents the results of correlation and prognostication in terms of the PC-SAFT model for the phenol–acetamide system, whose phase diagrams show crystallization curves of intermolecular compounds of stoichiometry 2 : 1 and 1 : 1; the crystallization curve of the 1 : 1 compound is very short. To evaluate ΔH^{ref} for both the compounds, we employed the method of weighted-average values of the entropy of melting of the starting substances [16]. The parameter k_{ij} was varied, but, unfortunately, the crystallization line of the 1 : 1 compound could not be described.

The phase diagram of the BPA–phenol system, in which an adduct of equimolar composition is formed, is shown in Fig. 3. The value of ΔH^{ref} of the incongruently melting compound was taken from [17]. This system shows nearly ideal behavior and the model rather well describes it for both zero and slightly negative values of the parameter k_{ij}. The solid–liquid equilibrium was calculated using the PC-SAFT equation of state for the amine–*n*-alkanol systems (Fig. 4), which are characterized by appearance of congruently melting compounds of 1 : 1 stoichiometry [22–24]; the enthalpies of melting of the adducts were determined in [20]. As demonstrated by Fig. 4a, the calculation correctly reproduces the general form of the diagram, but the calculated crystallization lines of the adduct somewhat differ from those obtained experimentally. This system exhibits strong negative deviations from the Raoult law. The results of prognostication by the PC-SAFT equation for the octylamine–octanol system (Fig. 4b), whose behavior is nearly ideal, coincide with the experimental data with good precision.

Recently, experimental data have been reported [25] on the solid–liquid equilibrium for the BPA–phenol–water ternary system in which an adduct of BPA and phenol is formed with a 1 : 1 stoichiometry. To prognosticate the phase diagram for this system, additional calculations of fusibility diagrams were performed for phenol–water and BPA–water binary subsystems.

As is known [26], the phase behavior of the phenol–water system is rather complex: the liquid solution stratifies and three-phase equilibria of different types appear. Figure 5 illustrates the phase diagram for this system under atmospheric pressure, with the solid–liquid, liquid–liquid, and liquid–vapor equilibria shown. It is noteworthy that the regions of coexistence of ice and the liquid phase (L_2) and of solid phenol

and liquid (L_2) are rather narrow and virtually invisible on the scale used in the figure. The PC-SAFT equation can reflect with an acceptable accuracy the full phase diagram of this system in a wide temperature range. Unfortunately, no experimental data on the solid–liquid equilibrium could be found in the literature, and, therefore, the fusibility diagram of this mixture was prognosticated (k_{ij} = 0). The predicted diagram was found to be similar to that for the phenol–water system.

Figure 6 shows the results of description of the phase diagram of the ternary system BPA–phenol–water for a constant mole fraction of water. The dependence of the melting point on composition was plotted for this system on the scale of a relative mole fraction of BPA (characterizing the composition of the BPA–water quasibinary mixture) at a prescribed content of water. The calculations for the ternary system used the same value of ΔH^{ref} as that for the BPA–phenol binary subsystem. T^{ref} were found by extrapolation from experimental data on the dependence of the melting point of the ternary mixture on its composition. The crystallization lines of the pure substances and adduct were prognosticated for the ternary aqueous-organic system for a zero value of the parameter k_{ij} for the BPA–water mixture; a calculation was also made with fitting of this parameter by using the data for the BPA–phenol–water system (k_{ij} = –0.018). The use of a corrected value of k_{ij} for the BPA–water binary subsystem made it possible to describe the experimental data with a good accuracy. As can be seen in Fig. 6, the crystallization curves in the ternary system shift to lower temperatures as the content of water increases.

CONCLUSIONS

(1) The PC-SAFT model describes, on the whole, successfully the solid–liquid equilibrium for binary and ternary systems (methanol–water, phenol–acetamide, bisphenol A–phenol, hexylamine–octanol, octylamine–octanol, and bisphenol A–phenol–water) in which intermolecular compounds are formed. Use of a single fitting parameter, that of the binary interaction, is sufficient for a satisfactory description of phase diagrams for all of the systems considered.

(2) The model reproduces with an acceptable accuracy the phase diagram of the phenol–water system at atmospheric pressure, in which various types of two- and three-phase equilibria are observed.

(3) The lines of crystallization lines of a chemical compound that completely dissociates in the liquid phase can be calculated using the method described in this study from data on the enthalpy of melting and the melting point of the compound.

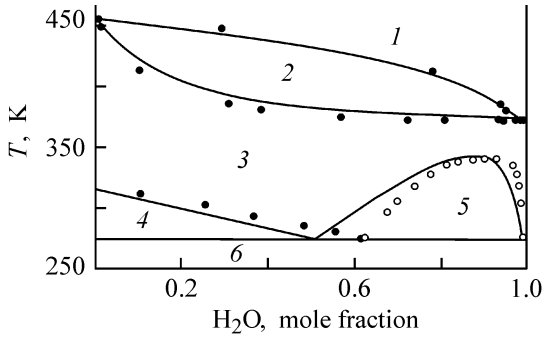

Fig. 5. Phase diagram of the phenol–water system under atmospheric pressure. (*1*) Vapor phase, (*2*) region of vapor–liquid equilibrium, (*3*) liquid phase, (*4*) region of coexistence of solid phenol and solution, (*5*) region of a liquid (L_1)–liquid (L_2) equilibrium, (*6*) region of coexistence of phenol crystals and ice. *Points*, experimental data [26]; *lines*, calculation by the PC-SAFT equation.

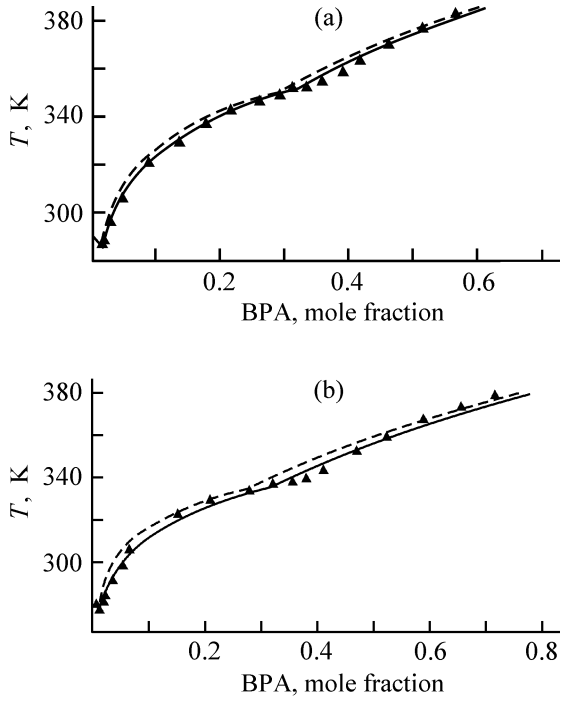

Fig. 6. Prognostication of the fusibility diagrams of the BPA–phenol–water ternary system at water content of (a) 30 mol % and (b) 50 mol %. (BPA) Relative content of bisphenol A in the BPA–phenol quasibinary system. *Points*, experimental data [25]; *lines*, calculation by the PC-SAFT equation for the following values of the parameter k_{ij} for the BPA–water binary subsystem: k_{ij} = –0.018 (*solid lines*) and k_{ij} = 0 (*dashed lines*).

ACKNOWLEDGMENTS

The authors thank N.A. Smirnova for discussion of the paper and valuable remarks.

The study was financially supported by a joint grant of the Ministry of Education and Science of the Russian Federation and German academic exchange service (DAAD) in the framework of the Program "Mikhail Lomonosov" (project no. A/05/05/05420), by the Russian Foundation for Basic Research (project no. 05-03-33267), and by the Grant of the President of the Russian Federation for support of leading scientific schools (project no. NSh-5557.2006.3).

REFERENCES

1. Gross, J. and Sadowski, G., *Ind. Eng. Chem. Res.*, 2001, vol. 40, pp. 1244–1260.
2. Barker, J.A. and Henderson, D., *J. Chem. Phys.*, 1967, vol. 47, pp. 2856–2861.
3. Tumakaka, F. and Sadowski, G., *Fluid Phase Equilibr.*, 2004, vol. 217, pp. 233–239.
4. Dominik, A., Chapman, W.G., Kleiner, M., and Sadowski, G., *Ind. Eng. Chem. Res.*, 2005, vol. 44, pp. 6928–6938.
5. Gross, J. and Vrabec, J., *Am. Inst. Chem. Eng. J.*, 2006, vol. 52, pp. 1194–1204.
6. Gross, J. and Sadowski, G., *Ind. Eng. Chem. Res.*, 2002, vol. 41, pp. 5510–5515.
7. Gross, J. and Sadowski, G., *Ind. Eng. Chem. Res.*, 2002, vol. 41, pp. 1084–1093.
8. Gross, J., Spuhl, O., Tumakaka, F., and Sadowski, G., *Ind. Eng. Chem. Res.*, 2003, vol. 42, pp. 1266–1274.
9. Kleiner, M., Tumakaka, F., Sadowski, G., et. al., *Fluid Phase Equilibr.*, 2006, vol. 241, pp. 113–123.
10. Tumakaka, F., Gross, J., and Sadowski, G., *Fluid Phase Equilibr.*, 2005, vol. 228–229, pp. 89–98.
11. Chapman, W.G., Gubbins, K.E., Jackson, G., and Radosz, M., *Ind. Eng. Chem. Res.*, 1990, vol. 29, pp. 1709–1721.
12. Huang, S.H. and Radosz, M., *Ind. Eng. Chem. Res.*, 1990, vol. 29, pp. 2284–2294.
13. Huang, S.H. and Radosz, M., *Ind. Eng. Chem. Res.*, 1991, vol. 30, pp. 1994–2005.
14. Wolbach, J.P. and Sandler, S.I., *Ind. Eng. Chem. Res.*, 1998, vol. 37, pp. 2917–2928.
15. Prausnitz, J.M., Lichtenthaler, R.N., and Azevedo, E.G., *Molecular Thermodynamics of Fluid–Phase Equilibria,* Prentice Hall PTR, 1998, 3rd ed.
16. Wales, S.M., *Phase Equilibria in Chemical Engineering*, Boston: Butterworth, 1985.
17. Wyrzykowska-Stankiewicz, D. and Palczewska-Tuliń ska, M., *Thermochim. Acta*, 1991, vol. 190, pp. 209–216.
18. Miller, G.A. and Carpenter, D.K., *J. Chem. Eng. Data*, 1964, vol. 9, pp. 371–373.
19. Folas, G.K., Gabrielsen, J., Michelsen, M.L., et al., *Ind. Eng. Chem. Res.*, 2005, vol. 44, pp. 3823–3833.
20. Domań ska, U. and Marciniak, M., *Fluid Phase Equilibr.*, 2005, vol. 235, pp. 30–41.
21. Ott, J.B., Goates, J.R., and Waite, B.A., *J. Chem. Thermodyn.*, 1979, vol. 11, pp. 739–746.
22. Domań ska, U. and Gtoskowska, M., *Fluid Phase Equilibr.*, 2004, vol. 216, pp. 135–145.
23. Domań ska, U. and Gtoskowska, M., *J. Chem. Eng. Data*, 2004, vol. 49, pp. 101–108.
24. Domań ska, U. and Gtoskowska, M., *Ind. Eng. Chem. Res.*, 2004, vol. 43, pp. 7647–7656.
25. Kwok, K.S., Chan, H.C., Chan, C.K., and Ng, K.M., *Ind. Eng. Chem. Res.*, 2005, vol. 44, pp. 3788–3798.
26. King, M.B., *Phase Equilibrium in Mixtures*, Oxford: Pergamon Press, 1969.

ISSN 1070-4272, Russian Journal of Applied Chemistry, 2007, Vol. 80, No. 4, pp. 549–552. © Pleiades Publishing, Ltd., 2007.
Original Russian Text © Sh.B. Kasenova, Zh.K. Tukhmetova, A.Zh. Abil'daeva, E.V. Burdel'naya, G.K. Mukusheva, B.K. Kasenov, S.M. Adekenov, A.Zh. Turmukhambetov, 2007, published in Zhurnal Prikladnoi Khimii, 2007, Vol. 80, No. 4, pp. 562–565.

PHYSICOCHEMICAL STUDIES OF SYSTEMS AND PROCESSES

Thermodynamic Properties of Alkaloids Lappaconitine and Glaucine

Sh. B. Kasenova, Zh. K. Tukhmetova, A. Zh. Abil'daeva, E. V. Burdel'naya, G. K. Mukusheva, B. K. Kasenov, S. M. Adekenov, and A. Zh. Turmukhambetov

Fitokhimiya Research-and-Production Center AO, Ministry of Education and Science of the Republic of Kazakhstan, Karaganda, Kazakhstan

Received June 27, 2006; in final form, December 2006

Abstract—Calorimetric methods were used to study the enthalpy of solution of the alkaloids glaucine $C_{21}H_{25}NO_4$ and lappaconitine $C_{32}H_{44}N_2O_8$ in 96% ethanol and their heat capacity in the temperature ranges 173–298.15 and 173–423 K. Equations describing the dependences $\Delta H^{m}_{sol} \sim f(\sqrt{m})$ (m is molal concentration) and $C^{0}_{p} \sim f(\sqrt{T})$ for the compounds under study were derived. The enthalpies of combustion, melting, and formation of $C_{21}H_{25}NO_4$ and $C_{32}H_{44}N_2O_8$ were estimated by means of theoretical calculations.

DOI: 10.1134/S1070427207040052

Alkaloids belong to promising natural compounds owing to their biological activity. An interesting area of study of these compounds is analysis of their therodynamic properties to obtain new physicochemical constants necessary for standardization and certification of biologically active compounds and for directed synthesis of their derivatives possessing a high physiological activity.

This communication presents the results of experimental studies and calculations of the enthalpies of combustion, melting, and formation of the alkaloids glaucine and lappaconitine and of the temperature dependence of their heat capacity. In [1, 2], the thermodynamic properties of lappaconitine hydrochloride, which is an antiarrhythmic pharmacopoeic preparation Allapinine, and glaucine hydrobromide, basis of an antitussive preparation, were examined.

Lappaconitine (**I**) and glaucine (**II**) subjected to a calorimetric analysis were isolated from plants and accumulated in sufficient amounts at the laboratory of chemistry of alkaloids at Fitokhimiya NPTs AO (Karaganda) and had chromatographic purity:

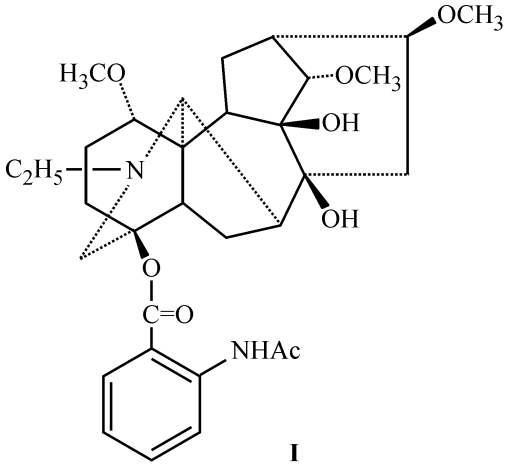

I

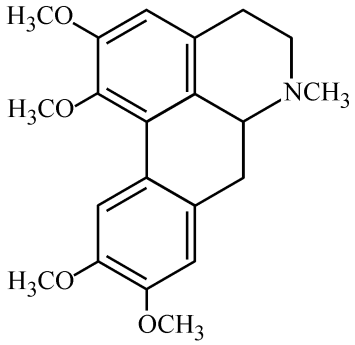

II

Table 1. Experimental values of the enthalpy of solution of lappaconitine $C_{32}H_{44}N_2O_8$ (M = 584.3654) and glaucine $C_{21}H_{25}NO_4$ (M = 355.4377) in 96% ethanol at various dilutions (T = 298.15 K)*

Alkaloid	Weighed portion, g	Dilution	Q_{sol}, J	ΔH^m_{sol}, kJ mol^{-1}
$C_{32}H_{44}N_2O_8$	0.0055	1 : 9000	0.1182	125.59
$C_{21}H_{25}NO_4$	0.0034	1 : 9000	0.2206	23.06
$C_{32}H_{44}N_2O_8$	0.0028	1 : 18000	0.0817	170.51
$C_{21}H_{25}NO_4$	0.0017	1 : 18000	0.1647	34.44
$C_{32}H_{44}N_2O_8$	0.0014	1 : 36000	0.0583	245.85
$C_{21}H_{25}NO_4$	0.0008	1 : 36000	0.1281	56.93

* Five independent determinations were made at each dilution.

Table 2. Experimental values of the specific $C_p \pm \bar{\delta}$ and molar $C^0_p \pm \mathring{\Delta}$ heat capacities of lappaconitine (mp 207–209°C) and glaucine (mp 115–119°C)

T, K	$C_p \pm \bar{\delta}$, J g^{-1} K^{-1}	$C^0_p \pm \mathring{\Delta}$, J mol^{-1} K^{-1}
	Lappaconitine	
173	0.5685 ± 0.0135	332 ± 22
198	1.8994 ± 0.0396	1110 ± 64
223	2.4411 ± 0.0467	1426 ± 76
248	2.1298 ± 0.0386	1245 ± 63
273	1.7993 ± 0.0513	1051 ± 83
298.15	1.5196 ± 0.0369	888 ± 60
323	2.1153 ± 0.0498	1236 ± 81
348	1.3504 ± 0.0391	789 ± 64
373	0.9662 ± 0.0239	565 ± 39
398	0.7192 ± 0.0242	420 ± 39
423	0.6679 ± 0.0155	390 ± 25
	Glaucine	
173	0.4250 ± 0.0106	151 ± 10
198	0.8985 ± 0.0156	319 ± 15
223	0.2430 ± 0.0231	441 ± 23
248	0.3707 ± 0.0328	487 ± 32
273	0.4580 ± 0.0411	518 ± 41
298.15	0.4996 ± 0.0290	532 ± 29

The heat of solution of compounds **I** and **II** in 96% ethanol at three dilutions of 1 : 9000, 1 : 18000, and 1 : 36000 (moles of alkaloid per moles of ethanol) was experimentally studied on a DAK-1-1A isothermal automated differential calorimeter. The experimental procedure was described in detail in [3–6]. The operation of the instrument was tested by measuring the heat of solution of a three times recrystallized potassium chloride at dilutions of 1 : 1600, 1 : 2400, and 1 : 3200 (moles of salt per moles of water). The average heat of KCl solution in water, equal to 17610 ± 333 J mol^{-1}, is in a good agreement with its recommended and reference values of 17577 ± 34 [7] and 17489 ± 371 J mol^{-1} [8].

Five parallel experiments were carried out at each dilution, and the results obtained were averaged. The experimental errors and the uniformities of their variances were calculated by methods of mathematical statistics with the use of Student's an Cochran's criteria [9]. The significance level of the criteria used was 5%. Results of the calorimetric measurements are listed in Table 1.

The experimentally obtained heats of solution of $C_{32}H_{44}N_2O_8$ and $C_{21}H_{25}NO_4$ in 96% ethanol at the dilutions specified were extrapolated to the infinite dilution, using the least-squares procedure. It was found on the basis of the relation $\Delta H^m_{sol} \sim f(\sqrt{m})$ [10] that the dependences of the enthalpies of solution of lappaconitine and glaucine on the molal concentration are described by the following equations (kJ mol^{-1}):

$$\Delta H^m_{sol}(C_{32}H_{44}N_2O_8) = 356.07 - 4845.92\sqrt{m}, \quad (1)$$

$$\Delta H^m_{sol}(C_{21}H_{25}NO_4) = 85.11 - 1302.28\sqrt{m}. \quad (2)$$

Equations (1) and (2) were used to calculate a fundamental thermochemical quantity, standard enthalpy of solution of these compounds in 96% ethanol at the infinite dilution, to be 356.07 ± 0.33 and 85.11 ± 1.53 kJ mol^{-1}, respectively.

The heat capacities of $C_{32}H_{44}N_2O_8$ and $C_{21}H_{25}NO_4$ were measured in the temperature ranges 173–423 and 173–298.15 K, respectively, at intervals of 25 K by the procedure described in [11], using an IT-s-400 calorimeter. The results obtained were averaged, subjected to mathematical processing, and used to calculate the molar heat capacity at each temperature. The instrument was calibrated by determining the heat capacity of α-Al_2O_3: the experimental value of $C^0_p(298.15)$ of α-Al_2O_3, equal to 76.0 J mol^{-1} K^{-1} was in a satisfactory agreement with the recommended value of 79.0 J mol^{-1} K^{-1} [12].

Table 2 lists experimental values of the specific and molar heat capacities of the compounds. The dependence $C^0_p \sim f(\sqrt{T})$ is plotted in the figure.

The curve describing the dependence $C^0_p \sim f(\sqrt{T})$ for lappaconitine in the temperature range 173–423 K shows sharp heat capacity peaks at 223 and 323 K. These effects are probably associated with structural

transformations of the molecule of this compound or with second order phase transitions. In this connection, for heat capacity equations related to different values of ΔT were derived for lappaconitine (J mol^{-1} K^{-1}):

$$C_{p1}^0 = -(3454 \pm 234) + (21886 \pm 1486) \times 10^{-3}T \quad (173\text{–}223\ \text{K}), \quad (3)$$

$$C_{p2}^0 = (3027 \pm 205) - (7179 \pm 487) \times 10^{-3}T \quad (223\text{–}298\ \text{K}), \quad (4)$$

$$C_{p3}^0 = -(3261 \pm 221) + (13924 \pm 945) \times 10^{-3}T \quad (298\text{–}323\ \text{K}), \quad (5)$$

$$C_{p3}^0 = -(9905 \pm 672) + (16226 \pm 1102) \times 10^{-3}T + (6156 \pm 418) \times 10^{5}T^{-2} \quad (323\text{–}423\ \text{K}). \quad (6)$$

The temperature dependence of the heat capacity of glaucine is monotonic in the temperature range under study and is described by the following equation (J mol^{-1} K^{-1}:

$$C_p^0 = (1642 \pm 101) - (2549 \pm 156) \times 10^{-3}T - (314.4 \pm 19.3) \times 10^{5}T^{-2}. \quad (7)$$

Further, the Karas and Frost equations [13] were used to estimate the standard enthalpy of combustion. The averaged values of the heats of combustion of $C_{32}H_{44}N_2O_8$ and $C_{21}H_{25}NO_4$, calculated by these two equations, are -18039 ± 708 and -11662 ± 382 kJ mol^{-1}, respectively. The Hess cycle for the reactions

$$C_{32}H_{44}N_2O_{8\,(l)} + 39O_{2\,(g)} = 32CO_{2\,(g)} + 22H_2O_{(l)} + N_{2\,(g)} - \Delta H_{comb}^0, \quad (8)$$

$$C_{21}H_{25}NO_{4\,(l)} + 50.5O_{2\,(g)} = 42CO_{2\,(g)} + 25H_2O_{(l)} + N_{2\,(g)} - \Delta H_{comb}^0, \quad (9)$$

was used to calculate the standard enthalpies of formation of the compounds in the liquid (molten) state to be -854.3 and -182.0 kJ mo^{-1}, respectively. The values of $\Delta_f H_{298.15}^0$ [$CO_{2\,(g)}$, $H_2O_{(l)}$], necessary for the calculation, were taken from [14].

In view of the fact that the compounds under study are in the crystalline state at the standard temperature (298.15 K), $\Delta_f H_{298.15}^0$ of their solid modification was calculated. For this purpose, ΔH_m of the compounds were evaluated using the empirical Gambill's equation

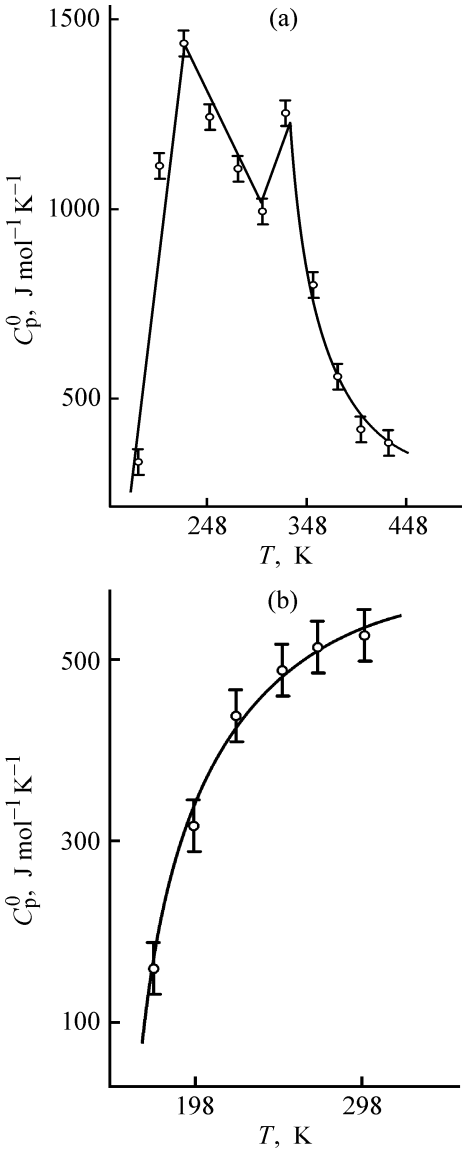

Heat capacity C_p^0 of (a) lappaconitine and (b) glaucine vs. temperature T.

[15] to be 766.7 and 110.5 kJ mol^{-1}, respectively. $\Delta_f H_s^0$ was calculated by the formula

$$\Delta_f H_{298.15\,(s)}^0 = \Delta_f H_{298.15\,(l)}^0 - \Delta H_m. \quad (10)$$

The standard enthalpies of formation of lappaconitine and glaucine in the crystalline state, calculated by substituting $\Delta_f H_{298.15\,(l)}^0$ and ΔH_m into (7), were -1621.0 and -293.5 kJ mol^{-1}, respectively.

CONCLUSIONS

(1) The heats of dissolution of natural alkaloids lappaconitine and glaucine in 96% ethanol were ex-

perimentally studied for the first time and the calorimetric data obtained were used to determine their standard enthalpies of solution in 96% ethanol at the infinite dilution.

(2) The temperature dependence of the heat capacity of $C_{32}H_{44}N_2O_8$ and $C_{21}H_{25}NO_4$ was studied in the temperature ranges 173–423 and 173–298.15 K, respectively. Sharp heat capacity peaks associated with second-order phase transitions were observed for lappaconitine at 223 and 323 K. Equations describing the temperature dependences of the heat capacity of the compounds were derived.

(3) The enthalpies of combustion, melting and formation of the compounds under study were estimated.

REFERENCES

1. Kasenov, B.K., Tukhmetova, Zh.K., Turmukhambetov, A.Zh., et al., *Zh. Prikl. Khim.*, 2003, vol. 76, no. 12, pp. 1971–1975.
2. Kasenov, B.K., Kasenova, Sh.B., Tukhmetova, Zh.K., et al., *Zh. Prikl. Khim.*, 2003, vol. 76, no. 8, pp. 1396–1397.
3. Skuratov, S.M., Kolesov, V.P., and Vorob'ev, A.F., *Termokhimiya* (Thermochemistry), Moscow: Mosk. Gos. Univ., 1964, vol. 1.
4. Calvet, E. et Prat, H., *Microcalorimetrie. Applications physico-chemiques et biologiques*, Paris: Masson, 1956.
5. Topor, N.D. and Suponitskii, Yu.L., *Usp. Khim.*, 1984, no. 9, pp. 1425–1462.
6. Recent Advances of Microcalorimetry, *Zh. Fiz. Khim.*, 1959, no. 6, pp. 1161–1175.
7. Mishchenko, K.P. and Poltoratskii, G.M., *Termodinamika i stroenie vodnykh i nevodnykh rastvorov elektrolitov* (Thermodynamics and Structure of Aqueous and Nonaqueous Electrolyte Solutions), Leningrad: Khimiya, 1977.
8. *Termicheskie konstanty veshchestv: Spravochnik* (Thermal Constants of Substances: Reference Book), Glushko, V.P., Ed., Moscow: Nauka, 1982, issue 10, part 2.
9. Spiridonov, V.P. and Lopatkin, A.A., *Matematicheskaya obrabotka eksperimental'nykh dannykh* (Mathematical Processing of Experimental Data), Moscow: Mosk. Gos. Univ., 1970.
10. Krestov, G.A., *Termodinamika ionnykh protsessov v rastvorakh* (Thermodynamics of Ionic Processes in Solutions), Leningrad: Khimiya, 1984.
11. Platunov, E.S., *Teplofizicheskie izmereniya v monotonnom rezhime* (Thermal Measurements in the Monotonic Mode), Moscow: Energiya, 1973.
12. Robie, R.A., Hewingway, B.S., and Fisher, J.K., *Thermodynamic Properties of Minerals and Related Substances at 298.15 K and 1 Bar (10^5 Pascals) Pressure and Higher Temperatures,* Washington, 1978, p. 456.
13. Kazanskaya, A.S. and Skoblo, V.A., *Raschety khimicheskikh ravnovesii* (Calculation of Chemical Equilibria), Moscow: Vysshaya Shkola, 1974.
14. Ryabin, V.A., Ostroumov, M.A., and Svit, T.F., *Termodinamicheskie svoistva veshchestv: Spravochnik* (Thermodynamic Properties of Substances: Reference Book), Leningrad: Khimiya, 1977.
15. Viktorov, V.V., *Metody vychisleniya fiziko-khimicheskikh velichin i prikladnye raschety* (Methods for Calculation of Physicochemical Quantities and Applied Calculations), Moscow: Khimiya, 1977.

ISSN 1070-4272, Russian Journal of Applied Chemistry, 2007, Vol. 80, No. 4, pp. 553–556. © Pleiades Publishing, Ltd., 2007.
Original Russian Text © A.I. Demidov, 2007, published in Zhurnal Prikladnoi Khimii, 2007, Vol. 80, No. 4, pp. 566–569.

PHYSICOCHEMICAL STUDIES OF SYSTEMS AND PROCESSES

Thermodynamics of Patina Formation

A. I. Demidov

St. Petersburg State Polytechnic University, St. Petersburg, Russia

Received December 12, 2006

Abstract—Changes in the standard Gibbs energies in reactions that occur in the interaction of copper and copper oxides with oxygen, water, and impurities contained in atmospheric precipitations were calculated.

DOI: 10.1134/S1070427207040064

It is known [1] that copper and copper-based alloys (brass, bronzes) exhibit moderate stability under atmospheric conditions. The average depth of corrosion penetration is 0.1 to 1, 0.6 to 4, and 1 to 8 μm yr^{-1} in a rural, marine, and industrial atmosphere. After several years of exposure to an urban or coastal atmosphere, a dense layer of patina is formed on copper and copper alloys and this layer hinders further development of corrosion. The patina is mostly composed of basic copper sulfates, with minor amounts of basic copper chloride present in coastal regions and minor amounts of malachite (basic cupric carbonate) formed in some cases [2].

The present paper reports the results of a thermodynamic analysis of the interaction of copper and copper oxides with oxygen, water, and impurities contained in atmospheric precipitations. The change in the standard Gibbs energy in the reactions was calculated per mole of atoms of the starting substances [3, 4]. The calculations used published values of changes in the standard Gibbs energies [5, 6] (see table). The interaction of copper with oxygen at the standard temperature of 298.15 K can be described by the reactions

$$[2Cu + 1/2O_2 = Cu_2O]/3,$$
$$\Delta G^0_{298} = -50.2 \text{ kJ mol}^{-1}; \quad (1)$$

$$[Cu + 1/2O_2 = CuO]/2,$$
$$\Delta G^0_{298} = -64.7 \text{ kJ mol}^{-1}. \quad (2)$$

The smallest change in the standard Gibbs energy is observed for reaction (2).

Copper(II) oxide is reduced by copper to copper(I) oxide:

$$[CuO + Cu = Cu_2O]/3,$$
$$\Delta G^0_{298} = -7.03 \text{ kJ mol}^{-1}. \quad (3)$$

In turn, copper(I) oxide can react with oxygen:

$$[Cu_2O + 1/2O_2 = 2CuO]/4,$$
$$\Delta G^0_{298} = -27.1 \text{ kJ mol}^{-1}. \quad (4)$$

Thus, copper(II) oxide is the most stable compound in the system Cu–O. The exceedingly thin oxide film formed on copper in the atmosphere of oxygen at room temperature may be composed of a single CuO layer or of two layers: outer CuO layer and inner Cu_2O one. A noticeable interaction of copper with oxygen begins at temperatures of about 500 K [7].

Changes in the standard Gibbs energies of various substances and ions according to [5, 6]

Formula	ΔG^0_{298}, kJ mol^{-1}	Formula	ΔG^0_{298}, kJ mol^{-1}
Cu	0	$CuSO_{4(s)}$	–661.8
Cu^{2+}	65.6	$CuSO_4 \cdot H_2O_{(s)}$	–918.6
O_2	0	$CuSO_4 \cdot 3H_2O_{(s)}$	–1400.2
CuO	–129.4	$CuSO_4 \cdot 5H_2O_{(s)}$	–1879.9
Cu_2O	–150.5	O_2	0
H_2O	–237.2	$CuSO_4 \cdot 3Cu(OH)_2$	–1818.8
$Cu(OH)_2$	–359.4	Cl^-	–131.2
H^+	0	$CuCl_2 \cdot 3Cu(OH)_2$	–1340.3
$CuOH^+$	–134.7	$CO_{2(aq)}$	–386.2
$Cu(OH)_{2(aq)}$	–328.5	$CuCO_3 \cdot Cu(OH)_2$	–900.9
$[Cu(OH)_3]^-$	–501.7	HS^-	12.6
$[Cu(OH)_4]^{2-}$	–657.7	CuS	–53.6
SO_4^{2-}	–742.0	Cu_2S	–86.3

The reactions of copper(I) and (II) oxides with deoxygenated water, written per mole of atoms of the starting substances,

$$[Cu_2O + H_2O = Cu(OH)_{2(s)} + Cu]/6, \quad \Delta G^0_{298} = 4.72 \text{ kJ mol}^{-1}; \quad (5)$$

$$[CuO + H_2O = Cu(OH)_{2(s)}]/5, \quad \Delta G^0_{298} = 1.44 \text{ kJ mol}^{-1}; \quad (6)$$

are characterized by a small positive changes in the standard Gibbs energy and, consequently, by a small yield of the reaction products.

In oxygen saturated with water vapor, water is involved in oxidation of copper and copper(I) oxide:

$$[Cu + 1/2O_2 + H_2O = Cu(OH)_2]/5, \quad \Delta G^0_{298} = -24.4 \text{ kJ mol}^{-1}; \quad (7)$$

$$[Cu_2O + 1/2O_2 + 2H_2O = Cu(OH)_2]/10, \quad \Delta G^0_{298} = -9.39 \text{ kJ mol}^{-1}. \quad (8)$$

In turn, copper(II) hydroxide can be reduced by copper to copper(I) oxide:

$$[Cu(OH)_2 + Cu = Cu_2O + H_2O]/6, \quad \Delta G^0_{298} = -4.72 \text{ kJ mol}^{-1}. \quad (9)$$

Thus, a film composed of copper(I) oxide and copper(II) hydroxide can be formed on the surface of copper in the presence of water vapor.

Impurities in the atmosphere are one of the most important factors making higher the corrosion rate of metals. Sulfur dioxide SO_2 is directly formed in eruptions of volcanoes, combustion of coal or other kinds of fuel, or oxidation of H_2S in decomposition of organic substances [8]. The process of formation of sulfur trioxide SO_3 in photochemical oxidation of SO_2 can be schematically represented as

$$2SO_2 + O_2 + h\nu \rightarrow 2SO_3.$$

Then, sulfur trioxide is dissolved in drops of atmospheric moisture to give sulfuric acid:

$$SO_3 + H_2O \rightarrow H_2SO_4.$$

Sulfur dioxide can dissolve in drops of atmospheric moisture to give sulfurous acid

$$SO_2 + H_2O \rightarrow H_2SO_3.$$

In turn, sulfurous acid is oxidized by oxygen dissolved in water to H_2SO_4. Thus, the presence of sulfur dioxide in air leads to the formation of sulfuric acid in thin films of moisture on the metal surface and markedly accelerates the corrosion processes:

$$[Cu(OH)_2 + 2H^+ = Cu^{2+} + 2H_2O]/7, \quad \Delta G^0_{298} = -7.06 \text{ kJ mol}^{-1}, \ pH_{10}\ 4.33; \quad (10)$$

$$[CuO + 2H^+ = Cu^{2+} + 2H_2O]/4, \quad \Delta G^0_{298} = -10.6 \text{ kJ mol}^{-1}, \ pH_{11}\ 3.7; \quad (11)$$

$$[Cu_2O + 2H^+ = Cu^{2+} + Cu + H_2O]/5, \quad \Delta G^0_{298} = -4.22 \text{ kJ mol}^{-1}, \ pH_{12}\ 1.85. \quad (12)$$

When calculating the pH, we took the activities of copper compounds and ions of copper and water to be unity. The presented values of ΔG^0_{298} and pH indicate that reaction (10) predominantly occurs in dilute sulfuric acid solutions (2×10^{-5} N), and reactions (11) and (12), in more concentrated solutions.

Metal cations are hydrated in aqueous solutions, and, therefore, the copper(II) ion Cu^{2+} should be written as $Cu(H_2O)_4^{2+}$ in an aqueous solution [9]. The copper(II) ion $Cu(H_2O)_4^{2+}$ can undergo hydrolysis [10]. The hydrolysis of copper(II) ions occurs in stages by the scheme

$$Cu(H_2O)_4^{2+} + H_2O = Cu(H_2O)_3OH^+ + H_3O^+.$$

If water molecules bound to a copper(II) ion are dropped from this equation, we have

$$Cu^{2+} + H_2O = CuOH^+ + H^+, \quad K_{13} = 3.4 \times 10^{-7}, \ pH_{13}\ 6.47\ [11]. \quad (13)$$

The values of the constant K_{13} and Gibbs energies of formation of Cu^{2+} and H^+ ions and water were used to calculate the Gibbs energy of formation of the $CuOH^+$ ion (see table):

$$Cu(H_2O)_3OH^+ + H_2O = Cu(H_2O)_2OH_{2(aq)} + H_3O^+,$$

or, in reduced form,

$$CuOH^+ + H_2O = Cu(OH)_{2(aq)} + H^+, \quad K_{14} = 2.5 \times 10^{-8}, \ pH_{14}\ 7.60; \quad (14)$$

$$Cu(H_2O)_2(OH)_{2(aq)} + H_2O = Cu(H_2O)OH_3^- + H_3O^+;$$

or, in reduced form,

$$Cu(OH)_{2(aq)} + H_2O = [Cu(OH)_3]^- + H^+,$$
$$K_{15} = 6.3 \times 10^{-12},\ pH_{15}\ 11.2; \quad (15)$$

and

$$Cu(H_2O)(OH)_3^- + H_2O = [Cu(OH)_4]^{2-} + H_3O^+,$$

or, in reduced form,

$$[Cu(OH)_3]^- + H_2O = [Cu(OH)_4]^{2-} + H^+,$$
$$K_{16} = 6.3 \times 10^{-15},\ pH_{16}\ 14.2. \quad (16)$$

If hydrolysis of copper(II) ions is accompanied by formation of a copper(II) hydroxide precipitate:

$$Cu(H_2O)_4^{2+} + 2H_2O = Cu(OH)_{2(s)} + 2H_3O^+$$

or, in reduced form,

$$Cu^{2+} + 2H_2O = Cu(OH)_{2(s)} + 2H^+,$$
$$K_{17} = 2.2 \times 10^{-9}, \quad (17)$$

then the calculated theoretical value of pH_{17} is 4.33. According to the results of [12], copper(II) hydroxide is formed as a jelly-like blue precipitate in processing of cold solutions of copper(II) salts with alkali solutions at pH 5.0–5.5.

Copper ions (Cu^{2+}) contained in thin films of water on the metal surface can interact with sulfate ions to give the corresponding crystal hydrates:

$$[Cu^{2+} + SO_4^{2-} + H_2O = CuSO_4 \cdot H_2O_{(s)}]/9,$$
$$\Delta G^0_{298} = -0.56\ kJ\ mol^{-1}; \quad (18)$$

$$[Cu^{2+} + SO_4^{2-} + 3H_2O = CuSO_4 \cdot 3H_2O_{(s)}]/15,$$
$$\Delta G^0_{298} = -0.81\ kJ\ mol^{-1}; \quad (19)$$

$$[Cu^{2+} + SO_4^{2-} + 5H_2O = CuSO_4 \cdot 5H_2O_{(s)}]/21,$$
$$\Delta G^0_{298} = -0.83\ kJ\ mol^{-1}. \quad (20)$$

Summing reactions (10) and (18)–(20), we obtain

$$[Cu(OH)_2 + 2H^+ + SO_4^{2-} = CuSO_4 \cdot H_2O_{(s)} + H_2O]/12,$$
$$\Delta G^0_{298} = -4.53\ kJ\ mol^{-1}; \quad (21)$$

$$[Cu(OH)_2 + 2H^+ + SO_4^{2-} + H_2O = CuSO_4 \cdot 3H_2O]/15,$$
$$\Delta G^0_{298} = -4.11\ kJ\ mol^{-1}; \quad (22)$$

$$[Cu(OH)_2 + 2H^+ + SO_4^{2-} + 3H_2O = CuSO_4 \cdot 5H_2O]/21,$$
$$\Delta G^0_{298} = -3.19\ kJ\ mol^{-1}, \quad (23)$$

i.e., the interaction of copper(II) hydroxide with sulfuric acid on the metal surface can give copper(II) sulfate crystal hydrates. Taking into account reaction (21), we can suggest that brochantite is formed by the reaction

$$[4Cu(OH)_2 + 2H^+ + SO_4^{2-} = CuSO_4 \cdot 3Cu(OH)_2 + 2H_2O]/27,$$
$$\Delta G^0_{298} = -4.21\ kJ\ mol^{-1}. \quad (24)$$

An important role is played in the atmospheric corrosion of metals by salts contained in air. It is commonly believed that the influence of salts is an order of magnitude weaker than that of sulfur oxides [13]. Mear the sea coast, basic copper chloride $CuCl_2 \cdot 3Cu(OH)_2$ (atacamite) can also be formed on the copper surface:

$$[CuSO_4 \cdot 3Cu(OH)_2 + 2Cl^- = CuCl_2 \cdot 3Cu(OH)_2 + SO_4^{2-}]/23,$$
$$\Delta G^0_{298} = -0.05\ kJ\ mol^{-1}. \quad (25)$$

However, the content of copper sulfate exceeds that of the chloride even in the immediate vicinity of sea. For example, the patina formed on the Freedom statue is composed of 95% brochantite and 5% atacamite [14].

As mentioned above, minor amounts of malachite are present in some cases in the composition of patina:

$$[CuSO_4 \cdot 3Cu(OH)_2 + 2CO_{2(aq)} = 2CuCO_3 \cdot Cu(OH)_2 + 2H^+ + SO_4^{2-}]/27,\quad \Delta G^0_{298} = 1.76\ kJ\ mol^{-1}. \quad (26)$$

Thus, the presence of contaminations in the atmosphere plays an important part in the formation of green patina.

Modern sculptures and art articles made of copper and its alloys are virtually everywhere treated, to form patina, with aqueous solutions of ammonium hydrosulfide or potassium and sodium polysulfides [15]. Dark brown or black films are formed on the metal surface if concentrated solutions are used, and golden-brown, in the case of diluted solutions:

$$[Cu + 1/2O_2 + H^+ + HS^- = CuS + H_2O]/5,$$
$$\Delta G^0_{298} = -60.7\ kJ\ mol^{-1}; \quad (27)$$

$$[2Cu + 1/2O_2 + H^+ + HS^- = Cu_2S + H_2O]/6,$$
$$\Delta G^0_{298} = -56.0\ kJ\ mol^{-1}. \quad (28)$$

Upon prolonged exposure to open air, copper sulfides and the metal are oxidized to give brochantite:

$$[CuS + 3Cu + 7/2O_2 + 3H_2O = CuSO_4 \cdot 3Cu(OH)_2]/21,$$
$$\Delta G^0_{298} = -50.2 \text{ kJ mol}^{-1}; \quad (29)$$

$$[Cu_2S + 2Cu + 7/2O_2 + 3H_2O = CuSO_4 \cdot 3Cu(OH)_2]/21,$$
$$\Delta G^0_{298} = -48.6 \text{ kJ mol}^{-1}. \quad (30)$$

Comparing the changes in the standard Gibbs energies of reactions (24), (29), and (30), we can conclude that the sulfide patination of bronze sculptures favors formation of green patina on the metal surface. Sodium chloride and carbon dioxide contained in atmospheric precipitations can slightly change the composition of the film [reactions (25) and (26)], but presumably do not noticeably affect its protecting properties.

CONCLUSION

Sulfide patination of bronze sculptures favors formation of green patina on the metal surface. Sodium chloride and carbon dioxide contained in atmospheric precipitations can slightly change the composition of the film, but presumably do not noticeably affect its protecting properties.

REFERENCES

1. Mikhailovskii, Yu.N., *Atmosfernaya korroziya metallov i metody ikh zashchity* (Atmospheric Corrosion of Metals and Methods for Their Protection), Moscow: Metallurgiya, 1989.
2. *Corrosion*, Shreir, L.L., Ed., 2d Ed., London: Newnes-Butterworths, 1976.
3. Demidov, A.I. and Markelov, I.A., *Zh. Prikl. Khim.*, 2005, vol. 78, no. 5, pp. 721–724.
4. Demidov, A.I. and Kokhatskaya, M.S., *Zh. Prikl. Khim.*, 2006, vol. 79, no. 8, pp. 1382–1384.
5. *Termicheskie konstanty veshchestv: Spravochik v 10 vypuskakh* (Thermal Constants of Subbstances: Reference Book in 10 Issues), Glushko, V.P., Ed., Moscow: VINITI, 1965, issue 1; 1966, issue 2; 1972, issue 6, part 1.
6. Garrels, R.M. and Christ, Ch.L., *Solutions, Minerals, and Equilibria*, New York: Harper and Row, 1965.
7. Nekrasov, B.V., *Osnovy obshchei Khimii* (Fundamentals of General Chemistry), Moscow: Khimiya, 1973, vol. 2.
8. *Environmental Chemistry*, Bockris, J.O'M., Ed., New York: Plenum, 1977. Translated under the title *Khimiya okruzhayushchei sredy*, Tsygankov, A.P., Ed., Moscow: Khimiya, 1982, pp. 260–275.
9. Peters, D.G., Hayes, J.M., and Hieftje, G.M., *Chemical Separations and Measurements: The Theory and Practice of Analytical Chemistry*, New York, W.B. Saunders, 1974.
10. Nazarenko, V.A., Antonovich, V.P., and Nevskaya, E.M., *Gidroliz ionov metallov v razbavlennykh rastvorakh* (Hydrolysis of Metal Ions in Dilute Solutions), Moscow: Atomizdat, 1979.
11. Yatsimirskii, K.B. and Vasil'ev, V.P., *Konstanty nestoikosti kompleksnykh ionov* (Instability Constants of Complex Ions), Moscow: Akad. Nauk SSSR, 1959.
12. Ripan, R. and Ceteanu, I., *Chemia metalelor*, Bucuresti: Editura didactica si pedagogica, 1968, vol. II.
13. Berukshtis, G.K. and Klark, G.B., *Korrozionnaya ustoichivost' metallov i metallicheskikh pokrytii v atmosfernykh usloviyakh* (Corrosion Stability of Metals and Metallic Coatings under Atmospheric Conditions), Moscow: Nauka, 1971.
14. *Sea Water Corrosion Handbook*, Schumacher, M.M., Ed., Park Ridge (New Jersey): Noyes Data, 1979.
15. Nikitin, M.K. and Mel'nikova, E.P., *Khimiya v restavratsii* (Chemistry in Restoration), St. Petersburg: Tsentr TEKhINFORM, 2002.

ISSN 1070-4272, Russian Journal of Applied Chemistry, 2007, Vol. 80, No. 4, pp. 557–561. © Pleiades Publishing, Ltd., 2007.
Original Russian Text © K.N. Semenov, N.A. Charykov, A.K. Pyartman, V.A. Keskinov, O.V. Arapov, N.I. Alekseev, and V.V. Lishchuk, 2007, published in Zhurnal Prikladnoi Khimii, 2007, Vol. 80, No. 4, pp. 570–574.

PHYSICOCHEMICAL STUDIES OF SYSTEMS AND PROCESSES

Polythermal Study of the Solubility of Fullerenes in Pelargonic and Caprylic Acids

K. N. Semenov, N. A. Charykov, A. K. Pyartman, V. A. Keskinov, O. V. Arapov, N. I. Alekseev, and V. V. Lishchuk

St. Petersburg State University, St. Petersburg, Russia

Innovations of Leningrad Institutions and Enterprises, Private Company, St. Petersburg, Russia

Received November 24, 2006; in final form, November 2006

Abstract—A polythermal study of the solubility of C_{60} and a fullerene mixture (60% C_{60} + 39% C_{70} + 1% C_{76}–C_{90}) in pelargonic and caprylic acids was carried out at 20–80°C. The solubility polytherms are given and discussed.

DOI: 10.1134/S1070427207040076

In this study, we examined the solubility polytherms of individual fullerenes and a fullerene mixture (60% C_{60} + 39% C_{70} + 1% C_{76}–C_{90}) in a series of *n*-alkanoic acids.

Studies of the solubility of fullerenes are of primary importance for developing methods for extraction separation of fullerenes from a fullerene-containing carbon black and for their purification prior to chromatographic isolation [1].

The topicality of this problem is evidenced by the fact that the solubility of C_{60} has been determined in more than 150 solvents, and that of C_{70}, in 20 solvents [2], including those belonging to various classes of organic and inorganic solvents (aromatic solvents, alkanes, cyclohexanes, alkyl halides, and alcohols). Furthermore, much attention has been given to correlations between the solubility and various molecular characteristics of solvents [3–6]. In particular, some of the authors attempted to find correlations between the mole fraction of C_{60} in a saturated solution with such solvent characteristics as the refractive index, molar volume, permittivity, and Hildebrand solubility factor. It appeared that none of the solvent parameters alone can serve as a universal factor controlling the solubility. Nevertheless, it was demonstrated that a set of empirical parameters allows a quite reliable prediction of the solubility. Thus, high solubility of fullerenes should be observed in solvents with high refractive index, dielectric constant of about 4, large molecular volume, Hildebrand solubility factor of about 20 $(J\ cm^{-3})^{1/2}$, and an intermediate nucleophilicity.

It should be pointed out that published data can only be used to describe binary systems, e.g., fullerene (C_{60} or C_{70})–solvent, being rather unsuitable for development of methods for extraction separation of fullerene mixtures because of the strong mutual solubility effects, such as salting-in and salting-out [7].

It is worth noting that there is very limited information in the literature on the mutual solubility of two different fullerenes in one solvent or of an individual fullerene in a mixed solvent. The polythermal dependences of the solubility in the ternary systems like C_{60}–C_{70}–solvent are lacking at all, despite that these data may be significant for optimization of the extraction separation of fullerene mixtures. The only exceptions are the papers [7, 8] dealing with the solid–liquid phase equilibria in ternary systems C_{60}–C_{70}–toluene and C_{60}–C_{70}–*o*-xylene at 25 and 80°C.

No systematic study has been made of the solubility of fullerenes in a series of *n*-alkanoic acids. Individual carboxylic acids and commercial mixtures of higher isomeric carboxylic acids (HICA) show promise because virtually any solution of the fullerene mixture in the indicated solvents is enriched in C_{70}, which considerably increases the efficiency of prechromatographic separation methods based on the solid–liquid, and probably, liquid–liquid phase

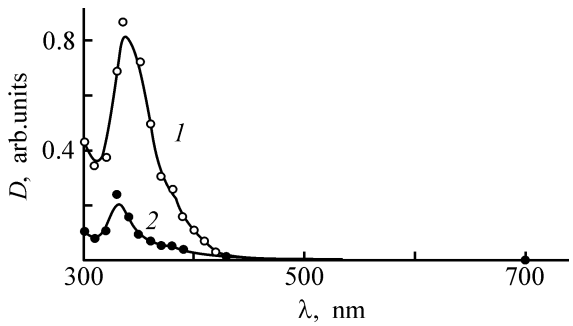

Fig. 1. Electronic absorption spectra of solutions of C_{60} in (*1*) pelargonic acid (c = 177.9 mg l^{-1}) and (*2*) caprylic acid (c = 58.3 mg l^{-1}). Carboxylic acid : *o*-xylene = 1 : 22 (by volume). (*D*) Optical density and (λ) wavelength; the same for Fig. 3.

equilibria. The higher solubility of C_{70} is associated with its higher polarizability (8×10^{-23} cm^3) as compared to C_{60} (6.4×10^{-23} cm^3) [9], which, in turn, is due to the less symmetrical structure of C_{70} (ellipsoid of revolution against a spheroid).

It was demonstrated in the preliminary experiments at 25°C that the most efficient extractants for C_{70} and C_{60} are caprylic and pelargonic acids, respectively. That is why we examined in this study the solubility polytherms of fullerenes just in these solvents.

EXPERIMENTAL

In the experiments we used fullerene C_{60} of 99.9% purity containing about 0.1% C_{70}, a fullerene mixture 60% C_{60} + 39% C_{70} + 1% C_{76}–C_{90} from ILIP Private Company (St. Petersburg), *o*-xylene (analytically pure grade), and pelargonic and caprylic acids (chemically pure grade).

The solubility of individual fullerene C_{60} and fullerene mixture, as influenced by the temperature, was studied by the isothermal saturation method. First, solutions of C_{60} and a fullerene mixture in pelargonic and caprylic acids were prepared (in all cases, fullerenes were taken in a considerable excess: 50 mg of fullerene per 10 ml of solvent). Then the solutions were equilibrated for 8–10 h at each temperature (maintained to within 0.05°C) in a temperature-controlled shaker in the range 20–80°C. Such a long time of the experiments is required for equilibrium to be attained in the systems carboxylic acid–fullerene. Finally, the liquid phase was separated by filtration through a Schott filter no. 16 and analyzed.

Fullerenes C_{60} and C_{70} in the liquid phase saturated at each temperature were determined spectrophotometrically on a Specord-32 instrument at wavelengths of 335.5 and 472.0 nm. The equilibrated solutions taken for analysis were diluted with *o*-xylene. In all determinations, we used as the reference a solution of the respective carboxylic acid in *o*-xylene at the same dilution as in the sample. Such a procedure of analysis is dictated by problems in recovery of fullerenes from high-boiling liquid phases (up to 260°C at 1 atm).

The fullerene concentrations were estimated using empirical relashionships derived for fullerene mixtures [10]:

$$c(C_{60}) = 13.10(D_{335} - 1.808D_{472}), \quad (1)$$

$$c(C_{70}) = 42.51(D_{472} - 0.0081D_{335}), \quad (2)$$

where D_{335} and D_{472} are the optical densities of solutions related to unit path (1 cm); and $c(C_{60})$ and $c(C_{70})$, concentrations of the respective fullerenes (mg l^{-1}).

Here and hereinafter the contribution of higher fullerenes C_n ($n > 70$) is neglected.

The solvent content of crystal solvates was determined as follows. The solid phase just precipitated from a carboxylic acid solution was washed twice with ethanol, dried at 20°C for 30 min, and weighed. Then the resulting solid was refluxed with ethanol in a Soxhlet's apparatus (78°C, 1 atm), vacuum-dried at 200°C (0.1 mm Hg) for 1 h, and weighed again. The solvent content of the initial crystal solvate (or solid solution of fullerenes on its basis) was determined as the weight loss.

Figure 1 shows electronic absorption spectra of the fullerenes and a fullerene mixture in pelargonic acid. Similar spectra were obtained in caprylic acid. It should be pointed out that the spectra in caprylic and pelargonic acids demonstrate no solvatochromic effects, i.e., no strong change in the spectrum induced by insignificant change in the solution concentration or solvent composition, as it was observed in binary solvents, such as acetonitrile–toluene, benzene–methanol, etc. [11–16]. Therefore, there is a full analogy between the spectra we recorded and the corresponding spectra in a series of one-component aromatic solvents (*o*-xylene, benzene, toluene, and *o*-dichlorobenzene), so that the use of empirical relationships (1) and (2) is quite reasonable in our case.

Figures 2 and 3 show the solubility polytherms of C_{60} and fullerene mixture in caprylic and pelargonic

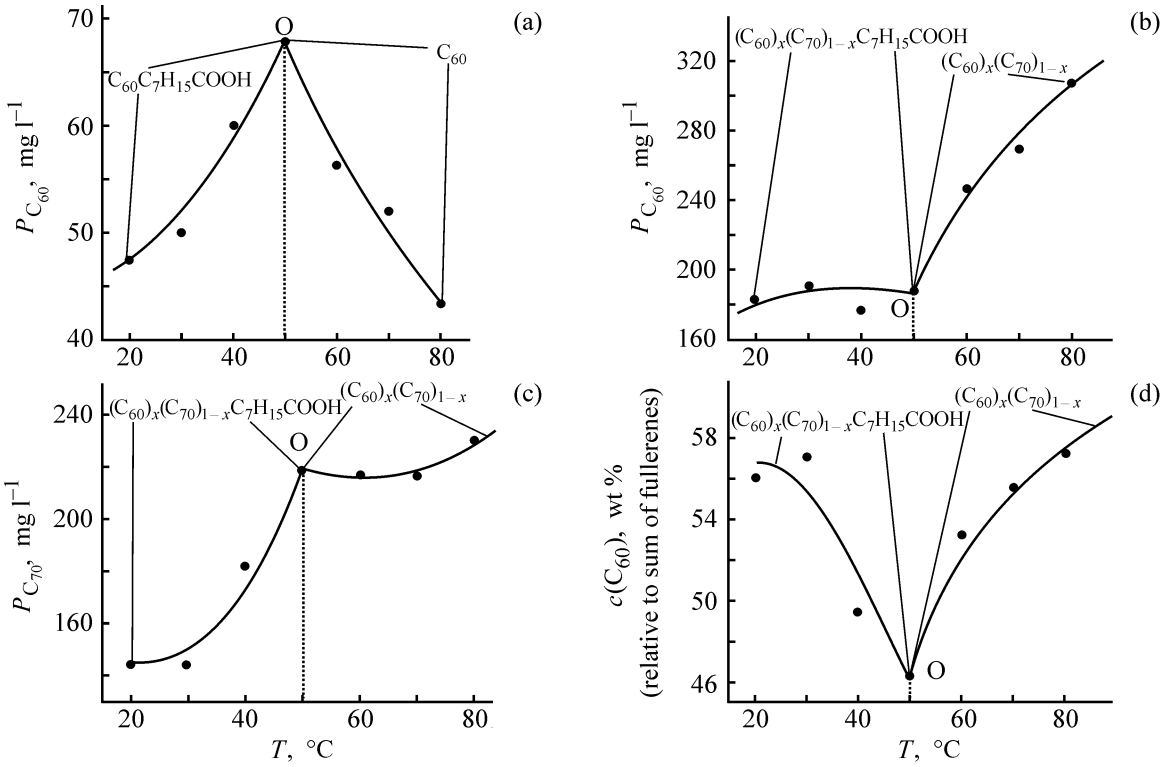

Fig. 2. Solubility polytherms of (a) C_{60}, (b) C_{60} from fullerene mixture, and (c) C_{70} from fullerene mixture in caprylic acid, and (d) polythermal dependence of the $c(C_{60})$ concentration (wt % relative to sum of fullerenes) in the saturated solution of the fullerene mixture in caprylic acid. (P) Solubility and (T) temperature.

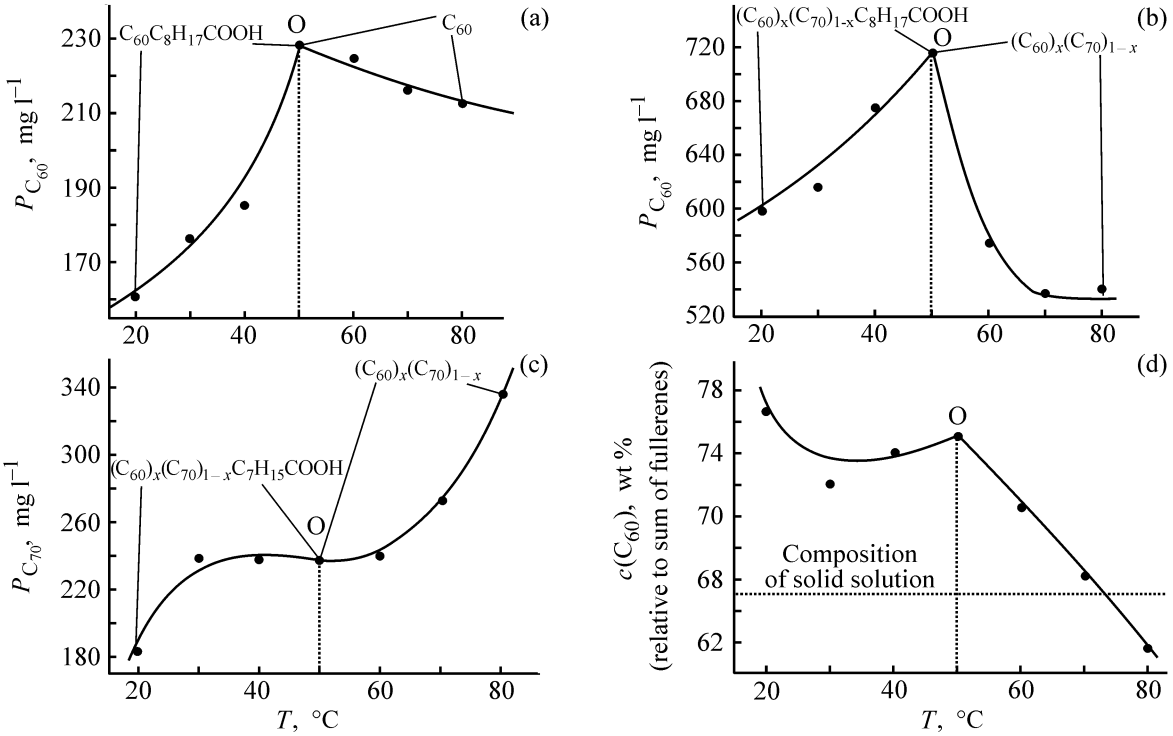

Fig. 3. Solubility polytherms of (a) C_{60}, (b) C_{60} from fullerene mixture, and (c) C_{70} from fullerene mixture in pelargonic acid, and (d) polythermal dependence of the $c(C_{60})$ concentration in the saturated solution of the fullerene mixture in pelargonic acid. (P) Solubility and (T) temperature.

Solubility of fullerenes in caprylic and pelargonic acids

T, °C	Solubility, mg l^{-1}					
	C_{60}	C_{60} from fullerene mixture	C_{70} from fullerene mixture	C_{60}	C_{60} from fullerene mixture	C_{70} from fullerene mixture
	caprylic acid			pelargonic acid		
20	47.3	183.4	143.9	160.5	597.8	182.4
30	49.7	190.4	143.7	176.3	615.0	238.4
40	60.0	176.4	181.4	184.8	675.0	237.4
50*	67.7	188.0	218.1	228.2	714.9	236.7
60	56.2	246.1	216.6	224.7	574.9	240.4
70	51.9	269.4	216.0	216.5	537.1	273.2
80	43.4	307.6	229.8	212.6	540.9	337.0

* Equilibrium solid phase at temperatures below 50°C represents C_{60} monosolvate or solid solutions based on monosolvates of light fullerenes C_{60} and C_{70}, and above 50°C, unsolvated C_{60} or solid solutions based on unsolvated light fullerenes C_{60} and C_{70}.

acids. The table lists polythermal data on the solubility of individual C_{60} and of C_{60} and C_{70} from the fullerene mixture in these acids.

The temperature dependences of the solubility of individual fullerene C_{60} and of C_{60} from the fullerene mixture are nonmonotonic in both acids (Figs. 2a, 2b; 3a, 3b), as well as the temperature dependence of the solubility of C_{70} from the fullerene mixture in caprylic acid (Fig. 2c). This kind of temperature dependences is frequently observed in binary water–salt systems, such as $NaF–H_2O$, $CaF_2–H_2O$, $NH_4HF_2–H_2O$, $ZrOCl_2–H_2O$, $MgSO_3–H_2O$, and $CuSO_4–H_2O$ [17].

An analysis of published data revealed that, in the cases of fullerenes C_{60} and C_{70}, such a dependence has been only found in few systems, such as C_{60}–toluene, C_{60}–benzene, $C_{60}–CS_2$, C_{60}–1,2-dimethylbenzene, C_{60}–1,2-dichlorobenzene, C_{60}–tetralin, C_{60}–1,2-diphenylacetone, C_{70}–1,2-dichlorobenzene, C_{70}–tetralin, and C_{70}–1,2-diphenylacetone [2, 16, 17]. Korobov [16, 17] has suggested a thermodynamic model describing this kind of the solubility polytherms. Thermodynamic analysis by Smith et al. [18] revealed that this shape of the solubility diagrams is caused by an unusual relationship between the enthalpy of formation of the crystal solvate and that of the saturated liquid solution.

Our analysis shows that, in all cases when the solubility polytherms demonstrate nonmonotonic temperature dependence for the branch characterized by $(dc/dT)_p > 0$, the fullerene saturated solution is in equilibrium with solid monosolvates of a definite composition $C_{60}–C_nH_{2n-1}COOH$ (in the systems C_{60}–caprylic acid and C_{60}–pelargonic acid) (Figs. 2a, 3a), and also with monosolvates of solid solutions $(C_{60})_x(C_{70})_{1-x} \cdot C_{2n-1}COOH$ (Figs. 2b, 2c, and 3b). At the nonvariant point of the extremum in the solubility diagram (Figs. 2 and 3, points O), incongruent melting of the solid crystal solvate (monosolvate in our case) occurs to give unsolvated individual fullerene C_{60} or unsolvated solid solution (in the case of the fullerene mixture).

Data on the temperature dependence of the C_{60} content of the liquid phase, obtained in dissolution of the fullerene mixture (Figs. 2d and 3d), show that, in the case of pelargonic acid, the maximal enrichment in C_{60} is attained at 20°C (compared to the initial solid phase, the C_{60} content in the solution is higher by 15%). By contrast, in the case of caprylic acid, the liquid phase is enriched in C_{70}, and the maximal fullerene concentration is attained at 50°C (20% enrichment of the liquid phase relative to the initial mixture). It is worth noting that the difference between the fullerene contents of the initial mixture and solution can be used as a basis for development of a method for more or less complete prechromatographic separation of fullerenes.

CONCLUSIONS

(1) Fullerene C_{60} and fullerene mixture (60% C_{60} + 39% C_{70} + 1% C_{76-C90}) are fairly readily soluble in pelargonic and caprylic acids at 20–80°C. The solubility ranges from 50 to 1000 mg l^{-1}.

(2) The solubility polytherms of C_{60} and fullerene mixture in both acids consist of two crystallization branches: a low-temperature branch (C_{60} monosolvates or solid solutions based on fullerene monosolvates) and a high-temperature branch (unsolvated C_{60} or solid solutions based on unsolvated fullerenes).

ACKNOWLEDGMENTS

The study was financially supported by the Target Federal Scientific Program "Research and Developments in Priority Areas of Science and Engineering in 2002–2006" (State Contract no. 02.467.11.7005, May 23, 2005).

REFERENCES

1. Arapov, O.V., Charykov, N.A., Semenov, K.N., et al., *Zh. Prikl. Khim.*, 2006, vol. 79, no. 2, pp. 203–206.
2. Korobov, M.V. and Smith, A.L., *Solubility of Fullerenes*, New York: Wiley, 2000, pp. 53–90.
3. Ruoff, R.S., Malhorta, R., Huestis, D.L., et al., *Nature*, 1993, vol. 362, no. 6416, pp. 140–141.
4. Ruoff, R.S., Tse, D.S., Malhorta, R., et al., *J. Phys. Chem.*, 1993, vol. 97, pp. 3379–3383.
5. Sivaraman, N., Dhamodaran, R., Kallippan, I., et al., *J. Org. Chem.*, 1992, vol. 57, pp. 6077–6079.
6. Hildebrand, J.H. and Scott, R.L., *Regular Solutions*, New York: Prentice-Hall, 1962.
7. Ponomarev, A.N., Aksel'rod, B.M., Barchenko, V.T., et al., *Zh. Fiz. Khim.*, 2000, vol. 74, no. 12, pp. 2134–2137.
8. Arapov, O.V., Aksel'rod, B.M., Pronkin, A.A., et al., *Zh. Prikl. Khim.*, 2003, vol. 76, no. 1, pp. 35–38.
9. Matsuzawa, N. and Dixon, D.A., *J. Phys. Chem.*, 1992, vol. 96, pp. 6241–6244.
10. Ponomarev, A.N., Yudovich, M.E., Charykov, N.A., et al., *Opt. Spectrosc.*, 2000, vol. 88, no. 2, pp. 195–197.
11. Hirenda, N., Avinash, V., and Jai, P., *J. Phys. Chem.*, 1996, vol. 100, pp. 9439–9443.
12. Sukhendu, N. and Haridas, P., *Chem. Phys. Lett.*, 2000, vol. 327, pp. 143–148.
13. Sukhendu, N. and Haridas, P., *Chem. Phys. Lett.*, 2002, vol. 360, pp. 422–428.
14. Hirenda, N. and Avinash, V., *J. Phys. Chem.*, 1996, vol. 100, pp. 9439–9443.
15. Kirgintsev, A.N., Trushnikova, L.N., and Lavrent'eva, V.G., *Rastvorimost' neorganicheskikh veshchestv v vode* (Solubility of Inorganic Compounds in Water), Leningrad: Khimiya, 1972.
16. Korobov, M.V., Mirakian, A.L., Avramenko, N.V., et al., *J. Phys. Chem.*, 1998, vol. 102, pp. 3712–3717.
17. Korobov, M.V., Mirakian, A.L., Avramenko, N.V., et al., *J. Phys. Chem.*, 1999, vol. 103, pp. 1339–1346.
18. Smith, A.L., Walter, E., Korobov, M.V., et al., *J. Phys. Chem.*, 1996, vol. 100, pp. 6775–6780.

ISSN 1070-4272, Russian Journal of Applied Chemistry, 2007, Vol. 80, No. 4, pp. 562–565. © Pleiades Publishing, Ltd., 2007.
Original Russian Text © M.P. Zverev, O.M. Zverev, Z.Z. Abdulkhakova, L.A. Polovikhina, E.V. Dovbii, D.G. Sil'chenkov, 2007, published in Zhurnal Prikladnoi Khimii, 2007, Vol. 80, No. 4, pp. 575–578.

SORPTION AND ION-EXCHANGE PROCESSES

Specific Features of Sorption of Chromium(VI) Anions by VION Fibrous Chemisorbents

M. P. Zverev, O. M. Zverev, Z. Z. Abdulkhakova, L. A. Polovikhina, E. V. Dovbii, and D. G. Sil'chenkov

Moscow State Regional University, Moscow, Russia

All-Russia Research Institute of Polymeric Fibers, Moscow, Russia

Military University of Radiation, Chemical, and Biological Protection, Moscow, Russia

Received July 15, 2005; in final form, July 2006

Abstract—Certain fundamental aspects of the process of sorption of chromium(VI) ions from aqueous solutions at pH 6 and 2 by VION fibrous anion-exchangers with varied basicity were revealed.

DOI: 10.1134/S1070427207040088

Sorption of metal anions with variable oxidation state from an aqueous medium by polymeric chemisorbents is accompanied in some cases by redox reacions between ions being recovered from solution and chemically active groups of the sorbent [1, 2]. A study of the role played by the chemical nature of functional groups of an ion exchanger and of the influence exerted by sorption conditions on the recovery of metal anions from solutions, complicated by the occurrence of redox reactions, is of not only theoretical, but also practical interest.

This study makes an attempt to solve this problem, with VION fibrous anion exchangers with varied basicity serving as the sorption material and chromate and dichromate ions as sorbates.

The materials under study contained pyridinium (AN-1, AS-1) and aliphatic (AN-5, AS-2) amino groups. AS-1 fiber was obtained by alkylation with epichlorohydrin of AN-1 fiber, which is alkylated by only 50% because of a steric hindrance. Therefore, AS-1 fiber contains tertiary pyridinium nitrogen in addition to the quaternary pyridinium nitrogen. The fibrous anion-exchangers used are characterized in Table 1, in which the dissociation constants pK_a are taken from the literature [3].

The static exchange capacity (SEC) was determined using a 0.1 N HCl solution for weakly basic anion exchangers (AN-1, AN-5) and a 0.1 N NaCl solution for strongly basic sorbents (AS-1, AS-2), with the experimental error not exceeding 5%. The sorption

Table 1. Parameters of VION fibrous chemisorbents

VION fiber	Chemically active group	pK_a	SEC, mmol g^{-1}	VION fiber	Chemically active group	pK_a	SEC, mmol g^{-1}
AN-1	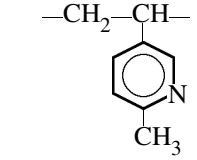	9–10	2.5	AN-5	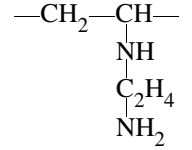	6–9	2.5
AS-1	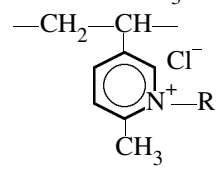	1–2	1.0	AS-2	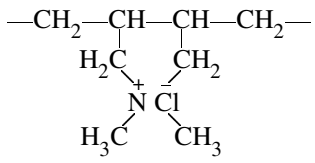	1–2	1.0

properties of the fibers to saturation were studied under static conditions at a pH value of the medium equal to 2 and 6. HNO_3 was used to acidify the solutions. The hydrogen index was measured with an EV-74 universal ion-meter, the pH value was maintained constant in the course of the experiments to within the device error (≤0.05 pH units). A 0.1-g portion of a fiber was placed in a conical vessel containing 1 dm^3 of an aqueous solution of $K_2Cr_2O_7$ (K_2CrO_4). The initial concentration of Cr(VI) in the form of $Cr_2O_7^{-2}$ or CrO_4^{-2} anions in solution was 0.15 g dm^{-3}. A fiber sample was kept in the solution agitated at regular intervals of time at a temperature of 18–20°C until sorption equilibrium was attained, which was judged from a constant value reached by the amount of sorption in the course of time.

The amount of sorption was calculated from the difference of the Cr(VI) concentrations in the initial solution and that after the study. The content of Cr(VI) in the solution before and after the sorption was monitored photometrically [4], using the reaction with diphenylcarbazide, specific to chromium(VI). The determination was made as follows: 10 cm^3 of a solution of a chromium(VI)-containing salt was diluted with distilled water in a 100-cm^3 volumetric flask, the mixture was agitated, and then three 20-cm^3 samples were taken. One of the samples was neutralized with a 0.1 N NaOH solution, with phenolphthalein as indicator, until a pale pink coloration appeared. To another sample, the same volume of NaOH was added without indicator, 0.5 cm^3 of H_2SO_4 and 0.4 cm^3 of diphenylcarbazide were poured in, and the optical density D of the solution was determined in 10–15 min, in comparison with the third portion of the same water, to which all the reagents except diphenylcarbazide were added. Cuvettes with a layer thickness of 50 mm (wavelength 540 nm) were used in the FEK-56 photoelectrocolorimeter. The measurements were repeated three times and the content of chromium(VI) was found using the average value of D from the calibration plot.

Electronic paramagnetic resonance (EPR) spectra were recorded on a Rubin spectrometer (working frequency ~10 GHz, modulation frequency ~100 kHz). A single crystal of synthetic ruby was used as the side standard; calibration samples of diphenyl picryl hydrazyl (DPPH) and Mn(II) in a solid solution in MgO served as the central standard. The content of paramagnetic Cr(VI) and Cr(III) ions was calculated from EPR spectra by the commonly accepted method [5, 6]. The number of spins in a sample being measured was calculated using the basic formula

$$N = N_{ref} S/S_{ref} h_{ref.st}/h_{st}.$$

Table 2. Sorption of Cr(VI) by fibrous sorbents

Sorbent	Sorption, mmol g^{-1}, at indicated pH	
	6	2
AN-1	0	2.2
AN-5	0.7	3.2
AS-1	1.8	3.2
AS-2	1.2	1.2

Here, N_{ref} is the number of spins in the central standard; S, number under the absorption curve of a sample; S_{ref}, area under the absorption curve of the central standard; $h_{ref.st}$ and h_{st}, amplitudes of the side standard in recording the central standard and a sample under study, respectively.

The $h_{ref.st}/h_{st}$ ratio makes it possible to take into account changes in the spectrometer sensitivity because of changes in the Q-factor of the resonator. To diminish the systematic error, the geometric dimensions of a sample are minimized: the diameter of the ampule for samples is about 2 mm with a filling of about 7 mm. The error in determining the absolute number of spins may be as large as 30–50%. However, this error remains constant if the same measurement mode is used. In the case of an invariable position of a sample in the resonator the scatter in multiple measurements with a set of samples of the same type does not exceed 2%.

IR spectra of the fibers under study before and after the sorption were measured with a Hitachi spectrometer. Samples were prepared in the form of pellets by compaction with KBr preliminarily dried in a desiccator with zero humidity for 48 h. The samples were ground in a ball mill.

The content of fibers in a sample was 1 wt %. The pellets with KBr were formed in a standard annular mold at a compaction pressure of 40 MPa.

Table 2 lists data on catching of Cr(VI) by strongly basic sorbents at pH 6, which markedly exceeds that by weakly basic sorbents. The insignificant amount of Cr(VI) sorption by AN-5 fiber is due to the higher basicity of the aliphatic amine, compared with the pyridinium amine (Table 1).

As can be seen from Table 2, the absorption of chromate and dichromate ions by AN-1, AN-5, and

Table 3. Content of paramagnetic ions Cr(V) and Cr(III) in fibrous sorbents after Cr(VI) sorption

Sorbent	pH 6				pH 2			
	Cr(V)		Cr(III)		Cr(V)		Cr(III)	
	$c \times 10^{-18}$, spins g^{-1}	$c \times 10^{2}$, mmol g^{-1}	$c \times 10^{-20}$, spins g^{-1}	c, mmol g^{-1}	$c \times 10^{-18}$, spins g^{-1}	$c \times 10^{-18}$, mmol g^{-1}	$c \times 10^{2}$, spins g^{-1}	$c \times 10^{-20}$, mmol g^{-1}
AN-1	0.0	0.0	0.0	0.0	0.3	0.2	0.8	0.1
AN-5	13.0	2.2	0.0	0.0	5.3	0.9	4.3	0.7
AS-1	14.0	2.3	1.8	0.3	3.4	0.6	8.3	1.4
AS-2	2.7	0.4	3.3	0.6	2.3	0.4	2.6	0.4

AS-1 fibrous sorbents increases at pH 2, which is due to protonation of low-basic pyridinium amines AN-1 and AS-1 and aliphatic amine AN-5. The protonation of the functional groups of the sorbents leads to addition of chromium(VI) anions to these groups to give the salt form, which is confirmed by IR spectral data. For example, absorption bands associated with vibrations of the pyridinium ring (747, 1500, and 1600 cm^{-1}) are characteristic of AN-1 fiber. After the sorption of chromate ions at pH 2, the band of stretching vibrations of the weakly basic group at 1500 cm^{-1} disappears and there appear bands at 774 and 942 cm^{-1}, related to deformation vibrations of chromate ions. Also observed are weak bands at 1350 and 1400 cm^{-1}, associated with the NO_3^- group.

Similar changes in IR spectra were observed for AN-5 and AS-1 fibers after Cr(VI) sorption at pH 2. It should be noted that AN-1 and AN-5 anion exchangers have the same SEC; however, AN-5 fiber sorbs a considerably larger amount of Cr(VI), which is due, as already noted, to the stronger basicity of the aliphatic amine, compared with the pyridinium amine. Probably, the degree of protonation of the active groups of AN-1 at pH 2 does not reach the necessary value.

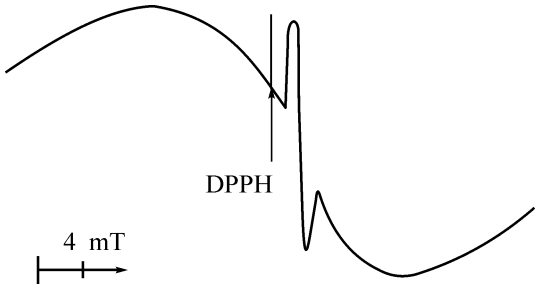

EPR spectrum of AS-1 sorbent at pH 2 after sorption of Cr(VI) to the maximum value.

As expected, AS-2 sorbent containing only the strongly basic quaternary nitrogen sorbs the same amount of Cr(VI) ions, irrespective of the solution pH.

No EPR spectra of all the fibers studied can recorded before Cr(VI) sorption from $K_2Cr_2O_7$ (K_2CrO_4) solutions. After Cr(VI) sorption, a superposition of EPR spectra is recorded with the sorbents (see figure).

The superposition comprises two EPR signals, a narrow ($\Delta H \approx 0.002$ T) and broad ($\Delta H \approx 0.05$ T). The intensity ratio of these signals depends on the nature of a sorbent and sorption conditions, but the intensity of the narrow signal is always high. The g-factors of the narrow and broad signal are virtually the same and equal to ~1.97. Analysis of the EPR spectra and published data [1] suggests that the narrow signal is associated with Cr(V) paramagnetic ions, and the broad signal, with Cr(III) ions. Consequently, the EPR method shows that redox reactions occur in the chemisorbents under study, which result in that Cr(VI) is reduced to Cr(V) and Cr(III).

Table 3 presents the content of paramagnetic ions in fibrous solvents after absorption of Cr(VI) at pH 6 and 2.

It follows from the data of Table 3 that, irrespective of the solution pH, the strongly basic chemisorbents AS-2 has in its structure virtually equal amounts of reduced ions of penta- and triple-charged chromium and sorbs equal amounts of Cr(VI) (Table 2). Analysis of the data in Tables 2 and 3 for the other sorbents suggests that the capacity for reduction of Cr(VI) depends on the degree of its catching by the sorbents. This is also confirmed by the data on the content of penta- and triple-charged chromium in

relation to the amount of Cr(VI) sorbed at pH 2 for AS-1 VION fiber (Table 4).

Indeed, the larger the amount of Cr(VI) caught by the sorbent, the higher the degree of its reduction, i.e., the amount of Cr(III) increases and the content of Cr(V) decreases.

As shown above, the sorption of Cr(VI) by the chemisorbents under study depends on the pH of the medium and on their basicity, and, therefore, the degree of Cr(VI) reduction to Cr(V) and Cr(III) is related to these factors (Table 3). At the same time, it is necessary to take into account the stability of the chemical groups of the sorbents against oxidation because of the occurrence of redox reactions. Probably, the higher the stability of a sorbent against oxidation, the smaller the amount of the reduced forms of chromium, Cr(V) and Cr(III), formed in sorption. The low content of paramagnetic ions Cr(V) and Cr(III) in AN-1 fiber after sorption of Cr(VI) at pH 2 is to a certain extent due to this circumstance.

Analysis of published data [1, 2] suggests that reduced chromium ions form complex compounds with the functional groups of the sorbents.

CONCLUSIONS

(1) It was shown that the sorption of chromate and dichromate ions by VION anion-exchange fibrous sorbents is determined by their basicity and the pH of the medium.

(2) It was found that, in contrast to strongly basic sorbents, weakly basic sorbents catch chromium(VI) ions when being protonated.

Table 4. Content of paramagnetic ions Cr(V) and Cr(III) in AS-1 VION fiber

Cr(VI) sorption, mmol g^{-1}	Cr(V)		Cr(III)	
	$c \times 10^{-18}$, spins g^{-1}	$c \times 10^{2}$, mmol g^{-1}	$c \times 10^{-20}$, spins g^{-1}	c, mmol g^{-1}
0.5	13.0	2.2	0.5	0.08
1.0	8.7	1.4	1.5	0.25
3.2	3.7	0.6	8.3	1.38

(3) The EPR method demonstrated that sorption of Cr(VI) anions on fibrous anion exchangers is accompanied by partial reduction of chromium(VI) to Cr(III) and Cr(V), whose content is determined by the amount of sorption.

REFERENCES

1. Molochnikov, L.S., Bakhus, E.N., et al., *Zh. Neorg. Khim.*, 1990, vol. 35, no. 2, pp. 389–393.
2. Andreeva, I.Yu., Drogobuzhskaya, S.V., and Kazakevich, Yu.E., *Vestn. Len. Gos. Univ., Ser. 4*, 1990, no. 1, pp. 67–71.
3. Zverev, M.P. and Abdulkhakova, Z.Z., *Voloknistye khemosorbenty* (Fibrous Chemisorbents), Moscow: Narodnyi Uchitel', 2001.
4. Lur'e, Yu.Yu., *Analiticheskaya khimiya promyshlennykh stochnykh vod* (Analytical Chemistry of Industrial Wastewater), Moscow: Khimiya, 1984.
5. Molin, Yu.N., Chibrikin, V.M., et al., *Zavod. Lab.*, 1966, vol. 32, no. 8, pp. 933–943.
6. Wertz, J.E. and Bolton, J.R., *Electron Spin Resonance. Elementary Theory and Practical Applications*, New York: McGraw–Hill, 1972.

ISSN 1070-4272, Russian Journal of Applied Chemistry, 2007, Vol. 80, No. 4, pp. 566–570. © Pleiades Publishing, Ltd., 2007.
Original Russian Text © M. Spasoević, M. Cvijović, L. Rybić-Zelenović, G. Aćamović-Joković, 2007, published in Zhurnal Prikladnoi Khimii, 2007, Vol. 80, No. 4, pp. 579–583.

APPLIED ELECTROCHEMISTRY AND CORROSION PROTECTION OF METALS

Electrochemical Deposition of Copper on Steel from a Solution of Diacido-1,3-Propylenediamine-*N*,*N*'-Diacetato-*N*,*N*'-Dipropionate Cuprate(II)

M. Spasoević, M. Cvijović, L. Rybić-Zelenović, and G. Aćamović-Joković

University of Kragujevac, Čačak, Serbia

Received February 14, 2006; in final form, November 2006

Abstract—The possibility of obtaining smooth homogeneous copper coatings with good adhesion and homogeneous copper coatings with poor adhesion by electrochemical deposition of copper on steel from a solution of nontoxic copper(II) complex with the ligands, 1,3-propylenediamine-*N*,*N*'-*diacetato-N*,*N*'-di-3-propionic acid, was analyzed. For both types of coatings, the optimum composition of the solution and the optimum deposition conditions were determined.

DOI: 10.1134/S107042720704009X

The quality of copper coatings on steel depends on the temperature and composition of the solution, electric current density of deposition, and difference between the equilibrium potential of the copper electrode, E_1, and the steady-state potential of steel electrode, E_2 [1, 2]. At a potential difference $E_1 - E_2 > 0.5$ V, fast cementation occurs. This process yields spongy coatings with poor adhesion and cohesion. In acid solutions of copper(II) sulfate, $E_1 - E_2$ is about 0.8 V, and the quality of copper coatings on steel is, therefore, poor. Smooth homogeneous copper coatings with good adhesion cannot be formed on steel and iron from a solution of copper(II) salts because of the fast cementation [1, 2]. A potential difference of 0.2 to 0.4 V is attained at a certain composition of the solution. At this potential difference the cementation is slow. In this case, smooth homogeneous coatings with weak adhesion, free from inner stresses, can be obtained on steel. These coatings are easily detached from steel, even if the steel was not passivated before coating deposition. Electrochemically produced copper foil free from inner stresses can be used in electrochemical industry for manufacture of printedcircuit boards. In copper foil formed by metal rolling, the inner stresses are considerable. At $E_1 - E_2 < 0.1$ V virtually no cementation occurs. Smooth homogeneous coatings with good adhesion can be electrochemically obtained on steel at an appropriate current density.

Copper coatings are commonly deposited on steel in a cyanide bath. The open-circuit potential of iron in a cyanide solution is more positive than the equilibrium potential of the copper(I) cyanide complex [2]. Therefore, copper can be deposited on steel when no cementation occurs. High-quality copper coatings on steel are deposited in cyanide baths [1].

Meanwhile, work with cyanide solutions involves a number of difficultes, primarily because cyanide complexes decompose in an acid medium to give toxic gaseous hydrogen cyanide. Therefore, it is necessary to replace copper(I) cyanide electroplating solutions with solutions of less toxic copper complexes [3].

It has been shown previously [4–8] that EDTA anions affect the electrochemical action of some metals, because they hinder reduction of the surface layer of oxygen compounds or provide dissolution of the surface oxide film being formed. Moreover, these species are involved in anodic dissolution of some metals and in cathodic evolution of hydrogen [4–8].

The goal of this study was to obtain quality copper coating on steel from a solution of diacido-1,3-propylenediamine-*N*,*N*'-diacetato-*N*,*N*'-dipropionate cuprate(II) (CuH_2L), with subsequent deposition of metallic nickel or chromium onto this coating, and to develop a formulation for deposition from this so-

lution of smooth homogeneous coating that are free from inner stresses and can easily detached from steel.

In aqueous solutions, H_4L exists in the ionic form [4]:

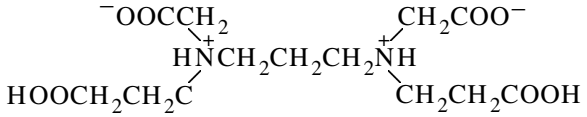

The ligand, 1,3-propylenediamide-*N*,*N*'-diacetate-*N*,*N*'-di-3-propionic acid (H_4L), forms with Cu(II) ions complexes of varied composition, depending on pH [9]. With allowance made for the various orientations of carboxylic groups in the Cu(II) complexes, geometric isomers of copper(II) compounds with the ligands under study may be also formed [9, 10].

EXPERIMENTAL

We measured the steady-state potential of the steel electrode and the equilibrium potential of the copper electrode in solutions with varied pH value and different Cu(II) to H_4L ratios. The polarization curves were obtained by the stationary potentiostatic method. We used in the study the standard electrochemical cell of an RDE potentiostat (Pine Instrument Co) and a 7035 BX-Y recording device (Hewlett Packard). A 2 × 2-cm steel (or copper) plate served as the working electrode, and a copper plate, as the counter electrode. A saturated calomel electrode was used as the reference.

The solutions were prepared from triple-distilled water and chemical substances purchased from Merck and used without additional purification.

The pH value of the electrolyte was adjusted in the range from 2.0 to 12.0 with a 2.0 mol dm^{-3} NaOH solution and 25% NH_4OH. The steel electrodes used to study the spontaneous deposition of copper were kept in the solutions for 20 h.

Coatings with a thickness of 1.0, 3.0, 5.0, or 10.0 μm were deposited, depending on the current density. All the experiments were performed at 295 K. The porosity of the coatings was determined by the standard technique [11], and their adhesion, by the cracking method [12].

The equilibrium potential of the copper electrode and the steady-state potential of the steel electrode in solutions of copper(II) complexes with H_4L are complex functions of the pH value (Fig. 1). In strongly acid solutions (2.0 < pH < 3.0) exist $[CuH_2L]$ complexes with $[CuHL]^-$ [9, 10]. At pH in the range from 3.0 to 6.0, the solution predominantly contains $[CuHL]^-$

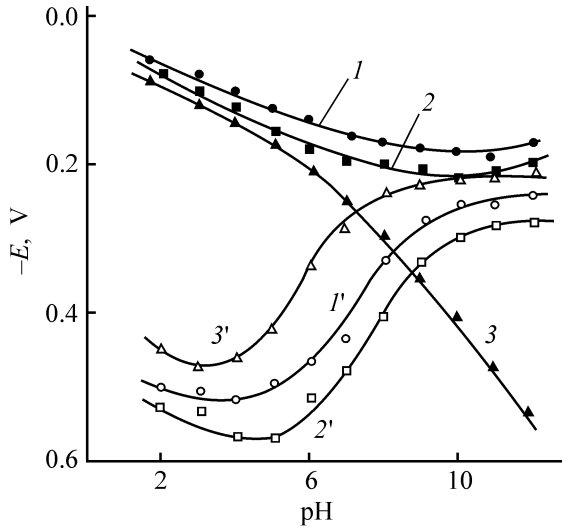

Fig. 1. (*1*–*3*) Equilibrium potential *E* of copper electrode and (*1'*–*3'*) open-circuit potential of steel electrode relative to a saturated calomel electrode vs the pH value and solution composition. Potentials are determined 10 min after submerging the electrodes in a solution. Solution composition (M): (*1*, *1'*) $CuSO_4$ 0.016, H_4L 0.016, Na_2SO_4 0.15, NaOH *x*, (*2*, *2'*) $CuSO_4$ 0.33, H_4L 0.33, Na_2SO_4 0.15, NaOH *x*, and (*3*, *3'*) $CuSO_4$ 0.1, H_4L 0.1, Na_2SO_4 0.15, NH_4Cl 0.1, NH_4OH *x*.

and $[CuL]^{2-}$ ions. The formation of the $[CuL]^{2-}$ complex starts at pH 3.0 and is virtually complete at pH 6.0. At pH 6.0–10.0, only the $[CuL]^{2-}$ complex is formed. At pH higher than 10.0, the complex is hydrolyzed by the reaction [9, 10]:

$$[CuL]^{2-} + H_2O \rightleftarrows [Cu(OH)L]^{3-} + H^+. \quad (1)$$

The hydrolysis reaction (1) is a result of the competition between OH^- ions and carboxy groups for the coordination site. The overall stability constant of a complex depends on its nature [9, 10]. The values of these constants show that the equilibrium concentrations of uncomplexed Cu^{2+} ions decrease as the solution pH becomes higher. This behavior is also confirmed by the run of curves *1* and *2* in Fig. 1. The potential of the copper electrode in a NH_4OH-containing solution is more negative (curve *3*). This is a consequence of the competition between NH_3 and carboxy groups for the coordination site. The open-circuit potential of the steel electrode also depends on pH (Fig. 1) [2, 13] and decreases in the course of time (Fig. 2). Copper is deposited in solutions with lower pH. Immediately after the steel electrodes are placed in solutions containing (mol dm^{-3}): $CuSO_4$ 0.1, H_4L 0.1, NH_4Cl 0.1, Na_2SO_4 0.4, NH_4OH *x* (a); $CuSO_4$ 0.2, NH_4L 0.2, NH_4Cl 0.2, Na_2SO_4 0.8, NH_4OH *x* (b); $CuSO_4$ 0.8, NH_4L 0.3, NH_4Cl 0.3, Na_2SO_4 1.2,

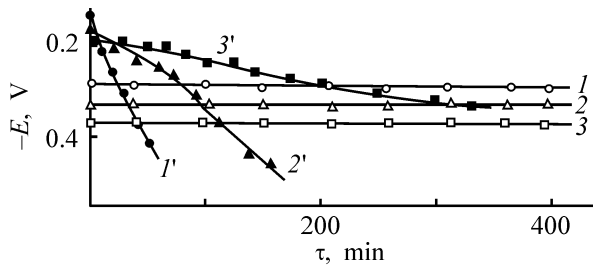

Fig. 2. (*1–3*) Equilibrium potential E of copper electrode and (*1′–3′*) open-circuit potential of steel electrode relative to a saturated calomel electrode in the solution vs. time τ. Solution composition (M): $CuSO_4$ 0.4, H_4L 0.4, NH_4Cl 0.4, Na_2SO_4 1.6, NH_4OH x. pH: (*1*, *1′*) 8.5, (*2*, *2′*) 9.0, and (*3*, *3′*) 9.5; the same for Fig. 3.

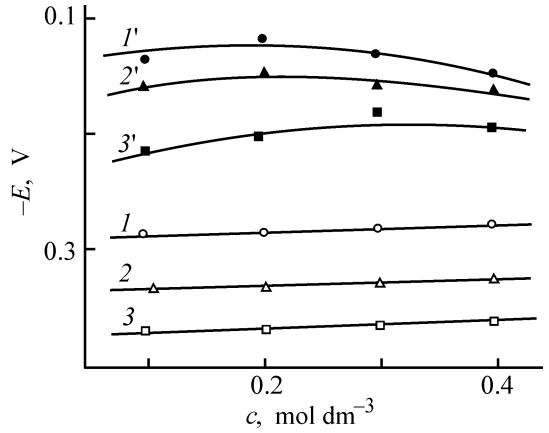

Fig. 3. (*1–3*) Equilibrium potential E of copper electrode and (*1′–3′*) open-circuit potential of steel electrode relative to a saturated calomel electrode vs. pH and $CuSO_4$ and H_4L concentrations c.

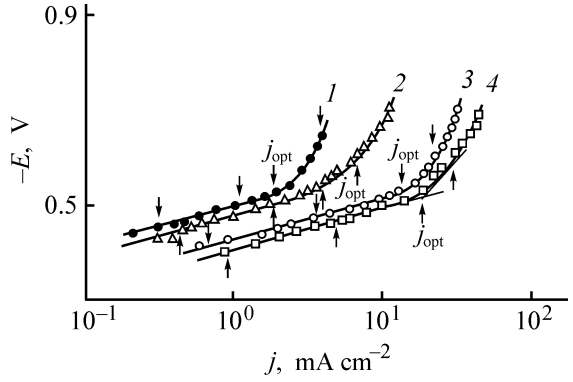

Fig. 4. Polarization curve of copper deposition. (E) Equilibrium potential and (j) current density; the same for Fig. 5. Solution composition (M): (*1*) $CuSO_4$ 0.04, H_4L 0.04, NH_4Cl 0.04, Na_2SO_4 0.1, NH_4OH x, (*2*) $CuSO_4$ 0.1, H_4L 0.1, NH_4Cl 0.1, Na_2SO_4 0.4, NH_4OH x, (*3*) $CuSO_4$ 0.3, H_4L 0.3, NH_4Cl 0.3, Na_2SO_4 1.2, NH_4OH x, (*4*) $CuSO_4$ 0.4, H_4L 0.4, NH_4Cl 0.4, Na_2SO_4 1.6, NH_4OH x, pH = 9.5, t = 295 K.

NH_4OH x (c); $CuSO_4$ 0.4, NH_4L 0.4, NH_4Cl 0.4, Na_2SO_4 1.6, and NH_4OH x (d), the open-circuit potential is more positive than the potential of the copper electrode (Figs. 2, 3). After a certain time, the open-circuit potentials of the steel electrode become equal to the potential of the copper electrode. When the potential of the steel electrode becomes more negative that that of the copper electrode, spontaneous deposition of copper on steel may occur. The time necessary for the equilibration of the potentials is independent of the concentration of $CuSO_4$ and H_4L, but depends on the solution pH. In 23 min, the open-circuit potential of the steel electrode in solutions (a)–(d) (pH 8.5) becomes equal to the equilibrium potential of the copper electrode (Fig. 2). Only after 2.5 h, a thin transparent copper coating is spontaneously deposited on steel.

At pH 9.0 the potentials become equal after 100 min of contact. A thin copper coating appears on steel in 4.2 h. At pH 9.5 the potentials do not equalize even in 400 min, and no copper coating appears on steel after 18 h of contact. Solutions with pH > 10.0 are unstable and no reliable experimental results can be obtained in this case. At pH < 6.0, spontaneous deposition of spongy copper coatings with poor adhesion to the steel starts immediately.

The optimal pH range for deposition of homogeneous smooth coatings strongly adhering to the steel support is 9.0 < pH < 9.8.

Figure 3 shows the equilibrium potential of the copper electrode (a) and the open-circuit potential of the steel electrode (b) as functions of the $CuSO_4$ and H_4L concentrations and the solution pH. The potentials were recorded 30 s after the electrode was submerged in a solution. The potentials of the copper and steel electrodes decrease as the solution pH increases from 8.5 to 9.5. In the process, the ammonia concentration and, consequently, the concentration of the complexes become higher.

The optimum current density for deposition of smooth homogeneous coatings with good adhesion lies at the beginning of the mixed region of the potentials. In this region, the control over the reaction passes from the charge transfer to diffusion [13–16].

Figure 4 shows polarization curves of copper deposition from solutions of various compositions (arrows indicate current densities corresponding to deposition of 1.0-, 3.0-, 5.0-, and 10.0-μm-thick coatings). The best-quality coatings were obtained at j_{opt} (Fig. 4). At current densities lower than the optimum value, the porosity and roughness of the coatings in-

creases as the current density decreases. The coating roughness also grows with the current density at current densities exceeding the optimum value. The results obtained are well consistent with the data of [13–16].

Figure 5 shows the polarization curve of copper deposition. This curve can be used to accurately determine the limiting diffusion current density j_L.

The optimum current density for deposition of high-quality coatings was found graphically (Fig. 4) as the initial current density corresponding to the onset of deposition in the region of the mixed control (about 0.3 j_L). This optimum current density linearly increases with the CuH_2L concentration (Fig. 6).

The experimentally obtained data confirmed the adequacy of the previously described theoretical approach [2, 14, 15]. The authors derived for the optimum current density j_{opt}, as the end point of the Tafel curve, the equations

$$\frac{j_L}{j_o} = \frac{1}{k}\left(\frac{1}{1-k}\right)^{10}, \quad (2)$$

$$j_{opt} = kj_L, \quad (3)$$

where j_L is the limiting diffusion current density; j_o, exchange current density; and k, proportionality coefficient ($0 < k \leq 1$).

The values of j_{opt} and k were determined for solutions of various compositions on the basis of the experimental data (Figs. 4–6) and Eqs. (2), (3). The coefficient k was found to be 0.3. These values of k and j_{opt} are in good agreement with the graphically determined values (table, Figs. 4, 6).

The data presented show the conditions at which smooth homogeneous copper coatings with good adhesion are formed on steel from a solution of the copper(II) complex with H_4L. Smooth homogeneous coatings with poor adhesion, easily detachable from the steel support, even though the support was not passivated prior to coating deposition, can be deposited from the same solutions.

To obtain coatings of this kind, the steel support should be subjected to "slow cementation" for 7 min before electrochemical deposition of a coating. The slow cementation occurs when the equilibrium potential of the copper electrode is approximately 0.3 V more positive that the open-circuit potential of the steel electrode in solutions of the copper(II) complex with H_4L at a concentration of the latter compound equal to 0.2–0.4 mol dm^{-3} [solutions (b)–(d)].

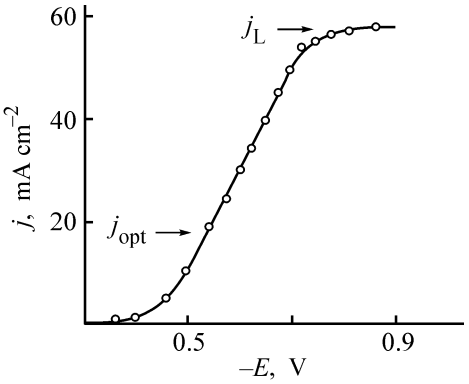

Fig. 5. Polarization curve of copper deposition. Solution composition (M): $CuSO_4$ 0.04, H_4L 0.04, NH_4Cl 0.4, Na_2SO_4 1.6, NH_4OH x; pH 9.5, T = 295 K.

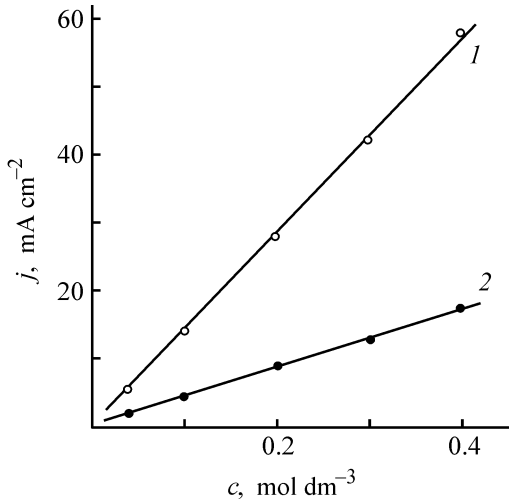

Fig. 6. (*1*) Limiting diffusion current density j and (*2*) optimum current density vs. the CuH_2L concentration c in solution. pH 9.5, T = 295 K.

Thus, high-quality coatings can be obtained at appropriate current densities in electrochemical deposition of copper on steel from a solution of the low-toxic copper(II) complex with the ligand, 1,3-propylene diamine-*N*,*N*'-diacetate-*N*,*N*'-di-3-propionic acid

Limiting diffusion current density j_L, exchange current density j_o, and their ratio at different concentrations of diacyde-1,3-propylenediamine-*N*,*N*'-diacetate-*N*,*N*'-dipropionate cuprate(II)

Parameter	CuH_2L concentration				
	0.4	0.3	0.2	0.1	0.04
j_L, mA cm^{-2}	58	42	28	1.4	5.6
j_{opt}, mA cm^{-2}	18	13	9.0	4.2	1.8
j_{opt}/j_L	0.31	0.31	0.32	0.30	0.33
j_o, mA cm^{-2}	0.44	0.32	0.20	0.10	0.042

(H_4L), as in the case of copper deposition from cyanide electrolytes [1, 2].

CONCLUSIONS

(1) Smooth homogeneous copper coatings can be deposited on steel from a solution of the copper(II) complex with a ligand, 1,3-propylene diamine-*N*,*N*'-diacetate-*N*,*N*'-di-3-propionic acid (H_4L).

(2) The quality of copper coatings depends on the difference between the copper electrode potential E_1 and the open-circuit potential of the steel electrode E_2. At $E_1 - E_2 < 0.1$ V, no cementation occurs, but smooth homogeneous copper coatings with good adhesion can be electrochemically obtained on steel at an appropriate current density.

(3) Smooth homogeneous copper coatings with poor adhesion, easily detachable from the steel support, are obtained if steel is subjected, prior to deposition, to slow cementation for 7 min at the potential $0.2 < E_1 - E_2 < 0.4$ V.

REFERENCES

1. Löwenheim, F.A., *Modern Electroplating*, New York: Wiley, 1974, pp. 6–165.
2. Popov, K.I., Grgur, B.N., and Vojnović, M.V., *J. Serb. Chem. Soc.*, 1993, vol. 58, no. 12, pp. 1085–1090.
3. Korovin, N.V., *Novye pokrytiya i elektrolity v gal'vanotekhnike* (New Coatings and Electrolytes in Electroplating), Moscow: Metallurgizdat, 1962.
4. Tunold, R., Brun, J., Johansen, B., and Jakšić, M., *Russ. J. Electrochem.*, 1995, vol. 31, pp. 638–643.
5. Jakšić, M., Brun, J., Johansen, B., and Tunold, R., *Russ. J. Electrochem.*, 1995, vol. 31, pp. 1187–1194.
6. Marinović, V. and Despić, A., *Russ. J. Electrochem.*, 1997, vol. 33, pp. 965–971.
7. Stanković, S., Grgur, B., Krstajić, N., and Vojinović, M., *Electroanal. Chem.*, 2003, vol. 549, pp. 37–47.
8. Stanković, S., Grgur, B., Krstajić, N., and Vojinović, M., *J. Serb. Chem. Soc.*, 2003, vol. 68, no. 3, pp. 207–218.
9. Durdević, P., Radanović, D., Cvijović, M., and Veselinović, D., *Talanta*, 1991, vol. 38, no. 4, pp. 455–460.
10. Durdević, P., Radanović, D., Cvijović, M., and Dimitrijević, M., *Polyhedron*, 1992, vol. 11, no. 2, pp. 197–204.
11. Jugoslovenski Standard, JUS CAI, 555 V–1969.
12. Borђxviћ, C., *Metalne prevlake* (Metal Coatings), Belgrad: Tekhnichka Kn'iga, 1992, pp. 136–154.
13. Radoshevіћ, N., *Khemijski i fizichki podatsi i velichine* (Chemical and Physical Data and Constants), Belgrad: Rad, 1987, pp. 706–707.
14. Popov, K.I., Krstajić, N.V., and Popov, S.R., *Surf. Techn.*, 1983, vol. 20, pp. 199–207.
15. Popov, K.I., Pavlović, Lj.J., Pavlović, M.G., and Čekerevać, N.J., *Surf. Coat. Techn.*, 1988, vol. 35, pp. 39–42.
16. Popov, K.I., Keča, D.N., Drašković, D.A., and Vuksanović, B.J., *J. Appl. Electrochem.*, 1976, vol. 6, pp. 155–160.

ISSN 1070-4272, Russian Journal of Applied Chemistry, 2007, Vol. 80, No. 4, pp. 571–575. © Pleiades Publishing, Ltd., 2007.
Original Russian Text © V.P. Boyarskii, T.E. Zhesko, E.V. Larionov, V.A. Polukeev, 2007, published in Zhurnal Prikladnoi Khimii, 2007, Vol. 80, No. 4, pp. 584–589.

CATALYSIS

Synthesis of Heteroaromatic Carboxylic Acids by Carbonylation of Hetaryl Halides with Catalysts Based on Cobalt Carbonyl Modified with Epoxides

V. P. Boyarskii, T. E. Zhesko, E. V. Larionov, and V. A. Polukeev

VNIIneftekhim Open Joint-Stock Company, St. Petersburg, Russia
NPF Gallar Limited Liability Company, St. Petersburg, Russia
St. Petersburg State University, St. Petersburg, Russia
Vekton Private Company, St. Petersburg, Russia

Received November 9, 2006

Abstract—A new method for the synthesis of heteroaromatic acids and their derivatives (esters and salts) by carbonylation of the corresponding halides was developed. Hetaryl halides were activated in alcoholic-alkali medium by highly active catalytic systems based on cobalt carbonyl modified with epoxides, developed previously for carbonylation of aryl halides.

DOI: 10.1134/S1070427207040106

Heteroaromatic acids are widely used in preparative organic chemistry and as a raw material in the production of a wide range of substances, mainly biologically active, and first of all of drugs and plant protection agents [1].

The traditional methods for preparing heteroaromatic acids, used today in the industry and laboratory practice, are diverse. They are based on a set of classical reactions of organic chemistry (alkylation, acylation, oxidation, cyanidation) and have a number of serious disadvantages: multistep synthesis, low selectivity, large consumption of raw materials, and complex process flowsheet. Some of these methods are environmentally unfavorable. Recently, the method of carbonylation of the corresponding halides has come into use for selective (one-step) introduction of the carboxy group into an aromatic core, i.e., for the synthesis of aromatic acids. Preparation of arenecarboxylic acids by carbonylation of aryl halides using cobalt carbonyl complex modified with alkyl halides as a catalyst has been known since the mid-1980s [2–6]:

$$\mathrm{ArHal + CO} \xrightarrow[\mathrm{ROH + B}]{\mathrm{Co(CO)_8 + A}} \mathrm{ArCOOR},$$

where A is an activator (alkyl halide) and B, base.

It was found that alkylcobalt carbonyl complexes $\mathrm{R'Co(CO)_4}$ formed in situ by the reaction of alkyl halides R'X, active in nucleophilic substitution (e.g., methyl iodide or methyl monochloroacetate $\mathrm{ClCH_2COOCH_3}$), with cobalt carbonyl in an alcoholic-alkaline medium can activate comparatively inert aryl halides in carbonylation reactions [2]. In the process, alkyl halides act as cocatalysts (activators) of cobalt carbonyl in aryl halide carbonylation. The reaction proceeds under very mild conditions: CO pressure of 1–3 atm and temperature of 60–65°C. We have shown [3, 4] that benzyl chloride forming the catalytic complex $\mathrm{PhCH_2Co(CO)_4}$ is the best activator (A) among alkyl halides.

Miura et al. [7] found that aryl halide carbonylation can proceed at room temperature and atmospheric pressure of CO, with the system cobalt(II) chloride–methyl iodide is used as a catalyst, but the reaction is slow. To accelerate the reaction in this catalytic system, Nindakova et al. [8] used reducing agents and, in particular, sodium borohydride or sodium naphthalenide. Nindakova et al. [8] believe that elimination of the stage of cobalt carbonyl preparation is an advantage of such an approach. However, in spite of the fact that such systems do not differ in activity from the systems studied in [2–6], additional reducing agents complicate the process.

In 1994, we discovered a new catalytic system for carbonylation of bromobenzene and chloronaphtalene, which consists of cobalt carbonyl, potassium carbonate, and olefin oxide (e.g., ethylene oxide or propylene oxide) [9]:

$$ArHal + CO + CHO^- \xrightarrow[\text{CH}_3\text{OH, } K_2CO_3, 60^\circ C, P_{CO} = 1 \text{ atm}]{Co(CO)_4^-,\ \text{epoxide}} ArCOOCH + Hal^-$$

We found that this catalytic system noticeably surpasses in activity the previously used system based on alkyl halides.

The new catalyst was used to prepare various aromatic carboxylic acids: 4-butylbenzoic, 4-acetylbenzoic, 4,4'-diphenyl- and 4,4'-(diphenyl oxide)dicarboxylic, and 2,6-naphtalenedicarboxylic. It was shown that this system can be successfully used for laboratory and commercial synthesis of a wide range of aromatic carboxylic acids of various structures [10].

At the same time, the synthesis, using this catalytic system, of aromatic carboxylic acids with a complex structure containing heterocyclic substituents has not been studied. At the same time, the exclusively high selectivity of the new catalytic system can become especially useful in the case of difficultly available and expensive heterocyclic compounds. Taking into account the fact that a number of various heteroaromatic halides can be prepared comparatively simply (by direct introduction of halogen into the aromatic core or by substitution with halogen of hydroxy group often formed in synthesis of the heterocycle), the use of cobalt carbonyl as an inexpensive and readily available catalyst of oxo synthesis, as applied to carbonylation of hetaryl halides, seemed very attractive from the practical and theoretical viewpoints. At the same time, this question required special consideration, because the majority of the heterocyclic compounds can potentially react as ligands and affect the catalytic properties of the cobalt complex.

First of all, we examined the possibility of using carbonylation to prepare acids derived from a nitrogen-containing heterocycle. It is well known that pyridine can form complexes with cobalt carbonyl, acting as a base ligand [11]. Therefore, it was necessary to check to what extent the catalytic activity of the carbonyl-base-propylene oxide system is preserved in the presence of the pyridine compound. We found that 2-chloropyridine undergoes carbonylation. Some important conclusions follow from this fact: (1) The system preserves the catalytic activity under the above conditions, i.e., in the presence of the potential heterocyclic ligand. (2) Hetaryl halides can undergo carbonylation. (3) As in usual reactions of nucleophilic substitution, halopyridine is more active than the corresponding halobenzene, i.e., the activating effect of the pyridine ring is preserved. This allows preparation of pyridinecarboxylic (and, apparently, also quinolinecarboxylic) acids by carbonylation of the corresponding hetaryl chlorides, which are substantially more readily available than the corresponding hetaryl bromides.

The synthesis of various quinolinecarboxylic acids, which are difficult to prepare by other methods, is of particular practical interest. We studied carbonylation of a series of halides containing tetrahydroquinoline (**I**), quinoline (**IV**, **V**), tetrahydroqiunazoline (**II**), and tetrahydroquinoxaline (**III**) rings:

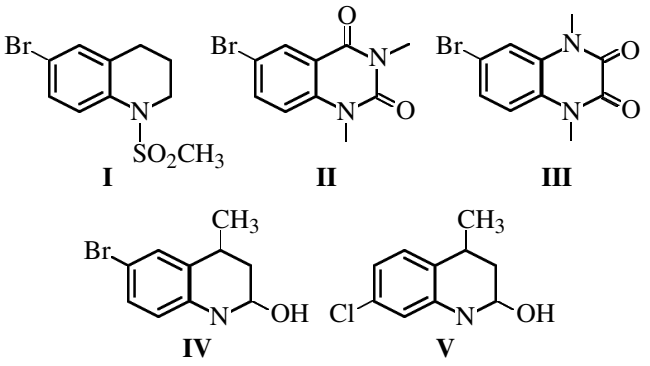

Table 1. Carbonylation of hetaryl halides containing fused nitrogen-containing heterocycles (T = 61–63°C, P_{CO} = 1 atm, reaction time 6 h)

Substrate	Substrate concentration, M	Molar ratio substrate : cobalt carbonyl : propylene oxide : potassium carbonate	Substrate conversion*	Product yield**
			%	
I	0.34	100 : 1 : 100 : 310	91	86 (95)
II	0.27	92 : 1 : 111 : 310	87	86 (99)
III	0.27	15 : 1 : 41 : 74	89	49
IV	0.2	22 : 1 : 107 : 40	23	–
V	0.34	65 : 1 : 91 : 196	85	81 (95)

* From the volume of carbon monoxide taken up.

** Preparation yield (in parenthese, taking into account isolated unchanged substrate); the same for Table 2.

Table 2. Influence of reaction conditions on carbonylation of hetaryl halide **I** (T = 63°C, P_{CO} = 1 atm, reaction time 4 h)

Substrate concentration, M	Molar ratio substrate : cobalt carbonyl : propylene oxide : potassium carbonate	Substrate conversion*	Product yield
		%	
0.17	50 : 1 : 50 : 130	87	83 (95)
0.34	100 : 1 : 100 : 310	91	86 (95)
0.69	200 : 1 : 200 : 600	28	26 (93)
0.34	200 : 1 : 200 : 635	52	51 (98)
0.34	194 : 1 : 200 : 620	52	52 (100)
0.34	190 : 1 : 190 : 600	75	71 (95)
0.34	194 : 1 : 400 : 620	68	64 (94)
0.48	200 : 1 : 200 : 600	78	75 (96)

* From ^{1}H NMR data.

The results obtained are listed in Table 1. As seen, all the hetaryl bromides studied readily undergo carbonylation with the catalytic system suggested. Moreover, chlorine derivatives of quinoline can also be, as expected, substrates in carbonylation. With the carbonylation of **I** as an example, we examined the influence of the reactant, catalyst, and activator concentrations on the reaction yield (Table 2).

The data obtained show that the method suggested is suitable for preparing heteroaromatic carboxylic acids.

To check whether the activity of the catalytic system is preserved with sulfur-containing heterocycles as substrates, we studied carbonylation of 2-bromo-5-(piperidyl-1-sulfo)thiophene **VI**:

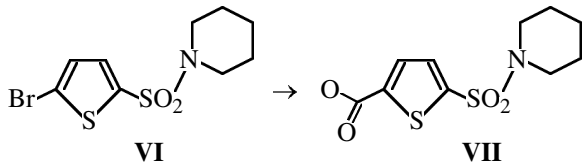

VI **VII**

We found that the substrate conversion in 4 h reached 94%, and the yield of isolated acid **VII** was 79%.

Preparation of 4-(4-carboxyphenyl)thiazoles **VIII**

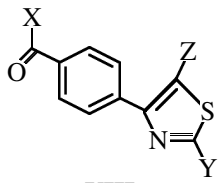

VIII

is of great interest. At present, such derivatives are studied as biologically active substances, e.g., potential COX-2 inhibitors [12]. Preparation of these derivatives involves the use of expensive starting compounds, 4-acylbenzoic acids, whereas carbonylation of aryl halides would allow the use of the substantially less expensive 4-bromoacylbenzenes.

The synthesis of 4-(2-methylthiazol-4-yl)benzoic acid **X** from 4-bromoacetophenone by carbonylation can be performed along two pathways:

A:

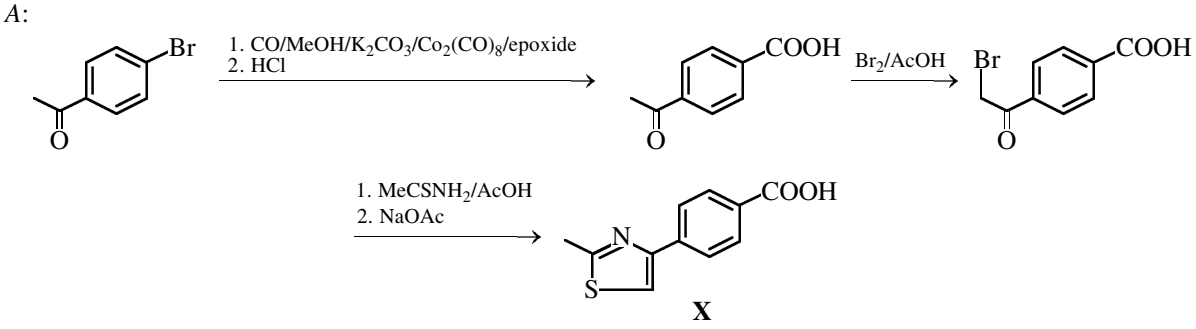

X

B:

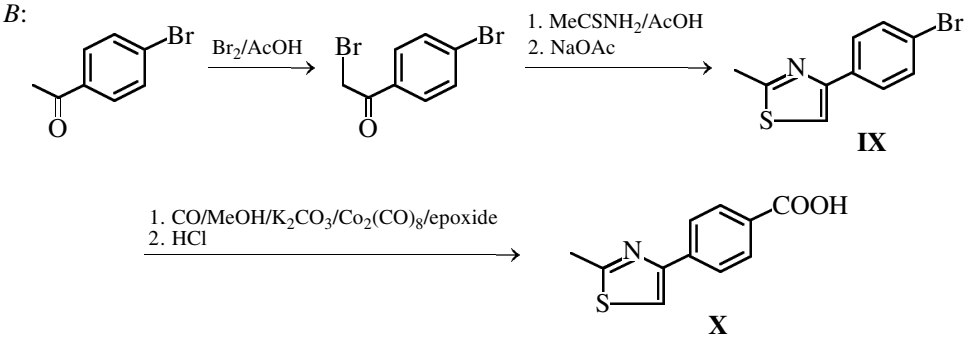

Pathway *A* involves carbonylation of aryl halide (4-bromoacetophenone) described in [10]. Pathway *B* includes the stage of carbonylation of halide **IX**, which required preliminary examination.

Carbonylation of 4-(4-bromophenyl)-2-methylthiazole **IX** catalyzed by the cobalt complex readily occurs in methanol with potassium carbonate as a base:

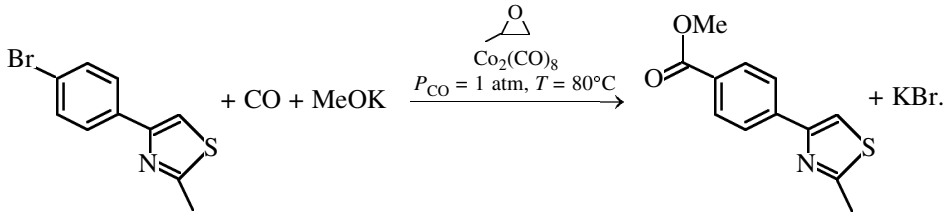

Analysis of the reaction mixture showed a high selectivity of carbonylation of this substrate and good preparation yield (Table 3).

Thus, we can synthesize **X** by two methods (*A* and *B*). The preparation yields are compared in Table 4. The data obtained show that the presence of thiazole fragment in the aryl halide molecule does not prevent carbonylation. Carbonylation after heterocycle formation (but not in the early stage of the synthesis) improves the overall parameters of the process.

As can be seen from the above data, the efficient catalytic system $Co(CO)_4$–propylene oxide–K_2CO_3 in metanol, developed previously for aryl halide carbonylation, can also be successfully used in the selective synthesis of various heteroaromatic carboxylic acids with a good yield and high selectivity under very mild

Table 3. Results of carbonylation of 4-(4-bromophenyl)-2-methylthiazole **IX** at various molar ratios of reactants

Molar ratio **IX** : $Co_2(CO)_8$: propylene oxide : K_2CO_3	Reaction time, h	Substrate conversion*	Product yield**
		%	
73 : 1 : 137 : 160	8.0	95	93
80 : 1 : 90 : 170	6.0	93	92
152 : 1 : 170 : 330	6.0	86	84

* Conversion is determined by NMR analysis of the reaction mixture.

** Yield of isolated 4-(2-methylthiazol-4-yl)benzoic acid **X** after carbonylation, base hydrolysis, and acidification of the reaction mixture.

Table 4. Comparison of the yields in the synthesis of 4-(2-methylthiazol-4-yl)benzoic acid **X** synthesis by methods *A* and *B*

Reaction step	Product yield, % of theory	
	pathway *A*	pathway *B*
Bromination of acetyl group	76	79
Formation of heterocycle by reaction with thioacetamide	78	94
Carbonylation*	74	84
Total product yield based on *p*-bromoacetophenone	44	62

* Equal conditions and reactant ratios for 4-bromoacetophenone and 4-(4-bromophenyl)-2-methylthiazole; without taking the probable recycle of the substrate into consideration.

conditions both in laboratory practice and on the commercial scale for production of raw materials required for fine chemistry.

EXPERIMENTAL

The carbonylation reactions were studied at CO atmospheric pressure in ordinary temperature-controlled glass apparatus with vigorous stirring in a CO atmosphere. The reaction products were analyzed by GLC and ^{1}H NMR. The identification of products was based on data of ^{1}H and ^{13}C NMR spectroscopy and mass spectrometry.

The mass spectra were recorded on an MKh-1321 mass spectrometer using direct sample inlet and ionization by electron impact (70 eV); the temperature of the ionization chamber was 200°C.

GLC analysis was performed on a Chrom-5 chromatograph with a flame ionization detector; the carrier gas was argon, flow rate 20–30 ml min^{-1}. Glass columns, 3 mm in diameter and 2500 mm long, were packed with SF-30 (10%) on Chromaton N-Super (80–100 mesh). The vaporizer and column temperature was 200°C.

The NMR spectra were recorded on a Bruker DPX 300 spectrometer [operating frequency 300.130 (^{1}H) and 75.03 (^{13}C) MHz]; solvent: 2 : 1 (by volume) mixture of CCl_4 with deuterated dimethyl sulfoxide.

A 2-l round-bottomed flask equipped with a power-driven stirrer, reflux condenser, thermometer, gas-feeding tube, and dropping funnel was purged with CO and charged with 200 g (1.4 mol) of K_2CO_3, 1200 ml of methanol, and 0.5 mol of a substrate. The reaction mixture was purged with CO under stirring for 0.5 h. Then, in a CO flow, 2.4 g of octacarbonyldicobalt (7 mmol) was added, and the temperature of the reaction mixture was elevated to 62°C. Then, the required amount of propylene oxide and 15–20 ml of methanol were added from a dropping funnel over a period of 10 min. After that, the temperature of the reaction mixture was elevated to 64°C, and the reaction was performed for 6 h at this temperature. Then the CO flow was stopped, the reaction mixture was cooled, 56 g of KOH (1 mol) was added, and methanol was distilled off at atmospheric pressure with stirring for several hours. After methanol distillation, water and diethyl ether were added into the reaction mixture, the organic phase was separated, and the aqueous phase was acidified with concentrated hydrochloric acid to pH 4–5 and kept until the acids precipitated. The precipitate was filtered off and dried.

CONCLUSIONS

(1) A new method was developed for synthesis of heteroaromatic acids and their derivatives by carbonylation of the corresponding hetaryl halides using highly active catalytic systems based on cobalt carbonyl, modified with epoxides.

(2) It was demonstrated that carbonylation of hetaryl halides proceeds under very mild conditions (CO pressure 1 atm) in alcohols in the presence of bases.

(3) It was shown that hetaryl halides with various structures, containing pyridine, quinoline, tetrahydroquinoline, tetrahydroquinazoline, thiophene, or thiazole fragments can be substrates in the above synthesis.

(4) A series of previously unknown heteroaromatic acids were synthesized.

REFERENCES

1. Mashkovskii, M.D., *Lekarstvennye sredstva* (Drugs), Moscow: Meditsina, 1998.
2. Foa, M. and Francalanci, F., *J. Mol. Catal.*, 1987, vol. 41, nos. 1–2, pp. 89–107.
3. Zhesko, T.E., Boyarskii, V.P., and Beletskaya, I.P., *Metalloorg. Khim.*, 1998, vol. 68, no. 1, pp. 385–387.
4. Zhesko, T.E., Boyarskii, V.P., and Nikitina, A.G., *Zh. Obshch. Khim.*, 1998, vol. 68, no. 1, pp. 85–89.
5. Miura, M., Itoh, K., and Nomura, M., *J. Mol. Catal.*, 1990, vol. 59, no. 1, pp. 11–15.
6. Shim, S.C., Lee, Y.D., Choi, H.J., et al., *Bull. Korean Chem. Soc.*, 1994, vol. 15, no. 9, pp. 772–774.
7. Miura, M., Itoh, K., and Nomura, M., *J. Mol. Catal.*, 1988, vol. 48, no. 1, pp. 11–13.
8. Nindakova, L.O., Shmidt, F.K., Reshetnikova, O.M., and Dmitrieva, T.V., *Zh. Org. Khim.*, 1991, vol. 27, no. 11, pp. 2276–2281.
9. Zhesko, T.E. and Boyarskii, V.P., *Kinet. Katal.*, 1994, vol. 35, no. 2, p. 320.
10. Zhesko, T.E., Boyarskii, V.P., and Lanina, S.A., *Zh. Prikl. Khim.*, 2005, vol. 78, no. 11, pp. 1875–1880.
11. Vigranenko, Yu.T., Vysokinskaya, A.T., Rybakov, V.A., et al., *Neftepererab. Neftekhim.*, 1987, no. 3, p. 21.
12. Woods, K.W., McCroskey, R.W., Michaelides, M.R., et al., *Bioorg. Med. Chem. Lett.*, 2001, vol. 11, no. 10, pp. 1325–1328.

ISSN 1070-4272, Russian Journal of Applied Chemistry, 2007, Vol. 80, No. 4, pp. 576–581. © Pleiades Publishing, Ltd., 2007.
Original Russian Text © V.M. Linkov, Yu.S. Dzyaz'ko, V.N. Belyakov, V.Yu. Atamanyuk, 2007, published in Zhurnal Prikladnoi Khimii, 2007, Vol. 80, No. 4, pp. 590–595.

ENVIRONMENTAL PROBLEMS OF CHEMISTRY AND TECHNOLOGY

Inorganic Composite Membranes for Electrodialytic Desaltination

V. M. Linkov, Yu. S. Dzyaz'ko, V. N. Belyakov, and V. Yu. Atamanyuk

University of Western Cape, Bellville, South Africa

Institute of General and Inorganic Chemistry, Ukrainian, National Academy of Sciences, Kiev, Ukraine

Received November 30, 2006

Abstract—Application of inorganic composite membranes in electrodialytic desaltination of dilute solutions containing Na^+, Ca^{2+}, Mg^{2+}, Cl^-, and SO_4^{2-} ions was studied. The membranes are based on an oxide ceramic containing hydrated zirconium(IV) oxide as an ion-exchange component. The limiting currents were estimated theoretically.

DOI: 10.1134/S1070427207040118

In recent decades, a considerable attention has been given to membrane methods for obtaining high-quality drinking water. A particular place among these methods is occupied by electrodialysis, which enables effective desalination of water containing 1 to 10 g l^{-1} of salts [1–4]. As a rule, ion-exchange membranes based on organic polymers are used for electrodialysis. However, low-soluble substances of organic origin and also colonies of microorganisms are concentrated on the surface of such membranes in the course of exploitation [5, 6]. This leads to gradual reduction of the efficiency of purification by electrodialysis and to an increase in power consumption. Replacement of organic membranes with those made of inorganic materials could solve this problem.

Inorganic ion-exchangers and, in particular, hydrated oxides of Group-IV metals are capable of ion exchange by acid or basic mechanism [7, 8], depending on the pH of the medium. The results reported in [9] show that composite ceramic membranes containing an inorganic cation-exchange component (zirconium hydrophosphate) are promising for electrodialytic extraction of cations from dilute solutions.

The aim of this study was to assess the possibility of using ceramic composite membranes containing an ion-exchange component (hydrated oxide of a Group-IV metal) for electrodialytic desaltination of subsaline water.

A flow of cations $N_{\mathrm{Cat,m}}$ across an ideal selective cation-exchange membrane is determined by their migration in the solution bulk and by diffusion across the near-membrane layer on the side of the desaltination chamber [10]:

$$N_{\mathrm{Cat,m}} = N^{\mathrm{migr}}_{\mathrm{Cat,s}} + N^{\mathrm{dif}}_{\mathrm{Cat,s}}. \quad (1)$$

Here, $N^{\mathrm{migr}}_{\mathrm{Cat,s}}$ and $N^{\mathrm{dif}}_{\mathrm{Cat},s}$ are the migration and diffusion components of the flow, with the subscripts "m" and "s" corresponding to the membrane and solution. In this case, the material balance equation (1) can be represented as

$$\frac{it_{\mathrm{Cat,m}}}{z_{\mathrm{Cat}}F} = \frac{it_{\mathrm{Cat,s}}}{z_{\mathrm{Cat}}F} + k_{\mathrm{Cat}}(c_{\mathrm{Cat,s}} - c^0_{\mathrm{Cat,s}}). \quad (2)$$

Here, i is the current density; $t_{\mathrm{Cat,m}}$ and $t_{\mathrm{Cat,s}}$, ion transport numbers across the membrane and solution, respectively; z_{Cat}, ion charge; F, Faraday constant; $c_{\mathrm{Cat,s}}$ and $c^0_{\mathrm{Cat,s}}$, ion concentrations in the solution bulk and near-membrane solution layer on the side of the desaltination chamber, respectively; and k_{Cat}, mass-transfer coefficient of cations, defined as D_{Cat}/δ, where D_{Cat} is the diffusion coefficient of cations in solution, and δ, the width of the solution layer near the membrane surface.

The diffusion and migration flows are related by

$$N^{\mathrm{dif}}_{\mathrm{Cat,s}} = \frac{|z_{\mathrm{Cat}}|}{|z_{\mathrm{An}}|} N^{\mathrm{migr}}_{\mathrm{Cat,s}}. \quad (3)$$

It follows from Eq. (2) that an increase in the current density should intensify the ion transfer across the membrane. At the same time, the current density has the limiting value $i_{\mathrm{lim,Cat}}$, which corresponds to

$c^0_{\text{Cat, s}} = 0$. If the concentration of the supporting electrolyte is insignificant, the limiting current is determined by both diffusion and migration [11]:

$$i_{\text{lim, Cat}} = z_{\text{Cat}}\left(1 + \frac{|z_{\text{An}}|}{|z_{\text{Cat}}|}\right)Fk_{\text{Cat}}c_{\text{Cat, s}}. \quad (4)$$

In the presence of more than a 10-fold excess of the supporting electrolyte in the solution (in mole ratios), Eq. (4) can be simplified to

$$i_{\text{lim, Cat}} = z_{\text{Cat}}Fk_{\text{Cat}}c_{\text{Cat, s}}, \quad (5)$$

It is necessary to note that the limiting current of transfer across the membrane is an additive quantity and includes the corresponding values of i_{lim} for all the cations. The above relations are also valid for anions.

In the case of a laminar flow along flat parallel membranes (it is assumed that the surface of the membranes is ideally smooth), the mass-transfer coefficient can be found from the correlation equation [12]:

$$\text{Sh} = 1.85\left(\text{Re}\,\text{Sc}\frac{d}{L}\right)^{0.33}. \quad (6)$$

Here, Sh, Re, and Sc are the dimensionless Sherwood, Reynolds, and Schmidt numbers, respectively; d, distance between membranes; and L, height of the working space of the membranes. Because

$$\text{Sh} = \frac{k_{\text{Cat}}d}{D_{\text{Cat, s}}},\ \text{Re} = \frac{du}{\nu},\ \text{Sc} = \frac{\nu}{D_{\text{Cat, s}}}$$

(ν is the kinematic viscosity of a solution), this enables us to calculate the limiting current due to the ion transfer across the membrane.

EXPERIMENTAL

We chose ceramic plates of composition Al_2O_3 (70%) and ZrO_2 (30%) with an average pore diameter of 0.19 μm and specific surface area of 4.5–5 $m^2\ g^{-1}$ as a starting matrix for preparation of ion-selective membranes. The matrix was filled in stages with hydrated zirconium dioxide (HZD). For this purpose, a membrane was impregnated with an HZD sol, kept in ammonia vapor, washed with deionized water, and dried at 423 K [13]. To fill matrix pores to a fuller extent, the ion-exchange component was introduced seven times.

The experimental installation, described in detail in [14, 15], comprised a three-chamber electrodialysis cell, three independent contours for solution feeding, a power source, and measuring devices. Platinum electrodes were placed in side compartments of the cell, and the cathode and anode spaces were separated from the central compartment by ceramic membranes. The effective area of the membranes and electrodes was 16 cm^3 (4 cm × 4 cm), and the distance between the membranes, 1 cm.

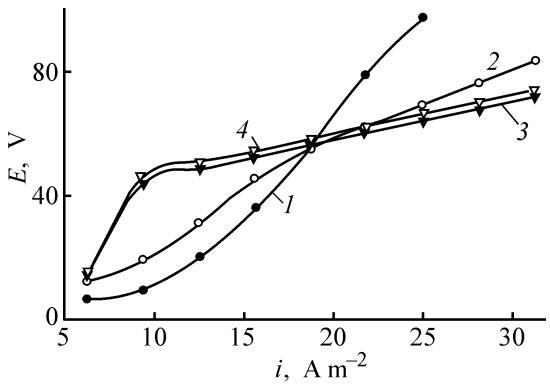

Fig. 1. Voltage E vs. the current density i for the electrodialytic system. Solution flow rate through the middle compartment ($m^3\ s^{-1}$): (*1*) 5×10^{-8}, (*2*) 1×10^{-7}, (*3*) 1.5×10^{-7}, (*4*) 2×10^{-7}; the same for Figs. 2 and 3.

The starting solution, containing (mol m^{-3}) Na_2SO_4 1.8, NaCl 5.9, $CaCl_2$ 3.9, and $MgCl_2$ 3.0, was delivered in a direct-flow mode into the central compartment of the cell (desaltination chamber) at a rate u of 5×10^{-8}, 1×10^{-7}, 1.5×10^{-7}, or 2×10^{-7} $m^3\ s^{-1}$ by SP-311 peristaltic pumps. The electrical conductivity of the solution at the cell output was measured with an HI 9932 conductometer, the pH was recorded wit an EV-40 ion meter. The electrical conductivity of the starting solution was 2.5 $m\Omega^{-1}\ cm^{-1}$, and pH 6.5. A 5 mol m^{-3} solution of H_2SO_4 (anolyte) and a solution with the initial composition corresponding to that of the solution to be purified (catholyte) were circulated through the electrode compartments (concentrating chambers). The initial volume of the solution in each compartment was 200 cm^3.

The experiments were carried out in the galvanostatic mode at current densities 6.2–31.2 A m^{-2}, using an IPPT 65-49 power source. The voltage was measured with an SHCH-1312 voltmeter, and the current, with an SHCH-4311 ammeter. The duration of each experiment at various flow rates and current strengths was about 8 h.

Samples were periodically taken from the compartment containing the catholyte and analyzed for the content of cations with a PYE UNICAM SP 9 atomic-absorption spectrometer (Ca^{2+} and Mg^{2+}) and a PFM-U4.2 flame photometer (Na^+).

Dependences of the voltage E on the current density are shown in Fig. 1. The values of E were re-

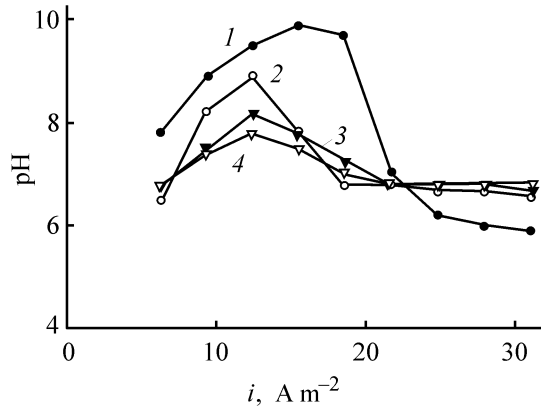

Fig. 2. pH value of the dialyzate vs. the current density i at various solution flow rates through the middle compartment.

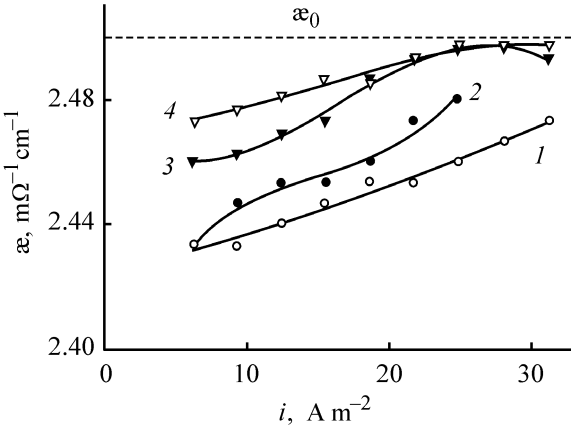

Fig. 3. Electrical conductivity of the dialyzate, æ vs. the current density i at various solution flow rates through the medium compartment.

corded 30 min after the beginning of each experiment. It was found that the current–voltage curve is S-shaped at a solution flow rate through the middle chamber of 5×10^{-8} m^3 s^{-1}. The voltage increases slowly in the range 6.2–9.4 A m^{-2} and sharply at $i > 9.4$ A m^{-2}. In the range 12.5–28.1 A m^{-2} the E–i dependence becomes linear, but tends to deviate from linearity as the current increases further. At a flow rate of 1×10^{-7} m^3 s^{-1}, four portions can be distinguished in the curve E–i: slow (6.2–9.4 A m^{-2}) and steep (9.4–15.6 A m^{-2}) rise in voltage, with the subsequent decrease in the slope of the curve slope (15.6–18.7 A m^{-2}) and a linear region at $i >> 18.7$ A m^{-2}. At flow rates of 1.5 10^{-7} and 2×10^{-7} m^3 s^{-1}, the voltage first sharply increases (6.2–9.4 A m^{-2}), and then decreases (9.4–12.5 A m^{-2}). At $i > 12.5$ A m^{-2} E–i, the curves become linear.

In the course of electrodialysis, the voltage difference tended to decrease at all currents, which is probably due to an increase in the solution concentrations in the electrode compartments because of the transfer of ions across the membranes and generation of H^+ and OH^- ions at the electrodes. The shape of the current–voltage curves in Fig. 1 is undoubtedly related to a change in the solution acidity in the central compartment.

Figure 2 shows how the pH value of the dialyzate depends on the current density (pH was measured 30 min after the beginning of an experiment). It is necessary to note that all the pH-vs.-current density curves exhibit an extremal behavior. At a solution flow rate through the medium chamber of 5×10^{-8} m^3 s^{-1}, the maximal pH value is reached at 15.6 A m^{-2}. Further increase in the current leads to a decrease in the dialyzate pH. At higher flow rates, the pH reaches a limiting value at 12.5 A m^{-2}, sharply decreased (12.5–21.8 A m^{-2}), and then stabilizes at 21.8 A m^{-2}.

Dependences of the electrical conductivity æ of the dialyzate on the current density are shown in Fig. 3. The value æ$_0$ corresponds to the electrical conductivity of the starting solution, with other æ values measured 30 min after the beginning of the experiment. In all the cases, the electrical conductivity of the dialyzate remained unchanged during each experiment. It is seen from Fig. 3 that æ increases with the current density.

It was found that, at a flow rate of 1×10^{-7} m^3 s^{-1} and a current density of 6.25 A m^{-2}, the rate of ion transfer reaches 1.67×10^{-8} (Na^+), 8.33×10^{-9} (Ca^{2+}), and 7.18×10^{-9} mol s^{-1} (Mg^{2+}). When the current density is raised to 25.1 A m^{-2}, these values decreases to 4.12×10^{-9} mol s^{-1} for Ca^{2+} and to 2.65×10^{-9} mol s^{-1} for Mg^{2+}, respectively; the rate of Na^+ transfer somewhat increases (1.8×10^{-8} mol s^{-1}).

We calculated the theoretical values of the limiting current due to transfer of each type of ions. In doing so, we took into consideration that the distance between the membranes was 1 cm, and the height of the central compartment, 4 cm. Because both single- and double-charged cations and anions were present in the solution, we determined the lower and upper bounds on the limiting current. Taking into consideration the concentration of each ion, we carried out the calculations by Eqs. (4) (Na^+ and Cl^-) and (5) (Ca^{2+}, Mg^{2+}, and SO_4^{2-}). In the calculations, we used the diffusion coefficients of ions in solution from

Calculation of the limiting current of the ion transfer across the membranes

Ion	c, mol g^{-3}	ω, m s^{-1} (u, m^3 s^{-1})	D, m^2 s^{-1}	Re	Sc	Sh	k, m s^{-1}	i_{lim}, A m^{-2}
Na^+	9.5	1.25×10^{-4} (5.0×10^{-8})	1.62×10^{-9}	1.39	555	10.50	1.71×10^{-6}	2.35–3.13
		2.50×10^{-4} (1.0×10^{-7})	1.62×10^{-9}	2.78	555	13.20	2.14×10^{-6}	2.94–3.92
		3.75×10^{-4} (1.5×10^{-7})	1.62×10^{-9}	4.17	555	15.09	2.44×10^{-6}	3.35–4.47
		5.00×10^{-4} (2.0×10^{-7})	1.62×10^{-9}	5.57	555	16.60	2.69×10^{-6}	3.70–4.93
Ca^{2+}	3.9	1.25×10^{-4} (5.0×10^{-8})	7.20×10^{-10}	1.39	1248	13.72	9.88×10^{-7}	0.74
		2.50×10^{-4} (1.0×10^{-7})	7.20×10^{-10}	2.78	1248	17.25	1.24×10^{-6}	0.94
		3.75×10^{-4} (1.5×10^{-7})	7.20×10^{-10}	4.17	1248	19.71	1.42×10^{-6}	1.07
		5.00×10^{-4} (2.0×10^{-7})	7.20×10^{-10}	5.57	1248	21.68	1.56×10^{-6}	1.17
Mg^{2+}	3.0	1.25×10^{-4} (5.0×10^{-8})	7.90×10^{-10}	1.39	1137	13.30	1.05×10^{-6}	0.61
		2.50×10^{-4} (1.0×10^{-7})	7.90×10^{-10}	2.78	1137	16.72	1.32×10^{-6}	0.76
		3.75×10^{-4} (1.5×10^{-7})	7.90×10^{-10}	4.17	1137	19.14	1.51×10^{-6}	0.85
		5.00×10^{-4} (2.0×10^{-7})	7.90×10^{-10}	5.57	1137	21.04	1.68×10^{-6}	0.97
Cl^-	19.7	1.25×10^{-4} (5.0×10^{-8})	2.03×10^{-9}	1.39	441	9.73	1.98×10^{-6}	5.64–7.53
		2.50×10^{-4} (1.0×10^{-7})	2.03×10^{-9}	2.78	441	12.24	2.48×10^{-6}	7.08–9.43
		3.75×10^{-4} (1.5×10^{-7})	2.03×10^{-9}	4.17	441	13.99	2.84×10^{-6}	8.08–10.78
		5.00×10^{-4} (2.0×10^{-7})	2.03×10^{-9}	5.57	441	15.38	3.12×10^{-6}	8.90–11.87
SO_4^{2-}	1.8	1.25×10^{-4} (5.0×10^{-8})	1.05×10^{-9}	1.39	870	12.18	1.28×10^{-6}	0.44
		2.50×10^{-4} (1.0×10^{-7})	1.05×10^{-9}	2.78	870	15.31	1.61×10^{-6}	0.56
		3.75×10^{-4} (1.5×10^{-7})	1.05×10^{-9}	4.17	870	17.50	1.84×10^{-6}	0.64
		5.00×10^{-4} (2.0×10^{-7})	1.05×10^{-9}	5.57	870	19.25	2.02×10^{-6}	0.70

the reference book [16]. The results obtained are listed in the table.

It was found that the total limiting current due to the cation transfer into the cathode compartment is 3.5–4.48, 4.64–5.62, 5.27–6.39, and 5.84–7.07 A m^{-2} at flow rates of 5×10^{-8}, 1×10^{-7}, 1.5×10^{-7}, and 2×10^{-7} m^3 s^{-1}, respectively. The limiting current of anions at the same flow rates is 6.08–7.97, 7.64–9.99, 8.64–11.42, and 9.60–12.57 A m^{-2}. It can be seen that $i_{lim,Cat} < i_{lim,An}$. It is necessary to note that these calculations disregarded the limiting current due to the transfer of OH^- or H^+ ions, because the content of these ions in the dialyzate is very low at low current densities.

The electrodialysis at $i < i_{lim,Cat}$ and $i < i_{lim,An}$ results in that cations and anions enter the cathode and

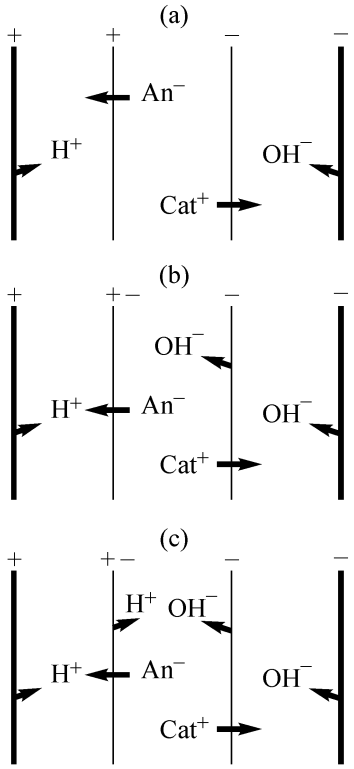

Fig. 4. Schematic of ion transfer across composite inorganic membranes under conditions of (a) sub-limiting current, (b) over-limiting current, and (c) acid leakage from the anolyte across the membrane.

anode chambers in equivalent amounts (Fig. 4a). In the process, equivalent amounts of OH^- and H^+ ions are generated at the cathode and anode; the acidity of the solution being purified remains unchanged. The constancy of the pH value of the dialyzate can serve as an indication that the limiting current is not reached in the system. The neutrality of the solution delivered into the central chamber and the acid character of the anolyte provide that the charge on the surface of the membrane that separates the anode and central compartments is positive and, accordingly, the membrane is permeable to anions. Similarly a neutral dialyzate and an alkaline catholyte favor formation of a negative charge of the membrane on the side of the cathode chamber and, accordingly, provide the selectivity of the membrane with respect to cations.

At flow rates of 1×10^{-7} $m^3\ s^{-1}$ and more, the real value of the total limiting current of cations is apparently higher than the theoretical value. This is demonstrated by the fact that the rate of transfer of Na^+ ions somewhat grows as the current increases from 6.25 to 25.1 A m^{-2}. In addition, the pH of the dialyzate is close to 7. This circumstance may be due to the surface roughness of membranes and, hence, to a certain intensification of the mass transfer. Taking into account that the reaction of the dialyzate is neutral, $u > 1 \times 10^{-7}$ $m^3\ s^{-1}$, and $i = 6.25$ A m^{-2}, we can calculate the current efficiency by cations, Q_{Cat}, from the change in the electrical conductivity of the solution:

$$Q_{Cat} = \frac{æ_0 - æ}{æ_0} u\tau\Sigma z_{Cat} c_{Cat} \frac{F}{Si\tau}. \quad (7)$$

Here u is the volumetric flow rate of the solution; τ, time; and S, membrane area.

The first term in Eq. (7) corresponds to the degree of solution purification, the second, to the dialyzate volume, the third, to the total equivalent concentration of ions in solution, and the fourth, to the amount of transferred ions, calculated by Faraday's law. The current efficiency by anions is determined similarly.

The values of Q_{Cat}, found using Eq. (7), are 68–70% for solution delivery rates of 1×10^{-7}–2×10^{-7} $m^3\ s^{-1}$ at a current not exceeding the limiting value (6.25 A m^{-2}). It is necessary to note that the current efficiency of 100% at $i << i_{lim}$ is, as a rule, not reached, either, in the case of heterogeneous organic membranes because of their polarization [17].

In the case when the current exceeds $i_{lim,Cat}$, an excess of cations is present is a solution being purified. The electroneutrality of the dialyzate is provided by hydroxide ions formed on the membrane surface via water dissociation, which makes the dialyzate more alkaline (Fig. 4b). In this case, the membrane retains the cation-exchange function on the cathode side. At the same time, the surface of the membrane separating the anode and central chambers is charged positively on the anode side and negatively on the side of the desaltination chamber, which hinders penetration of anions into the anolyte. This leads to a sharp rise in voltage. It is believed that, at $i > i_{lim,Cat}$, Ca^{2+} and Mg^{2+} ions are partially precipitated as difficultly soluble compounds on the surface of the membrane separating the cathode and central chambers. This assumption is confirmed by the decrease in the rates of transfer of Ca^{2+} and Mg^{2+} ions at high current densities.

After the limiting current for anions is reached, water starts to dissociate at the membrane separating the anode and central spaces, with H^+ ions generated on the membrane surface on the central chamber side, and the dialyzate pH decreasing to 7. The membrane acquires a positive charge on the anode side. The slope of the E–i curve decreases, which points to a decrease in the resistance of the electrodialytic system.

It is possible that the acid formed in the anolyte penetrates into the central chamber at high current densities (Fig. 4c). This is confirmed by the gradual increase in the electrical conductivity of the dialyzate, observed as the current becomes higher. The dialyzate is slightly acidified at high current densities, although an increase in pH would be expected in view of the inequality $i_{\mathrm{lim,Cat}} < i_{\mathrm{lim,An}}$. Thus, H^+ ions that penetrate from the anode chamber into the central chamber owing to an acid leakage are partly neutralized by OH^- ions generated on the membrane separating the central and cathode chambers. At the same time, the excess of acid anions is compensated by an excess of cations in the dialyzate.

CONCLUSIONS

(1) It was shown that inorganic composite membranes containing an ion-exchange component, hydrated zirconium dioxide introduced into a ceramic matrix, can be used for electrodialytic desaltination of dilute solutions containing Na^+, Ca^{2+}, Mg^{2+}, Cl^-, and SO_4^{2-} ions.

(2) The limiting currents were theoretically estimated for both cations and anions. For currents lower than the limiting value, the degree of desaltination was estimated by a change in the electrical conductivity of the solution.

(3) It was found that the current efficiency in the electrodialytic desaltination is 68–70%.

REFERENCES

1. Koryta, J., Dvorzhak, J., and Bogachkova, V., *Electrochemistry* (Translated from Czech), London, 1970.
2. Zabolotskii, V.I. and Nikonenko, V.V., *Perenos ionov v membranakh* (Transfer of Ions in Membranes), Moscow: Nauka, 1996.
3. Ortiz, J.M., Exposito, E., Gallud F., et al., *J. Membr. Sci.*, 2006, vol. 274, no. 2, pp. 138–149.
4. Dzyaz'ko, Yu.S. and Atamanyuk, V.J., *Naucnye Zapiski NAUKMA, Khim. Nauki i Tekhnologii*, 2004, vol. 28, pp. 50–62.
5. Lee, H.J., Moon, S.H., and Tsai, S.P., *Separ. Purif. Technol.*, 2002, vol. 27, no. 2, pp. 89–95.
6. Lindstrand, V., Jonsson, A.S., and Sundstrom, G., *Desalination*, 2000, vol. 130, no. 1, pp. 73–84.
7. Linkov, V.N. and Belyakov, V.N., *Separ. Purif. Technol.*, 2001, vol. 25, no. 1–3, pp. 57–63.
8. Amphlett, C.B., *Inorganic Ion Exchangers*, Amsterdam: Elsevier, 1964.
9. Sukharev, Yu.I., *Sintez i primenenie spetsificheskikh oksigidratnykh sorbentov* (Synthesis and Application of Specific Oxyhydrate Sorbents), Moscow: Energoatomizdat, 1987.
10. Walsh, F., *A First Course in Electrochemical Engineering*, London: Alresford, 1993.
11. Vetter, K.J., *Electrochemische Kinetik*, Berlin: Springer, 1961.
12. Ciborowski, J., *Podstawy Inzynierii Chemicznej*, Warsaw: Naukovo-Techniczne, 1965.
13. Dzyaz'ko, Yu.S., Belyakov, V.N., Stefanyak, N.V., and Vasilyuk, S.L., *Zh. Prikl. Khim.*, 2006, vol. 79, no. 5, pp. 778–782.
14. Dzyaz'ko, Yu.S., Rozhdestvenskaya, L.M., and Pal'chik, A.V., *Zh. Prikl. Khim.*, 2005, vol. 78, no. 3, pp. 418–424.
15. Dzyazko, Yu.S. and Belyakov, V.N., *Desalination*, 2004, vol. 162, pp. 179–189.
16. Parsons, R., *Handbook of Electrochemical Constants*, London: Butterworth Sci., 1959.
17. Balavadze, E.G., Bobreshova, O.V., and Kulintsov, P.I., *Usp. Khim.*, 1988, vol. 57, no. 6, pp. 1031–1041.

ISSN 1070-4272, Russian Journal of Applied Chemistry, 2007, Vol. 80, No. 4, pp. 582–585. © Pleiades Publishing, Ltd., 2007.
Original Russian Text © I.P. Sizeneva, V.A. Val'tsifer, V.N. Strel'nikov, 2007, published in Zhurnal Prikladnoi Khimii, 2007, Vol. 80, No. 4, pp. 596–599.

ENVIRONMENTAL PROBLEMS OF CHEMISTRY AND TECHNOLOGY

Concentration of Trace Amounts of Butyl Alcohol, Butyl Acrylate, and Acrylic Acid from Water by Distillation

I. P. Sizeneva, V. A. Val'tsifer, and V. N. Strel'nikov

Institute of Technical Chemistry, Ural Division, Russian Academy of Sciences, Perm, Russia

Received September 19, 2006

Abstract—A procedure for concentration of trace amounts of butyl alcohol, butyl acrylate, and acrylic acid from water by joint distillation with ethanol is suggested.

DOI: 10.1134/S107042720704012X

Measurement of the concentration of noxious impurities is one of the most important tasks of sanitary-chemical monitoring of natural and waste water. For most of organic compounds subject to regulations, the maximum permissible concentrations (MPC)) are below 1 mg l^{-1}, and, therefore, they cannot be always determined by the most versatile gas-chromatographic method.

The new requirements to wastewater treatment and the increasingly stringent parameters subject to regulations necessitate development of new high-sensitivity analytical procedures for determination of toxic substances. Presently, the production and consumption of acrylic monomers and polymers and formulations based on them is widely developing, which makes it necessary to monitor discharges from these industries. The wastewater from butyl acrylate (BAc) production contains toxic admixtures of butyl alcohol (BA), butyl acrylate, and acrylic acid (AA), whose MPC in potable water are 0.1, 0.01, and 0.5 mg l^{-1}, respectively [1]. Direct gas-chromatographic analysis of wastewater containing these impurities in amount of 0.5–10.0 MPC fails to provide the required detection limit. Therefore, it is necessary to preconcentrate the impurities in order to improve the determination sensitivity. Published data show that a limited number of methods are being used to concentrate trace amounts of organic substances in water. These include the following: sorption concentration on hydrophobic sorbents; liquid extraction; gas extraction, which is a variety of the vapor-phase concentration of volatile impurities contained in liquids [vapor-phase analysis (VPA)]; and distillation.

The compounds to be monitored are reactive, belong to different classes of organic compounds, and differ significantly in the MPC values. Therefore, application of any of these methods meets certain difficulties. In the case of the sorption concentration, it is necessary to remove water or to eliminate its interference in thermal desorption of impurities into a chromatographic column. The difference in polarity between the above compounds limits the choice and availability of effective sorbents. The liquid extraction is intended for removal of low-volatile substances with limited solubility in water. Therefore, its application is complicated by the need to work with large volumes of wastewater and organic substances because the distribution coefficients of BA and, especially AC, in the known extracting agents are low even upon salting-out and acidification. The main purpose of VPA is to determine readily volatile compounds with poor solubility in water. The method has high sensitivity and can provide the necessary detection limit of BA and BA impurities without any special concentrating procedures [2]. However, it is inefficient for analysis for AC a compound well soluble in water [3], at the MPC level.

Thus, development of a concentration procedure to provide chromatographic determination of BA, BAc, and AA impurities at the MPC level in the case of their simultaneous presence in water is a topical task.

EXPERIMENTAL

We chose for concentration the method of joint distillation of impurities from water with another solvent. The procedure consists in that a solvent with a comparatively low boiling point is added to water. Then, distillation of the solvent will involve simulta-

Table 1. Physicochemical characteristics of substances being analyzed

Compound	MPC, mg l^{-1}	T_b °C	Polarity	Solubility, g l^{-1} at 20°C		
				Water	Ethanol	Acetone*
BA	0.1	117.2	Polar	90	∞	w.s.
BAc	0.01	147.4	Low-Polarity	1.3	∞	s.
AA	0.5	141.6	High-Polarity	∞	∞	s.

* w.s., well soluble; s., soluble.

neous evaporation of trace components. The necessary condition for applicability of this procedure is that the components to be determined should be stable at the distillation temperature [4].

All the analyses were performed by the gas-chromatographic method on an LKhM-80 chromatograph with a flame-ionization detector. A 100 × 0.3-cm steel column preliminarily deactivated with concentrated orthophosphoric acid was packed with Chromaton N-AW-NMDS (0.020–0.025 cm), onto which 15% (by mass) of the stationary phase, polyehtylene glycol adipate (PEGA), was deposited. The chromatographic conditions were as follows. Temperature (°C): evaporator, 190; detector, 170; columns, isotherm at 53 for 16 min, rise in temperature from 53 to 170 at a rate of 25 deg min^{-1}, and then again isotherm for 10 min. Carrier gas: nitrogen at a flow rate of 30 cm^3 min^{-1}. To suppress the irreversible sorption of AA in the column, the carrier gas was mixed with a formic acid vapor in a flask connected to the carrier gas line, or 3 μml of 40% formic acid was introduced into the column prior to analysis. The quantitative determination was performed by the absolute calibration method. The calibrating solutions were prepared from accurately weighed portions of chemically pure BA, BAc, and AA by successive dilution. The detection limit on the scale 50×10^{-12} A (with a 10 μml sample introduced into the column) was 0.01, 0.01, and 0.03 mg ml^{-1} for BA, BAc, and AA, respectively. The analysis time was 30 min and the relative error did not exceed 20%.

The conditions of concentration were chosen using model wastewater solutions containing BA, BAc, and AA in an amount of 0.5–100 MPC.

Concentration by distillation: to wastewater were added sodium chloride (up to 20 wt %), orthophosphoric acid to pH 1–2 as indicated by universal indicator paper, and a low-boiling solvent. Then, the solvent with a vapor temperature equal to the boiling point of the solvent was evaporated into volumetric test tubes by rectification in a glass column packed with a glass pipe cut in pieces. This operation should be performed with great care, because the temperature of the water–alcohol mixture should be raised slowly to provide the vapor rectification mode. The concentration coefficient was calculated as a ratio of the wastewater volume to the volume of the distillate obtained.

Concentration by evaporation: into a test tube with a distillate was introduced a weighed portion of polyethylene glycol (0.01–0.025%), the test tube was connected to a refluxer through a Kuderny–Danishe evaporator, and the solvent was distilled-off. The concentration coefficient was calculated as a ratio of the distillate volume to the volume of the evaporated concentrate.

As solvent was chosen ethanol, because all three impurities have unlimited solubility in this alcohol and its boiling point is 40°C lower than that of the lowest-boiling impurity, BA (Table 1).

To provide complete evaporation of BA and AA from water, we used, by analogy with extraction, the effect of salting-out with an inorganic salt and acidification with a nonvolatile acid, thereby reducing the solubility of organic impurities in water and facilitating their transfer to the alcohol. Preliminarily, we determined that no acid hydrolysis of BA occurs under the experimental conditions. The salting-out also reduces the solubility of ethanol in water and facilitates its evaporation. We used as the salting-out agent the least expensive and readily available sodium chloride. Several explanations for the salting-out capacity of salts have been suggested in the literature, the principal of which is that the hydration of a salt diminishes the amount of unbound water, with the hydration of the organic substance, and, as consequence, its solubility in water, decreasing. This capacity of the ions of a salting-out agent is associated with their radii. Ions with a small radius have a large charge density and are better hydrated. The salting-out capacity of a salt is an additive sum of the effects of cations and anions, with anions having a higher salting-out capacity than cations, all other conditions being the same. This ability of ions of a dissolved salt to interact with water molecules of a solution is quantitatively characterized by the number of water

Table 2. Characteristics of concentration of BA, BAc, and AA from water

Solvent	Degree of extraction into distillate, rel %			Loss in evaporation, rel %		
	BAc	BA	AA	BAc	BA	AA
Methanol	None	99.8	30.5	–	–	–
Acetone		95–98		≤5	≤1	1–2
Ethanol		95–98		40–50	1–2	≤5
				With polyethylene glycol		
				≤5	≤1	1–2

molecules bound to the ion, or by the hydration number. Salts with small ions with a large charge, e.g., aluminum and iron salts, are stronger salting-out agents, but they are not easily available [5, 6]. In this case, a 95–98% extraction of components and the maximum concentration coefficient (100) are achieved (Table 2). However, analysis for BA, BAc, and AA at their concentrations in water in the range 0.5–10 MPC requires higher concentration coefficients.

To raise the concentration coefficients, we used a simple procedure of evaporation of organic solvents containing impurities. In some cases, evaporation results in loss of compounds with boiling points 30–50°C higher than that of the solvent (BA, AA) or in those with a high vapor pressure (BAc). To decrease the concentration loss, the alcohol distillate was evaporated using a Kuderny–Danishe evaporator, to which a refluxer was connected in series [7, 8]. The loss of BA in this evaporation process was the largest (Table 2), which is due to its volatility. In addition, the water–alcohol azeotrope (bp 78.4°C) is subject to evaporation together with the impurities and is distilled-off. Because BA is virtually insoluble in water, it is displaced from water and carried away by the alcohol vapor.

To diminish the BA loss in alcohol evaporation, ethanol was replaced with solvents having lower boiling points and forming no azeotropes with water (acetone and methanol). A single run was carried out with methanol, with a 100-fold concentration followed by evaporation. An analysis of the evaporated alcohol distillate demonstrated that virtually the whole amount of BA (99.8%) and 30.5% of AA were preserved, with BAc absent. This result can be accounted for by the possibility of transesterification of BAc into methyl acrylate (MAc) in an acid medium, with simultaneous esterification of AA and methyl alcohol, which also yields MAc. Because the boiling point of MAc (80.5°C) and its concentration are low, its peak in a chromatogram may be masked by that of the solvent (methanol). It can be carried away, similarly to the volatile ester, by the alcohol vapor in distillation. This result and the high toxicity of methanol make inadvisable its use as a solvent.

Experiments with acetone demonstrated that, to provide a 95–98% extraction of BA, BAc, and AA, it is necessary to add this solvent to wastewater in a 1 : 6–1 : 8 ratio (maximum concentration coefficient is 8). This is due to the lower solubility of BA, BAc, and AA in acetone, compared with their unlimited solubility in ethanol. Evaporation of the acetone distillate shows satisfactory results, with the loss of BAc not exceeding 5%. However, the need to use order of magnitude larger amounts of acetone for the distillation and the following concentration of impurities, compared with that of alcohol, leads to a considerable increase in the process time and makes this method inefficient.

Thus, ethanol is the most effective in extraction of all the three impurities. To minimize the loss of the extracted impurities in evaporation of the alcohol distillate, we introduced an additional solvent or compounds that facilitate retention of the trace component in the solution in the evaporation of the main solvent. Difficultly volatile polar compounds are commonly used for this purpose, whose interaction with molecules of the compound being analyzed makes lower the equilibrium concentration of the components being determined in the solution, i.e., diminishes their partial vapor pressures. The vapor pressure of the additive itself should be sufficiently low [8]. As additives were used ethylene glycol and polyethylene glycol (PEG-M-1500 brand, molecular weight 1500), which, being polar compounds, also have a salting-out effect. The best result was provided by polyethylene glycol added in an amount of 0.025–0.05% to the alcohol distillate in evaporation in a Kuderny–Danishe evaporator and a refluxer, with the loss of BAc not exceeding 5%.

To simplify measurements of the concentrate volume in evaporation of the alcohol distillate, we used

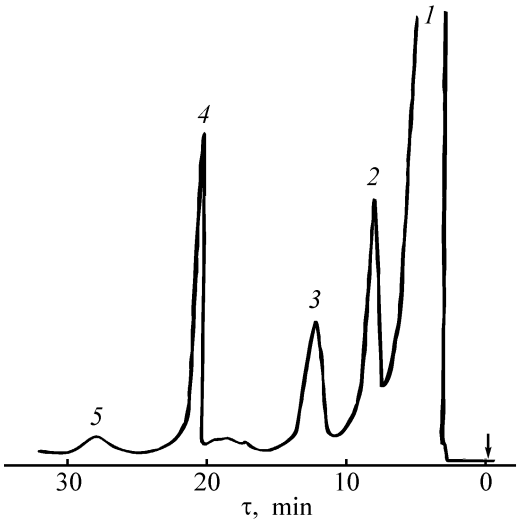

Chromatogram of impurities in wastewater from butyl acrylate production shops. (*1*) Ethanol (solvent), (*2*) BA, (*3*) BAc, (*4*) AA, and (*5*) butyl-β-butoxy propionate. (τ) Time.

graduated volumetric tubes or flasks with a volumetric finger-like arm of certain, calibrated volume. The concentration coefficient was calculated as the ratio of the volume of the initial wastewater, V_{ww}, to the that of the concentrate, V_c. The total time of concentration did not exceed 2 h.

The procedure we suggested was tested with real wastewater samples from butyl acrylate production shops (see figure).

CONCLUSIONS

(1) The procedure developed involves extraction of butanol, butyl acrylate, and acrylic acid from water by joint distillation with ethanol added to water being water in a 1 : 50–1 : 100 ratio.

(2) The procedure developed provides a 1000-fold concentration of butanol, butyl acrylate, and acrylic acid for gas-chromatographic determination in the range 0.5–10 MPC.

(3) The concentration coefficient is 500–1000.

REFERENCES

1. *Metodicheskie ukazaniya po vnedreniyu sanitarnykh pravil i norm SanPin 2.14.559–96* (Methodological Instructions on Introduction of Sanitary Rules and Regulations SanPin 2.14.559–96), Moscow: Goskomsanepidnadzor Rossii, 1977.
2. Baksanova, L.E., Val'tsifer, V.A., Budnikov, V.I., et al., *Zh. Anal. Khim.*, 2003, vol. 61, no. 1, pp. 78–82.
3. Baksanova, L.E., Val'tsifer, V.A., Budnikov, V.I., and Kondrashova, N.B., et al., *Zh. Prikl. Khim.*, 2002, vol. 75, no. 9, pp. 1459–1961.
4. Beyermann, K., *Organic Trace Analysis*, Translated Ed. R.A. Chalmers, Chichester: Ellis Horwood, 1984.
5. Korenman, I.M., *Ekstraktsiya v analize organicheskikh veshchestv* (Extraction in Analysis of Organic Substances), Moscow: Khimiya, 1974.
6. Sergeeva, V.F., *Usp. Khim.*, 1965, vol. 34, no. 4, pp. 717–732.
7. Leite, V., *Determination of Organic Contaminants in Potable Water, Natural Water, and Wastewater*, Moscow: Khimiya, 1975. [Russian Translation].
8. *Kontsentrirovanie sledov organicheskikh soedinenii: Sbornik nauchnykh trudov* (Concentration of Trace Amounts of Organic Compounds: Coll. of Sci. Works), Kuz'min, N.M., Ed., Moscow: Nauka, 1990.

ISSN 1070-4272, Russian Journal of Applied Chemistry, 2007, Vol. 80, No. 4, pp. 586–590. © Pleiades Publishing, Ltd., 2007.
Original Russian Text © S.A. Tsarenko, V.M. Kochkodan, N.G. Potapchenko, V.N. Kosinova, V.V. Goncharuk, 2007, published in Zhurnal Prikladnoi Khimii, 2007, Vol. 80, No. 4, pp. 600–604.

ENVIRONMENTAL PROBLEMS OF CHEMISTRY AND TECHNOLOGY

Use of Titanium Dioxide for Surface Modification of Polymeric Membranes to Diminish Their Biological Contamination

S. A. Tsarenko, V. M. Kochkodan, N. G. Potapchenko, V. N. Kosinova, and V. V. Goncharuk

Dumanskii Institute of Colloid and Water Chemistry, National Academy of Sciences of Ukraine, Kiev, Ukraine

Received November 30, 2006

Abstract—Adhesion of microorganisms to the surface of polymeric membranes and the efficiency of modification of the membrane surface by deposition of titanium dioxide to diminish biological overgrowth were studied.

DOI: 10.1134/S1070427207040131

Use of membrane techniques in water purification [1] involves a number of problems associated with accumulation of various substances (organic, inorganic, colloid, or suspended particles) or microorganisms on their surface. The contamination of membranes with microorganisms and products of their life activity leads to biological overgrowth (colonization of the membrane surface and formation of a biological film) [2]. Microorganisms can rapidly manyfold increase in abundance under favorable conditions, which makes the problem in question even more severe [3].

The process of biological overgrowth is primarily governed by the adhesion of microorganisms to the membrane surface. The key role is played by charges of the surface of microorganisms and functional groups of the working layer of a membrane; at opposite charges the electrostatic attraction makes the adhesion stronger.

To solve the biological contamination problem, thermal or chemical methods for disinfection of membranes can be used, but they failed to find wide application. For the thermal methods, the reason was that the thermal stability of most of the commercial brands of polymeric back-osmosis, ultra-, and nanofiltration membranes is low. In turn, use of chemical disinfectants, which are for the most part toxic and corrosive, changes the barrier layer of membranes and thereby impairs their selectivity [4].

Another approach to the problem of biological contamination of membranes consists in modification of their surface [4, 5] to improve their biological resistance [6] or in deposition of biocide substances, which exert by themselves or under the action of additional factors a disinfecting influence [7, 8]. As a rule, organic substances with a bactericide effect are used as modifying agents.

This paper reports on a study of the adhesion of various kinds of microorganisms to the surface of polymeric membranes of varied nature. Particular attention was given to the decrease in the membrane throughput upon adhesion of microorganisms and to analysis of the disinfecting action of a finely dispersed powder of titanium dioxide deposited onto the membrane surface, under exposure to UV light.

EXPERIMENTAL

Membranes of varied chemical nature: polysulfonic, PS-100H (Millipore) and 4F-PS-100H (Nadir); polysetersulfonic, P005F (Nadir); cellulose, C100F (Nadir); polyvinylidene fluoride, PVDF (Millipore); nylon, Nylon (Millipore); and cellulose acetate, MFA-Ma no. 3 (Vladipor).

The adhesion of microorganisms to the membranes was evaluated using a modified method [9, 10]. To obtain a comparatively size-uniform suspension of bacterial cells, cultures of one-day bacteria grown on a meat-peptone nutritive agar (NA) were placed in 3 cm^3 of a meat-peptone broth (MPB) and *Escherichia coli 1257* (*E. coli*) were cultivated at 37°C, and

Pseudomonas putida (*P. putida*) and *Acinetobacter calcoaceticus* (*A. calcoaceticus*), at 28°C for 24 h.

A 24-h-old broth culture was transferred into 200 cm^3 of MPB and grown at an appropriate temperature until the stationary growth phase commenced. After centrifugation at 2500 g for 10 min (K 26 D centrifuge), the cultures were three times washed with sterile distilled water and resuspended to a density of 10^8 CFU (colony-forming units) per cubic centimeter, as judged by the optical density measured on a KFK-2 photocolorimeter (λ = 540 nm, l = 0.5 cm). In filtration experiments, the initial suspension was diluted to a required density.

Membrane samples of area 1 cm^2 were submerged in 50 cm^3 of a bacterial suspension and kept for 4 h with agitation. When studying the effect of the time of contact on the number of adhered cells, membrane samples were removed from the suspension after a varied time of contact elapsed. The membrane samples removed from the suspension were two times washed, during 15 min, with 50 cm^3 of sterile distilled water on a rocker under mild agitation. Further, the membranes were placed in test tubes with 10 cm^3 of sterile distilled water and three specimens from each sample were treated with ultrasound for 15 min on a UM-4 installation, and three other speciments, shaken on a rocker for 15 min. The number of bacteria removed from the membrane in solution was calculated from the number of CFU on seeding *E. coli* on an *Endo's medium*, and other bacteria on a nutritive agar, and cultivation of *E. coli* at 37°C for 24 h and other bacteria at 28°C for 1–2 days. As the number of adhered bacteria on the membranes was taken the difference between the numbers of bacteria removed in ultrasonic treatment and in agitation.

To study the effect of biological overgrowth on the throughput of membranes, the *P. putida* microorganism was used as the test culture. River water preliminary inoculated with microorganisms was filtered across the membranes. The membranes were placed in Petri dishes and poured-over with sterile river water. After that the membranes were extracted from the solution at certain intervals of time and their throughput was measured. In parallel, the number of *P. putida* cells on the membrane surface was measured using the procedure described above. Additionally, a control run was performed without introduction of bacteria and with bacteria subjected to a lethal dose of UV irradiation (conditionally designated as "dead" bacteria). The extermination of microorganisms was effected by their exposure to light from an SVD-120A ultrahigh-pressure UV lamp (200–400 nm). The incident light power density was 1.89 W cm^{-2}, and the irradiation duration 0.5 h.

Membranes with bacteria were kept in river water or in a nutritive medium. The river water (Nivka river) had the following characteristics: color index 42–45°; content of phosphates, nitrates, and ammonium nitrogen 4–13, 0.5–0.7, and 0.12–0.3 mg dm^{-3}. The synthetic nutritive medium for *P. putida* contained (g dm^{-3}): glucose 3, NH_4Cl 1, KH_2PO_4 2.77, $Na_2HPO_4 \cdot 2H_2O$ 3.49; and 1 cm^3 dm^{-3} of a microelement solution; pH 6.8 [11]. The bacteria attached to the membranes under study were shaken-off by ultrasonic treatment for 15 min on a UM-4 installation.

To obtain modified samples, a PS-100H (Millipore) membrane was preliminarily kept in a suspension of titanium dioxide until its particles were deposited on the membrane surface. A TiO_2 suspension (Sigma-Aldrich, 5 μm) with a concentration of 2 g dm^{-3} was used. After the membrane surface was covered with titanium dioxide particles, a suspension of *P. putida* microorganisms (1.6×10^4 CFU cm^{-3}) was passed across the membrane. Membranes with and without deposited TiO_2 with living cells on their surface were irradiated with an SVD-120A UV lamp with UFS 6-3 and BS-7 light filters to select the wavelength of 365 nm. The irradiation power density was 153 μW cm^{-2}. For control, some of the membranes were not subjected to irradiation.

The number of *P. putida* colonies on the surface of control membranes and membranes subjected to irradiation was determined. When measuring the time dependence of the membrane throughput, samples were daily irradiated for 4 h, using the light filters mentioned above. The throughput of the membrane samples was measured every 24 h.

To photograph membranes with microorganisms, a TiO_2 powder was deposited on the surface of some of the membranes, with the surface of the rest of the membranes (control samples) remaining clean. *P. putida* suspensions with initial concentrations of 10 and 10^2 CFU cm^{-3} were passed across all the membranes. After that the membranes were irradiated with UV light for 4 h. Then the membranes were placed on NA and kept there until visible colonies were formed on their surface. The colonies were stained dark blue with a reagent used to stain oxidase-positive bacteria (dimethyl-*n*-phenylenediamine) [12]. The stained preparations were photographed with a digital camera.

In a study of the adhesion, the maximum time of contact was 4 h, and the concentration of bacteria in the suspension, $(1–6) \times 10^8$ CFU cm^{-3}. As can be seen

in Fig. 1, the test cultures studied can be arranged in order of increasing capacity for attachment to the MFA-Ma no. 3 and C100F membranes as follows: *E. coli* < *A. calcoaceticus* < *P. putida*. With respect to the P005F membrane, *A. calcoaceticus* and *P. putida* have approximately the same adhesion capacity. However, *P. putida* attached to the 4F-PS-100H membrane to a lesser extent than *A. calcoaceticus*, which adhered to this membrane and P005F in approximately equal amounts. *E. coli* bacteria exhibited the lowest adhesion capacity among the test cultured studied to all the membranes. Presumably, this is due to dissimilarities in the hydrophilic-hydrophobic nature of the surface between different bacteria. *P. putida* has a comparatively large wetting angle (38.5°), which indicates that the surface of its cells is hydrophobic. At the same time, this parameter varies for *E. coli* (different strains) within the range 16.7–24.7° [13]. With another method used to measure the hydrophobicity, from the adsorption of bacterial cells on the surface of a hydrophobic liquid (e.g., hexadecane), the K-12 strain of *E. coli* has a zero hydrophobicity index, and the *A. calcoaceticus* microorganism, 91.1% [13].

These data indicate that the capacity of cells for adhesion to the surface grows as the hydrophobicity of the cell surface becomes stronger. Because *P. putida* more widely occurs in natural water than *A. calcoaceticus*, just the former microorganism was used in further studies.

It was found in a study of the biological overgrowth of membranes by *P. putida* that the throughput of the membranes depends on the presence and state of bacteria on their surface. The most pronounced drop in throughput was observed for membranes with living cells (85% in 7 days); with dead bacteria present on the membrane surface, the drop was by 69%. The throughput of membranes that had no microorganisms on their surface decreased by 60% (Fig. 2).

The significant drop in the throughput of the membranes with living cells is due to an increase in the concentration of microorganisms and formation of various life-activity by-products. The change in the throughput of membranes without microorganisms points to a possible colonization of the membrane surface by other microorganism species coming from the environment. A layer of dead cells gave rise to an additional hydrodynamic resistance to the flow of water, which also adversely affected the throughput of membranes on which dead cells were deposited.

As can be seen in Fig. 3, filtration of water containing *P. putida* across membrane samples leads to a significant biological overgrowth of the surface

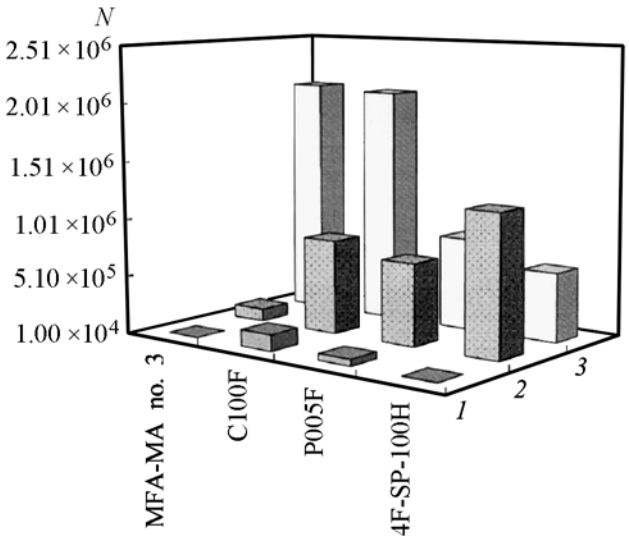

Fig. 1. Adhesion of test microorganisms to various membranes. Suspension density 1×10^8 CFU cm^{-3}, time of contact 4 h. (*N*) Number of bacteria per 1 cm^2 of membrane surface. (*1*) *E. coli*, (*2*) *A. calcoaceticus*, and (*3*) *P. putida*.

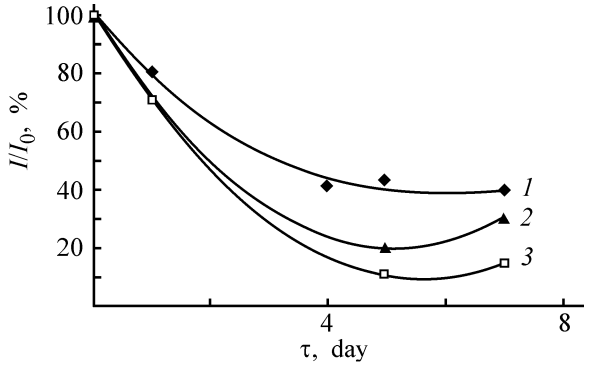

Fig. 2. Throughput of Nylon membranes covered with *P. putida* in contact with river water. (I/I_0) Relative throughput and (τ) process duration. Membrane: (*1*) without cells, (*2*) with dead cells, and (*3*) with living cells.

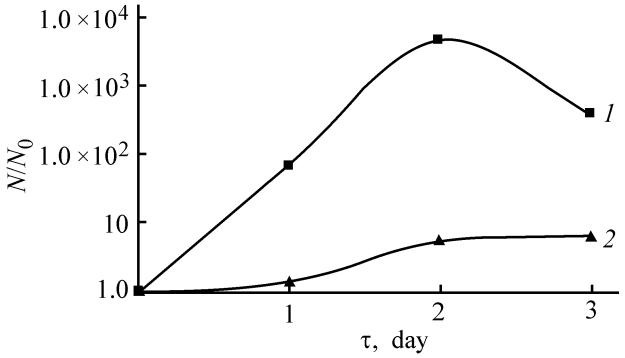

Fig. 3. Concentration of *P. putida* cells on (*1*) PVDF and (*2*) Nylon membranes vs. time τ of contact with river water. (N/N_0) Relative number of cells.

by these microorganisms. For example, the concentration of bacteria on Nylon and PVDF membranes increased in 3 days from 8.8×10^5 to 5.8×10^6 and from 1.4×10^4 to 5.5×10^6 CFU/membrane, respectively. These data indicate that the PVDF membrane is more susceptible to biological contamination than the Nylon membrane. As is known [14], the polyvinylidene fluoride membrane PVDF has a high hydrophobicity, in contrast to the Nylon membrane, which is more hydrophilic. The surface of a *P. putida* cell is also rather hydrophobic. Apparently, it is the hydrophobic interactions between the membrane and a cell that favor an increased adhesion of the microorganisms to the surface of the PVDF membrane.

To preclude biological overgrowth of membranes, experiments with deposition of a titanium dioxide powder on the surface were carried out. As can be seen in Fig. 4 (curves *1–3*), deposition of TiO_2 onto membrane samples without subsequent irradiation or irradiation of the initial membrane samples without deposition of TiO_2 on their surface has virtually no effect on the throughput of membranes. By contrast, a significant increase in the throughput was observed for membrane samples with deposited TiO_2 upon UV irradiation (Fig. 4, curve *4*). In particular, the throughput of modified irradiated membranes was 1.7–2 and 1.9–2.3 times higher in 1 and 2 days, respectively, than that of the other membranes. This is due to a significant decrease in the concentration of *P. putida* bacteria on the surface of membranes with TiO_2 upon UV irradiation: from 7.0×10^4 to 1.3×10^2 CFU/membrane in 4 days (Fig. 5). At the same time, the concentration of cells on the surface of other membranes remained virtually unchanged. These results indicate that the surface of modified membranes exhibits strong bactericide properties (the loss of microorganisms is about 99.8%).

The most vulnerable, to the biocide effect of substances, parts of bacterial cells are the cell wall, cytoplasmatic membrane, and cytoplasm [15]. Presumably, the mechanism of the bactericide action of TiO_2 under UV irradiation consists in the following. TiO_2 is excited by UV light and, as a result, electrons are generated in the conduction band, and holes, in the valence band. In the presence of water molecules, $OH^{\cdot}$, $O_2^{\cdot}$, and $HO_2^{\cdot}$ radicals are formed in the system [16]. Hydrophobic interactions and presence of a cell charge favor adhesion of bacterial cells to TiO_2 particles and enable active oxygen-containing radicals to reach the cell wall and to interact with it. Thus, the cell membrane is damaged in the presence of TiO_2 and the wall of the cell is disintegrated, which leads to its extinction [16].

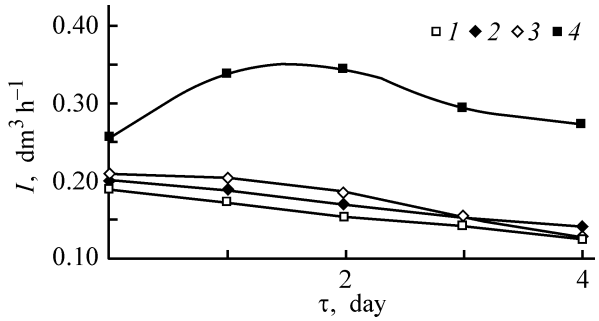

Fig. 4. Throughput *I* of PSSS-100H membrane samples with *P. putida* deposited on their surface vs. the time τ of contact with river water (ΔP = 0.3 MPa). Membrane samples: (*1*) without TiO_2 in the dark, (*2*) with TiO_2 in the dark, (*3*) without TiO_2 with UV, and (*4*) with TiO_2 with UV; the same for Fig. 5.

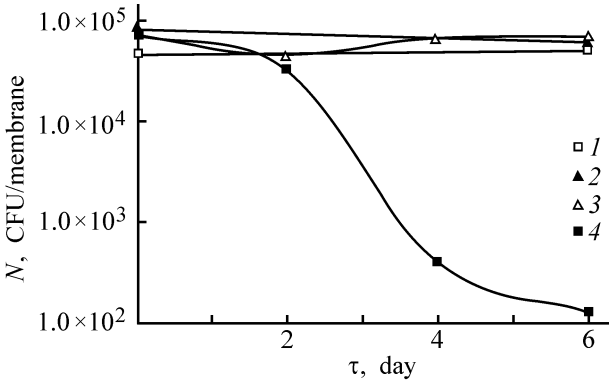

Fig. 5. Effect of TiO_2 deposition and UV irradiation on the concentration of *P. putida* cells on the PS-100H membrane. (*N*) Concentration of *P. putida* and (τ) process duration.

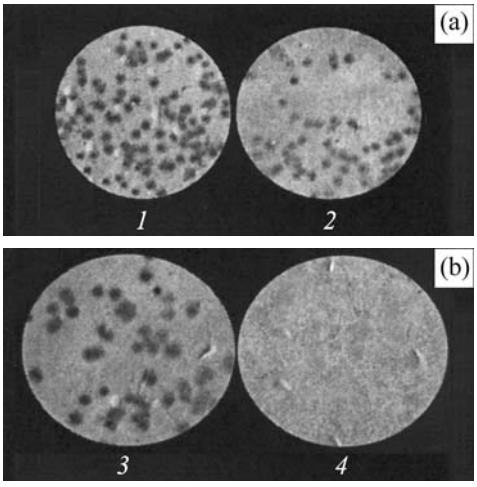

Fig. 6. Photograph of the surface of (*1*, *3*) initial PS-100H membrane and (*2*, *4*) its samples after deposition of TiO_2. *P. putida* suspensions with initial concentrations of (a) 10^2 and (b) 10 CFU cm^{-3} was filtered across the membranes, the samples were irradiated with UV light for 4 h.

Photographs of the surface of membranes across which *P. putida* suspensions with concentrations of 10^2 (Fig. 6a) and 10 CFU cm^{-3} (Fig. 6b) were passed demonstrate the efficiency of surface modification of polymeric membranes with a finely dispersed titanium dioxide powder. In each pair of samples, one membrane was covered with TiO_2 and irradiated with UV light for 4 h, and the other remained unchanged. The difference in the number of colonies on modified and untreated membranes is well noticeable even under visual inspection.

A calculation of the number of colonies gave the following values (FCU/membrane): (a) initial membrane 85, irradiated sample with TiO_2 43; (b) initial membrane 37, irradiated sample with TiO_2 0. Thus, in the case of filtration across membranes of a suspension of *P. putida* with an initial concentration of 10^2 CFU cm^{-3}, the number of bacteria on the membrane decreased because of the bactericide effect of TiO_2 and UV irradiation by 49.4%; at a concentration of 10 CFU cm^{-3}, the decrease was by 100%.

CONCLUSIONS

(1) The tendency of microorganisms to adhere to the surface of membranes becomes more pronounced as the hydrophobicity of the cell surface increases. In particular, the comparatively hydrophilic cells of *E. coli* show a considerably lower adhesion, compared with the more hydrophobic *A. calcoaceticus* and *P. putida*.

(2) The throughput of membranes with microorganisms deposited on their surface decreases in the course of their contact with river water because of the biological overgrowth of the membranes.

(3) Upon deposition of a finely dispersed TiO_2 powder and UV irradiation, the number of microorganisms on the membrane surface markedly decreases and the throughput of the thus treated membrane samples considerably increases, which indicates that the method described can be used to modify the surface of membranes to diminish their biological contamination.

ACKNOWLEDGMENTS

The authors thank A.O. Samsoni-Todorova (Institute of Colloid and Water Chemistry, National Academy of Sciences of Ukraine) for providing an SVD-120A UV lamp and UFS 6-3 and BS-7 light filters, and for measuring the intensity of light.

REFERENCES

1. Mulder M., *Basic Principles of Membrane Technology*, Dordrecht: Kluwer, 1991.
2. Vrouwenvelder, H.S., van Paassen, J.A.M., Folmer, H.C., et al., *Desalination*, 1998, vol. 118, pp. 157–166.
3. Kochkodan, V.M., Hilal, N., Goncharuk, V.V., et al., *Kolloid. Zh.*, 2006, vol. 68, no. 3, pp. 26–33.
4. Pieracci, J., Crivello, J.V., and Belfort, G., *J. Membr. Sci.*, 2002, vol. 202, pp. 1–16.
5. Hilal, N., Al-Khatib, L., Atkin, B.P., et al., *Desalination*, 2003, vol. 158, pp. 65–72.
6. Belfer, S., Gitron, J., Purinson, Y., et al., *Desalination*, 2001, vol. 139, pp. 169–176.
7. Leeming, K., Moore, C.P., and Denyer, S.P., *Int. Biodeter. Biodegrad.*, 2002, vol. 49, pp. 39–43.
8. Flemming, H.-C., *Experim. Therm. Fluid Sci.*, 1997, vol. 14, no. 4, pp. 382–391.
9. Ridgway, M.G. and Argo, D.G., *JAWWA*, 1985, no. 7, pp. 97–106.
10. Ridgway, H.F., Juctice, C.A., Whittaker, C., et al., *JAWWA*, 1984, no. 6, pp. 94–102.
11. *Manual of Methods for General Bacteriology*, Gerhardt, P., Ed., Washington: American Society for Microbiology, 1981.
12. *Enterobakterii* (Enterobacteria), Pokrovskii, V.I., Ed., Moscow: Meditsina, 1985.
13. Stebnikova, E.V., Gordienko, A.S., and Ivanova, V.N., *Vzaimodeistvie kletok s poverkhnost'yu razdela zhidkost'–gaz* (Interaction of Cells with the Liquid–Gas Interface), Kiev: Naukova Dumka, 1991.
14. Cornelissen, E.R., van den Boomgaard, Th., and Strathmann, H., *Colloids Surf. A, Physicochem. Eng. Aspects*, 1998, vol. 138, p. 283.
15. Denyer, S.P. and Stewart, G.S.A.B., *Int. Biodeter. Biodegrad.*, 1998, vol. 41, pp. 261–268.
16. Salih, F.M., *J. Appl. Microbiology*, 2002, vol. 92, pp. 920–926.

ISSN 1070-4272, Russian Journal of Applied Chemistry, 2007, Vol. 80, No. 4, pp. 591–594. © Pleiades Publishing, Ltd., 2007.
Original Russian Text © A.A. Gaile, G.D. Zalishchevskii, A.S. Erzhenkov, E.A. Kayfadzhyan, L.L. Koldobskaya, 2007, published in Zhurnal Prikladnoi Khimii, 2007, Vol. 80, No. 4, pp. 605–607.

PROCESSES AND EQUIPMENT OF CHEMICAL INDUSTRY

Extraction of Aromatic Hydrocarbons from Reformates with Mixtures of Triethylene Glycol and Sulfolane

A. A. Gaile, G. D. Zalishchevskii, A. S. Erzhenkov, E. A. Kayfadzhyan, and L. L. Koldobskaya

St. Petersburg State Technological Institute, St. Petersburg, Russia

OOO "Pa Kirishinefteorgsintez," Kirishi, Leningrad oblast, Russia

Received June 13, 2006

Abstract—Results are presented of a seven-stage counterflow extraction of C_6–C_8 aromatic hydrocarbons from the reformate of the gasoline fraction with a mixed extracting agent composed of triethylene glycol, sulfolane, and water, containing 37.6–57.6 wt % sulfolane.

DOI: 10.1134/S1070427207040143

A process for extraction of aromatic hydrocarbons from the reformate of the 62–105°C fraction with a mixed extractive agent composed of triethylene glycol (TEG) and sulfolane has been developed at St. Petersburg State Technological Institute in cooperation with OOO "Pa Kirishinefteorgsintez" [1–4]. The process developed was implemented on an LG-35-8/300B installation [5].

The use of a mixed selective solvent containing 15 wt % sulfolane, instead of aqueous TEG, made it possible to reduce the ratio of the extracting agent and recycle to the feed by 20% or, in another operation mode, raise the degree of recovery of arenes by 2.1%. In 2002, the use of the mixed extracting agent allowed additional isolation of 2.2 thousand tons of arenes, with an economic effect of about 18 million roubles, resulting from additional sales of products and a decrease in the energy expenditure [6].

With the content of sulfolane in the mixed extractive agent further raised to 25–30 wt %, it became possible, as a result of a decrease in the necessary ratio of the extractive agent to the feed, to use an additional source of raw material for the extracting unit, a part of the prexylene fraction from the installation for total xylenes, with recovery of an additional amount of toluene and benzene. The resulting economic effect obtained by OOO "Pa Kirishinefteorgsintez" was 34 million roubles in 2004 and 32.6 million roubles in the first eight months of 2005 [7].

Transfer of the installation from operation with a mixed solvent to that with pure sulfolane would require a substantial reconstruction of the extracting unit, which is due to the need to regenerate sulfolane from the extract phase by vacuum distillation, with the diameter of the stripping tower increasing.

The aim of this study was to determine the optimal conditions of extraction of C_6–C_8 arenes from the reformate with TEG–sulfolane mixtures containing 37.6–57.6 wt % sulfolane. The increased content of sulfolane in the mixed selective solvent should lead to an increase in its selectivity and dissolving power with respect to arenes and to the resulting possible decrease in the ratios of both the extractive agent and the recycle to the feed of extractor. Further decrease in the expenditure of the recycle and in the total flows in the extractor seems to be possible on replacing the recycle containing C_6–C_8 hydrocarbons with the pentane recycle. Because of the increased solubility of pentane in polar solvents, compared with C_6–C_8, the content of these alkanes in the extract phase should decrease. In addition, the higher relative volatility coefficients of pentane, with respect to benzene and toluene, will lead to a decrease in the content of these aromatic hydrocarbons in the recycle, which will also make lower the recycle expenditure and will improve the throughput of the extractor in terms of the raw material.

Table 1. Parameters of the raw material (reformate) and recycle from the LG-35-8/300B installation

Parameter	Reformate	Recycle
Standard distillation, °C:		
IBP	60	70
10%	69	75
20%	75	78
30%	79	80
40%	81	81
50%	83	83
60%	86	84
70%	90	86
80%	98	90
90%	107	98
FBP	123	120
Refractive index at 20°C	1.4251	1.4887
Density at 20°C, g cm^{-3}	0.736	0.833
Arenes, wt %, including:	37.6	84.9
benzene	20.6	66.6
toluene	16.5	18.3
xylenes	0.5	–

Table 2. Experimental conditions of seven-stage counterflow extraction of arenes from the reformate

Parameter	Run no.			
	1	2	3	4*
Temperature, °C	50	50	50	30
Composition of the extractive agent, wt %:				
sulfolane	37.6	47.7	57.6	57.6
TEG	56.4	47.7	38.4	38.4
water	6.0	4.6	4.0	4.0
Mass ratio: extractive agent : feed	4 : 1	3.5 : 1	3 : 1	3 : 1
recycle : feed	0.35 : 1	0.3 : 1	0.3 : 1	0.23 : 1

* A 65 : 35 (wt %) pentane–benzene mixture was used in run no. 4 as a recycle.

EXPERIMENTAL

A reformate sample from the LG-35-8/300B installation at OOO "Pa Kirishinefteorgsintez," combine with the prexylene fraction from the installation of total xylenes. The reformate is characterized in Table 1. The same table lists parameters of a factory sample of the recycle: recirculating flow returned into the extractor, in which saturated hydrocarbons remaining in the extract phase are concentrated.

The recycle contains a large amount of benzene, with toluene also present. The fact that even toluene finds its way into the recycle is due to a single-stage equilibrium in the single-evaporation chamber and to the low relative volatility coefficients of saturated hydrocarbons C_7–C_8, with respect to toluene, in the presence of a mixed TEG–sulfolane extractive agent.

The multistage extraction was performed in a set of thermostated separating funnels by the scheme of a counterflow process simulating the operation of the extraction column [9] (see Table 2).

The composition of the equilibrium phases was analyzed by means of gas-liquid chromatography using as fixed phases polyphenyl methyl siloxane and Carbowax-20M on a Chromaton-N-AW-HMDS inert solid support.

The raffinate phase was washed with water to complete removal of admixtures of selective solvents. The recycle was evaporated by rectification of the extract phase on a column with an efficiency of 15 theoretical plates, and then the aromatic extract was obtained by distillation with steam.

The parameters of the raffinates and extracts obtained are listed in Table 3, and the degrees of recovery of arenes, in Table 4.

As follows from the data in Tables 3 and 4 and previously published results [5], raising the content of sulfolane in the mixed extractive agent from 15 to 57.6 wt % makes it possible to reduce the mass ratio of the extractive agent to feed from 6.5 : 1 to 3 : 1, i.e., by more than a factor of 2 at a close degree of recovery and quality of aromatic hydrocarbons. The increased content of sulfolane (selective solvent with a high dissolving power and viscosity lower than that of TEG) makes it possible to lower the temperature of the extraction process, which leads to an additional increase in the separation selectivity and reduction of the recycle expenditure.

Use of a pentane recycle (run no. 4), instead of C_6–C_8 hydrocarbons results in that toluene is excluded from its composition and the recycle contains a con-

Table 3. Parameters of the raffinates and extracts obtained in run nos. 1–4

Parameter	Run no.							
	1		2		3		4	
	raffinate	extract	raffinate	extract	raffinate	extract	raffinate	extract
Yield, wt %	63.4	36.6	63.5	36.5	63.3	36.7	63.4	36.6
Arenes, wt %, including:	1.70	99.9	1.73	99.86	1.63	99.69	1.76	99.70
benzene	0.33	55.8	0.35	55.76	0.33	55.59	0.39	55.62
toluene	1.31	42.8	1.32	42.85	1.25	42.82	1.31	42.82
xylenes	0.06	1.3	0.06	1.23	0.05	1.28	0.06	1.26

Table 4. Degree of recovery of arenes in run nos. 1–4

Parameter	Run no.			
	1	2	3	4
Degree of recovery of arenes, wt %, including:	97.1	97.1	97.2	97.0
benzene	99.0	98.9	99.0	98.8
toluene	95.0	94.8	95.2	94.9
xylenes	92.0	90.0	93.7	92.0

siderably smaller amount of benzene, 15–30 wt %. The expenditure of the recycle decreases in this case to 23 wt % relative to the feed.

The considerable reduction of the recirculating flows of a mixed extracting agent with increased content of sulfolane and of the recycle makes it possible to improve the output capacity of the existing extractors in terms of the raw material. As an additional source of feed for the extractor of LG-35-8/300B installations can serve not only the prexylene fraction from the installation for total xylenes, but also the benzene fraction of the reformate of the broad gasoline fraction, which will solve the topical ecological problem of reducing the content of benzene in automotive gasolines.

Use of a mixed TEG–sulfolane–water extractive agent with increased content of sulfolane, instead of a switchover of the installation to pure sulfolane as selective solvent, does not require any significant reconstruction of the existing installations. The stripping of the extract to remove the mixed extractive agent does not require vacuum distillation, which is due to the absence of strong intermolecular interactions in the TEG–sulfolane system [2]. The weak hydrogen bonds in this system are due to the low basicity of sulfolane, compared with sulfoxides, amines, ketones, and amides [10]. In accordance with the conditions for azeotrope formation [11], the close saturated vapor pressures of TEG and sulfolane and positive deviations from Raoult law for the TEG–sulfolane system lead to formation of an azeotropic mixture with the minimum boiling point, which facilitates the regeneration of the mixed extractive agent.

CONCLUSIONS

(1) Raising the content of sulfolane in the mixed extractive agent composed of triethylene glycol and sulfolane from 15 to 57 wt % makes it possible to reduce the mass ratio of the extractive agent to the raw material by more than a factor of 2 and the expenditure of the recycle from 80–100 to 30 wt % relative to the raw material.

(2) Use of a pentane recycle instead of C_6–C_8 hydrocarbons results in that toluene is excluded from its composition, the content of benzene in the recycle

becomes considerably lower, and the expenditure of the recycle additionally decreases.

REFERENCES

1. Marusina, N.B., Gaile, A.A., and Semenov, L.V., *Zh. Prikl. Khim.*, 1994, vol. 67, no. 8, pp. 1311–1315.
2. Marusina, N.B., Gaile, A.A., and Semenov, L.V., *Zh. Prikl. Khim.*, 1996, vol. 69, no. 7, pp. 1163–1169.
3. RF Patent 2 127 718.
4. RF Patent 2 177 023.
5. Gaile, A.A., Erzhenkov, A.S., Semenov, L.V., et al., *Zh. Prikl. Khim.*, 2001, vol. 74, no. 10, pp. 1618–1621.
6. Zalishchevskii, G.D., *Trudy Mezhdunarodnogo foruma "Toplivno-energeticheskii kompleks Rossii: regional'nye aspekty", SPb, 8–11 aprelya 2003 g.* (Proc. of Int. Forum "Fuel-Energetic Complex of Russia: Regional Aspects," St. Petersburg, April 8–11, 2003), St. Petersburg, 2003, pp. 122–123.
7. Zalishchevskii, G.D., Development and Improvement of Extraction Technologies for Separation of Oil Products, *Doctoral Dissertation*, St. Petersburg, 2006.
8. Gaile, A.A., Somov, V.E., Varshavskii, O.M., and Semenov, L.V., *Sul'folan: svoistva i primenenie v kachestve selektivnogo rastvoritelya* (Sulfolane: Properties and Use as Selective Solvent), St. Petersburg: Khimizdat, 1998.
9. Alders, L., *Liquid–Liquid Extraction. Theory and Laboratory Practice*, Amsterdam: Elsevier, 1959.
10. Pal'm, V.A., *Osnovy kolichestvennoi teorii organicheskikh reaktsii* (Fundamentals of a Quantitative Theory of Organic Reactions), Leningrad: Khimiya, 1977.
11. Kogan, V.B., *Azeotropnaya i ekstraktivnaya rektifikatsiya* (Azeotropic and Extractive Distillation), Leningrad: Khimiya, 1971.

ISSN 1070-4272, Russian Journal of Applied Chemistry, 2007, Vol. 80, No. 4, pp. 595–599. © Pleiades Publishing, Ltd., 2007.
Original Russian Text © A.A. Gaile, A.S. Erzhenkov, L.L. Koldobskaya, E.A. Kayfadzhyan, 2007, published in Zhurnal Prikladnoi Khimii, 2007, Vol. 80, No. 4, pp. 608–611.

PROCESSES AND EQUIPMENT OF CHEMICAL INDUSTRY

Extraction of Toluene and Xylenes from the Toluene–Xylene Fraction of the Reforming Catalyzate with Mixtures of Triethylene Glycol with Sulfolane

A. A. Gaile, A. S. Erzhenkov, L. L. Koldobskaya, and E. A. Kayfadzhyan

St. Petersburg State Technological Institute, St. Petersburg, Russia

OOO "PA Kirishinefteorgsintez," Kirishi, Leningrad oblast, Russia

Received July 5, 2006

Abstract—Seven-stage counterflow extraction of aromatic hydrocarbons from the toluene–xylene fraction of the reforming catalysate with sulfolane and its mixtures with triethylene glycol was studied. A liquid–liquid phase equilibrium diagram is presented for a pseudoternary system that includes saturated and aromatic hydrocarbons of the toluene–xylene fraction of the reformate and a mixed extractive agent composed of triethylene glycol, sulfolane, and water (48.1 : 48.1 : 3.8 wt %).

DOI: 10.1134/S1070427207040155

It has been suggested to use a mixed selective solvent composed of triethylene glycol, sulfolane, and water as an agent for extraction of arenes C_6–C_8 from the reformate of the 62–105°C fraction [1–4]. In 2000, this method for extraction of arenes was implemented on an LG-35-8/300B installation at OOO "PA Kirishinefteorgsintez" [5].

In view of modern ecological requirements to the quality of automotive gasolines, the maximum permissible content of benzene in the gasolines is limited by 1 vol % [6]. Benzene can be effectively removed from the benzene fraction of the reformate by extractive distillation. For example, an installation for extractive distillation with a Tectiv-100 mixed extractive agent composed of industrially available selective solvents [7] is to be constructed at OOO "PA Kirishinefteorgsintez" under license from Glitsch Technology Co. After the new installation is put in operation, the extracting unit of the working LG-35-8/300B installation can be used to obtain toluene and total xylenes. In doing so, there will be no need to change the technological scheme of the installation, provided that the TEG–sulfolane mixed extractive agent will be used.

However, the activity coefficients and critical solution temperatures (CST) of xylene isomers in polar solvents markedly exceed those for benzene. For example, a mixed TEG–sulfolane extractive agent of 70 : 30 wt % composition forms a homogeneous system with benzene at 25°C, the CST with toluene is 58.3°C and those with C_8 arenes are even higher [2]. Therefore, it is desirable to extract xylenes with a mixed solvent with higher dissolving power, increased content of sulfolane.

The aim of this study was to compare the efficiencies of extraction of arenes from the toluene–xylene fraction with mixed TEG–sulfolane–water solvents of various compositions.

EXPERIMENTAL

Stable reformates from the LG-35-8/300B and LCh-35-11/600 installations of catalytic reforming of the benzene–toluene and xylene fractions at OOO "PA Kirishinefteorgsintez" were used as the starting raw material. A benzene fraction with IBP 90°C was distilled-off on a rectification column with an efficiency of 15 theoretical plates in yield of 64.0 and 11.5 wt %, respectively.

Table 1. Characteristics of the raw material

Parameter	Combined toluene–xylene fraction
Standard distillation, °C:	
IBP	97
10%	115
20%	118
30%	120
40%	122
50%	123
60%	125
70%	128
80%	133
90%	140
95%	145
FBP (98%)	161
Refractive index at 20°C	1.4661
Density at 20°C, g cm^{-3}	0.810
Arenes, wt %,	70.39
including toluene	24.6
Σ C_8	43.87
Σ C_9	1.92

Table 2. Experimental conditions of extraction of arenes from the toluene–xylene fraction

Parameter	Run no.		
	1	2	3
Number of extraction stages	7	7	7
Extraction temperature, °C	60	60	50
Composition of the extractive agent, wt %:			
TEG	62.3	48.1	–
sulfolane	32.8	48.1	99.5
water	4.9	3.8	0.5
Mass ratio:			
extractive agent : feed	5.0 : 1	5.0 : 1	5.0 : 1
recycle : feed	0.5 : 1	0.3 : 1	0.3 : 1

Still bottoms containing no benzene according to chromatographic data were combined in accordance with the output capacity of the installations and yield of toluene–xylene fractions after rectification, i.e., in a 1 : 4.9 mass ratio.

The parameters of the combined toluene–xylene fraction are listed in Table 1.

Multistage counterflow extraction of arenes was performed with a mixed extractive agent in the presence of a recycle (recirculating hydrocarbon flow distilled-off from the extract phase) in a set of thermostated separating funnels by the classical scheme [8]. The conditions of the extraction experiments are listed in Table 2. In run no. 1, a TEG–sulfolane–water mixture circulating in the LG-35-8/300B installation was used as the extractive agent. An addition of technical-grade sulfolane to this extractive agent yielded a mixed selective solvent with equal contents of TEG and sulfolane, used in run no. 2. A technical-grade sulfolane containing 0.5 wt % water was used in run no. 3.

The composition of the equilibrium raffinate and extract phases was analyzed by GLC: Carbowax and PFMS-4 on a Chromaton-N-AW-HMDS solid support as fixed phases; 3-m-long chromatographic columns with inner diameter of 3 mm; carrier gas helium; temperature (°C): columns 70–190, evaporator 280, detector (katharometer) 250. The following calibration coefficients were used: saturated hydrocarbons 0.80, benzene 1.00, toluene 1.02, C_8 arenes 1.04, C_9 arenes 1.06, sulfolane 1.3, TEG 1.6.

The extractive agent was many times re-extracted from the raffinate phase with water. The recycle was evaporated from the extract phase on a rectification column with an efficiency of 15 theoretical plates and then the extract was isolated from the still bottoms by steam distillation.

Table 3 present as an example the material balance of extraction run no. 2, calculated using the yields of the raffinate and extract phases and their composition. The characteristics of the raffinates and extracts obtained are listed in Table 4.

The liquid–liquid equilibrium in the pseudoternary system constituted by saturated hydrocarbons, arenes from the toluene–xylene fraction of the reformate, and TEG–sulfolane–water mixed extractive agent (48.1 : 48.1 : 3.8 wt %) was examined at 60°C by an analytical method: single-stage extractions of arenes

Table 3. Material balance of run no. 3 (per 100 mass units of the feed)

Component	Input	Output	
		raffinate phase	extract phase
Raw material,	100		
including saturated hydrocarbons	29.61	29.53	15.08
toluene	24.6	0.59	39.01
Σ C_8	43.87	1.14	42.74
Σ C_9	1.92	0.09	1.83
Recycle,	30		
including saturated hydrocarbons	15		
toluene	15		
Mixed extractive agent	500	1.78	498.22
Total	630	33.12	596.88

Table 4. Characteristics of the raffinates and extracts obtained in extractive purification of the combined toluene–xylene fraction in run nos. 1–3

Parameters	Raffinate			Extract		
	1	2	3	1	2	3
Yield in terms of the feed, wt %	32.82	31.34	30.82	67.18	68.66	69.18
Saturated hydrocarbons, wt %	90.0	94.19	95.84	0.1	0.11	0.1
Arenes, wt %,	10.0	5.81	4.16	99.9	99.89	99.9
including toluene	2.60	1.88	1.11	35.35	35.00	35.06
Σ C_8	7.01	3.64	2.79	61.88	62.23	62.17
Σ C_9	0.39	0.29	0.26	2.66	2.66	2.66
Degree of recovery, wt %,	–	–	–	95.31	97.43	98.18
including toluene	–	–	–	96.54	97.60	98.62
Σ C_8	–	–	–	94.75	97.42	98.04
Σ C_9	–	–	–	93.20	95.31	95.83

Table 5. Ternary liquid–liquid equilibrium diagram for the system constituted by saturated hydrocarbons (1), aromatic hydrocarbons from the toluene–xylene fraction (2), and mixed extractive agent (3) under the conditions of run no. 2

Initial composition, wt %			Composition of the raffinate phase, wt %			Composition of the extract phase, wt %			c_{ar}, wt %		Degree of extraction of arenes, α, wt %	Distribution coefficient of arenes, K_d	Separation coefficient β
									in the raffinate	in the extract			
(1)	(2)	(3)	(1)	(2)	(3)	(1)	(2)	(3)					
26.2	62.3	11.5	Homogeneous region										
2.9	6.8	90.3	69.7	27.5	2.8	0.7	5.8	93.5	28.3	89.2	81.4	0.211	21.01
4.9	11.6	83.5	51.5	44.4	4.1	1.2	9.4	89.4	46.3	88.7	75.9	0.212	9.10
7.4	17.6	75.0	42.0	52.5	5.5	1.6	11.7	86.7	55.3	88.0	57.1	0.225	5.91
8.5	20.2	71.3	39.3	54.7	6.0	1.9	12.9	85.2	58.2	87.2	53.0	0.236	4.88
13.7	32.5	53.8	30.6	59.4	10.0	2.2	14.4	83.4	66.0	86.7	26.4	0.242	3.37

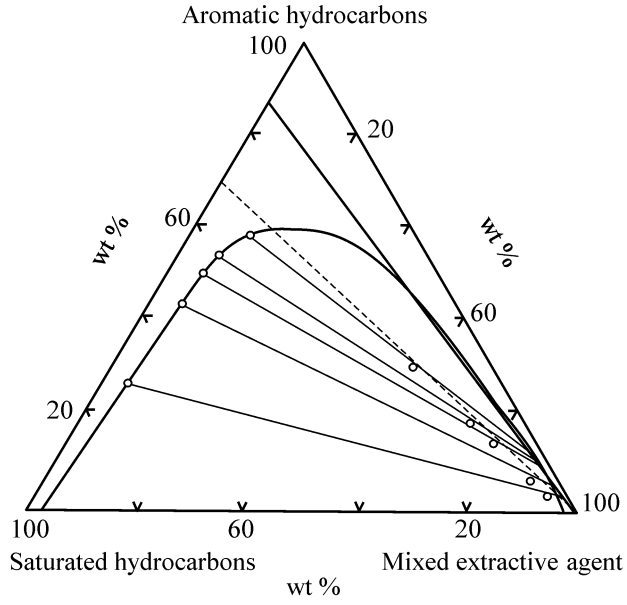

Liquid–liquid phase equilibrium diagram for a pseudo-ternary system constituted by saturated hydrocarbons, arenes from the toluene–xylene fraction of the reformate, and TEG–sulfolane–water mixed extractive agent (48.1 : 48.1 : 3.8 wt %) at 60°C.

were carried out in a hermetically sealed thermostated vessel with a magnetic rabble at various ratios between the extractive agent and feed (see figure, Table 5). Table 5 also lists the distribution coefficients of arenes, calculated as ratios of their concentrations in the extract and raffinate phases, and separation coefficients found as the ratio of the distribution coefficients of aromatic and saturated hydrocarbons.

The results of run no. 1 are inferior to the operation parameters of the LG-35-8/300B installation in extraction of arenes from the reformate of the 62–105°C fraction: the content of arenes in the raffinate is considerably higher, and the degree of extraction of toluene and xylene is lower. This occurs for the following reasons: the considerably higher content of arenes in the feed (>70 wt %); lower degree of extraction of toluene and xylenes, compared with benzene, in extraction with any extractive agent; and smaller ratio between the extractive agent and the combined reformate.

The best way to improve the degree of extraction of toluene and xylenes is to make higher the content of sulfolane in the mixed selective solvent.

Raising the sulfolane : TEG ratio in the mixed extracting agent from 34.5 : 65.5 wt % to 50 : 50 wt % at a smaller recycle : feed ratio and all other extraction conditions being the same makes it possible to reduce the content of arenes in the raffinate by a factor of 1.72 and to raise the degree of extraction by 2.1 wt %.

It follows from the phase equilibrium diagram that the maximum content of arenes in the extract, which can be achieved without use of the recycle at 60°C, is about 87 wt %. This value is in agreement with the material balance of run no. 2 (Table 3), according to which the content of arenes in seven-stage counterflow extraction, in terms of the hydrocarbon part of the extract phase, is as high as 85 wt %.

As demonstrated by capillary GLC, minor admixtures of saturated hydrocarbons, which remain in the extract after rectification removal of the recycle from the extract phase, are represented by octane and higher-boiling alkanes and cycloalkanes C_{8+}.

The extractive recovery of xylenes, used instead of the rectification method presently employed at OOO "PA Kirishinefteorgsintez," will extend the boiling limits of the raw material in catalytic reforming and raise the output of xylenes.

Even higher is the degree of extraction of arenes from the toluene–xylene fraction of the reformate in run no. 3, with sulfolane containing no TEG used as the extractive agent (Table 4). The overall degree of extraction of arenes increases by 0.75 wt %, compared with run no. 2. However, replacement of the mixed extractive agent with neat sulfolane would involve a substantial reconstruction of the extracting unit of the LG-35-8/300B installation because it would be necessary to create vacuum in the stripping column and to replace it with a larger-diameter column [9].

CONCLUSIONS

(1) Seven-stage counterflow extraction of arenes from the toluene–xylene fraction of the reformate with a mixed extractive agent composed of triethylene glycol, sulfolane, and water (48.1 : 48.1 : 3.8 wt %) at a 5 : 1 mass ratio between the extractive agent and the feed will provide a >97% degree of extraction of toluene and xylenes without reconstruction of the extracting unit of the working LG-35-8/300B installation.

(2) The maximum content of arenes in the extract, achieved in extraction from the toluene–xylene fraction of the reformate at 60°C with a mixed extractive agent of the composition specified, without use of the recycle, is as high as 87 wt %.

REFERENCES

1. Marusina, N.B., Gaile, A.A., and Semenov, L.V., *Zh. Prikl. Khim.*, 1994, vol. 67, no. 8, pp. 1311–1315.
2. Marusina, N.B., Gaile, A.A., and Semenov, L.V., *Zh. Prikl. Khim.*, 1996, vol. 69, no. 7, pp. 1163–1169.
3. RF Patent 2 127 718.
4. RF Patent 2 177 023.
5. Gaile, A.A., Erzhenkov, A.S., Semenov, L.V., et al., *Zh. Prikl. Khim.*, 2001, vol. 74, no. 10, pp. 1618–1621.
6. Kaminskii, E.F. and Khavkin, V.A., *Glubokaya pererabotka nefti: tekhnologicheskii i ekologicheskii aspekty* (Deep Processing of Oil: Technological and Ecological Aspects), Moscow: Tekhnika. OOO TUMA GRUPP, 2001.
7. Jentry, J.C., Kumar, C.S., Li, H.M., and Li, I.Kh., *Khim. Tekhnol. Topl. Masel*, 2003, nos. 1–2, pp. 12–17.
8. Alders, L., *Liquid–Liquid Extraction. Theory and Laboratory Practice*, Amsterdam: Elsevier, 1959.
9. Gaile, A.A., Somov, V.E., Varshavskii, O.M., and Semenov, L.V., *Sul'folan: svoistva i primenenie v kachestve selektivnogo rastvoritelya* (Sulfolane: Properties and Use as Selective Solvent), St. Petersburg: Khimizdat, 1998.

ISSN 1070-4272, Russian Journal of Applied Chemistry, 2007, Vol. 80, No. 4, pp. 600–604. © Pleiades Publishing, Ltd., 2007.
Original Russian Text © A.A. Gaile, A.S. Erzhenkov, E.A. Kayfadzhyan, L.L. Koldobskaya, 2007, published in Zhurnal Prikladnoi Khimii, 2007, Vol. 80, No. 4, pp. 612–616.

PROCESSES AND EQUIPMENT OF CHEMICAL INDUSTRY

Recovery of Arenes from the Reformate of Gasoline Fraction by Combined Method of Extraction and Azeotropic Distillation

A. A. Gaile, A. S. Erzhenkov, E. A. Kayfadzhyan, and L. L. Koldobskaya

St. Petersburg State Technological Institute, St. Petersburg, Russia
OOO "Pa Kirishinefteorgsintez," Kirishi, Leningrad oblast, Russia

Received July 5, 2006

Abstract—Recovery of arenes C_7–C_9 from the reformate of the gasoline fraction by a combined method was studied. The method consists in extraction with a mixed extractive agent composed of triethylene glycol, sulfolane, and water, followed by removal of saturated hydrocarbons from the extract phase by azeotropic distillation with ethanol.

DOI: 10.1134/S1070427207040167

In accordance with modern ecological requirements to the quality of automotive gasoline, the total content of aromatic hydrocarbons in the fuel should not exceed 30 vol %, and that of benzene, 1 vol % [1]. Previously, a combined method has been suggested for removal of excess benzene and its homologues from reformed gasoline by extraction with sulfolane, followed by removal of admixtures of nonaromatic hydrocarbons by extractive-azeotropic distillation with sulfolane and ethanol [2, 3]. As a result, a reformulated component of gasoline, which satisfies the requirements to the permissible content of benzene and total arenes, can be obtained. In this component, the decrease in the octane number is compensated for by the presence of a high-octane azeotrope-forming component, ethanol, which requires no regeneration. Simultaneously, commercial benzene, toluene, xylenes can be recovered with a low overall ratio of sulfolane to the feedstock in both stages of the process and, consequently, with a low specific energy expenditure.

To solve the priority problem, to diminish the benzene content of gasolines, it has been suggested to extract benzene from the benzene fraction of the reformate by extraction with sulfolane [4] or by extractive distillation with *N*-formylmorpholine [5]. It is planned by OOO "Pa Kirishinefteorgsintez" to extract benzene by extractive distillation with the use of a mixed selective solvent by the process developed by GTC Co. [6].

After a new installation for extractive distillation is put in operation, the already functioning LG-35-8/300B installation can be used for extractive lowering of the total content of arenes in automotive gasolines and simultaneous recovery of toluene and xylenes. OOO "Pa Kirishinefteorgsintez" employs a mixed extractive agent composed of triethylene glycol (TEG), sulfolane, and water is used for extraction of benzene and toluene. Therefore, it is appropriate to use the same extractive agent for extraction of arenes from a higher-boiling fraction of the reformate.

The aim of this study was to determine the efficiency of extractive removal of the excess amount of C_7–C_9 arenes from the reformed 95–180°C gasoline fraction with TEG–sulfolane–water mixtures with varied content of sulfolane, with the subsequent azeotropic distillation of the extract phase with ethanol.

EXPERIMENTAL

Reforming catalyzates produced in LG-35-8/300B, LCh-35-11/600, and LCh-35-11/1000 installation for catalytic reforming at OOO "Pa Kirishinefteorgsintez" were used as the starting raw material. The benzene fraction with IBP of 90°C was distilled-off from the catalyzates on a rectification column with an efficiency of 15 theoretical plates in 64, 11.5, and 20 wt % yields, respectively. The still bottoms

Table 1. Characteristics of the raw material

Parameter	Combined C_7–C_9 fraction	Parameter	Combined C_7–C_9 fraction
Standard distillation, °C:		Refractive index at 20°C	1.4719
IBP	95		
10%	111		
20%	115	Density at 20°C, g cm^{-3}	0.822
30%	118		
40%	121		
50%	125	Arenes, wt %,	70.41
60%	130	including toluene	30.00
70%	136	ΣC_8	36.90
80%	143	ΣC_9	3.51
90%	157		
95%	168		
FBP (98%)	189		

Table 2. Conditions of experiments on extraction of arenes from C_7–C_9 of the reformate fraction

Parameter	Run no.		
	1	2	3
Number of extraction stages	7	7	7
Extraction temperature, °C	60	60	50
Composition of the extractive agent, wt %:			
TEG	62.3	48.1	–
sulfolane	32.8	48.1	99.5
water	4.9	3.8	0.5
Mass ratio between the extractive agent and the feed	2.5 : 1	2.5 : 1	2.5 : 1

Table 3. Material balance of run no. 2 (per 100 units of mass of the feed)

Component	Input		Raffinate phase		Extract phase	
	mass	wt %	mass	wt %	mass	wt %
Saturated hydrocarbons:	29.59	8.45	23.47	68.01	6.12	1.94
Toluene	30.00	8.57	1.63	4.72	28.37	8.99
ΣC_8	36.90	10.55	5.46	15.82	31.44	9.95
ΣC_9	3.51	1.00	0.99	2.87	2.52	0.80
Mixed extractive agent	250	71.43	2.96	8.58	247.04	78.32
Total:	350	100	34.51	100	315.49	100

containing no benzene were combined in accordance with their yields and output capacities of the installations. The combined reformate containing C_7–C_9 hydrocarbons is characterized in Table 1.

A multistage counterflow extraction of arenes was performed with the mixed solvent without recycling in a system of thermostated separating funnels [7]. The conditions in which the extraction experiments were carried out are listed in Table 2. Table 3 presents, as an example, the material balance of extraction run no. 2.

To remove admixtures of saturated hydrocarbons from the extract phase, ethanol was added to this phase at a mass ratio between ethanol and saturated

Table 4. Material balance of azeotropic distillation of the extract phase obtained in run no. 2 (per 100 units of mass of the extract phase)

Component	Input	Output	
		distillate	still bottoms
Extract phase,	100	–	
including saturated hydrocarbons	1.94	1.78	0.16
toluene	8.99	0.45	8.54
ΣC_8	9.95	–	9.95
ΣC_9	0.80	–	0.80
Mixed extractive agent	78.32	–	78.32
Ethanol	4.8	4.8	–
Total	104.8	7.03	97.77

Table 5. Characteristics of the raffinate, extract, combined raffinate, and aromatic concentrate obtained upon extraction of C_7–C_9 arenes from the combined reformate in run nos. 1–3

Parameter	Raffinate			Extract			Combined raffinate			Aromatic concentrate		
	1	2	3	1	2	3	1	2	3	1	2	3
Yield relative to feed, wt %	47.5	34.55	23.3	52.5	65.45	76.7	54.09	53.76	48.74	50.83	61.36	67.46
Saturated hydrocarbons, wt %	59.0	77.02	92.79	2.97	4.55	10.39	54.18	54.11	59.52	0.77	0.81	0.86
Arenes, wt %,	41.0	22.98	7.21	97.03	95.45	89.61	36.72	17.77	7.24	99.23	99.19	99.14
including toluene	14.0	4.72	1.37	44.48	43.25	38.70	13.01	5.77	4.45	45.18	43.84	41.25
ΣC_8	24.0	15.40	4.98	48.57	48.04	46.60	21.07	10.16	2.38	50.17	51.24	52.98
ΣC_9	3.0	2.86	0.86	3.98	3.85	4.32	2.64	1.84	0.41	4.10	4.11	4.91
Ethanol, wt %	–	–	–	–	–	–	9.1	28.12	33.24	–	–	–
Recovery, wt %,	–	–	–	71.68	88.72	97.61	–	–	–	71.80	86.44	94.99
including that of toluene	–	–	–	76.27	94.57	98.93	–	–	–	74.03	89.67	92.77
ΣC_8	–	–	–	69.11	85.20	96.86	–	–	–	69.11	85.20	96.86
ΣC_9	–	–	–	59.54	71.79	94.30	–	–	–	59.54	71.79	94.30

Table 6. Ternary liquid–liquid equilibrium diagram for the system constituted by (1) saturated hydrocarbons, (2) aromatic hydrocarbons of the C_7–C_9 fraction of the reformate, and (3) mixed silvent for the conditions of run no. 2

Initial composition, wt %			Composition of the raffinate phase, wt %			Composition of the extract phase, wt %			c_{ar}, wt %		Degree of recovery of arenes, α, wt %	Distribution coefficient of arenes, K_d	Separation coefficient β
									in raffinate	in extract			
(1)	(2)	(3)	(1)	(2)	(3)	(1)	(2)	(3)					
25.0	59.4	15.6	Homogeneous region										
2.8	6.6	90.6	71.7	25.4	2.9	0.7	6.5	92.8	26.2	90.3	98.07	0.256	26.22
4.9	11.6	83.5	55.0	39.5	5.5	1.3	10.5	88.2	43.9	89.0	87.08	0.265	11.21
8.5	20.1	71.4	40.4	52.2	7.4	1.9	15.2	82.9	56.4	88.9	65.74	0.291	6.19
14.8	35.2	50.0	30.0	57.5	12.5	2.7	19.9	76.4	65.7	88.0	34.63	0.346	3.84
22.8	54.1	23.1	25.6	59.0	15.4	3.7	24.2	71.1	69.7	86.7	6.17	0.410	2.84

hydrocarbons of about 2.5 : 1 and the resulting azeotropic mixtures were distilled-off on a rectification column with an efficiency of 15 theoretical plates. Table 4 presents the material balance of the azeotropic distillation with ethanol of the extract phase produced in run no. 2. The distillate was combined with the raffinate obtained from the raffinate phase after washing with water to remove the extractive agent. An aromatic concentrate was removed by distillation with steam from the still bottoms formed in azeotropic distillation. The composition of the products obtained was analyzed by GLC [8].

The products isolated in run nos. 1–3 are characterized in Table 5.

The liquid–liquid phase equilibria in the pseudoternary system constituted by saturated hydrocarbons, C_7–C_9 arenes, and a mixed extractive agent (TEG–sulfolane–water, 48.1 : 48.1 : 3.8 wt %) were studied at 60°C by the analytical method [8] (Table 6, see figure).

It follows from the data in Table 5 that, under the conditions of run no. 1, a reformulated gasoline component satisfying the requirements of Euro-3 can be obtained at a sulfolane : TEG ratio of 34.5 : 65.5 wt % in the mixed solvent. According to these requirements, the total content of arenes in automotive gasolines should not exceed 42% [9]. Because deep rearomatization of the reformate is unnecessary in this case, the ratio between the extractive agent and the feed is as low as 2.5 : 1 (by mass) or 1.7 : 1 (by volume), which is markedly lower than that in industrial extraction processes used in manufacture of benzene and its homologues [10].

Run no. 2, at a sulfolane : TEG ratio of 50 : 50 wt % in the mixed solvent and the same ratio between the extractive agent and the feed yields a reformulated gasoline component satisfying with a safety margin the requirements of Euro-4 and Euro-5 to the total content of aromatic hydrocarbons.

As follows from the figure, the maximum concentration of arenes in the extract, which can be achieved at 60°C without recycling, is 91.5 wt %, in agreement with the results presented in Table 5.

An even deeper dearomatization of the reformate occurs under the conditions of run no. 3, with sulfolane used as the extractive agent. The combined ethanol-containing raffinate obtained in run nos. 2 and 3 can be compounded with the reformate of the gasoline fraction, which is not subject to extractive dearomatization.

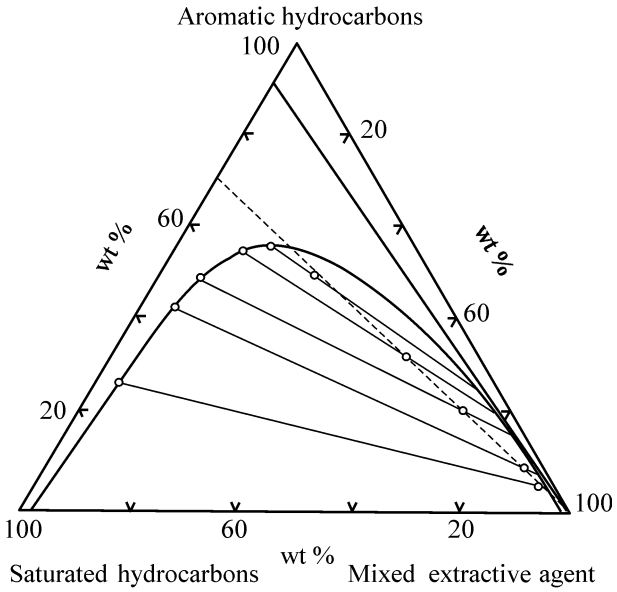

Liquid–liquid phase equilibrium diagram for the pseudoternary system constituted by saturated hydrocarbons, arenes from the C_7–C_9 fraction of the reformate, and a mixed solvent (TEG–sulfolane–water, 48.1 : 48.1 : 3.8 wt %) at 60°C.

The compounding of the combined raffinate with the reformate of the gasoline fraction as well as with alkylates and isomerizates, can be performed with account of the GOST (State Standard) 52 201–2004 in force in Russia, according to which the ethanol motor fuel should not contain more than 10% ethanol [11]. In order to homogenize the system, high-octane alcohols C_3–C_4 and, in particular, isobutyl alcohol, which exhibits a synergistic effect in mixtures with ethanol [12], can be added to fuel gasoline formulations.

The aromatic concentrates obtained contain a minor admixture of saturated hydrocarbons, mostly C_8–C_9. For example, according to capillary GLC, the contents of saturated hydrocarbons with different numbers of carbon atoms, which remain in the aromatic concentrate produced in run no. 2, are as follows (wt %): C_7 0.08, C_8 0.33, C_9 0.09. A fractionation of the aromatic concentrate yielded high-quality toluene, a minor amount of the prexylene fraction (about 0.5 wt %), in which admixtures of isooctanes and *n*-octane are concentrated, and C_8 arenes; C_9 arenes remain the still bottoms.

The advantages of the process suggested for diminishing the total content of arenes in automotive gasolines, with simultaneous recovery of toluene and xylenes, consist in the low ratio between the extractive agent and feed and in the absence of recycling flows impairing the output capacity of extraction apparatus.

CONCLUSIONS

(1) A combined method was suggested for extraction of C_7–C_9 arenes from the reformate of the gasoline fraction with a mixed solvent composed of triethylene glycol and sulfolane (50 : 50 wt %), with the subsequent removal of admixtures of saturated hydrocarbons from the extract phase by azeotropic distillation with ethanol, without regeneration of the alcohol. The method can produce a reformulated gasoline component satisfying the Euro-4 and Euro-5 requirements to the total content of arenes.

(2) Commercial toluene and total xylenes were recovered by distillation from the resulting aromatic concentrate. The process is characterized by low extractant-to-raw material ratio and absence of recycling flows.

REFERENCES

1. Kaminskii, E.F. and Khavkin, V.A., *Glubokaya pererabotka nefti: tekhnologicheskii i ekologicheskii aspekty* (Deep Processing of Oil: Technological and Ecological Aspects), Moscow: Tekhnika. OOO TUMA GRUPP, 2001.
2. Gaile, A.A., Zalishchevskii, G.D., Gafur, N.N., et al., *Khim. Tekhnol. Topl. Masel*, 2004, no. 4, pp. 11–14.
3. RF Patent 2256691.
4. *Petrotekku-Petrotech.*, 2000, vol. 23, no. 5, pp. 416–426.
5. Ranke, U. and Ennenbach, F., *Petrotekku=Petrotech.*, 1999, vol. 22, no. 5, pp. 406–411.
6. Gentry, J.K., Kumar, K.S., Li, H.M., and Li, I.H., *Khim. Tekhnol. Topl. Masel*, 2003, nos. 1–2, pp. 12–17.
7. Alders, L., *Liquid-liquid Extraction. Theory and Laboratory Practice*, Amsterdam: Elsevier, 1959.
8. Gaile, A.A., Erzhenkov, A.S., Koldobskaya, L.L, and Kaifadzhyan, E.A., *Zh. Prikl. Khim.*, 2007, vol. 80, no. 4, pp. 608–611.
9. Kaminskii, E.F. and Khavkin, V.A., *Sbornik Trudov 5-go Mezhdunarodnogo foruma "Toplivo-energeticheskii kompleks Rossii: regional'nye aspekty" Sankt-Peterburg, 4–7 aprelya 2005 g.* (Proc. 5th Int. Symp. "Russia's Fuel-and-Energy Complex: Regional Aspects," St. Petersburg, April 4–7, 2005), St. Petersburg, 2005, pp. 191–195.
10. Bittrich, H.-I., Gaile, A.A., Lempe, D., et al., *Razdelenie uglevodorodov s ispol'zovaniem selektivnykh rastvoritelei* (Separation of Hydrocarbons with the Use of Selective Solvents), Leningrad: Khimiya, 1987.
11. Shpak, V.S., Shapovalov, O.I., Kartashov, Yu.I., et al., *Khim. Prom–st.*, 2006, vol. 83, no. 2, pp. 89–96.
12. Danilenko, T.V., Development of Gasoline Fuel Formulations with Addition of Aliphatic Alcohols, *Cand. Sci. Dissertation*, Moscow, 2005.

ISSN 1070-4272, Russian Journal of Applied Chemistry, 2007, Vol. 80, No. 4, pp. 605–610. © Pleiades Publishing, Ltd., 2007.
Original Russian Text © A. Dionizy, P. Nowak, C. Mora, 2007, published in Zhurnal Prikladnoi Khimii, 2007, Vol. 80, No. 4, pp. 617–622.

PROCESSES AND EQUIPMENT OF CHEMICAL INDUSTRY

A Study of Effect of Agitation Intensification on the Size and External Shape of Silver Bromide Crystals Produced by Controlled Ostwald Growth in the Presence of Dimethyl Sulfoxide

A. Dionizy, P. Nowak, and C. Mora

Institute of Physical and Theoretical Chemistry, Wroclaw University of Technology, Wroclaw, Poland

Received September 26, 2006

Abstract—Results obtained in a study of the effect of agitation intensification on the granulometric properties of silver bromide crystals contained in photographic emulsions and produced by controlled Ostwald growth are presented.

DOI: 10.1134/S1070427207040179

Published and patent data of recent years point to the possibility of technological use of silver halide crystals produced in the form of strongly flattened plates by crystallization from solutions containing polar aprotic solvents [1–7]. The still presently used methods for production of silver halide crystals use aqueous-gelatin solutions as the reaction medium [8–10]. Planar crystals of silver halides (tabular crystals, T-crystals) are also obtained in an aqueous medium, but, in this case, complex organic compounds, the so-called growth directors or modifiers are most frequently used. Owing to the high sensitometric and structuremetric parameters of light-sensitive layers formed by tabular crystals, they are presently used in the technology of light-sensitive materials of nearly all types, especially in highly sensitive materials intended for diagnostics in medicine and industrial defectoscopy. However, wide use of these methods to obtain prescribed granulometric and crystallographic properties is exceedingly difficult because exhaustive data on the mechanism of formation of crystals of this kind in the presence of growth modifiers are still lacking [11–13].

Recently, several methods have been suggested for crystallization of silver halides in nonaqueous media, mostly with use of polar aprotic solvents (or mixtures of these) or aqueous media with other organic solvents, to give silver halide crystals with desirable crystalline shape and granulometric parameters [14–17]. Of particular interest are techniques for synthesis of tabular crystals [11, 13, 18–22]. The tabular silver halide crystals obtained under these conditions are characterized by presence of two or several twinning planes and a comparatively large number of crystal lattice defects. Presence of these defects is necessary for formation, in the course of chemical sensitization, of impurity sensitivity centers with precisely defined topography in the bulk of the crystal. They also act as the so-called sensitivity centers, which are highly efficient traps for holes and electrons.

Of certain importance is the high efficiency of the process of chemical sensitization of tabular silver halide crystals; it appears via formation of comparatively large dye aggregates on large undistorted {111} faces of the crystals. For example, high efficiency of the spectral sensitization is not observed in the case of compact (spherical) crystals. The advantage of the tabular crystals has aroused researchers' interest in methods for synthesis of crystals of this kind, despite the intensively developing technology of digital photography.

Recently, interesting experimental data have been published on synthesis of silver halide light-sensitive emulsions obtained in aqueous-gelatin solutions of aprotic polar solvents or mixtures of these and(or) protic solvents whose dissociation constant is lower than that of water. These results indicate that the efficiency of light-sensitive layers containing light detectors in the form of strongly flattened hexagonal or trigonal crystals of silver halides can be improved [1, 4–7, 23–25].

The results reported in these papers formed the basis for the present study, whose main goal was

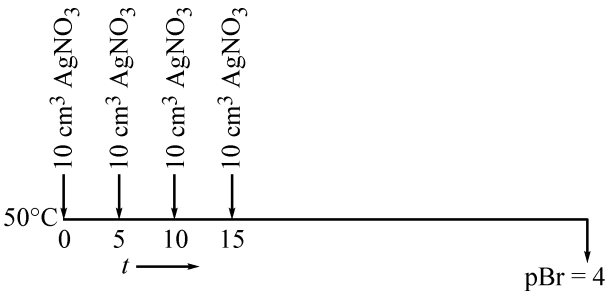

Fig. 1. Scheme of synthesis of the Lippmann emulsion.

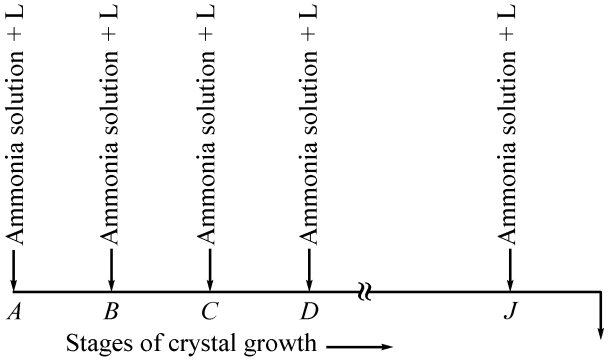

Fig. 2. Synthesis stages of the model emulsion by the COR method.

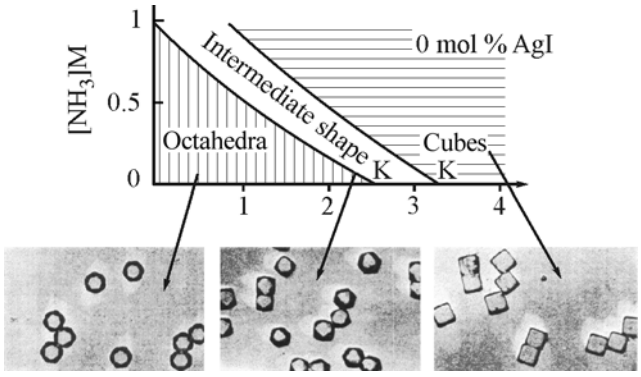

Fig. 3. Scheme of stability of the 3*D* shapes of silver bromide crystals obtained by the COR method in relation to the excess concentration of bromide ions and ammonia [26].

to determine whether or not dimethyl sulfoxide (DMSO) can be used to synthesize light-sensitive emulsions containing tabular crystals of silver bromides by controlled Ostwald ripening (COR). Particular attention was given to the influence exerted by the intensity of agitation of the reaction mixture on the growth rate of silver halide crystals and, consequently, on their size, polydispersity, and shape.

The COR method is a way to fabricate silver-halide model emulsions. It was developed by Romer and Markocki in 1962 [25]. This method is based on production of a certain ensemble of silver halide crystals in an aqueous solution of gelatin at a comparatively low supersaturation and permanent addition of combined ions necessary for crystal growth. Uniform ensembles of silver halide crystals are obtained at a certain constant excess of halide ions, whose concentration, as well as that of other ingredients that form complexes with silver halides, predetermines the shape of the growing crystals.

First, a Lippmann emulsion (L) containing AgHal crystals about 0.01–0.05 μm in size is synthesized at a final concentration of excess bromide ions c = 0.0001 M (pBr 4) (Fig. 1).

In the next stage, a nucleation emulsion with crystals about 0.1–0.3 μm in size is prepared from the Lippmann emulsion (Fig. 2). To this emulsion are successively added (Fig. 2, crystal growth stages *A*, B, *C*, ...) in certain proportions the Lippmann emulsion and solutions of ammonia and potassium bromide. In the presence of substances that enhance the solubility of silver chlorides, fine crystals of the Lippmann emulsion rapidly dissolve and are then precipitated on the surface of large, compared with thee crystals, growing crystals of the nucleation emulsion. The end of the successive stages of crystal growth, as well as that of the whole process of emulsion synthesis, is monitored with a microscope. This method can be used to rapidly obtain comparatively large silver halide crystals with properties similar to those of crystals produced by the double-jet technique.

The COR method can be used to obtain, using the stability conditions of certain forms of AgHal, known from the literature [26], model emulsions containing desired crystals by varying the concentration of ammonia and excess bromide ions. The stability scheme of the shapes of silver halide crystals [26] is shown in Fig. 3. The most recent published data indicate that the COR method can be used, which is considerably simpler than the conventional techniques for synthesis of tabular AgHal crystals with aprotic solvents, e.g., DMSO [27].

Several emulsions were synthesized at a constant excess concentration of bromide ions [c = 0.3 M (pBr 0.5)], constant ionic strength I = 0.54, and constant content of DMSO in the reaction mixture (50 vol %). These emulsions were synthesized in the same reaction vessel under constant topochemical conditions at a varied rotation rate of the rabble, without changes in its configuration. In contrast to the conventional methods for emulsion synthesis by

the COR method, the ammonia solution was replaced with an appropriate amount of DMSO. The scheme of emulsion synthesis is shown in Fig. 4. The next stages of emulsion synthesis were preceded by taking a 40-ml sample of the reaction mixture to maintain constant the liquid level in the conical reaction vessel (level height fluctuations of up to 6.7%; Fig. 5) and preserve to the maximum possible extent the exchange conditions in the entire volume of the reaction mixture. The agitation intensity was changed by varying the rotation rate of the two-blade impeller of the rabble. Three rabble rotation rates were used in the experiments: 430, 650, and 1050 rpm. After each synthesis stage (*A*, *B*, *C*, ...) the emulsion was sampled and preparations for inspection under a microscope were produced. Micrographs of AgBr crystals formed in a certain growth stage under various agitation conditions are shown in Fig. 6. Analysis of changes in the shape and size of the crystals demonstrates that the average size of silver bromide crystals grows and their shape changes as the agitation rate increases and in the course of recrystallization.

The emulsions obtained at the slowest rotation rate of the rabble (430 rpm) contain nearly exclusively planar hexagonal silver bromide crystals with well defined faces and vertices. This indicates that, under the given conditions, there occurs an exceedingly uniform recrystallization process leading to the formation of a nearly uniform ensemble of crystals. The average size of the AgBr crystals obtained under these conditions was about 40 μm. The crystals obtained under the identical conditions, but at a high rotation rate of the rabble (650 rpm), also grow as well-defined hexagonal plates. The average size of these crystals is about 55 μm, with the forming ensembles exhibiting a considerably higher polydispersity, compared with crystals obtained at a lower rotation rate of the rabble (430 rpm). Further increase in the rotation rate to 1050 rpm results in that the AgBr crystals become larger (up to 65 μm) and their polydispersity grows. In addition, undesirable changes of the shape of the crystals occur under the conditions of such an intensive mass exchange, which is manifested in rounding of the faces and vertices of the tabular AgBr crystals. Also observed is a mechanical damage to large tabular crystals, which occurs as a result of mutual friction of mostly large crystals; very thin tabular crystals are most easily mechanically deformed under the conditions of vigorous agitation.

An analysis of changes in the granulometric parameters of photographic emulsions produced by the COR method in the presence of DMSO at a variable rotation rate of the rabble demonstrated that an increase in the rotation rate, on which the rate of mass exchange in the reactor depends, affects the rate of recrystallization of tabular silver bromide crystals. This effect causes the following: (1) the average size of the crystals increases in each stage of the synthesis process; (2) the polydispersity of the crystals becomes more pronounced and noticeably grows with the recrystallization time; and (3) the crystallographic shape of the crystals is more distorted, which is manifested in rounding of the faces and vertices of tabular crystals and, in the final stage of the emulsion synthesis, in mechanical damage to the largest crystals and formation of bulk crystals.

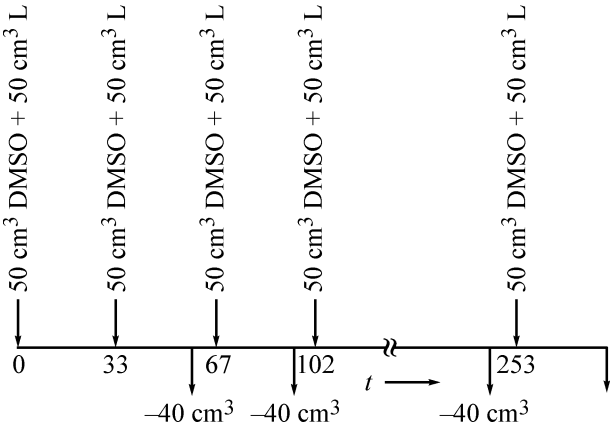

Fig. 4. Scheme of emulsion synthesis by the COR method with 50% DMSO.

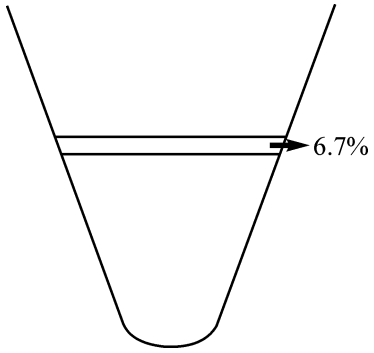

Fig. 5. Change in the level of the reaction mixture in the conical reactor during emulsion synthesis by the COR method by the scheme in Fig. 4. A change in the liquid volume by 30% at an initial volume of 120 cm^3 leads to a change in the height of the liquid level in the reactor by 6.7%.

In the course of emulsion synthesis and, consequently, during the occurring recrystallization, the size of tabular silver bromide crystals steadily grows at each agitation rate. The course of these changes is

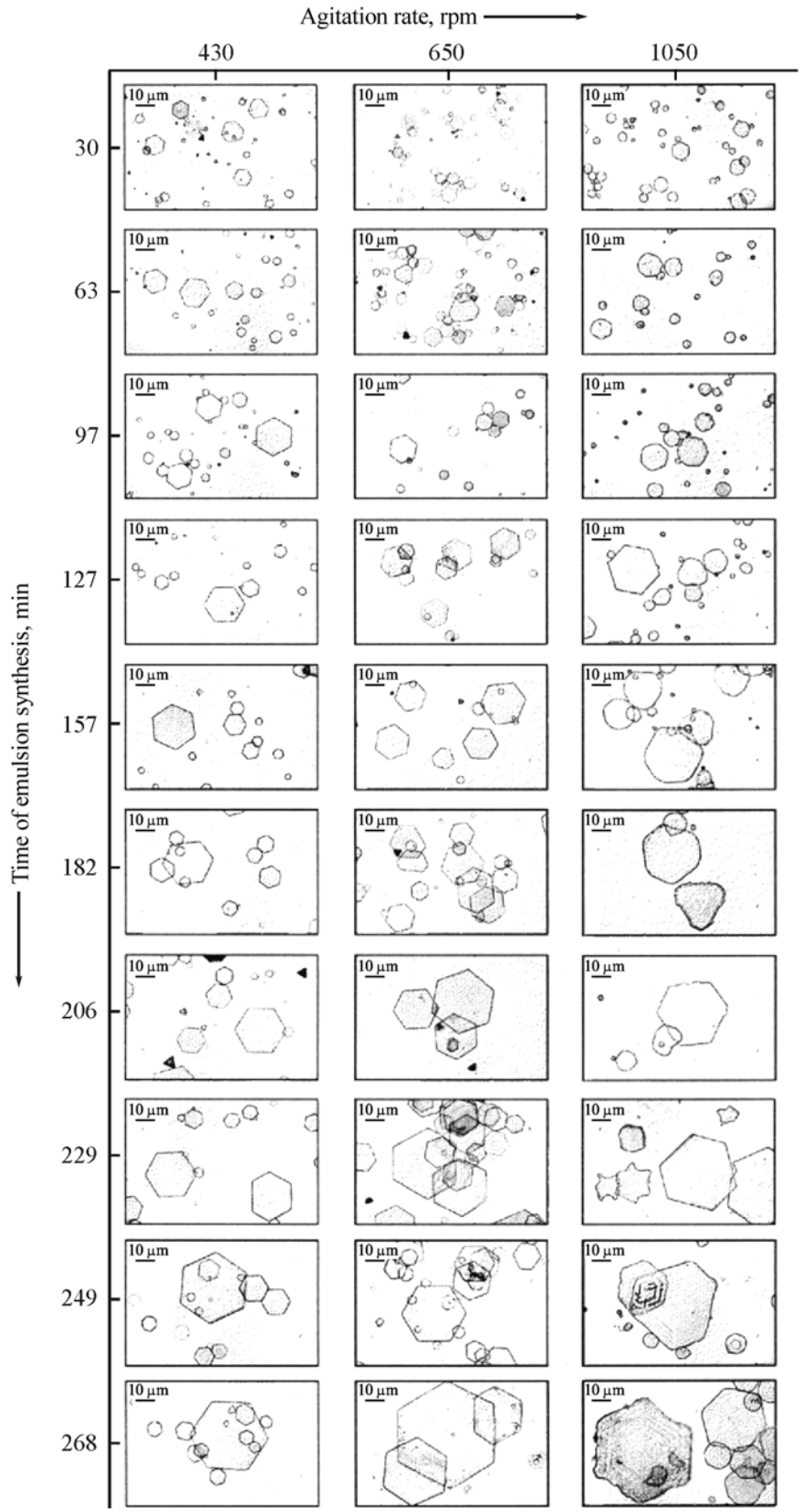

Fig. 6. Microphotographs of silver bromide crystals obtained in synthesis of photographic emulsions by the COR method in the presence of DMSO at various agitation intensities.

shown in Fig. 7. At an agitation rate of 1050 rpm, the crystals grow in size the most rapidly. It should, however, be remembered that, under these conditions, the shape of the crystals undergoes undesirable transformations and their polydispersity increases. Mostly rounded crystal shapes, frequently mechanically damaged and of the bulk type, are for the most part represented in the ensemble of crystals of thus prepared emulsions, with well-defined hexagonal tabular AgBr crystals contained in a minor amount. Making longer the recrystallization time at a vigorous agitation of the reaction mass also leads to a decrease in the shape factor, i.e., leads to formation of bulk-type crystals.

Analysis of the shape of tabular AgBr crystals formed in the final stage of synthesis of some emulsions prepared at different agitation rates (Fig. 6, 268 min of synthesis) shows that the finest, mostly hexagonal, tabular silver bromide crystals of the best shape are produced at a comparatively slow agitation. Intense mass-exchange during synthesis of photographic emulsions by the COR method in the presence of DMSO does not favor formation of tabular silver bromide crystals with well-pronounced granulometric properties, but results in an increase in the average size of the crystals.

No uniform, so-called monodisperse, emulsions were produced in the study. However, ensembles of hexagonal tabular crystals containing more than one twinning plane were obtained. The formation of tabular hexagonal crystals of silver bromide is due to the presence in the reaction mixture of molecular complexes of silver salts, stabilized by DMSO. Complexes of this kind favor formation of first a single type (trigonal crystals), and then a succession of twin crystals, which, in the end, promotes lateral growth of a crystal in the form of a hexagonal plate. Probably, during successive introduction of silver bromide portions in the form of a Lippmann emulsion, there occurs, in parallel with the Ostwald crystallization leading to growth of the already existing crystals, nucleation of a new ensemble of crystals. Under the conditions of emulsion synthesis, these latter are formed in the twin form and further grow via recrystallization and next twinning. Thus, presence of DMSO not only leads to an increase in the solubility of silver halides in the reaction medium and to lateral growth of tabular, but also, and above all, promotes constant twinning of AgBr crystals in each stage of their growth, despite that twinning planes are already present in the crystal. Just this circumstance hinders synthesis of monodisperse emulsions with hexagonal silver

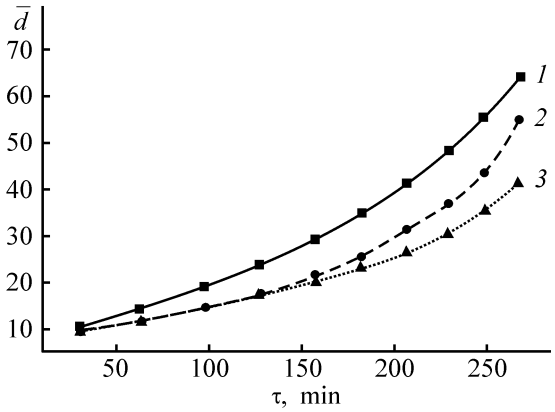

Fig. 7. Variation of the average size $\bar{d}$ of tabular silver bromide crystals, recorded in different stages of emulsion synthesis at three rotation rates of the rabble. (τ) Time of synthesis. ω (rpm): (*1*) 1050, (*2*) 650, and (*3*) 430.

halide crystals by controlled Ostwald growth in the presence of DMSO.

Undoubtedly, the method suggested for synthesis of photographic emulsions by controlled Ostwald growth in the presence of dimethyl sulfoxide opens up new opportunities in the technology of silver halide light-sensitive materials containing crystals having the shape of hexagonal plates.

ACKNOWLEDGMENTS

The authors thank Adam Zaleski for valuable remarks and discussion and Aleksandra Giszczak for assistance in laboratory experiments.

REFERENCES

1. Millan, A., *J. Crystal Growth*, 2000, vol. 208, pp. 592–598.
2. Millan, A., Bennema, P., Goessens, C., et al., *J. Imag. Sci. Technol.*, 1998, vol. 42, pp. 385–392.
3. US Patent 5 478 718.
4. US Patent 5 541 051.
5. US Patent 5 733 715.
6. Nowak, P., Mora, C., Rajkowski, B., et al., *The Imag. Sci. J.*, 2004, vol. 52, pp. 35–40.
7. Polish Patent Appl. 350 504.
8. Duffin, G.F., *Photographic Emulsion Chemistry*, London: Focal, 1966.
9. Sturmer, D.M. and Marchetti, A.P., *Imaging Processes and Materials*, Strurge, J., Walworth, V., and Shepp, A., Eds., New York: Van Nostrand Reinhold, 1989, p. 109.
10. Zwicky, H., *Einfürung in die Technologie photographischer Silberhalogenidschichten*, Burgdorf, 1979.

11. US Patent 5 320 938.
12. Berry, C.R. and Skillman, D.C., *Photogr. Sci. Eng.*, 1962, vol. 6, pp. 159–165.
13. Bennema, P., Bgels, G., Bollen, D., et al., *The Imag. Sci. J.*, 2001, vol. 49, pp. 1–32.
14. Millan, A., Bennema, P., Verbeeck, A., and Bollen, D., *J. Crystal Growth*, 1998, vol. 192, pp. 215–224.
15. Bgels, G., Buijnsters, J.G., Verhaegen, S.A.C., et al., *J. Crystal Growth*, 1999, vol. 203, pp. 554–563.
16. Goessens, C., Schryvers, D., Van Landuyt, J., et al., *J. Crystal Growth*, 1995, vol. 151, pp. 335–341.
17. Goessens, C., Schryvers, D., Van Landuyt, J., et al., *J. Crystal Growth*, 1997, pp. 172, pp. 426–432.
18. Plomp, M., Buijnsters, J.G., Bëgels, G., et al., *J. Crystal Growth*, 2000, vol. 209, pp. 911–923.
19. Ohzeki, K., Urabe, S., and Tani, T., *J. Imag. Sci. Technol.*, 1990, vol. 34, pp. 136–142.
20. Brust, T.B. and House, G.L., *IS&T's 49th Annual Conf.*, pp. 35–37.
21. Bëgels, G., *Growth Mechanism of (111)-Twinned fcc crystals: Application to Silver Halides: Doctor these*, Nijmegen, 1999.
22. Bëgels, G., Meekes, H., Bennema, P., and Bollen, D., *The Imag. Sci. J.*, 2001, vol. 49, pp. 33–43.
23. Nowak, P., Mora, C., Rajkowski, B., et al., *Synteza halogenków srebra w środowisku rozpuszczalników aprotonowych oraz ich zastosowanie jako wysokoefektywne detektory promieniowania elektromagnetycznego*, Wroclawš, 2001.
24. Nowak, P., Mora, C., Rajkowski, B., et al., *Badania warunków zarodkowania i wzrostu plaskich kryształow halogen ków srebra w formie sześciokatnych lub trójkatnych plytek o wysokim współczynniku AR (aspect ratio > 50), w środowisku wodno-żelatynowych roztworów wybranych rozpuszczalników aprotonowych ilub rozpuszczalników protonowych, których stala dysocjacji jest mniejsza od stalej dysocjacji wody*, Wroclawš, 2003.
25. Markocki, W. and Romer, W., *Vorträge u. Diskussionen auf dem IV Int. Kolloquium über Korpuskularphotographie: Korpuskularphotographie IV*, München, 1962, pp. 162–168.
26. Markocki, W. and Zaleski, A., *Photogr. Sci. Eng.*, 1973, vol. 17, pp. 289–294.
27. Dionizy, A., Nowak, P., and Mora, C., Abstracts of Reports, *Mezhdunarodnyi Simpozium "Fotografiya v XXI veke: traditsionnye i tsifrovye protsessy"* (Int. Symp. "Photography in the XXI Century; Conventional and Digital Processes").

ISSN 1070-4272, Russian Journal of Applied Chemistry, 2007, Vol. 80, No. 4, pp. 611–614. © Pleiades Publishing, Ltd., 2007.
Original Russian Text © R.L. Safiullin, L.R. Enikeeva, 2007, published in Zhurnal Prikladnoi Khimii, 2007, Vol. 80, No. 4, pp. 623–626.

ORGANIC SYNTHESIS AND INDUSTRIAL ORGANIC CHEMISTRY

Oxidation of 2-Methoxy-3,6-dichloropropenylbenzene with Ozone

R. L. Safiullin and L. R. Enikeeva

Institute of Organic Chemistry, Ufa Scientific Center, Ufa, Bashkortostan, Russia

Received June 27, 2006

Abstract—Oxidation of 2-methoxy-3,6-dichloropropenylbenzene with ozone in acetic acid and carbon tetrachloride was studied.

DOI: 10.1134/S1070427207040180

Ozonolysis is one of the most promising methods for oxidation of hydrocarbons containing double bonds. In this study, we examined the formation of 2-methoxy-3,6-dichlorobenzaldehyde by ozonation of 2-methoxy-3,6-dichloropropenylbenzene (DCPB). 2-Methoxy-3,6-dichlorobenzaldehyde can serve as a starting compound for preparing 2-methoxy-3,6-dichlorobenzoic acid and its derivatives used in agriculture as herbicides [1–3]. It is known that the efficiency of ozonolytic conversion of olefins is determined by the decomposition of intermediate ozonolysis products, ozonides. In this study, we examined the thermal stability of ozonides formed by ozonation of 2-methoxy-3,6-dichloropropenylbenzene and the effect of acidity on their decomposition.

EXPERIMENTAL

2-Methoxy-3,6-dichloropropenylbenzene was purified by vacuum distillation under argon. Carbon tetrachloride (CCl_4) was successively treated with ozone, dried over $CaCl_2$, and distilled in argon. Methanesulfonic acid (CH_3SO_3H) and *p*-toluenesulfonic acid (*p*-$TolSO_3H$) of chemically pure grade were used without purification. Ozone was prepared from oxygen in a ozonizer with an output capacity of 0.5 g of ozone per hour at an oxygen consumption of 4 l h^{-1}.

The ozonation of DCPB and isolation of products of its conversion were carried out as follows. A solution of the olefin in acetic acid or CCl4 was purged with an ozone–oxygen mixture fed into the lower part of a reactor. The ozone content at the inlet and outlet of the reactor was determined spectrophotometrically at λ = 300 nm (ozone extinction coefficient 95 l mol^{-1} cm^{-1}) [4]. After the breakthrough of ozone through the reactor, the ozonation was stopped.

The intermediate compounds containing peroxy groups were determined by spectrophotometric iodometric titration [5]. The concentration of intermediates containing peroxy groups (–O–O–) was calculated by the equation

$$[–O–O–] = AV_{as}/(\varepsilon l V_s),$$

The extinction coefficient of I_3^- at λ = 360 nm is ε = 28 000 l mol^{-1} cm^{-1}, the optical cell width is 1 cm, the volume of the solution being analyzed V_{as} = 2.5–3.0 ml, and the introduced sample volume V_s = 2–10 μl.

The decomposition products of ozonized compounds were examined by ^1H and ^{13}C NMR, IR, and UV spectroscopies, and also by GLC. The ^1H and ^{13}C NMR spectra were recorded in $CDCl_3$ on a Bruker AM-300 NMR spectrometer (300 and 75 MHz, respectively).

Ozonation of the olefin in acetic acid solutions. 2-Methoxy-3,6-dichloropropenylbenzene (27.4 mol, 6.06 g) was dissolved in glacial acetic acid (50 ml) and ozonized at 315 K. In the course of the ozonation, the reaction mixture was sampled at regular intervals and the samples were titrated iodometrically. The reaction mixture was ozonized for 3 h . After the ozonation was complete, the ozonide concentration in the reaction mixture was 0.12 M.

Ozonation of the olefin in acetic acid containing water and *p*-toluenesulfonic acid. The initial mix-

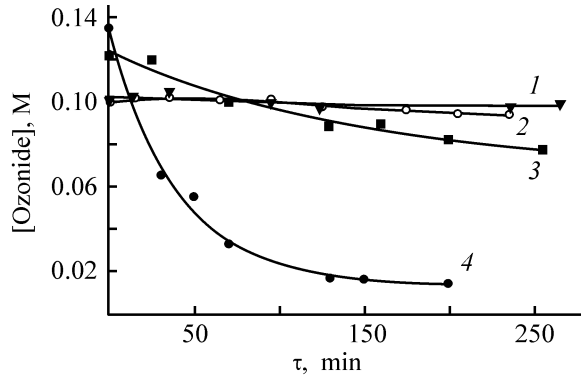

Fig. 1. Kinetic curves of ozonide decomposition in CH3COOH. (τ) Time. Temperature, K: (*1*) 298, (*2*) 326, (*3*) 347, and (*4*) 347 in the presence of $[CH_3SO_3H] = 1.1 \times 10^{-2}$ M.

ture to be ozonized (50 ml) contained olefin (6.06 g) dissolved in an acetic acid solution containing *p*-TolSO_3H (0.1 g) and H_2O (3.2 g). The ozonation was carried out at 315 K. After a lapse of 2 h 35 min, the ozonide concentration in the reaction mixture reached 0.2 M.

Ozonation of the olefin in CCl_4. In these experiments, solutions of the olefin in CCl_4 (50 ml) containing 6.06 g of the olefin were ozonized at 295 K. Although the ozone breakthrough occurred 40 min after the start of the reaction, the ozonation was continued for 3 h. Under these conditions, the ozonide content in the reaction mixture did not exceed 0.1 M.

Rate constant of ozonide decomposition in an acetic acid solution at various temperatures and sulfonic acid concentrations

T, K	$[RSO_3H]$, M	$[Ozonide]_0$, M	k_{eff}, s^{-1}
290	–	0.03*	$(5 \pm 0.2) \times 10^{-7}$
298	–	0.01	$(7.5 \pm 2.1) \times 10^{-7}$
347	–	0.04	$(2.3 \pm 0.4) \times 10^{-5}$
	[Methanesulfonic acid]:		
347	0.5×10^{-2}	0.12	$(4.0 \pm 0.5) \times 10^{-5}$
	0.9×10^{-2}	0.16	$(4.2 \pm 0.5) \times 10^{-5}$
	3.1×10^{-2}	0.07	$(7.3 \pm 0.5) \times 10^{-5}$
	5.0×10^{-2}	0.14	$(11.4 \pm 1.5) \times 10^{-5}$
	7.0×10^{-2}	0.14	$(12.9 \pm 1.6) \times 10^{-5}$
	[*p*-Toluenesulfonic acid]:		
347	0.6×10^{-2}	0.03	$(4.6 \pm 0.7) \times 10^{-5}$
	1.8×10^{-2}	0.07	$(7.5 \pm 0.7) \times 10^{-5}$
	2.9×10^{-2}	0.06	$(8.1 \pm 0.7) \times 10^{-5}$
	6.8×10^{-2}	0.07	$(14.7 \pm 0.8) \times 10^{-5}$

* In CCl_4.

The thermal stability of ozonides formed by ozonation of the olefin was examined as follows. A portion of the reaction mixture was taken from the reactor and dissolved in acetic acid. This solution was placed in a temperature-controlled reactor equipped with a water-cooled reflux condenser and a stirrer. At certain intervals, the reaction mixture was sampled drawn and the concentration of the peroxy groups in was determined iodometrically. This experiment was continued until the degree of decomposition of the ozonide reached no less than 70%. To elucidate how the acidity affects the kinetics of acid-catalyzed decomposition of ozonides, weighed portions of the sulfonic acid were added to the reaction mixture.

Thermal stability of 2-methoxy-3,6-dichloropropenylbenzene ozonide. The thermal decomposition of the ozonide was examined in acetic acid solutions at 288–347 K. As can be seen from Fig. 1, 2-methoxy-3,6-dichloropropenylbenzene ozonide is stable at room temperature for several hours. We found that the addition of water (3.3 M) does not affect the kinetics of degradation of the ozonide. With increasing temperature, the ozonide stability decreases. Noticeable decomposition of the ozonide begins at 347 K. The kinetic curve of thermal decomposition of the ozonide is linear in the coordinates of equation of a first-order reaction, which allows calculation of the effective rate constant k_{eff} of the ozonide decomposition (see table). These data show that this rate constant is independent of both the initial ozonide concentration and solvent type, and its value is close to that of decomposition of 1-hexene ozonide [4].

Acid-catalyzed decomposition of ozonide. We found that addition of methane and *p*-toluenesulfonic acids (RSO_3H) accelerates the decomposition of the ozonide. Acetic acid used as the solvent (pK_a 4.75) [6] is weaker than methane- and *p*-toluenesulfonic acids (pK_a 0 and 0.7, respectively) [7]. The table shows that the ozonide decomposition is noticeably accelerated in the presence of methanesulfonic acid. The kinetic curve of ozonide decomposition in the presence of methanesulfonic acid is linear in the coordinates of equation of a first-order reaction, which allows calculation of the effective rate constant k_{eff} of ozonide decomposition. The effective rate constants k_{eff} of ozonide decomposition in the presence of sulfonic acids at varied temperature are listed in the table. Thus, with the content of sulfonic acid in acetic acid solutions increasing within the entire concentration

range, the stability of ozonides decreases, with k_{eff} weakly dependent on the initial ozonide concentration. Figure 2 shows that k_{eff} linearly depends on the sulfonic acid concentration. These correlations suggest that the rate of ozonide decomposition is described by the linear equation

$$W = k_{eff}[\text{ozonide}] = (k_0 + k_c[RSO_3])[\text{ozonide}]_0,$$

where k_0 is the rate constant of ozonide decomposition in the absence of sulfonic acid, and k_c, the rate constant of ozonide decomposition catalyzed by sulfonic acid.

The rate constants of ozonide decomposition in acetic acid containing a sulfonic acid were calculated from our experimental data for $[\text{ozonide}]_0 = 0.16$–$0.03$ M and are as follows: in the presence of *p*-toluenesulfonic acid, $k_0 = (3.5 \pm 1.5) \times 10^{-5}$ s^{-1}, $k_c = (1.5 \pm 0.3) \times 10^{-3}$ l mol^{-1} s^{-1}; and in the presence of methanesulfonic acid, $k_0 = (2.8 \pm 1{,}5) \times 10^{-5}$ s^{-1} and $k_c = (1.5 \pm 1.3) \times 10^{-3}$ l mol^{-1} s^{-1}.

It should be noted that the rate constant of acid-catalyzed decomposition of 2-methoxy-3,6-dichloropropenylbenzene ozonide determined in this study reasonably agrees with the rate constant of decomposition of 1-hexene ozonide catalyzed by *p*-toluenesulfonic acid in the presence of the accumulated aldehyde, 7.4×10^{-4} s^{-1} [8].

After the completion of the ozonide decomposition, the products of oxidative conversion of DCPB were isolated by two different methods. In the first method, water was added to the reaction mixture and the resulting yellow oily precipitate was treated with saturated aqueous Na_2SO_4 and cooled to 273 K. A grayish precipitate formed under these conditions was filtered off, washed with benzene, and dried. The ^{1}H and ^{13}C NMR spectra of this product formed in a yield of 98% were found to be identical to those of 2-methoxy-3,6-dichlorobenzaldehyde.

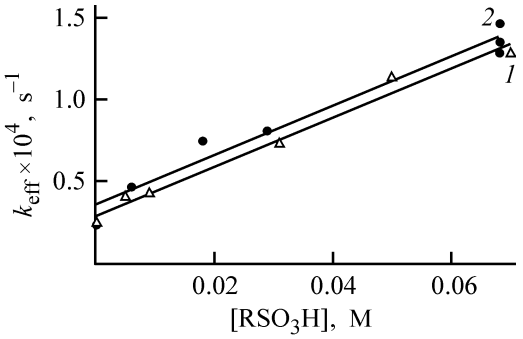

Fig. 2. Plot of k_{eff} vs. RSO_3H concentration at 347 K. (*1*) CH_3SO_3H and (*2*) *p*-TolSO_3H.

In the second method, acetic acid was distilled off from the reaction mixture, and the resulting precipitate was dissolved in CCl_4. This solution was filtered and CCl_4 was distilled off. The ^{1}H NMR spectrum of the resulting product formed in 96% yield contains a signal at 10.4 ppm belonging to the aldehyde group. The ^{13}C NMR spectra show that the product of oxidation of DCPB is 2-methoxy-3,6-dichlorobenzaldehyde.

^{1}H NMR spectrum of 2-methoxy-3,6-dichlorobenzaldehyde

Proton	–OCH$_3$	–C(O)H	≥CH	≥CH
δ, ppm:				
calculation	3.84	10.57	7.32	7.23
experiment	3.8–395	10.2–10.4	7.3–7.5	7.1–7.2

^{12}C NMR spectrum of 2-methoxy-3,6-dichlorobenzaldehyde

C atom	–OCH$_3$	H–C≤	H–C≤	≥C–Cl	≥C–Cl	≥C–OR	≥CH=O
δ, ppm:							
calculation	62.49	127.0	134.6	122.8	137.3	156.05	190.4
experiment	62.84	127.1	134.9	121.1	134.9	156.12	188.5

Our experimental results can be adequately described within the framework of the known mechanism of ozonation of unsaturated compounds [4]:

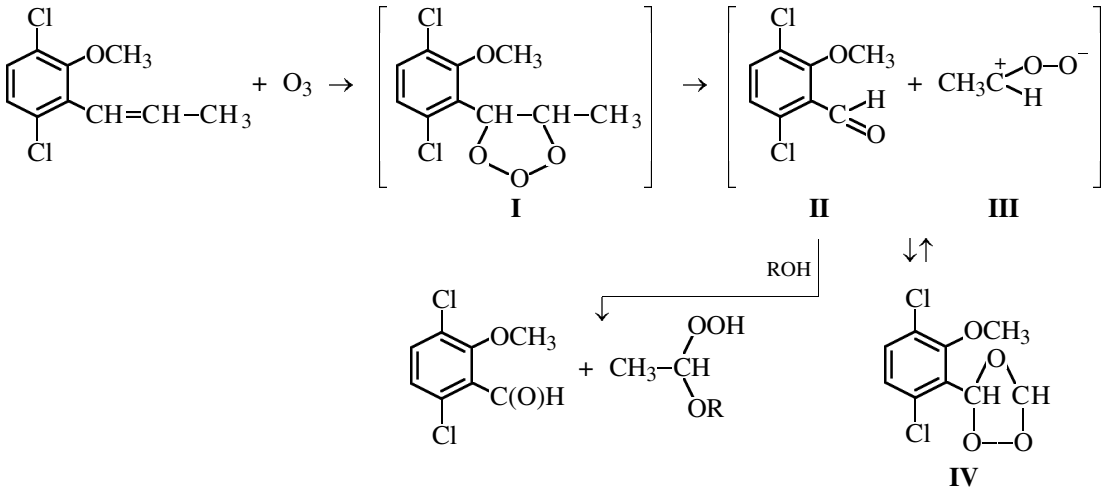

Chemical scheme of ozonation.

In this scheme, molozonide **I** formed by the reaction of ozone with the double bond is very unstable and decomposes to yield aldehyde **II** and carbonyl oxide **III**. Owing to the cell effect, some portion of carbonyl oxide has no time to escape into the bulk and reacts with the aldehyde to form more stable ozonide **IV**. This is evident from the fact that, if the components of the reaction mixture containing active oxygen are not decomposed, the aldehyde yield does not exceed 70%. At the same time, the yield of the product containing the –O–O– group increases in the course of ozonation and, after the reaction is complete, it is approximately 20% of the initial olefin amount.

Thus, the main part of aldehyde is formed by direct ozonation of 2-methoxy-3,6-dichlorobenzene. A small portion of the aldehyde (up to 20% of the initial olefin) is converted to ozonide by the reaction with the simultaneously formed carbonyl oxide. After decomposition of the ozonide in the presence of *p*-toluenesulfonic acid, 2-methoxy-3,6-dichlorobenzaldehyde is formed in a yield of up to 98%.

CONCLUSIONS

(1) The ozonation of 2-methoxy-3,6-dichloropropenylbenzene yields 2-methoxy-3,6-dichlorobenzaldehyde (up to 70%) and the corresponding ozonide.

(2) Strong acids catalyze the ozonide decomposition.

(3) The main ozonation product in acetic acid, formed in 98% yield after completion of decomposition of the ozonide, is 2-methoxy-3,6-dichlorobenzaldehyde.

REFERENCES

1. Mel'nikov, N.N., Novozhilov, K.V., and Belan, S.R., *Pestitsidy i regulyatory rosta rastenii: Spravochnik* (Pesticides and Plant Growth Regulators: Handbook), Moscow: Khimiya, 1995.
2. RF Patent 2106782.
3. RF Patent 2070877.
4. Razumovskii, S.D. and Zaikov, G.E., *Ozon i ego reaktsii s organicheskimi soedineniyami* (Ozone and Its Reactions with Organic Compounds), Moscow: Nauka, 1974.
5. Safiullin, R.L., Enikeeva, L.R., and Komissarov, V.D., *Kinet. Katal.*, 1989, vol. 30, no. 5, pp.1040–1044.
6. *Spravochnik khimika* (Chemist's Handbook), Nikol'skii, B.P., Ed., Moscow: Khimiya, 1964, vol. 3.
7. *Organic Chemistry of Sulfur, Oae, S.*, Ed., New York: Plenum, 1977.
8. Yur'ev, Yu.N., Razumovskii, S.D., Berezova, L.D., and Zelikman, E.S., *Zh. Org. Khim.*, 1975, vol. 11, no. 1, pp. 7–11.

ISSN 1070-4272, Russian Journal of Applied Chemistry, 2007, Vol. 80, No. 4, pp. 615–618. © Pleiades Publishing, Ltd., 2007.
Original Russian Text © A.E. Trofimov, I.S. Stepanova, A.V. Ten'kovtsev, 2007, published in Zhurnal Prikladnoi Khimii, 2007, Vol. 80, No. 4, pp. 627–631.

A New Approach to Synthesis of Organic/Inorganic Nanocomposites

A. E. Trofimov, I. S. Stepanova, and A. V. Ten'kovtsev

Institute of Macromolecular Compounds, Russian Academy of Sciences, St. Petersburg, Russia

Received September 20, 2006; in final form, January 2007

Abstract—The possibility of preparation of nanocomposite materials with improved physicomechanical properties by polycondensation of spirocyclic silicates and diisocyanates was elucidated. The thermomechanical, spectral, and thermogravimetric properties of the resulting materials were examined.

DOI: 10.1134/S1070427207040192

Polymer-based nanocomposite materials are today a subject of intensive research because particles <200 nm in size are promising as fillers for preparation of items with novel properties [1]. Owing to the large surface area of nanosized filler particles, the interaction between the polymeric matrix and the inorganic component is enhanced. This, in turn, substantially improves the mechanical characteristics of articles, compared to those prepared using conventional micron-sized fillers [2].

Nancomposites are typically prepared by (1) mechanically mixing or exfoliating an inorganic material in the polymer [3, 4]; (2) polymerization of a vinyl type monomer in a mixture with finely ground inorganic material [5]; or (3) formation of filler nanoparticles by sol–gel technique within a the polymeric matrix [6].

All the above-mentioned approaches have both advantages and major drawbacks. For example, mechanical mixing of the components and polymerization in the presence of a filler suspension typically makes problematic a uniform distribution of the particles in the bulk of the composite, which markedly affects the strain-strength characteristics of the articles, namely, the relative elongation and the tensile stress decrease [1]. An alternative approach utilizing the sol–gel technique for generation of nanoparticles of SiO_2 [7] or other oxides, e.g., TiO_2 [8], allows preparation of items with uniform distribution of the particles within the polymeric matrix. In this case, the most widely used synthetic procedure consists in dissolution of a polymer or oligomer, prepared in advance, in a solvent common to the macromolecular compound and tetraalkoxylsilane, with the subsequent initiation of hydrolysis of the orthosilicate [7]. Despite the mild reaction conditions, this method of preparation of nanocomposites also has major drawbacks. For example, its application is substantially restricted by the insolubility of most of polymers in aqueous-organic media required for sol–gel processes. Also, the very high shrinkage (typically 50–75%) results in disintegration of articles prepared from composites obtained by this method [9]. To avoid these difficulties, Ellsworth and Novak [9, 10] suggested to prepare the composites from monomers to be involved in concurrent sol–gel and polymerization processes when exposed simultaneously to radical initiators and water. This made it possible to reduce the shrinkage to 15–20% owing to the lack of volatiles. However, such an approach does not allow use of the polycondensation reaction, whereas a large number of plastics widely used in industry belong to polycondensation polymers.

In this study, we elucidated the possibility of preparing nanocomposite materials via two concurrent polycondensation processes: preparation of SiO_2 by hydrolysis of spirocyclic orthosilicates and synthesis of the polymeric matrix by the reaction of the diol being eliminated with diisocyanate.

As the model system we chose commercially available 1,6-hexamethylene diisocyanate and spirocyclic 2,2-dimethylpropane-1,3-diol orthosilicate [11]. The choice of this system was dictated by the facts that (1) the polycondensation of diols with diisocyanates is not accompanied by release of by-products and (2) the synthesis of polyurethanes and formation of silica gel particles by sol–gel technique proceed at close temperatures (80–100°C). This decreases the prob-

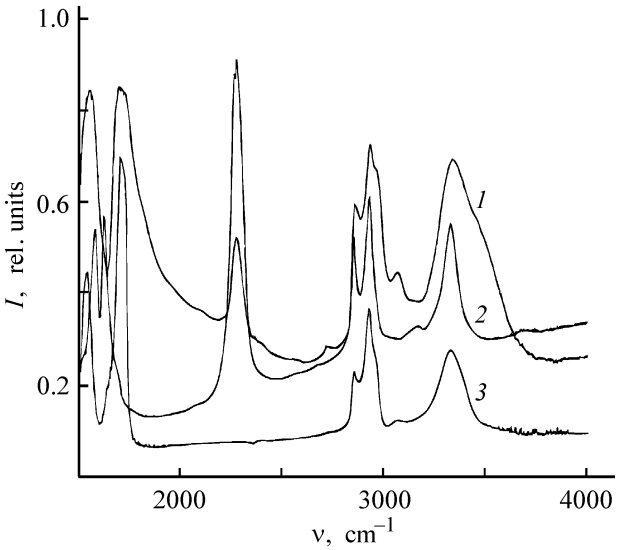

Fig. 1. IR spectra (KBr, IFS88 (Bruker) spectrometer). (*I*) Intensity and (ν) wavenumber. (*1*) Model polyurethane [poly-(2,2-dimethyl-1,3-propylene 1,6-hexamethylenecarbamate]; (*2*) model polyurea [poly(1,3-propylene-1,6-hexamethyleneurea]; and (*3*) nanocomposite.

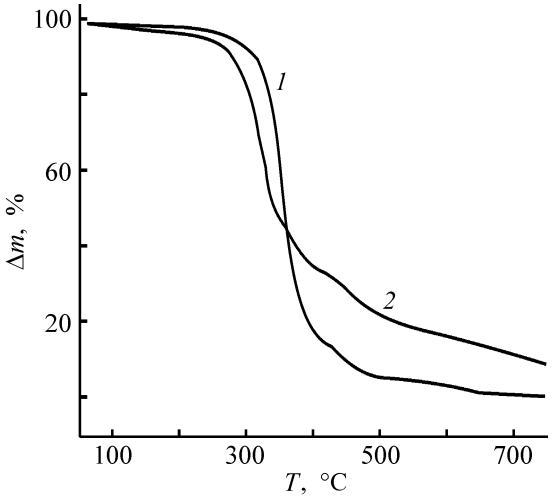

Fig. 2. Thermal gravimetric analysis curves. TGA-7 derivatograph (Perkin–Elmer); air; heating rate 10 K min^{-1}. (Δ*m*) mass loss and (*T*) temperature. (*1*) Model polyurethane [poly-(2,2-dimethyl-1,3-propylene 1,6-hexamethylenecarbamate] and (*2*) nanocomposite.

ability that the SiO_2 particles will grow in size because of an increase in the viscosity of the system and the diffusion limitations that preclude dehydration of the silanol groups on the filler surface.

Introduction of a controlled amount of water causes hydrolysis of the Si–O bonds of spirosilane and release of the diol, which further reacts with the diisocyanate. Heating the components at 100–120°C for 2–2.5 h yields a composite material suitable for preparation, under the reactive molding conditions, of transparent films and solid items. It should be noted that the shrinkage of the item being formed does not exceed 8–10%. Combined with strong adhesion to metal and glass, this makes the system of interest suitable for preparation of coatings.

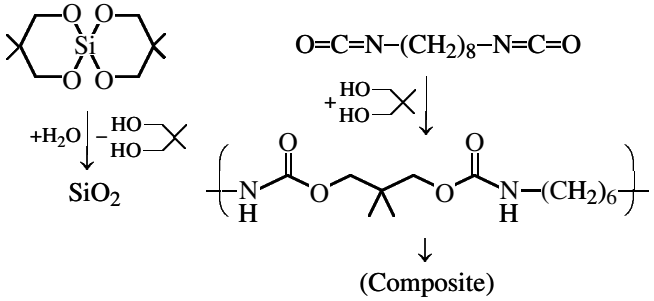

General reaction scheme.

Clearly, introduction of water into the reaction mixture containing hydrolyzable isocyanate groups can result in formation of urea and cyanurate fragments in the polymeric part of the composite. The IR spectra of the composite (Fig. 1) do not contain bands at 1620 and 2250 cm^{-1} corresponding to vibrations of the carbonyl from the urea and isocyanate fragments, respectively. At the same time, the spectrum of unfilled poly(2,2-dimethyl-1,3-propylene 1,6- hexamethylenecarbamate) contains a rather intense absorption band with a maximum at 2250 cm^{-1}. This suggests that, under the actual conditions, the rate of hydrolysis of the Si–O bonds and formation of urethane bonds is much higher than that of hydrolysis of the isocyanate groups. Thus, the resulting polyurethane matrix is virtually free of the ureide and cyanurate fragments:

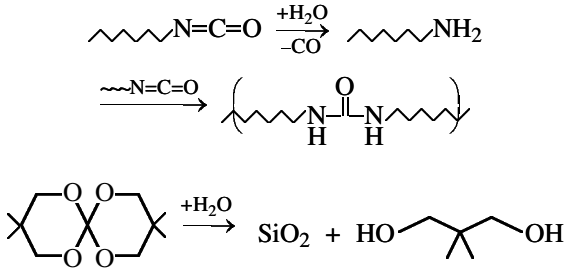

Comparison of the thermal properties of the model polymer and composite (Fig. 2) suggests that they are close in heat resistance. In both cases, upon heating in air, a 5% mass loss is observed near 295°C. However, upon further increase in temperature, the unfilled polymer virtually breaks down (mass loss 80%) at 345°C, while the composite loses 50% of its mass. In the latter case, the organic component completely disappears near 500°C, the residual mass being ~12%,

which approximately corresponds to the calculated amount of SiO_2 in the material.

Figure 3 presents a cross-sectional micrograph of the nanocomposite film, obtained by scanning electron microscopy. It is seen that the filler nanoparticles have a size of 50–100 nm and a spherical shape. Notably, the SiO_2 particles have blurred boundaries, evidently, due to the reaction between the surface silica gel groups with diisocyanate and formation of partially cross-linked or branched organic/inorganic hybrid structures:

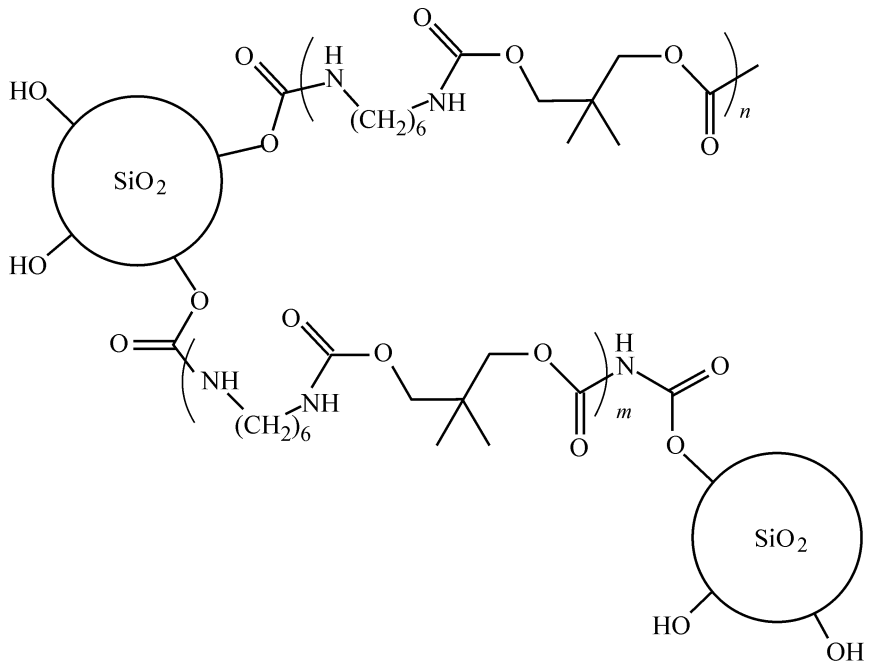

This is also evidenced by the results of an examination by polarization optical microscopy: The flow point of the composite material exceeds 260°C, while the model polymer prepared from hexamethylene diisocyanate and 2,2-dimethyl-1,3-propanediol transforms to the viscous-flow state already at 210°C.

The mechanical properties of the composite material significantly differ from those of the model polyurethane. As already noted, under the reactive molding conditions, optically transparent self-supporting films and solid items can be obtained from the nanocomposite, whose strain-strength characteristics are fairly high for this polymer type. In particular, the modulus of elasticity of the films was estimated at 1.0 GPa, tensile strength, at 35 MPa, and relative elongation, at 22%. Under analogous conditions, only brittle non-self-supporting films were prepared from the model polymer, whose mechanical properties could not be determined. However, we failed to prepare items by molding from the composite melt, whereas solid items can be prepared by this method from the model polyurethane. This observation also confirms the assumption that the nanocomposite has a branched and/or partially cross-linked nature.

Thus, the approach we suggest, which combines synthesis of SiO_2 by sol–gel technique with polycondensation of the released diol with diisocyanate, allows preparation of nanocomposite materials with filler

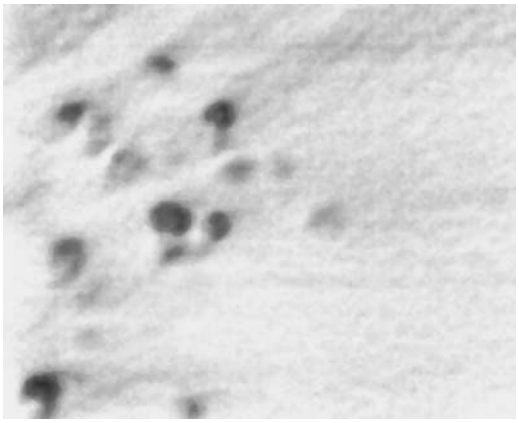

Fig. 3. Electron micrograph of the nanocomposite film cross section [S4800 field emission scanning electron microscope (Hitachi), 1 kV].

particles up to 100 nm in size, which greatly surpass materials based on unfilled polymer in the strain-strength characteristics.

EXPERIMENTAL

Synthesis of 3,3,9,9-tetramethyl-1,5,7,11-tetraoxa-6-silaspiro[5.5]undecane. To a solution of 20.8 g (0.2 mol) of 2,2-dimethyl-1,3-propanediol in 100 ml of absolute toluene, a solution of 11.5 g (0.1 mol) of silicon tetrachloride in 20 ml of absolute toluene was added with stirring. The mixture was refluxed in an argon stream for 4 h, then cooled to 5°C, kept for 3 h, and filtered. After the solvent was distilled off, 18.2 g (76%) of the target product was obtained as a colorless solid substance. Since the product polymerizes in storage, it was kept as a 20% solution in toluene at 5°C.

Found, %: C 58.49, H 8.20.

Calculated, % C 59.69, H 8.68.

^{1}H NMR (Bruker, DRX 500, $CDCl_3$, 25°C, δ, ppm: 0.85 (s, 12H, CH_3) and 3.45 (s, 8H, CH_2).

Synthesis of poly(2,2-dimethyl-1,3-propylene 1,6-hexamethylenecarbamate)-SiO_2 composite. To 1.15 g (0.005 M) of 3,3,9,9,-tetramethyl-1,5,7,11-tetraoxa-6-silaspiro[5.5]undecane, 1.62 g (0.01 M) of 1,6-hexamethylene diisocyanate was added, and the resulting mixture was heated to 80°C. Next, an equivalent amount of water was added, whereupon the mixture was left at 80°C for 3 h. To prepare a film, a viscous transparent melt was poured onto a glass substrate and kept at 80°C for 12 h. A uniform transparent composite film was detached from the substrate and subjected to mechanical tests.

Synthesis of poly(2,2-dimethyl-1,3-propylene 1,6-hexamethylenecarbamate) (model polymer). Hexamethylene diisocyanate [1.62 g (0.01 mol)] was mixed with 1.04 g (0.01 mol) of 2,2-dimethyl-1,3-propanediol, and the mixture was heated to 80°C. After 3 h, a viscous transparent melt was poured onto a glass substrate and kept at 80°C for 12 h. This yielded a transparent brittle polymer.

CONCLUSIONS

(1) A new method was suggested for preparation of transparent film-forming nanocomposites containing highly dispersed silicon dioxide.

(2) It was demonstrated that simultaneous sol–gel process yielding silica gel particles and polycondensation of the released diol with diisocyante yields a composite material with the filler particle size under 100 nm. The mechanical properties of items thereof significantly surpass those prepared from unfilled polyurethane.

REFERENCES

1. Moniruzzaman, M. and Winey, K.I., *Macromolecules*, 2006, vol. 39, no. 16, pp. 5194–5205.
2. Tan, E.P.S. and Lim, C.T., *Composites Sci. Technol.*, 2006, vol. 66, no. 9, pp. 1102–1111.
3. Plummer, C.J.G., Garamszegi, L., Leterrier, Y., et al., *Chem. Mater.*, 2002, vol. 14, no. 2, pp. 486–488.
4. Ishida, H., Campbell, S., and Blackwell, J., *Chem. Mater.*, 2000, vol. 12, no. 5, pp. 1260–1267.
5. Lee, Sung-Il, Hang, Y.B., Nham, K.S., and Lee, Y.-S., *Polym. Adv. Technol.*, 2005, vol. 16, no. 5, pp. 328–331.
6. Donghai Sun, Rui Zhang, Zhimin Liu, et al., *Macromolecules*, 2005, vol. 38, no. 13, pp. 5617–5624.
7. Bandyopadhyay, A., Sarkar, M., and Bhowmick, A.K., *J. Mater. Sci.*, 2005, vol. 40, no. 19, pp. 5233–5241.
8. Perrin, F.X., Nguyen, V.N., and Vernet, J.L., *Polym. Int.*, 2002, vol. 51, no. 10, pp. 1013–1022.
9. Ellsworth, M.W. and Novak, B.M., *J. Am. Chem. Soc.*, 1991, vol. 113, no. 7, pp. 2756–2758.
10. Ellsworth, M.W. and Novak, B.M., *Chem. Mater.*, 1993, vol. 5, pp. 839–844.
11. Andrianov, K.A., *Metody elementoorganicheskoi khimii: Kremnii* (Methods of Organometallic Chemistry: Silicon), Moscow: Nauka, 1968.

ISSN 1070-4272, Russian Journal of Applied Chemistry, 2007, Vol. 80, No. 4, pp. 619–622. © Pleiades Publishing, Ltd., 2007.
Original Russian Text © Yu.N. Sazanov, G.N. Fedorova, E.M. Kulikova, D.M. Kostycheva, A.V. Novoselova, A.V. Gribanov, 2007, published in Zhurnal Prikladnoi Khimii, 2007, Vol. 80, No. 4, pp. 632–636.

MACROMOLECULAR CHEMISTRY AND POLYMERIC MATERIALS

Cocarbonization of Polyacrylonitrile with Lignin

Yu. N. Sazanov, G. N. Fedorova, E. M. Kulikova, D. M. Kostycheva, A. V. Novoselova, and A. V. Gribanov

Institute of Macromolecular Compounds, Russian Academy of Sciences, St. Petersburg, Russia

Received February 8, 2007

Abstract—The boundary and parameters of the thermochemical reaction of lignin and polyacrylonitrile were determined by dynamic and isothermal thermal analysis. The time, temperature, and concentration effects of formation of composites, allowing preparation of new carbonizates with enhanced heat resistance and noticeably higher carbon residue, were studied.

DOI: 10.1134/S1070427207040209

In our previous papers concerned with the possibility of preparing new composite materials (CMs) based on polyacrylonitrile (PAN) and other synthetic polymers we noted the positive influence of PAN on the characteristics of the resulting CMs. However, we encountered in this line of investigation some technological and economical problems [1–3]. To avoid these difficulties, we made an attempt to prepare CMs with PAN on the basis of natural macromolecular compounds [4–6]. The possibility of preparing CMs based on binary mixtures of PAN with cellulose ethers, chitin, and chitosan with high heat resistance, mechanical strength, and ability to carbonization, has been shown. The results obtained allowed formulation of basic principles for preparation of carbon composites by thermochemical cocarbonization of polymers [7].

In this study, we used lignin (LG) as a component in combination with PAN. It is well known that LG is a component of wood (25–30 wt %) and is a complex aromatic substance with uncertain chemical structure [8–10] and molecular weight of $(2–6) \times 10^4$. This structure is based on various phenol derivatives randomly bound by oxymethylene bonds. As regards the reactivity, LG reacts with many organic substances along the pathways of electrophilic and nucleophilic substitution [8]. As regards polymers, there are some publications on modification of a series of thermosetting polymers, such as phenol–formaldehyde, melamine, urea, and epoxy resins and also rubbers. These data are concentrated in special literature (patents, technical reports, processing regulations) and mainly refer to description of the blending procedure and characteristics of the resulting CMs [11–13]. However, these data are insufficient for making certain conclusions on features of polymer-analogous transformations involving LG. Since there are no data on the reaction of PAN with LG, we studied thermochemical reactions of PAN with LG under the conditions of dynamic and isothermal heating of a blend of these polymers in order to elucidate the possibility of preparing CMs based on these substances with account of principles of cocarbonization of polymers [7].

EXPERIMENTAL

As the initial compounds we used PAN synthesized by the radical polymerization mechanism [14] and LG powder recovered using acid hydrolysis [15]. Dynamic thermal analysis was performed on an MOM derivatograph (model C, Hungary) at a heating rate of 10 deg min^{-1} in air; weighed portions 50–100 mg, ceramic crucibles. Dynamic and isothermal analyses of PAN, LG, and their mechanical mixtures in the form of powders at a PAN : LG ratio equal to 25 : 75, 50 : 50, and 75 : 25 were performed on an installation for thermovolumetric analysis (TVA) [16] in a nitrogen medium and in a vacuum.

The first stage of studying thermochemical reactions of LG, PAN, and their mixture was identification of the main thermal parameters characterizing the behavior of the samples during their heating from room temperature to the temperature of complete decomposition and evaporation of thermal degradation products or to a certain temperature limit. The TG curves of the integral weight loss in heating of the samples at a constant rate to 1000°C are shown in Fig. 1a.

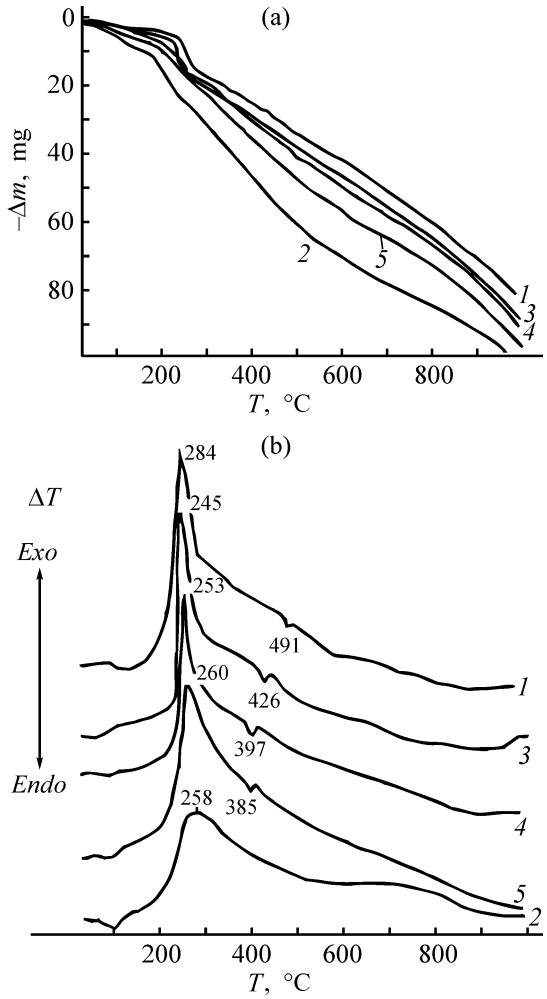

Fig. 1. (a) TG and (b) DTA curves of LG and PAN samples and their powder blends under dynamic heating at a rate of 10 deg min^{-1} in air. (Δm) Weight loss, and (T) temperature; the same for Fig. 3. (*1*) PAN, (*2*) LG; LG : PAN: (*3*) 25 : 75, (*4*) 50 : 50, and (*5*) 75 : 25.

The thermal effects accompanying thermochemical transformations of the samples in the same temperature range, recorded simultaneously with the TG curve, are presented in Fig. 1b (DTA curves). Comparison of the TG curves of the initial products and their blends shows that decomposition of the blend samples proceeds in the temperature range limited by the TG curves of LG and PAN; the curve shapes vary smoothly with the ratio of the initial reactants. The absence of abrupt changes in the kinetics of the weight loss during the entire period of thermal degradation suggests only a weak reaction of LG with PAN even in the period of the maximum thermal activity of both components in the temperature range 200–300°C. The DTA curves furnish more information; comparison of these curves reveals the occurrence of a certain chemical reaction of PAN with LG. The presence of LG in the mixture shifts the exothermic effect to lower temperatures; in this case, the temperature of the exothermic effect of PAN cyclization becomes lower as the concentration of LG decreases. It is likely that phenols formed by thermal decomposition of LG exert a catalytic effect on the cyclization of PAN; however, the possibility of these reactions is limited by the spatial arrangement of the components. For example, the dominating effect at high concentrations of LG is thermal degradation of LG, which is confirmed by broadening of the exothermic peak similar to degradation of pure LG (Fig. 1b, curve *5*). It is evident that, at low concentration of LG, the catalytic cyclization of PAN due to phenols released in degradation of LGs predominates. In this case, the peak of the exothermic effect of PAN cyclization is shifted to low temperatures by 39°C (Fig. 1b, curve *3*).

In addition, the temperature of the endothermic effect in the range 491–385°C decreases as the concentration of PAN becomes lower. The nature of this effect remains to be elucidated; however, it was assumed [17] that some ordered structure is formed in carbonization of PAN and this structure melts in the above temperature range. This phenomenon can be confirmed in an independent structural study using spectral analysis.

The shapes of TG and DTA curves in the initial stage of weight loss up to 230°C suggest that the removal of volatile products from LG–PAN mixtures proceeds due to thermal degradation of LG and the composition of these products (acidic water, traces of phenol and its substituted derivatives) confirms the prevalence of LG degradation. It is likely that the presence of phenols initiates cyclization of PAN at a lower temperature and thus shifts the equilibrium of feasible concurrent reactions of PAN thermal degradation toward cyclization, in comparison with the reactions of PAN with the products of thermal degradation of LG. Such a development of thermochemical reactions in the LG–PAN blend hampers realization of the first principle of cocarbonization: coincidence of temperature ranges of high thermal reactivity for both reacting components. To avoid the activation of low-temperature products of thermal degradation of LG, we performed experiments on isothermal storage of LG and its blends with PAN at different temperatures and compositions of the surrounding medium. These experiments also allowed determination of the limits of thermal stability of the samples with the aim to provide complete homogenization required for reliable contact of the reacting compounds under conditions of heterogeneous synthesis. Preliminary measurements of the thermal stability of LG in isothermal storage for 3 h at 150°C

showed that LG is fairly stable in air. During this period, with the 7% weight loss during heating to 150°C disregarded, the weighed portion of LG loses no more than 5% of its weight and this occurs only in the first hour of heating. Thus, this treatment allows removal of the major part of low-molecular-weight products of the initial thermal treatment of LG. Furthermore, with the aim to make the limits of LG thermal stability closer to the temperature range of a high thermal reactivity of both LG and PAN, we performed stepwise isothermal heating of the samples in a nitrogen medium. The results of this series of experiments (Fig. 2) show that, upon isothermal heating for 6 h at 200°C, LG losses approximately 17% of its weight without stabilization of this process. With further heating, thermal degradation proceeds at the same rate in isothermal and dynamic modes of heating of the sample (Fig. 2, curve *2*).

Addition of PAN powder to LG results in some thermal stabilization of LG, which is seen from a comparison of the curves of weight loss in the isothermal mode at 200 and 300°C for the LG–PAN mixtures at various concentrations of the initial polymers. It should be noted that, at the PAN content in the blend equal to 25%, the weight loss of LG at 200°C due to removal of low-molecular-weight products of thermal degradation is minimal. The effect of PAN is also noticeable at a heating temperature elevated to 300°C (Fig. 2, curve *5*). Thus, we can conclude that the influence of PAN on thermal stabilization of LG and the kinetics of thermochemical reactions of PAN with LG is positive. Further increase in the PAN concentration in the blend results in a gradual approach of the thermal characteristics of the blends to the characteristics of the pure PAN powder.

Typical curves of dynamic TG–DTA in air, which characterize the influence of isothermal heating of the blend LG : PAN = 75 : 25, are shown in Fig. 3. Comparison of these curves with those presented in Fig. 1 reveals a certain increase in the thermal stability of the blend in air and an insignificant variation of the kinetics of thermochemical reactions caused by preliminary removal of low-molecular products of LG degradation and partial cyclization of PAN. Isothermal heating results in a noticeable increase in the carbon residue (CR) to 62% at 600°C; for unheated samples this value is 43%, and at 1000°C the CR values are 15 and 0%, respectively. Figure 3 also shows the TG and TDA curves of the same blend with a large weighed portion (curves 7). A noticeable increase in all the thermal parameters of this sample suggests a significant influence of the "diffusion factor" on the kinetics of carbonization of the LG–PAN blend.

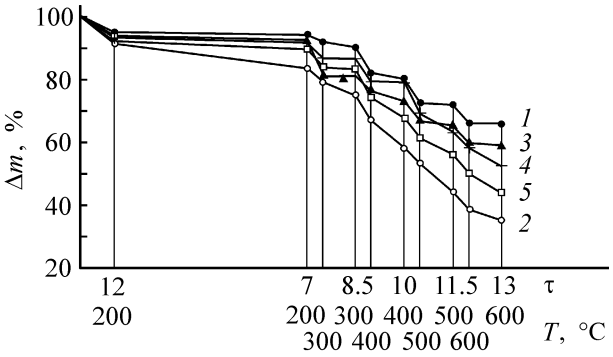

Fig. 2. TG curves in stepwise isothermal heating of (*1*) PAN, (*2*) LG, (*3*) LG : PAN = 25 : 75, (*4*) LG : PAN = 50 : 50, and (*5*) LG : PAN = 75 : 25 in a nitrogen medium. Heating rate in the transition stage 3 deg min^{-1}. (Δm) Weight residue, (T) temperature, and (τ) time of stepwise heating of the samples.

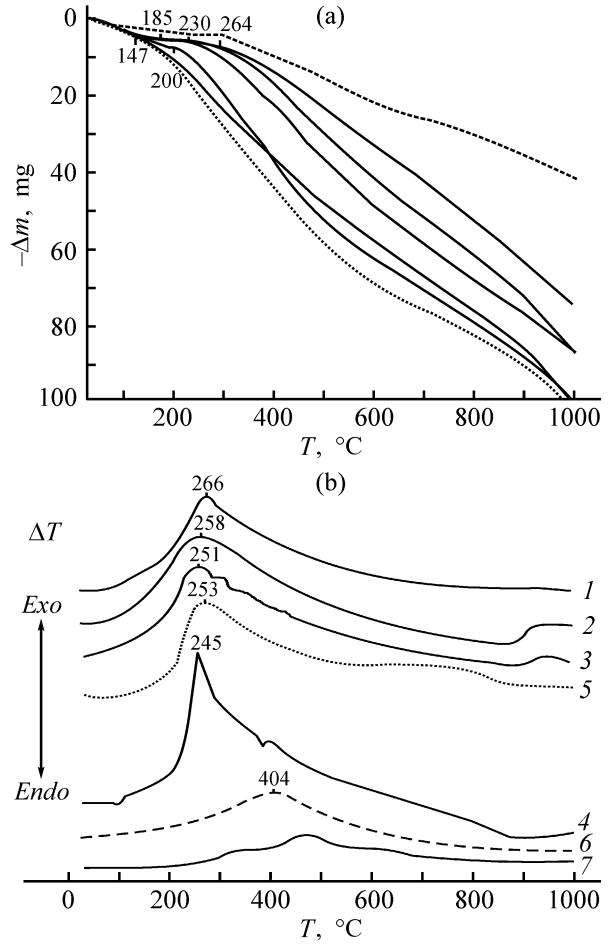

Fig. 3. (a) TG and (b) DTA curves of (*5*) LG and (*6*) PAN samples heated at 300°C for 6 h in N_2: (*1*) blend LG : PAN = 75 : 25, (*2*) blend LG : PAN = 75 : 25 heated at 400°C for 6 h in N_2, (*3*) LG heated at 200°C for 6 h in N_2, (*4*) unheated blen LG : PAN = 75 : 25, and (*7*) blend LG : PAN = 75 : 25 heated at 400°C for 6 h in N_2, weighed portion 500 mg.

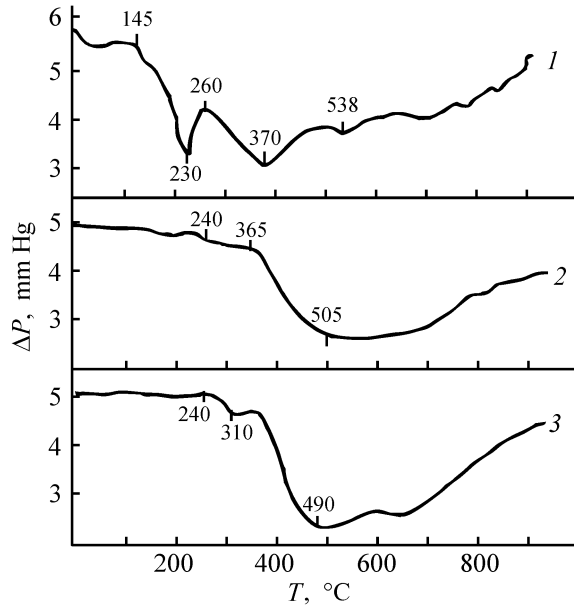

Fig. 4. TVA curves of the LG samples and LG : PAN = 75 : 25 blend, weighed portion 50 mg. (ΔP) Pressure differential and (T) temperature. (*1*) LG (weighed portion 50 mg), heating rate 3 deg min^{-1}, (*2*) LG + PAN after isothermal heating at 400°C for 1 h in N_2, and (*3*) LG + PAN after isothermal heating at 400°C for 6 h in N_2, weighed portion 600 mg.

It also demonstrates that procedures hindering diffusion of low-molecular-weight products of thermal decomposition from the blend samples are efficient in shifting the thermochemical reactions toward intermolecular structuring of the blend components.

This assumption is confirmed by the experiments on dynamic thermal analysis by the TVA method (Fig. 4). These data show that gas evolution in heating of the samples of the same LG–PAN blend noticeable decreases in comparison with pure LG both after additional isothermal heating and on making larger the weighed portion of the sample; accordingly, the CR increases from 15 for LG to 64% for the heated blend with a large weighed portion.

CONCLUSIONS

(1) A study of the thermochemical reaction of lignin with polyacrylonitrile in the temperature range 20–1000°C showed that the cyclization temperature of polyacrylonitrile decreases due to a catalytic effect of the products of thermal degradation of lignin.

(2) The thermal stability of lignin increases upon addition of limited amounts of polyacrylonitrile in isothermal heating of the composites in an inert medium at 200–300°C.

(3) Lignin–polyacrylonitrile carbonizates differing in their characteristics from those obtained from the initial polymers were prepared.

ACKNOWLEDGMENTS

The authors are grateful to the A.M. Bochek's laboratory for submitting the lignin samples.

REFERENCES

1. Sazanov, Yu.N., Novoselova, A.V., Amsharov, K.Yu., et al., *Zh. Prikl. Khim.*, 2005, vol. 78, no. 5, pp. 810–813.
2. Sazanov, Yu.N., Spirina, T.N., Shibaev, L.A., et al., *J. Therm. Anal.*, 1990, vol. 36, pp. 2329–2338.
3. Silinskaya, I.G., Spirina, T.N., Novoselova, A.V., et al., *Vysokomol. Soedin., Ser. A*, 1991, vol. 33, no. 8, pp. 1617–1624.
4. Sazanov, Yu.N., Nud'ga, L.A., Petrova, L.A., et al., *Zh. Prikl. Khim.*, 2004, vol. 77, no. 8, pp. 1366–1369.
5. Sazanov, Yu.N., Nud'ga, L.A., Novoselova, A.V., et al., *Zh. Prikl. Khim.*, 2004, vol. 77, no. 4, pp. 643–648.
6. Sazanov, Yu.N., Novoselova, A.V., Nud'ga, L.A., et al., *Zh. Prikl. Khim.*, 2005, vol. 78, no. 8, pp. 1344–1348.
7. Sazanov, Yu.N. and Gribanov, A.V., *Zh. Prikl. Khim.*, 2006, vol. 79, no. 3, pp. 440–445.
8. Kislitsyn, A.N., *Piroliz drevesiny* (Pyrolysis of Wood), Moscow: Lesn. Prom–st., 1990.
9. *Wood Structure and Composition*, Lewin, V. and Goldstein, L.S., Eds., New York: Marcel Dekker, 1991.
10. Kononov, G.N., *Khimiya drevesiny i ee osnovnykh komponentov* (Chemistry of Wood and Its Main Components), Moscow: Mosk. Gos. Univ. Lesa, 1999.
11. Arbuzov, V.V., *Kompozitsionnye materially iz lignininykh veshchestv* (Composite Materials from Lignin Substances), Moscow: Ekologiya, 1991.
12. Zakis, G.F., *Funktsional'nyi analiz ligninov i ikh proizvodnykh* (Functional Analysis of Lignins and Their Derivatives), Riga: Zinatne, 1987.
13. Kadla, J.F., Kubo, S., Venditti, R.A., et al., *Carbon*, 2002, vol. 40, pp. 2913–2930.
14. Sazanov, Yu.N., Shirokov, N.A., and Goltsin, B.E., *Thermochim. Acta*, 1978, vol. 24, pp. 81–88.
15. Obolenskaya, A.V., El'nitskaya, Z.P., and Leonovich, A.A., *Laboratornye raboty po khimii drevesiny i tsellyulozy* (Laboratory Works on Chemistry of Wood and Cellulose), Moscow: Ekologiya, 1991.
16. Sazanov, Yu.N. and Sysoev, V.A., *Eur. Polym. J.*, 1974, vol. 10, pp. 867–869.
17. Gribanov, A.V. and Sazanov, Yu.N., Abstracts of Papers, *2 Mezhdunarodnaya konferentsiya "Uglerod: fundamental'nye problemy nauki, materialovedeniya, tekhnologii"* (2nd Int. Conf. "Carbon: Fundamental Problems of Science, Materials Science, and Technology"), Moscow, 2003, p. 87.

ISSN 1070-4272, Russian Journal of Applied Chemistry, 2007, Vol. 80, No. 4, pp. 623–628. © Pleiades Publishing, Ltd., 2007.
Original Russian Text © B.A. Zaitsev, G.I. Khromova, I.D. Shvabskaya, 2007, published in Zhurnal Prikladnoi Khimii, 2007, Vol. 80, No. 4, pp. 637–642.

MACROMOLECULAR CHEMISTRY AND POLYMERIC MATERIALS

Acid-Catalyzed Oligomerization of Aromatic Ethers (Rolivsans) with Terminal Styrene and Methacrylate Groups

B. A. Zaitsev, G. I. Khromova, and I. D. Shvabskaya

Institute of Macromolecular Compounds, Russian Academy of Sciences, St. Petersburg, Russia

Received December 14, 2006

Abstract—Cationic mechanism of transformation of unsaturated aromatic monomers contained in Rolivsans into thermosetting aromatic oligoethers with increased molecular weight was analyzed. The composition and chemical structure of Rolivsans as influenced by catalytic systems with various donor-acceptor properties were studied.

DOI: 10.1134/S1070427207040210

Rolivsans are low-viscosity thermosetting resins of new type, formed by reactions of secondary aromatic diols, such as di-[4-(1-hydroxyethyl)phenyl] ether (**I**)

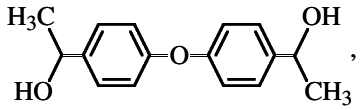

with methacrylic acid catalyzed by strong acids [1–5]. Their thermal treatment yields heat-resistant glassy network polymers [6–10] which are used in (micro)-electronics and electrical engineering.

It has been found previously that Rolivsans contain the following monomer aromatic ethers: 4,4'–CH_2=CH–PhOPh–CH=CH_2 (M1), 4,4'–CH_2=CH–PhOPh–CH(CH_3)OCO–C(CH_3)=CH_2 (M2), 4,4'–CH_2=C(CH_3)–COO(CH_3)CH–PhOPh–CH(CH_3)OCO–C(CH_3)=CH_2 (M3), and oligoethers (OL) with terminal styrene-like and methacrylate groups.

The monomer-oligomer composition and properties of Rolivsans can be varied in a wide range depending on the synthesis conditions [3–5]. Low-viscosity compositions (500–1500 mPa s^{-1}) containing no solvents and predominantly consisting of monomers M1, M2, and M3 and small amounts (15–30%) of low-molecular-weight unsaturated oligomers (dimers and trimers) can be used as heat-resistant insulating casting and impregnating compounds.

In this study, we examined the formation of monomer–oligomer formulations with molecular weight of components increased due to higher content of aromatic oligoethers with terminal unsaturated groups. These formulations yield thermosetting polymers with controlled network density and can be used to prepare heat-resistant coatings and binders [11–12].

EXPERIMENTAL

The IR spectra were recorded on a Specord 75-IR device (thin films or $CHCl_3$ solutions). The exclusion liquid chromatography (ELC) of Rolivsans was performed on a GPC Waters chromatograph equipped with Ultrastyrogel (500 Å) columns at 20°C, using toluene as eluent. The number-average molecular weights of oligomers $\overline{M}_n$ were determined with a Hitachi–Perkin–Elmer 115 vapor osmometer. The sample unsaturation was studied on a ADS-4 ozonizer at 0°C (CCl_4 solvent). The viscosity and viscoelastic properties of Rolivsan MV-1 and of the products of its oligomerization were studied on a PIRSP-1 rheogoniometer with a cone-plate working unit (cone diameter 2 cm, cone angle 1°). The velocity gradients were varied from 2×10^{-2} to 4×10^{2} s^{-1}, and circular frequencies, from 2×10^{-2} to 10 s^{-1}.

Samples of Rolivsan MV-1 (series I and II) were prepared in accordance with TU (Technical Specifications) 6-36-57-0–91 by condensation of di-[4-(1-hydroxyethyl)phenyl] ether (**I**) with methacrylic acid in the presence of *p*-toluenesulfonic acid monohydrate (TSA-M) [3–5]; their compositions and properties are listed in Table 1.

Oligomer no. 1 was isolated from the initial reaction mixture (Rolivsan VM-1, series I) after its dilution with chloroform and subsequent precipitation

Table 1. Properties of Rolivsan MV-1*

Series	Composition, wt %				>C=C<, mol g^{-1}	$\bar{M}_n$	n_D^{20}	η^{25}, mPa s^{-1}	d^{20}, g cm^{-3}	τ^{140}, h
	M1	M2	M3	OL						
I	13	31	23	33	0.0058	400	1.585	1500	1.09	1.5
II	13	26	18	43	0.0056	420	1.590	1800	1.09	2.5

* >C=C< is the degree of unsaturation of oligomer, mole of double bonds per gram of product; $\bar{M}_n$, number-average molecular weight; and τ^{140}, time of gelation at 140°C.

with ethanol. The efficiency of oligomer isolation was monitored chromatographically (ELC) by the absence of peaks belonging to monomers M1, M2, and M3 in the product isolated. After a fourfold reprecipitation, the oligomer contained insignificant amounts (2–4%) of the initial monomers; the monomer-free product was obtained only after an eightfold reprecipitation. The properties of oligomer no. 1 were as follows: mp ~80°C, $\bar{M}_n$ ~ 1650, content of dimers with $\bar{M}_n$ ~500 (ELC data) 2–4%; found (%): C 79.6, H 6.5.

The degree of unsaturation of oligomer no. 1 was 0.37 mole of double bonds per 100 g of the product.

Two catalytic systems (CS A and CS B) were tested in oligomerization of Rolivsans catalyzed by TSA-M. Catalytic system A [solution of TSA-M (19.80 wt %) in polyphenyl ether (PPE, *m*-$C_{30}H_{22}O_4$, analytically pure grade, 5F 4E brand, mp 28°C] was prepared by through trituration of TSA-M (8.7841 g, 99% main compound) with liquid PPE (35.1365 g). Catalytic system B is a glycerol-like solution of TSA-M (23.63 wt %) in Cellosolve.

The acid-catalyzed oligomerization was performed by thorough mixing of Rolivsan with CS and storage of the homogenized composition at room temperature or at elevated temperature for a given time; then the composition and properties of the resulting compound were analyzed (Table 2).

To prepare oligomer nos. 2 and 3, CS A (1.05 g) was added with stirring to Rolivsan MV-1, series I (98.95 g), the homogenized composition was heated at 80°c for 1 h 35 min, and a sample was taken for isolation of OL no. 2. The process was continued for 2 h 40 min, and OL no. 3 was isolated from the reaction mixture. The product compositions were studied by ELC and IR spectroscopy. The composition of the sample containing OL no. 2 before isolation was as follows, wt %: 9 M1, 18 M2, 17 M3, and 56 OL. The sample was diluted with chloroform; the oligomer was precipitated with ethanol and dried at 20°C at reduced pressure. The precipitated product contained (wt %): 3 M1, 4 M2, 6 M3, and 87 OL no. 2, it is soluble in acetone and chloroform, $\bar{M}_n$ 1000. Oligomer no. 3 isolated by the similar procedure contained (wt %): 1 M1, 2 M2, 4 M3, and 93 OL; $\bar{M}_n$ 1220.

To prepare oligomer nos. 4 and 5, CS B (0.80 g) was added with stirring to Rolivsan MV-1, series I (99.20 g), and then one portion (50 g) of the homogenized composition was heated at 80°C for 2 h 10 min, and another portion (50 g) was stored at 20°C for 21 days. The compositions of the resulting products were analyzed as described above. The composition of the sample containing OL no. 4 before isolation was as follows, wt %: 3 M1, 6 M2, 4 M3, and 87 OL. No monomers were found in OL no. 4 after an eightfold reprecipitation; mp 90–110°C; found (%): C 79.60, H 6.70; 0.0030 mol of double bonds per gram of product, $\bar{M}_n$ 3375. The composition of the sample containing OL no. 5 before isolation was as follows, wt %: 2 M1, 5 M2, 3 M3, and 90 OL (no. 5). After precipitation and drying, we obtained oligomer no. 5 as a light brown resin with mp 95–115°C. After reprecipitation in the presence of hydroquinone (1%), the melting point of OL no. 5 increased to 125–135°C; found (%): C 81.20, H 6.70; 0.0037 mol of double bonds per gram of product, $\bar{M}_n$ 2700.

As shown previously, cleavage of esters (such as methacrylates) [1–5] and cationic addition polymerization of divinyl aromatic monomers with proton transfer [13–18] are of particular importance in catalyzed reactions of aromatic ethers containing secondary alcohol groups with carboxylic acids, such as methacrylic acid (MAA). The cleavage of dimethacrylate of aromatic diol (**I**), which is the main component of Rolivsan M3, and subsequent dimerization of the resulting vinyl aromatic monomer M2 are typical examples of such transformations [19]:

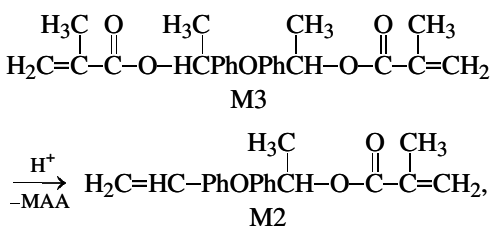

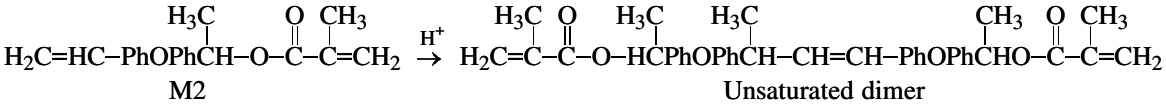

These data suggest that the intensified cleavage of methacrylates (M2, M3, and related compounds: dimers, trimers, etc.) and cationic addition polymerization of vinyl and divinyl aromatic compounds can yield linear unsaturated oligomers of the following type:

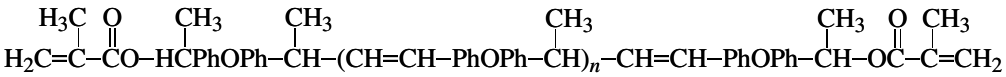

Oligomerization was studied using two series of Rolivsans with different compositions and properties (Table 1). It should be noted that homogenization (dissolution) of TSA-M powder by direct stirring with a resin was rather difficult, because a high local concentration of the catalyst sharply accelerates oligomerization in situ and causes encapsulation of the TSA-M particles with the oligomer formed. To improve the homogenization conditions, we suggested two catalytic systems (CS A and CS B) based on PPE and Cellosolve solvents with different donor-acceptor properties.

The conditions of the acid-catalyzed process and the composition and characteristics of the oligomerized compositions and oligomers are listed in Table 2. The oligomers were isolated by dilution of the compositions with chloroform and subsequent precipitation with ethanol. Changes in the monomer-oligomer composition under different conditions of oligomerization of Rolivsans were studied by ELC (Fig. 1), IR spectroscopy (Figs. 2, 3), and rheokinetics (Fig. 4).

Gel chromatograms (Fig. 1) show that the content of the monomers decreases with time, with a simultaneous increase in the content of oligomers (especially, dimers and trimers) with number-average molecular weights of 500 – 800. Oligomerization was performed at a fixed content of catalysts both at 20 ± 2°C and at elevated temperatures. With the temperature increasing from 60 to 80°C, the process rate grows by more than a factor of 4, which corresponds to the known empirical van't Hoff rule.

It should be noted that the characteristics of unsaturation, content of carbon (Table 2), and ^{1}H NMR spectra are not fully consistent with the chemical structure of the oligomers, given above. The calculated degrees of unsaturation and carbon content are slightly higher than the experimental values. This is probably due to formation of small amounts of saturated structures (e.g., 1-methyl-3-phenylindan), along with the main structure of 1,3-diphenyl-1-butene (*trans*) type, in the course of acid-catalyzed dimerization of styrene. We also cannot rule out the side

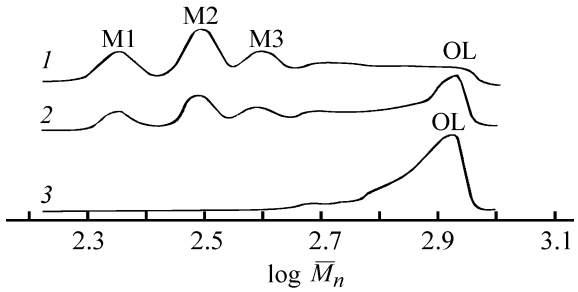

Fig. 1. Gel chromatograms of the (*1*) monomer–oligomer composition Rolivsan MV-1 (series I), (*2*) composition oligomerized by heating at 80°C for 1 h 35 min in the presence of CS A (content of TSA-M 1.19×10^{-2} M), and (*3*) oligomer no. 1 reprecipitated eight times to remove monomers. ($\overline{M}_n$) Molecular weight of oligomers.

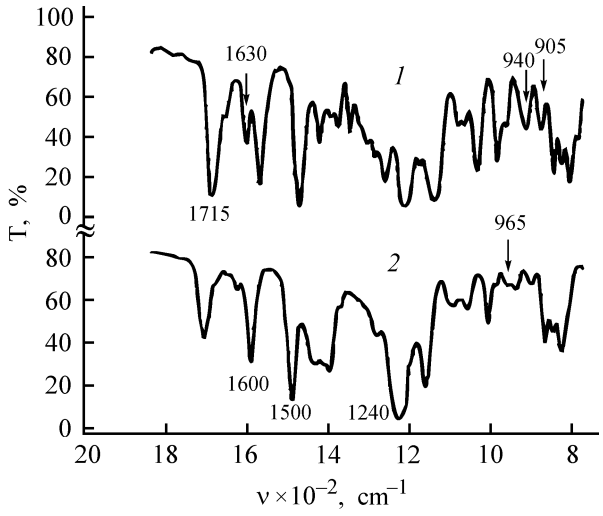

Fig. 2. IR spectra of the (*1*) monomer–oligomer composition Rolivsan MV-1 (series I) and (*2*) oligomer no. 3. (T) Transmission and (ν) wavenumber; the same for Fig. 3.

Table 2. Composition and properties of the reaction mixtures before and after oligomerization of Rolivsan MV-1 (series I)

Sample no.	Composition (oligomer)	CS	$c_{TSA-M} \times 10^2$, M	T, °C	τ, h	Composition, wt %				>C=C<, mol g^{-1}	Found, %		$\overline{M}_n$	mp, °C
						M1	M2	M3	OL		C	H		
1	Initial	–	–	–	–	13	31	23	33	0.0058	79.1	6.5	420	–
2	Oligomer no. 1*	–	–	–	–	1	2	6	91	–	–	–	–	–
3	Oligomer no. 1**	–	–	–	–	0	0	0	100	0.0037	79.6	6.5	1650	~80
4	Oligomerized	(A)	2.26	20	168	4	12	12	72	–	–	–	–	–
5	The same	(A)	2.26	80	1.2	4	8	7	81	–	–	–	–	–
6	〃	(A)	1.19	80	1.6	9	18	17	56	–	–	–	–	–
7	Oligomer no. 2	(A)	1.19	80	1.6	3	4	6	87	–	–	–	1000	–
8	Oligomer no. 3	(A)	1.19	80	2.7	1	2	4	93	–	–	–	1220	–
9	Oligomerized	(B)	2.02	80	0.45	4	8	7	81	–	–	–	–	–
10	The same	(B)	2.02	60	1.2	4	11	9	76	–	–	–	–	–
11	〃	(B)	1.08	20	504	3	6	4	87	–	–	–	–	–
12	Oligomer no. 4**	(B)	1.08	20	504	–	–	–	100	0.0030	79.6	6.7	3400	90–110
13	Oligomerized	(B)	1.08	80	2.2	2	5	3	90	–	–	–	–	–
14	Oligomer no. 5	(B)	1.08	80	2.2	–	–	–	–	0.0037	81.2	6.7	2700	125–135

* After fourfold reprecipitation; ** After eightfold reprecipitation.

reactions of oxidation on heating of unsaturated compounds in the presence of strong acids and of an addition of an aromatic solvent (toluene) and an inhibitor of the radical polymerization (hydroquinone) to the internal double bonds of the oligomer of Ar–CH(CH_3)–CH=CH–Ar type [16].

Similarly to the gel chromatograms, the IR spectra strongly change in the course of oligomerization. The initial IR spectrum of Rolivsan (Fig. 2, spectrum *1*) exhibits the absorption bands of the unsaturated and aromatic groups at 3080, 3060, 3030, 2975, 1630, 1600, 1500, 985, 965, 940, and 905 cm^{-1}, methyl and methylene groups at 2960, 2925, 2870, and 2850 cm^{-1}, methine group at 2900 cm^{-1}, and strong bands of the stretching vibrations of the carbonyl group in methacrylates at 1715 cm^{-1} and of aromatic ethers at 1240 cm^{-1} [4]. The IR spectrum of oligomer no. 3 (Fig. 2 spectrum *2*) isolated from the oligomerized composition (Table 2) shows the expected decrease in the intensity of the bands of the carbonyl groups at 1715 cm^{-1} and of out-of-plane bending vibrations H–C= at ~902 and 940 cm^{-1} belonging to the *p*–CH_2=CH–Ph–O–Ph and CH_2=C(CH_3)COO groups, respectively. Simultaneously, the band of H–C= out-of-plane bending vibrations of the –CH=CH– (*trans*) groups, whose concentration increases in the course of the stepwise dimerization reactions (cationic addition polymerization) of vinyl aromatic compounds [4, 19], grows in intensity.

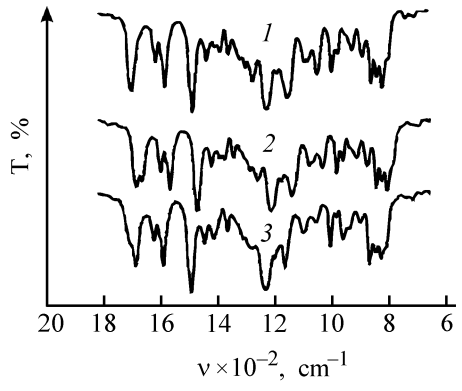

Fig. 3. IR spectra (20°C) of the monomer–oligomer composition Rolivsan MV-1 (series I) after its heating with CS B at a TSA-M content of 2.22×10^{-2} M. (*1*) 20°C (initial composition); (*2*) heated from 20 to 110°C over a period of 1 h and kept at 110°C for 2 h; (*3*) the same plus heating to 130°C over a period of 2 h.

Oligomerization was also performed at higher temperatures (110–180°C), at which the above reactions of addition polymerization are accompanied by crosslinking and cyclization. With heating, the intensity of the absorption bands of the terminal unsaturated groups at 1630, 940, and 905 cm^{-1} strongly decreases (Fig. 3, spectra *2*, *3*) owing to their consumption in copolymerization.

Another process of the cationic type, namely, cleavage of methacrylates to form vinyl aromatic compounds, methacrylic acid, and its copolymers, and also cationic addition polymerization of divinyl aromatic compounds occur simultaneously in the course of

oligomerization. With heating, the band of the stretching vibrations of the carbonyl group >C=O of the methacrylic ester at 1715 cm^{-1} splits, and a new band of the MAA carboxy group appears at 1700–1685 cm^{-1} (Fig. 3, spectra *2*, *3*) [19].

Since the viscosity and gelation time (viability) are the most important process characteristics of the thermosetting plastics, which determine the possibility of their processing into a polymeric material, we studied the rheological properties of Rolivsans in the course of their catalytic oligomerization.

As can be seen from Fig. 4, each curve can be divided into two portions: that with comparatively slowly increasing viscosity, corresponding to the initial stage of the process, and that with rapidly increasing viscosity at the final stage of oligomerization (gelation). The intersection point of the tangents to these portions characterizes the gelation onset time τ_r. Table 3 we present the comparative data on τ_r and gelation time τ_g, determined visually from the loss of fluidity.

The fact that τ_g appreciably exceeds τ_r can be explained as follows: The rheokinetic method allows determination of the start of formation of 3*D* structures (microgel) from a sharp increase in the viscosity more precisely than does the visual determination of the fluidity loss observed at higher microgel concentrations.

Comparison of curves *2* and *4* (Fig. 4) shows that the rate of viscosity growth owing to oligomerization at 60°C is significantly higher in the experiment with addition of CS B (1.5 wt %), although the concentration of TSA-M (2.02×10^{-2} M) is lower in this case in this case than that in the experiment with addition of CS A (2 wt %) and TSA-M concentration of 2.26×10^{-2} M. The effect of the donor-acceptor complexes PPE–TSA–M and Cellosolve–TSA–M on the acidity of CS A and CS B and, thus, on their catalytic activity in the course of the Rolivsan oligomerization is illustrated in Fig. 5.

As can be seen, CS B containing Cellosolve is more reactive than CS A, other oligomerization conditions being equal. This is probably due to the higher basicity of Cellosolve as compared to PPE in which the lone electron pair of the ether oxygen is delocalized and interacts with the electron-acceptor phenyl groups, whereas in Cellosolve it is localized and interacts with the electron-donor alkyl groups. Thus, the electron-acceptor properties of PPE and Cellosolve interacting with TSA-M are strongly different. The electron density on the protonation centers in Cellosolve is higher owing to the lone electron pairs of the oxygen atoms.

Table 3. Gelation time of Rolivsan MV-1 (series I) as influenced by the conditions of the acid-catalyzed oligomerization

CS	*C*, wt %	$c_{TSA\text{-}M} \times 10^2$, M	*T*, °C	τ_r	τ_g
				h	
–	0.00	0.00	140	1.3	1.5
A	1.00	1.14	80	2.5	3.5
A	2.00	2.28	80	0.75	1.0
A	3.30	3.76	80	0.5	0.7
A	2.00	2.28	60	3.0	>6.0
B	0.80	1.08	80	1.0	1.3
B	1.15	1.55	80	0.45	0.6
B	1.50	2.02	80	0.23	0.45
B	1.80	2.42	80	0.17	0.37
B	15.0	20.2	80	–	0.08
B	1.50	2.02	60	1.4	1.5
B	0.80	1.08	60	2.0	>5.0
B	1.50	2.02	20	–	72
B	15.0	20.2	20	–	>48

At a CS A content decreased by a factor of 2, the rate of viscosity growth can be preserved by rais-

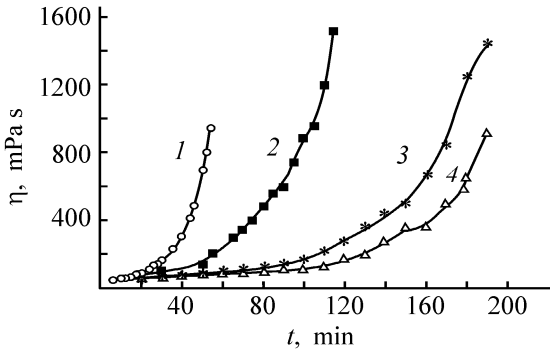

Fig. 4. Viscosity η of Rolivsan MV-1 (series I) vs. time *t* of oligomerization with addition of (*1*, *3*, *4*) CS A and (*2*) CS B. c_{CS}(wt %)/$c_{TSA\text{-}M}$, M: (*1*, *4*) 2/2.26, (*2*) 1.5/2.02, and (*3*) 1/1.14. Temperature, °C: (*1*, *3*) 80 and (*2*, *4*) 60.

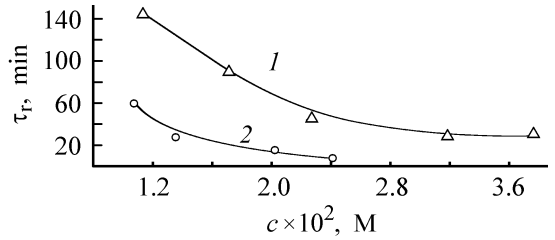

Fig. 5. Gelation time τ_r of Rolivsan MV-1 (series I) at 80°C vs. the TSA-M concentration *c*. Catalytic system: (*1*) A and (*2*) B.

ing temperature from 60 to 80°C (Fig. 3, curves *3*, *4*) which is also consistent with the van't Hoff rule.

CONCLUSIONS

(1) A procedure was developed for altering the composition and properties of Rolivsans by conversion of the monomer components [4,4'-divinyldiphenyl ether, 4-vinyl-4'-(1-methacryloyloxyethyl)diphenyl ether, and bis[4-(1-methacryloyloxyethyl)phenyl] ether] into linear unsaturated aromatic oligoethers with the terminal methacrylate groups .

(2) Under the conditions of the homogeneous catalytic oligomerization of Rolivsans at moderate temperatures (60–80°C), successive-parallel reactions of cleavage of methacrylates, formation of (di)vinylaromatic compounds, and addition polymerization of the latter with the proton transfer occur in 1–3 h.

(3) The catalytic systems with different donor-acceptor properties were developed, allowing variation of the rate Rolivsan oligomerization in a wide range.

(4) Low-melting oligoethers with the terminal methacrylate groups containing unsaturated and diphenyl oxide groups in the backbone were prepared and characterized.

REFERENCES

1. Zaitsev, B.A., Khramova, G.I., and Dantsig, L.L., *Macromolek. Soedin., Ser. A*, 1982, vol. 24, no. 12, pp. 2467–2474.
2. Zaitsev, B.A., Dantsig, L.L., and Khramova, G.I., *Zh. Org. Khim.*, 1983, vol. 19, no. 11, pp. 2340–2349.
3. Zaitsev, B.A., Relationships in Formation, Structure, and Properties of Heat-Resistant Network Polyarenes, *Doctoral Dissertation*, Leningrad, 1983.
4. Zaitsev, B.A., Khramova, G.I., and Tsygankova, T.S., *Zh. Prikl. Khim.*, 2003, vol. 76, no. 4, pp. 658–662.
5. Zaitsev, B.A., *Polyamides and High-Performance Polymers, STEPI 7 Book*, Sillion, B. and Abadie, M.J.M., Eds., Montpellier, May 2006, pp. 124–134.
6. Zaitsev, B.A., Khramova, G.I., and Dantsig, L.L., *Plast. Massy*, 1981, no. 9, pp. 12–13.
7. Zaitsev, B.A., Khramova, G.I., Tsygankova, T.S., et al., *Mekhn. Kompoz. Mater.*, 1982, no. 5, pp. 775–778.
8. Zaitsev, B.A., Khramova, G.I., Tsygankova, T.S., et al., *Plast. Massy*, 2003, no. 10, pp. 23–25.
9. Zaitsev, B.A. and Shvabskaya, I.D., *Polyamides and High Performance Polymers, STEPI 7 Book*, Sillion, B. and Abadie, M.J.M., Eds., Montpellier, May 2006, pp. 194–204.
10. Zaitsev, B.A. and Shvabskaya, I.D., *Polyamides and High Performance Polymers, STEPI 7 Book*, Sillion, B. and Abadie, M.J.M., Eds., Montpellier, May 2006, pp. 247–253.
11. Zaitsev, B.A., Tsygankova, T.S., Garkavi, S.L., et al., *Mekh. Kompoz. Mater.*, 1988, no. 4, pp. 579–584.
12. Lukasov, S.V., Zaitsev, B.A., Kenunen, I.V., et al., *Mekh. Kompoz. Mater.*, 1988, no. 5, pp. 771–778.
13. Zaitsev, B.A. and Kiseleva, R.F., *Vysokomol. Soedin., Ser. A*, 1981, vol. 23, no. 8, pp. 1783–1790.
14. Zaitsev, B.A. and Kiseleva, R.F., *Acta Polym.*, 1983, vol. 36, no. 10, pp. 527–530.
15. Zaitsev, B.A., Kiseleva, R.F., Denisov, V.M., et al., *Vysokomol. Soedin., Ser. A*, 1984, vol. 26, no. 8, pp. 1602–1609.
16. Zaitsev, B.A., Kiseleva, R.F., Denisov, V.M., et al., *Izv. Akad. Nauk SSSR, Ser. Khim.*, 1990, no. 11, pp. 2566–2574.
17. RF Patent 1 573 845.
18. Zaitsev, B.A., Kiseleva, R.F., and Gusarova, I.O., *J. Polym. Sci., Polym. Chem. Ed.*, 1996, vol. 34, pp. 1165–1181.
19. Zaitsev, B.A., Khramova, G.I., and Tsygankova, T.S., *Zh. Prikl. Khim.*, 2003, vol. 76, no. 10, pp. 1708–1714.

ISSN 1070-4272, Russian Journal of Applied Chemistry, 2007, Vol. 80, No. 4, pp. 629–633. © Pleiades Publishing, Ltd., 2007.
Original Russian Text © A.P. Voznyakovskii, E.M. Krivoruchko, V.M. Rodin, 2007, published in Zhurnal Prikladnoi Khimii, 2007, Vol. 80, No. 4, pp. 643–647.

MACROMOLECULAR CHEMISTRY AND POLYMERIC MATERIALS

Specific Features of the Molecular Organization of Solutions of Ethylene–Perfluorinated Ether Copolymers

A. P. Voznyakovskii, E. M. Krivoruchko, and V. M. Rodin

Lebedev Research Institute of Synthetic Rubber, Federal State Unitary Enterprise, St. Petersburg, Russia

Received October 12, 2006; in final form, December 2006

Abstract—Dilute and maximally concentrated solutions of ethylene–perfluorinated vinyl ether copolymers were studied.

DOI: 10.1134/S1070427207040222

Film-forming materials based on polyfluorinated elastomers can be successfully used in aggressive media at elevated temperatures. Depending on the supramolecular structure of polymer solutions, which is closely associated with the chemical structure of a macromolecular unit, such polymers can be used in diverse fields. An example is the use of polyfluorinated elastomers as protective coatings [1] or selectively permeable membranes.

In this study, we examined solutions of ethylene–perfluoroalkyl trifluorovinyl ether copolymers by dynamic light scattering and inverse gas chromatography.

EXPERIMENTAL

We studied copolymers of ethylene with perfluorinated vinyl ethers (EPFEs) of the general formula

$$[(CH_2{-}CH_2){-}(\underset{\displaystyle R}{\underset{|}{CF}}{-}CF_2)]$$

where R = O–CF_2–CF_2–CF_3 (EPFE-1), CF_2–O–CF_2–CF_2–CF_3 (EPFE-2), and CF_2O–$(CF_2)_2(OCF_2)_4OCF_3$ (EPFE-3).

The polymers were prepared by emulsion polymerization, using potassium persulfate as initiator. The majority of experiments were performed with EPFE-1.

According to the ^1H and ^{19}F NMR data, the EPFEs under consideration are alternating copolymers. However, about 15% of ethylene units form diads, and less than 0.01%, triads.

The structure of dilute solutions was studied by dynamic light scattering [2]. The specific features of the chemical structure of the EPFEs prepared sharply restrict the range of potential solvents. Whereas fluorinated elastomers derived from vinylidene fluoride show unlimited swelling in polar solvents (e.g., in acetone) [3], for EPFEs the degree of swelling does not exceed 15–20 wt %. The most suitable solvents for EPFEs are low-molecular-weight fluorinated compounds. For further experiments we chose 1,1,2-trifluorotrichloroethane. This solvent is more readily available than other related compounds and, therefore, is of greater interest for commercial production of film materials.

It should be noted that attaining the molecular solubility of fluorinated elastomers is a nontrivial problem. For example, only 30–60 wt % fraction of commercial fluorinated elastomers derived from vinylidene fluoride forms true solutions [4]. The remaining fraction of the polymer is the so-called globular fraction and consists of microgel particles formed by chemical bonds, including hydrogen bonds.

The structure of EPFE solutions was studied by dynamic light scattering. The distribution of the weight fractions of structural units of an EPFE polymer in 1,1,2-trifluorotrichloroethane solution, determined by this method, is shown in Fig. 1. The curves were obtained at polymer concentrations of 0.07, 0.15, and 0.5 wt %. Figure 1 shows that all the three curves have a bimodal distribution with the components separated by a large distance on the size scale. The fine fraction has a maximum at a size of ~30 nm. We identify this fraction with coils of individual polymer

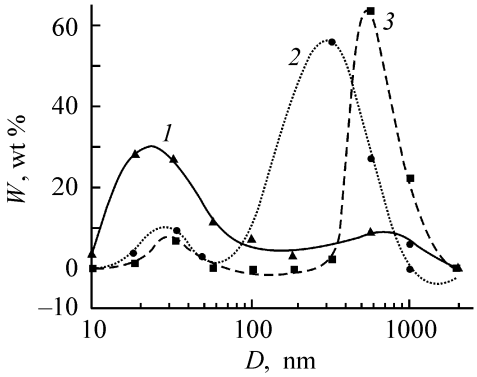

Fig. 1. Distribution of the weight fractions W of EPFE-1 structural units with respect to size D in 1,1,2-trifluorotrichloroethane at a polymer concentration c of (*1*) 0.07, (*2*) 0.15, and (*3*) 0.50 wt %.

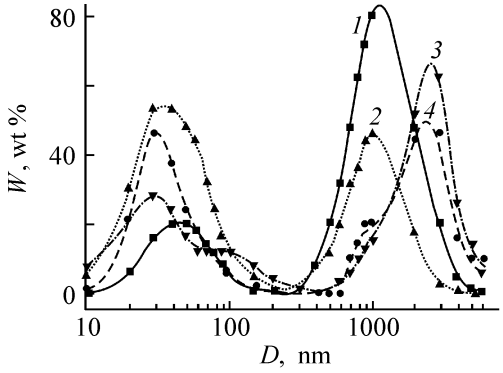

Fig. 2. Distribution of the weight fractions W of EPFE-1 structural units with respect to size D in 1,1,2-trifluorotrichloroethane with addition of (*1*) 5, (*2*) 1, (*3*) 0.5, and (*4*) 0.25 wt % acetone.

molecules. The coarse fraction corresponding to associates of macromolecules has a maximum at a size of the order of 1 μm. The mean size in this fraction is approximately 0.55 μm. The characteristics of the polymer fractions are listed in Table 1. These data show that a decrease in the polymer concentration in solution causes a decrease in the relative content of associated polymer coils and an increase in that of the nonassociated molecules. Figure 1 and Table 1 also show that the hydrodynamic sizes of the molecular coils and associates do not noticeably vary with the polymer concentration in solution.

The curves in Fig. 1 also demonstrate the tendency of EPFE molecules to associate. The weight fraction of associated polymer molecules is 90% in 0.5 wt % solution and only 22% in 0.07 wt % solution.

A dynamic light scattering study showed that a significant content of EPFE associates remains in 1,1,2-trifluorotrichloroethane solution even at low copolymer concentrations.

To determine what forces are responsible for the formation of EPFE associates, we examined the dispersion composition of this polymer in 1,1,2-trifluorotrichloroethane solutions modified with various low-molecular-weight substances (acetone, hexafluorobenzene, nitromethane, benzene). The choice of these additives was governed by our intention to reveal the donor–acceptor mechanism of solvation of EPFE molecules. The thermodynamic quality of the additives as EPFE solvents was estimated by inverse gas chromatography (IGC). Hexafluorobenzene appeared to be a good solvent (weight activity coefficient $\Omega_W < 4$). Benzene, acetone, and nitromethane do not noticeably dissolve EPFE ($\Omega_W \geq 20$; only low-molecular-weight substances with $\Omega_W < 10$ are regarded as solvents [5]). Benzene, acetone, and nitromethane show a tendency toward donor–acceptor interaction with hydrocarbon macrochains. Therefore, it can be expected that addition of small amounts of a modifier can raise the solubility of EPFE molecules in 1,1,2-trifluorotrichloroethylene. Figure 2 shows how the dispersion composition of EPFE molecules changes upon addition of various amounts of acetone.

Figure 2 shows that the general pattern of EPFE particle distribution in solution remained unchanged. However, the mean size of associates in the coarse fraction, equal to 2 μm in the solvent without acetone additions, decreases on adding minor amounts of acetone. The characteristics of the polymer fractions

Table 1. Characteristics of EPFE-1 fractions in 1,1,2-trifluorotrichloroethane solution

Polymer concentration, wt %	Mean particle diameter, nm	Weight fraction, %	Polymer concentration, wt %	Mean particle diameter, nm	Weight fraction, %
Fine fraction			Coarse fraction		
0.5	30	9	0.5	600	91
0.15	28	16	0.15	450	84
0.07	29	78	0.07	580	22

Table 2. Influence of the solvent composition on the characteristics of polymer fractions

Acetone concentration, wt %	Fraction of nonassociated polymer	Mean particle diameter in indicated fraction, nm		Acetone concentration, wt %	Fraction of nonassociated polymer	Mean particle diameter in indicated fraction, nm	
		fine	coarse			fine	coarse
0	0.31	40.4	1950	1.0	0.55	42.7	940
0.25	0.48	40	1780	5.0	0.20	49.4	1120

Table 3. Excess thermodynamic functions $\Delta\overline{H}_1^{E\infty}$ and $\Delta\overline{S}_1^{E\infty}$ at 60°C

Sorbate	EPFE-1		EPFE-2		EPFE-3	
	$\Delta\overline{H}_1^{E\infty}$, kJ mol^{-1}	$\Delta\overline{S}_1^{E\infty}$, J mol^{-1} K^{-1}	$\Delta\overline{H}_1^{E\infty}$, kJ mol^{-1}	$\Delta\overline{S}_1^{E\infty}$, J mol^{-1} K^{-1}	$\Delta\overline{H}_1^{E\infty}$, kJ mol^{-1}	$\Delta\overline{S}_1^{E\infty}$, J mol^{-1} K^{-1}
Pentane	4.06	16.80	1.38	21.79	2.13	19.31
Hexane	6.50	10.44	5.08	10.70	3.54	15.24
Heptane	8.08	6.97	6.57	7.26	2.51	17.19
Octane	8.59	6.73	7.48	5.37	5.79	10.42
Nonane	9.99	3.95	8.53	3.17	6.98	7.76
Decane	11.06	2.20	9.73	0.61	7.77	6.46
Cyclohexane	7.96	5.58	6.47	5.89	4.41	12.10
Benzene	7.23	6.15	4.61	8.58	3.36	13.83
HFB*	0.66	10.11	–0.04	9.75	0.58	8.44

* Hexafluorobenzene.

are given in Table 2. It is seen that addition of acetone causes, along with a decrease in the size of associates, also a small increase in the hydrodynamic size of the nonassociated coils (from 40 to 49 nm) and an increase in the amount of these species relative to associates. These trends are apparently due to the fact that acetone molecules solvate hydrocarbon units, thereby improving the solubility of EPFE as a whole. Furthermore, a part of molecules pass in this case from associates into the solution. In the process, the mean size of the associates decreases by a factor of approximately 2 at 1 wt % concentration of acetone.

As follows from the results of dynamic light scattering measurements, EPFE macromolecules show a strong tendency toward association. Modification of a solvent by addition of low-molecular-weight substances capable of specific interaction considerably increases the extent of molecular dispersity of the solutions, but does not fully suppress the tendency of EPFE molecules to associate. Nevertheless, the distribution of EPFE structural units in the modified solvent is considerably more uniform, which allows preparation of self-supporting EPFE films, i.e., of films exhibiting satisfactory strength characteristics without application onto a support. Modified EPFE solutions were used for preparing ultrathin films whose supramolecular structure was studied by IGC.

The supramolecular organization in maximally concentrated solutions was studied by IGC [6]. The possibilities of the method were used for characterizing the thermodynamics of sorption of low-molecular-weight EPFE associates and for calculating the thermodynamic parameters of mixing: $\Delta\overline{H}_1^{E\infty}$ and $\Delta\overline{S}_1^{E\infty}$ (excess partial molar enthalpy and entropy, respectively).

The excess partial molar enthalpy $\Delta\overline{H}_1^{E\infty}$ is the resultant of all intramolecular interactions in the infinitely dilute solutions formed [7]. It can be represented as a sum

$$\Delta\overline{H}_1^{E\infty} = \Delta H_{break} + \Delta H_{cav} + \Delta H_{disp} + \Delta H_{sp}, \quad (1)$$

where ΔH_{break} is the enthalpy of breaking of the bonds between the solute molecules; ΔH_{cav}, enthalpy of cavity formation in the structure of the pure solvent (polymer in the case of IGC); ΔH_{disp}, enthalpy of van der Waals interaction; and ΔH_{sp}, enthalpy of the specific interaction.

To calculate the thermodynamic functions of mixing in the systems EPFE–low-molecular-weight substance, we obtained the equations of the temperature dependences of the weight activity coefficients Ω_1^{∞} and the coefficients of these equations [8, 9].

$$\ln \Omega_1 = C \ln T + D/T + E.$$

where C, D, and E are constants.

The values of $\Delta\overline{H}_1^{E\infty}$ calculated on substituting the coefficients obtained in Eq. (1) are listed in Table 3. It is seen that all these quantities are positive

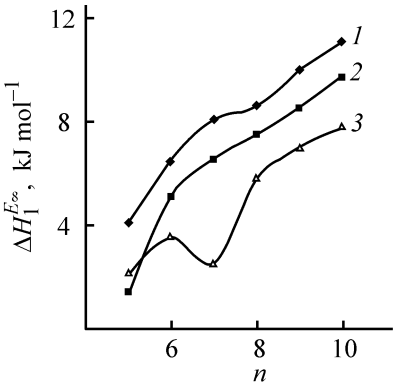

Fig. 3. Excess partial molar enthalpy $\Delta\bar{H}_1^{E\infty}$ vs. the number n of carbon atoms in the chain of a normal alkane: (*1*) EPFE-1, (*2*) EPFE-2, and (*3*) EPFE-3.

and appreciably larger than unity for all the sorbates except HFB.

As far as the solvating properties of HFB toward EPFE are concerned, it should be noted that HFB shows a tendency toward electrophilic addition, which is due to the considerably higher, compared to benzene, density of the π-electron system [10]. At the same time, HFB, like other perfluoroaromatic compounds, is active toward nucleophiles. Thus, HFB can solvate both methylene groups with a partial positive charge on the H atom and the perfluoromethylene groups of the linear chain. In turn, the alternating microstructure of the polymer and the self-organization processes leading to the formation of hydrocarbon clusters in the bulk of the polymer give rise to steric hindrance to solvation of methylene sequences with HFB (shielding with adjacent perfluorinated groups). Such a supramolecular organization should make the copolymers stable in polar solvents. According to our experiments, the polymers under consideration show only limited swelling in polar solvents, in contrast to copolymers derived from vinylidene fluoride, whose solubility in polar solvents is well known [3].

We studied how $\Delta\bar{H}_1^{E\infty}$ varies with increasing molecular mass of *n*-alkane (Fig. 3). The plot obtained for EPFE-1 is characterized by the ascending initial portion (from *n*-C_5 to *n*-C_7), followed by plateau (from *n*-C_7 to *n*-C_8) and second ascending portion (from *n*-C_8 to *n*-C_{10}). With an increase in the molecular mass of *n*-alkane, its absorption by the polymer becomes more difficult, which is reflected in an increase in $\Delta\bar{H}_1^{E\infty}$ (the contribution of ΔH_{cav} grows). At the same time, the dispersion forces acting in the solvation of macrochains increase, which partially compensates for the increase in ΔH_{cav} (plateau in the plot). As the molecular mass of an alkane is raised further, an increase in the dispersion forces no longer compensates for the increase in ΔH_{cav} (second ascending portion).

It could be expected that an increase in the length of the side substituent in EPFE-2, with incorporation of a flexible –OCF_2– unit, would lead to a considerable increase in the free volume and, correspondingly, to a considerable decrease in $\Delta\bar{H}_1^{E\infty}$ of sorbates. However, the absolute values of $\Delta\bar{H}_1^{E\infty}$ of sorbates on EPFE-2 appeared to be only slightly lower than those on EPFE-1. It should be noted that there is no pronounced plateau in the $\Delta\bar{H}_1^{E\infty} = f(n_C)$ curve for EPFE-2. Thus, the difference between EPFE-1 and EPFE-2 in the side substituents, though leading to an increase in the free fluctuation volume in EPFE-2, does not appreciably affect the supramolecular organization of the fluorinated elastomers.

A sharp increase in the length of the side substituent chain in EPFE-3, relative to EPFE-1 and EPFE-2, with alternation of rigid (–CF_2–CF_2–) and flexible (–OCF_2–) segments, apparently leads to an increase in the free volume and correspodingly to a decrease in $\Delta\bar{H}_1^{E\infty}$ of the sorbates. Also, a minimum (at $n_C = 7$) is observed in the curve $\Delta\bar{H}_1^{E\infty} = f(n_C)$. The first fact can be apparently attributed to a relative (compared to EPFE-1) increase in the fluctuation free volume, caused by differences in the geometry of side substituents in the EPFEs, namely, to a decrease in the contribution of ΔH_{cav} to $\Delta\bar{H}_1^{E\infty}$ and the corresponding decrease of the latter quantity. The local minimum in the $\Delta\bar{H}_1^{E\infty} = f(n_C)$ curve suggests that the mean size of elements of the free volume in EPFE-3 corresponds to the molecular size of *n*-heptane.

In the Flory–Huggins thermodynamics, the expression for the partial molar excess entropy of alkanes has the form [11]

$$\Delta\bar{S}_1^{E\infty} = R[\ln m - (m - 1)/m]. \quad (2)$$

where m is the ratio of the solid-core volumes of the polymer and low-molecular-weight substance. The equation is valid if there are no intermolecular interactions and the free volume remains constant on mixing. With these restrictions, Eq. (2) predicts a decrease in $\Delta\bar{S}_1^{E\infty}$ with an increase in the molecular volume of *n*-alkane. The $\Delta\bar{S}_1^{E\infty}$ values obtained are listed in Table 3. Table 3 shows that, with all the examined EPFEs, the $\Delta\bar{S}_1^{E\infty}$ values of *n*-alkanes do decrease with an increase in their molecular volume. It should be noted that Eq. (2) does not hold true for many elastomers [12], and more typical is independence of $\Delta\bar{S}_1^{E\infty}$ from the molecular volume of the al-

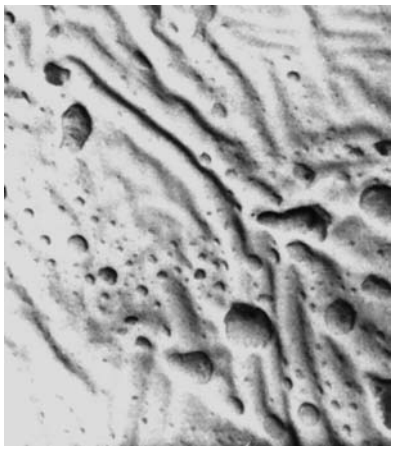

Fig. 4. Supramolecular organization of EPFE-1.

kane. A decrease in $\Delta\overline{S}_1^{E\infty}$ with the molecular volume of the alkane in the case of EPFEs may be due to the sorption mechanism involving accommodation of alkane molecules in the intraassociate voids (free volume elements) of the elastomer, which is characteristic of sorption with associated liquids [13].

We examined the supramolecular organization of thin polymer films. A SEM micrograph of EPFE-1 is shown as example in Fig. 4. The supramolecular organization of the polymer is characterized by the lamellar structure; the alternating microstructure of the chain does not prevent its formation.

CONCLUSIONS

(1) Macromolecules show a strong tendency toward aggregation in dilute solutions of ethylene–perfluorinated ether copolymers.

(2) Self-organization processes occurring in solutions of perfluorinated vinyl ethers directly affect the supramolecular organization of thin copolymer films.

(3) The driving force of self-organization is thermodynamic incompatibility of the hydrocarbon and perfluorinated constituents of perfluorinated vinyl ethers, leading to the formation of hydrocarbon clusters of methylene sequences in the prefluorinated matrix and of free volume elements.

(4) The structure of perfluorinated vinyl ethers, combinated with the specific features of the chain microstructure, ensures high stability of the films derived from these ethers in aggressive polar media, including alkaline solutions.

(5) The presence of free volume elements is a prerequisite for the development of selectively permeable membranes based on these copolymers.

REFERENCES

1. Mulin, Yu.A., Panshin, Yu.A., Bucherkova, M.A., and Yavzina, N.E., *Zashchitnye pokrytiya i futerovki na osnove termoplastov* (Protective Coatings and Linings Based on Thermoplastics), Leningrad: Khimiya, 1984.
2. Berne, B.J. and Pecora, R., *Dynamic Light Scattering*, New York: Wiley, 1976.
3. Novitskaya, S.P., Nudel'man, Z.N., and Dontsov, A.A., *Ftor-elastomery* (Fluoro Elastomers), Moscow: Khimiya, 1988.
4. Dontsov, A.A., *Protsessy strukturirovaniya elastomerov* (Structurization of Elastomers), Moscow: Khimiya, 1978.
5. Galin, M., *Macromolecules*, 1977, vol. 10, no. 6, pp. 1239–1244.
6. Nesterov, A.E., *Obrashchennaya gazovaya khromatografiya polimerov* (Inverse Gas Chromatography of Polymers), Kiev: Naukova Dumka, 1988.
7. Berezkin, V.G., *Gazo-zhidko-tverdofaznaya khromatografiya* (Gas–Liquid–Solid Phase Chromatography), Moscow: Khimiya, 1986.
8. Gray, D.G. and Guillet, J.E., *Macromolecules*, 1972, vol. 5, no. 3, pp. 316–321.
9. Genkin, A.N., Voznyakovskii, A.P., and Krivoruchko, E.M., *Zh. Fiz. Khim.*, 1998, vol. 72, no. 7, pp. 1303–1308.
10. Sheppard, W.A. and Sharts, C.M., *Organic Fluorine Chemistry*, New York: Benjamin, 1969.
11. Belousov, V.P. and Morachevskii, A.G., *Teploty smesheniya zhidkostei: Spravochnik* (Heats of Mixing of Liquids: Handbook), Leningrad: Khimiya, 1970.
12. Roth, M. and Novak, J., *Macromolecules*, 1986, vol. 19, no. 2, pp. 364–369.
13. Yampolskii, Yu.P., Kaluzhnyi, N.E., and Durgarjan, S.G., *Macromolecules*, 1986, vol. 19, no. 3, pp. 846–850.

ISSN 1070-4272, Russian Journal of Applied Chemistry, 2007, Vol. 80, No. 4, pp. 634–637. © Pleiades Publishing, Ltd., 2007.
Original Russian Text © D.N. Valeeva, F.Yu. Akhmadullina, V.F. Kurenkov, D.G. Pobedimskii, 2007, published in Zhurnal Prikladnoi Khimii, 2007, Vol. 80, No. 4, pp. 648–651.

MACROMOLECULAR CHEMISTRY AND POLYMERIC MATERIALS

Intermolecular Association of Tilan with Vinylpyrrolidone Copolymers

D. N. Valeeva, F. Yu. Akhmadullina, V. F. Kurenkov, and D. G. Pobedimskii

Kazan State Technological University, Kazan, Tatarstan, Russia
Moscow State Academy of Fine Chemical Technology, Moscow, Russia

Received June 6, 2006; in final form, March 2007

Abstract—The results of physicochemical studies of promising prolonging agents for Tilan antibiotic: polyvinylpyrrolidone and vinylpyrrolidone copolymers, are reported. The optimal component ratios of the drug formulation were determined by viscometry and conductometric titration. As determined by IR spectroscopy, the components are associated mainly via intermolecular hydrogen bonds.

DOI: 10.1134/S1070427207040234

As a continuation of our previous studies of prolonging agents for water-soluble antibiotics for veterinary purposes [1–4], we examined in this study polyvinylpyrrolidone (PVP) and various copolymers of vinylpyrrolidone (VP) with salts of 2-acrylamido-2-methylpropanesulfonic acid. Tilan, a broad-spectrum macrolide antibiotic [5], was used as the pharmaceutical.

The simplest way to prolong the action of pharmaceuticals is covalent and noncovalent binding of a pharmaceutical with hydrophilic polymers. For this purpose, a complex of a pharmaceutical with an auxiliary compound is mainly prepared by mechanical dispersion or mechanical activation of a solution of pharmaceuticals with macromolecular compounds (MMCs). Under these conditions, inter- and intramolecular bonds in polymer macromolecules are ruptured and their reactivity increases. Then, the activated macromolecules react with the pharmaceutical to form inclusion complexes or grafted complexes, depending on the polymer structure [6].

The association in the antibiotic-MMC systems was studied by viscometry, conductometric titration, and IR spectroscopy. These studies allowed more correct estimation of the binding strength in these systems and gave an insight into the mechanism and conditions of formation of polycomplexes of Tilan with PVP and vinylpyrrolidone copolymer.

The choice of vinylpyrrolidone copolymers as promising auxiliary compounds is caused by the fact that, among water-soluble synthetic polymers, PVP and its copolymers are the most widely used in pharmacy. The reason is that PVP is slowly taken in from the injection place, thus decelerating the intake of the pharmaceutical forming a complex with it.This effect is the most pronounced in the case of intramuscular injection of a pharmaceutical [7, 8].

We studied PVP and vinylpyrrolidone copolymers with calcium and sodium salts of 2-acrylamido-2-propanesulfonic acid, prepared by copolymerization of calcium 2-acrylamido-2-propanesulfonate and sodium 2-acrylamido-2-propanesulfonate (Ca-APS and Na-APS) with vinylpyrrolidone in concentrated alkaline aqueous solutions of the monomers at 50°C. The weight ratio of VP and Na-APS was 2 : 98, 6.2 : 93.8, and 12 : 88, and that of VP and Ca-APS, 85.2 : 14.8 [9].

Since the auxiliary compounds should be nontoxic, we performed a preliminary toxicological study of the vinylpyrrolidone copolymers.

EXPERIMENTAL

The complexation of Tilan with MMC was studied by viscometry and conductometric titration of isomolar series. The viscosity of by 0.2 mg ml^{-1} (0.02%)

Table 1. Complexation of Tilan with PVP and VP copolymers

Auxiliary compounds (composition)	Viscometry			Conductometric titration		
	$c_a - c_{ac}$, %	range of formation of the Tilan–AC complex, %	$(\eta/\Sigma\eta)_{min}$	$c_a - c_{ac}$, %	range of formation of the Tilan–AC complex, %	$(\chi/\Sigma\chi)_{min}$
PVP	5–3	(15–69) : (85–31)	0.55	0.1–0.1	–	–
Na-APS : VP:						
98 : 2	5–0.02	(97–99) : (3–1)	0.43	0.1–0.1	(17–83) : (83 : 17)	0.913
93.8 : 6.2	5–0.02	(97–99) : (3–1)	0.45	0.1–0.1	(17–83) : (83 : 17)	0.885
88 : 12	5–0.02	(97–99) : (3–1)	0.48	0.1–0.1	(17–83) : (83 : 17)	0.864
Ca-APS : VP = 14.8 : 85.2	5–0.02	(97–99) : (3–1)	0.51	0.1–0.1	–	–

aqueous solution of the polymers and a 50 mg ml^{-1} (5%) aqueous solution of the antibiotic (these concentrations are determined by features of the system examined) were measured on an Ubbelohde viscometer with a capillary diameter of 0.73 mm. In the case of the Tilan-PVP system, the initial monomer concentrations were 5 and 3%, respectively.

The electrical conductivity was measured with an R-5021 ac bridge using an Impul's high-sensitivity device as a zero gage and a cell with platinum electrodes. The concentration of Tilan, c_a, and vinylpyrrolidone copolymers in solutions was 1 mg ml^{-1} (0.1 wt %).

All measurements were performed at 25°C. We used both direct and back titration.

The IR spectra of the individual substances and their complexes were recorded on a Specord 75-IR spectrometer. The samples were prepared by uniform application of a paste obtained from solutions of the pure compounds and 4 : 1 antibiotic–VP copolymer mixtures (at this ratio the yield of the complex is maximal) onto a KRS-5 window, followed by prolonged drying at 40°C.

To determine the concentration range of association and to estimate the strength of the complexes between the antibiotic and the auxiliary compound, we used the procedure described in [10].

Our experimental data show that polycomplexes of the antibiotic and PVP and VP copolymers are formed in all the mixtures examined and in a wide range of weight ratios of the components (Table 1).

The substantial deviation of the reduced viscosity and conductometric parameters from unity suggests that strong and compact associates are formed. The results of viscometric measurements are well consistent with those of direct and back conductometric titration.

As can be seen from Table 1, the strength of the intermolecular interaction decreases with increasing fraction of vinylpyrrolidone units in the copolymers. The weakest complexes are formed in the Tilan–PVP system. Apparently, as the content of VP units in the copolymers increases, the contact between the antibiotic molecules and MMC becomes sterically hindered, thus weakening the association of the components. As expected, the reduced conductivity parameters decrease with an increase in the VP fraction, since the degree of dissociation of macromolecules decreases.

Unfortunately, the role of the metal cation in the structuring in the systems examined is difficult to estimate correctly, since the ratios of the monomer units in VP copolymers with calcium 2-acrylamido-2-propanesulfonate and sodium 2-acrylamido-2-propanesulfonate substantially differ.

The nature of intermolecular bonds in molecular complexes is of great significance. Since both proton-donor and proton-acceptor groups are present in the Tilan–PVP system (i.e., carbonyl and hydroxy groups of Tilan and amide and sulfonic groups of the copolymer), intermolecular hydrogen bonds should substantially contribute to the formation of Tilan–PVP polycomplexes. The contribution of the carbonyl groups of the pyrrolidone ring to the structuring is probably less significant since the binding of the antibiotic with PVP gets considerably weakened with an increase in the fraction of VP units.

To elucidate the complexation mechanism in the binary systems, we studied the IR spectra of Tilan,

Table 2. Characteristic IR bands of functional groups of the antibiotic and its prolonging agents

Bond (group)	ν, cm^{-1}	Bond (group)	ν, cm^{-1}	Bond (group)	ν, cm^{-1}	Bond (group)	ν, cm^{-1}	Bond (group)	ν, cm^{-1}
Tilan		PVP		Tilan–PVP		Na-APS : VP		Tilan–Na-APS : VP	
–OH	3428	–OH	3478	–OH	3428	–OH	3465	–OH	3420
–C=C–C=O	–	–C=O	1664	–C=O	1670	–C=O			
including:						Amide (I)	1664	–C=O	1660
–C=O	1673	–	–	–	–	–N–H			
–C=C–	1595	–	–	–C=C–	1595	(Amide II)	1540	–N–H	1540
–C=O						–S=O	1210	–S=O	1180
including							1040		1040
H									
C=O	1720			–C=O	1726				

PVP, VP copolymers, and 4 : 1 Tilan–Na-APS : VP mixture (Table 2).

The absorption in the range of stretching vibrations of hydroxy and amino groups (4000–2800 cm^{-1}), which characterizes the presence and type of hydrogen bonding, is of particular interest. A strong band at 3428 cm^{-1} in the Tilan spectrum in this range suggests association of this antibiotic in solutions through a system of hydrogen bonds. The band of carbonyl groups involved in the complexation appears at 1673 cm^{-1}. The band of the –C=C bond conjugated with this group is observed at 1595 cm^{-1}. The strong band at 1720 cm^{-1} is due to C=O vibrations in the aldehyde group.

The IR spectra of the binary systems and corresponding auxiliary compounds have the following features.

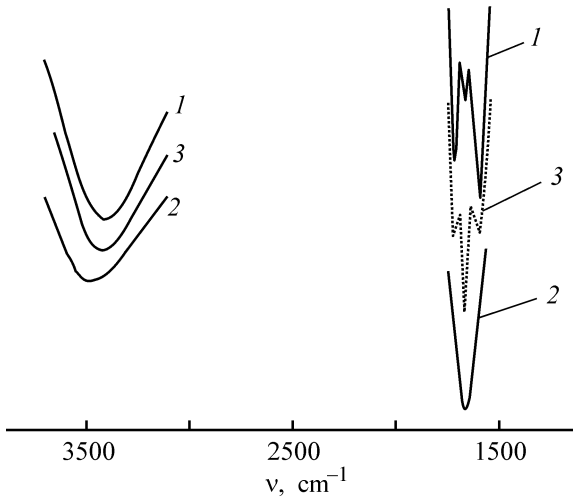

Fragment of IR spectra of (*1*) Tilan, (*2*) polyvinylpyrrolidone, and (*3*) Tilan–polyvinylpyrrolidone mixture. (ν) Wavenumber.

Tilan–PVP system. The band at 3478 cm^{-1} is present, along with the characteristic bands, in the spectrum of PVP. This band is mainly due to water impurities absorbed by hygroscopic PVP [11] or to the hydrolysis product of the amide bond in the pyrrolidone ring.

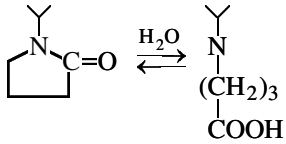

It is known that this product contains carboxy groups having characteristic $\nu_{C=O}$ absorption in the range 1760–1720 cm^{-1}. The intensity of this band is substantially higher than that of $\nu_{OH.}$ The absence of this band in the spectrum indicates that the main impurity is absorbed water.

THe strong difference between the spectrum of the associate and those of the pure components suggests a change in the state of their functional groups (see figure). The frequency of the OH stretching band in the spectrum of the complex is similar to that of Tilan (3428 cm^{-1}), but the intensity of this band in the spectrum of the complex is substantially higher. This suggests formation of a new H-bond network whose strength is higher than that of the hydrogen bonding between adsorbed water and PVP and comparable with that of the intermolecular hydrogen bond in the associates formed in aqueous solutions.

A significant increase in the intensity of the absorption of the carbonyl group in the associate, especially at 1670 cm^{-1}, as compared to that in the spectrum of Tilan not only confirms the formation of the antibiotic-auxiliary compound complex but also suggests the prevailing contribution of the –C=C–C=O group of Tilan

to the complexation. Such an increase in the intensity of the carbonyl band can be only due to an increase in the dipole moment of the C=O bond, caused by intermolecular bonding. The decrease in the intensity of the band of the –C=C bond confirms this assumption [7].

A slight high-frequency shift of the band of the carbonyl groups of PVP (1670 cm^{-1}) suggests its involvement in the complexation.

Thus, the results of this study are consistent with the previously published data [11] and show that complexation of hydrated PVP with various substances occurs via bound water. In this case, water can stabilize the intermolecular complexes.

Tilan–Na-APS : VP system. We studied the IR spectra of two samples of this system with component ratios of 2 : 98 and 6.2 : 93.8. The spectra were similar. The broad asymmetric band in the range 3600–3200 cm^{-1} can be assigned to both stretching vibrations of the NH bond of the secondary amide and to stretching OH vibrations of absorbed water, which causes its complex shape. In the range of absorption of the carbonyl groups, there are two bands: Amide I and Amide II. The first band is strong and is observed at 1664 cm^{-1}; the second band at 1540 cm^{-1} is assigned to bending vibrations of the NH group. The strong band at 1664 cm^{-1} is probably due to vibrations of the C=O bond in the pyrrolidone ring.

The symmetric and asymmetric stretching vibrations of the SO_2 group in the ranges 1260–1150 cm^{-1} and 1080–1010 cm^{-1} are typical of salts of sulfonic acids. In the spectrum of Na-APS : VP, these bands are observed at 1210 and 1040 cm^{-1}, respectively.

The IR spectra of the copolymer and Tilan substantially change after their association in the mixtures. The low-frequency shift of the stretching bands of OH and NH groups suggests the formation of a new stronger (especially as compared to Na-APS : VP) system of hydrogen bonds. The change in the intensity and insignificant shift of the C=O band to low frequencies as compared to the spectrum of the initial components of the system confirm the formation of the complexes. A strong (by 30 cm^{-1}) long-wave shift of the band of symmetrical stretching vibrations of the SO_2 group at 1180 cm^{-1} in the IR spectrum of the complex shows that the contribution of sulfonic groups of the copolymer to hydrogen bonding is maximal.

CONCLUSIONS

(1) It was found that comparatively strong and compact associates of Tilan with polyvinylpyrrolidone and VP copolymers are formed in a wide range of the component ratios.

(2) The optimal Tilan-prolonging agent ratios were determined.

(3) Significant contribution of intermolecular hydrogen bonds to structure formation in Tilan–macromolecular compound system was demonstrated.

REFERENCES

1. Krivenko, L.V., Vyatkina, I.V., Akhmadullina, F.Yu., and Pobedimskii, D.G., in *Khimiya i tekhnologiya elementoorganicheskikh soedinenii i polimerov: Mezhvuzovskii sbornik nauchnykh trudov* (Chemistry and Technology of Organoelemental Compounds and Polymers: Intercollegiate Coll. of Scientific Papers), Kazan, 2000, p. 97.
2. Valeeva, D.N., Vyatkina, I.V., Pavlukhina, E.A. et al., *Biologicheskaya aktivnost' modifitsirovannogo tilana* (Biological Activity of Modified Tilan), available from VINITI, February 12, 2002, no. 292V–2002.
3. RF Patent 2228743.
4. Valeeva, D.N., Akhmadullina, F.Yu., Makaev, Kh.N., and Pobedimskii, D.G., Abstracts of Papers, *XVII Mendeleevskii s''ezd po obshchei i prikladnoi khimii* (XVII Mendeleev Congr. on General and Applied Chemistry), Kazan, 2003, p. 211.
5. Sazonova, E.M., Violin, B.V., Kovalev, V.F., et al., *Veterinariya*, 1999, no. 5, pp. 54–57.
6. Zakharova, E.A. and Oktyabr'skii, F.V., *Khim.-Farm. Zh.*, 1993, vol. 23, no. 11, pp. 14–21.
7. Lebedeva, T.L., IR Spectroscopic Study of the Hydrogen Bond Structure in Aqueous and Nonaqueous Polymer Systems, *Doctoral Dissertation*, Moscow, 1995.
8. Kurenkov, V.F., *Sorovsk. Obraz. Zh.*, 1997, no. 5, pp. 48–53.
9. Kurenkov, V.F., Sirotkin, R.O., Beryachkova, E.A., and Khairullin, M.R., *Zh. Prikl. Khim.*, 1998, vol. 71, no. 9, pp. 1533–1537.
10. Zakirov, R.K., Intensification of Biological Purification of Wastewater by Reagent and Ultrasonic Treatment, *Cand. Sci. Dissertation*, Kazan, 2001.
11. Lebedeva, T.L., Fel'dshtein, M.M., Kuptsov, S.A., and Plate, N.A., *Vysokomol. Soedin., Ser. A*, 2000, vol. 42, no. 9, pp. 1504–1523.

ISSN 1070-4272, Russian Journal of Applied Chemistry, 2007, Vol. 80, No. 4, pp. 638–642. © Pleiades Publishing, Ltd., 2007.
Original Russian Text © S.M. Matusova, A.V. Pirogov, T.B. Tennikova, O.A. Shpigun, 2007, published in Zhurnal Prikladnoi Khimii, 2007, Vol. 80, No. 4, pp. 652–657.

MACROMOLECULAR CHEMISTRY AND POLYMERIC MATERIALS

Development of Principles of Controlled Synthesis of Monolithic Polymeric Sorbents for Ion Chromatography

S. M. Matusova, A. V. Pirogov, T. B. Tennikova, and O. A. Shpigun

Lomonosov Moscow State University, Moscow, Russia

Institute of Macromolecular Compounds, Russian Academy of Sciences, St. Petersburg, Russia

Received November 21, 2006; in final form, December 2006

Abstract—A series of monolithic macroporous sorbents based on glycidyl methacrylate and ethylene glycol dimethacrylate were prepared by free radical copolymerization. The effect of polymerization conditions and composition of reaction mixture on the pore structure of the monolithic material was studied by IR spectroscopy, intrusion mercury porosimetry, and scanning electron microscopy.

DOI: 10.1134/S1070427207040246

The idea of preparing macroporous copolymers as rigid monoliths, put forward in the late 1980s–early 1990s [1–5], has become a powerful tool in production of modern high-performance sorbents. At present, monolithic stationary phases are widely used in high-speed chromatographic separation of biological (macro)molecules, in modern enzyme reactors, and in other processes based on the dynamic interphase distribution of various compounds [6].

As compared to common chromatographic separation procedures using packed columns, the new separation method has certain significant advantages [6]. These advantages are primarily related to features of the mechanism of intraporous mass transfer controlled by the flow convection, rather than by molecular diffusion typical of chromatography and controlling the rate of the separation process. In the case of monolithic stationary phases, it is possible to use high rates of the eluent flow, which noticeably shortens the process time and significantly increases the separation performance at adsorption capacity and resolution that are comparable with HPLC. Despite the significant progress in application of monolithic sorbents to separation of various biological objects, this stage of development of this method requires improvement of its potential. For example, preparation and optimization of such stationary phases are necessary for development of efficient and highly selective procedures of separation of organic and inorganic ions [7–10]. Obviously, solution of this problem primarily requires an essential rearrangement of the pore structure of the known materials to provide controlled changes in the pore size and adsorption surface. It should be noted that, despite the significant number of papers on this question, there are almost no published data on the algorithm of changes in the pore structure as influenced by the conditions of the sorbent preparation.

In this study, we developed principles of controlled formation of the homogeneous pore structure of monolithic materials for the example of a known copolymer of 2,3-epoxypropyl methacrylate (glycidyl methacrylate, GMA) and ethylene glycol dimethacrylate (EDMA), using thermally initiated free-radical polymerization. For this purpose, we prepared a series of monolithic rods (HPLC columns) characterized by various morphologies and topographies of the sorbent surface, with the aim of finding a compromise sorbent with a high permeability to the liquid phase at relatively low pressure and large area of intraporous adsorption-active surface.

EXPERIMENTAL

In our study we used glycidyl methacrylate (Sigma-Aldrich GmbH, Germany), ethylene glycol dimethacrylate (Sigma-Aldrich GmbH, Germany), 2,2-azobis(isobutyronitrile) (AIBN) (Merck-Schuchard, Germany), dodecanol (D) (Reakhim, Russia), cyclohexanol (C) (Sigma-Aldrich GmbH, Germany), ethanol (Reakhim, Russia), acetonitrile (AN) (Sigma-Aldrich GmbH, Germany), bovine serum albumin (BSA) (Reakhim, Russia), acetone (Reakhim, Russia), *L*-tyrosine (Sigma-Aldrich GmbH, Germany), 25% aque-

ous ammonia (Reakhim, Russia), and sodium chloride (Reakhim, Russia).

The experiments on variation of the polymerization conditions were performed in special vessels (1-ml plastic syringes). The sorbents were prepared using a reaction mixture consisting of an initiator of the free-radical polymerization (AIBN, 1 wt %), a mixture of GMA and EDMA (0.4 ml) with varied volume ratios of these monomers, and a mixture of dodecanol and cyclohexanol (0.6 ml) as pore-forming solvents, with varied ratio of these solvents in the organic phase. Before polymerization, the mixture was purged with a nitrogen flow to remove oxygen acting as polymerization inhibitor. The polymerization was performed at 55–70°C for 12 h (constant time for all the experiments). After the reaction completion, the resulting polymer was washed several times with ethanol and dried at reduced pressure to constant weight. The morphological structure of the copolymer was studied by scanning electron microscopy (JSM-6700F microscope, Japan) and by intrusion mercury porosimetry (PASCAL 440 porosimeter, Thermoquest, Italia). The content of the epoxy groups was determined using a Bruker Tensor 27 IR Fourier spectrometer.

The monoliths prepared directly in stainless steel columns (60 × 2 mm) were washed with ethanol for 15 h on a Milikhrom 4 microcolumn liquid chromatograph (Russia) to remove unchanged monomers and inert porophores. Removal of porophores from the resulting polymer yields a macroporous polymeric material with a volume fraction of pores corresponding to the content of these agents in the initial reaction mixture.

The dependence of the pressure on the eluent flow rate was studied on an Akvilon liquid chromatograph (Russia). The fraction of pores accessible to various compounds was determined chromatographically using a Milikhrom 4 microcolumn liquid chromatograph equipped with a UV spectrophotometric detector (λ 254 nm); 0.05 M NaCl solution was used as a mobile phase. The pore fraction in the sorbents was calculated from the following equation:

$$V_{pore} = (V_R - V_m)/V_{rod},$$

where V_{pore} is the pore fraction in the sorbents (ml ml^{-1}); V_R, eluate volume required to remove the compound from the column; V_m, eluate volume required to remove the compound from the chromatographic system without the column (33 μl); and V_{rod}, volume of the monolithic rod (0.188 ml).

The adsorption amino groups were introduced by treatment of the monolithic porous stationary phases with 25% ammonia solution at 40°C for 5 h.

Table 1. Parameters varied in the course of the polymer synthesis

Monolith*	Content, wt %				Content of epoxy groups, mmol g^{-1}
	GMA	EDMA	C	D	
G-60-10	24	16	54	6	4.2
G-50-10	20	20	54	6	3.5
G-25-10	10	30	54	6	1.8
G-60-17	24	16	50	10	4.2
G-60-0	24	16	60	0	4.2
G-60-30	24	16	42	18	4.2
G-60-40	24	16	36	24	4.2
G-60-50	24	16	30	30	4.2

* G means glycidyl methacrylate; the first figure is its percentage in the monomer mixture, and the second, the percentage of dodecanol in the mixture of porophores.

The morphology (namely, the homogeneity of the pore structure, surface quality, total pore surface area depending on then pore size, and size distribution of the pores) is an important characteristic of a monolithic macroporous material [11–14]. In this study, we examined the effect of the polymerization conditions (e.g., ratio of monomers and porophores in the reaction mixture and temperature) on the pore structure of the GMA–EDMA model polymer in order to develop an algorithm for preparing a chromatographic sorbent with controllable properties.

The chemical structure of the GMA-EDMA copolymer is as follows:

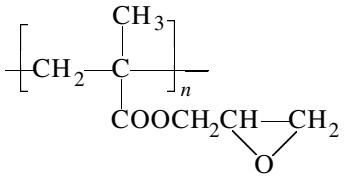

The resulting polymeric material has a microglobular texture and contains pores forming a network of interolaced channels with a bimodal pore size distribution. In accordance with the accepted classification of pores, the total pore space is subdivided into macropores [holes between microglobule clusters (>0.05 μm)], mesopores [gaps between microglobules (0.002–0.050 μm)], and micropores [gaps between the nuclei (<0.002 μm)] [15].

A comparative study of the formation of the pore structure in the monolith was performed by scanning electron microscopy (SEM). The parameters varied in the course of preparation of the initial polymeric mixture are listed in Table 1. As can be seen, raising

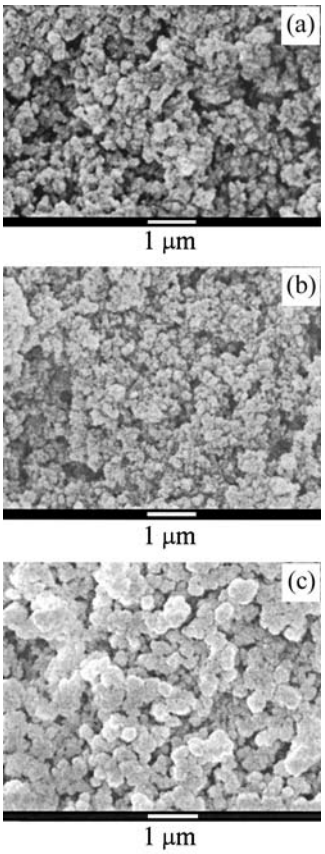

Fig. 1. Electron micrographs of chips of monoliths (a) G-60-10, (b) G-50-10, and (c) G-25-10 prepared by polymerization at 70°C, polymerization time 7 h.

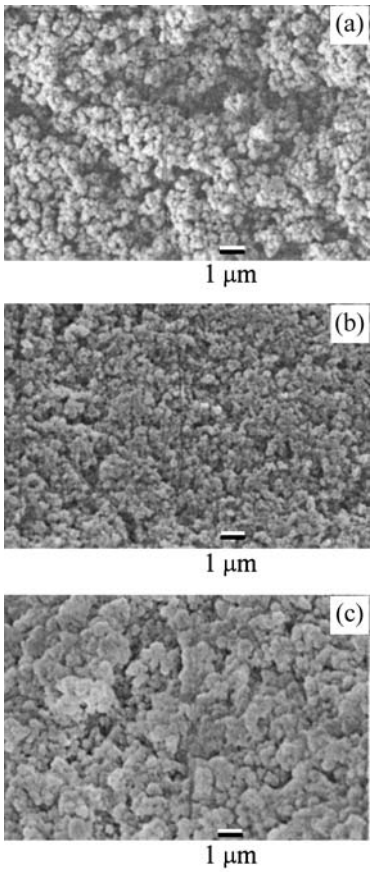

Fig. 2. Electron micrographs of chips of GMA–EDMA monolith (a) G-60-17, (b) G-60-10, and (c) G-60-0 prepared are varied porophore ratio in the reaction mixture.

the content of the cross-linking agent (EDMA) leads to an increase in the "density" of the resulting polymeric products and, thus, in the sorbent surface area and to a decrease in the average pore size (Fig. 1). At the same time, the high degree of cross-linking causes formation of almost impermeable areas on the surface of the porous polymer, which deteriorates its hydrodynamic properties.

It is known that formation of the structure of a monolithic polymer (in particular, GMA–EDMA copolymer) strongly depends on the nature and ratio of the thermodynamically poor solvents (porophores) in the organic phase [16]. We found that, with a mixture of cyclohexanol and dodecanol (C–D) used as the porophore, an increase in the cyclohexanol fraction up to complete substitution of dodecanol leads to a considerable decrease in the size of macropores, with the corresponding increase in the internal surface area of the monolith (Fig. 2).

Table 2. Properties of G-60-10 sorbent prepared at different polymerization temperatures

T, °C	τ, h	Surface area, $m^2 g^{-1}$	Pore size, μm
55	12	23.7	0.6
60	9	32.6	0.3
70	7	70.5	0.1

The polymerization temperature is an important parameter affecting the final morphology of the solid copolymer. Examination by intrusion mercury porosimetry quantitatively showed that the average pore size decreases as the process temperature is elevated (Table 2). It was found that gradient variation of the polymerization temperature, i.e., gradual linear heating from room temperature over a period of 1 h to a given temperature corresponding to the temperature of the initiator decomposition, makes the average pore size larger and the pore size distribution narrower as compared to the sorbents prepared at the same temperature, which was attained by quick

heating and then kept constant (Fig. 3). This phenomenon can be accounted for by the mechanism of radical polymerization: the higher the polymerization rate, the higher the rate of nucleus formation and the greater the number of these nuclei in the unit volume. As a result, the matrix formed is characterized by a higher structure density and, thus, by a smaller average pore size. The random distribution of the growing globules, associated with the high polymerization rate, also broadens the pore size distribution.

Based on the experimental data, we chose the polymerization conditions required to prepare a material with boundary properties, i.e., with the pore size providing unhindered liquid flow at low pressures and high specific surface area of pores. In this case, the GMA : EDMA monomer ratio was 6 : 4, and the porophore ratio C : D = 9 : 1. The polymerization was carried with linear heating from 20 to 55°C over a period of 1 h; the polymerization time was 12 h. The resulting monolith had high mechanical strength and chemical stability. The rigid structure of the monolithic sorbent allowed chromatographic experiments to be performed at a pressure of up to 200 bar in the mobile phase flow. The chemical stability of the stationary phase was confirmed by passing various organic solvents, inorganic and organic acids, buffer solutions, and other eluents through the column. The IR spectroscopic and SEM data showed no degradation of the monolith matrix.

The dependence of the pressure on the linear flow velocity of the mobile phase (water) (Fig. 4) was determined using the (60 × 2 mm) column packed with monolithic GMA–EDMA polymer prepared in situ. It can be seen that, at a water flow velocity of 2.0 ml min^{-1} (corresponding to F = 10.5 ml min^{-1} for a standard column 4.6 mm in diameter), the pressure was only 40 bar, whereas columns of the same size packed with a granular sorbent are characterized by a pressure drop of about 100 bar at an eluent flow rate of 1–2 ml min^{-1}.

The relative porosity of the monolithic stationary phases can be determined chromatographically from the elution of nonsorbable compounds [17]. Markers with different molecular sizes allow determination of the fraction of pores accessible to a given compound in the course of chromatographic separation. The results for the above column, determined from the elution volumes of low-molecular-weight (acetone, *L*-tyrosine) and high-molecular-weight (bovine serum albumin) compounds, are listed in Table 3.

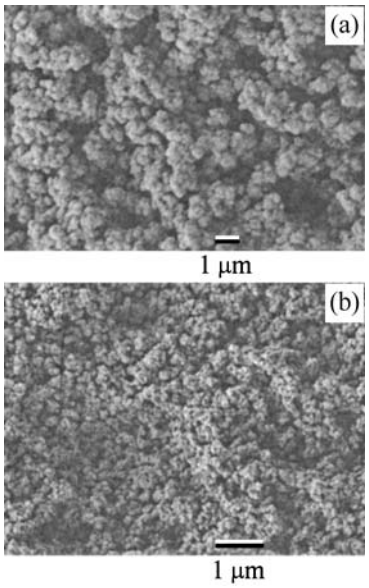

Fig. 3. Electron micrographs of chips of GMA–EDMA monolith prepared at a polymerization temperature of 55°C; (a) constant temperature and (b) temperature gradient.

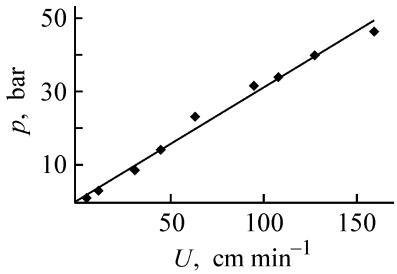

Fig. 4. Pressure P vs. the linear flow velocity U of the eluent (water).

Table 3. Fraction of accessible sorbent pores, calculated from the elution volumes of low-molecular-weight (acetone, *L*-tyrosine) and high-molecular-weight compounds (bovine serum albumin, BSA)

Compounds	Molecular weight	Elution volume V_R			Corrected elution volume V_R^*			Pore fraction V_{por}, ml ml^{-1}
		μl at indicated elution rate, μl $μl^{-1}$						
		20	100	200	20	100	200	
Acetone	58	120	120	120	87	87	87	0.46
L-Tyrosine	181	115	115	115	82	82	82	0.44
BSA	67 000	87	87	87	54	54	54	0.29

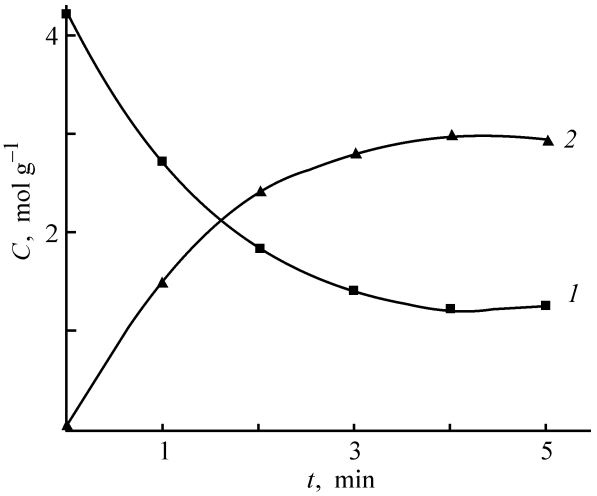

Fig. 5. Kinetic curve of conversion of epoxy groups by ammonia: (*t*) time of modification of the polymer with an ammonia solution and (*C*) conversion of epoxy groups by ammonia. Content, mmol g^{-1}: (*1*) epoxy groups and (*2*) nitrogen.

A significantly smaller pore volume was calculated for high-molecular-weight BSA, because it cannot occupy smaller pores. The chromatographic patterns recorded at various elution rates are typical of monolithic stationary phases; they are symmetric and independent of the elution rate.

To make the sorbents suitable for ion chromatography, we introduced a controlled amount of adsorption centers into the sorbent structure by chemical modification of the monolith with amino groups:

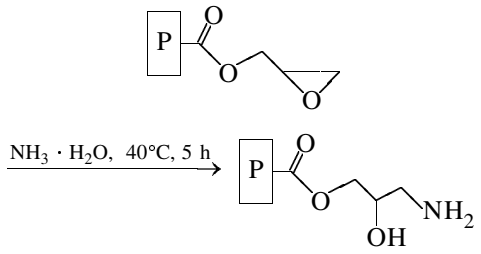

We found that the conversion of the epoxy groups upon polymer modification with 25% ammonia solution at 40°C for 5 h reaches 70–75%. The IR spectra showed that, under the static conditions, the kinetic curve of conversion of the epoxy groups by ammonia levels off in 4 h (Fig. 5). This kinetic dependence allows preparation of sorbents with various (even small) densities of the adsorption ligands, which is of particular importance for preparing stationary phases for ion chromatography.

CONCLUSIONS

(1) Matrices of a macroporous copolymer based on glycidyl methacrylate and ethylene glycol dimethacrylate exhibit rigid macroporous morphology controlled in the stage of synthesis and characterized by a large total surface area, chemical stability, mechanical strength, and unique hydrodynamic parameters.

(2) Direct tests in columns showed the efficiency of these materials as fixed phases for high-speed liquid chromatography.

REFERENCES

1. Tennikova, T.B., Belenkii, V.G., and Svec, F., *J. Liq. Chromatogr.*, 1990, vol. 13, no. 1, pp. 63–70.
2. Svec, F. and Tennikova, T.B., *J. Biocompat. Polym.*, 1991, vol. 6, no. 2, pp. 393–397.
3. Tennikova, T.B. and Svec, F., *J. Chromatogr.*, 1993, vol. 646, no. 2, pp. 279–288.
4. US Patent 4889632.
5. Tennikova, T.B. and Freitag, R., *J. High Resol. Chromatogr.*, 2000, vol. 23, no. 1, pp. 27–41.
6. *Monolithic Materials: Preparation, Properties, and Applications*, Svec, F., Tennikova, T.B., and Deyl, Z., Eds., Amsterdam: Elsevier, 2003, vol. 67.
7. Hutchinson, J.P., Hilder, E.F., Macka, M., et al., *J. Chromatogr. A*, 2006, vol. 1109, no. 1, pp. 10–18.
8. Novic, M. and Haddad, P.R., *J. Chromatogr. A*, 2006, vol. 1109, no. 1, pp. 19–28.
9. Augustin, V., Jardy, A., and Gareil, P., *J. Chromatogr. A*, 2006, vol. 1119, no. 1, pp. 80–87.
10. Riordan, C. and Barron, L., *J. Chromatogr. A*, 2006, vol. 1109, no. 1, pp. 111–119.
11. Svec, F. and Frechet, J.M.J., *Biotechnol. Bioeng.*, 1995, vol. 48, no. 5, pp. 476–480.
12. Svec, F. and Frechet, J.M.J., *Chem. Mater.*, 1995, vol. 7, no. 1, pp. 707–718.
13. Strancar, A., Barut, M., Podgornik, A., et al., *LC-GC Int.*, 1998, vol. 10, no. 11, pp. 660–668.
14. Strancar, A., Podgornik, A., Barut, M., et al., in *Advances in Biochemical Engineering/Biotechnology: Modern Advances in Chromatography*, Heidelberg: Springer, 2002, vol. 76, pp. 50–66.
15. Kun, K.A. and Kunin, R., *J. Polym. Sci.*, 1967, vol. 16, pp. 1457–1469.
16. Svec, F. and Frechet, J.M.J., *Ind. Eng. Chem. Res.*, 1999, vol. 38, no. 1, pp. 34–48.
17. Tennikov, M.B., Gazdina, N.V., Tennikova, T.B., and Svec, F., *J. Chromatogr. A*, 1998, vol. 798, no. 1, pp. 55–64.

ISSN 1070-4272, Russian Journal of Applied Chemistry, 2007, Vol. 80, No. 4, pp. 643–646. © Pleiades Publishing, Ltd., 2007.
Original Russian Text © E.E. Ergozhin, K.I. Imanbekov, E.R. Kendirzhanov, 2007, published in Zhurnal Prikladnoi Khimii, 2007, Vol. 80, No. 4, pp. 658–662.

MACROMOLECULAR CHEMISTRY AND POLYMERIC MATERIALS

Ion Exchangers Based on Homo- and Copolymers of Vinyloxyethylamine and Epoxy Compounds

E. E. Ergozhin, K. I. Imanbekov, and E. R. Kendirzhanov

Bekturov Institute for Chemical Sciences, Ministry of Education and Science of the Republic of Kazakhstan, Almaty, Kazakhstan

Received June 14, 2005; in final form, March 2007

Abstract—A method was developed for synthesis of highly permeable polyelectrolytes through the reaction of polyvinyloxyethylamine with various glycidyl derivatives of dihydroxybenzenes, aminophenols, and aromatic diamines. The physicochemical and sorption properties of the resulting polymers were examined.

DOI: 10.1134/S1070427207040258

Soluble and cross-linked ion exchangers produced on the basis of polyvinyloxyethylamine (PVOEA, monoethanolamine polyvinyl ether) demonstrate unique performance characteristics as sorbents, exhibiting high chemical, thermal, and radiation resistance. They are widely used in solving diverse problems of chemical technology, e.g., for recovery of noble, rare, and nonferrous metals and purification of medical products [1–7].

In this study, we synthesized polyfunctional ion-exchange resins by the reaction of di-, tri-, and tetraglycidyl derivatives of dihydroxybenzenes, *m*- and *p*-aminophenols, and aromatic diamines with VOEA homo- and copolymers and characterized their properties.

EXPERIMENTAL

Epoxy compounds (ECs): diglycidyl derivatives of resorcinol (DGR), hydroquinone (DGH), and aniline (DGA); triglycidyl derivatives of *m*- and *p*-aminophenols (TGmAP, TGpAP); and tetraglycidyl derivative of diaminodiphenylmethane (TGDADPM) were prepared as in [8].

VOEA-based polymers: homopolymer (PVOEA) and VOEA copolymers with *N*-vinylpyrrolidone (VOEA–NVP) and 2-methyl-5-vinylpyridine (VOEA–MVP) were synthesized at a monomer molar ratio of VOEA : vinylpyridine = 25 : 75 by the procedure described in [9].

The ion exchangers were synthesized by polycondensation of homo- and copolymers of VOEA with ECs [10] in isobutanol at 60–120°C for 8–10 h. The reaction mixture was poured on a tray and concentrated at 80°C. The resulting product was crushed and screened to obtain the 0.25-mm fraction by the standard procedure [11, 12].

The chemical resistance of the resins against acids and alkalis was studied according to [11, 13]. Two 1-g samples were placed in 250-ml round-bottomed flasks. One sample was poured over with 100 ml of 5 M H_2SO_4 and the other sample, with 100 ml of 5 M NaOH. The contents were heated for 30 min (water bath) with a reflux condenser and then cooled to room temperature. The sample was filtered off and, if needed, converted into the OH form. Finally, the sample was washed with distilled water and analyzed for the static exchange capacity (SEC). The chemical resistance of the resin X (%) was estimated as

$$x = \frac{\mathrm{SEC}}{\mathrm{SEC}_0} \times 100,$$

where SEC_0 and SEC are the static exchange capacities of the resin before and after treatment, respectively.

To determine the chemical resistance of the resins against oxidants [11, 13], a 1-g resin sample was poured over with 100 ml of 10% H_2O_2 and allowed to stand for 48 h at room temperature with intermittent stirring. Then the resin was filtered off, converted into the OH form, washed with distilled water, and analyzed for $\mathrm{SEC}_{\mathrm{HCl}}$. The chemical resistance was estimated by Eq. (1).

The kinetics of the reaction of DGEA with PVOEA was studied IR-spectroscopically on a Spec-

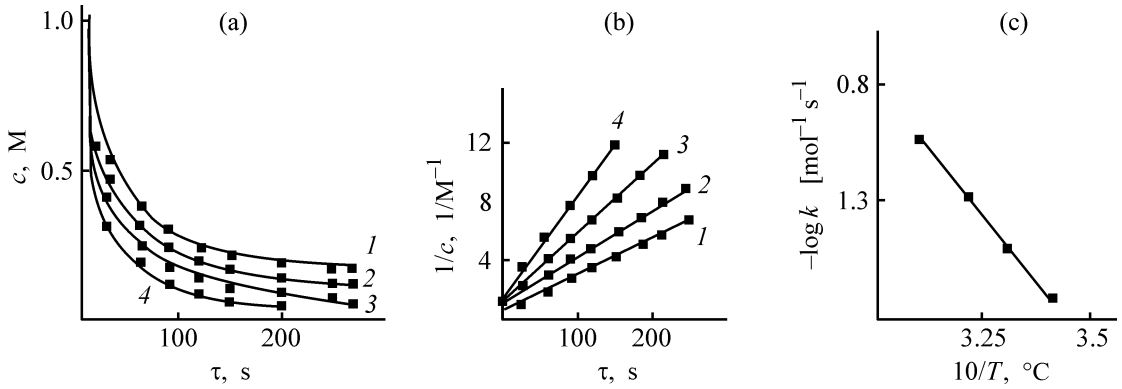

Fig. 1. (a) Kinetic curves for the decrease in the epoxy group content c, (b) their linearized forms, and (c) Arrhenius plot for the reaction of DGEA with PVOEA. (k) Rate constant and (τ) time. T (°C): (*1*) 20, (*2*) 30, (*3*) 40, and (*4*) 50.

ord M80 instrument (Carl Zeiss) with 0.04-mm cells [14, 15]. The reaction was monitored by the decrease in the intensity of the band at 917–920 cm^{-1} (asymmetric stretching vibrations of the DGA epoxy groups). The resulting transmission-vs.-time curves were converted to the curves of epoxy concentration against time.

It follows from Fig. 1 that, under ambient conditions, epoxy groups readily react with the primary amino groups of PVOEA. The linear dependence in the coordinates $1/c$ vs. τ suggests a second-order kinetics.

The activation energies of the reactions of DGA with PVOEA (Fig. 1), VOEA–MVP, and VOEA–NVP were estimated to be 28.04, 31.90, and 35.01 kJ mol^{-1}, respectively, which is well consistent with published data [16, 17]. Data on the influence of the starting reagent ratio, curing time, and temperature on SEC_{HCl} (0.1 M HCl) of the resulting resins, obtained in this study show (Table 1) that, in all cases, SEC grows as

Table 1. Influence of the nature and ratio of the starting components on SEC

EC	SEC (0.1 M HCl), mg-equiv g^{-1}											
	PVOEA				VOEA–MVP				VOEA–NVP			
	1 : 1	1 : 2	1 : 3	1 : 4	1 : 1	1 : 2	1 : 3	1 : 4	1 : 1	1 : 2	1 : 3	1 : 4
DGR	5.2	5.4	6.5	6.5	5.2	5.8	6.0	6.1	1.4	1.6	1.6	1.6
DGH	5.3	6.5	6.7	6.5	4.9	5.8	6.2	6.0	1.3	1.6	1.6	1.7
DGA	5.6	6.4	7.0	7.2	5.8	6.0	6.4	6.2	1.5	1.7	1.9	2.0
TGDADPM	6.0	6.5	6.9	7.1	6.2	6.4	6.7	6.7	1.5	1.6	1.9	1.9
TGpAP	5.8	6.5	6.9	6.9	5.8	5.9	6.3	6.4	1.5	1.6	1.7	1.7

Table 2. Static exchange capacity of anion-exchange resins synthesized at various temperatures

EC	SEC (0.1 M HCl), mg-equiv g^{-1}, at indicated temperature, °C											
	PVOEA				VOEA–MVP				VOEA–NVP			
	60	80	100	120	60	80	100	120	60	80	100	120
DGA	6.2	6.4	6.7	6.6	5.6	6.0	6.2	6.1	1.2	1.5	1.6	1.5
DGR	6.1	6.5	6.7	6.5	6.2	6.3	6.4	6.3	1.2	1.4	1.6	1.5
DGH	6.5	6.9	7.0	6.9	5.2	5.6	6.2	6.0	1.3	1.5	1.9	1.7
TGmAP	6.5	6.9	6.9	6.8	5.9	6.7	6.7	6.5	1.5	1.8	1.9	1.8
TGpAP	6.4	6.6	6.9	6.7	5.6	5.8	6.3	6.2	1.1	1.3	1.7	1.7

Table 3. Influence of the curing time τ on SEC of the resins

EC	SEC (0.1 M HCl), mg-equiv g^{-1}, at indicated time, h											
	PVOEA				VOEA–MVP				VOEA–NVP			
	4	6	8	10	4	6	8	10	4	6	8	10
DGA	6.8	7.4	7.7	7.8	5.9	6.5	6.8	6.8	1.5	1.8	2.1	2.1
DGR	5.7	5.9	6.5	6.7	4.8	5.6	6.2	6.2	1.2	1.3	1.5	1.6
DGH	5.4	6.0	6.6	6.7	6.2	6.3	6.4	6.4	1.3	1.4	1.6	1.6
TGmAP	5.6	6.1	6.8	7.0	4.8	5.4	6.1	6.2	1.4	1.5	1.8	1.9
TGpAP	5.3	5.8	6.9	6.9	5.3	5.9	6.7	6.7	1.3	1.5	1.9	1.9
TGDADPM	5.3	5.8	6.8	6.9	5.0	5.6	6.3	6.3	1.2	1.4	1.6	1.7

Table 4. Chemical resistance X of the resins*

EC	W, %	V, ml g^{-1}	SEC_0 (0.1 N HCl), mg-equiv g^{-1}	SEC_0/X, %, with indicated reagent		
				5 N H_2SO_4	5 N NaOH	10% H_2O_2
PVOEA						
DGR	93	2.6	6.4	6.4/100	6.3/98.4	6.3/98.4
DGH	95	3.0	6.4	6.4/100	6.4/100	6.4/100
DGA	94	3.3	6.5	6.5/100	6.4/98.5	6.5/100
TGDADPM	95	3.3	6.7	6.7/100	6.6/98.5	6.7/100
TGpAP	95	3.2	6.3	6.3/100	6.2/98.4	6.2/98.4
VOEA–MVP						
DGR	91	2.9	6.0	6.0/100	6.0/100	6.0/100
DGH	95	3.2	6.1	6.1/100	6.0/98.4	6.1/100
DGA	92	3.3	6.1	6.1/100	6.1/100	6.1/100
TGDADPM	90	3.4	6.3	6.3/100	6.2/98.4	6.2/98.4
TGpAP	95	2.9	6.2	6.2/100	6.1/98.4	6.1/98.4

* (SEC) Static exchange capacity (0.1 HCl) after treatment with 5 N H_2SO_4, 5 N NaOH, and 10% H_2O_2; (V) swellability of the resin in water; and (W) moisture content.

the VOEA to EC ratio increses from 1 : 1 to 4 : 1. The anion exchangers based on *m*- and *p*-dihydroxybenzenes are characterized by low SEC, since, in contrast to aromatic mono- and diamines, they contain no titratable amino groups. Introduction of the *N*-vinylpyrrolidone units into the copolymer considerably decreases SEC.

It is known that the properties of ion exchangers are strongly influenced by the prepolymer curing mode. Our results show (Tables 2 and 3) that the products should be cured for 8–10 h at 80–100°C, depending on the condensation temperature and nature of VOEA polymers.

The SEC of the resins prepared under optimal conditions ranges from 2.3 to 7.7 mg-equiv g^{-1}. These products demonstrate a limited swellability (Table 4). In this case, the yield of the target products is 88–95%. The SEC loss caused by treatment of the resins with 5 N H_2SO_4, 5 N NaOH, and 10% H_2O_2 was within 5%.

The polyelectrolytes obtained selectively extract Au ions from hydrochloric acid solutions over a wide concentration range (Fig. 2).

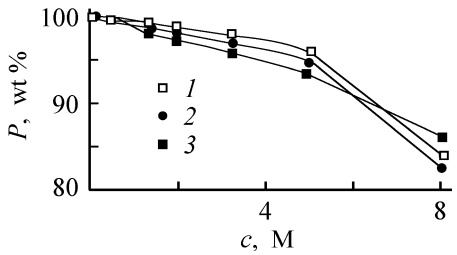

Fig. 2. Sorption P of Au ions on anion-exchange resins based on (*1*) PVOEA, (*2*) VOEA–MVP, and (*3*) VOEA–NVP vs. the HCl concentration c.

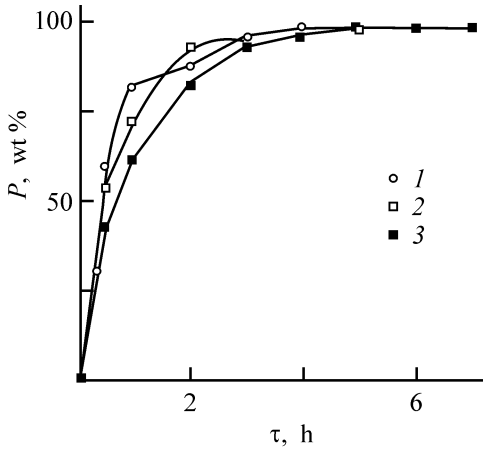

Fig. 3. Kinetic curves of Au sorption on anion-exchange resins based on (*1*) PVOEA, (*2*) VOEA–MVP, and (*3*) VOEA–NVP. (*P*) Degree of sorption and (τ) time.

Kinetic data on the sorption of anionic Au species on the anion-exchange resins show (Fig. 3) that the nature of the epoxy compound has no effect on the sorption rate. For the resins based on TGDADPM, the maximal sorption was attained in 3 h. In this case, a 50% sorption was attained in 0.5 h.

To conclude, anion exchangers based on VOEA polymers and various ECs are highly efficient sorbents for recovery of Au from hydrochloric acid solutions. The resins recover 98–99.9% of Au over a wide HCl concentration range, which points to their high selectivity and chemical resistance.

CONCLUSIONS

(1) Condensation of di-, tri-, and tetraglycidyl derivatives of dihydroxybenzenes, aminophenols, and aromatic mono- and diamines with homo- and copolymers of β-vinyloxyethylamine were studied.

(2) The activation energies of the reactions of aniline diglycidyl derivative with β-vinyloxyethylamine homopolymer and its copolymers with 2-methyl-5-vinylpyridine and *N*-vinylpyrrolidone were estimated to be 28.04, 31.90, and 35.01 kJ mol^{-1}, respectively, which is well consistent with the published data.

(3) It was found that the chemical resistance of ion exchangers synthesized on the basis of di-, tri-, and tetraglycidyl derivatives of aromatic compounds and β-vinyloxyethylamine polymers in 5 N sulfuric acid, 5 N NaOH, and 10% H_2O_2 is 98–100%.

(4) It was demonstrated that the polyelectrolytes obtained selectively recover Au from hydrochloric acid solutions over a wide HCl concentration range. The degree of sorption is as high as 98–99%.

REFERENCES

1. Imanbekov, K.I., Nusipova, A.M., and Erkasov, R.Sh., *Izv. Vyssh. Uchebn. Zaved., Khim. Khim. Tekhnol.*, 1998, vol. 41, no. 2, pp. 122–124.
2. Shatalov, V.V., Kharina, T.P., Balanovskii, N.V., et al., *Khim. Tekhnol.*, 2000, no. 7, pp. 19–23.
3. Ergozhin, E.E. and Imanbekov, K.I., *Zh. Prikl. Khim.*, 2006, vol. 79, no. 5, pp. 744–746.
4. Imanbekov, K.I. and Ergozhin, E.E., *Zh. Prikl. Khim.*, 2006, vol. 79, no. 8, pp. 1311–1314.
5. Ergozhin, E.E., Kenzaliev, B.K., Chalov, T.K., et al., *Tsvetn. Met.*, 2005, no. 2, pp. 43–46.
6. Chalov, T.K., Kovrigina, T.V., Akhmetova, K.Sh., et al., in *Materialy regional'noi nauchno-prakticheskoi konferentsii "Tekhnologiya organicheskikh veshchestv i vysokomolekulyarnykh soedinenii"* (Proc. Regional Scientific and Practical Conference "Technology of Organic Substances and Macromolecular Compounds"), Tomsk, 2003, pp. 164–166.
7. Garkusha-Bozhko, V.S. and Shvaika, O.P., *Khim. Geterotsikl. Soedin.*, 1990, no. 4, pp. 507–510.
8. Ergozhin, E.E. and Menligaziev, E.Zh., *Polifunktsional'nye ionoobmenniki* (Polyfunctional Ion-Exchange Resins), Alm-Ata: Nauka, 1986.
9. Nurkeeva, Z.S., Shaikhutdinov, E.M., and Seitov, A.Z., in *Geterogennye protsessy v vodnykh i organicheskikh sredakh* (Heterogeneous Processes in Aqueous and Organic Solutions), Alma-Ata: Kaz. Gos. Univ., 1984, pp. 79–89.
10. Kazakhstan Inventor's Certificate, no. 17988.
11. Polyanskii, I.P., Gorbunov, G.V., and Polyanskaya, N.L., *Metody issledovaniya ionitov* (Methods for Studying Ion Exchangers), Moscow: Khimiya, 1976.
12. *GOSTs* (State Standards) *10898–2.74*, *10896–78*, *10898–84*, *10898–5.84*, and *20255.1–89*.
13. Rakhmankulov, D.L., Kimsanov, B.Kh., Loktionov, N.A., et al., *Epikhlorgidrin: metody polucheniya, fizicheskie i khimicheskie svoistva, tekhnologiya proizvodstva* (Epichlorohydrin: Preparation, Physical and Chemical Properties, and Production Technology), Moscow: Khimiya, 2003.
14. Noskov, A.M. and Gogolev, V.N., *Zh. Prikl. Spektr.*, 1974, vol. 22, no. 1, pp. 88–91.
15. Sidyakin, P.V., *Vysokomol. Soedin., Ser. A*, 1972, vol. 14, no. 5, pp. 979–988.
16. Begenova, B.E., Ergozhin, E.E., Atshabarova, R.V., et al., *Dokl. Akad. Nauk SSSR*, 1987, vol. 292, no. 5, pp. 1154–1156.
17. Ergozhin, E.E., Bektenov, N.A., and Akimbaeva, A.M., *Polielektrolity na osnove glitsidilmetakrilata i ego sopolimerov* (Polyelectrolytes Based on Glycidyl Methacrylate and Its Copolymers), Almaty: Evero, 2004.

ISSN 1070-4272, Russian Journal of Applied Chemistry, 2007, Vol. 80, No. 4, pp. 647–653. © Pleiades Publishing, Ltd., 2007.
Original Russian Text © V.V. Semenov, N.V. Melenskova, N.F. Cherepennikova, Yu.A. Kurskii, O.V. Kuznetsova, M.A. Lopatin, 2007, published in Zhurnal Prikladnoi Khimii, 2007, Vol. 80, No. 4, pp. 663–669.

MACROMOLECULAR CHEMISTRY AND POLYMERIC MATERIALS

Functionalized Silicon-containing Imino Enols and Enamino Ketones Prepared by Hydrolytic Condensation

V. V. Semenov, N. V. Melenskova, N. F. Cherepennikova, Yu. A. Kurskii, O. V. Kuznetsova, and M. A. Lopatin

Razuvaev Institute of Organometallic Chemistry, Russian Academy of Sciences, Nizhni Novgorod, Russia
Lovachevsky State University, Nizhni Novgorod, Russia

Received July 24, 2006; in the final form, December 2006

Abstract—A mixture of two isomers of organosilicon carbofunctional compounds, 4-(3'-triethoxysilylpropylimino)pent-2-en-2-ol $(EtO)_3Si–CH_2CH_2CH_2–N=C(Me)–CH=C(Me)–OH$ (**Ia**, 83%) and 4-(3'-triethoxysilylpropylamino)pent-3-en-2-one $(EtO)_3–CH_2CH_2CH_2–NH–C(Me)=CH–C(O)Me$ (**Ib**, 17%) was prepared by reaction of 3-aminopropyltriethoxysilane with acetylacetone. The use of trimethylsilyl ether of acetylacetone instead of acetylacetone yields **Ia** (84%) and silylated derivatives $(Me_3SiO)_n(EtO)_{3-n}Si–CH_2CH_2CH_2–N=C(Me)CH=C(Me)OH$ (**II**) (16%). Solid, liquid, or resinous products were prepared by hydrolytic condensation of **I** and **II**. Compositions for preparing transparent sol-gel films were developed.

DOI: 10.1134/S107042720704026X

β-Diketones and their nitrogen derivatives (keto imines, enamino ketones, and imino enoles) [1] are conventional chelating ligands. Numerous complexes of *d* and *f* elements with these ligands have been prepared [2–5]. Organic polymers and mineral sorbents with grafted chelate groups are used for concentration, separation, and purification of metals [6–8]. In this study, we developed a procedure for preparing a silicon-containing imino enol from 3-aminopropyltriethoxysilane (APTES) and acetylacetone. The presence of triethoxysilyl groups in the product allows its use for hydrolytic polycondensation and grafting of a ligand to hydrated metal oxides and for preparation of organosilicon polymers, transparent films, and functionalized adsorbents.

A mixture of two isomers, 4-(3'-triethoxysilylpropylimino)pent-2-en-2-ol **Ia** and 4-(3'-triethoxysilylpropylamino)pent-3-en-2-one **Ib**, can be prepared by reaction of APTES with acetylacetone or its trimethylsilyl ether.

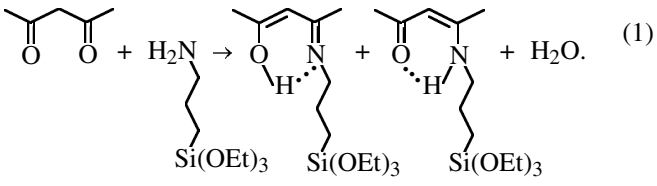

(1)

Ia **Ib**

Ia : **Ib** = 83 : 17

Water released in the course of the reaction reacts with APTES and compound **I**, thus decreasing the yield of **I** and increasing the yield of the oligomers.

The use of trimethylsilyl ether of acetylacetone for this purpose substantially increases the yield of the products distillable in a vacuum. However, preparation of pure compound **I** by this method is complicated by the reaction of the released trimethylsilanol with **I** to form products of substitution of one, two, and three EtO groups at the silicon atom by Me_3SiO: compounds **IIa**–**IIc**, respectively:

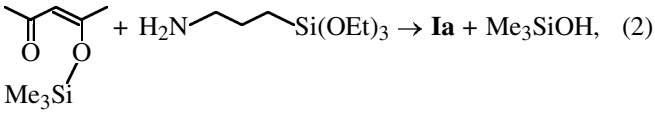

(2)

Ia + $n$$Me_3SiOH$

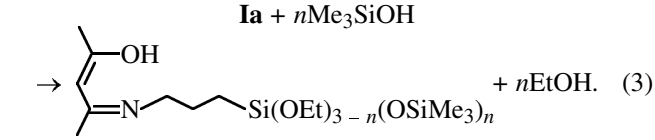

(3)

where n = 1 (**IIa**), n = 2 (**IIb**), n = 3 (**IIc**).

The **I** : **II** ratio calculated from the ^1H NMR data is 84 : 16.

The IR spectrum of compound **I** contains the stretching (2974, 2933, 2888 cm^{-1}) and bending (1441, 1391,

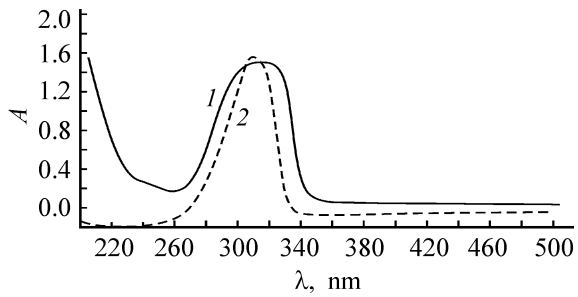

Fig. 1. UV spectrum of (*1*) compound **I** (film on a quartz support, λ_{max} = 310 nm) and (*2*) mixture **I/II** (1.82×10^{-4} M solution in EtOH, λ_{max} = 311 nm, ε = 17200 l mol^{-1} cm^{-1}). (*A*) Optical density and (λ) wavelength.

1355 cm^{-1}) bands of C–H bonds. A strong doublet at 1613 and 1583 cm^{-1} and the band at 1517 cm^{-1} are assigned to vibrations of the imino enol (HO–C=CH–C=N–) and enamino ketone (O=C–CH=C–N–) fragments. The strong bands of the triethoxysilyl group are observed at 1168, 1097, 961, and 784 cm^{-1}. The spectra of **I** and **II** are, on the whole, similar. The difference is that the spectrum of **II** contains two additional bands at 1254 and 845 cm^{-1}, typical of the trimethylsilyl group. The IR and NMR data show that compound **I** prepared by the reaction of acetylacetone with APTES mainly consists of imino enol **A** (83%) and enamino ketone **B** (17%). Synthesis via trimethylsilyl ether yield compounds **I** and **II** in the form of pure imino enols. The keto imine form **C** is not typical of compounds **I** and **II**

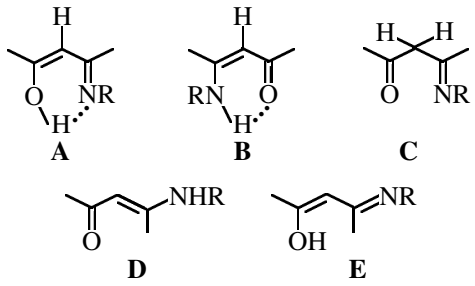

The IR spectrum of compound **I** contains a broad band of ν(O–H) in the range 3400–2600 cm^{-1}, which is superimposed by three strong ν(C–H) bands. The shape of the ν(O–H) band is typical of the hydrogen-bonded chelate ring. The ^{1}H NMR signals of the protons bound with oxygen and nitrogen atoms are observed in the low field (10.84 ppm for OH and 8.38 ppm for NH), with the signal of the OH group being stronger than that of NH. The signal of the methine hydrogen in the imino enol fragment is observed at 4.91 ppm and has a high-field shoulder due to impurity of tautomer **B**. The intensity ratio of the signal of the methine proton, hydrogen atoms of the methylene bridge $Si(CH_2)_3N$, and ethoxy groups $SiOCH_2CH_3$ is 1 : 2 : 6 : 9, which confirms the presence of tautomers **A** and **B** and the absence of the keto imine form **C** containing two protons at the central carbon atoms. The signals of the $CH_3C(O)$ and CH_3CN groups are observed in the form of two singlets of equal intensity at 1.97 and 1.89 ppm. The ^{1}H NMR spectrum of compound **I** contains similar signals and additional signals at –0.039, –0.021, and +0.003 ppm assigned to the Me_3Si group in $–CH_2–Si(OSiMe_3)_3$, $–CH_2–Si(OSiMe_3)_2(OEt)$, and $–CH_2–Si(OSiMe_3)(OEt)_2$. The electron-withdrawing power of the Me_3SiO substituent (σ_J = +0.05) is lower than that of EtO (σ_J = +0.26) [9]. The signals of the protons of the Me_3SiO groups were assigned on the assumption that they should be shifted upfield in going from **IIa** to **IIb** and then to **IIc**. The molar ratio of the products **IIa** : **IIb** : **IIc** = 31 : 24 : 45, calculated from the ^{1}HNMR spectrum, suggests that the nucleophilic substitution at the silicon atom is nonselective.

The ^{13}C NMR and DEPT spectra confirm the structure of compounds **IIa**–**IIc**. The signals of carbon atoms of the *C*H$_3$Si, *C*H$_3$CH$_2$O, *C*H$_3$CN, and *C*H$_3$C(O) groups and of the *CH* group of the central carbon atom of imino enol are observed at 1.99, 18.56, 19.03, 28.95, and 95.33 ppm, respectively; and the signals of the CH_2Si, CH_2CH_2N, and CH_2O groups, at 7.80, 24.28, 45.73, and 58.77 ppm, respectively. The two lowest-field signals of equal intensity at 162.96 and 194.31 ppm are assigned to the carbon atoms of the imino enol fragment bound to the oxygen and nitrogen atoms. The absence of splitting of these signals suggests the formation of a strong chelate ring. The ring closure through the OH···N hydrogen bond rules out formation of *trans* isomers **D** and **E**. The presence of these isomers should result in splitting of these signals. The results are, on the whole, consistent with the data of monograph [10], in which the imine–enamine tautomerism of the N derivatives of β-dicarbonyl compounds is considered in detail.

The UV spectra of compound **I** and **I/II** mixture (Fig. 1) contain a strong band at 310 nm and a very weak band at 230–240 nm. It is known that β-diketones also have two absorption bands: a short-wavelength band due to the $\pi \rightarrow \pi^*$ transition and a long-wavelength band assigned to the $n \rightarrow \pi^*$ transition. Two bands at 227 and 290 nm are observed in the spectrum of the triethoxysilyl derivative $(EtO)_3SiCH_2CH_2CH_2C[C(O)Me]_2$. The presence of the strong absorption band at 310 nm, which is red-shifted as compared to the band of the β-diketone, suggests the delocalization of π and *n* electrons in the hydrogen-bonded chelate ring. The weak band in the short-

Time of curing τ_{cur} and weight loss of films in the course of their cross-lonking in air and subsequent heating

Composition of initial mixture, wt %			τ_{cur}, h	Weight loss, %		
I/II	APTES	Oligodimethyl-siloxanediols		curing in air	heating for 0.5 h	
					100°C	150°C
15	31	54	12	25	28	30
39	31	30	20	8	13	21
49	25	26	28	25	31	40

wavelength range is due to the presence of a small amount of acyclic imino enol and enamino ketone.

Pure compound **I** and a **I/II** mixture prepared by reactions 2 and 3, respectively, are relatively stable with respect to atmospheric moisture. When thin films of these compounds were aged on a glass support for 48 h, no solid films were formed. Transparent 20–50-μm solid films were obtained from compositions containing **I** (or **I/II**), oligodimethylsiloxanediols $HO(SiMe_2O)_nH$ (n = 2–5), and APTES. The time of spontaneous curing at room temperature in air ranges from 15 to 30 h, depending on the composition of the initial liquid mixture. Turbid or strongly opalescent films were formed in 15–20 h in the absence of siloxanediols at **I** : APTES [(**I/II**) : APTES] weight ratio from 0.5 : 2 to 2 : 1. At the weight ratio of 4 : 1, the mixture is cured in 48 h incompletely; however, the viscosity of the liquid layer strongly increases.

The curing time and weigh loss of the films in the course of cross-linking in air and subsequent heating to 100 (0.5 h) and 150°C (0.5 h) are listed in the table. It is seen that the cross-linking duration grows from 12 to 28 h with an increase in the fraction of **I/II** in the initial mixture from 15 to 49 wt %. The weight loss in the course of curing and heat treatment is minimal at the **I/II** content of about 40 wt %. The films withstand heating to 100°C. At 150°C they become yellow, but remain transparent. The maximal weigh loss can reach 40%.

The presence of nonhydrolyzable Me_3SiO groups in compounds **IIa**–**IIc** should result in an increase in the fraction of linear polysiloxane fragments and a decrease in the degree of cross-linking in the course of curing in air as compared to the films prepared from **I**. Siloxanediols act as plasticizers and agents cross-linking tri- and bifunctional molecules of silylated imino enols **I** and **II** by the condensation mechanism. Molecules of APTES containing primary amino groups act as both a base catalyst and a trifunctional component along with **I**:

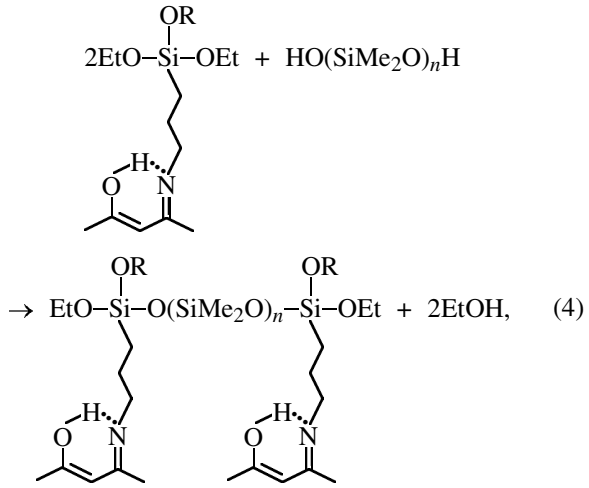

(4)

where R = Et, $SiMe_3$.

The structure of the solid film can be described as follows:

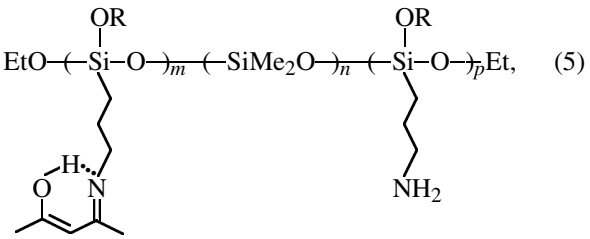

(5)

where R = Et, $SiMe_3$, –Si≡.

The IR spectra of the film prepared by curing a mixture containing 15 wt % **I/II**, 54 wt % siloxanediols, and 31 wt % APTES in air, followed by heating to 100 and 150°C, are shown in Fig. 2. The IR data can give insight into the curing mechanism. The spectrum of the initial liquid mixture (Fig. 2, curve *1*) contains weak bands at 3449, 3373, 3297, and 3171 cm^{-1} assigned to the O–H and NH vibrations in siloxanediols, compounds **I** and **II**, and APTES. A strong doublet at 1613, 1578 cm^{-1} is assigned to the imino enol group. The bands of $Si(OEt)_3$

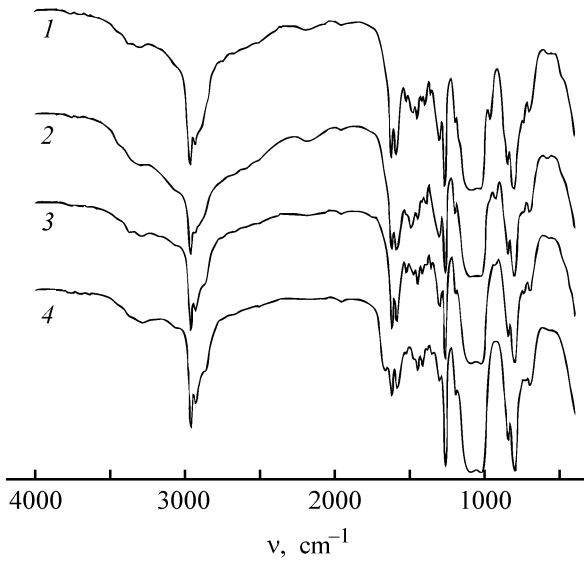

Fig. 2. IR spectra of a film prepared from a mixture of compounds **I/II**, APTES, and oligodimethylsiloxanediols taken in a weight ratio of 15 : 31 : 52. (ν) Wavenumber; the same for Fig. 3. Film: (*1*) initial, (*2*) cured in air for 15 h, (*3*) heated at 100°C for 30 min, and (*4*) heated at 150°C for 30 min.

and $Si(OEt)_{3-n}(OSiMe_3)_n$ are observed at 1260, 1168, 1098, 1027, 961, 845, and 804 cm^{-1}.

When a liquid film in kept in air for 15 h at room temperature (until curing) (Fig. 2, curve *2*), the bands in the range 3500–2700 cm^{-1} are broadened and become stronger. At the same time, the spectrum in the range 1150–840 cm^{-1} (SiOEt, $SiOSiMe_3$) changes insignificantly. The bands are broadened owing to the formation of quaternary ammonium cations giving broad N–H bands in the range 3000–2200 cm^{-1}. The spectrum in the range of vibrations of imino enol group and N–H bending vibrations (1700–1450 cm^{-1}) also changes substantially. The bands at 1583 and 1472 cm^{-1} are broadened and shifted toward low (the first band) and high (the second band) frequencies owing to superposition with the bending vibrations of the N–H bond in the ammonium cation. The intensity of the second band (1482 cm^{-1}, NH_3^+) substantially increases. Compounds **I** and **II** are weak protonic acids, whereas APTES is a base. The changes in the IR spectrum in the range 2900–2200 cm^{-1} can be described by the reaction

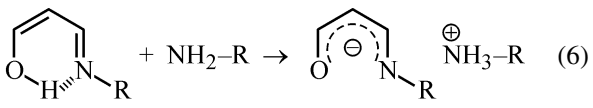

R = ∧∧Si(OEt)$_n$(OSiMe$_3$)$_{3-n}$

The broadening of the absorption bands in the range 3400–3050 cm^{-1} and an increase in their intensities can be due to association of the silanol groups with APTES:

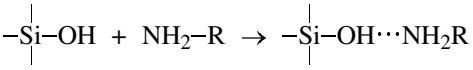

Thus, a quaternary ammonium salt is formed in the composition after introduction of APTES. These compounds are effective catalysts of hydrolysis of triethoxysilyl groups and condensation of silanol groups [11]:

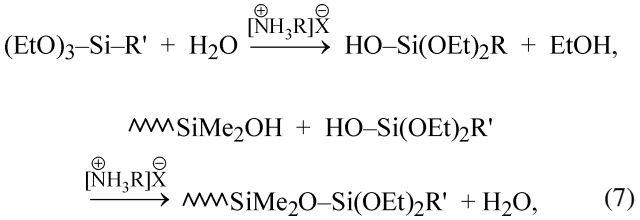

where R = ∧∧Si(OEt)$_3$, R' = ∧∧N=C(Me)CH=C(Me)OH, X = MeC(O)CHC(NR)Me.

Heating of the sample at 100°C for 1 h restores the initial shape of the spectrum (Fig. 2, curve *3*), with the transformation in the range 3500–2700 cm^{-1} being the most pronounced. This is due to decomposition of unstable ammonium derivatives shown in schemes (6) and (7). The main distinction between the spectrum of the film heated to 100°C and that of the initial liquid mixture is the lower intensity of the stretching (3000–2800 cm^{-1}) and bending (1400–1300 cm^{-1}) C–H bands after heating. The shape of the bands in the range 1200–950 cm^{-1} also changes due to a decrease in the content of the SiOEt fragments and an increase in the number of the SiOSi bonds. The intensity of the C–H bands decreases further after heating to 150°C (Fig. 2, curve *4*). The spectrum in the range 1660–1550 cm^{-1} noticeably changes owing to the reaction of the enamino ketone fragment with the primary amino group of APTES.

Thus, the following reactions occur in the course of film curing: formation of imino enol–APTES complex catalyzing the curing; condensation of the silanol groups with the ethoxysilyl groups of compound **I** and APTES; formation of polysiloxane fragments; and release of ethanol.

Organosilicon imino enols **I** and **I/II** were hydrolyzed in an ethanol solution with hydrochloric acid, ammonia, and water in the presence of Bu_4NF. The concentration of hydrochloric acid and ammonia

was 1 mol per mole of the compound. Tetrabutylammonium fluoride was introduced in catalytic amounts. An insoluble powdered polyorganosiloxane, transparent colorless resin, and transparent colorless oil were obtained from **I/II** in the presence of HCl, NH_4OH, and Bu_4NF, respectively. The IR spectra of the products are shown in Fig. 3. The strongest spectral transformations were observed in the spectrum of the samples prepared in the presence of hydrochloric acid (Fig. 3, curve *1*). The appearance of a strong broad band at 3408 cm^{-1} (CO–H) and a number of broadened bands in the range 2730–2400 cm^{-1} (N–H) and transformation of a doublet at 1613 and 1583 cm^{-1} (O–C=C–C=N) into a singlet at 1608 cm^{-1} suggest the protonation of the nitrogen atom and formation of a quaternary iminium cation, with cleavage of the intramolecular hydrogen bond:

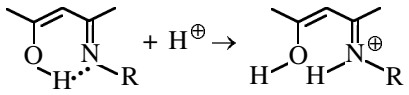

(8)

These substantial structural transformations of the chelate ring change the shape of the absorption band of the O–C=C–C=N fragment at 1600 cm^{-1}. The spectral changes in the range 1200–750 cm^{-1} suggest the conversion of the ethoxysilyl groups into disiloxane groups. The band at 1093 cm^{-1} is broadened and split into a doublet; the intensity of the bands at 1168, 956, and 774 cm^{-1} strongly decreases. It is known that organic silanols readily condense to form disiloxanes in the presence of an acid. The band 3408 cm^{-1} is assigned to the alcoholic group. The results of elemental analysis show that the carbon content of the hydrolysis product is underestimated by a factor of 1.5–1.7 and the silicon content is overestimated with respect to those calculated for organosilsesquioxane $O_{1.5}Si–CH_2CH_2CH_2–N=C(Me)–CH=C(Me)–OH \cdot HCl$ and found in the products of hydrolysis in neural and alkaline solutions. This can be due to partial defragmentation of organosilicon imino enol in the presence of a strong acid, formation of acetylacetone, and its removal from the solid products on drying in a vacuum.

Hydrolysis with ammonia and water in the presence of Bu_4NF results in less substantial transformation of the IR spectrum. The shape and intensity of the absorption bands in the range 1650–1200 cm^{-1} remain the same, which suggests the preservation of the chelate ring. The maximal amount of associated silanol groups is formed in hydrolysis of a **I/II** mixture and compound **I** by water in the presence of Bu_4NF (Fig. 3, curve *3*), which is confirmed by the presence of a strong and broad band at 3373 cm^{-1}

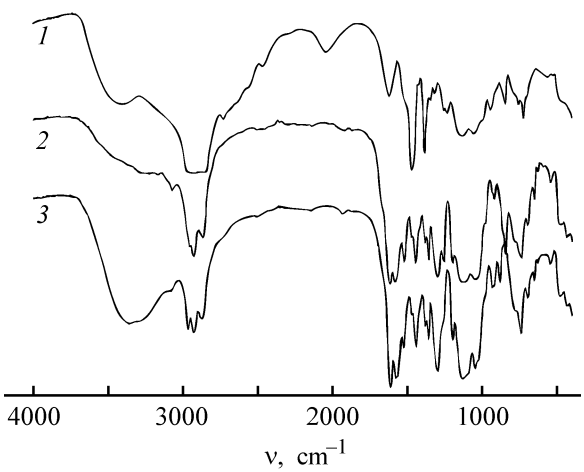

Fig. 3. IR spectra of products formed by hydrolysis of a **I/II** mixture with (*1*) HCl (Nujol mull) and (*2*) NH_4OH solution (liquid film) and (*3*) of compound **I** with water in the presence of Bu_4NF (liquid film).

with a shoulder at 3282 cm^{-1}. The lower intensity of the absorption in the range 3500–3150 cm^{-1} and the stronger broadening of the doublet at 1128 and 1047 cm^{-1} suggest the condensation of a significant number of the SiOH fragments in the presence of NH_4OH to form a high-molecular-weight polysiloxane with terminal silanol groups (Fig. 3, curve *2*).

Thus, solid, resinous, and liquid hydrolysis products with different contents of disiloxane and silanol groups can be prepared by hydrolysis of a **I/II** mixture and pure compound **I** under different conditions.

EXPERIMENTAL

The IR spectra of the samples in the form of a liquid film of Nujol mull between KBr or CaF_2 windows were recorded on an FSM 1201 Fourier IR spectrometer. The electronic absorption spectra were recorded on a Perkin–Elmer Lambda 25 spectrophotometer. The ^1H NMR spectra were recorded in $CDCl_3$ on a Bruker Avance DPX-200 (200 MHz) spectrometer at 25°C using Me_4Si as an internal reference.

Compounds **I** and **II** were analyzed on a Tsvet 530 chromatograph (0.3 × 200 cm stainless steel column, 5% SE-30 on Chromaton N-Super). Acetylacetone was distilled under reduced pressure and was analyzed on a 0.3 × 300-cm column packed with 15% Reoplex-400 on Chezasorb AW-HMDS. 3-Aminopropyltriethoxysilane (Altaikhimprom Production Association, Slavgorod, Altai krai, Russia) was distilled on a 1 × 50 cm column packed with Nichrome spirals and was analyzed on a 0.3 × 200 cm column packed with 5% XC-2-1 silicone on Chromaton-N-AW-DMCS.

The content of isomeric 2-aminopropyltriethoxysilane isomer was 2.0%. Glass (1 × 25 × 40 mm) and quartz (3 × 12 × 40 mm) supports used for film preparation were treated with a saturated NaOH solution in isopropanol for 10 h and then with a chromic acid mixture for 10 h, washed with water, and dried at 150–170°C.

Reaction of acetylacetone with APTES. To a solution of acetylacetone (5.1 g, 0.05 mol) in toluene (25 ml), a solution of APTES (13.3 g, 0.06 mol) in toluene (10 ml) was added. The mixture was refluxed for 4 h. The solvent was distilled off and the residue was subjected to fractional distillation in a vacuum. Compound **I** (5.8 g, 38%) was isolated in the form of a transparent liquid, bp 115–118°C (2 mm Hg), n_D^{20} = 1.4712. IR spectrum, ν, cm^{-1}: 3070 w (H–C=C), 2974 vs (CH), 2933 vs (CH), 2766 w (H–CN), 2736 w (H–CN), 1613 vs, 1583 vs, 1517 m, 1441 s (O–C=C–C=N), 1391 m (CH), 1355 m (CH), 1295 vs, 1194 m, 1168 s (SiOEt), 1097 vs (SiOEt), 1027 m, 961 vs (SiOEt), 784 vs (SiOEt), 648 w, 541 w, 491 m, 445 m. ^{1}H NMR spectrum, $CDCl_3$, δ, ppm (*J*, Hz): 0.63 t (2H, CH_2Si, *J* = 7.8), 1.18 t (9H, CH_3CH2O, *J* = 7.0), 1.59–1.74 quintet (2H, CH_2, *J* = 7.8), 1.89 s [3H, $CH_3C(N)$], 1.97 s [3H, $CH_3C(O)$], 3.15–3.26 q (2H, CH_2N, *J* = 7.0), 3.73–3.83 q (6H, CH_2O, *J* = 7.0), 4.91 s (1H, HC=C), 8.38 s (1H, NH, 17%), 10.84 s (1H, OH, 83%).

Found, %: C 54.81, H 9.33, Si 8.97.
$C_{14}H_{29}NO_4Si$.
Calculated, %: C 55.41, H 9.63, Si 9.26.

Reaction of 4-(trimethylsiloxy)pent-3-en-2-one with APTES. To a solution of (9.3 g, 0.054 mol) of 4-(trimethylsiloxy)pent-3-en-2-one in hexane (20 ml), APTES (12.0 g, 0.054 mol) was added. The mixture was refluxed for 5 h. The solvent was distilled off, and the residue was subjected to fractional distillation in a vacuum. A **I/II** mixture (84/16) was obtained (7.9 g, 49%); bp 110–112°C (1 mm Hg). IR spectrum, ν, cm^{-1}: 3226 vw, 3171 vw (OH), 3070 w (H–C=C), 2974 vs (CH), 2928 vs (CH), 2888 vs (CH), 2766 w (H–CN), 2736 w (H–CN), 1613 vs, 1583 vs, 1512 s, 1441 s (O–C=C–C=N), 1386 m (CH), 1355 s (CH), 1295 vs, 1254 s (CH_3Si), 1194 m, 1168 s (SiOEt), 1093 vs, br (SiOEt, SiOSi), 956 vs (SiOEt), 845 s (CH_3Si), 774 vs (SiOEt), 648 w, 592 vw, 514 w, 486 m, 430 m. ^{1}H NMR spectrum, $CDCl_3$, δ, ppm (*J*, Hz): –0.04 s (27H, CH_3Si), –0.02 s (18H, CH_3Si), 0.03 s (9H, CH_3Si), 0.49–0.57 t (2H, CH_2Si, *J* = 7.8), 1.08 t (9H, CH_3CH_2O, *J* = 7.0), 1.48–1.64 quintet (2H, CH_2, *J* = 7.5), 1.78 m [3H, $CH_3C(N)$], 1.85 s [3H, $CH_3C(O)$], 3.05–3.15 q (2H, CH_2N, *J* = 6.8), 3.62–3.73 q (6H, CH_2O, *J* = 7.0), 4.81 s (1H, HC=C), 10.73 br.s (1H, OH). ^{13}C NMR spectrum, DEPT, $CDCl_3$, δ, ppm: 1.6 (CH_3Si), 7.5 (CH_2Si), 18.2 (CH_3CH_2O), 18.6 (CH_3CH_2O), 23.7 (CH_2), 28.5 [$CH_3C(O)$], 45.3 (CH_2N), 58.3 (CH_2O), 94.9 [*HC*(=C)(C=N)], 163.0 (C=N), 194.3 (C=*C*–OH).

Found, %: C 50.03, H 9.72, Si 20.81.
$C_{16}H_{37}N_1O_4Si_3$.
Calculated, %: C 49.06, H 9.52; Si 21.51.

A typical procedure for preparation and heat treatment of the films was as follows. Compound **I/II** (0.1482 g), APTES (0.1158 g), and oligodimethylsiloxanediol (0.1135 g) were mixed. A weighed portion of this mixture was applied in the form of a thin film onto a weighed glass support. A solid transparent film was formed in 12 h. The film on the support was placed between two Petri dishes and heated in an air thermostat at 100°C for 30 min and then at 150°C for 30 min. The weight loss on curing and heating was determined by weighing the supported film. The results are listed in the table.

Hydrolysis of compounds I/II and I. (a) To a mixture of compounds **I/II** (1.20 g) in EtOH (3 ml), water (0.5 ml) and concentrated HCl (0.4 ml) were added. The mixture was stirred for 7 h and filtered. The filtrate was evaporated. The residue was heated in a vacuum for 30 min at 150°C. Light yellow powder of polyorganosiloxane (0.34 g) was obtained. Its IR spectrum is shown in Fig. 3.

Found, %: C 23.81, H 7.60, Si 19.00, Cl 16.38.

(b) To a mixture of compounds **I/II** (1.95 g) in EtOH (3 ml), H_2O (0.5 ml) and concentrated NH_4OH (0.97 ml) were added. The mixture was stirred for 7 h and filtered; the filtrate was evaporated, and the residue was heated for 30 min at 100°C. Polyorganosiloxane was obtained in the form of a yellow transparent resin; yield 0.30 g. Its IR spectrum is shown in Fig. 3.

(c) To a mixture of compounds **I/II** (0.71 g) in EtOH (10 ml), H_2O (0.2 ml) and Bu_4NF (0.0007 g) were added. The mixture was stirred for 7 h, kept at room temperature for 7 days, and filtered; the filtrate was evaporated at 40–50°C in a vacuum. A transparent colorless oily liquid (0.33 g) was obtained. The viscosity of this liquid increased with time.

Found, %: C 46.67, H 8.72, Si 17.13.

(d) To a solution of compound **I** (1.13 g) in EtOH (10 ml), H_2O (0.4 ml) and Bu_4NF (0.0007 g) were added. The mixture was stirred for 7 h and filtered; the filtrate was evaporated at 40–50°C in a vacuum. A transparent light-yellow viscous liquid (0.37 g) was obtained. The IR spectrum of this liquid is shown in Fig. 3.

Found, %: C 46.73, H 7.61, Si 16.15.

Elemental analyses were performed at the Analytical Center of the Razuvaev Institute of Organometallic Chemistry, Russian Academy of Sciences.

CONCLUSIONS

(1) Acetylacetone reacts with 3-aminopropyltriethoxysilane to form 4-(3'-triethoxysilylpropylimino)-pent-2-en-2-ol (**Ia**, 83%) and 4-(3'-triethoxysilylpropylamino)pent-3-en-2-one (**Ib**, 17%).

(2) Trimethylsilyl ether of acetylacetone reacts with 3-aminopropyltriethoxysilane to form **Ia** and compounds **II** in which the EtO groups at the silicon atom are substituted with Me_3SiO groups.

(3) Compositions containing compound **I**, **I/II** mixture, 3-aminopropyltriethoxysilane, and oligodimethylsiloxanediols can be used for preparing transparent sol–gel films.

(4) Hydrolysis of compounds **I/II** and **I** in ethanol solutions yields solid, liquid, or resinous products, depending of the hydrolysis conditions (HCl, NH_4OH, Bu_4NF).

ACKNOWLEDGMENTS

This study was financially supported by INTAS (project no. 03-51-5959), Russian Foundation for Basic Research (project nos. 05-03-32556, 06-03-81005 Bel, 06-03-08208), Grant of RF President (project no. NSh 8017.2006.3), State Contract no. 02.445.11.7365 of the Federal Agency on Science and Innovations, and Russian Academy of Sciences (Complex Programs of the Presidium of the Russian Academy of Sciences "Basic Problems of Physics and Chemistry of Nanosystems and Nanomaterials," "Directed Synthesis of Substances with Preset Properties and Preparation of Functionalized Materials Based on Them").

REFERENCES

1. Peshkova, V.M. and Mel'chakova, N.V., *Analiticheskie reagenty. β-Diketony* (Analytical Reagents. β-Diketones), Moscow: Nauka, 1986.
2. *β-Diketonaty metallov* (Metal β-Diketonates), Spitsyn, V.I., Ed., Moscow: Nauka, 1978.
3. *Stroenie, svoistva i primenenie β-diketonatov metallov* (Structure, Properties, and Applications of Metal β-Diketonates), Spitsyn, V.I., Ed., Moscow: Nauka, 1978.
4. *Problemy khimii i primeneniya β-diketonatov metallov* (Problems of Chemistry and Applications of Metal β-Diketonates), Spitsyn, V.I., Ed., Moscow: Nauka, 1982.
5. *Teoreticheskaya i prikladnaya khimiya β-diketonatov metallov* (Theoretical and Applied Chemistry of Metal β-Diketonates), Spitsyn, V.I. and Martynenko, L.I., Eds., Moscow: Nauka, 1985.
6. Pomogailo, A.D. and Uflyand, I.E., *Makromolekulyarnye metallokhelaty* (Macromolecular Metal Chelates), Moscow: Khimiya, 1991.
7. Ermakov, Yu.I., Zakharov, V.A., and Kuznetsov, B.N., *Zakreplennye kompleksy na oksidnykh nositelyakh v katalize* (Complexes Immobilized of Oxides in Catalysis), Nauka, 1980
8. Hartley, F.R., *Supported Metal Complexes. A New Generation of Catalysts*, Dordrecht: Reidel, 1985.
9. Vereshchagin, A.N., *Induktivnyi effekt: Konstanty zamestitelei dlya korrelyatsionnogo analiza* (Inductive Effect: Substituent Constants for Correlation Analysis), Moscow: Nauka, 1988.
10. Freimanis, Ya.F., *Khimiya enaminoketonov, enaminoiminov, enaminotionov* (Chemistry of Enamino Ketones, Enamino Imines, and Enamino Thiones), Riga: Zinatne, 1974.
11. Corriu, R.J.P. and Douglas, W., *Silicon-Based Polymers: The Science and Technology of Their Synthesis and Applications*, Jones, R.G., Ando, W., and Chojnowski, J., Eds., Dordrecht: Kluwer, 2000, pp. 667–695.

ISSN 1070-4272, Russian Journal of Applied Chemistry, 2007, Vol. 80, No. 4, pp. 654–659. © Pleiades Publishing, Ltd., 2007.
Original Russian Text © V.I. Chursin, 2007, published in Zhurnal Prikladnoi Khimii, 2007, Vol. 80, No. 4, pp. 670–675.

MACROMOLECULAR CHEMISTRY AND POLYMERIC MATERIALS

Features of Oxidative Degradation of Hydroxyethyl Cellulose

V. I. Chursin

Research Institute of Leather-Shoe Industry, Joint-Stock Company, Moscow, Russia

Received October 30, 2006; in final form, December 2006

Abstract—The kinetics of degradation of hydroxyethyl cellulose in its oxidation with hydrogen peroxide, sodium periodate, and potassium persulfate was studied. The effect of oxidation time and oxidant concentration on the properties of the oxidation products was analyzed.

DOI: 10.1134/S1070427207040271

The stringent requirements to the environmental safety of industries, including the leather-shoe industry, make it necessary to reject some of the traditionally used chemicals and processes. Therefore, one of the main trends in the development of modern techniques for treatment of leather raw materials is replacement of toxic chemicals with natural compounds and, in particular, with plant tanning extracts, polysaccharides, and other nontoxic tanning compounds.

A promising approach to synthesis of environmentally safe tanning agents from renewable plant raw materials is based on oxidative transformation of polysaccharides into their dialdehyde derivatives [1–3]. The tanning capacity of starch dialdehyde prepared by oxidation of starch with periodate was reported in [4]. It has been found, however, that polysaccharides (with polygalacturonic acid as an example) are resistant to oxidation at 20°C [5]. Their oxidative degradation occurs only in the presence of a catalyst or on heating to 95°C [6]. At the same time, it has been found [7] that chitosan polysaccharide macromolecules are oxidized with hydrogen peroxide at 30°C and their molecular weight decreases in the course of oxidation in proportion to the oxidant concentration. The possibility of oxidation of arabinogalactan with potassium persulfate with the formation of carboxy groups was reported in [2]. No data have been reported on oxidation of hydroxyethyl cellulose (HEC) with potassium persulfate.

The aim of the study was to analyze the kinetics of HEC oxidation and to obtain oxidation products with a tanning capacity for collagen.

EXPERIMENTAL

Hydroxyethyl cellulose (HEC) produced by the Politsell Private Company [TU (Technical Specifications) 2231-013-32957739–01] was used in our experiments in the form of a 4% aqueous solution. Sodium periodate, hydrogen peroxide (50%), and potassium persulfate were used as oxidants. The optical density of HEC solutions treated with sodium periodate was measured on an SF-46 spectrophotometer at a wavelength of 222 nm corresponding to the maximal absorption of periodate anions. The dynamic viscosity of solutions was measured on a Brookfield viscometer at a shear rate of 20 s^{-1}. The electrical conductivity of solutions was measured on a Hanna Instruments conductometer. The refractive index was measured on a URL-1 refractometer.

The oxidation of HEC was studied in the dark at room temperature. At regular intervals, an aliquot of the reaction mixture was taken and its viscosity, refractive index, and electrical conductivity were measured. The carboxy group content of solutions of oxidized HEC was determined by addition of aqueous barium acetate (0.2 N), followed by titration of the released acetic acid with NaOH (0.02 N). The spectroscopic characteristics of films prepared from oxidized HEC were measured by Fourier spectroscopy.

The variation of characteristics of HEC solutions in the course of oxidation is illustrated by Table 1. These data show that, with the sodium periodate concentration increasing over 0.5 wt %, the oxidative conversion of HEC sharply increases and viscosity

Table 1. Kinetics of oxidative degradation of HEC (initial characteristics: η = 870 mPa s, n = 1.540, and χ = 80×10^{-3} Ω^{-1} cm^{-1})

Oxidant concentration, %	Dynamic viscosity η, mPa s			Refractive index n			Electrical conductivity $\chi \times 10^{-3}$, Ω^{-1} cm^{-1}		
	Treatment time, min								
	30	90	180	30	90	180	30	90	180
Sodium periodate:									
1	580	500	349	1.545	1.549	1.559	76	68	72
0.5	621	596	580	1.544	1.546	1.555	65	49	43
0.25	621	621	600	1.541	1.544	1.552	74	71	30
Hydrogen peroxide:									
2	849	799	771	1.545	1.546	1.547	58	67	58
1	961	927	892	1.543	1.543	1.545	38	83	41
0.5	981	924	918	1.541	1.542	1.543	52	104	59
Potassium persulfate:									
2	946	820	770	1.542	1.544	1.546	161	421	552
1	853	750	731	1.543	1.544	1.546	127	333	123
0.5	879	853	791	1.543	1.545	1.547	77	86	163

of its aqueous solutions decreases by a factor of 2.5. It is also seen that, in treatment of HEC with 0.5 wt % and more concentrated sodium periodate, the viscosity first decreases for 30 min and then remains virtually constant.

It is known [1] that periodate breaks carbohydrate chains containing two or more hydroxy groups. This process is accompanied by an increase in the refractive index of the reaction mixture, caused by oxidative conversion of polysaccharide hydroxy groups into other groups. These groups are, most likely, carboxy groups [5], because it is known that the refractive index increases in oxidation of aldehyde groups to carboxy groups [8]. The dependence of the refractive index on the oxidation time is step-like, which is especially pronounced in oxidation with 1% aqueous sodium periodate. We believe that, in the first step of this process, the hydroxy groups of HEC are oxidized to aldehyde groups, which are then converted to carboxy groups. The first reaction step was complete within 60 min after introduction of the oxidant and the second step continued for 3.5 h until complete consumption of the oxidant (1%). At a lower oxidant concentration, the second step is not complete. The oxidative transformation of HEC can be represented by the following reaction scheme:

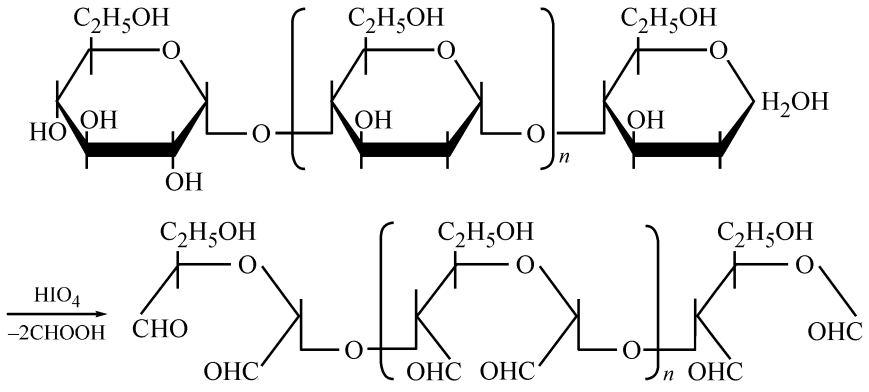

The variation of the electrical conductivity of HEC solutions, caused by HEC oxidation (Table 1), shows that the oxidation of HEC is a multifactor process involving breakdown of the polysaccharide polymeric chain, formation of new functional groups differing in χ, and also chemical conversion of the oxidant. At decreased sodium periodate concentrations, the electrical conductivity decreases in the course of the reaction. Furthermore, as the oxidant concentration decreases, a minimum in dependence of the electrical

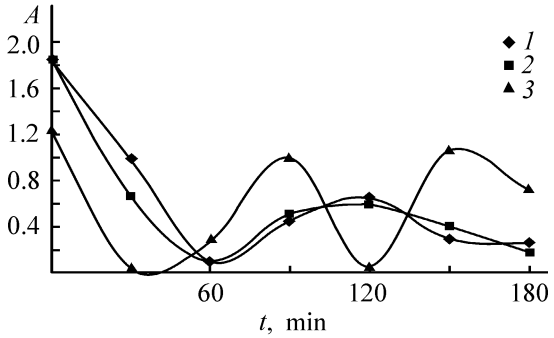

Fig. 1. Dependence of the optical density A of aqueous solutions of HEC on time t of oxidation with sodium periodate at its varied consumption. Sodium periodate consumption, wt %: (*1*) 1, (*2*) 0.5, and (*3*) 0.25.

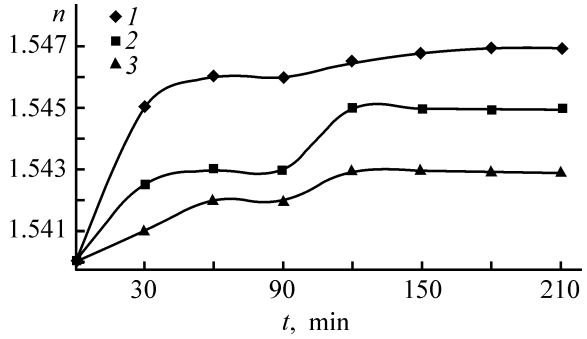

Fig. 2. Variation with time t of the refractive index n of aqueous HEC solutions HEC in the course of oxidation with hydrogen peroxide at its varied consumption. Hydrogen peroxide consumption, wt %: (*1*) 2, (*2*) 1, and (*3*) 0.5.

conductivity on the oxidation time shifts from 130 to 90 and 60 min. We believe that this effect is caused by reduction of periodate to iodide. The decrease in the electrical conductivity of the reaction mixture in the first oxidation step can be caused by formation of an unstable complex of periodate anions with oxygen atoms of the carbohydrate chain. The further increase in the electrical conductivity is apparently caused by decomposition of this complex, with the release of iodide.

Figure 1 shows that the trends in variation of the optical density of reaction mixtures in the course of oxidation of HEC with sodium periodate are similar to those observed for the electrical conductivity. In the first step of this process, the optical density sharply decreases owing to the formation of an intermediate complex between HEC and periodate anions. In the second step of HEC oxidation, this complex is broken down to yield iodide, which is manifested as an increase in the optical density of the reaction mixture.

Table 2 shows that the appearance and features of films prepared from aqueous solutions of HEC oxidized with sodium periodate are dependent on both the oxidation time and sodium periodate consumption.

In contrast to sodium periodate, hydrogen peroxide can oxidize the hydroxy groups bound to the second and third carbon atoms in the cellulose chain to form both the aldehyde and keto groups. Table 1 reveals the following trends in the variation of the viscosity of HEC solutions in the course of their treatment with hydrogen peroxide of various concentrations. First of all, there is an unexpected increase in the viscosity of the reaction mixture in the first oxidation step. At a hydrogen peroxide consumption of 0.5%, the largest increase in viscosity is observed 30 min after addition of hydrogen peroxide, and then the viscosity somewhat decreases. At a hydrogen peroxide concentration of 2%, the viscosity of solutions varies with time in the course of oxidation as follows: decreases within first 30 min, reaches a maximum, as in the case of lower oxidant consumption, and then gradually decreases.

These results suggest that, in oxidation of HEC with concentrated hydrogen peroxide, this biopolymer is subjected to oxidative degradation.

At hydrogen peroxide consumption of 0.5 and 1%, hydroxy groups in HEC are oxidized to carboxy groups only. This transformation increases the viscosity of aqueous HEC due to hydrogen bonding. A certain delay in the oxidation of HEC at a hydrogen peroxide concentration of 2% is caused by the accumulation of peroxy derivatives of HEC [2], which are subsequently consumed for the oxidation of HEC. The aldehyde groups formed in the first oxidation step are converted into carboxy groups.

Table 2. Appearance and features of films prepared from HEC oxidized with sodium periodate

Oxidant consumption, %	Film appearance at indicated oxidation time, h		
	1	2	4
0.25	Flexible transparent	Less flexible transparent	Not formed
0.5	Less flexible whitish	Rigid with frosty pattern	The same
1.0	Brittle with rod-like structure	Brittle with frosty pattern	Rigid and dull

Figure 2 shows how the refractive index of aqueous HEC varies in the course of its oxidation at various hydrogen peroxide consumptions. These curves consist of two portions corresponding to two different steps of HEC oxidation. The first and second steps are complete within 90 and 150–180 min, respectively. In the first step, the hydroxy groups are oxidized to aldehyde groups, and in the second step the aldehyde groups are oxidized to carboxy groups.

The dependence of the electrical conductivity of aqueous HEC solutions on the time of oxidation by hydrogen peroxide is qualitatively consistent with the trends observed for the viscosity and refractive index. The influence of the oxidation time and oxidant consumption on the electrical conductivity of aqueous HEC solutions is determined by the following processes: sequential oxidation of hydroxy and aldehyde groups, formation of complicated oxidation products of HEC, and their involvement in decomposition of hydrogen peroxide [2]. It was found that, at a low initial hydrogen peroxide content of the reaction mixture, the oxidation processes prevail and the degradation of HEC macromolecules is minor. With an increase in the hydrogen peroxide concentration to 2%, the polysaccharide degradation is intensified. The variation of the chemical composition of the reaction mixture in the course of oxidation is manifested as a considerable increase in the refractive index.

In oxidation of aqueous HEC with potassium persulfate, there is no distinct correlation between the oxidant consumption and the reaction mixture viscosity. However, at a persulfate consumption of 2%, an increase in the viscosity occurs, caused by oxidation of hydroxy groups to carboxy groups. With increasing oxidation time, the oxidative degradation of HEC prevails. The prevalence of the degradation processes is typical of systems with low persulfate consumption (0.5 and 1%).

The largest increase in the electrical conductivity of aqueous HEC solution is observed at the potassium persufate consumption of 2%, and this parameter changes insignificantly at lower persulfate concentrations. On treatment of aqueous HEC with persulfate, the refractive index somewhat increases, it does not show a steplike trend typical of the other oxidants. Thus, our results show that potassium persulfate oxidizes HEC and breaks its macromolecules in aqueous solutions to a lesser extent than do other oxidants under consideration. The effect of various oxidants on the dynamic viscosity of solutions of HEC at the same oxidant consumption (1%), shown in Fig. 3,

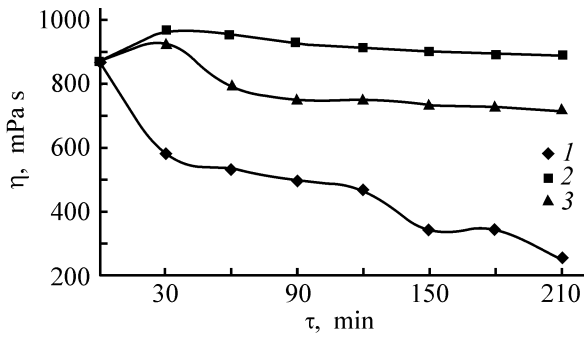

Fig. 3. Influence of the oxidant type on variation of the dynamic viscosity η of aqueous HEC solutions with oxidation time. (τ) Time. (*1*) Sodium periodate, (*2*) hydrogen peroxide, and (*3*) potassium persulfate.

allows comparison of their oxidative powers with respect to hydroxyethyl cellulose.

Based on our experimental kinetic data, the rate coefficients of degradation and oxidation of HEC were calculated by the equation

$$C = b/at,$$

where $b = 1/\eta_t(d_t) - 1/\eta_0(d_0)$; a, oxidant amount (g); and t, oxidation time (min).

Table 3 shows that, in treatment of aqueous HEC with sodium periodate, the rate of oxidative conversion of functional groups of HEC exceeds the rate of degradation of HEC macromolecules by an order of magnitude. In oxidation of HEC with hydrogen peroxide, the formation of aldehyde and carboxy groups

Table 3. Rate parameters of HEC degradation and oxidation with various oxidants

Oxidant, wt %	Degradation rate coefficient C_η, $mPa^{-1}\ s^{-1}\ g^{-1}\ min^{-1}$	Oxidation rate coefficient C_d, $unit^{-1}\ g^{-1}\ min^{-1}$
$NaIO_4$:		
1.0	9.0×10^{-6}	4.4×10^{-5}
0.5	6.0×10^{-6}	6.9×10^{-5}
0.25	1.1×10^{-5}	1.1×10^{-6}
H_2O_2:		
2.0	4.1×10^{-7}	8.2×10^{-6}
1.0	1.6×10^{-7}	1.2×10^{-5}
0.5	5.8×10^{-7}	1.4×10^{-5}
$K_2S_2O_8$:		
2.0	4.1×10^{-7}	7.0×10^{-6}
1.0	1.2×10^{-6}	1.4×10^{-5}
0.5	1.3×10^{-6}	3.3×10^{-5}

Table 4. Major absorption bands in the IR spectra of HEC before and after oxidation

Wavelength, cm^{-1}	Oxidant consumption, %				
	sodium periodate			hydrogen peroxide	potassium persulfate
	0.25	0.5	1.0	2.0	2.0
1020	1070	1070	–	1070	1070
1260	–	1300	–	–	1300
1350	–	–	–	–	1500
1650	1650	1650	1630	1650	1650

also prevails, whereas the oxidative degradation of polymeric chains is minor. In going to oxidation with potassium persulfate, the conversion of the hydroxy groups is virtually the same as that for hydrogen peroxide, but the degree of oxidative degradation of the carbohydrate polymer increases.

The appearance of protonated carboxy groups in oxidized HEC was confirmed by its back-titration with aqueous sodium hydroxide. The maximal content of carboxy groups was found in HEC treated with 0.25 wt % aqueous sodium periodate. Thus, sodium periodate is the most efficient oxidant for HEC. The high degree of formation of oxidized functional groups in HEC is also reached with the other oxidants at their low concentrations.

The additional information on oxidation of HEC by the oxidants under consideration was obtained from an IR study of the initial HEC and its oxidation products. The IR spectra of celluloses oxidized with periodic acid were published in [9]. Their analysis show that, even at a high degree of oxidative conversion of HEC into cellulose dialdehyde, the oxidation product contains no strong C=O absorption bands. These spectra contain ill-resolved bands at 1370, 1360, 1340, and 1320 cm^{-1} and a strong absorption band at 900 cm^{-1}. The major absorption bands in the Fourier IR spectra of the initial and oxidized HEC are listed in Table 4.

The IR spectrum of the initial HEC contains a broad absorption band of the stretching vibrations of the hydrogen-bonded hydroxy groups at 3000–3600 cm^{-1}, the absorption bands of internal bending vibrations of the CH, CH_2, and CH_2O groups (1350 cm^{-1}), the bands of the C–O–C stretching vibrations (1260 cm^{-1}) and the bands of the CH and CH_2 rocking vibrations (1020 cm^{-1}). The most noticeable changes in the IR spectra of oxidized HEC are observed in the range of the absorption bands at 1020–1070, 1260–1300, and 1350–1500 cm^{-1} (Table 4). The oxidized HEC shows an increased intensity of the absorption band of water of crystallization at 1650 cm^{-1}, and the absorption bands at 1260–1350 cm^{-1} change their shape and intensity, apparently due to oxidation of the CH_2OH groups. The cleavage of the C–C bonds in the carbohydrate chains caused by oxidative degradation of HEC is manifested as a shift of the absorption band at 1020 cm^{-1}, typical of the initial HEC, to 1070 cm^{-1}.

Our experiments showed that, on treatment of leather raw materials with products of oxidative transformation of HEC, the temperature of derma welding increases by 8–10°C, suggesting a strong intermolecular cross-linking in the collagen structure [4]. Thus, oxidative treatment of HEC allows substantial modification of its functionality and broadens the range of its application. The oxidized HEC can be used as an environmentally safe tanning agent and filler in production of leathers and furs.

CONCLUSIONS

(1) Oxidation of hydroxyethyl cellulose with sodium periodate, hydrogen peroxide, and potassium persulfate is accompanied by opening of the polysaccharide cyclic structure and formation of aldehyde and carboxy groups.

(2) Addition of oxidants to aqueous hydroxyethyl cellulose causes degradation of its polymeric structure. The strongest decrease in the molecular weight of polysaccharides occurs in their oxidation with sodium periodate at its concentration of 0.5% and higher.

(3) The maximal rate of oxidative transformation of hydroxyethyl cellulose occurs within the first hour of its oxidation. Depending on the type of oxidant and its concentration, either oxidation or degradation of polysaccharide prevails.

REFERENCES

1. Stepanenko, B.N., *Biokhimiya i khimiya uglevodov (Polisakharidy)* (Biochemistry and Chemistry of Carbohydrates (Polysaccharides)), Moscow: Vysshaya Shkola, 1978.
2. Borisov, I.M., *Dokl. Ros. Akad. Nauk*, 2002, vol. 383, pp. 774–777.
3. Filatov, V.N. and Ryl'tsev, V.V., *Biologicheski aktivnye materialy* (Biologically Active Materials), Moscow: Informelektro, 2002, vol. 1.

4. Mikhailov, A.N., *Kollagen kozhnogo pokrova i osnovy ego pererabotki* (Collagen of Coverlet and Fundamentals of Its Processing), Moscow: Legkaya Industriya, 1971.
5. Golova, O.P. and Mayat, N.S., *Izv. Akad. Nauk SSSR. Otd. Khim. Nauk*, 1955, no. 5, pp. 899–905.
6. Borisov, I.M., Shirokova, E.N., Musharipova, R.Kh., et al., *Izv. Vyssh. Uchebn. Zaved., Khim. Khim. Tekhnol.*, 2003, vol. 46, no. 4, pp. 29–31.
7. Galiaskarova, G.G., Mullagaliev, I.R., Kuz'min, I.A., et al., *Materialy XI Vserossiiskoi konferentsii po khimicheskim reaktivam "Reaktiv-98"* (Proc. XI Russian Conf. on Chemical Reagents "Reagent-98"), Ufa: Reaktiv, 1998, pp. 41–45.
8. Ioffe, B.V., *Refraktometricheskie metody khimii* (Refractometric Methods of Chemistry), Leningrad: Khimiya, 1983.
9. Zhbanov, R.G., *Infrakrasnye spektry tsellulosy i ee proizvodnykh* (Infrared Spectra of Cellulose and Its Derivatives), Minsk: Nauka i Tekhnika, 1964.

ISSN 1070-4272, Russian Journal of Applied Chemistry, 2007, Vol. 80, No. 4, pp. 660–664. © Pleiades Publishing, Ltd., 2007.
Original Russian Text © I.I. Goncharik, F.F. Mozheiko, T.P. Kulikova, Z.A. Gotto, 2007, published in Zhurnal Prikladnoi Khimii, 2007, Vol. 80, No. 4, pp. 676 – 680.

MACROMOLECULAR CHEMISTRY AND POLYMERIC MATERIALS

Stability and Structural and Rheological Properties of Rapeseed Oil-Based Emulsions in the Presence of Sodium Carboxylates

I. I. Goncharik, F. F. Mozheiko, T. P. Kulikova, and Z. A. Gotto

Institute of General and Inorganic Chemistry, National Academy of Sciences of Belarus, Minsk, Belarus

Redceived July 11, 2006; in final form, January 18, 2007

Abstract—Formation conditions and structural and rheological properties of rapeseed oil-based emulsions in the presence of sodium laurate and sodium palmitate were examined.

DOI: 10.1134/S1070427207040283

Formation of emulsions requires introduction into the water–oil system of an emulsifier to promote creation of a strong adsorption layer at the interface and to increase their stability. As oil phase can serve vegetable oils (linseed, hempseed, sunflower, rapeseed, etc.). In recent years, especially wide application has been enjoyed by rapeseed oil and emulsions thereof. We have elucidated previously [1] how the stability and structural and rheological properties of rapeseed oil-based emulsions is influenced by inorganic electrolytes. To prepare stable emulsions, emulsifiers (various surfactants) are typically introduced into the emulsion. The most widely used for these purposes are sodium carboxylates (soaps). Therefore, it was of interest to examine how the stability and structural and rheological properties of rapeseed oil-based emulsions are influenced by soaps. The increased interest in soaps is also due to the fact that they are components of wastes in many chemical productions. For example, adipates are alkaline waste from caprolactam production, and spent lye, the waste from soap manufacture; they can also serve as emulsifiers in preparation of emulsions. As is known [2], only high-molecular-weight soaps (alkaline salts of lauric and fatty acids with higher molecular weights) are used as emulsifiers.

EXPERIMENTAL

In this study, we used as emulsifiers chemically pure-grade sodium laurate and sodium palmitate, as well as rapeseed oil produced according to GOST (State Standard) 8988–77.

Emulsions were prepared by the procedure from [3]. After 15-min dispersing, a portion of the resulting emulsion was placed in calibrated test tubes, and the phase separation in the systems of interest was monitored visually. As the measure of stability we took the percentage ratio of the volume of the separated aqueous or oil phase to that of the entire initially prepared emulsion. The remaining emulsion was used for examining the structural and rheological properties and electrical conductivity. The structural and rheological examinations were carried out on a Rheotest 2 rotary viscometer in the coaxial-cylinder system at the strain rate within 3.0–1312 s^{-1}. Based on the measured data, we calculated, for each velocity gradient D, by standard procedures [4] the shear stress τ_r and the effective viscosity η. The examination of the equilibrium shear stress in relation to the strain rate yielded full rheological curves.

We found that the stability of the emulsions depends on the concentration of the oil phase and emulsifiers, as well as on the nature of the latter. The results are presented in Table 1. It is seen that sodium laurate stabilizes only the water–rapeseed oil system containing 75% oil phase. The stabilizing effect of sodium laurate is manifested even at low concentrations. For example, upon introduction of 0.4×10^{-3} and 0.8×10^{-3} M of the emulsifier, 36 and 40%, respectively, of the oil phase separates within 1 day from the resulting emulsion, whereas without the emulsifier, the emulsion completely separates within this time into the oil and aqueous phases. Upon increasing the sodium laurate concentration to $(8.0–56) \times 10^{-3}$ M, the emulsion preserves stability even for 10 days. Evidently, at these concentrations, the adsorption layer formation at the liquid–liquid interface is complete, which ensures high stability of the emulsions. Introduction of sodium laurate into the system containing 25, 50, and 90% oil phase leaves the emulsion stability virtually unaffected.

Table 1. Stability and structural and rheological properties of the emulsions prepared from rapeseed oil of different concentrations *s* in relation to the concentration *c* of sodium laurate and sodium palmitate

s, wt %	$c \times 10^3$, M	P_{k2},* Pa	η, Pa s	æ, S cm^{-1}	Solubility of emulsion in water	Emulsion type	Breakdown of emulsion within 1 day, %
				Sodium laurate			
25	–	2	0.05	0.7×10^{-4}	Soluble	1	Phase separation
25	28.2	5	0.05	0.7×10^{-4}	〃	1	60
50	–	25	0.05	0.8×10^{-4}	〃	1	25
50	0.4	40	0.10	1.0×10^{-4}	〃	1	24
50	4.4	40	0.10	1.1×10^{-4}	〃	1	30
50	13.2	40	0.10	1.2×10^{-4}	〃	1	28
50	28.4	50	0.10	2.1×10^{-4}	〃	1	27
50	56.8	65	0.10	3.0×10^{-4}	〃	1	30
75	–	40	0.5	1.3×10^{-7}	Insoluble	2	Phase separation
75	0.4	65	0.70	1.3×10^{-7}	〃	2	36
75	0.8	85	0.70	1.3×10^{-7}	〃	2	40
75	8.0	155	1.04	0.8×10^{-4}	Soluble	1	Stable
75	28.4	170	1.35	0.9×10^{-4}	〃	1	〃
75	56.0	225	1.04	0.8×10^{-4}	〃	1	〃
				Sodium palmitate			
50	0.4	30	0.10	1.2×10^{-4}	Soluble	1	29
50	2.1	370	3.20	1.3×10^{-7}	Insoluble	2	Stable
50	3.2	400	6.26	1.3×10^{-7}	〃	2	〃
75	2.1	60	0.52	1.3×10^{-7}	〃	2	Phase separation
90	2.1	40	0.52	1.3×10^{-7}	〃	2	〃

* P_{k2} Ultimate shear stress.

With sodium palmitate as the emulsifier, the stabilizing effect was attained only for the system containing 50 wt % rapeseed oil. Upon introduction of 2.1×10^{-3} M of the emulsifier, the stability of the resulting emulsion is preserved for 1 day, while without the emulsifier it breaks down within this period by 25%. Table 1 shows that, with increasing chain length of the soap molecule, the soap concentration corresponding to formation of a stable emulsion tends to decrease. For example, it was estimated at 8×10^{-3} M for sodium laurate and 2.1×10^{-3} M for sodium palmitate.

The rheological curves obtained for rapeseed oil based emulsions in the presence of different concentrations of sodium laurate and sodium palmitate (Figs. 1, 2) show that the emulsions exhibit properties of non-Newtonian fluids. Introduction of sodium laurate into the emulsions containing 50% rapeseed oil

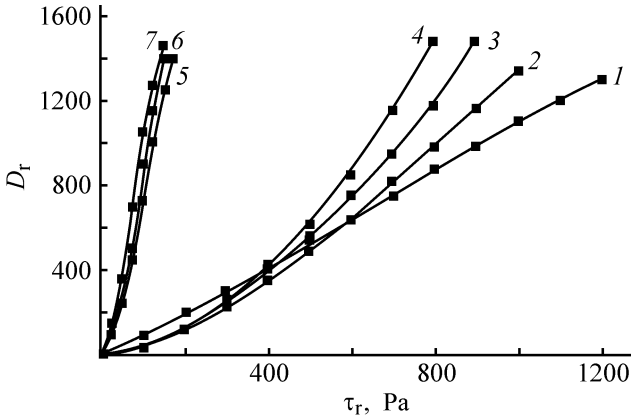

Fig. 1. Rheological flow curves of emulsions based on rapeseed oil and sodium laurate. (D_r) Velocity gradient and (τ_r) shear stress, the same for Fig. 2. Rapeseed oil concentration, %: (*1–4*) 75 and (*5–7*) 50. Sodium laurate concentration, M: (*1*, *7*) 0, (*2*, *6*) 0.028, (*3*, *5*) 0.056, and (*4*) 0.008.

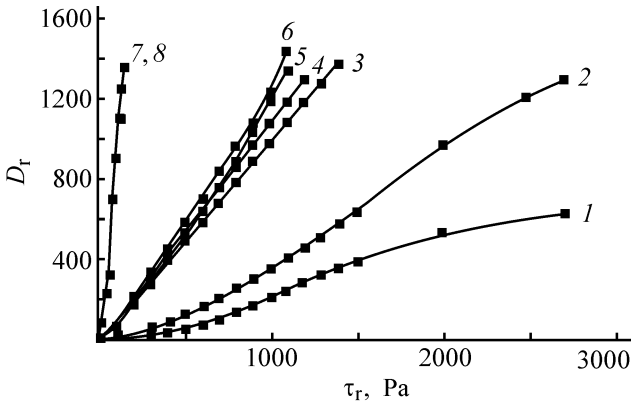

Fig. 2. Rheological flow curves of the emulsions based on rapeseed oil and sodium palmitate. Rapeseed oil concentration, wt %: (*1*, *2*, *7*, *8*) 50; (*3*, *4*) 75; and (*5*, *6*) 90. Sodium palmitate concentration, M: (*4*, *5*, *8*) 0, (*1*) 0.0032, (*2*, *3*, *6*) 0.0021, and (*7*) 0.0004.

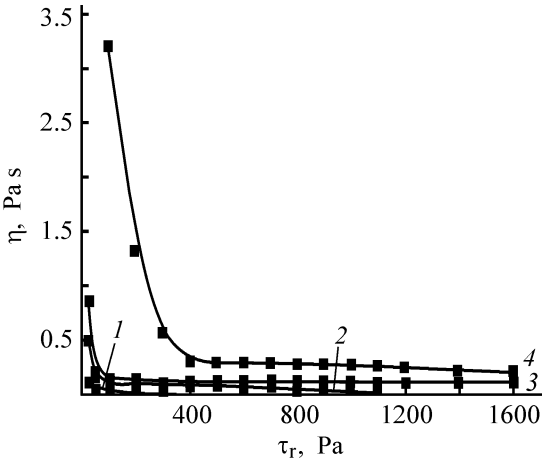

Fig. 3. Effective viscosity η vs. shear stress τ_r for rapeseed oil-based emulsions in the presence of (*3*) sodium laurate and (*4*) sodium palmitate. Rapeseed oil concentration, wt %: (*1*, *4*) 50 and (*2*, *3*) 75. Surfactant concentration, M: (*1*, *2*) 0, (*3*) 0.0284, and (*4*) 0.021.

leaves the rheological properties virtually unaffected. However, for the emulsions containing 75% oil phase in the presence of sodium laurate, the ultimate strength P_{k2} tends to increase with the sodium laurate concentration. This suggests strengthening of the emulsion structure. For example, at the sodium laurate content of 0.4×10^{-3} and 5.6×10^{-2} M, P_{k2} was estimated at 65 and 225 Pa, respectively, against 40 Pa without sodium laurate. Analysis of the rheological curves (Fig. 2) suggests that sodium palmitate strengthens the structure of the resulting emulsions containing 50% rapeseed oil. Upon introduction into the system of 2.1×10^{-3} and 3.2×10^{-3} M of this emulsifier the ultimate shear stress increases to 370 and 400 Pa, respectively, against 25 Pa without the emulsifier (Table 1). When 2.1×10^{-3} M of sodium palmitate is introduced into the system containing 75 and 90 wt % oil phase, the ultimate shear stress is 60 and 40 Pa, respectively. Thus, depending on their concentration and oil phase content, sodium carboxylates (laurate and palmitate) can act both as stabilizers and thinners of the water–rapeseed oil system. This is also confirmed by the growth of the initial effective viscosity of the emulsions stabilized by sodium salts of fatty acids against the initial rapeseed oil emulsion. The dependence of the initial effective viscosity on the sodium laurate concentration in the water–rapeseed oil system (Table 1) has a maximum at a concentration of 2.84×10^{-2} M and was estimated at 1.35 Pa s against 0.5 Pa s without sodium laurate (oil phase concentration 75 wt %). Evidently, at this concentration of sodium laurate its content in the interphase layer increases, thereby making higher the effective viscosity. Further increase in its concentration in the system of interest causes separation of the emulsifier from the interface layer, thereby leading to a decrease in the effective viscosity.

Similar results were obtained upon introduction of sodium palmitate into the water–rapeseed oil system. It should be noted that, in the presence of sodium palmitate, the initial effective viscosity is significantly higher than that in the presence of sodium laurate. For example, upon introduction of 2.1×10^{-3} M of sodium palmitate into the system containing 50% rapeseed oil the largest effective viscosity was 3.2 Pa s. At the same time, upon introduction into this system of 2.84×10^{-2} M of sodium laurate, this parameter was as low as 0.1 Pa s.

Figure 3 shows how the effective viscosity calculated from the flow rheograms varies with the shear stress for the emulsions prepared from rapeseed oil both in the presence of sodium laurate and sodium palmitate and in their absence. The $\eta = f(\tau_r)$ curves also suggest that these emulsions are non-Newtonian fluids, since their viscosity tends to decrease with increasing shear stress in the system. Figure 3 shows that, in the presence of sodium palmitate (curve *4*) and sodium laurate (curve *3*), both the initial and final viscosity tend to increase relative to those of the emulsions containing no emulsifiers. For example, at the sodium palmitate concentration of 2.1×10^{-3} M the former parameter was estimated at 3.2, and the latter, at 0.25 Pa s against 0.05 and 0.01 Pa s, respectively, without the emulsifier (50% rapeseed oil in the system). In the case of sodium laurate ($c = 2.84 \times 10^{-2}$ M), these parameters were as low as 1.35 and 0.15 Pa s, respectively, against 0.5 and 0.05 Pa s without the emulsifier (75% rapeseed oil in the system). These data suggest that sodium palmitate forms a stronger structure in the water–rapeseed oil system than does sodium laurate.

Since many of the emulsification processes occur in the presence of inorganic electrolytes, it was of interest to elucidate how the latter influence the stability and the structural and rheological properties of the rapeseed oil-based systems. As known, inorganic electrolytes as such do not act as emulsion stabilizers because of insufficient adsorption of their ions on the nonpolar hydrocarbon–water interface. However, in the presence of emulsifiers, their adsorption at the liquid–liquid interface can be enhanced. The object of our examinations was the emulsion containing 75% rapeseed oil at different concentrations of sodium laurate, 4.5×10^{-3} and 2.84×10^{-2} M. As inorganic salt we used sodium carbonate (Table 2).

Table 2. Stability and structural and rheological properties of rapeseed oil-based emulsions in relation to the concentrations of sodium laurate *s* and of sodium carbonate *c* (rapeseed oil concentration 75 wt %)

$s \times 10^2$	$c \times 10^2$	æ,	P_{k2},	Solubility of emulsion in water	Emulsion type	Breakdown of emulsion within 1 day, %
M		S cm^{-1}	Pa			
–	–	1.3×10^{-7}	60	Insoluble	2	Phase separation
–	0.8	1.2×10^{-5}	–	Soluble	1	0
–	4.7	6.3×10^{-4}	–	″	1	0
–	7.5	7.5×10^{-4}	80	″	1	0
–	11.0	4.5×10^{-4}	120	″	1	0
–	23.0	1.3×10^{-7}	–	Insoluble	2	75
–	28.0	1.3×10^{-7}	–	″	2	Phase separation
–	34.0	1.3×10^{-7}	–	″	2	″
0.45	–	1.3×10^{-7}	70	″	2	0
0.45	0.14	1.1×10^{-4}	140	Soluble	1	0
0.45	7.8	3.9×10^{-4}	130	″	1	0
0.45	23.0	1.3×10^{-4}	190	″	1	0
0.45	70.0	3.6×10^{-4}	150	″	1	0
0.45	140.0	4.5×10^{-4}	150	″	1	0
2.84	–	0.6×10^{-4}	150	″	1	0
2.84	0.14	1.1×10^{-4}	140	″	1	0
2.84	8.0	3.9×10^{-4}	130	″	1	0
2.84	23.0	1.3×10^{-4}	190	″	1	0
2.84	30.0	2.0×10^{-4}	150	″	1	10
2.84	50.0	1.3×10^{-7}	100	Insoluble	2	60
2.84	90.0	1.3×10^{-7}	110	″	2	76
2.84	190.0	1.3×10^{-7}	100	″	2	80

Table 2 shows that, when Na_2CO_3 is introduced into the water–rapeseed oil system in minor concentrations, the stability of the resulting emulsions increases. For example, at the Na_2CO_3 concentration of $(0.8–11.0) \times 10^{-2}$ M, the emulsion preserves stability for 1 day, while without Na_2CO_3 it breaks down completely within this period. The reason is that, in the presence of Na_2CO_3, rapeseed oil undergoes saponification into sodium salts of high-molecular-weight acids that are emulsifiers themselves, which favors formation of stable emulsions. With increasing concentration of the electrolyte, the salting-out of the emulsifier from the interface surface is intensified, which leads to breakdown of the emulsion. For example, upon introducing 0.23 M of sodium carbonate into the water–rapeseed oil system, the emulsion breaks down within 1 day by 75%, and at the sodium carbonate content of 0.28 and 0.34 M it breaks down completely within this period.

When Na_2CO_3 is introduced into the water–rapeseed oil–sodium laurate system at the sodium laurate concentrations below CMC, specifically, 4.5×10^{-3} M, the stability of the resulting emulsions is virtually unaffected by the content of the inorganic electrolyte. Even at the electrolyte concentration of 0.7 M the emulsion preserves stability for 1 day, like without the electrolyte. However, the structural and rheological properties somewhat change, as evidenced by an increase in the ultimate shear stress. For example, at the Na_2CO_3 concentration of 0.23 M, P_{k2} was estimated at 190 Pa, and without it, at 70 Pa.

It should be noted that, in the presence of sodium laurate, the range of inorganic electrolyte concentrations corresponding to formation of stable emulsions extends. For example, with 0.28 M Na_2CO_3 in the absence of sodium laurate, the emulsion breaks down within 1 day (Table 2), while in the presence of sodium laurate ($c = 4.5 \times 10^{-3}$ M) even with 1.4 M Na_2CO_3 the emulsion remains stable. In this case, sodium laurate favors creation of a more stable adsorption layer at the liquid–liquid interface, which increases the aggregation stability of the emulsion.

At the sodium laurate concentration equal to CMC (2.84×10^{-2} M), the emulsion undergoes phase separation only when large amounts of Na_2CO_3 are used. For example, up to the salt concentration of 0.23 M, the emulsions preserve stability for 1 day, while at the salt concentration of ≥0.3 M the emulsion begins to break down. With 1.9 M of the salt it breaks down

by 80%, while without emulsifier even with 0.28 M Na_2CO_3 the emulsion breaks down completely. A possible reason is that, in the presence of electrolytes, saturation of the adsorption layer is achieved at lower bulk concentrations of the surfactant [5, 6]. In this case, sodium laurate separates from the surface layer at the liquid–liquid interface, thereby breaking down the emulsion.

We identified the type of the resulting emulsions from the electrical conductivity and solubility in water. As known, the oil-in-water emulsions can be diluted with water and have a comparatively high electrical conductivity. Water-in-oil emulsions cannot be diluted with water and do not exhibit noticeable electrical conductivity. Tables 1 and 2 show that phases invert depending on the rapeseed oil, surfactant, and Na_2CO_3 concentrations in the system. At minor concentrations of sodium laurate, $(0.4–0.8) \times 10^{-3}$ M, in the system with 75% rapeseed oil (Table 1) the emulsion does not dissolve in water, and the electrical conductivity is not high and remains equal to that of rapeseed oil, 1.3×10^{-7} S cm^{-1}. In this case, a water-in-oil emulsion is formed. At high concentrations of sodium laurate, $(8–56) \times 10^{-3}$ M, the emulsion dissolves in water, and the electrical conductivity increases to 0.8×10^{-4} S cm^{-1}. In this case, an oil-in-water emulsion is formed. With increasing sodium palmitate concentration the phases invert as well. The emulsion type changes in the water–rapeseed oil–sodium laurate–sodium carbonate system depending on the composition as well (Table 2).

Thus, introduction into the water–rapeseed oil system of sodium laurate or sodium palmitate, as well as of sodium carbonate, opens up opportunities for raising its thickening power, with the amount of rapeseed oil to be spent for production of emulsions thereof reduced and the quality of structured dispersed systems improved.

CONCLUSIONS

(1) The rapeseed oil-based emulsions exhibit the highest stability upon introduction of sodium laurate and sodium palmitate into the system containing 75 and 50% oil phase, respectively.

(2) In the presence of sodium soaps, the structural and rheological properties of the water–rapeseed oil system, characterized by the ultimate shear stress P_{k2} and effective viscosity η, are enhanced; sodium palmitate forms in the water–rapeseed oil system a stronger structure than does sodium laurate.

(3) Sodium carbonate introduced into the water–rapeseed oil system exerts a stabilizing effect both in the presence and absence of sodium laurate.

(4) Phases invert in the water–rapeseed oil system. Depending on the oil phase, surfactant, and sodium carbonate concentrations in the system, oil-in-water and water-in-oil systems are formed.

ACKNOWLEDGMENTS

This study was financially supported by the Belarussian Republican Foundation for Basic Research (project code X06–182).

REFERENCES

1. Goncharik, I.I. and Mozheiko, F.F., *Zh. Prikl. Khim.*, 2002, vol. 75, no. 12, pp. 2046–2050.
2. Fridrikhsberg, D.A., *Kurs kolloidnoi khimii* (A Course of Colloid Chemistry), Leningrad: Khimiya, 1995.
3. *Laboratornye raboty i zadachi po kolloidnoi khimii* (Laboratory Works and Problems on Colloid Chemistry), Frolov, Yu.G. and Grodnenskii, A.S., Eds., Moscow: Khimiya, 1986.
4. Bibik, E.E., *Reologiya dispersnykh sustem* (Rheology of Disperse Systems), Leningrad: Leningr. Gos. Univ., 1981.
5. Aleksandrovich, Kh.M., Dikhtievskaya, L.V., Mitina, T.D., et al., *Kolloidn. Zh.*, 1990, vol. 52, no. 5, pp. 835–840.
6. Dikhtievskaya, L.V. and Mozheiko, F.F., *Dokl. Nats. Akad. Nauk Belarusi*, 1999, vol. 43, no. 5, pp. 58–61.

ISSN 1070-4272, Russian Journal of Applied Chemistry, 2007, Vol. 80, No. 4, pp. 665–668. © Pleiades Publishing, Ltd., 2007.
Original Russian Text © A.M. Magerramov, M.R. Bairamov, G.M. Mekhtieva, M.A. Agaeva, P.Sh. Mamedova, D.M. Kulieva, I.G. Mamedov, 2007, published in Zhurnal Prikladnoi Khimii, 2007, Vol. 80, No. 4, pp. 681–685.

CHEMISTRY OF FOSSIL FUEL

Synthesis of Aminomethylated Derivatives of Allylphenols and Study of Their Antimicrobial Characteristics in Motor Oil

A. M. Magerramov, M. R. Bairamov, G. M. Mekhtieva, M. A. Agaeva, P. Sh. Mamedova, D. M. Kulieva, and I. G. Mamedov

Baku State University, Baku, Azerbaijan

Institute of Chemistry of Fuel Additives, National Academy of Sciences of Azerbaijan, Baku, Azerbaijan

Received November 29, 2006

Abstract—A series of nitrogen-containing compounds was synthesized by Mannich condensation of allyl-substituted derivatives of phenol and *o*- and *p*-cresols with formaldehyde and secondary amines. These compounds were studied as antimicrobial additives to motor oil (at a content of 1–2 wt %).

DOI: 10.1134/S1070427207040295

Nitrogen-containing derivatives of phenols, and in particular Mannich's bases are the subject of systematic studies and, despite numerous papers in this field, still attract researchers' interest, which is caused by their useful functional characteristics [1–5].

With the aim to synthesize new nitrogen-containing phenols in whole structure an allyl fragment is present, along with aminomethyl group, we examined in this study the reactions of ternary Mannich condensation of 2-allyl-substituted derivatives of phenol and also *o*- and *p*-cresols with formaldehyde and secondary amines.

As can be suggested, the presence of the above substituents in the aromatic core of phenols should impart additional functional properties and, in particular, antimicrobial properties to phenols. Biological protection of oils, fuels, polymers, and other materials is topical problem, since the microbial corrosion of the above materials adversely affects the national economy [6].

EXPERIMENTAL

With the aim to synthesize phenol compounds simultaneously containing an allyl group and amine fragment, we carried out ternary condensation of allyl-substituted derivatives of phenol and *o*- and *p*-cresols with formaldehyde and secondary amines (under the conditions of Mannich's reaction).

Formaldehyde was used in the form of a 37% aqueous solution (Formalin). It was found that the above reaction proceeds well at the equimolar ratio of reactants at 70–75° and duration of 4–5 h to give the corresponding aminomethylated allyl-containing phenols. The target compounds were isolated from the reaction mixture by vacuum distillation. The reaction scheme is as follows:

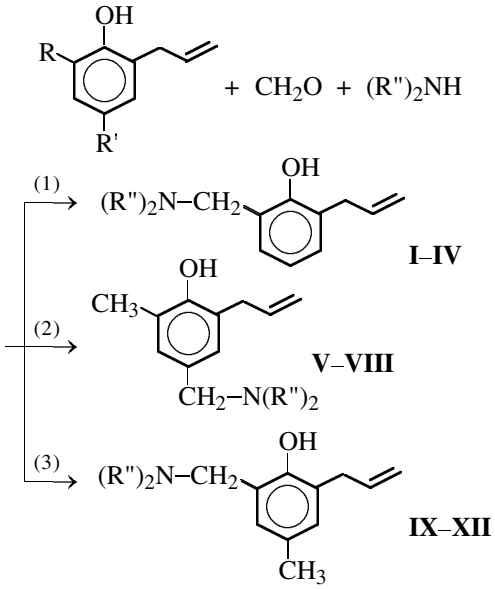

where (1) at R and R' = H; R" = $-CH_3$ (**I**), $-C_2H_5$ (**II**); $NR"_2$ = –N⟨⟩ (**III**), –N⟨⟩O (**IV**); (2) at R = $-CH_3$; R' = H; R" = $-CH_3$ (**V**), $-C_2H_5$ (**VI**); $NR"_2$ = –N⟨⟩ (**VII**), –N⟨⟩O (**VIII**); (3) at R = H; R' = CH_3; R' = CH_3; R" = $-CH_3$ (**IX**), $-C_2H_5$ (**X**); $NR"_2$ = –N⟨⟩ (**XI**), –N⟨⟩O (**XII**).

The initial allylphenols were synthesized by the well-known procedure [7], Claisen thermal rearrangement of allyl ethers of phenol and *o*- and *p*-cresols, within 3–6 h and were isolated from the reaction mixture by distillation in a high vacuum.

The characteristics of the compounds synthesized are listed in Table 1. Their yield varies from 48.0 to 70.6%, depending on the nature of amine and initial phenol compound. All these compounds, except 4-methyl-2-morpholinomethyl-6-allylphenol (**XII**), are

Table 1. Characteristics of aminomethylated allylphenols

Compound	Yeld, % of theoretical	bp, °C/*P*, mm Hg	n_D^{20}	d_4^{20}, kg m^{-3}
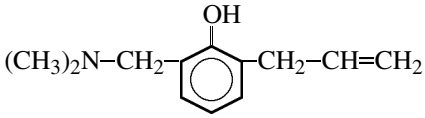 **I**	48.4	110–111/0.8	1.5298	1015.9
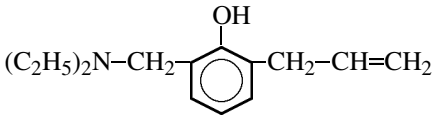 **II**	70.6	113–114/0.7	1.5285	993.4
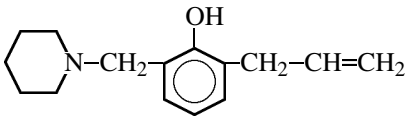 **III**	50.0	118–120/0.8	1.5010	1048.5
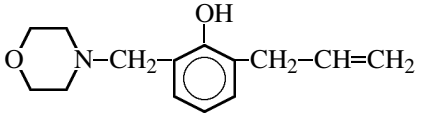 **IV**	70.8	118–119/0.6	1.5030	1091.3
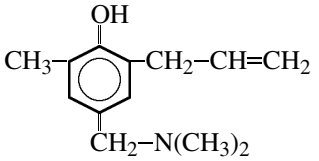 **V**	45.3	111–113/0.7	1.5012	1023.8
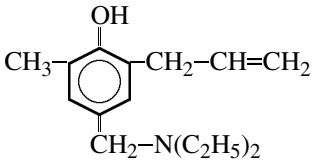 **VI**	60.0	119–120/0.7	1.5040	1007.9
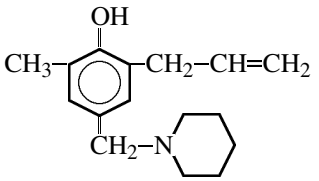 **VII**	58.5	124–126/0.6	1.5047	1051.4
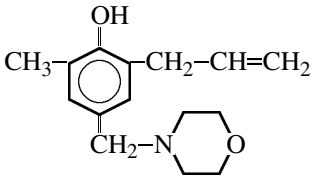 **VIII**	64.0	126–128/0.5	1.5040	1143.5
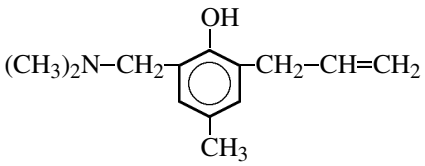 **IX**	48.0	110–112/0.6	1.5240	973.2

Table 1. (Contd.)

Compound	Yeld, % of theoretical	bp, °C/*P*, mm Hg	n_D^{20}	d_4^{20}, kg m^{-3}
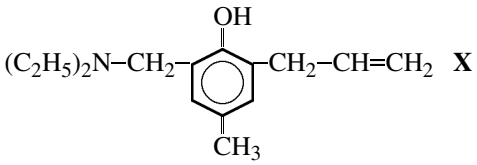 **X**	63.2	118–120/0.6	1.5210	971.8
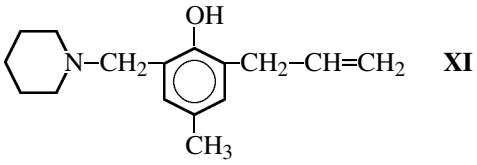 **XI**	52.7	127–129/0.7	1.5064	1033.4
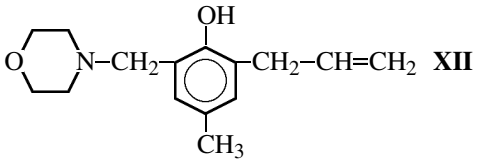 **XII**	65.2	128–130/0.6	–	–

Table 2. Results of studying antimicrobial characteristics of aminomethylated derivatives of allylphenols in M-12 motor oil

Compound	Concentration in oil, wt %	Area of bacterium annihilation	Area of fungus annihilation
		cm	
2-Dimethylaminomethyl-6-allylphenol (**I**)	1.0	+ +	0.8–1.0
	2.0	+ +	1.6–2.0
2-Diethylaminomethyl-6-allylphenol (**II**)	1.0	+ +	0.9–1.0
	2.0	+ +	1.9–2.0
2-Piperidinomethyl-6-allylphenol (**III**)	1.0	+ +	+ +
	2.0	+ +	1.0–1.2
2-Morpholinomethyl-6-allylphenol (**IV**)	1.0	0.9–1.0	0.7–0.8
	2.0	1.9–2.0	1.5–1.7
2-Allyl-4-dimethylaminomethyl-6-methylphenol (**V**)	1.0	+ +	0.8–1.0
	2.0	+ +	1.7–2.0
6-Methyl-2-allyl-4-diethylaminomethylphanol (**VI**)	1.0	+ +	0.6–0.7
	2.0	1.0–1.1	1.3–1.5
6-Methyl-2-allyl-4-piperidinomethylphenol (**VII**)	1.0	+ +	+ +
	2.0	+ +	1.0–1.1
6-Methyl-2-allyl-4-morpholinomethylphenol (**VIII**)	1.0	+ +	0.7–1.0
	2.0	+ +	1.5–2.1
4-Methyl-2-dimethylaminomethyl-6-allylphenol (**IX**)	1.0	+	+ +
	2.0	+ +	1.0–1.1
4-Methyl-2-diethylaminomethyl-6-allylphenol (**X**)	1.0	+ +	0.7–1.0
	2.0	+ +	1.4–2.0
4-Methyl-2-piperidinomethyl-6-allylphenol (**XI**)	1.0	+ +	0.6–0.9
	2.0	+ +	1.3–1.9
4-Methyl-2-morpholinomethyl-6-allylphenol (**XII**)	1.0	1.1–1.4	0.6–0.9
	2.0	2.2–2.9	1.3–1.9
8-Quinolinol (reference) (**XIII**)	1.0	0.7–1.0	+ +
	2.0	1.5–2.0	+ +
M-12 motor oil (**XIV**) (without additive)	–	+ +	+ +

viscous liquid substances colored from light yellow to brown and readily soluble in aromatic solvents. 4-Methyl-2-morpholinomethyl-6-allylphenol is a light-straw-colored crystalline substance with mp 43°C.

The structures of all the synthesized aminomethylated derivatives of allylphenols were confirmed by the IR and NMR data.

All the compounds were tested as antimicrobial additives to the M-12 motor oil at a content of 1 and 2 wt %. The operations were performed according to GOSTs (State Standards) 9.082–77 and 9.052–88. The nutrient medium for growing the bacterial culture was meat-extract agar (MEA), and for growing the fungus culture, wort agar (WA). The comparison was performed with 8-quinolinol (reference). The results of the tests are presented in Table 2.

As can be seen from Table 2, all the studied aminomethylated derivatives of allylphenols exhibit a fungicidal activity. The diameter of the area of depression of fungus growth, depending on the compound structure and its concentration, is, on the average, 0.8–1.0 (at a content of 1 wt %) and 1.4–2.0 cm (at a content of 2 wt %).

Morpholine-substituted allylphenols also have bactericidial properties and are second in these properties only to 8-quinolinol (reference). As can be seen from Table 2, the latter has no fungicidal activity and the fungus growth was not suppressed in its presence even at a content of 2 wt %. As regards spent M-12 oil, it shows no resistance to fungi and bacteria. The results of comparison tests show that the aminomethylated derivatives of allylphenols are of practical interest and can find application as antimicrobial additives to lubricating oils.

CONCLUSION

Aminomethylated derivatives of allylphenols synthesized by ternary Mannich condensation of allyl-substituted derivatives of phenol and *o*- and *p*-cresols with formaldehyde and secondary amines, when added at a content of 1–2 wt %, have high fungicidal activity with respect to mold fungi. Compounds **IV** and **XII** containing cyclic amine fragment in their structures have also high bactericidal properties (in comparison with the reference, 8-quinolinol).

REFERENECES

1. US Patent no. 6 179 885. Compositions Containing Mannich's Aromatic Compounds and Procedures of Their Synthesis, 2001, *Ref. Zh. Khim.*, 2002, 0202-19P187P.
2. Kondrat'ev, V.V., Kirillov, N.S., and Bobyr', O.V., *Khim. Tekhnol.*, 2005, no. 7, pp. 13–14.
3. Zui Baoyou and Xu Danqion, *J. Chem. Ind. Eng.*, 2004, vol. 55, no. 12, pp. 2043–2046.
4. Terada Masahiro, *J. Am. Chem. Soc.*, 2004, vol. 126, no. 17, pp. 5356–5357.
5. Kharitonova, N.I., Burilov, A.N., and Pudovik, M.A., *Izv. Ross. Akad. Nauk, Ser. Khim.*, 2003, no. 3, pp. 694–696.
6. Andreyuk, E.I., Bilai, V.M., and Koval', E.Z., *Mikrobnaya korroziya i ee vozbuditeli* (Microbial Corrosion and Its Pathogens), Kiev: Naukova Dumka, 1980.
7. Weygand-Hilgetag, *Organisch-Chemische Experimentierkunst*, Leipzig: Johann Ambrosius Barth, 1964.

ISSN 1070-4272, Russian Journal of Applied Chemistry, 2007, Vol. 80, No. 4, pp. 669–671. © Pleiades Publishing, Ltd., 2007.
Original Russian Text © B.V. Patrov, E.S. Chupina, 2007, published in Zhurnal Prikladnoi Khimii, 2007, Vol. 80, No. 4, pp. 686–688.

BRIEF COMMUNICATIONS

Activity of Components of Binary Chloride Melts

B. V. Patrov and E. S. Chupina

St. Petersburg State Polytechnic University, St. Petersburg, Russia

Received February 14, 2007

Abstract—Activities of components of the systems NaCl–AgCl, KCl–AgCl, NaCl–$FeCl_2$, and NaCl–$CoCl_2$ were calculated using the model of regular solutions and data on the enthalpies of mixing of binary chloride melts.

DOI: 10.1134/S1070427207040301

A calculation of the activities of components of melts of binary systems with a common anion from the enthalpies of mixing has been described earlier [1]. It has been shown that, in terms of the regular solution model [2], the activity coefficients of components of binary systems can be represented as

$$\ln \gamma_1 = \frac{A}{RT} x_2^2, \quad (1)$$

$$\ln \gamma_2 = \frac{A}{RT} x_1^2. \quad (2)$$

Here, A is an interaction parameter, and x_1 and x_2 are the mole fractions of the components.

Let us express the interaction parameter A in these equations through molar enthalpy of mixing of the components, ΔH^{M} (J mol^{-1}):

$$A = \frac{\Delta H^{\mathrm{M}}}{x_1 x_2}. \quad (3)$$

As is known, the activities of the components are related to the activity coefficients and mole fraction:

$$a_1 = \gamma_1 x_1, \quad (4)$$

$$a_2 = \gamma_2 x_2. \quad (5)$$

The validity of these equations for the melts under study was verified using Burylev's equation for regular solutions [3]

$$\sigma = \sigma_1 x_1 + \sigma_2 x_2 + C x_1 x_2. \quad (6)$$

Here, σ_1, σ_2 and x_1, x_2 are the surface tension and mole fractions of the components of the binary systems; C is the constant of Burylev's equation.

For the binary chloride melts NaCl–AgCl, KCl–AgCl, NaCl–$FeCl_2$, and NaCl–$CoCl_2$, experimental data on the surface tension [4] and enthalpies of mixing [5] are available, their phase diagrams correspond to simple solutions with an eutectic and to solid solutions [6].

The average values of the constant C in Burylev's equation and of the interaction parameter A of the systems under study are as follows:

System	T, K	$-C$, mJ m^{-2}	$-A$, J mol^{-1}
NaCl–AgCl	1083	57.0	–5496
KCl–AgCl	1083	97.3	8716
NaCl–$FeCl_2$	1083	90.6	25984
NaCl–$CoCl_2$	1083	38.8	28034

A comparison of the experimental values of the surface tension and those calculated by Burylev's equation demonstrated that the difference does not exceed the measurement error (2%). A stronger difference was found for two compositions of the system of potassium and silver chlorides. Hence, the melts under study are regular solutions and Eqs. (1)–(6) are applicable to them.

The activities of the melt components, calculated from the enthalpy of mixing, are listed in Table 1.

The choice of the systems NaCl–AgCl and KCl–AgCl for the study was based on the fact that the partial Gibbs energy of melt formation from the components is known for these systems [5]. It was determined by measuring the electromotive force of galvanic cells. As is known, the partial Gibbs energy is related to activities a_1 and a_2 of components by

Table 1. Enthalpy of mixing and activities of components of the systems under study at 1083 K

x_1	$-\Delta H^M$, J mol^{-1}	γ_1	a_1	γ_2	a_2	x_1	$-\Delta H^M$, J mol^{-1}	γ_1	a_1	γ_2	a_2
NaCl (1)–AgCl (2)						NaCl (1)–$FeCl_2$ (2)					
0.1	–350	1.5120	0.1512	1.0051	0.9046	0.1	1480	0.0966	0.0097	0.9716	0.8744
0.2	–650	1.3863	0.2773	1.0206	0.8165	0.2	3020	0.1577	0.0315	0.8910	0.7128
0.3	–890	1.2841	0.3852	1.0470	0.7329	0.3	4590	0.2431	0.0729	0.7713	0.5399
0.4	–1060	1.2017	0.4807	1.0851	0.6511	0.4	6000	0.3538	0.1415	0.6302	0.3781
0.5	–1150	1.1361	0.5680	1.1361	0.5680	0.5	6980	0.4860	0.2430	0.4860	0.2430
0.6	–1140	1.0851	0.6511	1.2017	0.4807	0.6	7270	0.6302	0.3781	0.3538	0.1415
0.7	–1040	1.0470	0.7329	1.2841	0.3852	0.7	6650	0.7713	0.5399	0.2431	0.0729
0.8	–820	1.0206	0.8165	1.3863	0.2773	0.8	5070	0.8910	0.7128	0.1577	0.0315
0.9	–480	1.0051	0.9046	1.5120	0.1512	0.9	2710	0.9716	0.8744	0.0966	0.0097
KCl (1)–AgCl (2)						NaCl (1)–$CoCl_2$ (2)					
0.1	870	0.4565	0.0457	0.9904	0.8913	0.1	1160	0.0803	0.0080	0.9693	0.8724
0.2	1510	0.5382	0.1076	0.9620	0.7696	0.2	2510	0.1363	0.0273	0.8829	0.7063
0.3	1930	0.6223	0.1867	0.9166	0.6416	0.3	4230	0.2175	0.0652	0.7556	0.5289
0.4	2150	0.7058	0.2823	0.8565	0.5139	0.4	6100	0.3260	0.1304	0.6076	0.3646
0.5	2180	0.7851	0.3926	0.7851	0.3926	0.5	7670	0.4592	0.2296	0.4592	0.2296
0.6	2030	0.8565	0.5139	0.7058	0.2823	0.6	8440	0.6076	0.3646	0.3260	0.1304
0.7	1730	0.9166	0.6416	0.6223	0.1867	0.7	7990	0.7556	0.5289	0.2175	0.0652
0.8	1280	0.9620	0.7696	0.5382	0.1076	0.8	6160	0.8829	0.7063	0.1363	0.0273
0.9	700	0.9904	0.8913	0.4565	0.0457	0.9	3220	0.9693	0.8724	0.0803	0.0080

Table 2. Partial Gibbs energy and activities of components of the systems under study at 1083 K

x_1	$-\Delta G_1$, J mol^{-1}	$-\Delta G_2$, J mol^{-1}	a_1	a_2	x_1	$-\Delta G_1$, J mol^{-1}	$-\Delta G_2$, J mol^{-1}	a_1	a_2
NaCl (1)–AgCl (2)					KCl (1)–AgCl (2)				
0.1	16920	900	0.1527	0.9049	0.1	26380	1020	0.0534	0.8929
0.2	11480	1820	0.2794	0.8170	0.2	18950	2290	0.1219	0.7754
0.3	8540	2790	0.3873	0.7335	0.3	14260	3840	0.2052	0.6528
0.4	6560	3840	0.4826	0.6528	0.4	10760	5710	0.3027	0.5304
0.5	5070	5060	0.5695	0.5701	0.5	7980	7990	0.4122	0.4117
0.6	3850	6550	0.6521	0.4831	0.6	5710	10760	0.5304	0.3027
0.7	2790	8530	0.7335	0.3878	0.7	3840	14260	0.6528	0.2052
0.8	1820	11480	0.8170	0.2794	0.8	2290	18950	0.7754	0.1219
0.9	900	16930	0.9049	0.1525	0.9	1020	26380	0.8929	0.0534

$$\Delta\overline{G}_1 = RT\ln a_1, \quad (7)$$

$$\Delta\overline{G}_2 = RT\ln a_2. \quad (8)$$

The activities of the components, calculated using the partial Gibbs energy, are listed in Table 2 for comparison with those found from the data on mixing enthalpies.

It is seen that, for NaCl–AgCl melts with a positive enthalpy of mixing and positive deviations from ideal solutions, the activity of the components, calculated from the enthalpy of mixing, coincides with that calculated from the partial Gibbs energy of melt formation. The difference in the activity values does not exceed 0.002. For the melts of potassium and silver chlorides with a negative enthalpy of mixing, the values of the activity of the components, calculated from the partial Gibbs energies or from the enthalpy of mixing, differ more widely (up to 0.02), presumably owing to the small number of studies concerned with this system.

CONCLUSIONS

(1) It was shown that the binary chloride melts studied are regular solutions.

(2) The activities of the components of chloride melts were calculated using data on the surface tension and enthalpy of mixing.

(3) It was demonstrated that the activities of the components, calculated from the enthalpies of mixing, satisfactorily coincide with those calculated from the partial Gibbs energy of melt formation.

REFERENCES

1. Patrov, B.V., *Zh. Prikl. Khim.*, 2006, vol. 79, no. 12, pp. 2052–2053.
2. Hildebrand, J.H., *Solubility of Non-Electrolytes*, New York: Reinhold, 1936, 2d ed.
3. Burylev, B.P. and Vasil'ev, V.V., *Fizicheskaya khimiya poverkhnostnykh yavlenii v rasplavakh* (Physical Chemistry of Surface Phenomena in Melts), Kiev: Naukova Dumka, 1971, pp. 144–149.
4. Stepanov, V.P., *Mezhfaznye yavleniya v ionnykh solevykh rasplavakh* (Interphase Phenomena in Ionic Salt Melts), Yekaterinburg: Nauka, 1993.
5. Markov, B.F., Volkov, S.V., Prisyazhnyi, V.D., et al., *Termodinamicheskie svoistva rasplavov solevykh sistem* (Thermodynamic Properties of Melts of Salt Systems), Kiev: Naukova Dumka, 1985.
6. Posypaiko, V.I. and Alekseeva, E.A., *Diagrammy plavkosti solevykh sistem. Chast' 1. Dvoinye sistemy s obshchim anionom* (Fusibility Diagrams of Salt Systems, Part 1, Binary Systems with a Common Anion), Moscow: Metallurgiya, 1977.

ISSN 1070-4272, Russian Journal of Applied Chemistry, 2007, Vol. 80, No. 4, pp. 672–674. © Pleiades Publishing, Ltd., 2007.
Original Russian Text © A.G. Kasikov, A.M. Petrova, 2007, published in Zhurnal Prikladnoi Khimii, 2007, Vol. 80, No. 4, pp. 689–690.

BRIEF COMMUNICATIONS

Effect of the Structure of Octanols on Their Extraction Capacity for Rhenium(VII) in Sulfuric Acid Solutions

A. G. Kasikov and A. M. Petrova

Tananaev Institute of Chemistry and Technology of Rare Elements and Mineral Resources, Kola Scientific Center, Russian Academy of Sciences, Apatity, Murmansk oblast, Russia

Received October 16, 2006

Abstract—Extraction of Re(VII) from sulfuric acid solutions with isomers of octanol was studied.

DOI: 10.1134/S1070427207040313

In their physicochemical characteristics, aliphatic alcohols C_8–C_{10} meet the basic requirements to industrial extractants. Furthermore, with these alcohols, there is no need to use some diluents and modifiers, which simplifies extraction systems. That is why intensive research is being conducted on extraction of inorganic acids and some chemical elements with alcohols, primarily with various isomers of octanol [1–8].

Despite that octanols differ in their physicochemical characteristics, in most of these studies no comparison has been made of the extraction capacity of the isomers. At the same time, Karamushko et al. [8] demonstrated that alcohols can differ significantly in their extraction capacity for Nb(V), depending on their structure, and they recommended 2-octanol for extraction processing of fluorometallate solutions.

The goal of this study was to examine the effect of the structure of octanols on their extraction capacity and to search for efficient extractants for Re(VII). For this purpose, we studied the extraction of Re(VII) from sulfuric acid solutions with isomers of octanol. The possibility of use of octanols for extraction of Re has been reported previously [5–7]. However, in these studies, the results were obtained under different experimental conditions and, generally, without control over the equilibrium concentration of sulfuric acid.

EXPERIMENTAL

In the experiments on extraction of Re(VII), we used 1-octanol and DL-2-octanol from Vekton Private Company, and 3-octanol (synthetic grade, Merck). To prepare the initial solutions, we used chemically pure grade NH_4ReO_4 and H_2SO_4. The extraction experiments were carried out at room temperature in 50-ml volumetric cylinders for 5 min at 1 : 1 organic to aqueous phase ratio. Rhenium in the raffinates was determined spectrophotometrically from the band of the thiourea complex of Re(IV), which is formed in the presence of Sn(II) as a reducing agent. The measurements were performed at λ = 390 nm on a KFK-3 photoelectric colorimeter [7]. The sulfuric acid concentration in the aqueous phase was determined by titration. The Re(VII) concentration in the organic phase was estimated as the difference between its concentrations in the initial solution and raffinate, with account taken of changing phase volumes.

The dependence of the Re(VII) distribution ratio D_{Re} on the H_2SO_4 concentration in the initial solution is shown in Fig. 1 for three octanol isomers. With increasing acid concentration, D_{Re} initially grows, passes through a maximum at 4–7 M H_2SO_4, depending on the isomer, and then decreases. The increase in the extraction capacity of the alcohols with the acid concentration is due to the fact that hydrogen ions are involved in the extraction by the hydration-solvation mechanism [7]:

$$ReO_4^- + H^+ + (n + 1)H_2O + qS \rightleftarrows [H_3O \cdot (H_2O)_n \cdot qS]ReO_4.$$

The subsequent decrease in the distribution coefficients can be attributed to a concurrent extraction of

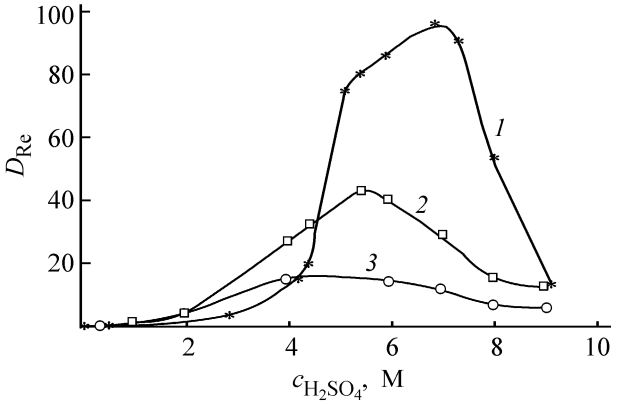

Fig. 1. Rhenium(VII) distribution ratio D_{Re} vs. the equilibrium concentration of H_2SO_4 in extraction with octanols: (*1*) 3-octanol, (*2*) DL-2-octanol, and (*3*) 1-octanol; the same for Fig. 2. ($c_{H_2SO_4}$) Initial H_2SO_4 concentration in the aqueous phase; the same for Fig. 2.

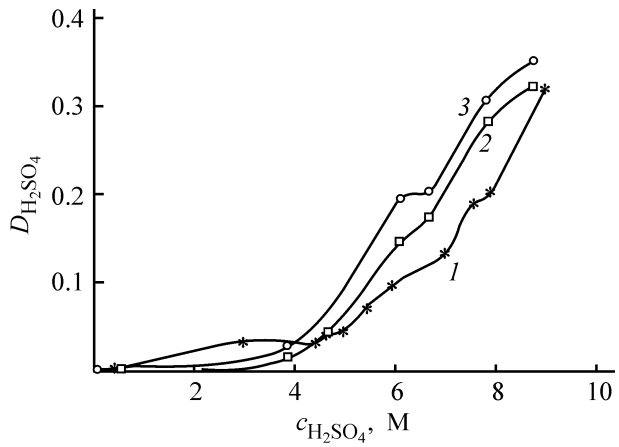

Fig. 2. H_2SO_4 distribution ratio $D_{H_2SO_4}$ vs. its concentration in the aqueous phase in extraction with octanols.

H_2SO_4, which increases with the acid concentration in the solution (Fig. 2). At high acid concentrations in the aqueous phase, the decrease in the extraction of ReO_4^- may be associated with the formation in the extractant phase of sulfuric acid esters [9] which virtually cannot extract Re(VII) [7].

Furthermore, the decrease in D_{Re} at $c_{H_2SO_4}$ above 7 M is caused by the formation of the sulfate complex $H[ReO_2(SO_4)_2]$ [10] which is considerably worse extracted to the organic phase, as we have shown previously for extraction of Re(VII) with triisooctylamine [11]. Evidently, this fact is responsible for the observed abrupt decrease in D_{Re} of 3-octanol at $c_{H_2SO_4} > 7$ M.

Figure 1 shows that the extraction capacity of the octanols depends not only on the H_2SO concentration, but it also strongly affected by their structure. This is clearly illustrated by the fact that the maximal D_{Re} for secondary 3-octanol is above 90, which is higher by about a factor of 5 that that for 1-octanol of the normal structure. Such effect of the structure can be attributed to different basicities of the isomers, which decrease in the order 1-octanol > 2-octanol > 3-octanol as a result of induction effects [12]. The higher D_{Re} values obtained for the secondary alcohols are also associated with the less pronounced effect of the concurrent extraction of sulfuric acid on the extraction of Re(VII) (Fig. 2). The inverse order of the extraction capacity of the alcohols for sulfuric acid is probably due to predominance of the steric factor in the secondary alcohols over the basicity factor.

CONCLUSIONS

(1) The extraction capacity of octanols for rhenium(VII) and sulfuric acid depends on the alcohol structure. It increases for Re(VII), but decreases for H_2SO_4 on passing from 1-octanol to 3-octanol.

(2) The dependences of D_{Re} on the acid concentration have maxima at 4–7 M, which are most clearly pronounced for the secondary alcohols.

(3) The abrupt decrease in the extraction capacity of octanols with increasing H_2SO_4 concentration above 7 M is caused by changes in the extractant composition and Re(VII) speciation in the solution.

ACKNOWLEDGMENTS

The study was financially supported under the program “Leading Scientific Schools” (project no. NSh-4383.2006.3).

REFERENCES

1. Sklokin, L.I., Tyuremnov, A.V., and Kalinnikov, V.T., *Khim. Tekhnol.*, 2002, no. 8, pp. 25–31.
2. RF Patent 2 159 293.
3. Kopkova, E.K. and Sklokin, L.I., *Khim. Tekhnol.*, 2001, no. 11, pp. 20–26.
4. Keskinov, V.A., Kudrova, A.V., Valueva, V.A., and Pyartman, A.K., *Zh. Prikl. Khim.*, 2004, vol. 77, no. 9, pp. 1571–1572.
5. Kasikov, A.G., Areshina, N.S., Kudryakov, M.V., and Khomchenko, O.A., *Khim. Tekhnol.*, 2004, no. 6, pp. 25–31.

6. Travkin, V.F., Kubasov, V.L., Ishchenko, A.A., et al., *Tsvetn. Metall.*, 2005, no. 1, pp. 5–10.
7. Borisova, L.V. and Ermakov, A.N., *Analiticheskaya khimiya reniya* (Analytical Chemistry of Rhenium), Moscow: Nauka, 1974.
8. Karamushko, E.V., Glubokov, Yu.M., and Travkin, V.F., Abstracts of Papers, *XII Rossiiskaya konferentsiya po ekstraktsii* (XII Russian Conf. on Extraction), Moscow, October 7–13, 2001, p. 36.
9. Tyuremnov, A.V., Sklokin, L.I., et al., *Materialy Mezhdunarodnoi konferentsii "Ekologicheskie problemy severnykh regionov i puti ikh resheniya"* (Proc. Int. Conf. "Environmental Problems of the Northern Areas and Ways to Their Solution," Apatity (Russia), August 31–September 3, 2004, pp. 136–138.
10. Bardin, V.A., Petrov, K.I., and Bol'shakov, K.A., *Zh. Neorg. Khim.*, 1966, vol. 21, no. 9, pp. 2101–2107.
11. Kasikov, A.G. and Petrova, A.M., *Zh. Prikl. Khim.*, 2006, vol. 79, no. 6, pp. 925–930.
12. Becker, H., *Einfuhrung in die Elektronentheorie organisch-chemischer Reaktionen*, Berlin: Verlag, 1964, 2nd ed.

ISSN 1070-4272, Russian Journal of Applied Chemistry, 2007, Vol. 80, No. 4, pp. 675–677. © Pleiades Publishing, Ltd., 2007.
Original Russian Text © R.I. Yurchenko, I.S. Pogrebova, T.N. Pilipenko, 2007, published in Zhurnal Prikladnoi Khimii, 2007, Vol. 80, No. 4, pp. 691–692.

BRIEF COMMUNICATIONS

1-Phenacylmethyl-2-(acylaminothiocarbonylamino)pyridinium Bromides as Protectors of Steel Acid Corrosion

R. I. Yurchenko, I. S. Pogrebova, and T. N. Pilipenko

Kiev Polytechnic Institute, National Technical University of Ukraine, Kiev, Ukraine

Received May 11, 2006; in final form, August 2006

Abstract—Inhibiting effect of 1-phenacylmethylpyridinium bromides containing acylthiourea substituents in the pyridine ring on corrosion of mild steel in sulfuric acid (3 M) was studied.

DOI: 10.1134/S1070427207040325

The inhibiting properties of 1-phenacylmethylpyridinium bromides containing, in the 2-position of the pyridine ring, the $–NH_2$ [1], –NH(C)OR [2], –NHC(O)NHR, and –NHC(S)NHR [3] groups have been studied previously. The thiourea derivatives were found to be the most active. In this study, we examined ureides **I**–**VIII** as a logical continuation of the above studies: 1-(2-oxo-2-phenylethyl)-2-(3-phenylureido)pyridinium bromide **I**, 1-(2-oxo-2-phenylethyl)-2-[3-(4-methylphenyl)ureido]pyridinium bromide **II**, 1-(2-oxo-2-phenylethyl)-2-[3-(4-methoxyphenyl)-ureido]pyridinium bromide **III**, 1-(2-oxo-2-phenylethyl)-2-[3-(4-bromomethylphenyl)ureido]pyridinium bromide **IV**, 1-(2-oxo-2-phenylethyl)-2-[3-(4-chloromethylphenyl)ureido]pyridinium bromide **V**, 1-(2-oxo-2-phenylethyl)-2-[3-(2-furyl)ureido]pyridinium bromide **VI**, 1-(2-oxo-2-phenylethyl)-2-[3-(adamant-1-yl)ureido]pyridinium bromide **VII**, and 1-(2-oxo-2-phenylethyl)-2-[3-(undec-1-yl)ureido]pyridinium bromide **VIII**.

These compounds are acyl derivatives of thiourea and contain RC(O)NHC(S)NH groups in the 2-position of the pyridine ring. It is known that β-dicarbonyl compounds are often used in organic chemistry as complexing agents. Therefore, we can expect that the structure of substituents taken will be favorable for the protective properties of the compounds studied.

Compounds **I**–**VIII** were synthesized by the reaction of acyl chlorides, ammonium thiocyanate, and 2-aminopyridine, followed by treatment of the compounds obtained with ω-bromoacetophenone:

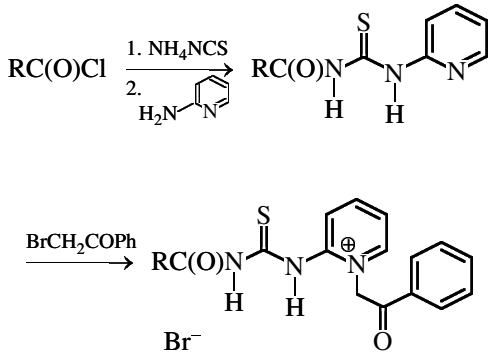

where R is Ph (**I**), 4-$CH_3C_6H_4$ (**II**), 4-$CH_3OC_6H_4$ (**III**), 4-BrC_6H_4 (**IV**), 4-ClC_6H_4 (**V**), 2-furyl (**VI**), 1-adamantyl (**VII**), and 1-undecyl (**VIII**).

The composition of the compounds obtained was confirmed by IR and ^1H NMR spectra.

EXPERIMENTAL

A mixture of an appropriate acid chloride prepared by reaction of the acid with thionyl chloride (2×10^{-2} mol), ammonium thiocyanate (2.5×10^{-2} mol), and anhydrous acetone (15 ml) was stirred for 30 min, after which 2-aminopyridine (2×10^{-2} mol) was added, and stirring was continued for an additional 1 h. The reaction mixture was treated with a small portion of water, and, the next day, the precipitate was separated. Equimolar amounts (1.5×10^{-3} mol) of the compound prepared and ω-bromoacetophenone were refluxed in 15 ml of ethyl acetate for 3 h, and the precipitate was separated. The yields (%) and

Corrosion inhibition coefficient γ and degree of protection, *Z*, for 08KP steel in 3 M H_2SO_4 in the presence of 1-phenacylmethylpyridinium bromides **I**–**VIII**

Compound	R	40°C		60°C		80°C	
		γ	*Z*, %	γ	*Z*, %	γ	*Z*, %
I	C_6H_5	23.90	95.82	129.40	99.22	41.70	97.60
II	4-$CH_3C_6H_4$	29.87	96.66	373.10	99.73	190.10	99.47
III	4-$CH_3OC_6H_4$	36.70	97.27	396.42	99.75	125.10	99.22
IV	4-BrC_6H_4	22.76	95.60	103.40	99.03	56.55	98.23
V	4-ClC_6H_4	22.76	95.60	121.20	99.17	103.60	99.03
VI	2-Furyl	41.56	97.59	218.70	99.54	119.00	99.16
VII	1-Adamantyl	39.80	97.48	380.56	99.73	192.75	99.48
VIII	1-Undecyl	38.24	97.38	328.10	99.69	102.90	99.02

melting points (°C) of **I**–**VIII** are as follows: **I**, 40, 229–232; **II**, 50, 198–200; **III**, 75, 195–205; **IV**, 70, 210–212; **V**, 71, 196–203; **VI**, 69, 218–220; **VII**, 35, 227–229; and **VIII**, 70, 212–215.

The corrosion-protective properties **I**–**VIII** were evaluated gravimetrically at 20, 40, 60, and 80°C by the inhibition coefficient γ and degree of protection, *Z*, of a 08KP steel in 3 M sulfuric acid [1]. Unfortunately, the poor solubility of the compounds obtained in 3 M H_2SO_4 prevented attaining the same concentration as for the previously studied 1-phenacylmethylpyridinium bromides.

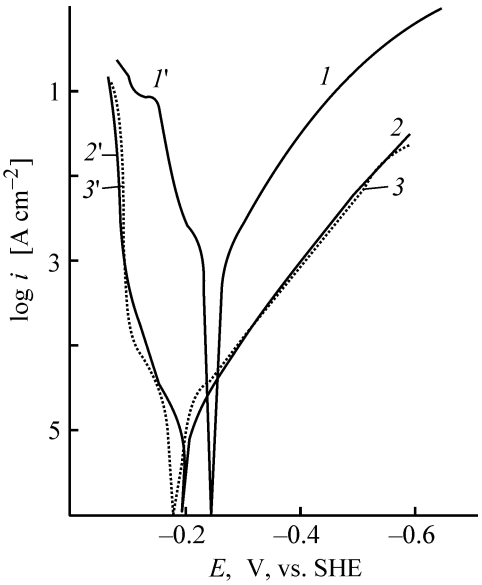

(*1*–*3*) Cathodic and (*1'*–*3'*) anodic polarization curves recorded at 20°C on 08 KP steel in 3 M H_2SO_4 and in solutions saturated with **VI** and **VII**. (*i*) Current density and (*E*) potential. Solution: (*1*, *1'*) supporting electrolyte, (*2*, *2'*) with **VI**, and (*3*, *3'*) with **VII**.

Nevertheless, the tests performed showed that compounds **I**–**VIII** are fairly efficient inhibitors of steel acid corrosion (see table). The corrosion inhibition coefficients found for saturated solutions in 3 M H_2SO_4 vary within the ranges 15.79–26.47 at 20°C, 22.76–41.56 at 40°C, 103.40–396.42 at 60°C, and 41.70–192.80 at 80°C. Voltammetric measurements on steel with **VI** and **VII** at 20°C showed that these compounds behave as mixed-type inhibitors affecting the rate of both anodic and cathodic processes (see figure). Calculations based on the "formal theory" of inhibition [4] indicate that corrosion is inhibited by these compounds at 40°C by the energy-blocking mechanism.

Introduction of MeO group into the *p*-position of the benzene ring in **I** or replacement of the phenyl substituent with a furyl group enhances the protective properties, which is in accordance with the chemical nature of the substituents introduced, but the extent of enhancement is substantially lower than that in the series of the previously studied compounds [2, 3]. At 60°C, the corrosion inhibition coefficient for ureide **III** is only three times higher, and for **VI**, two times higher than that for **I**.

CONCLUSIONS

(1) It was found that the steel corrosion inhibition coefficients for saturated solutions of 1-phenacylmethyl-2-(acylaminothiocarbonlylamino)pyridinium bromides in 3 M sulfuric acid vary within the ranges 15.79–26.47 at 20°C, 22.76–41.56 at 40°C, 103.40–

396.42 at 60°C, and 41.70–192.80 at 80°C; the degree of metal surface protection is 95.6–99.7%.

(2) Voltammetric measurements showed that the compounds studied behave as mixed-type inhibitors affecting the rates of both anodic and cathodic processes. Corrosion is inhibited by these compounds by the energy-blocking mechanism.

REFERENCES

1. Yurchenko, R.I., Pogrebova, I.S., Pilipenko, T.N., and Kras'ko, E.M., *Zh. Prikl. Khim.*, 2003, vol. 76, no. 11, pp. 1814–1818.
2. Yurchenko, R.I., Pogrebova, I.S., Pilipenko, T.N., and Shubina, T.E., *Zh. Prikl. Khim.*, 2004, vol. 77, no. 7, pp. 1132–1135.
3. Yurchenko, R.I., Pogrebova, I.S., Pilipenko, T.N., and Shubina, T.E., *Zh. Prikl. Khim.*, 2006, vol. 79, no. 12, pp. 1993–1997.
4. Antropov, L.I., *Zashch. Met.*, 1977, vol. 13, no. 4, pp. 387–399.

ISSN 1070-4272, Russian Journal of Applied Chemistry, 2007, Vol. 80, No. 4, pp. 678–681. © Pleiades Publishing, Ltd., 2007.
Original Russian Text © A.M. Syroezhko, 2007, published in Zhurnal Prikladnoi Khimii, 2007, Vol. 80, No. 4, pp. 693–696.

INFORMATION

Prospects for Chemical Processing of Fossil Fuels

DOI: 10.1134/S1070427207040337

The International Conference "Prospects for Chemical Processing of Fossil Fuels" was held from September 12 to 15, 2006 in St. Petersburg. The conference was timed with the 135th anniversary of foundation of the Department of Technology of Petro- and Coal-Chemical Works at the Russian's oldest institution for higher technological education, St. Petersburg State Technological Institute (Technical University).

There were presented more than 100 plenary reports and oral lectures, and their abstracts were published. The Conference organizers were the Ministry of Education and Science of the Russian Federation; Division of Chemistry and Materials Science, Russian Academy of Sciences; Joint Scientific Council for Chemistry of Oil, Gas, and Solid Fuels; Scientific Council for Chemistry of Solid Fossil Fuels; Mendeleev Russian Chemical Society; and St. Petersburg State Technological Institute (Technical University).

More than 500 scientists from Russia and other countries were conference participants. They represented 46 institutes of higher-school institutions, more than 90 firms and joint-stock companies from 6 countries, and 23 oil- and coal-processing enterprises.

The Conference included three sessions: (1) Chemical Processing of Oil and Gas, (2) Processing of Solid Fossil Fuels, and (3) Environmental Aspects of Fossil Fuel Processing. A roundtable "Training of Engineering and Scientific Specialists" was organized. The poster session included 98 presentations. Finally, abstracts of 72 correspondence participants were also published in the Proceedings.

In the opening session, Academician G.F. Tereshchenko and Professors A.S. Dudyrev and V.M. Potekhin outlined the great significance of the fuel and energy complex for the world and Russian economy and the contribution of a pleiad of researchers to organization and development of one of the oldest chairs of the St. Petersburg State Technological Institute, the chair of technology of petro- and coal-chemical industries.

Plenary lectures were delivered by such distinguished specialists in the field of processing of natural energy carriers as S.N. Khadzhiev, A.L. Lapidus, V.M. Potekhin, M.I. Levinbuk, A.S. Noskov, A.S. Dykman, V.M. Zakoshanskii, M.G. Rudin, V.M. Strakhov, and J. Soone.

The lecture presented by S.N. Khadzhiev was devoted to the use of promising nanotechnologies in oil refining, including their cost efficiency in relation to secondary processing of the oil stock.

A.L. Lapidus analyzed in his lecture the general processes for making hydrocarbon mixtures from synthesis gas by the Fischer-Tropsch method with cobalt catalysts. The process mechanism was considered as well as the relationships between the activity and selectivity of catalysts and their physicochemical characteristics. The hardware implementation was discussed. Finally, the lecturer reported methods for production of synthetic liquid fuel from alternative raw materials (shale, coal, biomass).

M.I. Levinbuk analyzed the strategy of development of the Russian oil and gas complex, including the changeover from sales of raw materials to sales of high-quality oil and gas processing products and up-to-date technologies, which is extremely topical today.

A.S. Noskov reported recent developments of the Institute of Catalysis, Siberian Division, Russian Academy of Sciences in design of catalysts and processes for deep desulfurization of crude oil, processing of oil gas into arenes, utilization of methane-containing rejects of coal mines for energy production, and catalytic combustion of low-concentrated carbon-containing wastes.

V.M. Zakoshanskii overwieved in his lecture the history and progress of the cumene process for production of phenol and acetone. New chemical and related environmental aspects of the formation and decomposition of cumyl hydroperoxide were considered. The great contribution of Soviet researchers and their priority in the development of this significant process of the basic organic synthesis were underlined.

A.S. Dykman analyzed the prospects for production of monomers for synthetic rubber, which is topi-

cal in the context of modernization of domestic synthetic rubber plants.

M.G. Rudin made an overview of the current status and prospects for oil processing in Russia. He clearly demonstrated the need to modernize domestic oil refineries and emphasized the increasing significance of such processes as catalytic cracking, hydrocracking, low-temperature isomerization, and heat-contact carbonization. The lecturer also reported the specific features of oil processing in the United States. He outlined the necessity for application of promising processes developed by US companies to modernization of domestic refineries.

J. Soone, Director, Oil Shale Research Institute, Tallinn Polytechnical Institute, reported the potentialities of his institute for training students in chemistry and technology of fuels. He demonstrated the need for close collaboration with Russian institutes in this area.

THe session "Chemical Processing of Oil and Gas" included 19 oral lectures, including those presented by professors and lecturers of the department whose anniversary was celebrated: A.A. Gaile, A.M. Syroezhko, Yu.V. Pokonova, D.A. Rozental', V.A. Proskuryakov, and V.V. Gromova.

E.A. Chernysheva (Moscow) considered the problem of exchange-resonance effect of the electromagnetic field on oil dispersions and the prospects for application of this effect to oil processing in both primary distillation and processing of black stock.

The lecture delivered by S.A. Akhmetov (Ufa, Bashkortostan) was devoted to analog simulation and search for physicochemical constants of individual hydrocarbons and oil fractions (these data are necessary for technologists and developers).

A.M. Syroezhko (St. Petersburg) considered features of processing of heavy oil residue in the presence of oil shales, to obtain top fractions and residual stock for production of modified bitumens, pitches, and water-fuel emulsions.

A.A. Gaile (St. Petersburg) devoted his presentation to development of extraction and combined processes for oil product refining.

V.V. Vasil'ev (St. Petersburg) reported the results of analysis of the commercial fraction of shale naphtha by chromatography-mass spectrometry. Out of 225 identified compounds, 69 were detected for the first time.

The problems of petrochemical industry of Algeria were overviewed by Professor Hamada Boudjema (Algeria).

The fundamental aspects of formation of carbon nanofibers and carbon black in the course of electrocracking of organic raw materials were reported by B.V. Peshnev (Moscow).

The lecture presented by D.L. Astanovskii (Moscow) was devoted to selection of the hardware implementation in processing of natural gas into petrol.

The experience gained at four refineries in use of new highly selective naphtha reforming catalysts (RB series), developed at the Olkat Research and Production Company, Limited Liability Company (St. Petersburg), was analyzed by V.B. Maryshev.

V.Z. Mordkovich (Moscow) shared his experience in use of reactors with high-performance composite membranes in production of synthetic liquid fuel.

V.Yu. Dolmatov (St. Petersburg) prospects for using nanodiamonds produced by explosion in oil and gas technology.

A many-year experience gained in utilization of oil residues was summarized by Yu.V. Pokonova (St. Petersburg).

New methods for processing of oil residues such as hydroviscosity breaking, hydrocarbonization, thermal deasphalting, tested at the State Petroleum Technical University (Ufa, Bashkortostan), were reported by A.F. Ishkal'din.

Formation of a carbon fiber by thermal treatment of petroleum pitches under an inert atmosphere in reactors made from various materials was reported by R.N. Gimaev (Ufa).

An interesting lecture delivered by T.E. Zhesko (St. Petersburg) was devoted to use of carbon oxide for carbonylation of aryl halides to obtain aromatic acids and their derivatives.

In other oral, poster, and correspondence presentations, such important problems of oil and gas processing were considered as oil preparation for processing; use of the membrane technology in oil processing; hydrofining; demetallization and dewaxing of various oil fractions; processing of oil gas; processes for petrol improvement; hydroisomerization and isomerization catalysts; dehydrogenation, hydrofining, and reforming catalysts; wax accumulation inhibitors and combined-action antioxidants; high-performance thermocatalytic processing of residual gas condensate and oil fractions; improvement of bitumens and polymer bitumastics; combined processing of peats and bitumen; production of refined petroleum coke; cutting fluids; addidives to gasoline and diesel oil; desul-

furization; oxidation and conversion of natural gas; Fischer-Tropsch production of a synthetic liquid fuel; production of hydrogen by catalytic pyrolysis of methane; improvement of the gas condensate processing technology; catalytic purification of phenol; synthesis of alkylphenols and cyclohexanones; aqueous bitumen and fuel emulsions; etc.

The session "Processing of Solid Fossil Fuels" also included 19 oral presentations. They covered such topics as the prospects for further development of coal fuel chemistry and shale chemistry [gasification in melts (V.N. Vorob'ev)], thermal solvolysis of coals (E.I. Andreikov), integrated processing of shale oils (Yu.A. Strizhakova), non-fuel use of coals (A.A. Knyazev), and transformation of coal under high-rate heating (V.D. Glyanchenko). The problems associated with the production of semicoke in Russia were discussed by V.M. Strakhov (Novokuznetsk) and S.G. Stepanov (Krasnoyarsk).

At the Institute of Fossil Fuels (Moscow), G.S. Golovin and coworkers have developed a concept of multidimensional supramolecular structure and also a model of average statistical structural unit of the organic matter of coal. Combined with quantum-chemical calculations of the electronic structure of model compounds (A.M. Gyul'maliev), this approach allows simulation of the decomposition of coal matter.

Among the Conference participants were coal fuel chemists from Ukraine: A.F. Dmitruk, V.I. Saranchuk, A.F. Popov, T.G. Shendrik, L.V. Pashchenko, I.B. Frolova, L.F. Butuzova, and I.G. Krut'ko (Donetsk). They all made interesting presentations on chemistry and technology of coal. The abstracts of these contributions have been published.

The problems of processing of mixtures of coals with oil products were considered in the presentations given by T.G. Shendrik, E.I. Andreikov, and E.A. Khukhrin. V.A. Proskuryakov with coworkers and I.L. Glezina reported on nonresiduum processing of oil shales.

The section also included 26 poster presentations. Their abstracts have been published.

The composition of alcohol-benzene extracts of coals, heated under high pressure, and transition of coals into the plastic state was considered by V.D. Glyanchenko (Yekaterinburg), with the theoretical concepts of the coal-sintering and carbonization mechanisms extended.

The rest of the oral, poster, and correspondent contributions covered such significant aspects of solid fuel processing as the prospects for development of novel technologies; low-temperature coking and high-temperature pyrolysis of coals; hydrogenation and thermal dissolution of coals and oil shales; gasification, liquation, and oxidation of coals; granulation and briquetting; carbonization of coals, wood, and oil-slime; chemical processing of coals; combined processing of coal, oil shale, and oil-slime; non-fuel coal processing; nonwaste oil shale processing; binders; pitches; carbonaceous reducing agents; sorbents and synthetic fuel from coal; wastewater treatment at by-product coke plants and utilization of wood-chemical resins and mining and coal-cleaning wastes; resource saving; exposure of coal and its processing products to microwave, cavitation-wave, and other treatments; NMR spectroscopy of coal resins; effect of sulfur on coke formation; and so on.

In particular, A.Ya. Eremin and coworkers devoted their presentation to a promising coke quenching technique. A combined process for thermal preparation of coal charges and coke cooling was reported by V.I. Sukhorukov and coworkers (Yekaterinburg).

Oxidative desulfurization of fiery coal was considered by Kh.V. Shevchuk (Lviv, Ukraine).

Microwave breakage of coal, followed by its briquetting with iron-ore concentrate, was reported by A.A. Khaidurov (Irkutsk). Thermal dissolution of younger coal of the Irkutsk coal fields was considered by G.G. Shevchenko (Irkutsk).

R.Sh. Mirzoev (Baku, Azerbaijan) and Dangaa Oyuunbold (postgraduate student from St. Petersburg) devoted their presentation to the development of fuel pressing technology. Dangaa Oyuunbold also reported specific features of fast pyrolysis of Kansk-Achinsk, Kirgiz, and Mongolian brown coals and oil shale.

The problems of coal slack and coal cleaning wastes were analyzed by V.S. Beletskii and I.A. Arovin (Donetsk, Ukraine). A.S. Torgashin (Novosibirsk) and M.I. Baikenov (Karaganda) reported features of hydrogenation of coal organic matter.

Dangaa Oyuunbold reported on a study of the structure and bioactivity of humic acids separated from Mongolian brown coals. She underlined that non-fuel aspects of brown coal processing (production of various humics) are very topical for Mongolia, where most of soils are poor in humus.

Properties of carbonaceous sorbents and reducing agents produced from coal and wood-chemical raw materials were considered by I.L. Glezin (St. Petersburg), Yu.O. Lesishina (Donetsk), and E.V. Veselovskaya (Novocherkassk).

The session "Environmental Aspects of Fossil Fuel Processing" included 14 oral presentations. They covered such problems as utilization of aerosol releases from heat-electric generating plants and mining wastes; refining of hydrocarbon raw materials to remove hydrogen sulfide, mercaptans, carbonyl sulfide, and carbon disulfide; remediation of areas contaminated with oil (L.P. Zaichenko); and monitoring of air and water in territories under the impact of oil and gas production complexes. The environmental problems of by-product coke works and ways to their solution were considered by V.I. Sukhorukov (Yekaterinburg).

The "Training of Engineering and Scientific Specialists" roundtable (chairman V.M. Potekhin) included three presentations.

The Conference's decisions were as follows:

(1) To hold the conference "Prospects for Chemical Processing of Fossil Fuels" every three years on the basis of the St. Petersburg State Technological Institute or related departments of other institutes.

(2) To promote application of nanoprocesses to oil refining and petro-, gas-, and coal- chemical syntheses.

(3) To promote more intensively utilization of alternative raw materials (coal, oil shale, natural gas, plant raw materials, biomass, and oil, gas, and oil shale processing wastes), to produce competitive and environmentally friendly high-performance petrol.

(4) To practice international specialist exchange programs, to train students and postgraduates in fossil fuel processing.

A. M. Syroezhko

ISSN 1070-4272, Russian Journal of Applied Chemistry, 2007, Vol. 80, No. 4, pp. 682–683. © Pleiades Publishing, Ltd., 2007.
Original Russian Text © A.G. Morachevskii, 2007, published in Zhurnal Prikladnoi Khimii, 2007, Vol. 80, No. 4, pp. 697–698.

BOOK REVIEWS

Sergeev, G.B., *Nanokhimiya: Uchebnoe posobie* (Nanochemistry: Textbook),

Moscow: University Book Publishing House (KDU), 2006, 336 pp.

DOI: 10.1134/S1070427207040349

In 2003, G.B. Sergeev, a professor of Lomonosov State University in Moscow and a known specialist in low-temperature chemistry, published the, in fact, first domestic monograph devoted to the new, rapidly developing area of research in modern science, nanochemistry [Sergeev, G.B., *Nanokhimiya* (Nanochemistry), Moscow: Mosk. Gos. Univ, 2003]. The textbook with the same title, brought to readers' notice, was for the most part written by the same author on the basis of this monograph, with account of very recent original studies (2003–2005) and lectures delivered by Sergeev at the chemical and materials science faculties of Moscow State University.

The book comprises a preface, eight chapters, conclusion, and extensive bibliography. The brief preface (pp. 6, 7) notes that the world's scientific community has recognized the development of nanotechnologies as the most promising area of research in science and technology of the XXI century. A new interdisciplinary area has formed: nanoscience, regarded as a body of knowledge about the fundamental properties of matter on the nanometer scale. The advances of this science are implemented in nanotechnologies by development of new materials, functional devices, and structures on the atomic, molecular, and nanometer levels. The author emphasizes that nanochemistry is now one of the leading areas of nanoscience.

The introduction (pp. 8–10) reminds that nanosize particles have started to attract researches' attention in various fields of science only in the last 15–20 years. Nevertheless, the sections "nanoparticles," "nanoclusters," and "nanocomposites" are already included to some extent in curricula, not to say about the congresses, conferences, and symposia devoted to this issue. The author convincingly substantiates the chemists' interest in nanoparticles and specially notes that particles less than one nanometer in size deserve special attention. The unusual chemical properties of particles composed of several atoms or several tens of atoms require a profound modification of the concepts previously developed for systems including thousands and millions of atoms. The textbook by Sergeev can be regarded, on the one hand, as an interestingly and lively written introduction to a novel field of chemistry, and on the other, as a thorough, and composed by a skilled author, guide to the vast material accumulated by nanochemistry by the year of 2005.

The first chapter (pp. 11–20) gives a general notion of the nanoscience developing at the intersection of physics, chemistry, and biology. The rapid advance of the nanoscience in the last decade is primarily due to the development of new methods for synthesis, study, and modification of nanoparticles and nanostructures. A considerable attention is given by the author in the first chapter to notions and terms used by the nanoscience and, in particular, by nanochemistry. A classification of nanoparticles by their size, number of atoms in a particle, and number ratio of surface to bulk atoms is given. The author believes that the key issue is to determine the influence exerted by the size of particles on their chemical activity. In conclusion of the chapter, Sergeev notes that he is convinced that the importance of nanochemistry in the development of nanotechnology will steadily increase in the nearest 5–10 years.

The second chapter (pp. 21–61) considers methods for synthesis and stabilization of nanoparticles. Most of elements of the Periodic table are metals, and, therefore, the primary attention in further presentation is given to metals. Methods for synthesis of nanoparticles are analyzed in detail and classified, and processes of their stabilization are discussed.

The third chapter (pp. 62–75) describes methods for analysis of the size and properties of nanoparticles in the gas phase, on a surface, in the bulk, or in a host. The following techniques are considered: transmission and scanning electron microscopy, probe microscopy, diffraction analysis, etc. The potentialities, advantages, and disadvantages of various methods of analysis are compared.

The fourth chapter (pp. 76–150) discusses problems of the cryochemistry of nanosize metal particles (nanocryochemistry). The author of the textbook,

Sergeev, has made a major contribution to the development of this field of nanochemistry. In most detail have been studied reactions of magnesium, silver, and rare-earth metal particles at low (77 K) and ultralow (4–7 K) temperatures. The possibility of modeling of the physicochemical properties and reactivity of metal nanoparticles is considered.

The fifth chapter of the textbook (pp. 151–215), named "chemical nanoreactors," mostly includes evidence concerning methods for stabilization of nanoparticles. The activity of metal clusters and particles is primarily due to uncompensated surface bonds. Systems of this kind can be regarded as chemical nanoreactors possessing a significant store of energy. The author considers in detail the method of matrix isolation, which enables stabilization of active particles. The sixth chapter (pp. 216–226) is devoted to the role of carbon in nanochemistry. The discovery of fullerenes and carbon nanotubes has been an important contribution to the development of the nanochemistry of nonmetals. This chapter also presents information about silicon clusters.

The seventh chapter (pp. 227–250) summarizes the evidence concerning dimension effects in nanochemistry. By the dimension effect is understood a fundamental change in the physicochemical properties and reactivity of particles of a substance, which occurs as the number of atoms or molecules in a particle decreases to less than about 100 atomic-molecular diameters. It can be regarded confirmed that the manifestation of dimension effects is one of the main distinctions of nanochemistry from chemical transformations under ordinary reaction conditions. A notion of the internal, external, and quantum dimension effects is given. It is once again emphasized in the final part of the chapter that analysis of the dimension effects and establishment of a relationship between the number of atoms involved in a reaction and the resulting fundamental changes is the primary goal of nanochemistry. The size, shape, and structure of metal particles in the nanosize range exert direct influence on the chemical activity of systems, stability and properties of the materials obtained, and opportunity of their application in nanotechnology.

The eighth chapter (pp. 251–297) discusses, on the basis of the most recent publications (2000–2005), the application of nanoparticles in various fields of science and technology: catalysis on nanoparticles, use of nanocrystalline oxides in various syntheses, nanoparticles in semiconductors and sensors, photochemistry (nanophotonics), carbon nanotubes, and nanoparticles in biology and medicine.

In the conclusion (pp. 298–306), the author formulates, based on an analysis of a vast body of diverse experimental data, promising avenues of development of fundamental and applied nanochemistry. The basic research is primarily aimed to establish relationships between the chemical and physical properties, size, and shape of nanoparticles. The goal of applied nanochemistry is to use nanoparticles to develop new materials with unique optical, electrical, magnetic, mechanical, sensor, and catalytic properties. In the context of these global tasks, the author discusses a number of special problems.

Each of the eight chapters of the textbook ends with control questions. The book is provided with a rather informative bibliographic list (pp. 307–333), composed separately for each of the chapters (a total of 335 references). The textbook by Sergeev is close in structure and contents to the already mentioned monograph by the same author. The bibliographic list in the textbook is less extensive than that in the monograph (606 references), but seems to be still exceedingly large for a textbook. A considerable part of foreign periodic publications of recent years, included in the list, are, unfortunately, nearly inaccessible to students who study outside Moscow. The textbook by Sergeev is of interest and can be recommended for students specialized in quite a number of areas, as well as for postgraduate students, research workers, and lecturers. The book luckily combines simplicity and high scientific level of presentation.

A. G. Morachevskii

ISSN 1070-4272, Russian Journal of Applied Chemistry, 2007, Vol. 80, No. 5, pp. 685–694. © Pleiades Publishing, Ltd., 2007.
Original Russian Text © G.M. Mikhailov, M.F. Lebedeva, 2007, published in Zhurnal Prikladnoi Khimii, 2007, Vol. 80, No. 5, pp. 705–715.

REVIEWS

Procedures for Preparing Chitin-Based Fibers

G. M. Mikhailov and M. F. Lebedeva

Institute of Macromolecular Compounds, Russian Academy of Sciences, St. Petersburg, Russia

Received October 4, 2006; in final form, March 2007

Abstract—Data on preparation of chitin threads for the fabrication of absorbable suture materials, dressings, and biodegradable substrates for the growth of human skin cells (keratinocytes and fibroblasts) are analyzed.

DOI: 10.1134/S1070427207050011

Chitin, poly-(1-4)-2-acetamido-2-deoxy-β-*D*-glucopyranose, is contained in shells and exoskeletons of Crustacea and insects. This natural renewable polysaccharide exhibits a set of unique biological properties: it is enzymatically cleaved with lysozyme to form *N*-acetylglucosamine and glucosamine; it shows antimicrobial activity; it is a hemostatic, an immunomodulator, etc. [1–4]. Like cellulose, which is the most widely used polysaccharide, chitin is a fiber-forming polymer.

The use of chitin as suture material was suggested by L.L. Balassa [5]. He noted the capability of chitin to promote wound healing. Studies of chitin-based sutures confirmed that they fix tissues until the wound is completely healed, after which they fully resolve without leaving a trace. The resulting stitches become cosmetic, without cicatrization of tissues [3, 4]. Chitin is resistant to hydrolysis and is therefore stable in prolonged storage. The sutures resolve in a patient's body in a time ensuring complete healing of a wound.

Despite apparent advantages of this polysaccharide, there is still no commercial production of chitin-based absorbable suture materials in the world because of insufficient elasticity of chitin threads and certain problems in the production process.

The information considered in this review concerns preparation of chitin threads for the fabrication of absorbable suture materials, wound textiles, and biodegradable substrates for the growth of human skin cells (keratinocytes and fibroblasts).

The first attempts to prepare chitin solutions to make fibers from them were made in the beginning of the XX century. In 1926, Kunike [6] reported on the first studies of chitin fibers. He dissolved chitin in cold concentrated sulfuric acid and obtained 6–10% solutions. He used a wet procedure for thread forming, with water, alcohols, or alkali as coagulants. After drying the filament,[1] he obtained chitin fibers with a density of 1.4 g cm^{-3} and a tensile strength of about 35 kg mm^{-2}.

Knecht and Hibbert [7] prepared films from a solution of chitin in concentrated HCl.

It is known that concentrated acids slowly dissolve chitin with the simultaneous hydrolysis of the polysaccharide to oligomers and monomers. Orthophosphoric acid containing 15% water dissolves chitin mildly, and in some cases brittle films can be prepared from the solution [8].

Saturated solutions of salts capable of intense hydration ($LiCNS > Ca(CNS)_2 > CaI_2 > CaBr_2 > CaCl_2$) were tested as chitin solvents. With these solvents, chitin was converted to a strongly swollen plastic paste from which a fiber-like material was prepared [9].

In 1936, Clark and Smith [10], using LiCNS as chitin solvent and aqueous acetone as coagulant, prepared a fiber; its characteristics, however, were not reported. Further search for a chitin solvent led to systems containing acids and organic solvents. Solutions of chitin in a mixture of chloroethanol and H_2SO_4 were used for forming fibers, with the precipitation into water, methanol, or aqueous ammonia [11].

Attempts were made to dissolve chitin in solutions of mono- and dichloroacetic acids; however, the resulting threads showed poor strain and strength characteristics because of strong hydrolyzing power of these acids.

In 1975, Brine and Austin suggested trichloroacetic

[1] Filament is the amount of fibers corresponding to the number of holes in a spinneret used for fiber forming; monofilament is a fiber prepared using a single-hole spinneret, and polyfilament, a thread prepared by twisting several filaments together.

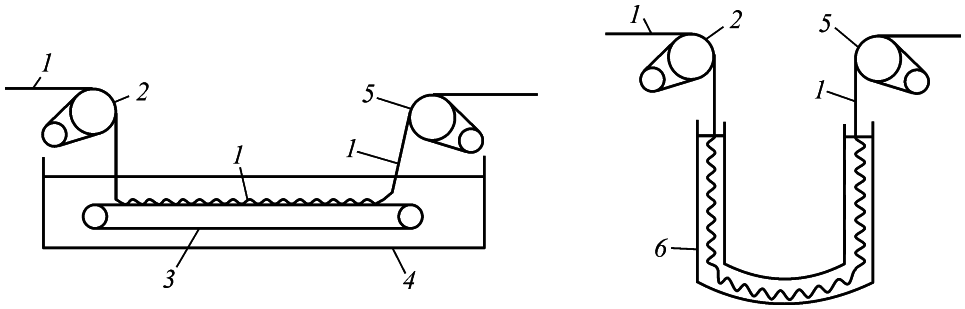

Fig. 1. Scheme of a unit for preparing chitin fibers: (*1*) chitin fiber, (*2*) feed roller, (*3*) belt conveyor, (*4*) second spinning bath, (*5*) transfer roller, and (*6*) U-shaped tube.

acid (TCA) for chitin dissolution. Because TCA is a very strong acid promoting hydrolysis of polysaccharides and has a high melting point (57°C), it becomes necessary to use it as solution and to dissolve chitin at low temperatures at which the hydrolysis is slow. A 2% chitin solution was prepared on adding to TCA 40% chloral hydrate and 20% methylene chloride. Acetone was used as coagulant. The precipitated fiber was neutralized with a solution of KOH in isopropanol and was washed with water. The fiber strength σ was 63 kg mm^{-2} (618 MPa), and elongation ε, 13%. It was claimed that the mechanical characteristics of threads could be substantially improved by controlling the extrusion rate and choosing appropriate coagulant [13].

In 1977, Austin and Brine [14] patented chitin films and fibers suggested for use for foodstuff protection and suture fabrication. In this case, they used for dissolving chitin TCA and chlorinated solvents like chloral or chloral hydrate. The spinning solutions obtained were used in chitin reclaiming for forming fibers and films. The strength of the fibers they obtained was 63 kg mm^{-2}, and breaking elongation, 13%; however, the filament contained 5.03% N and 9.455% Cl.

Preparation of high-strength chitin fibers for absorbable sutures was described by Inoue et al. [15]. To dissolve chitin, they used a 25 : 75 to 75 : 25 mixture of TCA with methylene chloride. The claimed chitin concentration in the spinning solution was from 1 to 10%; the setting bath was filled with acetone. The fiber draw ratio was from 0.4 to 1.4 (preferably from 0.6 to 1.1). Under these forming conditions, the strength of the dry fiber was 255 MPa and over. Kifune et al. [16] suggested a procedure for preparing chitin fiber intended for use as suture. To prepare chitin solutions, they used TCA in a mixture with chlorinated hydrocarbons (chloromethane, dichloromethane, chloroform, etc.). The fiber was characterized by a linear density of the filament of 0.5–20 denier[2] and a dry strength exceeding 384 MPa.

To prepare a spinning solution of chitin, Kifune et al. [17] used TCA solutions, with anhydrous acetone or anhydrous methanol as coagulant; the fibers were formed by adding the chitin solution to a setting bath with a coagulant temperature of 10–25°C and keeping in the bath for approximately 1 min. Since the fiber contained the solvent, it was fed with a belt conveyor to a second spinning bath where the solvent was removed. The residence time of the fiber in the second bath was ≥10 min. Then the fiber was fed to a U-shaped tube for more complete neutralization of the acid that had been the chitin solvent. The fiber was washed with distilled water and dried. The scheme of the equipment used is shown in Fig. 1.

Filament *1*, which was extruded to the first spinning bath from a spinneret with 40 holes 0.04–0.06 mm in diameter, from feed roller *2* was fed to conveyor *3* of the second spinning bath *4*, from which it was loaded through transfer roller *5* into U-shaped tube *6* containing a coagulant with an alkali. From this tube, the filament was withdrawn with a transfer roller and taken up by a reel at a tension of 64 or 38 MPa, or at a lower tension. The resulting fiber had a linear density of 0.5 to 20 denier. The fiber could be extended by 20–80%. The tensile strength of the fiber exceed 255 MPa.

Later a process for producing chitin fibers for suture materials was patented. The chitin fibers were plaited; the plait size met the US Pharmacopoeia standard for catgut sutures. A solution of TCA in chlorinated hydrocarbons (chloromethane, dichloromethane, 1,2-dichloroethane, 1,1,1-trichloroethane, 1,1,2-trichloroethane) was used as chitin solvent; the TCA concentration in solutions was 25–75 wt %. The dissolution of chitin was performed at a low tempera-

[2] 1 denier = 1 g/9000 m of fiber.

ture (5°C); the solution was filtered through a steel gauze (1480 mesh) under a pressure of 4 kg mm^{-2} and degassed in a vacuum to obtain 1–10% spinning solutions of chitin.

The equipment used for forming fibers is shown in Fig. 1. A spinneret with 40 holes 0.04–0.08 mm in diameter was used; the coagulant was acetone at 14°C (first setting bath). The temperature of the spinning solution before feeding to the spinneret was raised to 20°C. The spinning solution was fed at a rate of 2.3 ml min^{-1}. Then the filament was fed to a conveyor and washed in the second bath with methanol containing 0.3 g l^{-1} KOH, after which it was kept in a U-shaped tube filled with the same methanolic solution of KOH. Then the fiber was washed with distilled water and dried. The strength of the dried fiber was 215–400 MPa, and the breaking elongation, 8.7–20.0%. After keeping the fiber in 0.5% KOH solution, the fiber strength increased to 290–412 MPa, and the breaking elongation, to 19.2–27.3%. From the filaments thus prepared, plaited sutures were fabricated, and their knot strength and variation of the tensile strength in vivo were evaluated.

The characteristics of chitin fibers (polyfilament and monofilament) prepared under various conditions are listed in Table 1. It is seen that all the samples have good mechanical properties. The best of them is sample A exhibiting the highest values of the tensile strength (396 MPa) and breaking elongation (20.0%).

Twelve polyfilaments of each of these four samples were plaited to obtain sutures no. 3-0 (0.31 mm in diameter) in accordance with the US Pharmacopoeia standard (20th edition). The knot strengths of these materials are given in Table 2.

All the four samples were tested as sutures. Sample A showed good absorption properties in vivo.

A filament prepared similarly to sample A (Table 1) was subjected to an additional 1.4-fold extension (Table 3, sample 1). Its tensile strength was 523 MPa. The fibers were plaited to obtain suture material no. 4-0. Experiments with suture materials made of polyglycolic acid (sample 2) and chromic catgut (sample 3) were made for comparison. The results of a comparative study of the absorption properties of these materials in vivo are given in Table 3.

Table 3 shows that, with polyglycolic (sample 2) and catgut (sample 3) suture materials, the absorption is too fast. The chitin material (sample 1) resolves slowly in the first 10 days, after which the process accelerates; just such a behavior is required of an absorbable suture material.

Table 1. Characteristics of chitin fibers

Sample	Linear density, denier		Dry strength, MPa	Elongation, %
	polyfilament	monofilament		
A	72	1.80	396	20.0
B	68	1.70	211	8.7
C	66	1.65	213	8.8
D	71	35.5	370	18.0

Table 2. Strength characteristics of suture materials

Sample	Breaking load in knot,* kg	Knot tensile strength, MPa
A	1.87	235
B	0.80	106
C	0.79	107
D	1.97	222

* According to the Japanese Pharmacopoeia standard, the breaking load in knot should exceed 1.25 kg.

In 1990, Kifune et al. [19] took out a patent for chitin fibers and their fabrication procedure. They claimed that chitin fibers are intended for the production of chitin suture materials exhibiting high strength, elasticity, and good absorption properties.

With a reference to the previous patent [18], Kifune et al. reported that fabrication of sutures by the previously suggested procedures was complicated by large thickness of filaments. Patent [19] concerns production of threads with a dry filament strength exceeding 255 MPa at a linear density from 0.5 to 20 denier. The authors claimed that chitin fibers with such characteristics can be prepared by an additional treatment of filaments with a coagulant solution in a unit (Fig. 1) described as a second spinning bath with a belt conveyor, in which the fiber is in the free state.

In [19], Kifune et al. specified the parameters for preparing chitin fibers, in particular, for the fabrication of sutures of all sizes, from no. 1 to no. 9-0 in accordance with the US Pharmacopoeia standard for catgut; the characteristics of these threads in a knot were given. As chitin solvent Kifune et al. used TCA solutions. To minimize hydrolysis of chitin macromolecules, the spinning solution of chitin was prepared and used immediately before forming the fiber.

The above procedures for preparing spinning solutions of chitin involve the use of TCA with its solvents. This is a very aggressive medium causing not only corrosion of the equipment, but also, what is

Table 3. Strength of suture materials

Sample no.	Knot strength, kg	Residual knot strength, %				Tissue reaction (in 30 days)
		5 days	10 days	20 days	30 days	
1	1.31	76	52	13	0	Complete recovery
2	0.97	54	32	4	0	Complete recovery
3	0.79	25	12	0	0	Damage of capillaries in the area of suture resorption

more important, depolymerization of chitin in spinning solutions both during their preparation and in the course of storage and processing of a chitin solution into a thread. Furthermore, the fiber contains a large amount of chlorine, up to 9.455 wt %, which cannot be removed by washing the freshly formed fiber [14]. The chlorine content of threads can be reduced to 1% only by prolonged refluxing in *n*-propanol containing 1% NaOH.

The results of the above-mentioned studies suggest that the supramolecular organization and morphology of the fibers became nonuniform, as indicated by the large breaking elongation of the fiber (up to 20%). Presumably, TCA reacts directly with chitin, because washing with various solvents and even refluxing with an alkali do not ensure complete removal of chlorine from the target product.

To recover chitin from shells, the shells are heated with aqueous solutions of alkalis to remove protein. In so doing, chitin undergoes partial deacetylation with the formation of amino groups, which can react with TCA to form both salts and chlorinated amide groups. The latter groups can also be formed by displacement of the weaker acetic acid from acetamide groups with the stronger trichloroacetic acid. In contrast to Austin and Brine [14], Kifune did not determine the chlorine content of the fiber. These procedures have not yet found industrial application.

Thor and Henderson [20, 21] prepared chitin xanthates. The following protocol is given as example: 150 g of purified chitin was mixed at room temperature with a 31–40% NaOH solution. The mixture was allowed to stand for 2 h. After squeezing, approximately 450 g of alkali chitin was obtained; it was mixed in a sealed vessel with 60 ml of CS_2. The mixture was stirred at 25°C for 4 h and transferred into a vacuum flask. Crushed ice (1.6 kg) was added; the mixture was stirred for 1 h and allowed to stand for 12–16 h. Then it was filtered and degassed, and a spinning solution subsequently used for forming fibers was obtained.

The same method for preparing fibers was used by Balassa and Prudden [22]. A solution of chitin xanthate was fed to a precipitation bath containing 8% sulfuric acid, 25% sodium sulfate, 3% zinc sulfate, and water at 40°C. The filament was collected in skeins; its strength ranged from 77 to 128 MPa.

The fibers obtained were tested as dressings in studies of wound healing, performed on animals and humans. The authors claimed that the matherials efficiently promote wound healing.

The strength properties of chitin fibers were somewhat improved by Noguchi et al. [23]. The viscosity of a chitin xanthate solution aged for 14–18 h was 130 P. Addition of an equimolar amount of urea with respect to the *N*-acetylglucosamine group decreased the solution viscosity to 100 P. After filtration and degassing, a spinning solution was obtained. Forming was performed at room temperature into a spinning bath containing 10% sulfuric acid, 25% sodium sulfate, and 1% zinc sulfate. Ethanol was used in a stretch bath; after that, the fibers were washed with water and then, before drying, with ethanol and were dried on a roller at 110°C.

In patent [24], Yoshikawa et al. claimed preparation of chitin fibers and films to be used for fabrication of clothes, hygienic materials, fibers with antimicrobial activity, and items for everyday life. The authors treated chitin with a NaOH solution and obtained chitin containing 10–48% NaOH; after removing excess alkali by squeezing, this material was treated with a CS_2 solution to obtain a solution of chitin xanthate, similar to solutions of cellulose xanthate. From this solution, Yoshikawa et al. prepared by wet forming, as it is commonly done in production of viscose silk, "chitin" fibers with excellent antimicrobial characteristics. By mixing a solution with chitin xanthate with a solution of cellulose xanthate in various ratios, Yoshikawa et al. prepared composite fibers consisting of "chitin" and cellulose. These fibers exhibited a tensile strength of 240–304 MPa at

a breaking elongation of 24.3–16.7%. The chitin-to-cellulose ratio was varied from 5 : 95 to 95 : 5.

One of key factors governing the properties of chitin and its derivative chitosan (solubility, biological activity, etc.) is the degree of acetylation (DA). Treatment of chitin with a concentrated NaOH solution results not only in formation of alkali chitin, but also in elimination of acetate froups from acetamide fragments of glucopyranose units of the polysaccharide macromolecules, i.e., the degree of acetylation of chitin decreases. At 50% decrease in DA, the properties change so drastically that the product is no longer termed chitin and is termed chitosan. The chitin fibers prepared in [24] were not characterized by the degree of acetylation. Chitosan exhibits higher antimicrobial activity than chitin. Since the degree of acetylation is not indicated in these patents, it can be concluded that actually the fibers obtained in these studies were formed by chitosan (copolymer of glucosamine with *N*-acetylglucosamine) rather than chitin.

Since chitosan is cleaved by lysozyme more difficultly, and at high degrees of deacetylation is not cleaved by lysozyme at all, it is impossible to prepare absorbable suture materials from these fibers. The fibers should be tested for the cleavage with lysozyme.

It was discovered later that chitin forms stable solutions in *N*,*N*-dimethylacetamide (DMAA) and *N*-methylpyrrolidone (MP).

In 1977, Austin patented new chitin solvents [25] and their use for purification and reclaiming of chitin in the form of fibers or films [26]. The solvent was a solution of 2–5% LiCl in DMAA, MP, or their mixture. The dissolution of chitin was peformed at room temperature or at moderate heating (50°C). It was noted that the amount of the dissolved chitin depended on its molecular weight. Concentrations as high as 15% can be attained, but in this case the solution becomes so viscous that forming of fibers and films becomes impossible. Therefore, it is advisable to use 2–5% chitin solutions. Acetone was used as coagulant. However, in studies concerning chitin reclaiming, only films were prepared and characterized.

Rutherford and Austin [27] reported on forming of chitin fibers from solutions of chitin in aprotic solvents. The fiber forming procedure was not described; only the film preparation was reported in detail. The films were cut into strips which could be subjected to 75% extension.

Kibune et al. [28], with a reference to [25], reported on the preparation of fibers and films from solutions of chitin in dimethylacetamide or *N*-methylpyrrolidone containing LiCl; the chitin concentration in the spinning solution was 2–10 wt %.

Crab shells thoroughly washed and dried at 40°C were ground and sieved through a 180-mesh sieve. One portion (220 g of chitin powder) was treated with 2 l of 2 N HCl at room temperature for 5 h, and another portion (91 g), with 500 ml of 2 N HCl for 2 days. Both portions were subsequently washed with water and treated with 500 ml of 1 N NaOH at 100°C for 12 h, washed again with water, and dried. The resulting chitin was dissolved in a mixture of 92% DMAA (23 g) and 8% LiCl (2 g). The solution containing 0.2 g of chitin per 100 g of DMAA had a viscosity of 985 cP at 30°C. After additional treatment of chitin at 40°C with 1 N HCl for 1 h, the solution viscosity decreased to 305 cP. This chitin was dissolved at room temperature in a 20 : 1 mixture of DMAA with LiCl, taken in an amount required to obtain a 3 wt % chitin solution. The mixture was degassed, and the solution was used for spinning. The fibers were obtained using a 50/0.08 spinneret (50 holes 0.08 mm in diameter). The spinning bath contained isobutanol; the wind-up speed was 10 m min^{-1}. The fiber obtained had a linear density of 61 denier; the dry strength was 483 MPa. From a chitin sample whose solution had a viscosity of 985 cP, at a wind-up speed of 3 m min^{-1}, the fiber with a strength of 408 MPa was obtained. After an additional treatment of chitin with 1 N HCl for 1 h, the viscosity of the spinning solution was 24 cP, and the fiber prepared had a linear density of 63 denier and a strength of 331 MPa. LiCl was not removed from the fibers. Medical applications of the fibers were not considered.

Kibune et al. [29] used for dissolving chitin both DMAA and MP, both containing more than 5.5% LiCl. The reported chitin concentration in the spinning solution ranges from 0.5 to 10 wt % relative to DMAA or MP. The fiber forming procedure is similar to that given in [28]. The fibers have a linear density of 58 denier and a strength of 542 MPa.

As in the previously discussed patent, crab shells were washed with water, dried, and ground. The sieved chitin was treated with 1 N HCl at 40°C to control the molecular weight. The control system, a solution of 2 g of LiCl and 0.2 g of chitin in 25 g of DMAA, had a viscosity of 350 cP at 30°C. A 50/0.08 spinneret was used. The solution was fed at a pressure of 2 kg cm^{-2}. The spinning bath contained isobutanol at 25°C. The fiber wind-up speed was 10 m min^{-1}. The fiber had a linear density of 65 denier and a strength of 529.8 MPa. With MP + 5% LiCl used as chitin solvent, the dissolution was performed at 25°C.

The solution was filtered through a stainless steel gauze (1480 mesh), degassed, and formed as described above. The linear density of the fiber obtained was 62 denier, and the strength, 390 MPa. The drying conditions were not reported. Lithium chloride was not removed.

Kibune [30] patented a chitin spinning solution containing chitin, LiCl, and MP or DMAA; the LiCl weight exceeded that of chitin. The chitin amount relative to MP or DMAA containing LiCl was 0.5–10 wt %. Chitin was dissolved at 25°C in LiCl-saturated MP or DMAA. The fiber was formed using a 50/0.08 spinneret. The solution at 25°C was fed with a pump to a spinning bath (isobutanol, 70°C, contact time 2 min, wind-up speed 10 m min^{-1}). The fiber obtained had a linear density of 65 denier and a strength of 530 MPa. With DMAA replaced with MP, other conditions being the same, the linear density of the fiber was 65 denier, and the dry strength, 456 MPa. LiCl was not removed from the fibers. The breaking elongation and the degree of acetylation of the reclaimed chitin were not reported.

According to [31], crab shells were treated for 3 h with 5% aqueous NaOH at 80°C and for 3 h with 6% HCl at 60°C, after which they were washed with water and dried. Chitin flakes were ground and sieved through a 30-mesh sieve. The chitin powder was dissolved in DMAA + 8% LiCl; the viscosity of the 0.2% chitin solution was 31 cP at 30°C. From this chitin powder, 7% chitin solutions in DMAA + 8% LiCl were prepared. After degassing, the highly viscous spinning solution was extruded at 70°C through a spinneret with 6000 holes 0.1 mm in diameter into a spinning bath with a coagulant temperature of 70°C. The fiber was spooled at a speed of 5 m min^{-1} and then was treated for 8 h with hot (90°C) water, apparently, to remove LiCl. After drying, the linear density of the single fiber obtained was 2.0 denier. Fibers were cut into 5-mm pieces which were blended with a cut fibrous binder. The blend was dispersed in water, and sheets were formed as in paper production. The samples were calendered, and a 0.08-mm-thick nonwoven material was obtained. After sterilization with gaseous ethylene oxide, the nonwoven material was used for treatment of skin wounds after heavy thermal burns. Within 15 days, the damaged area of the skin was recovered and had an even surface.

In another procedure, a fiber was prepared by extrusion of a spinning chitin solution through a spinneret with 6000 holes 0.07 mm in diameter into water at 80°C. The fiber wind-up speed was 8 m min^{-1}. The fiber was washed with water at 90°C for 6 h to remove LiCl. The filament had a lustrous surface; the linear density was 1.8 denier. The fiber was cut into pieces 6 cm long, which were processed into a 5-mm-thick nonwoven material using a carding machine and a needle stem. The material was cut into 10 × 10-cm pieces which, after bactericidal treatment, were used for treating bedsores (removing the fluid, draining the wound).

However, the strain and strength characteristics of fibers were not reported in the patents. Probably, the fibers were too brittle to be used for preparing sutures.

Virtually 1 month after taking out patent [18], Kifune et al. patented a nonwoven dressing material [32] formed by chitin fibers with a linear density less than 1 denier and a strength of no less than 255 MPa, with a fibrous binder. As chitin solvents, along with TCA solutions, Kifune et al. claimed solutions of LiCl in DMAA and MP.

A chitin powder (100 mesh) was treated to remove calcium and protein with 1 N HCl for 1 h at 4°C and with 3% NaOH for 3 h at 90°C, after which it was washed and dried. A 0.2% solution of purified chitin in DMAA + 8% LiCl had a viscosity of 256 cP at 30°C.

Chitin was dissolved in DMAA containing 7% LiCl. The spinning solution contained 7% chitin. The solution was fed at a rate of 2.2 ml min^{-1} through a spinneret (200 holes 0.06 mm in diameter) to a spinning bath (butanol, 60°C). The precipitated chitin was wound up at a speed of 10 m min^{-1}. The filament was washed with water and dried. It had a linear density of 0.68 denier and a strength of 393 MPa; it was used for preparing nonwoven materials.

Agboh and Qin [33] prepared chitin solutions using DMAA + 7% LiCl. Prior to dissolution, chitin was treated with *p*-toluenesulfonic acid in isopropanol. As noted in [33], this pretreatment substantially facilitates the subsequent dissolution of chitin and preparation of a spinning solution. It leads to a decrease in the molecular weight of chitin from 2×10^6 to 1.5×10^5 Da. They found that the best composition of the spinning bath is H_2O + DMAA in 75 : 25 ratio, at a bath temperature of 40–75°C. The fibers had the following characteristics: diameter 8–20 μm, strength 97–306 MPa, and elongation 7–7.5%.

Examination of the forming conditions showed that the formability was improved with increasing temperature of the spinning bath and on adding a properly chosen plasticizer to the spinning solution. However, the content of chitin derivatives and toluenesulfonic acid in the spinning solution and ready fiber was not

Table 4. Strain and strength characteristics of chitin fibers

References	Publication year	Solvent	Fiber strength, MPa	Breaking elongation, %
[6]	1926	H_2SO_4	340	
[12]	1975	40% Cl_3CCOOH; 40% CCl_3CHO; 20 CH_2Cl_2	618	13
[14]	1977	40% Cl_3CCOOH...	618	13
[15]	1982	40% Cl_3CCOOH	≥255	
[16]	1987	40% Cl_3CCOOH	384	
[17]	1982	40% Cl_3CCOOH	≥255	
[18]	1984	40% Cl_3CCOOH	274–511	8.7–20.0
[19]	1990	40% Cl_3CCOOH	≥511	
[28]	1983	DMAA and LiCl	331	
[34]	1984	DMAA and LiCl	496	
[35]	1989	DMAA/MP + LiCl	390–540	3.0
[29]	1990	DMAA/MP + LiCl	542	
[30]	1990	DMAA/MP + LiCl	538.6–456	
[37]	1991	DMAA and LiCl	436	2.9
[33]	1996	DMAA and LiCl	97–306	7–7.5
		Fibers prepared via chitin derivatives		
[21]	1940	Chitin xanthate	77; 128	
[24]	1996	Xanthate (chitin + cellulose)	240–304	24.3–16.7
[38]	2003	Dibutyrylchitin fiber	226.68	5.9
		Reclaimed chitin fiber	370	9.8

reported. Treatment of chitin-containing raw materials to remove proteins results in formation of a certain amount of amino groups which, when reacting with toluenesulfonic acid, can form not only salts but also amides. These structures are inadmissible if the material is intended for use in surgery as suture material, because the release of free toluenesulfonic acid in patient's body can cause a pain shock.

Using DMAA + LiCl as solvent, Nakajima [34] prepared chitin fiber with a tensile strength of 496 MPa. Thin filaments ~5 μm in diameter were formed using a spinneret with a hole diameter of 0.05 mm. Butanol was used as coagulant.

The strain and strength characteristics of chitin fibers prepared in various periods using vaious solvents are listed in Table 4. In cases when the breaking elongation was not reported, the fibers, apparently, exhibited high crystallinity and were very brittle [29]. The high brittleness is commonly observed at high orientation stretching under the conditions when the chitin fiber acquired a highly crystalline structure [35].

Using DMAA and MP aprotic solvents with dissolved LiCl (up to 9%), we prepared stable chitin solutions. In these systems, chitin hydrolysis does not occur. We found that the chitin solution, if protected from the contact with atmospheric moisture, preserved its properties for more than 5 years, and the strain and strength properties of fibers prepared during this period were reproducible. In contrast to the previously used chitin solvent systems containing acids and causing hydrolysis of the polysaccharide, solutions in DMAA or MP containing LiCl are stable.

When studying the fiber-forming ability of chitin, we found that the high brittleness of chitin fibers is caused by its strong tendency to crystallize [35]. An increase in the structural heterogeneity of the system upon partialy heterogeneous deacetylation of chitin hinders crystallization of the polymer in the course of fiber preparation and allows the fiber elasticity to be enhanced. At a degree of chitin deacetylation of 0.30 and less, the fiber can be tied in a knot and preserves 40% of the initial elasticity [36]. Heterogeneous deacetylation involves severe treatment with a concentrated alkali (30–50%) at a high temperature and often yields products with poorly reproducible characteristics. Therefore, inclusion of this step in the production process is undesirable because of unstable characteristics of the resulting copolymer (solubility, gelation), complicating or even making impossible preparation of spinning solutions and fiber forming.

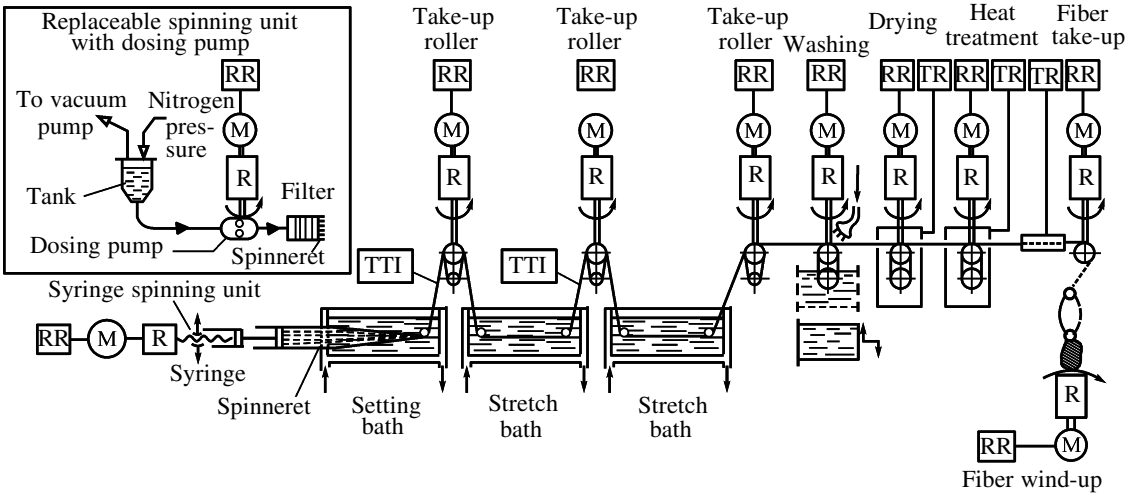

Fig. 2. Functional scheme of an installation for studying orientation forming of fibers from polymer solutions (PIFV-01): (RR) rotation speed regulator, (M) motor, (R) rotor, (TR) temperature regulator, and (TTI) thread tension indicator.

The forming of chitin fibers starts with the chitin recovery from shells of crabs, shrimps, and krill. To obtain strong fibers, it is necessary to use the high-molecular-weight polysaccharide from crab shells.

The chitin purification process should not significantly alter the molecular weight of the polymer. Therefore, removal of calcium and other ash components should be performed at low temperatures, preferably at 4–5°C. Shells of Far-Eastern crabs, thoroughly washed and dried at 60°C in a vacuum oven, were ground and sieved through a 180-mesh sieve. Then the powder was treated with 1 N HCl for 0.5 h at 4–10°C and solid-to-liquid ratio of 1 : 10 to remove ash elements. The liquid was removed by vacuum filtration, and the treatment was repeated under the same conditions. Then the chitin was washed with distilled water until the absence of Cl^- ions in the wash water.

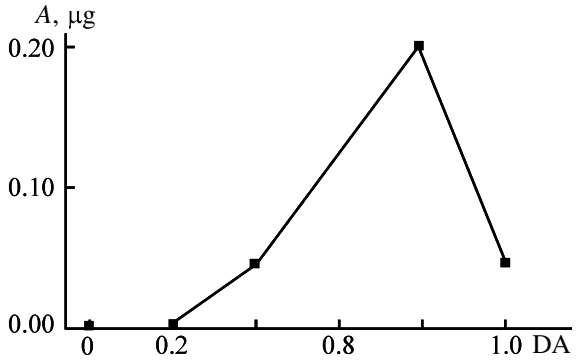

Fig. 3. Rate of enzymatic cleavage of chitosan with hen egg lysozyme as a function of the degree of *N*-acetylation of chitosan: (*A*) amount of reducing sugars (*N*-acetyl-*D*-glucosamine) and (DA) degree of chitosan *N*-acetylation.

To remove protein, chitin was subsequently treated with 1 N NaOH for 1 h at 40°C and solid-to-liquid ratio of 1 : 5, washed with distilled water, and again treated with 0.5% HCl for 30 min at 4–10°C and solid-to-liquid ratio of 1 : 5. After removing the liquid phase, the chitin was again washed with distilled water until the absence of Cl^- ions in the wash water and treated with a detergent solution (pH 11) with continuous stirring for 1 h at 40°C and solid-to-liquid ratio of 1 : 5. The solution was removed by vacuum filtration, and the chitin was washed with distilled water until pH of the wash water became neutral. After dehydration to the maximal extent, the chitin was washed two times with anhydrous acetone, with 10-min standing, and then was vacuum-dried at 60°C to constant weight.

After such treatment, chitin contained no protein and ash; its molecular weight was 170 kDa, and the degree of deacetylation, 5%.

LiCl was dissolved in DMAA on heating to 80°C with continuous stirring. A chitin sample was poured over with a solution of LiCl in DMAA. The mixture was stirred for 5 h with natural cooling to room temperature. After standing for 10–12 h, the solution was filtered under pressure through a filter made of a nonwoven material. The filtration was easy, and a colorless transparent solution was obtained. The solution was degassed in a vacuum, and the fiber was formed on the PIFV-01 installation (Fig. 2).

Dosing, take-up, and winding units were equipped with stroboscopic sensors interfaced with control units and a digital recorder.

Table 5. Radiation sterilization of chitin thread* (46.9 tex)

Sample no.	Dose, kGy	f_b, g	T, cN tex^{-1}	f_k, g	T_k, cN tex^{-1}	f_k/f_b, %	ε_b, %
Initial	0	736	15.38	340	7.11	46.2	7.8
2**	25	737	15.40	326	6.81	44.2	11.0
3***	44	702	14.67	299	6.25	42.6	7.9

* (f_b) Breaking load, (f_k) breaking load in knot, (T) thread strength, (T_k) thread strength in knot, and (ε_b) breaking elongation.
** Irradiation dose in kGy accepted for sterilization of polypropylene.
*** Irradiation dose in kGy accepted for sterilization of catgut.

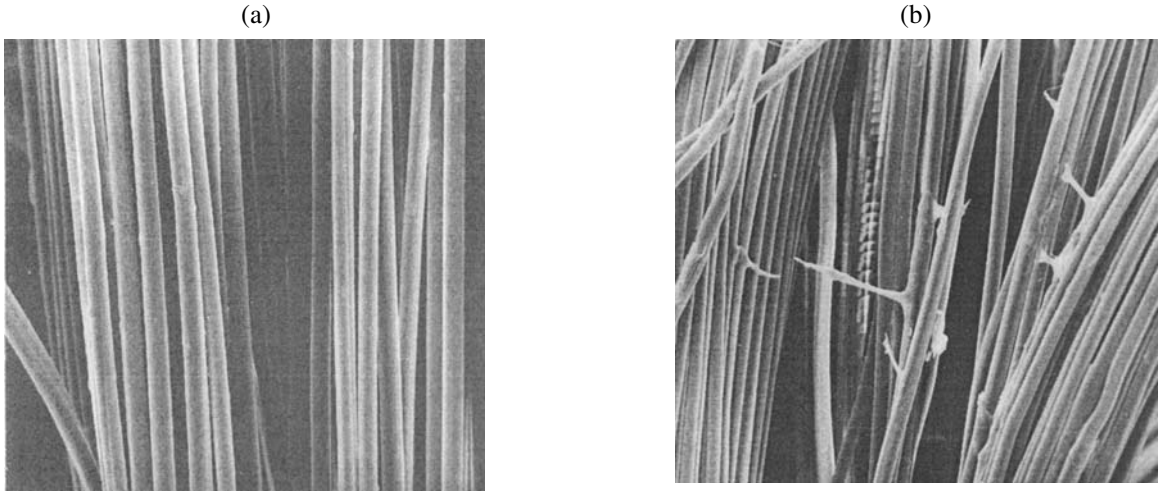

Fig. 4. (a) Initial chitin fibers without cells and (b) cultivation of fibroblasts for 5 days.

A spinning solution containing 3.2% chitin and 6.5% LiCl was extruded into an isopropanol bath through a 300/0.08 spinneret. The coagulant temperature was 18°C, and the temperature of the stretch and washing baths, 50°C. The fiber wind-up speed was 3 m min^{-1}. The filament was washed with hot (80–90°C) water, treated with acetone, and dried at room temperature.

The filament has the following characteristics: linear density 17.9 tex, strength 237 MPa, relative knot strength 70%, and breaking elongation 7.5%.

After keeping for 24 h in a desiccator over a concentrated solution of sodium acetate (relative humidity 65%), the fibers were tested with an Instron-110 device. The extension diagrams were obtained with a 50-mm specimen at a loading rate of 5 mm min^{-1}.

The material proved to be resistant to radiation sterilization at doses accepted for polypropylene and catgut (Table 5).

Figure 3 characterizes the enzymatic cleavage of chitin to the monomers with lysozyme isolated from egg white [39]. These results show that, by varying the degree of deacetylation of chitin from which the fiber was prepared, it is possible to control the rate of enzymatic cleavage of sutures and thus the time of their absorption. To this end, it is necessary to develop a procedure for homogeneous deacetylation of chitin and to determine the conditions of thread forming.

Another socially significant application field of chitin threads is production of woven fabrics (Fig. 4) on which human skin cells can be grown. These fabrics can be used for treating extensive burns and other skin damages that previously led to lethal outcome.

The above features make chitin thread very promising for production of absorbable materials for medicine.

ACKNOWLEDGMENTS

The authors are grateful to E.F. Panarin for the discussion of the paper.

REFERENCES

1. Zhogolev, K.D., Nikitin, V.Yu., and Bulan'kov, Yu.I., in *Aktual'nye problemy gnoino-septicheskikh infektsii* (Topical Problems of Purulent Septic Infections), St. Petersburg, 1996, pp. 36–37.

2. Zhogolev, K.D., Nikitin, V.Yu., and Tsygan, V.N., *Med. Immunol.*, 2001, vol. 3, no. 2, pp. 316–317.
3. Shigemasa, A. and Minami, S., *Kobunshi Kako*, 1997, vol. 46, no. 2, pp. 27–33.
4. Singh D.K. and Ray A.R., *J. Macromol. Sci. Rev. Chem. Phys.*, 2000, vol. C40, no. 1, pp. 60–83.
5. US Patent 3632754.
6. Kunike, G., *J. Soc. Dyers Colour.*, 1926, vol. 42, pp. 318–342.
7. Knecht, E. and Hibbert, E., *J. Soc. Dyers Colour.*, 1926, vol. 42, pp. 343–359.
8. Danilov, C.N. and Plisko, E.A., *Zh. Obshch. Khim.*, 1954, vol. 24, no. 10, pp. 1761–1769.
9. Von Veimarn, R.R., *Kolloid Z.*, 1926, vol. 40, no. 2, pp. 120–135.
10. Clark, G.L. and Smith, A.F., *J. Phys. Chem.*, 1936, vol. 40, pp. 863–872.
11. US Patent 3879377.
12. Brine, C.J. and Austin, P.R., *Am. Chem. Soc. Symp. Ser.*, vol. 18: *Marine Chemistry in the Coastal Environment*, Church, V.D., Ed., Washington: Am. Chem. Soc., 1975, pp. 505–508.
13. Austin, P.R. and Brine, C.J., FRG Patent 2615952, 1975, *Chem. Abstr.*, 86: 18653a.
14. US Patent 4029727.
15. JPN Patent 57–171712.
16. JPN Patent 62–078215.
17. JPN Patent 57–077310.
18. US Patent 4431601.
19. US Patent 4932404.
20. US Patent 2168374.
21. US Patent 2168375.
22. Balassa, L.L. and Prudden, J.F., *Proc. 1st Int. Conf. on Chitin and Chitosan*, Muzzarelli, R.A.A. and Pariser, E.R., Eds., Cambridge, Massachusetts: MIT, 1978, pp. 486–495.
23. Noguchi, J., Tokura, S., and Nishi, N., *Proc. 1st Int. Conf. on Chitin and Chitosan*, Muzzarelli, R.A.A. and Pariser, E.R., Eds., Cambridge, Massachusetts: MIT, 1978, pp. 315–326.
24. JPN Patent 80–92820.
25. US Patent 4059457.
26. US Patent 4062921.
27. Rutherford, E.A. and Austin, P.R., *Proc. 1st Int. Conf. on Chitin and Chitosan*, Muzzarelli, R.A.A. and Pariser, E.R., Eds., Cambridge, Massachusetts: MIT, 1978, pp. 479–485.
28. JPN Patent 58–127736.
29. JPN Patent 59–068347.
30. JPN Patent 59–071343.
31. JPN Patent 2001–254231.
32. US Patent 4651725.
33. Agboh, O.C. and Qin, Y., *Polym. Adv. Technol.*, 1996, vol. 8, pp. 355–365.
34. Nakajima, M., Atsumi, K. and Kifune, K., *Chitin, Chitosan and Related Enzymes*, Zikakis, J.P., Ed., Oxford: Academic, 1984, pp. 407–410.
35. Sukhanova, T.E., Sidorovich, A.V., Goryainov, G.I., et al., *Vysokomol. Soedin., Ser. B*, 1989, vol. 31, no. 5, pp. 381–384.
36. Nud'ga, L.A., Baklagina, Yu.G., Petropavlovskii, G.A., et al., *Vysokomol. Soedin., Ser. B*, 1991, vol. 32, no. 11, pp. 864–868.
37. Mikhailov, G.M., Lebedeva, M.F., Nud'ga, L.A., and Petrova, V.A., *Zh. Prikl. Khim.*, 2001, vol. 74, no. 9, pp. 1526–1529.
38. Szosland, L. and Struzczyk, H., in *Novye perspektivy v issledovanii khitina i khitozana: Materialy Pyatoi konferentsii* (New Prospects in Studies of Chitin and Chitosan: Proc. Fifth Conf.), Moscow: VNIRO, 1990, pp. 63–74.
39. Hirano, S., Hirochi, K., Hayashi, K., et al., *Cosmetic and Pharmaceutical Applications of Polymers*, Gebelein, C.G. et al., Ed., New York: Plenum, 1991, pp. 95–104.

ISSN 1070-4272, Russian Journal of Applied Chemistry, 2007, Vol. 80, No. 5, pp. 695–704. © Pleiades Publishing, Ltd., 2007.
Original Russian Text © A.B. Venediktov, S.V. Korenev, S.P. Khranenko, S.V. Tkachev, P.E. Plyusnin, S.N. Mamonov, L.V. Ivanova, V.A. Vostrikov, 2007, published in Zhurnal Prikladnoi Khimii, 2007, Vol. 80, No. 5, pp. 716–725.

INORGANIC SYNTHESIS AND INDUSTRIAL INORGANIC CHEMISTRY

Properties of Nitric Acid Palladium Solutions with a High Metal Concentration

A. B. Venediktov, S. V. Korenev, S. P. Khranenko, S. V. Tkachev, P. E. Plyusnin, S. N. Mamonov, L. V. Ivanova, and V. A. Vostrikov

Nikolaev Institute of Inorganic Chemistry, Siberian Division, Russian Academy of Sciences, Novosibirsk, Russia
Gulidov Krasnoyarsk Factory of Nonferrous Metals, Open Joint-Stock Company, Krasnoyarsk, Russia

Received May 4, 2006; in final form, September 2006

Abstract—Nitric acid solutions (c_{Pd} up to 3.2 M) with variable HNO_3 concentration were studied by electronic spectroscopy, ^{14}N and ^{17}O NMR, acid-base titration, gravimetry, and other methods. Solid phases that precipitated on storing these solutions were studied by X-ray phase analysis, thermogravimetry, and IR spectroscopy. The conditions for stability of particular Pd(II) species were determined, and specific features of aging of such highly concentrated palladium solutions were revealed. A procedure for palladium isolation as $[Pd(NH_3)_4](NO_3)_2$ from nitric acid solutions in 98% yield was developed.

DOI: 10.1134/S1070427207050023

The main body of the data on speciation of platinum group metals (PGMs) in media unconventional for their refining, in particular, in nitrate, sulfate, and phosphate solutions, were obtained by the middle of the 1970s. The results of these studies are summarized in reviews cited in [1]. According to the data obtained, PGMs in these acid solutions exist in the form of polynuclear or oligomeric species, and chemical processes occurring in the systems are extremely complicated and variable. It should be noted that the data obtained concerned solutions with low PGM concentrations (of the order of mM). In the subsequent decades, studies in this direction were not systematic.

At present, interest in such studies, mainly concerning the speciation and stability of PGM complexes in solutions other than hydrochloric acid, increased. It is caused by the need for expanding the assortment of commercially produced PGM compounds and catalytic systems based on them. Special attention is given to highly concentrated or saturated PGM solutions. The progress in this direction is limited by the lack of experimental data on the PGM behavior in such media.

The aim of this study was to examine the processes occurring in solutions maximally concentrated with respect to platinum metal, using the system Pd–HNO_3 as an example, to reveal the state of Pd and changes in the macrocomponents of the systems, and to evaluate the stability of solutions in their storage under various experimental conditions.

EXPERIMENTAL

The electronic absorption spectra (EAS) of all solutions without dilution were recorded on a Hewlett–Packard Vectra instrument in cells of 0.0019 cm thickness, and the NMR spectra, on a Bruker CXP-300 spectrometer with a working frequency of 21.865 MHz for ^{14}N and 40.700 MHz for ^{17}O, at natural abundance of the isotopes in solutions. The chemical shifts, which are positive in a weak field, are given in the δ scale and measured relative to conventional standards. The error in determining chemical shifts did not exceed ±0.05 ppm. Thermogravimetric studies were carried out on a Q-1000 device modified for operating in various gaseous media with numeralization of an analog signal. The other data were obtained using standard modern devices and equipment.

The starting nitric acid palladium solutions (NAPSs) were prepared as follows. A powder of metallic palladium containing no less than 99.97% Pd was dissolved at 90–95°C within 1 h in 40 ml of HNO_3 (ultrapure grade, density d = 1.419 g cm^{-3}) with addition of 0.02 ml HCl (chemically pure grade, d = 1.165 g cm^{-3}) per 10 g of Pd. Then the solution

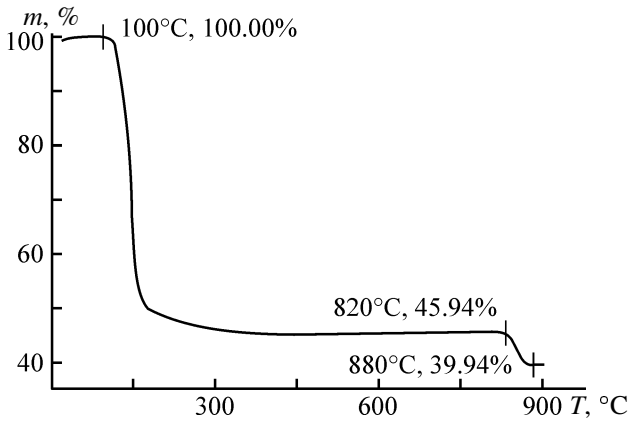

Fig. 1. Curve of $[Pd(NO_3)_2(H_2O)_2]$ weight loss in air. The weight of the starting sample is taken as 100%. (*m*) Sample weight and (*T*) temperature.

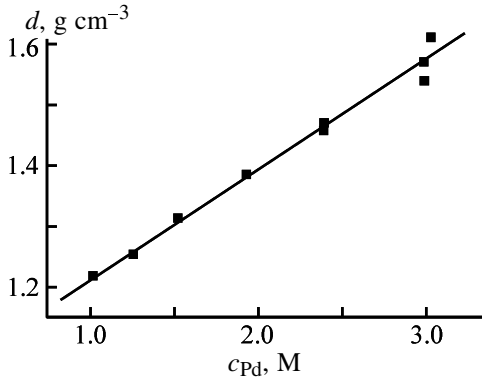

Fig. 2. Dependence of the density *d* of Pd(II) nitric acid solutions on the Pd(II) concentration c_{Pd}. Concentration of free nitric acid in solutions varied from 1.5 to 2.6 M.

was evaporated at the same temperature and diluted with water to c_{Pd} = 2–3 M; the concentration of free HNO_3 was varied from 3.8 to 5.6 M.

In certain experiments the starting substance for obtaining NAPS was crystalline $[Pd(NO_3)_2(H_2O)_2]$. It was prepared from NAPS by concentrating in air to wet crystals. Then the dish with the wet precipitate was placed for 1–2 days in a desiccator over KOH to complete removal of liquid phase traces, after which it was kept in a desiccator without a desiccant. The compound was identified by elemental analysis, IR spectroscopy, X-ray phase analysis, and thermogravimetry.

The curve of the weight loss of the synthesized $[Pd(NO_3)_2(H_2O)_2]$ on heating is shown in Fig. 1. It agrees well with the data [2]. Furthermore, the Pd(II) content in the crystalline product (39.9 wt %) determined from this curve corresponds to its content in $[Pd(NO_3)_2(H_2O)_2]$ (calculated 39.94 wt % Pd). Two endothermic effects are clearly detected in the DTA curves (in air) at 160 and 817°C. The first of them is caused by the reaction

$$[Pd(NO_3)_2(H_2O)_2] \rightarrow PdO + H_2O + 2HNO_3. \quad (1)$$

The theoretical weight loss for this reaction is 54.06, and the observed loss, 53.8%. The second effect is caused by PdO decomposition to the metal, as follows from the correspondence between the theoretical and experimental weight losses.

The data on the crystal structure of $[Pd(NO_3)_2 \cdot (H_2O)_2]$ obtained from the powder X-ray patterns by ab initio method were published in [3]. The starting substance was synthesized by dissolution of metallic palladium in concentrated HNO_3 with the subsequent evaporation of the solution. It is a light brown powder, relatively stable in air depending on atmospheric conditions. Dinitratodiaquapalladium(II) has an orthorhombic lattice, space group *Pbca*, $Z = 4$. Unit cell parameters: $a = 5.0036(3)$, $b = 10.6073(7)$, and $c = 11.7223(8)$ Å. The coordination surrounding of Pd(II) is square planar, and nitrato groups are monodentate. It is interesting that in the previous studies concerning the synthesis and properties of $[Pd(NO_2)_2(H_2O)_2]$ its geometric configuration was not discussed. Indirect data about its *trans* structure are known [4], and in [3] its *trans* configuration was clearly determined.

We have obtained EAS of $[Pd(NO_3)_2(H_2O)_2]$ solutions in 2–2.5 M HNO_3. The concentration of Pd(II) was varied from 0.00123 to 0.184 M. The spectrum of this compound has a very broad absorption band; therefore, accurate determination of its maximum is difficult: its position varies from 397 to 404 nm, and the extinction coefficient, from 138 to 145 $1\,mol^{-1}\,cm^{-1}$.

Determination of acidity. To determine c_{Pd} and acidity of NAPS, aliquots of solutions containing from 100 to 200 mg of Pd(II) were weighed. To obtain correct data, it was necessary to measure the densities of these solutions. The results of such measurements are shown in Fig. 2.

It is seen from Fig. 2 that the dependence of NAPS density on Pd(II) concentration is linear and is expressed by the equation $d = 1.03 \pm 0.18 c_{Pd}$. These data make it possible to determine accurately the palladium concentration. The measurement of NAPS density is also the simplest and the most effective method of estimating the state of solutions in their storage. The relatively low reproducibility of the data at c_{Pd} of about 3 M will be discussed below. It should be noted that the insignificant scatter of the experimental

data is caused by two reasons. The first of them is the fact that the concentration of free HNO_3 in solutions varied from 1.5 to 2.6 M. However, it is possible to estimate these deviations. In particular, it follows from the reference data on the HNO_3 density that its change is no more than 3.3 rel. % in this interval of concentrations, which is the maximal error of the measurements. The second reason consists in the fact that the NAPS density was measured at room temperature, which varied within the range 20–28°C. It was experimentally found that the density variation under these conditions was about 1.5%.

Several techniques were tested for the acidity determination. The first (method no. 1) consisted in that a NAPS aliquot diluted by a factor of 12.5 was treated with a tenfold amount of solid $NaNO_2$ relative to Pd(II) for quantitative binding of Pd(II) in the tetranitro complex, with the subsequent pH-metric titration to pH 6.8–7.0. Unreliability of this technique consisted, firstly, in the formation of small amounts of nitrogen oxides. Secondly, the titration curves of free HNO_3 and of the same amount of HNO_3 with an addition of $Na_2[Pd(NO_2)_4]$ and of the required excess of $NaNO_2$ differed essentially.

The second technique (method no. 2) was based on the results of [5–7] where it was proved that Pd(II) is quantitatively extracted as compounds $[Pd(NO_3)_2L_2]$ with sulfides according to Eq. (2), with the concentration of free HNO_3 remaining unchanged during the process:

$$\{Pd^{2+} + 2NO_3^-\}(aq) + 2L(org) \rightarrow [PdL_2(NO_3)_2](org), \quad (2)$$

where L designates a molecule of coordinated sulfide. Then the raffinate containing only HNO_3 was titrated with a standard alkali solution. This technique of the acidity determination could be close to ideal if it were possible to determine precisely the volume of the raffinate after the separation of Pd(II) by extraction. It appeared to be extremely difficult; therefore, for calculations we used eight parameters and six equations, which resulted in the accumulation of errors and low reproducibility.

The third technique (method no. 3) allowed us to determine simultaneously the content of free HNO_3 and also c_{Pd} during NAPS storage. Using the data of Fig. 2, we took NAPS weighed portions, diluted them with water approximately to 50 ml, and precipitated Pd(II) with dimethylglyoxime (DMG) by the standard procedure [8]. The difference from the technique [8] consisted in that the separated precipitate was washed only with hot water without its acidification. The main difference was that the excess of the precipitant did not exceed 10% of the Pd(II) : DMG = 1 : 2 stoichiometry. The mother liquor and the whole amount of the washing liquid were transferred to a 200-ml volumetric flask, and 50-ml aliquots were titrated with a standard NaOH solution, using a mixture of Phenol Red and Bromocresol Green indicators [9]. According to the data of [9], its color changes at pH 7.2 ± 0.2. It was found experimentally that the use of indicators with a higher pT results in regular overestimation of results. When calculating the concentration of free HNO_3, $2c_{Pd}$ was subtracted from the found total acidity, as two H^+ ions are released into solution upon Pd(II) precipitation with DMG.

Finally, a direct pH-metric titration of freshly prepared NAPS solutions resulted in the formation of dark brown precipitates. In this case, it was necessary to wait for no less than 1 h for reaching a stable potential; therefore, this technique is unacceptable.

To check the correctness of techniques for the acidity determination, we have carried out introduced–found experiments using model solutions. They were prepared by the dissolving accurately weighed portions of crystalline $[Pd(NO_3)_2(H_2O)_2]$ in a fixed volume of HNO_3 of precisely known concentration. The final volume of such solutions was always higher than the initial HNO_3 volume; therefore, to express concentrations in the M scale, we determined the densities of the model solutions.

Method no. 3 gives the maximum discrepancy of 1.5% between the found and introduced amounts. However, it is rather labor-consuming, and a DMG excess larger than 10%, as well as wrong choice of an indicator, result in the substantial overestimation of the NAPS acidity. These drawbacks are compensated by the possibility of the exact determination of both c_{Pd} and the concentration of free HNO_3 from a single NAPS sample. The causes of regular errors in the results obtained by method nos. 1 and 2 were considered above. For the other methods, the deviation of acidity from that of model solutions did not exceed –5.6 (no. 2) and +9.4% (no. 1).

NMR studies of NAPSs. The in situ determination of the concentration of components in nearly saturated solutions, like NAPSs under study, is a difficult problem. The NMR method seems to be the most informative in these cases. To elucidate its possibilities, we have carried out several series of experiments in which we varied the following parameters of solutions: concentrations of nitric acid and nitrate ions and the nature of a nitrate salt cation (Na^+ or Zn^{2+}). Taking

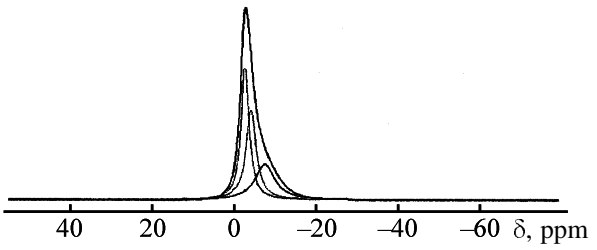

Fig. 3. Experimental ^{14}N NMR spectrum of NAPS-1 diluted by a factor of 2.5 with water and components of its resolution by the Simplex method. (δ) Chemical shift.

into account the facts that the ionic radii of palladium and zinc are close to each other and the Zn(II) complex formation with nitrate ions is, presumably, very weak, we chose zinc as a model simulating aqueous solutions of Pd(II) nitrate. The following regular trends were revealed. In 0.5–7 M solutions of $Na^{14}NO_3$, the factor defining $^{14}NO_3^-$ chemical shifts is the solution acidity. Further, as the acidity of solutions increases, the concentration dependence of the $Na^{14}NO_3$ chemical shift is displaced upfield and becomes linear with a slope of 0.70. However, the linear dependence of the chemical shift on the concentration of $Zn(NO_3)_2$ has a slope of 1.15 when the HNO_3 concentration is varied. Hence, the dependences of the chemical shift of free nitrate ions both on their concentration and on the acidity are individual for each specific cation. Thus, the determination of the concentration of nitrate ions based on the analysis of regular trends in variation of ^{14}N chemical shifts in nitrate solutions shows little promise.

The presence of nitrite ions in NAPSs is of a principle importance in their analysis. The identification of nitrite ions in concentrated nitric acid Pd(II) solutions can be rather simple when using the NMR method. It was found experimentally that, when the number of scans of the ^{14}N resonance is about 10^4 (experiment duration about 6000 s), a signal of nitrite ions can be readily seen at their content of 0.01 M. Such a detection limit of nitro groups is sufficient for determination of their content in the systems under consideration. In any case, when the content of nitro groups in NAPSs with a Pd(II) content of about 3.0 M is monitored by ^{14}N NMR, the contribution Pd(II) nitro complexes to the material balance is negligible.

To elucidate the nature of Pd(II) complex species and to determine the concentrations of certain NAP macrocomponents, we also used NMR. The overwhelming majority of such experiments were carried out with a sample hereinafter designated as NAPS-1. The content of Pd(II) in it is 20.07 wt % counting on the metal (or 3.042 M), and the density of this solution at 20°C is 1.613 g cm^{-3}.

In the ^{14}N NMR spectrum of NAPS-1 taken in the range from +460 to –560 ppm, only a symmetric signal with a chemical shift of –8.93 ppm is detected. This range essentially exceeds the range of 48–88 ppm characteristic of nitrite ins coordinated to Pd(II) in various amounts [10]. This fact confirms our earlier conclusion that Pd(II) nitrite complexes make a negligible contribution to the material balance of the NAPS system and allows us to rule out the presence of noticeable amounts of nitrite ions or nitrous acid (CS ~200 ppm [10]) in Pd(II) nitric acid solutions.

The spectrum of the same solution diluted by a factor of 2.5 with water, taken immediately after the dilution, is shown in Fig. 3. After the dilution of the starting NAPS-1 solution, a shoulder appears in the high field in all the spectra, and it is the more pronounced, the more diluted is the NAPS-1 solution (by a factor of 10 at most). This is apparently due to changes in the Pd(II) speciation. In this case, lines of irregular and unsymmetric shapes were resolved into a number of components specified by an operator. Then, using the Simplex method, we carried out the optimization of the following parameters of each component: position in the spectrum (chemical shift), amplitude, half-width, and Gaussian line contribution to the shape of the signal resolved after Lorentz. The optimization continued until the best fit of the experimental spectrum with the total envelope of all the components was attained. It should be noted that the line of undiluted NAPS-1 was resolved neither into two nor into three components, unlike the lines of diluted solutions. The correctness of this approach is illustrated by the fact that the experimental and optimized spectra of undiluted NAP-1 coincide to within 1%. This is a very good result for NMR spectroscopy.

The presence of a single symmetric line in the NMR spectrum of undiluted NAPS-1, which is not resolved into any number of signals, can be, in principle, associated with the closeness of the chemical shifts of Pd(II) species present in solution and of nitric acid, or with a high rate of exchange of coordinated and free nitrate ions, or with the fact that the ^{14}N NMR signals of NAPSs are considerably broader than those of nitrate ions. In our case, the line width is 95.8 Hz. To compare, the line width of the signal of ~3 M nitric acid is 9 Hz, and that of a nitric acid solution with a total concentration of nitrate ions of 7.0 M is 13.9 Hz. The presence of Pd(II) in a concentration of about 3 M in NAPS can affect the viscosity and

other parameters of solutions, but the comparison of the above-given data shows that it would hardly lead to an increase in the line width in the NAPS-1 spectrum by an order of magnitude.

This fact, together with the asymmetry of lines of NAP solutions diluted with water, was the reason why we attempted to resolve the NMR spectra of dilute solutions into components.

The change in the symmetry of lines in the spectra of solutions diluted with water and the presence of three resolved components of these spectra adequately describing the experimental spectra suggest either the appearance of hydrolyzed Pd(II) species upon lowering the acidity or the dissociation of complex Pd(II) nitrates resulting in an increase in the concentration of NO_3^- ions. These reasons are supported by the data on the stability Pd(II) nitratoaqua complexes and by the constants of $[Pd(H_2O)_4]^{2+}$ acid dissociation.

Stability constants of Pd(II) nitratoaqua complexes. There are only three publications [11–13] in which the constants of formation of Pd(II) nitratoaqua complexes are given. Shoittsov [11] reported that a bathochromic shift in EAS of Pd(II) aqua complexes with λ_{max} = 390 nm is observed at 2.1 : 1 ratio of concentrations of nitrate ions and Pd(II) at c_{Pd} = 0.008 M. In that study, the formation of Pd(II) nitrato complexes was examined spectrophotometrically up to 3.6 M NO_3^- concentration at a total ionic strength of 4.0 M. It was found that only the mononitrato complex $[Pd(H_2O)_3(NO_3)]^+$ with a stability constant $\beta_1 = 1.6 \pm 0.3$ is formed in the examined concentration range. The calculated EAS parameters of this species are as follows: λ_{max} = 415 nm and ε_{max} = 155 l mol^{-1} cm^{-1}. The formation constant of the mononitrato complex $\beta_1 = 1.2 \pm 0.4$ was also determined spectrophotometrically in [12]. Note that the β_1 values from [11, 12] completely agree with each other within the limits of the errors given in these papers. The parameters of $[Pd(H_2O)_3NO_3]^+$ EAS in these two papers also practically coincide. It was shown in [12] that the position of the maximum and its intensity in EAS of $[Pd(H_2O)_3NO_3]^+$ noticeably decrease both on replacement of HNO_3 by $NaNO_3$ and with a decrease in HNO_3 concentration. The procedures for preparing the nitrate solutions in [11, 12] are the same and are based on the dissolution of Pd powder in concentrated HNO_3 with the subsequent boiling to eliminate possible sources of NO_2 generation. The range of working Pd(II) concentrations in these studies was 0.001–0.01 M.

The stability constants of Pd(II) nitrato complexes determined from the extraction data sharply differ from the results of [11, 12]. This question is discussed in [13]. The approach to the estimation of the constants is based on the examination of the dependences of the Pd(II) distribution coefficient D_{Pd} on the concentration of HNO_3 in the aqueous phase in the case of the extraction from nitric acid media with neutral phosphoryl-containing compounds, nitrates of amines, and salts of quarternary ammonium bases. In so doing, it was postulated that the nonideality of the aqueous phase is caused solely by the formation of Pd(II) nitrato complexes. Such approach gives the β_1 value lying in the range 14–20. Moreover, the constants of formation of di- and trinitrato complexes were estimated at 2 and 6, respectively. However, Shmidt et al. [13] consider these estimates of β_i only as empirical parameters in the dependences of D_{Pd} on HNO_3 concentration in the aqueous phase, as there are no quantitative approaches to the determination of the activity coefficients in a wide range of conditions.

The first paper on the hydrolysis of Pd(II) aqua ions was published in 1967 [14]. In that paper, solutions of palladium aqua ions (c_{Pd} = 0.001–0.006 M) were prepared by dissolving in perchloric acid the palladium hydroxide precipitated from nitric acid solutions. Hydrolysis constants were determined both from the data of pH-metric titration and by spectrophotometry, and then extrapolated to zero ionic strength. Reaching constant pH values took about 5 h in each point of the titration curve. The constants $\beta_1 = [PdOH^+(aq)]/[Pd^{2+}(aq)][OH^-]$ and $\beta_2 = [Pd(OH)_2(aq)]/[Pd^{2+}(aq)][OH^-]^2$ were determined. The values of $\log\beta_1$ and $\log\beta_2$ at 25°C averaged by both methods are 12.7 ± 0.6 and 26.2 ± 0.7, respectively. The logarithm of the constant K_s of the equilibrium $[Pd(OH)_2(s)] = [Pd(OH)_2(s)]$ is –2.7. Combining this value with $\log\beta_2^{-1}$, we obtain the solubility product $Pd(OH)_2(s)$ equal to $10^{-28.9}$. The constant β_1 found for the reaction

$$[Pd(H_2O)_4]^{2+} + OH^- = [Pd(H_2O)_3OH]^+ + H_2O \quad (3)$$

can be readily converted to the constant K_d of $[Pd(H_2O)_4]^{2+}$ dissociation by the equation

$$[Pd(H_2O)_4]^{2+} = [Pd(H_2O)_3OH]^+ + H^+. \quad (4)$$

In this case, $K_d = \beta_1 K_w$. The values of pK_d calculated in such a way from the data of [11, 14] are 1.2 ± 0.1, which shows that the acid dissociation constants calculated using data from two independent sources actually coincide. It remains unclear why such an important quantity as the dissociation constant of

Pd(II) aqua ion has not been calculated previously. It follows from the value cited above that, first, the Pd(II) aqua ion is in fact a strong acid, and, second, in solutions without complexing ligands (e.g., perchlorate) at $[H]^+ = 1$ M approximately 10% of Pd(II) will be in the monohydroxo form, and at $[H]^+ = 10$ M this fraction will be about 1%. In the specified acidity range, the fraction of hydrolyzed Pd(II) will always be several percents.

The dissociation processes are very fast; hence, the subsequent slow changes in properties of solutions, mainly precipitation, are probably associated with slow polymerization of the hydrolyzed species. The presence of ligands capable of forming complexes with Pd(II) will lead to a decrease in the strength of acids such as $[Pd(H_2O)_3L]$; therefore, the degree of hydrolysis decreases. Hence, the contribution of polymerization processes to the common patztern of the occurring reactions also decreases.

Speciation of Pd(II) in nitric acid solutions. In view of the considered data on the stability of nitrate complexes and acid properties of Pd(II) aqua ions, using the NMR data for solutions, we can obtain the information on the nature of species present in NAPS. The regular trends in variation of the ^{14}N NMR spectra of NAPS-1 solutions on their 2.5-, 5-, and 10-fold dilution with water are as follows. For the species giving the lowest-field signal, the shift changes from –2.4 to –0.8 upon dilution, with the fraction of the species increasing by a factor of almost 2 with dilution. We can readily assign this signal to free NO_3^- ions on the basis of the previously obtained data on the resonance of concentrated $NaNO_3 + HNO_3$ solutions. Hence, on dilution nitrate ions are accumulated in solutions, which can be caused only by decomposition of the Pd(II) nitrate complex. The chemical shift of the next signal varies from –4.2 to –1.6 ppm, with the fraction of this species, 0.31 ± 0.05, remaining approximately constant. This signal presumably corresponds to the Pd(II) nitratotriaqua complex, which should be the most stable complex species at these concentrations. The highest-field signal has a stable chemical shift (-7.6 ± 0.1 ppm), with the fraction of the species decreasing from 0.24 to 0.12. It should be noted that the ratio of the concentration of coordinated nitrate ions to c_{Pd}, calculated from the integral intensities of lines, decreases on dilution from 1.9 to 1.4.

To confirm the absence of hydrolytic processes and the prevalence of dissociation reactions of complex Pd(II) nitrates, as indicated by all experimental data, we have carried our two series of experiments. The idea of the first series consisted in the following. In the NAPS material balance, only hydroxide and nitrate ions can be anions. To check it, we have taken the ^{14}N NMR spectrum of one of NAPSs with an internal reference, nitromethane (0.124 M) in NAPS with the initial concentration $c_{Pd} = 21.05$ wt %, diluted by a factor of 3. As a result, the difference between the calculated concentration of nitrate ions and the concentration found from the integral intensities of the total nitrate lines and the internal reference line appeared to be 3.5%, which is a very accurate result for the method in use. The second series of experiments consisted in measuring pH of freshly prepared solutions of the same NAPS with a dilution by a factor from 12.5 to 193. An important result is the fact that the measured pH values for the first solution were 0.56 ± 0.04, which agrees well with the concentration of hydrogen ions calculated on the basis of the acid dissociation constant of Pd(II) aqua ions.

The ^{17}O NMR spectra of both the starting NAPS-1 solution and solution after its dilution (at most tenfold) contain only two lines with chemical shifts of 412 ± 1 ppm and from –121 to –128 (variation with increasing dilution). The first signal exactly coincides with the spectrum of 3.12 M nitric acid. The comparison of the second signal with the data of [15] shows that it corresponds to the Pd(II) aqua ion with a good accuracy. It confirms the fact that the exchange of free nitrate ions with the nitrate groups coordinated to Pd(II) is very fast, and the difference between these ions cannot be detected by NMR.

Thus, the above-discussed results allow the following conclusion. The undiluted NAPS solution has a symmetric signal in the ^{14}N NMR spectrum (δ –8.9 ppm, half-width about 96 Hz), contains the dominating form $[Pd(NO_3)_2(H_2O)_2]$, and approximately equal low concentrations of $[Pd(NO_3)(H_2O)_3]^+$ and $[Pd(NO_3)_3(H_2O)]^-$ providing the line symmetry. The following processes occur on dilution of the solutions with water:

$$[(PdNO_3)_3(H_2O)]^- + H_2O \rightarrow [Pd(NO_3)_3(H_2O)_2] + NO_3^-, \quad (5)$$

$$[Pd(NO_3)_2(H_2O)_2] + H_2O \rightarrow [Pd(NO_3)(H_2O)_3]^+ + NO_3^-, \quad (6)$$

$$[Pd(NO_3)(H_2O)_3]^+ + H_2O \rightarrow [Pd(H_2O)_4]^{2+} + NO_3^-, \quad (7)$$

$$[Pd(H_2O)_4]^{2+} \rightarrow [Pd(OH)(H_2O)_3]^+ + H^+. \quad (8)$$

Reactions (5)–(7) result in increasing concentration of nitrate ions in solutions, which accounts for the

essence of the occurring processes. The occurrence of process (8) is proved without controversy by the fact that, in all NAPSs diluted with water, dark brown fine precipitates are formed within 5–7 days after the dilution. The data of IR spectroscopy, X-ray diffraction, and elemental analysis suggest that the precipitate is hydrated palladium oxide $Pd(OH)_2 \cdot xH_2O$, where x varies within the range 1.20–1.45. The greater the dilution, the higher x. The maximal dilution corresponded to the 25-fold decrease in c_{Pd}. Dilute acid HCl did not dissolve these precipitates, and concentrated HCl, only on boiling. This agrees completely with the data of [16].

Isolation of Pd(II) from NAPS in the form of $[Pd(NH_3)_4](NO_3)_2$. It should be noted that we were able to reach a nearly quantitative yield of $[Pd(NO_3)_2 \cdot (H_2O)_2]$ crystals. The $[Pd(NO_3)_2(H_2O)_2]$ obtained can be used as the starting compound in the synthesis of a very important product, $[Pd(NH_3)_4](NO_3)_2$. Owing to its high solubility, the compound can find use in the production of supported palladium catalysts or precursors of polymetallic powders. Furthermore, the use of $[Pd(NH_3)_4](NO_3)_2$ makes it possible to carry out syntheses in the presence of small amounts of HCl, in contrast to $[Pd(NH_3)_4]Cl_2$ whose application inevitably leads to the formation of *trans*-$[Pd(NH_3)_2 \cdot Cl_2]$. The complex $[Pd(NH_3)_4](NO_3)_2$ was obtained from $[Pd(NO_3)_2(H_2O)_2]$ in the presence of an excess of concentrated ammonia, after which the resulting reaction mixture was evaporated. As a result, $[Pd(NH_3)_4](NO_3)_2$ was obtained in a high yield:

$$[Pd(NO_3)_2(H_2O)_2] + 4NH_3 \rightarrow [Pd(NH_3)_4]^{2+} + 2NO_3^- + 2H_2O. \quad (9)$$

To optimize the synthesis procedure, a series of experiments with various starting conditions have been carried out. The reaction of solid $[Pd(NO_3)_2 \cdot (H_2O)_2]$ (~0.01 mol) with an excess of concentrated aqueous solution of ammonia (~0.5 mol) at room temperature or at 50–60°C yields a light brown solution containing a small amount of a voluminous brown precipitate. On further heating of the reaction mixture with the added ammonia, the color becomes lighter within several hours, and the solid practically completely precipitates on the bottom. Then the reaction mixture is filtered through a porous glass filter, and the mother liquor is evaporated to dryness. The target product $[Pd(NH_3)_4](NO_3)_2$ represents crystals in the form of colorless or slightly yellowish plates. The yield reaches 97%. The recrystallization of the substance from water allows us to obtain a high-purity product.

The reaction of 5 ml of $Pd(NO_3)_2 \cdot 2H_2O$ aqueous solution (~1 M) with an excess of concentrated aqueous solution of ammonia at room temperature yielded a light brown solution containing a small amount of a voluminous brown precipitate. The reaction mixture was heated with excess ammonia, the precipitate was filtered off, and the resulting solution was evaporated to dryness on a water bath. Yield 98%.

The reaction of 10 ml of an aqueous solution containing 0.8 M $Pd(NO_3)_2$ and 1.6 M free HNO_3 with an excess of concentrated aqueous solution of ammonia at room temperature proceeds as follows. At the first moment after the addition of the ammonia solution, a light yellow voluminous flocculent precipitate is formed, which completely dissolves on further adding ammonia. The resulting solution has a light brown color. No clear precipitate is observed. Then the solution is evaporated up to the formation of a film of crystals and is cooled. The precipitated crystals are separated by filtration. To remove an NH_4NO_3 impurity, the product is recrystallized from aqueous solution. Yield 70%. The reaction at room temperature with a solution containing 2.5 g of NH_4HCO_3 in concentrated ammonia proceeds similary.

Our experiments show that small amounts of a precipitate contaminating the target product are formed during the synthesis. In the synthesis from $Pd(NO_3)_2 \cdot 2H_2O$ solutions containing free HNO_3, such precipitate is not formed. We failed to determine the composition of the precipitate. However, data of IR spectroscopy and of X-ray phase and thermal analysis suggest that the precipitate composition can be expressed by the general formula $PdO(NH_3)_x(H_2O)_y$. In particular, this assumption is supported by the fact that the dried precipitates of this phase readily dissolve in dilute HCl without heating, which is quite uncharacteristic of dried $PdO(H_2O)_x$.

Variation of NAPS properties in time. We have obtained the following experimental data on the NAPS stability in time. First of all, it should be noted that freshly prepared NAPSs can contain solutions oversaturated with respect to Pd(II), which are fairly stable for a certain time. Depending on the Pd(II) concentration in solution, they remain homogeneous for a period from 2 to 24 h, but after that a crystalline phase of $[Pd(NO_3)_2(H_2O)_2]$ precipitates. We have obtained NAPS containing up to 26.22% Pd(II). If the precipitate is separated from it and the solution is stored further, crystalline $[Pd(NO_3)_2(H_2O)_2]$ precipitates again from the solution. It is most likely that the crystalline precipitates are formed due to limited solubility of $[Pd(NO_3)_2(H_2O)_2]$ in nitric acid.

Electronic absorption spectra of Pd(II) nitric acid solutions. Concentration of free HNO_3 in solutions 3.7–5.7 M

Solution no.	Solution*	c_{Pd}, M	λ of maxima, nm, at indicated keeping time, weeks				
			0	3	4	8	16
1	NAPS-1	3.042	397(220)**	397(272)	398(244)	398(247)	
2	NAPS-1	3.042	398(211)				393(244)
3	A	2.744	396(286)	398(294)	396(244)	396(283)	
4	B	2.070	419(160)	419(188)	421(170)	419(165)	
5	C	2.925	419(178)	421(172)	421(189)	419(172)	
6	D***	3.181	425(173)	421(198)	422(180)	419(170)	
7	E	2.706	428(194)	428(206)	427(180)	426(181)	

* Molar extinction coefficients.
** Solutions A, B, C, D, and E were prepared using the technique of acidity correction.
*** Prepared by dissoluving crystalline $[Pd(NO_3)_2(H_2O)_2]$ in HNO_3.

From the experimental data we concluded that NAPSs are the most stable if the Pd(II) content is 21–22%, or close to 3.0 M. Higher Pd(II) content results in the precipitation of crystalline products of the composition $[Pd(NO_3)_2(H_2O)_2]$. This fact is responsible for the above-mentioned low reproducibility of the data on the NAPS density in the region of c_{Pd} 3 M (Fig. 2). The most important conclusion from our experiments is the fact that NAPSs are stable in time if c_{Pd} does not exceed 21 wt % and the molar ratio of free HNO_3 and c_{Pd} is no less than 1 : 1.

This conclusion on the Pd(II) and HNO_3 concentrations ensuring the stability of NAPS solutions was supplemented by a series of other measurements. We have monitored the dynamics of variations of such solution parameters as palladium(II) concentration, acidity, and EAS taken in situ without dilution. These observations were carried out during a period of 3–9 months. The weight fraction of Pd(II) in the solutions studied was in the range 15.0–20.7 wt %, or 2.07–3.17 M. The content of free HNO_3 was from 172 to 316 g l^{-1}. All the solutions were prepared according to the technique described above, but after the evaporation to the necessary volume the acidity was corrected by adding certain amounts of concentrated HNO_3 to ensure the molar ratio of Pd(II) and free HNO_3 required for the NAPS stability.

It was found that the concentration of Pd(II) in solutions prepared in such a way remains unchanged in time within 0.1–0.6 rel. % and practically does not depend on the fact whether these solutions were held in the dark or in a scattered laboratory light. The latter conclusion was confirmed by an experiment on laser flash photolysis, carried out as follows. A solution was irradiated at a wavelength of 308 nm (the average position of the maximum of NAPS absorption) by 100 pulses of 20 mJ each, which corresponds to approximately a week storage under usual laboratory illumination. No difference was observed between the spectra of the irradiated and initial solutions.

The characteristics of the absorption spectra of the NAPSs under study are given in the table. All the solutions were kept in the dark, except for solution no. 2. The solutions designated by letters A, B, C, D, and E were prepared using the acidity correction. It should be noted that the contribution of nitric acid to the absorption in its fairly concentrated solutions does not give rise to an appreciable fixed error at wavelengths longer than 350 nm, which is very favorable for characterizing EAS of Pd(II) nitric acid solutions. Typical spectra of undiluted Pd(II) nitric acid solutions are shown in Fig. 4.

It is interesting that the EAS of the solutions are of two types. The spectra of NAPS-1 and solution A have a maximum at approximately 400 nm, which coincides in position with the maximum of $[Pd(NO_3)_2 \cdot (H_2O)_2]$, but these spectra are much more intensive. At the same time, solutions B, C, D, and E are characterized by a maximum at 425 ± 4 nm, and EAS are apparently superpositions of at least two spectra of different Pd(II) species in NAPS. Furthermore, the difference in the molar extinction coefficients of the spectra under consideration is about 30%. The comparison of the spectra of solutions C and E is especially characteristic, as they noticeably differ in c_{Pd}, but have almost the same shape.

It should be noted that the characteristics of EAS of Pd(II) nitric acid solutions depend, as follows from the published data [11–13, 17], on the concentration

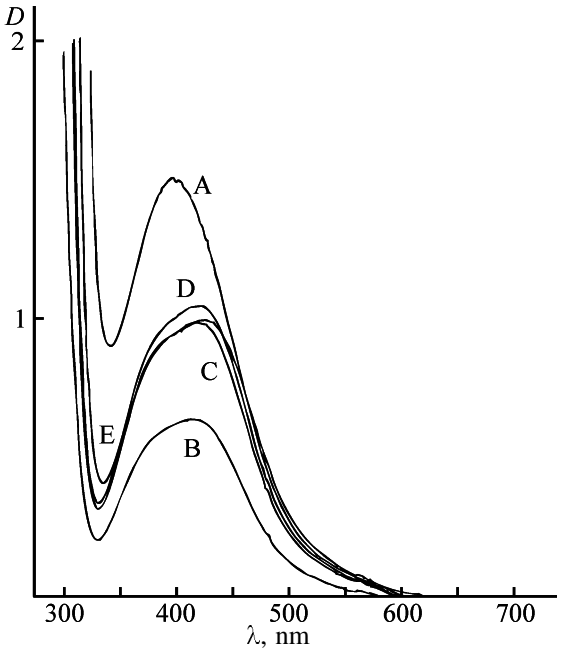

Fig. 4. EAS of Pd(II) nitric acid solutions. (*D*) Optical density and (λ) wavelength. (A–E) Solutions (see text).

of free nitric acid, which noticeably varied in different NAPSs. Solutions A, B, and C have almost equal acidity, but their spectra essentially differ in the shape. It is probable that differences in the NAPS spectra somehow depend on fine details of the solution preparation and acidity correction.

The most important conclusion consists in the fact that, when solutions are kept for three months, the positions and intensities of maxima in EAS remain constant within the limits of measurement errors, which first of all depend on the thickness of the absorbing layer of the cell in use and on specific features of its filling with solutions. This conclusion is also proved by the measurements of the solution densities, which, in spite of appreciable temperature variation during monitoring, were nevertheless more accurate and remained constant within 2%.

Along with recording EAS of solutions, we measured the acidity of solutions using NAPS-1 as an example of the most aged solution. This monitoring was carried out during a period of 10 months. In this period, the acidity remained constant and was 198 ± 3 g l^{-1} HNO_3 (confidence level 95%).

CONCLUSIONS

(1) The nature of solid phases precipitating from Pd(II) nitric acid solutions with c_{Pd} of up to 20.67 wt % (or 3.181 M) and the concentration of free HNO_3 of 3.7–5.6 M during their storage both in light and in the dark under various conditions was determined.

(2) At Pd(II) content higher than 21 wt %, the crystalline phase $[Pd(NO_3)_2(H_2O)_2]$ precipitates from solutions. It is hygroscopic and unstable to the action of light on storage. The technique of the preparation of $[Pd(NH_3)_4](NO_3)_2$ from this substance with a yield close to quantitative was suggested. Thanks to its specific properties, the product can be used for preparing supported palladium catalysts.

(3) The ratio of concentrations of palladium(II) and free nitric acid is important for the stability of Pd nitric acid solutions in storage. Solutions with c_{Pd} about 20 wt % can be stored for indefinitely long time if the ratio of concentrations of free HNO_3 and Pd(II) is no less than 1 : 1 (i.e., no less than 3 M HNO_3, or about 200 g l^{-1}).

(4) According to the data obtained, the Pd nitric acid solutions contain a mixture of palladium(II) nitroaqua compounds in the presence of free nitric acid. Nitrite ions or nitrous acid are present in negligible amounts or absent at all. One of the main conditions of the safe storage of nitric acid solutions containing about 20% Pd and about 3 M free HNO_3 is the exclusion of their dilution by water. Otherwise Pd(II) hydroxides precipitate from the solutions within several days.

(5) The comparison of properties of solutions kept in the light and in the dark shows that they are almost inert photochemically.

(6) To diagnose properties of nitric acid solutions in the course of their storage, it is suggested to use a combination of visual observation and measurement of solutions density. In this case, using calibration dependences of the density of nitric acid solutions on the Pd(II) concentration in them, it is possible to determine palladium concentration accurate to 3% without analytical measurements.

ACKNOWLEDGMENTS

The authors are grateful to A.V. Belyaev for useful discussion.

REFERENCES

1. *Khimiya platinovykh i tyazhelykh metallov* (Chemistry of Platinum and Heavy Metals), Ser.: *Problemy koordinatsionnoi khimii* (Problems of Coordination Chemistry), Shchelokov, R.N., Ed., Moscow: Nauka, 1975.

2. Shmidt, V.S., Shorokhov, N.A., Vashman, A.A., and Samsonov, V.E., *Zh. Neorg. Khim*, 1982, vol. 27, no. 5, pp. 1254–1255.
3. Laligant, Y., Ferey, G., and Le Ball A., *Mater. Res. Bull.*, 1991, vol. 26, no. 4, pp. 269–275.
4. Gatehouse, B.M., Livingstone, S.E., and Nyholm, R.S., *J. Chem. Soc.*, 1957, no. 10, pp. 4222–4225.
5. Torgov, V.G., Tatarchuk, V.V., Druzhinina, I.A., et al., *At. Energ.*, 1994, vol. 76, pp. 478–482.
6. Torgov, V.G., Tatarchuk, V.V., Druzhinina, I.A., et al., *At. Energ.*, 1996, vol. 80, pp. 267–273.
7. Tatarchuk, V.V., Druzhinina, I.A., Korda, T.M., and Torgov, V.G., *Zh. Neorg. Khim.*, 2002, vol. 47, no. 12, pp. 2082–2088.
8. Charlot, G., *Les methods de la chimie analytique. Analyse quantitative minerale*, Paris: Masson, 1961, 4th ed.
9. Butler, J.N., *Ionic Equilibrium (A Mathematical Approach)*, Reading, Massachusetts: Addison–Wesley, 1964.
10. Belyaev, A.V., Fedotov, M.A., and Korenev, S.V., *Koord. Khim.*, 1989, vol. 15, no. 11, pp. 1551–1555.
11. Shoittsov Rudi, A Spectrophotometric Study of Palladium(2+) State in Aqueous Solutions, *Cand. Sci. Dissertation*, Moscow, 1972.
12. Jorgensen, C.K. and Parthasarathy, V., *Acta Chem. Scand. A*, 1978, vol. 32, no. 10, pp. 957–963.
13. Shmidt, V.S., Mezhov, E.A., Rubisov, V.N., et al., *Radiokhim.*, 1986, vol. 28, no. 3, pp. 345–349.
14. Izatt, R.M., Eatough, D., and Christensen, J.J., *J. Chem. Soc. A*, 1967, pp. 1301–1304.
15. Fedotov, M.A., Troitskii, S.Yu., and Likholobov, V.A., *Koord. Khim.*, 1990, vol. 16, no. 12, pp. 1675–1677.
16. Giemser, O. and Peuschell, G., *Z. Anorg. Allg. Chem.*, 1955, vol. 281, no. 1, pp. 44–47.
17. Shmidt, V.S. and Shorokhov, N.A., *At. Energ.*, 1988, vol. 64, no. 2, pp. 103–110.

ISSN 1070-4272, Russian Journal of Applied Chemistry, 2007, Vol. 80, No. 5, pp. 705–710. © Pleiades Publishing, Ltd., 2007.
Original Russian Text © O.N. Kirsanov, 2007, published in Zhurnal Prikladnoi Khimii, 2007, Vol. 80, No. 5, pp. 726–731.

PHYSICOCHEMICAL STUDIES OF SYSTEMS AND PROCESSES

Specific Features of the Kinetics of Autocatalytic Combustion of Sodium Chlorate with Polyethylene in a Manometric Bomb

O. N. Kirsanov

Prikladnaya Khimiya Russian Scientific Center, Federal State Unitary Enterprise, St. Petersburg, Russia

Received March 24, 2006; in final form, March 2007

Abstract—Velocities of combustion and outflow of combustion products from the surface of formulations based on sodium chlorate and polyethylene in a constant-volume bomb were evaluated in relation to the aggregative state of polyethylene.

DOI: 10.1134/S1070427207050035

This study is a continuation of [1]. The principal goal of the study was to examine the kinetics of the combustion of sodium chlorate (SC) with polyethylene (PE) and to determine, on the basis of the previously derived analytical dependences, to what extent the combustion process is close to the critical conditions (to detonation). Good agreement of the results obtained in a calculation of the pressure in the bomb by equations of autocatalytic reactions with experimental data has been attained previously [1] for the combustion of SC with PE, with the coefficient of correlation between the calculation and experiment no less than 0.98.

EXPERIMENTAL

To make the previously obtained data more reliable, we carried out additional studies of formulations based on SC and PE in a constant-volume bomb by the method described in [1]. Polyethylene was used both as a powder (conventional scheme for explosives) and in the form of tubules (layered system). We also tested a layered system with addition of 9.1 wt % sodium chloride. As before [1], the measurement error was ±10% for pressure and ±0.001 s for time (time marker of an N117/1 loop oscilloscope). The formulations studied were charged into textolite cups with an inner diameter of 38 mm, and the cups were placed on the bomb bottom. The ignition was done with a weighed portion (2 g) of black powder. Table 1 lists the following parameters: charge mass M; oxidant excess factor α; induction time t_{ind}; combustion time t_{com}; fuel density ρ; combustion chamber volume V; maximum pressure P_m in combustion of the formulations; and specific strength of combustion products, RT, in comparison with the energy efficiency θ of the process. The process efficiency was evaluated by comparing the RT value found from experimental data with the calculation [1].

Analysis of these experimental data confirms the previously obtained results: the higher dynamic (t_{ind} and t_{com}) and energetic (RT and θ) process parameters of the powder system, compared with layered systems (with or without sodium chloride). In accordance with the aforesaid, we use the equations of autocatalytic reactions to describe the combustion process in the bomb. We assume that the final pressure in the bomb is determined by the mass of gaseous products of charge combustion (initial concentration [A] and "primer" concentration [B]). Then the starting expression for the autocatalytic reaction can be expressed in a modified form in terms of the process completeness as

$$d\alpha/dt = k_1(1 - \alpha)(\beta - \alpha), \quad (1)$$

where α is the completeness of the process (reduced pressure in the bomb); $\beta = [A]/[B]$, share of the primer in the total mass; and $k_1 = k[A]$.

Solution to differential equation (1) has the form

$$\alpha(t) = \frac{\beta[\exp(\beta + 1)k_1 t - 1]}{1 + \beta\exp(\beta + 1)k_1 t}. \quad (2)$$

For the powder system, oscillograms of the combustion processes in the bomb can be processed with the Mathcad software package, using the reduced equation because of the rapidity of the process. For

Table 1. Principal parameters of the process in the bomb

Formulation*	$M \times 10^3$, kg	α	ρ, kg m^{-3}	$V \times 10^6$, m^3	t_{ind}, s	t_{com}, s	P_m, MPa	RT, kJ kg^{-1}	θ
SC + PEP	60	1.0	1500	301.6	0.005	0.01	128.6	646.5	0.9
SC + PET	60.5	1.1	1500	283	0.02	0.29	109.7	513.4	0.72
SC + PETC	68.9	0.92	1390	291	0.01	0.28	980	413.9	0.56

* SC + PPE, sodium chlorate plus polyethylene powder; SC + PET, sodium chlorate plus polyethylene in the form of tubes; and SC + PETC, sodium chlorate plus a layered system with addition of 9.1 wt % sodium chloride.

the layered system (with or without sodium chloride), we use an equation that accounts for thermal loss (by Ya.B. Zel'dovich):

$$\alpha(t) = \frac{\beta[\exp(\beta + 1)k_1(t)t - 1]}{1 + \beta\exp(\beta + 1)k_1(t)t}, \quad (3)$$

$$k_1(t) = 1/(a/T_0 + bt), \quad (4)$$

where T_0 is the initial (calculated adiabatic) temperature of the system; t, time; and a and b, coefficients to be determined.

It was shown in [1] that the amount of primer was not determined for the powder system, although it was taken for the simple layered system as the limiting in accordance with GOST (State Standard). As a result, the coefficients of Eq. (1) may take different paired values at a virtually complete coincidence of the calculated curve with the experiment. Table 2 lists calculated values of the coefficients of Eqs. (2)–(4).

We use the equation parameters obtained to determine how the combustion velocity varies in the systems under consideration and to find, based on these results and on the mass conservation law, the outflow velocity of combustion products from the burning surface. The gas outflow velocity can be used to judge whether the subsonic combustion can pass to detonation. Let us make the following assumptions: the combustion products are described by equations for ideal gases, combustion occurs in the layer-by-layer mode (this is justified for atmospheric conditions [2]), diameter d_{com} of the combustion chamber of the bomb is equal to the charge diameter (d_{ch} = 38 mm), and RT = const during the process (further alternatives in which RT increases with time will be considered).

Table 2. Coefficients of Eqs. (2)–(4)

Formulation	β	k_1	a	b
SC + PEP	10^{-6}	1900		
	10^{-8}	2500		
	10^{-10}	3100		
SC + PET	0.003	52	33	0.06
SC + PETC	0.091	43	55	0.10

The pressure (Pa) developed in fuel combustion can be found, with account of the assumptions made, using the formula

$$P(t) = \frac{m(t)RT}{V(t)}, \quad (5)$$

where $m(t) = \rho\pi d^2 h(t)/4$ is the mass of the burnt fuel (kg), and $V(t) = V_{com} + V_f$ is the combustion chamber volume (m^3), equal to the initial volume plus that of the burnt fuel.

With account of the assumptions made, the total volume is given by

$$V(t) = \pi d^2[h_1 + h(t)]/4,$$

where h_1 is the height of the initial volume of the bomb, related by the charge diameter, and $h(t)$ is the height of the burnt fuel (m) (varies with time).

We substitute in Eq. (5) expressions for the mass and volume and, after cancellations, obtain

$$P(t) = \frac{\rho RT h(t)}{h_1 + h(t)}. \quad (6)$$

From expression (6) we find how the height of the burnt fuel bed depends on pressure:

$$h(t) = \frac{P(t)h_1}{\rho RT - P(t)}. \quad (7)$$

However, $P(t) = P_m\alpha(t)$ [1], where P_m is the maximum pressure developed in combustion of the whole amount of fuel in the bomb. This pressure can be, in turn, calculated by formula (6), with the initial charge height h_2 substituted instead of $h(t)$. Then, we obtain after simple rearrangements the dependence of the height $h(t)$ of burnt fuel as

$$h(t) = [h_1h_2\alpha(t)]/[h_1 + h_2 - h_2\alpha(t)]. \quad (8)$$

The derivative of $h(t)$ with respect to time is just the linear combustion velocity, i.e.,

$$u(t) = \mathrm{d}h(t)/\mathrm{d}t. \quad (9)$$

Now we calculate, using the data listed in Table 1, the reduced height of the initial volume of the bomb and the initial height of the fuel bed (Table 3).

Carrying out a single differentiation of Eq. (8), we obtain the dependence (9) of the linear velocity on the combustion time, and upon a double differentiation, we find the instant of time at which the maximum combustion velocity is reached, t_u. Figure 1a shows, as a typical example, how the combustion velocity of the powder system varies for the second pair of parameters from Table 2. Numerical values for all the three cases are given below. Figure 1b shows similar kinetic curves for the layered system with and without sodium chloride added. Numerical values of the maximum combustion velocities and instants of time at which these velocities are reached are listed in Table 4.

It follows from Fig. 1 that (i) all the curves of variation of linear combustion velocities are bell-shaped, (ii) linear combustion velocity of the powder system is 1–1.5 orders of magnitude higher than that of layered systems, (iii) the time in which the maximum combustion velocity is reached is an order of magnitude shorter than that of layered systems, (iv) combustion velocity of a layered system with NaCl additive somewhat exceeds that without the additive, and the time in which the maximum velocity is reached is two time shorter, and (v) initial combustion velocity for the layered system with a NaCl additive exceeds that without the additive. Autocatalytic reactions [2] are characterized by an extent of reaction at the initial instant of time that is dependent on the primer concentration [Eq. (1)]. It should be noted that Eq. (3) well describes the development of the process in the bomb with a correlation coefficient not lower than 0.98.

A characteristic feature of autocatalytic reactions is the position of the inflection point on the conversion vs. time curve [3]. At this instant of time, the rate of the chemical reaction reaches its maximum value. For example, in the case when the rate equation of the reaction is first-order with respect to the product and starting substance, the inflection point approximately corresponds to 50% conversion of the starting substance into reaction products. When the rate equation is second-order with respect to the conversion product and first-order with respect to the starting substance,

Table 3. Initial heights of the original volume of the bomb and of the fuel bed

Formulation	h_1, m	h_2, m
SC + PEP	0.266	0.035
SC + PET	0.25	0.035
SC + PETC	0.257	0.044

Table 4. Principal kinetic parameters of the process

β	k_1	u, m s^{-1}	t_u, s	h, mm	φ	z
10^{-6}	1900	16.6	0.0073	17.5	0.5	41.3
10^{-8}	2500	21.9	0.0074	17.5	0.5	55.8
10^{-10}	3100	27.1	0.0075	17.5	0.5	69.1
0.003	52	0.39	0.08	14.1	0.4	1

the inflection point corresponds to consumption of approximately two thirds of the starting substance. In the opposite situation with the reaction orders, the inflection point will correspond to consumption of an approximately one third of the starting product. It should be noted that the smaller the amount of primer, the closer the position of the inflection point on the kinetic curve to the limiting values (0.5, 0.66, and 0.33). Let us consider from this standpoint the combustion of a mixture of SC with PE powder for

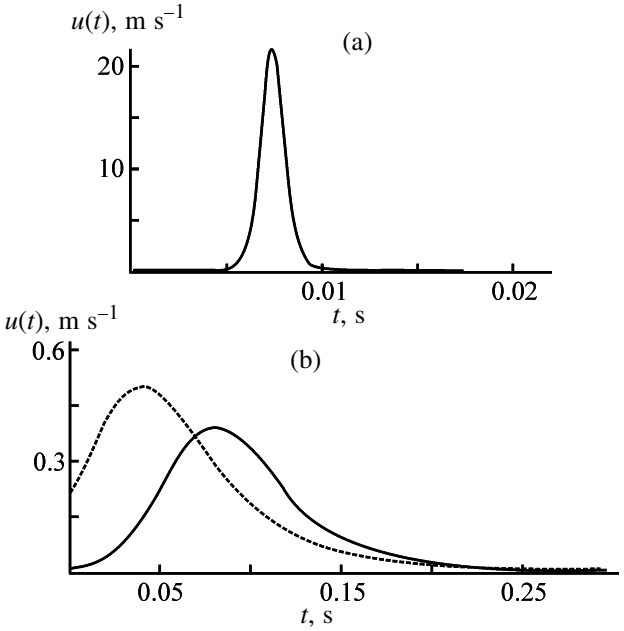

Fig. 1. Kinetic curves of variation of the linear combustion velocity $u(t)$ for (a) powder formulation (β = 10^{-8}, k_1 = 2500) and (b) layered system (*1*) without and (*2*) with addition of sodium chloride. (*t*) Time; the same for Fig. 2.

the three values of the equation parameters in Table 2, in comparison with the layered system. We determine the numerical values of the maximum linear combustion velocities and the instants of time at which these velocities are reached, using Eq. (8). To find the reaction order, it is necessary to calculate the fraction of fuel burnt by the instant of time when the maximum combustion velocity is reached. For this purpose, we integrate the expression for the linear combustion velocity from 0 to t_u, the time corresponding to the maximum combustion velocity:

$$h = \int_0^t u(t)\mathrm{d}t. \quad (10)$$

We divide the resulting value of the height of the burnt bed by the initial value of h_2 to obtain the degree of conversion:

$$\varphi = h/h_2. \quad (11)$$

Table 4 lists the results of these calculations and, in addition, the ratios z between this linear combustion velocity and the linear velocity for the layered system.

Analyzing the data in Table 4 and, primarily, those related to the powder system, we see that a decrease in the share β of the primer leads to an increase in the linear combustion velocity, although the inflection point on the kinetic curve remains constant and corresponds to 50% conversion of the fuel. Based on this circumstance, we can assume that this is the case in which the reaction equation is first-order with respect to both the starting substance and the reaction product (sodium chloride). Apparently, this assumption is also valid for the layered system, despite the difference in the degree of half-conversion (0.4 instead of 0.5), because it is rather improbable that the reaction mechanism would change because of differences in the aggregative state of polyethylene. This difference is probably accounted for by introduction of corrections for thermal loss introduced into Eq. (2) [Eq. (3)]. For the layered system with addition of NaCl, the degree of conversion is even lower (0.3) than that for the system without NaCl because of the even larger thermal loss (Table 1).

As shown previously [4], the combustion of the powder formulation of SC with PE occurs under kinetic control (activation energy E_p = 141 700 J mol^{-1}), and that of the layered system, under mixed (but closer to diffusion) control (activation energy E_s = 38 000 J mol^{-1}). If the preexponential factor is considered the same for these cases, the calculated ratio of the reaction rates (linear combustion velocities) can be expressed as

$$z_1 \approx \exp(E_p/R_\mu T_a)/\exp(E_s/R_\mu T_a), \quad (12)$$

where T_a is the adiabatic temperature of formulation combustion [3], and R_μ, the universal gas constant. Substituting the corresponding values of R_μ and T_a into expression (12), we obtain z_1 = 41.3. This value virtually coincides with the value of z in the first row of Table 4. Consequently, the first pair of parameters of Eq. (2) in Table 2 can be regarded as more appropriate for description of the combustion process of the powder system. Thus, the different linear combustion velocities are due to differences in the activation energies.

Knowing the law by which the linear combustion velocity varies with time and having made several additional assumptions, we can pass to determining the velocity of the gas outflow from the burning surface of the fuel. Let us first consider the case of the powder system (for the second pair of parameters in Table 2), whose tests by the UN-approved procedure demonstrated that such a system belongs to the class of explosives. Let us assess for this system to what extent the combustion process is close under our experimental conditions to transition to detonation. To find the outflow velocities, we use the mass conservation law

$$w(t)\rho_1(t) = u(t)\rho, \quad (13)$$

$$\rho_1(t) = p(t)/RT, \quad (14)$$

$$p(t) = p_k\alpha(t) + 101\,325, \quad (15)$$

where $\rho_1(t)$ is the density of the combustion products, and $p(t)$ is the absolute pressure in the bomb.

Let us assume that the specific strength of the combustion products, RT, is established instantaneously upon the onset of combustion and does not vary with time and, specifically, during the time shorter than, or equal to the induction period (t_{ind} = 0.005 s) to be RT = 785.50 kJ kg^{-1} (specific strength of air in the gas generator at the initial instant of time), otherwise RT = 646.500 kJ kg^{-1}. Figure 2a (curve *1*) shows how the outflow velocity of the combustion products from the burning surface (or, more precisely, from the combustion front) varies with time in this case.

It follows from an analysis of Eqs. (13)–(15) and Fig. 2a (curve *1*) that the maximum gas outflow velocity is 581.5 m s^{-1} 0.006 s after the onset of the combustion process.

Table 5. Velocity parameters of the combustion process

Formulation	β	k_1	u, m s^{-1}	t_u, s	w_{lin}, m s^{-1}	t_{lin}, s	w_v, m s^{-1}	t_v, s
SC + PEP	10^{-6}	1900	16.6	0.0073	413	0.006	442	0.006
	10^{-8}	2500	21.9	0.0074	573	0.007	582	0.006
	10^{-10}	3100	27.1	0.0075	720	0.007	721	0.0062
SC + PET	0.003	52	0.39	0.08	13.1	0.043	19.2	0.021
SC + PETC	0.091	43	0.48	0.039	23.9	0.011	24.2	0.011

Let us consider another case, when RT varies gradually (e.g., by a linear law) and reaches a steady value after half the combustion time, i.e., 0.005 s, elapses. We represent the linear dependence as $s(t) = 90\,000\,000t + 78\,550$. Figure 2a (curve *2*) shows the dependence obtained under these conditions.

It can be seen from Fig. 2a that the maximum outflow velocities and the instants of time at which the maximum values are reached are virtually only slightly different for these cases: 581.5 m s^{-1} at $t = 0.006$ s and 572.6 m s^{-1} at $t = 0.007$ s. It is interesting that the outflow velocity was 332.2 m s^{-1} at the instant of time at which the maximum combustion velocity is reached, $t_u = 0.0074$ s.

We now perform similar calculations for outflow velocities for the layered system. Let us first consider the case when RT is established immediately after the onset of combustion, or, more precisely, 0.001 s after the induction period (Fig. 2b, curve *1*).

In the case of a linear rise in RT as $f(t) = 10\,000\,000t + 78\,550$, we obtain a somewhat different value of the outflow velocity (Fig. 2b, curve *2*).

Analysis of the graphical dependences of the outflow velocities for the layered system shows that the absolute values of the velocities are only slightly different, and the difference is mostly determined by the adopted law of RT variation. The variation of the outflow velocities for the layered system with 9.1% NaCl is similar to that without this additive.

It follows from Table 5 that the linear combustion velocity of the powder systems exceeds by more than an order of magnitude that for the layered systems and reaches these values in an order of magnitude shorter time. For this reason, the combustion of the powder system occurs under virtually adiabatic conditions with a higher energetic completeness θ of the process and larger RT (Table 1). The outflow velocities of the combustion products of the powder system also exceed by 1.5–2 orders of magnitude those for the layered system and approach the critical velocity (equal to 940 m s^{-1} according to preliminary calculations) beyond which transition from the subsonic combustion mode to detonation is possible. Because the powder system belongs to explosives, the absence of detonation in the experiment under consideration is possibly accounted for by the small height of the fuel bed, low bulk density of the fuel, and its granulometric composition, or by all these factors taken together [5, 6]. It is known [3] that the kinetics of autocatalytic and branching chain reactions may be rather similar. Therefore, it is difficult to distinguish these reactions, although they differ in nature. Our attempt to describe the combustion of the powder system with a typical equation for branching chain reactions

$$U(t) = Ae^{\varphi t} \qquad (16)$$

failed to give any encouraging result: the total coef-

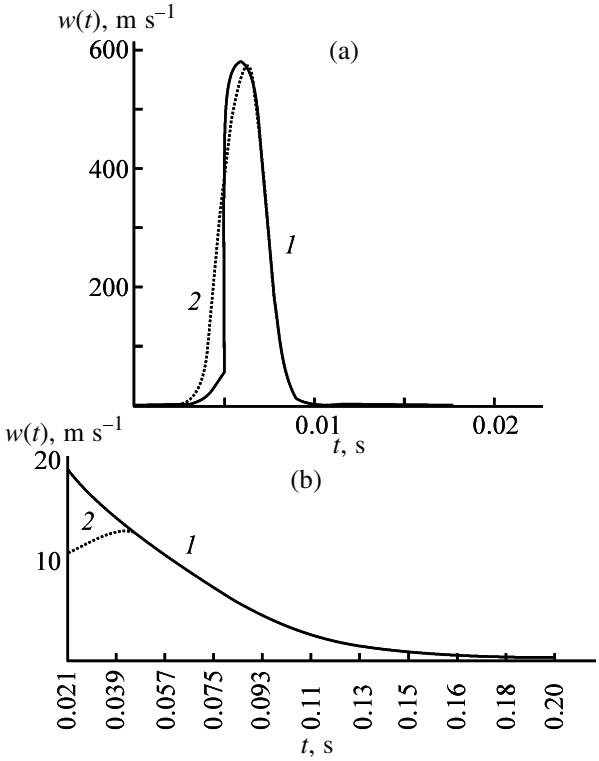

Fig. 2. Variation of the velocity $w(t)$ of gas outflow from the burning surface (reaction front) for (a) powder system and (b) layered system, with (*1*) instantaneous establishment of RT and (*2*) linear rise in RT.

ficient of correlation between the experiment and calculation does not exceed 0.8. Moreover, the exponential dependence well describes only the beginning of the process and disregards the burning-out of the substance in the course of the reaction, and, therefore, no graphical dependence by Eq. (16) is given here.

Because only the layered system can be considered for practical purposes, the fact that introduction of 9.1 wt % NaCl into the formulation not only does not impair the dynamic parameters of the process, but even somewhat improves them makes this fuel promising as being less expensive and having a lower hygroscopicity [7].

CONCLUSIONS

(1) The experiments performed in a constant-volume bomb and calculations demonstrate that the combustion of sodium chlorate with polyethylene in a closed volume is described by an equation of autocatalytic reactions of first-order with respect to both the starting substance and the reaction products.

(2) The linear combustion velocity in the powder system exceeds by more than an order of magnitude the combustion velocity of the layered system. This is attributed to difference in activation energies (reaction control modes).

(3) The outflow velocity of combustion products in the powder system approaches, under the given experimental conditions, the critical value, beyond which transition to detonation is possible.

(4) The layered systems are far from the critical conditions in both the maximum combustion velocities and outflow velocities of the combustion products from the burning surface (reaction front).

(5) Of practical interest is the layered system with a sodium chloride additive, which, not impairing the dynamic parameters of the process, is less expensive and has lower hygroscopicity.

ACKNOWLEDGMENTS

The author is sincerely grateful to V.S. Shpak for permanent attention and help in this area of research.

REFERENCES

1. Kirsanov, O.N., *Zh. Prikl. Khim.*, 2005, vol. 78, no. 11, p. 1813–1818.
2. Paramonov, G.P., Vinogradov, Yu.I., and Kirsanov, O.N., *Fizicheskie problemy razrusheniya gornykh porod: Sbornik trudov Tret'ei mezhdunardnoi konferentsii* (Proc. 3rd Int. Conf. on Physical Problems of Rock Disintegration), Abaza (Khakassiya, Russia), September 9–14, 2002, pp. 265–270.
3. Emanuel', N.M. and Knorre, D.G., *Kurs khimicheskoi kinetiki* (A Course of Chemical Kinetics), Moscow: Vysshaya Shkola, 1974.
4. Kirsanov, O.N., *Zh. Prikl. Khim.*, 2005, vol. 78, no. 8, pp. 1252–1257.
5. Bakhman, N.N. and Belyaev, A.F., *Gorenie geterogennykh kondensirovannykh system* (Combustion of Heterogeneous Condensed Systems), Moscow: Nauka, 1967.
6. Belyaev, A.F., Bobolev, V.K., Korotkov, A.I., et al., *Perekhod goreniya kondensirovannykh sistem vo vzryv* (Transition of the Combustion of Condensed Systems to Explosion), Moscow: Nauka, 1973.
7. Shraibman, S.S., *Proizvodstvo bertoletovoi soli i drugikh khloratov* (Manufacture of Berthollet's Salt and Other Chlorates), Moscow: GONTI NKTP, 1938.

ISSN 1070-4272, Russian Journal of Applied Chemistry, 2007, Vol. 80, No. 5, pp. 711–715. © Pleiades Publishing, Ltd., 2007.
Original Russian Text © V.G. Badelin, E.Yu. Tyunina, I.N. Mezhevoi, 2007, published in Zhurnal Prikladnoi Khimii, 2007, Vol. 80, No. 5, pp. 732–736.

PHYSICOCHEMICAL STUDIES OF SYSTEMS AND PROCESSES

Calorimetric Study of Dissolution of Amino Carboxylic Acids in Water at 298.15 K

V. G. Badelin, E. Yu. Tyunina, and I. N. Mezhevoi

Institute of Solution Chemistry, Russian Academy of Sciences, Ivanovo, Russia

Received July 3, 2006; in final form, December 2006

Abstract—The enthalpies of solution of glycine, *DL*-alanine, *D*-valine, and *L*-serine in water at 298.15 K were measured on a special ampule calorimeter equipped with an isothermal shell. The enthalpies of hydration of 12 α-amino acids differing in the steric configurations of the side radical were estimated using the measured values and the published data on the heats of solution and sublimation for biologically active substances. The influence of hydrophobicity of the substances on their dissolution and hydration was considered.

DOI: 10.1134/S1070427207050047

It is known that water plays the key role in structurization and functioning of proteins in a liquid medium [1, 2]. Therefore, study of interactions of protein model compounds with water is extremely important for the estimation of functional capabilities of active groups in biological and medicinal compounds (enzymes, pharmacological receptors), in genetic engineering, and for the development of remedies, new analytical and diagnostic procedures, and molecular sensors [3, 4]. Recently the development of new medicines advantageous in that they are identical to compounds inherent in human body became an important direction in pharmacology. Model protein compounds, such as amino acids, peptides, and their derivatives, can be classed with the above medicines. To develop the optimal processes of the synthesis of such substances and construct the thermodynamic cycles of formation of intermediates, it is necessary to know their thermodynamic constants, including enthalpies of sublimation and solution.

Here we report the experimental values obtained in a thermochemical study and the calculated enthalpies of solution, sublimation, and hydration for some amino carboxylic acids, which are used as remedies (glycine) or model catalytic or substrate centers of enzymes (alanine, *L*-phenylaniline, etc.). Each protein molecule involves the specific number of amino acids. Amino acids can be arranged in the following order with respect to abundance in the living nature: leucine, alanine, and serine [5]. Therefore, the above acids were chosen as objects of study. Note that amino acid molecules, in both solutions and crystals, are in the bipolar or zwitterionic form, NH_3^+–CH(R)–COO^- [5, 6]. Along with the NH_3^+ and COO^- groups bearing effective charges, different polar and hydrophobic groups are present in the amino acid structure. The chemical properties of amino acids in the proteins, i.e., their capability to enter into a particular reaction, are determined by the properties of a side radical –R. It was of interest to estimate how their hydrophobicity affects the energies of solution and hydration. In this respect, calorimetric methods are particularly important for studying thermodynamic properties of such systems [6].

EXPERIMENTAL

Isothermal calorimetry has been recommended as one of efficient methods providing direct thermodynamic information about interactions of various amino acids with water. The enthalpies of solution of glycine (Gly), *DL*-alanine (*DL*-Ala), *D*-valine (*D*-Val), and *L*-serine (Ser) were measured with a special four-ampule calorimeter with an isothermal shell. A series of thermal effects that occurred in dissolution of several weighed portions of a substance were measured in the same volume of the solvent without recharging the calorimetric cell. The reactor and all inner parts of the calorimeter in contact with the solution were made of VT-1 titanium alloy. A thin-walled calorimetric beaker *1* about 110 ml in volume, sealed with a silicone rubber gasket *2*, was placed into a massive brass shell *3* with insulated surface (see figure). Inertia-free heater *4* made of manganin wire and placed into a cylindrical thin-walled case, heat exchanger *5*, and a propeller stirrer *6* were

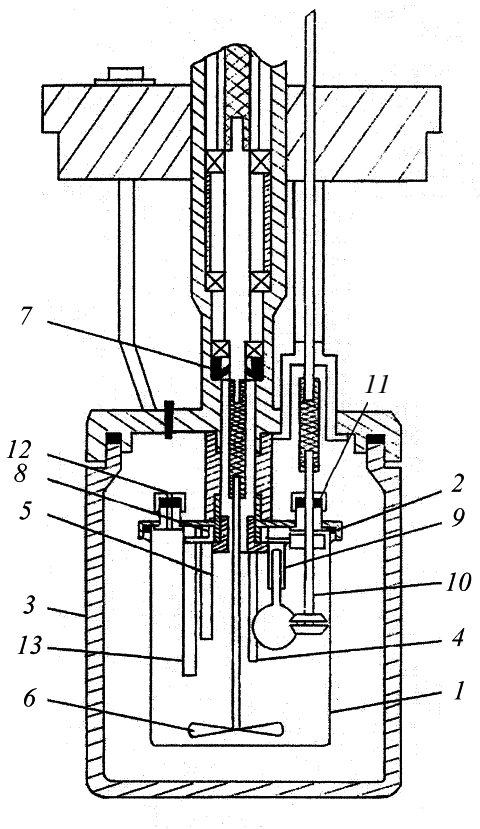

Scheme of a calorimetric cell: (*1*) Thin-walled beaker (V = 110 cm^3), (*2*) silicone gasket, (*3*) brass shell, (*4*) heater, (*5*) heat exchanger, (*6*) stirrer, (*7, 11*) stuffing boxes, (*8*) cogged bushing, (*9*) holder of ampules with a substance, (*10*) ampule breaker, (*12*) valve for filling the beaker with a solvent, and (*13*) temperature sensor (KMT-14).

located inside the calorimetric beaker. The inlet of the stirrer was sealed with a self-packing stuffing box *7*. The calorimeter was calculated for four ampules that are fixed to a cogged bushing *8* with holders *9*. A stuffing box *11* ensured tightness of the system in the course of rotation of ampule breaker *10*. The solvent was added to the calorimetric vessel through valve *12*. As temperature sensor was used a KMT-14 thyristor placed into case *13*. The Wood's alloy ensured secure heat contact between the thermistor and the walls of the case. The assembled massive unit was placed into a water bath of 16 l volume. In the course of the calorimetric measurement, the stability of the temperature-control system was maintained constant to within 10^{-3} K. The sensitivity of the calorimeter in measuring the temperature and energy was 2×10^{-4} K mm^{-1} and 1×10^{-3} J mm^{-1}, respectively, of the scale of the measuring device. The thermal effect was compensated by the electric current.

Each weighed portion of the substance examined was ground in an agate mortar to decrease the dissolution time and dried to constant mass. All ampules used for measuring the thermal effect of solution were weighed on a VLR-200 balance with an accuracy of 5×10^{-5} g. In the general case, the integral heat of solution was estimated in successive dilutions by the equation:

$$\Delta_{sol}H^m = \frac{\sum_1^n \Delta m_i/\Delta_{sol}H(m_{i-1} \to m_i)}{\sum_1^n \Delta m_i}, \quad (1)$$

where Δm_i is change in the molal concentration in ith measurement; $\Sigma \Delta m_i = m$, final molal concentration of the solution; and n, number of successive measurements.

The accuracy and reliability of operation of the calorimetric installation was estimated by measuring the thermal effect of solution of KCl at 298.15 K. Using 10 independently measured enthalpies of solution of KCl in water and the values from [7], we obtained the standard enthalpy of solution $\Delta_{sol}H^0$ = 17.23 ± 0.06 kJ mol^{-1}, in good agreement with the generally accepted value of 17.22 ± 0.33 kJ mol^{-1}.

The chromatographically homogeneous amino acids, Gly, *DL*-Ala, *D*-Val, and Ser (Reanal, Hungary) used in the study were dried in a vacuum oven at 343 K for 48 h immediately before use. Water was subjected to deionization and double distillation. The maximum error in determining the enthalpies of solution of amino acids was 0.5% at a confidence level of 0.95. In the concentration range studied, 0.003–0.012 mol kg^{-1}, $\Delta_{sol}H^m$ of all systems is concentration-independent within the experimental error. Therefore, the enthalpies of solution $\Delta_{sol}H^0$ were found as weighted averages of seven independent measurements.

Table 1 generalizes the measured values and the published data for the amino acids studied, which are used to compare the enthalpies of solution in water of amino acids differing in the structures of the side radical. As objects of study we chose linear and branched aliphatic amino acids (Gly, *L*-Ala, *DL*-Ala, Abu, *DL*-Nva, *DL*-Nle, *L*-Val, *D*-Val, and *L*-Leu), amino acids with a polar side chain (*L*-Ser, *L*-Thr), and those containing benzene ring (*L*-Phe). As follows from Table 1, the dissolution of amino acids in water is an endothermic reaction, which may be due to the fact that the energy spent for breaking a network of hydrogen bonds in water and crystal structure of

Table 1. Standard enthalpies of solution $\Delta_{sol}H^0$ in water and standard enthalpies of sublimation $\Delta_{subl}H$ of α-amino acids at 298.15 K

Substance $[NH_3^+–CH(R)–COO^-]$	R–	$\Delta_{sol}H^0$	$\Delta_{subl}H$
		kJ mol^{-1}	
Glycine (Gly)	H–	14.25 ± 0.06	136.5 ± 0.5 [12]
DL-Alanine (*DL*-Ala)	CH_3–	9.34 ± 0.04	146 ± 4 [8]
L-Alanine (Ala)	CH_3–	7.61 ± 0.08 [8]	138.1 ± 0.8 [13]
D-Valine (*D*-Val)	$(CH_3)_2CH$–	2.16 ± 0.05	162.7 ± 0.8 [8]
L-Valine (Val)	$(CH_3)_2CH$–	5.34 ± 0.06 [9]	162.8 ± 1.1 [12]
L-Leucine (Leu)	$(CH_3)_2CHCH_2$–	2.93 ± 0.2 [9]	150.6 ± 1.1 [13]
L-Phenylalanine (Phe)	$(C_6H_5)CH_2$–	7.69 ± 0.08 [9]	153.9 ± 0.9 [13]
L-Serine (Ser)	$CH_2(OH)$–	11.01 ± 0.09	148 ± 4 [8]
L-Threonine (Thr)	$CH_3CH(OH)$–	10.33 ± 0.06 [10]	159 ± 5 [8]
2-Aminobutanoic acid (Abu)	CH_3CH_2–	6.64 ± 0.09 [11]	132 ± 1 [12]
2-Aminopentanoic acid (norvaline, Nvl)	$CH_3(CH_2)_2$–	0.30 ± 0.08 [11]	120.8 ± 0.5 [13]
2-Aminohexanoic acid (norleucine, Nle)	$CH_3(CH_2)_4$–	–6.1 ± 0.2 [11]	114.4 ± 0.4 [13]

the substances is large and is not compensated by exothermic hydration effects. As the length of the side radical increases, the enthalpy of solution of amino acids becomes more negative. On passing from linear acids (Abu, Nva, Nle) to the more branched acids (Val, Leu), $\Delta_{sol}H^0$ increases. The heats of solution of the isomers (*DL*- and *L*-alanine, *D*- and *L*-valine) differ by 1.73 and 3.18 kJ mol^{-1}, respectively. The enthalpies of solution of Ser and Thr are more positive than the heats of solution of aliphatic amino acids, despite possible formation of hydrogen bonds between the OH polar group and water molecules. Introduction of the benzene ring into Ala (passing to Phe) affects the heat of solution only slightly.

It should be noted that, for all the amino acids, the nature of the reactive charged groups (COO^-, NH_3^+) is the same and, in all probability, the changes in the thermodynamic properties may be caused by the specific solvation and by the change in the molecule hydrophobicity. The logarithm of the coefficient of the substance distribution between two immiscible phases (in the *n*-octanol–water model system) $\pi = \log P$ [5] was accepted as the hydrophobicity coefficient. The π values calculated for the amino acids by the AM1 method [14] are listed in Table 2. The hydrophobicity coefficients π vary in the orders Gly < Ala < Val < Leu, Phe > Ala > Ser < Thr, and Ala < Abu < Nva < Nle. In other words, π grows with increasing length of side alkyl chains and with introducing additional CH_3 (Thr) or C_6H_5 (Phe) group. Note that, among the amino acids studied, Phe is the most hydrophobic. The π value is somewhat higher for linear compounds than for branched ones (Nvl > Val, Nle > Leu). Considerably less hydrophobic are Ser, Thr, and Gly, which is due to the influence of OH group on the interaction energy of Ser and Thr molecules with water (formation of hydrogen bonds) and to the electrostatic interaction of Gly zwitterions with water dipoles.

The variation of the hydrophobicity of amino acid molecules is reflected in the enthalpies of solution. An increase in the hydrophobicity makes the dissolution of biosubstances less endothermic and enhances the exothermic contribution, first of all, of hydrophobic

Table 2. Enthalpies of hydration $\Delta_{hydr}H^0$, specific volume enthalpies of hydration $\Delta_{hydr}H^0/V_2^0$, and coefficients of molecule hydrophobicity π and molecule packing D_{aq} in aqueous solutions of α-amino acids

Substance	$-\Delta_{hydr}H^0$	$-\Delta_{hydr}H^0/V_2^0$	π	D_{aq}
	kJ mol^{-1}			
Gly	122	2.83	–1.07	0.84
DL-Ala	137	2.28	–	0.77
Ala	131	2.16	–0.53	0.76
D-Val	161	1.75	–	0.72
Val	157	1.73	0.33	0.72
Leu	147	1.37	0.66	0.70
Phe	146	1.20	1.15	0.73
Ser	139	2.28	–1.32	0.80
Thr	149	1.95	–0.91	0.78
Abu	125	1.66	0.06	0.74
Nvl	120	1.31	0.34	0.71
Nle	120	1.12	0.73	0.69

hydration. However, correct estimation of the hydration contributions to the thermal effects of solution of amino acids can be done solely by taking into account the energies of their crystal lattices. As a measure of the interaction of a dissolved substance with water molecules we used the heat of hydration $\Delta_{hydr}H^0$ [15]:

$$\Delta_{hydr}H^0 = \Delta_{sol}H^0 - \Delta_{subl}H, \quad (2)$$

where $\Delta_{subl}H$ is the enthalpy of sublimation of amino acid (Table 1).

The calculated heats of hydration, $\Delta_{hydr}H^0$, of amino acids are presented in Table 2.

In model amino acid crystals, $\Delta_{subl}H$ decreases in a series of linear amino acids (Ala > Abu > Nva > Nle) and increases in a series of aliphatic acids (Leu < Val < Ala < Gly) with increasing length of the side alkyl chain. At the same number of carbon atoms, $\Delta_{subl}H$ is considerably higher for amino acids with branched side radicals than for linear acids. This may be due to the change in the degree of braking of the internal rotation about the C_α–N bond and to the contribution from the side radical. Introduction of the benzene ring into the side chain of alanine decreases, and the introduction of OH groups increases the specific volume enthalpy of sublimation, which is defined as $\Delta_{subl}H/V_w$ ratio and characterizes the "rigidity" of the crystal structure [16].

Tables 1 and 2 show that, along with electrostriction of the water molecules arranged close to effective charges on NH_3^+ and COO^- groups of amino acids, the complementary influence of the specific interaction of water with polar functional groups of biomolecules and the interaction of water with a nonpolar hydrophobic radical determine the enthalpies of solution and hydration of amino acids. Using the values of [17–19] for the partial molar volume V_2^0 of amino acids in water at infinite dilution at 298.15 K, we calculated the specific volume enthalpies of hydration, $\Delta_{hydr}H^0/V_2^0$ [20], of the compounds studied. The packing coefficients of amino acid molecules in water were calculated from the relation $D_{aq} = NV_w/V_2^0$ (where V_w is the van der Waals volume of molecule and N, number of molecules present in a cell, equal to the Avogadro number) [8, 21]. The results obtained are collected in Table 2. The relative error in calculating $\Delta_{hydr}H^0/V_2^0$ does not exceed 3.5%. The lower the $\Delta_{hydr}H^0/V_2^0$ of amino acids, the higher the coefficient D_{aq} and the degree of structurization of the aqueous solutions [8].

In a series of aliphatic amino acids having nonpolar side chains, the strongest electrostriction effect on the surrounding water is exerted by Gly. The fact that the effect of Thr is weaker than that of Ser is due to the presence of a methyl group. The ratio $\Delta_{hydr}H^0/V_2^0$ tends to increase with increasing π (Table 2). Increasing the nonpolar moiety of the molecule makes it more hydrophobic, with $\Delta_{hydr}H^0$ decreasing for branched amino acids and becoming less negative for linear acids. Apparently, this is accounted for by the state of molecules in the solid phase and by the contribution of the crystal lattice energy in dissolution of a compound in water. The introduction of the OH polar fragment into a nonpolar side chain of Ala decreases its hydrophobicity and is accompanied by a decrease in $\Delta_{hydr}H^0$ for Ser. In comparison with Ser, the presence of an additional methyl group in Thr increases the hydrophobicity and makes the hydration more exothermic. In some cases, the difference in the $\Delta_{hydr}H^0$ values of zwitterions is obscured by the difference in their $\Delta_{subl}H$ values. For example, in the case of *L*-Ala and *L*-Phe, the enthalpies of solution are virtually the same, whereas $\Delta_{hydr}H^0$ for Phe is more exothermic by 15.7 kJ mol^{-1}.

CONCLUSIONS

(1) The heats of solution of glycine, *DL*-alanine, *D*-valine, and *L*-serine in water at 298.15 K were determined experimentally on a special calorimeter equipped with an isothermal shell. The enthalpies of solution and hydration were determined for 12 α-amino carboxylic acids, containing linear or branched alkyl radicals, polar OH groups, or a benzene ring in a side chain, which simulate the properties of active centers of enzymes or remedies.

(2) The parameter $\Delta_{hydr}H^0/V_2^0$ can be used as a measure of the stabilizing effect exerted by amino acid on the aqueous solution. The lower its value, the more structured is the solution examined.

(3) The electrostriction compression of water in the vicinity of charge centers (NH_3^+, COO^-) in the molecules of different amino acids is the same. The hydrophobic interaction with water is accompanied by a decrease in $\Delta_{hydr}H^0$ (it becomes more negative) in a series of branched acids (from Ala to Leu) and by only slight its variation in a series of linear acids (Abu, Nva, Nle).

(4) From the energy standpoint, the thermal effects of solution of various amino acids in water can simulate the denaturation, which is considered as transfer of amino acid residues from the inner region of the

protein into water. In this case, balance between the hydrophobic and specific interactions and between the specific interactions and dehydration of amino acid is of great importance. It was demonstrated that hydrophobic hydration plays the key role in interaction of amino acids with water and is larger for more complex biomolecules.

ACKNOWLEDGMENTS

The study was financially supported by the Russian Foundation for Basic Research (project no. 06-03-96312-r_tsentr_a) and by a grant from the President of the Russian Federation (project no. MK-4905.2006.3).

REFERENCES

1. Kharakoz, D.P., *J. Phys. Chem. A*, 1991, vol. 95, pp. 5634–5642.
2. Chilikian, T.V., *J. Phys. Chem. B*, 2001, vol. 105, no. 50, pp. 12566–12578.
3. Raevskii, O.A., and Shnaider, G.I., *Zh. Org. Khim.*, 1995, vol. 31, no. 12, pp. 1793–1801.
4. Eggins, B., *Biosensors: An Introduction*, Chichester: Wiley, 1996.
5. Varfolomeev, S.D., *Khimicheskaya enzimologiya* (Chemical Enzymology), Moscow: Akademiya, 2005.
6. Rialdi, G., Battistel, E., and Barisas, B.G., *Thermochim. Acta*, 1991, vol. 192, pp. 349–352.
7. Bastos, M., Bai, G., Qvarnstrom, E., and Wadso, I., *Thermochim. Acta*, 2003, vol. 405, pp. 21–30.
8. Tyunina, E.Yu., and Badelin, V.G., *Biofizika*, 2005, vol. 50, no. 6, pp. 835–841.
9. Rodanter, F., *Thermochim. Acta*, 1989, vol. 149, p. 157.
10. Palecz, B., *J. Therm. Anal.*, 1998, vol. 54, pp. 257–263.
11. Catanzano, F., and Barone, G., *Thermochim. Acta*, 1996, vol. 273, pp. 43–52.
12. Arnautova, E.A., Zakharova, M.V., Pivina, T.S., et al., *Izv. Ross. Akad. Nauk, Ser. Khim.*, 1996, no. 12, pp. 2872–2886.
13. Lebedev, Yu.A., and Miroshnichenko, E.A., *Termokhimiya paroobrazovaniya organicheskikh veshchestv* (Thermochemistry of Vaporization of Organic Substances), Moscow: Nauka, 1981.
14. Dewar, M.J.S., Zoebisch, E.G., Healy, E.F., and Stewart, J.J.P., *J. Am. Chem. Soc.*, 1985, vol. 107, no. 13, pp. 3902–3909.
15. Belousov, V.P., and Panov, M.Yu., *Termodinamika vodnykh rastvorov neelektrolitov* (Thermodynamics of Aqueous Solutions of Nonelectrolytes), Leningrad: Khimiya, 1983.
16. Meyer, K., *Physikalische-chemische Kristallographie*, Leipzig: Grundstoffindustrie, 1968.
17. Kikuchi, M., Sakurai, M., and Nitta, K., *J. Chem. Eng. Data*, 1995, vol. 40, no. 4, pp. 935–942.
18. Natarajan, M., Wadi, R.K., and Gaur, H.C., *J. Chem. Eng. Data*, 1990, vol. 35, no. 1, pp. 87–93.
19. Rao, M.V.R., Atreyi, M., and Rajeswari, M.R., *J. Chem. Soc., Faraday Trans. I*, 1984, vol. 80, no. 8, pp. 2027–2032.
20. Reis, J.C.R., Blandamer, M.J., Davis, M.I., and Douheret, G., *Phys. Chem. Chem. Phys*. 2001, vol. 3, pp. 1465–1470.
21. Kitaigorodskii, A.I., *Molekulyarnye kristally* (Molecular Crystals), Moscow: Nauka, 1971.

ISSN 1070-4272, Russian Journal of Applied Chemistry, 2007, Vol. 80, No. 5, pp. 716–721. © Pleiades Publishing, Ltd., 2007.
Original Russian Text © V.N. Bekhterev, E.A. Kabina, 2007, published in Zhurnal Prikladnoi Khimii, 2007, Vol. 80, No. 5, pp. 737–742.

PHYSICOCHEMICAL STUDIES OF SYSTEMS AND PROCESSES

Technology of Vapor-Phase Extraction of Water-Soluble Organic Substances

V. N. Bekhterev and E. A. Kabina

Research Center for Health Resort Treatment and Rehabilitation, Black Sea Regional Administration of Specialized Sanatoria, Ministry of Public Health and Social Development of the Russian Federation, Sochi, Krasnodar krai, Russia

Received June 20, 2006; in final form, March 2007

Abstract—A method of vapor-phase extraction has been suggested for recovery of organic substances from an aqueous medium. The appropriate apparatus have been developed. The method enables use of both hydrophobic and hydrophilic organic liquids. The results of vapor-phase extraction of low-molecular-weight organic acids are discussed in terms of the kinetic model of the process mechanism.

DOI: 10.1134/S1070427207050059

Numerous technologies are based on extraction of target products. A considerable experience has been accumulated in liquid extraction of organic compounds, and theoretical foundations of the process have been developed, which enables prediction of the efficiency of extraction systems. At the same time, the distribution ratios ($K_d = c_{org} : c_{aq}$) of well soluble organic compounds do not exceed 50 even in the best solvent–water systems [1]. The use of hydrophobic alcohols (pentyl, decyl alcohols), acetic acid esters (butyl acetate, heptyl acetate) has shown that the extractive activity of solvents-homologs steadily grows as the number of carbon atoms in their molecules decreases. However, this leads to an increase in the solubility of an extractive agent in water, which does not allow (and even rules out) the use of low-molecular-weight homologs without a special "salting-out" procedure: introduction of large amounts of neutral salts into a water sample. A risk of side chemical processes arises, numerous technological difficulties are encountered, etc.

Here we suggest a possible solution to the problem of use of hydrophilic organic liquids for recovery of water-soluble organic substances: vapor-phase extraction (VPE). Aqueous solutions of low-molecular-weight carboxylic acids served as objects of study.

EXPERIMENTAL

To implement the method of vapor-phase extraction of dissolved organic substances from aqueous objects, we developed the device described in [2]. It served as a basis for creating the extraction unit schematically shown in the figure [3]. The extraction unit comprises, in addition to the necessary, but not shown in the figure, instrumentation for measuring

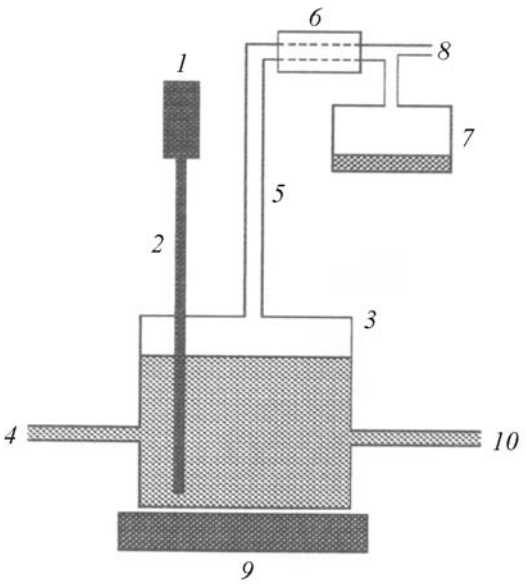

Device for vapor-phase extraction of organic substances (VPE unit): (*1*) liquid batching pump for delivery of the extractive agent, (*2*) pipeline for supply of the extractive agent, (*3*) distillation vessel, (*4*) pipeline for feed, (*5*) steam line, (*6*) condenser for condensing the vapor of the extractive agent with target components, (*7*) vessel for collection of the extract, (*8*) pipe for connecting a compressor or a vacuum pump, (*9*) heater, and (*10*) discharge pipe.

process parameters (temperature, pressure, level and feeding rate of liquids, etc.), the following basic units and parts: liquid batching pump *1* (NNR-5001, former Czechoslovakia), which delivers the extractive agent via pipeline *2* into a liquid sample in the distillation vessel *3*; steam line *5* for discharge of the extractive agent vapor with organic substances being recovered and its delivery to condenser *6* for condensing the vapor and obtaining an extract collected in vessel *7*; pipe *8* for connecting a compressor or a vacuum pump; heater *9*; and pipe *10*, through which the spent liquid is delivered to the next stage of the overall production scheme. At an industrial plant this may be discharge or a further stage in the process chain, as well as delivery to the input of a next VPE unit with another extractive agent.

To perform vapor-phase extraction, the extractive agent used should have a boiling point lower than that of the sample. The sample is heated to the boiling (distillation) point of the extractive agent added. When necessary, for recovery of thermally unstable substances, the distillation temperature can be lowered by reducing the pressure with a vacuum pump via pipe *8*. In the case of vapor-phase extraction under elevated pressure, the vacuum pump is replaced with a compressor.

The vapor-phase extraction can be carried out in the above-described installation in the static mode. In this case, a hydrophilic organic liquid or an immiscible extractive agent with a density exceeding that of the sample is delivered by batcher *1* into the sample volume *3*. Then the sample is heated and the extract-condensate is collected. The extraction may be single-stage or steplike multistage successive, when, before adding the next portion of the extractive agent, the sample is cooled below the boiling point of the extractive agent. A series of successive vapor-phase extracts is obtained, which makes it possible to raise the degree of recovery.

The temperature of the steplike successive VPE, i.e., the boiling point of a sample after addition of a hydrophilic solvent, was gradually raised in the course of the extraction procedure as the solvent evaporated from the sample. The recovery was terminated when the volume of the cocondensate exceeded that of the solvent added by approximately 50%. This corresponded to a VPE temperature of 96 ± 2°C.

The vapor-phase extraction in the dynamic mode involves continuous delivery of the extractive agent by a liquid pump *1* into a sample preliminarily heated to the boiling point of the extractive agent, with this temperature further maintained by heater *9*. Continuous feeding of the starting sample can also be additionally carried out in this mode.

The content of organic acids in the samples being analyzed was found by gas chromatography on an M-3700 chromatograph with a flame-ionization detector and glass column with a length of 1.25 m and inner diameter of 4 mm, packed with Chromaton N-AW-DMCS (0.16 – 0.20) with 15% Carbowax 20M, and a Meta-Khrom analog-digital signal processing system.

We found in the course of the experiment that the degree of recovery depends on individual physicochemical characteristics of dissolved organic substances, amount of the extractive agent used, etc. To explain the results obtained, we suggested a theoretical model that regards the phenomenon under study as a process of distribution of the target substance among two phases: liquid (water) and vapor of the organic extractive agent added.

Gas extraction, in which a target component is transferred into a gas medium (nitrogen, argon, etc.) in contact with a liquid, is widely used in chemical analysis [4, 5]. It should, however, be noted that the vapor-phase extraction as extraction with a vapor of an organic liquid differs from gas extraction (extraction with a gas, blowing-out, bubbling with a gas). The vapor is the gaseous state of a substance, into which it passes upon evaporation, but, in contrast to a gas, it is below the so-called critical temperature. This circumstance indicates that the vapor and the condensed phase have a number of common physicochemical properties. It is known, in particular, that the vapor of individual organic substances and mixtures of these is composed of separate molecules and various associates of these molecules. The critical temperatures of the organic extractive agents used in this study substantially exceed the experimental temperatures. With account of the established terminology and commonly accepted classification, the aforesaid makes it possible to name the extraction of target components from water with a vapor of an organic liquid the vapor-phase extraction (VPE).

As a direct confirmation that the vapor of a solvent added to a sample is involved in recovery of organic substances from an aqueous medium can serve the experimental results listed in Table 1. Experiments on vapor-phase extraction with ethanol, i.e., in the presence of ethanol in an aqueous solution of organic acids, showed that, all other conditions being the same, their equilibrium concentrations in the vapor-and-gas phase noticeably increase, compared with those in gas extraction. Collecting and condensing in

Table 1. Results of a comparative study of gas (air) and vapor-phase (ethanol) extraction of carboxylic acids from water at 100°C

Extraction	Content of indicated organic acid in vapor-and-gas phase,* μg ml^{-1}				
	C_2	C_3	C_4	C_5	C_6
Gas	70 ± 17.4	150 ± 13.8	190 ± 16.8	260 ± 29.9	320 ± 34.0
Vapor-phase (with addition of 3% ethanol to sample)	114 ± 6.0	280 ± 31.7	340 ± 44.9	480 ± 36.6	590 ± 52.5
Initial concentration in water	324	368	287	304	305

* Acid: C_2, acetic; C_3, propionic; C_4, butyric; C_5, valeric; and C_6, caproic.

a separate vessel the vapor of the organic solvent added, formed in evaporation from the sample, i.e., by performing VPE, we can obtain the extract-cocondensate containing the target substances.

In our opinion, the PVE mechanism is as follows. In evaporation of the organic solvent (alcohol) added to the aqueous solution from this solution, it forms a separate phase, the vapor in the bulk of the sample (bubbles) and over the solution in the distillation vessel, to give a heterogeneous liquid–vapor system.

Molecules of the organic substances dissolved in water permanently pass from one phase into another and back. In our case, the vapor of the organic solvent is an extractive agent with respect to water.

The rates of migration of the substances from one phase into another are proportional to the concentrations of the component being recovered in these phases. Accordingly, the following expression is valid for the rates of transfer of molecules from the liquid phase to vapor (v_L) and back (v_V):

$$v_L = k_L c_L, \quad (1)$$

$$v_V = k_V c_V, \quad (2)$$

where k_L and k_V are the corresponding rate constants, determined by the physicochemical parameters of a component and the heterogeneous system under consideration; c_L, concentration of the component in the liquid phase; and c_V, that in the vapor phase.

Under the dynamic equilibrium conditions, the number of substance molecules that passed from the liquid into the vapor in unit time is equal to the number of its molecules returning from the vapor to the liquid:

$$v_L = v_V, \quad (3)$$

$$k_L c_L = k_V c_V, \quad (4)$$

$$c_V/c_L = k_L/k_V = K_{eq}. \quad (5)$$

The validity of the assumption that equilibrium can be attained in VPE is confirmed by the following. It is known that, under the conditions of the dynamic mode of gas extraction, the equilibrium conditions of liberation of the substances into the gas phase are provided at gas flow rates of up to 0.5 l min^{-1} [4], or, recalculated to the amount of the gaseous extracting agent, 0.5/22.4 = 0.022 mol min^{-1}. In our case, e.g., in dynamic vapor-phase extraction with 95 vol % ethanol fed into the sample at a rate of 1 ml min^{-1}, we have the following rate mode: (0.95 ml × 0.7893 g ml^{-1})/46 g mol^{-1} = 0.016 mol of the extractive agent per minute. Consequently, taking into account a certain analogy between the gas and vapor-phase extraction, we believe that our experiment is performed under equilibrium conditions of transboundary transfer of molecules of the components being recovered.

The equilibrium constant K_{eq} characterizes the extractive properties of the organic solvent added. At $K_{eq} < 1$, the equilibrium concentration of the substance being recovered is higher in the liquid (water), and, conversely, at $K_{eq} > 1$, in the vapor phase.

Taking into account the material balance in the case when the target substance is completely concentrated in water at the beginning of an experiment, we can write

$$m_0 = m_L + m_V, \quad (6)$$

where m_0 is the initial mass of the substance in a sample (water); m_L, mass in the liquid phase (water) after the equilibrium is attained; and m_V, mass in the vapor phase (ethanol vapor) after the equilibrium is attained.

Taking into account (6), we can rewrite (5) as

$$K_{eq} = (m_0 - m_L)V_L/m_L V_V = (m_0/m_L - 1)V_L/V_V, \quad (7)$$

where V_L is the volume of the liquid phase, and V_V, that of the vapor phase.

Table 2. Triple successive vapor-phase extraction of carboxylic acids with ethanol, methanol, and isopropanol from water (pH 3–4).* Initial concentration of acids in water: acetic 50–170, propionic 50–150, butyric 35–180 μg ml^{-1}

V_{org}/V_{aq}	n	N/fr	V_D, ml	$c_{ethanol}$, vol %, after VPE		$*K_{eq}$ of indicated acid		
				in condensate	in sample	acetic	propionic	butyric
Ethanol								
1 : 30	11	1	15 ± 2.3	39 ± 2.3	1.2 ± 0.21	0.32 ± 0.036	1.1 ± 0.13	2.1 ± 0.20
	10	2	16 ± 1.2	49 ± 2.6	1.8 ± 0.24	0.26 ± 0.045	1.0 ± 0.10	1.8 ± 0.21
	10	3	17 ± 1.4	52 ± 2.5	2.0 ± 0.44	0.27 ± 0.038	0.9 ± 0.10	1.8 ± 0.22
2 : 30	3	1	36 ± 5.8	40 ± 6.8	1.7 ± 0.65	0.31 ± 0.095	0.7 ± 0.30	1.3 ± 0.52
	3	2	32 ± 1.1	50 ± 3.6	2 ± 1.2	0.2 ± 0.10	0.6 ± 0.32	1.0 ± 0.62
	3	3	35 ± 1.1	53 ± 2.2	3 ± 2.2	0.18 ± 0.090	0.5 ± 0.33	1.1 ± 0.66
3 : 30	3	1	44 ± 6.0	52 ± 1.8	2.2 ± 0.68	0.25 ± 0.046	0.7 ± 0.16	1.1 ± 0.18
	3	2	48 ± 4.9	58 ± 5.1	3.2 ± 0.78	0.22 ± 0.064	0.6 ± 0.11	1.08 ± 0.053
	3	3	49 ± 6.8	63 ± 4.8	4 ± 1.8	0.21 ± 0.053	0.64 ± 0.035	1.1 ± 0.20
Methanol								
1 : 30	4	1	16.2 ± 0.5	28 ± 2.4	1.9 ± 0.13	0.5 ± 0.12	1.7 ± 0.40	3.1 ± 0.57
	4	2	16 ± 2.7	37 ± 4.0	3.33 ± 0.068	0.38 ± 0.053	1.2 ± 0.12	2.3 ± 0.22
	4	3	16 ± 1.5	39 ± 9.9	4.7 ± 0.59	0.32 ± 0.060	1.1 ± 0.27	2.1 ± 0.55
Isopropanol								
1 : 30	3	1	14 ± 1.5	49 ± 8.7	0.8 ± 0.22	0.38 ± 0.078	1.30 ± 0.088	2.5 ± 0.13
	3	2	16 ± 2.5	50 ± 10.8	1.0 ± 0.35	0.32 ± 0.080	1.21 ± 0.077	2.4 ± 0.19
	3	3	16 ± 1.9	57 ± 7.0	1.2 ± 0.41	0.33 ± 0.064	1.1 ± 0.14	2.2 ± 0.49

* V_{org}/V_{aq}, volume ratio of an alcohol and an aqueous solution of organic acids before VPE; n, number of determinations; N/fr, ordinal number of a vapor-phase extract; V_D, volume of the condensate produced in VPE; $c_{ethanol}$, content of alcohol; and $*K_{eq}$, distribution coefficient of an indicated acid between the vapor and liquid.

It is noteworthy that Eq. (7) can be transformed by simple mathematical operations into the expression derived in [4] for calculating the concentration of a substance in the liquid phase in gas extraction.

In VPE, the whole amount of the vapor is condensed and the condensate is collected in a receiving flask, i.e., the mass of the forming vapor (M_V) is equal to that of the distillate obtained (M_D):

$$M_V = M_D, \quad (8)$$

$$V_V\rho_V = V_D\rho_D, \quad (9)$$

$$V_V = (\rho_D/\rho_V)V_D, \quad (10)$$

where ρ_D is the density of the distillate obtained, and V_D, volume of the distillate.

Taking into account (8)–(10), we can write the following expression:

$$K_{eq} = K_{eq}(\rho_D/\rho_V) = V_L/(m_0/m_D - 1)V_D, \quad (11)$$

where m_0 is the mass of the substance being extracted in the condensate, and $m_D = m_V$ because the whole amount of the vapor and, accordingly, the entire mass of the target component is collected in the condensate.

In Eq. (11), the constant quantity ρ_D/ρ_V, because the vapor and the distillate obtained from this vapor are composed in equal proportions of water and an organic extractive agent, is combined with K_{eq}. The content of the components being recovered is incommensurably small and their contribution to the density of the vapor and condensate can be neglected. Expression (11) is a kind of integral characteristic of the VPE procedure, because fluctuations of the composition and density of the vapor and collected condensate are possible in recovery of target components. Nevertheless, the experiment demonstrated (Table 2) that Eq. (11) derived using the above-described theoretical concepts of the VPE mechanism is well observed. The calculated distribution ratio $*K_{eq}$ is a kind of the extraction equilibrium constant and it should depend neither on the concentration of the components being recovered nor on the volumes of the water sample and extractive agent, taken for vapor-phase extraction. A slight decrease in this coefficient in triple succes-

Table 3. Vapor-phase extraction of low-molecular-weight organic acids with ethanol from water in the dynamic mode

Substance being extracted	Ethanol feed rate 1 ml min^{-1}		Ethanol feed rate 2 ml min^{-1}	
	τ, min	$^*K_{eq}$	τ, min	$^*K_{eq}$
Acetic acid	25	0.35 ± 0.031	20	0.37 ± 0.033
	20	0.36 ± 0.039	20	0.22 ± 0.020
			20	0.18 ± 0.024
			20	0.18 ± 0.022
			20	0.17 ± 0.022
			20	0.19 ± 0.026
Propionic acid	25	0.69 ± 0.067	20	0.82 ± 0.089
	20	0.71 ± 0.079	20	0.53 ± 0.063
			20	0.46 ± 0.063
			20	0.45 ± 0.069
			20	0.44 ± 0.062
			20	0.42 ± 0.055
Butyric acid	25	1.36 ± 0.098	20	1.4 ± 0.16
	20	1.4 ± 0.11	20	0.81 ± 0.084
			20	0.72 ± 0.086
			20	0.67 ± 0.072
			20	0.69 ± 0.077
			20	0.68 ± 0.075

sive VPE with ethanol of C_2–C_4 acids, observed as the volume of the extractive agent grows, is presumably due to a rise in the alcohol concentration remaining in the sample after a VPE procedure.

The coefficient $^*K_{eq}$ is determined by the physicochemical properties of a component being recovered and extractive agent. Indeed, replacement of ethanol with methanol leads, as can be seen from a comparison of the results listed in Table 2, to a pronounced increase in this coefficient. Isopropanol exhibited approximately the same activity as ethanol in VPE. If a hydrophobic solvent, carbon tetrachloride, is chosen for vapor-phase extraction of the aliphatic acids mentioned above, the coefficient of vapor-phase extraction decreases dramatically. On replacing ethanol with CCl_4, the value of $^*K_{eq}$ for butyric acid decreases by a factor of more than 30 to be 0.06 ± 0.009. If we remain within the range of acid concentrations in water, used in this study, determination of $^*K_{eq}$ for acetic and propionic acids is difficult under these conditions because of the low sensitivity of the method (GLC-FID). The constant $^*K_{eq}$ in vapor-phase extraction with CCl_4 is 0.005 ± 0.0014 for acetic acid and 0.013 ± 0.0032 for propionic acid. In our opinion, these data open up prospects for the development of a method for selective vapor-phase extraction of target products for technological purposes.

The vapor-phase extraction in the dynamic mode involves continuous feed of the extractive agent by a liquid pump *1* (see figure) into a sample preliminarily heated to the boiling point of the extractive agent. The results obtained in determining the coefficient $^*K_{eq}$ of vapor-phase extraction of a mixture of low-molecular-weight aliphatic acids with ethanol from water at different alcohol feed rates are listed in Table 3. In the experiment, the collected portion of the extract-condensate was delivered after a certain interval of time (extraction time), without interrupting the process, to GLC to determine $^*K_{eq}$. As follows from the data obtained (Tables 2, 3), the constants of vapor-phase extraction of acetic, propionic, and butyric acids with ethanol from water under static (steplike successive extraction) and dynamic conditions virtually coincide. In other words, the extraction equilibrium in the vapor–liquid system, assumed to exist in the theoretical analysis of the VPE mechanism, presumably has enough time to be attained in the course of dynamic VPE at extractive agent feed rates in the range 1–2 ml min^{-1}.

Thus, the mechanism of vapor-phase extraction can be hypothetically represented, in the case of water-soluble extractive agent, as the classical liquid–liquid extraction from a water volume into that of an organic solvent additive, collected as a cocondensate with target components. Being infinitely miscible with water, the cocondensate in fact forms no interface with water.

Hence, in contrast to the conventional liquid extraction, the vapor-phase extraction makes it possible to recover organic compounds from aqueous solutions with water-soluble organic liquids without any additional treatment of a sample. Moreover, compared with the gas extraction, which can only use a limited number of gaseous extractive agents, the vapor-phase extraction can, with a proper choice of an extractive agent from the extremely wide variety of organic solvents, selectively recover separate classes or groups of organic compounds. This is so because the VPE apparatus and the dynamic mode of VPE make it possible to introduce into the system also hydrophobic water-insoluble organic extractive agents. Successive use of VPE and back extraction can potentially provide selective isolation of separate chemical compounds.

An additional number of advantageous properties of VPE should be noted. In contrast to the case of gas extraction, the apparatus to be used in the VPE experi-

ment is considerably simpler because there is no need to use hermetical sealing, compressed gases, pressure gages, etc. Moreover, the vapor-phase extracts obtained can be used in the production chain virtually without any additional procedures.

CONCLUSIONS

The process suggested for vapor-phase recovery of water-soluble organic substances extends the capacity of extraction techniques by making possible use of hydrophilic solvents. The results obtained for the example of low-molecular-weight organic acids indicate that, in the case in question, the efficiency of recovery from aqueous solutions exceeds that in gas extraction. The kinetic model of the mechanism of vapor-phase extraction, presented here, is in satisfactory agreement with the experiment.

REFERENCES

1. Korenman, Ya.I., *Koeffitsienty raspredeleniya organicheskikh soedinenii: Spravochnik* (Distribution Coefficients of Organic Compounds: Reference Book), Voronezh: Voronezh. Gos. Univ., 1992.
2. RF Patent 51 997.
3. RF Patent 58 049.
4. Vitenberg, A.G., *Zh. Anal. Khim.*, 2003, vol. 58, no. 1, pp. 7–21.
5. Rodinkov, O.V., Moskvin, L.N., and Rathour, J.K., *Zh. Anal. Khim.*, 2004, vol. 59, no. 11, pp. 1188–1193.

ISSN 1070-4272, Russian Journal of Applied Chemistry, 2007, Vol. 80, No. 5, pp. 722–725. © Pleiades Publishing, Ltd., 2007.
Original Russian Text © N.P. Kakurkin, A.D. Kirillov, V.V. Shcherbakov, 2007, published in Zhurnal Prikladnoi Khimii, 2007, Vol. 80, No. 5, pp. 743–746.

PHYSICOCHEMICAL STUDIES OF SYSTEMS AND PROCESSES

Solutions in the Calcium Oxide–Ethylene Glycol–Water System

N. P. Kakurkin, A. D. Kirillov, and V. V. Shcherbakov

Mendeleev Russian University of Chemical Engineering, Moscow, Russia

Received May 6, 2006; in final form, March 2007

Abstract—A comprehensive study of solutions formed in dissolution of calcium oxide in ethylene glycol and in its mixtures with water was carried out. The major form of compounds in the solutions was established. The maximum attainable concentration of Ca(II) in solutions was determined in relation to the temperature and composition of the mixed solvent.

DOI: 10.1134/S1070427207050060

Metal alkoxides and their alcoholic solutions find increasing application as intermediate products in fine inorganic synthesis. They are used for the production of simple and complex metal oxides, ceramics, dielectrics, and other substances and materials [1]. Not-too-viscous alkoxide solutions with a reasonably high concentration of base substance are superior to other reagents, in particular, in sol–gel synthesis [2].

Among such calcium-containing compounds, a solution of calcium glycolate in ethylene glycol (EG) shows much promise. It is, for example, successfully used for the production of hydroxylapatite [3, 4]. Ethylene glycol has a higher boiling point compared to other alcohols, which makes it possible to extend the temperature interval of synthesis of various calcium glycolate products. The drawback of the known compound consists in its relatively high cost associated with the use of calcium metal in its synthesis. Therefore, the study of the possibility of using a cheaper and more readily available compound, i.e., calcium oxide, is topical. In this work, the solutions formed by reaction of CaO with EG and with a mixture of EG and water were studied with the aim to substantiate the synthesis conditions.

The reaction of calcium metal with EG, accompanied by hydrogen evolution, yields calcium glycolate solvated with two alcohol molecules [3]:

$$4HOCH_2CH_2OH + Ca \rightarrow Ca(OCH_2CH_2OH)_2 \cdot 2HOCH_2CH_2OH + H_2.$$

The direction and character of reactions proceeding in alkaline-earth metal oxide–alcohol–water systems are still poorly understood. Their study is complicated by the reaction of the above oxides with water, yielding the corresponding hydroxides. For example, preparation of calcium glycolate by dissolution of CaO in anhydrous EG at normal temperature, proceeding with water release,

$$CaO + 2HOCH_2CH_2OH \rightarrow Ca(OCH_2CH_2OH)_2 + H_2O,$$

can be accompanied by the formation of $Ca(OH)_2$. Therefore, it is likely that basic salt, calcium hydroxy glycolate, may be preferentially formed under these conditions:

$$CaO + HOCH_2CH_2OH \rightarrow Ca(OH)(OCH_2CH_2OH).$$

The salt formed can also be solvated with solvent molecules.

The assumption that the second scheme of the process (formation of basic calcium glycolate) is more probable is also supported by the same character of the reactions proceeding in the $CaO–CH_3OH$ [5] and $BaO–CH_3OH$ systems [6]. Also, it may be suggested that, depending on the process temperature and duration, any of the suggested reactions may proceed. In this case, it should be taken into account that EG has low volatility in comparison with water and monohydric alcohols.

The dissolution of CaO in the $EG–H_2O$ mixture containing a fairly large amount of H_2O yields poorly soluble in water $Ca(OH)_2$ as the major product. At the same time, taking into account the behavior of the metal oxide–methanol systems, the reaction of calcium hydroxide with anhydrous EG is likely to yield

other products, i.e., the reaction

$$Ca(OH)_2 + 2HOCH_2CH_2OH \rightleftarrows Ca(OCH_2CH_2OH)_2 + 2H_2O$$

can proceed in both directions depending on the synthesis conditions.

EXPERIMENTAL

We used freshly prepared calcium oxide, EG, and water. Calcium oxide was prepared from analytically pure grade calcium carbonate by calcination at 1000°C for 4 h. The degree of calcination was no less than 99.5%. The concentration of CaO in the compound was no less than 98.5 wt %. Ethylene glycol (analytically pure grade) was dried over sodium sulfate and then distilled in vacuum. Freshly distilled water used for preparing solutions was decarbonated by boiling to remove 1/3 of the initial volume. The specific electrical conductivity of both pure solvents and their mixtures did not exceed 2×10^{-6} S cm^{-1}.

The most promising for use in syntheses are solutions with high concentrations of Ca(II) ions. In this connection, it is appropriate to study in more detail the physicochemical properties of the system under consideration and the interactions in it in the region of the maximal Ca(II) concentration in the liquid phase. Therefore, in the first stage of the study it was necessary to obtain data on the solubility, coexisting equilibrium solid phases, and equilibration time in the CaO–EG–H_2O system. In many cases, determination of the solubility in systems containing organic solvents is known to meet serious difficulties associated with a long time of attainment of the liquid–solid equilibrium. This is especially true for highly viscous solvents, EG in particular. In addition, the true solubility in oxoalkoxide alcoholic solutions is difficult to attain, and their solid phase is mostly a noncrystalline mass [2].

The same characteristic features were revealed in studying the solubility in the CaO–EG–H_2O system. In particular, it was established that, with approaching saturation, the solutions become viscous gel-like systems, and no coexisting equilibrium solid phases can be separated from them by traditional methods. In the context of the above problems, we attempted to determine the maximum attainable concentration of Ca(II) in EG and its aqueous solutions.

The CaO dissolution in EG and its aqueous solutions was performed with vigorous agitation at a preset temperature. We used in the experiments a glass vessel equipped with a thermostating jacket and a stirrer with a liquid seal. The rotation rate of the stirrer was 300 rpm. By gradual addition of CaO we reached the state when the dissolution in the system virtually ceased, which was controlled visually.

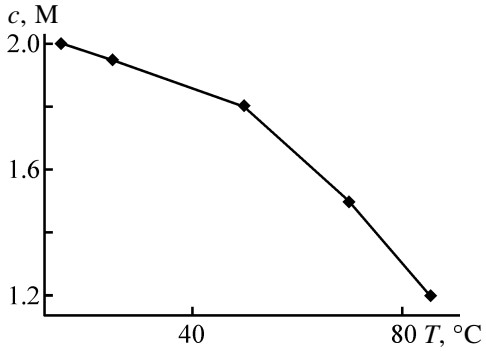

Fig. 1. Maximum attainable Ca(II) concentration c in solutions of the CaO–EG system vs. temperature T.

The CaO dissolution in EG was studied in the 25–90°C range, and that in its aqueous solutions, at 25°C. The calcium(II) concentration in the solutions prepared was determined by complexometric titration [7], with the relative determination error not exceeding 0.5%.

It was established that the Ca(II) concentration in the solution is maximal (about 2 M) at 25°C, the lowest temperature studied (Fig. 1). The Ca(II) concentration in the solution decreases with increasing temperature and attains a value of about 1.2 M at 90°C, i.e., the temperature coefficient of the CaO solubility in EG is negative. It should be noted that the similar properties are exhibited by alkoxides of alkali and alkaline-earth metals, whose solubility in the corresponding alcohols decreases with increasing temperature [8, 9]. The obtained values of the Ca(II) concentration in the solution are higher by two orders of magnitude than those in saturated aqueous solutions of calcium hydroxide at the same temperatures. It was also found that the viscosity suitable for practical use is exhibited by the solutions containing no more than 0.5 M Ca(II), which corresponds to its concentration in solutions prepared from calcium metal and used for inorganic synthesis [3].

In studying the CaO dissolution in aqueous EG solutions at 25°C, we determined the region of existence of solutions in the CaO–EG–H_2O system at the ethylene glycol concentration in the mixed solvent varied from 5 to 100 vol %. As expected, the Ca(II) concentration in the solution increases with increasing concentration of the organic component in the mixed

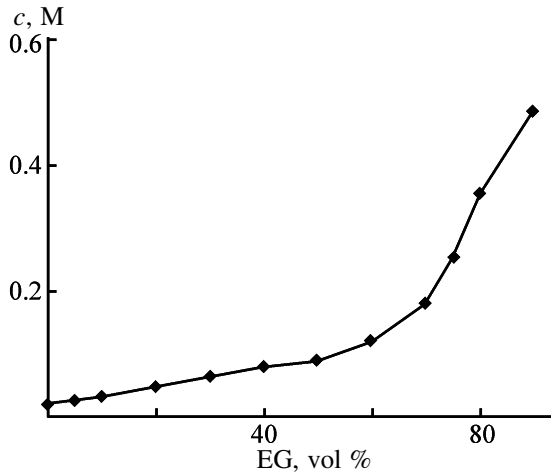

Fig. 2. Maximum attainable Ca(II) concentration c vs. EG concentration in the mixed solvent.

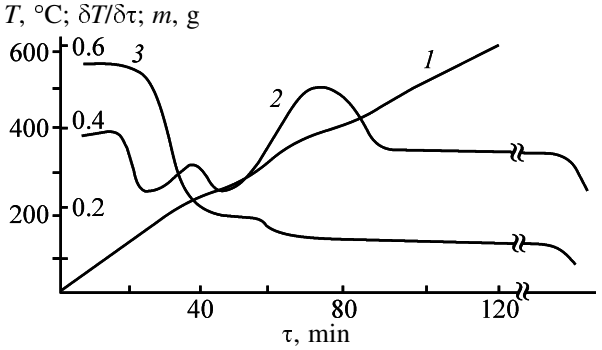

Fig. 3. Curves reflecting variation with time τ of (*1*) temperature T, (*2*) differential change in temperature $\delta t/\delta\tau$, and (*3*) sample weight m.

solvent (Fig. 2). It should be noted that the bend in the plot at 65 vol % concentration of EG approximately corresponds to the composition of the solvate $HOCH_2CH_2OH \cdot 2H_2O$ formed in the EG–H_2O mixture.

The composition of the compounds formed in the CaO–EG system was determined by NMR spectroscopy. The ^1H NMR spectra were recorded on a Tesla BS-467 NMR spectrometer (60 MHz) at 20°C. The chemical shift was determined relative to an external reference (tetramethylsilane). The ^{13}C NMR spectra were recorded on a Bruker WP-200 NMR spectrometer. Deuterated acetone was used as external reference. The Ca(II) concentration in the solutions examined was 0.5 M.

Along with the signal at 64.3 ppm from the CH_2 groups of ethylene glycol, the ^{13}C NMR spectra of the solution formed in the CaO–EG system contain weaker signals at 65.7 and 69.8 ppm, which are probably due to calcium hydroxy glycolate. The ^1H NMR spectrum also confirms the presence of hydroxy glycolate in the solution. In the presence of electrolyte in the solution, the spectral line at 4.3 ppm, assigned to OH groups of the pure solvent, becomes broadened and asymmetrical, which confirms the presence of different types of OH groups. Thus, NMR data show that the main species formed in solutions of the CaO–EG system at ambient temperature is calcium hydroxy glycolate, which is also confirmed by the previous pH-metric studies of these solutions [10]. The presence of hydroxy group in the composition of the dissolved substance should be taken into account in synthesis of calcium-containing compounds based on these solutions. For example, the conditions of the hydroxylapatite preparation may differ from those when calcium glycolate is used as intermediate [3, 4].

As shown above, the fact that the boiling point of ethylene glycol is higher than that of other alcohols makes it possible to considerably extend the temperature interval in which different glycolate products can be synthesized. To get insight into the processes occurring in the CaO–EG system at higher temperature and obtain additional information about the composition and properties of the solutions in this system, a thermogravimetric study was also performed. The dissolved substance was salted-out from concentrated solutions of the CaO–EG system by addition of dioxane. The substrate obtained was analyzed on an OD-102 derivatograph (MOM, Hungary). The derivatograms of the concentrate containing 25 wt % Ca(II) were recorded in the 20–1000°C range.

The DTA curves have endothermic and exothermic peaks (Fig. 3). The endothermic peak at about 190°C is associated with removal of EG molecules of solvation, which is in agreement with the observed weight loss.

As known, above 150°C monosubstituted alkali metal glycolates disproportionate with the formation of disubstituted glycolates and release of EG. In our case, the effect observed corresponds to the transformation of calcium hydroxy glycolate into disubstituted glycolate:

$$Ca(OH)OCH_2CH_2OH \xrightarrow{\Delta} Ca(OCH_2CH_2O) + H_2O.$$

The exothermic effect without weight change is observed at 320°C and is likely due to the oxidation of disubstituted calcium glycolate to calcium carbonate by the reaction

$$Ca(OCH_2CH_2O) + 2.5O_2 \xrightarrow{\Delta} CaCO_3 + CO_2 + 2H_2O,$$

which proceeds without change in the weight of the condensed phase.

Thus, the results of the derivatographic study also show that the solvated basic calcium glycolate exists in solutions of the CaO–EG systems up to 150°C. The transformations occurring in the system at higher temperatures should be taken into account when choosing synthesis conditions of calcium-containing compounds.

CONCLUSIONS

(1) The maximum attainable concentration of Ca(II) in solutions of the CaO–EG system was determined. With increasing temperature from 25 to 90°C, it decreases from 2 to 1.2 M.

(2) The maximum attainable concentration of Ca(II) in solutions of the CaO–ethylene glycol–H_2O ternary system at 25°C was determined. The solubility of calcium oxide increases with increasing ethylene glycol concentration in the mixed solvent. The region of the solution concentrations recommended for the use in inorganic synthesis was determined (concentration up to 0.5 M).

(3) The NMR and thermogravimetric analyses show that calcium hydroxy glycolate is the major species in the solutions formed by dissolution of calcium oxide in ethylene glycol.

(4) The transformations in the calcium oxide–ethylene glycol system at elevated temperature were studied. Calcium hydroxy glycolate is preserved in the system up to 150°C. At higher temperatures, disubstituted calcium glycolate is formed, which is then oxidized to calcium carbonate.

REFERENCES

1. Turevskaya, E.P., Yanovskaya, M.I., and Turova, N.Ya., *Neorg. Mater.*, 2000, vol. 36, no. 3, pp. 265–274.
2. Turova, N.Ya., *Usp. Khim.*, 2004, vol. 73, no. 11, pp. 1131–1154.
3. Weng, W.Y., Yang, H., and Ge, M., *Mater. Chem. Phys.*, 1998, vol. 55, no. 2, pp. 102–107.
4. Weng, W.Y., Huang, L., and Han, G., *Appl. Organomet. Chem.*, 1999, vol. 13, no. 8, pp. 555–564.
5. Berner, E., *Ber. Deutsch. Chem. Ges.*, 1938, vol. 71, no. 9, pp. 2015–2021.
6. Scholder, R. and Kreutz, M., *Justus Liebigs Ann. Chem.*, 1965, vol. 653, no. 1, pp. 1–11.
7. *GOST* (State Standard) *10398–76: Complexometric Method for Determining the Main Substance Content.*
8. Turova, N.Ya. and Novoselova, A.V., *Izv. Akad. Nauk SSSR, Neorg. Mater.*, 1967, vol. 3, no. 2, pp. 351–360.
9. Turova, N.Ya., *Zh. Neorg. Khim.*, 2000, vol. 45, no. 2, pp. 243–249.
10. Zav'yalova, E.M., Kakurkin, N.P., and Kirillov, A.D., *Usp. Khim. Khim. Tekhnol.: Tr. Ross. Khim.-Tekhnol. Univ. im. D.I. Mendeleeva*, 2004, vol. 18, no. 5, p. 103.
11. Turova, N.Ya., and Novoselova, A.V., *Usp. Khim.*, 1965, vol. 74, no. 3, pp. 385–433.

ISSN 1070-4272, Russian Journal of Applied Chemistry, 2007, Vol. 80, No. 5, pp. 726–729. © Pleiades Publishing, Ltd., 2008.
Original Russian Text © A.P. Yaroshenko, M.V. Savos'kin, N.I. Lazareva, V.N. Mochalin, A.N. Magazinskii, 2007, published in Zhurnal Prikladnoi Khimii, 2007, Vol. 80, No. 5, pp. 747–750.

SORPTION AND ION-EXCHANGE PROCESSES

A New Method for Production of Composites Consisting of Expanded Graphite and Amorphous Carbon

A. P. Yaroshenko, M. V. Savos'kin, N. I. Lazareva, V. N. Mochalin, and A. N. Magazinskii

Litvinenko Institute of Physicoorganic and Coal Chemistry, National Academy of Sciences of Ukraine, Donetsk, Ukraine

Received May 25, 2006

Abstract—A new method was developed for production of composites constituted by expanded graphite and amorphous carbon from residual graphite hydrosulfate and a precursor of amorphous carbon, sucrose.

DOI: 10.1134/S1070427207050072

At present, the problem of water treatment to remove contaminants is exceedingly topical [1]. It is frequently solved using sorption methods. Floating carbon–carbon sorbents based on expanded graphite (EG) and amorphous carbon (AmC) are among the most promising sorbents because they combine the valuable properties of the individual components: large surface area and high sorption activity of amorphous carbon with the buoyancy of expanded graphite. The methods for production of EG–AmC composites, described in the literature, are multistage processes performed in an inert atmosphere (He, Ar) and employ expensive raw materials, organic solvents, and a binder for combining the components of the composite [3, 4]. Procedures of this kind are laborious and energy-intensive and have an increased impact on the environment. Consequently, industrial manufacture of EG–AmC composite sorbents requires that methods for their production should be improved and simplified.

Rather attractive in this regard is a single-stage process for production of EG–AmC composites, in which expansion of a graphite intercalation compound, its impregnation with a precursor of amorphous carbon, and carbonization of the precursor would occur simultaneously, in the same process stage, without organic solvents and inert atmosphere. Until now, a process of this kind could not be performed because the commonly used graphite intercalation compounds are effectively expanded only at 900–1200°C, whereas amorphous carbon is strongly oxidized in air at these temperatures, which leads to irrational utilization of raw materials.

Recently, an industrial method for manufacture of residual graphite hydrosulfate, which can be effectively expanded even at temperatures of about 500°C, has been developed [5]. With this compound, it was possible to perform for the first time a single-stage process for production of EG–AmC composites at comparatively low temperatures and, as a result, to discard the inert atmosphere. A successful choice of a precursor of amorphous carbon, sucrose, also made it possible to avoid use of an additional binder for combining the components of a composite.

EXPERIMENTAL

To obtain EG–AmC composites, we used residual graphite hydrosulfate [TU (Technical Specification) U 26.8-20 372 011-001–2002] produced from a GSM-1 flake graphite from Zaval'evskoe deposit (Ukraine) and sucrose (Merck) with an ash residue of 0 wt % as a precursor of amorphous carbon. Sucrose was ground into a fine powder and mixed in the course of several minutes with residual graphite hydrosulfate in a glass vessel on an MPW-300 stirrer. After that, distilled water was added in an amount equal to the mass of graphite and agitation was continued for an additional 10 min. The content of components of the mixture was varied, but its total mass remained constant (25 g). After the mixing stage, the composite was kept at 105°C for 2 h for partial caramelization of sucrose. After that, the mixture was transferred in 3-g portions to cold stainless steel cells placed for 4 min in a Fisher Scientific Isotemp® Model 650 programmable muffle furnace heated to 650°C. The thermal treat-

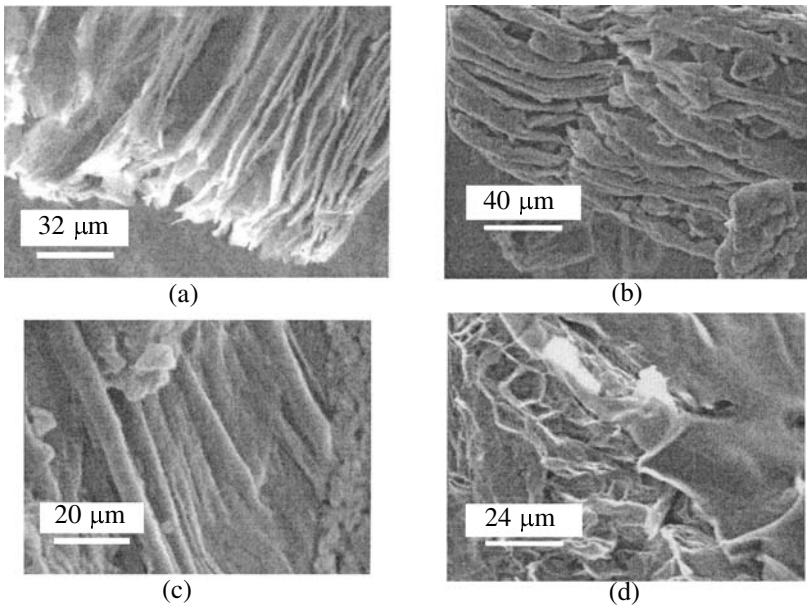

Fig. 1. SEM micrographs of products formed in different stages of synthesis of the EG–AmC composite material. RGH: (a) starting, (b) after mixing with sucrose, (c) after keeping in an oven at 105°C for 2 h; (d) EG–AmC composite.

ment yielded a finished product in 25 to 70% yield, depending on the composition of the starting mixture. The specific surface area was found by the method of low-temperature adsorption of argon (BET) in accordance with GOST (State Standard) 13 144–79. The composites obtained were studied by scanning electron microscopy (SEM) on a JEOL JSM-T300 instrument.

The sorption of phenol from its aqueous solutions with a concentration of 10–50 mg l^{-1} by composite samples was studied in a temperature-controlled (25°C) glass vessel with a ground-in glass cover and a magnetic stirrer. A 500-ml portion of a phenol solution was poured into the reactor, 0.35–0.40 g of a composite (1–2-mm grains) was placed on the surface of the solution, and agitation was switched on. The liquid phase was sampled at regular intervals of time and the content of phenol in the samples was determined by the standard photoelectrocolorimetric method with 4-aminoantipyrine [6]. The experiment was carried out in the course of 12–48 h until the sorption equilibrium was attained, which was indicated by the fact that the phenol concentration in the solution ceased to vary.

Figure 1a shows a micrograph of the starting residual graphite hydrosulfate (RGH) produced by the method described in [5]. It can be seen that, in contrast to other graphite intercalation compounds [7], the RGH used shows a considerable separation into layers. This results in that the second component of the composite easily penetrates, even under simple mechanical agitation, into spaces between graphite stacks. As a result, graphite flakes are homogeneously and densely filled with particles of the second component, precursor of amorphous carbon (sucrose particles in the given case) (Fig. 1b).

Further keeping in an oven at 105°C for 2 h leads to partial caramelization of sucrose and spreading of the melt to give a uniform thin layer over the surface of RGH flakes (Fig. 1c).

The caramelization of sucrose under mild conditions is accompanied by polycondensation reactions, which favors an increase in the yield of amorphous carbon in the course of its subsequent carbonization [8, 9].

The material obtained upon caramelization of sucrose is subjected to heat treatment at 300–900°C, which leads to swelling of the graphite intercalation compound, which is conjugated in space and time with the progressing melting and caramelization of sucrose, impregnation of the cellular structure of swollen graphite with molten caramel, and carbonization of the precursor of amorphous carbon, to give the final product, EG–AmC composite. The heat treatment parameters (in particular, temperature and time of treatment) exert a strong influence on the properties of the material obtained. In special-purpose experiments, we determined the optimal values of these parameters, with production of composite materials

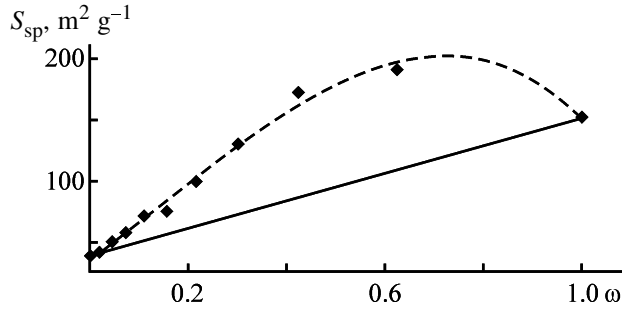

Fig. 2. Specific surface area S_{sp} of EG–AmC composites vs. their composition ω (mass fraction of amorphous carbon in a composite). Straight line, calculation in terms of the additive model with account of the yield of amorphous carbon.

having the most developed surface used as the target condition. Values of the specific surface area of EG–AmC composites in relation to the temperature and time of treatment are listed below.

Specific surface area S_{sp} of an EG–AmC composite with 16 wt % amorphous carbon in relation to the temperature and time of swelling

T, °C	300	400	450	500	550	600
S_{sp}, m^2 g^{-1}	0.4	2	8	29	50	29
T, °C	650	700	750	800	850	900
S_{sp}, m^2 g^{-1}	27	27	27	31	21	19

S_{sp}, m^2 g^{-1}	22	70	89	90	66	53	52
τ, min	2	3	4	5	7	10	30

The maximum surface area is obtained at 550°C, with keeping at this temperature for 4 min. Any further increase in the temperature or time of treatment is inadvisable. Moreover, it follows from the data presented here that this leads to burning-out of the amorphous carbon phase. The yield of the composite at the optimal composition and time and temperature of treatment is about 50%.

Figure 1d shows a SEM micrograph of one of the EG–AmC composites obtained. The micrograph well shows the macroporous structure of the composite with coarse mouth-like pores belonging to the graphite matrix and the amorphous carbon phase coating the vermicules of expanded graphite. The texture of the material in Fig. 1d is typical of composites produced from expanded graphite and in situ prepared activated carbon [10, 11].

The partial melting of sucrose in the production of the composite, accompanied by spreading of the melt over the surface of the graphite substrate, provides an intimate contact between the two phases in the product obtained. This structure imparts a sufficient mechanical strength to the EG–AmC composite. An EG–AmC composite with an AmC content of 16 wt %, placed on the surface of water, remained intact for a month.

Figure 2 compares specific surface areas of the EG–AmC composites obtained, measured by the method of low-temperature sorption–desorption of argon, with those calculated in terms of the additive model. The additive model presumes that the specific surface area of the composite is the sum of the specific surface areas of its individual components:

$$S_{sp} = \omega_{AmC} S_{sp.AmC} + \omega_{EG} S_{sp.EG}, \quad (1)$$

where S_{sp} is the specific surface area of an EG–AmC composite of composition $\omega_{AmC} : \omega_{EG}$ (m^2 g^{-1}); ω_{AmC} and ω_{EG}, mass fractions of AmC and EG in a composite; and $S_{sp.AmC}$ and $S_{sp.EG}$, specific surface areas of the individual components (m^2 g^{-1}).

In the entire range of sucrose concentrations, except at the end points corresponding to the individual components, the measured specific surface areas of the composites obtained markedly exceed the values calculated by Eq. (1). The deviations grow as the content of amorphous carbon in the composite increases. This behavior can be attributed to a concerted effect of two factors: (i) acid catalysis of condensation reactions that occur upon heating of sucrose and (ii) activation of the forming amorphous carbon by gaseous components (H_2SO_4, SO_2, SO_3, etc.) and water, liberated in expansion of residual graphite hydrosulfate.

Because the composites obtained were intended from the very beginning for use as high-efficiency floating sorbents for purification of natural and waste water, we studied their behavior in sorption of a real contaminant, phenol, from aqueous solutions. The measured values of the limiting sorption of the composites for phenol grow as the fraction of amorphous carbon increases (Fig. 3) to reach a maximum at an AmC content of the composite equal to 63 wt %. A clearly pronounced correlation is observed between the limiting sorption capacities of the composites for phenol and their specific surface areas, with a correlation coefficient ρ = 0.953 (Fig. 3). In this case, despite the small specific surface area of the composite with 63 wt % AmC (S_{sp} = 192 m^2 g^{-1}), it shows a rather high limiting sorption capacity for phenol (A = 23.7 mg g^{-1}), i.e., it is virtually as good in this regard as commercial samples of granulated activated carbons [12]. At the same time, the EG–AmC composite, in contrast to activated carbon, has buoyancy, which

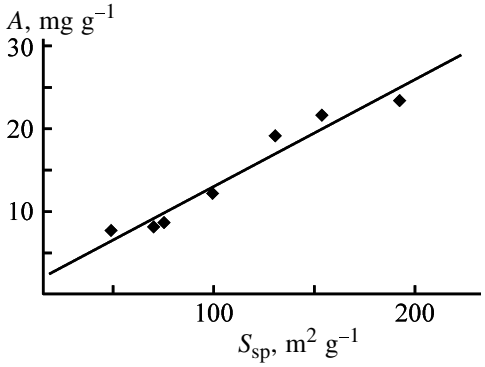

Fig. 3. Sorption capacity A of the EG–AmC composite for phenol vs. the specific surface area S_{sp} of the composite.

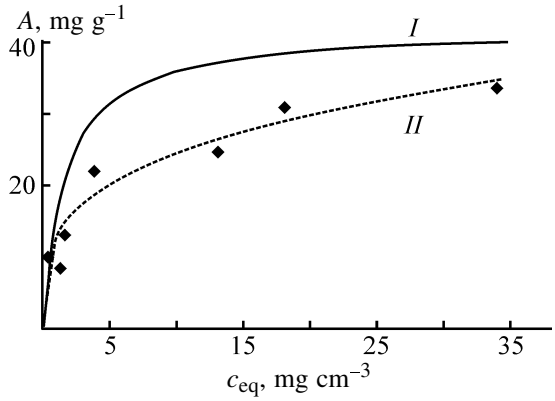

Fig. 4. Isotherm of phenol sorption A by a composite containing 63 wt % amorphous carbon. (c_{eq}) Equilibrium concentration of phenol. Points, experimental data; calculation: (*I*) by Langmuir equation and (*II*) by Freundlich equation.

markedly facilitates purification of large open aquatic surfaces and, in particular, natural water basins.

Figure 4 shows an isotherm of phenol sorption at 25°C by a composite containing 63 wt % amorphous carbon. The Langmuir and Freundlich equations were used as models in experimental data processing. The data obtained are better described by the Freundlich isotherm, which is characteristic of adsorption on surfaces with an exponential energy distribution of active centers. This indicates that, in all probability, there occur both chemical (chemisorption involving surface functional groups) and physical types of adsorption [13].

CONCLUSIONS

(1) A new method for production of composite materials composed of expanded graphite and amorphous carbon from residual graphite hydrosulfate and sucrose was suggested. The method is distinguished from the presently existing techniques by lower time and energy expenditure and better availability of raw materials.

(2) It was shown by scanning electron microscopy that the products obtained are indeed composite materials composed of expanded graphite and amorphous carbon, in which an intimate contact between the solid phases of graphite and amorphous carbon is provided by specific features of the synthesis of the composite. This yields a sufficient mechanical strength of the materials obtained.

(3) Synthesis of composites by the method suggested leads to an additional increase in their surface area, compared with the additive value. This increase is provided by acid catalysis of the condensation reactions occurring in heating of sucrose and activation of the forming amorphous carbon by gaseous acid products evolved in expansion of residual graphite hydrosulfate.

(4) The sorption activity of the materials obtained in absorption of phenol from its aqueous solutions is comparable with that of commercial activated carbons. The composites obtained are favorably distinguished from activated carbons by their capacity to remain on the surface of a liquid for a long time.

REFERENCES

1. Liu, D.H.R. and Liptak, B.G., *Wastewater Treatment*, Boca Raton: Lewis, 2000.
2. Tryba, B., Tsumura, T., Janus, M., et al., *Appl. Catal. B, Environ.*, 2004, vol. 50, p. 177.
3. US Patent 5228701.
4. Mareche, J.F., Begin, D., Furdin, G., et al., *Carbon*, 2001, vol. 39, no. 5, pp. 771–773.
5. Yaroshenko, A.P., Savos'kin, M.V., Magazinskii, A.N., et al., *Zh. Prikl. Khim.*, 2003, vol. 76, no. 8, pp. 1269–1272.
6. Lur'e, Yu.Yu. and Rybnikova, A.I., *Khimicheskii analiz proizvodstvennykh stochnykh vod* (Chemical Analysis of Industrial Wastewater), Moscow: Khimiya, 1974, pp. 259–261.
7. Park, S.-J., Kim, K.-S., and Hong, S.-K., *Hwahak Konghak*, 2003, vol. 41, no. 6, pp. 802–807.
8. US Patent Appl. 03/0066523.
9. Ukrainian Patent 74868.
10. Menard, D., Py, X., and Mazet, N., *Carbon*, 2003, vol. 41, pp. 1715–1727.
11. Py, X., Daguerre, E., and Menard, D., *Carbon*, 2002, vol. 40, pp. 1255–1265.
12. Buzanova, G.N., Tubolkin, A.F., Gaenko, A.V., et al., *Zh. Prikl. Khim.*, 1999, vol. 72, no. 8, pp. 1328–1330.
13. Butt, H.J., Graf, K., and Kappl, M., *Physics and Chemistry of Interfaces*, Chichester: Wiley, 2003.

ISSN 1070-4272, Russian Journal of Applied Chemistry, 2007, Vol. 80, No. 5, pp. 730–733. © Pleiades Publishing, Ltd., 2007.
Original Russian Text © L.F. Kozin, N.V. Mashkova, F.D. Manilevich, B.I. Danil'tsev, 2007, published in Zhurnal Prikladnoi Khimii, 2007, Vol. 80, No. 5, pp. 751–754.

APPLIED ELECTROCHEMISTRY AND CORROSION PROTECTION OF METALS

Electrochemical Behavior of Manganese in Chloride–Bromide–Ammonium Electrolytes

L. F. Kozin, N. V. Mashkova, F. D. Manilevich, and B. I. Danil'tsev

Vernadsky Institute of General and Inorganic Chemistry, National Academy of Sciences of Ukraine, Kiev, Ukraine

Received November 30, 2006

Abstract—Halide–ammonium electrolytes were developed for electrochemical production of high-purity manganese.

DOI: 10.1134/S1070427207050084

Metallic manganese of purity 99.7–99.8% [GOST (State Standard) 6008–90] is produced by electrolysis, as a rule, from sulfate–ammonium solutions with the use of insoluble lead cathodes [1]. A major disadvantage of this technique is that cathode deposits of manganese contain inclusions of sulfur (0.03–0.1%) and alloying components of lead anodes: tin, antimony, and cobalt [1, 2].

High-purity manganese is necessary for obtaining new semimagnetic semiconductors, single- and polycrystalline ferrites, materials with magnetooptical properties and luminophores, high-purity metal oxide catalysts and inorganic sorbents, and precision alloys. High-purity manganese can be obtained by electrolysis on replacing sulfate–ammonium electrolytes with those of halide–ammonium composition [3, 4]. Development of promising electrolyte compositions requires detailed information about the electrochemical behavior of manganese in these electrolytes, including that concerning the kinetics and mechanism of anodic dissolution of manganese and cathodic reduction of manganese ions. Published data on fundamental aspects of these electrode processes are rather contradictory.

The standard electrode potential of manganese is –1.185 V [5]. Therefore, it is necessary to take into account corrosion processes in cathodic deposition of manganese, which may govern the current efficiency by the metal. At low current densities, the rate of electroreduction of Mn^{2+} ions may be comparable with the rate of corrosion dissolution of cathode deposits of manganese.

The aim of this study was to determine cathode current efficiencies by manganese in its deposition from chloride–bromide–ammonium electrolytes on various cathode supports and to analyze the kinetics and mechanism of discharge–ionization of manganese.

The cathode current efficiencies by manganese were found from changes in the mass of cathodes thoroughly washed after electrolysis and dried with ethanol and diethyl ether and from the theoretical amounts of manganese that would be deposited on the cathodes at a 100% current efficiency by manganese. Polarization curves were measured on a smooth rotating disc electrode (RDE) made of electrolytic manganese, with a PI-50-1 potentiostat and PR-8 programmable unit at a potential sweep rate of 4 mV s^{-1} and electrode rotation rate of 980 rpm. The cathode and anode spaces of a glass cell were separated by a glass filter. The atmospheric oxygen dissolved in the electrolyte was removed with a flow of high-purity nitrogen. The electrolyte temperature was maintained with a U-4 thermostat. The potentials of the working electrode were measured relative to a saturated silver chloride reference electrode. A plate of electrolytic manganese served as the auxiliary electrode. The electrolytes were prepared from $MnCl_2$ of chemically pure grade, NH_4Br of ultrapure grade, and water double-distilled in a quartz apparatus. In the electrolytes studied, the exchange equilibrium with the electrode was attained in the course of 3–5 min, after which the pH value of the solution was 5.5 ± 0.1.

Figure 1 shows the dependences of the current efficiency by manganese, η (%), on the cathode current density, measured at 25°C in $MnCl_2$ + NH_4Br solutions of various quantitative compositions on several metals used as cathode supports. It can be seen that the current efficiency by manganese depends on the

electrolyte composition. Changing the NH_4Br concentration within the range 0–0.5 M only slightly affects the value of η, which is as high as 40% in a solution composed of 1.0 M $MnCl_2$ + 0.5 M NH_4Br. As the NH_4Br concentration is raised to 2.0 (curve *5*) and 3.0 M (curve *6*) in a solution containing 1.0 M $MnCl_2$, the value of η on a titanium support increased to 70 and 73%, respectively.

Gamali et al. [6] found that η depends on the atomic radius of the metal of a cathode support. Manganese is deposited with a high current efficiency on metals whose atomic radii are close to that of manganese (1.30 Å). From this standpoint, the most promising metals for use as cathode supports are Ni (1.24 Å), Co (1.25 Å), Fe (1.26 Å), Cu (1.28 Å), Ir (1.35 Å), Pt (1.38 Å), and Zn (1.39 Å), as well as Cr (1.27 Å) and Rh (1.34 Å) [7]. It is known that titanium has a high chemical resistance in electrolyte solutions, but its atomic radius (1.46 Å) [7] is markedly different from that of manganese. In this study we compare the values of η obtained in an electrolyte of the composition 2 M $MnCl_2$ + 2 M NH_4Br on titanium (Fig. 1, curve *7*) and nickel (Fig. 1, curve *8*) supports at various current densities. In the current density range 160–300 mA cm^{-2}, these values were 83–86% on titanium and 94–96% on nickel, despite that the overvoltage of hydrogen evolution on titanium (0.97 V) exceeds that on nickel (0.62 V) [8]. The overvoltage of hydrogen evolution on mercury is very high (1.40 V) [8], and, therefore, η values as high as 99.5–100% were obtained on a manganese amalgam cathode (Fig. 1, curve *9*).

Figure 2 shows experimental anodic and cathodic polarization curves measured on a manganese RDE in an electrolyte composed of 2.0 M $MnCl_2$ + 2.0 M NH_4Br at pH 5.5±0.1 and temperatures of 18, 40, and 60°C (Fig. 2a) and the same curve in the semilog coordinates. It can be seen that the anodic polarization curves are smooth, whereas the cathodic curves have inflections indicating that the cathodic process is hindered in certain range of potentials. As the temperature is elevated, the rates of the anodic and cathodic processes grow and the regions of current delay on the cathodic curves are shifted to more negative potentials and higher current densities.

Inflections in the cathodic polarization curves of manganese are attributed in the literature to attainment of limiting currents of kinetic or diffusion nature [9, 10] or to occurrence of corrosion processes [11]. However, beyond the region of limiting currents, the rate-determining electrode reaction responsible for the limiting current should change. For example,

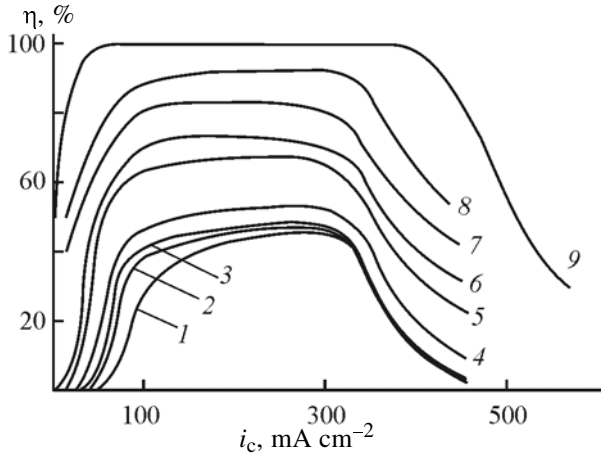

Fig. 1. Current efficiency by manganese η vs. the cathode current density i_c in (*1–6*) 1.0 M $MnCl_2$ and (*7–9*) 2.0 M $MnCl_2$ solutions at various NH_4Br concentrations (25°C). Cathode support: (*1–7*) Ti, (*8*) Ni, and (*9*) Hg. NH_4Br concentration, M: (*1*) 0, (*2*) 0.1, (*3*) 0.5, (*4*) 1.0, (*5, 7–9*) 2.0, and (*6*) 3.0.

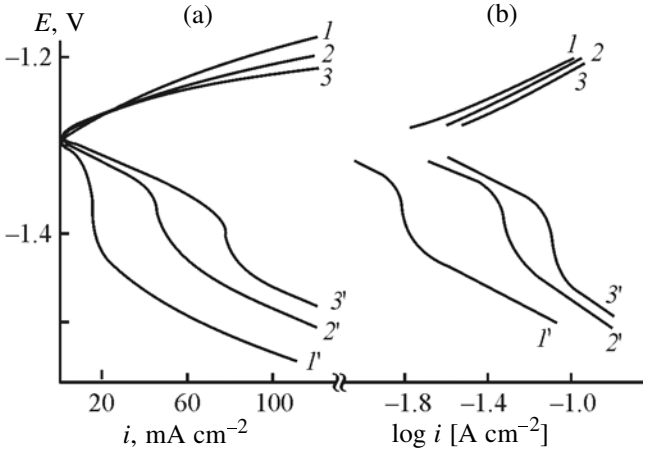

Fig. 2. (a) *E–i* and (b) *E*–log *i* dependences obtained on manganese RDE (980 rpm) in a solution composed of 2.0 M $MnCl_2$ + 2.0 M NH_4Br (pH 5.5±0.1) at various temperatures. (*E*) Potential and (*i*) current density. Polarization curves: (*1–3*) anodic and (*1'–3'*) cathodic. Temperature, °C: (*1*) 18, (*2*) 40, and (*3*) 60.

the discharge of Mn^{2+} ions can be replaced with hydrogen liberation from water, or discharge of high-ligand complexes $[MnCl_4]^{2-}$ may occur instead of the discharge of low-ligand complexes [$MnCl^-$] or [$MnCl_2$] [12]. Such changes of the mechanism of the electrode process at the manganese cathode have not been confirmed experimentally, despite being postulated by numerous authors for explaining the "anomalous" run of polarization curves [1, 9–11].

Inflections in the cathodic polarization curves of manganese are attributed in the literature to attainment of limiting currents of kinetic or diffusion nature

[9, 10] or to occurrence of corrosion processes [11]. However, beyond the region of limiting currents, the rate-determining electrode reaction responsible for the limiting current should change. For example, the discharge of Mn^{2+} ions can be replaced with hydrogen liberation from water, or discharge of high-ligand complexes $[MnCl_4]^{2-}$ may occur instead of the discharge of low-ligand complexes $[MnCl^-]$ or $[MnCl_2]$ [12]. Such changes of the mechanism of the electrode process at the manganese cathode have not been confirmed experimentally, despite being postulated by numerous authors for explaining the "anomalous" run of polarization curves [1, 9–11].

Probably, the occurrence of an inflection in the cathodic polarization curves of manganese in solutions of its salts is due to a change in the surface charge of the electrode after the attainment of the zero-charge potential E_{zc}. As can be seen in Fig. 2, the potential of the onset of the inflection in the polarization curve obtained at 18°C is –1.332 V (relative to silver chloride electrode), which corresponds to the reference value of E_{zc} for manganese (–1.11 V relative to standard hydrogen electrode [13]). As the temperature is raised, the potential of the onset of the inflection shifts in the negative direction to –1.349 V relative to silver chloride electrode at 40°C and –1.398 V at 60°C.

It should be noted that inflections in the cathodic polarization curves at a potential of an uncharged electrode surface were first observed by Kolotyrkin and co-workers in a study of the hydrogen evolution on a lead electrode, and later also on thallium and cadmium electrodes, in a sulfuric acid solution [14].

Clearly pronounced linear portions are seen in the polarization curves plotted in the semilog coordinates (Fig. 2b), with portions of this kind present in the cathodic curves both before and after the inflections. The only electrode process occurring on manganese anodes in the region of linear portions of the polarization curves is ionization of manganese. The slope of the linear portion of the anodic curve obtained at 18°C is 0.116 V per $\log i$ unit; on raising temperature to 60°C, this parameter slightly increases. The linear portions of the anodic polarization curves shown in Fig. 2b can be regarded as Tafel portions, because it is apparent that the anodic ionization of the manganese RDE (980 rpm) in the region of these portions occurs with kinetic hindrance.

The theoretical values of the slope of the Tafel portions of the anodic polarization curves were calculated by the formula

$$b_a = 2.303RT/\beta zF, \quad (1)$$

where R is the universal gas constant; T, absolute temperature; β, transport coefficient of the anodic process; z, number of electrons involved in an elementary event of the rate-determining step of the electrode process; and F, Faraday number.

At 18°C, the theoretical value of b_a is 0.1156 V at $z = 1$ and $\beta = 0.5$. Such a value of b_a is virtually equal to its experimental value and, consequently, a single electron is involved in the elementary event of the rate-determining step of anodic ionization of manganese, and the electrode process occurs in steps:

$$Mn^0 \rightarrow Mn^+_{ads} + e, \quad (2)$$

$$Mn^+_{ads} \rightleftarrows Mn^{2+} + e. \quad (3)$$

Intermediate ions Mn^+_{ads} formed by reaction (2) can be further oxidized by reaction (3) or interact with each other within the electrical double layer (disproportionation reaction):

$$2Mn^+_{ads} \rightleftarrows Mn^0 + Mn^{2+}. \quad (4)$$

The rate of the anodic ionization of manganese is determined by the rate of the slow step of abstraction of the first electron from surface manganese atoms and is described by the equation

$$i_a = k_a \exp(\beta FE/RT), \quad (5)$$

where k_a is the rate constant of the anodic process, and E is the electrode potential.

The adsorbed intermediate species Mn^+_{ads} are rather unstable and are rapidly consumed by concurrent reactions (3) and (4). The high chemical activity of the Mn^+_{ads} species points to their high energy capacity. The formation of just these species is, in all probability, the slowest step of the electrode process and the reason for the electrode polarization.

As shown above, the current efficiency by manganese on various cathode supports, except that composed of an amalgam, from an electrolyte of composition 2.0 M $MnCl_2$ + 2.0 M NH_4Br is lower than 100%. A possible reason may be both corrosion-induced dissolution of manganese cathode deposits and hydrogen evolution at the cathode, concurrent with manganese deposition. According to data of various authors, the pH value of the electrolyte solution near the surface of the manganese electrode differs from that in the bulk of the electrolyte and falls within the range 8.1–10.5 [9]. At these pH values, the concentration of hydroxonium ions in solution is negligibly low. Being a salt of a weak base and strong acid, ammonium chloride is hydrolyzed in solution to give ammonia hydrates whose dissociation constant is

1.81×10^{-5} at 25°C [15]. Consequently, the content of ammonium ions in the solution is also exceedingly low. Under these conditions, the only possible source of hydrogen ions that discharge at the cathode is water, whose decomposition requires high values of the cathodic polarization of manganese. Therefore, it may be considered that only manganese ions are discharged at the cathodes at low polarization values and the corresponding linear portions of the cathodic polarization curves reflect only this process.

The slope of the initial linear portion of the cathodic polarization curve measured at 18°C and shown in Fig. 2b is 0.117 V per $\log i$ unit. As the temperature is raised, the slope of these linear portions changes only slightly. Such a value of the slope of the Tafel portion of the polarization curve indicates that a single electron is involved in an elementary event of the rate-determining step of discharge of manganese ions.

The reasoning behind the above analysis of the anodic ionization of manganese suggests that the discharge of manganese ions also occurs in steps

$$Mn^{2+} + e \rightarrow Mn^{+}_{ads}, \quad (6)$$

$$Mn^{+}_{ads} + e \rightleftarrows Mn^{0} \quad (7)$$

by a branched mechanism, because chemical disproportionation (4) may proceed in parallel with reaction (7). The rate of the electrode process, determined by the rate of formation of unstable intermediate species Mn^{+}_{ads}, is given by

$$i_c = k_c a_{Mn^{2+}} \exp(-\alpha FE/RT), \quad (8)$$

where k_c and α are the rate constant and transport coefficient of the cathodic process, respectively; and $a_{Mn^{2+}}$ is the activity of manganese ions.

It should be noted, however, that the real mechanisms of the anodic and cathodic processes are apparently more complex because it is quite probable that other components of the electrolyte solution are involved in these processes.

CONCLUSIONS

(1) Manganese can be cathodically recovered from chloride–bromide–ammonium electrolytes with high current efficiency, especially in those cases when metals whose atomic radii are close to that of manganese are used as cathode supports.

(2) The most probable reason for the appearance of inflections in the polarization curves describing the discharge of manganese ions is that the charge of the electrode surface changes after the zero-charge potential is reached.

(3) The mechanisms of the anodic ionization of manganese and cathodic discharge of manganese ions are multistep and branching: the chemical reaction of disproportionation of intermediate species Mn^{+}_{ads} can occur in parallel with the single-electron electrochemical reactions of discharge–ionization. The rate-determining step for both the anodic and cathodic processes is that in which Mn^{+}_{ads} species are formed.

REFERENCES

1. Gasik, M.I., *Marganets* (Manganese), Moscow: Metallurgiya, 1992.
2. Sadunishvili, O.S., Lomiya, T.A., Seperteladze, D.Ya., and Gofman, N.T., in *Elektrokhimiya margantsa* (Electrochemistry of Manganese), Tbilisi: Metsniereba, 1979, vol. 8, pp. 103–107.
3. Agladze, R.I., in *Gidrometallurgiya khloridov* (Hydrometallurgy of Chlorides), Kiev: Naukova Dumka, 1964, pp. 43–57.
4. Kozin, L.F., Mashkova, N.V., and Manilevich, F.D., *Zh. Prikl. Khim.*, 1998, vol. 71, no. 3, pp. 400–406.
5. Milazzo, G. and Caroli, S., *Tables of Standard Electrode Potentials*, New York: Wiley, 1978.
6. Gamali, I.V., Danilov, F.I., and Stender, V.V., *Zh. Prikl. Khim.*, 1964, vol. 37, no. 2, pp. 337–342.
7. Vainshtein, B.K., Fridkin, V.M., and Indenbom, V.L., *Sovremennaya kristallografiya* (Modern Crystallography), vol. 2: *Struktura kristallov* (Structure of Crystals), Moscow: Nauka, 1979.
8. Kheifets, V.L., Krasikov, B.S., and Rotinyan, A.L., *Elektrokhimiya*, 1970, vol. 6, no. 7, pp. 916–924.
9. Gofman, N.T. and Sadunishvili, O.S., in *Elektrokhimiya margantsa* (Electrochemistry of Manganese), Tbilisi: Metsniereba, 1975, vol. 6, pp. 164–202.
10. Gamali, I.V. and Vorozhko, A.V., *Elektrokhimiya*, 1980, vol. 16, no. 6, pp. 835–839.
11. Loshkarev, Yu.M., *Ukr. Khim. Zh.*, 1963, vol. 29, no. 9, pp. 918–925.
12. Kozin, L.F., *Elektroosazhdenie i rastvorenie mnogovalentnykh metallov* (Electrodeposition and Dissolution of Multivalent Metals), Kiev: Naukova Dumka, 1989.
13. Trasatti, S., *Electroanal. Chem.*, 1971, vol. 33, no. 2, pp. 351–378.
14. Kolotyrkin, Ya.M. and Medvedeva, L.A., *Trudy soveshchanya po elektrokhimii* (Proc. Symp. on Electrochemistry), Moscow: Akad. Nauk SSSR, 1953, pp. 369–379.
15. Spitsyn, V.I. and Martynenko, L.I., *Neorganicheskaya khimiya* (Inorganic Chemistry), Moscow: Mosk. Gos. Univ., 1991, part 1.

ISSN 1070-4272, Russian Journal of Applied Chemistry, 2007, Vol. 80, No. 5, pp. 734–739. © Pleiades Publishing, Ltd., 2007.
Original Russian Text © L.A. Voropanova, L.P. Khomenko, 2007, published in Zhurnal Prikladnoi Khimii, 2007, Vol. 80, No. 5, pp. 755–760.

APPLIED ELECTROCHEMISTRY AND CORROSION PROTECTION OF METALS

Kinetic Parameters of Electroextraction of Cobalt from Aqueous Solutions of Cobalt and Manganese Sulfates

L. A. Voropanova and L. P. Khomenko

North-Caucasian Institute of Mining and Metallurgy (State Technological University), Vladikavkaz, North Ossetia, Russia

Received March 24, 2006; in final form, September 2006

Abstract—The effect exerted by cobalt(II) concentration in the initial solution and temperature on the kinetics of cobalt(II) electroextraction from cobalt(II) and manganese(II) sulfate solutions was studied. The kinetic parameters of the process were determined.

DOI: 10.1134/S1070427207050096

The known methods of treatment of sulfate and chloride–sulfate solutions of cobalt(II) to remove manganese(II) are manganese(II) oxidation with gaseous chlorine and sorption of cobalt(II) on an anion exchanger followed by its desorption with an acid solution [1, 2]. One of promising methods is the electrochemical treatment [3]. Cathodic cobalt obtained from sulfate and chloride–sulfate solutions of cobalt(II) and manganese(II) using this method has high purity, lustrous smooth surface, and, according to the spectral and X-ray phase analyses, contains virtually no manganese.

This study is concerned with the effect exerted by cobalt concentration in the initial solution and electroextraction temperature on the kinetic parameters of cobalt electroextraction from the sulfate solutions of cobalt(II) and manganese(II).

The electrolytic separation of cobalt(II) from solution is known. According to reference data of [4], the standard electrode potential of the reaction E^0 is

$$Co^{2+} + 2e \rightarrow Co,\ E^0 = -0.277\ V.$$

The manganese anions move toward the anode and are separated on the lead anode with the anodic sludge. According to the reference data of [4],

$$MnO_2 + 4H^+ + 2e \rightarrow Mn^{2+} + 2H_2O,\ E^0 = +1.23\ V;$$

$$MnO_4^- + 8H^+ + 5e \rightarrow Mn^{2+} + 4H_2O,\ E^0 = +1.51\ V;$$

$$MnO_4^- + 2H_2O + 3e \rightarrow MnO_2 + 4OH^-,\ E^0 = +0.588\ V.$$

Thus, the Mn^{2+} cation is oxidized on the anode by the reactions

$$Mn^{2+} - 2e + 6H_2O = MnO_2 + 4H_3O^+,$$

$$Mn^{2+} - 5e + 2O_2 = MnO_4^-.$$

The MnO_4^- ion is reduced on the cathode by the reaction

$$MnO_4^- + 5e + 8H_3O^+ = Mn^{2+} + 12H_2O; \quad (1)$$

however, the Mn^{2+} ion is not reduced on the cathode, because $E^0(Mn^{2+}/Mn^0) = -1.18$ V.

The scheme of the electrolyzer is shown in Fig. 1. The solution was fed into the anode cell and removed from the cathode space. The anode was made of lead containing 1% silver, and the cathode was made of

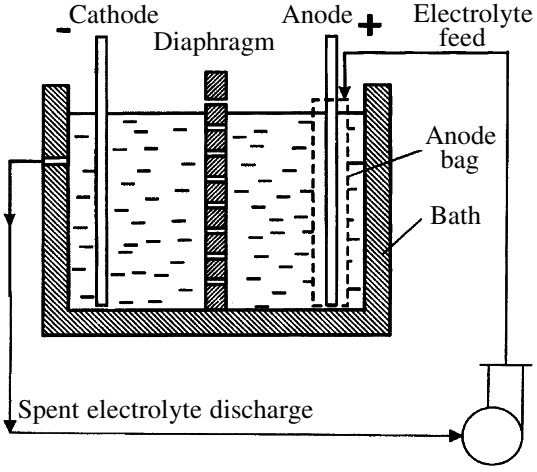

Fig. 1. Scheme of the electrolyzer.

Table 1. Results obtained in electrolysis from Co(II) and Mn(II) sulfate solutions. Solution volume 1300 cm^3, electrolyte volume 400 cm^3; pH 1; temperature 23–25°C; cathode and anode surface areas 33 and 36 cm^2, respectively; interelectrode spacing 7.8 cm; cathodic and anodic current densities 303 and 278 A m^{-2}, respectively

Electrolysis time, h	Residual concentration of ions in solution, g dm^{-3}			U, V	Mass, g		Current efficiency, %	Specific consumption of electric power, kW h kg^{-1}
	Co(II)	Mn(II)	Co : Mn		cathodic cobalt	anodic sludge		
0	62.60	8.59	7.29	–	0	0	0	0
6	58.20	7.25	8.03	14.3	3.903	0.687	59.2	22.0
12	55.30	6.30	8.78	12.8	6.787	1.499	51.5	22.6
18	52.80	5.45	9.69	10.2	9.027	2.371	45.6	20.3

Table 2. Results obtained in electrolysis from Co(II) and Mn(II) sulfate solutions at constant volume. Electrolyte volume 100 cm^3; pH 1; cathode and anode surface areas 14 and 37 cm^2, respectively; cathodic current density 86 A m^{-2}; interelectrode spacing 5.1 cm

Run no.	Concentration in initial solution, g dm^{-3}			T, °C	U, V	Mass, g		Current efficiency, %	Specific consumption of electric power, kW h kg^{-1}
	Co(II)	Mn(II)	Co : Mn			cathodic cobalt	anodic sludge		
1*	11.20	1.02	11	27	5	0.7	0.5	22	21
2*	11.40	1.04	11	22	7	0.7	0.4	22	28
3**	35.91	0.99	36	20	5	1.5	0.4	63	7
4**	37.00	1.01	37	15	6	1.2	0.3	51	11

* Initial solution volume 250 cm^3, τ 1440 min, solution flow rate 0.2 cm^3 min^{-1}.
** Initial solution volume 500 cm^3, τ 1080 min, solution flow rate 0.5 cm^3 min^{-1}.

aluminum. The supply and removal of the electrolyte were performed in a closed loop using a pump.

In such method of the electroextraction, MnO_4^- anions forming on the anode are unlikely to appear in the cathode space, because, for example, Mn^{2+} ions present in the initial solution and MnO_4^- ions can react with each other:

$$3Mn^{2+} + 2MnO_4^- + 2H_2O = 5\ MnO_2 + 4H^+. \quad (2)$$

Thus, the manganese(II) ion is removed to the anodic sludge in the form of MnO_2 by reaction (2) or in the form of other difficultly soluble compounds. This makes penetration of MnO_4^- anions into the cathode space and, consequently, their recovery on the cathode by reaction (1) impossible. Difficultly soluble manganese compounds incorporated into anodic sludge are accumulated on a dense filter cloth, anode bag, and do no not enter the cathode space. Passage of the anodic sludge particles toward the cathode is also impeded with a porous diaphragm.

This method for feeding initial solution into an electrolyzer and removing spent electrolyte makes quality of the cathodic cobalt surface better and decreases the concentration of manganese in it. In this method, the concentration of manganese(II) ions is not limited, especially if, according to reaction (2), the molar ratio of Mn^{2+} ions in the initial solution to MnO_4^- ions in the anolyte $Mn^{2+}/MnO_4^- \geq 3/2$.

At many plants for the electrolytic production of cobalt, the electroextraction is performed at pH 1.1–1.4 or 4.6–6.5 [2]. The studies show that the mechanism of the cathodic process is different in the following pH ranges: 0.5–2.2, 2.5–4.0, and from pH 4.0 to a value corresponding to the onset of cobalt hydr°lysis [2]. At pH 0.5–2.2, Co^{2+} ions are discharged on a negatively charged surface of the cathode by addition of two electrons to a discharging simple Co^{2+} ion [2].

We studied the cobalt electroextraction at pH 1 (Tables 1, 2).

As follows from these data, at a constant current density and the same concentration of manganese(II) ions in the initial solution, the results of the electrolysis depend on the concentration of the initial solution, temperature, electrolyte flow rate, voltage, time, and other electrolysis parameters (Tables 1, 2). The current

Table 3. Phase composition of anodic sludges according to X-ray phase analysis

Electro-extraction time, h	Content, vol %								
	$PbSO_4$	PbO_2	PbO	$CoSO_4$	$MnSO_4$	$Mn(OH)_4$	$(Co, Mn)(CoMn)_2O_4$	$MnPbMn_6O_{14}$	others
6	19	22	11	10	10	4	12	–	12
12	17	28	10	14	7	9	11	4	0
18	16	22	14	13	10	8	8	9	0

efficiency by cathodic cobalt increases, whereas the specific consumption of the electric power decreases with increasing concentration of the cobalt(II) ions in the electrolyte and temperature. The loss of cobalt in the anodic sludge is 9.62, 11.77, 1.08, and 5.78% in run nos. 1, 2, 3, and 4, respectively (Table 2). The loss increases with decreasing temperature and significantly decreases as the number of strippings of the anodic sludge and cathodic cobalt decreases. In runs of Table 1 and in run nos. 1 and 2 of Table 2, the interval at which the cathode and anode were stripped was 6 h; in run no. 3 (Table 2), it was 18 h for the cathode and 6 h for the anode; and in in run no. 4 (Table 2), it was 18 h for the cathode and 12 and 6 h for the anode. Decreasing the number of anodic sludge strippings increases the bath voltage.

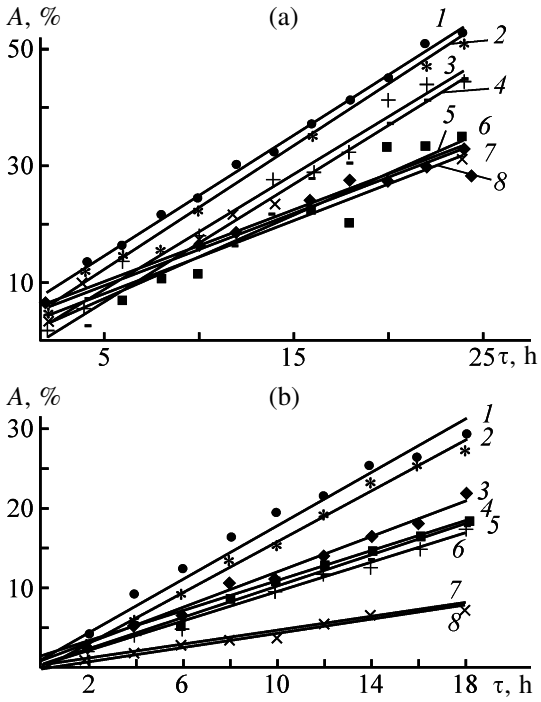

Fig. 2. Dependence of the degree of extraction A of cobalt and manganese on the electrolysis time τ in runs of Table 2: (a) nos. 1 (27°C) and 2 (22°C); (b) nos. 3 (20°C) and 4 (15°C). (a) (*1*) Mn-22a, (*2*) Mn-22c, (*3*) Mn-27c, (*4*) Mn-27a, (*5*) Co-22a, (*6*) Co-27a, (*7*) Co-22c, and (*8*) Co-27c; (b) (*1*) Mn-20a, (*2*) Mn-20c, (*3*) Co-20c, (*4*) Co-20a, (*5*) Mn-15a, (*6*) Mn-15c, (*7*) Co-15c, and (*8*) Co-15a.

The spectral analysis revealed no more than 0.01 wt % manganese in the cathodic cobalt. Unlike a box-type batch electrolyzer, the given electrolyzer, suitable for continuous electroextraction, also ensures decrease in the concentration of manganese impurity in the cathodic cobalt by more than an order of magnitude.

According to the X-ray phase analysis, anodic sludges obtained by electrolysis in aqueous solutions of cobalt(II) and manganese(II) sulfates in runs indicated in Table 1 contain compounds of lead, cobalt, and manganese and their double salts (Table 3).

Figure 2 shows how the cobalt(II) and manganese(II) extraction depends on the electrolysis time under the conditions of (a) runs no. 1 (27°C), 2 (22°C), and (b) run nos. 3 (20°C) and 4 (15°C) (Table 2).

Table 4 lists the coefficients of the regression

Table 4. Coefficients of the regression equation adequate to dependences in Figs. 2a, 2b

Runs of Figs. 2a, 2b	$E = a\tau + b$		R
	a	b	
Co-22c	1.2398	3.3327	0.9802
Co-22a	1.4295	0.1979	0.9389
Mn-22c	2.1065	1.9450	0.9879
Mn-22a	2.0618	4.3236	0.9960
Co-27c	1.2537	1.7823	0.9533
Co-27a	1.2238	4.2659	0.9664
Mn-27c	1.9719	–1.0352	0.9814
Mn-27a	2.0073	–3.1789	0.9907
Co-20c	1.1276	0.7373	0.9852
Co-20a	1.0147	0.2470	0.9931
Mn-20c	1.6132	–0.3476	0.9942
Mn-20a	1.6960	0.8200	0.9651
Co-15c	0.4354	0.3227	0.9710
Co-15a	0.4540	–0.3020	0.9687
Mn-15c	0.9297	0.2227	0.9858
Mn-27a	0.9369	1.3991	0.9834

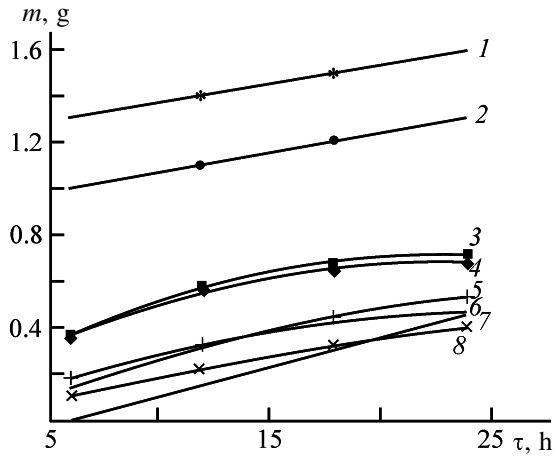

Fig. 3. Variation with time τ of the mass *m* of cathodic cobalt and anodic sludge (as) formed during the electroextraction: (*1*) Co-20, (*2*) Co-15, (*3*) Co-27, (*4*) Co-22, (*5*) as-27, (*6*) as-22, (*7*) as-20, and (*8*) as-15.

equation adequate to the dependences of Figs. 2a and 2b. Figures 2a and 2b and Table 4 show that the degree of manganese and cobalt extraction increases with increasing electrolyte temperature and the increase in the cobalt(II) concentration facilitates its extraction on the cathode.

Variation with time of the masses of the electroextracted cathodic cobalt and anodic sludge is shown in Fig. 3. As seen, the masses increase as the concentration of cobalt(II) ions in the electrolyte and the temperature increase.

The electroextraction of manganese ions can be considered in terms of equations of formal kinetics by taking into account that, in the course of the process, the pH and electrolyte volume are constant, the cobalt concentration varies only slightly, the concentrations of manganese ions are far from saturation, and the concentration of manganese ions is lower by an order of magnitude than the cobalt(II) concentration during the whole process.

Table 5 shows how the residual concentration of manganese(II) ions varies with time and temperature in run nos. 1–4 (Table 2).

The data of Table 6 characterize the $c = f(\tau)$, $\ln(c_{in}/c) = f(\tau)$, $c^{-1} = f(\tau)$, and $c^{-2} = f(\tau)$ dependences obtained for manganese ions from data of Table 5.

As follows from the data obtained, under the conditions of run nos. 1 and 2 the $c = f(\tau)$ functions are linear and have the form

$$c = a_1\tau + b_1. \quad (3)$$

Table 5. Residual concentration of manganese(II) ions at various times and temperatures in runs of Table 2

τ, h	*c*, mmol dm^{-3}			
	Mn-c	Mn-a	Mn-c	Mn-a
	Run nos. 1, 2			
	T = 300 K		*T* = 295 K	
0	18.5455	18.5455	18.9091	18.9091
2	17.6364	17.2727	18.5455	18.7273
4	16.3636	16.0000	17.8182	18.3636
6	15.8182	15.4545	16.4500	17.6364
8	14.9091	14.5455	15.8182	16.0000
10	14.3637	14.0000	15.4545	15.8182
12	13.2727	12.9091	15.0909	15.2727
14	12.5455	12.5454	13.6364	14.1818
16	12.0000	11.6364	13.4545	13.6364
18	10.9548	10.9091	12.7273	13.0909
	Run nos. 3, 4			
	T = 293 K		*T* = 288 K	
0	18.0545	18.0545	18.3091	18.3091
2	17.6364	18.0000	17.7818	17.5091
4	17.0909	16.3636	17.6364	17.2727
6	16.3636	15.8182	17.4545	16.9091
8	15.6364	15.0909	16.7273	16.7273
10	15.2727	14.5455	16.5455	16.3636
12	14.5455	14.1818	16.1818	16.0000
14	13.8182	13.4545	16.0000	15.8182
16	13.6364	13.2727	15.6364	15.2727
18	13.2727	12.7273	15.2727	15.0909

For run nos. 3 and 4, the $c^{-1} = f(\tau)$ functions are linear and have the form

$$c^{-1} = a_2\tau + b_2. \quad (4)$$

The coefficients of the linear regression equations (3) and (4), calculated by the least-squares method, are listed in Tables 7 and 8. It is seen that the correlation coefficients are close to unity, i.e., functions (3) and (4) are adequate to the experimental data.

A slight difference in temperatures did not result in the change in the process mechanism, and, consequently, in the order of the electroextraction reaction. Under these conditions, the rate with respect to the extracted manganese can be expressed by the equation

$$V = -dc/d\tau = kc^n, \quad (5)$$

Table 6. Correlation coefficients for the concentration vs. time dependences obtained for manganese ions from data of Table 5

T, K	Mn	$c = f(\tau)$	$\ln(c_{in}/c) = f(\tau)$	$c^{-1} = f(\tau)$	$c^{-2} = f(\tau)$
			Run nos. 1, 2		
300	Mn-c	0.9860	0.9719	0.9426	0.9014
	Mn-a	0.9913	0.9597	0.9241	0.9828
295	Mn-c	0.9952	0.9948	0.9789	0.9494
	Mn-a	0.9960	0.9893	0.9641	0.9235
			Run nos. 3, 4		
293	Mn-c	0.9899	0.9832	0.9910	0.9870
	Mn-a	0.9651	0.9787	0.9872	0.9476
288	Mn-c	0.9871	0.9858	0.9878	0.9863
	Mn-a	0.9824	0.9860	0.9869	0.9863

Table 7. Coefficients of linear regression equation (3)

T, °C	Mn	a_1	b_1	R
27	Mn-c	–0.4092	18.324	0.9860
	Mn-a	–0.4050	18.026	0.9913
22	Mn-c	–0.3534	18.971	0.9952
	Mn-a	–0.3521	19.332	0.9960

Table 8. Coefficients of linear regression equation (4)

T, °C	Mn	a_2	b_2	R
20	Mn-c	0.0012	0.0545	0.9910
	Mn-a	0.0013	0.0550	0.9872
15	Mn-c	0.0006	0.0545	0.9878
	Mn-a	00006	0.0555	0.9869

Table 9. Coefficients of Eq. (6)

T, °C	Mn	c_{in}, mmol dm^{-3}	k, mmol dm^{-3} h^{-1}
27	Mn-c	18.324	0.4092
	Mn-a	18.026	0.4050
22	Mn-c	18.971	0.3534
	Mn-a	19.322	0.3521

where k is the rate constant; τ, electroextraction duration; and c, residual concentration of manganese ions to a time moment τ.

The solution of differential equation (5) at $n = 0$ is the relationship

$$c = c_{in} - k\tau, \quad (6)$$

and at $n = 2$, the relationship

$$c^{-1} = c_{in}^{-1} + k\tau. \quad (7)$$

From Eqs. (3) and (6) we obtain the relationships $a_1 = -k$, $b_1 = c_{in}$, and from Eqs. (4) and (7), the relationships $a_2 = k$ and $b_2 = c_{in}^{-1}$. The results are given in Tables 9 and 10.

Table 10. Coefficients of Eq. (7)

T, °C	Mn	c_{in}^{-1}, dm^3 mmol^{-1}	k, dm^{-3} mmol^{-1} h^{-1}
20	Mn-c	0.0545	0.0012
	Mn-a	0.0550	0.0013
15	Mn-c	0.0545	0.0006
	Mn-a	0,0555	0.0006

The reaction order ($n = 0.15$) (Table 2, run nos. 1, 2) was also calculated by the half-conversion method.

The reaction order $n \approx 0$ shows that the manganese electroextraction depends only slightly on the initial concentration of manganese ions (Table 2, run nos. 1, 2), whereas the reaction order $n = 2$ confirms the existence of the above dependence (Table 2, runs nos. 3, 4).

The activation energy E can be calculated by the Arrhenius equation

$$\ln k = \ln k^0 - ER^{-1}T^{-1},$$

where T is temperature (K).

The activation energies of the manganese electroextraction, as estimated from the experimental data (Table 10) obtained within 15–20°C, are $E_c = 97.3$ kJ on the cathode and $E_a = 108.5$ kJ on the anode.

The reaction order $n \approx 0$ and the activation energy $E = 20.6$–21.6 kJ suggest that the manganese electroextraction under the conditions of run nos. 1, 2 (Table 2) is controlled by internal diffusion.

The reaction order ($n = 2$) and the activation energy $E = 97.3$–108.5 kJ suggest that the manganese electroextraction in run nos. 3, 4 (Table 2) is controlled by the chemical redox reactions.

CONCLUSIONS

(1) In production of metallic cobalt, the electrochemical treatment of cobalt solutions to remove

manganese has a number of advantages such as high degree of purification, good quality of the surface of cathodic cobalt, the possibility of utilizing anodic sludge, i.e., developing wasteless technology, and environmental safety of the process.

(2) The degree of manganese and cobalt extraction increases with increasing electrolyte temperature. The increase in the cobalt concentration facilitates its extraction on the cathode.

(3) With increasing concentration of the cobalt ions in the electrolyte, the processes associated with the extraction of manganese ions pass from the diffusion to kinetic control.

REFERENCES

1. Khudyakov, I.F., Klyain, S.E., and Ageev, N.G., *Metallurgiya medi, nikelya, soputstvuyushchikh elementov i proektirovanie tsekhov* (Metallurgy of Copper, Nickel, and Concomitant Elements and Design of Shops), Moscow: Metallurgiya, 1993.
2. Reznik, I.D., Sobol', S.I., and Khudyakov, V.M., *Kobal't* (Cobalt), Moscow: Mashinostroenie, 1995, part 2.
3. RF Patent 2212460.
4. *Kratkii spravochnik fiziko-khimicheskikh velichin* (Concise Handbook on Physicochemical Quantities), Ravdel', A.A. and Ponomareva, A.M., Eds., Leningrad: Khimiya, 1983.

ISSN 1070-4272, Russian Journal of Applied Chemistry, 2007, Vol. 80, No. 5, pp. 740–745. © Pleiades Publishing, Ltd., 2007.
Original Russian Text © I.V. Sheveleva, L.A. Zemskova, A.V. Voit, S.V. Zheleznov, V.G. Kuryavyi, 2007, published in Zhurnal Prikladnoi Khimii, 2007, Vol. 80, No. 5, pp. 761–766.

APPLIED ELECTROCHEMISTRY AND CORROSION PROTECTION OF METALS

Relationship between Electrochemical and Structural Properties of Modified Carbon Fibers

I. V. Sheveleva, L. A. Zemskova, A. V. Voit, S. V. Zheleznov, and V. G. Kuryavyi

Institute of Chemistry, Far-Eastern Division, Russian Academy of Sciences, Vladivostok, Russia

Received September 29, 2006

Abstract—Effect of modification conditions on the electrochemical and structural properties of fibrous carbon materials was studied.

DOI: 10.1134/S1070427207050102

Having a well-developed surface, large porosity, and high electrical conductivity, fibrous carbon materials find wide use in widely diverse processes of chemical technology [1, 2]. A promising application of carbon fibers is that as electrodes and sorption materials [3]. Activated fibrous carbon (AFC) is used as electrodes in high-sensitivity electrochemical analytical methods [4], electrochemical treatment of wastewater, and manufacture of supercapacitors [5]. The efficiency of use of fibrous materials in sorption processes is due not only to their large surface area and high adsorption rate, but also to the possibility of carrying out a process at a prescribed polarization potential. The possibility of implementation of liquid-phase adsorption methods based on use of carbon materials under electrochemical polarization conditions largely depends on the efficiency of charging of porous carbon electrodes whose structure strongly affects the course of an electrochemical process.

Structural characteristics of fibers can be changed by various kinds of modification by electrochemical or chemical methods. For example, the size of the existing pores can be adjusted by electrochemical treatment of fibers to make larger the specific volume of mesopores [6]. A developed system of pores in activated carbon fibers and their surface groups can be formed by steam-and-gas activation or by deposition of metal oxides and hydroxides or various polymers [2, 3]. Modification of the surface of carbon materials with, e.g., titanium hydroxide, which forms mechanically strong and biologically inert coatings and is stable in a wide range of pH values, makes it possible to vary the surface properties and the pore structure of AFC. These latter, in turn, affect the conditions of carbon fiber charging [8].

The electrochemical properties of a carbon material brought in contact with an electrolyte solution allow evaluation of changes in its structural and surface characteristics [9]. Structural changes in AFC can be directly examined by atomic-force and electron microscopy [10].

The aim of this study was to determine by the electrochemical method how the surface characteristics of activated carbon fibers vary with the conditions of their modification and to supplement these measurements with analysis by atomic-force and electron microscopies.

EXPERIMENTAL

We used as electrode materials Aktilen B bundle fibers (AFC-B) and 709-P granulated mesoporous carbon, whose specific surface area, pore volume, and average pore radius are, respectively, 700 and 200 $m^2 g^{-1}$, 0.4 and 0.4 $cm^3 g^{-1}$, and 4 and 100 Å. In addition, we used modified carbon fibers obtained by chemical [11] and electrochemical [7] deposition of titanium hydroxide. We used as electrolytes saline (0.9% NaCl) and a universal buffer solution (sodium phosphate–acetate–borate). The choice of the electrolytes was due to further use of composite materials in sorption and electrosorption of protein molecules.

Electrochemical measurements were made using cyclic voltammetry [8, 9]. A sample of a carbon material was placed on a gold grid serving as a current lead. A silver chloride electrode was used as reference. The auxiliary electrode, made of a porous carbon material, was separated from the working electrode by an MB-2 bipolar membrane. Cyclic voltam-

metric curves were measured at potentials of ±50 mV [8] relative to the immersion potential of the working electrode at potential sweep rates of 4×10^{-5}–1×10^{-3} V s^{-1}. The electrode capacitance C (F g^{-1}) was calculated by the formula [12]

$$C = (I_a + I_c)/2mv, \quad (1)$$

where I_a and I_c are the anode and cathode polarization currents (A): m, mass of the carbon material (g); and v, potential sweep rate (V s^{-1}).

The degree (fraction) α of utilization of the electrode surface in the electrochemical process was calculated using the relation

$$\alpha = C/C_{max}, \quad (2)$$

where C and C_{max} are the electrode capacitances at a given and minimum potential sweep rates.

In processing the potentiodynamic curves by the least-squares method, we calculated the characteristic charging time τ and ohmic resistance R of the electrolyte in pores ($R = \tau/C$) by the formula [13]

$$I = Cv\{1 - (2/\pi^2)\sum_{n=0}(n + 1/2)^{-1}\exp[-\pi^2(n + 1/2)^2(t/\tau)]\}, \quad (3)$$

where I is current (A g^{-1}); v, potential sweep rate (V s^{-1}); t, time; and n, summation index.

The structure of the fibers was studied on an LEO430 scanning electron microscope (Germany) and an atomic-force microscope (AFM) (Zelenograd, Russia). The AFM measurements were made in contact and tapping modes, with images chosen in the most representative presentations.

For effective use of AFC as an electrode material in various processes, it is necessary to reveal specific features of the influence exerted by their pore structure on the electrochemical properties of fibers. Carbon, including fibrous, electrodes with a well-developed system of pores have a large-area interface between the carbon matrix and the electrolyte solution. However, the polarization of porous electrodes may lead to hindrance associated with a slow supply of ions (diffusion hindrance) and changes in potential in pores (ohmic hindrance). As a result, not the whole internal surface is equally accessible to the electrochemical process. For microporous materials, in which the pore radius is smaller than 1.5–2.0 nm, there may also occur difficulties in formation of the electrical double layer (EDL) in pores [8, 9], which hinders polarization of the internal space and impairs the efficiency of operation of the porous electrode. Modification of the carbon matrix can also change its surface properties and structure and, as a result, also alter the accessibility of the surface to the electrochemical process.

A basic characteristic of an electrode is the capacitance of the electrical double layer, whose value depends on conditions of its formation in the pore structure of a carbon material, including a modified material. Use of data on the EDL capacitance of porous electrodes makes it possible to calculate their charging conditions [14] determining the efficiency of application of AFC and AFC-based composite materials as electrodes in various processes occurring under polarization conditions.

One of methods used to determine the EDL capacitance of porous carbon and fibrous electrodes is cyclic voltammetry [8], because it makes it possible to assess the effect of structural and surface properties of carbon materials on the conditions of their charging. Figure 1 shows as an example voltammograms measured at different electrode polarization rates in saline (0.9% NaCl) and buffer solutions. The voltammograms obtained at the minimum potential sweep rate (0.4 mV s^{-1}) are virtually rectangular (curves *1* and *2*), which indicates that, in this case, there are no hindered charging processes, which appear upon a significant increase in the electrode polarization rate (curves *3* and *4*). The occurrence of the hindered charging processes may be due to pore structure parameters of the fiber, phase-boundary phenomena at the electrode–solution interface, and properties of the conduction band of the carbon material [15], which are all dependent on the conditions of its synthesis.

It should be noted that the electrolyte composition affects the process of electrode charging. In polarization in a buffer solution (especially at high potential sweep rates), hindered charging processes are manifested to a greater extent, in contrast to similar processes in polarization of the electrodes in saline. This difference is possibly due to the presence of larger ions in the multicomponent buffer solution, which hinder EDL formation in a porous electrode at high potential sweep rates. It is also not improbable that specific adsorption of phosphate ions on the surface of a titanium-containing fiber is important, which may affect the charging of composite electrodes.

The differences in charging and the specific structural features of carbon materials can be judged from how their capacitance varies with the potential sweep rate. At a slow polarization, when the potential sweep rate corresponds to the supply rate of ions forming

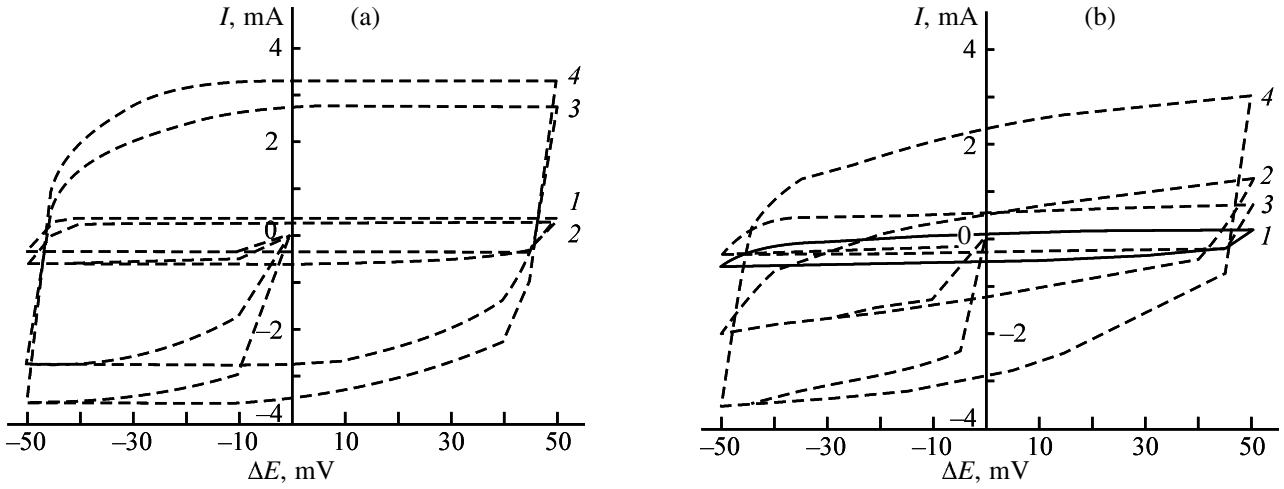

Fig. 1. Cyclic voltammograms measured on carbon electrodes at different potential sweep rates v in (a) saline and (b) buffer solution. (I) Current strength and (ΔE) shift of the potential relative to the steady-state value. v, mV s^{-1}: (*1, 2*) 0.04 and (*3, 4*) 0.4. (*1, 3*) AFC and (*2, 4*) AFC-Ti(ECh).

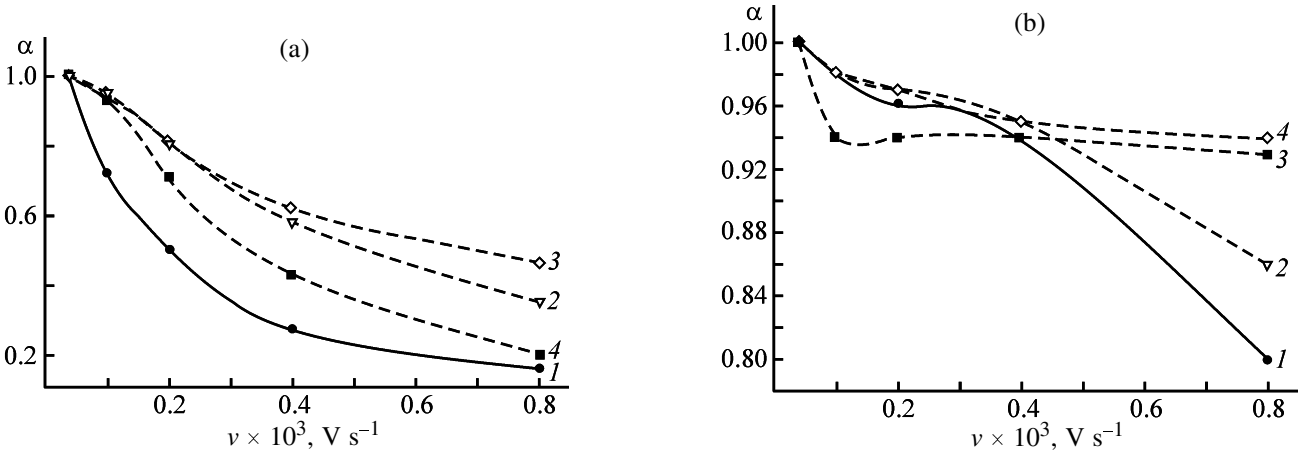

Fig. 2. Surface fraction α involved in the electrochemical process vs. the potential sweep rate v in (a) buffer solution and (b) saline. (*1*) AFC, (*2*) AFC-Ti(Ch), (*3*) AFC-Ti(ECh), and (*4*) 709-P.

the EDL "plate," the capacitance corresponds to the entire surface area that can be involved in charging of the electrode in a given electrolyte. An increase in the rate of polarization of the microporous material makes the ohmic potential drop higher and the diffusion hindrance to the rate of the electrode process stronger. This leads to a decrease in the capacitance, because the value measured corresponds only to the surface area that is involved in the electrochemical process and constitutes a certain fraction of the total surface area.

As follows from the dependences in Fig. 2a, the EDL capacitances (and, consequently, the surface fractions involved in the electrochemical process) of the starting fiber and granulated carbon steeply decrease as the rate of electrode polarization in the buffer solution is raised and reach rather small values, which indicates that the charging process is displaced to the outer surface. However, modification of fibers results in that the capacitances of fibrous electrodes reach higher values in polarization. This indicates that the fiber structure changes in preliminary chemical and electrochemical treatment with titanium hydroxide.

Changing the electrolyte composition (replacing the buffer solution with saline) (Fig. 2b) affects the polarization of carbon materials in the entire range of potential sweep rates. This may be due to the fact that, in a low-component solution (saline), the surface of porous electrodes is more accessible to smaller ions forming the EDL plate. As a result, fibrous electrodes

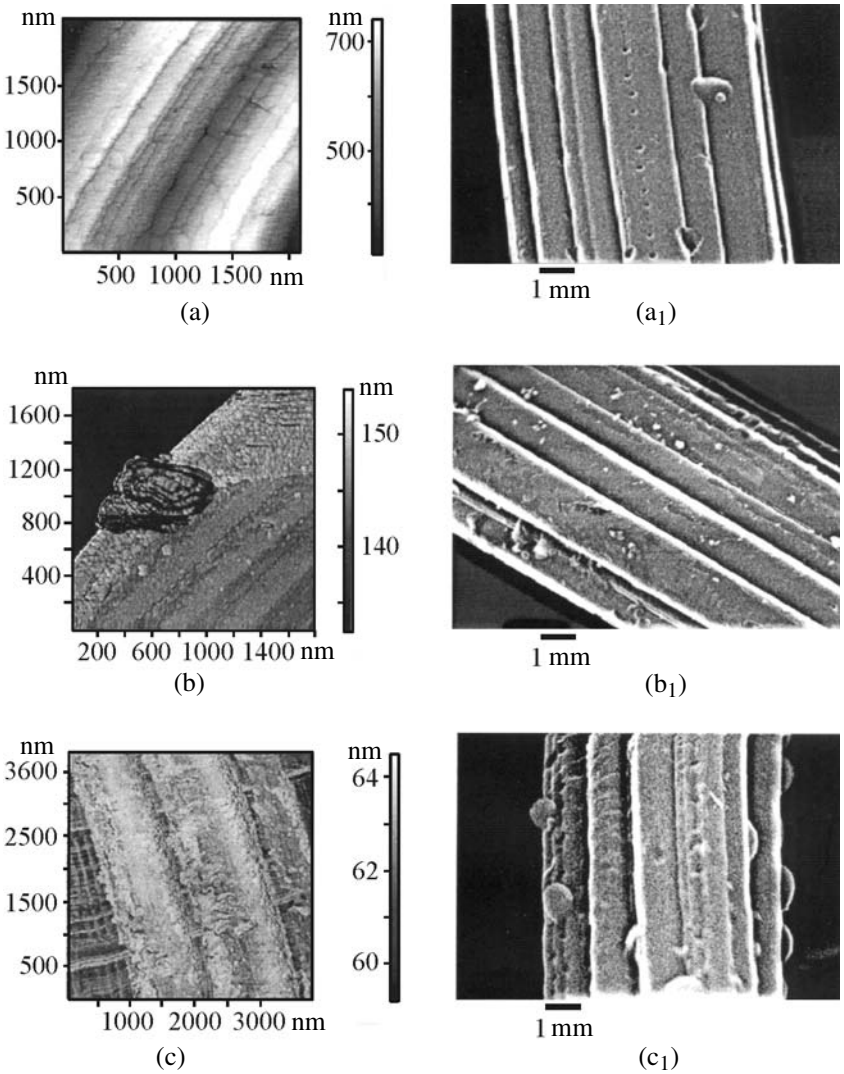

Fig. 3. (a–c) AFM and (a_1–c_1) SEM images of carbon fibers: (a, a_1) AFC, (b, b_1) AFC-Ti(ECh), and (c, c_1) AFC-Ti(Ch).

are polarized similarly to mesoporous granulated carbon. The fact that high values of the AFC capacitance are preserved in the entire range of potential sweep rates may also be due to the lability of the fiber structure under the polarization conditions. The effect of lability of the carbon fiber is manifested in a change in its pore structure upon polarization, which consists in parting of fibrils of the fiber and in an increase in the size of transport pores [6, 14, 16]. The manifestation of this effect results in that the hindering influence exerted by the porous medium on the process of EDL formation is weakened and rather high rates of current and mass transport are preserved. It should be noted that, irrespective of the electrolyte composition, the surface of modified AFC is more accessible to the electrochemical process than the starting fiber. The behavior of this kind is due to structural changes in AFC in the course of its modification.

Figure 3 shows AFM and SEM images of unmodified and titanium-containing AFC. It follows from the AFM data obtained that the unmodified AFC (Fig. 3) is composed of fibers 1000–1500 nm in diameter, which are, in turn, constituted by even thinner microscopic fibrils [2] 100–300 nm in diameter. The carbon fiber is formed by microcrystalline blocks aligned along the fiber axis. Pores of various sizes are present on the surface. Micropores with a transverse size of about 10 nm are formed, according to the AFM data obtained, at joining places of blocks constituting the fiber. The SEM image in Fig. $3a_1$ shows some micropores with sizes of up to 100 nm, formed between microfibrils or at places of their transverse rupture.

Figures 3b and $3b_1$ show AFM and SEM images of an AFC modified by electrochemical deposition of

Charging parameters of porous carbon electrodes

Material	τ, s	*R*, Ω	τ, s	*R*, Ω
	solution			
	buffer, pH 4.7		saline	
AFC-B	1285.9	130.7	413.5	60.1
AFC-B Ti(Ch)	578.2	90.8	353.9	49.5
AFC-B Ti(ECh)	547.6	74.6	327.3	44.4
709-P	1543.8	533.2	540.7	180.4

titanium hydroxide, which forms a coating in the form of separate island-like particles-blocks with a size of up to 300 nm. Possibly, island particles are formed at micropores, which are rather sparsely situated in the starting fiber. Micropores are formed in the titanium-containing fiber among the blocks. It follows from the AFM data that the system of pores constitutes a double sieve in the modified fiber at places in which it is coated with titanium hydroxide. This sieve is formed by pores in the titanium hydroxide film at the top, and by pores in the fiber itself, below.

Figures 3b and $3b_1$ show AFM and SEM images of an AFC modified with titanium hydroxide by chemical modification. As also in the case of the electrochemically produced coating, the images demonstrate particles of about micrometer size. In this case, however, the particles are not of the island type, but adhere to each other so as to form, on large areas, a solid coating with a thickness of up to tenths of a micrometer. According to the AFM data, the chemically deposited coating has a more profiled surface and is composed of conglomerates of about micrometer particles. Thus, comparison of the results obtained shows that different methods of titanium hydroxide deposition can give structurally different composite fibers, which, in turn, leads to dissimilar charging conditions of modified AFCs.

A mathematical processing of the data on variation of the capacitance of the electrodes with the rate of their polarization in terms of Eq. (3) made it possible to calculate the resistance *R* of the electrolyte in the pores and the characteristic electrode charging time τ. The table lists the calculated values, which enabled evaluation of the efficiency of utilization of carbon materials under the polarization conditions. Analysis of the data obtained shows that, in contrast to granulated carbon, both the starting and modified fibers are charged faster and with lower electrolyte resistance. Presumably, this is due to changes in the structure of the fibers both in the course of AFC polarization [6, 14, 16] and in deposition of a modifier onto the carbon matrix. In the process, the radii of pores in the labile AFC structure increase [16], which leads to a decrease in the diffusion and ohmic resistance and makes it possible to achieve a more uniform polarization of fibrous electrodes. Moreover, it should be noted that the AFC modified with titanium hydroxide by electrochemical deposition is among fibers with the lowest electrolyte resistance within pores. Presumably, this is due both to an increase in the size of pores in the fiber itself in the course of polarization and the forming pore structure of the hydroxide being deposited. Thus, a study of the relationship between the structural and electrochemical properties of modified fibrous electrodes can determine the most promising materials to be used in electrochemical processes.

CONCLUSIONS

(1) It was shown by cyclic voltammetry that carbon fibers are polarized more uniformly when electrodes are charged in physiological saline.

(2) Deposition of titanium hydroxide onto a carbon matrix changes its structure and the charging conditions of composite fibers.

(3) The composite material produced by electrochemical deposition of titanium hydroxide onto a carbon fiber is more suitable in its electrochemical characteristics for use in electrodes.

REFERENCES

1. Varentsov, V.K. and Varentsova, V.I., *Elektrokhimiya*, 2001, vol. 37, pp. 811–820.
2. Ermolenko, I.N., Lyubliner, I.P., and Gul'ko, N.V., *Elementosoderzhashchie ugol'nye voloknistye materially* (Element-Containing Fibrous Carbon Materials), Minsk: Nauka i Tekhnika, 1982.
3. Zemskova, L.A., Sheveleva, I.V., and Glushchenko, V.Yu., *Khim. Tekhnol.*, 2004, no. 7, pp. 6–11.
4. Druzhinina, T.V., Tolmachev, A.V., Volodin, Yu.Yu., and Nazar'ina, L.A., *Zh. Prikl. Khim.*, 1999, vol. 72, no. 8, pp. 1303–1306.
5. Conway, B.E., Niu, J., and Pell, W.G., *Kem. Ind.*, 2005, vol. 54, no. 4, pp. 187–198.
6. Bondareva, G.V., Gul'ko, N.V., and Kitikova, N.V., *Zh. Prikl. Khim.*, 1997, vol. 70, no. 3, pp. 415–419.
7. RF Patent 2075170.

8. Kinoshita, K., *Carbon: Electrochemical and Physicochemical Properties*, New York: Wiley, 1988.
9. Calas-Blanchard, C., Comtat, M., Marty, J.-L., and Mauran, S., *Carbon*, 2003, vol. 41, pp. 123–130.
10. Gusev, A.I., *Nanomaterialy, nanostruktury, nanotekhnologiii* (Nanomaterials, Nanostructures, Nanotechnologies), Moscow: Fizmatlit, 2005.
11. RF Patent 2026732.
12. Wang, C.-C. and Hu, C.-C., *Carbon*, 2005, vol. 43, pp. 1926–1937.
13. Posey, F.A. and Morozumi, T., *J. Electrochem. Soc.*, 1966, vol. 113, no. 2, pp. 176–184.
14. Artem'yanov, A.P. and Sheveleva, I.V., *Zh. Prikl. Khim.*, 2004, vol. 77, no. 11, pp. 1811–1814.
15. Oren, Y. and Soffer, A., *J. Electroanal. Chem.*, 1985, vol. 186, pp. 63–77.
16. Sheveleva, I.V., Khabalov, V.V., and Gul'ko, N.V., *Ukr. Khim. Zh.*, 1990, vol. 56, no. 6, pp. 605–609.

ISSN 1070-4272, Russian Journal of Applied Chemistry, 2007, Vol. 80, No. 5, pp. 746–753. © Pleiades Publishing, Ltd., 2007.
Original Russian Text © I.V. Stolyarova, I.B. Kovban', R.V. Prikhod'ko, A.O. Kushko, M.V. Sychev, V.V. Goncharuk, 2007, published in Zhurnal Prikladnoi Khimii, 2007, Vol. 80, No. 5, pp. 767–774.

CATALYSIS

Relationship between the Catalytic Behavior of FeZSM-5 Zeolites in Oxidative Degradation of Dyes and the Nature of Their Active Centers

I. V. Stolyarova, I. B. Kovban', R. V. Prikhod'ko, A. O. Kushko, M. V. Sychev, and V. V. Goncharuk

Dumanskii Institute of Colloid and Water Chemistry, National Academy of Sciences of Ukraine, Kiev, Ukraine

Received June 20, 2006; in final form, March 2007

Abstract—Catalytic activity of FeZSM-5 zeolites in oxidative degradation of Rhodamine 6G and Methyl Orange dyes was studied in relation to the nature, localization, and dispersity of active centers and on the reversibility of the oxidation–reduction of iron contained in the zeolites.

DOI: 10.1134/S1070427207050114

Millions of tons of dye-contaminated wastewater formed in textile and paint-and-varnish industries and in manufacture of finishing materials pose a severe environmental problem [1]. Use of adsorptive, biological, electrochemical, and oxidative technologies makes it possible to clarify contaminated water, but only catalytic methods provide complete degradation of dyes [2]. Of particular interest in this regard is the oxidizing system based on the homogeneous Fenton reagent ($Fe^{2+}/Fe^{3+}/H_2O_2$) [3, 4]. However, a number of disadvantages, such as impossible regeneration of the catalyst, narrow range of pH values at which the reaction occurs, and necessity for removal of iron compounds from purified water strongly restrict the possible application field of this system [3–5]. Most of these problems can be resolved by using heterogeneous catalysts and, in particular, zeolites, whose recovery from water and regeneration are not too difficult [6]. Fe-containing zeolites show redox properties because iron can change its oxidation state (Fe^{2+}, Fe^{3+}, Fe^{4+}) [7]. These materials are effective catalysts for oxidative breakdown of phenol [6], a number of carboxylic acids [8], and ethanol [9] in water. Their efficiency in the Fenton reaction may strongly depend on the structural topology, surface chemistry, and preparation method. However, this issue and the question as to whether the FeZSM-5 zeolite can be used as a catalyst for dye degradation in aqueous media have been poorly elucidated.

The aim of this study was to analyze the relationship between the nature of active centers and the catalytic properties of the FeZSM-5 zeolite in oxidative degradation of a diaminoxanthene dye Rhodamine 6G and an azo dye Methyl Orange. The choice of these model objects is due to the presence in their structure of different functional groups and other reactive centers, which can enter into redox reactions.

EXPERIMENTAL

The FeZSM-5(A) zeolite containing Fe^{3+} ions in the zeolite framework (Si^{4+}/Fe^{3+} = 40) was synthesized under hydrothermal conditions by the method described in [10, 11], using the reaction mixture $TEOS : TPAOH : Fe_2O_3 : H_2C_2O_4 = 1.0 : 0.312 : 0.0125 : 0.0823$, where TEOS is tetraethyl orthosilicate, and TPAOH is tetrapropylammonium hydroxide (20% aqueous solution). A [Fe, Al]ZSM-5(B) sample isomorphically substituted with iron and aluminum cations (Si^{4+}/Fe^{3+} = 50, Si^{4+}/Al^{3+} = 200, Fe^{3+}/Al^{3+} = 4.0) was synthesized in a similar way. Composition of the reaction mixture (g): TEOS 10.24, TPAOH 15, $Fe(NO_3)_3 \cdot 9H_2O$ 0.383, $Al(NO_3)_3 \cdot 9H_2O$ 0.089, and $H_2C_2O_4 \cdot 2H_2O$ 0.493. The template (TPAOH) was removed from both the zeolites by calcination in a flow of N_2 for 8 h and then in a flow of dried air at 823 K for 4 h at a heating rate of 1.0 deg min^{-1}. The FeZSM-5(C) catalyst was prepared by ion exchange in the medium of in situ generated Fe^{2+} ions [12, 13] using NH_4ZSM-5 zeolite (atomic ratio Si^{4+}/Al^{3+} = 40, Akzo-Nobel). The FeZSM-5(D) sample was synthesized by modification of the same zeolite with iron acetylacetonate in toluene [14].

The content of iron in the materials under study was determined by the ICP-AES method (Perkin–Elmer Optima, DV-3300, ICP-AES Instrument). Their X-ray diffraction analysis was made on a Rigaku RINT-2000 diffractometer (CuK_α radiation, λ = 1.54178 Å) at Bragg angles 2θ = 5°–50°. Electronic diffuse reflection spectra (EDRS) of the catalysts were measured on a Shimadzu UV 2401 spectrophotometer (spectral range 190–800 nm), with $BaSO_4$ as reference. The IR spectra were recorded on a Nicolet Avatar 360 FT-IR spectrophotometer with pelletized samples prepared by compaction of a material under study with thoroughly dried KBr (taken in 1 : 60 ratio). A thermally programmed reduction of the catalysts with hydrogen (H_2-TPR) in the temperature range 298–1073 K was performed in a flow-through reactor at a heating rate of 10 deg min^{-1} in a flow of a hydrogen–argon mixture (5 vol % H_2) passed through the reactor at a flow rate of 30 cm^3 min^{-1}. The absorption of H_2 was determined using a thermal conductivity detector calibrated against CuO. Prior to experiments, the samples (100 mg, grain size 0.3–1.0 mm) were heated in a flow of Ar at 473 K to remove physically sorbed water. Part of the samples were calcined for 2 h at 623 K in an Ar/N_2O mixture (5 vol % N_2O), cooled to 298 K in a flow of the same mixture, and blown-through with argon for 1 h, and then a TPR experiment was carried out. Isotherms of nitrogen adsorption–desorption at 77 K were recorded with preliminarily vacuum-treated samples (5 h, 673 K) on a Micromeritics ASAP 2010 installation. The isotherms obtained were analyzed using Langmuir and Dubinin–Astakhov equations [15]. This was so done because the BET method based on the polylayer model of N_2 adsorption inadequately describes adsorption processes in zeolite channels owing to the small size of these channels (<0.7 nm) [16].

The oxidative degradation of the dyes (0.1 g dm^{-3}) was performed at a catalyst concentration of 1 g dm^{-3} in isothermal conditions (298–323 K) under permanent agitation in a shaded temperature-controlled glass reactor. Fifteen minutes after the catalyst was introduced into the dye solution, addition of 30% H_2O_2 at a constant rate was started. The degree of decolorization of the dyes was measured colorimetrically (Specord M-40 spectrophotometer or FEK56 colorimeter, λ = 540 nm) with an aliquot from which the catalyst was removed by centrifugation (7000 rpm). To assess the operation stability of the catalysts, they were recovered from the solution after the reaction was complete and their activity was again measured, with the ratio between the catalyst mass and dye concentration remaining the same as that in experiments with a fresh sample. The effect of iron ions leached-out from FeZSM-5 samples on the degradation of the dyes was determined as follows. After the activity was measured, the catalysts were recovered from the reaction mixture by filtration at a temperature equal to the reaction temperature. Then, the dye and H_2O_2 were introduced into the filtrate in the same amounts as those in the heterogeneous catalytic process, after which the reaction was again carried out. The specific activity A_{sp} of the catalysts and the activity A_{Fe} of leached-out iron cations were expressed as the molar ratio of a dye decolorized in unit time to the iron content of the samples. The content of the total organic carbon in water was measured using a Shimadzu TOC-VCSN analyzer, with the reaction preliminarily terminated by addition of a fixed volume of a 10% $NaHSO_3$ solution (pH 9–10). The reaction products were analyzed with a Tsvet 3006 ion chromatograph with an Elsian 6 column.

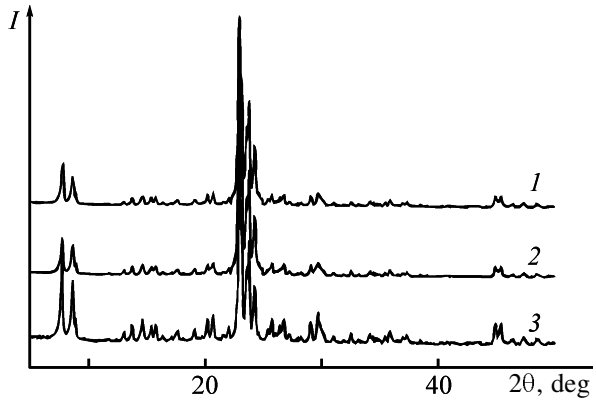

Fig. 1. X-ray diffraction patterns of the samples. (*I*) Intensity and (2θ) Bragg angle. (*1*) FeZSM-5(A), (*2*) [Fe, Al]ZSM-5(B), and (*3*) FeZSM-5(C).

The FeZSM-5(A) and [Fe,Al]ZSM-5-5(B) catalysts have an MFI (ZSM-5) structure [17], which follows from the presence in their X-ray diffraction patterns of basal reflections characteristic of highly crystalline zeolites of this type (Fig. 1). The IR spectra of these samples show a weak absorption band at around 650 cm^{-1} (stretching vibrations in ≡Si–O–Fe= structural fragments [10, 11]), which indicates that iron(III) is present in the zeolite framework. Introduction of iron cations into channels of the NH_4ZSM-5 zeolite via ion exchange has virtually no effect on its crystallinity (Fig. 1). However, this changes the coordination state and distorts the ligand surrounding of a part of Al^{3+} structural ions, which was revealed by ^{27}Al NMR spectroscopy in preliminary studies. This occurs under the action of a strongly acidic medium used to perform the given process. The adsorption isotherms

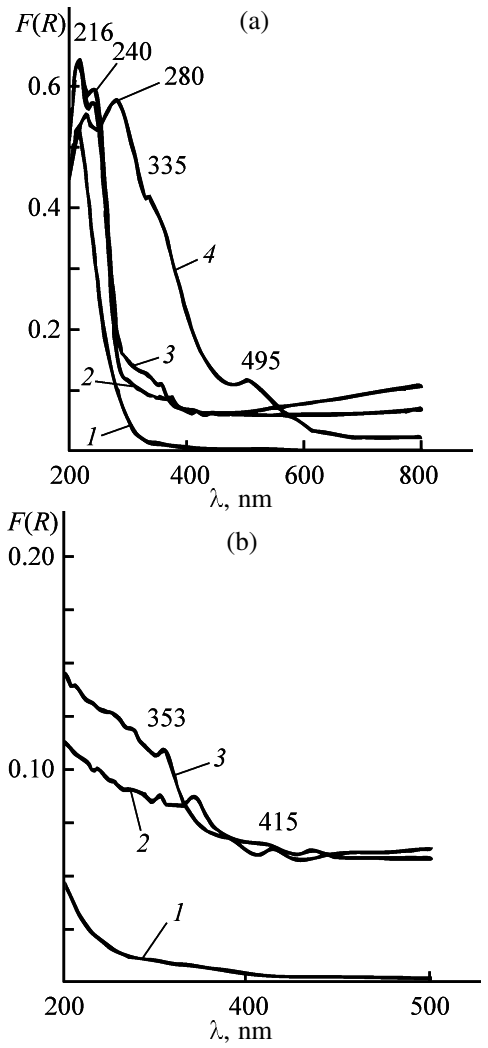

Fig. 2. EDR spectra of FeZSM-5 samples. [$F(R)$] Kubelka–Munk function and (λ) wavelength. (a) Full range and (b) region of *d–d* transitions. (*1*) FeZSM-5(A), (*2*) [Fe, Al]-ZSM-5(B), (*3*) FeZSM-5(C), and (*4*) FeZSM-5(D); the same for Fig. 3.

of all the samples can be attributed to type I by IUPAC classification [15, 16], which points to their microporous structure characteristic of MFI-type zeolites [18]. The pore structure parameters of the [Fe]ZSM-5(A) and [Fe, Al]ZSM-5(B) catalysts differ only slightly (Table 1) because of the similar conditions of their synthesis. The smaller values of the specific surface area and micropore volume of FeZSM-5(C) and FeZSM-5(D) samples, compared with the starting material (Table 1), can be attributed to the blocking role of iron compounds localized within pores and on the surface of zeolite crystals.

The coordination and oxidation states of iron and the dispersity of its oxides in the catalysts under study were determined by EDRS [11, 19]. The EDR spectra of [Fe]ZSM-5(A) and [Fe, Al]ZSM-5(B) samples (Fig. 2) show a band at around 250 nm, which reflects charge transfer between a ligand and a metal atom [19, 20], tetrahedrally coordinated iron(III) [11, 19], which points to its localization in the zeolite structure. A similar conclusion also follows from an analysis of the spectra in the range of *d–d* transitions (300–500 nm). However, the [Fe, Al]ZSM-5(B) sample contains a smaller number of Fe^{3+} ions in its framework, which follows from the lower intensity of bands at 350 and 415 nm (absorption by isolated Fe^{3+} ions [21]) (Fig. 2). This is a consequence of competition between Al^{3+} and Fe^{3+} in the formation of the crystal lattice of the zeolite, with the result that a larger number of Fe^{3+} ions occupy out-of-framework positions [22]. The FeZSM-5(C) catalyst mostly contains iron(II) because its spectrum contains no clearly pronounced bands in the range of absorption by Fe^{3+} ions (224, 278, 350, and 495 nm) [19]. The spectrum of the FeZSM-5(D) sample shows, together with bands characteristic of dispersed oxide clusters of iron(III) (230, 280, and 335 nm), also absorption by aggregated Fe_2O_3 particles (at 500 nm) [19, 20].

The catalysts were also characterized by their temperature-programmed reduction with hydrogen (H_2-TPR), which can be used to determine the structural localization and dispersity of oxide clusters of iron and the reversibility of its reduction–oxidation [23–25]. The H_2-TPR curves of [Fe]ZSM-5(A) and [Fe, Al] ZSM-5(B) samples contain each two peaks of hydrogen uptake at 640, 670 and 960, 1020 K, respectively (Fig. 3). The first peak reflects the reduction of out-of-framework compounds of the Fe_xO_y and $(Fe_xO_y)_n$ types [23], whereas the higher-temperature peak corresponds to reduction of structural ions of iron(III) [23, 24]. The shift of the peaks to higher temperatures, observed for the [Fe, Al]ZSM-5(B) catalyst, is apparently due to the lower content of iron and to the effect of structural ions of aluminum. Oxidative treatment of these samples in NO_2 leads to an increase in the intensity of the low-temperature peak, its shift, and rise in the H_2/Fe molar ratio from 0.38–0.40 to 0.50–0.53 (Fig. 3). This effect is commonly attributed to the presence of readily oxidizable out-of-framework iron(II), which is formed via the $Fe^{3+} \rightarrow Fe^{2+}$ conversion in thermal degradation of the organic template to give [Fe]ZSM-5 [21, 23]. The presence of two high-temperature peaks in the H_2-TPR curves points to existence of different kinds of the framework iron. For the FeZSM-5(C) catalyst, the temperature of the maximum absorption of H_2 is about 770 K (H_2/Fe $\approx$ 1.0), which corresponds to the $FeO \rightarrow Fe^0$

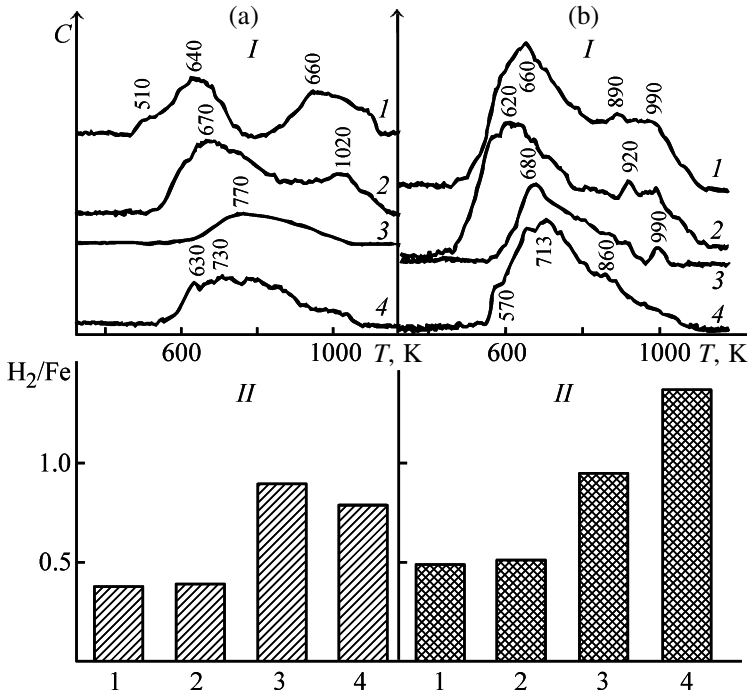

Fig. 3. Temperature-programmed reduction of catalysts: (*C*) H_2 uptake, (*T*) temperature, and (H_2/Fe) hydrogen-to-iron molar ratio. (*I*) TPR curves and (*II*) H_2/Fe molar ratio. (a) Starting samples and (b) N_2O-treated samples.

conversion [25], and decreases by 90 K after its oxidation (Fig. 3). In all probability, the appearance in the process of a peak at about 990 K reflects the reduction of an admixture of the framework iron(III), which is commonly present in industrial zeolites. The reduction of iron(III) in the FeZSM-5(D) sample occurs in a very wide temperature range (Fig. 3), which points to a considerable inhomogeneity of composition and strong nonuniformity of the aggregative state of the oxide phase. This phase is predominantly localized at the external surface of the zeolite, because iron acetylacetonate used in synthesis of the given sample does not penetrate into the channels of ZSM-5 because of the large molecular size (~1.0 nm). This is also confirmed by the adsorption data (Table 1). The shoulder at about 570 K in the H_2-TPR curve of an oxidized [Fe]ZSM-5(D) sample (Fig. 3) can be attributed to the presence of binuclear oxo cations of iron $[OH–Fe–O–Fe–OH]^{2+}$ [25].

The H_2 uptake at 600–1000 K reflects the conversion $Fe_2O_3 \rightarrow Fe_3O_4 \rightarrow FeO \rightarrow Fe^0$ [25], and the weak peak at about 800 K points to existence of aggregated Fe_2O_3 particles, which is consistent with the EDRS data. The noticeable rise in the H_2/Fe ratio, observed for [Fe]ZSM-5(D) after its treatment with N_2O (Fig. 3), also points to a considerable inhomogeneity of the composition of the oxide phase. The results obtained make it possible to assess the capacity of iron for reversible reduction–oxidation [23–25]. For the materials studied, this capacity decreases in the following order: FeZSM-5(C) > [Fe]ZSM-5(A) ≥ [Fe, Al]ZSM-5(B) > FeZSM-5(D).

Thus, the data obtained suggest that the [Fe]ZSM-5(A) and [Fe, Al]ZSM-5(B) catalysts contain iron in framework position and in the form of dispersed Fe_xO_y and $(Fe_xO_y)_n$ clusters mostly localized in zeolite channels. In the FeZSM-5(C) sample, iron is in the cationic form, whereas in FeZSM-5(D), oxo cations, $(Fe_xO_y)_n$ clusters, and Fe_2O_3 particles are mostly situated on the external surface of the zeolite. The so widely diverse nature and composition of

Table 1. Iron content of the catalysts studied and parameters of their pore structure

Catalyst	Si/Al	c_{Fe}, mmol g^{-1}	Fe/Al	S_{Lang}, m^2 g^{-1}	V_{micro}, cm^3 g^{-1}
FeZSM-5(A)	–	0.30	–	470	0.157
[Fe,Al]ZSM-5(B)	200	0.24	4.0	465	0.163
NH_4ZSM-5	40	–	–	440	0.168
FeZSM-5(C)	40	0.09	0.27	435	0.140
FeZSM-5(D)	40	0.07	0.23	410	0.128

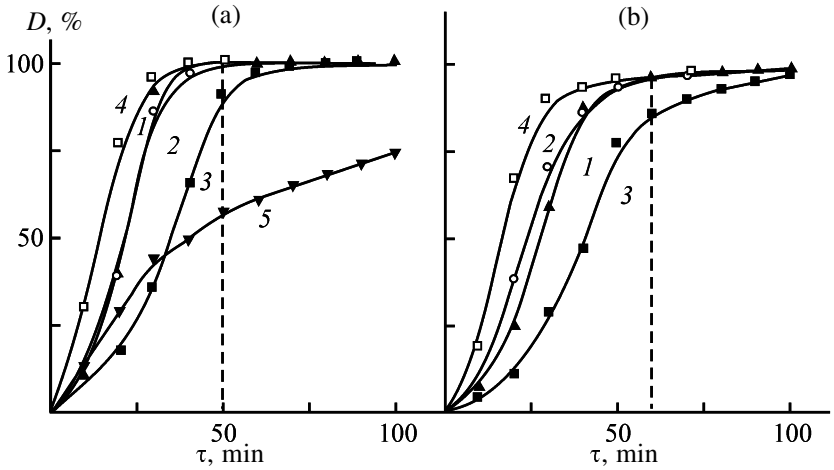

Fig. 4. Kinetics of dye decolorization in the presence of FeZSM-5 catalysts. (*D*) Decolorization and (τ) reaction duration. (a) Rhodamine 6G and (b) Methyl Orange. (*1*) FeZSM-5(A), (*2*) [Fe, Al]ZSM-5(B), (*3*) FeZSM-5(C), (*4*) FeZSM-5(D), and (*5*) 0.3 M $Fe(NO_3)_3$ solution.

active centers and the surface chemistry may strongly affect the behavior of these catalysts in the reaction under study.

It can be seen from the schematic of the structures that the dyes used differ in the size and shape of the carbon skeleton, as well as in the number of reactive centers and functional groups sensitive to the action of oxidizing agents and pH.

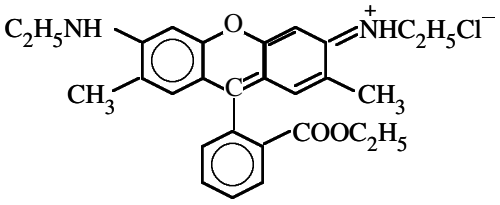

Rhodamine 6G

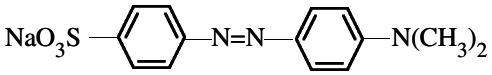

Methyl Orange

It was found that, irrespective of the iron content and nature of active centers of the catalysts, variation of the initial pH value of the reaction medium within the range 3.0–6.0 has virtually no effect on the rate of their decoloration. This is possible at a considerably higher pH value than the pK_a of organic compounds in water [26]. In the presence of the catalysts under study, the pH of water decreases to 3.5–4.0, depending on the content of iron and aluminum compounds in the catalysts. Hence follows that the acid centers of the zeolites, i.e., bridging hydroxy groups of the structural fragments ≡Si–OH–Al= or ≡Si–OH–Fe= or hydrated exchange cations of iron, can control the pH value. Therefore, further experiments were performed at a pH value natural to the dyes.

The lower activity of the homogeneous catalyst, compared to the heterogeneous analogs (Fig. 4), can be attributed to the absence of Fe^{2+} ions. As is known [27, 28], the initial stage of H_2O_2 decomposition catalyzed by iron(III) is its reduction accompanied by the formation of hydroperoxy radicals $HO_2^{\bullet}$ [5]:

$$Fe^{3+} + H_2O_2 \rightarrow Fe(OOH)^{2+} + H^+, \quad (1)$$

$$Fe(OOH)^{2+} \rightarrow Fe^{2+} + HO_2^{\bullet}. \quad (2)$$

The oxidizing capacity of $HO_2^{\bullet}$ is considerably lower than that of $OH^{\bullet}$ radicals [29] generated by H_2O_2 decomposition in the presence of Fe^{2+}. The higher activity of the heterogeneous catalysts may also be due to the specific structure and composition of their active centers, which depend on the structural topology of a zeolite [23–25]. It should, however, be taken into account that iron cations washed-out in the course of the reaction can contribute to the total activity of the catalysts [9]. This effect is the most pronounced for the FeZSM-5(C) sample (Table 2). This seems to be reasonable because this zeolite contains cations retained within its pores by electrostatic interaction with uncompensated negative charges of the crystalline framework. In the rest of the catalysts, iron is in a more bound state, i.e., is partly localized in the structure or in out-of-framework positions in the form of oxide clusters, which leads to a decrease in its leaching-out rate. Nevertheless, even in the case of the Fe-exchange zeolite, the contribution of this process to its activity does not exceed 9%.

Table 2. Specific activity A_{sp} of the catalysts and the activity A_{Fe} of iron cations leached-out from them

Catalyst	A_{sp}	A_{Fe}	A_{sp}	A_{Fe}
	activity, h^{-1}			
	Rhodamine 6G		Methyl Orange	
FeZSM-5(A)	0.79	0.063	0.66	0.029
FeZSM-5(B)	0.66	0.082	0.70	0.069
FeZSM-5(C)	2.82	0.178	2.71	0.150
FeZSM-5(D)	2.73	0.010	3.0	0.048

The deactivation of the catalysts may also be due to loss of the active phase in the course of the reaction. The activity of samples that were used and then dried at room temperature is markedly lower than that of the fresh samples. However, it is virtually completely restored on washing of the catalysts with methanol, followed by drying at 383 K. Consequently, the decrease in activity is mostly due to blocking of surface centers, rather than to loss of iron cations in the course of the reaction. These results clearly demonstrate the relationship between the catalytic function of the materials under study and the nature of their active centers.

Elevation of the temperature from 298 to 323 K leads to a noticeable increase in the rate of dye decolorization in the presence of the catalysts under study. However, the loss of total organic carbon (TOC) depends on temperature to a lesser extent. This is apparently due to formation of intermediates whose mineralization is hindered [8]. The rate at which H_2O_2 is introduced can strongly affect the degree of degradation of the organic substratum [3, 4]. At H_2O_2 addition rates of 21, 41, and 82 mmol h^{-1}, the dye decolorization in the initial period of time (~20 min) only slightly depends on this parameter (Fig. 5). As the reaction proceeds, their degradation slows down at a less vigorous addition of H_2O_2, which points to an insufficient content of the oxidizing agent in the reaction medium. Only for the FeZSM-5(C) catalyst the loss of total organic carbon grows as the rate of H_2O_2 addition is raised (Fig. 5). In all probability, the reason is that, in the case of H_2O_2 deficiency, the forming $OH^{\bullet}$ radicals [Eq. (3)] are partly consumed for oxidation of Fe^{2+} ions [Eq. (4)] [27, 28]:

$$Fe^{2+} + H_2O_2 \rightarrow Fe^{3+} + OH^{\bullet} + OH^-, \quad (3)$$

$$Fe^{2+} + OH^{\bullet} \rightarrow Fe^{3+} + OH^-. \quad (4)$$

Therefore, further experiments were performed at an H_2O_2 addition rate of 82 mmol h^{-1}, because the

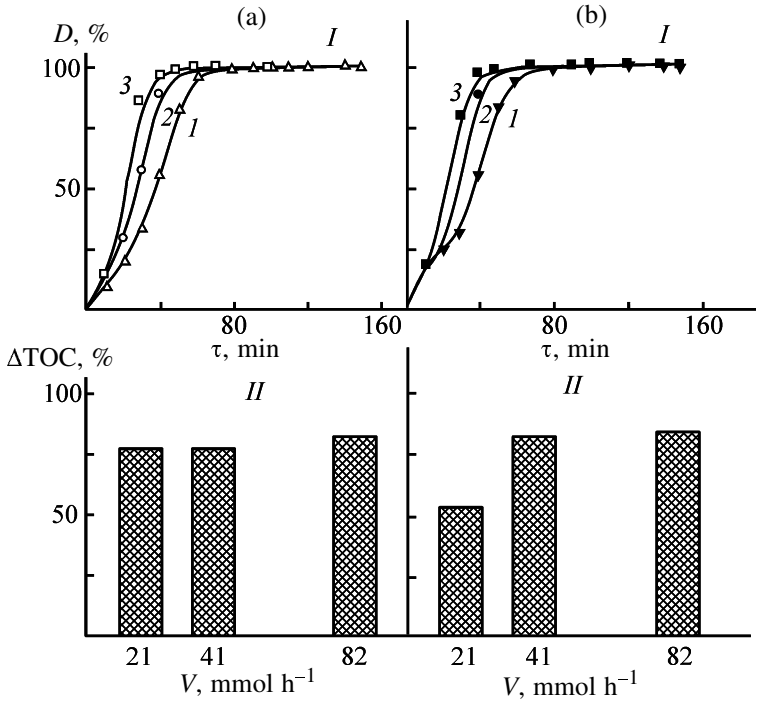

Fig. 5. Effect of the rate V of H_2O_2 addition on the dye decolorization D and TOC loss ΔTOC in the presence of the catalysts under study. (τ) Reaction duration. (*I*) Decoloration curves and (*II*) TOC loss. (a) FeZSM-5(A) and (b) [Fe, Al]ZSM-5(C). V, mmol h^{-1}: (*1*) 21, (*2*) 41, and (*3*) 82.

performance of the catalysts is the highest in this case. Despite the different iron contents (Table 1) and the varied nature of active centers, the total activities of FeZSM-5(C) and FeZSM-5(A) samples are approximately the same (Fig. 5). However, the specific activity of the first of them is considerably higher (Table 2). This can be accounted for by the increased content in this material of Fe^{2+} ions, which catalyze formation of $OH^{\bullet}$ radicals [Eq. (3)] [28], with the result that their concentration in the reaction medium will be high. The [Fe]ZSM-5(A) catalyst contains a larger amount of iron(III) and, therefore, it generates, in addition to $OH^{\bullet}$, the less reactive radicals $HO_2^{\bullet}$ [29], which adversely affects their specific activity. However, the higher concentration of the forming $HO_2^{\bullet}$ radicals compensates for the influence of this factor, and, as a result, the performance of the FeZSM-5(C) and [Fe]ZSM-5(A) samples becomes equal. The dispersity of the active centers may also be a reason for the difference in the catalytic properties of the materials under study. In the FeZSM-5(C) sample, iron is in the highly dispersed cationic form, which leads to an increased reactivity of an individual center. This is reflected in the high specific activity of this catalyst.

The validity of the aforesaid is confirmed by the results obtained with the FeZSM-5(D) catalyst, in whose presence the dye decolorization rate is the highest. However, the loss of TOC is only 40% in this case. This is possibly because the given sample can mostly generate $HO_2^{\bullet}$ radicals and O_2 [28] owing to the fact that the role of its active centers is played by dispersed and aggregated Fe_2O_3 particles. The oxidizing power of these agents was sufficient for decolorization of dyes, but not for their deep degradation. Another important factor is the reversibility of the oxidation–reduction of iron, which is the dominant cycle in the formation of $OH^{\bullet}$ radicals from H_2O_2 [27–29]. According to the H_2-TPR data, the FeZSM-5(D) catalyst contains the smallest amount of active centers exhibiting this property, which totally correlates with its low performance, as indicated by the loss of TOC.

At the optimal rate of H_2O_2 addition (82 mmol h^{-1}) and temperature of 323 K, the deepest degradation (TOC loss of 85%) is observed in the presence of the FeZSM-5(C) and [Fe]ZSM-5(A) catalysts at H_2O_2/dye molar ratios of 860 and 520 for Rhodamine 6G and Methyl Orange, respectively. This result seems to be reasonable because the molecule of Rhodamine 6G has a more branched carbon skeleton and contains a larger number of centers that can enter into reactions involving free radicals. Its degradation catalyzed by FeZSM-5 is more complex, compared to that of Methyl Orange. This process can include a number of competing stages, e.g., degradation of the chromophore and formation of *N*-dealkylation products, which then undergo hydroxylation to give the final products of the reaction, mostly lower carboxylic acids, as indicated by a chromatographic analysis. The change in the oxidation state of iron in the course of the reaction [Eqs. (1)–(4)] and the interaction of the radicals being generated with intermediate products of dye degradation [28] also necessitate use of an excess amount of H_2O_2.

CONCLUSIONS

(1) The nature, localization, and dispersity of active centers predetermine the catalytic behavior of FeZSM-5 zeolites in oxidative degradation of dyes.

(2) Materials containing iron(II) in the cationic form or highly dispersed clusters of the Fe_xO_y and $(Fe_xO_y)_n$ types in zeolite channels have an increased reactivity. The most stable are the catalysts in which iron is localized in both out-of-framework and structural positions.

(3) The catalytic properties of FeZSM-5 strongly depend on the reversibility of the oxidation–reduction of iron forming the active centers. Complete decolorization of Rhodamine 6G and Methyl Orange dyes, accompanied by a 80–85% decrease in the content of total organic carbon, is achieved at a reaction duration of 50–70 min and not-too-high temperature (323 K). The degradation of these compounds can be effected at a nearly neutral pH value, which is an important advantage over the homogeneous system (Fe^{2+}/Fe^{3+} : H_2O_2).

REFERENCES

1. Kim, S.C., Jeong, B.-Y., and Lee, D.K., *Topics Catal.*, 2005, vol. 33, nos. 1–4, pp. 149–154.
2. Pirkanniemi, K. and Sillanpaa, M., *Chemosphere*, 2002, vol. 48, no. 10, pp. 1047–1060.
3. Neamtu, M., Zaharia, C., Catrinescu, C., et al., *Appl. Catal. B: Environ.*, 2004, vol. 48, no. 4, pp. 287–294.
4. Guelou, E., Barrault, J., Fournier, J., and Tatibouet, J.M., *Appl. Catal. B: Environ.*, 2003, vol. 44, no. 1, pp. 1–8.
5. Martinez, F., Calleja, G., Malero, J.A., and Molina, R., *Appl. Catal. B: Environ.*, 2005, vol. 60, nos. 3–4, pp. 185–194.
6. Fajerwerg, K. and Debellefontaine, H., *Appl. Catal. B: Environ.*, 1996, vol. 10, pp. L229–L235.

7. Kiwi-Minsker, L., Bulushev, D.A., and Renken, A., *J. Catal.*, 2003, vol. 219, no. 2, pp. 273–275.
8. Centi, G., Perathoner, S., Torre, T., and Verduna, M.G., *Catal. Today*, 2000, vol. 55, nos. 1–9, pp. 61–69.
9. Kuznetsova, E.V., Savinov, E.N., Vostrikova, L.A., and Parmon, V.N., *Appl. Catal. B: Environ.*, 2004, vol. 51, no. 3, pp. 165–170.
10. Szostak, R., Nair, V., and Thomas, T.L., *J. Chem. Soc., Faraday Trans. 1*, 1987, vol. 83, pp. 487–494.
11. Ratnasamy, P. and Kumar, R., *Catal. Today*, 1991, vol. 9, no. 4, pp. 329–416.
12. Long, R.Q. and Yang, R.T., *Catal. Lett.*, 2001, vol. 74, nos. 3–4, pp. 201–205.
13. Schwidder, M., Santhosh Kumar, M., Bruckner, A., et al., *Chem. Commun.*, 2005, pp. 805–807.
14. Ledenev, I.A., Zorin, V.E., Prikhod'ko, R.V., et al., *Zh. Prikl. Khim.*, 2005, vol. 78, no. 11, pp. 1853–1858.
15. Webb, P.A. and Orr, C., *Analytical Methods in Fine Particles Technology*, Norcross (the United States): Micromeritics Instrument, 1997, pp. 59–73.
16. Zhu, Q., Teeffelen, R.M. van, Santen, R.A. van, et al., *J. Catal.*, 2004, vol. 221, no. 2, pp. 575–583.
17. Treacy, M.M.J., Higgins, J.B., and Ballmoos, R. von, *Zeolites*, 1996, vol. 16, nos. 5–6, pp. 522–525.
18. Cundy, C.S. and Cox, P.A., *Micropor. Mesopor. Mater.*, 2005, vol. 82, nos. 1–2, pp. 1–78.
19. Murturano, P., Drozdova, L., Kogelbauer, A., and Prins, R., *Stud. Surf. Sci. Catal.*, 2001, vol. 135, pp. 143–151.
20. Centi, G., Fazzini, F., Fierro, J.L.G., et al., *Stud. Surf. Sci. Catal.*, 1998, vol. 118, pp. 577–585.
21. Ferretti, A.M., Oliva, C., Forni, L., et al., *J. Catal.*, 2002, vol. 208, no. 1, pp. 83–88.
22. Lobree, L.J., Hwang, I.-C., Reimer, J.A., et al., *J. Catal.*, 1999, vol. 186, no. 2, pp. 242–253.
23. Perez-Ramirez, J., Mul, G., Kapteijn, F., et al., *J. Catal.*, 2002, vol. 207, no. 1, pp. 113–126.
24. Zhilinskaya, E.A., Delahay, G., Mauvezin, M., et al., *Langmuir*, 2003, vol. 19, pp. 3596–3602.
25. Mauvezin, M., Delahay, G., Coq, B., et al., *J. Phys. Chem. B*, 2001, vol. 105, no. 5, pp. 928–935.
26. Goi, A. and Trapido, M., *Proc. Estonian Acad. Sci., Chem.*, 2001, vol. 50, pp. 5–6.
27. Kavitha, V. and Palanivelu, K., *Water Res.*, 2005, vol. 39, no. 13, pp. 3062–3072.
28. Sychev, A.Ya. and Isak, V.G., *Usp. Khim.*, 1995, vol. 64, no. 12, pp. 1183–1198.
29. Ramirez, J.H., Costa, C.A., and Madeira, L.M., *Catal. Today*, 2005, vol. 107–108, pp. 68–76.

ISSN 1070-4272, Russian Journal of Applied Chemistry, 2007, Vol. 80, No. 5, pp. 754–756. © Pleiades Publishing, Ltd., 2007.
Original Russian Text © A.P. Yaroshenko, M.V. Savos'kin, V.N. Mochalin, N.I. Lazareva, 2007, published in Zhurnal Prikladnoi Khimii, 2007, Vol. 80, No. 5, pp. 775–777.

CATALYSIS

New Floating Photocatalysts Based on Expanded Graphite and Anatase

A. P. Yaroshenko, M. V. Savos'kin, V. N. Mochalin, and N. I. Lazareva

Litvinenko Institute of Physical Organic and Coal Chemistry, National Academy of Sciences of Ukraine, Donetsk, Ukraine

Received May 30, 2006

Abstract—A new method for production of composites constituted by expanded graphite, amorphous carbon, and titanium dioxide was suggested. The structure of the materials obtained was studied, and it was demonstrated that they show promise as photocatalysts for water treatment to remove organic contaminants.

DOI: 10.1134/S1070427207050126

Photocatalytic processes of contaminant decomposition involving titanium dioxide are presently regarded as one of the most promising methods for water treatment [1]. This is due to the high photocatalytic activity, longevity, stability in aqueous media, comparatively low cost, and low toxicity of this material [2]. Beginning in the second half of the 1990s, when TiO_2 deposited on expanded graphite (EG) was first described [3, 4], this composite material is of interest because of the unique combination of the photocatalytic activity of TiO_2 and the buoyancy of EG [5]. This combination provides the most complete utilization of UV light by titanium dioxide particles and substantially simplifies the procedure of removal of a spent photocatalyst from the water surface. Recently, it has been reported that EG–TiO_2 composites can effectively decompose such dangerous water contaminants as petroleum [6], heavy oil [7], pesticides [8], and phenols [9].

However, wide-scale use of EG–TiO_2 floating composites is still hindered by the lack of simple and inexpensive methods for their manufacture. The few procedures described in the literature [3, 4, 7] are primarily oriented to laboratory production and are hardly suitable for industrial manufacture because they are complicated and require that expensive and hazardous reagents should be used, including organometallic compounds, organic solvents, and organosilicon binders.

Recently, we have suggested [10] a simple method for production of composites composed of expanded graphite and amorphous carbon (EG–AmC) from inexpensive and readily available starting materials: graphite intercalation compounds (residual graphite hydrosulfate) and a renewable source of amorphous carbon, sucrose. The procedure includes a considerably smaller number of stages and does not require any organometallic and organosilicon compounds, organic solvents, and an inert atmosphere, which enables industrial manufacture of EG–AmC composites with low energy and labor expenditure. In this study, the previously suggested approach is extended and used to obtain new EG–AmC–TiO_2 photocatalysts to be used in water treatment.

EXPERIMENTAL

EG–AmC–TiO_2 composites were produced from residual graphite hydrosulfate [TU (Technical Specification) U 26.8-20372011-001–2002] synthesized by the method described in [11] from GSM-1[1] flake graphite and sucrose (Merck) as a precursor of amorphous carbon. The procedure for synthesis of EG–AmC–TiO_2 composites is similar to that described in [10] with the only difference that a TiO_2 powder (anatase 99.9 wt %, Aldrich, particle size 10 nm) was added to the starting mixture of residual graphite hydrosulfate and sucrose. A detailed description of the methods used to obtain EG–AcM–TiO_2 composites can be found in [12]. The specific surface areas (by BET) of the materials obtained, determined by the method of low-temperature adsorption of argon in conformity with GOST 13144–79, varied from 30 to 200 $m^2 g^{-1}$, depending on the composite composition. The structure and composition of the samples were

[1] Zaval'evskoe deposit (Ukraine).

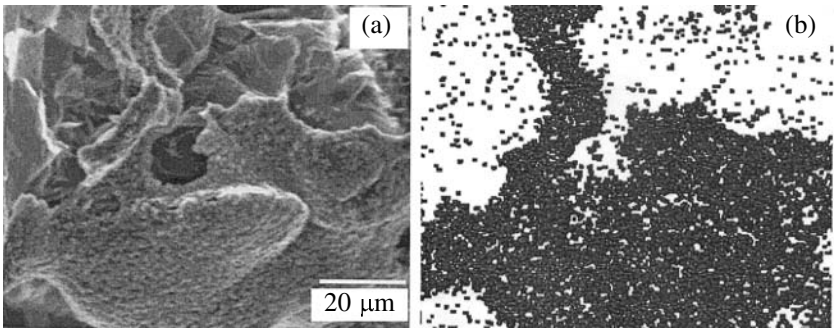

Fig. 1. SEM images of the same part of an EG–AmC–TiO_2 composite, obtained (a) by the conventional method with secondary electrons and (b) with the TiK_α radiation.

analyzed by scanning electron microscopy (SEM) on a JEOL JSM-1300 instrument.

The photocatalytic activity of the EG–AmC-TiO_2 composites in photodegradation of phenol was studied by the method described in [13]. A 100-W DRSh-100-2 high-pressure mercury lamp with a continuous emission spectrum was used as a source of UV light. To preclude photolysis of phenol under the action of absorbed photons, the spectral range 310–410 nm was used [13]. The intensity of light that entered the reactor, found by the standard procedure with a ferrisilicate actinometer [14], was $(3.0 \pm 0.3) \times 10^{-4}$ E s^{-1}.

Kinetic measurements were performed as follows. A freshly prepared aqueous solution of phenol, with a concentration of 50–200 mg l^{-1}, was placed in a thermostated reactor (25°C) and 0.4 g of the EG–AmC–TiO_2 composite was added so that it uniformly covered the entire surface of the solution. To reach sorption equilibrium before the beginning of irradiation, the solution was agitated in the dark for 48–60 h. Then, the UV source was switched on and the loss of phenol in the liquid phase was determined using the standard photoelectrocolorimetric method with 4-aminoantipyrine [15] after prescribed intervals of time under continuous agitation.

SEM micrographs of a sample of the composite synthesized are shown in Figs. 1a and 1b. The image in Fig. 1a clearly demonstrates the multicomponent structure of the material, with a macroporous cellular matrix of expanded graphite, covered with a layer of amorphous carbon formed in situ by carbonization of sucrose. It is noteworthy that a similar structure is also characteristic of previously obtained EG–AmC composites [10]. It can also be well seen in Fig. 1a that the amorphous carbon phase coating particles of expanded graphite has a rough surface. This is due to inclusions of titanium dioxide particles in the layer of amorphous carbon. The image in Fig. 1b confirms that these embedded particles are TiO_2 particles. The same figure shows at the same magnification the same part of the surface of the composite material as that in Fig. 1a, but obtained with TiK_α radiation. The dark spots in Fig. 1b correspond to places of localization of TiO_2 particles on the sample surface, from which photons with energy of the K_α line of titanium are emitted.

Thus, amorphous carbon produced in situ by carbonization of sucrose not only acts as an effective sorbent [10], but also binds together the individual components of the material, which makes unnecessary use of any additional binder. The intimate contact between EG and TiO_2 particles, provided by amorphous carbon, imparts to the composite obtained a disintegration resistance sufficient for its use as a floating photocatalyst. It was found in a separate experiment that particles of the EG–AmC–TiO_2 composite placed on the surface of water retain buoyancy under laboratory conditions and do not disintegrate into individual components, at least during several weeks.

It should be noted that the procedure suggested can give stable floating EG–AmC–TiO_2 composites with high content of TiO_2, in contrast to the previously suggested methods. For example, the technique described in [7], which uses titanium isopropoxide as a TiO_2 precursor without any additional binder, gives no way of making the titanium dioxide content of the composite higher than 14.5 wt %. Ramanathan et al. [3], who were the first to suggest a method for synthesis of EG–TiO_2 materials with an organosilicon binder, reported nothing about composites containing more than 45 wt % TiO_2. The method suggested in this paper allows easy production of EG–AmC–TiO_2 composites with titanium dioxide content of up to 70 wt %.

Preliminary data on the kinetics of photocatalytic

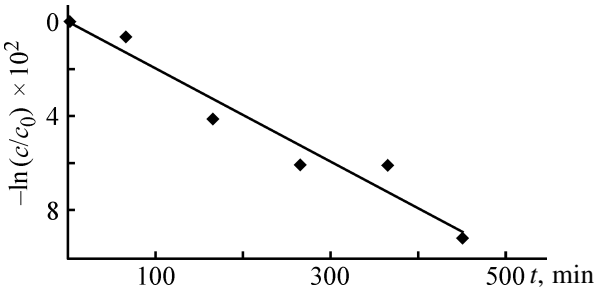

Fig. 2. Photodegradation of phenol in an aqueous solution, catalyzed by an EG–AmC–TiO_2 composite (68 wt % TiO_2). Initial concentration of phenol in solution 195 mg l^{-1}. (c) Phenol concentration and (t) reaction duration.

degradation of phenol in aqueous solutions with the materials obtained is satisfactorily described by pseudo-first-order equations. The apparent rate constant for a composite with TiO_2 content of 68 wt % is $(3.3 \pm 0.4) \times 10^{-6}$ s^{-1} (Fig. 2), which agrees in order of magnitude with published data for AmC–TiO_2 composites [13].

CONCLUSIONS

(1) A new method is suggested for synthesis of composite materials composed of expanded graphite, amorphous carbon, and titanium dioxide from residual graphite hydrosulfate, sucrose, and titanium dioxide in the form of anatase. The method is distinguished from the presently existing techniques by low time and energy consumption, readily available raw materials, and easy scaling-up to industrial manufacture.

(2) The results of a study of the composites by scanning electron microscopy confirm their multicomponent structure and demonstrate that TiO_2 is predominantly localized on the surface of the amorphous carbon phase, which serves not only as a sorbent, but also as a binder of the individual components of the composite material.

(3) Preliminary data on the photocatalytic activity of new composite materials composed of swollen graphite, amorphous carbon, and titanium dioxide, obtained in the study, make it possible to regard these materials as readily available effective floating photocatalysts for water treatment and environment protection.

REFERENCES

1. Zaleska, A. and Hupka, J., *Advanced Oxidation Techniques in Environmental Protection*, Lodz: Polska Akad. Nauk, Oddzial w Lodzi, 2002.
2. Hoffmann, M.R., Martin, S.T., Choi, W., et al., *Chem. Rev.*, 1995, vol. 95, no. 1, pp. 69–96.
3. Ramanathan, K., Anvir, D., Modestov, A., et al. *Chem. Mater.*, 1997, vol. 9, no. 11, pp. 2533–2540.
4. Modestov, A., Glezer, V., Marjasin, I., et al., *J. Phys. Chem. B*, 1997, vol. 101, no. 23, pp. 4623–4629.
5. Toyoda, M., Umemura, H., and Inagaki, M., *New Carbon Mater.*, 2002, vol. 17, no. 2, pp. 1–3.
6. Grzechulska, J., Hamerski, M., and Morawski, A.W., *Water Res.*, 2000, vol. 34, no. 5, pp. 1638–1644.
7. Tsumura, T., Kojitani, N., Umemura, H., et al., *Appl. Surface Sci.*, 2002, vol. 196, nos. 1–4, pp. 429–436.
8. Modestov, A. and Lev, O., *J. Photochem. Photobiol., A, Chem.*, 1998, vol. 112, nos. 2–3, pp. 261–270.
9. Tryba, B., Morawski, A.W., and Inagaki, M., *Appl. Catal. B, Environ.*, 2003, vol. 41, no. 4, pp. 427–433.
10. UA Patent 74868.
11. Yaroshenko, A.P., Savos'kin, M.V., Magazinskii, A.N., et al., *Zh. Prikl. Khim.*, 2003, vol. 76, no. 8, pp. 1269–1272.
12. UA Patent 74688.
13. Tryba, B., Tsumura, T., Janus, M., et al., *Appl. Catal. B, Environ.*, 2004, vol. 50, no. 3, pp. 177–183.
14. Kuhn, H.J., Braslavsky, S.E., and Schmidt, R., *Pure Appl. Chem.*, 2004, vol. 76, no. 12, pp. 2105–2146.
15. Greenberg, A.E., Clesceri, L.S., and Eaton, A.D., *Standard Methods for the Examination of Water and Wastewater*, Washington: APHA, AWWA, WEF, 1992, 18th ed.

ISSN 1070-4272, Russian Journal of Applied Chemistry, 2007, Vol. 80, No. 5, pp. 757–760. © Pleiades Publishing, Ltd., 2007.
Original Russian Text © V.Z. Kuz'min, I.I. Safarova, T.M. Prokudina, V.A. Shepelin, R.R. Sharifullin, 2007, published in Zhurnal Prikladnoi Khimii, 2007, Vol. 80, No. 5, pp. 778–781.

ORGANIC SYNTHESIS AND INDUSTRIAL ORGANIC CHEMISTRY

Surface Activity of Oxyethylated Alkylphenols

V. Z. Kuz'min, I. I. Safarova, T. M. Prokudina, V. A. Shepelin, and R. R. Sharifullin

Nizhnekamskneftekhim Joint-Stock Company, Nizhnekamsk, Tatarstan, Russia

Received June 13, 2006; in final form, January 2007

Abstract—Pilot samples of oxyethylated products derived from octylphenol, isononylphenol, and isododecylphenol were synthesized. Their colloidal characteristics were studied and compared with the characteristics of ethoxylates of higher aliphatic alcohols.

DOI: 10.1134/S1070427207050138

Surfactants are widely used in many modern processes and materials. The assortment of natural and synthetic surfactants is very wide. With respect to the characteristics, structure, and composition, the most diverse are nonionic surfactants, whose share in the whole commercial production of surfactants reaches 20% [1].

Oxyethylated isononylphenols, Neonols, produced by the Nizhnekamskneftekhim Joint-Stock Company are nonionic surfactants. Oxyethylated isononylphenols are mixtures of oligomers-homologs, whose average degree of oxyethylation can vary in a wide range. The fields of application of Neonols are the same as those for oxyethylated aliphatic alcohols, but they are more widely used for technical purposes. Being adsorbed at the phase boundary, surfactants play a significant role in wetting, dispersion, emulsification, foaming, and other phenomena.

One of the main characteristics of surfactant performance is surface tension σ. There are numerous data on surface and interfacial tension of aqueous surfactant solutions, showing that the structure of surfactant molecule significantly affects its ability to decrease the interfacial tension. The other important characteristic of the surfactant performance is the critical micellization concentration C_{cmc}, i.e., concentration at which micelles are formed, causing abrupt changes in other characteristics of surfactant. The C_{cmc} value corresponds to the minimum surface tension. For homologous series of surfactants it was established that, the lower C_{cmc}, the more efficient is the surfactant [2].

The study of the surface tension of aqueous solutions of oxyethylated primary aliphatic alcohols as an example showed [2] that an increase of the length of alkyl chain increases the surface tension. With respect to decreasing surface tension, a branched alkyl group is more preferable than a linear radical. The general regularity of decreasing surface activity with increasing number of oxyethyl groups was elucidated. The individual values of surface tension for some samples of oxyethylated octylphenols and nonylphenols were determined. The influence of the hydrocarbon radical and the length of the polyoxyethylene chain of polyglycol ethers of alkylphenols was studied in [3, 4] for alkylphenols with CH_3, C_4H_9, C_9H_{19}, $C_{12}H_{25}$, and $C_{18}H_{37}$ radicals having normal hydrocarbon chains and degree of oxyethylation from 2 to 28.

This study was aimed to compare of colloidal-chemical characteristics of commercial Neonols produced by the Nizhnekamskneftekhim Joint-Stock Company and specially synthesized pilot samples of oxyethylated isononylphenols with degree of oxyethylation higher than 12 and also oxyethylated products derived from oxyphenol and isododecylphenol (alkylphenol derived from propylene tetramers).

EXPERIMENTAL

Alkylphenols were synthesized on a laboratory installation for alkylation of phenol at 110°C using two- or threefold molar excess of phenol in the presence of Lewatit SPC-108 HG sulfonated ion-exchange resin as a catalyst. α-Olefins C_8 and trimers and tetramers of propylene produced by the Nizhnekamskneftekhim Joint-Stock Company were used as alkylating agents. These products were suited to the require-

Table 1. Composition of alkylphenols used for oxyethylation

Component	Composition, wt %		
	octylphenol	isononylphenol	isododecylphenol
Olefin	0.01	–	0.23
Phenol	0.06	0.01	0.15
Alkyl phenyl ether	0.44	–	–
Monoalkylphenol	99.48	99.79	99.03
Dialkylphenol	0.01	0.20	0.59

ments of the technical specifications and were used without additional purification. Alkylphenols were recovered from the reaction mixtures by vacuum distillation. The compositions of the resulting alkylphenols used for oxyethylation are presented in Table 1.

Oxyethylene derivatives were synthesized on a laboratory installation for oxyethylation at a temperature of 120–125°C and a pressure of 5–6 kgf cm^{-2}. A 30% aqueous solution of sodium hydroxide [GOST (State Standard) 2263–79] or potassium hydroxide (GOST 24368–80) in an amount of 0.12–0.20% relative to the final product was used as a catalyst. After addition of alkali to the initial alkylphenol, the moisture was removed from the starting system. The starting system was dried for 60–90 min at 80–90°C and residual pressure of 2660–3990 Pa. Polyethylene glycol ethers were neutralized with acetic acid (GOST 19814–74) to pH 6.5–7.5.

Physicochemical characteristics of polyethylene glycol ethers of alkylphenols of the general formula $C_mH_{2m+1}C_6H_4O(CH_2–CH_2–O)_nH$ are presented in Table 2.

For water-soluble samples of the alkylphenols studied, we measured the surface tension at the water–air interface by the ring detachment method on a du Nouy tensiometer at 24 ± 1°C for surfactant concentration in aqueous solution in the range 0.4–10^{-6} wt %. From the experimental data, we plotted the isotherms of surface tension at the interface of aqueous solution of nonionic surfactant and air (Fig. 1), and from the

Table 2. Physicochemical characteristics of polyethylene glycol ethers of alkylphenols

Product AF_n-m*	Aggregative state	Melting point, °C	Cloud point, °C	Density ρ, g cm^{-3}	Kinematic viscosity $\eta \times 10^{-6}$, m^2 s^{-1}	EO content, wt %		PEG content, %
						calculated	found	
AF_8-8	Liquid	2–10	55	1.0398^{40}	67.2^{40}	63.1	62.5	0.2
AF_8-10	Liquid	11–18	73.5	1.0468^{40}	69.6^{40}	68.1	65.0	0.7
AF_8-20	Solid	32	86.5**	1.0642^{50}	81.6^{50}	81.0	–	3.0
AF_8-25	Solid	35	89.5**	1.0729^{50}	106.3^{50}	84.2	–	3.0
AF_9-2	Liquid	–22	50***	0.9859^{20}	137^{40}	28.6	–	0.2
AF_9-3	Liquid	–23	53.9***	1.0003^{40}	113^{40}	37.5	–	0.2
AF_9-4	Liquid	–24	56***	1.025^{40}	101.0^{40}	44.4	44.2	0.3
AF_9-6	Liquid	–20	68***	1.027^{40}	–	54.5	53.5	0.5
AF_9-8	Liquid	–2–2	77.5	1.062^{20}	–	61.5	61.0	0.5
AF_9-9	Liquid	3–8	54.2	1.045^{40}	–	64.3	64.0	0.5
AF_9-10	Liquid	6–10	66.3	1.040^{50}	–	66.7	67.0	0.6
AF_9-12	Liquid	13–17	86.0	1.046^{50}	70.0^{50}	70.6	69.6	0.8
AF_9-14	Liquid	17–20	76**	1.061^{40}	122^{40}	73.7	72.0	1.0
AF_9-16	Paste	21–29	82.5**	–	45.7^{70}	76.2	75.1	1.0
AF_9-25	Solid	31–36	91.5**	–	–	83.3	81.0	2.2
AF_{12}-6	Liquid	<20	63.3***	1.0128^{40}	125.2^{40}	50.2	44.5	1.2
AF_{12}-8	Liquid	5	74.1***	1.0256^{40}	119.5^{40}	57.3	56.0	1.3
AF_{12}-10	Liquid	8–10	80.0***	–	141.0^{40}	62.3	65.5	1.3
AF_{12}-14	Paste	21–23	86.5	0.9616^{20}	124.7^{40}	70.2	73.0	1.5
AF_{12}-16	Paste	21–29	98.0	1.0469^{40}	159.7^{40}	72.9	75.5	2.0

* *n* is the number of carbon atoms in hydrocarbon radical of alkylphenol and *m* is the number of moles of added EO (ethylene oxide).

** Cloud point was determined in aqueous saline solution.

*** Cloud point was determined in 25% aqueous solution of *n*-butyl diglycol.

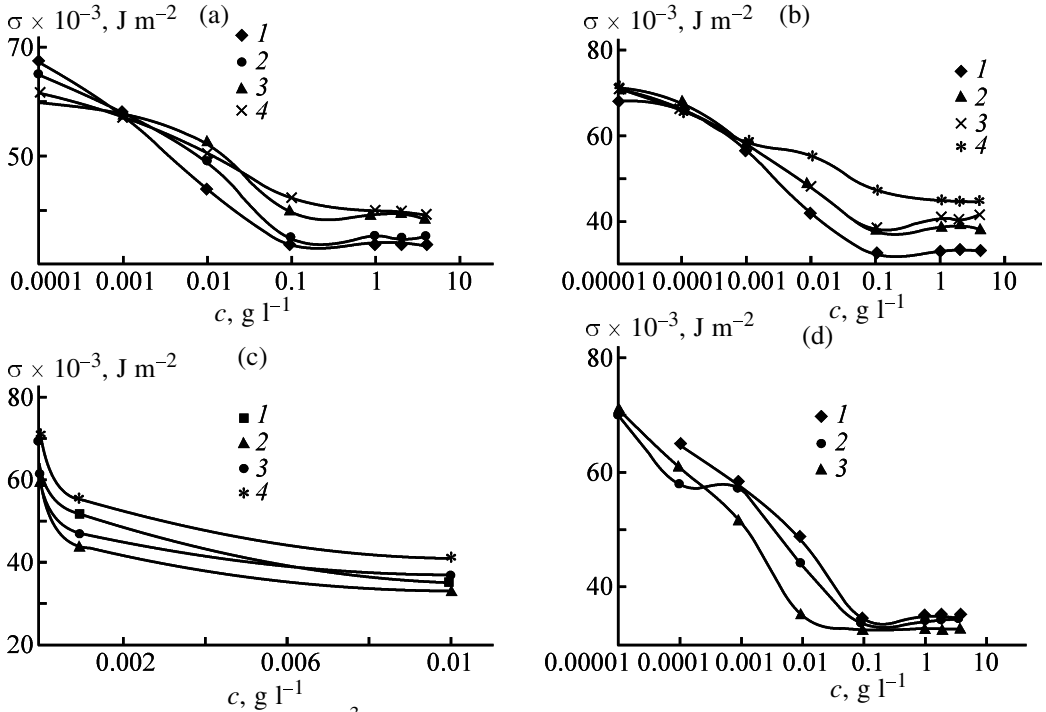

Fig. 1. Isotherms of surface tension $\sigma \times 10^{-3}$ of (a) aqueous solutions of oxyethylated octylphenols, (b) isononylphenols, (c) isododecylphenols, and (d) alkylphenols oxyethylated by 10 mol of ethylene oxide. (*c*) Concentration of nonionic surfactant, g l^{-1}. Product: (a) (*1*) AF_8-8, (*2*) AF_8-10, (*3*) AF_8-12, and (*4*) AF_8-20; (b) (*1*) AF_9-8, (*2*) AF_9-14, (*3*) AF_9-18, and (*4*) AF_9-25; (c) (*1*) AF_{12}-10, (*2*) AF_{12}-12, (*3*) AF_{12}-14, and (*4*) AF_{12}-16; (d) (*1*) AF_8-10, (*2*) AF_9-10, and (*3*) AF_{12}-10.

coordinates of the inflection points of the resulting dependences we determined the C_{cmc} for a series of samples of oxyethylated products.

The results of our experiments showed that the regular trends determined for oxyethylated adducts, including ethoxylates of aliphatic alcohols, are also observed with oxyethylated alkylphenols.

For all the three groups of the alkylphenols in hand, the surface tension increases with increasing degree of oxyethylation (Figs. 1a–1c) and, on the contrary, decreases with increasing length of hydrocarbon chain of alkylphenol (Fig. 1d).

For comparison, we determined the surface characteristics of pilot samples of polyethylene glycol ethers of higher aliphatic alcohols (HAAs, C_{12}–C_{14} fraction) produced by the Procter and Gamble Company and oxyethylated with 2 (AE-2), 3 (AE-3), and 7 (AE-7) mol of ethylene oxide.

The surface tension values determined experimentally and the critical micellization concentration are presented in Table 3.

Some researchers believe that in their surface characteristics ethoxylates of aliphatic alcohols are more efficient than their analogs based on alkylphenols; this, however, is not quite correct. The surface characteristics of oxyethylated adducts based on alkylphenols are governed by the ratio of hydrophilic and hydrophobic parts (hydrophilic-lipophilic balance, HLB) and by the structure of the hydrocarbon substituent of the benzene ring of alkylphenol.

Table 3. Surface tension and critical micellization concentration of oxyethylated adducts

Oxyethylated product	C_{cmc}, wt %	$\sigma_{cmc} \times 10^{-3}$, J m^{-2}
AF_8-8	0.01	33.6
AF_8-10	0.01	35.3
AF_8-20	0.01	42.5
AF_8-25	0.01	45.1
AF_9-9	0.01	32.9
AF_9-10	0.01	34.0
AF_9-12	0.01	35.4
AF_9-14	0.01	37.7
AF_9-16	0.01	39.3
AF_9-25	0.1	47.4
AF_{12}-8	0.001	33.3
AF_{12}-10	0.001	33.1
AF_{12}-14	0.001	36.3
AF_{12}-16	0.001	38.3
AE-2	0.001	32.8
AE-3	0.001	32.0
AE-7	0.001	33.0

The experimental data showed that polyethylene glycol ethers derived from alkylphenols and HAAs having close values of HLB have also close values of surface tension. Oxyethylated alkylphenols derived from tetramers of propylene and ethoxylates of HAAs have low C_{cmc}, which suggests their higher surfactant performance. For Neonols based on octylphenol and isononylphenol, the C_{cmc} values are lower, and approximately constant, 0.01 wt %. For isododecylphenols oxyethylated with 8 and 10 mol of ethylene oxide and for aliphatic alcohol of C_{12}–C_{14} fraction oxyethylated with 7 mol of ethylene oxide (57.3, 62.7, and 60.6 wt % ethylene oxide, respectively), close values of surface tension were obtained.

CONCLUSIONS

(1) The main physicochemical characteristics of polyethylene glycol ethers of octyl-, isononyl-, and isododecylphenols were determined and variation of the surface tension as a function of the length of the oxyethylene chain at constant alkyl radical and of the radical length at a constant length of oxyethylene chain was studied.

(2) At a certain combination of fractions of alkyl and oxyethyl components in the structure of polyethylene ethers of alkylphenols and depending on the structure of alkyl substituent in the aromatic ring, adducts based on alkylphenols, well competing in the performance with ethoxylates of higher aliphatic alcohols, can be synthesized.

REFERENCES

1. Pletnev, M.Yu., *Khim. Prom–st*., 2001, no. 1, pp. 48–61.
2. Schönfeldt, N., *Grenzflachenaktive Äthyleneoxid-Addukte*, Stuttgart: Wissenschaftliche, 1976.
3. Petrov, A.A. and Pozdyshev, G.N., *Kolloidn. Zh*., 1966, vol. 28, no. 6, pp. 858–865.
4. Pozdyshev, G.N. and Petrov, A.A., *Kolloidn. Zh*., 1967, vol. 29, no. 4, pp. 569–575.

ISSN 1070-4272, Russian Journal of Applied Chemistry, 2007, Vol. 80, No. 5, pp. 761–766. © Pleiades Publishing, Ltd., 2007.
Original Russian Text © V.V. Lisitskii, Z.A. Akhmetchenko, I.E. Alekhina, Yu.I. Murinov, 2007, published in Zhurnal Prikladnoi Khimii, 2007, Vol. 80, No. 5, pp. 782–787.

ORGANIC SYNTHESIS AND INDUSTRIAL ORGANIC CHEMISTRY

Hydrolysis of 2-Substituted and 1,2-Disubstituted Imidazolines

V. V. Lisitskii, Z. A. Akhmetchenko, I. E. Alekhina, and Yu. I. Murinov

Bashir State University, Ufa, Bashkortostan, Russia
Institute of Organic Chemistry, Ufa Scientific Center, Russian Academy of Sciences, Ufa, Bashkortostan, Russia

Received July 14, 2006

Abstract—The mechanism and kinetics of hydrolysis of 2-substituted and 1,2-disubstituted imidazolines in acid, neutral, and alkaline solutions were studied. The influence of the substituents at the 1- and 2-positions of the imidazoline ring on the hydrolytic resistance of these compounds was demonstrated.

DOI: 10.1134/S107042720705014X

2-Substituted and 1,2-disubstituted imidazolines are widely used for preparing cationic and ampholytic surfactants [1–6] and as corrosion inhibitors in production, transportation, and refining of oil [1, 7–13]. The possibility and advisability of industrial application of imidazolines depend significantly on their hydrolytic resistance.

Since preparation of ampholytic surfactants from imidazolines is performed in aqueous solutions at a high excess of alkali metal hydroxide [1–5], hydrolysis of 2-substituted and 1,2-disubstituted imidazolines in alkali solutions was studied most extensively [1, 14–24]. The kinetics of base hydrolysis of 1-hydroxyethyl-2-nonyl-2-imidazoline at 40–90°C was studied in [16–18, 24]. The content of 1,2-disubstituted imidazoline in the hydrolysis products was estimated by IR and UV spectroscopy. Taking into account a large water excess, the experimental results were treated by the pseudo-first-order rate equation. The calculated rate constants of hydrolysis show that hydrolysis of 1-oxyethyl-2-nonyl-2-imidazoline is extremely temperature-sensitive. For examples, at 40°C $K_{hydr} = 1.22 \times 10^{-4}$ and at 90°C $K_{hydr} = 8.42 \times 10^{-4}$ s^{-1} [16]. The apparent activation energy of hydrolysis in the temperature range 40–90°C is very low (5.73 kJ mol^{-1}). The hydrolysis rate constant of 1-hydroxyethyl-2-nonyl-2-imidazoline is almost independent of its concentration. The hydrolysis rate constant varies within the limits of the experimental error when the molar excess of water ranges from 11- to 50-fold and in the presence of *N*-capryl-*N*'-(β-hydroxyethyl)ethylenediamine (hydrolysis product of 1-hydroxyethyl-2-nonyl-2-imidazoline, up to 10 wt %) [16].

The influence of the pH of the solution on the hydrolysis rate is stronger than that of temperature [17–19, 24]. The hydrolysis rate constant at 50°C increases by a factor of more than 40 (from 0.078×10^{-4} to 3.14×10^{-4}) with increasing pH from 8.05 to 12.5. The dependence of $\log K_{hydr}$ on pH is linear and has a bend at pH 9.7. The linearity of the $\log K_{hydr}$–pH dependence suggests that the rate-determining step of the process is nucleophilic attack of OH^- ions on protonated 1-hydroxyethyl-2-nonyl-2-imidazoline:

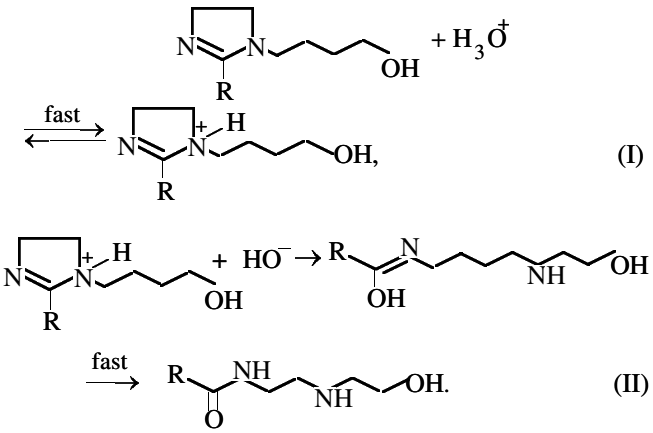

At pH 9.7, equilibrium (I) is shifted to formation of the neutral product, the fraction of protonated imidazoline decreases, and hence the relative hydrolysis rate decreases [17]. The hydrolysis rate constant decreases also with an increase in the ionic strength of the solution.

A study of the influence of OH^- and imidazoline concentrations on the hydrolysis rate constant showed that the reaction was of the first order with respect to

OH^- and imidazoline. Hence, the overall reaction order of 1-hydroxyethyl-2-nonyl-2-imidazoline hydrolysis is second [17].

Savignac et al. [19] studied, with 1-aminoethyl-2-decyl-2-imidazoline and 2-nonyl-2-imidazoline as examples, the influence of the substituent at position 1 of the imidazoline ring on the kinetics of base hydrolysis at 25–50°C. As determined by UV spectroscopy, an increase in the concentration of hydroxide ions in the reaction mixture accelerates substantially hydrolysis of 1,2-disubstituted imizazoline and has virtually no effect on the hydrolysis rate of the 2-substituted imidazoline, irrespective of the temperature. It should be noted that the apparent rate constants of hydrolysis at similar pH differ by approximately an order of magnitude, especially in strongly alkaline solutions (pH > 10) [19]. Substantially lower stability of 1,2-disubstituted imidazoline as compared to that of 2-substituted imidazoline is confirmed by the activation energies of base hydrolysis of these compounds: for 1-aminoethyl-2-decyl-2-imidozaline E_{act} = 69.5 kJ mol^{-1}, and for 2-nonyl-2-imidazoline E_{act} = 75.2 kJ mol^{-1}.

The experimental results show that the amphoteric surfactants prepared by alkylation of 1,2-disubstituted imidazolines with monochlorinated aliphatic carboxylic acids in aqueous alkali solutions (pH 9.5–13.5) at 40–100°C are the reaction products of hydrolyzed imidazolines rather than substituted imidazolines [1–6].

Experiments on alkylation of 1-hydroxyethyl-2-alkyl-2-imidazolines show that at pH ~13.5 their base hydrolysis products but not the initial compounds are alkylated [18, 24].

The absorption at 230 nm completely disappears and a new band at 206 nm appears after reaction of 1-hydroxyethyl-2-nonyl-2-imidazoline with sodium monochloroacetate in the presence of sodium hydroxide. The IR spectrum of the reaction product contains a band of bending vibrations of the N–H bond of secondary amides at 1565 cm^{-1} and the C=O band of the amide group at 1645 cm^{-1}. The bands at 1605 and 1415 cm^{-1} are due to symmetric and antisymmetric vibrations of the carboxy group (COO^-), respectively [18]. The results of elemental analysis, the aggregation state, and the physicochemical and colloidal properties of the products prove the absence of imidazoline ring in the amphoteric surfactants prepared in aqueous alkali solutions and the linear structure of these products. Thus, the first step of alkylation of 1-hydroxyethyl-2-nonyl-2-imidazoline with sodium monochloroacetate is hydrolysis of imidazoline [18, 24] to form acyclic *N*-acyl-(β-hydroxyethyl)ethylenediamine:

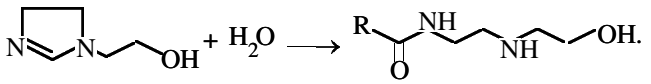

(III)

This is followed by consecutive reactions of nucleophilic substitution in sodium monochloroacetate

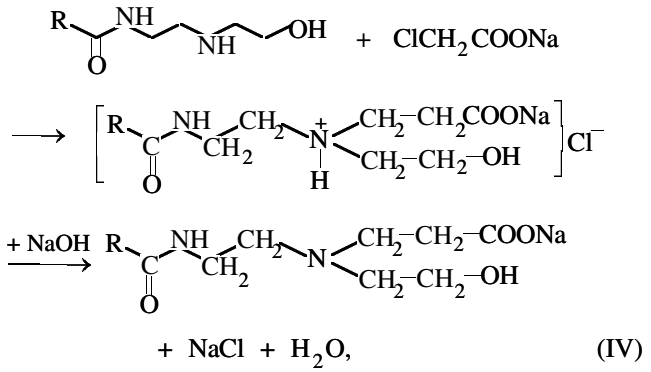

(IV)

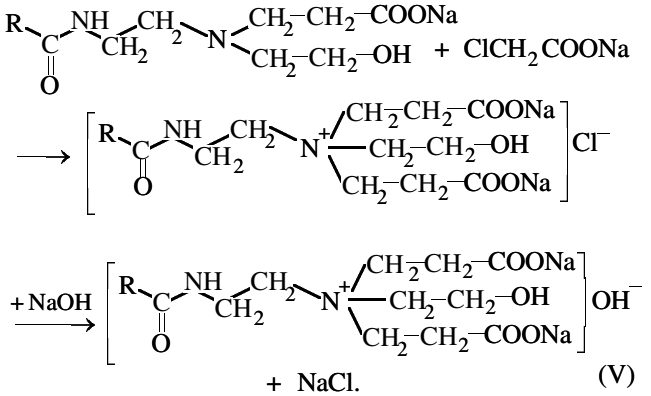

(V)

The main reactions (III)–(V) are accompanied by side hydrolysis of sodium monochloroacetate to form sodium glycolate [24]:

$$ClCH_2COONa + NaOH \rightarrow HOCH_2COONa + NaCl.$$

Since the rate of this reaction is close to that of hydrolysis of 1-hydroxyethyl-2-nonyl-2-imidazoline, these reactions are competitive. The experimental results show that the content of sodium glycolate in the reaction products increases with an increase in pH of the solution [24].

Poly(2-vinyl-2-imidazoline) is more stable in an alkaline solution and is hydrolyzed by the mechanism similar to that of 1-hydroxyethyl-2-alkyl-2-imidazoline [20]:

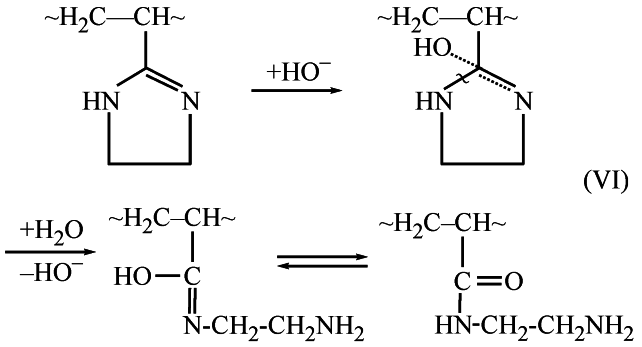

(VI)

The UV and IR spectra of aqueous solutions of poly(2-vinyl-2-imidazoline) show that this compound is completely hydrolyzed in an alkaline solution within 2 months. The apparent activation energy of hydrolysis at pH 10.7 and 12.0 is 65.2 and 68.6 kJ mol^{-1}, respectively.

It should also be noted that, in the course of hydrolysis, the reactivity of the imidazoline units in the polymer decreases owing to formation of amido amine units in the macromolecules. The amido amine units contain highly polarized carbonyl groups, which promotes shielding and decrease in the positive charge on the second carbon atom of the imidazoline ring:

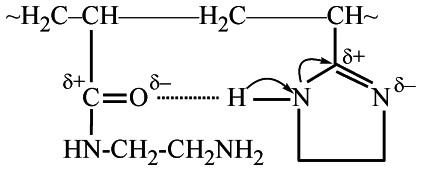

(VII)

Introduction of a branched substituent at the α-position of the reaction site noticeably complicates addition of hydroxide ion, which can significantly decrease the imidazoline hydrolysis [23].

The apparent hydrolysis rate constant of 1-(2-aminoethyl)-2-(1-ethylpentyl)-2-imidazoline at 50°C and pH 12.4 [$K_{hydr} = (2.8 \pm 0.1) \times 10^{-5}$ s^{-1}] is approximately one order of magnitude lower than that of 1-hydroxyethyl-2-nonyl-2-imidazoline ($K_{hydr} = 30 \times 10^{-5}$ s^{-1}). At 90°C, the apparent hydrolysis rate constant of the imidazoline increases by a factor of approximately 7.5. However, the hydrolysis rate at this temperature is lower by a factor of 25 than that of imidazolines with linear alkyl substituents [21, 23]. The activation parameters of hydrolysis of 1,2-disubstituted imidazolines containing branched substituent at the position 2 of the imidazoline ring were determined from the temperature dependence of $\ln K_{hydr}$. At pH 12, E_{act} for imidazoline with branched alkyl substituents is noticeably higher (53.8 kJ mol^{-1}) than that for imidazolines with linear substituents (44.6 kJ mol^{-1}), with the preexponential factor A being the same ($\log A = 4.1$). As determined by ^{13}C NMR and IR spectroscopy and gas–liquid chromatography, the hydrolysis product of 1-(2-aminoethyl)2-(1-ethylpentyl)-2-imidazoline is *N*-(5-amino-3-azapentyl)-2-ethylhexanamide [23].

The published data on the stability of the imidazoline ring in neutral and acid solutions are rather contradictory [1, 22, 23, 25–29]. Belov et al. [1] state that higher 1,2-disubstitued imidazolines are stable in acid solutions (pH ≤ 7) at elevated temperatures. At the same time, it was shown [14, 15] that in acid solutions the imidazoline ring underwent slow hydrolysis to form the initial acid and the amine.

We studied the stability of the imidazoline ring with 1-hydroxyethyl-2-nonyl-2-imidazoline as example in acid and neutral solutions at 50 and 140°C [26]. The products of hydrolysis at pH ≤ 7 were analyzed by UV spectroscopy and physicochemical methods. At relatively low temperatures (50°C), hydrolysis is noticeably accelerated with increasing acidity, and at high temperatures (140°C) 1-hydroxyethyl-2-nonyl-2-imidazoline is hydrolyzed almost completely to form capric acid and β-hydroxyethylethylendiamine hydrochloride. The experimental data on acid hydrolysis of 2-methylimidazoline at 99.9°C in the presence of 0.1–6.0 M HCl and 4.0–16.0 M H_2SO_4 [27] show that the apparent hydrolysis rate constant increases by a factors of tens with decreasing pH of the solution irrespective of the chemical structure of the acid. An increase in the ionic strength of the solution also decreases the resistance of 2-methylimidazoline to hydrolysis [27].

It should also be noted that the hydrolysis is accelerated with increasing concentration of H_2SO_4 from 4.0 to 11–12 M. In more acidic solutions, the hydrolysis rate decreases, with the final hydrolysis products being acetic acid and ethylenediamine. Haake and Watson [27] suggested a mechanism of acid hydrolysis of 2-methylimidazoline via protonation of the nitrogen atom, followed by rupture of the C–N bond of the imidazoline ring:

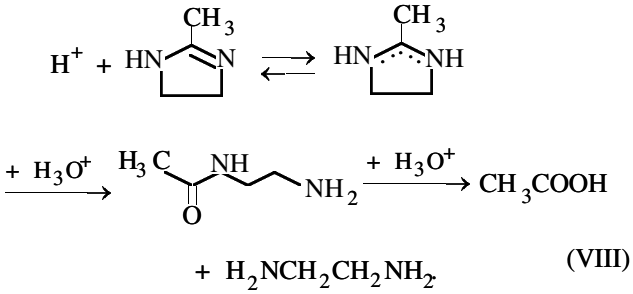

(VIII)

The kinetics of acid hydrolysis of 1-aryl-2-phenyl-2-imidazoline and the influence of electron-acceptor substituents on the hydrolysis rate were studied in [28]. It was found that the hydrolysis was accelerated with decreasing pH of the solution (increasing H_2SO_4 concentration). At the H_2SO_4 concentration lower than 1 M, the reaction is of the first order with respect to both imidazoline and H^+. In solutions with higher acid concentration, the hydrolysis rate does not increase.

The basicity of the substituents at position 1 of the imidazoline ring also affects the acid hydrolysis rate of 1,2-disubstituted imidazolines. The acid hydrolysis rate of imidazolines containing benzene substituents with electron-acceptor groups at position 1 of the imidazoline ring is higher by two orders of magnitude that that of imidazolines with electron-donor substituents, which agrees with the Hammett equation [28]

$$\log K_{hydr} = -1.14pK - 6.56.$$

Introduction of an alkyl substituent at the α-position relative to the reaction site enhances, as in the case of base hydrolysis [23], the hydrolytic resistance of the imidazoline ring in neutral and acid solutions. A study of hydrolysis of 1-(2-aminoethyl)-2-(1-ethylpentyl)-2-imidazoline in the pH range 2.0–12.7 showed that the $\log K_{hydr}$ vs. pH dependence measured at 90°C consisted of two linear portions and a bend at pH 10 [23]. At pH 10, the content of imidazoline with protonated primary amino group is the highest. At pH < 6, 1-(2-aminoethyl)-2-(1-ethylpentyl)-2-imidazoline is not noticeably hydrolyzed, although the content of 1,2-disubstituted imidazoline with protonated tertiary nitrogen atom of the imidazoline ring is the highest [23]. Probably, the positive charge on the tertiary nitrogen atom prevents hydrolysis, since no positive charge is formed on the carbon atom in this case.

EXPERIMENTAL

1-[2-(2-Aminoethyl)aminoethyl]-2-alkyl(C_8–C_{18})-2-imidazoline was prepared by condensation of triethylenetetramine with α,α'-branched C_{10}–C_{19} monocarboxylic acids at 250–280°C in a nitrogen atmosphere. The imidazoline content in the condensation products in the course of hydrolysis was estimated by the intensity of the $\pi \rightarrow \pi^*$ band of the C=N bond in the heterocycle at 230–235 nm [23]. The pH of the solutions was measured with an OR211/1 pH meter with a combined glass electrode. The pH of the solution was adjusted with 0.1 N HCl or 0.1 N NaOH.

The facts that the =C–N= bond in 1,2-disubstituted imidazolines prepared from α,α'-branched C_9–C_{19} monocarboxylic acids

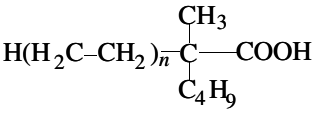

(IX)

(n = 1–6) and triethylenetetramine is strongly shielded and the rate of cyclocondensation of the corresponding 1-*N*-monoacyltriethylenetetramine into imidazoline is lower by an order of magnitude than that of linear 1-*N*-monoacylpolyethylenepolyamines [23, 25] suggest that the hydrolytic resistance of 1,2-disubstituted imidazoline prepared from α,α'-branched acids should be higher than that of 1,2-disubstituted imidazolines prepared from linear acids [25]:

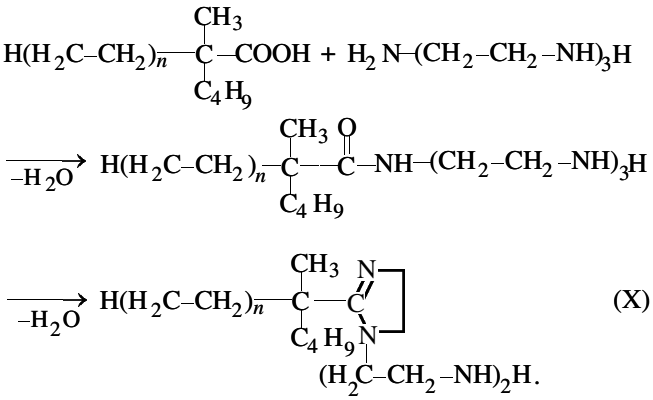

(X)

The kinetic curves of hydrolysis of 1-[2-(2-aminoethyl)aminoethyl]-2-alkyl(C_8–C_{18})-2-imidazoline in alkaline solutions (pH 10) are shown in Fig. 1. Analysis for the 1-[2-(2-aminoethyl)aminoethyl]-2-alkyl-(C_{10}–C_{18})-2-imidazoline content in the course of base hydrolysis of 30 wt % solutions containing 2.0 and 1.0 M imidazoline shows no hydrolysis in a period of 30 days. Thus, the imidazoline ring containing branched alkyl radicals at the α-position shows high hydrolytic resistance. An insignificant decrease in the imidazoline content during the first days of storage is probably due to the presence in the condensation products of imidazolines with short (C_2–C_9) linear alkly substituents which are always present in 1-[2-(2-aminoethyl)aminoethyl]-2-alkyl(C_8–C_{18})-2-imidazoline (Fig. 1). The hydrolytic resistance of shielded 1,2-disubstitued imidazolines X in neutral and acid solutions is still higher.

The kinetic curves of acid hydrolysis of 1,2-disubstituted imidazolines are similar (Fig. 2). These compounds are stable at pH 2.

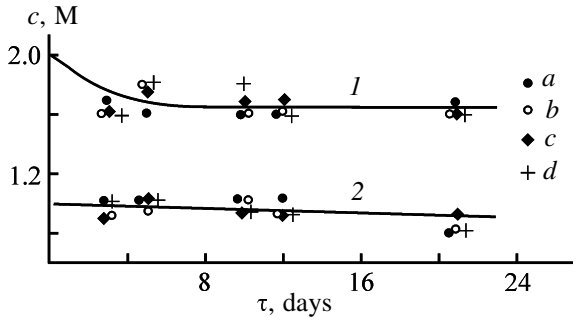

Fig. 1. Kinetic curves of hydrolysis of cyclocondensation products containing (*1*) 65.0 and (*2*) 35.0 wt % of appropriate 1-[2-(2-aminoethyl)aminoethyl]-2-alkyl(C_{10}–C_{18})-2-imidazoline in alkaline solutions (pH 10). (*c*) Concentration and (τ) time; the same for Fig. 2. Water content, %: (*a*) 0–3, (*b*) 0–5, (*c*) 0–10, and (*d*) 0–2; the same for Fig. 2.

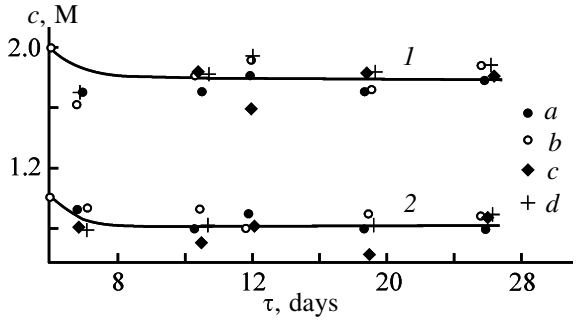

Fig. 2. Kinetic curves of hydrolysis of cyclocondensation products containing (*1*) 65.0 and (*2*) 35.0 wt % of appropriate 1-[2-(2-aminoethyl)aminoethyl]-2-alkyl(C_{10}–C_{18})-2-imidazoline in acid solutions (pH 2).

Thus, comparison of the apparent hydrolysis rate constants in alkaline (~10^{-3} s^{-1}) [17, 19, 23] and acid solutions shows that hydrolysis of the imidazoline ring in acid solutions even at 90–100°C is substantially slower than that in alkaline solutions. The hydrolytic resistance of 1,2-disubstituted imidazolines depends on the type and chemical structure of the substituents at the first and especially second position of the imidazoline ring. Significant shielding of the C–N bond in the condensation products of α,α'-branched saturated monocarboxylic acids with polyethylenediamines sharply enhances the hydrolytic resistance of the imidazoline ring, which is hydrolyzed neither in acidic or neutral nor in alkaline solutions.

CONCLUSION

Shielded 1,2-disubstituted imidazolines prepared by condensation of α,α'-branched saturated monocarboxylic acids with polyethylenepolyamines are resistant to hydrolysis and can be used as effective corrosion inhibitors in production, transportation, and refining of oil and in preparation of cationic and ampholytic surfactants.

REFERENCES

1. Belov, P.S., Frolov, V.I., and Chistyakov, B.E., *Novye poverkhnostno-aktivnye veshchestva na osnove zameshchennykh imidazolinov* (New Surfactants Based on Substituted Imidazolines), Moscow: TsNIITEneftekhim, 1975.
2. US Patent 02 781 357.
3. Swiss Patent 373 047.
4. US Patent 02 820 043.
5. USSR Inventor's Certificate no. 502 886.
6. DE Patent 19 524 265.
7. Altsybeeva, A.I. and Levin, S.Z., *Ingibitory korrozii metallov* (Inhibitors of Metal Corrosion), Leningrad: Khimiya, 1968.
8. US Patent 02 668 100.
9. US Patent 02 851 415.
10. US Patent 02 920 030.
11. US Patent 02 927 080.
12. US Patent 06 475 431.
13. Szyprowski, A.J., *Corrosion*, 2003, vol. 59, no. 2, pp. 130–138.
14. Hill, A. and Aspinal, R., *J. Am. Chem. Soc.*, 1939, vol. 61, pp. 822–825.
15. German, V.K., Kolomiets, B.S., Sherbik, L.K., and Suchkov, V.V., *Zh. Prikl. Khim.*, 1975, vol. 48, no. 7, pp. 1586–1589.
16. Kolomiets, B.S., German, V.K., Suchkov, V.V., et al., *Zh. Prikl. Khim.*, 1975, vol. 48, no. 5, pp. 1094–1097.
17. Kolomiets, B.S., German, V.K., and Suchkov, V.V., *Zh. Prikl. Khim.*, 1978, vol. 51, no. 5, pp. 1141–1145.
18. Kolomiets, B.S., German, V.K., Suchkov, V.V., and Kudryavtseva, M.I., *Zh. Prikl. Khim.*, 1978, vol. 51, no. 12, pp. 2758–2762.
19. Savignac, A., Kabbage, T., Dupin, P., and Calmon, M., *J. Heterocyclic Chem.*, 1978, vol. 15, no. 5, pp. 897–905.
20. Kasperchik, V.P., Sergeev, G.I., and Soldatov, V.S., *Dokl. Akad. Nauk Bel. SSR*, 1988, vol. 32, no. 7, pp. 621–623.
21. Bondareva, S.O., Lisitskii, V.V. and Murinov, Yu.I., Abstracts of Papers, *III Regional'noe soveshchanie respublik Srednei Azii i Kazakhstana po khimicheskim reaktivam* (III Regional Meet. of Central Asia and Kazakhstan on Chemicals), Tashkent, October 16–19, 1990, vol. 1, part 2.

22. Watts, M.M., *J. Am. Oil Chem. Soc*., 1990, vol. 67, no. 12, pp. 993–995.

23. Bondareva, S.O., Lisitskii, V.V., Yakovtseva, N.I., and Murinov, Yu.I., *Izv. Ross. Akad. Nauk, Ser. Khim*., 2004, no. 4, pp. 767–771.

24. German, V.K., *Cand. Sci. Dissertation*, Moscow, 1986.

25. Lisitskii, V.V., Matalinov, V.I., and Rasulev, Z.G., *Zh. Prikl. Khim*., 1992, vol. 65, no. 6, pp. 1368–1373.

26. Kolomiets, B.S., German, V.K., and Suchkov, V.V., *Zh. Prikl. Khim*., 1978, vol. 51, no. 9, pp. 2119–2120.

27. Haake, P. and Watson, J.W., *J. Org. Chem*., 1970, vol. 35, no. 12, pp. 4063–4068.

28. Fernandes, B.M., Reverdito, A.M., Perillo, I.A., and Lamdan, S., *J. Heterocyclic Chem*., 1983, vol. 20, no. 6, pp. 1585–1588.

29. Bondareva, S.O., Lisitskii, V.V., Murinov, Yu.I., et al., *Izv. Akad. Nauk SSSR, Ser. Khim*., 1991, no. 4, pp. 878–882.

ISSN 1070-4272, Russian Journal of Applied Chemistry, 2007, Vol. 80, No. 5, pp. 767–770. © Pleiades Publishing, Ltd., 2007.
Original Russian Text © A.V. Radushev, T.Yu. Nasrtdinova, A.G. Drozdetskii, M.G. Shcherban', I.N. Koval'chuk, 2007, published in Zhurnal Prikladnoi Khimii, 2007, Vol. 80, No. 5, pp. 788–791.

ORGANIC SYNTHESIS AND INDUSTRIAL ORGANIC CHEMISTRY

Physicochemical Properties of 1,1-Dimethyl-1-alkylhydrazinium Chlorides

A. V. Radushev, T. Yu. Nasrtdinova, A. G. Drozdetskii, M. G. Shcherban', and I. N. Koval'chuk

Institute of Technical Chemistry, Ural Division, Russian Academy of Sciences, Perm, Russia
Prikladnaya Khimiya Russian State Scientific Center, St. Petersburg, Russia
Perm State University, Perm, Russia

Received January 30, 2007

Abstract—With the aim of widening the applications of 1,1-dimethyl-1-alkylhydrazinium chlorides, the physicochemical properties (solubility, hygroscopicity, thermal and chemical stability, distribution between aqueous and organic phases) of their homologs with the alkyl radicals $C_{10}H_{21}$–$C_{18}H_{37}$ were studied.

DOI: 10.1134/S1070427207050151

Quaternary hydrazinium salts (QHSs) are known for a long time [1, 2]. The increased current interest in them is caused both by urgency of problem of utilization of 1,1-dimethylhydrazine DMG used as a component of rocket propellant [3] and useful properties of QHS (in particular, 1,1-dimethyl-1-alkylhydrazinium chlorides DMAHCs which can be readily prepared from DMG) [4]. These compounds are cationic surfactants, bactericides [1, 2, 5], and polyfunctional [3, 6] and flotation [7] reagents. The wide application of DMAHCs stimulates study of their physicochemical properties. In available literature we found only data on surface-active properties of a few DMAHCs [1, 2, 5, 7, 8].

In this study we examined the physicochemical characteristics of DMAHC homologs with the alkyl radicals $C_{10}H_{21}$–$C_{18}H_{37}$.

EXPERIMENTAL

1,1-Dimethyl-1-alkylhydrazinium chlorides of the general formula $[C_nH_{2n+1}(CH_3)_2NNH_2]Cl$, where n = 10, 12, 14, 16, 18, and 12 + 14 mixture, were prepared by quaternization of DMH by the reaction with primary chloroalkanes [9]

$$C_nH_{2n+1}Cl + (CH_3)_2NNH_2 \rightleftarrows \underset{\mathbf{I}}{[C_nH_{2n+1}(CH_3)_2NNH_2]Cl}, \quad (1)$$

The product of reaction (1) was doubly or triply recrystallized from acetone, and the main compound content in the final product was determined by the modified volumetric method as follows [10]. A weighed portion of the product to be analyzed (about 0.05 g) was dissolved in 0.1 N HCl and then chloroform (20 ml), and 1–2 drops of a mixed indicator (0.1% alcoholic solution of Dimethyl Yellow + 0.1% alcoholic solution of Methylene Blue in their volume ratio of 2 : 1) were added; the resulting mixture was titrated at stirring with 0.015 M aqueous sodium lauryl sulfate until the color of the chloroform layer changed from yellow-green to pink-violet. The DMAHC content c_{DMAHC} was calculated by the equation

$$c_{DMAHC} = \frac{V_{ls}N_{ls}M_{DMAHC}}{m_w 1000} \times 100, \quad (2)$$

where V_{ls} is the volume of aqueous lauryl sulfate consumed for titration (cm^3); N_{ls}, lauryl sulfate concentration in the titrant (g-equiv l^{-1}); M_{DMAHC}, DMAHC molecular weight; and m_w, DMAHC weighed portion.

The hygroscopicity of DMAHCs was determined as follows. A DMAHC portion was dried at 80°C and then weighed (P_0, g). This weighed sample was kept at room temperature (20°C) at controlled humidity and then weighed again. The relative increase in the moisture content of DMAHCs, ΔH_2O (%), was calculated by the equation

$$\Delta H_2O = \frac{P - P_0}{P_0} \times 100. \quad (3)$$

Table 1. Characteristics of $[(CH_3)_2RNNH_2]Cl$

R	*M*	Main compound content, wt %	mp, °C	
			experiment	data of [9]
$C_{10}H_{21}$	236.5	96	75–78	108–114
$C_{12}H_{25}$	264.5	100	118–126	–
$C_{14}H_{29}$	292.5	97	124–132	116–118
$C_{16}H_{33}$	320.5	99	125–131	83–87
$C_{18}H_{37}$	348.5	93	135–138	93–96
$(C_{12}–C_{14})$	278.5	96	73–77	60–70

Table 2. Solubility of $[(CH_3)_2RNNH_2]Cl$ in various solvents

R	Solubility, g l^{-1}			
	H_2O	toluene	2-EG	C_6H_{14}
$C_{10}H_{21}$	>330	0.025	–	2.0
$C_{12}H_{25}$	343	0.3	217	1.2
$C_{14}H_{29}$	268	0.28	76	0.25
$C_{16}H_{33}$	19.7	0.9	44	0.2
$C_{18}H_{37}$	2.0	1.1	38	–
$(C_{12}–C_{14})$	>100	0.4	–	0.15

The solubility of DMAHCs in water and organic solvents was determined gravimetrically. To do this, an aliquot of a saturated solution of DMAHC was heated to evaporate the solvent and the resulting residue was kept in an oven at 105–110°C to constant weight.

The thermal stability of DMAHCs was examined thermogravimetrically on a Q-1500D derivatograph (MOM, Hungary) in air (weighed portion 190–200 mg, temperature range 20–500°C, heating rate 10 deg min^{-1}).

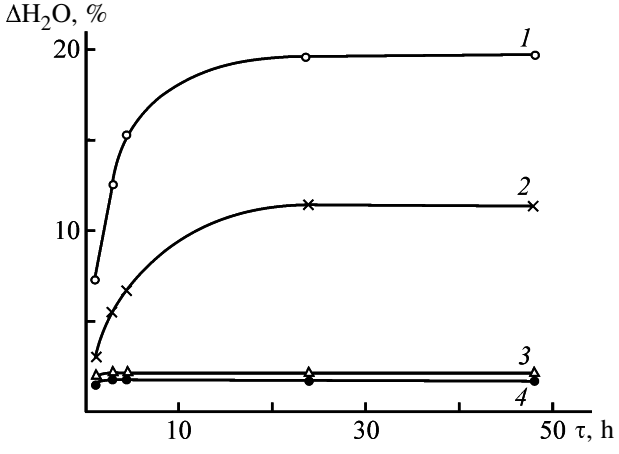

Fig. 1. Water content ΔH_2O in DMAHCs $[(CH_3)_2RNNH_2]Cl$ vs. the time of keeping in air of 96% humidity. (τ) time. R: (*1*) C_{10}, (*2*) $C_{12} + C_{14}$, (*3*) C_{12}, and (*4*) C_{16}.

The IR spectra of DMAHCs (mull in Vaseline oil) were recorded on a UR-20 spectrophotometer.

The chemical stability was determined by two different techniques. In the first method, a weighed portion of DMAHC was dissolved in 1 M aqueous HCl or NaOH, and the DMAHC content was determined by titration with aqueous sodium lauryl sulfate. In the second method, DMAHC was dissolved in water and its content was determined at regular intervals during a period of 154 days.

The distribution of DMAHCs between aqueous and organic phases was determined as follows. A 0.072–0.100 M DMAHC in an organic solvent (5 ml) was shaken with 0.1 N aqueous H_2SO_4 at $V_o : V_{aq} = 1 : 10$ for 3 min. Upon standing for 30 min, an aliquot of the aqueous phase (10 ml) was sampled and analyzed for DMAHC by microvolumetric titration with aqueous sodium lauryl sulfate. The distribution ratio of DMAHCs between the aqueous and organic phases *D* was calculated by the equation

$$D = [c_0 - c_{aq}(V_{aq}/V_o)]c_{aq}^{-1}, \quad (4)$$

where c_0 is the initial DMAHC concentration in the organic phase (M); c_{aq}, equilibrium DMAHC concentration in the aqueous phase (M); and V_{aq} and V_o, volumes (cm^3) of the aqueous and organic phases, respectively.

The average distribution ratios D_{av} of DMAHCs under consideration were determined from five successive contacts of the initial organic solution with fresh portions of water after complete removal of the previous aqueous phase equilibrated with the organic phase.

The DMAHCs under consideration (Table 1) are white crystalline compounds. The lower homolog (n = 10) deliquesces in air. Figure 1 shows the kinetics of absorption of water with various DMAHCs from air at a relative humidity of 96%.

Figure 1 shows that the hygroscopicity of individual DMAHCs strongly depends on the radical length and sharply decreases in going from DMAHC with $R = C_{10}H_{21}$ to that with $R = C_{18}H_{37}$. The commercial DMAHC ($C_{12} + C_{14}$) has relatively high hygroscopicity: after 48-h keeping in air, its weight increased by 9%.

Table 2 shows the solubility of DMAHCs in various solvents. It is seen that DMAHCs with $R = C_{10}$,

C_{12}, and C_{14} readily dissolve in water. However, with further lengthening radicals, the solubility sharply decreases. The solubility of DMAHC with R = C_{18} is as low as 2.0 g l^{-1}. The dependence of the solubility of DMAHCs in 2-ethylhexanol on the radical length is similar. In toluene and hexane all the DMAHCs are poorly soluble.

Three DMAHC samples (individual DMAHCs with R = C_{12} and R = C_{14} and a commercial mixture with R = C_{12} + C_{14}) were tested for their thermal stability in air. Figure 2 shows as an example the thermogravimetric diagram of DMAHC with R = C_{14}. The other individual DMACHs show similar thermal behavior.

We observed no weight loss of individual DMAHCs on their heating up to 190°C, i.e., within this temperature range these compounds are thermally stable. At the same time, the mixed DMAHC with R = C_{12} + C_{14} slowly loses its weight (by 10% in heating from 20 to 190°C). On heating above 200°C, all the DMAHCs begin to decompose, and this process is accompanied by heat evolution, formation of white gaseous products, and considerable weight loss.

The IR spectra of DMAHCs with R = C_{12} and C_{14} and of their commercial mixture contain absorption bands of medium intensity of the ν_{NH_2} vibrations (3200–3190, 3080–3065 cm^{-1}), δ_{NH_2} bands (1635–1630 cm^{-1}), the ν_{NN} bands (1100–1090 cm^{-1}) and a weak absorption band of the ν_{N^+C} vibrations (1400–1410 cm^{-1}). These spectroscopic characteristics of DMAHCs agree with those reported in [11].

Table 3 illustrates the stability of 26.7 and 29.3% aqueous solutions of DMAHCs in their storage in a polyethylene flask for 154 days. Two samples of mixed commercial DMAHC with R = C_{12} + C_{14} were tested. In the course of these experiments, the solution of DMAHCs was sampled at regular intervals and analyzed for the DMAHC content. Table 3 shows that throughout the storage time the main compound content remains constant within the determination error (5 rel. %).

The DMAHCs with R = C_{10} and R = C_{16} were tested for their chemical stability. To do this, the first compound was kept at a constant temperature of 60°C for 4 h, and the second DMAHC was refluxed in 1 M aqueous HCl and NaOH for 2 h. We found that such a treatment did not alter the chemical composition of the compounds under consideration. These results disagree with the data reported in [11] which show that under identical conditions DMAHC with R = C_{12} decomposes to give dodecylmethylamine and dodecene.

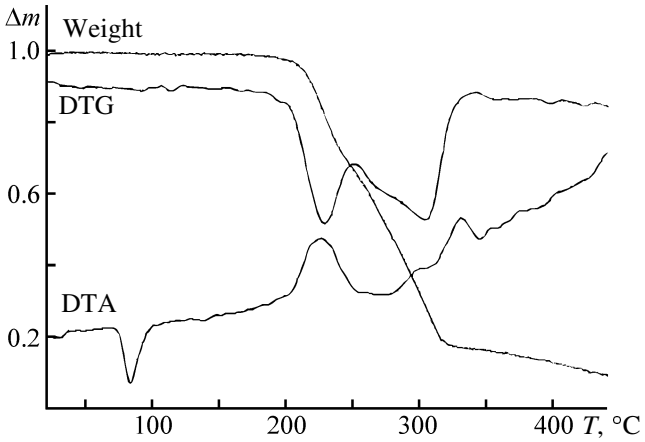

Fig. 2. Thermogravimetric diagram of DMAHC (R = C_{14}). (Δm) Weight loss and (T) temperature.

It is possible that this difference is caused by higher alkali concentration used in [11].

Table 4 shows the distribution ratios of DMAHCs between 0.1 M aqueous H_2SO_4 and 2-ethylhexanol

Table 3. Stability of aqueous DMAHC (R = C_{12} + C_{14}) in prolonged storage at room temperature*

Storage time, days	Main compound content, wt %	
	sample no. 1	sample no. 2
0	26.7	29.3
7	26.4	28.5
56	26.8	29.2
84	26.5	29.3
140	26.7	29.0
154	26.6	29.2

* Evaluated as the average from results of two determinations; the main compound content was determined by potentiometric titration of ~0.3–0.5-ml aliquots with 0.01 M aqueous $AgNO_3$ in 0.01 M aqueous HNO_3 using silver and silver chloride electrodes.

Table 4. Average distribution ratios D_x of DMAHCs between 0.1 M aqueous H_2SO_4 and 2-ethylhexanol (2-EG). $V_0 : V_{aq} = 1 : 10$

R	M	DMAHC concentration, M		D_x*
		initial in 2-EG, $c_0 \times 10^2$	after phase separation, $c_{aq} \times 10^3$	
$C_{14}H_{29}$	292.5	10.0	1.42	60
$C_{16}H_{33}$	320.5	9.3	0.44	201
$C_{18}H_{37}$	348.5	7.20	0.106	659

* Average from five experiments.

(2-EG). It is seen that, with lengthening radicals from C_{14} to C_{18}, the distribution ratio increases from 60 to 659.

It is known [12] that the distribution ratio of homologous extractable organic species correlates with their radical length:

$$\log D_x = \log D_0 + hn, \quad (5)$$

where D_0 and D_x are the distribution ratios of the reference and tested extractable species depending on particular organic solvent; n, number of methylene groups in homologous extractable species; and h, contribution of the CH_2 group to the distribution ratio.

The factor h calculated from the experimental data listed in Table 4 was found to be 0.26. This value is smaller than h ~0.52 reported in [12] for homologous series of aliphatic amines.

With the mixed solvent 2-EG-xylene (2-EG to xylene ratio 1 : 1), D_x of DMAHC with R = $C_{18}H_{37}$ was found to be 1150, i.e., the loss of the reagent with the aqueous phase is smaller than in the system with straight 2-EG.

CONCLUSIONS

(1) In homologous series of 1,1-dimethyl-1-alkylhyldrazinium chlorides $[(CH_3)_2NNH_2]Cl$, the relatively high hygroscopicity is shown only by homologs with R = C_{10} and commercial mixture with R = C_{12} + C_{14}, and the hygroscopicity sharply decreases in going to longer alkyl substituents.

(2) Among the solvents tested, 1,1-dimethyl-1-alkylhydrazinium chlorides readily dissolve in 2-ethylhexanol and especially in water; the solubility rapidly decreases with increasing length of radical.

(3) 1,1-Dimethyl-1-alkylhydrazinium chlorides are stable in 1 M aqueous NaOH and HCl and are thermally stable on heating to 190 °C. Their aqueous solutions remain stable in the course of no less than 6-month storage.

(4) The distribution ratio of 1,1-dimethyl-1-alkylhydrazinium chlorides between aqueous and 2-ethylhexanol phases increases from 60 to 659 with increasing length of the alkyl radical (going from $C_{14}H_{25}$ to $C_{18}H_{37}$).

(5) The physicochemical properties of 1,1-dimethyl-1-alkylhydrazinium chlorides obtained in this study allow their wider applications.

REFERENCES

1. Harris, C. and Hag, T., *Ber.*, 1898, vol. 31, p. 56.
2. Westphal, O., *Ber.*, 1941, vol. 74, p. 759.
3. Lopyrev, V.A., Dolgushin, G.V., and Laskin, B.M., *Ross. Khim. Zh.*, 2001, vol. 46, nos. 5/6, pp. 149–156.
4. Aleksandrova, G.A., Drozdetskii, A.G., Koval'chuk, I.N., et al. in *Doklady Mezhdunarodnogo seminara "Nauchno-tekhnicheskii potentsial Zapadnogo Urala v oblasti konversii voenno-promyshlennogo kompleksa"* (Proc. Int. Workshop "Scientific and Technical Potential of West Urals for Conversion of Military-Industrial Complex"), Perm, June 17–23, 2001, Perm: Permsk. Nauchn., Tsentr Ural'sk. Otd. Ross. Akad. Nauk, 2001, pp. 18–22.
5. US Patent 2 929 847.
6. Tul'bovich, B.I., Kazakova, L.V., Radushev, A.V., et al., *Neft. Khoz.*, 1995, no. 11, pp. 44–45.
7. RF Patent 2123 893.
8. Shcherban', M.G., Radushev, A.V., Nasrtdinova, T.Yu., et al., *Zh. Prikl. Khim.*, 2004, vol. 77, no. 11, pp. 1861–1864.
9. RF 2 074 174.
10. Siggia, S. and Hanna, J.G., *Quantitative Organic Analysis via Functional Groups*, New York: Wiley–Interscience, 1979.
11. Kamayama, E., and Minegishi, Y., *J. Chem. Soc. Jpn., Ind. Chem. Sect.*, 1968, vol. 71, no. 10, pp. 1671–1674.
12. Shmidt, V.S., *Ekstraktsiya aminami* (Extraction with Amines), Moscow: Atomizdat, 1980.

ISSN 1070-4272, Russian Journal of Applied Chemistry, 2007, Vol. 80, No. 5, pp. 771–776. © Pleiades Publishing, Ltd., 2007.
Original Russian Text © L.I. Kutsenko, Yu.G. Santuryan, E.B. Karetnikova, I.V. Gofman, A.M. Bochek, E.F. Panarin, 2007, published in Zhurnal Prikladnoi Khimii, 2007, Vol. 80, No. 5, pp. 792–797.

MACROMOLECULAR CHEMISTRY AND POLYMERIC MATERIALS

Properties of the Methyl Cellulose–Polyvinylpyrrolidone Binary System in Solution and in the Solid State

L. I. Kutsenko, Yu. G. Santuryan, E. B. Karetnikova, I. V. Gofman, A. M. Bochek, and E. F. Panarin

Institute of Macromolecular Compounds, Russian Academy of Sciences, St. Petersburg, Russia

Received March 21, 2007

Abstract—Rheological properties of dilute and moderately concentrated aqueous solutions of methyl cellulose–polyvinylpyrrolidone blends, as well as the conditions of gelation in them, were studied. Films were obtained from solutions of the polymer blends, and their physicomechanical properties were examined. The range of the compositions corresponding to thermodynamic compatibility of methyl cellulose with polyvinylpyrrolidone was identified by the solvent vapor sorption method and by thermomechanical examinations of the films.

DOI: 10.1134/S1070427207050163

Preparation of cellulose materials with novel or improved properties through combining cellulose ethers with synthetic polymers is of scientific and practical interest. Structural modification of polymers by combining two polymers of different chemical structures in a common solvent allows preparation of polymer blends with controllable properties. Depending on the chemical composition, rigidity of the macromolecular chain, degree of polymerization, and kind of solvent, the blended polymers can form in solution structures of different organization and stability.

Increased attention is given today to self-associated polymer systems based on environmentally safe and biodegradable natural polymers [1]. Among these polymers are water-soluble compounds of cellulose: sodium salt of carboxymethyl cellulose (NaCMC), methyl cellulose (MC), and other ethers [2, 3]. Methyl cellulose is widely used as thickener of muds in oil extraction, as well as in textile, pulp and paper, food, and pharmaceutical industries [4]. The rheological properties of MC solutions and conditions of gelation in them, as well as the physicomechanical properties of the films obtained from solutions, can also be varied by introducing a different water-soluble polymer into solutions [5–7].

Polyvinylpyrrolidone (PVP) is used in production of tableted medicines and also serves as blood substitute and blood detoxifier. It is used for preparing prolonged-action agents with a wide activity spectrum [8].

In this study we examined the rheological properties of dilute and moderately concentrated solutions of MC–PVP blends, as well as the thermodynamic compatibility of these polymers and the physicomechanical and thermomechanical properties of the films obtained from their solutions.

Examination of the properties of MC–PVP blends was motivated by a search for new modifiers of methyl cellulose intended for encapsulation of medicines, as well as by the possibility for preparing film materials containing PVP which, in turn, is suitable as the basis for medicines.

EXPERIMENTAL

The objects of our study were commercial samples of MC with the degree of substitution of 1.7 and molecular weight (MW) of 150000 and PVP with MW of 14200. The solutions of the MC–PVP blends were prepared by mixing equiconcentrated solutions of the two polymers at different component ratios. Distilled water served as the solvent. The viscosity of the dilute solutions was measured on an Ubbelohde capillary viscometer at 20°C.

The rheological properties of moderately concentrated solutions (2 wt %) were studied on a Rheotest-2.1 rheoviscometer at shear stresses within 3–600 Pa at 20–50°C. The gelation onset temperature T_{gel} in solutions was determined from the change of the viscosity of the solutions on a Hoeppler viscometer.

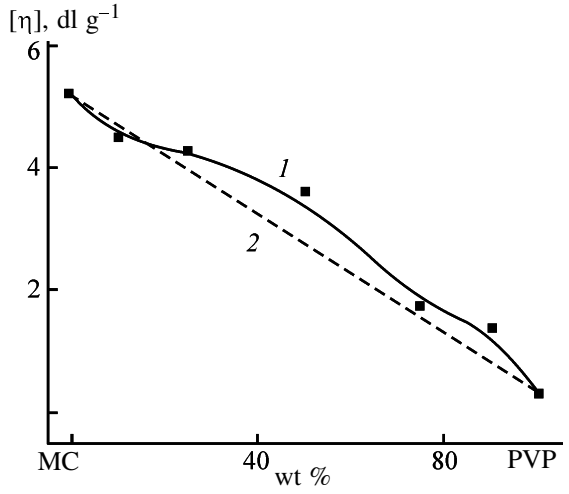

Fig. 1. (*1*) Experimental $[\eta]_e$ and (*2*) calculated $[\eta]_c$ intrinsic viscosities $[\eta]$ of the MC–PVP blends as functions of the composition at 20°C.

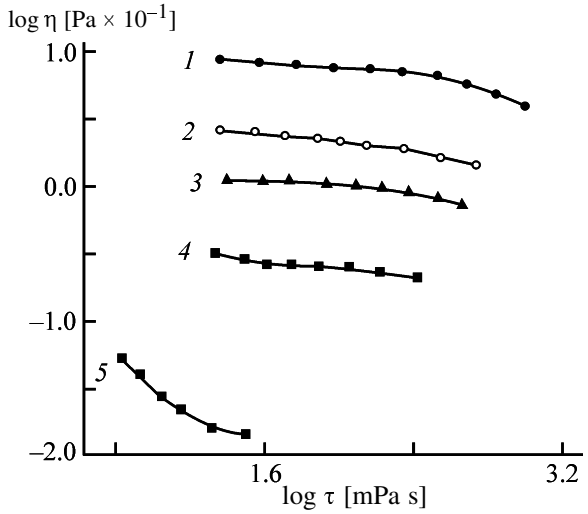

Fig. 2. Flow curves of 2% solutions of (*1*) MC, (*2–4*) MC–PVP blends, and (*5*) PVP at 20°C. (η) Viscosity and (τ) shear stress. PVP content, wt %: (*2*) 30, (*3*) 50, and (*4*) 70.

The compatibility of the polymers, depending on the blend composition, was determined by the solvent vapor sorption on films formed from 2% solutions, as well as from the change in the glass transition points of the polymers T_g in films. The films from the polymer blend solutions were formed by the dry method using a laboratory draw plate with controlled slit.

The mechanical characteristics of the films formed from blends were determined at room temperature in the uniaxial stretching mode on a UTS 10 (UTS-testsysteme, Germany) universal setup for mechanical tests. The samples were stretched at a rate of 20 mm min^{-1} (100% of the initial length of the sample per minute). We recorded the sample stretching diagram, which allowed estimation of the modulus of elasticity E, elastic limit σ_e, tensile strength σ_t, and breaking elongation ε_b.

The glass transition point T_g was determined by a thermomechanical method on a UMIV-3 setup; the sample heating rate was 50 deg min^{-1} at a constant stretching load of 0.5 MPa.

To characterize the mutual influence of the MC and PVP macromolecules in solutions, we examined variation of the intrinsic viscosity $[\eta]_e$ of blends of different compositions. We recorded deviation of $[\eta]_e$ of the blends from the calculated ideal values $[\eta]_c$. This deviation can be treated as a measure of intermolecular interactions of different kinds of polymers [9].

The ideal $[\eta]_c$ values were calculated by the formula

$$[\eta]_c = [\eta]_1 W_1 + [\eta]_2 W_2, \quad (1)$$

where $[\eta]_1$ and $[\eta]_2$ are the experimental intrinsic viscosities of the first and second components of the blend, and W_1 and W_2, their mass fractions, respectively.

Figure 1 shows how the experimental $[\eta]_e$ and calculated $[\eta]_c$ intrinsic viscosities vary with the MC–PVP blend composition. For all the compositions, except for the blend containing 10 wt % PVP, the experimental viscosity exhibits a positive deviation from the calculated viscosity.

A positive deviation of the experimental viscosity of the blends of dilute solutions from the calculated viscosity suggests predominance in the solution of intermolecular interactions of the different kinds of macromolecules, yielding structures whose hydrodynamic volume exceeds the weighted-average hydrodynamic volumes of the two components taken separately. A negative deviation of the $[\eta]_e$ parameters of the blends from the additive values can be due both to compaction of the polymer macromolecules in the case of their incompatibility and to formation of mixed complexes whose hydrodynamic volume is smaller than those of the macromolecules of the two polymeric components taken separately.

The intermolecular interactions in moderately concentrated solutions were analyzed through examination of the rheological properties of the 2% solutions of MC–PVP blends at 20–50°C. Figure 2 presents as an example the flow curves for the solutions of MC and PVP and their blends of different compositions at 20°C. The flow curves of the solutions of MC, PVP, and their blends are partial flow curves of non-

Table 1. Amount of the water sorbed Q, volume fractions of the solvent φ_1 and polymer φ_2, and polymer–solvent χ_1 and polymer–polymer χ_{23} interaction parameters

Composition, wt %		Q, g g^{-1}	φ_1	φ_2	χ_1	χ_{23}
MC	PVP					
100	0	0.824	0.519	0.481	0.753	–
90	10	0.854	0.526	0.474	0.747	–0.04
75	25	0.822	0.513	0.487	0.759	–0.162
60	40	0.885	0.528	0.472	0.744	–0.126
50	50	0.898	0.529	0.471	0.701	0.011
40	60	1.087	0.574	0.426	0.710	0.066
30	70	1.366	0.626	0.374	0.653	0.012
10	90	1.489	0.641	0.359	0.658	0.076
0	100	1.600	0.656	0.344	0.655	–

Newtonian fluids. The structural viscosity branch for the MC solution becomes prominent at shear stresses over $\log\tau = 2.4$ ($\tau > 250$ Pa $\times 10^{-1}$). The viscosity of the PVP solution is much lower than that of the MC solution because of a lower molecular weight of the synthetic polymer.

The temperature dependences of the viscosities of the solutions of the blends (20–45°C) were used for calculating the heat of activation of viscous flow of solutions E_a. Figure 3 shows how the viscosity of concentrated solutions of the blends, heat of activation of viscous flow E_a, and gelation onset temperature T_{gel} vary with the composition of the 2% solutions. It is seen that the viscosity of the concentrated solutions of the blends exceeds the additive value; the same is true of E_a. The observed positive deviations of the viscosity and E_a can be due to formation in solutions of the blends of a new three-dimensional system of hydrogen bonds and of new mixed structural units due to interaction of different kinds of polymer macromolecules.

With increasing PVP fraction, the gelation onset temperature T_{gel} tends to increase, presumably due to a decrease in the fraction of the gel-forming polymer, MC. At the PVP content over 90 wt %, no gelation is observed in solutions.

To estimate the thermodynamic compatibility of MC with PVP, as well as the affinity of the polymer for the solvent, we used the solvent vapor sorption method [10]. Samples of films prepared from the solutions were vacuum-dried to constant weight, placed into a closed vessel containing water, and kept in the atmosphere of saturated vapor at 20°C until the equilibrium was attained, whereupon the samples were weighed, and the degree of swelling of the films was determined.

Table 1 presents data on the water vapor sorption by the films. Based on the experimental degrees of swelling of the films we calculated the polymer–solvent interaction parameter χ_1 and the polymer–polymer interaction parameter χ_{23}; χ_1 was calculated by the Flory–Huggins equation [11]

$$\ln a_1 = \ln(P_1/P_1^0) = \ln(1 - \varphi_2) + \varphi_2 + \chi_1\varphi_2^2, \quad (2)$$

where a_1 is the solvent activity, and P_1/P_1^0, relative pressure of the solvent vapor.

The experiments were performed at the saturated solvent vapor pressure, i.e., at $a_1 = P_1/P_1^0 = 1$, $\ln a_1 = 0$. The volume proportion of the polymer was calculated by the expression

$$\varphi_2 = 1/[1 + (d_2/d_1)W], \quad (3)$$

where d_1 is the solvent density; d_2, polymer density; and W, amount of the solvent sorbed, g g^{-1}.

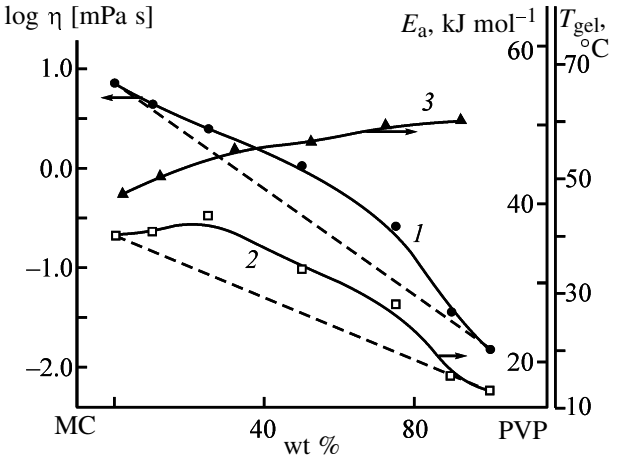

Fig. 3. (*1*) Viscosity η, (*2*) viscous flow activation energy E_a, and (*3*) gelation onset temperature T_{gel}, °C, as functions of the composition of 2% MC–PVP solutions.

Table 2. Mechanical characteristics and relaxation transition temperatures in the MC and MC–PVP blend films

Composition, wt %		E, GPa	σ_e, MPa	σ_t, MPa	ε_b, %	T_g, °C
MC	PVP					
100	0	4.03 ± 0.09	82 ± 1	156 ± 3	28 ± 2	191
90	10	3.64 ± 0.05	78 ± 3	137 ± 4	28 ± 3	190
80	20	3.71 ± 0.12	79 ± 3	138 ± 2	26 ± 2	188
75	25	3.66 ± 0.09	78 ± 3	136 ± 4	29 ± 2	185
70	30	3.59 ± 0.13	79 ± 2	138 ± 6	32 ± 2	178
60	40	3.02 ± 0.11	77 ± 2	126 ± 4	40 ± 5	176
50	50	3.09 ± 0.07	76 ± 2	102 ± 2	30 ± 1	172

The density of the samples was determined by hydrostatic weighing in heptane.

The polymer–polymer interaction parameter χ_{23} was calculated by the Patterson relationship [12]:

$$\chi_{23} = \chi_{12}\varphi_a + \chi_{13}\varphi_b - \chi_{1(23)}/\varphi_a\varphi_b, \quad (4)$$

where χ_{12}, χ_{13}, and $\chi_{1(23)}$ are the Flory–Huggins parameters of interaction with water of individual polymers MC and PVP and their blends, respectively, and φ_a and φ_b, volume proportions of MC and PVP in the blend, respectively. For blends of compatible polymers $\chi_{23} < 0$ [13].

Table 1 shows that, in the solid state (films), MC is compatible with PVP in the polymer blends containing up to 40% PVP. At the PVP content above 60% the polymers are incompatible.

It should be noted that the data on the compatibility of MC with PVP, derived from water vapor sorption experiments, do not always correlate with the measured viscosities of dilute solutions of polymer blends (Fig. 1) As mentioned above, in the case of compatibility of different kinds of polymers in dilute solutions (in our case, with up to 10 wt % PVP), negative deviations of $[\eta]_e$ from $[\eta]_c$ can be due to formation of mixed structural units whose hydrodynamic volume is smaller than those of the macromolecules of both polymeric components taken separately. With over 10% PVP in the solutions, the experimental viscosity exhibits a positive deviation from the calculated data. This is also due to formation of mixed structural units whose hydrodynamic volume exceeds the weighted-average hydrodynamic volumes of the two components taken separately because of the predominance of intermolecular interactions of different kinds of macromolecules. In the case of the polymer blends in the solid state, the polymers are compatible only in films with up to 40–50 wt % PVP. These contradictions between the data on the compatibility of the same polymers, obtained by two different methods, are due to changes in the affinity of the different kinds of polymers, observed with variation of the total concentration of the polymers in solution. As known, the compatibility of polymers can decrease with increasing concentration of solutions. Presumably, in dilute solutions, MC and PVP are compatible throughout the composition range examined. During formation of the films, the solvent evaporates, and the range of the compositions of the polymers within which they are compatible tends to decrease with increasing concentration of the solution.

It was of interest to examine the physicomechanical properties and characteristics of the relaxation transitions of the MC–PVP blend films. As known, PVP, though exhibiting a biological activity, is not a film-forming polymer. However, film materials (films, coatings) can be prepared from blends of PVP with other polymers having film-forming properties. Methyl cellulose is suitable for these purposes because its films exhibit a high strength, are elastic, and do not exert harmful or irritating effect on human body [14].

In mechanical tests we used MC films and films of blends with up to 50% PVP. It should be noted that, throughout the composition range examined, we obtained uniform transparent films. Further increase of the PVP concentration in the blends resulted in formation of turbid nonuniform films whose appearance suggested the onset of phase segregation in the material. The results of the tests are summarized in Table 2.

Analysis of the trends in variation of the modulus of elasticity E with the composition of the composite films revealed a marked decrease in the film rigidity with increasing PVP fraction in the blends: The Young modulus decreases by 25% with increasing

PVP fraction from 0 to 0.50. Similar, through less prominent, trend is exhibited by the elastic limit σ_e.

The dependences of the mechanical characteristics of the films on their composition are determined by the combined action of several factors. On the one hand, the deformability of the films does not decrease with increasing PVP content in the blend to 50%. By contrast, the breaking elongation clearly grows with increasing PVP fraction in the blend to 0.40. It should be emphasized that, even at a fairly high content of PVP in the blend (up to 50%), we obtained nonbrittle elastic films suitable for practical application. At the same time, increase in the PVP content in the blend within the limits mentioned causes the strength of films to decrease by 1/3 of that of films of pure MC. Combined with an increase in the tensile strain and the slightly varying elastic limit, this decrease can be attributed only to the change in the nature of the deformation processes in films with increasing PVP content. Indeed, this is suggested by the change in the appearance of the deformation curves of the film in changing from MC to blends with a substantial content of PVP (Fig. 4).

The MC film exhibits a stretching diagram typical for rigid-chain polymers with initially stretched unfolded chains, while, upon introducing PVP, the deformation of the film after passing through the elastic limit (at 5–10% strain) acquires a prominently plastic nature. The diagram contains a prominent section in which the film deformation proceeds without marked increase in the force, i.e., orientation and unfolding of the macromolecular chains are observed. This section is not long, i.e., introduction of PVP into the material causes only a small growth of the folding of the supporting macrochains, but this growth is specifically responsible for deterioration of the strength characteristics of the films of the blends.

Examination of the characteristics of the relaxation transitions in the films of blends is a very important stage of the study, since specifically these data furnish information on the compatibility of the components of the MC–PVP blends in the condensed state. These characteristics were determined by the thermomechanical method (Fig. 5). The temperatures of the transitions recorded during thermomechanical tests of the films of different compositions are presented in Table 2.

It is seen that no individual temperatures of phase transitions characterizing each of the blend components can be identified in the thermomechanical curves of the blends.

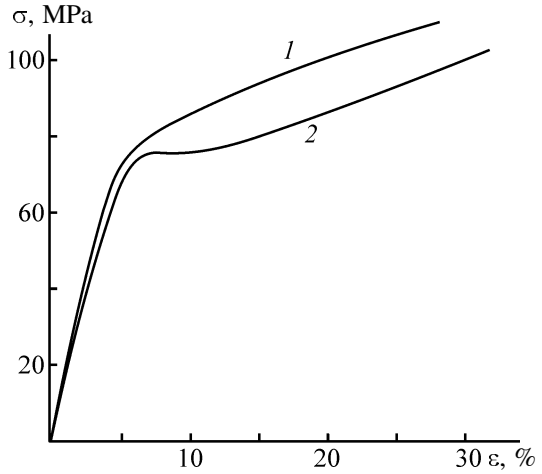

Fig. 4. Stretching diagrams of the (*1*) MC films and (*2*) films of MC–PVP blends with 50% PVP. (σ) Stretching stress and (ε) relative elongation.

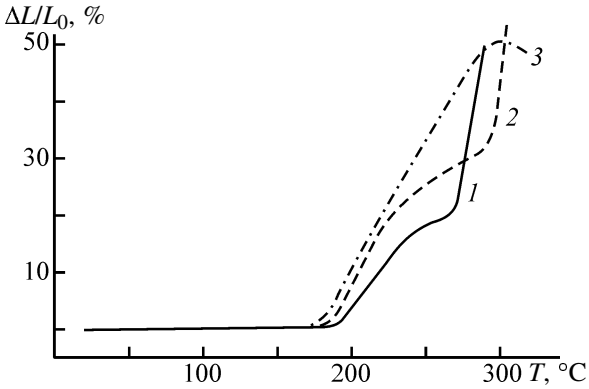

Fig. 5. Thermomechanical curves of the (*1*) MC films and (*2, 3*) films of MC–PVP blends with (*2*) 30% and (*3*) 50 wt % PVP. ($\Delta L/L_0$) Relative strain and (*T*) temperature.

The MC films exhibit two temperature transitions: The mobility of the macrochains sharply increases near 190°C (glass transition point of MC) and, upon further increase of temperature, the mobility increases once again near 270°C (Fig. 5). Evidently, this high-temperature transition reflects melting of the ordered domains in MC; the temperature range within which it is observed agrees well with the melting points of MC, reported in [15]. Further heating leads to degradation of the MC film virtually immediately after this transition.

Upon changing from MC to MC–PVP blends, no additional transitions appear in the thermomechanical curves in the range of temperatures corresponding to the glass transition point of PVP, near 150°C [8]. At the same time, the glass transition gradually shifts to lower temperatures with increasing PVP content in the blend (increase in the PVP content in the blend

to 50% causes the glass transition point to shift by over 15°C). These features of thermal behavior is indicative of both a high compatibility of the blend components throughout the composition range examined, i.e., of blends with the PVP content of up to 50% (the polymers do not form individual phases and exist as a solid molecular solution) and of strong intermolecular interaction. Thus, the range of the MC–PVP compositions in which the polymers are compatible, determined by thermomechanical method, is identical to that revealed by the solvent vapor sorption method.

CONCLUSIONS

(1) Viscous properties of dilute and moderately concentrated aqueous solutions of methyl cellulose, polyvinylpyrrolidone, and their blends of different compositions were examined. For moderately concentrated solutions of the polymer blends, the viscosity of the solutions and the heat of activation of viscous flow exhibit positive deviations from the additive values. This can be due to intermolecular interaction of the polymers, resulting in formation of mixed structures with a new hydrogen bond system.

(2) The gelation onset temperature in the solutions increases with increasing PVP fraction in the blends.

(3) The compatibility of methyl cellulose with polyvinylpyrrolidone in films was examined by the solvent vapor sorption method. In composite films with up to 50% polyvinylpyrrolidone, the polymers are thermodynamically compatible.

(4) Transparent uniform composite films of methyl cellulose with polyvinylpyrrolidone, containing up to 50% of the latter and exhibiting high deformation and strength properties, were obtained. Thermomechanical tests of the resulting films showed that, by varying the quantitative composition over a wide range, from pure methyl cellulose to blends with up to 50% polyvinylpyrrolidone, it is possible to obtain polymeric composite materials with a high degree of dispersion of the components forming solid molecular solutions.

REFERENCES

1. Nikolaev, A.F. and Okhrimenko, G.I., *Vodorastvorimye polimery* (Water-Soluble Polymers), Leningrad: Khimiya, 1979.
2. Matveeva, N.A., Ostrovskaya, L.D., Klenkova, N.I., et al., *Cellulose Chem. Technol.*, 1984, vol. 18, pp. 155–168.
3. Nikolaev, O.V., Budtova, T.A., Kalyuzhnaya, L.M., et al., *Vysokomol. Soedin., Ser. A*, 1999, vol. 41, no. 7, pp. 1176–1182.
4. Bytenskii, V.Ya. and Kuznetsova, E.P., *Proizvodstvo efirov tsellyulozy* (Production of Cellulose Ethers), Leningrad: Khimiya, 1974.
5. Kutsenko, L.I., Ivanova, N.P., Karetnikova, E.B., et al., *Zh. Prikl. Khim.*, 2002, vol. 75, no. 2, pp. 314–318.
6. Kutsenko, L.I., Karetnikova, E.B., Bochek, A.M., and Kalyuzhnaya, L.M., *Zh. Prikl. Khim.*, 2003, vol. 76, no. 10, pp. 1720–1724.
7. Kutsenko, L.I., Bochek, A.M., and Karetnikova, E.B., in *Materialy 10-oi Vserossiiskoi nauchno-tekhnicheskoi konferentsii "Efiry tsellyulozy i krakhmala: sintez, svoistva, primenenie"* (Proc. 10th Russian Scientific and Technical Conf. "Cellulose and Starch Ethers and Esters: Synthesis, Properties, and Application"), Suzdal, May 5–8, 2003, pp. 162–165.
8. Kirsh, Yu.E., *Poli-N-vinilpirrolidon i drugie poli-N-vinilamidy* (Poly-*N*-vinylpyrrolidone and Other Poly-*N*-vinylamides), Moscow: Nauka, 1988.
9. Staikos, G.B., *Makromol. Chem.*, 1991, vol. 192, pp. 1073–1087.
10. *Eksperimental'nye metody v adsorbtsii i molekulyarnoi khromatografii* (Experimental Methods in Adsorption and Molecular Chromatography), Kiselev, A.V. and Dantsig, V.P., Eds., Moscow: Mosk. Gos. Univ., 1973.
11. Tager, A.A., *Fiziko-khimiya polimerov* (Physical Chemistry of Polymers), Moscow: Khimiya, 1978.
12. Su, C.S. and Patterson, D., *Macromolecules*, 1974, vol. 10, pp. 708–712.
13. Scott, R.L., *J. Polym. Sci.*, 1952, vol. 9, pp. 423–432.
14. Petropavlovskii, G.A., *Gidrofil'nye chastichno zameshchennye efiry tsellyulozy i ikh modifikatsiya putem khimicheskogo sshivaniya* (Hydrophilic Partially Substituted Cellulose Ethers and Their Modification by Chemical Cross-Linking), Leningrad: Nauka, 1988.
15. *Entsiklopediya polimerov* (Encyclopedia of Polymers), Moscow: Sov. Entsiklopediya, 1977, vol. 3.

ISSN 1070-4272, Russian Journal of Applied Chemistry, 2007, Vol. 80, No. 5, pp. 777–782. © Pleiades Publishing, Ltd., 2007.
Original Russian Text © G.M. Pavlov, E.V. Korneeva, N.P. Ivanova, O.A. Pavlova, E.F. Panarin, 2007, published in Zhurnal Prikladnoi Khimii, 2007, Vol. 80, No. 5, pp. 798–803.

MACROMOLECULAR CHEMISTRY AND POLYMERIC MATERIALS

Synthesis and Hydrodynamic and Molecular Characteristics of *N*-Methacryloylglucosamine–*N*-Vinylformamide Copolymers

G. M. Pavlov, E. V. Korneeva, N. P. Ivanova, O. A. Pavlova, and E. F. Panarin

Institute of Macromolecular Compounds, Russian Academy of Sciences, St. Petersburg, Russia
Fock Institute of Physics, St. Petersburg State University, St. Petersburg, Russia

Received February 28, 2007

Abstract—Random 50 : 50 *N*-methacryloylglucosamine–*N*-vinylformamide copolymers were synthesized, and their hydrodynamic and molecular characteristics were examined. For the copolymers with the molecular weight $70 < M \times 10^{-3}$ g mol^{-1} < 570 in 0.2 M NaCl, the Kuhn–Mark–Houwink–Sakurada equations were obtained, which relate the intrinsic viscosity and the translational diffusion and centrifugal sedimentation coefficients, on the one hand, to the molecular weight, on the other. The length of the statistical segment of the copolymer chains was estimated.

DOI: 10.1134/S1070427207050175

Interaction of biopolymer macromolecules plays an important role in biological processes, in particular, in intercellular recognition. In these interactions, of key importance are glycoprotein molecules containing both the peptide and carbohydrate moieties. The mechanisms of intercellular recognition are examined for various model polymeric systems of a simpler chemical structure than glycoproteins, whose structure can be controlled. Possible models of glycoproteins include, e.g., carbon-chain polymers containing in their side chain the characteristic functional groups, carbohydrate moieties and amide groups. Examples of such model systems are vinylsaccharide–vinylamide copolymers, e.g., *N*-vinylformamide (VFA)–*N*-methacryloylglucosamine (MAG) copolymers [1]. The presence of carbohydrate moieties and amide groups in the same macromolecule, able of forming hydrogen bonds under intra- and interchain contacts, can substantially affect their conformational properties. We examined earlier the conformational properties of homopolymers, poly-*N*-methacryloylglucose (PMAG) [2, 3] and poly-*N*-vinylformamide (PVFA) [4]. We found that both belong to flexible-chain polymers and revealed a difference between them, consisting in a slightly larger equilibrium rigidity of the PMAG chains. The potential tendency of the PMAG and PVFA macromolecules to intrachain interactions with hydrogen bonding between the –CO–NH– and OH– groups makes of interest elucidation of how the intrachain hydrogen bonds can affect the conformational properties of the MAG–VFA copolymers simulating glycoproteins.

In this study we synthesized 50 : 50 MAG–VFA copolymers with different molecular weights and examined their molecular and conformational characteristics by the molecular hydrodynamics methods.

EXPERIMENTAL

The MAG–VFA copolymers were synthesized as described earlier [1]. To obtain the copolymers with a wide range of molecular weights, we varied the nature of the initiator and its content in the polymerization medium and the concentrations of the comonomers, and also used various solvents. The synthesis conditions for the copolymers are presented in Table 1.

The hydrodynamic characteristics of the copolymers were studied in 0.2 M NaCl with the following

Table 1. MAG : VFA = 50 : 50 copolymerization at T = 60°C

Solvent, %	Initiator, %	Time, h	Yield, %
H_2O, 10	Guanide, 1.0	4	90
DMF, 15	AIBN, 1.0	5	70
H_2O, 10	Guanide, 1.5	4	84
DMF, 15	AIBN, 1.0	24	70

Table 2. Hydrodynamic and molecular characteristics of MAG : VFA = 50 : 50 copolymers in 0.2 M NaCl at 20°C

Sample no.	$[\eta]$, $cm^3\ g^{-1}$	k'	$D_0 \times 10^7$, $cm^2\ s^{-1}$	$s_0 \times 10^{13}$, s	k_s, $cm^3\ g^{-1}$	$M_{sD} \times 10^{-3}$, $g\ mol^{-1}$	$A_0 \times 10^{10}$	$\beta_s \times 10^{-7}$	$k_s/[\eta]$
1	77	0.45	1.15	9.2	165	566	3.00	1.30	2.14
2	36	0.65	1.35	6.8	80	357	2.30	1.00	2.22
3	32.3	0.80	1.60	5.7	60	252	2.40	1.00	1.86
4	11.6	2.4	3.55	3.6	33	72	2.45	1.15	2.84
						Average	2.5 ± 0.2	1.1 ± 0.1	2.3 ± 0.3

characteristics at 20°C: density $\rho_0 = 1.007\ g\ cm^{-3}$ and dynamic viscosity $\eta_0 = 1.0 \times 10^{-2}$ P. The translational diffusion was studied on a Tsvetkov diffusometer [5] in a glass cell, 3 cm in length along the beam path. The solution with the concentration no higher than $c = 0.10 \times 10^{-2}\ g\ cm^{-3}$ was introduced under the solvent layer. The variance of the diffusion boundary σ^2 was calculated from the area and the maximal ordinate of the symmetrical diffusion curve. From the variance vs. diffusion time t plot we estimated the translational diffusion coefficient D (Fig. 1) by the relationship

$$\delta^2 = \sigma_0^2 + 2Dt. \quad (1)$$

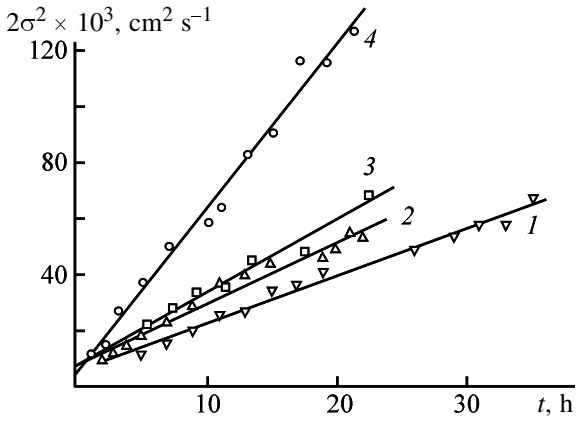

Fig. 1. Diffusion boundary variance σ^2 vs. the diffusion time t. Digits at straight lines correspond to the copolymer sample nos. in Table 2; the same for Fig. 3.

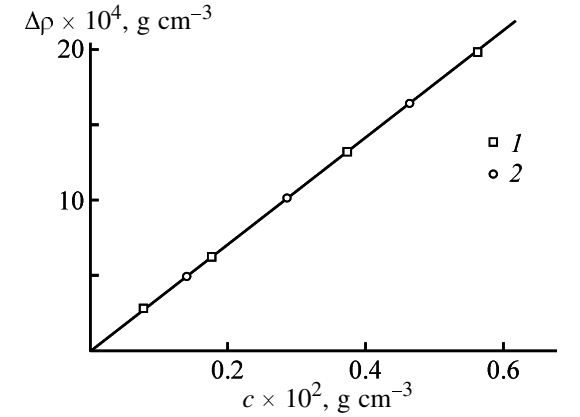

Fig. 2. Difference in density between the solution and solvent $\Delta\rho$ vs. the concentration c of the aqueous solution for sample no. (*2*) 1 and (*1*) 3 (Table 2).

The solutions were diluted and satisfied the condition of virtually limiting dilution $c[\eta] \ll 0.1$, where $[\eta]$ is the intrinsic viscosity. Hence, we took the parameter D equal to that corresponding to the limiting dilution D_0, which was further used for calculating the molecular weight.

The density increment $\Delta\rho/\Delta c$ or the buoyancy factor $(1 - v\rho_0)$ of the copolymer solutions in straight water was determined from the concentration dependence of the density (Fig. 2). The density of the solutions was measured on a Kratky densitometer (A. Paar, Austria) at 20°C [6]. Based on the $\Delta\rho/\Delta c = (1 - v\rho_0)$ parameter, we estimated the partial specific volume v of the copolymer at $0.651 \pm 0.003\ cm^3\ g^{-1}$.

The viscometric measurements were carried out on an Ostwald viscometer (Fig. 3). The intrinsic viscosities $[\eta]$ and Huggins parameters k' are listed in Table 2.

The sedimentation experiments were carried out on a Beckman XLI analytical ultracentrifuge at the rotor rotation rate of 57 000 rpm in two-sector cells (12 mm in length along the beam path), placed into a four-cell rotor. The sedimentation boundary was monitored using interference optical devices (a Rayleigh interferometer). The sedimentograms were processed using a Sedfit routine [7]. We preliminarily selected in the framework of the routine the parameter f/f_0 [where f and f_0 are the coefficients of translational friction of the macromolecule (particle) and a rigid sphere of the identical molecular weight, respectively], which minimizes the divergence between the calculated and experimental sedimentation profiles (Fig. 4). The

sedimentation coefficients were determined for each sample at three concentrations from within $0.10 < c \times 10^2$ g cm^{-3} < 0.65, which yielded reliable coefficients s_0 and k_s from the linear approximation

$$s^{-1} = s_0^{-1}(1 - k_s c + ...). \quad (2)$$

The experimental hydrodynamic characteristics are listed in Table 2.

Analysis of the s_0 and k_s parameters showed that they are correlated as $k_s = Ks_0^{\gamma} = 3.55s_0^{(1.7\pm0.2)}$. The exponent γ is related to the corresponding exponent b_s in the Kuhn–Mark–Houwink–Sakurda (KMHS) relationships [8] as $\gamma = (2 - 3b_s)/b_s$; the parameter b_s can be estimated at (0.43 ± 0.02). Also, we compared the parameters k_s with parameters [η] having identical dimensionalities. The average $k_s/[\eta]$ was estimated at 2.3 ± 0.3, which exceeds ~1.7 typical for flexible-chain homopolymers [9]. Further analysis of the system of the hydrodynamic data involves estimation of the hydrodynamic invariant A_0 [5, 10] and the sedimentation parameter β_s [11, 12]. These hydrodynamic invariants were calculated using the following relationships:

$$A_0 = (R[D]^2[s][\eta])^{1/3}, \quad (3)$$

$$\beta_s = N_A(R^{-2}[D]^2[s]k_s)^{1/3}, \quad (4)$$

where R is the universal gas constant; N_A, Avogadro number; $[D] \equiv \eta_0 D_0/T$; and $[s] \equiv s_0\eta_0(1 - v\rho_0)$.

The parameters A_0 and β_s for each sample and their average values are presented in Table 2. The fact that these parameters fluctuate around a certain average value suggests that the hydrodynamic characteristics are consistent. It should be noted, however, that A_0 is smaller than the parameter typical for flexible-chain homopolymers, $(3.2\pm0.2)\times10^{-10}$ g cm^2 s^{-2} deg^{-1} × mol$^{-1/3}$ [10]. At the same time, the average β_s agrees well with the parameters characteristic for flexible-chain homopolymers [12].

The molecular weights M were estimated on the basis of the sedimentation and diffusion analysis using the Svedberg formula

$$M_{sD} = R[s]/[D]). \quad (5)$$

By comparing the molecular weights and hydrodynamic characteristics, we established a complete set of KMHS relationships $C_i = K_i M^{b_i}$, where $C_i \equiv [\eta]$, D_0, or s_0 (Fig. 5). The coefficients K_η–b_η, K_D–b_D, and K_s–b_s are listed in Table 3.

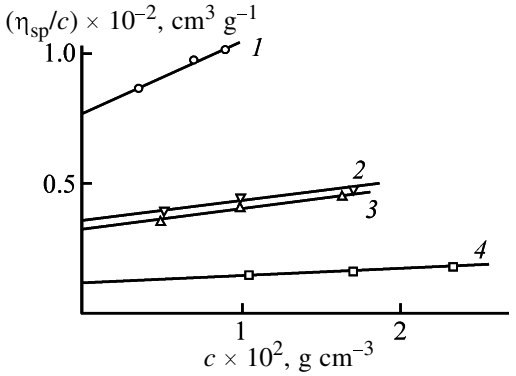

Fig. 3. To determination of the intrinsic viscosity η_{sp}/c of the MAG : VFA = 50 : 50 copolymers in 0.2 M NaCl. (*c*) Concentration.

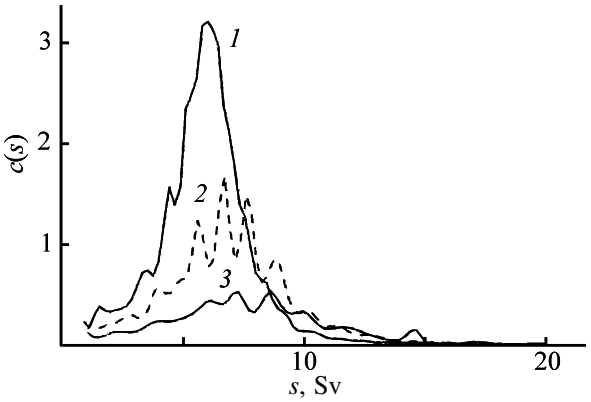

Fig. 4. Distribution with respect to the sedimentation coefficients, $c(s)$ vs. s, for sample no. 1 at concentrations of (*1*) 0.351, (*2*) 0.210, and (*3*) 0.106×10^{-2} g cm^{-3}.

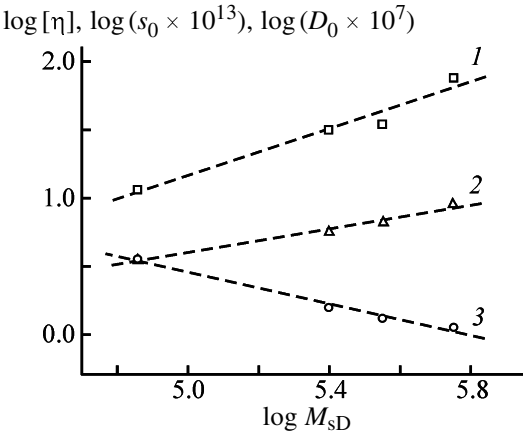

Fig. 5. Kuhn–Mark–Houwink–Sakurada plots for MGA : VFA = 50 : 50 copolymers in 0.2 M NaCl: (*1*) intrinsic viscosity, (*2*) sedimentation coefficient, and (*3*) translational diffusion coefficient.

The errors in determination of the b_i parameters, especially of b_η, are fairly high. Within the accuracy of determination holds a relationship between b_η and b_D module, derived assuming the equivalence of

Table 3. Parameters of the Kuhn–Mark–Houwink–Sakurada relationships obtained for the MAG : VFDA = 50 : 50 copolymers in 0.2 M NaCl at 20°C

Parameter	b_i	K_i	r_i
$[\eta]$–M	$0.86 \pm 0.1_2$	7.10×10^{-4}	0.9808
D_0–M	$-(0.56 \pm 0.04_6)$	1.85×10^{-4}	–0.9933
s_0–M	$0.44 \pm 0.04_6$	2.57×10^{-15}	0.9892

the chain dimensions in translational and rotational frictions in solutions [13, 14]:

$$|\beta_D| = (b_\eta + 1)/3. \quad (6)$$

Expression (6) was used for correcting the KMHS relationships. Within the accuracy, we selected such b_i values at which relationship (6) strictly holds. It should be noted that, when the molecular weight is determined by the Svedberg formula, the b_s and b_D parameters are unambiguously related as $b_s + |b_D| = 1$. By rocking the straight lines around the middle points we estimated further the parameters K_i, which yielded

$$[\eta] = 2.25 \times 10^{-3} M^{0.77},$$

$$D_0 = 2.61 \times 10^{-4} M^{-0.59},$$

$$s_0 = 3.69 \times 10^{-15} M^{0.41}.$$

In view of the carbon-chain structure of the backbone of the copolymer and the molecular properties of the corresponding homopolymers [2–4], we can suggest that the deviation of the parameters b_i from 0.50 is due to the occurrence of volume interactions in the copolymer macromolecules. The parameter characterizing the thermodynamic quality of the solvent was estimated as $\varepsilon = (2b_\eta - 1)/3 = (2|b_D| - 1) = 0.18 \pm 0.06$ [15].

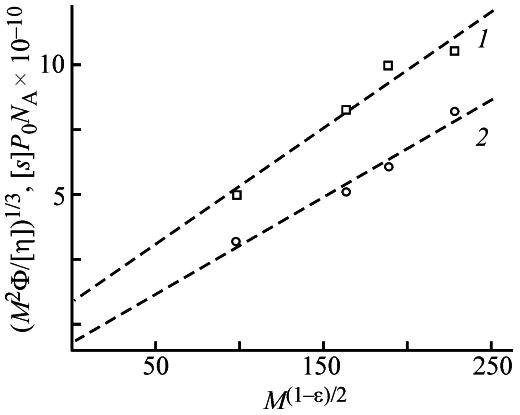

Fig. 6. To determination of the statistical Kuhn segment A of the MAG : VFA = 50 : 50 copolymer macromolecules: (*1*) intrinsic viscosity and (*2*) translational friction.

The hydrodynamic data were further interpreted using the relationships that can be derived from the Gray–Bloomfield–Hearst theory [16] taking into account both the volume interaction and the intramolecular permeation in the macromolecules [17]:

$$[s]P_0N_A = (M^2\Phi_0/[\eta])^{1/3} = [3/(1 - \varepsilon)(3 - \varepsilon)]M_L^{(1+\varepsilon)/2} \times M/A^{(1-\varepsilon)/2} + (M_L P_0/3\pi)[\ln A/d - (3A/d)^{-1} - \varphi(\varepsilon)], \quad (7)$$

where $P_0 = 5.11$ and $\Phi_0 = 2.87 \times 10^{23}$ are the hydrodynamic Flory parameters; M_L, linear density of the polymer chain; A, statistical Kuhn segment length; d, hydrodynamic cross section of the macromolecule; and $\varphi(\varepsilon) = 1.431 + 2.64\varepsilon + 4.71\varepsilon^2$.

Relationships (7) were used for estimating the statistical Kuhn segment of the chains simulating the macromolecules of the random copolymer. Figure 6 presents the corresponding plots, and Table 4, the coefficients characterizing the linear approximations of the experimental points: $y = ax + b$, where $x = M^{(1-\varepsilon)/2}$; a, section cut in the ordinate; and b, slope of the straight line. The latter parameter allows estimation of the Kuhn segment length characterizing the equilibrium rigidity of the chain:

$$b = d([s]P_0N_A)/d(M^{(1-\varepsilon)/2}) = d\{(M^2\Phi_0/[\eta])^{1/3}\}/d\{M^{(1-\varepsilon)/2}\} = [3/(1 - \varepsilon)(3 - \varepsilon)]M_L^{(1+\varepsilon)/2}A^{-(1-\varepsilon)/2}. \quad (8)$$

Based on the copolymer composition, we estimated the average linear density of the chains $M_L = 629$ g nm^{-1} mol^{-1} to be used in estimating the parameters A from Table 4.

The section cut in the ordinate corresponds to the second term in the right-hand part of Eq. (7); it describes the intramolecular permeation in the chains and, in principle, allows estimation of the hydrodynamic cross section of the macromolecule. However, Table 4 shows that, in our case, a limited number of the samples and possible heterogeneity of their composition, as well as a limited range of the molecular weights, are responsible for the fact that the error in determining the parameter exceeds the parameter itself, and, hence, the hydrodynamic diameter remains uncertain.

We compared the equilibrium rigidity of the chains of the random MAG–VFA copolymers, estimated in this study, with those for the corresponding homo-

Table 4. To estimation of the equilibrium rigidity of the chains of the MAG : VFA = 50 : 50 random copolymer

Parameter	$(b \pm \Delta b) \times 10^{-8}$	$(a \pm \Delta a) \times 10^{-10}$	r	$A \pm \Delta A$, nm
Translational friction	$3.75 \pm 0.4_5$	$-(0.72 \pm 0.7_9)$	0.9859	3.1 ± 0.9
Intrinsic viscosity	$4.50 \pm 0.6_5$	$0.83 \pm 1.1_5$	0.9797	2.0 ± 0.7

polymers [2–4] on the basis of the concept of normalized KMHS relationships [18]. The translational friction was plotted as $\log [s]/M_L$ vs. $\log L$, and the intrinsic viscosity, as $\log [\eta]M_L$ vs. $\log L$, where L is the contour chain length $L = M/M_L$ (Fig. 7). It is seen that the hydrodynamic dimensions of the copolymer macromolecules are intermediate between those of the initial homopolymers with the corresponding contour lengths.

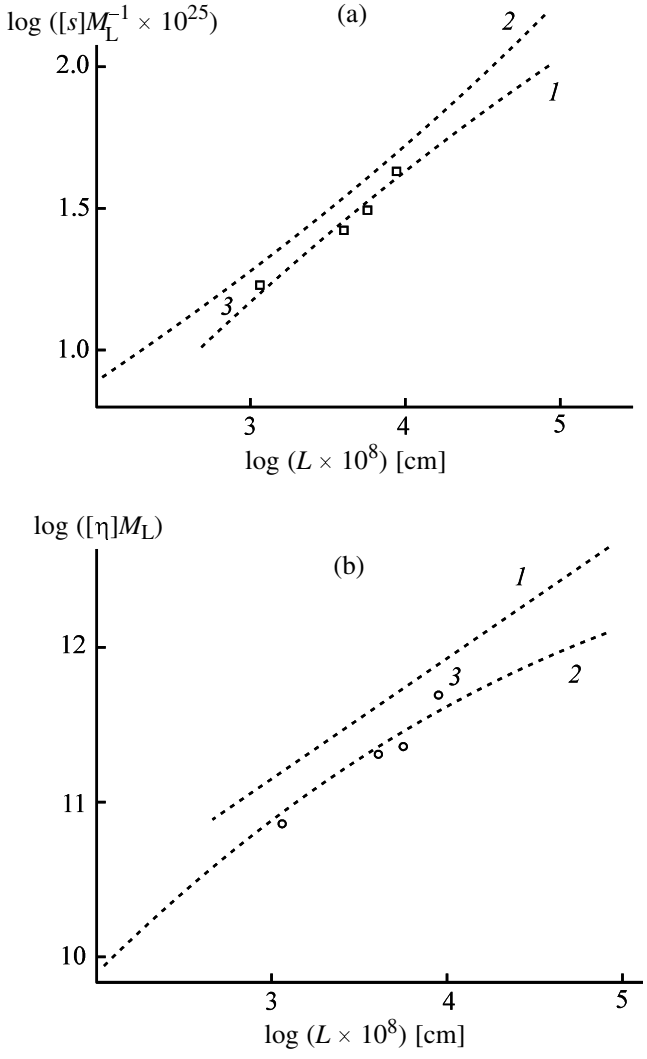

Fig. 7. Log–log plots of the (a) centrifugal sedimentation coefficient and (b) intrinsic viscosity, normalized to the linear density, vs. the contour length of the macromolecules L. (*1*) Poly-*N*-methacryloylglucose [2, 3]; (*2*) poly-*N*-vinylformamide [4]; and (*3*) points corresponding to the MAG : VFA = 50 : 50 copolymer, according to Table 2.

CONCLUSIONS

(1) Random 50 : 50 *N*-methacryloylglucosamine–*N*-vinylformamide copolymers were synthesized by radical polymerization.

(2) The diffusion and sedimentation analysis allowed estimation of the molecular weights of the copolymers and determination of the parameters of the Kuhn–Mark–Houwink–Sakurada relationships.

(3) The length of the statistical segment of the copolymer chains lies within $2.0 < A < 3.1$ nm and is actually intermediate between the values of the corresponding homopolymers.

ACKNOWLEDGMENTS

This study was financially supported in part by the Russian Foundation for Basic Research (project no. 05-0333210).

The authors are grateful to C. Ebel (Institut de Biologie Structurale, Grenoble, France) for the opportunity to carry out the sedimentation experiments in the Laboratoire de Biophysique Moleculaire.

REFERENCES

1. Panarin, E.F. and Ivanova, N.P., *Zh. Prikl. Khim.*, 2005, vol. 78, no. 8, pp. 1340–1343.
2. Pavlov, G.M., Korneeva, E.V., Mikhailova, N.A., et al., *Vysokomol. Soedin., Ser. A*, 1993, vol. 35, no. 10, pp. 1646–1651.
3. Pavlov, G.M., Ivanova, N.P., Korneeva, E.V., et al., *Carbohydrate Chem.*, 1996, vol. 15, no. 4, pp. 417–433.
4. Pavlov, G.M., Korneeva, E.V., Ebel, C., et al., *Vysokomol. Soedin., Ser. A*, 2004, vol. 46, no. 10, pp. 1732–1737.
5. Tsvetkov, V.N., Eskin, S.Ya., and Frenkel, S.Ya., *Struktura makromolekul v rastvorakh* (Structure of Macromolecules in Solutions), Moscow: Nauka, 1964.

6. Kratky, O., Leopold, H., and Stabinger, H., *Meth. Enzymol.*, 1973, vol. 27, pp. 98–110.
7. Schuck, P., *Biophys. J.*, 2000, vol. 78, pp. 1606–1619.
8. Pavlov, G.M. and Frenkel, S.Ya., *Vysokomol. Soedin., Ser. B*, 1982, vol. 24, no. 3, pp. 173–180.
9. Skazka, V.S., *Sedimentatsionno-diffuzionnyi analiz polimerov v rastvore* (Sedimentation and Diffusion Analysis of Polymers in Solution), Leningrad: Leningr. Gos. Univ., 1985.
10. Tsvetkov, V.N., *Zhestkotsepnye polimernye molekuly* (Rigid-Chain Polymer Molecules), Leningrad: Nauka, 1986.
11. Pavlov, G.M. and Frenkel, S.Ya., *Vysokomol. Soedin., Ser. B*, 1986, vol. 28, no. 5, pp. 353–357.
12. Pavlov, G.M., *Eur. Biophys. J.*, 1997, vol. 25, nos. 5/6, pp. 385–397.
13. Budtov, V.P., *Fizicheskaya khimiya rastvorov polimerov* (Physical Chemistry of Polymer Solutions), St. Petersburg: Khimiya, 1992.
14. Pavlov, G.M., *Prog. Colloid. Polym. Sci.*, 2002, vol. 119, pp. 149–157.
15. Ptitsyn, O.B. and Eizner, Yu.E., *Zh. Tekh. Fiz.*, 1959, vol. 29, no. 9, pp. 1105–1112.
16. Gray, G., Bloomfield, V., and Hearst, J., *J. Chem. Phys.*, 1967, vol. 46, pp. 1493–1500.
17. Pavlov, G.M., Panarin, E.F., Korneeva, E.V., et al., *Vysokomol. Soedin., Ser. A*, 1990, vol. 32, no. 6, pp. 1190–1192.
18. Pavlov, G.M., *Vysokomol. Soedin., Ser. A*, 2004, vol. 46, no. 10, pp. 1872–1878.

ISSN 1070-4272, Russian Journal of Applied Chemistry, 2007, Vol. 80, No. 5, pp. 783–789. © Pleiades Publishing, Ltd., 2007.
Original Russian Text © B.A. Zaitsev, G.I. Khramova, I.D. Shvabskaya, 2007, published in Zhurnal Prikladnoi Khimii, 2007, Vol. 80, No. 5, pp. 804–811.

MACROMOLECULAR CHEMISTRY AND POLYMERIC MATERIALS

Synthesis of Rolivsans Containing Unsaturated Biphenyl Units by Acid-Catalyzed Transformations of 4,4'-Di(1-hydroxyethyl)biphenyl

B. A. Zaitsev, G. I. Khramova, and I. D. Shvabskaya

Institute of Macromolecular Compounds, Russian Academy of Sciences, St. Petersburg, Russia

Received February 9, 2007

Abstract—The mechanism and kinetics of formation, and also the structure, composition, and properties of thermosetting resins of a new class, Rolivsans with biphenyl units, were studied.

DOI: 10.1134/S1070427207050187

Rolivsans are thermosetting polyfunctional resins exhibiting high thermal and chemical resistance and containing diphenyl ether units with terminal vinyl and methacrylate groups. They are used as insulating materials operating under extreme conditions [1–4]. Rolivsans are prepared from various aromatic compounds and unsaturated carboxylic acids [5–8]. Rolivsan MV-1 resin has been developed and has found practical application. Its synthesis is based on transformations of methacrylic acid and bis[4-(1-hydroxyethyl)phenyl] ether, catalyzed by strong acids. The starting ether, in turn, is prepared from diphenyl ether [9, 10].

The goal of this study is detailed examination of the conditions of synthesis, structure, and properties of unsaturated biphenyl compounds and of compositions and resins of Rolivsan type based on them.

It is known that biphenyl is a readily available starting compound and that biphenyl units incorporated in some heat-resistant polymers are characterized by high resistance to thermal oxidation and hydrolysis; they also tend to form mesomorphic structures. The synthesis and molecular design of Rolivsans [6–8] determine in this case the choice of 4,4'-di(1-hydroxyethyl)biphenyl as the starting compound. This compound is prepared in two steps. The first step is Friedel–Crafts acetylation of biphenyl **I**, giving 4,4'-diacetylbiphenyl **II** in quantitative yield [8, 11]. In the second step, compound **II** is subjected to catalytic hydrogenation on Raney nickel to obtain 4,4'-di(1-hydroxyethyl)biphenyl, also in quantitative yield. Rolivsans with bifunctional units were prepared by heating of bisecondary diol **III** with methacrylic acid **IV** in an aromatic solvent in the presence of *p*-toluenesulfonic acid monohydrate **V** and polymerization inhibitors:

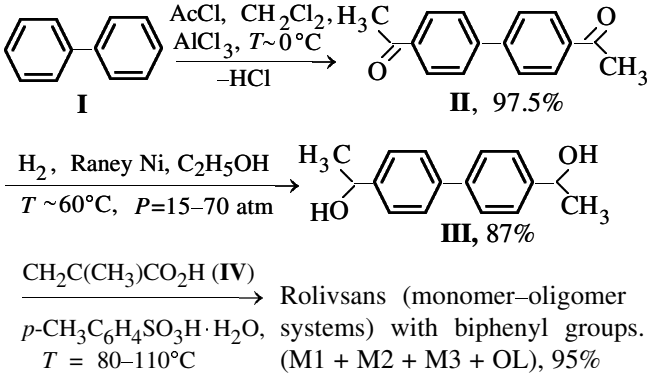

Previously we studied in detail acid-catalyzed dehydration of di[4-(1-hydroxyethyl)phenyl] ether **VI** both in the presence of carboxylic acids (mainly methacrylic acid) and without them. The reaction was performed with refluxing in an aromatic solvent, with azeotropic distillation of the released water [6–10]. Comprehensive studies showed that the process involves consecutive-parallel reactions: polycondensation of the bisecondary diol, its esterification with methacrylic acid, dehydration of this diol and its polycondensation products, cleavage of (di)methacrylates with the formation of a (di)vinylaromatic compound and methacrylic acid, and dimerization of (di)vinylaromatic compounds by the polyaddition mechanism with the proton transfer (oligomerization) [12–16].

However, first we studied a simpler process, polycondensation of 4,4'-di(1-hydroxyethyl)biphenyl (**III**) itself without a carboxylic acid. Based on the previ-

Table 1. Synthesis conditions and composition of divinylbiphenyl systems obtained

Run no.	Concentration, M		T_{react},* °C	τ, h	Product composition,** wt %				T_m, °C	Found, %	
	$c_{diol\ III}$	$c_{cat\ V} \times 10^3$			M1	$(m_1)_2$	$(m_1)_3$	$(m_1)_{n>3}$		C	H
1	0.2173	5.0	111	2.0	75	19	5	1	135–151	91.7	7.0
2***	0.1588	10.1	111	1.0	70	15	5	10	135–151	91.7	7.0
3	0.1585	10.1	111	1.5	35	25	10	30	132–134	91.6	7.5
4	0.2392	19.7	111	0.2	15	17	17	51****	–	–	–
5	0.2392	19.7	111	0.3	42	25	10	23****	–	–	–
6	0.2582	4.9	144	0.8	77	17	4	2	135–145	–	–
7	0.2173	3.0	144	1.0	89	8	2	1	150–153	–	–

* Refluxing in toluene (111°C) or *o*-xylene (144°C).
** $(m_1)_2$, $(m_1)_3$, and $(m_1)_{n>3}$ refer to dimers, trimers, and higher oligomers, respectively.
*** The degree of unsaturation of the product (run no. 3), determined by ozonolysis, is 0.00773 mol of double bonds per gram.
**** Mixture of unsaturated oligoethers (OL) and produtcs of imcomplete dehydration (cleavage) of oligoerthers described previously [6, 7, 13].

ously suggested mechanism [6, 7, 8, 11–16], after the polycondensation of bisecondary aromatic diols [13] catalyzed by strong acids and the subsequent dehydration of oligoethers **VII** [12], formation of divinylbiphenyl monomer–oligomer systems of various compositions could be expected:

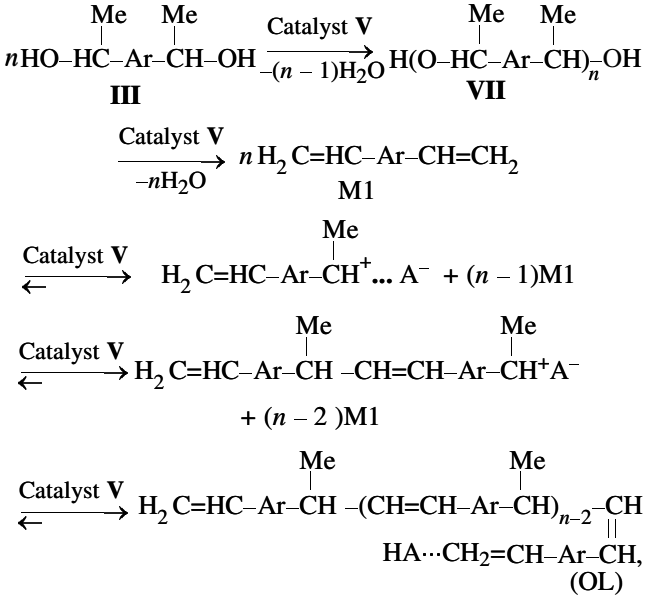

where Ar = 4,4'-Ph–Ph; n = 0, 1, 2, 3, etc.; HA is catalyst **V**.

Indeed, as seen from Table 1 and Fig. 1, acid-catalytic transformations of diol **III** lead to compositions consisting of 4,4'-divinylbiphenyl (M1), its unsaturated dimer, trimer, tetramer, and oligomers of higher molecular weights. The product composition strongly depends on the synthesis conditions. For example, refluxing of diol **III** in *o*-xylene at a relatively high temperature (run no. 7) and low c_{cat} results in the formation of 4,4'-divinylbiphenyl (M1) in almost quantitative yield. This monomer, like low-melting divinylarene compositions listed in Table 1, is readily miscible with the known thermosetting resins and is of interest as a heat-resistant and chemically stable cross-linking agent. Pure divinylbiphenyl monomer M1 (melting point 152–154°C) can be readily separated from such compositions by sublimation.

In accordance with the established mechanism, in the case of similar "polycondensation" of biphenyl diol **III** with carboxylic acid **IV** we could expect formation of divinylarene monomer–oligomer systems of the following compositions:

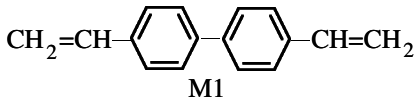

M1

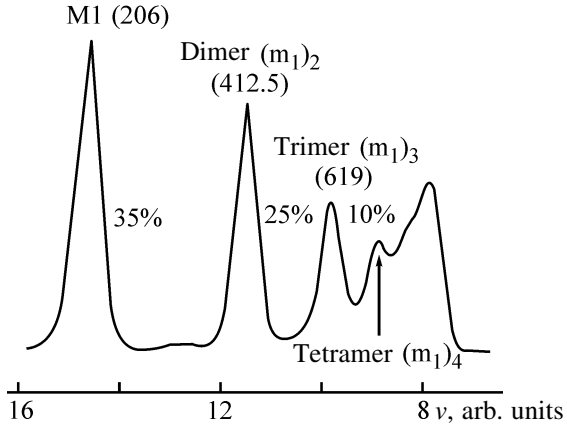

Fig. 1. Gel chromatogram of the monomer–oligomer system prepared in toluene (Table 1, run no. 3). Eluent toluene; sample concentration 2 g per 100 ml of solvent. (*v*) Retention volume; the same for Figs. 3 and 4.

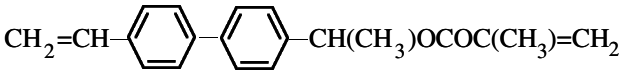

M2

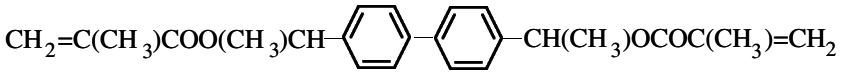

M3

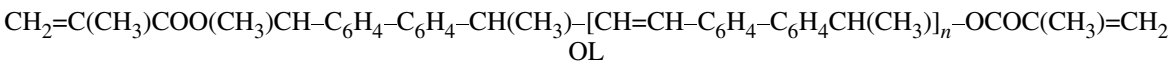

OL

The results of these transformations are given in Tables 2 and 3. The composition and structure of Rolivsans containing biphenyl units were examined by exclusion liquid chromatography, IR spectroscopy, elemental analysis, and analysis for functional groups (ester numbers, ozonolysis). As seen from Fig. 2, the initial rates of the dehydration of aromatic diols with biphenyl (**III**) and diphenyl ether (**VI**) groups on heating with methacrylic acid are essentially different. Despite the fact that the concentration of acid catalyst **V** in the system with biphenyl diol **III** is approximately 2.5 times higher, the initial dehydration rate in this system is considerably lower. To compare the rates of both processes, the kinetic data can be reduced to the same synthesis conditions, taking into account the fact that the initial dehydration rate is proportional to the concentration of the acid catalyst [6–8, 17]. Calculation shows that in this case the rate of water release from the start of the process to 70–80% conversion is approximately five times higher for the system with diphenyl ether diol **VI**. This effect, apparently, cannot be assigned to the influence of the chemical structure of diols **III** and **VI** on the reactivity of terminal hydroxy groups in the dehydration. The difference in the electronic effects seems to be insignificant in this case. The difference in the catalyst acidity in these media is considerably more pronounced. The acidity of catalyst **V** in the medium of diphenyl ether diol **VI** is considerably higher, because it forms a protonated species with the lone electron pair of the ether oxygen atom [17].

It should be noted that monomer M1 can also be prepared by sublimation from methacrylate compositions; however, in this case it contains an impurity of jointly subliming methacrylate M2 (Fig. 3).

As seen from Tables 2 and 3, and from Figs. 4 and 5, the composition and properties of products formed by reaction of diol **III** with carboxylic acid **IV** regularly vary in accordance with the established mechan-

Table 2. Synthesis conditions and characteristics of unsaturated monomer–oligomer systems containing biphenyl compounds with terminal vinyl and methacrylate groups*

Run no.** (sample)	Concentration, M			T_{react},*** °C	τ, h	>C=C<	EN	Found, %		T_m, °C	n_D^t
	$c_{diol\,III}$	c_{IV}	$c_{catV} \times 10^3$					C	H		
8	0.3687	0.9207	11.7	81	3.5	–	–	82.5	7.2	–	–
9	0.4160	1.0241	13.2	81	1.7	–	156	81.5	7.5	30–35	1.590^{40}
10	0.2393	0.5763	19.7	111	0.5	–	–	81.6	7.5	–	1.595^{40}
11(1)	0.2390	0.5756	19.7	111	0.5	0.540	–	81.7	7.0	30–32	–
11(2)	0.2390	0.5756	19.7	111	1.5	0.708	–	84.1	6.9	112–118	–
11(4)	0.2390	0.5756	19.7	111	3.5	0.755	–	90.5	7.1	132–134	–
12	0.2393	0.5763	19.7	111	2.2	–	–	91.5	7.0	123–128	–
13	0.2373	0.5714	19.5	111	0.7	–	–	–	–	95–110	–
14	0.2373	0.5714	19.5	111	1.5	–	–	–	–	110–115	–
15	0.2373	0.5714	19.5	111	2.5	–	–	–	–	80–108	–
16	0.3815	1.9121	12.1	111	1.5	0.552	250	79.9	7.2	35–45	1.588^{40}

* (>C=C<) Degree of unsaturation, mol of double bonds per 100 g of product; (EN) ester number, mg KOH per gram of product.
** c_{III}/c_{IV} = 1 : 2.5 (run nos. 8, 9), 1 : 2.4 (run nos. 10–15), or 1 : 5 (run no. 16).
*** In refluxing benzene (81°C) or toluene (111°C).

Table 3. Composition of Rolivsans containing biphenyl units and prepared at various catalyst concentrations and synthesis times*

Run no.	$c_{cat\,\mathbf{V}} \times 10^3$, M	τ, h	Composition, wt %			
			M1	M2	M3	OL
11(1)	19.7	0.5	6	35	38	21
11(2)	19.7	1.5	24	42	30	6
11(3)	19.7	2.5	37	38	23	2
11(4)	19.7	3.5	45	30	20	5
17(2)	19.7	0.3	10	45	34	11
17(5)	19.7	1.0	29	30	31	10
17(13)	19.7	4.5	10	8	22	60
18(6)	7.0	6.0	30	45	22	3
18(8)	7.0	8.0	38	42	17	3
18(10)	7.0	10.0	48	34	14	4
18(12)	7.0	12.0	54	29	12	5

* The products were prepared by refluxing the reaction mixtures containing 0.239 M diol **III** and 0.576 M methacrylic acid **IV** in toluene (111°C).

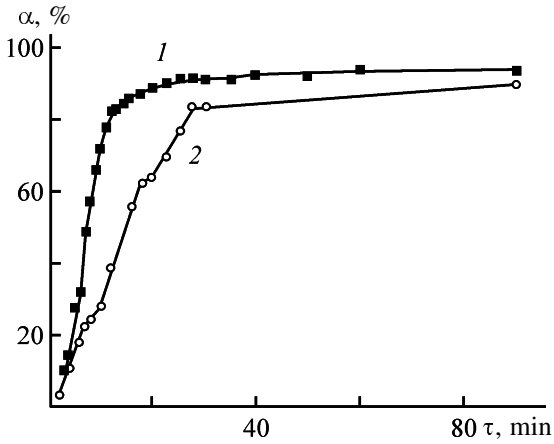

Fig. 2. Kinetics of dehydration of the system bisecondary aromatic diol–methacrylic acid in toluene at 111°C. (α) Degree of dehydration and (τ) time. (*1*) Molar ratio diol **VI** : acid **IV** = 1 : 2.47, $c_{cat\,\mathbf{V}} = 7.86 \times 10^{-3}$ M; (*2*) molar ratio diol **VI** : acid **IV** = 1 : 2.41, $c_{cat\,\mathbf{V}} = 19.7 \times 10^{-3}$ M.

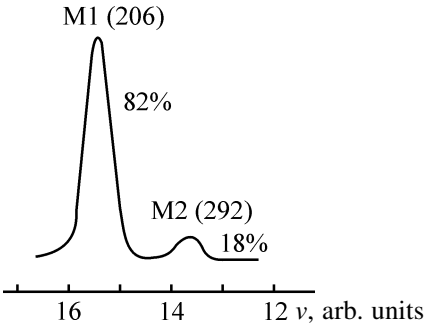

Fig. 3. Gel chromatogram of components M1 and M2 (mp 122–123°C) sublimed from the monomer–oligomer composition (Table 2, run no. 12).

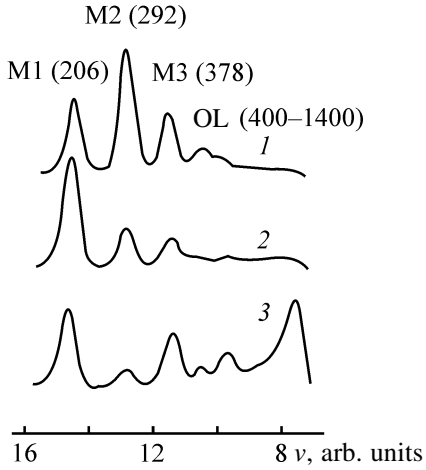

Fig. 4. Gel chromatograms of samples taken (*1*) 20, (*2*) 60, and (*3*) 270 min after the start of the synthesis of the monomer–oligomer system (Table 3, run no. 17, samples 2, 5, and 13). The molecular weights of the components are given in parentheses.

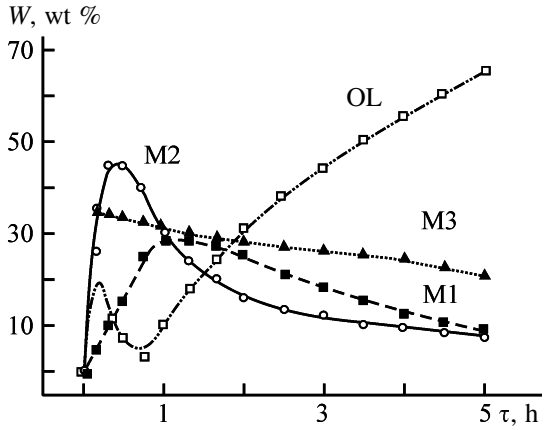

Fig. 5. Kinetics of formation of components *W* of the monomer–oligomer system (Table 3, run no. 17). (τ) Synthesis time.

ism and kinetics of the process. In the initial and middle steps of the process, primary oligoethers undergo dehydration, and the maximal amounts of vinyl- and divinylaromatic monomers (M1, M2) and of methacrylates (M2, M3) are formed. Further steps involve consecutive-parallel cleavage of methacrylates (M2, M3) to form again monomers M1 and M2, which, in turn, enter into stepwise dimerization reactions (cationic polyaddition with the proton transfer), etc. The final products of these transformations are oligomers (OL) of type m_2–$(m_1)_n$–m_2, where m_1 and m_2 are units of monomers M1 and M2, respectively.

The IR spectra of unsaturated biphenyl compounds containing terminal vinyl and methacrylate groups and internal double bonds (Fig. 6) exhibit bands of unsaturated and aromatic groups at 1630, 1600, 1495, 990,

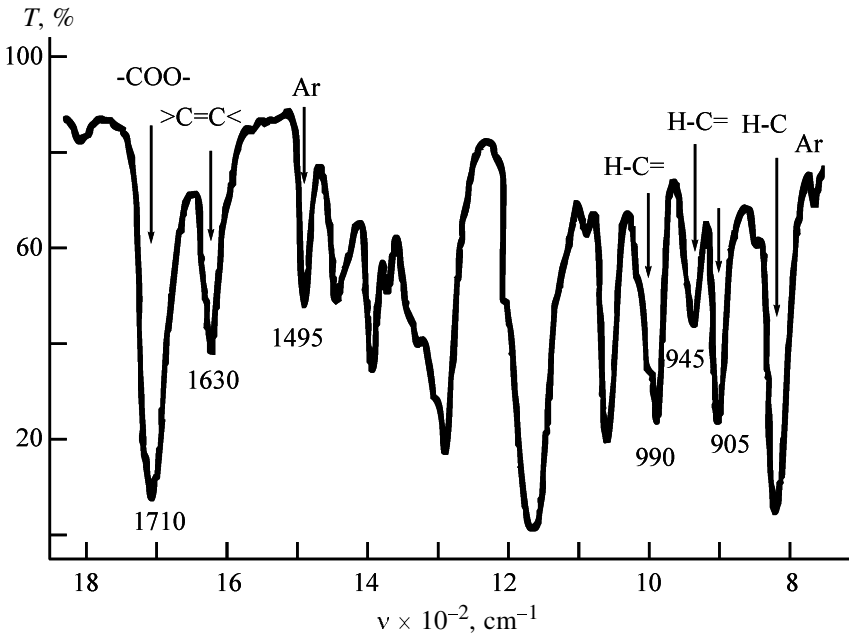

Fig. 6. IR spectrum of the monomer–oligomer composition [Table 3, run no. 11 (2)]. (*T*) Transmission and (ν) wavenumber.

965, 945, and 905 cm^{-1}, bands of methyl and methylene groups at 2960, 2925, 2870, and 2850 cm^{-1}, bands of methine groups at 2900 cm^{-1}, and also strong bands of stretching vibrations of the carbonyl group, characteristic of methacrylates, at 1710 cm^{-1} [18, 19]. With the progress of the reaction, the carbonyl band at 1710 cm^{-1} and of the out-of-plane vibration bands of the H–C= group in *p*-CH_2=CH–Ph–Ph– and CH_2=C(CH_3)COO fragments at ~902 and 940 cm^{-1}, respectively, decrease in the intensity, whereas the band at 965 cm^{-1}, belonging to the out-of-plane vibrations of the H–C= group in *trans*-–CH=CH– fragments, increases; the concentration of these fragments grows in the course of stepwise dimerization (cationic polyaddition) of vinylaromatic compounds [14–16, 20]. The unsaturated compositions obtained are pasty or low-melting compounds curing on heating and forming monolithic network polymers and plastics with a high softening point (Table 4).

EXPERIMENTAL

4,4'-Di(1-hydroxyethyl)biphenyl III was prepared by Friedel–Crafts acetylation of biphenyl **I** [8, 11] followed by catalytic hydrogenation or reduction of the resulting aromatic diketone **II**. Diketone **II** was prepared as follows. To a mixture of 80 ml of CH_2Cl_2 and 133.2 g (1.0 mol) of anhydrous $AlCl_3$, cooled to approximately 0°C, 85.2 ml (94.2 g, 1.20 mol) of acetyl chloride was added with stirring over a period

Table 4. Thermal and physicomechanical properties of glass fiber laminates based on Rolivsans with biphenyl units*

Run no.	T_m, °C	θ, °C	DTGA		Ultimate bending stress, MPa			
			$T_{5\%}$, °C	$T_{10\%}$, °C	$\sigma_b^{20°C}$	$\sigma_b^{320°C}$	$\sigma_b^{20°C}$**	$\sigma_b^{320°C}$**
9***	30–35	405	400	430	260	160	160	240****
11(1)	30–32	–	–	–	460	300	–	220
11(2)	112–118	–	–	–	300	240	–	220
11(4)	132–134	407	420	450	290	200	–	220
12	123–128	–	–	–	320	–	220	180

* (θ) Softening point of the cured compound (binder); ($T_{5\%}$, $T_{10\%}$) temperatures of 5 and 10% weight loss, respectively.
** After thermal oxidative aging in air at 320°C for 10 h.
*** Gelation time 2 h at 140°C.
**** Weight loss 1.7 or 5.8% for binder (counting on its ~30% content in the glass fiber laminate).

of 15–20 min. To the resulting acetylating complex, a solution of 61.6 g of biphenyl **I** in 80 ml of CH_2Cl_2 was added over a period of 1 h at 0±5°C with vigorous stirring; the released HCl was absorbed by an alkaline solution. The resulting complex of the acetylated product with $AlCl_3$ in methylene chloride was stirred for 0.5 h at ~0°C and for an additional 3 h at ~40°C. Diketone **II** was isolated by decomposing the complex with a mixture of 900 g of finely crushed ice, 2 l of distilled water, and 1.2 l of 20% HCl, which was followed by washing with water and drying at 60–70°C. The yield of dry diketone **II** was 95.8 g (97.5%), mp 165–170°C; after recrystallization from ethanol and repeated recrystallization from toluene, the melting point of **II** increased to 185–190 and 193–195°C, respectively (published data [21]: 190–192°C). The content of acetyl groups in **II** was determined by oximation.

Found, %: >C=O 24.1.
$C_{16}H_{14}O_2$.
Calculated, %: 23.5.

4,4'-Di(1-hydroxyethyl)biphenyl III was prepared by two procedures: (*A*) hydrogenation of **II** on Raney nickel and (*B*) reduction of **II** with sodium borohydride. In procedure *A*, a mixture of 250 ml of ethanol, 5.0 g of Raney nickel (Merck–Schuchardt) containing about 88% Ni and 12% Al, and 30.0 g (0.126 mol) of **II** was stirred in a pressure vessel at 60–70°C at initial hydrogen pressure of 50–70°C for approximately 1 h. Then the catalyst was separated by decanting and centrifugation of the solution of the hydrogenated product in ethanol; the alcohol was distilled off at reduced pressure, and the residue was recrystallized from toluene. Yield of aromatic diol **III** 26.5 g (87%), mp 158–159.5°C (published data [21]: 159–161°C).

Found, %: C 79.2; H 7.4.
$C_{16}H_{18}O_2$.
Calculated, %: C 79.3; H 7.5.

The content of hydroxy groups was determined by acetylation.

Found, %: OH 13.7.
$C_{16}H_{18}O_2$.
Calculated, %: OH 14.

In procedure *B*, a mixture of 200 ml of absolute ethanol, 5.0 g (0.13 mol) of sodium borohydride, and 25.8 g (0.11 mol) of diketone **II** was heated at 60°C for 2 h. The reaction mixture was treated with 50 ml of water, the precipitated hydroxides were filtered off, the solvent was distilled off at reduced pressure, and the residue was recrystallized from toluene. Yield 18.6 g (70%), mp 160–161°C.

4,4'-Divinylbiphenyl (M1). A mixture of 5.0020 g (0.02064 mol) of diol **III**, 0.0500 g of *tert*-butylcatechol, 0.0742 g of catalyst **V**, and 75 ml of *o*-xylene was refluxed (~144°C) for 50 min with azeotropic distillation of the released water. Then the mixture was worked up as described above. Yield of unsaturated monomer–oligomer composition containing about 75% monomer M1 (data of exclusion liquid chromatography) 3.8 g, mp 135–145°C. Sublimation of 0.500 g of the composition at a bath temperature of 160°C and residual pressure of 1–2 mm Hg for 7–10 min gave 0.33 g of pure monomer M1, mp 152–154°C (published data [21, 22]: 152.5–153°C).

Biphenyl compounds with terminal vinyl and methacrylate groups, and also their oligomerization products containing unsaturated dimers, trimers, tetramers, and higher oligomers were prepared as follows. A solution of biphenyl diol **III** in an aromatic solvent (benzene, toluene, *o*-xylene), containing inhibitors of radical polymerization (hydroquinone, CuCl) and a catalyst (*p*-toluenesulfonic acid monohydrate, **V**) was refluxed in the presence of methacrylic acid **VI** or without it in a flask equipped with a Dean–Stark trap. Water formed by polycondensation, esterification, and dehydration was removed by azeotropic distillation. Then the mixture was cooled and, after filtering CuCl off, washed successively with water, 5% $NaHCO_3$ solution, and again water, after which it was dried over $CaCl_2$ and passed through a 2–3-cm Al_2O_3 bed; the solvent was distilled off at reduced pressure. The conditions of synthesis, composition, and properties of the unsaturated biphenyl compounds [4,4'-divinylbiphenyl (M1), dimethacrylate of diol **III** (M3), 4-vinyl-4'-(1-hydroxyethyl)biphenyl methacrylate (M2)] and of unsaturated aromatic monomer–oligomer systems containing Rolivsans with biphenyl-containing units are listed in Tables 1–3. The IR spectra were recorded on a Specord 75-IR device from thin films or solutions in $CHCl_3$. Exclusion liquid chromatography was performed on a KhZh-1307 chromatograph at 20°C; the column was packed with Ultrastyrogel sorbent (500 Å); the eluent was toluene; the product concentration was 0.20–0.50 g in 100 ml of a solvent. The degree of unsaturation was determined on an ADS-4 ozonizer at 0°C (solvent CCl_4). The ester number was determined by dissolving a resin sample in dioxane purified by distillation from KOH and Na, which was followed by adding a 0.1 N solution of KOH in ethanol–dioxane, refluxing the mixture for 7 h (in so doing, the reflux condenser was equipped with a soda

lime tube), and titrating with 0.1 N HCl. Samples of glass fiber laminates in the form of 1.6–2.0-mm-thick plates were prepared by hot pressing of prepregs (eight sheets of T-10-80 glass fiber fabric impregnated with a melt of the unsaturated composition) in a mold at a pressure of 1 kgf cm^{-2}, followed by thermal curing of the stack at 120–250°C (heating rate 10 deg h^{-1}). The ultimate bending stress at three-point bending was determined with 3–4-mm-wide samples at a support spacing of 15 min and a loading rate of 15 mm min^{-1}. Dynamic thermogravimetric analysis (DTGA) was performed in air on a C derivatograph (MOM, Hungary) at a heating rate of 4.5 deg min^{-1}. The softening point was determined on a Vicat-type device designed at the Institute of Macromolecular Compounds, Russian Academy of Sciences at an indenter load of 1 kg and an indenter cross section of 1 mm^2.

CONCLUSIONS

(1) The previously suggested method for preparing polyfunctional aromatic compounds, divinylaromatic monomer–oligomer compositions, and heat-resistant thermosetting resins of a new type (Rolivsans), based on acid-catalyzed transformations of bisecondary aromatic diols, was applied to biphenyl derivatives.

(2) Previously unknown unsaturated monomeric and oligomeric compounds with biphenyl groups, e.g., 4,4'-di(1-hydroxyethyl)biphenyl dimethacrylate, 4-vinyl-4'-(1-hydroxyethyl)biphenyl methacrylate, and difficultly accessible 4,4'-divinylbiphenyl, and their compositions can be prepared in high yield by a one-pot process: dehydration of 4,4'-(1-hydroxyethyl)biphenyl and of the system 4,4'-di(1-hydroxyethyl)biphenyl–methacrylic acid.

(3) Rolivsans containing biphenyl units and based on the above (di)vinylbiphenyl compounds and methacrylates of secondary alcohols form heat-resistant network polymers and plastics on curing.

REFERENCES

1. Zaitsev, B.A., Khramova, G.I., Dantsig, L.L., et al., *Plast. Massy*, 1981, no. 9, pp. 12–13.
2. Zaitsev, B.A., Khramova, G.I., Tsygankova, T.S., et al., *Mekh. Kompoz. Mater.*, 1982, no. 5, pp. 775–778.
3. Zaitsev, B.A., *Sintez, struktura i svoistva polimerov: Sbornik trudov Inst. vysokomolekulyarnykh soedinenii AN SSSR* (Synthesis, Structure, and Properties of Polymer: Coll. of Papers of Inst. of Macromolecular Compounds, USSR Acad. Sci.), Koton, M.M., Ed., Leningrad: Nauka, 1989, pp. 66–77.
4. Zaitsev, B.A., Khramova, G.I., Tsygankova, T.S., et al., *Plast. Massy*, 2003, no. 10, pp. 23–25.
5. USSR Inventor's Certificate no. 794026.
6. Zaitsev, B.A., Khramova, G.I., and Dantsig, L.L., *Vysokomol. Soedin., Ser. A*, 1982, vol. 24, no. 12, pp. 2467–2474.
7. Zaitsev, B.A., Dantsig, L.L., and Khramova, G.I., *Zh. Org. Khim.*, 1983, vol. 19, no. 11, pp. 2340–2349.
8. Zaitsev, B.A., Regular Trends in Formation, Structure, and Properties of Heat-Resistant Network Polyarylenes, *Doctoral Dissertation*, Leningrad, 1983.
9. Zaitsev, B.A., Khramova, G.I., and Tsygankova, T.S., *Zh. Prikl. Khim.*, 2003, vol. 76, no. 4, pp. 658–662.
10. Zaitsev, B.A., Khramova, G.I., and Shvabskaya, I.D., *Zh. Prikl. Khim.*, 2007, vol. 80, no. 4, pp. 637–642.
11. Zaitsev, B.A., Dantsig, L.L., Khramova, G.I., et al., *Zh. Prikl. Khim.*, 1977, vol. 50, no. 2, pp. 411–415.
12. Zaitsev, B.A. and Kiseleva, R.F., *Vysokomol. Soedin., Ser. A*, 1981, vol. 23, no. 8, pp. 1783–1790.
13. Zaitsev, B.A., Fedorova, A.V., Kiseleva, R.F., et al., *Vysokomol. Soedin., Ser. A*, 1983, vol. 25, no. 5, pp. 1076–1081.
14. Zaitsev, B.A. and Kiseleva, R.F., *Acta Polym.*, 1983, vol. 36, no. 10, pp. 527–530.
15. Zaitsev, B.A., Kiseleva, R.F., Denisov, V.M., et al., *Vysokomol. Soedin., Ser. A*, 1984, vol. 26, no. 8, pp. 1602–1609.
16. Zaitsev, B.A., Kiseleva, R.F., and Gusarova, I.O., *J. Polym. Sci., Polym. Chem. Ed.*, 1996, vol. 34, pp. 1165–1181.
17. Denisov, E.T., *Kinetika gomogennykh khimicheskikh reaktsii* (Kinetics of Homogeneous Chemical Reactions), Moscow: Vysshaya Shkola, 1978.
18. Zaitsev, B.A., Khramova, G.I., and Tsygankova, T.S., *Zh. Prikl. Khim.*, 2003, vol. 76, no. 10, pp. 1708–1714.
19. Bellamy, L.J., *The Infra-Red Spectra of Complex Molecules*, New York: Wiley, 1957.
20. Zaitsev, B.A., Kiseleva, R.F., Denisov, V.M., et al., *Izv. Akad. Nauk SSSR, Ser. Khim.*, 1990, no. 11, pp. 2566–2574.
21. Wiley, R.H. and Mayberry, G.L., *J. Polym. Sci., Part A*, 1963, vol. 1, no. 1, pp. 217–226.
22. Drefahl, G., Plotner, G., and Rudolph, F., *Chem. Ber.*, 1960, vol. 93, pp. 998–1005.

ISSN 1070-4272, Russian Journal of Applied Chemistry, 2007, Vol. 80, No. 5, pp. 790–798. © Pleiades Publishing, Ltd., 2007.
Original Russian Text © Yu.P. Kuznetsov, E.V. Kruchinina, Yu.G. Baklagina, A.K. Khripunov, O.A. Tulupova, 2007, published in Zhurnal Prikladnoi Khimii, 2007, Vol. 80, No. 5, pp. 812–820.

MACROMOLECULAR CHEMISTRY AND POLYMERIC MATERIALS

Deep Desalination of Water by Evaporation through Polymeric Membranes

Yu. P. Kuznetsov, E. V. Kruchinina, Yu. G. Baklagina, A. K. Khripunov, and O. A. Tulupova

Institute of Macromolecular Compounds, Russian Academy of Sciences, St. Petersburg, Russia
St. Petersburg State Technological University of Plant Polymers, St. Petersburg, Russia

Received February 14, 2007

Abstract—Transport properties and structural features of a number of already known and new types of polymeric membranes in desalination of aqueous salt solutions by membrane distillation and pervaporation were studied. The possibility of obtaining distilled water in a single stage by pervaporation from dilute or concentrated aqueous salt solutions was examined for the example of membranes fabricated from celluloses of varied origin (wood, cotton, bacterial).

DOI: 10.1134/S1070427207050199

In view of the steadily increasing deficit in fresh water, development of new methods and improvement of the already existing ones for water desalination and treatment to remove other undesirable impurities is a topical scientific and applied task. An important place in solving the problem is occupied by membrane technologies using mostly porous polymeric membranes (of micro-, ultra-, or nanofiltration type, as well as reverse-osmotic and ion-exchange membranes). Depending on the initial salt content and required degree of water treatment, multistage process schemes are commonly used, which include various combinations of the above-mentioned types of membranes and sorptive treatment to remove organic impurities.

Of interest in this context are alternative single-stage methods for deep desalination of water, based on evaporation of polymeric membranes. To these methods belong membrane distillation (water evaporation through porous membranes based on hydrophobic polymers) and pervaporation (evaporation of liquid substances through nonporous membranes of the diffusion type). The membrane distillation has been used for production of distilled water from aqueous salt solutions [2] and concentration of alcohols or organic acids from dilute aqueous solutions [3, 4]. The pervaporation method is more versatile and can be used for separation or concentration of mixtures of aqueous–organic or organic liquids, including those of azeotropic composition [5–7]. At the same time, there is virtually no published information about application of this method to water desalination. Previously, the possibility of application of the membrane technique to production of distilled water from aqueous salt solutions has been demonstrated for the example of a methanol-selective multilayer composite pervaporation membrane [8].

This paper presents a comparative analysis of specific features of the mass-transfer mechanism, structure, and transport characteristics of the already known and new types of membranes in water desalination by pervaporation and membrane distillation. Also, the possibility of pervaporation concentration of aqueous-salt dispersions of proteins in the over-membrane space under mild temperature conditions was examined.

EXPERIMENTAL

We performed the membrane distillation with industrial ultrafiltrates of MFFK brand, based on Ftoroplast-42 (analog of Teflon) manufactured by Vladipor Private Co. (Vladimir), with average pore diameter on the surface equal to 0.05, 0.1, or 0.2 μm.

The pervaporation was done with nonporous films of hydrated cellulose (HC) produced from plant cellulose (wood or cotton) of thickness 30 ± 5 μm and bacterial cellulose (BC) synthesized in surface cultivation of *Acetobacter xylinum* of VKM V-880 strain.

We studied samples of gel films of BC, containing 10% residual water (GFBC-10) or dried to constant weight (BC-D), with thicknesses of 240 and 40 μm, respectively [9]. Also, we used composite membranes produced by forming a thin layer (3–5 μm) of cellulose diacetate (CDA) on the surface of substrates composed of MFFK or UPM-20 (based on aromatic polyamide manufactured by Vladipor Private Co.), with the subsequent saponification of the coating layer in a 1 : 1 NaOH–CH_3COONa buffer solution at 50°C.

The degree of equilibrium swelling (%) of film membranes was found from the difference of masses of swollen and dry membranes, related to the mass of a dry membrane (measurement error ±7%).

An X-ray diffraction analysis of the film membranes was made on a DRON-2 diffractometer (CuK_α radiation).

The membranes were tested in a laboratory cell of the flange type with a useful membrane surface area of 7×10^{-4} m^2.

The permeability was evaluated at 20–40°C after a steady-state mode of mass transfer across the membrane was attained at a pressure below the membrane equal to 0.2 mbar. We used solutions of NaCl or sea salt in distilled water, with an initial salt content of 4–20 wt %, and aqueous-salt protein dispersions with initial concentrations of 10–100 g l^{-1}. All experiments with aqueous-salt solutions or dispersions were performed with their agitation over the membrane in order to minimize the undesirable effect of concentration polarization [5].

The water vapor passed through the membranes was condensed in a vacuum in a glass receiver with liquid nitrogen and weighed, with the flow rate subsequently calculated (kg m^{-2} h^{-1}).

The salt content of the water obtained was evaluated using a refractometer or by electrical resistance.

After each experiment, the absence of a salt in the submembrane space was determined, because the salt that passes across the membrane virtually does not reach the receiver and is accumulated in the bottom part of the cell.

1. MEMBRANE DISTILLATION

As noted above, this method can be implemented using porous membranes based on hydrophobic polymers, such as polypropylene, polytetrafluoroethylene, or polyvinylidene fluoride, with average pore size on the membrane surface of 0.1–0.45 μm [2]. As a result of the poor wetting, water forms menisci on the surface of pores in these membranes. On application of a driving force (temperature or pressure gradient), mass transfer of water occurs via evaporation across the menisci, with its intensity controlled by the equilibrium between the liquid and vapor phases, similarly to the distillation process. There are no published examples of application of MFFK membranes to membrane distillation, and, therefore, the membranes were tested in desalination of water from 4–10 wt % NaCl solutions, with the membranes operating in the pressure-gradient mode. The results obtained are listed in Table 1.

Table 1. Permeability of MFFK membranes in desalination of aqueous NaCl solutions in relation to the average pore size (37°C)

Membrane no.	Average pore diameter, μm	Initial salt concentration, wt %	Flow rate, kg m^{-2} h^{-1}	Salt content, %
1	0.05	4	4.2	100
2	0.1	4	5.6	100
3	0.1	10	5.4	100
4	0.2	4	7.3	Trace amounts*

* Trace amounts of the salt in the bottom part of the cell.

Table 1 shows that the permeability increases with the average pore size of the membranes and somewhat decreases as the salt content of the starting solution is raised to 10 wt %. The latter may be of practical interest for desalination of more concentrated aqueous salt solutions, which cannot be done with reverse-osmosis membranes.

A membrane with an average pore size of 0.1 μm was also tested in concentration of a 10% aqueous solution of ethanol at 20°C. Under these conditions, a stable permeability (3.8 kg m^{-2} h^{-1}) was observed during a 10-day experiment, with the degree of enrichment with ethanol of the flow that passed through the membrane being 39%. This value is somewhat lower that the content of ethanol in the vapor phase (45.1%) in distillation of a mixture of the same initial composition [10].

At the same time, the membrane distillation failed to find wide use in the applications considered above, which is due to the narrow variety of industrial membranes of this type, gross loss of heat in mass transfer, and comparatively high cost of these membranes [2]. In addition, the surface tension forces of water may be insufficient, in the case of a broad pore size distribution, for menisci to be formed in coarser pores. For this reason, the mass transfer in this zone will occur

Table 2. Transport characteristics of film HC membranes in desalination of aqueous salt solutions (40°C)

Membrane no.	Type of cellulose	Pretreatment and experimental conditions	Initial salt concentration, %	Flow rate, kg m^{-2} h^{-1}	Salt retention, %
1	CDA*	Without activation	4	0.91	100
2	WC	Without activation	4	1.7	100
2.1	WC	Without activation	0	1.8	–
3	CC	Without activation	0	1.95**	–
4	CC	Without activation	0	3.7→4.7	–
		Activation with water:			
5	CC	20 min	0	8.2→6.4	–
6	CC	12 h	0	8.7→6.5	–
7	CC	20 min, without agitation	0	5.3	–
8	CC	Without activation	4	4.55	100
9	CC	Without activation	4***	4.5	100
10	CC	Activation with water for 20 min	4	6.7→6.05	100
11	CC	Activation with water	20	3.7	100
12	GFBC-10	Without activation	4	21.9	0
13	BC-D	Without activation	0	2.0	–
14	BC-D	Without activation	4	1.85	100
15	BC-D	Activation with water for 12 h	4	1.9	100

* WC-based CDA.
** At 20°C.
*** Sea salt (salt concentrations, g l^{-1}: NaCl 27.2, MgCl 3.8, $CaSO_4$ 1.3, $MgSO_4$ 1.6, $CaCO_3$ 0.1, $MgBr_2$ 0.1).

by flow through pores. Apparently, such an effect partly takes place in membrane no. 4 (Table 1) and occurs in concentration of an aqueous–alcoholic solution. In operation of these membranes, periodic rupture of the menisci formed can also be favored by the presence of mechanical impurities in the starting solution and by intense turbulization of the solution over the membrane surface. The mass-transfer process can also be complicated by capillary condensation of water vapor in transverse pores in the membranes. This undesirable effect becomes more probable as the temperature gradient increases or the pressure gradient across the opposite sides of a membrane decreases. The transport parameters of the MFFK membranes (Table 1) will be used for comparison with those for the membranes fabricated in this study in pervaporation desalination of water, which was our basic goal.

2. PERVAPORATION

The mechanism of mass transfer of liquids across diffusion-type (nonporous) polymeric membranes is more complex and includes successive stages of sorption of a liquid and its diffusion through the free volume of the polymeric material. In the process, the phase state of the liquid changes to a vapor. This mechanism indicates that the physicochemical properties of membrane-forming polymers and of components of liquid mixtures exert a decisive influence on the selectivity of membranes and intensity of mass transfer. Apparently, a higher water permeability in pervaporation desalination should be observed for membranes based on hydrophilic polymers, to which hydrated cellulose also belongs. The pervaporation of an aqueous salt solution can be regarded as separation of a pseudo-liquid mixture containing free water molecules and bulkier hydrated ions formed in solution upon dissociation of the salt in water. The possibility of selective separation of such a mixture depends on the competitive diffusion of its constituent components through unit elements of the free volume. Apparently, for high-selectivity separation to be possible, the size of these elements should be very small and comparable with the kinetic diameter of water molecules (2.7 Å). For this reason, it is preferable that the membrane-forming polymer should be highly structurally ordered on the supramolecular level. In the case of HC, this is favored by the dense packing of polymer chains, provided by the network of intermolecular hydrogen bonds. It should also be noted that any possibility of transport of bacteria, viruses, and other pathogenic species across diffusion membranes is completely ruled out by the very small size of free-volume elements.

2.1. Transport characteristics of film membranes fabricated from hydrated cellulose. Table 2

lists transport parameters of two HC films based on wood (WC) and cotton (CC) cellulose and films of bacterial cellulose, GFBC-10 and BC-D. We tested membranes fabricated from HC of varied origin for distilled water and aqueous salt solutions under various experimental conditions. Irrespective of their origin, membranes of all the types, except GFBC-10 (Table 2, no. 12), demonstrated 100% salt retention at significant differences in their water permeability. Among the membranes studied, those based on WC and its CDA derivative had lower permeability. A possible reason for the difference in permeability between these membranes (Table 2, nos. 2 and 1) may be the lower hydrophilicity of CDA, compared with WC, evaluated by the equilibrium swelling of the corresponding membranes at 20°C (6.5 and 28 wt %, respectively).

The equilibrium swelling in water of the CC-based membrane is 44 wt %, and, as a result, it has higher water permeability. All other experimental conditions being the same, the permeability of the CC membrane is 2.6 times that of the WC membrane (Table 2, nos. 4 and 2.1). The significant difference between the permeabilities of HC membranes of varied origin may also be due to their structural features on the supramolecular level.

It is known that the permeation of gases or liquids across diffusion-type polymeric membranes increases with temperature. This can also be seen in comparison of the water permeabilities of membrane nos. 3 and 4 (Table 2) at 20 and 40°C. It was found that the permeability of CC-based membranes can be raised to an even greater extent if samples are preliminarily activated in contact in water directly in the cell without applying the driving force of the mass transfer (Table 2, nos. 5 and 6). Under these conditions, the water permeability was as high as 8.2–8.7 kg m^{-2} h^{-1} in the initial stage of the pervaporation experiment and then decreased with time to stabilize at a flow rate of 6.4–6.5 kg m^{-2} h^{-1} in approximately 1.5 h. It can be seen from Table 2 that the stabilized flow rate for membrane nos. 5 and 6 markedly exceeds that for membrane no. 4 (4.7 kg m^{-2} h^{-1}). For membrane no. 4, which operated from the very beginning with a driving force applied, the flow, by contrast, steadily increased with time and stabilized approximately 30 min after the beginning of an experiment, after the steady-state mass-transfer mode was attained.

In all probability, the strong difference in the stabilized flow rates is due to the position of the lower boundary of the concentration gradient of water vapor relative to the cross section of membranes activated and nonactivated with water. The vapor concentration decreases in the direction of mass transfer, and, therefore, the working surface of the membrane is always plasticized with water to a greater extent in the course of pervaporation, compared with its back, "drier" side. This suggests that, under conditions of preliminary activation with water, the lower boundary of the concentration gradient for membrane nos. 5 and 6 lies, after the steady-state mass-transfer mode is attained, closer to their backside, compared with membrane no. 4, which is plasticized to a smaller depth in accordance with the experimental conditions. Thus, preliminary activation of HC membranes with water can be used to intensify the mass transfer. A similar effect can also be obtained by making the membranes thinner, which will be demonstrated below for the example of composite membranes.

It should be noted that the permeability markedly decreased in an experiment without agitation (Table 2, no. 7) because of the well-known effect of temperature-related polarization at the interface between the membrane and water, caused by a decrease in temperature at this interface upon a change in the aggregative state of water to a vapor [5]. For this reason, we carried out the rest of the experiments with vigorous agitation of solutions over the membranes.

Comparison of the permeabilities of CC membrane nos. 4 and 8, and also 5 and 10 (Table 2), confirms that the nature of the process of water mass transfer is the same in pervaporation of distilled water and aqueous salt solutions. It should be noted that, in the latter case, the water permeability of membrane no. 8 (not activated with water) somewhat decreases to 4.55 kg m^{-2} h^{-1}, and that of membrane no. 10 (activated with water), to 6.05 kg m^{-2} h^{-1}, compared with membrane nos. 4 and 5, respectively. The decrease in permeability can be primarily attributed to introduction into the starting mixture of a component (salt) that cannot penetrate across the membrane and to the known effect of concentration-related polarization near the membrane surface. The effect of the concentration- and temperature-related polarizations can be minimized by turbulization of the salt solution over the membrane surface. Apparently, the influence of all the above-mentioned effects is manifested to a greater extent in separation of a more concentrated aqueous salt solution of NaCl (Table 2, no. 11), when the permeability decreases to 3.7 kg m^{-2} h^{-1}. It should also be noted that quantitative desalination of an aqueous solution of sea salt is also possible (Table 2, no. 9). This seems to be reasonable on the background of the positive results obtained in desalination of aqueous solutions of NaCl, because the size of hydrated

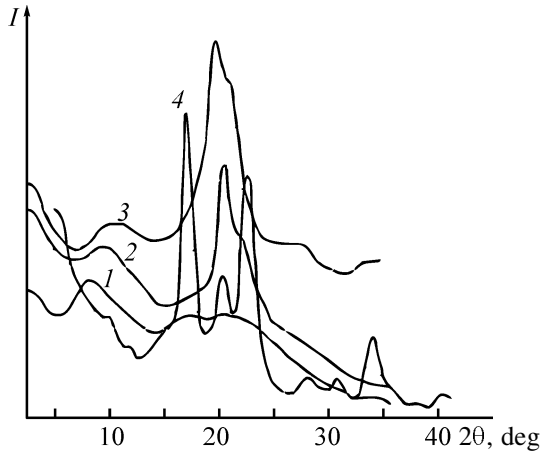

X-ray diffraction patterns of film membranes made of (*1*) WC-based CDA, (*2*) saponified CDA, (*3*) CC, and (*4*) BC. (*I*) Intensity and (2θ) Bragg angle.

Ca^{2+} and Mg^{2+} ions markedly exceeds that of not only water molecules, but also hydrated Na^{+} ions.

The positive, as regards the salt retention, results were obtained for BC membranes only with completely dried samples (Table 2, nos. 13–15). The bacterial cellulose produced in biosynthesis is a bulky gel film containing 99 g of water per gram of the polymer. Most part of water can be removed from the gel film by squeezing under a press. The thus obtained GFBC-10 membrane contains 10% residual water, has a thickness of about 240 μm, and shows a very high water permeability (21.9 kg m^{-2} h^{-1}) at a total absence of salt retention (Table 2, no. 12). Apparently, this is due to its exceedingly loose structure even at so low content of water. At the same time, complete removal of water in further drying of GFBC-10 results in 100% salt retention for BC-D membrane at a comparatively low permeability (Table 2, no. 14) comparable with that of the WC-based membrane. Preliminary activation of the BC-D membrane with water does not lead to any increase in its water permeability (Table 2, no. 15). Apparently, this is due to the fact that, in contrast to WC and CC membranes, it virtually does not sorb water, which is due to the specific supramolecular structural organization of bacterial cellulose, formed in the stage of its synthesis [9], and to compaction of the starting gel film of BC in drying. The latter is confirmed by the significant difference between the thicknesses of the GFBC-10 and BC-D membranes (240 and 40 μm, respectively).

Comparative analysis of the data in Tables 1 and 2 shows that the permeabilities of CC-based membranes and those of the MFFK type are of the same order of magnitude. At the same time, the pervaporation mode of desalination seems to be preferable as regards the stability of the selectivity parameter, because, for porous hydrophobic membranes, several above-mentioned factors (broad pore size distribution, possible partial absence or menisci or their being damaged) may lead to a decrease in, or loss of, selectivity.

2.2. Structural features of hydrated cellulose membranes of varied origin. The figure shows X-ray diffraction patterns of film membranes fabricated from WC-based CDA (curve *1*) and saponified form of CDA (curve *2*) and a WC membrane (curve *3*). On the whole, the structure of WC- and CC-based membranes can be classed on the basis of the diffraction patterns as mesomorphic. A strong difference in the structural organization of cellulose chains on passing from CDA (curve *1*) to its saponified form (curve *2*) is seen when comparing the corresponding diffraction patterns. It is manifested in the appearance of a clearly pronounced reflection peaked at 2θ = 21°20′ in curve *2*. The positions and intensities of the reflections at 2θ = 19°–23° for WC- and CC-based membranes are close (curves *2* and *3*, respectively). At the same time, the decrease in the intensity of the reflection at 2θ = 8°–14°, demonstrated by comparison of curves *1–3*, and the tendency toward its shift to a reflection angle characteristic of the CC membrane can be attributed to transformation of acetate groups into hydroxy groups in the course of CDA saponification. Comparison of the reflection intensities in curves *1–3* in this range of Bragg angles shows that the content of OH groups in the CC-based membrane is higher. This is quantitatively confirmed by the data on the water permeability and equilibrium swelling in water for CC membranes, compared with those for the membranes made of CDA and its saponified form. This comparison is justified because the water affinity of cellulose of varied origin and their derivatives primarily depends on the content of hydroxy groups [11]. At the same time, it is known that the supramolecular structure of CC is close to that of cellulose II characterized by a more disordered 3D structure and the resulting weakened hydrogen bonding. According to IR data, cellulose II has a wide variety of intermolecular hydrogen bonds in which the distances between oxygen atoms in the O–H···O bonds are larger than those in the crystal structure of cellulose I. The positions of OH groups are not strictly fixed and easily change in interaction with water or water vapor, accompanied by partial rupture of hydrogen bonds.

This suggests that the supramolecular organization of HC-based membranes and their transport properties

not only depend on the origin of a cellulose material, but also can change for membranes of the same type in their interaction with water. For the series of the membranes studied, this conclusion is confirmed by the strong difference in their water permeabilities and by the increase in the permeability of the CC membrane after its preliminary activation with water, with this effect not observed for BC-D membranes.

The figure also shows an X-ray diffraction pattern of the BC-D membrane (curve *4*). Comparison of the diffraction patterns in the figure points to a particular supramolecular organization of BC-D. The presence of distinct reflections at $2\theta = 17°$, 21°, 23°, and 35° is an indication of the highly crystalline structure of BC-D, similar to that of cellulose I [9]. According to [9, 11, 12], BC is composed of nanosize crystalline microfibrillar ribbons with an axial-planar texture, with the microfibrils having a 13×7 nm rectangular cross section. The formation of GFBC with very high water content in the stage of BC synthesis is determined by the presence of a large number of primary OH groups on the surface of the ribbons and on their lateral faces. This creates conditions for interaction of the initial crystalline nanofibrillar BC ribbons with water, which can be sorbed by GFBC and be contained in it both in the free and hydrogen-bonded states [13].

Apparently, even upon removal of about 90% of water from the starting gel film of BC by squeezing, the structure of the GFBC-10 film remains rather loose. This is confirmed by the high water permeability of the latter at a totally lacking salt retention (Table 2, no. 12) and by the possibility of introduction into a matrix of this kind of silver or selenium nanoparticles stabilized by polyvinyl pyrrolidone by sorption from aqueous solutions [12]. Because of the crystallinity of the BC microfibrils, their cross section cannot be a zone of mass transfer for water molecules. Probably, the free volume is constituted in BC by voids formed in the textured network of microfibrillar ribbons. Comparison of the salt retention data for the GFBC-10 and BC-C membranes (Table 2) and of their thicknesses suggests that, only for the latter, in which the packing density of microfibrils is considerably higher, the size of free-volume elements is comparable with the kinetic diameter of free water molecules. As a consequence, only the BC-D membrane can provide 100% salt retention.

At the same time, the close flow rates for WC and BC-D membranes indicate that their free volumes in mass transfer are comparable. It should be noted in this context that, for HC membranes of plant origin, the manner in which the free volume varies fundamentally differs from that for BC membranes. In the first case, the free volume of the starting dry samples grows via swelling in preliminary activation of membranes with water or in the initial stage of their operation, before the steady-state mode of mass transfer is attained. In this case, reversible changes of the free volume are possible, after drying of the membranes and a repeated pervaporation experiment. By contrast, in the second case, the free volume irreversibly decreases already in the stage of GFBC-10 drying (in air on the surface of a glass plate) and remains unchanged under the conditions of a pervaporation experiment for the BC-D membrane. It can be assumed that the morphology and free volume of the GFBC-1-membrane can be additionally varied by changing the method of its drying (squeezing, drying in air in the free state or upon successive treatments with organic liquids).

2.3. Composite membranes. Problems of membrane separation are, as a rule, solved using composite membranes (CM) composed of a microporous polymeric or inorganic substrate and thin (0.1–0.5 μm) diffusion cover layers formed by polymers of another chemical nature, which show selectivity for accomplishing a specific separation task. Minimization of the thickness of the selective layer diminishes its resistance to mass transfer, which makes it possible to considerably raise the permeability of membranes. To obtain CM on the above-mentioned two types of substrates, we used as a selective layer WC-based CDA and its saponified form. Table 3 lists transport characteristics of the corresponding CM in pervaporation of distilled water or aqueous salt solutions.

Data for membrane nos. 1 and 2 (Table 3) with selective layers composed of CDA and its saponified form show that the water permeability of CM on an MFFK substrate is low and comparable with that for the corresponding film membranes (Table 2). This indicates that a CDA layer is formed not only on the surface of the MFFK substrate, but also within pores of its cross section. For this reason, the total thickness of the CDA layer in CM approaches the thickness of the films whose properties were considered above (Table 2), which makes higher the overall resistance of CM to mass transfer. In addition, an increase in the resistance to mass transfer can also be favored by the possibly hindered saponification of that part of the CDA layer which lies within the substrate pores. In this case, mass transfer will occur successively via the saponified and nonsaponified forms of CDA, which have different water permeabilities

Table 3. Transport properties of composite membranes at 40°C

Membrane no.	Type of cellulose	Pretreatment and experimental conditions	Initial salt concentration, %	Flow rate, kg m^{-2} h^{-1}	Salt retention, %
1	MFFK* (0.2 μm)	Without saponification of CDA layer and activation	0	1.05	–
2	MFFK	After saponification of CDA layer, without activation	0	2.0	–
3	UPM-20*	Without saponification of CDA layer and activation	0	2.9	–
4	UPM-20	After saponification of CDA layer, without activation	0	6.8	–
5	UPM-20	After saponification of CDA layer, activation with water for 20 min	0	9.7→7.1	–
6	UPM-20	After saponification of CDA layer, without activation	4	5.1	100
7	UPM-20**	Without saponification of CDA layer and activation	0	3.0	–
8	UPM-20	After saponification of CDA layer, without activation	0	4.9	–
9	UPM-20	After saponification of CDA layer, without activation	4	4.1	100
10	UPM-20	After saponification of CDA layer, activation with water or 4% aqueous solution of NaCl for 20 min	4	5.1	Trace amount of the salt in the bottom part of the cell

* Formation of a cover layer from a 6% solution of CDA.
** Formation of a cover layer from a 4% solution of CDA.

(Table 2). The results obtained with a CM based on an MFFK substrate are also markedly inferior to those of MFFK membranes in membrane distillation (Table 1). The best results were obtained for CM on UPM-20 substrates. The smaller average size of pores on the surface of these substrates makes it possible, all other conditions of cover layer formation (concentration of the CDA solution) being the same, to produce a thinner selective layer because of its formation mostly on the substrate surface. This leads to a considerable increase in the permeability of CM with cover layers composed of both CDA and its saponified form (Table 3; nos. 3 and 4, respectively). Preliminary activation of the selective cover layer of CM leads, as in the case of film membranes, to a sharp increase in the water permeability in the initial stage of a pervaporation experiment, with its subsequent decrease (Table 3, no. 5). However, the stabilized flow rate is close in this case to that for membrane not activated with water (Table 3, no. 4). It should also be noted that the CM nonactivated with water provides a 100% salt retention at a permeability of 5.1 kg m^{-2} h^{-1} (Table 3, no. 6) This value is three times that for the film WC membrane (Table 2, no. 2) and is comparable with the flow rate across the film version of the CC membrane (Table 2, no. 8). A decrease in the CDA concentration in formation of a cover layer on the UPM-20 substrate does not lead to any increase in the permeability of CM. It is apparent that an undesirable effect of filling of substrate pores by the cover polymer, also observed in the case of the MFFK substrate, but to a greater extent, is manifested in this case, accompanied by hindrance to saponification of the polymer. This is confirmed by comparison of the permeabilities of membrane nos. 4 and 8 (Table 3). It should be noted separately that the small thickness of the selective layer in CM (3–5 μm) gives no way of achieving 100% salt retention under the conditions of a preliminary activation of their selective layer with water or a NaCl solution (Table 3, no. 10). In so thin films, activation can lead to a nearly equilibrium swelling across the entire thickness of the selective layer, with partial transport of the salt across the activated membrane probably occurring only in the initial stage of the pervaporation experiment (before the steady-state mode of mass transfer is reached), when the flow rate across the CM is at a maximum.

2.4. Concentration of aqueous-salt protein dis-

Table 4. Transport properties of a film CC membrane in concentration of aqueous–salt protein dispersions

Initial concentration, g l^{-1}	T, °C	Experiment duration, min	Flow rate, kg m^{-2} h^{-1}		Final concentration, g l^{-1}
			beginning of experiment	end of experiment	
0	40	120	6.4	6.4	0
10	20	310	2.14	1.52	21.2
10	40	160	5.26	4.28	24.1
50	40	210	4.42	3.24	121.3
100	40	330	2.35	1.63	194.5

persions. The sufficiently high water permeability of the membranes studied in desalting of aqueous salt solutions justified a test of the pervaporation method for concentration of aqueous-salt (NaCl) protein dispersions in the over-membrane space. Commonly, solutions or dispersions of various substances, including proteins, are concentrated with microporous membranes. However, this method is unacceptable, similarly to the evaporation technique, for achieving a sufficiently high degree of concentration because of the rapid decrease in the permeability of membranes, caused by blocking of pores or by thermal degradation of proteins. The undesirable effect of pore blocking is totally ruled out for diffusion-type membranes because of the absence of physical pores in the selective layer of such membranes. An example is known of use of a polysulfone pervaporation membrane fabricated for concentration of a liquid radioactive waste [14].

As shown above, CC-based membranes exhibit a fairly high water permeability under mild conditions. The properties of a film version of such a membrane in concentration of aqueous-salt protein dispersions with various total initial concentrations of dry substance are listed in Table 4. The results obtained confirm the possibility of achieving high degrees of concentration (up to 194 g l^{-1}). In this case, the permeability decreases both in the course of time and on raising the initial concentration of the dispersion. This occurs because of an increase of the fraction of the component that cannot penetrate across the membrane in the starting mixture and as a result of concentration- and temperature-related polarization effects. The concentrates can be brought to the dry-residue state in a shorter time with a rotary evaporator. It should be noted that, in all the experiments on dispersion concentration, the permeate was composed of distilled water. In addition, the adsorption of proteins on the membrane surface was insignificant, as indicated by visual inspection.

The study we performed demonstrated the possibility of using the pervaporation method for deep single-stage desalination of dilute or concentrated aqueous salt solutions to give distilled water. Owing to their high hydrophilicity, HC-based membranes have a throughput that is sufficiently high for the pervaporation method (up to 6–7 kg m^{-2} h^{-1} at 40°C). This value substantially exceeds that of the known analog for the same purpose [15], for which the throughput in pervaporation treatment of water from underground sources to remove dissolved salts is 2.35 kg m^{-2} h^{-1} at 82°C. At the same time, it should be noted that all the desalination experiments were carried out under model conditions with salt solutions in distilled water. Under real conditions, water can contain, in addition to salts, impurities of organic substances and various pathogenic species. Permeation of these latter via diffusion through nanosize free-volume elements of pervaporation membranes is totally ruled out. A qualitative prognosis can be made regarding noxious impurities of organic liquids. The most probable is mass transfer of molecules, close in polarity and size to water, of organic substances, such as aliphatic alcohols (methanol), aldehydes (acetaldehyde), acetonitrile, and some others. At the same time, joint mass transfer with water of weakly polar or high-boiling substances, or those having bulky molecules, such as phenol, chlorophenol, chloroform, and aromatic and aliphatic hydrocarbons, is hardly possible. Additional studies in this area require high-sensitivity methods for analysis of permeates.

CONCLUSIONS

(1) A comparative study was carried out of desalination of aqueous salt solutions with microporous hydrophobic fluoroplastic membranes in membrane distillation and with film or composite membranes fabricated from celluloses of varied origin in pervaporation processes.

(2) High efficiency of both the methods as regards the quality (distilled water) and throughput of desali-

nation (up to 6–7 kg m^{-2} h^{-1} at 40°C) was demonstrated.

(3) The possibility of controlling the throughput by varying the structural organization of cellulose, type of membranes, and experimental conditions, including preliminary activation of the membranes with water, was demonstrated for the example of film and composite membrane based on celluloses of varied origin.

(4) The possibility of pervaporation concentration of aqueous-salt protein dispersions in the over-membrane space to high concentrations under mild temperature conditions was shown.

ACKNOWLEDGMENTS

The study was financially supported by the Russian Foundation for Basic Research (project no. 06-03-32493).

The authors are grateful to P.A. Vdovin for provision of microporous fluoroplastic membranes.

REFERENCES

1. Pervov, A.G., Khakhanov, S.A., and Dudkin, E.V., *Kritich. Tekhnol., Membr.*, 2001, no. 11, pp. 3–11.
2. Schneider, K., Holz, W., and Wollbeck, R., *J. Membr. Sci.*, 1988, vol. 39, no. 1, pp. 25–42.
3. Kimura, S., Nakao, S.-I., and Shimatani, S.-I., *J. Membr. Sci*. 1987, vol. 33, no. 3, pp. 285–288.
4. Kokugan, T., Wakatsuki, M., Shimizu, M., and Kikukawa, H., *J. Chem. Eng. Jpn.*, 1996, vol. 29, no. 4, pp. 717–720.
5. Mulder M., *Basic Principles of Membrane Technology*, Dordrecht: Kluwer, 1991.
6. Kuznetsov, Yu.P., Kononova, S.V., Kruchinina, E.V., et al., *Zh. Prikl. Khim.*, 2001, vol. 74, no. 8, pp. 1302–1307.
7. Staudt-Bickel, C. and Lichtenthaler, R.N., *Vysokomol. Soedin.*, 1994, vol. 36, no. 11, pp. 1924–1945.
8. Kononova, S.V., Kuznetsov, Yu.P., Romashkova, K.A., et al., *Zh. Prikl. Khim.*, 1995, vol. 68, no. 8, pp. 1361–1368.
9. Baklagina, Yu.G., Khripunov, A.K., Tkachenko, A.A., et al., *Zh. Prikl. Khim.*, 2003, vol. 76, no. 6, pp. 1017–1024.
10. Kogan, V.B., Fridman, V.M., and Kafarov, V.V., *Ravnovesie mezhdu zhidkost'yu i parom* (Liquid–Vapor Equilibrium), Moscow: Nauka, 1966, p. 50.
11. Klenkova, N.I., *Struktura i reaktsionnaya sposobnost' tsellyulozy* (Structure and Reactivity of Cellulose), Leningrad: Nauka, 1976.
12. Baklagina, Yu.G., Khripunov, A.K., et al., *Kristallografiya*, 2006, vol. 51, no. 4, pp. 659–666.
13. Hatakeyma, H., Hatakeyma, T., and Nakamura, K., *J. Appl. Polym. Sci., Appl. Polym. Symp.*, 1983, vol. 37, pp. 979–991.
14. Krysinskaya, N.V. and Varezhkin, A.V., *Kritich. Tekhnol., Membr.*, 2005, no. 4, pp. 16–20.
15. FRG Patent Appl. 19910549.

ISSN 1070-4272, Russian Journal of Applied Chemistry, 2007, Vol. 80, No. 5, pp. 799–804. © Pleiades Publishing, Ltd., 2007.
Original Russian Text © D.O. Kirsanov, A.V. Legin, A.P. Kulikova, E.N. Pol'shin, Yu.G. Vlasov, 2007, published in Zhurnal Prikladnoi Khimii, 2007, Vol. 80, No. 5, pp. 821–826.

MACROMOLECULAR CHEMISTRY AND POLYMERIC MATERIALS

Polymeric Sensors for Determination of Anions of Organic Acids

D. O. Kirsanov, A. V. Legin, A. P. Kulikova, E. N. Pol'shin, and Yu. G. Vlasov

St. Petersburg State University, St. Petersburg, Russia

Received March 13, 2007

Abstract—New polymeric electrochemical sensors based on various neutral and charged organic ionophores were suggested. The new sensors have a high sensitivity to anions of various organic acids (acetic, oxalic, lactic, malic, succinic, tartaric, and citric) in a wide concentration range. The selectivity and the detection limit of the developed sensors with respect to anions of the acids were studied.

DOI: 10.1134/S1070427207050205

Rapid development of such branches as pharmaceutics, food-processing industry, and various biotechnological productions both in Russia and abroad pose a number of new problems in the fields of industrial and environmental analytical chemistry. One of the most important tasks is the development of fast, convenient, and reliable methods of monitoring industrial processes on-line and of monitoring various industrial emissions. The problem of the determination of organic components of various solutions and mixtures, in particular, organic acids is of prime importance. Available methods of the determination of these organic compounds, such as high-performance liquid chromatography, some kinds of ionic chromatography, etc., are characterized by high prices of equipment, complexity of the analyses, and are insufficiently quick. An attractive solution of the problem is the use of chemical sensors, for example, ion-selective electrodes and(or) arrays of selective and nonselective chemical sensors ("electronic tongue"), measurements with which are simple and fast, do not require complicated equipment and highly skilled staff, and can be readily automated. This brings up a problem of searching for new active components of sensory membranes which would ensure a high reproducible sensitivity to various organic acids and selectivity in the presence of inorganic and organic anions.

Published compositions of polymeric sensory membranes for the determination of anions of organic acids are limited in number. The majority of the studies are devoted to the determination of salicylate, benzoate, and citrate anions. Metal porphyrins with various central atoms were used as membrane-active compounds in sensors for salicylate ions [1, 2]. To determine benzoate ions, sensors based on derivatives of trifluoroacetylbenzoic acid were applied [3]. Citrate ions in aqueous solutions were determined using sensors with membranes containing various dibenzyltin derivatives [4]. Sensors with membranes containing phenylporphyrins and uranyl salophen complexes were used as acetate-sensitive electrodes [5, 6]. It should be noted that the determination of salicylate, for example, is of a low practical value, and more often it is used as an illustration of sensitivity and selectivity of sensors to this ion. At the same time, in real media organic acids, as a rule, are present in complicated mixtures both with each other and with inorganic ions.

The aim of this study was to develop compositions and to study properties, in particular, sensitivity and selectivity, of a wide set of solid-contact potentiometric polymeric anion sensors based on various metal porphyrins, quarternary ammonium bases, and derivatives of trifluoroacetylbenzoic acid for the determination of several practically most important organic acids, namely, acetic, citric, oxalic, lactic, malic, succinic, and tartaric, which in various combinations and proportions are contained in the overwhelming majority of drinks, foodstuffs, process liquids of food and pharmaceutical productions, and other important real objects. As the organic acids under study dissociate in aqueous solutions, at least partially, for the determination of organic residues of these acids in liquids it is appropriate to develop and study potentiometric chemical sensors sensitive to anions.

The final aim of such studies is the development of not one, but a number of chemical sensors with reproducible sensitivity to several organic acids (cross sensitivity), and also with various selectivity toward anions of organic acids and widespread inorganic anions, such as, e.g., chloride, bromide, and nitrate. Combination and use of such sensors in multisensory systems like "electronic tongue" will make it possible to solve the problem of simultaneous quantitative determination of several organic acids in mixtures and in a number of real media.

EXPERIMENTAL

All the components for making sensory membranes were purchased from Fluka (Switzerland). We also used Merck (Germany) analytical grade organic acids, chemically pure grade inorganic salts and organic solvents from Reaktiv (St. Petersburg), and double-distilled water.

The polymeric sensory membranes studied (a total of more than 15 different compositions) contained various membrane-active components: metal porphyrins differing in the nature of the central metal atom, quarternary ammonium bases with various length of alkyl radicals, and derivatives of trifluoroacetylbenzoic acid. Seven of them are the most promising for the analysis of anions of organic acids, namely: types 1–3 based on metal porphyrins with manganese and rhodium central atoms and substituents in the porphyrin ring; types 4 and 5 based on quarternary ammonium salts; types 6 and 7 based on neutral organic complexing agents, structural analogs of trifluoroacetylbenzoic acid.

Sensory membranes were prepared by a standard technique. Weighed samples of membrane components were poured over with tetrahydrofuran (THF) and mixed using a magnetic stirrer until the dissolution was complete. The resulting cocktail was poured in a Teflon weighing bottle with a flat bottom and allows to stand until THF evaporated completely (~48 h). Disks 7 mm in diameter were cut out from the resulting membrane, and a solid contact (a composite conducting material) was deposited onto one of disk sides. Depositing the composite material results in the formation on the membrane surface of a layer with a mixed conductivity: ionic due to the membrane composition and electronic due to the composite. A current lead (a copper wire) was immersed into the deposited composition. The structure was allowed to stand until the composite conducting material dried completely; then the membrane was pasted in a plastic electrode case. We have made at least three sensors with membranes of each type. The numerical characteristics of electrodes given below are averaged values for sensors of the same type.

Potentiometric measurements were carried out in the voltaic cell

Cu	Ag	AgCl, KCl_{sat}	Test solution	Membrane	Solid contact	Cu.

Readings were taken using a multichannel electronic digital voltmeter with a high input resistance connected to a personal computer for data collection and processing. An EVL 1M 3.1 silver chloride reference electrode was used.

The sensitivity of sensors was studied by the method of calibration measurements in the range of concentrations of organic acids 10^{-6}–10^{-2} M. The slopes of the linear portions of the electrode functions were calculated for the concentration range 10^{-5}–10^{-2} M.

The pH values of all the calibrating solutions for all the organic acids were fixed by adding sodium hydroxide to pH 6 to eliminate the effect of acidity variation on the electrode functions. The selectivity coefficients were determined by the method of mixed solutions (MMS). The pH values of solutions were monitored with a standard ESL 43-07 pH glass electrode.

To check whether the sensors under study are sensitive to anions of organic acids, we made a series of calibrations with respect to solutions of the following acids: oxalic, acetic, citric, lactic, malic, succinic, and tartaric. The calibrations were carried out over the range of organic acid concentrations 10^{-6}–10^{-2} M at a constant pH 6 in all solutions, which was adjusted with sodium hydroxide solution.

A typical shape of calibrating plots for various sensors in tartaric acid solutions is shown in Fig. 1.

Experimental data on the slopes of the linear portions of the electrode functions of sensors in solutions of organic acids are given in the table.

The above data show that the majority of sensors under study have a high sensitivity to anions of organic acids. The slopes of the electrode functions of the majority of the sensors towards anions of oxalic, succinic, malic, and tartaric acids are in the range 24 ± 3 mV decade^{-1}, which agrees well with the theoretical value for double-charged anions. The sensitivity of sensors of types 1 and 2 in solutions of acetic acid also approaches the theoretical value of

Slopes of the electrode functions of sensors in solutions of organic acids. Average error of the determination of the electrode function slope ±2 mV

Sensor type	Slope of electrode function for indicated acid						
	acetic	citric	lactic	malic	oxalic	succinic	tartaric
1	–53	–38	–33	–26	–23	–26	–27
2	–53	–40	–34	–28	–24	–27	–28
3	–50	–39	–33	–28	–24	–27	–28
4	–31	–24	–23	–20	–18	–20	–20
5	–32	–20	–23	–20	–20	–20	–21
6	–43	–25	–27	–22	–21	–22	–23
7	–35	–22	–25	–22	–21	–22	–22

59 mV decade^{-1} for single-charged anions. As a whole, the sensitivity of the sensors based on metal porphyrins to anions of organic acids is slightly higher as compared to other types of sensors. All the types of sensors under consideration are the least sensitive to oxalic acid anions, which is apparently due to high hydrophilicity of oxalate anions ($\log K_{o/w} = -0.7$). On the whole, sensors of types 4 and 5 based on quarternary ammonium salts of various structures show the lowest electrode sensitivity, as their response is of the ion-exchange nature and is not connected with specific complex formation.

The selectivity of sensors was determined by the method of mixed solutions. The results obtained are presented in Fig. 2.

The sensors studied show the highest selectivity toward citric acid anions. For all the types of sensors, the values of $\log K_{sel}$(Acetate/Citrate) are less than –1.0, and in case of sensors of type 6, $\log K_{sel}$(Acetate/Citrate) = -4.3 ± 0.1, i.e., sensors of type 6 are capable of determining citrate in the presence of 10000-fold excess of acetate anions.

The selectivity to anions of tartaric and succinic acids in the presence of acetate is also fairly high, and the corresponding values of $\log K_{sel}$(Acetate/X) lie in the range 0.5–1.

The selectivity of sensors with respect to lactate and oxalate in the presence of acetate is low, and the logarithms of the corresponding selectivity coefficients of the majority of sensors are close to zero.

For several structurally related acids, succinic, malic, and tartaric, differing only in the number of hydroxy groups at atoms in the carbon skeleton, we have carried out a special experiment on studying their selectivity. The selectivity coefficients were determined by the MMS method at a fixed tartaric acid concentration. The experimental data are given in Fig. 2b.

Sensors of types 4 and 5 based on quarternary ammonium bases do not exhibit significant selectivity to any of the three acids. A similar pattern takes place for sensors of type 7 based on a neutral transporting agent.

The selectivity of the sensors based on metal porphyrins (types 1–3) clearly increases as the number of hydroxy groups in the carbon skeleton of an acid molecule decreases. These sensors exhibit the highest selectivity to succinic acid anions, which have no hydroxy groups in the carbon chain; then the selectivity decreases to malate (one hydroxy group in the carbon skeleton) and then to tartaric acid anions (two hydroxy

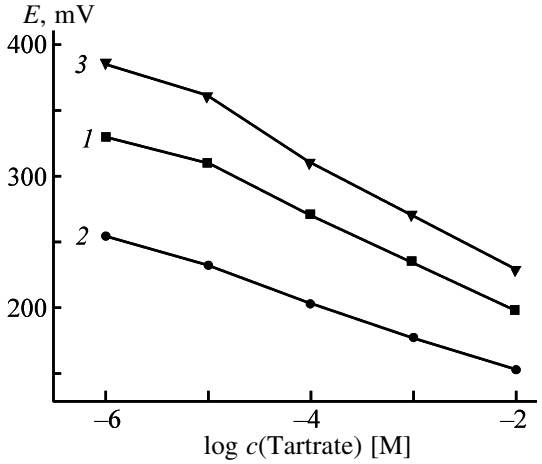

Fig. 1. Typical shape of calibrating plots for various sensors in tartaric acid solutions (constant pH 6). (*E*) Potential and (*c*) concentration. Sensor type: (*1*) 1, (*2*) 3, and (*3*) 7.

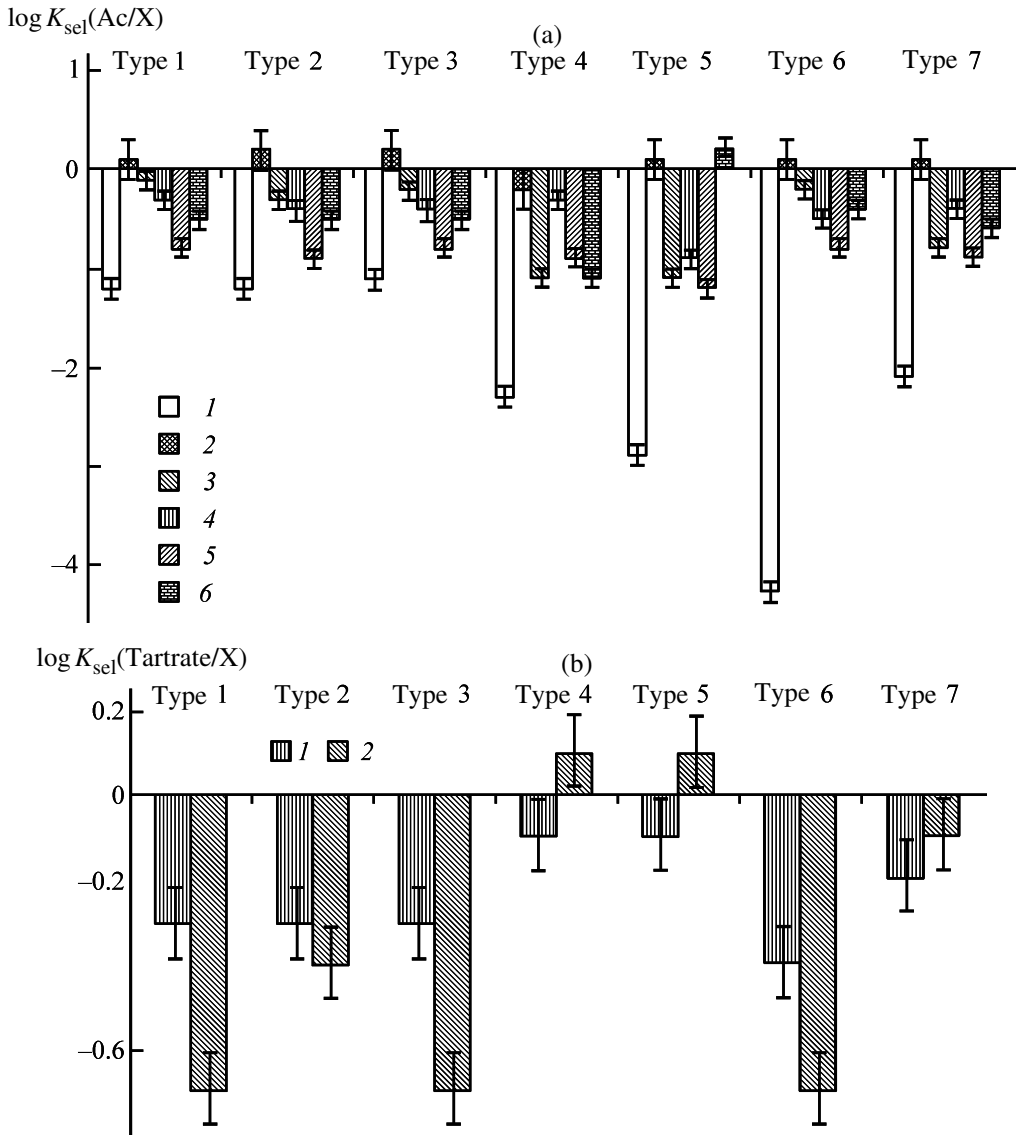

Fig. 2. Logarithms of selectivity coefficients K_{sel} of sensors (MMS, constant pH 6). Fixed concentration of (a) acetate, (b) tartrate, (c) chloride, and (d) nitrate. (a) (*1*) citrate, (*2*) lactate, (*3*) oxalate, (*4*) malate, (*5*) succinate, and (*6*) tartrate; (b) (*1*) malate and (*2*) succinate; (c, d) (*1*) acetate, (*2*) citrate, and (*3*) oxalate.

groups). Sensors of type 6 based on a neutral complexing agent behave similarly. The membranes containing quarternary ammonium salts show no selectivity to any of structurally related acids.

It is known that inorganic anions, in particular, chloride and nitrate, can be present in many real analytical objects in noticeable concentrations along with anions of organic acids. Their influence on the electrode function can hinder the determination of organic acids in real solutions. To estimate this influence, we have carried out a series of experiments on studying the selectivity toward the most wide-spread organic acids (acetic, citric, oxalic) in the presence of inorganic anions. The data obtained are shown in Figs. 2c and 2d.

Sensors based on quarternary ammonium bases and neutral transporting agents (types 4–7) allow citrate ions to be determined in the presence of a tenfold excess of chloride [$\log K_{sel}(Cl^- : \text{citrate}) \approx -1$]. In the case of sensors based on metal porphyrins (types 1–3), chloride ions exert a very strong interfering effect on the determination of organic acids, and the logarithms of the corresponding selectivity coefficients are either positive or close to zero (sensors of types 2 and 3, in a citrate–chloride pair).

The interfering effect of nitrate ions (Fig. 2e) is

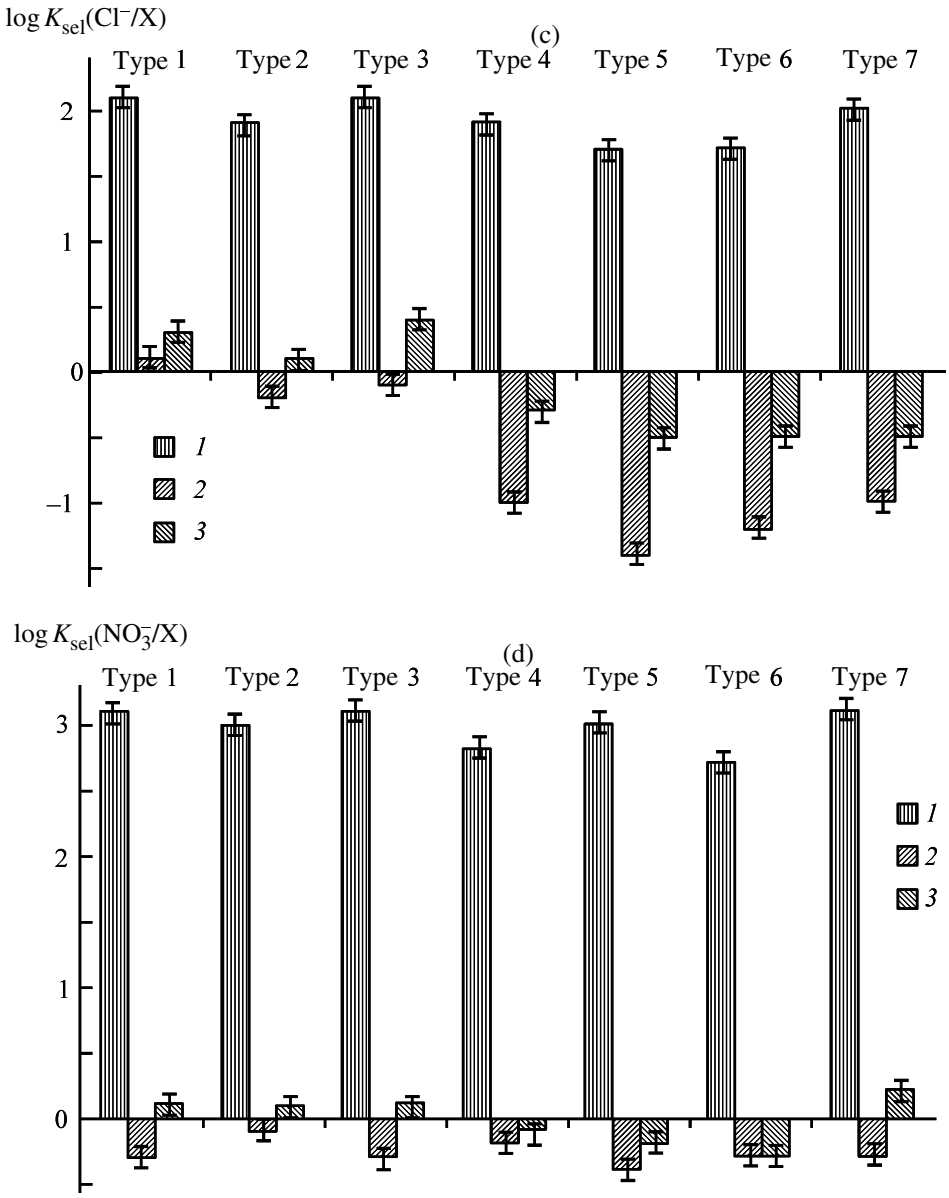

Fig. 2. (Contd.)

stronger than that of chloride ions, which is evidently due to the higher lipophilicity of nitrate. However, the determination of citrate (sensors of types 1, 3–7) and oxalate (type 6) in the presence of a small (2–3-fold) excess of nitrate ions is possible.

It should be particularly noted that essentially different selectivities of sensors with different compositions open prospects for their successful and differentiated analytical applications, and also for effective use of a set of such sensors with different sensitivities and selectivities (cross sensitivity) in the composition of multisensor systems like "electronic tongue."

CONCLUSIONS

(1) New polymeric sensors based on membrane-active components of various nature have been developed.

(2) The new sensors have a high sensitivity to anions of widespread organic acids (acetic, citric, oxalic, lactic, malic, succinic, and tartaric) over a wide concentration range at pH 6.

(3) The slope of the linear portion of the electrode function of the sensors, e.g., those based on metal porphyrins, in solutions of singly charged anions, in particular acetate, is 53–54 mV decade^{-1}, and for

anions of dibasic acids it is 24 ± 3 mV decade^{-1} for the majority of sensors.

(4) The selectivity of sensors both in solutions of organic acids and in solutions containing inorganic anions (chloride and nitrate) has been studied. The selectivities of sensors of various composition toward the same ion differ essentially (by a factor of more than 100), which opens prospects for their successful analytical application in various conditions, and also for the use of a set of such sensors in the composition of multisensor systems.

ACKNOWLEDGMENTS

This study was financially supported in part by the Russian Foundation for Basic Research (project no. 05-03-34824).

REFERENCES

1. Chaniotakis, N.A., Park, S.B., and Meyerhoff, M.E., *Anal. Chem.*, 1989, vol. 61, pp. 556–570.
2. Li, J.Z., Pang, X.Y., Gao, D., and Yu, R.Q., *Talanta*, 1994, vol. 41, pp. 881–890.
3. Katsu, T. and Hanada, N., *Anal. Chim. Acta*, 1996, vol. 321, pp. 21–25.
4. DeMuelenaere, R.L., Onsrud, P., and Arnold, M.A., *Electroanalysis*, 1993, vol. 5, pp. 833–838.
5. Amemiya, S., Buhlmann, P., and Umezawa, Y., *Anal. Chem.*, 1999, vol. 71, pp. 1049–1054.
6. Antonisse, M.M.G., Snellink-Ruel, B.H.M., Ion, A.C., et al., *J. Chem. Soc., Perkin Trans. 2*, 1999, pp. 1211–1218.

ISSN 1070-4272, Russian Journal of Applied Chemistry, 2007, Vol. 80, No. 5, pp. 805–809. © Pleiades Publishing, Ltd., 2007.
Original Russian Text © V.F. Kurenkov, I.N. Nadezhdin, A.V. Kurenkov, H.-G. Hartan, F.I. Lobanov, 2007, published in Zhurnal Prikladnoi Khimii, 2007, Vol. 80, No. 5, pp. 827–831.

MACROMOLECULAR CHEMISTRY AND POLYMERIC MATERIALS

Effect of Cationic Praestols on Sedimentation of Concentrated Suspensions of Calcium Carbonate

V. F. Kurenkov, I. N. Nadezhdin, A. V. Kurenkov, H.-G. Hartan, and F. I. Lobanov

Kazan State Technological University, Kazan, Tatarstan, Russia
Ashland Eurasia Limited Liability Company, Moscow, Russia

Received October 30, 2006

Abstract—Using photosedimentation procedure, the sedimentation stability of 60% suspension of calcium carbonate was studied in relation to the concentration, molecular weight, chemical composition, and conformation of macromolecules of cationic Praestol and to the concentration and nature of mineral coagulants (NaCl and $CaCl_2$).

DOI: 10.1134/S1070427207050217

Suspensions of calcium carbonate are used in production of paper, ceramics, soda, and sugar. The stability of suspensions can be controlled by water-soluble polymers, whose performance is determined by molecular and adsorption characteristics of polymers and by the nature of the disperse phase particles and solvent [1–3]. The data on the behavior of $CaCO_3$ suspensions, presented in reviews [4–6], are ambiguous. The effect of cationic Praestols on sedimentation stability of dilute suspensions of sodium carbonate was studied previously in [7].

Here we report on the sedimentation stability of 60% $CaCO_3$ suspension as influenced by the concentration, molecular weight, chemical composition, and conformation of macromolecules of cationic Praestol and by mineral coagulants (NaCl and $CaCl_2$).

EXPERIMENTAL

We used cationic Praestols [copolymer of acrylamide (AA) with *N*-acrylamidopropyl-*N,N,N*-trimethylammonium chloride (AAPTMAC)] purchased from Moscow–Stockhausen–Perm Private Company (Perm, Russia). The properties of Praestols studied are listed in the table. In the experiments we also used pure grade $CaCO_3$, chemically pure grade NaCl and $K_2S_2O_8$, and distilled water.

The samples of cationic Praestol with intrinsic viscosities [η] of 100, 68, 57, 46, and 25 $cm^3\ g^{-1}$ and constant chemical composition were prepared according to [8] by radical degradation of Praestol 655 in 0.1% aqueous solutions at 50°C in the presence of potassium persulfate (PP) radical degradation agent ([PP]/[polymer] = 0.6). The content of ionic units in cationic Praestol macromolecule was evaluated from the content of chloride ions, determined by mercurimetric titration [9].

The molecular weight *M* of cationic Praestols was calculated from the intrinsic viscosities using the Mark–Houwink equation. The intrinsic viscosity [η]

Properties of cationic Praestols*

Brand	[η], $cm^3\ g^{-1}$	Content of ionic units, mol %	
		AA	AAPTMAC (β)
611	920	91	9
650	690	80	20
644	620	73	27
655	555	67	33
	100	67	33
	68	67	33
	57	67	33
	46	67	33
	25	67	33

* Structure of the macromolecule unit:

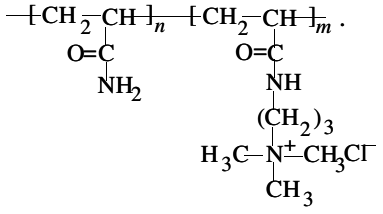

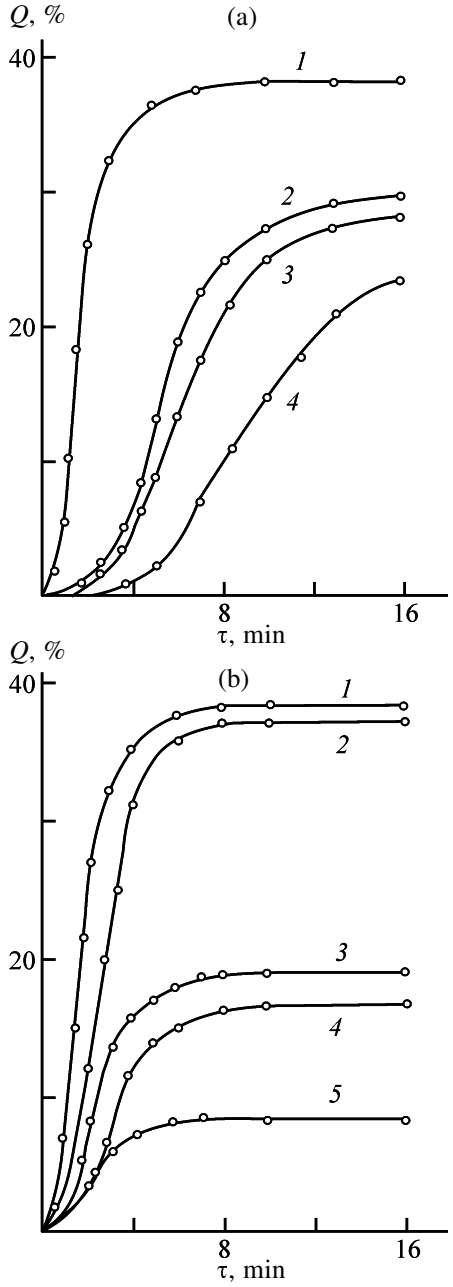

Fig. 1. Degree of clarification of calcium carbonate suspension Q at various concentrations of (a) dispersed phase c_d and (b) cationic Praestol 650, as a function of time τ. (a) c_d, %: (*1*) 40, (*2*) 50, (*3*) 55, and (*4*) 60. (b) c_d = 60%; $c_p \times 10^3$, %: (*1*) 0, (*2*) 1, (*3*) 2, (*4*) 3, and (*5*) 5.

of copolymer solutions was measured in a 0.5 M NaCl solution at 30°C on a VPZh-3 viscometer (d_c = 0.56 mm). The [η] values were determined from the experimental linear dependence of the reduced viscosity $\eta_{sp}/c_p = f(c_p)$, where c_p is the copolymer concentration:

$$[\eta] = \lim(\eta_{sp}/c_p) \text{ at } c_p \to 0.$$

The effective size of the macromolecule globules $(\bar{r}^2)^{1/2}$ of cationic Praestol in aqueous solutions was evaluated from the reduced viscosity η_{sp}/c_p, because at small c_p $(\bar{r}^2)^{3/2} \sim \eta_{sp}/c_p$ in accordance with the Flory–Fox equation.

The sedimentation tests were out carried using 60% $CaCO_3$ suspensions at 20°C in a 150 cm^3 cylinder. After addition of all the reagents, the system was mixed for 1 min with a perforated stirrer (ten back-and forth movements), and variation in the optical density of the resulting suspension with time was recorded. The measurements were carried out in the upper section of the cylinder at a depth of 60 mm from the surface and thickness of the absorption layer of 40 mm using an FS-1 photosedimentometer.

The ζ potential of the $CaCO_3$ particles was determined by electrophoretic procedure and calculated from the Smoluchowski equation.

First we determined the stability of the $CaCO_3$ suspension as influenced by the concentration of the dispersed phase c_d. The tests were performed in the c_d range from 40 to 60% in the absence of polymer additives (Fig. 1a). As seen, in the entire concentration range studied the degree of clarification Q increases with time, which suggests that the concentrated suspensions are unstable and the sedimentation rate v_0, which was determined from the curve slopes, decreases with increasing c_d. This is obviously due to the enhancement of sedimentation hindrance with increasing c_d. All the further tests were performed at c_d = 60%.

To evaluate the effect of the cationic Praestol concentration c_p on the $CaCO_3$ suspension stability, the sedimentation tests were performed at c_p $(1–5) \times 10^{-3}$. Several kinetic curves of $CaCO_3$ suspension clarification are shown in Fig. 1b. Using these data, we calculated the rates of sedimentation in the presence of polymer and the flocculation activity of cationic Praestols D:

$$D = (v - v_0)/v_0,$$

where v and v_0 are the sedimentation rates of the $CaCO_3$ suspension in the presence of the polymer and without it.

The increase in D values indicates an increase in the flocculation activity of the polymer, whereas their decrease suggests enhancement of the stabilizing effect on the suspension sedimentation stability.

The dependence of the flocculation effect D of cationic Praestol 655 on the polymer concentration c_p

is shown in Fig. 2 (curve *2*). As seen, this dependence passes through a maximum. First, with increasing c_p the flocculation effect increases (ascending branch), which is due to the enhanced adsorption of the polymer on $CaCO_3$ particles owing to charge neutralization. With addition of positively charged polymer to negatively charged $CaCO_3$ particles, the overall particle charge decreases and their recharging is observed. This is confirmed by the data on changes in ζ potential of the particles (Fig. 3). As a result, the electrostatic repulsion between the $CaCO_3$ particles decreases, which improves binding between the particles. Increase in the polymer adsorption on the $CaCO_3$ particles with increasing c_p makes higher the concentration of macromolecular bridges between the $CaCO_3$ particles, providing formation of coarse floccules and thus accelerating their sedimentation. Further increase in c_p (after passing a maximum) causes saturation of the particle surface with the polymer, hinders mobility of the dispersed particles and, thus, stabilizes $CaCO_3$ suspension (descending branch, Fig. 2). As seen from Fig. 2, at $c_p > 1 \times 10^{-3}$% D decreases for both Praestol 644 (curve *1*) and Praestol 611 (curve *3*).

The dependence of the flocculation parameter D on the chemical composition of cationic Praestol macromolecules is also illustrated in Fig. 2. Comparison of experimental data at c_p = const shows nonmonotonic variation of D: Praestol 655 < Praestol 644 > Praestol 611. Our experimental results are probably due to the fact that $(\bar{r}^2)^{1/2}$ varies in the same direction as β (content of the ionic units in cationic Praestols). This fact is indirectly confirmed by the dependence $\eta_{sp}/c_p = f(\beta)$ at c_p = const. (Fig. 4). The viscosity data obtained at various c_p well agree with each other (Fig. 4, curves *1* and *2*). The maximal flocculation effect D is observed at β 27 mol% (Fig. 2, curves *1* in comparison with curves *2, 3*). We assumed that in this case the macromolecules are characterized by the optimal ratio of the charge density and chain flexibility, providing the highest $(\bar{r}^2)^{1/2}$ values. As a result, binding of two and more $CaCO_3$ particles with macromolecular bridges makes the globules coarser and accelerates their sedimentation.

The effect of the molecular weight M of polymers on the flocculation effect D was evaluated using the samples (see table) with [η] changing in the 25–555 $cm^3\ g^{-1}$ range and constant chemical composition of macromolecules prepared by radical degradation of Praestol 655. The results of these experiments are shown in Fig. 5. As seen, all the dependences $D = f([\eta])$ determined at various c_p pass through a mini-

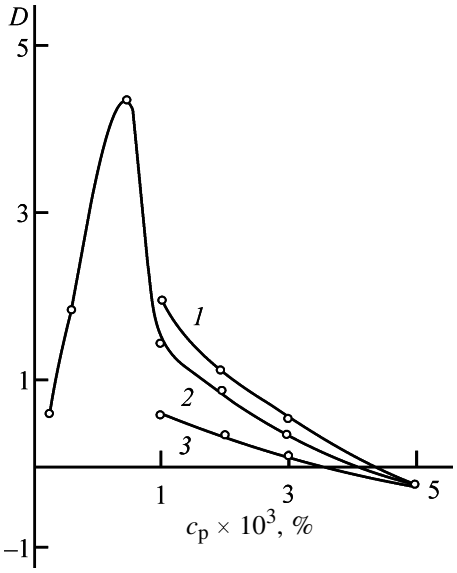

Fig. 2. Flocculation parameter D as a function of the concentration c_p of cationic Praestol (c_d = 60%). Praestol: (*1*) 644, (*2*) 655, and (*3*) 611.

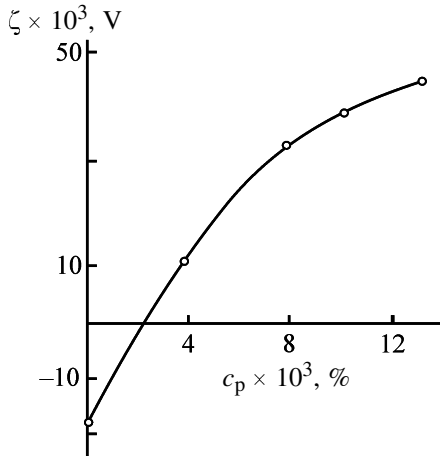

Fig. 3. ζ Potential (V) of the $CaCO_3$ particles as a function of the concentration c_p of cationic Praestol 650.

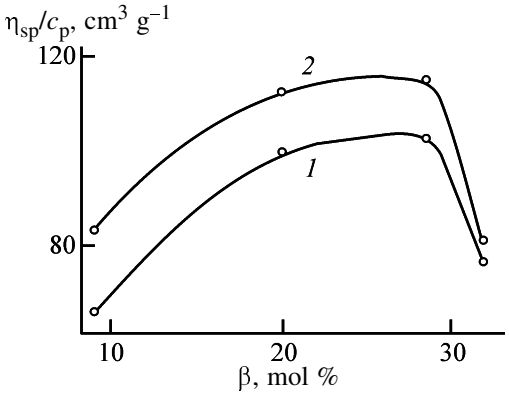

Fig. 4. Reduced viscosity η_{sp}/c_p as a function of the content of ionic units β in the cationic Praestol macromolecules. c_p, %: (*1*) 0.002 and (*2*) 0.004.

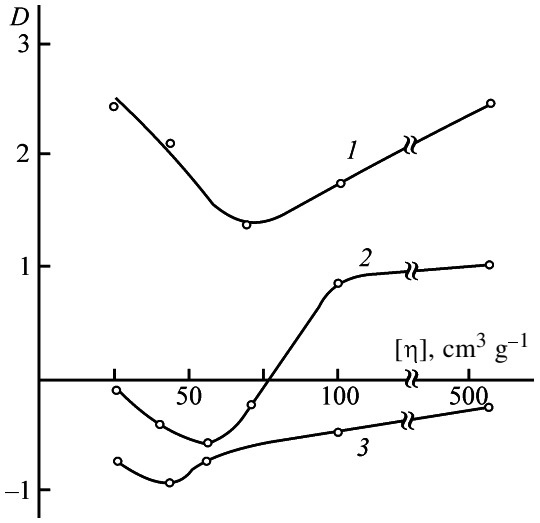

Fig. 5. Flocculation parameter D as a function of intrinsic viscosity [η] of cationic Praestol (c_d = 60%). $c_p \times 10^3$, %: (*1*) 0.8, (*2*) 2, and (*3*) 5.

mum (Fig. 5). This suggests changes in the nature of interaction of the $CaCO_3$ particles with polymer. First, D decreases with increasing [η] (descending branches of the curves). This phenomenon is obviously due to an increase in the number of contacts between macromolecules and $CaCO_3$ particles, when separate macromolecules are adsorbed on the particle surface owing to the charge neutralization. Adsorption layers arising in this case make weaker the contacts between particles and improve the suspension stability. After passing through a minimum of the dependence $D = f([\eta])$, D increases with increasing [η] (ascending branches of the curves). This is probably due to the adsorption of not only separate macromolecules on the particle surface but also of their aggregates, which are formed under the given experimental conditions [10]. In this case, macromolecules unrolling over the particle surface form greater number of contacts with $CaCO_3$ particles. As a result, owing to charge neutralization and formation of bridges between the suspension particles, globules become coarser and precipitate, which is confirmed by the increase in the flocculation parameter D.

As seen from Fig. 5, at [η] = const D decreases with increasing c_p at all the M values, This is due to an increase in the sedimentation stability of $CaCO_3$ suspension (passing from curve *1* to curve *3*) owing to a decrease in the particle charge and probable formation of bridges between the $CaCO_3$ particles through adsorbed macromolecular ions.

The effect of salt additions on sedimentation of $CaCO_3$ suspension was evaluated using the sample of

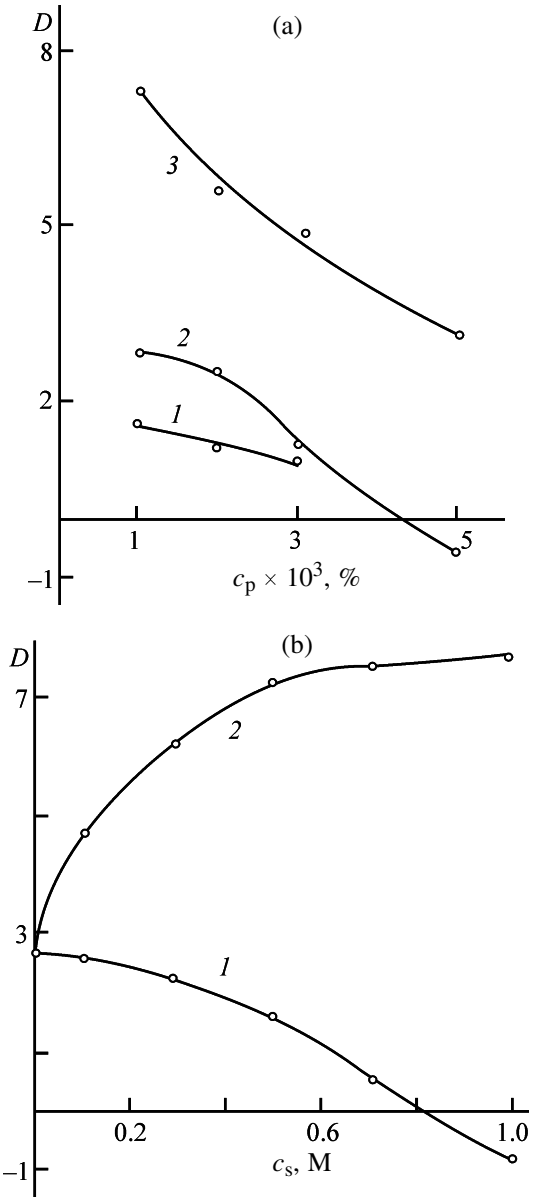

Fig. 6. Flocculation parameter D as a function of (a) concentration c_p of cationic Praestol 650 and (b) concentration c_s of (*1*) NaCl and (*2*) $CaCl_2$. (a) c_d = 60%; 0.5 M salt added: (*1*) NaCl and (*2*) $CaCl_2$; (*3*) no salt added. (b) c_d = 60%, $c_p = 1 \times 10^{-3}$%.

cationic Praestol 655 in the presence of NaCl and $CaCl_2$. In this case, D was determined taking into account changes in v_0 determined in sedimentation of the polymer-free suspension in the presence of these salts. The effect of salt additions on D is shown in Fig. 6. As seen, with (a) addition of NaCl and (b) increase in its concentration D decreases (Fig. 6, curves *1*). This is obviously due to the compression of the electrical double layer around the $CaCO_3$ particle, which decreases the distance between the particles

owing to strengthening of the van der Waals interaction, causes their aggregation, and decreases the sedimentation stability of the $CaCO_3$ suspension. As seen, with (a) addition of $CaCl_2$ and (b) increase in its concentration D increases (Fig. 6, curves *2*). This is obviously due to the hydrolysis of $CaCl_2$ in aqueous solutions to form the hydroxide poorly soluble in water. Positively charged hydroxy complexes neutralize negatively charged $CaCO_3$ particles, which then form aggregates and precipitate. In the presence of the polymer, formation of complex bridges (such as particle–macromolecular ion–Ca^{2+}) also causes aggregation and sedimentation of the dispersed particles. The effect of NaCl and $CaCl_2$ additions on the behavior of $CaCO_3$ suspension in the presence of cationic Praestol was observed at various c_p (Fig. 6a).

Our experimental data suggest that the above relationships of the $CaCO_3$ suspension sedimentation in the presence of cationic Praestol can be used not only to promote the flocculation but also to stabilize the suspension.

CONCLUSIONS

(1) The data on sedimentation stability of 60% suspension of calcium carbonate in the presence of cationic Praestol showed that at polymer concentration $c_p > 1 \times 10^{-3}$% D decreases with increasing c_p upon addition of NaCl and increases upon addition of $CaCl_2$, and the dependence of D on the intrinsic viscosity $[\eta]$ of the polymer passes through a minimum with minimal value at $[\eta] = 50–75$ cm^3 g^{-1}.

(2) The dependences of the flocculation parameter D and reduced viscosity η_{sp}/c_p on the content of the ionic units β in the macromolecule of cationic Praestol pass through a maximum at $\beta = 27$ mol %, which is due to the parallel variation of $(\bar{r}^{-2})^{1/2}$.

REFERENCES

1. Aripov, E.A., Glekel', F.L., and Khamraev, S.S., *Zh. Vses. Khim. O–va. im. D.I. Mendeleeva*, 1989, vol. 34, no. 2, pp. 219–223.
2. Napper, D.H., *Chemical Technology of Water Soluble Polymers*, Finch, C.A., Ed., New York: Plenum, 1985, 2nd ed., pp. 245–248.
3. Samasundaran, Yu.P., *Colloids Surf. A: Phys. Eng. Asp*., 1994, vol. 89, pp. 277–281.
4. Duplop-Jones, N. and Jaycock, M.J., *Paper Trade J*., 1981, vol. 34, no. 20, pp. 169–173.
5. Siffert, B. and Fimbel, P., *Colloids Surf*., 1984, vol. 377, nos. 3–4, pp. 11–18.
6. Huang, Y.A., Fowkes, F.M., Lloyd, T.B., and Sanders, N.D., *Langmuir*, 1991, no. 7, pp. 1742–1750.
7. Kurenkov, V.F., Nadezhdin, I.N., Kurenkov, A.V., et al., *Khim. Tekhnol*., 2006, no. 5, pp. 12–16.
8. Kurenkov, V.F., Len'ko, O.A., Snigirev, S.V., and Lobanov, F.I., *Zh. Prikl. Khim*., 2002, vol. 75, no. 7, pp. 1164–1168.
9. *Rukovodstvo po khimicheskomu i tekhnologicheskomu analizu vody* (Manual on Chemical and Technological Analysis of Water), Moscow: Khimiya, 1982.
10. Lipatov, Yu.S. and Sergeeva, L.M., *Adsorbtsiya polimerov* (Adsorption of Polymers), Kiev: Naukova Dumka, 1972.

ISSN 1070-4272, Russian Journal of Applied Chemistry, 2007, Vol. 80, No. 5, pp. 810–812. © Pleiades Publishing, Ltd., 2007.
Original Russian Text © E.I. Kulish, L.G. Kuzina, A.G. Chudin, R.Kh. Mudarisova, S.V. Kolesov, Yu.B. Monakov, 2007, published in Zhurnal Prikladnoi Khimii, 2007, Vol. 80, No. 5, pp. 832–835.

MACROMOLECULAR CHEMISTRY AND POLYMERIC MATERIALS

Transport Properties of Chitosan Films

E. I. Kulish, L. G. Kuzina, A. G. Chudin, R. Kh. Mudarisova, S. V. Kolesov, and Yu. B. Monakov

Bashkir State University, Ufa, Bashkortostan, Russia
Institute of Organic Chemistry, Ufa Scientific Center, Russian Academy of Sciences, Ufa, Bashkortostan, Russia

Received October 16, 2006; in final form, January 2007

Abstract—Effect of the history of chitosan films on their transport characteristics in relation to elimination of drugs from the body is studied.

DOI: 10.1134/S1070427207050229

Unique properties of the natural polysaccharide chitosan (Cht), which is produced from renewable natural raw materials, such as its compatibility with human body tissues, biodegradability, moisture permeability, etc. [1, 2], make this polymeric product suitable for medical use. The above useful properties of Cht, on the one hand, and the possibility of modifying its structure and, therefore, the structure of its derivatives, on the other hand, suggest that Cht can be used as a polymer matrix for systems with controlled elimination of drugs. The elimination of a drug associated with a polymer film is controlled primarily by the supramolecular structure of the polymer, which is preset even in the course of film preparation by, e.g., varying the thermodynamic quality of the solvent. Therefore, the film preparation procedure may considerably influence the elimination rate of drugs from the film. The goal of this study was to prepare chitosan films with controllable transport characteristics.

EXPERIMENTAL

In the study we used chitosan [TU (Technical Specifications) 6-09-05-296–76] from the Khimmed Company (Russia), prepared by alkaline deacetylation of crab chitin (degree of deacetylation ~75%, M_η 120 000); polyvinyl alcohol (PVA) of 16/1 grade [GOST (State Standard) 10 779-78] with M_η 25 000; and antibiotic Levomycetin (LC) as a 3% alcoholic solution. The films of Cht and blends of Cht with PVA in the salt form were prepared by casting a polymer solution in acetic acid (1–70 wt %) onto glass. The weight concentration of the polymers in the initial solution was 2 g dl^{-1}. The solution of LC was added to the solution of Cht just prior to film preparation. The LC concentration was varied from 0.0082 to 0.063 mol mol^{-1} Cht. The film thickness was 0.1 mm in all experiments. The kinetics of elimination of LC from the films was studied UV-spectrophotometrically at λ = 270 nm. To prevent dissolution of the Cht salt film in water, it was treated for 15, 30, or 60 min with aqueous sodium dodecyl sulfate (SDS) of 0.5 wt % concentration, which is above CMC [3]. Finally, the film was heat-treated at 120°C. The swellability of the films was determined gravimetrically.

It is known that dissolution of Cht in acetic acid (HAc) is accompanied by the protonation of its amino groups. The degree of protonation and the thermodynamic quality of the solvent depend on the HAc concentration in the solution [4]. The maximal unfolding of the macromolecular chains and the minimal degree of structurization of the solution were observed in the Cht solutions in 10% HAc. Both decrease and increase in the HAc concentration in the solution lead to a decrease in the degree of protonation of the amino groups and, correspondingly, to an increase in the level of structurization. Whereas in more dilute HAc solutions (1–2%) intramolecular bonding dominates, a different situation takes place in concentrated solutions. Taking into account that, according to the published data [5], a 70% HAc solution demonstrates the best thermodynamic quality with respect to Cht, it becomes clear that, in this case, structurization occurs through intermolecular bonding. Evidently, the difference in the structure of the initial solution is reflected in the kinetics of elimination of LC from the film.

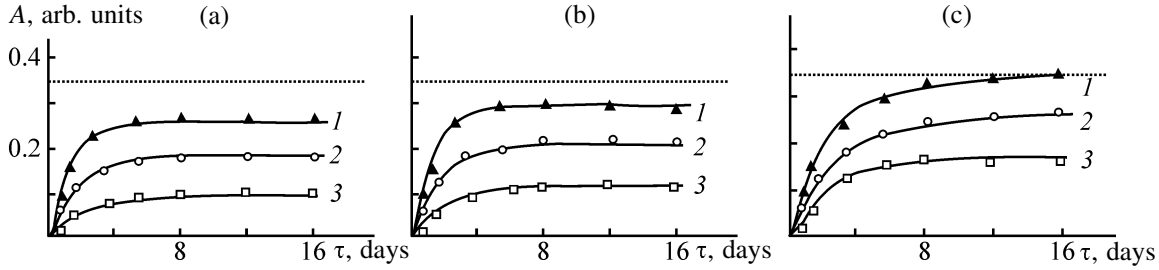

Fig. 1. Kinetics of LC elimination from the film obtained from solution in (a) 1, (b) 10, and (c) 70% HAc. (*A*) Optical density and (τ) time. Treatment time with the SDS solution, min: (*1*) 15, (*2*) 30, and (*3*) 60. LC concentration in the film 0.0163 mol mol^{-1} Cht; the optical density corresponding to this LC concentration is shown as a dotted line.

Table 1. Equilibrium elimination of LC (%) from Cht films

[HAc] in initial solution, wt %	Exposure time in SDS, min	Equilibrium elimination of LC, %, at indicated LC content in film, mol mol^{-1} Cht				
		0.0082	0.0163	0.0314	0.049	0.063
1	15	100	72	60	52	50
	30	75	69	49	40	33
	60	48	33	28	21	17
	Heat-treated films	100	74	71	69	67
10	15	100	78	75	72	70
	30	91	65	54	52	51
	60	54	39	26	24	22
70	15	100	82	78	75	73
	30	98	63	55	53	52
	60	73	51	34	30	25

Figure 1 shows typical dependences of the elimination of LC on the exposure time in water. The features of the elimination curves are as follows. Firstly, the most intensive elimination of LC is observed in the initial 2–3 days. By the 10th–12th day, the elimination of LC reaches its equilibrium value. Secondly, the higher the HAc concentration in the initial solution, the more complete is the elimination of LC from the film. Thirdly, the elimination of LC from the Cht film decreases with increasing time of the film treatment with SDS. For the film prepared from a solution in 70% HAc and treated for 15 min with the SDS solution, we observed practically complete elimination of LC in two weeks. In all other cases, the elimination was incomplete. Furthermore, as seen from Table 1, the lower the LC concentration in the film, the higher the probability of its complete elimination. LC in high concentration (>0.07 mol mol^{-1} Cht) deteriorates mechanical characteristics of the film, making it brittle and decreasing its moisture absorption (Fig. 2).

An additional tool for controlling the degree of elimination of drugs from the polymer matrix is formation of films from polymer blends. Comparison of Tables 1 and 2 shows that the elimination of LC from Cht–PVA film is lower than that from the individual Cht films, evidently, as a result of higher packing density in the polymer blend [4]. Note that the elimination of LC from blend films is an additive function of the blend composition (Fig. 3), and the moisture absorption of Cht–PVA film is considerably lower as compared to individual Cht film. However, treatment

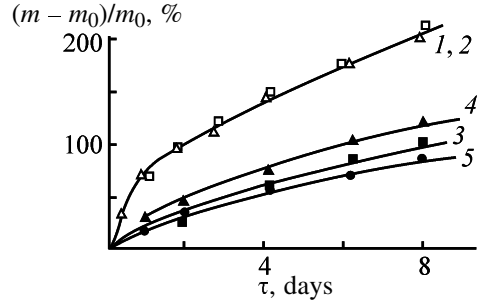

Fig. 2. Swellability $(m - m_0)/m_0$ of films of (*1–4*) Cht and (*5*) Cht–PVA blend (80 : 20), all prepared from solutions in 1% acetic acid, as a function of the swelling time in water vapor τ. Films contain (*1–3, 5*) no LC and (*4*) 0.063 mol LC mol^{-1} Cht; films (*2*) heat-treated or (*3*) treated with the SDS solution for 30 min.

Table 2. Equilibrium elimination of LC from 80 : 20 Cht–PVA films obtained from solutions in 1% acetic acid

Treatment time with SDS, min	Equilibrium elimination of LC, %, at indicated LC/Cht molar ratio			
	0.0163	0.0314	0.049	0.063
15	60	54	48	47
30	40	43	32	26
60	27	25	18	15
Heat-treated films	62	58	55	53

of the films with SDS solution practically eliminates this difference: all the films after treatment swell weakly.

Insolubility of the SDS-treated films in water is without question advantageous, as increasing the durability of the polymer matrix under conditions of medical use. However, the fact that these films demonstrate low moisture absorption is a significant disadvantage. Furthermore, treatment of Cht films with SDS solution strongly deteriorates their mechanical properties, which is reflected in clearly pronounced surface irregularity of the films. At the same time, heat treatment at 120°C for 3 h allows preparation of water-insoluble films demonstrating high moisture absorption well comparable with that of individual Cht (Fig. 2) and satisfactory mechanical characteristics. The elimination of LC from these heat-treated films is only slightly higher as compared to the untreated films.

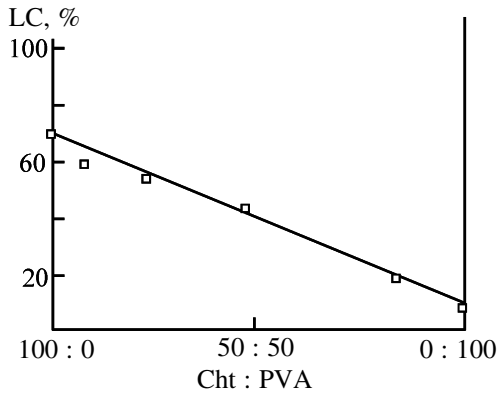

Fig. 3. Equilibrium elimination of LC from the films obtained from solutions in 10% acetic acid as a function of the Cht : PVA ratio in the polymer blend. LC concentration in the film 0.049 mol mol^{-1}; treatment time with the SDS solution 15 min.

Finally, the elimination of a drug from the polymer matrix can be controlled by varying film composition and by using heat treatment or treatment with surfactant solution.

CONCLUSION

The elimination of Levomycetin from chitosan films can be controlled by several ways such as (a) variation of the Levomycetin concentration in the film, (b) variation of the acetic acid concentration in the initial solution for film preparation, (c) introduction of the second polymer into the film, (d) treatment of the film surface with surfactant solution, and (e) heat treatment.

REFERENCES

1. Skryabin, K.G., Vikhoreva, G.A., and Varlamov, V.P., *Khitin i khitozan: Poluchenie, svoistva, i primenenie* (Chitin and Chitosan: Preparation, Properties, and Applications), Moscow: Nauka, 2002.
2. Muzzarelli, R.A., *Chitin*, Oxford: Pergamon, 1977.
3. Kil'deeva, N.R., Babak, V.G., Vikhoreva, G.A.,, et al., *Vestn. Mosk. Univ., Ser. 2: Khim.*, 2000, vol. 42, no. 6, p. 423.
4. Vikhoreva, G.A., Rogovina, S.Z., Pchelko, O.M., et al., *Vysokomol. Soedin., Ser. B*, 2001, vol. 43, no. 6, p. 1079.
5. Ageev, E.P., Vikhoreva, G.A., Matushkina, N.N., et al., *Vysokomol. Soedin., Ser. A*, 2000, vol. 42, no. 2, p. 333.

ISSN 1070-4272, Russian Journal of Applied Chemistry, 2007, Vol. 80, No. 5, pp. 813–817. © Pleiades Publishing, Ltd., 2007.
Original Russian Text © N.A. Storozhakova, Kh.Kh.N. Akhmed, A.I. Rakhimov, R.G. Fedunov, 2007, published in Zhurnal Prikladnoi Khimii, 2007, Vol. 80, No. 5, pp. 836–840.

MACROMOLECULAR CHEMISTRY AND POLYMERIC MATERIALS

Oligomerization and Polymerization of ε-Caprolactam in the Presence of the System 1,1,5-Trihydroperfluoropentanol–Acetic Acid

N. A. Storozhakova, Kh. Kh. N. Akhmed, A. I. Rakhimov, and R. G. Fedunov

Volgograd State Technical University, Volgograd, Russia
Institute of Chemical Problems of Ecology, Russian Academy of Natural Sciences, Volgograd, Russia

Received May 12, 2006; in final form, March 2007

Abstract—Catalytic oligomerization and hydrolytic polymerization of ε-caprolactam in the presence of the system 1,1,5-trihydroperfluoropentanol–acetic acid was studied.

DOI: 10.1134/S1070427207050230

Perfluorinated low-molecular-weight compounds, oligomers, and polymers are widely used to impart water-, oil-, and dust-repellent properties to polymers [1]. Introduction of small amounts of polyfluorinated derivatives of unsaturated polyesters (0.05–1 wt part per 100 wt parts of the formulation) into polyamides improves their tribological properties [2, 3].

It was shown previously that addition of 1,1,5-trihydroperfluoropentanol (TPFP) into polycaproamide (PCA) in the step of granule processing enhances the heat resistance, inhibits UV-induced oxidative degradation, and enhances the resistance of PCA to oxidative degradation in the dark [4–6]. It is also known [7] that acetic acid (AA) catalyzes oligomerization of ε-caprolactam (CL).

N-Acyl derivatives of ε-aminocaproic acid and its oligomers were isolated from the reaction of AA with CL [8–11]. Without a carboxylic acid, polymerization of CL occurs with an induction period [12], which is attributed to accumulation of ε-aminocaproic acid and its subsequent participation in opening of the lactam ring.

Korshak et al. [13] studied the hydrolytic polymerization of CL using $H_2{}^{18}O$ and supportred the opinion [14] that the reaction occurs by an ionic mechanism with the protonation of the NH group of the lactam ring. In this connection, it becomes necessary to study the modification of PCA by adding TPFP in the step of ε-caprolactam polymerization.

In this study we examined the features of oligomerization and polymerization of ε-caprolactam in the presence of the system 1,1,5-trihydroperfluoropentanol–acetic acid and the processing characteristics, heat resistance, and physicomechanical parameters of the resulting PCA.

EXPERIMENTAL

The IR spectra of liquid substances (Specord M82) were recorded from thin films, and the spectra of solid substances, from mulls in mineral oil. The rates of reactant consumption and oligomer formation were estimated by the ampule method. A 8–10 cm^3 glass ampule was charged with 0.02 mol of CL and 0.02 mol of dried acetic acid, after which a catalytic amount (0.001 mol) of a saturated monohydric alcohol (butanol, pentanol) and TPFP was added. The mixture was heated to 200°C. For TPFP, the concentration was varied within 0.025–0.1 mol % (Fig. 1). The ampule was withdrawn from the thermostat after the lapse of the required period (60-min steps) and cooled at room temperature. Then the mixture from the ampule was transferred into a beaker, 15–20 ml of chloroform was added, and the mixture was thoroughly stirred to separate the forming oligomer from the starting compounds. The oligomer was filtered off, washed successively with 5 ml of chloroform and 10 ml of diethyl ether, and dried. The oligomer prepared in 4 h was filtered off and recrystallized from ethanol. The results are given in Tables 1 and 2 and in Fig. 1.

The higher-molecular-weight oligomers remained on the filter and were separated using their different solubilities in hot water and ethanol.

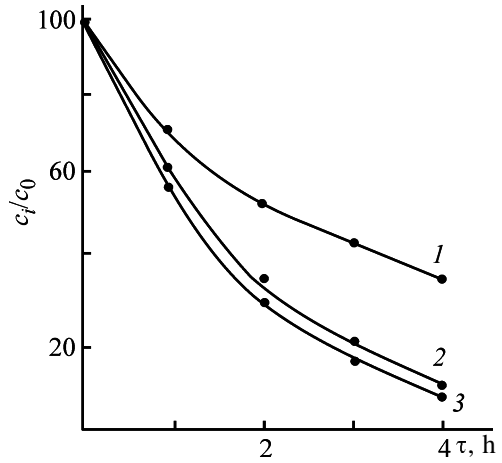

Fig. 1. Consumption of ε-caprolactam in the reaction with acetic acid at different TPFP concentrations. (c_i/c_0) Percent ratio of the running and initial concentrations of ε-caprolactam and (τ) time. TPFP concentration, mol %: (*1*) 0.025, (*2*) 0.05, and (*3*) 0.1.

The molecular weight was determined cryoscopically in glacial acetic acid. In particular, the molecular weight of the oligomer prepared using TPFP, determined in acetic acid, is 2447, which corresponds to 21 monomeric units (calculated: 2443) (Tables 1, 2). Nitrogen content: found 11.98%, calculated for $CH_3C(O)[HN(CH_2)_5C(O)]_{21}OH$ 11.99%.

The structure of the reaction products was proved by IR spectroscopy. The IR spectra contain amide I (1636 cm^{-1}) and amide II (1546 cm^{-1}) absorption bands. The band of hydrogen-bonded NH groups (NH···O=C) is observed at 3292 cm^{-1}. The hydrogen-bonded COOH groups give the bands $\nu_{C=O}$ at 1708 and ν_{OH} at 3112 cm^{-1}. The composition was determined by elemental analysis.

Table 1. Effect of alcohol on the oligomerization parameters, number of monomeric units *n*, and properties of oligomers. Temperature 200°C, thermostating for 4 h

Alcohol	CL conversion, %	Oligomer yield, % based on CL	T_m, °C, of oligomer	*n*
None	40	35	163–165	12
Butanol	65	61	177–180	14
Pentanol	70	68	183–187	15
TPFP	90	82	193–194	21

Table 2. Influence of the TPFP amount on the CL oligomerization parameters

TPFP amount, mol %	Conversion, %		Oligomer yield, %	*n* in 4 h
	CL	AA		
0.025	65	15	61	14
0.05	90	25	82	21
0.1	92	30	82	21

Addition of TPFP in the step of hydrolytic polymerization of CL was performed in an ANP-12 commercial apparatus for continuous polymerization. CL (16 t day^{-1}) and a mixture containing water (1.24–1.32%), AA (0.04–0.05%), thermostabilizer {1,2-di-[4-(*N*-phenylamino)phenoxy]ethane (N1) or 2-hydroxy-1,3-di[4-(*N*-phenylamino)phenoxy]propane (N2), 0.05–0.07%}, and TPFP (0.001 wt %) [15] were continuously fed in a nitrogen flow. The reaction temperature was 265–270°C. The polymer was analyzed for the content of low-molecular-weight compounds, and the relative viscosity of PCA was determined. The heat resistance was evaluated by changes in the thread strength before and after heating for 2 h at 200°C; the heat resistance of the granulate was studied derivatographically [15].

Quantum-chemical calculations were performed by the AM1 method allowing the associative interactions in the system to be taken into account [16, 17].

We studied the hydrolytic polymerization of CL in the presence of the TPFP–AA system. The step of the lactam ring opening (studied also by the AM1 method) and the step of oligomer formation were considered with the CL–AA–TPFP system as model, in comparison with the systems with *n*-butanol and *n*-pentanol. Experiments on hydrolytic polymerization revealed the effect of TPFP on the content of low-molecular-weight compounds (LMC), relative viscosity of the polymer, and amount of thin extrudate (bristle) returned to reprocessing.

First we performed experiments at a minimal concentration of TPFP (8.8×10^{-4} wt %) and as low concentration of thermal stabilizer as possible. As seen from Table 3, a decrease in the concentration of the thermal stabilizer from 7.1×10^{-2} to 5.8×10^{-2} wt % causes a certain decrease in the relative viscosity of the granulate after casting and the amount of thin extrudate (bristle) returned to reprocessing (2.1–2.6%). However, further decrease in the amount of the thermal stabilizer, as well as an increase in the TPFP amount, deteriorate the processing parameters and cause a drastic increase in the amount of bristle returned to reprocessing: with 9.2×10^{-4} wt % TPFP and 1×10^{-2} wt % thermal stabilizer, the amount of thin extrudate (bristle) increases to 6.0%. In the absence of TPFP, the volume of bristle returned to re-

processing increases to 9.4–9.9%. Hence, further decrease in the thermal stabilizer concentration and increase in the TPFP concentration are not appropriate, resulting in worsening of the polymer properties. It should also be noted that the absence of the polyfluorinated alcohol in the polymerization system results in an increase in the LMC content to 11.62% and in the amount of thin extrudate (bristle) returned to reprocessing, to 9.4–9.9%. The relative viscosity of the granulate is also an important parameter. Introduction of TPFP increases the relative viscosity from 2.81–2.84% without TPFP to 2.91–2.95% with TPFP added (8.8×10^{-4} wt %).

To elucidate the character of the reaction of CL with AA and with the AA–TPFP system, we examined the rate of CL oligomerization in these systems in comparison with that in the presence of saturated monohydric alcohols.

We found (Table 1) that the CL conversion in the course of oligomerization strongly depends on the structure of the alcohol added (0.05 mol %) and decreases in the order TPFP > 1-pentanol > 1-butanol.

The highest conversion of CL (temperature 200°C) is attained with TPFP: 90% in 4 h (Table 1). Introduction of TPFP also increases the oligomer yield (to 82%) and the number of monomer units in the oligomer (from 12 without catalyst to 21 with TPFP).

To determine the optimal amount of the most effective catalyst, TPFP, we examined how the TPFP concentration varied in the range 0.025–0.1 mol % affects the CL transformation rate (Fig. 1). Table 2 and Fig. 1 show that the optimal concentration of TPFP is 0.05 mol %: CL conversion 90, AA conversion 25, oligomer yield 82%. Further increase in the TPFP concentration only slightly affects the conversion of CL and AA and the oligomer yield. At the same time, at the catalyst concentration decreased to 0.025 mol %, the CL conversion decreases to 65, AA conversion, to 15, and oligomer yield, to 61%.

Table 3. Effect of the TPFP–AA system on the LMC content, relative viscosity of the granulate, and amount of bristle returned to processing

Run no.	$c_{TPFP} \times 10^4$, wt %	PCA granulate		Thin extrudate (bristle)
		η, %	LMC content, %	
1	8.8(1)*	2.91–2.95	10.56	2.1
2	8.8(2)	2.86–2.89	10.85	2.6
3	9.2(3)	2.85–2.87	10.40	6.0
4	None(1)	2.81–2.83	11.62	9.4
5	None(3)	2.81–2.84	11.25	9.9

* The reaction mixture contained 1,2-di[4-(*N*-phenylamino)-phenoxy]ethane (N1) in an amount of 7.1×10^{-2} (1) or 5.1×10^{-2} (2) wt %, or 2-hydroxy-1,3-di[4-(*N*-phenylamino)phenoxy]-propane in an amount of 5.1×10^{-2} wt % (3).

Simultaneous participation of alcohols and AA in the opening of the lactam ring can be represented by the scheme taking into account the electrophilic properties of the acid protonating the amide nitrogen atom and the acidity and nucleophilicity of the alcohol participating in the interaction with the lactam carbonyl carbon atom and simultaneously in the release of AA from the forming complex:

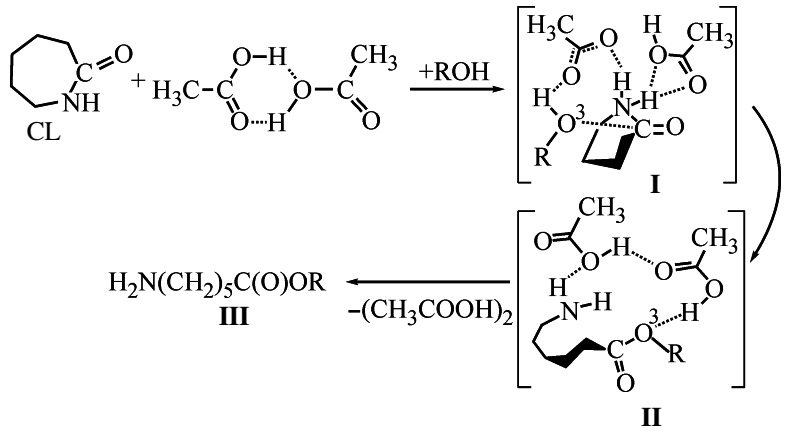

where R = C_4H_9, C_5H_{11}, or $CH_2(CF_2CF_2)H$.

This scheme was analyzed by the AM1 method. As the reaction coordinate we chose the O^3–C bond formed as the hydroxyl oxygen atom (O^3) of the alcohol approaches the carbonyl carbon atom of the lactam ring. In the first step of the reaction, the anion–cation complex is attacked by another acetic acid mol-

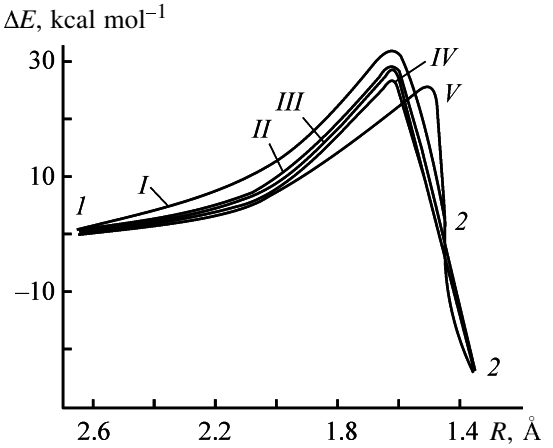

Fig. 2. Variation of the relative energy $\Delta E = E_0 - E_R$ of the systems ε-caprolactam–AA and ε-caprolactam–alcohol along the reaction coordinate R: (*I*) AA, (*II*) C_4H_9OH, (*III*) $C_5H_{11}OH$, (*IV*) $H(CF_2)_2CH_2OH$, and (*V*) $H(CF_2)_4CH_2OH$. (*1*, *2*) Points corresponding to the initial and final states of the reaction system, respectively. The reaction coordinate R is the length of the O^3–C bond.

ecule or by an alcohol molecule (HOR) (structure **I**). This results in the ring opening via structure **II** with the simultaneous formation of ester **III** in the case of participation of ROH and acetic acid dimer.

It is important that, in the case of attack with acetic acid, the energy of the products coincides with that of the reactants (Fig. 1), i.e., a situation arises when the ring opening does not occur completely (N–C bond length about 0.17 nm). Attack with alcohol leads to an appreciable gain in the energy of the final product, with the complete ring opening (N–C bond length about 0.46 nm). The energy barrier of this reaction is about 28 kcal mol^{-1} (Fig. 2).

The experiment and quantum-chemical calculations show that TPFP is more reactive than 1-butanol or 1-pentanol.

The formation of the intermediate polyfluoroalkyl esters of the oligomers was detected by ^1H NMR spectroscopy: The intermediate product, 1,1,5-trihydroperfluoropentyl esters (identified in the initial step of the reaction of CL with AA in the presence of TPFP after recrystallization from water), gives a triplet of triplets of the $H–CF_2CF_2$ proton at $\delta = 6.4$ ppm. Synthesis of polyfluoroalkyl esters of ε-aminocaproic acid oligomers was described in [18, 19].

Table 4. Effect of TPFP on the physicomechanical characteristics and heat resistance of PCA fiber (200°C, 2 h)

Run no.*	Tex	Tensile strength, N	Relative elongation, %	Residual fiber strength, %
1	187	13.4	15.3	85.7
2	185	12.5	16.0	88.8
3	183	12.5	16.1	90.7
4	185	12.5	16.0	80.3
5	183	12.4	16.5	81.0

* The numbering is the same as in Table 3.

In the presence of the polyfluorinated alcohol, the oligomers are formed faster and have a considerably higher molecular weight, compared to the synthesis in the presence of unsubstituted alcohols.

An increase in the oligomer molecular weight and regeneration of the catalyst (alcohol) are due to the reaction of the ester with the amino group of the adjacent molecule:

$$R–C(O)[NH(CH_2)_5C(O)]_nOCH_2(CF_2CF_2)_2H$$

$$+ H_2N(CH_2)_5\sim \rightarrow R–C(O)[NH(CH_2)_5C(O)]_nO(CH_2)_5\sim$$

$$+ H(CF_2CF_2)_2CH_2OH.$$

Introduction of the perfluorinated group into the ester moiety (in the case of TPFP) increases the positive charge on the carbonyl carbon atom, which favors its attack by the lone electron pair of the amine nitrogen atom of the adjacent oligomer molecule, with the regeneration of TPFP.

The reaction between the ester group of the oligomer and the amino group of the PCA macromolecule in the course of hydrolytic polymerization of CL in the presence of TPFP leads to a decrease in the LMC content and to an increase in the viscosity of the granulate melt (Table 3), confirming the occurrence of the above reactions. These transformations lead to a decrease in the content of reactive functional groups in the polymeric system. All these factors favor enhancement of the heat resistance of PCA. The heat resistance of PCA was judged from changes in the residual strength of the PCA fiber and in the granulate weight upon heat treatment [15]. The residual tensile strengths of the PCA fiber samples upon heat treatment for 2 h at 200°C with TPFP introduced into the polymerization system and without it (commercial polymer) are compared in Table 4. It is seen that the residual strength of the PCA sample prepared in the presence of TPFP decreases insignificantly upon heat treatment at 200°C, whereas without TPFP (commercial PCA) it decreases by almost 20% (the variation of the PCA fiber upon heat treatment is the most important parameter for evaluation of the heat resistance of the fiber in the production process). Consistent data were

Table 5. Decrease in the granulate weight in time in the course of heating to 400°C

T, °C	Time of reaching indicated temperature, min	Weight loss of granulate, %	
		commercial	with TPFP added
150	17.8	1.1	0.4
330	34.2	6.0	2.0
355	36.6	7.7	4.0
380	39.0	11.0	6.0
400	41.5	20.2	12.7

also obtained in evaluation of the heat resistance by derivatographic examination of the thermolysis of the PCA granulate (Table 5). For example, on heating to 330°C over a period of 34.2 min, the weight loss of the granulate prepared in the presence of TPFP was three times smaller, compared to the commercial granulate.

Thus, introduction of 1,1,5-trihydroperfluoropentanol in polymerization of ε-caprolactam favors opening of the ε-lactam ring, and participation of the intermediate ester in the chain propagation step leads to an increase in the molecular weight of poly-ε-caprolactam and to the enhancement of the heat resistance of the polymer.

CONCLUSIONS

(1) The system 1,1,5-trihydroperfluoropentanol–acetic acid catalyzes opening of the lactam ring more efficiently than acetic acid or polyfluorinated alcohol.

(2) The mechanism of catalysis of caprolactam oligomerization and polymerization in the steps of ring opening and chain propagation, with the regeneration of 1,1,5-trihydroperfluoropentanol, was considered.

(3) The processing characteristics (decrease in the content of low-molecular-weight compounds and in the amount of bristle returned to reprocessing) and heat resistance of polycaproamide are improved by using the system 1,1,5-trihydroperfluoropentanol–acetic acid.

REFERENCES

1. *Fluorine Compounds: Modern Technology and Applications*, Ishikawa, N., Ed., Tokyo: CMC, 1987.
2. Krasnov, A.P., Afonicheva, O.V., Popov, V.N., et al., *Tren. Iznos*, 2000, vol. 21, no. 5, pp. 566–570.
3. Novakov, I.A., Storozhakova, N.A., Morozova, M.Yu., and Artemenko, S.E., Abstracts of Papers, *Perspektivnye polimernye kompozitsionnye materialy: Al'ternativnye tekhnologii. Pererabotka. Primenenie. Ekologiya: Mezhdunarodnaya konferentsiya "Kompozit-2004"* (Promising Polymeric Composites: Alternative Technologies. Processing. Applications. Ecology: Int. Conf. "Composite-2004"), Saratov, 2004, pp. 316–317.
4. Novakov, I.A., Storozhakova, N.A., Krasnov, A.P., et al., *Vysokomol. Soedin., Ser. B*, 2005, vol. 47, nos. 11–12, pp. 335–338.
5. Novakov, I.A., Storozhakova, N.A., Ivanov, V.B., and Priimak, V.V., *Vysokomol. Soedin., Ser. B*, 2006, vol. 48, no. 1, pp. 121–125.
6. Storozhakova, N.A., Golovanchikov, A.B., Tatarnikov, M.K., et al., *Khim. Tekhnol. Khim. Volokon*, 2002, no. 4, pp. 41–45.
7. Korshak, V.V. and Frunze, T.M., *Sinteticheskie geterotsepnye poliamidy* (Synthetic Heterochain Polyamides), Moscow: Nauka, 1962.
8. Storozhakova, N.A., Akhmed, Kh.Kh.N., and Rakhimov, A.I., *Zh. Prikl. Khim.*, 2005, vol. 78, no. 7, pp. 1139–1141.
9. Storozhakova, N.A., Akhmed, Kh.Kh.N., and Rakhimov, A.I., Abstracts of Papers, *9-ya Mezhdunarodnaya konferentsiya po khimii i fizikokhimii oligomerov "Oligomery-2005"* (9th Int. Conf. on Chemistry and Physical Chemistry of Oligomers "Oligomers-2005"), Odessa, September 13–16, 2005.
10. US Patent 2956068.
11. US Patent 5414099.
12. Wiloth, F., *Kolloid Z.*, 1955, vol. 143, pp. 129–135.
13. Korshak, V.V., Kudryavtsev, R.V., and Sergeev, V.A., *Izv. Akad. Nauk SSSR, Otd. Khim. Nauk*, 1962, no. 8, pp. 1468–1470.
14. Majury, T.G., *Polym. Sci.*, 1958, vol. 31, no. 3, pp. 383–397.
15. RF Patent 2187517.
16. Voets, R. and François, J.P., *J. Comput. Chem.*, 1989, vol. 10, no. 4, pp. 449–467.
17. Voets, R. and François, J.P., *J. Comput. Chem.*, 1990, vol. 11, no. 3, pp. 269–290.
18. Storozhakova, N.A., Efanova, E.Yu., Fedunov, R.G., and Rakhimov, A.I., *Zh. Fiz. Khim.*, 2002, vol. 76, no. 12, pp. 2260–2263.
19. Storozhakova, N.A., Efanova, E.Yu., and Rakhimov, A.I., *Zh. Prikl. Khim.*, 2002, vol. 75, no. 10, pp. 1749–1751.

ISSN 1070-4272, Russian Journal of Applied Chemistry, 2007, Vol. 80, No. 5, pp. 818–821. © Pleiades Publishing, Ltd., 2007.
Original Russian Text © N.B. Valetova, L.L. Semenycheva, I.S. Il'ichev, A.N. Artemov, D.F. Grishin, 2007, published in Zhurnal Prikladnoi Khimii, 2007, Vol. 80, No. 5, pp. 841–844.

MACROMOLECULAR CHEMISTRY AND POLYMERIC MATERIALS

Features of Polystyrene Synthesis in the Presence of (Diphenylbutadiene)tricarbonylchromium

N. B. Valetova, L. L. Semenycheva, I. S. Il'ichev, A. N. Artemov, and D. F. Grishin

Lobachevsky Institute of Chemistry, Nizhnii Novgorod State University, Nizhni Novgorod, Russia

Received October, 16, 2006; in final form, December 2006

Abstract—Features of radical polymerization of styrene in the presence of (diphenylbutadiene)tricarbonylchromium were studied.

DOI: 10.1134/S1070427207050242

New approaches to control over the kinetic parameters of synthesis of polymers attract a great attention. These methods involve formation of stable radicals controlling chain propagation by the mechanism of reversible inhibition directly in the polymerization system (in situ) [1–3]. Under these condition, polymerization is faster and the reaction temperature is lower (50–80°C) than those in the presence of stable nitroxyl radicals introduced directly into the polymerizate.

Metal-containing monomers including chromium complexes can be used as chain-terminating agents formed in situ under the conditions of radical initiation [3]. Organochromium compounds react with initiator radicals or with growing macroradicals to form relatively stable metal-containing carbon radicals affecting directly the polymerization rate and the molecular weight of the polymers [3–5].

The aim of this study was to develop a procedure of gel-free polymerization of one of the most practically important monomers, styrene, in the presence of (diphenylbutadiene)tricarbonylchromium (DPB). This complex can accept an initiator radical to form in situ a relatively stable sterically hindered carbon radical stabilized additionally by the arenetricarbonylchromium group.

EXPERIMENTAL

(Diphenylbutadiene)tricarbonylchromium was prepared by the procedure described in [6]. Its physicochemical properties were similar to the published data. Styrene was purified by the conventional procedure [7]. Commercial azobis(isobutyronitrile) (AIBN) used as an initiator was recrystallized from methanol. Di-*tert*-butylperoxytriphenylantimony (DPS) was prepared by the procedure described in [8]. Triisobutylboron was a commercial product. Physicochemical properties of all the compounds used in this study were similar to the published data.

Styrene was polymerized in temperature-controlled evacuated ampules. The polymerization kinetics was studied by gravimetric and thermographic methods. To remove unchanged monomer from the polymerization product, the polymers were precipitated with hexane from an ethyl acetate solution under argon. The molecular weight (MW) and molecular weight distribution (MWD) were estimated by gel permeation chromatography (GPC) [10]. Chromatographic analysis was performed on a Knauer liquid chromatograph with a Linear-2 column ("Phenomenex"). An R-2301 Knauer differential refractometer was used as a detector. The eluent was chloroform.

The study of the kinetics of styrene radical polymerization initiated by AIBN in the presence of DPA showed that DPB substantially affected propagation of the polymeric chain and significantly decreased the gel effect (Fig. 1). Autocatalytic polymerization is almost completely suppressed at a DPB concentration of 0.3 mol %. In this case, the time dependence of the styrene conversion is almost linear (Fig. 2, curve *2*), which is typical for controlled radical polymerization [11–13]. Styrene polymerization initiated by the radical initiator in the absence of the chromium complex is characterized by the S-shaped time dependence of the conversion (Fig. 2, curve *1*), which is typical for polymerization with gel effect. In this case the MW increases spontaneously.

Our previous ESR studies [14] showed that DPB reacted with radicals to form a sterically hindered chromium-containing radical with the unpaired electron localized at the carbon atom:

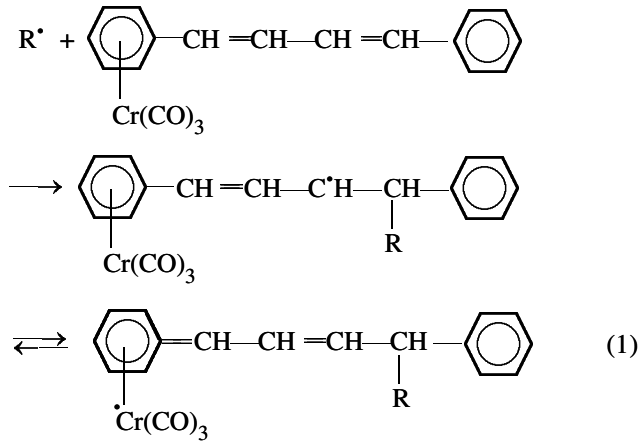

(1)

1,4-Diphenyl-1,3-butadiene, an organic analog of DPB, readily forms diphenylbutadienyl anions in the presence of *sec*-butyllithium in toluene at 70°C [15]. Although diphenylbutadienyl anions are readily formed by the reaction of diphenylbutadiene with *sec*-BuLi, this diene does not polymerize and copolymerize with styrene. As shown by Barson et al. [16], 1,4-diphenyl-1,3-butadiene (organic analog of DPB) is almost inert to 1-cyano-1-methylethyl radical formed by thermolysis of AIBN initiator. Thus, introduction of the bulky tricatbonylchromium group into diphenylbutadiene results in redistribution of the electron density in the molecule so that DPB becomes capable of entering into radical reactions.

Previously we showed [14] that DPB did not polymerize under the conditions of radical-initiated polymerization in a polar solvent (ethyl acetate) at 70°C for 50 h. No poly[(diphenylbutadiene)tricarbonylchromium] was formed when the polymerization was performed for 33 days in the presence of binary organometallic initiator [di-*tert*-butylperoxytriphenylantimony + triisobutylboron]. This initiator was used as an effective initiator of polymerization of various monomers, including dienes, in a wide temperature range [13].

As seen from the table and Fig. 3, the viscosity-average and number-average MW (M_n) linearly increase with the monomer conversion after introduction of the organochromium compound in the amount comparable with the initiator concentration. The dependences of the molecular weight of PS on the conversion with AIBN initiator in the absence of DPB are shown in Fig. 3 for comparison. As seen from these data, in the absence of the organometallic monomer,

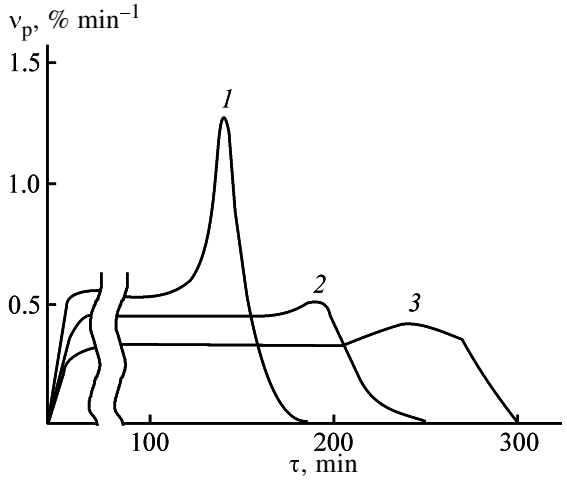

Fig. 1. Differential kinetic curves of ST polymerization in the presence of (*1*) 0, (*2*) 0.2, and (*3*) 0.3 mol % DPB at 80°C. Initiator AIBN (0.8 mol); the same for Fig. 2. (ν_p) Polymerization rate and (τ) time.

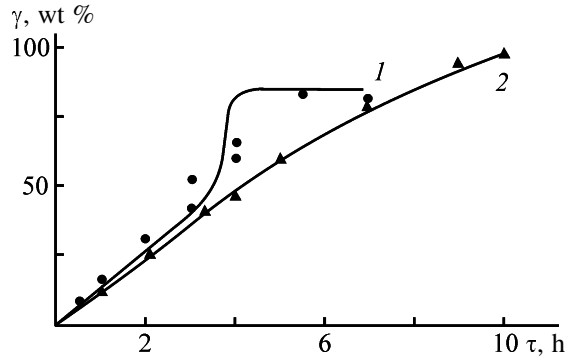

Fig. 2. Integral kinetic curves of ST polymerization in the presence of (*1*) 0 and (*2*) 0.3 mol % DPB at 80°C. (γ) Conversion and (τ) time.

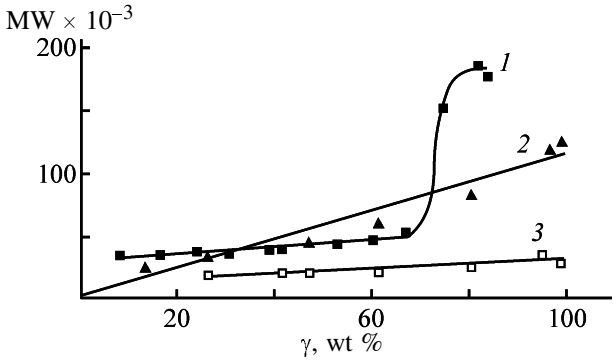

Fig. 3. (*1, 2*) Viscosity-average and (*3*) number-average MW of polystyrene formed in the presence of (*1*) 0, (*2*) 0.2, and (*3*) 0.3 mol % DPB as a function of the conversion γ. Initiator AIBN (0.8 mol). T = 70°C.

MW increases spontaneously in the course of the polymerization.

Introduction of DPB into the polymerizate substantially affects the kinetics of ST polymerization. This is

Molecular-weight parameters of polystyrene prepared at T = 70°C in the presence of (diphenylbutadiene)tricarbonylchromium. Initiator AIBN (0.8 mol %)

DPB, mol %	Monomer conversion, wt %	$M_n \times 10^{-3}$	$M_w^* \times 10^{-3}$	M_w/M_n
0	84	77	246	3.2
0.3	42	20	36	1.8
	48	21	39	1.9
	62	23	45	2.0
	81	27	107	4.1
	95	37	182	4.9

* M_w is weight-average MW.

probably due to reaction of the propagating radical with the chromium-containing monomer to form sterically hindered carbon radical stabilized by the arenetricarbonylchromium group [Eq. (1)]. We suggest that these stabilized radicals formed in the system can affect the kinetic parameters of polymerization and molecular weight parameters of the polymer by the mechanism of reversible inhibition:

$$\sim P_n^{\bullet} + {}^{\bullet}X \rightleftharpoons \sim P_n \cdots X \qquad (2)$$

$$\sim P_n\text{–}X \underset{k_c}{\overset{k_d}{\rightleftharpoons}} \sim P_n^{\bullet} \overset{k_p}{\circlearrowright} + {}^{\bullet}X \qquad (3)$$

where $\sim P_n$ is the propagating radical; X, chromium-containing carbon radical; k_d, dissociation rate constant of the adduct; k_r, recombination rate constant; and k_p, rate constant of chain propagation.

In addition, the shift of MWD curves of PS samples prepared in the presence of DPB to higher MWs with an increase in the monomer conversion suggests

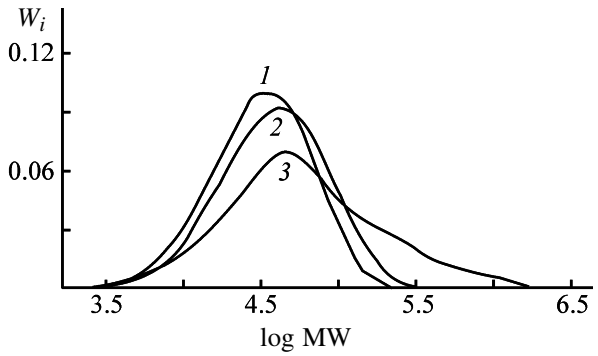

Fig. 4. Molecular weight distribution of PS samples prepared at 70°C in the presence of 0.8 mol % AIBN and 0.3 mol % DPB. (W_i) Weight fraction of molecules with the given MW. Conversion γ, wt %: (*1*) 42, (*2*) 62, and (*3*) 99.

that polymerization of styrene in the presence of DPB occurs by the mechanism of controlled chain propagation [scheme (3)].

Thus, styrene polymerization in the presence of the chromium-containing monomer in the amount comparable with the initiator concentration has features of "living" polymerization, in particular, linear dependence of the molecular weight of the polymer on the conversion. This is an indirect evidence that the molecular weight of the polymer increases continuously in the course of polymerization [13, 17, 18] and hence the MWD shifts to higher MWs with increasing polymer conversion from small conversions owing to fragmentary propagation of the polymeric chain.

It should be noted that the MWD curves are broadened and the polydispersity coefficients of the samples increase (see table) at high conversions, which is atypical for controlled radical polymerization by the mechanism of reversible inhibition. Clearly, this can be due to reactions increasing the polydispersity coefficient (isomerization, disproportionation, and chain transfer to monomer and polymer), i.e., formation in the system of "dead" polymer by bimolecular chain termination. These reactions occur concurrently with the reactions of reversible inhibition.

Similar features of controlled polymerization were observed when sterically hindered (α-methylstyrene)-tricarbonylchromium radical was used as a chain-terminating agent [3].

CONCLUSIONS

(1) Introduction of (diphenylbutadiene)tricarbonylchromium into the polymerization system affects the kinetics parameters of styrene polymerization and molecular-weight properties of the polymer and suppresses the gel effect. Under these conditions, the molecular weight of the polymer increases linearly and the molecular-weight distribution shifts to higher molecular weight with the monomer conversion.

(2) The chain-terminating agent substantially affects the chain propagantion at temperatures of industrial preparation of polystyrene (70–80°C). The disadvantage of this agent under conditions of radical initiation is relatively high polydispersity of the resulting polymer.

ACKNOWLEDGMENTS

This study was financialy supported by the Russian Foundation for Basic Research (project no. 32668).

REFERENCES

1. Grishin, D.F., Semyonycheva, L.L., and Kolyakina, E.V., *Mendeleev Commun.*, 1999, no. 6, pp. 250–252.
2. Detrembleur, C., Sciannamea, V., and Koulic, C., *Macromolecules*, 2002, vol. 35, no. 19, pp. 7214–7223.
3. Grishin, D.F., Semenycheva, L.L., Telegina, E.V., and Cherkasov, V.K., *Vysokomol. Soedin., Ser. A*, 2003, vol. 45, no. 2, pp. 211–216.
4. Grishin, D.F., Semyonycheva, L.L., Artemov, A.N., et al., *Appl. Organomet. Chem.*, 2003, vol. 17, pp. 717–722.
5. Grishin, D.F., Valetova, N.B., Ul'ichev, I.S., et al., *Vysokomol. Soedin., Ser. B*, 2005, vol. 47, no. 6, pp. 1029–1033.
6. Cais, M. and Feldkimel, M., *Tetrahedron Lett.*, 1961, no. 13, pp. 444–447.
7. Smith, L.J. and Taylor, F.L., *J. Am. Chem. Soc.*, 1935, vol. 57, no. 8, pp. 2461–2463.
8. USSR Inventor's Certificate no. 1567584.
9. Arulin, V.I. and Efimov, L.I., *Tr. Khim. Khim. Tekhnol.* (Gor'kii), 1970 no. 2, pp. 74–77.
10. Belen'kii, B.G. and Vilenchik, L.Z., *Khromatografiya polimerov* (Chromatography of Polymers), Moscow: Khimiya, 1978.
11. *Controlled Radical Polymerization*, Matyjaszewski, Kr., Ed., Oxford: Univ. Press, 1988.
12. Hawker, C.J., Bosman, A.W., and Harth, E., *Chem. Rev.*, 2001, vol. 101, no. 12, pp. 3611–3688.
13. Grishin, D.F. and Semenycheva, L.L., *Usp. Khim.*, 2001, vol. 70, no. 5, pp. 486–510.
14. Valetova, N.B., Semyonycheva, L.L., Ilitchev, I.S., et al., *Appl. Organomet. Chem.*, 2005, vol. 19, pp. 971–974.
15. Hsieh, H.L. and Kraus, G., *J. Polym. Sci. Polym. Chem. Ed.*, 1973, vol. 11, no. 2, pp. 453–466.
16. Borson, C.A., Bevington, J.C., and Huckerby, T.N., *Polymer*, 1990, vol. 31, no. 1, pp. 145–149.
17. Chernikova, E.V., Garina, E.S., Zaremskii, M.Yu., et al., *Vysokomol. Soedin., Ser. A*, 1995, vol. 37, no. 10, pp. 1638–1643.
18. Grishin, D.F., Semenycheva, L.L., and Kolyakina, E.V., *Vysokomol. Soedin., Ser. A*, 1999, vol. 40, no. 4, pp. 609–614.

ISSN 1070-4272, Russian Journal of Applied Chemistry, 2007, Vol. 80, No. 5, pp. 822–827. © Pleiades Publishing, Ltd., 2007.
Original Russian Text © V.P. Lesnyak, D.I. Shiman, L.V. Gaponik, S.V. Kostyuk, F.N. Kaputskii, 2007, published in Zhurnal Prikladnoi Khimii, 2007, Vol. 80, No. 5, pp. 845–850.

MACROMOLECULAR CHEMISTRY AND POLYMERIC MATERIALS

Radical Copolymerization of the C_9 Hydrocarbon Fraction of Liquid Pyrolysis Products with Maleic Anhydride

V. P. Lesnyak, D. I. Shiman, L. V. Gaponik, S. V. Kostyuk, and F. N. Kaputskii

Research Institute of Physicochemical Problems, Belarussian State University, Minsk, Belarus

Received September 12, 2006; in final form, March 2007

Abstract—Radical copolymerization of the C_9 hydrocarbon fraction of liquid pyrolysis products with maleic anhydride was studied. The influence of reaction conditions on the copolymer yield, its molecular mass, and maleic anhydride content was elucidated. Hydrophilic products showing promise as modifying additives to paper stock, binding agents, dispersants, and compatibilizers were prepared.

DOI: 10.1134/S1070427207050254

Oligomerization of the C_9 fraction, a by-product from production of ethylene and propylene, yields petroleum polymeric resins (PPRs) which are widely used in production of synthetic drying oils and oil varnishes, and also as plasticizing, sizing, and other additives to various composites. The hydrophobicity of PPRs restricts their applications. Chemical modification of PPRs by carboxylation [1–6] and sulfonation allows not only variation of their physicochemical properties but also preparation of hydrophilic products, thus expanding the PPR application area. Maleinization of hydrocarbon resins by the reaction of PPR with maleic anhydride (MA) at a high temperature (≥200°C) with the formation of hydrophilic carboxyl-containing oligomers (MA content c ≥ 15 wt %) has been described in detail [1–5]. We believe that radical copolymerization of the C_9 fraction with MA, allowing preparation of resins with an MA content of up to 50%, is more promising. However, virtually no data on this process are available. On the contrary, copolymerization of binary mixtures of individual vinylaromatic monomers (in particular, styrene and its derivatives) and dicyclopentadiene, present in the C_9 fraction, with MA, maleic acid, or fumaric acid has been extensively studied [8–38].

The goals of this study were to perform copolymerization of the C_9 fraction with MA, examine the effect of reaction conditions (nature and content of initiator and solvent; reaction temperature and time) on the yield and composition of the products, and prepare hydrophilic copolymers promising as additives to stock in paper production, as binders, dispersants, compatibilizers, etc. To prepare the copolymers, we used the C_9 fraction of the composition given in Table 1. It is known that the copolymerization of monomers of the electron-donor (vinylaromatic monomers, DCPD) and electron-acceptor (MA) types in the presence of radical initiators occurs by the radical-complex mechanism with the formation of predominantly alternating copolymers [11].

To determine how the initiator affects the copolymer yield and its MA content, we tested as copolymerization initiators such commonly used agents as benzoyl peroxide (BP), cumyl peroxide, and 2,2'-azobis(isobutyronitrile). Table 2 shows that the most effective initiators of the copolymerization of the C_9

Table 1. Composition of the C_9 fraction (bp 94–175°C)

Component	Content, wt %
Dicyclopentadiene (DCPD)	23
Styrene	14
o-, *m*-, *p*-Vinyltoluenes	9
Indene	8
α-Methylstyrene	3
Cyclopentadiene	2
DCPD derivatives	2
Total monomers	61
m-, *p*-Xylenes	10
1,2,3-Trimethylbenzene	6
o-Xylene	5
Isopropylbenzene	2
1,3,5-Trimethylbenzene	1
Indan	1
Benzene	1
Unidentified	13

Table 2. Influence of the initiator on the copolymer yield and its MA content. Copolymerization conditions: weight ratio of monomers of the C_9 fraction to MA 1 : 1, solvent dioxane, volume ratio of dioxane to the C_9 fraction 1 : 1, initiator amount 1 wt % relative to the monomers, reaction time 3 h

Initiator	*T*, °C	*T*, °C, at which the initiator half-life is 10 h [12]	Copolymer yield based on monomers, wt %	MA content of copolymer, wt %
2,2'-Azobis(isobutyronitrile)	65	64	49	22
	65 + 115*		61	31
Benzoyl peroxide	80	71	75	34
	115		91	31
Cumyl peroxide	120	112	87	30

* 2.5 h at 65°C + 0.5 h at 115°C.

fraction with MA are benzoyl and cumyl peroxides; in their presence, the copolymers are formed in a high yield. In the presence of 2,2'-azobis(isobutyronitrile), even at elevated temperatures, the copolymer yield is lower than in the presence of BP and cumyl peroxide. With BP, at the synthesis temperature increased to 115°C, it is possible to prepare copolymers in a high yield, due to accelerated decomposition of the initiator. Since too high copolymerization temperatures distort the alternation of the monomer units [12, 13], it is not appropriate to heat the reaction mixture above 120°C. Therefore, in the further studies we used BP; furthermore, it ensured the highest, compared to the other initiators tested, content of MA in the resulting copolymers. It is interesting that the nature of the initiator and its content in the reaction mixture do not noticeably affect the molecular mass of the copolymer; the molecular masses show a large scatter in different experiments, and the molecular-mass distribution (MMD) is broad.

When studying the effect of the initiator amount on the copolymer yield and its MA content, we found that the copolymer yield regularly increased with an increase in the initiator concentration. The MA conversion did not noticeably change (64 wt %) with an increase in the BP concentration in the reaction mixture (starting from 1 wt %), and the content of the anhydride in the copolymer was 31 wt %.

A study of how the copolymerization time affects the copolymer yield and its MA content showed that, at a BP concentration of 1 wt %, the highest (for these conditions) yield of the product (85%) is attained in 3 h, whereas in the presence of 0.5 wt % BP the highest yield (76%) is attained in a longer time, 6 h (Fig. 1). The MA content of the copolymer does not noticeably vary with the conversion of the monomers. The number-average molecular mass of the copolymer decreases with an increase in the reaction time (Fig. 2), and the products prepared show very broad

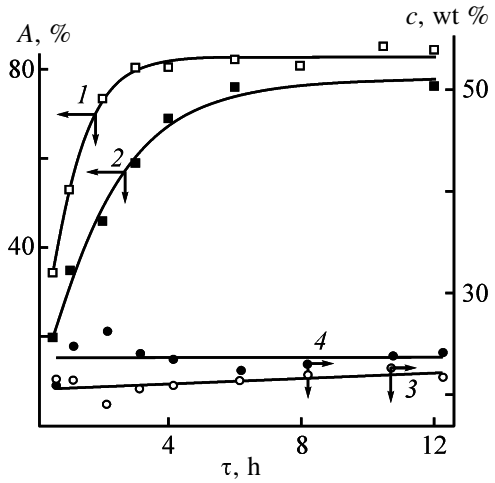

Fig. 1. (*1, 2*) Copolymer yield *A* (% based on monomer) and (*3, 4*) its MA content *c* as functions of the synthesis time τ. Copolymerization conditions: weight ratio of monomers of the C_9 fraction to MA 1 : 1, initiator BP, solvent dioxane, volume ratio of dioxane to the C_9 fraction 2 : 1, temperature 80°C; the same for Fig. 2. BP content, % of monomers: (*1, 3*) 1 and (*2, 4*) 0.5.

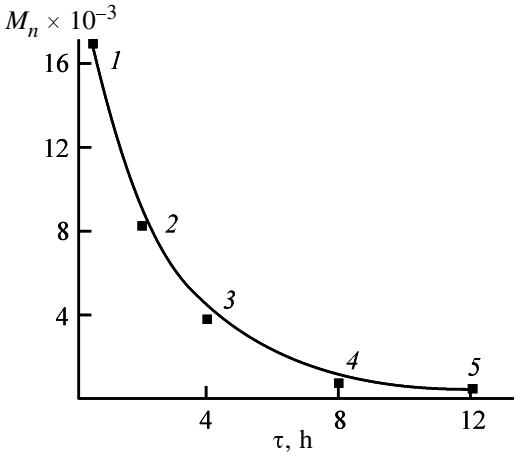

Fig. 2. Number-average molecular mass M_n of the copolymer as a function of the synthesis time τ. BP content 1% relative to the monomers. M_w/M_n: (*1*) 5.8, (*2*) 8.1, (*3*) 5.6, (*4*) 24.4, and (*5*) 12.9.

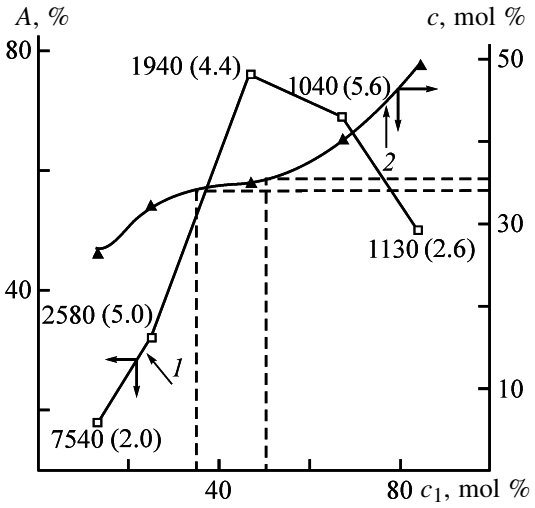

Fig. 3. (*1*) Copolymer yield *A* (% based on monomer) and (*2*) its MA content *c* as functions of the MA content of the monomer mixture c_1. Copolymerization conditions: initiator BP, 1% of the monomers; solvent dioxane, volume ratio of dioxane to C_9 fraction 1 : 1; 80°C, 3 h. The figures denote the M_n values; the M_w/M_n ratios are given in parentheses.

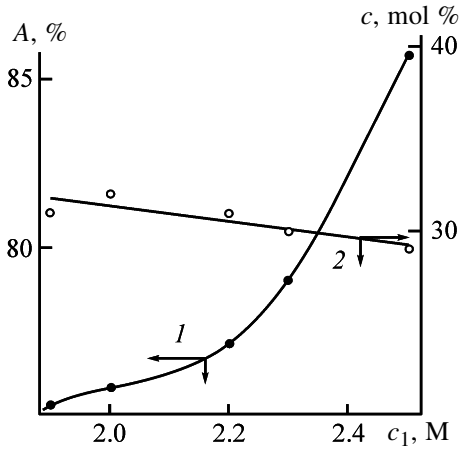

Fig. 4. (*1*) Copolymer yield *A* (% based on monomer) and (*2*) its MA content *c* as functions of the concentration of the monomers in the starting mixture c_1. Copolymerization conditions: initiator BP, 1% of the monomers; weight ratio of the monomers of the C_9 fraction to MA 1 : 1; solvent dioxane; 80°C, 3 h.

MMD even at low conversion of the monomers. This may be due to the presence of a large number of monomers of different activities in the system.

A study of how the ratio of the monomers of the C_9 fraction to MA in the reaction mixture affects the copolymer composition (Fig. 3) showed that the 1 : 1 copolymer can be prepared only from a mixture with a large excess of the anhydride (MA content 84 mol %). At 50 : 50 molar ratio of the monomers, no more than 36 mol % MA is incorporated into the copolymer. On the contrary, the copolymerization of binary mixtures styrene (or styrene derivative)–MA and DCPD–MA (molar ratio 50 : 50) yields copolymers whose composition does not noticeably differ from that of the monomer mixture, i.e., 50 : 50 [14–17]. It should be noted that neither MA nor DCPD homopolymerize under the copolymerization conditions [14].

Despite the fact that the mixture of monomers of the C_9 fraction is complex and multicomponent, a certain tendency to alternation of monomers of different nature in the copolymers is observed. As seen from Fig. 3, this tendency is particularly pronounced in the copolymerization of mixtures with an MA content of up to 35 mol %, from which copolymers with the anhydride content exceeding that in the starting mixture are formed. The copolymer with the relative content of anhydride units equal to the MA content in the starting mixture is formed only from a mixture with 35 mol % MA. When the MA content in the starting mixture exceeds 35 mol %, the resulting copolymers are depleted of the MA units. This trend may be due to exhaustion of the most active electron-donor monomers present in the C_9 fraction (styrene, vinyltoluenes) and increase in the contribution to the chain propagation of separate monomers rather than of relatively stable monomeric donor–acceptor complexes. As a result, the distribution of units in the copolymer becomes random.

The copolymer yield also depends on the composition of the monomer mixture, and the reaction rate is the highest at the molar ratio of the monomers of the C_9 fraction to MA of approximately 50 : 50 (Fig. 3). Apparently, at this monomer ratio the concentration of monomeric donor–acceptor complexes in the system is the highest, and it is well known that the rate of the copolymerization involving complexes is higher than that of the process involving separate monomers [11]. A study of how the concentration of the monomers affects the copolymerization rate showed that the reaction rate increased with the monomer concentration, and the MA content of the copolymer slightly decreased (by approximately 2%) (Fig. 4).

Figure 3 shows that the number-average molecular mass of the copolymers decreases with an increase in the MA content of the starting monomer mixture. From a mixture with 9 mol % MA, we obtained a copolymer with the highest molecular mass (7540). Apparently, an increase in the ratio of MA to monomers of the C_9 fraction in the starting monomer mixture increases the probability of chain transfer. It is interesting that, at both low (9 mol %) and high

Table 3. Effect of solvent on the copolymer yield and its MA content. Copolymerization conditions: weight ratio of the monomers of the C_9 fraction to MA 1 : 1; volume ratio of the solvent to the C_9 fraction 1 : 1; initiator BP, 1 wt % relative to the monomers; 3 h

Solvent	Dielectric permittivity of solvent	Copolymer yield based on monomers, wt %	MA content of copolymer, wt %	M_n	M_w/M_n
1,4-Dioxane	2.2	76	32	1820	15.6
Toluene	2.4	55	21	–	–
1,2-Dichloroethane	10.4	63	34	4670	6.4
Cyclohexanone	18.2	44	21	1200	4.1
Dimethylformamide	36.7	18	34	–	–

(84 mol %) MA content of the reaction mixture, the resulting copolymers have a narrower MMD than those prepared at the intermediate monomer ratios.

The copolymerization of monomers of the electron-donor and electron-acceptor types is strongly influenced by the solvent [9, 10, 18–20]. Some solvents used in the copolymerization of MA with vinylaromatic monomers can form donor–acceptor complexes with the anhydride (tetrahydrofuran, dioxane, etc.), affecting the formation of complex monomer pairs and correspondingly contributing to the overall copolymerization process [9, 10]. For example, in the photopolymerization of a mixture of styrene with MA, the copolymerization rate and molecular mass of the copolymer decrease with an increase in the donor power of the solvent.

Experiments on the copolymerization of MA and C_9 fraction in various solvents showed that the dependence of the copolymer yield (and hence copolymerization rate) on the solvent polarity was common (Table 3). The lowest yield was observed in the most polar solvent, dimethylformamide. This is due to the fact that, among the solvents tested, dimethylformamide has the highest dielectric permittivity and the highest Gutmann donor number (26.6 [22]); therefore, it forms with electron-acceptor MA a stronger complex than do monomers of the C_9 fraction, which leads to suppression of the copolymerization, the more so as the solvent is in excess relative to the electron-donor monomers. With low-polarity toluene, a deviation from the common trend is observed, probably due to the fact that the arising copolymer forms a separate phase. The solvent affects not only the reaction rate but also the copolymer composition. In toluene and cyclohexanone, copolymers with a lower MA content were obtained. However, no clear correlation is observed between the solvent polarity and the MA content of the copolymer. Table 3 also shows that the copolymers formed in various solvents have low M_n and broad MMD.

Thus, our studies of how the copolymer yield and MA content depend on the composition of the starting monomer mixture, nature of the initiator and solvent, and reaction conditions showed that the copolymerization of the C_9 fraction with MA in the presence of radical initiators somewhat differs from the copolymerization of the binary monomer mixtures. No clear dependence of the molecular mass of the copolymers on the reaction conditions (initiator concentration, temperature, solvent) is observed. The copolymers obtained from equimolar monomer mixtures contain considerably less than 50 mol % MA. Apparently, the observed deviations from certain regular trends characteristic of radical copolymerization are primarily associated with the multicomponent composition of the system, leveling off the effect of various reaction parameters on the copolymerization. The copolymers prepared have M_n from 500 to 17 000; they are soluble in acetone, dioxane, tetrahydrofuran, and cyclohexanone, and in the form of ammonium and sodium salts, in water.

EXPERIMENTAL

The copolymerization was performed in a glass reactor equipped with a power-driven stirrer, a thermometer, and a reflux condenser. The reactor was purged with an inert gas, after which it was charged with 10 ml of a solvent (dioxane, cyclohexanone, dichloroethane, toluene, or dimethylformamide), 5.7 g of MA (at 1 : 1 weight ratio of MA to monomers of the C_9 fraction), 10 ml of the C_9 fraction, and 0.114 g (1 wt % relative to monomers) of an initiator [benzoyl peroxide, cumyl peroxide, or 2,2'-azobis(isobutyronitrile)]. The mixture was heated with vigorous stirring to 85 (with BP), 120 (with cumyl peroxide), or 65°C [with 2,2'-azobis(isobutyronitrile)] for a prescribed

time (usually 3 h). The resulting mixture was poured into a four- to fivefold excess of a precipitant (80–100 mol of a mixture of petroleum ether and benzene, 1 : 1 by volume). The precipitated copolymer was separated and dried. The product was dissolved in acetone and reprecipitated, after which it was vacuum-dried (90–100°C, 2 mm Hg) to constant mass.

The number-average and weight-average molecular masses and the molecular-mass distribution of the copolymers prepared were determined by gel permeation chromatography on a Spectra Physics device equipped with two columns (PL gel, length 300 mm, diameter 5 μm, pore size 100 and 500 Å) and an SP8430 differential refractometer as detector. The elution was performed at 30°C with tetrahydrofuran at a rate of 1 ml min^{-1}. The values of M_n and M_w/M_n of the polymer were calculated from the elution curves using the calibration plots obtained with close-cut polystyrene references.

The MA content was determined by back-titration with phenolphthalein as indicator. A copolymer sample (0.1–0.2 g) was dissolved in 10 ml of acetone, and 10 ml of water and 10 ml of 0.2 N KOH were added. After standing for 2–3 h, the resulting solution was titrated with 0.1 N HCl.

The C_9 fraction was analyzed with a Shimadzu GC-17A-QP-5000 gas chromatograph–mass spectrometer equipped with an HP-5ms detector. The fraction was separated on a 50 m × 0.2 mm capillary column coated with a 0.33-μm layer of the stationary phase. Measurement conditions: electron impact (70 eV), column temperature 60–300°C (10 deg min^{-1}), carrier gas He (1 ml s^{-1}).

The C_9 fraction was dried over $CaCl_2$ and distilled under reduced pressure. Maleic anhydride was recrystallized from chloroform and then distilled under reduced pressure. The initiators and solvents were purified by standard procedures.

CONCLUSIONS

(1) Copolymerization of the C_9 fraction of liquid pyrolysis products with maleic anhydride in the presence of various initiators [benzoyl peroxide, cumyl peroxide, 2,2'-azobis(isobutyronitrile)] was performed. The dependence of the copolymer yield and content of maleic anhydride in it on the composition of the starting monomer mixture, nature and concentration of the initiator, solvent, and reaction temperature and time was elucidated. As compared to the copolymerization of binary mixtures of individual electron-donor monomers with electron-acceptor maleic anhydride, copolymerization of the C_9 fraction with maleic anhydride is characterized by weaker tendency to alternation of different units. The copolymers prepared from monomer mixtures containing 50 mol % maleic anhydride contained only 36 mol % anhydride units.

(2) Based on the regular trends revealed, hydrophilic copolymers containing 25–50 mol % maleic anhydride with M_n from 500 to 17 000 and a broad molecular-mass distributoin were prepared.

REFERENCES

1. Mokrii, E.M., Dzinyak, B.O., and Kichura, D.B., *Ukr. Khim. Zh.*, 2002, vol. 68, no. 1, pp. 54–58.
2. Ukrainian Patent 44 605.
3. Ermilova, T.A., Mogilevich, M.M., and Budanov, N.A., *Lakokras. Mater. Ikh Primen.*, 1991, no. 2, pp. 3–6.
4. RF Patent 2 177 959.
5. Dumskii, Yu.V., Cherednikova, G.F., Ivolin, V.V., et al., *Neftepererab. Neftekhim.*, 1999, no. 4, pp. 23–25.
6. Bondaletov, V.G., Bondaletova, L.I., and Troyan, A.A., *Izv. Vyssh. Uchebn. Zaved., Khim. Khim. Tekhnol.*, 2003, vol. 46, no. 2, pp. 43–45.
7. Lesnyak, V.P., Gaponik, L.V., Mardykin, V.P., and Kaputskii, F.N., *Zh. Prikl. Khim.*, 2003, vol. 76, no. 11, pp. 1921–1923.
8. Rzaev, Z.M.O., *Prog. Polym. Sci.*, 2000, vol. 25, pp. 163–217.
9. Rätzsch, M., *Prog. Polym. Sci.*, 1988, vol. 13, pp. 277–337.
10. Yablon'ko, B.M. and Tanchuk, Yu.V., *Neftepererab. Neftekhim.*, 1990, no. 39, pp. 45–55.
11. Kabanov, V.A., Zubov, V.P., and Semchikov, Yu.D., *Kompleksno-radikal'naya polimerizatsiya* (Radical Complex Polymerization), Moscow: Khimiya, 1987.
12. Semchikov, Yu.D., *Vysokomolekulyarnye soedineniya* (Macromolecular Compounds), Moscow: Akademiya, 2003.
13. Terteryan, D.A. and Khrapov, V.S., *Vysokomol. Soedin., Ser. A*, 1983, vol. 25, no. 9, pp. 1850–1854.
14. Rzaeva, Z.I., Medyakova, L.V., and Agaev, U.Kh., *Vysokomol. Soedin., Ser. A*, 1986, vol. 27, no. 5, pp. 1089–1094.
15. Briššová, M. and Štaudner, E., *Eur. Polym. J.*, 1996, vol. 32, no. 4, pp. 529–533.
16. Shashi, D.B. and Narayan, C.L., *J. Appl. Polym. Sci.*, 1996, vol. 60, pp. 649–656.
17. Zerroukhi, A., Cincu, C., and Montheard, J.-P., *J. Appl. Polym. Sci.*, 1999, vol. 71, pp. 1447–1454.

18. Brown, P.G. and Fujimori, K., *Polymer*, 1995, vol. 36, no. 5, pp. 1053–1059.
19. Rätzsch, M., Schicht, G., Arnold, M., et al., *Chem. Zvesti*, 1984, vol. 38, no. 6, pp. 823–838.
20. Klumperman, B. and Brown, P.G., *Macromolecules*, 1994, vol. 27, pp. 6100 – 6101.
21. Cincu, C. and Montheard, J.-P., *J. Appl. Polym. Sci*., 1996, vol. 61, pp. 1847–1851.
22. Reichardt, Ch., *Solvents and Solvent Effects in Organic Chemistry*, Weinheim: VCH, 1988.
23. Butler, G.B., Do Choon, H., and Zerner, M.C., *J. Macromol. Sci., Part A*, 1989, vol. 26, no. 8, pp. 1115–1135.
24. Deb, P.C. and Meyerhoff, G., *Polymer*, 1985, vol. 26, no. 4, pp. 629– 635.
25. Deb, P.C. and Meyerhoff, G., *Eur. Polym. J*., 1984, vol. 20, no. 7, pp. 713–719.
26. Rataj, A. and Nowak, D., *Przem. Chem*., 1989, vol. 68, no. 10, pp. 460 – 462.
27. Sembai, E.I., Lazarev, E.M., and Smelyanskii, P.S., *Vestn. L'vovsk. Politekh. Inst*., 1986, no. 201, pp. 39–40.
28. Chen Show-An and Chang Gwo-Yang, *Macromol. Chem*., 1986, vol. 187, no. 7, pp. 1597–1602.
29. Hill, D.J.T., O'Donnell, J.H., and O'Sullivan, P.W., *Macromolecules*, 1985, vol. 18, no. 1, pp. 9–17.
30. Światla-Żeliakow, M., *Eur. Polym. J*., 1999, vol. 35, pp. 83–88.
31. Ottenbrite, R.M. and Jones, J., *Am. Chem. Soc. Polym. Prepr*., 1985, vol. 26, no. 1, pp. 128–129.
32. Zhen Yao, Bo-Geng Li, Kun Cao, and Zu-Ren Pan, *J. Appl. Polym. Sci*., 1998, vol. 67, pp. 1905–1912.
33. Zhen Yao, Bo-Geng Li, Wen-Jun Wang, and Zu-Ren Pan, *J. Appl. Polym. Sci*., 1999, vol. 73, pp. 615–622.
34. Belkhiria, S., Meyer, T., and Renken, A., *Chem. Eng. Technol*., 1994, vol. 66, no. 4, pp. 513–516.
35. Gnutenko, V.A., Tsvetkov, N.S., and Plakhtii, O.A., *Vestn. L'vovsk. Univ., Ser. Khim*., 1989, no. 30, pp. 8–11.
36. Benoit, D., Craig, J.H., Elbert, E.H., et al., *Macromolecules*, 2000, vol. 33, pp. 1505–1507.
37. Park Eun-Soo, Kim Mal-Nam, Lee Ik-Mo, et al., *J. Polym. Sci., Part A*, 2000, vol. 38, no. 12, pp. 2239–2244.
38. Ye-Zi You, Chun-Yan Hong, and Cai-Yuan Pan, *Eur. Polym. J*., 2002, vol. 38, pp. 1289–1295.

ISSN 1070-4272, Russian Journal of Applied Chemistry, 2007, Vol. 80, No. 5, pp. 828–832. © Pleiades Publishing, Ltd., 2007.
Original Russian Text © I.V. Pimkov, O.G. Lutsenko, O.A. Golubchikov, 2007, published in Zhurnal Prikladnoi Khimii, 2007, Vol. 80, No. 5, pp. 851–855.

MACROMOLECULAR CHEMISTRY AND POLYMERIC MATERIALS

Immobilization of Cobalt Disulfophthalocyanine Complex on Polypropylene

I. V. Pimkov, O. G. Lutsenko, and O. A. Golubchikov

Ivanovo State University of Chemical Engineering, Ivanovo, Russia
Institute of Solution Chemistry, Russian Academy of Sciences, Ivanovo, Russia

Received November 20, 2006

Abstract—Procedures were developed for chemical activation of polypropylene materials and subsequent immobilization on them of the cobalt disulfophthalocyanine complex. Factors affecting these processes were examined, and the state of the phthalocyanine on the surface of the polypropylene fiber was determined.

DOI: 10.1134/S1070427207050266

Because of the absence of polar groups on the surface and in the bulk of the polymer, polypropylene materials are very poorly dyed with all the types of dyes, and their coloration is possible only through structural modification [1].

The goals of this study were to develop methods for modification of a nonwoven polypropylene material and for immobilization of the cobalt disulfophthalocyanine complex (CoP) on activated polypropylene, and also to examine how the concentrations of the electrolyte and CoP affect the adsorption of the dye.

EXPERIMENTAL

We used distilled water, *o*-xylene, H_2O_2, NaOH, Br_2 (pure grade), HNO_3 (d = 1.36, chemically pure grade), sodium peroxocarbonate (Khimprom Joint-Stock Company, Novocheboksarsk, Chuvashia, Russia), and CoP (Zavolzhsk Chemical Plant, Joint-Stock Company, Russia). We also used geotextile nonwoven polypropylene material (GPP) produced by the Kamenskvolokno Joint-Stock Company with the surface density of 400 g m^{-2} and thickness of 4 mm, and a 20-μm film of biaxially oriented isotactic polypropylene of molecular mass 400–700 kDa [TU RB (Technical Specifications of Belarus Republic) 00204079.164-97]. The absorption spectra were recorded on a U-2000 spectrophotometer, and the IR MATIR spectra, on an Avatar 360 FT-IR spectrometer. The specific surface area of GPP was determined on a Sorbtometr-M surface area analyzer. The photomicrographs of polypropylene films were obtained with an Axiostar plus microscope. Polypropylene was activated by different procedures.

Activation with hydrogen peroxide. A round-bottomed flask equipped with a reflux condenser was charged with 100 ml of 35% aqueous H_2O_2 and 2 g of GPP (four 0.5-g specimens), after which 5 mg of $FeSO_4$ was added (larger amounts impart a brown color to polypropylene, and smaller amounts do not ensure efficient catalysis of H_2O_2 decomposition). The reaction mixture was heated to boil and refluxed for various periods. The start of boiling was considered as the start of the reaction. After the activation, the specimens were washed with distilled water, dried in air, and analyzed by IR MATIR spectroscopy. The results obtained with different activating agents and at different activation times are listed in Table 1.

Activation with sodium peroxocarbonate. A 500-ml round-bottomed flask equipped with a reflux condenser was charged with 2 g of GLL (four 0.5-g specimens) and 200 ml of 5% NaOH. The mixture was heated to boil, and 10 g of sodium peroxocarbonate was added in small portions over a period of 1 h, so as to ensure continuous evolution of oxygen. The specimens were withdrawn and immersed in a fresh 5% NaOH solution, after which another 10 g of sodium peroxocarbonate was added over a period of 1 h. The thus treated specimens were washed with distilled water.

Activation in NaBrO solution. The activation procedure is based on the NaBrO synthesis protocol [2]. A 250-ml flask equipped with a reflux condenser was charged with 2 g of GPP, and 100 ml of 40% NaOH

Table 1. Reduced peak heights in the IR spectra in relation ot the procedure and time of treatment of polypropylene materials

Treatment time, min	Activation	Polypropylene film			GPP		
		absorption band in IR spectrum, cm^{-1}					
		3300	1740	1635	3300	1740	1635
5	H_2O_2	0.1	2.0	2.10	3.1	2.9	2.9
15		0.7	1.8	2.50	4.0	1.0	4.5
30		1.0	w	3.00	5.2	w	5.3
60		1.6	w	3.22	5.6	w	5.7
90		1.7	w	3.81	5.8	w	5.8
120		1.8	w	4.00	6.1	w	6.0
5	Na_2CO_4	1.0	2.0	2.0	3.3	3.0	5.0
15		4.0	1.6	5	10.0	3.0	15.0
30		5.0	w	7	16.0	w	20.4
60		7.3	w	10.2	26.3	w	36.2
90		7.8	w	12.3	27.0	w	38.0
120		8.2	w	13	29.0	w	40.0
5	NaBrO	2.0	4.0	8.0	3.8	10.0	4.0
15		9.0	7.0	15.1	7.0	25.0	7.0
30		10.0	9.0	19.0	9.0	29.0	9.0
45		26.0	10.0	28.3	10.0	32.0	11.0
15	HNO_3	1.2	1.3	5.0	5.0	4.2	4.5
30		3.0	2.9	8.0	8.0	7.5	8.0
60		4.4	4.3	10.0	12.0	12.0	13.6

and 25 ml of Br_2 were added. The mixture was heated to boil and refluxed for various periods. The start of boiling was considered as the start of the reaction. The activated specimens were washed with distilled water.

Activation by nitration. Nitration is seldom used for the modification of polypropylene and is the least studied [3]. We used a procedure based on data from [4]. A flask equipped with a reflux condenser was charged with 100 ml of HNO_3 (d = 1.36) and 2 g of GPP. The reaction was performed at the boiling point of the acid for various periods.

To perform the immobilization and determine the surface concentration of CoP on geotextile polypropylene, a 1-g specimen of GPP preliminarily wetted in distilled water was placed in a flask equipped with a reflux condenser, and 100 ml of an aqueous solution of CoP and electrolyte was added. The mixture was heated to boil and then left at room temperature for 12 h. Then the specimen was washed (until the wash water became transparent) and dried in air.

The CoP amount on the polypropylene surface was determined similarly to [5]. A dyed 0.5-g specimen was placed in a 100-ml flask equipped with a reflux condenser; 20 ml of 20% aqueous solution of pyridine was added, and the mixture was heated for 30 min on a boiling water bath. The solution was separated, and the dye retained on the fiber was washed out with an additional portion of aqueous pyridine. The solutions were transferred into a 50-ml volumetric flask and brought to the mark with aqueous pyridine, after which the optical density at 670 nm ($\log\varepsilon = 4.82$) was determined. The dependence of the surface concentration of CoP on its and NaCl concentrations in solution is presented in Table 2.

The state of CoP on the GPP surface was examined by spectrophotometry [6]. A dyed specimen was placed in a cell and poured over with *o*-xylene whose refractive index is virtually equal to that of polypropylene. The light scattering in the dispersion of polypropylene in *o*-xylene is absent, which allows correct recording of the electronic absorption spectra.

The procedures used for activation of a polypropylene film and immobilization of CoP on its surface were similar to those described above.

Alkaline treatment of the material was performed as follows. A 150 × 10-mm strip of the geotextile material with immobilized CoP was placed in a cy-

Table 2. Surface concentration of CoP on GPP at various solution compositions

Material	NaCl concentration, g l^{-1}, at c_{CoP} = 2.31 g l^{-1}						
	0	5	50	100	150	300	350
	CoP concentration on GPP surface, mg g^{-1}						
Initial material	0.056	0.38	1.66	3.60	5.53	5.59	5.64
Activated with H_2O_2	0.28	0.52	2.3	3.85	5.62	5.73	5.73
Material	CoP concentration, g l^{-1}, at c_{NaCl} = 300 g l^{-1}						
	0.0924	0.231	0.462	1.115	2.31	4.62	–
	CoP concentration on GPP surface, mg g^{-1}						
Initial	0.24	1.69	2.82	4.80	5.64	5.65	–
Activated with:							
H_2O_2	0.40	2.18	3.15	5.04	5.73	5.73	–
HNO_3	0.45	2.20	3.54	5.07	5.73	5.73	–
NaBrO	0.65	2.39	4.21	5.12	5.81	5.82	–
Na_2CO_4	0.71	2.54	4.64	5.20	5.85	5.87	–

lindrical vessel 350 mm high and 35 mm in diameter and fixed on the bottom, after which 200 ml of 0.2 M NaOH was added. A glass tube reaching the bottom was inserted, and air was passed at a rate of 2 l min^{-1}. The CoP concentraiton of the fiber was determined at the initial moment and after the treatment for 20, 40, 60, and 80 h.

The IR MATIR spectra of the activated polypropylene films and GPP show that the suggested activation procedures result in formation of oxygen-containing groups on the surface. The appearing absorption bands at 1635, 1740, and 1710 cm^{-1} correspond to stretching vibrations of C=O groups in various surroundings, and those at 3200 and 3300 cm^{-1}, to stretching vibrations of OH groups involved in hydrogen bonding [7, 8] (Fig. 1). The IR spectra show that the initial polypropylene film and GPP contain a small amount of oxygen-containing groups. The band at 1555 cm^{-1} in the spectrum of the specimen activated with nitric acid can be unambiguously assigned to the $-NO_2$ stretching vibrations [7].

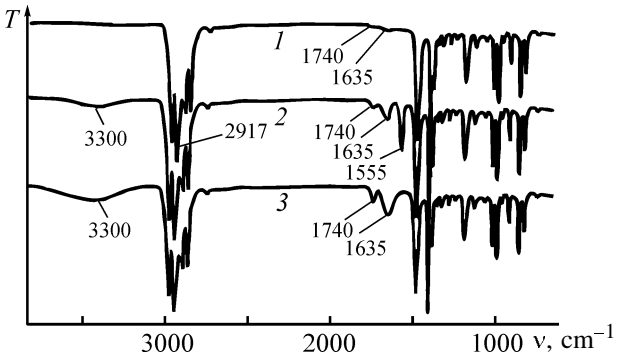

Fig. 1. IR MATIR spectra. Polypropylene film: (*1*) initial, (*2*) activated in HNO_3, and (*3*) activated in NaBrO. (*T*) Transmission amnd (ν) wavenumber.

It is appropriate to estimate the amount of oxygen-containing groups on the polypropylene surface from the relative (reduced), rather than absolute, heights of the corresponding peaks in the IR MATIR spectra (Table 1):

$$h = (T_i/T_{2917}) \times 100,$$

where T_i is the transmission at a given wavenumber and T_{2917}, that at 2917 cm^{-1}.

This peak of the C–H stretching vibrations was chosen as internal reference, because its intensity is affected by any kind of treatment of polypropylene materials to the least extent.

Table 1 shows that GPP undergoes chemical modification somewhat more readily than does the polypropylene film. The degree of modification increases with an increase in the activation time. The most efficient modification procedure for GPP is treatment in a sodium peroxocarbonate solution, and for polypropylene film, activation with NaBrO.

All attempts to immobilize CoP on a polypropylene film activated by one or another procedure failed.

The electronic absorption spectra of films, even after folding in six, demonstrate the presence of only traces of CoP on the surface. However, on GPP (both activated and initial) CoP is adsorbed readily. This difference is caused by the fact that the specific surface area of polypropylene film is considerably lower than that of nonwoven polypropylene: 0.054 $m^2 g^{-1}$ for polypropylene film, 3.84 $m^2 g^{-1}$ for the initial GPP, and 5.11 $m^2 g^{-1}$ for GPP treated with NaBrO.

It should be noted that the presence of oxygen-containing groups (–COOH, –OH, etc.) on the GPP surface promotes the adsorption of CoP. For example, the surface concentration of CoP was 0.056 mg g^{-1} on the initial material and as high as 0.28 $m^2 g^{-1}$ on that activated in H_2O_2. Furthermore, preliminary activation of polypropylene enhances the strength of CoP binding to the surface. This can be judged from the dynamics of variation of the surface concentration of the complex on treatment of the modified GPP with aqueous solutions of alkalis (Fig. 2). Apparently, CoP molecules form intermolecular hydrogen bonds with oxygen-containing centers on the GPP surface.

It is known [9] that the presence of an electrolyte in the solution increases the degree of adsorption of dyes on the fiber surface. Since the suggested procedure of CoP immobilization is similar to dyeing, we examined how the CoP and NaCl concentrations affect the degree of adsorption of cobalt disulfophthalocyanine. Table 2 shows that, with an increase in the electrolyte concentration, the CoP amount on GPP increases by an order of magnitude, reaching a limit at c_{NaCl} = 150 g l^{-1}. With an increase in the CoP concentration in solution, the degree of its immobilization on the fiber also increases (Table 2). The optimal CoP concentration is 2.31 g l^{-1}.

An increase in the temperature also favors the immobilization of the complex on GPP. Apparently, heating causes expansion of microcracks (potential sites for CoP fixation) on the GPP surface [10].

To check this assumption, we made photomicrographs of polypropylene fibers before and after the activation and after the immobilization of the phthalocyanine. We found that oxidative treatments make the fiber surface rough and cause formation of shallow ckacks in which the local concentration of CoP is increased.

Figures 3 and 4 show the CoP spectra recorded under different conditions. In dilute solutions, the complex exists in the monomeric form characterized by the bathochromic shift of the long-wave absorption maximum (Fig. 3): 667 nm in aqueous solution,

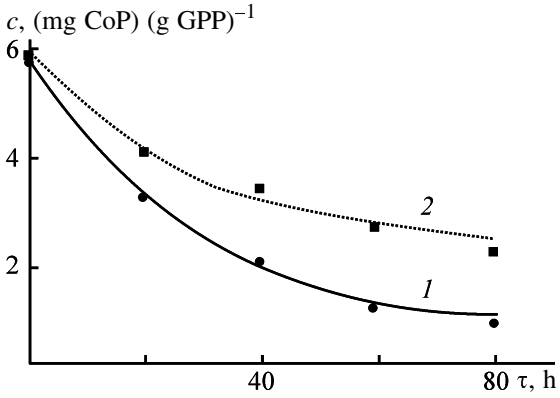

Fig. 2. Variation with time τ of the CoP surface concentration *c*: (*1*) without chemical pretreatment and (*2*) after treatment in NaBrO.

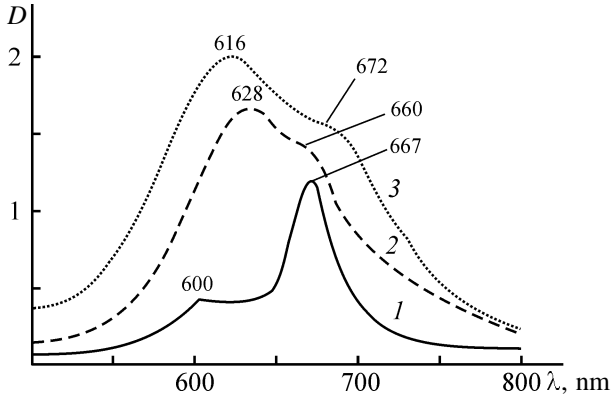

Fig. 3. Electronic absorption spectra: (*1*) aqueous CoP solution, pH 12, monomeric form; (*2*) aqueous CoP solution, pH 4, dimeric form; (*3*) polycrystalline CoP coating on glass. (*D*) Absorption and (λ) wavelength; the same for Fig. 4.

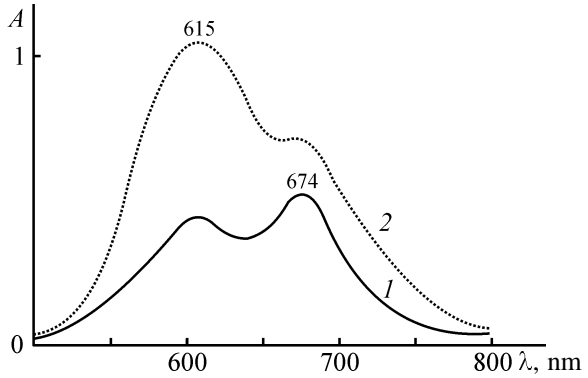

Fig. 4. Influence of the surface concentration of immobilized CoP on its electronic absorption spectrum: (*1*) 0.40 and (*2*) 5.73 mg of CoP per gram of GPP.

669 nm in DMF, and 670 nm in pyridine–water mixture. With an increase in the CoP concentration or with a decrease in pH, favoring association of sulfo derivatives of phthalocyanines [11], dimeric species

(λ_{max} 628 nm) are accumulated in aqueous solution (Fig. 3). The CoP polycrystals prepared by evaporation of an aqueous solution of the phthalocyanine on glass are characterized by an absorption maximum at 616 nm. The complex immobilized on polypropylene at its surface concentration less than 0.40 mg of Co per gram of GPP, as judged from the spectrum (Fig. 4), occurs to a large extent in the monodisperse form. At the surface concentration on polypropylene exceeding 5.73 mg of Co per gram of GPP, the polycrystalline form of CoP prevals.

Thus, experiments with the cobalt complex of a sulfonated phthalocyanine, chosen as a model, show that chemical activation of polypropylene fibrous materials is a promising pretreatment procedure for the subsequent immobilization of dyes and of catalytically and biologically active substances.

CONCLUSIONS

(1) The best procedure for chemical activation of nonwoven polypropylene is treatment with sodium peroxocarbonate, and in the case of polypropylene film, treatment with a NaBrO solution.

(2) The optimal conditions for immobilization of cobalt disulfophthalocyanine on geotextile polypropylene material are as follows: concentration of the complex in solution 2.31 g l^{-1} and NaCl concentration 300 g l^{-1}.

(3) At a surface concentration of 5.73 mg of CoP per gram of geotextile nonwoven polypropylene material, the phthalocyanine occurs on the fiber mainly in the form of microcrystals, and at a concentration of 0.40 mg of CoP per gram, in the monomeric form.

ACKNOWLEDGMENTS

The study was financially supported by the Russian Federation President's grant for the state support of young Russian scientists (MK-1534.2006.3), project no. RNP 2.1.1.1180 within the framework of the analytical departmental target program "Development of the Scientific Potenial of Higher School (years 2006–2008)," and program no. 8 of the Presidium of the Russian Academy of Sciences "Purposeful Synthesis of Inorganic Substances with Preset Properties and Development of Functional Materials Based on Them. Catalytically Active Polypropylene Materials. Synthesis, Usage, and Applications."

REFERENCES

1. Krichevskii, G.E., *Khimicheskaya tekhnologiya tekstil'nykh materialov: Uchebnik dlya vuzov* (Chemical Technology of Textile Materials: Textbook for Higher Schools), Moscow: Mir, 2000, vol. 1.
2. *Handbuch der präparativen anorganischen Chemie*, Brauer, G., Ed., Berlin: Akademie, 1952.
3. Filimoshkin, A.G. and Voronin, N.I., *Khimicheskaya modifikatsiya polipropilena i ego proizvodnykh* (Chemical Modification of Polypropylene and Its Derivatives), Tomsk: Tomsk. Univ., 1988.
4. Topchiev, A.V., *Izbrannye trudy: Nitrovanie* (Selected Works: Nitration), Moscow: Nauka, 1965.
5. *Laboratornyi praktikum po khimicheskoi tekhnologii voloknistykh materialov: Uchebnoe posobie dlya studentov vuzov tekstil'noi promyshlennosti* (Laboratory Course of Chemical Technology of Fibrous Materials: Textbook for Students of Higher Schools Specialized in Textile Industry), Moscow: Legkaya Industriya, 1976.
6. Golubchikov, O.A., Pimkov, I.V., and Lutsenko, O.G., *Izv. Vyssh. Uchebn. Zaved., Khim. Khim. Tekhnol.*, 2006, vol. 49, no. 8, pp. 14–17.
7. Nakanishi, K., *Infrared Absorption Spectroscopy*, Tokyo: Nankido, 1962.
8. Bellamy, L.J., *The Infra-Red Spectra of Complex Molecules*, London: Methuen, 1954.
9. Krichevskii, G.E., *Khimicheskaya tekhnologiya tekstil'nykh materialov: Uchebnik dlya vuzov* (Chemical Technology of Textile Materials: Textbook for Higher Schools), Moscow: Mir, 2001, vol. 2.
10. Gordon, P.F. and Gregory, P., *Organic Chemistry in Colour*, Berlin: Springer, 1983.
11. Farina, R.D., Halko, D.J., and Swinehart, J.H., *J. Phys. Chem.*, 1972, vol. 76, no. 17, pp. 2343–2348.

ISSN 1070-4272, Russian Journal of Applied Chemistry, 2007, Vol. 80, No. 5, pp. 833–837. © Pleiades Publishing, Ltd., 2007.
Original Russian Text © B.A. Zhubanov, R.M. Iskakov, R.B. Sarieva, M.J.M. Abadie, 2007, published in Zhurnal Prikladnoi Khimii, 2007, Vol. 80, No. 5, pp. 856–861.

MACROMOLECULAR CHEMISTRY AND POLYMERIC MATERIALS

New Film Composites Based on Alicyclic Polyimide

B. A. Zhubanov, R. M. Iskakov, R. B. Sarieva, and M. J. M. Abadie

Institute of Chemical Sciences, Almaty, Kazakhstan
University of Montpellier, France

Received June 19, 2006; in final form, November 2006

Abstract—New film composites based on alicyclic polyimide with polyethylene terephthalate and polycarbonate plasticizers were prepared. The thermodynamic parameters of mixing of film materials were determined by differential scanning calorimetry and thermogravimetry. The structure and composition of the resulting materials were studied by IR spectroscopy and X-ray diffraction analysis.

DOI: 10.1134/S1070427207050278

Polyimides (PIs) are of particular importance owing to the development of nanotechnologies which are widely used in production of light plastics applied in instrument-making industry, e.g., in design of large devices to be unrolled in the outer space [1].

Films based on aromatic polyamides (produced by Du Pont, the United States), which exhibit high thermal and radiation resistance, are most often used as supports for further metal plating of their surface. However, these films do not promote rapid and profound penetration of metal ions into the polymer [2–4]. Therefore, to obtain materials with improved physicochemical properties, new polymeric films were prepared, which are based on alicyclic polyimide prepared by high-temperature single-stage polycondensation of tricyclododecenetetracarboxylic acid dianhydride (adduct of benzene and maleic anhydride) with oxydianiline in *m*-cresol and DMF [5].

The choice of plasticizers is governed by the fact that the degree of crystallinity in polyethylene terephthalate (PET) and polycarbonate (PC) reaches 60 and 40%, respectively, which strongly improves the material strength [6]. Moreover, PET and PC are film-forming, thermally stable, and frost-resistant compounds and can operate in a wide temperature range from –60 to 200°C and from –150 to 200°C, respectively [7].

The aim of this work was to prepare film polymeric composites with improved mechanical properties based on an alicyclic polyimide.

EXPERIMENTAL

Initial PI was prepared by high-temperature single-stage polycondensation of dianhydride of tricyclo-(4.2.2.$0^{2,5}$)dec-7-ene-3,4,9,10-tetracarboxylic acid (adduct of benzene and maleic anhydride) with oxydianiline in *m*-cresol–DMF (40%) solution with pyridine catalyst [8, 9] at gradual heating to 140–170°C over a period of 5 h:

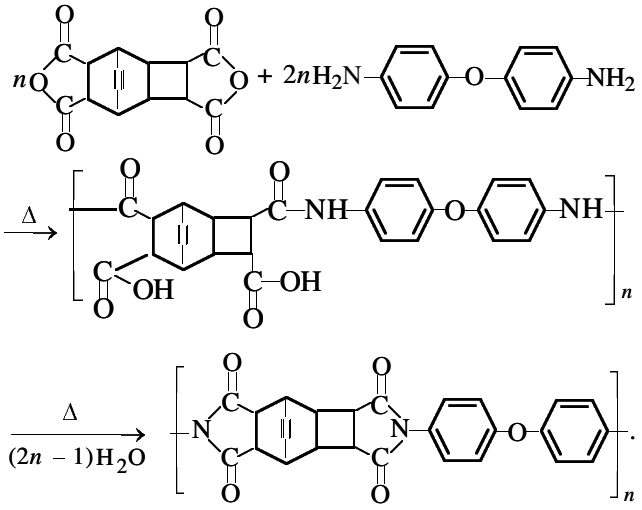

Commercial PET and PC (Aldrich and Bayer Material 5 brand, respectively) stabilized with phosphine (3%) were used. The composites were prepared by reaction and mechanical mixing at various initial component ratios [10, 11].

The viscosities of the polymer solutions in *m*-cresol were determined on an Ubbelohde viscometer at 20°C [12]. The IR spectra were recorded on a Nexus-Nicolet 5700 Fourier spectrometer.

The films on a support were fixed in a holder which was placed in a spinner of a D8 Advance (Bruker AXS) diffractometer (CuK_α radiation, λ 1.5406 Å). When the Kapton films were inelastic or

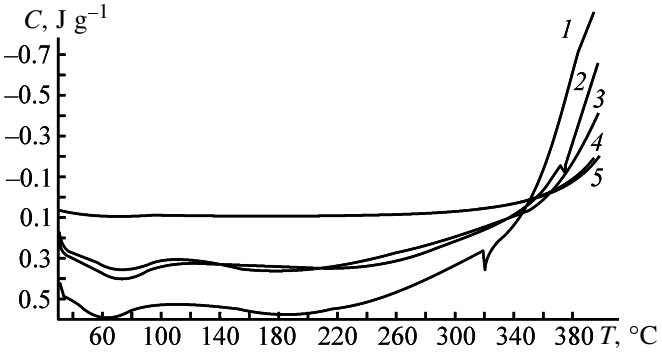

Fig. 1. Heat capacity C of PI–PET composites as a function of temperature T. PI : PET, wt % : wt %: (*1*) 85 : 15, (*2*) 95 : 5, (*3*) 98 : 2, (*4*) 99 : 1, and (*5*) pure PI.

buckled, they were glued to the support using a Ramsay paste invisible in X-ray diffraction.

The thermogravimetric (TGA) analysis and evaluation of the heat capacity of the polymers in question were performed by the procedures of thermal degradation and differential scanning calorimetry (DSC) on a Mettler Toledo TGA/SDTA 851^c and an FP85 TA Cell devices at constant heating rates of 4 and 8 deg min^{-1}, respectively.

The mechanical properties of the film samples (60×10 mm) determined out on a Com-Ten Testing Equipment tensile-testing machine (the United States).

The polymer blends based on PI and PET were prepared in *m*-cresol solutions by the reaction mixing at PET concentration varied from 1 to 20 wt %. The reaction mixing provides preparation of the polymers completely thermodynamically compatible with formation of molecularly homogeneous blends [13]. However, owing to specific smell, *m*-cresol cannot be widely used as high-temperature solvent for mechanical mixing of the initial components.

The polymeric composites based on PI and PC were prepared by mechanical mixing of the components in DMF at PC concentration varied from 0.5 to 2 wt %. Such narrow concentration range is due to relatively low solubility of PC in DMF; moreover, at PC concentration higher than 5 wt % the films become thermodynamically incompatible with PI.

The data on the polymeric compositions of PI and PET showed that the compatible films are formed at a PET concentration of 1–5 wt %; with increasing PET content to 15 wt %, the polymeric material becomes turbid, but its physicomechanical properties remain, on the whole, unchanged.

To evaluate the thermodynamic compatibility of the polymers (films), we determined the heat capacities of PI–PET and PI–PC systems and initial PI in *m*-cresol and DMF. From the temperature dependences of the heat capacities (Fig. 1), the glass transition points T_g were determined (Table 1).

The observed decrease in T_g in the PI–PET system with increasing PET content is probably due to the nature of the plasticizer, which in the presence of water released above 100–120°C in the course of cyclization of the amide groups is partially hydrolyzed with breakdown of the ester group, thus decreasing the degree of crystallinity and glass transition point of the polymer. With increasing PC content in the PI–PC composites, the glass transition point of the polymeric films increases.

This increase in the glass transition temperature T_g with increasing PC content in the PI–PC composites is probably due to the fact that these polymers are characterized by strong interchain interaction through H bonds owing to high polarity of the carbonyl groups in PC [7]. As a result, the crystal structure in the PI–PC polymers is more stable as compared to the PI–PET composites.

It is known [5] that PI is an amorphous polymer whose morphology is described as an ideal melt with irregular supramolecular structure. On transformation from hyperelastic into rigid glassy state, amorphous polymers remain in the disordered glassy state. Mutual transformations of amorphous polymers from one state into another are not phase transitions. In contrast to real phase transitions, these transformations proceed gradually and continuously within a given temperature range and only in the transition area the behavior of the polymer glasses resembles the thermodynamic transition of the second kind when an abrupt change in the thermodynamic properties is observed [13].

Temperature dependences of the heat capacity of the polymer blends given in Fig. 1 involve no breaking points, which corresponds to the thermodynamic transition of the first type, e.g., given polymers are characterized by the short-range ordering.

It should be noted that the heating rate can strongly affect T_g of the amorphous polymers [6], and this is probably typical for their blends when the content of the additive is relatively small. For example, at a heating rate of 4 deg min^{-1} no T_g is observed on the DSC curves for PI in *m*-cresol (Fig. 1), whereas at a heating rate of 8 deg min^{-1} (Fig. 2) certain jump at 114°C in the curve of the weight loss is observed, which corresponds to T_g of PI.

Also, the glass transition point is an important criterion for evaluating the compatibility of the poly-

Table 1. Physicochemical properties of the PI–PET and PI–PC composites

Initial component ratio PI : P_2, wt % : wt %	[η], dl g^{-1}	Tensile strength, δ_t, MPa	Relative elongation, %	T_m	T_g
				°C	
100/0 (*m*-cresol)	1.51	100	15.4	380	114
100/0 (DMF)	1.44	71	30	393	93.7
PI–PET:					
0/100	[4]	14–29		255–265	70–80
99/1	1.50	106	15.2	368	
98/2	1.49	101.5	17.2	363	92
95/5	1.46	91	15.3	360	85
85/15	1.42	80	13.3	355	78
PI–PC:					
0/100	[4]	–	–	–	–
99.5/0.5	1.42	100	9.0	390	97.0
99/1.0	1.4	95	10.4	387	97.5
98.5/1.5	1.35	85	11.0	384	98.0
98/2	1.33	72	11.6	380	98.7

mer blends. If a composite is characterized by two glass transition points corresponding to the polymeric components, then this system is incompatible; and the system is compatible if it is characterized by a single glass transition point.

As seen from experimental results (Fig. 1, Table 1), the polymeric composites based on PI and containing PET (1–15 wt %) or PC (0.5–2.0 wt %) exhibit only one glass transition point, which indicates that all the polymeric films are thermodynamically compatible.

Thus, we succeeded in preparing compatible polymeric films based on PI containing the above amounts of PET and PI plasticizers; T_g of PI–PET composites is lower than that of PI–PC composites. The main parameters affecting T_g are the chain flexibility and the nature of intermolecular packing [6]. With a decrease in the chain flexibility, T_g increases owing to steric hindrance, which is typical for PI–PC systems. The observed decrease in T_g for PI–PET composites is probably due to higher degree of freedom in macromolecules causing higher mobility and flexibility of the polymer sections owing to the plasticizing affect of PET. Based on the resulting thermodynamic parameters we assumed that the composites with PET plasticizer show more promise for further modification of the film material, namely, for implantation of metal ions such as Ag^+, Cu^{2+}, Ni^{2+}, or Co^{2+} [15].

In this work we studied the structure and physicochemical properties of the film materials, because addition of partially crystalline PET and PC into the amorphous PI matrix improves the composite morphology [16] and probably enhances the strength of the polymer film.

The assumption that the packing in PI–PC composites is more rigid than in PI–PET systems is confirmed by X-ray diffraction data, namely, by the presence of PC crystallites in PI halo (Fig. 3). This fact confirms the presence of a crystalline area in the polymer, in contrast to the PI–PET films, for which the crystalline area is rather diffuse.

The presence of the PET ester group in the PI–PET polymers is confirmed by the IR spectra. As seen from Fig. 4a, with increasing content of PET from 1 to 5 wt % the intensity of the stretching vibrations of the ester group ν_{C-O} at 1000 cm^{-1} increases, and at 15 wt % content of the PET plasticizer in the polymer blend the intensity of these vibrations is close to that

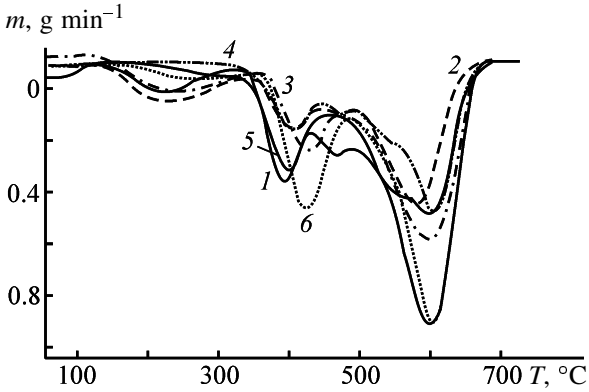

Fig. 2. DTG curves of composites based on (*1*) neat PI and PI–PET with PET content of (*2*) 2, (*3*) 5, (*4*) 10, (*5*) 15, and (*6*) 20 wt %. (*m*) Weight loss rate and (*T*) temperature.

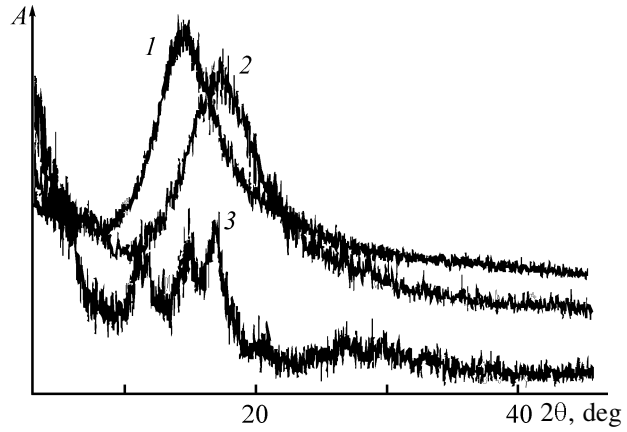

Fig. 3. Diffraction patterns of (*1*) pure PI and its composites containing (*2*) 5 wt % PET and (*3*) 1.5 wt % PC, sliding angle 2 deg. (*A*) Intensity and (2θ) Bragg scattering angle.

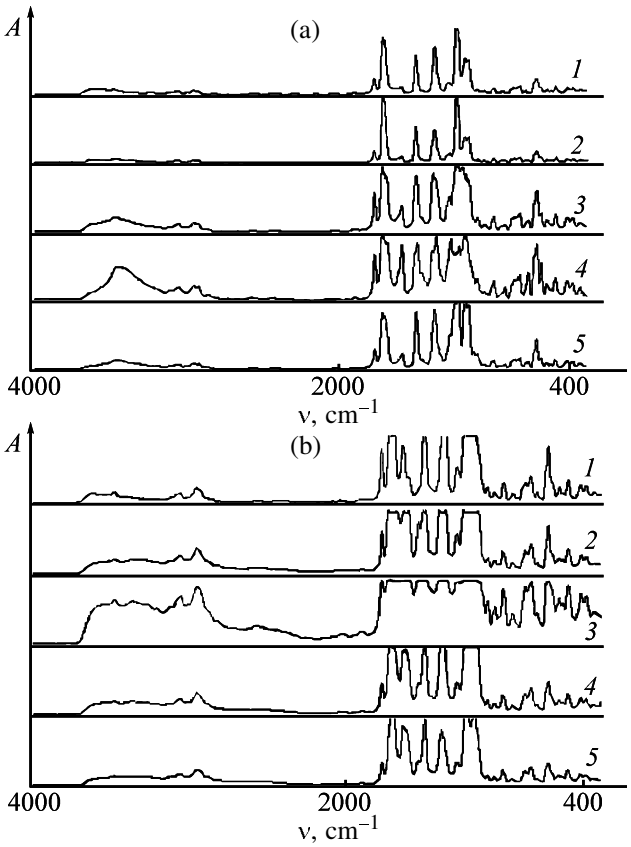

Fig. 4. IR spectra of (*1*) neat PI and (a) PI–PET composites with PET content of (*2*) 1, (*3*) 2, (*4*) 5, and (*5*) 15 wt % and (b) PI–PC with PC content of (*2*) 0.5, (*3*) 1.0, (*4*) 1.5, and (*5*) 2.0 wt %. (*A*) Adsorption and (ν) wavenumber.

in the initial PI. This is probably due to the fact that at 15 wt % content of PET the polymer blend undergoes phase segregation making the polymer film turbid; this corresponds to the second weak peak in the temperature dependence of the heat capacity of the PI–PET composite (Fig. 1). In the IR spectra of the PI–PET composite, the bands of the carbonyl group of the initial PET at 1735 cm^{-1} and of the carbonyl group of PI at 1700 cm^{-1} are shifted by 35 and 20 cm^{-1}, respectively, probably due to the formation of a hydrogen bond between the carbonyl group of PET and hydroxy group of the amido acid fragment [17] formed in the course of PI synthesis. The presence of this acid in the PI–PET systems is confirmed by thermogravimetric analysis. The content of the imide groups and amido acid fragment appearing in the polymer with addition of PET is shown in Table 2. These results correspond to the theoretical ratio of the components.

Table 2. Composition of polyimide systems

Composite	Content, wt %		Content of PET, wt %	
	imide	amido acid	gravimetry	TGA data
PI	89.8	10.2		
PI–PET, PET, %:				
1%	86.1	12.4	1.05	1.15
2%	83.8	12.0	2.1	2.25
5%	80.5	11.8	5.1	7.7
15%	74.0	10.9	15.3	14.9

The above data suggest that there are no chemical interactions in the PI–PET polymer films, which are physical blends associated through hydrogen bonds.

No chemical interactions were observed in the PI–PC composites. The characteristic band belonging to the PC carbonyl group at 1740 cm^{-1} is found in all the IR spectra of PI–PC composites with various component ratios (Fig. 4b). No shifts by more than 200 cm^{-1} were observed. Hence, PI–PC composites are also probably formed due to the hydrogen bonds. This is indirectly confirmed by the fact that after heating at temperatures higher than 50°C the film becomes turbid and brittle.

We also tested the mechanical properties of new PI–PET and PI–PC composites; the data on the tensile strength and relative elongation at constant deformation rate are listed in Table 1. As seen, the tensile strength of the PI–PET composites decreases with increasing PET content (similarly to T_g) but remains significantly higher than that of the individual PET (14–29 MPa). As for PI–PC systems, T_g and δ_t vary in the opposite directions. This is probably due to the

fact that, in contrast to PET with linear polymeric structure and more compact packing, PC contains bulky side groups, which make the polymeric films brittle. Nevertheless, addition of partially crystalline PET and PC polymers improves the strength of the polymer films; upon mixing of PI and PC, δ_t increases from 71 to 100 MPa. For PI–PET (99 : 1) composites δ_t increases from 100 to 106 MPa; at the other component ratios, when the tensile strength of the polymer films slightly decreases, their relative elongation remains fairly high (15.2–17.2%), i.e., all the PI–PET polymer films are characterized by high rupture strength and relative elongation. Since the melting points of the composite materials are 355–393°C at high reduced viscosities of the polymer solutions, these polymers can be classed with thermally stable composites with high physicochemical and mechanical properties.

Thus, polymeric films with thermally controlled and high strength properties were prepared using PI–PET and PI–PC polymer blends with various ratios of the initial components.

CONCLUSIONS

(1) The thermodynamic parameters of mixing of the film materials were determined by differential scanning calorimetry and thermogravimetry; these data show that the films based on polyimide containing polyethylene terephthalate (1.0–15.0 wt %) or polycarbonate (0.5–2.0 wt %) have a single glass transition point, i.e., the resulting polymer films are thermodynamically compatible.

(2) The absence of chemical interaction between polyimide and polyethylene terephthalate or polycarbonate was confirmed by IR spectroscopy.

(3) Addition of polyethylene terephthalate (1.0–15.0 wt %) or polycarbonate (0.5–2.0 wt %) into the polyimide matrix enhances the film strength. Their tensile strength increases from 71 to 100 and from 72 to 106 MPa for PI–PET and PI–PC systems, respectively, whereas the thermal properties of the composites (T_m 355–393°C) remain essentially unchanged.

ACKNOWLEDGMENTS

This study was financially supported by the International Science and Technology Center (project no. K-1117).

REFERENCES

1. Kudaikulova, S.K., Iskakov, R.M., Kravtsova, V.D., et al., *Polimery spetsial'nogo naznacheniya* (Specialty Polymers), Almaty: Inst. Khim. Nauk im. A.B. Bekturova, 2006.
2. Kudaikulova, S.K., *Izv. Nats. Akad. Nauk Resp. Kaz., Ser. Fiz.-Mat.*, 2001, vol. 2, no. 6, pp. 186–193.
3. Stoakley, D.M. and Clair, A.K., *J. Polym. Prepr.*, 1996, vol. 37, no. 1, pp. 541–546.
4. Souhward, R.E., Bogges, C.M., et al., *J. Chem. Mater.*, 1998, vol. 10, no. 2, pp. 1409–1414.
5. Zhubanov, B.A., Arkhipova, I.A., and Alimbekov, O.A., *Novye geterotsiklicheskie polimery* (New Heterocyclic Polymers), Alma-Ata: Nauka, 1979.
6. Rabek, J.F., *Experimental Methods in Polymer Chemistry. Physical Principles and Applications*, Chichester: Wiley, 1980.
7. *Entsikopediya polimerov* (Encyclopedia of Polymers), Moscow: Sov. Entsikopediya, 1977.
8. Zhubanov, B.A., Boiko, G.I., Shaikhutdinov, E.M., and Maimakov, T.P., *Kataliz polikondensatsionnykh protsessov* (Catalysis of Polycondensation Processes), Almaty: UNAT, 1999.
9. Zhubanov, B.A., Kravtsova, V.L., Almabekov, O.A., and Bekmagambetova, K.Kh., *Galogensoderzhashchie poliimidy* (Halogen-Containing Polyimides), Almaty: Inst. Khim. Nauk im. A.B. Bekturova, 2004.
10. Kravtsova, V.L., Zhubanov, B.A., Iskakov, R.M., et al., Kazakh Prepatent 50062, Astana, December 8, 2004.
11. Kudaikulova, S. et al., *J. Eurasian Chem. Technol.*, 2004, vol. 6, pp. 11–15.
12. Zhubanov, B.A., Iskakov, R.M., Sarieva, R.B., and Abilova, M., Abstracts of Papers, *III Mezhdunarodnyi simpozium "Fizika i khimiya uglerodnykh materialov: Nanoinzheneriya"* (III Int. Symp. "Physics and Chemistry of Carbon Materials: Nanoengineering"), 2004, pp. 63–65.
13. Baranov, A.O., Kotova, A.V., Zelinskii, A.N., and Prut, E.V., *Usp. Khim.*, 1997, vol. 66, no. 2, pp. 972–984.
14. Bernshtein, A.V. and Egorov, V.M., *Differentsial'noskaniruyushchaya kalorimetriya v fizikokhimii polimerov* (Differential Scanning Calorimetry in Physical Chemistry of Polymers), Leningrad: Khimiya, 1990.
15. Kudaikulova, S.K., Iskakov, R., Vecherkina, E., et al., in *7 European Technical Symp. on Polyimides: High Performance Functional Polymers*, 2005, pp. 183–193.
16. Kudaikulova, S.K., Musapirova, Z., Syzdykova, A.G., et al., *Khim. Zh. Kaz.*, 2003, no. 1, p. 76–84.
17. Kabanova, V.A., Semchikov, Yu.D., and Zubov, V.P., *Kompleksno-radikal'naya polimerizatsiya* (Complex Radical Polymerization), Moscow: Khimiya, 1987.

ISSN 1070-4272, Russian Journal of Applied Chemistry, 2007, Vol. 80, No. 5, pp. 838–841. © Pleiades Publishing, Ltd., 2007.
Original Russian Text © A.A. Gorbatovskii, D.A. Rozental', S.V. Dronov, 2007, published in Zhurnal Prikladnoi Khimii, 2007, Vol. 80, No. 5, pp. 862–865.

MACROMOLECULAR CHEMISTRY AND POLYMERIC MATERIALS

Structure and Composition of Polymer–Bitumen Composites

A. A. Gorbatovskii, D. A. Rozental', and S. V. Dronov

St. Petersburg State Technological Institute, St. Petersburg, Russia

Received January 25, 2007

Abstract—Features of the composition and structure of polymer–bitumen composites are examined, including the effects of the amount and quality of the basic components on the characteristics of the final product. The effect of butadiene–styrene thermoplastic elastomer on the properties of the cold applied polymer–bitumen mastic is considered. Typical component mixing schemes are analyzed, and a flowsheet for production of polymer–bitumen mastic is presented.

DOI: 10.1134/S107042720705028X

Polymer–bitumen composites are widely used in production of mastics for various purposes and advanced paving mixes, and in repair of critical sections of highways and airfield paving. Presently, there are a lot of patents on the composition of such materials. However, no general theory substantiating the processes for their production is developed yet, since there is no common view of the behavior of bitumen and polymers in preparation of composites.

It is a common view that heavy oil residues including bitumens are colloid systems: the dispersion medium is represented by oils and resins (so-called malthenes), and the dispersed phase, by solid lamellar-block asphaltene particles. According to the modern views, molecules of practically all components of petroleum bitumens are built on the same principle. Molecules of both hydrocarbons and their hetero derivatives are hybrid compounds with a polycyclic core containing 4–6 rings, mostly six-membered. This polycyclic system may have several methyl and one long-chain (C_3–C_{12}) alkyl substituents. The cyclic part of the molecule may include sulfur- or nitrogen-containing rings, the oxygen-containing functional groups being arranged mostly at the periphery of the molecule [1, 2].

The feature of the structure of asphaltene molecules is that they have three aromatic or heteroaromatic rings. This ensures the practically planar structure of asphaltene molecules; as a result of interaction of π-electron clouds with polar groups, they build associates in the form of stacks of parallel planar molecules. Therefore, asphaltenes of bitumen occur as extremely fine solid particles (1.2–2.5 nm) surrounded by solvate shells, which are spread among oil and resin molecules [2, 3].

The structure of a colloid system controls its characteristics. Therefore, the properties of bitumens are controlled by the concentration of asphaltenes (dispersed phase), component composition of malthenes (dispersion medium), and degree of their aromaticity. This is clearly demonstrated by the dependence of the softening point on the composition of bitumen: the softening point increases with increasing asphaltene concentration.

Depending on the asphaltene content, bitumens form sols, sol–gel structures, and gel-like structures (at the maximal asphaltene content). Different energy is required to destroy these structures. This energy is indirectly characterized by the softening point, which is higher for bitumens having a gel structure. In all the indicated structures, asphaltene particles are surrounded by solvate shells, preventing their adhesion. The higher the asphaltene concentration, the smaller is the dispersion medium space between the particles. At a certain asphaltene content, their solvate shells are brought in contact with each other to form clusters, which, in turn, are surrounded by a solvate shell of the molecules of the dispersion medium. Further increase in the asphaltene content results in adhesion of the clusters with formation of a rigid framework in bitumen (bitumens of structural and some special grades). However, in this case, when practically the entire dispersion medium is converted into a solvation shell, asphaltenes do not form an individual phase. Therefore, it is asphaltenes that most significantly affect the strength and softening point of bitumen [4].

Effects of the composition of bitumen on its brittle point and penetration are more complex, since these parameters depend primarily on the characteristics of the dispersion medium, like such parameters as plasticity, frost resistance, cohesion, viscosity, tendency to exudation, and many others.

To make commercial bitumen suitable for use as a structural material, its properties are modified by adding various polymers (so-called bitumen modifiers). The resulting composites are characterized by a wide plastic temperature range (high softening point and, at the same time, high plasticity at low temperatures). The use of bitumen modifiers also improves the plasticity of the material as well as its capability to withstand periodic stress without damage. The latter properties can be characterized in part by such parameters as the relative and residual elongation.

Thus, upon addition of only 4 wt % of styrene–butadiene–styrene (SBS) thermoplastic elastomer Kraton (Kraton Polymers Co.), the ring-and-ball softening point [GOST (State Standard) 11 506–73] of BND 60/90 viscous paving bitumen increased from 52 to 75°C, and the relative elongation (GOST 2678–87), from 94 to 400%.

As an illustration for the effect of bitumen modifiers on the properties of the composites we may present the results of testing obtained for cold applied mastics with various Kraton polymer contents (see table and Figs. 1–3). Cold applied mastics are distinguished in the lack of the need in warming prior to use, which is attained by adding a special solvent, making it possible to use the viscous-flow composite at relatively low temperatures.

Note that as bitumen modifiers there were tested practically all existing polymers, but the spectrum of applicable polymers appears to be rather limited.

To improve the elastic characteristic of bitumens, styrene–butadiene–styrene (SBS) thermoplastic elastomers are used. Butadiene–styrene rubbers are prepared by bulk polymerization of styrene and butadiene; they are block copolymers with spatial nodes and linear chains with the polybutadiene phase in the center and polystyrene phase at the ends [4]. Addition of the polymer into bitumen alters the structure of the latter, but not its dispersion medium. It is a common view that polymer–bitumen composites are physical blends, although at high temperatures their components can form a small amount of chemical bonds, which has no significant effect on properties of the composite.

It is advisable to consider the polymer–bitumen composites as three-component systems containing a solvent (malthenes) in which more rigid particles of bitumen and polymer are spread. The polymer dissolved in bitumen mostly thickens the dispersion medium, thus increasing the softening point of bitumen. Furthermore, the solutions generally have a lower freezing point than the solvent, thus decreasing the brittle point [4].

Effect of Kraton content on performance characteristics of cold applied mastic

Kraton, wt %	T_s (ring and ball), °C	Elongation, %	
		relative	residual
1	32	197	127
3	50	333	142
5	55	454	155
7	68	621	273
10	72	1414	476

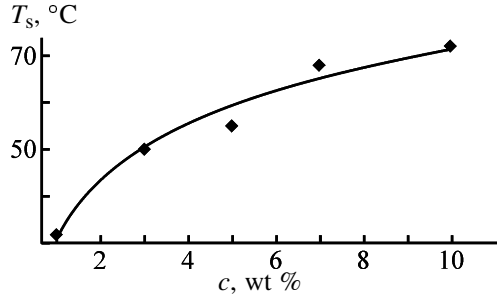

Fig. 1. Softening point T_s as a function of Kraton content c.

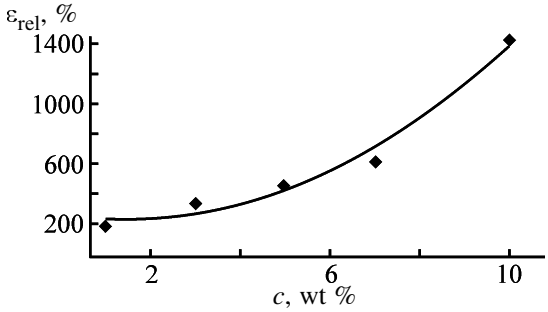

Fig. 2. Relative elongation ε_{rel} as a function of Kraton content c.

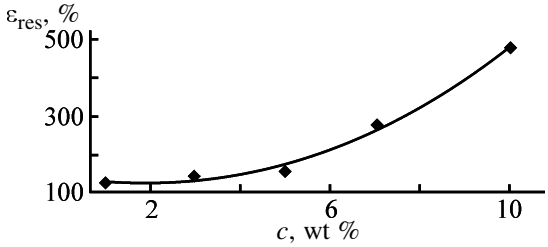

Fig. 3. Residual elongation ε_{res} as a function of Kraton content c.

Scheme 1. Flowsheet for production of polymer–bitumen composites.

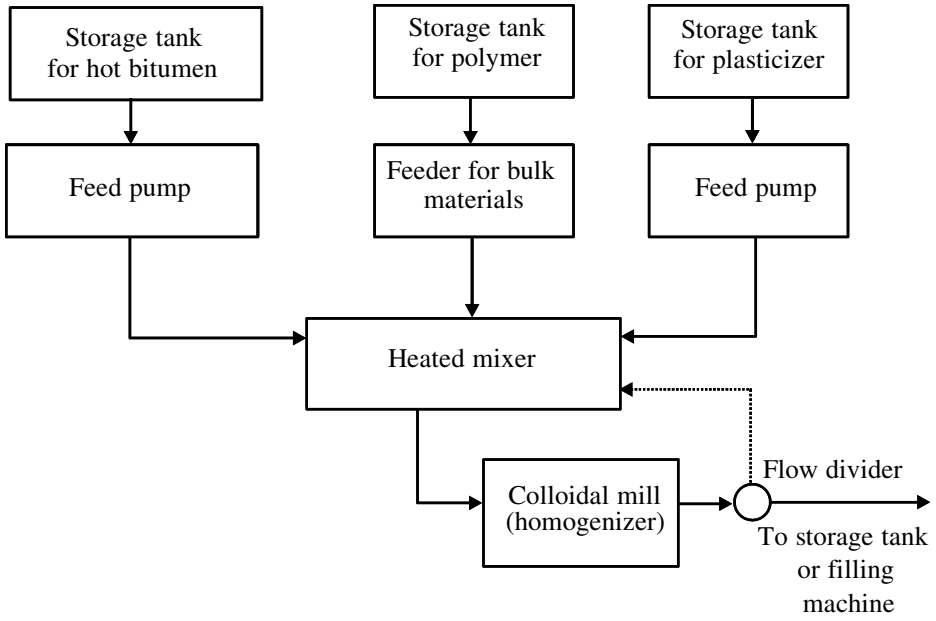

Depending on the concentration, the polymer first affects the dispersion medium and, through it, bitumen as a whole; then, at higher concentration, the polymer forms a new (the third) phase in the system, becoming a filler for bitumen. At high polymer concentrations, inversion of the phases takes place, and the polymer turns from filler into a material to be filled, and bitumen turns into filler. The phase inversion follows the coexistence state of the two continuous phases of the polymer and bitumen (in this state, the polymer fibers penetrates throughout bitumen, thus reinforcing it).

Since the polymer is dissolved just in the malthene fraction of bitumen, the relative content of this fraction should be taken into account: at an insufficient content of oils in bitumen, the modifier can locally coagulate, thus deteriorating the performance characteristics of the composite. To avoid this, bitumen is additionally modified with so-called plasticizers, which eliminate the shortcomings of the dispersion medium. The decision on the plasticizer should be made taking into account their nature, compatibility with other bitumen components, and the ability to dissolve the polymer. The plasticizer should be aromatic; otherwise, exudation of some of its components from the body of the composite will occur, like that in the case of using machinery oil.

In producing polymer–bitumen composites, of a great importance is to optimize a flow chart (Scheme 1). In the use of three basic components, bitumen, oil, and polymer, the following versions of the process are feasible in principle.

(1) Introduction of the polymer into temperature-stabilized oil, followed by mixing of the resulting mass with heated bitumen. This operation can be performed at 150–160°C, which is below the melting point of the polymer (190–200°C). In this version, it takes shorter time to complete mixing of the polymer with a softener and then with bitumen.

(2) Premixing of heated oil and bitumen, followed by addition of the modifier. Generally, this version is distinguished by longer time of mixing required to attain complete dissolution of the polymer, but it would be the best choice under certain circumstances.

In addition to the above-indicated components, polymer–bitumen composites may include diverse additives for various purposes, e.g., to improve the adhesion, to stabilize the dispersion system, to inhibit oxidation processes, etc. Generally, such additives are quite efficient, but their use considerably increases the cost of the products.

By now, some problems remain to be understood in the area of bitumen composites modified with polymers, including those concerning interaction of the components, aging of the composites, and some properties of bitumen itself.

Nevertheless, polymer–bitumen composites stand well among diverse construction materials, the field of their application being steadily expanding.

CONCLUSIONS

(1) Characteristics of bitumens and, therefore, polymer–bitumen composites depend primarily on the relative content of asphaltenes, which, along with the polymer additive, exert a structuring effect on bitumen.

(2) There is a well-defined limit of the modifier content in the composite, beyond which the performance characteristics of the product deteriorate as a result of phase inversion, when the polymer, initially acting as filler, becomes a material to be filled, and bitumen turns into filler.

(3) In formulation of the polymer–bitumen composite, a special attention should be paid to the nature of a plasticizer and its compatibility with bitumen and polymer additive.

REFERENCES

1. Posadov, I.A., Abstracts of Papers, *Khimicheskii sostav neftei i nefteproduktov: Vsesoyuznaya konferentsiya* (Chemical Composition of Oils and Petroleum Products: All-Union Conf.), Tbilisi, October 1–5, 1984, pp. 21–24.
2. Posadov, I.A., Rozental', D.A., Abramovich, G.V., and Borisova, L.A., *Kolloidn. Zh.*, 1985, vol. 47, no. 2, pp. 315–322.
3. Kam'yanov, V.F., Aksenov, V.S., and Titov, V.I., *Geteroatomnye komponenty neftei* (Heteroatomic Components of Oils), Novosibirsk: Nauka, 1983.
4. Rozental', D.A., Tabolina, L.S., and Fedosova, V.A., *Modifikatsiya svoistv bitumov polimernymi dobavkami: Obzornaya informatsiya* (Modification of Bitumen Properties with Polymeric Additives: A Review), Ser.: *Pererabotka nefti* (Oil Refining), Moscow: TsNIITEneftekhim, 1988, issue 6.

ISSN 1070-4272, Russian Journal of Applied Chemistry, 2007, Vol. 80, No. 5, pp. 842–845. © Pleiades Publishing, Ltd., 2007.
Original Russian Text © A.V. Kurzin, A.N. Evdokimov, O.S. Pavlova, V.B. Antipina, 2007, published in Zhurnal Prikladnoi Khimii, 2007, Vol. 80, No. 5, pp. 866–870.

CHEMISTRY OF FOSSIL FUEL

Synthesis and Characterization of Biodiesel Fuel Based of Esters of Tall Oil Fatty Acids

A. V. Kurzin, A. N. Evdokimov, O. S. Pavlova, and V. B. Antipina

St. Petersburg State Technological University of Plant Polymers, St. Petersburg, Russia

Received February 14, 2007

Abstract—Synthesis of esters from tall oil fatty acids and lower aliphatic alcohols is studied, and characteristics of the products as substitutes or components of diesel fuel are determined.

DOI: 10.1134/S1070427207050291

Biofuel is a renewable environmentally friendly power source, which could compete with fossil fuel. Liquid biofuel is used in spark-ignition engines (ethanol and methanol) and in diesel engines (vegetable oils and their methyl esters as well as their mixtures and mixtures with conventional diesel fuel). Biodiesel is synthesized from renewable resources by ester interchange of fats and oils with lower aliphatic alcohols using acid, base, or enzymatic catalysis [1–3]. The sources of fatty acids can be vegetable oils, animal oils, and by-products and wastes from production of edible fats and oils [1–6].

Currently, the common view is that the most promising biodiesel, whose characteristics are close to those of hydrocarbon fuel, is a mixture of methyl esters of colza oil fatty acids (COFAs). It is known that even a small addition of biodiesel to the conventional fuel reduces exhaust [1, 2].

Biodiesel produced using the traditional processes has a higher cost (by 10–20%), requiring consumption of common kinds of energy, which pollute the environment. The viscosity of COFA-based biodiesel is twice that of the conventional diesel fuel, resulting in incomplete combustion of fuel aerosols. Another limitation of using oils and their derivatives is high oxygen content (8–10%), causing a decrease in the low heat value of this fuel as compared to hydrocarbon fuel and, correspondingly, an increase in the biodiesel consumption.

Despite the indicated drawbacks, the biodiesel output steadily increases. Investigators are improving the processes for its production and searching for new raw materials including esters having higher caloric value.

Among the available sources of fatty acids is tall oil, a by-product of craft pulp production. In vacuum distillation of crude tall oil (its yield amounts to 60 kg per ton of bone-dry cellulose), along with other components, fatty acids (TOFAs) constituting 30–60% of tall oil, depending on the kind of wood to be processed, are separated [7]. The fatty-acid composition of tall oil resembles that of vegetable oils, being represented primarily by unsaturated acids C_{16}–C_{18} (oleic, linoleic, linolenic, etc.) [8].

Presently, the conventional application fields of TPFAs are being reduced. Among the ways to their chemical modification is esterification. In their characteristics the resulting esters are well comparable with petroleum gas oil, so that they can be used, like COFAs, as individual fuel or depressor additive to black oil, to improve its performance characteristics [9, 10]. It should be pointed out that tall oil and distilled tall oil was suggested to be used as an additive to low-sulfur fuel for diesel engines [11].

In this study we examined esterification of TPFAs with lower aliphatic alcohols (methanol, ethanol, and isopropanol) in the presence of various catalysts, and also properties of the resulting esters characterizing them as biodiesel.

As known, the reaction can be catalyzed by mineral acids, sulfonic acids, Lewis acids, or solid acid catalysts, among them ion-exchange resins in the H form [3, 12–14]:

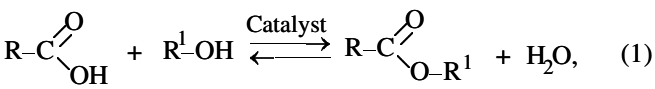

where R is the hydrocarbon radical of TOFA and R^1 = Me, Et, *i*-Pr.

Table 1. Influence of the catalyst concentration on the yield of alkyl esters of TOFAs (alcohol : TOFAs = 3 : 1, reaction time 3 h)

TOFA ester	Catalyst	Ester yield, %, at indicated catalyst concentration, wt %			
		0.5	1.0	2.0	4.0
Methyl	Sulfuric acid	54.4	63.6	68.9	70.1
	p-Toluenesulfonic acid	62.8	67.3	83.0	85.5
	Zinc(II) chloride	12.0	17.1	23.2	24.5
	Amberlyst-15	57.0	65.2	75.0	76.0
Ethyl	Sulfuric acid	56.7	64.0	69.2	71.8
	p-Toluenesulfonic acid	64.7	69.2	80.4	83.2
	Zinc(II) chloride	13.2	18.6	24.5	26.3
	Amberlyst-15	60.5	67.2	74.0	75.1
Isopropyl	Sulfuric acid	52.1	57.4	64.7	65.2
	p-Toluenesulfonic acid	62.8	68.6	79.8	81.0
	Zinc(II) chloride	11.9	17.5	22.9	24.1
	Amberlyst-15	58.0	63.8	73.8	74.1

As catalysts we used sulfuric acid, *p*-toluenesulfonic acid, $ZnCl_2$, and Amberlyst-15 ion-exchange resin.

Table 1 shows how the catalyst nature and concentration and also the alcohol structure influence the ester yield. Practically, the decision on the catalyst is made taking into account such parameters as the product yield, catalyst availability and practicability, and regenerability. The catalysts in hand are widely used on commercial scale, being, therefore, available. For reasons of economy, sulfuric acid is most widely used, even though it does not provide the maximal yield. We obtained the best results with *p*-toluenesulfonic acid (2 wt %) and Amberlyst-15. In the case of *p*-toluenesulfonic acid, increase in the catalyst concentration from 1.0 to 2.0 wt % increased the ester yield to 85.5%. Further increase in the catalyst concentration did not increase the conversion. Additionally, the indicated catalysts do not cause dehydration of alcohols and sulfonation of double bonds in fatty acids. At the same time, the catalyst based on an ion-exchange resin is more practicable and regenerable.

Therefore, it is insufficient to only optimize the catalyst to ensure the maximal ester yield. Another way is to remove one of the products from the reaction zone. Performing the reaction with simultaneous azeotropic distillation of water with benzene allowed increase of the product yield by 6%. However, in this case, the hardware implementation of the process becomes more complex.

To increase the yield, we developed a system in which methanol vapor passes through a heated catalyst unit, where it reacts with fatty acids, and the resulting esters stream down to a receiver. The use of this system increased the conversion of TOFAs by 10%.

The composition of the esters, determined by GLC, resembles that of the initial acids, suggesting that their reactivity is similar under the esterification conditions.

In Table 2, a comparison is made of the properties of the esters obtained and commercial diesel fuel (Diesel Motor Fuel Euro, Lukoil). The kinematic viscosity of the TOFA esters is no more than 4.6×10^{-6} $m^2 s^{-1}$, which is lower than the maximal value of 5.0×10^{-6} $m^2 s^{-1}$ fixed in European EN 14214 Standard. On passing from the methyl ester to isopropyl ester, the refractive index increases, and the pour point decreases. The iodine number, acid number, saponification number, sulfur content, flash point (closed cup), cloud point, and filtration termination temperature for the TOFA esters obtained are close to each other. In these parameters (except for sulfur content) the esters meet the requirements of EN 14214 standard.

As known [15], biodiesel additive based on methyl esters of vegetable oils increases the lubricity. We studied the lubricity of the TOFA methyl esters (HFR2, PCS Instruments). The results showed that the wear scar diameter (WSD) decreases from 374 μm for the hydrocarbon fuel to up to 330 μm for diesel fuel containing 10% TOFA esters, which can be attributed to increasing stability of the film on the metal surface.

EXPERIMENTAL

The IR spectra of the esters were recorded in a thin film on an IKS-29 instrument. The final product was characterized by GLC [Chrom-5 chromato-

Table 2. Characteristics of hydrocarbon diesel fuel and alkyl esters of TOFAs

Characteristics	Diesel fuel	TOFA ester		
		methyl	ethyl	isopropyl
Cetane number	45–55	48.5	48.8	49.2
Kinematic viscosity $\nu \times 10^6$, $m^2\ s^{-1}$:				
at 20°C	Up to 5.85	7.0	6.9	6.7
at 40°C	Up to 3.8	2.5	2.4	2.3
Pour point, °C, not above	–15	–22	–24	–23
Cloud point, °C, not above	–6	–8	–8	–8
Filtration termination temperature on cold filter, °C, not above	–11	–14	–15	–15
Flash point, Pensky Martens Closed Cup, °C	77	178	180	181
Fire point, °C, not below	–	55	57	59
Carbon residue (10% bottoms), %, no more than	–	0.4	0.3	0.3
Copper strip corrosion	–	Stands	Stands	Stands
Low heat value, $MJ\ kg^{-1}$	–	36.5	37.0	37.3
Total glycerol, %, maximally	–	0	0	0
Ash content, %	No standard	No more than 0.01	No more than 0.01	No more than 0.01
Filtration factor	–	No more than 3	No more than 3	No more than 3
Density at 20°C, $kg\ m^{-3}$	800–870	No more than 880	No more than 880	No more than 880
Particulate contamination	–	No	No	No
Moisture content, %	No standard	0.008	0.007	0.007
Sulfur content, wt %, no more than	0.05–0.3	0.005	0.005	0.005
Acid number, mg KOH/g	No standard	0.284	0.280	0.278
Saponification number, mg KOH/g	–	112.9	114.2	114.2
Iodine number, mg I_2/g	–	124.3	125.0	125.3
Refractive index n_D^{20}	–	1.4712	1.4822	1.4830

graph, flame-ionization detector, column 50 m × 0.22 mm (stationary phase BP×70), carrier gas helium (30 $ml\ min^{-1}$)]; solvent hexane.

Characteristics of the final product such as density, refractive index, acid number, saponification number, iodine number, ester content, sulfur content, closed-crucible flash point, flow point, cloud point, lower filtration temperature, and lubricity number were determined by the standard procedures. TOFAs from Segezha Pulp and Paper Combine (FA content 96.5%) were used as received. Alcohols (methanol, ethanol, and 2-propanol) and catalysts [sulfuric acid, *p*-toluenesulfonic acid, zinc(II) chloride, and Amberlyst-15 cation-exchange resin (Rohm & Haas)] were of chemically pure grade. Methyl esters of individual FAs (analytically pure grade) were purchased from Merck, Sigma, Aldrich, and Fluka. All the chemicals were used without additional purification.

In all the experiments, the reaction time was 3 h and the alcohol to TOFAs molar ratio was 3 : 1. The catalysts were added in amount from 0.5 to 4.0 wt % relative to the total weight of reactants.

Alkyl esters of TOFAs were synthesized by refluxing the acids with a threefold excess of an alcohol in the presence of various amounts of catalyst [16, 17].

The esterification was carried out in a 500-ml flask equipped with a reflux condenser and a mechanical stirrer. The flask was charged with 200 g of TOFAs and appropriate amounts of an alcohol and a catalyst. The mixture was vigorously stirred and heated to the boiling point of the alcohol (70, 80, or 85°C). At fixed intervals, a 2-ml portion of the reaction mixture was taken for IR analysis. The amounts of esters formed was determined by the intensity of the absorption band at 1165–1185 cm^{-1}. Additionally, the conversion of TOFAs was characterized by the acid number determined by the standard procedure. After completion of the experiment, the reaction mixture was analyzed for esters by GLC. The mixture was transferred into a separating funnel and washed three

times with 5% $NaHCO_3$ and then with distilled water to pH 7 of the wash water. The resulting esters were dried over $MgSO_4$. Then esters were separated from the unchanged acids by vacuum distillation. The ester content in the resulting product was determined by the IR spectra and GLC analysis. The ester yield was from 12.0 to 85.5%.

The product, TOFA esters, was obtained as a yellowish liquid soluble in nonpolar organic solvents and poorly soluble in water.

CONCLUSIONS

(1) Methyl, ethyl, and isopropyl esters of tall oil fatty acids were synthesized using various acid catalysts. The highest ester yield was obtained with *p*-toluenesulfonic acid.

(2) A specially designed reactor was developed to increase the yield of the methyl esters.

(3) Esters of tall oil fatty acids can be used as a substitute for, or an additive to hydrocarbon diesel fuel.

REFERENCES

1. Kulkarni, M.G. and Dalai, A.K., *Ind. Eng. Chem. Res*., 2006, vol. 45, no. 9, pp. 2901–2913.
2. Ma, F.R. and Hanna, M.A., *Bioresource Technol*., 1999, vol. 70, no. 1, pp. 1–15.
3. Lotero, E., Liu, Y., Lopez, D.E., et al., *Ind. Eng. Chem. Res*., 2005, vol. 44, no. 14, pp. 5353–5363.
4. Cetinkaya, M. and Karaosmanoglu, F., *Energy Fuels*, 2004, vol. 18, no. 6, pp. 1888–1895.
5. Wang, P.S., Tat, M.E., and Van Gerpen, J., *J. Am. Oil Chem. Soc*., 2005, vol. 82, no. 11, pp. 845–849.
6. Canakci, M. and Van Gerpen, J., *Trans. ASAE*, 2001, vol. 44, no. 6, pp. 1420–1436.
7. Golovin, A.I., Trofimov, A.N., Uglov, G.A., et al., *Lesokhimicheskie produkty sul'fattsellyuloznogo proizvodstva* (Wood-Chemical Products from Sulfate Pulping), Moscow: Lesnaya Prom–st., 1977.
8. Kogan, V.B. and Trofimov, A.N., *Poluchenie karbonovykh kislot na osnove drevesiny* (Production of Carboxylic Acids from Wood), Moscow: Lesnaya Prom–st., 1977.
9. Kurzin, A.V., Evdokimov, A.N., Golubeva, Yu.M., et al., in *Mezhdunarodnaya nauchno-prakticheskaya konferentsiya "Resurso- i energosberezhenie v tsellyulozno-bumazhnoi promyshlennosti i gorodskom kommunal'nom khozyaistve"* (Int. Scientific and Practical Conf. "Resource and Energy Saving in Pulp and Paper Industry and Municipal Economy," St. Petersburg (Russia), October 27–28, 2005, pp. 283–286.
10. Altiparmak, D., Keskin, A., Koca, A., and Guru, M., *Bioresource Technol*., 2007, vol. 98, pp. 241–246.
11. RF Patent 2289612.
12. Sonntag, N.O.V., *J. Am. Oil Chem. Soc*., 1979, vol. 56, no. 11, pp. 751–754.
13. Farris, R.D., *J. Am. Oil Chem. Soc*., 1979, vol. 56, no. 11, pp. 770–773.
14. Heidekum, A., Harmer, M.A., and Hoeldrich, W.P., *J. Catal*., 1999, vol. 181, no. 2, pp. 217–222.
15. Bhatnagar, A.K., Kaul, S., Chhibber, V.K., and Gupta, A.K., *Energy Fuels*, 2006, vol. 20, no. 3, pp. 1341–1344.
16. Soboleva, L.M., Solov'ev, V.V., Chernova, I.K., et al., *Vestn. Yaroslavl. Gos. Tekh. Univ*., 1999, no. 2, pp. 80–83.
17. Solov'ev, V.V., Bychkov, B.N., Koshel', G.N., et al., *Zh. Prikl. Khim*., 1989, vol. 62, no. 9, pp. 2128–2131.

ISSN 1070-4272, Russian Journal of Applied Chemistry, 2007, Vol. 80, No. 5, pp. 846–850. © Pleiades Publishing, Ltd., 2007.
Original Russian Text © S.A. Semenova, Yu.F. Patrakov, 2007, published in Zhurnal Prikladnoi Khimii, 2007, Vol. 80, No. 5, pp. 871–875.

CHEMISTRY OF FOSSIL FUEL

Effect of Ozonation on the Composition of Crude Coal-Tar Benzene

S. A. Semenova and Yu. F. Patrakov

Institute of Coal and Coal-Tar Chemistry, Siberian Division, Russian Academy of Science, Kemerovo, Russia

Received July 3, 2006; in final form, January 26, 2007

Abstract—The effect of ozonation on the composition of crude benzene produced by the coal-tar chemical industry was studied.

DOI: 10.1134/S1070427207050308

One of the most urgent problems of coal-tar chemical industry is improvement of crude benzene quality. The main impurities deteriorating characteristics of crude benzene are sulfur-containing, unsaturated, and saturated hydrocarbons. At present, among procedures of benzene purification are conventional sulfuric acid treatment and also fairly expensive catalytic hydrofining [1]. The latter combines in one process hydrogenolysis of sulfur-contaning compounds and hydrogenation of unsaturated hydrocarbons, which allows production of the pure product, an important raw material for synthesis of organic compounds [2].

Difficulties in utilization of wastes formed in sulfuric acid purification and high capital and operation costs of hydrofining processing [3] require development of simple and environmentally safe procedures of purification of crude benzene.

Along with conventional procedures, oxidation (e.g., with hydrogen peroxide) [4], ultrasonic treatment [3], and biotechnologies [6] are also used for purification of oil fractions for which the main detrimental impurities are unsaturated and sulfur-containing compounds.

Ozonation [7, 8] is suggested as one of oxidation procedures of purification of diesel fractions. The feature of ozone is its selective electrophilic addition to both sulfur-containing and unsaturated compounds and polycyclic arenes [9]. Unique chemical activity of ozone allows the reactions to be efficiently performed at moderate temperatures without catalysts.

Considering similar composition of undesirable target products of oil refining and coal-tar chemical industries, ozonation can be one of the feasible procedures of purification of crude coal-tar benzene. In this connection, our study was aimed to determine how ozonolysis affects the composition of crude coal-tar benzene.

EXPERIMENTAL

Crude benzene produced by coal-tar shop at the Novokuznetsk Metallurgic Plant was used as a subject of the study. The characteristics of the initial product are presented in Table 1.

Ozonation was performed at 25°C and atmospheric pressure in a bubbling-type reactor with uninterrupted feeding of ozone–oxygen mixture (1.5 vol % ozone). After the process completion, tar products accumulated at the reactor walls and dissolved in benzene were extracted with 5% KOH. Then, the product purified to remove tar was treated with 50% H_2SO_4 in

Table 1. Characteristics of crude benzene

Index	Characteristic
External appearance	Transparent yellow-orange liquid without suspended particles
Density, g cm^{-3}	0.87
Temperature, at which 97% of the product is distilled, °C	Not higher than 140
Content, wt %:	
benzene	32.3
toluene	37.1
xylene	13.5
carbon disulfide	0.24
Acidity, mg g^{-1}	1.10
Bromine number, %	5.66

the 2 : 1 ratio to remove sulfones and sulfoxides. The samples treated with acid were decanted in a separating funnel and washed with distilled water to neutral reaction.

Alkali-soluble ozonation products were acidified with dilute sulfuric acid. The precipitate containing macromolecular acids (MMAs) was separated on a filter. Low-molecular-weight products were recovered from acidic aqueous solution by extraction with methyl ethyl ketone. The products were dried, and their yield was determined.

The acid number was determined by the reaction of crude benzene with KOH, and the bromine number, by iodometric titration [10]. The elemental analysis of the products was performed by the procedure described in [11]. Chromatographic mass-spectrometric analysis was performed on a Hewlett–Packard device comprised of an HP-5890 gas chromatograph (series II) and an HP-5971 mass-selective detector. Capillary column HP-5MS (5% diphenyl-, 95% dimethylsiloxane) 30 m × 0.25 mm × 0.26 μm. Carrier gas helium, flow rate 1 ml min^{-1}. Heating mode of the column: 2 min at 50°C, from 50 to 300°C at a rate of 10 deg min^{-1}, 30 min at 300°C. The vaporizer temperature was 280°C; temperature of ion source, 175°C. The scanning rate in the range 30–650 amu was 1.2 scan s^{-1}. The IR spectra were recorded on a System-2000 Perkin–Elmer Fourier spectrometer.

Ozonation of crude benzene is accompanied by variation of its total acidity (Fig. 1). The cause of its decrease at the beginning of ozonation can be oxidation of phenolic impurities in the product. An increase in the ozonation duration over 1 h promotes intense formation of oxygen-containing products, which results in increasing acid number of crude benzene. It is likely that, after treatment with ozone for 2 h, the resulting products are subjected to secondary oxidation and the product acidity decreases again. In this case, the product color changes from the initial yellow to bright orange. After base hydrolysis, the acidity of crude benzene decreases from 1.1 to 0.2 mg g^{-1} (Fig. 1a).

The content of unsaturated and sulfur-containing compounds in the product decreases after its ozonation. For example, the bromine number of crude benzene decreased by 60% (Fig. 1b), and the content of carbon disulfide, the main component of sulfur-containing impurities in benzene [1], by 80% (Fig. 2). The effect of treatment corresponds to ozonation for 2 h. Then, the process decelerates due to saturation of crude benzene with oxidation products.

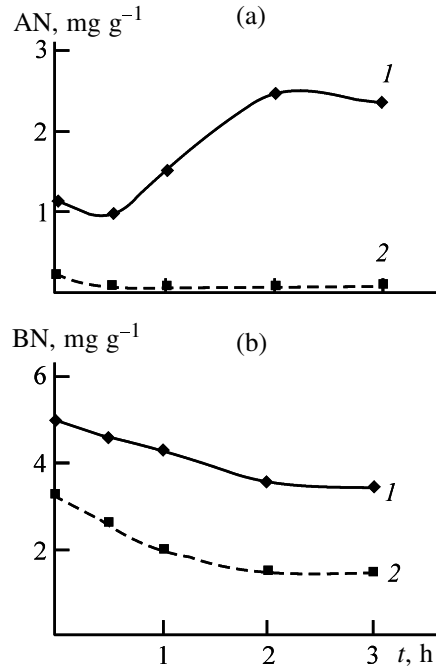

Fig. 1. (a) Acid number AN and (b) bromine number BN of crude benzene (*1*) before and (*2*) after purification, as functions of ozonation time *t*.

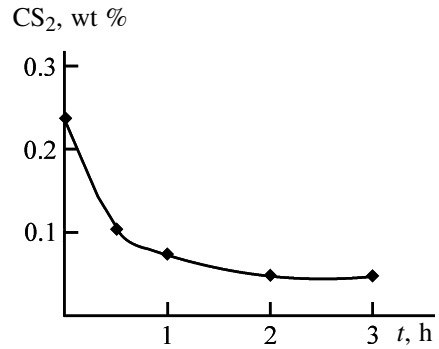

Fig. 2. Content of carbon sulfide CS_2 in crude benzene as a function of ozonation time *t*.

In the initial crude benzene, 46 individual compounds were identified by the chromatography–mass spectroscopy with a probability of identification higher than 90% (Table 2). Among these compounds, for approximately 60% substances the content of each component was more than 0.1 wt %. The content of main components of the product, benzene, toluene, and xylenes, is approximately 83% of the total compounds accessible for chromatographic analysis. The other aromatic hydrocarbons (approximately 1%) include ethyl- and trimethylbenzenes. The content of unsaturated hydrocarbons (linear and cyclic alkenes and alkadienes) is approximately 11.5%. It is likely that the presence of some low-boiling compounds

Table 2. Composition of crude benzene

Compound no.	Compound	Content in crude benzene, wt %		
		1*	2*	3*
1	Formaldehyde	–	–	0.05
2	Furan	–	–	0.08
3	1,3-Butadiene	0.03	0.06	–
4	Acetonitrile	0.18	–	–
5	2-Methyl-1,3-butadiene	0.07	0.12	0.02
6	1,3-Cyclopentadiene	0.73	1.03	0.21
7	Cyclopentene	0.07	0.08	0.03
8	1-Pentene	0.05	0.06	0.04
9	Propionitrile	0.05	–	–
10	Hexane	0.07	0.07	0.06
11	Methylcyclopentane	0.11	0.12	0.10
12	Methylcyclopentene	0.06	0.06	0.03
13	1-Methylcyclopentadiene	0.03	0.03	–
14	Benzene	32.28	32.95	34.02
15	Thiophene	1.33	1.34	1.11
16	Cyclohexene	0.10	0.11	0.07
17	1,2-Dimethylcyclopentane	0.12	0.12	0.11
18	Heptane	0.11	0.12	0.11
19	Methylcyclohexane	0.61	0.62	0.60
20	Ethylcyclopentane	0.04	0.04	0.04
21	1,2,4-Trimethylcyclopentane	0.04	0.04	0.04
22	Pyridine	0.33	–	–
23	1,2,3-Trimethylcyclopentane	0.07	0.03	0.03
24	2-Methylheptane	0.04	0.04	0.04
25	Toluene	37.06	36.76	38.95
26	2-Methylthiophene	0.19	0.19	0.17
27	3-Methylthiophene	0.19	0.19	0.19
28	2,4-Dimethylheptane	0.16	0.16	0.16
29	1,3-Dimethylcyclohexane	0.21	0.21	0.21
30	2-Methylpyridine	0.07	–	–
31	Ethylcyclohexane	0.07	0.06	0.07
32	Ethylbenzene	0.39	0.39	0.43
33	*o, p*-Xylene	13.46	13.17	14.61
34	Phenylethyne	0.20	0.20	0.19
35	Styrene	3.77	3.76	3.57
36	Nonane	0.04	0.04	0.04
37	Benzaldehyde	0.04	–	0.35
38	1,2,3-Trimethylbenzene	0.25	0.25	0.36
39	1,3,5-Trimethylbenzene	0.23	0.23	0.34
40	Benzofuran	0.10	0.10	0.10
41	4,7-Methano-3*a*,4,7,7*a*-tetrahydro-1*H*-indene	4.08	4.22	1.19
42	Indan	0.07	0.08	0.08
43	Indene	1.05	1.07	0.69
44	Bicyclo[2.2.1]hept-5-ene-2-carbonitrile	0.99	0.99	0.82
45	2-Methylbicyclo[2.2.1]hept-2-ene	0.14	0.16	0.06
46	8-Methylene-3-oxabicyclo[3.3.0]octan-2-one	0.15	0.15	0.07
47	Naphthalene	0.43	0.42	0.50
48	8-Phenylbicyclo[2.2.1]hept-2-ene	0.14	0.16	0.06

* (1, 2, 3) Initial crude benzene treated successively with NaOH and H_2SO_4 and ozonized for 2 h, respectively.

Table 3. Composition of ozonation products of coal

Product	Treatment duration, h	Elemental composition, wt %			H/C	O/C	Functional composition, mg-equiv g^{-1} (COOH + OH)
		C	H	O			
LMC	1	31.3	3.1	65.6	1.19	1.57	5.12
	2	52.5	4.8	42.7	1.10	0.61	7.72
	3	50.5	4.5	45.0	1.07	0.67	8.13
MMS	2	63.8	5.2	31.0	0.98	0.36	6.17

(1,3-butadiene with bp –4.5°C, 1-pentene with bp 30°C, etc.), present in crude benzene in trace amounts (less than 0.05 wt %), is caused by their solubility in the mixture of higher-boiling components. Linear, cyclic, and structural isomers of paraffins are contained in insignificant amounts (approximately 1.7%). Nitrogen-, sulfur-, and oxygen-containing compounds together account for approximately 2.6%.

It should be noted that successive treatment of crude benzene with alkali and sulfuric acid solutions is favorable to removal of nitrogen-containing compounds, acetonitrile and pyridine, from the product (Table 2). This operation does not significantly affect the content of other substances.

As a result of ozonation, the ratio of individual compounds in the crude product changes. Treatment with ozone exerts the most noticeable influence on the content of unsaturated compounds (Table 2), which is in good agreement with the results of determination of the bromine number (Fig. 2). Their fraction in the initial product decreased to 6.8%. To a greater extent this concerns dienes of linear (butadiene) and cyclic (cyclobutadiene, cyclopentadiene) structures, and to a lesser extent, compounds containing one double bond (pentene, cyclohexene, etc.). Among sulfur-containing components, unsaturated thiophene reacts with ozone more actively than do its methyl derivatives. It is likely that the presence of alkyl substituents poses steric hindrance to ozone molecules, which leads to a decrease in the reaction rate. Paraffin (hexane, heptane, nonane) and naphthene (cyclohexane) hydrocarbons and their isomers are not noticeably involved in the reaction because of low rate constants (k = 0.02–0.03 $1\,ml^{-1}\,s^{-1}$) [9]. It is likely that the increase in the fraction of neutral oxygen-containing compounds not extracted with alkali (formaldehyde, benzaldehyde) is a result of ozonolytic rupture of the C=C bonds in unsaturated hydrocarbons [9]. Removal of by-products from crude benzene results in a relative increase in the content of the main components: benzene, toluene, and xylene.

The results of extraction of oxygen-containing products of ozonolysis of crude benzene are presented in Fig. 3. The most active formation of the extractable products corresponds to ozonation for 2 h. In the extract composition, low-molecular-weight compounds (LMC) soluble in acidic medium predominate. With increasing process duration, the fraction of macromolecular insoluble substances (MMS) increases (Fig. 3).

The fraction of LMC is characterized by higher content of oxygen and higher O/C ratio (Table 3). The fraction of MMS is characterized by increased carbon content and decreased H/C ratio, which suggests prevalence of insoluble oxygen-containing products of aromatic structure.

With increasing ozonation time, the O/C ratio in LMC composition decreases and the amount of acidic groups increases (Table 3). A high content of oxygen

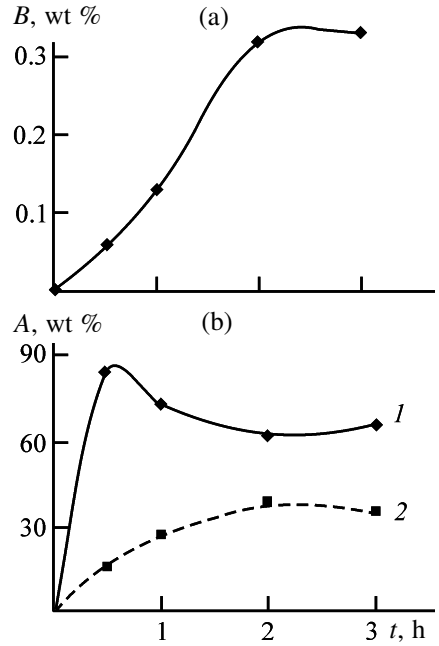

Fig. 3. (a) Yield of extract B and (b) fraction of (*1*) LMC and (*2*) MMS as functions of duration of ozonation of crude benzene t.

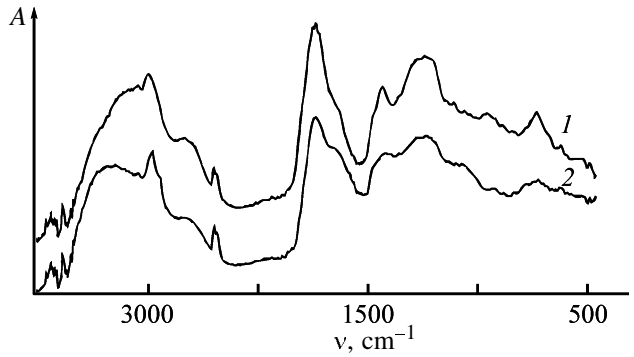

Fig. 4. IR spectra of (*1*) LMC and (*2*) MMS. (*A*) Absorption and (ν) wavenumber.

in soluble products in the initial stage of ozonation can be caused by primary oxidation of diene hydrocarbons with ozone with formation of low-molecular-weight acids and aldehydes as a result of degradation of C=C bonds. It is likely that subsequent increase in the content of carbon and hydrogen in LMC is caused by formation of compounds with longer or branched alkyl chain in the course of ozonation. This is possible due to the reaction of ozone with hydrocarbons of linear and cyclic structure containing one double bond (e.g., 1-pentene, cyclohexene) and also hydrocarbons having bulky substituents at the C=C bond (e.g., 2-methylbicyclo[2.2.1]hept-2-ene).

In the IR spectrum of extracted products (Fig. 4), the strongest absorption bands are those of oxygen-containing groups: for example, in the range 3100–3500 cm^{-1}, the bands corresponding to the OH groups of alcohols and carboxylic acids, involved in formation of hydrogen bonds; in the range 2500–2800 cm^{-1}, the bands corresponding to stretching modes of OH groups of acid dimers bonded with stronger intramolecular hydrogen bonds. The absorption bands in the range 1610–1780 cm^{-1} correspond to the –C=O groups of aromatic and aliphatic acids, aldehydes, and ketones. In the range 1100–1300 cm^{-1}, a broad band with a maximum at 1260 cm^{-1} characterizes in-plane bending vibrations of OH groups and stretching vibrations of the C–O groups of alcohols and acids.

In the spectrum of LMC, the strongest are the bands of oxygen-containing OH– (3400, 2500–2800 cm^{-1}), C=O– (1610–1780 cm^{-1}), and C–O (1100–1300 cm^{-1}) groups and also aliphatic CH_3 groups (2920 and 1380 cm^{-1}). On the contrary, MMS components are characterized by a wide variety of aliphatic bonds (CH_3 at 2920 and 1380 cm^{-1} and CH_2 group at 2920, 2850, and 1460 cm^{-1}) and the presence of aromatic structures (C=C– at 1600 cm^{-1} and CH_{ar} group in the range 690–870 cm^{-1}). These data suggest prevalence of low-molecular-weight saturated mono- and dicarboxylic acids in low-molecular-weight products and more complicated composition of macromolecular substances containing aromatic nuclei with a high degree of substitution.

CONCLUSIONS

(1) Crude coal-tar benzene can be purified by ozonation to remove unsaturated and sulfur-containing hydrocarbons.

(2) In the composition of extractable oxygen-containing substances, low-molecular-weight products prevail. These products can serve as the raw materials for synthesis of individual chemical compounds.

REFERENCES

1. *Spravochnik koksokhimika* (Handbook of Coal-Tar Chemist), Shelkov, A.K., Ed., Moscow: Metallurgiya, 1966.
2. Kovalev, E.T., Chernovol, P.A., Zhuravlev, V.I., and Serik, D.T., *Koks Khim.*, 2003, no. 11, pp. 21–22.
3. Titushkin, V.A. and Frolovnin, Yu.V., *Koks Khim.*, 2006, no. 3, pp. 43–46.
4. Sharipov, A.Kh., and Nigmatullin, V.R., *Neftekhimiya*, 2005, vol. 45, no. 6, pp. 403–409.
5. Innovations, *Neftegaz. Tekhnol.*, 2001, no. 1, pp. 78–80.
6. Linguist, L. and Pacheeo, M., *Oil Gas J.*, 1999, vol. 8, pp. 45–49.
7. Likhterova, N.M., Lunin, V.V., Torkhovskii, V.N., et al., *Neftekhimiya*, 2005, vol. 45, no. 1, pp. 3–14.
8. Kam'yanov, V.F., Sivirilov, P.P., Litvintsev, I.Yu., and Antonova, T.V., *Khim. Interes. Ust. Razv.*, 1999, vol. 7, pp. 141–155.
9. Razumovskii, S.D. and Zaikov, G.E., *Ozon i ego reaktsii s organicheskimi soedineniyami* (Ozone and Its Reactions with Organic Compounds), Moscow: Nauka, 1974.
10. Gluzman, L.D. and Edel'man, I.I., *Laboratornyi kontrol' koksokhimicheskogo proizvodstva* (Laboratory Monitoring of Coal-Tar Chemical Industry), Kharkov: Metallurgizdat, 1957.
11. Klimova, V.A., *Osnovnye mikrometody analiza organicheskikh soedinenii* (Main Methods of Organic Microanalysis), Moscow: Khimiya, 1975.

ISSN 1070-4272, Russian Journal of Applied Chemistry, 2007, Vol. 80, No. 5, pp. 851–852. © Pleiades Publishing, Ltd., 2007.
Original Russian Text © A.G. Morachevskii, I.N. Beloglazov, 2007, published in Zhurnal Prikladnoi Khimii, 2007, Vol. 80, No. 5, pp. 876–877.

BOOK REVIEWS

Turaev, N.S. and Zherin, I.I., *Khimiya i tekhnologiya urana* (Chemistry and Technology of Uranium)

Moscow: Ruda i Metally, 2006, 396 pp.

DOI: 10.1134/S107042720705031X

The book is based on the course of lectures on chemistry of radioactive elements and technology of uranium, delivered to students of Tomsk Polytechnic University (TPU), supplemented with materials from domestic and foreign monographs, periodic literature, and works of staff members of the chair of chemical technology of rare, scattered, and radioactive elements at TPU. All this makes it possible to regard the book as an extended and in-depth textbook for study of chemistry and technology of uranium.

The book comprises an introduction, twelve chapters, and bibliographic list. The introduction (pp. 3–11) briefly presents historical evidence about studies of uranium and other radioactive elements and development on nuclear power engineering in various countries. Chapter 1 (pp. 12–37) presents a general characterization of the physicochemical properties of uranium and its main compounds: hydride, oxides, fluorides, and a number of other compounds of uranium in various oxidation states. The very small Chapter 2 (pp. 38–40) gives a general scheme of uranium ore processing from mining to production of metallic uranium. Chapter 3 (pp. 41–56) considers formation of uranium deposits, most important uranium-containing minerals, and main uranium ore deposits. It is noted, in particular, that about 19% of reliably surveyed resources is concentrated in Kazakhstan, with 70% of the uranium ore resources suitable for underground leaching.

Chapter 4 (pp. 57–105) summarizes evidence about mechanical treatment of uranium ore raw materials, methods for dressing of uranium ores, and their high-temperature treatment (oxidative calcination, sulfatizing calcination, chlorination of ore concentrates, and sintering with sodium chloride). Chapter 5 (pp. 106–168) is devoted to leaching of uranium ores with acid or carbonate solutions. Together with the conventional technology of leaching of ores, processes of heap, underground, and well-underground leaching are considered. Chapter 6 (pp. 169–184) discusses processes of separation of the solid and liquid phases (thickening, filtration) as applied to processing of uranium ores. Chapter 7 (pp. 185–308) presents in ample detail methods for uranium recovery from solutions: chemical precipitation, ion-exchange processes, extraction.

In Chapter 8 (pp. 309–326), the authors substantiate the limiting content of various groups of impurities in uranium compounds used in nuclear technologies. To the most dangerous impurities having the largest cross sections of thermal neutron capture are attributed boron, cadmium, and lanthanides of the yttrium group. Various methods for refining of uranium compounds are discussed. Chapter 9 (pp. 328–346) contains evidence concerning production of uranium trioxide from various compounds of uranium. Also described are reduction of higher uranium oxides with hydrogen, thermodynamics and kinetics of the processes, and the apparatus used.

One of the most important intermediate products in uranium industry is uranium tetrafluoride UF_4, used to manufacture both metallic uranium and uranium hexafluoride UF_6. Synthesis of UF_4 by reaction of uranium dioxide with hydrogen fluoride is considered in detail in Chapter 10 (pp. 347–365). Chapter 11 (pp. 366–376) is devoted to the theory and technology of manufacture of uranium hexafluoride UF_6. The final Chapter 12 (pp. 377–389) briefly considers methods for manufacture of metallic uranium: electrolysis of chloride–fluoride melts, reduction of uranium oxides with calcium, and reduction of uranium tetrafluoride with magnesium or calcium. Also described is refining melting of raw uranium ingots in vacuum induction furnaces. The bibliographic list contains references to 75 nearly exclusively Russian publications.

The entire technology for processing of uranium-containing raw materials, beginning from ore mining to production of most important uranium compounds and pure metal, has probably been for the first time described in so ample detail and so thoroughly in the domestic literature. A major advantage of the book

is, in our opinion, presentation of examples of some technologies used not only in Australia or Canada, but on the territory of CIS countries as well. Having unquestionable advantages, the book is not devoid of certain shortcomings, which could be eliminated in a close scientific editing. It seems that it was not too successful idea to make a rather detailed presentation of physicochemical issues, to which belong thermodynamics of leaching processes, theoretical foundations of extraction, and thermodynamics of reduction processes.

Long ago, it was a professor of TPU, A.G. Stromberg (1910–2004), who wrote (together with D.P. Semchenko) one of the best domestic textbooks on physical chemistry for students of chemical higher school institutions. Since the time when it was written (1973), the textbook ran into five editions (4th in 2001 and 5th in 2003). The authors of the, on the whole, technological book about uranium should have kept in mind this textbook and followed its terminology and representation of thermodynamic characteristics of processes and reactions under consideration. It is impossible to discuss details of presentation in this brief review of N.S. Turaev and I.I. Zherin's book. We note only that, widely using the terms "activity" and "activity coefficient," the authors never mention that some standard state is to be chosen. The form in which heat effects are written for reactions (12.1)–(12.4) is unacceptable. The aggregative state of the substances involved should be specified for reactions occurring at high temperatures. It is necessary to use the same terminology for thermodynamic functions throughout the text.

The book by Turaev and Zherin is provided with a large number of illustrations. However, the plentiful of details of secondary importance complicates understanding of the operation principles of apparatus. If the book is primarily regarded as a textbook, it seems that schematic representation of apparatus (e.g., Figs. 4.20, 4.25) would be more appropriate than their detailed circuits (Figs. 4.5, 4.6). As regards the polygraphic quality of the book, it is very well published.

A. G. Morachevskii and I. N. Beloglazov

ISSN 1070-4272, Russian Journal of Applied Chemistry, 2007, Vol. 80, No. 6, pp. 853–859. © Pleiades Publishing, Ltd., 2007.
Original Russian Text © B.G. Sukhov, D. Enkhtuyaa, Zh. Amgalan, T.I. Vakul'skaya, L.N. Novikova, Zh.G. Bazarova, B.G. Bazarov, 2007, published in Zhurnal Prikladnoi Khimii, 2007, Vol. 80, No. 6, pp. 881–886.

INORGANIC SYNTHESIS AND INDUSTRIAL INORGANIC CHEMISTRY

Effect of Mechanical Activation on Structural-Chemical Properties of Phosphorites

B. G. Sukhov, D. Enkhtuyaa, Zh. Amgalan, T. I. Vakul'skaya, L. N. Novikova, Zh. G. Bazarova, and B. G. Bazarov

Favorskii Institute of Chemistry, Siberian Division, Russian Academy of Sciences, Irkutsk, Russia

Railway Institute, Ulan Bator, Mongolia

Institute of Chemistry and Chemical Engineering, Mongolian Academy of Sciences, Ulanbator, Mongolia

Baikal Institute of Nature Management, Siberian Division, Russian Academy of Sciences, Ulan-Ude, Russia

Received December 19, 2006

Abstract—Effect of mechanochemical activation of mono- and mid-fraction of phosphorites from the Burenkhan deposit was studied by IR and ESR spectroscopies in vibration and planetary mills.

DOI: 10.1134/S1070427207060018

Phosphate raw materials occupy one of the first places among the plentiful mineral resources of Mongolia and are the most important for manufacture of fertilizers [1]. The Burenkhan deposit contains medium-quality ores of a carbonate-siliceous composition: 60–70% apatite minerals, 20% SiO_2, 13.01% $CaCO_3$, and 6.51% $MgCO_3$ [2].

A promising area in decomposition of mineral raw materials is their mechanochemical activation [3, 4]. This way of processing of phosphate ores is ecologically safe and allows use of phosphate raw materials containing 15% P_2O_5 and more. The thus produced activated phosphate fertilizers are not carried away from plow fields into water reservoirs and exhibit a prolonged effect [1]. It is known that treatment of natural phosphorites in power-intensive mills results in amorphization of their structure because of the crystal lattice deformation, defect formation, and intensification of chemical processes, which, in turn, raises the activity of phosphate minerals [3–5]. In this case, the solubility of phosphates in weak acids imitating humic acids increases [6]. The reasons for the high solubility of the Burenkhan phosphates in citric acid solutions are still unclear and may be related to structural changes in mechanical activation. The nature of structural disturbances of natural apatites, which occur as a result of amorphization and rupture of inter- and intramolecular bonds in the course of mechanical activation, may depend on changes in both the functional and radical compositions, as it has been confirmed by numerous studies [7]. Of present interest are studies concerned with the effect of the activator type on the degree of phosphorus conversion to a form assimilable by plants. Introduction into soil of a phosphorite treated in a vibration mill promotes, to a greater extent than that in the case of a planetary mill, an increase in the cellulose-decomposing activity, oats yield (by 28%), and weight of wheat grains (by 8.5%), compared with superphosphate [2].

In this study, we made a comparative analysis of changes in the structural-chemical properties of mono- and mid-fraction of Burenkhan phosphates in their mechanical activation in vibration and planetary mills, by IR and ESR spectroscopies.

Along with medium technological sample (3), we used mono-fraction (I) as an object of study. It was isolated from natural phosphorite (II) by elutriation and centrifugation in a mixture of heavy liquids under an X-ray purity control [2]. According to [8], the mono-fraction can be classed, as regards the $F : H_2O$ weight ratio (Table 1), with the FOH type apatite, and the phosphorite, with the OHF-type apatite. The total content of organic substances in phosphorites is low (0.5–2%). Impurities present in the phosphorite, namely, SiO_2 (20%), K_2O (0.06%), Na_2O (0.04%), MgO (2.02%), Fe_2O_3 (0.55%), Al_2O_3 (0.32%), and S_{total} (0.11%), are contained in the monophosphate in insignificant amounts.

Table 1. Main components of Burenkhan phosphorite and its monophosphate

Sample	Composition, %				
	P_2O_5	CaO	CO_2	F	H_2O
Phosphorite (II)	25.00	40.60	9.16	1.80	0.78
Monophosphate (I)	40.98	52.82	1.72	2.92	0.61

Based on the chemical composition of the monophosphate (Table 1) and on results of X-ray and derivatographic analyses, we found the crystal-chemical formula of Burenkhan phosphorites: $Ca_{9.83}(PO_4)_{5.66} \cdot (CO_3)_{0.41}F_{1.59}(OH)_{0.34}$, which allows us to assign them to fluorocarbonatehydroxoapatites.

The monophosphate with the empirical formula $Ca_{9.9}P_{5.66}O_{24}F_{1.49}$ has F/P_2O_5 and CO_2/P_2O_5 ratios of 0.070 and 0.023, respectively [2].

A qualitative analysis of the IR spectra of phosphorite samples was carried out in the following three spectral ranges most important for the mineral: 4000–3000, 1800–800, and 700–400 cm^{-1} [9]. The quantitative analysis of the IR spectra is based on a comparison of the absorption band intensities measured relative to the baseline line and internal standard: absorption by the P–O–P bond in the range 748–730 cm^{-1} characteristic of fluorohydroxoapatites. This absorption band is related to the crystallinity and is sensitive to various substitutions in the phosphorite [10]. The variation of the intensity of the absorption band at 748–730 cm^{-1} between samples I (0.8), 3 (1.3), 1 (1.0), 2 (0.8), 4 (0.7), and 5 (0.6), relative to the absorption in phosphorite II, indicates that this band is sensitive to external treatments.

The isolation of monophosphate and phosphorite 3 from mother raw materials II and their mechanical activation result in certain changes in the position and relative optical absorption intensities ($ROA\nu/\nu_{748-730}$) of IR bands (Tables 2 and 3). The IR spectra of sam-

Table 2. Characteristics of IR spectra of phosphorite (II), its mono- (I) and mid- (3) fractions, and also of products of their mechanical activation in vibration (1, 4) and planetary (2, 5) mills

Absorption band, cm^{-1}	Assignment of absorption bands	Relative optical absorption $\nu/\nu_{748-730}$						
		II	I	1	2	3	4	5
3547–3534	OH…F-Hydrogen bonds	1.8	2.2	3.1	2.4	1.3	3.1	3.7
3441–3429	OH…O-Hydrogen bonds	2.0	2.6	3.4	2.6	1.5	3.8	4.7
2920	CH_3-Groups	0.6	1.0	1.2	0.4	0.4	1.2	1.0
2850	CH_2-, CH-Groups	0.3	0.8	0.9	0.3	0.3	1.0	0.6
2089–2085	CN-, C–F-Bonds	0.2	0,3	0.3	0.3	0.2	0.3	0.2
2002–1996	–OCN, –SCN-Groups	0.3	0.5	0.5	0.4	0.3	0.5	0.3
1649	Water molecules, COO-Groups	1.3	2.1	2.4	1.2	0.7	2.4	1.9
1634–1626	C–H-Bonds	1.3	2.2	2.6	1.5	1.1	2.6	2.2
1503–1502	CO_3^{2-}-Groups	2.6	3.5	3.9	1.9	1.1	3.6	1.8
1458–1453	CO_3^{2-}-Groups	3.7	4.8	5.1	2.4	1.8	5.0	3.1
1430–1421	CO_3^{2-}-Groups	3.4	4.5	5.0	2.2	1.7	4.8	2.7
1161–1158	P–O–C-Bonds	4.6	8.9	10.8	4.9	3.9	11.8	7.5
1095–1094	P–C-, C–F-, P–S-Bonds	9.0	14.0	14.9	13.4	8.2	17.8	15.9
1048–1044	PO_4^{3-}-, HPO_4^{2-}-, $H_2PO_4^-$-Groups	10.1	14.8	15.2	15.7	9.3	18.3	17.0
966–961	H–O–P-Groups	5.1	10.2	11.1	5.9	4.6	11.8	7.7
878–873	Carbonate	2.9	4.8	5.1	2.2	2.1	4.8	2.2
799–798	C–S-, S–O-, P–S-Bonds	2.9	2.9	3.2	1.3	2.0	5.3	3.4
780–775	Quartz, kaolinite	1.9	2.1	2.4	0.9	1.6	4.3	2.4
696–692	SiO-, C–F-Bonds	0.3	0.2	0.3	0.1	0.4	1.0	1.0
604–602	C–S-, S–O-, P–S-, S–S-Bonds	5.9	12.1	13.0	10.1	5.6	13.7	12.2
576–570	Fe_2O_3, Carbonate	5.3	11.6	12.5	9.4	5.1	12.8	10.9
530–514	SO_4^{2-}-Groups	2.1	2.4	3.1	1.3	2.2	4.8	3.1
473–466	F^--, Cl^--Ions	2.8	3.0	4.1	1.5	2.5	7.2	4.7

Table 3. Change in the intensity of relative optical absorption in the IR spectra of mono- and mid-fractions of phosphorites after mechanical treatment in vibration (1, 4) and planetary (2, 5) mills

Absorption band, cm^{-1}	Relative optical absorption $\nu/\nu_{748-730}$, %					
	I	3	1	2	4	5
3547–3534	31	–23	29	–2	120	181
3441.3–3428.8	33	–23	25	–4	137	213
2920	80	–35	17	–57	221	175
2850	150	–18	0	–66	267	144
2089–2085	50	–18	0	–14	83	–8
2002–1996	50	–18	0	–14	83	22
1649	63	–45	8	–47	221	175
1634–1626	75	–18	7	–39	129	114
1503–1502	43	–57	5	–49	221	68
1458–1453.4	36	–50	0	–54	166	74
1430–1421	35	–50	4	–54	170	64
1161–1158	105	–12	13	–49	188	96
1094.7–1094	63	–7	–1	–11	107	97
1047.8–1044.3	53	–6	–4	–1	89	87
966–961	109	–8	2	–46	143	69
878–873	73	–28	0	–57	123	12
798.9–798.3	4	–31	6	–57	158	75
779.9–775	15	–13	8	–60	155	53
748–730	0	0	0	0	0	0
696–692	–50	9	100	–14	175	175
603.8–602.5	115	–3	0	–22	133	121
575.7–570.3	128	–3	0	–25	141	119
530–514.4	18	8	20	–49	105	39
473–466	14	–8	26	–55	175	90

ples under study contain a broad absorption band with peaks at 3547–3534 and 3441–3428 cm^{-1}, which are associated with hydrogen bonds with fluorine or oxygen [11]. The variation of the intensity of the absorption by hydrogen bonds with fluorine and oxygen makes it possible to judge about surface disturbances of the phosphorite structure. The peaks of the absorption bands associated with hydrogen bonds in samples I (3547 and 3436 cm^{-1}) and 3 (3537 and 3441 cm^{-1}) are shifted relative to those in the starting sample II (3542 and 3440 cm^{-1}), as well as the peaks of the absorption bands of the products of mechanical activation of monophosphates 1 (3540 and 3429 cm^{-1}) and 2 (3534 and 3440 cm^{-1}), which indicates that some types of hydrogen bonds are ruptured and other types are formed. In the products formed upon treatment of phosphorite 3, the peaks of absorption by hydrogen bonds are not shifted, but the intensity of absorption by the O–H...F bond in sample 4 (3537 cm^{-1}) somewhat decreases upon a vibration mill treatment. After a planetary mill, the intensity of absorption by hydrogen bonds with fluorine and oxygen in sample 5 increases.

It can be seen from Table 3 that hydrogen bonds are ruptured only in the monophosphate upon activation in a planetary mill. The activation of monophosphate in a vibration mill and that of phosphorite in mills of both types favor formation of hydrogen bonds, which may be due to sorption of water on the surface of crushed phosphorite (predominant grain size of 0.5 to 5–10 μm [12]). In the monophosphate and in the products of its treatment in a vibration mill (sample 1), and also in samples 4 and 5 obtained upon both types of treatment of phosphorite 3, the intensity of absorption by methyl and methylene groups (2920 and 2850 cm^{-1}) increases, which may be due to disintegration of organomineral complexes. The decrease in the intensity of absorption by these groups in phosphorite 3 and sample 2 points to destruction of the organic component. The decrease in the intensity of the absorption by C–F bonds (2089–2085 cm^{-1}) upon

treatment of phosphorites in a planetary mill confirms the data of [12], which indicate that the position of fluorine in the fluorapatite structure is more easily affected by mechanical treatment.

The absorption by the functional groups of phosphorite is observed at 1800–800 and 700–400 cm^{-1}. In the same IR spectral ranges, there are absorption bands of minerals entering into the phosphorite composition: quartz (1170, 1090, 795, 770, and 695 cm^{-1}), carbonate (1640, 1520, 1450, 1420, 880, 855, and 700–705 cm^{-1}), and calcite (1425, 875, and 715 cm^{-1}) [9]. The change in the $ROA\nu/\nu_{748-730}$ intensity of the doublet at 799–798 and 777–775 cm^{-1} shows that Si–O– bonds are present in the samples. The presence of quartz and kaolinite is characterized by the absorption near 696 cm^{-1}, and that of calcite, at 878–873 cm^{-1}. According to the electron-microscopic data [12], the mineral component of the Burenkhan phosphorite mainly consists of quartz and fluorapatite.

Mechanical activation of phosphorites leads to an increase in the intensities of absorption by impurities, especially upon a treatment in a vibration mill, whereas their decrease is characteristic only of a monophosphate treated in a planetary mill (Table 3). The absorption by structurally bound carbonates, with peaks of stretching vibrations at about 1450 and 1425 and 880–870 cm^{-1}, is weaker in samples I and 3, compared with the starting phosphorite II. However, treatment in a vibration mill results in that the absorption intensity increases, especially in the phosphorite sample 4 containing a larger amount of bound water. The weaker bands at 1996 and 2000 cm^{-1} can be assigned to vibrations of CO_3^{2-} ions formed upon the absorption of carbon dioxide from air [11], and the band at 1500 cm^{-1} points to a shift of the carbonate group toward fluorapatite (type B) [13]. The strongest bands in the monophosphate and phosphorite samples under study are observed at 1000–1100 cm^{-1}, with peaks at 1095 and 1045 cm^{-1}. These bands are associated with stretching vibrations of P–C-, C–F-, and P–S bonds and PO_4^{3-}-, HPO_4^{2-}-, and H_2PO^--groups. Absorption bands associated with the H–O–P– bonds are observed at 966–961 cm^{-1}; bands related to P–O–P– bonds, at 740 cm^{-1}; and those associated with bending vibrations of P–O– and –P–O–Me, at 600–400 cm^{-1}. It should be noted that the intensities of $ROA\nu/\nu_{748-730}$ of phosphate groups of the monophosphate and of products of its mechanical activation are about the same, and those for products of mechanical activation of sample 3 are 2–3 times higher (Table 2). In the range of vibrations of the complex PO_4^{3-} ion, five absorption bands have been observed [4, 14]. These bands are related to fully symmetric stretching vibrations ν_1 at 966–961 cm^{-1}, asymmetric stretching vibrations ν_3 near 1045 and 1095 cm^{-1}, and bending vibrations ν_4 at 575 and 603 cm^{-1}. The occurrence of the ν_1 vibrations points to a decrease in the symmetry of the PO_4^{3-} anion for sample I upon its isolation and mechanical treatment in a vibration mill, and for sample 3 subjected to both types of activation. The intensity of the ν_3 absorption does not change for sample 1 upon its treatment in a vibration mill, but slightly decreases in sample 2 upon treatment in a planetary mill. The ν_3 range of sample 3 is activated as a result of mechanical treatment, and this occurs to a greater extent after treatment in a vibration mill (sample 4). Similar changes were observed in the vibration intensities of the C–F–, C–S–, and S–P– bonds (1160–1158, 693–696 cm^{-1}) and in the intensities of bending vibrations ν_4 of PO_4^{3-} anions (Table 2, 3). Therefore, the type of mechanical activation strongly affects the type of structural changes in the monophosphate and phosphorite.

The $ROA\nu/\nu_{748-730}$ data on vibrations of the bridging P–O–P bond point to an increase in the content of water, hydrogen bonds, and carbonate and phosphate groups in samples under study upon their treatment in a vibration mill. A more severe treatment in a planetary mill also activates the above-mentioned structures in phosphorite, but does so to a lesser extent, and, according to the changes in the monophosphate absorption, results in a pronounced disintegration of the structure, including phosphate groups. Adsorbed water molecules are involved in the formation of hydrogen bonds, which is confirmed by the identical changes in $ROA\nu/\nu_{748-730}$ at 3547–3534, 3441–3429, and 1649 cm^{-1} (Table 2). An analysis of the monophosphate subjected to mechanical activation in a vibration mill demonstrated that its composition remains virtually unchanged; however, there occurs isomorphous substitution of elements. Various isomorphous impurities (Mn^{2+}, Cu^{2+}, Fe^{3+}, Ti^{3+}, V^{4+}, Au^{3+}, Ag^+, Sr^{2+}, Si^{4+}, C^{4+}, S^{6+}, and O^{2-}) result in a compositional disorder, structural disturbances and distortions (especially of nonisovalent types), and formation of various centers of electron and hole types [12, 15].

The samples studied are paramagnetic and give complex ESR spectra consisting of several superimposed signals related to different paramagnetic centers (Figs. 1 and 2). The content of radicals in the samples is comparatively low, about 10^{16} spins g^{-1}.

Several types of paramagnetic centers were detected in sample II, among which CO_2^-, CO_3^-, and

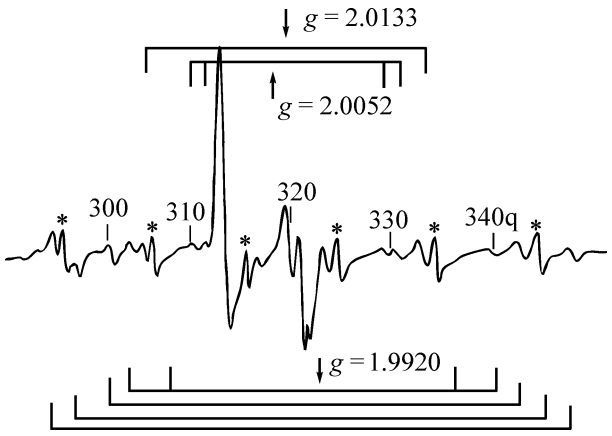

Fig. 1. ESR spectrum of natural phosphorite from the Burenkhan deposit (doublets of phosphorus radicals are shown in the spectrum; $^{55}Mn^{2+}$ lines are marked by asterisks).

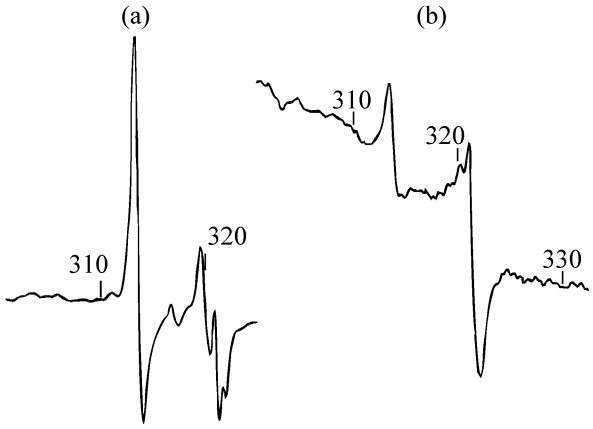

Fig. 2. ESR spectra of phosphorites, recorded in the magnetic field scanning range of 70 mT. (a) mid sample 3, (b) monophosphate I.

CO_3^{2}- centers, oxygen radicals, $^{55}Mn^{2+}$ ions, and phosphorous-containing radicals were identified (Table 4 and Fig. 1). The signals with a *g*-factor of 2.052–2.055 and a noticeable contribution of spin-orbit interactions are associated with oxygen paramagnetic centers OH^-–O^-–HO^- or F^-–O^-–F^- [15, 16]. Lines at *g*-factors of 2.010–1.998 can be assigned to overlapping signals of CO^{2-}-, CO_3^--, and CO_3^{2-}- centers [7, 15–22]. The sextet with a splitting of 9.3 mT and *g*-factor of 2.002(6) is due to interaction of an unpaired electron with the nucleus with a spin 5/2 and can be attributed to $^{55}Mn^{2+}$ ions. In the ESR spectrum of the starting phosphorite II, the signals with *g*-factors of 1.992, 2.005, and 2.013 and with stronger (20 to 50 mT) doublet splittings were also recorded (Fig. 1), related to various types of phosphorus radicals PO_3^{2-} and PO_4^{3-} [22, 23]. The starting phosphorite also contains paramagnetic centers (g = 1.988), which are absent in both mono- and mid-fractions of phosphorite and, apparently, are impurity-related. In addition, a narrow line with ΔH = 0.4 mT and g = 2.028 is present in the ESR spectrum of the starting phosphorite, which may be associated with the presence in apatites of either uranium ions [23] or anion-radicals S_4^- [24].

As a result of production of the mid-fraction phosphorite 3 and isolation of monophosphate I from the natural phosphorite II, the paramagnetic centers responsible for the sextet are lost. This can be accounted for by structural disordering or by ionization of Mn^{2+} to give diamagnetic Mn^{3+} [26]. At the same time, carbon radicals CO_2^-, CO_3^-, CO_3^{2-}, and oxygen radicals OH^-–O–HO^- and F^- –O^-–F^- (g = 2.055) are retained in mono-fraction I, and also a new type of paramagnetic centers appears, which gives a very broad (> 40 mT) absorption line with a *g*-factor of about 2.0 (Fig. 2b).

In the samples subjected to a mechanical treatment, some paramagnetic centers disappear, and new centers appear. In the process, a very high-intensity broad absorption line, absent in the spectrum of the starting phosphorite, appears in the ESR spectrum of the monophosphate. Treatment of monophosphate I in a vibration mill (sample 1) does not lead to changes in the structure of the ESR spectrum. In turn, treatment of I in a planetary mill changes the relative contents of various carbon radicals in sample 2, which is confirmed by the appearance of a signal with g = 1.998 in the ESR spectrum.

By contrast, mechanical activation of the mid-fraction phosphorite 3 in a vibration mill results in that the signal with g = 1.998 (9) (sample 4) disappears from the ESR spectrum, whereas treatment in a planetary mill does not lead to any changes in the spectrum (sample 5). All of the mechanically activated sam-

Table 4. Characteristics of ESR signals of carbon and oxygen paramagnetic centers

Sample	O-Radicals	C-Radicals		
	g_1 (ΔH = 0.27–0.93 mT)	g_2 (ΔH = 0.67–0.90 mT)	g_3 (ΔH = 0.32–0.98 mT)	g_4 (ΔH = 0.25 mT
II	2.055(0)	2.010(2)	2.004(9)	1.998(3)
3	2.055(2)	2.008(3)	2.002(7)	1.998(9)
I	2.055(0)	2.008(9)	2.003(3)	
1	2.053(0)	2.011(0)	2.003(9)	
2	2.054(0)	2.008(0)	2.003(8)	1.998(0)
4	2.051(5)	2.008(5)	2.003(6)	
5	2.055(2)	2.008(2)	2.003(9)	1.997(0)

ples contain, similarly to the monophosphate, paramagnetic centers responsible for a broad absorption line in the ESR spectra at a *g*-factor of 2.0, which are, presumably, defects or vacancies that captured an electron.

Thus, according to the IR and ESR spectral data, mechanical activation in mills of different types leads to unequal changes in the phosphorite structure, although spectral changes are observed already in the stage of isolation of the mono- and mid-fractions from the starting phosphorite. A strong activation of phosphates is observed upon a mechanical treatment in a vibration mill, which is accompanied by a breakdown of the symmetry of the PO_4^{3-} anion and does not lead to disintegration of the monofraction, as is the case of treatment in a planetary mill.

EXPERIMENTAL

Phosphorite was treated in a DRM-75T vibration mill in steel cups with balls with a weight of 500 g for 30 min. The activation of phosphorite in an EI-2 × 150 planetary mill was performed in steel drums with steel balls 3 mm in diameter with a total weight of 200 g for 15 min. The treatment time was chosen experimentally so as to obtain approximately equal degrees of amorphization (64% of particles smaller than 20 μm in size). In this way, we obtained monophosphate (1 and 2) and phosphorite (4 and 5) samples, respectively.

The IR spectra were measured in the spectral range 400–4000 cm^{-1} on an IFS 25 instrument in KBr pellets containing 2 wt % phosphorite. The inaccuracy in the positions of absorption bands was ±1 cm^{-1}.

The ESR spectra were measured on an SE/X-2547 Radiopan spectrometer (Poland) equipped with a magnetometer and a high-frequency meter at room temperature in the magnetic field scanning range 10–300 mT. The amplitude of HF modulation was 100 kHz. The content of paramagnetic centers was calculated using the known techniques with diphenylpicrylhydrazyl (DPPH) and ultramarine as calibrated standards [20, 21].

CONCLUSIONS

(1) Mechanical treatment of phosphorite in a vibration mill favors an increase in the relative content of phosphate groups.

(2) In the more severe conditions of a planetary mill, the activation of phosphate groups is less effective because of the destruction of the monophosphate.

(3) Irrespective of the type of a mechanical treatment, the relative content of carbon and oxygen radicals is 2 : 1 for monophosphate and 1 : 2 for phosphorites.

REFERENCES

1. Chaikina, M.V., Amgalan J., Battsetseg F., et al., *Khim. Interes. Ustoich. Razv.*, 2002, vol. 10, no. 4, pp. 503–517.
2. Enkhtuyaa, Z., *Cand. Sci. Dissertation*, Ulan Bator, 1999.
3. Boldyrev, V.V., *Usp. Khim.*, 2006, vol. 75, no. 3, pp. 203–216.
4. Chaikina, M.V., *Mekhanokhimiya prirodnykh i sinteticheskikh apatitov* (Mechanochemistry of Natural and Synthetic Apatites), Novosibirsk: Izd. Geo, Sib. Otd. Ross. Akad. Nauk, 2002.
5. Molchanov, V.I., Selezneva, O.G., and Zhirnov, E.N., *Aktivatsiya mineralov pri izmel'chenii* (Activation of Minerals in Grinding), Moscow: Nedra, 1988.
6. Boldyrev, V.V., Lyakhov, N. Z., Chaikina, M.V., and Avvakumov, E.G., Abstracts of Papers, *XVI Mendeleevskii s"ezd po obshchei i prikladnoi khimii* (XVI Mendeleev Congress on General and Applied Chemistry), Moscow: PIK VINITI, 1998, pp. 244–245.
7. Gilinskaya, L.G. and Zanin, Yu.N., *Zh. Strukt. Khim.*, 1998, vol. 39, no. 5, pp. 821–842.
8. Gilinskaya, L.G., *Neorg. Mater.*, 2005, vol. 41, no. 5, pp. 585–591.
9. Orlov, D.S., *Khimiya pochv* (Chemistry of Soils), Moscow: Mosk. Gos. Univ., 1985, pp. 159–161.
10. Knubovets, R.G. and Kislovskii, L.D., *Fizika apatita* (Physics of Apatite), 1975, pp. 63–88.
11. Stolpovskaya, V.N. and Zanin, Yu.N., *Issledovanie fosfatov kal'tsiya fizicheskimi metodami* (Study of Calcium Phosphates by Physical Methods), Novosibirsk: Nauka, 1979, pp. 29–33.
12. Dorzhieva, S.G., Bazarova, Z.G., Enkhtuyaa, Z., et al., *Vestn. Buryat. Univ., Ser. 1, Khim.*, Ulan-Ude, 2005, no. 2, pp. 170–175.
13. Kustova, G.N., Yurchenko, E.N., Burgina, E.B., et al., *Zh. Strukt. Khim.*, 1979, vol. 20, no. 6, pp. 1019–1023.
14. Nakamoto, K., *Infrared and Raman Spectra of Inorganic and Coordination Compounds*, New York: John Wiley, 1986.
15. Gilinskaya, L.G. and Shcherbakova, M.L., *Fizika apatita* (Physics of Apatite), Novosibirsk: Nauka, 1975, pp. 7–63.

16. Gilinskaya, L.G., *Zh. Strukt. Khim.*, 2001, vol. 42, no. 3, pp. 446–453.
17. Vestad T.A., Gustafsson H., Lund A., et al., *Phys. Chem. Chem. Phys.*, 2004, vol. 6, pp. 3017–3022.
18. Bartoll, J. and Rink, W.J., *Advances in ESR Applications*, 2002, vol. 18, pp. 83–86.
19. Shapkin, V.L., Gilinskaya, L.G., Chaikina, M.V., *Izv. Sib. Otd. Akad. Nauk SSSR, Ser. Khim.*, 1985, vol. 8, no. 3, pp. 48–52.
20. Inoue, K., Hirai, M., and Ikeda, M., *Advances in ESR Applications*, 2002, vol. 18, pp. 87–92.
21. Zdravkova, M., Vanhaelewyn, G., Callens, F., et al., *Spectrochim. Acta*, 2005, part A 61, pp. 3131–3138.
22. Gilinskaya, L.G., *Zh. Strukt. Khim.*, 1990, vol. 31, no. 6, pp. 51–58.
23. Gilinskaya, L.G., *Issledovanie fosfatov kal'tsiya fizicheskimi metodami* (Study of Calcium Phosphates by Physical Methods), Novosibirsk: Nauka, 1979, pp. 39–48.
24. Levillain, E., Leghii, P., Gobeltz, N., and Lelieur, J.P., *New J. Chem.*, 1997, vol. 21, pp. 335–341.

ISSN 1070-4272, Russian Journal of Applied Chemistry, 2007, Vol. 80, No. 6, pp. 860–863. © Pleiades Publishing, Ltd., 2007.
Original Russian Text © A.I. Nikolaev, V.B. Petrov, Yu.V. Pleshakov, Yu.G. Bychenya, G.I. Kadyrova, 2007, published in Zhurnal Prikladnoi Khimii, 2007, Vol. 80, No. 6, pp. 887–890.

INORGANIC SYNTHESIS AND INDUSTRIAL INORGANIC CHEMISTRY

Purification of Sphene Concentrate to Remove Phosphorus Impurity with Dilute Mineral Acids

A. I. Nikolaev, V. B. Petrov, Yu. V. Pleshakov, Yu. G. Bychenya, and G. I. Kadyrova

Tananaev Institute of Chemistry and Technology of Rare Elements and Mineral Resources, Kola Scientific Center, Russian Academy of Sciences, Apatity, Murmansk oblast, Russia

Apatit Open Joint-Stock Company, Apatity, Murmansk oblast, Russia

Received December 26, 2006

Abstract—Methods of crystal-optic, X-ray phase, chemical, and IR spectroscopic analyses were used to study the interaction of sphene and fluorapatite concentrates with dilute mineral acid solutions. The conditions under which the sphene concentrate can be purified to remove admixtures of phosphorus-containing compounds were found.

DOI: 10.1134/S107042720706002X

Sphene ($CaTiSiO_5$) is a rock-forming mineral in apatite-nepheline ores of the Khibiny deposits. The sphene concentrate obtained in dressing of these ores is regarded as a promising raw material for production of titanium pigments and for use in coatings of welding electrodes [1]. Presence of phosphorus in the concentrate intended for manufacture of the titanium dioxide pigment leads to a pronounced decrease in the yield of titanium into the final product [2] and precludes direct use of the concentrate in coatings of welding electrodes. According to technical specifications for the sphene concentrate for welding electrodes [TU (Technical specification) 1715-069-00203938–2000], the content of phosphorus should not exceed 0.1% in terms of P_2O_5. The presence of phosphorus is due to the fact that the sphene concentrate contains an admixture of a fluorapatite mineral, $Ca_5(PO_4)_3F$, both as aggregations with sphene and separately.

Phosphorus compounds cannot be removed to the required extent in the dressing stage. Therefore, chemical purification methods based on decomposition of fluorapatite with dilute solutions of mineral acids (sulfuric acid, for the most part) have been suggested [3]. In this process, sphene remains unchanged.

The content of phosphorus in the initial sample of the sphene concentrate used to develop the purification procedure was 1.88% in terms of P_2O_5.

The conditions of the given process require an additional study to substantiate the choice of an acid and minimize its expenditure at satisfactory purification parameters. The mineralogical[1] and chemical compositions of the starting sphene and fluorapatite concentrates used in this study are listed in Tables 1 and 2, respectively.

Chemical purification to remove fluorapatite can be performed not only with sulfuric acid, but also with hydrochloric and nitric acids [3]. With H_2SO_4 used,

Table 1. Mineralogical composition of sphene and fluorapatite concentrates

Mineral	Sphene concentrate	Apatite concentrate
	content, wt %	
Sphene	86.0	0.4
Fluorapatite	4.5	95.1
Nepheline	3.2	1.8
Aegirine	4.5	0.8
Feldspars	1.5	
Microcline		0.1
Hydromicas	0.5	0.1
Titanomagnetite		0.1

[1] Mineralogical analysis was made by V.F. Fedchenko at the Central laboratory of Apatit Open Joint-Stock Company.

Table 2. Chemical composition of sphene and apatite concentrates

Concentrate	Content, wt %							
	TiO_2	SiO_2	CaO	Fe_2O_3	P_2O_5	MgO	Na_2O	F
Sphene	35.9	30.4	25.1	1.7	1.88	0.6	0.7	0.4
Fluorapatite	0.4	2.3	49.6	0.4	39.2	0.2	0.2	3.1

the purified sphene concentrate is contaminated with an additional impurity to be controlled, sulfur. Nevertheless, use of this acid can be justified by the simpler utilization of spent sulfuric acid solutions, compared with those of hydrochloric and nitric acids. To choose rational purification conditions, the behavior of fluorapatite and sphene concentrates in their interaction with dilute mineral acids was studied.

Samples of apatite and sphene concentrates, taken from the dressing stage, were treated with acids of various concentrations and subjected to chemical, crystal-optic, X-ray phase, and IR spectroscopic analyses. The behavior of aegirine, feldspars, and nepheline was not studied because they contain no phosphorus. In addition, the first two of these minerals are stable against dilute acids and the decomposition of nepheline has been studied in sufficient detail [4].

Because it is fluorapatite that is the source of phosphorus impurity limited in the sphene concentrate, its interaction with mineral acids was studied separately.

To determine the behavior of fluorapatite under sphene concentrate purification conditions, experiments on fluorapatite decomposition with dilute sulfuric, hydrochloric, and nitric acids were performed at room temperature and s : l = 1 : 3. The chosen expenditure of the acids was lower than the stoichiometric value even for 5% solutions. The interaction of fluorapatite with dilute mostly occurs under the chosen conditions by the reactions

$$2Ca_5(PO_4)_3F + 3H_2SO_4 = 6CaHPO_4 + 3CaSO_4 + CaF_2,$$

$$2Ca_5(PO_4)_3F + 6HCl = 6CaHPO_4 + 3CaCl_2 + CaF_2,$$

$$2Ca_5(PO_4)_3F + 6HNO_3 = 6CaHPO_4 + 3Ca(NO_3)_2 + CaF_2.$$

The degree of apatite decomposition was judged from the increase in the phosphorus concentration in solutions in the course of time. The results obtained (Table 3) characterize the kinetics of fluorapatite decomposition. It follows from these data that the decomposition of fluorapatite by sulfuric and hydrochloric acids occurs at approximately equal rates exceeding that for nitric acid. The choice of nitric acid is also undesirable because of the more difficult utilization on nitrate waste solutions.

The data furnished by chemical, crystal-optic, X-ray phase, and IR spectroscopic analyses of precipitates formed in decomposition of fluorapatite with dilute H_2SO_4 at an acid expenditure exceeding the stoichiometric value show that these precipitates are composed of anhydrite, $CaSO_4$. The IR spectra of precipitates not washed to remove the mother liquor and dried at room temperature and at 90°C also coincide with the spectrum of anhydrous calcium sulfate [5] (see figure, curves *1* and *2*).

At the same time, the spectra of the precipitates washed with water and dried at room temperature show that anhydrite is converted into gypsum in the course of washing. The IR spectrum reveals the appearance of a doublet of absorption bands in the ranges of both stretching (3400–3600 cm^{-1}) and deformation vibrations (1630–1690 cm^{-1}) of water molecules (see figure, curve *3*).

In drying of washed precipitate at 90°C, gypsum loses 1.5 molecules of water and is converted into a semihydrate $CaSO_4 \cdot 0.5H_2O$. This is indicated by the disappearance of splitting in the region of deformation vibrations and a shift of the absorption bands

Table 3. Decomposition of fluorapatite with dilute acids

Treatment time, h	P_2O_5 concentration, g l^{-1}, in treatment with indicated acid, wt %					
	H_2SO_4		HCl		HNO_3	
	2	5	2	5	2	5
1	8.1	25.2	8.8	26.5	5.1	14.9
2	8.4	26.5	9.2	27.6	5.6	15.6
3	8.5	26.8	9.3	28.4	6.5	20.5

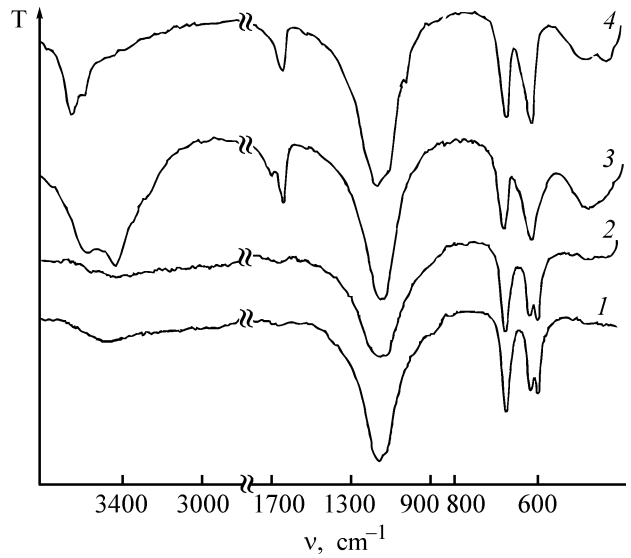

IR spectra of calcium sulfates. (ν) Wave number. (*1*) $CaSO_4$ not washed to remove the mother liquor with water and dried at room temperature, (*2*) $CaSO_4$ not washed to remove the mother liquor with water and dried at 90°C, (*3*) $CaSO_4 \cdot 2H_2O$ washed to remove the mother liquor with water and dried at room temperature, and (*4*) $CaSO_4 \cdot 0.5H_2O$ washed to remove the mother liquor with water and dried at 90°C.

in the range of stretching vibrations of water to higher frequencies (see figure, curve *4*).

The methods used in this study did not reveal any content of calcium phosphate in the precipitates.

Similarly to experiments on apatite decomposition with dilute acid solutions, the purification of the sphene concentrate to remove phosphorus (fluorapatite) was studied. The results obtained are listed in Table 4.

Table 4. Kinetics of purification of the sphene concentrate to remove fluorapatite (s : l = 1 : 3)

Treatment time, h	Residual content of P_2O_5, wt %, upon treatment with indicated acid, wt %					
	H_2SO_4		HCl		HNO_3	
	2	5	2	5	2	5
1	1.1	0.25	0.9	0.18	1.15	0.17
2	0.41	0.09	0.38	0.083	0.51	0.10
3	0.24	0.056	0.19	0.042	0.27	0.061
4	0.14		0.12		0.16	
5	0.094		0.081		0.11	

The results of purification of the sphene concentrate to remove the phosphorus impurity confirm the data obtained in fluorapatite decomposition and demonstrate that nitric acid is less effective than hydrochloric and sulfuric acids. The efficiency of the acids decreases in the order HCl > H_2SO_4 > HNO_3. In the same order grows the overstoichiometric expenditure of the acid for fluorapatite decomposition. At equal percentage concentrations of the acids, nitric acid has the lowest concentration in gram-equivalents. Nevertheless, the characteristics obtained with any of the three acids can give a sphene concentrate satisfying the requirements of TU 1715-069-00 203 938–2000 to the content of phosphorus (less than 0.1% in terms of P_2O_5).

From the ecological standpoint, use of nitric acid for purification of the sphene concentrate to remove phosphorus is less attractive because the maximum permissible concentration (MPC) of nitrate ions is lower than that for sulfate and chloride ions. The MPC is most simply provided in purification of waste solutions containing sulfate ions. Use of H_2SO_4 solutions leads to contamination of the concentrate with calcium sulfate having low solubility, and the technical specification for welding materials does not limit the content of sulfur. It is necessary to take into account that the expenditure of water for washing of the purified sphene concentrate to remove mother liquor containing sulfate ions is approximately 2–3 times that for washing to remove chloride ions. The real expenditure of water for purification to remove phosphorus is at a minimum for hydrochloric acid.

It follows from the data in Table 4 that purification to remove fluorapatite is sufficiently effective and the content of phosphorus in the target product decreases to the required level already in 3–5 h, depending on the acid concentration.

Starting from the assumption that there exist aggregations of sphene and fluorapatite [3], it was decided to check the effectiveness of the purification conditions for a finely ground sphene concentrate, in which the content of aggregations is virtually zero. The sphene concentrate was ground in a ball mill to grain size of –28 μm and treated with 2% hydrochloric acid. The choice of the acid was due to its higher efficiency, compared with sulfuric and nitric acids.

The reactivity of sphene in its interaction with the acid grows with the grinding fineness, and the higher the acid concentration, the stronger the interaction. Simultaneous decomposition of sphene and fluorapatite may lead to formation of a poorly soluble

titanium phosphates, i.e., to lower degree of purification to remove phosphorus. Therefore, 2% hydrochloric acid was taken for the treatment in order to reduce the degree of sphene decomposition. The finely ground sphene concentrate was processed using the procedure described above. The results of the experiments are presented below

Treatment time, h	1	2	3
Residual content of P_2O_5, wt %	0.14	0.029	0.024

Comparison with the data in Table 4 shows a considerably higher efficiency of purification to remove phosphorus for the finely ground sphene concentrate.

The final stage in preparation of the sphene concentrate is its washing with water to remove the mother liquor. Because of the low solubility of the precipitated calcium sulfate (~2 g l^{-1}), its removal by washing requires a water volume exceeding that of the acid by a factor of 6–8. At the same time, the expenditure of water to removal of chloride and nitrate ions by washing is 2–3 times smaller than that for calcium sulfate.

The problem of utilization of solutions formed in decomposition of fluorapatite and washing solutions requires an additional analysis. One of suggestions is to purify the sphene concentrate in fluidized-bed apparatus, which will enable fuller consumption of the acid and lower expenditure of water for washing of the purified concentrate. In this case, the acid will be consumed nearly completely. With hydrochloric acid used for purification, the waste solution will be a solution of $CaCl_2$, which can be utilized, e.g., by electrodialysis [6, 7].

With sulfuric acid used for purification to remove phosphorus, the forming finely crystalline $CaSO_4$ will be carried away from the apparatus by the washing solution and then can be separated by hydroclassification, which was confirmed in the stage of pilot industrial tests at Apatit Open Joint-Stock Company.

CONCLUSION

The efficiencies of purification of the sphene concentrate to remove a phosphorus impurity with hydrochloric and sulfuric acids are close, but preference should be given to hydrochloric acid, which rules out any contamination of the concentrate with sulfur impurity and makes it possible to reduce the expenditure of water for washing by a factor of 2–3.

ACKNOWLEDGMENTS

The study was financially supported by the program “Leading Scientific Schools” (grant no. NSh-4383.2006.3).

REFERENCES

1. Fedorov, S.G., Nikolaev, A.I., Brylyakov, Yu.E., et al., *Khimicheskaya pererabotka mineral’nykh kontsentratov Kol’skogo poluostrova* (Chemical Processing of Mineral Concentrates from Kola Peninsula), Apatity: Kola Nauch. Tsentr Ross. Akad. Nauk, 2003.
2. Gerasimova, L.G., *Pigmenty i napolniteli iz prirodnogo titansoderzhashchego syr’ya i tekhnogennykh otkhodov* (Pigments Produced from Natural Titanium-containing Raw Materials and Technological Wastes), Apatity: Kola Nauch. Tsentr Ross. Akad. Nauk, 2001.
3. Motov, D.L. and Maksimova, G.K., *Sfen i ego khimicheskaya pererabotka na titanovye pigmenty* (Sphene and Its Chemical Processing To Give Titanium Pigments), Leningrad: Nauka, 1983.
4. Kalinnikov, V.T., Nikolaev, A.I., and Zakharov, V.I., *Gidrometallurgicheskaya kompleksnaya pererabotka netraditsionnogo titano-redkometall’nogo i alyumosilikatnogo syr’ya* (Integrated Hydrometallurgical Processing of Unconventional Titanium–Rare-Earth and Aluminosilicate Raw Materials), Apatity: Kola Nauch. Tsentr Ross. Akad. Nauk, 1999.
5. Plyusnina, I.I., *Infrakrasnye spektry mineralov* (IR Spectra of Minerals), Moscow: Mosk. Gos. Univ., 1977.
6. RF Patent 2 174 561.
7. Todorov, S.A., Lainer, Yu.A., and Medvedev, A.S., *Izv. Vyssh. Uchebn. Zaved., Tsv. Metall.*, 2004, no. 3, pp. 37–39.

ISSN 1070-4272, Russian Journal of Applied Chemistry, 2007, Vol. 80, No. 6, pp. 864–867. © Pleiades Publishing, Ltd., 2007.
Original Russian Text © L.P. Firsova, 2007, published in Zhurnal Prikladnoi Khimii, 2007, Vol. 80, No. 6, pp. 891–893.

INORGANIC SYNTHESIS AND INDUSTRIAL INORGANIC CHEMISTRY

Leaching-out of Biologically Active Elements from Enriched Granulated Phosphogypsum

L. P. Firsova

Moscow State University, Moscow, Russia

Received December 8, 2005

Abstract—Leaching-out of biologically active microelements (Mn^{2+}, Zn^{2+}) from grains of phosphogypsum enriched with macro- and microadditives introduced into its composition before granulation was experimentally studied.

DOI: 10.1134/S1070427207060031

The main product of sulfuric acid processing of phosphorites, with dissolution of mineral raw materials in mixtures of sulfuric and phosphoric acids, is, together with phosphoric acid, calcium sulfate (phosphogypsum) in the form of semihydrate, dihydrate, or anhydrite. The less stable under ordinary conditions is semihydrate, which transforms in the presence of an excess amount of moisture, including that of atmospheric origin, into a dihydrate [1–3]. Under conditions that favor dehydration, the semihydrate transforms into anhydrous calcium sulfate.

As shown in [4, 5], phase transitions between various forms of calcium sulfate also occur in phosphogypsum grains. The forms of phosphogypsum differ not only in stability, but also in other physical and chemical properties and, accordingly, in application methods and areas. Purified dihydrate (gypsum) with low content of phosphorus and fluorine is used in manufacture of building materials, special types of paper, and gypsum board. Unpurified (to remove phosphorus and other impurities) phosphogypsum is mostly used in agriculture as a meliorating agent. To extend the application area of phosphogypsum in plant growing, it seems advisable to enrich it with biologically active macro- and microadditives (phosphorus, nitrogen, boron, manganese, zinc, cobalt, copper, molybdenum, etc.), which make phosphogypsum an integrated mineral fertilizer of prolonged action [6–9]. A necessary condition in this case is development of methods for granulation of phosphogypsum in the presence of specially introduced admixtures imparting to grains such properties as, e.g., sufficient mechanical strength and low dusting, which enable prolonged storage and transportation. Important characteristics of phosphogypsum for agriculture are its stability against moisture and parameters of impurity leaching-out from grains by water and aqueous solutions, including soil moisture.

This study is concerned with leaching-out of biologically active chemical elements, manganese and zinc, from phosphogypsum grains prepared by various methods, including those with specially introduced macro- and microadditives.

EXPERIMENTAL

In the experiments, calcium sulfate semihydrate powders with phase composition stabilized by treating phosphogypsum (industrial waste from phosphoric acid production) with several portions of acetone to remove hygroscopic moisture in order to preclude conversion of $CaSO_4 \cdot 0.5H_2O$ into $CaSO_4 \cdot 2H_2O$. Phosphogypsum washed with acetone was dried in air. The stabilized phosphogypsum contained (wt %): water 6.8 (theoretical value for semihydrate 6.2), CaO 39–40, SO_3 56–57, P_2O_5 0.9–1.1, F 0.3–0.4, SiO_2 0.7–0.8, and oxides of rare-earth elements 0.5–0.6. The content of zinc and manganese was less than 0.1 wt %. The bulk density of the powder was 0.94–1.0 g cm^{-3}. According to the results of a microscopic analysis, the phosphogypsum powder was composed of druses 10 to 300 μm in size, constituted by hexagonal prisms of the semihydrate of lengths in the range from 1 to 30 μm, with their (001) edges for the most part sticking together.

Immediately before granulation, an air-dry powder of the semihydrate was wetted with distilled water or aqueous solutions containing various specially introduced components, including manganese or zinc sulfates in an amount of 1–5 wt %, urea (up to 60–80 wt %), or urea phosphate $m\mathrm{CO(NH_2)_2} \cdot n\mathrm{H_3PO_4}$ (up to 40 wt %). To wet the taken weighed portions of the powder, the amount of a moistening solution was chosen so as to provide production of the maximum amount of grains with diameter in the range 2–6 mm in stock pelletization. The humid powder was transferred to the steel plate of the granulator and the stock was palletized for several minutes. The rotation rate of the granulator plate was varied from 50 to 80 rpm at a plate inclination angle of 20°–40°.

After the pelletization was complete, grains into whose composition no urea or urea phosphate was introduced, which had an initial strength of about 1–2 kg cm^{-2}, were carefully transferred for several hours into a humid atmosphere of a desiccator for "ripening," to be strengthened via a change in the phase composition in the transition from $\mathrm{CaSO_4} \cdot 0.5\mathrm{H_2O}$ to $\mathrm{CaSO_4} \cdot 2\mathrm{H_2O}$. After many hours of ripening the grains were dried in air. The degree of phase transformation of the semihydrate, found from the content of crystallization water, depended on the ripening time and composition of the moistening solution. For example, it was 35–45% if aqueous solutions of manganese or zinc sulfates (1–5 wt %) were used for moistening of the semihydrate, whereas in the case of wetting with solutions of manganese sulfate in 5% sulfuric acid, the degree of transformation increased to 80 ± 3% in about the same ripening time. The degree of phase transformation in ripening correlated with the grain strength. According to the results of measurements on an IPG-1 device (Russia), the strength of ripened air-dry grains (without urea) under uniaxial compression varied from 4 ± 1 to 12 ± 2 kg cm^{-2}, depending on the content of impurity components, manganese ions. Grains obtained from suspensions containing urea or urea phosphate, which have, immediately after pelletization, a considerably higher initial strength than urea-fee grains, were dried in air, without the ripening stage. The air-dry grains with urea sustained load on the order of 20 kg cm^{-2} without disintegration. The bulk density of these grains was 10 ± 2% higher than that of grains containing no urea. A study with an MBI-14 microscope (USSR) demonstrated that grains containing urea or urea phosphate were less friable and had a smaller number of pores than grains with addition of manganese(II) or zinc(II) salt, but without urea. Table 1 lists data on the content of chemical additives in the grains and on their mechanical strength θ.

Table 1. Content of chemical additives in phosphogypsum grains and their mechanical strength

Content, wt %			θ, kg cm^{-2}
$(NH_2)_2CO$	P_2O_5	Mn	
–	1.0	<0.1	11 ± 2
–	1.0	1.8	8 ± 1
22	0.8	1.0	19 ± 2
7.8	7.8	1.5	20 ± 2

X-ray spectra previously obtained [10] on an ARL X*TRA X-ray diffractometer (USA–Switzerland) demonstrated that the phase compositions of grains with and without urea are different. In grains produced in wetting of calcium sulfate semihydrate with aqueous solutions containing urea or urea phosphate, the main form of calcium sulfate is anhydrite. In grains that contained no urea and were ripened in a humid atmosphere, calcium sulfate semihydrate is present.

The leaching-out of impurities (manganese and zinc compounds) from phosphogypsum grains was studied under static or dynamic conditions at a temperature of 19 ± 20°C. Grains of size 2, 4, or 6 mm were taken for experiments. In static experiments, weighed portions of equal-size grains were placed in glass vessels and poured over with distilled water at s : l = 1 : 5. The grains were in contact with water for 24 h. During this time, the vessels were periodically turned upside down. After the time of contact between grains and water was over, the liquid was separated by centrifugation or filtration. The content of manganese or zinc ions in the filtrate was determined spectrophotometrically. In the dynamic experiment, a weighed portion of grains was introduced into a glass column with an inner diameter of 10 mm, the grain layer was densified by tapping and its height was measured. Bidistillate, taken in an amount of up to 30 volumes of the grain layer, was passed at a rate of 8 ± 0.5 ml h^{-1} through the column filled with grains by UNIPAN-335A micropumps (Poland). The solutions collected were filtered and the content of zinc or manganese ions was spectrophotometrically determined. The number of parallel experiments on leaching in static and dynamic modes was 10–12. It was visually noticed that grains containing no urea or urea phosphate are destroyed by water more rapidly under both static and dynamic conditions.

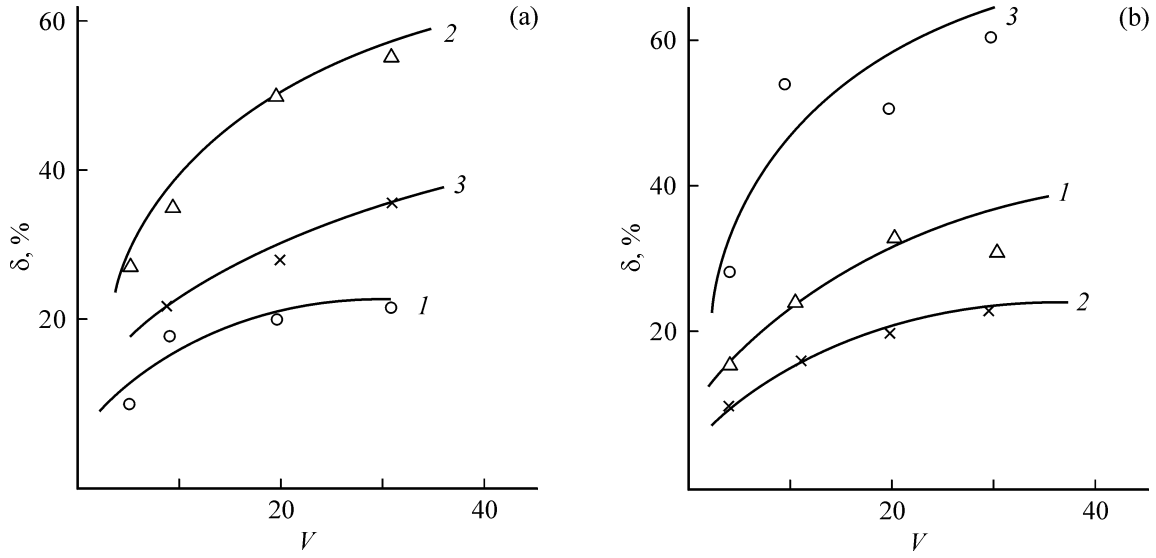

Fig. 1. Fraction δ of manganese(II) and zinc(II) leached-out from phosphogypsum grains produced by moistening with aqueous solutions containing various additives. Additive: (a) (*1*) manganese sulfate, (*2*) manganese sulfate and urea sulfate, and (*3*) manganese sulfate and urea phosphate; (b) (*1*) zinc sulfate, (*2*) zinc sulfate and urea sulfate, and (*3*) zinc sulfate and urea phosphate.

The content of manganese in the filtrates was determined by the peroxodisulfate method, with Mn^{2+} ions converted into permanganate ions, and that of zinc was found by the dithizone technique [10]. The optical densities of the solutions under study and standard colored solutions were compared using a KF–77 (Poland) or FEK-56 M photocolorimeter (USSR). The data obtained were used to calculate the degrees δ of microelement recovery from the solid phase on the assumption that the concentrations of manganese and zinc ions in distilled water can be taken to be zero. The experimental data on the degree of Mn(II) and Zn(II) leaching-out from phosphogypsum grains of various compositions are listed in Table 2 and shown in Fig. 1.

Table 2. Degree of leaching-out of Mn(II) and Zn(II) from phosphogypsum

Additives to $CaSO_4 \cdot 0.5H_2O$	Degree of leaching, δ	
	Mn(II)	Zn(II)
$MnSO_4$	0.74 ± 0.31	–
$MnSO_4$ + urea	0.65 ± 0.28	–
$MnSO_4$ + urea phosphate	0.52 ± 0.24	–
$ZnSO_4$	–	0.71 ± 0.25
$ZnSO_4$ + urea	–	0.64 ± 0.34
$ZnSO_4$ + urea phosphate	–	0.49 ± 0.27

The data in Table 2 demonstrate that Mn(II) and Zn(II) are leached-out from grains enriched in urea or urea phosphate at a considerably slower rate. The slowing-down of Mn(II) and Zn(II) leaching-out from grains with urea or urea phosphate may occur for several reasons. First, the moisture resistance and mechanical strength of grains whose skeleton is formed in the presence of urea by crystals of anhydrous calcium sulfate [10], which also has lower solubility than hydrated forms $CaSO_4 \cdot xH_2O$. Such grains more slowly disintegrate under the action of water or soil moisture. Second, a visual analysis with an MBI-14 microscope and measurements of bulk density demonstrated that grains with urea or urea phosphate have a less friable structure and lower porosity, which may also lead to a decrease in the fraction of impurities washed-out from pores. In addition, the rate of washing-out of Mn(II) and Zn(II) ions from pores may decrease because of the presence in the pore space of ions of orthophosphoric acid and urea forming with sulfates MSO_4 adduct, e.g., of composition $MSO_4 \cdot 2CO(NH_2)_2 \cdot 4H_2O$ [12]. Thus, presence of urea and phosphate ions may lead both to an increase in the mechanical strength and moisture resistance of grains and to a decrease in the rate of leaching-out of bioactive microcomponents, including manganese or zinc ions, from grains.

CONCLUSIONS

A study of the leaching of phosphogypsum grains enriched in various biologically active macro- and microcomponents demonstrated that urea and phosphate ions, including those in the form of urea phosphate, introduced into the composition of the grains can markedly improve the mechanical strength and moisture resistance of the grains. Simultaneously, they make lower the rate of washing-out of manganese(II) and zinc(II) from the grains and prolong the action of integrated fertilizers based on industrial wastes from sulfuric acid processing of phosphorites.

REFERENCES

1. Melikhov, I.V., Rudin, V.N., and Vorob'eva, L.I., *Neorg. Mater.*, 1988, no. 3, pp. 488–452.
2. Melikhov, I.V., Rudin, V.N., and Vorob'eva, L.I., *Teor. Osn. Khim. Tekhnol.*, 1985, vol. 19, no. 6, pp. 742–748.
3. Teylor, H.F.W., *Cement Chemistry*, London: Academic, 1990.
4. Firsova, L.P., *Vestn. Mosk. Univ., Ser. 2, Khim.*, 2003, vol. 44, no. 5, pp. 352–355.
5. Firsova, L.P., *Zh. Prikl. Khim.*, 2003, vol. 76, no. 3, pp. 353–355.
6. USSR Inventor's Certificate, no. 724654.
7. USSR Inventor's Certificate, no. 724655.
8. Firsova, L.P., *Vestn. Mosk. Univ., Ser. 2, Khim.*, 2004, vol. 45, no. 3, pp. 204–207.
9. Firsova, L.P., *Zh. Prikl. Khim.*, 2004, vol. 77, no. 2, pp. 179–183.
10. Firsova, L.P., *Zh. Prikl. Khim.*, 2006, vol. 79, no. 12, pp. 2049–2051.
11. Peshkova, V.M. and Gromova, M.A., *Prakticheskoe rukovodstvo po spektrofotometrii* (Manual of Spectrophotometry), Moscow: Mosk. Gos. Univ., 1965.
12. Kucheryavyi, V.I. and Lebedev, V.V., *Sintez i primenenie karbamida* (Synthesis and Use of Carbamide), Leningrad: Khimiya, 1970.

ISSN 1070-4272, Russian Journal of Applied Chemistry, 2007, Vol. 80, No. 6, pp. 868–873. © Pleiades Publishing, Ltd., 2007.
Original Russian Text © N.I. Kasikova, A.G. Kasikov, V.T. Kalinnikov, 2007, published in Zhurnal Prikladnoi Khimii, 2007, Vol. 80, No. 6, pp. 894–898.

INORGANIC SYNTHESIS AND INDUSTRIAL INORGANIC CHEMISTRY

Effect of Diluents on the Extractive Capacity of Organophosphoric Acids in Vanadium(V) Recovery from Sulfuric Acid Solutions

N. I. Kasikova, A. G. Kasikov, and V. T. Kalinnikov

Tananaev Institute of Chemistry and Technology of Rare Elements and Mineral Resources, Kola Scientific Center, Russian Academy of Sciences, Apatity, Murmansk oblast, Russia

Received October 2, 2006

Abstract—The extractive capacity of di(2-ethylhexyl)phosphoric and di(2,4,4-trimethylpentyl)phosphinic acids for vanadium(V) in its extraction from individual sulfuric acid solutions with the use of kerosene, a number of aliphatic alcohols, and octanone as diluents was studied. The most effective organic mixtures for extraction of vanadium(V) were determined in relation to the concentration of sulfuric acid.

DOI: 10.1134/S1070427207060043

One of sources of vanadium are sulfuric acid solutions obtained in aqueous or acid leaching of vanadium-containing raw materials [1, 2]. Extraction methods are frequently used for recovery of vanadium from solutions of this kind and its concentration and purification. The extent to which the metal passes into the organic phase depends on its state in aqueous solutions. In contrast to niobium and tantalum, which are present as cations in dilute solutions of the mineral acid and form anionic complexes as the concentration of sulfuric acid increases, vanadium(V) typically forms a wide variety of ion forms at both low and high contents of H_2SO_4 [3–13].

Analysis of published data shows that the ionic state of V(V) in H_2SO_4 solutions is determined by the concentrations of vanadium(V) and H_2SO_4. It was shown in [3] that, in dilute H_2SO_4 solutions, vanadium(V) is in the form of mono- and polynuclear complex ions whose composition depends on the solution pH.

It has been found [4–8] that, at a concentration of less than 10^{-4} g-ion l^{-1}, vanadium exists in the monomeric state, irrespective of the solution pH, and at vanadium concentrations exceeding 1×10^{-4} g-ion l^{-1}, polycondensation of ions occurs in solution, with degrees of polycondensation of 2, 3, 4, and 10 [8]. The structures of the ionic forms of vanadium have been determined in relation to the solution pH. As the pH value increases from 1 to 14, the following species are found in solutions: VO^{2+}, VO^{3-}, $V_2O_7^{4-}$, VO_4^{3-}, $V_3O_9^{3-}$, $V_3O_{10}^{5-}$, $V_4O_{12}^{4-}$, $V_4O_{13}^{6-}$, HVO_4^{2-}, $HV_2O_8^{5-}$, $H_aV_{10}O_{28}^{(6-a)-}$ ($a = 0-6$) [8, 9].

In concentrated H_2SO_4 solutions, the following species have been found: VO^{2+} [8], HVO_3 [3], and VO^{3+} [10]. A decrease in the acidity of the medium, causes conversion of VO^{2+} into other ionic forms, whose formation depends on the vanadium concentration. It was shown in [11] that, at high V(V) concentrations (≥0.12 M) in solutions containing more than 9 M of H_2SO_4, dimeric species are formed, and at H_2SO_4 concentration of 13–16 M, vanadium(V) exists only in the dimeric form [12]. At H_2SO_4 concentrations of 9 M and less, vanadium forms monomeric complexes whose central group is a vanadium(V) dioxocation [13].

The wide variety of forms of vanadium(V) in sulfuric acid solutions poses certain difficulties in preparation of selective extractive systems for separation of vanadium from accompanying impurities.

There is published evidence about use of a wide variety of extractive agents, such as amines [1], ketones [14], tributyl phosphate [15], alcohols [16, 17], di(2- ethylhexyl)phosphoric acid (D2EHPA) [11], and mixtures of extractive agents for recovery of vanadium(V) from sulfuric acid solutions.

Of particular interest among the reagents listed above are polydentate extractive agents having in their composition several extraction-active groups and, in

particular, organophosphoric acids (OPA), to which belongs D2EHPA. Extracting agents of this class contain two functional groups: hydroxy (–OH) and phoshoryl (P=O), which makes it possible to regard these groups as cation-exchange groups, on the one hand, and neutral oxygen-containing extractants, on the other.

Data on extraction of vanadium(V) with OPA are scarce. There have been several reports of extraction of vanadium(V) in the weakly acidic region [18] and in concentrated H_2SO_4 [11], with undiluted purified D2EHPA used as an extractive agent. It is known, however, that OPA are dimerized in pure form and in solutions of inert solvents [19, 20], which is due to the simultaneous presence in their composition of proton-donor and proton-acceptor groups (–OH and P=O). This gives rise to a system of hydrogen bonds and leads to a decrease in the thermodynamic activity of the extractive agent, because, in this case, the access to the functional groups of the extractive agent of particles being distributed is hindered.

In recent years, a considerable attention has been given to the choice of extractant mixtures having synergetic properties with respect to a metal being recovered [1, 21, 22]. It is known that active solvents, to which belong neutral oxygen-containing reagents, such as TBP, sulfoxides. DMSO, ketones and alcohols, make lower the degree of dimerization of organic acids [19, 20, 22], which should raise their extractive power. It was shown in [20] by IR spectroscopy that D2HPA is completely monomerized in methanol because of the formation of H-complexes of D2HPA with the alcohol molecule.

Because extractive systems with alkylphosphoric acids and neutral ligands are commonly regarded as systems that typically exhibit synergism [22], of particular interest is a study of the effect of neutral oxygen-containing reagents as diluents on the extraction characteristics of OPA.

Previously, the extractive properties of two organophosphoric acids, D2EHPA and di(2,4,4-trimethylpentyl)phosphinic acid (Cyanex 272) with respect to titanium, niobium, and tantalum in extraction from hydrochloric solutions have been studied [23–25]. It was found that replacement of an inert diluent with a neutral oxygen-containing reagent positively affects the extractive properties of both organophosphoric acids, whereas the extractive power of OPA with respect to rare-earth elements shows pronounced differences.

The aim of this study was to compare the extractive properties of D2EHPA and Cyanex 272 with respect to vanadium(V) on replacement of inert diluents with neutral oxygen-containing compounds.

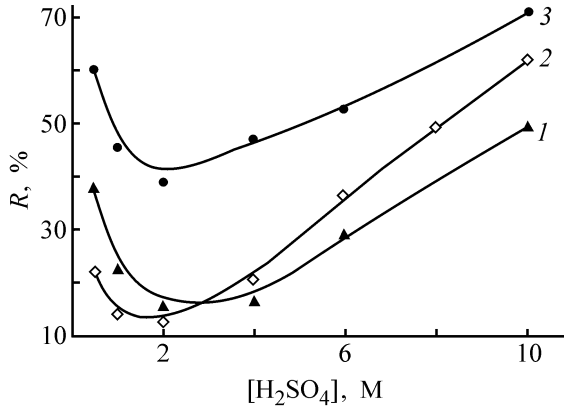

Fig. 1. Effect of H_2SO_4 on the recovery R of vanadium(V) with (*1*) $D2HPA_{techn}$, (*2*) $D2HPA_{pur}$ (manufactured by Bayer), and (*3*) Cyanex 272 in a diluent, kerosene, at a constant concentrations of vanadium in the starting solutions (1.5×10^{-2} M V_2O_5) and of the extractive agent in the diluent (1.2 M).

EXPERIMENTAL

The following OPA were used as extractive agents: D2EHPA manufactured by Bayer (Germany), with 97.3% main substance, technical-grade D2EHPA of domestic manufacture (Volgograd), with the content of the main substance of 65% and more; and Cyanex 272 manufactured by Cytec (Canada), with 85–90% main substance. The following diluents were used: an inert diluent, aviation kerosene; long-chain aliphatic alcohols, octanol, isooctanol, and decanol; and a ketone, octanone-2. All the neutral oxygen-containing reagents were of pure grade.

Vanadium solutions were prepared by dissolution of V_2O_5 of special purity grade in 1–10 M of H_2SO_4 of chemically pure grade. The extraction was performed in calibrated test tubes. After volume measurements, the phases were separated. The concentration of sulfuric acid was determined by titration with NaOH in the presence of Methyl Orange. The concentration of vanadium(V) in the starting solutions and in equilibrium aqueous phases after extraction was found using the phosphorus-tungstate method [26] and also a Plasma-400 ICP spectrometer with inductively coupled plasma. The content of vanadium(V) in extracts was calculated from the difference of the concentrations in aqueous solutions before and after extraction.

Figure 1 shows data on the influence exerted by the concentration of sulfuric acid on vanadium(V)

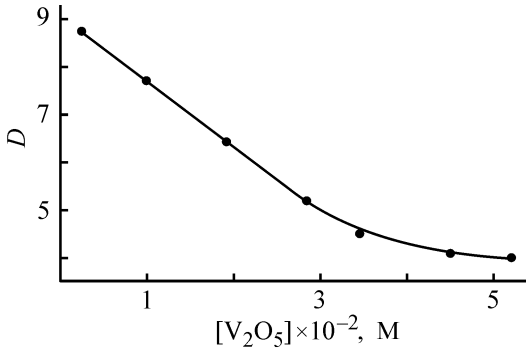

Fig. 2. Vanadium distribution coefficient D vs. the V_2O_5 concentration in the starting solution at $pH_{in} \approx 3$. Extractive agent: 1.2 M $D2EHPA_{techn}$ in kerosene.

recovery with technical-grade (curve *1*) and purified (curve *2*) D2EHPA and with Cyanex 272 (curve *3*) in an inert diluent, kerosene, at concentrations in the range 0.5–10 M. It was found that the dependences of the extraction of vanadium(V) on the H_2SO_4 concentration show minima at 1–4 M (Fig. 1, curves *1–3*). Previously, data on extraction of niobium(V), tantalum(V), and titanium(IV) with D2EHPA of various brands in the same inert diluent have been obtained [27]. The existence of minima was only noticed in recovery of niobium, tantalum, and titanium with purified D2EHPA in kerosene.

The data obtained indicate that the mechanism of extraction of rare-earth elements becomes more complex as the H_2SO_4 concentration increases. This occurs because, in the case of chelating extractive agents of acid nature (to which belong OPA), both the functional groups, –PO and –OH, are involved in coordination and the coordination mechanism, whose contribution increases with the solution acidity, operates in addition to the cation exchange, which complicates the extraction process [28].

Previously, differences in the extraction characteristics of pure and technical-grade D2EHPA with respect to niobium, tantalum, and titanium have been revealed [27]. It was shown that, in contrast to the pure extractive agent, technical-grade D2EHPA extracts rare elements with high distribution coefficients in the entire range of acidities (1.5–10 M H_2SO_4). The high degree of recovery of niobium, tantalum, and titanium with technical-grade D2EHPA has been attributed to the synergic effect [22, 27] appearing in the presence of monoalkylphosphoric acid contained in technical-grade D2EHPA [28]. In the case of vanadium(V) extraction with OPA in inert diluents (Fig. 1, curves *1–3*), no synergic effect of was observed.

Thus, OPA in inert diluents can be arranged in order of increasing capacity for vanadium(V) extraction in acid solutions containing 0.5 M of H_2SO_4 and more as follows: D2EHPA (technical grade) < D2EHPA (purified) < Cyanex 272.

It is known that branching of carbon chains in OPA can affect both the extractive power and the selectivity of extraction of separate elements [29]. The acids D2EHPA and Cyanex 272 possess, respectively, ethyl and methyl radicals in the β-position. In contrast to D2EHPA, phosphonic acid has two more substituents (methyl radicals) at the fourth carbon atom, which suggests a higher selectivity of Cyanex 272 with respect to vanadium, compared with D2EHPA.

An opposite pattern was observed in extraction of vanadium(V) from weakly acidic solutions, in which the cation-exchange mechanism is operative. In recovery of vanadium with technical-grade D2EHPA (pK_a 2.12) in kerosene from solutions with pH 3, the vanadium(V) distribution coefficient was, at vanadium(V) concentration in the aqueous solution equal to 2.8×10^{-2} M, $D = 5.2$ in contrast to $D = 0.08$ for Cyanex 272 (pK_a 6.4). These differences are probably due to the fact that two ester groups (–OR) are present in the structure in the case of D2EHPA [structural formula $(RO)_2POOH$] and absent in the case of Cyanex 272 (structural formula R_2POOH). These groups favor extraction of metals by the cation-exchange mechanism because they withdraw the electron density from the hydroxy group –OH and thereby make higher the proton mobility. The occurrence of the extraction by the cation-exchange mechanism is indicated by a considerable change in the pH value of the aqueous solution in the course of extraction.

Figure 2 shows how the vanadium distribution coefficient depends on the concentration of vanadium in the starting solution in the range $(0.25–5.2) \times 10^{-2}$ M V_2O_5 at pH_{in} 3 in the case of technical-grade D2EHPA in kerosene.

The dependence obtained indicates that the distribution coefficients decrease as the vanadium(V) concentration in the starting solutions becomes higher. This is probably due to polymerization in the aqueous phase and agrees with published data [8, 9], according to which polycondensation of vanadium occurs under these conditions.

Replacement of an inert diluent with a neutral oxygen-containing reagent leads to substantial changes in the extractive properties of organophosphoric acids.

Figures 3 and 4 show how the vanadium(V) distribution coefficients depend on the H_2SO_4 concentration in extraction with OPA in oxygen-containing diluents. The dependences obtained with purified D2EHPA virtually coincide with the results for technical-grade D2EHPA, and, therefore, are not shown here. For comparison, the same figures show data on extraction of vanadium with OPA in inert diluents (Figs. 3 and 4, curves *2*) and with an individual aliphatic alcohol, 100% isooctanol (Fig. 3, curve *5*). The data obtained indicate that oxygen-containing diluents differently affect the extraction of vanadium(V) from dilute and concentrated solutions with alkylphosphoric acids.

In extraction of vanadium(V) with D2EHPA from solutions containing less than 2 M H_2SO_4, the following dependence of the effect of the diluents used on the extractive properties of alkylphosphoric acid was obtained: kerosene > octanol ≈ isooctanol ≈ decanol > octanone. A somewhat different dependence was obtained in vanadium extraction with phosphonic acid Cyanex 272: kerosene > octanone > decanol = isooctanol = octanol.

It follows from the data obtained that is kerosene the best diluent for D2EHPA at H_2SO_4 concentrations of less than 2 M.

The long-chain ketone has a positive effect as a diluent at low H_2SO_4 concentrations only when it is used in a mixture with phosphonic acid (Fig. 4, curve *1*). Because, in contrast to D2EHPA, Cyanex 272 contains no electron-donor ester groups, the acceptor C=O group of the ketone possibly withdraws the electron density from the hydroxy group of OPA and thereby makes higher the mobility of a proton and promotes its exchange for a metal cation.

It was found that, as the H_2SO_4 concentration is raised from 0.5 to 4 M, the distribution coefficient of vanadium in its extraction with 100% isooctanol changes from 0.06 to 0.08 and the degree of vanadium extraction in this range does not exceed 8% (Fig. 3, curve *5*).

In recovery of vanadium from H_2SO_4 solutions concentrated in mineral acid (c > 4 M), a significant increase in the extractive power of OPA was observed in such diluents as aliphatic alcohols, compared with inert diluents. In this case the maximum effect was observed with isooctyl alcohol (2-ethyl-1-hexanol) (Fig. 3, curve *6*; Fig. 4, curve *5*), compared with alcohols of normal structure. The degrees of vanadium(V) recovery in extraction with OPA in mixtures with octanol and decanol virtually coincide (Figs. 3 and 4, curves *3* and *4*).

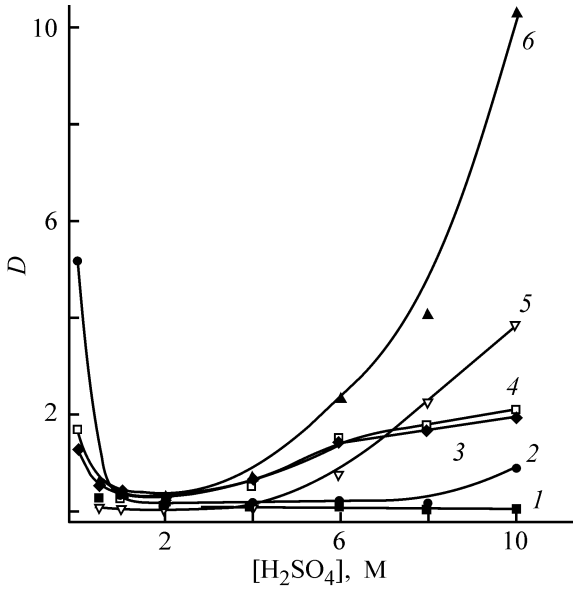

Fig. 3. Vanadium distribution coefficient D vs. H_2SO_4 concentration in the starting solution in extraction with 1.2 M D2EHPA in the following diluents: (*1*) octanone, (*2*) kerosene, (*3*) decanol, (*4*) octanol, and (*6*) isooctanol; and (*5*) in extraction with pure isooctyl alcohol.

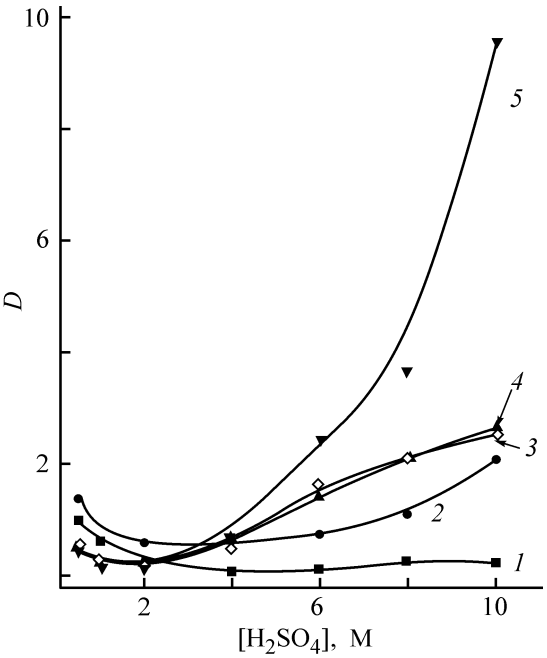

Fig. 4. Vanadium distribution coefficient D vs. H_2SO_4 concentration in the starting solution in extraction with 1.2 M Cyanex 272 in the following diluents: (*1*) octanone, (*2*) kerosene, (*3*) decanol, (*4*) octanol, and (*5*) isooctanol.

With isooctyl alcohol used as diluent for organophosphoric acids, there probably occurs a synergic effect, because the extraction of vanadium with a pure alcohol or OPA in an inert diluent is considerably lower.

CONCLUSIONS

(1) A study of the extractive properties of a number of industrial organophosphoric acids in an inert and neutral oxygen-containing diluents with respect to vanadium(V) in its extraction from individual sulfuric acid solutions revealed differences in the extraction behavior of vanadium(V) and other rare elements: niobium(V), tantalum(V), and titanium(IV).

(2) The influence exerted by the sulfuric acid concentration in the starting solutions on the extraction characteristics of extractive agents was determined. It was found that, at low H_2SO_4 concentrations (<2 M), the most effective diluent for all of the organophosphoric acids under study is kerosene. Use of octanone under these conditions has a positive effect only on the extractive properties of phosphonic acid.

(3) The optimal conditions of vanadium recovery with technical-grade di(2-ethylhexyl)phosphoric acid in kerosene at pH 2.8–3.0 were found. It was shown that use of phosphonic acid under these conditions is inefficient.

(4) Advantages of neutral oxygen-containing reagents as diluents in vanadium(V) recovery with organophosphoric acids from concentrated (in sulfuric acid) solutions were demonstrated. The conditions were found and the composition of extractive mixtures based on organophosphoric acid and isooctanol was suggested for effective recovery of vanadium from solutions containing H_2SO_4 in concentrations of 9 M and more.

ACKNOWLEDGMENTS

The study was financially supported by the Russian Foundation for Basic Research–North (grant no. 05-03-97502).

REFERENCES

1. Ritcey, G.M. and Ashbrook, A.W., *Solvent Extraction. Principles and Applications to Process Metallurgy*, Amsterdam: Elsevier, 1979.
2. Palant, A.A., *Metally*, 1996, no. 5, pp. 43–45.
3. Mirolyubov, V.R., Podval'naya, N.V., and Volkov, V.L., *Zh. Neorg. Khim.*, 2005, vol. 50, no. 1, pp. 111–116.
4. Morachevskii, Yu.V. and Belyaeva, A.I., *Zh. Anal. Khim.*, 1956, no. 11, p. 672.
5. Babko, A.K. and Gridchina, G.I., *Zh. Neorg. Khim.*, 1968, no. 13, p. 3029.
6. Sannikov, Yu.I., Zolotavin, V.L., and Bezrukov, I.Ya., *Zh. Neorg. Khim.*, 1963, vol. 8, p. 923.
7. Ivakin, A.A. and Fotiev, A.A., *Tr. Ins. Khim. Ural. Nauchn. Tsentra Akad. Nauk SSSR*, 1971, no. 24.
8. Dudarev, V.I., Morgen, E.A., and Vlasov, N.A., *Issledovanie vodnykh rastvorov vanadatov metodom elektronnoi spektroskopii* (A Study of Aqueous Solutions of Vanadates by Electron Spectroscopy), 1978, Irkutsk, Dep. no. 1764/78.
9. Rozantsev, G.M., Sazonova, O.I., and Kholin, Yu.V., *Zh. Neorg. Khim.*, 1999, vol. 44, no. 12, pp. 2099–2104.
10. Muzgin, V.N., Khamzina, L.B., Zolotavin, V.L., and Bezrukov, I.Ya., *Analiticheskaya khimiya vanadiya. Ser. "Analiticheskaya khimiya elementov"* (Analytical Chemistry of Vanadium, Series "Analytical Chemistry of Elements"), Moscow: Nauka, 1981.
11. Kurbatova, L.D., Kurbatov, D.I., and Medvedev, N.I., *Zh. Prikl. Khim.*, 2004, vol. 77, no. 4, pp. 680–683.
12. Madic, C., Begun, G.M., Hahn, R.L., et al., *Inorg. Chem.*, 1984, vol. 23, pp. 469–476.
13. Kurbatova, L.D. and Kurbatov, D.I., *Zh. Neorg. Khim.*, 2006, vol. 51, no. 5, pp. 908–910.
14. Kaveney, Mc. and Freiser, H., *Analyt. Chem.*, 1958, vol. 30, p. 52.
15. Zharovskii, F.G., Vyazovskaya, L.M., and Kostova, R.V., *Ukr. Khim. Zh.*, 1968, no. 34, p. 181.
16. Kopach, S. and Paidovski, L., *Zh. Neorg. Khim.*, 1971, vol. 16, no. 2, pp. 451–456.
17. Ivakin, A.A., Petunina, N.I., and Gamburov, V.G., *Tr. Inst. Khim. Ural. Otd. Akad. Nauk SSSR*, 1966, no. 10, p. 3.
18. Kurbatova, L.D., Medvedeva, N.I., and Kodess, M.I., *Zh. Neorg. Khim.*, 1997, vol. 42, no. 11, pp. 1927–1929.
19. Komarov, E.V., Kopyrin, A.A., and Proyaev, V.V., *Teoreticheskie osnovy ekstraktsii assotsiirovannymi reagentami: Uchebnoe posobie dlya vysshikh uchebnykh zavedenii* (Theoretical Foundations of Extraction with Associated Reagents: Textbook for Higher School Institutions), Moscow: Energoatomizdat, 1984.
20. Stoyanov, E.S., Popov, V.M., and Mikhailov, V.A., *Zh. Prikl. Spektrosk.*, 1984, vol. 40, no. 1, pp. 77–84.
21. Kuznetsov, V.A., *Metall. Tsv. Redk. Met.*, 1979, vol. 6, pp. 56–135.
22. Rublev, V.V., *Zh. Anal. Khim.*, 1983, vol. 38, no. 5, pp. 922–930.
23. Kasikova, N.I., Kasikov, A.G., Nikolaev, A.I., et al., *Nedelya khimicheskikh tekhnologii v Sankt-Peterburge: Sbornik materialov konferentsii "50 let Rossiiskoi ekstraktsii", SPb, 28–31 oktyabrya 2002 g.* (Week of Chemical Technologies in St. Petersburg: Proc. Conf. "50 Years of Extraction Technology in Russia," St. Petersburg, October 28–31, 2002), pp. 94–99.

24. Kasikova, N.I., Kasikov, A.G., and Kalinnikov, V.T., *Innovatsionnyi potentsial Kol'skoi nauki* (Innovation Potential of the Kola Science), Apatity: Kola Nauchn. Tsentr Ross. Akad. Nauk, 2005, pp. 180–184.
25. Kasikova, N.I. and Kasikov, A.G., *Materialy mezhdunarodnoi konferentsii "Kompleksnaya pererabotka netraditsionnogo titano-redkometall'nogo i alyumosilikatnogo syr'ya: Sovremennoe sostoyanie i perspektivy", Apatity, 4–8 aprelya 2006 g.* (Proc. Int. Conf. "Integrated Processing of Unconventional Titanium–Rare-Earth and Aluminosilicate Raw Materials: Modern State and Prospects," April 4–8, 2006), pp. 102–104.
26. Ponomarev, A.I., *Metody khimicheskogo analiza zheleznykh, titano-magnetitovykh i khromovykh rud* (Methods for Chemical Analysis of Iron, Titanium-Magnetite, and Chromium Ores), Moscow: Nauka, 1966, pp. 100–111.
27. Kasikova, N.I., Extraction of Niobium, Tantalum, and Titanium from Sulfuric Acid and Fluoride-Sulfate Solutions with Oxygen-containing Extractive Agents, *Cand. Sci. Dissertation*, Moscow, 1987.
28. Ignatenko A.V., Pastukhova I.V., Petrov K.A. et al., *Zh. Anal. Khim.*, 1982, vol. 37, no. 4, pp. 744–747.
29. Rozen, A.M. and Krupnov, B.V., *Usp. Khim.*, 1996, vol. 65, pp. 1052–1079.

ISSN 1070-4272, Russian Journal of Applied Chemistry, 2007, Vol. 80, No. 6, pp. 874–878. © Pleiades Publishing, Ltd., 2007.
Original Russian Text © V.G. Maiorov, A.I. Nikolaev, B.Ya. Zil'berman, V.M. Shcherbakov, 2007, published in Zhurnal Prikladnoi Khimii, 2007, Vol. 80, No. 6, pp. 899–902.

INORGANIC SYNTHESIS AND INDUSTRIAL INORGANIC CHEMISTRY

Utilization of Waste Solutions in Perovskite Technology

V. G. Maiorov, A. I. Nikolaev, B. Ya. Zil'berman, and V. M. Shcherbakov

Tananaev Institute of Chemistry and Technology of Rare Elements and Mineral Resources, Kola Scientific Center, Russian Academy of Sciences, Apatity, Murmansk oblast, Russia

Khlopin Radium Institute, St. Petersburg, Russia

Russian Federal Nuclear Center, All-Russia Research Institute of Experimental Physics, Sarov, Nizhni Novgorod oblast, Russia

Received September 4, 2006; in final form, December 2006

Abstract—A scheme for utilization of chloride solutions of complex composition with α- and β-activity of up to 35 and 28 kBq l^{-1}, respectively, is suggested.

DOI: 10.1134/S1070427207060055

In Russia, there is a stable deficit of titanium(IV), niobium(V), and tantalum(V) compounds, which is due to the lack of a surveyed resources of the conventional raw materials (ilmenite, columbite-tantalite, pyrochlore, and microlite ores). At the same time, Russia possesses a considerable part of world's resources of titanium–rare-earth raw materials, of which the Kola Peninsula has about half of the national resources. The largest stock of titanium–rare-earth materials are concentrated in loparite ores of the Lovozero deposit and perovskite ores of the Afrikand and Vuoriyarvi deposits. The loparite concentrate is manufactured in limited amounts and is the only source of raw materials in the country for manufacture of niobium–tantalum and rare-earth products. Deposits of perovskite ores for manufacture of these deficient products deserve a greater attention.

The total resources of ores at only the Afrikand deposit (best prepared for industrial use) constitute 626.2 million tons (52.2 million tons of TiO_2). A characteristic feature of perovskite is the complex multicomponent composition. For example, perovskite from the Afrikand deposit contains (wt %): $(Nb + Ta)_2O_5$ 0.64–2.50, TiO_2 50.8–56.8, SiO_2 0.12–1.93, Al_2O_3 0.15–1.30, Fe_2O_3 0.43–2.00, FeO up to 1.44, Ln_2O_3 2.18–10.7 (here and hereinafter Ln_2O_3 is a sum of oxides of rare-earth elements, REE), CaO 26.3–38.1, Na_2O 0.10–2.35, and ThO_2 0.07–0.14. Various schemes for integrated processing of perovskite have been developed [1, 2], which are mostly based on decomposition of a concentrate with mineral acids: sulfuric, nitric, or hydrochloric, followed by separation of the main components of the systems by hydro- and pyrometallurgical methods. These technologies can produce 0.41–0.47 ton of pigment titanium dioxide, up to 100 kg of a rare-earth concentrate, 7.7–9.3 kg of Nb_2O_5, and 0.42–0.50 kg of Ta_2O_5 from a ton of the concentrate. A promising technique is decomposition of perovskite with hydrochloric acid, with calcium(II), REE(III), and thorium(IV) transferred to solution, and titanium(IV), niobium(V), and tantalum(V), to a precipitate further processed into commercial products by known techniques [1–3].

A difficult problem in the hydrochloric acid technology of perovskite is posed by utilization of waste solutions containing radionuclides, mostly thorium(IV), and also U(VI) and Ra(II). These solutions have a complex multicomponent composition and contain chemical elements with markedly different properties and a large amount of $CaCl_2$, which strongly affects the recovery and separation of components of the system. The processing of solutions of this kind has virtually not been studied at all. The utilization of these solutions, with their purification to remove radionuclides and to obtain valuable components as commercial products, has been analyzed [4–9]. In this communication, the results of these studies are used when choosing a utilization scheme (see scheme; *n* is the number of stages in the continuous counterflow process) and evaluating the main material flow rates.

The radioactive contamination of the solutions being processed is mainly due to presence of thorium(IV). Th(IV) can be recovered by both extraction and pre-

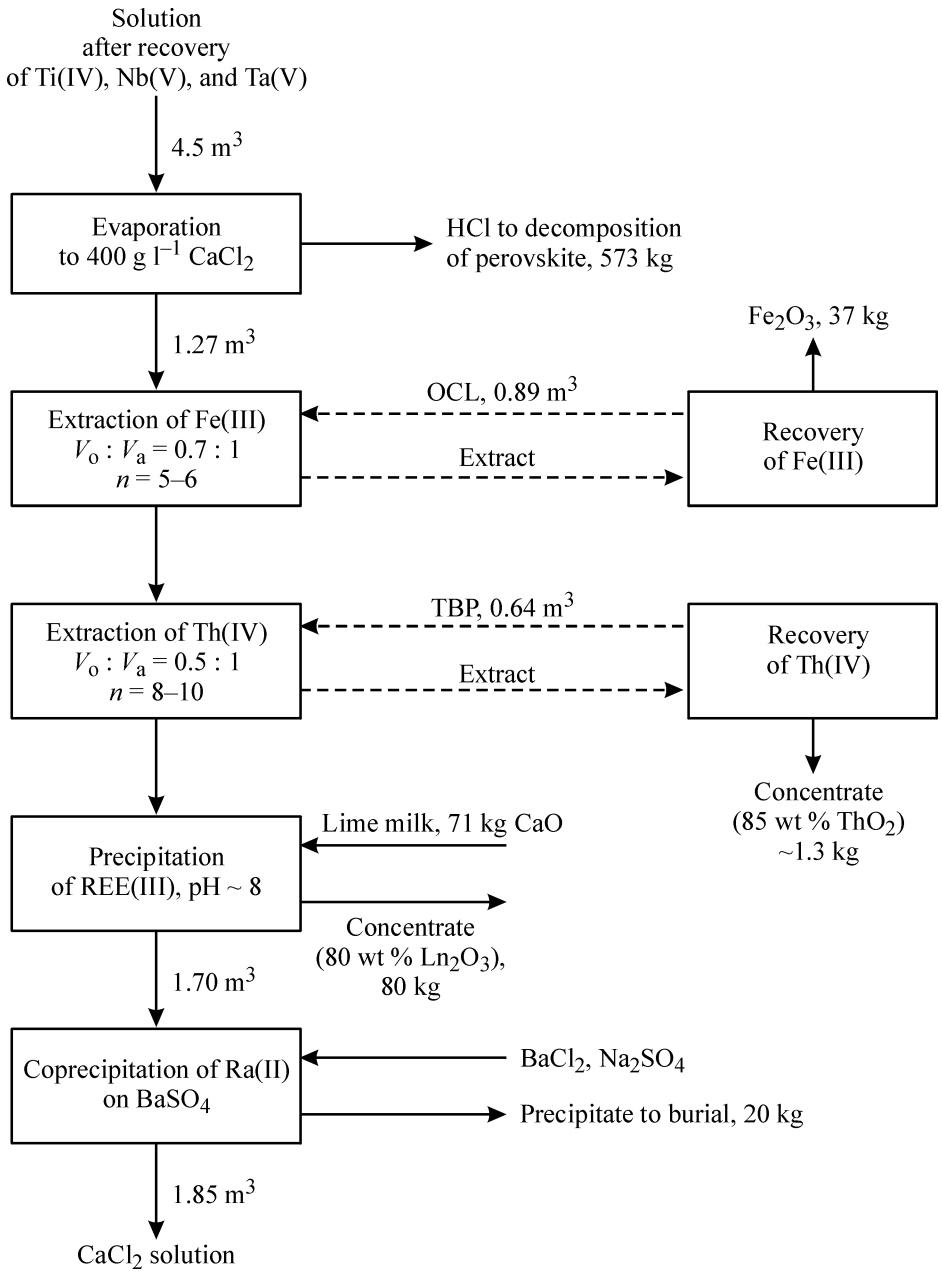

cipitation methods, which have been tested previously [6–8]. Preference was given to extraction because this technique can more selectively recover Th(IV) from technological solutions to give concentrates rich in this element. It was taken into account that the interest in thorium(IV) as an energy-containing raw material has revived: at a deficiency of natural uranium(VI), thorium(IV) can markedly improve the resource potential of the nuclear power engineering of the future. As the most important source of thorium(IV) is recommended its accompanying recovery in processing of rare-metal ores [10].

Solution obtained upon extraction of Ti(IV), Nb(V), and Ta(V), which contained 100–200 g l^{-1} of HCl and 100–150 g l^{-1} of $CaCl_2$ were preliminarily evaporated to a $CaCl_2$ concentration exceeding 400 g l^{-1} in order to reduce technological flow rates, regenerate HCl (returned to perovskite decomposition), and improve the extraction of thorium(IV). According to published data [11] and results obtained in the present study, the extraction of Th(IV) with tributyl phosphate steeply increases with the $CaCl_2$ concentration, especially at $[CaCl_2] > 400$ g l^{-1}. The scheme shows the solution volumes before and after evaporation and the mass of

regenerated hydrochloric acid (in terms of 100% acid); here and hereinafter the material flow rates were calculated (per ton of the perovskite concentrate) using average values of the composition of perovskite and the starting and intermediate solutions.

After the evaporation, the solutions had the following composition (g l^{-1}): HCl 70–90, $CaCl_2$ 430–470, ThO_2 0.54–1.38, Ln_2O_3 25–30, Fe_2O_3 27–32 [Fe(II) + Fe(III) in terms of Fe_2O_3], TiO_2 1–5, ZnO 0.5–1.5, Al_2O_3 2–6, V_2O_5 0.1–0.4, and MnO 0.5–1.3, with α- and β-activities of up to 35 and 28 kBq l^{-1}, respectively. Preliminarily, prior to recovery of Th(IV), Fe(III) was selectively extracted with octanol-1 (OCL) in order to reduce the mass of the further obtained concentrates of Th(IV) and REE(III) [4, 5]. Because Fe(II) cannot be extracted in the given system [11], it was oxidized to Fe(III) by the known methods. A virtually complete recovery of Fe(III) is achieved at a ratio of organic to aqueous phases $V_o : V_a \approx 0.7 : 1$. Under these conditions, the transfer of titanium(IV), thorium(IV), and REE(III) into the organic phase does not exceed 50, 2, and 0.1%, respectively. After washing and re-extraction of iron(III) with water [at $V_o : V_a$ of 10 : 1 and (2–3) : 1, respectively], neutralization with an ammonia solution yielded pure iron(III) hydroxide. According to the results of an emission spectral analysis, the content of impurities in Fe_2O_3 (after calcination) was as follows (wt %): Cu, Al, and Mn < 0.001; Mg ≤ 0.001; Si and Ti ≤ 0.003; Ca, Ce, La, and Pb < 0.03; Cr ≤ 0.03; and Zn, Sn, and Zr < 0.1. Pure iron(III) compounds are widely used in various fields of technology [12].

In Th(IV) recovery were tested di(2-ethylhexyl)-phosphoric acid, OCL, and TBP, with good results obtained in the case of TBP. In a system with TBP, the influence exerted on the Th(IV) distribution by the content of HCl and $CaCl_2$, and $V_o : V_a$ values in extraction, washing, and re-extraction has been studied. A conclusion was made that a high Th(IV) recovery is favored by an increase in the $CaCl_2$ concentration at a minimum content of HCl in the system. At $[CaCl_2] > 400$ g l^{-1} and $V_o : V_a \approx 1 : 1$, the degree of Th(IV) recovery in a single stage is 92–94%. However, the $V_o : V_a$ ratio was lowered to approximately 0.5 : 1 in order to diminish the co-extraction of impurities (see scheme). Under these conditions, the recovery of Th(IV) decreases to 78%, but the extraction of the main accompanying impurities, Ca(II) and REE(III), decreases to an even greater extent (severalfold), to 5 and 2.6%, respectively. The low recovery of impurities made it possible to eliminate the stage of extract washing. The re-extraction of Th(IV) is performed with a solution of 10 g l^{-1} HCl ($V_o : V_a$ = 1 : 1), with thorium(IV) precipitated from the re-extract at pH 5. The content of ThO_2 in the concentrate is about 85%; the recovery of Th(IV) from the starting solution into the product obtained is about 75% (with recycles disregarded).

Uranium(VI), whose content in perovskite is approximately 0.01 wt % [an order of magnitude lower than that of Th(IV)], is extracted from hydrochloric solutions better than Th(IV) [11, 13] and is concentrated together with Th(IV). In the scheme under consideration, U(VI) can be isolated from the filtrate after precipitation of Th(IV).

After extraction of Th(IV), the activity of the solution, naturally, decreases dramatically, to values of about 7.5 and 9.0 kBq l^{-1} for α- and β-radiation, respectively; however, these values still remain high and considerably exceed the levels specified by sanitary regulations.

The raffinate obtained after extraction of Th(IV) contains Ti(IV), Nb(V), and other elements precipitating in a more acidic medium than do REE(III). To separate these elements from REE(III), neutralization with lime milk (20 wt % CaO) to pH 2–4 is carried out. A precipitate of hydroxides (up to 10 kg per ton of perovskite) is returned to the stage of concentrate decomposition. Further processing of the solution includes recovery of the REE(III) concentrate at pH ~8 and coprecipitation of radium(II) with $BaSO_4$ [6–9, 14]. If purification to remove Ra(II) is performed before precipitation of REE(III), REE(III) are partly precipitated (lost), which presumably occurs because of the formation of poorly soluble double sulfates with Na_2SO_4 [15] introduced into solution in recovery of radium(II).

The REE(III) concentrate is contaminated with radioactive impurities, mostly radium(II) and products of its decay, because of the sorption of radionuclides on REE(III) hydroxides in the course of their precipitation; the α- and β-activities of the product are 6.4 and 21.7 kBq kg^{-1}, respectively; the content of ThO_2 is about 0.1 wt %. According to sanitary regulations, the concentrate does not belong to radioactive solid waste, but its use as a raw material in subsequent processing requires a permission by sanitary control [16]. The concentrate is further processed by the known methods, including (when necessary) an additional purification to remove radionuclides [1, 2, 17–20].

After the precipitation of REE(III), the α- and β-activities of the solution, approximately equal to 3 and 2.2–4 kBq l^{-1}, respectively, are mostly determined by the presence of radium(II) and products of its decay. To remove Ra(II) by coprecipitation with $BaSO_4$, $BaCl_2$ and Na_2SO_4 were successively introduced into

the solution. The conditions of radium(II) recovery: solution acidity, expenditure of $BaCl_2$ and Na_2SO_4, temperature, and other precipitation parameters, were studied in detail. The most complete purification to remove radionuclides is achieved at an expenditure of 0.068 m^3 of a solution containing 170 g l^{-1} of $BaCl_2$ per 1 m^3 of the technological solution and a 180% expenditure (relative to the amount stoichiometrically necessary for $BaSO_4$ formation) of a solution of a 180 g l^{-1} solution of Na_2SO_4, temperature $T \approx 20°C$, and pH 7–9. The expenditure of $BaCl_2$ and Na_2SO_4 per ton of the concentrate is 12 and 14 kg, respectively.

In this stage, the specificity of the technological solutions being processed, with a high content of $CaCl_2$, was manifested the most clearly. It is known [14] that Ra(II) is precipitated the most completely with $BaSO_4$ from acid solutions. In the case in question, however, it is necessary to make the acidity of the system lower. It has been noted [14] that the degree of precipitation of a microcomponent in cocrystallization of isomorphous compounds is the higher, the more complete is the precipitation of a macrocomponent. It can be concluded that the solubility of $BaSO_4$ [and $CaSO_4$ on which Ra(II) also partly coprecipitates] in a system with high $CaCl_2$ concentration is at a minimum at pH 7–9. Accordingly, a higher degree of purification to remove radium(II) is observed just in this region.

After the final purification to remove radionuclides, the α- and β-activities of the solution are less than 0.18 and 0.08 kBq l^{-1}, respectively. The final solution is not dangerous for the environment in radiation regard.[1] Methods for processing of a solution containing virtually only $CaCl_2$ were considered in [1–3, 17]; a possible way is addition of H_2SO_4 to obtain gypsum, with HCl regeneration. The expenditure of H_2SO_4 and the yield of gypsum and HCl (100% acid) per ton of the concentrate are, respectively, 622, 864, and 464 kg.

On the whole, the scheme suggested is virtually waste-free. Among disadvantages of the scheme are the comparatively high flow rate of TBP in Th(IV) recovery and contamination of the REE(III) concentrate with radionuclides.

CONCLUSION

A scheme for utilization of solutions formed in perovskite processing, which have complex composition and high content of $CaCl_2$ and other salts, was suggested. The scheme includes extraction of iron(III) with octanol-1 ($V_o : V_a = 0.7 : 1$) and extraction of thorium(IV) with tributyl phosphate ($V_o : V_a = 0.5 : 1$) to give a Th(IV) concentrate (ThO_2 content of about 85 wt %), neutralization with recovery of a concentrate of rare-earth elements (80–90 wt % Ln_2O_3), and coprecipitation of radium(II) with $BaSO_4$. The final solutions are radiation-safe and suitable for production of gypsum and other calcium(II) compounds.

[1] According to the data obtained at Khlopin Radium Institute.

REFERENCES

1. Nikolaev, A.I., *Pererabotka netraditsionnogo titanovogo syr'ya Kol'skogo poluostrova* (Processing of Unconventional Titanium-containing Raw Materials of the Kola Peninsula), Apatity: Kola Nauchn. Tsentr Ross. Akad. Nauk, 1991.
2. Kalinnikov, V.T., Nikolaev, A.I., and Zakharov, V.I., *Gidrometallurgicheskaya kompleksnaya pererabotka netraditsionnogo titano-redkometall'nogo i alyumosilikatnogo syr'ya* (Integrated Hydrometallurgical Processing of Unconventional Titanium–Rare-Earth and Aluminosilicate Raw Materials), Apatity: Kola Nauchn. Tsentr Ross. Akad. Nauk, 1999.
3. Nikolaev, A.I., Gerasimova, L.G., Maiorov, V.G., et al., Abstracts of Papers, *XVII Mendeleevskii s"ezda po obshchei i prikladnoi Khimii, Kazan, 21–26 sentyabrya 2003 g.* (XVII Mendeleev Congress on General and Applied Chemistry, Kazan, September 21–26, 2003), vol. 3, *Materialy i nanotekhnologii*, (Materials and Nanotechnologies), Kazan, 2003, p. 313.
4. Maiorov, V.G., Nikolaev, A.I., Kopkov, V.K., et al., *Zh. Prikl. Khim.*, 2004, vol. 77, no. 5, pp. 715–719.
5. Maiorov, V.G., Nikolaev, A.I., Avsaragov, Kh.B., et al., *Tsv. Met.*, 2005, no. 3, pp. 85–87.
6. Maiorov, V.G., Avsaragov, Kh.B., Kopkov, V.K., et al., *Zh. Prikl. Khim.*, 2005, vol. 78, no. 10, pp. 1596–1599.
7. Maiorov, V.G., Avsaragov, Kh.B., Nikolaev, A.I., et al., *Tsv. Met.*, 2006, no. 1, pp. 21–26.
8. Maiorov, V.G., Avsaragov, Kh.B., Popova, T.V., et al., *Khim. Tekhnol.*, 2006, no. 2, pp. 24–28.
9. Maiorov, V.G., Nikolaev, A.I., and Zil'berman, B.Ya., *Kompleksnaya pererabotka netraditsionnogo titano-redkometall'nogo i alyumosilikatnogo syr'ya: Sovremennoe sostoyanie i perspektivy. Materialy mezhdunarodnoi konferentsii, 4–8 aprelya 2006 g.* (Proc. Int. Conf. on Integrated Processing of Unconventional Titanium–Rare-Earth and Aluminosilicate Raw Materials: Modern State and Prospects, April 4–8, 2006), Apatity: Kola Nauchn. Tsentr Ross. Akad. Nauk, 2006, pp. 161–166.
10. Kosynkin, V.D., Kotova, V.M., and Shatalov, V.V., *Khim. Tekhnol.*, 2004, no. 3, pp. 30–35.
11. Zolotov, Yu.A., Iofa, B.Z., and Chuchalin, L.K., *Ekstraktsiya galogenidnykh kompleksov metallov*

(Extraction of Halide Complexes of Metals), Moscow: Nauka, 1973.

12. Kopkova, E.K. and Sklokin, L.I., *Khim. Tekhnol.*, 2001, no. 11, pp. 20–26.
13. Markov, V.K., Vernyi, E.A., Vinogradov, A.V., et al., *Uran: Metody ego opredeleniya* (Uranium: Methods for Its Determination), Moscow: Atomizdat, 1964.
14. Vdovenko, V.M. and Dubasov, Yu.V., *Analiticheskaya khimiya radiya* (Analytical Chemistry of Radium), Leningrad: Nauka, 1973.
15. Ryabchikov, D.I. and Ryabukhin, V.A., *Analiticheskaya khimiya redkozemel'nykh elementov i ittriya* (Analytical Chemistry of Rare-Earth Elements and Yttrium), Moscow: Nauka, 1966.
16. *Sanitarnye pravila obrashcheniya s radioaktivnymi otkhodami (SPORO–2002)* [Sanitary Regulations Concerning Radioactive Waste Handling (SPORO–2002)], Moscow: Minzdrav Rossii, 2003.
17. Lebedev, V.N., Asseretskova, O.V., and Smirnova, I.P., *Khimiya i tekhnologiya mineral'nogo syr'ya Kol'skogo poluostrova* (Chemistry and Technology of Mineral Resources of the Kola Peninsula), St. Petersburg: Nauka, 1992, pp. 54–60.
18. Mikhailichenko, A.I., Mikhlin, E.B., and Patrikeev, Yu.B., *Redkozemel'nye metally* (Rare-Earth Metals), Moscow: Metallurgiya, 1987.
19. Kosynkin, V.V., Makarov, V.D., and Shatalov, V.I., *Razvitie redkometall'noi promyshlennosti Rossii na baze loparita: Sbornik trudov IV nauchnoi konferentsii, Sankt-Peterburg, 22–24 maya 2001 g.* (Proc. of Int. Conf. on Development of Russia's Rare-Metal Industry on the Basis of Loparite, St. Petersburg, May 22–24, 2001), St. Petersburg, 2001, pp. 153–158.
20. Karmannikov, V.P., Klimenko, M.A., Mikhlin, E.B., et al., *Razvitie redkometall'noi promyshlennosti Rossii na baze loparita: Sbornik trudov IV nauchnoi konferentsii, Sankt-Peterburg, 22–24 maya 2001 g.* (Proc. of Int. Conf. on Development of Russia's Rare-Metal Industry on the Basis of Loparite, St. Petersburg, May 22–24, 2001), St. Petersburg, 2001, pp. 113–114.

ISSN 1070-4272, Russian Journal of Applied Chemistry, 2007, Vol. 80, No. 6, pp. 879–882. © Pleiades Publishing, Ltd., 2007.
Original Russian Text © V.M. Ogenko, L.V. Dubrovina, O.V. Goldun, S.V. Volkov, 2007, published in Zhurnal Prikladnoi Khimii, 2007, Vol. 80, No. 6, pp. 903–906.

INORGANIC SYNTHESIS AND INDUSTRIAL INORGANIC CHEMISTRY

Porous Inorganic Materials Modified with Pyrolytic Carbon Producted from Polystyrene

V. M. Ogenko, L. V. Dubrovina, O. V. Goldun, and S. V. Volkov

Vernadsky Institute of General and Inorganic Chemistry, National Academy of Sciences of Ukraine, Kiev, Ukraine

Received January 16, 2006

Abstract—Microporous materials were obtained by pyrocarbon modification of matrices based on a highly dispersed silicon dioxide. The modification involved polystyrene carbonization at 400 and 700°C in an argon flow. The possibility was elucidated of varying the properties of porous materials (density, porosity, sorption of organic solvents, and compression strength) by varying the way of introduction of polystyrene solutions into the matrix and their concentrations.

DOI: 10.1134/S1070427207060067

Direct carbonization of carbon-containing compounds yields carbonizates with low strengths, which prevents preparation of fairly large articles therefrom. This problem can be solved by carrying out carbonization in an inorganic matrix. Pyrocarbon modification of inorganic porous materials is widely used for preparation of carbon-mineral adsorbents and gas-separation membranes [1–3]. Recently, pyrocarbon modification has been characterized by ever widening use of carbonization of polymers in a solid matrix, yielding porous carbon structures. In solid-phase carbonization, the resulting carbon is concentrated in the volume or on the surface of the pores; its structures are distinguished by high density and microporosity. The structure of the resulting carbonizate depends on the concentration and composition of the polymer and intermediates, carbonization conditions, rate of the process, etc. The difference in the structure of the carbonizates governs their properties: strength, density, total and closed porosities, and sorption properties [4–5].

We examined here the properties of porous materials based on highly dispersed silicon dioxide with a pyrocarbon coating formed from polystyrene carbonization.

EXPERIMENTAL

The structure-forming components were highly dispersed silicon dioxides (particle size 5–80 nm): hydrophilic Aerosils (A-300, S_{sp} = 300 $m^2 g^{-1}$; A-175, S_{sp} = 175 $m^2 g^{-1}$; A-50, S_{sp} = 50 $m^2 g^{-1}$) and hydrophobic Aerosils (AM, with modifying methyl groups on the surface, with S_{sp} = 175 $m^2 g^{-1}$; AO, with trimethylsilyl modifying groups on the surface, with S_{sp} = 195 $m^2 g^{-1}$). In the presence of a liquid dispersion medium, highly dispersed silicon dioxides form gels [6] which, after drying, were used as matrices for preparation of pyrocarbon. The precursor for carbon preparation was polystyrene (PS) with the molecular weight (MW) of 240 000. We used ethyl acetate solutions of PS with various concentrations for impregnation of the matrix obtained from silicon dioxide or as the dispersion medium. The carbonization of PS was carried out at 400 and 750°C in an argon flow. For technique of preparation of matrices and carbonized samples, see [7, 8].

Sorption of organic solvents by the composites was examined under static conditions at room temperature. The true density of the composites was determined pycnometrically, the porosity of the composites, from sorption of carbon tetrachloride [9]; and adsorption of Methylene Blue, by UV spectroscopy. [10]. The compression strength was determined for 1.0 × 1.0 × 0.5 cm samples.

Polystyrene is a virtually noncarbonizable polymer: Heating causes its degradation with breakdown of the backbone of the macromolecule and formation of low-molecular-weight volatiles. However, in carbonization in an inert gas atmosphere, removal of volatiles formed by PS degradation and their diffusion in the bulk of the samples are decelerated to such an extent that they get involved into secondary reac-

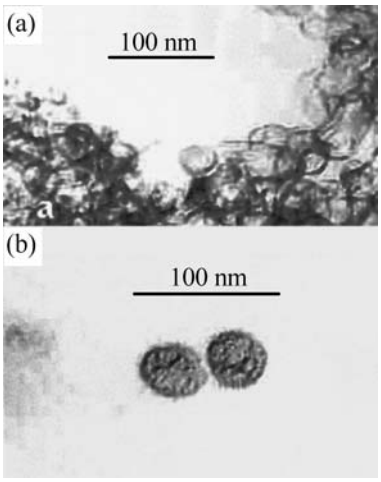

Fig. 1. TEM images of the carbon structures formed from carbonization of polystyrene introduced together with the dispersion medium into the pores of the composite based on A-50 silicon dioxide. Concentration of the polystyrene solutions in ethyl acetate, g per 100 ml: (a) 1.5 and (b) 5.

tions. Therefore, a coke residue can remain in the pores of the matrix composite.

The intermediates formed in thermal degradation in a vacuum of PS with MW of 230000 are compounds with MW of 264 at 500°C and 476 at 800°C, which evaporate before degradation. In thermal degradation in an inert gas atmosphere, these compounds decompose mainly to styrene; also formed are benzene, toluene, and minor amounts of other compounds [11]. It can be assumed that, in the composites of interest, the thermal degradation products formed when PS is carbonized at 750°C in an argon atmosphere undergo further transformations into carbon. The resulting samples were black. An elemental analysis confirmed that carbonizate was virtually pure carbon.

Madorsky [11] examined the amount of volatiles as influenced by the thermal degradation time at $T < 400$°C for PS with MW of 230000 and revealed a mass loss of 20–50% within 30 min. Thus, the yellow color of the samples in which PS was carbonized at 400°C is presumably due to formation of structures containing double bonds conjugated with the benzene ring [12]:

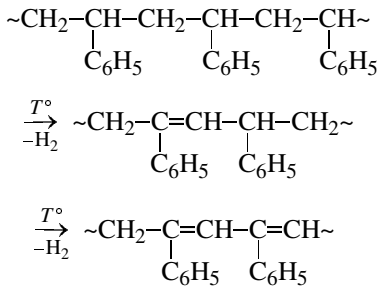

An elemental analysis confirmed that the carbonizate consisted of carbon (~95%) and hydrogen (~4 wt %).

As is known [13], the size of aggregates of the PS macromolecules in ethyl acetate at the concentration $c = 0.25$ g per 100 ml is 1000 Å; at $c = 1.5$ g per 100 ml, 4000 Å; and at $c = 5.0$ g per 100 ml, 890 Å, and their number is 0.017×10^9, 0.27×10^9, and 6.88×10^9, respectively. We have found earlier [7, 8] that the pore size of matrices based on A-50 silicon dioxide is such that the PS molecules with the conformation formed in a solution with the concentration of 5.0 g per 100 ml penetrate into these pores without hindrance during impregnation. To obtain composites with other concentrations of PS, its solutions were used as the dispersion medium for formation of polymer-containing gels carbonized after drying. Figure 1 shows TEM images of the carbon nanostructures formed in these composites. These are up to 5-nm-thick spherical segments with a diameter of up to 60 nm (Fig. 1a), or segmented spheres with a diameter of up to 60 nm (Fig. 1b).

Table 1 presents the properties of the carbon-containing composites obtained at 750°C. It is seen that these are highly porous materials, since their apparent

Table 1. Properties of carbon-containing composites obtained by introducing PS with the dispersion medium (carbonization at 750°C)

c_{PS}, g per 100 ml	Compression strength σ, kg cm^{-2}	d_{eff}	d_{true}	Volume of the solvents sorbed, ml g^{-1}, at indicated d^*, nm [14]			
		g cm^{-3}		water	benzene	toluene	hexane
				0.35	0.59	0.63	0.67
1.5	37.5	0.41	2.20	1.71	1.79	1.76	1.76
5.0	20.0	0.43	2.17	1.81	1.82	1.78	1.76

* Van der Waals diameter of the molecules.

Table 2. Formulation and properties of the matrix composites used for impregnation with polystyrene solutions

Composite	Composite formulation	d_{eff}, g cm^{-3}	Porosity W, %	Composite	Composite formulation	d_{eff}, g cm^{-3}	Porosity W, %
1	A-50 + A-300	0.53	61	3	A-50 + AM	0.50	58
2	A-50 + A-175	0.49	55	4	A-50 + AO	0.47	81

Table 3. Properties of carbon-containing composites obtained by introduction of PS via impregnation

Matrix composite	Concentration of PS solution used for impregnation, g per 100 ml								
	5.0			1.5			0.25		
	d_{eff}, g cm^{-3}	v, ml g^{-1}		d_{eff}, g cm^{-3}	v, ml g^{-1}		d_{eff}, g cm^{-3}	v, ml g^{-1}	
		benzene	hexane		benzene	hexane		benzene	hexane
Carbonization at 750°C									
1	0.52	1.10	1.10	0.53	1.12	1.08	0.53	1.14	1.13
2	0.40	1.08	1.13	0.43	1.12	1.06	0.45	1.11	1.09
3	0.51	1.09	1.08	0.53	1.12	1.04	0.57	1.09	1.03
4	0.53	1.16	1.12	0.54	1.17	1.13	0.60	1.18	1.15
Carbonization at 400°C									
1	0.51	1.09	1.05	0.52	1.11	1.11	0.47	1.17	1.11
2	0.51	1.07	1.07	0.53	1.08	1.07	0.53	1.13	1.07
3	0.54	1.03	1.02	0.48	1.10	1.04	0.55	1.07	1.23
4	0.52	1.16	1.11	0.51	1.14	1.09	0.53	1.16	1.15

density d_{eff} is much lower than that of amorphous silicon dioxide and graphite (2.20 and 2.27 g cm^{-3}, respectively), and their structure depends on the concentration of PS being introduced into the matrix.

A decrease in the volume of the solvents sorbed v, ml g^{-1}, with increasing size of their molecules can be associated with the molecular sieve effect. An increase in the amount of the solvents sorbed on going from one composite sample to another is indicative of an increase in the porosity for the composites obtained from PS solutions of a higher concentration, and also of a change in the carbon coating structure. This is confirmed by a decrease in the true density of the composites with increasing precursor solution concentration. The adsorption of Methylene Blue by the composite prepared from A-50 silicon dioxide, using ethyl acetate as the dispersion medium was estimated at 17 mg g^{-1}. The fact that Methylene Blue is not sorbed by carbon-containing composites, whose properties are summarized in Table 1, suggests that these are microporous composites with a pore size under 1.3 nm [15].

Water sorption does not provide adequate information on the porosity of hydrophobic composites [14], but is indicative of the presence in the carbon composition of a large number of polar groups.

To prepare carbon-containing composites by introducing a carbonization precursor by the impregnation method, we obtained matrix composites from mixtures of highly dispersed silicon dioxides. Table 2 lists the composition and properties of these composites.

Table 3 summarizes the properties of the carbon-containing materials obtained from these composites. It is seen that these are highly porous materials whose properties vary with the matrix composition and PS solution concentration. A decrease in the PS concentration causes the effective density of the carbon-containing composites to increase. This is due to the change in the structure of the carbon coating, depending on the conformation of the PS macromolecules in the solution and, hence, on their interaction with silicon dioxide [13]. Introduction into the matrix of smaller, compared to A-50, silicon dioxide particles results in a denser packing [13]. On the one hand, this is responsible for an increase in the effective density of the composites, and on the other, the porosity increases due to additional formation of carbon from

the modifying groups when the modified silicon dioxides are introduced during carbonization.

Table 3 shows that the composites prepared by carbonization at 400°C differ only slightly in the properties from those carbonized at 750°C. The practical use of the former should take into account the presence in them of incompletely carbonized PS residues.

Comparison of the properties of the composites into which PS was introduced by impregnation (Table 3) and with the dispersion medium (Table 1) shows that the former have a smaller porosity, sorb smaller volumes of organic solvents, and the molecular-sieve effect is less pronounced or lacking.

The sorption characteristics of the obtained carbon-containing porous composites are by approximately an order of magnitude higher than those of commercial active carbons. The high sorption power and mechanical strength make these composites promising for practical application. A drawback of these composites is that, like commercial active carbons, they burn out at temperatures above 250°C.

CONCLUSIONS

(1) Polystyrene carbonization in matrices based on highly dispersed silicon dioxide yielded monolithic porous composites, which are, essentially, a pyrocarbon-coated silicon dioxide skeleton.

(2) Physicomechanical and sorption properties of the composites can be changed by varying the size and composition of the surface of the SiO_2 particles constituting the matrix, as well as the polystyrene concentration and the way of its introduction into the matrix.

REFERENCES

1. Alekseeva, O.K. and Amirkhanov, D.M., *Ross. Khim. Zh.*, (*Zh. Poss. Khim. O–va. im. D.I. Mendeleeva*), 2004, vol. 48, no. 5, pp. 82–89.
2. Soldatov, A.P., Rodionova, I.A., Shkol'nikov, E.I., et al., *Zh. Fiz. Khim.*, 2004, vol. 78, no. 9, pp. 1659–1664.
3. Komarov, V.S., *Adsorbenty: voprosy teorii, sinteza i struktury* (Adsorbents: Theory, Synthesis, and Structure), Minsk: Belaruskaya Navuka, 1997.
4. Gribanov, A.V. and Sazanov, Yu.N., *Zh. Prikl. Khim.*, 1997, vol. 70, no. 6, pp. 881–902.
5. Ostrovskii, V.S., *Khim. Tverd. Topl.*, 1980, no. 5, pp. 134–137.
6. Iler, R.K., *The Chemistry of Silica*, New York: Wiley–Interscience, John Wiley & Sons, 1979.
7. Ogenko, V.M., Dubrovina, L.V., Goldun, O.V., et al., *Neorg. Mater.*, 2006, vol. 42, no. 5, pp. 575–578.
8. Volkov, S.V., Ogenko, V.M., Dubrovina, L.V., et al., *NATO Security through Science, Ser. A: Chemistry and Biology, V. Hydrogen Materials Science and Chemistry of Carbon Nanomaterials,* Springer Science + Business Media B.V., 2006, pp. 497–504.
9. Grigorov, O.N., Karpov, I.F., Koz'mina, Z.P., et al., *Rukovodstvo k prakticheskim rabotam po kolloidnoi khimii* (Guide on Practical Works on Colloid Chemistry), Moscow: Khimiya, 1964.
10. Brooks, C.S., Kolloid-Z. *Z. Polym.*, vol. 199, no. 1, pp. 31–36.
11. Madorsky, S.L., *Thermal Degradation of Organic Polymers*, New York: Interscience, 1964.
12. Grassie, N. and Scott, G., *Polimer Degradation and Stabilisation*, Cambridge: Cambridge Univ., 1985.
13. Lipatov, Yu., Todosijchuk, T., and Chornaya, V., *J. Colloid. Interface Sci.*, 1993, vol. 155, pp. 283–289.
14. Koganovskii, A.M., Klimenko, N.A., Levchenko, T.M., and Roda, I.G., *Adsorbtsiya organicheskikh veshchestv iz vody* (Adsorption of Organic Substances from Water), Leningrad: Khimiya, 1990.
15. Kel'tsev, N.V., *Osnovy adsorbtsionnoi tekhniki* (Fundamentals of Adsorption Technique), Moscow: Khimiya, 1984.

ISSN 1070-4272, Russian Journal of Applied Chemistry, 2007, Vol. 80, No. 6, pp. 883–886. © Pleiades Publishing, Ltd., 2007.
Original Russian Text © A.K. Pyartman, V.A. Keskinov, V.V. Lishchuk, Ya.A. Reshetko, 2007, published in Zhurnal Prikladnoi Khimii, 2007, Vol. 80, No. 6, pp. 907–910.

PHYSICOCHEMICAL STUDIES OF SYSTEMS AND PROCESSES

Phase Equilibria in the Liquid Ternary System $[Th(NO_3)_4(TBP)_2]$–$[Gd(NO_3)_3(TBP)_3]$–TBP–Isooctane at Different Temperatures

A. K. Pyartman, V. A. Keskinov, V. V. Lishchuk, and Ya. A. Reshetko

St. Petersburg State Institute of Technology (Technical University), St. Petersburg, Russia

Received November 13, 2006; in final form, January, 2007

Abstract—The phase diagrams of the ternary system $[Th(NO_3)_4(TBP)_2]$–$[Gd(NO_3)_3(TBP)_3]$–TBP–isooctane in the temperature range 298.15–333.15 K were constructed.

DOI: 10.1134/S1070427207060079

The mutual solubility of components in the binary systems decane (tetradecane)–REM(III) nitrate solvates with tri-*n*-butyl phosphate $[Ln(NO_3)_3(TBP)_3]$ at different temperatures was studied in [1, 2]. The phase diagrams of these systems contain the field of homogeneous solutions and the field of separation into two liquid phases. The upper critical solution temperature of these systems depends on the kind of a rare-earth metal(III).

The phase diagrams of the ternary systems $[Th(NO_3)_4(TBP)_2]$–$[UO_2(NO_3)_2(TBP)_2]$–decane (tetradecane) in the tempetrature range 298.15–333.15 K were constructed in [3, 4]. These diagrams contain a field of homogeneous solutions and a field of separation into two liquid phases (I, II). Phase I is enriched in $[Th(NO_3)_4(TBP)_2]$ and $[UO_2(NO_3)_2(TBP)_2]$, and phase II is enriched in saturated hydrocarbon diluent. In extraction of actinides and lanthanides with organic solutions of TBP, not only saturated hydrocarbon of normal structure, but also their isomeric derivatives, for example isooctane, are of interest as diluents.

No data have been reported on the phase diagram of the system $[Th(NO_3)_4(TBP)_2]$–$[Gd(NO_3)_3(TBP)_3]$-isooctane, which is of interest for extractive separation of thorium and REM.

Before use, TBP was distilled in a vacuum. The densities of TBP and isooctane $\rho_{298.15}$ were 0.9727 and 0.6868 g cm^{-3}, respectively. The solvates $[Th(NO_3)_4(TBP)_2]$ and $[Gd(NO_3)_3(TBP)_3]$ were prepared by three- or fourfold contact of TBP with concentrated aqueous solutions of Th(IV) and Gd(III) nitrates. The molar content of the stoichiometric solvates $[Th(NO_3)_4(TBP)_2]$ and $[Gd(NO_3)_3(TBP)_3]$, c (mol dm^{-3}), was 1.80 ± 0.01 and 1.10 ± 0.01, respectively. Their densities, $\rho_{298.15}$ (g cm^{-3}) were 1.7022 ± 0.0013 and 1.2755 ± 0.015, respectively.

The binodal curves were obtained by Alekseev's visual polythermal technique [1–4]. The content of $[Th(NO_3)_4(TBP)_2]$ and $[Gd(NO_3)_3(TBP)_3]$ in organic solutions was determined by complexometric titration [5, 6]. In preliminary experiments, we found that the volumes of solution of Th(IV) and Gd(III) nitrate solvates in isooctane are additive quantities within the limits of 0.3 vol %. The experimental compositions of the coexisting phases (vol %) were recalculated to the weight fractions, taking into account the solution densities. The binodal curves were approximated with polynomials of third and fourth degrees.

Our experimental results were represented as the phase diagram constructed in the form of the second Roozeboom's triangle in rectangular coordinates with weight fractions of two components along the coordinate axes (the weight fraction of the third component is calculated as the difference $\omega_3 = 1 - \omega_1 - \omega_2$). The determination error of the weight fraction of the components did not exceed $\pm(0.001 - 0.002)$. The determination error of temperature was ± 0.2 K.

The components of the binary system $[Gd(NO_3)_3 \cdot (TBP)_3]$-*iso*-$C_8H_{18}$ have infinite mutual solubility over the entire temperature range studied (298.15–333.15 K). By contrast, the similar system with satu-

Composition of coexisting phases in the ternary system $[Th(NO_3)_4(TBP)_2]$–$[Gd(NO_3)_3(TBP)_3]$–*iso*-C_8H_{18} at 288.15–333.15 K

$[Th(NO_3)_4(TBP)_2]$	$[Gd(NO_3)_3(TBP)_3]$	*i*-C_8H_{18}	*T*, K	Node
wt. fraction				
0.176	0	0.824	298.15	0
0.190	0.016	0.794		1
0.225	0.043	0.732		2
0.247	0.063	0.690		3
0.264	0.078	0.658		4
0.566	0.160	0.274		4
0.630	0.150	0.220		3
0.700	0.132	0.168		2
0.841	0.061	0.098		1
0.932	0	0.068		0
0.189	0	0.811	318.15	0
0.206	0.013	0.781		1
0.225	0.024	0.751		2
0.250	0.037	0.713		3
0.289	0.053	0.658		4
0.630	0.112	0.258		4
0.711	0.101	0.188		3
0.787	0.075	0.138		2
0.833	0.053	0.114		1
0.919	0	0.081		0
0.196	0	0.804	333.15	0
0.211	0.004	0.785		1
0.233	0.011	0.756		2
0.257	0.018	0.725		3
0.296	0.028	0.676		4
0.659	0.058	0.283		4
0.747	0.048	0.205		3
0.806	0.036	0.158		2
0.867	0.017	0.116		1
0.912	0	0.088		0

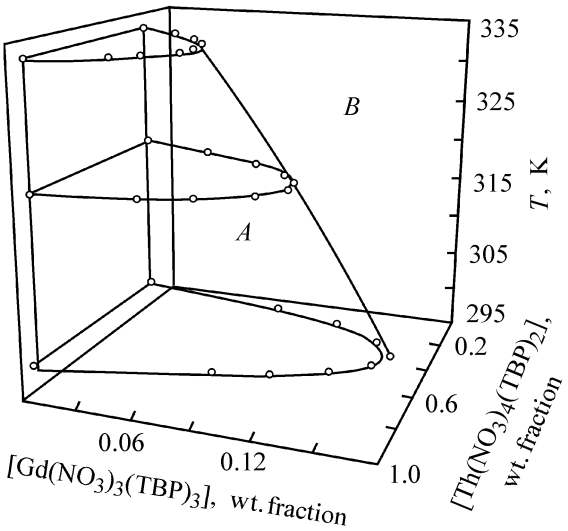

Fig. 1. Phase diagram of the ternary system $[Th(NO_3)_4(TBP)_2]$–$[Gd(NO_3)_3(TBP)_3]$–isooctane at different temperatures. (*A*) Field of separation into two liquid phases and (*B*) field of homogeneous solutions.

rated normal hydrocarbon separate into two phases. The binary system $[Th(NO_3)_4(TBP)_2]$–isooctane is a two-phase system over the entire temperature range studied (see table, Figs. 1, 2). It can be seen that, with increasing temperature, the mutual solubility of components in the binary system $[Th(NO_3)_4(TBP)_2]$–isooctane grows only slightly. We failed to determine the upper critical solution temperature in this binary system since, with the temperature increasing above 353.15 K, the system loses isooctane because of its evaporation.

At all the temperatures studied, the phase diagram of the ternary system $[Th(NO_3)_4(TBP)_2]$–$[Gd(NO_3)_3(TBP)_3]$–*iso*-C_8H_{18} contains a field of homogeneous solutions (*B*) and a two-phase field (*A*). These fields are bounded by binodal curves. With the tem- perature increasing from 298.25 to 333.15 K, the two-phase fields somewhat contract. The nodes in these diagrams show that one of the coexisting phases is enriched in both $[Th(NO_3)_4(TBP)_2]$

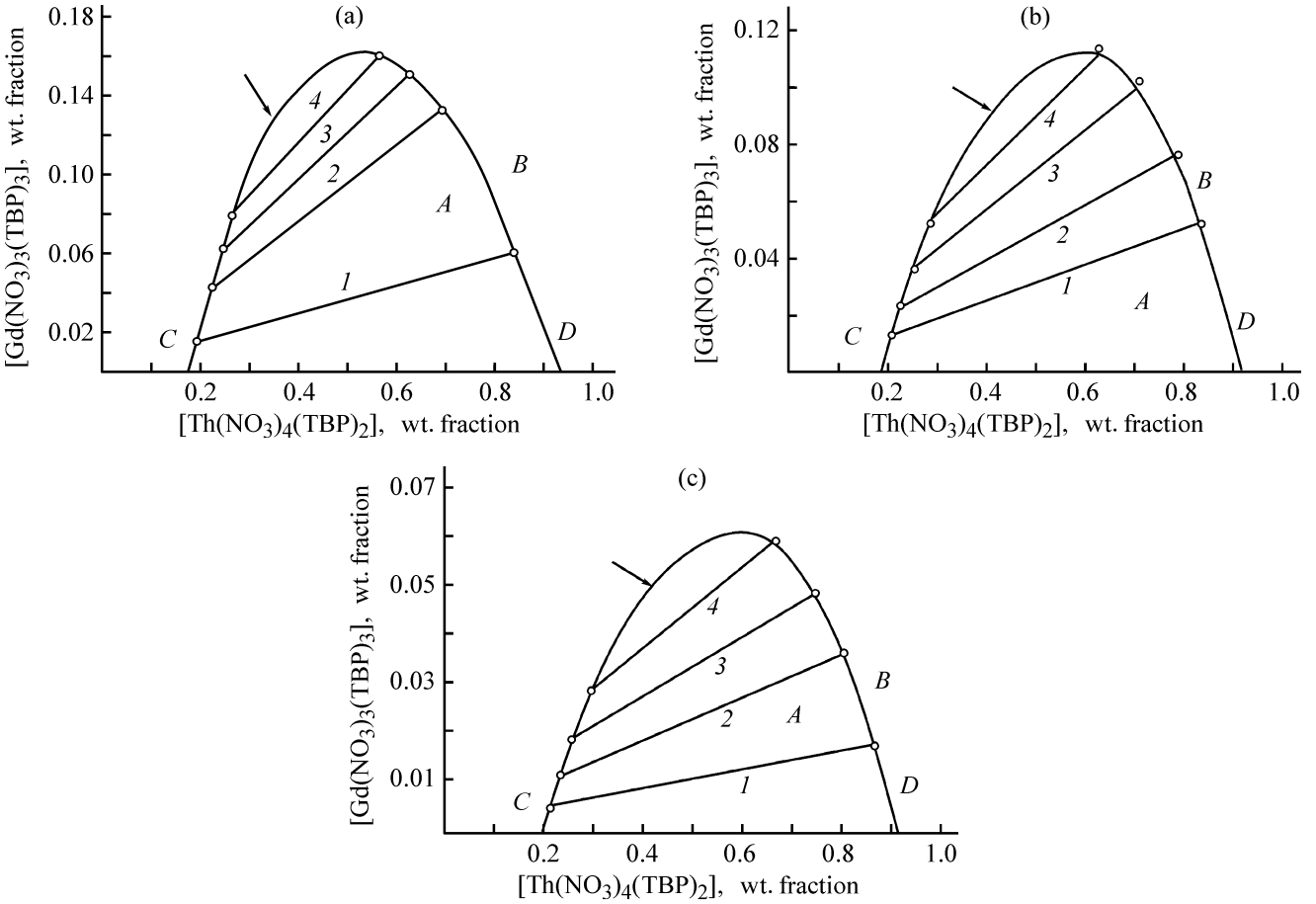

Fig. 2. Isothermal sections of the phase diagram of the ternary system $[Th(NO_3)_4(TBP)_2]$–$[Gd(NO_3)_3(TBP)_3]$–*iso*-C_8H_{18}. (*1*)–(*4*) Nodes of the binodal curves. The arrow shows the critical point in a binodal curve. (*A*) Field of separation into two liquid phases, (*B*) field of homogeneous solutions, and (*CD*) binodal curve. Temperature, K: (a) 298.15, (b) 318,15, and (c) 333.15.

and $[Gd(NO_3)_3(TBP)_3]$ (phase I), and the other is enriched in isooctane (phase II).

Figure 2 shows that, with the temperature increasing from 298.15 to 333.15 K, the $[Th(NO_3)_4(TBP)_2]$ concentration at the critical point grows (from 0.35 to 0.43 wt fraction), the $[Gd(NO_3)_3(TBP)_3]$ concentration decreases (from 0.13 to 0.051 wt fraction), and the isooctane content remains virtually constant (~0.52–0.53 wt fraction). This means that, with increasing temperature, $[Gd(NO_3)_3(TBP)_3]$ and isooctane dissolve in phase I to a greater extent, whereas phase II becomes enriched in $[Th(NO_3)_4(TBP)_2]$.

It should be noted that, whereas the binary systems $[Gd(NO_3)_3(TBP)_3]$–decane (tetradecane) containing normal saturated hydrocarbon separate into two phases, the binary system $[Gd(NO_3)_3(TBP)_3]$-isooctane is homogeneous over the entire composition range.

Addition of $[Gd(NO_3)_3(TBP)_3]$ to the heterogeneous system $[Th(NO_3)_4(TBP)_2]$–isooctane homogenizes the resulting ternary system at the temperature-dependent critical points.

Thus, to prevent formation of the second organic phase in extraction of Th and Gd nitrates with solution of TBP in isooctane in the temperature range 298.15–333.15 K at saturation of the extractant with metals, the content of Th nitrate solvates with TBP in the organic phase should be lower than 0.30, and the content of Gd nitrate solvate, no less than 0.13 wt fraction. Taking into account that REM(III) nitrate solvates and isomeric saturated hydrocarbons have infinite mutual solubility at all the temperatures, these solvents are more preferable in extraction than normal saturated hydrocarbons.

CONCLUSIONS

(1) The binary system $[Gd(NO_3)_3(TBP)_3]$–decane (tetradecane) containing normal saturated hydrocarbon solvents separates into two phases, whereas the binary

system $[Gd(NO_3)_3(TBP)_3]$–isooctane is homogeneous over the entire composition range. The binary system $[Th(NO_3)_4(TBP)_2]$–isooctane separates into two phases over the entire temperature range studied (T = 288.15–333.15 K).

(2) At all the temperatures studied the phase diagram of the ternary system $[Th(NO_3)_4(TBP)_2]$–$[Gd(NO_3)_3(TBP)_3]$–*iso*-C_8H_{18} contains a field of homogeneous solutions (*B*) and a two-phase field (*A*). These fields are bounded by binodal curves. With the temperature increasing from 298.25 to 333.15 K, the two-phase fields slightly contract. The nodes in these diagrams show that one of the coexisting phases is enriched in both $[Th(NO_3)_4(TBP)_2]$ and $[Gd(NO_3)_3(TBP)_3]$ (phase I), and other phase is enriched in isooctane (phase II).

(3) Addition of $[Gd(NO_3)_3(TBP)_3$ to the heterogeneous binary system $[Th(NO_3)_3(TBP)_3]$–isooctane homogenizes the ternary system at the temperature-dependent upper critical points. Thus, to prevent formation of the second organic phase in extraction of Th and Gd nitrates with a solution of TBP in isooctane at saturation of the extractant with metals, the content of Th nitrate solvates with TBP in the organic phase should be lower than 0.30, and the content of Gd nitrate solvate, no less than 0.13 wt. fraction. Taking into account that REM(III) nitrate solvates and saturated isomeric hydrocarbons have infinite mutual solubility at all the temperatures, these solvents are more preferable in extraction than normal saturated hydrocarbons.

REFERENCES

1. Pyartman, A.K., Keskinov, V.A., Mishina, N.E., and Kudrova, A.V., *Radiokhimiya*, 2005, vol. 47, no. 5, pp. 443–444.
2. Keskinov, V.A., Kudrova, A.V., and Pyartman, A.K., *Zh. Neorg. Khim.*, 2005, vol. 50, no. 5, pp. 895–896.
3. Keskinov, V.A., Mishina, N.A., and Pyartman, A.K., *Radiokhimiya*, 2005, vol. 47, no. 5, pp. 520–522.
4. Keskinov, V.A., Lishcuk, V.V., and Pyartman, A.K., *Zh. Neorg. Khim.*, 2006, vol. 51, no. 6., pp. 1050–1052.
5. Pyartman, A.K., Kopyrin, A.A., Berinskii, A.E., and Keskinnov, V.A., *Radiokhimiya*, 2000, vol. 42, no. 2, pp. 128–130.
6. Pribil, R., *Analytical Application of EDTA and Related Compounds*, Oxford: Pergamon, 1972.

ISSN 1070-4272, Russian Journal of Applied Chemistry, 2007, Vol. 80, No. 6, pp. 887–890. © Pleiades Publishing, Ltd., 2007.
Original Russian Text © A.V. Golounin, V.A. Sokolenko, O.V. Zakharova, E.A. Shor, M.S. Tovbis, 2007, published in Zhurnal Prikladnoi Khimii, 2007, Vol. 80, No. 6, pp. 911–914.

PHYSICOCHEMICAL STUDIES OF SYSTEMS AND PROCESSES

Complexes of *ortho*-Nitrophenols with Aluminum Bromide in Nonaqueous Solutions

A. V. Golounin, V. A. Sokolenko, O. V. Zakharova, E. A. Shor, and M. S. Tovbis

Institute of Chemistry and Chemical Technology, Siberian Division, Russian Academy of Sciences, Krasnoyarsk, Russia

Received February 2, 2006; in final form, February 2007

Abstract—The reactions of 2-nitro-, 2-nitro-4,6-dichloro-, 2,4-dinitro-, and 2,4,6-trinitrophenols with aluminum bromide in nitromethane solution were studied by calorimetry and by ^{1}H and ^{13}C NMR.

DOI: 10.1134/S1070427207060080

The reactions of methylated phenols, naphthols, and polyphenols with strong Lewis acids in nonaqueous solutions frequently result in tautomeric transformations [1–4]. Data on the reactions of nitrophenols with Lewis acids are searce. For example, it has been found that the reaction of 4-nitrophenol with $TiCl_4$ in benzene at room temperature yields the salt NO_2–C_6H_4–O–$TiCl_3$ [5]. In dry methanol, iron(III) chloride forms a coordination compound with 4-nitrophenol via OH group [6]. Complexes of 2-nitrophenol with gallium, aluminum, and boron halides in organic solutions were studied in [7, 8]. It was concluded that a coordination bond of metal halides with the nitro group is formed; however, in [9] this conclusion was to questioned.

The most complete data on the structure of complexes of nitrophenols with metal halides can be obtained by NMR spectroscopy. Therefore, we synthesized complexes of *o*-nitrophenols with aluminum bromide and recorded ^{1}H and ^{13}C NMR spectra of these complexes.

It is well known that metal halides are bonded in nonaqueous solutions with aromatic nitro compounds via nitro group [10, 11]. In the presence of other donor groups, such as hydroxy, carbonyl, or amino group, the coordination site may change. In the case of *o*-nitrophenol, nitro-aci tautomerism **I** : **II** is also possible

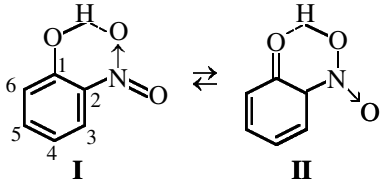

I **II**

Furthermore, formation of complexes of different compositions is possible; thus, the pattern becomes complicated.

To determine the stoichiometry of complexes of *o*-nitrophenol **I** with aluminum bromide, we performed calorimetric measurements. First, an 0.01 M solution of *o*-nitrophenol in bromobenzene was titrated with an $AlBr_3$ solution at 100°C and then back-titration was performed. The experimental procedure has been repeatedly described in the literature [9, 10]. In the dependence of the enthalpy of reaction on the molar ratio of donor and acceptor $m_D : m_A$, there are two inflections: at the ratios of 1 : 1 and 1 : 2. The heat effects were evaluated by the procedure described in [9], assuming that the enthalpy of reaction is expressed by the equation

$$\Delta H_c = \Delta H_e + 0.5\Delta H Al_2Br_6 - \Delta H_{solv},$$

where ΔH_c is the heat of complexation; ΔH_e, enthalpy determined experimentally; $\Delta H Al_2Br_6$, enthalpy of dimer dissociation; and ΔH_{solv}, enthalpy of solvation [4].

The first portion of the curve corresponds to ΔH_c = 31.5, and the second, to 20.1 kJ mol^{-1}. The total thermal effect is 51.6 1 kJ mol^{-1}.

To estimate the energy of *o*-nitrophenol transformation into an aci tautomer, we performed a quantum-chemical calculation. The molecular configurations of **I** and **II** were optimized using the restricted Hartree–Fock method. The energies were estimated by considering correlation effects in the framework of the Møller–Plesset method (MP-2) [13]. In the cal-

^{1}H Chemical shifts of nitrophenols and complexes in nitromethane

Nitrophenol	$AlBr_3$	H-2	H-3	H-4	H-5	H-6	OH
2-Nitrophenol	1 : 0		8.12	7.08	7.69	7.17	10.4
	1 : 1		7.89	6.92	7.75	6.92	8.37
	1 : 2		7.89	6.92	7.75	6.92	8.13
2-Nitro-4,6-dichlorophenol	1 : 0		8.14		7.84		10.7
	1 : 1		7.84		7.81		8.54
					7.80		
	1 : 2		7.84		7.81		8.28
					7.80		
2,4-Dinitrophenol	1 : 0		9.05		8.49	7.45	10.7
	1 : 1		8.79		8.55–8.62	7.29	8.98
						7.24	
	1 : 2		8.79		8.55–8.62	7.29	8.65
						7.24	
2,4,6-Trinitrophenol	1 : 0		9.10		9.10		11.0
	1 : 1		8.91		8.91		8.64
	1 : 2		8.91		8.91		8.40
Nitrobenzene	1 : 0	8.11	7.50	7.66	7.50	8.11	
	1 : 1	8.09	7.48	7.72	7.48	8.09	

culations, we used the 6-31G* basis set. The calculated ΔH_t was 72.7 kJ mol^{-1}.

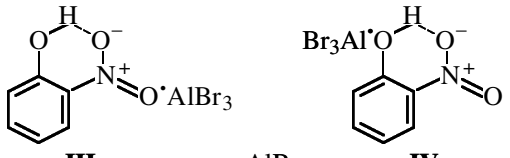

III

IV

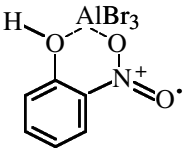

V

To find the structure of the complexes, we recorded their ^{1}H and ^{13}C NMR spectra. The ^{1}H chemical shifts of the initial phenols and complexes are listed in the table. The specific feature of the spectra of free *o*-nitrophenols is that the signals of hydroxylic protons are shifted downfield (10–11 ppm) due to the presence of intramolecular hydrogen bond [10], contrary to phenols associated by intermolecular bonds (4–5 ppm) [2].

Attempts to obtain a complex of 2-nitrophenol with $AlBr_3$ in inert solvents at room temperature failed, since the reaction is complicated by the release of gaseous hydrogen bromide. The most suitable solvent was nitromethane.

The influence of $AlBr_3$ on the chemical shifts of nitro compounds bound into in a complex was demonstrated for nitrobenzene as an example. The ^{1}H NMR spectrum of its complex shows no differences from that of free nitrobenzene, except a certain broadening of the signals. This fact suggests that, in coordination with aluminum bromide, the charge on the nitrogen atom of the nitro group does not noticeably change [11].

In the spectrum of a solution of 2-nitrophenol with $AlBr_3$ the ^{1}H signals are noticeably shifted upfield (not downfield, as it is observed for complexes of methylated phenols and naphthols) relative to the signals of the initial phenol. Hence, it can be assumed that the coordination mode of 2-nitrophenol differs from that of nitrobenzene and phenols. The signals with chemical shifts of 8.37 and 8.13 ppm (approximately 3 : 1) were assigned to hydroxyl protons of complex compounds, since they have integral intensities corresponding to one hydrogen atom each. Accidentally, the chemical shifts of the 1 : 1 and 1 : 2 complexes almost coincide; as a result, all the signals in the spectrum are broadened. The ^{1}H signal of 3-H (8.12 ppm, $J_{3,4}$ 8.55; $J_{3,5}$ 1.64 Hz in the initial phenol) is a doublet at 7.89 ppm; in this case, no Moler remote coupling is observed. The split triplet of 5-H gives broadened signal at 7.75 ppm. The hydrogen atoms 4-H and 6-H appearing in the form of a split doublet at 7.17 and triplet at 7.08 in the initial *o*-nitrophenol in the complex give an unresolved multiplet in the range 6.8–7.1 ppm.

On heating, hydrogen bromide is released from the solution as a result of formation of 2-NO_2–C_6H_4–O–Al_nBr_{3n-1}, and the intensities of the signals at 8.37 and 8.13 ppm decrease. All other signals remain unchanged. This fact indicates that the chemical shifts of the complexes and aluminum salts are close. A similar fact has been noted previously [14]. After recording the spectrum, hydrogen bromide was passed with cooling through the resulting solution until its saturation. As a result, the intensities of signals of hydroxyl protons increased to the initial value. The absence of any other changes in the ^{1}H NMR spectrum after saturation of the solution with HBr suggests that the complex compounds are protonated neither via the ring nor via the functional groups.

To elucidate whether the complexes obtained are actually complexes of aci form **II**, we recorded the ^{13}C NMR spectrum of a solution of 2-nitrophenol with $AlBr_3$. We did not find a signal at 170–190 ppm (coordinated carbonyl group [15]), which suggests the absence of a system of double bonds >C=O and >C=N–. This fact is in good agreement with calculations and calorimetric measurements.

The effect of substituents on the complexation of *o*-nitrophenols was determined in the reactions of 2-nitro-4,6-dichloro-, 2,4-dinitro-, and 2,4,6-trinitrophenols with $AlBr_3$ in nitromethane.

In the spectrum of a solution of 2-nitro-4,6-dichlorophenol with $AlBr_3$, the signal of 3-H protons is shifted upfield from 8.14 to 7.84 ppm, the signal of 5-H proton is split into two (7.81 and 7.80 ppm) but remains virtually at the same place. In addition, instead of the low-field (10.7 ppm) signal of the hydroxyl proton, two signals whose intensity corresponds to one proton appear in higher field at 8.54 and 8.28 ppm (ratio approximately 3 : 1).

The signal of 3-H in the spectrum of a solution of 2,4-dinitrophenol with $AlBr_3$ is shifted upfield from 9.05 to 8.79 ppm. The doublet of 6-H (7.45 ppm) is shifted to 7.25 ppm. The doublet of 5-H (8.49 ppm) transforms into a complex set of signals in the range 8.55–8.62 ppm, suggesting the existence of several complexes in the solution. Two signals of hydroxyl protons appear in the spectrum: at 8.86 ppm and in the range of the 5-H signal at 8.65 ppm. In the ^{13}C NMR spectrum of the 2,4-dinitrophenol complex, there are signals at 162.8 (C_1), 131.0 (C_2), 134.3 (C_3), 137.0 (C_4), 125.3 (C_5) and 125.3 ppm (C_6). As in the preceding case, the signals in the range 170–190 ppm corresponding to the coordinated C=O group [15] were not found.

A similar pattern is observed in the reaction of 2,4,6-trinitrophenol with $AlBr_3$. It is the common opinion that the yellow color of 2,4,6-trinitrophenol solution is caused by appearance of an aci structure (type **II**) [16]. However, both ^{1}H and ^{13}C NMR signals correspond to picric acid in the phenolic form. Upon addition of $AlBr_3$, the color of the solution becomes deeper and the signal of aromatic protons is insignificantly shifted upfield. In parallel, two signals appear at 8.65 and 8.40 ppm, whose intensity corresponds to one proton.

Thus, the NMR spectra show that, irrespective of the structure of *o*-nitrophenols, two complexes in which the aromaticity of the benzene ring is preserved are formed with $AlBr_3$.

The whole set of the results obtained is well accounted for by formation of chelate complexes. When considering a model of chelate complex 1 : 1 **V** (complex 1 : 2 has apparently the same structure excluding the fact that aluminum bromide is dimer), it is seen that $AlBr_3$ should be situated between OH and NO_2 groups. This arrangement of $AlBr_3$ will result in rupture of the intramolecular hydrogen bond. Due to the formation of a chelate, the fractional positive charge on the oxygen atom of the hydroxy group will be lower than that in the oxonium complex; therefore, the shift of hydroxyl proton in the NMR spectra will be intermediate between the shift in free phenols and oxonium complexes, which is actually observed. The upfield shift of aromatic protons in complexes is apparently caused by the anisotropic effect of aluminum atom in the resulting six-membered ring.

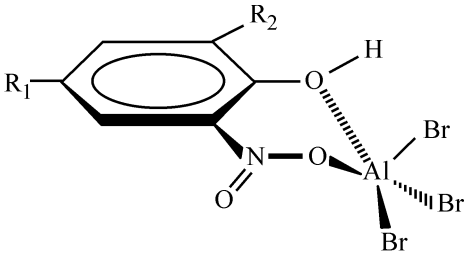

V

The model suggested is additionally confirmed by the ^{17}O NMR spectra obtained previously for the complex 2-NO_2–C_6H_4–OH · BCl_3 [8]. In the spectrum of the complex, two signals appear at 560 and 406 ppm, instead of one signal of two oxygen atoms of nitro group (569 ppm). The signal of oxygen atom of the hydroxy group is shifted after coordination from 94 to 144 ppm, i.e., one oxygen atom of nitro group and oxygen atom of hydroxy group are involved in

the coordination. This fact can be explained by assuming that a chelate complex of *o*-nitrophenol with BCl_3 is formed.

EXPERIMENTAL

The phenols used had the following mp (°C): 2-nitrophenol 45.3–45.7, 4-nitrophenol 113–114, 2-nitro-4,6-dichlorophenol 124–125, and 2,4-dinitrophenol 115–116. Nitromethane was dried and distilled at bp 102–103°C. The complexes were prepared by dissolution of aluminum bromide in nitromethane with subsequent addition of nitrophenols in a molar ratio of 2 : 1 to the suspension cooled to –20°C. The enthalpy of the reaction of 2-nitrophenol with aluminum bromide was determined by the procedure described in [12]. The solutions of complexes were saturated with hydrogen bromide at 0°C. The ^1H NMR spectra were recorded on a Bruker Avance 200 spectrometer. In recording the spectra of free nitrophenols, TMS was used as an internal reference; the spectra of complexes were recorded using nitromethane as a reference (4.28 ppm).

CONCLUSIONS

(1) Calorimetric measurements show that *o*-nitrophenol forms 1 : 1 and 1 : 2 complexes with aluminum bromide, with the enthalpy of formation of 31.6 and 20.1 kJ mol^{-1}, respectively.

(2) Quantum-chemical calculation estimates the enthalpy of transition of *o*-nitrophenol into the aci form at 72.7 kJ mol^{-1}.

(3) The experimental data obtained indicate that *o*-nitrophenols in complexes with the chelate structure remains aromatic.

REFERENCES

1. Golounin, A.V. and Koptyug, V.A., *Zh. Org. Khim.*, 1970, vol. 6, no. 12, pp. 2555–2558.
2. Golounin, A.V. and Koptyug, V.A., *Zh. Org. Khim.*, 1972, vol. 8, no. 2, pp. 607–610.
3. Golounin, A.V., Sokolenko, V.A., and Shakirov, M.M., *Izv. Ross. Akad. Nauk, Ser. Khim.*, 1997, no. 6, pp. 1158–1160.
4. Golounin, A.V., Shchedrin, Yu.S., and Fedorov, V.A., *Zh. Org. Khim.*, 2001, vol. 37, no. 9, pp. 1170–1172.
5. Luchinskii, G.P., *Zh. Obshch. Khim.*, 1937, vol. 7, no. 7, pp. 2044–2047.
6. Silver, J., Morrison, I.E.J., and Rees, L.V.C., *Inorg. Nucl. Chem. Lett.*, 1979, vol. 15, nos. 11–12, pp. 433–436.
7. Suvorov, B.A., Orlova, L.I., and Dzhigaspanyan, R.V., *Zh. Obshch. Khim.*, 1982, vol. 52, no. 4, pp. 749–754.
8. Suvorov, B.A., *Zh. Prikl. Spektrosk.*, 1990, vol. 53, no. 6, pp. 1023–1026.
9. Golounin, A.V., Rubailo, A.I., and Pavlenko, N.I., *Zh. Obshch. Khim.*, 1998, vol. 68, no. 4, pp. 562–565.
10. Gorenbein, E.Ya., *Zh. Neorg. Khim.*, 1959, vol. 4, no. 7, pp. 1643–1648.
11. Schmidt, M.W. et al., *J. Comput. Chem.*, 1993, vol. 14, pp. 1347–1363.
12. *The chemistry of the Nitro and Nitroso Groups*, Feuer, H., Ed., New York: Interscience, 1969, part 1.
13. Alpatova, N.M., Gavrilenko, V.V., Kessler, Yu.M., et al., *Kompleksy metalloorganicheskikh gidridnykh i galoidnykh soedinenii alyuminiya* (Complexes of Organometallic Aluminum Hydrides and Halides), Moscow: Nauka, 1970.
14. Golounin, A.V., *Zh. Prikl. Khim.*, 1997, vol. 70, no. 10, pp. 1750–1752.
15. Golounin, A.V., Rezvukhin, A.I., Mamatyuk, V.I., and Koptyug, V.A., *Zh. Org. Khim.*, 1973, vol. 9, no. 11, pp. 2359–2363.
16. Hantsch, A., *Ber.*, 1906, vol. 39, pp. 1084–1090.

ISSN 1070-4272, Russian Journal of Applied Chemistry, 2007, Vol. 80, No. 6, pp. 891–903. © Pleiades Publishing, Ltd., 2007.
Original Russian Text © R.I. Ibragimova, A.I. Mil'chenko, N.V. Vorob'ev-Desyatovskii, 2007, published in Zhurnal Prikladnoi Khimii, 2007, Vol. 80, No. 6, pp. 919–931.

SORPTION AND ION-EXCHANGE PROCESSES

Criteria for Choice of a Brand of Activated Carbon for Hydrometallurgical Recovery of Gold from Ore Pulps in Carbon-in-Leaching and Carbon-in-Pulp Processes

R. I. Ibragimova, A. I. Mil'chenko, and N. V. Vorob'ev-Desyatovskii

JSC Polymetal Engineering, St. Petersburg, Russia

Received January 24, 2007

Abstract—Criteria used to choose activated carbons suitable for sorption recovery of the $[Au(CN)_2]^-$ anion from cyanide ore pulps are considered. Results obtained in the development of authors' own tests for determining the mechanical strength and loss of carbons via their disintegration in this technological process are presented. Changes occurring on the surface of grains of activated carbon in its agitation in abrasive media and specific features of the design of sorption apparatus that can be used for rationally carrying out carbon-in-pulp and carbon-in-leaching processes are discussed.

DOI: 10.1134/S1070427207060092

One of the most important events of the last quarter of the XX century in hydrometallurgy of gold was the introduction of sorption technologies employing activated carbons (AC). These sorbents can be used for recovery of gold from clarified solutions in column apparatus (carbon-in-column, CIC process) or be introduced into the pulp. Depending on the ore composition, AC can be delivered into the pulp together with the leaching agent (carbon-in-leach, CIL process) or after preliminary leaching of gold (carbon-in-pulp, CIP process). As a rule, the CIL process is used in those cases when the ore contains natural sorption-active materials that can adsorb $[Au(CN)_2]^-$ anions from solution. In the second edition of the widely known monograph by Marsden and House [1], the introduction of the CIP technology into the world practice of gold mining in 1972–2000 was named the "CIP revolution." Indeed, more than 50% of world's gold production is presently done with the use of AC [2]. The main advantages of the carbon sorption technologies consist in the economics of the process, which is determined not in the last turn by avoiding the procedures of thickening, counter–current decantation washing of cakes, and filtration. This is particularly important in processing of poorly thickening and poorly filterable pulps and solutions.

In Russia, modern carbon technologies started to be introduced into gold mining practice only in the late 1990s. In the fraction of gold recovered by carbon sorption technologies, Russia occupied, in the end of 2004, 12th place among the 15 largest manufactures of this metal, being only ahead of China, Peru, and Chile [3]. At the same time, the Russian Federation firmly held fifth place in overall manufacture of gold. Presently, use of carbon technologies in domestic gold mining is hindered by a number of objective and subjective factors. Among these is the lack of the relevant literature accessible to most of domestic specialists and insufficient experience in choice and optimal use of AC in CIL and CIP processes. In this communication, we dwell on the last of the problems mentioned above.

When choosing an AC brand for CIL or CIP processes, the following carbon characteristics are commonly taken into account [1, 4]:

kinetic parameters of gold(I) sorption on carbons;

mechanical strength;

adsorptive capacity;

shape and size of adsorbent particles;

bulk density;

content of fine and dust particles in the carbons;

loss of the material in reactivation and conditioning;

ash content after burning of the starting materials;

cost of the adsorbent.

The first two parameters are believed [4] to be the most important and predetermine the choice of an AC brand. The rest are related to the first two, or to conditions of a technological process, or, as shown below, bear no relation to solution of the problem under consideration.

The adsorption kinetics of the $[Au(CN)_2]^-$ anion on AC particles, which governs the principles of process simulation and the choice of an AC brand, are rather difficult in analysis and mathematical description. It is commonly believed [5, 6] that, in the first stage of sorption (far from carbon saturation), gold(I) is adsorbed on the surface of macro- and mesopores in AC at a high rate and the process itself occurs under outer-diffusion control and is described by the film-diffusion mechanism. In this stage, pseudo-equilibrium is attained rather rapidly (in 2–48 h [6, 7]). The rate constant k_1 of $[Au(CN)_2]^-$ ion adsorption on AC corresponds in the case in question to a first-order reaction and is described by the following equation

$$d[Au]_c/dt = k_I[Au]_s, \quad (1)$$

where $[Au]_c$ and $[Au]_s$ are, respectively, the concentrations of gold(I) in the carbon and solution phases.

The adsorption rate constant k_I depends on a multitude of parameters [5, 6]:

pulp agitation intensity (increases to a certain limit with the agitation intensity);

pulp viscosity and density (decreases as either of these increases);

temperature (increases with temperature);

NaCN concentration and pH value (decreases as either of these increases);

AC particle size (inversely proportional to the carbon particle size);

total and relative numbers of macro-, meso-, and micropores in the AC structure;

presence in the liquid phase of the pulp of organic and inorganic compounds and ions that can block sorption centers of the carbon;

ionic strength of the solution (increases with the ionic strength of the solution to a certain limit and then falls).

With account of the parameters listed above, CIL and CIP processes are, as a rule, carried out in the turbulent mode of pulp agitation at pH not exceeding 10.8 and as low sodium cyanide concentration as possible. The last requirement is also due to the fact that, after adsorption cyanidation, the pulp is commonly subjected to detoxication and high concentrations of the residual cyanide in the pulp will lead to an increase in expenditure for detoxication. In addition, AC catalyzes oxidation of the cyanide anion by atmospheric oxygen [8]. This process is the most intense if copper(I) compounds are present in solution [9], which also leads to unjustified loss of sodium cyanide.

In a real industrial sorption process performed in the counter–current mode, the value of k_I is not lower than 80–100 h^{-1} and should remain approximately constant in all tanks of the cascade, irrespective of the concentration of the $[Au(CN)_2]^-$ anion in the liquid phase in each vessel [7].

The most acceptable from the standpoint of adsorption kinetics would be carrying out the process in dilute, as regards the content of the solid phase, pulps. However, the economics of the process, necessity for precluding carbon segregation in too liquid or too thick pulps, and requirements to the sedimentation stability of the pulps themselves result in that sorption is commonly performed with pulps with a content of the solid phase equal to 40–50 wt %.

In the second stage of adsorption, $[Au(CN)_2]^-$ anions slowly diffuse into the micropores of AC. This process occurs under inner-diffusion control. The duration of the adsorption process in the second stage may exceed that of the first stage by a factor of 10 and more. Although the content of gold(I) in the AC phase grows in the second stage of sorption, this stage makes difficult the subsequent desorption of gold(I) from carbon micropores and impairs the economics of the process.

The variation of the gold(I) concentration in the liquid and solid phases of the pulp in adsorption of the $[Au(CN)_2]^-$ anion from solution onto activated carbon can be described by the equations [6]:

$$-d[Au]_s/dt = (kM_c/M_s)(K[Au]_s - [Au]_c), \quad (2)$$

$$d[Au]_c/dt = k(K[Au]_s - [Au]_c). \quad (3)$$

Here, $k = k_s k_c A/(k_c K + k_s)$; k_s and k_c are the mass-transfer coefficients of Au(I) in solution and in carbon pores; K, equilibrium constant; A, surface area of a unit volume of AC; and M_c and M_s, masses of carbon and solution, respectively.

The adsorption rate of Au(I) on AC particles in a stage of the industrial counter–current process is

commonly evaluated using the following simple empirical equation [6]:

$$\Delta[\mathrm{Au}]_c = k''[\mathrm{Au}]_s t^n. \quad (4)$$

Here, $\Delta[\mathrm{Au}]_c$ is the change in the gold(I) concentration on carbon (g ton^{-1}) in a time t (h) elapsed after the transfer of AC from the preceding stage; $[\mathrm{Au}]_s$, gold(I) concentration in solution (mg l^{-1}); and k'' rate constant of the process.

For each industrial plant, the parameters k'' and n take their own values.

In view of the wide diversity of factors affecting the adsorption kinetics of the $[Au(CN)_2]^-$ anion on AC, the suitability of a carbon for use in sorption processes in laboratory is occasionally assessed on the basis of pseudokinetic constants k' [10]. The method for determining k' is based on the test in which an AC sample (0.5 g) is agitated at a certain frequency (100 min^{-1}) in a 0.5-l bottle roll agitator in contact with a solution containing gold(I) in the form of the $[Au(CN)_2]^-$ ion and NaCN in concentrations of 10 and 250 mg l^{-1}, respectively, at pH 10.0. Samples for determining the Au(I) content are taken in 0, 0.5, 1.0, 2.0, and 3.0 h. The value of k' is found from Eq. (4), which is transformed for convenience to

$$\log \Delta[\mathrm{Au}]_c^t/[\mathrm{Au}]_s^t = n\log t + \log k'. \quad (5)$$

Here, $\Delta[\mathrm{Au}]_c^t$ is the change of the Au(I) concentration on the carbon relative to $t = 0$ (g ton^{-1}); $[\mathrm{Au}]_s^t$, Au(I) concentration in solution at a time t (mg l^{-1}); n, experimentally found parameter ($0.6 < n < 1.2$); and t, time (h).

For good-quality AC, the value of k' at 25°C is within the range 800–1300 h^{-1} [10]. Comparison of various AC brands in the value of k' enables choice of the best, among several brands, carbon having the highest adsorption rate under the standard conditions. However, these conditions do not correspond to the real conditions characteristic of industrial CIP or CIL processes. The method considered here may be of use in preliminary screening of ACs. It is convenient to compare the constant k' of an AC under study with that of the reference carbon during the same period of time, e.g., in $t = 1$ h, with the following simple equation used instead of (4) [10]:

$$[\mathrm{Au}]_s^t = 10000/(k' + 1000). \quad (6)$$

The working experience of South-African plants shows that the average time of contact of an AC with the $[Au(CN)_2]^-$ anion in CIP processes commonly does not exceed 24 h in each sorption apparatus [24]. An economical criterion of the necessity for carbon transfer between apparatus in the counterflow scheme is the ratio between the gold(I) concentration in the carbon phase, $[\mathrm{Au}]_c$ (g ton^{-1}), to that in solution, $[\mathrm{Au}]_{aq}$ (mg l^{-1}):

$$[\mathrm{Au}]_c/[\mathrm{Au}]_{aq} = 750–1000. \quad (7)$$

It has been found [7] that mechanical agitation of a pulp with AC is substantially better than pneumatic agitation as regards the effect on the adsorption kinetics of gold(I).

One of the principal disadvantages of the CIL and CIP processes is the accompanying wear of carbon particles, whose part is lost in the form of fine fractions with a particle size of less than 1 mm. Particles of AC disintegrate in all stages of its existence, from transportation to a consumer to carbon reactivation at a gold mining plant (GMP). Among the factors leading to wear of carbon particles and loss of carbon, we can mention the following:

damage to and disintegration of carbon particles upon collisions with impeller blades and other members of adsorptive cyanidation apparatus;

mechanical disintegration of carbon in its transport by pumps and abrasion against pipeline walls and screen grids;

abrasion of AC particles by solid particles of the pulp;

cracking of carbon under sharp temperature changes in autoclave desorption and quenching after reactivation in a kiln;

loss of carbon for oxidation and abrasive wear in the regeneration kiln (5–10%);

abrasion of carbon by carbon particles themselves in preliminary conditioning and subsequent screening of carbon (1.5 to 30%).

It is important to emphasize that the first four reasons for carbon loss are accompanied by removal of fine AC particles containing adsorbed gold(I) from the technological process. This may lead to loss of up to 0.85 kg of Au per ton of carbon fines [2].

The loss of AC at GMPs is directly associated with the strength of AC particles. At present there exist three approaches to determination of the strength properties of AC [10, 11]. Abroad, “dry” methods of abrasion in a rod mill (abrasion index, AI) or on

a vibrating sieve with balls (ball-pan hardness, BPH) are used for this purpose [11, 12].

In Russia, the mechanical strength of AC is evaluated in conformity with GOST (State Standard) 16188–70 [13] by grinding a dry weighed portion in a rod mill for 3 min, followed by sieving of the sorbent and determination of its mechanical strength Π (%) by the formula

$$\Pi = \frac{m}{M} \times 100. \quad (8)$$

Here, M and m are, respectively, the masses (g) of a dry weighed portion of carbon, with preliminarily removed fine fractions, and that after grinding.

This procedure, which is largely similar to the foreign method for determining the abrasion index AI [11], has been developed for evaluating the mechanical strength of catalysts.

For example, it is known that the value of Π is 85% for a domestic carbon of IPI-T brand and 91.5% for a TAIKO CW 814 Japanese carbon. It is clear that the information importance of these figures is rather poor, because they give no way of prognosticating the working life of a sorbent and furnish no evidence concerning the control over the particle comminution process in industrial apparatus with intensive pulp motion under the action of mechanical agitating devices (MAD). These methods for testing of AC samples can only reveal differences in their mechanical properties under the conditions of a particular test. Carbons with good mechanical properties according to tests performed in conformity with GOST 16188–70 have Π exceeding 90%. The parameter Π is commonly several units lower than the AI and BPE parameters obtained using foreign methods [11, 12].

Specialists of a Dutch company Norit introduced into the practice of mechanical testing of AC the so-called "wet" method. This technique is based on mixing of AC grains with a water-sand pulp simulating the CIP or CIL process [10, 11, 15]. Comparison of the results of dry and wet tests for AC shows that the strength of carbon increases with the size of its grains in dry tests and the reverse pattern is observed with the wet method [10]. However, the varieties of wet tests considered in the literature [10, 11, 15] for AC samples, as applied to real industrial hydrometallurgical processes, have similar disadvantages, because the technical characteristics of laboratory apparatus, granulometric parameters of sand, and concentration of AC particles in AC conditioning are taken without regard for specific features of real apparatus in which the test results will be used.

In this communication, we suggest to perform laboratory tests of the adsorbent under conditions that are closer to the real industrial process. This will enable not only correct prognostication of the loss of activated carbon and precious metals, but also control over the abrasion rate of the sorbent by making a rational choice of the design and basic parameters of apparatus for sorption cyanation.

The problems of abrasion (disintegration) of solid materials have been actively studied in recent decades as regards the appearance of secondary particles in crystallizers with stirrers [16] and bead mills in manufacture of pigments [17], erosion wear of stirrer blades [18, 19], specific features of floccule disintegration in microbiological industry [20], etc. The process of particle abrasion in apparatus with stirrers is rather complex and has not been reliably mathematically substantiated so far. However, the already accumulated experimental information indicates that the most important parameters governing the kinetics of particle abrasion are the following:

specific agitation power introduced from the outside into the process under study and the shear stresses dependent on this power [18, 20];

properties of the materials of moving particles and apparatus members interacting with these particles [18, 20];

size and number of solid particles [18–21];

design of the apparatus and its technical characteristics [17–21].

It is noteworthy that this multitude of important parameters should be considered simultaneously with the requirement of complete suspension of precipitated particles of the ore being cyanidated at the so-called determining rotation frequency of the stirrer [22]

$$n_0 = 10.4\frac{D}{d^2}\left[\frac{(\rho_{sol} - \rho_{liq})\delta(1 - \varepsilon_{pr})f\Gamma_D}{\rho_{ss} K_N}\right]^{0.5} \quad (9)$$

at which the power N expended for agitation is calculated using the known formula [23]:

$$N = K_N \rho_{ss} n_0^3 d^5. \quad (10)$$

Here, D and d are the diameters of the apparatus and stirrer, respectively; Γ_D and K_N, simplex of geometric similarity of the stirrer and its power coefficient; f, internal friction coefficient of particles; ρ_{liq}, ρ_{sol}, and ρ_{ss}, density of liquid and solid phases and suspension, respectively; δ, particle size; and ε_{pr}, precipitate porosity.

Simulation studies of the abrasion kinetics of activated carbon particles should be governed by the condition necessary for suspension: the shear stresses in shear of a monolayer of particles of the industrial pulp in model (τ_m) and industrial (τ_{ind}) apparatus should be equal:

$$\tau_m = \tau_{ind} = (\rho_{sol} - \rho_{liq})\delta f g(1 - \varepsilon_{pr}), \quad (11)$$

where g is the acceleration of gravity.

As is known [24], from (11) results formula (9) and the following scaling rules for smooth-wall apparatus with MAD:

$$n_0 D^q = \text{idem}, \quad (12)$$

$$PD^q = \text{idem}, \quad (13)$$

$$T = \text{const}, \quad (14)$$

where $P = N/V$ is the specific power expended for pulp agitation in an apparatus of volume V; $T = [N/(2\pi n_0)]/V$, specific rotational moment of the MAD; and q, constant dependent of the stirrer type and suspension agitation mode [23]. In the case of a three-blade stirrer with a blade angle $\alpha = 24°$, considered here, q is 0.9.

Let us consider as an example of application of relations (9)–(14) to simulation of the process of carbon particle abrasion the apparatus for sorption cyanation, working at one of Russia's GMPs. The sorption apparatus and the pulp in these apparatus have the following parameters: $V_{ind} = 280$ m^3, $D_{ind} = 7$ m, $d_{ind} = 2.8$ m, $n_{ind} = 0.5$ s^{-1}, $x = 0.474$; $\delta = 0.074$ mm, $\rho_{sol} = 2860$ kg m^{-3}, and $\rho_{liq} = 1000$ kg m^{-3}.

The volume concentration of activated carbon is maintained within the range 5%. All the AC samples used at the GMP and in laboratory experiments were of industrial manufacture. An AC sample produced from the coconut shell by its carbonization and activation (henceforth, coconut carbon) had an average particle size d_C 3.35 × 1.70 mm (6 × 12 mesh). Extruded (molded) AC obtained from a complex composite material had cylindrical particles with a diameter $d_C = 1.5$ mm and length equal to two to three diameters. The model laboratory apparatus geometrically similar to the industrial apparatus had the following parameters: $V_m = 0.003$ m^3, $D_m = 0.150$ m, $d_m = 0.060$ m. The chemically active ore was replaced in laboratory experiments on abrasion of AC grains with neutral sand of the corresponding granulometric composition and concentration, and distilled water was used as dispersion phase.

The rotation frequency of MAD on the model stand was calculated in accordance with the scaling rule (12):

$$n_{ind} D_{ind}^{0.9} = n_m D_m^{0.9} \quad (15)$$

to be

$$n_m = 0.5\left(\frac{7}{0.15}\right)^{0.9} = 15.9 \text{ s}^{-1}.$$

In the first stage of the study, only $z = 15$ of coarse grains of the carbon, rather than 5 vol %, was charged into a water-sand pulp with a mass fraction of sand, $x = 0.474$. Such a small number of grains can be readily separated after a certain time, together with the fragments formed, from the pulp with a sieve with a 0.5-mm mesh, washed, dried, and weighed on an analytical balance, after which changes in grains agitated together with the pulp can be visually analyzed. To reveal the main reason for abrasion and comminution of grains, experiments were carried out two times for each carbon brand: with steel stirrer blades in one experiment and rubber-coated blades in the second, with the latter leading to an elastic interaction between a grain and a rotating blade.

The run of the curves in Fig. 1 and the number of coarse grains (number z near the corresponding curve

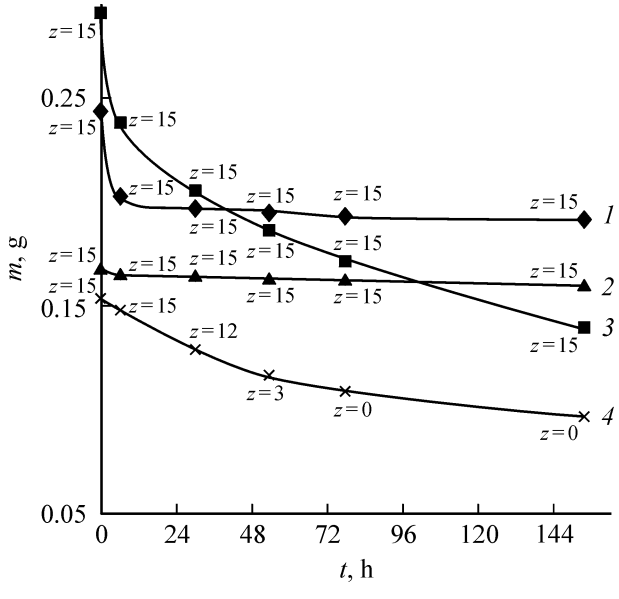

Fig. 1. Mass m of a sample vs. the abrasion time t for abrasion of 15 particles at a clockwise rotation of stirrer blades with $d = 60$ mm. (z) Number of intact grains. Carbon: (*1*) coconut, rubber-coated blades; (*2*) molded, rubber-coated blades; (*3*) coconut, steel blades; and (*4*) molded, steel blades.

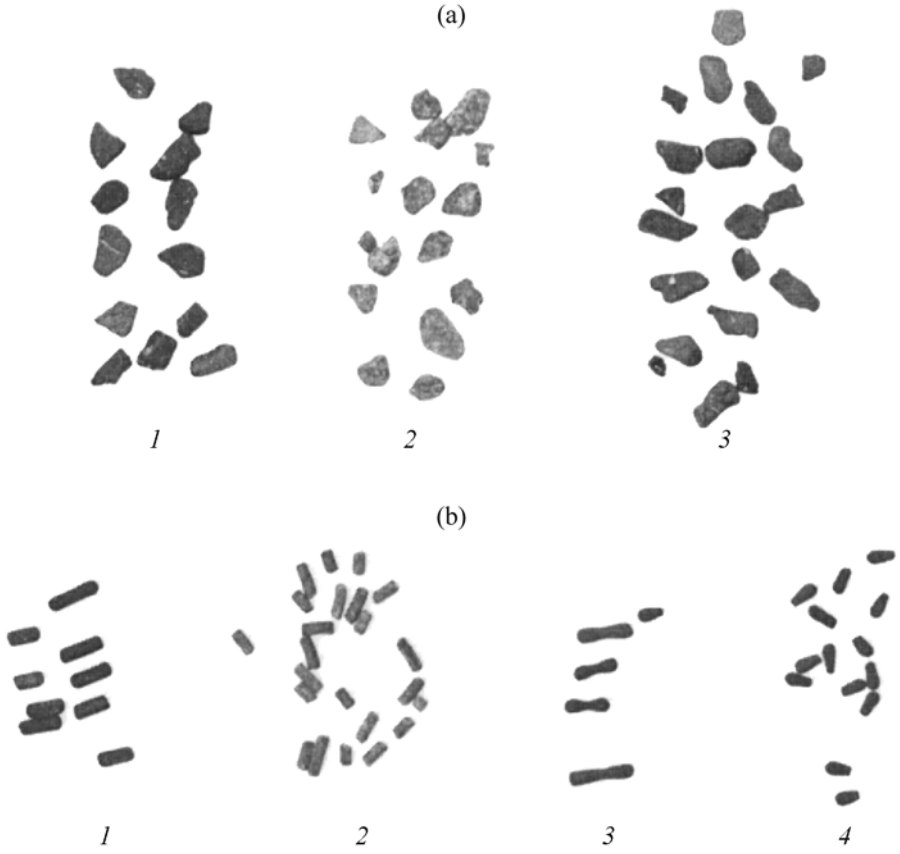

Fig. 2. Photographs of (a) coconut and (b) molded carbons. Carbon: (*1*) starting, (*2*) taken from the technological process, and (*3*, *4*) abraded.

of each curve), as well as their photographs in Fig. 2 before and after experiments, indicate that the mechanisms of disintegration of grains of the two brands of carbon under study are fundamentally different and lead to practical conclusions about how the loss of carbon and, consequently, of precious metals, too, can be diminished. In grains of the coconut carbon, sharp edges are first rounded.

Then the grains slowly delaminate into coarse plates of smaller thickness, which do not pass through a sieve with a 0.5-mm mesh. In the final stage of abrasion, thin flakes are mechanically disintegrated and the resulting fragments form tailings.

The cylindrical grains of the molded carbon first acquire a dumb-bell shape and then disintegrate nearly in two halves. Subsequently, these halves become spheres with a gradually decreasing size, which penetrate through the screen grid and find their way into the waste. These observations are in agreement with previous reports [15].

Comparison of the wear of AC grains with steel and rubber-coated blades indicates that the main reason for wear of carbon particles under the experimental conditions is their strong impact interaction with steel blades of the stirrer, whose circumferential velocity may be as high as 3–5 m s^{-1}. It is of interest to emphasize here that this conclusion is in agreement with numerous publications, according to which a larger part of the agitation power is dissipated in a small volume of the medium, $V_{ag} = \pi/4d^2h$ (h, height of the blade projection onto the diametral plane) near the stirrer blades [25]. As confirmed by the experiments performed in [20], intense disintegration of floccules in agitation in fermenters occurs just in this zone. It is also natural to believe that the most erosion-vulnerable place of MAD is the blade periphery moving at the highest circumferential velocity, which is indicated by the experiments and calculations reported in [18, 19, 26]. It is also reasonable to note the published suggestions that the circumferential velocity of stirrer blades in the CIP process should be limited to a value of 4–5 m s^{-1} [27]. Thus, it is possible to markedly depress a reason for loss of carbon and precious metals and, simultaneously, to make longer the service life of the stirrer by coating blades with rubber, which is typically done with hydrometallurgical equipment.

In the second stage of the study, we analyzed the abrasion of carbon particles with a concentration of 5 vol % in a water-sand pulp. As follows from Figs. 3 and 4, at a considerably higher concentration of carbon grains, too, the influence exerted on their abrasion by an antiabrasive rubber coating of blades, which positively affects the dynamics of interaction between grains and the rapidly rotating stirrer, is still strong. At the same time, even though the difference in wear resistance between carbons of two brands is in favor of molded carbon particles, it is rather insignificant. In this case, the final choice of the carbon brand should be governed by other important criteria, such as kinetic characteristics of adsorption, adsorptive capacity, cost, etc. [2, 10].

The empirical dependence of the loss of mass by an AC sample (Δm) on the time of its agitation with a pulp (t), which can be used to describe the abrasion of carbons in the model experiment, has the form ($t \le 30$ h)

$$\Delta m = at^b, \qquad (16)$$

and the values of the coefficient a and exponent b are shown in Fig. 4 at the corresponding curves.

The abrasion of particles of the extruded carbon of industrial concentration in the water-sand pulp was also studied with other MAD parameters (d = 80 mm, n = 8.33 s^{-1}, rubber-coated blades), at which the energy dissipation decreases by approximately a factor of 2, compared with the previously tested variant. In this case, a slower wear of AC particles would be expected. These MAD parameters approximately conform to requirements (11) and (14), which is important for elucidation of the wear pattern of carbon under model and industrial conditions. Figure 5 compares the results of abrasion of molded carbon particles for two MADs, which confirm the conclusion that, in the case of particle disintegration in apparatus with stirrers, it is necessary to take into account the energy dissipation not only in the total working volume of an apparatus, but also in the conditional volume V_{st} of a cylinder formed in rotation of stirrer blades [20]. Thus, the dependence (16) we obtained can be extended with a large safety margin to prognostication of particle abrasion under industrial conditions, because $P_{ind} \ll P_m$. It is noteworthy that the loss of AC in smooth-wall sorption apparatus must be considerably lower than that in energy-intensive apparatus with a baffles.

We also experimentally studied the influence exerted by the direction of axial rotation on the abrasion of carbon particles by standard three-blade stirrers

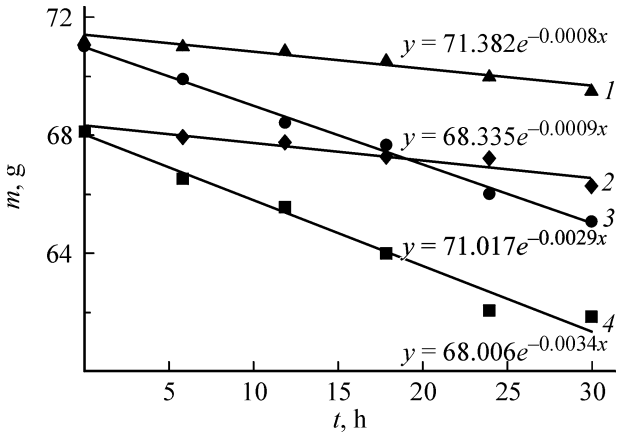

Fig. 3. Sample mass m vs. abrasion time t at a 5 vol % content of activated carbon in the pulp and clockwise rotation of stirrer blades with d = 60 mm. Carbon: (*1*) molded, rubber-coated blades; (*2*) coconut, rubber-coated blades; (*3*) molded, steel blades; and (*4*) coconut, steel blades; the same for Fig. 4.

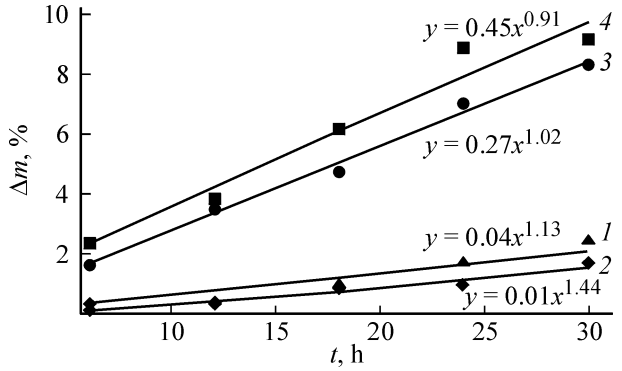

Fig. 4. Relative mass loss $\Delta m = [m_0 - m_t)/m_0] \times 100$ by a sample vs. abrasion time t at a 5 vol % content of activated carbon in the pulp and clockwise rotation of stirrer blades with d = 60 mm. (m_0) Mass of the starting sample and (m_t) that after abrasion for a time t.

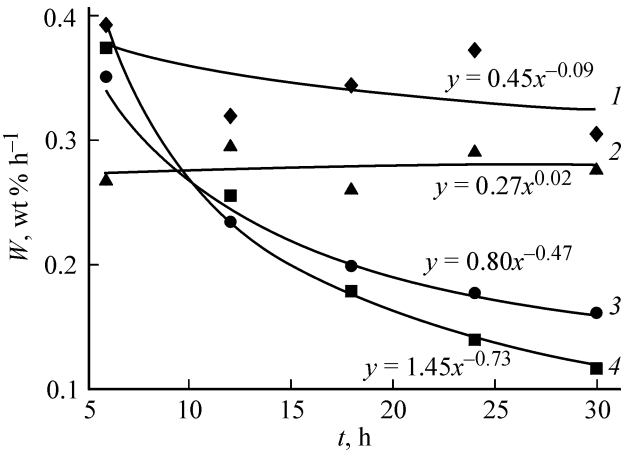

Fig. 5. Rate of mass loss by a sample, $W = (\Delta m/m_0 t) \times 100$ vs. abrasion time in the case of a clockwise rotation of steel blades of various diameters. Carbon, d (mm): (*1*) coconut, 60; (*2*) molded, 60; (*3*) molded, 80; and (*4*) coconut, 80.

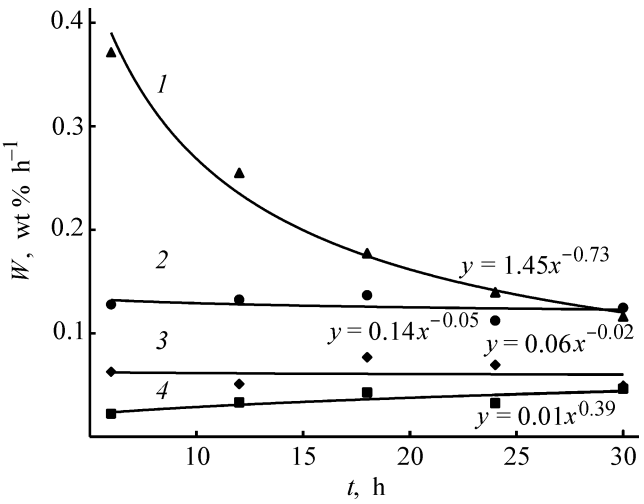

Fig. 6. Rate of mass loss by a sample, *W*, vs. abrasion time *t* for coconut carbon at different directions of meridian circulation of the pulp at d = 80 mm. Blades: (*1*) steel, clockwise; (*2*) steel, anticlockwise; (*3*) rubber-coated, clockwise; and (*4*) rubber-coated, anticlockwise.

with a blade angle with respect to the horizon equal to 24°. As it can be seen from Fig. 6, the upward suspension motion in the central zone of the apparatus (anticlockwise rotation) is accompanied by lower abrasion of sorbent particles, compared with the conventionally taken [28] downward motion of the suspension to the bottom. This preferable upward direction of suspension motion is accompanied, as Japanese researchers have demonstrated [19], by a more uniform distribution of the number of collisions of solid particles with each of the 25 small elements of area, marked out on the working surface of a blade (5 areas across the width of a blade and 5 along its radius). At the same time, in the case of suspension motion in the central zone toward the bottom (on reverting the direction of stirrer rotation), the distribution of collisions among these 25 areas is exceedingly nonuniform. For example, five and more areas adjacent to the stirrer hub do not interact with particles at all, and five peripheral areas having the highest circumferential velocity may experience 50–80% of the total number of collisions with solid particles [19]. Naturally, not only intensive crushing of particles, but also rapid erosion wear of the blade periphery occur in this case [18, 19, 26, 29].

Comparison of the curves describing the loss of mass via mechanical abrasion (Fig. 1) shows that, in the course of time, the rate of carbon loss via mechanical abrasion for coconut carbon markedly decreases to become virtually equal to that for extruded carbon. This indicates that the loss of precious metals with carbon fines can be substantially diminished if each portion of carbon is subjected, before being fed into the sorption process, to mechanical conditioning. This procedure consists in agitation of a concentrated water-carbon suspension in an apparatus with baffles, followed by classification of the resulting mass on a screen. As a result of this conditioning, carbon particles that are predisposed to disintegration because of the presence of pronounced mechanical defects (cracks), as well as long and thin AC fragments, will be separated from coarse and firm particles because of the comminution in this apparatus. This precludes loss of precious metals adsorbed on fine AC fragments in CIL and CIP processes and, as shown below, activates to a certain extent the adsorbent surface.

As shown by studies of agitation of water-carbon suspensions with a mass concentration $X \le 0.25$ (kg of carbon per kg of water), standard apparatus with a conical bottom, baffles, and three-blade stirrer are well suitable for mechanical conditioning of carbon [30].

The apparatus was successively charged, at a working stirrer, first with water and then with a preliminarily weighed portion of carbon. The conditioning time (1–3 h) and the degree of abrasion ($\Delta m \le 10\%$) depended on the brand of carbon and parameters of MAD and the apparatus [24] at the optimal specific agitation power $P = N/V \approx 2$ kW m^{-3}.

The stirrer blades and baffles, near which nearly the whole amount of power is dissipated, should be rubber-coated to preclude excessive crushing of carbon particles. As usual in agitation of suspensions whose solid phase particles markedly differ in shape from the well-studied spherical particles, tests of a geometrically similar model of an industrial apparatus are necessary, with transfer of the experimental data obtained to a full-scale apparatus by means of the known scaling rules [24].

Thus, it is desirable to subject AC to preliminary mechanical conditioning, with sieving and removal of particles of the fine fraction (<1.0–1.2 mm). This will substantially diminish the loss of both carbon itself and gold in apparatus for sorptional cyanidation. With this simple technological method implemented, the difference in mass loss between the two AC brands considered here is largely eliminated.

It should be noted that, as the concentration of AC particles in the pulp increases, the time of their residence in the cascade of counter–current sorption apparatus becomes longer, which, among other things,

enhances the abrasion interaction of carbon particles with each other. Therefore, the reasonable range of volume concentrations of AC in the pulp is commonly 1–5%, but the problem of optimization of this concentration is economical.

A mistake widely occurring among specialists is that the concentration of AC in the last, along the pulp flow, counter–current apparatus for adsorptive cyanidation should exceed that in the others. The studies performed demonstrated that the best results in the CIP process are achieved in the case of a uniform distribution of the carbon concentration along the entire sorption scheme [6].

In addition to the AC characteristics described above, the choice of a carbon brand is occasionally based on such parameter as its adsorptive capacity (SC) for the $[Au(CN)_2]^-$ anion. In real industrial processes, only several percent of this capacity is used, and therefore, it is believed [5, 6, 10] that the value of SC is not a key characteristic in AC choice. The capacity of AC decreases as the concentration of a free CN^- anion in solution, temperature, and pH value grow, and increases with the ionic strength of the solution [6]. The pseudoequilibrium value of SC may exceed 100 mg of Au(I) per gram of carbon [31]. Under industrial conditions, the content of gold(I) on a saturated carbon delivered to desorption is, as a rule, 3 to 10 mg g^{-1}.

At low concentrations of the $[Au(CN)_2]^-$ anion in the liquid phase, characteristic of the CIL and CIP processes, the dependence of the SC of activated carbons on the Au(I) concentration is commonly well described by the Freundlich isotherm equation

$$SC = K'[Au]_{sol}^{1/\beta}, \quad (17)$$

where $[Au]_{sol}$ is the equilibrium concentration of gold(I) in solution (M or mg l^{-1}). The coefficient K' and exponent β in Eq. (17) depend on the state of the AC surface.

Figure 7 shows isotherms of adsorption of the $[Au(CN)_2]^-$ anion on samples of molded and coconut carbons, fresh and taken after 152 h of agitation with a water-sand mixture, and the table lists the corresponding values of K' and β. As follows from the data we obtained, the values of K' and β in the Freundlich isotherm equation decrease upon mechanical abrasion of the adsorbent surface, but the influence exerted by the exponent β on SC is stronger than that of the slope ratio K'. As a result, all other conditions being the same, the capacity of samples of both coconut and extruded carbons subjected to abrasive wear exceeds that of "fresh" samples.

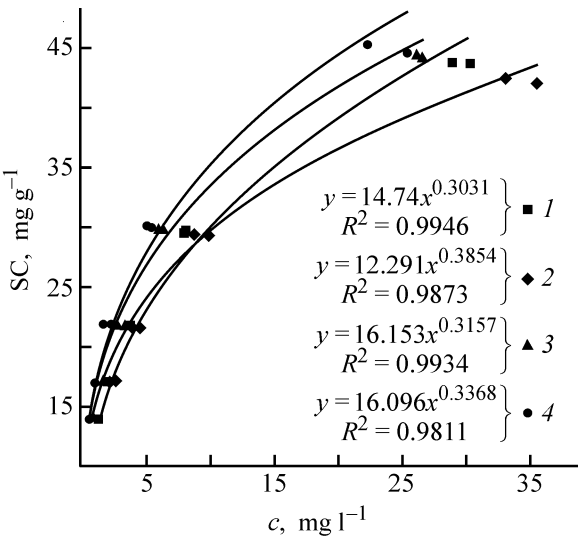

Fig. 7. Isotherms of adsorption of cyanide complexes of Au by various ACs. (SC) Sorption capacity of AC and (*c*) concentration of $[Au(CN)_2]^-$. Carbon: (*1*) coconut fresh, (*2*) coconut abraded, (*3*) molded fresh, and (*4*) molded abraded.

In adsorption of the $[Au(CN)_2]^-$ ion from aqueous solutions and pulps under real conditions, oppositely directed processes occur. Part of these processes lead to a decrease in the adsorptive capacity of the carbon. The following can be distinguished among these processes: (1) deactivation of the AC surface via deposition of organic (flocculants, flotation reagents, combustible and lubricant substances, natural humic acids, etc.) [32–34] and insoluble inorganic [$CaCO_3$, $MgCO_3$, $Fe(OH)_3$, $(MgOH)_2CO_3$, etc.] substances [31] and adhesion of solid ore particles to the surface {the strongest negative influence is exerted on the Au(I) sorption by organic substances, and primarily by flotation reagents [7]}; (2) rapid oxidation of sorption-active centers, which gives rise to surface oxygen complexes of carbon and, to a lesser extent, to nitrogen-containing fragments [35] (the sorption capacity of AC for the $[Au(CN)_2]^-$ ion decreases as the content of oxygen in the carbon adsorbent increases [36]); and (3) saturation of accessible adsorption centers by cyanide complexes of Au(I), Ag(I), and other metals [37].

Values of K' and β in the Freundlich equation at varied abrasion of activated carbon samples

Sample	K'	β
Carbon:		
coconut fresh	14.740	3.3
coconut abraded	12.291	2.6
molded fresh	16.153	3.2
molded abraded	16.096	3.0

At the same time, mechanical contact of carbon particles with each other and solid particles in the pulp, as well as with the stirrer blades and vessel walls, leads to formation of new defects on their surface, and primarily on the basal planes of AC particles. These defects have the form of new macro- and mesopores whose mouths can sorb an additional amount of $[Au(CN)_2]^-$ ions, which leads to an increase in the sorption activity of the surface of AC particles for the cyanide complex anion of gold(I). Such a change in the behavior of AC particles may evidence in favor of a mechanical activation of the sorbent in the course of abrasion, with this referring to a greater extent to the sample produced from the coconut shell. A similar increase in the adsorbent capacity as a result of its mechanical activation has been observed in a study of the sorption of Zn(II) ions on calcite [38].

The positive influence of mechanical abrasion on the adsorption process is nearly eliminated in industrial CIP and CIL processes by loss of gold(I) with carbon, but not completely because a larger part of AC is lost in the form of fine fractions with particles less than 1 mm in size.

It is occasionally recommended to be oriented, when choosing AC samples, to a number of accessible, but indirect characteristics of carbons, such as their specific surface area, capacity for adsorption of some organic or inorganic substances, bulk density of AC, size of AC particles, and ash content [1, 6, 10, 39]. We emphasize that, strictly speaking, these quantities cannot serve as a reliable basis for determining the suitability of a carbon for use in the technological process under consideration.

Commonly, AC samples used for adsorption of gold(I) have a specific surface area S_{sp} of 800 to 1200 $m^2 g^{-1}$, which can be found from the low-temperature sorption of Ar or N_2 by the BET method. If we determine the specific surface area of AC from the adsorption of carbon dioxide by calculation with the Dubinin–Polany equation and subtract from the value obtained the specific surface area furnished by the BET method, the resulting value gives notion of the specific surface area of micropores in the sample [40]. The relative amount of micro-, meso-, and macropores in AC is largely determined by the nature of a material from which the sample is fabricated. The AC fabrication technology affects this amount and, consequently, the possible value of the SC of a carbon for gold(I) to a lesser extent [41]. The specific surface area of AC samples is determined by the content of meso- and micropores in these samples. These same types of pores sorb the main amounts of gold(I). However, it has been demonstrated on the basis of a vast statistical material that, at S_{sp} of 484 to 1861 $m^2 g^{-1}$, the linear correlation coefficient between the equilibrium capacity of a carbon for gold(I) and its specific surface area is as low as 0.137 [42].

In practice, attempts to characterize the quality of AC samples as regards their suitability as sorbents for gold(I) recovery from cyanide pulps are frequently based on such characteristics of these samples as the iodine number and capacity to absorb CCl_4 vapor or organic dyes, e.g., Methylene Blue, from aqueous solutions [10]. For carbons best suitable for the CIL and CIP processes, the published values of the iodine number and activity with respect to CCl_4 vapor are, respectively, 1100–1200 mg g^{-1} [1] and 55–70% [39]. These parameters of carbons are indirectly related to their specific surface area S_{sp}. However, the linear correlation coefficient between the specific surface area of AC samples and their capacity for the $[Au(CN)_2]^-$ anion has, as already noted, a rather low value. Special studies [42] have shown that the linear correlation coefficients between the equilibrium capacities of AC for the $[Au(CN)_2]^-$ anion, on the one hand, and the capacities for Methylene Blue and the iodine number, on the other hand, are negative and equal to -0.133 and -0.393. On the whole, two AC samples having equal specific surface areas or iodine numbers may strongly differ in their capacity for adsorption of Au(I) [39]. The larger the specific surface area of an AC, the lower, at the same particle size, its bulk density and mechanical strength, which should also be taken into account when choosing a carbon. A usual value of the bulk density of activated carbons with a specific surface area in the range 800–1200 $m^2 g^{-1}$ is approximately 420–520 kg m^{-3} at an average AC grain size of 1.7–2.5 mm for coconut carbons and 490–510 kg m^{-3} for extruded carbons [1]. The bulk density of carbons in the range 500 ± 10 kg m^{-3}, as a rule, provides a good combination of kinetic and strength properties of AC and a good segregation stability of a carbon in ore pulps. In this case, the true pycnometric density of various AC samples falls within the range 1800–2100 kg m^{-3}.

The size of AC grains is also important in selection of AC brands suitable for CIL or CIP processes. Naturally, small particles (passing through a sieve with a 1-mm mesh) will have better kinetic characteristics, compared with larger particles. However, their lifetime is shorter because of the mechanical abrasion, and, consequently, the loss of precious metals with these particles substantially exceeds that with coarser particles. As a result, it is advisable to remove small

particles from the process in the stage of carbon reactivation. At the same time, AC particles retained in classification by a sieve with a 3-mm mesh are considerably less active in sorption of the $[Au(CN)_2]^-$ anion than smaller particles [10]. This circumstance will make necessary a longer contact of these particles with the pulp to reach the same degree of gold recovery as that with finer particles. This leads either to an increase in the number and volume of sorption apparatus or to a higher AC concentration in the pulp, which is undesirable. Therefore, the optimal size of AC particles presently used in CIL and CIP processes is 1.5–3.0 mm, and the desirable particle shape is spherical.

The ash content of the best AC samples used for gold recovery from cyanide pulps is 2–4% [1].

Finally, one more characteristic of carbons, which determines their suitability for gold mining, is their capacity for reactivation. Reactivation of ACs primarily restores their kinetic activity with respect to gold(I) adsorption, but involves a noticeable loss of mass by the adsorbents via oxidation and mechanical disintegration. The variation of the adsorptive properties of a carbon with the time of its contact with deactivating impurities and the degree of restoration of the adsorptive activity of the AC upon reactivation can be determined in laboratory. It has been suggested to use for this purpose electrochemical methods [43, 44], thermogravimetry, determination of the specific surface area of ACs [44], and kinetic parameters of adsorption of a saturated or regenerated carbon samples under study in comparison with the similar characteristics of the starting carbon. The last method consists in determining the pseudokinetic rate constant of sorption, k', and was described above.

Comparison of the curves describing the loss of mass by the starting sample and that under study in an inert atmosphere in the temperature range 150–600°C suggests that the ACs are contaminated with various compounds [44].

As the surface of an AC sample is saturated, its steady-state electrochemical potential shifts in the negative direction, compared with that of the starting sample, and its specific surface area decreases. The method of cyclic voltammetry shows that the currents of the cathodic and anodic peaks and the areas under the current peaks in a redox process involving a 0.05 M solution of $Fe(NO_3)_3$ in an acid medium (HNO_3, pH 1) on an AC powder electrode [43] depends on the degree of adsorbent saturation with various impurities of organic and inorganic nature.

EXPERIMENTAL

In simulation of the mechanical disintegration of AC particles, we used a quartz sand with a content of the –0.071-μm fraction of 95 ± 2%, which corresponds to the granulometric composition of the ore. The granulometric composition of the sand was determined on a Fritsch Alalysette 22 Compact laser granulometer (Germany). The water-sand pulp was agitated with an Ekros PE-8000 device (Russia). The stirrer rotation frequency was monitored with a tachometer and maintained constant during the entire experiment (152 h). The parameters of a polypropylene laboratory vessel and a stirrer were specified ented above.

The isotherm of gold(I) adsorption was measured using the method of varied weighed portions. The capacity of a carbon for Au(I), A (mg g^{-1}), was calculated by the formula $A = (c - c_0)V/m'$, where c_0 is the initial concentration of gold(I) in the solution (mg l^{-1}); c, its equilibrium concentration in the solution (mg l^{-1}); V, solution volume; and m', sorbent mass (g).

The concentration of Au(I) in solution was determined on a Varian SpectrAA 110 spectrometer (Australia).

CONCLUSIONS

(1) Direct and indirect characteristics of activated carbons were considered from the standpoint of their choice for use in CIL and CIP processes. The most important characteristics of carbons, which determine their suitability for hydrometallurgical processes, are the pseudokinetic rate constant of adsorption of the dicyanoaurate(I) anion on an activated carbon sample and its mechanical strength in agitation in an abrasive medium.

(2) A procedure for testing carbon sorbents for abrasion, made closer to the conditions of a real pulp process, was developed. The method is based on the assumption of geometrical similarity of the industrial and model smooth-wall apparatus and on the requirement that the shear stresses in these apparatus should be equal for providing an effective agitation of particles of the ore being cyanidated. The method was tested in a study of the abrasion of activated carbons of two brands differing in the fabrication technology, adsorptive capacity, and cost.

(3) Mechanisms of abrasion (comminution) of particles of the coconut and molded sorbents in a compact and energy-saturated volume of the medium, in

which occurs dynamic interaction of grains with rapidly rotating blades, were suggested. It was shown that the detrimental effect of the dynamic interaction on the particle abrasion and, simultaneously, on the blade erosion can be suppressed to a considerable extent by rubber coating of the stirrer blades.

(4) The available published evidence that the dissipation of the suspension agitation energy is the key factor in carbon abrasion was confirmed. As a result, it becomes possible, when designing apparatus of this kind, to make their technical characteristics conform to, among other things, the requirement of the minimum loss of the sorbent. In this case, it is preferable to use smooth-wall apparatus with three-blade stirrers at a simplex $\Gamma_D = D/d = 2–3$, which consume a considerably lower power than apparatus with baffles, more popular abroad and more energy-intensive.

(5) It was shown that the rotation direction of the three-blade stirrer studied affects the degree of abrasion of activated carbon particles. A stirrer rotation causing an ascending central-zone axial flow of a material being agitated is preferable to the descending flow.

(6) A comparison of the results of a simulation model with industrial data on abrasion of carbon particles demonstrated that a kinetic dependence of the type (16) can be used to evaluate the loss of activated carbon with a wide safety margin dependent on the considerable excess of the specific agitation power in a model apparatus over that in its industrial analogue.

(7) A design and technical characteristic of an apparatus for conditioning of activated carbon to diminish the loss of precious metals with carbon fines were suggested.

(8) It was found that mechanical treatment on carbon particles in CIL and CIP processes activates the adsorbent surface because of the formation of new defects on the surface of activated carbon.

ACKNOWLEDGMENTS

The authors are deeply grateful to Uwe Pashke and Victor Baborovich-Hansen (Republic of South Africa) for help in preparation of this communication.

REFERENCES

1. Marsden, J.O. and House, C.I., *The Chemistry of Gold Extraction*, Littleton: Soc. For Mining, Metallurgy, and Exploration, 2006.
2. Kotlyar, Yu.A., Meretukov, M.A., and Strizhko, L.S., *Metallurgiya blagorodnykh metallov* (Metallurgy of Noble Metals), Moscow: Ruda i Metally, 2005, vol. 1, p. 296.
3. Marsden, J.O., *Min. Metall. Processing*, 2006, vol. 23, no. 3, pp. 121–125.
4. Beatty, R.L., *Eng. Mining J.*, 1994, no. 6, pp. 30–35.
5. Fleming, C.A. and Nicol, M.J., *J. S. Afr. Inst. Min. Metall.*, 1984, vol. 84, no. 4, pp. 85–93.
6. McDougall, G.J. and Fleming, C.A., *Ion-Exchange and Sorption Processes in Hydrometallurgy*, Streat, M. and Naden, D., Eds., Chichester: John Wiley & Sons, 1987, vol. 19, pp. 57–126.
7. Laxen, P.A., Fleming, C.A., Holtum, D.A., and Rubin, R., *Proc. 12th CMMI Congress*, Johannesburg: S. Afr. Inst. Min. Metall., 1982, pp. 551–560.
8. Bernardin, F.E., *J. Water Poll. Control. Fed.*, 1973, vol. 45, no. 2, pp. 221–231.
9. Adams, M.D., *Miner. Eng.*, 1994, vol. 7, no. 9, pp. 1165–1177.
10. Avraamides, J., *Proc. Randol Perth Internat. Gold Conf.*, Golden: Randol Int., 1988, pp. 261–263.
11. van Dam, H.E., *Eng. Mining J.*, 1994, no. 8, pp. 34–35.
12. *ASTM Standard* D3892–79. *Ball-Pan Hardness of Activated Carbon*, in *ASTM Book of Standards, Refractories, Activated Carbon, Advanced Ceramics*, ASTM International, 2006, vol. 15.01–06.
13. *GOST* (State Standard) *16188–70, Sorbents, Methods for Determining the Abrasion Resistance*.
14. Chernov, V.K., Voiloshnikov, G.I., Elshin, V.V., and Rashchenko, A.F., in *Analiz, dobycha i pererabotka poleznykh iskopaemykh* (Analysis, Mining, and Processing of Mineral Resources), Lodeishchikov, V.V., Ed., Irkutsk: IRGIREDMET, 1998, pp. 290–298.
15. van Dam, H.E., *Eng. Mining J.*, 1993, no. 2, pp. 44–45.
16. Shamlou, P.A., Jones, A.G., and Djamarani, K., *Chem. Eng. Sci.*, 1990, vol. 45, no. 5, pp. 1405–1416.
17. Shter, N., *Lakokras. Mater. Ikh Primen.*, 2002, nos. 2–3, pp. 24–30.
18. Nienow, A.W. and Conti, R., *Chem. Eng. Sci.*, 1978, vol. 33, no. 8, pp. 1077–1086.
19. He, Y., Takahashi, K., and Nomura, T., *J. Chem. Eng. Japan*, 1995, vol. 28, no. 6, pp. 786–789.
20. Henzler, H.J. and Biederman, A., *Chem. Ing. Tech.*, 1996, vol. 68, no. 12, pp. 1546–1561.
21. Kee, K.C. and Rielly, C.D., *Chem. Eng. Res. Des.*, 2004, vol. 82, no. 9, pp. 1237–1249.
22. Mil'chenko, A.I, Domanskii, I.V, and Vorob'ev–Desyatovskii, N.V., *Zh. Prikl. Khim.*, 2005, vol. 78, no. 12, pp. 2002–2007.
23. *Novyi spravochnik khimika i tekhnologa: Protsessy i apparaty khimicheskikh tekhnologii* (New Reference

Book of a Chemist and Technologist: Processes and Apparatus of Chemical Technology), Ostrovskii, G.M., Ed., St. Petersburg: Professional, 2004, part 1.

24. Domanskii, I.V. and Mil'chenko, A.I., *Khim. Prom–st.*, 2003, vol. 80, no. 12, pp. 608–614.
25. *Handbook of Industrial Mixing, Science and Practice*, Paul, E.L., Atiemo-Obeng, V.A., and Kresta, S.M., Eds., Hoboken: John Wiley & Sons, 2004.
26. Kipke, K.D., *Chem. Ing. Tech.*, 1980, vol. 52, no. 8, pp. 658–659.
27. Shaw, J.A., *Chem. Eng. Prog.*, 1992, no. 5, pp. 34–41.
28. Braginskii, L.N., Begachev, V.I., and Barabash, V.M., *Peremeshivanie v zhidkikh sredakh* (Agitation in Liquid Media), Leningrad: Khimiya, 1984.
29. Nienow, A.N. and Bujalski, W., *Trans. I, Chem. Eng.*, 2004, vol. 82, part A, no. 9, pp. 1073–1081.
30. *GOST* (State Standard) *20680–2002, Apparatus with Mechanical Devices.*
31. Syna, N. and Valix, M., *Miner. Eng.*, 2003, vol. 16, no. 5, pp. 421–427.
32. La Brooy, S.R., *Proc. Randol Perth Internat. Gold Conf.*, Golden: Randol Int., 1988, pp. 264–267.
33. Voiloshnikov, G.I., Chernov, V.K., Kaigorodova, N.S., and Vasil'eva, I.I., *Analiz, dobycha i pererabotka poleznykh iskopaemykh* (Analysis, Mining, and Processing of Mineral Resources), Lodeishchikov, V.V., Ed., Irkutsk: IRGIREDMET, 1998, pp. 298–308.
34. Fisher, N.G., *Identification of Organic Fouling Agents on Activated Carbon by Evolved Gas Analysis*, Thesis, Ph.D., Ed., Perth: Curtin Univ. of Technol., 2000.
35. Vorob'ev-Desyatovskii, N.V., Ibragimova, R.I., Gordeev, S.K., and Nikolaev, B.P., *Zh. Obshch. Khim.*, 2006, vol. 76, no. 6, pp. 988–998.
36. Ibrado, A.S. and Fuerstenau, D.W., *Hydrometallurgy*, 1992, vol. 30, nos. 1–3, pp. 243–256.
37. Ibrado, A.S. and Fuerstenau, D.W., *Miner. Metall. Process.*, 1989, vol. 6, no. 2, pp. 23–28.
38. Balac, P., Alacova, A., and Briancin, J., *Chem. Eng. J.*, 2005, vol. 114, nos. 1–3, pp. 115–121.
39. Smit, R.W., Die Adsorption von Gold und Silber an Aktivkohle: *Dissertation zur Erlangung des Grades eines Doktor–Ingenieurs*, Technischen Universitat Clausthal, 1987.
40. Mahajan, O.P. and Walker, P.L., *Analytical Methods for Coals and Coals Products*, Karr, C., Jr., Ed., New York: Acad., 1978, vol. 1, pp. 125–162.
41. Satya Sai, P.M. and Krishnaiah, K., *Ind. Eng. Chem. Res.*, 2005, vol. 44, no. 1, pp. 51–60.
42. Davidson, R.G., Douglas, W.D., and Tumilty, J.A., *Seminar on Carbon-in-Pulp Technology for the Extraction of Gold*, Kalgoorlie: Australian Inst. of Mining and Metallurgy, 1982, pp. 193–212.
43. Biniak, S., Swiatkowski, A., and Pakula, M., *Chemistry and Physics of Carbon*, Radovic, L.R., ED., New York: Marcel Dekker, 2001, vol. 27, pp. 125–226.
44. Swiatkowski, A., Biniak, S., Pakula, M., and Trykowski, G., *Ochora Srodowiska*, 2005, vol. 27, no. 1, pp. 3–6.

ISSN 1070-4272, Russian Journal of Applied Chemistry, 2007, Vol. 80, No. 6, pp. 904–908. © Pleiades Publishing, Ltd., 2007.
Original Russian Text © V.M. Kuznetsov, A.M. Toikka, Yu.P. Kuznetsov, 2007, published in Zhurnal Prikladnoi Khimii, 2007, Vol. 80, No. 6, pp. 928–931.

SORPTION AND ION-EXCHANGE PROCESSES

Pervaporation Selectivity as a Function of Pressure and Sorption Properties of a Polymeric Film Membrane

V. M. Kuznetsov, A. M. Toikka, and Yu. P. Kuznetsov

St. Petersburg State University, St. Petersburg, Russia

Institute of Macromolecular Compounds, Russian Academy of Sciences, St. Petersburg, Russia

Received October 14, 2004; in final form, October 2006

Abstract—Results obtained in an experimental study of the pervaporation of binary solutions with a cellulose hydrate (cellophane) nonporous film membrane are discussed. A primary attention is given to the sorption and the effect of the residual pressure of the permeate on the separation characteristics.

DOI: 10.1134/S1070427207060109

Researchers' interest in pervaporation (evaporation across a membrane) is due to the possibility of application of this process in the separation technology in those cases when the conventional methods, such as distillation or rectification, are inapplicable or inefficient [1]. By now, a number of methods for simulation and calculation of pervaporation parameters have been developed, with the dissolution–diffusion model being commonly accepted [1–4]. At the same time, the concepts of the process mechanisms are widely diverse and, occasionally, contradictory [5]. Therefore, the existing methods are insufficiently versatile, which impairs their practical value as compared with the methods of thermodynamics of the liquid–vapor equilibrium, used in the case of distillation and rectification [6]. Development of the pervaporation theory requires that additional physicochemical information about various stages of the process should be invoked.

A study of the sorption as an equilibrium between a feed mixture and a membrane has been the subject of extensive research [7]. In [8], the equilibrium between a liquid ternary mixture of benzene, cyclohexene, and cyclohexane and films of polyurethane and polyetherblockamide was studied. In [9], a study of the sorption of aqueous solutions of ethanol, methanol, and 2-propanol by a film of polyvinyl alcohol was reported. The sorption of gaseous oxygen, carbon dioxide, ethylene, dimethyl sulfide, trichloroethylene, and toluene by a film of polydimethylsiloxane was examined in [10]. These data can be used to calculate the equilibrium solubility factor of a component in a membrane, defined as the ratio of the component concentration in the membrane to the concentration in solution. This factor reflects the pervaporation properties of the membrane material and makes it possible to prognosticate, to a certain extent, the pervaporation selectivity [8]. In the vacuum mode, pervaporation is an open phase process [11], because the forming permeate is continuously removed. In this case, the pervaporation substantially differs from the evaporation of a liquid from a free surface. It is known that direct evaporation from a free surface occurs considerably faster, compared with the subsequent diffusion of the vapor, and just this stage is the rate-determining stage of the process as a whole [12]. Accordingly, the vapor formed is in a prolonged contact with the solution, which favors attainment of a dynamic equilibrium. In the case of pervaporation, the vapor is rapidly removed by evacuation, which precludes attainment of an equilibrium. As the residual pressure increases, the flux of substances across the membrane decreases and the permeate composition changes.

It is noteworthy that the dependence of pervaporation parameters on the residual pressure has been the subject of only a small number of reports. This is due to the practical purpose of the pervaporation: a low permeate pressure is necessary for creating technologically attractive high transmembrane fluxes. In [13], the concept of a vapor–liquid "pseudo-equilibrium" in pervaporation was discussed as the state of the process at a zero transmembrane flux and unequal pressures on the sides of the feed solution and the vapor. However, the concept suggested was verified at a the same permeate pressure in all the exper-

iments and no data on fluxes were reported. Moreover, the initial amount of the feed solution was so small that its composition substantially changed in the course of an experiment because of the loss of substances into the permeate. Therefore, the experimental conditions correspond to a nonsteady-state mode and do not satisfy the requirements of the concept suggested in [13].

In [14], the recovery of isomeric butanols from dilute (~1 wt %) binary aqueous solutions with various membranes was studied. It was shown that, for a polyetherblockamide membrane, an increase in the residual pressure (decrease in the flux) differently affects the content of butanol isomers in the permeate, which partly correlates with their vapor pressures (or boiling points). In the case of *n*-butanol (bp 117.7°C), its content in the permeate moderately decreased as the residual pressure became higher, whereas for tertiary butanol (bp 82.5°C), it steeply increased. It should be noted that evaporation of butanol solutions across the membranes studied leads to a poorer separation, compared with open equilibrium evaporation. Only with a polydimethylsiloxane (PDMS) film the content of alcohols (with the exception of tertiary butanol) in the vapor was somewhat higher than that at the liquid–vapor equilibrium.

A mathematical simulation of the pervaporation process with organophilic membranes in terms of the dissolution–diffusion model was performed in [15]. The model developed makes it possible to take into account the effect of the residual pressure of the permeate on its composition, which must correspond in the limiting case of high pressures to the liquid–vapor equilibrium. To confirm the adequacy of the model, the results of the calculations were compared with experimental data on recovery, from aqueous solutions, of phenol (5 wt % phenol) with an acetate–PDMS membrane [16] and ethanol (5–50 wt % ethanol) with a PDMS membrane [17]. Upon an increase in the residual pressure from nearly zero values to 110 mm Hg, the content of phenol in the permeate decreased from 15 to 4 mol % at $T = 75$°C; for the liquid–vapor equilibrium the content of phenol in the vapor is 1.16 mol % [18]. Upon an increase in the residual pressure to 50 mm Hg in the case of aqueous–ethanolic solutions, the content of the alcohol in the vapor reaches values corresponding to the liquid–vapor equilibrium. Thus, it is confirmed [7] that polydimethylsiloxane, a known hydrophobic polymer, is unsuitable for recovery of such strongly polar compounds as alcohols from aqueous solutions.

This communication reports the results of an experimental study of the sorption properties of a hydrophilic nonporous membrane and of the dependence of the pervaporation selectivity on the permeate pressure in separation of liquid aqueous–organic mixtures.

Pervaporation experiments were carried out with binary systems constituted by water and acetic acid and water and ethanol with the use of a film membrane (thickness 70 μm) made of cellulose hydrate (cellophane manufactured by Tsellofan Open Joint-Stock Company, Balakovo, Saratov oblast), which is a hydrophilic polymer. The setup for pervaporation experiments has been described previously [19]. The fluxes were calculated from gravimetric data with account of the membrane area and experiment duration. The temperature of the liquid mixtures used was 30 ± 0.1°C. The residual pressure in the vacuum chamber was maintained at 1, 20, 30, or 50 mm Hg with an accuracy of ±0.1 mm Hg. The mixtures were prepared from distilled water, ethanol, and acetic acid (chemically pure grade). The equilibrium sorption of a liquid by cellophane was studied at 30 ± 0.1°C, using the procedure described in [8]. For this purpose, cellophane strips with a mass of 0.6–0.7 g were placed in thermostated aqueous-organic solutions. In the course of sorption there occurs swelling of a polymeric film, with its weight, accordingly, increasing. After the mass of a swollen polymer reached a constant value, the compositions of the solution and liquid sorbed by cellophane were considered equilibrium. For the solutions and membranes studied, equilibrium was attained in 10–14 days. Further, the free liquid was removed from the surface of a membrane sample with a filter paper and the sample was placed in a flask thermostated at 60°C. The flask was connected to a vacuum pipeline and a liquid-nitrogen-cooled trap in which a condensate of the desorbed vapor was collected after evacuation. The residual pressure was 1 mm Hg. The completeness of liquid extraction from the polymeric membrane was monitored by comparing its mass before and after the desorption experiment. The liquid was completely removed from the membrane after 2 h of vacuum treatment. The compositions of the solutions and vapor condensates were determined in all the experiments by gas chromatography; changes in the membrane mass were monitored gravimetrically.

The results obtained when studying the pervaporation process and the sorption equilibrium for a mixture of water and acetic acid are presented in Figs. 1–3.

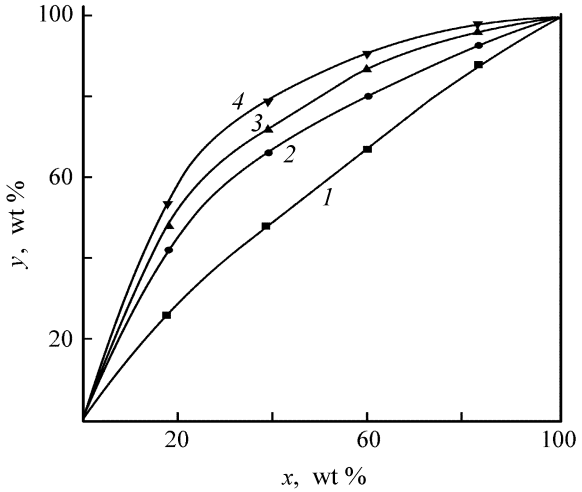

Fig. 1. Water content y of the vapor (permeate) vs. the water content x of the feed solution in pervaporation at residual permeate pressures of (*2*) 1, (*3*) 10, and (*4*) 300 mm Hg. System constituted by water and acetic acid, $T = 30 \pm 0.1$°C; the same for Figs. 2, 3. Line *1* corresponds to the liquid–vapor equilibrium; the same for Fig. 4.

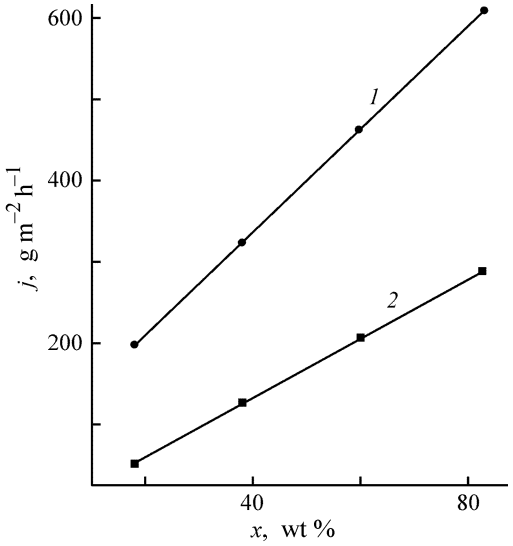

Fig. 2. Flux J in pervaporation vs. the water content x of the solution at residual vapor pressures of (*1*) 1 and (*2*) 10 mm Hg.

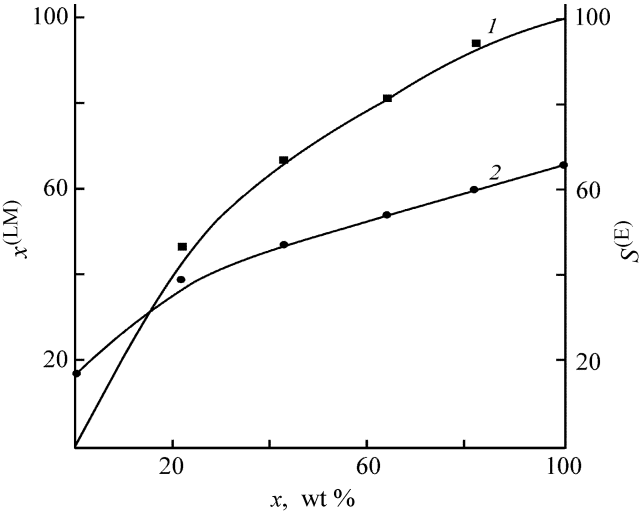

Fig. 3. (*1*) Equilibrium water content $x^{(LM)}$ of the liquid sorbed by a cellophane film membrane and (*2*) degree of membrane swelling, $S^{(E)}$, vs. the water content x of the solution.

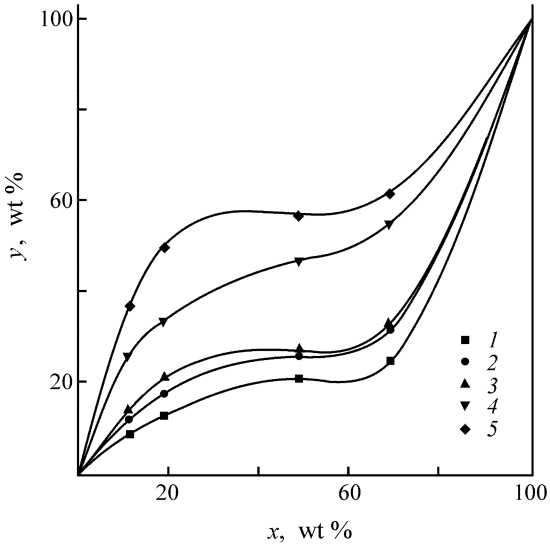

Fig. 4. Water content y of the vapor vs. the water content x of the feed solution in pervaporation at residual permeate pressures of (*5*) 1, (*4*) 10, (*3*) 40, and (*2*) 50 mm Hg. Water–ethanol system, $T = 30 \pm 0.1$°C; the same for Fig. 5.

Figure 1 demonstrates how the water content of the permeate depends on the composition of the liquid at different residual pressures of the permeate. The same figure shows for comparison a curve for the liquid–vapor equilibrium [18]. As the residual pressure increases from 1 to 30 mm Hg for the entire range of compositions of the feed solution, the water content of the permeate grows and differs to an increasingly great extent from the values corresponding to the liquid–vapor equilibrium. As the residual pressure increases further (from 30 to 50 mm Hg), the composition of the permeate remains virtually unchanged. Under the conditions of increasing residual pressure, the transmembrane flux decreases (Fig. 2) to become as low as 2–7 g m^{-2} h^{-1} at 30–50 mm Hg (the last line is not shown in Fig. 2). As equilibrium is attained, the liquid absorbed by the cellophane membrane is strongly enriched in water, compared with the starting solution. This plot is shown in Fig. 3. The same figure presents data on the effect of the solution composition on the degree of swelling $S^{(E)}$. This quantity is defined [7] as the percentage ratio of the mass of liquid ab-

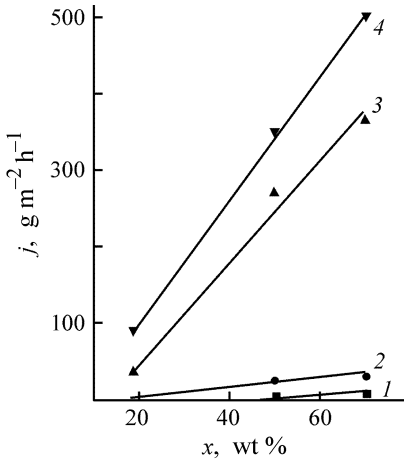

Fig. 5. Flux J in pervaporation vs. the water content x of the solution at residual permeate pressures of (*4*) 1, (*3*) 10, (*2*) 40, and (*1*) 50 mm Hg.

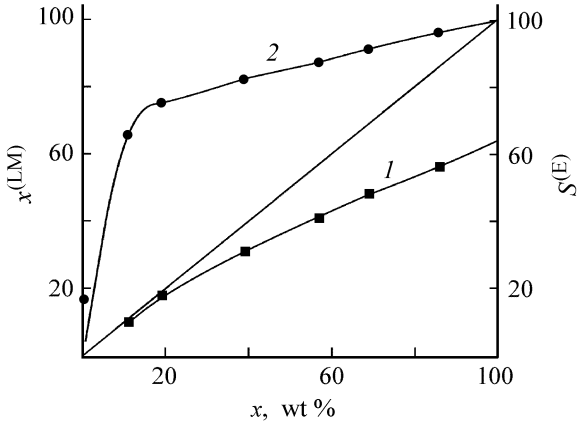

Fig. 6. (*2*) Equilibrium water content $x^{(LM)}$ of the liquid sorbed by a cellophane film membrane and (*1*) degree of membrane swelling, $S^{(E)}$, vs. the water content x of the solution of ethanol.

sorbed by a membrane to the mass of the membrane. As can be seen in Fig. 3, the degree of swelling increases with the content of water, x, in the solution, to reach a value of 64%. This dependence becomes linear at $x > 20$ wt %.

In contrast to the case of aqueous solutions of acetic acid, an increase in the residual pressure in pervaporation separation of water and ethanol leads to a decrease in the water content of the permeate (Fig. 4), and, in the case of low fluxes, the hydrophilic film mainly permeates the alcohol, so that the selectivity of pervaporation falls. As the value of 50 mm Hg is reached, the permeate composition becomes independent of any further increase in pressure; however, it differs from the values corresponding to the liquid–vapor equilibrium (Fig. 4, line *1*). As also in the case of the system constituted by water and acetic acid, the flux of substances increases as the residual pressure becomes lower and the water content of the starting solution of ethanol grows (Fig. 5). As can be seen in Fig. 5, the fluxes in membrane evaporation of a mixture of water and ethanol are substantial and equal to 5–30 g m^{-2} h^{-1} at 40–50 mm Hg. Figure 6 illustrates the dependence of the equilibrium water content $x^{(LM)}$ of the water–ethanol mixture sorbed by the membrane on the water content of the solution. Figure 6 also shows how the degree of film swelling, $S^{(E)}$, depends on the solution composition. The values of $x^{(LM)}$ and $S^{(E)}$ increase as the water content becomes higher, with the water content of the liquid sorbed by the membrane exceeding that in the case of solutions composed of water and acetic acid.

CONCLUSIONS

(1) The sorption characteristics (equilibrium swelling and composition of sorbates) in pervaporation of water–ethanol and water–acetic acid mixtures of various compositions were studied.

(2) It was shown that, in pervaporation of these mixtures at residual under-membrane pressures of 1–50 mm Hg, the membrane exhibits dehydrating properties for the mixture constituted by water and acetic acid at any water content of the starting mixture, and for the water–ethanol mixture, at a water content not exceeding 40 wt %.

(3) It was demonstrated that, as the residual under-membrane pressure increases, the permeability decreases in all cases, with the separation selectivity for acid-containing mixtures increasing and that for ethanol-containing mixtures decreasing because of the difference in the volatilities of acetic acid and ethanol relative to that of water.

ACKNOWLEDGMENTS

The study was performed in the framework of the Federal target program "Integration" (project. B0028/1365), with financial support by the Russian Foundation for Basic Research (grant nos. 03-03-32379 and 06-03-32493).

REFERENCES

1. Baker, R.W., *Membrane Technology and Applications*, New York: McGraw–Hill, 2000.

2. Rautenbach, R. and Albrecht, R., *J. Membr. Sci.*, 1980, vol. 7, pp. 203–215.
3. Mulder M., *Basic Principles of Membrane Technology*, Dordrecht: Kluwer, 1991.
4. Lipnizki, F. and Tragardh, G., *Separ. Purif. Rev.*, 2001, vol. 30, pp. 4–125.
5. Feng, X. and Huang, R.Y.M., *Ind. Eng. Chem. Res.*, 1997, vol. 36, pp. 1048–1066.
6. Zharov, V.T. and Serafimov, L.A., *Fiziko-khimicheskie osnovy distillyatsii i rektifikatsii* (Physicochemical Foundations of Distillation and Rectification), Leningrad: Khimiya, 1975.
7. Jounqueres, A., Clement, R., and Lochon, P., *Prog. Polym. Sci.*, 2002, vol. 27, pp. 1803–1877.
8. Enneking, L., Heintz, A., and Lichtenthaler, R.N., *J. Membr. Sci.*, 1996, vol. 115, pp. 161–170.
9. Hauzer, J., Reinhardt, G.A., Stumm, F., and Heintz, A., *J. Membr. Sci.*, 1989, vol. 47, pp. 261–276.
10. De Bo, J., Van Langenhove, H., and De Keijser, J., *J. Membr. Sci.*, 2002, vol. 209, pp. 39–52.
11. Storonkin, A.V., *Termodinamika geterogennykh sistem* (Thermodynamics of Heterogeneous Systems), Leningrad: Len. Gos. Univ., 1967, parts 1 and 2.
12. Nicolis, G and Prigogine, I., *Self-organisation in Non-equilibrium Systems: From Dissipative Structures to Order Through Fluctuations*, New York: Wiley, 1977.
13. Sarkhel, R., Bandyopadhyay, M., and Bhattacharya, P., *Sep. Pur. Techn.*, 2003, vol. 30, pp. 89–96.
14. Boddeker, K.W., Bengtson, G., and Pingel, H., *J. Membr. Sci.*, 1990, vol. 54, pp. 1–12.
15. Ten, P.K. and Field, R.W., *Chem. Eng. Sci.*, 2000, vol. 55, pp. 1425–1445
16. Bennett, M., Bridson, B.J., England, R., and Field, R.W., *J. Membr. Sci.*, 1997, vol. 137, pp. 63–88.
17. Blume, I., Wijmans, J.G., and Baker, R.W., *J. Membr. Sci.*, 1990, vol. 49, pp. 253–286.
18. Kogan, V.B., Fridman, V.M., and Kafarov, V.V., *Ravnovesie mezhdu zhidkost'yu i parom: Spravochoe posobie* (Liquid–Vapor Equilibrium: Reference Book), Moscow: Nauka, 1966, part 1.
19. Kuznetsov, V.M., Toikka, A.M., and Kuznetsov, Yu.P., *Zh. Prikl. Khim.*, 2004, vol. 77, no. 4, pp. 554–559.

ISSN 1070-4272, Russian Journal of Applied Chemistry, 2007, Vol. 80, No. 6, pp. 909–914. © Pleiades Publishing, Ltd., 2007.
Original Russian Text © V.G. Berezkin, E.V. Kormishkina, 2007, published in Zhurnal Prikladnoi Khimii, 2007, Vol. 80, No. 6, pp. 932–937.

SORPTION AND ION-EXCHANGE PROCESSES

A Variation of Circular Thin-Layer Chromatography with Closed Adsorbent Layer

V. G. Berezkin and E. V. Kormishkina

Topchiev Institute of Petrochemical Synthesis, Russian Academy of Sciences, Moscow

Received August 18, 2006; in final form, April 2007

Abstract—A new variation of circular thin-layer chromatography with an adsorbent layer closed during the experiment and a simple dismountable device for implementation of this technique are suggested.

DOI: 10.1134/S1070427207060110

Thin-layer chromatography (TLC) is a variation of planar chromatography, in which substances are separated on a planar, commonly open adsorbent layer, which makes a chromatographic experiment simple and convenient.

An efficient variation of TLC is circular TLC (CTLC) [1–3]. In this variant, samples to be analyzed are deposited at a certain distance from the plate center along a circle and an eluent is fed into the central part of the plate. In CTLC, substances with low and moderate mobilities R_f are well separated. At the starting area, the zones of the compounds being separated are more symmetric and compact, whereas closer to the front, these zones contract in the elution direction and are simultaneously elongated along the circumference. Circular chromatography is the simplest variation of planar chromatography. Its most important advantage is the automatic contraction of zones in the motion direction of the mobile phase as a result of the existence of the velocity gradient of the mobile phase in the direction of zone motion.

However, a disadvantage of both this method and the TLC technique in general is the comparatively slow course of the experiment and poor reproducibility. This is mostly due, in the opinion of numerous researchers [4], to the influence exerted on the chromatographic process by the gas phase commonly present in the chromatographic chamber. In this context, it seemed appropriate to suggest and implement a new variation of TLC with a closed sorption layer, in which the adsorbent layer virtually does not come in contact with the gas phase.

It is noteworthy that use of chromatography with a closed layer has been known previously, but only in connection with a single problem, development of a quasi-column thin-layer system operating at high pressures. In [5–7], high-pressure TLC was suggested for the first time. This method is implemented on a special device in which the adsorbent layer of a TLC plate is covered with a polymeric film forced against the plate by a high pressure. Consequently, the system used for development of a TLC plate has no free gas volume. The concept, method, and device suggested in [5–7] have been successfully used in TLC for more than 25 years; the system suggested is actually a planar column. However, some researchers justly note as the principal disadvantage of this interesting, useful, and original system its intricate design and comparatively high cost. Therefore, the main goal of our studies of recent years has been to develop new approaches to design of simple dismountable low-cost devices for performing the process of chromatographic separation on standard plates under conditions of a closed adsorbent layer and to perform an experimental study of the possibility and advisability of carrying out the chromatographic process under the conditions of a new TLC variation with a closed layer.

Previously, a new simple device has been suggested for linear chromatography, in which a TLC plate is compressed between two glass plates, with a layer of Parafilm M polymeric film [8] placed between the adsorbent layer of the TLC plate and the glass plate and no high-pressure system employed. This approach has been successfully used in a variation of the conventional linear chromatography with a closed layer under conditions of ascending elution [8, 9].

The main goal of the present study was to implement the new approach to CTLC with a closed (for

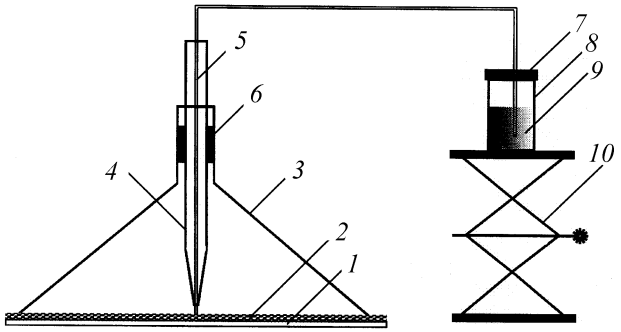

Fig. 1. Installation for the conventional CTLC (a similar solution was suggested in [2]). (*1*) Aluminum substrate for the TLC plate, (*2*) adsorption layer of the plate, (*3*) transparent polymeric funnel (angle 60°, tube diameter 1 cm), (*4*) glass tube used to center the capillary, (*5*) quartz capillary (diameter 0.32 μm) serving for delivery of the mobile phase, (*6*) rubber seal, (*7*) cover, (*8*) vessel for the mobile phase, (*9*) mobile phase, and (*10*) support for the vessel with the mobile phase (with variable height).

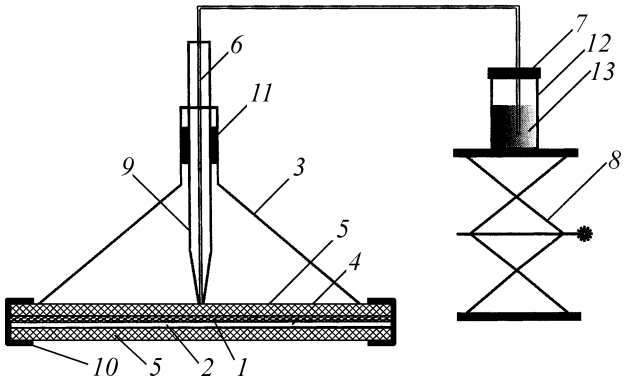

Fig. 2. Installation for CTLC with a closed sorption layer. (*1*) Adsorption layer of the TLC plate, (*2*) aluminum substrate for the plate, (*3*) transparent polymeric funnel (angle 60°, tube diameter 1 cm), (*4*) Parafilm M sealing polymeric film, (*5*) rectangular glass plates, (*6*) fused silica capillary (diameter 0.32 μm) serving for delivery of the mobile phase, (*7*) cover, (*8*) support for the vessel with the mobile phase (with variable height), (*9*) glass tube used to center the capillary, (*10*) clumps, (*11*) rubber seal, (*12*) vessel for the mobile phase, and (*13*) mobile phase.

the time of an experiment) adsorption layer and to analyze this concept experimentally.

EXPERIMENTAL

The design of the device (chamber), previously described for the conventional CTLC and used in this study, is shown in Fig. 1 [2].

The CTLC process with an open layer was implemented as follows: a mixture to be chromatographically separated was circularly deposited onto a plate at a distance of 1 cm from the plate center. Then the plate with a flexible substrate was placed on a glass plate (base) and covered with a polymeric funnel into which a glass tube serving to center the capillary was inserted. This capillary was passed through the tube so as to touch the adsorbent layer of the chromatographic plate. A vessel with the mobile phase was situated above the plate level at a height of approximately 15 cm.

Circular chromatography with a closed adsorbent layer (Fig. 2) was performed as follows: a mixture of standard compounds was circularly deposited onto a TLC plate at a distance of 1 cm from the plate center. Then the plate was covered with a Parafilm M sealing polymeric film and pressed between glass plates with special metallic clumps along the entire TLC plate length. Then the mobile phase was delivered to the plate through a fused silica capillary (diameter 0.32 μm) and the separation process was performed.

The chromatographic process under conditions of a closed layer were performed on plates with silica gel on a 100×100 mm aluminum support for high-efficiency TLC with a UV indicator (STKh-1VE silica gel, grain size 8–12 μm, layer thickness 110 μm, UF-254 UV indicator), manufactured by Sorbpolimer Private Company (Krasnodar, Russia).

As a seal served a Parafilm M transparent polymeric film (thickness 0.12 mm), manufactured by Pechiney Plastic Packing, Inc. (Chicago, USA).

Characteristics of the conventional CTLC and of the variation with a closed adsorption layer, suggested here, were studied in separation of a mixture of the following dyes: (i) Brilliant Green, Rhodamine S, and Erythrosine, taken in a ratio of 1 : 1 : 1 (chromatographed with rectified ethanol as mobile phase) and (2) Rhodamine G, Neutral Red, and Methyl Red in a ratio of 1 : 1 : 1 [separated with a mixture of acetonitrile of pure grade, TU (Technical Specification) 6-09-3534–87, with ethanol in a volume ratio of 10 : 1]. The samples were deposited with a microsyringe.

The distance to which the front of the mobile phase moved in the experiments was 35 mm, with this height measured from the starting line at which the samples containing the substances under study were deposited. In parallel with the experiments in the CTLC variation with a closed layer, we carried out experiments in the conventional circular variation by the procedure described above.

On completion of an experiment, the device was disassembled and the TLC plate was dried in air and scanned on a Genius Color Page-Vivid3x flatbed scanner (KYE Systems Corp., China). The scanning was done with Sorbfil Videodensitometr TLC Quantitative Evaluation software (v. 1.7.0.216) developed by Sorbpolimer Private Company (Krasnodar, Russia). The statistical processing of the results obtained was carried using Excel software (Microsoft, USA).

When performing the chromatographic experiments, we used as parameters of the process under study the following chromatographic quantities: (1) dye mobility R_f

$$R_f = l/Z_f, \quad (1)$$

where l is the largest distance traveled by the spot center from the point of sample deposition, and Z_f is the distance (35 mm in our experiments) traveled by the eluent front from the starting line; and (2) height equivalent to a theoretical plate (HETP or H), calculated for each compounds by the equation

$$H = l/N, \quad (2)$$

where N is the number of theoretical plates; N was found using the Sorbfil Videodensitometr TLC Quantitative Evaluation software.

We estimated the reproducibility of the mobilities R_f in variations of the conventional chromatography and TLC with a closed layer with the use of commonly accepted methods [10].

We first estimated the rough deviation (miss). The miss was estimated by the τ-criterion. In this case, we calculated the average $\bar{x}$ and the standard deviation s for the whole set of measurements (including "doubtful" values) and then found the confidence interval

$$\bar{x} \pm \Delta x = \bar{x} \pm \tau s, \quad (3)$$

in which all the values of the set, except misses (τ-coefficient), can be found with a prescribed confidence probability.

The average value of the quantity being measured, R_f, was calculated using the formula

$$\bar{x} = \frac{\sum_{i=1}^{n} x_i}{n}, \quad (4)$$

where x_i is a single random measurement, and n is the number of repeated measurements.

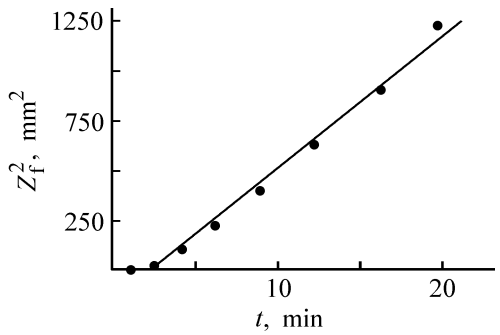

Fig. 3. Z_f^2 for the CTLC variation with a closed sorption layer vs. time t. Mobile phase ethanol.

To evaluate the variance of a random quantity, we used the selected variance s^2, which is a sum of squared deviations of the measurement results from the selected mean, divided by $(n - 1)$:

$$s^2 = \frac{\Sigma(x_i - \bar{x})^2}{n - 1}. \quad (5)$$

The standard deviation s characterizing the scatter of the results in the selected data set was calculated by the formula

$$s = \sqrt{s^2}. \quad (6)$$

The standard deviation is a measure of scatter and characterizes the random error in R_f measurement.

To characterize the reproducibility of the results of our quantitative analysis, we also used the relative determination error

$$\varepsilon = \Delta X/X_{av}. \quad (7)$$

We also studied specific features of the chromatographic process in variations of the conventional CTLC and the CTLC with an adsorption layer covered with a Parafilm M polymeric film. It was found that it is advisable to use, for describing the time dependence of motion of the front of the mobile phase for CTLC with a closed layer, a quadratic equation of motion [3]

$$Z_f^2 = kt + a, \quad (8)$$

where Z_f is the distance from the starting line to the front line of the mobile phase on the plate; k, flow-rate constant; t, time of motion of the mobile phase front from the starting line to a distance $Z_f(t)$; and a, constant.

Figure 3 shows the time dependence of the position of the mobile phase front for a CTLC variation with

Table 1. Front motion distance Z_f in relation to time t for the conventional CTLC and the CTLC with a closed adsorption layer, with a binary acetonitrile : ethanol = 10 : 1 mobile phase (polymeric seal Parafilm M $Z_{f.max}$ = 35 mm)

Distance Z traveled by the binary phase front, mm	Time t, min		Distance Z traveled by the binary phase front, mm	Time t, min	
	conventional CTLC	CTLC with a closed layer		conventional CTLC	CTLC with a closed layer
0	0.43	0.38	20	4.61	3.38
5	1.09	0.84	25	6.02	4.61
10	2.14	1.48	30	7.41	6.05
15	3.27	2.34	35	8.59	7.61

a closed adsorption layer and ethanol used as a mobile phase. It can be seen that the motion time of the mobile phase front is 20 min.

Table 1 lists data on the motion of the front of a binary mobile phase (acetonitrile–ethanol) in the course of time for the conventional CTLC and a CTLC variation with a closed adsorption layer. It can be seen that the motion velocity of a low-viscosity mobile phase in the variation with a closed layer is 10% higher than that in the conventional case.

The smaller difference in the time of the chromatographic process between the conventional CTLC and the CTLC with a closed adsorption layer is due to the use of low-viscosity mobile phases.

If we take into account that, in the case of motion of the mobile phase front along a plate in the conventional CTLC (especially with a volatile mobile phase), there may occur its noticeable evaporation, it seems advisable to use for describing the front motion an equation that accounts for the volatility of the mobile phase. An equation of this type was suggested in [11], whose authors believed that the motion of the front of the liquid mobile phase along the plate is combined with the saturation of the dry adsorption layer of the plate with the mobile phase vapor:

$$Z_f^2 = \chi t + \chi(V_v/\Sigma_0 d)t^2, \quad (9)$$

where Z_f^2 is the position of the mobile phase front; χ, flow rate constant,

$$\chi = 2k_0 d_p \gamma \eta^{-1}, \quad (10)$$

γ, surface tension; η, liquid viscosity; d_p, particle diameter; k_0, permeability parameter dependent of the structure of outer pores; V_v, fraction of the capillary volume, occupied in the preliminarily saturated layer by the liquid phase; $\Sigma_0 = V_m/V_e$; V_m, total pore volume; and V_e, geometric volume of the layer (total).

Then

$$Z_f^2/t = \chi + \chi(V_v/\Sigma_0 d)t = a + bt. \quad (11)$$

In accordance with Eq. (9), we obtained time dependences of the motion of the mobile phase front in the (Z_f^2/t)–t coordinates for the conventional circular chromatography with ethanol or an acetonitrile–ethanol mixture as a mobile phase (Fig. 4). It can be seen that Eq. (9) well describes experimental data for the conventional CTLC.

It also follows from Fig. 4 that the time of motion of the mobile phase in the conventional CTLC is about 35 min for ethanol, which is approximately 40% higher than that in circular chromatography with a closed adsorption layer.

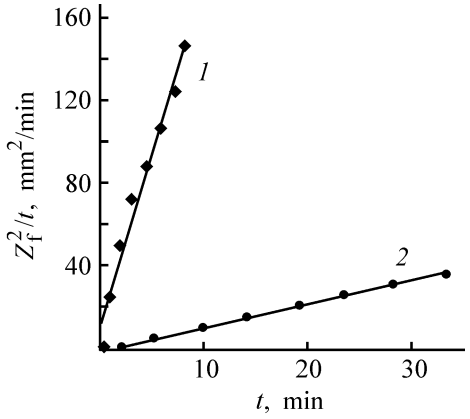

Fig. 4. Z_f^2/t in the conventional CTLC vs. time t. Mobile phase: (*1*) acetonitrile : ethanol = 10 : 1 (by volume) and (*2*) ethanol.

Table 2. Mobilities and efficiencies (R_f and H) for dyed compounds chromatographed by the conventional CTLC and the CTLC with a closed adsorption layer, with ethanol as the mobile phase (polymeric seal Parafilm M, $Z_{f.max}$ = 35 mm, AF-V-UF plates)

Chromatography variation	Parameter	Brilliant Green	Rhodamine S	Erythrosine
Conventional CTLC	R_f	0.07	0.50	0.81
	H, μm	14	13	8
CTLC with a closed layer	R_f	0.08	0.49	0.94
	H, μm	19	14	5

Table 3. Mobilities and efficiencies (R_f and H) in the conventional CTLC and the CTLC with a closed adsorption layer [polymeric seal Parafilm M, acetonitrile : ethanol = 10 : 1 (by volume) mobile phase, $Z_{f.max}$ = 35 mm, AF-V-UF plates]

Chromatography variation	Parameter	Rhodamine G	Neutral Red	Methyl Red
Conventional CTLC	R_f	0.05	0.55	0.63
	H, μm	29	26	22
CTLC with a closed layer	R_f	0.04	0.40	0.61
	H, μm	32	28	26

Table 4. Statistical estimates of the experimentally measured mobilities in the conventional CTLC and the CTLC with a closed layer (n = 10, p = 0.95)

Sorbate	$\overline{X}$	ΔX	S	S	ε, %
			Conventional CTLC		
Brilliant Green	0.07	0.0001	0.00002	0.005	0.15
Rhodamine S	0.50	0.0004	0.00042	0.021	0.08
Erythrosine	0.81	0.0006	0.00090	0.030	0.07
			CTLC with a closed layer		
Brilliant Green	0.08	0.0002	0.00007	0.008	0.25
Rhodamine S	0.49	0.0007	0.00096	0.031	0.15
Erythrosine	0.94	0.0009	0.00145	0.038	0.10

We also estimated the mobilities and efficiencies in the CTLC with a closed adsorption layer and the conventional CTLC with ethanol as the mobile phase (Table 2). It can be seen that the mobility of compounds is higher in a CTLC variation with a closed adsorption layer and the efficiency is somewhat higher in the conventional method.

Table 3 lists the mobility and efficiency characteristics for the conventional CTLC and a CTLC variation with a closed adsorption layer, with an acetonitrile–ethanol mixture as the mobile phase. It follows from these data that the mobilities are somewhat higher in the conventional CTLC, compared with the variation with a closed layer. The efficiency in CTLC with a closed adsorption layer is, as a rule, somewhat lower, and the selectivity, somewhat higher than those in the conventional CTLC.

Using the data obtained, we estimated the reproducibility of the mobilities R_f and efficiencies (HETP). The statistical estimates of the results obtained, by values of R_f for the conventional CTLC and the CTLC with a closed adsorption layer, are listed in Table 4. It should be noted that the average values of R_f are only slightly different between the two variations of chromatography. A somewhat wider difference between values of R_f for erythrosine are due to the closeness of the zone of this compound to the mobile phase front, i.e., erythrosine is eluted in the region of a vir-

tually nonsteady-state flux of the mobile phase. The standard deviation S and the relative error ε for the CTLC with a closed adsorption layer exceed those for the conventional chromatography. However, the wider scatter of R_f for the circular chromatography variations under study is not a factor leading to a negative assessment of the method we suggested, because the CTLC with a closed adsorption layer is an express technique (the separation duration decreases in the case of this variation by 10–40%).

CONCLUSIONS

(1) Use of a circular thin-layer chromatography with a closed adsorption layer can markedly simplify the chromatographic process at an insignificant change in efficiency, with the device for implementation of the variation suggested being rather simple and convenient in operation.

(2) Implementation of the new variation of circular thin-layer chromatography somewhat reduces the expenditure of the mobile phase and its evaporation into the ambient medium.

ACKNOWLEDGMENTS

The study was supported by a grant of the Department of Chemical Sciences, Russian Academy of Sciences, in the framework of the program "Development of efficient methods for chemical and structural analyses of substances and materials."

REFERENCES

1. Sumina, E.G., Shtykov, S.N. and Tyurina, N.V., *Tonkosloinaya khromatografiya: Teoreticheskie osnovy i prakticheskoe primenenie: Uchebno-metodochiskoe posobie* (Thin-Layer Chromatography: Theoretical Foundations and Practical Use: Manual), Saratov: Saratov. Univ., 2002.
2. *HPTC: High Performance Thin-Layer Chromatography*, Zlatkis, A. and Kaiser, R.E., Eds., Amsterdam: Elsevier Scientific, 1977.
3. Geiss, F., *Fundamentals of Thin Layer Chromatography*, Heidelberg: Alfred Huthig, 1987.
4. Siouffi, A.M., *A Century of Separation Science*, Issaq, H., Ed., New York: Dekker, 2002, pp. 69–85.
5. Tyihak, E., Mincsovics, E., and Kalasz, H., *J. Chromatogr.*, 1979, vol. 174, p. 75.
6. Tyihak, E. and Mincsovics, E., *J. Planar Chromatogr.*, 1988, vol. 1, p. 6.
7. Mincsovics, E., Ferenczi-Fodor, K., and Tyihak, E., *Handbook of Thin-Layer Chromatography*, Sherma, J. and Fried, H.B., Eds., New York: Dekker, 1996, pp. 171–203.
8. Berezkin, V.G. and Kormishkina, E.V., *Zh. Anal. Khim.*, 2006, vol. 61, no. 10, pp. 1074–1080.
9. Berezkin, V.G. and Kormishkina, E.V., *J. Planar Chromatogr.*, 2006, vol. 19, pp. 81–85.
10. *Sistematicheskie i sluchainye pogreshnosti khimicheskogo analiza: Uchebnoe posobie dlya vuzov* (Systematic and Random Errors of Chemical Analysis: Textbook for Higher-School Institutions), Chernov'yants, M.S., Ed., Moscow: IKTs Akademkniga, 2004.
11. Guiochon, G. and Siouffi, A., *J. Chromatogr. Sci.*, 1978, vol. 16, p. 598.

ISSN 1070-4272, Russian Journal of Applied Chemistry, 2007, Vol. 80, No. 6, pp. 915–919. © Pleiades Publishing, Ltd., 2007.
Original Russian Text © B.M. Kats, R.M. Dlubovskii, 2007, published in Zhurnal Prikladnoi Khimii, 2007, Vol. 80, No. 6, pp. 938–942.

SORPTION AND ION-EXCHANGE PROCESSES

Selective Sorption of Water Vapor from Gas Mixtures Containing H_2S, SO_2, NO_2, NO, and CO on KU-2 Sulfonic Styrene Cation Exchanger in Different Ion Forms

B. M. Kats and R. M. Dlubovskii

Mechnikov National University, Odessa, Ukraine

Received August 2, 2006; in final form, March 2007

Abstract—Sorption of water vapor and some acid gases (H_2S, SO_2, NO_2, NO, and CO) on KU-23-15/100 macroporous sulfonic cation exchanger in different ion forms and on commercial KSM silica gel and NaX artificial zeolite was studied under equilibrium and dynamic conditions. The equilibrium isotherms of water vapor sorption were measured for all the adsorbents examined. The mechanism of water sorption on the sulfonic cation exchanger was discussed.

DOI: 10.1134/S1070427207060122

Adsorption and gas-chromatographic properties of macroporous ion exchangers are due to their high porosity, i.e., to the presence of macro- and mesopores permeable to molecules of gaseous adsorbates [1, 2]. These molecules can be irreversibly sorbed on the internal surface of ion exchanger grains. The sorption is caused by specific interaction of gases with the functional groups of the ion exchanger [3]. Selective sorption of a gas can be provided by introduction of appropriate functional groups into the sorbent. For example, the sorption capacity of particular ion forms of KU-23 sulfonic action exchanger for some gases (e.g., ammonia and amines [4, 5]) is fairly high, with the sorption being mainly determined by the type of the exchangeable cation.

The aim of this study was to examine the possibility of using KU-23 macroporous sulfonic cation exchanger as selective desiccant for gas mixtures containing hydrogen sulfide and oxides of sulfur, nitrogen, and carbon. These substances are the main atmospheric pollutants whose detection on gas-analyzers is complicated by the interfering effect of water vapor present in a gas–air mixture (GAM) [6, 7].

EXPERIMENTAL

We used commercial KU-23-15/100 macroporous sulfonic styrene cation exchanger (Azot Production Association, Cherepovets, Russia) [8]. The static exchange capacity of the sample for 0.1 M NaOH, determined by the procedure described in [9], was 3.8 mg equiv g^{-1}. We studied the sulfonic cation exchanger in the hydrogen, sodium, copper, and cobalt forms. The hydrogen form was prepared by successive washing of the initial sample with 5% solutions of NaOH and HCl to their constant concentration in the filtrate and then with distilled water to the neutral reaction. The salt (sodium, copper, and cobalt) forms were prepared by washing of the hydrogen form of the cation exchanger with a 5% solution of the appropriate metal salt until the concentration of the metal ion in the solution became equal to that in the filtrate. Commercial desiccants of various gases (artificial NaX zeolite and KSM silica gel) [10] were studied for comparison.

We used as adsorbates gaseous H_2S, SO_2, NO_2, NO, and CO prepared from analytically pure grade chemicals and purified by know procedures. Twice distilled water was used to produce the water vapor.

The equilibrium sorption was studied with a vacuum unit equipped with a MacBain–Bakr quartz spring balance [12]. The sorbent was placed in the unit and kept at 293 K and a residual pressure of 0.133 Pa until the sample weight became constant, i.e., the sorption equilibrium was attained. Prior to the experiment, NaX zeolite was kept at 620 K for 2 h, and KSM silica gel at 570 K for 2 h. The measurements were performed with the aid of a cathetometer. The water vapor pressure gradually increased to p/p_s ~0.95.

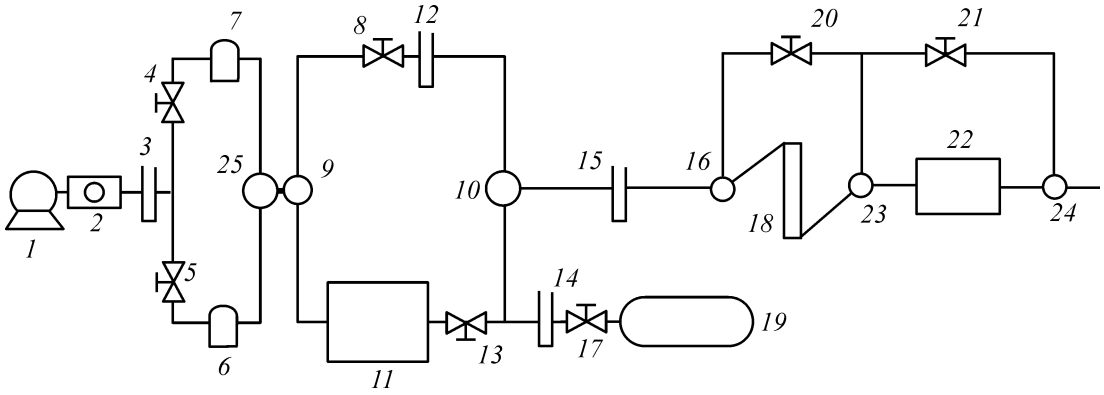

Fig. 1. Scheme of the unit for dynamic sorption: (*1*) pump, (*2*) flow-rate stabilizer, (*3*, *12*, *14*, *15*) flowmeters, (*4*, *5*, *8*, *13*, *17*, *20*, *21*) control valves, (*6*) air humidifier, (*7*) air drier, (*9*) hygrometer, (*10*, *25*) mixers, (*11*) gas mixture generator, (*16*, *23*, *24*) two-way stopcocks, (*18*) filter with adsorbent, (*19*) cylinder with a gas mixture, (*22*) gas analyzer .

The relative determination error of the adsorption, calculated in accordance with the recommendations of [12], did not exceed 6.0% in the whole range of p/p_s.

The dynamic sorption capacity for water vapor and indicated gases was measured with a bench unit schematically shown in Fig. 1. Prior to the measurements, the sorbents were dried at 393 K for 2 h.

To determine the moisture capacity of the gas-vapor mixture with a relative humidity of 20 to 95% at 298 K, it was passed at a flow rate of 60 $dm^3\ h^{-1}$ through a sorbent bed packed in a 25 cm^3 transparent filter body. The water vapor content at the inlet and outlet of the filter was measured with a Volna-5 piezosorption hygrometer (2.5 grade of accuracy). The humidity of more than 1% at the outlet was taken as a breakthrough. The water adsorbtion was determined gravimetrically.

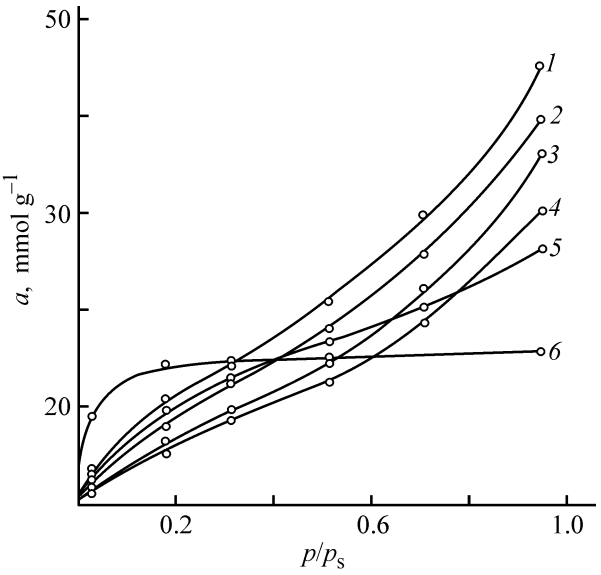

Fig. 2. Isotherm of water vapor sorption on KU-23-15/100 sulfonic cation exchanger in the (*1*) H^+, (*2*) Co^{2+}, (*3*) Cu^{2+}, and (*4*) Na^+ forms and on (*5*) KSM silica gel and (*6*) NaX zeolite. (*a*) Adsorption and (p/p_s) partial pressure.

To determine the selectivity of the sorbents, we prepared gas-air mixtures of purified air and a gaseous adsorbate. The adsorbate content was controlled with a Mikrogas diffusion generator of calibrating gases (H_2S, SO_2, NO_2) or with gas cylinders (NO and CO). The experiments were performed at 298 K, flow rate of gas-air of 60 $dm^3\ h^{-1}$, 50% humidity, and weight concentration of the adsorbate of 20 mg m^{-3}. A 100-mm column 15 mm in diameter was packed with sorbents. The gas concentrations at the inlet (c_{in}) and outlet (c_{out}) of the column were measured. The retention time τ defined as the time for which the c_{out} was no less than 0.9 c_{in} was determined. The H_2S and SO_2 concentrations were measured with a GAU-2 electrochemical gas analyzer, and the CO concentration, with Palladii electrochemical gas analyzer. The NO and NO_2 concentrations were determined with a coulometric cell with a working electrode made of a platinum gauze immersed in a KBr solution. The cell was calibrated using conventional colorimetric procedures [13]. To construct the outlet curves, we used in all cases an appropriate gas analyzer measuring continuously the sorbate concentration at the column outlet. The relative determination error of the gas concentrations was no higher than 20%.

The isotherms of water vapor sorption on all of the sorbents examined are shown in Fig. 2. As can be seen from Fig. 2, the relative position of the isotherms substantially changes with increasing p/p_s. The sorption capacity of NaX zeolite is the highest in the p/p_s range from 0 to 0.3. However, at p/p_s = 0.8–0.95, the sorption capacity of the sulfonic cation exchanger

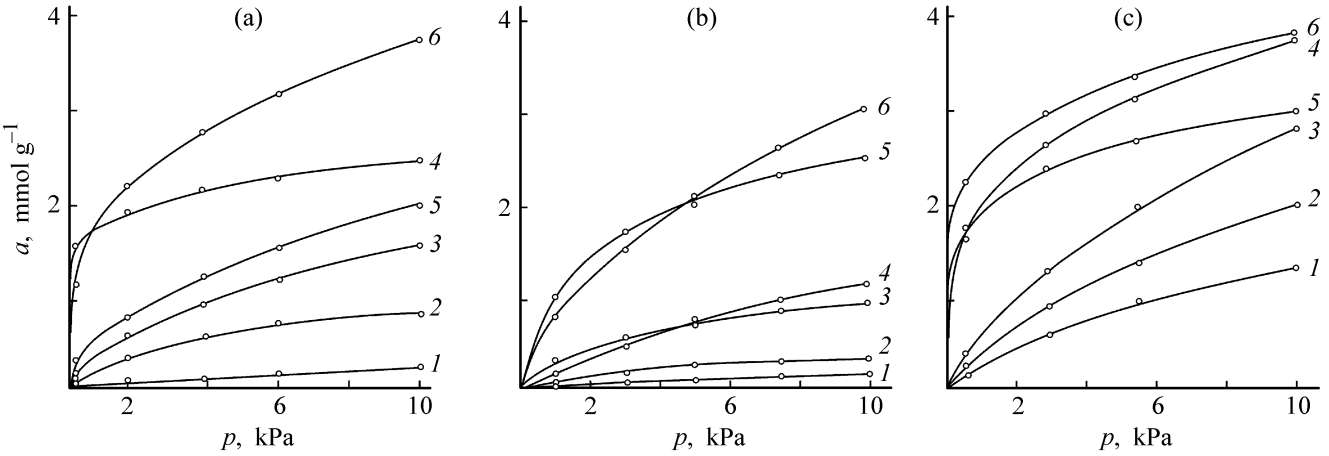

Fig. 3. Sorption isotherm of (a) H_2S, (b) SO_2, and (c) NO_2 on KU-23-15/100 sulfonic cation exchanger in the (*1*) H^+, (*2*) Co^{2+}, (*3*) Na^+, and (*4*) Cu^{2+} form and on (*5*) KSM silicagel and (*6*) NaX zeolite. (*a*) Adsorption and (*p*) pressure.

in the hydrogen and cobalt forms exceeds by a factor of more than 2 that of the other sorbents. The sorption capacity of KSM silica gel at $p/p_s > 0.6$ is higher than that of the zeolite, but significantly lower than that of the sulfonic cation exchanger in the hydrogen and salt forms in the whole range of the partial pressures. These sorption features are due to different mechanisms of water vapor sorption on inorganic sorbents, NaX zeolite, and KSM silica gel. It is known [10] that the microporous zeolite structure is filled even at low p/p_s, whereas the hydrophilic silica gel sorbs water vapor in a wide range of p/p_s.

The isotherms of water vapor sorption on all the ion forms of the sulfonic cation exchanger are S-shaped, which is typical of hydrophilic strongly polar polymers [14]. The fist sorption steps consist in hydration of sulfonic groups to form a monolayer of adsorbed water molecules. Next, some adlayers are formed by binding of water molecules with exchangeable cations. Finally, the sample swells owing to osmotic water absorption caused by capillary condensation of water vapor [15]. Clearly, this multistep mechanism causes high sorption capacity of the cation exchanger, which makes it promising as a desiccant of gas mixtures.

The moisture capacity of the zeolite under the dynamic conditions in the humidity range of 20–40% is the highest. However, as the p/p_s ratio increases, the adsorption of water vapor on the sulfonic cation exchanger and silica gel grows, especially at $p/p_s > 0.9$ (see table).

It should be noted that the dynamic sorption capacities of the zeolite and silica gel are underestimated as compared to published data [16]. This is probably due to the fact that, in small filters, whose length (10–15 cm) is comparable to the height of the working bed of the desiccant, the sorption capacity is saturated incompletely. This is not the case for the cation exchanger whose effective particle size is approximately 0.5 mm, i.e., is an order of magnitude smaller than that of grains of the mineral sorbents. In this case, the height of the working sorbent bed does not exceed 1 cm, so that the sorption occurs in the mode of frontal chromatography and hence the sorption capacity is comparatively high. It should also be noted that the color of the sulfonic cation exchanger in the cobalt form changes layerwise from blue to pink during saturation of the sorbent with water vapor. This is due to formation of cobalt(II) aqua complexes on the surface of the cation exchanger.

To assess the possibility of preparing a selective sorbent for drying of gas mixtures containing H_2S, SO_2, NO_2, NO, and CO, we studied the equilibrium sorption of these compounds on KU-23-15/100 cation exchanger in different ion forms and on KSM silica gel and NaX zeolite. The sorption isotherms of H_2S, SO_2, and NO_2 are shown in Figs. 3a–3c, respectively. As can be seen from Figs. 3a–3c, the sorption capacity

Dynamic sorption capacity of the adsorbents for water vapor

GAM, Humidity, %	Dynamic sorption capacity, mg cm^{-3}			
	KU-23-H^+	KU-23-Co^{2+}	NaX zeolite	KSM silica gel
20	96	90	115	70
40	110	106	122	98
60	125	110	125	110
80	143	126	126	115
95	150	130	128	118

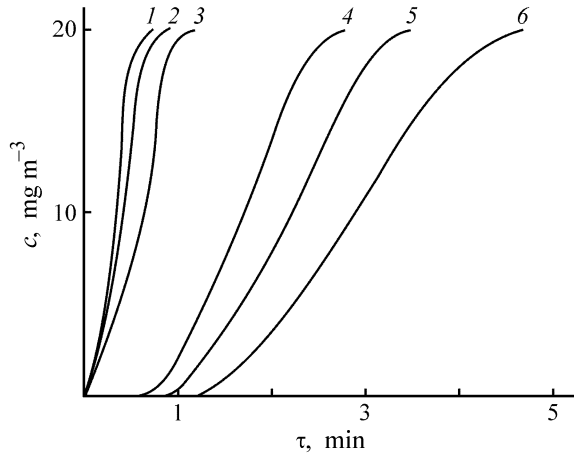

Fig. 4. Breakthrough curves of (*1*, *4*) H_2S, (*2*, *5*) SO_2, and (*3*, *6*) NO_2 on KU-23-15/100 sulfonic cation exchanger in the (*1–3*) hydrogen and (*4–6*) cobalt forms. (*c*) Sorbate concentration and (τ) time.

of the salt form of the cation exchanger for these gases is comparatively high and is comparable to that of the mineral adsorbents. The sorption capacity of the hydrogen form is substantially lower.

It is known [2] that the mechanism of specific interaction of ion exchangers with gases depends on the presence of water in the system. For example, the water content of the cation exchanger samples after attainment of the sorption equilibrium at 293 K and a residual pressure of 0.133 Pa is up to 5% [17]. As a result, the first step of sorption of H_2S, SO_2, and NO_2 on the salt forms of the cation exchanger occurs by the conventional ion-exchange mechanism between the cation of the sulfonic group and the proton of the mineral acid formed. It is clear that this is not the case for the hydrogen form of the sulfonic cation exchanger and hence the sorption capacity of this form for all of the compounds examined is significantly lower. Since NO and CO cannot form strong mineral acids, they are not noticeably sorbed by any of the ion forms of the sulfonic cation exchanger.

Taking into account the results obtained under equilibrium conditions, we studied further KU-23-15/100 sulfonic cation exchanger in the hydrogen and cobalt forms. The breakthrough curves of H_2S, SO_2, and NO_2 on these samples are shown in Fig. 4. It can be seen that the retention time in the case of the hydrogen form of the cation exchanger is as short as 30–50 s. Hence, this sorbent can be used for selective adsorption of water from mixtures of water vapor with H_2S, SO_2, and NO_2. The sorption properties of the spent sorbent are completely restored after heating at 393 K for 2 h. The zeolite and silica gel completely sorb these gases for several hours. The retention time τ_r for the cobalt form of the cation exchanger is 2.5–4.5 min. Thus, these sorbents cannot be used as selective desiccants.

CONCLUSIONS

(1) Macroporous KU-23-15/100 sulfonic cation exchanger in different ion forms was used for the first time as a selective desiccant for analytical pretreatment of gas samples containing water vapor in a mixture with H_2S, SO_2, NO_2, NO or CO. The specific sorption of water vapor on the sulfonic cation exchanger at $p/p_s > 0.5$ (this range is of the most practical interest) is higher than that on commercial desiccants, NaX zeolite and KSM silica gel.

(2) The advantages of KU-23-15/100 sulfonic cation exchanger in the H form as a selective desiccant of gas mixtures containing H_2S, SO_2, NO_2, NO and CO were demonstrated.

(3) It was shown that the cobalt form of KU-23-15/100 sulfonic cation exchanger can be used as indicator selective desiccant for gas mixtures containing NO and CO.

REFERENCES

1. Belyakova, L.D., *Usp. Khim.*, 1991, vol. 60, no. 2, pp. 374–397.
2. Ashirov, A. *Ionoobmennaya ochistka vod, rastvorov i gazov* (Ion-Exchange Treatment of Water, Solutions, and Gases), Leningrad: Khimiya, 1983.
3. Tarasevich, Yu.I. and Kats, B.M., *Visn. Akad. Nauk Ukr. RSR*, 1983, no. 12, pp. 55–62.
4. Varenko, V.P., Kondrasheva, A.L., Plachenov, T.G., et al., Zh. *Prikl. Khim.*, 1979, vol. 52, no. 10, pp. 2199–2203.
5. Kats, B.M., Kutovaya, L.M., and Al'tshul', V.Ya., *Zh. Prikl. Khim.*, 1987, vo. 60, no. 4, pp. 731–735.
6. Jimnez, I., Villa, A., Calveras, A.C., and Moranta, J.R., *IEEE Sensors J.*, 2005, vol. 5, no. 3, pp. 385–391.
7. Talanchuk, P.M., Golubkov, S.P., and Maslov, V.P., *Sensory v kontrol'no-izmeritel'noi tekhnike* (Sensors in Control and Measuring Equipment), Kiev: Tekhnika, 1991.
8. *Ionity: Katalog* (Ion Exchangers: Catalog), Cherkassy: NIITEKhIM, 1980.
9. Polyanskii, N.G., Gorbunov, G.V., and Polyanskaya, N.L., *Metody issledovaniya ionitov* (Methods for Studying Ion Exchangers), Moscow: Khimiya, 1976.
10. Neimark, I.E., *Sinteticheskie mineral'nye adsorbenty i nositeli katalizatorov* (Synthetic Mineral Adsorbents and Catalyst Supports), Kiev: Naukova Dumka, 1982.
11. Karayakin, Yu.V. and Angelov, I.I., *Chistye khimi-*

cheskie veshchestva (Pure Chemical Substances), Moscow: Khimiya, 1974.

12. *Eksperimental'nye metody v adsorbtsii i khromatografii* (Experimental Methods in Adsorption and Chromatography), Kiselev, A.V. and Dreving, V.P., Eds., Moscow: Mosk. Gos. Univ., 1973.
13. Murav'eva, S.I., Bukovskii, M.I., and Prokhorova, E.K., *Rukovodstvo po kontrolyu vrednykh veshchestv v vozdukhe rabochei zony* (Manual of Determinatiion of Hazardous Substances in Air of Working Zone), Moscow: Khimiya, 1991.
14. Zundel, G., *Hydration and Intermolecular Interaction, Infrared Investigation with Polyelectrolyte Membranes*, New York: Academic, 1969.
15. Kats, B.M., Lazarev, M.Yu., and Malinovskii, E.K., *Ukr. Khim. Zh.*, 1981, vol. 46, no. 12, pp. 1337–1339.
16. Kel'tsev, N.V., *Osnovy adsorbtsionnoi tekhniki* (Fundamentals of Adsorption Techniques), Moscow: Khimiya, 1984, 2nd ed.
17. Sherman, F.B., Kats, B.M., and Evenko, G.N., *Talanta*, 1986, vol. 33, no. 5, pp. 429–434.

ISSN 1070-4272, Russian Journal of Applied Chemistry, 2007, Vol. 80, No. 6, pp. 920–923. © Pleiades Publishing, Ltd., 2007.
Original Russian Text © S.I. Tsyganova, A.N. Mel'nikov, I.V. Korol'kova, N.V. Chesnokov, B.N. Kuznetsov, 2007, published in Zhurnal Prikladnoi Khimii, 2007, Vol. 80, No. 6, pp. 943–945.

SORPTION AND ION-EXCHANGE PROCESSES

Synthesis of Porous Carbon Materials from Birch Sawdust Modified with $ZnCl_2$

S. I. Tsyganova, A. N. Mel'nikov, I. V. Korol'kova, N. V. Chesnokov, and B. N. Kuznetsov

Institute of Chemistry and Chemical Technology, Siberian Division, Russian Academy of Sciences, Krasnoyarsk, Russia

Received July 18, 2006; in final form, March 2007

Abstract—Carbonization of birch sawdust modified with zinc chloride and selected properties of the resulting porous carbon materials were studied.

DOI: 10.1134/S1070427207060134

Birch wood is the conventional raw material for manufacture of carbon sorbents. Industrial technologies for production of activated carbon include stages of wood carbonization and subsequent activation of raw carbon with steam. With account of the low yield of activated carbon (5–12% relative to the mass of the starting raw material), a topical task is to raise the yield of activated carbon and to extend the resources of raw materials for manufacture of sorbents by using waste wood.

It is known that modification of plant polymers with various chemical reagents can be used to control the yield of the carbon product and its texture characteristics [1–3]. A promising way to produce carbon materials is modification of plant polymers with compounds of transition metals [1, 3–6]. In pyrolysis of metal-substituted plant materials, carbonization and chemical activation simultaneously occur [3–9]. It is believed that a modifying reagent activates aliphatic groups, with aryl–aryl C–C bond nearly unaffected at all, and leads to selective removal of oxygen, hydrogen, and other heteroatoms, accompanied by carbonization and activation at temperatures that are commonly below 650°C [4–8].

The goal of this study was to analyze fundamental aspects of thermochemical transformations of birch wood (BW) modified with zinc chloride and examine properties of the resulting porous carbon materials.

EXPERIMENTAL

Birch sawdust of the 0.25–0.50-mm fraction was used as object of study. The sawdust was activated by impregnation with an aqueous solution of $ZnCl_2$, followed by drying to constant weight. The content of $ZnCl_2$ in the samples obtained was 5 and 10 wt % (BW-5 and BW-10, respectively).

The samples were carbonized in an installation with a horizontal flow-through reactor in a flow of argon supplied at a rate of 130 $cm^3\ min^{-1}$. The heating was performed in a programmed mode at a rate of 10 deg min^{-1} to a temperature of 800°C, with a 30-min keeping at the final temperature.

The specific surface area of the carbon products was measured by the method of thermal desorption of nitrogen on a Gazometr-1 analyzer. The elemental composition was determined with a Flash EA 1112 instrument. Thermogravimetric studies were carried out on an MOM Q-1500D derivatograph (Hungary) by heating a sample in a flow of helium, delivered at a rate of 1200 $cm^3\ min^{-1}$, at a heating rate of 10 deg min^{-1} to a final temperature of 1000°C. IR spectra of the samples under study were recorded on a Vector 22 IR Fourier spectrometer.

Figure 1 shows how the yield and specific surface area of the carbon product (CP) depend on temperature. Up to a treatment temperature of 200°C, the yield of CP from unmodified sawdust exceeds that from

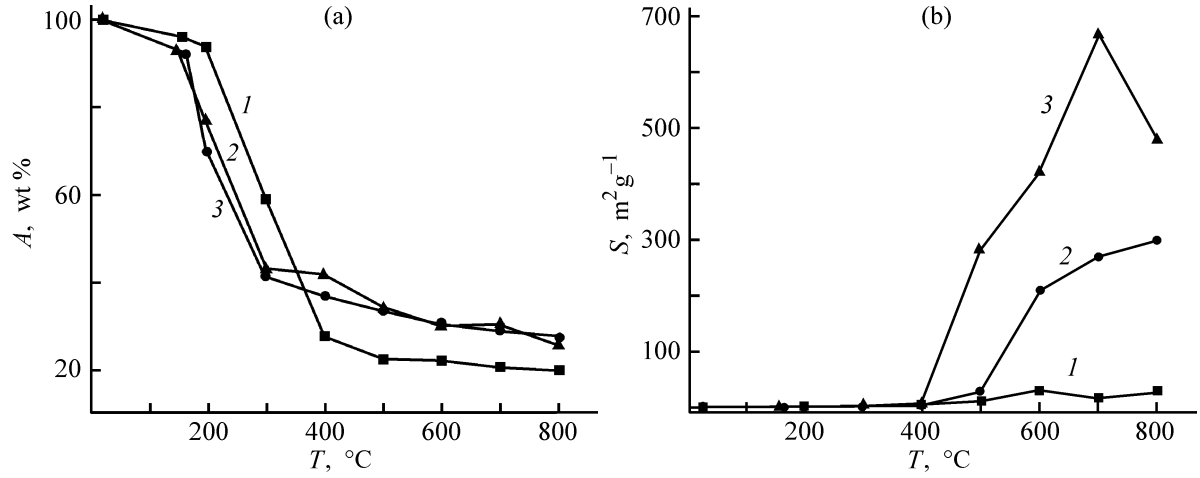

Fig. 1. (a) Yield *A* and (b) specific surface area *S* of the carbon product formed from (*1*) starting birch wood and (*2*, *3*) wood modified with solutions containing (*2*) 5 and (*3*) 10% $ZnCl_2$ vs. the carbonization temperature *T*.

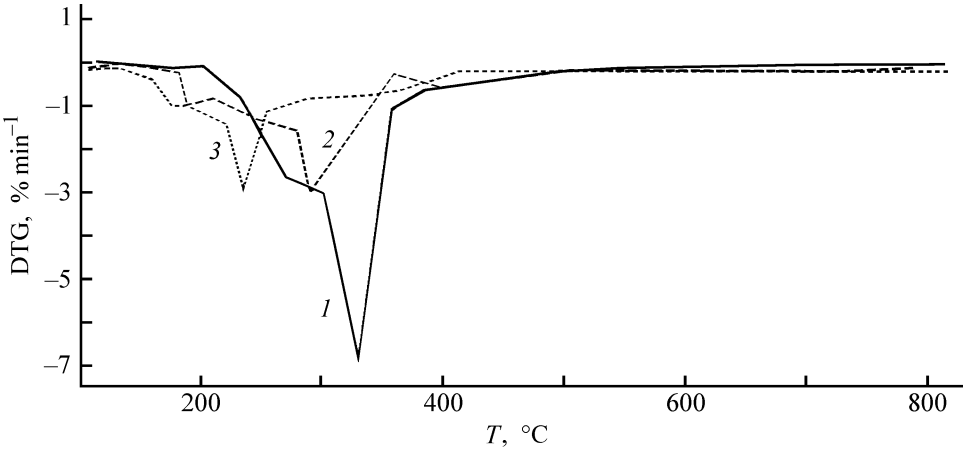

Fig. 2. Differential thermogravimetric (DTG) curves for (*1*) BW, (*2*) BW-5, and (*3*) BW-10 samples, obtained at a heating rate of 10 deg min^{-1}. (*T*) Temperature; the same for Fig. 3.

the samples promoted with $ZnCl_2$ (Fig. 1a). A major decrease in the yield of CP occurs in the range 200–400°C for a sample of the starting birch wood and in narrower range 200–300°C for samples of wood modified with zinc chloride. The yield of the carbon product from zinc-containing wood samples is 5–10 wt % higher than that from unmodified wood, with a change in the content of zinc chloride in the samples from 5 to 10 wt % having virtually no effect of the CP yield.

The specific surface area of the carbon product strongly changes in the course of carbonization of modified samples (Fig. 1b), whereas the specific surface area of the carbon product formed from unmodified birch wood increases with temperature only slightly: from 1.0 $m^2 g^{-1}$ at 25°C to 27.0 $m^2 g^{-1}$ at 800°C. The specific surface area of CP produced from BW-5 sample markedly grows at treatment temperatures exceeding 500°C, to reach a value of 300 $m^2 g^{-1}$ at 800°C. In carbonization of BW-10 sample, the specific surface area starts to grow at lower temperatures (400°C), to reach the maximum value of 670 $m^2 g^{-1}$ at 700°C. Thus, chemical activation of birch wood with $ZnCl_2$ leads to an increase in the yield and specific surface area of the carbon product in the course of carbonization. As the content of zinc chloride in BW increases, the yield of the carbon residue remains virtually unchanged and the specific surface becomes 1.5–2 times larger.

The thermograms in Fig. 2 demonstrate that the onset temperature and rate of thermochemical transformation of birch wood markedly decrease in the presence of $ZnCl_2$. The most intense thermochemical

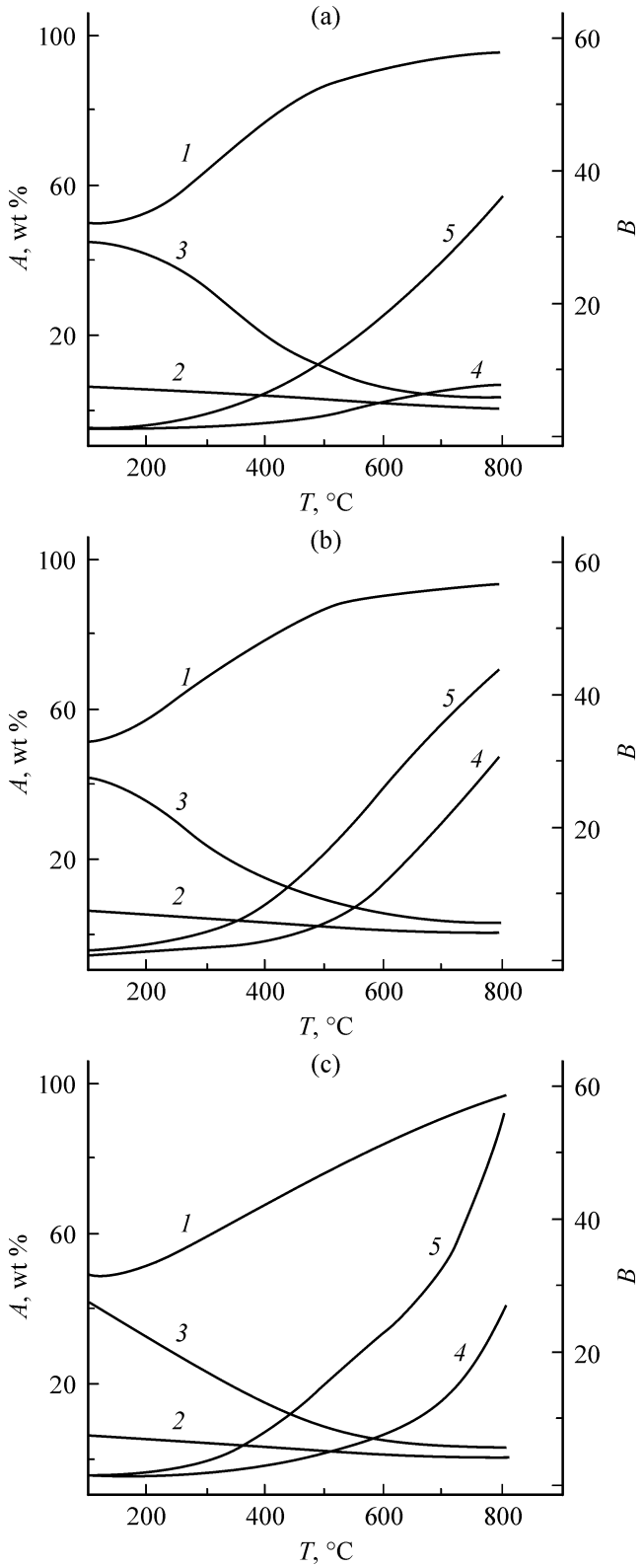

Fig. 3. Variation of the content *A* of (*1*) C, (*2*) H, and (*3*) O and of atomic ratios B (*4*) C/H and (*5*) C/O in the course of carbonization of birch sawdust. Sample: (a) BW, (b) BW-5, and (c) BW-10.

transformations are observed at 330°C for unmodified wood and at 290 and 235°C for BW-5 and BW-10, respectively.

According to the results of an elemental analysis, the content of carbon in carbon products obtained from modified and unmodified wood increases and the content of hydrogen and oxygen decreases as the treatment temperature becomes higher (Fig. 3). At carbonization temperatures exceeding 500°C, the C/O and C/H ratios markedly increase, especially for modified samples (Figs. 3b, 3c). The decarboxylation, decarbonylation, and aromatization processes are presumably intensified at temperatures exceeding 500°C in the presence of $ZnCl_2$ in a sample. This leads to formation of a developed porous structure of the carbon product.

Results of an IR spectral study of BW, BW-5, and BW-10 samples also indicate that the composition of unmodified wood changes at a treatment temperature of 300°C, and that of wood samples modified with $ZnCl_2$, at 200°C. In the process, the content of hydroxy and ester groups increases and an ordered cellulose structure starts to be observed. In the high-temperature region, there probably occur aromatization and condensation processes leading to removal of oxygen and hydrogen and to formation of a porous structure of the carbon product.

CONCLUSIONS

(1) Modification of birch wood with zinc chloride leads to a slight increase in the yield of the carbon product and to a rise in its specific surface area by a factor of 10–25. It is found that $ZnCl_2$ shifts the onset of intense thermochemical transformations of wood to lower temperatures by 100°C.

(2) In the course of pyrolysis, $ZnCl_2$ promotes reactions of deoxygenation and condensation of components of the organic matter of wood and favors development of a porous structure of the carbon product.

REFERENCES

1. Fenelonov, V.B., *Vvedenie v fizicheskuyu khimiyu formirovaniya supramolekulyarnoi struktury adsorbentov i katalizatorov* (Introduction to Physical Chemistry of Formation of the Supramolecular Structure of Adsorbents and Catalysts), Novosibirsk: Sib. Otd. Ross. Akad. Nauk, 2002.
2. Khokhlova, G.P., Shishlyannikova, N.Yu., and Patrakov, Yu.F., *Khim. Inter. Ustoich. Razv.*, 2005, no. 13, pp. 103–111.

3. Kuznetsov, B.N., Chesnokov, N.V., Mikova, N.M., et al., *Khim. Inter. Ustoich. Razv.*, 2002, no. 10, pp. 421–430.
4. Benaddi, H., Bandosz, T.J., Jagiello, J., et al., *Carbon*, 2000, no. 38, pp. 669–673.
5. Khalili, N.R., Campbell, M., Sandi, G., and Golas, J., *Carbon*, 2000, no. 38, pp. 1905–1915.
6. Gonzalez-Serano, E., Cordero, T., Rodriguez-Mirasol, J., and Rodriguez, J.J., *Ind. Chem. Res.*, 1997, no. 36, pp. 4832–4845.
7. Caturla, F., Molina-Sabio, M., and Rodriguez-Reinoso, F., *Carbon*, 1991, no. 29, pp. 999–1003.
8. Ahmadpour, A. and Do, D.D., *Carbon*, 1997, no. 35, pp. 1723–1732.
9. Tsyganova, S.I., Chesnokov, V.N., Mel'nikov, A.N., et al., *Sbornik nauchykh trudov "25 let Institutu khimii i khimicheskoi tekhnologii Sib. Otd. Ross. Akad. Nauk: itogi i perspektivy"* (Coll. of Sci. Works Devoted to 25th Foundation Anniversary of the Institute of Chemistry and Chemical Technology, Siberian Division, Russian Academy of Sciences), Krasnoyarsk, 2006, vol. 2, pp. 153–156.

ISSN 1070-4272, Russian Journal of Applied Chemistry, 2007, Vol. 80, No. 6, pp. 924–929. © Pleiades Publishing, Ltd., 2007.
Original Russian Text © I.V. Sheveleva, L.A. Zemskova, S.V. Zheleznov, A. Voit, N.N. Barinov, S.V. Sukhoverstov, V.I. Sergienko, 2007, published in Zhurnal Prikladnoi Khimii, 2007, Vol. 80, No. 6, pp. 946–951.

APPLIED ELECTROCHEMISTRY AND CORROSION PROTECTION OF METALS

Effect of Modification on Electrochemical and Sorption Properties of Woven Carbon Materials

I. V. Sheveleva, L. A. Zemskova, S. V. Zheleznov, A. Voit, N. N. Barinov, S. V. Sukhoverstov, and V. I. Sergienko

Institute of Chemistry, Far-Eastern Division, Russian Academy of Sciences, Vladivostok, Russia

Received December 18, 2006; in final form, February 2007

Abstract—Relationship between electrochemical, structural, and sorption properties of woven carbon materials modified with chitosan was studied.

DOI: 10.1134/S1070427207060146

Carbon materials, including activated carbon fibers (ACF), are used in technical electrochemistry for fabrication of energy accumulators [1] and as sorbents and electrosorbents in sorption processes for purification of technological solutions, potable water, and biological liquids [2, 3]. Carbon fibers having high electrical conductivity are used in both electrochemical and electrosorption processes [3, 4]. To raise the working surface area, capacity, and selectivity of fibers, they are modified with metal oxides and hydroxides, by chemical and electrochemical oxidation, and by deposition of films of synthetic and natural polymers [5]. A promising modifying agent is chitosan, which can form membranes, has high selective permeability to water, good bioadhesion, high mechanical strength, and is susceptible to chemical modification because of the presence of chemically active amino and hydroxy functional groups [6]. Chitosan can serve as a support or sorbent for biological substances [7]. The maximum unfolded state of the chitosan surface and accessibility of all the active ionogenic groups can be achieved on depositing the biopolymer onto the surface of a porous support [8]. Carbon materials having chemical stability in acid and alkaline media, electrical stability and conductivity, and highly developed porosity and surface, are best suitable for this purpose. The best among various methods for deposition of a modifier onto a solid surface are electrochemical methods, which allow control over the growth and size of particles being deposited onto the support surface [9]. Use of chemical and(or) electrochemical modification methods enables, with account of the properties of chitosan and carbon fibers, targeted synthesis of chitosan–carbon materials with controllable properties [10]. It is necessary, however, when using materials of this kind as electrodes, to primarily take into account the fact that the operation efficiency of an electrode depends on the accessibility of its surface to the electrochemical process. In turn, the course of the electrochemical is strongly affected by the porous structure of the carbon material [11].

The electrochemical properties of a carbon material brought in contact with an electrolyte solution make it possible to assess changes of its structural and surface characteristics [12]. The porous structure of the carbon matrix affects formation at the interface of an electric double layer (EDL), within which charge redistribution and adsorption of ions or molecules occur [13]. Therefore, elucidation of the relationship between the electrochemical, structural, and sorption properties of fibers will enable us to characterize the modified materials under study to a fuller extent.

The aim of this study was to examine the possibility of using woken carbon materials modified with chitosan as electrodes and sorbents.

EXPERIMENTAL

We used as an electrode a Busofit T-055 activated woven carbon fiber, whose specific surface area, pore volume, and average pore radius are 700 $m^2 g^{-1}$, 0.55 $cm^3 g^{-1}$, and 3.5–8 Å, respectively. In addition, we used modified carbon fibers produced by deposition of chitosan onto the surface of the starting Busofit in the absence of polarization [ACF(w/o/p)] and

at potentials of +0.9 V [ACF(900)] and –0.9 V [ACF(900)] [10].

Electrochemical measurements were performed using methods of cyclic voltammetry and charging curves in solutions of 0.9% NaCl (physiological solution) and 3.5% NaCl. The solutions were vigorously agitated and bubbled with inert gas. The choice of the electrolytes was governed by further studies of sorption processes for protein recovery with chitosan–carbon materials (CCM). The fiber samples under study were placed on a gold grid serving as an inert current lead. A silver chloride electrode was used as reference. The auxiliary electrode made of a porous carbon material was separated from the working electrode by an MB-2 bipolar membrane. Potentiodynamic curves were obtained with a P-5848 potentiostat in the double-layer region of potentials in the range ±50 mV relative to the immersion potential of the working electrode [14]. The capacitance of the EDL was calculated by the formula [14, 15]:

$$C = I/mv = (I_c + I_a)/2mv. \quad (1)$$

Here, C is the electrode capacitance (F g^{-1}); I_c and I_a, cathode and anode polarization currents (A); and v, potential sweep rate (mV s^{-1}).

The degree (fraction) α of utilization of the electrode surface in the electrochemical process was calculated using the relation

$$\alpha = C/C_{max}, \quad (2)$$

where C and C_{max} are the electrode capacitances at a given and the minimum potential sweep rates.

When processing the potentiodynamic curves by the least-squares method, we calculated the characteristic charging time of the EDL (τ) and the ohmic resistance of the electrolyte within pores ($R = \tau/c$) by the formula [16]:

$$I = Cv\left[1 - \frac{2}{\pi^2}\sum_{n=0}\frac{1}{\left(n+\frac{1}{2}\right)^2}\right]e^{-\pi^2(n+\frac{1}{2})^2\frac{t}{\tau}}. \quad (3)$$

Here, I is the current (A g^{-1}); v, potential sweep rate (V s^{-1}); t, time; and n, summation index.

In galvanostatic measurements, the polarizing current density was chosen experimentally. In all cases, the charging current density was varied within the range 10^{-11}–10^{-10} A cm^{-2}. The capacitance C (F g^{-1}) was calculated by the formula

$$C = I\Delta t/m\Delta E, \quad (4)$$

where I is the polarization current (A); Δt, electrode charging time (s); m, electrode mass (g); and ΔE, shift of the electrode potential (V).

The sorption properties of the fibers for bovine serum albumin (BSA) was studied in recovery of the protein from a physiological solution (0.9% NaCl) with a BSA concentration of 1 mg ml^{-1} under static conditions in a standard three-electrode cell. The protein was analyzed by HPLC on a Shimadzu LC-10Avp liquid chromatograph (Japan) with a Shimadzu SPD-10Avp UV detector (wavelength 280 nm). The amount Γ of sorbed BSA (mg g^{-1}) was calculated by the formula

$$\Gamma = (c_{in} - c_{eq})V/m,$$

where c_{in} and c_{eq} are the initial and equilibrium concentrations of the protein in a solution (mg cm^{-3}); V, solution volume (ml); and m, sorbent mass (g).

BSA was desorbed by changing the charge of the electrically conducting carbon matrix in the same solution from which the protein was preliminarily recovered at the open-circuit potential. The measurements were made relative to the silver chloride electrode. The potentials at which the BSA desorption was carried out were chosen in the range in which no chemical transformations occurred with the protein. For this purpose, preliminary voltammetric measurements were performed in a system constituted by the protein and carbon fibers.

Microscopic studies were carried out with an EVO-50XVP scanning electron microscope in the secondary-electron mode at accelerating voltages ranging from 20 to 30 kV. The materials to be studied were glued with a conducting silver glue to an aluminum table.

The use of porous carbon electrodes with a highly developed surface markedly improves the efficiency of the electrochemical process. However, the electrode polarization may hinder the charging process. This hindrance is due to slow supply of ions (diffusion hindrance) or to changes in the potential within pores (ohmic hindrance). In addition, presence of micropores less than 1.5–2.0 nm in size, within which EDL formation is difficult [14, 17], can complicate polarization of the intrapore space and impair the operation efficiency of the porous electrode. Also, the modification of the carbon surface can change its structure and, as a result, alter the accessibility of the surface to the electrochemical process.

Effect of ACF modification on the capacitances and charging parameters of the electrodes in various NaCl solutions

Sample	C_1	C_2	R, ohm	τ, s
	F g^{-1}			
0.9% NaCl				
Starting	50.89	51.09	79.2	434
(+900)	64.85	64.97	198.3	1529
(w/o/p)	58.46	58.7	233	1929
(–900)	43.45	43.64	68.5	389
3.5% NaCl				
Starting	50.42	50.32	27	129
(+900)	69.79	69.58	28.3	189
(w/o/p)	60.5	60.18	42.8	255
(–900)	47.37	47.14	28	162

Note. C_1 was found from the results of voltammetric measurements at the minimum potential sweep rate, and C_2, from galvanostatic data.

To find out whether the chitosan film is permeable and the surface is accessible to electrolyte ions forming the EDL plate, we preliminarily determined the capacitances of unmodified and chitosan-coated glassy carbon electrodes. We obtained that the capacitances of such electrodes are the same and equal to 8 μF cm^{-2}. This value is comparable with the data of other researchers who measured the capacitances of glassy carbon electrodes in various solutions [14, 17]. The results obtained suggest that the chitosan film does not prevent electrolyte ions from penetrating to the carbon surface to form an EDL. It was shown in [6] by various methods, including cyclic voltammetry, that a chitosan film deposited on glassy carbon has good permeability and favors fast penetration of electrolyte ions to the surface of the carbon material.

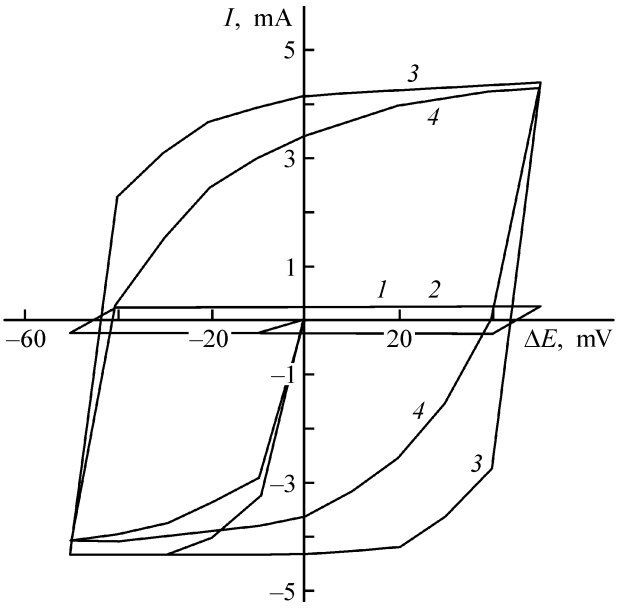

Fig. 1. Cyclic voltammetric curves obtained on (*1*, *3*) initial and (*2*, *4*) modified ACF(–900) in a solution of 0.9% NaCl at various potential sweep rates *v*. (*I*) Current and (Δ*E*) shift of the potential from the steady-state value. *v* (mV s^{-1}): (*1*, *2*) 0.04 and (*3*, *4*) 0.1.

The capacitance of the electric double layer is one of the main electrochemical characteristics of an electrode. The capacitance of EDL depends on the conditions of its formation in the porous structure of carbon materials, including those modified. Data on the EDL capacitance make it possible to calculate the charging conditions of porous fibrous electrodes [18] and to evaluate the efficiency of utilization of ACF and ACF-based composites in processing occurring under polarization.

One of methods for determining the EDL capacitance of porous carbonic and fibrous electrodes is cyclic voltammetry [14], which can evaluate the effect of the structural and surface properties of carbon materials on the conditions of their charging. We compared the electrode capacitances found by cyclic voltammetry and galvanostatic measurements. The values obtained are listed in the table. The good agreement of the results indicates that these two methods can be equally successfully used to determine the capacitance of porous electrodes.

The effect of the porous structure on the charging of carbon materials can be judged from the shape of voltammetric curves. Figure 1 shows as an example voltammograms obtained at different polarization rates in a solution with 0.9% NaCl. The shape of the cyclic curves, with equal areas under the anodic and cathodic portions indicates that no irreversible Faraday processes occur [19]. The voltammograms obtained at the minimum potential sweep rate of 0.04 mV s^{-1} (curves *1*, *2*) have a virtually rectangular shape, which indicates that there are no hindered charging processes, which appear upon a considerable increase in the electrode polarization rate (curves *3*, *4*). The occurrence of hindered charging processes may be due to porous structure parameters of the fiber, surface phenomena at the electrode–solution interface, and properties of the conduction band of the carbon material [20], dependent on the preparation conditions of the carbon fabric. In turn, modification of the carbon fiber predetermines changes of its porous structure, which will affect the charging conditions of chitosan–carbon materials.

The differences in charging and the structural features of modified fibers can be judged from the dependence of the electrode capacitance on the potential sweep rate (Fig. 2). The EDL capacitance calculated at the minimum potential sweep rates is close to that found from galvanostatic measurements (see table). As the load on the electrode increases, the capacitance decreases, which is due to diffusion and ohmic limitations appearing in a structure whose specific features are determined by the modification conditions of the carbon matrix. Deposition of chitosan onto the surface of a porous support in the absence of polarization and under an anodic potential gives CCM in which the capacitance is larger compared with that for an unmodified fabric. The capacitance of the composite material obtained upon chitosan deposition at cathodic potentials is lower than that of the unmodified electrode (see table). However, the CCM obtained at cathodic potentials is polarized more uniformly, compared with the composites produced at anodic potentials. An increase in the charging rate of an electrode does not lead to any sharp decrease in its capacitance and in the fraction of its working area that is involved in the electrochemical process (Figs. 2 and 3, curves *4*). It should be noted that, in the case of polarization in a solution with 3.5% NaCl, the capacitance of the electrodes under study does not decrease considerably and the fraction of the surface involved in the electrochemical process remains rather large. Presumably, this is favored by a substantial increase in the concentration gradient of charged particles promoting faster EDL formation in an electrode subjected to charging.

A mathematical processing by Eq. (3) of the dependences of the capacitance of the electrodes on the rate of their polarization made it possible to calculate the charging time of the electrodes and the electrolyte resistance in the intrapore space. Analysis of the data presented in the table shows that charging of CCM (especially in the 0.9% NaCl solution) depends on the preparation conditions of these materials. A faster charging with a lower electrolyte resistance within pores is observed for modified electrode materials obtained in cathodic deposition of chitosan onto a carbon matrix. Presumably, this method of modifier deposition gives a structure that favors better EDL formation and more uniform charging of the chitosan–carbon electrode.

The use of scanning electron microscopy (SEM) revealed structural differences between the starting and modified carbon matrices. It was found that meso- (~25 to 50 nm) and rounded macropores not exceeding 320 nm in size are present on the surface of the

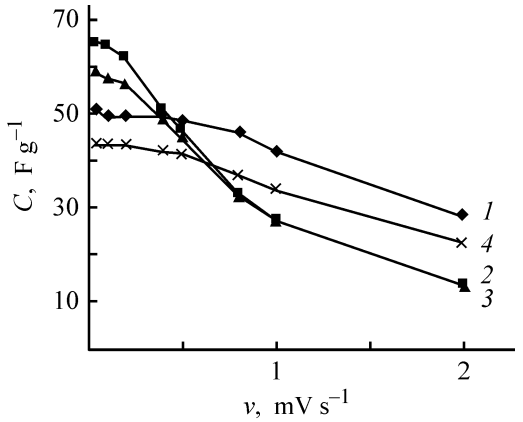

Fig. 2. Capacitance C vs. the potential sweep rate v in polarization in the double-layer range of potentials in a solution with 0.9% NaCl. (*1*) ACF, (*2*) ACF(+900), (*3*) ACF(w/o/p), and (*4*) ACF(–900); the same for Fig. 3.

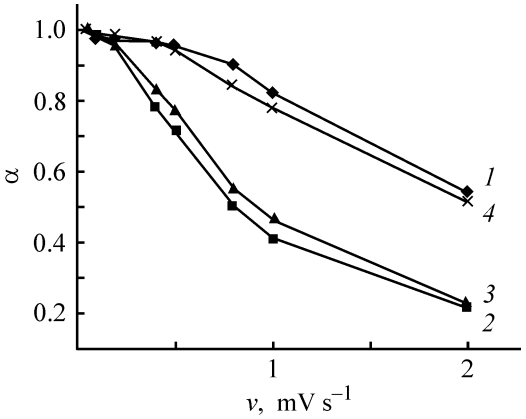

Fig. 3. Surface fraction α vs. the potential sweep rate v for carbon electrodes in a solution of 0.9% NaCl.

starting woven fiber. The surface is mostly covered by mesopores.

Modification of a carbon fiber at cathodic potentials leads to deposition onto the ACF surface of an insoluble chitosan as a result of solution alkalinization in the near-electrode space. In the cathodic polarization, the porous structure of the carbon matrix changes, with the depth of pore penetration into the fiber increasing. Finer pores merge in the course of their development into macropores of complex structure, which have the form of a sieve combining meso- and macropores of size not exceeding 300 nm. Presumably, the formation of just this kind of hierarchic structure across the depth of the porous electrode affects the charging conditions of the modified electrode.

In anodic polarization, a large number of macropores, absent in the starting fiber, are formed in the surface layer of the modified fiber. This is due to

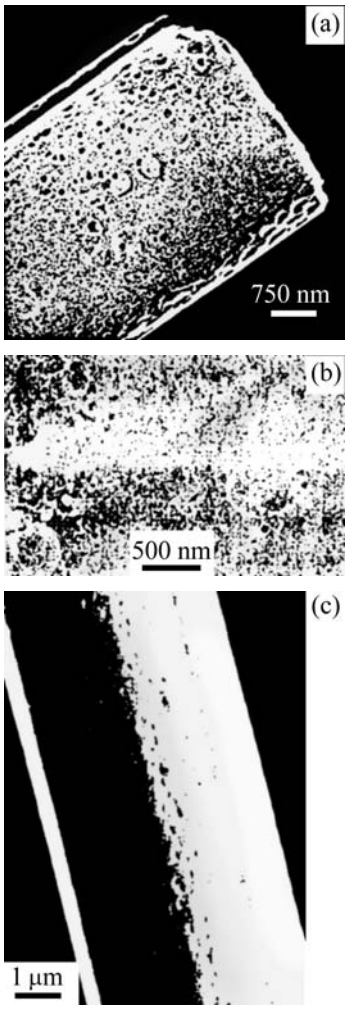

Fig. 4. SEM images of (a) starting and (b, c) modified carbon fibers. (b) ACF(–900) and (c) ACF(+900).

an additional electrochemical oxidation of the surface [21]. Thus, according to SEM data, the morphology of the carbon surface strongly varies with the conditions of ACF treatment.

Figure 4 shows SEM images of the surface of the starting and modified fibers.

Having determined the electrochemical characteristics of CCM, we can judge about changes in the structure of the carbon matrix in modifier deposition, whereas determination of sorption characteristics of CCM allows evaluation of changes in the surface parameters of the carbon fiber upon its modification. We studied the sorption properties of CCM in recovery of BSA from a physiological solution (0.9% NaCl). For the unmodified fiber and chitosan–carbon materials obtained at potentials of –0.9 and +0.9 V, the sorption capacities are 20.4, 73.7, and 36.7 mg g^{-1}, respectively, i.e., the absorption capacity of CCM for albumin depends on the preparation conditions of the sorbents. In chitosan deposition onto a carbon matrix, the chemical nature of the surface significantly changes, with hydrophilic-hydrophobic areas with different densities of ionogenic groups formed as a result of chitosan deposition onto the surface of a charged fiber at different polarization potentials [10]. This, in turn, determines the sorption capacity of the composite materials.

Changing the surface charge of a chitosan–carbon fiber with preliminarily sorbed BSA, with the surface potential shifted into the cathodic region, leads to desorption of the protein from the surface of the carbon material and can serve as a method for sorbent regeneration [22]. By electrodesorption of BSA under cathodic polarization (ΔE = –0.3 V), 42.7, 72.6, and 35.2% of the preliminarily sorbed protein can be removed from the surface of, respectively, unmodified sorbent and chitosan–carbon sorbents obtained at cathodic and anodic potentials. BSA is removed from the surface because of the generation of OH^- ions under the cathodic polarization of the carbon material [14, 17], and these ions substantially change the pH in the nearelectrode layer. This, in turn, leads to ionization of protein molecules and to repulsion of like-charged ions from the sorbent surface. Thus, cathodic polarization of the CCM makes it possible to remove BSA from its surface and to restore the absorption capacity of the sorbent.

We found in a study of the sorption properties of CCM that chitosan is firmly retained on the carbon matrix and is washed into solution neither in protein adsorption nor in sorbent polarization. This was indicated by the results of an analysis by HPLC of solutions formed upon adsorption and desorption of BSA from the CCM surface. The absence of even trace amounts of chitosan in the liquid phase indicates that chitosan is firmly fixed to the fiber surface. In addition, the absence in chromatograms of additional peaks corresponding to appearance of albumin decomposition products suggests that protein molecules do not undergo any destructive changes when in contact with the modified surface.

CONCLUSIONS

(1) It was shown that modification conditions affect the process of charging of chitosan–carbon electrodes. The modified fabric produced in chitosan deposition onto an electrically conducting matrix in the range of cathodic potentials is a promising electrode material and can be successfully used in an electrosorption process.

(2) The adsorption of bovine serum albumin was studied and it was demonstrated that the fiber modification conditions affect both the absorption capacity of the chitosan–carbon sorbent and the removal of albumin from the fiber surface.

ACKNOWLEDGMENTS

The study was supported by a grant from the Far-Eastern Division of the Russian Academy of Sciences (no. 06-1-P8-013).

REFERENCES

1. Shi Hang, *Electrochim. Acta*, 1996, vol. 41, no. 10, pp. 1633–1639.
2. Ermolenko, I.N., Lyubliner, I.P., and Gul'ko, N.V., *Elementosoderzhashchie ugol'nye voloknistye materialy* (Element-containing Fibrous Carbon Materials), Minsk: Nauka i Tekhnika, 1982.
3. Zemskova, L.A., Sheveleva, I.V., and Glushchenko, V.Yu., *Khim. Tekhnol.*, 2004, no. 7, pp. 6–11.
4. Varentsov, V.K., *Intensifikatsii elektrokhimicheskikh protsessov* (Intensification of Electrochemical Processes), Moscow: Nauka, 1988, pp. 94–118.
5. Zemskova, L.A. and Sheveleva, I.V., *Ros. Khim. Zh.*, 2004, vol. 48, no. 5, pp. 53–57.
6. Cruz, J. and Kawasaki, V., *J. Electroanal. Chem.*, 2000, vol. 72, pp. 680–686.
7. *Khitin i khitozan: poluchenie, svoistva i primenenie* (Chitin and Chitosan: Production, Properties, and Use), Skryabin, K.G., Vikhoreva, G.A., and Varlamov, V.P., Eds., Moscow: Nauka, 2002.
8. Samonin, V.V., Amelina, I.Yu., Vedernikov, Yu.N., and Dail'nitsyn, V.A., *Zh. Fiz. Khim.*, 1999, vol. 73, no. 5, pp. 880–883.
9. Gubin, S.P., Yurkov, G.Yu., and Kataeva, N.A., *Neorg. Mater.*, 2005, vol. 41, no. 10, pp. 1159–1175.
10. RF Patent 2281160.
11. Ksenzhek, O.S., Shembel', E.M., Kalinovskii, Yu.A., and Shustov, V.A., *Elektrokhimicheskie protsessy v sistemakh s poristymi matritsami* (Electrochemical Processes in Systems with Composite Matrices), Kiev: Vishcha Shkola, 1983.
12. Calas-Blanchard, C., Comtat, M., Marty, J.-L., and Mauran, S., *Carbon*, 2003, vol. 41, pp. 123–130.
13. Conway, B.E., Niu, J., and Pell, G., *Kem. Ind.*, 2005, vol. 54, no. 4, pp. 187–198.
14. Kinoshita, K., *Carbon: Electrochemical and Physicochemical Properties*, New York: Wiley, 1988.
15. Wang, C.-C. and Hu, C.-C., *Carbon*, 2005, vol. 43, pp. 1926–1935.
16. Posey, F.A. and Morozumi, T., *J. Electrochem. Soc.*, 1966, vol. 113, pp. 176–184.
17. Tarasevich, M.R., *Elektrokhimiya uglerodnykh materialov* (Electrochemistry of Carbon Materials), Moscow: Nauka, 1984.
18. Artem'yanov, A.P. and Sheveleva, I.V., *Zh. Prikl. Khim.*, 2004, vol. 77, no. 11, pp. 1811–1814.
19. Koresh, J. and Soffer, A., *J. Electroanal. Chem.*, 1983, vol. 147, pp. 223–237.
20. Oren, Y. and Soffer, A., *J. Electroanal. Chem.*, 1985, vol. 186, pp. 63–77.
21. Bondareva, G.V., Gul'ko, N.V., and Kitikova, N.V., *Zh. Prikl. Khim.*, 1984, vol. 70, no. 3, pp. 415–419.
22. Sheveleva, I.V., Zemskova, L.A., and Golikov, A.P., *Khim. Tekhnol. Vody*, 2005, vol. 27, no. 3, pp. 227–236.

ISSN 1070-4272, Russian Journal of Applied Chemistry, 2007, Vol. 80, No. 6, pp. 930–933. © Pleiades Publishing, Ltd., 2007.
Original Russian Text © S.A. Chulovskaya, V.I. Parfenyuk, 2007, published in Zhurnal Prikladnoi Khimii, 2007, Vol. 80, No. 6, pp. 952–955.

APPLIED ELECTROCHEMISTRY AND CORROSION PROTECTION OF METALS

Effect of Isopropyl Alcohol on Cathodic Deposition of Ultradispersed Copper-containing Powders from Electrolyte Solutions

S. A. Chulovskaya and V. I. Parfenyuk

Institute of Solution Chemistry, Russian Academy of Sciences, Ivanovo, Russia

Ivanovo State University of Chemical Engineering, Ivanovo, Russia

Received October 16, 2006; in final form, March 2007

Abstract—The possibility of cathodic deposition of copper-containing powders of nanosize dispersity from solutions of copper dichloride in a mixed water–isopropanol solvent was studied.

DOI: 10.1134/S1070427207060158

By now, a large number of techniques for production of nanomaterials with prescribed size, shape, and other particle parameters have been developed [1–3]. All methods for synthesis of highly dispersed materials, including ultradispersed powders of metals and metal-containing compounds, can be conditionally subdivided into those of mechanical and condensation types [4, 5]. The former involve comminution of starting raw materials without, as a rule, changes in their chemical composition. In processes of the latter type, both the aggregative state and chemical composition of the starting components change.

Powders of copper and copper oxides are of particular interest for chemical technology and industry. Ultradispersed copper-containing powders can be used as additives to metal-ceramic sealants and to lubricants for various friction units [6].

A promising area of modern technologies is electrochemical cathodic deposition of metal-containing nanosize powders from electrolyte solutions [7–9]. In this technique, a metal and its compounds pass from the dissolved state into a solid state in the form of loose deposits. To important advantages of this method belong the simplicity of the apparatus used and the possibility of controlling the process by changing the electrical modes.

The formation of a cathodic deposit in electrolysis is governed by the occurrence and competition of two parallel processes: nucleation and dynamics of nucleus growth. If the number of nucleation centers formed exceeds that of developing centers, the resulting deposit is finely dispersed. Therefore, an important factor governing the mechanism and kinetics of these reactions is the required balance of the rates of these processes. A high dispersity of electrodeposited particles can be achieved in the presence of surfactants. The effect of surfactants introduced into an electrolyte is primarily manifested in a redistribution of the rates of formation and growth of a new phase via blocking of active centers and change in surface energies at interfaces. Performing an electrochemical synthesis at the limiting current density makes it possible to recover metal-containing products from electrolyte solutions directly as highly dispersed powder.

This study is concerned with the effect of organic additives to an electrolyte on the dispersity of copper-containing powders produced by electrochemical cathodic reduction from copper dichloride solutions with a concentration of 0.1 mol kg^{-1} solvent (m) in mixed water–isopropanol solutions of various compositions.

EXPERIMENTAL

The electrochemical deposition of copper-containing powders was performed in a glass cell. A steel rod served as a cathode. As anodes were used ruthenium-titanium oxide plates. Current was switched on several seconds after the electrodes were submerged in the electrolyte. During this time, a thin homogeneous layer of contact copper was formed, in which the ripening of active centers and the subsequent growth of ultradispersed cathodic deposits were considerably

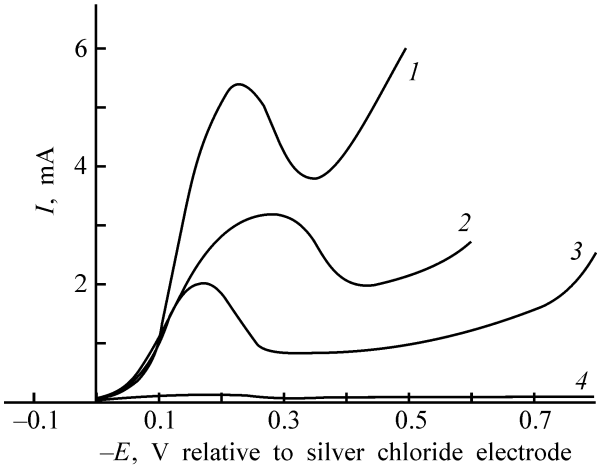

Fig. 1. Cathodic polarization curves of copper deposition from water–isopropanol solutions with varied content of copper dichloride. Content of i-C_3H_7OH 0.04 mole fractions. (*1*) Current and (*E*) potential; the same for Fig. 2. Copper dichloride concentration (mol kg^{-1}): (*1*) 0.4, (*2*) 0.2, (*3*) 0.1, and (*4*) 0.01.

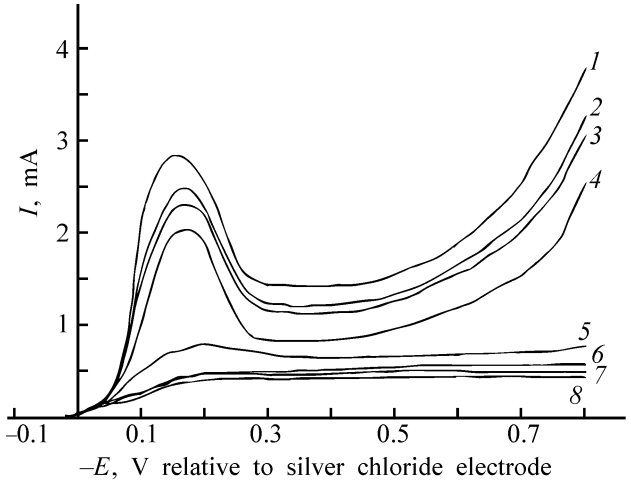

Fig. 2. Cathodic polarization curves of copper deposition from 0.1 m copper dichloride solutions with varied content i-C_3H_7OH. Content of i-C_3H_7OH (mole fraction): (*1*) 0.00, (*2*) 0.01, (*3*) 0.03, (*4*) 0.04, (*5*) 0.08, (*6*) 0.12, (*7*) 0.23, and (*8*) 0.5.

faster than those in the case of direct deposition onto a steel rod.

The electrocrystallization of copper was performed from solutions without forced agitation and removal of dissolved oxygen. A minor amount of hydrogen evolving in the accompanying process provided natural agitation of the solution in the near-cathode space and favored loosening of the growing deposit. A criterion for termination of the process was vigorous hydrogen evolution, and, therefore, the duration of deposition varied between the experiments. The evolving hydrogen had no effect on the quality of the forming deposit and did not enter into its composition. The electrolytic deposit was formed on the cathode as a sponge at T = 25°C. The deposit formed upon completion of the electrolysis was three times washed with twice-distilled water and then with isopropyl alcohol and dried to a powdered state. The electrolyte was prepared from reagents of chemically pure grade. Isopropyl alcohol i-C_3H_7OH (0.00–0.80 mole fraction) served as an organic component.

To determine the working concentration ranges of copper dichloride and the initial current density corresponding to the limiting mode of diffusion mass transfer, polarization studies were carried out in the potentiodynamic mode with a PI-50-1 potentiostat with a PR-8 programming unit. The potential sweep rate was 5 mV s^{-1}. The working electrode had the form of a cylindrical copper disc embedded in fluoroplastic. A platinum electrode served as auxiliary electrode, and a saturated silver chloride electrode, as reference. The cathodic polarization curves were measured in the model solutions under study. Because of the increase in the cathode surface area in the course of electrolysis, the polarization curves are plotted with currents, rather than current densities.

It can be seen from Fig. 1 that the optimal concentration of copper dichloride for electrochemical synthesis of ultradispersed powders is 0.1 mol kg^{-1}. Carrying out the electrolysis at higher salt concentrations is difficult in view of the instability of the electrolysis mode, because the range of formation of finely dispersed deposits is very narrows. In 0.1 m copper dichloride solutions, the range of potentials in which the rate of ion delivery into the near-cathode space lags behind the rate of their discharge (and just this is one of the main reasons why finely dispersed copper-containing deposits are formed) is sufficient for the formation of crystallization centers and their subsequent growth. At lower salt concentrations, electrochemical deposition is inadvisable for several reasons: low deposition rate, low yield of the product, and increase in the size of particles contained in the cathodic deposits obtained.

Figure 2 shows the results of polarization studies in 0.1 m aqueous-organic solutions of copper dichloride with various concentrations of isopropyl alcohol. The polarization curves have the classical shape characteristic of multistage processes occurring under the diffusion control. This is manifested in the appearance of plateaus corresponding to limiting currents. A steep rise in current, which follows these plateaus

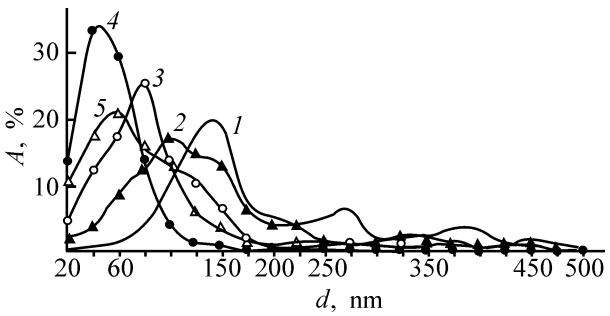

Fig. 3. Size distribution of copper-containing particles obtained in solutions with varied content of i-C_3H_7OH. (*A*) Fraction of particles and (*d*) particle diameter. i-C_3H_7OH content (mole fraction): (*1*) 0.00, (*2*) 0.01, (*3*) 0.03, (*4*) 0.04, and (*5*) 0.08.

in the polarization curves, is due to vigorous evolution of hydrogen.

Analysis of the results of the polarization studies suggests that carrying out electrolysis at isopropanol concentrations exceeding 0.12 mole fraction is inadvisable because of the pronounced coarsening of particles. The peaks observed in the polarization curves are due to formation of difficultly soluble chlorine-containing compounds of copper(I) [10]. As the concentration of the organic component increases, the cathodic polarization curves shift to more electronegative values and the peak heights and cathode currents decrease, which can be attributed to an increase in the viscosity of the aqueous-alcoholic electrolyte [11] and to the resulting decrease in the diffusion coefficients of copper ions.

Size distribution of ultradispersed particles at varied content of isopropyl alcohol

Particle size, nm	Fraction of particles, %, at indicated content of i-C_3H_7OH, mole fraction				
	0.00	0.01	0.03	0.04	0.08
20–39	0.35	2.00	4.60	13.75	10.30
40–59	0.94	3.83	12.37	33.47	17.52
60–79	1.17	8.95	17.54	29.43	20.91
80–99	3.98	12.46	25.23	13.75	15.50
100–124	10.19	17.17	13.52	4.04	13.06
125–149	17.80	14.70	10.93	1.46	5.94
150–174	19.20	13.10	6.47	0.96	3.50
175–199	7.73	6.55	2.16	0.12	1.59
200–224	5.27	4.23	0.72	0.39	0.74
225–249	4.22	3.83	0.43	0.58	1.70
250–274	5.27	1.28	1.29	0.31	1.59
275–299	6.32	1.04	1.44	0.15	1.27
300–324	2.11	1.68	0.78	0.39	0.53
325–349	2.46	2.54	0.86	0.24	0.42
350–374	2.22	2.00	0.43	0.19	0.55
375–399	3.63	1.28	0.14	0.31	1.70
400–424	3.39	0.40	0.29	0.08	0.85
425–449	1.29	1.12	0.36	0.19	1.06
450–474	1.76	1.20	0.22	0.15	0.74
475–500	0.70	0.64	0.22	0.04	0.53
Total	100	100	100	100	100

The data previously obtained in measurements of the surface potentials of organic and aqueous-organic solvents of various classes [12–14] (on reaching a certain concentration of the nonaqueous component in an aqueous-organic mixture, the surface potential changes its sign on passing from water to nonaqueous solvents) suggest that the diffusion layer in the near-electrode space is virtually completely composed of alcohol molecules after an isopropanol content of 0.12 mole fraction is reached. This leads to a decrease in the dielectric constant and the electrical conductivity of this part of the solution, and, as a consequence, in the cathodic currents.

The particle size of the deposited powders was found from micrographs obtained with an EMV-100 L transmission electron microscope in the high-resolution mode at an accelerating voltage of 75 kV [15]. Electron-microscopic measurements were performed for several preparations of each of the samples, immediately after they were made up. For each preparation, several micrographs of its various microscopic areas were taken, which provided a statistical sample sufficient for reliable construction of histograms characterizing the dispersion composition of the powders. Data on the size distribution of electrolytically deposited nanosize copper-containing powders in relation to the composition of the nonaqueous solvent are listed in the table. The distribution curves plotted using these data (Fig. 3) confirm the conclusion that isopropanol additives affect the powder particle size. The maximum amount of 20–100-nm powder particles was obtained at an isopropanol content of 0.04 mole fraction. The maximum lies at around 50 nm. The amount of coarser particles is small and equal to about 10–15% of the total.

CONCLUSIONS

(1) The study performed demonstrated that nanosize copper-containing powders can be produced by electrochemical reduction from aqueous-organic electrolyte solutions.

(2) It was found that the electrochemical crystallization of copper-containing deposits from copper dichloride solutions in water–isopropanol mixtures is strongly affected by the composition of the aqueous-organic solvent.

(3) It was shown that addition of low-molecular-weight surfactants to aqueous electrolyte solutions lead to a decrease in the limiting cathodic currents, which favors formation of finely dispersed deposits and ultradispersed powders.

(4) It was demonstrated that use of organic solvents as additives to water opens up promising opportunities for optimization of the size characteristics of metal-containing powders obtained from electrolyte solutions by cathodic reduction.

REFERENCES

1. Gubin, S.P., Koksharov, Yu.A., Khomutov, G.B., and Yurkov, G.Yu., *Usp. Khim.*, 2005, vol. 74, no. 6, pp. 539–574.
2. Sergeev, G.B., *Nanokhimiya* (Nanochemistry), Moscow: Mosk. Gos. Univ., 2003.
3. Pomogailo, A.D., Rozenberg, A.S., and Uflyand, I.E., *Nanochastitsy metallov v polimerakh* (Metal Nanoparticles in Polymers), Moscow: Khimiya, 2000.
4. Rusanov, A.I., *Zh. Obshch. Khim.*, 2002, vol. 72, no. 4, pp. 532–549.
5. Mikubaeva, E.V., Kobotaeva, N.S., and Sirotkina, E.E., *Zh. Prikl. Khim.*, 2004, vol. 77, no. 12, pp. 1937–1941.
6. Mel'nikov, V.G., *Zashch. Met.*, 2005, vol. 41, no. 2, pp. 168–181.
7. Zagorovskii, G.M., Prikhod'ko, G.P., Ochenko, V.M., and Sidorenko, I.G., *Zh. Prikl. Khim.*, 2001, vol. 74, no. 3, pp. 416–418.
8. Chulovskaya, S.A., Balmasov, A.V., Lilin, S.A., and Parfenyuk, V.I., *Zashch. Met.*, 2006, vol. 42, no. 4, pp. 430–433.
9. Murashova, I.B., Taushkanov, P.V., and Burkhanova, N.G., *Elektrokhimiya*, 1999, vol. 35, no. 7, pp. 835–840.
10. *Spravochnik khimika* (Chemist's Handbook), Nikol'skii, B.P., Ed., Leningrad: Khimiya, 1971, vol. 2.
11. Afanas'ev, V.N., Efremova, L.S., and Volkova, T.V., *Fizikokhimicheskie svoistva binarnykh rastvoritelei: Vodosoderzhashchie sistemy* (Physicochemical Properties of Binary Solvents: Water-containing Systems), Ivanovo, 1988, part 2.
12. Parfenyuk, V.I., *Colloid J.*, 2002, vol. 64, no. 5, pp. 588–596.
13. Chankina, T.I. and Parfenyuk, V.I., Russ. *J. Phys. Chem.*, 2004, vol. 78, no. 9, pp. 1396–1399.
14. Chankina, T.I., Chulovskaya, S.A., and Parfenyuk, V.I., *Russ. J. Phys. Chem.*, 2004, vol. 78, no. 6, pp. 856–859.
15. Chulovskaya, S.A., Parfenyuk, V.I., Lilin, S.A., and Girichev, G.V., *Izv. Vyssh. Uchebn. Zaved., Khim. Khim. Tekhnol.*, 2006, vol. 49, no. 1, pp. 35–39.

ISSN 1070-4272, Russian Journal of Applied Chemistry, 2007, Vol. 80, No. 6, pp. 934–940. © Pleiades Publishing, Ltd., 2007.
Original Russian Text © K. K. Kalnin'sh, 2007, published in Zhurnal Prikladnoi Khimii, 2007, Vol. 80, No. 6, pp. 956–962.

CATALYSIS

Electron and Proton Transfer in Acid–Base Catalysis

K. K. Kalnin'sh

Institute of Macromolecular Compounds, Russian Academy of Sciences, St. Petersburg, Russia

Received April, 12 2007

Abstract—The role of electron and proton transfer in acid–base catalysis is discussed, with two reactions as examples, in one of which (polymerization of cyclobutenes) an acid, and in another (nitramide decomposition), a base acts as the catalyst.

DOI: 10.1134/S107042720706016X

The conventional theory of acid–base catalysis regards proton transfer as the basic elementary process [1]. These views originate early papers by Brønsted and Pedersen [2, 3], who established the catalytic law in the simple form

$$k_A = G_A K_a^{\alpha} \quad (1a)$$

for an acid and

$$k_B = G_B (1/K_a^{\beta}) \quad (1b)$$

for a base. Here k_A, k_B are the reaction rate constants; K_a, acid dissociation constant; G_A and G_B, constants; and indices A and α refer to the acid, and B and β, to the base.

Equations (1a) and (1b) are usually represented in the linear logarithmic form:

$$\log k_A = -\alpha \, pK_a + \text{const}, \quad (2a)$$

$$\log k_B = \beta \, pK_a + \text{const}. \quad (2b)$$

Linear dependences (2a) and (2b) have been obtained for a number of systems and many acids and bases, but they are not universal. Bell [4, 5] advanced (apparently for the first time) a concept stating that the acid–base catalysis is based on proton transfer. It is believed that the cleavage of a covalent bond is much easier when one of the reacting molecules is protonated [1]. The general acid–base catalysis theory was also applied to enzymatic catalysis, whose extremely high efficiency is attributed to high concentrations of acids and bases in the enzymatic active site and proper orientation of the reacting groups [1].

We have suggested a totally different approach to the mechanism of acid–base catalysis [6–11] and demonstrated that, like any other chemical reaction, a catalytic reaction is based on by electron transfer (excitation), and proton transfer (or hydrogen bonding) facilitates, catalyzes, this process. We believe that proton transfer itself does not cause a structural rearrangement of the molecule, and a chemical bond is actually cleaved only via subsequent electron transfer, yielding chemically active radical species. The proton transfer, combined with transfer of electron in an electronically excited state, underlies the fundamental electron–proton effect [12]. The latter consists in a decrease in the lifetime and a huge decrease in the energy of the electronically excited states of the molecular complexes (associates) down to thermal energies, due to interrelated transfers of the electron and proton.

This paper discusses the mechanism of acid–base catalysis with two reactions as examples, using data of nonempirical quantum-chemical calculation. For the calculation technique, see [13, 14].

Electron-donor–acceptor and proton-donor–acceptor interactions in the reaction complex. Among the elementary stages of acid–base catalysis, electron transfer (excitation) is of special importance, as it immediately precedes the chemical transformation of the molecules. The probability of thermal transfer of an electron depends on the state of the proton-donor–acceptor (PDA) interactions between the molecules of the reactants, and the latter, in turn, are directly exposed to the third species, a catalyst. This requires a combined analysis of the electron-donor–acceptor (EDA) and PDA properties of the molecules of the reactants in the presence of an acid or base catalyst.

There are two important factors governing the catalytic effect of acids and bases in reactions in which the reactants are not identical: one acts as electron donor, and the other, as electron acceptor.

(1) An acid (generally, a proton donor) activates one of the reactants acting as an electron acceptor in such a manner that its electron affinity increases.

(2) A base (generally, a proton acceptor), by contrast, activates the electron donor via hydrogen bonding or deprotonation, thereby making lower its ionization potential.

These effects, taken separately (acid or base catalysis) or in combination (bifunctional catalysis), enhance the EDA power of the molecules of the reactants, thereby lowering (in terms of the approach taken here) the energy of the excited level of the reaction complex and the energy barrier of the reaction. The strength of the interaction of the acid or base with the reactant widely varies from weak hydrogen bond, which can be discussed in terms of the continuum approach, to complete proton transfer: proton addition to (protonation), or detachment from (deprotonation) the reactant molecule. Only the latter case, protonation/deprotonation of reactants, is typically regarded as catalysis, whereas weak interactions are qualified as the influence of the environment. The acid–base catalysis theory being developed considers all these cases from a common standpoint: In all of them the PDA interactions are responsible for the lowering of the energy of the excited level of the reaction complex.

The proton transfer in the DH + Y system, where Y is a proton acceptor, takes place only in the limiting case of strong interactions; a more common case is hydrogen bonding D–H…Y. Importantly, the H bond is stronger and the probability of the proton transfer in the excited state of the complex, much higher, compared to the ground state because of an increase in the acidity of the OH groups in the radical-cation state yielded by the electron transfer. The energy of stabilization of the excited levels via hydrogen bonding is very significant and, according to our data, can exceed 1.5 eV. In the case when proton transfer precedes electron transfer, and, hence, occurs in the ground state, the role of the base catalyst consists in lowering the ionization potential of the reagent, down to 1–3 eV in the case of complete deprotonation of DH.

In base catalysis, the catalyst Y activates the electron and proton donor DH via deprotonation [Eq. (3a)] of DH or hydrogen bonding [Eq. (3b)]

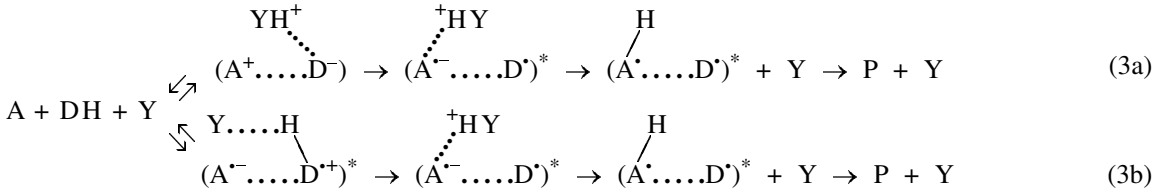

(3a)

(3b)

The resulting enhancement of the electron-donating power of DH makes higher the electron transfer probability. Of key importance in the given context is the formation of excited levels with low energies (<1 eV), as specifically these levels can be thermally populated under ordinary conditions.

In acid catalysis [Eq. (4)], an acid HX that acts as a catalyst (a strong proton donor) interacts with both the electron acceptor A and the electron donor DH. The latter interaction is energetically more favorable, but yields hydrogen-bonded X–H…..DH or protonated $DH_2^+X^-$ species, which are not involved in the reaction, because of the weakening of the electron-donating power in the reaction of DH with acid HX. In acid catalysis, the basic initiating event is the activation of the acceptor A:

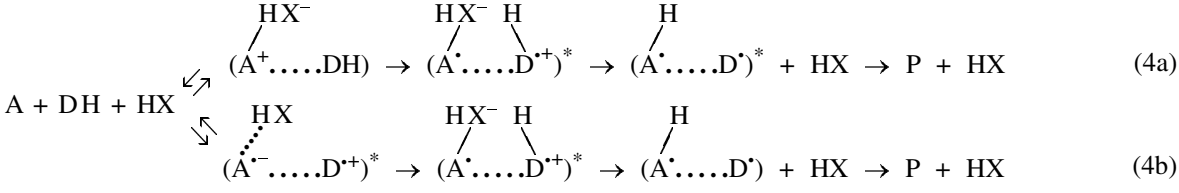

(4a)

(4b)

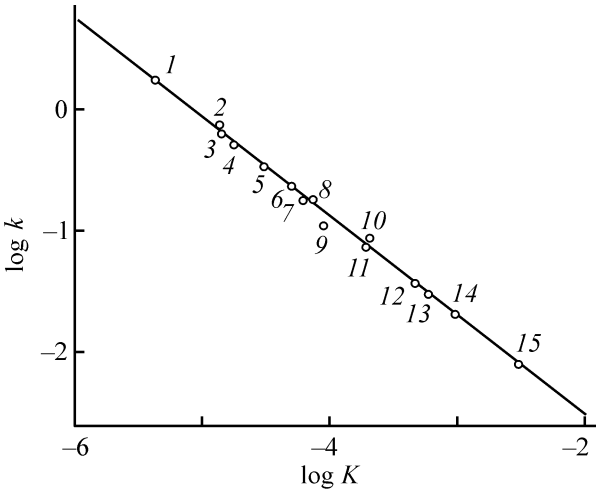

Fig. 1. Brønsted plots for the catalytic reaction of nitramide decomposition [2]: (*1*) succinate II, (*2*) malate II, (*3*) propionate, (*4*) acetate, (*5*) succinate I, (*6*) phenyl acetate, (*7*) benzoate, (*8*) tartrate II, (*9*) oxalate II, (*10*) formate, (*11*) malate I, (*12*) tartrate I, (*13*) phthalate I, (*14*) salicylate, and (*15*) phosphate I.

Formation of the A.....HX hydrogen bond and protonation of the electron acceptor AH^+X^- raise its electron affinity, thereby lowering the energy of the excited level of the reaction complex. According to Kampar [15], the electron affinity E_A of organic cations is 5–7 eV, which is responsible for the low charge-transfer energies. In real systems, the counterion makes lower the electron affinity of the cations, which is to be taken into account in theoretical analysis.

Base catalysis of the nitramide decomposition. The key role of proton transfer in acid–base catalysis is typically confirmed by the reaction of nitramide (NA) decomposition into water and dinitrogen oxide molecules, proceeding in water in the presence of bases:

$$H_2N–NO_2 \rightleftarrows H_2O + N_2O. \quad (5)$$

For this reaction, the logarithm of the rate constant $\log k_r$, shows a linear correlation with the logarithm of the constant of the base added, pK_a (Fig. 1), which is consistent with Eq. (2a). A good linear correlation is observed over three units of pK_a and two decimal orders of the rate constants. The straight line has a slope $\beta = 0.66$. Similar Brønsted dependences were obtained for many other reactions and a much greater number of experimental points than in Fig. 1. At first glance, these data suggest that the chemical catalytic process is controlled by proton transfer, which is easily recorded experimentally and can be described quantitatively.

Presumably, a proton is transferred in the first stage of nitramide decomposition catalyzed by base B from nitramide to the base molecule:

$$H_2N–NO_2 + B \rightleftarrows HN–NO_2^- + BH^+,$$

and the proton transfer is a rate-limiting stage. It is believed that the nitramide anions $HN–NO_2^-$ formed in an aqueous solution have enhanced reactivities and decompose into dinitrogen oxide N_2O and hydroxide ion OH^-, which is easily converted into a water molecule: $OH^- + BH^+ \rightarrow H_2O + B$. The decomposition rate for deprotonated HA molecules is unambiguously determined by the strength of the base, i.e., by pK_a, which is responsible for observed the linear dependence $\log k_r \sim pK_a$.

The above concept does not specially consider the mechanism of decomposition of the deprotonated nitramide molecule. Without discussing the mechanism, it is taken for granted that the nitramide anions, or anions of any other substance, yielded by the reaction with a base, are unstable and acquire a new quality, which is responsible for their decomposition or chemical transformations in subsequent reactions.

A new approach to the mechanism of catalysis, suggested in this paper, implies that, in the specific case of reaction (5), an enhanced chemical activity is exhibited by complexes of the nitramide anions with the initial HA molecules, rather than by nitramide anions proper. In the ground electronic state in solutions, such EDA complexes are in dynamic equilibrium with the reactants and do not exhibit any chemical activity:

$$H_2N–NO_2 + HN–NO_2^- \overset{K_{eq}}{\rightleftarrows} (H_2N–NO_2...HN–NO_2^-). \quad (6)$$

By contrast, excited states of the EDA complex, and above all the lowest singlet S_1 and the lowest triplet T_1 states, are highly reactive. This is due to a specific feature of the excited states of the complexes: These states result from intermolecular electron transfer, which occurs between the anion and the neutral HA molecule in our case. Similar states generate radical (radical ion) species involved in chemical transformations following the nitramide deprotonation events.

We can state that decomposition of an isolated deprotonated nitramide molecule in the ground state is unlikely. This follows from the available data on the nature of the molecular bonding and dissociation curves demonstrating that passing to the dissociation

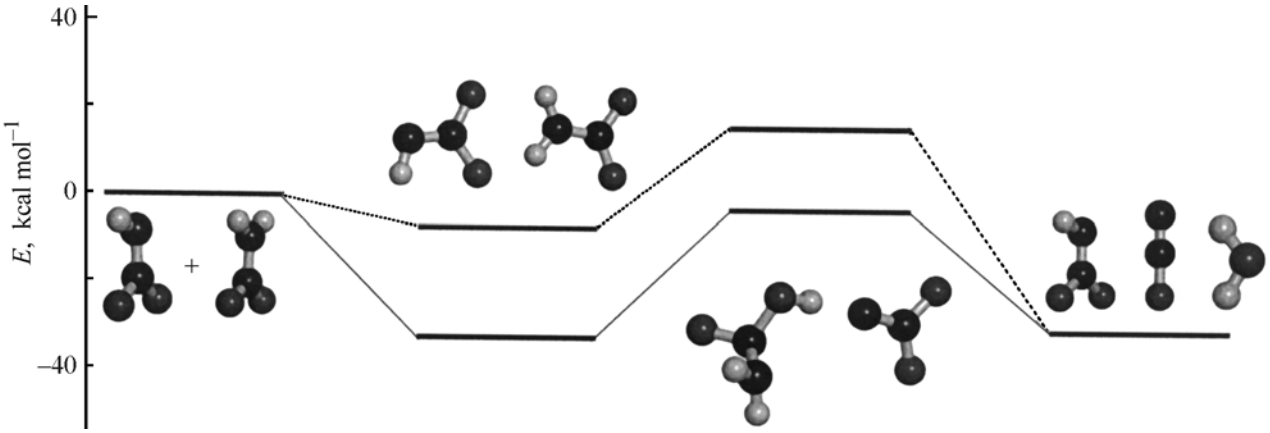

Fig. 2. Energy diagram for *E* of the catalytic reaction of nitramide decomposition, calculated by RHF, ROHF, and MCSCF/DH methods. (*Dashed lines*) Calculation in the PCM approximation for an aqueous medium; insets demonstrate the optimized structures of the molecules and complexes.

potential curve leading to cleavage of the chemical bond can result only from excitation of the molecule. Such an excitation cannot be achieved in thermal experiments because of the high energies of the electronic states (>3 eV). However, it can be observed in a system of two reacting nitramide molecules, one of which turns into a strong electron donor upon deprotonation making it negatively charged, and the other acts as electron acceptor. Intermolecular electronic levels are located much below the intramolecular levels, and specifically in this system of short-lived excited low-lying states, yielded by collision events, thermal reactions can proceed.

The initial nitramide is not a strong electron acceptor: ROHF/6-31G* calculations gave 1.03 eV for its electron affinity (PM3/GAMESS calculations, 0.85 eV). However, in a complex with deprotonated molecule ($HA\ldots HA^-$), electron transfer can take place and an $(N_2O_2H_2^{\cdot -}\ldots N_2O_2H^{\cdot})^*$ radical-ion pair can be formed. In an excited state of the complex, electron transfer transforms the nitramide molecule to the $N_2O_2H_2^{\cdot -}$ radical anion, and the deprotonated molecule, to the $N_2O_2H^{\cdot}$ neutral radical.

In this context, however, of principal importance is the probability of thermal population of the excited state of the complex, which depends on the energy of the state. If these levels are located significantly above 1 eV, their population at room temperature is insignificant. This is responsible for the insignificant rate of the thermal transfer of an electron. Therefore, the excitation energy should be correctly estimated.

Figure 2 shows the energy diagram of the nitramide decomposition reaction, obtained by nonempirical calculations by RHF, ROHF, and MCSCF/DH methods, which adequately describe the structure and properties of excited states of reaction complexes. Calculations were performed for vacuum conditions and in the PCM approximation for a water medium. For convenience of comparison, the energy levels of the reactants for these two cases are superposed. It is seen that the excitation (electron transfer) energy is negative relative to that of the free molecules in a vacuum, –2.45 kcal mol^{-1}, and takes a small positive value of +16.7 kcal mol^{-1} in an aqueous medium. Thus, spontaneous electron transfer in a vacuum is possible. In water, this requires a certain thermal activation, but, because of the low energy, the corresponding T_1 excited level can be populated under ordinary conditions. The heats of reaction (5), calculated from the difference of the total energies of the end reaction products (H_2O and N_2O) and the reactant, nitramide, are identical for these two cases and take a large negative value of –30 kcal mol^{-1}. Hence, nitramide decomposition is thermodynamically favorable.

There can be different arrangements of the molecules in the excited complex $(N_2O_2H_3^{\cdot}\ldots N_2O_2^{\cdot -})^*$, differing in the energy and spin density distribution. The lowest excitation energy of –2.45 kcal mol^{-1} is characteristic of the complex shown in Fig. 2, in which both molecules are linked by a strong hydrogen bond N...H–O ($R_{N\ldots H}$ = 1.82 Å). Along with electron transfer in the excited state of the complex, quantum-chemical optimization implies a proton transfer from the $N_2O_2H^{\cdot}$ radical to the $N_2O_2H_2^{\cdot -}$ radical anion. The resulting new structure is a complex of $N_2O_2H_3^{\cdot}$ radical with $N_2O_2^{\cdot -}$ neutral double-deprotonated radical anion. This chemical transformation can be regarded as reduction of nitramide with a similar,

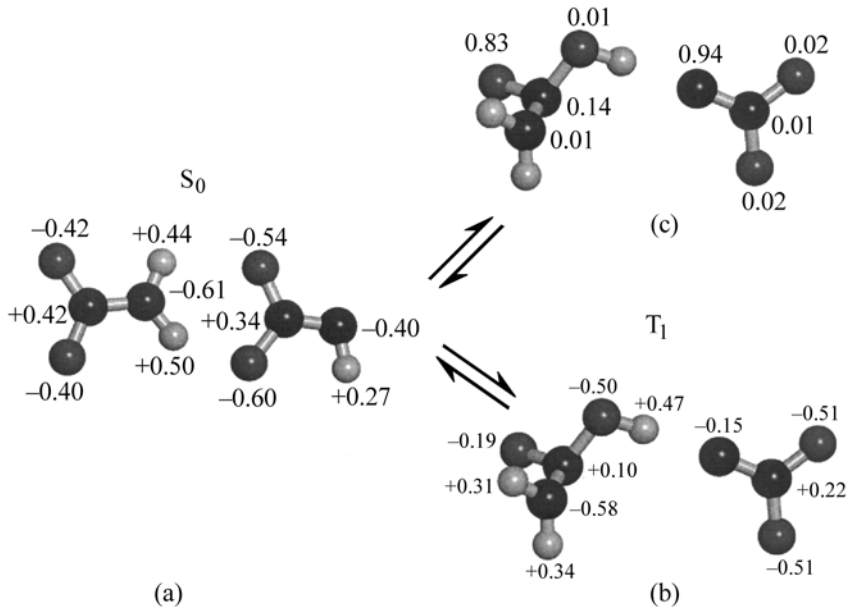

Fig. 3. (a, b) Atomic charges for (a) S_0 ground singlet and (b) T_1 excited triplet state and (c) spin populations for the triplet state.

though deprotonated, molecule, which yields an unstable biradical pair $(N_2O_2H_3^{\cdot}...N_2O_2^{\cdot -})^*$. A probable pathway of its chemical transformations is dissociative decomposition of $N_2O_2H_3^{\cdot}$ radical species, with cleavage of the N–O bond and splitting of a hydroxyl radical, which is further converted to a water molecule.

Of certain interest is analysis of the atomic charge and spin population distributions. Figure 3a shows that, in the ground state of the EDA complex, the electron density is only slightly ($\Delta q = -0.07$) withdrawn from the $N_2O_2H^-$ anion by the nitramide molecule. In the excited state (Fig. 3b), complete electron transfer is accompanied by a proton transfer. As a result, the HA molecule loses two protons and turns into a negatively charged ion $N_2O_2^{\cdot -}$. The spin populations S_p in the triplet state (Fig. 3c) are localized on the oxygen ($S_p = 0.94$) and nitrogen ($S_p = 0.83$) atoms in each of the interacting molecules. These atoms are separated by 4.4 Å and cannot be involved in recombination events to form a chemical bond, but fragmentation of the generated radical species is highly probable.

Our calculations show that, in the above-considered cases, the excited levels of the $(N_2O_2H_3^{\cdot}...N_2O_2^{\cdot -})^*$ complex can be thermally populated under ordinary conditions. The chemical transformations in the excited state of the reaction complex of nitramide are driven by dissociative attachment of the electron, resulting in the fragmentation of the molecule and formation of stable reaction products. Our calculations confirm the original concept stating that base-catalyzed reactions proceed via an electronically excited state of the reaction complex. The excitation energies of such complexes fall within the thermal energy range, which favors their thermal population at room temperature.

Acid catalysis of polymerization of cyclobutenes. The concept of the leading role of proton transfer in acid–base catalysis has been applied in various areas of organic chemistry and, in particular, to cationic polymerization [16]. The conventional theory states that, in reactions initiated by Brønsted (HX) or Friedel–Crafts ($AlCl_3 \cdot HX$) acids, protonation of a monomer molecule enhances its chemical activity and facilitates addition of a new monomer molecule M in the chain propagation event:

$$M \overset{HX}{\rightleftarrows} M\text{–}H^+ \overset{M}{\rightleftarrows} M_2\text{–}H^+, \qquad (7)$$

However, no details concerning the chemical activation are typically provided. A specific feature of polymerization is that an acid promotes formation of a new bond, rather than cleavage of the chemical bond, as is usually indicated for the activating role of protonation of the molecule. In this context, we cannot state that addition of a proton to the molecule weakens the chemical bonds and promotes their cleavage. The cationic polymerization practice suggests that acids activate the propagating polymeric chain in such a manner that a monomer molecule can add to the positively charged chain end.

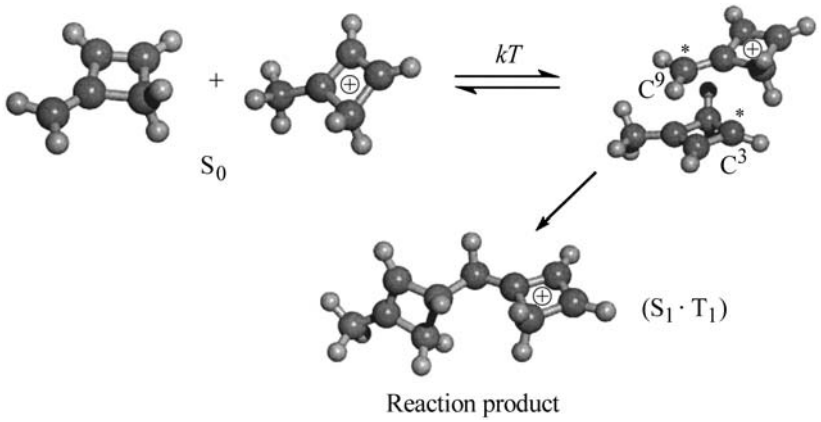

Fig. 4. Molecular scheme of the first stage in addition of methylenecyclobutene to the protonated analog. $(S_1 \cdot T_1)$ Electronically excited complex; asterisks mark atoms with the maximum spin population, involved in chemical bonding.

A contradiction is inherent in traditional views, as evident from a consistent application of the concept of the leading role played by proton transfer in catalysis to various chemical reactions. The concept postulating that proton transfer is the basic elementary chemical process, in fact, reflects only one aspect of the chemical reaction, and simply ignores the other aspect, electron transfer (excitation). The latter is not so prominent in ordinary chemical experiments as proton transfer, due to difficulties in observation of short-lived radical species. However, specifically this stage and the subsequent rearrangement of the electronic structure of the molecules are responsible for the actually observed changes of the chemical structure of the substance.

In this context, the nature of the activating role of an acid should be elucidated so as to more comprehensively disclose the mechanism of acid–base catalysis. An illustrative example of the interrelation between the proton and electron transfer stages can be found in cationic polymerization catalyzed by a Brønsted acid.

Hall and Ykman [17] carried out detailed experiments on cationic polymerization of cyclobutenes and demonstrated that it can be catalyzed by both anionic and cationic agents to form different polymeric products from the same monomers. Previously [18], we have carried out quantum-chemical analysis of the mechanism of polymerization of cyclobutenes. In this study, we consider another aspect of this reaction, modeling of acid catalysis.

As in the conventional theory of acid catalysis, it is believed that the first stage of the reaction consists in addition of proton to the 3-methylenecyclobutene (MCB) molecule at the exocyclic carbon atom of the double bond:

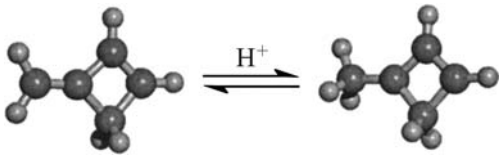

(8)

Methylenecyclobutene exhibits a high proton affinity of 220.7 (RHF, ROHF/6-31G* calculations) or 212.5 kcal mol^{-1} (RHF, ROHF/DH calculations) and a rather low ionization potential of 8.9 eV (PM3/GAMESS semiempirical calculation). The positive charge in the MCB–H^+ cation is distributed primarily over the hydrogen atoms; therefore, MCB–H^+ can be regarded as a positive single-charged bulky species. In the second stage, a collision of a strong electron acceptor MCB–H^+ (E_A = 7.9 eV) with the electron donor MCB results in the formation of an electron-donor–acceptor complex which, at a favorable mutual orientation and sufficient energy, passes into an electronically excited state (Fig. 4). Such collision complexes have a short life, but, within this period, the main elementary process, intermolecular electron transfer with formation of chemically active radical species, takes place.

The energy of the excited state is one of the basic factors: Only at low (<1 eV) energies, the population of excited states can be sufficient for providing the experimentally observed reaction rate. According to an ROHF/DH quantum-chemical calculation for vacuum conditions, the excited triplet state energy of the $^3(MCB^{\cdot+}...MCB–H^{\cdot})^*$ reaction complex is 26.6 kcal mol^{-1} relative to the energy level of the free molecules of the reactants. This is close to the thermal energy boundary and, evidently, if the initial geometry and environmental conditions are adequately accounted for, this energy can be lower (<1 eV), which corresponds to the reaction rates observed.

According to Hall and Ykman [17], the reaction product (Fig. 4) is a polymer containing cyclobutene units linked by methylene bridges. A polymer with such a structure is obtained in the case when a bond is formed between the exocyclic carbon atom C^9 of the double bond in the monomer and the carbon atom C^3 of the ring in the terminal moiety (Fig. 4). However, specifically this line of attack of the propagating polymer end of MCB–H^+ species by a monomer molecule is predicted by calculation of the spin densities (or free valence indices), characterizing the chemical activity of atoms in the excited states of the reaction complex.

The calculated atomic charges additionally confirm the original concept of electron transfer in the reaction. A complete electron transfer ($\Delta q = 0.06$) occurs between the MCB monomer molecule and its protonated analogue MCB–H^+ in an excited state: The monomer molecule is converted to the $MCB^{\cdot+}$ radical cation, and the protonated molecule, to the MCB–$H^{\cdot}$ neutral free radical. A stable product is formed in the final stage after recombination events with the radical centers that can be regarded as independent free radicals with all their inherent properties, of which the main is an extremely high chemical activity. In the product molecule, the positive charge is shifted to the terminal unit (Fig. 4), which acts as an electron acceptor in the subsequent stage of the polymerization reaction, whereupon the sequence of elementary events is repeated.

CONCLUSIONS

(1) Deprotonation of the nitramide molecules under the action of bases sharply raises their electron-donating power and favors electron transfer to the initial nitramide molecules. The energies of the excited levels of the complexes fall within the thermal energy range.

(2) Cationic polymerization of cyclobutenes proceeds via protonation of the monomer molecule and subsequent electronic excitation of the complex formed by the resulting cation and the initial cyclobutene molecule.

REFERENCES

1. Bender, M.L., Bergeron, R.J., and Komiyama, M., *The Bioorganic Chemistry of Enzymatic Catalysis*, New York: Wiley, 1984.
2. Brønsted, J.N. and Pedersen, K., *Z. Phys. Chem.*, 1924, vol. 108, pp. 185–235.
3. Brønsted, J.N., *Chem. Rev.*, 1928, vol. 5, pp. 231–338.
4. Bell, R.P., *Acid–Base Catalysis*, Oxford: Clarendon, 1941.
5. Bell R.P., *The Proton in Chemistry*, Ithaca: Cornell Univ., 1973.
6. Kalnin'sh, K.K., *Elektronnoe vozbuzhdenie v khimii* (Electronic Excitation in Chemistry), St. Petersburg: Sankt-Peterb. Gos. Univ. Tekhnol. Dizaina, 1998.
7. Kalnin'sh, K.K., *Dokl. Akad. Nauk SSSR*, 1988, vol. 299, no. 1, pp. 143–147.
8. Kalnin'sh, K.K., *Teor. Eksp. Khim.*, 1991, no. 6, pp. 710–714.
9. Kalnin'sh, K.K. and Panarin, E.F., *Dokl. Akad. Nauk SSSR*, 1991, vol. 321, no. 4, pp. 756–759.
10. Kalnin'sh, K.K., *Izv. Ross. Akad. Nauk, Ser. Khim.*, 1992, no. 5, pp. 1048–1055.
11. Kalnin'sh, K.K., *Dokl. Akad. Nauk SSSR*, 1987, vol. 293, no. 5, pp. 1066–1068.
12. Kalnin'sh, K.K., *Zh. Prikl. Khim.*, 2005, vol. 78, no. 11, pp. 1761–1779.
13. Kalnin'sh, K.K. and Semenov, S.G., *Zh. Prikl. Khim.*, 2003, vol. 76, no. 10, pp. 1585–1600.
14. Kalnin'sh, K.K. and Panarin, E.F., *Vozbuzhdennye sostoyaniya v khimii polimerov* (Excited States in Polymer Chemistry), St. Petersburg: Sankt-Peterb. Gos. Univ. Tekhnol. Dizaina, 2007.
15. Kampars, V.E., *Izv. Akad. Nauk Latv. SSR, Ser. Khim.*, 1984, pp. 585–601.
16. Kennedi, J. *Kationnaya polimerizatsiya olefinov* (Cationic Polymerization of Olefins), Moscow: Mir, 1978.
17. Hall, H.K., Jr. and Ykman, P., *J. Polym. Sci., Macromol. Rev.*, 1976, vol. 11, pp. 1–44.
18. Kalnin'sh, K.K. and Semenov, S.G., *Zh. Prikl. Khim.*, 2006, vol. 79, no. 9, pp. 1501–1509.

ISSN 1070-4272, Russian Journal of Applied Chemistry, 2007, Vol. 80, No. 6, pp. 941–944. © Pleiades Publishing, Ltd., 2007.
Original Russian Text © I.L. Glazko, Yu.A. Druzhinina, S.V. Levanova, 2007, published in Zhurnal Prikladnoi Khimii, 2007, Vol. 80, No. 6, pp. 963–966.

ORGANIC SYNTHESIS AND INDUSTRIAL ORGANIC CHEMISTRY

Performance and Selectivity of Organic Solvents in Extraction of Caprolactam from Lactam Oil

I. L. Glazko, Yu. A. Druzhinina, and S. V. Levanova

Samara State Technical University, Samara, Russia

Received December 14, 2006; in final form, February, 2007

Abstract—The extraction of lactam from lactam oil with benzene, toluene, cyclohexane, and cyclohexane-benzene and cyclohexane-cyclohexanol mixtures, followed by its backwashing with water, was studied. The distribution ratios of caprolactam and main characteristics of the resulting aqueous lactam (permanganate number, content of volatile bases) were determined.

DOI: 10.1134/S1070427207060171

Caprolactam is one of the most marketable chemicals. Approximately 98% of the world production of caprolactam is consumed for manufacture of a polyamide (Nylon-6) [1].

The characteristics of the polyamide are sensitive to the purity of the initial caprolactam. The presence of even minor impurities negatively affects the polymerization. Therefore, the quality of caprolactam must meet stringent requirements [2–4].

The purification of caprolactam to remove impurities involves extraction, ion-exchange treatment, and distillation. In extractive purification step, caprolactam is recovered with an organic solvent from lactam oil prepared by Beckmann rearrangement of cyclohexanone oxime [5]. In the second step, caprolactam is backwashed with water and the resulting aqueous solution is subjected to ion-exchange treatment. The efficiency of extraction is dependent on the kind of organic solvent used as extractant and its physicochemical characteristics: solubility in the aqueous phase and selectivity with respect to caprolactam.

It is known that organic compounds can be recovered from aqueous solutions with organic solvents of various types: alcohols, ethers, esters, ketones, phosphorus-, nitrogen-, and sulfur-containing organic oxides, nitro- and halo-substituted aromatic hydrocarbons [6].

Data on extraction of caprolactam from aqueous media, available from published papers and patents, are insufficiently comprehensive. As a rule, these studies are restricted to determination of the distribution ratios and do not analyze the selectivity of solvents to caprolactam [7, 8].

In the modern chemical industry, caprolactam is extracted from lactam oil with trichloroethylene (TCE). This extractant is characterized by high distribution ratio of caprolactam, good phase separation, and fire safety. However, TCE has the following significant drawbacks: in the course of regeneration, TCE partially decomposes to give corrosion-active hydrogen chloride; in oxidation and also in prolonged storage without protection from light, TCE is converted to phosgene; and, in combustion of trichloroethylene-containing waste at 700 °C, environmentally hazardous dioxins are formed.

In this study, we tested a series of environmentally acceptable chlorine-free organic solvents to choose extractants that would be suitable for effective recovery of caprolactam from aqueous-organic mixtures and have technical and economic characteristics comparable to, or even exceeding those of TCE. This extractant must meet the following requirements: high distribution ratio of caprolactam, high selectivity for caprolactam (evaluated by the permanganate number PN), low solubility in water, commercial availability, and hazard class not worse than 3–4. Furthermore, to simplify the regeneration, this extractant must be involved into existing industrial cycle of caprolactam production.

EXPERIMENTAL

In this study, we examined the extraction of caprolactam from lactam oil with benzene, toluene, cyclo-

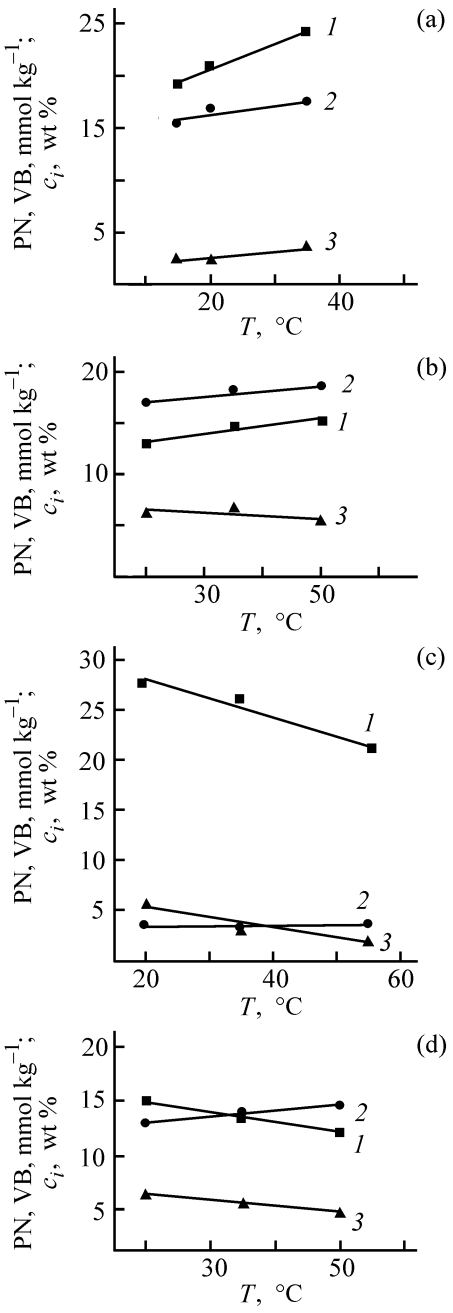

Fig. 1. Influence of the temperature T of caprolactam extraction from lactam oil with (a) trichloroethylene, (b) benzene, (c) cyclohexane, and (d) toluene on the characteristics of the resulting aqueous caprolactam: (*1*) permanganate number PN, (*2*) concentration of caprolactam c_i, and (*3*) concentration of volatile bases VB.

hexene, and also with cyclohexane–benzene and cyclohexane–cyclohexanol mixtures.

The extraction was carried out at a constant weight ratio of organic solvent to lactam oil of 2 : 1. The temperature was varied from 20 to 50°C. The characteristics of lactam oil used in our experiments were as follows: caprolactam content not lower than 70%, PN 153 units, content of volatile bases 149 mmol kg^{-1} caprolactam.

Weighed samples of lactam oil and an immiscible organic solvent were placed in a separating funnel temperature-controlled with an aqueous thermostat. These liquids were vigorously stirred for 30 min and then allowed to settle to complete separation of the extract (solution of caprolactam in organic solvent) from the raffinate (depleted aqueous caprolactam solution). To reach complete recovery of caprolactam from the organic extract, the latter was triply washed with distilled water specially pretreated to remove oxidants (PN no higher than 0.02), with pH from 6.2 to 6.5 [9].

In backwashing caprolactam with water, a portion of the organic solvent inevitably passes to the aqueous phase, and its content in the resulting aqueous solution may reach 3–4%. The presence of an organic solvent in the backwash increases the permanganate number of caprolactam. To remove the organic solvent, the backwash was mixed with an equal volume of distilled water and then the aqueous azeotrope was distilled off under moderate boiling. The residual content of the organic solvent in the purified aqueous phase was monitored on a Kristall-2000 gas chromatograph with an OV-101 capillary column (50 m) equipped with a flame ionization detector. The gas-chromatographic analysis of caprolactam in these solutions was performed at a column temperature of 200°C and vaporizer temperature of 300°C, with helium as carrier gas at a flow rate of 10 ml min^{-1}. In quantitative determination of caprolactam and solvents, the detector was calibrated with respect to substance volume. We found that the residual content of solvents in the resulting aqueous caprolactam did not exceed 0.001 wt %. The content of caprolactam in these solutions was determined refractometrically. The PN and content of volatile bases were found by standard techniques [9, 10].

Figure 1 shows how the main characteristics of the resulting aqueous caprolactam (permanganate number, concentrations of volatile bases, and concentration of caprolactam) depends on the temperature of caprolactam extraction from lactam oil with various organic solvents. It is seen that, with increasing temperature of extraction of caprolactam with cyclohexane and toluene, the PN of aqueous caprolactam containing 3% caprolactam decreases, whereas in extraction of caprolactam with benzene, and especially with trichloroethylene, PN increases. This means that, with increasing temperature of extraction, the selectivity

of caprolactam recovery with benzene and trichloroethylene decreases, whereas the selectivity of caprolactam recovery with cyclohexane and toluene increases. In accordance with the permanganate number, the smallest amounts of oxidizable impurities are present in aqueous backwashes from benzene extracts obtained at 20°C (PN = 12.9 units) and in those from toluene extracts obtained at 50°C (PN = 12 units). These PN values are less by factors of 1.5–2.0 than those of aqueous backwashes from extracts of caprolactam with the other solvents [PN 20–44].

The smallest content of volatile bases in aqueous backwashes (2.3–3.5 mmol kg^{-1}) was found in extraction of caprolactam with trichloroethylene. In extraction with other organic solvents, the content of volatile bases was as follows: benzene 6.2–10.1, toluene 2.7–4.7, cyclohexane 2.3–5.8, cyclohexane–benzene 6.2–6.9, and cyclohexane-cyclohexanol 11.6 mmol kg^{-1}. However, in extraction with trichloroethylene, hydrogen chloride can be liberated. Hydrogen chloride binds volatile amine impurities present in caprolactam [reactions (1) and (2)], which leads to their underestimation.

$$CHCl{=}CCl_2 \rightarrow CCl{\equiv}CCl + HCl, \quad (1)$$

$$RNH_2 + HCl \rightleftarrows [RNH_3]^+Cl^-. \quad (2)$$

The distribution ratio of caprolactam between the organic extract and aqueous raffinate was calculated by the equation

$$K_d = c_e/c_r, \quad (3)$$

where c_e and c_r are the equilibrium concentrations of caprolactam (wt %) in the extract and raffinate, respectively.

Figure 2 shows that the extraction of caprolactam from lactam oil (K_d) with cyclohexane, toluene, trichloroethylene, and benzene only slightly depends on temperature. The highest distribution ratios at 20°C were reached in extraction with trichloroethylene and benzene.

In this study, the binary solvents cyclohexane-cyclohexanol and benzene–cyclohexane were also tested as extractants for caprolactam. These mixed solvents are used in caprolactam production. Straight cyclohexanol cannot be used as extractant because of its high polarity, high boiling point (161°C), and high solubility in water (5.7 g per 100 g of water at 15°C), which causes its large loss with wash waters. This solvent is also difficult to remove from aqueous backwashes.

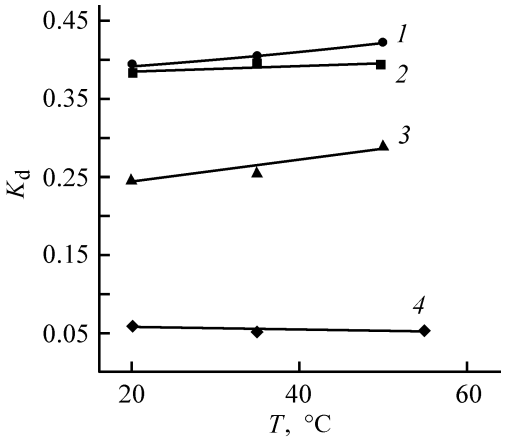

Fig. 2. Effect of temperature T on the extraction (distribution ratio K_d) of caprolactam from lactam oil with (*1*) trichloroethylene, (*2*) benzene, (*3*) toluene, and (*4*) cyclohexane.

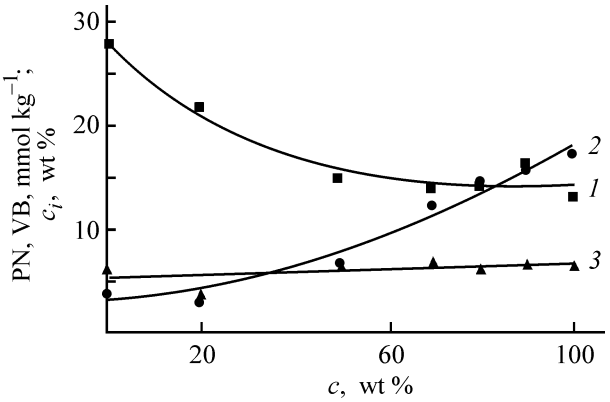

Fig. 3. Effect of benzene concentration c in benzene–cyclohexane mixed solvent on characteristics of final aqueous caprolactam: (*1*) permanganate number PN, (*2*) caprolactam concentration c_i, and (*3*) concentration of volatile bases VB.

The addition of cyclohexanol (10 wt %) to cyclohexane did not improve the recovery of caprolactam. In this case, K_d = 0.13, and the characteristics of aqueous backwash were as follows: PN = 45 units, content of volatile bases 11.6 mmol kg^{-1}, and caprolactam concentration in the resulting aqueous solution 4.43 wt %.

Figure 3 shows the effect of the benzene content of the benzene-cyclohexane extract on the characteristics of the aqueous backwash of caprolactam at 20°C: permanganate index PN, concentration of volatile bases VB (mmol kg^{31}), and caprolactam content c_i (wt %). It is seen that, with increasing benzene content in the mixed extractant, the capolactam content in the final aqueous backwash increases to 17 wt %, the permanganate index decreases to 12.9 units, and the content

Influence of temperature on the distribution ratio of caprolactam in its extraction from lactam oil with various solvents and the main characteristics of the resulting aqueous solutions of caprolactam: permanganate number, concentration of volatile bases, and caprolactam concentration c_i (wt %) (weight ratio of solvent and lactam oil 2 : 1)

Extractant	Temperature of extraction, °C	PN, units	Content of volatile bases, mmol kg^{-1}	Caprolactam content of the extract, wt %	K_d
Trichloroethylene	15	19.0	2.3	15.3	0.39
	20	20.9	2.2	16.3	0.40
	35	24.1	3.5	17.3	0.42
Benzene	20	12.9	6.2	16.9	0.38
	35	14.8	6.8	18.2	0.40
	50	15.2	5.3	18.5	0.39
Cyclohexane	20	27.5	5.9	3.7	0.06
	35	26.2	3.4	3.5	0.05
	55	21.3	2.4	3.6	0.06
Toluene	20	14.7	6.4	12.9	0.25
	35	13.4	5.6	13.9	0.26
	50	12.0	4.7	14.5	0.29
Cyclohexane–benzene, wt %:					
0*	20	27.5	6.2	3.7	0.06
20*	20	21.6	3.7	3.2	0.05
50*	20	14.7	6.9	6.6	0.11
70*	20	13.7	6.7	11.9	0.21
80*	20	14.1	6.0	14.3	0.27
90*	20	16.2	6.5	15.7	0.32
100*	20	12.9	6.2	16.9	0.38
Cyclohexane–cyclohexanol 10*	20	44.9	11.6	4.4	0.07

* Benzene (cyclohexanol) content of the mixture.

of volatile bases remains approximately constant (6.2–6.8 mmol kg^{-1}). The distribution ratio of caprolactam gradually increases with the benzene content of the mixed cyclohexane–benzene extractant (from pure cyclohexane to pure benzene). Taking into account that benzene is more selective extractant for caprolactam, the extraction of caprolactam with cycloxane-benzene mixtures is unsuitable. The experimental data obtained in this study are listed in the table.

CONCLUSIONS

(1) The extraction powers of benzene and trichloroethylene in extraction of caprolactam from lactam oil at 20–30°C are close, but the extraction with neat benzene allows the extraction selectivity to be increased by a factor of 1.5–2 at a close consumption of the extractant. The extraction of caprolactam with toluene is also feasible, but this solvent is less efficient because of the lower distribution ratio.

(2) Substitution of trichloethylene with chlorine-free benzene in industrial extraction of caprolactam from lactam oil allows improvement of the economic and environmental characteristics of the process by excluding formation of dioxin in waste incineration, decreasing corrosion of equipment, and improving the caprolactam quality.

REFERENCES

1. Kim, S., *Khim. Zh.*, 2006, nos. 7–8, pp. 54–56.
2. Karaseva, S.Ya., Krasnykh, E.L., Levanova, S.V., et al., *Ross. Khim. Zh.*, 2006, vol. 50, no. 3, pp. 54–58.
3. *GOST* (State Standard) *7850–86: Caprolactam.*
4. Lupanov, P.A. et al., *Khim. Prom–st.*, 1975, no. 5, pp. 336–338.
5. Ovchinnikov. V.I. and Ruchinskii, V.P., *Proizvodstvo kaprolaktama* (Caprolactam Production), Moscow: Khimiya, 1977.
6. JPN Patent Appl. 62–149 665.
7. Dutch Patent 170 630.
8. Lenden, M.L. van, Kuipers, N.J.H., Haan, A.B. de, and Lerner, O., in *Advances in Chemical Engineering in Nuclear and Process Industries*, 2002, pp. 668–673.
9. *GOST* (State Standard) *26 743.7–86: Caprolactam: Method of Determination of the Permanganate Number.*
10. *GOST* (State Standard) *26 743.8–86: Caprolactam: Method of Determination of Volatile Bases.*

ISSN 1070-4272, Russian Journal of Applied Chemistry, 2007, Vol. 80, No. 6, pp. 945–950. © Pleiades Publishing, Ltd., 2007.
Original Russian Text © T.E. Zhesko, V.P. Boyarskii, A.G. Nikitina, 2007, published in Zhurnal Prikladnoi Khimii, 2007, Vol. 80, No. 6, pp. 967–972.

ORGANIC SYNTHESIS AND INDUSTRIAL ORGANIC CHEMISTRY

A Versatile Procedure for Synthesis of Organic Acids by Cobalt Carbonyl Catalyzed Carbonylation of Organic Halides

T. E. Zhesko, V. P. Boyarskii, and A. G. Nikitina

VNIIINeftekhim Joint-Stock Company, St.Petersburg, Russia
Galar Limited Liability Company, St. Petersburg, Russia

Received November 9, 2006

Abstract—A versatile procedure for synthesis of a broad range of fatty-aromatic and aromatic acids by carbonylation of the corresponding halides under very mild conditions in the presence of cobalt carbonyl as a catalyst was suggested. The main principles of a flexible process for production of practically significant acids and their derivatives were developed.

DOI: 10.1134/S1070427207060183

Aromatic and fatty-aromatic acids and their derivatives (ethers, salts) have a wide application area. They are used in paint and varnish industry and in production of pharmaceuticals, plant-protecting agents, fragrance compounds, lubricants, and corrosion inhibitors. In addition, aromatic carboxylic acids find growing application in production of liquid-crystal materials. Di- and polyarenecarboxylic acids are used in production of liquid crystal thermoplastics, nanomaterials, and electroluminescent compounds applied in development of new kinds of equipment.

The conventional synthesis of these acids is based on classical organic reactions: alkylation, acylation, oxidation, and cyanation and has serous disadvantages. The methods are multistage, low-selective, expensive, and environmentally hazardous.

An alternative method is carbonylation of organic halides, which finds growing application for synthesis of fatty-aromatic and aromatic acids [1]. For example, phenylacetic acid (FAA) can be readily prepared by carbonylation of benzyl chloride under very mild conditions (1–5 atm, 40–80°C) in the presence of the conventional catalyst for oxo synthesis, cobalt carbonyl. The reaction is performed in an alkaline-alcoholic (mainly in methanol) solution, in which the catalyst exists in the salt form $MCo(CO)_4$. Since benzyl chloride readily enters into nucleophilic substitutions, it is activated in the course of carbonylation owing to the substitution of chlorine by the $Co(CO)_4$ anion to form alkylcobalt carbonyl (**1**). Then the CO molecule is inserted to form acylcobalt carbonyl complexes (**2**). The target methyl phenylacetate (**3**) is reductively eliminated under the action of the methylate anion [1]:

$$PhCH_2Cl \xrightarrow{Co(CO)_4^-} \underset{\mathbf{1}}{PhCH_2Co(CO)_4} \xrightarrow{CO} \underset{\mathbf{2}}{PhCH_2COCo(CO)_4}$$

$$\xrightarrow{O(CH)_3^-} \underset{\mathbf{3}}{PhCH_2COO(CH)_3}$$

The optimization of PAA synthesis allowed us to obtain this compound in a yield of no less than 95% [2]. We also developed a procedure for preparing the cobalt catalyst in the form of $Co(CO)_4^-$ in methanol under relatively mild conditions (at pressures of up to 50 atm) [2]. This procedure can be used instead of the reaction of benzyl chloride with highly toxic sodium cyanide. A batch of PAA (~40 kg) was prepared by this method for the first time in Russia and was tested in production of antibiotics. Naphthylacetic acid was prepared similarly. This compound is an intermediate product in production of Naphthizin pharmaceutical, Heteroauxin plant growth stimulant, and a valuable monomer, phenylenediacetic acid (Table 1).

Methyl monochloroacetate enters into this reaction at a higher CO pressure (up to 10 atm) to form malonic acid. Practically significant fatty-aromatic and

Table 1. Acids produced by the versatile process for carbonylation of organic halides

Product	Application
	Fatty-aromatic and aliphatic acids
X-C_6H_4CHRCOOH X, R = Phenylacetic acid	Antibiotic precursor; used in production of dyes, optical brighteners, and fragrance compounds
X = *p*-OH, *o*,*p*,-Cl; R=CH_3	Production of pharmaceuticals
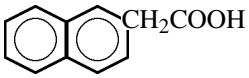 α-Naphthylacetic acid	Heteroauxin plant growth stimulant; in pharmaceutical production
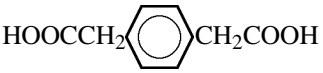 *p*-Phenylenediacetic acid	Monomer in production of aviation oils and polymers
$PhCH_2COCOOH$ Phenylpyruvic acid	In production of phenylalanine and synthetic sweetener, aspartame
$CH_2(COOH)_2$ Malonic acid $PhCH(COOH)_2$ Phenylmalonic acid	Intermediates in production of pharmaceuticals, vitamins, and dyes
	Aromatic acids
 p-Butylbenzoic acid (X = *p*-C_4H_9) X = R, RO, RCO, R , R	Liquid crystals and components of liquid–crystal systems
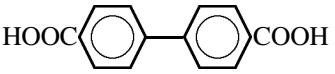 4,4'-Diphenyldicarboxylic acid 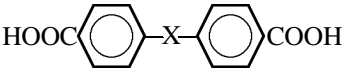 X = O, SO_2 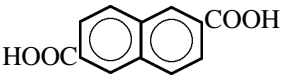 2,6-Naphthalenedicarboxylic acid	Monomers in production of highly heat-resistant liquid-crystal thermoplastics used in preparation of modern composites
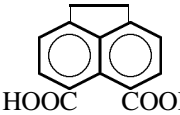 5,6-Acenaphthenedicarboxylic acid	Intermediate in synthesis of 1,4,5,8-naphthalenetetracarboxylic acid used in production of high-quality vat dyes (Vat Crimson 2Zh) and highly heat-resistant fibers

aliphatic (malonic) acids prepared by carbonylation of the corresponding halides by the above procedure are represented in Table 1.

Of particular interest is a modification of the method for carbonilation of benzyl chloride with calcium hydroxide in isopropanol serving as a base:

$$PhCH_2Cl + CO \xrightarrow[Ca(OH)_2]{Co_2(CO)_8/Isopropanol} \underset{\mathbf{1}}{(PhCH_2COCOO)_2Ca} + \underset{\mathbf{2}}{(PhCH_2COO)_2Ca}$$

We found [2] that the product of double carbonylation of benzyl chloride (calcium phenylpyruvate) is formed in large amounts along with PAA under mild conditions (atmospheric CO pressure and 30–40°C) (Fig. 1). Phenylpyruvic acid can be used for preparing an important amino acid, phenylalanine, which is a precursor for production of a valuable sweetener, aspartame (Table 1).

Carbonylation of aromatic halides. It is known that, unlike fatty aromatic halides, nonactivated aryl halides do not enter into nucleophilic substitution. That is why, apparently, these compounds are not activated with the $Co(CO)_4^-$ anion by the S_N2 mechanism under the conditions of benzyl chloride carbonylation.

First we activated more reactive aryl bromides and aryl iodides by oxidative addition of low-valent metal complexes [1]. We studied the preparation of acenaphthenedicarboxylic acid by carbonylation of 5,6-dibromoacenaphthene [3] under the conditions of phase-transfer catalysis by palladium halophosphine complexes. As determined by IR spectroscopy, the active catalytic species was the intermediate zero-valent palladium complex $PdCOP_3$ formed in the presence of carbon monoxide. The mechanism of this reaction was described in our previous paper [3]. It should be noted that palladium complexes have also been recently used to catalyze carbonylation of less active aryl chlorides with acceptor substituents. In this case, complex ligands (e.g., cyclohexyl-substituted ferrocenylphosphines) were developed to activate palladium [4]. However, these catalytic systems are difficultly available and expensive and can be used only for fine synthesis of small amounts of expensive compounds.

Although aryl halides are completely inactive in carbonylation catalyzed by cobalt carbonyl under ordinary conditions [in alcohols in the presence of bases (B)], the making possible use of cobalt carbonyl (the cheapest and the most available catalyst of oxo synthesis) in carbonylation of aryl halides is a very attractive practical and theoretical task.

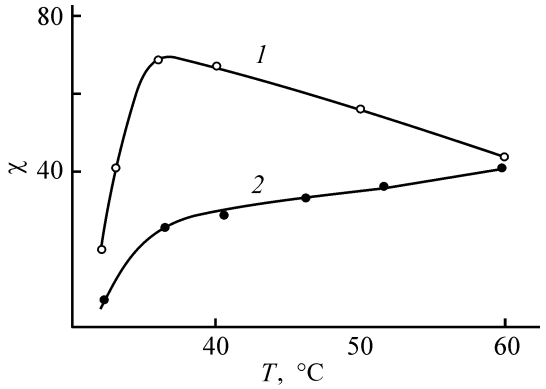

Fig. 1. Yield χ of (*1*) phenylpyruvic and (*2*) phenylacetic acids vs. temperature T (P = 1 atm).

Some alklylcobalt carbonyl complexes $RCo(CO)_4$ formed in situ in the course of carbonylation of alkyl halides RX can catalyze carbonylation of low-active aryl halides [5]. In this case, alkyl halides are cocatalysts (A) (activators) of cobalt carbonyl in carbonylation of aryl halides. The reaction occurs under very mild conditions (CO pressure 1 atm, 60–65°C):

$$ArHal + CO \xrightarrow[ROH + B]{Co_2(CO)_8 + A} ArCOOR \qquad (I)$$

We have shown previously [2, 6] that the most reactive catalytic complex, $PhCH_2Co(CO)_4$, is formed in the reaction with benzyl chloride as a cocatalyst [A, scheme (I)].

The results of a study of the catalytic effect of acceptor substituents on carbonylation of substituted bromobenzenes and of the inhibition of aryl halide carbonylation with one-electron acceptors (nitrobenzene, anthraquinone) [7] suggest the $S_{RN}1$ radical anion mechanism of aryl halide activation. The active catalytic species of carbonylation is the anionic complex $[RCo(CO)_3COOCH_3]^-$ [5, 7] formed by nucleophilic attack of the methylate anion on the carbon atom of the carbonyl group of alkylcobalt carbonyl. The nucleophilic power of this complex is very high. Because benzyl chloride is also carbonylated under these conditions [scheme (I)], we determined the mode and rate of feeding the cocatalyst, benzyl chloride, to maintain the catalyst in the active form, thus providing an almost complete conversion [7]. The catalytic cycle of the reaction in the presence of benzyl chloride as a cocatalyst has been suggested and analyzed [7].

A series of practically significant aromatic acids was prepared for the first time by carbonylation in the presence of a new effective catalytic system, cobalt carbonyl–benzyl chloride–base, in methanol (Table 1). This catalytic system is the most suitable

Table 2. Main process parameters of carbonylation in the presence of benzyl chloride

Product	Solvent	Base	CO pressure, atm	*T*, °C	Yield, %	By-product
Na-PAA	Methanol	NaOH	1–3	60–65	94–97	MBE*
Ca-PPA	Isopropanol	$Ca(OH)_2$	1–5	35–40	75–85	PAA
K-ADA	Methanol	KOH	1–1.5	55–62	90–95	PAA

* MBE is methyl benzyl ether.

for synthesis of preparing acenaphthendicarboxylic acid (potassium salt K-ADA) by carbonylation of 5,6-dichloroacenaphthene. This acid is used for production of a valuable commercial product, 1,4,5,8-naphthalenetetracarboxylic acid (Table 1) [2, 8]. The technical documentation for this process was developed. A pilot batch of the product (50 kg) was produced for the first time by the carbonylation procedure and was tested in production of a valuable heat-resistant dye, Vat Crimson 2Zh.

Some implementations of the developed versatile process in carbonylation in the presence of benzyl chloride as both reagent and cocatalyst are shown in the scheme below. The process was tested in practice. The main process parameters are listed in Table 2.

The process for synthesis of a valuable aromatic compound, phenylethanol, an analog of rose oil, by carbonylation (hydroformylation) of benzyl chloride via intermediate formation of phenylacetaldehyde is also shown in the scheme.

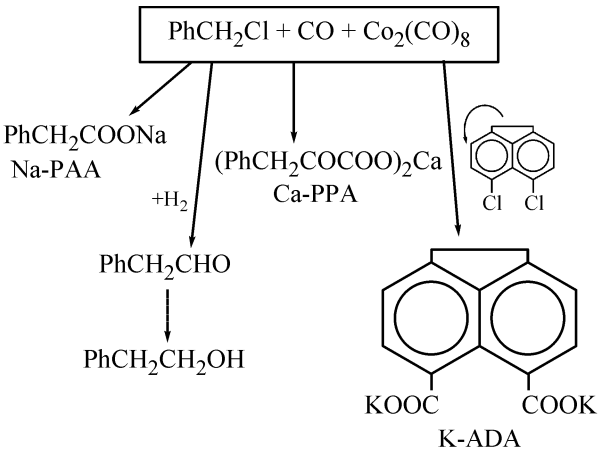

Process scheme based on benzyl chloride.

To improve the efficiency of the catalytic system for carbonylation of aryl halides, we studied other cocatalysts of cobalt carbonyl. The main requirements to the cocatalyst are the low self-carbonylation rate and the absence of chlorine in their composition, to decrease the consumption of a base required for halide binding. We developed new catalytic systems [7, 9, 10] containing ethylene chlorohydrin, olefin oxides, and epichlorohydrin as cocatalysts. The catalytic activity of these systems was higher by a factor of approximately 2 that that of the system containing benzyl chloride [7, 9]. These cocatalysts are not carbonylated under the reaction conditions but can undergo methanolysis, which, however, is insignificant in the presence of weak bases (B), alkali metal carbonates.

Epoxy cocatalysts are halogen-free compounds, and, hence, additional consumption of a base for halide binding is not required. The most available, low-cost, and convenient in use cocatalyst is propylene oxide. The mechanism of aryl halide carbonylation catalyzed by a cobalt carbonyl–epoxide system was analyzed in our previous paper [9].

Thus, cobalt carbonyl–epoxide–base system [9, 10] is a highly active and readily available catalytic system for selective carbonylation of aryl halides in a high (frequently quantitative) yield. This system, along with the catalytic system containing benzyl chloride as a cocatalyst, can be used as a highly efficient catalyst for both industrial production of many valuable products (Table 1) and fine laboratory synthesis [9]. This system is the most convenient for low-active substrates such as stable organic pollutants, polychlorobiphenyls [10].

A fundamentally new versatile process for synthesis of valuable industrial products by halide carbonylation was developed, based on the results of a study of new catalytic systems containing cobalt carbonyl. It should be noted that preparation of fatty-aromatic acids by carbonylation of the corresponding halides was described in [1], whereas the synthesis of aromatic acids is our original development.

A technological development of these processes showed that they can be performed using the same equipment. The preparation of the catalyst and carbonylation are performed with common units (Fig. 2). The units for feed preparation and isolation of the reaction products differ (depending on the properties

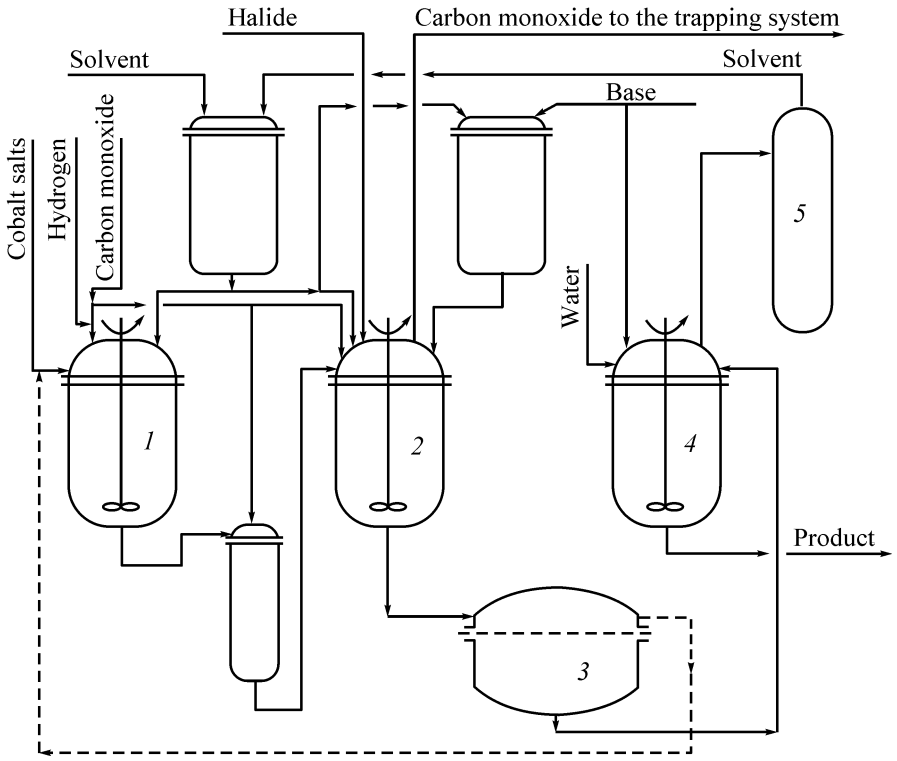

Fig. 2. Schematic of the installation for carbonylation of halides.

and aggregative state). The carbonylation is performed under mild conditions, which can be varied in a narrow range [CO pressure 1–5 atm, 35–70°C, alkali or alkaline-earth metal hydroxides and carbonates as bases, alcohols as solvents (we used methanol as the solvent in all processes except double carbonylation)]. To devise a process for sythesis of key products (fatty-aromatic and aromatic acids, namely, phenylacetic, penylpyruvic, and 5,6-acenaphthendicarboxylic acids) and thus the main units for the versatile process, we developed and fabricated an original pilot installation for carbonylation of halides [2] (Fig. 2). The installation consists of a reactor for preparing catalyst *1* (alcoholic solution of cobalt carbonyl), reactor for carbonylation *2*, pressure filter *3* (product isolation step), reactor for hydrolysis *4*, and collector of the solvent to be recycled *5*. A pilot batch of the product in an amount of 10 to 50 kg was produced on this installation. The reactor volume is 100 l. The design productivity of the unit is 10 tons year^{-1}.

The aim of further studies is to broaden the range of compounds involved in the carbonylation, including, in particular, heteroaromatic compounds [pyridines, furans, thiophenes, polychlorobiphenyls (PCB)] and to develop processes for synthesis of new products and utilization of stable organic pollutants (PCB) [10] as highly heat-resistant industrial insulators and polybromodiphenyl ethers as fire-retardants.

EXPERIMENTAL

All laboratory carbonylation experiments were performed under atmospheric pressure of CO in temperature-controlled glass reactors under vigorous stirring in a CO flow. The experimental procedure was described in detail in [7]. The reaction products were analyzed by GLC, chromatography-mass spectrometry, and NMR spectroscopy, including 2*D* COSY spectroscopy, for identification of complex products.

The industrial process was developed using a 1-l pressure vessel and the pilot unit described above (Fig. 2).

CONCLUSIONS

(1) Fatty-aromatic and aromatic carboxylic acids were prepared by carbonylation of the corresponding halides in alcohols in the presence of cobalt carbonyl as the catalyst and of bases under very mild conditions (CO pressure, up to 3 atm; temperature, up to 65°C).

(2) It was shown that the reaction is highly selective and occurs with a high yield. To carbonylate chemically stable aryl halides, benzyl chloride and epoxides were added as cocatalysts (promoters).

(3) A novel versatile and economically efficient process for producing a wide range of organic acids (mainly aromatic and fatty-aromatic carboxylic acids) and their derivatives by carbonylation of the corresponding organic halides was developed.

REFERENCES

1. Sheldon, R.A., *Chemicals from Synthesis Gas: Catalytic Reactions of CO and H_2*, Dordrecht: Reidel, 1987.
2. Zhesko, T.E., Boyarskii, V.P., Nikitina, A.G., et al., in *Protsessy neftepererabotki i neftekhimii* (Oil Refining and Petrochemical Processes), St. Petersburg: Giord, 2005, pp. 216–226.
3. Zhesko, T.E, Shygalevsky, V.A., and Novikova, E.G., in *Fundamental Research in Homogeneous Catalysis*, New York: Gordon and Breach, 1986, vol. 3, pp. 1141–1152.
4. Magerlein, W. and Indolese, A., *J. Organomet. Chem.*, 2002, vol. 641, pp. 30–40.
5. Francalanci, F., Gardano, A., and Foa, M., *J. Organomet. Chem.*, 1983, vol. 251, p. C5.
6. Zhesko, T.E, Boyarskii, V.P., and Beletskaya, I.P., *Metalloorg. Khim.*, 1989, vol. 2, no. 2, pp. 385–387.
7. Zhesko, T.E, Boyarskii, V.P., and Nikitina, A.G., *Zh. Obshch. Khim.*, 1998, vol. 68, no. 1, pp. 85–89.
8. RF Patent 1825488.
9. Boyarskii, V.P., Zhesko, T.E, and Lanina, S.A., *Zh. Prikl. Khim.*, 2005, vol. 78, no. 11, pp. 1875–1880.
10. RF Patent 2215729.

ISSN 1070-4272, Russian Journal of Applied Chemistry, 2007, Vol. 80, No. 6, pp. 951–954. © Pleiades Publishing, Ltd., 2007.
Original Russian Text © S.M. Azarov, I.L. Shashkova, A.I. Rat'ko, T.A. Azarova, N.V. Mil'vit, S.V. Shemchenok, V.V. Dmitriev, 2007, published in Zhurnal Prikladnoi Khimii, 2007, Vol. 80, No. 6, pp. 973–976.

ENVIRONMENTAL PROBLEMS OF CHEMISTRY AND TECHNOLOGY

Regeneration of Ceramic Filter Cells for Water Purification

S. M. Azarov, I. L. Shashkova, A. I. Rat'ko, T. A. Azarova, N. V. Mil'vit, S. V. Shemchenok, and V. V. Dmitriev

Institute of General and Inorganic Chemistry, National Academy of Sciences of Belarus, Minsk, Belarus

Received January 16, 2007

Abstract—Regeneration of ceramic aluminosilicate filter cells for water purification by chemical methods and, in particular, by acid dissolution of the deposit formed in filter pores was studied.

DOI: 10.1134/S1070427207060195

Filter cells are regenerated to restore their rated service characteristics. In this case, a filtering body is to be regarded as a combination of two phases: a ceramic and a contaminating substance, i.e., as a specific state associated with the dispersity of particles forming the porous body and with phenomena in pores, caused by their appreciable curvature and by the nature of interactions at interfaces between the material of a filter cell and a contaminant. Specific features of the regeneration are determined in the case under consideration by the specificity of the dispersed state of the contaminant in pores of the ceramic and should be manifested in kinetic dependences of the influence exerted by the regenerating medium on the mechanism of restoration of the service characteristics.

Ceramic aluminosilicate filter cells are used for removal of mechanical admixtures of varied origin and colloid particles of iron hydroxide from drinking and return water. Ceramic filter cells have a multilayer porous structure, with the pore size successively decreasing from layer to layer.

In this communication, we present the results obtained in a study of the process of regeneration of ceramic filter cells for water purification, manufactured in Belarus and used at various plants of the Republic. The chemical composition of deposits filtered-off from drinking and return water was studied, and possibility of regeneration of ceramic filter cells by chemical methods and, in particular, by acid dissolution of the deposit formed in filter pores was demonstrated.

EXPERIMENTAL

The regeneration was experimentally studied on segments of tubular filter cells with an external diameter of 70 mm and height of 50 mm, built in the water supply system of the Institute, using a laboratory bench.

The working capacity of a filter is defined as the volume of water passed before loss of 95% of the initial throughput of filter cells. The ratio of the initial throughput and working capacity after regeneration to the values of these characteristics before regeneration was taken as the degree of regeneration (%).

In the study, we used filter cells selected after tests at industrial plants and at housing and communal facilities, as well as those used in water recycling systems at industrial plants.

The initial throughput and working capacity of starting filter cells before exploitation were measured for a set of witness samples to be, on the average, 0.38 $l\ s^{-1}$ and 960 l, respectively.

In chemical regeneration, a filter cell segment was steeped in a 1–20% hydrochloric acid solution and kept in this solution for 2–24 h. Then the filter cell was washed with water, and its restored initial throughput and working capacity were measured.

Table 1. Results of X-ray fluorescent determination of the mineral composition of the deposit from the filter

Sample no.*	Content of oxides in a sample, wt %										
	K_2O	CaO	Fe_2O_3	SiO_2	P_2O_5	MgO	Al_2O_3	TiO_2	S	Cl	MnO
1	2.5	4.3	24.4	49.1	1.1	1.5	9.4	0.6	0.2	0.1	3.0
2	0.3	15.2	58.1	4.5	3.0	2.0	0.6	0.0	0.1	0.0	0.06

* Sample: no. 1, return water; no. 2, drinking water (typical examples).

To determine the chemical composition of the deposit filtered-off by ceramic filter cells from drinking and return water, it was separated from the filter, dried to constant weight at room temperature in air, thoroughly homogenized, and then its chemical composition was determined by the quantitative X-ray fluorescent analysis on an SRM-18 instrument.

The averaged results of the chemical analysis of the deposits filtered-off from drinking and return water, obtained using the X-ray fluorescent method, are listed in Table 1 in terms of element oxides. As can be seen from Table 1, the main components of the deposit taken from the filter are silicon, iron, calcium, and aluminum. The deposit also contains minor amounts of potassium and manganese, with the total content of their oxides being about 5%. The content of other components is insignificant and does not exceed 1%. The elements represented in Table 1 are contained in water as hydroxides and salts in a colloid-dissolved state, and silicon may be in the form of insoluble silicates and oxides.

The mineral composition of the filtered-off deposit is determined by the composition of underground water used for water supply in a given region and also by the chemical nature of the reagents employed in water treatment. In particular, the presence of such elements as Al, S, Mn, and Cl in the deposit may be due to use of aluminum sulfate $Al_2(SO_4)_3$ as a coagulant and also of permanganate and chlorine oxidants in water treatment.

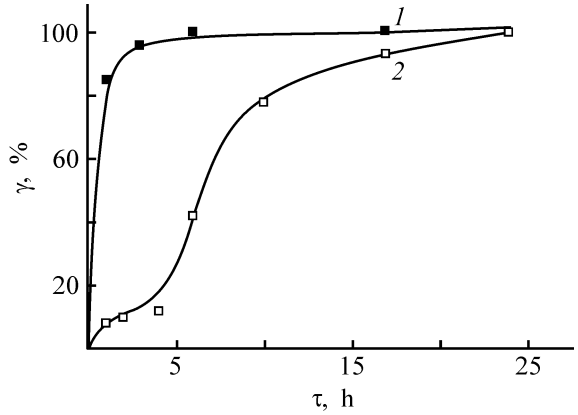

Fig. 1. Degree of filter cell regeneration, γ, with respect to (*1*) initial throughput and (*2*) working capacity vs. time τ.

All the minerals listed in Table 1, except silicon oxide, are readily soluble in inorganic acids and, in particular, hydrochloric acid. Silicon-containing admixtures insoluble in acids (SiO_2) can be separated from the surface of a filter cell in dissolution of other components.

To determine the optimal conditions of dissolution of the oxides represented in Table 1, we used hydrochloric acid in a wide range of concentrations (1–20%), with the treatment time varied from 1–2 to 24 h.

Figure 1 shows curves describing the degree of filter cell regeneration with respect to initial throughput and working capacity by treatment with a 5% HCl solution. It can be seen that these curves strongly differ in shape.

In the first case, the curve steeply rises and, having reached the maximum values of the degree of regeneration, rapidly flattens out to form a plateau. The curve describing the degree of regeneration with respect to the working capacity is markedly different. It has an S-shape characteristic of diffusion-dependent processes.

The process of dissolution of colloid particles of aluminum and iron hydroxides in hydrochloric acid is rather fast and complete in several minutes [1]. However, particles being dissolved are, in this case, within pores of the aluminosilicate ceramic, and, therefore, the diffusion of hydrogen ions requires a certain time.

The influence of the chemical treatment conditions (treatment time and HCl concentration) on the degree

Table 2. Influence of chemical treatment conditions on the degree of filter cell regeneration

c_{HCl}, wt %	τ, h	Initial throughput after regeneration	Degree of regeneration with respect to the initial throughput, %	Working capacity after regeneration, l	Degree of regeneration of the working capacity, %
≤5	1	0.32	85	–	8
≤5	3	0.33	96	–	11
≤5	6	0.38	100	404	42
≤5	17	0.38	100	900	94
≤5	24	0.38	100	960	100
10	3	0.31	81.8	346	36
10	5	0.42	~100*	350	36
10	8	0.42	~100*	500	52
10	16	0.42	~100	–	–
10	24	0.38	100	960	100
20	2	0.36	94.7	400	42
20	5	0.33	86.8	400	42
20	15	0.42	~100*	900	94
20	24	0.42	~100*	960	100

* The degrees of regeneration with respect to the initial throughput exceed 100%, but fall within the range of the initial throughputs measured for a set of witness samples.

of filter cell regeneration is illustrated by Table 2. It can be seen that particles in the coarsest pores of outer layers of a filter cell are dissolved within 1–2 h, which is sufficient for a 85–95% restoration of the initial throughput. In contrast to the initial throughput, the working capacity of the filter cell is not restored so rapidly and requires at least 15 h. Even when the initial throughput of filter cells reached 100% upon a treatment for 1–10 h, the working capacity of the regenerated filter cells did not exceed 50% of the initial value. For example, filters with the initial working capacity of 960 l had, after regeneration in a 10% HCl solution for 5 h, a working capacity of 404–379 l.

The data presented indicate that the key factor in chemical regeneration of filter cells is the kinetics of diffusion of hydrogen ions into pores of deep layers of the filter. Therefore, the process requires a rather long time, and only the working capacity of a filter cell, but not the degree of restoration of the initial throughput, can serve as a measure of regeneration.

It was also of interest to study the capacity of filter cells for multiple regeneration. For this purpose, we carried out the following experiment. A segment of a mullite-quartz filter cell was built in the water supply system of the Institute, using a laboratory bench, and water was passed until the filter was clogged. Then the filter was regenerated, its initial throughput and working capacity were measured, and the filter was again built in the water supply system.

The results obtained are plotted in the form of histograms (Figs. 2a and 2b). It can be seen that the working capacity of a filter cell after three regenerations for 17 h still has sufficiently high values (up to 870 l).

According to the data obtained, a prolonged acid treatment of filter cells has no effect on the strength

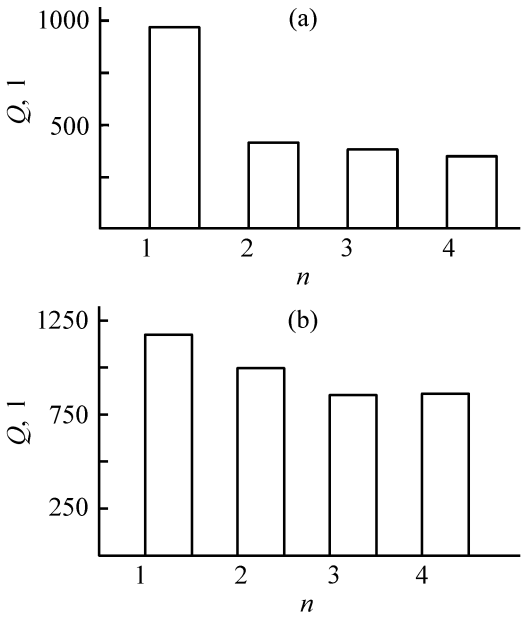

Fig. 2. Variation of the working capacity Q of a filter cell in cyclic operation and regeneration under various conditions. (n) Cycle number. Regeneration duration (h): (a) 5 and (b) 17.

Table 3. Effect of the acid treatment duration on strength properties of the aluminosilicate ceramic

HCl content, wt %	Time of keeping in HCl, h	Breakdown pressure of a filter cell, atm
1	2	3
1	2	2.8
1	5	2.9
5	2	3.2
5	5	3.1
5	10.5	2.9
5	16.5	3.2
5	24	3.0
10	3	4.8
10	5	5.0
10	8	5.2
10	16.5	5.0
10	24	3.2
20	2	4.2
20	5	3.0
20	15	4.0
20	24	2.6

properties of ceramic filter cells. Table 3 lists average values of inside-to-outside load gradients leading to breakdown of filter cells after regeneration. The breakdown pressure of aluminosilicate ceramic filter cells not subjected to chemical treatment is 2.9–7.0 atm, depending on the size of initial particles and sample wall thickness. Thus, chemical treatment only slightly affects the strength properties of filter cells.

CONCLUSIONS

(1) The results of the study indicate that the degree of recovery of the working capacity of filter cells, but not the initial throughput, can serve as a measure of the regeneration of aluminosilicate ceramics.

(2) The process of the chemical regeneration of ceramic filter cells based on aluminosilicates is diffusion-dependent. The principal factor governing the degree of filter cell regeneration is the diffusion kinetics of hydrogen ions within pores of inner layers of the aluminosilicate ceramics.

(3) A rather prolonged treatment (for no less than 10–15 h) of filter cells with hydrochloric acid solutions is necessary for the optimal regeneration of the filter cells. The concentration of hydrochloric acid has no significant effect on the regeneration rate, which enables use of dilute acids (1–5%) in this process.

REFERENCE

1. Frolov, Yu.G., *Kurs kolloidnoi khimii: poverkhnostnye yavleniya i dispersnye sistemy* (A Course of Colloid Chemistry: Surface Phenomena and Dispersed Systems), Moscow: Khimiya, 1989.

ISSN 1070-4272, Russian Journal of Applied Chemistry, 2007, Vol. 80, No. 6, pp. 955–959. © Pleiades Publishing, Ltd., 2007.
Original Russian Text © Ya.I. Korenman, N.N. Popova, T.A. Kuchmenko, 2007, published in Zhurnal Prikladnoi Khimii, 2007, Vol. 80, No. 6, pp. 977–982.

ENVIRONMENTAL PROBLEMS OF CHEMISTRY AND TECHNOLOGY

Determination of Formic and Acetic Acids in Air by Piezoelectric Microweighing

Ya. I. Korenman, N. N. Popova, and T. A. Kuchmenko

Voronezh State Technological Academy, Voronezh, Russia

Received August 3, 2006; in final form, February 2007

Abstract—The quantitative and kinetic parameters of sorption of formic and acetic acids on thin films of various modifiers of piezoelectric quartz resonator electrodes are determined. Parameters of film formation on the electrodes (application procedure and thickness) are optimized. Methods for joint and separate determination of formic and acetic acids in air by piezoelectric microweighing with single- and double-sensor devices are developed.

DOI: 10.1134/S1070427207060201

Development of microsensors for determination of toxic compounds in air is a topical problem of modern analytical instrument making. Formic and acetic acid are a health hazard not only when occurring at a level close to the maximum permissible concentration (MPC) (1–5 mg m^{-3}), but also in lower concentrations as a result of the cumulative effect [1–4]. In emergencies, emission sources of carboxylic acid are classified with stable rapid damage sites [2]. Carboxylic acids are to be determined in air in working areas at hazardous works and factory laboratories and for risk assessment. The limitations to use of such common methods as gas and liquid chromatography are caused by large consumption of chemicals (sometimes no less hazardous than the acids to be determined) and by the need in expensive and sophisticated equipment and highly skilled staff. Piezoelectric quartz microbalances [piezoelectric quartz bulk acoustic wave resonators (PQRs) with film-coated electrodes] are widely used for determination of toxic compounds in air. The sensitive films on the PQR electrodes are recyclable, in contrast to dosimeters and indicator tubes, which can be used only once [4, 5].

EXPERIMENTAL

The experiments were carried out on a laboratory setup consisting of electric power unit, detector cell with rigidly mounted PQRs with electrodes preliminarily modified with sorbents, compressor, and F5137 two-channel digital frequency meter connected to a computer. In the study, we used an AT-cut PQR with a resonance frequency of 10–15 MHz. The 5-mm electrodes were fabricated from Al_2O_3 [6].

The sorbents were selected taking into account the selectivity criteria (McReynolds constants, Rohrschneider coefficients) with respect to the acids to be determined, and also the nature of the sorbent and sorbate and their polarities. As sorbents we examined such commonly used chromatographic phases as polystyrene (PS), Triton X-100 (TX-100), poly(ethylene glycol) esters [adipate (PEGA), succinate (PEGS), and sebacate (PEGSb)], pentaerythritol tetrabenzoate (PETB), poly(vinylpyrrolidone) (PVP), Apiezon N (A-N), Apiezon L (A-L), squalane (Sq), and Tween-40 (Tw-40) [7, 8].

In addition to the chromatographic phases, we used for modification of the electrodes β-alanine, glycine, ethylenediaminoazobenzenesulfonic acid sodium salt (EDBSA), dibenzo-18-crown-6 (DB18C6), bee-glue (BG), and beeswax (BW) [7]. These modifiers were selected taking into account the physicochemical properties of the sorbents and acids to be determined.

Films on the PQR electrodes were prepared by the following methods: (I) static evaporation of a drop of a sorbent solution or layer-by-layer application of solutions of two sorbents and (II) immersing of PQR in a sorbent solution or in a mixed solution of two sorbents (III).

Table 1. Selected metrological characteristics of PQR electrodes with modifiers applied by various methods* ($m_f = 20 \pm 1.5$ μg, $n = 3$, $P = 0.95$)

Sorbent	Method I			Method II		
	$\bar{X} \pm \Delta X$	$S^2_{X_i}$	Δ, %	$\bar{X} \pm \Delta X$	$S^2_{X_i}$	Δ, %
PEGA	22.4 ± 0.2	0.05	2.46	20.1 ± 0.2	0.03	2.18
PEGS	20.7 ± 0.2	0.04	2.42	19.7 ± 0.2	0.03	2.03
PEGSb	19.3 ± 0.3	0.06	3.21	19.4 ± 0.2	0.06	2.69
TX-100	22.3 ± 0.2	0.04	2.24	19.7 ± 0.2	0.04	1.91
PETB	22.3 ± 0.3	0.06	2.78	23.3 ± 0.2	0.06	2.24
A-L	21.5 ± 0.3	0.09	3.30	21.7 ± 0.2	0.05	2.73
A-N	23.9 ± 0.3	0.07	2.76	20.9 ± 0.2	0.05	2.73
Sq	24.4 ± 0.3	0.08	2.91	20.3 ± 0.3	0.08	2.55
PVP	23.2 ± 0.3	0.07	2.93	19.7 ± 0.2	0.04	2.54
PS	24.5 ± 0.2	0.04	2.04	24.4 ± 0.1	0.01	1.02
Tw-40	22.9 ± 0.3	0.06	2.70	22.5 ± 0.2	0.03	1.95
β-Alanine	22.2 ± 0.2	0.03	2.03	–	–	–
Glycine	24.2 ± 0.3	0.06	2.56	–	–	–
EDBSA	23.5 ± 0.3	0.09	3.15	23.5 ± 0.2	0.05	2.43
DB18C6	23.8 ± 0.3	0.07	2.77	23.8 ± 0.2	0.04	2.18

* $\bar{X}$, average value of the analytical signal ΔF_f; dash means that a film cannot be formed by this method.

To enhance the analytical response, improve the reproducibility of results, and reduce the measuring error, the modifiers were bound to a polymer support (polystyrene).

In film fabrication by method I, the solution was applied onto the PQR electrode using a microsyringe. The thickness of the films was controlled by the volume of the sorbent solution applied onto the electrode surface. In fabricating the films by method II, the thickness was controlled by varying the solution concentration. As solvents we used distilled water, acetone, and alcohol (analytically pure grade).

The solvents were removed from the films in an oven at 40–50°C for 20–30 min, except for PQRs modified with BW and amino acids. In the case of amino acids, the drying time was 30–50 min, since water is evaporated more slowly than the organic solvents. Beeswax irreversibly degrades above 30°C [8, 9]. The BW-modified resonator was dried in a desiccator over a desiccant bed for 1.0–1.5 h at 20°C. The drying time of the films fabricated by immersing PQRs into sorbent solutions was 10–15 min at 40–50°C.

The film weight m_f (μg) was estimated by the Sauerbrey equation [10]:

$$m_f = \frac{\Delta F_f s}{K_f F_0^2},$$

where $\Delta F_f = (F_0 - F_f)$ is the change in the resonator frequency after coating (Hz); K_f, calibration factor of the piezoelectric microbalance (under normal conditions, $K_f = 2.3 \times 10^{-6}$ cm^2 g^{-1}); F_0, resonance frequency of PQR (Hz); s, surface area of the PQR electrodes (cm^2); and F_f, oscillation frequency of film-coated PQR (Hz).

The sorption efficiency was estimated from the analytical signal (maximum frequency difference of the sensor in sorption) ΔF_s^{max} (Hz) [6, 9, 11–13]. The acid concentration in the detection cell before sorption c_0 (mg m^{-3}) was estimated by the reduced Mendeleev–Clapeyron equation, taking into account the dilution with laboratory air [6, 9, 11–13]. The sensitivity of the piezosensors S_M (Hz dm^3 mol^{-1}) with respect to the acids was calculated as the ratio of the signal of the film-coated PQR sensor (piezosensor) to the acid concentration in the sample [6]. The kinetic parameters of sorption were estimated from the time of establishment of the sorption equilibrium under isothermal conditions (time elapsed from sample injection in the detection cell until the maximum analytical signal was obtained [12]).

The procedure of film application onto PQR electrodes was optimized in the experiments with sorbent solutions of the same concentration by measuring δGF_f (Table 1), using the reproducibility of the film weight and sorption capacity as criteria.

In deposition of the films by method II, the uncertainty in the stage of film application was lower than in method I. Therefore, in all further experiments, the films were deposited by immersing the PQR electrodes in the sorbent solutions, except the films of amino acids, which were dissolved in water. Because of the poor wetting of the quartz plate and PQR electrodes with water, it is impossible to obtain a uniform thin film. The films obtained from the solutions of amino acids, DB18C6, and EDBSA are air-sensitive and the response of an unloaded piezosensor is unstable (drift more than 100 Hz min^{-1}). Therefore, the films were bound to the polymer support (polystyrene film), which is stable and demonstrates the minimal drift of the piezosensor baseline. The films of amino acids and DB18C6 were applied by method I onto a preformed support. To obtain a PS–EDBSA film, the 10 mg cm^{-3} solutions of the modifiers were mixed at a 4 : 1 volume ratio, and the PQR electrodes were immersed in the resulting solution.

The optimal film weight was found to be 20.0 ± 1.5 μg, and the injected sample volume, 3 cm^3 [11–13]. The samples were injected in a closed cell at 20 ± 1°C.

It is known that chromatographic data cannot be used as a unique criterion for characterization of the selectivity of sorbents with respect to the compounds to be determined (or their group). These data are not always consistent with the results obtained by piezoquartz microweighing [11]. Therefore, to make a decision on the films, we determined the quantitative and kinetic parameters of sorption of individual acid vapors. PEGA, PS–β-alanine, PS–glycine, PS–EDBSA, TX-100, and PS–DB18C6 appeared to be the most selective sorbents for formic and acetic acids (Fig. 1).

Virtually all the air samples contained both formic and acetic acids in various proportions, which made necessary experiments on sorption of the acids from their mixtures. In exposure of PQRs with the most sensitive films (Fig. 1), it was demonstrated that the sorption is an additive value, with the calculated analytical responses from the acid mixtures being lower than those obtained experimentally (Fig. 2). Statistical data processing revealed that the difference between the calculated and experimental values is statistically significant. This is due to the fact that, after the sorption sites on the film surface are covered, the molecules of amino acids adsorbed on the film and those occurring in the gas phase form dimers. The total acid concentration in air was determined with the PS– β-alanine film, which is highly sensitive to both acids (Fig. 1); the sorption time was 10 s.

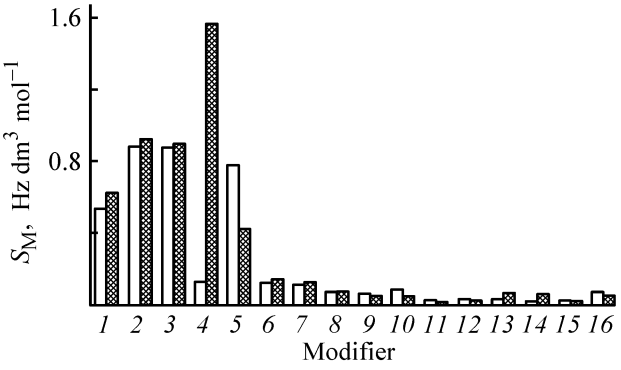

Fig. 1. Molar sensitivity histograms of the modifiers with respect to formic (white bars) and acetic (cross-hatched bars) acids: (*1*) PS–DB18C6 (I), (*2*) PS–β-alanine (I, layer-by-layer), (*3*) PS–glycine (I, layer-by-layer), (*4*) PS–EDBSA (II, mixed sorbent solution), (*5*) TX-100 (II), (*6*) PEGA (II), (*7*) PEGS (II), (*8*) PEGSb (II), (*9*) PETB (II), (*10*) PVP (II), (*11*) BG (II), (*12*) BW (II), (*13*) A-N (II), (*14*) A-L (II), (*15*) Sq (II), and (*16*) Tw-40 (II). (S_M) Sensitivity of the piezosensor.

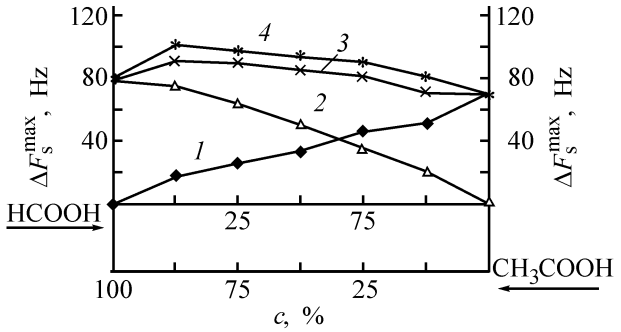

Fig. 2. Analytical signal of the sensor, ΔF_s^{max}, vs. (*1*) formic and (*2*) acetic acid concentration c. (*3*) Theoretical and (*4*) experimental analytical signals obtained in joint sorption of formic and acetic acids (1–10 mg m^{-3}) on the PS–β-alanine film.

When exposed to individual acid vapors, the sensor modified with the PS–β-alanine film demonstrated a linear response over the acid concentration range from 1 to 10 mg m^{-3}. The calibration curves for determination of formic and acetic acid concentrations by microweighing with this sensor are described by Eqs. (1) and (2), respectively:

$$\Delta F_1 = 7.0c_{HCOOH} + 7.2, \quad (1)$$

$$\Delta F_2 = 6.5c_{CH_3COOH} + 4.1, \quad (2)$$

where ΔF_1 and ΔF_2 are the analytical responses (Hz) of the sensor exposed to individual formic and acetic acid vapors, and c_{HCOOH} and c_{CH_3COOH}, the acid concentrations (mg m^{-3}).

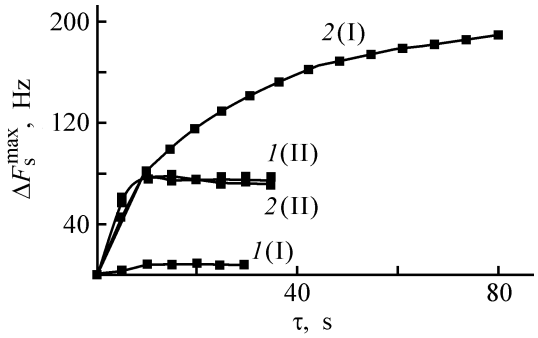

Fig. 3. Analytical signal of the sensor, ΔF_s^{max}, vs. time τ in sorption of (*1*) formic and (*2*) acetic acids on (I) PS–EDBSA and (II) PS–β-alanine films. Acid concentration $c = 10$ mg m^{-3}.

The modifiers used are characterized by cross sensitivity to formic and acetic acids. Therefore, two piezosensors are required for their separate determination, provided that one of them is selective. This condition is met for the sensors with electrodes modified with the PS–EDBSA and PS–β-alanine films (Fig. 1).

It was demonstrated that the sorption time of formic and acetic acids on the PS–EDBSA film should be 20–175 and 40–215 s, respectively, depending on their concentrations. It is seen from the time dependence of the analytical signal (Fig. 3) that, in exposure of the piezosensor modified with the PS–β-alanine film to the acid vapors, the signals are virtually indistinguishable (5–10 s). The detection limits of formic acid with the piezosensors modified with PS–EDBSA and PA–β-alanine films are 10 and 1 mg m^{-3}, and that with both piezosensors, 1 mg m^{-3}. The piezosensor with the PS–EDBSA film is selective with respect to the acetic acid (its molar sensitivity to formic acid is lower by an order of magnitude than for acetic acid [14]).

The calibration curves for determination of formic and acetic acid concentrations by microweighing with a piezosensor with the PS–EDBSA film are described by Eqs. (3) and (4), respectively:

$$\Delta F_1 = 1.6c_{HCOOH} - 0.8, \quad (3)$$

$$\Delta F_2 = 15.8c_{CH_3COOH} + 1.3. \quad (4)$$

The sorption isotherm of acetic acid on the PS–EDBSA film shows two linear sections, one being described by Eq. (4) (over the concentration range 1–15 mg m^{-3}) and another, by Eq. (5) (15–30 mg m^{-3}):

$$\Delta F = 37.4c_{CH_3COOH} - 278.7. \quad (5)$$

Two linear portions were also found in the sorption isotherm of formic acid on the PS–EDBSA film in the region of low concentrations, one being described by Eq. (3) (1–10 mg m^{-3}) and another, by Eq. (6) (10–70 mg m^{-3}):

$$\Delta F = 5.4c_{HCOOH} - 4.8. \quad (6)$$

Therefore, the acids can be determined separately both at the MPC level and at higher concentrations. At concentrations close to MPC, it is quite enough to expose the sensors to the acid vapor for 20 s, and at higher concentrations, for 1.5–2 min, since the sorption time of acetic acid on the PS–EDBSA film increases with the acid concentration.

From regression equations (1)–(4), obtained for PQRs modified with the PS–EDBSA and PS–β-alanine films, we derived equations allowing joint determination of formic and acetic acids in air:

$$c_{HCOOH} = \frac{(b_{2.2} + \Delta F_{tot.2} - b_{2.1})a_{1.1} - (\Delta F_{tot.1} + b_{1.1} + b_{1.2})a_{2.1}}{a_{2.2}a_{1.1} - a_{1.2}a_{2.1}}, \quad (7)$$

$$c_{CH_3COOH} = \frac{(\Delta F_{tot.1} + b_{1.1} + b_{1.2})a_{2.2} - (b_{2.2} + \Delta F_{tot.2} - b_{2.1})a_{1.2}}{a_{2.2}a_{1.1} - a_{1.2}a_{2.1}}, \quad (8)$$

where $a_{1.1}$, $a_{1.2}$, $a_{2.1}$, $a_{2.2}$, $b_{1.1}$, $b_{1.2}$, $b_{2.1}$, and $b_{2.2}$ are the regression coefficients in Eqs. (1)–(4); $\Delta F_{tot.1}$ and $\Delta F_{tot.2}$, integral analytical signals from the sensors with the PS–β-alanine and PS–EDBSA films, respectively, exposed to a mixed acid vapor.

To check the analytical procedure for consistency, the piezosensors were calibrated in individual acid vapors, and the experimental regression coefficients were introduced into Eqs. (7) and (8). Then we prepared gas mixtures with fixed acid concentrations of 1 to 10 mg m^{-3}. A sample of the equilibrium gas phase was injected into the detection cell equipped with two piezosensors. The exposure time was 20 s. Finally, the acid concentrations were estimated

Table 2. Joint and separate determination of (1) formic and (2) acetic acids with the piezoelectric sensor ($n = 3$, $P = 0.95$)

Separate determination					Joint determination		
introduced, mg m^{-3}		found, mg m^{-3}		Δ, %	introduced, mg m^{-3}	found, mg m^{-3}	Δ, %
(1)	(2)	(1)	(2)				
1.0	5.0	1.0 ± 0.1	5.1 ± 0.2	22.7	1.00	1.1 ± 0.1	15.3
5.0	1.0	5.2 ± 0.2	1.0 ± 0.1	19.8	5.00	4.9 ± 0.2	12.1
2.5	2.5	2.6 ± 0.2	2.4 ± 0.2	14.6	8.00	7.9 ± 0.2	10.3

using the above equations. The results are listed in Table 2.

CONCLUSIONS

(1) Based on data on the sorption of formic and acetic acid and their mixtures from the gas phase on thin film-coated electrodes of bulk-acoustic-wave piezoelectric quartz resonators, methods for joint and separate determination of the acids were developed, using single- and double-sensor devices, respectively. The polystyrene–β-alanine film is recommended for joint determination of the acids, and the polystyrene–sodium ethylenediaminoazobenzenesulfonate film for separate determination.

(2) It was shown that the response time of the piezosensors depends on the formic and acetic acid concentrations in the mixed vapor.

(3) Regression equations for determination of formic and acetic acids in air were derived from the linear portions of the sorption isotherms of the acids on the modifier films.

REFERENCES

1. *Khimicheskaya entsiklopediya* (Chemical Encyclopedia), Knunyants, I.A., Ed., Moscow: Bol'shaya Ross. Entsiklopediya, 1992, vol. 3.
2. Bespamyatnov, G.P. and Krotov, Yu.A., *Predel'no dopustimye kontsentratsii khimicheskikh veshchestv v okruzhayushchei srede: Spravochnik* (Maximum Permissible Concentrations of Chemicals in the Environment: A Handbook), Leningrad: Khimiya, 1985.
3. Peregud, E.A., Bykhovskaya, M.S., and Gernet, E.V., *Bystrye metody opredeleniya vrednykh veshchestv v vozdukhe* (Express Methods for Determination of Hazardous Compounds in Air), Moscow: Khimiya, 1970.
4. Zolotov, Yu.A., Ivanov, V.M., and Amelin, V.G., *Khimicheskie test-metody analiza* (Chemical Testing Methods), Moscow: Editorial URSS, 2002.
5. Otto, M., *Analytische Chemie*, Weinheim: Wiley–VCH, 2000.
6. Kochetova, Zh.Yu., Determination of Volatile Organic Compounds in the Gas Phase with Piezosorption Sensors Based on Synthetic and Natural Polymers, *Cand. Sci. Dissertation*, Saratov, 2002.
7. Petsev, N. and Kotsev, N., *Nar''chnik po gazova khromatografiya* (Handbook of Gas Chromatography), Sofia: Nauka i Izkustvo, 1984.
8. Korol', A.N., *Nepodvizhnaya faza gazozhidkostnoi khromatographii* (Stationary Phase in Gas-Liquid Chromatography), Kiev: Naukova Dumka, 1969.
9. Kuchmenko, T.A., Kudinov, D.A., and Korenman, Ya.I., *Sorbts. Khromatogr. Prots.*, 2001, vol. 1, no. 6, pp. 1092–1100.
10. Sauerbrey, G.G., *Z. Phys.*, 1964, vol. 178, no. 2, pp. 457–463.
11. Silina, Yu.E., Determination of Volatile Components of Building Materials in Indoor Air Using Mass-Metric Sensors, *Cand. Sci. Dissertation*, Saratov, 2005.
12. Korenman, Ya.I., Kuchmenko, T.A., and Smagina, N.N., *Sensor*, 2005, no. 1, pp. 27–29.
13. Korenman, Ya.I., Kuchmenko, T.A., Suleimanov, S.M., and Smagina, N.N., *Sensor*, 2005, no. 2, pp. 19–24.
14. Kuchmenko, T.A., *Primenenie metoda p'ezokvartsevogo mikrovzveshivaniya v analiticheskoi khimii* (Application of Piezoelectric Quartz Microweighing in Analytical Chemistry), Voronezh: Voronezh. Gos. Tekhnol. Akad., 2001.

ISSN 1070-4272, Russian Journal of Applied Chemistry, 2007, Vol. 80, No. 6, pp. 960–964. © Pleiades Publishing, Ltd., 2007.
Original Russian Text © M.N. Malanin, E. Moeller, P.M. Pakhomov, 2007, published in Zhurnal Prikladnoi Khimii, 2007, Vol. 80, No. 6, pp. 983–987.

NANOTECHNOLOGY AND NANOMATERIALS

Formation of the Pore Structure in Xerogel Films Based on Ultra-High-Molecular-Weight Polyethylene and Multiwall Carbon Nanotubes

M. N. Malanin, E. Moeller, and P. M. Pakhomov

Tver State University, Tver, Russia
University of Osnabruck, Osnabruck, Germany

Received August 29, 2006; in final form; January 2007

Abstract—The fundamental aspect of the pore structure formation in composite films based on ultra-high-molecular-weight polyethylene and multiwall carbon nanotubes were studied by IR spectroscopy, mercury porosimetry, scanning electron microscopy, and differential scanning calorimetry in relation to the degree of filling.

DOI: 10.1134/S1070427207060213

Preparation, structural studies, and search for new applications fields of polymeric composites (in particular, nanocomposites) are important problems of modern materials science. Nanotubes receive particular attention today as a polymer filler. Such fillers, when added to a polymer, change its structure (often causing its ordering) and, thus, its properties, such as melting point, mechanical and thermoelastic characteristics, diffusion coefficients, etc. Although papers on this problem have been published [1, 2], data on the structure and some properties of the polymer composites with nanotubes in the form of fibers are scarce.

It has been found recently [3, 4] that addition of some fillers (strontium ferrite, vermiculite, etc.) to a solution of ultra-high-molecular-weight polyethylene (UHMWP) increases the porosity of the xerogel structure, which is of particular importance in synthesis of highly absorbing materials. The fraction of pores in a material determines not only its sorption properties, but also its mechanical characteristics (e.g., strength), which are impaired at large free volumes in the composite. This dependence should be taken into account in production of polymeric fibers [5]. Thus, evaluation of the conditions of the pore structure formation in the course of preparation of the final material (e.g., fibers and films with high strength characteristics) is a topical problem.

In this study, we examined the formation of the pore structure in the UHMWP xerogel films in relation to the concentration of multiwall carbon nanotubes as filler.

EXPERIMENTAL

In the experiments, we used films of UHMWP xerogels with a molecular weight M_w 1.7×10^6, filled with multiwall carbon nanotubes (MWCNT) [6]. The average diameter and length of the nanotubes were 20 nm and 5 μm, respectively. The allotropic modification of carbon used was purchased from the Carbon Nano-Material Technology Co., Ltd. (Germany, South Korea). An electron micrograph of MWCNT is shown in Fig. 1. The films were prepared as follows. First, the polymer was dissolved in a solid paraffin and the filler was added to the true solution obtained. The resulting heterogeneous system was slowly cooled

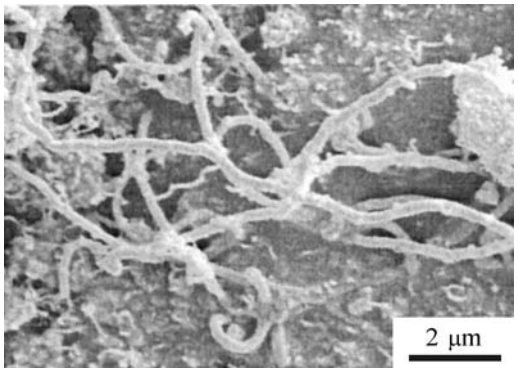

Fig. 1. Electron micrograph of MWCNT.

to room temperature, forming a filled xerogel film. Then, paraffin was washed out with hexane in a Soxhlet apparatus in the course of 24 h. The method used to prepare xerogel films is described in detail elsewhere [3, 4]. As a result, we obtained filled UHMWP xerogel films with a thickness of 20 to 60 μm; the degree of film filling was varied from 0 to 15%. We failed to prepare xerogel films with a higher degree of filling because of their mechanical breakdown in the course of preparation.

The dependences of the pore structure of the composites on the degree of their filling were studied by IR Fourier spectroscopy [7]. The IR spectra were recorded on an Equinox 55 Fourier IR spectrometer (Bruker). The IR evaluation of the porosity parameters, such as total porosity, average pore size, and pore size distribution, was described in [8, 9]. It is known that the overall extinction coefficient (attenuation factor) ε consists of the extinction coefficient related to absorption ε_A and extinction coefficient related to scattering ε_S, i.e., $\varepsilon = \varepsilon_A + \varepsilon_S$. The total porosity of the material α (%), which is the ratio of the total pore volume in the sample to the sample volume, was calculated using the following equation [8, 9]:

$$\alpha = \frac{\varepsilon_A^M - \varepsilon_A}{\varepsilon_A^M} \times 100, \quad (1)$$

where ε_A^M is the absorption-related extinction coefficient (ratio of the optical density at the absorption peak to the sample thickness in centimeters) of the most intense IR band (for polyethylene we used the absorption band at 730 cm^{-1}, associated with rocking vibrations of the CH_2 groups in the monolithic sample) and ε_A is the absorption extinction coefficient of the same band in the porous sample. In other words, ε_A decreases, with increasing pore volume in the material, i.e., the absorption-related extinction coefficient is inversely proportional to the total porosity.

When the sample contains heterogeneities (e.g., pores or filler particles) whose size is comparable with the wavelength of the incident radiation, this radiation is scattered in the system, which is manifested in the transmission or absorption spectra as a typical S-shaped inflection [8, 9]. The scattering-related extinction coefficient ε_S depends on the concentration, size, and shape of the scattering particles [10]. The larger the scattering S in the sample, the lower the light transmission and the greater the inflection curvature. By subtracting the IR spectrum of the monolithic sample of the same thickness, containing no scattering particles, from the IR spectrum of the scattering sample, we can obtain the dependence of scattering S (or directly the dependence of the size of scattering particles) on the wavelength λ. Subsequent differentiation of the resulting dependence of $S(\lambda)$ with respect to λ gives data on the size distribution of the scattering particles (in our case, pores) in the sample [8, 9].

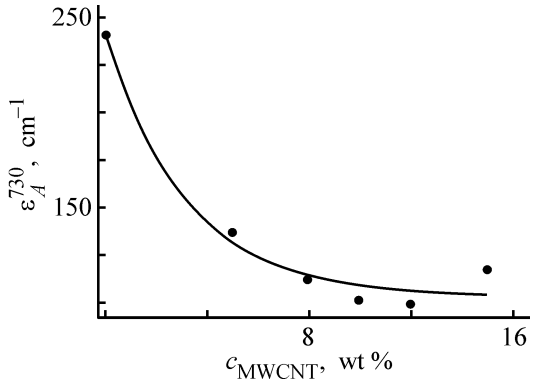

Fig. 2. Absorption-related extinction coefficient ε_A^{730} of UHMWP xerogel film vs. the degree of filling, c_{MWCNT}.

As independent methods for studying the composite pore structure, we used scanning electron microscopy [11] and mercury porosimetry (measurement of the mercury volume penetrating into the material at given pressures and evaluation of the size of pores filled with mercury) [12]. The samples for microscopic studies were prepared as follows. A sample was placed on a support coated with sputtered gold and dried in a vacuum [13]. Micrographs of the composite film surface were obtained with a Zeiss DSM 962 scanning electron microscope. The porosity (average pore diameter and total porosity determined only by micro- and nanopores) of the samples was determined on a Pascal 140 mercury porosimeter (Thermo Electron Corporation). Thermograms of melting of the polymer composites were recorded on a Diamond DSC 700 differential scanning calorimeter (Perkin–Elmer) at a heating rate of 10 deg min^{-1}; the weight of the xerogel film samples was 1.0–1.5 mg. Then, using the above thermal data, we calculated the degree of crystallinity æ (%) from the following equation:

$$æ = (\Delta H_m/\Delta H_m^0) \times 100, \quad (2)$$

where ΔH_m is the specific heat of melting of the given sample, and ΔH_m^0 is the calorific heat of melting of the ideal polyethylene crystal (293 J g^{-1} [10, 11]).

As shown above, the absorption-related extinction coefficient is inversely proportional to the free volume in the sample. The dependence of the extinction coefficient ε_A^{730} (or total porosity) of the composite on the filler concentration is shown in Fig. 2. As can be seen, the total porosity gradually increases with

Table 1. Total porosity α, average pore diameter d_{av}, and pore concentration c_{mac} in relation to the degree of filling, c_{MWCNT}, (based on IR data)

c_{MWCNT}, wt %	α, %	d_{av}, μm	c_{mac}, arb. units
0	8.8	5.7	171
5	48.0	9.9	50
8	57.3	9.9	41
10	61.5	3.1	87
12	62.3	6.1	41
15	55.1	3.4	119

the filler content of the sample. However, the corresponding curve flattens out at a filler concentration of 10–12 wt %, and at filler concentration of 15 wt % the total porosity even slightly decreases. A possible explanation is that the filler first leads to disordering of the polymer system, but, at its content exceeding 12 wt %, the sample becomes more compact owing to filling of the pores with the filler particles added. The results obtained using Eq. (1) are listed in Table 1. With account of the fact that ε_A^{730} for the monolithic polymer is 262.8 cm^{-1}, these data suggest that the total porosity is the highest (~62.0%) at an MWCNT content of 10–12%. Further increase in the filler content causes breakdown of the sample.

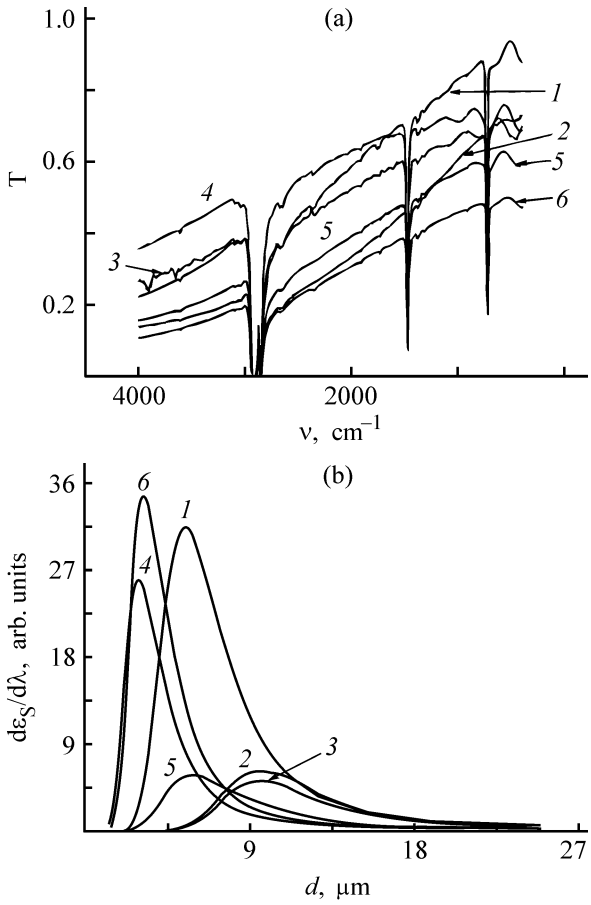

Fig. 3. (a) Transmission IR spectra of the composite UHMWP xerogel films with various degrees of filling and (b) pore size distribution in the composite films vs. the degree of filling. (T) Transmission, (ν) wavenumber, (*d*) pore diameter, and ($d\varepsilon_S/d\lambda$) first derivative of the scattering-related extinction coefficient with respect to the wavelength λ. Degree of filling, c_{MWCNT}, wt %: (*1*) 0, (*2*) 5, (*3*) 8, (*4*) 10, (*5*) 12, and (*6*) 15.

The transmission IR spectra of the composite polyethylene films with various degrees of filling are shown in Fig. 3a. As can be seen, the previously observed trend [3, 4] toward an increase in the pore size with the filler content of UHMWP is preserved. However, at a 8% degree of filling, the average size of the scattering sites (in particular, pores) decreases, which is confirmed by a shift of the characteristic S-shaped bend in the IR spectra toward shorter wavelengths [7, 8] (Table 1).

The size distribution curves of the scattering particles (pores, nanotubes), determined from the IR spectra using the procedure given in [8], are shown in Fig. 3b. As can be seen, a sharp increase in the porosity and a shift of the size distribution toward larger pore diameters are observed at 5 and 8% degrees of filling. With a further increase in the degree of filling, the sample with a smaller pore diameter is formed (10%) and the pore size distribution curves shift toward smaller values.

However, the total content of macropores, i.e., pores of micrometer size, which is determined as the integral of the pore size distribution curves or the area under these curves in Fig. 3b [15]), changes nonmonotonically. As can be seen from Table 1, the concentration of macropores in the xerogel film decreases in the initial stage (5 and 8% filling), as the total porosity of the sample increases. This can be attributed to an increase in the average pore size owing to merging of fine pores in the course of formation of the pore structure, promoted by the filler addition. At a 10% filling, the amount of macropores first grows, and as the degree of filling increases further, it decreases again. Presumably, both the size and concentration of nanopores contributing to the total porosity increase along with changes in macropores. Moreover, with increasing filler content, nanotubes can penetrate in the pore volume, thus changing the number and size of macropores.

Addition of one-wall carbon nanotubes changes such important system parameters as the melting point of the material [16]. It was found that multiwall carbon nanotubes, when added to the xerogel, affect not only the pore structure of the polymer, but also

the degree of polymer crystallinity [4]. In this case, the melting point of the xerogel films changes insignificantly (by 2–3°C). On the whole, the degree of crystallinity of the composite decreases with an increase in the degree of filling of the polymer. Comparison of the data of IR spectroscopy and differential scanning calorimetry (Figs. 3 and 4, respectively) shows that, when the degree of crystallinity in the system decreases, the average size of macropores (5, 8, and 12 wt % filling) increases, and vice versa. This is probably due to deceleration of the polymer crystallization upon addition of a filler. When carbon nanotubes are used as a filler, the composite can be regarded as a polymer layer between two planes formed by nanotubes. In accordance with [17, 18], the volume of the crystalline areas formed upon cooling correlates with the thickness of this polymer layer; it should be noted that this dependence passes through a maximum. If the thickness of the polymer layer is small, then the crystalline phase is formed predominantly on the surface (12, 15%). We assume that, in this case, changes in the crystallization process should leads to a decrease in the fraction of the surface pores At some intermediate layer thickness, corresponding to 10% filling, the volume of the crystalline phase is the largest, which is illustrated by a certain increase in the degree of crystallinity (Fig. 4). Further increase in the polymer layer thickness (5 and 8 wt % filling) accelerates formation of amorphous regions (film bulk), which ultimately leads to an increase in the fraction of pores in the material.

The data of mercury porosimetry are listed in Table 2. As can be seen, a certain decrease in macroporosity is observed at 10 wt % filling, which agrees with IR (Fig. 3a, the IR spectra are less distorted at 10% filling) and calorimetric data. However, as can be seen from Fig. 2, the sample porosity steadily increases with the degree of filling. This suggests that, in this case, the porosity is due to closed pores. The average diameter of macropores, d_1, increases with the degree of filling (Table 2), which also disagrees with Fig. 3b. This can be explained as follows. Mercury porosimetry characterizes only open and through pores in the sample, whereas IR spectroscopy reveals all the pores present in the sample. Along with the pores of micrometer size (1.0–100.0 μm), which can be studied by IR spectroscopy [8, 9], sample also contains nanopores (thinner than 1 μm). Changes in the total nanoporosity α_2 are proportional to changes in the total microporosity α_1 (Table 2). Changes in the average diameter of nanopores are expectable, because especially this fraction of the pore volume should be sensitive to an increase in the degree of crystallinity of the sample. Less porous structures are formed owing to disappearance of nanopores.

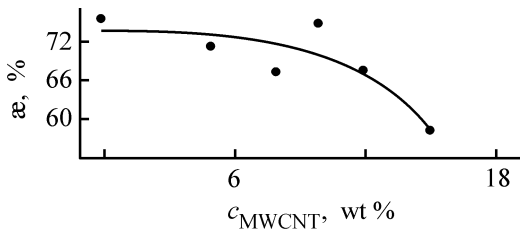

Fig. 4. Degree of crystallinity æ of the UHMWP xerogel films vs. the degree of filling, c_{MWCNT}.

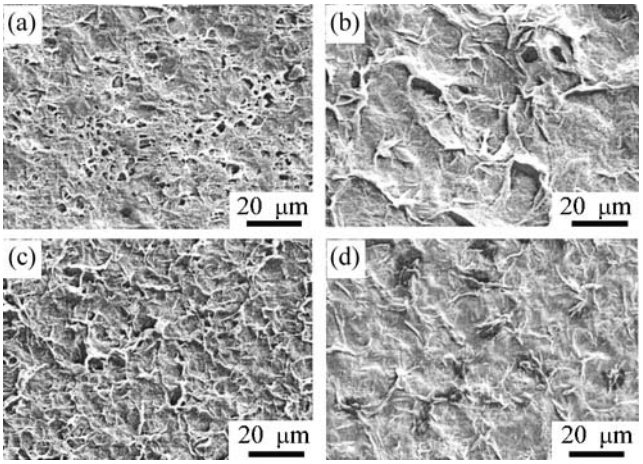

Fig. 5. Electron micrographs of the composite UHMWP xerogel surface at various degrees of filling, c_{MWCNT}, wt %: (a) 0, (b) 5, (c) 10, and (d) 15.

Electron micrographs of the surface of the composites with various degrees of filling are shown in Fig. 5. With increasing content of the filler (Figs. 5a, 5b; 0, 5 wt % filling), the average size of pores on the sample surface grows. When the content of nanotubes reaches 10–15 wt % (Fig. 5c, 5d), the sample

Table 2. Average volume of macro- (d_1) and micropores (d_2), and fraction (relative to total sample volume) of macro- (α_1) and micropores (α_2) in relation to the degree of filling of the composite, c_{MWCNT} (mercury porosimetry data)

c_{MWCNT}, wt %	α_1, %	α_2, %	d_1, μm	d_2, nm
0	13.2	15.2	26.8	39.1
10	2.1	0.8	39.4	25.0
15	44.6	14.8	36.7	87.4

surface becomes smoother and the content of the surface pores decreases, which agrees with the data shown in Fig. 2. The electron-microscopic data confirm that the porosity in the surface polymer layers varies with the degree of filling.

CONCLUSION

The data on the formation of the pore structure in composite xerogel films of ultra-high-molecular-weight polyethylene filled with multiwall carbon nanotubes showed that, with increasing filler content, the porosity of the system grows. As the degree of filling increases to more than 10 wt %, the system becomes more compact owing to the filling of the pores by the carbon nanotubes added.

ACKNOWLEDGMENTS

The authors are grateful to S.D. Khizhnyak for assistance in experiments and to S.A. Gribanov for recording the thermal data.

This study was financially supported by the Russian Foundation for Basic Research (project nos. 06-03-32609a and 06-03-08111 ofi) and by the German Service of Academic Exchange and Ministry of Science and Education of the Russian Federation within the framework of the Joint Russian–German Program "Mikhail Lomonosov" (2005/2006, project code 999998.)

REFERENCES

1. Mahfuz, H., *Int. J. Nanosci.*, 2005, vol. 4, no. 1, pp. 55–72.
2. McNally, T. et al., *Polymer*, 2005, vol. 46, pp. 8222–8232.
3. Mikhailova, Yu.N., Nazarova, E.V., Khizhnyak, S.D., et al., *Zh. Prikl. Khim.*, 2002, vol. 75, no. 1, pp. 107–112.
4. Pakhomov, P.M., Nazarova, E.V., Anan'eva, T.A., et al., *Zh. Prikl. Khim.*, 2003, vol. 76, no. 3, pp. 479–482.
5. *Karbotsepnye sinteticheskie volokna* (Carbon-Chain Synthetic Fibers), Perepelkin, K.E., Ed., Moscow: Khimiya, 1973.
6. Iijima, S., *Nature*, 1991, vol. 354, pp. 56–58.
7. Pakhomov, P.M., Malanin, M.N., Kuznetsov, A.Yu., et al., *Zh. Prikl. Khim.*, 2006, vol. 79, no. 6, pp. 1014–1017.
8. Pakhomov, P.M., Khizhnyak, S.D., Malanin, M.N., Kuznetsov, A.Yu., and Mikhailova, Yu.N., *Zavod. Lab. Diagn. Mater.*, 2002, vol. 68, no. 5, pp. 31–33.
9. Pakhomov, P.M., Malanin, M.N., and Khizhnyak, S.D., *Vysokomol. Soedin., Ser. B*, 2005, vol. 45, no. 6, pp. 1066–1072.
10. Bohren, C.F. and Huffman, D.R., *Absorption and Scattering of Light by Small Particles*, New York: Wiley, 1983.
11. Luk'yanovich, V.M. and Radushkevich, L.V., in *Metody issledovaniya struktury vysokodispersnykh i poristykh tel* (Methods for Analysis of the Structure of Highly Dispersed and Porous Bodies), Moscow: Akad. Nauk SSSR, 1953, pp. 39–46.
12. Kamakin, N.M., in *Metody issledovaniya struktury vysokodispersnykh i poristykh tel* (Methods for Analysis of the Structure of Highly Dispersed and Porous Bodies), Moscow: Akad. Nauk SSSR, 1953, pp. 47–58.
13. Goldstein J.I., Newbury, D.E., Echlin, P., Joy, D.C., Fiori, C.E., and Lifshin, E., *Scanning Electron Microscopy and X-ray Microanalysis*, New York: Plenum, 1981.
14. Mandelkern, L., *Crystallization of Polimers*, New York: McGraw–Hill, 1964.
15. Isimaru, A., *Wave Propagation and Scattering in Random Media*, New York: Academic, 1978.
16. Xie, X.L., Aloys, K., Zhou, X.P., and Zheng, F.D., *J. Therm. Anal. Calorim.*, 2003, vol. 74, pp. 317–323.
17. Lipatov, Yu.S., *Fiziko-khimicheskie osnovy napolneniya polimerov* (Physicochemical Foundations of Polymer Filling), Moscow: Khimiya, 1991.
18. Solomko, V.P., *Napolnenie kristallizuyushchikhsya polimerov* (Filling of Crystallizing Polymers), Kiev: Naukova Dumka, 1980.

ISSN 1070-4272, Russian Journal of Applied Chemistry, 2007, Vol. 80, No. 6, pp. 965–970. © Pleiades Publishing, Ltd., 2007.
Original Russian Text © A.E. Zaikin, R.S. Bikmullin, I.A. Gorbunova, 2007, published in Zhurnal Prikladnoi Khimii, 2007, Vol. 80, No. 6, pp. 988–993.

NANOTECHNOLOGY AND NANOMATERIALS

Characterization of the Adhesion Interaction of Polymers with the Surface of Filler Nanoparticles

A. E. Zaikin, R. S. Bikmullin, and I. A. Gorbunova

HighTech Consulting Ltd., Kazan, Tatarstan, Russia
Kazan State Technological University, Kazan, Tatarstan, Russia

Received October 10, 2006; in final form, February, 2007

Abstract—A method for characterization of the adhesion interaction of polymers with the surface of filler nanoparticles is suggested.

DOI: 10.1134/S1070427207060225

Undoubtedly, the adhesion of a polymer to the surface of filler particles is among factors substantially influencing the structure and properties of filled polymers. Therefore, it is important to have a technique allowing characterization of such an adhesion interaction. Numerous papers concerning this problem have been published [1–13]. However, it appeared difficult to develop a sufficiently reliable method for measuring the efficiency of adhesion interaction of a polymer with the surface of filler nanoparticles, because of the extremely small particle size of the filler and the high viscosity of the polymers [1–13].

The existing methods can be subdivided into two groups. The first group includes those based on determination of parameters characterizing the energy of interaction of a polymer with the surface of filler particles (true cohesion energy) [1–6]. Being based on sorption techniques for determination of thermodynamic parameters and on construction of thermodynamic cycles, these methods are very complex.

The second and the most numerous group covers the methods based on direct or indirect determination of the mechanical strength of adhesion of the polymer to the filler particles [8–13]. All the indirect methods allow estimation of only the relative efficiency of the adhesion interaction. The major drawback of the direct mechanical methods is the uncertainty about the adhesive fracture area and, frequently, even about the fracture mode.

Because of the lack of simple and reliable methods for determination of the adhesion strength, published data on the effect of the filler and polymer on the adhesion strength between them are scarce. Therefore, development of new adequate methods for determination of this characteristic appears to be a very topical task.

EXPERIMENTAL

We used in the study the following commercial thermoplastics: 15803-020 grade high-pressure low-density polyethylene (LDPE) [GOST (State Standard) 16337–77]; 11708–1250 grade ethylene/vinyl acetate copolymer (EVA) [TU (Technical Specifications) 6-05-1636–97] containing 28 wt % VA; PSM-115 polystyrene (PS) (GOST 20282–86); D-50 poly(vinyl acetate) (PVA) (GOST 18992–90); and 01 003 grade polypropylene (PP) (GOST 26996–86); and also commercial elastomers: P-118 polyisobutylene (PIB) (GOST 13303–67); 1,4-*cis*-polybutadiene (SKD) (GOST 14924–75); SKN-40m butadiene/acrylonitrile random copolymer (SKN) (GOST 7738–65, Mooney viscosity 54) containing 39 wt % AN; Nairit-M polychloroprene (PCP) (Mooney viscosity 62); SKT poly(dimethylsiloxane) (PDMS) (GOST 14680–79, number-average molecular weight 560000); and Urelan urethane thermoplastic elastomer (UTPE) (TU 38-403-0006–77) based on polyfurite, 4,4'-diphenylmethane diisocyanate, and 1,4-butanediol (0.5 : 1.0 : 0.5 molar ratio).

As fillers we used P267 crude oil furnace carbon black (CB) (GOST 7885–86, specific adsorption surface area S_{sp} = 225 $m^2 g^{-1}$, mean size of primary aggregates 28 nm) and A175 pyrogenetic amorphous silica in the form of Aerosil (GOST 14922–77, S_{sp} = 175 $m^2 g^{-1}$, particle size 10–40 nm). Prior to determination of the heat of wetting, the fillers were vacuum-

dried for 1 h in to remove physisorbed water. Carbon black was dried at 120°C, and Aerosil, at 200°C.

All the solvents used were of chemically or analytically pure grade, and they were additionally distilled before use.

The heats of wetting of the fillers with low-molecular-weight liquids were determined on a DAK1-1A automatic differential calorimeter. A weighed portion (40 mg) of a dried filler was placed in a thin-wall ampule, and the ampule was slowly evacuated and sealed. The ampule, wetting liquid (2 ml), and glass stick for breaking the ampule were placed in both cells of the calorimeter. After the desired temperature in the cells was reached, the ampule in one of them was broken. The liberated heat was recorded with an automatic potentiometer. The specific heat of wetting, ΔH, was estimated as

$$\Delta H = Q/S_{ads},$$

where S_{ads} is the specific adsorption surface of the filler, and Q, heat of wetting, determined from the calorimetric curves by the equation

$$Q = AS,$$

where S is the area under the curve recorded by the potentiometer, and A, calorimeter constant at a fixed sensitivity. The determination error was within 2%.

The specific heat of wetting, ΔH, was determined at 30.2°C, because the thermostat of the calorimeter operates reliably only at temperatures several degrees above the ambient temperature, whereas at higher temperatures, the volatility of the solvents increases.

To determine the peeling resistance of the polymer from the powdered filler, the latter was added to polypropylene by mixing on roll mills at 190 ± 5°C. The resulting filled polymer was compacted into a plate on a hydraulic press at 200 ± 5°C.

A thin polymer layer was then removed from the surface of the filled PP by treatment with an abrasive paper (grain size 50 μm). To avoid warming-up of the plate surface, the abrasive treatment was carried out in a cooling water stream at a very low processing speed. A plate made of unfilled PP was processed similarly.

Finally, the thus prepared plates were covered with a layer of the test polymer from a solution. The coating was carried out step-by-step, with each preceding layer dried. In the course of coating, the polymer layer was reinforced with a cotton fabric. The resulting sample was air-dried at room temperature for 1 day and then in a vacuum oven to final dryness.

The polymer solutions were prepared using the following solvents: toluene for SKD and PS; THF for UTPE; and chloroform for SKN, PCP, EVA, and PVA. A PE layer was applied onto a filled PP plate step-by-step at 160°C for 15 min.

After applying and drying a layer, all the rubber coatings were cured. For this purpose, the standard sulfurous curing agent [14] was added to SKN-40, SKD, and PCP using a roll mill prior to solution preparation. In the case of PDMS, K-18 hardener (5 wt %) was added prior to coating. The filled PP plates coated with the indicated rubbers were cured at 160°C for 20 min in an oven.

The peeling resistance was measured on a tensile-testing machine at a holder speed of 25 mm min^{-1}, temperature of 23°C, and peeling angle of 90°. Three parallel series of tests were performed with five samples in each series.

As mentioned above, the existing methods for determination of the interaction energy of polymers with a solid surface are very complex. At the same time, it is clear that the energy of adsorption interaction of liquids with a solid surface at a fixed temperature mostly depends on the chemical natures of the adsorbent and adsorbate [15–17]. Therefore, the energy of adsorption interaction of low-molecular-weight analogs of polymers with a solid surface should be well comparable with that of the corresponding polymers with the same surface, allowing evaluation of the efficiency of adsorption interaction of polymers with the surface of filler particles from model experiments with low-molecular-weight analogues.

The energy of adsorption of liquids on the surface of filler particles can be estimated from the heat of wetting ΔH. Since the adsorption of a liquid on a solid surface is not accompanied by changes in the aggregative state of the substances, the entropy of the system only slightly changes. Therefore, in this case, the integral heat of wetting is virtually equal to the energy of adhesion of the liquid to the surface [15].

It appeared interesting to measure the heat of wetting of the fillers not only with some low-molecular-weight analogues of the polymers, but also with a broader spectrum of liquids, in order to study the effect of the nature of liquids on ΔH. Our results showed that the ΔH values of carbon black and Aerosil

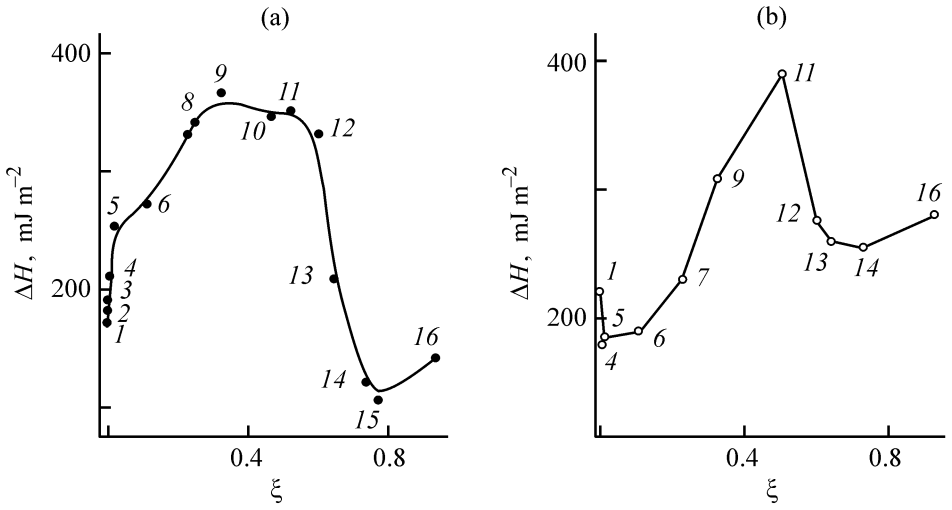

Fig. 1. Heat of wetting, ΔH, of (a) carbon black and (b) Aerosil vs. the polarity ξ of the liquids: (*1*) carbon tetrachloride, (*2*) *n*-hexane, (*3*) 2,2,4-trimethylpentane, (*4*) ethylbenzene, (*5*) toluene, (*6*) 1-chlorobutane, (*7*) MMA, (*8*) THF, (*9*) ethyl acetate, (*10*) 1-hexanol, (*11*) DMF, (*12*) acetonitrile, (*13*) ethanol, (*14*) ethylene glycol, (*15*) glycerol, and (*16*) water.

depend in a certain way on the polarity of liquids ξ (Fig. 1). The polarity of the polymers and liquids was estimated from the polar (δ_p) and hydrogen-bonding (δ_h) terms of the solubility parameter δ [18–21]:

$$\xi = (\delta_p^2 + \delta_h^2)/\delta^2.$$

The results showed that, with increasing polarity of the liquid, ΔH of carbon black and Aerosil passes through a maximum in a certain ξ range. The initial increase in ΔH is caused by the formation of hydrogen and polar bonds on the surface of carbon black with oxygen-containing groups, in addition to dispersion bonds. The increase in ΔH with the polarity of the liquid has been reported for carbon black previously [15, 22]. Furthermore, it was reported that the dependence of the adhesion of organic liquids to the surface of a number of metal oxides on the polarity of the liquids, determined from the soaking rate of the powders, is also nonmonotonic [23].

The maximal ΔH for such a filler as P267-grade carbon black is observed at $\xi \sim 0.33$, which is in satisfactory agreement with published data on the polarity of the surface of two other types of carbon black, determined from data on their dispersibility in liquids (0.43 and 0.38 for gas and furnace carbon blacks, respectively [18, 19]). P267-grade carbon black is distinguished by a relatively low concentration of the carboxy groups on the surface (9 mg-equiv g^{-1} on the average [24]). As a result, it has a slightly lower ξ.

Similar results were obtained for A175-grade Aerosil (pyrogenetic silica). For this material, the maximal ΔH was observed at $\xi = 0.51$ (Fig. 1), suggesting a higher polarity of the Aerosil surface as compared to carbon black, which is well consistent with the chemical structure of the surfaces of the fillers investigated.

Our results show that an increase in the polarity of the polymers to $\xi = 0.33$ enhances their adhesion to carbon black. Similar trend should also be observed for Aerosil with the polarity of the polymer increasing to 0.51.

It was of interest to examine how the above results correlate with the adhesion of the polymers to the fillers. However, the existing methods for determination of the adhesion of polymers to fine powders suffer from significant disadvantages [9]. For example, Yagnyanenskaya and Voyutskii [11] suggested to embed a powder in a polymeric binder, e.g., by mixing the filler power with a solution of polyvinyl alcohol, followed by removal of the solvent, and then to measure the peeling resistance of the surface of the polymeric binder with encapsulated filler particles with respect to the polymer investigated. However, the filler surface is covered in this case with the polymeric binder, so that a change in the peeling resistance could be detected only at a very high degree of filling. Savel'ev et al. [13] suggested to apply filler to the surface of a PS polymeric support pretreated with an organic solvent (chloroform). After the removal of the solvent, a part of the filler was glued to

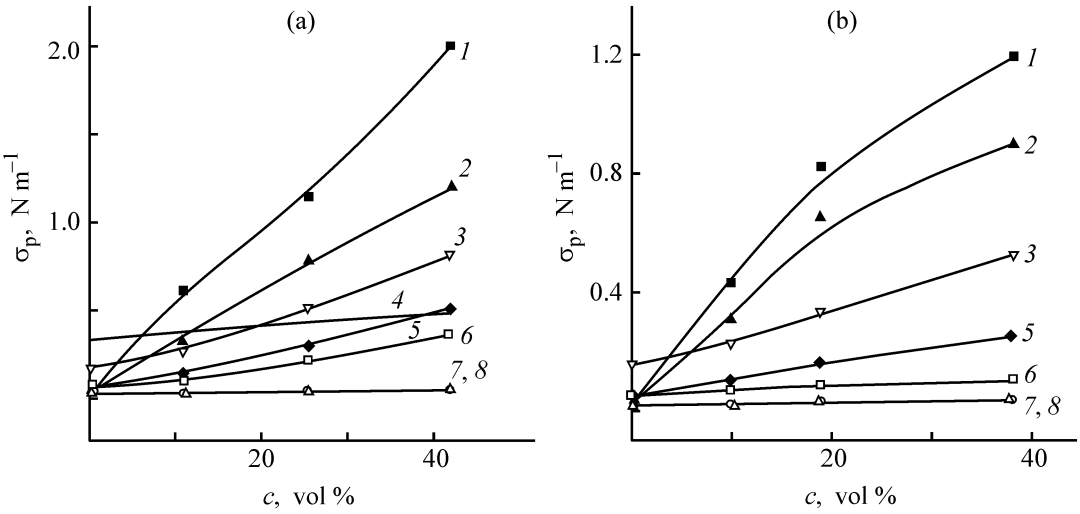

Fig. 2. Peeling resistance σ_p of (a) carbon black and (b) Aerosil fixed in polypropylene with respect to polymers vs. the filler content c: (*1*) PVA, (*2*) UTPE, (*3*) PCP, (*4*) SKD, (*5*) SKN-40m, (*6*) EVA-28, (*7*) PS, and (*8*) LDPE.

the support. The residual filler was removed with a brush. Then the polymer investigated was applied as a melt to the plate by pressing, and the peeling resistance of the filler particles fixed on the support was measured with respect to the polymer investigated. It is noteworthy that, in this method, the filler surface remained partly open. However, some doubt is cast in this case upon the strength of fixation in the matrix of all the remaining filler particles. Furthermore, the surface concentration of the filler is unknown.

To overcome these drawbacks, we suggest in this study a somewhat different technique for fixation of the filler to the polymer matrix. The filler was introduced into a polymer melt and the resulting mixture was compacted into plates. In this case, as mentioned above, the surface of the filler particles appears to be coated with a polymer layer. To strip the surface of the filler particles, a thin layer of the polymer was removed from the plate surface using an abrasive. Then a layer of the polymer investigated was applied to the wafer by spraying, followed by removal of a solvent, and the peeling resistance was measured. Analysis of the experimental results becomes simpler if the polymeric binder used as a matrix for the filler is characterized by very low adhesion to the polymer investigated. In this case, the adhesion of the binder to the polymers can be neglected. In this study, we used polypropylene as a binder, as having a very low adhesion to the most of the investigated polymers and low room-temperature solubility in liquids.

In this sample preparation procedure, the fraction of stripped surface of the filler particles should be in proportion to its volume fraction in the binder, as demonstrated by the almost linear dependence of the peeling resistance σ_p on the filler content (Fig. 2). In the case when the filled polymer plates have not been processed with an abrasive prior to application of the adhesive, σ_p started to increase only at a filler (carbon black or Aerosil) content of about 30 vol %. Evidently, at such a high degree of filling, the surface of carbon black or Aerosil is incompletely wetted with the polymer in the mixture, so that the mixture adsorbs the adhesive.

To adequately characterize the adhesion of the polymer to the filler, it is necessary to know what mode [adhesion (along boundaries) or cohesion (though the bulk of the material)] of peeling occurs in the tests. An optical-microscopic examination of the surfaces of the adhesive and supporting wafer after testing suggested that the filler particles are not transferred from PP to the surface of the polymer film being peeled. Only at the filler content in PP as high as approximately 40 vol %, we observed transfer of small amount of the filler particles onto the adhesive. The microscopic examination revealed no residual adhesive on the plate surface coated with the binder. All these facts allow characterization of the relative efficiency of the adhesion interaction of the polymers with the filler by the increase in the peeling resistance $\Delta\sigma_p$, resulting from a higher filler content of PP.

Data on σ_p (Fig. 2) show that, with increasing polarity of the polymer (see table), its adhesion to the filler grows. Qualitatively, this result is well consistent with data obtained from the heat of wetting

Characteristics of the interaction of polymers and their low-molecular-weight analogues with carbon black and Aerosil

Polymer				Low-molecular-weight analogue			
kind of polymer	ξ [18–21]	$\Delta\sigma_p^*$, kN m^{-1}		compound	ξ [18–21]	ΔH, mJ m^{-2}	
		carbon black	Aerosil A-175			carbon black	Aerosil A-175
PE	0.0	0.02	0.01	*n*-Hexane	0	170	220
PIB	0.0	0.02	0.01	2,2,4-Trimethylpentane	0	175	225
PS	0.012	0.02	0.01	Ethylbenzene	0.01	205	180
SKD	0.003	0.15	0.05	1-Hexene	–	180	–
PDMS	0.041**	0.03	–	Octamethylcyclotetrasiloxane	0.04	200	–
EVA-28	–	0.32	0.05	–	–	–	–
SKN-40	–	0.46	0.21	–	–	–	–
PCP	0.112**	0.65	0.37	1-Chlorobutane	0.11	270	190
UTPE	–	1.17	0.87	–	–	–	–
PVA	0.333	2.12	1.17	Ethyl acetate	0.33	365	308

* ($\Delta\sigma_p$) Increase in σ_p with an increase in the carbon black content of PP from 0 to 42 vol % and in the Aerosil A-175 content of PP from 0 to 38 vol %.

** Estimated from the ratio of the polar and dispersion terms of the surface tension of the polymer [25].

(see table and Fig. 1). Therefore, with increasing fraction of the polar and hydrogen constituents of the solubility parameter of the polymers from 0 to 0.33, their adhesion to carbon black and Aerosil becomes stronger.

Data on ΔH and σ_p show that PE, PIB, SKD, PP, PS, and PDMS have the lowest and close energies of adsorption interaction with the surface of carbon black and Aerosil. The adhesion of the other polymers to carbon black and Aerosil increases in the order EVA-28 < SKN-40 < PCP < UTPE < PVA.

CONCLUSIONS

(1) Data on the efficiency of adsorption interaction of a series of polymers with the surface of finely dispersed fillers, determined from data on the heat of wetting of the fillers with low-molecular-weight analogs, agree well with those obtained by measuring the peeling resistance of the fillers with respect to the polymers.

(2) With the fraction of the polar and hydrogen constituents of the solubility parameter of the polymers increasing from 0 to 0.33, their adhesion to carbon black and Aerosil becomes stronger.

REFERENCES

1. Kwei, T., *J. Appl. Polym. Sci.*, 1964, no. 8, p. 1483.
2. Kwei, T., *J. Polym. Sci., Ser. A3*, 1965, p. 3225.
3. Uskov, I.A., Galinskaya, V.I., and Artyukh, L.V., *Vysokomol. Soedin.*, 1966, no. 10, p. 1853.
4. Bessonov, Yu.S., Tager, A.A., Yushkova, S.M., et al., *Vysokomol. Soedin., Ser. A*, 1978, vol. 20, no. 1, pp. 99–105.
5. Tager, A.A., Yushkova, S.M., Bessonov, Yu.S., et al., *Vysokomol. Soedin., Ser. A*, 1979, vol. 21, no. 5, pp. 1051–1058.
6. Tager, A.A., Yushkova, S.M., and Safronov, A.P., *Plast. Massy*, 1987, no. 5, pp. 26–27.
7. Tsvetkova, M.N., *Zh. Prikl. Khim.*, 1985, vol. 58, no. 6, pp. 43–45.
8. Hess, W.M., *Reinforcement of Elastomers*, Kraus, G., Ed., New York: Interscience, 1965. Translated under the title *Usilenie elastomerov*, Moscow: Khimiya, 1968, ch. 6, pp. 168–187.
9. Lupinovich, L.N. and Garshin, A.P., *Plast. Massy*, 1986, no. 5, pp. 43–45.
10. Lazukin, A.I. and Val'tsifer, V.A., *Zavod. Lab.*, 1984, vol. 50, no. 2, p. 46.
11. Yagnyanenskaya, S.M. and Voyutskii, S.S., *Kauchuk Rezina*, 1971, no. 1, pp. 19–20.
12. Dorofeev, T.V., Grigor'ev, L.N., and Sergeev, V.I., *Vysokomol. Soedin., Ser. A*, 1985, vol. 27, no. 2, p. 374.
13. Savel'ev, A.V., Vnukova, V.G., Kiselev, V.Ya., and Tutorskii, I.A., *Kauchuk Rezina*, 1986, no. 6, pp. 38–39.
14. Zakharchenko, P.I., *Spravochnik rezinshchika: Materialy rezinovogo proizvodstva* (A Handbook of Rubber Worker: Materials for Rubber Production), Moscow: Khimiya, 1971.
15. Adamson, A.W., *Physical Chemistry of Surfaces*, New York: Wiley, 1976.

16. Dannenberg, E.M., *Rubber Chem. Technol.*, 1975, vol. 48, no. 2, p. 410.
17. Waddell, W.H., in *The Second Int. Conf. on Carbon Black, Mulhouse* (France), September 1993, pp. 147–150.
18. Hansen, C.M., *J. Paint. Technol.*, 1967, vol. 39, no. 505, pp. 104–113.
19. Hansen, C.M., *J. Paint. Technol.*, 1967, vol. 39, no. 511, pp. 505–510.
20. Kinloch, A. J., *Adhesion and Adhesives: Science and Technology*, London: Chapman and Hall, 1987. Translated under the title *Adgeziya i adgezivy: Nauka i tekhnologiya*, Moscow: Mir, 1991, pp. 42–45.
21. Skaarup, K., *Skand. Tidskr. Fang och Lack*, 1968, vol. 14, no. 3, pp. 45–51.
22. Lavelle, J.A. and Zettlemoer, A.S., *J. Phys. Chem.*, 1967, vol. 71, no. 2, pp. 414–417.
23. Stepin, S.N., Bogatov, F.V., and Svetlakov, N.V., *Zh. Prikl. Khim.*, 1991, vol. 64, no. 10, p. 2107.
24. Gul', V.E. and Shenfil', L.Z., *Elektroprovodyashchie polimernye kompozitsii* (Electrically Conducting Polymeric Composites), Moscow: Khimiya, 1984.
25. Wu, S., *Polymer Blends*, Paul, D.R. and Newman, S., Eds., New York: Academic, 1978, vol. 1. Translated under the title *Polimernye smesi*, Moscow: Mir, 1981, ch. 6, pp. 283–336.

ISSN 1070-4272, Russian Journal of Applied Chemistry, 2007, Vol. 80, No. 6, pp. 971–978. © Pleiades Publishing, Ltd., 2007.
Original Russian Text © G.A. Shagisultanova, M.S. Masalovich, L.P. Ardasheva, 2007, published in Zhurnal Prikladnoi Khimii, 2007, Vol. 80, No. 6, pp. 994–1001.

MACROMOLECULAR CHEMISTRY AND POLYMERIC MATERIALS

Electrically Conducting Polymers Based on *trans*-[Pt(qol)$_2$] Complex

G. A. Shagisultanova, M. S. Masalovich, and L. P. Ardasheva

Herzen Russian State Pedagogical University, St. Petersburg, Russia

Received November 14, 2006; in final form, March 2007

Abstract—Oxidative electrochemical synthesis and formation kinetics of electrically conducting polymeric platinum(II) complexes with 8-quinolinol was studied. Spectroscopic and electrochemical properties of the polymers were characterized.

DOI: 10.1134/S1070427207060237

The chemistry of electroactive polymers is rapidly developing. These materials are widely used as corrosion protectors, catalysts, electrochromic materials, materials for chemical sensors and voltaic cells [1].

The so-called redox polymers, which are characterized by regular alternation of oxidized and reduced molecular fragments, occupy a particular place among polymeric materials. Organometallic redox polymers have a number of advantages over organic polymers with uniform electronic structure. Some of them are analogues of biocatalysts, e.g., peroxidase and oxygenase, and are characterized by high efficiency and selectivity. In addition, the properties of these materials can be controlled by varying the nature of metal centers, which opens up new prospects for control over optical properties of polymers by electric signals or protons [2]. Recent studies of production of transparent light-emitting diodes demonstrated the advisability of using electroluminescent polymers based on [Al(qol)$_3$] in LED devices, which are elements of flat-panel display screens of the next generation [3].

Redox polymers based on transition metal complexes are among the most important polymers of this type [4–10]. Among them, thin-layer electrically conducting, photosensitive, and luminescence-active polymers based on Pt(II) complexes with various polychelate ligands including *N*,*N*'-bis(salicylidene)ethylenediamine (Salen) and its derivatives [11] are of particular interest.

In this study, we used *trans*-[Pt(qol)$_2$] (Hqol is 8-quinolinol) as a monomeric unit in synthesis of multifunctional polymers [12]. The formula of this complex is as follows:

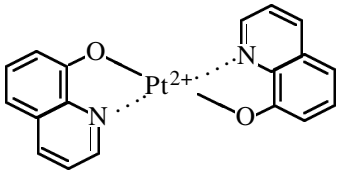

The optical, photophysical, and catalytic properties of [Pt(qol)$_2$] have been well studied [3, 13–16]. However there are no data on electrochemical synthesis of thin electrically conducting polymeric films on its basis.

In contrast to the previously used meSal ligand [17], containing imine nitrogen atom bound with the methyl group, in the qol ligand, the nitrogen atom is incorporated in the pyridine ring of 8-quinolinol. Thus, one of our main goals was to examine the influence of the chelate ring size (five-membered ring in Pt complex with qol in contrast to six-membered cycles with Salen and meSal) on the electropolymerization of the metal complex. The structural formulas of Salen and meSal are as follows:

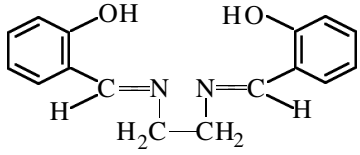

Salen

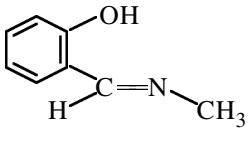

meSal

The complex [Pt(qol)$_2$] was synthesized by the modified method [13]. Potassium tetrachloroplatinate(II), K_2PtCl_4 and 8-quinolinol C_9H_7ON (Merck), recrystallized from ethanol, were used.

Potassium tetrachloroplatinate(II) (0.6 g) was dissolved in water (6 ml), and the solution was added

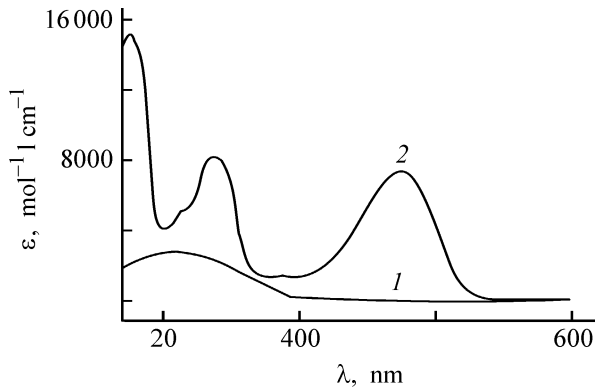

Fig. 1. Electronic absorption spectra of 1×10^{-4} M solutions of (*1*) 8-quinolinol ligand Hqol and (*2*) complex $[Pt(qol)_2]$ in DMF. (ε) Extinction coefficient and (λ) wavelength.

to a solution of 8-quinolinol (1 g) in 10 ml of glacial acetic acid (pH 4). The reaction mixture was stirred for 1 h at 70°C. After cooling, the orange-brown precipitate formed was filtered off, washed with plentiful of dilute acetic acid, then with ethanol, and recrystallized from DMF. The yield was 86%.

Because $[Pt(qol)_2]$ is photochemically labile in the presence of atmospheric oxygen [3, 13], all solutions were prepared in the dark.

The ligand and complex were identified by electronic absorption spectroscopy (EAS) and X-ray photoelectron spectroscopy (XPES).

The electronic absorption spectra of the ligand and complex in DMF (ultra-pure grade) and of the polymer (both oxidized and reduced forms) were recorded on an SF-2000 spectrophotometer at 293 K.

Table 1. Binding energy of photoelectrons and atomic concentrations of the XPES components of the ligand Hqol and complex $[Pt(qol)_2]$

Line	Hqol		$[Pt(qol)_2]$	
	E_b, eV	atomic concentration, %	E_b, eV	atomic concentration, %
C1*s*	285.0	45.2	285.0	17.3
	286.0	27.3	285.9	53.44
	289.3	2.3	286.8	7.57
	291.3	2.8		
O1*s*	531.7	3.0	531.9	6.62
	532.9	9.8	532.9	1.66
			534.2	0.84
N1*s*	399.3	5.9	400.9	6.59
	400.3	0.7	401.7	1.47
			402.8	0.44
Pt4*f*			73.7	4.07

The absorption spectra of the ligand Hqol and complex $[Pt(qol)_2]$ are shown in Fig. 1. As can be seen, the spectrum of Hqol is characterzed by a strong absorption band at 314 nm (ε = 2630) corresponding to intraligand π–π^* transition [13].

The complexation of $[Pt(qol)_2]$ is accompanied by pronounced changes in the EAS. For instance, the strong π–π^* band shows a batochromic shift to λ_{max} = 345 nm (ε = 8000). In addition, a new strong band at λ_{max} = 478 nm (ε = 6900) appears. This band was assigned, according to published data [3], to intraligand charge transfer (ILCT) from oxygen to nitrogen atom, or from phenolic to pyridine ring. At the same time, the mixed type of this absorption band associated with overlap of the ILCT band with the metal-to-ligand charge transfer (MLCT) band cannot be ruled out.

X-ray photoelectron spectra were recorded on an Axis Ultra (Kratos Alalytical, the United Kingdom) electron spectrometer with excitation by Al_{K_α} (1486.6 eV)[1] radiation. During measurements, the residual pressure in the spectrometer was 5×10^{-7} Pa. The spectra were processed using Vision 2 software, Kratos Analytical. The energy scale was calibrated against the C1*s* line of aromatic carbon as a reference (E_b = 285.0 eV).

The binding energy of photoelectrons and the atomic concentrations of the components (in at.%) for Hqol and $[Pt(qol)_2]$ are listed in Table 1.

The presence of two lines at 531.7 and 532.9 eV in the O1*s* spectrum and of two lines at 399.1 and 400 eV in the N1*s* spectrum for protonated ligand Hqol is probably caused by equilibrium proton transfer from the O atom to the N atom and back, with the equilibrium being shifted to formation of hydroxy groups.

The formation of $[Pt(qol)_2]$ is accompanied by changes in the binding energy of the highest-intensity components of O1*s* and N1*s* spectra as compared to Hqol. The N1*s* energy decreases from 399.3 to 400.9 eV, while the O1*s* energy decreases from 532.9 to 531.9 eV, respectively.

The observed chemical shifts (+1.6 eV for N1*s* and –1.0 eV for O1*s*) show that the binding energy of N1*s* electron increases because of the formation of the σ-donor bond in the complex with the participation of the unshared electron pair of the nitrogen atom belonging to the polycyclic ligand. In the process,

[1] Spectra was obtained by A.V. Shchukarev, St. Petersburg State University.

a part of the electron density shifts to the oxygen atom via the metal center.

In the complex, the platinum atom has the 4*f* electron binding energy of 73.7 eV, which corresponds to Pt(II) [18]. The Pt : N : O ratio is about 1 : 2 : 2, which indicates a virtually complete coordination of the metal center with the ligands via two nitrogen atoms and two oxygen atoms.

The electrochemical properties of the ligand and complex [Pt(qol)$_2$] and the synthesis and the redox properties of polymeric compounds obtained from monomeric [Pt(qol)$_2$] were studied by cyclic voltammetry.

The electrochemical measurements were carried out on an IPC-PRO potentiostat-galvanostat in a hermetic beaker with a common space for the working, auxiliary, and reference electrodes. A platinum wire (99.99% purity) with a surface area of 0.27 cm^2, soldered in a Pyrex holder, platinum plates, and optically transparent quartz plates with a layer of Sn(IV) oxide deposited on their surface served as working electrodes. A platinum grid was an auxiliary electrode. All potentials are given relative to a glass AgCl/Ag reference electrode filled with a NaCl saturated solution. A 0.1 M solution of tetrabutylammonium perchlorate (Bu_4NClO_4) in ultrapure grade dichloromethane (CH_2Cl_2) served as the supporting electrolyte. The concentration of the complex in the solution was 1 mM.

To find the optimal conditions of the synthesis of electrically conducting and photoactive [Pt(qol)$_2$] polymers, polymeric films were formed on an electrode in two modes: potentiodynamic and potentiostatic.

In the potentiodynamic mode, the polymer was accumulated under the conditions of cycling of the working electrode potential within the range 0.0–1.2 ± 0.1 V in the solution of the initial monomeric compound at a sweep rate of 0.05 V s^{-1}. The cycloammogram (CVA curve) obtained by single potential cycling in the solution of the complex [Pt(qol)$_2$] in CH_2Cl_2 is shown in Fig. 2 and is characterized by two oxidation waves with features at potentials of 0.9 (shoulder) and 1.0 V (peak). Two broad unresolved cathode waves with current peaks at 0.75 and 0.15 V appear when sweep direction is changed.

At the same time, only one oxidation wave is observed on a CVA curve of the ligand solution, with a peak at 1.1 V, whereas the back reduction wave is absent. Thus, there is no reversible charge transport, i.e., free ligand (8-quinolinol) in CH_2Cl_2 (and in acetonirile [19]) does not form active polymeric substances on the electrode surface. This was also confirmed visually. The close potentials of the anodic oxidation peak of the ligand and of the second peak of oxidation of the complex suggest that the orbitals of predominantly ligand type participate in the electrooxidation of the complex. At the same time, the first oxidation potential of the complex at E = 0.9 V can be attributed to the transfer of electron predominantly belonging to metal orbitals.

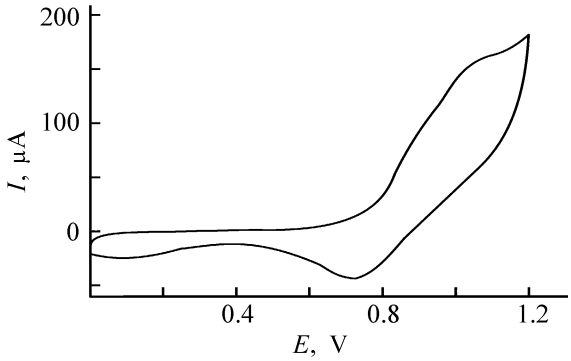

Fig. 2. CVA curve of the first cycle of electrode sweep potential in 1 mM solution of the complex [Pt(qol)$_2$] in 0.1 M solution of Bu_4NClO_4 in CH_2Cl_2. v_p = 0.05 V s^{-1}. (*I*) Current strength and (*E*) potential; the same for Figs. 3 and 6.

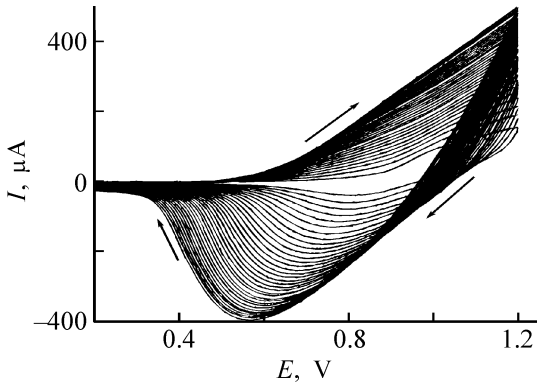

Fig. 3. CVA curves reflecting the dynamics of precipitation of the electroactivesubstance on the electrode surface from 1 mM [Pt(qol)$_2$] in 0.1 M solution of Bu_4NClO_4 in CH_2Cl_2. v_p = 0.05 V s^{-1}; 35 scans.

The subsequent cycling of the potential within the range from 0.0 to +1.2 V at a sweep rate of 0.05 V s^{-1} is accompanied by an increase in the height of the current peaks on both anodic and cathodic branches of the CVA curves, and also by overlap and leveling of the peaks and by the shift of the cathodic peak at E = 0.75 V to the negative region. By the 35th cycle, when an increase in current peak stops, we can note a cathodic peak at E_p = 0.6 V and appearance of an unresolved broad anodic wave with a feature at E = 0.9 V (shoulder) (Fig. 3).

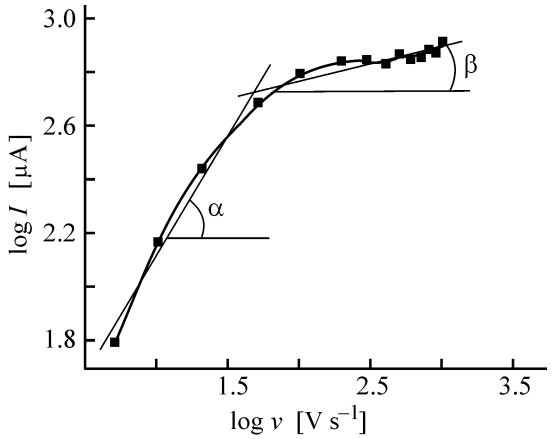

Fig. 4. Dependence of the logarithm of the cathode peak current I on the logarithm of the sweep rate of the potential of the electrode modified with a 1.4 μm layer of $[Pt(qol)_2]$ in 0.1 M solution of Bu_4NClO_4 in CH_2Cl_2.

A red film insoluble in water and organic solvents is detected visually on the electrode surface which confirms the formation of a stable solid product of $[Pt(qol)_2]$ oxidation. The transition from the reduced to oxidized form is accompanied by an electrochromic effect, with the film color changing from red to black. A calculation [20] showed that the polymer film thickness increases by 100 nm after each potential sweep.

To study the electrochemical stability and determine certain quantitative characteristics of polymeric films, we transferred the electrodes with poly$[Pt(qol)_2]$ obtained by polymerization in various potential sweep ranges into a solution of the pure supporting electrolyte and cycled the potential within the range from 0.0 to +1.2 V. It was found that the CVA curves remained unchanged for a long time. This fact confirms the stable character of the reversible charge transport in the bulk of the polymer solid phase.

A study of CVA curves at various sweep rates (from 0.005 to 1.0 V s^{-1}) allowed us to determine such quantitative characteristics of the polymer as thickness h (μm) and diffusion coefficient D_{ct} (cm^2 s^{-1}). As is known [20, 21], at low potential scanning rates, the film function in the mode of thin-layer voltammetry (TVA), which is accompanied by oxidation or reduction of all molecular fragments of the polymer chain. At high rates, only certain fragments of the polymeric chain are active, so that we have the mode of semiinfinite diffusion (SID). Thus, SID allows estimation of the charge transport rate in the polymeric phase, whereas we can approximately estimate by thin-layer voltammetry the thickness of the electrically conducting layer. As can be seen from the dependence of the logarithm of the cathode current peak on the logarithm of the potential sweep rate (Fig. 4), redox processes occur at sweep rates of 0.005 to 0.05 V s^{-1} in the TVA mode, as judged from the slope of the straight line ($\tan\alpha = 1$). The increase in the potential sweep rate for the electrode modified with poly$\{Pt(qol)_2]$ from 0.05 to 1.0 V s^{-1} causes transition to the diffusion mode of the polymer functioning ($\tan\beta = 0.5$).

The thickness of the polymer film and charge diffusion coefficient in the bulk of poly$[Pt(qol)_2]$ were calculated by the known methods [20]. The values obtained in the dynamic mode for films differing in synthesis conditions are listed in Table 2.

It should be noted that widening of the range of the electrode potential sweep in the complex solution to 1.4 V sharply changes the shape of the CVA curve already in the second cycle: the anode and cathode current peaks disappear.

Vilas–Boas et al. [22] suggest that the fact the current peaks cease increase during polymerization can be caused by "overoxidation" due to irreversible ligand oxidation with increasing potential. It was also found that narrowing of the potential sweeping range in oxidation of the complex under the dynamic conditions from 0.1–1.2 to 0.9–1.2 V does not change the quan-

Table 2. Thickness of the polymer film and charge diffusion coefficient in the bulk of poly$[Pt(qol)_2]$ synthesized under the dynamic conditions

Electrode potential, E^*, V	Number of cycles	$D_{ct} \times 10^{-11}$,** cm^2 s^{-1}	h,*** μm
0.0…+1.1	35	4.7	0.8
0.0…+1.2	35	7.3	1.4
0.0…+1.3	35	4.0	1.4

* 1 mM solution of $[Pt(qol)_2]$, supporting electrolyte 0.1 M Bu_4NClO_4 in CH_2Cl_2.

** Calculated from CVA curves obtained by sweeping the potential of the electrode modified with poly$[Pt(qol)_2]$ in pure supporting electrolyte at a sweep rate of 0.05–1.0 V s^{-1}.

*** Calculated from CVA curves in the pure supporting electrolyte at potential sweep rates of 0.005–0.05 V s^{-1}.

titative characteristics of the polymer synthesized, whereas sweeping within the 1.0–1.2 V and 1.1–1.2 V ranges decreases the thickness of the polymeric film. This can be caused by the fact that a sharp change of the direction of the potential sweeping with the corresponding alternation of the redox processes, prevents formation of a homogeneous polymer structure and, hence, increase in the film thickness.

The static mode involves formation of the polymer at a constant accumulation potential E_a. The optimal E_a is that at which the maximal amount of the electrochemically active polymer is deposited on the electrode surface in unit time.

To determine the optimal potential of accumulation and specific features of the poly[Pt(qol)$_2$] formation, we studied the dependence of the polymer layer thickness on E_a and process time τ_a.

The optimal values of E_a were determined as maxima of functions $h = f(E_a)$ and $h = f(\tau_a)$ (Fig. 5). The thickness of the polymer film at various E_a is listed below (accumulation time τ_a is 5 min):

E_a, V	0.8	0.9	1.0	1.1	1.2	1.3	1.4
h, μm	0	0.06	0.8	0.65	0.5	0.25	0.25

The increase in h values on raising the potential from 0.8 to 1.0 V may be due to an increasing rate of electrooxidation of complexes. The decrease in the film thickness after attaining the optimal potential or formation time is probably due to loss of the polymer electroactivity because of the irreversible oxidation and decomposition of the π-conjugation chain in the ligands.

As can be seen from Fig. 5, the extremum of the function $h = f(\tau_a)$ exceeds, under static conditions of synthesis, the extremum of the similar function for dynamic conditions. This indicates that it is economically advisable to prepare films in the static mode, because a larger film thickness can be attained in a shorter time and the synthesis can be performed for a longer time as compared to dynamic conditions.

The CVA curves obtained at a single potential sweep for poly[Pt(qol)$_2$] films with various thicknesses in a solution of pure supporting electrolyte (sweep rate 0.01 V s^{-1}) are shown in Fig. 6. As can be seen, the anodic and cathodic waves characterizing the reversible charge transport in the bulk of the polymer phase are observed in the CVA curves. An increase in the synthesis time to 45 and 60 min is accompanied by termination of the growth and decrease in the reduction wave, respectively, whereas the anodic peaks continue to increase. Alpatova et al. [23] and Vorotyntsev et al. [24] explained the decrease in the polymer redox activity by existence of the residual structural units of the polymer in the oxidized form which act as of electron "traps," or areas with "inhibited core".

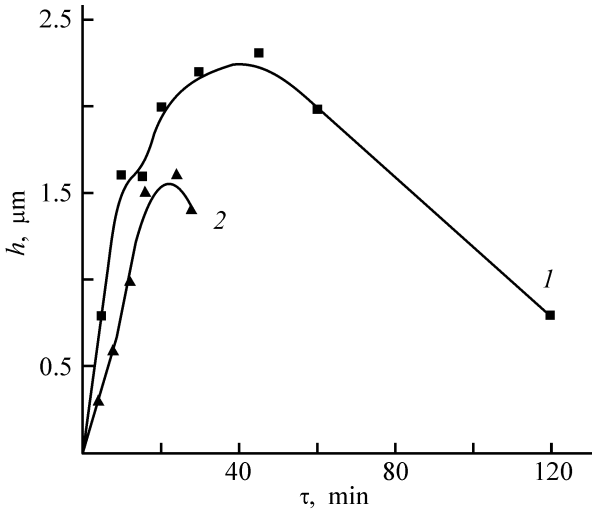

Fig. 5. Thickness h of poly[Pt(qol)$_2$] layer vs. the accumulation time τ in the (*1*) potentiostatic (E_a = 1.0 V) and (*2*) potentiodynamic modes.

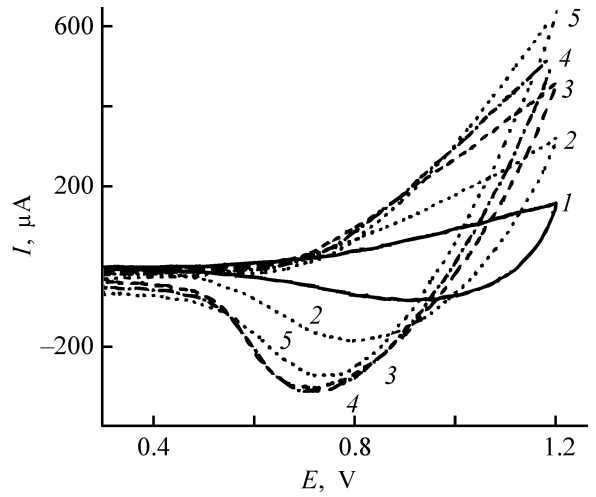

Fig. 6. CVA curves describing solid-phase redox processes in samples of poly[Pt(qol)$_2$] synthesized in the potentiostatic mode at E_a = 1.0 V. 0.1 M solution of Bu_4NClO_4 in CH_2Cl_2, v_p = 0.01 V s^{-1}. Synthesis time, min: (*1*) 5.0, (*2*) 15.0, (*3*) 30.0, (*4*) 45.0, and (*5*) 60.0.

Thus, accumulation in the static mode at E_a = 1.0 V for τ_a = 30–40 min is the optimal condition of synthesis of poly[Pt(qol)$_2$].

As mentioned above, the diffusion coefficient D_{ct} is the most important characteristic of the charge transfer rate in the polymeric matrix. The D_{ct} values

Table 3. Influence of the potential and accumulation time on D_{ct} of poly[Pt(qol)$_2$]

E_a, V	τ, min	$D_{ct} \times 10^{-11}$,* cm^2 s^{-1}
0.9	5	0.6
1.0	5	7.9
1.1	5	7.1
1.2	5	2.1
1.3	5	0.6
1.4	5	0.04
1.0	5	8.0
1.0	10	8.2
1.0	15	4.6
1.0	20	6.1
1.0	30	4.9
1.0	45	4.9
1.0	60	2.7
1.0	120	0.4

* Calculated from CVA curves obtained by sweeping the potential of the electrode modified with poly[Pt(qol)$_2$] in the pure supporting electrolyte at a sweep rate of 0.2 V s^{-1}.

of poly[Pt(qol)$_2$] prepared in the static mode at various times and accumulation potentials are listed in Table 3.

As can be seen, D_{ct} is constant for thin films, but begins to decrease as the film thickness increases. These data are consistent with the concept that the number of the chain cross-links increases with the thickness [25]. The calculated values of D_{ct} suggest that the rate of diffusion of counterions is the rate-determining stage of the charge transport in poly[Pt(qol)$_2$].

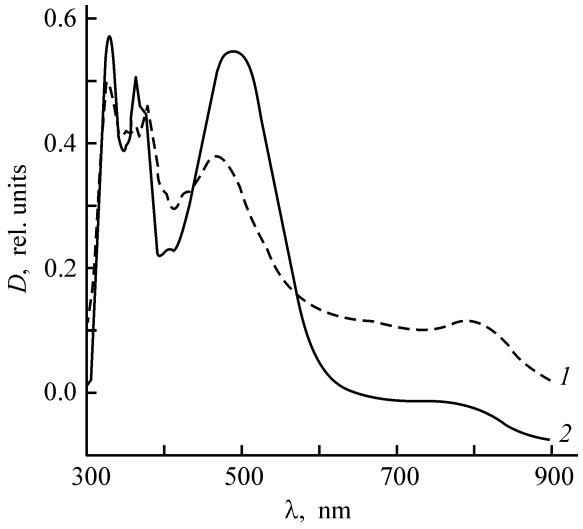

Fig. 7. Electronic absorption spectra of poly[Pt(qol)$_2$] in the (*1*) oxidized (1.0 V) and (*2*) reduced (0.2 V) forms. (*D*) Optical density and (λ) wavelength.

Probably, an increase in the number of cross-links of the polymeric chains with the synthesis time hinders the diffusion of ClO_4^- counterions stabilizing the oxidized form of the polymer, which, in turn, decreases D_{ct}.

A comparative analysis of XPES data for monomeric and polymeric platinum complexes allowed characterization of the poly[Pt(qol)$_2$] composition. In going from monomeric to polymeric compound, a new line with E_b = 75.2 eV appears in the XPES spectrum, which suggest partial oxidation of Pt(II) to Pt(IV) during electropolymerization. The ratio of the atomic concentrations of the corresponding components depends on whether the complex is predominantly in the oxidized or reduced forms.

In the XPES spectrum of the polymer, a Cl2$p^{3/2}$ line at 208.0 eV indicates the presence of the ClO_4^- ion in the film. Thus, the ClO_4^- ion plays the role of a counterion providing the electroneutrality of the polymer. It should be noted that additional lines at 198.5 and 200.6 eV, belonging to the chloride ion, also appear in the XPES spectrum. This fact can be accounted for by partial reduction of the ClO_4^- counterion during recording of the XPES spectrum. The XPES data for the polymer confirm previous conclusions about oxidation of the metal centers of platinum complexes in the course of the polymerization, in contrast to the related nickel(II), palladium(II), and copper(II) compounds. In the process, the unstable Pt(III) disproportionates to give Pt(II) and Pt(IV) centers.

Samples of poly[Pt(qol)$_2$] were prepared for recording the electronic absorption spectra on optically transparent electrodes [quartz plates coated with a Sn(IV) oxide layer] by anodic polymerization. The thickness of the polymer layer was about 1.2 μm.

The electronic absorption spectra (EAS) of poly-[Pt(qol)$_2$] in the oxidized (curve *1*) and reduced (curve *2*) forms are shown in Fig. 7. The EAS of the initial monomeric complex (solution in DMF) and polymeric films are similar within the 300–400 nm range and show a strong absorption caused by π–π^* type electronic transitions.

The presence of an isobestic point at 440 nm suggest that two equilibrium forms of the polymer coexist: oxidized and reduced.

The EAS of both poly-[Pt(qol)$_2$] and the monomeric complex contain strong low-energy bands peaked at λ = 465 and λ = 485 nm for the oxidized and reduced forms, respectively. The blue shift of the band belonging to the oxidized form of the poly-

mer is probably caused by an increase in the energy gap between the adjacent polymeric chains because of polymer swelling due to incorporation of charge-compensating ClO_4^- ions into the polymer phase [26].

At the same time, the EAS of the oxidized form contain a new broad absorption band peaked at λ = 800 nm is observed. Based on published data on EAS of organic polymers [6, 27–30], this band in the red spectral range can be attributed to the existence of mobile charge carriers, radical-cations. At a high degree of oxidation and simultaneous incorporation of the supporting electrolyte into the polymeric membrane cavities, the number of free charge carriers (radical-cations) increases, which, in turn, makes higher the conductivity of the polymer and causes its transition from an insulator to a substance with semiconducting properties. The accumulation of radical-cations leads to adecrease in the energy level of the conduction band and causes an increase in the conductivity of the polymeric compound.

To confirm the existence of radical-cations in the oxidized form of the polymer, we studied the near-IR spectra of the initial monomeric complex and polymeric compounds.

The IR absorption spectrum of the complex (KBr pellet) and IR reflection spectra of polymer films deposited onto quartz plates with a platinum mirror coating were recorded on an IFS-88 IR Fourier spectrometer within the 4000–15000 cm^{-1} range.

The dependences of the transmission T (%) on the wave number ν (cm^{-1}) are shown in Fig. 8. As can be seen, the polymer in the oxidized form is characterized by virtually complete absorption ($T \sim 0$) within the above wave-number range, which confirms the presence of free charge carriers in the polymeric matrix of the oxidized form. At the same time, the transmission increases in the spectrum of the partially reduced form, which suggests a decrease in the radical-cation concentration and the loss of conductivity.

CONCLUSIONS

(1) The electrochemical polymerization of a Pt(II) complex with pyridine-type ligand, 8-quinolinol, in the potentiodynamic and potentiostatic modes was performed for the first time.

(2) The optimal conditions of poly-[Pt(qol)$_2$] synthesis were found, under which polymeric films with the maximum thickness of the electroactive layer are formed in unit time, are accumulation in the static mode at a potential E_a = 1.0 V for τ_a = 30–40 min.

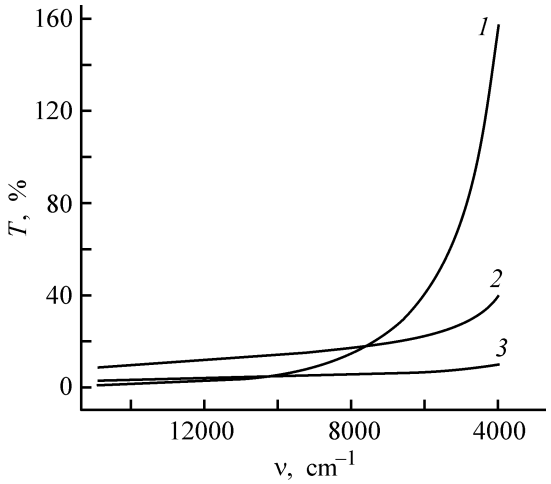

Fig. 8. Transmission T vs. the wavenumber ν. Sample: (*1*) [Pt(qol)$_2$], (*2*) poly[Pt(qol)$_2$] in the reduced form, and (*3*) poly[Pt(qol)$_2$] in the oxidized form.

(3) It was shown that an increase in the time of the polymer synthesis can lead to a decrease in the rate of charge transport in the polymer phase.

(4) The data of electronic and IR spectroscopy confirmed that only oxidized and partially oxidized forms of the polymer exhibit electroconducting properties.

ACKNOWLEDGMENTS

The authors are grateful to A.V. Shchukarev (St. Petersburg State University) for recording the XPE spectra.

REFERENCES

1. Reddinger, J. L. and Reynolds, J.R., *Chem. Mater.*, 1998, vol. 10, pp. 1236–1243.
2. Nikolaeva, E., *Khim. Zh.*, 2002, December, pp. 28–31.
3. Donges, D., Nagle, J.K., and Yersin, H., *Inorg Chem.*, 1997, vol. 36, pp. 3040–3048.
4. Balzani, V., Juris, A., Venturi, M., et al., *Chem Rev.*, 1996, vol. 96, p. 759.
5. Vilas-Boas, M., Freire, C., de Castro, B., et al., *Chem. Eur. J.*, 2001, vol. 7, no. 1, pp. 139–150.
6. Goldsby, K.A., *J. Coord. Chem.*, 1988, vol. 19, no. 3, pp. 83–90.
7. Shagisultanova, G.A., and Ardasheva, L.P., *Zh. Prikl. Khim.*, 2003, vol. 76, no. 10, pp. 1669–1674.
8. Shagisultanova, G.A., Ardasheva, L.P., and Orlova, I.A., *Zh. Prikl. Khim.*, 2003, vol. 76, no. 10, pp. 1675–1681.

9. Shagisultanova, G.A., *Teor. Prikl. Khim.*, 1991, vol. 27, pp. 330–338.
10. Shagisultanova, G.A. and Kuznetsova, N.N., *Koord. Khim.*, 2003, vol. 29, no. 9, pp. 1–8.
11. Ardasheva, L.P., Spectral-Luminescent, Photochemical, and Electrochemical Properties of Platinum(II) and Palladium(II)complex Compounds with Schiff Bases, *Cand. Sci. Dissertation*, Moscow, 1999.
12. Bergamini, P., Bertolasi, V., Ferretti, V., and Sostero, S., *Inorg. Chim. Acta*, 1987, vol. 126, pp. 151–155.
13. Ballardini, R., Varani, G., Indelli, M.T., and Scandola, F., *Inorg Chem.*, 1986, vol. 25, pp. 3858–3865.
14. Ballardini, R., Indelli, M.T., Varani, G., et al., *Inorg. Chim. Acta*, 1978, vol. 31, pp. L423–L424.
15. Bartocci, C., Sostero, S., Traverso, O., et al., *J. Chem. Soc.*, Faraday Trans., 1980, vol. 76, pp. 797–803.
16. Borgarello, E.,Pelizzetti, E., Ballardini, R., and Scandola, F., *Nouv. J. Chim.*, 1984, vol. 8, pp. 567–569.
17. Gubasola, T.N., Synthesis and Study of Polymers Based on Nickel(II), Palladium(II), Platinum(II), and Copper(II) Complex Compounds with Schiff Bases, *Cand. Sci. (Chem.) Dissertation*, St. Peresburg, 2002.
18. Shchukarev, A.V., Ardasheva, L.P., and Shagisultanova, G.A., *Zh. Neorg. Khim.*, 1999, vol. 44, no. 5, pp. 790–794.
19. Masalovich, M.S., Ardasheva, L.P., and Shagisultanova, G.A., *Zh. Neorg. Khim.*, 2006, vol. 51, no. 9, pp. 1591–1596.
20. Abruna, H.D., *Coord. Chem. Rev.*, 1988, vol. 86, no. 1, pp. 135–189.
21. Galyus, Zb., *Teoretyczue Podstawy Elektroanalisy Chemicznej*, Warszawa: Naukowe, 1971.
22. Vilas-Boas, M., Freire, C., de Castro, B., et al., *Inorg. Chem.*, 1997, vol. 36, no. 22, pp. 4919–4929.
23. Alpatova, N.M., Semenikhina, O.A., Ovsyannikova, E.V., et al., *Elektrokhimiya*, 2000, vol. 36, no. 9, pp. 1045–1052.
24. Vorotyntsev, M.A. and Badiali, J.P., *Electrochim. Acta*, 1994, vol. 39, no. 2, pp. 289–306.
25. Alpatova, N.M., Ovsyannikova, E.V., Semenikhina, O.A., et al., *Elektrokhimiya*, 2000, vol. 36, no. 2, pp. 173–179.
26. Jiang, J. and Kucernak, A., *J. Electroanal. Chem.*, 2000, vol. 490, p. 17–30.
27. Touillon, G. and Garlner, F., *J. Phys. Chem.*, 1983, vol. 87, pp. 2289–2292.
28. Patil, A.O., Heeger, A.J., and Wudl, F., *Chem. Rev.*, 1988, vol. 88, no. 1, pp. 183–200.
29. Geskin, V.M. and Letuchii, Ya.A., *Electrokhimiya polimerov* (The Electrochemistry of Polymers), Tarasevich, M.R. and Khrushcheva, E.I., Eds., Moscow: Nauka, 1990, pp. 121–145.
30. Ovsyannikova, E.V., Crosheva, M.Yu., and Alpatova, N.M., *Short Commun.*, 2004, vol. 40, no. 10, pp. 1089–1091.

ISSN 1070-4272, Russian Journal of Applied Chemistry, 2007, Vol. 80, No. 6, pp. 979–982. © Pleiades Publishing, Ltd., 2007.
Original Russian Text © Yu.V. Frantsuzova, A.Yu. Neverovskaya, A.P. Voznyakovskii, 2007, published in Zhurnal Prikladnoi Khimii, 2007, Vol. 80, No. 6, pp. 1002–1006.

MACROMOLECULAR CHEMISTRY AND POLYMERIC MATERIALS

Specific Features of Formation of 3*D* Chemical Networks in Siloxane Block Copolymers

Yu. V. Frantsuzova, A. Yu. Neverovskaya, and A. P. Voznyakovskii

Lebedev Research Institute of Synthetic Rubber, Federal State Unitary Enterprise, St. Petersburg, Russia

Received November 27, 2006; in final form, December 2006

Abstract—The formation of 3*D* chemical networks in siloxane block copolymers in the course of room-temperature vulcanization (RTV) was studied. The influence of the moisture content of the reaction medium on the RTV of the systems under consideration was analyzed for the case of preparation of films from solutions.

DOI: 10.1134/S1070427207060249

Siloxane copolymers whose macrochains consist of "rigid" and "flexible" blocks are characterized by a physical network formed by rigid block domains, which improves their physicomechanical properties as compared to linear silicone robbers. To attain the required level of elasticity and strength, it is necessary to form a 3*D* chemical network in the polymer. This network is formed in the course of vulcanization.

The well-known procedure for curing of two-component systems based on siloxane rubber involves the use of a cross-linking agent, e.g., $Si(OEt)_4$, and a curing catalyst [as a rule, dialkyltin dicarboxylates of the general formula $R_2Sn(OCOR')_2$, where R, R' = –Alk]. The process occurs via a series of successive reactions of heterofunctional condensation with the formation of Si–O–Si bonds [1].

Severnyi [2] suggested a model of the RTV process, which involves moisture sorbed by the polymer from the surrounding medium. The catalyst is activated by water and, in turn, activates the cross-linking agent. Molecules of the activated cross-linking agent react with hydroxy groups of the macrochains, thus forming a 3*D* chemical network.

For homopolyorganosiloxanes, self-vulcanizing (one-component) systems curable in the presence of atmospheric moisture have also been developed. In such systems, various cross-linking agents are used, e.g., trifunctional compounds of the general formula $RSiX_3$, where R = –Alk, X = –OAc, $–ONCR_2$, etc. [3, 4]. Severnyi [5] considers the formation of a 3*D* chemical network under the RTV conditions. It is assumed that, after the polymer and cross-linking agent are mixed, the reaction occurs until the OH groups of the polymer are completely exhausted; as a result, a system consisting of a siloxane polymer with functional X groups and excess cross-linking agent is obtained. Such systems can be stored in a hermetically sealed volume for a long time. On their contact with the environment, atmospheric moisture induces hydrolytic polycondensation to give Si–O–Si bonds, and a 3*D* chemical network is formed in a thin polymer layer.

The goal of this study was to examine the mechanism of formation and the parameters of the 3*D* chemical network in film-forming materials based on siloxane block copolymers.

The parameters of the 3*D* chemical network can be determined with a reasonable accuracy from the experimental data on the elastic strain of polymers under uniaxial extension. In this case, as a rule, the stress–strain relationship is described by the Mooney–Rivlin equation [6]

$$f^* = \sigma/(\lambda^2 - 1/\lambda) = C_1 + C_2\lambda^{-1}, \qquad (1)$$

where f^* is the reduced mechanical stress; C_1 and C_2, constant coefficients; $\lambda = 1 + \varepsilon$, relative elongation; and ε, relative strain.

From the initial portion of the dependence of f^* on λ^{-1}, in the range of initial strains, it is possible to determine the initial value of $f_0^* = C_1 + C_2$, char-

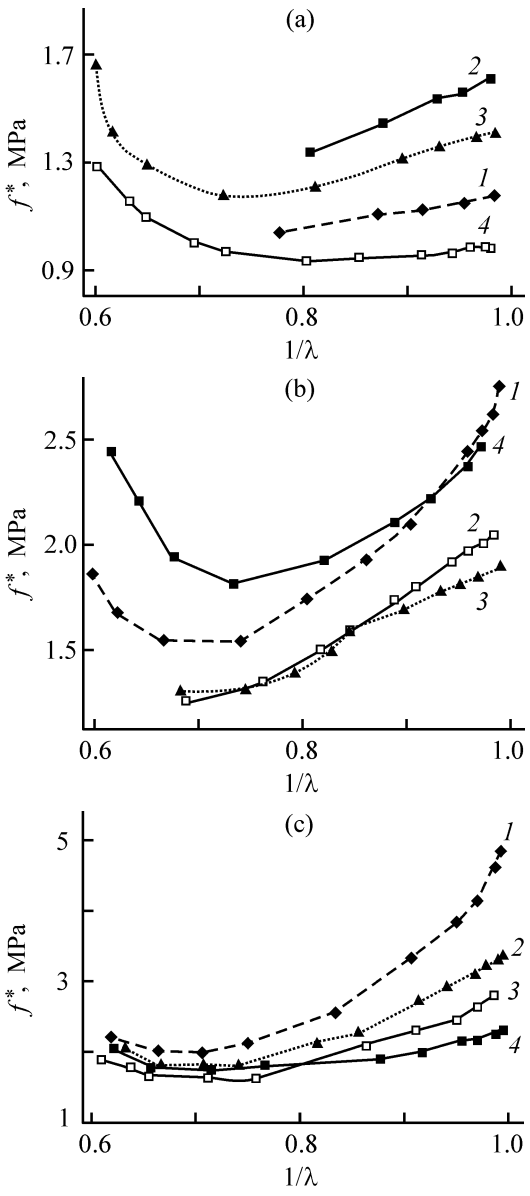

Fig. 1. Reduced mechanical stress f^* vs. reciprocal relative elongation $1/\lambda$ for films prepared by casting from various solvents. Cross-linking agent; (a) none, (b) **A**, and (c) **C**. Solvent: (*1*) toluene, (*2*) ethyl acetate, (*3*) chloroform, and (*4*) CCl_4.

acterizing the network density, by the extrapolation $\lambda^{-1} \to 1$ ($\varepsilon \to 0$); the coefficient C_2 related to the deviation of the network from the ideal state can be estimated from the slope of the linear portion, for which the Mooney–Rivlin equation is valid.

EXPERIMENTAL

We used polysiloxane block copolymer of ladder polyphenylsilsesquioxane and polydimethylsiloxane (PPSSO–PDMS)[1] with >42 wt % fraction of flexible PDMS blocks:

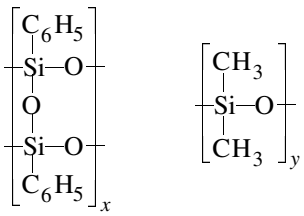

We used the following cross-linking agents: vinyltris(isopropylidenaminooxy)silane CH_2=CH–Si–[O–N=C$(CH_3)_2]_3$ (vinyl oxime, **A**) and aminopropyltriethoxysilane NH_2–$(CH_2)_3$–Si–(O–CH_2–$CH_3)_3$ (**C**).

The use of other cross-linking agents does not involve the moisture in the formation of the 3*D* chemical network. Curing occurs by heterofunctional polycondensation throughout the bulk of the polymer.

Organosilanes used as cross-linking agents and the solvents (toluene, ethyl acetate, chloroform, CCl_4) were distilled before use and dried over zeolites. The block copolymer PPSSO–PDMS was dried in an oven at 120°C to constant weight.

To a solution of PPSSO–PDMS in one of the above-indicated solvents, we added 5 wt % cross-linking agent and stirred on a magnetic stirrer for 15 min. Films were formed from the solution on a cellophane support at a constant temperature of 30°C. The samples were baked for 2.5 h at 200°C.

The deformation behavior of films of the block copolymer were studied on an installation described in [7]. The installation design provided use of loads starting from 1 g. The extension was determined with a KM-6 cathetometer (accuracy 0.01 mm) from the positions of marks preliminarily made on the sample. With the aim to reduce the error of calculation of f_0^* and C_2, the data set for statistical treatment was constructed for strains $\varepsilon > 3\%$.

PPSSO–PDMS films were formed from solution. Naturally, it could be expected that the solvent would significantly affect both the mechanism of formation and the parameters of the network.

The elastic strain curves in the coordinates of the Mooney–Rivlin equation for films formed from the compounds without cross-linking agent are shown in Fig. 1a. It is seen that all the extension curves have a portion of a linear dependence $f^*(\lambda^{-1})$ described by

[1] Produced on the semicommercial scale by the Lebedev Research Institute of Synthetic Rubber.

Coefficients of the Mooney–Rivlin equation for films formed from various solvents with various cross-linking agents

Solvent	No cross-linking agent			Cross-linking agent **A**			Cross-linking agent **C**		
	f_0^*	C_2	$N \times 10^{21}$, cm^{-3}	f_0^*	C_2	$N \times 10^{21}$, cm^{-3}	f_0^*	C_2	$N \times 10^{21}$, cm^{-3}
	MPa			MPa			MPa		
CCl_4	1.00	0.33	0.5299	2.50	3.51	1.3244	2.30	3.34	1.1278
Toluene	1.19	0.67	0.6301	2.66	5.30	1.4107	4.68	13.80	2.4803
Chloroform	1.43	1.19	0.7606	1.89	2.36	1.0029	3.35	7.20	1.7750
Ethyl acetate	1.64	1.63	0.8675	2.07	3.28	1.0959	2.78	5.52	1.4726

Eq. (1). We determined the corresponding parameters C_1, C_2, and f_0^* (reduced mechanical stress at zero strains) in various solvents, and also the number of active chains in 1 cm^3 of the network N (see table). The table shows that, without a cross-linking agent, the solvent affects the density of the physical network. The coefficient C_2 is also solvent-dependent, which indicates that the network deviates from the ideal state owing to the solvent effect. Our results show that the density of the physical network for the films formed without a cross-linking agent increases in the order CCl_4 < toluene < chloroform < ethyl acetate. The calculated values of C_2 show that the deviations from the ideal state of the physical networks of polymer films formed from various solvents without a cross-linking agent are relatively small. Nevertheless, it can be noted that the extent of these deviations and the density of the physical network vary in the same direction.

Studies of the systems containing cross-linking agents show that the solvent affects also the 3*D* chemical network (Figs. 1b, 1c). With cross-linking agent **A**, the network density increases in the order chloform < ethyl acetate < CCl_4 < toluene, and with cross-linking agent **C**, in the order CCl_4 < ethyl acetate < chlroforom < toluene. It is seen from this table that the structure of films prepared with a cross-linking agent strongly differs from the ideal structure. The largest deviation of the network parameters is observed with films formed with cross-linking agent **C**. The solvent effect on the parameters of the 3*D* chemical network strongly depends on the cross-linking agent used, except ofr the films cast from CCl_4; in the latter case, an essentially similar supramolecular structure is obtained with cross-linking agents **A** and **C**.

As the RTV systems under consideration include solvents, it is necessary to analyze the effect of dissolved water on the formation of a chemical network. In particular, the solubility of water in toluene is very low, and films with high strength and good elastic and strain properties are formed from toluene solutions. As for the diffusion of water into a block copolymer after the solvent removal, it occurs via penetration of moisture into the free fluctuation volume of the polymer and is limited by the diffusion coefficient and water solubility in the block copolymer.

We performed a series of experiments on the formation of a chemical network in PPSSO–PDMS block copolymer containing moisture that remained in the polymer after the synthesis (~0.1 wt %), with gradual removal of moisture in the course of drying (samples of the block copolymer were taken at definite intervals). The films were cast from a solution in toluene. We found that the lower the initial content of water in the block copolymer, the higher the strength of the films prepared from it (Fig. 2a). With toluene replaced with ethyl acetate, the films prepared under

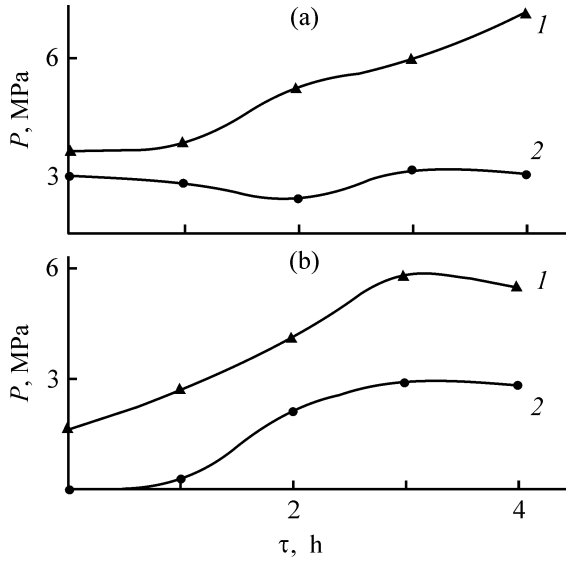

Fig. 2. Strength P of film materials vs. the time of drying of the block copolymer τ. Films cast from solutions in (a) toluene and (b) ethyl acetate. Cross-linking agent: (*1*) **A** and (*2*) **C**.

the same conditions showed worse elastic and strength parameters (Fig. 2b). Nevertheless, the trend toward improvement of the film properties in the course of drying was observed, too. These experiments show that even a small content of water in the systems negatively affects the formation of the 3*D* chemical network.

To refine the mechanism of the network formation, we analyzed the effects of the solvent and cross-linking agent on the strength characteristics of films at low (100%) strains. We found that, in the strain range examined, the parameters varied had no appreciable effect on the strength characteristics. This fact suggests that "rigid" blocks within the domains are not involved in the formation of the 3*D* chemical network. At the same time, if PDMS blocks were involved the network formation, the elastic strain would considerably increase, with the tensile strength remaining virtually the same. Thus, it can be assumed that in PPSSO–PDMS the 3*D* chemical network is mainly formed via OH groups arranged in defects of rigid blocks, not involved in the domain structure. The presence of such blocks is due to steric features of structures of polyblock copolymers. Since the system contains a solvent, the OH groups of the polymer are initially solvated either by water present in the system or by the solvent. Hence, to react with a functional group of the block copolymer, the cross-linking agent should enter into the competitive exchange, as shown in schemes I and II:

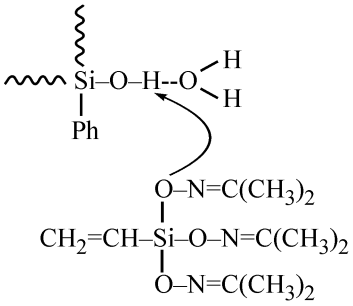

Scheme I.

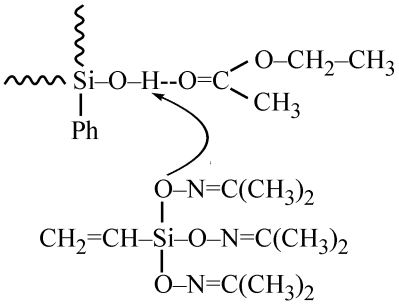

Scheme II.

A more polar solvent forms more stable solvation complexes with a functional group of the block copolymer, hindering the access to it of cross-linking agent molecules. This fact accounts for differences in the formation of the 3*D* chemical network in films cast from different solvents.

CONCLUSIONS

(1) A study of the elastic strain at uniaxial extension showed that the solvent affects not only the supramolecular structure of the block copolymer itself, but also the structure of 3*D* chemical networks formed in the RTV process.

(2) In the synthesis of polyphenylsilsesquioxane–polydimethylsiloxane block copolymer, it is necessary to control the moisture content of the final product, because even a small content of moisture in the block copolymer negatively affects the set of elastic and strength parameters of films prepared from this copolymer.

(3) The 3*D* chemical network is formed in the ternary system polymer–solvent–cross-linking agent under the conditions of competitive solvation of the functional groups of rigid blocks in the interphase layer.

REFERENCES

1. Weij, F.W. van der, *Macromol. Chem.*, 1980, vol. 181, pp. 2541–2548.
2. Severnyi, V.V., *Kauchuk Rezina*, 1998, no. 4, pp. 14–17.
3. Schätz, M., *Silikonový Kaučuk*, Praha: SNTL–Technické Literatury, 1971.
4. Dolgov, O.N., Voronkov, M.G., and Grinblat, M.P., *Kremnii-organicheskie zhidkie kauchuki i materialy na ikh osnove* (Organosilicon Liquid Rubbers and Materials Based on Them), Leningrad: Khimiya, 1975.
5. Severnyi, V.V., *Khim. Prom–st.*, 1995, no. 11, pp. 686–691.
6. *Sovremennye fizicheskie metody issledovaniya polimerov* (Modern Physical Methods for Studying Polymers), Slonimskii, G.L., Ed., Moscow: Khimiya, 1982.
7. Ramsh, A.S., Segregation Effects and Phase–Aggregation State of Siloxane-Containing Block Copolymers, *Cand. Sci. Dissertation*, Leningrad, 1985.

ISSN 1070-4272, Russian Journal of Applied Chemistry, 2007, Vol. 80, No. 6, pp. 983–987. © Pleiades Publishing, Ltd., 2007.
Original Russian Text © V.V. Il'in, S.K. Filippov, A.Yu. Bilibin, 2007, published in Zhurnal Prikladnoi Khimii, 2007, Vol. 80, No. 6, pp. 1007–1012.

MACROMOLECULAR CHEMISTRY AND POLYMERIC MATERIALS

Synthesis of Polyoxyethylene Block Copolymers and Their Aggregation in Water

V. V. Il'in, S. K. Filippov, and A. Yu. Bilibin

St. Petersburg State University, St. Petersburg, Russia

Received January 18, 2007

Abstract—The possibility of thermal degradation of polyoxyethylene in the course of high-temperature polycondensation was examined. Conditions were suggested for the low-temperature synthesis of ABA block copolymers whose molecules contain a polyoxyethylene central block and *p*-aromatic ester terminal blocks. The aggregation of the block copolymers in water was studied by dynamic light scattering and electron microscopy.

DOI: 10.1134/S1070427207060250

Micellization of block copolymers in water aroused increased researchers' interest in the mid-1980s. Studies of this phenomenon were stimulated by papers concerning the use of block-copolymeric micelles in pharmacology. Bader et al. [1] were the first to demonstrate that aqueous solutions of nontoxic block copolymers can be used as means for delivery of drugs in a living body. For this purpose, a hydrophobic drug can be introduced into the micell core in one of the following ways: (1) by covalent binding with functional groups of the core-forming block or (2) by noncovalent interactions within the core (van der Waals forces, hydrogen bonding). The pioneering studies concerned specifically the first alternative; polyoxyethylene-σ-poly(*L*-lysine) [1] and polyoxyethylene-σ-poly(aspartic acid) [2] were tested. Covalent binding makes the drug–micelle system stable to external effects; however, this mode of binding hinders the interaction with the target molecules in vivo, with partial loss of the biological activity of the drug. Recent studies mainly concerned the second mode of binding of a hydrophobic drug, involving noncovalent interaction with the core-forming block [3–5]. The structural stability of block-copolymeric micelles is primarily determined by the critical micelle concentration (CMC), and also by the stability to substances present in the surrounding medium (in a living body, e.g., to proteins and lipids). A novel approach to enhancement of the micelle stability has been suggested by Iijima et al. [6]: Cross-linking of a polylactide block after micellization of polyoxyethylene-σ-polylactide allows stabilization of the micelle core with covalent bonds. The constituent parts of micelles, core and shell, have definite functions. The core is used for loading and release (if required) of a drug. The shell is responsible for the surface interaction with the environment, which may be respondible for the delivery kinetics. The diameter of polymeric micelles (usually from 10 to 100 nm) is suited for long-term circulation in blood, because it appreciably exceeds the renal filtration threshold, but is lower than the sensitivity threshold for nonspecific capture with monocytes.

The goal of this study was to synthesize block copolymers capable of aggregation[1] in water and to examinae of this phenomenon by various methods. As objects of the study we chose ABA triblock copolymers whose macromolecules contain a polyoxyethylene central block and aromatic terminal blocks consisting of *p*-hydroxybenzoic acid residues. Strictly speaking, these substances are not block copolymers in the classical sense, because the terminal "blocks" are very short; in some cases, they consist of a single monomeric unit strongly differing in polarity from the remaining part of the macromolecule. To some extent, these substances can be regarded as compounds intermediate between true amphiphilic block copolymers capable of forming unimolecular micelles and common surfactants. There are examples in the literature when substances of similar molecular architecture are classed with ABA block copolymers. For example, in HEUR-type polymers, the terminal blocks

[1] The term "aggregation" expands the range of species under consideration. In contrast to micelles, which should have a definite structure, there are no structural requirements for aggregates.

are $-C_{16}H_{33}$ radicals [7]; in polyoxybutylene-σ-polyoxyethylene-σ-polyoxybutylene, the degree of polymerization of the terminal blocks is 4 [8]. Here we summarize raw data obtained by ^{1}H NMR spectroscopy for the polymers synthesized and also report the results furnished by the methods of dynamic light scattering and electron microscopy.

EXPERIMENTAL

The block copolymers were prepared by a multistep assembling–disassembling process tested in [9, 10] for the synthesis of liquid crystal multiblock copolymers. The assembling step involves esterification of diols with di(4-chlorocarbonylphenyl) oxalate, and the disassembling step, selective hydrolysis of oxalate ester groups with an aqueous solution of sodium hydrogen carbonate. Thus, after each assembling–disassembling step, a *p*-hydroxybenzoic acid residue is added to each terminus of the molecule of poly(ethylene glycol) or its derivative. The sequence involving two assmebling–disassembling steps and the conventional designations of the investigation objects are given in the scheme:

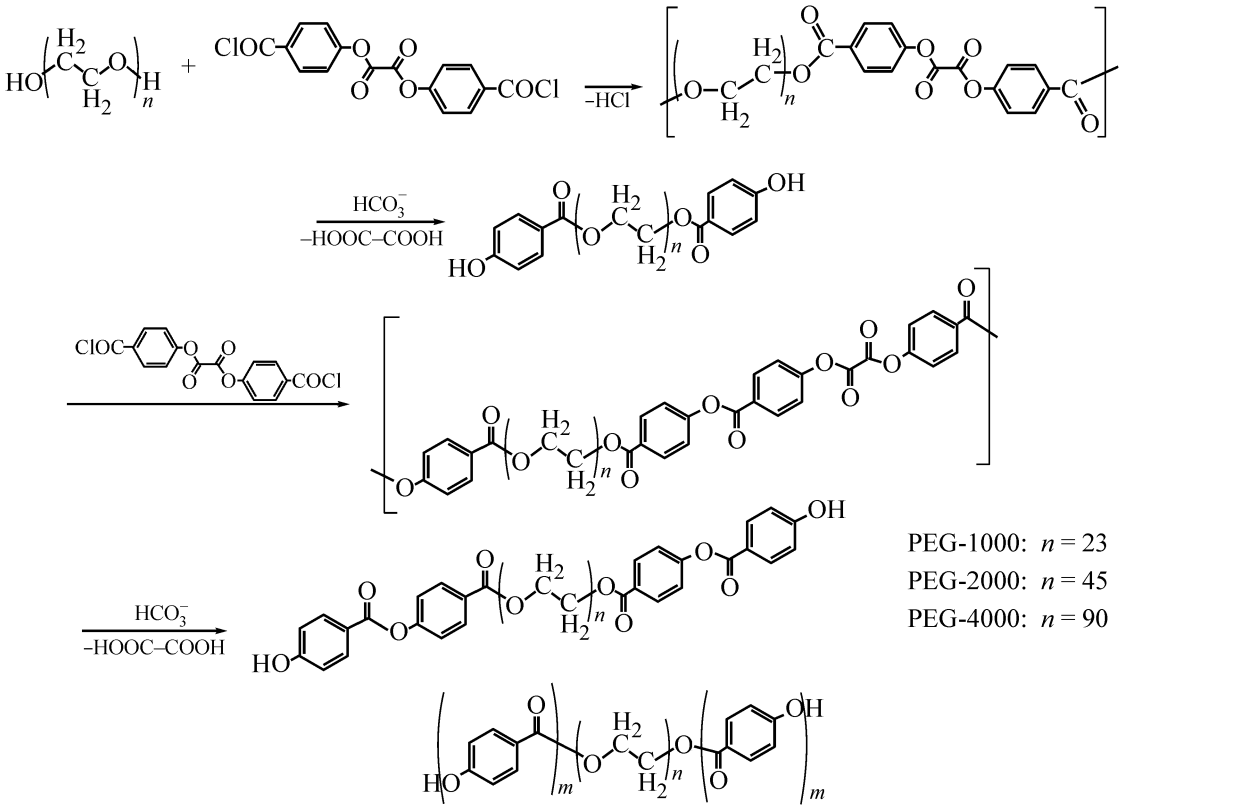

By successively performing several steps, the rigid-chain (*p*-aromatic) block is lengthened. An important advantage of this approach is that the terminal blocks show no polydispersity. Commercial poly(ethylene glycol) used in the study had molecular weights of 1000, 2000, and 4000 (PEG-1000, PEG-2000, and PEG-4000, respectively).

Initially, we performed the synthesis in the high-temperature mode for the PEG-2000 series. In this mode, the assembling is performed at 180°C for 2 h in an α-chloronaphthalene solution. In the ^{1}H NMR spectra recorded in $CDCl_3$, for all the polymers (triblock copolymers and their precursors, oxalyl-containing multiblock copolymers), three regions of signals can be distinguished (Fig. 1), corresponding to (1) nonterminal polyoxyethylene protons (with satellite signals), 3.5–4 ppm; (2) terminal protons of polyoxyethylene, adjacent to the ester bond, 4.4–4.5 ppm; and (3) aromatic protons, 6.8–8.5 ppm.

As a reference for the integration we chose the first region, because the signal of nonterminal protons of polyoxyethylene undergoes the least significant

changes in the course of the synthesis. It should be taken into account, however, that the multistep synthesis can be accompanied by changes in the molecular-weight distribution of polyoxyethylene. In this case, the pattern will be somewhat distorted. Figure 1 shows as an example the spectrum of B–(2000)–B. The ^{1}H NMR spectra of the PEG-2000 derivatives show that the polycondensation yields aromatic derivatives of poly(ethylene glycol). This is confirmed by the appearance of signals from polyoxyethylene protons adjacent to the ester group (terminal protons). As judged from the relative intensities of these signals, the esterification yield is as high as 70–100%. However, viscometric data cast doubt on the success of the syntheses. The intrinsic viscosity [η] of the initial PEG-2000 (chloroform, 25°C) is 0.10 dl g^{-1}; in going to the polymers of the first and second steps of assembling, [(2000)–BOxB–] and [(2000)–B–BOxB–B–], the intrinsic viscosity becomes 0.13 and 0.10 dl g^{-1}, respectively. The lack of increase in [η] suggests that the high-temperature polycondensation is accompanied by degradation of the polyoxyethylene chain. To confirm this assumption, we performed a model experiment with poly(ethylene glycol). PEG-4000 was heated under the conditions of high-temperature polycondensation (Ar, 180°C, 2 h). This treatment resulted in a decrease in the intrinsic viscosity from 0.18 to 0.13 dl g^{-1}. This fact indicates that polyoxyethylene undergoes degradation under the conditions of high-temperature polycondensation. Comparison of the ^{1}H NMR spectra of PEG-4000 before and after heating shows that the intensity of the signals corresponding to protons of the OH groups becomes several times higher after heating. The IR data are also consistent: The intensity of the O–H stretching band sharply increases after the heat treatment of poly(ethylene glycol). Thus, thermal degradation of poly(ethylene glycol) is accompanied by the appearance of hydroxy groups.

Because of the poor heat resistance of polyoxyethylene, we suggested and optimized a procedure for low-temperature acceptor polycondensation. In this procedure, the polycondensation of poly(ethylene glycol) with di(4-chlorocarbonylphenyl) oxalate was performed at room temperature in tetrahydrofuran (THF). As HCl acceptor we used 4-(dimethylamino)-pyridine (DMAP). The derivatives were prepared with all the three PEG samples: PEG-1000, PEG-2000, and PEG-4000. The ^{1}H NMR spectra in $CDCl_3$ solutions of poly(ethylene glycol) derivatives prepared under the conditions of low-temperature polycondensation fundamentally differ from the ^{1}H NMR spectra of the above-considered compounds. In the spectrum of the polymer [(2000)–BOxB–], the integral intensity of the signals of aromatic protons decreases by a factor of 10. At the same time, the ^{1}H NMR spectrum of this compound contains a triplet at 4.44 ppm from two methylene groups of polyoxyethylene, adjacent to the ester bond. The integral intensity of this triplet corresponds to 4H, suggesting the 100% functionalization of poly(ethylene glycol). Viscosity measurements give consistent results. In going from the starting PEG-2000 to the product of low-temperature polycondensation, the intrinsic viscosity in chloroform increases from 0.10 to 0.59 dl g^{-1}.

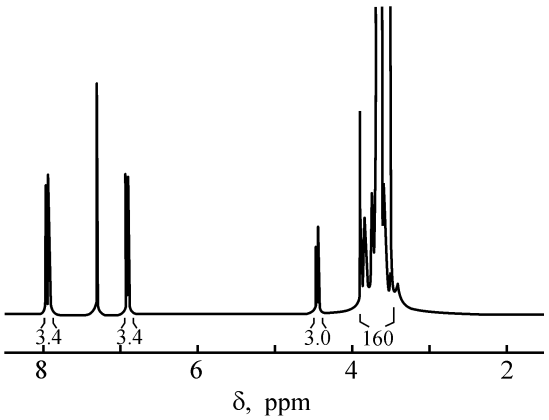

Fig. 1. ^{1}H NMR spectrum of B–(2000)–B in $CDCl_3$ (the signal at 7.28 ppm belongs to residual protons of the solvent). (δ) Chemical shift.

The abnormally low intensity of aromatic proton signals is caused by aggregation of the polymer in the solvent (chloroform). The possibility of solvation of the oxalylbis(oxybenzoic) fragment of macromolecular chains is strongly limited. Therefore, core–shell associates are formed. The cores consisting of aromatic fragments are surrounded by the polyoxyethylene shell. Because of the dense packing inside the cores, the protons of core fragments have relatively long relaxation times, which results in the disappearance of the aromatic proton signals from the ^{1}H NMR spectra. Similar examples can be found in the literature [11, 12].

In the ^{1}H NMR spectrum of the oligomer B–(2000)–B prepared by hydrolysis of the low-temperature polymer, the aromatic proton signals are also strongly suppressed. The total integral of multiplets in the range 6.8–8.4 ppm is as low as 1.0 (10% of the theoretical value). The occurrence of the hydrolysis is confirmed by the intrinsic viscosity [η] = 0.13 dl g^{-1} (before hydrolysis, [η] = 0.59 dl g^{-1}). In the ^{1}H NMR spectrum of the B–(2000)–B sample recorded in D_2O, the aromatic proton signals are suppressed to a still

Table 1. ^{1}H NMR data ($CDCl_3$) for samples prepared at low temperatures

Compound	Intensity		Intensity of signals with $\delta < 3$ ppm
	terminal protons of polyoxyethylene	aromatic protons	
B–(1000)–B	80	5	5.9
B_2–(1000)–B_2	87	6	6.7
[(2000)–BOxB–]	100	11	5.6
B–(2000)–B	93	10	6.1
B_2–(2000)–B_2	93	5	9.6
[(4000)–BOxB–]	100	35	30
B–(4000)–B	92	1	12.3
B_2–(4000)–B_2	94	11	17.1
B_3–(4000)–B_3	91	9	18.4

Table 2. Dynamic light scattering data for aqueous solutions of the samples

Compound	R, nm		
B–(1000)–B	–	21 ± 1	159 ± 8
B_2–(1000)–B_2	Does not dissolve		
B–(2000)–B	5 ± 1	29 ± 2	166 ± 8
B_2–(2000)–B_2	–	–	175 ± 12
B–(4000)–B	3.0 ± 0.5	39 ± 2	228 ± 11
B_2–(4000)–B_2	1.8 ± 0.3	39 ± 1	252 ± 4
B_3–(4000)–B_3	1.9 ± 0.1	37 ± 3	252 ± 8

greater extent, to less than 1% of their theoretical intensity. The ^{1}H NMR data ($CDCl_3$) for the block copolymers of all the three series are summarized in Table 1. As can be seen, the intensity of the aromatic proton signals is strongly underestimated in all the cases.

It should be noted that the ^{1}H NMR spectra of all the block copolymers prepared at low temperature contained anomalous high-field ($\delta < 3$ ppm) signals. The appearance of such signals is also attributed to aggregation. The polyethylene block forming the micelle shell should occur in the loop conformation. In this conformation, there are bending sites in the molecular chain. Furthermore, aggregation may be accompanied by interweaving of the molecules. The protons at the sites of bending and of chain contact may have particular properties and give rise to signals shifted relative to typical positions.

The method of dynamic light scattering (DLS) allows determination of the diffusion coefficient of the particles in solution. The hydrodynamic radius R_h can be calculated from the Stokes–Einstein equation:

$$D = \frac{kT}{6\pi\eta_0 R_h},$$

where D is the translational diffusion coefficient; k, Boltzmann constant; T, absolute temperature; and η_0, solvent viscosity.

We studied aqueous solutions of the concentration $c = 0.7$ g l^{-1}. All the modes revealed had the diffusion character. The hydrodynamic radii of particles observed in DLS measurements are listed in Table 2. It is seen that, in most cases, the size distribution is multimodal. Along with particles whose hydrodynamic radius is several nanometers, there are particles with R_h on the order of tens and hundreds of nanometers. This fact conclusively confirms the tendency of the polymers prepared toward association, because the distribution function of the initial poly(ethylene glycol) is unimodal, with particle sizes R_h on the order of nanometers. It is well seen that the sizes of intermediate and coarse particles detected in the polymer solutions correlate with the molecular weight of both polyoxyethylene block and aromatic blocks. An increase in the molecular weight leads to a rise in the aggregate size. It should be noted that particles of the smallest size (on the order of several nanometers) are also detected in solutions of the compounds studied. However, because of the small contribution of these particles to the overall scattering, quantitative determination of their diffusion coefficients requires long time for accumulation of the correlation function and is therefore difficult.

The hydrodynamic radii of particles consisting of molecules of structurally related ABA block copolymers (polyoxyethylene central block and hydrophobic terminal blocks) can be found in [7, 8, 11, 13–15]. The reported values correspond to particles of three types: (1) separate molecules, (2) flower-type micelles, and (3) aggregates (often termed intermicellar clusters). Comparison of the published data allows a conclusion that the hydrodynamic radius of separate molecules of the block copolymers studied here is within 1–2 nm (for PEG-1000 series, most probably, even smaller than 1 nm). The radius of flower-type micelles is 2 to 7 nm. Particles with the radius on the order of tens of nanometers and over are, apparently, intermicellar clusters. Thus, the large (hundreds of nanometers) and intermediate (tens of nanometers) hydrodynamic radii should be assigned to intermicellar clusters. The particles with R_h = 2–5 nm are, most probably, micelles.

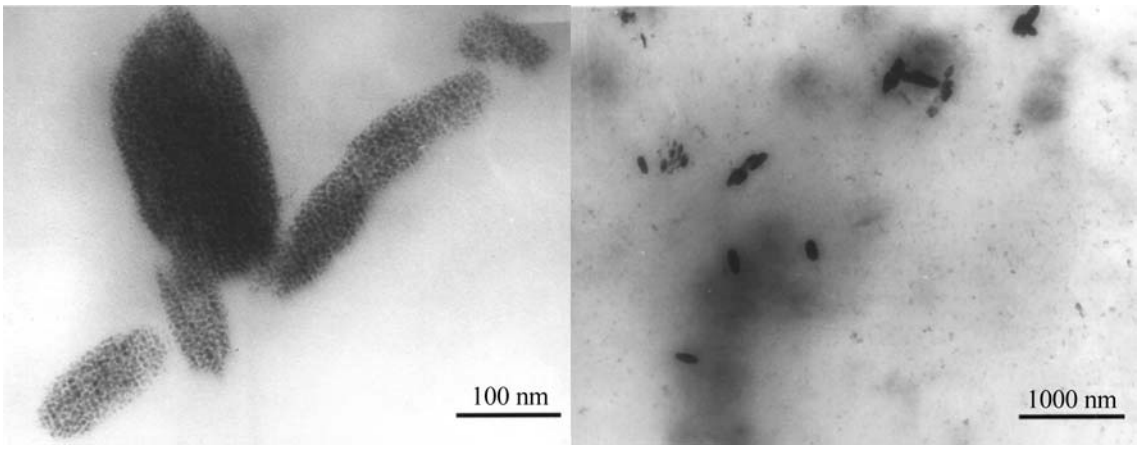

Fig. 2. Electron micrographs of aqueous solution of B–(4000)–B.

Electron microscopy. For the samples under consideration, we obtained TEM images. The specimens were prepared by solvent evaporation from 1 g dl^{-1} solutions. The general structural features of aggregates formed in aqueous solution are similar for all the compounds. Figure 2 shows as an example the electron micrographs of the B–(4000)–B sample. It is seen that the particles have an elliptic shape. Coarse aggregates are composed of a set of small particles (structural units). The structural units are spheres 5–10 nm in diameter, presumably the flower-type micelles. The size of structural units depends on a particular sample.

Coarse elliptic particles are intermicellar clusters. Turning back to the DLS results, we see that there are two or three values of the hydrodynamic radius on the order of hundreds (coarse particles) and tens (intermediate particles) of nanometers. Simple comparison with the particle size in the electron micrographs shows that specifically the intermediate value of R_h corresponds to intermicellar clusters. The correlation between the cluster size and the length of the polyoxyethylene chain, already mentioned when discussing the DLS data, is also seen from the electron micrographs. The micrographs taken with a smaller magnification show that intermicellar clusters tend to associate. The associates thus formed are apparently the coarse particles (R_h of hundreds of nanometers) that were detected in DLS experiments.

CONCLUSIONS

(1) A procedure was developed for low-temperature synthesis of ABA block copolymers whose molecules contain the polyoxyethylene central block.

(2) It was found that terminal blocks of triblock copolymer molecules, consisting of *p*-hydroxybenzoic acid residues, promote aggregation in water and chloroform.

(3) Particles of the size corresponding to micelles and intermicellar clusters were detected in aqueous solution.

REFERENCES

1. Bader, H., Ringsdorf, H., and Schmidt, B., *Angew. Makromol. Chem.*, 1984, vol. 123/124, pp. 457–485.
2. Yokoyama, M., Inoue, S., Kataoka, K., et al., *Makromol. Chem., Rapid Commun.*, 1987, vol. 8, pp. 431–435.
3. Calvo, P., Remunan-Lopez, C., Vila-Jato, J.L., and Alonso, M.J., *Pharm. Res.*, 1997, vol. 14, pp. 1431–1436.
4. Kim, S.Y. and Lee, Y.M., *Biomaterials*, 2001, vol. 22, pp. 1697–1704.
5. Bhattarai, N., Bhattarai, Sh.R., Yi, H.K., et al., *Pharm. Res.*, 2003, vol. 20, pp. 2021–2027.
6. Iijima, M., Nagasaki, Y., Okada, T., et al., *Macromolecules*, 1999, vol. 32, pp. 1140–1146.
7. Pham, Q.T., Russel, W.B., Thibeault, J.C., and Lau, W., *Macromolecules*, 1999, vol. 32, pp. 2996–3005.
8. Yang, Y.-W., Yang, Zh., Zhou, Z.-K., et al., *Macromolecules*, 1996, vol. 29, pp. 670–680.
9. Bilibin, A.Yu. and Piraner, O.N., *Makromol. Chem.*, 1991, vol. 192, pp. 201–214.
10. Bilibin, A.Yu., Girbasova, N.V., and Tenkovtsev, A.V., *Macromol. Symp.*, 1998, vol. 128, pp. 131–143.
11. Bhattarai, N., Bhattarai, Sh.R., Khil, M.S., et al., *Eur. Polym. J.*, 2003, vol. 39, pp. 1603–1608.
12. Yuan, J., Xu, Z., Cheng, Sh., and Feng, L., *Eur. Polym. J.*, 2002, vol. 38, pp. 1537–1546.
13. Kim, M., Choi, Y.-W., Sim, J.-H., et al., *J. Phys. Chem. B*, 2004, vol. 108, pp. 8269–8277.
14. Mai, Sh.-M., Ludhera, S., Heatley, F., et al., *J. Chem. Soc., Faraday Trans.*, 1998, vol. 94, pp. 567–572.
15. Chu, B., *Langmuir*, 1995, vol. 11, pp. 414–421.

ISSN 1070-4272, Russian Journal of Applied Chemistry, 2007, Vol. 80, No. 6, pp. 988–991. © Pleiades Publishing, Ltd., 2007.
Original Russian Text © S.E. Mitrofanova, E.N. Cherezova, 2007, published in Zhurnal Prikladnoi Khimii, 2007, Vol. 80, No. 6, pp. 1014–1017.

MACROMOLECULAR CHEMISTRY AND POLYMERIC MATERIALS

Synthesis of Polyfunctional Sulfur-containing Oligomers and Their Effection SKI-3 Rubber and Its Vulcanizates

S. E. Mitrofanova and E. N. Cherezova

Kazan State Technological University, Kazan, Tatarstan, Russia

Received November 20, 2006; in final form, February 2007

Abstract—Polysulfide oligomers with sterically hindered phenolic fragments were prepared. Their effect on the antioxidative stability and kinetics of vulcanization of rubber stocks based on SKI-3 rubber was examined.

DOI: 10.1134/S1070427207060262

Polysulfide oligomers (PSOs) are widely used as components of sealants. The use of PSOs as effective vulcanizing agents for unsaturated rubbers has been reported [1]. When used as vulcanizing agents, PSOs provide formation of more flexible cross-links compared to rigid sulfur bonds, thus imparting enhanced elasticity to the vulcanizates.

Along with acting as vulcanizing agents, polysulfide oligomers are potentially capable, owing to the presence of sulfide and terminal hydrosulfide groups, of inhibiting oxidation of polymers by decomposing hydroperoxides (HPs), i.e., can act as secondary antioxidants (AOs) [2]. It has been shown that terminal hydrosulfide groups of sulfur-containing oligomers can be used for introduction of functional groups [3], e.g., sterically hindered phenolic (SHP) fragments scavenging peroxy radicals. Apparently, combination in one molecule of centers inhibiting oxidation of organic substrates by different mechanisms will substantially enhance the stabilizing function of the oligomers.

The goal of this study was to develop a procedure for preparing polysulfide oligomers with terminal SHP fragments and evaluate their antioxidative and vulcanizing properties.

EXPERIMENTAL

The starting chemicals were 4-dimethylaminomethyl-2,6-di-*tert*-butylphenol (Mannich base, MB), mp 93–95°C, and commercial PSO NVB-5, TU (Technical Specification) 38.50309–93, content of total sulfur 37.20 and of SH groups 4.74 wt %.

The PSOs were prepared as follows. A flask equipped with a stirrer, reflux condenser, thermometer, and bubbler was charged with the synthesized polysulfides (PSs) and MB. The mannich base was taken in an amount theoretically required for the conversion of all the SH groups in the PS. The mixture was stirred at 110–120°C in a nitrogen flow for 3–3.5 h. The reaction course was monitored by the release of dimethylamine, which was absorbed by a 0.1 N H_2SO_4 solution, using Methyl Orange as indicator. When the release of dimethylamine ceased, the reaction was assumed to be complete.

The weight percentage of the SH groups was determined by a laboratory procedure according to GOST (State Standard) 12812–80.

The IR spectra were recorded in the range 4000–400 cm^{-1} with a Perkin–Elmer 16PC-FT-IR device.

Autooxidation of the polymer was performed in oxygen (P_{O_2} = 250 mm Hg) at 135°C (polymer sample weight 0.1 g). To introduce PSO into the rubber, 5% solutions of SKI-3 in toluene were prepared; the mixtures were stirred to complete homogenization, after which the solvent was vacuum-evaporated.

The rate and degree of vulcanization of rubber stocks were determined with a Monsanto 100 S rheometer at 151°C; the test time was 60 min.

In our study, we prepared PSs with different extents of branching at the molar ratio monomer : sodium tetrasulfide = 1 : 1, with the aim to examine the effect of the structure on the PS properties. As the starting monomer we used dichlorodiethyl formal, pure or with additions of other chlorinated monomers (molar ratios: dichlorodiethyl formal : 1,2,3-trichloropropane = 98 : 2; dichlorodiethyl formal : diethane : 1,2,3-trichloropropane = 84.5 : 15 : 0.5).

The high-molecular-weight PSs obtained were washed with water to remove excess sodium tetrasulfide and then cleaved to obtain oligomers. To do this, the washed dispersion was heated with continuous stirring at 65°C for 40–60°C in the presence of a cleaving agent (1 : 1 mixture of Thiuram D with zinc stearate, 5% of the total product weight). After that, the cleaved dispersion was coagulated with 20% H_2SO_4 to pH 4–5. The precipitated polymer was repeatedly washed with cold water and vacuum-dried at 80°C to constant weight.

The products obtained were yellowish oils. Their molecular weights and contents of total sulfur and SH groups are listed in Table 1.

Among our goals was synthesis of polyfunctional compounds exhibiting AO properties along with vulcanizing power. For this purpose, we performed the reactions of the PSOs with 4-dimethylaminomethyl-2,6-di-*tert*-butylphenol (MB), which allowed introduction of SHP fragments into the oligomer:

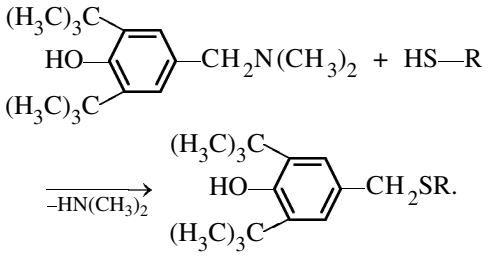

In accordance with this equation, the content of SH groups in the products was close to zero (Table 2).

The IR spectra of the PSOs contained absorption bands at 2600–2800, 1040–1200, and 600–800 cm^{-1}, characteristic of the stretching vibrations of the HS–, –OC–, and –SS– groups, respectively. The polysulfides SHP-PSO-4–SHP-PSO-6 also contained a well-defined peak at about 3600 cm^{-1}, corresponding to the OH group in the sterically hindered phenolic fragment, whereas the SH band at 2000–2800 cm^{-1} was absent.

The AO performance of the oligomers prepared was evaluated manometrically from the induction periods of oxidation of SKI-3 polymer at elevated temperatures. To compare the stabilizing performance of the PSOs prepared with that of the previously known polysulfides, we also determined the induction periods for the rubber containing commercial PSO NVB-2 widely used as a component of sealants, and also NVB-2 modified with SHP fragments.

We found that the PSOs under consideration increase the induction period (Table 3), well competing in the AO power with NVB-2. The most branched additive, PSO-3, surpassed NVB-2 by 15%.

Introduction of SHP fragments into PSOs led to a considerable increase in the induction period of the polymer oxidation. The most branched additive, SHP-PSO-6, showed the highest performance.

In the next stage of our study, the PSOs obtained were tested as vulcanizing agents in unfilled rubber

Table 1. Physicochemical characteristics of the compounds obtained

Polysulfide oligomer	Molecular weight	Content, wt %	
		SH groups	total sulfur
PSO-1	4400	1.48	27.80
PSO-2	3448	1.91	32.10
PSO-3	2857	2.61	51.40

Table 2. Content of SH groups in the synthesized SHP derivatives

PSO	Content, wt %			
	initial	final		total sulfur
		calculated	experimental	
SHP-PSO-4	1.48	0	0.030	25.44
SHP-PSO-5	1.91	0	0.066	27.86
SHP-PSO-6	2.61	0	0.060	43.68

Table 3. Induction period τ of thermal oxidation of SKI-3 rubber in relation to the type and concentration of the stabilizer added (P_{O_2} = 250 mm Hg, 135°C)

Stabilizer	τ, min, at indicated concentration of additive, wt %		
	1	2	3
NVB-2	15	20	50
PSO-1	20	30	60
PSO-2	20	30	60
PSO-3	25	40	70
SHP-NVB-2	60	80	100
SHP-PSO-4	50	70	90
SHP-PSO-5	60	80	100
SHP-PSO-6	80	100	120
–	10		

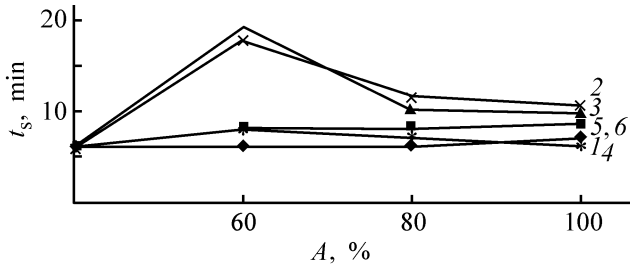

Fig. 1. Vulcanization onset time t_s vs. the amount and type of the polysulfide oligomer added. (*A*) Degree of replacement of sulfur with the oligomer; the same for Figs. 2, 3. Oligomer: (*1*) PSO-1, (*2*) PSO-2, (*3*) PSO-3, (*4*) SHP-PSO-4, (*5*) SHP-PSO-5, and (*6*) SHP-PSO-6.

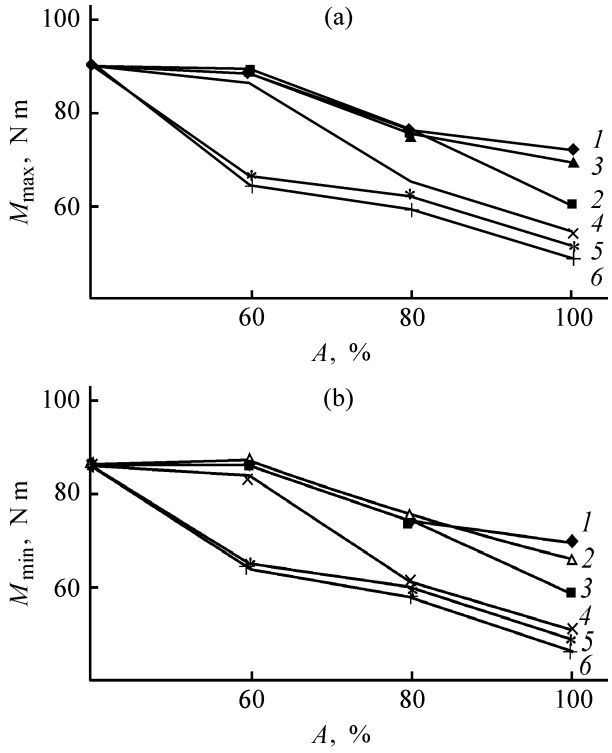

Fig. 2. (a) Maximal torque M_{max} and (b) minimal torque M_{min} vs. the amount of polysulfide added.

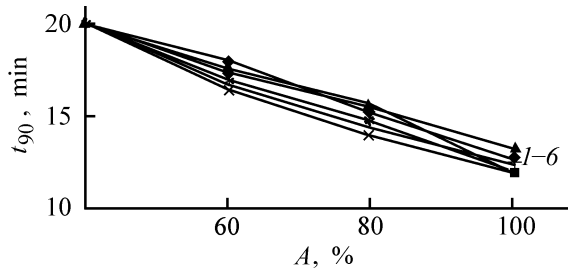

Fig. 3. Optimal vulcanization time t_{90} vs. the amount and type of polysulfide oligomer added.

stocks based on SKI-3 rubber, of the standard composition (wt parts): 100 SKI-3, 5 ZnO, 1 stearic acid, 0.6 altax, 3 diphenylguanidine, 1 Diafen FP, 1–0 sulfur, and 1–0 additive synthesized. In these stocks, 50–80–100% of sulfur was replaced with a PSO in such an amount that the total amount of sulfur was 1%.

Upon addition of the most branched PSOs (PSO-2, PSO-3) in a relative amount of 50%, the vulcanization onset time t_s sharply increased; however, further increase in the concentration of the additive affected t_s insignificantly (Fig. 1). Additions of linear oligomers, PSO-1 and SHP-PSO-4, did not appreciably alter t_s. The presence of the SHP fragment in branched PSOs led to an increase in the vulcanization onset time at the relative content of the additive exceeding 80% (SHP-PSO-5, SHP-PSO-6). Apparently, the additives inhibit the radical process.

The addition of the synthesized PSOs without SHP fragments in a relative amount exceeding 50% led to a decrease in both the maximal (Fig. 2a) and minimal (Fig. 2b) torques. The most pronounced decrease in these parameters was observed with the most branched oligomer, PSO-2.

Introduction of SHP fragments into the PSO molecules led to a more significant decrease in M_{max}. With SHP-PSO-5 and SHP-PSO-6, the torque sharply decreased even on replacement of 50% of sulfur in the stock.

Addition of the synthesized PSOs without SHP fragments made the optimal vulcanization time shorter (Fig. 3). This fact suggests that the polysulfides are good vulcanizing agents.

In the next stage of our study, we determined the main elastic and strength characterisitcs of the unfilled vulcanizates.

Experimental data show that introduction of the PSOs synthesized into the rubber stock cause an increase in the relative breaking elongation, compared to the control sample containing NVB-2. Upon addition of SHP-PSOs, the relative breaking elongation increased when more than 50% of sulfur was replaced with the additive. The strength of the PSO-containing vulcanizates appeared to be considerably higher than that of the control sample. In the vulcanizates with SHP-PSOs, these parameter also increased upon 50% replacement of sulfur and then varied linearly with a further increase in the content of the additive. The highest strength was attained with the branched additives: PSO-2, PSO-3, SHP-PSO-5, and SHP-PSO-6. It should be noted that the elongation set was observed only upon complete replacement of sulfur in

the vulcanizates with SHP-PSOs. In all the other cases, the elongation set was zero. Thus, the copolymers under consideration improved the plastoelastic properties of the vulcanizates relative to the composition with sulfur as vulcanizing agent.

The physicomechanical properties of vulcanizates prepared with the PSOs and SHP-PSOs synthesized were compared with those of vulcanizates prepared with sulfur and with commercial PSO NVB-2. It was found that the additives synthesized well compete with NVB-2 and even surpass it in some parameters. For example, with PSO-2, PSO-3, SHP-PSO-5, and SHP-PSO-6, the tear resistance and strength increased by 83–240% relative to the vulcanizate prepared with sulfur, whereas with NVB-2 and SHP-NVB-2 the increase was less pronounced (20–40%).

Since the synthesized PSOs contained SHP fragments enhancing the resistance to oxidation, we performed aging of vulcanizates (72 h, 100°C) and evaluated the stabilizing performance of the additives from the aging coefficients. The aging coefficients increased by 10–30% with the copolymers added to the stock, relative to the control sample. The most branched additives PSO-2, PSO-3, SHP-PSO-5, and SHP-PSO-6 ensured the best physicomechanical properties and aging coefficients of the vulcanizates.

CONCLUSIONS

(1) The synthesized polysulfide oligomeric additives containing sterically hindered phenolic fragments make longer the induction period of SKI-3 rubber oxidation.

(2) The synthesized polysulfide oligomers decrease the maximal and minimal torques and optimal vulcanization time and increase the vulcanization onset time.

REFERENCES

1. Rylova, M.V. Copolymers of Dicyclopentadiene and Elemental Sulfur with Decreased Sulfidity: Formation Mechanism, Structure, and Possible Fields of Application, *Cand. Sci. Dissertation*, Kazan, 2004.
2. Averko-Antonovich, I.Yu., Averko-Antonovich, L.A., Gonyukh, A.V., et al., Abstracts of Papers, *IV Vsesoyuznaya konferentsiya po khimii i fizikokhimii oligomerov* (IV All-Union Conf. on Chemistry and Physical Chemistry of Oligomers), Chernogolovka, 1990, p. 239.
3. Mitrofanova, S.E., Girfanova, E.N., Averko-Antonovich, I.Yu., and Cherezova, E.N., *Zh. Prikl. Khim.*, 2006, vol. 79, no. 1, pp. 139–143.

ISSN 1070-4272, Russian Journal of Applied Chemistry, 2007, Vol. 80, No. 6, pp. 992–994. © Pleiades Publishing, Ltd., 2007.
Original Russian Text © R.Yu. Mitrofanov, P.N. Bochkarev, V.P. Sevodin, 2007, published in Zhurnal Prikladnoi Khimii, 2007, Vol. 80, No. 6, pp. 1018–1020.

MACROMOLECULAR CHEMISTRY AND POLYMERIC MATERIALS

A Chemical Procedure for Reprocessing of Poly(Ethylene Terephthalate) Waste

R. Yu. Mitrofanov, P. N. Bochkarev, and V. P. Sevodin

Biisk Technological Institute, Branch of Polzunov Altai State Technical University, Biisk, Altai krai, Russia

Received October 10, 2006; in final form, March 2007

Abstract—A procedure was developed for degradation of poly(ethylene terephthalate) waste with water to the starting monomers. The possibility of preparing diethyl terephthalate without a catalyst in a rocking cylindrical pressure vessel with the rocking axis passing through the geometric center was examined.

DOI: 10.1134/S1070427207060274

Poly(ethylene terephthalate) (PET) patented in 1941 was initially intended for production of fibers; however, thanks to its unique properties, it is also widely used today as a structural material. As the volume of PET production grows, the amount of industrial and domestic PET waste increases also; only in Russia it amounts to 300–400 thousand tons annually.

The existing mechanical procedures for utilization of spent PET containers allow preparation of only a secondary raw material for production of finished items. However, the demand for items prepared in this way is low. Furthermore, the use of secondary raw materials in Russia and EU countries for packaging of foodstuffs is prohibited by the legislation.

An alternative solution is chemical reprocessing of spent PET containers and articles. The existing chemical methods for PET reprocessing can be subdivided into three types: (1) reprocessing to obtain the primary monomers, namely, ethylene glycol (EG) and terephthalic acid (TPA) or dimethyl terephthalate (DMT); (2) glycolysis of PET with ethylene glycol to obtain bis(hydroxyethyl) terephthalate and other oligomers, which are then either subjected to polycondensation to obtain PET or brought into reactions with dicarboxylic acids to obtain "polyester polyols" used in production of polyurethane foam or elastomers; (3) depolymerization of PET with propylene glycol, followed by the reaction of the decomposition product with maleic anhydride to obtain "unsaturated polyesters" used in production of reinforced fibers.

Methods of types 2 and 3 have been fairly well studied. These methods are mainly applicable to large-tonnage process waste. The final products obtained using methods of type 1 are TPA + EG or DMT + EG.

Degradation of PET waste into TPA can be performed in three modes: pressure hydrolysis, acid hydrolysis in the presence of strong mineral acids, and alkaline saponification. In all the cases, almost theoretical yields are attained. However, acid and base hydrolysis of PET waste exclude the possibility of EG regeneration and require use of aggressive chemicals, which causes drastic increase in the capital investments required for auxiliary reagents and effluent treatment.

In the 1960–1970s, a procedure for recycling of substandard PET [1] formed in the course of production was developed and commercially implemented. The process involves depolymerization of the waste in excess methanol in the presence of a catalyst at a pressure of 20–25 kgf cm^{-2} and 180°C for 3–5 h. The process is intended for large-scale use; it is sophisticated, involves a large number of operations, and requires regular supply of waste of the preset quality. Therefore, this process is inapplicable to small volumes of domestic wastes which are, as a rule, strongly contaminated with mineral and organic impurities.

Furthermore, there are fragmentary published data [2] that PET can be decomposed under appropriate

conditions with alcohols, esters, and amines, with the cleavage of the ester bond. These reactions are considerably accelerated at elevated temperatures and higher catalyst acidities. Aminolysis of PET yields polyamido esters. The extent of aminolysis depends on the amount and kind of the diamine.

A possible alternative solution to the problem of reprocessing of domestic PET waste into a valuable raw material for chemical, paint-and-varnish, or pharmaceutical industry is setting up small- or medium-scale shops.

For example, procedures have been suggested for preparing various paint-and-varnish materials, including powders (hydroxyl- and carboxyl-containing components for epoxy–polyester compounds), insullacs, alkyd oligomers, materials for road marking, etc. [3–5]. Film-forming agents are prepared by ester interchange of PET with various polyols [3]. The reaction occurs in two steps. The first step is destructive alcoholysis to give unsymmetrical oligomers; the second step, cross-linking, starts simultaneously, yielding a 3*D* polymer. Depending on the reaction time and PET : polyol ratio, it is possible to prepare oligomers with the prescribed softening and dropping points and with predictable solubility in organic lacquer solvents.

Along with the symmetrical polymer, it is possible to prepare polymers with various combinations of comonomers (terephthalic acid, ethylene glycol, *p*-hydroxybenzoic acid). Such polymers exhibit increased shrinkage and are well dyed with dispersible dyes without applying a pressure [6]. Polymers with prescribed properties can be prepared by varying the comonomer ratio.

Published data on the chemical processing methods show that the most widely used, economically feasible, and environment friendly method is hydrolysis of PET in a neutral medium to TPA and EG. The process is performed in excess water at 180–220°C for 5–6 h; it is fairly simple and requires no additional chemicals.

EXPERIMENTAL

To prepare crude TPA, we used spent TPE containers; their pretreatment involved removal of labels and adhesives, followed by shredding. No sorting by color was performed.

The process was carried out in a rocking pressure vessel [7] (a steel cylinder 1.1 m long, 0.065 m i.d.). The degree of filling was 0.6. The rocking rate was 20 min^{-1} [8].

The purity of the compounds obtained was monitored by TLC on Silufol UV-254 plates (Czechia), eluent benzene–acetone, 3 : 1. The melting points of the products were measured with a PTP(M) capillary device for melting point measurements and were not corrected.

Terephthalic acid. The pressure vessel was charged with 500 g of PET and 2000 ml of distilled water. The vessel was hermetically sealed. Agitation was switched on; the mixture was heated to 280–285°C, kept at this temperature for 10 min, and cooled to 30–35°C. The vessel was opened, and the TPA obtained was filtered off, washed with distilled water (4 × 250 ml), and dried at 100–120°C. Yield of TPA 431.42 g (99.8%); light brown crystals subliming in an open capillary without melting at approximately 300°C.

Diethyl terephthalate (DET). The pressure vessel was charged with 240 g of terephthalic acid and 2200 ml of 96% ethanol. The vessel was hermetically sealed, agitation was switched off, and the contents were heated to 230–240°C, kept at this temperature for 6 h, and cooled to 25–30°C. Then the vessel was opened, and the mixtrue was filtered and evaporated to 1/3 of the initial volume. The residue was refluxed for 30 min with addition of 2 g of activated carbon and then filtered. The filtrate was cooled in an ice bath with stirring; in so doing, the major fraction of the diethyl ester crystallized. An additional amount of the product was obtained by the filtrate evaporation.

The product was stirred with 1000 ml of 5% sodium hydrogen carbonate at 10–20°C for 30 min, filtered off on a Büchner funnel, and washed with distilled water (3 × 250 ml). The alkaline filtrate was acidified on cooling with sulfuric acid; as a result, a mixture of the monoester and TPA was obtained, which was delivered to the esterification step with addition of pure TPA.

The crystalline diethyl ester obtained was dried at 30–35°C for 48 h. Yield 279.36 g (87.3%), mp 43–44°C.

As a method of PET waste utilization, we examined hydrolysis without a catalyst. It is known [9] that, at temperatures exceeding 280°C, PET undergoes virtually instantaneous hydrolysis with cleavage of the ester bonds. As the reaction time is varied from 2 to 120 min, the TPA yield varies insignificantly (95.5–96.9%), which is consistent with published data.

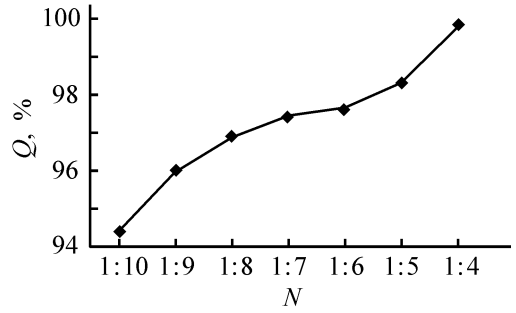

Fig. 1. TPA yield Q vs. the PET : water ratio N.

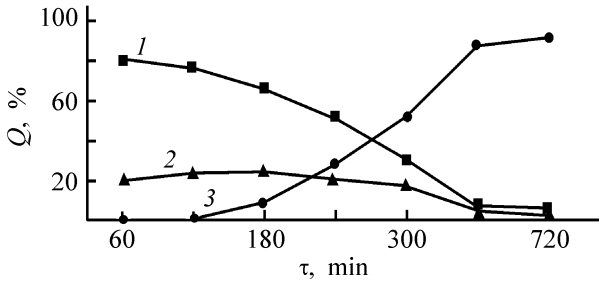

Fig. 2. Yield of esterification products, Q, vs. reaction time τ: (*1*) TPA, (*2*) ethyl hydrogen terephthalate, and (*3*) DET.

The influence of the PET : water ratio on the TPA yield is shown in Fig. 1.

The acid obtained is of low purity and cannot be returned to the polymer production. Purification by reprecipitation is labor-consuming and involves use of alkalis and strong mineral acids. According to published data [10, 11], TPA is a valuable raw material for preparation of compounds used in fine organic synthesis. One of such compounds is diethyl terephthalate (DET).

To prepare DET, we esterified crude TPA with ethanol in the pressure vessel at 230–240°C. The dependence of the yield of the esterification products on the reaction time is shown in Fig. 2.

The esterification results demonstrated that at a TPA : C_2H_5OH ratio of 1 : 9 the maximal DET yield was 87.3%. With an increase in the reaction time from 6 to 12 h, the yield increased by no more than 4%; therefore, it is not appropriate to perform the reaction for a time exceeding 6 h.

Advantages of the method are the high reaction yield and the absence of a catalyst. The mixture obtained after the reaction completion is a homogeneous transparent solution which can be readily purified by filtration to remove mechanical impurities and label paper; the costs for pretreatment of PET waste can thus be reduced.

CONCLUSIONS

(1) A convenient procedure was suggested for utilization of heavily contaminated domestic poly(ethylene terephthalate) waste, allowing its reprocessing on small and medium scales using nonstandard equipment.

(2) The process involves formation of an insignificant amount of waste.

REFERENCES

1. US Patent 3 403 115.
2. Pilunov, A.G., Mikhitarova, Z.A., and Tseitlin, G.M., *Khim. Prom–st.*, 2001, no. 6, pp. 22–28.
3. Kudyukov, Yu.P., Maslosh, V.Z., Savitskaya, A.V., and Litvinova, E.V., *Lakokras. Mater. Ikh Primen.*, 1993, no. 3, pp. 3–4.
4. Klosowska-Wolkewicz, Z., *Wlock. Chem.*, 1982, vol. 8, no. 4, pp. 412–418.
5. Ostrish, R., Penchek, P., and Snezhko, A., *Khim. Ind.*, 1982, no. 2, pp. 50, 51, 75–78.
6. Petukhov, B.V., *Poliefirnye volokna* (Polyester Fibers), Moscow: Khimiya, 1976.
7. RF Industrial Model 2518.
8. Sevodina, G.I., A Study of Heterogeneous Processes in Rocking Autoclaves, *Cand. Sci. Dissertation*, Biisk, 1998.
9. *Entsiklopediya polimerov* (Polymer Encyclopedia), Kabanov, V.A., Ed., Moscow: Sov. Entsiklopediya, 1977, vol. 3.
10. US Patent 4 399 303.
11. US Patent 3 931 210.

ISSN 1070-4272, Russian Journal of Applied Chemistry, 2007, Vol. 80, No. 6, pp. 995–998. © Pleiades Publishing, Ltd., 2007.
Original Russian Text © N.I. Polezhaeva, A.A. Nefedov, L.A. Kruglyakova, I.V. Polezhaeva, V.A. Fedorov, 2007, published in Zhurnal Prikladnoi Khimii, 2007, Vol. 80, No. 6, pp. 1021–1024.

MACROMOLECULAR CHEMISTRY AND POLYMERIC MATERIALS

Kinetics of Thermal Oxidative Degradation of a Polyester Resin and of Its Formulation with Diethyldibenzylammonium Bromide

N. I. Polezhaeva, A. A. Nefedov, L. A. Kruglyakova, I. V. Polezhaeva, and V. A. Fedorov

GOU VPO Siberian State Technological University, Krasnoyarsk, Russia

Received September 21, 2006; in final form, January 2007

Abstract—The kinetics of thermal oxidative degradation of a polyester resin and of its formulation with diethyldibenzylammonium bromide was studied. The rate constants of the thermal decomposition were determined.

DOI: 10.1134/S1070427207060286

This study further examinates the developed formulations of low-temperature noncorrosive solder creams based on a polyester resin modified with rosin and quaternary ammonium salts [1, 2].

The temperature and time limits of the working capacity are important characteristics of polymers. These limits are determined by the occurrence of physical or chemical transformations of polymers [3].

A thermal analysis can be performed in isothermal and dynamic modes. In the first case, the thermal degradation is monitored at a constant temperature, which allows comparison of the degradation rates of various materials at a given temperature. This mode is suitable when the working temperature range of a material is known.

To estimate the heat resistance of a material, it is necessary first to determine the temperature ranges of the occurrence of transformations that irreversibly alter the chemical nature of the polymer. This is done using dynamic thermal analysis.

EXPERIMENTAL

The parameters of thermal oxidative degradation of a polyester resin (sample no. 1) and its formulation with diethyldibenzylammonium bromide (DEDBAB) (sample no. 2) were determined by dynamic thermogravimetry [4]. For more accurate determination of the temperatures at which the samples start to decompose, we recorded along with the TG curves the DTG and DTA curves (Figs. 1a, 1b). Experiments were performed with an MOM Q-1000 derivatograph (Hungary) in the programmed-heating mode. Samples (0.05 g) were heated in a platinum crucible in air at rates of 5 and 10 deg min^{-1}. The sensitivities were as follows: balance, 100 mg; DTA galvanometer, 1/3; DTG galvanometer, 1/10.

When heated in air, sample no. 1 decomposes in three steps in the interval 80–600°C (Fig. 1a). The first step (80–250°C) involves removal of the residual solvent and free volatile components boiling in this range: water formed in the course of the resin synthesis, residual alcohol, and unsaponifiable substances. The second step (310–400°C) involves endothermic decomposition of the polyester resin and simultaneously occurring exothermic oxidation of a part of the products formed [1, 3, 5]. The third step is characterized by a complex exothermic effect with characteristic temperatures of 420 (onset of exothermic peak corresponding to the oxidation in the DTA curve) and 540°C. The strong peak at 540°C corresponds to oxidation of the gaseous products released in the course of the thermal decomposition of the polyester resin [1, 3, 5].

Sample no. 2, when heated in air, decomposed in three steps in the interval 100–560°C (Fig. 1b). The first step (100–220°C) is of the same origin as for sample no. 2. The second step (250–400°C) involves

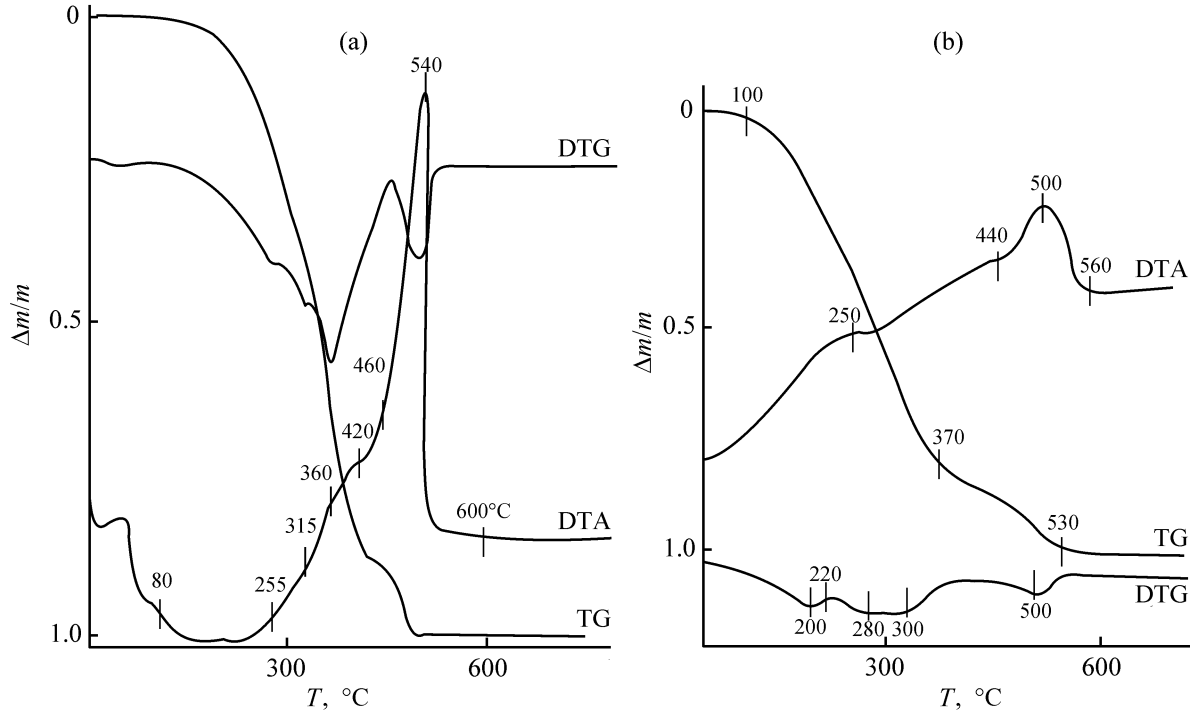

Fig. 1. Thermogram of (a) a polyester resin modified with rosin and (b) its formulation with diethyldibenzylammonium bromide. ($\Delta m/m$) Relative weight loss and (T) temperature.

endothermic decomposition of DEDBAB and simultaneously occurring exothermic oxidation of a part of the products formed [2, 5]. The third step is characterized by a complex exothermic effect with characteristic temperatures of 440 (onset of exothermic peak corresponding to the oxidation in the DTA curve) and 500°C. The strong peak at 500°C corresponds to oxidation of the gaseous products released in the course of the thermal decomposition of the polyester resin [2, 5].

The kinetics of thermal degradation was studied in the static mode by the manometric method, using a glass Bourdon zero gage at a residual pressure in the reaction volume of 10^{-1}–10^{-2} mm Hg in the temperature range 100–300°C. The temperature in the thermostat was maintained with an accuracy of ±(0.2–0.5)°C. The scheme of the installation and the experimental procedure were described in [6, 7].

To make the data comparable, the results of the manometric study were converted to the normal volume of gaseous products per gram of the starting compounds:

$$V_t = (T_0 V_r P_t)/(T P_0 m),$$

where V_r is the volume of the reaction space in the manometer (cm^3); P_t, pressure of decomposition products by the instant of time t (mm Hg); V_t, volume of gaseous decomposition products released by the instant of time t (cm^3); T_0, temperature corresponding to the normal conditions (273.15 K); T, experimental temperature (K); m, sample weight (g); and P_0, pressure corresponding to normal conditions (760 mm Hg).

The experimental data were plotted as the volume of the released gases per gram of the starting substance vs. time. The value of the maximal gas release V_∞ required for determining the reaction rate constant by a first-order equation, $k = (1/t)\ln[V_\infty/(V_\infty - V_t)]$, was taken from the experimental manometric curves. The quantity V_∞ is specific to each temperature, because, as the temperature is raised, the growing number of components become volatile. The character of the thermal degradation can be judged from the shape of the smoothed kinetic curve. For the decomposition by a first-order reaction, the dependence $V_i = f(t_i)$ is described by a flattening-out curve (which was actually observed in the experiment). In this case, the rate constant of the thermal decomposition (s^{-1}) was calculated by the formula

$$k = (1/t)\ln[V_\infty/(V_\infty - V_t)],$$

where V_∞ is the total volume of gaseous decomposition products under normal conditions, released from 1 g of the starting substance (cm^3).

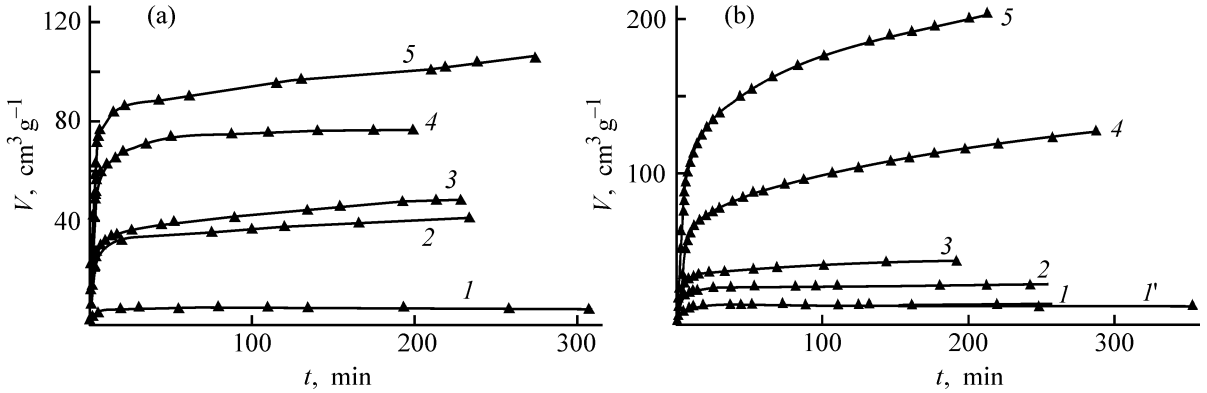

Fig. 2. Manometric curves of gas evolution from sample nos. (a) 1 and (b) 2 at temperatures of up to 300°C. (*V*) Volume of gaseous products per gram of the starting substance and (*t*) time; the same for Fig. 3. Temperature, °C: (*1*) 100, (*1*') 120, (*2*) 150, (*3*) 180, (*4*) 250, and (*5*) 300.

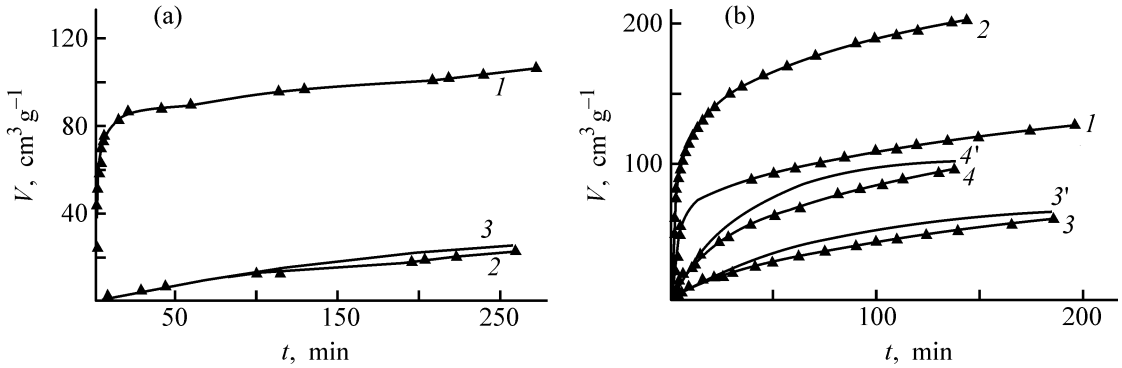

Fig. 3. Manometric curves of the gas release from (a) sample no. 1 at 300°C and (b) sample no. 2 at 250 and 300°C. (a) (*1*) Initial experimental curve, (*2*) curve with subtracted initial volume of gas release, and (*3*) approximating curve corresponding to a first-order reaction equation. (b) (*1*, *2*) Initial experimental curves, (*3*, *4*) curves with subtracted initial volume of gas release, and (*3*', *4*') approximating curves corresponding to first-order reaction equations; temperature, °C: (*1*, *3*, *3*') 250 and (*2*, *4*, *4*') 300.

The working reflow temperatures of low-temperature solder creams (°C) are as follows: POIn-52, 120; 45% Sn + 29% Pb + 17% Cd + 9% In, 140–150; POSK 50/18, 170–180; POS-61, 220–250. Therefore, manometric studies of sample nos. 1 and 2 were performed at 100, 120, 150, 180, 250, and 300°C [8].

Manometric studies of sample nos. 1 and 2 showed that the resins are thermally stable up to approximately 250°C (Figs. 2a, 2b). The gas release observed in the course of the experiment is caused by the removal of residual solvent and free volatile components: water formed in the course of the resin synthesis, residual alcohol, and unsaponifiable substances. The gas release was up to 60 ml per gram of the sample (depending on the experimental temperature).

Thermal degradation of sample nos. 1 and 2 starts at approximately 250°C. The initial portion of the manometric curve corresponds to the removal of the residual solvent, and this is followed by the thermal degradation proper (Figs. 3a, 3b). Thermal degradation of sample nos. 1 and 2 is described by a first-order reaction equation. The calculated rate constants of the thermal degradation are as follows: sample no. 1, 300°C, 6.9×10^{-5} s^{-1}; sample no. 2, 250°C, 2.2×10^{-4} s^{-1}; 300°C, 4.51×10^{-4} s^{-1}. That is, the samples are fairly heat-resistant. The higher resistance of sample no. 1 to thermal oxidation, compared to sample no. 2, may be due to acid catalysis of the resin decomposition, observed in the presence of DEDBAB (its hydrolysis leads to acidification of the reaction medium).

CONCLUSION

Isothermal and dynamic thermal analyses of a polyester resin and its formulation with diethyldibenzylammonium bromide showed that these substances are

resistant to thermal oxidative degradation at the reflow temperatures of low-temperature solder creams.

REFERENCES

1. Polezhaeva, N.I., Polezhaeva, I.V., Levdanskii, V.A., et al., *Zh. Prikl. Khim.*, 2001, vol. 74, no. 4, pp. 684–685.
2. Polezhaeva, N.I., Polezhaeva, I.V., Levdanskii, V.A., and Kuznetsov, B.N., *Zh. Prikl. Khim.*, 2002, vol. 75, no. 4, pp. 689–690.
3. Pavlova, S.-S.A., Zhuravleva, I.V., and Tolchinskii, Yu.I., *Termicheskii analiz organicheskikh i vysokomolekulyarnykh soedinenii* (Thermal Analysis of Organic and Macromolecular Compounds), Moscow: Khimiya, 1983.
4. Wendlandt, W.Wm., *Thermal Methods of Analysis*, New York: Interscience, 1964.
5. Kovarskaya, B.M., Blyumenfel'd, A.B., and Levantovskaya, I.I., *Termicheskaya stabil'nost' geterotsepnykh polimerov* (Heat Resistance of Heterochain Polymers), Moscow: Khimiya, 1977.
6. Stepanov, R.S. and Kruglyakova, L.A., *Kinet. Katal.*, 1996, vol. 37, no. 3, pp. 316–317.
7. Gol'binder, A.I., *Laboratornye raboty po kursu vzryvchatykh veshchestv* (Laboratory Works for the Course of Explosives), Moscow: Rosvuzizdat, 1963.
8. Krasov, V.G., Petrauskas, G.B., and Chernozubov, Yu.S., *Tolstoplenochnaya tekhnologiya v SVCh mikroelektronike* (Thick-Film Technology in UHF Microelectronics), Moscow: Radio i Svyaz', 1985.

ISSN 1070-4272, Russian Journal of Applied Chemistry, 2007, Vol. 80, No. 6, pp. 999–1001. © Pleiades Publishing, Ltd., 2007.
Original Russian Text © G.V. Akopyan, R.A. Karamyan, R.N. Engibaryan, M.L. Eritsyan, 2007, published in Zhurnal Prikladnoi Khimii, 2007, Vol. 80, No. 6, pp. 1024–1026.

MACROMOLECULAR CHEMISTRY AND POLYMERIC MATERIALS

Water-Absorption Capacity of Cross-Linked Copolymers of Acrylic Acid and Acrylamide, Containing Various Ionic Groups

G. V. Akopyan, R. A. Karamyan, R. N. Engibaryan, and M. L. Eritsyan

Abovyan State Pedagogical University, Yerevan, Armenia

Received August 2, 2006; in final form, February, 2007

Abstract—Radical copolymerization of acrylic acid with acrylamide in the presence of sodium 1,3-diallyl isocyanurate cross-linking agent was studied.

DOI: 10.1134/S1070427207060298

Water-absorbing copolymers based on acrylic acid (AA) and its derivatives have been examined in numerous studies. Some papers consider in detail the relationship between the structural features and water-absorption capacity of copolymers [1–4].

At the same time, data on the effect of the counterions of the ionic groups in homo- and copolymers of AA and its derivatives and of the ionic strength of their aqueous solutions on the rate of water absorption of these polymers are virtually lacking. Therefore, we examined in this study the dependence of the amount of water absorbed by AA copolymer with acrylamide on the nature and concentration of counterions of the ionic groups in copolymers.

We studied NH_4^+, Li^+, Na^+, and K^+ cations as counterions of the acrylate groups in the copolymer. Copolymers with these counterions were prepared by treatment of AA copolymers with acrylamide (AM) with alkalis containing the above counterions. The macromolecular chains formed by copolymerization of AA and acrylamide were cross-linked with sodium 1,3-diallyl isocyanurate (Na-DAIC).

In all the copolymerization experiments, the total concentration of AA and its salts was 2 M (30% acrylates relative to AA in the monomer mixture). In preparing copolymers, the content of acrylamide was 30% relative to the total concentration of the other monomers.

Copolymerization of AA and acrylamide in the presence of Na-DIAC yielded cross-linked polymers, which acquire high water-absorption capacity upon treatment with appropriate alkalis.

The data on the amount of water absorbed by the copolymers in relation to the content of Na-DIAC and nature of counterions of the ionic groups in the copolymer are listed in Table 1.

Table 1. Water-absorption capacity of copolymers as influenced by the density of cross-linking and nature of counterions of the ionic groups

Monomer molar ratio [AK]+[M-AA]*+[AA]/ [Na-DIAC] in copolymer	Water-absorption capacity, mg H_2O/gram copolymer								
	NH_4^+	Li^+	Na^+	K^+	NH_4^+/Li^+	NH_4^+/Na^+	Li^+/Na^+	Li^+/K^+	Na^+/K^+
5	200	150	130	100	180	150	125	110	90
10	350	220	200	150	280	210	190	180	160
30	580	450	400	330	500	460	430	380	350
50	630	500	450	400	570	530	490	460	420
60	750	650	580	500	690	630	600	560	520

Note. Counterions M are NH_4^+, Li^+, Na^+, K^+, and their equimolar mixtures NH_4^+/Li^+, NH_4^+/Na^+, Li^+/Na^+, Li^+/K^+, and Na^+/K^+.

Table 2. Rate of water absorption in relation to the nature of counterions of the ionic groups in copolymers and to the concentration of aqueous salt solutions

Salt, wt %	Rate of water absorption, mg min^{-1}									
	NH_4^+	Li^+	Na^+	K^+	NH_4^+/Li^+	NH_4^+/Na^+	NH_4^+/K^+	Li^+/Na^+	Li^+/K^+	Na^+/K^+
0	0.5	0.35	0.2	0.18	0.3	0.25	0.23	0.21	0.2	0.18
NaCl:										
0.1	0.4	0.27	0.18	0.16	0.23	0.21	0.2	0.19	0.18	0.17
0.3	0.37	0.19	0.11	0.1	0.21	0.2	0.18	0.16	0.15	0.13
0.5	0.35	0.17	0.08	0.06	0.19	0.17	0.14	0.11	0.1	0.09
$CaCl_2$:										
0.1	0.33	0.21	0.16	0.06	0.28	0.19	0.17	0.14	0.095	0.05
0.3	0.25	0.125	0.075	0.02	0.16	0.12	0.095	0.08	0.07	0.03
0.5	0.2	0.085	0.025	0.008	0.09	0.06	0.04	0.03	0.02	0.01

As can be seen, copolymers whose ionic groups contain NH_4^+ counterions exhibit the highest water-absorption capacity. This is probably due to a higher hydrolytic activity of NH_4^+ ions as compared to the activity of the other counterions.

Moreover, copolymers containing ionic groups with different counterions exhibit lower water-absorption capacity than copolymers with the ionic groups containing the more active counterion only (NH_4^+ or Li^+).

It is known that the water-absorption capacity of cross-linked homo- and copolymers decreases with increasing concentration of dissolved salts [5]. In this context, we studied the water-absorption capacity of AA copolymers with acrylamide cross-linked with Na-DIAC in the presence of NaCl and $CaCl_2$ aqueous solutions of various concentrations.

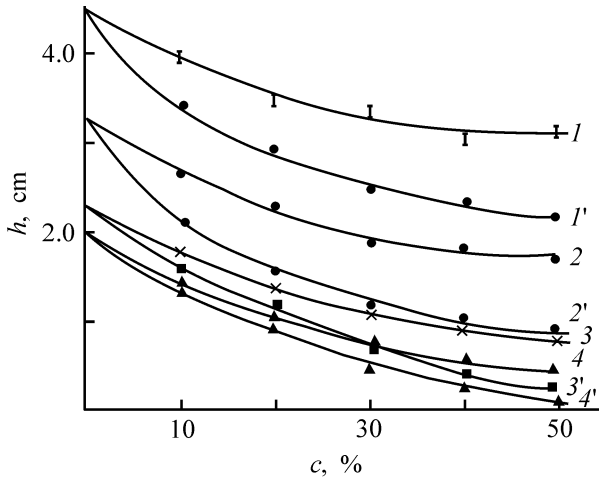

Water absorption h of copolymers, as influenced by the salt concentration c and nature of counterions of the ionic groups. (*1*–*4*) NaCl and (*1'*–*4'*) $CaCl_2$. (*1*, *1'*) NH_4^+, (*2*, *2'*) Li^+, (*3*, *3'*) Na^+, and (*4*, *4'*) K^+.

The dependences of the amount of water absorbed by the copolymers on the nature and concentration of the aqueous solutions (NaCl and $CaCl_2$) and on the nature of counterions of the carboxy groups in copolymer are shown in the figure. The results were obtained using copolymers with the monomer molar ratio AA : M-AA : AM : Na-DIAC = 0.7 : 0.3 : 0.3 : 0.02. Ammonium acrylate was used as M-AA. It should be noted that the copolymer of the above composition can absorb up to 750 g of water per gram. Irrespective of the nature of the counterions of the ionic groups in the copolymer, absorption of water proceeds at a constant rate during 15 min after the being of the experiment.

Our experimental data showed that the counterions of the ionic groups in the copolymers affect not only the water-absorption capacity of copolymers but also the absorption rate.

The rates of water absorption, as influenced by nature of counterions of the ionic groups and by the concentrations of aqueous salt solutions, are listed in Table 2. As can be seen, copolymers containing NH_4^+ counterions exhibit not only high water-absorption capacity but also high rate of water absorption.

EXPERIMENTAL

Na-DIAC was prepared and purified by the procedure described elsewhere [6]. The fraction of AA with bp 141°C and n_D^{20} = 1.4224 was used. Acrylamide (mp 85°C) and ammonium persulfate were recrystallized from methanol and ethanol, respectively.

The ionic (carboxy) groups in copolymers were prepared using LiOH, NaOH, and KOH, of analytically pure grade and 18% NH_4OH. The copolymerization was carried out at 70 ± 0.5°C [3].

Copolymers with ionic groups and the corresponding counterions (NH_4^+, Li^+, Na^+, and K^+ and their mixtures) were prepared by addition of the required amount of an aqueous alkali solution of a definite concentration (wt %) to a preliminarily swollen copolymer gel. Then the mixture was thoroughly mixed and stored for 24 h. The swollen mass was first dried in air to completely remove water and then in a vacuum (1.5–2.0 mm Hg) at 65–70°C to constant weight. The degree of neutralization of the carboxy groups in the copolymer with the corresponding alkalis was determined by titration of the filtrate after neutralization of the repeatedly swollen copolymer gel with 0.1 N HCl solution.

The amount V (ml) of absorbed water in copolymers was calculated from the equation $V = \pi R^2 h$, where R is the capillary radius and h is the level of absorbed water in the capillary.

The rate of water absorption (ml min^{-1}) in copolymers was determined using the kinetic dependences of water absorption.

To determine the water-absorption capacity of copolymers, a weighed portion of a copolymer (0.125 g) was placed in a graduated cylinder (0.5 cm in diameter and 30 cm high); then water was added up to the upper mark, the mixture was thermostated at a required temperature, and the upward shift of the swollen gel boundary was monitored.

CONCLUSIONS

(1) The nature of counterions of the carboxy groups in copolymers affects both the water-absorption capacity and the rate of water absorption by copolymers of acrylic acid and acrylamide, cross-linked with sodium 1,3-diallyl isocyanurate and containing various ionic groups.

(2) The concentration and nature of the aqueous salt solutions (NaCl and $CaCl_2$) strongly affect both the water-absorption capacity and the rate of water absorption. With increasing concentrations of these salts in aqueous solutions, both the water-absorption capacity of the copolymers considerably decreases.

REFERENCES

1. Doseva, V.N., Shenkov, S.D., Brychkov, Khr.I., et al., *Vysokomol. Soedin., Ser. B*, 2002, vol. 44, no. 8, pp. 1444–1449.
2. Philipova, O.E., Karibyants, N.S., and Starodubtsev, S.E., *Macromolecules*, 1994, vol. 27, no. 9, pp. 2398–2405.
3. Eritsayn, M.L., Galstyan, G.G., and Karamyan, R.A., *Vysokomol. Soedin., Ser. A*, 2003, vol. 45, no. 7, pp. 1202–1204.
4. Suleimenov, I.E., Budtova, T.V., and Bekturov, E.A., *Vysokomol. Soedin., Ser. A*, 2002, vol. 44, no. 9, pp. 1571–1577.
5. Lee Wen-Fu and Yeh Pao-Li, *J. Appl. Polym. Sci.*, 1997, vol. 64, no. 12, pp. 2371–2378.
6. Chovnik, L.N., Pazenko, Z.N., Kornev, K.A., and Khomenkova, K.K., *Zh. Org. Khim.*, 1965, vol. 1, no. 10, pp. 742–743.

ISSN 1070-4272, Russian Journal of Applied Chemistry, 2007, Vol. 80, No. 6, pp. 1002–1006. © Pleiades Publishing, Ltd., 2007.
Original Russian Text © R.G. Makitra, G.G. Midyana, O.I. Romanyuk, E.Ya. Pal'chikova, 2007, published in Zhurnal Prikladnoi Khimii, 2007, Vol. 80, No. 6, pp. 1028–1032.

MACROMOLECULAR CHEMISTRY AND POLYMERIC MATERIALS

Swelling of a Sulfamide Polymer in Alcohols

R. G. Makitra, G. G. Midyana, O. I. Romanyuk, and E. Ya. Pal'chikova

Institute of Geology and Geochemistry of Fossil Fuels, National Academy of Sciences of Ukraine, Lviv, Ukraine

Division of Physical Chemistry of Fossil Fuels, Litvinenko Institute of Physical Organic and Coal-Tar Chemistry, National Academy of Sciences of Ukraine, Lviv, Ukraine

Received August 10, 2006; in final form, March 12, 2007

Abstract—Swelling of a sulfamide polymer of UPM brand in a series of alcohols was studied gravimetrically. Correlation analysis with multiparameter equations showed that solvation processes exert a decisive effect on the swelling.

DOI: 10.1134/S1070427207060304

The resistance of polymers to organic liquids is one of their important service characteristics. It is not surprising that, since the 1940–1950s, numerous papers concerning swelling of synthetic rubbers and other polymers have been published. Today, because of the increasing use of membrane technologies, studies of the resistance of polymers to the surrounding medium, of the membrane permeability, and of diffusion of liquids across membranes become more and more topical [1]. However, mostly carbon-chain polymers have been studied; heterochain polymers, showing much promise as membrane materials, are understood to a considerably lesser extent.

It should be noted that the published values of the degree of swelling (Q), diffusion coefficients (D), and permeability (P) have been obtained from data on the kinetics of the polymer weight gain in the solvents examined, monitored until an equilibrium was attained. At the same time, no reliable correlations between these quantities and physicochemical characteristics of organic liquids have been found. The most widely used Flory–Huggins approach based on the regular solution theory gives only fuzzy bell-shaped correlations of the maximal swelling $\log Q$ with the Hildebrand solubility parameter δ^2, with numerous outliers [2, 3]. This inadequacy is caused by the fact that specific solvation processes are disregarded. However, attempts to characterize the swelling solely by parameters of solvation processes, e.g., by the Reichardt electrophilicity parameter E_T or by the difference between the donor and acceptor numbers of the solvent DN – AN, have either failed or led to equations applicable to only homologous series of solvents [4]. A similar pattern has been observed with the diffusion coefficients: Chalykh [5, 6] has shown that the correlations between the diffusion coefficients of low-molecular-weight substances in polymers and their molecular weights or molar volumes are linear only within separate homologous series.

Aparently, penetration of a liquid into a polymer structure depends on many factors and cannot be described by a single characteristic of a liquid. The approach commonly used in the modern solution chemistry is based on the linear free energy relationship; within this approach, the solvent effect on the occurring processes is regarded as a sum of all the occurring effects [7]. In particular, this approach has been effectively applied to swelling of polyethylene and other hydrocarbon polymers [8], polyurethanes [9], and coals [10]. Therefore, it seemed appropriate to check its applicability to polymers containing bulky sulfamide groups capable of donor–acceptor interactions.

EXPERIMENTAL

In this study, we examined swelling in alcohols at 15°C of films of UPM sulfamide polymer, which is the product of polycondensation of 4,4'-diaminodiphenyl sulfone with terephthalic acid dichloride. To reveal the possible effect of hydroxy group on the swelling, we also studied the swelling in aprotic ethyl acetate. The degree of swelling as a function of time was determined gravimetrically with samples 105 μm

Limiting degrees of solvent absorption Q_∞, constants k of Eq. (2), and rate constants k' of swelling of UPM polymer (**I**) at 15°C and of polyurethane B600 (**II**) at 25°C [12]

Sample no.	Solvent	UPM (**I**)			Polyurethane (**II**)	
		Q_∞, mol/100 g	k, min^{-1}	$\log k'$	Q_∞, mol/100 g	$k \times 10^2$, min^{-1}
1	Methanol	–	–	–	0.7781	2.394
2	Ethanol	0.85	0.455	2.1510	0.7261	1.598
3	1-Propanol	–	–	–	0.6333	1.345
4	2-Propanol	0.94	0.371	2.0038	0.4183	1.138
5	1-Butanol	–	–	–	0.6392	1.061
6	2-Butanol	–	–	–	0.4500	1.043
7	2-Methyl-1-propanol	–	–	–	0.5257	0.797
8	2-Methyl-2-propanol	0.44	0.269	1.6903	–	–
9	2-Methyl-1-butanol	–	–	–	0.4705	0.703
10	1-Hexanol	0.63	0.481	2.0645	–	–
11	1-Nonanol	0.28	0.191	1.2944	–	–
12	Ethyl acetate	0.66	0.488	2.2652	–	–

thick, with a mean pore size of 50 nm. Polymer samples (1 g) were placed in weighing bottles filled with 30 ml of an appropriate solvent; at regular intervals, the samples were withdrawn, dried with a filter paper, and weighed. The swelling was monitored until complete saturation was attained. The temperature was measured with an accuracy of ±0.5°C. Weighing was performed with an accuracy of ±0.2 mg. However, it is hardly possible to ensure complete removal of high-boiling, relatively viscous alcohols from the sample surface; therefore, we estimated the actual accuracy at ±0.01 g. The limiting degrees of solvent absorption Q_∞ are listed in the table.

Figure 1 plots the amount of absorbed solvent Q vs. square root of time $\tau^{1/2}$ for a series of solvents. The curves have similar shapes: After the initial rapid absorption of a solvent, they flatten out, as in the case of other polymers [1, 11]. This shape of the curves is consistent with the well-known relationship found by Einstein, according to which the diffusion coefficient D is inversely proportional to the radius of the penetrating particle, r, and its viscosity η:

$$D = \text{const} r^{-1}\eta^{-1}. \quad (1)$$

The quantity Q_∞ and absorption rate decrease with an increase in the molecular weight and degree of branching (*tert*-butanol) of the alcohol; for ethyl acetate (four carbon and two oxygen atoms), Q_∞ is close to that of *n*-hexanol.

To compare the sorption power of the sulfamide polymer with that of polyurethane, also containing amide groups, we also included in the table data on the sorption of alcohols with a film of Vibrathane B600, a product of the condensation of poly(propylene oxide) with toluylene diisocyanate, cross-linked with 4,4'-methylenebis(*o*-chloroaniline) [12]. Similar experiments were performed with 0.25-mm-thick film samples. As can be seen, the data obtained are of the same order of magnitude as those obtained for the sulfamide polymer and show the same trend: Q_∞ regularly decreases with an increase in the molecular weight and in the degree of branching of the alcohol.

The shape of the curves of liquid absorption by the polymer up to 50% saturation can be generally described by the equation [11, 13]

$$Q_\tau/Q_\infty = k\tau^n, \quad (2)$$

where the constant k characterizes the structural features of the polymer and n depends on the mechanism of liquid penetration.

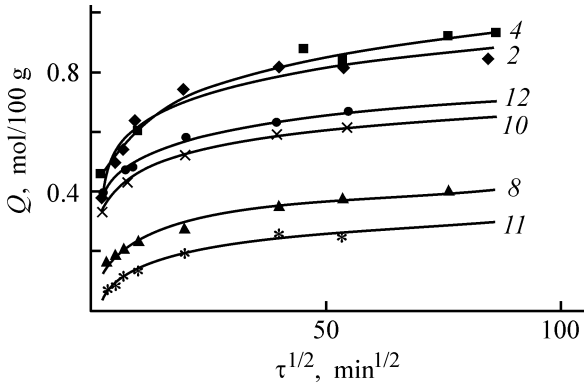

Fig. 1. Degree of swelling of sulfamide polymer in solvents, Q vs. time τ. *Figures at curves* are sample nos. in the table; the same for Figs. 2 and 3.

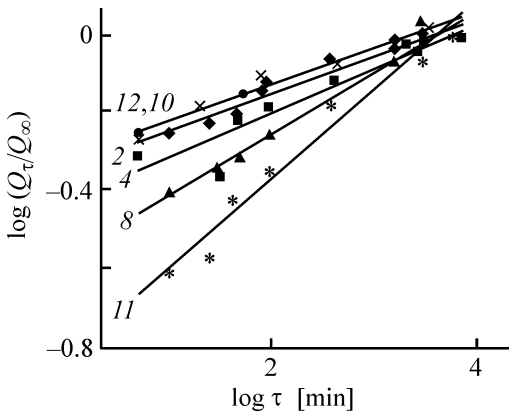

Fig. 2. Plot of $\log(Q_\tau/Q_\infty)$ vs. $\log(\tau)$ (τ is time).

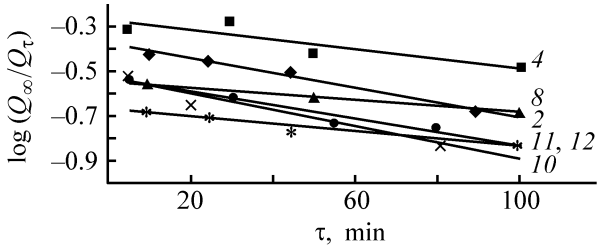

Fig. 3. Determination of the kinetic order of swelling from the plot of $\log(Q_\infty/Q_\tau)$ vs. time τ.

Without specific interactions of the system components, $n \sim 0.5$, i.e., the process is described by Fick's law. If the penetration kinetics is complicated by such interactions, n is in the range $0.5 < n < 1$. However, application of Eq. (2) to the experimental results obtained did not give positive results. Although there are linear correlations between $\log(Q_\tau/Q_\infty)$ and $\log\tau$, with the correlation coefficients R as high as 0.95–0.99 (Fig. 2), the values of $n < 0.5$ calculated from these correlations are of no real sense. This fact suggests a complex mechanism of sorption, apparently determined by the presence in the polymer of amide groups capable of donor–acceptor interactions with alcohol protons.

In accordance with [11], the constants k reflect the structural features of a polymer; hence, for a given polymer, they should be equal for all the solvents. These constants were determined for the sulfamide polymer from our sorption data, and taken from [12] for the polyurethane. However, k actually varies in the range $k = 0.27–0.49$, and for n-nonanol showing the maximal sorption k is even lower. Thus, apparently, depends not only on k particular polymer, but also on the sorbate.

The k values calculated for the sulfamide polymer are an order of magnitude higher than those for the sorption of esters (0.02–0.04) [11] and alcohols (0.007–0.02) [12] by polyurethane films, which also confirms the difference in the mechanism of absorption by these two polymers. In both cases, k decreases with an increase in the molecular weight of the alcohol (an exception is n-hexanol) and in the degree of its branching. The constants k for the sorption of alcohols with the polyurethane are also listed in the table.

Since the sorption rate of liquids is proportional to the difference between the osmotic pressures inside and outside the polymer film, i.e., is approximately determined by the corresponding vapor pressures, the sorption kinetics can be described by a first-order equation

$$dQ/dt = k'(Q_\infty - Q_\tau) \quad (3)$$

for which the rate constant is

$$k' = \{2.303\log[Q_\infty/(Q_\infty - Q_\tau)]\}/\tau. \quad (4)$$

Indeed, the correlation in the coordinates $\log(Q_\infty - Q_\tau)$–τ is linear (Fig. 3), but only in the initial period of the process, up to approximately 50% saturation. The corresponding values of k' (min^{-1}) for the sulfamide film, determined by Eq. (4), are listed in the table; they are of the same order of magnitude as those for the penetration of esters into a polyurethane membrane at 25°C [11].

As can be seen from the table, the quantities Q_∞, k, and k' are appreciably dependent on the organic solvent; however, these quantities do not clearly correlate with any separate property of the liquids. It has been shown recently that a good correlation for Q_∞ can be obtained with a multiparameter equation taking into account the capacity of solvents for both specific and nonspecific solvation, and also the structural characteristics of the solvents [7, 8]:

$$\log Q_\infty = a_0 + a_1(n^2 - 1)(n^2 + 2)^{-1} + a_2(\varepsilon - 1)(2\varepsilon + 1)^{-1} + a_3\delta^2 + a_4B + a_5E_T + a_6V_m, \quad (5)$$

where n is the refractive index; ε, dielectric permittivity of organic solvents (these parameters are related to the polarizability and polarity of solvents, responsible for nonspecific solvation of a substrate); B, Palm basicity [14]; E_T, Reichardt electrophilicity [15] (these parameters describe the capability of a solvent for acid–base interaction, i.e., for specific solvation); δ^2, Hildebrand solubility parameter squared, characterizing the cohesion energy of a solvent (its tendency to self-association), proportional to the energy required for accommodation of a foreign molecule in the solv-

ent structure, i.e., for cavity formation; and V_m, molar volume of the liquid.

Equation (5) allowed successful correlation of data on Q_∞ of polyethylene in 27 solvents [8], butyl rubber in 18 solvents [16], and polyurethane Vibrathane B601 in 36 solvents [9]. Therefore, it would be appropriate to apply the same approach to data from the table. In this case, however, the number of the examined solvents is small and equal to the number of parameters of the equation. Therefore, it becomes necessary to reveal insignificant factors by the leave-one-out procedure and construct equations with a smaller number of parameters. By so doing, we found that the factors δ^2 and V_m are insignificant for Q, despite relatively high pair correlation coefficient between Q and V_m (r = 0.851). The data on Q_∞ of the sulfamide polymer in alcohols are satisfactorily fitted by a four-parameter equation

$$\log Q_\infty = -8.047 + (13.94 \pm 1.80) f(n^2) + (24.13 \pm 1.76) f(\varepsilon) - (17.08 \pm 1.17) \times 10^{-3} B - (4.75 \pm 0.55) \times 10^{-2} E_T,$$
$$R = 0.996, \quad s = \pm 0.017. \qquad (6)$$

The factors of polarizability and electrophilic solvation also appeared to be of relatively low significance. Their exclusion led to an equation ensuring acceptable accuracy, although R was somewhat lower than the recommended value R = 0.95:

$$\log Q_\infty = -2.602 + (11.11 \pm 1.93) f(\varepsilon) - (8.66 \pm 1.55) \times 10^{-3} B - (1.15 \pm 1.07) \times 10^{-2} E_T,$$
$$R = 0.948, \quad s = \pm 0.062; \qquad (7)$$

$$\log Q_\infty = -2.498 + (9.83 \pm 1.68) f(\varepsilon) - (9.01 \pm 1.68) \times 10^{-3} B,$$
$$R = 0.936, \quad s = \pm 0.069. \qquad (8)$$

Thus, the factors determining the degree of swelling of the polymer are the polarity and basicity of solvents; their exclusion leads to a decrease in R to approximately 0.5, i.e., fully breaks the correlation. Here the positive effect of polarity is quite natural, taking into account the presence of sulfone and amide groups in the polymer. At the same time, amide groups containing tertiary nitrogen atom are incapable of solvation with electron-donor basic solvents, and the interaction is repulsive, as indicated by the negative sign of the coefficient at B.

The negative (though relatively insignificant) effect of the capacity of alcohols for specific electrophilic solvation of solutes is somewhat surprising; it may be associated with the acidic character of the proton of sulfamide groups. At the same time, with polyurethane, the effect of this factor is positive (promoting swelling), though also weak. The following equation was obtained for eight alcohols on the basis of data from [12]:

$$\log Q_\infty = -28.310 + (26.50 \pm 8.89) f(n^2) + (41.63 \pm 13.68) f(\varepsilon) + (4.05 \pm 1.76) \times 10^{-3} B + (0.93 \pm 2.31) \times 10^{-2} E_T + (1.60 \pm 1.13) \times 10^{-3} \delta^2 + (3.63 \pm 4.17) \times 10^{-3} V_m,$$
$$R = 0.985, \quad s = \pm 0.017. \qquad (9)$$

After exclusion of insignificant terms, we obtain

$$\log Q_\infty = -21.93 + (25.21 \pm 3.80) f(n^2) + (32.29 \pm 5.91) f(\varepsilon) + (1.47 \pm 0.31) \times 10^{-3} \delta^2,$$
$$R = 0.970, \quad s = \pm 0.024. \qquad (10)$$

Thus, absorption by polyurethane films involves nonspecific solvation of polar carbamate groups, mainly favoring the process. Note that, for swelling of the same polymers in 36 solvents of different nature, the decisive factors in the general correlation equation were the same [9].

By a similar procedure, we treated the constants k of Eq. (2), and for polysulfamide, also the swelling rate constants k'. For polysulfamide, we obtained the following equation:

$$\log k = -2.974 + (40.88 \pm 0.79) f(n^2) - (16.55 \pm 0.29) f(\varepsilon) + (5.23 \pm 0.13) \times 10^{-2} E_T - (2.30 \pm 0.03) \times 10^{-2} V_m,$$
$$R = 0.999, \quad s = \pm 0.003. \qquad (11)$$

In this case, further exclusion of any term makes R lower than 0.9, i.e., breaks the correlation.

For polyurethane, we obtain a simpler equation with different levels of significance of separate terms:

$$\log k = 0.486 + (0.178 \pm 0.330) \times 10^{-3} \delta^2 - (0.66 \pm 0.19) \times 10^{-3} V_m,$$
$$R = 0.972, \quad s = \pm 0.040. \qquad (12)$$

In this case, however, only the electrophilic solvation factor E_T is decisive; its pair correlation coefficient r is 0.970. The difference in the nature of factors governing R confirms the above assumption that the solvents interact with polysulfamide and polyure-

thane films essentially differently, primarily because of the different nature of the sulfamide and carbamate groups. For the swelling rate constants k' (min^{-1}) of the sulfamide film in alcohols, we obtained the correlation equation

$$\log k' = 0.429 + (56.12 \pm 5.61)f(n^2) - (29.11 \pm 2.07)f(\varepsilon) + (98.00 \pm 9.27) \times 10^{-3}E_T - (35.22 \pm 2.48) \times 10^{-3}V_m,$$
$$R = 0.995, \quad s = \pm 0.076. \qquad (13)$$

Thus, the swelling rate, i.e., rate of penetration of alcohol molecules into the structure of the sulfamide polymer, is favored by solvation interactions between the system components. At the same time, an increase in the size of solvent molecules leads to a decrease in the penetration rate, which is quite reasonable.

CONCLUSIONS

(1) The rate of swelling of UPM sulfamide polymer in alcohols is not described by Fick's law.

(2) The values of limiting swelling of UPM polymer can be correlated with solvent properties with multiparameter equations; the capacity of solvents for nonspecific solvation favors swelling, and their capacity for specific solvation exerts a negative effect.

REFERENCES

1. Aminabhavi, T.M., Harogoppad, S.B., Khinnavar, R.S., and Balundgi, R.H., *JMS-Rev. Macromol. Chem. Phys.*, 1991, vol. C31, no. 4, pp. 433–498.
2. Flory, P.J., *J. Chem. Phys.*, 1945, vol. 13, no. 6, pp. 453–465.
3. Bristow, J.M. and Watson, W.F., *Trans. Faraday Soc.*, 1958, vol. 54, no. 11, pp. 1731–1740.
4. Jonquieres, A., Roizard, D., and Lochon, P., *J. Appl. Polym. Sci.*, 1994, vol. 54, no. 11, pp. 1673–1682.
5. Chalykh, A.E., *Diffuziya v polimernykh sistemakh*, (Diffusion in Polymer Systems), Moscow: Khimiya, 1987, pp. 74–108.
6. Chalykh, A.E., *Vysokomol. Soedin.*, 2001, vol. 43, no. 12, pp. 2304–2328.
7. Makitra, R., Turovskiy, A., and Zaikov, G.E., *Correlation Analysis in Chemistry of Solutions*, Utrecht: VSP, 2004.
8. Makitra, R., Pyrih, Y., Zagladko, E., et al., *J. Appl. Polym. Sci.*, 2001, vol. 81, no. 7, pp. 3133–3140.
9. Makitra, R.G., Pristanskii, R.E., and Evchuk, I.Yu., *Vysokomol. Soedin., Ser. A*, 2005, vol. 47, no. 11, pp. 1987–1992.
10. Makitra, R.G. and Pristanskii, R.E., *Khim. Tverd. Topl.*, 2001, no. 5, pp. 3–16.
11. Khinnavar, R.S. and Aminabhavi, T.M., *J. Appl. Polym. Sci.*, 1992, vol. 46, no. 5, pp. 909–920.
12. Aithal, U.S. and Aminabhavi, T.M., *J. Chem. Eng. Data.*, 1990, vol. 35, no. 3, pp. 298–303.
13. Lucht, L.M. and Peppas, N.A., *J. Appl. Polym. Sci.*, 1987, vol. 33, no. 5, pp. 1557–1566.
14. Koppel, I.A. and Paju, A.I., *Reakts. Sposobn. Org. Soedin.*, 1974, vol. 11, no. 1, pp. 121–138.
15. Reichardt, Ch., *Solvents and Solvent Effects in Organic Chemistry*, Weinheim: VCH, 1988, pp. 359–371.
16. Makitra, R., Turovskiy, A., Zagladko, E., and Zaikov, G., in *Trends in Molecular and High Molecular Science*, New York: Nova Science, 2005, pp. 143–147.

ISSN 1070-4272, Russian Journal of Applied Chemistry, 2007, Vol. 80, No. 6, pp. 1007–1011. © Pleiades Publishing, Ltd., 2007.
Original Russian Text © L.A. Zemnukhova, L.G. Kolzunova, E.D. Shkorina, 2007, published in Zhurnal Prikladnoi Khimii, 2007, Vol. 80, No. 6, pp. 1033–1036.

MACROMOLECULAR CHEMISTRY AND POLYMERIC MATERIALS

Extractive Substances Formed from Buckwheat Grain Production Waste

L. A. Zemnukhova, L. G. Kolzunova, and E. D. Shkorina

Institute of Chemistry, Far-Eastern Division, Russian Academy of Sciences, Vladivostok, Russia

Received December 14, 2006; in final form, february 2007

Abstract—Properties of liquid and dry extracts produced in treatment of buckwheat fruit shells (husk) and straw with water or an acid solution were studied. The conditions of pigment concentration from aqueous extracts by ultrafiltration were determined.

DOI: 10.1134/S1070427207060316

A promising resource of raw materials for synthesis of various multifunctional products (chemical substances, pharmaceutical and cosmetic preparations, food additives, natural pigments, fillers, sorbents) is the presently poorly used waste from manufacture of buckwheat grain: fruit shells [husk (BH) or hull] and straw (BS). Analysis of published evidence shows that a large body of data has been accumulated for development of a versatile and economically feasible technology for deep processing of this waste: new methods have been devised for crushing of the starting plant material [1], extraction [2, 3], and production of dispergates (dry extracts) [4] and natural food pigments [5]. The conditions of synthesis of the following products from BH and BS have been studied: flavonoids [6], food additives [7, 8], cellulose [9, 10], polysaccharides [11], sorbents [12, 13], and inorganic components [14, 15]. It has also been found that aqueous extracts of buckwheat straw and husk inhibit corrosion of low-carbon steel [16]. However, not all of the products formed in processing of buckwheat waste, including extracts, have been studied in sufficient detail, which probably hinders organization of a modern industry on the basis of these products.

The present study continues the analysis of the possibility of integrated processing of buckwheat grain production waste [10–16] and is concerned with the composition of water-soluble extractive substances produced from buckwheat husk and straw and with the conditions of their concentration by ultrafiltration.

EXPERIMENTAL

The hull of the buckwheat of Pri-7 brand (BH-11) and straw (BS-4) of buckwheat of Izumrud brand, taken in Primorsky krai in 2002, served as objects of study (the numbering corresponds to that in the collection of the Institute of Chemistry, Far-Eastern Division, Russian Academy of Sciences). Samples of husk, with particle size of no less than 2 mm, and straw, shredded into fragments of up to 10 mm in size, were preliminarily washed with water and dried in air.

A weighed portion of the raw material, with volume ratio s : l = 1 : 25, was subjected to extraction with water or a hydrochloric acid solution of varied concentration (0.1 and 1.0 N) at 80–90°C in the course of 1 h. The extracts formed were filtered through a filter paper (blue ribbon) and analyzed for the content of inorganic components on a Nippon Jarrel Ash AA-780 flame atomic-absorption spectrometer (Japan). The data obtained are listed in Table 1. K^+, Na^+, Ca^{2+}, Mg^{2+}, Cu^{2+}, Zn^{2+}, Mn^{2+}, and Fe^{3+} ions were found in the solutions. The yield of extractive substances, which varies within the range 10–35% relative to the mass of dry raw materials, and the coloration of the extracts depend on treatment conditions and type of a waste (husk or straw). Aqueous and acid treatment of BH and BS results in that polysaccharides, whose content and composition have been studied previously [11], polyphenols determining the coloration of the extracts, and other water-soluble substances [7] are recovered into solution.

Table 1. Yield of water-soluble substances and content of metal ions in these substances

Raw material	Extractive agent	Yield of extractive substances, %	Solution color	Content of metal ions in solution, μg ml^{-1}							
				K^+	Na^+	Ca^{2+}	Mg^{2+}	Cu^{2+}	Zn^{2+}	Mn^{2+}	Fe^{3+}
BH	H_2O	10	Brown	240	10.0	11.0	37.0	1.40	0.4	0.4	0.4
	HCl, 0.1 N	22	Apricot	110	1.9	19.0	48.0	0.14	0.3	1.6	1.4
	HCl, 1 N	35	Red	114	2.1	23.0	59.0	0.15	0.9	1.5	3.0
BS	H_2O	21	Brown	525	7.5	10.0	30.5	0.02	0.9	1.4	2.2
	HCl, 0.1 N	30	Light	800	1.5	160	86.0	0.10	0.2	1.8	1.4
	HCl, 1 N	34	red	450	2.5	150	120	0.08	0.6	1.3	2.4

Samples of a dry extract (DE) were obtained by evaporation of liquid extracts on a water bath or by lyophilic drying. In the experiments carried out in this study, the DE yield, dependent on the concentration of extractive substances in solution, was no less than 2% relative to the mass of the starting raw material. Such a low DE yield, compared with the amount of extractive substances in solution, may be due to presence of volatile components in the extract. The DE samples produced by lyophilic drying were light brown, and those formed by drying on a water bath, dark brown, which indicates that substances extracted from buckwheat waste are thermally labile and more modern drying techniques are necessary [4]. The structure of the samples, studied by X-ray diffraction analysis (DRON-2 diffractometer, Cu_{K_α} radiation) was amorphous for DE produced from aqueous extracts of BH and BS, and crystalline in the case of acid extracts. Figure 1 shows typical X-ray diffraction patterns of DE samples. However, the crystalline phase could not be identified using the powder database (PDF-2).

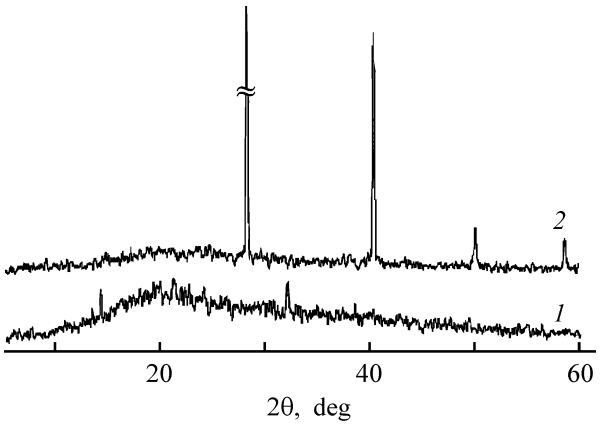

Fig. 1. X-ray diffraction pattern of DE samples produced from (*1*) buckwheat husk treated with water and (*2*) buckwheat straw treated with an acid (2θ) Bragg angle.

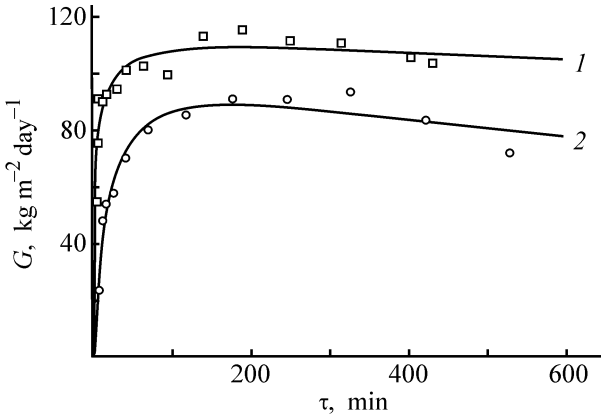

Fig. 2. Membrane throughput G in relation to pore diameter at ΔP = 0.2 MPa. (τ) Time; the same for Fig. 3. Membrane: (*1*) UAM-150P and (*2*) UAM-100P.

To intensify the process of DE synthesis, the ultrafiltration (UF) technique was employed. This method enables concentration and purification of substances with minimum energy expenditure and no need to use any reagents. The conditions of separation and concentration of pigments in solutions were optimized for the example of an aqueous extract of BH. The solutions were monitored for the content of polyphenols with an SF-256 UVI spectrophotometer by the optical density at 220–300 nm, with preliminary calibration by the standard procedure [17]. Baromembrane filtration of the aqueous extract of BH was carried out with cellulose acetate membranes with various pore diameters (UAM-100P and UAM-150P) at a pressure drop ΔP = 0.2–0.4 MPa and T = 20°C on an installation described in [18]. In the process, a filtrate (solution after ultrafiltration) and concentrate (or retentate, i.e., the residue of the starting solution over the membrane) were obtained.

The dynamics of ultrafiltration is shown in Fig. 2. It can be seen that the UAM-150P membrane reaches the steady-state mode in 10 min (curve *1*), whereas the UAM-100P membrane requires for this a longer time (curve *2*). It was found that the selectivity of separation of the starting solution (density d = 0.996 g cm^{-3}) into a colorless filtrate (d = 0.995 g cm^{-3}) and colored concentrate (d = 0.997 g cm^{-3}) at ΔP = 0.2 MPa is

Table 2. Content of metal ions in various fractions of the aqueous extract from buckwheat husk

UF conditions		Content, μg ml^{-1}								
ΔP, MPa	membrane pore diameter, Å	starting extract			filtrate			concentrate		
		K^+	Ca^{2+}	Mg^{2+}	K^+	Ca^{2+}	Mg^{2+}	K^+	Ca^{2+}	Mg^{2+}
0.2	150	150	8.0	16.0	100	7.0	9.0	340	50.0	78.0
0.2	100	96	6.9	8.0	30.0	2.9	0.7	150	11.9	15.0
0.4	100	110	6.6	12.0	24.0	1.0	0.6	300	15.0	33.0

Table 3. Elemental chemical analysis of DE samples produced from buckwheat husk and straw with (+) or without (–) ultrafiltration

Raw material	Extractive agent	UF	Content, %			Raw material	Extractive agent	UF	Content, %		
			C	H	N				C	H	N
BH	H_2O	–	37.9	4.8	5.1	BH	HCI, 0.1 N	–	33.2	4.2	5.0
		+	38.7	4.3	5.1	BS		–	32.8	4.2	5.0

higher for the UAM-100P membrane, compared with that of the UAM-150P type, but the former is inferior in the throughput G and the time in which the maximum degree of concentration is reached (6–10 h for UAM-100P and 3 h for UAM-150P). The throughput of the UAM-100P membrane increases by a factor of 4–5 on raising the pressure to ΔP = 0.4 MPa (Fig. 2, curve *2* and Fig. 3, curve *1*). However, the dynamics of ultrafiltration of an aqueous extract of BH changes in this case. The observe extremal behavior of the G–τ dependence (Fig. 3, curve *1*) may be due to a higher concentration rate, stronger membrane densification under pressure, and partial pore clogging by pigment particles.

It was also demonstrated that, under identical conditions of baromembrane filtration, the throughput for freshly prepared extracts is lower than that for extracts kept for $\tau \geq 10$ days (Fig. 3, curve *3*). A possible reason is that pigment molecules associate in the course of time into coarser particles, which diminishes the clogging of pores in the membrane and improves its throughput. The data obtained indicate that accumulation and storage of extracts before the ultrafiltration stage is admissible and can serve as a positive factor for the technological process.

The degree of pigment concentration was evaluated by a change in the dry residue mass in the over-membrane solution (retentate). The maximum (fivefold) increase in the mass of the substance was achieved on the UAM-100P membrane (ΔP = 0.4 MPa) at the best combination of throughput/selectivity parameters and minimum loss of the dispergate (about 2%).

A twofold increase in the concentration of the starting extract (to s : l = 1 : 12.5) leads to a decrease in the filtration rate (Fig. 3, curves *1*, *2*), but provides a faster attainment of the steady-state mode and makes shorter the total time of concentration.

The distribution of K^+, Ca^{2+}, and Mg^{2+} ions among fractions in ultrafiltration of an aqueous extract of BH is illustrated by Table 2. The data in the table indicate that these ions are accumulated in the extract.

The color of the dry extract produced by ultrafiltration (DE_{uf}) and by lyophilic drying of the concentrate was brown (similarly to the color of the starting extract) and its structure was amorphous. The results of a chemical analysis for the content of carbon, hydrogen, and nitrogen, made using the standard procedures [19], are listed in Table 3. The DE_{uf} sample differs from the others in a higher content of carbon. The thermal behavior of the sample, studied using

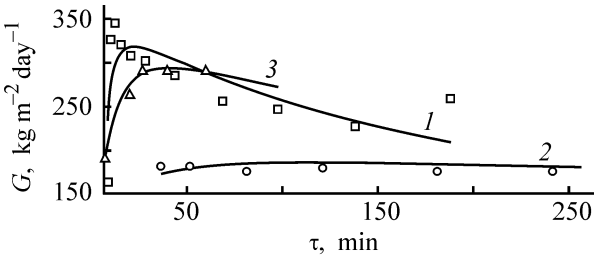

Fig. 3. Membrane throughput G in relation to pressure and concentration of the extract from buckwheat husk. ΔP (MPa): (*1*, *2*) 0.4 and (*3*) 0.2. s : l: (*1*, *3*) 1 : 25 and (*2*) 1 : 12.5.

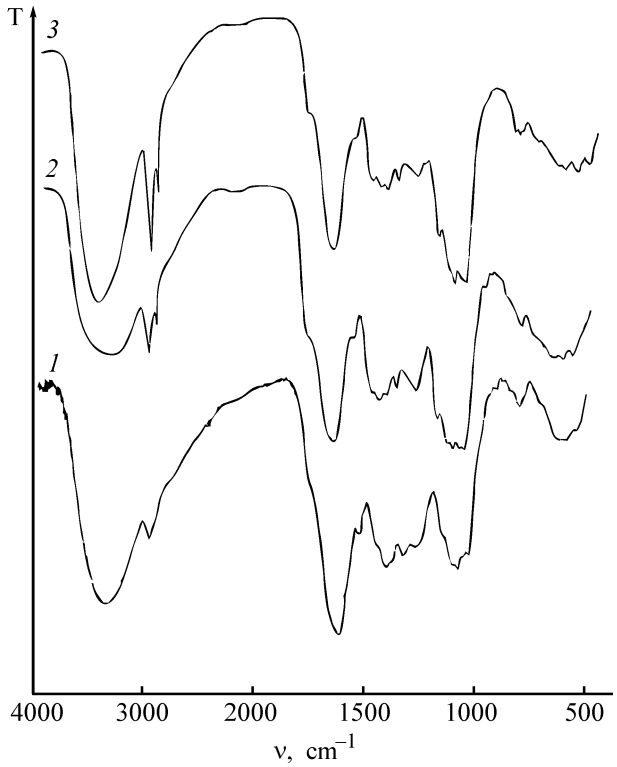

Fig. 4. IR spectra of DE samples obtained from an aqueous extract from buckwheat husk with (*1*) drying on a water bath, (*2*) ultrafiltration and lyophilic drying, and (*3*) lyophilic drying. (T) Transmission and (ν) wave number.

a Q-1000 derivatograph (Hungary) shows that the product starts to slowly decompose in the range 50–140°C. Further heating to 700°C leads to intensive continuous decomposition.

Figure 4 show IR absorption spectra measured in the range 400–4000 cm^{-1} on a Shimadzu IR Prestige 21 spectrophotometer (Japan) for three DE samples obtained from aqueous extracts of BH under different conditions. Analysis shows that the spectra contain groups of bands of different intensities in the following frequency ranges (cm^{-1}): 3600–2935, 1750–1516, 1450–1260, 1150–1020, and ~700–400, which is typical of polysaccharides of plant origin, including the buckwheat waste [11]. The use of baromembrane filtration and lyophilic drying in the extract processing yields a purer final product (DE), which is reflected by the IR spectra: absorption bands of dry substance, and especially those at 1242–1444 cm^{-1} (where frequencies of stretching and deformation vibrations of CH_2, CH, C–O and C–C groups appear), 2935–2850 cm^{-1} (region of stretching vibrations of CH bonds), and 3402–3248 cm^{-1} (stretching vibrations of OH groups), are more clearly pronounced and better resolved (Fig. 4, spectra *2*, *3*).

CONCLUSIONS

(1) It was shown that the yield of water-soluble substance from buckwheat husk and straw varies within the range 10–35% relative to the mass of a dry raw material, and the content of a dry extract at raw material to water ratio of 1 : 25 is not less than 2%.

(2) It was demonstrated that ultrafiltration (UAM-100P membrane at ΔP = 0.4 MPa) can be of use for concentration of pigments from aqueous extracts from buckwheat husk.

(3) Aqueous solutions with extractive substances and dry extracts were characterized by chemical, X-ray phase, and thermographic analyses and by IR spectroscopy.

REFERENCES

1. Oparin, S.A., Soroka, P.I., Shishkov, N.I., and Zrazhevskii, V.I., *Vopr. Khim. Khim. Tekhnol.*, 2002, no. 4, pp. 115–118.
2. Mertvetsov, N.P., Ramazanov, Yu.A., Repkov, A.P., et al., *Gazovikhrevye bioreaktory "BIOK": Ispol'zovanie v sovremennoi biotekhnologii* (BIOK Gas-Whirl Reactors: Use in Modern Biotechnology), Novosibirsk: Nauka, 2002.
3. Kirillova, N.P., Kuznetsov, M.G., Petrushenkov, P.A., et al., *Materialy II Vserossiskoi konferentsii "Khimiya i tekhnologiya rastitel'nykh veshchestv", Kazan, 24–27 iyunya, 2002 g.* (Proc. II All-Russia Conf. "Chemistry and Technology of Plant Substances," Kazan, June 24–27, 2002), Kazan, 2002, p. 82.
4. Aleinikov, I.N., Sergeev, V.N., Rusakov, A.V., et al., *Moloch. Prom–st.*, 2000, no. 5, pp. 18–19.
5. Katserikova, N.V. and Poznyakovskii, V.M., *Prirodnye pishchevye krasiteli: Obzornaya informatsiya* (Natural Food Pigments: Review Information), Novosibirsk: EKOR, 1999.
6. Kiselev, V.E., Kovalenko, V.I., and Minaeva, B.G., *Grechikha – kak istochnik flavoniodov* (Buckwheat as a Source of Flavonoids), Novosibirsk: Nauka, 1985.
7. Aleinikov, I.N., Sergeev, V.N., Rusakov, A.V., and Aganyan, V.E., Pishch. Ingred., *Syr'e Dobavki*, 2001, no. 1, pp. 30–31.
8. Korystin, S.I., Tarasevich, T.V., and Doroshev, S.A., Abstracts of Papers, *IV Vserossiiskaya nauchnaya konferentsiya "Khimiya i tekhnologiya rastitel'nykh veshchestv", Syktyvkar, 25–30 iyunya 2006 g.* (All-Russia Conf. "Chemistry and Technology of Plant Substances," Syktyvkar, June 25–30, 2006), Syktyvkar: Inst. Khim., Komi Nauchn. Tsentr Ural'sk. Otd. Ross. Akad. Nauk, 2006, p. 392.
9. Dudkin, M.S., Ozolina, S.A., and Shkantova, N.G., *Khim. Drevesiny*, 1980, no. 4, pp. 18–22.

10. Brovkina, O.V., Shkorina, E.D., Zemnukhova, L.A., et al., *Zh. Prikl. Khim.*, 2006, vol. 79, no. 3, pp. 488–492.
11. Zemnukhova, L.A., Tomshich, S.V., Shkorina, E.D., and Klykov, A.G., *Zh. Prikl. Khim.*, 2004, vol. 7, no. 7, pp. 1192–1196.
12. Zemnukhova, L.A., Shkorina, E.D., and Filippova, I.A., *Khim. Rastit. Syr'ya*, 2005, no. 2, pp. 51–54.
13. RF Patent 2031849.
14. Zemnukhova, L.A., Shkorina, E.D., and Fedorishcheva, G.A., *Zh. Prikl. Khim.*, 2005, vol. 78, no. 2, pp. 329–333.
15. Polyakova, N.V., Shkorina, E.D., Kovekhova, A.V., and Zemnukhova, L.A., *Int. Cong. on Analytical Sciences (ICAS-2006), June 25–30, 2006*, Moscow, Russia, Book of Abstracts, Moscow, 2006, vol. 1, p. 420.
16. Zemnukhova, L.A., Chernov, B.B. , Shkorina, E.D., and Shchetinina, G.P., *Transportnoe delo Rossii. Spetsial'nyi vypusk no. 7* (Transportation in Russia, Special Issue no. 7), Moscow, 2006, pp. 149–152.
17. Pilipenko, A.T. and Pyatnitskii, I.V., *Analiticheskaya khimiya* (Analytical Chemistry), Moscow: Khimiya, 1990, vol. 1.
18. Kozunova, L.G., Zemnukhova, L.A., Fedorishcheva, G.A., et al., *Zh. Prikl. Khim.*, 2000, vol. 73, no. 10, pp. 1644–1651.
19. Klimova, V.A., *Osnovy mikrometoda analiza organicheskikh soedinenii* (Fundametals of a Micromethod for Analysis of Organic Compounds), Moscow: Khimiya, 1967.

ISSN 1070-4272, Russian Journal of Applied Chemistry, 2007, Vol. 80, No. 6, pp. 1012–1014. © Pleiades Publishing, Ltd., 2007.
Original Russian Text © S.A. Shoinbekova, A.I. Nikitina, E.E. Ergozhin, B.A. Mukhitdinova, N.I. Razuvaeva, 2007, published in Zhurnal Prikladnoi Khimii, 2007, Vol. 80, No. 6, pp. 1037–1039.

MACROMOLECULAR CHEMISTRY AND POLYMERIC MATERIALS

Activity of Mono- and Disubstituted Derivatives of 1,4-Benzoquinone and Allylamine in Cationic Polymerization

S. A. Shoinbekova, A. I. Nikitina, E. E. Ergozhin, B. A. Mukhitdinova, and N. I. Razuvaeva

Bekturov Institute of Chemical Sciences, Ministry of Education and Science of Kazakhstan Republic, Almaty, Kazakhstan

Received August 4, 2006; in final form, January 2007

Abstract—Cationic polymerization of mono- and disubstituted derivatives of 1,4-benzoquinine and allylamine in the presence of hydrochloric acid was studied. The optimal conditions were found and the kinetic parameters of the process were evaluated.

DOI: 10.1134/S1070427207060328

Allyl monomers, among them allylamine, polymerize difficultly [1]. It is well known [2–4] that their activity in radical polymerization increases upon introduction of electron-acceptor substituents directly bonded to the nitrogen atom. This is due to the fact that with increasing electron-acceptor power of substituents the rate constant of degradation chain transfer decreases.

From 1,4-benzoquinone, which is a strong electron acceptor [5], and allylamine, mono- and disubstituted derivatives of the following structures were obtained under mild conditions by the procedures developed previously [6]:

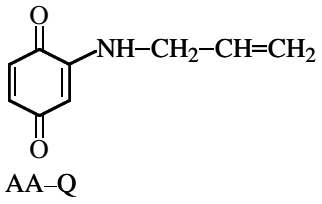

AA–Q

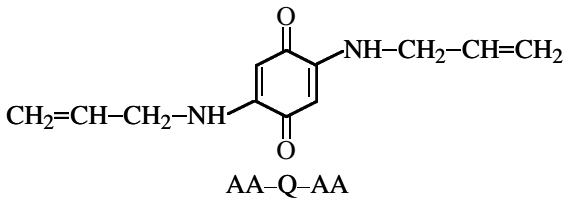

AA–Q–AA

Their activity in radical polymerization in the presence of benzoyl peroxide has been studied previously [7], and it was established that AA–Q monomer is more reactive than AA–Q–AA.

In this study, we examined the activity of mono- and disubstituted derivatives of 1,4-benzoquinone and allylamine in cationic polymerization.

EXPERIMENTAL

Redox monomers AA–Q and AA–Q–AA were prepared by the procedure described in [6]. Concentrated hydrochloric acid of ultrapure grade was used, d = 1.179 g cm^{-3}. Dimethylformaide (DMF) was purified by the procedure described in [8].

The polymerization of AA–Q and AA–Q–AA was performed by the ampule method in the presence of hydrochloric acid in DMF. Weighed portions of monomers AA–Q and AA–Q–AA were charged into glass ampules, DMF was added, and, after dissolution of the monomers, hydrochloric acid was added. The reaction conditions were varied in the following ranges: concentration of monomers 10–50 g l^{-1}, HCl concentration 0.04–0.29 M, temperature 7–28°C, and duration 0.5–5.0 h. The degree of polymerization was determined by the polarographic method from the amount of the residual nonpolymerized monomer.

The polarograms were recorded in a temperature-controlled cell at 25–0.5°C on a PU-1 polarograph, using a mercury drop electrode with a capillary char-

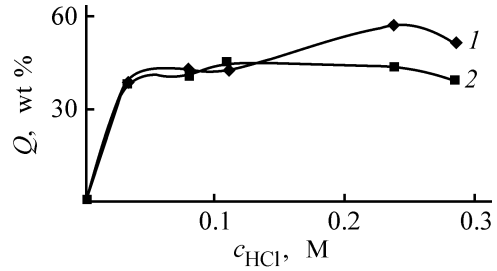

Fig. 1. Yield of polymer, Q, vs. the catalyst amount c_{HCl} in cationic polymerization of (*1*) AA–Q and (*2*) AA–Q–AA at 21°C for 5 h.

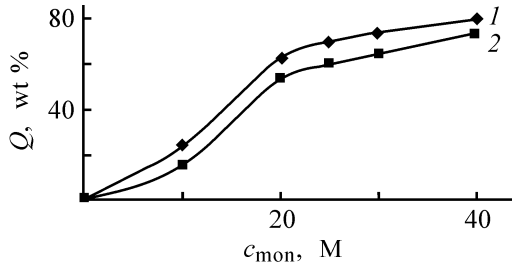

Fig. 2. Yield of polymer, Q, vs. monomer concentration in the solution c_{mon} in cationic polymerization of (*1*) AA–Q and (*2*) AA–Q–AA at 21°C for 5 h.

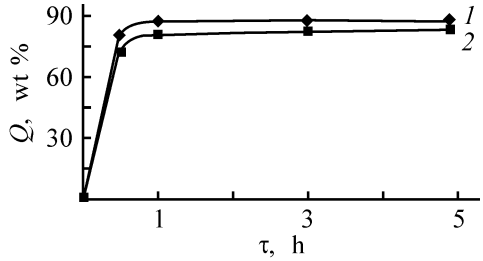

Fig. 3. Yield of polymer, Q, vs. the synthesis duration τ in cationic polymerization of (*1*) AA–Q and (*2*) AA–Q–AA at 7°C.

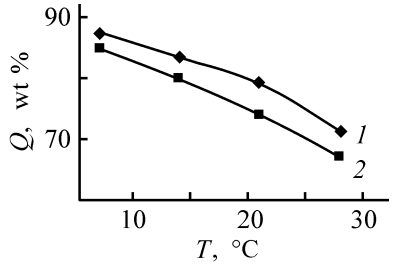

Fig. 4. Influence of temperature T on the yield of polymer, Q, in cationic polymerization of (*1*) AA–Q and (*2*) AA–Q–AA at synthesis duration of 5 h.

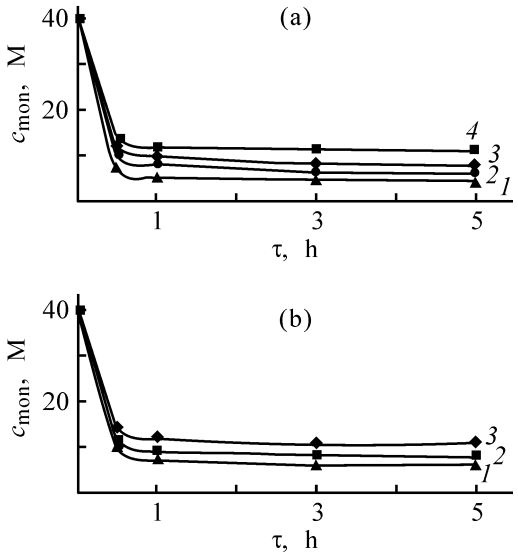

Fig. 5. Kinetic curves of consumption of monomers in cationic polymerization of (a) AA–Q and AA–Q–AA at concentration of monomers of 40 g l^{-1} and temperature (°C): (*1*) 7, (*2*) 14, (*3*) 21, and (*4*) 28. (c_{mon}) Monomer concentration and (τ) time.

acteristic at open circuit $m^{2/3}t^{1/6}$ = 4.38 $mg^{2/3}\ s^{1/6}$; the supporting electrolyte was phosphate buffer solution with pH 7.4 in 25% DMF. Oxygen was removed from the solution by bubbling with argon for 5 min.

The catalysts of cationic polymerization are strong mineral acids [9]. It is well known [10] that, upon addition of protonic acids to allyl monomers that are Lewis bases, the rates of their radical polymerization and molecular weights of the resulting polymers significantly increase. In this case, the conservation of the radical nature of the process is confirmed by the fact that the process occurs only in the presence of a source of free radicals (γ-radiation) and is inhibited by radical inhibitors. We found that monomers AA–Q and AA–Q–AA are fairly easily involved in the polymerization in the presence of hydrochloric acid without radical initiators or additional action on the system. The yield of the polymer as a function of the catalyst amount is plotted in Fig. 1. It is seen that, to attain the maximum yield of the redox polymer based on AA–Q, a larger amount of hydrochloric acid (0.238 M) than that for AA–Q–AA (0.142 M) is required. It was found (Fig. 2) that the maximum permissible concentration of AA–Q and AA–Q–AA in their polymerization in DMF solution is 40 g l^{-1}. Use of more concentrated solutions of the monomers for polymerization is impossible because of their limited solubility in DMF.

The optimal reaction duration is 0.5 h (Fig. 3). In this case, the yield of polymers based on AA–Q and AA–Q–AA is 88 and 85%, respectively. For both monomers, the yield of the polymer decreases almost linearly as temperature increases in the temperature range studied (Fig 4). From the kinetic curves (Fig. 5) it was concluded that, in the initial period of the process, cationic polymerization is a first-order

Kinetic parameters of cationic polymerization of AA–Q and AA–Q–AA monomers in the presence of hydrochloric acid

Monomer	T, K	k, s^{-1}	log k	E_a, kJ mol^{-1}	Monomer	T, K	k, s^{-1}	log k	E_a, kJ mol^{-1}
AA–Q	280	0.000675	–3.17	–8.41	AA–Q–AA	280	0.000902	–3.05	–19.10
	287	0.000616	–3.21			287	0.000705	–3.15	
	294	0.000565	–3.25			294	0.000587	–3.22	
	301	0.000510	–3.29						

reaction with respect to the monomer concentration. Based on this fact, we evaluated the rate constants at various temperatures and found from the Arrhenius plot (Fig. 6) the activation energies of the process for AA–Q and AA–Q–AA (see table).

As can be seen from the table, the activation energies of cationic polymerization of AA–Q and AA–Q–AA are negative. It is well known [11] that, for cationic polymerization, the total activation energy E_{tot} determined from the reaction rate is

$$E_{tot} = E_i + E_p - E_t,$$

where E_i, E_p, and E_t are the activation energies of initiation, chain propagation, and chain termination, respectively.

The negative values of E_{tot} can be explained assuming that E_p is low and E_t is high. This is possible when the termination reaction is the reaction between solvated ionic pairs. In the common case, E_{tot} of cationic polymerization is in the range from –42 to 63 kJ mol^{-1}. The activation energies we found agree well with these values.

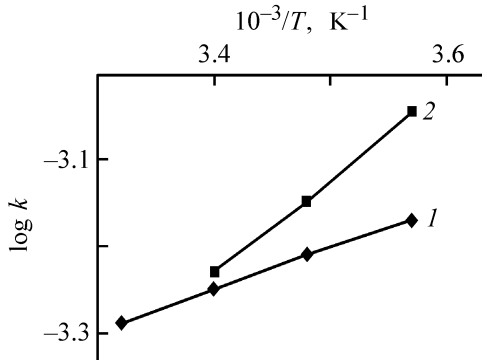

Fig. 6. Logarithm of the rate constant of cationic polymerization of (*1*) AA–Q and (*2*) AA–Q–AA monomers vs. T^{-1}.

CONCLUSIONS

(1) New allyl redox monomers AA–Q and AA–Q–AA can polymerize not only by free-radical mechanism but also by the cationic mechanism.

(2) A more promising procedure for synthesis of polymers from these monomers is cationic polymerization, since, in this case, the synthesis temperature and synthesis duration significantly decrease: from 87 to 7°C and from 21 to 0.5 h, respectively.

REFERENCES

1. Volodina, V.I., Tarasov, A.I., and Spasskii, S.S., *Usp. Khim.*, 1970, vol. 39, no. 2, pp. 276–303.
2. Vorob'eva, Yu.A., Prochukhan, Yu.A., and Monakov, Yu.B., *Vysokomol. Soedin., Ser. C*, 2003, vol. 45, no. 12, pp. 2118–2136.
3. Shcherbina, F.F., Fedorova, I.P., and Gorlov, Yu.I., *Vysokomol. Soedin., Ser. A*, 1970, vol. 12, pp. 2042–2045.
4. Matsoyan, S.G., Pagosyan, G.M., Dzhigamen, A.O., and Mushegyan, A.V., *Vysokomol. Soedin.*, 1963, vol. 5, no. 6, pp. 854–860.
5. Pullman, B. and Pullman, A., *Quantum Biochemistry*, New York: Interscience, 1963.
6. Kazakhstan Patent no. 9729.
7. Moldagazyeva, Zh.Y., Ergozhin, E.E., and Mukhitdinova, B.A., *Khim. Zh. Kaz.*, 2003, no. 1, pp. 67–75.
8. Weissberger, A. and Proskauer, E.S., *Organic Solvents. Physical Properties and Methods of Purification*, Riddick, J.A. and Toops, E.E., Eds., New York: Interscience, 1955.
9. Vaculik, P., *Chemie monomeru*, Prague: Ceskoslov. Akad., 1956, vol. 1.
10. Kabanov, V.A., Zubov, V.P., and Semchikov, Yu.D., *Kompleksno-radikal'naya polimerizatsiya* (Complex-Radical Polymerization), Moscow: Khimiya, 1987.
11. *The Chemistry of Cationic Polymerization*, Plesch, P.H., Ed., Oxford: Pergamon, 1963.

ISSN 1070-4272, Russian Journal of Applied Chemistry, 2007, Vol. 80, No. 6, pp. 1015–1017. © Pleiades Publishing, Ltd., 2007.
Original Russian Text © A.V. Golounin, V.A. Sokolenko, M.S. Tovbis, O.V. Zakharova, 2007, published in Zhurnal Prikladnoi Khimii, 2007, Vol. 80, No. 6, pp. 1040–1042.

BRIEF COMMUNICATIONS

Complexes of Nitronaphthols with Aluminum Bromide

A. V. Golounin, V. A. Sokolenko, M. S. Tovbis, and O. V. Zakharova

Institute of Chemistry and Chemical Technology, Krasnoyarsk, Russia

Received June 20, 2006; in final form, February 2007

Abstract—The structure of complexes of nitronaphthols with aluminum bromide in nitromethane was studied by NMR.

DOI: 10.1134/S107042720706033X

It is assumed that mesomeric structures of the type of *N*-oxybenzoquinone oximes are involved in some reactions of nitrophenols. In particular, both phenol and oxime ethres are formed in methylation of nitrophenols with diazomethane [1]. Oxime ether is also formed by treatment of 9-nitro-10-hydroxyphenanthrene [2]. The intense color of nitrophenol salts is caused by mesomerism [3]. One would expect that mesomeric species can be fixed by complexation of nitronaphthols with strong Lewis acids.

It is well known that, in the reaction with aluminum halides, methylated phenols [4] and some alkyl- and phenylnaphthols [5–7] are quantitatively transformed into complexes of the keto form. The strong electron acceptor group ($-NO_2$) significantly decreases the basicity of the aromatic ring; therefore, formation of a complex of the keto form is difficult to expect, but formation of a complex of the aci form is not improbable.

To continue the studies of the complexation of phenols, we performed the reaction between 1-nitro-2-naphthol or 2-nitro-1-naphthol and aluminum bromide in nonaqueous solutions with the aim to elucidate the structure of the complexes.

Since nitronaphthols in contact with $AlBr_3$ in nonpolar solvents (benzene, petroleum ether, cyclohexane) are readily converted into salts, we selected nitromethane as a solvent in which fairly stable strongly colored complexes can be obtained at lowered temperatures.

To determine the structure of adducts, we recorded NMR spectra of nitronaphthols before and after the reaction with $AlBr_3$. The ^1H NMR chemical shifts are listed in Table 1. Since the ^1H NMR signals of H-4 and H-8 atoms of 1-nitro-2-naphthol in the nitromethane solution overlap, we additionally recorded the ^1H NMR spectrum of a solution in acetone-d_6, in which the signals of H-8 and H-4 are well resolved.

The existence of a mesomeric complex of the aci form can be confirmed by the ^{13}C NMR spectrum, because it is well known that the signal of the carbonyl

Table 1. Chemical shifts in the ^1H NMR spectra of nitronaphthols and complexes with $AlBr_3$

Compound	Solvent	Chemical shift, ppm							
		H-2	H-3	H-4	H-5	H-6	H-7	H-8	OH
1-Nitro-2-naphthol	$CDCl_3$		7.25	8.01	7.62	7.51	7.74	7.92	12.12
	CH_3NO_2		7.43	8.15	8.01	7.59	7.74	8.15	10.75
Complex with $AlBr_3$	$CDCl_3$		6.84	8.19	7.74	7.50	7.69	8.65	8.43
	CH_3NO_2		6.84	8.28	7.85	7.61	7.80	8.77	8.52
2-Nitro-1-naphthol	CH_3NO_2		8.00	7.34	7.81	7.62	7.73	8.51	12.24
Complex with $AlBr_3$	CH_3NO_2		7.59	7.39	7.79	7.92	7.65	8.27	8.63
4-Nitro-1-naphthol	CH_3NO_2	6.68	8.20		8.30	7.53	7.73	8.71	6.15
Complex with $AlBr_3$	$CDCl_3$	6.67	8.10		8.36	7.62	7.51	8.70	12.7

Table 2. Spin–spin coupling constants

Compound	$J_{3,4}$	$J_{5,6}$	$J_{6,7}$	$J_{7,8}$	$J_{5,7}$	$J_{6,8}$
	Hz					
1-Nitro-2-naphthol						
Ligand	9.0	7.6	7.2	8.4	1.4	1.2
Complex	9.0	7.6	7.2	8.4	–	–
2-Nitro-1-naphthol						
Ligand	9.2	7.8	6.8	8.2	1.2	1.2
Complex	9.7	7.8	7.6	8.2	–	–

carbon atom should appear in the range 180–200 ppm in the spectra of the keto form [4]. However, we did not find this signal in the spectrum of the complex.

The coordination of $AlBr_3$ with 1-nitro-2-naphthol results in a downfield shift of the NMR signals of aromatic protons; the signals of H-8 are the most shifted. The significant downfield shift of H-8 is apparently caused by the formation of intramolecular hydrogen bond between H-8 and oxygen atom of the nitro group. This bond can be formed when nitro group is fixed in the plane of the naphthalene ring, i.e., in complexes **I** or **II**:

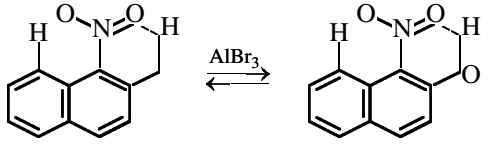

I

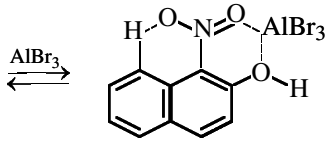

II

When complex **I** is formed, i.e., $AlBr_3$ is coordinated via hydroxy group, the intramolecular hydrogen bond between OH and NO_2 should be strengthened [8]. The ^1H signal of OH group should be downfield shifted, as it is observed in the complexes of the oxy form of methylated phenols [6]. Actually the ^1H NMR signal of the OH group is shifted upfield from 10.75 to 8.52 ppm.

A series of the effects observed can be explained by assuming that chelate complex **II** is formed in nitromethane solution. In this case, the oxygen atoms of the nitro and hydroxy groups lie in the plane of the naphthalene ring, and the intramolecular hydrogen bond with the nitro group is ruptured; therefore, the signal of hydroxyl proton is shifted upfield. It whould be expected that, in the complex of 2-nitro-1-naphthol with $AlBr_3$, the downfield shift of the H-8 signal should be absent because of the absence of a suitable partner for intramolecular hydrogen bond in the vicinity of peri-hydrogen.

In mixing of cooled solutions of $AlBr_3$ and 2-nitro-1-naphthol in nitromethane, a bright-colored complex is formed (C^{13} chemical shifts of the complex: C_1 137.248, C_2 135.621, C_3 116.099, C_4 124.602, C_5 126.611, C_6 126.846, C_7 126.850, C_8 127.076, C_9, C_{10} 124.668). Since in the ^{13}C NMR spectrum of the complex the signal in the range 180–200 ppm (signals of carbonyl carbon atoms) is absent, formation of a complex of the aci form can be excluded:

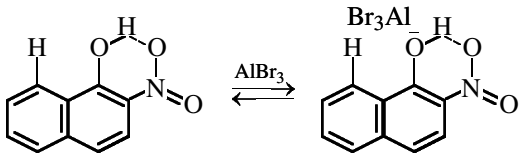

III

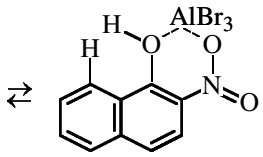

IV

Irrespective of whether the complex of 2-nitro-1-naphthol has structure **III** or **IV**, the hydrogen atom H-8 cannot form an intramolecular hydrogen bond; therefore, its chemical shift varies insignificantly, from 8.51 to 8.27 ppm, respectively.

As in the preceding case, the ^1H NMR signal of hydroxy group in the complex is shifted upfield (not downfield), from 12.24 ppm in 2-nitro-1-naphthol to 8.63 ppm in the complex.

The upfield shift of the ^1H NMR signal of the hydroxy group is apparently caused by the formation of chelate **IV**. Actually, the signal of the coordinated hydroxy group is shifted downfield to 12.7 ppm in the complex of 4-nitro-1-naphthol with $AlBr_3$ in $CDCl_3$ solution, in which formation of the chelate is impossible.

It should also be noted that the coordination of nitronaphthols with $AlBr_3$ does not noticeably affect the spin-spin coupling constants (Table 2).

EXPERIMENTAL

The ^{1}H NMR spectra were recorded on a Bruker Avance 200 spectrometer. We used TM as an internal reference, in recording spectra of free nitrophenols, and nitromethane (4.33 ppm) in recording spectra of complexes. The presence of $AlBr_3$ in a solution results in the shifts of the ^{1}H NMR signal of nitromethane by 0.1–0.2 ppm; mp (°C): 1-nitro-2-naphthol 103, 2-nitro-1-naphthol 128, 4-nitro-1-naphthol 164. The complexes were synthesized in a dry box at 0°C. The spectra were recorded at 20°C.

CONCLUSION

In the reaction with aluminum bromide in nitromethane solution, 2-nitro-1-naphthol and 1-nitro-2-naphthol form bright-colored chelate complexes, whereas 4-nitro-1-naphthol forms a typical complex of the oxy form.

REFERENCES

1. Choen, L.A. and Jones, W.M., *J. Am. Chem. Soc.*, 1963, vol. 85, no. 21, pp. 3397–3402.
2. Meek, J.S., Folver, J.S., Monroe, P.A., and Clark, T.Y., *J. Org. Chem.*, 1968, vol. 33, no. 1, pp. 226–229.
3. Hantzsch, A. and Gorkin, H., *Ber.*, 1906, vol. 39, pp. 1073–1084.
4. Golounin, A.V. and Koptyug, V.A., *Zh. Org. Khim.*, 1972, vol. 8, pp. 607–611.
5. Koptyug, V.A., Andreeva, T.P., and Mamatyuk, V.I., *Izv. Akad. Nauk SSSR, Ser. Khim.*, 1968, vol. 12, pp. 2844–2845.
6. Koptyug, V.A., Andreeva, T.P., and Mamatyuk, V.I., *Zh. Org. Khim.*, 1970, vol. 7, pp. 1148–1153.
7. Andreeva, T.P., Tregub, G.P., Mamatyuk, V.I., and Koptyug, V.A, *Zh. Org. Khim.*, 1972, vol. 8, pp. 1271–1276.
8. Baitinger, W.F., Schleyer, P.R., Murty, T.S., and Robinson, L., *Tetrahedron*, 1964, vol. 20, pp. 1635–1638.

ISSN 1070-4272, Russian Journal of Applied Chemistry, 2007, Vol. 80, No. 6, pp. 1018–1019. © Pleiades Publishing, Ltd., 2007.
Original Russian Text © N.A. Sklyarova, K.B. Grekov, E.A. Andreeva, 2007, published in Zhurnal Prikladnoi Khimii, 2007, Vol. 80, No. 6, pp. 1043–1044.

BRIEF COMMUNICATIONS

Detoxication of Spent Bleaching-Fixative Solutions

N. A. Sklyarova, K. B. Grekov, and E. A. Andreeva

St. Petersburg State University of Cinematography and Television, St. Petersburg, Russia

Received February 16, 2007

Abstract—Various technological schemes for detoxication of spent bleaching-fixative solutions, with sodium peroxocarbonate as an oxidizing agent and multistage acid-alkaline treatment making possible recovery of separate valuable components, were studied. A method for minimization of the expenditure of the oxidizing agent was chosen.

DOI: 10.1134/S1070427207060341

A particular place among waste solutions formed in chemical-photographic processing of various photographic materials (primarily, modern color photographic paper) is occupied by bleaching-fixative solutions (BFS). These solutions present the most severe difficulties in utilization and recycling, as well as in detoxication in those cases when utilization is impossible or hindered. Modern color motion-picture and photographic materials are processed with BFS of various compositions, e.g.: Fe(III) EDTA · $2H_2O$ 35 g l^{-1}, $(NH_4)_2S_2O_3$ (70% solution) 150 ml l^{-1}, Na_2SO_3 10 g l^{-1}, and EDTA 30 g l^{-1}; with a pH value of up to 6.7 [1]. In addition, spent BFS commonly contain up to several grams of silver (in the form of dissolved complex compounds). Also, various agents activating the bleaching process, e.g., thiourea, thiosemicarbazide, or potassium (ammonium) bromide or iodide, are frequently introduced into the composition of various BFS based on an iron complexone in order to diminish the concentration of free silver ions in the reaction volume. Many of these compounds are reducing agents, and, therefore, they lead, when present in wastewater, to an increase in the chemical oxygen demand and biochemical oxygen demand.

A technological scheme for detoxication of solutions of this kind has been developed. This scheme is recommended for large regional centers engaged in regeneration of spent photographic solutions. After recovery of silver by an electrolytic or a reagent method, BFS are subjected to multistage acid-alkaline treatment, which enables successive extraction from these solutions of a number of valuable components (iron hydroxide, ammonia, sulfur, ethylenediaminetetraacetic acid). It has been suggested to use hydrogen peroxide for oxidation of organic and residual sulfur-containing compounds [2, 3].

However, the high cost, inflammability, and insufficient storage stability led us to an attempt to replace Perhydrol with an alternative oxidizing agent, sodium peroxocarbonate, which is largely devoid of the disadvantages mentioned above. Moreover, oxidation of a number of compounds, including those containing sulfur, requires alkalinization of the solution, and, therefore, presence of sodium carbonate in the composition of the oxidizing agent can diminish the expenditure of an alkali.

We performed preliminary studies of the oxidation efficiency with a model solution containing 16.5 g l^{-1} of sodium thiosulfate. It was shown that, at a sodium peroxocarbonate dose of 40 g l^{-1} (oxidizing agent is introduced in an excess amount), the duration of thiosulfate oxidation does not exceed 30–45 min.

As noted above, spent BFS are subjected for detoxication, after silver recovery by an electrolytic or a reagent method, to an acid-alkaline treatment. In this case, iron in the form of a hydroxide, ammonia, sulfur, and ethylenediaminetetraacetic acid are successively extracted, and organic and residual sulfur-containing compounds are oxidized by the oxidation method. To choose the simplest, convenient, economical, and safe detoxication technique, we compared various schemes of this process, in which sodium peroxocarbonate was used as an oxidizing agent:

(1) Treatment with an oxidizing agent after recovery of iron hydroxide by addition of sodium hydroxide to pH 13, followed by keeping and filtering.

(2) Treatment with an oxidizing agent after recovery of iron hydroxide (scheme 1), removal of ammonia by addition of sulfuric acid and calcium hydroxide to pH 10, followed by keeping of the resulting solution for several hours and decomposition of the thiosulfate by addition of concentrated sulfuric acid to pH 1, with the subsequent keeping and separation of precipitated sulfur by filtration.

(3) Treatment with an oxidizing agent after recover of iron hydroxide, decomposition of the thiosulfate with a strong acid (scheme 2) and isolation of EDTA in the crystalline form by addition of sodium hydroxide to pH 2, keeping for EDTA crystals to be formed, and separation of the solution by decantation or filtration.

(4) Solidification in the form of gypsum of the liquid waste produced by scheme 3, by addition of calcium hydroxide to pH 6–7.

A study of the technological schemes for BFS detoxication demonstrated that the degree of oxidation of BFS components by different detoxication schemes is the same: 98–99% and more. This enables us to recommend the first scheme for use in small photographic mini laboratories.

However, the most efficient and economically favorable is scheme 3, in which sodium peroxocarbonate used as oxidizing agent is introduced after a preliminary recovery of components. The chosen method provides the minimum expenditure of the oxidizing agent ($\leq$ 3–5 g l^{-1}) and recovery of valuable components. If the total dose of acid and alkali is raised in this scheme from 50 to 300–400 g l^{-1}, the most complete solution detoxication (up to 99.9%) is achieved in BFS processing.

Because BFS show, after detoxication, an acid reaction (pH 1–2) and contain a large amount of sulfate ions, calcium hydroxide can be used for neutralization of this solution. This reaction will yield gypsum and this, in turn, will totally preclude formation of any liquid waste.

REFERENCES

1. Iwano, H., Hatano, T., and Matsushita, S., *J. Appl. Phot. Eng.*, 1976, vol. 2, no. 2, pp. 65–69.
2. Grekov, K.B. and Lebedev, S.A., *Nov. Tekhnol. Ikh Primen.*, 2005, no. 1, pp. 68–70.
3. Knorre, H., Maenning, D., and Stuetzel, K., *J. Imaging Technology*, 1988, vol. 14, no. 6, pp. 154–156.

ISSN 1070-4272, Russian Journal of Applied Chemistry, 2007, Vol. 80, No. 6, pp. 1020–1022. © Pleiades Publishing, Ltd., 2007.
Original Russian Text © N.O. Zulumyan, A.R. Isaakyan, Z.G. Oganesyan, 2007, published in Zhurnal Prikladnoi Khimii, 2007, Vol. 80, No. 6, pp. 1047–1049.

BRIEF COMMUNICATIONS

A New Promising Method for Processing of Serpentinites

N. O. Zulumyan, A. R. Isaakyan, and Z. G. Oganesyan

Institute of General and Inorganic Chemistry, National Academy of Sciences of the Republic of Armenia, Yerevan, Armenia

Received November 18, 2005; in final form, March 2007

Abstract—A new thermal-acid method for processing of serpentinized ultrabasic rocks was developed. The method makes it possible to recover, in a very short time and in good yield, magnesium and iron(III) in the form of salts (hydroxides or oxides) and two varieties of SiO_2 as an aqua silica gel and light silica.

DOI: 10.1134/S1070427207060353

Of particular importance for the development of national economies of numerous countries is elaboration of new methods for processing of such complex rocks as ultramafites. For example, such rocks as dunites, peridotites, pyroxenites, and their varieties form large mountain massifs in various continents of the Earth. It should be noted that serpentinized rocks widely occur in the Caucasian region. In Armenia, they, in particular, contain (%): 38–40 SiO_2, 37–41 MgO, 4 FeO_2 and about 15 Fe_2O_3, Al_2O_3, Cr_2O_3, NiO, CoO, etc. [1].

Recently, a new technique for thermal-acid processing of serpentinized ultrabasic rock has been developed [2]. Processing of rock by this method results in that salts of magnesium and iron(III) and a major part of SiO_2 in the form of orthosilicic acid pass into solution, and the acid is recovered using a sol–gel technique.

Production of an aqua silica gel by the method suggested can be regarded as a new, third method, because only two widely used techniques for synthesis of aqua silica gels by means of sol–gel processes have been known until recently: from soluble silicates and such silicon-containing compounds as SiH_4, $SiCl_4$, and $Si(OR)_4$ [3].

EXPERIMENTAL

The essence of the method developed consists in that serpentinite preliminarily calcined at 650–700°C is treated with dilute acid during several minutes. The resulting sludge is decanted and filtered [4, 5]. In the process, up to 95% of MgO and up to 80–90% of Fe_2O_3 pass into solution, as also does SiO_2 whose amount depends on the degree of rock serpentinization and on the variety of the primary mineral [6].

It has been believed until recently that, in thermal treatment of serpentinized rock at 600–800°C, there simultaneously occur two processes: removal of the constitution water and amorphization of serpentinite [7]. It has been found that the removal of the constitution water in this temperature range is accompanied by disintegration of the silicate network of serpentinite, and just the latter is the reason why orthosilicic acid passes into solution in acid treatment [4]. The degree of disintegration varies with the type of the primary rock (dunite, peridotite, pyroxenite) subjected to serpentinization. This is confirmed by the fact that different amounts of orthosilicic acid are obtained in solution. The table lists the percentage content of orthosilicic acid obtained from various

Degree of recovery of orthosilicic acid from various samples

Sample	SiO_2, %
Apodunite serpentinite:	
4135*	31.0
4246	37.6
4248	30.2
Apopyroxenite serpentinite 4147B	10.4
Partly serpentinized variety:	
4247	17.3
4254	9.80

* Number assigned by the authors.

samples of serpentinites. It can be seen that the yield of SiO_2 in thermal-acid processing of apodunite serpentinites exceeds that for apopyroxenite or other partly serpentinized varieties. It is noteworthy that, occasionally, the degree of SiO_2 recovery into solution is as high as 60%.

Numerous studies have shown that oxidation of Fe^{2+} ions, present in a mineral, to Fe^{3+} also favors disintegration of silicate networks of serpentinite. It is quite natural that, in this state, the interaction of silicate anions with ions of magnesium and iron(III) is unstable, and, therefore, the mineral readily enters into an ion-exchange reaction with both strong and weak acids.

One of the simplest variants of the disintegration of serpentines $Mg_6(Si_4O_{10})(OH)_8$ in the temperature range 600–800°C can be represented as

$$n\mathrm{Mg_6(Si_4O_{10})(OH)_8} \rightarrow 2n\mathrm{Mg_2SiO_4} + \mathrm{Mg_{2n}(Si_2O_6)_n} + 4n\mathrm{H_2O}. \quad (1)$$

Occasionally, forsterite Mg_2SiO_4 and enstatite $Mg_2(Si_2O_6)$ may be in the crystalline state [7], as indicated by X-ray diffraction patterns of calcined samples, but this does not affect the rate of ion-exchange reactions between forsterite, enstatite, and acids, which occur in accordance with the equations,

$$\mathrm{Mg_2SiO_4} + 4\mathrm{H^+} \rightarrow \mathrm{H_4SiO_4} + 2\mathrm{Mg^{2+}}, \quad (2)$$

$$\mathrm{Mg_{2n}(Si_2O_6)_n} + 4n\mathrm{H^+} \rightarrow \mathrm{H_{4n}(Si_2O_6)_n}\downarrow + 2n\mathrm{Mg^{2+}}. \quad (3)$$

It was demonstrated that, after a chemical reaction, metal salts, orthosilicic acid, and part of oligosilicic acid easily penetrate into solution through a filter. The resulting solution may contain about 8 g l^{-1} of SiO_2 and can remain in a stable state for a long time. It was also found that Fe^{3+} ions strongly affect the stability of this solution.

The aqua gel of orthosilicic acid can be easily recovered from solution, and, after filtration and washing at pH 6.5–7, a stable gel mass is formed with $\nu(SiO_2)/\nu(H_2O) \approx 1 : 65$. It was found that, depending on the method used to remove water from this mass, $SiO_2 \cdot nH_2O$ with different physical characteristics are formed.

The specific surface area of $SiO_2 \cdot nH_2O$ produced by one of these methods and treated at 300°C is 542 m^2 g^{-1}, and the particle size distribution is as follows (%): 10, up to 4.1 μm; 50, up to 30 μm; and 90, up to 146 μm. The measurements were made by the BET technique (see figure).

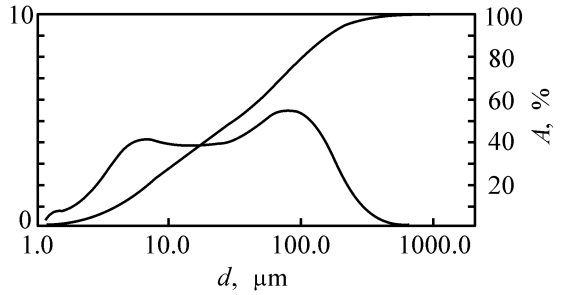

Differential particle size distribution of SiO_2 particles. (*d*) Particle size and (*A*) content of particles.

It can be seen from the data presented above that there exists a certain disagreement between the values of the specific surface area and the calculated particle sizes. A possible reason is that orthosilicic acid undergoes polycondensation in the acid medium and a high concentration of Mg^{2+} and Fe^{3+} ions is present, which probably leads to formation of specific aqua silica gel units. Heating of these units, with removal of bound water, leads to agglomeration of the forming highly dispersed $SiO_2 \cdot nH_2O$ particles. It should be noted that, owing to the polycondensation of orthosilicic anions, uniform acid centers are formed in the silica gel. This fact was taken into account when using this silica gel as a catalyst support.

The specificity and high purity of the silica gel obtained also enable its use in manufacture of optical glass and synthesis of nanocomposite materials [8].

After decantation and filtration of the solution obtained, silica containing 12% MgO and 8% Fe_2O_3 remains on the filter. Subsequent acid treatment of this silica gives an active light silica powder with a purity exceeding 99.5%.

According to preliminary calculations, the method suggested can produce up to 400–420 kg of MgO, 70–80 kg of Fe_2O_3, 120–150 kg of SiO_2 in the form of an aqua silica gel, and 280–300 kg of active silica powder from a ton of thermally treated serpentinite.

CONCLUSIONS

The suggested thermal-acid treatment method opens up new opportunities for processing of serpentinized ultramafites. It is not only a new technologically convenient and economically feasible method for production of magnesium and iron(III) compounds, but also new technique for production of a special silica gel and light silica powder.

If compounds of chromium, cobalt, and nickel and other compounds are originally present in the rock,

the unreacted residue obtained after decantation can serve as a concentrate of these compounds.

REFERENCES

1. Abovyan, S.B., *Geologiya i poleznye iskopaemye severovostochnogo poberezh'ya ozera Sevan* (Geology and Mineral Resources of the northwestern Coast of Lake Sevan), Yerevan: Akad. Nauk ArmSSR, 1961.
2. Republic of Armenia Patent 1339.
3. Neimark, I.E. and Sheinfain, R.Yu., *Silikagel', ego svoistva i primenenie* (Silica Gel: Properties and Use), Kiev: Naukova Dumka, 1973.
4. Zulumyan, N.O., Oganesyan, Z.G., Oganesyan, E.B., and Karakhanyan, S.S., *Dokl. Nats. Akad. Nauk Resp. Armenia*, 2002, no. 3, pp. 238–242.
5. Republic of Armenia Patent 1576.
6. Zulumyan, N.O., Abovyan, S.B., Oganesyan, Z.G., and Kazaryan, S.E., *Izv. Nats. Akad. Nauk Resp. Armenia, Ser. Nauk. Zemle*, 2003, vol. 56, no. 3, pp. 29–34.
7. Ivakova, V.P., Kasatov, B.K., Krasavina, T.N., and Rozinova, E.A., *Termicheskii analiz mineralov i gornykh porod* (Thermal Analysis of Minerals and Rocks), Leningrad: Nedra, 1974.
8. Zulumyan, N.H., Torosyan, A.R., Hovhannisyan, Z.H., and Ghazaryan, S.E., *TMS 2005 Annual Meeting & Exhibition*, 13–17 February 2005, San Francisco, Ca, USA, p. 65.

ISSN 1070-4272, Russian Journal of Applied Chemistry, 2007, Vol. 80, No. 6, pp. 1023–1025. © Pleiades Publishing, Ltd., 2007.
Original Russian Text © A.I. Levinskii, 2007, published in Zhurnal Prikladnoi Khimii, 2007, Vol. 80, No. 6, pp. 1048–1049.

BRIEF COMMUNICATIONS

Relationship between Fluid and Vapor Densities and Enthalpy of Evaporation

A. I. Levinskii

21629, Neu Wulmstorf, Germany

Received April 12, 2006; in final form, January 2007

Abstract—A simple semiempirical formula relating the enthalpy of vaporization to the densities of a fluid and a vapor in equilibrium with this fluid is derived.

DOI: 10.1134/S1070427207060365

It is known [1] that the interaction energy of two molecules is well described by the Lennard–Jones potential, which can be represented as

$$\psi(r) = a/r^6 - b/r^{12}, \quad (1)$$

where r is the distance between molecules, and a and b are constants.

Let us consider a molecule in a fluid that is in equilibrium with its vapor. This molecule interacts with all other molecules of the fluid in accordance with formula (1), and the interaction energy is equal to the sum of energies of interaction with all molecules of the given volume of the fluid. Let us denote the molar volume of the fluid by V_f. Then the number of molecules in unit volume $n = N_A/V_f$, where N_A is the Avogadro number. The number of molecules in a spherical layer of radius r and thickness dr is d$n = (N_A/V_f)4\pi r^2 dr$. The energy of interaction of a molecule with molecules from this layer is given by

$$dE = \left(\frac{a}{r^6} - \frac{b}{r^{12}}\right)\frac{N_A}{V_f}4\pi r^2 dr,$$

and the full interaction energy, by

$$E = 4\pi\frac{N_A}{V_f}\int_R^\infty\left(\frac{a}{r^6} - \frac{b}{r^{12}}\right)r^2 dr = 4\pi\frac{N_A}{V_f}\left(\frac{a}{3R^3} - \frac{b}{9R^9}\right),$$

where R is the distance to the nearest-neighbor molecule.

The distance between the nearest molecules can be related to the volume v occupied by a single molecule by $v = kR^3$, where k is the structural factor close, in order of magnitude, to unity (for the cubic packing of molecules, $k = 1$; $k = \sqrt{3} \approx 1.732$ if the volume occupied by a molecule is tetrahedral, and $k = \pi/6 \approx 0.524$ if it is spherical). Then the molar volume of the fluid $V_f = kN_AR^3$, whence follows that $R^3 = V_f/kN_A$ and the interaction energy $E = 4\pi\frac{N_A}{V_f}\left(\frac{akN_A}{3V_f} - \frac{bk^3N_A^3}{9V_f^3}\right)$. If we introduce designations $A' = 4\pi N_A^2 ak/3$ and $B' = 4\pi N_A^4 bk/9$, the interaction energy can be represented as $E = A'/V_f^2 - B'/V_f^4$. Taking into account that the fluid density $\rho_f = M/V_f$, where M is the molecular weight and introducing designations $A = A'/M^2$ and $B = B'/M^4$, we finally obtain

$$E = A\rho_f^2 - B\rho_f^4. \quad (2)$$

Formula (2) is valid for a real gas.

The vaporization of a molecule can be represented as occurring in two stages: (1) removal of the molecule from the fluid volume into a vacuum, with an energy $A\rho_f^2 - B\rho_f^4$; and (2) transfer of the molecule from a vacuum into the vapor volume, with an energy $A\rho_v^2 - B\rho_v^4$ released. Thus, the enthalpy of vaporization can be represented as the difference of these two energies:

$$\Delta H = A(\rho_f^2 - \rho_v^2) - B(\rho_f^4 - \rho_v^4). \quad (3)$$

To compare the values calculated by formula (3) with those obtained experimentally, we used published data [2]. We chose seven fluids: homologous series of methane (methane, nonpolar nearly spherical molecules; ethane, propane, and butane, virtually non-

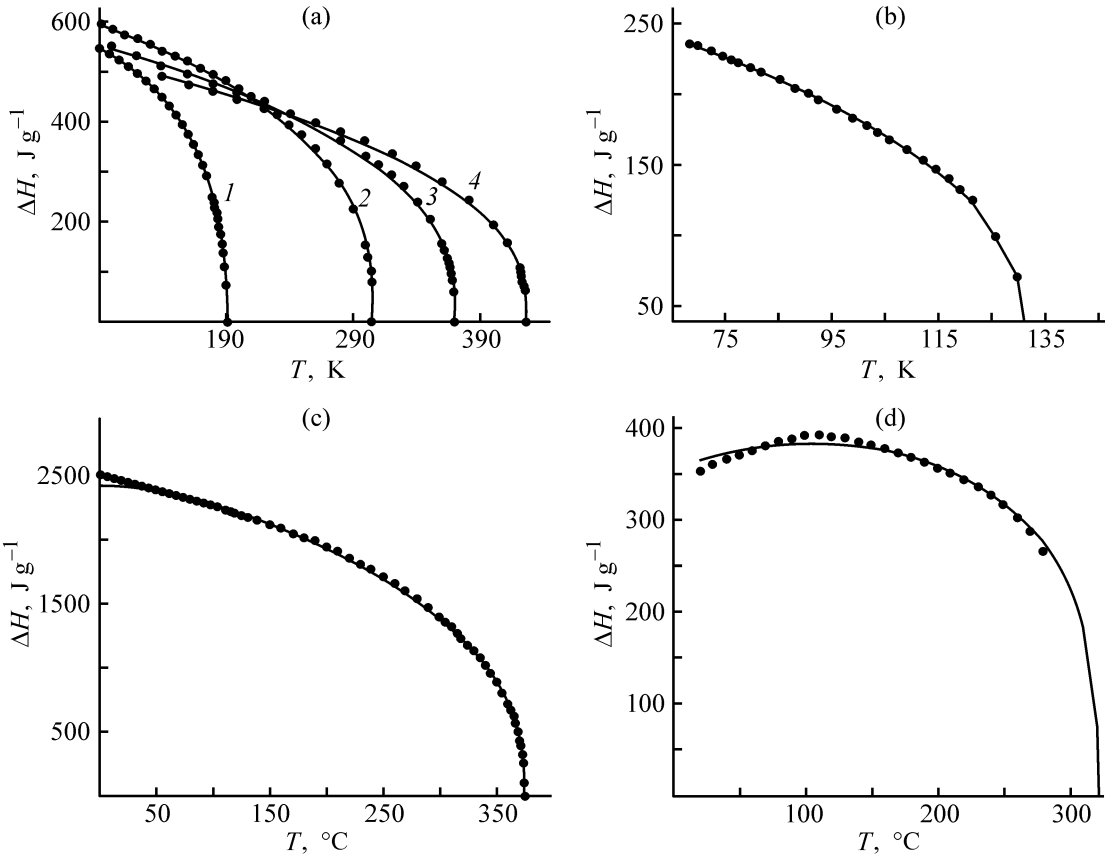

Enthalpy of vaporization, ΔH, vs. temperature T for various fluids. (a) (*1*) methane (A = 4079.65, B = 6904.1), (*2*) ethane (A = 2213.33, B = 1925.62), (*3*) propane (A = 1634.26, B = 1124.35), (*4*) butane (A = 1350.45, B = 809.45); (b) carbon dioxide (A = 460.28, B = 184.37); (c) water (A = 3069.93, B = 647.72); and (d) acetic acid (A = 846.73, B = 469.50). *Lines*, calculation by formula (3); *points*, experimental data [2]. For rms deviations of the calculated curves from the experimental points, see text.

polar nonspherical molecules), carbon monoxide (polar molecules), water, and acetic acid (preence of a hydrogen bond). The results obtained are shown in the figure. Parameters A and B were found by the generalized least-squares method, i.e., so as to minimize the root-mean-square deviation of the calculated curve from experimental data (discrepancy). It can be seen that formula (3) is in good agreement with the experiment for fluids whose molecules have a nearly spherical shape and contain no hydrogen bonds: the rms deviation from the theoretical curve from the experimental points is 1.2 J g^{-1}, or 0.22% relative to the highest enthalpy of vaporization, for methane and 1.4 J g^{-1}, or 0.58%, for carbon monoxide). The agreement is somewhat poorer in the presence of a hydrogen bond (rms deviation of 26 J g^{-1}, or 1.0%, for water and 5.4 J g^{-1}, or 1.4%, for acetic acid) or in the case of strongly nonspherical molecules (4.9 J g^{-1}, or 0.83%, for ethane; 4.3 J g^{-1}, or 0.78%, for propane; and 5.4 J g^{-1}, or 1.1%, for butane). This is presumably accounted for by the fact that the dependence of the hydrogen bond energy on the intermolecular distance differs from the function specified by the Lennard–Jones potential, which is also the case in interaction of strongly nonspherical molecules.

Formula (3) can be used for practical purposes. To do so, it is necessary to know a single function (temperature dependence of the fluid density ρ_f) and two parameters, A and B. There is no need to know the temperature dependence of the vapor density, because it can be readily calculated using the known empirical rule: the sum of fluid and vapor densities linearly depends on temperature.

Also known are other formulas making it possible to calculate the enthalpy of vaporization, e.g., the Wattson formula [3]:

$$\frac{\Delta H_2}{\Delta H_1} = \left(\frac{1-\tau_2}{1-\tau_1}\right)^n.$$

This formula compares the calculated enthalpy of vaporization, ΔH_2, with the enthalpy of vaporization of a chemically related fluid, ΔH_1; τ_2 and τ_1 are "reduced" temperatures. This means that only a single function, $\Delta H_1(T_1)$, and three parameters (n, triple point temperature T_2^0, and critical temperature T_2^*) should be known for a practical calculation. In this case, the calculation error is 8–13% [3]. Thus, the accuracy of formula (3) suggested for calculating the enthalpy of vaporization is an order of magnitude better.

REFERENCES

1. McQuarrie, D. and Simon, J.D., *Physical Chemistry: a Molecular Approach*, Sausalito, California: Univ. Sci. Books, 1997.
2. Vargaftik, N.B., *Handbook of Physical Properties of Liquids and Gases*, Washington, 1983.
3. Poling, B.E., Prausnitz, J.M., and O'Connel, J.P., *The Properties of Gases and Liquids*, New York: McGraw–Hill, 2001.

ISSN 1070-4272, Russian Journal of Applied Chemistry, 2007, Vol. 80, No. 6, p. 1026. © Pleiades Publishing, Ltd., 2007.
Original Russian Text © A.G. Morachevskii, M.S. Kokhatskaya, 2007, published in Zhurnal Prikladnoi Khimii, 2007, Vol. 80, No. 6, p. 1050.

BOOK REVIEWS

Teplinskii, Yu.A. and Mamaev, N.I., *Korrozionnaya povrezhdaemost' podszemnykh truboprovodov* (Vulnerability of Underground Pipelines to Corrosion Damage),

St. Petersburg: Info-da, 2006, 406 pp.

DOI: 10.1134/S1070427207060377

The lack of an efficient corrosion protection of metallic members of apparatus and machines and of underground metallic constructions leads to a huge loss of metals. By 1990, the annual corrosion loss of metals in our country was estimated at 20 million tons [*Zashchita podzemnykh metallicheskikh sooruzhenii ot korrozii* (Corrosion Protection of Underground Metallic Constructions), Moscow: Stroiizdant, 1990]. A considerable fraction of this loss is associated with underground pipelines. The corrosion damage to important underground communications has a strongly detrimental effect on the country's economy and lead to irreversible ecological consequences. In view of the steadily expanding network of underground pipelines, their protection from various corrosion effects is of primary importance.

The industrial-technological book by Yu.A. Teplinskii and N.I. Mamaev is devoted to the problem of corrosion protection of underground natural-gas pipelines, primarily in the North-West region of the country. The book comprises an introduction, ten chapters, list of designations, and bibliographic list.

In the introduction (pp. 3–7), the authors mention extension of the service life of various kinds of metalwork and prevention of accidents as the most important task for specialists engaged in corrosion protection. In 2003, the total length of underground gas pipelines used by Gazprom Open Joint-Stock Company was 178.3 thousand kilometers. Of these pipelines, 44.7% have been in service for more than 20 years. The first chapter (pp. 8–36) considers in a rather popular form main kinds of corrosion damage, typical of underground pipelines. Stress corrosion, leakage-current corrosion, and methods and means of protection are discussed.

The second chapter (pp. 37–92) is devoted to analysis of the state of the corrosion protection of underground pipelines in the North-West region of Russia, working zone of Severgazprom Ltd. The existing methods for protection of main pipelines, principal reasons for damage to pipelines and the nature of this damage, and various corrosion-caused accidents are described. The third (pp. 93–134) and fourth (pp. 135–166) chapters are concentrated on cases of pitting of pipes of main gas pipelines. The fifth chapter (pp. 167–208) presents examples of stress-induced corrosion cracking of pipes made of various steels. The sixth chapter (pp. 209–231) analyzes corrosion processes associated with leakage currents.

The small seventh chapter (pp. 232–245) discusses accidents on neighboring objects, caused by corrosion of pipelines. The eighth chapter (pp. 246–297) contains evidence about laboratory tests of pipeline steels for corrosion resistance, corrosion-mechanical properties, and susceptibility to stress-induced corrosion cracking. The ninth chapter (pp. 298–342) considers the possibility of assessing the working capacity of pipes that suffered from various kinds of corrosion damage. The tenth chapter (pp. 343–389) is devoted to methods for maintenance of long-working gas pipelines. These are primarily aimed to reveal damage to insulating coatings and their repair.

The bibliographic list (pp. 393–404) contains references to 131 publications, including various regulation documents. In view of the steadily expanding network of gas pipelines, wear of pipes, and necessity for their corrosion protection, the usefulness of publication of the book is beyond any doubt. The book presents a large number of particular examples of corrosion damage to underground gas pipelines, analyzes accidents, and includes a widely diverse illustrative material and photographs.

A.G. Morachevskii and M.S. Kokhatskaya

ISSN 1070-4272, Russian Journal of Applied Chemistry, 2007, Vol. 80, No. 7, pp. 1027–1031. © Pleiades Publishing, Ltd., 2007.
Original Russian Text © V.Ya. Khentov, L.N. Velikanova, V.V. Semchenko, A.B. Slabinskaya, 2007, published in Zhurnal Prikladnoi Khimii, 2007, Vol. 80, No. 7, pp. 1057–1062.

INORGANIC SYNTHESIS AND INDUSTRIAL INORGANIC CHEMISTRY

Recovery of Metals from Raw Materials of Industrial Origin

V. Ya. Khentov, L. N. Velikanova, V. V. Semchenko, and A. B. Slabinskaya

South-Russia State Technical University, Novocherkassk, Rostov oblast, Russia

Received May 4, 2006; in final form, May 2007

Abstract—Interaction of *d* elements and their compounds (oxides, sulfides, carbonates, and other compounds poorly soluble in water) with organic ligands in aprotic solvents was studied. Methods for recovery of metals from nonaqueous solutions of the resulting complex compounds are suggested.

DOI: 10.1134/S1070427207070014

The capability of metal compounds for donor–acceptor interaction with organic ligands dissolved in organic solvents can be used as a basis for a technique for recovery of metals from mining tailings, spent catalysts from organic synthesis, and wastes from breakdown of finely disseminated ores.

Compounds of *d* elements (oxides, sulfides, carbonates, and other compounds poorly soluble in water) readily enter into donor–acceptor interaction with organic ligands dissolved in aprotic solvents [1, 2]. The resulting complex compound of a metal is in the dissolved state. The metal can be recovered from the solution by reduction [3]. Surface oxide compounds are involved in the interaction of *d* elements with ligands [4]. The logarithm of the reaction rate constant is directly proportional to the electrophilicity parameter E_T [5] characterizing the solvent. Values of E_T have been obtained for different solvents by studying the effect of a solvent on the electronic spectra of a standard solvatochromic dye, *N*-(4-oxy-3,5-diphenyl)phenyl-2,4,6-triphenylpyridinium betaine.

The aim of this study was to examine the effect of the nature of a metal, concentration and nature of a ligand, temperature, and introduction of proton-donor additives in order to develop a technique for processing of raw materials of industrial origin. We studied the following *d* metals: copper, nickel, iron, manganese, chromium, vanadium, titanium, molybdenum, tungsten, cadmium, and cobalt; as well as oxides, hydroxides, sulfides, phosphates, and carbonates of the *d* metals. Benzene, 1,4-dioxane, hexane, ethyl acetate, trichloroethylene, trichloroethane, dimethylformamide (DMF), dimethyl sulfoxide, acetone, acetonitrile, carbon tetrachloride, and methylpyrrolidone were used as aprotic solvents. The solvents were dried over molecular sieves. As ligands served salicylalaniline (SA) $C_6H_4OHCNC_6H_5$, α-benzoin oxime $C_6H_5CH(OH)C{=}NOH(C_6H_5)$, tetracyanoquinodimethane $(CN)_2C{=}C_6H_4{=}C(CN)_2$, and 1-nitroso-2-naphthol $NOC_{10}H_6OH$.

EXPERIMENTAL

We chose for study those *d* elements and their compounds which are contained in raw materials of industrial origin. These are wastes from abrasive processing of steel at machine-building plants and dust wastes, mining tailings, spent catalysts from organic synthesis, and finely disseminated ores. In chemical composition, these are *d* elements and their compounds poorly soluble in water (oxides, sulfides, carbonates, phosphates).

Metals in the form of 30 × 20 × 1 mm plates with a total surface area of 13 cm^2 (calculated as the sum of areas of all faces of a rectangular parallelepiped) or dispersed particles and compounds of these metals were treated in 60 ml portions of ligand solutions at a working propeller mixer (200 rpm). DMF was used as a solvent. To determine the effective surface area of dispersed particles, we measured their size with a measuring microscope, plotted a histogram, and found the most probable effective diameter of a particle. This enabled us to calculate the specific surface area of the powder and find the total surface area of the powder for each weighed portion. The rate of the chemical reaction (mol cm^{-2} h^{-1}) was calculated with account of the total surface area of a compact or powdered sample.

The concentration of the solution of the complex compound obtained was determined from the optical

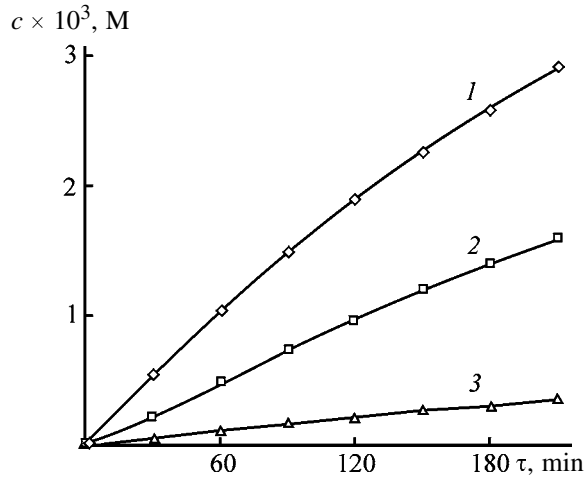

Fig. 1. Variation of the concentration of a complex compound with time τ. Powder: (*1*) copper with an oxide surface film, activated in a 30 g l^{-1} HCl solution for 30 s; (*2*) copper(I) oxide; and (*3*) copper(II) oxide.

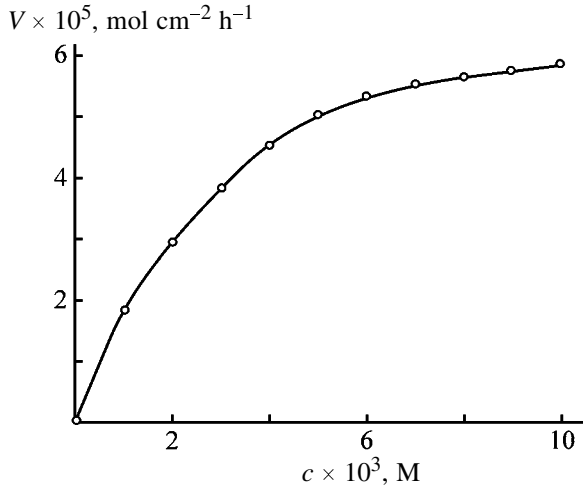

Fig. 2. Interaction rate *V* vs. the salicylalaniline concentration *c*.

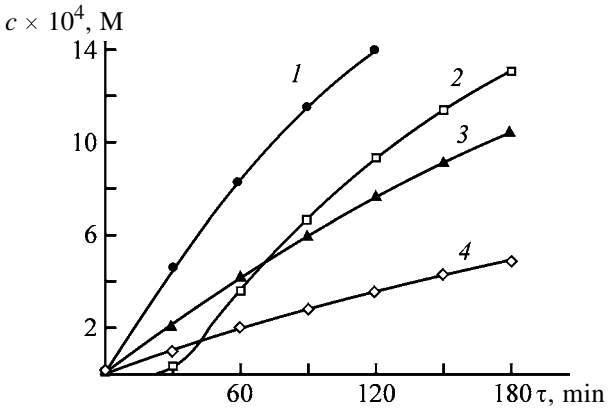

Fig. 3. Variation of the concentration of complex compounds *c* with time τ at varied ligand nature. Powdered copper, dimethylformamide as solvent. Ligand: (*1*) salicylalaniline, (*2*) α-benzoin oxime, (*3*) 1-nitroso-2-naphthol, and (*4*) tetracyanoquinodimethane.

density of the solution. Preliminarily, we plotted the corresponding calibration dependences. For this purpose, we synthesized complex compounds by the classical techniques. To identify the complex compounds synthesized by these techniques and those obtained in this study, we measured IR spectra in the range 3700–400 cm^{-1} on a Specord 75-IR instrument. Simultaneously, we determined the weight loss by the samples under study.

Metals react with solutions of a ligand in an aprotic solvent only in the presence of atmospheric oxygen, with no chemical reaction occurring in nitrogen. Hence follows that the surface oxide film enters into a reaction with the ligand. The oxide film is involved in the formation of a complex compound, this compound passes from the reaction zone into the solution, dissolved oxygen oxidizes the metal surface, and the process of formation of the complex compound is repeated [6].

It should be noted that the surface oxide reacts with the ligand at a higher rate, compared with the bulk oxide phase. Figure 1 shows how the concentration of the complex compound formed in the interaction of powdered copper and copper oxides with an SA solution in DMF varies with time. Similar results were obtained for copper sulfide.

A study of the temperature dependence of the process rate enabled us to calculate the activation energy of the reaction between copper or its oxides and SA. The activation energy was (kJ mol^{-1}) 36 ± 3 for the copper powder with an oxide film, 54 ± 4 for copper(I) oxide, and 71 ± 3 for copper(II) oxide.

Figure 2 shows how the rate of the donor–acceptor interaction of compact copper depends on the concentration of SA in DMF. The process rate is described by the equation of a first-order reaction. We determined the reaction order using the van't Hoff and Ostwald–Noyes method. The leveling-off run of the curve suggests that, as the ligand concentration increases and the complex compound is accumulated in solution, this hinders the removal of the complex compound from the reaction zone and the supply of oxygen to the metal surface through the solvent to form an oxide film. Thus, there exists a range of optimal ligand concentrations at which the rate of metal dissolution is high.

The effect of the ligand nature on the reactivity of metals is illustrated for the example of copper by Fig. 3. The rate of interaction between copper and a ligand decreases in the following order: SA > α-benzoin oxime > 1-nitroso-2-naphthol > tetracyanoquinodimethane.

Table 1. Relationship between the activation energy of interaction between metals and salicylalaniline, E_a (kJ mol^{-1}), and physical parameters of metals

Parameter	Functional dependence	R	Significance level
Binding energy E_b [7], kJ mol^{-1}	$E_a = -426.380 + 5.396E_b$	0.90	0.098
Melting point T_m, °C	$E_a = -333.323 + 0.315T_m$	0.96	0.172
Boiling point T_b, °C	$E_a = -1008.945 + 0.401T_b$	0.83	0.172
Surface energy of a crystallization nucleus, W [8], erg cm^{-1}	$E_a = -278.004 + 1.695W$	0.96	0.042
Atomic concentration of elements, $c_{at} \times 10^{-22}$ [7], cm^{-3}	$E_a = -1334.403 + 162.576c_{at}$	0.92	0.078

We revealed within a single period a relationship between the activation energy of the interaction of metals with SA and the physical parameters of the metals (Table 1). Presumably, all the physical parameters are related to oxidation of the metal surface. Indeed, there exist reliable linear relationships, with high correlation coefficients R, between the standard heat ΔH^0 of formation of oxides of metals in the lowest oxidation state (Cu_2O, FeO, CoO, NiO) and such physical parameters of metals as internuclear distance a, characteristic Debye temperature θ, and surface tension of a metal in the liquid state σ:

$$\Delta H^0 = -915.552 + 342.713a, \quad R = 0.98;$$

$$\Delta H^0 = 28.338 - 0.197\theta, \quad R = -0.98;$$

$$\Delta H^0 = 13.810 - 0.041\sigma, \quad R = -0.92.$$

Te rate of dissolution of the surface metal oxide film in an SA solution in an aprotic solvent is determined by the nature of a metal. Table 2 lists the dissolution rates of an oxide film on the metal surface and the activation energies of the process.

We obtained linear dependences of the logarithm of the reaction rate constant, $\log k$, on the electrophilicity parameter E_T characterizing a solvent. For oxygen-free solvents,

$$\log k = -14.43 + 0.31E_T, \quad R = 0.98.$$

For oxygen-containing solvents,

$$\log k = -10.49 + 0.19E_T, \quad R = 0.97.$$

In view of the aforesaid, prospects open up for removal of oxide films from the surface of a metal and metallic substrates, e.g., from the surface of optical materials. In addition, it seems possible to recover metals from wastes formed in abrasive processing at machine-building plants and from dust wastes. As the main reagent serve solutions of an organic ligand in an aprotic solvent.

To examine the possibility of metal recovery from ores, we analyzed dissolution of oxides, spinels, and preliminary ground finely disseminated minerals in solutions of SA in DMF. The iron–copper spinel was synthesized by sintering oxides at 1200°C. The composition of the spinel was confirmed by X-ray diffraction analysis. Table 3 lists the rates and activation energies of dissolution of preliminarily compacted pellets of area 1 cm^2.

It should be noted that the dissolution rate and the degree of recovery increase if the ligand solution is bubbled with air. This may be due to enhancement of mass-exchange processes at the solid–liquid phase boundary.

A topical problem is utilization of spent catalysts from industrial organic synthesis, composed of metal oxides and organometallic compounds of copper, bismuth, nickel, and chromium. For example, the re-

Table 2. Rate V of interaction between powdered metals and salicylalaniline (0.01 M solution in dimethylformamide) and the activation energy of the process, E_a

Metal	$V \times 10^5$, mol cm^{-2} h^{-1}	E_a, kJ mol^{-1}
Titanium	5.42	171 ± 4
Vanadium	5.65	–
Chromium	0.72	43 ± 3
Manganese	3.01	–
Iron	1.06	69 ± 3
Cobalt	0.99	141 ± 4
Nickel	0.44	136 ± 4
Copper	2.02	36 ± 3
Zinc	0.79	–
Molybdenum	1.4	101 ± 4
Cadmium	0.55	41 ± 3
Tungsten	0.38	127 ± 4
Mercury	0.18	–

Table 3. Rate V and activation energy of dissolution of the spinel, oxides, and ores in a solution of salicylalaniline in dimethylformamide (0.01 M)

Material being dissolved	$V \times 10^6$, mol cm^{-2} h^{-1}	E_a, kJ mol^{-1}
Spinel $CuFe_2O_4$	33.3	171 ± 4
Cuprite Cu_2O	63.6	54 ± 3
Hematite Fe_2O_3	2.2	98 ± 3
Magnetite Fe_3O_4	3.0	87 ± 3
Siderite $FeCO_3$	21.7	69 ± 3
Bornite Cu_5FeS_4	41.8	117 ± 4

Table 4. Formation rates of a complex compound in supply of a finely dispersed powder with a dust–gas flow (V_1) and in direct introduction of a powder into the reaction bath (V_2), and the respective degrees of recovery (α_1, α_2)

Dust particles	V_1, mol cm^{-2} h^{-1}	α_1, %	V_2, mol cm^{-2} h^{-1}	α_2, %
Cu	5.0×10^{-6}	94.3	5.57×10^{-7}	10.5
CuS	5.6×10^{-6}	96.6	2.59×10^{-7}	43.7
V_2O_3	9.0×10^{-6}	90.6	4.6×10^{-6}	46.2
VO_2	8.99×10^{-6}	94.3	4.28×10^{-6}	45.1

covery of copper in treatment of a copper–bismuth catalyst (150.1 g kg^{-1} copper and 26.3 g kg^{-1} bismuth) in a system composed of SA (0.01 M) and DMF occurs at a rate of 97.3 g h^{-1} m^{-2}, with a degree of recovery equal to 78%. For the copper–nickel–chromium catalyst (124.4 g kg^{-1} copper, 81.0 g kg^{-1} nickel, and 29.9 g kg^{-1} chromium), the rate and degree of recovery were, respectively, 78.7 g h^{-1} m^{-2} and 77% for copper, 20.6 g h^{-1} m^{-2} and 81% for nickel, and 29.9 g h^{-1} m^{-2} and 84% for chromium.

Of particular interest is recovery of metals from dust discharged from industrial plants. This can be done by bubbling washing of a dusty gas, with a simultaneously occurring chemical reaction. For this purpose, a dust–gas flow was directed into a solution of SA in DMF. Dust particles had an average size of 160 μm. The SA concentration was 0.1 M, and the solution volume, 60 ml. Air was supplied at a rate of 4 l min^{-1} (average bubble size 8 mm, depth of bubble floating-up 10 cm), and the solid phase, at a rate of 0.008 g min^{-1}. Table 4 lists the results obtained in a study of dissolution of dust particles delivered into the ligand solution directly with a dust–gas flow by bubbling or introduced directly into the solution.

It should be noted that the dissolution rate and, especially, the degree of metal recovery appreciably increase if the solution is bubbled with the dust–gas flow. The activation energy of the chemical reaction in activation of copper particles in the dust–gas flow was 18 ± 1 kJ mol^{-1} against 28 ± 2 kJ mol^{-1} in the direct interaction of the copper powder with the solution. The activated nature of the interaction of copper particles may be associated with tribocharging in the dust–gas flow. We determined the charge of dust particles. When passing the dust–gas flow between oppositely charged plates, we observed adhesion of the powder to one of these plates. Cu particles were positively charged, whereas CuS, V_2O_3, and VO_2 particles carried a negative charge. When passing powders taken from the reaction vessel between the capacitor plates, no powder adhesion was observed. The increase in the rate of the chemical reaction may be due to a rise in the chemical potential of dust particles upon their charging. In accordance with the Guggenheim equation, the chemical potential of a charged particle is given by

$$\mu = \mu_0 + ZF\Psi,$$

where μ is the chemical potential of a particle in the gas flow; μ_0, chemical potential of a particle; Z, number of electrons attached to the particle; F, Faraday constant; and Ψ, potential acquired by the particle in the flow.

Table 5 summarizes the results of our studies of metal recovery from raw materials of industrial origin. A metal can be recovered by decomposition of a complex compound, reduction with hydrazine, and electrochemical reduction from nonaqueous solutions of a complex compound [3]. Use of nonaqueous solvents may be of considerable interest, especially for recovery of those metals that cannot be, in principle, obtained in the free state from aqueous solutions. With hydrazine used as a reducing agent, it is thermodynamically possible to perform chemical reduction by the scheme

$$M^{z+}_{DMF-SA} + N_2H_4 \rightarrow M\downarrow + N_2\uparrow + 4H^+_{DMF-SA}$$

In reduction with hydrazine, metals are in an ultradispersed state and exhibit a high chemical activity. In this case, all operations should be performed in an inert atmosphere.

Of particular interest is the possibility of regeneration of spent catalysts from industrial organic synthesis. For this purpose, a catalyst is preliminarily treated with a solution of SA in DMF. In the process, the oxide and organometallic phases of the catalyst are

Table 5. Reaction rates in introduction of the substance into a solution (V_1) and supply of the substance into the solution with the dust–gas flow (V_2), and the respective degrees of metal recovery (α_1, α_2)

Type of waste	Substance	Metal content, %	Treatment time, h	$V_1 \times 10^2$, mol cm^{-2} h^{-1}	α_1, %	$V_2 \times 10^2$, mol cm^{-2} h^{-1}	α_2, %
Dust carry-over	Cu	19.2	4	5.6	10.2	50.1	94.3
Carry-over in chalcopyrite dressing	CuS	12.8	1	5.2	43.7	5.7	96.6
Waste from processing of vanadium bronzes	V_2O_3	15.0	2	4.6	46.2	9.0	90.6
	VO_2	12.4	2	4.3	45.1	8.9	94.3
Spent catalyst	V_2O_5	50.4	3	35.8	61.3	90.6	93.0

Table 6. Metal content c of the catalyst, metal recovery rate V, and degree α of metal recovery

Catalyst	c, g kg^{-1}	V, g h^{-1} m^{-2}	α, %
Copper–bismuth	Cu 150.1,	97.28	78
	Bi 26.3	–	–
Copper–nickel–chromium	Cu 24.4,	78.7	77
	Ni 81.0,	20.6	81
	Cr 84.0	29.9	84

dissolved. The catalyst support (silica gel, graphite, kaolin) is impregnated with a solution of the complex compounds obtained and then thermally treated at 180°C. Metals are formed on the support surface in the ultradispersed state and are easily oxidized by atmospheric oxygen to oxides. In catalyst regeneration, there is no need to recover each metal. The percentage ratio of metals in the solution of the complex compound corresponds to their content on the catalyst surface. Table 6 lists the rates and degrees of recovery of the metals.

CONCLUSIONS

(1) Metals and their compounds poorly soluble in water can be transferred to the soluble state by interaction with salicylalaniline in nonaqueous solvents.

(2) There exists a linear relationship between the oxidation rate of metals, activation energy of the process, electrophilicity parameter E_T characterizing the solvent, and physical parameters of metals (boiling and melting points, binding energy, atomic concentration of an element).

(3) Metals can be recovered from ores, dust waste, and spent catalysts via complexation with organic ligands in nonaqueous solvents.

(4) The charging of solid particles in their interaction with the liquid reagent accelerates the process.

REFERENCES

1. Semchenko, V.V., Velikanova, L.N., Khentov, V.Ya., and Pugovkina, E.V., *Bezopasnost' zhiznedeyatel'nosti, okhrana truda i okruzhayushchei sredy: Mezhvuzovskii sbornik* (Safety of Life Activities, Labor and Environment Protection: Intercollegiate Coll.), Rostov-on-Don: Rostov. Gos. Akad. Sel'khozmashinostroeniya, 1998, issue 2, pp. 76–77.
2. Khentov, V.Ya., Lipkina, T.V., Lipkin, M.S., et al., *Izv. Vyssh. Uchebn. Zaved., Sev.-Kavk. Reg., Tekh. Nauki*, 2001, no. 4, pp. 97–100.
3. Lipkina, T.V., Use of Nonaqueous Solutions Based on Dimethylformamide in Electrodeposition of Metals and Synthesis of Thin-Film Sulfide Materials, *Cand. Sci. Dissertation*, Novocherkassk, 2002.
4. Khentov, V.Ya., Semchenko, V.V., and Velikanova, L.N., *Izv. Vyssh. Uchebn. Zaved., Sev.-Kavk. Reg., Tekh. Nauki*, 1998, no. 3, pp. 78–80.
5. Khentov, V.Ya., Velikanova, L.N., and Semchenko, V.V., *Izv. Vyssh. Uchebn. Zaved., Sev.-Kavk. Reg., Tekh. Nauki*, 1998, no. 2, pp. 55–58.
6. *Neorganicheskaya khimiya* (Inorganic Chemistry), Tret'yakov, Yu.D., Ed., Moscow: Akademiya, 2004, vol. 1.
7. Kittel, Ch., *Introduction to Solid State Physics*, New York: Wiley, 1971.
8. Missol, V., *Energia powierzchni rozdzialu faz w metalach*, Katowice: Šlask, 1974.

ISSN 1070-4272, Russian Journal of Applied Chemistry, 2007, Vol. 80, No. 7, pp. 1032–1035. © Pleiades Publishing, Ltd., 2007.
Original Russian Text © E.M. Bayan, T.G. Lupeiko, M.O. Gorbunova, 2007, published in Zhurnal Prikladnoi Khimii, 2007, Vol. 80, No. 7, pp. 1063–1066.

INORGANIC SYNTHESIS AND INDUSTRIAL INORGANIC CHEMISTRY

Interaction of a Carbonate-Containing Reagent with Heavy Metal Ions in Aqueous Solutions

E. M. Bayan, T. G. Lupeiko, and M. O. Gorbunova

Rostov State University, Rostov-on-Don, Russia

Received December 19, 2006; in final form, March 2007

Abstract—Results of interaction of a carbonate-containing water-treatment waste with ions of copper(II), zinc(II), nickel(II), iron(III), and chromium(III) in aqueous solutions are compared.

DOI: 10.1134/S1070427207070026

Modern domestic and foreign technologies for wastewater treatment can provide virtually any required degree of purification, with the economical feasibility of the corresponding methods acquiring primary importance. Of particular interest are low-cost techniques of wastewater treatment. A promising method of this kind is that using water-treatment waste.

Preliminary studies with waste formed in water treatment at a thermal power plant have shown that this material can efficiently remove quite a number of heavy metal ions [1–5]. An analysis of the waste has demonstrated that it is mainly composed of calcium and magnesium carbonates, is homogeneous and finely dispersed, has a comparatively constant composition, and is safe in chemical and radiation regards [6].

In this study, we made a comparative analysis of the results of interaction between this carbonate-containing reagent (CCR) and aqueous solutions of Fe(III), Cr(III), Cu(II), Zn(II), and Ni(II) heavy metal (HM) ions most frequently occurring in wastewater.

EXPERIMENTAL

We studied processes of recovery of HM ions with CCR as follows: a weighed portion of CCR with a particle size of 0.25–0.50 mm was added to 100 ml of a solution being purified, with a prescribed concentration c_{in} (mg l^{-1}) of a metal ion, and the mixture was vigorously agitated for a time τ (min). After that the solutions were filtered. The pH value and the concentration of metal ions in solution were measured before and after contact with the reagent. The degree of recovery of metal ions, DR (%), and the amount of a metal per gram of the reagent, A (mg g^{-1}), were calculated from the difference of the initial and residual concentrations.

The concentration of HM in solution was determined spectrophotometrically by the commonly accepted techniques [7]. The optical density was measured on a KFK-2MP photometer with an error not exceeding 5%. The pH value of the solutions was monitored potentiometrically with an I-120M ion meter with an accuracy as good as ± 0.05 pH units. The phase composition of the starting waste and solid phases obtained in purification was determined by X-ray diffraction analysis on a DRON-2 installation with CuK_α radiation.

We used as starting solutions those with HM concentrations of 50 and 100 mg l^{-1}, typical of wastewater.

The results of our experimental study of recovery of HM ions are listed in Table 1 and shown in Figs. 1 and 2 in relation to time.

The carbonate-containing reagent is based on calcium and magnesium carbonates and just these compounds apparently determine the nature of the interaction between CCR and solutions containing heavy metal ions. Because of the hydrolysis of the carbonate phases, the pH value of an aqueous solution of CCR (CCR : water = 1 : 5) is 8.7 [1]. Therefore, this solution acts as a "soft" neutralizer of acid HM solutions. In this case, the possible final product of HM precipitation is the hydroxide of the corresponding metal.

To achieve virtually complete recovery of metal ions from acidic aqueous solutions in the form of

Table 1. CCR activity in relation to the time of contact with a solution being purified. CCR added in an amount of 1 g l^{-1}

Time of contact, h	A, mg g^{-1}				
	Fe^{3+}	Cr^{3+}	Cu^{2+}	Zn^{2+}	Ni^{2+}
Concentration of starting solutions 50 mg l^{-1}					
0.05	48.7	46.8	2.7	2.7	0.1
0.12	50.0	48.2	4.5	3.5	0.1
0.4	–	49.7	10.2	8.6	0.8
0.5	–	50.0	17.8	15.7	1.8
1	–	–	32.8	29.5	4.2
6	–	–	42.7	41.1	8.0
12	–	–	47.1	45.4	8.4
24	–	–	48.4	47.2	8.6
48	–	–	49.2	48.3	9.0
72	–	–	49.7	49.4	9.6
Concentration of starting solutions 100 mg l^{-1}					
0.25	100.0	89.5	13.6	12.4	1.3
0.5	–	96.2	32.8	28.5	3.1
1	–	100.0	59.6	52.6	6.7
6	–	–	79.4	76.5	13.7
12	–	–	83.7	83.5	14.1
24	–	–	90.7	88.3	14.4
48	–	–	94.5	90.6	15.1
72	–	–	99.3	92.7	15.5

Table 2. pH of precipitation of metal hydroxides

Hydroxide	pH		
	precipitation onset	virtually complete precipitation*	precipitate dissolution onset
$Fe(OH)_3$	2.3	4.1	14.0
$Cr(OH)_3$	4.7	6.8	9.4
$Cu(OH)_2$	6.2	7.1	14.0
$Zn(OH)_2$	6.4	8.0	10.5
$Ni(OH)_2$	7.7	9.5	13.2

* Residual metal concentration is lower than 10^{-6} M.

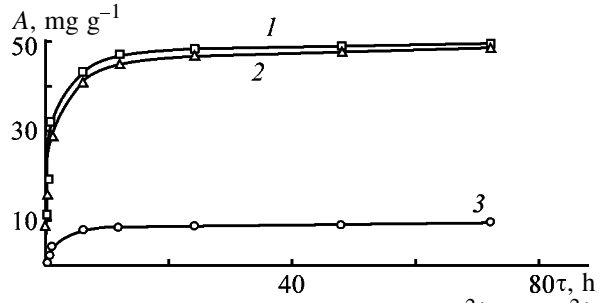

Fig. 1. CCR activity A vs. time τ for (*1*) Cu^{2+}, (*2*) Zn^{2+}, and (*3*) Ni^{2+} ions in purification of solutions containing 50 mg l^{-1} metal ions. CCR added in an amount of 1 g l^{-1}; the same for Fig. 2.

poorly soluble hydroxides, it is necessary to use a definite range of pH values (Table 2) [8]. Taking into account the pH values for a CCR solution, we expect that it can be used for efficient treatment of aqueous solutions to remove Fe^{3+}, Cr^{3+}, Cu^{2+}, Zn^{2+}, and Ni^{2+} ions. In this case, we can predict a number of specific features of the processes that occur with CCR as a precipitating agent. For example, it is apparent that the pH value at which precipitated hydroxides of these metals dissolve is not reached when CCR is used. This precludes "return" of metal ions into solution in the case of an overdose of the reagent.

However, the interaction of the carbonate-containing reagent with HM solutions may involve, in addition to "pure" hydrolysis, also other concurrent processes yielding, together with hydroxides, other poorly soluble compounds. Their solubility products (SP) are as follows: $SP_{MgCO_3} = 2.1 \times 10^{-5}$, $SP_{CaCO_3} = 3.8 \times 10^{-9}$, $SP_{ZnCO_3} = 1.45 \times 10^{-11}$, $SP_{CuCO_3} = 2.5 \times 10^{-10}$, and $SP_{NiCO_3} = 6.6 \times 10^{-9}$ [7], and, consequently, the interaction of CCR with aqueous solutions of these HM may involve an exchange interaction of calcium and magnesium carbonates to give zinc, copper, and nickel carbonates.

In the case of the Cu(II) ion, a basic carbonate of the type $Cu_2(OH)_2CO_3$ may precipitate together with the carbonate, by analogy with the malachite mineral widely occurring in nature, for which the solubility product is 1.7×10^{-34}. Probably, formation of basic carbonates is also possible for the Zn^{2+} and Ni^{2+} ions; however, no reliable data on the structure and solubility products of phases formed in this case can be found in reference books.

In addition to these compounds, mixed carbonates with anions from solution (e.g., Cl^-, SO_4^{2-}) and poorly soluble sulfates (in purification of sulfate solutions) can be formed and other reactions may occur between

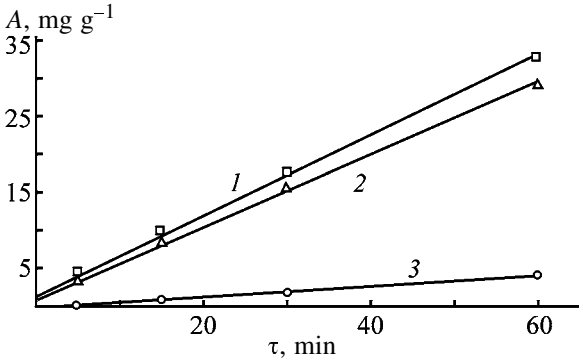

Fig. 2. CCR activity A vs. time τ for (*1*) Cu^{2+}, (*2*) Zn^{2+}, and (*3*) Ni^{2+} ions in the τ range 0–60 min in purification of solutions containing 50 mg l^{-1} metal ions.

CCR components and ions from a solution being purified [1].

The removal of heavy metal ions from solutions with the use of CCR can be represented as a set of the following possible schematic reactions.

Partial dissolution of the carbonate components of CCR to give hydroxy anions:

$$CO_3^{2-} + H_2O \rightleftarrows HCO_3^- + OH^-. \quad (1)$$

Mutual enhancement of the hydrolysis of HM salts and carbonates from CCR, to the point of carbon dioxide evolution and precipitation of poorly soluble HM hydroxides:

$$HCO_3^- + H_2O \rightarrow OH^- + H_2CO_3,\ H_2CO_3 \rightarrow H_2O + CO_2 \quad (2)$$

$$M^{n+} + nHOH \rightarrow M(OH)_n\downarrow + nH^+,\ n = 2, 3. \quad (2)$$

Formation of poorly soluble copper, zinc, and nickel carbonates:

$$CaCO_3(s) + M^{2+} \rightarrow MCO_3(s) + Ca^{2+}. \quad (3)$$

Formation of poorly soluble basic carbonates (in the case of Cu^{2+}, Zn^{2+}, Ni^{2+}):

$$CaCO_3(s) + 2M^{2+} + 2HOH \rightarrow M_2(OH)_2CO_3(s) + Ca^{2+} + 2H^+. \quad (4)$$

Formation of mixed carbonates, with anions from solution possibly involved, e.g.:

$$CaCO_3(s) + 2M^{2+} + 2Cl^- \rightarrow M_2(CO_3)Cl_2(s) + Ca^{2+}. \quad (5)$$

Other side reactions of the CCR components with ions from a solution being purified, e.g., gypsum formation from the carbonate-containing component itself is possible in the case of high-concentration sulfate solutions:

$$CaCO_3(s) + SO_4^{2-} + 5H_2O \rightarrow CaSO_4 \cdot 5H_2O(s) + CO_3^{2-}. \quad (6)$$

Reactions (2)–(6) can occur in parallel in the initial period to give a nonequilibrium mixture of poorly soluble products. This process of initial precipitation from solutions occurs rather rapidly. The composition of the products obtained is primarily determined by the SP of the possible poorly soluble reaction products, with the product with a lower SP predominant in the precipitate composition.

Further conversion of the initial mixture into an equilibrium solid phase will consist in dissolution of mixture components having lower SP and in crystallization of those with higher SP. This process will occur at a considerably lower rate, compared with the processes of the first stage.

Thus, the time in which the precipitation of HM with CCR is complete and the final products of their interaction may widely vary from one HM to another.

It can be seen from the results of our study (Table 1) that the precipitation of Fe(III) and Cr(III) compounds from solutions is fast. Fe(III) compounds are virtually completely precipitated from starting solutions with concentrations of 50 and 100 mg l^{-1} in 5 and 15 min, respectively. For Cr(III), these times are 30 and 60 min, respectively.

In these processes, CCR acts as a neutralizing agent and precipitates iron(III) and chromium(III) ions in the form of hydroxide phases (aqua hydroxo complexes).

The hydroxide phases of iron(III) and chromium(III) are poorly soluble and have solubility products ($SP_{Fe(OH)_3} = 6.3 \times 10^{-38}$, $SP_{Cr(OH)_3} = 6.3 \times 10^{-31}$) many orders of magnitude lower than those of the other possible phases. Therefore, virtually no parallel formation of other phases occurs in the interaction of CCR with solutions of iron and chromium salts. Thereby, the subsequent slow processes of mutual transformation of the coprecipitated phases are automatically precluded. Presumably, the somewhat longer time required for the completion of chromium(III) precipitation, compared with precipitation of iron(III), can be attributed to the SP ratio of their hydroxides. As a result, diffusion of ions to and from the CCR surface is the rate-determining stage of the precipitation of hydroxide phases in these systems. Because the precipitation occurs under vigorous stirring, the diffusion rate is rather high and iron(III) and chromium(III) compounds are precipitated in several minutes.

As an indirect confirmation of the mechanism of this kind serve, in the case of iron(III) and chromium(III) ions, X-ray diffraction data. The following phases: $CaCO_3$ (calcite), $MgCO_3 \cdot 3H_2O$, and β-, γ-$Fe_2O_3 \cdot H_2O$, present in the starting reagent (CCR) [1], were found in samples of a precipitate obtained upon solution purification. It should also be noted that a strong background is present in X-ray diffraction patterns, which indicates that amorphous noncrystallized phases are present in the samples.

At the same time, the processes occurring in the case of copper, zinc, and, especially, nickel ions

require a substantially longer time for completion. The difference of copper, zinc, and nickel precipitation processes from those for triply charged metal ions presumably consists in that, in the latter, the precipitation of hydroxide phase is accompanied by concurrent precipitation and subsequent mutual conversion of hydroxide, hydroxo carbonate, carbonate, and other solid phases. The conversion of one solid phase into another is a prolonged process, and, in all probability, just this process is the rate-determining stage in the given case. This explanation is supported by the fact that the solubility products of the hydroxide phases of copper, zinc, and nickel ($SP_{Cu(OH)_2} = 5.6 \times 10^{-20}$, $SP_{Zn(OH)_2} = 4.6 \times 10^{-16}$, $SP_{Ni(OH)_2} = 1.6 \times 10^{-14}$) markedly exceed those of iron(III) and chromium(III) hydroxides. Therefore, formation of other solid phases, in addition to the hydroxide phases, is quite possible in these systems.

CONCLUSIONS

(1) The processes of interaction of a carbonate-containing reagent with copper(II), zinc(II), nickel(II), iron(III), and chromium(III) ions in aqueous solutions were compared and it was demonstrated that the metals can be ranked in the order of decreasing precipitation rate as follows: $Fe^{3+} > Cr^{3+} > Cu^{2+} > Zn^{2+} > Ni^{2+}$.

(2) The main, and the only in the case of iron(III) and chromium(III) ions, process occurring in the precipitation of the ion group under study is the formation of poorly soluble aqua hydroxo complexes because of the mutual enhancement of hydrolysis. Also possible for copper, zinc, and nickel ions is, in addition to hydrolytic precipitation, exchange of calcium(II) and magnesium(II) ions from the carbonate-containing reagent in an aqueous solution for the corresponding doubly charged metal ion to give a less soluble carbonate. In addition to those mentioned above, mixed hydroxo carbonate phases, solid solutions, etc. can also be formed. Also, metal ions can adsorb on the surface of an undissolved reagent and on freshly formed particles.

(3) The results obtained in purification of solutions to remove heavy metal ions with a carbonate-containing reagent demonstrate that this method can be recommended for implementation at industrial plants producing acid wastewater and wastewater containing iron(III), chromium(III), zinc(II), and copper(II) ions.

REFERENCES

1. Lupeiko, T.G., Ivleva, T.I., and Solov'ev, L.A., *Zh. Prikl. Khim.*, 2001, vol. 74, no. 4, pp. 567–570.
2. Lupeiko, T.G., Gorbunova, M.O., and Bayan, E.M., *Zh. Prikl. Khim.*, 2001, vol. 74, no. 10, pp. 1648–1650.
3. Lupeiko, T.G., Gorbunova, M.O., and Bayan, E.M., *Zh. Prikl. Khim.*, 2004, vol. 77, no. 1, pp. 83–86.
4. Lupeiko, T.G., Gorbunova, M.O., and Bayan, E.M., *Zh. Prikl. Khim.*, 2004, vol. 77, no. 1, pp. 87–91.
5. Lupeiko, T.G., Gorbunova, M.O., and Bayan, E.M., *Zh. Prikl. Khim.*, 2005, vol. 78, no. 9, pp. 1482–1486.
6. Lupeiko, T.G., Bayan, E.M., Gorbunova, M.O., and Tsapkova, N.N., *Izv. Vyssh. Uchebn. Zaved., Sev.-Kavk. Reg., Estestv. Nauki*, 2003, supplement, no. 3, pp. 75–79.
7. Lur'e, Yu.Yu., *Analiticheskaya khimiya promyshlennykh stochnykh vod* (Analytical Chemistry of Industrial Wastewater), Moscow: Khimiya, 1984.
8. Lur'e, Yu.Yu., *Spravochnik po analiticheskoi khimii* (Handbook of Analytical Chemistry), Moscow: Khimiya, 1989.

ISSN 1070-4272, Russian Journal of Applied Chemistry, 2007, Vol. 80, No. 7, pp. 1036–1039. © Pleiades Publishing, Ltd., 2007.
Original Russian Text © L.E. Pustovaya, 2007, published in Zhurnal Prikladnoi Khimii, 2007, Vol. 80, No. 7, pp. 1067–1070.

INORGANIC SYNTHESIS AND INDUSTRIAL INORGANIC CHEMISTRY

Optimization of the Process for Synthesis of a Ceramics Based on Lead Ferroniobate

L. E. Pustovaya

Don State Technical University, Rostov-on-Don, Russia

Received October 30, 2006; in final form, January 2007

Abstract—Microstructure, phase transitions, and electrical properties of a ceramics based on lead ferroniobate were considered. The possibility of optimizing the process for synthesis of this ceramics by using a glass-forming additive of lithium carbonate in synthesis via an intermediate phase with a columbite structure in order to provide steadily high pyroelectric properties was analyzed.

DOI: 10.1134/S1070427207070038

It is known that lead ferroniobate $PbFe_{0.5}Nb_{0.5}O_3$ (LFN) is an antiferromagnetic and a ferroelectric with a perovskite structure and exhibits a ferroelectric phase transition with a Curie temperature of 385 K and a transition into a state with magnetic ordering with a Néel temperature of 143 K. As a result, its activity is manifested in posistor, magnetoresistive, ferroelectric, and relaxor properties. The interest in materials based on LFN is due to its multifunctionality [5, 6]. However, the pyroelectric properties of this material have not been examined despite the large number of varied-purpose studies; the occurrence of the $R3m \rightarrow R3c$ phase transition in the ferroelectric range has not been confirmed, either. This circumstance can be attributed to shortcomings of the procedure for synthesis of lead ferroniobate, which result in its high conductivity and dielectric loss tangent and thereby preclude any detailed electrical studies.

EXPERIMENTAL

We chose as object of study the ceramics of the composition: $PbFe_{0.5}Nb_{0.5}O_3$ (LFN); $PbFe_{0.5}Nb_{0.5}O_3$–1 wt % Li_2CO_3, (LFN–Li); $(1 - x)PbFe_{0.5}Nb_{0.5}O_3$–$xPbTiO_3$, where $0.04 < x < 0.09$ mol % (LFN–Ti); $(1 - x)PbFe_{0.5}Nb_{0.5}O_3$–$xPbTiO_3$–1 wt % Li_2CO_3, where $0.02 < x < 0.1$ mol % (LFN–Ti–Li); $(1 - x)PbFe_{0.5}Nb_{0.5}O_3$–$xPbZrO_3$–1 wt % Li_2CO_3, where $0.1 < x < 0.35$ mol % (LFN–Zr–Li). The ceramics was synthesized in the following ways.

(1) Conventional solid-phase technique with varied degree of grinding (grinding time 2, 6, and 24 h).

(2) "Columbite" technique, which consists in that the synthesis is performed via an intermediate phase with a columbite structure:

$$Fe_2O_3 + Nb_2O_5 \rightarrow 2FeNbO_4,$$

$$2PbO + FeNbO_4 \rightarrow Pb_2FeNbO_6.$$

(3) "Semiceramic" method, in which various compounds are precipitated from solutions onto solid oxides, hydroxides, or carbonates of metals, preliminarily suspended in these solutions. In this study, niobium oxide and stoichiometric amounts of iron and lead hydroxides, precipitated with an ammonia solution from solutions of respective salts, served as starting substances.

(4) Hot compaction method. The synthesis was performed in two stages: (i) for 2 h at 700°C and (ii) for 2 h after regrinding (800°C); sintering was carried out at 1100°C for 2 h. The hot compaction was done at 800°C under a pressure of 150 kg cm^{-2} for 40 min.

The materials synthesized were subjected to X-ray diffraction analysis on a DRON-3M diffractometer (U = 35 kV, I = 36 mA) with filtered CuK_α radiation.

The microstructure was studied on polished surfaces with an MI-2E optical microscope. The fine structure of the material was determined with an EVM-100B transmission electron microscope by the method of single-step platinum–carbon replicas [7–9].

Temperature dependences of the pyroelectric constant were studied by the dynamic pyroelectric effect method [10–12].

A microstructural study of the pore distribution demonstrated that addition of lead zirconate or titanate to the LFN ceramics markedly impairs the course of sintering. The number of pores per unit area increases.

Microstructural studies of the LFN ceramics modified with 1 wt % Li_2CO_3 revealed trace amounts of a liquid phase formed at the sintering temperatures (Fig. 1). This phase forms rather thick (up to 0.5 μm) smooth films at grain boundaries and separate grains of the same type at joints between the grains of the main phase. All these facts indicate that the liquid phase is involved in sintering processes: it executes a transport function and facilitates diffusion processes.

The domain structure of the LFN–Li ceramics (Fig. 2) has the form conventional for the rhombohedral symmetry, i.e., it is represented by series of 70(110)-degree domains arranged in two of the eight crystallographic directions possible for rhombohedral modifications. The width of domains in a series is in the range from 0.03–0.05 to 0.1–0.2 μm. The domains have a lamellar shape, their wedging-out frequently occurs along their length. A typical phenomenon is splitting of the domains into thinner wedges. There occur structures of the 180-degree type in the form of arbitrary configurations crossing the 70(110)-degree boundaries.

The LFN ceramics synthesized by the same methods and under the same sintering conditions, but not modified with Li_2CO_3 has high porosity, which is occasionally of the through type because of the connected pores, which hinders studies of both the microstructure (different degrees of recrystallization give no way of selecting an efficient etching mode for all grains) and the electrical properties because of the impossibility of high-quality polarization.

We also examined the effect of stock dispersity on the microstructure and properties of the resulting ceramics. The ceramics obtained from a stock synthesized by methods 2–4 has a homogeneous finely grained structure with grain sizes of 0.1–1.5 μm and uniformly distributed low porosity. In the ceramics obtained from a stock synthesized by method 1 at different degrees of grinding (10–40, 6–10, and <1 μm for 2, 6, and 24 h of grinding, respectively), the grains are coarser (10, 1–5, and 0.5–1.5 μm). Simultaneously, the pores become coarser and their distribution density decreases. On the whole, the granular structure is comparatively homogeneous; however, the pore distribution type reveals a tendency toward development of secondary recrystallization areas, well seen from the distribution of pores and from their sparseness and rejection to the periphery of these areas.

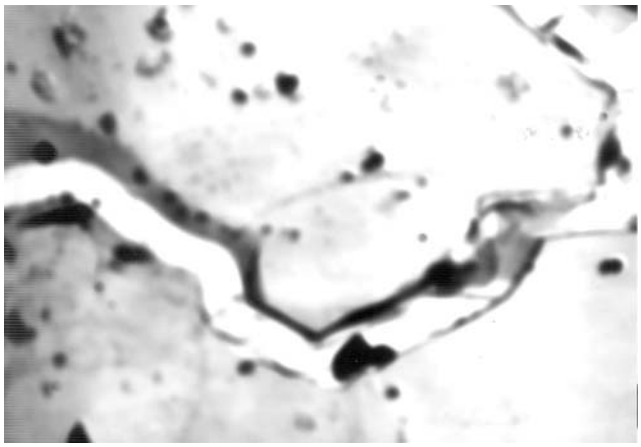

Fig. 1. Film of the glassy phase at grain boundaries in the LFN–Li ceramics. Magnification 16000.

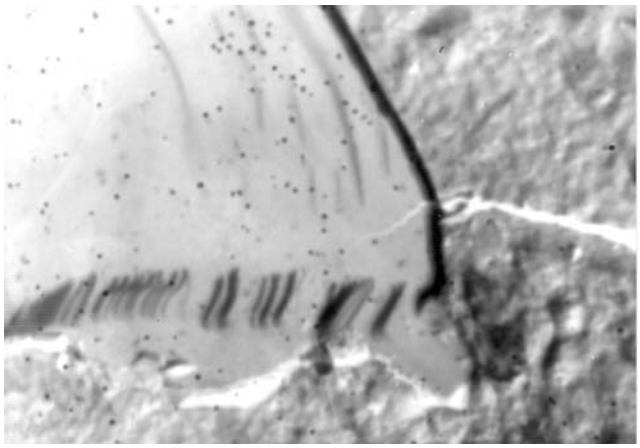

Fig. 2. Domain structure of the LFN–Li ceramics. Magnification 16500.

The ceramics sintered from a stock ground for 2 h (~10 μm) is markedly inhomogeneous and has a coarse-grained structure and a porosity of up to 15–20%. Analysis of the results obtained shows that diffusion processes are combined here, as a driving force of sintering, with interphase processes of dissolution and recrystallization. This is confirmed by the presence of growth steps on the surface of grains of the coarse-porous ceramic (Fig. 3).

Based on the results of X-ray diffraction analyses, we found the unit cell parameters for LFN with 1 wt % Li_2CO_3: a = 4.016 Å and α = 89°54′.

We studied hysteresis loops, from which we determined the residual polarization P_s and coercive field E_c (see table). The table also lists Curie temperatures T_C, dielectric constants ($\varepsilon^{sol}/\varepsilon_0$), dielectric loss tangent $\tan\delta$, and dynamic pyroelectric constant γ_d. The most pronounced pyroelectric properties are ob-

Electrical properties of ceramics based on lead ferroniobate, synthesized by the columbite method

Material	$\varepsilon^{sol}/\varepsilon_0$	$\tan\delta$	T_C, °C	$\gamma_d \times 10^{-4}$, C m^{-2} K^{-1}	$P_s \times 10^{-6}$, C cm^{-2}	E_c, kV cm^{-1}
LFN–Li	1500	0.02	118	15	6	0.63
(1 – *x*)LFN–*x*Ti, *x*, mol %:						
0.04	1750	0.016	122	5.4		
0.06	2200	0.011	126	13	5.8	0.8
0.07	2700	0.016	130	3.8		
0.09	2800	0.025	135	3.8		
(1 – *x*)LFN–*x*Ti–Li, *x*, mol %:						
0.02	2000	0.025	139	7.2		
0.04	2700	0.03	150	7.2	6	0.78
0.06	3200	0.03	155	10		
0.08	3800	0.025	160	7		
0.1	4300	0.025	170	5		
(1 – *x*)LFN–*x*Zr–Li, *x*, mol %:						
0.10	1120	0.03	145	5		
0.15	940	0.025	154	4.6		
0.20	770	0.025	167	4.4	5	0.5
0.25	520	0.02	183	4.4		
0.30	500	0.02	196	4.5		
0.35	370	0.02	207	3.9		

served for the ceramics synthesized by the columbite method with addition of Li_2CO_3. An analysis of the hysteresis loops demonstrated that the reason for the poorer pyroelectric properties of the other types of the LFN ceramics is their high electrical conductivity, especially for the ceramics produced by methods 3 and 4, rather than presence of phases having a cubic symmetry.

The table shows that the ways in which the dielectric constant varies in modification of the lead ferroniobate ceramics with lead titanate and zirconate are different. Upon introduction of titanium ions, the dielectric constant and the Curie temperature substantially increase, which is presumably due to approach to the morphotropic region of the phase transition to the tetragonal symmetry. Addition of zirconium ions leads to a gradual decrease in the dielectric constant and T_C, which indicates that no phase transformations occur in the $PbZrO_3$ concentration range studied. We can also note a significant decrease in the pyroelectric constant at T = 20°C upon LFN–Li modification with lead zirconate, with an increase in the content of the additive having only slight effect on this coefficient. We found that the LFN–Ti–Li and LFN–Zr–Li ceramics have very low coercive field energies, which makes them promising for use in a number of electronic devices.

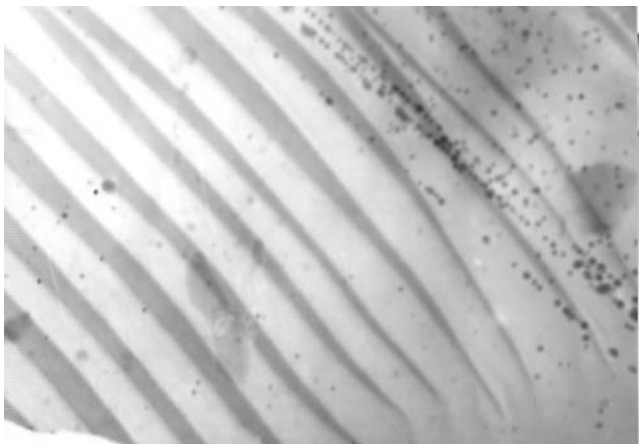

Fig. 3. Growth steps in the LFN–Li ceramics. Magnification 21 000.

We observed no visible anomalies in the temperature dependences of the conductance (*G*–*T*) and capacitance (*C*–*T*) for the materials under study. The temperature dependences of the dynamic pyroelectric constant (γ_d–*T*) and discharge current (*i*–*T*) of the LFN–Li ceramics (Fig. 4) show two distinct peaks: the first at around 97°C, which corresponds to a transition from the low- to high-temperature rhombohedral phase ($R3m \rightarrow R3c$), and the second at 118°C, associated with a transition to the cubic

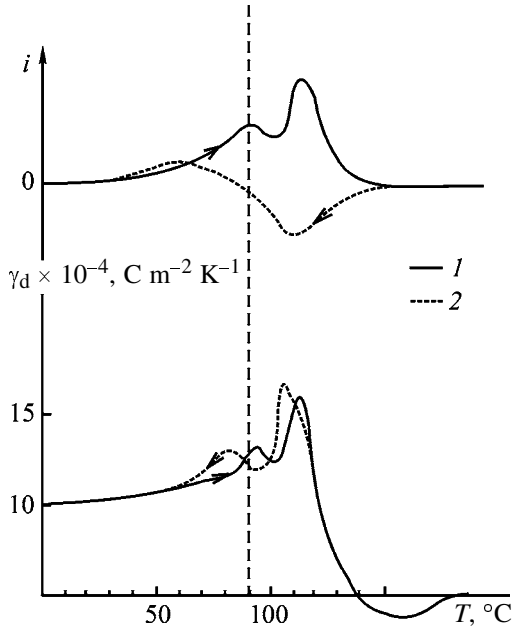

Fig. 4. γ_d and i vs. temperature T for the $PbFe_{0.5}Nb_{0.5}O_3$ + 1 wt % Li_2CO_3 ceramics. Curves: (*1*) heating and (*2*) cooling.

symmetry. The transition $R3m \rightarrow R3c$ is rather broad and shows a temperature hysteresis of approximately 10–15°C, which enables us to identify it as a second-order phase transition of the displacement type. The materials of the systems LFN–Ti, LFN–Ti–Li, and LFN–Zr–LI show in these temperature dependences only a single peak corresponding to a phase transition from the rhombohedral to the cubic crystal system.

We also observed for the LFN–Li ceramics a change in the sign of the γ_d–T dependence after passing the Curie point, which points to existence of fluctuation regions ("dipole glass"). The method of the dynamic pyroelectric effect enabled us to determine the existence range of complexes of this kind in the paraelectric phase.

CONCLUSIONS

(1) The optimal combination of pyro- and dielectric properties of a ceramics based on lead ferroniobate was provided by the columbite technology, with lithium carbonate used as a modifying additive.

(2) The method of the dynamic pyroelectric effect made it possible to determine the temperature ranges of existence of ferroelectric phases and of regions of a "dipole glass" in the paraelectric phase.

REFERENCES

1. Fesenko, E.G., Dantsiger, A.Ya., and Razumovskaya, O.N., *Novye p'ezokeramicheskie materialy* (New Piezoceramic Materials), Rostov-on-Don: Rostov Gos. Univ., 1983.
2. Fesenko, E.G., *Semeistvo perovskita i segnetoelektrichestvo* (Perovskite Family and Ferroelectricity), Moscow: Atomizdat, 1972, pp. 248–263.
3. Jaffe, B., Cook, B.W.R., Jr., and Jaffe, H., *Piezoelectric Ceramics*, London: Academic, 1971. Translated under the title *P'ezoelektricheskaya keramika*, Moscow: Mir, 1974, pp. 51–88.
4. Venevtsev, Yu.N., Politova, E.D., and Ivanov, S.A., *Segneto- i antisegnetoelektriki semeistva titanata bariya* (Ferro- and Antiferroelectrics of Barium Titanate Family), Moscow: Khimiya, 1985, p. 193.
5. Isupov, V.A., Agranovskaya, A.I., and Khuchua, N.P., *Izv. Akad. Nauk SSSR, Ser. Fiz.*, 1960, vol. 24, no. 10, pp. 1271–1274.
6. Bol'shakova, N.N., Chereshneva, N.N., and Rudyak, V.M., Abstracts of Papers, *Mezhdunarodnaya nauchno-tekhnicheskaya konferentsiya po fizike tverdykh dielektrikov* (Int. Scientific and Technical Conf. on Physics of Solid Insulators), St. Petersburg, 1997, vol. 2, p. 133.
7. Okazaki, K., *Ceramic Engineering for Dielectrics*, Tokyo: Gakkensya, 1969.
8. Budnikov, P.P. and Gistling, A.M., *Reaktsii v smesyakh tverdykh veshchestv* (Reactions in Solid Mixtures), Moscow: Stroiizdat, 1965, pp. 27–49.
9. Kingery, W.D., *Introduction to Ceramics*, New York: Wiley, 1960.
10. Pustovaya, L.E., Synthesis and Properties of Pyroelectric Materials Based on Lead Zirconate–Titanate and Ferroniobate, *Cand. Sci. Dissertation*, Rostov-on-Don, 1999.
11. Bogdanov, Ya.S., Zakharov, Yu.N., and Shpital'nik, B.Ts., Abstracts of Papers, *X Vsesoyuznaya konferentsiya po segnetoelektrichestvu i primeneniyu segnetoelektrikov v narodnom khozyaistve* (X All-Union Conf. on Ferroelectricity and Use of Ferroelectrics in National Economy), Minsk, 1982, part 2, p. 139.
12. Pustovaya, L.E., Zakharov, Yu.N., Raevski, I.P., et al., *Ferroelectrics*, 2000, vol. 247, nos. 1–3, pp. 47–52.

ISSN 1070-4272, Russian Journal of Applied Chemistry, 2007, Vol. 80, No. 7, pp. 1040–1044. © Pleiades Publishing, Ltd., 2007.
Original Russian Text © A.G. Morachevskii, E.Yu. Kolosova, L.Sh. Tsemekhman, L.B. Tsymbulov, 2007, published in Zhurnal Prikladnoi Khimii, 2007, Vol. 80, No. 7, pp. 1071–1075.

PHYSICOCHEMICAL STUDIES OF SYSTEMS AND PROCESSES

Application of Wilson's Method to the Calculation of Thermodynamic Properties of Liquid Ternary Metallic Systems from the Data on Boundary Binary Systems

A. G. Morachevskii, E. Yu. Kolosova, L. Sh. Tsemekhman, and L. B. Tsymbulov

St. Petersburg State Polytechnic University, St. Petersburg, Russia
Gipronikel' Institute, Limited Liability Company, St. Petersburg, Russia

Received May 4, 2007

Abstract—The possibility of applying Wilson's polynomial to the description of concentration dependences of thermodynamic functions in binary liquid metallic systems and to the calculation of thermodynamic properties of ternary systems from the data on boundary binary systems was considered.

DOI: 10.1134/S107042720707004X

At present, calculation methods based on the data on boundary binary systems are widely used to estimate integral thermodynamic functions of ternary and more complicated liquid metallic systems. Both integral values and activities of components in liquid alloys of the Ni–Fe–Co, Ni–Cu–Co, Ni–Cu–Fe, and Fe–Cu–Co systems were calculated in a series of studies aimed to simulate the thermodynamic functions of the Cu–Ni–Co–Fe system [1–6]. Numerous geometric models and a model based on Redlich–Kister's polynomial were used in these calculations. Irrespective of the model applied, the calculated integral thermodynamic functions, full and excess Gibbs energies ΔG and ΔG^{exc} and enthalpies of mixing ΔH, as a rule, agree fairly well with each other. All the models, both geometrical and polynomial, are based on the idea that the thermodynamic properties of ternary and more complicated liquid metallic systems are mainly determined by pair interactions of the components. Ternary interactions do not play an essential role. It is accepted that each binary system makes its independent contribution to the integral thermodynamic characteristic of the mixing process when a ternary or multicomponent system is formed. The difference between rather numerous geometric models consists only in the mode of considering contributions of each of the boundary binary systems. It should be noted that, when Redlich–Kister's polynomial for ternary systems is applied to liquid metal alloys, there is no need in considering coefficients calculated from the data related to the ternary system.

Experimental study of thermodynamic properties of the group of systems under consideration at high temperatures (1350–1600°C) is difficult, which restricts the possibility of direct comparison of the calculated and experimental data. Sufficiently reliable experimental data on thermodynamic properties of liquid alloys are available only for the Ni–Fe–Co [7] and Ni–Cu–Fe [8, 9] systems. In the study of both systems, mass-spectrometric analysis of the vapor phase with Knudsen's cell was applied. The calculations of the integral thermodynamic functions and activities of components in liquid alloys of the Ni–Fe–Co system at 1600°C [5, 10] are in very good agreement with the data of Tomiska [7]. The calculated activities of components in liquid alloys of the Cu–Ni–Fe system at 1350°C [2, 6] are close to the data of Pagador et al. [8, 9].

In studying two other metallic systems, Ni–Cu–Co [3] and Fe–Cu–Co [4], the only reliability criterion was the closeness of the thermodynamic properties calculated using six to eight different geometric models and the polynomial Redlich–Kister's method. Along with the calculation of integral values, the software tools provided an estimation of the corresponding partial quantities and the activity of each of liquid alloy components. This operation was based on the application of the Gibbs–Duhem equation to ternary and multicomponent systems by Darken's method [11].

$$\Delta G_1(x_1,x_2/x_3) = \Delta G(x_1,x_2/x_3) + (1 - x_1)(\partial\Delta G/\partial\Delta x_1)_{x_2/x_3},$$

$$\Delta G_1 = RT\ln a_1. \quad (1)$$

The activities of the two other components can be calculated similarly. The spline function method was used in the differentiation for the analytical representation of the dependence of an integral quantity on the composition along one or another cross section. The program provided also a possibility of estimating partial molar quantities and activities of each of ternary system components in the liquid state on the basis of the corresponding data for boundary binary systems without preliminary calculation of the integral quantities using expressions following from certain geometrical models (Toop's and Kohler's models). The same task can also be solved with the application of Redlich–Kister's polynomial.

As shown previously [12], Redlich–Kister's polynomial of form (2)

$$\Delta G_{12}^{\text{exc}}/RT = x_1x_2[b_{12} + c_{12}(x_1 - x_2) + d_{12}(x_1 - x_2)^2 + ...] \quad (2)$$

is well applicable to the description of the concentration dependences of the thermodynamic functions and to the estimation of the limiting activity values for the components γ_1^∞ and γ_2^∞ in liquid metallic systems with various types of interactions between components. It was shown by the example of a wide group of liquid alloys that the increase in degree of polynomial (2) over two, as a rule, does not appreciably affect the difference between the experimental value of ΔG^{exc} and the approximated value [13, 14]. In the case of a ternary system, Redlich–Kister's equation takes form (3).

$$\begin{aligned}\Delta G_{123}^{\text{exc}}/RT = {} & x_1x_2[b_{12} + c_{12}(x_1 - x_2) + d_{12}(x_1 - x_2)^2] \\ & + x_2x_3[b_{23} + c_{23}(x_2 - x_3) + d_{23}(x_2 - x_3)^2 \\ & + x_1x_3[b_{13} + c_{13}(x_2 - x_3) + d_{13}(x_1 - x_3)^2 \\ & + x_1x_2x_3[c_1 + d_1x_1 + d_2x_2]. \end{aligned} \quad (3)$$

As noted above, we may neglect the last term in the right part of Eq. (3) containing coefficients c_1, d_1, and d_2 determined from experimental data for a ternary system. Good agreement between the data calculated using Redlich–Kister's polynomial and the experimental data (3) was confirmed in the case of a series of ternary systems [5, 12, 15].

It seems reasonable to expand the number of polynomial models used for the description of concentration dependences of thermodynamic functions in liquid binary metallic systems and for the calculation of thermodynamic properties of ternary and more complicated systems. The polynomial expression offered by Wilson [16] and then modified by Orye and Prausnitz [17] is of interest in this respect. Wilson's equation is applicable to systems with organic components, has a small number of coefficients, and takes the following forms for components of a binary system and a system as a whole.

$$\ln\gamma_1 = -\ln(x_1 + \Lambda_{12}x_2) + x_2\left[\frac{\Lambda_{12}}{x_1 + \Lambda_{12}x_2} - \frac{\Lambda_{21}}{x_2 + \Lambda_{21}x_1}\right], \quad (4)$$

$$\ln\gamma_2 = -\ln(x_2 + \Lambda_{21}x_1) + x_1\left[\frac{\Lambda_{12}}{x_1 + \Lambda_{12}x_2} - \frac{\Lambda_{21}}{x_2 + \Lambda_{21}x_1}\right], \quad (5)$$

$$\Delta G^{\text{exc}} = RT[\ln(x_1 + \Lambda_{21}x_2) + \ln(x_2 + \Lambda_{21}x_1)]. \quad (6)$$

The coefficients Λ_{12} and Λ_{21} are estimated from the experimental values of γ_1 and γ_2 at several compositions, and for ideal systems $\Lambda_{12} = \Lambda_{21} = 1$. At x_1 (or x_2) tending to zero, the activity coefficients γ_1 (or γ_2) approach their limiting values (γ_1^∞ and γ_2^∞). The coefficients Λ_{12} and Λ_{21} are positive at any type of the deviation of a binary system from the ideal behavior and depend on temperature. It is noted in Turkdogan's monograph [18] that Wilson's polynomial well describes the concentration dependences of γ_1, γ_2, and ΔG^{exc} only when a system shows moderate deviations from the ideal behavior, and the best results are obtained at positive deviations.

Tarby and Stein [19] have applied Wilson's model to two liquid binary metallic systems (Cu–Fe, 1550°C; Fe–Ni, 1600°C). In the first system, positive deviations from the ideal behavior were observed, whereas the second system is close to ideal. The calculated activities of the components are close to the experimental data.

The application of certain polynomial expressions with small numbers of fitting coefficients to binary liquid metallic systems with various kinds of the interaction between components was discussed by Choi and Hucke [20]. They confirmed the fact that Wilson's equation better describes the concentration dependences of thermodynamic functions in systems with positive deviations from the ideal behavior.

In this study we consider the application of Wilson's polynomial to six liquid binary metallic systems at 1600°C: Cu–Fe, Cu–Co, Cu–Ni, Fe–Ni, Fe–Co, and Co–Ni. The accepted values of thermodynamic functions for these systems are based on the analysis

Table 1. Coefficients of Eqs. (4)–(6) and correlation coefficients r

System	Λ_{12}	Λ_{21}	r
Cu–Fe	0.2467	0.2195	0.9979
Cu–Co	0.3734	0.1746	0.9999
Cu–Ni	0.7196	0.2790	0.9984
Fe–Ni	0.2930	3.4138	0.9850
Fe–Co	0.2478	1.7444	0.9609
Co–Ni	1.0827	1.0821	0.9996

of the whole set of the corresponding experimental data. These values were used previously in the calculations of thermodynamic properties of ternary systems [2–6]. The resulting values of the coefficients Λ_{12} and Λ_{21} and the correlation coefficients are given in Table 1.

Table 2 shows that Eq. (6) well describes the concentration dependence of the integral molar excess Gibbs energy for all the six binary systems under

Table 2. Integral molar excess Gibbs energies of binary systems (I) recommended on the basis of experimental data (1600°C) and (II) described by Eq. (6)

x,* mole fraction	ΔG^{exc}, kJ mol^{-1}											
	I	II	I	II	I	II	I	II	I	II	I	II
	Cu–Fe		Cu–Co		Cu–Ni		Fe–Ni		Fe–Co		Co–Ni	
0.1	3.05	2.90	2.49	2.50	1.33	1.50	–1.41	–1.46	0.66	0.75	–0.22	–0.23
0.2	4.98	4.99	4.41	4.41	2.68	2.73	–2.40	–2.31	1.06	1.14	–0.40	–0.40
0.3	6.44	6.41	5.81	5.80	3.69	3.68	–2.93	–2.75	1.32	1.30	–0.52	–0.53
0.4	7.28	7.24	6.68	6.68	4.39	4.33	–3.02	–2.88	1.42	1.30	–0.60	–0.60
0.5	7.49	7.53	7.03	7.07	4.73	4.66	–2.76	–2.77	1.35	1.21	–0.63	–0.63
0.6	7.11	7.28	6.95	6.95	4.67	4.64	–2.33	–2.47	1.09	1.04	–0.61	–0.60
0.7	6.36	6.48	6.30	6.30	4.20	4.24	–1.80	–2.02	0.73	0.83	–0.53	–0.53
0.8	5.17	5.08	5.04	5.03	3.33	3.40	–1.25	–1.45	0.40	0.58	–0.41	–0.40
0.9	3.26	2.99	3.01	3.02	2.04	2.03	–0.66	–0.77	0.14	0.30	–0.23	–0.23

* x is the content of the component indicated first.

Table 3. Integral molar thermodynamic characteristics (1600°C) of ternary systems calculated by Wilson's method from the data on boundary binary systems

x_2,* mole fraction	ΔG^{exc}, kJ mol^{-1}	ΔH, kJ mol^{-1}	ΔG^{exc}, kJ mol^{-1}	ΔH, kJ mol^{-1}	ΔG^{exc}, kJ mol^{-1}	ΔH, kJ mol^{-1}
	$x_1 : x_3 = 1 : 3$		$x_1 : x_3 = 1 : 1$		$x_1 : x_3 = 3 : 1$	
			Ni–Cu–Fe			
0.2	2.92	3.55	1.53	0.97	1.18	0.16
0.4	5.43	6.01	4.09	3.71	3.53	2.66
0.6	5.97	6.15	4.94	4.53	4.39	3.61
0.8	4.40	4.23	3.85	3.43	3.48	2.87
			Ni–Cu–Co			
0.2	3.58	5.44	3.02	4.64	2.74	3.73
0.4	5.80	7.48	5.11	6.36	4.62	5.14
0.6	6.21	7.26	5.58	6.14	5.05	4.94
0.8	4.57	4.92	4.14	4.10	3.75	3.25
			Fe–Cu–Co			
0.2	5.39	5.50	5.53	5.69	5.33	7.26
0.4	7.31	7.90	7.46	7.92	7.40	8.61
0.6	7.25	7.79	7.35	7.67	7.34	7.50
0.8	5.08	5.36	5.10	5.19	5.10	5.18
			Ni–Fe–Co			
0.2	–0.01	–1.51	–0.95	–2.04	–1.08	–2.71
0.4	0.25	–2.08	–0.92	–2.74	–2.03	–3.48
0.6	0.17	–1.87	–0.71	–2.43	–1.55	–3.02
0.8	–0.02	–1.13	–0.44	–1.45	–0.86	–1.77

* x_2 is the content of the component indicated second.

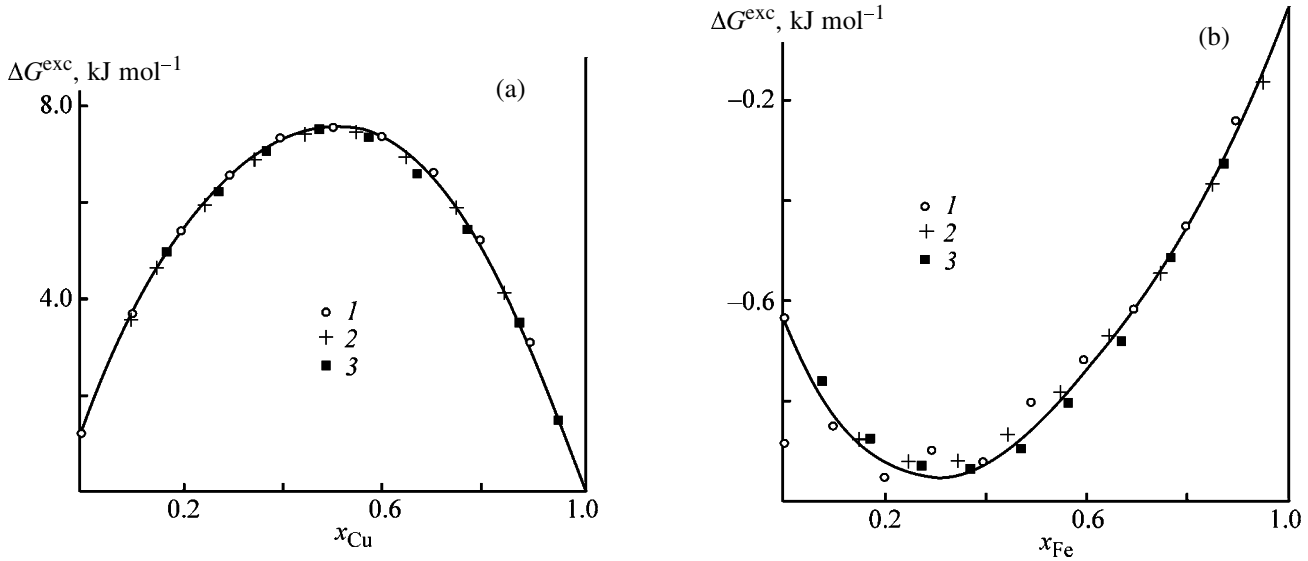

Fig. 1. Composition dependences of the integral molar excess Gibbs energy ΔG^{exc} for ternary systems (a) Fe–Cu–Co ($x_{Fe} : x_{Co}$ = 1 : 3) and (b) Ni–Fe–Co ($x_{Ni} : x_{Co}$ = 1 : 1) at 1600°C, calculated using (*1*) geometric models, (*2*) Redlich–Kister's method, and (*3*) Wilson's method; the same for Fig. 2.

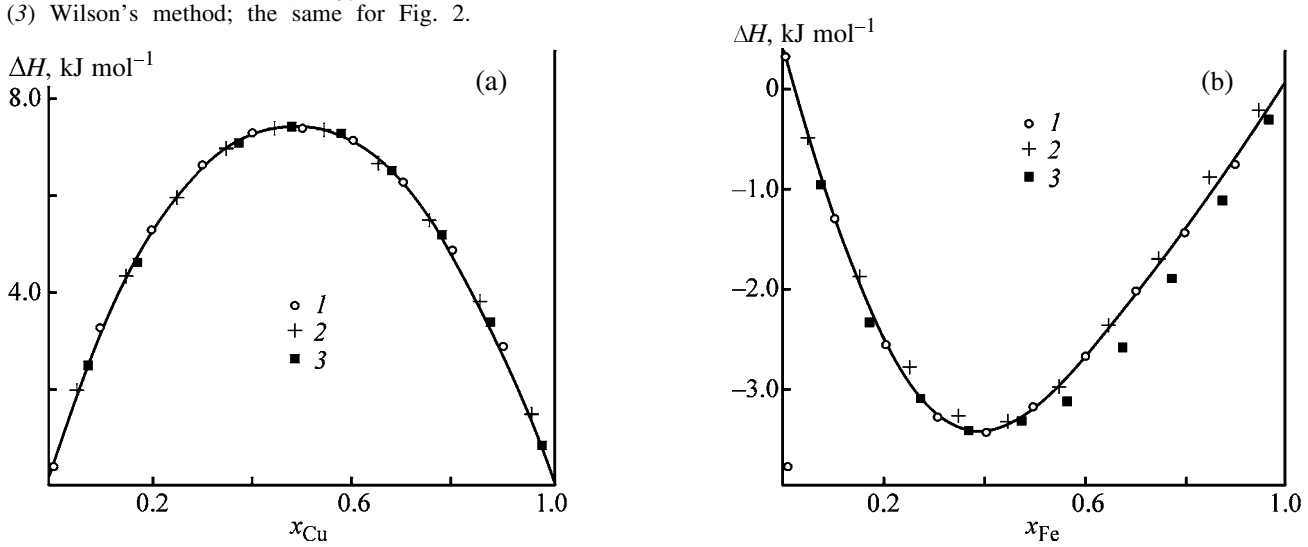

Fig. 2. Composition dependences of the integral molar enthalpy of mixing ΔH of ternary systems (a) Ni–Cu–Co ($x_{Ni} : x_{Co}$ = 1 : 3) and (b) Ni–Fe–Co ($x_{Ni} : x_{Co}$ = 3 : 1) at 1600°C.

consideration. According to [17], expression (7) based on Wilson's polynomial can be written for multicomponent systems:

$$\Delta G_{12}^{exc}/RT = -\sum_{i=1}^{n} x_i \ln\left[\sum_{j=1}^{n} x_j \Lambda_{ij}\right], \quad (7)$$

where ΔG^{exc} is the integral molar excess Gibbs energy of the system including n components, and Λ_{ij} are the positive fitting coefficients ($\Lambda_{ii} = \Lambda_{jj} = 1$).

A similar equation can be written also for the enthalpy of mixing of a multicomponent system.

The values of ΔG^{exc} and ΔH at 1600°C for four ternary systems under consideration, calculated on the basis of the data on boundary binary systems using Wilson's polynomials, are given in Table 3.

As noted above, the thermodynamic functions for this group of ternary systems were calculated previously from the data on boundary binary systems using a large number of geometric models (up to 6–8) and polynomial Redlich–Kister's method [2–6]. The results of the calculation of ΔG^{exc} and ΔH for certain cross sections of ternary systems based on geometric models (averaged values) and on Redlich–Kister's and Wilson's polynomials are compared with each other in Figs. 1 and 2. The agreement between these data can be considered as quite satisfactory.

CONCLUSIONS

(1) Wilson's polynomial method can be applied to the description of the concentration dependences of thermodynamic functions in liquid binary metallic systems with moderate deviations from the ideal behavior: Cu–Fe, Cu–Co, Cu–Ni, Fe–Ni, Fe–Co, and Co–Ni.

(2) The integral thermodynamic characteristics of mixing of liquid ternary systems Ni–Cu–Fe, Ni–Cu–Co, Fe–Cu–Co, and Ni–Fe–Co calculated using the data on boundary binary systems, certain geometric models, and Redlich–Kister's and Wilson's polynomial models agree with each other fairly well.

REFERENCES

1. Morachevskii, A.G., Kolosova, E.Yu., Tsymbulov, L.B., and Tsemekhman, L.Sh., *Zh. Fiz. Khim.*, 2006, vol. 80, no. 11, pp. 2006–2010.
2. Morachevskii, A.G., Tsymbulov, L.B., and Kolosova, E.Yu., *Zh. Prikl. Khim.*, 2004, vol. 77, no. 9, pp. 1438–1441.
3. Morachevskii, A.G., Tsymbulov, L.B., Kolosova E.Yu., and Tsemekhman, L.Sh., *Zh. Prikl. Khim.*, 2005, vol. 78, no. 1, pp. 59–65.
4. Morachevskii, A.G., Tsymbulov, L.B., Kolosova, E.Yu., and Tsemekhman, L.S., *Zh. Prikl. Khim.*, 2005, vol. 78, no. 7, pp. 1074–1079.
5. Morachevskii, A.G., Tsymbulov, L.B., Kolosova E.Yu., and Tsemekhman, L.Sh., *Zh. Prikl. Khim.*, 2005, vol. 78, no. 12, pp. 1963–1966.
6. Morachevskii, A.G., Kolosova, E.Yu., and Tsymbulov, L.B., *Zh. Prikl. Khim.*, 2006, vol. 79, no. 8, pp. 1379–1381.
7. Tomiska, J., *J. Alloys Comp.*, 2004, vol. 373, nos. 1–2, pp. 142–150.
8. Fujita, Y., Pagador, R.U., Hino, M., and Azakami, T., *J. Jpn. Inst. Met.*, 1997, vol. 61, no. 7, pp. 619–624.
9. Itagaki, K., Hino, M., Pagador, R.U., and Surapunt, S., *Ber. Bunsenges. Phys. Chem.*, 1998, vol. 102, no. 9, pp. 1304–1308.
10. Morachevskii, A.G., Ryabko, A.G., and Tsemekhman, L.Sh., *Termodinamika zhidkikh splavov sistemy nikel'–med'–kobal't* (Thermodynamics of Liquid Alloys of the Nickel–Copper–Cobalt System), St. Petersburg: Sankt-Peterb. Gos. Politekh. Univ., 2004.
11. Darken, L.S., *J. Am. Chem. Soc.*, 1950, vol. 72, no. 7, pp. 2009–2014.
12. Maiorova, E.A. and Morachevskii, A.G., *O primenenii metoda Redlikha–Kistera pri opisanii termodinamicheskikh svoistv zhidkikh splavov* (Application of Redlich–Kister's Method to the Description of Thermodynamic Properties of Liquid Alloys), Available from VINITI, Akad. Nauk SSSR, 1976, no. 724–76 Dep.
13. Morachevskii, A.G. and Erofeev, K.B., *Zh. Prikl. Khim.*, 1999, vol. 72, no. 11, pp. 1913–1914.
14. Erofeev, K.B., Computer Simulation of Thermodynamic Properties of Liquid Binary Alloys of Magnesium with Elements of Groups II–V of the Periodic System, *Cand. Sci. Dissertation*, St. Petersburg, 2005.
15. Morachevskii, A.G. and Gerasimenko, L.N., *Zh. Fiz. Khim.*, 1971, vol. 45, no. 8, pp. 1951–1953.
16. Wilson, G.M., *J. Am. Chem. Soc.*, 1964, vol. 86, no. 1, pp. 127–130.
17. Orye, R.V. and Prausnitz, J.M., *Ind. Eng. Chem.*, 1965, vol. 57, no. 5, pp. 18–26.
18. Turkdogan, E.T., *Fizicheskaya khimiya vysokotemperaturnykh protsessov* (Physical Chemistry of High-Temperature Processes), Moscow: Metallurgiya, 1985.
19. Tarby, S.K. and Stein, F.P., *Met. Trans.*, 1970, vol. 1, August, pp. 2354–2356.
20. Choi, S.-D. and Hucke, E.E., *CALPHAD*, 1990, vol. 14, no. 4, pp. 367–376.

ISSN 1070-4272, Russian Journal of Applied Chemistry, 2007, Vol. 80, No. 7, pp. 1045–1047. © Pleiades Publishing, Ltd., 2007.
Original Russian Text © Yu.A. Ferapontov, D.V. Zhdanov, M.A. Ul'yanova, 2007, published in Zhurnal Prikladnoi Khimii, 2007, Vol. 80, No. 7, pp. 1076–1078.

PHYSICOCHEMICAL STUDIES OF SYSTEMS AND PROCESSES

Physicochemical Properties of $KOH–H_2O_2–H_2O$ Solutions

Yu. A. Ferapontov, D. V. Zhdanov, and M. A. Ul'yanova

Roskhimzashchita Corporation, Open Joint-Stock Company, Tambov, Russia

Received October 30, 2006; in final form, March 2007

Abstract—Density, viscosity, and surface tension of $KOH–H_2O_2–H_2O$ solutions used to synthesize potassium superoxide in sprayer apparatus were studied with various relative amounts of the components in the temperature range 0–30°C. Analytical dependences of the above-mentioned quantities on temperature and solvent (water) content of the system were found.

DOI: 10.1134/S1070427207070051

Carrying out any process of chemical technology requires that the properties of the materials involved should be known. It has been found in the development of apparatus for a technological line for manufacture of potassium superoxide (KO_2) from hydrogen peroxide and potassium hydroxide in a sprayer apparatus [1–5] that most of physicochemical properties of the system $KOH–H_2O_2–H_2O$ (henceforth, an alkaline solution of hydrogen peroxide) for the ranges of interest of the concentrations of the starting components and temperatures cannot be found in the literature. As input data in calculations of spraying processes and apparatus serve those properties of a solution being dispersed, which determine the atomization spectrum of the nozzle employed. According to [6–10], these properties include the kinematic and dynamic viscosities, density, and surface tension. The reported [11] values of the dynamic viscosity and density of $KOH–H_2O_2–H_2O$ solutions lie outside the range of our interest, and, therefore, it was necessary to obtain the lacking experimental data.

EXPERIMENTAL

We prepared an alkaline solution of hydrogen peroxide by the previously described procedure [1–5, 12, 13] by mixing potassium hydroxide and hydrogen peroxide of various concentrations with the subsequent recalculation to the solvent (water) content of the solution. To preclude catalytic decomposition of peroxide products, we introduced magnesium sulfate as a stabilizing agent [14] into the alkaline hydrogen peroxide solutions under study. The molar ratios $H_2O_2/KOH = 1.7$ (at this ratio of the starting components, the final product obtained by the previously suggested technology contains the maximum amount of KO_2 [12]) and $MgSO_4 : H_2O_2 = 1/750$ remained the same for all of the solutions studied. The densities, viscosities, and surface tensions changed upon introduction of the stabilizing agent in the amount specified above within the experimental error. All the substances we used were of ultrapure grade.

The physicochemical properties of the solutions were studied in the temperature range 0–30°C at a solvent (water) content of 0.29 to 0.5 kg of water per 1 kg of a solution. We chose the water content as a criterial parameter in determining the density, viscosity, and surface tension in the system under study. This choice is due to the fact that it is the content of water to be removed from the reaction zone that is the dominant factor in further use of the data obtained in engineering calculations of apparatus for, and process parameters of potassium superoxide production in a sprayer apparatus. Recalculation of the density, viscosity, and surface tension of the solution under study as functions (as it is commonly accepted) of the contents of KOH and H_2O_2 in this solution, rigidly related by the molar ratio $H_2O_2/KOH = 1.7$, is not a complicated mathematical task.

The chosen range of variation of the temperature and the concentrations of the starting components is due to the economical feasibility of the process under study for synthesis of potassium superoxide, on the one hand, and to the possibility of mixing of the starting reagents without any significant loss of active oxygen by the system (temperature factor) at a high safety of the process, on the other hand [12, 13].

The density of the alkaline solution of hydrogen peroxide was determined pycnometrically with

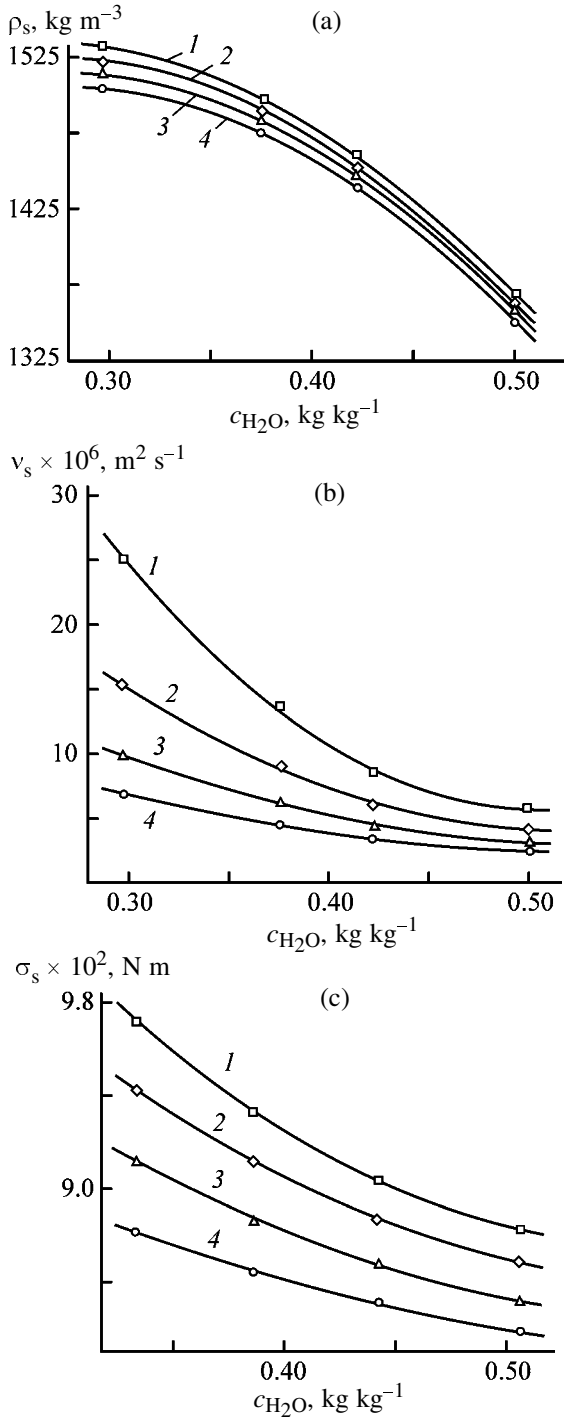

Fig. 1. (a) Density ρ_s, (b) kinematic viscosity ν_s, and (c) surface tension σ_s of an alkaline solution of hydrogen peroxide vs. the solvent concentration c_{H_2O}. Temperature, °C: (*1*) 0, (*2*) 10, (*3*) 20, and (*4*) 30.

an error not exceeding 0.3% [13]. The data obtained in determining the solution density, calculated as an arithmetic mean of the results of five parallel runs, are shown in Fig. 1a.

The experimental data are well described by a power series of the form

$$\rho_s = a_0 + a_1 c_{H_2O} + a_2 c_{H_2O}^2, \quad (1)$$

whose coefficients linearly depend on temperature:

$$a_0 = 1900.04 - 1.07878T_s, \quad (1a)$$

$$a_1 = 48.1161 + 5.44812T_s, \quad (1b)$$

$$a_2 = -1561.93 - 4.97642T_s. \quad (1c)$$

The maximum disagreement between the calculated and experimental densities did not exceed 1.2%.

We studied the kinematic viscosity of solution samples with a VPZh-2 glass capillary viscometer in conformity with GOST (State Standard) 33–66, using the results of the individual factory calibration of the viscometer. The required temperature was maintained by thermostating the viscometer within ±0.1°. The kinematic viscosity of the solution, ν_s, was found from the arithmetic-mean outflow time τ_{am} in five parallel runs by the formula

$$\nu_s = gk\tau_{am}/9.807, \quad (2)$$

where $g = 9.813$ m s^{-2} is the acceleration of gravity at the measurement site (Tambov), and $k = 3.136 \times 10^{-7}$ m^2 s^{-2} is the viscometer constant.

The results of an experimental study of the kinematic viscosity of the alkaline solution of hydrogen peroxide are shown in Fig. 1b as a family of isothermal curves.

For convenience of further use of the results of our study in engineering calculations, the dependence $\nu_s = f(c_{H_2O}, T_s)$ was represented in the analytical form as

$$\nu_s = 10^{-6}(a_0 + a_1 + a_1 c_{H_2O} + a_2 c_{H_2O}^2). \quad (3)$$

The coefficients a_0, a_1, and a_2 in expression (3) were calculated as functions of temperature by the formulas

$$a_0 = 9413.54 - 61.9307T_s + 0.10213T_s^2, \quad (3a)$$

$$a_1 = -38026.39 + 250.9153T_s - 0.4180T_s^2, \quad (3b)$$

$$a_2 = -39320.46 - 259.9735T_s + 0.43053T_s^2, \quad (3c)$$

where T_s is the solution temperature (K), and c_{H_2O} is the concentration of water in the solution (kg kg^{-1}).

The resulting approximating polynomial satisfactorily describes experimental data. The maximum

discrepancy between the calculated and experimental values does not exceed 2%.

The surface tension of the solution was determined by the method of the highest pressure in a bubble, developed by P.A. Rebinder [15]. The results obtained are shown in Fig. 1c and represented in the analytical form as

$$\sigma_s = a_0 + a_1 c_{H_2O} + a_2 c_{H_2O}^2, \quad (4)$$

$$a_0 = 49.6879 - 0.12943T_s, \quad (4a)$$

$$a_1 = -138.045 + 0.43386T_s, \quad (4b)$$

$$a_2 = 129.015 - 0.40980T_s. \quad (4c)$$

The maximum discrepancy between the calculated and experimental values of surface tension does not exceed 1.5%.

The coefficients in the functional dependences for density, kinematic viscosity, and surface tension were found using the least-squares method [16].

The results we obtained suggest that the density, viscosity, and surface tension increase as the solvent (water) content of the system under consideration becomes lower. This is in good agreement with the conclusions made by Loginov et al. [11], who studied these parameters of the KOH–H_2O_2–H_2O system in other temperature and concentration ranges.

CONCLUSIONS

(1) The density, viscosity, and surface tension of the KOH–H_2O_2–H_2O system were studied in the temperature range 0–30°C at a fixed molar ratio H_2O_2/KOH = 1.7 and various concentrations of the starting components (water content of 0.29 to 0.5 kg per 1 kg of solution). The results obtained were used to derive analytical dependences for these parameters. The dependences can be used to calculate apparatus and parameters of the process for synthesis of potassium superoxide from hydrogen peroxide and potassium hydroxide in a sprayer apparatus.

(2) Under the experimental conditions, the density, kinematic viscosity, and surface tension of an alkaline solution of hydrogen peroxide increase as the solvent (water) content of the system decreases.

ACKNOWLEDGMENTS

The study was supported by the Russian Foundation for Basic Research (project no. 07-08-12018).

REFERENCES

1. Ferapontov, Yu.A., Gladyshev, N.F., Simanenkov, S.I., et al., *Vestn. Tambov. Gos. Tekh. Univ.*, 2001, vol. 7, no. 3, pp. 422–434.
2. Ferapontov, Yu.A., Zhdanov, D.V., and Gladyshev, N.F., *Materialy XV Mezhdunarodnoi nauchnoi konferentsii "Matematicheskie metody v tekhnike i tekhnologiyakh"* (Proc. Int. Conf. "Mathematical Methods in Technology"), Tambov, 2002, vol. 3, pp. 161–166.
3. RF Patent 2210416.
4. Zhdanov, D.V., Ferapontov, Yu.A., and Ul'yanova, M.A., *Zh. Prikl. Khim.*, 2005, vol. 78, no. 2, pp. 191–194.
5. Dvoretskii, S.I., Gladyshev, N.F., Zhdanov, D.V., et al., *Vestn. Tambov. Gos. Tekh. Univ.*, 2005, vol. 11, no. 3, pp. 658–672.
6. Dolinskii, A.A. and Ivanitskii, G.K., *Optimizatsiya protsessov raspylitel'noi sushki* (Optimization of Processes for Spray Drying), Kiev: Naukova Dumka, 1984.
7. Pazhi, D.G. and Galustov, V.S., *Osnovy tekhniki raspylivaniya zhidkostei* (Fundamentals of Liquid Atomization Techniques), Moscow: Khimiya, 1984.
8. Pazhi, D.G., Koryagin, A.A., and Lamm, E.L., *Raspylivayushchie ustroistva v khimicheskoi promyshlennosti* (Spraying Devices in Chemical Industry), Moscow: Khimiya, 1975.
9. Borodin, V.A., Dityakin, Yu.F., Klyachko, L.A., and Yagodkin, V.I., *Raspylivanie zhidkostei* (Atomization of Fluids), Moscow: Mashinostroenie, 1967.
10. Golovkov, L.G., *Inzh.-Fiz. Zh.*, 1964, vol. 7, no. 11, pp. 55–58.
11. Loginov, S.V., Kutuzov, V.L., and Pilipenko, G.P., *Zh. Prikl. Khim.*, 1989, vol. 62, no. 3, pp. 702–704.
12. Ferapontov, Yu.A., Development of New Techniques for Production of Potassium Superoxide, *Cand. Sci. Dissertation*, St. Petersburg, 2002.
13. Zhdanov, D.V., Kinetics of, and Apparatus for a Resource-Saving Process for Potassium Superoxide Synthesis, *Cand. Sci. Dissertation*, Tambov, 2003.
14. Ferapontov, Yu.A., Zhdanov, D.V., Ul'yanova, M.A., et al., *Zh. Prikl. Khim.*, 2003, vol. 76, no. 11, pp. 1909–1910.
15. Sheludko, A., *Kolloidnaya khimiya* (Colloid Chemistry), Moscow: Mir, 1984.
16. Bezdenezhnykh, A.A., *Inzhenernye metody sostavleniya uravnenii skorostei reaktsii i rascheta kineticheskikh constant* (Engineering Methods for Making-up Reaction Rate Equations and Calculating Kinetic Constants), Leningrad: Khimiya, 1973.

ISSN 1070-4272, Russian Journal of Applied Chemistry, 2007, Vol. 80, No. 7, pp. 1048–1054. © Pleiades Publishing, Ltd., 2007.
Original Russian Text © V.I. Maksin, O.Z. Standritchuk, 2007, published in Zhurnal Prikladnoi Khimii, 2007, Vol. 80, No. 7, pp. 1079–1085.

PHYSICOCHEMICAL STUDIES OF SYSTEMS AND PROCESSES

Solubility Diagrams of the Systems Nickel Sulfamate–Water and Cobalt Sulfamate–Water

V. I. Maksin and O. Z. Standritchuk

National Agrarian University of Ukraine, Kiev, Ukraine

Received July 14, 2006; in final form, February 2007

Abstract—Solubility diagrams of nickel and cobalt sulfamates in water in the temperature range from –40 to 145°C are presented.

DOI: 10.1134/S1070427207070063

The solubility of metal sulfamates is comparable with that of nitrates and acetates [1–8], which is essential for their applications [6–14]. The solubilities of sulfamic acid and ammonium sulfamate [1, 2, 15] are the most extensively studied, and those of sulfamates of lanthanides [4–7], silver, and lead [3] are less investigated. The solubilities of sodium, magnesium, calcium, barium, and nickel sulfamates was determined only at 20–25°C [1, 2, 8], and the experimental data for cobalt, iron, copper, and chromium sulfamates are lacking. Previously [16, 17], an attempt was made to substantiate theoretically the solubility values of sulfamates, the thermodynamic aspects were considered, and standard solubilities of the majority of sulfamates were calculated and compared to the known experimental data. However, no systematic experimental studies in this direction were carried out, and further studies of the solubility of sulfamates in water remain topical.

In this study we examined the temperature dependences of the solubility of nickel and cobalt sulfamates in water and constructed two-component phase diagrams in the systems $Ni(SO_3NH_2)_2$–H_2O and $Co(SO_3NH_2)_2$–H_2O.

EXPERIMENTAL

In the experiments we used nickel and cobalt sulfamates synthesized from sulfamic acid (chemically pure grade) and the corresponding metal carbonates (analytically pure grade) according to [16], and also preliminarily recrystallized commercial chemicals. We studied the solubility as follows. We used a Pyrex reactor with a temperature-control jacket, equipped with a propeller stirrer (50 rpm) and seats for a mercury thermometer and for sampling. The reactor was charged with 250 ml of double-distilled water and a metal sulfamate in an amount sufficient to obtain a saturated solution with a small excess of undissolved crystals. Then the vessel was closed with a lid equipped with a hydroseal, a thermometer was inserted, and the system was brought to a desired temperature using a thermostat. Thermal insulation supported a constant temperature within the limits of 0.1–0.2°C. After stirring for 2 h, 1 cm^3 of the resulting solution was sampled at 10-min intervals using a temperature-controlled pipet with a filtering tip. The metal content of the samples was determined chelatometrically [18]. The equilibrium in the systems under study was reached within 2–8 h, and then the bottom phase and the mother liquor were analyzed. To find the most reliable result, the data obtained from several parallel experiments at the same temperature were treated by the least-squares method.

It should be noted that constructing solubility diagrams of salts tending to form several crystal hydrates is a rather complicated task [19], especially in the case of studying phase diagrams of the systems $Ni(SO_3NH_2)_2$–H_2O and $Co(SO_3NH_2)_2$–H_2O where two isomeric and several tautomeric modifications characteristic for sulfamate ions can exist [20, 21], and at temperatures higher than 85°C sulfamate ions can, in addition, undergo hydrolysis [15]. Therefore, to simplify the experiment, we studied the temperature dependence of the solubility in the range from –15 to 85°C with the subsequent construction of the corresponding portions of the diagrams $S = f(T)$, where S is the solubility (wt %) at a temperature T (°C). Then the obtained portions of experimental curves $S = f(T)$ were superimposed, using a computer, on the

Table 1. Solubility S in binary systems $Ni(SO_3NH_2)_2$–H_2O and $Co(SO_3NH_2)_2$–H_2O

$Ni(SO_3NH_2)_2$–H_2O		$Co(SO_3NH_2)_2$–H_2O	
T, °C	S, wt %	T, °C	S, wt %
–14.2	41.2	–14.7	39.8
–0.5	44.0	–1.2	41.3
10.3	47.8	8.3	47.0
19.0	50.5	19.3	49.4
25.0	53.7	25.0	53.0
29.5	55.1	28.0	54.1
38.9	57.3	31.1	55.2
47.3	59.8	52.7	58.3
59.8	62.0	61.2	59.8
77.9	63.6	79.6	62.9
83.5	64.1	83.2	65.0

analogous solubility diagrams of other inorganic salts (chlorides, sulfates, nitrates, etc.) of nickel and cobalt [19] and of sulfamic acid [15] to reveal by comparative analysis correlations in the arrangement of singular points (eutectics and peritectics) and common features of the curve shapes. After that, Further missing portions of the diagrams above 85 and below –15°C were constructed on the basis of the revealed regular trends by extrapolating the experimental portions of $S = f(T)$ curves to probable peritectics and also to eutectics of stable and metastable forms of sulfamates under study in the calculated ebullioscopic and cryoscopic curves, respectively.

The results of studying solubility of nickel and cobalt sulfamates in water in the range from –15 to 85°C, given in Table 1, were used to build up the corresponding $S = f(T)$ diagrams. Analysis of bottom phases according to the lever rule (Schreinemakers' method of wet residues) shows that nickel and cobalt sulfamates form several crystal hydrates (containing 4, 3.5, 3, and 2 water molecules). The formation of these crystal hydrates in the systems under study was confirmed by thermographic studies.

The total solubility diagram of the $Ni(SO_3NH_2)_2$–H_2O system is shown in Fig. 1a. The shape of the experimental portion of the $S = f(T)$ curve shows that two more singular points *a* and *b* appear behind the eutectic in the range of the existence of the crystal hydrate with four water molecules. These peritectics in the curves near 8.7 and 26.8°C can be due to phase transitions from the zwitterionic $[^{+\delta}H_2NSO_3^{-(\delta+1)}]$ to the open ($H_2NSO_3^-$) structure, characteristic also for sulfamic acid in this temperature range [15, 16, 20, 21]. Correspondingly, this portion of the $S = f(T)$ curve from the eutectic to the peritectic in point *b* is divided into three regions of the existence of α-, β-, and γ-$Ni(SO_3NH_2)_2 \cdot 4H_2O$ modifications. The possibility of such transitions and also exact temperatures of their occurrence are proved by the conductometric studies. For example, the temperature dependences $\chi = f(T)$ of the conductivity χ of nickel sulfamate solutions contain bends in points *a, b, c, d*, and *g* (Fig. 2, curve *1*) in the regions of peritectic temperatures, which, in turn, well correlate with the corresponding transitions in the solubility diagrams (Fig. 1). A similar temperature dependence $\chi = f(T)$ is given in Fig. 2 (curve *1*) for the well-studied system sulfamic acid–water with pronounced manifestation of the regions of existence of several tautomeric and isomeric forms [15]:

$$\alpha\text{-}^+H_3NSO_3^- \rightleftarrows \beta\text{-}^+H_3NSO_3^- \rightleftarrows \gamma\text{-}^+H_3NSO_3^-.$$

Examination of the curves $\chi = f(T)$ (Fig. 2, curves *1* and *2*, regions *A–D*) shows that the revealed temperature ranges of existence of singular points practically coincide with the peritectics in the diagram $S = f(T)$ (Fig. 1a) and are associated with the following transitions:

$$\alpha\text{-}Ni(SO_3NH_2)_2 \cdot 4H_2O \rightleftarrows \beta\text{-}Ni(SO_3NH_2)_2 \cdot 4H_2O$$

$$\rightleftarrows \gamma\text{-}Ni(SO_3NH_2)_2 \cdot 4H_2O.$$

When comparing the two experimental methods, in addition to "true" eutectics and peritectics, we detected singular points (Figs. 1 and 2, points *e, d*, and *g*) in the regions of metastable existence of all the forms of sulfamates shown in Table 2.

In particular, the peritectic temperature $T_p = 84 \pm 2$°C (Fig. 1a, point *h*) associated with the transitions $Ni(SO_3NH_2)_2 \cdot 3H_2O \rightleftarrows Ni(SO_3NH_2)_2 \cdot 2H_2O$ is the boundary of the metastable existence of the γ-$Ni(SO_3NH_2)_2 \cdot 4H_2O$ modification and the onset of intense hydrolysis, whereas $T_p = 53 \pm 2$°C (Fig. 1a, point *c*) is the boundary of the region of the metastable existence of α- and β-$Ni(SO_3NH_2)_2 \cdot 4H_2O$. The temperature $T_p = 53 \pm 2$°C is the boundary corresponding to noticeable acceleration of the chemical reactions between sulfamic acid and metals, their oxides, and carbonates [1, 2, 9–14]. The latter conclusion also agrees well with the results of [15, 22]. In these studies it was suggested that the open structures of sulfamic acid, HSO_3NH_2, are more active than the zwitterionic structures, $^+H_2NSO_3^-$.

The occurrence of phase tautomeric transitions in metal sulfamates can also be confirmed by structural

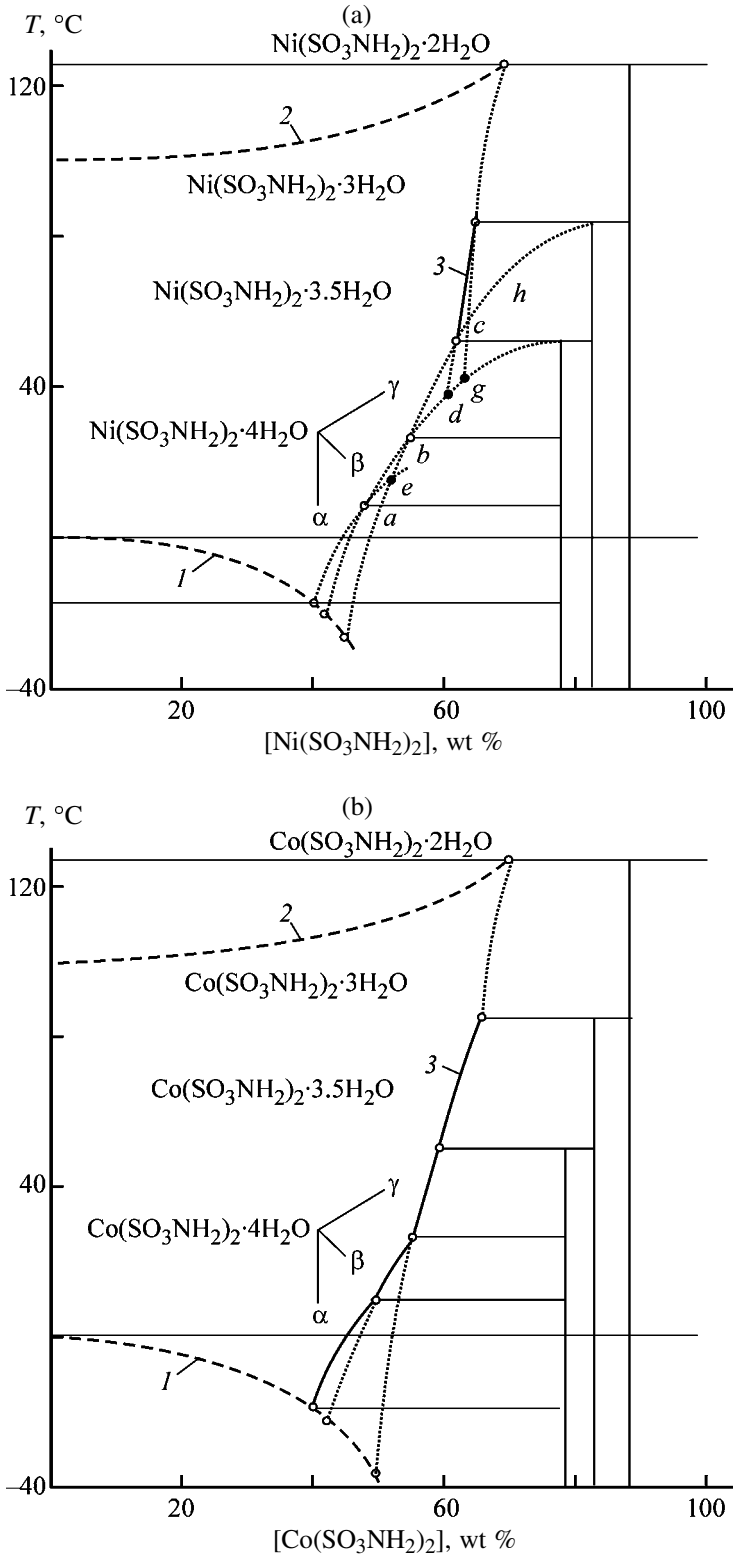

Fig. 1. Total solubility diagrams of the systems (a) $Ni(SO_3NH_2)_2$–H_2O and (b) $Co(SO_3NH_2)_2$–H_2O in the coordinates concentration of $Ni(SO_3NH_2)_2$ or $Co(SO_3NH_2)_2$–temperature *T*. Curves: (*1*) cryoscopy, (*2*) ebullioscopy, and (*3*) solubility. Solid lines, experiment; dashed lines, calculation; dotted lines, graphical extrapolation in metastable regions.

Table 2. Composition of bottom phases and parameters of singular points in binary systems $Ni(SO_3NH_2)_2$–H_2O and $Co(SO_3NH_2)_2$–H_2O

Point no.	Most probable bottom phase composition	T, °C	Weight fraction, %
	$Ni(SO_3NH_2)_2$–H_2O system		
1	Ice + α-$Ni(SO_3NH_2)_2 \cdot 4H_2O$	–17	40.5
2	α-$Ni(SO_3NH_2)_2 \cdot 4H_2O$ + β-$Ni(SO_3NH_2)_2 \cdot 4H_2O$	8.7	47.8
3	β-$Ni(SO_3NH_2)_2 \cdot 4H_2O$ + γ-$Ni(SO_3NH_2)_2 \cdot 4H_2O$	28.8	54.6
4	β-$Ni(SO_3NH_2)_2 \cdot 4H_2O$ + $Ni(SO_3NH_2)_2 \cdot 3.5H_2O$	{53}*	{61.6}
5	$Ni(SO_3NH_2)_2 \cdot 3H_2O$ + $Ni(SO_3NH_2)_2 \cdot 2H_2O$	{84}	{64.2}
6	Vapor + $Ni(SO_3NH_2)_2 \cdot 2H_2O$	(128)**	(69)
7	Ice + α-$Ni(SO_3NH_2)_2 \cdot 4H_2O$ + β-$Ni(SO_3NH_2)_2 \cdot 4H_2O$(met)	(–21)	(42)
8	Ice + α-$Ni(SO_3NH_2)_2 \cdot 4H_2O$ + β-$Ni(SO_3NH_2)_2 \cdot 4H_2O$(met) + γ-$Ni(SO_3NH_2)_2 \cdot 4H_2O$(met)	(–27)	(45)
9	β-$Ni(SO_3NH_2)_2 \cdot 4H_2O$ + α-$Ni(SO_3NH_2)_2 \cdot 4H_2O$(met) + γ-$Ni(SO_3NH_2)_2 \cdot 4H_2O$(met)	(17)	(52)
10	γ-$Ni(SO_3NH_2)_2 \cdot 4H_2O$ + β-$Ni(SO_3NH_2)_2 \cdot 4H_2O$(met) + $Ni(SO_3NH_2)_2 \cdot 3H_2O$(met)	(37)	(60)
11	γ-$Ni(SO_3NH_2)_2 \cdot 4H_2O$ + β-$Ni(SO_3NH_2)_2 \cdot 4H_2O$(met) + $Ni(SO_3NH_2)_2 \cdot 2H_2O$(met)	(42)	(63)
12	$Ni(SO_3NH_2)_2 \cdot 3.5H_2O$ + γ-$Ni(SO_3NH_2)_2 \cdot 4H_2O$(met) + $Ni(SO_3NH_2)_2 \cdot 2H_2O$(met)	(57.5)	(63.5)
	$Co(SO_3NH_2)_2$–H_2O system		
1	Ice + α-$Co(SO_3NH_2)_2 \cdot 4H_2O$	–16	39
2	α-$Co(SO_3NH_2)_2 \cdot 4H_2O$ + β-$Co(SO_3NH_2)_2 \cdot 4H_2O$	10.4	49
3	β-$Co(SO_3NH_2)_2 \cdot 4H_2O$ + γ-$Co(SO_3NH_2)_2 \cdot 4H_2O$	27.1	54.2
4	γ-$Co(SO_3NH_2)_2 \cdot 4H_2O$ + $Co(SO_3NH_2)_2 \cdot 3.5H_2O$	51.2	58.5
5	$Co(SO_3NH_2)_2 \cdot 3H_2O$ + $Co(SO_3NH_2)_2 \cdot 2H_2O$	{86}	{64.7}
6	Vapor + $Co(SO_3NH_2)_2 \cdot 2H_2O$	(126)	(68)
7	Ice + α-$Co(SO_3NH_2)_2 \cdot 4H_2O$ + β-$Co(SO_3NH_2)_2 \cdot 4H_2O$(met)	(–22)	(41.5)
8	Ice + α-$Co(SO_3NH_2)_2 \cdot 4H_2O$ + β-$Co(SO_3NH_2)_2 \cdot 4H_2O$(met) + γ-$Co(SO_3NH_2)_2 \cdot 4H_2O$(met)	(–37)	(49)

* Positions of characteristic points determined with a probability of no more than 80% are given in braces.

** Probable positions of characteristic points found by extrapolation of experimental portions of curves for metastable forms are given in parentheses.

methods. In particular, when the temperature of an aqueous solution of lead sulfamate is increased from 4 to 40°C, the corresponding lines in its NMR spectra recorded at H_0 = 200.13 MHz (i.e., in the region of the $–NH_2$ absorption) were shifted downfield, and the line intensities increased. Similar splitting of the spectrum and the downfield shift are characteristic for the rearrangement $–NH_3 \rightleftarrows –NH_2 + H^+$ [23, 24]. Therefore, at T_p = 26.8°C (the temperature of the transition of zwitterion structures into open forms of sulfamate ions), the NMR spectrum was strongly split. If water molecules, which facilitate the transition from $^+H_3NSO_3^-$ to HSO_3NH_2 [15, 17], are involved in the exchange processes, separate stages of such transitions can be detected even as independent modifications. Thus, the coincidence of peritectic temperatures in points *a* (T_p = 8.7°C) and *b* (T_p = 26.8°C) in the curve $S = f(T)$ (Fig. 1a) with the conductometric analysis data [$\chi = f(T)$ (Fig. 2)] and the NMR data convincingly confirms the existence of α, β, and γ modifications of $Ni(SO_3NH_2)_2 \cdot 4H_2O$.

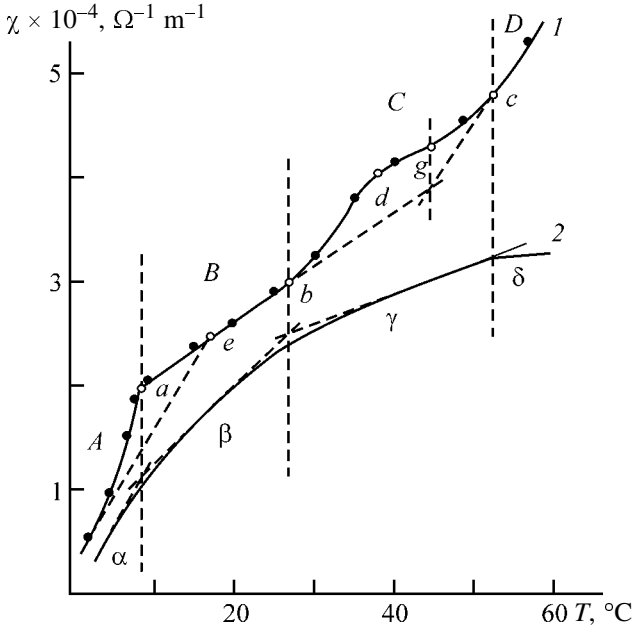

Fig. 2. Temperature dependences of the conductivities χ of (*1*) 25% $Ni(SO_3NH_2)_2$ solution and (*2*) HSO_3NH_2. Points, discrete measurements; solid line, automatic recording.

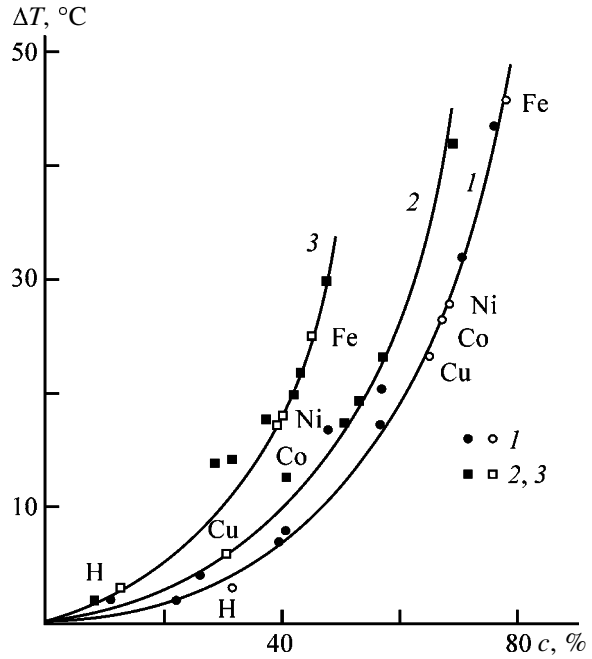

Fig. 3. Temperature shifts ΔT (°C) for (*1*) boiling (ebullioeutectics) and (*2, 3*) ice crystallization (cryoeutectics) points in saturated solutions of (filled squares and circles) chlorides, sulfates, and nitrates and (hollow squares and circles) sulfamates of double-charged metal ions, as functions of their limiting concentration c relative to the corresponding parameters of water.

The experimental study of the solubility above 85°C, especially construction of ebullioscopic curves by boiling points of saturated solutions, is strongly complicated by the onset of the hydrolysis of sulfamate ions according to the scheme

$$3M(SO_3NH_2)_2 + 4H_2O = [M(NH_3)_4](SO_3NH_2)_2 + 2M(HSO_4)_2,\ M = Ni,\ Co.$$

In this case, despite certain measures (performing saturation for shorter time, increasing the number of replicate experiments), the results were rather approximate. At the same time, the experimental determination of the eutectic was strongly complicated by the tendency of nickel sulfamate to supersaturation at low temperatures. Therefore, we calculated the courses of the ebullioscopic and cryoscopic curves and found the most probable variants by graphical comparison of the experimental portions of the $S = f(T)$ curves for the sulfamates under study (Fig. 1) with the known solubility diagrams of various inorganic salts (chlorides, sulfates, nitrates, etc.) of nickel, cobalt, and other double-charged metal ions [19]. As a result of the comparative analysis, we revealed correlations in the structures of such two-component diagrams. In particular, we found that the boiling and freezing curves of salt solutions and the arrangement of eutectics and peritectics clearly correlate with weight concentrations of the solutes. As an example we plotted in Fig. 3 the shifts of the boiling (curve *1*) and ice crystallization (curves *2, 3*) points vs. weight concentration of the salt dissolved in water for MA_2–N_2O systems ($M = Ni^{2+}$, Co^{2+}, and other double-charged metal cations; $A = Cl^-$, Br^-, ClO_4^-, NO_3^-, SO_4^{2-}, and $SO_3NH_2^-$ anions). Thus, the results obtained allowed us to correct the calculated portions of the total solubility diagram of the system $Ni(SO_3NH_2)_2$–H_2O (Fig. 1a) and also to refine positions of singular points which are presented in Table 2.

The solubility diagram of the cobalt sulfamate–water system (Fig. 1b) was constructed similarly using the data of Table 1; the parameters of singular points are given in Table 2. The comparison of both diagrams (Figs. 1a, 1b), and also of the results presented in Table 2, shows that cobalt sulfamate crystal hydrate with four water molecules, as well as the related nickel sulfamate, shows tautomerism with the formation of α, β, and γ modifications of $Co(SO_3NH_2)_2 \cdot 4H_2O$. Three more crystal hydrates of cobalt sulfamate $Co(SO_3NH_2)_2 \cdot 3.5H_2O$, $Co(SO_3NH_2)_2 \cdot 3H_2O$, and $Co(SO_3NH_2)_2 \cdot 2H_2O$ are also formed in this system.

Slow isohydric crystallization at room temperature makes it possible to obtain $Co(SO_3NH_2)_2 \cdot 4H_2O$ in the form of large (up to 5–10 mm in a diagonal) transparent dark pink prismatic single crystals with a refraction index of $N_{av} = 1.517$. Cobalt sulfamate crystal hydrate with four water molecules, which is very unstable in air, is gradually eroded to form light pink powders by gradual passing from $Co(SO_3NH_2)_2 \cdot 3.5H_2O$ to the most stable in air crystal hydrate $Co(SO_3NH_2)_2 \cdot 3H_2O$.

Unlike cobalt sulfamate, nickel sulfamate tends to form supersaturated solutions. When seed crystals are introduced into a dark green supersaturated solution of nickel sulfamate, a blue-green crystalline ($N_{av} = 1.583$) powder of $Ni(SO_3NH_2)_2 \cdot 4H_2O$, which is stable in air and to vacuum drying, precipitates from the solution.

The general view of the solubility diagrams of the nickel sulfamate—water and cobalt sulfamate–water systems correlates well with the solubility diagram of sulfamic acid HSO_3NH_2–H_2O [15]. Furthermore, all these diagrams are characterized by a phase transition from zwitterionic structures to open forms at 26.7–27.1°C and by the onset of hydrolysis of sulfamate ions at 84 ± 2°C.

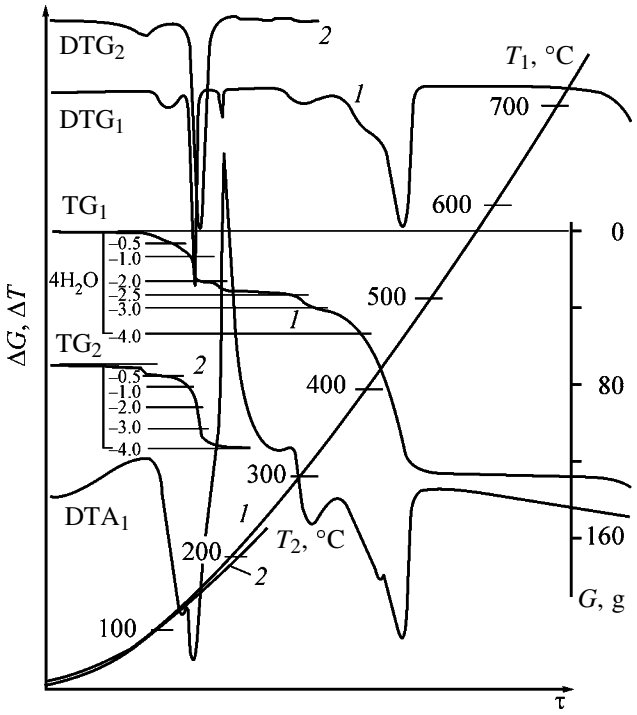

Fig. 4. Thermograms of crystalline samples of (*1*) nickel and (*2*) cobalt sulfamates. Automatic mode, heating rate 10 deg min^{-1}, DTA/DTG = 1/10, samples 250 mg of $Ni(SO_3NH_2)_2 \cdot 4H_2O$ (subscript *1*) and 185 mg of $Co(SO_3NH_2)_2 \cdot 4H_2O$ (subscript *2*). (ΔG) Weight loss rate, (ΔT) temperature difference, (T) temperature, (G) sample weight loss, and (τ) time.

The results of a thermographic study (Q-1500D derivatograph) of crystalline samples of $Ni(SO_3NH_2)_2 \cdot 4H_2O$ and $Co(SO_3NH_2)_2 \cdot 4H_2O$ at a heating rate of 10 deg min^{-1} are shown in Fig. 4. It is clearly seen (for obviousness, the region of loss of crystal hydrate water is specially denoted in Fig. 4) that nickel and cobalt sulfamates lose crystal water in several steps. First the processes go equally for both samples with successive of elimination of $0.5H_2O$ in two steps, and then, at temperatures close to ebullioscopic eutectics, the second molecule is lost with the formation of readily crystallizing crystal hydrates with two water molecules:

$$M(SO_3NH_2)_2 \cdot 4H_2O - 0.5H_2O = M(SO_3NH_2)_2 \cdot 3.5H_2O,$$

$$M(SO_3NH_2)_2 \cdot 3.5H_2O - 0.5H_2O = M(SO_3NH_2)_2 \cdot 3H_2O,$$

$$M(SO_3NH_2)_2 \cdot 3H_2O - 0.5H_2O = M(SO_3NH_2)_2 \cdot 2H_2O.$$

Then, long before the onset of sulfamate ion decomposition, cobalt sulfamate successively loses the third and the fourth H_2O molecules, forming anhydrous crystals, and nickel sulfamate continues to retain water up to the onset of sulfamate ion decomposition involving the fourth molecule of crystal hydrate water. These are the processes responsible for easier removal of supersaturation in the case of cobalt sulfamate, as compared to nickel sulfamate, in the course of vacuum-thermal crystallization.

It should be noted in conclusion that in the diagrams shown (Figs. 1a, 1b) the temperature dependences of the sulfamate solubility in water (curves *3*) denoted by solid lines were obtained experimentally, whereas the portions designated by dashed and dotted lines are tentative, as they were obtained on the basis of calculations and indirect theoretical studies. Nevertheless, our results were fruitfully used in the development of processes for producing electroplating electrolytes and crystalline nickel and cobalt sulfamates [14, 22].

CONCLUSIONS

(1) The solubilities of $Ni(SO_3NH_2)_2$ and $Co \cdot (SO_3NH_2)_2$ show strong temperature dependences, and the compounds exhibit tautomerism.

(2) The formation of tautomeric modifications of sulfamates is associated with multistage transformations from the zwitterionic form $^{+\delta}H_2NSO_3^{-(\delta+1)}$ to the open form $H_2NSO_3^-$.

(3) The diagrams obtained closely correlate with the solubility diagram of the HSO_3NH_2–H_2O system.

REFERENCES

1. Cupery, M.E., *Ind. Eng. Chem.*, 1938, vol. 30, no. 6, pp. 627–631.
2. Patron, M., *J. Ind. Chim.*, 1955, vol. 42, no. 457, pp. 237–243.
3. Odehnal, M., *Chem. Listy*, 1955, vol. 49, no. 10, pp. 1571–1573.
4. Mustaev, A.K. and Yakovenko, R.T., *Izv. Akad. Nauk Kirg. SSR*, 1963, vol. 5, no. 4, pp. 5–8.
5. Krakovskaya, T.A., Pireks, O.B., and Vasil'ev, S.V., *Zh. Neorg. Khim.*, 1986, vol. 31, no. 3, pp. 617–624.
6. Kreinberg, J., Taedel, W.A., and Audrieth, L.F., *Ind. Eng. Chem., Anal. Ed.*, 1939, vol. 11, pp. 368–369.
7. King, G.B. and Hooper, I.F., *J. Phys. Chem.*, 1941, vol. 45, no. 5, pp. 938–941.
8. Levin, A.I. and Zhang Go-Heng, *Zh. Prikl. Khim.*, 1960, vol. 33, no. 3, pp. 667–674.
9. Benningof, H., *Metalloberflache*, 1982, vol. 36, no. 11, pp. 561–565.
10. US Patent 3 321 273.

11. US Patent 3620669.
12. USSR Inventor's Certificate no. 322316.
13. USSR Inventor's Certificate no. 452543.
14. Maksin, V.I., Standritchuk, O.Z., Vakhnin, I.G., et al., *Khim. Tekhnol. Vody*, 1989, vol. 11, no. 3, pp. 630–636.
15. Standritchuk, O.Z., Maksin, V.I., and Zapol'skii, A.K., *Zh. Obshch. Khim.*, 1990, vol. 60, no. 2, pp. 253–258.
16. Standritchuk, O.Z., Maksin, V.I., and Zapol'skii, A.K., *Zh. Fiz. Khim.*, 1989, vol. 63, no. 9, pp. 2332–2339.
17. Standritchuk, O.Z., Maksin, V.I., and Zapol'skii, A.K., *Ukr. Khim. Zh.*, 1991, vol. 57, no. 5, pp. 458–462.
18. Schwarzenbach, G. und Flaschka, H., *Die komplexometrische Titration*, Stuttgart: Ferdinand Enke, 1965.
19. Kirgintseva, A.I., Trushnikova, L.N., and Lavrent'eva, V.G., *Rastvorimost' neorganicheskikh veshchestv v vode. Spravochik* (Solubility of Inorganic Substances in Water. Handbook), Leningrad: Khimiya, 1972.
20. Garrett, M., Tao, T., and Jolly, W.L., *J. Phys. Chem.*, 1964, vol. 68, no. 4, pp. 624–626.
21. Hicking, S.J. and Wolley, R.G., *Chem. Phys. Lett.*, 1990, vol. 166, no. 1, pp. 43–48.
22. Maksin, V.I. and Standritchuk, O.Z., *Khim. Tekhnol. Vody*, 2001, vol. 23, no. 6, pp. 583–596.
23. Emsley, J.W., Feeney, J., and Sutcliffe, L.H., *High Resolution Nuclear Magnetic Resonance Spectroscopy*, Oxford: Pergamon, 1965.
24. Drago, R.S., *Physical Methods in Chemistry*, Philadelphia: Saunders, 1977.

ISSN 1070-4272, Russian Journal of Applied Chemistry, 2007, Vol. 80, No. 7, pp. 1055–1057. © Pleiades Publishing, Ltd., 2007.
Original Russian Text © N.S. Shaglaeva, S.V. Amosova, R.G. Sultangareev, L.M. Stanevich, E.F. Voropaeva, 2007, published in Zhurnal Prikladnoi Khimii, 2007, Vol. 80, No. 7, pp. 1086–1088.

SORPTION AND ION-EXCHANGE PROCESSES

Gold(III) Sorption with Copolymers Derived from Divinyl Sulfide

N. S. Shaglaeva, S. V. Amosova, R. G. Sultangareev, L. M. Stanevich, and E. F. Voropaeva

Favorskii Irkutsk Institute of Chemistry, Siberian Division, Russian Academy of Sciences, Irkutsk, Russia
Irkutsk State Technical University, Irkutsk, Russia
Irkutsk State Medical University, Irkutsk, Russia

Received June 27, 2006; in final form, February 2007

Abstract—Sorption recovery of gold(III) from aqueous mineral acids with copolymers of 4-vinylpyridine and 2-methyl-5-vinylpyridine with divinyl sulfide was studied.

DOI: 10.1134/S1070427207070075

Preconcentration of trace amounts of precious metals in analysis of natural and industrial objects and recovery of these elements from hydrometallurgical waste with ion-exchange resins find growing use. The corresponding ion-exchange resins should have high sorption capacity and distribution coefficients [1, 2]. Previously [3, 4] we developed methods for preparing network copolymers of divinyl sulfide (DVS) with 4-vinylpyridine (VP) and 2-methyl-5-vinylpyridine (MVP) and examined the physicochemical properties of these macromolecular compounds.

In this study, we examined the sorption activity of copolymers of divinyl sulfide with vinylpyridines with respect to gold(III).

EXPERIMENTAL

Divinyl sulfide was separated from the stabilizer by distillation (bp 83–84°C/720 mm Hg). 4-Vinylpyridine and 2-methyl-5-vinylpyridine, which are commercial monomers, were purified by repeated distillation in a vacuum. Their purity was monitored chromatographically.

Radical copolymerization of DVS with VP or MVP was performed in dimethylformamide (DMF) by an ampule method in the presence of azobis(isobutyronitrile) (AIBN) at 60°C under argon. The copolymers were washed with solvents (benzene, acetone, water) and dried to constant weight in a vacuum. The copolymer composition was calculated from the data of elemental analysis, which was performed on a Thermo Finnigan gas analyzer. The IR spectra of compounds in KBr pellets and mineral oil were recorded on an IFS-25 spectrometer.

The reference Au(III) solution was prepared by dissolution of $H[AuCl_4]$ in water and standardized by the standard procedure [5]. The working solutions were prepared by dilution of the initial solutions just before experiments. The sorption ability of the copolymers with respect to gold(III) chloro complexes was studied in the static mode at room temperature as follows: 10 mg of a copolymer was introduced into a beaker, the required acidity of the solution was adjusted, and a definite amount of an Au(III) solution was added. The metal sorption was performed from 20 ml of solution in the static mode with vigorous stirring. After a definite time, the copolymer was filtered off. The Au(III) content was determined by atomic absorption spectroscopy.

The radical copolymerization of DVP with VP gives insoluble products in any case. In the DVS–MVP system, copolymerization in the presence of AIBN gives an insoluble copolymer only at a low content of the sulfur-containing monomer (<5 mol %). The maximal sulfur content of the sample is 1.2 wt % (Table 1). At a further increase in the DVS content of the initial mixture, soluble reaction products are formed. The yield of the copolymer decreases with increasing DVS content. The scheme of formation of network copolymers is shown below:

Table 1. Copolymers of DVS with VP and MVP

Copolymer	Composition of starting mixture, wt %		Content, wt %		Copolymer composition, mol %		Yield, %
	VP or MVP	DVS	N	S	VP or MVP	DVS	
DVS–VP	50.00	50.00	8.78	12.67	61.23	38.77	92
DVS–MVP	95.00	5.00	11.52	1.20	96.04	3.97	79

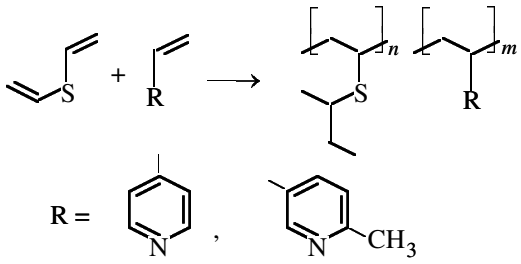

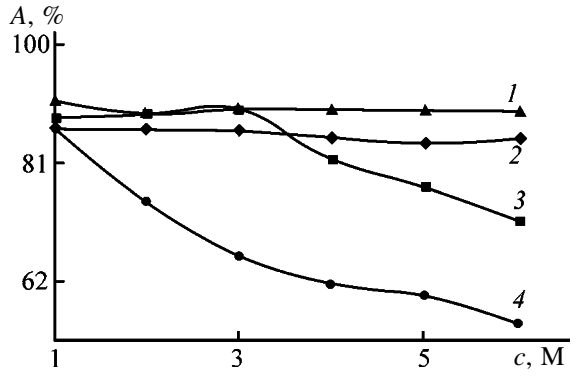

Fig. 1. Influence of the kind and concentration c of acid on the degree of gold recovery A from solution. m_{sorb} = 1.62 mg, sorption time 2 h. Copolymer: (*1, 3*) DVS–VP and (*2, 4*) DVS–MVP. Acid: (*1, 2*) H_2SO_4 and (*3, 4*) HCl; the same for Fig. 2.

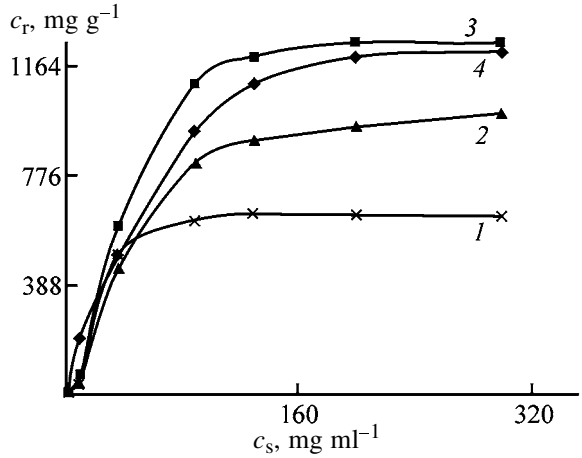

Fig. 2. Equilibrium distribution of gold(III) in its recovery from 1 M acids. m_{sorb} = 10 mg, sorption time 2 h. (c_s) Equilibrium gold(III) concentration in the solution and (c_r) equilibrium gold(III) content in the resin. Copolymer: (*1, 4*) DVS–VP and (*2, 3*) DVS–MVP.

The copolymers taken for studying the sorption activity are listed in Table 1. Among samples of DVS–VP copolymer, we chose that with a sulfur content of 12.67 wt %, prepared in the maximal yield at equimolar composition of the initial mixture.

The dependence of the efficiency of gold(III) recovery with DVS–VP or DVS–MVP copolymer on the nature and concentration of mineral acids is shown in Fig. 1. As seen, the degree of gold recovery decreases with increasing HCl concentration and is virtually independent of the sulfuric acid concentration. The first trend can be attributed to the competition of the Cl^- ion and anionic metal chloro complex for the resin. Such influence of the HCl concentration suggests an ion-exchange mechanism of gold(III) interaction with the resin in HCl, although the coordination mechanism cannot be ruled out either. The lack of any influence of sulfuric acid concentration on the gold sorption shows that in this case the sorption occurs mainly by the coordination mechanism. In the IR spectrum of the sorbent with sorbed gold (concentrate), a broad band in the 3000–2600 cm^{-1} range characteristic of the ammonium cation is observed. The shift of the absorption band maximum from 1600 to 1630 cm^{-1} is attributable to the coordination via nitrogen atom [2–6].

The curves of gold(III) distribution between the sorbent and solution in sorption from 1 M acids are shown in Fig. 2, and the calculated sorption capacities (SC) and distribution coefficients of gold D are listed in Table 2.

Table 2. Sorption capacities of copolymers based on DVS and gold(III) distribution coefficients in sorption from 1 M acids

Copolymer	SC, mg g^{-1}	D, cm^3 g^{-1}
	HCl	
DVS–VP	730	1.5×10^5
DVS–MVP	980	2.2×10^4
	H_2SO_4	
DVS–VP	1200	1.6×10^4
DVS–MVP	1190	1.5×10^4

The copolymers show high sorption capacities for the Au(III) chloro complex, which is probably caused by two types of interactions: ion-exchange and coordination. High distribution coefficients allow the use of these sorbents in analytical chemistry.

CONCLUSIONS

(1) Static sorption capacities and distribution coefficients of gold(III) in its recovery from aqueous solutions of sulfuric and hydrochloric acids with copolymers of divinyl sulfide with 4-vinylpyridine or 2-methyl-5-vinylpyridine were determined.

(2) These copolymers exhibit high sorption capacities for gold(III) chloro complexes and can recover small amounts of gold(III) from solutions.

ACKNOWLEDGMENTS

The study was financially supported by the Russian Foundation for Basic Research (project no. 06-08-00320).

REFERENCES

1. Myasoedova, G.V. and Savvin, S.B., *Khelatoobrazuyushchie sorbenty* (Chelating Sorbents), Moscow: Nauka, 1984.
2. Saldadze, K.M. and Kopylova-Valova, V.F., *Kompleksoobrazuyushchie ionity* (Complexing Ion Exhangers), Moscow: Khimiya, 1980.
3. Shaglaeva, N.S., Amosova, S.V., Shaulina, L.P., et al., *Vysokomol. Soedin., Ser. B*, 2004, vol. 46, no. 5, pp. 905–911.
4. Shaglaeva, N.S., Amosova, S.V., Shaulina, L.P., et al., *Zh. Prikl. Khim.*, 2005, vol. 78, no. 8, pp. 1296–1298.
5. Ginzburg, S.I., Gladysheva, S.A., Ezerskaya, N.A., et al., *Rukovodstvo po khimicheskomu analizu platinovykh metallov i zolota* (Manual on Chemical Analysis of Platinum Metals and Gold), Moscow: Nauka, 1965.
6. Dechant, J., Danz, R., Kimmer, W., et al., *Ultrarotspektroskopische Untersuchungen an Polymeren*, Berlin: Akademie, 1972.

ISSN 1070-4272, Russian Journal of Applied Chemistry, 2007, Vol. 80, No. 7, pp. 1058–1062. © Pleiades Publishing, Ltd., 2007.
Original Russian Text © A.A. Blokhin, N.D. Abovskii, Yu.V. Murashkin, 2007, published in Zhurnal Prikladnoi Khimii, 2007, Vol. 80, No. 7, pp. 1089–1093.

SORPTION AND ION-EXCHANGE PROCESSES

Ion-Exchange Recovery of Palladium(II) from Multicomponent Chloride Solutions

A. A. Blokhin, N. D. Abovskii, and Yu. V. Murashkin

St. Petersburg State Institute of Technology (Technical University), St. Petersburg, Russia

Received March 16, 2007

Abstract—Ion-exchange sorption of palladium(II) from both concentrated aqueous hydrochloric acid solution containing Fe(III), Sn(II), Zn(II), and Cu(II) and weakly acidic concentrated aqueous ammonium chloride solution containing Zn(II) and Cu(II) was studied. The Purolite S920, Purolite S924, and Purolite S984 macroporous resins with the thiourea, thiol, and polyethylenepolyamine functional groups, respectively, were used as sorbents. Strongly basic Purolite A500 anion exchanger was also tested. The desorption of palladium(II) with aqueous ammonia, hydrochloric acid, and acidified aqueous thiourea was examined.

DOI: 10.1134/S1070427207070087

In refining platinum metals (PMs), large volumes of spent PM-containing solutions are formed. The palladium(II) content in them can be as large as 150 mg l^{-1}. The platinum metals are commonly recovered from spent refining solutions by precipitation in the form of poorly soluble compounds and also by cementation or electrolysis [1]. However, these methods do not ensure the required completeness of PM recovery. Furthermore, their use leads to the formation of poorly soluble products depleted of PMs, whose further processing to recover PMs is difficult.

Extensive published data on ion-exchange sorption of PMs show that resins with the thiourea, thiol, and polyethylenepolyamine functional groups selectively sorb these metals [1–3]. Therefore, we can expect that application of these resins will allow more complete recovery of PMs from spent refining solutions. However, currently ion-exchange sorption is rather seldom used for this purpose. The ion-exchange methods are mainly used for preconcentrating PMs before their chemical analysis [4–6]. Studies concerning industrial processing of PM-containing solutions mainly dealt with commercial resins nonselective to PMs [7–11].

The modern chemical industry produces a large number of resins with various selective functional groups, which allows selection of sorbents suitable for more complete recovery of PMs from spent multicomponent refining solutions.

In this study we examined the possibility of more complete selective ion-exchange recovery of palladium(II) from two kinds of spent refining solutions: after precipitation of ammonium hexachloroplatinate(IV) and *trans*-dichlorodiamminepalladium(II).

EXPERIMENTAL

We tested the following commercial macroporous complexing resins produced by Purolite Int. Ltd. company: Purolite S920, Purolite S924, and Purolite 984 with the thiourea, thiol, and polyethylenepolyamine functional groups, respectively. For comparison, Purolite A500 strongly basic anion exchanger was also tested.

In the static sorption experiments, weighed portions of a resin were brought in contact with solutions containing a constant amount of macrocomponents and impurity metals and variable amount of palladium(II) at 1 : 200 ratio of the dry resin (g) and liquid (ml). On attainment of the sorption equilibrium (5–7 days), the solution was separated from the resin and analyzed for palladium. The amount of palladium sorbed on the resin was determined by the difference between its concentrations in the initial and equilibrium solutions, taking into account the weighed portion of the resin, its specific volume, and the solution volume. In determining the degree of palladium desorption from the resin, its weighed sample preliminarily saturated with palladium(II) was washed with 0.3 M aqueous hydrochloric acid and then brought in contact with a desorbing solution.

The experiments on ion-exchange sorption of palladium(II) under dynamic conditions were carried out with a series of identical columns packed with an ion exchanger (8 ml) of commercial granulation. The ratio of the resin bed height to the column diameter was 9 : 1. After completion of the sorption of palladium(II), the column was washed with acidified water (11 g HCl l^{-1}), and then palladium was desorbed from the column. In sorption and desorption steps, the corresponding solutions were passed through the column at a rate of 1.0–1.5 and 0.7–1.0 column volumes per hour, respectively. The palladium(II) content in the desorbates was determined photocolorimetrically from the light absorption of a colored complex of palladium(II) with tin(II) chloride [12]. Before determination of iron(III) and copper(II) in the desorbate, the latter was treated with sulfuric and perchloric acids on heating to decompose thiourea. In the resulting solutions iron(III) was determined photocolorimetrically from the light absorption of its yellow complex with sulfosalicylic acid in aqueous ammonia (pH 8–10) [13]. Copper(II) was determined from the light absorption of its blue complexes with ammonia.

In this study we examined the ion-exchange recovery of palladium(II) from two solutions simulating the average chemical composition of the real mother liquors formed after precipitation of ammonium hexachloroplatinate(IV) (solution I) and *trans*-dichlorodiamminepalladium (solution II) from the refining shop at one of the domestic enterprises. Their salt and elemental composition was as follows (g l^{-1}): solution I: NH_4Cl 53.5, HCl 1.10, Cu(II) 3.2, Zn(II) 3.3, Fe(III), 2.8, and Sn(IV) 6.0; solution II: NH_4Cl 160, Cu(II) 3.2, Zn(II) 3.3, pH 3.3.

First we obtained the sorption isotherms of palladium(II) from solutions I and II (Figs. 1a, 1b).

Figure 1a shows that complexing resins with the thiourea (S920) and thiol (S924) functional groups sorb palladium(II) from strongly acidic solutions I containing large amounts of hydrochloric acid and ammonium chloride, and also fairly large amount of hydrolyzable metal cations Fe(III), Sn(IV), Zn(II), and Cu(II) tending to form negatively charged chloride complexes. It is seen that the sorption selectivity of S920 and S924 resins to palladium(II) is noticeably higher than that of both the A500 strongly basic anion exchanger poorly sorbing palladium(II) and S984 weakly basic anion exchanger. The sorption capacity of S920 resin for palladium(II) is higher than that of S924 over the entire concentration range studied.

As seen from Fig. 1b, in sorption of palladium from the weakly acidic solution (pH ~3) with a high

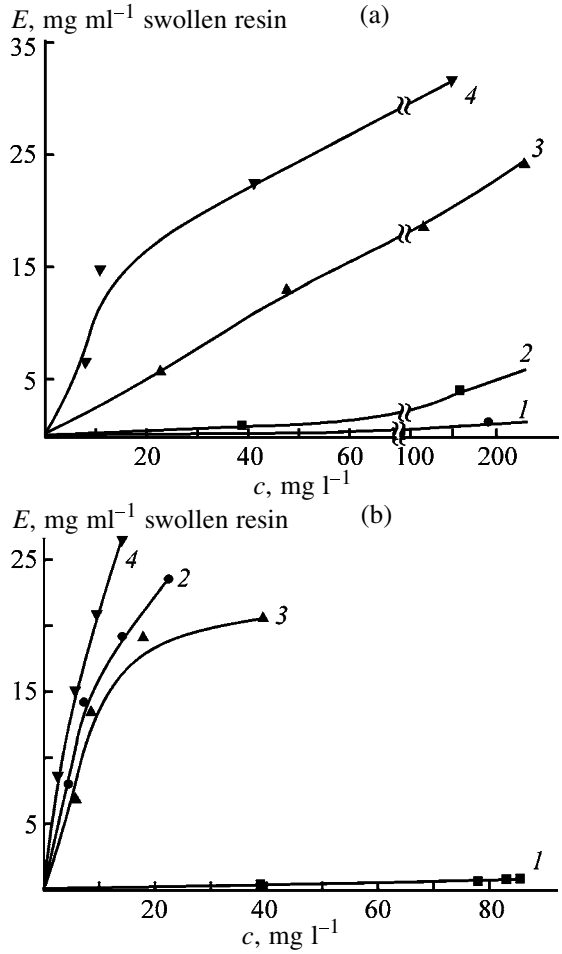

Fig. 1. Sorption isotherms of palladium(II) from solutions of various compositions on (*1*) A500, (*2*) S984, (*3*) S924, and (*4*) S920 resins. (*E*) Sorption capacity of resins for palladium(II) and (*c*) palladium concentration in the equilibrium solution. Solutions composition, g l^{-1}: (a) NH_4Cl 53.5, HCl 110, Cu(II) 3.2, Zn(II) 3.25, Fe(III) 2.8, and Sn(IV) 6.0; (b) NH_4Cl 160, Cu(II) 3.2, Zn(II), 3.3, pH ~3.3.

content of salts (solution II), high selectivity to palladium(II) is exhibited not only by S920 and S924 resins, but also by S984 weakly basic anion exchanger with the polyethylenepolyamine functional groups. Its sorption capacity for palladium(II) is only slightly lower than that of S920 resin.

On the contact of S984 anion exchanger with concentrated aqueous hydrochloric acid, its functional groups are protonated. Under these conditions, S984 loses its selectivity to palladium(II), because Pd(II) can be sorbed in this case only by the anion-exchange (onium) mechanism in the form of $[PdCl_4]^{2-}$, which is the major palladium species in solution. In going to weakly acidic solutions, the sorption selectivity of S984 sharply increases, apparently due to deprotonation of its functional groups and their strong inner-

Table 1. Desorption of palladium(II) from resins under static conditions

Resin	Desorbing solution composition, M	Degree of desorption, %
S920	HCl 12.0	24
	NH_4OH 6.0	~1
	$(NH_2)_2CS$ 0.66, HCl 0.3	98
S924	HCl 12.0	12
	NH_4OH 6.0	~1
	$(NH_2)_2CS$ 0.66, HCl 0.3	65
S984	HCl 12.0	35
	NH_4OH 6.0	10
	$(NH_2)_2CS$ 0.66, HCl 0.3	~100

sphere comlexation with palladium(II). As for S920 and S924, their thiourea and thiol groups are apparently capable of binding palladium(II) through inner-sphere complexation from strongly acidic solutions also.

The suitability of resins for practical application is governed not only by their sorption power and selectivity, but also by the feasibility of desorption of the sorbed component. It is known that desorption of PMs from ion-exchange resins often involves problems [8–14]. Analysis of data on the desorption of PMs from ion exchangers under static conditions [1, 7, 8, 12, 15] (Table 1) allows us to predict the possibility of palladium(II) desorption from S920, S924, and S984 resins with aqueous hydrochloric acid, ammonia, and thiourea.

Table 1 shows that neither concentrated aqueous hydrochloric acid nor concentrated aqueous ammonia are capable of desorbing palladium(II) from any of the resins under consideration. At the same time, treatment of resins with aqueous thiourea ensures virtually complete desorption of palladium(II) from S920 and S984 resins. At the same time, the degree of palladium desorption from S924 resin with aqueous thiourea does not exceed 65%.

The dynamic experiments on sorption of palladium(II) on resins were carried out taking into account our data on sorption of palladium(II) on the same resins under static conditions. The sorption of palladium(II) from solution I was studied on S920 and S924 resins, and the sorption from solution II {mother liquors after precipitation of *trans*-$[Pd(NH_3)_2Cl_2]$}, on S920 and S984 resins. Figures 2 and 3 show the breakthrough and desorption curves of palladium(II). The main characteristics of sorption and desorption of palladium(II) under dynamic conditions are listed in Table 2.

Our results show that, when solutions I and II are passed through the columns packed with the resins under consideration, palladium is sorbed virtually completely (taking into account the detection limit, 2 mg l^{-1}). In sorption of palladium from solution I on S920 resin, its DEC for palladium to breakthrough and the TDEC for palladium exceed the corresponding parameters of S924 resin by a factor of 3. Another advantage of S920 resin is that palladium(II) can be virtually completely desorbed with aqueous thiourea. The average palladium(II) concentration in the desorbate from S920 exceeds its concentraion in the initial solution by a factor of approximately 20. For several fractions of the desorbate, especially those highly enriched in palladium, this factor exceeds 70.

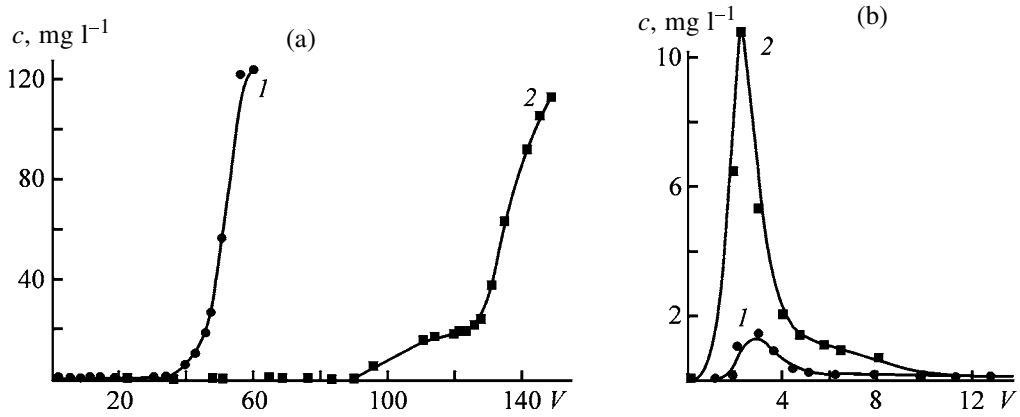

Fig. 2. (a) Breakthrough curves for palladium(II) sorption on resins (*1*) S924 and (*2*) S920, and (b) curves of palladium(II) desorption from the same resins with aqueous thiourea. (*c*) Palladium concentration in the (a) eluate and (b) desorbate and (*V*) eluate volume passed through the column (number of column volumes); the same for Fig. 3. Solution composition, g l^{-1}: Pd 0.150, HCl 109.5, NH_4Cl 53.5, Cu(II) 3.2, Zn(II) 3.25, Fe(III) 2.8, and Sn(IV) 6.

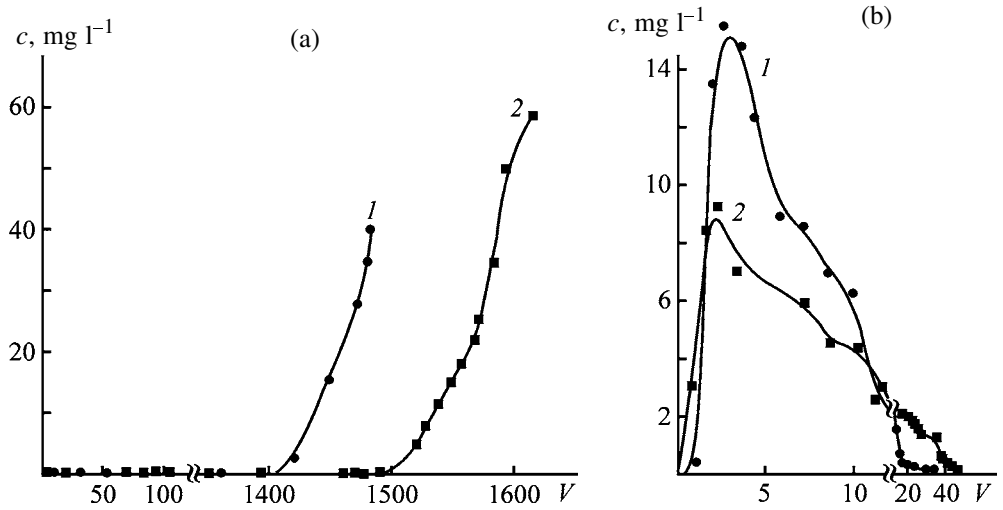

Fig. 3. (a) Breakthrough curbes for palladium(II) sorption on (*1*) S984 and (*2*) S920 resins from weakly acidic solution (pH 5.5) and (b) curves of palladium desorption from (*1*) S984 and (*2*) S920 resins with aqueous thiourea. (a) Solution composition, g l^{-1}: Pd 0.066, NH_4Cl 160, Cu(II) 3.2, and Zn(II) 3.25.

In these fractions, yellow crystalline complexes of palladium(II) with thiourea precipitate. As opposed to S920 resin, from S924 resin palladium is desorbed with aqueous thiourea incompletely (to less than 65%). Therefore, S924 resin was excluded from further experiments.

The S920 and S984 resins efficiently sorb palladium from solution II. In spite of the fact that the palladium(II) concentration in solution II is lower than in solution I, the sorption capacity of S920 for palladium(II) in sorption from solution II is higher than that in sorption from the solution I by a factor of 5. In agreement with the sorption isotherms, S984 anion exchanger exhibits almost the same sorption capacity. Although palladium is fairly completely desorbed with aqueous thiourea from both resins, its desorption from S984 anion exchanger is easier. In desorption of palladium from S920 resin, the mean palladium concentration in the desorbate exceeds its concentration in the initial solution by a factor of 50, and in the desorbate fractions most enriched in palladium this factor exceeds 140. For comparison, in desorption of palladium from S984 resin, these factors are 100 and 230, respectively. In desorption of palladium from both resins, a yellow crystalline complex of palladium(II) with thiourea precipitates.

Analysis of the desorbates for iron and copper shows that the content of these metals is below the detection limit (0.5 and 2.0 mg l^{-1}, respectively).

Table 2. Characteristics of sorption and desorption of palladium from resins under dynamic conditions

Solution composition, g l^{-1}	Resin	Sorption capacity for Pd(II),* mg ml^{-1}		Desorption of palladium(II), mg ml^{-1} resin	c_{Pd} in desorbate, g l^{-1}		Concentration factor	
		DEC	TDEC		average	maximal	average	maximal
Pd 0.150, HCl 109.5, NH_4Cl 53.5, Cu(II) 3.2, Zn(II) 3.3, Fe(III) 2.8, Sn(IV) 6	S920	15	21.4	21.6	3.0	10.8	20	73
	S924	5.8	8.1	3.7	0.26	1.4	1.8	9.5
Pd 0.066, NH_4Cl 160, Cu(II) 3.2, Zn(II) 3.3; pH ~ 3.3	S920	100.4	104.9	104.8	6.1	9.2	54	140
	S984	97.9	98	97.2	6.9	15.5	106	234

* (DEC) Dynamic exchange capacity of resin for palladium to breakthrough; (TDEC) total dynamic exchange capacity of resin for palladium.

CONCLUSIONS

(1) Among resins tested for sorption of palladium from strongly acidic chloride solutions containing nonferrous metal ions and iron(III) (Purolite S920, Purolite S924, Purolite S984, and Purolite A500), Purolite S920 and Puriolte S924 resins with thiourea and thiol functional froups, respectively, show the best selectivity to palladium(II). In sorption of palladium from weakly acidic chloride solutions (pH ~3), the highest selectivity to palladium(II) is shown by Purolite S984 weakly basic anion exchanger with the polyethylenepolyamine functional groups.

(2) Aqueous thiourea virtually completely desorbs palladium(II) from the resins with the thiourea and polyethylenepolyamine functional groups, but from the resin with thiol functional groups the degree of desorption does not exceed 65%.

(3) The Purolite S920 resin efficiently sorbs palladium(II) from strongly acidic solutions simulating the chemical composition of mother liquors formed after precipitation of ammonium hexachloroplatinate(IV) from spent refining solutions. In the case of weakly acidic solutions simulating the chemical composition of the mother liquor after the precipitation of *trans*-dichlorodiamminepalladium from spent refining solutions, the sorption recovery of palladium can be performed with both Purolite S920 and Purolite S984 resins. The palladium can be readily desorbed from these resins with acidified aqueous thiourea.

REFERENCES

1. Meretukov, M.A. and Orlov, A.M., *Metallurgiya blagorodnykh metallov* (Metallurgy of Precious Metals), Moscow: Metallurgiya, 1991.
2. Simanova, S.A., Kukushkin, Yu.N., Kolontarev, I.Ya., et al., *Zh. Prikl. Khim.*, 1978, vol. 51, no. 8, pp. 1871–1874.
3. Blokhin, A.A., Abovskii, N.D., Murashkin, Yu.V., et al., *Sorbts. Khromatogr. Protsessy*, 2004, vol. 4, pp. 40–49.
4. Fan Zhefeng, *Chem. Mag.*, 2004, vol. 6, no. 4, p. 23.
5. Myasoedova, G.V. and Malofeeva, G.I., *Zh. Anal. Khim.*, 1979, vol. 34, no. 8, pp. 1626–1638.
6. *Analiticheskaya khimiya metallov platinovoi gruppy* (Analytical Chemistry of Platinum Metals), Zolotov, Yu.A., Varshal, G.M., and Ivanov, V.M., Eds., Moscow: URSS, 2003.
7. *Ionity v tsvetnoi metallurgii* (Ion Exchangers in Nonferrous Metallurgy), Lebedev, K.B., Ed., Moscow: Metallurgiya, 1975.
8. Krashenina, S.V., Saburbaeva, L.Yu., and Sukhanova, O.M., *Tsvetn. Met.*, 1997, no. 10, pp. 42–43.
9. Skorokhodov, V.I., Goryaeva, O.Yu., and Naboichenko, S.S., *Tsvetn. Met.*, 2004, no. 5, pp. 38–41.
10. Bogdanov, V.I., Gorbatova, L.D., Grokhovskii, S.V., et al., *Tsvetn. Met.*, 2001, nos. 9–10, pp. 33–37.
11. Grokhovskii, S.V., Gorbatova, L.D., Konik, K.P., et al., Abstracts of Papers, *XVII Mezhdunarodnoe Chernyaevskoe soveshchanie po khimii, analizu i tekhnologii platinovykh metallov* (XVII Int. Chernyaev Meet. on Chemistry, Analysis, and Technology of Platinum Metals), Moscow: GEOKhI, 2001, p. 230.
12. Ginzburg, S.I., *Analiticheskaya khimiya platinovykh metallov* (Analytical Chemistry of Platinum Metals), Moscow: Nauka, 1972.
13. Marczenko, Z., *Kolorymetryczne oznaczanie pierwiastkow*, Warsaw: Naukowa-Techniczne, 1968.
14. Simanova, S.A., Bobritskaya, L.S., Kukushkin, Yu.M., and Kolontarov, I.Ya., *Zh. Prikl. Khim.*, 1981, vol. 54, no. 3, pp. 514–517.
15. US Patent 5 256 187.

ISSN 1070-4272, Russian Journal of Applied Chemistry, 2007, Vol. 80, No. 7, pp. 1063–1067. © Pleiades Publishing, Ltd., 2007.
Original Russian Text © N.D. Abovskii, A.A. Blokhin, Yu.V. Murashkin, 2007, published in Zhurnal Prikladnoi Khimii, 2007, Vol. 80, No. 7, pp. 1094–1098.

SORPTION AND ION-EXCHANGE PROCESSES

Kinetics of Platinum(II) and Platinum(IV) Sorption from Hydrochloric Acid Solutions with a Complexing Ion Exchanger Containing Thiourea Functional Groups and with a Strongly Basic Anion Exchanger

N. D. Abovskii, A. A. Blokhin, and Yu. V. Murashkin

St. Petersburg State Institute of Technology (Technical University), St. Petersburg, Russia

Received March 16, 2007

Abstract—The kinetics of platinum(II) and platinum(IV) sorption from 2 M HCl with Purolite S920 complexing ion exchanger containing thiourea functional groups and Purolite A500 strongly basic anion exchanger was studied in relation to the resin granule size, stirring intensity, and temperature.

DOI: 10.1134/S1070427207070099

Ion exchange is one of the most efficient methods for recovery of platinum metals (PM) from multicomponent chloride solutions [1, 2]. Among known ion exchangers, complexing ion exchangers containing thiourea functional groups exhibit particularly high selectivity to PM, including platinum [3–5]. However, choice of an ion exchanger is governed not only by its selectivity, but also by the sorption rate. The majority of papers on platinum sorption with ion exchangers containing thioamide functional groups [5–7] dealt with experimental samples of ion exchangers (in particular, fibrous sorbents, whose use involves certain problems). By now, many complexing ion exchangers with various functional groups (including thiourea groups) have become commercially available. In this study, we examined the kinetics of sorption of platinum(II) and platinum(IV) chloride complexes from hydrochloric acid solutions with Purolite S920 commercial ion exchanger containing thiourea functional groups and (for comparison) with Purolite A500 strongly basic anion exchanger.

EXPERIMENTAL

Experiments were performed with commercial macroporous ion exchangers on a polystyrene matrix, produced by the Purolite Int. Ltd. company: Purolite S920 with thiourea functional groups and strongly basic anion exchanger Putolite A500 (hereinafter S920 and A500, respectively). S920 was in the protonated form, and A500, in the chloride form. The ion exchangers were preliminarily separated into 0.16–0.25-, 0.25–0.5-, and 0.5–1.0-mm fractions (in the swollen state).

The kinetics of platinum(II) and platinum(IV) sorption was studied by the method of the restricted volume at s : l 1 : 1000 (gram of absolutely dry ion exchanger : milliliter of solution). The sorption was performed from a 2 M HCl solution with the initial platinum concentration of 0.5 mM. In the experiments, we varied the ion exchanger granulation, rate of stirrer rotation (from 100 to 500 rpm), and temperature (20, 30, 40, and 50°C). As it will be shown, the rate of platinum(II) and platinum(IV) sorption in all the systems studied is mainly controlled by inner diffusion. To calculate the apparent diffusion coefficient, we used the Boyd–Adamson–Myers equation [8]. In spite of the fact that this equation was intended for calculation of diffusion coefficients under conditions of renewable solution (method of thin layer), in our case its use is justified by the fact that the quantity $\omega' = \bar{c}\bar{V}/(cVK_u)$ parameter ($\bar{c}$ and c are the platinum concentrations in the ion exchanger phase and in solution; $\bar{V}$ and V are the volumes of the ion exchanger and contacting solution, respectively; and K_u, metal distribution coefficient) is 0.005–0.01 depending on the ion exchanger, i.e., is close to zero [9]. For each experimental value of F (degree of equilibrium attainment), using the table in [10], we found the corresponding value of dimensionless time $B\tau$ and constructed the dependence of $B\tau$ on τ. The effective diffusion coefficients were determined by the equation

$$D = B\tau^2/\tau\pi^2, \quad (1)$$

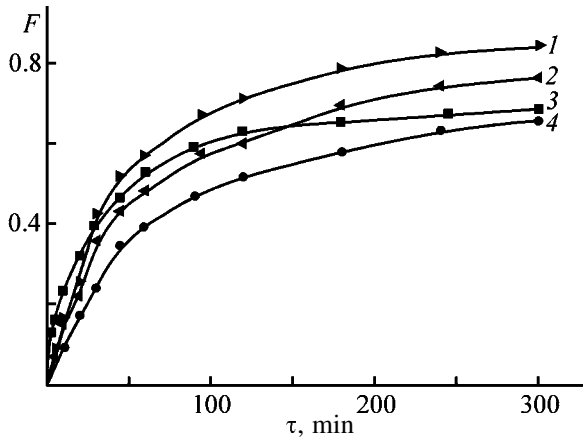

Fig. 1. Degree of the equilibrium attainment F as a function of time τ in Pt(II) sorption with (*1, 2*) A500 and (*3, 4*) S920 ion exchangers. Ion exchanger granulation: (*1, 3*) 0.16–0.25 and (*2, 4*) 0.5–1.0 mm. 20°C; Stirrer rotation rate 200 rpm; the same for Fig. 3.

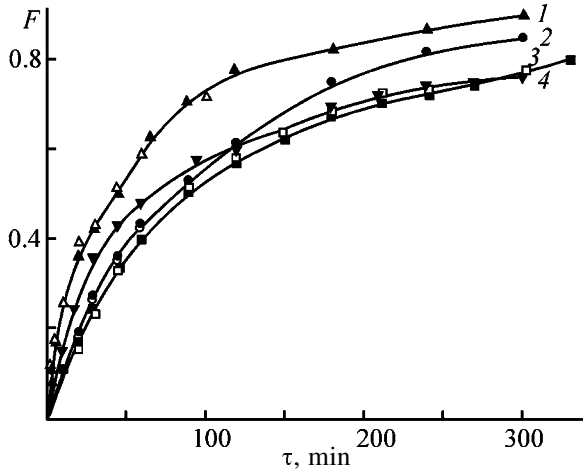

Fig. 2. Degree of the equilibrium attainment F as a function of time τ in sorption of (*1, 2*) Pt(IV) and (*3, 4*) Pt(II) with ion exchangers (*1, 3*) A500 and (*2, 4*) S920 at 20°C. Stirrer rotation rate, rpm: filled points, 60; hollow points, 400.

where r is the average radius of swollen ion exchanger grains.

The apparent activation energies E_a were calculated from the temperature dependences of the apparent diffusion coefficients by the Arrhenius equation

$$D = D_0 e^{-E_a/RT}. \quad (2)$$

The Biot criterion was estimated from the time dependences of $-\log(1 - F)$ [11], which at relatively large τ become straight lines cutting off $\log B_1$ segments on the ordinate axis. From the lengths of these segments, using the table in [12], we found the Biot criterion values.

The platinum concentration in the solution was determined photocolorimetrically from the intensity of the color of the Pt complex with tin(II) chloride [13]. The amount of sorbed platinum was found as the difference between the platinum concentrations in the initial solution and in the solution after contact with the sorbent, taking into account the amount of the ion exchanger and the volume of the contacting solution. The equilibrium capacity of the ion exchangers was determined through the change in the platinum concentration in the solution after stirring with the ion exchanger for 40–80 h depending on temperature. The preliminary experiments showed that this time is sufficient to attain the equilibrium.

The specific surface area of dried samples of the ion exchanger was estimated by the method of low-temperature argon adsorption [14]; total pore volume, by isooctane sorption [15]; and the mean pore radius, from the equation [16]

$$r = 2V/S, \quad (3)$$

where V is the total pore volume ($m^3\ g^{-1}$) and S, specific surface area ($m^2\ g^{-1}$).

First we studied how the resin granule size affects the rate of platinum(II) and platinum(IV) sorption. Figure 1 illustrates the influence of the resin granule size on the kinetics of attainment of the equilibrium for the platinum(II) sorption with A500 and S920 ion exchangers.

As can be seen, an increase in the granule size leads to a decrease in the rate of platinum(II) sorption on both ion exchangers. The same result is observed for platinum(IV) sorption.

Thus, the platinum(II) and platinum(IV) sorption with both A500 strongly basic anion exchanger and S920 complexing ion exchanger depends on the granule size. This fact shows that diffusion, rather than chemical reaction, is the slowest and hence the rate-determining step of the sorption.

Then we examined the influence of the stirring intensity on the platinum sorption kinetics (Fig. 2). As can be seen, the rate of equilibrium attainment in the sorption of both platinum(II) and platinum(IV) with both ion exchangers is virtually independent of the stirring intensity. This fact indicates that the sorption rate is controlled mainly by inner diffusion.

This conclusion is confirmed by the shape of the dependences F–$\tau^{0.5}$, $-\log(1 - F)$–τ, and $B\tau$–τ for the sorption of platinum(II) and platinum(IV) with S920 and A500 ion exchangers (Fig. 3).

Indeed, at degrees of equilibrium attainment F 0.3–

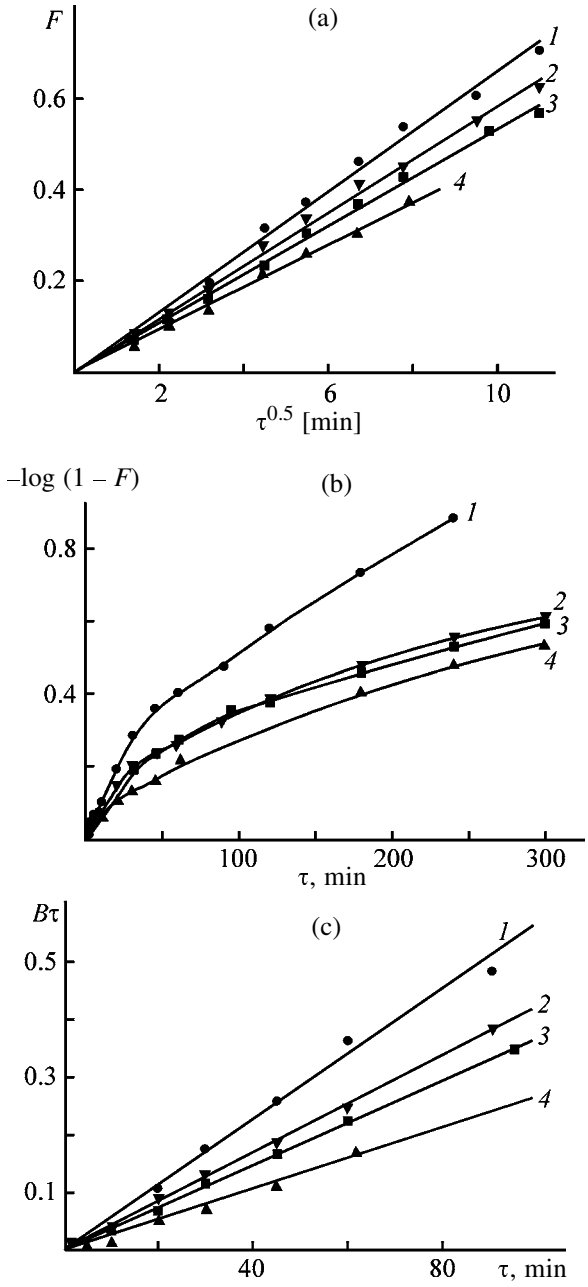

Fig. 3. Plots (a) F–$\tau^{0.5}$, (b) $-\log(1 - F)$–τ, and (c) B_t–τ for (*1, 2*) Pt(IV) and (*3, 4*) Pt(II) sorption with (*1, 3*) A500 and (*2, 4*) S920 ion exchangers. (F) Degree of equilibrium attainment, (τ) time, and ($B\tau$) dimensionless time parameter.

0.7, the F–$\tau^{0.5}$ dependences are straight lines issuing from the origin. The dependences $-\log(1 - F)$–τ deviate from linearity at low F (0.2–0.4) and become straight lines at high F, whereas the $B\tau$–τ dependences are straight lines at low F. Such a shape of the above dependences is characteristic for ion-exchange processes whose kinetics is controlled by inner diffusion [8].

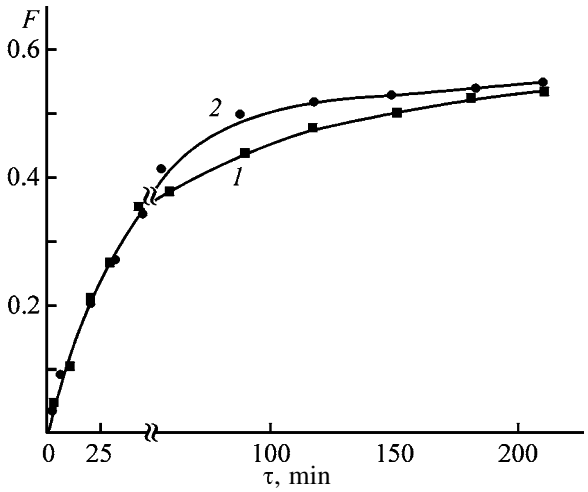

Fig. 4. Degree of the equilibrium attainment F as a function of time τ (*1*) without interruption and (*2*) with interruption of Pt(IV) sorption with S920 ion exchanger.

The interruption technique is considered as the most reliable method of revealing the rate-determining step of ion exchange (outer or inner diffusion) [8]. In such an experiment, when the kinetics of platinum(IV) sorption with S920 was studied, 45 min after starting the sorption the sorbent grains were separated from the contacting solution and then, after 90 min, these grains were again placed into the same solution. Immediately after the contact was resumed, the sorption rate increased (Fig. 4), which is characteristic of ion exchange processes whose kinetics is determined by inner diffusion. The absolute values of Biot criterion listed in the table lead to the same conclusion.

At a fixed rotation rate (200 rpm) and the same granulation (0.5–1.0 mm), we examined the influence of temperature on the rate of the equilibrium attainment in platinum(II) and platinum(IV) sorption with both ion exchangers. The temperature dependences of the apparent coefficients of platinum(II) and platinum(IV) inner diffusion are shown in Fig. 5.

The data on sorption kinetics for both S920 and A500 are summarized in the table.

As can be seen, the apparent diffusion coefficients of both platinum(II) and platinum(IV) vary within the $n \times 10^{-9}$–$n \times 10^{-8}$ $cm^2\ s^{-1}$ range depending on ion exchanger and temperature. The apparent activation energies we determined are typical of ion-exchange processes controlled by inner diffusion [8, 10].

In general, platinum(II) and platinum(IV) sorption on A500 strongly basic anion exchanger can occur only through exchange of negatively charged chloride complexes $[PtCl_4]^{2-}$ or $[PtCl_6]^{2-}$ with chloride ions neutralizing the charge of anion exchanger functional

Parameters of platinum(II) and platinum(IV) sorption kinetics with S920 and A500 ion exchangers

Ion exchanger	Pt oxidation state	T, °C	$\tau_{1/2}$, min	Bi	D, $cm^2\ s^{-1}$	E_a, $kJ\ mol^{-1}$
S920	Pt(IV)	20	74	>50	$(2.8\pm0.2)\times10^{-9}$	40±6
		30	42	>50	$(4.2\pm0.2)\times10^{-9}$	
		40	29	>50	$(8.0\pm0.1)\times10^{-9}$	
		50	23	>50	$(12\pm0.3)\times10^{-9}$	
	Pt(II)	20	124	>50	$(1.2\pm0.1)\times10^{-9}$	39±14
		30	65	>50	$(1.5\pm0.1)\times10^{-9}$	
		40	33	>50	$(3.7\pm0.1)\times10^{-9}$	
		50	12	>50	$(1.5\pm0.1)\times10^{-8}$	
A500	Pt(IV)	20	46	>50	$(9.4\pm0.4)\times10^{-9}$	15±3
		30	49	>50	$(1.0\pm0.1)\times10^{-8}$	
		40	34	>50	$(1.3\pm0.1)\times10^{-8}$	
		50	31	>50	$(1.4\pm0.1)\times10^{-8}$	
	Pt(II)	20	84	>50	$(6.6\pm0.2)\times10^{-9}$	29±4
		30	43	>50	$(9.9\pm0.2)\times10^{-9}$	
		40	42	>50	$(1.4\pm0.1)\times10^{-8}$	
		50	31	>50	$(1.6\pm0.1)\times10^{-8}$	

groups. On S920 ion exchanger with thiourea functional groups, the platinum(II) and platinum(IV) sorption should proceed through complex formation with thiourea functional groups of the ion exchanger, i.e., by exchange of chloride ions initially located in the inner coordination sphere of platinum for fixed ligands (ion exchanger functional groups) with the formation of complexes in the ion exchager phase [17]. In the process, platinum(IV) can be reduced with thiourea groups to platinum(II) [17]. However, the rates of these reactions are probably fairly high and, in any case, higher than the rate of diffusion inside ion exchanger granules. Therefore, in spite of the difference in the mechanism of platinum(II) and platinum(IV) sorption with A500 strongly basic anion exchanger (ion exchange) and S920 complexing resin (complex formation with ion exchanger functional groups and probably redox reaction), in all the systems studied, inner diffusion is the rate-determining step.

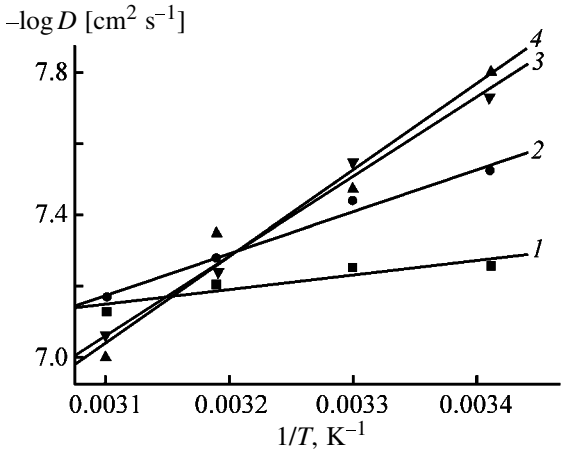

Fig. 5. Effective coefficients of inner diffusion D of (*1, 4*) Pt(IV) and (*2, 3*) Pt(II) as functions of temperature T in sorption with (*1, 2*) A500 and (*3, 4*) S920 ion exchangers.

At the same time, the rate of both platinum(II) and platinum(IV) sorption with A500 strongly basic anion exchanger and the effective diffusion coefficients of Pt(II) and Pt(IV) are noticeably higher than the rate of sorption with S920 complexing ion exchanger, whereas the effective activation energy is lower. This is probably caused by stronger hindrance of platinum(II) and platinum(IV) diffusion inside S920 grains because of their specific interaction with the sorbent functional groups. Differences in the pore structure of the sorbent matrixes can also cause differences in the kinetic characteristics of the ion exchange. The specific surface area of dry S920 and A500 ion exchangers is 6.8 and 23 $m^2\ g^{-1}$; total pore volume, 0.63 and 0.36 $cm^3\ g^{-1}$; and mean pore radius, 185 and 31 nm, respectively. Of course, it should be taken into account that, after swelling of macroporous ion exchangers in aqueous solution, their specific surface area and mean pore radius can change substantially. Furthermore, the characteristics of the pore structure of the dried ion exchangers were estimated by the simplified method. Nevertheless, we can suggest that certain differences in the pore structure of S920 and A500 matrices do exist, which can affect the permeability of these ion exchangers to chloride complexes of platinum(II) and platinum(IV).

In general, we believe that, although the rate of platinum(II) and platinum(IV) sorption with S920 and

A500 ion exchangers is moderate, the kinetic factor in their recovery in the dynamic mode will not lead to essential complications.

CONCLUSIONS

(1) The influence exerted by the ion exchanger grain size and stirring rate on the time dependence of the degree of the equilibrium attainment in platinum(II) and platinum(IV) sorption from 2 M hydrochloric acid with Purolite A500 strongly basic anion exchanger and Purolite S920 complexing ion exchanger with thiourea functional groups was examined. The sorption rate of both platinum(II) and platinum(IV) is mainly limited by inner diffusion.

(2) The apparent diffusion coefficients [$n \times (10^{-8}$–$10^{-9})$ $cm^2\ s^{-1}$], apparent activation energies (15–40 kJ mol^{-1}), and Biot criterion (>50) in platinum(II) and platinum(IV) sorption with Purolite A500 and Purolite S920 ion exchangers were estimated.

(3) Both platinum(II) and platinum(IV) are sorbed with Purolite A500 anion exchanger at a higher rate than with Purolite S920 complexing ion exchanger.

REFERENCES

1. *Ionity v tsvetnoi metallurgii* (Ion Exchangers in Nonferrous Metallurgy), Lebedev, K.B., Ed., Moscow: Metallurgiya, 1975.
2. Meretukov, M.A. and Orlov, A.M., *Metallurgiya blagorodnykh metallov (zarubezhnyi opyt)* (Metallurgy of Noble Metals (Foreign Experience)), Moscow: Metallurgiya, 1991.
3. Warshawsky, A., in *Hydrometallurgy: Research, Development, and Plant Practice: Proc. 3rd Int. Symp. on Hydrometallurgy, 112 AIME Annual Meet.*, Atlanta, 1983, pp. 517–527.
4. Warshawsky, A., Fieberg, M.M.B., Michalik, P., et al., *Sep. Purif. Meth.*, 1980, vol. 9, no. 2, pp. 209–265.
5. Simanova, S.A., Kolontarov, I.Ya., Bobritskaya, L.S., and Lysenko, A.A., *Zh. Prikl. Khim.*, 1989, vol. 62, no. 8, pp. 1840–1844.
6. Pozhidaev, Yu.N., Belousova, L.I., Vlasova, N.N., and Voronkov, M.G., *Dokl. Ross. Akad. Nauk*, 2000, vol. 370, no. 5, pp. 636–637.
7. Simanova, S.A., Kukushkin, Yu.N., Kolontarov, I.Ya., et al., *Zh. Prikl. Khim.*, 1978, vol. 51, no. 8, pp. 1872–1874.
8. Helfferich, F., *Ionenaustauscher*, Weinheim: Chemie, 1959, vol. 1.
9. Samsonov, G.V., Trostyanskaya, E.B., and El'-kin, G.E., *Ionnyi obmen: Sorbtsiya organicheskikh veshchestv* (Ion Exchange: Sorption of Organic Substances), Leningrad: Nauka, 1969.
10. Reichenberg, D., *J. Am. Chem. Soc.*, 1953, vol. 75, pp. 589–597.
11. Kokotov, Yu.A. and Pasechnik, V.A., *Ravnovesie i kinetika ionnogo obmena* (Equilibrium and Kinetics of Ion Exchange), Moscow: Khimiya, 1970.
12. Lykov, A.V., *Teoriya teploprovodnosti* (Theory of Heat Conductivity), Moscow: Vysshaya Shkola, 1967.
13. Ginzburg, S.I., Ezerskaya, N.A., Prokof'eva, I.V., et al., *Analiticheskaya khimiya platinovykh metallov* (Analytical Chemistry of Platinum Metals), Moscow: Nauka, 1972.
14. *GOST* (State Standard) *23401–90: Metal Powders: Catalysts and Supports. Determination of Specific Surface Area*, Moscow: Izd. Standartov, 1991.
15. Polyanskii, N.G., Gorbunov, G.V., and Polyanskaya, N.L., *Metody issledovaniya ionitov* (Methods for Studying Ion Exchangers), Moscow: Khimiya, 1976.
16. Gregg, S.J. and Sing, K.S.W., *Adsorption, Surface Area, and Porosity*, New York: Academic, 1982, 2nd ed.
17. Koster, G. and Schmuckler, G., *Anal. Chim. Acta*, 1967, vol. 38, pp. 179–184.

ISSN 1070-4272, Russian Journal of Applied Chemistry, 2007, Vol. 80, No. 7, pp. 1068–1072. © Pleiades Publishing, Ltd., 2007.
Original Russian Text © B.N. Afanas'ev, E.A. Mozhzherina, Yu.P. Akulova, O.V. Proskurina, A.M. Timonov, 2007, published in Zhurnal Prikladnoi Khimii, 2007, Vol. 80, No. 7, pp. 1099–1103.

SORPTION AND ION-EXCHANGE PROCESSES

Determination of Thermodynamic Parameters Characterizing the Adsorption of Nickel Complexes with Schiff Bases from Acetonitrile Solution at the Air–Solution Interface and on an Uncharged Graphite Surface

B. N. Afanas'ev, E. A. Mozhzherina, Yu. P. Akulova, O. V. Proskurina, and A. M. Timonov

St. Petersburg State Institute of Technology (Technical University), St. Petersburg, Russia
Herzen State Pedagogical University, St. Petersburg, Russia

Received October 30, 2006

Abstract—Adsorption of a nickel(II) complex with a ligand *N,N'*-2,3-dimethylbutane-2,3-diylbis(salicylidenimine) on a powdered thermally expanded natural graphite and at the air–solution interface from an acetonitrile solution was studied at 283 and 293 K.

DOI: 10.1134/S1070427207070105

The chemistry of conducting polymeric compounds is a vigorously developing area of modern chemical science [1, 2]. Polymerization is always accompanied by adsorption of monomers on the electrode surface. In [3], the adsorption of a nickel(II) complex Ni(SalEn) on a powdered thermally expanded natural graphite from acetonitrile solutions was studied in the temperature range 273–313 K and thermodynamic parameters characterizing the adsorption of this compound were determined. This study is concerned with the adsorption on a nickel(II) complex with *N,N'*-2,3-dimethylbutane-2,3-diylbis(salicylidenimine) [Ni(SaltmEn)] at the air–solution interface and on powdered thermally expanded graphite at 283 and 293 K.

The structures of the compounds studied are presented below:

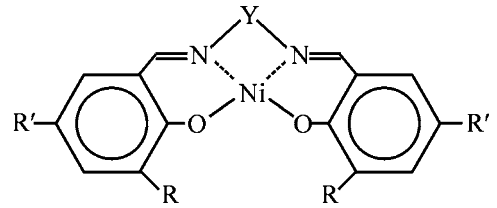

where R, R' = H, Y = $-CH_2-CH_2-$ [Ni(SalEn)] and R, R' = H, Y = $-C(CH_3)_2-C(CH_3)_2-$ [Ni(SaltmEn)].

The aim of our study was to determine parameters that characterize the binding of Ni(SaltmEn) molecules to the graphite surface.

If a surfactant is adsorbed at the air–solution interface and the adsorption is described by a Frumkin or Langmuir isotherm, then, as demonstrated in [4], the following equation is valid:

$$\Delta G_B^{\infty} = (\Delta G_{ads}^0)^s + RT\ln\gamma_{org}^s/\nu - RT\ln\gamma_{org}^{\infty}, \qquad (1)$$

where ΔG_B^o is the standard Gibbs energy of adsorption, which corresponds to an asymmetric choice of the standard state; ν, number of solvent moles displaced from the surface upon adsorption of 1 mol of the surfactant; γ_{org}^{∞} and γ_{org}^s, activity coefficients of the surfactant in an infinitely dilute solution and in the surface layer, which correspond to a symmetric choice of the standard state.

The activity coefficient γ_{org}^{∞} characterizes the properties of a very dilute solution and may vary, depending on the surfactant and solvent properties, within the range from unity (ideal solution) to 10^3–10^5 [5].

The standard Gibbs energy of adsorption $(\Delta G_{ads}^0)^s$, corresponding to the symmetric choice of the standard state in the solution bulk and in the near-surface layer, can be calculated using the equation [6]

$$(\Delta G_{ads}^0)^s = (\Gamma_{max})^{-1}(\sigma_{org} - \sigma_{solv}), \qquad (2)$$

where σ_{org} and σ_{solv} are the surface tensions of the surfactant and solvent, and Γ_{max}, maximum number of surfactant moles adsorbed on unit surface area.

If a surfactant is adsorbed on the surface of a metal M, graphite, or oxide, it is necessary to take into account the Gibbs energy of the interaction of the surfactant with the adsorbent surface. Because the Gibbs energy is an additive quantity, Eq. (2) should be written as

$$(\Delta G^0_{ads})^s_M = \Delta(\Delta G^0_{M-SA}) + (\Gamma'_{max})^{-1}(\sigma_{org} - \sigma_{solv}), \quad (3)$$

where $\Delta(\Delta G^0_{M-SA})$ is that component of the standard Gibbs energy $(\Delta G^0_{ads})^s_M$ which appears if an adsorbed surfactant molecule interacts with solvent molecules on the adsorbent surface,

$$\Delta(\Delta G^0_{M-SA}) = \Delta G^0_{M-SA} - \Delta G^0_{solv}, \quad (4)$$

where $\Delta(\Delta G^0_{M-SA})$ and $\Delta(\Delta G^0_{M-solv})$ are the standard Gibbs energies of adsorption, which characterize the adsorbent–surfactant and adsorbent–solvent binding.

It follows from Eqs. (1) and (3) that the following equation is valid for the adsorpiton of a surfactant on the adsorbent surface:

$$\Delta G^0_A = \Delta(\Delta G^0_{M-SA}) + (\Gamma'_{max})^{-1}(\sigma_{org} - \sigma_{solv}) + RT\ln(\gamma^\infty_{org})'/\nu' - RT\ln\gamma^\infty_{org}, \quad (5)$$

where ΔG^0_A is the experimental Gibbs energy of adsorption, calculated using the known equation [7]:

$$\ln(B\Sigma n) = -\Delta G^0_A/RT; \quad (6)$$

Σn, number of solvent moles in 1 l; B, adsorption constant in the Frumkin or Langmuir isotherm; (γ^s_{org}), ν', and Γ_{max}, parameters characterizing the adsorption of the surfactant on a metal, graphite, or oxide.

Subtraction of Eq. (1) from (5) gives

$$\Delta(\Delta G^0_A) = \Delta G^0_A - \Delta G^0_B = \Delta(\Delta G^0_{M-SA}) + [(\Gamma'_{max})^{-1} - (\Gamma_{max})^{-1}](\sigma_{org} - \sigma_{solv}) + RT\ln(\gamma_{org})'/\gamma_{org} - RT\ln\nu'/\nu. \quad (7)$$

If the surfactant orientation remains unchanged on passing from the air–solvent interface to that between a metal (oxide) and a solution, then

$$\Gamma'_{max} \approx \Gamma_{max} \text{ and } \nu' \approx \nu. \quad (8)$$

In this case, the following approximate equation is valid:

$$\Delta(\Delta G^0_A) = \Delta(\Delta G^0_{M-SA}) + RT\ln(\gamma^s_{org})'/\gamma^s_{org}. \quad (9)$$

EXPERIMENTAL

The procedure we used in studies with powdered thermally expanded graphite was the same as that described in [3]. The concentration of a saturated monomer solution was determined from a calibration plot of the optical density against concentration. We found that the saturation concentration of Ni(SaltmEn) in acetonitrile c^{sat}_{org} = 0.064 M at T = 293 K and 0.046 M at T = 283 K.

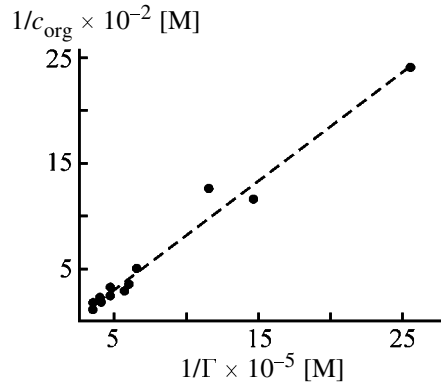

Fig. 1. Experimental dependence in the $1/c_{org}$–$1/\Gamma$ coordinates, described by the Langmuir isotherm (10), which characterizes the adsorption of the nickel complex Ni(SaltmEn) dissolved in acetonitrile on the graphite surface at T = 293 K. (c_{org}) Concentration of the complex in acetonitrile and (Γ) amount of monomer adsorbed on 1 m^2 of the graphite surface.

We studied the adsorption of Ni(SaltmEn) at the air–solution interface using several methods. In the first of these, the surface tension was determined by measuring the reflection of light (laser beam) from the meniscus [8], and in the second, the modified method of a Wilhelmy plate was used [9]. The absolute error in determining the surface tension by these methods was 0.5 mN m^{-1}.

The experimental data we obtained in a study of Ni(SaltmEn) adsorption on powdered graphite were described by the Langmuir isotherm

$$(c_{org})^{-1} = B\Gamma'_{max}/\Gamma_{max} - B \quad (10)$$

and by the Frumkin isotherm

$$\Gamma(\Gamma'_{max} - \Gamma_{max})^{-1}\exp(-2a\Gamma/\Gamma'_{max}) = Bc_{org}, \quad (11)$$

where Γ is the number of monomer moles adsorbed on 1 m^2 of the graphite surface, and a is the attraction constant in the Frumkin isotherm.

Figure 1 shows the experimental dependence of $1/c_{org}$ on $1/\Gamma$, obtained at T = 293 K. It can be seen that the experimental data are well described by the Langmuir isotherm. We used Origin software [3, 4] to find the parameters Γ'_{max}, a, and B in the Frumkin isotherm.

Table 1. Parameters characterizing the Ni(SaltmEn) adsorption at different temperatures

T, K	Frumkin isotherm			Langmuir isotherm	
	B, l mol^{-1}	$2a$	$\Gamma'_{max} \times 10^6$, mol m^{-2}	B, l mol^{-1}	$\Gamma'_{max} \times 10^6$, mol m^{-2}
283	600 ± 200	0.56	3.2 ± 0.2	700 ± 200	3.3 ± 0.2
293	220 ± 50	–0.3	4.0 ± 0.6	200 ± 40	4.5 ± 0.5

Table 2. Thermodynamic parameters characterizing the Ni(SaltmEn) adsorption

T, K	$-\Delta G^0_A$, kJ mol^{-1}	$\Delta(\Delta G^0_A)$, kJ mol^{-1}	$RT\ln\gamma^\infty_{org}$, kJ mol^{-1}	$-\Delta G^0_{ads}$, kJ mol^{-1}
283	22.5 ± 0.6	–19.0 ± 0.6	14.0	8.5 ± 0,6
293	20.5 ± 0.5	–17.5 ± 0.5	13.9	6.6 ± 0.5

The adsorption parameters characterizing the adsorption of Ni(SaltmEn) are listed in Table 1. It can be seen that the values of B and Γ'_{max}, found by processing the experimental data in terms of the Frumkin and Langmuir isotherms, are in agreement within the experimental error. This is due to the fact that the attraction constant $a \le 0.5$. At T = 283 K, the Γ'_{max} for Ni(SaltmEn) molecules virtually coincides with the value $\Gamma'_{max} = (3.5 \pm 0.5) \times 10^{-6}$ mol m^{-2}, obtained in [3] for adsorbed Ni(SalEn) molecules. The area occupied on the graphite surface by a Ni(SaltmEn) molecule at T = 283 K is $(55 \pm 0.5) \times 10^{-20}$ m^2 (molecule)$^{-1}$, which corresponds to the predominantly planar orientation of the adsorbed molecules. As temperature increases, Γ'_{max} slightly grows.

Equation (6) was used to calculate the values of ΔG^0_A, which characterize the monomer adsorption on the surface of the graphite powder. One liter contains 19.024 mol of acetonitrile at T = 298 K. Therefore, we took that $\Sigma n \approx 19$ in ΔG^0_A calculations. The values obtained are listed in Table 2. The parameters are in good agreement with the values of ΔG^0_A, found in [3] for Ni(SalEn), which means that replacement of the $-CH_2-CH_2-$ group with $-C(CH_3)_2-C(CH_3)_2-$ in the monomer molecule has virtually no effect on the Gibbs energy of adsorption.

A study of the Ni(SaltmEn) adsorption at the interface between air and an acetonitrile solution demonstrated that the monomer is very poorly adsorbed, because the change in the surface tension on passing from neat acetonitrile to a solution saturated with Ni(SaltmEn) is within 1 mN m^{-1}, which is comparable with the experimental error. Therefore, we cannot plot an experimental adsorption isotherm. If we assume that the Ni(SaltmEn) adsorption at the air–solution interface is described by the Henry isotherm, we can calculate ΔG^0_B by the equation [4]

$$\Delta G^0_B = -RT\ln[\Delta\sigma(x_{org})^{-1}(RT\Gamma_{max}\nu)^{-1}], \qquad (12)$$

where $\Delta\sigma$ is the change in the surface tension (assumed to be $\Delta\sigma$ = 0.5 mN m^{-1} on passing from neat acetonitrile to a saturated solution); x_{org}, mole fraction of the saturation solution; and ν, number of acetonitrile moles displaced from the surface layer upon adsorption of 1 mol of the surfactant. Taking into account the area occupied on the surface by a Ni(SaltmEn) molecule, we can take that ν = 3. Our calculations demonstrated that $\Delta G^0_B \approx 3$ kJ mol^{-1} at T = 293 K and –3.5 kJ mol^{-1} at T = 283 K. The values of $\Delta(\Delta G'_A)$, calculated by Eq. (7), are listed in Table 2.

It was shown in [10] that the hydrophilicity of a substance is related to its surface tension. The surface tension of graphite is low and close to that of mercury and bismuth [11]. Therefore, we can assume that the parameters characterizing the adsorption of a surfactant on the surface of mercury, bismuth, and graphite should be close to each other [10]. At the same time, it has been found in a study of the adsorption of acetonitrile from an aqueous solution that the value of $\Delta(\Delta G^0_A)$, calculated by Eq. (7), is close to zero [12]. In this case, it follows from Eq. (4) that

$$\Delta G^0_{Hg-CH_3C\equiv N} \approx \Delta G^0_{Hg-H_2O}. \qquad (13)$$

This gives reason to believe that the interaction of an acetonitrile molecule with the Hg surface is approximately the same as that of ν water molecules. In acetonitrile adsorption on the mercury surface, two water molecules are displaced [12]. Consequently, we can compare the value of $\Delta(\Delta G^0_A)$, found in a study of

the adsorption of the monomer from acetonitrile on the graphite surface, with those obtained in an analysis of the adsorption of other surfactants from aqueous solutions on the surface of mercury and bismuth.

The vast body of the available published data [12, 13] demonstrates that, in adsorption of organic molecules from aqueous solutions on an uncharged surface of mercury or bismuth, the values of $\Delta(\Delta G^0_A)$ fall within the range from +5 to –20 kJ mol^{-1}.

Thus, the large negative values of $\Delta(\Delta G^0_A)$ for Ni(SaltmEn) (Table 2) point to a rather strong interaction between an adsorbed monomer molecule and the graphite surface. If we take that $\gamma^\infty_{org}/\gamma_{org} \approx 1$, then, using the values of $\Delta(\Delta G^0_A)$ from Table 2 and the known thermodynamic equation [14]

$$\Delta(\Delta G^0_A) = \Delta(\Delta H^0_A) - T\Delta(\Delta S^0_A), \quad (14)$$

we can calculate the enthalpy of adsorption:

$$\Delta(\Delta H^0_A) = \Delta(\Delta H^0_{M-SA}) - \nu\Delta(\Delta H^0_{M-solv}). \quad (15)$$

Because the parameters $\Delta(\Delta H^0_A)$ and $\Delta(\Delta S^0_A)$ are temperature-independent in a narrow temperature range, calculations by Eq. (14) show that $\Delta(\Delta S^0_A) = -150$ J mol^{-1} and $\Delta(\Delta H^0_A) = -63$ kJ mol^{-1}.

It is commonly believed in studies of the surfactant adsorption on a solid surface from the gas phase that chemisorption is observed if the enthalpy of adsorption falls within the range –(50–400) kJ mol^{-1} [14].

If acetonitrile molecules interact with the graphite surface, then $\Delta(\Delta H^0_{M-solv}) < 0$ and, consequently, $\Delta(\Delta H^0_{M-SA}) > 63$ kJ mol^{-1}. These results point to a weak chemisorption binding of the monomer molecule to the graphite surface.

In [3], experimental data were analyzed in terms of the standard Gibbs energy of adsorption (Γ^0_{ads}), which corresponds to adsorption of the surfactant from a hypothetical ideal solution, calculated using the formula

$$\Delta G^0_{ads} = \Delta G^0_A + RT\ln\gamma^s_{org}. \quad (16)$$

If a surfactant poorly dissolves in the solvent, then the activity coefficient is given by

$$\gamma^0_{org} = (x^{sat}_{org})^{-1}, \quad (17)$$

where x^{sat}_{org} is the saturated surfactant concentration (mole fraction) [7].

Table 2 lists the values of $RT\ln\gamma^\infty_{org}$ and ΔG^0_{ads}. It can be seen that the difference $\Delta G^0_{ads} - \Delta(\Delta G^0_A)$ is

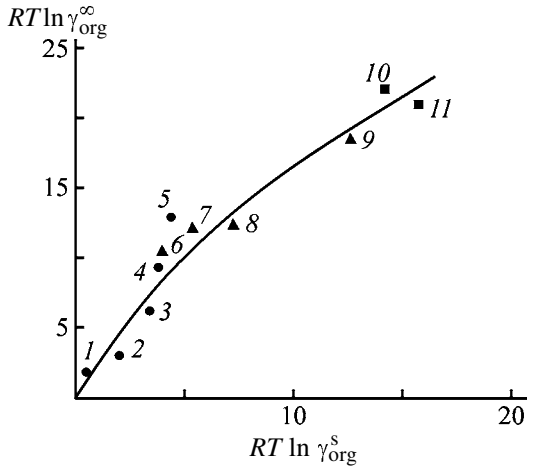

Fig. 2. $RT\ln\gamma^\infty_{org}$ vs. $RT\ln\gamma^s_{org}$ at T = 298 K for various classes of organic compounds. γ^∞_{org} and γ^s_{org} are the surfactant activity coefficients in the infinitely dilute solution and in the surface layer, respectively. (*1*) Methanol, (*2*) ethanol, (*3*) propanol, (*4*) butanol, (*5*) pentanol, (*6*) phenol, (*7*) aniline, (*8*) benzyl alcohol, (*9*) benzoic acid, (*10*) toluene, and (*11*) benzene.

10.5 kJ mol^{-1}. It follows from Eqs. (5), (7), and (8) that

$$\Delta G^0_{ads} - \Delta(\Delta G^0_A) \approx \Delta(\Delta G^0_{ads})^s + RT\ln\gamma^s_{org} - RT\ln\nu. \quad (18)$$

It was shown in [15] that an increase in the size of the hydrophobic part of a molecule results in that the activity coefficients γ^∞_{org} and γ^s_{org} become larger.

Figure 2 shows the dependence of $RT\ln\gamma^\infty_{org}$ on $RT\ln\gamma^s_{org}$. It can be seen that there is a certain correlation between the activity coefficients in the solution bulk and in the surface layer.

The Ni(SaltmEn) molecule contains two benzene rings and a –C(CH$_3$)$_2$–C(CH$_3$)$_2$–carbon chain, and its activity coefficient γ^∞_{org} = 305. All this suggests that $\gamma^s_{org} \gg 1$. Using the plot in Fig. 2, we can easily find that, for the monomer, $RT\ln\gamma^s_{org}$ = 7.5 kJ mol^{-1} and $\gamma^s_{org} \approx 20.5$. Then it follows from Eq. (18) that $(\Delta G^0_{ads})^s \approx 5.7$ kJ mol^{-1} at ν = 3, and we find from Eq. (2) that $\sigma_{org} \approx 50 \times 10^{-3}$ J m^{-2} for the monomer, because $\sigma_{solv} = 29 \times 10^{-3}$ J m^{-2} for acetonitrile [16].

The value of γ^s_{org} points to a strong positive deviation from the Raoult law [14]. This means that the energy of interaction between monomer and acetonitrile molecules substantially exceeds that for the monomer and solvent molecules. If the energy of interaction between the monomer and graphite atoms is not too high, stratification of the surface layer is

possible, with the result that islands of monomer molecules and solvent molecules can be formed.

CONCLUSIONS

(1) A study of the adsorption of the monomer on the graphite powder demonstrated that the experimental data can be described in terms of the Langmuir and Frumkin isotherms.

(2) It was found that the monomer is virtually not adsorbed at all at the air–solution interface.

(3) A calculation of the thermodynamic parameters characterizing the adsorption of the monomer on the graphite powder demonstrated that at least a weak chemisorption occurs.

(4) The activity coefficient of Ni(SaltmEn) in the surface layer $\gamma^{s}_{org} \gg 1$.

REFERENCES

1. Borisov, A.N., Timonov, A.M., and Shagisultanova, G.A., *Zh. Strukt. Khim.*, 1995, vol. 41, no. 2, pp. 333–334.
2. Rodyagina, T.Yu., Chepurnaya, I.A., Vasil'eva, S.V., and Timonov, A.M., *Zh. Prikl. Khim.*, 2005, vol. 78, no. 9, pp. 1416–1422.
3. Afanas'ev, B.N., Aleksandrova, E.A., Akulova, Yu.P., and Logvinov, S.A., *Zh. Prikl. Khim.*, 2004, vol. 77, no. 10, pp. 1643–1646.
4. Afanas'ev, B.N. and Aleksandrova, E.A., *Zh. Fiz. Khim.*, 2004, vol. 78, no. 7, pp. 1130–1135.
5. Morachevskii, A.G., Smirnova, N.A., Balashova, I.M., and Pukinskii, I.B., *Termodinamika razbavlennykh rastvorov neelektrolitov* (Thermodynamics of Dilute Nonelectrolyte Solutions), Leningrad: Khimiya, 1982.
6. Afanas'ev, B.N., Akulova, Yu.P., and Yakovleva, O.R., *Zh. Fiz. Khim.*, 2003, vol. 77, no. 4, pp. 722–731.
7. Damaskin, B.B., Petrii, O.A., and Batrakov, V.V., *Adsorbtsiya organicheskikh soedinenii na elektrodakh* (Adsorption of Organic Compounds on Electrodes), Moscow: Nauka, 1968.
8. Levichev, S.A., *Vestn. Leningr. Gos. Univ.*, 1978, no. 16, pp. 85–89.
9. Noskov, B.A., Akintyev, A.V., Bilibin, A.Yu., and Miller, R.A., *Adv. Colloid Interface Sci.*, 2003, vol. 104, pp. 245–271.
10. Afanas'ev, B.N. and Akulova, Yu.P., *Zashch. Met.*, 2000, vol. 36, no. 1, pp. 29–34.
11. Mezey, L.Z. and Giber, J., *Jpn. J. Appl. Phys.*, 1982, vol. 21, no. 11, pp. 1569–1571.
12. Afanasyev, B.N., Akulova, Yu.P., and Kotlyar, M.M., *J. Solid State Electrochem.*, 1997, vol. 1, no. 1, pp. 68–76.
13. Palm, U.V. and Damaskin, B.B., *Itogi Nauki Tekh., Ser.: Elektrokhim.*, 1977, vol. 12, pp. 99–140.
14. Atkins, P.W., *Physical Chemistry*, Oxford: Oxford Univ. Press, 1978.
15. Afanas'ev, B.N., Akulova, Yu.P., Mozhzherina, E.A., and Proskurina, O.V., *Termodinamika poverkhnostnykh yavlenii i adsorbtsiya: Trudy seminara 4–10 iyulya 2005 g.* (Thermodynamics of Surface Phenomena and Adsorption: Proc. Workshop, July 4–10, 2005), Ivanovo, 2005, pp. 12–15.
16. *Kratkii spravochnik fiziko-khimicheskikh velichin* (Concise Reference Book of Physicochemical Quantities), Ravdel', A.A. and Ponomareva, A.M., Eds., Leningrad: Khimiya, 1983, p. 20.

ISSN 1070-4272, Russian Journal of Applied Chemistry, 2007, Vol. 80, No. 7, pp. 1073–1077. © Pleiades Publishing, Ltd., 2007.
Original Russian Text © V.V. Sidorchuk, V.A. Zazhigalov, V.S. Aleksandrova, L.S. Kuznetsov, 2007, published in Zhurnal Prikladnoi Khimii, 2007, Vol. 80, No. 7, pp. 1104–1108.

SORPTION AND ION-EXCHANGE PROCESSES

Synthesis of $H_3PW_{12}O_{40}$ Based Heteropoly Compounds Chemically Fixed on Silica Surface

V. V. Sidorchuk, V. A. Zazhigalov, V. S. Aleksandrova, and L. S. Kuznetsov

Institute of Sorption and Endoecology Problems, National Academy of Sciences of Ukraine, Kiev, Ukraine

Received September 12, 2006

Abstract—Possibility of activating the silica surface for chemical fixation of tungsten heteropoly compounds of the 12th series on its surface was analyzed.

DOI: 10.1134/S1070427207070117

Thanks to a combination of valuable properties, heteropoly compounds (HPCs) find wide use in numerous practically important processes. On the one hand, heteropoly acids (HPAs) are very strong Brønsted acids in both dissolved and solid states [1–3], which predetermines their successful use in homo- and heterogeneous acid–base catalyses [2–4] and also as solid electrolytes [5]. For this reason, both HPAs and their salts are promising in ion-exchange processes [6, 7]. On the other hand, HPCs include in their composition such elements as molybdenum, tungsten, and vanadium, which imparts redox properties to these compounds and enables their use in catalytic oxidation of organic compounds [2–4, 8, 9]. Thus, HPCs are clearly pronounced bifunctional catalysts. Also known are numerous examples of their use in adsorption [3, 6, 7, 10], membrane [11, 12], and other processes.

Together with possessing a wide variety of valuable properties, compounds of this class also have a number of shortcomings, mostly of technological nature. For example, HPCs have a small specific surface area, up to 5 $m^2 g^{-1}$ [2, 3], and a poorly developed porous structure, mainly represented by micropores [3], which restricts their applications in heterogeneous catalysis and adsorption. At the same time, HPA salts exhibit higher porosity and larger specific surface area, even though they most frequently belong to microporous materials [3, 13, 14] and this leads to slow attainment of equilibrium and impossibility of access of large reagent molecules to the inner surface of pores (diffusion hindrance). Another disadvantage is the comparatively low thermal stability: for HPCs of the 12th series, the Keggin structure disintegrates at 400–450°C [2], which restricts their applicability in some gas-phase catalytic processes.

The purely technological disadvantages of HPCs is their difficult granulation, poor filterability of finely crystalline HPC salts in processes performed in the liquid phase, and low mechanical strength [6]. In economical regard, HPC are rather expensive chemicals, which can also hinder their practical use. However, industrial processes in which HPCs are used as catalysts already exist [2–4].

One way to eliminate these disadvantages of HPCs is their deposition on porous solid supports, both inorganic and organic. Silicas of varied origin are the most frequently used supports for HPCs, as well as for the majority of catalysts.

This study is devoted to synthesis of HPCs on the surface of silica activated by groups that can bind phosphotungstic acid (PTA).

EXPERIMENTAL

A mesoporous aerosilogel with cylindrical grains was used as the starting silica [15]. This aerosilogel was preliminarily activated in two ways.

(1) Reaction of surface silanol groups with 3-aminopropylthriethoxysilane (APTES). It should be noted that this compound has already been used in HPC deposition onto the SiO_2 surface [16, 17]. The reaction itself between APTES and the silica surface is well understood [18]. In the present study, we obtained, by modifying the aerosilogel in an autoclave at 70 and 150°C (preliminarily the aerosilogel was vacuum-treated at 250°C), surface concentrations of amino groups of 0.34 and 0.68 mmol g^{-1}, or 2.2 and 5.9 μmol m^{-2} (supports 1 and 2, respectively).

(2) Reaction of silanol groups with polyhydric alcohols, butanediol and glycerol. The resulting con-

Table 1. Selected physicochemical parameters of supported samples with PTA

Sample no.	Treatment conditions	PTA content, wt %	S, $m^2 g^{-1}$	V_σ, ml g^{-1}	d, nm	c,* μmol m^{-2}
1	Bulk PTA	100	5	–	–	0.780
2	Starting SiO_2	–	303	1.10	14.5	0.009
3	Starting SiO_2, impregnation with PTA	1.65	192	0.96	20.0	0.035
4	Support 1	–	155	0.78	20.1	–
5	Support 1, 20°C, PTA in acetone	0.30	118	0.51	17.5	0.033
6	Support 1, 150°C, PTA in acetone	0.40	96	0.41	17.0	0.045
7	Support 1, 150°C, PTA in water	0.37	90	0.43	19.0	0.047
8	Support 2		115	0.69	24.0	–
9	Support 2, 20°C, PTA in acetone	0.91	60	0.43	28.5	0.043
10	Support 2, 150°C, PTA in acetone	1.11	49	0.39	32.0	0.070
11	Support 2, 150°C, PTA in water	1.15	45	0.40	35.5	0.074
12	Support 2, mechanochemical treatment, water, 2 h	0.90	40	0.39	39.0	0.050
13	Support 3		190	0.90	19.0	–
14	Support 3, 250°C, PTA in acetone	–	285	1.10	15.5	0.009
15	Support 4		181	0.92	20.5	–
16	Support 4, 250°C, PTA in acetone	–	291	1.08	15.0	0.010

* c is the total acidity of the samples synthesized.

centrations of grafted groups were, respectively, 0.42 (support 3) and 0.31 mmol g^{-1} (support 4); in both cases, the reaction was carried out in an acetone solution in an autoclave at 200°C.

Then, PTA ($H_3PW_{12}O_{40}$) was deposited onto the activated supports from solutions at room temperature or in an autoclave at 150–250°C. After the deposition, the samples were thoroughly washed with acetone a room temperature and refluxed in methanol [19]. The course of silica activation and subsequent PTA deposition was qualitatively monitored by IR spectroscopy, on the basis of changes in the absorption intensity and appearance of new absorption bands (Specord M-80 spectrophotometer, double-beam mode, spectral range 4000–400 cm^{-1}, KBr pellets). In addition, the total pore volume of the supports V_σ and the specific surface area S were measured for the same purpose in all stages by impregnation with ethanol and by the method of thermal desorption of argon, respectively. As noted in [20], the total pore volume and the specific surface area steadily decrease in the case of grafting. The amount of grafted groups was found by an integrated derivatographic analysis in air [18] (Q-1500D instrument, temperature range 20–900°C, heating rate 10 deg min^{-1}). The concentration of the deposited PTA was calculated from the results of an X-ray fluorescence analysis (ElvaX spectrometer). The total acidity of the surface of samples with PTA was found from the chromatographically monitored pyridine adsorption at 130°C [21].

It should be primarily noted that the methods suggested for activation of the silica surface lead to different results in the subsequent attempts to immobilize PTA. For example, preliminary modification of the aerosilogel with polyhydric alcohols was followed by its treatment in an autoclave at 200–250°C with 20% PTA solutions in order to involve the OH groups of the grafted alcohol into the reaction that yields an ester bond with PTA, as it occurs in synthesis of phosphoric acid esters. However, formation of this kind of compounds could not be observed in the given case by the methods employed, and IR spectroscopy failed to reveal bound PTA on the surface even upon a treatment under rather severe conditions, at 250°C and a pressure of 55 atm. The same is suggested by the trends in variation of S and V_σ: they steadily decrease upon modification of the starting silica with alcohols (Table 1, sample nos. 13 and 15), but increase as a result of treatment of supports 3 and 4 with PTA solutions, to virtually reach the values for the starting aerosilogel (sample nos. 14 and 16). It has been found [18] that the acid catalyzes the rupture of the Si–O–C bond by which the diol or triol residue is attached to the surface. It is this behavior that is indicated by the run of the TG and DTA curves in the derivatogram. For example, an exothermic effect peaked at 390°C and mass loss in the same range, which corresponds to the content of grafted alcohol groups, are observed when heating glycerol-modified silica (support 4). At the same time, neither thermal effects associated with

Table 2. Absorption bands in IR spectra of supported samples with PTA

Assignment	Sample					
	pure PTA	no. 9	no. 10	no. 11	no. 12	support 2
Stretching modes of $[PO_4]$	1088	1100	1100	1100	1093	
Stretching modes of W=O	980	950	950	983	952	
Stretching modes of W–O–W	897	888	895	895	900	
	795	800	805	805	785	
Bending modes of $[PO_4]$	595	595	600	595	575	
	465	463	462	465	465	
Bending modes of W=O	375	367	370	390	370	
	337					
Stretching modes of C–H		2835	2825	2825	2830	2890
		2950	2930	2965	2955	2945
Stretching modes of N–H		3260	3250	3240	3235	3415
		3350	3350	3360	3360	3495

removal of organic groups or PTA decomposition (which, according to the data obtained, ends for bulk samples in crystallization of tungsten trioxide at 615°C), nor any significant mass loss are observed for sample no. 15 (Table 1) at temperatures above 250°C.

If PTA is deposited onto SiO_2 with amino groups on the surface, it is chemically fixed in all cases. This is indicated by the IR spectra in Fig. 1 and by the band assignment in Table 2. As seen from Fig. 1, the spectra of samples with deposited PTA show, even after thorough washing of the samples, bands typical of the Keggin structure of PTA, which are also present in spectra of bulk PTA (Fig. 1, curve *1*): 1088, 975, 887, 800, 595, 525, 375, and 337 cm^{-1} [1, 22, 23]. The shift of the absorption bands from these positions for supported samples is due to the interaction of PTA with active centers of the support [24]. Apparently, the HPA forms surface compounds of the salt type with amino groups, which is also indicated by the strong shift to lower frequencies of the bands associated with stretching vibrations of the N–H bond. For example, the band at 3495 cm^{-1} shifts after the reaction of amino silica with PTA to 3360–3350 cm^{-1}, and the band at 3415 cm^{-1}, to 3260–3240 cm^{-1}. Similar results have been obtained in the case of interaction of NH_2 groups with surface silanol groups [18, 25].

For all the samples synthesized on supports 1 and 2, a sharp decrease in the specific surface area and total pore volume is observed in the stage of PTA deposition (Table 1), which confirms that PTA is chemically grafted. Interestingly, both the starting silica (aerosilogel) and supported PTA-containing samples obtained on its basis have a mesoporous structure, which is indicated by the values of d (nm).

It is known that the thermal decomposition of 3-aminopropyltriethoxysilyl groups occurs on the silica surface in a wide temperature range, with exo-

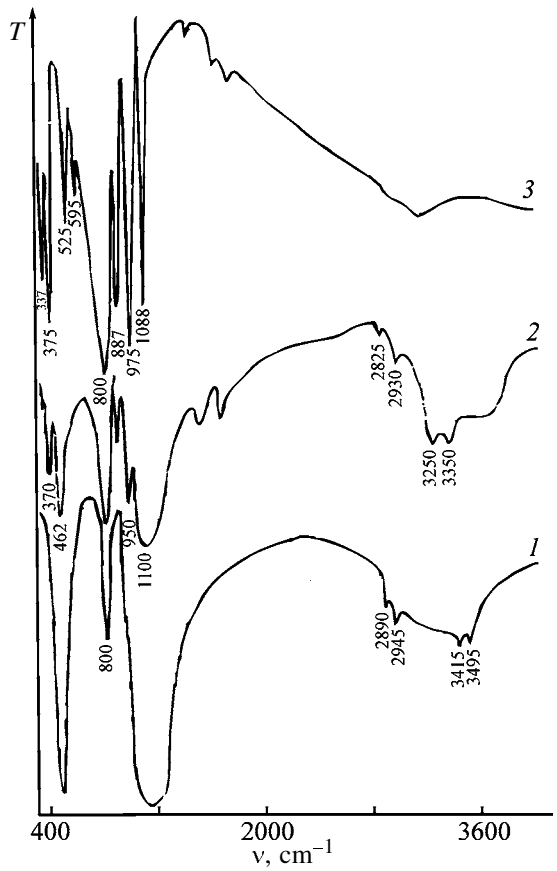

Fig. 1. IR spectra of the samples studied. Sample no.: (*1*) 8 (support 2), (*2*) 10, and (*3*) 1 (pure PTA).

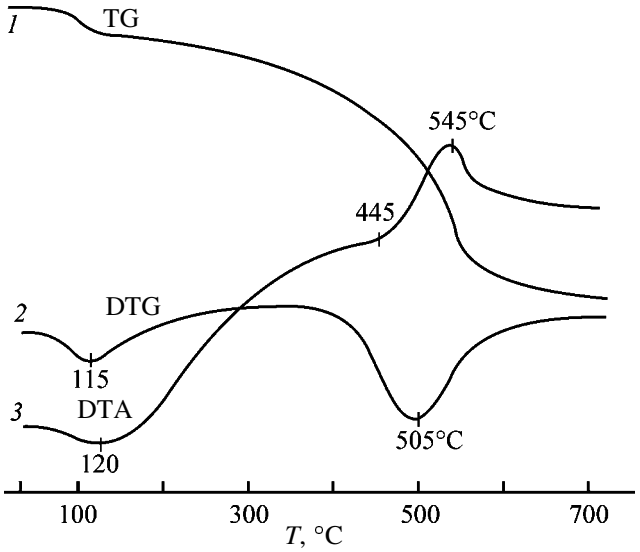

Fig. 2. Derivatographic curves for sample no. 10. (*T*) Temperature. (*1*) TG, (*2*) DTG, and (*3*) DTA.

thermic effects at 315°C (removal of pendant ether groups, with rupture of the Si–O–C bond) and 510°C (rupture of the Si–C bond) [26]. For the amino silicas obtained in this study, the modifying layer is removed from the surface at 250–600°C, with exothermic effects at 330 and 540°C. As found in a study of the supported samples, the surface compounds formed by grafted amino groups and PTA decompose in the same temperature range, with the effect at 330°C lacking in the TG and DTA curves (Fig. 2). As already mentioned, this may be due to decomposition of pendant ethoxy groups by the acid in the step of its deposition. In all probability, the exothermic effect at 545°C and the corresponding mass loss are associated with elimination of the whole modifying fragment, together with the supported PTA. A thermographic analysis of separately synthesized bulk samples in the PTA–3-aminopropyltriethoxysilane system confirmed that such salt decomposes in virtually the same temperature range as that for bulk PTA, at 615–645°C. Thus, it can be assumed that the thermal decomposition of the Keggin structure occurs in supported samples in parallel with the degradation of the organic layer above 400°C without crystallization of tungsten oxide, because the whole fragment is eliminated together with PTA at 540–550°C. This is the difference of the systems in question from those produced by impregnation, in which an increase in the thermal stability of supported HPA, compared to bulk acids, has been observed [2, 3, 27].

Table 1 also lists the total acidities c (μmol m^{-2}) of the synthesized supported samples. As is known [2], solid HPA show a purely Brønsted activity, which, apparently, is largely true for the case under consideration. Also consistent with published data is the sharp decrease in acidity upon PTA deposition onto a support [2, 28]. As seen from Table 1, the acidity c decreases by more than an order of magnitude upon impregnation of a pure (starting) silica with PTA. At the same time, c remains higher upon deposition of PTA onto a silica activated by amino groups. In all probability, the reason for such a behavior is in the extent of PTA interaction with the support surface. For example, on modified supports 1 and 2, the amino group to which PTA is bound lies rather far from the surface, at a distance of at least three $–CH_2–$ links. Therefore, even reacting via one or two protons with an NH_2 group, PTA still has unbound protons to exhibit acid properties. In this case, the acidity depends both on the concentration of amino groups on the support surface and on the conditions of PTA deposition. For example, the amount of PTA fixed on support 2, in which the density of NH_2 groups is 2.7 times that on support 1, is 2.5–3 times higher and the acidity increases by a factor of only 1.3–1.6. The latter may be due to a stronger interaction between the PTA molecule and binding centers (amino groups in the case in question) at their higher concentration (this interaction leads to a shift of the IR absorption bands of amino groups by 135–165 cm^{-1}). For example, it is known [5] that an HPA molecule can interact with five OH groups on the silica surface.

The conditions of PTA deposition (temperature, medium) also affect in a certain way the physicochemical parameters of the resulting samples. For example, an increase in temperature leads to a larger amount of deposited PTA and, accordingly, the acidity grows. In this case, both the specific surface area and the total pore volume decrease. Close values were obtained for all the parameters mentioned above in organic (acetone, ethanol) and aqueous media.

Mention should also be made of a test experiment on mechanochemical deposition of PTA onto support 2 in an aqueous medium (Fritch planetary mill, 700 rpm, agate balls; Table 1, sample no. 12). It can be seen that PTA is also fixed on the surface, but its acidity is somewhat lower, compared to samples produced in an autoclave.

Table 1 also lists the properties of supports 3 and 4 before and after an attempt to deposit PTA. It can be seen that their acidities are about the same and, naturally, close to the values for the starting aerosilogel.

Interestingly, 1- and 2-substituted "salts" synthesized for comparison purposes from PTA and 3-aminopropyltriethoxysilane at 20°C in acetone had a

rather high acidity (0.51 and 0.20 μmol m^{-2}, respectively), which was, however, naturally lower than that of bulk PTA.

CONCLUSIONS

(1) Samples with phosphotungstic heteropoly acid chemically fixed on their surface were produced by interaction of the heteropoly acid with silica modified with amino groups. The sample had the following properties: (i) Keggin structure of the heteropoly anion; (ii) presence of organic and inorganic groups on the surface; (iii) developed mesoporous structure; (iv) not too high, but widely controllable total acidity; (v) stability in aqueous and organic media; and (vi) rather high thermal stability, up to 550°C.

(2) The properties listed above suggest that such materials can serve as adsorbents and ion exchangers, and also can be used in liquid- and gas-phase (with certain limitations) catalysis.

REFERENCES

1. Pope, M.T., *Heteropoly and Isopoly Oxometalates*, Berlin: Springer, 1983.
2. Kozhevnikov, I.V., *Usp. Khim.*, 1993, vol. 62, no. 5, pp. 510–528.
3. Moffat, J.B., *The Surface and Catalytic Properties of Heteropoly Oxometalates, Fundamental and Applied Catalysis*, New York: Kluwer, 2001.
4. Kozhevnikov, I.V., *Catalysis by Polyoxometalates*, Chichester: Wiley, 2002.
5. Akhorukomeie, Zh. and Pak, V.N., *Zh. Prikl. Khim.*, 1992, vol. 65, no. 8, pp. 1757–1760.
6. Pushkarev, V.V. and Nikiforov, A.F., *Sorbtsiya radionuklidov solyami geteropolikislot* (Sorption of Radionuclides by Salts of Heteropoly Acids), Moscow: Energoatomizdat, 1982.
7. Murthey, G.S., Sivceiah, M.V., Kumar, S.S., et al., *J. Radioanal. Nucl. Chem.*, 2004, vol. 260, no. 1, pp. 109–114.
8. Song In, K. and Barteau, M., *J. Mol. Catal.*, 2004, vol. 212, nos. 1–2, pp. 227–236.
9. Okuhara, T., Mizuno, N., and Misono, M., *Appl. Catal. A*, 2001, vol. 222, no. 1, pp. 63–77.
10. Rykova, A.I., Burkat, T.M., and Pak, V.N., *Zh. Prikl. Khim.*, 2000, vol. 63, no. 6, pp. 1038–1040.
11. Liu, Q., Jia, P., and Chen, H., *J. Membr. Sci.*, vol. 159, nos. 1–2, pp. 233–241.
12. Belyakov, V.N., Pal'chik, A.V., Kotvitskii, A.G., and Rozhdestvenskaya, A.M., *Ukr. Khim. Zh.*, 2004, vol. 70, nos. 7–8, pp. 38–45.
13. Corma, A., *Chem. Rev.*, 1997, vol. 97, no. 6, pp. 2373–2419.
14. Okuhara, T., *Catal. Today*, 2002, vol. 73, no. 1, pp. 167–176.
15. Maidannik, D.G., Sidorchuk, V.V., and Tertykh, V.A., *Zh. Prikl. Khim.*, 1993, vol. 66, no. 9, pp. 2054–2058.
16. Mrowiec-Bialon, J., Turek, W., and Jarzebski, A.B., *React. Kinet. Catal. Lett.*, 2002, vol. 76, no. 2, pp. 213–219.
17. Zhu, K., He, H., Xie, S., et. al., *Chem. Phys. Lett.*, 2003, vol. 377, nos. 3–4, pp. 317–321.
18. Tertykh, V.A. and Belyakova, L.A., *Khimicheskie reaktsii s uchastiem poverkhnosti kremnezema* (Chemical Reactions Involving Silica Surface), Kiev: Naukova Dumka, 1991.
19. Rac, B., Mulas, G., Csongradi, A., et al., *Appl. Catal. A*, 2005, vol. 282, pp. 255–265.
20. Sidorchuk, V.V., *Zh. Prikl. Khim.*, 2006, vol. 79, no. 1, pp. 66–70.
21. Bautista, F.M., Campelo, J.M., Garcia, A., et al., *J. Catal.*, 1994, vol. 145, no. 1, pp. 107–125.
22. Okuhara, T., Mizuno, N., and Misono, M., *Adv. Catal.*, 1996, vol. 41, pp. 113–252.
23. Kazanskii, L.P., *Izv. Akad. Nauk SSSR, Ser. Khim.*, 1975, no. 3, pp. 502–507.
24. Fisun, L.A., Akhorukomeie, Zh., and Pak, V.N., *Zh. Prikl. Khim.*, 1992, vol. 65, no. 1, pp. 91–95.
25. Tertykh, V.A., Chuiko, A.A., Khranovskii, V.A., and Neimark, I.E., *Zh. Fiz. Khim.*, 1968, vol. 42, no. 7, pp. 1758–1761.
26. Belyakova, L.A., Tertykh, V.A., and Bortun, A.I., *Khim. Tekhnol.*, 1987, no. 2, pp. 3–10.
27. Goncharova, O.I., Yur'eva, T.M., and Davydov, A.A., *Kinet. Katal.*, 1986, vol. 27, no. 4, pp. 942–949.
28. Kapustin, G.I., Brueva, T.R., Klyachko, A.L., et al., *Kinet. Katal.*, 1990, vol. 31, no. 5, pp. 1017–1021.

ISSN 1070-4272, Russian Journal of Applied Chemistry, 2007, Vol. 80, No. 7, pp. 1078–1081. © Pleiades Publishing, Ltd., 2007.
Original Russian Text © L.A. Kupchik, M.P. Kupchik, O.L. Alekseev, E.S. Bogdanov, 2007, published in Zhurnal Prikladnoi Khimii, 2007, Vol. 80, No. 7, pp. 1109–1112.

SORPTION AND ION-EXCHANGE PROCESSES

Effect of Electrosurface Properties of Pectin Substances on Their Sorption Capacity for Water and Heavy Metals

L. A. Kupchik, M. P. Kupchik, O. L. Alekseev, and E. S. Bogdanov

Institute of Sorption and Endoecological Problems, National Academy of Science of Ukraine, Kiev, Ukraine
National University of Alimentary Technologies, Kiev, Ukraine
Ovcharenko Institute of Biocolloid Chemistry, National Academy of Science of Ukraine, Kiev, Ukraine

Received July 11, 2006; in final form, March 2007

Abstract—Three industrial pectins, viz., citrus, apple, and beet pectins were examined for the chemical composition, sorption, and electroosmotic transfer. The gelation concentrations, charge, and binding of the pectins to water and heavy metals were determined.

DOI: 10.1134/S1070427207070129

Pectins are natural components of plant tissues. They are commercially produced from various kinds of wastes from the food industry such as pomace, citrus peel, beet pulp, and sunflower heads [1–3].

The application of pectins as therapeutic, prophylactic, and detoxicant agents is based on their ability to form hydrogels and insoluble complexes with heavy metals [4–6]. These properties of pectin depend on such factors as the source, preparation route, and physicochemical characteristics of pectin itself. However, in the literature we found no systematic data on the relationship between the physicochemical and performance (hydrophilic, sorption, and electrosurface) characteristics of industrial pectins, which makes it difficult to optimize the dosage and therapeutic approach for these promising natural detoxicants in prophylactic and medical practice.

In this study we examined correlations between the chemical, sorption, and electrosurface properties of various industrial pectins.

We used tree kinds of pectins: PEKTOWIN citrus pectin (type NEC-A2), PEKTOWIN apple pectin (type NEJ-A2), and lab-made beet pectin. The characteristics of these pectins obtained by the standard analytical methods [7] are summarized in Table 1. Particularly, the uronic fraction, total carboxy group concentration, and free and methoxylated carboxy group concentrations were determined titrimetrically.

The electrosurface characteristics of pectins (maximal electroosmotic transfer, ζ potential, and charge of pectin molecules) were determined according to the procedures described in [8]. The gelling and sorption properties (sol/gel point, bound water, and sorption capacity for water and heavy metals) were characterized using the methods described in [9].

In all the experiments we observed the transport of the fluid across the pectin gel toward the cathode, suggesting a positive charge of the counterions, and, correspondingly, a negative charge on the pectin macromolecules. The experimental dependence of the electroosmotic transfer rate (ETR) on the pectin concentration in a gel membrane represents a curve with a maximum (Fig. 1, curves *1–3*), the initial section of which characterizes the increase in ETR with decreasing concentration of the dispersed phase. However, with further dilution, the disperse system passes into the free-disperse state. In this case, ETR abruptly decreases ((Fig. 1, curves *1–3*, the left branch of the curves). Therefore, the maximum point corresponds to the transition from the bound-disperse to the free-disperse state (sol/gel transition). This dependence can be described by Eq. (1):

$$P = \frac{k}{\alpha d c_T} - \frac{k(1+\beta)}{ad}, \quad (1)$$

where P is ETR ($cm^3\ C^{-1}$); c_T, pectin concentration (wt %); α, specific charge of the pectin particles ($C\ g^{-1}$); β, specific concentration of pectin-bound water ($g\ g^{-1}$); d, density of the dispersion medium ($g\ cm^{-3}$); and k, coefficient reflecting the ratio between the speeds of the fluid and counterions (it is close to unity in our case).

Table 1. Chemical characteristics of industrial pectins

Pectin source	Uronic fraction, wt %	Heavy metal content, μg kg^{-1}	Degree of esterification, wt %	Carboxy group content, wt %		
				total	free	methoxylated
Apple	57.9	>50	39.03	16.02	9.72	6.30
Citrus	50.5	>50	42.90	17.82	10.17	7.65
Beet	62.2	>20	52.30	18.90	9.00	9.90

The value of charge may characterize the ion-exchange and sorption capacities of pectin, and the fraction of bound water β (g g^{-1}), its hydrophilicity.

The maximal ETR can be used to determine the electrokinetic potential (mV) on the dispersed particles of pectin by Smoluchowski's equation (2):

$$\zeta = \eta KP/\varepsilon\varepsilon_0, \quad (2)$$

where K is the conductivity of the solution, and η and $\varepsilon\varepsilon_0$ are the viscosity and permittivity of the dispersion medium, respectively.

It follows from Eq. (2) that P is a linear function of $1/c_T$, allowing estimation of the charge on the pectin macromolecules and bound water concentration from experimental data. In so doing, from single series of ETR measurements in relation to c_T, we gained information on the charge and gelling point in the system pectin–water (Table 2).

As mentioned above, the gelling ability is among the most important characteristics of pectins. It increases with decreasing gelling concentration. Table 2 shows that, for the investigated pectins, the gelling concentration increases in the order apple < citrus < beet.

Table 1 shows that this order well correlates with the methoxy group content, total carboxy group content, and degree of esterification, suggesting that it is these chemical characteristics that control the gelling ability of pectins, which decreases on passing from apple pectin to beet pectin.

Binding of water on the surface of hydrophilic materials, particularly, pectins is caused by ionized carboxy groups and also by hydrogen bonding with a great amount of hydroxy groups. The number of bound water molecules per charged functional group can be estimated from the ratio of the above functional groups. The charged surface of pectin binds a considerable number of water molecules, making it a continuum. This imparts new properties to the surface, among them the ability to sorb metal cations.

Table 2. Sorption characteristics of industrial pectins with respect to heavy metals*

Ion	Pectin source					
	apple		beet		citrus	
	a_0	n	a_0	n	a_0	n
Ni^{2+}	0.177	0.981	0.158	1.055	0.196	0.896
Co^{2+}	0.411	0.560	0.224	0.973	0.346	0.800
Cu^{2+}	0.299	0.508	0.435	0.484	0.265	0.469
Zn^{2+}	0.068	1.168	0.063	1.219	0.074	1.149
Cd^{2+}	0.082	1.481	0.146	0.954	0.060	0.965
Pb^{2+}	0.409	0.507	0.400	0.277	0.554	0.377

* (a_0) Standard sorption capacity of pectins and (n) capacity factor.

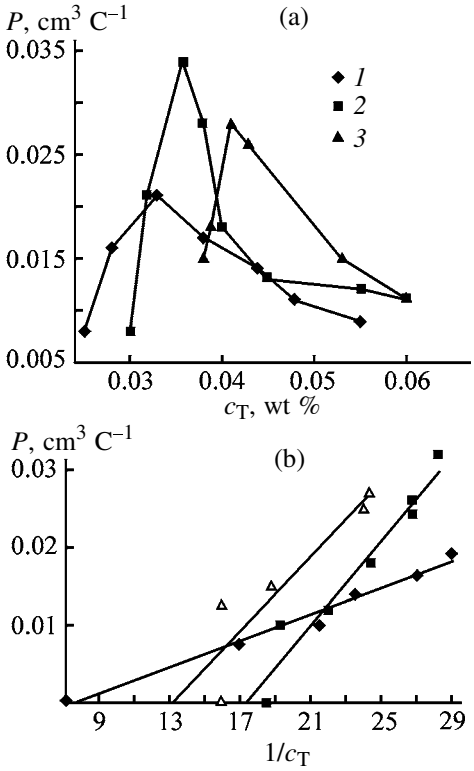

Fig. 1. Electroosmotic transfer rate P in pectin gels as a function of (a) dispersed phase concentration c_T and (b) $1/c_T$. Pectin: (*1*) apple, (*2*) citrus, and (*3*) beet.

Table 3. Sorption and electrosurface characteristics of pectins

Characteristic	Pectin		
	apple	citrus	beet
Sol/gel point, wt %	3.00	4.40	4.06
Maximal ETR, $cm^3\ C^{-1}$	0.022	0.035	0.028
ζ, mV	9.03	16.5	5.0
Charge on pectin molecules, $C\ g^{-1}$	1150	320	460
Adsorbed water β, $g\ g^{-1}$	6.5	17.3	10.8
Sorption of heavy metals per unit charge on pectin, mg-equiv C^{-1}:			
Ni^{2+}	1.54	6.11	3.43
Co^{2+}	3.57	10.80	4.87
Cu^{2+}	2.60	8.28	9.46
Zn^{2+}	0.59	2.32	1.37
Cd^{2+}	0.71	1.88	3.17
Pb^{2+}	3.56	17.3	8.70

The sorption characteristics of the industrial pectins were determined in the static mode. Sorption was studied from 0.1–10 mM aqueous solutions of $NiCl_2$, $CoCl_2$, $CuSO_4$, $ZnSO_4$, $CdCl_2$, and $Pb(NO_3)_2$, prepared using Ringer's solution as a supporting electrolyte at a sorbent to solution ratio of 1 : 250 and pH 6.2–6.5. The metal concentrations in the initial and equilibrium solutions were determined by atomic absorption spectroscopy on a Varian automatic analyzer (the United States). The sorption capacity of pectins for heavy metal ions A (mmol g^{-1}) was determined as

$$A = (c_0 - c_{eq})V/m, \quad (3)$$

where c_0 and c_{eq} are the initial and equilibrium concentrations of a heavy metal in the solution; V, solution volume; and m, sorbent weight.

The experimental data fit to the Freundlich isotherm (Table 3):

$$A = a_0 c_{eq}^n \quad \text{and} \quad \log A = \log a_0 + n \log c_{eq}, \quad (4)$$

where a_0 is the initial (standard) sorption capacity of pectins at $c_{eq} = 1$ M ($\log c_{eq} = 0$).

Analysis of the results obtained (Table 2) shows that apple pectin has the highest affinity (a_0) for cobalt(II); beet pectin, for copper(II) and cadmium(II); and citrus pectin, for nickel(II), zinc(II), and lead(II). However, judging from the fact that this characteristic does not correlate with the capacity factor n, one may expect that, at low metal concentrations, the sorption characteristics of pectins could be strongly different.

Comparison of the sorption, hydrophilic, and electrosurface properties of the industrial pectins shows that they are well correlated, and citrus pectin ranks first in all performance characteristics (Table 3).

As seen, free carboxy groups play a crucial role in both charging and sorption capacity of pectins. It should be pointed out that there is no common view of the binding mechanism of heavy metals to pectin. Most likely, it involves the formation of pectates through complexation of metal ions with the carboxy groups of the polysaccharide matrix. Also some inclusion compounds can be formed through uptake of a metal ions by the swollen macromolecule of the polysaccharide. Another possible mechanism is ion exchange involving functional groups of pectins.

CONCLUSIONS

(1) All the pectins studied are characterized by similar sol/gel points (3–4 wt %).

(2) A relationship is found between the chemical, electrosurface, and sorption characteristics of industrial pectins. The free carboxy group concentration is the key factor controlling both the charge on pectin and its sorption capacity for heavy metals.

REFERENCES

1. *Virobnitstvo ta vikoristannya pektiniv v kharchovii promislovosti* (Production and Application of Pectins in Food Industry), Guloi, I.S. and Kupchik, M.P., Eds., Kiev: Shust, 2001.
2. Bakasov, Z.B., *Nauchnye osnovy tekhnologii pektina* (Scientific Foundations of Pectin Technology), Frunze: Ilim, 1988.
3. Donchenko, L.V., *Tekhnologiya pektina i pektinoproduktov: Uchebnoe posobie* (Technology of Pectin and Pectin-Derived Products: A Handbook), Moscow: DeLi, 2000.
4. Trakhtenberg, I. and Krasnyuk, O., *Probl. Pit. Zdorov.*, 1997, no. 2, pp. 17–20.
5. Velichko, B.A. and Venkovskii, N.I., *Fitosorbenty tyazhelykh metallov* (Phytosorbents for Heavy Metals),

Moscow: Ross. Univ. Druzhby Narodov, 2002, part 2.

6. Rudichenko, V., *Prirodnye pishchevye sorbenty – faktor zdorov'ya sovremennogo cheloveka* (Natural Food Sorbents: A Health Factor for the Present-Day Humans), Kiev: Vishcha Shkola, 1997.
7. Nelina, V.V., Donchenko, L.V., Karpovich, N.L., and Ignat'eva, G.N., *Pektin: Metody kontrolya v pektinovom proizvodstve* (Pectin: Monitoring Methods in Pectin Production), Kiev: Osnova, 1992.
8. Alekseev, O.L. and Ovcharenko, F.D., *Elektropoverkhnostnye yavleniya i gidrofil'nost' dispersnykh system* (Electrosurface Phenomena and Hydrophilicity in Disperse Systems), Kiev: Naukova Dumka, 1992.
9. Kartel, M.T., Kupchik, L.A., and Veisov, V.K., *Chemosphere*, 1999, vol. 38, no. 11, pp. 2591–2596.

ISSN 1070-4272, Russian Journal of Applied Chemistry, 2007, Vol. 80, No. 7, pp. 1082–1086. © Pleiades Publishing, Ltd., 2007.
Original Russian Text © K.I. Tikhonov, G.K. Burkat, V.Yu. Dolmatov, E.A. Orlova, 2007, published in Zhurnal Prikladnoi Khimii, 2007, Vol. 80, No. 7, pp. 1113–1116.

APPLIED ELECTROCHEMISTRY AND CORROSION PROTECTION OF METALS

Use of Diamond Stock in Chromium Plating

K. I. Tikhonov, G. K. Burkat, V. Yu. Dolmatov, and E. A. Orlova

St. Petersburg State Institute of Technology (Technical University), St. Petersburg, Russia

Received February 27, 2007

Abstract—Cathodic deposition of a chromium coating from the standard electrolyte in the presence of a diamond stock was analyzed. The microhardness and wear resistance of chromium–diamond coatings and the effect of the diamond stock on the electrical conductivity and throwing power of the electrolyte were studied.

DOI: 10.1134/S1070427207070130

Chromium plating is one of the most commonly employed electroplating processes. Chromium coatings are widely used to impart a decorative appearance to articles, to protect parts subject to wear (shafts and pistons) and molds that should have a high surface hardness, and to restore worn components. As a rule, articles of this kind are coated with a thick chromium layer (200–500 μm).

Because the deposition of thick chromium layers is a rather high-cost process, a topical task is to develop a procedure for deposition of composite chromium–diamond coatings (CDC) with the use of nanodiamonds (ND) in order to diminish the thickness and improve the physicochemical properties of chromium coatings. The possibility of codeposition of chromium and ND was first reported in [1], with the amount of ND in the chromium plating electrolyte varied from 5 to 40 g l^{-1}.

A method for CDC deposition on blade tools has found wide use. This method was industrially implemented at Elektrokhimpribor combine (Lesnoi), Cherepovets steel works, and others. Therefore, this process has been the subject of extensive research work with rather contradictory results, from enthusiastic to negative [1–3].

At present, composite electroplated coatings (CEC) with ND are not widely used because of the high cost of diamond synthesis. Therefore, it is suggested to consider, in order to lower the production cost of chromium–diamond coatings, use of the raw material from which ND are obtained, diamond stock (DS). Detonation conversion of high-power explosives with a negative balance in a nonoxidative medium (i.e., in that with an oxygen content lower than the stoichiometric value) yields a condensed ND-containing carbon phase. Such a condensed carbon, named the diamond stock, may contain up to 75% ND [4]. DS exhibits adsorption capacity and high chemical activity.

The aim of this study was to examine the effect of DS on the mechanism of the chromium plating process, electrical conductivity and throwing power of the electrolyte, physicomechanical properties of coatings (microhardness, wear resistance), and outward appearance of chromium coatings obtained in various modes.

EXPERIMENTAL

A versatile chromium plating electrolyte of the following composition (g l^{-1}): CrO_3 230–260 and H_2SO_4 2.3–2.6 (electrolyte no. 1), was chosen for the study.

This choice was due to the following: its composition is more stable than that of a diluted chromium plating electrolyte; can be used to produce both wear-resistant and hard chromium deposits; has a rather high throwing and covering power; causes no difficulties in determination of the ND and DS content of the electrolyte (in contrast to the self-regulating electrolyte).

The deposition was performed from the above-mentioned solution, with DS introduced in amounts of 1, 2.5, 5, and 10 g l^{-1} (electrolyte nos. 2, 3, 4, and 5, respectively). The optimal DS concentrations in the chromium plating electrolyte was determined by

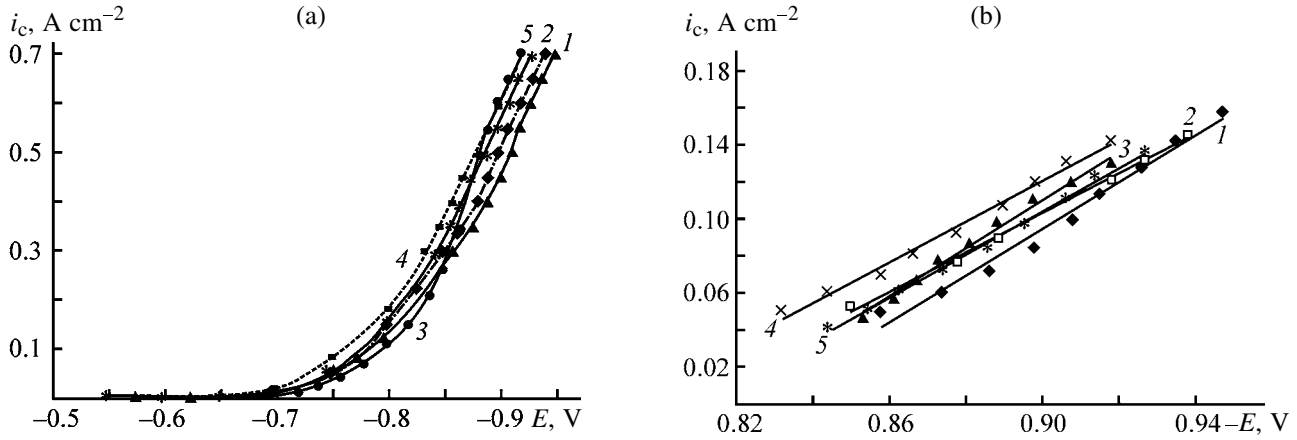

Fig. 1. (a) Overall and (b) partial polarization curves of chromium deposition from DS-containing electrolytes at 50 ± 1°C. (i_c) Current density and (E) potential; the same for Fig. 2. (*1*) Without additive; DS additive, g l^{-1}: (*2*) 1, (*3*) 2.5, (*4*) 5, and (*5*) 10.

analyzing the quality of the outward appearance of coatings and physicomechanical properties of chromium–diamond coatings obtained in various electrolysis modes. Experiments were carried out in the following modes: cathode current density (A dm^{-2}): 30, 40, 50, 60, 70; electrolyte temperature (°C): 45 ± 1, 50 ± 1, 55 ± 1.

The cathodic polarization curves were measured in a three-electrode cell with separated 50-ml electrode spaces with a P-5848 potentiostat by the potentiostatic method. A silver chloride reference electrode was used. The potentials were recalculated to the hydrogen scale. The current was measured with an M1104 milliammeter with an accuracy of 0.2%. The experiments were performed at 50 ± 1°C.

The throwing power (TP) of the electrolyte was evaluated using an indirect method by calculating the electrochemical similarity coefficient (Γ) defined as a product of the electrical conductivity of the solution (χ) and the electrode polarizability ($\Delta E/\Delta i_c$), which is a secondary distribution in determining the TP of an electrolyte [5, 6]. For this purpose, polarization curves were measured and the electrical conductivities of the solutions in the presence of DS and without it were determined. The electrical conductivity was found by measuring the voltage with a V7-40/4 voltmeter. Steel coated with chromium with a thickness of no less than 40 μm served as the working electrode (cathode), a lead plate was used as an auxiliary electrode (anode), and a silver chloride electrode served as reference.

The microhardness was measured with a PMT-3 microhardness meter. To obtain comparable data, the hardness was measured at a coating thickness of 45–50 μm and a constant load of 100 g. St. 20 steel plates were used as a support. The hardness was measured not earlier than 24 h after a coating was deposited.

Wear-resistance tests were performed on a machine with a reciprocal motion of samples under dry-friction conditions. The friction pair had the form of a brass disc with a 3.5–5-μm-thick coating to be tested, which rubs against a plane-parallel steel plate covered with hard chromium. All the tests were made under a constant load of 130 g in the course of 20 h, the wear resistance was evaluated by the mass loss by the samples upon abrasion [7].

The potentiostatic curves obtained in electrolytes in the presence of a diamond stock and without it, which reflect the overall electrode processes, are shown in Fig. 1a. Upon introduction of DS into the standard chromium plating electrolyte, the polarization curves somewhat shift in the positive direction (the polarization shift is up to 30 mV, which lies within the experimental error).

Figure 1b shows partial polarization curves of chromium deposition in solutions with and without DS additives. It can be seen that the slope of the polarization curves remains virtually unchanged. To plot partial polarization curves of chromium deposition from the standard chromium plating electrolyte with and without DS additive, the current efficiencies were measured at working current densities and a temperature of 50°C (Table 1). As seen from Table 1, addition of DS leads to a slight increase in the current efficiency (CE) by chromium. The maximum increase in CE relative to that for an electrolyte

Table 1. Effect of the cathode current density on the current efficiency by chromium at varied DS content of the electrolyte

c_{DS}, g l^{-1}	Current efficiency, %, at indicated cathode current density, A m^{-2}								
	0.3	0.35	0.4	0.45	0.5	0.55	0.6	0.65	0.7
0	16.8	17.5	18.1	19.1	20.1	20.9	21.6	22.1	22.5
1	19.9	20.8	21.8	22.3	22.6	23.5	24.6	25.4	26.3
2.5	17.9	19.0	20.2	21.4	22.8	23.7	24.7	25.2	25.8
5	18.6	18.9	19.3	20.1	20.6	21.8	23.0	23.4	23.8
10	18.0	19.6	21.4	21.7	22.1	22.7	23.2	23.8	24.4

without additives (up to 3%) is observed in an electrolyte with a DS content of 2.5 g l^{-1}.

Upon addition of DS to the electrolyte, the hydrogen evolution curves shift in the negative direction (Fig. 2), because the discharge of hydrogen ions on the electrolyte surface with adsorbed DS particles is hindered, in agreement with an increase in the current efficiency by chromium.

The electrical conductivity of the chromium plating electrolyte somewhat increases in the presence of DS, which, in turn, should affect the throwing power of the solution. Table 2 shows that the electrochemical similarity factor for DS-containing electrolytes somewhat exceeds that for additive-free electrolytes, and, consequently, the throwing power of DS-containing solutions should be higher than that of an electrolyte without additives.

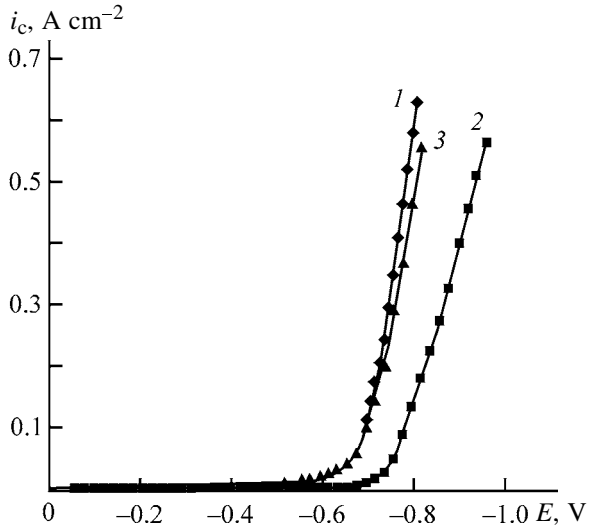

Fig. 2. Hydrogen curves measured in chromium anhydride with and without diamond stock on a chromium electrode at 50 ± 1°C. (*1*) Without additives; additive (g l^{-1}): (*2*) 2.5 and (*3*) 5.

The effect of DS on the microhardness of chromium coatings deposited at different temperatures is shown in Fig. 3. It can be seen that the microhardness of the chromium coatings increases with the cathode current density at the temperatures studied. The optimal concentration of DS in the electrolyte is 5 g l^{-1} (further increase in concentration has virtually no effect on the microhardness of the chromium coatings).

Table 2. Effect of the DS additive on the electrode polarizability $\Delta E/\Delta i_c$, electrical conductivity χ, and electrochemical similarity coefficient Γ (throwng power of the electrolyte)

c_{DS}, g l^{-1}	$\Delta E/\Delta i_c$, Ω cm^2	χ, S cm^{-1}	Γ, cm
0	0.203	0.647	0.131
1	0.207	0.676	0.140
5	0.207	0.685	0.142
10	0.2	0.674	0.135

Table 3. Effect of the DS additive on the wear resistance of chromium coatings deposited in various chromium plating modes

Additive, g l^{-1}	Loss of mass by a coating (wt %) at indicated temperature, °C					
	45 ± 1		50 ± 1		55 ± 1	
	and current density, A dm^{-2}					
	40	50	40	50	40	50
0	3.5	5.4	4.8	5.0	6.2	4.3
1	3.2	3.25	3.1	3.5	3.1	2.0
2.5	2.4	2.55	2.6	2.0	3.0	2.4
5	2.4	2.8	2.2	1.9	2.4	2.6
10	2.5	3.2	2.9	2.0	2.8	2.7

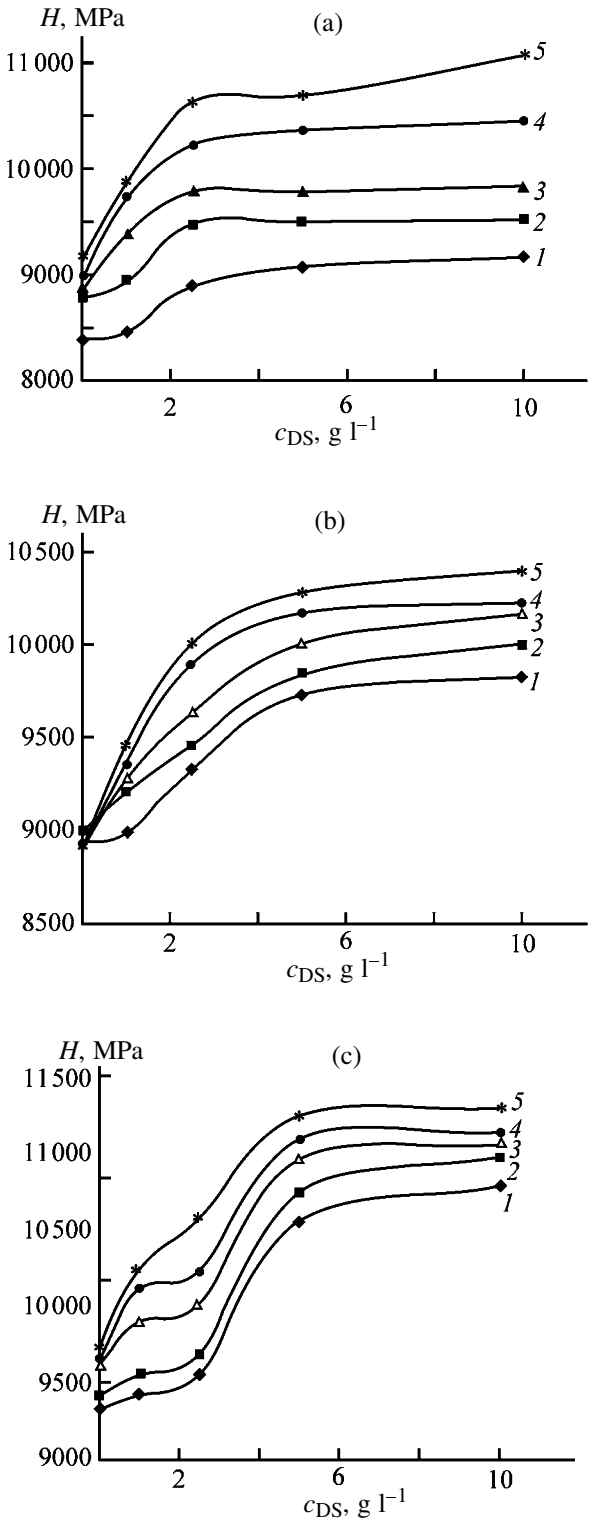

Fig. 3. Effect of DS concentration c_{DS} on the microhardness H of chromium coatings obtained at different temperatures and current densities. Temperature, °C: (a) 45 ± 1, (b) 50 ± 1, and (c) 55 ± 1. Current density, A dm^{-2}: (*1*) 30, (*2*) 40, (*3*) 50, (*4*) 60, and (*5*) 70.

The microhardness of chromium–diamond coatings is 15–20% higher. The increase in the microhardness of the chromium coatings in the presence of DS can be attributed to introduction of DS particles into the coatings via adsorption and to deposition of more finely crystalline coatings.

The microhardness of thermally treated coatings was also measured. The thermal treatment was carried out at 200 ± 20°C for 2 h. It was found that the microhardness of the chromium coatings regularly decreases upon thermal treatment. For example, the decrease in microhardness upon thermal treatment is 10–15% for a purely chromium coating and that deposited in the presence of 1 g l^{-1} of DS and 6–10% for the coating obtained from an electrolyte with 10 g l^{-1} of the stock.

It should be noted that lustrous chromium coatings can be deposited from an electrolyte containing 2.5 g l^{-1} of DS in a wide range of current densities without any preliminary polishing of a support. The coatings obtained upon a further increase in the DS concentration to 10 g l^{-1} are not lustrous and identical in outward appearance to those deposited from an additive-free electrolyte.

Table 3 lists data on the effect of the additives on the wear resistance of the resulting chromium coatings. It can be seen that, on the average, the wear resistance of chromium–diamond coatings is 2–3 times that of pure chromium. The best wear resistance is observed for coatings deposited from electrolytes containing 2.5–5 g l^{-1} of DS.

CONCLUSIONS

(1) Introduction of the DS additive into the standard chromium plating electrolyte has virtually no effect on the hydrogen evolution overvoltage and the polarizability of the process.

(2) The electrical conductivity and throwing power of DS-containing solutions somewhat exceed those of the standard chromium plating electrolyte. At DS concentrations of 1–2.5 g l^{-1}, the deposition range of lustrous coatings becomes wider.

(3) Introduction of DS into the electrolyte can improve the microhardness and wear resistance of chromium coatings. The microhardness increases by 15–20%. The optimal DS concentration is 5 g l^{-1}. The best wear resistance is observed for coatings deposited in the presence of 2.5–5 l^{-1} of DS.

REFERENCES

1. USSR Inventor's Certificate no. 1 694 710.
2. RF Inventor's Certificate no. 1 813 812.
3. Vashchenko, S.V. and Solov'eva, Z.A., *Gal'vanotekh. Obrab. Poverkhn*., 1992, vol. 1, nos. 5–6, pp. 45–48.
4. Lyamkin, A.I., Petrov, E.A., Ershov, A.P., et al., *Dokl. Akad. Nauk SSSR*, 1988, vol. 302, pp. 611–613.
5. Shul'gin, V.G., *Raspredelenie toka i povyshenie ravnomernosti osazhdeniya metallov v gal'vanotekhnike i gal'vanoplastike* (Current Distribution and Improvement of the Uniformity of Metal Deposition in Electroplating and Electroforming), Leningrad: Leningr. Dom Nauchno-Tekh. Propagandy, 1983.
6. Gamburg, Yu.D., *Gal'vanotekh. Obrab. Poverkhn*., 1993, vol. 2, no. 2, pp. 32–36.
7. Vyacheslavov, P.M. and Shmeleva, N.M., *Metody ispytanii elektrokhimicheskikh pokrytii* (Methods for Testing of Electrochemical Coatings), Leningrad: Mashinostroenie, 1977.

ISSN 1070-4272, Russian Journal of Applied Chemistry, 2007, Vol. 80, No. 7, pp. 1087–1089. © Pleiades Publishing, Ltd., 2007.
Original Russian Text © M.Z. Muldakhmetov, A.M. Gazaliev, I.V. Kirilyus, S.D. Fazylov, 2007, published in Zhurnal Prikladnoi Khimii, 2007, Vol. 80, No. 7, pp. 1117–1119.

APPLIED ELECTROCHEMISTRY AND CORROSION PROTECTION OF METALS

Electrolytic Synthesis of Nipecotic Acid Ethyl Ester

M. Z. Muldakhmetov, A. M. Gazaliev, I. V. Kirilyus, and S. D. Fazylov

Kazakhstan–Russia University, Astana, Kazakhstan
Institute of Organic Synthesis and Coal-Tar Chemistry of the Kazakhstan Republic, Karaganda, Kazakhstan

Received October 30, 2006; in final form, March 2007

Abstract—An electrolytic method was suggested for the synthesis of nipecotic acid ethyl ester in a diaphragm electrolytic cell on a copper cathode in aqueous–alcoholic alkali solution.

DOI: 10.1134/S1070427207070142

Nipecotic (3-piperidinecarboxylic) acid and its various esters are widely used in medicine as agents preventing thrombus formation, and also in clinical practice as an antiepileptic (Tiagabin).

No data on electrocatalytic synthesis of nipecotic acid and its esters have been reported. Osadchenko and Tomilov [1] prepared isonipecotic acid with a current efficiency of 60% by electrolytic reduction of the pyridine ring of isonicotinic acid on a copper cathode.

Reduction of the pyridine ring has been studied to a greater extent on electrodes with a low hydrogen overvoltage, e.g., on silver, and on those with a high overvoltage (lead, mercury). The course of pyridine reduction depends on the process conditions and structural features of pyridine derivatives; bis(piperidines) are frequently formed [2]. It is advisable to perform pyridine reduction in an electrocatalytic system on cathodes activated with Raney nickel or cobalt. At a current density of 2–8 kA m^{-2} and a pyridine concentration of 0.2–0.3 kmol m^{-3}, the piperidine yield based on the hydrogen uptake is 90% [3].

With the aim to develop an electrocatalytic procedure for preparing isonipecotic acid ethyl ester, we examined in this study exhaustive hydrogenation of nicotinic acid ethyl ester in aqueous and aqueous–alcoholic solutions.

EXPERIMENTAL

Electrolytic hydrogenation of nicotinic acid ethyl ester **I** was performed in a diaphragm electrolytic cell with the anode and cathode compartments separated by an MK-40 membrane. The cell volume was 60 ml (Fig. 1). As anode we used platinum grid, and as cathode, a cooper plate (support) with a visible surface area of 0.05 dm^2, closely adjoining the electrolyzer bottom. For cathode activation we used Raney nickel which was held on the electrode surface with a permanent magnet arranged outside the electrolyzer [1].

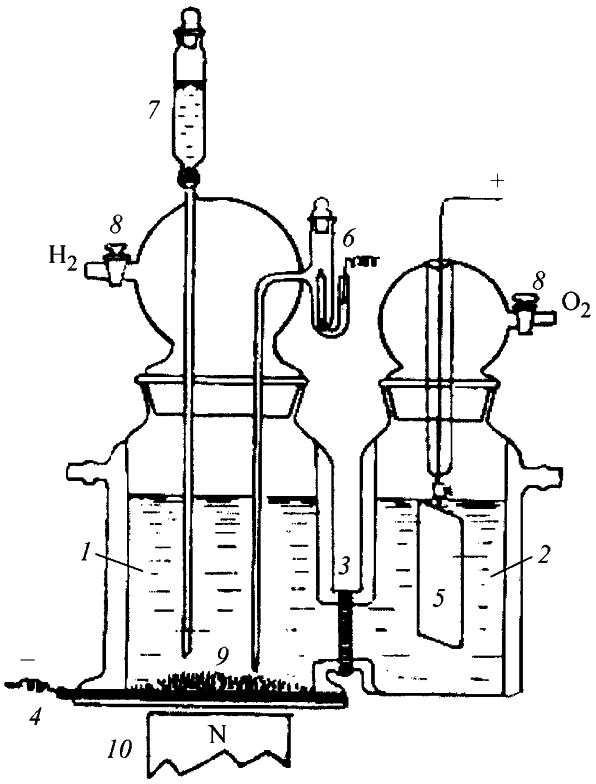

Fig. 1. Cell for electrocatalytic processes: (*1*) catholyte, (*2*) anolyte, (*3*) diaphragm, (*4*) cathode support, (*5*) anode, (*6*) calomel electrode, (*7*) funnel, (*8*) hydrogen and oxygen outlet, (*9*) catalyst, and (*10*) magnet.

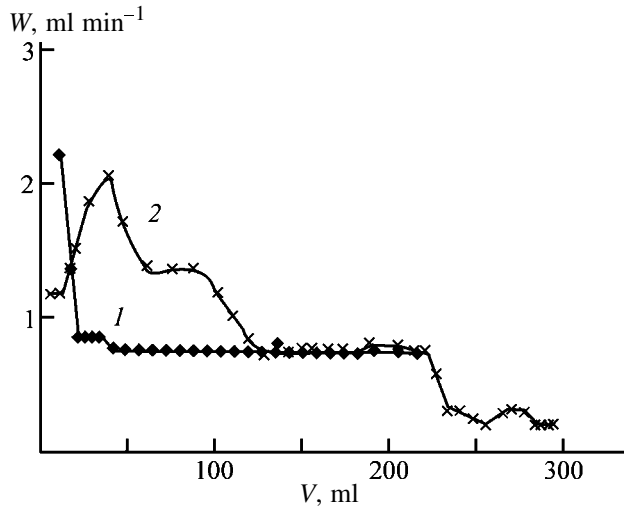

Fig. 2. Hydrogen uptake rate W as a function of volume V of hydrogen taken up in (*1*) aqueous and (*2*) aqueous–alcoholic NaOH solutions.

As organic solvent we used ethanol. The catholyte was a 1 : 1.5 mixture of alcohol with 20% aqueous NaOH, and the anolyte was 20% NaOH. The electrolysis was performed with gentle stirring (50–60 rpm) at a current of 1.0 A and solution temperature of 20–40°C, until the hydrogen uptake ceased; the amount of Raney nickel on the cathode surface was 1.0 g dm^{-2}. After the electrolysis completion, the target product was extracted from the catholyte with ether and purified by common procedures. According to Faraday's law, 300 ml of hydrogen should be absorbed by 0.78 g of the ester. The system was sealed, and gases evolving from the cathode and anode compartments could be collected in 500-ml graduated gas burets.

From the volume of the released oxygen and hydrogen, we calculated the reduction rate W, hydrogen uptake percentage, hydrogen utilization coefficient η, and current efficiency.

The reduction rate, (ml H_2) min^{-1}, was calculated by the equation

$$W = k(2V_O - V_H)/\Delta\tau,$$

where V_O and V_H are the volumes (ml) of the released oxygen and hydrogen, respectively; Δt, process time (min); and k, barometric coefficient for converting the gas volumes to normal conditions.

The hydrogen utilization coefficient, i.e., the ratio of hydrogen added to the organic substrate (pyridine ring) to the total volume of hydrogen released at the cathode, was calculated by the formula

$$\eta = (2V_O - V_H)/2V_O.$$

The best results were obtained when the electrolytic reduction of nicotinic acid ethyl ester was performed in aqueous–alcoholic solution (Fig. 2), which may be due to higher solubility of the starting ester in an aqueous–organic solution.

The pyridine molecule is not a regular hexagon: it has a dipole moment due to nonuniform charge distribution [4]. The nitrogen atom in pyridine is an electron acceptor withdrawing the electron density from the ring. Furthermore, formation of two σ bonds and one π bond between the *o*-C atoms and N atom of the ring results in orientation of the nitrogen lone electron pair outside the ring, which favors complexation with Lewis acids and solubility in proton-donor solvents.

In aqueous alkali, the hydrogen uptake does not go to completion (it does not exceed 74–78%), and the mean hydrogenation rate is 0.8 (ml H_2) min^{-1}. On adding ethanol to the catholyte, the hydrogen uptake accelerates [2 (ml H_2) min^{-1}] and reaches 100%. An analysis shows that electrocatalytic hydrogenation of **I** on the cathode occurs with a substance yield of 98% and current efficiency of 63%, following the scheme

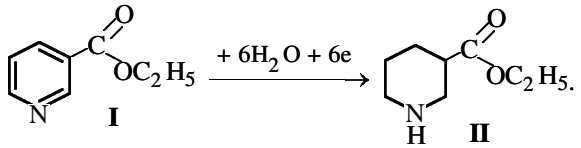

The structure of nipecotic acid ester **II** was proved by IR and ^{1}H NMR data, and the composition was confirmed by elemental analysis. The IR spectra were recorded on an Avatar-320 spectrometer from mulls in mineral oil, and the ^{1}H NMR spectra, on a Tesla BS-587 spectrometer (80 MHz) in DMSO-d_6 relative to HMDS. The IR spectrum of **II** contains a strong band at about 1740 cm^{-1} caused by stretching vibrations of the C=O group and a broad absorption band at about 3440 cm^{-1} belonging to NH stretching vibrations. In the ^{1}H NMR spectrum, the methylene protons of the piperidine core give a multiplet at 1.5–2.0 ppm, and the methyl protons of the ethoxy group give a triplet at 1.25 ppm (J 7.0 Hz).

CONCLUSION

A procedure was developed for electrolytic synthesis of nipecotic acid ethyl ester in aqueous–alcoholic alkali solution on a copper cathode with Raney nickel. The target product is prepared with almost

quantitative substance yield and 63% current efficiency.

REFERENCES

1. Osadchenko, I.M. and Tomilov, A.P., *Zh. Prikl. Khim.*, 2006, vol. 79, no. 3, pp. 508–509.
2. Kirilyus, I.V., *Elektrokataliticheskoe gidrirovanie* (Electrocatalytic Hydrogenation), Alma-Ata: Nauka, 1981.
3. Tomilov, A.P. and Kirilyus, I.V., *Katodnye sintezy organicheskikh preparatov* (Cathodic Syntheses of Organic Compounds), Alma-Ata: Nauka, 1982.
4. Ivanskii, V.I., *Khimiya geterotsiklicheskikh soedinenii* (Chemistry of Heterocyclic Compounds), Moscow: Vysshaya Shkola, 1978.

ISSN 1070-4272, Russian Journal of Applied Chemistry, 2007, Vol. 80, No. 7, pp. 1090–1096. © Pleiades Publishing, Ltd., 2007.
Original Russian Text © V.P. Boyarskii, T.E. Zhesko, S.A. Lanina, G.F. Tereshchenko, 2007, published in Zhurnal Prikladnoi Khimii, 2007, Vol. 80, No. 7, pp. 1120–1126.

ENVIRONMENTAL PROBLEMS OF CHEMISTRY AND TECHNOLOGY

Dechlorination of Persistent Organic Pollutants Polychlorobiphenyls by Catalytic Carbonylation

V. P. Boyarskii, T. E. Zhesko, S. A. Lanina, and G. F. Tereshchenko

VNIIneftekhim Open Joint-Stock Company, St. Petersburg, Russia
Galar Scientific and Production Firm, Limited Liability Company, St. Petersburg, Russia
St. Petersburg Scientific Center, Russian Academy of Sciences, St. Petersburg, Russia

Received April 19, 2007

Abstract—A new approach to dechlorination of "dioxin-like" ecotoxicants, polychlorinated biphenyls, based on carbonylation, was suggested. The weakly reactive aryl halides are activated by effective catalytic systems based on epoxide-modified cobalt carbonyl in alcoholic alkali solutions.

DOI: 10.1134/S1070427207070154

Polychlorinated biphenyls (PCBs) have a set of unique physicochemical properties and are widely used as dielectrics in transformers and capacitors, as hydraulic fluids, and as heat carriers. At the same time, PCBs are highly toxic; they damage the immune, endocrine, and nervous systems and exhibit carcinogenic properties [1, 2]. Because of the high vapor pressure and noticeable volatility, they are capable of transboundary transport to long distances. Being lipophilic, these compounds accumulate in adipose tissues of animals and humans and get involved in food chains. Polychlorobiphenyls are extremely resistant to biological and chemical degradation and can exist in the environment for centuries. Therefore, along with superecotoxicants, dioxins (polychlorodibenzodioxins) and polychlorodibenzofurans, they are included in the main list of persistent organic pollutants (POPs). According to Stockholm convention on POPs, which came into force in 2004, these compounds are to be destroyed or utilized [1].

Today the production of PCBs has been stopped. However, by the beginning of the 1990s, more than 1.5 mln tons of technical PCB mixtures (including approximately 180 thousand tons in the former Soviet Union) have been produced in the world. In Russia, up to 35 000 t of PCBs are still in use, including more than 1000 t in St. Petersburg and Leningrad oblast (according to incomplete data) [1].

Much attention is given today to the development of procedures for rendering polychlorobiphenyls harmless. It is known that spent technical oils that are not subjected to regeneration are commonly incinerated, but this procedure is unacceptable for PCB-containing oils, because of formation of dioxins in the process. The most promising way to decrease the amount of PCBs in the environment is their chemical reprocessing into environmentally safe products. Much attention is given to the development of methods for PCB reduction with alkali metals and alkali metal hydrides [2, 3], and also of safer and more feasible methods of catalytic reductive dehalogenation [2, 4]. It is also suggested to treat PCBs with alkali metal polyglycolates with the formation of ethers [5].

In this study we examined the principal possibility of reprocessing technical PCB mixtures by carbonylation, with the aim to subsequently develop a process for PCB utilization and conversion into useful products (acids and their derivatives: salts, esters, amides). These products can find wide use in production of dyes and pigments, polymers and resins, lubricants, surfactants, corrosion inhibitors, and additives to oils and bitumens.

The suggested procedure is based on the previously developed [6–8] principally new catalytic systems based on modified cobalt carbonyl, capable of activating aromatic halides and involving them in carbonylation with the formation of carboxylic acids and their derivatives. For the carbonylation of PCBs, which are inert aryl chlorides, we chose the most active catalytic systems promoted with propylene oxide (PO). The advantages of this procedure are the use of cheap and available raw materials and low power consumption

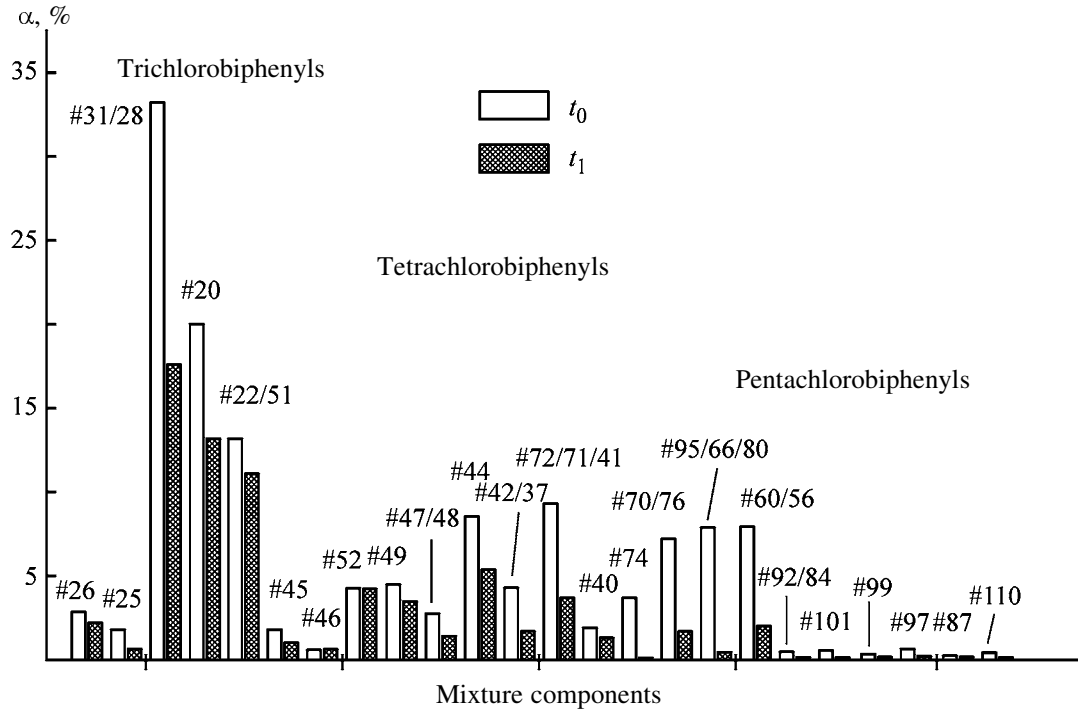

Fig. 1. Conversion α of tri-, tetra-, and pentachlorobiphenyls in carbonylation of technical-grade trichlorobiphenyl mixture: (t_0) before the start of the reaction and (t_1) in 5 h. (#) Congener no. according to IUPAC nomenclature.

due to the mild reaction conditions (CO pressure 1 atm, temperature 60–65°C).

To check the principal possibility of using this procedure, we performed carbonylation of technical-grade trichlorobiphenyl (TCB) mixture containing 43 wt % Cl and consisting, according to [9], of 14% di-, 49% tri-, 32% tetra-, 4% penta-, and 1% hexachlorobiphenyls. The chlorine content corresponds to the mean composition $C_{12}H_{6.8}Cl_{3.2}$, i.e., slightly more than three H atoms per biphenyl molecules are replaced by Cl. The reaction was performed at 60°C and atmospheric pressure of CO in methanol in the presence of K_2CO_3. As activator we used PO at the molar ratio [TCB] : [$Co_2(CO)_8$] : [PO] = 20 : 1 : 20 and $Co_2(CO)_8$ concentration of 0.015 M. The degree of dechlorination was determined from the Cl^- concentration in the solution after the reaction completion; it was about 30% in 5 h.

After the reaction, we analyzed the organic residue of the unchanged PCB mixture by gas chromatography. The compositions of the recycled PCB mixture and the starting mixture are compared in Fig. 1.

It can be seen that the conversion of various trichlorobiphenyl isomers ranges from 5 to 80%; that of tetrachlorobiphenyls, from 20 to 100%; and that of the minor components, penta- and hexachlorobiphenyls, is close to 100%. The reaction products, mixtures of methyl esters of polychlorobiphenylcarboxylic acids, were converted to the corresponding acids by hydrolysis in aqueous–alcoholic KOH, followed by acidification with HNO_3. According to elemental analysis, the Cl content in the final reaction product is 29 wt %. This means that approximately one chlorine atom per molecule is replaced by the carboxy group under the reaction conditions.

Our next series of experiments was performed with Sovtol-10 technical dielectric. Sovtol-10 consists of 90% Sovol technical mixture and 10% trichlorobenzene. The chlorine content of Sovtol-10 is about 55 wt %.

The major components of technical mixtures of Sovol type are pentachlorobiphenyls (53%). They also contain tri- (1%), tetra- (23%), hexa- (22%), and heptachlorobiphenyls (1%) [9], i.e., on the average, approximately five hydrogen atoms per biphenyl molecule are replaced by chlorine. The reaction was performed under the same conditions as with TCB (Table 1).

The degree of dechlorination was determined from the concentration of the Cl^- ion in the solution after the reaction completion. Also, the conversion was determined by GLC analysis of the reaction mixture

Table 1. Carbonylation of Sovtol-10 technical mixture with different amounts of the catalyst. 60°C, P_{CO} = 0.1 MPa, solvent methanol, base K_2CO_3, reaction time 5 h

Run no.	Loaded, M			Degree of dechlorination, % ([Cl^-])	PCB conversion (GLC)	Yield,* wt %
	Sovtol-10	$Co_2(CO)_8$, $c \times 10^3$	propylene oxide			
1	0.17	1.7	0.034	35	60	50
2	0.17	1.7	0.08	50	80	78
3	0.17	1.7	0.42	62	96	89
4	0.17	1.7	0.58	30	35	60
5	0.17	3.4	0.34	58	90	82
6	0.17	3.4	0.67	64	99	91
7	0.17	6.8	2.5	42	45	35

* Yield of polychlorobiphenylcarboxylic acids based on converted PCBs.

from the sum of the intensities of peaks belonging to all the residual congeners relative to the peak of the least reactive congener (Fig. 2).

Figure 2 illustrates not only the extent of the reaction, but also complete disappearance from the reaction mixture of the most toxic PCB congeners, dioxin-like coplanar tetra- and pentachlorobiphenyls, which was also confirmed by gas chromatography–mass spectrometry. The degree of dechlorination, estimated from the concentration of mineral chlorine in the solution after performing the reaction to 99% conversion of Sovtol-10, is about 60%.

To isolate the carbonylation product and separate it from the unchanged PCB residue, the mixture was hydrolyzed in an aqueous–alcoholic KOH solution and then was treated with HNO_3. The resulting mixture of polychlorobiphenylcarboxylic acids was separated and dried.

The mixture of acids from run no. 3 (almost complete PCB conversion) was treated with diazomethane. The resulting mixture of methyl esters of polychlorobiphenylcarboxylic acids (Fig. 3) was studied by gas chromatography–mass spectrometry.

The substances giving peak nos. 1–5 in the chromatogram (Fig. 3) have peaks with m/z = 314 (M^+) in the mass spectra, corresponding to Cl_3Ph_2COOMe

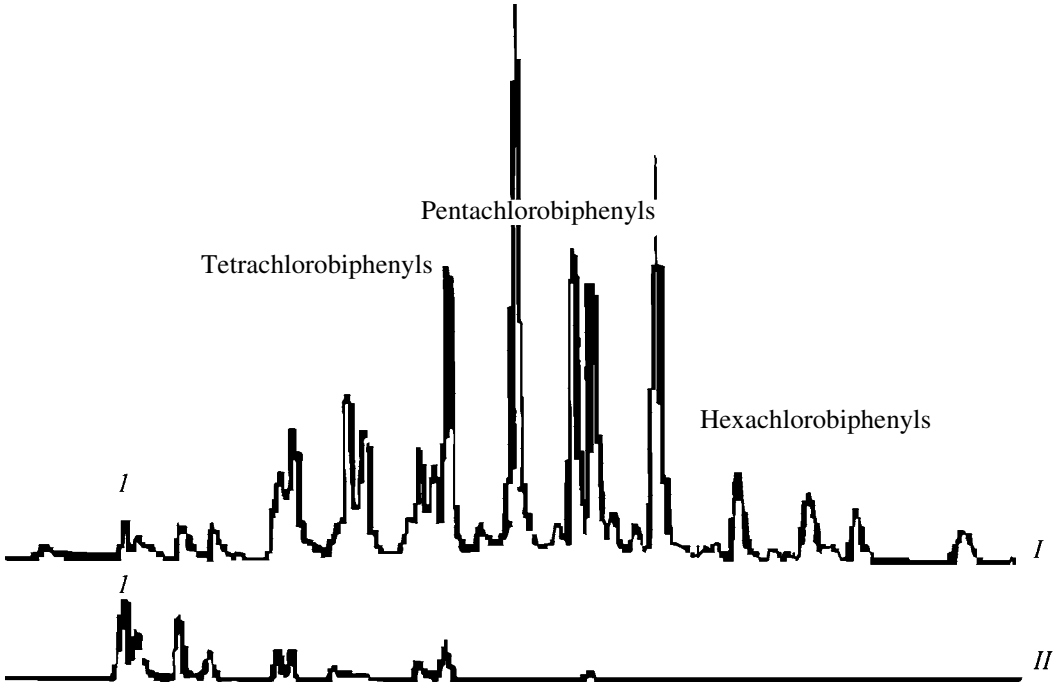

Fig. 2. Typical chromatograms of Sovtol-10 technical mixture (*I*) before and (*II*) after carbonylation. (*1*) Peak of the least reactive congener.

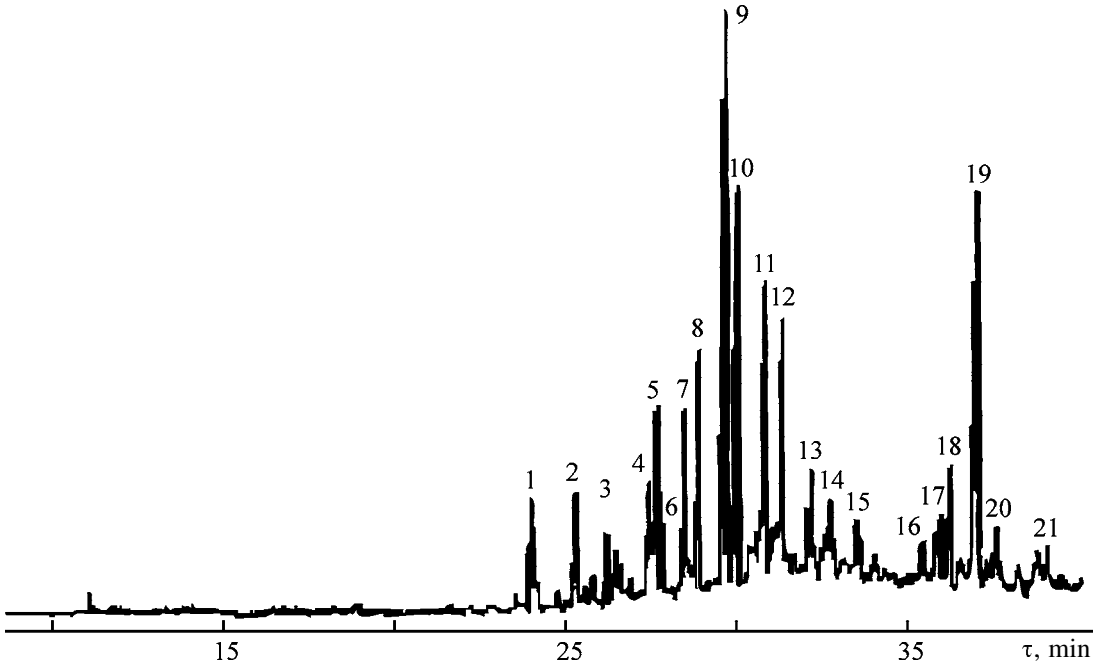

Fig. 3. Chromatogram of methyl esters of polychlorobiphenylcarboxylic acids formed by carbonylation of Sovtol-10 PCB mixture in the system $Co_2(CO)_8$–propylene oxide–K_2CO_3. (τ) Time. For comments, see text.

(considering ^{35}Cl), with the consistent isotopic pattern (m/z = 316, 318, 320).

Substances giving peak nos. 6–8 and 12 in the chromatogram have peaks with m/z = 338 (M^+) in the mass spectrum, corresponding to $Cl_2Ph_2(COOMe)_2$. Substances giving peak nos. 9–11 and 13–15 in the chromatogram have peaks with m/z = 372 (M^+) in the mass spectrum, corresponding to $Cl_3Ph_2(COOMe)_2$. Substances giving peak nos. 16–21 in the chromatogram have peaks with m/z = 372 (M^+) in the mass spectrum, corresponding to $Cl_2Ph_2(COOMe)_3$.

An NMR analysis of the mixture of methyl esters of polychlorobiphenylcarboxylic acids also revealed the presence of two, on the average, ester groups per substituted biphenyl molecule, which coresponds to 40% conversion with respect to chloride ion, whereas analysis for mineral chlorine gives 60%. This discrepancy may be due to hydrodechlorination of highly chlorinated congeners. This process was observed previously in studies of the carbonylation of individual congeners [8, 10, 11]. Analysis of the reaction mixtures by gas chromatography–mass spectrometry (GC–MS) revealed formation of reductive dechlorination products (Scheme 1) along with products of mono- and polycarbonylation.

The absence of monochlorobiphenyls among the reaction products and their inertness in carbonylation suggest that the carbonylation of PCBs precedes the hydrodechlorination.

In all cases when the hydrodechlorination occurs, the starting substrate contains two Cl atoms in the *o*-position relative to each other. As the PCB mixture contains a large amount of highly chlorinated congeners with such structural fragments, the occurrence of hydrodechlorination in the system should be confidently expected. This is also confirmed by the results of elemental and GC–MS analyses [11]. Comparison of the conversions estimated from the NMR data (40%) and analysis for Cl^- (60%) shows that the contribution of hydrodechlorination to the total conversion with respect to Cl^- ions in carbonylation of Sovtol-10 under the examined conditions is about 30%.

With the aim to develop principles of a technology for reprocessing of commercial PCB mixtures, we worked through a process for carbonylation of Sovtol-10 mixture using a 1-l pressure vessel (Table 2).

The results obtained show that the use of Na_2CO_3 as a base instead of K_2CO_3 leads to a decrease in the degrees of dechlorination and carbonylation (run no. 3). An increase in the process temperatrue and working pressure (run no. 5) does not lead to an increase in the PCB conversion. In this case, increased CO uptake is due to the occurrence of a side reaction, carbonylation of propylene oxide, as shown by analysis of the reaction mixture after isolation of the reaction products.

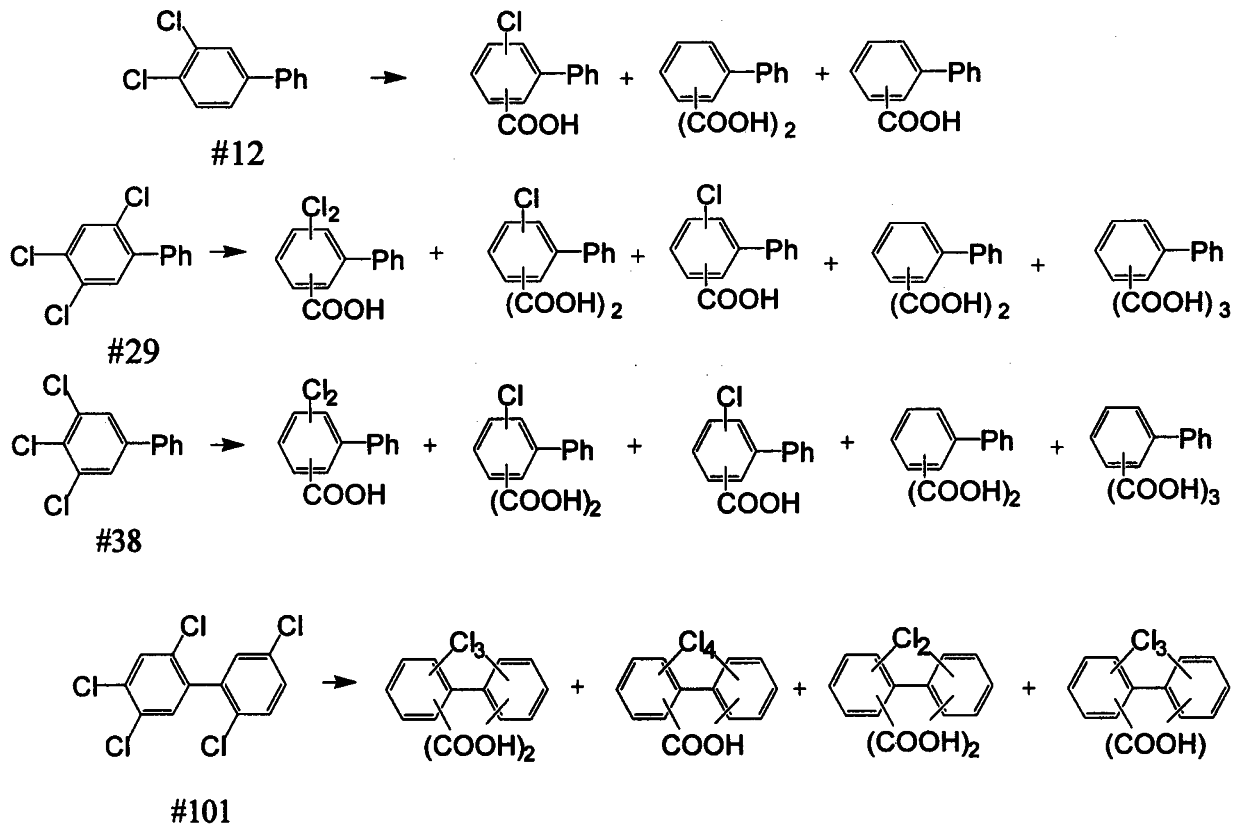

Scheme 1. Products of carbonylation of some individual congeners present in Sovtol-10 technical PCB mixture (data of mass spectrometry)

Sequence of transformations suggested for 3,4-dichlorobiphenyl (#12)

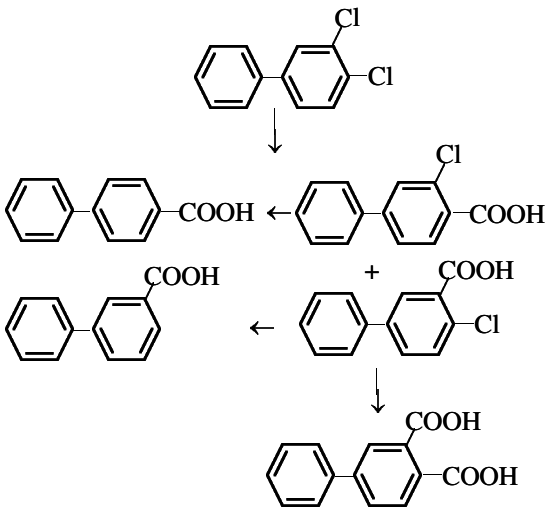

Reductive hydrodechlorination under similar conditions was observed previously in laboratory experiments performed in glassware (Table 1). The results obtained in experiments at elevated pressure (Table 2) show that the hydrodechlorination is pronounced only in those experiments when decomposition of the catalyst was followed by base hydrolysis. This fact indicates that, firstly, carbonylation and hydrodechlorination under the examined conditions occur by different catalytic mechanisms; secondly, subjected to hydrodechlorination are carbonylation products rather than the initial polychlorobiphenyls, and in the form of salts rather than esters.

In contrast to other procedures for reprocessing polychlorobiphenyls, the suggested procedure does not involve formation in the reaction mixture of other hazardous ecotoxicants: polychlorodibenzodioxins and polychlorodibenzofurans.

At the same time, technical PCB mixtures virtually always contain as microimpurities polychlorodibenzodioxins and polychlorodibenzofurans. Some of them strongly exceed PCBs in the toxicity. They can be formed in the course of both PCB production and their operation at elevated temperatures, and also upon photolysis of PCBs with sunlight [1, 2]. Therefore, in developing a procedure for detoxication of technical PCB mixtures by carbonylation, it is necessary to check whether this catalytic system is applicable to

Table 2. Carbonylation of Sovtol-10 technical mixture in a pressure vessel. 64–66°C, P_{CO} = 0.15–0.18 MPa, solvent methanol, base K_2CO_3

Run no.	Loaded, M			Degree of dechlorination, (g-equiv Cl^-) $(mol\ PCB)^{-1}$	CO uptake, mol mol^{-1} PCB	τ, h
	Sovtol-10	$Co_2(CO)_8$, $c \times 10^3$	propylene oxide			
1	0.25	0.013	1.8	2.8	2.2	9
2	0.48	0.0075	1.45	1.6	1.8	18
3	0.35	0.0075	2.23	0.9	0.6	9
4	0.28	0.0075	2.08	1.8	1.9	10
5	0.28	0.0075	2.28	1.9	2.5	11

* Run nos. 1–3: reaction products were additionally hydrolyzed after carbonylation completion; run no. 3: base Na_2CO_3; run no. 4: 74–75°C, P_{CO} = 0.25 MPa.

dechlorination of polychlorodibenzodioxins and polychlorodibenzofurans.

With 2,4,8-trichlorodibenzofuran as example, we showed that polychlorodibenzodioxins and polychlorodibenzofurans can also be readily dechlorinated with this catalytic system. Carbonylation of 2,4,8-trichlorodibenzofuran is highly selective. The reaction product is 2,8-dichlorodibenzofuran-4-carboxylic acid:

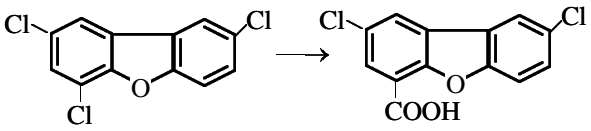

The structure of the product obtained confirms the relationship found previously for carbonylation of polychlorobiphenyls [10, 11]: The halogen atom located in the most substituted ring of a polycyclic aromatic system is replaced first.

The new economical carbonylation procedure that we developed for dechlorination, detoxication, and utilization of PCBs was protected by a patent [12].

EXPERIMENTAL

Carbonylation of Sovtol-10 technical mixture and technical-grade TCB was performed under atmospheric pressure of CO at 60°C in temperature-controlled glass installations with vigorous stirring. The reaction completion was judged from the results of GLC analysis of samples taken in a CO flow, treated with KOH, and extracted with ether. After the reaction completion, the aqueous-alkaline layer was acidified with HCl, and the precipitate of the mixture of reaction products, polychlorobiphenylcarboxylic acids, was filtered off, washed with water, and dried. The acids obtained were treated with diazomethane, and the resulting methyl esters were analyzed by GC–MS and ^1H NMR.

Chromatographic identification was made on a QO-500 Shimadzu device equipped with a capillary column (60 m × 0.25 mm, stationary phase SE-54) in the programmed heating mode: 40°C, 1 min; 40–180°C, 20 deg min^{-1}; 180–300°C, 5 deg min^{-1}. Vaporizer temperature 260°C; detector (ECD) temperature 250°C.

The ^1H NMR spectra of reaction mixtures and methyl esters of polychlorobiphenylcarboxylic acids were measured on a Bruker spectrometer (300 MHz) in $CDCl_3$ and 1 : 2 DMSO-d_6–CCl_4 mixture.

GLC analysis of technical-grade TCB and Sovtol-10, and of PCB mixtures after the carbonylation was performed with a Varian chromatograph equipped with an electron capture detector and a quartz capillary column (40 m × 0.25 mm); carrier gas N_2. The column temperature schedule was as follows: 160°C, 5 min; heating to 280°C, 20 deg min^{-1}. The analysis time was 40 min.

The carbonylation of technical PCB mixtures in a pressure vessel was described previously [13].

Structural analysis of 2,8-dichlorodibenzofuran-4-carboxylic acid was made by two-dimensional NMR correlation techniques (PFG, DQF) ^1H, ^1H COSY; PFG ^1H, ^{13}C (HMQC); and PFG ^1H, ^{13}C (HMBC). The spectra were taken in acetone-d_6 at 30°C on a Bruker Avance DRX 500 device (500 MHz). The molecular formula of 2,8-dichlorodibenzofuran-4-carboxylic acid was determined by mass spectrometry with electrospray ionization (ESI-TOF MS) with a TOF Micromass LCT mass spectrometer.

The content of mineral chlorine in aqueous solution of PCB carbonylation products was determined by argentometric titration.

CONCLUSIONS

(1) A novel procedure, based on carbonylation, was suggested and developed for detoxication and utilization of ecotoxicants, polychlorobiphenyls.

(2) Chemically stable polychlorobiphenyls can be activated with available catalytic systems based on epoxide-modified cobalt carbonyl and can be involved in carbonylation under mild conditions (atmospheric pressure of CO, 60–65°C).

(3) All the toxic components of the technical mixture of polychlorobiphenyls enter into the carbonylation to form a mixture of derivatives of aromatic carboxylic acids (esters, salts) containing two or three carboxy groups per molecule. The conversion of polychlorobiphenyls reaches 99%. The organic residue of polychlorobiphenyls (up to 1–2%) contains no initial toxic ("dioxin-like") polychlorobiphenyl congeners.

(4) It was demonstrated by the example of 2,4,8-trichlorodibenzofuran that polychlorodibenzodioxins and polychlorodibenzofurans can be readily dechlorinated with the suggested catalytic system.

REFERENCES

1. Khudolei, V.V., Gusarov, E.E., Klinskii, A.V., et al., *Stoikie organicheskie zagryazniteli: Puti resheniya problemy* (Persistent Organic Pollutants: Ways to Solve the Problem), St. Petersburg: Nauchno-Issled. Inst. Khimii Sankt-Peterb. Gos. Univ., 2002, p. 363.
2. Zanaveskin, L.N. and Aver'yanov, V.A., *Usp. Khim.*, 1998, vol. 67, no. 8, pp. 788–800.
3. Miyoshi, K. and Nishio, T., *Chemosphere*, 2000, vol. 41, pp. 819–824.
4. Lunin, V.V. and Lokteva, E.S., *Izv. Ross. Akad. Nauk, Ser. Khim.*, 1996, no. 7, pp. 1609–1624.
5. Gorbunova, T.I., Zapevalov, A.Ya., Saloutin, V.I., and Chupakhin, O.N., *Zh. Prikl. Khim.*, 2002, vol. 75, no. 5, pp. 832–835.
6. Zhesko, T.E. and Boyarskii, V.P., *Kinet. Katal.*, 1994, vol. 35, no. 2, p. 320.
7. Zhesko, T.E., Boyarskii, V.P., and Nikitina, A.G., *Zh. Obshch. Khim.*, 1998, vol. 68, no. 1, pp. 85–89.
8. Boyarskii, V.P., Zhesko, T.E., and Lanina, S.A., *Zh. Prikl. Khim.*, 2005, vol. 78, no. 11, pp. 1875–1880.
9. Ivanov, V. and Sandel, E., *Environ. Sci. Technol.*, 1992, vol. 26, no. 10, pp. 2012–2117.
10. Zhesko, T.E., Boyarskiy, V.P., Lanina, S.A., and Nikiforov, V.A., *Organohalogen Comp.*, 2001, vol. 54, pp. 226–229.
11. Boyarskiy, V., Nikiforov, V., Zhesko, T., Lanina, S., Kolehmainen, E., and Virtanen, E., *Organohalogen Comp.*, 2002, vol. 56, pp. 409–412.
12. RF Patent 2215729.
13. Boyarskii, V.P., Zhesko, T.E., and Nikitina, A.G., *Zh. Prikl. Khim.*, 2007, vol. 80, no. 5, pp. 967–972.

ISSN 1070-4272, Russian Journal of Applied Chemistry, 2007, Vol. 80, No. 7, pp. 1097–1100. © Pleiades Publishing, Ltd., 2007.
Original Russian Text © E.V. Ivanov, M.A. Artemova, A.A. Maslov, 2007, published in Zhurnal Prikladnoi Khimii, 2007, Vol. 80, No. 7, pp. 1127–1130.

PROCESSES AND EQUIPMENT OF CHEMICAL INDUSTRY

Extraction from Raw Materials with a Two-Phase System of Extractants in an Apparatus for Oscillating Vacuum Boiling

E. V. Ivanov, M. A. Artemova, and A. A. Maslov

St. Petersburg State Academy of Pharmaceutical Chemistry, St. Petersburg, Russia

Received January 23, 2007

Abstract—Extraction of hydrophilic and lipophilic compounds from vegetable raw materials with a two-phase system of extractants in an apparatus for oscillating vacuum boiling was studied. Dependences of the yield of target components on the time and hydrodynamic mode of the process were obtained.

DOI: 10.1134/S1070427207070166

If a raw material contains several groups of compounds with widely different solubilities, extraction is, as a rule, performed in several stages, with different solvents used in each stage. Recently, a new method has found use for extraction of hydrophilic and lipophilic compounds from vegetable raw materials with a two-phase system of extractants [1–4]. Hydrophilic compounds well dissolve in one of these, e.g., in an aqueous solution of ethanol, and lipophilic compounds, in the other, e.g., in vegetable oil. It has been shown that both hydrophilic and lipophilic compounds are extracted from raw materials mostly by the alcoholic-aqueous phase, from which lipophilic compounds subsequently pass into the oil phase [2, 4]. Thus, two main consecutive-paallel processes occur simultaneously: extraction of target components from vegetable raw materials with the alcoholic–aqueous phase and extraction of lipophilic compounds from the alcoholic–aqueous phase into the oil phase. The third process, extraction of lipophilic compounds from raw materials with oil, is insignificant.

Despite the strong interest in the given extraction technique, the effect of hydrodynamic mode in apparatus on the process intensity has been insufficiently studied, and, therefore, studies in this area are topical.

The aim of this study was to examine the extraction of hydrophilic and lipophilic compounds from vegetable raw materials with a two-phase system of extractants in an apparatus for oscillating vacuum boiling of the extractant.

The boiling-up of an extractant in an apparatus for oscillating vacuum boiling occurs as a result of periodic changes in the volume of a thermostated system constituted by a suspension being processed and a vapor [5]. As the volume of the system increases, the pressure in it decreases, the alcoholic–aqueous phase becomes superheated and boils up, with vapor bubbles forming and growing. As the volume of the system decreases, the pressure in it grows, vapor bubbles collapse, boiling terminates, and the heat of evaporation (condensation) is returned into the system. Vapor bubbles are formed throughout the volume of the alcoholic–aqueous phase. Their number and size depend on the frequency of boiling-up of the extractive agent and on the amplitude of oscillations in the suspension, which characterizes the variation amplitude of the volume of the system. As the frequency of boiling-ups of the extractant grows, the number of vapor bubbles increases and their size decreases. As the amplitude of suspension oscillations grows, the growth rate of vapor bubbles and, consequently, the intensity of their hydrodynamic impact on the suspension become higher.

The process was carried out at 50 to 90°C. The boiling-up frequency of the extractant was varied in the range 1–7.5 s^{-1}, and the amplitude of suspension oscillations, from 0.005 to 0.035 m.

A finely divided (2–3 mm) grass of common John's wort satisfying the requirements of State Pharmacopoeia [6] was used as a raw material. The two-phase system of extracting agents was composed of vegetable oil (low-polarity solvent) and a 70% aqueous solution of ethanol (polar solvent). The use of the alcoholic–aqueous mixture of the given concentration provides the most complete recovery of lipophilic substances from vegetable raw materials [2]. As tracers characterizing the rate and extent of the process were chosen chlorophyll derivatives (in terms of

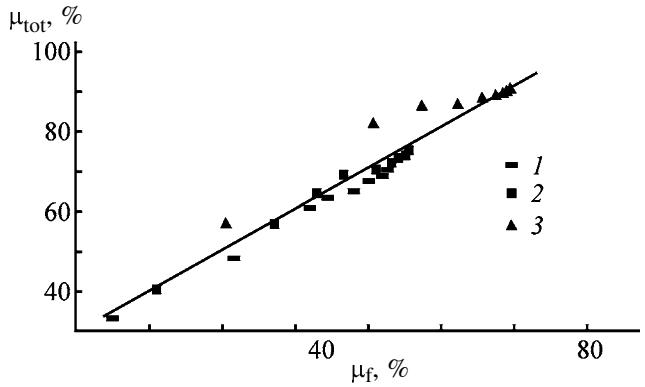

Fig. 1. Comparison of the total yield (into the alcoholic–aqueous and oil phases) of chlorophyll derivatives (μ_{tot}) and of the yield of flavonoid compounds (μ_f) at the same instants of time. Amplitude of suspension oscillations 0.035 m, boiling-up frequency of the alcoholic–aqueous phase 2.5 s^{-1}. *T*, °C: (*1*) 50, (*2*) 60, and (*3*) 90.

pheophytin A) and flavonoid compounds (in terms of rutin). The sum of flavonoids was quantitatively determined by spectrophotometry [6]. The content of chlorophyll derivatives in oil extracts was found spectrophotometricaly at a wavelength λ = 668 nm [7, 8]. Alcoholic–aqueous extracts were analyzed for the content of chlorophyll derivatives as follows: to 2 ml of an extract was added 5 ml of 70% ethanol, the mixture was agitated, and the optical density of the solution was measured at a wavelength of 668 nm. As a reference solution served a 70% aqueous solution of ethanol. The ratio between the raw material, oil, and ethanol was 1 : 10 : 10.

The extraction was performed in the course of 3 h. Samples of the two-phase system of extractants were separated into the alcoholic–aqueous and oil phases and then the content of chlorophyll derivatives in both phases and that of flavonoids in the alcoholic–aqueous phase were determined spectrophotometrically.

It was found that each 10°C increase in the process temperature is accompanied by a rise in the "apparent" equilibrium yield of flavonoid compounds by 5–10% and in that of chlorophyll derivatives by 8–12%. This is presumably due to a decrease in the viscosity of the vegetable oil and to an increase in the coefficients of transfer of target components in particles of the vegetable raw material. The highest process rate was observed at 90°C. In this case, the yield of the target components approached 90% and the "apparent" equilibrium was attained in 120–140 min.

An increase in the amplitude of suspension oscillations from 0.005 to 0.035 m was accompanied by a 20% rise in the yield of the target components, and the extraction time decreased to 60–80 min. Raising the frequency of boiling-ups of the alcoholic–aqueous phase from 1 to 7.5 s^{-1} led to a 15% increase in the apparent equilibrium yield, and the process duration decreased to 60–80 min. It should be noted for comparison that, all other conditions being the same, the equilibrium yield of 85% was reached in extraction from the grass of St. John's wort in an apparatus with an agitator in 120–180 min.

Thus, the best results were obtained when the extraction was performed, with the process parameters varied in the range under study, at 90°C, amplitude of suspension oscillations equal to 0.035 m, and boiling-up frequency of the alcoholic–aqueous phase of 7.5 s^{-1}.

A comparison of the total yield (into the alcoholic–aqueous and oil phases) of chlorophyll derivatives (μ_{tot}) and of the yields of flavonoid compounds (μ_f) at the same instants of time (Fig. 1) demonstrated that they are virtually equal. Therefore, to determine the total yield of some target components (hydrophilic or lipophilic), it suffices to know the total yield of other components, e.g., compounds whose analytical determination is less labor-consuming. In addition, Fig. 1 demonstrates that both flavonoid compounds and chlorophyll derivatives are extracted simultaneously and at equal rates.

Experimental data on the kinetics of two-phase extraction were processed using the relations suggested in [9, 10]. In the initial stage of the process ($0 \le \theta \le 0.25$), when the content of the target components in the main volume of the extractive agent has no effect on the extraction rate and the process rate is determined by the convective mass transfer in coarse pores, the following relation was used:

$$\mu = u_1\theta^{1/2}, \quad (1)$$

where μ is the yield of the target components (%); θ, dimensionless extraction time equal to the ratio of the running time to the time of attainment of the apparent equilibrium (80 min in this study); and u_1, parameter dependent on the hydrodynamic situation in the apparatus (%).

Experimental data on the extraction kinetics in the final stage of the process ($0.25 \le \theta \le 1$), in which the content of the target components in the main volume of the extractive agent affects the process rate, were approximated with the relation

$$\mu = w - u_2\theta^{-1/2}, \quad (2)$$

where w is an empirical coefficient (%), and u_2 is

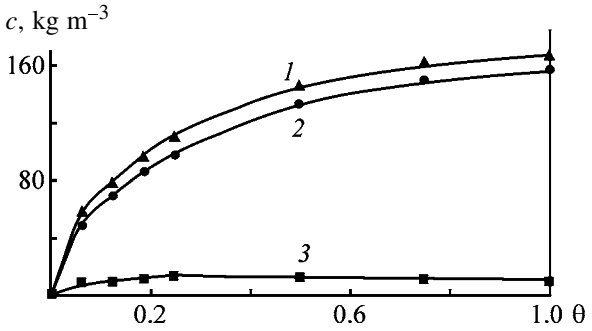

Fig. 2. Variation of the content c of chlorophyll derivatives in the extractants with time θ. Amplitude of suspension oscillations 0.035 m, boiling-up frequency of the alcoholic–aqueous phase 2.5 s^{-1}. (*1*) Sum in alcohol and oil, (*2*) in oil, and (*3*) in alcohol. Solid lines, calculation; points, experimental data.

a parameter dependent on the hydrodynamic situation in the apparatus.

The dependences of the total yield of chlorophyll derivatives into the alcoholic–aqueous and oil phases (with account of the aforesaid and the yield of flavonoid compounds into the alcoholic–aqueous phase) on the dimensionless time have the form

$$\mu_{tot} = [74 + 173.7(A\nu)]\theta^{1/2}, \quad 0 \le \theta \le 0.25; \quad (3)$$

$$\mu_{tot} = 118.8 - [40.9 - 43.4(A\nu)]\theta^{-1/2}, \quad 0.25 \le \theta \le 1, \quad (4)$$

where A is the amplitude of suspension oscillations (m), and ν is the boiling-up frequency of the alcoholic–aqueous phase (s^{-1}).

Experimental data on the extraction kinetics of chlorophyll derivatives from the alcoholic–aqueous phase into the oil phase were processed using the equations

$$dM/dt = k_{vo}V_o(c_o^* - c_o), \quad (5)$$

$$dM/dt = k_{va}V_a(c_a^* - c_a), \quad (6)$$

where M is the mass of chlorophyll derivatives that passed from the alcoholic–aqueous into the oil phase (kg); τ, time (s); k_{vo} and k_{va}, volumetric (related to the volume of the respective phase) coefficients of mass transfer of chlorophyll derivatives from the alcoholic–aqueous phase into the oil phase (s^{-1}); V_o and V_a, volumes of the oil and alcoholic–aqueous phases (m^3); c_o and c_a, concentrations of chlorophyll derivatives in the oil and alcoholic–aqueous phases (kg m^{-3}); and c_o^* and c_a^*, equilibrium concentrations of chlorophyll derivatives in the oil and alcoholic–aqueous phases (kg m^{-3}).

It was found that, in Eq. (5), $c_o^* = 159$ kg m^{-3} and $k_{vo} = 3.08 + 14.1A\nu$ (s^{-1}). Chlorophyll derivatives are poorly soluble in the alcoholic–aqueous phase and are present in this phase "in the form of an emulsion," and, therefore, their equilibrium concentration c_a^* depends on the hydrodynamic situation in the apparatus. The dependence of the mass-transfer coefficient on the complex $A\nu$ in Eq. (6) is described with the same accuracy by the formulas $k_{va} = 0.59 - 0.354\ln(A\nu)$ and $k_{va} = 0.78(A\nu)^{-1/4}$.

The yield of chlorophyll derivatives into the oil phase can be found with high precision without solving differential equations (5) and (6). Processing of the experimental data in terms of (1) and (2) gave the following dependences:

$$\mu_o = [65 + 153(A\nu)]\theta^{1/2}, \quad 0 \le \theta \le 0.25; \quad (7)$$

$$\mu_o = 115.1 - [41.3 - 38.3(A\nu)]\theta^{-1/2}, \quad 0.25 \le \theta \le 1. \quad (8)$$

For the adopted ratio between the raw material and extractants, the concentration of chlorophyll derivatives in the alcoholic–aqueous phase is related to their total yield into the alcoholic–aqueous and oil phases, μ_{tot}, and to the yield into the oil phase, μ_o, by $c_a = 1.87(\mu_{tot} - \mu_o)$. Therefore, expressions (3), (4), (7), and (8) can be used to obtain

$$c_a = [16.8 + 39.7(A\nu)]\theta^{1/2}, \quad 0 \le \theta \le 0.25; \quad (9)$$

$$c_a = 6.9 + [0.75 + 9.54(A\nu)]\theta^{-1/2}, \quad 0.25 \le \theta \cong 1. \quad (10)$$

The precision of these relations is illustrated by Fig. 2, in which calculated and experimental data are represented by solid lines and points, respectively.

CONCLUSIONS

(1) The total yield (into the alcoholic–aqueous and oil phases) of chlorophyll derivatives is virtually equal to that of flavonoid compounds at the same instants of time. The extraction of both flavonoid compounds and chlorophyll derivatives occurs simultaneously and at equal rates.

(2) Each 10°C increase in the temperature of two-phase extraction in an apparatus for oscillating vacuum boiling of the extractive agent is accompanied by a rise in the apparent equilibrium yield of flavonoid compounds by 5–10% and in that of chlorophyll derivatives by 8–12%. The highest process rate is observed at 90°C. In this case, the yield of target components approaches 90% and an apparent equilibrium is attained in 120–140 min.

(3) An increase in the amplitude of suspension oscillations from 0.005 to 0.035 m leads to a rise in the yield of recovered target components by 20% and to a decrease in the process duration to 60–80 min. An increase in the boiling-up frequency of the alcoholic–aqueous phase from 1 to 7.5 s^{-1} leads to a rise in the apparent equilibrium yield by 15% and to a decrease in the process duration to 60–80 min.

(4) The dependences describing the kinetics of extraction of chlorophyll derivatives from the raw material and the alcoholic–aqueous phase are in good agreement with experimental data. The model parameters depend on the hydrodynamic situation in the apparatus through the complex $A\nu$.

REFERENCES

1. Ivanova, S.A., Skochipets, S.E., Skochipets, M.E., et al., *Farmatsiya*, 2003, no. 6, pp. 22–25.
2. Ivanova, S.A., Vainshtein, V.A., and Kaukhova, I.E., *Khim.-Farm. Zh.*, 2003, vol. 37, no. 8, pp. 30–33.
3. Khazzaa, I.Kh., Vainshtein, V.A., and Chibilyaev, T.Kh., *Khim.-Farm. Zh.*, 2003, no. 7, pp. 20–23.
4. Artemova, M.A., Ivanov, E.V., and Maslov, A.A., *Razrabotka, issledovanie i marketing novoi farmatsevticheskoi produktsii: Sbornik nauchnykh trudov* (Development, Study, and Marketing of New Pharmaceutical Products: Coll. of Scientific Works), Pyatigorsk: Pyatigorsk. Gos. Farm. Akad., 2006, issue 61, pp. 67–72.
5. Ivanov, E.V., Shvyrev, M.V., Artemova, M.A., et al., *Khim.-Farm. Zh.*, 2006, vol. 40, no. 6, pp. 39–43.
6. *Gosudarstvennaya farmakopeya SSSR* (USSR State Pharmacopoeia), issue 2: *Obshchie metody analiza. Lekarstvennoe rastitel'noe syr'e* (General Analytical Methods, Medicinal Plant Raw Materials), Moscow: Meditsina, 1989, 11th ed.
7. Grinkevich, N.I. and Safronich, L.N., *Khimicheskii analiz lekarstvennykh rastenii* (Chemical Analysis of Medicinal Plants), Moscow: Vysshaya Shkola, 1983.
8. Dawson, R., Elliot, D.C., Elliot, W.H., and Jones, K.M., *Data for Biochemical Research*, Oxford: Clarendon, 1986.
9. Ivanov, E.V., *Khim. Prom–st.*, 2006, vol. 83, no. 6, pp. 271–276.
10. Ivanov, E.V. and Babenko, Yu.I., *Zh. Prikl. Khim.*, 2005, vol. 78, no. 9, pp. 1487–1492.

ISSN 1070-4272, Russian Journal of Applied Chemistry, 2007, Vol. 80, No. 7, pp. 1101–1104. © Pleiades Publishing, Ltd., 2007.
Original Russian Text © N.G. Kozlov, S.L. Bondarev, B.A. Odnoburtsev, L.I. Basalaeva, 2007, published in Zhurnal Prikladnoi Khimii, 2007, Vol. 80, No. 7, pp. 1131–1134.

ORGANIC SYNTHESIS AND INDUSTRIAL ORGANIC CHEMISTRY

Synthesis of Arylmethylpyrimidinetriones and Pyrimidoquinolinediones with Fluorescent and Nonlinear-Optical Properties

N. G. Kozlov, S. L. Bondarev, B. A. Odnoburtsev, and L. I. Basalaeva

Institute of Physical Organic Chemistry, National Academy of Sciences of Belarus, Minsk, Belarus
Institute of Molecular and Atomic Physics, National Academy of Sciences of Belarus, Minsk, Belarus

Received February 28, 2006

Abstract—5-Arylmethyl-2,4,6-(1*H*,3*H*,5*H*)pyrimidinetriones and 12-aryl-8,12-dihydrobenzo[*f*]pyrimido-[4,5-*b*]quinoline-9,11-(7*H*,10*H*)diones were synthesized, and their spectral-luminescence and nonlinear-optical properties were examined.

DOI: 10.1134/S1070427207070178

Organic luminophores containing a carbonyl group, either in the open chain or incorporated into the cyclic system, are of great practical significance. These compounds include, in particular, arylmethylpyrimidinetriones, both known and new, and pyrimidoquinolinediones prepared by the scheme

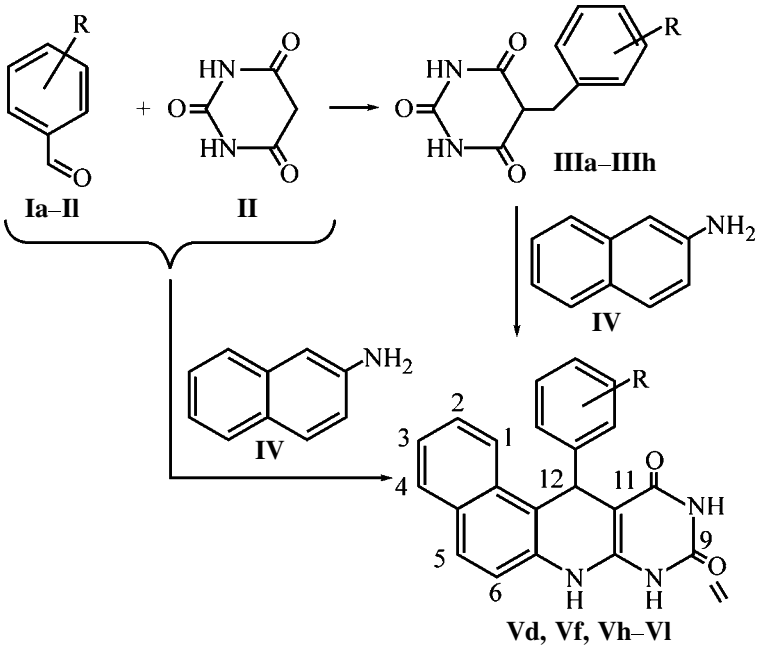

where R = $N(CH_3)_2$ (**a**), $N(C_2H_5)_2$ (**b**), 3,4-di-(OH) (**c**), 2,4-di-OMe (**d**), 3,4-di-OMe (**e**), 3-OEt-4-OH (**f**), 3-OMe-4-OCOEt (**g**), 3-OMe-4-$OCO(CH_2)_2Me$ (**h**), 2,4-di-Cl (**i**), 3-OMe-4-OH (**j**), 3-OMe-4-$OCOC_6H_5$ (**k**), and 2-F-6-Cl (**l**).

Refluxing equimolar amounts of appropriate benzaldehyde **Ia**–**Ih** and 2,4,6-(1*H*,3*H*,5*H*)pyrimidinetrione (barbituric acid) **II** in an alcohol solution resulted in selective formation of 5-arylmethyl-2,4,6-(1*H*,3*H*,5*H*)pyrimidinetriones **IIIa**–**IIIh.**

Table 1. Properties of 5-arylmethyl-2,4,6-(1*H*,3*H*,5*H*)pyrimidinetriones **IIIf–IIIh** and 12-aryl-8,12-dihydrobenzo[*f*]-pyrimido[4,5-*b*]quinoline-9,11-(7*H*,10*H*)diones **Vd, Vf,** and **Vh–Vl**

Compound	Yield, %	mp, °C	Found, %			Formula	Calculated, %		
			C	H	N		C	H	N
IIIf	75	275	56.55	4.34	10.12	$C_{13}H_{12}N_2O_5$	56.52	4.35	10.14
IIIg	70	283	54.92	4.58	9.15	$C_{14}H_{14}N_2O_6$	54.90	4.57	9.15
IIIh	63	292	56.24	5.02	8.77	$C_{15}H_{16}N_2O_6$	56.25	5.00	8.75
Vd	40	>350	68.77	4.78	10.50	$C_{23}H_{19}N_3O_4$	68.82	4.74	10.47
Vf	59	>350	68.87	4.76	10.51	$C_{23}H_{19}N_3O_4$	68.82	4.74	10.48
Vh	52	>350	68.25	5.00	9.21	$C_{26}H_{23}N_3O_5$	68.27	5.03	9.19
Vi	61	>350	61.58	3.15	10.3	$C_{21}H_{13}Cl_2N_3O_2$	61.61	3.18	10.27
Vj	62	>350	68.24	4.42	10.88	$C_{22}H_{17}N_3O_4$	68.20	4.39	10.85
Vk	37	>350	70.88	4.27	8.58	$C_{29}H_{21}N_3O_5$	70.87	4.28	8.55
Vl	64	>350	64.14	3.36	10.71	$C_{21}H_{13}FClN_3O_2$	64.12	3.31	10.68

Pyrimidoquinolinediones **Vd, Vf, Vh** and **Vi–Vl** can be prepared both by the reaction of arylmethylpyrimidinetriones with 2-naphthylamine and three-component condensation of benzaldehydes **Ii–Il**, barbituric acid, and 2-naphthylamine via formation of arylidenetriones which further react with 2-naphthylamine. The latter, having the highest electron density on the carbon atom in the α position with respect to the amino group, enters into the addition reaction at the double bond of arylmethylpyrimidinetriones **III**. Previously [1] we reported that this pathway is possible for multicomponent condensation of benzaldehydes, 1,3-diketones, and 2-naphthylamine. In this study, we prepared pyrimidoquinolinediones by two pathways: **Vd, Vf, Vh** by the first pathway, and **Vi–Vl**, by the second pathway. Physicochemical constants of arylmethylpyrimidinetriones **IIIa–IIIe** are identical to those published in [2–4]; for constants of **IIIf–IIIh** and **Vd, Vf, Vh** and **Vi–Vl**, see Table 1.

The position and multiplicity of the aromatic proton signals in the ^{1}H NMR spectra of arylmethylpyrimidinetriones **IIIa–IIIh** and pyrimidinequinolinediones **Vd, Vf,** and **Vh–Vl** correspond to the structures of compounds of this kind [5].

The IR spectra of arylmethylpyrimidinetriones **IIIa–IIIh** and pyrimidinequinolinediones **Vd, Vf,** and **Vh–Vl** contain bands associated with the stretching vibrations of secondary amines (a band at 3520–3185 cm^{-1}) and carbonyl groups (a band at 1729–1701 cm^{-1}). Pyrimidoquinolinediones **Vi** and **Vl** exhibit an intense absorption band at 860 and 830 cm^{-1}, respectively, associated with the stretching vibrations of the C–Cl bond.

The mass spectra of arylmethylpyrimidinetriones **IIIa–IIIh** synthesized contain a molecular peak $[M]^+$, which is the strongest (I_{rel} 100%), and several fragment peaks. The mass spectra of pyrimidoquinolinediones **Vd, Vf,** and **Vh–Vl** contain a peak with the maximal intensity (I_{rel} 100%) at *m*/*z* 264, corresponding to the $[M - C_6H_4]^+$ ion, a peak with *m*/*z* 265 corresponding to the $[M - C_6H_4 + 1]$ + ion (I_{rel} 65–70%), and peaks of the molecular ion M^+ (28–35%) and positive ions with *m*/*z* 111 (29–33%), 134 (56–60%), 139 (90–96%), 148 (72–78%), 153 (47–55%), 166 (32–39%), and 222 (18–23%) formed from the $[M - C_6H_4]^+$ fragment ion and constant for all these compounds.

The electronic absorption spectra of arylmethylpyrimidinetriones **IIIa–IIIh** and pyrimidinequinolinediones **Vd, Vf,** and **Vh–Vl** in ethanol are characterized by a number of vibronic bands (their λ_{max} and relative intensities are listed in Table 2); the spectra of **IIIa** and **Vl** are shown in the figure.

Pyrimidoquinolinediones **Vd, Vf,** and **Vh–Vl** in an ethanol solution exhibit a weak fluorescence with a maximum near 380 nm. Arylmethylpyrimidinetriones **IIIa–IIIh** in an ethanol solution also exhibit weak fluorescence, with the spectra shifted to long waves relative to those of **Vd, Vf,** and **Vh–Vl**.

All the compounds examined in the crystalline state at room temperature exhibit fluorescence of different intensities. The fluorescence spectra were recorded at λ_{exc} = 340 nm. Arylmethylpyrimidinetriones **IIIa, IIIb, IIIe** and pyrimidinequinolinediones **Vd, Vf, Vh, Vl** are characterized by intense fluorescence, and the remaining compounds examined, by weak fluorescence. The maxima in the fluorescence spectra vary over a wide spectral range. Fluorescence of polycrystals of **Vd, Vf,** and **Vh–Vl** is charac-

Table 2. Spectral-luminescence properties of arylmethylpyrimidinetriones **IIIf–IIIh** and pyrimidoquinolinediones **Vd, Vf,** and **Vh–Vl** in ethanol solution and as polycrystals at room temperature

Compound	Absorption λ_{max}, nm (I_{rel}), ethanol	Fluorescence, λ_{max}, nm (I_{rel})	
		ethanol	polycrystals
IIIa	465(1.0), 275(0.12), 244(0.23)	522	590(0.37), 634(1.0)
IIIb	470(1.0), 278(0.14), 239(0.26)	529	637
IIIc	410(1.0), 256(0.46), 233(0.53)	443(1.0), 517(0.83)	609
IIId	410(1.0), 252(0.45)	460	515
IIIe	395(0.83), 259(1.0), 230(0.86)	452(0.3), 573(0.9), 604(1.0)	588
IIIf	483(0.55), 407(1.0), 256(0.71), 232(0.67)	461	524
IIIg	358(0.59), 257(1.0)	420	401
IIIh	396(0.40), 257(1.0)	458	403(0.46), 547(1.0)
Vd	323(0.43), 284(1.0)	382	400
Vd	320(0.42), 279(1.0)	379	393
Vh	320(0.39), 285(1.0), 275(0.96)	378	393
Vi	323(0.34), 286(1.0), 275(0.88)	380	405(1.0), 550(0.32)
Vj	320(0.43), 263(1.0)	380	398(0.73), 426(1.0)
Vk	319(0.34), 284(0.96), 274(1.0)	377	394
Vl	322(0.30), 384(1.0)	381	410

terized primarily by maxima near 400 nm, while that of **IIIa–IIIh**, by maxima varying within 400–650 nm (see figure and Table 2).

Polycrystals of some compounds display nonlinear-optical properties, i.e., are able of converting the laser radiation frequency. For example, when excited by the first harmonics of radiation of a YAG : Nd^{3+} laser (λ_{exc} = 1.06 μm, E_{exc} = 80 mJ, pulse length 20 ns) polycrystalline arylmethylpyrimidinetriones **IIIa** and **IIIb** exhibited bright red two-photon-excited fluorescence (TEF) with λ_{max} ~640 nm, and arylmethylpyrimidinetrione **IIIa**, less intense yellow TEF at 600 nm.

Arylmethylpyrimidinetriones **IIIf** and **IIIg** exhibited a different nonlinear-optical effect, generation of the second harmonics of laser radiation (GSG). It consists in converting the wavelength of the first harmonics of a neodymium laser (1.06 μm) into the second harmonics wavelength (532 nm) by the polycrystals. Thus, both these substances emit bright red luminescence at 532 nm when irradiated with intense invisible IR radiation (1.06 μm). For arylmethylpyrimidinetrione **IIIh** we recorded a weak GSG effect.

The nonlinear-optical effects revealed for arylmethylpyrimidinetriones **IIIa, IIIb, IIIe** (TEF) and **IIIf–IIIh** (GSG) make these compounds candidate materials for preparing elements for visual imaging of invisible IR laser radiation, optical recording of information, and development of nonlinear-optical elements for GSG.

EXPERIMENTAL

The IR spectra of the arylmethylpyrimidinetriones and pyrimidoquinolinedions examined were recorded on a Nicolet Protege-460 Fourier spectrophotometer from a thin layer or KBr pellets, and mass spectra, on a Hewlett–Packard 5890/5979 Chrommas GC/MS chromatograph–mass spectrometer, HP-5MS column (70 eV). The absorption spectra of the solutions were measured at room temperature on a Cary-500 (Varian, the United States) spectrophotometer, and the fluores-

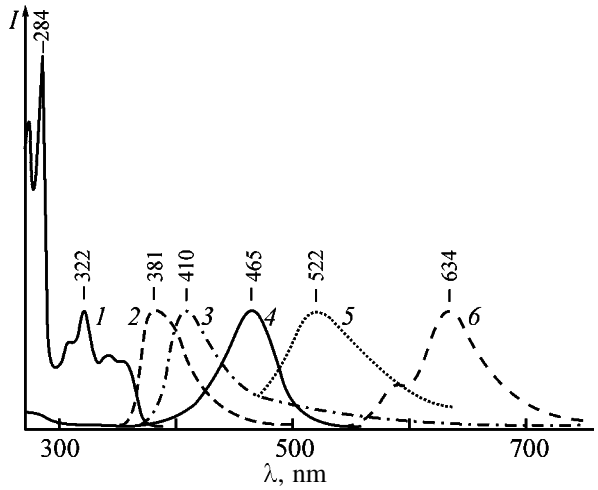

(*1, 4*) Absorption and (*2, 3, 5, 6*) fluorescence spectra of (*4–6*) **IIIa** and (*1–3*) **Vl** in (*1, 2, 4, 5*) ethanol and (*3, 6*) polycrystals at 293 K. (*I*) Intensity and (λ) wavelength.

cence spectra, on a wide-aperture setup [6]. Two-photon excitation was achieved with the first harmonics of a YAG : Nd^{3+} pulse laser with the wavelength of 1.06 μm.

5-Arylmethyl-2,4,6-(1*H*,3*H*,5*H*)pyrimidinetriones IIIf–IIIh. Barbituric acid **II** [1.3 g (0.01 mol)] and 0.01 mol of appropriate aldehyde **Ia**–**Ih** in an alcohol solution were refluxed for 20–30 min. The precipitate formed after cooling the reaction mixture was filtered off and recrystallized from alcohol.

12-Aryl-8,12-dihydrobenzo[*f*]pyrimido[4,5-*b*]-quinoline-9,11-(7*H*,10*H*)diones Vd, Vf, Vh. A solution of 0.01 mol of appropriate 5-(4-arylmethyl)-2,4,6-(1*H*,3*H*,5*H*)pyrimidinetrione **IIId, IIIf, IIIh** and 0.01 mol of 2-naphthylamine **IV** in 20 ml of butanol was refluxed until crystals formed. The precipitate was filtered off and recrystallized from a 1 : 1 alcohol–benzene mixture.

12-Aryl-8,12-dihydrobenzo[*f*]pyrimido[4,5-*b*]-quinoline-9,11-(7*H*,10*H*)diones Vi–Vl. A solution of 1.43 g (0.01 mol) of 2-naphthylamine **IV**, 0.01 mol of appropriate aromatic aldehyde **Ii**–**Il**, and 1.3 g (0.01 mol) of barbituric acid **II** in 20 ml of butanol was refluxed until crystals formed (30–60 min). The precipitate formed after cooling the reaction mixture was filtered off, washed with hot water and ether, and recrystallized from a 1 : 1 alcohol–benzene mixture.

CONCLUSIONS

(1) 5-Arylmethyl-2,4,6-(1*H*,3*H*,5*H*)pyrimidinetriones **IIIa**, **IIIb**, **IIIe** and 12-aryl-8,12-dihydrobenzo[*f*]pyrimido[4,5-*b*]quinoline-9,11-(7*H*,10*H*)diones **Vd, Vf, Vh, Vl** exhibit intense fluorescence.

(2) These compounds exhibit nonlinear-optical effects. Specifically, two-photon-excited fluorescence was revealed for already known 5-dimethylamino- (**IIIa**), 5-diethylamino- (**IIIb**), and 5-(3,4-dimethoxy)-phenylmethyl-2,4,6-(1*H*,3*H*,5*H*)-pyrimidinetriones (**IIIe**)], and generation of the second harmonics of the laser radiation, for previously unknown 5-(4-hydroxy-3-ethoxy- (**IIIf**), (4-carboxy-3-methyoxy)-(**IIIg**), 5-(4-carbpropoxy-3-methoxy)phenylmethyl-2,4,6-(1*H*,3*H*,5*H*)pyrimidinetriones (**IIIh**). The effects revealed make these compounds candidate materials for preparing elements for visual imaging of invisible IR laser radiation, optical recording of information, and development of nonlinear-optical elements for generation of the second harmonics of laser radiation.

ACKNOWLEDGMENTS

The authors are grateful to I.I. Kalosha from the Institute or Atomic and Molecular Physics, National Academy of Sciences of Belarus, for assistance in carrying out the nonlinear-optical measurements.

REFERENCES

1. Kozlov, N.G., Basalaeva. L.I., and Dikusar, E.A., *Zh. Org. Khim*., 2005, vol. 41, no. 11, pp. 1671–1680.
2. Geng, L.S., Wang, S.X., Li, Ji-Tai, and Liu, Ch.H., *Chin. J. Org. Chem*., 2002, vol. 22, no. 12, pp. 1047–1049.
3. Gao, Y., Tu, Shu-Jiang, and Zhou, J.F., *Chin. J. Appl. Chem*., 2002, vol. 19, no. 5, pp. 499–500.
4. Li, Jing-ci, Li, Gui-shen, Wang, C., and Feng, S., *J. Hebei Univ. Natur. Sci*., 2001, vol. 21, no. 3, pp. 269–272.
5. Dyer, J.R., *Applications of Absorption Spectroscopy of Organic Compounds*, Englewood Cliffs, New Jersey: Prentice-Hall, 1965.
6. Borisevich, E.A., Knyukshto, V.N., Kozyrev, A.N., and Solov'ev, K.N., *Opt. Spektrosk*., 1993, vol. 74, no. 1, pp. 210–218.

ISSN 1070-4272, Russian Journal of Applied Chemistry, 2007, Vol. 80, No. 7, pp. 1105–1110. © Pleiades Publishing, Ltd., 2007.
Original Russian Text © Z.R. Khasanova, M.Yu. Vozhdaeva, N.N. Kabal'nova, E.A. Kantor, 2007, published in Zhurnal Prikladnoi Khimii, 2007, Vol. 80, No. 7, pp. 1135–1140.

ORGANIC SYNTHESIS AND INDUSTRIAL ORGANIC CHEMISTRY

Chlorination and Oxidation Products Formed from 1,2,4-Trimethylbenzene in Aqueous Solution under the Action of Chlorine Dioxide

Z. R. Khasanova, M. Yu. Vozhdaeva, N. N. Kabal'nova, and E. A. Kantor

Ufa State Petroleum Technical University, Ufa, Bashkortostan, Russia
Ufavodokanal Municipal Unitary Enterprise, Ufa, Bashkortostan, Russia
Institute of Organic Chemistry, Ufa Scientific Center, Russian Academy of Sciences, Ufa, Bashkortostan, Russia

Received October 30, 2006; in final form, April 2007

Abstract—Products of the reaction of 1,2,4-trimethylbenzene with chlorine dioxide in aqueous solution were studied. A scheme of 1,2,4-trimethylbenzene transformations was suggested. The influence exerted on the number of the reaction products by the ClO_2 dosage and time of its contact with the substrate was examined.

DOI: 10.1134/S107042720707018X

Disinfection of water with chemical reagents improves its microbiological parameters. Water disinfection is usually performed with molecular chlorine, sodium hypochlorite, chloramine, ozone, or chlorine dioxide, or by UV irradiation [1–3]. Today it is important to find a method that would combine the advantages of various disinfection methods and reduce the formation of secondary toxicants [4].

Chlorine dioxide, which is an available and effective oxidant, finds growing use both in industry and in water preparation [5]. It improves the microbiological and organoleptic parameters of water and considerably reduces the amount of toxic disinfection products such as trihalomethanes, which are the main by-products in chlorination of water with molecular chlorine. This is particularly important in disinfection of water containing not only natural humic compounds but also manmade organic pollutants. According to published data, chlorine dioxide is a mild oxidant. Benzene and its simplest alkyl derivatives (toluene, ethylbenzene, xylenes, diphenylmethane) do not react with chlorine dioxide under the conditions of potable water treatment in the absence of traces of molecular chlorine [6].

In this study we examined transformations of organic compounds of industrial origin in aqueous solution under the action of chlorine dioxide. As organic substrate we chose 1,2,4-trimethylbenzene (1,2,4-TMB), which is a possible water pollutant in regions adjacent to petrochemical enterprises.

Our main analytical procedure for determining organic compounds was gas chromatography with mass-selective detector (GS–MSD), which is one of the most reliable methods for identification of components of complex organic mixtures [7].

EXPERIMENTAL

Chlorine dioxide was prepared by the reaction of sodium chlorite with hydrochloric acid [8]. Sodium chlorite (main substance content 80%) was purchased from Aldrich. The sodium chlorite concentration was determined by titration [9, 10]. The chlorine dioxide concentration was determined spectrophotometrically with a Specord M40 device (Carl Zeiss, Jena) in quartz cells (l = 0.1 cm) in the range of the ClO_2 absorption maximum (354–362 nm) just before each experiment.

In the experiments we used 1,2,4-TMB [GSO (State Reference Sample) 3309–85] and deionized water (Milli-Q Gradient). To attain 25 : 1 molar ratio of ClO_2 to the organic substrate, to Milli-Q water (V = 1 dm^3) containing 1,2,4-TMB (10 mg dm^{-3}, 8.32×10^{-5} M) we added ClO_2 to a concentration of 2.08×10^{-3} M. To attain 40 : 1 ratio, to Milli-Q water (V = 1 dm^3) containing the substrate (1 mg dm^{-3}, 8.32×10^{-6} M) we added ClO_2 to a concentration of 3.33×10^{-4} M. The exposure time was 6 and 24 h, respectively. The water treatment with ClO_2 was performed at room temperature. The reaction was stopped by

Table 1. Main parameters of devices for analysis of products of the reaction of 1,2,4-TMB with ClO_2 aqueous solution

Gas chromatograph	Agilent 5890N	G6000 Vega Series 2	HRGC Mega Series
Detector	MSD	FID	ECD
Column type	HP-5MS 30 m × 0.25 mm × 0.25 μm	DBWAX 30 m × 0.25 mm × 0.25 μm	DB-5 30 m × 0.32 mm × 1 μm
Carrier gas	Helium	Helium	Nitrogen
Carrier gas flow rate, $cm^3\ min^{-1}$	2	2	2
Temperature schedule, °C	35 to 60, 30 deg min^{-1}; 60 to 280, 6 deg min^{-1}; 280, 10 min	60, 9 min; 60 to 120, 10 deg min^{-1}; 120, 4 min	70
Temperature, °C:			
vaporizer	250	120	120
detector	–	300	330
ion source	230	–	–
quadrupole	150	–	–
transition channel	280	235	–
Ionization mode	Electron impact	–	–
Electron energy, eV	70	–	–

adding sodium thiosulfate which deactivates excess ClO_2 [11]:

$$5Na_2S_2O_3 + 8ClO_2 + 9H_2O \rightarrow 10NaHSO_4 + 8\ HCl.$$

To study the dynamics of formation of volatile organic compounds, at 15-min intervals we took from the reaction volume (V = 1 dm^3) 10 cm^3 samples of water into specially prepared vials with sodium thiosulfate and analyzed the samples by GC–MSD. Volatile aromatic hydrocarbons (VAHs) were determined by head space analysis with a flame ionization detector (GC–FID; Vega chromatograph, Carlo Erba Instruments). Volatile halogenated hydrocarbons (VHHs) were determined similarly using an electron capture detector (GC–ECD; Mega device, Carlo Erba Instruments, Head Space 850 unit).

The 1,2,4-TMB transformation products were extracted from aqueous solution with methylene chloride (Merck, 2 × 10 cm^3). The extract was dried over anhydrous sodium sulfate and analyzed on a 6890N gas chromatograph with a mass-selective detector (5973, Agilent). The characteristics of the quartz capillary columns used and the analysis and detection conditions for all the three methods are given in Table 1. The components were identified by comparing the experimental mass spectra with those from the Wiley 138 and NBS 75 libraries (coincidence quality 70–90% on the average) and by interpreting the fragmentation patterns under electron impact, taking into account well-known relationships [7].

For the chloro derivatives of 1,2,4-TMB, the response factors, reflecting the extraction coefficient, ionization cross section, contributiopn of the characteristic ion to the total ion current, and mass discrimination of the mass spectrometer used, were taken equal to unity. The concentrations of chloro derivatives of 1,2,4-TMB, c_{comp}, were quantitatively estimated with an external reference by the formula $c_{comp} = S_{comp}c_{ref}/S_{ref}$, where S_{comp} and S_{ref} are the areas of the chromatographic peaks of the product and external reference, respectively (mV s), and c_{ref} is the 1,2,4-TMB concentration (M). As external reference we used a 1,2,4-TMB solution. The analysis results are given in Table 2.

Analysis of the concentrates prepared after extraction of products of the reaction of 1,2,4-TMB with chlorine dioxide shows that the 1,2,4-TMB conversion in 1.75 h at 25-fold molar excess of ClO_2 is 90.2%. The possible transformation pathways of 1,2,4-TMB under the action of ClO_2 are shown in Scheme 1.

Among chlorinated transformation products (pathway II), we identified two compounds formed by monochlorination of the benzene ring (5-chloro-1,2,4-trimethylbenzene, **2**; 3-chloro-1,2,4-trimethylbenzene, **3**) and three compounds formed by chlorination of the methyl group: 1-(chloromethyl)-2,4-dimethylbenzene (**4**), 2-(chloromethyl)-1,4-dimethylbenzene (**5**), and 4-(chloromethyl)-1,2-dimethylbenzene (**6**). These compounds are virtually indistinguishable by mass spectrometry, which complicates the peak assignment. However, low intensity of the peak

Table 2. Content of products of 1,2,4-TMB transformations on treatment with ClO_2 aqueous solution

Product	Content $c \times 10^7$, M		Characteristic ions, %
	25-fold excess of ClO_2, 6 h	40-fold excess of ClO_2, 24 h	
1,2,4-TMB (**1**)	–	0.083	105(100), 120(45), 91(12)
5-Chloro-1,2,4-trimethylbenzene (**2**)	9.91	13.4	119(100), 154(50), 139(22), 91(16)
3-Chloro-1,2,4-trimethylbenzene (**3**)	6.98	8.94	119(100), 154(45), 139(19), 91(16)
1-(Chloromethyl)-2,4-dimethylbenzene (**4**)	–	1.08	119(100), 154(24), 139(2), 91(13)
2-(Chloromethyl)-1,4-dimethylbenzene (**5**)	1.54	3.53	119(100), 154(21), 139(4), 91(14)
4-(Chloromethyl)-1,2-dimethylbenzene (**6**)	0.82	1.37	119(100), 154(23), 139(3), 91(13)
5-Chloro-1-(chloromethyl)-2,4-dimethylbenzene (**7**)	2.53	1.84	153(100), 188(52), 115(34)
5-Chloro-2-(chloromethyl)-1,4-dimethylbenzene (**8**)	1.51	1.53	153(100), 188(54), 115(30)
1,4-Bis(chloromethyl)-2-methylbenzene (**9**)	–	0.072	153(100), 115(23), 188(9)
1,2-Bis(chloromethyl)-4-methylbenzene (**10**)	–	0.86	153(100), 115(19), 188(14)
1,1,5-Trichloro-1-pentene (**11**)	+	+	65(100), 137(90), 172(17)
Dichloroacetyl chloride (**12**)	–	+	83(100), 111(17), 146(2)
2,4-Dimethylbenzaldehyde (**13**)	–	+	134(100), 105(57), 77(25)
2,4-Dimethylbenzoic acid (**14**)	–	+	132(100), 150(89), 105(52)

Scheme 1.

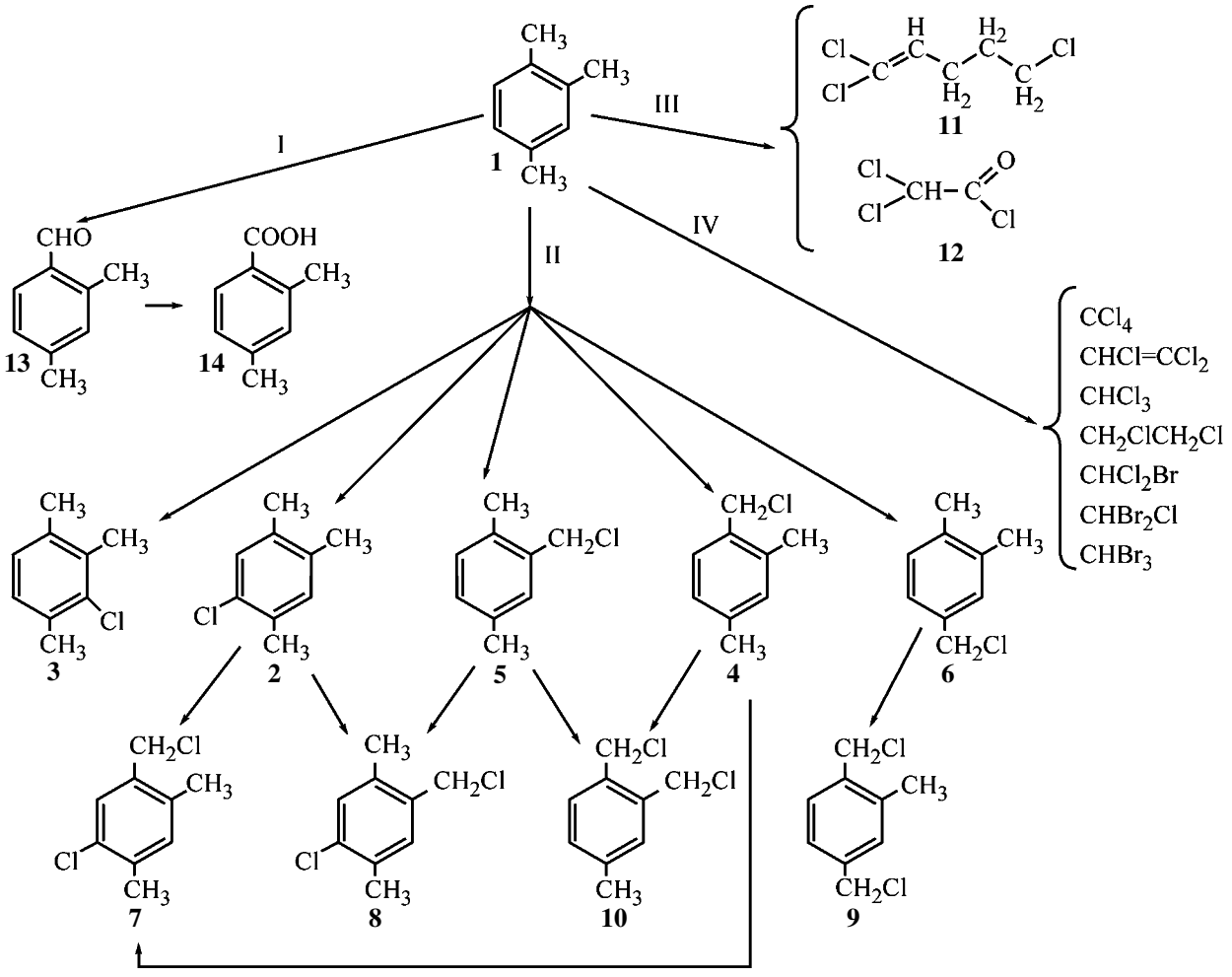

Scheme 2.

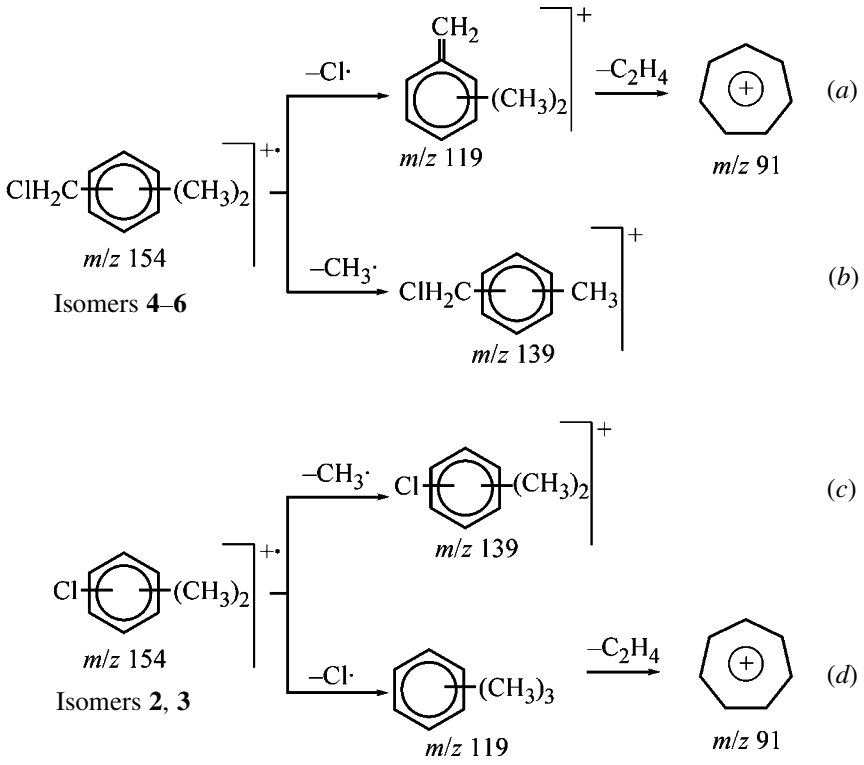

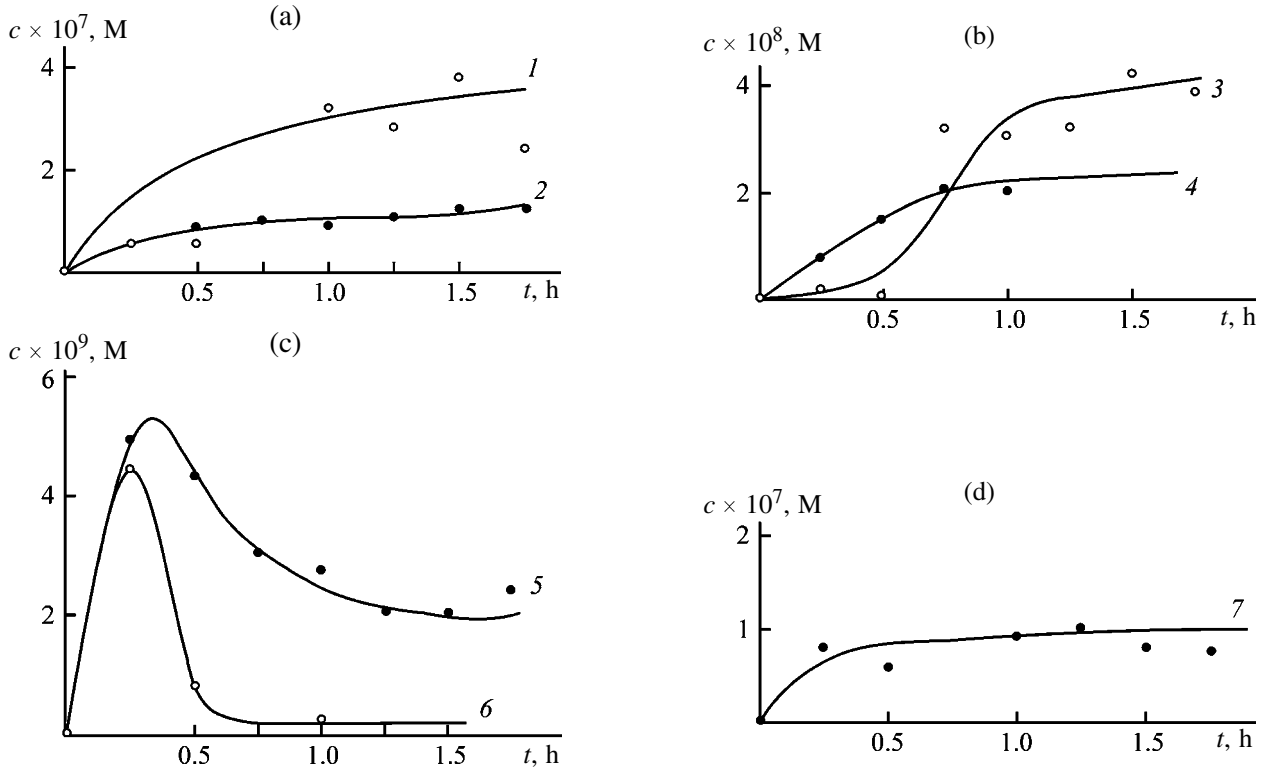

Fig. 1. Variation of VHH concentrations c with time t. [1,2,4-TMB] = 8.32×10^{-5} M; 25-fold excess of ClO_2. (a) (*1*) 1,2-Dichloroethane and (*2*) chloroform; (b) (*3*) bromoform and (*4*) tetrachloromethane; (c) (*5*) bromochloromethane and (*6*) dibromochloromethane; (d) (*7*) trichloroethylene.

Scheme 3.

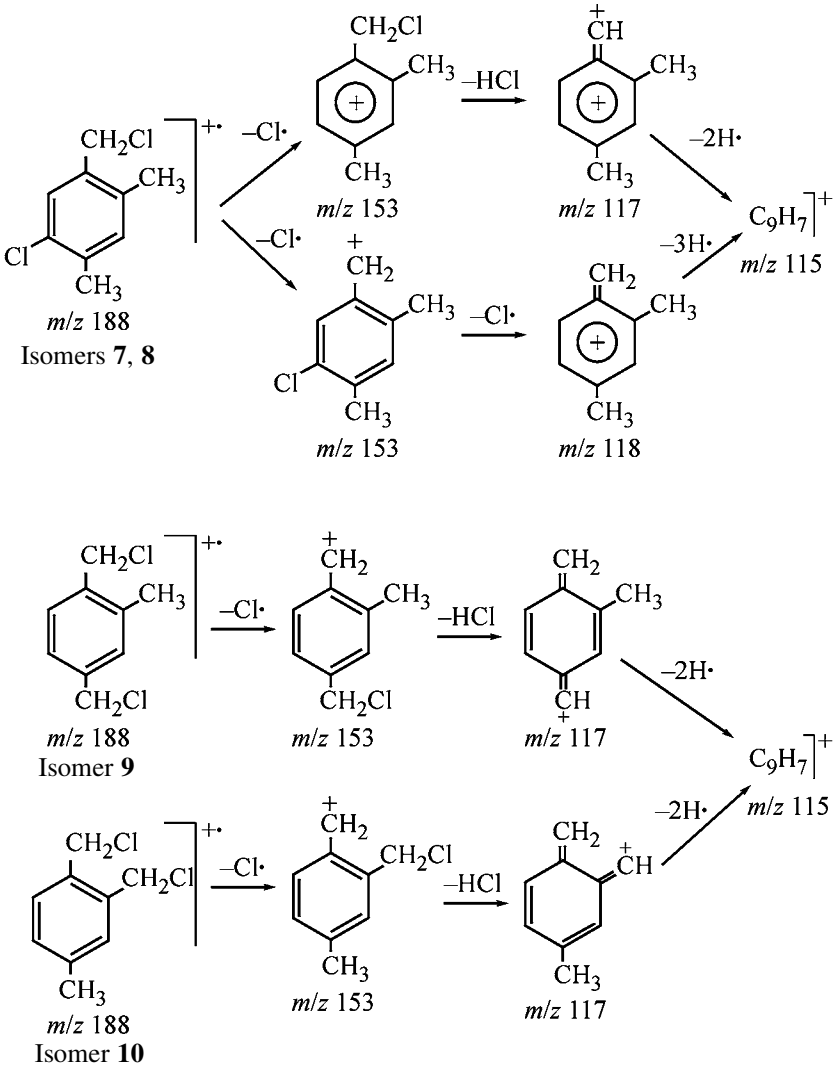

at m/z = 139 in the mass spectra of **4**–**6** indicates that their fragmentation mainly occurs through elimination of halogen atom and ethylene molecule from the molecular ion, with the subsequent formation of the tropylium cation (Scheme 2, pathway *a*). According to the fragmentation rules, this pathway is more probable for the 1,2,4-TMB monochloro derivatives containing the Cl atom in the side chain.

The higher intensity of the peak at m/z = 139 in the mass spectra of **2** and **3** (Table 2; Scheme 2, pathway *c*) indicates that the electron density distribution in these isomers facilitates the loss of the methyl groups as compared to **4**–**6** (pathway *b*).

Among dichlorinated products, we identified 5-chloro-1-(chloromethyl)-2,4-dimethylbenzene (**7**), 5-chloro-2-(chloromethyl)-1,4-dimethylbenzene (**8**), 1,4-bis(chloromethyl)-2-methylbenzene (**9**), and 1,2-bis(chloromethyl)-4-methylbenzene (**10**). The strongest peaks correspond to $[M - Cl]^+$, $[M - HCl]^+$, and some other ions formed by dehydrogenation characteristic of all steps of fragmentation of aromatic compounds under electron impact (Scheme 3) [12].

A distinctive feature of the mass spectra of **9** and **10** is approximately three times lower intensity of the molecular peak (m/z = 188) compared to **7** and **8**. This is due to the lower ionization potential of the molecule, its more intense fragmentation, and formation of the larger number of rearranged ions.

In the extracts we also identified 1,1,5-trichloro-1-pentene **11** and dichloroacetyl chloride **12** (pathway III).

In view of the fact that one of major advantages in chlorination of water with chlorine dioxide is forma-

tion of insignificant amounts of VHHs, we determined the content of tetrachloromethane, trichloroethylene, chloroform, 1,2-dichloroethane, bromodichloromethane, dibromochloromethane, and bromoform (pathway IV) in relation to the ClO_2 to substrate ratio and contact time. The results are given in the Fig. 1.

The presence of trihalomethanes among 1,2,4-TMB transformation products is apparently caused by an impurity of molecular chlorine, because the procedure for preparing ClO_2 did not involve removal of traces of Cl_2. The formation of brominated compounds (bromoform, bromodichloromethane, dibromochloromethane) is most probably associated with the presence of bromine-containing salts in sodium chlorite.

At a larger excess of ClO_2, the concentration of the reaction products increases (Table 2). Oxidation occurring on treatment of 1,2,4-TMB with ClO_2 results in the formation of oxygen-containing compounds (Scheme 1, pathways I and III): 2,4-dimethylbenzaldehyde **13**, 2,4-dimethylbenzoic acid **14**, and dichloroacetyl chloride, which were identified in an experiment with a large excess of ClO_2 and a long contact time.

CONCLUSIONS

(1) 1,2,4-Trimethylbenzene reacts with ClO_2 in aqueous solution to form chlorinated and oxygen-containing products.

(2) A scheme of transformations of 1,2,4-trimethylbenzene under the action of ClO_2 in aqueous solution was suggested.

(3) An increase in the ClO_2 to substrate ratio and in the time of contact of the substrate with ClO_2 results in larger number of reaction products, including oxygen-containing compounds and products formed by cleavage of the aromatic ring.

REFERENCES

1. Abdrakhmanova, A.R., Suvorkina, E.S., Yakupov, M.Z., et al., *Bashkir. Khim. Zh.*, 2000, vol. 7, no. 3, pp. 9–12.
2. Kuzubova, L.I. and Kobrina, V.N., *Khimicheskie metody podgotovki vody (khlorirovanie, ozonirovanie, ftorirovanie): Analiticheskii obzor* (Chemical Methods of Water Preparation (Chlorination, Ozonation, Fluorination): Analytical Review), Ser.: *Ekologiya* (Ecology), Novosibirsk, 1996, issue 42.
3. Shaidullina, G.M. and Lebedev, A.T., in *Biotekhnologiya v okhrane i reabilitatsii okruzhayushchei sredy: Sbornik nauchnykh trudov* (Biotechnology in Environment Protection and Remediation: Coll. of Scientific Papers), Moscow: Fiz. Inst. Ross. Akad. Nauk, 2003, pp. 241–247.
4. Bakhir, V.M., *Pit'ev. voda*, 2003, no. 1, pp. 13–20.
5. Prokopov, V.A., Tolstopyatova, G.V., and Maktaz, E.D., *Khim. Tekhnol. Vody*, 1997, vol. 19, no. 3, p. 283.
6. Rav-Acha, C. and Chosen, E., *Environ. Sci. Technol.*, 1987, vol. 21, no. 11, pp. 1069–1074.
7. Lebedev, A.T., *Mass-spektrometriya v organicheskoi khimii* (Mass Spectrometry in Organic Chemistry), Moscow: Binom, 2003.
8. Korzhenyak, I.G., *Vodosnabzh. Sanit. Tekh.*, 2000, no. 10, pp. 5–7.
9. *Unifitsirovannye metody analiza vod* (Unified Methods for Water Analysis), Lur'e, Yu.Yu., Ed., Moscow: Khimiya, 1973, 2nd ed.
10. Frumina, N.S., Lisenko, N.F., and Chernova, M.A., *Khlor* (Chlorine), Moscow: Nauka, 1983.
11. Horvath, A.K. and Nagypal, I., *J. Phys. Chem. A*, 1998, vol. 102, no. 37, pp. 7267–7272.
12. Polyakova, A.A. and Khmel'nitskii, R.A., *Mass-spektrometriya v organicheskoi khimii* (Mass Spectrometry in Organic Chemistry), Leningrad: Khimiya, 1972.

ISSN 1070-4272, Russian Journal of Applied Chemistry, 2007, Vol. 80, No. 7, pp. 1111–1115. © Pleiades Publishing, Ltd., 2007.
Original Russian Text © T.E. Sukhanova, S.V. Bronnikov, A.I. Grigor'ev, G.N. Gubanova, M.P. Perminova, N. Marangoci, M. Pinteala, V. Harabagiu, B. Simionescu, 2007, published in Zhurnal Prikladnoi Khimii, 2007, Vol. 80, No. 7, pp. 1141–1146.

MACROMOLECULAR CHEMISTRY AND POLYMERIC MATERIALS

Synthesis, Structure, and Thermal Properties of Polyrotaxanes Derived from β-Cyclodextrin and Polydimethylsiloxane

T. E. Sukhanova, S. V. Bronnikov, A. I. Grigor'ev, G. N. Gubanova, M. P. Perminova, N. Marangoci, M. Pinteala, V. Harabagiu, and B. Simionescu

Institute of Macromolecular Compounds, Russian Academy of Sciences, St. Petersburg, Russia
Petru Poni Institute of Macromolecular Chemistry, Iaşi, Romania

Received March 12, 2007

Abstract—Supramolecular inclusion complexes, polyrotaxanes, of β-cyclodextrin with modified polydimethylsiloxane were prepared. The structure and thermal properties of these complexes were studied as influenced by the preparation conditions, component ratio, and molecular weight of the polymer.

DOI: 10.1134/S1070427207070191

Synthesis and preparation of polymeric supramolecular complexes, polyrotaxanes (PRot), containing macromolecular rins strung on linear polymers with bulky terminal groups (blockers) attracts great attention [1–3].

Cyclodextrins (CDs), cyclic oligosaccharides consisting of *D*-glucopyranoside units bound by α-1,4-glucoside bond [4], are widely used as the cyclic component in matrix synthesis of PRot [1–3]. CD molecules have a shape of truncated cone 7 Å long and from 4.5 to 8.5 Å in internal diameter (depending on the modification: α-, β-, and γ-CD). These compounds contain hydroxy groups on the internal and external sides of their molecules and hydrocarbon and ether groups inside the cone. The internal surface of CD molecules is hydrophobic and the external surface is hydrophilic [4]. The linear components used for preparation of inclusion complexes of CD usually have two hydrophilic terminal groups and their internal part is hydrophobic. When both components are dissolved in a polar solvent (e.g., in water), the hydrophobic part of the linear macromolecule is strung on CD, whereas its hydrophilic parts do not enter inside the ring.

Supramolecular host–guest complexes formed by stringing CD (host) on linear polymer chains (guest) of different structure and molecular weights, such as poly(ethylene oxide) [5], poly(propylene oxide) [6], poly-ε-caprolactam [7], etc., have been prepared and characterized. These complexes are used as supports for preparing silicate materials whose pore size depends on the pH of the reaction mixture [8], delivering pharmaceuticals to required parts of stomach [9], as molecular switches [10, 11], etc.

Polyrotaxanes of β-CD and polydimethylsiloxane (PDMS) were prepared for the first time by Harada et al. [12–14]. They found that the geometrical size of α-CD cavity did not match the cross section diameter of PDMS macromolecule and hence the α-CD–PDMS complexes were not formed. At the same time, β-CD forms inclusion complexes with low-molecular-weight PDMS (M_n < 700). γ-CD can be strung on PDMS of higher molecular weight (up to M_n = 3300). The maximal ratio of CD to monomer units of the polymer in the inclusion complexes is 1.5 [12–14].

The aim of this study was to prepare PRots of β-CD with PDMS modified with epoxy groups (PDMSE) and to examine their supramolecular structure, morphology, and thermal properties by physical methods.

EXPERIMENTAL

The main component of the inclusion complex, linear PDMSE, was prepared by stepwise synthesis shown in Scheme 1.

The first step is the reaction of octamethylcyclotetrasiloxane with 1,1,3,3-tetramethyldisiloxane at room temperature for 4 h in the presence of 2 vol % H_2SO_4 to form PDMS with different molecular weights, having reactive Si–H terminal group.

Scheme 1. Stepwise synthesis.

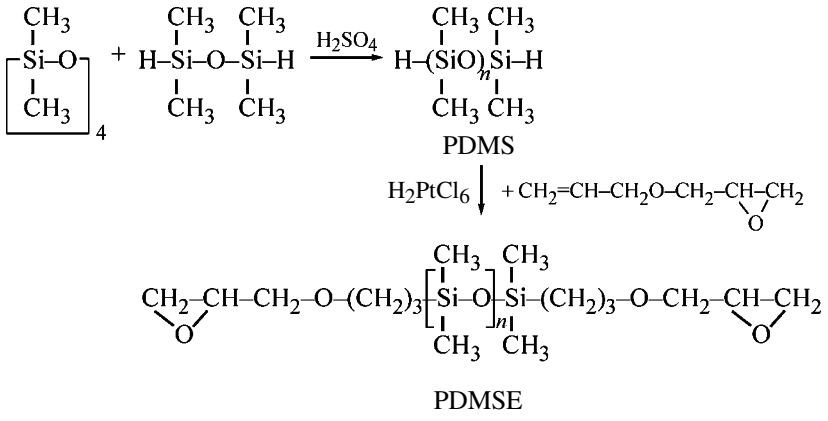

Scheme 2. PRot preparation.

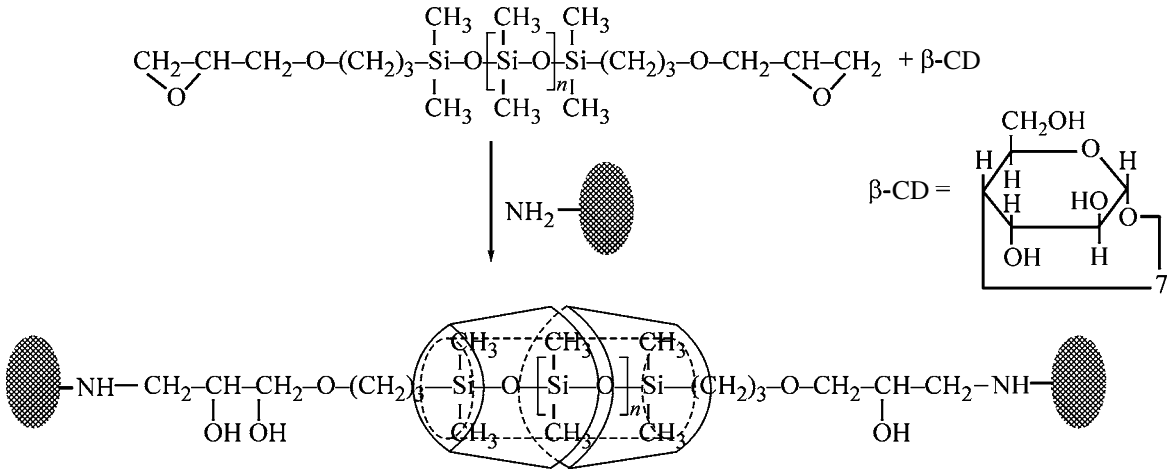

The second step involves hydrosilylation of vinyl glycidyl ether with 50 wt % PDMS solution in toluene in the presence of hexachloroplatinic(IV) acid (2% solution in isopropanol) at 100–110°C for 6 h to form PDMSE. The polymer precipitate was heated at 150°C in a vacuum (0.1 mm Hg) to remove impurities and unchanged components. Polymers with molecular weight M_n = 1250 (PDMSE-1) and M_n = 3310 (PDMSE-2) determined by exclusion chromatography were prepared.

The procedure for preparing PRot of β-CD and PDMSE is shown in Scheme 2.

In the first stage, saturated solutions of β-CD and PDMSE in DMF were mixed. The PRot structure was stabilized by reaction of the epoxy groups with the blocker (4-aminophenyltriphenylmethane) dissolved in isopropanol (saturated solution). To determine the influence of the ratio of the PRot components on the structure and physical properties of the complexes, we studied the samples with the following β-CD/SiO molar ratio: 0.253 (PRot-1a), 0.140 (PRot-1b), 0.069 (PRot-1c) and 0.058 (PRot-2) (Table 1). The ratios per Si–O bond were calculated from the ^{1}H NMR spectra. To prepare the PRot-1a sample, the mixture was stirred at 65°C for 72 h, after which the complex was precipitated with water, washed with ethanol, and dried with diethyl ether. To prepare the PRot-1b and PRot-1c samples, the mixture was additionally precipitated two times with aqueous DMF (Table 1).

The ^{1}H and ^{13}C NMR spectra of the intermediates and PRot were recorded on a Bruker DRX spectrometer (400 MHz). The X-ray diffraction analysis of β-CD and PRot was performed on a DRON-3 diffractometer (Burevestnik Research and Production Association, Russia) in the range 2θ = 3°–37° (CuK_α radiation, Ni filter). The thermal properties of the samples were studied on DSM-2M differential scanning calorimeter (Specialized Design Office of Instrument Making, Pushchino, Russia). The sample was heated at a rate of 16 deg min^{-1}. The morphology of the

Table 1. Preparation conditions and properties of PDMSE and PRot

Polymer	M_n	Poly-rotaxane	β-CD Content		Yield, %
			β-CD/SiO molar ratio	free β-CD, %	
PDMSE-1	1250	PRot-1a	0.253	54.1	–
	1250	PRot-1b	0.140	0	96
	1250	PRot-1c	0.069	0	55
PDMSE-2	3310	PRot-2	0.058	5.0	99

samples was studied on a Tesla BS-3001 scanning electron microscope (Czech Republic). The electron micrographs were treated with the aid of the Image-Tool 3.0 software (Texas University, United States).

The X-ray diffraction patterns of β-CD (curve *1*), PRot-1a (curve *2*), and PRot-2 (curve *3*) are shown in Fig. 1. The presence of a large number of reflections in the X-ray diffraction patterns of the samples (interlayer spacings *d* (Å) are summarized in Table 2) suggests their crystallinity. Comparison of *d* of supramolecular inclusion complexes PRot-1a and PRot-2 prepared at a β-CD excess (Table 1) and those of the initial β-CD shows that their crystal structures differ. Complex PRot-1c prepared at a deficiency of β-CD (β-CD/SiO = 0.069) is amorphous. Its X-ray diffraction pattern contains a halo with d = 6.8 Å which is preserved even after heating of the sample at 180°C. Thus, the β-CD/SiO molar ratio and the molecular weight of PDMSE affect the structure of the PRot complexes.

The thermal analysis curves of β-CD and PRot-1a, PRot-2, and PRot-1b complexes are shown in Fig. 2. The thermal analysis curve of β-CD (Fig. 2, curve *1*) is characterized by a sharp endo effect at 100°C due to elimination of bound water, which is consistent with data of [15, 16]. On heating above 250°C, β-CD melts simultaneously with its decomposition [15], which complicates determination of the melting point of the sample by DSC.

Table 2. Interplanar spacings of β-CD and PRot samples

Sample	*d*, Å
β-CD	18.6, 13.6, 8.25, 6.93, 5.80, 4.99, 4.49, 4.28, 3.90, 3.82, 3.30, 3.18, 2.58
PRot-1a	13.6, 9.30, 8.03, 6.67, 5.62, 5.21, 4.99, 4.73, 4.43, 4.18, 3.95, 3.59, 3.27, 2.93, 2.79
PRot-2	12.6, 8.62, 7.22, 6.00, 5.71, 5.06, 4.79, 4.28, 3.74, 2.95

The thermal analysis curve of PRot-1a (Fig. 2, curve *2*) also contains the endothermic effect at 100°C. In addition, an endo effect at 165 and an exo effect at 200°C are observed. We suggest that this complex undergoes polymorphous transformations on

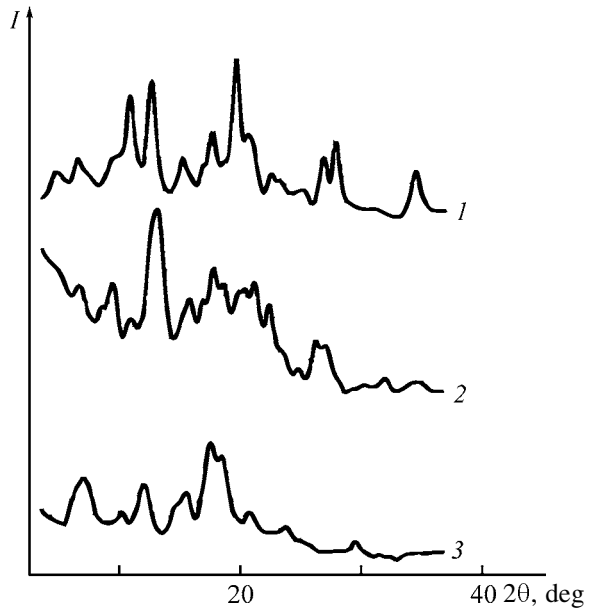

Fig. 1. X-ray patterns of (*1*) β-CD, (*2*) PRot-1a, and (*3*) PRot-2. (*I*) Intensity and (2θ) Bragg angle.

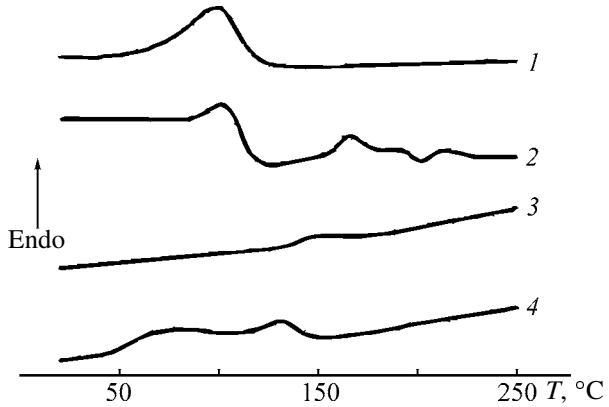

Fig. 2. DSC curves of (*1*) β-CD, (*2*) PRot-1a, (*3*) PRot-2, and (*4*) PRot-1b. (*T*) Temperature.

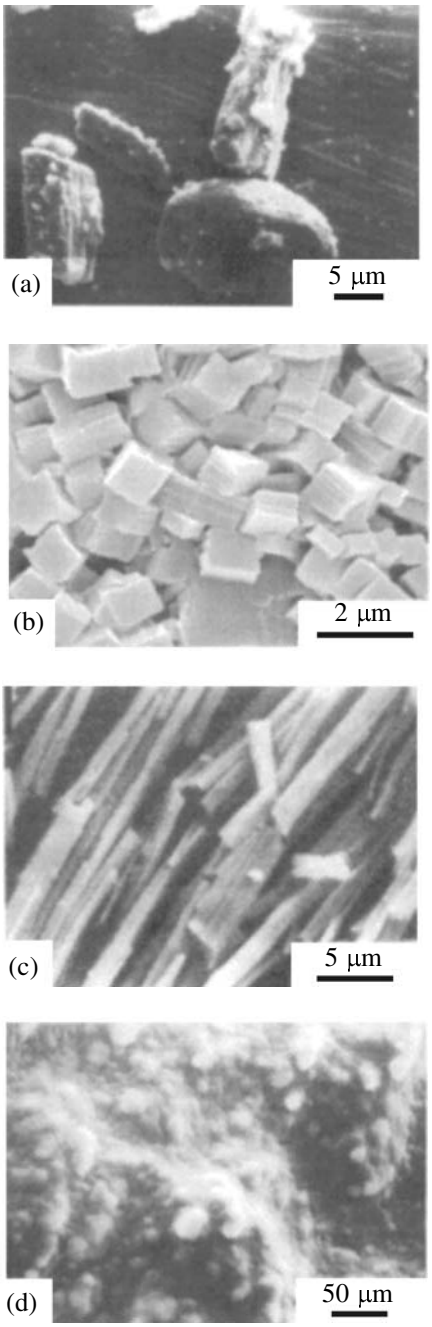

Fig. 3. Electron micrographs of (a) β-CD, (b) PRot-1a, (c) PRot-1b, and (d) PRot-1c.

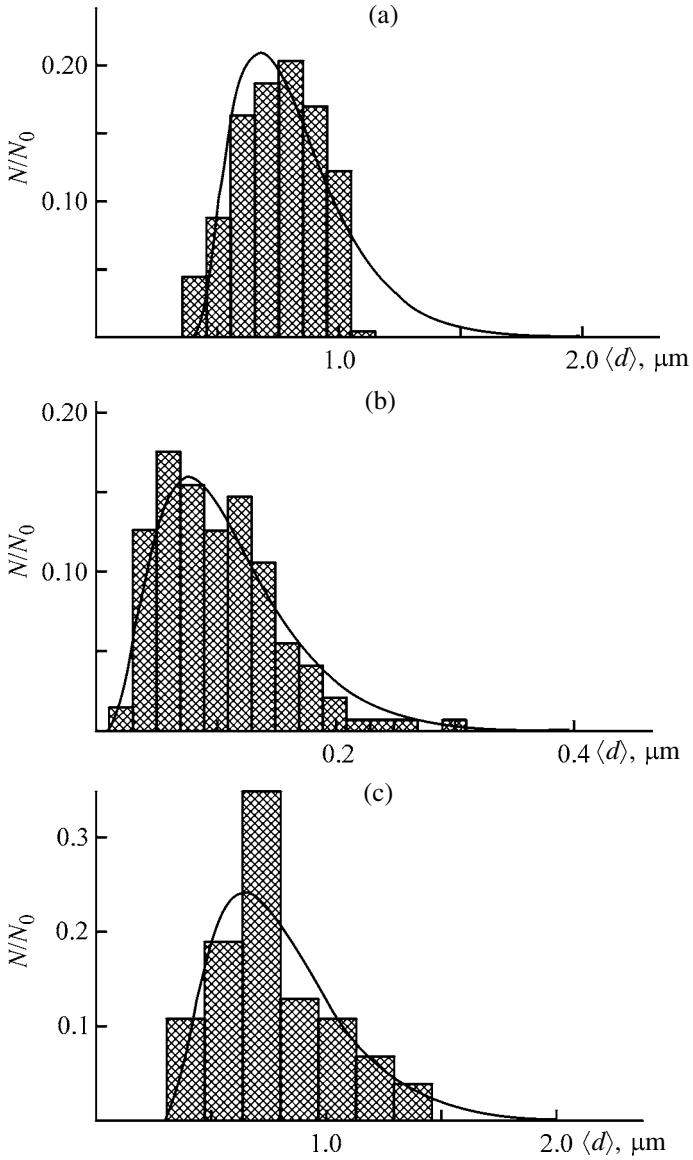

Fig. 4. Particle size distribution N/N_0 in (a, b) PRot-1a and (c) PRot-1c.

heating. The thermal analysis curve of PRot-2 in the range 50–150°C has two sharp endo effects caused by water elimination from the complex (Fig. 2, curve *3*). The thermal analysis curve of PRot-1c (Fig. 2, curve *4*) prepared at a deficiency of β-CD has a very weak endo effect (the enthalpy of the transition is no higher than 3 J g^{-1}) at 150°C due to melting of the sample, i.e., the complex is almost amorphous, which agrees with the X-ray diffraction data. It should be noted that this curve is similar to that of PRot-1a shifted to lower temperatures and having a sharp maximum at 165°C (Fig. 2, curve *2*).

The electron micrograph of β-CD is shown in Fig. 3a. It is seen that β-CD consists of lamellar particles of different shapes, whose size ranges from 1 to 40 μm. Different particle size and the absence of well-defined prevalent shape prevent quantitative analysis of the sample morphology.

Unlike pure β-CD, crystals of PRot-1a complex (Fig. 3b) have a shape of well-edged rectangular parallelepipeds. The results of statistical analysis of the particle size distribution are shown in Fig. 4a.

The particle size distribution is described well by the equation derived in the framework of the reversible aggregation model [17–19]. That is, the aggregates form thermodynamically optimized statistical ensemble [17, 18] with the most probable edge size of 0.81 μm (Fig. 4a). Each aggregate is a stack of square lamellar crystals (lamellas) whose average thickness is 0.1 μm (Fig. 4b).

Analysis of micrographs of well purified PRot-1b complex (Fig. 3c) show that the morphology of this sample is different: it consists of long rod-like crystals whose most probable thickness is approximately 0.8 μm (Figs. 4b, 4c). Interestingly, the most probable thickness of the rods is similar to the face size of crystalline aggregates of PRot-1a (0.81 μm). Complex PRot-1b consists of irregular-shaped amorphous particles whose size ranges from 0.5 to 3 μm (Fig. 3d). As seen from electron micrographs of PRot-2, this complex is crystallized in the form of a dispersion of small particles agglomerated in aggregates, which are difficult to characterize quantitatively.

CONCLUSIONS

(1) The supramolecular structure, morphology, and phase composition of inclusion complexes of β-cyclodextrin with polydimethylsiloxane modified with epoxy groups depends on the preparation conditions (purity and ratio of the components) and the molecular weight of the polymer.

(2) When the polyrotoxanes are prepared at an excess of unchanged β-cyclodextrin, well-edged lamellar crystals with the shape of rectangular parallelepipeds are formed, whereas at the optimal amount of β-cyclodextrin and high degree of purification of the product, rod-like crystalline aggregates are formed. Polyrotaxanes prepared at a deficiency of β-cyclodextrin are amorphous.

REFERENCES

1. Schill, G., *Catenanes, Rotaxanes, and Knots*, New York: Academic, 1971.
2. Panova, I.G. and Topchieva, I.N., *Usp. Khim.*, 2001, vol. 70, no. 1, pp. 28–51.
3. Huang, F. and Gibson, H.W., *Prog. Polym. Sci.*, 2005, vol. 30, no. 10, p. 982–1010.
4. Szejtli, J., *Pure Appl. Chem.*, 2004, vol. 76, no. 10, pp. 1825–1832.
5. Harada, A., Li., J., and Kamachi, M., *Macromolecules*, 1993, vol. 26, pp. 5267–5268.
6. Harada, A., Okada, M., Li., J., and Kamachi, M., *Macromolecules*, 1995, vol. 28, pp. 8406–8411.
7. Harada, A., Kawaguchi, Y., Nishiyama, T., and Kamachi, M., *Macromol. Rapid Commun.*, 1997, vol. 18, pp. 535–539.
8. Han, B.H. and Antonietti, M., *Chem. Mater.*, 2002, vol. 14, pp. 3477–3485.
9. Ooya, T., Eguchi, M., Ozaki, A., and Yui, N., *Int. J. Pharm.*, 2002, vol. 242, pp. 47–52.
10. Balzani, V., Gumez-Lipez, M., and Stoddart, J.F., *Acc. Chem. Res.*, 1998, vol. 31, pp. 405–411.
11. Bissell, R.A., Cordova, E., Kaifer, A.E., and Stoddart, J.F., *Nature* (London), 1994, vol. 36, pp. 133–142.
12. Okumura, H., Okada, M., Kawaguchi, Y., and Harada, A., *Macromolecules*, 2000, vol. 33, p. 4297–4298.
13. Okumura, H., Okada, M., Kawaguchi, Y., and Harada, A., *Macromol. Radid Commun.*, 2002, vol. 23, pp. 781–785.
14. Okumura, H., Kawaguchi, Y., and Harada, A., *Macromolecules*, 2001, vol. 34, pp. 6338–6343.
15. Manca, M.L., Zaru, M., Ennas, G., et al., *AAPS PharmSciTech.*, 2005, vol. 6, no. 3, article 58, pp. 464–472.
16. Mukne, A.P. and Nagarsenker, M.S., *AAPS PharmSciTech.*, 2004, vol. 5, no. 1, article 19, pp. 83–90.
17. Kilian, H.G., Metzler, R., and Zink, B., *J. Chem. Phys.*, 1997, vol. 107, pp. 8697–8714.
18. Kilian, H.G., Bronnikov, S., and Sukhanova, T., *J. Phys. Chem. B*, 2003, vol. 107, no. 49, pp. 13 575–13 582.
19. Bronnikov, S.V., Sukhanova, T.E., and Laius, L.A., *Vysokomol. Soedin., Ser. A*, 2002, vol. 44, no. 6, pp. 940–946.

ISSN 1070-4272, Russian Journal of Applied Chemistry, 2007, Vol. 80, No. 7, pp. 1116–1119. © Pleiades Publishing, Ltd., 2007.
Original Russian Text © A.I. Kuzaev, S.I. Solomko, O.M. Ol'khova, G.A. Mirontseva, A.E. Tarasov, M.N. Tyapkina, 2007, published in Zhurnal Prikladnoi Khimii, 2007, Vol. 80, No. 7, pp. 1147–1150.

MACROMOLECULAR CHEMISTRY AND POLYMERIC MATERIALS

Oligomerization of Substituted Oxetanes and Parameters of Their Molecular Heterogeneity

A. I. Kuzaev, S. I. Solomko, O. M. Ol'khova, G. A. Mirontseva, A. E. Tarasov, and M. N. Tyapkina

Institute of Problems of Chemical Physics, Russian Academy of Sciences, Chernogolovka, Moscow oblast, Russia

Received November 21, 2006

Abstract—Cationic oligomerization of disubstituted oxetanes promoted by trifluoroboron etherate in the presence of ethylene glycol was studied. The parameters of molecular-weight and functionality distribution of the resulting oligooxetane diols were determined by gel-permeation and liquid chromatography.

DOI: 10.1134/S1070427207070208

Polyurethane thermoplastic elastomers (TPs) are commercially produced today using diisocyanates, low-molecular-weight glycols, and oligomeric diols based on polyoxyalkylenes, polytetramethylene, and polyesters [1–3]. Oligoether diols derived from disubstituted oxetanes seem to be a promising alternative to low-molecular-weight glycols in the stage of TP synthesis [4]. Therefore, oligomerization of disubstituted oxetanes to prepare polyoxetane diols with given functionality and number-average molecular weight is a topical problem. Data on preparation of oligooxetane diols and, the more so, on the parameters of molecular-weight distribution (MWD) and distribution with respect to functionality types (DFT) of the resulting oligooxetane diols are lacking.

In this work we studied cationic oligomerization of disubstituted oxetanes, prepared oligooxetane diols of various chemical compositions, and evaluated their MWD and DFT parameters.

EXPERIMENTAL

As monomers we used 3,3-bis(azidomethyl)oxetane (BAMO), 3-azidomethyl-3-methyloxetane (AMMO), 3-methyl-3-nitratomethyloxetane (MNMO), and 3-azidomethyl-3-nitratomethyloxetane (AMNMO). The monomer purity was checked by liquid chromatography and IR spectroscopy. Before experiments 1,2-dichloroethane (DCE), ethylene glycol (EG), tetrahydrofuran (THF), heptane, and methyl ethyl ketone (MEK) were purified by standard procedures [5].

Oligooxetane diols were prepared by cationic oligomerization catalyzed by trifluoroboron etherate in the presence of ethylene glycol with continuous addition of the monomer dissolved in DCE [6]. The synthesis was carried out in a glass reactor equipped with a stirrer and a water-cooling jacket. First, the catalyst, EG, and solvent were added into the reactor. Then, oxetane was fed into the reactor using a batcher at a rate at which its current concentration in the system did not exceed the catalyst concentration. After completion of the monomer supply, the reaction mixture was stirred for 3 h at room temperature and kept at the same temperature for 120 h without stirring to attain the quantitative yield of the desired product. The reaction was terminated with water, the mixture was washed to remove the catalyst, and then water and the solvent were removed by the known procedure [6].

The gel-chromatographic study was performed on a Waters gel chromatograph equipped with three Styrogel columns (200, 500, and 1000 Å) using THF eluent at an elution rate of 1.2 ml min^{-1}. The polymer solution with a concentration of 0.2–0.3 wt % was added in one portion (the loop volume was 2 ml). The MWD parameters were calculated from the universal calibration dependence [7], which was used to evaluate the calibration dependences for each oligomer type. The DFT parameters of the resulting oligooxetanes were studied on a GPS II Waters liquid chromatograph using three columns: 250×4 mm (Separon 200 SGX), 150×3 mm (Separon SGX), and 150×3 mm (Separon SGX) [8]. The conditions of

chromatographic analysis of oligooxetane diols were as follows: MEK–heptane volume ratio 34.5 : 65.5 and 26.5 : 73.5 for 3,3-bis(azidomethyl)oxetane diol and 3-azidomethyl-3-methyloxetane diol, respectively.

Our experimental data (Table 1) show that the process with continuous supply of the monomer, developed previously for oxiranes [6], is applicable to cationic oligomerization of substituted oxetanes. Irrespective of the initial monomer type, the yield of the target products is quantitative. It should be noted that the measured molecular weights M_n are close to those calculated from the following equation:

$$M_n = M[\mathrm{Ox}]/[\mathrm{G}],$$

where M is the molecular weight of the monomer and [Ox] and [G] are the concentrations of oxetane and glycol, respectively.

However, polymerization of oxetanes proceeds more slowly than that of epoxides, and complete conversion is attained only after prolonged additional storage of the reaction mixture. This is confirmed by data on the polymerization kinetics. The time dependences of the reaction rates for epichlorohydrin (ECH) and AMNMO are shown in Fig. 1; for ECH the apparent rate constant of polymerization is 6.6×10^{-2} l mol^{-1} s^{-1} (Table 2). As seen, in the case of ECH the steady-state concentration of the monomer at its continuous feeding into the reactor is attained in a short period, and the reaction can be terminated at any moment by stopping of the monomer supply without deterioration of the target polyether quality. The molecular weight of the product thus obtained corresponds to the above ratio.

In the case of AMNMO, attainment of the steady-state mode of the polymerization requires a longer period, which suggests slower process initiation. Moreover, longer reaction is required to attain quantitative yield. The apparent rate constants for oxetanes studied are lower than that for ECH by 1.5–2 orders of magnitude.

The gel chromatograms of polyoxetane diols prepared in the presence of EG and without it are shown in Fig. 2. These data confirm the absence of cyclic products in the resulting oligooxetane diols. Hence, Rose's statement [9] on formation of cyclic tetramers in the course of polymerization of oxetane and its 3,3-dimethyl derivative requires additional verification. Moreover, in a later study [10], no cyclic compounds were found among the products of oxetane polymerization (GPC data).

Table 1. Results of cationic polymerization of oxetanes with the general formula $CH_2CR^1R^2OCH_2$. [Monomer] = 2.6 M, [EG] = 0.2 M, [BF_3] = 0.2 M; oligomerization was performed in DCE at 10°C

R^1	R^2	Yield, %	M_n^{exp}	M_n^{calc}
CH_2N_3	CH_2N_3	94	2200	2470
CH_2N_3	CH_3	90	2300	2220
CH_2N_3	CH_2ONO_2	97	2230	2300
CH_3	CH_2ONO_2	99	1300	1430

Table 2. Apparent rate constants of polymerization of epichlorophydrin and oxetanes studied

Monomer	Concentration, M		Propagation constant $K_p \times 10^3$, l mol^{-1}
	EG	catalyst	
ECH	0.40	0.02	66.0
BAMO	0.415	0.414	0.48
	0.415	0.414	0.47
	0.43	0.52	0.28
AMNMO	0.30	0.20	1.84
MNMO	0.30	0.30	1.10

Using the universal calibration dependence for oligomers [7], we plotted the absolute calibration dependences for oligo-3-azidomethyl-3-methyloxetane diol (oligo-AMMO) and oligo-3,3-bis(azidomethyl)-oxetane diol (oligo-BAMO) (Fig. 3). The calcu-

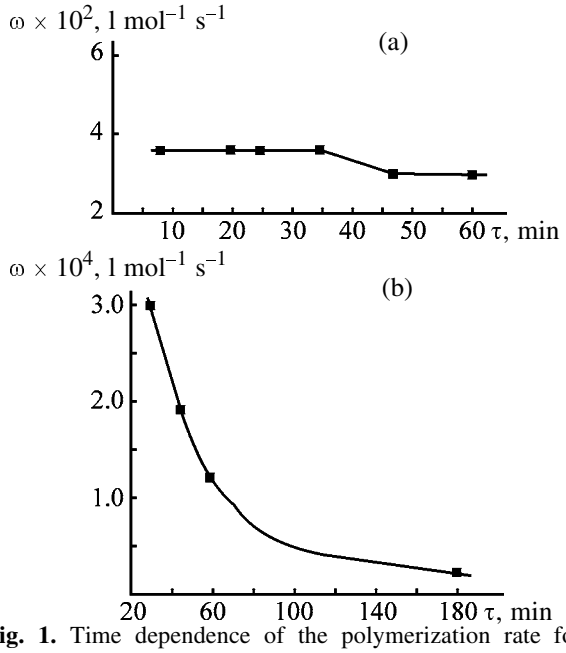

Fig. 1. Time dependence of the polymerization rate for (a) epichlorohydrin and (b) 3-azidomethyl-3-nitratomethyloxetane; c_0 0.02 M, 293 K. (τ) Time and (ω) apparent rate constant of polymerization.

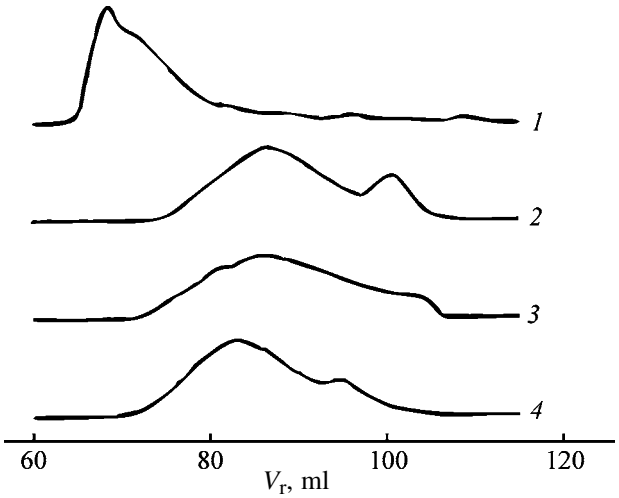

Fig. 2. Gel chromatograms of (*1*) oligo-3,3-bis(azidomethyl)oxetane and (*2–4*) 3-azidomethyl-3-methyloxetanes. (V_r) Retention volume; EG concentration, M: (*1*) 0, (*2*) 0.45, and (*3, 4*) 0.52.

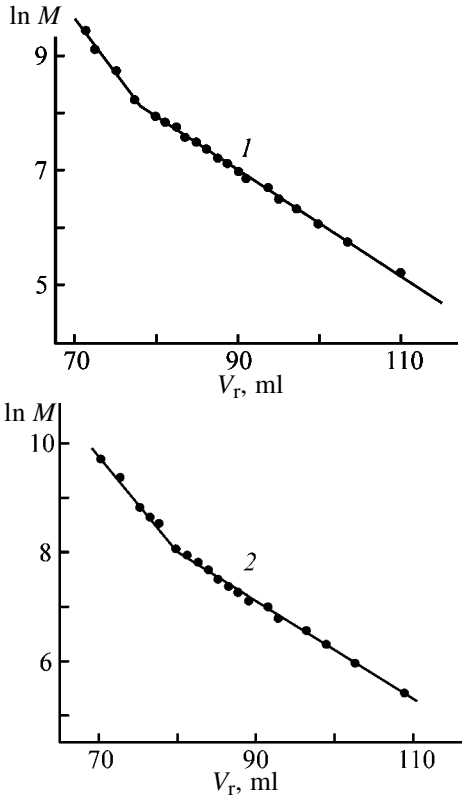

Fig. 3. Absolute calibration dependences of the logarithms of the molecular weights ln$M$ for (*1*) oligo-3,3-bis(azidomethyl)oxetane diol and (*2*) oligo-3-azidomethyl-3-methyloxetane diol vs. the retention volumes V_r.

lated MWD parameters for all the oxetanes studied (Table 3) are absolute and can be used to evaluate functionality from the following equation:

$$f_n = M_n/M_e,$$

Table 3. MWD parameters of oligo-3,3-bis(azidomethyl)-oxetane diol and oligo-3-azidomethyl-3-methyloxetane diol

Monomer	Concentration, M			M_n	M_w/M_n
	monomer	catalyst	EG		
AMMO	4.17	0.2	0.52	1020	1.57
AMMO	4.18	0.2	0.52	1400	1.41
AMMO	4.05	0.46	0.45	950	1.46
BAMO	3.69	0.2	–	3200	1.91

Table 4. DFT parameters of oligo-3,3-bis(azidomethyl)-oxetane diol and oligo-3-azidomethyl-3-methyloxetane diol

Oligomer	Concentration, M		DFT		
	EG	catalyst	$f = 0$	$f = 1$	$f = 2$
AMMO	0.45	0.45	0.4	7.9	91.7
	0.52	0.2	1.4	1.9	96.7
BAMO	0.41	0.41	6	9.8	83.5
	0.52	0.2	2.6	4.3	92.6

where M_e is determined form the content of the functional groups.

The DFT parameters of the resulting oligomers were studied by liquid chromatography. The results for oligo-AMMO and oligo-BAMO are listed in Table 4. As seen, in formation of oligo-AMMO the content of bifunctional macromolecules reaches 96.7% and the content of the molecules without functional groups is negligible. In oligo-BAMO the content of bifunctional macromolecules is smaller, and the content of the macromolecules without functional groups reaches 10%.

Thus, our experimental data show that synthesis of oligomers with continuous feeding of the monomer, developed previously for oxiranes, is applicable to oxetanes and allows preparation of oligomers with required properties.

CONCLUSION

(1) Cationic oligomerization of 3,3-bis(azidomethyl)oxetane, 3-azidomethyl-3-methyloxetane, 3-methyl-3-nitratomethyloxetane, and 3-azidomethyl-3-nitratomethyloxetane was studied, the corresponding oligoether diols were prepared, and the possibility of preparing oligooxetane diols using the procedure developed previously for oxiranes was confirmed.

(2) Parameters of the molecular-weight distribution of the resulting oligooxetane diols were determined, their polydispersity index is $M_w/M_n = 1.4–1.6$.

(3) The content of bifunctional macromolecules in oligooxetane diols derived from 3-azidomethyl-3-methyloxetane and 3,3-bis(azidomethyl)oxetane is 92–97 and 85–90%, respectively.

REFERENCES

1. *Termoelastoplasty* (Thermoplastic Elastomers), Moiseev V.V., Ed., Moscow: Khimiya, 1985.
2. Lipatov, Yu,.S., Kercha, Yu.Yu., and Sergeeva, L.M., *Struktura i svoistva poliuretanov* (Structure and Properties of Polyurethanes), Kiev: Naukova Dumka, 1970.
3. Wright, P. and Cumming, A.P.C., *Solid Polyurethane Elastomers*, London: Maclaren, 1969.
4. Badamshina, E.R., Kuzaev, A.I., Ol'khova, O.M., et al., *Vopr. Khim. Khim. Tekhnol*., 2003, no. 4, p. 17.
5. Weissberger, A. and Proskauer, E.S., *Organic Solvents. Physical Properties and Methods of Purification*, Riddick, J.A. and Toops, E.E., Eds., New York: Interscience, 1955.
6. Kuzaev, A.I., Ol'khova, O.M., and Baturin, S.M., *Vysokomol. Soedin., Ser. A*, 1986, vol. 28, no. 4, pp. 739–743.
7. Kuzaev, A.I., *Heterophase Network Polymers: Synthesis, Characterization, and Properties*, Londion: Taylor and Francis, 2002, pp. 27–32.
8. Kuzaev, A.I., Ol'khova, O.M., Solomko, S.I., and Baturin, S.M., *Zh. Fiz. Khim.*, 1994, vol. 68, no. 10, pp. 1794–1796.
9. Rose, J.B., *J. Chem. Soc*., 1956, p. 542.
10. Quzeski, M.Y. and Ochel, M., *Eur. Polym. J*., 1996, vol. 32, no. 6, pp. 691–693.

ISSN 1070-4272, Russian Journal of Applied Chemistry, 2007, Vol. 80, No. 7, pp. 1120–1125. © Pleiades Publishing, Ltd., 2007.
Original Russian Text © V.V. Bestuzheva, N.V. Sirotinkin, A.V. Tokarev, 2007, published in Zhurnal Prikladnoi Khimii, 2007, Vol. 80, No. 7, pp. 1151–1155.

MACROMOLECULAR CHEMISTRY AND POLYMERIC MATERIALS

Adhesive Compounds Based on Polyurethane Waste

V. V. Bestuzheva, N. V. Sirotinkin, and A. V. Tokarev

St. Petersburg State Institute of Technology (Technical University), St. Petersburg, Russia

Received March 13, 2007

Abstract—Formulations of adhesives and film materials from polyurethane waste were suggested, and the characteristics of these materials and conditions of their preparation were examined. A versatile resource-saving and environmentally sound procedure was suggested for the reuse of polyglycol adipate urethanes of dense and microcellular structure. The procedure allows transformation of a polymer waste into a reclaim with a high level of service parameters.

DOI: 10.1134/S107042720707021X

Polyurethanes (PUs) of various structures find wide and diverse applications in the modern engineering. However, increase in the production of polyurethane articles is accompanied by formation of hundreds of tons of industrial waste annually, giving rise to environmental problems and requiring undesirable resource expenditure. The diversity of commercially produced PUs additionally complicates the situation, because utilization of different kinds of cured materials requires different approaches. For each material, it is necessary to develop a nondestructive and cost-efficient procedure for reprocessing into valuable products.

Among widely used polyurethanes are poly(ethylene butylene glycol adipate urethanes), segmented ester thermoelastoplastics used in machine-building (integral and foamed PUs), in shoe industry (microcellular PUs), and in load-bearing units (monolithic PUs). The simplified structure of such polymers is as follows:

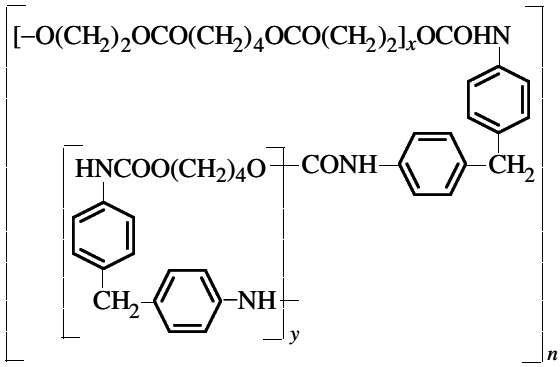

(1)

The elastomer is formed by addition to an isocyanate pseudoprepolymer of a mixture of a polyester component and a glycol acting as chain-terminating agent. The reaction of the diisocyanate with the glycol yields rigid segments imparting high strength to the material, whereas polyester fragments provide high elasticity [1]. Such products are commonly obtained by the pseudoprepolymer method using high-output casting machines. The amount of waste produced daily by each of these machines reaches 100 kg.

Polyurethane thermoelastoplastics exhibit high level of physicomechanical properties due to cross-linking of the macromolecules by hydrogen bonds formed in the course of curing [2]. This fact complicates reprocessing of PU waste of this type by contact molding methods. Additional problems arise from the porosity of the material and narrow interval between the flow point (at which the reprocessing is possible) and decomposition point.

The physicomechanical transformations of the PUs under consideration in the temperature interval from –40 to +150°C are shown in Fig. 1.

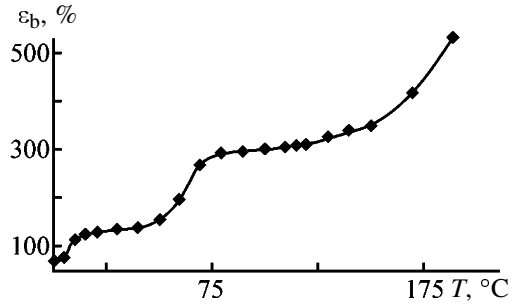

Fig. 1. Thermomechanical curve of monolithic poly(ethylene butylene glycol adipate urethane): (ε_b) relative elongation and (T) temperature.

The curve shape demonstrates the occurrence in the range 40–75°C of the hyperelastic strain of the segments formed by flexible, less oriented and hence more mobile units of polyurethane. At 122–137°C, crystalline units acquire mobility, and an induced plastic state of the thermoplastic is manifested. In the range 140–145°C, the material transforms into a viscous-flow state. Under these conditions, the material is capable of changing shape, and its molding becomes possible.

However, DTA data for commercial poly(ethylene butylene glycol adipate urethanes) show that even at 140–150°C the samples lose weight with the gas evolution.

At a flow temperature, hydrogen and then covalent bonds are broken, i.e., the polymer degrades with drastic deterioration of the physicomechanical properties of the reclaim. Therefore, high-temperature waste reprocessing does not allow preparation of a secondary material with high service characetristics.

Thus, to develop a procedure for utilization of polyurethanes with the preparation of molded articles, it is primarily necessary to decrease the flow point of the starting product. One of the simplest, most widely used, and most efficient ways to do this is plasticization of the material.

EXPERIMENTAL

In the experiments we used the following starting compounds: polyurethanes (monolithic, density 1150 kg m^{-3}, relative elongation 920%; microcellular, density 600 kg m^{-3}, tensile strength 7.5 MPa, relative elongation 450%; integral, density 75 and 800 kg m^{-3}, tensile strength 0.3 and 70 MPa, bending strength 0.2 and 15 MPa for core and crust, respectively); plasticizers [commercially available compounds of various classes meeting GOSTs (State Standards): dimethylformamide (DMF), GOST 20289–74; dimethyl sulfoxide (DMSO), TU (Technical Specification) 6-09-3818–77; cyclohexanone (CH), GOST 24615–81; glycerol (Gl), GOST 6259–75; toluene, GOST 5789–78; and dibutyl phthalate (DBP), GOST 2102–67].

For polymers of the same structure, the plasticization parameters primarily depend on the plasticizer properties. Available data on the thermodynamic behavior of segmented polyurethanes are ambiguous and do not allow prediction of their deformation behavior in one or another medium. We examined the interaction of monolithic polyurethane with plasticizers by the method of equilibrium swelling [3] with simultaneous determination of physicomechanical characteristics at regular intervals. The results are shown in Fig. 2.

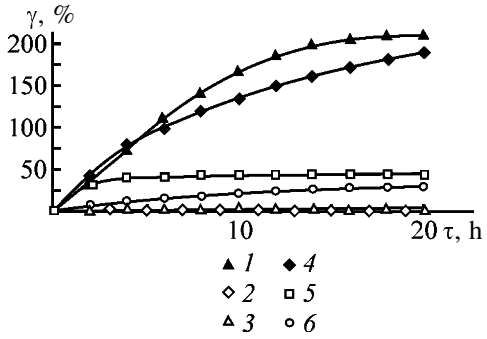

Fig. 2. Degree of swelling γ of STEP as a function of swelling time τ at 20°C. Plasticizer: (*1*) DMF, (*2*) Gl, (*3*) DBP, (*4*) CH, (*5*) DMSO, and (*6*) toluene.

Dibutyl phthalate is moderately absorbed by the polyurethane, and the thermodynamic equilibrium in the system is attained in 5 h at 20°C, 15 h at 40°C, and 20 h at 60°C. In glycerol, the similar state is attained at a concentration of 0.4–0.5%. DBP and Gl only slightly affect the microphase state of the segmented thermoelastoplastic (STEP); practical use of these plasticizers involves problems with ensuring uniform distribution of small amounts of the additive in the cured thermoplastic.

Toluene selectively breaks hydrogen bonds. It is concentrated in the flexible STEP matrix, leaving the structure of domains intact. Monolithic polyurethane can absorb up to 40 wt % toluene. Spectroscopic analysis shows that cleavage of interchain H bonds in the process leads to an increase in the relative content of free NH groups in the elastomer (a band appears at 3390 cm^{-1}, characteristic of associates of NH groups with the π-electron system of the aromatic ring of the solvent). As a result, the physicomechanical characteristics of the polymeric material are drastically deteriorated. Toluene decreases the structural glass transition point of flexible blocks, whereas the rigid microphase remains essentially intact in the process. Thus, the swollen polymer is inhomogeneous and nonuniform in properties.

Cyclohexanone, in contrast to aromatic toluene, contains a carbonyl group in the molecule and occupies an intermediate place between toluene and typical hydrogen acceptors (DMSO, DMF) with respect to processes occurring in its presence. Weakly pronounced proton-acceptor properties facilitate its active insertion into the interchain space of the flexible matrix with the cleavage of hydrogen bonds, but these

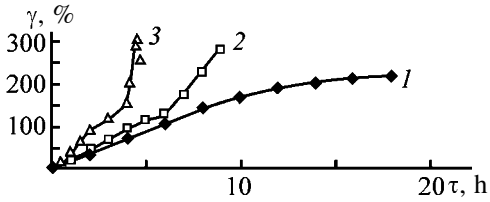

Fig. 3. Degree γ of STEP swelling in DMF as a function of time τ. Temperature, °C: (*1*) 20, (*2*) 40, and (*3*) 60.

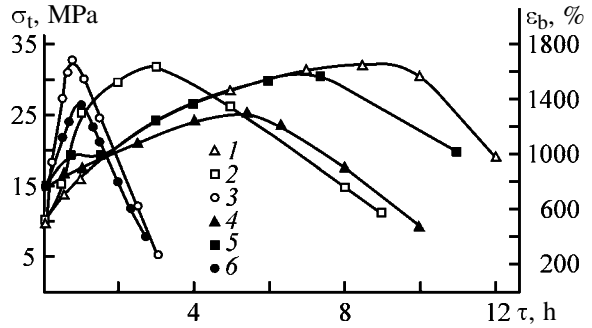

Fig. 4. (*1–3*) Ultimate tensile strength σ_t and (*4–6*) relative elongation ε_b of STEP as functions of swelling time τ in DMF. Temperature, °C: (*1*, *4*) 20, (*2*, *5*) 40, and (*3*, *6*) 60.

bonds are not restored after attainment of the thermodynamic equilibrium in the system. Therefore, the strength and elasticity of STEP in CH decrease from the very beginning of the process, and after keeping for 14 h at 60°C the polymer passes into the solution. Therefore, CH can be used for facilitating the breakdown of polyurethane in its utilization in the form of finely dispersed crumb as an additive to building mixes.

The proton-acceptor groups S=O and C=O present in DMSO and DMF interact with NH groups of the polymer. The breakdown and formation of hydrogen bonds in this case can be considered as a set of concurrent equilibrium processes. In swelling of STEP in DMSO, initially the physical network of molecular chains gets ordered, which enhances the strength of the polymer. Then, because of the exceedingly high penetrating power of the solvent, the whole volume of the polymer is nonselectively diluted and homogenized with the breakdown of both the network of chains formed by hydrogen bonds and the physical network of segmented domains. As a result of breakdown of the polymer matrix of both levels, it ceases to retain the plasticizer and degrades into short-chain fragments, forming a nearly true solution. This is manifested as an extreme decrease in the strength and breaking elongation. Dimethylformamide is more sensitive to steric hindrance and therefore is concentrated in amorphous regions for a longer time and more slowly penetrates into crystalline regions; therefore, the broken bonds have time to be partially restored.

Thus, each of the compounds studied shows, to different extents, the plasticizing power with respect to polyurethane, but the thermodynamic equilibrium is observed at different concentrations and hence the deformation properties are manifested to different extents. Preference should be given to aprotic compounds, and in particular to dimethylformamide, which is fairly active, cheap, and readily available.

The influence of temperature on the behavior of monolithic polyurethane in DMF is illustrated by Fig. 3.

In swelling of real networks in aprotic liquids, the following processes occur in succession: "dilution" of the network, rupture of physical bonds of polymer chains, and rupture of the physical network in segmented domains by molecules of the liquid. The latter process is manifested in the curves illustrating the polymer swelling with time as a characteristic inflection clearly pronounced in the whole temperature range examined.

The degree of swelling of PU after keeping for 5 h in DMF at 40°C is 1.5 times higher, and at 60°C, 4 times higher than at 20°C. Thus, by varying the time and temperature of treatment of the polymer with dimethylformamide, it is possible to vary in a wide range the degree of its swelling and hence the capability for deformation under external loads.

It should be determined, however, to what extent treatment with DMF destroys the polyurethane structure and whether the polyurethane strength can be restored after removal of the plasticizer.

To evaluate the level of physicomechanical properties of the cured monolithic polyurethane treated with DMF at different concentrations, samples in the form of "blades" with the length of the working zone of 2 cm were immersed in the plasticizer and kept there at a prescribed temperature. At equal time intervals, samples were withdrawn from the solvent, dried at 60°C to constant weight, and then tested with an RMI-250 tensile-testing machine. Experiments were continued until a thermodynamic equilibrium was attained in the system. The weight and volume of the swollen samples increased, but after drying the samples fully restored their shape and were suitable for tests.

Figure 4 shows how the ultimate tensile strength σ_t and relative breaking elongation ε_b vary in the course of plasticization at various temperatures. The network

Table 1. Properties of KLEUR liquid viscous adhesives

Parameter	Parameter value	Determination method
Viscosity (outflow time from VZ-246 viscometer at 20±2°C), s	240–480	GOST 8420–74
Weight fraction of nonvolatile substances, %	45–50	GOST 17537–72
Drying time, h, at *T*, °C:		GOST 19007–73
20±2	24	
60±2	10	
120±2	1	
150±2	0.2	
Strength of glued joint, peel (N m^{-1})/shear* (MPa):		GOST 6763–78
for calico	105/0.5	
for leather and polyurethane	860/0.7	
for leather and porous rubber	1960/0.8	
for leather and Steranip	1576/0.7	
for leather and TEP	180/0.4	
for linoleum	405/0.2	
for polyvinyl chloride	20/0.4	

* In all the cases, the shear strength tests of glued joints were accompanied by failure of the support material.

breakdown is manifested as extreme decrease in the strength and breaking elongation.

Thus, the PU structure can significantly change upon introduction of various kinds of modifiers. Addition of plasticizers alters the whole set of properties of the polymer, including the glass transition and flow points, and enhances the capability for strain transformations under given conditions, which is important for processing. Aprotic compounds are the most effective in this respect. Moderate plasticization with dimethylformamide for 7–10 h at 20°C, which corresponds to 130–170% swelling, leads to an increase in the strength and elasticity of the polymer after the removal of the plasticizer.

With an increase in the plasticizer concentration over the equilibrium concentration, the strength and elasticity of the material decrease: For each combination of a polymer and a liquid medium, there is a definite quantitative limit of the plasticizer content in the polyurethane, above which the polymer matrix is destroyed and the plasticized system loses the thermodynamic stability.

Under these conditions, it is possible to prepare from a finely ground vigorously stirred powder a homogeneous viscous-flow mass exhibiting adhesive and film-forming properties. This concerns not only monolithic polyurethane, but also polymeric sheets by rolling microcellular or integral PUs [4–9].

An increase in the polyurethane temperature at its contact with DMF, as well as stirring, decreases the time required for plasticization of the compound. Therefore, homogeneous concentrated solutions of poly(butylene glycol adipate urethane) were prepared in a horizontal mixer with Z-shaped blades at 90°C within 10 h.

The KLEUR adhesives thus obtained are concentrated (60–75%) solutions of polyurethane in DMF; their characteristics are given in Table 1. With respect to the strength of the glued joint, the compound meets typical requirements specification for shoe adhesives.

The compound also shows promise for gluing wood. Wood bars of size 120 × 30 × 8 mm were glued in the butt (via 30 × 8-mm faces) or lap (via 120 × 30-mm planes, length of glued joint 25 mm) modes. The results are given in Table 2 in comparison with the results obtained for the same joints with an epoxy resin as adhesive. After gluing, the specimens were kept for 24 h under a pressure of 0.2 MPa.

It is seen that, with respect to the strength of the

Table 2. Strength of wood glued joints

Adhesive formulation	Strength, MPa, for indicated joint	
	lap	butt
ED-20 + PEPA (125 : 7.5)	26.7	21.3
KLEUR with viscosity, min:		
8	29.2	23.6
6	24.0	22.1
4.3	22.1	20.8

Table 3. Properties of decorative-protective coatings based on polyurethane waste

Parameter	Parameter value	Determination method
Weight fraction of nonvolatile substances, %	40	GOST 17537–72
Viscosity (outflow time from VZ-246), s	45	GOST 8420–74
Degree of grinding, μm, no more than	20	GOST 6589–74
Covering power, g m^{-2}	175	GOST 8784–75
Drying time at 20°C, h:		GOST 19007–75
to degree 3	2	
to degree 4	20	
Film luster, %	45	GOST 896–69
Bending elasticity, mm	1	GOST 6806–71
Hardness (M-3 pendulum device), arb. units	0.27	GOST 5233–67
Adhesion, points:		GOST 15140–78
to aluminum	3	
to St.3 steel	3	
Water resistance at 20°C, days	No changes	GOST 9403–80
Oil resistance at 20°C, months	No changes	GOST 9403–80
Benzine resistance at 20°C, months	No changes	GOST 9403–80

wood glued joint, the compound we developed well competes with the epoxy resin [10]. As the joint made with KLEUR adhesive is highly elastic, in many cases it can be preferable over the joint made with an epoxy resin.

The film formed on dryingt of KLEUR adhesive has the ultimate tensile strength of 12 MPa, relative elongation of 920%, tear resistance of 0.6 kN m^{-1}, and Shore hardness of 72 units. Such parameters allow the viscous liquid compounds based on polyurethane waste to be used for preparing film coatings. We developed filled compounds containing (i) polyurethane acting as a binder for powdered components and providing formation of a protective film on a surface to be treated; (ii) plasticizer imparting the flowability to the compound and allowing application of the mastic onto a support; (iii) filler introduced to enhance physicomechanical characteristics, improve the fire safety, reduce stresses arising in the course of film formation, and decrease possible shrinkage; and (iv) pigment added to provide the required optical and decorative effects (Table 3).

CONCLUSIONS

(1) Waste of cured poly(ethylene butylene glycol adipate urethanes) should be plasticized to decrease the flow point and make it possible to use a low-destructive molding procedure to obtain items with satisfactory service characteristics.

(2) The macrokinetic parameters of equilibrium swelling of monolithic polyurethanes in various kinds of plasticizers were determined.

(3) Dimethylformamide was chosen as a plasticizer decreasing the temperature of reprocessing monolithic and microcellular polyurethane. In dimethylformamide, the material passes into the viscous-flow state within 24 h at 20°C. The resulting adhesive compound has good consumer's properties; it ensures the glued joint strength similar to that reached with epoxy resins.

(4) Preparation conditions and properties of film materials based on plasticized polyurethane waste were determined, and the possibility of using these materials as paint-and-varnish coatings was demonstrated.

REFERENCES

1. Kercha, Yu.Yu., *Fizicheskaya khimiya poliuretanov* (Physical Chemistry of Polyurethanes), Kiev: Naukova Dumka, 1979.
2. Moiseev, V.V., *Termoelastoplasty* (Thermoelastoplastics), Moscow: Khimiya, 1985.
3. Lazarev, S.Ya. and Ravnov, N.P., *Laboratornyi praktikum po sinteticheskim kauchukam* (Practical Laboratory Course of Synthetic Rubbers), Leningrad: Khimiya, 1991.
4. RF Patent 2069675.
5. Bestuzheva, V.V., Nalimova, N.K., and Kruteleva, G.V., *Vestn. Verkhne-Volzhsk. Otd. Akad. Tekh. Nauk Ross. Feder.* (Yaroslavl), 1996, no. 1, pp. 127–133.

6. Bestuzheva, V.V. and Nalimova, N.K., in *Khimiya vysokoorganizovannykh veshchestv i nauchnye osnovy nanotekhnologii: Sbornik trudov 2-oi Mezhdunarodnoi konferentsii* (Chemistry of Highly Organized Substances and Scientific Principles of Nanotechnology: Proc. Second Int. Conf.), St. Petersburg: Sankt-Peterb. Gos. Univ., 1998, p. 279.
7. Bestuzheva, V.V., Nalimova, N.K., Omel'chuk, Yu.V., and Sirotinkin, N.V., *Zhizn' Bezopasn.*, 2003, nos. 1–2a, pp. 112–114.
8. Bestuzheva, V.V., Nalimova, N.K., Omel'chuk, Yu.V., and Sirotinkin, N.V., *Upravlenie i obrashchenie s otkhodami: Sbornik trydov Nedeli khimicheskikh tekhnologii* (Waste Management: Proc. Week of Chemical Technologies), St. Petersburg, 2003, pp. 28–32.
9. Bestuzheva, V.V., Nalimova, N.K., Omel'chuk, Yu.V., and Sirotinkin, N.V., *Khim. Prom–st.*, 2004, vol. 81, no. 1, pp. 42–48.
10. Kardashov, D.A. and Petrova, A.P., *Polimernye klei* (Polymeric Adhesives), Moscow: Khimiya, 1983.

ISSN 1070-4272, Russian Journal of Applied Chemistry, 2007, Vol. 80, No. 7, pp. 1126–1129. © Pleiades Publishing, Ltd., 2007.
Original Russian Text © N.I. Kurbanova, A.M. Kuliev, 2007, published in Zhurnal Prikladnoi Khimii, 2007, Vol. 80, No. 7, pp. 1156–1159.

MACROMOLECULAR CHEMISTRY AND POLYMERIC MATERIALS

Composite Materials Based on Modified Butadiene–Styrene Rubber

N. I. Kurbanova and A. M. Kuliev

Institute of Polymeric Materials, Azerbaijan National Academy of Sciences, Sumgait, Azerbaijan

Received November 27, 2006

Abstract—Effect of fabrication procedure of rubber stocks on the strength and fatigue performance of composite materials based on modified butadiene–styrene rubber was examined.

DOI: 10.1134/S1070427207070221

For more than a century scientists attempted to obtain a synthetic elastomer with the structure and physical properties close to those of natural rubber (NR). Modern rubber industry uses essentially butadiene–styrene copolymer (SKS) as a source, because of its availability and low cost.

SKS is an elastomer suitable for fabrication of tires and other rubber goods. However, SKS exhibits some disadvantages as compared to NR, primarily, high hysteresis (strong heat liberation in multiple bending) [1].

SKS-based rubbers stocks are prepared at high temperatures. As a result of increased elastic recovery, the stocks exhibit a relatively high shrinkage. Furthermore, oil-filled stocks are characterized by uneven surface. These drawbacks may be overcome through optimization of the formulation, e.g., by combining unfilled with oil-filled SKS, introducing phenol–formaldehyde resins (to improve the adhesiveness) and special plasticizers and carbon black (to improve the workability) [2, 3].

The drawback of all types of synthetic rubber (SR), complicating their use in tire industry, is lower strength (cohesion strength) of raw compounds on their bases as compared to those based on NR, which is due to more perfect macroscopic structure of NR, which facilitates its crystallization at low deformation, and also to the lack of low-molecular-weight fractions [4].

The cohesion strength of SR-based stocks can be considerably improved through functionalization of the macromolecules and also by blending two or more polymers [5–7].

Conditions of fabrication and processing of rubber stocks as well as the use of additives strongly affect their structure and properties [8–10].

In this study we examined the effect of fabrication procedure of rubber stocks on the mechanical characteristics of composites based on modified SKS.

In the experiments we used SKS-30 ARKM-15 (up to 30% styrene, MW 320 000, unsaturation 70 mol %, Mooney viscosity 45); SKI-3 (94% *cis* units, MW 550 000, unsaturation 96 mol %, Mooney viscosity 61); SKS modified with trichloroacetic acid (SKS-I) (chlorine content 0.8 wt %, carboxy group content 0.5 wt %); and SKS modified with alkyl trichloroacetate (SKS-II) (chlorine content 0.6 wt %, carbonyl group content 0.3 wt %). SKS-I and SKS-II were prepared in benzene in the presence of benzoyl peroxide [11].

The rubbers were mixed under laboratory conditions using 160×320 mm rollers at a friction ratio of 1 : 1.24 and a temperature not exceeding 40°C.

The stocks were vulcanized in an electrically heated vulcanizing press at 143°C and hydraulic pressure of 110 ± 5 atm, using 1-mm-thick molds. The tensile tests were carried out on a tensile-testing machine at a strain rate of 200 mm min^{-1}.

We tested the following vulcanizates of polymer blends: (*1*) standard stocks consisting of 100% SKS (mod. SKS) or SKI-3 with 50 wt parts of S301 carbon black (vulcanizing system: sulfur + zinc oxide + Altax + diphenylguanidine); (*2*) standard stocks based on SKS (mod. SKS)/SKI-3 (50 : 50 wt/wt), filled with N242 high-structure carbon black (55 wt %) (vulcanizing system: sulfur + Oktofor-10 alkylphenol–sulfide–formaldehyde oligomer + zinc oxide + *N*-oxadiethylene-2-benzothiazolylsulfenamide (OBTS).

Table 1. Crack resistance under multiple flexures in blend rubbers, as influenced by the fabrication procedure

Rubber	Rubber mixing sequence	N_r, thousand cycles
SKS	–	50
SKI-3	–	85
SKS/SKI-3	Addition of SKS to SKI-3 master batch containing all ingredients	100
SKS/SKI-3	Combination of SKS and SKS-3, followed by introduction of ingredients	140
SKS/SKI-3	Combination of master batches of SKS and SKI-3	152
SKS/SKI-3	Addition of SKI-3 to SKS master batch containing all ingredients	305

Diversification of SRs opened the door for progress in developing composite rubbers based on blends of two or more elastomers. On this way, there were obtained blend rubbers with synergetically improved mechanical characteristics, which can be illustrated by an example of the fatigue behavior of rubbers based on *cis*-polyisoprene and *cis*-polybutadiene, as influenced by the component ratio [12]. Another example is the filler or modifier effect on the strength and elastic-relaxation behavior of rubbers based on binary blends of elastomers [13–15].

We studied the mechanical properties of the initial and modified vulcanizates of the resulting formulations, as influenced by the fabrication procedure. The results (average of five measurements) are listed in Tables 1 and 2.

The rubbers to be blended generally differ in their modulus, i.e., the system formed as a result of their combination exhibits different modules of the dispersed and continuous phases. Fracture of a sample upon multiple deformation starts from microcrack growth. If a microcrack is developed in a medium with a lower modulus, approaching a particle of a high-modulus rubber decelerates or even terminates its growth through overstrain relaxation at the crack tip. If a microcrack is developed in a medium with a higher modulus (modulus of the continuous phase is higher than that of the dispersed phase), the overstrains at the tip of the growing crack are readily relaxed on approaching a dispersed phase particle having higher elastic compliance. If a blend rubber consists of two continuous phases, there is no way to fracture of the sample without breakdown of the particles themselves, i.e., only along the phase boundaries [12]. Therefore, most likely, both above crack propagation mechanisms are realized.

Since blended polymers differ in their modulus and strength, an optimal inhomogeneous (microheterogeneous) system is formed, exhibiting a higher breaking strength. This hypothesis is supported by the direct measurements of the crack propagation rate under multiple flexure of a vulcanizate plate with a perforation applied, and also by the fact that the fracture surface of individual rubber vulcanizates appears smoother as compared to that of vulcanizates of polymer blends, especially against the samples with the highest dynamic strength.

The phase transfer of fillers and their transition from the free-disperse state to the state of dispersion in a viscous polymer occur during mechanical mixing. Therefore, the mixing conditions and filler addition mode exert a decisive effect on its phase distribution. An optimal set of mechanical characteristics of a filled polymer blend is provided by the optimal phase distribution of the filler. Note that the optimal distribution is not always equivalent to the uniform distribution. A directed phase distribution of the filler sets such a degree of microheterogeneity that provides the best suited conditions for strain relaxation,

Table 2. Mechanical characteristics of vulcanizates of blend rubbers*

Formulation	Rubber mixing sequence	M_{300}	σ_t	ε, %
		MPa		
SKS/SKI-3	I	8.1	26.8	500
	II	8.7	27.5	510
	III	9.5	28.1	520
	IV	7.6	26.0	480
SKS-I/SKI-3	I	11.5	32.1	665
	II	11.8	32.5	672
	III	12.5	33.2	680
	IV	10.4	31.5	659
SKS-II/SKI-3	I	10.9	29.5	640
	II	10.2	29.1	635
	III	11.7	30.5	650
	IV	9.8	28.7	625

* Carbon black addition mode: (I) (SKI-3 + carbon black) + (SKS + carbon black); (II) (SKI-3 + SKS) + carbon black; (III) (SKS + carbon black) + SKI-3; and (IV) (SKI-3 + carbon black) + SKS.

Table 3. Mechanical characteristics of standard rubbers based on SKS/SKI-3 blends and of the initial and modified SKS and SKI-3

Characteristic	Formulation						
	SKS	SKS-I	SKS-II	SKI-3	SKS/SKI-3	SKS-I/SKI-3	SKS-II/SKI-3
Modulus at 300% elongation, MPa	6.8	8.8	7.9	13.5	9.5	12.5	11.7
Tensile strength, MPa	25	30	32	32.5	28.1	33.2	30.5
Relative elongation, %	550	830	770	490	520	680	650
Elongation set, %	30	27	25	22	26	23	23
Tear resistance, kN m^{-1}	56	79	75	89	63	98	95
Coefficient of friction on wet concrete	0.52	0.58	0.57	0.60	0.56	0.65	0.63
Endurance of rubber in multilayer systems with bonding to SKI-3 rubber, cycles	2150	3320	3040	–	2500	4410	3560
Crack resistance under multiple flexures, thousand cycles	50	100	80	85	305	550	420
Adhesion strength to steel, MPa	2.5	7.5	5.2	0.03	2.0	6.6	3.5

thus eliminating crack propagation and improving the strength and fatigue behavior, as demonstrated in Tables 1 and 2.

As seen from Tables 1 and 2, the best results were obtained for the third mode of filler addition, i.e., on addition of SKI-3 to the SKS master batch containing all the ingredients.

The mechanical characteristics of the vulcanizates of the standard rubbers based on SKI-3, initial and modified SKS, and standard rubbers based on SKS/SKS-3 are summarized in Table 3.

As can be seen, the strength performance of the rubbers based on SKI-3 blend with the initial SKS is worse or the same as the additive values. With the use of modified SKS, the strength performance characteristics are slightly above the additive values (modulus at 300% elongation, tensile strength, relative elongation, and elongation set), the tear resistance being considerably above the additive value.

As expected, blending improved the performance: the crack resistance in the absence of fatigue substances increased by a factor of 7–10, the endurance of rubbers in multilayer systems with bonding to SKI-3 rubber increased, as well as the rubber adhesion to wet surface. The adhesive characteristics of the blend elastomers with respect to St.3 steel with the use of Leikonat glue were found to be much better (by a factor of 2–3) as compared to the initial components.

It is known that introduction of the carboxy groups into the rubber macromolecules improves the mechanical and elastic properties of the products. However, rubber stocks on their basis tend to overcure, and vulcanizates, to scorching. Therefore, it appears preferable to use compounds containing reactive ester groups as elastomer modifiers. The presence of the carboxy and ester groups in the structure of modifiers facilitates their conversion into ionic groups during vulcanization [4].

The observed high performance of vulcanizates of the modified rubbers can be attributed to the formation of bonds of different types (covalent and ionic) in the vulcanization network structure. Compared to the cross-linking via sulfur, the energy of ionic bonds is lower. The ability of these bonds to rearrange provides a possibility of stress relaxation in the vulcanization network and in deformation of the resulting vulcanizates. Stress relaxation is responsible for increasing resistance of rubbers to aging, tear, and multiple deformations.

The effect of improvement of the fatigue and adhesion behavior of the rubbers based on SKS/SKI-3 blends can find practical application in manufacture of rubbers for various purposes, and also of adhesives and specialty coatings.

CONCLUSIONS

(1) Data on the effect of the fabrication procedure of rubber stocks on the properties of composite materials showed that the best strength and fatigue performance were obtained upon adding SKI-3 to the SKS master batch containing all the ingredients.

(2) Introduction of the chlorine atoms, carboxy, or ester groups in the elastomers alters the structure

of the vulcanization network through development of a combination of strong valence and labile ionic bonds, thus improving performance characteristics of rubber.

(3) Preparation of the composites, based on modified SKS, with improved performance characteristics extends the application area of these materials in various branches of industry.

REFERENCES

1. Golding, B., *Polymers and Resins: Their Chemistry and Chemical Engineering*, Princeton: Van Nostrand, 1959.
2. Bogdanov, V.V., *Smeshenie polimerov* (Blending Polymers), Leningrad: Khimiya, 1982.
3. Pomogailo, A.D., *Usp. Khim.*, 2002, vol. 71, no. 1, pp. 5–38.
4. *Sinteticheskii kauchuk* (Synthetic Rubber), Garmonov, I.V., Ed., Leningrad: Khimiya, 1976.
5. Arkhireev, V.P., Perukhin, V.P., and Kochnev, A.M., *Vestn. Kazan. Tekhnol. Univ.*, 1998, no. 1, pp. 57–70.
6. Kiprova, A.V., Averko-Antonovich, I.Yu., and Marina, A.A., *Materialy Yubileinoi nauchno-prakticheskoi konferentsii "Kirpichnikovskie chteniya", posvyashchennoi 90-letiyu P.A. Kirpichnikova i 70-letiyu kafedry tekhnologii sinteticheskogo kauchuka KGTU* (Proc. Jubilee Scientific and Methodological Conf. "Kirpichnikov Readings" Dedicated to the Ninetieth Birthday Anniversary of P.A. Kirpichnikov and the Seventieth Anniversary of the Foundation of the Department of Technology of Synthetic Rubber, Kazan State Technological University), Kazan, March 25–28, 2003, pp. 509–510.
7. Prut, E.V. and Zelenetskii, A.N., *Usp. Khim.*, 2001, vol. 70, no. 1, pp. 72–87.
8. Ranimol, S., Raji, K.V.S.N., Nair Sobha, V., et al., *J. Appl. Polym. Sci.*, 2003, vol. 87, no. 11, pp. 2639–2648.
9. Xie, Hong Quan, Pan, Yong Jun, and Guo, Jun-Shi, *J. Macromol. Sci.*, 2003, vol. 42, no. 2, pp. 257–268.
10. Yin, D.H., Zhan, Y., Peng, Z.I., and Zhang, Y.X., *Eur. Polym. J.*, 2003, vol. 39, no. 1, pp. 99–105.
11. Kurbanova, N.I., *Proc. Petrochem. Oil Refin.*, 2004, no. 4, pp. 64–68.
12. Kuleznev, V. I., *Smesi polimerov* (Polymer Blends), Moscow: Khimiya, 1980.
13. Kurbanova, N.I., *Zh. Prikl. Khim.*, 2004, vol. 77, no. 6, pp. 1041–1043.
14. Taylor, R.E. and Register, R.A., *J. Polym. Sci., part B*, 1994, vol. 32, no. 12, pp. 2105–2114.
15. Zhovner, N.A., *Kauchuk Resina*, 2003, no. 3, pp. 44–45.

ISSN 1070-4272, Russian Journal of Applied Chemistry, 2007, Vol. 80, No. 7, pp. 1130–1134. © Pleiades Publishing, Ltd., 2007.
Original Russian Text © V.Z. Mingaleev, V.P. Zakharov, Yu.B. Monakov, 2007, published in Zhurnal Prikladnoi Khimii, 2007, Vol. 80, No. 7, pp. 1160–1164.

MACROMOLECULAR CHEMISTRY AND POLYMERIC MATERIALS

Polymerization of Butadiene on a Titanium Catalyst in Formation of a Reaction Mixture in Turbulent Flows

V. Z. Mingaleev, V. P. Zakharov, and Yu. B. Monakov

Institute of Organic Chemistry, Ufa Scientific Center, Russian Academy of Sciences, Ufa, Bashkortostan, Russia
Bashkir State University, Ufa, Bashkortostan, Russia

Received November 21, 2006

Abstract—Fundamental aspects of the polymerization of butadiene in the presence of a titanium catalyst under intensive agitation of the reaction mixture in the initial stage of polymerization, provided by use of a tubular turbulent divergent–convergent prereactor, were examined.

DOI: 10.1134/S1070427207070233

The stereospecific polymerization of dienes on complex Ziegler–Natta catalysts includes a number of complex physicochemical processes, some of which occur at high rates. To these processes belongs the stage of formation of active centers, which includes a redox reaction of a transition metal compound with an organoaluminum compound, formation of the surface structure of a microheterogeneous catalyst, addition of a first monomer molecule to the active center, etc. It was shown in [1–3] that the occurrence of fast stages in the polymerization process makes advisable use of tubular turbulent divergent–convergent prereactors. In this case, optimal conditions are created, under the conditions of a preliminary turbulent agitation of the reaction mixture, for occurrence of fast processes in the absence of diffusion limitations, with the chain propagation stage subsequently performed in a large-volume mixer with a long residence time of reagents in the reaction zone.

The aim of this study was to examine the fundamental aspects of the polymerization of butadiene in the presence of a $TiCl_4$–Al(i-C_4H_9)$_3$ catalyst under vigorous agitation of the reaction mixture in the initial stage of polymerization because of the use of a tubular turbulent divergent–convergent prereactor.

Butadiene was polymerized in toluene on an experimental installation including the tubular turbulent prereactor described in [3]. The starting reactants were purified by a standard procedure commonly accepted for stereospecific polymerization of dienes on Ziegler–Natta catalysts. The separately prepared catalytic complex $TiCl_4$–Al(i-C_4H_9)$_3$ was kept at 273 K for 30 min. The concentrations of the catalyst and monomer were c_{Ti} = 5 mM and c_m = 1.5 mM. The molar ratio of the components of the catalytic system, which provided the maximum polymerization rate and highest content of 1,4-*cis* links (~75–78%), was Al/Ti = 1.8.

The polymerization process was performed by two methods.

Method 1. The components of the reaction mixture (separately prepared catalytic complex and monomer solution) were mixed directly in the large-volume apparatus (500 cm^3 flask) under slow agitation with a magnetic stirrer. This method modeled the conventional way of polymerization under industrial conditions [4].

Method 2. A preliminarily kept catalytic complex was mixed with a butadiene solution in a tubular turbulent divergent–convergent prereactor in the course of 2–3 s. Then the reaction mixture was delivered into a large-volume apparatus, in which conditions similar to those in method 1 were created.

The number-average (M_n) and weight-average (M_w) molecular weights (MW) and the molecular-weight distribution (MWD) of polybutadiene were determined by gel-permeation chromatography on a Waters chromatograph at 80±0.5°C, with toluene as solvent and elution rate of 1 ml min^{-1}, The chromatograph was calibrated against close-cut (M_w/M_n = 1.1) polystyrene references. A correction for the in-

Kinetic parameters of butadiene polymerization on $TiCl_4$–$Al(i\text{-}C_4H_9)_3$*

Method	W_p	AC type	$c_a \times 10^4$	k_{cp}	k_{al}	k_m
1	0.0175	1	1.77	26.0	0.59	0.0130
		2	0.62	60.5	0.53	0.0126
		3	0.0740	533.0	0.36	0.0034
		4	0.0037	2042.0	0.0072	0.0002
		Σ	2.47	52.8	0.57	0.0126
		Σ**	2.50	55.0	–	–
2	0.08	1	–	–	–	–
		2	4.18	56.8	0.55	0.0130
		3	0.0187	519.0	0.36	0.0032
		4	0.00076	2050.0	0.0075	0.0002
		Σ	4.20	59.2	0.55	0.0130
		Σ**	4.20	58.0	–	–

* W_p is the initial polymerization rate (mol l^{-1} min^{-1}); c_a, concentration of active centers (M); k_{cp}, k_{al}, and k_m, rate constants of chain propagation and chain transfer to the organoaluminum compound and to the monomer, respectively (l mol^{-1} min^{-1}); Σ, kinetic parameter, which is an arithmetic mean for the constants and a sum for concentration of separate AC types.
** Σ is the kinetic parameter calculated from the data of [5].

strumental broadening was made. The error of the technique was 15–20%. The conversion dependences were obtained using the gravimetric method, with an error not exceeding 1%.

Raising the intensity of agitation of the reaction mixture in the initial stage of the polymerization process because of the use of a tubular turbulent prereactor makes the polymer yield higher (Fig. 1). In order to explain the observed acceleration of the polymerization process, the rate constant k_{cp} of chain propagation and the concentration of active centers (AC) were evaluated as described in [5]. The calculations demonstrated that the rate of polymerization, which is first-order with respect to the catalyst and the monomer, grows because of the 1.7-fold increase in the AC concentration in the polymerization system (see table). Changing the polymerization procedure has virtually no effect on the rate constant of the polymeric chain propagation. At the same time, the initial polymerization rate increases by a factor of up to 4.6 if the tubular turbulent prereactor is used, which can be attributed not only to an increase in the AC concentration, but also to the formation of a homogeneous reaction mixture and uniform particle distribution of the microheterogeneous catalyst.

It is well known that a change in the reaction rate on raising the agitation intensity indicates that the elementary stages of the process occur under diffusion control. Apparently, preliminary agitation of the reaction mixture in the turbulent mode in butadiene polymerization on a microheterogeneous titanium-based catalytic system diminishes the diffusion hindrance in the stage of formation of the surface structure of the catalyst.

According to the kinetic scheme of polymerization of dienes, an increase in the AC concentration should lead to a decrease in the average values of the molecular weight of polybutadiene [5, 6], which is confirmed by the experimental data obtained. In the preliminary forming of the reaction mixture in turbulent flows (method 2), the weight-average MW of polybutadiene substantially decreases (Fig. 2). In this case, a slight change in the number-average MW favors synthesis of a polymer with a narrow MWD (Fig. 3). In the conventional polymerization technique, the MWD curves

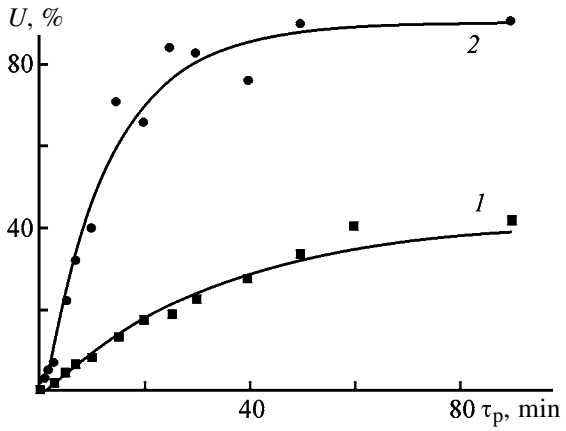

Fig. 1. Polybutadiene yield U vs. the polymerization time τ_p in the presence of the $TiCl_4$–$Al(i\text{-}C_4H_9)_3$ catalyst. (*1, 2*) Method numbers; the same for Figs. 3 and 4.

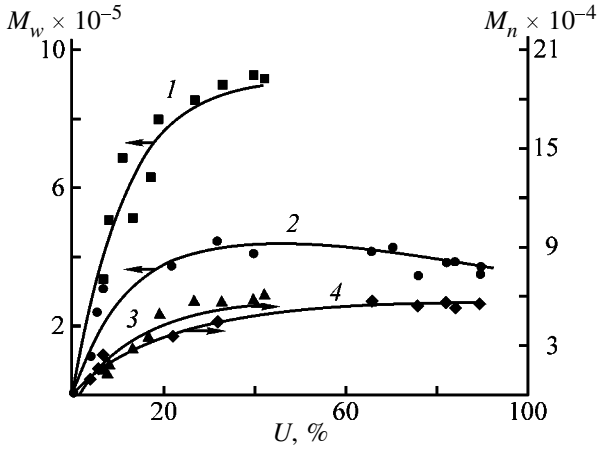

Fig. 2. (*1, 2*) Weight-average (M_w) and (*3, 4*) number-average (M_n) molecular weigts vs. the polybutadiene yield *U*. Method number: (*1, 3*) 1 and (*2, 4*) 2.

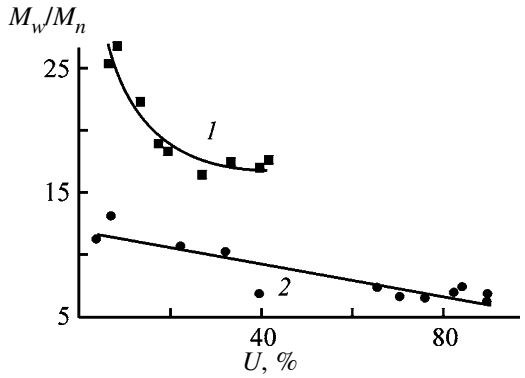

Fig. 3. Polydispersity index M_w/M_n vs. the polybutadiene yield *U*.

of polybutadiene have a unimodal shape and shift, as the monomer conversion increases, into the high-molecular-weight region without any significant change in the distribution width.

The hydrodynamic impact on the reaction mixture in turbulent flows in the initial stage of polymerization predetermines formation of a polymer with a unimodal MWD and a conversion shift of the corresponding curves into the low-molecular-weight region.

It is known that the MWD width is one of the most important and decisive factors determining the service parameters of synthetic rubbers [7], because the M_w/M_n ratio affects such parameters as the Mooney viscosity and cold-flow capacity and predetermines the properties of vulcanized rubbers. The latter is due to the fact that vulcanizates based on polybutadienes with broad MWD have a nonuniform and less dense vulcanization network, which leads to poor physicomechanical characteristics of vulcanized rubbers. It can be assumed that a decrease in the weight-average MW of polybutadiene at an insignificant change in the number-average MW must lead to an increase in the vulcanization network density.

However, the presence of low-molecular-weight fraction enables, because of their plasticizing effect, a flow at high shear stresses. Thus, it seems plausible that the observed decrease in the polydispersity index of polybutadiene, caused by the use of a tubular turbulent divergent–convergent prereactor, will make it possible to enhance the flow capacity of the polymer at high shear stresses and, simultaneously, improve the physicomechanical properties of vulcanizates.

It is known that the reason why the MWD of polydienes synthesized on Ziegler catalytic systems is broad is the polycentric nature of the polymerization AC [8–10]. A solution of the inverse MWD problem by the Tikhonov regularization method demonstrated that, with the conventional polymerization technique (method 1), the catalytic system is characterized by the presence of four types of active centers. The peak positions in the kinetic nonuniformity curves correspond to the following ranges of molecular weights: $\ln M$ = 9.2–10.4 (type I), 11.2–11.4 (type II), 12.9–13.2 (type III), and 14.1–14.7 (type IV), i.e., each type produces its own fraction of the polymer.

In the case of the conventional polymerization method, the kinetic activity of the macromolecule propagation centers of types I and II decreases as the conversion becomes higher, and that of type III and IV centers increases (Fig. 4). Upon a hydrodynamic impact on a separately prepared catalytic complex $TiCl_4$–$Al(i\text{-}C_4H_9)_3$ (method 2), the type I active center producing the low-molecular-weight fraction of polybutadiene ($\ln M$ = 9.2–10.4) disappears (Fig. 4). The kinetic activity of the type II AC in a reaction mixture formed in turbulent flows is substantially higher, compared with method 1. In the course of polymerization, the activity of type III centers changes only slightly, and that of type IV AC producing the high-molecular-weight fraction of polybutadiene remains unchanged and is lower than that in method 1.

The kinetic parameters of butadiene polymerization were calculated for each type of active centers by the method previously described in [11]. It can be seen from the table that the kinetic parameters of the polymerization process estimated in terms of the polycentric model well coincide with the calculations made in accordance with [5]. Upon a hydrodynamic impact on the reaction mixture in the initial stage of polymerization, the concentration of type II AC substantially increases to 99.5% of the total

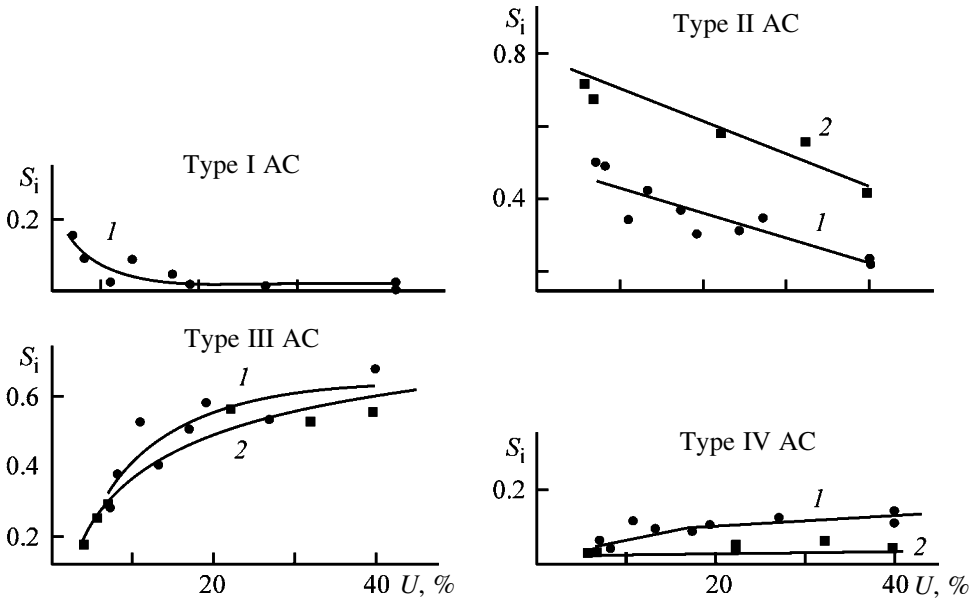

Fig. 4. Kinetic activity S_i of macromolecule propagation centers of various types vs. the polybutadiene yield U.

number of propagation centers in the polymerization system.

Each AC is characterized by a certain ratio of polymer chain termination and propagation constants, i.e., synthesizes macromolecules of certain length. As a consequence, the changes in the MW and MWD of polybutadiene, observed in the case of a preliminary treatment of the reaction mixture in a tubular turbulent prereactor, can be attributed not only to an increase in the total AC concentration, but also to a change in the number of types of AC with a certain set of kinetic constants. For example, presence of the low-molecular-weight fraction in the polymer, which primarily affects the number-average molecular weight, is determined by the reactions of chain transfer to the monomer and organoaluminum compound, whose rate constants are the largest for type I and II AC (see table). These active centers have comparable rate constants for chain transfer reactions, but markedly different rate constants for the chain propagation reaction. Upon a hydrodynamic impact on the reaction mixture (method 2), a pronounced increase in the concentration of type II AC is observed. These centers have a higher rate constant of the chain propagation reaction than type I center, which disappears. In accordance with the kinetic scheme of the process, this results in that the number-average molecular weight of polybutadiene changes only slightly on varying the polymerization method.

The presence of the high-molecular-weight fraction in the polymer is mostly due to type III and IV centers, whose initial concentration in the polymerization system decreases upon a preliminary hydrodynamic impact on the reaction mixture (see table). In addition, in the case of a hydrodynamic impact on the reaction mixture in turbulent flows, the kinetic activity of type IV centers does not change as the conversion increases, whereas an increase in the activity of this type of centers is observed (Fig. 4) in polymerization by the standard method. As a result, preliminary forming of the reaction mixture in the turbulent mode yields a polymer with a lower weight-average molecular weight.

Thus, if the reaction mixture for butadiene polymerization in the presence of $TiCl_4$–$Al(i\text{-}C_4H_9)_3$ is treated in the turbulent mode, the concentration of active centers increases and, as a result, the process rate grows. Use of a tubular turbulent prereactor has virtually no effect on the rate constants of the reactions of chain propagation and chain transfer to the organoalunimum compound and the monomer. Changing the polymerization method leads to disappearance of the active center producing the low-molecular-weight fraction of the polymer ($\ln M$ = 9.2–10.4), with an increase in the number of centers that synthesize a polymer with a molecular weight $\ln M$ in the range 11.2–11.4. In this case, the weight-average molecular weight of the resulting polybutadiene decreases and its molecular-weight distribution becomes narrower.

Use of a tubular turbulent prereactor in preliminary forming of the reaction mixture for butadiene polymerization makes it possible to reduce the expenditure of the titanium catalyst, compared with the conventional

polymerization technique. In particular, the polymerization occurs at an initial rate of 0.0175 mol l^{-1} min^{-1} in a conventional process with c_{Ti} = 5 mM, and use of a prereactor enables a 1.7-fold decrease in the catalyst expenditure (to the extent to which the AC concentration increases). A redistribution of the types of active centers occurs in this case, which results in that a polymer is obtained with a weight-average molecular weight equal to that of the polymer produced by method 1 at a higher catalyst concentration c_{Ti} = 5 mM. The decrease in the polydispersity index of polybutadiene on lowering the catalyst concentration and forming the reaction mixture in the turbulent mode is predetermined by its higher number-average molecular weight.

CONCLUSIONS

(1) Preliminary vigorous agitation of the reaction mixture in a tubular turbulent divergent–convergent prereactor in butadiene polymerization on a titanium catalyst leads to a rise in the process rate because of the increase in the concentration of active centers and a uniform catalyst distribution throughout the reaction volume. Under industrial conditions, this enables a decrease in the expenditure of the catalytic complex.

(2) The partial elimination of diffusion limitations in the stage of formation of the reaction mixture leads to disappearance of the active center responsible for synthesis of the low-molecular-weight fraction of the polymer ($\ln M$ = 9.2–10.4) and to an increase in the concentration of centers that produce macromolecules with molecular weights in the range 73 000–89 000. The redistribution of macromolecule propagation centers leads to a decrease in the weight-average molecular weight of polybutadiene and in the polydispersity index.

ACKNOWLEDGMENTS

The study was financially supported by the Russian Foundation for Basic Research (project no. 06-03-32 240), RF Presidential grant no. MD-1427.2005.3, and Foundation for Support of Leading Scientific Schools (grant no. NSh-9342.2006.3).

REFERENCES

1. Minsker, K.S., Zakharov, V.P., Berlin, Al.Al., and Monakov, Yu.B., *Dokl. Ross. Akad. Nauk*, 2001, vol. 381, no. 3, pp. 373–376.
2. Takhavutdinov, R.G., Mukhametzyanova, A.G., D'yakonov, G.S., et al., *Vysokomol. Soedin., Ser. A*, 2002, vol. 44, no. 7, pp. 1094–1100.
3. Zakharov, V.P., Sadykov, I.V., Minsker, K.S., et al., *Vysokomol. Soedin., Ser. B*, 2004, vol. 46, no. 10, pp. 1765–1769.
4. Kirpichnikov, P.A., Beresnev, V.V., and Popova, L.M., *Al'bom tekhnologicheskikh skhem osnovnykh proizvodstv promyshlennosti sinteticheskogo kauchuka* (Album of Flowsheets of Basic Synthetic Rubber Industries), Leningrad: Khimiya, 1986.
5. Chirkov, N.M., Matkovskii, P.E, and D'yachkovskii, F.S., *Polimerizatsiya na kompleksnykh metalloorganicheskikh katalizatorakh* (Polymerization on Complex Organometallic Catalysts), Moscow: Khimiya, 1976.
6. Gaylord, N.G. and Mark, H.F., *Linear and Stereoregular Addition Polymers*, London: Wiley, 1959.
7. *Sinteticheskii kauchuk* (Synthetic Rubber), Garmonov, I.D., Ed., Leningrad: Khimiya, 1983.
8. Sigaeva, N.N., Usmanov, T.S., Budtov, V.P., and Monakov, Yu.B., *Zh. Prikl. Khim.*, 2001, vol. 74, no. 7, pp. 1110–1116.
9. Sigaeva, N.N., Usmanov, T.S., Budtov, V.P., et al., *Vysokomol. Soedin., Ser. B*, 2000, vol. 42, no. 1, pp. 112–118.
10. Sigaeva, N.N, Usmanov, T.S., Shirokova, E.A., and Budtov, V.P., *Dokl. Ross. Akad. Nauk*, 1999, vol. 365, no. 2, pp. 221–225.
11. Saitova, F.F., Kinetic Nonuniformity of Active Polymerization Centers of Vanadium and Titanium Catalytic Systems and Molecular Characteristics of Isoprene, *Cand. Sci. Dissertation*, Ufa, 2005.

ISSN 1070-4272, Russian Journal of Applied Chemistry, 2007, Vol. 80, No. 7, pp. 1135–1139. © Pleiades Publishing, Ltd., 2007.
Original Russian Text © F.N. Kaputskii, N.K. Yurkshtovich, T.L. Yurkshtovich, N.V. Golub, R.I. Kosterova, 2007, published in Zhurnal Prikladnoi Khimii, 2007, Vol. 80, No. 7, pp. 1165–1169.

MACROMOLECULAR CHEMISTRY AND POLYMERIC MATERIALS

Preparation and Physicochemical and Mechanical Properties of Low-Substituted Cellulose Phosphate Fibers

F. N. Kaputskii, N. K. Yurkshtovich, T. L. Yurkshtovich, N. V. Golub, and R. I. Kosterova

Research Institute of Physicochemical Problems, Belarussian State University, Minsk, Belarus

Received November 27, 2006; in final form, February 2007

Abstract—Mechanical and physicochemical properties of cotton and viscose fibers esterified with aqueous solutions containing orthophosphoric acid and urea in different ratios were studied.

DOI: 10.1134/S1070427207070245

More than 50 types of suture filaments made of synthetic and natural polymers are widely used in modern world surgery. At the same time, none of the known materials are universal. Each of them has its own advantages and disadvantages, which not only requires their differential and purposeful application but also makes urgent preparation of new types of suture filaments.

Cellulose fibers are the most promising natural polymers for preparing suture filaments. Biocompatible materials resorbable in a living body can be prepared by modification of cellulose fibers. The physicochemical and medicobiological properties of cellulose phosphate with a degree of substitution with the phosphate groups of more than 0.2 (the phosphorus content is higher than 1.1 mmol g^{-1}) were extensively studied. The sorption capacity of the modified polysaccharide for inorganic and organic cations is high and this sorbent is not toxic [1, 2]. At the same time, highly substituted cellulose phosphates are prepared under rigid conditions (concentrated orthophosphoric acid, temperature above 145°C), which deteriorates their mechanical properties and makes these polymers unsuitable as suture materials.

The aim of this study was to prepare low-substituted phosphorylated viscose and cotton fibers, to study their physicochemical and mechanical properties, and to determine the possibility of their use for preparing suture materials.

EXPERIMENTAL

We studied viscose cordage (Svetlogorsk, Khimvolokno Production Association) and cotton (Grodno, Groniteks) fiber with the line density of 184 and 100 tex, respectively.

The cellulose fiber was phosphorylated in several steps [1]. The main steps are as follows: preliminary impregnation of the fiber with an esterifying mixture for 30 min at 80±2°C and a 1 : 10 liquor ratio (g ml^{-1}); squeezing to remove excess mixture down to 100% weight gain; drying to constant weight at room temperature; chemical modification at 145±2°C for 1 h; washing; treatment with 0.1 N HCl and drying to the air-wet state.

As esterifying agent we used aqueous solutions of orthophosphoric acid containing urea. The anhydroglycoside unit (AGU) : H_3PO_4 : $CO(NH_2)_2$ molar ratio was varied. The phosphorus content c_P (mmol g^{-1}) in the modified cellulose fiber was determined by the molybdate procedure [3]. The nitrogen content was determined by the Kjeldahl method [4]. The exchange capacity (EC) (mg-equiv g^{-1}) was measured by potentiometric titration with a sodium hydroxide solution [1]. The degree of swelling Q (g g^{-1}) was determined gravimetrically [1]. The IR spectra of the samples in the form of KBr pellets were recorded on a Thermo Nicolet FT-IR Nexus spectrophotometer. The X-ray diffraction analysis of cellulose samples was performed on a Carl Zeiss diffractometer (CuK_α, Ni filter, HZGb-4A). The crystallinity index was calculated using an internal reference [5]. The mechanical properties were estimated from the relative strength (ratio of the tensile strengths of dry and wet phosphorylated cellulose fibers and the fiber tied in a knot, measured on a PM-3-1 tensile-testing machine, to the linear density) and relative elongation ε (%) [6]. The linear density was deter-

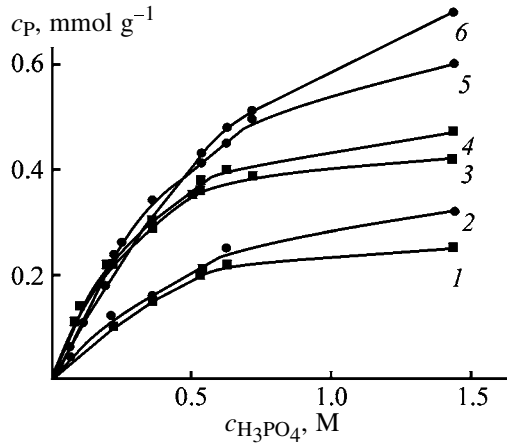

Phosphorus content c_P of (*1, 3, 4*) cotton and (*2, 5, 6*) viscose fibers as a function of the orthophosphoric acid concentration $c_{H_3PO_4}$. Urea concentration in the solution, M: (*1, 2*) 0.83, (*3, 5*) 3.33, (*4, 6*) 4.17.

mined from the data of [6]. Each relative strength P (sN tex^{-1}) and T is an average of no less than 10 measurements. The scatter of the relative strength did not exceed 10%. The strength loss ΔP (%) of the fibers after their phosphorylation was calculated by the equation

$$\Delta P = (P_{in} - P_{ph}) \times 100/P_{in},$$

where P_{in} and P_{ph} is the relative strength of the initial and phosphorylated fibers, respectively (cN tex^{-1}).

The phosphorus content of cellulose fibers rapidly increases during the first hour of their heat treatment at 145±2°C. Then the esterification substantially decelerates. This is typical for the heterogeneous reaction of cellulose and is due to different reactivity of the hydroxy groups of the polymer. It should be noted that the optimal time of phosphorylation of cellulose fibers is 1 h. Longer heat treatment deteriorates the mechanical properties of the polymer.

The content of fixed phosphorus in cellulose fibers depends on the concentration of orthophosphoric acid and urea in the solution (see figure), all other conditions (time and temperature of impregnation and heat treatment, squeezing, washing) being the same. The phosphorus content of the sample c_P ranges from 0.05 to 0.5 mmol g^{-1} when the concentration of orthophosphoric acid changes from 0.15 to 0.63, and that of urea, from 0.83 to 3.33 M. The content of fixed nitrogen in the fibers prepared under these conditions is fairly high. This is due to the fact that cyanic acid formed during heat treatment at temperatures higher than the melting point of urea reacts with hydroxy groups of cellulose to form carbamate groups [1, 7].

Formation of carbamate groups under these conditions is confirmed by IR spectroscopy. The IR spectra of phosphorylated cellulose fibers prepared at different AGU : H_3PO_4 : $CO(NH_2)_2$ ratios, unlike the IR spectra of the initial cellulose, contain the band of carbonyl group (C=O) at 1710 cm^{-1}. The intensity of this band increases with an increase in the fixed nitrogen content. It should be noted that the content of fixed nitrogen and hence of carbamate groups in the samples of low-substituted cellulose phosphates is equal to, or even higher than that of phosphorus (Table 1). The c_N increases with increasing concentration of both orthophosphoric acid and urea in the esterifying solution.

The bands at 790 (out-of-plane bending band of the P–O–H groups) and 830 cm^{-1}, the shoulder at 980 cm^{-1} (stretching vibration of the P–O bonds), and a complex band with the maximum in the range 1200–1220 cm^{-1} (P=O vibrations) in the IR spectra of the samples unambiguously confirm the presence of phosphate groups in the samples [7, 8].

As seen from Table 1, the phosphorus content of the phosphorylated fibers is lower by a factor of 2 than their exchange capacity determined by potentiometric titration. This can be due to the fact that the main esterification product is monosubstituted cellulose phosphate [1].

The content of functional groups in cellulose modified at low concentrations of orthophosphoric acid (0.5 M) and urea (0.83 M) in the solution is almost independent of the structural features of the fiber. The fact that at higher orthophosphoric acid concentration (0.5–1.5 M) in the impregnating solution the content of the phosphate groups in the viscose fibers is higher than that in cotton fibers can be caused by features of supramolecular structure of the initial cellulose fibers whose hydroxy groups are accessible to the esterifying agent.

The structural differences of the cotton and viscose fibers are clearly seen from their X-ray diffraction patterns. The X-ray diffraction pattern of the cotton fiber is typical of cellulose I (C–I), and its index of crystallinity (IC) calculated using internal references is 0.69. The X-ray pattern of the initial viscous fiber contains reflections at $2\theta = 22°$ (strong) and $2\theta = 12°$ and is similar to that of cellulose II (C-II). The index of crystallinity of these cellulose samples is in the range 0.35–0.38.

The X-ray patterns of phosphorylated cotton cellulose and viscose fiber are similar to those of the initial

Table 1. Composition of cellulose fibers modified at different concentrations of orthophosphoric acid and urea in the esterifying solution

Sample	Concentration, M		AGU : H_3PO_4 : $CO(NH_2)_2$ molar ratio	Content, mmol g^{-1}		Exchange capacity, mg-equiv g^{-1}
	H_3PO_4	$CO(NH_2)_2$		phosphorus	nitrogen	
Viscose fiber	–	–	–	0.01	0.01	0.01
	0.22	0.83	1 : 0.7 : 2.7	0.1	0.1	0.2
	0.63	0.83	1 : 2.0 : 2.7	0.3	0.3	0.5
	1.44	0.83	1 : 4.7 : 2.7	0.3	0.4	0.6
	0.25	3.33	1 : 0.8 : 10.8	0.3	0.2	0.6
	0.63	3.33	1 : 2.0 : 10.8	0.5	0.6	0.9
	0.22	4.17	1 : 0.7 : 13.5	0.2	0.5	0.4
	0.63	4.17	1 : 4.7 : 13.5	0.5	0.7	1.0
	1.44	4.17	1 : 4.7 : 13.5	0.7	0.9	1.4
Cotton fiber	–	–		0.01	0.01	0.01
	0.22	0.83	1 : 0.7 : 2.7	0.1	0.1	0.2
	0.63	0.83	1 : 2.0 : 2.7	0.2	0.2	0.4
	1.44	0.83	1 : 4.7 : 2.7	0.3	0.8	0.6
	0.22	3.33	1 : 0.7 : 10.8	0.2	0.2	0.4
	0.63	3.33	1 : 2.0 : 10.8	0.4	0.4	0.9
	0.22	4.17	1 : 0.7 : 13.5	0.2	0.4	0.4
	0.63	4.17	1 : 2.0 : 13.5	0.4	0.4	0.7

cellulose samples. The IC of the cotton fiber phosphorylated at c_P = 0.7 mmol g^{-1} is 0.67.

Some broadening and blurring of the reflections at 2θ 15° and 16° [(101) and (10$\bar{1}$)] suggests that these interplanar spaces of the cellulose fiber are the most accessible to the esterifying mixture. The results of a comparative IR study of the supramolecular structure of cellulose phosphate are completely consistent with the X-ray diffraction data. The index of asymmetry of the OH band in the range 3100–3600 cm^{-1} in the IR spectra of the phosphorylated samples changes insignificantly, and the maximum of this band remains the same. These transformations of the IR spectra of the modified cellulose samples suggest [10] insignificant change of the supramolecular structure during the modification.

Thus, the content of phosphate and carbamate group in the amorphous fraction of the cotton fiber is higher by a factor of 2 than that in the viscose fiber at the same degree of phosphorylation. Hence, the chemical composition of the viscose fibers esterified under all the conditions is more uniform, which undoubtedly affects their mechanical properties.

Data on the loss of the relative strength of the cellulose fiber after modification at different concentrations of orthophosphoric acid and urea in the esterifying solution are summarized in Table 2. It is seen that phosphorylation of the cellulose fibers decreases their relative strength, with the decrease being stronger for the cotton fiber. An increase in the concentration of phosphoric acid and urea in the esterifying solution affects in different manners mechanical properties of the phosphorylated fibers: the relative strength of

Table 2. Loss of the relative strength Δ*P* of dry cotton and viscose fibers phosphorylated at different concentrations of orthophosphoric acid and urea in the esterifying solution. Impregnation at 80±2°C for 0.5 h, heat treatment at 145±2°C for 1 h

$c_{H_3PO_4}$, M	Δ*P*, % at indicated $c_{CO(NH_2)_2}$, M			
	0.83	1.67	3.33	4.17
Cotton fiber				
0.20	62.0	55.9	52.5	49.8
0.35	70.1	59.3	55.2	52.5
0.52	75.6	67.4	57.9	56.5
0.60	79.6	71.5	62.0	59.0
1.50	100.0	87.8	62.0	62.0
Viscose fiber				
0.20	25.3	15.0	10.0	10.0
0.35	35.4	25.0	18.6	15.0
0.52	45.7	30.0	25.3	21.9
0.60	52.5	35.5	25.3	25.3
1.50	100.0	–	66.0	66.0

Table 3. Physicomechanical properties of cellulose fibers, phosphorylated at 145 ± 2°C for 1 h, with different content of phosphate groups

Parameter	Viscose fiber				Cotton fiber			
Urea concentration, M	–	0.83	3.33	0.33	–	0.83	3.33	0.33
c_P, mmol g^{-1}	Initial fiber	0.3	0.3	0.5	Initial fiber	0.3	0.3	0.5
P_{dry}, cN tex^{-1}	46.4	24.8	37.4	32.0	22.4	3.5	9.0	8.3
ε, %	11.0	11.0	17.6	17.3	10.7	5.0	8.1	7.0
P_{wet}, cN tex^{-1}	26.7	6.0	17.4	13.9	25.1	2.1	11.1	9.5
ε_{wet}, %	16.4	7.3	17.8	16.8	12.2	5.4	10.3	9.0
P_{knot}, cN tex^{-1}	29.0	16.8	22.6	18.7	14.1	3.6	8.1	5.9
ε_{knot}, %	4.3	5.5	12.5	9.8	7.8	4.3	7.0	7.4
Q, g g^{-1}	0.9	1.0	1.1	–	0.3	0.3	0.5	0.5
P_{knot}/P_{in}	0.63	0.68	0.61	0.58	0.63	1.03	0.90	0.71

the fiber decreases with increasing H_3PO_4 concentration and increases with increasing urea concentration. The maximal preservation of the relative strength of dry cellulose fibers that have similar content of the phosphate groups but were prepared at a higher urea concentrations in the esterifying solution corresponds to the higher relative elongation and degree of swelling (Table 3). These data suggest that at least two competing processes affecting the mechanical properties of the fiber [11, 12] occur at a higher urea concentration in the impregnating solution. The fiber strength (1) decreases owing to a decrease in the strength of intermolecular bonds in the cellulose structure and (2) does not change owing to a decrease in the degree of cellulose degradation with increasing urea concentration in the solution.

In addition, it should be noted that weakening of the hydrogen bond network has a dual affect on the mechanical properties of cellulose fibers. Weakening of intermolecular interactions can favor more uniform distribution of stresses in the bulk of the fiber and increase the flexibility of the macromolecules [11]. The increase in the mobility of the structural elements and hence an increase in the degree of ordering before rupture increase the fiber strength.

These processes are parallel, but their intensity differs. As a result, as determined experimentally, the loss of the relative strength of phosphorylated cellulose fibers decreases with increasing urea concentration in the esterifying solution.

Comparison of the mechanical properties of cellulose phosphate fibers prepared from viscose and cotton fibers under the optimal conditions (0.25–0.72 M H_3PO_4 and 3.33 M urea) show that the strength of low-substituted phosphorylated viscose and cotton fiber is lower than that of the initial fibers by 25.3 and 62.0%, respectively. We suggest that stronger loss of the relative strength of the cotton fibers phosphorylated in the H_3PO_4–$(NH_2)_2CO$–H_2O system is caused by their structural and chemical nonuniformity which promotes degradation and disordering of macromolecules in the amorphous fraction and increases tension in the bulk of the polymer. An increase in the strength of wet cotton fibers confirms the influence of the internal tensions on the decrease in the mechanical strength of the fibers. Water molecules plasticize cellulose, affect the mobility of the macromolecules in the bulk of the polymer, change the mechanism of stress relaxation, and promote ordering of the macromolecules along the external force.

It should be noted that the tensile strength of low-phosphorylated viscose fibers in a dry knot is similar to that of the know absorbable suture filaments such as catgut, collagen, Oktselon, Katselon, etc. To increase the strength of low-phoshporylated cotton fibers, stronger initial fibers should be used and additional cross-linking of cellulose macromolecules is required.

CONCLUSIONS

(1) Monosubstituted cellulose phosphates with the phosphate content from 0.1 to 0.7 mmol g^{-1} were prepared from viscose and cotton fibers. The conditions for phosphorylating cellulose fibers with the maximal preservation of the relative strength in the dry and wet state (heat reatemnt for 30 min, 0.22–0.72 M orthophosphoric caid, 3.33 M urea) were determined.

(2) The content of carbamate groups in phosphorylated fibers is equal to, or higher than that of the phosphate groups and increases with increasing con-

centration of both orthophosphoric acid and urea in the impregnating solution.

REFERENCES

1. Ermolenko,, I.N., Buglov, E.D., Lyubliner, I.P., and Dovgalev, S.I., *Novue voloknistye sorbenty meditsinskogo naznacheniya* (New Fibrous Sorbents for Medical Purposes), Minsk: Nauka i Zhizn', 1978.
2. Frecain, J.C., Granja, P.L., Borbosa, M.A., et al., *Biomaterials*, 2002, vol. 23, pp. 971–980.
3. *Colorimetric Determination of Nonmetals*, Boltz, D.F., Ed., New York: Interscience, 1958.
4. Houben-Weyl, *Methoden der organischen Chemie*, vol. 2: *Analytische Methoden*, Stuttgart: Georg Thieme, 1953.
5. Ielovich, M.Ya. and Veveris, G.P., *Khim. Drev*., 1980, no. 2, pp. 10–14.
6. Demina, N.V., Motorina, A.V., Nemchenko, Z.A., et al., *Metody fizikokhimicheskikh ispytanii khimicheskikh volokon, nitei i plenok* (Methods of Physicomechanical Tests of Chemical Fibers, Filaments, and Films), Moscow: Legkaya Industriya, 1969.
7. Heinze, U., Klemm, D., Under, E., and Pieschel, F., *Starch/Starke*, 2003, vol. 55, pp. 55–60.
8. Ermolenko, I.N., Gusev, S.S., and Lyubliner, I.P., *Zh. Prikl. Khim*., 1969, vol. 42, no. 10, pp. 2302–2306.
9. Papkov, S.P., *Fiziko-khimicheskie osnovy proizvodstva iskustvennykh i sinteticheskikh volokon* (Physicochemical Foundations of Production of Artificial and Synthetic Fibers), Moscow: Khimiya, 1972.
10. Petropavlovskii, G.A., *Gidrofil'nye chastichno zameshchennye efiry tsellyulozy i ikh modifikatsiya putem sshivaniya* (Hydrophilic Partially Substituted Cellulose Ethers and Esters and Their Modification by Cross-Linking), Leningrad: Nauka, 1988.
11. Perepelkin, K.E., *Struktura i svoistva volokon* (Structure and Properties of Fibers), Moscow: Khimiya, 1985.
12. Gul', V.E., *Struktura i prochnost' polimerov* (Structure and Strength of Polymers), Moscow: Khimiya, 1971.

ISSN 1070-4272, Russian Journal of Applied Chemistry, 2007, Vol. 80, No. 7, pp. 1140–1144. © Pleiades Publishing, Ltd., 2007.
Original Russian Text © S.B. Selyanina, N.V. Selivanova, 2007, published in Zhurnal Prikladnoi Khimii, 2007, Vol. 80, No. 7, pp. 1170–1174.

MACROMOLECULAR CHEMISTRY AND POLYMERIC MATERIALS

Hydrophilic–Oleophilic Properties of Sulfate Lignin

S. B. Selyanina and N. V. Selivanova

Institute of Environmental Problems of the North, Ural Division, Russian Academy of Sciences, Arkhangelsk, Russia

Received October 2, 2006; in final form, December 2006

Abstract—Effects of extractive resinous substances, type of wood, and pH on the hydrophilic–oleophilic behavior of solid lignin recovered from sulfate delignification liquors were evaluated.

DOI: 10.1134/S1070427207070257

Pulp industry is a primary consumer of wood, the yield of the final product being as low as about 50%. The sulfate cooking provides for total utilization of spent cooking liquors. This process necessarily involves recovery of sulfate soap as micellar aggregates, followed by production of tall oil by acid treatment. In this case, kraft lignin transferred into the soap emulsion with black liquor forms an insoluble solid product [1–3]. In the presence of lignin, a stable heterogeneous system (so-called lignotall emulsion or lignin phase) is formed. According to the modern views [4, 5], the lignin phase represents an oil-in-water emulsion. Lignin tends to concentrate at the interface, screening the surface of the oil droplets distributed throughout the bulk of the liquid and thus preventing their coalescence, i.e., stabilizing the emulsion. Therefore, the stability of such systems appears to be controlled by the characteristics of the stabilizer surface [6].

In this study, we examined the hydrophilic–oleophilic behavior of kraft lignins, as one of their most important characteristics as emulsion stabilizers.

Generally, the hydrophilic–oleophilic properties of surfaces are characterized by the ratio of the work of adsorption of a substance from the hydrocarbon (oil) and aqueous phases using the Bancroft rule [7], or by the conventional Rebinder relationship [8] for saturated hydrocarbons and water.

The classical method for determination of the gas adsorption on the surface of solid lignin is the gravimetric method with the use of a McBain quartz spring balance. This method is quite descriptive, being, however, characterized by complex hardware implementation and long time of analysis. The vacuum-static method is simpler and allows analysis of several samples in parallel [9]. This method is widely used for characterization of various sorbents. However, we found no indications in the literature for its use in analysis of lignin.

The lignin samples were allowed to stand in an adsorption cell until saturation, i.e., to constant weight of the sample. The final result was obtained as an average of three replicate experiments; the data scatter did not exceed 10% relative to arithmetic mean ($P = 0.95$).

The degree of hydrophilicity α was estimated by Eq. (1):

$$\alpha = \Gamma_w/(\Gamma_w + \Gamma_h), \quad (1)$$

where Γ_w and Γ_h are the limiting adsorptions of water vapor and hexane, respectively (mol g^{-1}).

The degree of oleophilicity β was estimated as the difference

$$\beta = 1 - \alpha. \quad (2)$$

When the adsorption cell was not evacuated prior to the experiment, the degree of oleophilicity estimated from the experimental specific adsorptions of hexane and water was within 0.13–0.16, while that determined with the McBain balance was 0.53–0.58 and 0.65–0.70 in coniferous and deciduous lignins, respectively [5].

As seen from Fig. 1, preliminary evacuation of the adsorption cell does not affect the specific adsorption of water vapor on the lignin surface, being, however, a crucial factor in adsorption of hexane, which is probably due to the difference in the vapor pressure.

The specific adsorption of hexane vapor approaches the equilibrium value at a residual pressure in the ad-

sorption cell of 0.07 MPa and lower. In this case, the hydrophilicity and oleophilicity differ by no more than 10% from those obtained using the McBain balance.

Therefore, the adsorptions of water and hexane vapors can be used as parameters for characterization of lignin samples and selection of samples with remarkably different hydrophilic–oleophilic properties, to clearly elucidate the effect of the lignin origin on the stability of emulsions.

To study the effect of extractive substances on the surface properties of lignin, distilled tall oil obtained from the distillation plant of the Solombala Pulp and Paper Combine (SPPC) was added stepwise to semiconcentrated black liquor [density 1200 kg m^{-3}, dry residue 38.1%, residual gummosity (recalculated to dry residue) 0.80%] after recovery of sulfate soap until complete dissolution. Distilled tall oil was selected as an additive, because it is a pure product similar in the composition to extractive resinous substances of black liquor. Lignin was precipitated from the resulting solution by acidification with 30% sulfuric acid to pH 2.1–2.5 with heating on a water bath. Then lignin was separated by centrifugation, washed, and dried at 50±1°C, to avoid its degradation [10].

Analysis of the hydrophilic–oleophilic behavior of lignins recovered in the presence of tall oil shows (Fig. 2) that increasing concentration of extractive resinous substances in black liquor from 0.8 to 2.2% (recalculated to dry residue) decreases the hydrophilic–lipophilic ratio by more than an order of magnitude by virtue of simultaneous decrease in the hydrophilicity and increase in the oleophilicity. The dependences of the specific adsorption of water and hexane vapors on kraft lignin on the concentration of extractive resinous substances in the initial liquor are nonlinear, which is more clearly pronounced in the case of water sorption, being reflected in the hydrophilic–oleophilic ratio.

Thus, we may conclude that the presence of extractive resinous substances in black liquors causes some uncertainty in characterization of the hydrophilic–oleophilic properties of lignin recovered from them, considerably increasing the oleophilicity and decreasing the hydrophilicity.

To eliminate this uncertainty, in the subsequent experiments, lignin samples were recovered from the liquors obtained in laboratory cooking of preliminary deresined wood chips of sound wood of pendent white birch and common spruce. The deresination was carried out in two steps. In the first step, wood chips were treated with an organic solvent (ligroin) to remove a part of resin and fatty acids along with neutral compounds. Then the residual solvent was removed by steam distillation, and extraction chips were soaked in aqueous sodium hydroxide to remove oxidized substances (readily soluble in alkali) and residual resin and fatty acids.

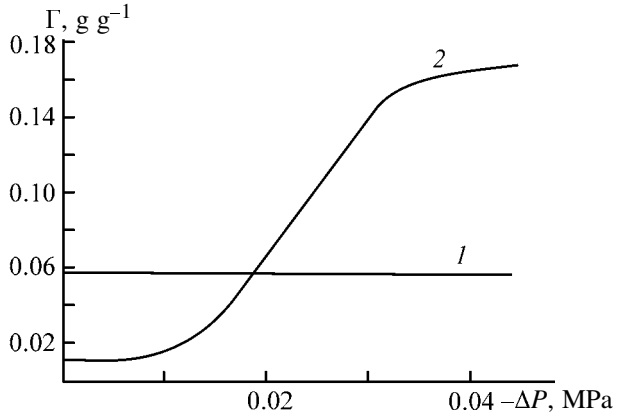

Fig. 1. Specific adsorption Γ of (*1*) water and (*2*) hexane vapor on the surface of kraft spruce lignin as a function of the rarefaction $-\Delta P$ in the adsorption cell.

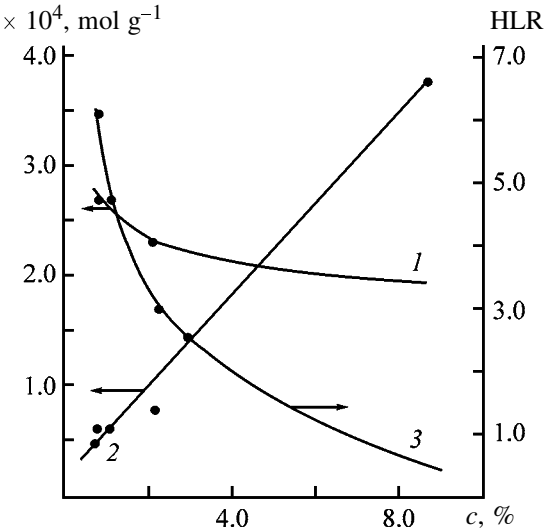

Fig. 2. Effects of the concentration of extractive resinous substances in black liquor *c* (recalculated to absolutely dry sample) on the specific adsorption of (*1*) water and (*2*) hexane vapors Γ, and on (*3*) hydrophilic–lipophilic ratio HLR in kraft lignin.

As known, lignins recovered from different kinds of wood differ considerably in the molecular weight distribution and functional composition [11], which can affect their hydrophilic–oleophilic and, therefore, emulsifying properties. The birch and spruce lignin samples recovered by the above procedure were characterized by the composition, molecular weight distribution (MWD), and hydrophilic–oleophilic properties [9, 12, 13] (Table 1, Fig. 3).

Table 1. Characteristics of spruce and birch lignin samples

Characteristic	Lignin	
	birch	spruce
Moisture content,* %	7.6	10.2
Adsorption of vapor $\Gamma \times 10^3$, mol g^{-1}:		
hexane $\Gamma_h \times 10^3$	7.6	10.2
water $\Gamma_w \times 10^3$	0.12	0.38
Hydrophilic–lipophilic ratio	53.7	17.2
Molecular weight M_w	2000	9300
Degree of polydispersity M_n/M_w	4.1	3.9
Ash content,* %	2.0	1.6
Klason lignin content, %	85.8	93.0
Elemental composition C : H : O	66.0 : 7.8 : 26.2	63.1 : 5.8 : 31.1

* Recalculated to absolutely dry sample.

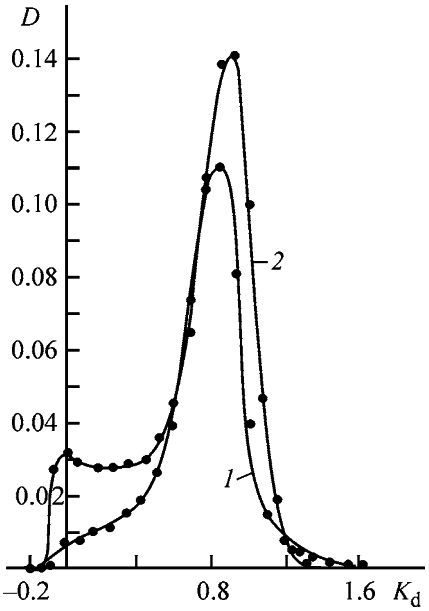

Fig. 3. Gel chromatograms of kraft lignins: (*1*) spruce and (*2*) birch. (*D*) Optical density at 280 nm and (K_d) distribution coefficient.

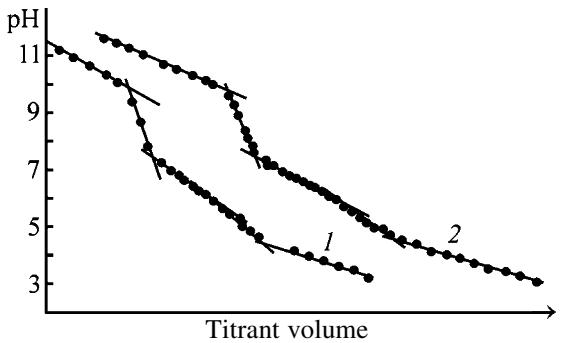

Fig. 4. Potentiometric titration curve of black liquor obtained in sulfate cooking with 0.1 HCl: (*1*) birch and (*2*) spruce.

The C, O, and H contents in our samples were well consistent with the published data obtained for similar lignins [11]. The oxygen content was found to be higher in the spruce lignin, which is due to the difference in the guaiacyl, syringyl, and *p*-hydroxyphenylpropane units in coniferous and deciduous lignins. The decreased Klason lignin content [14] in the sample recovered from birch wood can be attributed to a higher content of the acid-soluble fraction, which is typical of birch lignins.

It follows from the MWD curves (Fig. 3) that the samples in hand are polydisperse, the spruce lignin being characterized by a higher content of the high-molecular-weight fraction. As a result, spruce lignin has a higher weight-average molecular weight as compared to birch lignin (Table 1).

Differences in the composition of birch and spruce lignins are reflected in their hydrophilic–oleophilic properties. The absolute value of the adsorption of hexane vapor on higher-molecular-weight spruce lignin is higher by a factor of 3 than that on birch lignin, the adsorption of water being practically the same on both lignins. As a result, the hydrophilic–lipophilic ratio in birch lignin is higher by a factor of 3.1.

It is commonly accepted that properties of lignins are strongly affected by the recovery procedure, particularly pH. As seen from the potentiometric titration curves of black liquor (Fig. 4), substitution of the sodium ions for hydrogen in the acidic groups of kraft lignin proceeds after neutralization of excess alkali at pH 6.2–4.3. Despite the fact that, in sulfate cooking, lignin passes into the solution as various sodium compounds (lignosulfonates, lignophenolates, and lignoenolates), it appears impossible to distinguish some

Table 2. Characteristics of lignin samples recovered at various pH values

Characteristic	Lignin											
	birch						spruce					
pH of precipitation*	1.0	2.3	3.3	4.1	4.6	5.0	1.0	1.5	3.0	3.5	3.9	4.9
Moisture content,** %	4.4	7.6	8.5	9.1	8.3	4.3	4.8	10.2	10.2	9.2	11.5	4.6
Adsorption of vapor $\Gamma \times 10^3$, mol g^{-1}:												
hexane $\Gamma_h \times 10^3$	0.30	0.12	0.14	0.12	0.12	0.07	0.38	0.38	0.37	0.32	0.35	0.16
water $\Gamma_w \times 10^3$	8.90	6.44	6.50	6.33	6.17	6.17	8.28	6.55	6.50	6.55	6.55	7.00
Molecular weight M_w	2700	2000	1900	1800	1700	1170	9700	9300	8200	8500	8000	9600
Klason lignin content, %	93.4	85.8	85.2	84.0	83.8	83.8	88.2	93.0	92.5	93.5	92.3	90.7

* Measured with a laboratory pH-meter after cooling.
** Recalculated to absolutely dry substance.

sections in the potentiometric titration curves corresponding to the interaction of different groups with the acid. The solution becomes slightly turbid at about pH 6, but a precipitate can be separated only at pH 5 and below. Therefore, to study the effect of pH on the surface properties of lignin, the pH of precipitation was varied from 1 to 5 (Table 2).

Differences in the structure of native birch and spruce lignins [11] cause the need in more stringent cooking conditions for birch wood, to obtain the same degree of delignification as for spruce wood. In this case, birch lignin passes into the solution as finer species. All the spruce lignin samples have higher MW as compared to birch lignins (Table 2). It should be pointed out that, in the investigated biopolymers, the change in the weight-average molecular weight by 1000–1700 au corresponds to the change in the size of their macromolecules by 5–8 phenylpropane units. Keeping in mind the polydispersity of the investigated samples (Fig. 3), such a change in the weight-average molecular weights could not be considered as significant. Nevertheless, one could establish a fact of slight increase in MW of the samples recovered under more stringent conditions.

Analysis of the sorption characteristics of lignins shows (Table 2, Fig. 4) that, upon acidification to pH ~5, molecules having the minimal sorption capacity for hexane and increased adsorption of water are primarily recovered. In this case, the yield of lignin is rather low, and the mother liquor retains a darkbrown coloration, because of incomplete precipitation of lignin. Evidently, in this stage, sodium is replaced primarily in the phenol groups that contribute considerably to the hydrophilicity of the sample.

At pH < 4, the precipitation is more complete, and the mother liquor after recovery of lignin is light in color. In this case, lignin samples exhibit practically the same sorption capacities for both water and hexane. With decreasing pH to about 1, the adsorption of water increases in both birch and spruce lignins. The samples are highly hydrophilic, as demonstrated by the water sorption experiments. Taking into account that the molecular weights of all the investigated samples of birch and spruce lignins are similar, one may conclude that the ratio of the hydrophilic and hydrophobic fragments in the lignin molecule depends on both the functional group content and effect of modification of the lignin surface after sulfuric acid treatment.

CONCLUSIONS

(1) Lignin samples, recovered from sulfate liquors obtained in cooking of deresined wood, are characterized by an increased hydrophilic–oleophilic ratio. Increase in the content of extractive resinous substances in black liquor decreases this ratio through decreasing hydrophilicity and increasing oleophilicity of the lignin surface.

(2) The kind of wood has a considerable effect on the surface properties: birch lignin exhibits an increased sorption capacity for water vapor and decreased sorption capacity for hexane vapor, as compared to spruce lignin.

(3) The sorption capacity of lignins for hexane and water vapors depends on pH of their recovery. Lignins recovered at pH ~5 (incomplete precipitation), as well as lignins whose properties were altered by strong acid treatment, exhibit enhanced hydrophilicity.

ACKNOWLEDGMENTS

The authors are grateful to N.A. Makarevich for his help in design and organization of the experiments.

REFERENCES

1. Bogomolov, B.D., Sapotnitskii, S.A., Sokolov, O.M., et al., *Pererabotka sul'fatnogo i sul'fitnogo shchelokov: Uchebnoe posobie dlya vuzov* (Processing of Sulfate and Sulfite Liquors: A Textbook for Higher School), Moscow: Lesnaya Prom–st., 1989.
2. Chudinov, S.V., Trofimov, A.N., Uzlov, G.A., et al., *Spravochnik lesokhimika* (Wood Chemist's Handbook), Moscow: Lesnaya Prom–st., 1987.
3. *Tekhnologiya tsellyulozno-bumazhnogo proizvodstva: Spravochnye materialy* (Technology of Pulp and Paper Works: Reference Materials), St. Petersburg: Politekhnika, 2003, vol. 1, part 2.
4. Selyanina, S.B., Bogolitsyn, K.G., and Yanglyaeva, N.Zh., *Lesn. Zh.*, 2000, no. 3, pp. 123–129.
5. Selyanina, S.B., Afanas'ev, N.I., and Makarevich, N.A., *Zh. Prikl. Khim.*, 2000, vol. 73, no. 12, pp. 1986–1991.
6. Abramzon, A.A., Zaichenko, L.P., Faingol'd, S.I., et al., *Poverkhnostno-aktivnye veshchestva. Sintez, analiz, svoistva, primenenie* (Surfactants: Synthesis, Analysis, Properties, and Applications), Leningrad: Khimiya, 1988.
7. Shchukin, E.D., Pertsov, A.V., and Amelina, E.A., *Kolloidnaya khimiya* (Colloid Chemistry), Moscow: Vysshaya Shkola, 1992.
8. Rebinder, P.A., *Poverkhnostnye yavleniya, adsorbtsiya i svoistva adsorbtsionnykh sloev: Izbrannye trudy* (Surface Phenomena, Adsorption, and Properties of Adsorption Layers: Selected Works), Moscow: Nauka, 1978, pp. 74–121.
9. Baranova, V.I., *Praktikum po kolloidnoi khimii: Uchebnoe posobie dlya khimiko-tekhnologicheskikh spetsial'nostei vuzov i dr.* (Practical Course of Colloid Chemistry: A Handbook for Chemical Engineering Students), Moscow: Vysshaya Shkola, 1983.
10. Tiranov, P.P. and Bogomolov, B.D., Abstracts of Papers, *Vsesoyuznaya nauchno-prakticheskaya konferentsiya* (All-Union Scientific and Practical Conf.), 1983, pp. 28–29.
11. Karmanov, A.P., *Samoorganizatsiya i strukturnaya organizatsiya lignina* (Self-Organization and Structural Organization of Lignin), Yekaterinburg: Ural. Otd. Ross. Akad. Nauk, 2004, p. 269.
12. Sokolov, O.M., *Opredelenie molekulyarnoi massy ligninov na ul'tratsentrifuge i metodom gel'-fil'tratsii: Uchebnoe posobie* (Determination of the Molecular Weight of Lignin on an Ultracentrifuge and by Gel Filtration: Textbook), Leningrad: Lesotekh. Akad., 1978.
13. Bogolitsyn, K.B., Aizenshtadt, A.M., and Popova, N.R., *Mezhfaznye yavleniya: Uchebno-metodicheskoe posobie* (Interfacial Phenomena: Textbook), Arkhangelsk: Arkhangel'sk. Gos. Tekh. Univ., 1997.
14. Obolenskaya, A.V., El'nitskaya, Z.P., and Leonovich, A.A., *Laboratornye raboty po khimii drevesiny i tsellulozy* (Laboratory Course of Chemistry of Wood and Cellulose), Moscow: Ekologiya, 1991.

ISSN 1070-4272, Russian Journal of Applied Chemistry, 2007, Vol. 80, No. 7, pp. 1145–1150. © Pleiades Publishing, Ltd., 2007.
Original Russian Text © M.A. Krayukhina, S.A. Kozybakova, N.A. Samoilova, V.G. Babak, S.Z. Karaeva, I.A. Yamskov, 2007, published in Zhurnal Prikladnoi Khimii, 2007, Vol. 80, No. 7, pp. 1175–1180.

MACROMOLECULAR CHEMISTRY AND POLYMERIC MATERIALS

Synthesis and Properties of Amphiphilic Maleic Acid Copolymers

M. A. Krayukhina, S. A. Kozybakova, N. A. Samoilova, V. G. Babak, S. Z. Karaeva, and I. A. Yamskov

Nesmeyanov Institute of Organoelement Compounds, Russian Academy of Sciences, Moscow, Russia

Received November 9, 2006; in final form, March 2007

Abstract—New amphiphilic polymers derived from maleic acid copolymers and containing stearyl or oleyl residues were prepared. Their physicochemical properties were studied, and the possibility of using them as carriers for antifungal agents was examined with Amphotericin B as example.

DOI: 10.1134/S1070427207070269

Amphiphilic polymers (APs) contain in their chains both hydrophilic and hydrophobic groups. Many biopolymers (phospholipids, nucleic acids, proteins) are polyampholytes and amphiphiles. The association ability of APs in aqueous solutions opens prospects for using APs, e.g., in petroleum production, biotechnology, and also in production of pharmaceuticals to solubilize drugs and stabilize micro- and nanoaggregates containing bioactive substances [1]. There are two synthetic approaches to such APs: (co)polymerization of amphiphilic monomers or introduction of hydrophobic groups into hydrophilic polymers. The second approach seems preferable because of the possibility of varying the degree of hydrophobic substitution of a polymer without affecting the length of macromolecules. In this case, the hydrophobic ligand is randomly distributed along the macromolecular chain. Preparation and use of water-soluble carbon-chain APs were reported recently [2–4].

The goal of this study is synthesis of new APs based on maleic acid copolymers with *N*-vinylpyrrolidone, styrene, or ethylene by introducing into these copolymers stearyl or oleyl groups and examination of the physicochemical properties of the products and of the possibility of using them as carriers for antifungal agents:

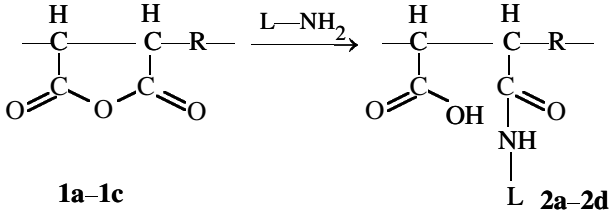

1a–**1c** **2a**–**2d**

where R = —H_2C—CH— (N, O), L = $C_{18}H_{37}$ (**a**);

R = —H_2C—CH— (C$_6$H$_5$), L = $C_{18}H_{37}$ (**b**);

R = —H_2C—CH_2—, L = $C_{18}H_{37}$ (**c**);

R = —H_2C—CH— (N, O), L = $C_{18}H_{35}$ (**d**).

It is well known [5] that copolymers of maleic acid or anhydride have a constant composition (1 : 1), with strict alternation of monomeric units in the polymer chain. The anhydride groups of the maleic anhydride fragments can react with amino groups of an introduced hydrophobic ligand under mild conditions without condensing agents. Maleic anhydride copolymers were widely used previously as a base for preparing various polymeric reagents and carriers, in particular, for developing affine sorbents [6].

EXPERIMENTAL

Copolymer of maleic anhydride with *N*-vinylpyrrolidone **1a** was prepared according to [5] (*M* 40 kDa); copolymer **1b** (*M* 50 kDa) was produced by Sterlitamak Chemical Combine; **1c** (*M* 25 kDa), by Monsanto (the United States); and stearyl- and oleylamines,

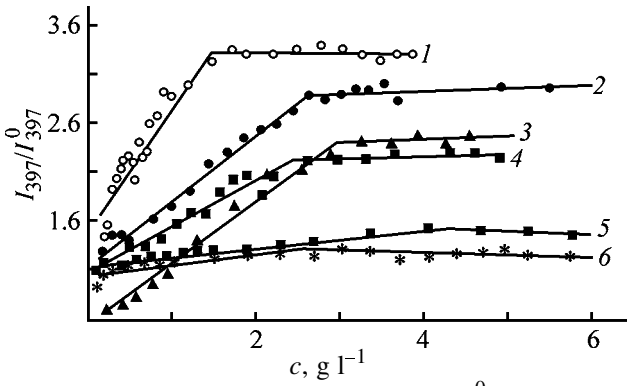

Fig. 1. Relative fluorescence intensity I_{397}/I_{397}^0 of pyrene solubilized with amphiphilic polymers **2a**–**2d** as a function of the AP concentration c. Emission wavelength 397 nm. (*1*) **2c** (DS 5%), (*2*) **2a** (DS 10%), (*3*) **2a** (DS 5%), (*4*) **2d** (DS 10%), (*5*) **2d** (DS 5%), and (*6*) **2b** (DS 5%).

by Aldrich. Pyridine (Khimspektr Limited Liability Trading Company) was purified by distillation from BaO; dimethylformamide was distilled from toluylene diisocyanate. For physicochemical studies we used deionized dust-free water. Hydrophobic ligand was introduced into polymers in an amount of 1–15 wt %.

The typical procedure for preparing AP is as follows: 3 g of copolymer **1a, 1b,** or **1c** was dissolved in 10 ml of dimethylformamide, and a solution of 0.3 g (10 wt %) of stearyl- or oleylamine in 5 ml of pyridine was added. After stirring for 2 h at room temperature, the mixture was poured with stirring into 100 ml of acetone (or chloroform for **1b, 1c**). The precipitate was filtered off and dissolved in water. The solution was filtered and dialyzed against an acetic acid solution (pH 5) and then against water, after which it was freeze-dried. Yield of polymers **2a**–**2d** 70–80%.

The structures of polymers **2a**–**2d** were confirmed by IR spectroscopy (KBr, ν, cm^{-1}): 3300 (N–H), 3200 (O–H), 1720–1730 (C=O), 1650 (C–N of pyrrolidone ring for **2a**). The characteristic frequencies of alkylamides, 1570 (C–N) and 1650 (C=O), were the most pronounced in the spectra of **2b** and **2c**.

The amount of the introduced hydrophobic ligand was confirmed by ^{1}H NMR spectroscopy (250 MHz, D_2O). Signals of stearyl residue, ppm: 0.74–0.97 (CH_3), 1.15–1.33 [$(CH_2)_{16}$], 1.58–1.61 (CH_2–N); the oleyl residue also gives a signal at 5.3 ppm (CH=CH).

It is well known that in aqueous solutions the behavior of charged AP macromolecules is affected by competing attraction (hydrophobic, van der Waals interactions, hydrogen bonds) and repulsion (Coulomb interactions) forces. The association and subsequent aggregation of APs are intensified with an increase in their concentration in solution to a threshold level, so-called critical aggregation concentration (CAC).

In this study, CAC was determined by the Wilhelmy method and by fluorescence spectroscopy with water-insoluble pyrene as a probe.

As seen from the table, CAC decreases with an increase in the degree of hydrophobic substitution of AP. As the major contribution to the formation of polymeric aggregates is made by the interaction of hydrophobic domains, an increase in the lipophilicity of a macromolecule can lead to enhancement of the hydrophobic interactions. Figure 1 shows how the relative fluorescence intensity depends on the concentrations of APs differing in the chain structure and hydrophobic ligand.

It can be noted that APs based on copolymers of *N*-vinylpyrrolidone (**2a**) and styrene (**2b**) with maleic acid, containing the octadecyl group as hydrophobic ligand (degree of substitution DS 5%), have approximately equal CAC (0.34 and 0.39 g dl^{-1}, respectively). The copolymer of ethylene with maleic acid (**2c**), with octadecyl groups introduced (DS 5%), has a more flexible macromolecular chain, with less pronounced conformation hindrance; therefore, its CAC is appreciably lower (0.7 g dl^{-1}).

Comparison of the copolymers of *N*-vinylpyrrolidone and maleic acid with various ligands (stearyl, **2a**, 5%; oleyl, **2d**, 5%) shows that the AP with the oleyl residue has a higher CAC (0.54 g dl^{-1}). Since the length of the hydrocarbon chain in the substituents in these APs is the same (C_{18}), this difference can be attributed to the higher rigidity of the ligand chain in **2d** (presence of double bond).

The dependence of the relative fluorescence intensity on the AP concentration in solution (Fig. 1) shows that, at $c \le$ CAC, two processes, association and aggregation, occur simultaneously, with the hydrophobic interactions making the major contribution to the aggregation. The further slight increase in the quantum yield of the fluorescence, continuing at $c >$ CAC, is attributable fo the continuing intermolecular aggregation.

A turbidimetric study of the stability of the associated polymeric systems at concentrations exceeding CAC revealed gradual occurrence of the further aggregation of AP particles, accompanied by coagulation and precipitation. For example, at a 2 g dl^{-1} concentration of AP **2a** (DS 15%), the precipitation started after keeping the system at room temperatrue for

12 days; with **2a** (DS 10 and 5%), it started in 13 and 16 days, respectively.

The hydrodynamic radius of AP particles in solution in CAC points was determined by dynamic light scattering (see table). As seen from the table, particles of **2a** with different degrees of substitution have similar size. At the same time, particles of the *N*-vinylpyrrolidone copolymers containing an oleyl group (**2d**) in the CAC point have a larger hydrodynamic radius, suggesting formation of an aggregate consisting of polymer macromolecules with a looser, less compact structure compared to macromolecules of **2a** with octadecyl (stearyl) residues, or of an aggregate containing a larger number of macromolecules.

A considerable increase in the weight of AP particles in solution relative to hydrolyzed polymers **1a**–**1c** was revealed by static light scattering. For example, at a concentration of AP **2a** (DS 5%) of 0.25 g dl^{-1} (below CAC), the particle weight increased by almost an order of magnitude, to 360 kDa (0.1 N NaCl).

In the Zimm diagram, we observed no curvatures of scattering indicatrices at small angles, typical of polymer systems whose polydispersity is determined by the presence of very large particles. That is, in the sample under consideration, the particle-size distribution is presumably quasiunimodal, without formation of very large aggregates.

Taking into account the fact that the aggegation can be governed not only by hydrophobic interactions, but also by the capability of carboxy and amide groups of the polymers for hydrogen bonding, we can suggest the occurrence of both intramolecular and intermolecular aggregation in the solution under consideration (0.1 N NaCl). This assumption accounts for a considerable increase in the AP particle weight. To confirm it, it was necessary to examine the rheology of AP solutions.

It is known that the interaction of hydrophobic groups affects the rheological properties of polymers. In aqueous solutions, hydrophobic groups of amphiphilic polymers containing no charged groups can favor formation of both intramolecular associates and intermolecular aggregates. The probability of coil overlap in a dilute solution is low, and therefore mainly intramolecular associates are formed. Their formation results in contraction of the polymeric coil (and hence in a decrease in its radius), which results in lower viscosity of a solution of an associating polymer compared to that of solution of the related polymer containing no associating groups. In a semidilute solution, polymer coils start to overlap, and intermolecular contacts become prevalent, which results in a sharp increase in a solution viscosity and formation of a physical gel in which polymeric chains play the role of cross-links between the aggregates.

Critical aggregation concentrations and mean hydrodynamic radii of particles of amphiphilic copolymers in CAC points

Sample	Amount of hydrophobic ligand, wt %	CAC,* g dl^{-1}	Hydrodynamic radius of particles *r*, nm
2a	2	0.58/0.60	276.7
2a	5	0.39/0.34	253.4
2a	10	0.22/0.26	255.3
2a	15	0.11/0.09	280.3
2d	5	0.50/0.41	424.7
2b	5	0.39/0.35	–
2c	5	0.17/0.20	–

* Wilhelmy method/pyrene method.

For strongly charged polymer chains, long-range Coulomb interactions of chains are prevalent and determine the rheological behavior of the system. However, in weakly charged polyelectrolytes, nonelectrostatic interactions efficiently compete with Coulomb interactions. To reveal the major factors affecting the rheological behavior of the APs under consideration in aqueous solutions, we measured the viscosity of AP solutions by capillary viscometry. The viscosity was measured in the concentration range 0.1–1.0 g dl^{-1}; the solutions whose concentration exceeded CAC were diluted.

In aqueous solutions of APs at pH 5 in the absence of a low-molecular-weight electrolyte, the isotherms of the reduced viscosity had a shape classical for polyelectrolytes: With dilution, the viscosity increased owing to polyelectrolytic swelling of the polymer macromolecules. With increasing degree of hydrophobic substitution, the effect of polyelectrolytic swelling became less pronounced: The slope of the linear portion of the isotherms relative to the abscissa decreased.

For AP solutions containing a low-molecular-weight salt (0.1 N NaCl), at the same pH, we obtained the reduced viscosity isotherms and calculated the intrinsic viscosity [η] of the amphiphilic copolymer samples by extrapolation to infinite dilution:

Sample	**1a**	**2a**	**2a**	**2a**	**2a**	**2a**
DS, wt %	0	1	2	5	10	15
[η], dl g^{-1}	0.17	0.23	0.25	0.36	0.44	0.48

As seen from the above data, with an increase in the degree of hydrophobic substitution (in the series

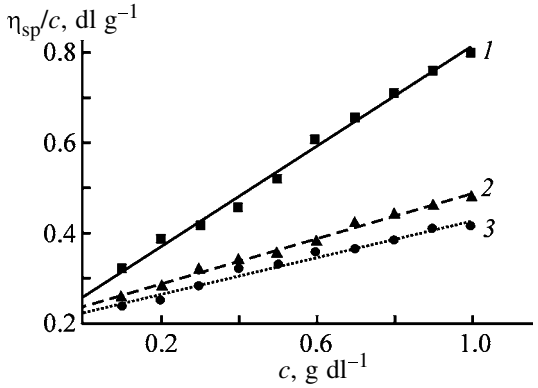

Fig. 2. Isotherms of reduced viscosity η_{sp}/c vs. AP concentration c in solution: (*1*) **2a** (DS 0), (*2*) **2a** (DS 5%), and (*3*) **2a** (DS 10%).

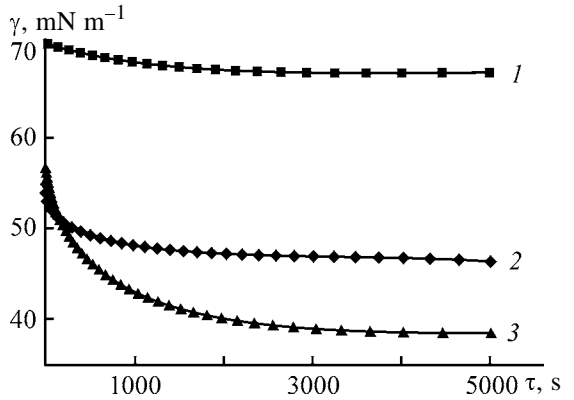

Fig. 3. Variation of the surface tension γ with time τ for APs with different nature of macromolecular chain. AP concentration 0.3 g dl^{-1}. (*1*) **2c** (DS 5%), (*2*) **2b** (DS 5%), and (*3*) **2a** (DS 5%).

of AP **2a**) [η] increased, indirectly suggesting an increase in the polymer coil size. Since in our study the Coulomb (electrostatic) interactions were not decisive, this trend should be attributed to changes in the nonelectrostatic interactions.

However, an increase in the amount of hydrophobic groups (and hence enhancement of hydrophobic interactions) should make the macromolecular coil more compact and thus decrease the hydrodynamic radius of the particle and the viscosity. The opposite trend we observed can be accounted for as follows: With an increase in the degree of hydrophobic substitution of carboxy groups in AP in the initial aqueous solutions, at concentrations above CAC, strong intermolecular aggregates were formed. These aggregates were not broken down under the conditions of dilution and shear deformations to which the system was subjected in the course of measurements with a capillary viscometer. The size of these aggregates and, apparently, their strength increased with an increase in the degree of hydrophobic substitution of AP, i.e., the major factors determining the hydrodynamic state of AP particles in solutions were hydrophobic intermolecular interactions, and also the presence of a complex network of hydrogen bonds between macromolecules. In other words, the rheological behavior of the APs in solution at pH 5 is determined by the integral effect of the above-indicated factors on the system.

To eliminate the effect exerted on the association by hydrogen bonds involving carboxy groups, we performed an experiment in which viscometric measurements were performed at the same ionic strength of the solution (0.1 M) in a glycine buffer (pH 9), in which the carboxy groups of the maleic acid units of the copolymer were virtually completely ionized. The reduced viscosity isotherms we obtained are shown in Fig. 2. As can be seen, the outflow pattern observed with AP solutions in the buffer with pH 9 differs from that observed with the solutions in 0.1 M NaCl with pH 5: With an increase in the degree of hydrophobic substitution, the slope of the isotherms decreases, i.e., the viscosity of the systems is the lower, the higher the degree of substitution. In infinitely dilute solutions (extrapolation to zero concentration), the effect of the hydrophobic substituent on the polymer particle size is levelled off: The intrinsic viscosities of the starting unmodified polymer **1a** and its hydrophobic derivatives **2a** with DS 5 and 10% are close.

Thus, at pH 9 in semidilute AP solutions we revealed the effect exerted on the hydrodynamic state of the system by hydrophobic interactions, namely, the dominating role of these interactions in the molecular aggregation of AP.

Self-organizing systems of water-soluble amphiphilic polymers are adsorbed on the water|air phase boundary, decreasing the surface tension of water. The driving force of such adsorption is hydrophobic interaction of the hydrophobic segments of polymer macromolecules with the air phase, accompanied by an increase in the entropy of the system due to break of the ordered structure of hydration shells formed around polymer chains. Figure 3 shows typical surface tension isotherms for a series of APs with the same degree of substitution. Two portions can be distinguished in these curves: the first portion in which the surface tension sharply decreases and the second portion in which the surface tension decreases more slowly and flattens out.

In the first portion of the isotherm, the polymer macromolecules take a more unfolded conformation on the interface and are adsorbed on it, with the hydrophobic groups oriented toward the nonpolar phase (air). Further decrease in the surface tension during

a longer time is controlled by the diffusion of macromolecules and their aggregates (associates) from the bulk of the solution to the phase boundary surface, their adsorption, and diffusion of surface-active segments of the adsorbed macromolecules inside the adsorption layer.

The APs under consideration showed higher interphase activity compared to the starting polymers without hydrophobic substituents. As expected, with an increase in the AP concentration and in the degree of hydrophobic substitution, the surface tension of polymer solutions decreased. In particular, for samples **2a** (0.2 g dl^{-1} in water) with DS 5, 10, and 15 wt %, the surface tension was 64.0, 62.0, and 61.0 mN m^{-1}, respectively.

It should be noted that the surface tension increased with an increase in the hydrophobicity of the macromolecular chain (Fig. 3). For example, the AP based on copolymer **2b** of maleic acid with styrene showed higher surface tension than the AP based on the more hydrophilic copolymer of *N*-vinylpyrrolidone with maleic acid (**2a**). Apparently, in **2b** the intramolecular hydrophobic aggregation occurs via hydrophobic interaction involving both hydrocarbon substituents and hydrophobic domains of the chain (styrene residues). At such aggregation, the macromolecule is adsorbed on the interface by its core, with the hydrophilic sites oriented inside the polar phase (water). The same reasoning is apparently applicable also fo AP **2c**.

In the case of **2a**, as already mentioned, the interphase adsorption of the macromolecules apparently occurred via hydrophobic interactions of hydrocarbon ligands with the air phase; as a result, the surface tension was lower compared to polymers **2b** and **2c**. From the viewpoint of thermodynamics, such adsorption mechanism is more favorable energetically for the "looser" macromolecule of **2a** containing, along with maleic acid residues and hydrophobic ligand, also *N*-vinylpyrrolidone fragments.

Thus, the surface properties of the samples correlated with their composition: higher interphase activity was exhibited by more hydrophobic samples whose higher hydrophobicity was determined both by the higher content of hydrophobic ligand and by the contribution from the hydrophobic comonomer (styrene and, to a lesser extent, ethylene).

Preparation of stable foams and emulsions is extremely important for their use in various branches of industry. Amphiphilic polymers decreasing the surface tension favor formation of foams and can act as foam and emulsion stabilizers.

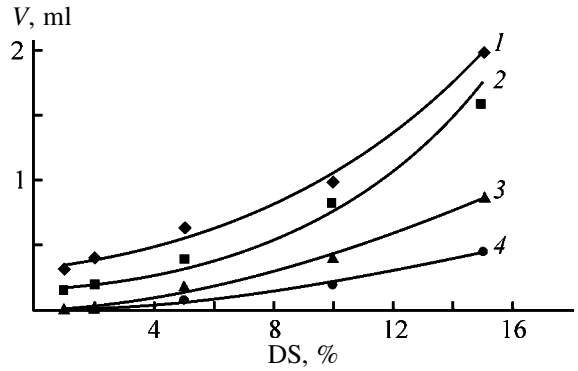

Fig. 4. Foam formation (foam volume *V*) as a function of the degree of substitution DS of amphiphilic copolymer **2a** with the hydrophobic ligand. Time, min: (*1*) 0, (*2*) 15, (*3*) 210, and (*4*) 1590.

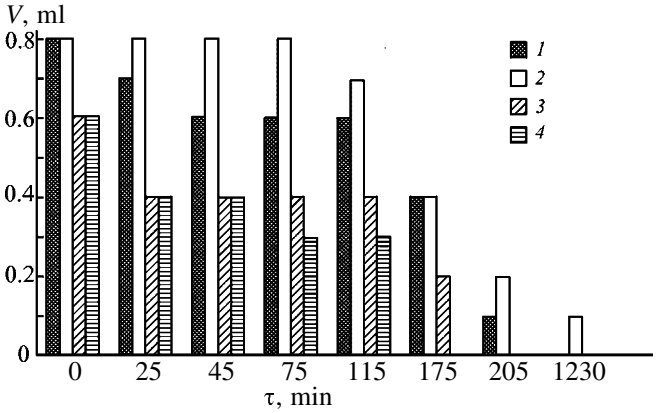

Fig. 5. Data on foam stability for copolymer **2d** (DS 5%) at its different concentrations. (*V*) Foam volume and (τ) time. *c*, g dl^{-1}: (*1*) 0.5, (*2*) 0.25, (*3*) 0.17, and (*4*) 0.08.

As expected, the foaming power of APs increased with an increase in the content of the hydrophobic ligand (Fig. 4). This parameter also depended on the AP concentration (Fig. 5).

The set of properties of the suggested amphiphilic polymers allows their use, e.g., for preparing water-soluble noncovalent conjugates with Amphotericin B antibiotic (AmB), which is virtually insoluble in water. The procedure for evaluating the antifungal activity (AA) is described elsewhere [7]. Figure 6 shows how the antifungal activity of the conjugates of the amphiphilic copolymers with Amphotericin B varies with time. It is seen that these conjugates affect the micellar growth of *Fusarium oxysporum* plant pathogen.

The activity of the polymer unmodified with the antibiotic, compared to complexes of AP with AmB, was relatively low and tended to decrease with time. Polymeric fungicides derived from **2a** (DS 2%) and **2c** (DS 5%) showed the highest antifungal activity within

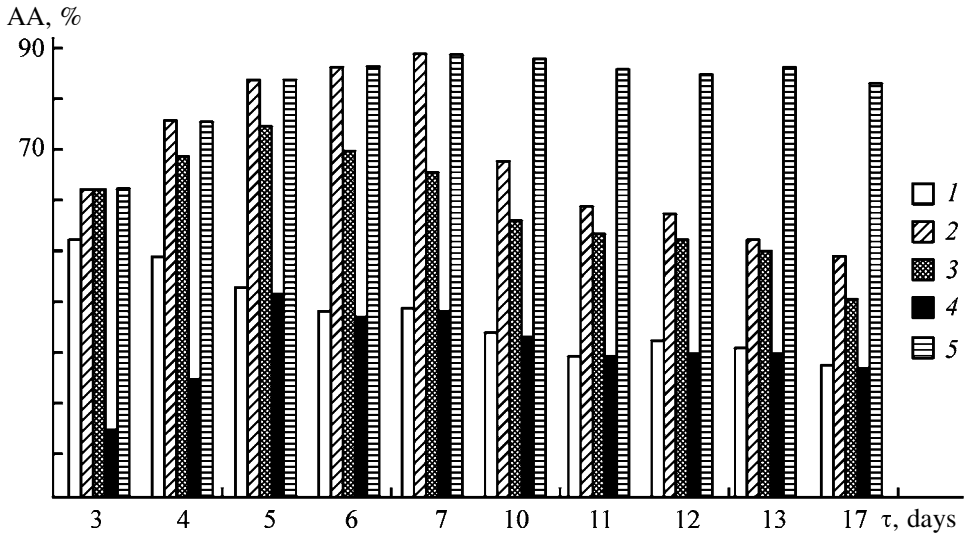

Fig. 6. Antifungal activity AA of polymeric conjugates of Amphotericin B (AmB) toward *Fusarium oxysporum* as a function of time τ. (*1*) Conjugate of hydrolyzed polymer **1a** with AmB (**1a**–AmB), (*2*) **2a** (DS 2%)–AmB, (*3*) **2a** (DS 5%)–AmB, (*4*) **2b** (DS 5%)–AmB, and (*5*) **2c** (DS 5%)–AmB. AmB content of complexes with amphiphilic copolymers 0.5 wt %.

the first seven days of the experiment. Then AA of **2a** (DS 2%)–AmB and **2a** (DS 5%)–AmB decreased to 46.8 and 38.3%, respectively (by the 17th day), whereas polymeric fungicide **2c** (DS 5%)–AmB showed high activity (~80%) up to the end of the experiment. Polymeric fungicide **2b** (DS 5%)–AmB suppressed the micellar growth to a considerably lesser extent; its AA by the 17th day was similar to that of **1a**–AmB (~25%). Higher activity of **2c** (DS 5%)–AmB is apparently associated with the faster release of AmB from the polymer matrix, which provided higher AmB concentration in the system.

CONCLUSION

New amphiphilic polymers, hydrophobically modified copolymers of maleic acid with *N*-vinylpyrrolidone, styrene, and ethylene, show much promise.

REFERENCES

1. Lin, S.-S., Chen, K.-S., and Run-Chu, L., *J. Control. Release*, 2000, vol. 68, pp. 343–350.
2. Torchilin, V.P., Levchenko, T.S., Whiteman, K.R., et al., *Biomaterials*, 2001, vol. 22, no. 15, pp. 3035–3044.
3. Volpert, E., Selb, J., and Candau, F., *Polymer*, 1998, vol. 39, no. 5, pp. 1025–1033.
4. Vilemson, A.M., Kuskov, A.N., Shtil'man, M.I., et al., *Biokhimiya*, 2004, vol. 69, no. 6, pp. 621–629.
5. Conix, A., Smets, G., and Johnson, B., *J. Polym. Sci.*, 1955, vol. 15, no. 79, pp. 221–229.
6. Samoilova, N.A., Krayukhina, M.A., and Yamskov, I.A., *J. Chromatogr. B*, 2004, vol. 800, pp. 263–269.
7. Charvalos, E., Tsatsakis, A., Tsatzarakis, M., et al., *Mycopathologia*, 2001, vol. 153, pp. 15–19.

ISSN 1070-4272, Russian Journal of Applied Chemistry, 2007, Vol. 80, No. 7, pp. 1151–1153. © Pleiades Publishing, Ltd., 2007.
Original Russian Text © E.V. Novikova, V.M. Smychenko, A.A. Iozep, 2007, published in Zhurnal Prikladnoi Khimii, 2007, Vol. 80, No. 7, pp. 1181–1183.

MACROMOLECULAR CHEMISTRY AND POLYMERIC MATERIALS

Sulfation of Dextran with Chlorosulfonic Acid in Organic Solvents

E. V. Novikova, V. M. Smychenko, and A. A. Iozep

St. Petersburg State Academy of Pharmaceutical Chemistry, St. Petersburg, Russia

Received November 7, 2006; in final form, March 2007

Abstract—Solutions of chlorosulfonic acid in dichloroethane and formamide are suggested for incorporation of sulfo groups into macromolecules of polysaccharides. The influence of temperature, reaction duration, and reactant ratio on the yield of sulfated dextran and also the influence of the reaction conditions on hydrolytic stability of the polymer were studied.

DOI: 10.1134/S1070427207070270

Polysaccharides containing sulfo groups are widely used in medicine. Among the existing procedures of production of these valuable polymers, the best known procedure is sulfation of polysaccharides with solutions of sulfuric anhydride in organic solvents or its complexes with tertiary amines, pyridine, and other related bases [1]. However, SO_3 should either be prepared from sulfurous anhydride or desorbed from oleum, which complicates the process equipment and makes the process hazardous. In this connection, chlorosulfonic acid produced on the industrial scale and widely used in synthesis of various drugs (saccharin, thrombovar, sulfanilamides, etc.) is of great interest. Chlorosulfonic acid found application for production of dextran sulfate [2]. However, that study involved the use of toxic pyridine [maximum permissible concentration (MPC) 5 mg m^{-3}], whose exhaustive removal from the target product presents difficulties.

The aim of this study was to develop a procedure of sulfation of polysaccharides with chlorosulfonic acid in the medium of less toxic (MPC 10 mg m^{-3}) and readily removable 1,2-dichloroethane (DCE) in the presence of formamide (FA).

EXPERIMENTAL

Chemical modification of polysaccharides was performed by the scheme

$$[C_6H_7O_2(OH)_3]_n$$
$$\xrightarrow{HSO_3Cl} [C_6H_7O_2(OH)_2(OSO_3H)]_k[C_6H_7O_2(OH)_3]_{n-k}$$
$$\xrightarrow{MOH} [C_6H_7O_2(OH)_2(OSO_3M)]_k[C_6H_7O_2(OH)_3]_{n-k},$$

where M is Na or K.

Sulfation of polysaccharides was studied by the example of the reaction of dextran with chlorosulfonic acid.

A suspension of polysaccharide in a mixture of DCE and FA was stirred for 1 h at room temperature; then, a solution of chlorosulfonic acid in DCE was added, and the mixture was heated at 35–65°C for 1–4 h. After the reaction completion, the mixture was neutralized with a solution of potassium hydroxide and dialyzed against water to remove low-molecular-weight impurities. The dialyzate was concentrated in a vacuum, and the product was precipitated with ethanol. The precipitate was washed with ethanol and dried in a vacuum.

The reaction product was a white amorphous powder soluble in water and insoluble in ethanol.

In the IR spectrum of dextran sulfate, the absorption bands at 1250 cm^{-1} can be assigned to stretching modes of sulfo group $\nu_{S=O}$ [3].

The degree of sulfation C_s (number of sulfo groups per monosaccharide unit) was evaluated from the results of conductometric titration and acid hydrolysis of sulfo groups [4].

An attempt of dextran sulfation with chlorosulfonic acid in DCE without FA at 3–5°C by the procedure developed previously for sulfuric anhydride [4] resulted in tarring of the reaction mixture. A decrease in temperature of the reaction mixture to –5°C allowed us to avoid polymer blackening, but C_s appeared to be 3 times lower than that after the reaction

Degree of sulfation of dextran C_s at various times and FA : chlorosulfonic acid ratios (T = 50°C)

Run no.	τ, h	FA : chlorosulfonic acid molar ratio	Degree of sulfation C_s
1	1	5 : 1	0.22
2	2	5 : 1	0.31
3	3	5 : 1	0.42
4	4	4 : 1	0.64
5	4	8 : 1	0.51
6	4	12 : 1	0.44
7	4	15 : 1	0.22
8	4	20 : 1	0.16

with sulfuric anhydride under the similar conditions (0.24 against 0.79).

This result may be due to the fact that active species in sulfation of alcohols with chlorosulfonic acid in DCE is sulfuric anhydride [5] formed by dissociation of chlorosulfonic acid:

$$HSO_3Cl \rightleftarrows SO_3 + HCl.$$

Apparently, in nonpolar DCE the degree of dissociation is low; therefore, sulfation proceeds slowly, and at temperatures above zero chlorosulfonic acid decomposes the polysaccharide.

Addition of formamide, which forms a complex with sulfuric anhydride, promotes dissociation of chlorosulfonic acid. In this case, the probable active species in the sulfation of the polysaccharide are both sulfur trioxide and its complex with formamide.

The use of formamide allowed the temperature of dextran sulfation with chlorosulfonic acid to be increased to 50°C without tarring of the reaction mixture. However, the rate of dextran sulfation by this procedure is lower than the rate of the similar process with sulfur trioxide in DCE. For example, the use of sulfuric anhydride allows preparation of the polymer with C_s = 0.79 at 5°C, and in the case of chlorosulfonic acid C_s is 0.64 at 50°C. This is apparently caused by the fact that the active species in sulfation of the polysaccharide with chlorosulfonic acid in DCE–FA is mainly the complex FA–SO_3, which is less active than free SO_3. The complex FA–SO_3 readily dissociates, but in the presence of a large excess of FA dissociation of the complex is suppressed, which results in decreased concentration of free SO_3 and lower reaction rate.

To prove this assumption, we studied the influence of the chlorosulfonic acid : formamide ratio on the amount of sulfo groups incorporated into the polymer. The results are presented in the table.

We found that, with increasing amount of formamide N_{FA} from 5 to 20 mol per mole of chlorosulfonic acid, C_s decreases from 0.64 to 0.16. The dependence is linear:

$$C_s = -0.033N_{FA} + 0.7894; \quad R^2 = 0.9388, \ n = 5.$$

The procedure we suggest allows the reaction to be performed in a wide temperature range without tarring of the reaction mixture. In addition, we studied the effect of temperature on the amount of sulfo groups incorporated into the polymer.

As expected, with increasing reaction temperature from 35 to 65°C C_s increases; however, because of possible degradation of the polymer most of the experiments were performed at 50°C.

Variation of sulfation duration τ in the range from 1 to 4 h also allows incorporation of different amounts of sulfo groups into the polymer (see table):

$$C_s = 0.148\tau + 0.022; \quad R^2 = 0.974, \ n = 4.$$

One of the most important requirements in the development of a procedure for modification of polysaccharides is avoiding their depolymerization. Under the suggested conditions of polysaccharide sulfation, chlorosulfonic and hydrochloric acids can promote rupture of glycoside bonds of the polymer, especially under heating. In this connection, we performed a comparative analysis of dextran and dextran sulfate by gel chromatography.

Commercial dextran is a mixture of fractions with various molecular weights and cannot be used for such a comparison. Therefore, it was fractionated with ethanol [6], and the homogeneity of fractions was estimated by gel chromatography on a column packed with Sephadex G-200. The eluate was collected in portions and analyzed quantitatively by the photometric method based on a color reaction of sugars in the presence of sulfuric acid [6].

The homogeneous fraction of dextran was sulfated with chlorosulfonic acid by the procedure we developed, at 50°C for 4 h at the molar ratio FA : chlorosulfonic acid = 5 : 1. The product was isolated and analyzed as described above. We obtained a sample of dextran sulfate containing 0.35 sulfo group per monomer fragment of the polysaccharide.

The results of gel chromatography of the homo-

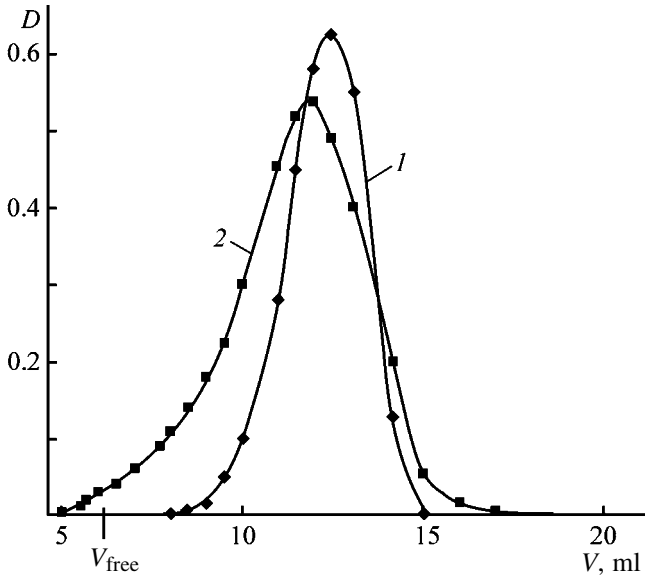

Fig. 1. Gel chromatogram of homogeneous fraction of dextran (*1*) before and (*2*) after sulfation. (*D*) Optical density and (*V*) eluate volume.

geneous fraction of dextran and its sulfated derivative are presented in the figure. As seen from the gel chromatograms, sulfation of dextran with chlorosulfonic acid does not distort the homogeneity of the fraction, which indicates that the polysaccharide does not degrade in the process.

CONCLUSIONS

(1) Chlorosulfonic acid in the formamide–dichloroethane medium can be used for sulfation of polysaccharides without their degradation.

(2) Addition of formamide to the reaction mixture allows sulfation of polysaccharides at 35–65°C; the maximum degree of sulfation is observed at the formamide : chlorosulfonic acid ratio equal to 5 : 1.

(3) The obtained dependences of the degree of sulfation on the reaction duration and amount of formamide allow control over the amount of sulfo groups incorporated into the polymer.

REFERENCES

1. Bochkareva, T.P., Passet, B.V., and Popov, K.R., *Khim. Geterotsikl. Soedin.*, 1987, no. 10, pp. 1353–1359.
2. Mahner, C., Lecner, M.D., and Nordmeter, E., *Carbohydr. Res.*, 2001, vol. 331, pp. 203–206.
3. Gordon, A.J. and Ford, R.A., *The Chemist's Companion. A Handbook of Practical Data, Techniques, and References*, New York: Wiley, 1972.
4. USSR Inventor's Certificate no. 1 420 908.
5. Chizhik, S.M., Passet, B.V., Musakin, A.P., and Smirnov, E.V., *Zh. Org. Khim.*, 1974, vol. 10, no. 9, p. 1908.
6. *Methods in Carbohydrate Chemistry*, Bemiller, R.L., Ed., vol. 6: *General Carbohydrate Methods*, New York: Academic, 1972.

ISSN 1070-4272, Russian Journal of Applied Chemistry, 2007, Vol. 80, No. 7, pp. 1154–1159. © Pleiades Publishing, Ltd., 2007.
Original Russian Text © A.V. Pestov, N.A. Zhuravlev, Yu.G. Yatluk, 2007, published in Zhurnal Prikladnoi Khimii, 2007, Vol. 80, No. 7, pp. 1184–1189.

MACROMOLECULAR CHEMISTRY AND POLYMERIC MATERIALS

Synthesis in a Gel as a New Procedure for Preparing Carboxyethyl Chitosan

A. V. Pestov, N. A. Zhuravlev, and Yu. G. Yatluk

Postovskii Institute of Organic Synthesis, Ural Division, Russian Academy of Sciences, Yekaterinburg, Russia
Institute of Solid State Chemistry, Ural Division, Russian Academy of Sciences, Yekaterinburg, Russia

Received October 10, 2006; in final form, January 2007

Abstract—A fundamentally new procedure of synthesis of carboxyethyl chitosan in a physical gel, ensuring higher degree of substitution at lower temperatures and lower consumption of time and chemicals, compared to the existing procedures, was developed. The structure of the resulting products was examined by diffuse reflection IR and ^{1}H NMR spectroscopy in solutions and also ^{1}H and ^{7}Li broad line NMR.

DOI: 10.1134/S1070427207070282

Chitosan, a natural amino polysaccharide, has a unique set of useful characteristics, such as environmental safety, biological activity, and high sorption characteristics and therefore finds wide use [1–2]. With respect to these characteristics and applications, chitosan derivatives are highly competitive with the initial polymer and in some cases surpass it. For example, carboxyethyl chitosan (CEC) has a number of additional useful characteristics: solubility in water in a wide pH range [3], excellent antioxidant characteristics, significant antimutagenic activity [4], high sorption selectivity to transition metal ions [5], and better biodegradability [6] than chitosan proper. CEC turned out to be a suitable mediator for transport of hydrophilic drugs through the skin [7] or a substrate for introduction of nitrogen oxide for medical purposes [8].

Well-known methods of synthesis of this compound, based on addition of acrylic acid (AA) and its derivatives, have certain drawbacks. When using AA in a dilute solution of chitosan (concentration approximately 0.5–1%), significant time expenditures are required; in this case, the degrees of substitution (DS) remain low [6]. An increase in the concentrations of chitosan and AA decreases the synthesis duration, but DS remains less than 1 [9]. An increase of the reactivity of acrylic reactant by using it as ethyl ester does not solve the problem, since in this case the degree of substitution equal to 1 is reached only in 240 h (in so doing, the product should be saponified) [10]. The common drawback of the above procedures is the need to use dilute solutions (due to low concentration of chitosan solutions in aqueous acids and limited solubility of methyl or ethyl acrylate in water), which requires large consumption of solvents (water or aqueous methanol) and decreases the product yield per unit volume of the apparatus. Thus, the existing procedures show little promise for commercial use.

EXPERIMENTAL

The following chemicals were used: chitosans Sonat (degree of deacetylation DD = 0.84, molecular weight MW = 250 kDa, ash residue 0.19%), Aldrich low (DD = 0.84, MW = 40 kDa), Aldrich medium (DD = 0.91, MW = 200 kDa); AA, potassium hydroxide, and lithium, sodium, potassium, and cesium carbonates of analytically pure grade. The degree of deacetylation was estimated by ^{1}H NMR spectroscopy, and the molecular weight, viscometrically by the procedure described in [11].

The ^{1}H NMR spectra of the mother liquors and model compounds in D_2O (reference DSS) were recorded on a Bruker DRX 400 spectrometer; the ^{1}H and ^{7}Li broad line NMR spectra, on an upgraded Tesla BS-477 spectrometer; and the IR diffuse reflection spectra, on a Perkin–Elmer Spectrum-One spectrometer. The C,H,N analysis was performed on a Perkin–Elmer automatic analyzer. The thermograms were obtained on a Netzsch STA-409PC derivatograph.

The synthesis was performed by three procedures:

(1) 3.3 g (0.02 mol) of chitosan was dissolved with stirring in 230 ml of water containing 2.7 ml (0.04 mol) of AA. The solution was heated with continuous stirring at 60°C for 24 h, cooled, and 2.24 g

of potassium hydroxide in 20 ml of water was added. The product was precipitated with acetone and dried in a vacuum at 25°C to constant weight.

(2) A mixture of 3.3 g (0.02 mol) of chitosan and 2.7 g (0.04 mol) of AA in 11 ml of water was kept at room temperature until a gel formed, heated at a required temperature for a required time, and cooled; then, 80 ml of 2.8% aqueous potassium hydroxide was added. The product was precipitated with acetone and dried in a vacuum at 25°C to constant weight.

(3) 0.33 g (0.002 mol) of chitosan was added to 20 ml of water in which 0.14 ml (0.002 mol) of AA was preliminarily dissolved. 0.54 ml (0.008 mol) of AA was dissolved in 10 ml of water, and 0.0046 mol of appropriate alkali metal (lithium, sodium, potassium, or cesium) carbonate was added. After the release of carbon dioxide, the resulting mixture was added to the chitosan solution, stirred, and allowed to stand at 60°C for 2 days. The product was precipitated with acetone, reprecipitated two times, and dried in a vacuum at 25°C to constant weight.

The degrees of substitution of the resulting products, determined from the ^{1}H NMR spectra (total DS, degree of monosubstitution DS_m, and degree of disubstitution DS_d), were evaluated by the formulas

$$DS = (m + 2n)/(1 - DD + m + n),$$

$$DS_m = m/(1 - DD + l + m + n),$$

$$DS_d = 2n/(1 - DD + l + m + n),$$

where m is the mole fraction of monocarboxyethylated glucosamine units; n, mole fraction of dicarboxyethylated glucosamine units; and l, mole fraction of glucosamine units.

The signal assignment and evaluation of m, n, and l from the corresponding integral intensities were performed according to [9] (due to the high viscosity of the solutions, the spectra were recorded in D_2O/DCl_{conc} at 343 K, polymer concentration 15 mg ml^{-1}).

The degree of substitution was also determined by elemental analysis of the resulting products using the formula

$$DS = [(n_C/n_N)_{product} - (n_C/n_N)_{chitosan}DS_{an}]/3,$$

where n_C/n_N is the molar ratio of elements in the product and in the initial chitosan, respectively.

Initially, to prepare the product with a higher degree of substitution, i.e., to prevent deactivation of amino groups of chitosan due to formation of the ammonium salt, we neutralized a part of AA with alkali metal carbonates (60°C, 48 h). Thus, in fact chitosan was treated with a mixture of AA and the corresponding acrylate, which increased pH of the solution:

M_2CO_3	Without base	Li	Na	K	Cs
DS*	0.44	0.33	0.31	0.33	0.37

* Only monosubstitution was observed.

As seen from these data, with increasing pH the degree of substitution decreases; in this case, the type of the base does not noticeably affect its value. This fact indicates that the reactivity of AA decreases faster than increases the nucleophilicity of the amino group of chitosan. Thus, the total reactivity of AA and ammonium salt of chitosan is higher than the total reactivity of the acrylate and amino group of chitosan, i.e., partial neutralization of AA does not give a positive effect.

The principal improvement of the process is parallel increase in the concentrations of AA and chitosan. Considering valuable characteristics of CEC and the lack of published data on convenient and cost-efficient procedures of its synthesis, we suggested a fundamentally new procedure of polymer-analogous transformations by the reaction of chitosan with acrylic acid in mixtures with high concentration of reactants, i.e., synthesis in a gel. Chitosan was modified by the scheme

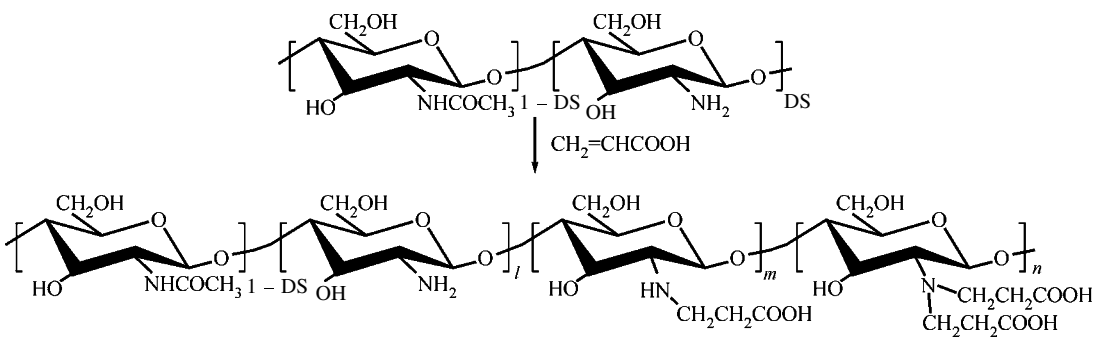

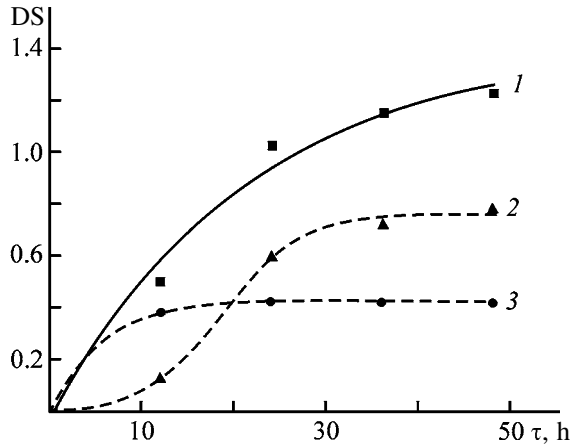

Fig. 1. Degree of substitution DS as a function of duration of chitosan treatment with AA τ at a ratio of 1 : 5 at 50°C. Degree of substitution: (*1*) total, (*2*) DS_d, and (*3*) DS_m.

Table 1. Carboxyethylation conditions and degree of substitution of the isolated product

AA : chitosan ratio	*T*, °C	τ, h	DS_m	DS_d	DS_{tot}
Increase in temperature					
2 : 1	50	12	0.49	0.2	0.69
2 : 1	70	12	0.63	0.49	1.12
2 : 1	90	12	0.66	0.68	1.34
Increase in AA excess					
2 : 1	50	24	0.50	0.46	0.96
3 : 1	50	24	0.48	0.58	1.06
4 : 1	50	24	0.41	0.60	1.11
Increase in chitosan concentration					
2 : 1 (1%)	60	24	0.31	0	0.31
2 : 1 (10%)	60	24	0.62	0.26	0.88
2 : 1 (20%)	60	24	0.52	0.44	0.96
5 : 1 (20%)	60	24	0.45	0.87	1.32
Twofold treatment					
2 : 1+2 : 1	70	12+12	0.55	0.9	1.45
5 : 1+5 : 1	70	24+24	0.46	1.08	1.54
5 : 1+5 : 1	90	12+12	0.51	0.97	1.48
Chitosan brand					
2 : 1 (Aldrich low)	70	12	0.66	0.55	1.21
2 : 1 (Aldrich medium)	70	12	0.62	0.58	1.20
2 : 1 (Sonat)	70	12	0.63	0.49	1.12

Contrary to the existing methods, we suggest to perform the reaction at a concentration of approximately 20%. In this case, the reaction mixture is a rigid gel in which this conversion is realized under heating. After the reaction completion, the mixture was treated with aqueous alkali and CEC was isolated in the form of the corresponding salt.

Table 2. Degree of substitution of CEC, according to ^{1}H NMR data and elemental analysis (EA)

Sample no.	Found, %			DS according to	
	C	H	N	EA	^{1}H NMR
1	41.45	5.81	5.86	0.61	0.51
2	39.94	5.52	4.70	1.15	1.1
3	39.49	5.02	4.43	1.30	1.15
4	38.90	4.70	4.11	1.57	1.45

It is seen from the dependence of the degree of substitution via nitrogen on the duration of chitosan treatment with AA (DS was determined by ^{1}H NMR [9]) that with increasing reaction duration the degree of substitution increases (Fig. 1); in this case, the degree of monosubstitution has a limit of saturation after 12 h of treatment. The subsequent increase in the total degree of substitution is caused only by addition of AA to the already carboxyethylated amino groups. It is likely that further formation of the disubstitution product is limited by the long-chain nature of the polymeric reagent (interaction between neighboring units, configuration, conformation of molecules in gel).

The influence of other reaction parameters on the degree of substitution of the product is presented in Table 1. Heating accelerates the addition reaction. An increase in the molar excess of AA increases the degree of substitution insignificantly. At a higher temperature this difference is leveled out. Passing from the solution to gel (increase in the chitosan concentration) abruptly increases the degree of substitution. Twofold treatment provides the highest DS. On the whole, to reach the degree of substitution of the order of 1, it will suffice to use a twofold molar excess of AA. The result of the process is only slightly influenced by particular brand of chitosan.

The degree of substitution determined by elemental analysis is somewhat higher (by 4–16%), which suggests partial addition via hydroxy groups (Table 2).

An important feature of this transformation is the occurrence of side processes, which to a certain extent prevent the addition process and affect the structure of the resulting product.

The ^{1}H NMR data for mother liquors suggest that the side products are β-hydroxypropionic acid and 2,2-dicarboxydiethyl ether (correlation of signals was performed by comparison with the spectra of model

compounds), i.e., water molecules are added to AA molecules. The occurrence of these reactions results in no-purpose consumption of AA and, taking into account the law of mass action, restricts the possibility of its addition. The side process in conversion of the polymer is formation of a small amount of bridging amide bonds; therefore, the crude product is insoluble in water:

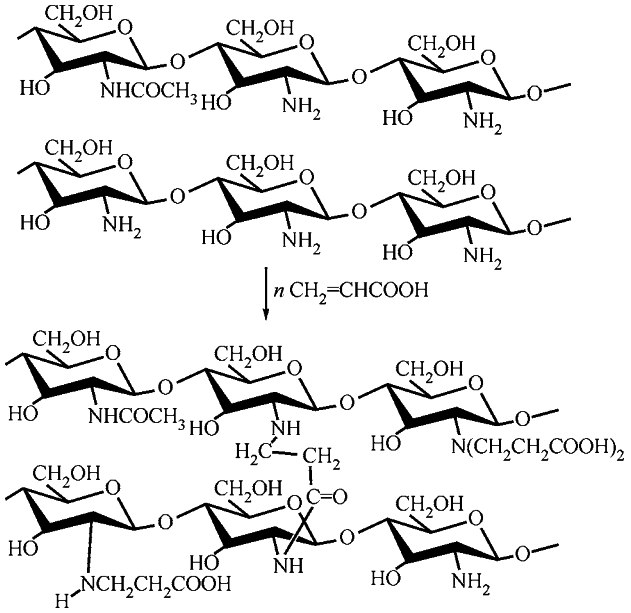

To break the cross-links of the macromolecules, the product isolation should involve treatment with an alkali. As known, amide bonds can also be ruptured using hydrazine; in so doing, excess AA is also removed. After extraction of CEC with hydrazine hydrate in a Soxhlet apparatus, the product is insoluble in water. Apparently, new cross-links are formed via terminal aldehyde groups. The crude product can be dissolved in hydrochloric acid under heating. However, in so doing, hydrolysis of glycoside bonds is possible, leading to a decrease in the molecular weight.

To confirm formation of amide bonds, we recorded the IR diffuse reflection spectrum of $CEC_{DS=1.0}$ untreated with alkali. It is impossible to reveal a new amide bond against the background of the strong absorption band of the amide bond of the residual acetyl groups (1655 cm^{-1}) at DD = 0.84. However, on subtraction of the spectrum of $CEC_{DS=1.0}$, obtained in the solution and containing no amide groups [3], from the given spectrum, the absorption band corresponding to a new amide bond at 1652 cm^{-1} is observed in the differential spectrum. Formation of an amide bond is additionally proved by the appearance of the signal at 169 ppm in the ^{13}C NMR spectra of the resulting products. This signal corresponds to the carbonyl carbon of the acrylamide group, contrary to the signal corresponding to the carbonyl carbon atom of acetamide group at 176 ppm.

For additional estimation of the structure of the resulting solid compounds we used broad line ^1H NMR spectroscopy. The spectrum of $CEC_{DS=1.0}$ in the form of lithium salt and resolution of the spectrum into components corresponding to the lines of one-, two-, and three-spin proton groups are presented in Fig. 2. The assignment of these components to

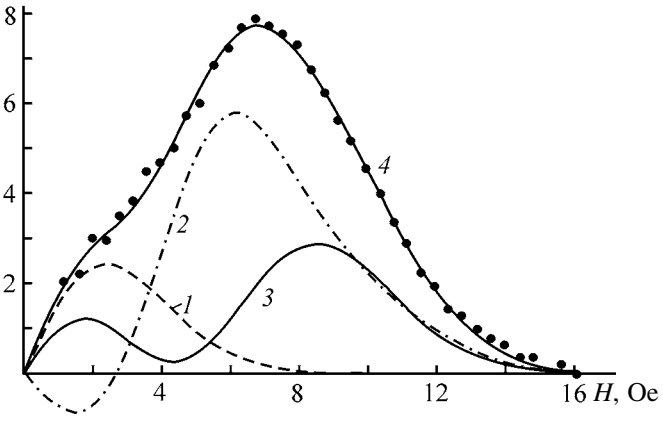

Fig. 2. ^1H NMR spectrum of a sample of lithium salt of $CEC_{DS=1.0}$ (85 MHz, –150°C). (*I*) Intensity and (*H*) magnetic field strength. Lines: (*1*) H^+, R_3NH^+, (*2*) H_2O, (*3*) OH_3^+, and (*4*) sum of components of the spectrum resolution. Points: experimental data.

Table 3. ^{1}H broad line NMR data

Line	Assignment	Content of protons of given group, % of total amount in sample				
		chitosan HCl	$CEC_{DS=0.5}$	$CEC_{DS=1.0}$	$CEC_{DS=0.5}$ (Li)	$CEC_{DS=0.5}$ (Li)
1	H^+, R_3NH^+	5.5 (H^+)	10.7 (H^+)	8.7	7.6(H^+)	7.0
2	H_2O	63.7 (H_2O)	67.8	62.1	60.1	57.2
3	OH_3^+, $ChNH_3^+$	30.8	21.5	29.2	32.3	35.8
Total contribution of lines 1 and 3		36.3	32.2	37.9	39.9	42.8

the corresponding proton groups entering into composition of the samples studied is given in Table 3.

The above data suggest that a decrease in the fraction of two-spin systems with a parallel increase in the fraction of the sum of one- and three-spin systems corresponds to an increase in the degree of substitution, i.e., in the amount of alkylammonium groups. The variation of the amount of three-spin systems is also of interest. In passing from chitosan hydrochloride to hydrochloride of $CEC_{DS=0.5}$, a part of protons of the amino group of chitosan are replaced by the carboxyethyl group, and protons of the carboxy group are bonded with excess amino groups. As a result, the total content of alkylammonium and hydroxonium ions decreases. In passing to hydrochloride of $CEC_{DS=1.0}$, the increased amount of carboxy groups results in significant increase in the amount of hydroxonium ions, which results in increased contribution of the sum of lines 1 and 3. At first glance, the presence of hydrogen ions in the structure of lithium salts of CEC seems paradoxical. Considering polyampholytic nature of the polymer [3], in this case, significant buffer power of CEC should be assumed. With the aim to study these characteristics in more detail, data on measurements of local pH should be used [12].

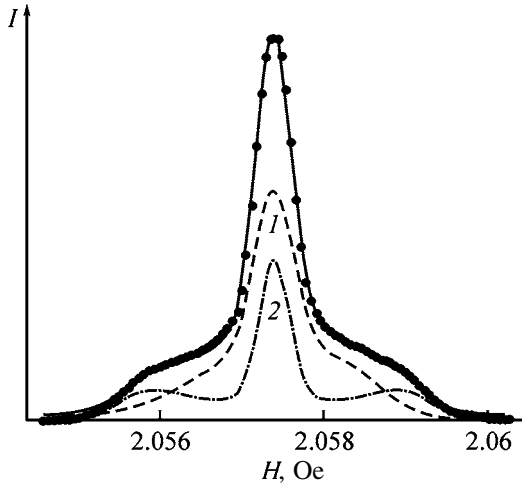

Fig. 3. ^{7}Li broad line NMR spectrum of the lithium salt $CEC_{DS=1.0}$ (Li) (33 MHz, 20°C). (*1*, *2*) Components of spectrum resolution.

A comparison of the data for two-spin systems with the data of thermal gravimetric analysis of the samples of chitosan and CEC hydrochlorides shows that, for both hydrochlorides and lithium salts, with increasing degree of substitution the absorption power with respect to water slightly decreases, which is apparently caused by better crystallinity of the polymer [13]:

Compound	Water loss, % (approximately to 150°C)
Chitosan HCl	10.59
$EC_{DS=0.5}$	6.63
$CEC_{DS=1.0}$	6.00
$CEC_{DS=0.5}$ (Li)	4.49
$CEC_{DS=1.0}$ (Li)	5.10

It is interesting that a calculation of the amount of hydrogen ions using ^{1}H broad line NMR data for chitosan hydrochloride gives 0.51 mol kg^{-1}. The actual concentration of HCl is 5.06 mol kg^{-1}, which suggests 10% dissociation of the hydrochloride. For the other compounds, the given mole fractions correspond to the sum of the signals of two different groups; therefore, more detailed conclusions about their concentration are impossible.

A comparison of the ^{7}Li broad line NMR spectra (Fig. 3) for lithium salts of $CEC_{DS=0.5}$ and $CEC_{DS=1.0}$ shows that lithium in each sample is located in the same crystallographic position, since the central line is the same, but positions of lithium atoms are different in their charge surrounding: in each spectrum there are two pairs of satellites. These spectra were resolved into components.

As follows from Table 4, the content of lithium ions with less symmetrical charge surrounding somewhat increases in passing to the sample of CEC with a higher degree of carboxyethylation, since lower quadrupole interaction constant corresponds to more symmetrical charge surrounding. It is well known that polycarboxylic amino acids form complexes even with

Table 4. Parameters of hyperfine interaction of lithium nuclei obtained from the ^{7}Li NMR spectra

Parameter	$CEC_{DS=0.5}$ (Li)		$CEC_{DS=0.5}$ (Li)	
	line 1	line 2	line 1	line 2
Isotropic shift K_{iso}	–0.0046	–0.0046	–0.005	–0.005
Quadrupole interaction constant (ν_Q), MHz	0.028	0.056	0.028	0.056
Integral intensity of component S, %	60.49	39.51	55.56	44.44

lithium and sodium [14]. Thus, the phenomenon observed suggests the presence of a complex of not only mono-, but also disubstituted derivative, which decreases the symmetry of the charge surrounding of lithium:

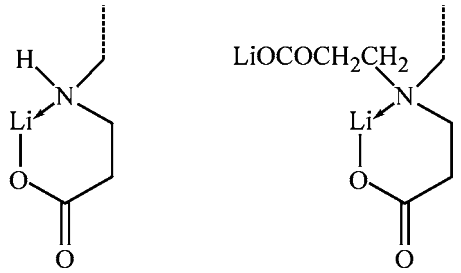

It should be noted in conclusion that chemical characteristics of carboxyethyl chitosan are close to those of carboxymethyl chitosan. The suggested procedure of CEC synthesis is undoubtedly simpler in practice than any methods of synthesis of the carboxymethyl derivative. The initial raw material for the synthesis of the first product is AA, and for the synthesis of the second product, chloroacetic acid: these compounds are equally available, but chloroacetic acid is somewhat more toxic. A set of these advantages makes carboxyethyl chitosan more advantageous for further applications.

CONCLUSIONS

(1) The suggested procedure for preparing carboxyethyl chitosan by synthesis in a gel allows the volume of the reaction mixture to be decreased by a factor of 50 compared to the synthesis in aqueous solution. The reaction does not require stirring and use of organic solvents and occurs under mild conditions (50–90°C). These advantages make the procedure very convenient.

(2) A study of mother liquors and the resulting polymers by ^{1}H NMR and IR Fourier spectroscopy showed that, during the reaction, a part of acrylic acid adds water to form β-hydroxypropionic acid and 2,2-dicarboxydiethyl ether. In addition, polymer molecules are cross-linked via amide bonds.

(3) A ^{1}H broad line NMR study of carboxyethyl chitosan hydrochlorides showed that an increase in the degree of substitution corresponds to a decrease in the fraction of two-spin systems with a parallel increase in the fraction of sum of one- and three-spin systems. The ^{7}Li broad line NMR data suggest the presence of different lithium complexes in carboxyethyl chitosan salts with different degrees of substitution.

REFERENCES

1. Lubben, I.M., Verhoet, J.C., Borchard, G., et al., *Eur. J. Pharm. Sci*., 2001, vol. 14, pp. 201–207.
2. Felse, P.A. and Panda, T., *Bioprocess Eng*., 1999, vol. 20, pp. 505–512.
3. Shorik, Y.A., Gomes, C.A.R., Vasconcelos, T.M.S.D., and Yatluk, Y.G., *Carbohydr. Res*., 2003, vol. 338, pp. 271–276.
4. Kogan, G., Skorik, Yu.A., Zitnanova, I., et al., *Toxicol. Appl. Pharmacol*., 2004, vol. 201, pp. 303–310.
5. Pestov, A.V., Skorik, Yu.A., and Yatluk, Yu.G., *Vestn. Ural. Gos. Tekh. Univ.–Ural. Politekh. Inst., Ser. Khim*., 2004, vol. 37, no. 7, pp. 53–55.
6. Sashiwa, H., Yamamori, N., Ichinose, Y., et al., *Macromol. Biosci*., 2003, vol. 3, no. 5, pp. 231–233.
7. Orienti, I., Luppi, B., and Zecchi, V., *J. Cosmetic Sci*., 1999, vol. 50, pp. 307–313.
8. US Patent 6261594.
9. JPN Patent 2002308901.
10. Aoi, K., Seki, T., Okada, M., et al., *Macromol. Chem. Phys*., 2000, vol. 201, pp. 1701–1703.
11. Gamzazade, A.I., Slimak, V.M., Skljar, A.M., et al., *Acta Polym*., 1985, vol. 36, pp. 420–424.
12. Molochnikov, L.S., Kovalyova, E.G., Grigor'ev, I.A., et al., *J. Phys. Chem. B*, 2004, vol. 108, pp. 1302–1307.
13. Chen, L., Du, Y., Wu, H., and Xiao, L., *J. Appl. Polym. Sci*., 2002, vol. 83, pp. 1233–1241.
14. Grinberg, A.A., *Vvedenie v khimiyu kompleksnykh soedinenii* (Introduction to Coordination Chemistry), Moscow: Khimiya, 1966.

ISSN 1070-4272, Russian Journal of Applied Chemistry, 2007, Vol. 80, No. 7, pp. 1160–1169. © Pleiades Publishing, Ltd., 2007.
Original Russian Text © A.N. Krasovskii, V.N. Filippov, D.V. Novikov, 2007, published in Zhurnal Prikladnoi Khimii, 2007, Vol. 80, No. 7, pp. 1190–1199.

MACROMOLECULAR CHEMISTRY AND POLYMERIC MATERIALS

Scale-Invariant Cluster Structure of the Chemical Network of Epoxy–Phenol Polymer

A. N. Krasovskii, V. N. Filippov, and D. V. Novikov

St. Petersburg State University of Motion Pictures and Television, St. Petersburg, Russia

Received October 30, 2006; in final form, April 2007

Abstract—The concentration dependences of the relative viscosity of a mixture of precondensates of epoxy–4,4'-isopropylidenediphenol and phenol–formaldehyde resins in a Cellosolve solution were examined. The surface tension curves at the solution–air interface at concentrations c = 0.5–45 % were obtained. The optimal concentration modes of preparation of coatings from solutions of precondensates of the resin mixture were calculated on the basis of the cluster model. Using electron microscopy with silver chloride surface decoration, the cluster structure parameters of the chemical network of the epoxy–phenol polymer were determined for coatings with high protective performance.

DOI: 10.1134/S1070427207070294

We found earlier [1, 2] that a transition from dilute to concentrated solutions of mixtures of epoxy–4,4'-isopropylidenediphenol and phenol–formaldehyde oligomers (EO and PO, respectively) is accompanied by formation of discrete aggregates and an infinite molecular cluster. Such transition causes changes of the density ρ and fractal dimension D of the aggregates, as well as of the degree of aggregation of the molecules in solution near the threshold concentration c^* with formation of an infinite cluster [2, 3]. In solutions of the EO–PO mixture in Cellosolve, stable hetero complexes are formed via intermolecular hydrogen bonding between the oligomers [4]. The size and structure of the EO–PO aggregates are determined by the molecular weight (MW), composition of the oligomer mixture, and thermal history of the solution [1–5].

Preparation of polymer coatings on metals via thermal curing of the EO–PO mixtures involves preliminary precondensation of the oligomers in solution in the presence of orthophosphoric acid [6]. Upon introduction of H_3PO_4 into the EO–PO mixture, dihydrogen phosphate, hydrogen diphosphate, and triphosphate esters of EO and PO are formed in the initial stage [4]. Mixed EO–PO dihydrogen phosphate is the most stable "elementary" aggregate of these molecules, yielded by the reaction of the H_3PO_4 molecule with the epoxy group in EO and hydroxy group in PO at the molar ratio $N_1(\text{EO})/N_2(\text{PO}) \approx 1$ [4, 5]. Thermal curing of the precondensates of the oligomer mixture involves chemical reactions between the methylol (butoxy) groups of PO and epoxy (hydroxy) groups of EO in the coating [5].

Earlier [7–10] we suggested a cluster mechanism of precondensation of oligomers in solution, comprising three stages of precondenstion of the EO–PO mixture and the corresponding topologic types of the chemical network of the epoxy–phenol polymer prepared by curing of EO and PO in various stages of the process [2]. These stages are as follows: breakdown of individual aggregates of EO and PO molecules, formation of mixed EO–PO aggregates, and formation of an infinite cluster of the molecules [9].

The cluster model of aggregation of oligomers allows substantiation of the concentration and kinetic regimes of pecondensation of the EO–PO mixture in solution [10]. We found earlier [7] that the run of the curves corresponding to the time dependences of the viscosity $\eta(t)$ and the precondensation time for the EO–PO mixture vary with the $N_1(\text{EO})/N_2(\text{PO})$ molar ratio and the orthophosphoric acid concentration N_3. In the final stage of precondensation of the EO–PO mixture ($N_1/N_2 = 1$) at the molar ratio $N_3/(N_1 + N_2) \approx 0.1$ we revealed the minima for the viscosity η and density ρ of the EO–PO aggregates in Cellosolve solutions [8].

The cluster structure of the epoxy–phenol polymer prepared by thermal curing of the EO–PO mixture is predetermined by the lattice density ρ of the chemical

Table 1. Molecular characteristics of E-05 epoxy–4,4'-isopropylidenediphenol and DFFr phenol–formaldehyde resins and samples of precondensates (PCs) of E-05 and DFFr mixtures in a Cellosolve solution at 298 K

Sample no.	Oligomer	N_1/N_2	c_1/c_2	[η], dl g^{-1}, ±5%	M_n, ±10%	M_w/M_n	σ(c*), mN m^{-1}
1	E-05	–	–	0.134	2850	2.7	28.6
2	DFFr	–	–	0.061	1030	3.8	31.8*
3	PC	0.7	2.2	0.115	2320	2.4	–
4	PC	0.8	2.4	0.131	2400	2.5	–
5	PC	1.0	2.9	0.148	2700	2.8	30.8
6	PC	1.5	4.5	0.154	3490	4.0	31.5

Notes: The parameters M_n and M_w/M_n for sample nos. 3–6 at precondensation time of 2 h. For sample no. 5, precondensation of E-05 and DFFr in a Cellosolve solution was carried out at c_1 = 26.7 and c_2 = 9.12 g dl^{-1}; σ(c*) is the surface tension at the threshold concentration c* of the oligomers (Table 2).

* For the DFFr concentration in solution c = 26 g dl^{-1}.

network cross-links [1, 2, 8]. The uniform chemical network of the epoxy–phenol polymer is characterized by the EO-to-PO molecular weight ratio close to 3 : 1 and the optimal M_n(EO) = 2800–3500 [1].

The lattice density of two infinite clusters of the decorating silver chloride particles, representing the cross-links of the uniform chemical network of the epoxy–phenol polymer based on the precondensate of the EO–PO mixture (N_1/N_2 = 1), is close to the percolation threshold of the particles on a triangular lattice at $N_3/(N_1 + N_2) \approx 0.1$ [7, 8]. In this case, the degrees of filling of the coating surface with these clusters are nearly identical, which suggests formation of a uniform chemical network for the two components, EO and PO [8].

It should be noted that the density of the EO–PO aggregates in solution and the structural parameters of the chemical network of the epoxy–phenol polymer vary both with the composition of the EO–PO mixture and the concentration c of the precondensate in solution [7–10]. At the same time, the relationships in formation of EO–PO aggregates in solution and of the chemical network of the epoxy–phenol polymer with varying N_1(EO)/N_2(PO) ratio and the precondensate concentration in solution c still remain to be elucidated in detail [6–8]. This hinders reliable optimization of the concentration modes in formation of protective coatings with high performance characteristics.

We report here the results of examination of the concentration dependences of the relative viscosity of the EO–PO precondensates and of the surface tension at the solution–air interface. Based on the fractal cluster model, the structural parameters of formation of the EO–PO aggregates were calculated, as well as the threshold concentrations of formation of an infinite cluster in solutions of precondensates of different compositions. Using electron microscopy with silver chloride surface decoration, the characteristics of the cluster structure of the uniform chemical network of the epoxy–phenol polymer were determined. Also, the concentration modes of formation of epoxy–phenol coatings with high protective performance were elucidated.

EXPERIMENTAL

The characteristics of E-05 epoxy–4,4'-isopropylidenediphenol and DFFr phenol–formaldehyde resins (Pigment Holding Company) were determined by capillary viscometry and gel-permeation chromatography [11]. The number-average MW M_n and the M_w/M_n ratios (M_w is the weight-average MW) for samples of E-05 and DFFr, as well as of the precondensates of the resins, are listed in Table 1.

Precondensation of a mixture of E-05 and DFFr resins was carried out in a Cellosolve solution at 333 K. The N_1(E-05)/N_2(DFFr) molar ratio was varied from 0.7 to 1.5 (c_1/c_2 = 2.4–4.5) (Table 1, sample nos. 3–6); the precondensation time was 2 h. Phosphoric acid was introduced into the mixture in the initial stage of the process; the H_3PO_4 concentration was 85 rel % (100% was taken for 0.25 g of H_3PO_4, calculated for 36 g of the E-05–DFFr mixture [6]), which corresponds to $N_3/(N_1 + N_2) \approx 0.1$ [7, 8].

The relative η_{rel} and intrinsic [η] viscosities of sample nos. 1–6 in Cellosolve solutions were measured on an Ubbelohde capillary viscometer (solvent outflow time 81 s, shear rate 100 s^{-1}) at 298 K with the relative error of 3%. The concentration curves of the relative viscosity $\eta_{rel}(c)$ of the precondensate sample nos. 3–6 in a Cellosolve solution were examined at concentrations c = 5–45% (Fig. 1, Table 1).

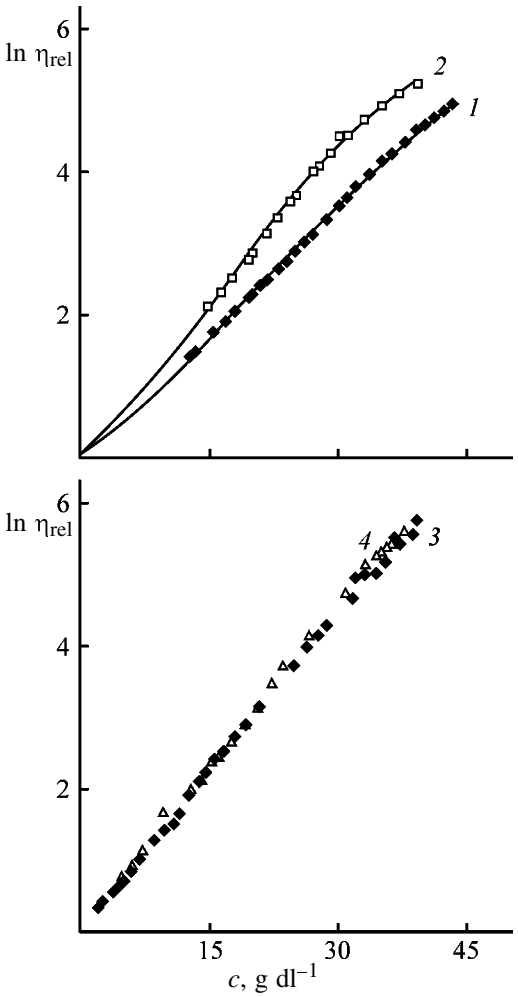

Fig. 1. Concentration dependences of the relative viscosity η_{rel} of the precondensates of a mixture of E-05 and DFFr resins in a Cellosolve solution in the $\ln \eta_{rel}$–c coordinates at 298 K. Sample no: (*1*) 3, (*2*) 4, (*3*) 5, and (*4*) 6; the same for Figs. 4 and 5. N_1/N_2: (*1*) 0.7, (*2*) 0.8, (*3*) 1.0, and (*4*) 1.5; the same for Figs. 4 and 5.

The surface tension σ of the EO and PO solutions at the solution–air interface was measured with a Du Nouy tensometer at 298 K [12, 13]. The relative error of 10 replicate measurements of σ was 0.3%.

The epoxy–phenol coatings with a thickness of 6–20 μm were obtained by casting the precondensate solution in Cellosolve with the concentration c = 18–30% (N_1/N_2 = 1, Table 1, sample no. 5) onto the electrolytic tin-plated sheet metal. Next, the coating was cured in air for 15 min at 483 K [5, 6]. The protective characteristics of the epoxy–phenol coatings were determined by the procedure from [6] in the following model media: 3% aqueous solutions of sodium chloride and acetic acid and 2% aqueous solution of tartaric acid and distilled water for 1 h at 393 K and pressure of 120 Pa.

To examine the cluster structure of the epoxy–phenol polymer, we carried out thermal sputtering of silver chloride on the coating surface at 1.33×10^{-3} Pa to the effective layer thickness of 0.4 nm. Coal replicas with the AgCl decorating particles, prepared by the procedure from [8], were examined with an EVM 100 L electron microscope. The mechanism of interaction of AgCl with the functional groups of PO consists in partial reduction of AgCl with quinonemethide groups of the epoxy–phenol polymer [14], yielded by thermal curing of the precondensates [5]. The silver particle nuclei are the nucleation sites for large AgCl particles.

Computer processing of the electron micrographs of the polymer coating surface (Figs. 2a–2e) was carried out on the basis of the cluster model [3]. We calculated the function of the radial distribution of the AgCl particles over the surface $g(R)$ [15] and the dependences of the lattice density ρ_l of the clusters on the radius R of the circumference incorporating the particle cluster. The correlation radius ξ and fractal dimension D of the clusters were estimated from the $\rho_l(R)$ curves using the expression $\rho_l(R) \sim R^{D-2}$ on the $R < \xi$ and $R > \xi$ scales [3]; the coordination number of the lattice m was determined from the area enclosed by the first maximum of the $g(R)$ function (Fig. 3).

The concentration dependences of the relative viscosity $\eta_{rel}(c)$ of the EO–PO mixture precondensates in Cellosolve solutions at c = 5–45% are described by the expression $\ln \eta_{rel} = ([\eta]c)^{(3-D/D)}$ [2], where $[\eta]$ is the intrinsic viscosity of sample nos. 3–6 in solution; c, concentration, g dl^{-1}; and D, fractal dimension of the aggregates of the mixed EO–PO molecules (Fig. 1 and Tables 1, 2). To estimate the threshold concentration c^* near which the degree of aggregation of the EO–PO molecules in Cellosolve solutions increases, we calculated the $f(x)$ parameter by the expression

$$f(x) = [\eta]c/\ln \eta_{rel} = x^{(2D-3)/D}, \quad x = [\eta]c. \qquad (1)$$

As expected [2], the $f(x)$ curves in the logarithmic coordinates, plotted for Cellosolve solutions of sample nos. 3–6 of EO–PO precondensates, consist of several portions differing in the slope and fractal dimension D of the aggregates of particles (Fig. 4, Table 2).

The degree of aggregation of the oligomers s and dimensionless lattice density ρ of the mixed EO–PO aggregates in Cellosolve solutions were calculated

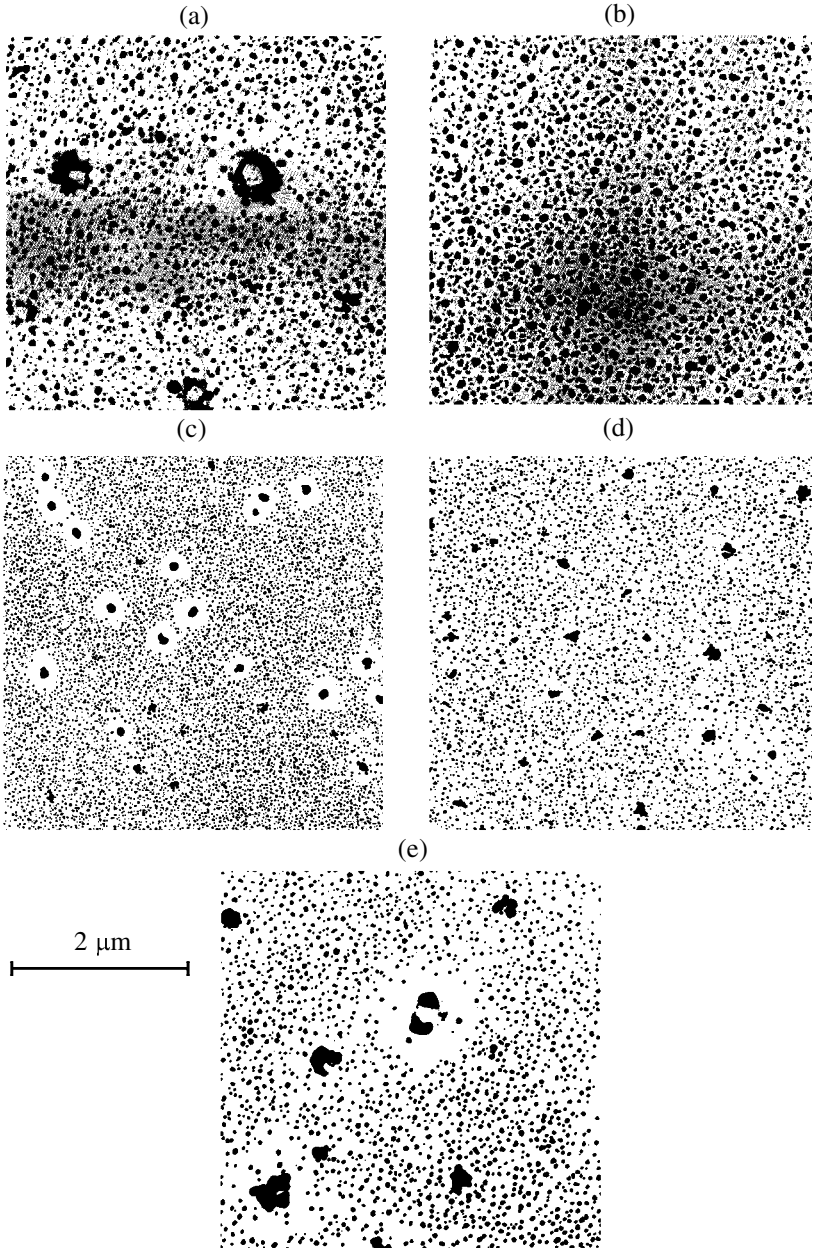

Fig. 2. Electron micrographs of the decorating silver chloride particles on the surface of epoxy–phenol coatings on sheet metal (sample no. 5). Magnification × 10000. Precondensate concentration in Cellosolve solution c, %: (a) 18, (b) 19, (c) 20, (d) 23, and (e) 25.

by the expressions [2, 10]

$$s = (\langle R\rangle/R_0)^D \approx [f(x)]^{D/(2D-3)}, \quad (2)$$

$$\rho = sR_0^3/\langle R\rangle^3 = w^{(1-3D)/D}[f(x)]^{(3-D)/(3-2D)}, \quad (3)$$

where R_0 is the radius of the "elementary" aggregate of E-05 and DFFr molecules of 2.1 nm, and w = 0.637, random packing coefficient of rigid spheres [3].

The average radius of the E-05–DFFr aggregates was determined by the expression [2]

$$\langle R\rangle = R_0 w^{-1/D}[f(x)]^{1/(2D-3)}. \quad (4)$$

It should be noted that formation of an infinite cluster in Cellosolve solutions is characterized by infinite growth of the degree of aggregation s of EO near the threshold concentration c^* = 26.7 g dl^{-1} (Table 2, sample no. 1). The degree of aggregation s of the EO molecules in Cellosolve solution near c^* is

Table 2. Parameters of the aggregates of the oligomer molecules in E-05 and DFFr solutions, as well as of the mixed EO–PO molecular aggregates in Cellosolve solutions of precondensates of the E-05–DFFr mixture at 298 K

Sample no.	c_{min}, g dl^{-1}	ρ_{min}, ±5%	D_1, ±7%	s_1	$\Delta\sigma(c_{min})$, mN m^{-1}	c^*, g dl^{-1}	ρ_{max}, ±5%	D_3, ±7%	s_3	$\Delta\sigma(c^*)$, mN m^{-1}
1	12.3	0.40	1.56	92	1.2	26.7	0.53	1.83	340	–3.2
2	19.8	0.22	1.34	1.3	1.5	26	0.20	1.25	~3	0.0
3	25.0	0.15	1.44	2	–	36	0.28	1.80	14	–
4	24.4	0.20	1.51	2	–	26	0.25	1.67	11	–
5	14.0	0.22	1.57	2	3.4	20.5	0.67	1.67	18	–1.0
6	17.0	0.12	1.47	8	2.0	29.0	0.40	2.04	34	–0.3

Note: Fractal dimension D of the aggregates and degree of aggregation s of the oligomer molecules are given in the first and third portions of the $f(x)$ curves. The density of the aggregates for the Euclidean dimensionality $E = 3$ are given for the minimum and maximum of the curves $\rho(c)$, characterized by c_{min} and c parameters. The $\Delta\sigma(c) = \sigma(c) - \sigma_1$ parameters were calculated for σ_1(Cellosolve) $= 31.8 \times 10^{-3}$ N m^{-1} [13].

two orders of magnitude higher ($s > 300$) than that of the PO molecules in solution at $c = 26$ g dl^{-1} ($s \approx 3$, sample no. 2).

Three portions in the $f(x)$ curves for Cellosolve solutions of the precondensates at $x = 0.4–4.5$ are associated with the fractal–fractal transitions from elementary EO–PO molecular aggregates with $D_1 = 1.57$ ($s_1 \approx 2$, aggregate radius $\langle R \rangle = 3.1$ nm at $c \le 14$ g dl^{-1} [2]) to larger and denser EO–PO aggregates with $D_3 \approx 1.7$ ($s_3 = 18$, $\langle R \rangle$ 18 nm at $c = 20$ g dl^{-1}) and infinite cluster of particles at $c \ge 20.5$ g dl^{-1} ($s \to \infty$, $c > c^*$) (Table 2, precondensate sample no. 5). In these portions of the $f(x)$ curves, the degree of aggregation s of the EO and PO molecules in the mixed aggregate is much lower than that in the EO solution in Cellosolve but much higher than that in the PO solution [2].

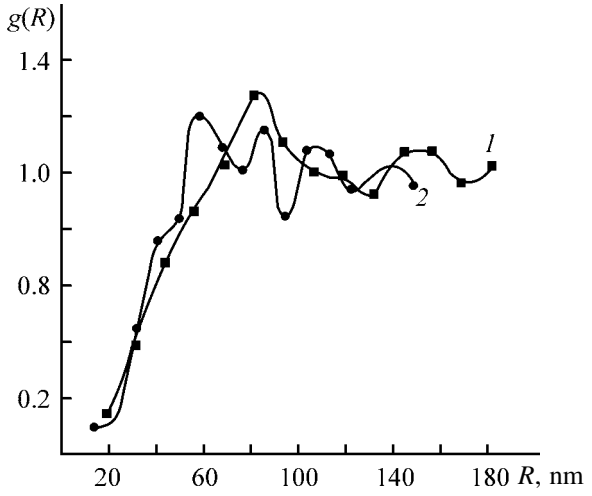

Fig. 3. Radial distribution function $g(R)$ for the decorating silver chloride particles on the surface of epoxy–phenol coatings on sheet metal (sample no. 5). (R) Particle radius, nm. Precondensate concentration in Cellosolve solution c, %: (*1*) 19 and (*2*) 30.

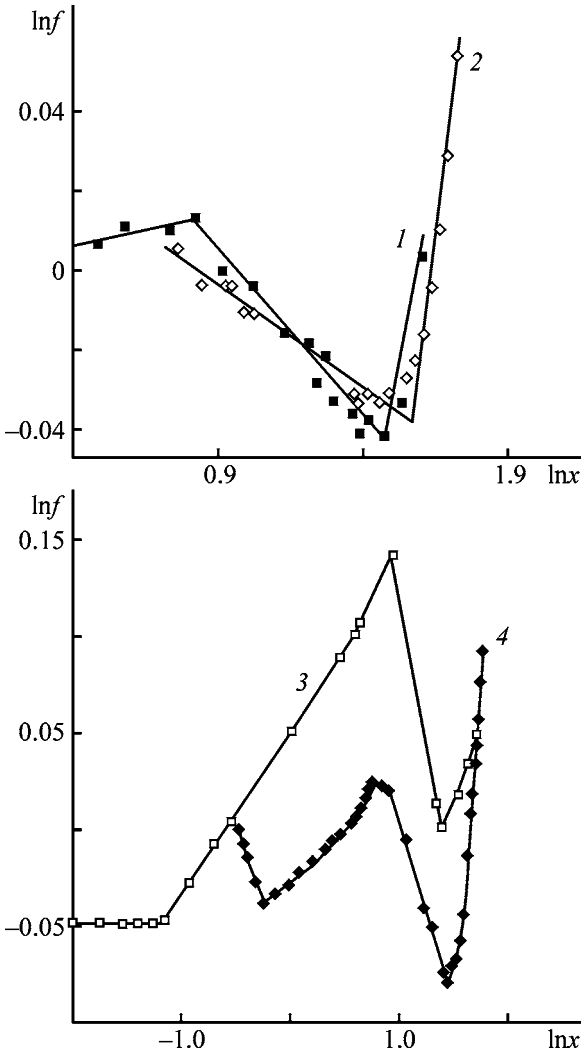

Fig. 4. $f([\eta]c)$ curves for precondensates of the mixture of E-05 and DFFr resins in Cellosolve solution in the ln$f$–ln$x$ coordinates ($x = [\eta]c$ is a dimensionless parameter). (*1–4*) See caption to Fig. 1.

In the first portion of the $f(x)$ curves, the degree of aggregation s_1 of the EO and PO molecules is nearly 2 for all the precondensate samples, except for sample no. 6 (N_1/N_2 = 1.5). In the third portion of the $f(x)$ curves, the degree of aggregation s_3 of the EO and PO molecules depends on the N_1/N_2 ratio, being much higher at N_1/N_2 = 1.5 than at N_1/N_2 = 0.7–1.0 (Table 2, Fig. 4).

The density ρ of the aggregates of the EO molecules and of mixed EO–PO aggregates varies nonmonotonically with growing concentration of the oligomers in solution at $[\eta]c$ = 0.5–6. The position of the extrema in the $\rho(c)$ curves for the EO–PO precondensates in the concentration c scale depends on the N_1/N_2 ratio (Fig. 5). The minimum of the density $\rho(c)$ of the mixed EO–PO aggregates corresponds to c_{min} which is at a minimum at N_1/N_2 = 1 (Table 2).

The density ρ is at a maximum near the threshold concentration c^* of the EO–PO precondensates in solution and then attains saturation at $c > c^*$. For sample no. 5 (N_1/N_2 = 1, Table 2) we revealed a maximal density $\rho(c^*)$ of the aggregates close to 0.69 and corresponding to percolation of the particles in a simple cubic lattice [3]. In other cases ($N_1/N_2 \neq 1$), the density of the aggregates ρ near c^* is much lower due to the departure from the optimal (1 : 1) composition of the mixed EO–PO aggregates (Fig. 5).

The concentration curves of the surface tension $\sigma(c)$ at the EO–PO solution–air interface are characterized by local extrema (Fig. 6). These curves can be described in terms of the Flory–Huggins–Prigogine lattice model by the expression [12]

$$\sigma(c) = \sigma_1 + (kT/\omega q)[\ln(1 - \varphi_2^{sur})/(1 - \varphi_2^{vol})], \quad (5)$$

where σ_1 and σ_2 are the surface tensions of the solution and solvent, respectively; ω, area of the particle in the surface phase; φ_2^{sur} and φ_2^{vol}, volume fractions of the oligomer in the surface phase and solution, respectively, and k, Boltzmann's constant (q = 1 for the oligomers).

The cluster model [3, 16] states that the area ω occupied by a particle in the aggregate is $\pi\langle R\rangle^2 s^{-1}$, where $\langle R\rangle$ is the aggregate radius. For the degree of aggregation s of the particles near the threshold concentration c^*, $s \approx (\langle R\rangle/R_0)^D$, where R_0 is the particle radius [2, 3]. Hence, the area ω occupied by a molecule in the aggregate is equal to $\pi\langle R\rangle^{2-D}R_0^D$. In the surface phase near the threshold concentration c^*, the fractal dimension of the aggregates D is close to 2 ($D \approx 1.89$ at the percolation threshold $p_c \approx 0.5$, the Euclidean dimensionality E = 2 [3]), hence ω

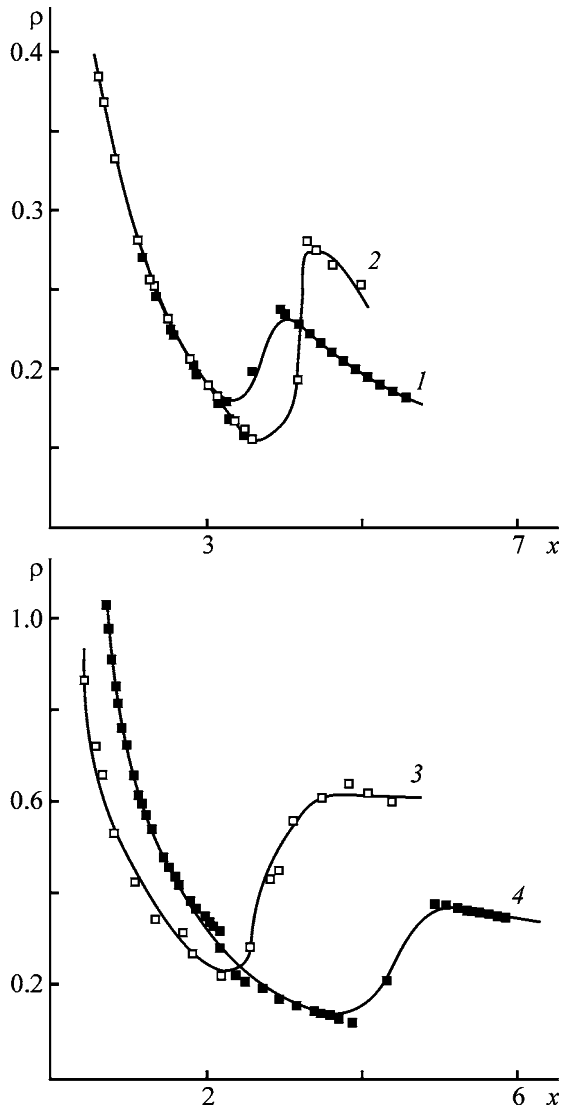

Fig. 5. Density ρ of the aggregates of the oligomer molecules vs. $x = [\eta]c$ for precondensates of the E-05–DFFr mixtures in Cellosolve solution. (*1*–*4*) See caption to Fig. 1.

$\approx \pi R_0^2$. Since at $c < c^*$ the fractal dimension of the particle aggregates $D < 2$, $\omega = \pi\langle R\rangle^{2-D}R_0^D$ exceeds πR_0^2.

Based on the relationship for the density of the particle aggregates in solution $\rho \sim (\langle R\rangle/R_0)^{D-3}$ (E = 3) [3], we can relate $\Delta\sigma(c)$ to the density ρ of the aggregates and the dimensionless parameter $x = [\eta]c$

$$\Delta\sigma(c) = \sigma(c) - \sigma_1 = kT\pi^{-1}\rho^{(D-2)/(D-3)}R_0^{-2} \times [\ln(1 - \varphi_2^{sur})/(1 - \varphi_2^{vol})], \quad (6)$$

$$\Delta\sigma(c) = kT\pi^{-1}w^{(2-D)/D}x^{(D-2)/D}R_0^{-2}[\ln(1 - \varphi_2^{sur})/(1 - \varphi_2^{vol})]. \quad (7)$$

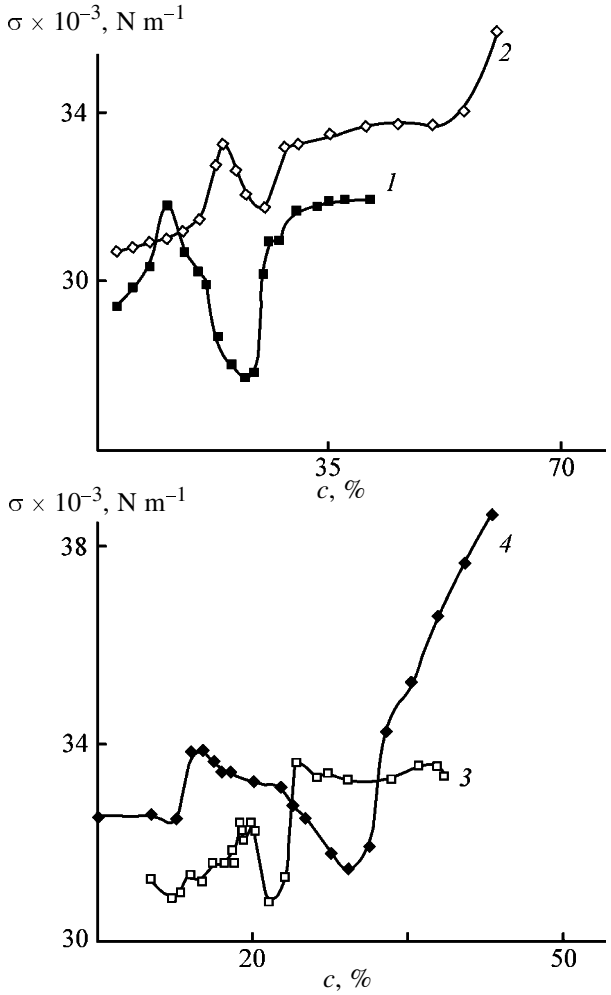

Fig. 6. Surface tension σ, at the solution–air interface vs. the concentration c of (*1*) E-05 and (*2*) DFFr and (*3, 4*) of the precondensates of the E-05–DFFr mixture in Cellosolve solution at 298 K. Precondensate sample no. (*3*) 5 and (*4*) 6.

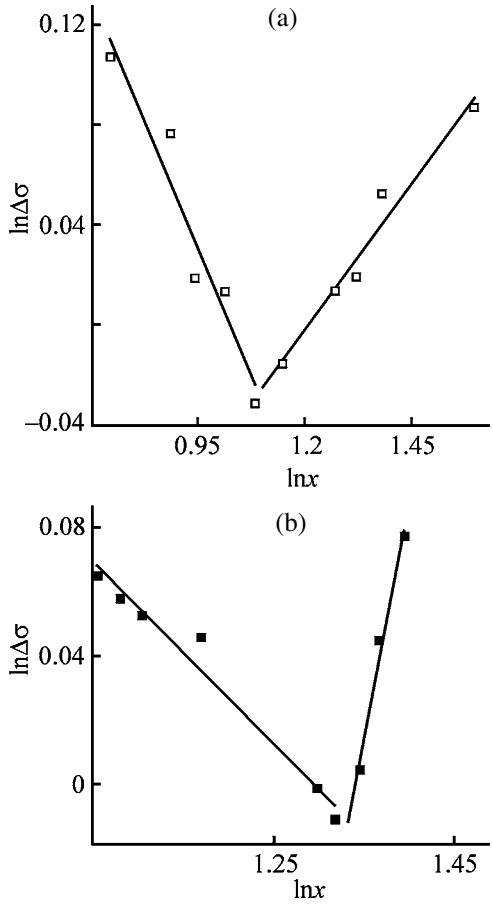

Fig. 7. Surface tension increment Δσ as a function of $x = [\eta]c$ in the $\ln \Delta\sigma$–$\ln x$ coordinates. Precondensate sample no. in a Cellosolve solution: (a) 5 and (b) 6. Fractal dimension D of the aggregates, calculated from the slope of the curves by expression (7), is equal to (a) 1.4 and (b) 1.8 at $c < c^*$, and (a, b) 2.6 at $c > c^*$.

Near the local maximum of the surface tension curves $\sigma(c)$ at $c < c^*$, $d\sigma/dc < 0$ and $\Delta\sigma(c) > 0$ ($D < 2$), for the minimum $\sigma(c)$ near c^*, $d\sigma/dc = 0$ and $\Delta\sigma(c) \approx 0$ ($D = 2$), and at $c > c^*$, $d\sigma/dc > 0$ and $\Delta\sigma(c) > 0$ ($D > 2$) (Fig. 7). The maximum in the $\sigma(c)$ curve corresponds to the minimum of the density $\rho(c)$ of the aggregates at c_{min}, and the minimum in the $\sigma(c)$ curve, to the maximum of the density $\rho(c)$ of the aggregates near c^* (Figs. 5, 6).

Data in Table 2 for the EO and PO solutions in Cellosolve support these predictions of the cluster model. The minima in the $\sigma(c)$ curves are due to the fact that the second derivative of the Gibbs free energy d^2F/dc^2 is equal to zero at the threshold concentration c^* ($D = 2$). The increment in the Gibbs free energy $\Delta F(c) = \Delta\sigma\omega\varphi_2^{sur}N_A$ (N_A is the Avogadro number) [12] is at a minimum near c^* ($d\sigma/dc = 0$). This is consistent with the thermodynamic criterion of stability of multicomponent systems [17]. At $c < c^*$, ΔF has a maximum coinciding with that of the concentration c_s of the aggregates of particles with $D < 2$ [2], and at $c > c^*$, $\Delta F > 0$ ($\Delta\sigma > 0$).

This fact suggests that the optimal concentration of the precondensate in formation of the coatings should correspond to the conditions of formation of an infinite cluster of particles and wetting of the substrate surface, $\sigma(c) \le \sigma_1$ [12]. For sample no. 5, the threshold concentration c^* of the precondensate in solution fully satisfies these conditions (Table 2).

The patterns of distribution of the decorating particles on the surface of the epoxy–phenol coatings reveal the cluster structure of the polymer, represented by the areas of localization of fractions of small (20–

Table 3. Parameters of the cluster structure of the chemical network of epoxy–phenol coatings on canning metal sheet, obtained by curing precondensate no. 5 in Cellosolve solution with concentrations c = 18–30%

Sample no.	$c \pm 0.5\%$	$\rho_l \pm 0.02$	ξ, nm, ± 10	D, $\pm 7\%$	m, ± 0.3	Lattice type
7	18	0.90	700	1.95	5.0	Two sublattices
		0.44	400	1.70	1.8	
		0.25*	1200	1.45		
8	19	0.92	300	1.96	5.6	Two sublattices
9	20	0.86	480	1.94	3.1	Two sublattices
		0.25	900	1.67	1.8	
		0.11*	1500	1.40		
10	23	0.82	480	1.93	4.2	Two sublattices
		0.50	550	1.67	2.2	
		0.30*	1200	1.40		
11	25	0.75	650	1.93	5.5	One lattice
12	30	0.90	500	1.95	4.5	One lattice

Notes: For sample nos. 7, 9, 10, the first row refers to homogeneous segments, and the second, to microheterogeneous segments.
* Lattice densities ρ_l (Euclidean dimensionality E = 2) are given for large AgCl crystals.

30 nm) and large (150–500 nm) AgCl particles (Figs. 3a–3e). Nonuniform energy microrelief of the coating surface is due to different strengths of the bond linking the AgCl particles with the substrate, as well as to the characteristics of distribution of the functional groups of E-05 and DFFr. Accumulations of small AgCl particles strongly bound to the polymer surface predominantly reflect the distribution of the functional groups of E-05 [1, 2]. Accumulations of large particles are formed by the mechanism of coalescence of small particles and topologically correspond to distribution of the functional groups of DFFr [8].

Microdecorograms of the coatings show that the most uniform distribution of the small and large AgCl particles corresponds to the precondensate in the Cellosolve solution with c = 19% (Table 3, sample no. 8; Fig. 2b). With departure from c = 19% the average distance between the large AgCl particles and their size tends to increase for all the samples, except for samples of coatings obtained at c = 25–30% (Table 3). At c = 18, 20, and 23% the coatings contain microheterogeneous segments lacking in the coatings at c = 19, 25, and 30%. For coating samples at c = 18–23%, the homogeneous segments correspond to clusters of the particles forming two sublattices, and the clusters of the particles in microheterogenous segments form only one lattice.

We estimated the dimensionless lattice density ρ_l, correlation radius ξ, coordination number m, and fractal dimension D of the clusters [1] in the microheterogeneous segments of the coatings from the data for the small fraction of AgCl particles. In the epoxy–phenol coatings (Table 3, sample nos. 7, 9–10), for which we revealed segregation into two phases, those of small and large particles, the small-sized fraction particles form only one lattice. The $\rho_l(R)$ curves corresponding to microheterogeneous segments of the coatings consist of three portions and are characterized by two values of the correlation radius ξ and fractal dimension D of the clusters in the first two portions (Fig. 8).

The most uniform structure of the chemical network of the epoxy–phenol polymer is characteristic for the coating formed at c = 19%. It can be represented as two infinite clusters forming two sublattices of small and large AgCl particles and reflecting, respectively, the distribution of the functional groups in the network segments containing E-05 and DFFr moieties (Fig. 3). In this case, the $\rho_l(R)$ curves for the small and large fractions of the decorating AgCl particles consist of two portions, and the correlation radius ξ is at a minimum, the lattice density of the clusters ρ_l is at a maximum, and the coordination number of the quasilattice $m \approx 6$ corresponds to the triangular lattice [3] (Fig. 8, Table 3).

Thus, at c = 19%, two infinite clusters are formed that are inserted into each other and contain two types of the decorating particles. The lattice densities of the two clusters are close. The topological structure of the infinite clusters suggests formation of a uniform and common for the two oligomeric components chemical network of the epoxy–phenol polymer [8, 17]. Such a structure of the chemical network of the epoxy–phenol polymer should provide high protecting characteristics of the corresponding coatings in aggressive media [6].

Table 4. Characteristics of the protective and adhesion-strength properties of the epoxy–phenol coatings on canning sheet metal, prepared by curing of the solution of precondensate sample no. 5. Relative error in determining the concentration c of the precondensate in solution ±0.5%

Sample no.	c, %	Thickness, μm	Model medium				Adhesion, points
			H_2O	NaCl	CH_3COOH	tartaric acid	
7	18	6.8	Satisfactory	Satisfactory	Weak roughness	Weak lightening	2_1
9	20	9.5	Satisfactory	Satisfactory	Very weak roughness	Satisfactory	1_1
9a	20*	10.3	Satisfactory	Satisfactory	Weak lightening	Satisfactory	1_1
10	23	11.1	Dull	Satisfactory	Lightening	Dull	Unsatisfactory
11	25	12.1	Satisfactory	Satisfactory	Lightening	Satisfactory	Unsatisfactory
12a	30*	23.5	Dull	Satisfactory	Dull	Unsatisfactory	

Notes: The adhesion characteristic is given in points: (1_1) high adhesion and (2_1) medium adhesion.
* Upon introduction into the precondensate solution of additional 0.3% of KO-815 oligomer according to the formulation of the EP-547 lacquer [6].

To support this conclusion, we studied the protective characteristics of the coatings obtained by curing of the precondensate (sample no. 5) in a Cellosolve solution at c = 18–30% (Table 4). The maximal resistance of the coatings in aggressive media and high adhesion to the support are achieved at c = 20% (sample no. 9) which is virtually identical to the threshold c* derived using other methods (Tables 2, 3).

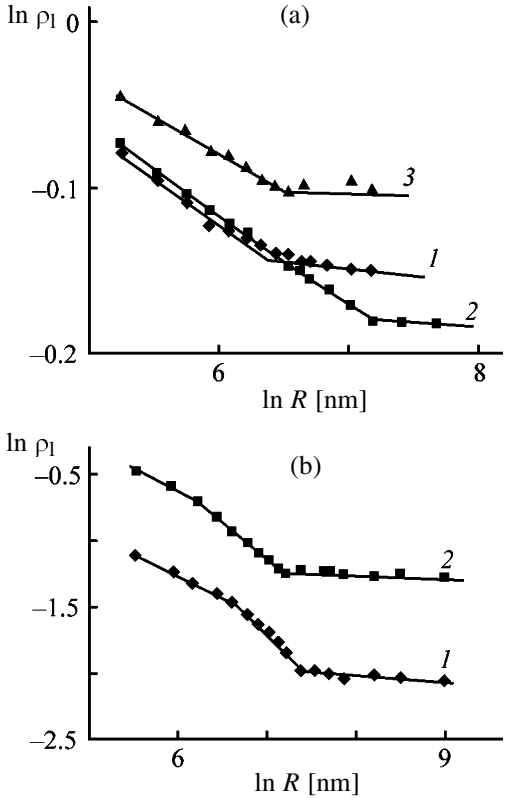

Fig. 8. Lattice density ρ_l of the decorating AgCl particles vs. the scale of the radius of the circumference R incorporating the cluster, nm. Segments of the epoxy–phenol coatings on sheet metal: (*1*) homogeneous and (*2*) heterogeneous. Sample no. 5, concentration c of the precondensate in a Cellosolve solution, %: (*1*) 18, (*2*) 20, and (*3*) 19.

Worsening of the protective and strength characteristics of the coatings (Table 4, sample nos. 7, 10–12), as well as of their ability for pressing [6] upon departure from the optimal concentration c* can be due to the breakdown of the uniform and common for the two components chemical network of the epoxy–phenol polymer into fairly long segments of the chemical network of epoxy–4,4'-isopropylidenediphenol resin, and discrete and microheterogeneous fragments of the chemical network of phenol–formaldehyde resin (Table 3, sample nos. 7, 9, 10). Such breakdown of the chemical network of the epoxy–phenol polymer upon departure from the threshold concentration c* of the precondensate in solution, deteriorating the structural uniformity of the coatings, can be predicted on the basis of viscometric and surface tension data.

CONCLUSIONS

(1) Near the threshold concentration c* of formation of an infinite cluster of particles in solutions of precondensates, the density of the mixed aggregates of epoxy–4,4'-isopropylidenediphenol and phenol–formaldehyde oligomers is at a maximum for the N_1/N_2 molar ratio of 1. In this case, the density is close to 0.69, which corresponds to percolation of the particles in a simple cubic lattice. In other cases ($N_1/N_2 \neq 1$) the density of the aggregate is much lower due to the departure from the optimal (1 : 1) composition of the mixed aggregates.

(2) The formulation concentrations of the oligo-

mers in formation of coatings from the solutions of the precondensates of a mixture of epoxy–4,4'-isopropylidenediphenol and phenol–formaldehyde oligomer should correspond to the concentration mode of formation of an infinite cluster, as well as to the condition for wetting of the substrate surface with the precondensate solution.

(3) The most uniform distribution of the decorating AgCl particles on the surface of epoxy–phenol coatings corresponds to the threshold concentration c^* of the precondensate in solution, with two infinite clusters of small and large AgCl particles formed that are inserted into each other. The lattice densities of such clusters are close, and their coordination numbers correspond to a triangular lattice. Such a structure of infinite clusters is due to formation of a homogeneous and common for the two components (epoxy–4,4'-isopropylidenediphenol and phenol–formaldehyde oligomers) chemical networks of the cross-linked polymer.

(4) The maximal resistance of the polymer coatings in aggressive media and high adhesion to the support are achieved at the threshold concentration c^* of the precondensate in solution. Upon departure from the threshold concentration c^*, the uniform and common for the two oligomeric component chemical networks of the epoxy–phenol polymer break down into discrete and microheterogeneous segments. Breakdown of such network disturbs the structural uniformity and deteriorates the protective and strength characteristics of the polymer coatings.

REFERENCES

1. Krasovskii, A.N., Novikov, D.V., Krasheninnikov, V.A., et al., *Zh. Prikl. Khim.*, 2001, vol. 74, no. 1, pp. 124–134.
2. Krasovskii, A.N., Novikov, D.V., Filippov, V.N., et al., *Zh. Prikl. Khim.*, 2003, vol. 76, no. 2, pp. 304–312.
3. Feder, J., *Fractals*, New York: Plenum, 1988.
4. Sorokin, M.F., Kochnova, Z.A., Nikolaev, L.P., et al., *Tr. Mosk. Khim.-Tekhol. Inst. im. D.I. Mendeleeva*, 1980, no. 110, pp. 63–67.
5. Kochnova, Z.A., Khrisanova, T.A., and Sorokin, M.F., *Lakokras. Mater. Ikh Primen.*, 1989, no. 2, pp. 82–89.
6. *Lakokrasochnye materialy dlya konservnoi tary* (Paint and Varnish Materials for Cans), Lyalyushko, S.M., Ed., Moscow: NIITEKhIM, 1981.
7. Krasovskii, A.N. and Filippov, V.N., *Zh. Prikl. Khim.*, 2003, vol. 76, no. 6, pp. 1000–1005.
8. Krasovskii, A.N., Novikov, D.V., and Filippov, V.N., *Zh. Prikl. Khim.*, 2004, vol. 77, no. 8, pp. 1382–1388.
9. Krasovsky, A.N., Novikov, D.V., Philiipov, V.N., et al., Abstracts of Papers, *4th Int. Symp. "Molecular Order and Mobility in Polymer Systems,"* St. Petersburg, 2002, p. 257.
10. Filippov, V.N., Application of the Cluster Lattice Model to Substantiating the Concentration and Kinetic Modes of Preparation of Poly(Ether Imide) and Epoxy–Phenol Coatings, *Cand. Sci. Dissertation*, St. Petersburg, 2004.
11. Gorshkov, A.V., Verenish, S.S., Evreinov, V.V., and Entelis, S.G., *Chromatographia*, 1988, vol. 26, pp. 338–342.
12. Pugachevich, P.P., Beglyarov, E.M., and Lavygin, I.A., *Poverkhnostnye yavleniya v polimerakh* (Surface Phenomena in Polymers), Moscow: Khimiya, 1982.
13. Drinberg, S.A. and Itsko, E.F., *Rastvoriteli dlya lakokrasochnykh materialov* (Solvents for Paint and Varnish Materials), St. Petersburg: Khimizdat, 2003.
14. Betcher, H.G.O. und Epperlein, J., *Moderne Photographische Systeme*, Leipzig: Grundstoffindustrie, 1990.
15. Skryshevskii, A.F., *Strukrurnyi analiz zhidkostei i amorfnykh tel* (Structural Analysis of Liquids and Amorphous Bodies), Moscow: Nauka, 1980.
16. Krasovkii, A.N. and Belousova, I.A., *Zh. Prikl. Khim.*, 1995, vol. 69, no. 1, pp. 142–147.
17. Ziman, J.M., *Models of Disorder: The Theoretical Physics of Homogeneously Disordered Systems*, Cambridge: Cambridge Univ. Press, 1979.

ISSN 1070-4272, Russian Journal of Applied Chemistry, 2007, Vol. 80, No. 7, pp. 1170–1174. © Pleiades Publishing, Ltd., 2007.
Original Russian Text © L.A. Zemnukhova, S.V. Tomshich, A.V. Kovekhova, L.Yu. Greben', 2007, published in Zhurnal Prikladnoi Khimii, 2007, Vol. 80, No. 7, pp. 1200–1205.

MACROMOLECULAR CHEMISTRY AND POLYMERIC MATERIALS

Polysaccharides Prepared from Sunflower Production Waste

L. A. Zemnukhova, S. V. Tomshich, A. V. Kovekhova, and L. Yu. Greben'

Institute of Chemistry, Far-Eastern Division, Russian Academy of Sciences, Vladivostok, Russia
Pacific Institute of Bioorganic Chemistry, Far-Eastern Division, Russian Academy of Sciences, Vladivostok, Russia
Institute of Chemistry and Applied Ecology, Far-Eastern State University, Vladivostok, Russia

Received October 23, 2006; in final form, February 2007

Abstract—The composition and content of polysaccharides recovered from various samples of sunflower husks by their sequential treatment with water, ammonium oxalate (or oxalic acid), and alkali were examined. The products were analyzed by X-ray diffraction and IR spectroscopy.

DOI: 10.1134/S1070427207070300

Agricultural wastes are a promising source of chemical compounds, as in most cases recovery of natural biologically active substances from these materials is more profitable than the chemical synthesis. Among such secondary resources is sunflower (*Helianthus annuus L.*) production waste.

Sunflower seeds are mainly used by food industry for the production of vegetable oil. Their processing at oil-extracting plants (OEPs) is accompanied by accumulation of husks. This is a large-tonnage waste, and each enterprise solves the problem of its utilization independently. Usually a part of this waste is incinerated in steam boilers and the other part is dumped, deteriorating the environmental situation in the region. Numerous procedures have been suggested for processing of sunflower husks, but the majority of them involve incineration or utilization in the hydrolytic industry for the production of xylose, furfural, and protein yeast [1]. It is also suggested to produce sorbents [2, 3], fertilizers [4–7], forage additives [8], and products exhibiting ion-exchange and bactericidal properties [9]. However, the lack of exhaustive information on many processes involved in treatment of sunflower husks prevents the development and application of efficient (flexible and low-waste) technologies.

To reveal how sunflower strain features affect the composition of husks as a promising raw material for chemical industry, we collected a series of husk samples from OEP waste in various regions of Russia and examined their compositions (organic and inorganic components).

The goal of this study was to analyze the composition and structure of carbohydrates recovered by various extraction procedures from sunflower husks (SH).

EXPERIMENTAL

We examined four SH samples from OEPs in Rostov-on-Don (SH-1, 2003), Altai krai (SH-2, 2004), Krasnodar krai (SH-3, 2004), and Uryupinsk, Volgograd oblast (SH-4, 2004). Visual examination of husks showed that they belonged to different strains.

Husk samples with the particle size no less than 2 mm were washed with water and air-dried to constant weight.

Polysaccharides (PSs) were recovered from SH by sequential extraction with water, ammonium oxalate solution, and alkali solution, after which their qualitative and quantitative compositions were determined. For this purpose, an SH sample (70 g) was poured over with water (solid : liquid weight ratio ~1 : 10) and heated on a water bath for 3 h. The residue was filtered off, the solution was concentrated on a rotary evaporator and centrifuged to remove residual raw material (4500–5000 rpm, 210–25 min), after which the polysaccharides were precipitated with acetone (volume ratio of the solutions 1 : 4). The polysaccharide precipitate was separated by centrifugation, dissolved in water, and freeze-dried to obtain water-extracted polysaccharides [PS(H_2O)]. Depending on the sampling site (and hence on the plant strain), the yield of these polysaccharides was 1.46–2.11 wt % (Table 1).

Table 1. Content, structure, and monosaccharide composition of PSs recovered from SH extracts. Extractant: (1) H_2O, (2) $(NH_4)_2C_2O_4$, and (3) NaOH

Raw material	Extractant	PS characteristics			Method 1*							
					monosaccharide composition,** mol %							GalA, mol %
		yield, wt %	color	structure***	Rha	Ara	Xyl	Man	Glc	Gal	Int	
SH-1	1	1.78	Brown	a	19	21	+	10	25	25	+	+
	2	3.09	Gray-brown	a + c	31	26	–	–	16	27	–	+
	3	4.98	Gray-brown	a	22	33	20	+	7	18	–	+
SH-2	1	1.46	Brown	a	24	21	+	8	23	24	+	+
	2	2.76	Gray-brown	a	28	24	–	–	25	23	–	+
	3	4.58	Gray-brown	a + c	22	34	22	–	7	15	–	+
SH-3	1	1.76	Brown	a	14	16	+	9	18	44	+	+
	2	2.46	Gray-brown	a	37	33	6	–	7	17	–	+
	3	5.63	Dark brown	a	10	19	61	+	+	10	–	+
SH-4	1	2.11	Light brown	a	14	27	+	8	22	29	+	+
	2	2.80	Gray-brown		41	28	+	+	10	21	–	+
	3	5.57	Brown	a	8	28	53	+	3	8	–	+

Raw material	Extractant	Method 2*			
		monosaccharide composition,** mol %			GalA, mol %
		Rha	Pen (Ara : Xyl)	Hex (Man : Glc : Gal)	
SH-1	1	9	21 (1 : 0)	28 (1 : 2.5 : 2.5)	42
	2	11	12 (1 : 0)	6 (0 : 1 : 2)	71
	3	9	74 (1.5 : 1)	7(0 : 1 : 2.5)	10
SH-2	1	12	21 (1 : 0)	22 (1 : 3 : 3)	45
	2	9	10 (1 : 0)	11 (0 : 1 : 1)	70
	3	9	72 (1.5 : 1)	8 (0 : 1 : 2)	11
SH-3	1	10	17 (1 : 0)	25 (1 : 3 : 3)	48
	2	10	14 (6.5 : 1)	12 (0 : 1 : 2.5)	64
	3	8	70 (1 : 3)	10 (0 : 0 : 1)	12
SH-4	1	10	19 (1 : 0)	24 (1 : 2 : 3)	47
	2	11	12 (1 : 0)	22 (0 : 1 : 2)	55
	3	6	77 (1 : 2)	9 (0 : 1 : 3)	8

* Monosaccharides were determined in the form of polyol acetates (method 1) and methyl glycoside acetates (method 2).
** Monosaccharides: (Rha) rhamnose, (Ara) arabinose, (Xyl) xylose, (Man) mannose, (Glc) glucose, (Gal) galactose, and (Int) inositol; (GalA) galacturonic acid; (Pen) pentoses and (Hex) hexoses. (+) Detected as traces.
*** Structure (X-ray diffraction data): (a) amorphous and (c) crystalline.

The residue after the aqueous extraction was poured over with a 0.5 N solution of ammonium oxalate (solid : liquid weight ratio ~1 : 10) and heated on a water bath for 3 h. The undissolved raw material was filtered off. The filtrate was dialyzed against running water for 2–3 days and then against distilled water for 1 day, after which it was concentrated on a rotary evaporator, and a fourfold volume of acetone was added. The precipitate was separated by centrifugation, dissolved in water, and freeze-dried to obtain oxalate-extracted polysaccharides. Their yield was 2.46–3.09 wt % (Table 1).

The SH solid residue after the treatment with water and ammonium oxalate was suspended in 0.5 N NaOH and heated on a water bath for 2 h. The solution was separated by centrifugation and worked up as described above to obtain alkali-extracted polysaccharides in a yield of 4.58–5.67 wt % (Table 1).

The qualitative and quantitative monosaccharide

compositions of the recovered PSs were determined, after acid hydrolysis of the samples with 1 N trifluoroacetic acid (TFA) at 100°C for 4–5 h, by paper chromatography (PC), gas–liquid chromatography (GLC), and GLC–mass spectrometry (GLC–MS) in the form of polyol acetates (method 1). Descending PC was performed on Filtrak FN-12 paper in the solvent system 1-butanol–pyridine–water, 6 : 4 : 3 (by volume). Monosaccharides were detected with an alkaline solution of silver nitrate. Gas–liquid chromatography was performed on an Agilent 6850 chromatograph (the United States) equipped with a flame-ionization detector, using an HP 5 MS capillary column (30 m × 250 μm × 0.25 μm) coated with poly(methyl–5% phenyl)siloxane. The column temperature was as follows: 150°C, 1 min; heating to 230°C, 3 deg min^{-1}; 230°C, 10 min. The GLC–MS analysis was performed with a Hewlett–Packard 6890 chromatograph (the United States) equipped with the similar capillary column and interfaced with a Hewlett–Packard 5973 mass spectrometer (the United States); the temperature conditions were similar.

Uronic acids were detected by GLC in the form of methyl glycoside acetates after methanolysis of PSs (acetyl chloride–methanol, 1 : 10 by volume, 100°C, 7–8 h), followed by acetylation.

Data on water-, oxalate-, and alkali-extracted polysaccharides recovered from SH samples are given in Table 1. All the SHs are brown or gray-brown. The total PS yield ranges from 8.80 (SH-2) to 10.48% (SH-4) relative to the raw material weight and depends on the plant strain and extraction procedure. The highest yield of polysaccharides from all the samples was ensured by alkaline extraction, and the lowest yield, by aqueous extraction.

It should be noted that neutral monosaccharides (rhamnose, arabinose, xylose, glucose, galactose, and mannose) were identified and quantitatively determined by GLC and GLC–MS in the form of polyol acetates. Uronic acids do not give polyols under these conditions; therefore, their qualitative and quantitative determination was performed in the form of methyl glycoside acetates (method 2). Neutral monosaccharides, especially if there are several of them (Table 1), in analysis in the form of methyl glycoside acetates give a complex difficult-to-identify mixture of anomers (from two to four for each monosaccharide); therefore, at best, it is possible to determine only the total content of pentoses and hexoses, rather than the content of separate (individual) monosaccharides.

The qualitative and quantitative monosaccharide composition of the recovered polysaccharides is diverse and depends on the origin of the raw material and on the recovery procedure. For example, in water- and oxalate-extracted PSs xylose is present in trace amounts, and in alkali-extracted PSs its content sometimes exceeds 50% (SH-3, SH-4). Mannose and inositol in small amounts were detected only in water-extracted PSs. Residues of rhamnose, arabinose, glucose, and galactose are present in all the PSs in different ratios. Uronic acids are represented only by galacturonic acid and are present in small amounts in all the recovered polysaccharides (Table 1); their content is maximal in oxalate-extracted PSs (55–71 mol %). In water-extracted PSs, their content is 2–3 times higher (40–47 mol %) than that of arabinose, and in alkali-extracted PSs their content is the lowest (8–12 mol %).

Comparison of the monosaccharide composition of PS samples from sunflower husks with that of the related substances recovered previously from rice husks and meal, buckwheat husks, and buckwheat straw [10, 11] shows that extracts from sunflower husks have a richer qualitative composition and contain large amounts of galacturonic acid.

The structures of the PSs were examined by X-ray phase analysis (DRON-2 diffractometer, CuK_α radiation) and IR spectroscopy (IR Prestige spectrophotometer, Shimadzu, Japan) in the range 400–4000 cm^{-1} by standard procedures. Samples for IR measurements were prepared as KBr pellets.

The X-ray diffraction data (Table 1) show that the PSs recovered from various SH samples have amorphous or amorphous-crystalline structure.

The IR absorption maxima of the examined polysaccharides are given in Table 2, and typical spectra of the substances recovered by extraction of sunflower husks with water, oxalate, and alkali are shown in Fig. 1. The absorption bands were identified using the available structural-spectroscopic data on polysaccharides [12, 13].

The structure and intensity of absorption bands in the IR spectra (400–4000 cm^{-1}) of polysaccharides recovered from sunflower husks noticeably vary depending both on the procedure for polysaccharide recovery (Fig. 1) and on the plant strain (Fig. 2).

Comparison of the characteristic bands of natural polysaccharides recovered by similar procedure but from different raw materials (buckwheat husks) also shows that hydrocarbons having different monosaccharide compositions (Table 1) [10, 11] can be characterized in relation to the kind of the raw material.

Table 2. IR absorption maxima of polysaccharides recovered from sunflower husks

Assignment [12, 13]*	ν, cm^{-1}			
	SH-1	SH-2	SH-3	SH-4
	Water-extracted polysaccharides			
1	3419 s.br	3419 s.br	3452 s	3385 s
2	2931 m	2926 m	2926 m	2937 m
3	1627 s	1616 s	1633 s	1633 s
4	1415 m	1419 m	1402 m	1419 m
	1249 m	1328 w, 1249 m	1236 m	1319 w, 1251 w
5	1099 m	1143 m	1099 m	1076 s
	1026 m	1099 m, 1022 m	1031 m	1047 s
6	(763, 536) s.br	(763, 640, 536) s.br	468 s.br	603 s.br
	Oxalate-extracted polysaccharides			
1	3446 br.s	3446 br.s	3446 s	3449 s
2	2933 m	2926 m	2927 w	2927 w
3	1734 m, 1616 s	1739 m, 1616 s	1627 s	1625 s
4	1404 s, 1328 m, 1242 m	1406 s, 1328 m, 1242 m	1402 m, 1330 w, 1240 w	1421 m, 1327 m, 1246 w
5	1143 m, 1099 m, 1016 m	1143 m, 1099 m, 1014 m	1141 m, 1099 s, 1022 m	1143 m, 1099 s, 1024 m
	954 m	954 m	958 w	958 m
6	(835, 765, 640, 538) m.br	(835, 765, 640, 538) m.br	(767, 646, 538) m.br	(777, 642, 540) m.br
	Alkali-extracted polysaccharides			
1	3419 br.s	3419 br.s	3417 s.br	3421 s
2	2922 m	2918 m	2924 m	2924 m
3	1627 s	1637 s	1631 s	1637 s
4	1411 m	1419 m	1421 m	1423 m
5	1041 s	1041 s	1076 m, 1043 s	1087 s, 1045 s
6	536 m.br	540 m.br	543 m.br	(798, 582, 468) m.br

* (1) OH stretching vibrations in CHOH and CH_2OH groups; (2) CH stretching vibrations; (3) OH bending vibrations, C=O stretching vibrations in carbonyl and carboxy groups; (4) group of bands including C–H bending modes: in-plane, internal (scissor), and external (wagging); (5) stretching vibrations of C–OH and C–O–C bonds in polysaccharides; (6) group of bands including out-of-plane bending modes of OH groups and pulsation vibrations of pyranose rings.

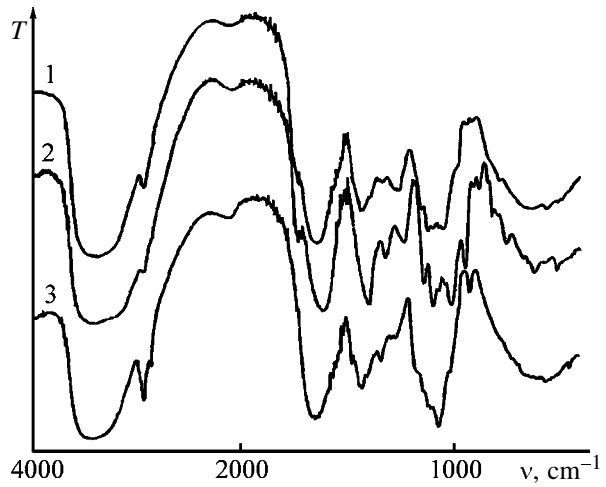

Fig. 1. IR absorption spectra of acetate residues of SH-1 polysaccharides after (*1*) aqueous, (*2*) oxalate, and (*3*) alkaline extraction. (*T*) Transmission and (ν) wavenumber; the same for Fig. 2.

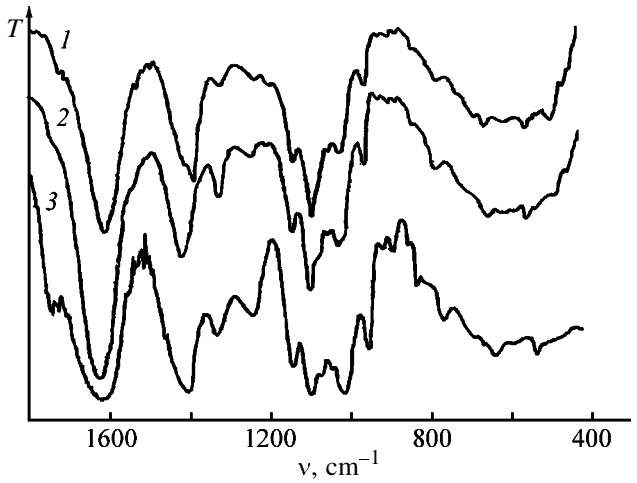

Fig. 2. IR absorption spectra of oxalate-extracted polysaccharides from samples (*1*) SH-1, (*2*) SH-2, and (*3*) SH-3.

The properties of PSs from sunflower husks are poorly studied yet, although it was found that, as a rule, the biological activity is exhibited by carbohydrates with medium and low degree of polymerization [14]. The strongest inhibiting effect is shown by samples recovered from rice husks by oxalate and alkaline extraction [15].

CONCLUSIONS

(1) The chemical composition of polysaccharides recovered by sequential extraction from sunflower husks differs from that of polysaccharides recovered similarly from buckwheat and rice husks in the richer qualitative composition of the monosaccharides. The quantitative ratio of monosaccharides depends on the raw material (plant strain, vegetation site), extraction procedure, and extractant used. The total yield of polysaccharides from sunflower husks varies from 8.8 to 10.5 wt % based on dry raw material. The largest amount of polysaccharides is recovered by alkaline extraction, and the smallest amount, by aqueous extraction.

(2) Uronic acids consist of galacturonic acid only. Its content is comparable to, or exceeds the total content of neutral monosaccharides incorporated in the examined polysaccharides. The highest yield of galacturonic acid was attained in oxalate extracts from sunflower husks.

(3) The polysaccharides are amorphous or amorphous-crystalline substances. IR spectroscopy allows prompt preliminary characterization of the carbohydrate product in relation to the processing conditions and origin (plant strain).

REFERENCES

1. Sharkov, V.I. and Kuibina, N.I., *Khimiya gemitsellyuloz* (Chemistry of Hemicelluloses), Moscow: Lesnaya Prom–st., 1972.
2. Stavitskaya, S.S., Mironyuk, T.I., Kartel', N.T., and Strelko, V.V., *Zh. Prikl. Khim.*, 2001, vol. 74, no. 4, pp. 575–578.
3. Shcherbakov, V.G., Aleksandrova, A.V., and Ksandopulo, S.Yu., *Izv. Vyssh. Uchebn. Zaved., Pishch. Tekhnol.*, 2003, no. 5/6, pp. 27–28.
4. Efanov, M.V. and Zabelina, A.V., *Khim. Prirodn. Soedin.*, 2002, no. 6, pp. 482–483.
5. Fedorova, T.E., Dudkin, D.V., Rokhin, A.V., et al., *Khim. Rastit. Syr'ya*, 2003, no. 4, pp. 25–29.
6. Efanov, M.V., Dudkin, D.V., Galochkin, A.I., and Shott, P.R., *Khim. Rastit. Syr'ya*, 2002, no. 2, pp. 47–51.
7. Efanov, M.V. and Dudkin, D.V., *Khim. Rastit. Syr'ya*, 2004, no. 1, pp. 65–66.
8. Mel'nikov, K.A., Ol'shanskii, V.A., Solokha, D.I., et al., *Kormoproizvodstvo*, 2000, no. 10, pp. 31–32.
9. Lagutkina E.F., Dolgikh N.V., and Kozyreva, N.Yu., Abstracts of Papers, *Vserossiiskaya konferentsiya "Khimiya i tekhnologiya rastitel'nykh veshchestv"* (All-Russia Conf. "Chemistry and Technology of Vegetable Substances"), Syktyvkar, September 25–30, 2000, p. 212.
10. Zemnukhova, L.A., Tomshich, S.V., Shkorina, E.D., et al., *Zh. Prikl. Khim.*, 2004, vol. 77, no. 7, pp. 1192–1196.
11. Zemnukhova, L.A., Tomshich, S.V., Mamontova, V.A., et al., *Zh. Prikl. Khim.*, 2004, vol. 77, no. 11, pp. 1901–1904.
12. Zhbankov, R.G., *Infrakrasnye spektry i struktura uglevodov* (IR Spectra and Structure of Carbohydrates), Minsk: Nauka i Tekhnika, 1972.
13. Filippov, M.P., *Infrakrasnye spektry pektinovykh veshchestv* (Infrared Spectra of Pectin Substances), Chisinau: Shtiintsa, 1978.
14. Ovodov, Yu.S., *Bioorg. Khim.*, 1998, vol. 24, no. 7, pp. 483–501.
15. Mamontova, V.A., Tomshich, S.V., Komandorova, N.A., and Zemnukhova, L.A., in *Materialy III Mezhdunarodnoi konferentsii "Mediko-sotsial'naya ekologiya lichnosti: sostoyanie i perspektivy"* (Proc. III Int. Conf. "Medical and Social Ecology of Human Person: Status and Prospects"), Minsk, 2005, part 2, pp. 132–135.

ISSN 1070-4272, Russian Journal of Applied Chemistry, 2007, Vol. 80, No. 7, pp. 1175–1177. © Pleiades Publishing, Ltd., 2007.
Original Russian Text © E.I. Kulish, R.R. Fatkullina, V.P. Volodina, S.V. Kolesov, Yu.B. Monakov, 2007, published in Zhurnal Prikladnoi Khimii, 2007, Vol. 80, No. 7, pp. 1206–1208.

MACROMOLECULAR CHEMISTRY AND POLYMERIC MATERIALS

Degradation of Enzyme-Containing Chitosan Films

E. I. Kulish, R. R. Fatkullina, V. P. Volodina, S. V. Kolesov, and Yu. B. Monakov

Bashkir State University, Ufa, Bashkortostan, Russia
Institute of Organic Chemistry, Ufa Scientific Center, Russian Academy of Sciences, Ufa, Bashkortostan, Russia

Received September 19, 2006; in final form, May 2007

Abstract—The features of degradation of the chitosan films prepared from acetic acid solutions using Collagenase KK enzyme preparation were studied.

DOI: 10.1134/S1070427207070312

The use of chitosan (CH) as a drug seems rather promising [1, 2]. Incorporation of proteolytic enzymes into CH can improve its pharmaceutical properties. It is believed that, in the absence of chemical bonding with the polymer, the enzymes will be released owing to the diffusion of the protein macromolecules from the polymer matrix into the environment and owing to the enzymatic degradation of chitosan.

In this work we simulated biodegradation of chitosan films containing a proteolytic enzyme.

EXPERIMENTAL

In this study we used chitosan [TU (Technical Specifications) 6-09-05-296–76, Khimmed Company, Russia] prepared by alkaline deacetylation of the crab chitin (75% degree of deacetylation, M_η 120000) and Collagenase KK proteolytic enzyme preparation from hepatopancreas of commercial crab species (Immunopreparat State Unitary Enterprise, Ufa, Bashkortostan, Russia). CH films were prepared by casting a polymer solution onto the glass surface. The weight concentration of CH in the initial solution was 2 g dl^{-1} in 1% acetic acid. In all the experiments the film thickness was constant, 0.1 mm. The enzyme preparation preliminarily dissolved in a small amount of water was added into the CH solution just before casting. The content of the enzyme in the film was varied from 0.5 to 10 wt% with respect to CH weight.

Biodegradation of chitosan under the effect of the enzyme added into the film was studied by viscometric method in a buffer solution containing 0.3 M acetic acid and 0.2 M sodium acetate according to the standard procedure [3]. The experimental error was no more than 5%. To simulate the enzymolysis, the chitosan film was placed on a support wetted with a solution of the enzyme preparation and kept at 35°C for a certain period (up to 1 h). The concentration of the enzyme preparation in the solution being in contact with the chitosan film was varied from 0.1 to 50 wt %. The degradation kinetics was evaluated from the viscometric data. The enzymolysis of chitosan with the enzyme preliminarily added into the films was also studied by viscometric procedure.

Addition of the Collagenase KK enzyme into the CH solution in the stage of the film preparation leads to the following results. As seen from Fig. 1a, with increasing content of collagenase in the film, the intrinsic viscosity of CH gradually decreases, which suggests that the molecular weight of chitosan decreases owing to biodegradation under the effect of the enzyme added.

Using viscometric data and Mark–Kuhn equation for CH solutions [4] in acetate buffer ($[\eta] = 1.38 \times 10^{-4} M^{0.85}$), we can evaluate a relative decrease in the intrinsic viscosity and in the molecular weight of CH (see table).

A similar decrease in the intrinsic viscosity is also observed in the case when the chitosan film prepared without enzyme in placed on a support wetted with a collagenase solution (Figs. 1b and 2a). The following trends are observed.

(1) Sharp decrease in the intrinsic viscosity is observed only in the first 10–15 min of the film contact with the enzyme solution (Fig. 2a). Longer enzymolysis does not noticeably affect the intrinsic viscosity of the CH solutions.

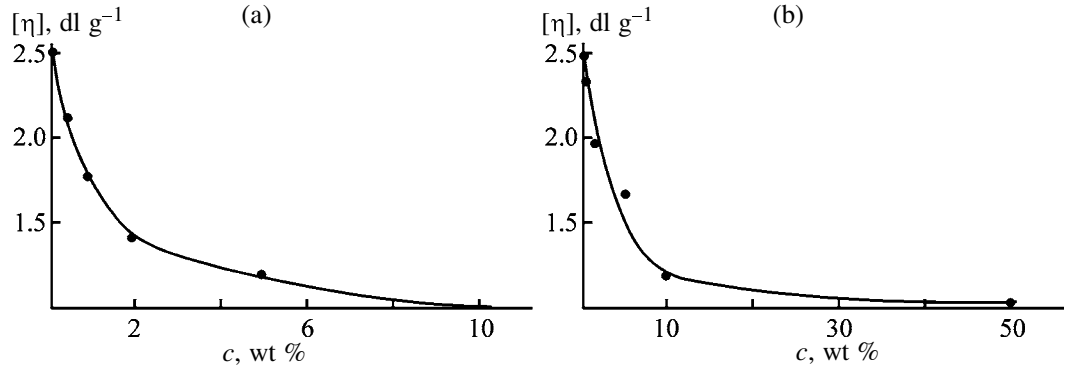

Fig. 1. Intrinsic viscosity [η] of CH recovered (a) from the enzyme-containing film, as a function of the content of Collagenase KK enzyme preparation in the film *c*, and (b) from the enzyme-free film after its contact with a solution of Collagenase KK enzyme preparation for 1 h, as a function of its content in the solution *c*.

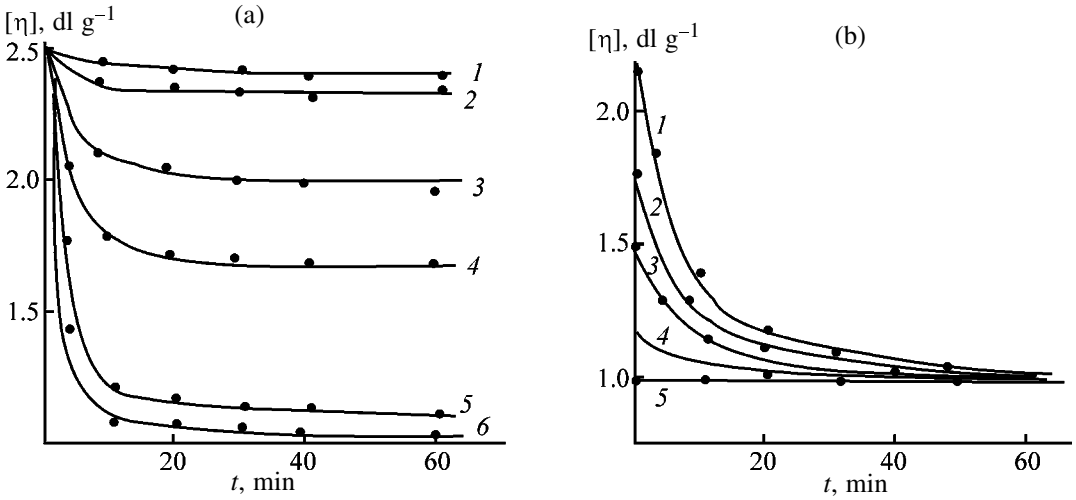

Fig. 2. (a) Variation with time of the intrinsic viscosity [η] of CH recovered (a) from the film at its contact with a solution of Collagenase KK enzyme preparation and (b) from the enzyme-containing film contacting with the solution of Collagenase KK enzyme preparation (4 wt %). (*t*) Contact time of the film and enzyme. (a) Enzyme concentration in solution (wt % with respect to CH weight): (*1*) 0.1, (*2*) 1, (*3*) 2, (*4*) 4, (*5*) 10, and (*6*) 50. (b) Enzyme concentration in the film (wt % with respect to CH weight): (*1*) 0.5, (*2*) 1, (*3*) 3, (*4*) 5, and (*5*) 10.

Degradation of CH as influenced by Collagenase KK enzyme preparation

Biodegradation		Enzymolysis	
c,* wt %	$\Delta M_\eta/M_\eta$, %	*c*,** wt %	$\Delta M_\eta/M_\eta$, %
0.5	11.0	0.1	1.2
1	22.4	1	5.1
3	34.0	2	18.7
5	46.4	4	27.0
10	54.9	10	46.4
		50	54.9

* *c* is the concentration of Collagenase KK in the CH film.
** *c* is the concentration of Collagenase KK in the solution being in contact with CH (contact time 1 h).

(2) Increase in the collagenase concentration in solution that is in contact with the CH film leads to faster decrease in the intrinsic viscosity and molecular weight (see table). Enzymolysis of the CH film for 1 h at a high concentration of the enzyme in solution decreases the molecular weight of chitosan by a factor of about 2.

In principle, proteolytic enzyme should not cause degradation of CH, which is a polysaccharide. However, the Collagenase KK preparation is a complex of enzymes and this complex exhibits high glycosidase activity. Thus, enzymatic degradation of chitosan films in the presence of collagenase is most probably due to the reaction of enzymes with a glycosidase function on CH. For example, collagenase is accompanied by hyaluronidase enzyme, which can split

the glycoside bond not only in hyaluronic acid but also in CH.

These features of the CH degradation are probably due to the fact that the accessibility of the CH units for interaction with enzyme is low, the more so as the enzyme is also a polymer. As a result, the intrinsic viscosity of the CH solutions changes nonmonotonically and flattens out. This fact can be explained as follows. Glycosidase reacts only with accessible CH units and subsequent increase in the concentration of Collagenase KK preparation (and, correspondingly, of glycosidases) or in the contact time of the film and solution does not affect the CH unit accessibility.

To simulate the process of biodegradation of the enzyme-containing preparation, the film (in which the enzyme was introduced in the course of formation) was placed on a support wetted with a collagenase solution. It was found that the rate of decrease in the CH intrinsic viscosity and, thus, in its molecular weight is determined by the amount of the enzyme contained in the film.

As seen from Fig. 2b, with increasing amount of the enzyme in the film the degree of the CH degradation at its contact with the enzyme solution decreases. At a relatively high content of the enzyme in the film (~5–10 wt %), contact of the CH film with a support wetted with a collagenase solution does not provide further decrease in the intrinsic viscosity of the solution. Apparently, in such films glycosidases already break down all the accessible glycoside bonds in CH and, thus, addition of new portions of the enzyme does not lead to the film enzymolysis. It should be noted that an increase in the enzyme concentration in a solution occurring in contact with the film from 4 to 10 wt % and more does not provide additional decrease in the intrinsic viscosity.

Thus, when the enzyme-containing film is placed on the wetted support, the film skeleton is broken across the glycoside bonds and, as a result, the introduced collagenase passes from the film into the solution.

The released collagenase does not lose its proteolytic activity, which is confirmed by enzymolysis of denatured albumin (after Tugolukov). This fact suggests that the CH films containing collagenase enzyme are promising for medical purposes.

CONCLUSIONS

(1) The intrinsic viscosity of chitosan in the form of films prepared from acetic acid solutions decreases under the effect of the Collagenase KK enzyme preparation both upon incorporation of the enzyme directly into the film and upon contact of the film with a support wetted with the enzyme-containing solution.

(2) The enzymatic degradation of chitosan was attributed to the action of glycosidases present in the Collagenase KK enzyme preparation.

(3) Degradation of the films under the effect of glycosidases leads to liberation of the proteolytic enzymes (collagenases), which retain their activity, for example, with respect to enzymolysis of denatured albumin.

REFERENCES

1. *Khitin i khitozan: Poluchenie, svoistva i primenenie* (Chitin and Chitosan: Preparation, Properties, and Use), Skryabin, K.G., Vikhoreva, G.A., and Varlamova, V.P., Eds., Moscow: Nauka, 2002.
2. Muzzarelli, R.A., *Chitin*, Oxford: Pergamon, 1977.
3. Rafikov, S.R., Budtov, V.P., and Monakov, Yu.B., *Vvedenie v fizikokhimiyu rastvorov polimerov* (Introduction to Physical Chemistry of Polymer Solutions), Moscow: Nauka, 1978.
4. Medvedev, V.V., Myasnikov, L.I., and Semchikov, Yu.D., *Vysokomol. Soedin., Ser. A*, 2000, vol. 42, no. 5, p. 840.

ISSN 1070-4272, Russian Journal of Applied Chemistry, 2007, Vol. 80, No. 7, pp. 1178–1180. © Pleiades Publishing, Ltd., 2007.
Original Russian Text © E.I. Kulish, R.R. Fatkullina, V.P. Volodina, S.V. Kolesov, Yu.B. Monakov, 2007, published in Zhurnal Prikladnoi Khimii, 2007, Vol. 80, No. 7, pp. 1209–1212.

MACROMOLECULAR CHEMISTRY AND POLYMERIC MATERIALS

Enzymatic Degradation of Modified Chitosan Films

E. I. Kulish, R. R. Fatkullina, V. P. Volodina, S. V. Kolesov, and Yu. B. Monakov

Bashkir State University, Ufa, Bashkortostan, Russia
Institute of Organic Chemistry, Ufa Scientific Center, Russian Academy of Sciences, Ufa, Bashkortostan, Russia

Received September 19, 2006; in final form, November 2006

Abstract—The features of enzymatic degradation of modified chitosan films prepared from acetic acid solutions using Collagenase KK enzyme preparation was studied.

DOI: 10.1134/S1070427207070324

The possibility of enzymatic degradation of chitosan (CH) is one of its advantages in preparing various medical-purpose materials such as films, sutures, coatings, and gels [1, 2]. However, too rapid enzymatic degradation, which decreases their operation life, can restrict their use.

In this work we studied enzymatic degradation of chitosan films and procedures of the film modification to improve their operation life. At least two ways to solve this problem are known. The first way is to change the supramolecular structure of CH, increase its packing density, and decrease accessibility of the CH units and, thus, degree of biodegradation. The second way is to prepare CH in water-insoluble form.

EXPERIMENTAL

In this work we used chitosan [TU (Technical Specifications) 6-09-05-296–76, Khimmed Company, Russia] prepared by alkaline deacetylation of the crab chitin (75% degree of deacetylation, M_η 120000) and Collagenase KK proteolytic enzyme preparation prepared from hepatopancreas of commercial crab species (Immunopreparat State Unitary Enterprise, Ufa, Bashkortostan, Russia).

CH films were prepared by casting a polymer solution onto the glass surface. The concentration of CH in the initial solution was 2 g dl^{-1}; 1–70 wt % acetic acid was used as solvent. In all the experiments the film thickness was constant, 0.1 mm. Films were dried to constant weight. To simulate the biodegradation process, a chitosan film was placed on a support wetted with a collagenase solution and kept at 35°C for a certain period (up to 1 h). The biodegradation kinetics was studied by the viscometric method in a buffer solution containing 0.3 M acetic acid and 0.2 M sodium acetate. Chitosan was converted into the alkaline form by keeping of the formed film in 0.1 M NaOH for 1 h with subsequent washing in distilled water. Thermal modification of the film was performed by heating of the formed film to 120°C. The degree of swelling of the film samples was studied gravimetrically.

Principal possibility of the CH enzymatic degradation under the effect of Collagenase KK enzyme preparation was shown previously in [3]. It was found that the conformation and supramolecular state of chitosan in the film and the rate of its enzymatic degradation strongly depend on the degree of protonation of the CH amino groups, which, in turn, is determined by the concentration of the acid used. Certain differences in the CH states in acetic acid solu-

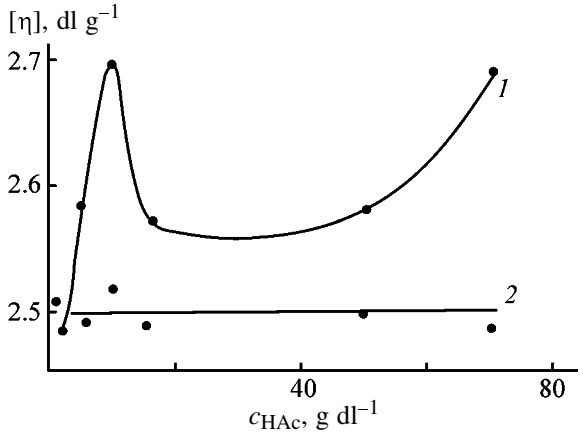

Fig. 1. Intrinsic viscosity of CH films [η] occurring in the (*1*) salt and (*2*) alkaline forms (before degradation) as a function of the acetic acid concentration in the initial solution *c*.

Properties of the CH film samples prepared from acetic acid solutions of various concentrations; keeping time in collagenase solution 1 h, molecular weight of the initial chitosan 1.26×10^5 ([η] 3.0 dl g^{-1})

Film form	Δ[η], dl g^{-1}, after enzymolysis at indicated concentration of acetic acid in the initial solution, %						
	1	5	10	15	20	50	70
Salt	1.03	1.28	1.33	1.15	1.08	1.12	1.59
Alkaline	0.51	0.46	0.63	0.51	0.60	0.65	0.72

tions of various concentrations are confirmed by differences in the intrinsic viscosity of CH before its contact with the enzyme (Fig. 1, curve *1*).

For all the CH films, the dependences of the intrinsic viscosity on the time of contact with the enzyme preparation are similar (Fig. 2). The most significant decrease in the intrinsic viscosity is observed in the first 15–20 min. With a further increase in the treatment time, changes in the intrinsic viscosity are insignificant. It should be noted that, both at short and long contact times, only one trend is observed: the changes in the molecular weight of the polymer are the smallest for the films prepared from 1% acetic acid, whereas molecular weights of the polymers prepared from 10 and, especially, 70% acetic acid change significantly (see table).

The CH films prepared in the salt form (sodium acetate) are highly soluble in water and exhibit high water-absorbing capacity (Fig. 3). Undoubtedly, high water-absorbing capacity is an advantage of chitosan; however, high solubility promotes rapid mechanical failure of the polymer film.

Chitosan in the salt form can be converted into the alkaline form by keeping in 0.1 M NaOH solution for 1 h [4]. This conversion into the alkaline form is characterized by strong increase in the packing density of the CH macromolecules with the corresponding decrease in the accessibility of the CH units for enzymes. The consequences of these changes in the chemical and supramolecular structure of CH in the films are as follows. (1) Conversion of the CH films into the alkaline form strongly decreases the degree of swelling of the film samples (Fig. 3, curve *2*). (2) The intrinsic viscosities of the CH films are leveled (Fig. 1, curve *2*), whereas for CH films in the salt form the intrinsic viscosities vary in a wide range (Fig. 1, curve *1*). (3) Although the shape of the dependence of the intrinsic viscosity on the time of contact with the solution of Collagenase KK preparation (Fig. 4) is similar to that for the films prepared in the salt form, the degree of degradation of the film samples noticeably decreases (see table).

It should be noted that, as in degradation of the salt films, the strongest decrease in the polymer molecular weights is observed for alkaline films prepared from 70% acetic acid. However, the overall degree of degradation of CH prepared in the alkaline form is significantly smaller as compared to CH in the salt form.

Smaller degree of enzymatic degradation of CH films in the alkaline form is their indubitable advant-

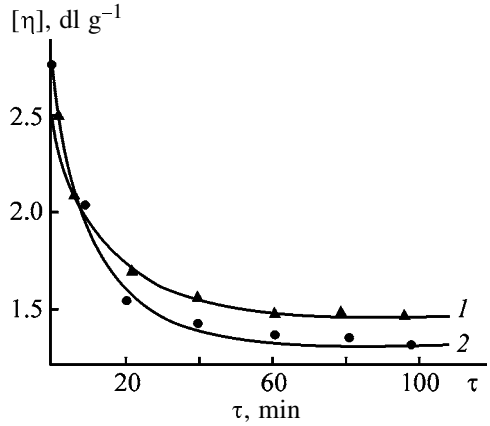

Fig. 2. Intrinsic viscosity of CH solutions [η] obtained from the film samples in the salt form prepared from (*1*) 1 and (*2*) 10% acetic acid as a function of the time of contact with the enzyme τ.

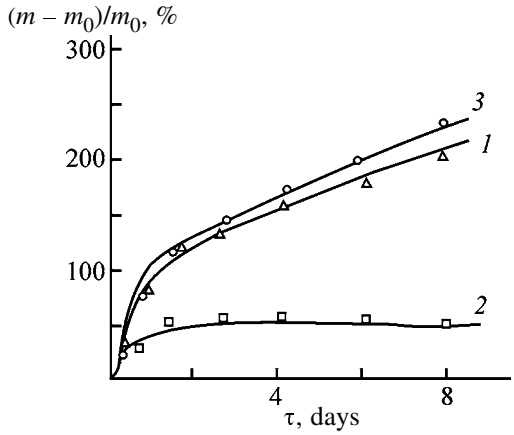

Fig. 3. Kinetics of swelling in water vapor $(m - m_0)/m_0$ of the CH films prepared from 1% acetic acid solution in the (*1*) salt and (*2*) alkaline forms and (*3*) subjected to thermal treatment. (τ) Time.

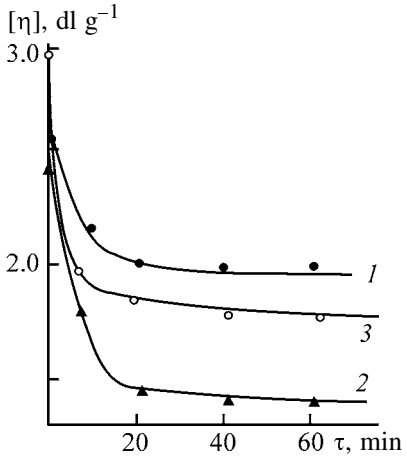

Fig. 4. Intrinsic viscosity of CH solutions [η] obtained from the film samples prepared from 1% acetic acid solution in the (*1*) salt and (*2*) alkaline forms and (*3*) heated at 120°C for 1 h, as a function of the time of contact with the enzyme solution τ.

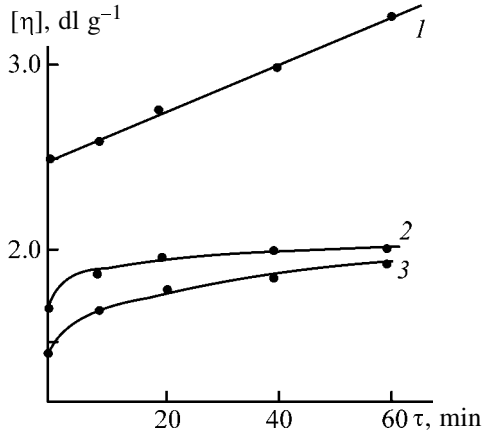

Fig. 5. Intrinsic viscosity of CH film samples [η] prepared from 5% acetic acid solution as a function of the time of thermal treatment τ. (*1*) Films not subjected to contact with the enzyme; contact time, min: (*2*) 10 and (*3*) 30.

age. At the same time, mechanical properties of these films are very poor; they are brittle and inelastic. Moreover, the water-absorption capacity of these films is low, which suggests their small absorption capacity with respect to the separated liquid and makes these films unsuitable.

It should be noted that thermal modification allows preparation of films that are poorly soluble in water but retain high degree of swelling. It is known [5] that heating to the CH films for 3 h at ~120°C causes strong rearrangement of its chemical structure, but does not even affect its swellability (Fig. 3, curve *3*). Since the resistance to degradation of the films insoluble in water cannot be analyzed, we studied the samples subjected to thermal treatment for 1 h, after which the films remain water-soluble. Nevertheless, as seen from Fig. 5, the intrinsic viscosity of the initial CH films noticeably increases with increasing time of thermal treatment (Fig. 5, curve *1*). This increase in the intrinsic viscosity is obviously due to the cross-linking of CH on heating. Moreover, with increasing time of thermal treatment, the stability of the modified films to enzymatic degradation also increases. In fact, degradation of such modified films proceeds down to viscosities close to that of the alkaline films (Fig. 4, curve *3*), but, in contrast to them, modified films are characterized by high mechanical properties.

Thus, both chemical modification of chitosan films by treatment of the formed film with alkaline solution and its thermal treatment allow preparation of polymer coatings with enhanced resistance to enzymatic degradation.

CONCLUSIONS

(1) Modified films of chitosan in the alkaline form exhibit poor solubility and small water-absorption capacity as compared to unmodified samples. These films are highly stable to enzymatic degradation, which is essentially independent on the features of the film preparation.

(2) The chitosan films modified by thermal treatment are virtually insoluble in water and are characterized by high levels of water-absorption capacity, mechanical strength, and elasticity. With increasing time of thermal treatment, the stability of the chitosan films to enzymatic degradation increases.

REFERENCES

1. *Khitin i khitozan: Poluchenie, svoistva i primenenie* (Chitin and Chitosan: Preparation, Properties, and Use), Skryabin, K.G., Vikhoreva, G.A., and Varlamova, V.P., Eds., Moscow: Nauka, 2002.
2. Muzzarelli, R.A., *Chitin*, Oxford: Pergamon, 1977.
3. Kulish, E.I., Volodina, V.P., Fatkullina, R.R., and Kolesov, S.V., Extended Abstracts, *Vos'maya Mezhdunarodnaya konferentsiya "Sovremennye perspektivy v issledovanii khitina i khitozana"* (Eighth Int. Conf. "Modern Prospects in Studies of Chitin and Chitosan"), Moscow: VNIRO, 2006, pp. 290–292.
4. Ageev, V.P., Vikhoreva, G.A., Matushkina, N.N., et al., *Vysokomol. Soedin., Ser. A*, 2000, vol. 42, no. 2, pp. 333–339.
5. Zotkin, M.A., Vikhoreva, G.A., and Kechek'yan, A.S., *Vysokomol. Soedin., Ser. B*, 2004, vol. 46, no. 2, pp. 359–363.

ISSN 1070-4272, Russian Journal of Applied Chemistry, 2007, Vol. 80, No. 7, pp. 1181–1182. © Pleiades Publishing, Ltd., 2007.
Original Russian Text © A.I. Demidov, 2007, published in Zhurnal Prikladnoi Khimii, 2007, Vol. 80, No. 7, pp. 1213–1215.

BRIEF COMMUNICATIONS

Thermodynamics of Reactions Involving Zinc and Cadmium Ions in Alkaline Solutions

A. I. Demidov

St. Petersburg State Polytechnic University, St. Petersburg, Russia

Received February 28, 2007

Abstract—The standard Gibbs energies of assumed reactions in aqueous solutions involving zinc and cadmium ions were calculated.

DOI: 10.1134/S1070427207070336

Zinc(II) ions $Zn(H_2O)_4^{2+}$ and cadmium(II) ions $Cd(H_2O)_4^{2+}$ can be hydrolyzed [1] to form the ions $ZnOH^+$, $[Zn(OH)_3]^-$, $[Zn(OH)_4]^{2-}$, $CdOH^+$, $[Cd(OH)_3]^-$, and $[Cd(OH)_4]^{2-}$. Zinc(II) and cadmium(II) hydroxides are formed as a gelatinous white precipitate when solutions of zinc and cadmium salts are treated with solutions of alkalis [2]. In the crystalline state $Zn(OH)_2$ exists in the form of five (α, β, γ, δ, and ε) modifications, of which only ε-$Zn(OH)_2$ is stable in water at room temperature.

Equilibria (1)–(4) are shifted toward the formation of Zn^{2+}, $[Zn(OH)_4]^{2-}$, Cd^{2+}, and $[Cd(OH)_4]^{2-}$ ions and zinc and cadmium hydroxides, as shown by our thermodynamic calculations of these reactions carried out using the data of [3, 4]:

$$2ZnOH^+ = Zn^{2+} + \varepsilon\text{-}Zn(OH)_{2(s)},\ \Delta G^0_{298} = -36.5\ \text{kJ};\quad (1)$$

$$2[Zn(OH)_3]^- = \varepsilon\text{-}Zn(OH)_{2(s)} + [Zn(OH)_4]^{2-},\quad \Delta G^0_{298} = -21.3\ \text{kJ};\quad (2)$$

$$2CdOH^+ = Cd^{2+} + Cd(OH)_{2(s)},\ \Delta G^0_{298} = -38.1\ \text{kJ};\quad (3)$$

$$2[Cd(OH)_3]^- = Cd(OH)_{2(s)} + [Cd(OH)_4]^{2-},\quad \Delta G^0_{298} = -25.7\ \text{kJ}.\quad (4)$$

Thus, Zn^{2+}, Cd^{2+}, $[Zn(OH)_4]^{2-}$, and $[Cd(OH)_4]^{2-}$ ions are the most stable forms of zinc and cadmium in aqueous solutions. Zinc(II) and cadmium(II) ions can be hydrolyzed according to schemes (5) and (6):

$$Zn^{2+} + 2H_2O = \varepsilon\text{-}Zn(OH)_{2(s)} + 2H^+,\ \Delta G^0_{298} = 65.7\ \text{kJ}.\quad (5)$$

At unit activities of ε-$Zn(OH)_{2(s)}$, Zn^{2+}, and water, pH is 5.75.

$$Cd^{2+} + 2H_2O = Cd(OH)_{2(s)} + 2H^+,\ \Delta G^0_{298} = 78.3\ \text{kJ}.\quad (6)$$

At unit activities of $Cd(OH)_{2(s)}$, Cd^{2+}, and water, pH is 6.86. In turn, the hydrolysis of zinc and cadmium hydroxides is accompanied by the formation of minor amounts of $[Zn(OH)_4]^{2-}$ and $[Cd(OH)_4]^{2-}$ ions:

$$\varepsilon\text{-}Zn(OH)_{2(s)} + 2H_2O = [Zn(OH)_4]^{2-} + 2H^+,\quad \Delta G^0_{298} = 169.5\ \text{kJ}.\quad (7)$$

At unit activities of $[Zn(OH)_4]^{2-}$, ε-$Zn(OH)_{2(s)}$, and water, pH is 14.8.

$$Cd(OH)_{2(s)} + 2H_2O = [Cd(OH)_4]^{2-} + 2H^+,\quad \Delta G^0_{298} = 191.3\ \text{kJ}.\quad (8)$$

At unit activities of $[Cd(OH)_4]^{2-}$, $Cd(OH)_{2(s)}$, and water, pH is 16.8.

As noted above, the treatment of solutions of zinc(II) and cadmium(II) salts with solutions of alkalis results in the formation of zinc and cadmium hydroxides:

$$Zn^{2+} + 2OH^- = \varepsilon\text{-}Zn(OH)_{2(s)},\ \Delta G^0_{298} = -94.1\ \text{kJ}.\quad (9)$$

$$Cd^{2+} + 2OH^- = Cd(OH)_{2(s)},\ \Delta G^0_{298} = -81.5\ \text{kJ}.\quad (10)$$

The reactions of zinc and cadmium hydroxides with hydroxide ions are accompanied by the formation of minor amounts of tetrahydroxozincate and tetrahydroxocadmate ions:

$$\varepsilon\text{-}Zn(OH)_{2(s)} + 2OH^- = [Zn(OH)_4]^{2-},\ \Delta G^0_{298} = 9.7\ \text{kJ}.\quad (11)$$

$$Cd(OH)_{2(s)} + 2OH^- = [Cd(OH)_4]^{2-},\ \Delta G^0_{298} = 31.5\ \text{kJ}.\quad (12)$$

The comparison of the equilibrium constants of reactions (5)–(12) suggests that reactions (9)–(12) bring the main contribution to the precipitation of zinc and cadmium hydroxides. When a zinc electrode is

ionized in an alkaline solution, tetrahydroxozincate ions are formed [5]:

$$Zn + 4OH^- = [Zn(OH)_4]^{2-} + 2e,\ E^0 = -1.200\ V. \quad (13)$$

These ions can dissociate by reaction (14):

$$[Zn(OH)_4]^{2-} = \varepsilon\text{-}Zn(OH)_{2(s)} + 2OH^-,\ \Delta G^0_{298} = -9.7\ kJ. \quad (14)$$

The standard potential of reaction (13) calculated in this study agrees well with the analogous value $E^0 = -1.196 \pm 0.01$ V found on the basis of experimental data of various authors [6]. The solubility of potassium zincate $K_2[Zn(OH)_4]$ in potassium hydroxide solutions (6–10 M) is 1–2 M [7]. When the solution is saturated with potassium zincate, the equilibrium of reaction (14) is shifted to the right, and its product, zinc hydroxide, covers an electrode surface, which results in a sharp increase in the polarization owing to difficult access of hydroxide ions to the electrode surface. The standard potential of reaction (15) calculated in this study agrees well with the reference data [8]:

$$Zn + 2OH^- = \varepsilon\text{-}Zn(OH)_2 + 2e,\ E^0 = -1.250\ V. \quad (15)$$

Zinc oxide ZnO is the most stable form and the final product of all transformations at alkali concentrations in solution higher than 8 M [7]. The results of thermodynamic calculations of reactions (16) and (17) support this experimental fact:

$$[Zn(OH)_4]^{2-} = ZnO + H_2O + 2OH^-,\ \Delta G^0_{298} = -11.7\ kJ; \quad (16)$$

$$\varepsilon\text{-}Zn(OH)_2 = ZnO + H_2O,\ \Delta G^0_{298} = -2.0\ kJ. \quad (17)$$

The theoretical value of the emf of nickel–zinc battery, calculated on the basis of standard potentials of the reactions occurring on positive [9] and negative electrodes, is 1.741 V. This value agrees well with the theoretical emf value of 1.74 V given in Bagotskii and Skundin's monograph [7].

The solubility of $Cd(OH)_2$ in alkaline solutions is insignificant and increases from 9×10^{-6} to 1.5×10^{-4} M on increasing potassium hydroxide concentration in solution from 1 to 10 M [10]. Hence, on the ionization of a cadmium electrode, the alkaline solution becomes practically immediately saturated with cadmium hydroxide. Therefore, the electrode reaction should be written as

$$Cd + 2OH^- = Cd(OH)_{2(s)} + 2e,\ E^0 = -0.825\ V. \quad (18)$$

The resulting standard potential of the cadmium electrode in alkaline solution considerably differs from that given in the handbook [8], $E^0 = -0.809$ V. This is apparently due to the fact that usually the standard Gibbs energy of the formation of amorphous (active) cadmium hydroxide is used in the calculation:

$$Cd + 2OH^- = Cd(OH)_{2(amorph)} + 2e,\ E^0 = -0.807\ V. \quad (19)$$

The theoretical values of the emf of a nickel–cadmium battery, calculated on the basis of standard potentials of the reactions occurring on positive and negative electrodes [reactions (18) and (19)], are 1.316 and 1.298 V, respectively. The theoretical emf value of a nickel–cadmium battery given in Bagotskii and Skundin's monograph is 1.30 V [7].

CONCLUSIONS

(1) The most stable species of zinc and cadmium in aqueous solutions are Zn^{2+}, Cd^{2+}, $[Zn(OH)_4]^{2-}$, and $[Cd(OH)_4]^{2-}$ ions.

(2) The standard potentials of the reactions occurring on the discharge of zinc and cadmium electrodes in an alkaline solution were calculated.

REFERENCES

1. Nazarenko, V.A., Antonovich, V.P., and Nevskaya, E.M., *Gidroliz ionov metallov v razbavlennykh rastvorakh* (Hydrolysis of Metal Ions in Dilute Solutions), Moscow: Atomizdat, 1979.
2. Ripan, R. and Ceteanu, I., *Chimia metalelor*, Bucharest: Didactica sai Pedagogica, 1967.
3. *Termicheskie konstanty veshchestv: Spravochnik* (Thermal Constants of Substances: Handbook), Glushko, V.P., Ed., Moscow: VINITI, 1972, issue 6, part 1.
4. Garrels, R.M. and Christ, C.L., *Solutions, Minerals, and Equilibria*, New York: Harper and Row, 1965.
5. *Khimicheskie istochniki toka: Spravochnik* (Chemical Power Sources: Handbook), Korovin, N.V. and Skundin, A.M., Eds., Moscow: MEI, 2003.
6. Revina, E.M., Rotinyan, A.L., and Shoshina, I.A., *Zh. Prikl. Khim.*, 1973, vol. 46, no. 12, pp. 2654–2659.
7. Bagotskii, V.S. and Skundin, A.M., *Khimicheskie istochniki toka* (Chemical Power Sources), Moscow: Energoizdat, 1981.
8. *Spravochnik po elektrokhimii* (Handbook of Electrochemistry), Sukhotin, A.M., Ed., Leningrad: Khimiya, 1981.
9. Demidov, A.I., Kokhatskaya, M.S., and Chernovets, B.V., *Zh. Prikl. Khim.*, 2006, vol. 79, no. 3, pp. 506–507.
10. Rozentsveig, S.A., Ershler, B.V., Shtrum, E.L., and Ostanina, M.M., in *Trudy soveshchaniya po elektrokhimii* (Proc. Meet. on Electrochemistry), December 19–25, 1950, Moscow: Akad. Nauk SSSR, 1953, pp. 571–578.

ISSN 1070-4272, Russian Journal of Applied Chemistry, 2007, Vol. 80, No. 7, pp. 1183–1184. © Pleiades Publishing, Ltd., 2007.
Original Russian Text © A.F. Gogotov, V.A. Babkin, A.A. Levchuk, L.A. Ostroukhova, 2007, published in Zhurnal Prikladnoi Khimii, 2007, Vol. 80, No. 7, pp. 1216–1217.

BRIEF COMMUNICATIONS

Vegetable Phenols as Effective Inhibitors of Thermal Polymerization for Petrochemical Plants

A. F. Gogotov, V. A. Babkin, A. A. Levchuk, and L. A. Ostroukhova

Irkutsk State Technical University, Irkutsk, Russia
Favorskii Institute of Chemistry, Siberian Division, Russian Academy of Sciences, Irkutsk, Russia

Received September 12, 2006

Abstract—A new source of effective polymerization inhibitors for petrochemical industry was suggested: polyphenols recovered from wood and other vegetable raw materials.

DOI: 10.1134/S1070427207070348

Structural reorganization of the chemical industry of the Russian Federation after disintegration of the Soviet Union led to the loss of such an important line as production of inhibitors and/or inhibiting formulaitions for various petrochemical processes. The revival of the Russian industry of effective and relatively cheap polymerization inhibitors is based, as previously in the Soviet Union, on the primary use of by-products or wastes from chemical industry. The most widespread raw materials for the synthesis of this class of auxiliary reagents for petrochemistry are phenols [1] and phenol-containing fractions of coal and wood processing [2, 3]. The experience of using the sum of phenolic fractions from thermal processing of coal and wood as inhibitors of undesirable thermal polymerization in the distillation processing of pyrocondensates showed that the fractions obtained, known as FCh-16 and DSI, have serious drawbacks making their use in the modern petrochemical industry virtually impossible.

For by-product coke phenols [2], an engineering solution was found that opens prospects for the development of a new generation of effective inhibitors: directional cross-linking of phenols to obtain oligomers that are insoluble in water but soluble in organic solvents and exhibit, compared to the starting unmodified phenols, increased inhibiting activity and higher level of other process characteristics [4].

As for phenols prepared from wood, it was found experimentally that the drawbacks of DSI [3], especially the low inhibiting activity of pyrolytic wood phenols, are inherent and it is necessary to develop novel processes for recovery of phenolic compounds from vegetable tissues, not involving pyrogenic treatment of the raw material. Since vegetable phenols contain a significant fraction of polyhydric phenols [5], the development of a process for their selective recovery seems promising. For example, DFV agent (dihydroquercetin) was experimentally tested as inhibitor of industrial radical processes (undesirable thermal polymerization) [6]. This natural condensed phenolic compound, belonging to flavonoids, contains two dihydric phenolic fragments: pyrocatechol and resorcinol fragments. Dihydroquercetin showed a very high inhibiting effect in thermal processing of the pyrocondensate from EP-300 installation of the Angarsk Polymer Plant under the laboratory conditions (130°C, 1 h). The inhibiting effect reaches 67.3% even at the inhibitor content as low as 0.01 wt %. The highest inhibiting activity of DKV, 77.8%, is observed at its content of 0.03 wt %. These parameters of the inhibiting activity are close to those of the known imported individual synthetic inhibitors, e.g., *tert*-butylpyrocatechol [7].

Dihydroquercetin is widely used today in medical, pharmaceutical, and food industry as the most effective natural antioxidant, nontoxic preservative, and prophylactic agent for strengthening the cardiovascular system [8–10]. As the source of raw materials for this product in Russia is virtually inexhaustible (coniferous wood) and the process for its extractive recovery from wood tissues is relatively simple [11–13], we can speak of a new source of effective inhibitors for petrochemical processes. Experimental trials showed, however, that wide application of this product to petrochemical industry requires elimination of certain drawbacks of DKV as inhibitor of industrial polymerization processes. In particular, it should be modified

to make it insoluble in hot water. Phenolic compounds of vegetable origin are environmentally safe products considerably differing in the organoleptic and toxicological properties from technogenic phenolic fractions. In particular, they are odorless and tasteless and have low toxicity and low solubility in cold water.

CONCLUSION

Dihydroquercetin, a well-known vegetable polyphenol and effective antioxidant, exhibits high antiradical activity, which makes this class of compounds promising as polymerization inhibitors for industrial petrochemical processes.

ACKNOWLEDGMENTS

The study was financially supported by the Russian Foundation for Basic Research (project no. 05-08-50097).

REFERENCES

1. Kurbatov, V.A., Liakumovich, A.G., and Kirpichnikov, P.A., *Neftekhimiya*, 1983, vol. 23, no. 1, pp. 118–120.
2. Berents, A.D., Vol'-Epshtein, A.V., Mukhina, T.N., et al., *Pererabotka zhidkikh produktov piroliza* (Processing of Liquid Pyrolysis Products), Moscow: Khimiya, 1985, pp. 59–60.
3. Zav'yalov, A.N., Gol'dshmidt, Yu.M., Zav'yalova, Z.A., and Kasilova, L.V., *Drevesnosmolyanyi i drugie ingibitory tsepnykh protsessov* (Wood-Resin and Other Inhibitors of Chain Processes), Moscow: VNIPIEIlesprom, 1978.
4. RF Patent 2265005.
5. Blažej, A., *Rastlinne fenolove zluceniny*, Bratislava: Alfa, 1973.
6. RF Patent 2270204.
7. Gogotov, A.F., Turova, A.V., Chertkov, A.M., et al., *Proizv. Ispol'z. Elastom.*, 2004, no. 4, pp. 7–11.
8. Tyukavkina, N.A., Rulenko, I.A., Kolesnik, Yu.A., et al., *Vopr. Pitan.*, 1996, no. 2, pp. 33–38.
9. Kolkhir, V.K., Tyukavkina, N.A., Bykov, V.A., et al., *Khim.-Farm. Zh.*, 1995, no. 9, p. 61.
10. Babkin, V.A., Ostroukhova, L.A., Malkov, Yu.A., et al., *Khim. Inter. Ustoich. Razv.*, 2001, no. 3, pp. 363–367.
11. RF Patent 2000797.
12. RF Patent 2034559.
13. RF Patent 2158598.

ISSN 1070-4272, Russian Journal of Applied Chemistry, 2007, Vol. 80, No. 7, pp. 1185–1186. © Pleiades Publishing, Ltd., 2007.
Original Russian Text © M.G. Voronkov, V.P. Baryshok, G.A. Kuznetsova, N.N. Vlasova, 2007, published in Zhurnal Prikladnoi Khimii, 2007, Vol. 80, No. 7, pp. 1218–1219.

BRIEF COMMUNICATIONS

Fungistatic Polyphenylmethylsiloxane Resin Prepared from the Phenyltrichlorosilane Production Bottoms

M. G. Voronkov, V. P. Baryshok, G. A. Kuznetsova, and N. N. Vlasova

Favorskii Institute of Chemistry, Siberian Division, Russian Academy of Sciences, Irkutsk, Russia
Irkutsk State Technical University, Irkutsk, Russia

Received March 16, 2007

Abstract—Polyphenylmethylsiloxane resin exhibiting a strong fungistatic effect was prepared by hydrolysis of phenyltrichlorosilane production bottoms with addition of phenyltrichlorosilane and methyltrichlorosilane.

DOI: 10.1134/S107042720707035X

Phenyltrichlorosilane is an intermediate in the production of lacquers based on phenylsiloxane resins and used, in particular, in electrotechnical industry [1–4]. The bottoms from the production of phenyltrichlorosilane, which is synthesized in Russia by high-temperature condensation of chlorobenzene with trichlorosilane, account for 1.5–3 wt % of the condensate [5, 6].

In this study we developed a procedure for utilization of the bottoms by their conversion to a heat-resistant phenylmethylsiloxane resin exhibiting fungistatic activity. The composition of the bottoms was determined by gas chromatography–mass spectrometry:

Composition of phenyltrichlorosilane production bottoms*

Component	Content, wt %
Phenyltrichlorosilane	24.0
Monochlorodiphenyl	26.3
Diphenyl	15.4
Dichlorodiphenyl	11.0
Trichlorosilyldiphenyls	17.6
Trichlorosilyldichlorodiphenyls	3.1
Chlorobenzene	2.6

* From Sibirskii Silikon Joint-Stock Company, Usol'e-Sibirskoe, Irkutsk oblast.

The procedure is based on the cohydrolysis of the bottoms with phenyltrichlorosilane and methyltrichlorosilane in aqueous butanol. The toluene solution of the resin (F-XIV) thus prepared is a transparent viscous dark brown liquid (KO-XIV organosilicon lacquer). In the physicochemical and technical parameters, the lacquer meets the requirements of GOST (State Standard) (Table 1) [7].

Lacquer coatings prepared from a solution of F-XIV resin exhibit high fungistatic activity. For F-XIV polyphenylsiloxane resin, it is 1 point against mold fungi in a humid chamber over water plane and 2 points in Petri dishes with Czapek medium (in the 6-point scale, Table 2). The tests were performed according to GOST 9.050–75; infection with an aqueous suspension of *Aspergillus flavus* + *Aspergillus niger* + *Cladosporium herbarum* + *Fusarium moniliforme* + *Paccilomyces varioti* + *Trichoderma viride* spores.

EXPERIMENTAL

A 2-l four-necked flask equipped with a stirrer, a reflux condenser, a dropping funnel, and a thermometer was charged with 320 ml of butanol, 320 ml of toluene, and 320 ml of water. The mixture was stirred for 30 min, after which a mixture of 30 ml of bottoms, 150 ml of phenyltrichlorosilane, and 7.5 ml of methyltrichlorosilane was slowly added over a period of 2 h, keeping the temperature at approximately 10°C (cooling with water). The mixture was stirred for an additional 2 h at 60–65°C and allowed to stand for 2 h at 20–22°C without stirring. The upper toluene layer was separated and washed three times with water to pH 6. The solvent was distilled off. The residue was heated for 30 min at 125–130°C. Yield of polyphenylmethylsiloxane resin 186.4 g.

Table 1. Main characteristics of KO-XIV organosilicon lacquer

Parameter	Standard (GOST 11066–74 with revisions 1, 2, 3, 4)	Analysis results
External appearance	Transparent dark brown liquid with minor mechanical inclusions	Transparent dark brown liquid
Weight fraction of nonvolatile substances, %	33–37	52
Viscosity (outflow time) at 20.0±0.5°C	12–16*	–
	10–13**	11.3
Acid number, mg KOH/g lacquer, no more than	10	1.3
Time of film drying to degree 3, no more than:		
in air, h	2	2
at 150±2°C, min	10	10

* VZ-1 viscometer (2.5-mm tip).
** VZ-4 viscometer (4-mm tip).

Table 2. Fungus resistance of F-XIV resin at 28°C*

Exposure conditions	Exposure time	Results
Resin in suspension of fungus association	48 h	3.2% germination (in control, 87.6%)
Resin applied onto brick in humid chamber (90% humidity)	14 days	No germination
Resin in Petri dishes with Czapek medium	14 days	All fungi (except *Trichoderma viride*) are fully suppressed; 68–80% inhibition of *Trichoderma viride* growth

* According to data of the Research Institute of Biology, Irkutsk State University.

CONCLUSIONS

(1) A procedure for utilization of phenyltrichlorosilane production bottoms was developed.

(2) Lacquers based on F-XIV polyphenylmethylsiloxane resin can be used for protecting various materials from the damage by mold fungi at a humidity of up to 100%.

ACKNOWLEDGMENTS

The study was supported by the Grant Council at the President of the Russian Federation (project no. NSh-4575.2006.3).

REFERENCES

1. Karyakina, M.I., Maiorova, N.V., and Viktorova, M.I., *Lakokrasochnye materialy: Tekhnicheskie trebovaniya i kontrol' kachestva: Spravochnoe posobie* (Paint-and-Varnish Materials: Requirements Specification and Quality Control: Handbook), Moscow: Khimiya, 1984.
2. *Paint and Surface Coatings: Theory and Practice*, Lambourne, R., Ed., Chichester: Ellis Horwood, 1987.
3. Sobolevskii, M.V., Skorokhodov, I.I., Grinevich, K.P., et al., *Oligoorganosiloksany: Svoistva, poluchenie, primenenie* (Oligoorganosiloxanes: Properties, Preparation, Applications), Sobolevskii, M.V., Ed., Moscow: Khimiya, 1985.
4. Sobolevskii, M.V., Muzovskaya, O.A., and Popeleva, G.S., *Svoistva i oblasti primeneniya kremniiorganicheskikh produktov* (Properties and Fields of Application of Organosilicon Products), Sobolevskii, M.V., Ed., Moscow: Khimiya, 1975.
5. Molokanov, Yu.K., Korablina, T.P., Kleinovskaya, M.A., and Shchelkunova, M.A., *Razdelenie smesei kremniiorganicheskikh soedinenii* (Separation of Mixtures of Organosilicon Compounds), Moscow: Khimiya, 1974.
6. Andrianov, K.A., *Metody elementoorganicheskoi khimii* (Methods of Organometallic Chemistry), Moscow: Nauka, 1968, pp. 104–105.
7. *GOST* (State Standard) *11066–74 with Revisions 1, 2, 3, 4: Heat-Resistant Organosilicon Lacquers and Enamels: Technical Specification*, Moscow: Izd. Standartov, 1997.

ISSN 1070-4272, Russian Journal of Applied Chemistry, 2007, Vol. 80, No. 7, pp. 1187–1193. © Pleiades Publishing, Ltd., 2007.
Original Russian Text © A.G. Morachevskii, 2007, published in Zhurnal Prikladnoi Khimii, 2007, Vol. 80, No. 7, pp. 1220–1228.

HISTORY OF CHEMISTRY AND CHEMICAL TECHNOLOGY

To Eightieth Anniversary of *Zhurnal Prikladnoi Khimii* (Russian Journal of Applied Chemistry)

DOI: 10.1134/S1070427207070361

On December 28, 1867, in St. Petersburg was opened the First Congress of Russian Natural Scientists and Physicians. By the initiative of the chemical section of the Congress, the question about organization of the Russian Chemical Society was raised on January 3, 1868. The participants of the Congress supported this idea and an appropriate resolution was adopted at the final plenary meeting of the Congress on January 4, 1868 [1]. The statute of the society, worked out at the organizational meetings on February 15 and September 19, 1868, was submitted to approval by the Minister of public education. Thanks to the vigorous efforts of D.I. Mendeleev (1834–1907) and N.A. Menshutkin (1843–1907), the first meeting of the Russian Chemical Society at St. Petersburg Imperial University was held already on November 6, 1868. N.N. Zinin (1812–1880), professor of Medical-Surgical Academy in St. Petersburg, academician of St. Petersburg Academy of Sciences since 1865, outstanding scientist in the field of organic chemistry, and organizer of a prominent scientific school, was elected the first president of the society [1, 2]. Menshutkin was entrusted with edition of *Zhurnal Russkogo Khimicheskogo Obshchestva* (Journal of the Russian Chemical Society).

In 1876, the Russian Chemical Society merged, at Mendeleev's suggestion, with the Russian Physical Society founded in 1872 and the Russian Physicochemical Society (RFKhO) was formed with two departments and a common journal having physical and chemical parts. In 1906, the RFKhO journal was divided into two independent journals of the physical and chemical departments.

The RFKhO journal (chemical department) was long the only chemical journal in Russia, with both theoretical and applied articles published. World War I (1914–1918) strongly affected the development of scientific studies in Russia. Despite the noticeable advances in chemical science and development of scientific schools, the level of the chemical industry in the country was insufficient. Russia had vast mineral resources, but their mining and processing were not organized. In 1904–1914, a rather rapid rise in the industrial production was observed in Russia, but, on the whole, it remained insufficient and Russia was not prepared to long war in many respects [3, 4]. It was understood already in the first months of war that the dramatically increased demand for powders and explosives cannot be satisfied because of the deficiency of nitric and sulfuric acids, as well as of benzene and toluene, lack of chemical warfare, deficiency of medicinals, and shortage of fuels and lubricants. Urgent and drastic measures were necessary.

On the initiative of Academician V.I. Vernadsky (1863–1945), an outstanding scientist and public figure, supported by a number of other scientists at St. Petersburg Academy of Scientists, the Permanent commission for study of natural productive forces of Russia (KEPS) was organized in February 1915. Vernadsky was elected its chairman, and A.E. Fersman (1883–1945, academician since 1919) became the secretary of the Commission. The main tasks of the Commission were to study natural resources and enable their industrial use. The Military-chemical committee was formed in October 1915 in Petrograd at the Russian Physicochemical Society in order to "unite the efforts of Russian chemists for joint systematic work on problems related to the needs of the State defense" [4, 5]. Particular mention should be made of the activities of the Chemical committee at Chief artillery department. Academician V.N. Ipat'ev (1867–1952), one of the most outstanding chemists of the first half of the XX century, was appointed head of this Committee in April 1915. Ipat'ev became world known because of his fundamental works in catalysis and catalytic organic synthesis [6–9]. He was the first who started use of high pressures and temperatures in heterogeneous catalytic processes, introduced a large number of previously unused catalysts into laboratory and technological practice, and demonstrated for the first time that use of mixed catalysts dramatically improves the potentialities of heterogeneous catalysis and enables purposeful modification of the properties of solid catalysts. During the years of World War I, professor of the Artillery Academy in St. Petersburg and lieutenant-general

Vyacheslav Evgen'evich Tishchenko.

Ipat'ev supervised the reforming and development of military-chemical industry in Russia. Data demonstrating the fast rise in the manufacture of explosives, war gases, and other most important chemical products already by the end of 1916 can be found in [7, 10]. The vigorous scientific and organizational activities of Ipat'ev also continued in the post-war period. V.I. Lenin named Ipat'ev "head of our chemical industry" [8]. In 1917–1926, Ipat'ev controlled the organization of chemical research, functioning of chemical industries, and development of new technologies.

The development of chemical research in Russia in the early XX century (1901–1917) and in the later period (1918–1941) was the subject of D.N. Trifonov's essays [11–14].

In 1918–1920, a number of scientific institutions, which later became the basis for most prominent research institutes, were created in Petrograd and Moscow on the initiative of KEPS despite the difficulties caused by the civil war. In particular, the Russian Institute of Applied Chemistry [later, State Institute of Applied Chemistry (GIPKh) and then Prikladnaya Khimiya Russian Scientific Center] was founded in 1919 in Petrograd for solution of most important problems in chemistry and chemical technology. The exploitation of natural resources of the country (Verkhnekamskoe deposit of potassium and magnesium salts, Tikhvin bauxites, Khibiny apatites, and phosphorite and mirabilite deposits), which was commenced soon after, and the need to solve other problems (synthesis of ammonia, industrial manufacture of synthetic rubber, production of plastics and artificial fibers, etc.), which required that the research in applied chemistry should be expanded, made coordination of these works in a specialized scientific journal an imperative necessity.

At the meeting of the chemical department of RFKhO on December 2, 1926, an appeal of a large group of scientists and staff members of industrial plants, concerning organization of the Department of Applied Chemistry in RFKhO, was considered. The appeal, in particular, said that the Department could unite active workers in the field of applied chemistry on the all-Union scale and would enable organization of a journal for publication of the relevant original research works. It was pointed out as an example that the American Chemical Society publishes, together with the main chemical journal (Journal of the American Chemical Society, published since 1879), also a journal devoted to problems of applied chemistry (Industrial and Engineering Chemistry, published since 1909). Among those who signed the appeal that the Department of Applied Chemistry should be organized in RFKhO were most prominent chemists of that time: M.S. Vrevskii, A.I. Gorbov, I.V. Grebenshchikov, S.N. Danilov, V.I. Ipat'ev, I.A. Kablukov, S.V. Lebedev, A.E. Porai-Koshits, V.E. Tishchenko, A.E. Favorskii, and others (a total of 95 signatures). Later, all those who signed the appeal became founder-members of the Department.

The general meeting of RFKhO on January 23, 1927, decided that organization of the Department of Applied Chemistry is rather desirable and timely. After the necessary authorizations, the decision to organize the Department of Applied Chemistry in RFKhO was made in April 1927. The organization meeting of the Department was held on May 12, 1927, eighty years ago. V.E. Tishchenko (1861–1941), one of the oldest members of RFKhO (since 1883), disciple of Mendeleev and A.M. Butlerov (1828–1886) was elected the Chairman of the Department [16, 17]. A scientist with broad interests, Tishchenko was equally successful in theoretical and applied chemistry. He was a prominent specialist in organic and technical chemistry and forest chemistry and paid a considerable attention to the history of chemistry. Tishchenko was among those who initiated the organization of the Institute of Applied Chemistry and worked for a long time (1919–1939) at this institute. He became a member of the Academy of Sciences of the USSR in 1935.

On November 17, 1927, at the first meeting of the Department of Applied Chemistry Tishchenko reported the agreement with state organizations about publication of *Zhurnal Prikladnoi Khimii* (ZhPKh), beginning in 1928. Most prominent scientists of that time: Ipat'ev, I.A. Kablukov (1857–1942), E.I. Orlov (1865–1944), V.E. Tishchenko, and A.E. Chichibabin (1871–1945), became members of the Editorial Board of the journal.

Academician Ipat'ev's achievements were already mentioned. Kablukov, professor of Moscow University and honorary member of the Academy of Sciences of the USSR since 1932, who became a member of the Editorial Board, was a known physical chemist with broad scientific interests, author of textbooks on inorganic and physical chemistry, and science popularizer. Electrochemistry of nonaqueous solutions was the preferred area of his scientific studies. E.I. Orlov (academician of the Academy of Sciences of the Ukrainian SSR since 1929) was a chemist-technologist with rather broad interests, engaged in the technology of manufacture of both organic (ethylene, formaldehyde) and inorganic materials (silicates, mineral pigments). In 1911–1927, he was a professor at Kharkov Technological Institute, and in 1932, he became professor at Moscow Institute of Chemical Engineering. The main object of interest of A.E. Chichibabin, one of the most prominent Russian organic chemists and academician of the Academy of Sciences of the USSR since 1928, was the chemistry of heterocyclic compounds, and primarily that of pyridine [18]. In 1909–1930, Chichibabin was a professor of Moscow Higher Technical College, he created a prominent scientific school and was the author of the known textbook *Osnovy organicheskoi khimii* (1925) (Fundamentals of Organic Chemistry), which ran into seven editions. Chichibabin made a major contribution to the creation of chemical-pharmaceutical industry in Russia. Professor A.I. Gorbov (1859–1939), an active propagandist of chemical science in our country, Butlerov's and Mendeleev's disciple, prominent scientist, and broadly educated man, was appointed executive secretary of ZhPKh. Main Gorbov's scientific studies were performed in military technology: analysis of properties of concretes and other materials used in construction of defense fortifications, development of methods for production, purification, and storage of hydrogen for aerostatic purposes, and participation in the development of gas masks. According to the recollections of contemporaries [19–21], Gorbov paid his undivided attention to his duties as editor of ZhPKh and to work with Journal's authors.

Aleksandr Ivanovich Gorbov.

In 1928, 60 printer's sheets were allocated for the Journal, and the first issue was published in February 1928 (1200 copies). The structure of the Journal provided publication of original papers, review articles, abstracts, chronicles, bibliography, personalia, and reference materials. On the whole, this structure has been preserved during all the 80 years of publication of *Zhurnal Prikladnoi Khimii*.

In the first issue of the first volume of ZhPKh were published materials concerning the history of RFKhO, organization of the Department of Applied Chemistry in the society, articles written by known scientists: "On Aging of Caoutchouc" by B.V. Byzov, "On Dyeing with Dyes Substantive for Cotton" by Porai-Koshits, and papers about new methods for analysis of platinum metals by O.E. Zvyagintsev and E.Kh. Fritsman. The chronicles section presented information about memorable days: centennial anniversaries of the birthdays of a French chemist M. Berthelot and Butlerov, and about the forthcoming V Mendeleev Congress on pure and applied chemistry and other scientific conferences. The bibliography section presented a brief list of chemical books published in 1927.

Beginning in the first years of publication of the Journal, the subjects of the articles it contained were rather diverse. Together with technological papers (basic chemical technology, technology of silicates and organic substances), it published results of topical

Sitting (from right to left): Editor-in-chief N.I. Nikitin; executive secretary L.K. Simonova; members of the editorial board: P.P. Budnikov, N.P. Fedot'ev, V.V. Pigulevskii, and D.V. Tishchenko; L.D. Anisimova, head of the editorial staff. Standing (from right to left): members of the editorial board: M.E. Pozin, Yu.A. Gorin, M.M. Koton, P.G. Romankov, N.A. Toropov, and V.V. Skorcheletti (mid-1960s.)

studies in analytical chemistry, applied electrochemistry, and physicochemical analysis of salt, metallic, and other systems. In the first decade of existence of the Journal, its authors included Ipat'ev, Kurnakov, Vrevskii, S.Z. Roginskii, P.F. Antipin, and other prominent scientists and their coworkers. A considerable attention was given to the Mendeleev Congress held in 1934 (and devoted to the centennial anniversary of Mendeleev's birthday). Detailed information about all meetings of the Congress was published [22].

Already in the first decade of publication of the Journal, its editorial board was substantially expanded. In different years, it included the following academicians: N.S. Kurnakov (1860–1941), N.D. Zelinskii (1861–1953), D.N. Pryanishnikov (1865–1948), A.A. Baikov (1870–1946), S.V. Lebedev (1874–1934), E.V. Britske (1877–1953), A.E. Porai-Koshits (1877–1949), I.V. Grebenshchikov (1887–1953), and a number of younger scientists.

Till 1931, ZhPKh was published by the Russian Physicochemical Society, and after 1931, by the State Technical-Theoretical Publishing House (Moscow, Leningrad). Since 1938, the Journal has been under authority of the Academy of Sciences of the USSR (later, Russian Academy of Sciences). At present, the publication of the Journal is supervised by the Department of Chemistry and Materials Science of the Russian Academy of Sciences).

Gorbov headed ZhPKh during 10 years and did much for its becoming a well-known journal. During this time, the number of journal issues increased to 12 in a year (the journal has been published monthly since 1936). Later, this periodicity was preserved, and only during the war years (1941, 1942, and 1945) there were several violations of this rule [23]. In 1939, Professor O.E. Zvyagintsev (1894–1967) became executive editor. Beginning in the first years of publication of the Journal, he was personal secretary of the executive editor, and became a member of the editorial board of the Journal in 1931. Many years, his scientific activities were associated with chemistry of noble metals and with the creation and development of the national industry of platinum metals [4, 24]. Zvyagintsev was the author of a number of monographs on refining of gold, silver, and platinum metals and paid much interest to the history of chemistry and scientific activities of Russian scientists. A known chemist, he remained an active member of the Editorial Board of ZhPKh till 1967. Zvyagintsev was also an organizer of *Zhurnal Neorganicheskoi Khimii* (Russian Journal of Inorganic Chemistry), deputy editor-in-chief of this journal, and member of the Editorial-Publishing Council of the Academy of Sciences of the USSR.

In 1942, Academician Porai-Koshits, a known scientist in the field of organic chemistry, organizer of a prominent scientific school of chemical technology of dyeing and fibrous substances [24], was appointed editor-in-chief of ZhPKh. Beginning in 1905 and till the end of his life, the pedagogical and scientific activities of Porai-Koshits were associated with the Technological Institute in St. Petersburg.

In 1949, N.I. Nikitin (1890–1975, corresponding member of the Academy of Sciences of the USSR since 1939), an organic chemist and prominent specialist in wood chemistry, was appointed editor-in-chief of ZhPKh. In 1925, he created at the Forestry Academy in Leningrad the first chair of wood and cellulose chemistry and headed this chair during many years. Nikitin is the author of quite a number of monographs devoted to wood chemistry. Beginning in 1959, he supervised, together with working at the Forestry Academy, research in the field of wood chemistry at the Institute of Macromolecular Compounds, Academy of Sciences of the USSR. Nikitin was editor-in-chief of ZhPKh during 25 years. In the interesting book of recollections written by him, he mentioned with high respect the prominent specialists who were members of the Editorial Board of the Journal in those years; L.K. Simonova, executive secretary of the Editorial Board; and L.D. Anisimova, head of the Editorial Office.

In 1976–1988, the Editorial Board of the Journal was headed by P.G. Romankov (1904–1990, corresponding member of the Academy of Sciences of the USSR since 1964), a prominent specialist in the field of processes and apparatus of chemical technology. He worked at the chair of processes and apparatus at the Leningrad Technological institute beginning in 1934 and headed the chair in 1943. In 1950–1980, he was pro-rector for scientific work at the Technological institute.

In 1989, Academician V.S. Shpak, a known scientist in the field of organic and technical chemistry, prominent science organizer, and member of the editorial board of the journal since 1976, was appointed Editor-in-Chief of ZhPKh. Beginning in 1931, he was engaged in pedagogical and research activities at the Leningrad Technological Institute; in 1953–1977, he was director of GIPKh. He became Chief chemist for heavy organic synthesis at the Ministry of Chemical Industries in 1977, and advisor of the director general of Prikladnaya Khimiya Russian scientific center in 1993. In 2006, the duties of the Editor-in-Chief of ZhPKh were entrusted to Academician G.F. Tereshchenko (Russian Academy of Sciences).

Aleksandr Evgen'evich Porai-Koshits.

Petr Grigor'evich Romankov.

In the post-war years, the editorial board of ZhPKh included academicians: S.I. Vol'fkovich (1896–1980), N.V. Ageev (1903–1983), I.V. Tananaev (1904–1993), and M.M. Shul'ts (1919–2006); and corresponding members of the Academy of Sciences of the USSR: P.P. Budnikov (1885–1968), N.A. Toropov (1908–1968), M.M. Koton (1908–2005), and V.B. Aleskovskii (1912–2006). During many years, professors V.V. Pigulevskii, M.E. Pozin, V.A. Proskuryakov, A.L. Rotinyan, V.V. Skorcheletti, M.M. Sychev, D.V. Tishchenko, and N.P. Fedot'ev took active part in the work of the Editorial Board of the Journal and in refereeing of the submitted articles.

At present, ZhPKh is the only Russia's wide-scope journal devoted to applied chemistry. In the breadth of the issues covered, the Journal has no analogs among world's periodic editions. In the last fifteen years, the following classification of the articles published, which clearly reflects the scope of the Journal, has been was introduced:

Inorganic Synthesis and Industrial Inorganic Chemistry;
Physicochemical Studies of Systems and Processes;
Sorption and Ion-Exchange Processes;
Applied Electrochemistry and Corrosion Protection of Metals;
Catalysis;
Environmental Problems of Chemistry and Technology;
Processes and Equipment of Chemical Industry;
Nanomaterials and Nanotechnologies;
Organic Synthesis and Industrial Organic Chemistry;
Macromolecular Compounds and Polymeric Materials;
Chemistry of Fossil Fuels;
Brief Communications;
History of Chemistry and Chemical Technology;
Book Reviews;
Information.

At present, ZhPKh annually publishes 440–450 articles (abstracts of papers submitted by the editorial board for deposition at VINITI, Russian Academy of Sciences, not included). Scientometric analysis of the publications of the last five years (2002–2006) demonstrates that the rubric devoted to macromolecular compounds contains 25–27% of the total number of the papers. The rubrics devoted to inorganic technology, sorption and ion-exchange processes, and applied electrochemistry show about the same in the number of the articles published: each covers 9 to 13% of the total number of papers.

After the geopolitical changes of 1991, 76 to 82% of papers come in the following years from scientific institutions of Russia. The shares of Ukraine and Belarus are 8–12 and 4–8%, respectively.

A considerable attention is paid by ZhPKh to publication of review articles that systematize, analyze, and generalize studies in a topical area of chemical technology and its theoretical foundations. In the last ten years (1997–2006), 47 reviews have been published, of which the following can be mentioned: "Integrated Processing of Deposits of the Kola Peninsula" [27], "Niobium in Molten Salts: State in Melts and Electrochemical Behavior" [28], "Physicochemical and Technological Studies of Desulfation of Lead-Containing Materials" [29], "High-Temperature Protonic Solid Electrolytes: Possible Applications" [30], "Lithium-Conducting Polymeric Electrolytes for Chemical Power Cells" [31], "Fullerene-Containing Chalcogenide Glass-Forming Materials" [32], "Electron–Proton Effect in Chemistry of Catalysis" [33], "New Methods for Control over Chain Growth in Polymerization of Vinyl Chloride" [34], "Hydrogen Bonds in Cellulose and Their Influence on Its Solubility in Aqueous and Nonaqueous Media" [35], "Applied Importance of Polyimides" [36], and "Laser Initiation of High-Energy-Capacity Compounds in Science and Technology" [37]. The topics covered by the reviews point to the wide diversity of problems discussed in ZhPKh.

According to the tradition established from the beginning of publication of the Journal, it continues to pay attention to various jubilee dates. In particular, the following articles have been published in the last decade: those devoted to the role played by the Academy of Sciences in the development of research in the field of chemistry and chemical technology in Russia (in connection with the 275th foundation anniversary of the Academy) [38], involvement of chemists of St. Petersburg in the development of science and industry in Russia (in connection with the 300th anniversary of St. Petersburg) [39], 80th anniversary of the State Institute of Applied Chemistry [40], 70th anniversary of the Apatit Combine [41], and 100th anniversary of the first Nobel Prize in chemistry [42]. Quite a number of papers have been devoted to Russian and foreign chemists in connection with various memorial dates.

During many years, *Zhurnal Prikladnoi Khimii* has been completely translated into English and published under the title Russian Journal of Applied Chemistry (Translation of *Zhurnal Prikladnoi Khimii*). Since 1993, the Journal has been simultaneously published in Russian and English in accordance with the License agreement between the Russian Academy of Sciences and Pleiades publishing house (the United States). The English version of the Journal is prepared in St. Petersburg.

The author is grateful to Academician Vladimir Stepanovich Shpak (Russian Academy of Sciences) for his permanent interest in studies in the field of history of chemistry and chemical technology.

REFERENCES

1. Solov'ev, Yu.I., *Istoriya khimii v Rossii* (History of Chemistry in Russia), Moscow: Nauka, 1985.

2. Figurovskii, N.A. and Solov'ev, Yu.I., *Nikolai Nikolaevich Zinin: Biograficheskii ocherk* (Nikolai Nikolaevich Zinin: a Biographical Essay), Moscow: Akad. Nauk SSSR, 1957.
3. Morachevskii, A.G. and Shpak, V.S., *Zh. Prikl. Khim.*, 2003, vol. 76, no. 5, pp. 705–716.
4. Morachevskii, A.G., *Ocherki ob uchenykh-khimikakh Sankt-Peterburga. XIX vek i pervaya polovina XX veka* (Essays about Chemists of St. Petersburg: XIX Century and the First Half of the XX Century), St. Petersburg: Politekh. Univ., 2004.
5. Solov'ev, Yu.I., *Nikolai Semenovich Kurnakov: 1860–1941*, Moscow: Nauka, 1986.
6. *K 35-letiyu nauchnoi deyatel'nosti V.N. Ipat'eva* (To 35th Anniversary of V.N. Ipat'ev's Scientific Activities), Leningrad: Nauch. Khim.-Tekh. Izd., 1929.
7. Loktev, S.M., *Vestn. Akad. Nauk SSSR*, 1990, no. 1, pp. 104–118.
8. Kuznetsov, V.I. and Maksimenko, A.M., *Vladimir Nikolaevich Ipat'ev: 1867–1952*, Moscow: Nauka, 1992.
9. Morachevskii, A.G., *Ocherki ob uchenykh-khimikakh Rossii i zarubezhnykh stran. XIX vek i pervaya polovina XX veka* (Essays about Chemists of Russia and Foreign Countries: XIX Century and the First Half of the XX Century), St. Petersburg: Politekh. Univ., 2005.
10. Ipat'ev, V.N., *Khimicheskii komitet pri Glavnom artilleriiskom upravlenii i ego deyatel'nost' dlya razvitiya otechestvennoi khimicheskoi promyshlennosti* (Chemical Committee at Chief Artillery Department and Its Activities in the Development of National Chemical Industry), Petrograd: Nauch. Khim.-Tekh. Izd., 1921, Part 1.
11. Trifonov, D.N., *Khim. Rossii*, 2000, February, pp. 17–20.
12. Trifonov, D.N., *Khim. Rossii*, 2000, April, pp. 12–15.
13. Trifonov, D.N., *Khim. Rossii*, 2000, May–June, pp. 15–17.
14. Trifonov, D.N., *Istoriya khimii v Rossii. Kratkie ocherki* (History of Chemistry in Russia: Brief Essays), Moscow: Ross. Khim.-Tekhnol. Univ. im. D.I. Mendeleeva, 2002.
15. *Organizatsiya i razvitie otraslevykh nauchno-issledovatel'skikh institutov Leningrada (1917–1977)* [Organization and Development of Research Institutes of Various Branches of Industry in St. Petersburg (1917–1977)], Kozlov, B.I., Ed., Leningrad: Nauka, 1979.
16. Tishchenko, V.V., *Vyacheslav Evgen'evich Tishchenko*, Leningrad: Leningr. Univ., 1968.
17. Gavrilov, B.G. and Emel'yanov, A.Yu., *Zh. Prikl. Khim.*, 1986, vol. 59, no. 12, pp. 2752–2754.
18. Evteeva, P.M., *Tr. Inst. Ist. Estestvozn. Tekh.*, 1958, vol. 18, pp. 296–356.
19. Okatov, A.P., *Zh. Prikl. Khim.*, 1939, vol. 12, no. 6, pp. 795–799.
20. Mladentsev, M.N., *Priroda*, 1939, vol. 28, no. 12, pp. 114–115.
21. Tishchenko, V.E., *Zh. Prikl. Khim.*, 1934, vol. 7, no. 8, pp. 1329–1332.
22. Fritsman, E.Kh., *Zh. Prikl. Khim.*, 1934, vol. 7, no. 8, pp. 1555–1563.
23. Kurochkina, M.I., *Zh. Prikl. Khim.*, 1988, vol. 61, no. 2, pp. 225–227.
24. Morachevskii, A.G., *Zh. Prikl. Khim.*, 1998, vol. 71, no. 1, pp. 3–6.
25. Porai-Koshits, B.A., Abozin, V.G., Perekalin, V.V., and Efros, L.S., *Materialy po istorii otechestvennoi khimii* (Materials on History of Domestic Chemistry), Moscow: Akad. Nauk SSSR, 1954, pp. 103–122.
26. Nikitin, N.I., *Na puti nauchnogo rabotnika-khimika* (Course of Life of Research Chemist), Leningrad: Nauka, 1969.
27. Kalinnikov, V.T., *Zh. Prikl. Khim.*, 1997, vol. 70, no. 5, pp. 705–712.
28. Polyakov, E.G., *Zh. Prikl. Khim.*, 1998, vol. 71, no. 2, pp. 181–191.
29. Morachevskii, A.G., *Zh. Prikl. Khim.*, 1998, vol. 71, no. 6, pp. 881–890.
30. Pal'guev, S.F., *Zh. Prikl. Khim.*, 1998, vol. 71, no. 1, pp. 7–16.
31. Kolosnitsyn, V.S., Dukhanin, G.P., Dumler, S.A., and Novakov, I.A., *Zh. Prikl. Khim.*, 2005, vol. 78, no. 1, pp. 3–21.
32. Blinov, L.N., *Zh. Prikl. Khim.*, 2003, vol. 76, no. 5, pp. 716–727.
33. Kalnin'sh, K.K., *Zh. Prikl. Khim.*, 2005, vol. 78, no. 11, pp. 1761–1779.
34. Semenycheva, L.L. and Grishin, L.F., *Zh. Prikl. Khim.*, 2003, vol. 76, no. 6, pp. 881–887.
35. Bochek, A.M., *Zh. Prikl. Khim.*, 2003, vol. 76, no. 11, pp. 1761–1770.
36. Sazanov, Yu.N., *Zh. Prikl. Khim.*, 2001, vol. 74, no. 8, pp. 1217–1234.
37. Ilyushin, M.A. and Tselinskii, I.V., *Zh. Prikl. Khim.*, 2000, vol. 73, no. 8, pp. 1233–1240.
38. Morachevskii, A.G. and Shpak, V.S., *Zh. Prikl. Khim.*, 1999, vol. 72, no. 5, pp. 705–717.
39. Morachevskii, A.G. and Shpak, V.S., *Zh. Prikl. Khim.*, 2003, vol. 76, no. 5, pp. 705–715.
40. Bazanov, A.G., *Zh. Prikl. Khim.*, 1999, vol. 73, no. 12, pp. 1937–1943.
41. Morachevskii, A.G. and Beloglazov, I.N., *Zh. Prikl. Khim.*, 2000, vol. 73, no. 5, pp. 869–872.
42. Morachevskii, A.G., *Zh. Prikl. Khim.*, 2001, vol. 74, no. 7, pp. 1205–1210.

A. G. Morachevskii

ISSN 1070-4272, Russian Journal of Applied Chemistry, 2007, Vol. 80, No. 7, p. 1194. © Pleiades Publishing, Ltd., 2007.
Original Russian Text © A.G. Morachevskii, I.N. Beloglazov, 2007, published in Zhurnal Prikladnoi Khimii, 2007, Vol. 80, No. 7, pp. 1229.

BOOK REVIEWS

Andrievskii, R.A. and Ragulya, A.V., *Nanostrukturnye materialy: Uchebnoe posobie dlya studentov vysshikh uchebnykh zavedenii* (Nanostructured Materials: Textbook for Higher School Students)

Moscow: Akademiya, 2005, 192 pp.

DOI: 10.1134/S1070427207070373

An important component of nanotechnology as an interdisciplinary research area formed in the world science in recent 15–20 years is the development of nanostructured materials (nanomaterials). Thanks to a unique set of properties, these materials occupy the leading position in modern materials science. The information flow constituted by the educational and monographic literature, reviews, and original papers concerned with nanotechnologies and nanomaterials has substantially increased, quite a number of specialized international scientific journals have appeared, and numerous conferences and symposia are being held.

The textbook offered to the readers' attention was written on the basis of the courses of lectures delivered by the authors in quite a number of domestic and foreign higher school institutions. The book comprises a foreword, five chapters, and supplements. Brief Chapter 1 (pp. 5–11) presents general evidence concerning the history of appearance of the nanotechnology, lists its priority areas, and explains certain terms.

Chapter 2 (pp. 12–44) presents a general structural characterization of nanomaterials. Particular attention is given by the authors to the structure of polymeric, biological, and carbon nanomaterials. Chapter 3 (pp. 45–113) discusses specific physical, mechanical, and chemical nanomaterials and gives notion of dimensional effects. Elucidation of the nature of dimensional effect is one of the most important problems of the materials science of nanostructured objects. Chapter 4 (pp. 114–149) describes the fundamentals of technologies for synthesis of nanomaterials of various kinds: consolidated nanomaterials, nanosemiconductors (nanoparticles, heterostructures, porous silicon), and polymeric, porous, tubular, and biological nanomaterials. Chapter 5 (pp. 150–179) considers various application fields of nanomaterials.

Each of the chapters is provided with control questions and rather extended lists of basic and supplementary literature. These lists are important by themselves because they contain detailed bibliographic descriptions of monographs, reviews, and original papers of domestic and foreign authors, which, as a rule, have been published in the last five to ten years.

The supplement presents information about the most important instruments used to study nanomaterials: scanning tunnelling microscope, atomic-force microscope, high-resolution transmission and scanning electron microscopes, and nanoindenters.

The book is recommended as a textbook for students specialized in physical materials science, it may be of use for students of other allied specialties.

A. G. Morachevskii and I. N. Beloglazov

ISSN 1070-4280, Russian Journal of Applied Chemistry, 2007, Vol. 80, No. 7, pp. 1195–1200. © Pleiades Publishing, Ltd., 2007.
Original Russian Text © V.I. Zhukov, G.V. Val'kovich, B.N. Skorik, Yu.M. Petrov, G.P. Belov, 2005, published in Khimicheskaya Promyshlennost', 2005, Vol. 82, No. 8, pp. 382–388.

TECHNOLOGY OF ORGANIC AND INORGANIC SUBSTANCES

Selective Dimerization of Ethylene to But-1-ene under the Conditions of Industrial Process. I. Influence of Temperature and Pressure on the Rate of the Process in a Bubbling Type Reactor

V. I. Zhukov[a], G. V. Val'kovich[a], B. N. Skorik[a], Yu. M. Petrov[a], and G. P. Belov[b]

[a]*Lukoil-Neftekhim Group, Stavrolen Co., Budenovsk, Russia*
[b]*Institute of Probems of Chemical Physics, Russian Academy of Sciences, Chernogolovka, Russia*
e-mail: gbelov@cat.icp.ac.ru

Received April 19, 2005

Abstract—Analysis of mass and heat balance in the reaction node of the process of ethylene dimerization into but-1-ene under the industrial conditions is performed. It is found that ethylene concentration in the reactor liquid phase by a complex way depends on the reactor temperature, pressure and but-1-ene concentration in the liquid phase. Optimal process temperature is 80–90°C, operating pressure in the reactor is 0.6–0.8 MPa. Increase in pressure above 1 MPa practically excludes heat withdraw via but-1-ene evaporation and makes the system of heat withdrawing ineffective.
DOI: 10.1134/S1070427207070385

But-1-ene is the most widespread, after ethylene and propylene, monomer of olefin series and it is more and more used in the plastics industry for the synthesis of linear medium and low density polyethylene, isotactic polybutene, polybutylene oils and copolymers with propylene. For the solving a problem of obtaining but-1-ene of polymerization purity grade, a new technology of high-selective catalytic dimerization of ethylene into but-1-ene has been developed.

Now in the world industrial practice two variants of technology for manufacturing but-1-ene of polymerization purity are in application:

—The variant "Alfa-okhtol" [1–3] developed in the Institute of Probems of Chemical Physics, Russian Academy of Sciences in cooperation with industrial branch institutions and applied in the beginning of 80th of 20th century in the biggest plants in Kazan and Budenovsk for manufacturing polyethylene; its principal scheme is shown in Fig. 1.

—The variant "Alfa-butol" of the French Oil Institute, applied in 80th of 20th century [4], based on the investigations of the Institute of Probems of Chemical Physics, Russian Academy of Science.

In both these variants the process of ethylene dimerization is perrgformed in liqid phase with the homogenous catalytic system tetrabutoxytitan–tralkylaluminum–modificator. As a solvent basically is applied a mixture of isohexenes (hereinafter in the text hexenes) formed as by-products in the process of ethylene dimerization, or a mixture of but-1-ene and hexenes. In the process of dimerization a mixture of but-1-ene and hexenes of the following composition is formed: hex-1-ene 10 wt %, 2-ethylbut-1-ene 60 wt %, 3-methylpent-1-ene 30 wt %. Besides hexenes, as a side product in a small amount are formed octenes and a polymer, which in the further consideration are not accounted for.

Mathematic model of the reaction of ethylene dimerization into but-1-ene on the $Ti(OR)_4$–AlR'_3 catalytic system has been considered in [5].

The technology of dimerization in the "Alfa-okhtol" variant (Fig. 1) assumes *heat withdrawing* by circulation of evaporating liquid phase from the reactor I as a vapor-gas mixture (g_3 flow) through condenser II with further returning of the gas phase (g_6 flow) and a part of liquid phase (g_9 flow) from the condenser II into reactor I. The material flows by this scheme are shown in Fig. 2.

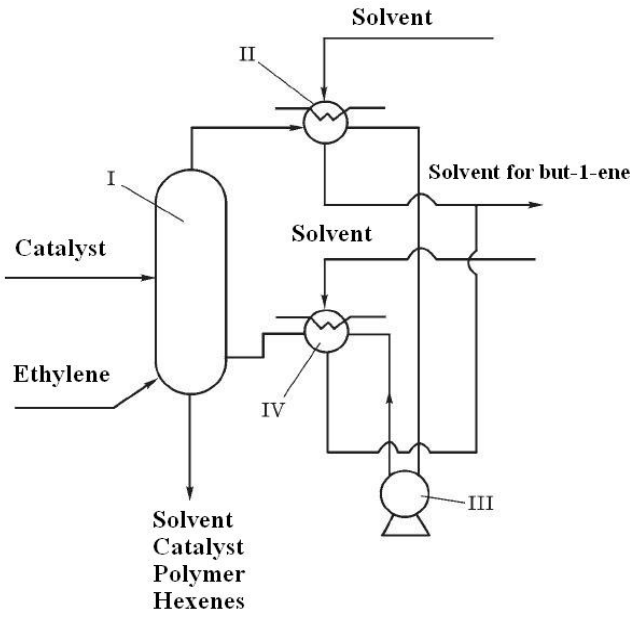

Fig. 1. Principal technological scheme of reaction node for ethlene to but-1-ene dimerizationaccording in "Alfa-okhtol" process. (I) reactor, (II, IV) condensers, (III) circulation compressor.

Such a technology is used in the processes of polymerization of low molecular weight olefins [6] and in suspension ethylene and propylene copolymerization [7].

When liquid phase presents in the reactor and condenser, all abovementioned hydrocarbons are in equilibrium. The ethylene, but-1-ene and hexenes concentrations in gas and liquid phases depend on several factors:

The process temperature,
Pressure in the reactor I,
The process selectivity,
Values of the flows g_2, g_5 and g_6, (Fig. 2),
Ratio of the flows g_3/g_4 and g_9/g_7.

Taking into account a large number of variables defining composition of liquid and gas phases, it was attempted to develop algorithms of mass and heat balances proceeding from the suggestion that gas and liquid phase are in equilibrium and the relations below are fulfilled.

For the reactor I:

$$Y^p_{c2} + Y^p_{c4} + Y^p_{c6} = 1, \quad (1)$$

$$X^p_{c2} + X^p_{c4} + X^p_{c6} = 1, \quad (2)$$

$$K^p_i = Y^p_i / X^p_i . \quad (3)$$

$$g_4 = g_3 (I - E^p) / E^p, \quad (4)$$

where g_3, g_4 denote amount of gas and liquid, respectively, leaving reactor I, kgmol/h; Y^p_{c2}, Y^p_{c4}, Y^p_{c6}, X^p_{c2}, X^p_{c4}, X^p_{c6} are molar fractions of ethylene, but-1-ene and hexenes in gas (Y) and liquid (X) phases of the reactor, K^p_i are the constants of phase equilibrium for ethylene, but-1-ene and hexenes at the temperature and pressure that occurred in the reactor (elucidated by

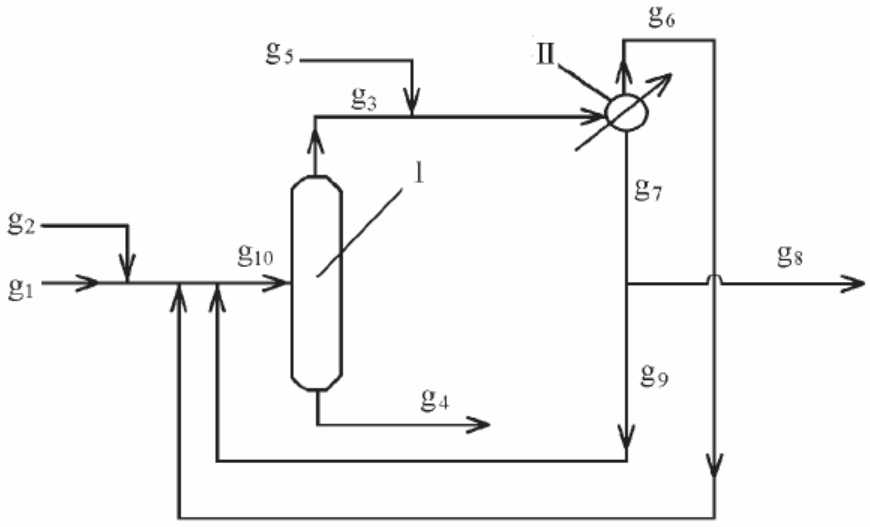

Fig. 2. Scheme of material flows in the reaction node for ethylene to but-1-ene dimerization by "Alfa-okhtol" process. (I) reactor, (II) condenser. Flows: (g_1) ethylene, (g_2, g_5) hexenes, (g_3) vapor-gas mixture from the reactor to condenser, (g_4) liquid phase from the reactor bottom, (g_6) gas phase from condenser to the reactor, (g_7) liquid phase from condenser, (g_8) liquid phase from condenser to rectification, (g_9) liquid phase from condenser to reactor, (g_{10}) the sum of flows g_1, g_2, g_6, and g_7.

calculation or from published data); E^p is mole fraction of distillate of the g_{10} flow feeding into the reactor

$$g_{10} = g_3 / E^p. \quad (5)$$

For the determination of olefins (ethylene, but-1-ene and hexenes) concentrations in the reactor liquid or gas phase it should be defined concentration of one of them and operating conditions in the reactor, e.g.:

$X^p_{c4} = 0.1; 0.25; 0.5; 0.75$

Temperature 50, 60, 70, 80, 90°C

Pressure 0.6, 0.8, 1.0 MPa

For condenser II:

$$Y^x_{c2} + Y^x_{c4} + Y^x_{c6} = 1, \quad (6)$$
$$X^x_{c2} + X^x_{c4} + X^x_{c6} = 1, \quad (7)$$
$$K^x_i = Y^x_i / X^x_i, \quad (8)$$
$$g_7 = g_6 (I - E^x) / E^x, \quad (9)$$

where g_6, g_7 denote amount of gas and liquid, respectively, leaving condenser II, kgmol/h; Y^x_{c2}, Y^x_{c4}, Y^x_{c6}, X^x_{c2}, X^x_{c4}, X^x_{c6} are molar fractions of ethylene, but-1-ene and hexenes in gas (Y) and liquid (X) phases of the condenser, K^x_i are the constants of phase equilibrium for ethylene, but-1-ene and hexenes at the given temperature and pressure 0.6, 0.8, 1.0 MPa; E^x is mole fraction of distillate of the g_{11} flow (under the conditions occurred in the condenser), hence

$$g_{11} = g_6 / E^x, \quad (10)$$
$$g_{11} = g_3 + g_5, \quad (11)$$
$$g_5 = g_3 \cdot A. \quad (12)$$

The A value can vary in the range 0–1.0, optimally 0–0.1.

The liquid phase from the condenser (g_7 flow) is devided into two flows:

1. The flow g_8 is directed to rectification.

2. The flow g_9 is returned to the reactor for heat withdrawing

$$g_9 = B \cdot g_7. \quad (13)$$

The B value can vary from 0 to 1, and further we take it equal to 0.1; 0.5; 0.9.

Relations between the concentrations of components in the reactor gas phase and condenser liquid phase are expressed as follows:

$$X^x_{C2} = Y^p_{C2}/(I+A)[E^x(K^x_{C2} - 1) + 1], \quad (14)$$
$$X^x_{C4} = Y^p_{C4}/(I+A)[E^x(K^x_{C4} - 1) + 1], \quad (15)$$
$$X^x_{C6} = Y^p_{C6} + A/(I+A)[E^x(K^x_{C6} - 1) + 1]. \quad (16)$$

The reactor mass balance of dimerization on the but-1-ene is expressed as:

$$g_3 \cdot Y^p_{C4} + g_4 \cdot X^p_{C4} = g_6 \cdot Y^x_{C4} + g_9 \cdot X^x_{C4} + G_{C4} \quad (17)$$

where G_{C4} is amount of the formed but-1-ene in kgmol/h, other flows are shown in Fig. 2 and by relations (1, 2, 6, 7).

Using above relations (1)–(16) we transform relation (17) to otain the following dependence:

$$G_{C4} = g_3 X^p_{C4} \cdot [E_p(K^p_{C4} - 1) + 1/E_p - K^p_{C4} \cdot E_x(K^x_{C4} - B) + B/E_x(K^x_{C4} - 1) + 1] \quad (18)$$

The amount of ethylene g^{C4}_{C2} consumed for the formation of but-1-ene in kgmol/h equals:

$$g^{C4}_{C2} = 2G_{C4} \quad (19)$$

The total amount of ethylene used for the formation of but-1-ene and hexenes g^{C4+C6}_{C2} is expressed by the relation:

$$g^{C4+C6}_{C2} = 2G_{C4} \quad (20)$$

where S is the process selectivity of dimerization on but-1-ene.

The mass balance on ethylene is expressed as:

$$g_1 = g_{эт}{}^{C4+C6} + g_4 X^p_{C2} + g_8 X^x_{C2} \quad (21)$$

The mass balance on hexenes is expressed by the relations below:

Amount of the formed hexenes

$$G_{C6} = 2G_{C4}(1-S)/3S. \quad (22)$$

$$g_1 = g_3 \left(\frac{2X^P_{C_4}}{S} \left[\frac{E^P \left(K^P_{C_4} - 1\right) + 1}{E^P} - \frac{K^P_{C_4} E^X \left(K^X_{C_4} - B\right) + B}{E^X \left(K^X_{C_4} - 1\right) + 1} \right] + X^P_{C_2} \left[\frac{1 - E^P}{E^P} + \frac{K^P_{C_2} (1 - B)(1 - E^X)}{E^X \left(K^X_{C_2} - 1\right) + 1} \right] \right),$$

$$g_2 = g_3\left(X^P_{C_6}\left[K^P_{C_6} + \frac{1 - E^P}{E^P}\right] - \left(K^P_{C_6}X^P_{C_6} + A\right)\left[B\left(1 - E^X\right)(1 + A) + \frac{E^X}{E^X\left(K^X_{C_6} - 1\right) + 1}\right]\right) -$$
$$- g_3\frac{2X^P_{C_4}(1 - S)}{3S}\left[\frac{E^P\left(K^P_{C_4} - 1\right) + 1}{E^P} - K^P_{C_4}\frac{E^X\left(K^X_{C_4} - B\right) + B}{E^X\left(K^X_{C_4} - 1\right) + 1}\right] .$$

Amount of hexenes G_{C6}^{g3+g4} leaving reactor with the flows g_3 and g_4:

$$g_{C6}^{g3+g4} = g_3 \cdot Y^p_{C6} + g_4 X^p_{C6}. \quad (23)$$

Amount of hexenes formed in the dimerization process and incoming with the flows g_6 and g_9

$$g_{C6}^{g6+g9+Gc6} = g_9 X^x_{C6} + g_6 Y^x_{C6} + G_{C6}. \quad (24)$$

and

$$g_2 = g_{C6}^{g3+g4} - g_{C6}^{g6+g9+Gc6}. \quad (25)$$

Transforming relations 21 and 25 and using (1) to (20) we obtain expressions for g_1 and g_2 showing (see Fig. 2) that they are functions of the flow g_3, but-1-ene concentration in the liquid phase of the reactor X^p_{c4}, phase equilibrium constants K_i at the temperatures in the reactor and in condenser, and of B value:

The flow value g_1 will be shown to depend also on ethylene concentration in the reactor liquid phse X^p_{c2} and flow g_2 on the hexenes concentration X^p_{c6}, A value and the process selectivity.

Such a system has many solutions, and for obtaining certain relations it is necessary:

define flow g_3 = 1 kgmol/h

define molar concentration X^p_{c4} = 0.1, 0.25, 0.5

define A = 0, 0.1

define B = 0.1, 0.5, 0.9

At the given dimerization conditions on temperature and pressure, the values of all flow can be calculated. These values will be true when the reactor heat balance is fulfilled.

Income of heat into the reactor is expressed by the relation

$$Q_{income} = Q_1 + Q_6 + Q_9 + Q_2 + Q_{reaction}, \quad (26)$$

where Q_{income}, Q_1, Q_6, Q_9, Q_2 and $Q_{reaction}$, are the amount of heat incoming to the reactor totally, of the flows g_1, g_2, g_6, g_9, and of the reaction heat, respectively.

The heat outcome from the reactor is expressed by the relation:

$$Q_{outcome} = Q_3 + Q_4 + Q_{loss}, \quad (27)$$

where $Q_{outcome}$, Q_3, Q_4, and Q_{loss} are respectively total outcoming heat, the heat of flows g_3, and g_4 and the

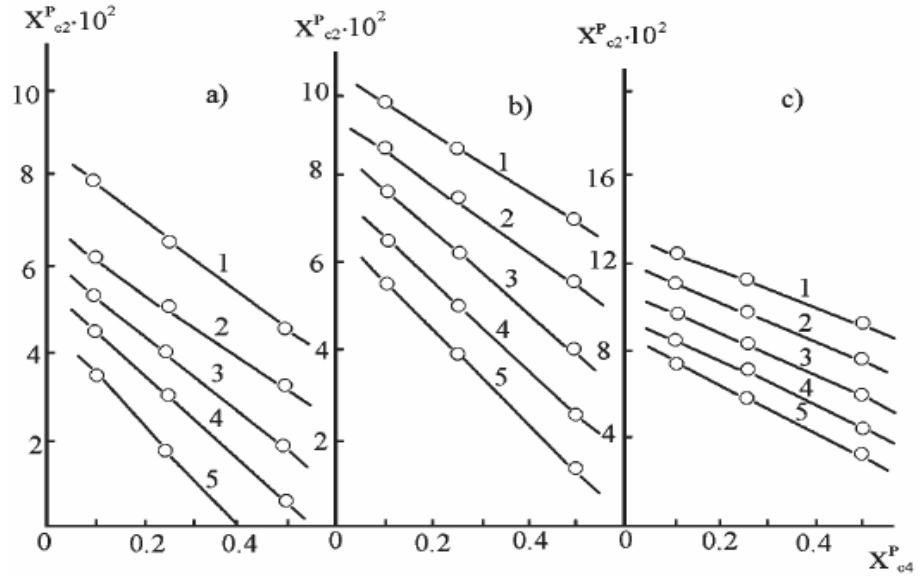

Fig. 3. Plots of ethylene concentration in the reactor liquid phase on but-1-ene concentration in the reactor liquid phase at different temperature and pressure. Pressure, MPa: (a) 0.6, (b) 0.8, (c) 1.0. Temperature, ºC: (1) 50, (2) 60, (3) 70, (4) 80, (5) 90.

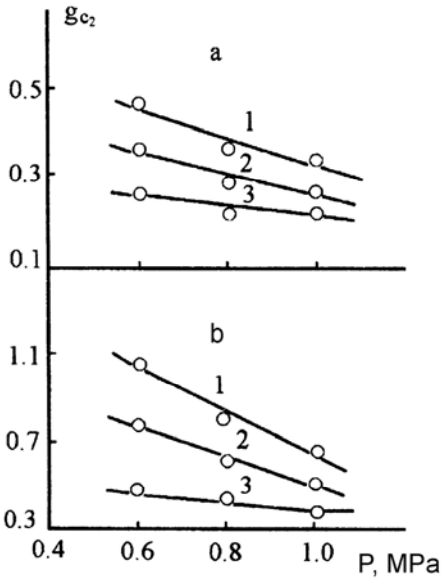

Fig. 4. Plots of ethylene amount g_{C2} consumed for the formation of but-1-ene and hexenes, on the process pressure, at $X^{p}_{C4} = 0.1$; B= 0.1, 0.5, 0.9; (a) at the temperature 80ºC, (b) at the temperature 90ºC.

Fig. 5. Dependence of maximum productivity of reaction node G on the pressure; (1) A = 0; (2) A = 0.1.

losses of heat to environment.

$$Q_{income} = Q_3 + Q_4 + Q_{outcome}\,. \qquad (28)$$

Join solution of the above relations allows to analyze influence of temperature and pressure on the process rete in the bubble type reactor.

The rate and selectivity of the dimerization process an hence the values of g_1, g_2 flows are affected by the concentration of ethylene in the recator liquid phase which in turn, as seen from Fig. 3, depends on the following factors: pressure, temperature and but-1-ene concentration in the reactor liquid phase.

Analysis of the data obtained shows that increase in pressure from 0.6 to 1.0 MPa increases ethylene concentration by the factor 1.5 to 2; increase in the process temperature from 50°C to 90°C decreases ethylene concentration in the reactor liquid phase by the factor 1.5 to 3, increase in but-1-ene concentration in the reactor liquid phase leads to decrease in ethylene concentration by the factor 1.5 to 2. Hence, maximum ethylene concentration occurs at the pressure 1.0 MPa, Δt = 50°C, and at mimimum concentration of but-1-ene in the reactor liquid phase.

Further analysis shows that temperature and pressure affect oppositely the ethylene concentration in the reactor liquid phase and on the amount of consumed ethylene.

Despite the increase of ethylene concentration in the reactor liquid phase, the amount of ethylene consumed for the formation of but-1-ene and hexenes falls down. The plots obtained are shown in Fig. 4.

The reaction node productivity as a dependence on the pressure is defined by the expression:

$$G = \frac{g_6 \cdot g_{c2} \cdot P_{work}}{E_x\,(1 + A)}\ \text{kgmol/h},$$

where g_6 is is circulation compressor discharge (flow g_6), Ex is the distillate fraction in condenser, g_2 is amount of ethylene consumed in the process of ethylene dimerization at the value of flow g_3 = 1 kgmol/h, P_{work} is working pressure.

The calculations show that maximum output of the reaction node falls by factor more than 3 in the pressure range 0.6 to 1.0 MPa (Fig. 5). Hence, it can be said that increase in pressure over 1.0 MPa practically excludes heat withdraw in account of evaporation of but-1-ene and makes this system of heat withdraw ineffective.

The dependence of ethylene amount on the temperature in the reactor or on the temperature difference between reactor and condenser Δt ($t_{condenser}$ = 40ºC), which can be consumed for the dimerization reaction

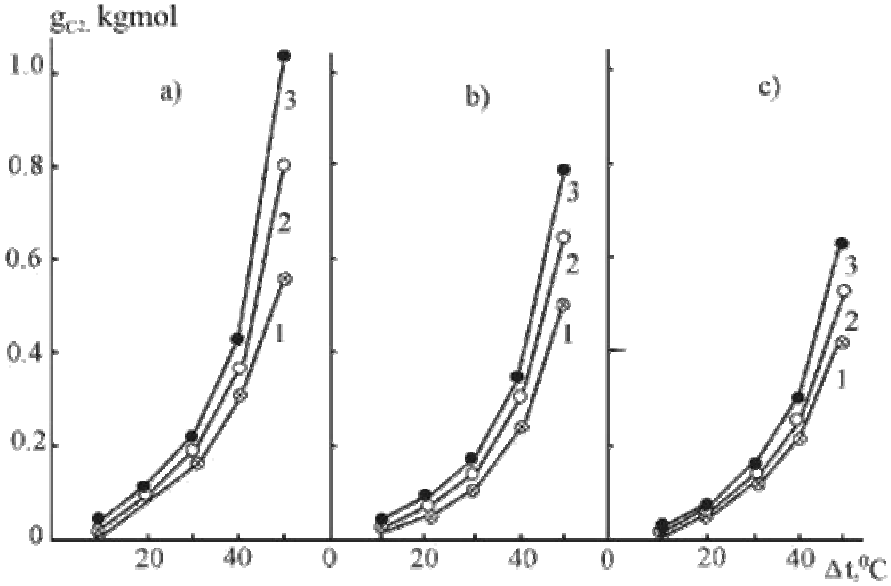

Fig. 6. Plots of ethylene amount g_{C2} consumed for the formation of but-1-ene and hexenes, on the difference in the reactor and condenser temperatures Δt. Pressure, MPa: (a) 0.6, (b) 0.8, (c) 1.0; parameters: X^{p}_{C4} = 0.1; A = 0; B: (1) 0.1, (2) 0.5, (3) 0.9.

without disturbance of heat and mass balances, is shown in Fig. 6. As seen, at Δt = 10°C the reaction node maximum output is minimal, while at Δt = 40 to 50°C it increases sharply. Depending on the pressure and B value the output at Δt = 40°C grows by the factor 10 to 20, at Δt = 50°C by factor 20 to 70. It should be noted that B value does not affect output at the Δt = 10°C, while at Δt = 50°C increase in B from 0.1 to 0.9 leads to increase in output by factor 1.5 to 2.

Thus, considering two characteristics of the industrial process of ethylene to but-1-ene dimerization in the bubble type reactor, the reactor productivity (amount of ethylene consumed g_1) and ethylene concentration in the reactor liquid phase it possible to conclude:

– Increase in the process temperature to 90°C leads to grow in amount of consumed ethylene.
– Increase in pressure is not reasonable because grow in the reaction node productivity is much lower than increase in ethylene concentration in the reactor liquid phase and besides is restricted by the conditions of heat withdraw.
– Ethylene concentration in the reactor liquid phase by complicate way depends on the reactor temperature, pressure and but-1-ene concentration in liquid phase.

Hence, for the considered scheme of technological process the optimum temperature in the reactor is 80 to 90°C, the optimum pressure is 0.6 to 0.8 MPa.

REFERENCES

1. Ivanchev, S.S., Zhukov, V.I., Belov, G.P., Ivolgina, S.R., Germashev, A.I., Gabutdinov, M.S., and Shestak, N.P., *Plasticheskie Massy*, 1990, vol. 10, p. 82.
2. Zhukov, V.I., Belov, G.P., Germashev, A.I., and Saushkin, Yu.I., *Plasticheskie Massy*, 1996, no. 5, p. 6.
3. Belov, G.P., Borodin, A.M., Val'kovich, G.V., Zhukov, V.I., Polevshchikov, N.P., Petrov, Yu.M., and Skorik, I.N., *Summa tekhnologii* (Review of Russian Technologies), 2001, no. 1, p. 79.
4. *Neftegazovye Tekhnologii*, 1995, no. 5, p. 39.
5. Belov, G.P., Psikha, B.L., Furman, G.A., Davtyan, S.P., and Agasaryan, A.V., *Neftekhimiya*, 1990, vol. 30, no. 5, p. 609.
6. Zhukov, V.I., Sergienko, G.S., and Frid, M.M., *Plasticheskie Massy*, 1986, no. 2, p. 15.
7. Arutyunov, I.A., Zhuravlev, V.P., Markosov, P.I., Dannik, V.P., and Rezumenko, Z.Ya., *Promyshlennost' Sinteticheskogo Kauchuka,* 1971, no. 2, p. 10.

ISSN 1070-4280, Russian Journal of Applied Chemistry, 2007, Vol. 80, No. 7, pp. 1201–1206. © Pleiades Publishing, Ltd., 2007.
Original Russian Text © V.I. Zhukov, G.V. Val'kovich, B.N. Skorik, Yu.M. Petrov, G.P. Belov, 2007, published in Khimicheskaya Promyshlennost', 2007, Vol. 84, No. 1, pp. 1–7.

TECHNOLOGY OF ORGANIC AND INORGANIC SUBSTANCES

Selective Dimerization of Ethylene to But-1-ene under the Conditions of Industrial Process. II. Selection of a Solvent for the Process of Ethylene to But-1-ene Dimerization

V. I. Zhukov[a], G. V. Val'kovich[a], B. N. Skorik[a], Yu. M. Petrov[a], and G. P. Belov[b]

[a]*Lukoil-Neftekhim Group, Stavrolen Co., Budenovsk, Russia*
[b]*Institute of Probems of Chemical Physics, Russian Academy of Sciences, Chernogolovka, Russia*
e-mail: gbelov@cat.icp.ac.ru

Received February 5, 2007

Abstract—A comparative economical analysis of reasons for application the solvents of various type in the process of ethylene to but-1-ene dimerization and of technological schemes of rectification of the products of ethylene dimerization with use of different solvents. The optimal solvent for the currently working industrial process of ethylene to but-1-ene dimerization is hexane fraction forming in the process of ethylene dimerization.
DOI: 10.1134/S1070427207070397

The highly selective process of manufacturing but-1-ene by catalytic dimerization of ethylene has been first developed in the Institute of Problems of Chemical Physics RAS and in cooperation with joint-stock companies Stavrolen and Kazanorgsynthes realized in industry [1–3]. In [4] we performed analysis of mass and heat balances of the reaction node for the process of ethylene dimerization under industrial conditions.

The process of ethylene dimerization is performed with homogenous catalyst $Ti(OR)_4 - AlR|_3 -$ modificator in the medium of hydrocarbon solvent. As the solvent can be used individual or mixed hydrocarbons, including the products of dimerization.

The solvent in the process of dimerization bears several functions:

–as a reaction medium for the process,
–solving ethylene and dimerization products,
–maintaining required temperature regime,
–promoting heat withdraw.

In this connection, the solvent should obey the following requirements:

–it should be chemically inert to the catalyst components, monomer and dimerization products,
–should contain minimum admixtures reacting with the catalyst components and the catalyst whole,
–should have certain composition on hydrocarbons providing stable proceeding of the process in time,
–should provide simple by technology method of separation of the dimerization products,
–should be accessible, accepted in the industrial scale and advantageous economically.

Taking into account these requirements, investigations for evaluation of various solvents and selecting the perfect one have been conducted.

Among the solvents for the ethylene to but-1-ene dimerization could be used the following solvents:

–individual paraffin hydrocarbons (hexane, heptane and others and their mixtures),
–naphthene solvents (cyclohexane),
–aromatic solvents (benzene, toluene and others),
–unsaturated hydrocarbons (but-1-ene, hexenes),
–halohydrocarbons (chloroethane, bromoethane),
–ethers (diethyl, diisopentyl),
–industrial hydrocarbon fractions C6 or C7 (Nefras "A", Nefras "C", BR-1, BR-2 and others).

In [5] was reported that the solvent nature affects

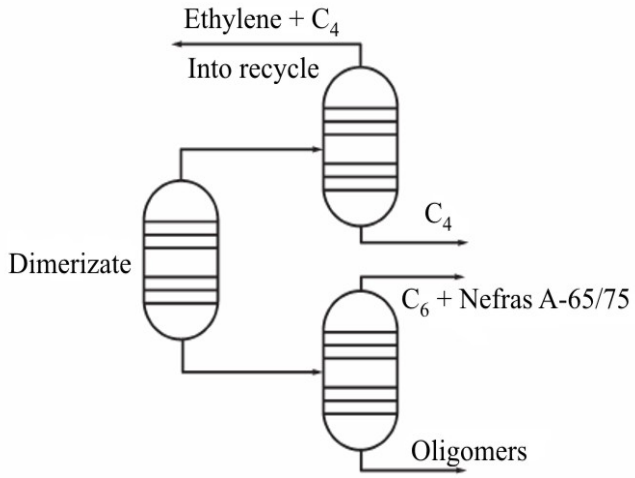

Fig. 1. Scheme of separation of the products of ethylene dimerization with Nefras "A" 65/75 as a solvent.

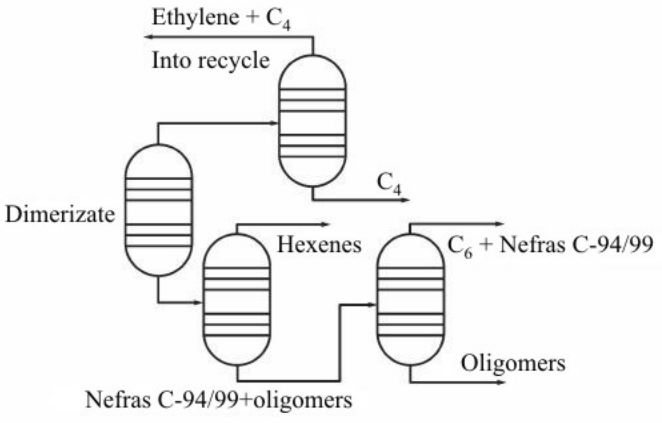

Fig. 2. Scheme of separation of the products of ethylene dimerization with Nefras "C" 94/99 as a solvent.

activity and selectivity of the process and increases them in the order: aromatic hydrocarbons; naphthene, paraffin hydrocarbons and industrial hydrocarbon fractions; chlorinated hydrocarbons, unsaturated hydrocarbons, ethers. This order can vary with increase in the process temperature.

From the viewpoint of the catalyst discharge, use of ethers as the solvent is disadvantageous due to enhanced consumption of organoaluminum component owing to necessity in higher $AlR'_3/Ti(OR)_4$ ratio, up to (10–20):1 instead of (4–3):1 in all other cases, explained by their chemical interaction with formation of strong $AlR_3 \cdot R_2O$ complex. The cost of halohydrocarbons such as bromoethane or chloroethane is too high and therefore their application is also unreasonable.

The most accessible solvents produced industrially are Nefras "A" 65/75 and Nefras "C" 94/99, and but-1-ene and hexenes formed in the process of ethylene dimerization as well. Estimating all the abovesaid, we have analyzed for the industrial application the possibility of use of hydrocarbon solvents of Nefras type, isopentane, and hexanes forming in the process of dmerization, and their mixtures.

Certain choice can be made after comparison of various schemes for isolation of but-1-ene, hexenes and polymer. The choice becomes the simplest when technological scheme of separation of the products of dimerization is analyzed.

ANALYSIS OF THECNOLOGICAL SCHEMES FOR THE SEPARATION OF THE PRODUCTS OF DIMERIZATION

In the process of ethylene dimerization various olefins are formed: but-1-ene, but-2-ene, hexenes (hex-

Table 1. Boiling points of solvents and hexanes

No.	Solvent or hexane component	Boiling point or boiling temperature range
1	Nefras "A"	65–75
2	Nefras "C"	94–99
3	3-Methylpent-1-ene	54.2
4	2-Ethylbut-1-ene	64.6
5	Hex-1-ene	63.4
6	Isopentane	27.8

1-ene 10%, 3-methylpent-1-ene 30%, 2-ethylbut-1-ene 60% of the sum of hexenes), little amounts of oligomers (C_8 and higher) and of polymer (less than 0.5 weight %). The fraction of each component depends on the process conditions and catalytic system. Besides, the reaction mixture contains dissolved ethylene, the solvent selected for the process and (when triisobutylaluminum is used as a component of catalytic system) certain amounts of isobutene and isobutylene.

In the further analysis of various technological

Table 2. Operating parameters of the column for separation ethylene and C4 fraction

No.	Parameter or characteristic	Units	Value
1	Operating pressure	kg/cm^2	4–10
2	Column top temperature	ºC	20–40
3	Column bottom temperature	ºC	130–150
4	Column efficiency	Ntp*	12
5	Column top composition	wt %	ethylene 3.0, but-1-ene 96.0, *n*-butane 1.0
6	Column bottom composition	wt %	Solvent 53.3, hexenes 38.2, oligomers 2.0, butene up to 2.5

Ntp* - Number of theoretical plates

Table 3. Operating characteristics of the column for ethylene separation

No.	Parameter or characteristic	Units	Value
1	Operating pressure	kg/cm^2	4–8
2	Column top temperature	ºC	25–30
3	Column bottom temperature	ºC	40–60
4	Column efficiency	Ntp*	10
5	Column top composition	wt %	ethylene 50, but-1-ene 50
6	Column bottom composition	wt %	but-1-ne 99.5, *n*-butane 0.2, but-2-ene 0.3

Table 4. Operating characteristics of the column for Nefras “A” 65/75 and hexenes separation from oligomers

No	Parameter or characteristic	Units	Value
1	Operating pressure	kg/cm^2	0.1–0.2
2	Column top temperature	ºC	70–80
3	Column bottom temperature	ºC	130–150
4	Column efficiency	Ntp*	33
5	Column top composition	wt %	Nefras “A” 45.5, but-1-ene 4.0
6	Column bottom composition	wt %	Hexenes 40.0, Nefras 50.0, oligomers 10.0

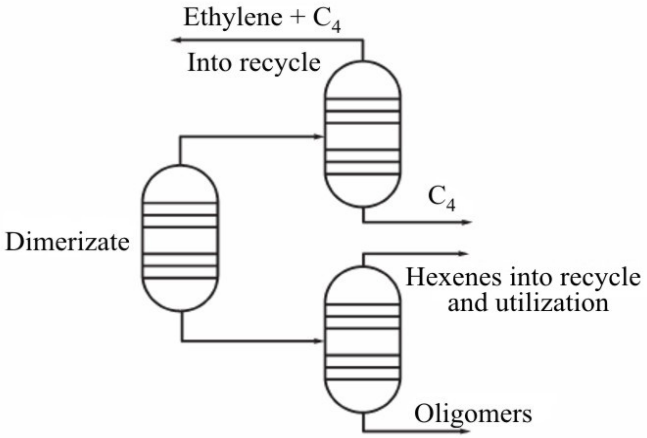

Fig. 3. Scheme of separation of the products of ethylene dimerization with hexenesas a solvent.

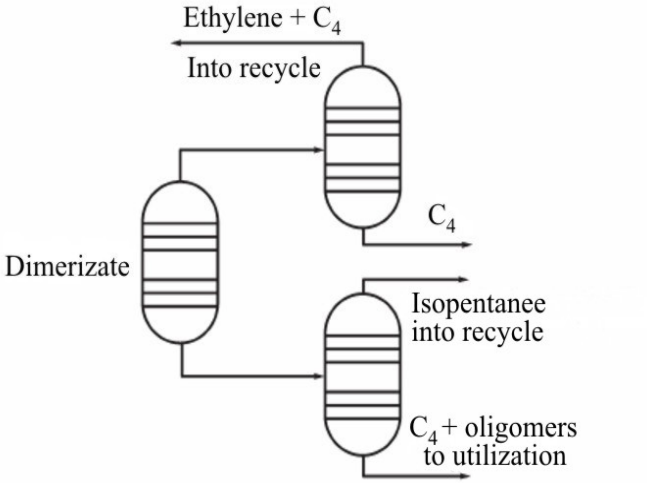

Fig. 4. Scheme of separation of the products of ethylene dimerization with isopentane as a solvent.

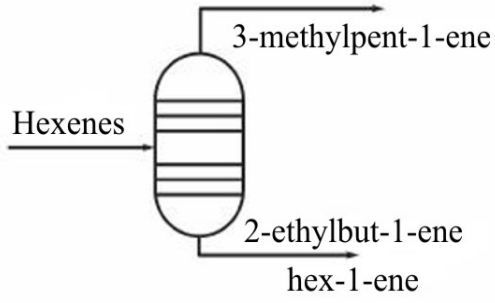

Fig. 5. Principal technological scheme for separation of hexenes.

schemes we omit separation into components of C_4 fraction, which composition is controlled by the dimerization process.

Depending on the nature of the chosen solvent, the principal technological schemes of rectification appear as seen in Figs. 1–5. As seen from the schemes, when Nefras "A" 65/75 is taken as a solvent in the ethylene dimerization, it can not be separated from the forming hexenes due to closeness of their boiling temperatures (Table 1, Fig. 1).

Application of Nefras "C" 94/99 allows isolation of hexenes, but additional column should be installed for its separation from oligomers (Fig. 2).

The most rational scheme is seems which uses hexenes (Fig. 3) or isopentane (Fig. 4) as a solvent. In these cases individual 3-methylpent-1-ene and 2-ethylbut-1-ene with hexane admixture can be isolated (Fig. 5).

For the drying reaction node and separation nodes, a node for azeotropic drying of solvent is needed; its principal scheme is shown in Fig. 6.

The drying node can operate continuously or in periodical regime.

All the schemes include first a column for separation of ethylene and C_4 fraction. Its characteristics are listed in Table 3. The characteristics of the column for separation Nefras "A" 65/75 and hexenes from oligomers are listed in Table 4, for Nefras "C" 94/99 in Table 5. The characteristics of the column for separation of hexenes from Nefras "C" are given in Table 6.

For separation of 3-methylpent-1-ene and 2-ethylbut-1-ene is used a column which characteristics

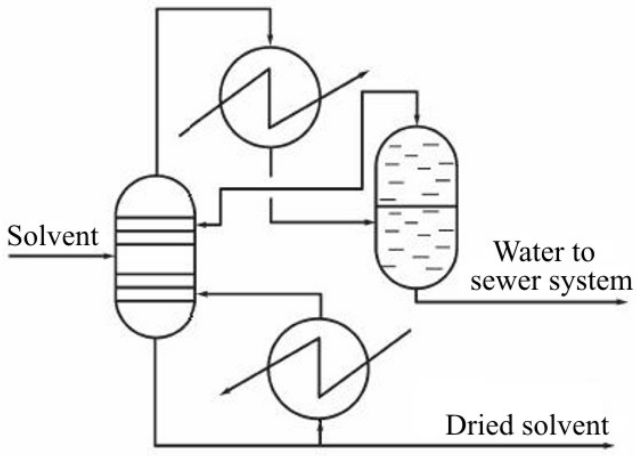

Fig. 6. Principal technological scheme for drying the solvent.

Table 5. Operating characteristics of the column for Nefras "C" 94/99 and hexenes separation from oligomers

No.	Parameter or characteristic	Units	Value
1	Operating pressure	kg/cm^2	No more than 0.5
2	Column top temperature	ºC	100–110
3	Column bottom temperature	ºC	130–150
4	Column efficiency	Ntp*	33
5	Column top composition	wt %	Nefras "C" 100%
6	Column bottom composition	-"-	Nefras "C" 98.0, oligomers 2.0

Table 6. Operating characteristics of the column for hexenes separation from Nefras "C"

No.	Parameter or characteristic	Units	Value
1	Operating pressure	kg/cm^2	No more than 0.5
2	Column top temperature	ºC	70–80
3	Column bottom temperature	ºC	125–135
4	Column efficiency	Ntp*	28
5	Column top composition	wt %	Hexenes 80.3, but-1-ene 4.4, Nefras "C" 15.3
6	Column bottom composition	wt %	Nefras "C" 98.5, oligomers 1.5

Table 7. Operating characteristics of the column for separation of 3-methylpent-1-ene and 2-ethylbut-1-ene

No.	Parameter or characteristic	Units	Value
1	Operating pressure	kg/cm^2	No more than 0.5
2	Column top temperature	ºC	60–70
3	Column bottom temperature	ºC	70–80
4	Column efficiency	Ntp*	35
5	Column top composition	wt %	3-methylpent-1-ene 95.0, 2-ethylbut-1-ene 5.0
6	Column bottom composition	wt %	2-ethybut-1-ene 85.0, 3-methylpent-1-ene 5.0, hex-1-ene 10.0

are listed in Table 7. The characteristics of the column for separation of hexenes from oligomers are listed in rerererre Table 9 lists characteristics of the column for azeotropic solvent drying.

Thus, consideration of technological schemes of rectification at the application of various solvents allows to select two type of solvents for the process of ethylene to but-1-ene dimerization:

Table 8. Operating characteristics of the column for separation of hexanes from oligomers

No.	Parameter or characteristic	Units	Value
1	Operating pressure	kg/cm^2	No more than 0.5
2	Column top temperature	°C	70–80
3	Column bottom temperature	°C	130–150
4	Column efficiency	Ntp*	33
5	Column top composition	wt %	hexenes 100%
6	Column bottom composition	wt %	hexenes 98.9, oligomers up to 2.0

Table 9. Operating characteristics of the column for azeotropic drying of solvent

No.	Parameter or characteristic	Units	Value
1	Operating pressure	kg/cm^2	No more than 0.7
2	Column top temperature	°C	95–100
3	Column bottom temperature	°C	105–110
4	Column efficiency	Ntp*	12
5	Column top composition	wt %	solvent 99.9, water (steam condensate) 0.1
6	Column bottom composition	wt %	solvent 100.0

–those forming hexenes in the process of dimerization
–isopentane.

Use of hexenes rather than isopentane is economically advantageous because the hexenes formed in the process of ethylene dimerization after their separation from but-1-ene do not require any drying to remove water or purification for removing other admixtures which could partially deactivate the catalyst.

REFERENCES

1. Ivanchev, S.S., Zhukov, V.I., Belov, G.P., Ivolgina, S.R, Germashev, A.I., Gabutdinov, M.S., and Shestak, N.P. *Plasticheskie Massy*, 1990, vol. 10, p. 82.
2. Zhukov, V.I., Belov, G.P., Germashev, A.I., and Saushkin, Yu.I., *Plasticheskie Massy*, 1996, no. 5, p. 6.
3. Belov, G.P., Borodin, A.M., Val'kovich, G.V., Zhukov, V.I., Polevshchikov, N.P., Petrov, Yu.M., and Skorik, I.N., *Summa Technologii* (Review of Russian Technologies), 2001, no. 1, p. 79.
4. Zhukov, V.I., Val'kovich, G.V., Skorik, B.N., Petrov, Yu.M., and Belov, G.P., *Khim. Promyslennost'*, 2005, vol. 82, no. 8, p. 382.
5. Belov, G.P., *Kinetika protsessov dimerizatsii i polimerizatsii etilena pod deistviem Ti-soderzhashchikh katalizatorov i svoistva obrazuyushchikhsya produktov* (Kinetics of ethylene dimerization and polymerization with Ti-containing catalysts and properties of the products formed). Doctorate dissertation, chemistry, Moscow: Inst. Khim. Fiziki RAN, 1984.

ISSN 1070-4280, Russian Journal of Applied Chemistry, 2007, Vol. 80, No. 7, pp. 1207–1212. © Pleiades Publishing, Ltd., 2007.
Original Russian Text © M.P. Yunusov, T.B. Molodozhenyuk, M.M. Ergashev, Sh.B. Dzhalalova, G.A. Gashenko, B.M. Saidulaev 2007, published in Khimicheskaya Promyshlennost, 2007, Vol. 84, No. 2, pp. 55–61.

TECHNOLOGY OF ORGANIC AND INORGANIC SUBSTANCES

Investigation of a System of Protecting Layer for the Process of Hydrorefining Oily Distillates of Uzbekistan's Petroleum

M. P. Yunusov[a], T. B. Molodozhenyuk[a], M. M. Ergashev[a], Sh. B. Dzhalalova[a], G. A. Gashenko[a], and B. M. Saidulaev[b]

[a]*Sultanov Uzbekistan Research Chemical Pharmaceutical Institute, Tashkent, Uzbekistan*
[b]*Fergana's Petroleum Processing Plant, Fergana, Uzbekistan*

Received February 19, 2007

Abstract—Complex investigation is conducted, directed to development of contacting materials (forcontacts) and catalysts for the protecting layer in the process of hydrorefining petroleum distillates taking into account their specificity and extensively attracting local raw materials. Forcontact FZS-7 is developed which, besides the function of uniform distribution of crude material over the reactor section, diminishes tarring and performs, owing to low nickel content, mild hydrogenation of unsaturated compounds. The proposed kaolin-bset catalyst of the protecting layer with low content of molybdenum oxide works reliably with the residual crude material with high content of iron and displays high enough demetallization activity.
DOI: 10.1134/S1070427207070403

Currently in Fergana's oil refining plant (FORP) is refined rather heavy hydrocarbon raw material from various fields in Uzbekistan, which is characterized by high content of paraffin, sulfur, and tarring compounds mixed with gas condensate. The refining scheme is defined by the local conditions: chemical composition of the petroleum distillates, nomenclature of demand by market petroleum products, and by technological potential of the facility for refining petroleum fractions.

Among the targeted processes in FORP a significant is producing basic lubricating oils with certain set of exploitation characteristics. The most problematic are enhanced colorization, compatibility with addition agents and low viscosity index. Correction of principal parameters of basic oils is performed at hydrorefining on G-24 installation where fractions of deparaffined distillate and deasphalted residue are treated in separate cycles. The tar-asphaltene substances colorizing petroleum products are mostly removed at deasphalting, but due to their volatility they contaminate oil distillates where they are undiserable due to high corrosion activity and deactivating effect on alumocobalt-molybdenum catalyst of hydrorefining. Design of the currently opertaing installation does not allow regeneration of deactivated catalyst directly in the reactor, therefore when reactor os sealed by deposits the process shold be interrupted. From the reactor after cooling are removed ceramic rings and upper, the most wasted and damaged part of catalyst. Then fresh catalyst is loaded and on it the ceramic rings cleaned from edges and deposits are placed. Thus, the main mass of catalyst is used for long time without regeneration, and raw material often containing admixture of unsaturated compounds feeds into the zone of relative high temperature and active catalyst. Unsaturated compounds initiates formation of sealing products which leads to faster increase in pressure difference and poisoning of hydrorefining catalyst. To improve quality of lubricating oil and the process parameters it is reasonable to perform multilayer loading of catalytic pacjage with additional forcontact and protecting catalyst layers.

Successful experimental-industrial testing of kaolin-phosphate forcontact (KPC) [1] in the reactor of Diesel distillate hydrodesulfrization in Fergana petroleum plant allowed considering of its application as front layer in treatment of heavier raw material. However, testing on a pilot-plant installation showed progressing grow of tarring components concentration in oil distillate, in residual fraction in particular, after contact with KPC under the process parameters analogous to those at the oil hydorefining (Table 1).

One probable reason for this observation is acceleration of polymerization reactions under the action of strong Bronsted acid centers [2] at lower hydrogen pressure compared to hydrodesulfurization of Diesel fuel. Really, testing the catalytic properties of KPC forcontact on a flow-type microinstallation in the temperature range 523–573 K revealed its ability of accelerating steric isomerization reactions of α-olefins and double bond migration into molecule followed by oligomerization. Yield of the products of intermolecular interaction of isomeric hexenes grows with temperature (Table 2), however, no surface coking was detected in the studied samples. Therefore for lowering the catalyst surface acidity excess to retard undesired reactions of to enhance hydrogenating function the KPC granules were impregnated with nickel compounds followed by thermal treatment. Studying showed that synthesis at lov pH values leads to dectrease in size of both large and small pores while impregnation of KPC by neutral solution increases fraction of pores 12-18 nm in diameter which leads to increase in sorption activity of the sample toward the largest test-molecules [3].Taking into account the coarse-pored structure and low specific surface of KPC, their impregnation conditions were taken to provide maximumm nickel concentration 1.3–1.5% inthe granules surface layer at the total NiO content 0.4–0.5% (sample FZS-7). IR spectrum of scrap from KPC granule surface showed decrease in the fraction of acid phosphites correlating with the change in acidity of the acid centers from $pK_a > 1.5$ on the surface to $pK_a < -3$ on the internal slice of granule. Modification of the forcontact with nickel compounds in neutral medium leads to relative increase in activity toward backbone isomerization of hex-1-ene and hydrogenation of forming unsaturated compounds.

Use of nickel salt solution with lower pH at impregnating KPC provides three-fold increase in concentration of surface acid centers with $pK_a < -3$ and more homogenous distribution of nickel compounds in the bulk granule (sample FZS-1). This leads to obvious strengthening of polymerization function in a model

Table 1. Testing protecting layer contacts on a pilot-plant installation. Temperature 523 K, pressure 2 MPa, volume rate 2.0 h^{-1}, hydrogen to raw material ratio 100 : 1

Sample	Change in properties of oil fractions on various contacts						Deposits on contacts, %	
	Color, CNT units	Viscosity, cSt at 40°C	Viscosity index	Iodine number, iodine grams per 100 g of oil	Sulfur total, %	Ash residue, $\%10^{-4}$	Cake	Tar
Oil distillate fraction III								
	2.4	41.6	87.0	0.80	0.67	15		
KPC	3.7	42.9	89.3	0.82	0.65	13	5.8	1.2
FZS-7	2.2	43.6	91.4	0.48	0.56	9	2.6	0.8
FZS-1	5.2	40.2	90.7	0.74	0.66	12	11.2	2.0
AKBM	2.0	39.2	94.3	0.35	0.43	7	4.2	1.8
Oil distillate fraction III								
	4.5	61.0	93.5	0.35	0.91	23		
FZS-7	3.8	62..3	96.3	0.19	0.78	17	Did not define	
AKBM	2.3	53.6	104	0.03	0.73	12	Did not define	
Residual fraction								
	7.8	343.4	89.1	0.56	1.23	63		
FZS-7	7.2	366.2	90.1	0.32	1.18	51	11.4	3.7
AKBM	5.2	296.0	99.5	0.13	0.97	29	6.9	4.5

reaction and sharp fall in colorization of oil fractions at hydrorefining due to intense tarring. On the contrary, passing residual fraction through FZS-7 layer leads to decolorizatiun of product by 1-2 TsNT (colorimetric standard) units. Besides, occurs certain increase in hydrocarbon chain branching, probably owing to isomerization followed by hydrogenation of unsaturated components, which leads in some increase in viscosity (Table 1) and decreases freezing temperature by 1–2°C. Appearance of hydrogen sulfide in gas phase together with practical absence of C_1–C_5 hydrocarbons attests proceeding of hydrogenation of the less stable sulfur compounds in oil fraction without C–C bond cleavage. Investigation of KPC samples and modified forcontact FZS-7 after their application to hydrorefining fraction III of oil distillate under the same condi-

Table 2. Comparative testing forcontact and catalyst activity in the model reaction of hex-1-ene conversion. Hydrogen pressure 0.001 MPa, volume rate 0.5–0.05 h^{-1}

Sample	Vpore, cm3/g (Rpore, nm)	T;K	Yield of reaction products, %				
			Cracking	Isomerization		Hydrogenation	Oligomerization
				steric	carcass		
KPC	0.14 (5÷6; > 10^4)	523	0	56.8	0.11	0	7.2
		573	0	57.4	0.63	0	12.6
		623	0.9	60.2	11.5	0	13.8
FZS-7	0.21 (7÷9; > 10^4)	523	0	37.2	19.3	0.3	2.1
		573	1.4	46.6	20.3	3.4	3.2
		623	1.6	49.7	23.3	7.9	3.7
FZS-1	0.18 (6÷8; > 10^3)	523	0	55.7	0.15	0	7.6
		573	0.05	58.0	0.76	0.9	14.3
		623	1.0	62.2	9.7	2.4	20.3
AK	0.31 (2÷3; > 10^4)	523	0	11.5	4.6	0	9.0
		573	0.03	19.0	12.2	0	7.0
		623	1.5	20.6	13.4	1.0	10.0
AB	0.58 (2÷3; 6÷8 > 10^4)	523	0	55.8	9.3	0.2	1.4
		573	1.0	52.3	14.8	4.5	2.8
		623	1.2	48.5	27.1	11.6	4.5
AKB	0.68 (4÷5; 7÷8 > 10^4)	523	3.4	44.3	13.4	0.5	1.5
		573	6.8	45.9	23.4	3.7	1.5
		623	8.9	47.9	22.3	4.8	2.3
AKM	0.68 (4÷7; > 10^4)	523	0.37	20.2	10.9	2.4	2.5
		573	1.4	20.3	13.5	14.8	3.7
		623	1.9	32.0	17.3	22.7	5.8
AKBM	0.65 (4÷8 > 10^4)	523	1.2	15.8	17.2	3.2	1.2
		573	1.5	17.3	19.2	15.4	1.6
		623	3.3	21.1	19.9	30.6	2.8

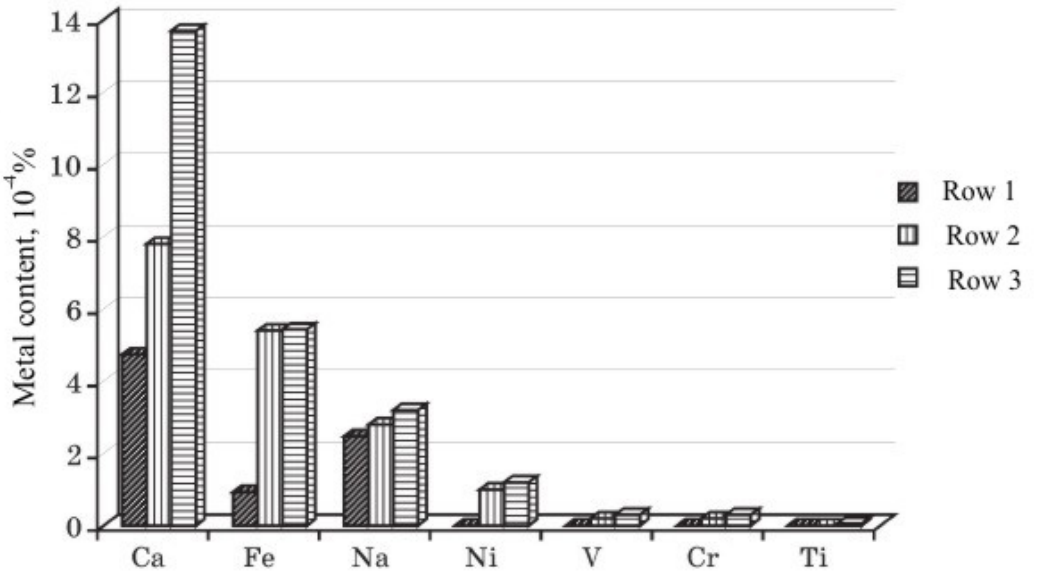

Fig. 1. Changes in metal content: 1 – in residual fraction, 2 – after hydropurification on FZS-7 forcontact, 3 – on AKBM protecting layer catalyst

tion in a pilot-plant installation revealed decrease in content of dry cake from 5.76% to 2.6 and of tar-asphalt substances extractable with benzene-alcohol mixture from 1.2% to 0.8%. On the FZS-1 forcontact surface was detected 11.2% of insoluble carbon-containing compounds. Comparison of decrease in concentration of metals in starting material and in the hydrogenizates (Fig. 1)with their distribution in "dry" cake and in extracts of caked samples allows to conclude that the forconacts partially trap alkaline and alkaline-earth metals, probably in the form of corresponding naphthenates dissolving in hydrocarbons. By the method of electron-sounding analysis we registered presence of sodium, potassium and calcium, mainly in ashed residues of oil fractions and in extracts of used up forcontact and catalyst of protecting layer (below). Concentration of typical catalyst poisons in the residual fraction, the vanadium, nickel and iron organic metallocomplexes, remains practically unchanged after passing oil through FZS-7 layer at hydrorefining, which attest low demetalliation function of this forcontact.

To avoid deactivation of cobaltmolybdenum catalyst in the process of work up heavy fractions, we prepared and studied a series of molybdenum-containing catalysts of protecting layer on the ground of clay minerals of Uzbekistan origin with by-products of local plants for their transformations. When carrier is prepared from bsevdobemit with 25% of kaolin, new very strong Si–O–Al bonds are formed between SiO_4 fragments of kaolinit and AlO_6 octahedrons of aluminum hydroxide. Optimal combination of strength and porous characteristics was achieved, in our opinion, with alumokaolin carrier modified with boric acid (Table 2).

The process of applying active metal from aqueous solution is significantly affected by state of hydroxyl shell of carrier, because change in solution pH is defined by dissociation of water molecules at the action of field strength of dominating aprotic adsorption centers. Study of acid-base properties of the smples dehydroxylated at 823 K showed that introducing kaolin to psevdobemit composition in strong acid medium enhances concentration of coordination-unsaturated aluminum ions on the surface of the calcined carrier, but on the other hand this promotes formation of Bronsted acid centers typical for alumosilicates [1]. Thus, the dehydroxylated alumokaolin carrier (AK) surface ears simultaneously fixed not mutually interacting strong aprotic and protic acid centers ($pK_a \leq -5$) and weak aprotic basic centers. On immersing the AK sample into water occurs emphasized alkalization of the medium (pH from 5.9 to 6.8) rather than at the hydration of aluminum γ-oxide prepared by pseudobemit calcination at 873–923 K [4], that is, the ratio of primary (acid) and secondary (basic) Lewis centers is shifted in favor of the latter and surface pK_a grows to 8.2. This is stipulated by formation of additional basic centers at the thermal decomposition of doped alkaline-earth

metal hydrocomplexes which in the process of plasticizing of the kaolin – bseudobemit mixture with nitric acid are washing out from kaolinit interpackage space, and further at thermal treating they are passed to the granule surface through capillary canals. De to irregular distribution of different type OH groups on the alumokaolin carrier surface, before formation of required monolayer, an "island" polymolybdate film is formed which contains up to 20% of water soluble molybdenum in the catalyst composition (AKM). The high content of water soluble mixed structures Mo^{6+}_{Td}–O–Mo^{6+}_{Oh} manifests itself as a bend at 33.3 kcm−1 in electronic diffuse reflectance spectrum, attesting weak enough interaction of active component with the carrier.

For strengthening granules and admitting proton-donor property to surface of hydrorefining catalyst for facilitating desorption of hydrogenolysis reaction products, to the catalyst compositionis introduced boric acid. Modifying aluminum oxide with boric acid in the absence of kaolin leads to formation of carrier (AB) with high concentration of Bronsted acid centers ($-8 < pK_a < -4$) on its dehydroxylated surface. In the first moment its hydration proceeds presumably by basic type affording H+ ions to the surrounding medium and decreasing pH value from 5.9 to 5.6. Then pH grows to 6.0, which points to the presence of two hydroxyl centers of two sorts capable of ion exchange, as well as Lewis acid centers capable of binding active component by sorption. Acidification of the medium due to ion exchange between surface groups of AB carrier and ammonium para-molybdate water solution shifts equilibrium to the side of formation in solution of polymolybdate structures, while fraction of water-soluble oxidomolybdene clusters in the final sample achieves 15%.

Modified alumokaolin carrier with optimal B_2O_3 concentration (AKB) the surface alumoborates formed after calcination at 773 K cover ¼ of monolayer. In couple with alumosilicate structures they provide formation of bronsted acid centers in the pK_a range from –4 to –1.5, regularly distributed on the carrier surface. At the contact of AKB with water the medium pH begins to change from 5.9 to 5.6, then becomes constant on 6.3 level, while pH of the carrier surface after hydration becomes equal to 7.2. Intoduction to this system of ammonium para-molybdate ammonia solution results in ion exchange reactions with surface structures and formation of Mo–O–Al, Mo–O–Si and Al–O–B–O–Mo bonds fied on the surface at thermal treatment. Applying of molybdenum oxide does not change spectrum of distribution by strength of acid centers on the AKB carrier, but increases concentration of Bronsted acid centers on the catalyst surface (AKBM).

Extraction treatment of the prepared catalyst showed absence of molybdenum water-soluble forms, although the fraction of active molybdenum extracted by ammonia is high enough. IR spectrum of AKBM in KBr pellet registered with reference KBr containing equivalent amount of AKB for compensation of the carrier bands contain bands near 920 cm^{-1}, which in conjunction with the data of electron diffuse reflectance spectroscopy evidences that molybdenum ions are in tetrahedral coordination and its significant part is in the composition of associates Mo_{Td}–O–Mo_{Td}, which are characterized by inflection point at 33.7 kcm^{-1}. Clear absorption band in the region of 40.0–43.3 kcm^{-1} is assigned to formation of amorphous alumomolybdenborates revealing high catalytic activity in the process of hydrocracking of heavy petroleum [5].

Express testing of catalytic properties of the catalyst on a microcatalytic installation of flow type, on the samples not containing molybdenum in the temperature range 473 – 673 K predominantly occurs reactions of stereoisomerization and double bond shift into the chain of normal acyclic α-olefin. Increase in concentration of acid centers pKa –5.6 leads to increase in the rate of formation of branced olefins due to backbone isomerization, but concentration of products of their hydrogenation decreases.

Hydrogenation of cyclohexene is accompanied with backbone isomerization with formation of methylcyclopentane and methylcyclopentenes. The same reaction products: cyclohexane, methylcyclopentane and various methylcyclopentene were formed bof in hydrohenation reaction and due to hydrogen redistribution in the experiments with inert gas. Although in the second case the products of backbone isomerization were formed in much less amount, their enhanced concentration on the samples with maximum acidity evidences unequivocally the principal role of strong acid centers in this process. We found that hydrogenating function of the catalysts correlates with concentration of water insoluble molybdenum, the maximal activity showed the catalyst on the carrier with the predominating strength of acid centers in the range $-4.5 < pKa < -1.5$. On the carries with stronger acidity (pKa below –5) the hydrogenation reaction are less successful and in the hydrogenizate increases fraction of undesired products of oligomerization.

We performed continuously testing of optimal forcontact samples FZS-7 and of protecting layer catalyst AKBM on a pilot-plant installation of high pressure hydrorefining fractions III and resifual fraction af oil distillates. The forcontact FZS-7 improves characteristics on color and iodine number of oil fraction before their passing on the catalyst of hydrorefining. Depending on the process parameter, on the protecting layer catalyst AKBM stable decreases colorization and sulfur content, increases viscosity index at minimal decrease in viscosity, and effectively trapped iron and other metal ions.

ABBREVIATIONS

FORP – Fergana oil refining plant,
G-24 – Installation for hydrorefining oil distillates,
KPC – Caolin-phosphate forcontact,
FZS-1 – Caolin-phosphate forcontact modified with nickel ions in acid medium,
FZS-7 – Caolin-phosphate forcontact modified with nickel ions in neutral medium,
AB – Alumoborate carrier,
AK – Alumocaolin carrier,
AKB – Alumocaolinborate carrier,
AKBM – Molibdenum-containing catalyst on the alumocaolinborate carrier.

REFERENCES

1. Yunusov, M.P., Molodozhenyuk, T.B., and Dzhalalova, Sh.B. *Chim. Promyshl*., 2005, vol. 82, no. 3, p. 121.
2. Sklyar, V.T., Lebedev, E.V., Zakupra, V.A. *Vyshie olefiny* (High olefins), Kiev, Tekhnika, 1964.
3. Yunusov, M.P., Molodozhenyuk, T.B., Dzhalalova, Sh.B., Ergashev, M.M., Gashenko, and Saidulaev, B.M. *International Scientific and Technological Conference "High technologies, education, perspectives of integration of science and industry"*, Tashkent, Conference proceedings, 2006, p. 112.
4. Nechiporenko, A.P., Vlasov, E.A., and Kudryashov, A.N. *Zh. Prikl. Khim*., 1986, vol. 59, no. 3, p. 689.
5. Rasikov, K.Kh., Vorobiev, V.N., and Abidova, M.F. *On the role op transition metal ion surface species in oil hydrocrecking. The 6 th Japan-Soviet Catalysis Seminar Catalysis for Coping with Oil Shortage*, 1981, Osaka, Japan, p. 139.

ISSN 1070-4280, Russian Journal of Applied Chemistry, 2007, Vol. 80, No. 7, pp. 1213–1217. © Pleiades Publishing, Ltd., 2007.
Original Russian Text © O.N. Filimonova, 2007, published in Khimicheskaya Promyshlennost, 2007, Vol. 84, No. 2, pp. 62–67.

TECHNOLOGY OF ORGANIC AND INORGANIC SUBSTANCES

Copolymer from the Waste Products of Styrene and Maleic Acid Production

O. N. Filimonova

Voronezh State Tecchnological Academy, Voronezh, Russia

Received February 9, 2007

Abstract—Influence of the process conditions on the production of "STAM" copolymer from waste products formed at join producing of styrene and propylene oxide, the acetophenone bottom residue at styrene rectification, with maleic acid. Effects of temperature, copolymerization process duration, weight ratio of acetophenone bottom residue to maleic acid and styrene content in the bottom residue are studied.
DOI: 10.1134/S1070427207070415

Solving the problem of targeted treatment of waste products require introduction of new processes based on the knowledge of composition and properties of the waste product as a physicochemical system, and mechanisms of their stimulated targeted reactions. The novelty consists in control over the process via kinetic modeling on the ground of chemical processes leading to predictable correlation of the model of initial physicochemical system and the copolymer quality as a reaction product. All steps of the process were studied in the sense of their interrelations.

We considered and solved the following problems: Maximum use of whole mass of bottom residue at styrene rectification, the waste product at the styrene manufacturing, that is, to minimize wastes at the treatment the bottom residue. Producing not toxic product in respect of residual styrene and other dangerous compounds [1].

Reaction of styrene with maleic acid in the presence of methylphenylcarbinol and acetophenone, the main components of the bottom residue in the join production of styrene and propylene oxide, leads to formation of polymer product ("STAM") which can show properties of a film forming material [2]. This is a multistep and multifactor process. Study of its steps allows to get a basis for the process separate steps and to reveal the most significant factors affecting yield and quality of the "STAM" copolymer.

The aim of this study is producing the "STAM" copolymer from the waste products at the styrene manufacturing, with maleic acid, namely, study if influence of the process temperature and duration, weight ratio of acetophenone bottom residue and maleic acid, styrene content in the bottom residue on the copolymer "STAM" yield. However, estimation of join effect of these factors on the producing the targeted substance in view of complexity in the study of this process requires application of the methods of mathematical modeling. Study of these factors and creation of the model require careful experiment planning.

The plan of experiments on the synthesis of "STAM" copolymer was based on the Greek-Latin 4-th order squire. The advantage of this method of planning is a significant diminishing the scope of experiments for revealing and estimating effects of certain factors and obtaining regression equations allowing simultaneous estimation of the effects of all factors and elucidating the range of each factor within limits of its varying, providing best experimental results in respect of a certain criterion that characterize the product quality or process efficiency. This is especially important in the cases where there is no interactions between the factors or such interaction is negligible. Structure of the squire is defined by the theory of planning experiments.

Experimental study of the copolymer production included the following:

–choice of the process temperature and synthesis duration, reagents ratio and styrene content in the initial bottom residue, as the principal parameters influencing the copolymerization process;

–estimating the basic parameters of the copolymerization process providing within a given range of their varying the highest yield of copolymer with required quality;

–revealing the dependence of the factors characterizing the polymer, on the condition of the synthesis.

The "STAM" copolymer synthesis was performed in a glass reactor equipped with reflux condenser, Dean-Stark trap and stirrer and located into a thermostat for maintaining required process temperature. The initial acetophenone bottom residue had the following composition (wt%): acetophenone 35, methylphenylcarbinol 14, styrene content was varied from 15 to 45 according to the plan of experiment, and all other was the tar which included polystyrene and other high-boiling compounds. Acetophenone bottom residue and maleic acid in a given ratio were loaded to the reactor simultaneously and then the reactor was heated stepwise to a given temperature which then was maintained within ±2.5°C. Reaction proceeding was monitored by the methods of chromatography and viscosimetry. After completing the synthesis, acetophenone and not polymerized compounds were distilled off in a vacuum at residual pressure 5–8 mm Hg and temperature 165–170°C.

As the factors affecting the process we consider: factor *A*, temperature of the synthesis, °C (*t*); factor *B*, the synthesis duration, h (τ); factor *C*, styrene content in the initial acetophenone bottom residue, wt% (*c*); factor *D*, amount of loaded maleic acid, wt%(*d*). The plan of experiment is shown in Table 1.

According to the plan of experiment, the coplymerization process consists of three steps, each step has its own temperature and duration. As response functions are taken: copolymer yield, its molecular weight, acid and ester numbers. Choice of these target functions is defined by the fact that they define the copolymer main properties and areas of its application. For estimation of the target functions and for prognosis of their values the experiment results were represented as regression equations,

$$Y = SF_1(t)\, F_2(\tau)\, F_3(c)\, F_4(d), \qquad (1)$$

where Y is the target function, S is a coefficient, $t=t_2t_3/t_1\text{-}(t_2t_3/t_1)_{min}$, t_1, t_2, t_3 are temperatures in first, second and third reaction steps, respectively, °C; $\tau = \tau_2\tau_3/\tau_1 - (\tau_2\tau_3/\tau_1)_{min}$, τ_1, τ_2, τ_3 are the durations of first, second and third steps, respectively, h; index min means that the minimal of possible values of monomials t_2t_3/t_1 and $\tau_2\tau_3/\tau_1$ are taken; *c* is styrene content in the acetophenone bottom residue, wt%; *d* is maleic acid doze, wt%; F_n is a function of one variable: $F_1=F_1(t)$, $F_2=F_2(\tau)$, $F_3=F_3(c)$, $F_4=F_4(d)$, F_1–F_4 characterize influence of temperature and duration regimes, styrene content and maleic acid dozing on the target function value.

Table 1. Plan of experiment

A	*B*			
	τ_1 — 2, 3, 5 (10)	τ_2 — 2, 4, 6 (12)	τ_3 — 3, 4, 7 (14)	τ_1 — 3, 5, 8 (16)
t_1 — 115 140 165	c_1 — 15 d_1 — 1 y_1	c_2 — 25 d_2 — 4 y_2	c_3 — 35 d_3 — 7 y_3	c_4 — 45 d_4 — 10 y_4
t_2 — 120 145 170	c_2 — 25 d_3 — 7 y_5	c_1 — 15 d_4 — 10 y_6	c_4 — 45 d_1 — 1 y_7	c_3 — 35 d_2 — 4 y_8
t_3 — 125 150 175	c_3 — 35 d_4 — 10 y_9	c_4 — 45 d_1 — 7 y_{10}	c_1 — 15 d_2 — 4 y_{11}	c_2 — 25 d_1 — 1 y_{12}
t_4 — 130 155 180	c_4 — 45 d_2 — 4 y_{13}	c_3 — 35 d_1 — 1 y_{14}	c_2 — 25 d_4 — 10 y_{15}	c_1 — 15 d_3 — 7 y_{16}

Note: the process temperature and duration relate to separate steps. Total process time is given in parentheses.

Table 2. Initial data for regression equations

Variable	Notation	Range of varying
Temperature, ºC, in first step	t_1	115–130
in second step	t_2	140–155
in third step	t_3	165–180
Duration, h, in first step	τ_1	2–3
in second step	τ_2	3–5
in third step	τ_3	5–8
Temperature index	t	0; 4.54; 9.11; 13.80
Duration index	τ	0; 4.50; 1.83; 5.83
Styrene content, wt%	c	15–45
Maleic acid content, wt%	d	1–10

Functions $F_1(t)$ and $F_2(\tau)$ in the equation (1) are discrete, and obey t and τ values within the ranges shown in Table 2.

The t and τ values are chosen taking into account convenience in calculation of $F_1(t)$ and $F_2(\tau)$, and are approximated by third degree equations. As far as levels of A and B factors are represented by scope of three values each, it is insufficient to characterize them by one value. Functions $F_1(t)$ and $F_2(\tau)$ in the accepted interpretation are discrete ones and reproduce experimental results only. Functions $F_3(c)$ and $F_4(d)$ are continuous ones, the possible experimental errors are smoothed assuming that this function can be represented by a second order polynomial.

Actual regression equations (2) – (5) for calculation of copolymer yield Y_{YD}, average molecular weight Y_{MW}, acid number Y_{AN} and ester number Y_{EN}, after mathematical treatment by means of computers with accounting for geometric mean values over the factors look as follows:

$$Y_{YD} = 2.14\cdot10^{-6}(75.3+0.335t—7.69\cdot10^{-2}t^2+ +6.24\cdot10^{-3}t^3)(76.8+7.47\tau—3.40\tau^2+0.375\tau^3)\times \times(42.0+2.05c—0.0251c^2)(69,1+2.91d—0.187d^2), \quad (2)$$

$$Y_{MW} = 8.51\cdot10^{-5}(17.4+4.53t–0.542t^2+1.63\times \times10^{-2}t^2)(22.5–0.108\tau–0.775\tau^2+0.162\tau^3)\times \times(29.3–0.449c+6.80\cdot10^{-3}c^2)(19.4+1.17d– –6.44\cdot10^{-2}d^2), \quad (3)$$

$$Y_{AN} = 6.85\cdot10^{-4}(12.6–0.571t+8.06\cdot10^{-2}t^2– –3.72\cdot10^{-3}t^3)(10.5+1.77\tau–0.239\tau^2– –1.39\cdot10^{-2}\tau^3)(5.92+0.287c–3.03\cdot10^{-3}c^2)\times \times(5.73+0.148d+0.151d^2), \quad (4)$$

$$Y_{EN} = 4.16\cdot10^{-5}(37.9–5.22t+0.691t^2– –2.72\cdot10^{-2}t^3)(22.2+13.2\tau–3.83\tau^2+ +0.299\tau^3)(18.6+0.517c– –4.95\cdot10^{-3}c^2)(11.8+2.78d+0.122d^2), \quad (5)$$

Average divergence of experimental values and the values calculated with the regression equations describing the process are, %: for copolymer yield 5.0, for average molecular weight 16.4, for acid number 3.6, for ester number 8.4. The ranges of response functions values according to the plan of experiment are given in Table 3.

The equations gives enough reliable prognosis of the possible results under the conditions differ from those used by the Greek–Latin 4th order squire and

Table 3. Experimental values ranges corresponding to the response functions

Data	Value
Copolymer yield, wt%	60–90
Copolymer average molecular weight, MW	12120–42660
Acid number, mg KOH / g	5–25
Ester number, mg KOH / g	11–81

allow varying the technology parameters and polymer composition depending on the conditions and area of its application to attain higher yield and necessary commercial properties.

The results of experiments allow assuming the polymer chain composition: it includes carboxyl, anhydride and ester functions. In all the cases the ester number defining presence of ester groups in the substance predominates over the acid number. This allows a suggestion that the ester groups are formed both in the process of reaction of maleic acid with methylphenylcarbinol and in reaction of methylphenylcarbinol with carboxylic groups in the polymer chain. Presence of all three groups of polymer chain is confirmed by the data of IR spectroscopy.

The presence of anhydride and carboxylic groups in the copolymer is defined not only by the presence of maleic acid in the reaction mixture. Number of such groups also is affected by the presence and content of styrene, to the side of increase. The effect of styrene content on the number of anhydride and carboxyl groups can be explained by the fact that the copolymer chain is formed as a result of reaction of styrene with maleic acid and anhydride. It is obvious that the more chains and longer each chain, the more anhydride and carboxylic groups they bear. Although, if we characterize effect of temperature defined as weighted average logarithms of temperature over synthesis steps, a tendency to decrease in the content of anhydride and carboxylic groups in the copolymer chain is revealed. It is very probably that this results from the insignificant changes in temperature (5°C) characterizing temperature regime and from reversibility of the copolymerization reaction [4].

Analysis of experimental data shows a significant increase in content of anhydride and carboxylic groups in the copolymer with increase in content of maleic acid in the initial reaction mixture.

Thus, the evidenced presence of anhydride and carboxylic groups in the copolymer is a direct sequence of copolymerization of styrene with the maleic acid and anhydride, and analysis of the results aimed at the elucidation of the copolymer chain structure shows, proceeding from the data on ester number, presence of ester groups in the copolymer. Formation of the ester groups can be stipulated by two circumstances: ester formation directly from maleic acid and methylphenylcarbinol and their exclusive formation in the reaction of methylphenylketone with carboxylic and anhydride groups belonging to the copolymer chain, because only one source of these groups is reaction of alcohol with carboxylic and anhydride groups [5].

The principal possibility of the first process has been substantiated for various modes of esterification reaction [6]. Being formed, the ester is involved into copolymerization similarly to the maleic acid itself or anhydride. The second mode which assumes reaction of methylphenylcarbinol with carboxylic and anhydride groups involved into copolymer chain also takes place. The possibility of ester formation is evidenced by both direct experiments using model mixtures in acetophenone medium and on the acetophenone bot-

Table 4. Chemical analysis of functional groups in the raw material and copolymers

Product	Acid number mg KOH/g	Bromine number g Br_2/100	Hydroxyl number mg NaOH/g	Iodine number g I_2/100	Ester number mg KOH/g	Carbonyl number mg NaOH/g
Initial acetophenone bottom residue	4.21	72.01	74.60	64.72	56.10	68.70
Copolymer without a coreagent	0.85	14.72	36.08	16.92	14.72	21.00
"STAM" copolymer	9.26	28.02	20.08	16.75	78.54	59.80
Copolymer with maleic anhydride	10.38	36.01	19.04	19.04	14.03	32.72

tom residue at styrene rectification.

Chemical analysis on functional groups of initial acetophenone bottom residue and copolymers based on it is shown by Table 4. It also confirms formation of esters. Also, it is confirmed by the data of IR spectroscopy: a series of bands at 1270, 1220 and 1180 cm^{-1} evidences presence of ester group, ν(C–O–C).

In a typical spectrum of the copolymer obtained on an IKS-29 instrument in the region 600–3200 cm^{-1} the presence of polystyrene ground is confirmed by the absorption bands at 1640, 1030, 906, 750 and 700 cm^{-1}. Strong absorption in the region of 1820 and 1770 cm^{-1} is characteristic of anhydride bands (styrene – anhydride conjunction in the polystyrene chain) and of maleic anhydride. The band 1710 cm^{-1} characterizes the maleic acid itself, ν(C – O), dimer. The shoulder on this band at 170–1660 cm^{-1} confirms existence of double bond ν(C=C) with *cis* arrangement of substituents. Anhydride band in the region of 1800–1500 cm^{-1} and absorption at 1740 cm^{-1} are due to ester group [7].

On the basis of chemical analysis and IR spectroscopy data we can assume structure of the obtained "STAM" copolymer as follows:

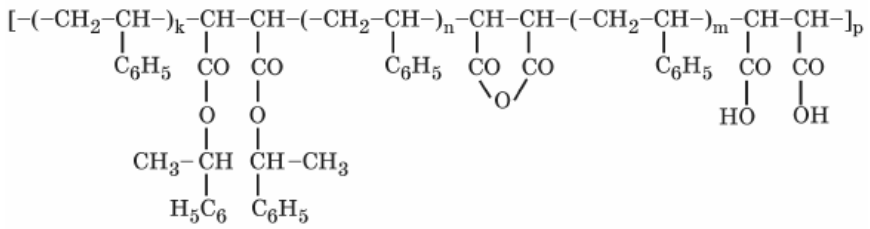

Thus, the experimental results which allow elucidate conditions for joint treatment of acetophenone bottom residue of styrene distillation and maleic acid for producing "STAM" copolymer are taken as a base for the technology operational description at the projecting experimental pilot-plant installation for producing "STAM" lacquer.

CONCLUSIONS

1. Using waste products at joint production of styrene and propylene oxide, the acetophenone bottom residue at styrene rectification, and maleic asid bcan be produced a copolymer possessing film-forming properties.
2. By experimental investigations is established that for producing this copolymer a three-step model of synthesis with the steps differ by temperature and duration is technologically reasonable.
3. The highest yield of the copolymer obeying commercial requirements can be achieved under the following conditions: in the first step temperature is 125–130°C and duration 2–3 h, in the second step temperature is 150–160°C and duration 4–5 h, in the third step temperature is 175–180°C and duration 7–8 h.
4. Content of styrene and methylphenylcarbinol in the acetophenone bottom residue should be not less than 25 and 4 wt%, respectively.
5. Content of maleic acid in the reaction mixture for copolymerization should be 4 to 7 wt%of the amount of acetophenone bottom residue.

REFERENCES

1. Petykhin, Yu.M. and Kontsova, L.V., Moscow: TsNIITE Neftekhim (proceedings), 1991, no. 6.
2. Yukelson, I.I., Butenko, T.R., and Berdutin, A.Ya., *Lakokrqasochnye Materialy i Ikh rimenenie*, 1979, no. 4, p. 9.
3. Akhnazarova, S.L. and Kafarov, V.V., *Optimizatsiya experimenta v khimii i khimicheskoi tekhnologii* (Experiment optimization in chemistry and chemical technology), Moskow: Vysshaya Shkola, 1985.
4. Berlin, A.A., Vol'fson, S.A., and Enikolopyan, N.S., *Kinetika polimerizatsionnykh protsessov* (Kinetics of polymerization processes), Moscow: Khimiya, 1978.
5. Emanuel', N.M. and Knorre, D.G., *Kurs khimicheskoi kinetiki: Uchebik dlya khimicheskikh fakultetov univesitetov* (The course of chemical kinetics, textbook for the students of university chemical faculties), 4-th edition, Moskow: Vysshaya Shkola, 1984.
6. Ingold, K., *Theoretical Grounds of Organic Chemistry* (Russian translation), Moscow: Mir, 1973.
7. Vest, V., *Application of Spectroscopy in Chemistry* (Russian translation), Moscow: Inostrannaya literatura, 1959.

ISSN 1070-4280, Russian Journal of Applied Chemistry, 2007, Vol. 80, No. 7, pp. 1218–1224. © Pleiades Publishing, Ltd., 2007.
Original Russian Text © M.B. Generalov 2007, published in Khimicheskaya Promyshlennost, 2007, Vol. 84, No. 2, pp. 68–78.

TECHNOLOGY OF ORGANIC AND INORGANIC SUBSTANCES

Technology of Plastic Industrial Explosives

M. B. Generalov

Received February 6, 2007

DOI: 10.1134/S1070427207070427

PLASTIC COMPOSITE EXPLOSIVES (OR PLASTIC EXPLOSIVES)

These explosives are a cross-linked polymer composition with polymer material as a continuous binding phase (matrix). In the polymer matrix a solid disperse mixture of explosives and specific additives is distributed like a filler.

Preparing the binding compounds consists in the following. As a binder in the polymer compositions usually are used various resins, which simultaneously are combustible components. A resin in viscous-flowing state is mixed with additives: plasticizers, vulcanizer, catalyst, dye and other special additives. The use of special additives is connected with the necessity of admitting required physico-mechanical properties to the commodity.

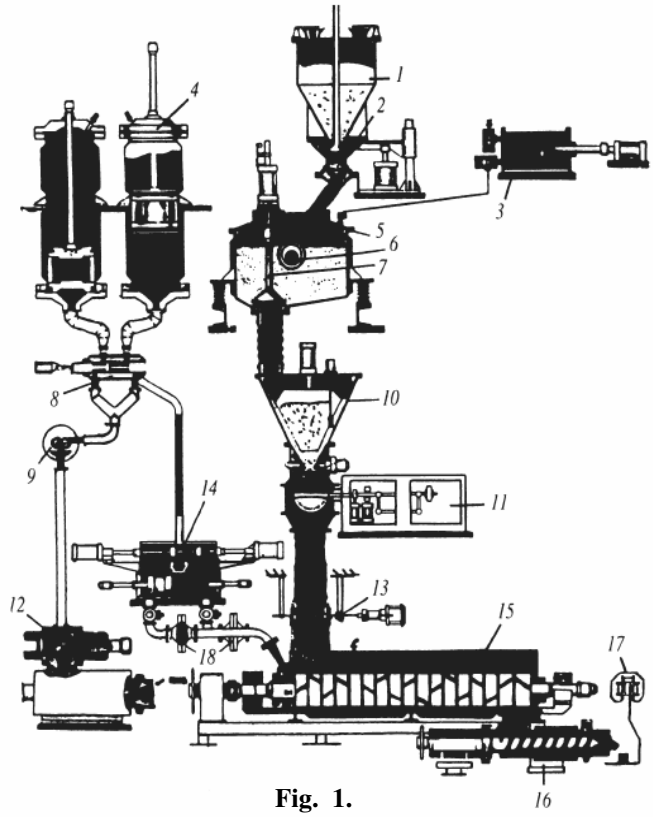

Fig. 1.

Preparation of friable substances is performed alongside the traditional technology considered earlier for the friable compositions of industrial explosives.

For preparation of explosive mass, a mixture of brisant explosive with additives is mixed with liquid binder in a mixer with periodical loading (blade, anchor or planetary type) or continuously operating (auger, two-screw type, two-blade type, rolls, etc.). Mechanical properties of the filled polymer explosives in a great extent depend on the size, distribution on size of the filler particles, their shape, homogeneity in distribution in the polymer matrix, degree of orientation (for anisotropic fillers) and interface properties. Content of filler in plastic explosives can vary in a wide range. In high-filled compositions it sometimes is over the polymer content. For example, the explosive "Hexoplast GP-87K" contains, %: hexogen 82.5, butyl rubber 13, fluoroplast 1.5, zinc white pigment 3, lecithin 0.1 [3].

The filled polymer explosive material in a general case can be solid amorphous (with partial crystallization) or in glass-like state, in solid highly elastic state, or in liquid viscous-flow state. The physical state of explosive material, partial or full bulk crystallinity and depending on it complex of its mechanical properties defines character of its application. The plastic explosive which are glass-like at ambient temperature or the explosives partially or fully crystalline are as a rule rigid materials and are known as plastics or plastids.

Plastic explosives in high-elastic state are known as elastomers or elastids, and posses properties of gum. The main advantage of the viscous-flow state polymer compositions is ability of most this type compositions to be molded and thus converted into a commercial mechanically shaped product.

The elastid charges are shaped as cords, tapes, plates by means of pressing, extrusion, rolling, pressure-die casting and by other methods.

Fig. 1 shows technological scheme of an installation for continuous producing plastic explosives [6].

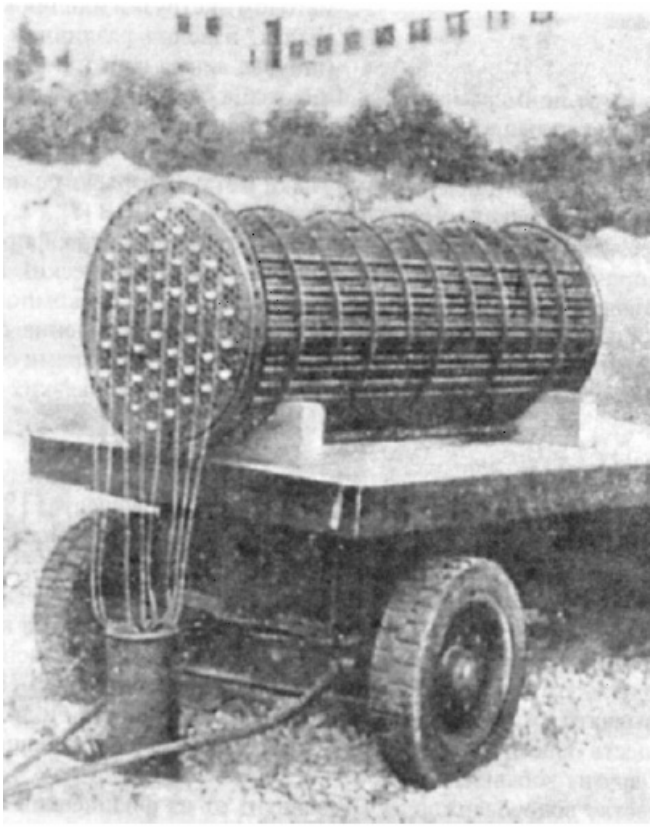

Fig. 2.

The power-saturated material from a hopper 1 through a loading unit 2 feeds into vibration mixer 5 equipped with a disbalance shaft 6. To the same mixer from a feeder (by volume) 3 is sprayed industrial oil. In the mixer the solid particles are covered by thin oily layer providing retardation, but the mixture remains friable. After completion the mixing process, through open ram 7 the friable mixture is passed into hopper 10 and then by vibrating feeder is passed into the unit for dozing by weight 11. Passing vibration screen 3, the friable mixture enters into the double spindle mixer 15 for stirring with plasticized polymer binder which feeds into the mixer from the feeder 14 dozing ratio by volume through filters 18. Into the feeder the polymer binder is loaded from alternately operating bunkers 4 via plunger pump distributer 8, volume pump 9 and ratio dozing feeder 12.

Before achieving the outlet of operating double spindle mixer the polymer binder and friable filler are transformed into homogenous two-component explosive mixture with a given ratio of components. In the auger unloading unit 16 the explosive plastic material is formed as separate blocks which are passed to loading unit of transporter 17.

Further the blocks are used for molding ware of different shape (cords, tapes, etc.) by, e.g., extrusion or rolling. As an example, Fig. 2 shows installation for rolling out tubes in the face lattice of a heat exchanging unit using cord charges of plastic explosive. Fig. 3 shows schematically cutting of metal by cumulative tape-shaped charges of plastic explosive.

Explosives containing nitric esters. The nitroester-containing (precaution) explosives ("Uglenit") are produced by two-step technology. Initially, friable components are mixed and hydrophobized by stearates. Final mixing of friable components with poorly gelatinized nitric esters is performed in a double blade mixers for plastic high-viscous materials [3].

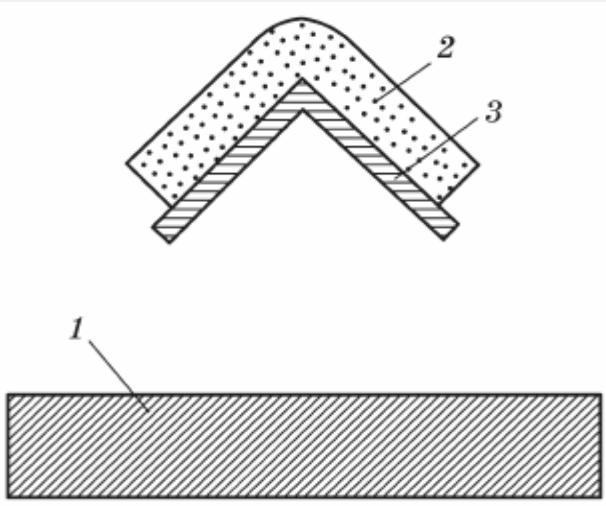

Fig. 3.

WATER-CONTAINING INDUSTRIAL EXPLOSIVES

Gel-like explosive mixtures. Basic idea in the technology of water-containing explosives consists in the use of saturated aqueous solution of an oxidizer (ammonium, potassium or sodium nitrate or mixtures of these compounds) as a continuous dispersion medium. In this water-containing composition is dispersed a mixture of friable material (TNT, alumotol, hexogen), combustible compound (aluminum powder), thickening agent (gel forming compound) and other additives.

Quality of the water-containing explowsives depends on their stability. Stability distortion appears as a stratification with formation of two layers leading to

unsteady detonation or even to failures. A reliable mean for stabilization explosives is introducing high-molecular thickening agents to increase viscosity of liquid phase.

Stabilization of water-containing explosives consisting of ammonium nitrate, granulated TNT and water can be achieved by introduction of 4% solution of carboxymethyl cellulose pure grade or 7% solution of carboxymethyl cellulose technical grade, and 1-2% of polyacrylamide [8, 10].

To provide stability of explosive containing 85% solution of ammonium nitrate as liquid phase its temperature should be below 68°C. For explosives with 80% solution temperature should be below 50°C. At lower temperature viscosity grows sharply. The lower temperature limit (critical temperature) is defined by pour point of the gel-like structure.

The method of keeping stability of gel-like explosives by maintaining optimal temperature is simply accomplishing: the required temperature of explosive mixture can be easily achieved by varying temperature of ammonium nitrate solution at mixing with solid components.

Among the most important parameters of gel-like explosives is considered their consistency, that is, content of solid phase by volume or weight. The system consistency defines explosive and technological properties of the gel-like explosives. It affects the explosion heat and power, the explosive mixture rheology (viscosity, shear stress yield), hydrodynamic parameters of transportation and thermal properties of the explosive.

Technological process of producing gel-like explosive includes the following principal phases [10]:

preparation of oxidizer solution,

preparation of solid friable components (TNT, granutol, alumotol and others),

preparation of combustible additives (aluminum powder),

mixing the components with binder to form gel-loke explosive or loading the components separately into mixing-charging device.

EMULSION EXPLOSIVES

All water-emulsion explosives contain high concentration solution of ammonium nitrate (sometimes with addition of sodium or calcium nitrate) and liquid petroleum product (Diesel fuel, industrial oil, mazut, etc.). The oxidizer solution heated to 60–90°C is dispergated and emulsified by adding small amount of a dispersing agent dissolved in the petroleum product achieving covering of each solution droplet by the petroleum product film.

Approximate composition of emulsion explosive components is as follows [8, 9], (wt %):

Ammonium nitrate	60–63
Sodium nitrate	16–19
Emulsifier	1–1.5
Oil (petroleum product)	7
Water	15
Nitric acid	below 0.3

The technological process of producing emulsion explosives is shown in Fig. 4 [8, 10].

The installation includes several modules: (1) preparing and loading oxidizers, including technological blocks for preparation water solutions of ammonium or sodium nitrate, the solution keeping and dozing; (2) preparing petroleum product, emulsifier and their mixture and the mixture dozing; (3) (additionally) the blocks for keeping and purifying cleaning sewers and the blocks of hydro-, electro- and pneumatic equipment; (4) preparing sodium nitrite and gas-generating additive (GGA); (5) emulsifying; (6) mixing-charging unit (MCU).

Preparing and loading oxidizer. Ammonium nitrate (GOST 2-85) from 60 kg bags in a treading down unit with a screw (auger) conveyers is loaded alternatively to one of dissolving units. Sodium nitrate (GOST 828-77) when necessary is loaded into dissolv-

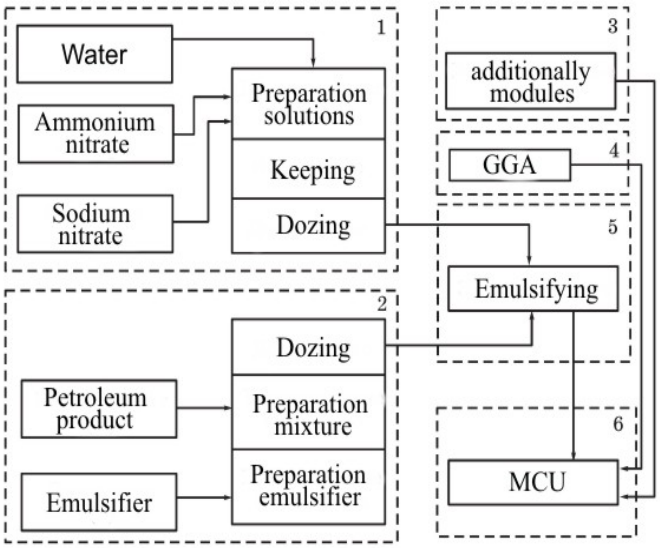

Fig. 4.

ing unit similarly.

A dissolving unit is vertical cylindrical receiver with a snake-like steam heater and equipped with a stirrer with electric motor. To the receiver loaded consecutively water by a pump up to required level and at working stirrer oxidizer (ammonium and sodium nitrate) in required amount. Then the mixture is stirred and heated until it achieves temperature 80ºC and required density, and thus prepared solution pumped into accumulating receivers. For preparing emulsion of commercial quality the solution of oxidizer(s) is passed to the module for preparing emulsion by dozing pumps.

Preparing petroleum product and emulsifier. A petroleum product (e.g., industrial oil, GOST 20799-88) from the receiver where it stored is pumped into mixing unit where it is heated to 40 – 70ºC. Emulsifier from a barrel is passed into the mixing unit uploaded by petroleum product by means of a sucking device which includes receiver and sucking pipe. If environmental temperature is below 10ºC, the barrel with emulsifier should be heated in a chamber.

To the mixing unit the petroleum product and emulsifier are pumped in a required ratio. The mixture is heated to 65–70ºC and stirred for a few minutes. From the mixer the petroleum product with emulsifier is passed by dozing pump into the module for preparing emulsion.

Preparation of solution of gas-generating additives (GGA). Sodium nitrite from 40 kg bags by screw transporter via inlet funnel is loaded into a dissolving unit filled preliminary up with water in required amount. Solution is prepared at the temperature 75–80ºC. The prepared solution of GGA is pumped into the bunker of mixing-charging device when necessary.

Emulsifying. To the mixer for preparing emulsion, solution of oxidizer and mixture of petroleum product with emulsifier are loaded continuously through dozing units. The products are dispersed at 80–85ºC to achieve formation of emulsion of "water in oil" type. The emulsion obtained by a special pump is passed to a storage tank or directly to mixing-charging machine.

Loading material into mixing-charging machine. The mixing-charging machine has tanks for filling it with hot water, GGA solution and emulsion. Loading emulsion is performed by pump in the emulsifying module or by gravity feed from storage tank. Filling with GGA solution is allowed also after loading emulsion. At low external temperature (below −10ºC) prior to loading material into the machine its tanks are heated by live steam.

As an example, Fig. 5 shows loading components of emulsion explosive into mixing-charging machine [8]. The final explosive mixture is formed directly in a bore hole.

TECHNOLOGY OF INDUSTRIAL EXPLOSIVES IN MINES AND OPEN PITS

Methods of producing plastic explosives. Water-containing and simplest explosives can be produced applying one of the following technology: (i) in a plant with packaging; (ii) in a stationary installation near a mine, an open pit, a well, with transportation of prepared mixtures from a charging machine to the place of blasting; (iii) separate transporting of the explosive components to the place of blasting, preparing the ex-

Fig. 5.

plosive mixture in a movable mixing-charging machine and charging.

The first method does not allow change the mixture recipe in a wide range, expensive and dangerous. The water-containing gel-like explosives made in a plant and used for charging bore hole under pressure are often more diluted and more sensitive, otherwise they are rather difficultly pumped through a hose into the bore hole. The sensitive explosive are transported by common roads without a binder, the latter is added prior to charging into bore hole for providing required viscosity and avoiding the slurry stratification at the charging.

By the second technology, the industrial explosive is produced near the user in a small scale mobile modules. The modules include chemical laboratory, tanks for saving the explosive components, a rolling train for preparation of the explosive (crushers, sieves, dozers, mixers), and are completed as a rule by the means for transporting explosives to the place of blasting. Such mobile modules allow easier varying content of explosive depending on the user query and conditions of blasting. For scaling up, an additional module line can be assembled in such a mini-plant.

The third technology is much more useful and safe, because not an explosive, but its separate components are transported. In a field work area near the pit is provided separate feeding the mixing-charging machine with friable components, nitrate solution (for emulsion explosives), emulsion gas-generating additives (for emulsion explosives), or by granulated ammonium nitrate and petroleum product or petroleum suspension with combustible material (for simplest industrial explosives of AN-DF type). The explosive mixture is formed only after mixing the ingredients and charging them into the bore hole.

Current statistics shows increase in consuming and extension of types of the explosives produced from nonexplosive ingredients near the blasting places. In 2001 their fraction was a half of all mass of the explosives consumed for blasting work [11].

TECHNOLOGY OF SIMPLEST INDUSTRIAL EXPLOSIVES

Producing of simplest industrial explosives, e.g., granulites and igdanites, includes a step of preparing ammonium nitrate and Diesel fuel or petroleum oil, and disperse combusting material (aluminum powder or alloys) [8,10].

Ammonium nitrate preparing consists in the operations of disclosing bags, sieving, crushing, loading into the saving bunker. For unpacking, a few types of devices are used:

vibration devices moving a bag with ammonium nitrate by oriented vibration and cutting by a knife,

rotating drums where the bag is moved through fixed knifes.

Simultaneously in these devices the granulated ammonium nitrate is sieved and crushed. The devices can also be used for preparing granulated explosives of TNT, granulotol and alumotol types and others.

Preparing combustible materials consists in the following. Tank of a hydrovacuum mixer is filled with Diesel oil and evacuated. The cans containing aluminum powder are disclosed and by vaccuum transport the aluminum powder is passed to mixer through flexible pipe. Then Diesel fuel and aluminum powder are circulated using a pump to formation of homogenous suspension with the fuel as continuous dispersion medium and solid aluminum as the disperse phase.

The final operation is mixing the components. The suspension is passed to auger mixer where suspension or fuel is sprayed over disperse particles of ammonium nitrate in the process of continuous mixing.

The process of producing granulits (igdanits) is monitored by measuring level of suspension (Diesel fuel) in the hydrovacuum mixer and by quantity of ammonium nitrate at its feeding from bunker into auger mixer and when necessary the quantity is controlled by a feeder slide bar driven with electric motor.

Complexes for producing water-containing explosives. The complex includes sections for preparing oxidizer solution and dry components, the line for preparing disperse metallic combustible additives, sections of charging and transportation [10].

Mixing-charging machines. For blasting in open pits are used charging machines for moving explosives from store into bore hole and mixing-charging machines for the transporting ingredients which are not explosive before mixing. In the mixing-charging machines the explosives are produced in the process of charging the bore hole.

The machines depending on the type of the used explosive are classified as working with explosives made of ammonium nitrate – Diesel fuel mixture and those working with water-containing explosives (gel-like or emulsion).

By the type of used explosive, all the charging and mixin-charging machines are classified into those

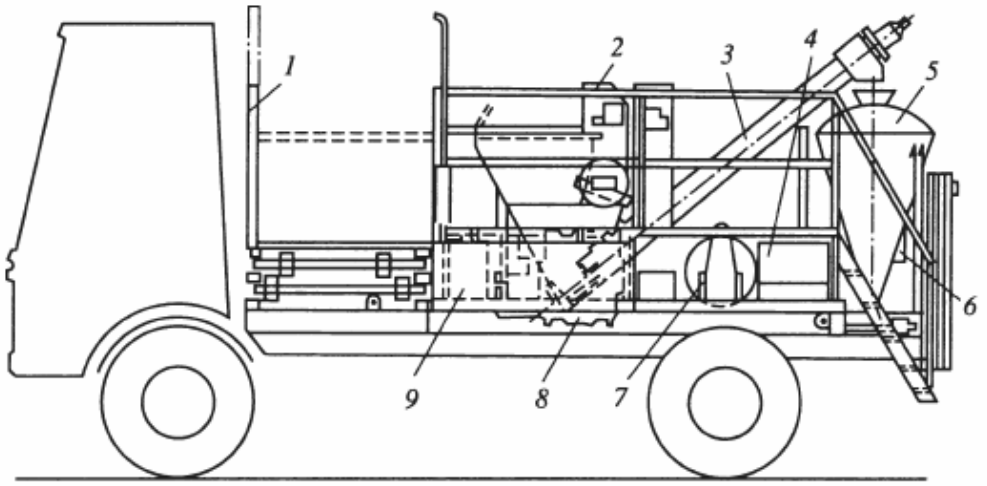

Fig. 6. "Emico" installation for preparation of AN–DF (ammonium nitrate – Diesel fuel) type explosives (1) lifting platform, (2) receiving container for ammonium nitrate, (3) auger loader, (4) system for Diesel fuel feeding, (5) charger, (6) control point, (7) compressor, (8) oil station, (9) hydraulic system.

working with explosives of AN-DF (ammonium nitrate – Diesel fuel) type and with water-containing explosives (gel-like and emulsion).

Mixing-charging machine for explosives of AN-DF type. By the method of feeding explosive mixture into the bare hole these machines are classified as pneumatic and auger type. Ingredients, e.g., ammonium nitrate and Diesel fuel placed to tanks in the process of charging are passed simultaneously into mixing chamber in a required ratio. The mixer is a chamber with sprayers spraying Diesel fuel at the moment when ammonium nitrate is feeding to the chamber by means of auger or vibrating transporter from the bunker through a closing device with hydraulic gear. Prepared mixture is passed into bare hole by compressed air or unloading auger.

The machine can be mounted on a trailer (Fig. 6) or as a stationary unit (Fig. 7).

Mixing-charging machine for explosives for water-containing explosives are based on the same principle of transportation of the non-explosive ingredients and saving them in separate tanks and bunkers. Feeding with the solid components is performed through feeders (auger or vibration type) with constant or controlled rate into a mixing unit. Feeding of liquid components is conducted by pumps.

For gel-like explosives of required consistency to the mixer is added binder. For emulsion explosives to the blending chamber is added sodium nitrite as a gas generating additive and dry components.

The most widely known suppliers of mixing-charging machines are the companies: Ireco hemicals (USA), Canadian Industries, Ltd. (Canada), African Explosives and Chemicals (SAR), Nitro Nobel (Sweden) and others. The machines as a rule are equipped with instruments showing consistency of explosive mixture, flow rate and consumption of explo-

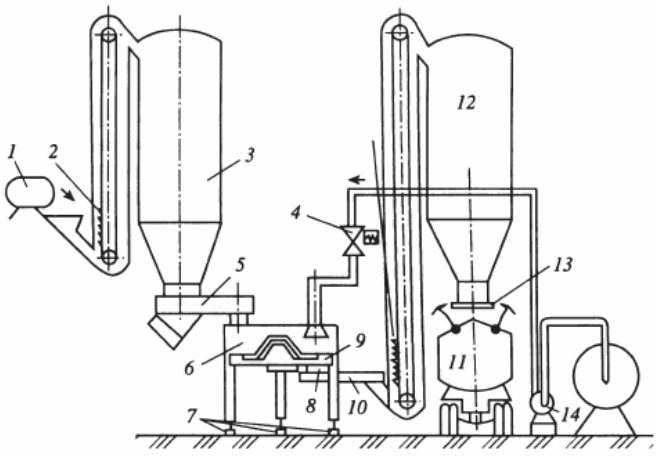

Fig. 7. Mechanized complex for explosive mixture of AN–DF type: (1) ammonium nitrate in bags, (2) elevator, (3) receiving container, (4) dozing valve, (5) vibration feeder, (6,10) augers, (7) vibrators, (8,9) node for preparing AN + DF mixture, (11) transporting–charging machine, (12) receiver for AN-DF mixture, (13) feeder, (14) pump for Diesel fuel.

sive. Control of the processes of blending, pumping, aeration, passing the mixture into bare hole is realized in automatic regime from electronic panel in cabin or in back part of machine. The machines allow varying ingredients ratio in the process of charging, forming charges differ by structure and programmable varying components ratio in the process of charging.

Additional details concerning charge-transporting and charge-mixing devices allowed for using in Russian Federation are described in [10, 11].

REFERENCES

1. Butnikov, M.A., Levkovich, N.A., and Bystrov, B.V., *Vzryvchatye veshchestva i porokha* (Explosives and propellants), Moscow: Gos. Izdatel'stvo Oboronnoi Promyshlennosti, 1955.
2. Vasil'ev, M.G., *Khimicheskii kompleks Rossii* (Chemical complex of Russia), Moscow, NIITEKHIM, 2002.
3. Dubnov, L.V., Vakharevich, N.S., and Romanov, A.I., *Promyshlennye vzryvchatye veshchestva* (Industrial explosives), Moscow, Nedra, 1973.
4. Orlova, E.Yu., *Khimiya i tekhnologiya brizanthykh vzryvchatykh veshchestv* (Chemistry and technology of brisant explosives), Moscow, Khimiya, 1981.
5. Zabarskii, V.L. and Zhilin, V.F., *Toluol i ego nitroproizvodnye* (Toluene and its nitro derivatives) Moscow: Editorial URSS, 2000.
6. *Vzryvcatye veshchestva, pirotekhnika, sredstva initsiirovaniya v poslevoennyi period* (Explosives, pyrotechnics, initiators in the after-war period), ed. N.G. Puzyrev, St. Petrersburg: Gumanistik, 2001.
7. Stepanov, V.G. and Shavrov, I.A., *Vysokoenergeticheskie impul'snye metody obrabotki metallow* (High-energy pulse methods of treatment metals), Leningrad: Mashinostroenie, 1975.
8. Kuk, M.A., *Nauka o promyshlennykh vzryvchatykh veshchestvakh*, Moscow: Nedra, 1975.
9. Zhuchenko, E.I., Ioffe, V.B., and Kukib, B.N., *Emulsionnye vzryvchatye veshchestva* (Emulsion explosives), Collection of scientific proceedings, Mendeleev Rus. Chem.-Technol. University, Moscow, 2000, p. 339.
10. Beisabaev, A.M., Erofeev, I.E., and Egupov, A.A., *Mekhanizatsiya vzryvnykh rabot: Spravochnoe posobie* (Mechanization of blasting: Handbook), Moscow: Nedra, 1992.
11. *Perechen' vzryvchatykh materialov, oborudovaniya i priborov vzryvnogo dela, dopushchennykh k primeneniyu v Rossiiskoi Federatsii* (List of explosive materials, equipment and instrumentation for blasting works allowed for application in Russian Federation), Ser. 13, Issue 2, Moscow: State Agency "Scientific Research Center on Safety in Industry", Gostekhnadzor, Russian Federation, 2002.

ISSN 1070-4280, Russian Journal of Applied Chemistry, 2007, Vol. 80, No. 7, pp. 1225–1234. © Pleiades Publishing, Ltd., 2007.
Original Russian Text © V.N. Skobelev, V.M. Yablokov, V.V. Serdyuk, L.A. Ashkinazi, 2007, published in Khimicheskaya Promyshlennost, 2007, Vol. 84, No. 2, pp. 79–91.

TECHNOLOGY OF ORGANIC AND INORGANIC SUBSTANCES

Amines as Antiknock Compounds. Phenomenological Approach

V. N. Skobelev[a], V. M. Yablokov[a], V. V. Serdyuk[b], and L. A. Ashkinazi[b]

[a]*St. Petersburg State Technological Institute, St. Petersburg, Russia*
[b]*Academy of Apply Research, St. Petersburg, Russia*

Received March 14 , 2007

Abstract—For enhancing octane number and improving ecological characteristics of internal combustion engines nitrogen-containing compounds of amine class are applied. Although these additives are inferior to the additives based on iron and manganese organoelement compounds (iron dicuyclopentadienyl, manganese methylcyclopentadienyltricarbonyl and others), but superior to oxygen-containing additives (low alcohols, methyl tert.-butyl ether and alone and mixed with tert-butanol and others). The nitrogen-containing compounds are ashess addition agents, thus they are advantageous over the addition agents based on organometallic compounds. A significant advantage of these additives is polyfunctionality. Being effective enough antiknock agents, they also possess antioxidant, stabilizing and anticorrosive properties.
DOI: 10.1134/S1070427207070439

This work is denoted to:

–Elucidation of mechanism of amine action with various fuels in the combustion chamber,
–Comparative analysis of efficiency of different amines in dependence of their molecular structure,
–Revealing the possibility of prognosis of most effective compounds for application, not inferior and even superior to the well known antiknock agents as aniline and monomethylaniline.

The initial position proceeds from the statement proceeding from the theory of chain reactions that over the pistion the preflame reactions on the frontier in going from combustion to explosion and detonation of the combustion products develop too vigorously. This leads to accumulation of many radicals developing and branching the chain reaction.

Development of chains [1] in time $n(t)$ depends on the probability ratio of interrupting (b) and continuing (a) the chain. It is therefore naturally that in the fuel charge the process of increase in the reaction rate below the critical value is closely connected with the ratio of these probabilities:

$$n(t) = \frac{n_0}{a - b}\left(e^{(a-b)t} - 1\right), \qquad (1)$$

where n_0 is initial rate of generation of radicals.

It is naturally that in each group of fuel the process of growing of reaction rate to critical value is connected with own probability ratio.

For increasing detonation resistance of fuel it is necessary to introduce the additives trapping radicals, thus increasing probability of chain interruption, which leads to smooth process of combustion the fuel charge. That is, efficiency of an additive is defined completely by the value of probability (b).

Due to fast exponential accelerating and, respectively, decelerating reaction in cylinder, even small increase in probability (b) leads to sharp deceleration of the process and respectively to increase in duration of growing number of radicals $n(t)$ in (1) to critical value (Fig. 1).

From relation (1) follows and in Fig. 1 is seen that in very beginning of the chain process of chain propagation the concentration of active radicals $n(t)$ is proportional to time and rate of increase in reaction rate to critical value depends significantly on the initial, start-up concentration of radicals n_0. Start-up radicals appear in the fuel charge spontaneously as a small portion of active high-energy particles in Maxwell distribution, or are created artificially, e.g. at illumination in photochemical processes.

The authors of out-of-engine express-method of estimation of octane number [6, 7] established experimentally that induction period of spontaneous ignition well correlates with octane number and symbasic cor-

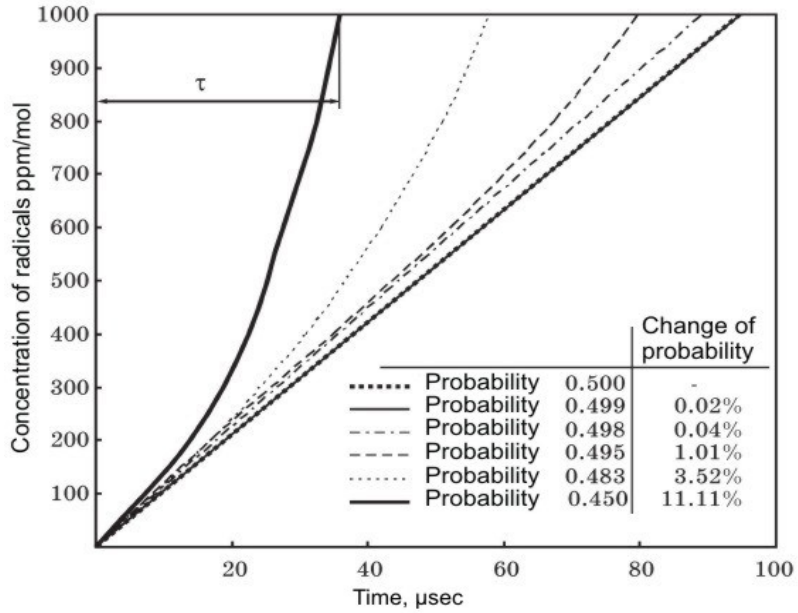

Fig. 1. Increase in radical concentration plotted against probability of chain break.

relation of these parameters is valid.

From relation (1) for short time period can easily be found connection of spontaneous ignition induction period τ and start-up rate of radical generation n_0.

$$E\tau = \frac{C}{n_0}, \quad (2)$$

where C is critical reaction rate at ignition, individual for each engine.

This indicates opposite correlation, now between induction period and n_0 value, and, eventually, similar correlation between octane number and n_0.

Thus, twice-triple increase in start-up generation rate (n_0) leads to reciprocal decrease in time of increase reaction to critical. This explain physical sense of octane numbers for various fuels. Increase in start-up rate of generation of radicals (n_0) is connected directly with shortening in time for achieving critical combustion rate which defines decrease in octane number of a fuel.

Further we have to classify fuels in correspondence with experimental data on the effect of amines on octane number. By this parameter three groups of fuel can be distinghished:

(1) fuel with octane number 86–90 relates to group I with low initial value n_0,

(2) fuel with medium octane number value 60–70 relates to group II characterized by n_{02} value,

(3) fuel with very low octane number 42 relates to group III characterized by large n_{03} value.

As is known, active particles in the process of combustion are atomic hydrogen, hydroxyl radical, hydrogen peroxide, various hydroperoxides and others. All these kinetical units either activate combustion by acceleration spreading of the flame front or lead to chain propagation and branching. The introduced additives should serve as traps for these units.

Relation (2) corresponds to correlation between additive-free fuel. In the case of additives, their influence on octane number should be taken into account. It can be made by taking into account three terms in expansion of exponent into a series, which shows the following relation between induction period and characteristics of radical, namely start-up rate of their generation n0 and probabilities of chain interruotion:

$$\tau \gg \frac{2}{a-b} + \frac{C}{n_0}. \quad (3)$$

Here a and b are probabilities of chain propagation and interruption, respectively.

This relation differs from (2) by appearance of a new term and it has transparent physical sense. First, it does not depend on conditions of combustion in the engine. Second, it characterizes only the radical and only the additive which we introduce to the fuel.

The additives increasing value of probability (a) are promoters of combustion, they decrease τ and hence decrease octane number. The additives increas-

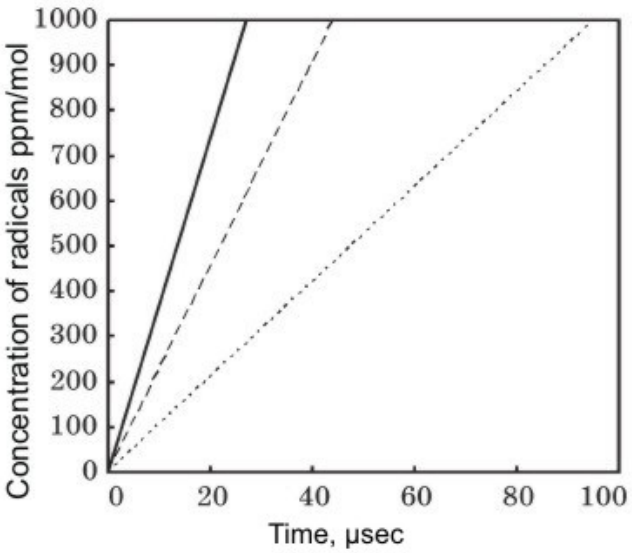

Fig. 2. Time shortening for achieving critical rate of radicals formation at decrease in the fuel octane number and, respectively, of increase in start rate of their generation, $n_0 = 10$, $n_{02} = 20$, $n_{03} = 30$.
.···· Start generation rate n_0,
- - - - Start generation rate n_{02},
—— Start generation rate n_{03}.

ing value of probability (b) increase induction period τ and eventually increase octane number.

Thus, the situation is simple in the case of model fuel (mono-fuel, for example pure heptane or pure isooctane). In a practical case the fuel consists of a complicated mixture of hydrocarbon fractions differ by nature. Thus at combustion of such mixture of hydrocarbons the ingredients convert with different rates, and integral experimental induction period is defined by the rate of "leading" reaction; in a process can be a few such reactions. In such a case the effective induction period is the sum of partial ones:

$$\frac{1}{t} = \sum_i \frac{1}{t_i} \quad . \tag{4}$$

Following to the idea in [6] we can say that if octane number in linear approximation is in line with induction period, it can be represented by the following relation:

$$ON = Kt = \frac{K}{\sum_i \frac{1}{t_i}} \quad , \tag{5}$$

Where K is proportionality factor between induction period and octane number (ON), is partial induction period, I is number of start-up chain (n_{0i}).

As follows from experiments and from this model approach, regime of fuel combustion can be controlled by both selection of hydrocarbon composition of the fuel and intoductio of antiknock additives.

Now, going back to influence of amines on the fuel combustion we have to note that mechanism of this process is defined by the effect of additive on the radical promoter. The additive "trap" for some time binds active radical and thus excludes it from the process. This is equivalent to increase in probability of chain interruption (b).

Our further consideration is based on the process of binding active particles by amines via electrostatic interaction or formation coordination and hydrogen bonds between amine hydrogen atoms aned oxygen atoms of hydroperoxides or between hydroperoxide protons and amine nitrogen atoms. An answer to the question "which bonds are more probable?" should be obtained from statistical correlation analysis.

Among whole array of amines (aliphatic and alicyclic, heterocyclic and aromatic) we have to select the most typical groups. As a first model approximation it is reasonable to consider two large groups differ by two typical structural attributes:

(1) primary amines,

(2) secondary amines.

Of course, such approach neglects fine physicochemical characteristics of these compounds, however, the further analysis will show that this is reasonable.

Let us consider influence of primary amines on the octane numbers of gasoline. Initial experimental data on primary amines are taken from publications [2–4]. All data on additives are recalculated and assigned to 2% concentration and normalized per mole. The datqa are listed in Table 1. Physico-chemical characteristics of some compounds were calculated using package of application programs ChemSiteSW [5] and also are listed in Table 1.

We consider the fuel of group II, for which there are many experimental data on octane number for individual compounds.

Increase in octane number for fuel with various amines as additives was attempted to correlate with certain molecular characteristics to find an approach to elucidation of mechanism of actions of amines. The following phenomenological correlations were attained:

–with molecular weight of amine (M), correlation

Table 1. Properties of primary amines

No.	Additive	Mol. weight	ON gain at the additive conc. 2 vol%			ΔON /mol·100		ON gain at the additive conc. 0.1 mol		L max molecule diameter	Rg molecule inertia radius	δqN charge value on nitrogen	δqH charge value on hydrogen
			Fuel group I	Fuel group II	Fuel group III	Fuel group I	Fuel group II	Fuel group I					
			ON-M	ON-I	ON-M	ON-M	ON-I	ON-M	ON-I				
1	Aniline	93.1	4.6	14	3.7	4.95	15	2.8	4.5	6.020	1.787	-0.863	0.352
2	Toluidines (mixed)	107.2	5.1	-	4.1	4.25	-	-	-				
3	*p*-Toluidine	107.2	-	14	-	-	13.1	-	-	6.917	2.036	-0.863	0.352
4	*m*-Toluidine	107.2	-	9	-	-	8.4	-	-	6.726	1.990	-0.863	0.352
5	*o*-Toluidine	107.2	5.1	7	4.1	-	6.55	-	-	5.930	1.912	-0.863	0.352
6	1,3-Diaminopropane	74.1	2.80	-	-	3.78	-	-	-	5.176	1.994	-0.539	0.224
7	*m*-Xylidine	121.2	3.6	-	2.4	2.97	-	-	-	6.170	2.184	-0.863	0.352
8	*p*-Xylidine	121.2	3.4	-	2.2	2.8	-	-	-	6.894	2.162	-0.863	0.352
9	Ethylenediamine	58.1	1.6	-	-	2.75	-	-	-	3.819	1.424	-0.528	0.228
10	1,4-Diaminobutane	88.1	2.0	-	-	2.7	-	-	-	6.531	2.190	-0.539	0.224
11	*t*-Butylamine	73.1	2.4	-	0.8	1.98	-	-	-	5.027	1.525	-0.542	0.223
12	*o*-Xylidine	121.2	1.04	-	-	1.4	-	-	-	6.606	2.046	-.0863	0.351
13	Methylamine	31.1	-	-	-	-	-	0.6	2.62	2.381	0.906	-.0537	0.225
14	Ethylamine	45.1	-	-	-	-	-	0.4	1.33	4.173	1.241	-0.539	0.224
15	*n*-Butylamine	73.1	-	-	-	-	-	0	0	6.110	1.855	-0.539	0.224
16	Isopropylamine	59.1	-	-	-	-	-	0.4	1	4.1823	1.419	-0.541	0.223
17	Benzylamine	107.2	0.56	-	-	0.5	-	-	-	6.000	2.017	-0.538	0.224
18	Isobutylamine	73.1	-	2.4	-	-	5.4	-	-	4.720	1.692	-0.539	0.224
19	Cyclohexylamine	99.2	-	-	-	-	2.3	-	-	4.970	1.702	-0.541	0.223
20	*t*-Octylamine	129.2	0.33	-	-	0.25	-	-	-	5.534	2.138	-0.542	0.223
21	2-Ethylhexylamine	129.2	-	0.3	-	-	0.23	-	-	8.510	2.787	-0.539	0.224

coefficient 0.911;

– with the value proportional to the rate of heat motion of molecules ($M^{0.5}$), correlation coefficient 0.907;

– with the value proportional to relative rate ($M^{0.5} - M_0{}^{0.5}$) of molecular motion of trapping molecule (amine) (M) and rate of motion of active radicals (M_0) (hydroperoxides with molecular weight M_0=40) with correlation coefficient 0.907.

The uncertainty in the promoter molecular weight appears due to the fact that the process of combustion affords a spectrum of the chain propagating radicals. Therefore the M_0 parameter means a molecular weight averaged over all radicals involved in the process by the proposed mechanism.

The proposed methodology operates with a parameter which is proportional to relative rates of the molecules:

$$\frac{1}{\sqrt{M_0}} - \frac{1}{\sqrt{M}}, \qquad (6)$$

where M_0 is molecular weight of promoter molecule, M is that of amine molecule.

For the most typical amines we performed correlation analysis for elucidation of the most probable representative among all possible promoters. From publications [7, 8] is known that as the promoters can be considered O–, HO–, H_2O_2, CH_3OOH and others, with their molecular weights M_0 = 16, 17, 34, 48 and higher. For all the array of amines for the fuel of group I we varied M_0 value with increment equal to 4 and calculated correlation coefficients. The results obtained showed (see Fig. 4) that correlation coefficients fall to a wide bell-shaped curve with the maximum in the region of promoter weight equal to 42. Hence it can be concluded that at combustion of this group fuel in the fuel charge occur pre-flame chain processes with all abovementioned compounds as promoters, but statistical weights of hydrogen peroxide and methane hydroperoxide, 34 and 48 respectively, predominate over all others.

Thus, the analysis shows that it is most probable that amines capture hydrogen peroxide and radical of methane hydroperoxide. The mechanism of amine effect thus consists in appearance of H-bonds between amine hydrogen atoms and peroxide oxygen atoms.

It seems reasonable to assume that the probability of chain breaking is the probability of the process of creation a bond between the molecules moving relatively to each other, and it is higher when the rate of relative motion is lower and the contact period is longer, $L/(M_0^{-0.5} - M^{-0.5})$. In a first approcimation it can be defined as a quotient at dividing molecule size (L is maximal diameter) by their relative motion rate.

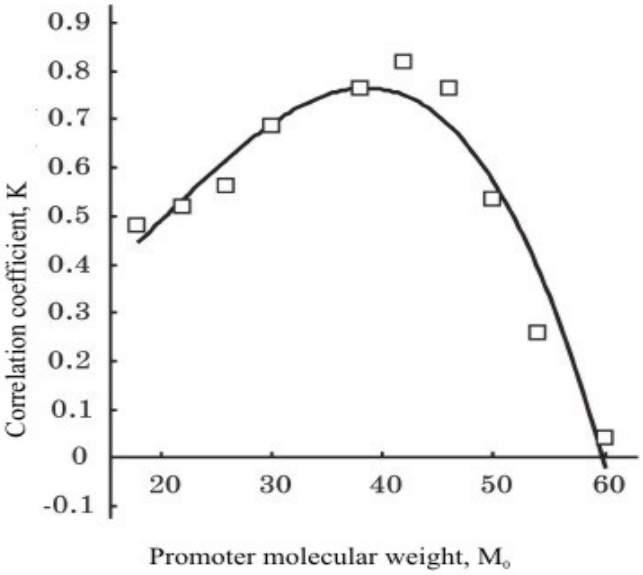

Fig. 3. Correlation coefficient plotted against the promoter molecular weight.

The molecule sizes are calculated by means of ChemSiteCW program. For the reaction proceeding is necessary realization of both imperative and adequacy conditions, respectively saturation of chemical bonding and steric conformity. The active zones of reacting molecules should coincide: a reagent molecule has to not only reach its partner, but also turn to it by active site. Therefore the process is expected to correlate clearly with the rate of rotation of molecules. This value is reciprocal to squire root of the molecule inertia moment ($M^{05}R_{g1}$). Actually, analysis shows that such correlation occurs, with correlation coefficient 0.862.

For the considered series of amines this is not surprisingly, but this factor will be shown to be very important in the case of diamines.

Above correlations show that the most active amines are those with the highest negative charge on nitrogen atom or, respectively, highest positive charge on the amine proton. Therefore for elucidation of the hydrogen bonds really involved in the process it seems reasonable to consider correlation accounting for these charges. Fig. 4 shows dependence of increase in octane number on contact period multiplied by the value of charge on the amine hydrogen atom.

Similar correlation analysis was carried out for the

charge on nitrogen atom. Here also occurs good enough correlation with coefficient equal to 0.918.

Comparison of the correlations allows to conclude that probably for this series of amines the most significant are hydrogen bonds between amine protons and peroxide oxygen atoms.

As to sequence of positions of the additives in toluidine series (3*, 4, 5, see Table 1), it can be simply explained by stability of molecule rotation around main inertia axis which is directly related to the molecule inertia moment $J=2/5\ M\cdot R_{g2}$ (the ball inertia moment). Rg is so-called inertia radius, a parameter in a program which puts ball with radius R_g in correspondence to the real molecule with the same inertia moment.

The higher inertia moment, the more stable motion of molecule in space. Among toluidine isomers (see Table 1), from R_g values follows that ortho-isomer (5) owing to its low symmetry moves in space the most irregularly.

Similar situation occurs in xylidine series (Fig. 5).

Comparison of correlations allows to conclude that probably in this series of amines is significant the appearance of hydrogen bonds between amine hydrogen and peroxide oxygen atoms.

The fuels of group I (octane numbers 86 to 91) were also tested on similar correlations, and expected correlation was actually found for this large group of amines.

Among the features of the studied group of amines we note, first, that fuel with high octane number show small increments of octane numbers, in correspondence with the proposed mechanism: at high octane number and, respectively, low n_0 values the bimolecular reaction rate of trapping promoter falls down. This situation lowers effect of adding additional quantity of additive.

Further, considering monoamines for the fuel of II group, they were compared also with diamines. Naturally, the diamines found more active and they fall well to the proposed correlation. This group includes the amines with rather wide spectrum of molecular weight and thermal motion rates. By the same methodology we correlated octane number increments with:

–molecular weight M, correlation coefficient is 0.271,

–rate of thermal motion (from the mas $M^{0.5}$) , correlation coefficient 0.213,

Further correlations accounting for:

–relative motion rate $M_0^{-0.5} - M^{-05}$, correlation coefficient 0.213,

–contact period $L/(M_0^{-0.5} - M^{-05})$, correlation coefficient 0.233,

–contact period multiplied by amine proton charge (Fig. 4), correlation coefficient 0.797 showed significantly improved correlation.

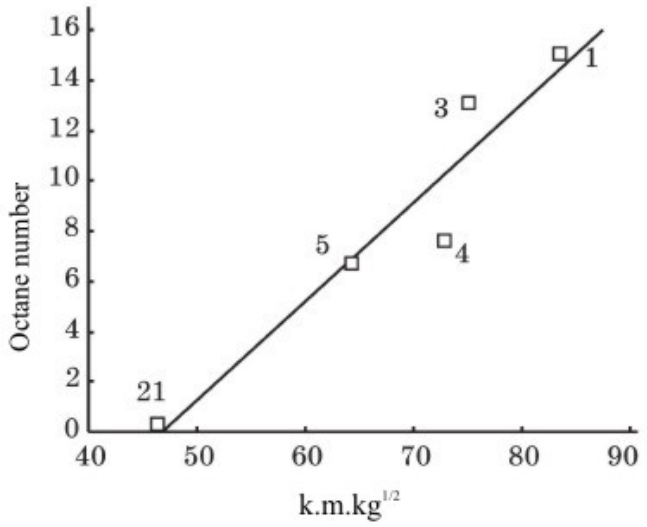

Fig. 4. Correlation of octane number gain with the charge on the amine proton multiplied by molecular contact duration for the radical C_2H_5COO – with molecular weight $M_0 = 61$. Points in the diagram correspond to numbers of the amines in Table 1. Correlation coefficient K = 0.969.

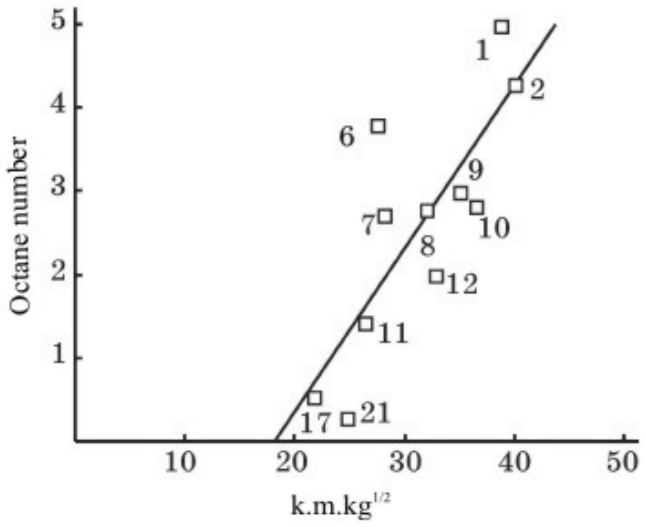

Fig. 5. Correlation of octane number gain with the charge on amine proton multiplied by molecular contact duration, $M_0 = 48$. Correlation coefficient K = 0.818.

Accounting for the charge on nitrogen atom leads to significant loses in correlation. This fact again confirms the statement that the main role in binding "bad" radicals in pre-flame processes play the hydrogen bonds between amine protons and peroxide oxygen atoms.

Consideration of symmetry allows setting xylidines in a sequence by efficiency. Here the situation is quite different compared to toluidines. Actually, the inertia moments of xylidines fall in in correspondence with R_g values in the order *meta* → *para* → *ortho*, thus defining their positions by increase in octane number.

The correlation shown in Fig. 4 shows that amines with large charge on the proton are comparatively more efficient. This statement seems to be not obeying by diamines which compete successfully with amines while possess less charge.

This inconsistence is avoided when steric factor is taken into account. To enter in a reaction, the reagent should occupy certain steric position at the partner, that is, the molecule has to be turned. The correlation shown below just is for such a case. The turning rate or rotation frequency is reciprocal to its inertia moment, therefore for such symmetrical molecules as diamines the statement is true that thy should not turn around not completely, but by half turn only. Formally this means twice increase in rotation rate, thus contact duration or charge increases by squire root of two.

This consideration explains anomalous "castling" of diamines, as shown in Fig. 6where correction of diamine rotation rates sharply improved correlation to the coefficient 0.887. Even more, when unsymmetrical ortho-xylidine molecule (12) is excluded from the data array, the correlation achieves to coefficient value 0.95.

In this array of amines another notable situation concerns ethylene diamine. Similar correction of ethylene diamine rotation frequency does not improve correlation, and therefore it was considered without taking into account its bifunctionality.

For $M_0 = 48$ (methane hydroperoxide) the correlation coefficient fall down to 0.483. Thus, the resilts of correlation shows that it is better conforms to the assumption that amines capture pure hydrogen peroxide rather than alkylhydroperoxide radicals.

Using the data of [4] we analyzed fuels with octane number 91.5 with the following amines as additives: aniline, methylamine, ethylamine, isopropylamine and *n*-butylamine in concentration 0.1 mol. For the group of the amines we also performed correlation analysis

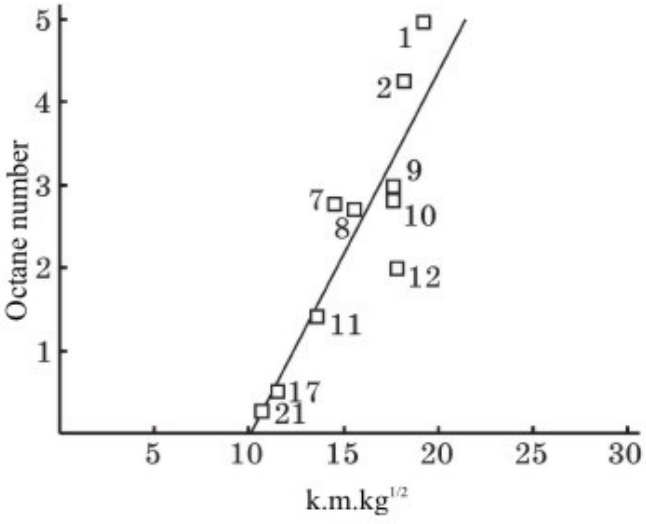

Fig. 6. Correlation of octane number gain with the charge on amine proton qH multiplied by molecular contact duration at relative rotation ($R_g\,{}^1M_0^{0.5} - R_g\,{}^1M^{0.5}$) for molecular weight $M_0 = 34$. Correlation coefficient 0.887. Points in the diagram correspond to numbers of the amines in Table 1.

for elucidation nature of promoters. We varied M_0 values with increment 4 withinnthe range from 16 to 68 weight units and calculated correlation coefficient. The results are shown in Table 7.

Consideration of correlation coefficient in dependence on the promoter molecular weight shows 4 maxima at M_0 = 16, 36, 48, and 64. These data with correlation coefficient 0.976 shows that we most probably deal with atomic oxygen or hydroxyl radical. With low statistic weight into the pre-flame processes can also be involved pure hydrogen peroxide and higher peroxide radicals. In this case also correlation of gain in octane number in dependence on charge on the amine proton multiplied by duration of molecular contact $\delta q \cdot L/(M_0^{-05} - M^{-05})$ shows correlation coefficient 0.885 and it is much better than correlation with the charge on nitrogen atom.

Comparison of correlations allows for this fuel group also conclude that or this series of amines significant are hydrogen bonds between amine protons and peroxide oxygen atoms. The correlations obtained (Fig. 8) lead to one more conclusion: the correlations are improved when M_0 value is taken equal 17 (which corresponds OH radical). The correlation coefficient is maintained on the level 0.885 for amine proton and 0.951 or 0.714 for nitrogen atom. When $M_0 = 34$ (hydrogen peroxide), then correlation coefficient falls down to complete absence of any correlation, k = 0.042.

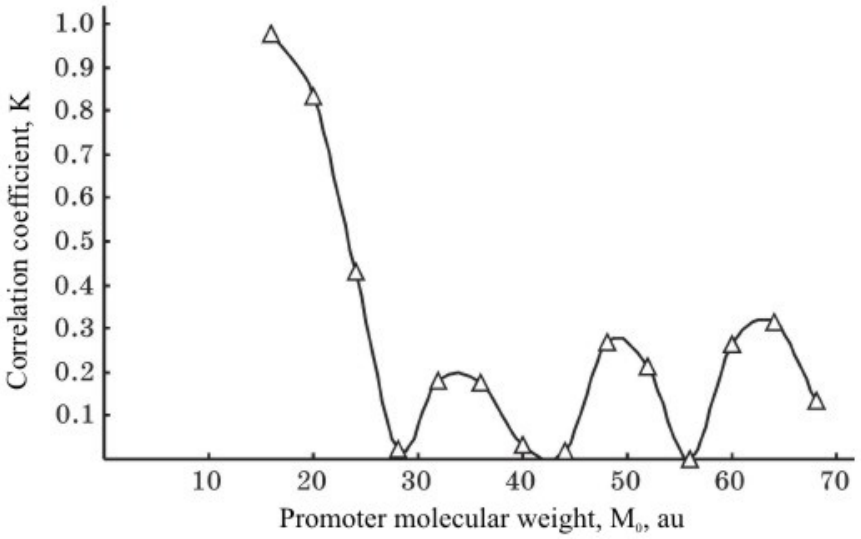

Fig. 7. Dependence of correlation coefficient on the promoter molecular weight.

The possibility of same mechanism of additives influence was tested for secondary amines. All required properties of the amines are listed in Table 2 [2–4]. By above considered methodology was revealed correlation for the fuels of group I at the adding amines.

Correlation of gain in octane number with amine proton charge multiplied by contact duration showed much lower correlation coefficient, for M_0 = 34 it was 0.541 only. Here interesting to note castling of t-butylfurfurylamine and piperidine. In the first compound the charge on proton is much lower, but structure of its molecule shows a feature: nitrogen atom and oxygen of keto group are close together, the distance is approximately corresponds to the length of hydrogen peroxide molecule. This fragment of the molecule can bind hydrogen peroxide molecule by two hydrogen bonds simultaneously: between peroxide proton and ketone oxygen and between the amine hydrogen and peroxide oxygen atoms. That is, this amine is bifunctional one.

The amines listed in Table 2 were added to the fuel in concentratiion 0.1 mol. The results of correlation alongside the abothe methodology showed that the best correlation coefficient is attained with hydrogen peroxide, M_0 = 34. In other words, the trapping compounds bind better hydrogen peroxide.

To a conclusion we note that we failed to explain high efficiency of dimethyl-*t*-butylamine which has anomalously low charge δq = 0.046 in the framework of the proposed mechanism. A feature of this molecule is its branched structure. In [7] with moderfuels was studied the process of pre-flame oxidation of a mixture of linear (*n*-heptane) and branched (isooctane) hydrocarbons and it was found that branched hydrocarbon under the conditions of pre-flame temperature does not oxidize due to its higher temperature of oxidative cracking. In a direct experiment was established that adding isooctane to n-heptane leads to proportional decrease in the tempera-

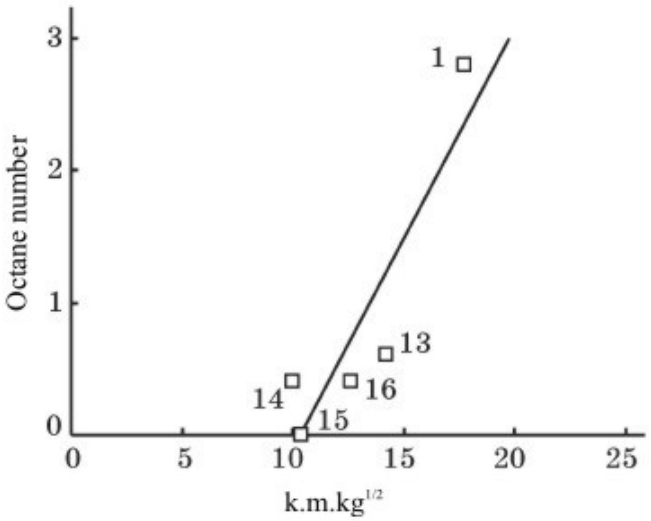

Fig. 8. Correlation of octane number gain with the charge on amine proton multiplied by molecular contact duration. Correlation coefficient K = 0.885 for molecular weight M_0 = 34. Points in the diagram correspond to numbers of the amines in Table 1.

Table 2. Properties of secondary amines

No.	Additive	Mol. weight	ON gain at the additive conc. 2 vol%			ΔON /mol·100		ON gain at the additive conc. 0.1 mol		L max molecule diameter	Rg molecule inertia radius	δqN charge value on nitrogen	δqH charge value on hydrogen
			Fuel group I	Fuel group II	Fuel group III	Fuel group I	Fuel group II	Fuel group I					
			ON-M	ON-I	ON-M	ON-M	ON-I	ON-M	ON-I				
1	*N*-Methylaniline	107.2	6.2	4.6	18	5.79	16.8	5.3	3.8	7.319	2.040	-0.662	0.317
2	*N*-Methyl-*p*-toluidine	121.2	-	-	18	-	15	-	-	8.178	2.290	-0.662	0.317
3	*N*-Methyl-*o*-toluidine	121.2	-	-	12.4	-	10.3	-	-	7.075	2.047	-0.348	0.317
4	Pyrrolidine	71.1	-	-	8	-	11.3	-	-	4.155	1.439	-0.742	0.314
5	*N,N*-Dimethylamine	41.1	-	-	-	-	-	6.66	2	4.213	1.223	-0.357	0.206
6	*N,N*-Disopropylamine	101.2	-	-	-	-	-	1.33	0.9	6.19	1.940	-0.360	0.200
7	*N,N*-Dipropylamine	101.2	-	-	-	-	-	0.44	0.3	7.697	2.316	-0.360	0.200
8	*NN*-Diethylamine	73.1	-	-	-	-	-	-	0.6	5.512	1.704	-0.361	0.205
9	*t*-Butylfurfurylamine	153.4	3.2	-	-	1.9	-	-	-	8.712	2.708	-0.332	0.212
10	Piperidine	85.2	1.26	-	5	1.48	5.95	1.23-1.94	0.7-1.11	4.974	1.630	-0.742	0.314
11	*NN*-Dimethyl-t-butylamine	101.2	1.26	-	-	1.24	-	-	-	5.625	1.826	-0.204	0.046
12	Nethylbenzylamine	121.2	0.74	-	-	0.64	-	-	-	8.304	2.385	-0.357	0.205
13	Dibenzylamine	197.3	1.0	-	-	0.51	-	-	-	10.37	3.311	-0.358	0.205
14	Diisobutylamine	129.2	1.2	-	-	0.85	-	-	-	7.589	2.603	-0.362	0.204

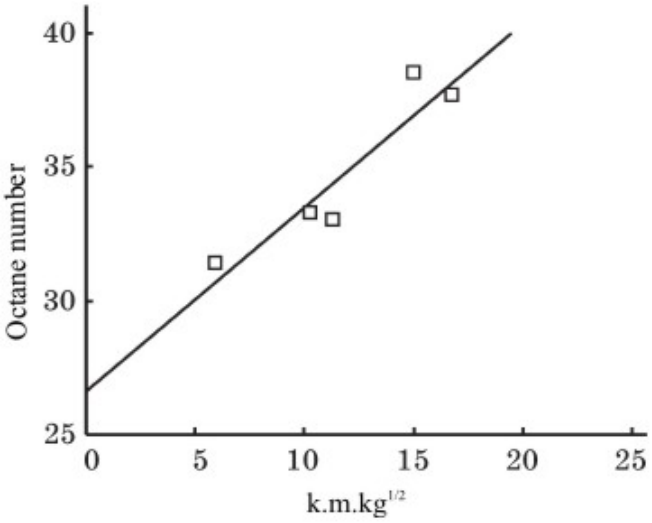

Fig. 9. Correlation of octane number gain with the charge on amine proton multiplied by molecular contact duration. Correlation coefficient K = 0.951 for molecular weight M_0 = 34. Points in the diagram correspond to numbers of the amines in Table 2.

ture for the mixed fuel. This can be considered as dilution of reactive *n*-heptane with chemically inert under same conditions isooctane. Thus isooctane in this case plays the role of inhibitor of pre-flame oxidation process. In [9] also was considered difference between *n*-heptane and isooctane which have polar values of octane number. Here chemical passivity of compact branched molecules is explained with low value of collision section and hence the pre-exponential factor in the rate constant of chemical reaction much increases.

It may be therefire concluded that brancged molecules practically are not involved into pre-flame oxidation processes due to both high activation energy and low pre-exponent in the reaction rate constant. Probably the considered tertiary amine wirks by this mechanism. By the mechanism of formatinon of hydrogen bonds it can not work at all because it does not possess labilehydrogen atoms in its molecule. Affecting octane number by dimethyl-*t*-butylamine is probably connected with local decrease in temperature and therefore by decrease in the initial rate of generation chains of radical promoters n_0 [see (3)–(5)].

Similar correlations were calculated for the fuels of group II. Fig. 9 shows correlation of gain in octane number with charge on amine proton multiplied by contact duration for molecular weight of hydrogen peroxide M_0 = 34. As seen from Fig. 9, the proposed mechanism as not bad for this case also.

SUMMARY

1. A well-founded mechanism of action of amines as additives to fuel for motors with spark ignition.

2. A procedure for analysis of comparative efficiency of various nitrogen-containing additives working alogside tis mechanism is proposed.

3. The regularities established and appearing exclusions can be naturally explained on the basis of consideration fine features of molecular dynamics, structure and properties of the amine molecules.

4. The correlation analysis is performed that allows to conclude that the most probable promoters are hydrogen peroxide and hydroxyl radical, and the amines are the traps just for these promoters.

REFERENCES

1. Semenov, N.N., *To the theory of the burning processes. In: "Theory of burning and explosion"*, Moscow: Nauka, 1981, p. 16.
2. Batrin et al., *Neftepererabotka i neftekhimiya*, 1999, no. 3.
3. Lerner, M.O., *Khimicheskie regulyatory goreniya motornykh topliv* (Chemical controllers of burning motor fuel), Moscow: Khimiya, 1979.
4. Lyle D. Burns, *Organic antiknock chemicals*, 1984, p. 744.
5. http://www.chemsw.com/
6. Azatyan, V.G., Kartashov, Yu.I., and Rumyancev, V.N., *International scientific and technological conference "New fuels with additives"*, Proceedings Collection, St. Petersburg, Academy of Apply Study, 2004, p. 359.
7. Melnikov, S.L., Kiselev, Yu.V., and Vyhrestyuk, N.I., *International scientific and technological conference "New fuels with additives"*, Proceedings Collection, St. Petersburg: Academy of Apply Study, 2006, p. 269.
8. Kolesnikov, I.M., Vinokurov, V.A., Kolesnikov, S.I., and Yablonskiy, A.V., *Khimiya i Tekhnologiya Topliva i Masel* (journal), 2001, no. 5, p. 23.
9. Skobelev, V.N., Hotuncova, S.V, Serdyuk, V.V., and Ashkinazi, L.A. *International scientific and technological conference "New fuels with additives"*, Proceedings Collection, St. Petersburg: Academy of Apply Study, 2004, p. 135.

ISSN 1070-4280, Russian Journal of Applied Chemistry, 2007, Vol. 80, No. 7, pp. 1235–1248. © Pleiades Publishing, Ltd., 2007.
Original Russian Text © N.A. Samoilov, I.A. Mnushkin, O.A. Mnushkina, 2007, published in Khimicheskaya Promyshlennost, 2007, Vol. 84, No. 1, pp. 24–39.

PROCESSES AND DEVICES OF CHEMICAL MANUFACTURES

Fractionation Step in the Technological Process on Reaction-Rectification Column of Ethylene Glycol Manufacturing

N. A. Samoilov[a], I. A. Mnushkin[a], and O. A. Mnushkina[b]

[a]*State Petroleum Technical University of Ufa City, Ufa, Russia*
[b]*Peton Co., Russia*

Received December 14, 2006

Abstract—Features of fractionation of reaction mixture in the synthesis of ethylene glycol by hydration of ethylene oxide in a reaction-rectification column are studied. Adequacy of the mathematical model applied to the process is evidenced. The ethylene glycol purity is shown depending on the process chemistry mainly. Side reaction of polyglycols formation restrict obtaining of high purity ethylene glycol: it can be isolated only as sideway stream in the bottom section of the reaction-rectification column.
DOI: 10.1134/S1070427207070440

The most widespread method of manufacturing ethylene glycol is direct hydration of ethylene oxide according to the reaction:

$$C_2H_4O + H_2O = HO–C_2H_4–OH, \quad (1)$$

Simultaneously with the main reaction occur side reactions of glycols with ethylene oxide resulting in formation of diethyleneglycol

$$C_2H_4O + HO–C_2H_4–OH = HO–C_2H_4–O–C_2H_4–OH, \quad (2)$$

trietyleneglycol

$$C_2H_4O + HO–C_2H_4–O–C_2H_4–OH = HO–C_2H_4–O–C_2H_4–O–C_2H_4–OH, \quad (3)$$

and tetraethyleneglycol

$$C_2H_4O + HO–C_2H_4–O–C_2H_4–O–C_2H_4–OH = HO–C_2H_4–O–C_2H_4–O–C_2H_4–O–C_2H_4–OH. \quad (4)$$

For depressing side reaction, the process is performed commonly in liquid phase at elevated temperature (ca. 200°C) and pressure (1.5–2 MPa) with water excess [1].

Technological scheme of the process is enough cumbersome. Besides reactor it includes three evaporation units for removing water excess from the reaction mixture and a block of rectification columns for removing admixture of di-, tri- and tetraethylene glycols from the product to achieve commercial quality. In this process all components except tetraethylene glycol are consecutively evaporated and condensed except; tetraethylene glycol is outlined from the bottom of the last column as liquid phase [1].

In the recent years interest to development of reaction-rectification units [2–4] joining chemical process and separation of products formed has markedly increased. This method gives rise to simplification of technological scheme of the process which allows to decrease basic investment for the facility construction and optimize the whole process [5–11]. The reaction-rectification columns can be also used in such technological processes as esterification, hydrolysis, oxidation, alkylation, isomerization and others, where chemical step proceeds in the temperature range of the components boiling points on the several contact mass exchange units in the column [2], in part, in the process of manufacturing ethylene glycol.

A feature of operating a reaction-rectification column at the ethylene glycol manufacturing is the necessity of circulation of water excess at the practically complete conversion of ethylene oxide [12–14], that is, top part of the column should work eventually in the regime of complete reflux for enhancing fractionation efficiency.

For the investigation of features of reaction-rectification column operating at the ethylene glycol manufacturing, we developed mathematical model of the device.

PRINCIPLES OF MODELING

As a basis for the model of reaction-rectification column we used a model of rectification process in a complex composed column which is equal to a set of simple columns [15]. At the developing this model we provided inlet of raw material to each theoretical plate and partial or full withdrawing vapor and liquid phases from the plate after mass exchange. These phases are passed out as final products or introduced as raw material on the other plates of composition column (Fig. 1, *a*). Such structure of the model allows simultaneous calculation of the system forming basis for optimization whole system. The model of theoretical plate for application to the considered problem is supplemented by blocks of mixing streams of raw and circulating materials and blocks for calculation of chemical process on the theoretical plate bearing simultaneously the function of reaction unit (Fig. 1, *b*). In such a case it is possible to withdraw reflux (which contains circulating water mainly) from an upper plate, mix it with raw material (ethylene oxide) and water stream, perform chemical reaction and separate reaction products on this reaction plate and on all other fractionating plates of the column. Therefore in the calculation of column two methods are joined: analysis of static fractionation on a theoretical plate providing determination of quality of products after separation in the vapor-liquid system via mass exchange, and analysis of kinetics of the chemical process on the reaction plate which allows determination of the contribution of components into composition of reaction mixture and time necessary for determination of acceptable deep of conversion of the raw material. This mathematic model was adapted to the synthesis of glycols by hydratation of ethylene oxide.

At the development of mathematic model of reaction-rectification column the following assumption were accepted:

– Hydrodynamics of contact unity is described by the model of ideal displacing,

– Average relative volatility of the separated components of the mixture in respect of reference component is taken constant along the column height. As the reference component is taken ethylene glycol, as board component of fractionated mixture: along the column, water with some admixture of organic compounds moves up, ethylene glycol containing some water and higher glycols, the products of side reaction, moves down.

The mathematic model of reaction-separation process on a contact unit consists of three blocks: mixing block, block of chemical reaction kinetics, and block of steady state rectification.

The model of mixing block of raw material with circulating water (reflux) in amounts corresponding to

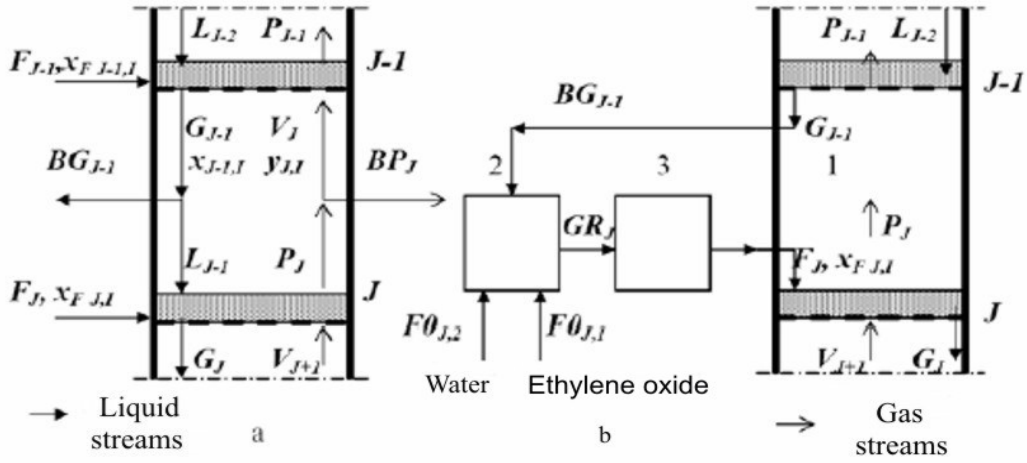

Fig. 1. Block-scheme of streams at the calculation of reaction-rectification column. (a) rectification zone, (b) reaction-rectification zone: (1) fractionating part, (2) mixing of raw material and circulating water streams, (3) reaction part.

overall balance incoming from the upper plate and containing small admixture of all other components, with definition of amount for each of six components (ethylene oxide, water, athylene glycol, diethylene glycol, triethylene glycol and tetrathylene glycol) incoming into reaction block, is performed as material balance equations for each component.

The model of reaction block is a system of differential equations accounting for influence of hydrodynamic situation on the kinetics of chemical process on each component of reaction mixture.

Reaction rate constants K_M is performed according to Arrhenius equation:

$$K_M = K_{M,0}\exp(-E_M/RT), \quad M = 1, 2, 3, 4, \qquad (5)$$

where $K_{M,0}$ is preexponential factor, E_M is activation energy for M-th reaction, T is the process temperature, R is universal gas constant.

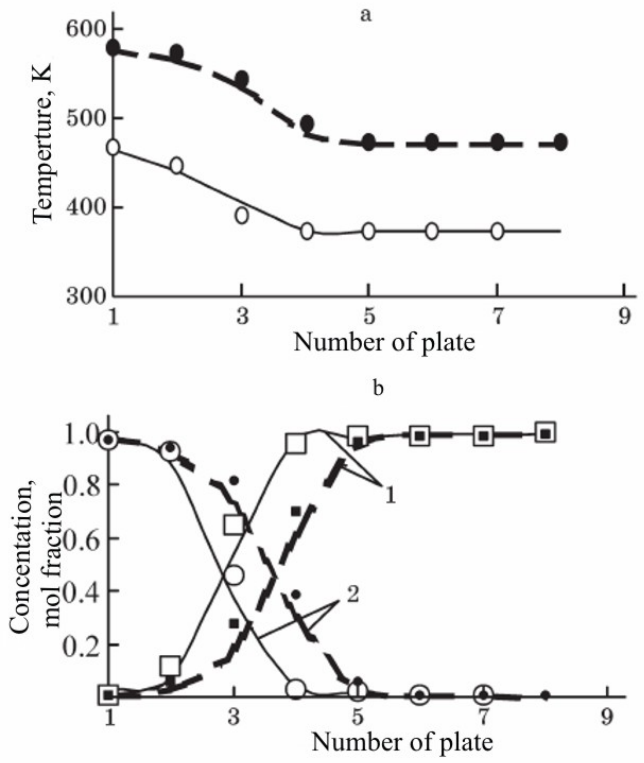

Fig. 2. Variations in temperature (a) and concentration (b) of ethylene glycol (1) and water (2) along the plates of reaction-rectification column (numbering from top to bottom). *Solid curves* – calculation according to the model at the pressure 0.1 MPa, *dashed curves* – calculation according to the model at the pressure 1.5 MPa, *dots* – data of [16].

The values of $K_{M,0}$ and E_M for the reactions (1)–(4) are taken according data of [1].

As a result of calculations of reaction block the quantity was determined of reaction products incoming on the corresponding theoretical plate for the separation of water and ethylene glycol containing admixtures of di-, tri- and tetraethylene glycols.

The model of rectification steady state assumes determination of the mixture composition on a plate after mixing incoming raw material (reaction mixture) with the streams of vapor and liquid incoming from neighboring plates placed below and above, calculation of the fraction of initial mixture outgoing as vapor, determination of the value of phase equilibrium constant of reference component (ethylene glycol) necessary for providing attaining of the given outgoing fraction on the theoretical plate, followed by calculation of composition of the equilibrium streams of liquid and vapor phases and their temperatures.

Calculation of chemical step of the process was performed by the first order Runge–Kutta method with obtaining the kinetic plots on all components of reaction mixture and determination of time for attaining maximum yield of ethylene glycol.

Calculation of rectification step is performed by relaxation method, the task was solved assuming filling the column with pure water as initial conditions. Starting data for the calculation include number of theoretical plates, molar streams of vapor moving up from each plate, positions of raw material inlet, the raw material quantity and composition. Algorithm of the task solution is featured by fast convergence (one variant of the column work takes 102 h for solution) with providing high accuracy of the calculation (one step of integration in calculation chemical step of the process consumes 0.0001 min at the reaction duration 1.5 to 0.5 min, equilibrium constant in the calculation of rectification steady state is calculated with accuracy 0.00001). Calculation is completed when in two consecutive iterations the difference in composition of vapor and liquid on all plates of the column was 10^{-8} mol fraction. For estimation of reliability of the mathematic model we compared results of calculation of manufacturing ethylene glycol alongside reactions (1)–(4) in the reaction-rectification column in the regime of complete reflux with the data obtained in [16] where besides the principal reaction (1) was taken into account the side reaction (2) only, with practically the same starting data (Table 1). As follows from Fig. 2, acceptable coincidence of temperature and concentra-

Table 1. Operating parameters of reaction-rectification columns for producing ethylene glycol

Parameter	Column operating at the pressure:			
	0.1 MPa		1.5 MPa	
	calculation of model	data of [16]	calculation of model	data of [16]
Accounting for number of side reaction	3	1	3	1
Number of theoretical plates	7	7	8	8
Raw material feeding, mol/s: ethylene oxide water	 7.30 7.30	 7.30 7.41	 7.30 7.30	 7.30 7.16
Reflux on plates, mol/s	591.2–598.4	594.9–598.4	624.5–631.6	626.8–631.6
Vapor streams on plates, mol/s	591.2	591.2–605.5	624.5	624.5–638.8
Top temperature, K	372.24	372.2	470.37	472.4
Bottom temperature, K	465.99	468.7	576.39	578.7
Column diameter, m	3.4	2.5	1.9	2.6
Heat supply, MWt	28.69	23.6	30.62	25.0
Heat withdraw, MWt	24.05	24.2	25.39	25.6
Ethylene glycol content in residue, mol fraction	0.981	0.97	0.979	0.97
Water content in residue, mol fraction	0.009	0.01	0.01	0.01

Table 2. Characteristics of flows in the considered modes of operation of reaction-rectification column at the reflux to ethylene oxide feeding ratio 90:1

Streams	Number of a variant					
	1 (Fig. 1, a)	2 (Fig. 1, b)	3 (Fig. 1, c)	4 (Fig. 1, d)	5 (Fig. 1, e)	6 (Fig. 1, f)
Raw material: ethylene oxide, mol water, mol	 10 10	 10 10	 10 810	 10 910	 5/3, 5/4* 5/3, 5/4*	 10 10
Distillate, mol	0	0.1	800	900	0	0.1
Residue, mol	10	9.9	10	10	10	0.08
Side distillate, mol	0	0	0	0	0	9.82

* Denominator shows number of plates with raw material inlet (3 and 4).

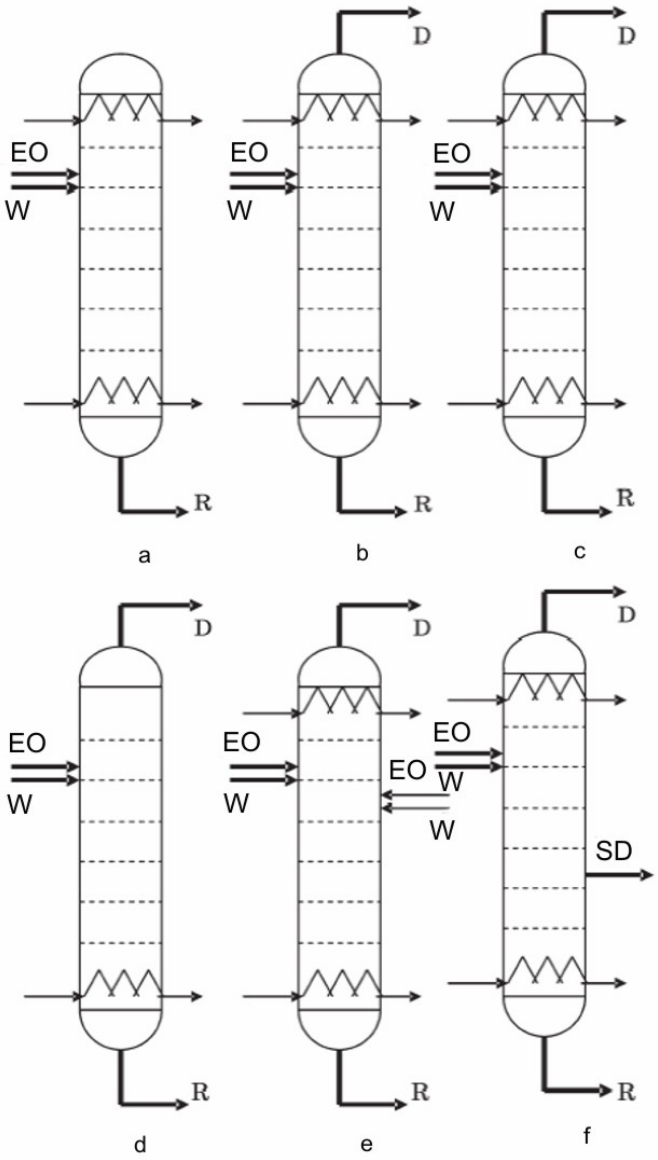

Fig. 3. Principal scheme of reaction-rectification column operating: (a) complete reflux, (b) withdrawing water admixture in residue as distillate, (c) withdrawing water excess loaded with raw material as distillate, (d) distillation column, (e) full reflux with dual inlet of raw material, (f) withdrawing final product as side distillate. Streams: (EO) ethylene oxide, (W) water, (SD) side distillate, (D) distillate, (R) residue.

tion of water and ethylene glycol profile along the column is obtained which attests adequacy of the static-kinetic model of reaction-rectification column.

RESULTS AND DISCUSSION

Preliminary calculations [12–14] showed that solving the task of performing controlled synthesis of ethylene glycol in a reaction-rectification column achieving low content of higher glycols in the reaction mixture and in residue is possible only under conditions of significant increase of water to ethylene oxide ratio in the raw material and, respectively, in the reaction mixture. For example, ethylene glycol concentration in the residue after complete removing water from it can be 0.97–0.99 mol fraction at the water:ethylene oxide ratio in raw material (30 to 100) : 1. Thus, a significant feature in the reaction-rectification column operating is the presence in the device of water in much excess; ethylene oxide converts practically completely; there is necessity of water separation from organic compounds. For estimation of the possibility to perform the process in the reaction-rectification column with obtaining highly pure ethylene glycol, we considered a series of modes of the column operation:

1) Column top part works in the regime of complete reflux without withdrawing distillate at the circulation of water in the column; feeling the column with raw material (water and ethylene oxide) in stoichiometric ratio of components.

2) Withdrawing water as a distillate in amount corresponding to residue in mode 1, water excess circulates in the column, raw material (water and ethylene oxide) is introduced to the column in stoichiometric ratio.

3) Water excess is introduced partially with raw material and is withdrawing as a distillate.

4) Water excess is introduced whole with raw material and is withdrawing as a distillate; from the fractionation viewpoint the device works as a distilling off column.

5) The column top part works in the regime of complete reflux without withdrawing a distillate, water circulates in the column, raw material (water and ethylene oxide) are introduced in stoichiometric ratio of components in parallel streams onto two plates.

6) As distillate, water is withdrew in amount corresponding to residue in mode 1, water excess circulates in the column, raw material (water and ethylene oxide) is introduced in stoichiometric ratio of components, commercial quality ethylene glycol (liquid phase) is taken as the side outflow.

Quantitative characteristics of streams in the reaction-rectification column for consideration of basic modes of the column operation are listed in Table 2. In

Table 3. Effect of reflux to ethylene oxide ratio on the variations in temperature (T, K) and equilibrium concentrations (mol fraction) of ethylene oxide (x1), water (x2), ethylene glycol (x3), diethylene glycol (x4), triethylene glycol (x5) and tetraethylene glycol (x6) in liquid phase on the theoretical plates of reaction-rectification column (pressure in column 1.5 MPa)

Plate No.	Parameters	Mole ratio reflux : ethylene oxide					
		10:1	30:1	50:1	70:1	90:1	110:1
1	x_2	0.9995223	0.9998326	0.9998954	0.9999226	0.9999364	0.9999449
	x_3	4.298059×10^{-4}	1.627555×10^{-4}	1.027627×10^{-4}	7.73026×10^{-5}	6.345109×10^{-5}	5.501843×10^{-5}
	T	470.35	470.35	470.35	470.35	470.35	470.35
2	x_2	0.9936638	0.9976256	0.9984976	0.9988709	0.9990734	0.9991968
	x_3	6.234771×10^{-3}	2.36092×10^{-3}	1.497407×10^{-3}	1.126789×10^{-3}	9.250583×10^{-4}	8.02227×10^{-4}
	T	470.54	470.42	470.39	470.38	470.38	470.37
3	x_2	0.9100021	0.9657198	0.9782393	0.9836266	0.9865587	0.9883449
	x_3	8.331473×10^{-2}	3.334836×10^{-2}	2.140724×10^{-2}	1.619075×10^{-2}	1.332923×10^{-2}	1.15792×10^{-2}
	T	473.22	471.41	471.01	470.85	470.75	470.70
4	x_2	0.9061879	0.9564369	0.9636677	0.9644922	0.9633694	0.9613062
	x_3	0.08711634	0.0426247	0.0359735	0.0353061	0.0365139	0.03861407
	T	473.35	471.70	471.47	471.44	471.48	471.54
5	x_2	0.8570021	0.841636	0.7940789	0.7533671	0.7191783	0.68866
	x_3	0.1355953	0.1570836	0.2052870	0.2462123	0.2804986	0.3110726
	T	475.05	475.59	477.37	478.98	480.41	481.75
6	x_2	0.6931023	0.5132733	0.4043546	0.3408169	0.2985947	0.2668504
	x_3	0.2967255	0.4833854	0.5934493	0.657537	0.7000708	0.7320198
	T	511.01	519.95	526.79	531.49	534.99	537.87
7	x_2	0.3248726	0.155714	0.1004253	0.07764918	0.0645316	0.0554636
	x_3	0.6490795	0.8375432	0.8926124	0.9172886	0.931416	0.9411289
	T	533.00	550.86	558.27	562.08	564.44	566.15

Table 3. (Contd.)

Plate No.	Parameters	Mole ratio reflux : ethylene oxide					
		10:1	30:1	50:1	70:1	90:1	110:1
8	x_1	7.538601×10^{-10}	2.921642×10^{-11}	6.529308×10^{-12}	2.420741×10^{-13}	1.139108×10^{-13}	6.380723×10^{-14}
	x_2	7.578363×10^{-5}	2.8171182×10^{-5}	1.767669×10^{-5}	1.335746×10^{-5}	1.095794×10^{-5}	9.350294×10^{-5}
	x_3	**0.8515911**	**0.9432899**	**0.9645234**	**0.9738445**	**0/9789782**	**0.9823374**
	x_4	0.068825	2.7988×10^{-2}	1.758945×10^{-2}	1.26917×10^{-2}	9.999026×10^{-3}	8.26861×10^{-3}
	x_5	3.66431×10^{-3}	5.4308×10^{-4}	2.088294×10^{-4}	1.057142×10^{-4}	6.469682×10^{-5}	4.366223×10^{-5}
	x_6	1.309195×10^{-4}	6.92473×10^{-6}	1.621758×10^{-6}	5.67165×10^{-7}	2.681317×10^{-7}	1.469047×10^{-7}
	T	563.81	572.53	574.71	575.62	576.13	576.49

all the considered modes the balance water – ethylene oxide ratio is taken equal to 90 : 1, which provides high concentration of ethylene glycol in the reaction mixture. When necessary for completeness of analysis of the problem, this ratio was changed, the number of theoretical plates and pressure in the column were also varied.

Varying water – ethylene ratio in the column working in the regime of complete reflux confirmed that owing to depression of side processes, the efficiency of whole process is enhanced (Table 3) and ethylene glycol content rises from 0.851 to 0.982 mol fraction at increase water – ethylene oxide ratio from 10 : 1 to 110 : 1, therewith it is sufficient to maintain water – ethylene oxide ratio 90 : 1. In the considered regime of the column operating, the raw material, water and ethylene oxide are introduced in 1 : 1 stoichiometric ratio on one of contact units (plate) in the medium part of the column, and mixed with reflux consisting of water with small content of admixtures. Here it enters to chemical reaction to afford ethylene glycol and small admixture of higher glycols. Thus, the process of rectification in the column in essence consists in separation of reaction products from circulating reflux.

A feature of the column working in the regime of complete reflux is virtual independence of quality of the obtained residue from the number of theoretical plates when the number of the plates is 5–6 or higher, because increase in the number of plates leads to formation on some theoretical plates of the peculiar region of constant concentrations where temperature and vapor and liquid compositions remain constant (Table 4). The pressure of vapor in the column does not affect practically efficiency of separation and relative content of glycols in the formed reaction mixture, but an increase in pressure leads to acceleration of chemical reactions which are completed within one – two real plates in the zone of raw material inlet. That is, we can assume that chemical transformation proceeds completely within one theoretical plate.

The variants of column working with complete reflux and as distilling column (Fig. 3) were analyzed with the purpose of diminishing water concentration in the residue, because in the regime of complete reflux it equals 0.008 mol fraction. The best results were obtained for the regime with withdrawing in the top of 0.1 mol of distillate, the water concentration in residue falls to 0.007, ethylene glycol content grows to 0.985 mol fraction (Table 5).

A possible way of diminishing the energy consuming in this process is replacement of discrete feeding the raw material to one reaction plate by distributing feeding over several plates in the column zone where change in the quality of reflux and vapor

Table 4. Dependence of temperature (T) and concentrations of water (x2) and ethylene glycol (x3) in liquid phase flowing down from plates of reaction-rectification column. Pressure in column 0.1 MPa, reflux to ethylene oxide (inlet on 3-rd plate) ratio is 90:1

Plate No.	Parameters	Number of plates in column			
		6	8	10	12
1	x_2	0.9999901	0.9999916	0.9999916	0.9999916
	x_3	6.42501×10^{-6}	4.9808×10^{-6}	4.97333×10^{-6}	4.97343×10^{-6}
	T	372.24	372.24	372.24	372.24
2	x_2	0.9996935	0.9997638	0.9997642	0.9997642
	x_3	3.04005×10^{-4}	2.35713×10^{-4}	2.35357×10^{-4}	2.35376×10^{-4}
	T	372.26	372.24	372.24	372.24
3	x_2	0.985711	0.9888626	0.9888790	0.9888788
	x_3	1.41865×10^{-2}	1.10364×10^{-2}	1.10199×10^{-2}	1.10202×10^{-2}
	T	372.52	372.45	372.45	372.45
4	x_2	0.8595069	0.9881128	0.9888635	0.9888674
	x_3	0.1403606	1.17861×10^{-2}	1.10354×10^{-2}	1.10315×10^{-2}
	T	375.17	372.47	372.45	372.45
5	x_2	0.1226969	0.9542174	0.98881579	0.98883245
	x_3	0.8756662	4.56777×10^{-2}	1.17401×10^{-2}	1.15735×10^{-2}
	T	415.55	373.14	372.47	372.47
6	x_2	9.45093×10^{-3}	0.6499565	0.9858908	0.9883142
	x_3	**0.9812574**	0.3498251	1.40071×10^{-2}	1.15838×10^{-2}
	T	465.76	405.97	390.13	390.13
7	x_2		0.1150408	0.9540226	0.98881598
	x_3		0.8833290	4.58725×10^{-2}	1.17381×10^{-2}
	T		440.84	397.83	397.09
8	x_2		8.78999×10^{-3}	0.6486488	0.9859213
	x_3		**0.9820252**	0.3511326	1.39766×10^{-2}
	T		466.02	405.01	397.13
9	x_2			0.1144457	0.9544424
	x_3			0.8839234	4.54527×10^{-2}
	T			440.93	397.82

Table 4. (Contd.)

Plate No.	Parameters	Number of plates in column			
		6	8	10	12
10	x_2			7.73897×10^{-2}	0.6514865
	x_3			**0.9820768**	0.3483957
	T			466.04	405.92
11	x_2				0.1157427
	x_3				0.8826284
	T				440.74
12	x_2				8.85012×10^{-2}
	x_3				**0.9819659**
	T				465.99

Table 5. Concentration (mol fraction) of ethylene oxide, water, ethylene glycol, diethylene glycol, triethylene glycol and tetraethylene glycol in residue for various modes of operation of reaction-rectification column.

Parameters	Variant			
	1 (Fig.1, a)	2 (Fig.1, b)	3 (Fig.1, c)	4 (Fig.1, d)
Structure of the rest:				
Ethylene oxide	1.55×10^{-16}	1.36×10^{-16}	5.01×10^{-16}	1.45×10^{-15}
Water	**0.008270**	**0.007256**	**0.026308**	**0.074102**
Ethylene glycol	**0.984175**	**0.985181**	**0.966488**	**0.919694**
Diethylene glycol	0.007525	0.007533	0.007176	0.006185
Triethylene glycol	2.854×10^{-5}	2.857×10^{-5}	2.614×10^{-5}	1.850×10^{-5}
Tetraethylene gelycol	5.677×10^{-8}	5.683×10^{-8}	4.993×10^{-8}	2.387×10^{-8}
Temperature of the rest	576.65	576.99	572.40	562.73

streams does not practically occur (Fig. 1, e). In the opinion of Cardoso and co-authors [16] this allow to provide much lower reflux quantity while the reflux to initial ethylene oxide ratio in the column remains unchanged. For example, while at the discrete inlet of 100 moles of ethylene oxide, to provide reflux – initial ethylene oxide ratio 100 : 1 the needed reflux stream should be 10000 moles, the inlet of 100 moles of raw material distribution over 2 plates 50 moles on each the necessary reflux is reduced to 5000 moles, the reflux to initial ethylene oxide ratio remains 100 : 1, that is, energy consuming is reduced to a half. However, the ideas in [16] have not been confirmed by calculations or experiments. Therefore we considered a task of comparison the reaction-rectification column operating with discrete (Fig. 3, a) and distributed (Fig. 3, e) inlet of raw material into the column. Table 6 contains results of column calculation according these two regimes.

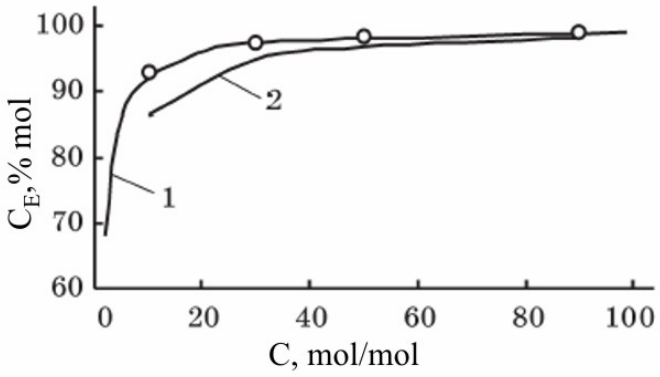

Fig. 4. Dependence of ethylene glycol concentration in residue (C_E) on the reflux to ethylene oxide ratio (C) at the pressure 1.0 MPa. (1) potential content of ethylene glycol in residue plotted against composition of reaction mixture on the plate with discrete inlet (C is water:ethylene oxide ratio); (2) calculated content of ethylene glycol after fractionation of reaction mixture on eight theoretical plates (C is reflux to ethylene oxide ratio); *circles* show potential content of ethylene glycol in residue after precise fractionation of reaction mixture (C is reflux to ethylene oxide ratio) for the curve 2.

first case we considered a possibility of three times reducing the consumed energy. In the second mode of calculation for the column with eight theoretical plates we presumed also a possibility of raw material inlet to third plate at the reflux – initial ethylene oxide ratio 10:1, equal distribution of raw material over five plates (third to seventh) providing real reflux to initial ethylene oxide ratio 50:1, and for comparison discrete inlet of raw material on third plate at the reflux – ethylene oxide ratio 50:1. The second regime would provide possibility of 5-fold energy saving.

The results of calculations (Table 6) show that discrete inlet of raw material does not provide expected energy saving because purity of residue on ethylene glycol at the distributed inlet of raw material is some below than at discrete inlet with the same actual reflux – ethylene oxide ratio. For example, at the actual reflux – initial ethylene oxide ratio 90:1 with discrete inlet of raw material on third plate the ethylene glycol concentration in the residue is 98.20 mol %, while distribution of raw material in equal portions over plates 3,4 and 5 it becomes 95.07 mol %, only slightly higher

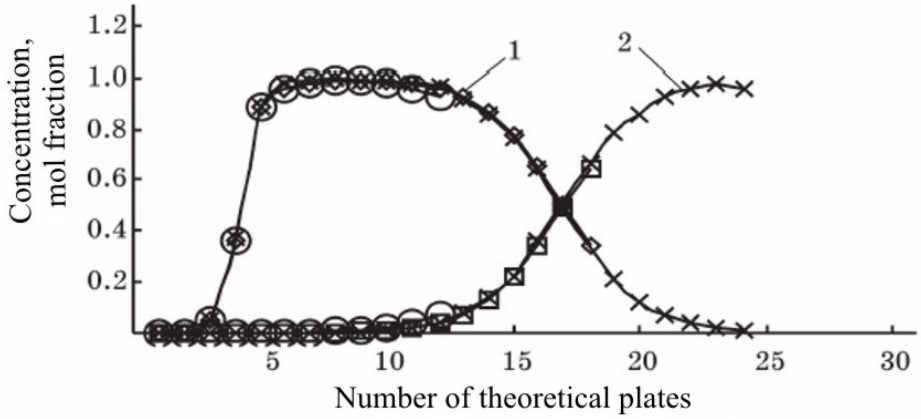

Fig. 5. Changes in ethylene glycol (1) and diethylene glycol (2) concentrations along the reaction-rectification column height at different numbers of theoretical plates in the device. Pressure in column 1.5 MPa, reflux to ethylene oxide ratio is 90 : 1, raw material inlet at third plate, ethylene glycol withdrawing from 8th plate at the total number of plates 12 (circles), and from 9th plate at 18 (rhombs) and 25 (crosses) plates in the column.

In the first mode we performed calculation of a column with 8 theoretical plates and considered discrete feed on third plate at the reflux to ethylene oxide ratio 30:1, equal distribution of raw material over three plates, the third, the fourth and the fifth, which provides real reflux – initial ethylene oxide ratio 90 : 1, and for comparison discrete feed at third plate with reflux to initial ethylene oxide ratio 90 : 1. Thus, in the than at discrete inlet and reflux to ethylene oxide ratio 30 : 1. When raw material is distributed equally over plates 3 to 7 with reflux to initial ethylene oxide ratio 50 : 1 the ethylene glycol content in the residue (86.1 mol %) is found not only below those at discrete inlet, but ever worse than at discrete inlet and reflux to ethylene oxide ratio 10 : 1. This situation can be explained by the fact that at distributed inlet the ethylene

Table 6. Influence of the method of raw material inlet on temperature (T) and concentrations of water (x_2) and ethylene glycol (x_3) in liquid phase (mole fraction) flowing down from plates of reaction-rectification column (pressure in the column 0.1 MPa) at different reflux:initial ethylene oxide ratios on the plate of raw material inlet

Plate No.	Parameter	First mode			Second mode		
		Discrete inlet of raw material on 3 th plate, C=30:1	Distributed inlet of raw material over 3–5 th plates, C=90:1	Discrete inlet of raw material on 3 th plate, C=90:1	Discrete inlet of raw material on 3 th plate, C=10:1	Distributed inlet of raw material over 3–7 th plates, C=50:1	Discrete inlet of raw material on 3 th plate, C=50:1
1	x_2	0.9999514	0.9997558	0.9999916	0.9996701	0.9995704	0.9999801
	x_3	0.00001440	0.0002404	0.0000045	0.00003909	0.0004262	0.0882952
	T	372.24	372.25	372.24	372.17	372.25	372.24
2	x_2	0.9993144	0.9886746	0.9997638	0.998114	0.9799041	0.9995806
	x_3	0.0006810	0.0125113	0.00023571	0.00184757	0.01977575	0.0004177
	T	372.25	372.46	372.24	372.27	372.64	372.25
3	x_2	0.967932	0.9779690	0.98888626	0.9137998	0.9615877	0.9802928
	x_3	0.0312252	0.0216428	0.01103642	0.08006782	0.0372169	0.01938972
	T	372.87	372.87	372.45	373.98	373.00	372.63
4	x_2	0.9676381	0.9676037	0.9881128	0.9136201	0.9943224	0.9798542
	x_3	0.0315190	0.0315582	0.0178608	0.08024848	0.0531756	0.01982829
	T	372.87	372.87	372.47	373.98	373.35	372.63
5	x_2	0.9544140	0.9534198	0.95421174	0.9057601	0.9203952	0.9598667
	x_3	0.0447330	0.0457954	0.04567777	0.0804240	0.0754080	0.0398092
	T	373.14	373.16	373.14	374.15	373.85	373.03
6	x_2	0.8197104	0.8094786	0.6499565	0.857952	0.8575766	0.7574481
	x_3	0.1792806	0.1895072	0.3498251	0.135796	0.1357771	0.2420914
	T	401.03	401.30	405.97	400.08	400.09	402.71
7	x_2	0.2710750	0.2557751	0.1150408	0.4964561	0.4934001	0.186847
	x_3	0.7245300	0.7397839	0.8833290	0.4915599	0.4940189	0.8103677
	T	424.44	425.63	440.84	411.74	411.87	431.89
8	x_1	2.398×10^{-13}	1.998×10^{-13}	9.207×10^{-15}	6.307×10^{-12}	3.859×10^{-14}	5.290×10^{-14}
	x_2	0.025106	0.02323033	0.0087899	0.0695667	0.0684885	0.015080
	x_3	**0.9487944**	**0.9507786**	**0.9820252**	**0.8630900**	**0.8610084**	**0.968322**
	x_4	0.025628	0.0254803	0.0091278	0.0646198	0.0701150	0.015991
	x_5	4.649×10^{-4}	5.047×10^{-4}	5.676×10^{-5}	3.211×10^{-3}	3.587×10^{-3}	1.770×10^{-4}
	x_6	5.506×10^{-6}	6.006×10^{-6}	2.288×10^{-7}	1.069×10^{-4}	1.520×10^{-4}	1.274×10^{-6}
	T	460.58	461.198	466.02	449.65	449.92	463.65

Table 7. Concentration (mol fraction) of ethylene oxide (x_1), water (x_2), ethlene glycol (x_3), diethlene glycol (x_4), triethlene glycol (x_5), tetraethlene glycol (x_6) and temperature (T) on the plates of rection-rectification column with ethylene glycol withdraw from 9th theoretical plate as side fractionation. Pressure in column 1.5 MPa, reflux to ethylene oxide ratio 90 : 1, 12 theoretical plates

Plate No.	Parameters	Value of parameters	Plate No.	Parameters	Value of parameters
1	x_2	0.9997586	10	x_2	8.35805×10^{-4}
	x_3	2.414401×10^{-4}		x_3	0.9921799
	T	470.35		T	588.10
2	x_2	0.9964869	11	x_2	3.0567×10^{-4}
	x_3	3.511317×10^{-3}		x_3	0.9868287
	T	470.43		x_4	1.2865×10^{-2}
3	x_2	0.9509767		T	588.24
	x_3	4.889155×10^{-2}	12	x_3	0.976180
	T	471.60		x_4	0.023708
4	x_2	0.6305962		T	588.44
	x_3	0.369237	13	x_3	0.9565451
	T	481.88		x_4	0.0431411
5	x_2	0.1075181		T	588.80
	x_3	0.8919769	14	x_3	0.921679
	T	521.97		x_4	0.078307
6	x_2	0.04289356		T	589.42
	x_3	0.9563395	15	x_3	0.8626716
	T	585.39		x_4	0.1373228
7	x_2	1.637595×10^{-2}		T	590.51
	x_3	0.9823784	16	x_3	0.7701812
	T	587.02		x_4	0.2298164
8	x_2	6.13666×10^{-3}		T	592.29
	x_2	0.991726	17	x_3	0.6412353
	T	587.67		x_4	0.3587633
9	x_1	$\mathbf{5.389623\times10^{-17}}$		T	594.93
	x_2	$\mathbf{2.2276998\times10^{-3}}$	18	x_3	0.4879973
	x_3	**0.9939049**		x_4	0.5120007
	x_4	$\mathbf{3.817291\times10^{-3}}$		T	598.36
	x_5	$\mathbf{7.26432\times10^{-7}}$	19	x_3	0.3369654
	x_6	$\mathbf{1.51701\times10^{-9}}$		x_4	0.6630294
	T	**587.95**		T	602.10

Table 7. (Contd.)

Plate No.	Parameters	Value of parameters
20	x_3	0.2132032
	x_4	0.7867794
	T	605.49
21	x_3	0.1262321
	x_4	0.8737044
	T	608.09
22	x_3	0.0715116
	x_4	0.9282892
	T	609.83
23	x_3	0.03942670
	x_4	0.95991660
	T	610.90
24	x_3	0.0213838
	x_4	0.9764874
	T	611.55
25	x_1	$1.1101 \cdot 10^{-34}$
	x_2	$2.932636 \cdot 10^{-12}$
	x_3	0.01146175
	x_4	0.9817087
	x_5	0.006814015
	x_6	$1.552932 \cdot 10^{-5}$
	T	602.10

oxide feeding into another except first plate in the feeding zone (according to calculation, this is third plate) is contacted with the reaction medium on the plate which contains a considerable amount of ethylene glycol, which enters to the reaction with ethylene oxide affording diethylene glycol, thus yield of ethylene glycol on the fourth, fifth and next plates falls. As follows from data of table 6, content of diethylene glycol in the residue at the distributed feeding increases by factor 2–4 compared to discrete feeding, all other conditions are equal. Potential concentrations of ethylene glycol in residue (that is, at complete distilling water off from the residue) were obtained the same regardless the method applied for the estimation, by calculation either the process in the reaction-rectification column or composition of reaction mixture on a reaction plate (Fig. 4).

Thus, quality of residue at the fractionation of reaction mixture depends, first of all, on the completeness and quality of chemical process in the reaction zone of the device. Purity of ethylene glycol can be higher only if polyglycols are separated from it. This problem can be solved by withdrawing ethylene glycol from side outlet in the medium part of the column between the zones of raw material inlet and residue outlet (Fig. 1, *F*). The calculations show that purity of both side output and residue depends on the number of theoretical plates N between the feeding zone and residue outlet (Fig. 5). At N values 4, 9 and 16 plates the ethylene glycol concentration in side outlet equals respectively 0.987, 0.991 and 0.994 mol fraction, and diethylene glycol concentration in reidue is 0.069, 0.646 and 0.981 mol fraction, respectively. This allows producing ethylene glycol and diethylene glycol in one column containing 25 theoretical plates (Table 7).

CONCLUSION

1. By the method of mathematical modeling were studied various modes of operating a reaction-rectification column in a wide range of pressure and reflux to initial ethylene oxide ratio.

2. At the operating column in the regime of complete reflux the quality of obtained residue practically does not depend on the number of theoretical plates between the zones of raw material inlet and residue outlet where a ragion of constant concentrations is formed.

3. Discrete and distributed modes of raw material inlet into the reaction-rectification column for ethylene glycol producing is analyzed. It is shown that distributed inlet can not result in energy saving because quality of residue at fractionation of reaction mixture depends first of all on the completeness and quality of the chemical process realization in the reaction zone of device: distributed inlet leads to lower ethylene glycol

concentration in the residue as compared with discrete feeding.

It is shown that better quality of ethylene glycol can be achieved at withdrawing ethylene glycol from the medium part of column and diethylene glycol from column bottom part.

REFERENCES

1. Dyment, O.N., Kazanskii, K.S., and Miroshnikov, F.M., *Glikoli i drugie proizvodnye okisei etilena i propilena* (Glycols and other ethylene and propylene oxides deivatives), Moscow: Khimiya, 1976, p. 373.
2. Astarita, J., *Mass transfer in chemicqal reaction* (Ruswsian translation), Leningrad: Khimiya, 1978, p. 223.
3. Katalov, A.I., *Teor. Osnovy Khim. Tekhnol.*, 1985, no. 3, p. 308.
4. Komissarov, Yu.A., Gordeev, L.S., and Vent, D.P., *Nauchnye osnovy protsessov rektificatsii* (Stientific Basis of Rectification Processes), vol. 1, Moscow: Khimiya, 2004.
5. Okasinski, M.J. and Doberty, M.F., *Ind. and Eng. Chem. Research*, 1998, no. 7, p. 2821.
6. Buzad, G. and Doherty, M.F., *Computers and Chem. Eng*., 1995, no. 4, p. 395.
7. Cardoso M.F., Salcedo R.L., and Feyo de Azevedo, *Computers and Chem. Eng*., 1996, no. 9, p. 1065.
8. Venkataraman S., Chan W.K., and Boston, J., *Chem. Engineering Progress*, 1990, no. 8, p. 45.
9. Chang, Y.A. and Seader, J.D., *Computers and Chem. Eng*., 1988, no. 12, p. 1243.
10. Stein, E., Kienle, A.R.J., Mohl, K.D. et al., *Computers and Chem. Engineering* (Suppl.), 1999, vol. 23, p. 903.
11. Ciric, A.R. and Gu, D., *AIChE Journal*, 1994, no. 9, p. 1479.
12. Samoilov, N.A., Mnushkin, I.A., and Mnushkina, O.I., *Khimicheskaya promyshlennost'*, 2006, no. 1, p. 1.
13. Samoilov, N.A., Mnushkin, I.A., and Mnushkina, O.I., *Mathematical modeling of reactive distillation column for the production of ethylene glycol. XVII International Conference on Chemical Reactors "CHEMREACTOR-17",* May 15–19, 2006, Athene-Crete, Greece, p. 694.
14. Samoilov, N.A., Mnushkin, I.A., and Mnushkina, O.I., *Matematicheskoe modelirovanie reakcionno-rektifikacionnoi kolonny dlya proizvodstva etilenglikolya (Mathematical modeling of reactive distillation column for the production of ethylene glycol). Conference proceedings "Perspektivy razvitiya khimicheskoi pererabotki goryuchih iskopaemyh (HGPI-2006)"*(Perspectives of development of chemical working up of combustible mineral resources), Sept. 12–15, 2006, St. Petersburg, 2006, p. 294.
15. Kondrat'ev, A.A. and Samoilov, N.A., *Zh. Prikl. Khim*., 1997, vol. 70, no. 9, p. 1512.
16. Cardoso M.F., Salcedo R.L., Feyo de Azevedo S. et al., *Chem. Engineering Sci*., 2000, vol. 55, p. 5059.

ISSN 1070-4280, Russian Journal of Applied Chemistry, 2007, Vol. 80, No. 7, pp. 1249–1255. © Pleiades Publishing, Ltd., 2007.
Russian Text © , A.V. Zubov, K.V. Zubov, V.A. Zubov, 2007, published in Khimicheskaya Promyshlennost, 2007, Vol. 84, No. 1, pp. 40–48.

PERSPECTIVE TECHNOLOGIES

Mechanism of Sodium Chloride Diossolving in Water and the Process of the Solution Aging

A. V. Zubov, K. V. Zubov and V. A. Zubov

Humbold University, Institute of Informatics, Berlin, Germany
A IST H&C Co.

Received December 16, 2006

Abstract—By the method of Flicker Noise Spectroscopy (FNS) we studied the process of sodium chloride dissolving in water (3.5 wt %) at 294 K on the level of long-range order formation in liquid. It is established that the process of dissolving the salt includes the following steps: formation of instable colloid particles, instable solvate clusters of the salt ion pairs (iSCIP), instable dissolved polymers of globular type, and 12 h later beginning of a new process of formation stable solvate clusters of the salt ion pairs (sSCIP) and stable polymer globules on their basis. Stroke diagrams of the cluster nano-structure and a model of aging the salt solution are presented. Influence of atmospheric pressure on the SCIP average weight is demonstrated. It is concluded that on the SCIP surface there is a porous layer of solvate water with membrane properties. The cluster structure of the 3.5 wt % solution prepared by dissolving the salt is shown to differ from that of the solution obtained by dilution. The solutions long-range order is formed by the nano dispersion of the water solvated salt crystal nuclei. The mechanism of the solution aging is discussed.
DOI: 10.1134/S1070427207070452

INTRODUCTION

The methods of preparing solutions, the dissolving processes and the solution keeping are of great importance in the chemical technology processes. First of all this concerns stabilization of quality, rational consumption of resources, knowledge of the role of salt state in solution, understanding the dissolving and solution aging processes.

The mechanism of dissolution of sodium chloride and the state of the salt ions in solution are considered in many publications [1–6]. However, there is no publications denoted to understanding this mechanism in view of long-range order formation and evolution on the level of static assembles (clusters) in water and in the solution of the salt in the initial steps of formation of thermodynamically stable solution as well as on the dynamics of the process of solution aging. Understanding this mechanism would allow to attain a new quality in performing technological processes, in understanding the processes in geochemistry, biochemistry and even in cookery.

This work is aimed at the study of the mechanism of sodium chloride dissolving in distilled water and the solution aging using the method of Flicker Noise Spectroscopy (FNS) [7, 8].

This method allows to measure weight fractions of cluster type formations by short period action of weak energy fields thus introducing minimum of possible distortion in the formation of static assembles in the liquid.

EXPERIMENTAL

As an object of the study was taken rapidly cooled water ($\chi = 20 \pm 5 \times 10^{-8}$ Ω^{-1} cm^{-1}) and crystalline NaCl (99.9%) with average crystal size 100 μ. A vessel for the salt dissolving is made of polyethylene (500 ml), the liquid was stirred by magnetic stirrer. The FN (flicker noise) spectra were registered on and Aist H&C GmbH (Germany) instrument [7, 8] three times with 15 sec intervals and distortions induced by $2000 \times 3 = 6000$ shock waves passed through the studied liquid were analyzed. The FNS sensor analyzing long-range order in the solution sample of 1.25 cm^3 volume was located in the center of the vessel and 3 cm from walls. The measurements were performed before stirring (Fig. 2, *1*, water before salt adding),

then at stirring (Fig. 2, *2*, water before salt adding), after adding salt powder (Fig. 2, *3*), after ending the stirring of the salt solution (Fig. 2, *4*), after completing the solution stirring (Fig. 2, *5*, beginning of solution aging) and then after 9, 10, 20 min, 0.5, 3.5, 12.5, 280, 320, 500 h of the solution formation. During all the experiment time the cell was maximum isolated from the influence of external energy fields (light, shaking, heat flows). At the moment of a FNS registration the stirrer was switched off. The temperature control accuracy was ±1K. The oscillator mass was calculated with the equation $T=2\pi(m/c)^{0.5}$ using our found constant $c=(6.2\pm0.8)\cdot10^{-15}$ N/m [8]. The instrument calibrating on the oscillator mass was made on the oscillation band of the cluster $(H_2O)_{280\pm1}$ (m=5.040) in twice-distilled water at 4350±50 Hz in the region of small clusters (http://www.lsbu.ac.uk/water/index.html), on the oscillations at 2451 Hz of the lisocime ferment globule with m=15.754 Da for the medium area of the spectrum and on the ocillations of polystyrene cluster [9] and silicon carbide globules [10] (m=3139.886 Da, 173.4 Hz) in the far part of the spectrum. Error in the determination of an oscillator mass can be 15% in the range of lg m from 0 to 2, less than 6% in the lg m range from 2.5 to 4.5 and up to 15% in the lg m range from 5.5 to 6.5.

The FNS method is based on the known methods of statistical treatment of weak signals [11,12]. The principal approach is application of fast Fourier transformation algorithm (FFT) in conjunction with mathematical analysis (authocorrelation) of ordered sequence of correlated random values (hip:// en.wikipedia.org/wiki/Fast_Fourier_Transform). The digraph of extraction of real signals of the clusters assumes saving initial signals from both the cells containing substance and without it, refining these signals, abstracting the cell signal from the signal of the cell with the sample, and saving thus obtained spectrum of the sample itself.

The positive signal (*f*) in the FNS method results from the energy release by expanded cluster, their compacting and crystallization. The negative signal (*–f*) corresponds to the energy absorption at the interaction of the shock wave with a dense cluster and melting the cluster. The fraction of the dense clusters is taken conveniently with minus while the fraction of expanded clusters with plus. This is made also for better understanding and separation of the clusters by their density in graphics. The fraction (*f*) of a cluster is the ratio of its signal intensity to the sum of absolute values of the signal intensities of all detected signals of clusters in the spectrum [8]. Each point of measuring energy release/absorption for a given range of oscillator mass is obtained as a result of statistical analysis of the noise from 6000 of weak shock waves passed through the sample. The broad band (by energy) weak shock waves were generated by a film, the film energetic characteristics (vibration frequency and intensity) were used for detection. The *f* value reflects energy of interaction of a series of shock waves from the spectrometer with condensed masses in the studied sample. Note that interaction of shock wave with a hinder describes density, strength and energy characteristics of the latter and allows to reveal its shape. The nonlinear character of the oscillators interaction with shock waves however restricts observation of principal results of such interaction in the trend of development of nonlinearity for a given case and material [13, p. 32]. It turns out that individual deviations from the nonlinearity of some of multitude oscillators shows stable reproducibility, and for a family of relative oscillators can be created quasi-linear algorithm of their evolution. "Enhancement" of the data obtained using chemistry logics and published data give rise to successful identification of clusters by means of FNS method. However, the key problem remains in concern the energetic description of the clusters oscillation and energy of their formation. It also can be solved because the number of the cluster types is not too high (40 – 160) and the number of the most significant types is a few units. A not trivial task is calibrating SN spectra on energy due to the absence of reliable internal reference, especially in complicated systems (solutions, gels, biological systems). It is more so, because the energy depends on many factors, first of all on the character of interaction with environment: the stronger interaction, the smaller is their formation energy, the mass cluster is more "spread", not condensed. Energy of clusters formation in water have been published [8]. For natural water and for solutions of various salts it is difficult to make the instrument calibration due to absence of reliable internal reference or starting point, therefore we represent the FNS data as *f* values.

As a criterion of globular structure of the clusters was the harmonization of the physical model of oscillating ball (the rotating ball inertia moment $J = (2/5)mr^2$, where *m* is mass, *r* is radius and *J* is inertia moment) with the data of computer modeling of water clusters by Chaplin (http://www.lsbu.ac.uk/water/ index.html) for the clusters consisting of 280 and 1890 water molecules, and unsatisfactorily correlation at the

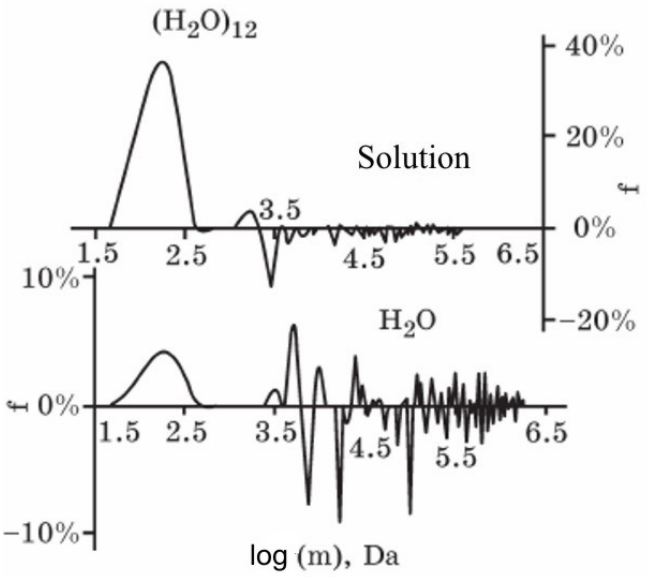

Fig. 1. Survey FN spectra of distilled water after fast cooling of vapor to 294 K and of 3.5 weght % solution after salt adding and 3-min stirring, 294 K. *f* is ratio of signal intensities of an oscillator (*f*i) in the spectrum to the sum of all signals modulo $\Sigma|fj|$ detected in the spectrum (*–f* are conventionally negative values for dense clusters, *+f* for extended clusters), m is oscillator mass, Da.

modeling with other rotation figures including full or empty cylinder, cone or free-rotating body (J=0.5π·ρ·∫·r4·dx, where ρ is the density of the rotating body, π = 3.14, integration (∫) is fom x_1 to x_2). A criterion of globular structure of the salt ion pairs (SCIP) is the same but in respect of the possible models of rotating dimers, tetramers, etc. [7]. These criterions obey successfully the general thermo-dynamic view on the minimization of body surface for a cluster in liquid.

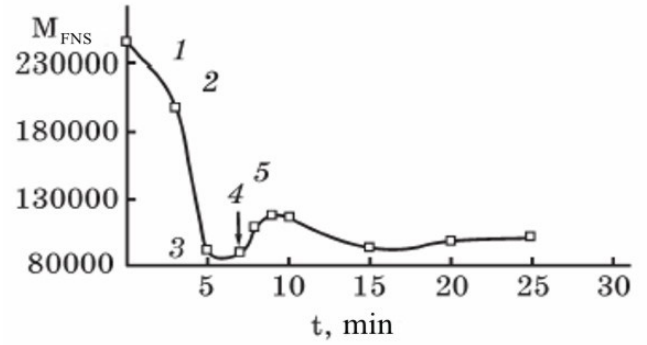

Fig. 2. Plots of average mass variation of clusters (M_{FNS} = $\Sigma|f{\cdot}m|$) in water and in solution in time. (*1*) parent water without stirring with magnet stirrer, (*2*) water at stirring with magnet stirrer, (*3*) solution after adding powdered salt and 1 min stirring with magnet stirrer, (*4*) solution 3 after 3 min stirring, (*5*) solution without stirring (t = 0, start of aging).

DISCUSSION

Fig. 1 shows FNS data for water and salt solution. As seen, both water and salt solution are nanodisperce systems. The clusters distribution oscillating at the action of weak shock wave is not homogenous. Adding the salt to water leads to distortion of cluster structure of the latter and to almost complete disappearance of expanded clusters (+*f*) except water clusters consisting of the molecular associates up to $(H_2O)_{12}$ [14]. The salt ions which are represented by a wide set of SCIP [7] allows water to form small clusters only, while medium and large statistical forms in the bulk solution are distorted. The spectrum of water shown in the figure differs slightly from that of distilled water obtained by water melting and heating to 300 K [8] due to bigger number of instable clusters (carcass clusters) and due to difference in the history of the liquid. Such water is mostly used in chemical technology at the preparation of salt solutions.

Fig. 2 shows dependence of average oscillator mass in water and in the salt solution in the process of its formation. It is seen that mechanical action in the process of stirring leads to sharp decrease in the average cluster mass and adding of the salt powder accelerates this process. The value of M_{FNS} falls down by factor more than 3.

Dissolving the salt stabilizes the process of strong change in M_{FNS} even at stirring the solution. Then stir is stopped, after 1 min occurs some increase in average oscillator mass, which then again decrease and stabilizes at the level of 96 ± 5 kDa with certain trend to the growing M_{FNS}. This curve running shows that occurs the process of redistribution in cluster structure of solution, its evolution and further aging. These processes can be visualized by representation of FNS data as dash codes (Fig. 3). The dash codes represent presence or absence of a cluster with given mass regardless intensity of corresponding signal in the FN spectrum.

From Fig. 3 is seen that in the process of saltdissolving occur the processes of change in cluster structure of the liquid. Adding the salt leads to appearance in water of giant oscillators with the size comparable with colloid particles (> log m = 6.31). It can be suggested that they are oscillating colloid particles, the fragments of difficultly dissolving fragments of solid

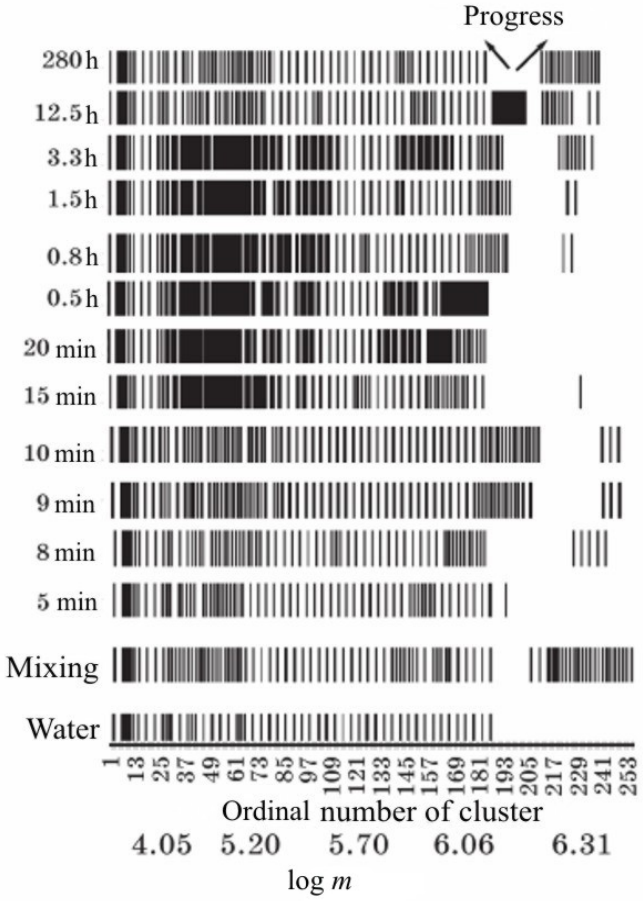

Fig. 3. Dashed representation of presence/absence of clusters in a liquid in the process of formation and aging its statistical structure (long-range order). The clusters ordinal numbers correspond to their order in FN spectra tentatively (step of observation raster).

salt with minimum defects in their crystal structure.

In the region of medum size clusters (log m from 4.05…5.25) is seen appearance of new oscillators, not typical for water. They can be polymeric solvate clusters of the salt ion pairs (pSCIP) [7, 15].

Stirring the solution for next 3 min leads to disappearance of the giant oscillators and to establishing of new thermodynamic equilibrium of SCIPs in the regions of mefium and big clusters. This equilibrium however is intermediate and not stable.

When stirring is stopped, the solution cluster structure evolution still continues. The dash spectrum (Fig. 3) expands to the side of appearance of very large oscillators with simultaneous compression of dashes in the region of medium and large clusters. Such a phenomenon continues for 2–3 min after stopping stirring and it can be explained by the formation of instable SCIPs (iSCIP) and their polymerization with formation of polymer globular and oscillating structures.

The iSCIPs after 15th minute become quickly aging and destroying (Fig. 3). The process of aging is accompanied with restructuring due to depolymerization of the most instable globules ad formation of oscillating low molecular weight stable SCIPs (sSCIP) of new structure which is in better harmony wih the clusters of mass between log m = 4.62 and log m = 5.6. In Fig. 3 this process is seen as disappearance of dashes in the region of giant clusters and strong increase in density of the dashes in the medium region (oligomeric clusters).

From 7th min to 12.3 h another trend occurs – the process of distribution of dashes over all the spectrum. This phenomenon we connect with formation of new thermodynamic equilibrium in the region of oligomeric clusters (numbers 77 to 100) leading to polymerization of iSCIPs and formation of new, more stable, high molecular oscillators with numbers 130 to 185.

After 0.8 h in the spectra again appear giant clusters whose number increases with the solution aging. The reasons for their appearance can be polymerization of new low molecular thermodynamically stable SCIPs.

After 3.5 h aging of the solution, occurs certain decrease in the number of SCIPs in the medium area of spectrum and increase in the number of oscillators in the region of big clusters. To 12.5 h these changes become obvious and dominating. In the region of oligomeric (medium) clusters the dashes density decreases to the level occurred at the moment of mixing salt and water, but in the region of giant clusters the dashes density increased sharply.

Note that the cluster dashes Nos. 70 to 150 remain the most stable during all the experiment. They can be assigned to the carcass clusters of the solution forming its long range order structure.

To 500 h the solution structure becomes mainly formed, but the process does not stops. In the solution the processes of attaining thermodynamic equilibrium continue, which are accompam\nied by the dividing of cluster structure into two big groups: wit the masses < log m = 6.2 and > log m = 6.36 (Fig. 3, progress vectors). The formation of two big groups of submicro particles has been reported in [15]. These data confirm that there are no ideal solutions and the old theory of ideal solutions should be declined. This, liquids can

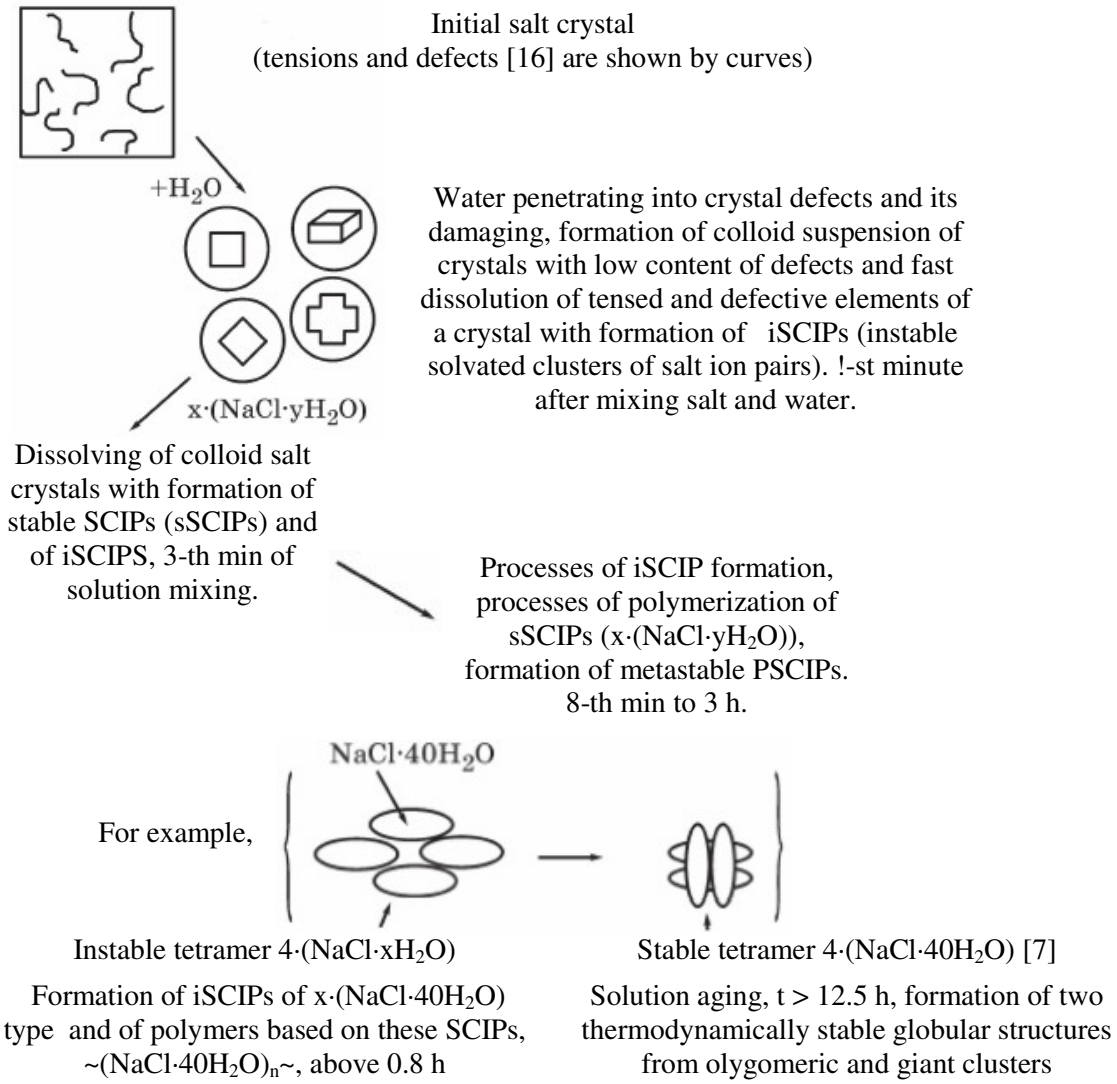

Fig. 4. Model of dissolution of salt in water.

not be considered as homogenous systems, they are heterogenic on the nano level, the level defining sensible chemical and biochemical processes which will be dominating in the 21th century technologies.

The processes of SCIP formation and their polymerization (polycondensation) pass a few steps in their evolution which can be represented as dissolving of salt in water (Fig. 4). The evolution of dashes represented in Fig. 3 also attests the presence of fluctuations in formation of thermodynamically stable salt solution.

The signals of oscillating clusters in FNS prove globular structure of the latter. Therefore the structure of completely formed solution of salt can be considered as thermodynamically stable nanodisperse suspension of polymer solvate cluster ion pair (PSCIP) in water. Therewith, the salt solution long-range order is defined on the level of structural constru cting of PSCIP and associates based on it.

The PSCIP should differ by anisotropy at least in surface layers contacting with the bulk solution. In [5] was found that solvate shell of an alkali metal in water has layers in two levels, internal and external, the external layer is rather porous (expanded) and differ by structure from both internal layer and surrounding solution. In [17] was reported that in NaCl solutions the h-bond bridges between water molecules are much longer than in pure water. These facts attest in favor of presence in SCIP of ex[anded surface layer consisting of water molecules.

It seems logically that at polymerization of SCIPs they approach each other up to the level of internal (condensed) layers of solvating water while expanded layer will be formed on the surface of the polymer globule at the solution frontier. Similar phenomenon which is characteristic of claster structure of water was described by Yoshiteru [18]. He found that 22% of water molecules have one H-bond bridge only and 77% have two bridges. We also modeled water clusters which allowed us to understand that surface layer consists of the molecules with one H-bridge (22%) and internal layers of the molecules with two H-bridges (78%). In other words, the density of the SCIP surface layers should differ by density from the overall liquid density and from the density of clusters inside construction.

It seems possible to detect this layer by, for example, changing pressure over the solution. If the layer exists, then, according to the osmosis laws (van't Hoff's equation, $\pi = icRT$, where π is osmotic pressure, R is gas constant, T is absolute temperature, c is the solution molar concentration) it should response to the change in pressure. In this equation the i factor is connected with the electrolyte degree of dissociation (α) in a diluted solution ($i = 1 + \alpha(\nu - 1)$, where ν is number of ions formed at the dissociation of the electrolyte) [19] and can reflect changes in the SCIP structure. The influence of pressure on the clusters distribution and their average mass can be reliably measured using the FNS method.

We found that weak changes in atmospheric pressure correlate with the character of SCIP distribution in the solutions of salt, values of M_{FNS} parameter and the number of oscillators in the solution (Fig. 5). Thus, the change in pressure of atmospheric air over the solution (+10%) for 1 sec results in significant changes of these parameters after tens of minutes and brings the system to the new thermodynamic equilibrium on hours. These parameters vary adequately with the change in pressure. The correlation of solutions physical properties (osmotic pressure, vapor pressure over the solution) with the ion hydration numbers was also reported earlier [20, 21].

Thus, SCIP has surface solvate shell which can play the role of membrane commutating with environment, e.g., for the tetramer $4(NaCl{\cdot}40\ H_2O)$ it can be represented by the following model (this layer is dashed, Scheme 1).

Scheme 1.

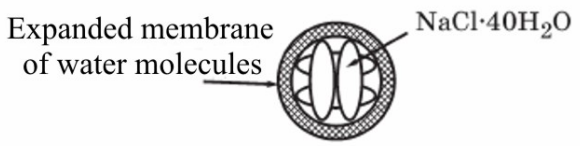

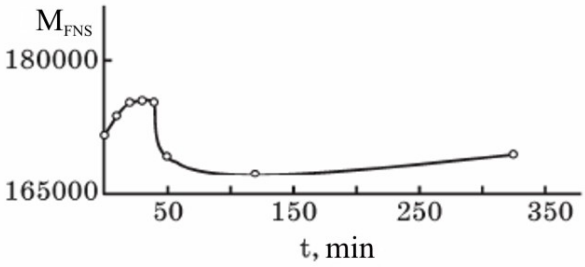

Fig. 5. M_{FNS} responce of 0.1 wt % salt solution (analogue of physiological salt solution) on sharp change in air pressure over the solution, ΔP=11%. Number of oscillators after 30 min increases by 35%.

We detected dependence of the cluster ordering hierarchy of the salt solution on the method of preparation of the solution.

In [7] the salt solutions were prepared by us by means of consecutive dilution of concentrated (26%) solution and keeping them for 2 weeks excluding carefully action of light, shaking and changes of temperature, while in the current work the 3.5% salt solution (Fig. 1) was prepared directly by dissolving salt in water. Comparison of FN spectra of the prepared in current work 3.5% salt solution after 328 h keeping with the spectrua in [7] showes that they are not completely identical in the region of small clusters (lg m from 2.6 to 3.6), but it is identical with the spectrum of 26% salt concentration below lg m = 3.7 which also was prepared by direct dissolving of the salt and keeping it for 320 h.

In the 3.5% solution obtained by direct dissolving of salt were found dimeric SCIPs $2(NaCl{\cdot}40H_2O)$ only in expanded form. The number of oscillators in the solution obtained by salt dissolving is by 56% higher than in the solution obtained through dilution.

Thus, the FNS method allows to obtain some data on the solution origin, namely, did it obtain by either diluting or direct dissolving.

Technologists long ago noted that many processes of chemical technology with solutions depend not only on the order of mixing, conditions of stirring, duration of "ripening," etc., but also on weather situation

(pressure jumping). We suggest that solutions of salts have long-range order analogous to that found in [7] and represented in the scheme 1 structure of SCIP. Such SCIPs are sensitive to change in pressure in apparatus and in vessels with open surface, and their changes can be used in fine chamical synthesis, for enhancing quality of products and certain reactions selectivity. Long time for establishing thermodynamic equilibrium in a salt solution can be used by technologists for protection of inventions and formation of "know how."

Advance biological systems are known to be very sensitive to pressure changes. Probably atmospheric pressure affects solvate shells of not only SCIPs, but also of dissolved compounds involved into biochemical processes and as a sequence to distorts metabolism in people organism (head-ache, joint-ache). Modern medicine still can not explain source of such diseases.

Evolutionary aging of salt solution according to the model shown in Fig. 4 and found by us phenomenon of dependence of cluster arrangement on the solution origin can assist understanding of existence in ocean stable layers and streams of water with equal salt content by differ in temperature which are not mixing together.

CONCLUSION

The process of salt dissolving in water is multistep one and includes the following steps: formation of instable colloid systems, metastable solvate clusters of the salt ion pairs, formation of instable globular polymeric structures in the solution, formation of thermodynamically stable structures SCIP and globular polymers based on them. This process for 3.5 weight % salt solution at 294 K requires basically hundreds hours. The SCIP surface consists of expanded layer ofsolvate molecules behaving as a membrane in the osmotic processes of informational interaction of clusters with environment. Dash codes of lon-range cluster organization in liquids can be used for estimation of their quality, archiving and modelling physical, chemical, hydrochemical and biochemical processes. FNS method allows obtaining certain data on the solution origin history (is it obtained by diluting or by direct dissolving). The salt solution is not an ideal solution, as has been suggested earlier.

ACKNOWLEDGMENT

We are grateful to "Aist H&C GmbH" company for financial support of this study.

REFERENCES

1. Zahn, D., *Physical Review Letters,* 2004, vol. 92, no. 4, p. 040801/1.
2. *Water and aqueous solution*, Horne, R.A., Ed., Willey-Interscience, 1972, p. 838.
3. Karazhanov, N.A., *Osnovy kinetiki rastvoreniya solei,*, Alma-Ata: Nauka, 1989, p. 189.
4. Peslherbe, G.H., Ladanyi, B.M., and Hynes, J.T., *Chem. Phys*., 2000, vol. 258, p. 201.
5. Karpov, G.V., *Chemical Physics Letters*, 2005, vol. 402, p. 300.
6. Maraňón, Di Leo and Maraňón, J., *K+ Ions in an Chemical Physics Letters*, 2005, vol. 404, p. 257.
7. Zubov, K.V., Zubov, A.V., and Zubov, V.A., *Zh. Prikl. Spektr*., 2005, vol. 72, no. 6, p. 766.
8. Zubov, K.V., Zubov, A.V., and Zubov, V.A., *Zh. Prikl. Spektr*., 2005, vol. 72, no. 3, p. 305.
9. Zysman, Viviane, Nguyen, Tuan Q., and Kausch, Henning, H., *J. Polymer Science, Part B: Polymer Physics*., 1994, vol. 32, no. 7, p. 1257.
10. Zubov, V.A., Sholc, R., Braun, M., Zubova, H.-L., Kolbanovskii, Yu.A., Ovsyannikov, A.A., and Shipachev, V.S., *Zh. Neorg. Khim.,* 1994, vol. 39, no. 11, p. 1784.
11. Müller, E., *Digitale Signalanalyse in der Hydroakustik (Teil 2): Angewandte Akustik*, no. 3, p. 34, Berlin: VEB Verlag Technik, 1989, 1 Auflage.
12. Dadzhion, D. and Mersero, P., *Tsifrovaya obrabotka mnogomernyh signalov*, Moscow: Mir, 1988, p. 488.
13. Horsthemke, V. and Lefevr, R., *Indutsirovannye shumom perehody: Teoriya i primenenie v fizike, khimii i biologii*, Moscow: Mir, 1987, p. 400.
14. Lenz, A. and Ojamäe, L., *Chemical Physics Letters.,* 2006, vol. 418, p. 361.
15. Georgalis, Y., Kierzek, A.M., and Saenger, W., *J. Phys. Chem., B,* 2000, vol. 104, no. 15, p. 3405.
16. *Khimicheskaya Entsiklopediya (Chemical Encyclopaedia),* Moscow: Sovetskaya Enciklopediya, 1990, vol. 2, p. 29.
17. Masuda, K., Haramaki, T., Nakashima, S., Habert, B., Martinez, I., and Kashiwabara, S., *Applied Spectroscopy.,* 2003, vol. 57, no. 3, p. 274.
18. Yoshiteru, Y., *Chemical Physics Letters*., 2005, vol. 406, p .49.
19. *Khimicheskii enciklopedicheskii slovar'* (Chemical Encyclopaedia), Moscow: Sovetskaya Entsiklopediya, 1983, p. 419.
20. Spangberg, D., Wojcik, M., and Hermansson, K., *Chemical Physics Letters*., 1997, vol. 276, nos. 1, 2, p. 114.

ISSN 1070-4280, Russian Journal of Applied Chemistry, 2007, Vol. 80, No. 7, pp. 1256–1269. © Pleiades Publishing, Inc., 2007.

POLYMER TECHNOLOGY

Applications of Unsaturated Polyester Resins[1]

Muhammad Ihsan Ul Haq

Paints Business I C I Pakistan Limited, 346-Ferozepur Road Lahore 54600, Pakistan
e-mail: - insane_ul_haq@ici.com

Received June 19, 2007

Abstract—Unsaturated polyester resins containing long chain fatty acids and styrene as cross-linking agents are easily available in Pakistan. I have made use of these resins in the preparation of overprint varnish, ornaments, synthetic marble and other related substances. The octates of manganese, cobalt, calcium and lead along with peroxide were used for jelling and drying of the resins. The effects of metal driers, aluminium stearate , peroxides and unsaturated long chain fatty acids in the composition as mentioned in the experimental section were also studied. The merits and demerits developed in the end products resulting from the variation of these chemicals in the compositions were also noted at their respective places.
DOI: 10.1134/S1070427207070464

INTRODUCTION

Polyester. Polyester is a class of polymer containing reoccurring −C(=O)−O− group in the main chain and generally are prepared from dihydric alcohols and dicarboxylic acids.

The polyesters are classified in to the following types:

(1). Linear unsaturated polyesters.
(2). Linear saturated polyesters of low molecular weights.
(3). Linear saturated polyesters of high molecular weight.
(4). Network polyesters.

1. Linear Unsaturated Polyesters

Linear unsaturated polyesters are generally prepared from a saturated acid such as phthalic, isophthalic, adipic or azelic and an unsaturated acid i.e. maleic anhydride or fumarolic anhydride, which are condensed with dihydric alcohols. A three dimensional structure is formed by cross linking polyester back ground with a vinyl monomer, most commonly styrene is used.

2. Linear saturated polyesters of low molecular weight

The polyesters, which are formed in a linear saturation chain having molecular weight less than 10,000, belong to this type. These are mainly used as plasticides. They are obtained by condensation of diol-dicarboxylic acids. Often a mono-hydric alcohol or a mono carboxylic carboxylic acid is used as to control the molecular weight.

3. Linear saturated polyester of high molecular weight

Poly (ethylene terephthalate) is of significant importance in this category. Poly (ethylene terephthalate) fiber is being used extensively as Mylar, Terylene, Dacron, and Terepak.

4. Net work Polyesters

The network polyesters are mainly used in surface coatings. The most important polyesters of this type are derived from phthalic anhydride and glycerin.

HISTORY

It was the beginning of the Second World War, which accelerated research work in the field of fundamental and applied chemistry. It was about the same period when important work was carried out on understanding chemistry of polyesters and their technical uses, although they know polyester a kind since seventeenth century.

Berzelius in 1847 pioneered work on synthesis of polyester from tartaric acid and glycerol. Lorenzo was successful in 1863 to manufacture polyester by heating

[1] The article was submitted by the author in English.

ethylene glycol with succinic acid, having the following formula.

$$-(-OCH_2\,CH_2\,OCOCH_2\,CH_2\,CO-)-$$

Kraut after about six years was able to produce a concept of polyester chain structure. Blaise and Marcilly in 1904 gave a chain formula to polyesters prepared from hydroxide pivalic acid. In 1916 the product prepared by the reaction of phthalic anhydride and glycerin was used for coating both wood and metals. It was in 1927 the term Alkyd (derived from Alcohol and Acid) was introduced by R.H.Kienle.

Standingers 27,28, and Carothers were able to prepare polyesters with well-defined polymeric structure. Carothers carried out fundamental research work on polymers including polyesters and established their importance in industry.

In the late thirties Broadly together with Kropa and Johnston reported that unsaturated polyester become insoluble and infusible on drying because of the presence of unsaturated double bonds in polyester chains. At the same time Ellis discovered that the rate of cure of unsaturated polyester could be increased by more than thirty times if unsaturated monomers were used. This discovery lead to the commercial application of unsaturated polyester on a wide scale.

Unsaturated polyester resin prepared from maleic anhydride-2-napthol, maleic anhydride and propylene glycol, may be co polymerized with styrene was reported by Jedlinsk. This unsaturated polyester had a regular net work structure.

The cross linking of an unsaturated linear polyester by means of a vinyl monomer such as styrene is presented as follows:

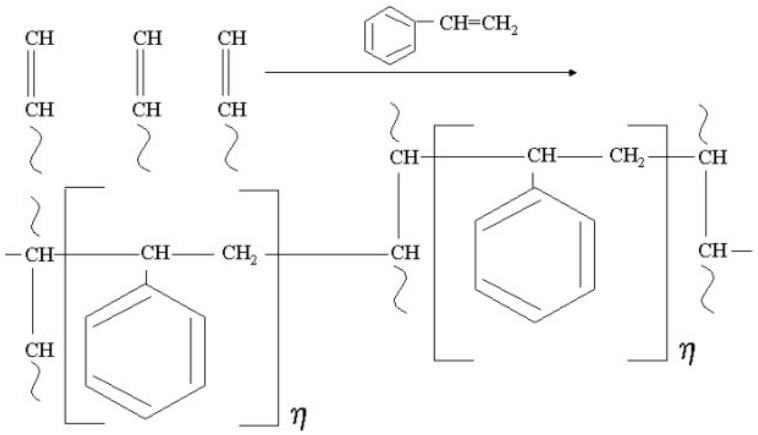

The average value of n in the above structure may be deduced from both spectroscopic and degradation studies.

USES

United States Rubber Company in 1942 used polyester made from diethylene glycol and maleic anhydride in the presence of styrene for reinforcing glass fibre.21.

The commercial production of glass fiber reinforcing polyester laminates was established in 1947 and become very important for preparation of boat hulls, lorry cabs, roofing plans, chemical plants and several seaplane floats and similar mouldings were made. It is used as thermosetting moulding compositions, casting resins and solvent less lacquers.

Polyester is further used in aircraft industry, protective covering over radar scanning apparatus for electrical industry. It is being used for the measurement of the concentration of abnormal red blood cells in human blood by preparing microprobes membrane for blood filtration.

These are useful as moulding compounds having good resistance to wrap and cracks. The sheet-moulding compound is prepared by using unsaturated polyester resin syrup, which has an excellent tensile strength.

It is used for the production of serving trays, lampshade, flat sheets, and corrugated sheets for building industry, ammunition boxes, disposable glass tanks and various containers.

Of the total resin use in reinforcing plastics market 93% is polyester 36.

Chemistry of polyester resin. The monomers, which are required for the production of polyester resins, are dicarboxcylic acid, anhydride, dihydric alcohols, monomers for cross linking and an inert solvent for refluxing. Catalyst is sometimes used to accelerate the reaction and reduce the reaction time. Inhibitors are also required.

The reaction between a hydroxide compound and anhydride proceeds in two distinct steps. In the first step, esterification of the anhydride occurs to form a free acid group, which is then esterified in the second step. The following reaction between maleic anhydride and propylene glycol is given as follows.

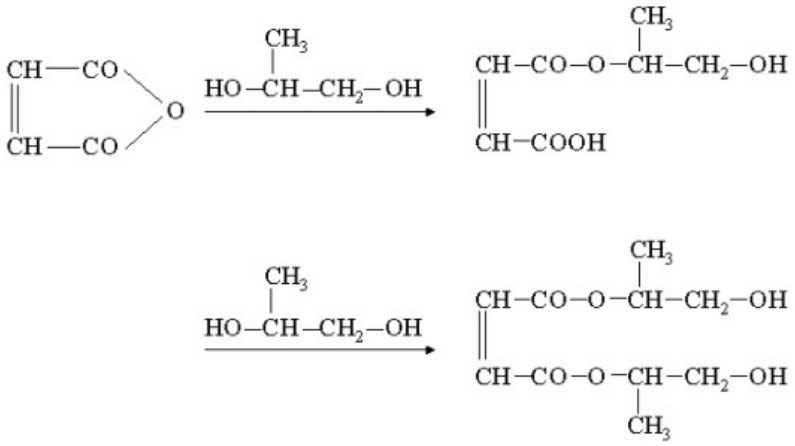

The first step proceeds more rapidly than the second since the anhydride group is more reactive than the free acid group. A glycol and anhydride may react through a sequence of reaction to yield linear polyester.

A segment of the polyester obtained from propylene glycol, maliec anhydride and phthalic anhydride may have the following structure.

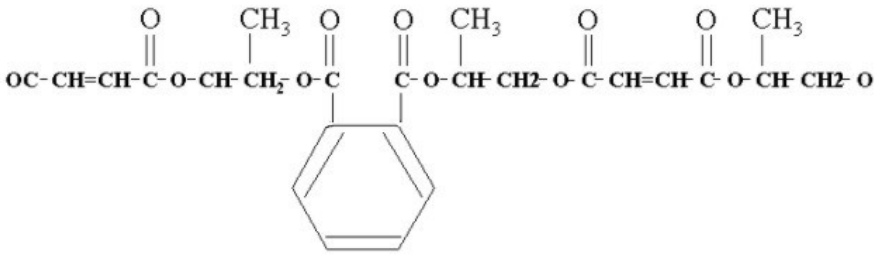

The cross linking of unsaturated linear polyester involves the reaction of the unsaturated sites in the polymer chain with a monomer which may be of vinyl type such as styrene or acrylonitrile etc. Cross-linking of unsaturated polyesters is a free radical reaction. These types of initiating systems are commonly employed for this reaction, namely

Those, which are effective at, elevated temperatures.

Those, which are effective at room temperatures.

The initiators, which are used at elevated temperatures, are peroxides such as benzyl peroxide. For the reaction at room temperature, methyl ethyl ketone peroxide is used as an initiator. Moreover peroxides along with octates of cobalt and manganese can initiate the reaction at room temperature.

The aim of this work is to utilize the unsaturated polyester resins, which are being manufactured in Pakistan. Every year Pakistan imports a huge amount of lacquers and varnishes. Unsaturated polyester resins

are the basic raw materials to manufacture a large variety of lacquers and varnishes. Moreover, these resins can be used for many other purposes e.g. in the manufacturing of artificial pearls and ornaments. The synthetic marble is another application of this resin. The author had worked on the aforesaid projects and hopes that if proper attention is given to these projects, and then a large amount of foreign exchange can be saved.

EXPERIMENTAL

Preparation of overprint varnish *1. General procedure*). Resins based on linseed oil, pentaernthrol, glycerin and unsaturated long chain fatty acids were taken in a 100ml beaker. Several kinds of driers like octates of manganese, cobalt, calcium, zirconium and aluminium stearate of different concentrations as shown in the following compositions were added in the resin mixture. They were thoroughly stirred and the resulting mixture was applied as a very thin layer on the different kinds of printing papers. The resin-coated papers were kept at room temperature to see their drying times. The drying time of each composition was noted.

2. Compositions based on manganese drier. In this experiment, the amounts of resins and linseed oil were fixed while the amount of manganese was varied from 0.3ml to 1.0 ml. The varnish was prepared using the method given in the general procedure.

2,a	Linseed oil	3 ml
	Resin	10 gm
	Manganese drier (10%)	0.3 ml (0.03 gm metal)
2,b	Linseed oil	3 ml
	Resin	10 gm
	Manganese drier (10%)	0.5 ml (0.05 gm metal)
2,c	Linseed Oil	3 ml
	Resin	10 gm
	Manganese drier (10%)	0.7 ml (0.07 gm metal)
2,d	Linseed Oil	3 ml
	Resin	10 gm
	Manganese drier (10%)	1.0 ml (0.1 gm metal)

Result: No one composition worked well. In all compositions results were found be unsatisfactory.

3. Compositions based on aluminium stearate and manganese drier. In this experiment, the amount of stearate was fixed, while the amount of manganese octate was varied from 0.3ml to 1.0ml.the instructions given in the general procedure were followed for its preparation and application.

3,a	Linseed oil	3 ml
	Resin	10 gm
	Aluminium stearate	0.3 gm
	Manganese drier (10%)	0.3 ml (0.03 gm metal)
3,b	linseed oil	3 ml
	Resin	10 gm
	Aluminium stearate	0.3 gm
	Manganese drier (10%)	0.5 ml (0.05 gm metal)
3,c	linseed oil	3 ml
	Resin	10 gm
	Aluminium stearate	0.3 gm
	Manganese drier (10%)	0.7ml (0.07gm metal)
3,d	linseed oil	3 ml
	Resin	10 gm
	Aluminium stearate	0.3 gm
	Manganese drier (10%)	1.0 ml (0.1gm metal)

Result: It was found that the viscosity of each compound has increased very much. All compositions failed to work and the resulting product did not dried even after 24 hours.

4. Experiment number 3 was repeated using fixed amount of aluminium stearate (0.1gm) in order to control the viscosity of the product. The amount of manganese octates was varied to increase the drying power of the varnish.

4,a	linseed Oil	3 ml
	Resin	10 gm
	Aluminium stearate	0.1 gm
	Manganese drier (10%)	0.3 ml (0.03 gm metal)
4,b	linseed Oil	3 ml
	Resin	10 gm
	Aluminium stearate	0.1 gm
	Manganese drier (10%)	0.5 ml (0.05 gm metal)
4,c	linseed Oil	3 ml
	Resin	10 gm
	Aluminium stearate	0.1 gm
	Manganese drier (10%)	0.7 ml (0.07 gm metal)
4,d	linseed Oil	3 ml
	Resin	10 gm
	Aluminium stearate	0.1 gm
	Manganese drier (10%)	1.0 ml (0.1 gm metal)

Result: Unsatisfactory results were obtained.

5. Compositions based on manganese and calcium driers. In this experiments the amount of calcium octate was fixed (0.3 ml) and the amount of manganese octates was varied from 0.3 ml to 1.oml.

5,a	Linseed oil	3 ml
	Resin	10 gm
	Calcium drier (10%)	0.3 ml (0.03 gm metal)
	Manganese drier (10%)	0.3 ml (0.03 gm metal)
5,b	Linseed oil	3 ml
	Resin	10 gm
	Calcium drier (10%)	0.3 ml (0.03 gm metal)
	Manganese drier (10%)	0.5 ml (0.05 gm metal)
5,c	Linseed oil	3 ml
	Resin	10 gm
	Calcium drier (10%)	0.3 ml (0.03 gm metal)
	Manganese drier (10%)	0.7 ml (0.07 gm metal)
5,d	Linseed oil	3 ml
	Resin	10 gm
	Calcium drier (10%)	0.3 ml (0.03 gm metal)
	Manganese drier (10%)	1.0 ml (0.1 gm metal)

Result: Unsatisfactory results were obtained

6. This experiment is very similar to experiment no.5. In this case, we have raised the amount of calcium octate (0.6 ml) in each composition. The manganese octate was varied from 0.3ml to 1.0ml.

6,a	Linseed oil	3 ml
	Resin	10 gm
	Calcium drier (10%)	0.6 ml (0.06 gm metal)
	Manganese drier (10%)	0.3 ml (0.03 gm metal)
6,b	Linseed oil	3 ml
	Resin	10 gm
	Calcium drier (10%)	0.6 ml (0.06 gm metal)
	Manganese drier (10%)	0.5 ml (0.05 gm metal)
6,c	Linseed oil	3 ml
	Resin	10 gm
	Calcium drier (10%)	0.6 ml (0.06 gm metal)
	Manganese drier (10%)	0.7 ml (0.07 gm metal)
6,d	Linseed oil	3 ml
	Resin	10 gm
	Calcium drier (10%)	0.6 ml (0.06 gm metal)
	Manganese drier (10%)	1.0 ml (0.1 gm metal)

Result: The results appeared to be good.

7. In this case, the amount of calcium octate was fixed to 0.9ml and manganese octate was varied. Here, I used the same instructions as given in experiment no.5.

7,a	Linseed oil	3 ml
	Resin	10 gm
	Calcium drier (10%)	0.9 ml (0.09 gm metal)
	Manganese drier (10%)	0.3 ml (0.03 gm metal)
7,b	Linseed oil	3 ml
	Resin	10 gm
	Calcium drier (10%)	0.9 ml (0.09 gm metal)
	Manganese drier (10%)	0.5 ml (0.05 gm metal)
7,c	Linseed oil	3 ml
	Resin	10 gm
	Calcium drier (10%)	0.9 ml (0.09 gm metal)
	Manganese drier (10%)	0.7 ml (0.07 gm metal)
7,d	Linseed oil	3 ml
	Resin	10 gm
	Calcium drier (10%)	0.9 ml (0.09 gm metal)
	Manganese drier (10%)	1.0 ml (0.1 gm metal)

Result: Unsatisfactory results were obtained.

8. Composition based on calcium, manganese & lead driers. In this experiment, the amount of manganese metal was made equivalent to the amount of lead metal. The amount of calcium drier was fixed to 0.3 ml. The manganese drier was varied from 0.3ml to 1.0ml.

8,a	Linseed oil	3 ml
	Resin	10 gm
	Calcium drier (10%)	0.3 ml (0.03 gm metal)
	Manganese drier (10%)	0.3 ml (0.03 gm metal)
	Lead drier (36%)	0.08 ml (0.03 gm metal)
8,b	Linseed oil	3 ml
	Resin	10 gm
	Calcium drier (10%)	0.3 ml (0.03 gm metal)
	Manganese drier (10%)	0.5 ml (0.05 gm metal)
	Lead drier (36%)	0.138 ml (0.05 gm metal)
8,c	Linseed oil	3 ml
	Resin	10 gm
	Calcium drier (10%)	0.3 ml (0.03 gm metal)
	Manganese drier (10%)	0.7 ml (0.07 gm metal)
	Lead drier (36%)	0.19 ml (0.07 gm metal)
8,d	Linseed oil	3 ml
	Resin	10 gm
	Calcium drier (10%)	0.3 ml (0.03 gm metal)
	Manganese drier (10%)	1.0 ml (0.1 gm metal)
	Lead drier (36%)	0.27ml (0.1 gm metal)

Result: Satisfactory results were obtained. Good shining layer of the resin deposited on the papers. The layer appeared to be water resistant.

9. In this experiment, the amount of calcium metal was fixed while the manganese and lead metal contents in the compositions were varied.

9,a	Linseed oil	3 ml
	Resin	10 gm
	Calcium drier (10%)	0.3 ml (0.03 gm metal)
	Manganese drier (10%)	0.3 ml (0.03 gm metal)
	Lead drier (36%)	0.04 ml (0.015 gm metal)

9,b	Linseed oil	3 ml
	Resin	10 gm
	Calcium drier (10%)	0.3 ml (0.03 gm metal)
	Manganese drier (10%)	0.5 ml (0.05 gm metal)
	Lead drier (36%)	0.07 ml (0.025 gm metal)
9,c	Linseed oil	3 ml
	Resin	10 gm
	Calcium drier (10%)	0.3 ml (0.03 gm metal)
	Manganese drier (10%)	0.7 ml (0.07 gm metal)
	Lead drier (36%)	0.097 ml (0.035 gm metal)
9,d	Linseed oil	3 ml
	Resin	10 gm
	Calcium drier (10%)	0.3 ml (0.03 gm metal)
	Manganese drier (10%)	1.0 ml (0.1 gm metal)
	Lead drier (36%)	0.13 ml (0.05 gm metal)

Result: Results obtained were unsatisfactory. The drying time of varnish reduced to 4-5 hours.

10. Use of castor oil in place of linseed oil. In this experiment, linseed oil was replaced by castor oil. The amount of calcium drier was fixed (0.3ml) while the amount of manganese and lead driers were varied.

10,a	Castor oil	3 ml
	Resin	10 gm
	Calcium drier (10%)	0.3 ml (0.03 gm metal)
	Manganese metal (10%)	0.3 ml (0.03 gm metal)
	Lead drier (36%)	0.125 ml (0.045 gm metal)
10,b	Castor oil	3 ml
	Resin	10 gm
	Calcium drier (10%)	0.3 ml (0.03 gm metal)
	Manganese metal (10%)	0.5 ml (0.05 gm metal)
	Lead drier (36%)	0.208 ml (0.075 gm metal)
10,c	Castor oil	3 ml
	Resin	10 gm
	Calcium drier (10%)	0.3 ml (0.03 gm metal)
	Manganese metal (10%)	0.7 ml (0.07 gm metal)
	Lead drier (36%)	0.29 ml (0.105 gm metal)
10,d	Castor oil	3 ml
	Resin	10 gm
	Calcium drier (10%)	0.3 ml (0.03 gm metal)
	Manganese metal (10%)	1.0 ml (0.1 gm metal)
	Lead drier (36%)	0.4 ml (0.15 gm metal)

Result: The drying time of the varnish had reduced to 2-3 hours. The results of the compositions appeared to be good.

11. In this case, the amount of calcium octate was increased from 0.3ml to 0.6ml while the quantities of other driers were varied. Moreover, castor oil was also replaced with China wood oil.

11,a	China wood oil	3 ml
	Resin	10 gm
	Calcium drier (10%)	0.6 ml (0.06 gm metal)
	Manganese metal (10%)	0.3 ml (0.03 gm metal)
	Lead drier (36%)	0.08 ml (0.03 gm metal)
11,b	China wood oil	3 ml
	Resin	10 gm
	Calcium drier (10%)	0.6 ml (0.06 gm metal)
	Manganese metal (10%)	0.5 ml (0.05 gm metal)
	Lead drier (36%)	0.138 ml (0.05 gm metal)
11,c	China wood oil	3 ml
	Resin	10 gm
	Calcium drier (10%)	0.6 ml (0.0 6gm metal)
	Manganese metal (10%)	0.7 ml (0.07 gm metal)
	Lead drier (36%)	0.19 ml (0.07 gm metal)
11,d	China wood oil	3 ml
	Resin	10 gm
	Calcium drier (10%)	0.6 ml (0.06 gm metal)
	Manganese metal (10%)	1.0 ml (0.01 gm metal)
	Lead drier (36%)	0.27 ml (0.1 gm metal)

Result: Excellent results were obtained. The drying times of thin layers yielded from compositions 11(a-d) fall within 2 to 4 hours.

12. In this experiment, the amount of lead metal was made half the amount of manganese metal. The amount of calcium drier was fixed to 0.6 ml. China wood oil was replaced by Soya been oil.

12,a	Soya been	3 ml
	Resin	10 gm
	Calcium drier (10%)	0. 6ml (0.06 gm metal)
	Manganese metal (10%)	0.3 ml (0.03 gm metal)
	Lead drier (36%)	0.04 gm (0.015 gm metal)
12,b	Soya been	3 ml
	Resin	10 gm
	Calcium drier (10%)	0.6 ml (0.06 gm metal)
	Manganese metal (10%)	0.5 ml (0.05 gm metal)
	Lead drier (36%)	0.07 gm (0.025 gm metal)
12,c	Soya been	3 ml
	Resin	10 gm
	Calcium drier (10%)	0.6 ml (0.06 gm metal)
	Manganese metal (10%)	0.7 ml (0.07 gm metal)
	Lead drier (36%)	0.097 gm (0.035 gm metal)
12,d	Soya been	3 ml
	Resin	10 gm
	Calcium drier (10%)	0.6 ml (0.06 gm metal)
	Manganese metal (10%)	1.0 ml (0.1 gm metal)
	Lead drier (36%)	0.13 gm (0.05 gm metal)

Result: The drying time of each composition was between 2 to 3 hours.

13. In this experiment, the amount of lead metal is 1.5 times to manganese metal. The amount of calcium drier was fixed to 0.6 ml, while the amount of manganese was varied from 0.3 ml to 1.0 ml. Soya

been oil was also replaced with linseed oil. Polyethlene wax was also added in the varnish to facilitate the application.

13,a	Linseed oil	3 ml
	Resin	10 gm
	Polyethylene wax.	0.5 gm
	Calcium drier (10%)	0.6 ml (0.06 gm metal)
	Manganese metal (10%)	0.3 ml (0.03 gm metal)
	Lead drier (36%)	0.125 gm (0.045 gm metal)
13,b	Linseed oil	3 ml
	Resin	10 gm
	Polyethylene wax.	0.5 gm
	Calcium drier (10%)	0.6 ml (0.06 gm metal)
	Manganese metal (10%)	0.5 ml (0.05 gm metal)
	Lead drier (36%)	0.208 gm (0.075 gm metal)
13,c	Linseed oil	3 ml
	Resin	10 gm
	Polyethylene wax.	0.5 gm
	Calcium drier (10%)	0.6 ml (0.06 gm metal)
	Manganese metal (10%)	0.7 ml (0.07 gm metal)
	Lead drier (36%)	0.29 gm (0.105 gm metal)
13,d	Linseed oil	3 ml
	Resin	10 gm
	Polyethylene wax.	0.5 gm
	Calcium drier (10%)	0.6 ml (0.06 gm metal)
	Manganese metal (10%)	1.0 ml (0.1 gm metal)
	Lead drier (36%)	0.4 gm (0.15 gm metal)

Result: Excellent and compromising results were obtained. The drying times lay in-between 2 to 3 hours.

14. In this experiment, the amount of calcium drier was increased from 0.6ml to 0.9ml. The amount of manganese metal is made equivalent to the amount of lead metal in the following compositions. The amount of manganese drier was also varied from 0.3ml to 1.0ml.Polyethlene wax was also removed from the composition.

14,a	Linseed oil	3 ml
	Resin	10 gm
	Calcium drier (10%)	0.9 ml (0.09 gm metal)
	Manganese metal (10%)	0.3 ml (0.03 gm metal)
	Lead drier (36%)	0.08 gm (0.03 gm metal)
14,b	Linseed oil	3 ml
	Resin	10 gm
	Calcium drier (10%)	0. 9ml (0.09 gm metal)
	Manganese metal (10%)	0.5 ml (0.05 gm metal)
	Lead drier (36%)	0.138 gm (0.05 gm metal)
14,c	Linseed oil	3 ml
	Resin	10 gm
	Calcium drier (10%)	0.9 ml (0.09 gm metal)
	Manganese metal (10%)	0.7 ml (0.07 gm metal)
	Lead drier (36%)	0.19 gm (0.07 gm metal)
14,d	Linseed oil	3 ml
	Resin	10 gm
	Calcium drier (10%)	0.9 ml (0.09 gm metal)
	Manganese metal (10%)	1.0 ml (0.1 gm metal)
	Lead drier (36%)	0.27gm (0.1 gm metal)

Result: Results obtained in all these cases seemed to be good. The drying times of all compositions found to be in-between 2 to 3 hours.

15. I have repeated the experiment No.12. The only difference in this case is that the amount of calcium drier is increased to 0.9 ml.

15,a	Linseed oil	3 ml
	Resin	10 gm
	Calcium drier (10%)	0.9 ml (0.09 gm metal)
	Manganese metal (10%)	0.3 ml (0.03 gm metal)
	Lead drier (36%)	0.0 4gm (0.015 gm metal)
15,b	Linseed oil	3 ml
	Resin	10 gm
	Calcium drier (10%)	0.9 ml (0.09 gm metal)
	Manganese metal (10%)	0.5 ml (0.05 gm metal)
	Lead drier (36%)	0.07 gm (0.025 gm metal)
15,c	Linseed oil	3 ml
	Resin	10 gm
	Calcium drier (10%)	0.9 ml (0.09 gm metal)
	Manganese metal (10%)	0.7 ml (0.07 gm metal)
	Lead drier (36%)	0.097 gm (0.035 gm metal)
15,d	Linseed oil	3 ml
	Resin	10 gm
	Calcium drier (10%)	0.9 ml (0.09 gm metal)
	Manganese metal (10%)	1.0 ml (0.1 gm metal)
	Lead drier (36%)	0.13 gm (0.05 gm metal)

Result: The drying times of the compositions

15,a	2 hrs 48 minutes
15,b	2 hrs 57 minutes
15,c	3 hrs
15,d	3 hrs

Results were satisfactory.

16. I have repeated the experiment No. 13.
The only difference in this case is that the amount of calcium drier is increased to 0.9 ml.

16,a	Linseed oil	3 ml
	Resin	10 gm
	Calcium drier (10%)	0.9 ml (0.09 gm metal)
	Manganese metal (10%)	0.3 ml (0.03 gm metal)
	Lead drier (36%)	0.125 gm (0.045 gm metal)
16,b	Linseed oil	3 ml
	Resin	10 gm
	Calcium drier (10%)	0.9 ml (0.09 gm metal)
	Manganese metal (10%)	0.5 ml (0.05 gm metal)
	Lead drier (36%)	0.208 gm (0.075 gm metal)

16,c	Linseed oil	3 ml
	Resin	10 gm
	Calcium drier (10%)	0.9 ml (0.09 gm metal)
	Manganese metal (10%)	0.7 ml (0.07 gm metal)
	Lead drier (36%)	0.29 gm (0.105 gm metal)
16,d	Linseed oil	3 ml
	Resin	10 gm
	Calcium drier (10%)	0.9 ml (0.09 gm metal)
	Manganese metal (10%)	1.0 ml (0.1 gm metal)
	Lead drier (36%)	0.4 gm (0.105 gm metal)

Result: The drying time of each composition falls in-between 2 to 3 hours.

17. In this experiment, the amounts of manganese and calcium octates were fixed to 0.3 ml and 0.6 ml respectively. The amount of lead drier was varied as shown in the following compositions.

17,a	Linseed oil	3 ml
	Resin	10 gm
	Calcium drier (10%)	0.6 ml (0.0 gm metal)
	Manganese metal (10%)	0.3 ml (0.03 gm metal)
	Lead drier (36%)	0.21 gm (0.06 gm metal)
17,b	Linseed oil	3 ml
	Resin	10 gm
	Calcium drier (10%)	0.6 ml (0.06 gm metal)
	Manganese metal (10%)	0.3 ml (0.03 gm metal)
	Lead drier (36%)	0.316 gm (0.09 gm metal)
17,c	Linseed oil	3 ml
	Resin	10 gm
	Calcium drier (10%)	0.6 ml (0.06 gm metal)
	Manganese metal (10%)	0.3 ml (0.03 gm metal)
	Lead drier (36%)	0.42 gm (0.12 gm metal)

Result: The results are good. The drying time of each composition is approximately 3 hours.

18. Experiment no.18 is very similar to experiment no.16. In this case, the amount of calcium octate is fixed to 0.9 ml.

18,a	Linseed oil	3 ml
	Resin	10 gm
	Calcium drier (10%)	0.9 ml (0.09 gm metal)
	Manganese metal (10%)	0.3 ml (0.03 gm metal)
	Lead drier (36%)	0.21 gm (0.06 gm metal)
18,b	Linseed oil	3 ml
	Resin	10 gm
	Calcium drier (10%)	0.9 ml (0.09 gm metal)
	Manganese metal (10%)	0.3 ml (0.03 gm metal)
	Lead drier (36%)	0.316 gm (0.09 gm metal)
18,c	Linseed oil	3 ml
	Resin	10 gm
	Calcium drier (10%)	0.9 ml (0.09 gm metal)
	Manganese metal (10%)	0.3 ml (0.03 gm metal)
	Lead drier (36%)	0.42 gm (0.12 gm metal)

Result: The drying time of each composition is between 4 to 5 hrs.

PREPARATION OF ARTIFICIAL PEARLS AND ORNAMENTS.

Key words: (MEK) Methyl ethyl ketone, (MEKP) Methyl ethyl ketone peroxide, (Ca) Calcium, (Pb) Lead, (Mn) Manganese, (Co) Cobalt**,** (DOP) Dioctyl phthalate.

19. General procedure. In order to prepare artificial pearls and ornaments, styrene based unsaturated polyesters was used. Peroxides of different kinds like benzyl peroxide, methyl ethyl ketone peroxide were used along with Ca, Pb, Mn, Co octates to jell the polyester resins. Pigments of different kinds along with various types of dyes were also used. To prepare any composition, polyester resin of known weight was taken in a beaker. Calculated amounts of pearls and dyes were added in it. Mixed the contents well, and then added peroxides and metal octate.

20. Determination of jelling time of polyester resin. In this experiment, the quantities of polyester resin and cobalt drier were fixed, while the amount of methyl ethyl ketone peroxide is varied from 0.1 gm to 1.0 gm. Then the jelling time of each composition is noted.

20,a	Polyester resin	10 gm
	Cobalt drier (1%)	0.05 ml (0.0005 gm metal)

Fig. 1. Papers having coating of over print varnish.

	MEKP	0.1 gm
20,b	Polyester resin	10 gm
	Cobalt drier (1%)	0.05 ml (0.0005 gm metal)
	MEKP	0.2 gm
20,c	Polyester resin	10 gm
	Cobalt drier (1%)	0.05 ml (0.0005 gm metal)
	MEKP	0.3 gm
20,d	Polyester resin	10 gm
	Cobalt drier (1%)	0.05 ml (0.0005 gm metal)
	MEKP	0.4 gm
20,e	Polyester resin	10 gm
	Cobalt drier (1%)	0.05 ml (0.0005 gm metal)
	MEKP	0.5 gm
20,f	Polyester resin	10 gm
	Cobalt drier (1%)	0.05 ml (0.0005 gm metal)
Cobalt drier (1%)		0.05 ml (0.0005 gm metal)
Methyl ethyl ketone peroxide		0.3 gm

21. Effects of DOP on polyester resin sheet. In this experiment, the amount of polyester resin, MEKP and cobalt drier were fixed, while the amount of DOP was increased from 0.1gm to 1.0 gm.

Polyester resin	10 gm
Cobalt drier (1%)	0.05 ml (0.0005 gm metal)
Methyl ethyl ketone peroxide	0.3 gm

22. Removal of bubbles problem in polyester resin sheet. The polyester resin sheets obtained from previous two experiments sustained bubbles of gases produced during the reaction. To eliminate the bubble problem, a small centrifugal machine was made. The polyester resin and other materials were added in this machine. The machine was allowed to revolve horizontally at a speed of 100,200,300,400,500,600 revolutions per minute respectively. The inner walls of the centrifugal machine were lubricated with DOP in order to produce anti sticking properties against polyester resin sheet.

The following composition was tried in this experiment.

22,a	Polyester resin	10 gm
	Cobalt drier (1%)	0.05 ml (0.0005 gm metal)
	MEKP	0.3 gm

Result: The polyester resin sheet obtained at the speed of 600 revolutions per minute was fine and free from any kind of blisters, cracks etc.

23. Selection of proper quantity of polyester resin. The basic purpose of this experiment is to select a proper quantity of polyester resin to obtain a suitable width of the walls of the polyester sheet.

23,a	Polyester resin	40 gm
	Cobalt drier (1%)	0.2 ml (0.0002 gm metal)
	MEKP	1.2 gm
23,b	Polyester resin	60 gm
	Cobalt drier (1%)	0.3 ml (0.0003 gm metal)
	MEKP	1.8 gm
23,c	Polyester resin	80 gm
	Cobalt drier (1%)	0.4 ml (0.0004 gm metal)
	MEKP	2.4 gm
23,d	Polyester resin	100 gm
	Cobalt drier (1%)	0.5 ml (0.0005 gm metal)
	MEKP	3.0 gm

Result: Composition 23,d gives a suitable width of the polyester sheet. So it was selected for further experimentation.

24. Addition of different pigments. In this experiment, different types of pigments were used to make large varieties of polyester resin sheets for multiple purposes. The following compositions were conceived and tried.

Polyester resin	100 gm
Cobalt drier (1%)	0.5 ml (0.0005 gm metal)
MEKP	3.0 ml

25. Problems relating to pigment distribution. Solid pigments settled down in the polyester resin and made the distribution uneven in the resin sheet. In this connection, various kinds of thickening agents were

Sr#	Amount of DOP	Remarks
1	0.1 gm	By increasing the amount of DOP, the softness and shining of the polyester sheet was also increased.
2	0.2 gm	
3	0.3 gm	
4	0.4 gm	
5	0.5 gm	
6	0.6 gm	
7	0.7 gm	
8	0.8 gm	
9	0.9 gm	
10	1.0 gm	

used to increase the viscosity of the resin in the following compositions.

Polyester resin	100 gm
Cobalt drier (1%)	0.5 ml (0.0005 gm metal)
MEKP	3.0 ml
Silver Pigment	1.0 gm

26. Use of Zinc drier in polyester resin. Cobalt drier gives its blue ting in the end product of polyester resin. So Zn drier was used in the following composition in order to eliminate the Colour.

Polyester resin	100 gm
MEKP	3.0 gm
Zn drier (1%)	0.5 ml

Result: Zn drier is found to be ineffective and no jelling of polyester resin occurs.

27. Addition of coloring agents and fillers. In this experiment, different types of coloring agents and fillers are mixed in polyester resin.

Polyester resin	100 gm
MEKP	3.0 gm
Cobalt drier (1%)	0.5 ml (0.005 gm metal)

Sr#	Pigment Quality	Pigment Quality	Remarks
1	Silver Pigment	0.025 gm	The amount of pigment controls the quality, attraction and uses of the polyester sheet. It is also found that the distribution of the pigment is not uniform.
2	Silver Pigment	0.25 gm	
3	Silver Pigment	0.5 gm	
4	Silver Pigment	0.75 gm	
5	Silver Pigment	gm	
6	Silver Pigment	1.25 gm	
7	Silver Pigment	1.50 gm	
8	Silver Pigment	1.75 gm	

Sr#	Amount of silicon dioxide.	Remarks.
1	0.5 gm	Silicon dioxide increases the viscosity of the polyester and make the pigment distribution more even but the shining of the final product is decreased. SiO_2 also imparts its own Colour. It is good for the opaque polyester resin sheets.
2	gm	
3	1.5 gm	
4	gm	
5	2.25 gm	
6	2.5 gm	
7	3.0 gm	

Sr#	Filler Quality	Filler Quantity	Remarks.
1	Graphite	gm	Black colored sheet having very good shinning.
2	Carbon black	gm	Black colored sheet.
3	Talcum powder	gm	Slightly greenish colored sheet.
4	Aluminium oxide	gm	White colored sheet.
5	Nitrocellulose	gm	Nitrocellulose did not dissolve in polyester resin.
6	DOP	gm	Flexible sheet was obtained.
7	Barium sulphate	2.0 gm	Slightly greenish colored sheet.

28. Use has more than one pigment. In this experiment, two or more than two types of pigments were added in the polyester resin.

28,a	Polyester resin	100 gm
	MEKP	3.0 gm
	Cobalt drier (1%)	0.5 ml (0.005 gm metal)
	Blue pigment paste	0.53 gm
	Pink pigment paste	0.26 gm
28,b	Polyester resin	100 gm
	MEKP	3.0 gm
	Cobalt drier (1%)	0.5 ml (0.005 gm metal)
	Blue pigment paste	0.35 gm
	Pink pigment paste	0.35 gm
	Golden pigment paste	1.0 gm
28,c	Polyester resin	100 gm
	MEKP	3.0 gm
	Cobalt drier (1%)	0.5 ml (0.005 gm metal)
	Golden pigment paste	0.8 gm
	Blue pigment paste	0.35 gm
	Pink pigment dye	0.35 ml
	Dissolved in MEK	
28,d	Polyester resin	100 gm
	MEKP	3.0 gm
	Cobalt drier (1%)	0.5 ml (0.005 gm metal)
	Copper pigment paste	0.8 gm
	Yellow transparent dye	0.5 ml
	Dissolved in MEK	

Results: The polyester resin sheets obtained are very beautiful and give multicolor shades.

PREPARATION OF SYNTHETIC MARBLE

29. General procedure. In order to prepare synthetic marble, styrene based unsaturated polyester was used. Peroxides of different kinds like benzyl peroxide, methyl ethyl ketone peroxide were used along with octates of Ca, Pb, Mn, Co in order to jell the polyester resin. Fillers of different kinds along with various types of dyes were also used.

30. Addition of different fillers in polyester resin. In this experiment, different kinds of fillers were added in the polyester resin in different quantities. The general procedure was adopted to prepare compositions. The following three inputs have the fixed quantities throughout the experimentation.

Polyester resin	80 gm
MEKP	2.4 gm
Cobalt drier (0.5%)	0.8 ml (0.004 gm metal)

The fillers and their quantities were varied as shown below.

Fig. 2. Artificial ornaments prepared from unsaturated polyester resin.

Sr#	Amount of Cao	Remarks
1	10 gm	By increasing the amount of CaO , the hardness of polyester resin sheet increases.
2	20 gm	
3	30 gm	
4	40 gm	
5	50 gm	
6	60 gm	
7	70 gm	

Sr#	Filler	Quantity	Remarks
8	Titanium dioxide	20 gm	Every filler shows its characteristic properties in synthetic marble e.g. mica gives the insulating properties to the synthetic marble. One major drawback of the synthetic marble was lack of weight and coloring agents.
9	Graphite	20 gm	
10	Al_2O_3	72 gm	
11	Heavy Kaolin	64 gm	
12	$CaCO_3$	35 gm	
13	Mica	35 gm	
14	Vulkasilk	30 gm	
15	Talcum Powder	64 gm	
16	$BaSO_4$	30 gm	

31. Use of different colored chips and pigments. The synthetic marble obtained from the experiment no.30 was lightweight and had no coloring agents. In this experiment, different kinds of colors were used individually and also in combination with the different colored chips.

Sr#	Pigment	Quantity	Remarks
1	Blue	5 gm	Every pigment is soluble in polyester resin and gives its characteristic beauty in the synthetic marble.
2	Red	5 gm	
3	Yellow	5 gm	
4	Brown	5 gm	
5	Green	5 gm	

Sr#	Chips	Quantity	Remarks
6	White	110 gm	By adding chips, the weight of the synthetic marble increased. Chips also increased the strength of the synthetic marble. After polishing the synthetic marble, the chips gave its characteristic designing.
7	Green	110 gm	
8	Yellow	110 gm	
9	Brown	110 gm	
10	Red	110 gm	

Sr#	Dyes	Qty.	Chips	Qty.	Remarks.
1	Yellow	5 gm	White	100 gm	Every composition has its characteristic beauty. Especially when the synthetic marble is polished, then the designing f the chips is very charming.
2	Red	5 gm	White	100 gm	
3	Orange	5 gm	White	100 gm	
4	Green	5 gm	White	100 gm	
5	Brown	5 gm	White	100 gm	
6	Green	5 gm	Yellow	100 gm	
7	Green	5 gm	Yellow	100 gm	
8	Yellow	5 gm	Green	100 gm	
9	Yellow	5 gm	Green	100 gm	
10	Yellow	5 gm	Red	100 gm	

32. Synthetic marble based on chips, filler and dyes. In this experiment, the following inputs have the fixed quantities throughout the work.

Polyester resin	80 gm
MEKP	2.4 gm
Cobalt drier (0.5%)	0.8 ml (0.004 gm metal)
Vulkasilk	20 gm

Fig. 3. Synthetic marble prepared from unsaturated polyester resin.

RESULTS AND DISCUSSION

The aim of this work is to find the various uses of industrial resins that are being manufactured in Pakistan. In this connection, two types of unsaturated resins based on unsaturated long chain fatty acids and styrene are selected. They are easily available from market. The resin, which we like to use in printing industry, is made of linseed oil, glycerin, erythretol and phthalic anhydride.

In Pakistan, there is more than fifty thousands printing press of various sizes. They use lacquers and varnishes to protect the printings on various substrates. The substrate may be in the form of books, decorating sheets, eid cards, wedding cards, packing materials and calendars etc. A huge amount of foreign exchange is being spent for the import of these lacquers and varnishes. In this connection, I have prepared a varnish from local raw materials, which is being used in the offset printing machines.

In this connection, several compositions were prepared and tried. In compositions 2(a-d), 3(a-d), 4 (a-d), I used manganese octate and a mixture of manganese octate and aluminium stearate. We found that aluminium stearate increased the viscosity and slippery power of the varnish. On the other hand, the drying of thin layer obtained from this varnish took a long time. In addition manganese octate did not help so much in the drying of varnish. The results obtained after the application of each composition on printing system were mentioned at the end of each experiment.

In compositions 5(a-d), 6(a-d), 7(a-d), a mixture of manganese octate and calcium octate was used. Their quantities were varied from minimum to maximum but none of them was found to be useful.

Thereafter lead octate was incorporated with the octates of manganese and calcium. The amount of each metal was varied keeping other factors constant. In this way, I have conceived several compositions as mentioned in the experimental section. I found that the compositions 12 (a-d) appeared to be the best and gave good results in terms of reflection, durability, water and light resistance. Moreover, I found that addition of Soya been oil, china wood oil and polyethylene waxes had enhanced the quality of varnish.

Driers and drying. Varnish driers are organic acid soaps or salts of certain metals. This act as catalysts to accelerate the drying of surface coatings, either by oxidation or polymerization.

The activity of a drier depends largely on the particular metal and its quantity. The organic acid radical functions as a carrier for the metal quantity. The organic acid radical functions as a carrier for the metal and contributes to its solubility in oils, solvents and paint media.

Air drying films. The catalytic action of a drier is a function of oxidation and reduction equilibrium and hence involves valency changes in the metal. In the case of air-drying films, oxidation and polymerization are accelerated greatly by the use of driers of certain

metal types. These metals, which are known as primary driers, are cobalt, lead and manganese. Certain other metals are used to provide auxiliary drier compounds. These when used with the primary driers, perform useful functions in a varnish film drying mechanism. Some important auxiliary driers are those based on zirconium, calcium and zinc.

Drying mechanism. The drying mechanism of unsaturated oils proceeds along with free radical reaction. The mechanism involves two steps.

1. Oxidation on the surface of film.
2. Polymerization throughout the depth of the film.

The oxidation at the surface of film produces hydroperoxides, the methylene groups in the fatty acid chain. This decomposition reaction produces free radicals, which initiate polymerization of the molecules via the unsaturated bonds in the fatty acid chains. Reactions taking place during polymerization are not thoroughly understood but there seems to be an indication that the fatty acid chains are linked together both directly and via oxygen.

Unsaturated polyester resins based on styrene has been extensively used in various fields e.g. the manufacturing of buttons, water storage tanks, lamination of wood and steel structures, plastic sheets, electric goods etc. Now this resin is also available in our country and I would like to use in the manufacturing of ornaments and synthetic marble. Several kinds of peroxides were reported for it's jelling. I used methyl ethyl ketone peroxide in my experiments. I found that it did not jell the resin whatever its amount might be. On the other hand, when it was incorporated with cobalt drier, then it became very effective and jelling of the resin did occur. In order to find the optimum amount of MEKP and cobalt octate, I performed a series of experiments as had mentioned in the experimental section. I found that increase in amount of MEKP dramatically decreased the jelling time of the resin but the quality of the end product was badly affected. Contrary, increase or decrease in amount of cobalt octate did not effect the jelling time of the resin. So after adjusting the amount of MEKP and cobalt octate in compositions 20 (a-d), I concluded that 5 to 6 % MEKP and 0.6 to 1.0 % cobalt drier were the optimum quantities that jell the unsaturated polyester resin within 15 to 20 minutes. The plastic sheets obtained in this connection had excellent properties in all characters. Moreover various kinds of pigments like silver, gold, copper, pink etc were mixed in the resin and centrifuged in the rotary drum. Excellent shinning colored sheets were obtained. In this connection, several kinds of compositions 24, 25, 26 (a), 27, 28 (a-d) as shown in the experimental section were tried.

Compositions 28 (a-d) were found to be excellent and end products were attractive. The results obtained in each case were mentioned at the bottom of each composition respectively. In this way, any substrate of any shape could be made using polyester resin of aforesaid composition in the desired mould.

Similarly synthetic marble, tiles and related things were also prepared. In this case, we used various kinds of fillers like calcium carbonate, calcium oxide, vulkasilk, barium sulphate, kaolin, marble chips etc. In each case, a good quality of end product was obtained. It was seen that natural marble and other ceramic material used in the construction of building, especially at the seashore were badly effected with the gases coming off seawater. The use of synthetic marble had eliminated this problem to a considerable extent. The tiles made of unsaturated polyester appeared to be good in every respect when used in acidic and basic environment. The role of peroxide and cobalt octate was found to be crucial in jelling the polyester resin. The variation from the exact quantities of methyl ethyl ketone peroxide and cobalt octate used in the composition had badly affected the properties of the final product.

REFERENCES

1. Kienle, R.H.,US Patent 1 893 873, 1933.
2. Berzelius, J., Rapport Annual, 26, 1847.
3. Smith ,W.J., *Soe.Chemistry Ind.,* 1901, no. 20, p. 1075.
4. Challahan, M.J., US.Patent 1 108 329, 1914.
5. Friedburg, L.H., US Patent 1 119 592, 1914.
6. Howell, K.B., US Patent 1 098 728, 1914.
7. Kienle, R.H., US Patent 1 893 873, 1933.
8. Martine, S.R.W., *Synthetic Resin Chemistry Champman and Hall.*
9. Richardson, M., *Fundamental of Plastic*, p.338.
10. Ronald Fleek, H., *Plastic Scientific and Technology,* p.200
11. Forguson Chemical Mat.Eng.39 599, 1939.
12. Fairbourne J.C.S.129, 1929.
13. Krumbhaar, *Paint Oil Chem.Rev*., 1931, no. 91 35 25.
14. Saunders, K.J., *Organic Polymer Chemistry Edition,* 1976.
15. *Encyclopedia of Polymer Science and Technology*.

ISSN 1070-4272, Russian Journal of Applied Chemistry, 2007, Vol. 80, No. 8, pp. 1271–1274. © Pleiades Publishing, Ltd., 2007.
Original Russian Text © I.M. Batyaev, A.V. Leonov, 2007, published in Zhurnal Prikladnoi Khimii, 2007, Vol. 80, No. 8, pp. 1233–1236.

INORGANIC SYNTHESIS AND INDUSTRIAL INORGANIC CHEMISTRY

Specific Features of Methods for Obtaining Ti(III) and Its Concentration Effect on Optical Properties of Potassium-Aluminum Phosphate Glass

I. M. Batyaev and A. V. Leonov

Herzen Russian State Pedagogical University, St. Petersburg, Russia

Received June 29, 2006; in final form, March 2007

Abstract—Potassium-aluminum phosphate glasses with different concentrations of Ti(III) activator were prepared and their spectral properties were studied.

DOI: 10.1134/S1070427207080010

Crystals based on Al_2O_3 remain among the most widely used compounds in quantum electronics. They possess a unique combination of physical and chemical properties.

Methods for growth of activated Al_2O_3 crystals are well developed, but require special conditions and expensive equipment. In this context, an attempt to obtain glass-based lasing substances might be promising. Glasses are inferior to crystals in certain physicotechnical parameters; however, most of glasses are considerably more technologically convenient than crystals.

The goal of this study was to obtain titanium(III) oxide for preparing multicomponent oxide glasses.

EXPERIMENTAL

We studied series of multicomponent oxide glasses containing potassium, aluminum, silicon, and phosphorus oxides [potassium-aluminum silicophosphate (PASP) glasses, e.g., glasses based on the oxides, Al_2O_3–P_2O_5, Al_2O_3–SiO_2–P_2O_5, and K_2O–Al_2O_3–SiO_2–P_2O_5].

In this study, we examined glasses of composition $33.5\,K_2O$–$14.01\,Al_2O_3$–$38\,P_2O_5$ (mol %), activated with trivalent titanium in concentrations varied within the range 0.1–0.9 mol %. The greatest attention was paid to obtaining trivalent titanium and its introduction into glasses.

A review of the literature [1–16] and preliminary experiments allowed us to select the most convenient and promising procedure for obtaining trivalent titanium.

We tested and compared the following methods for $Ti^{4+} \rightarrow Ti^{3+}$ reduction in glassy systems K_2O–Al_2O_3–SiO_2–P_2O_5 and Al_2O_3–SiO_2–P_2O_5: reduction with ammonia (NH_3), ammonium tartrate, and hydrogen. The reduction of tetravalent titanium to trivalent titanium with hydrogen was found to be the most promising method. The other methods for obtaining titanium(III) oxide proved to be unsuitable for solving the basic problem of creating glassy lasing materials activated with trivalent titanium.

We constructed a special-purpose installation for reduction of tetravalent titanium with hydrogen. The installation is shown schematically in Fig. 1. All

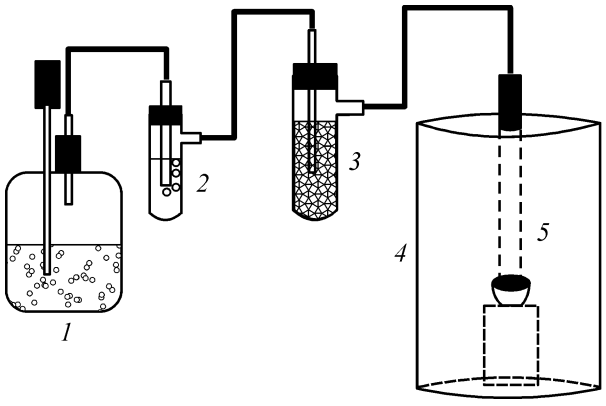

Fig. 1. Schematic of the installation for titanium reduction: (*1*) hydrogen gas generator, (*2*) gas-meter with an alkaline solution for H_2 purification, (*3*) tube with silica gel for drying of H_2, (*4*) furnace, and (*5*) crucible with TiO_2.

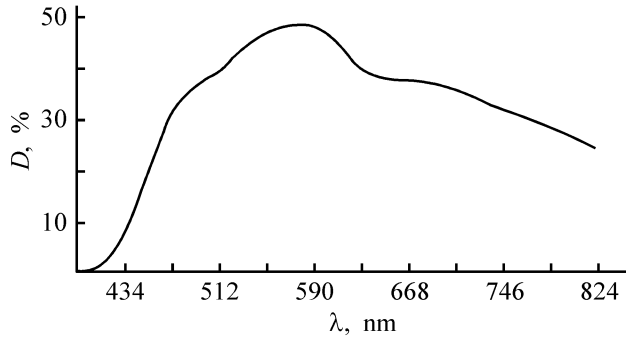

Fig. 2. Absorption spectrum of the $33.5\,K_2O$–$14.01\,Al_2O_3$–$38\,P_2O_5$ (mol %) glass activated with Ti^{3+}. Concentration $c_{Ti^{3+}} = 2.6$ M. (D) is optical density and (λ) wavelength.

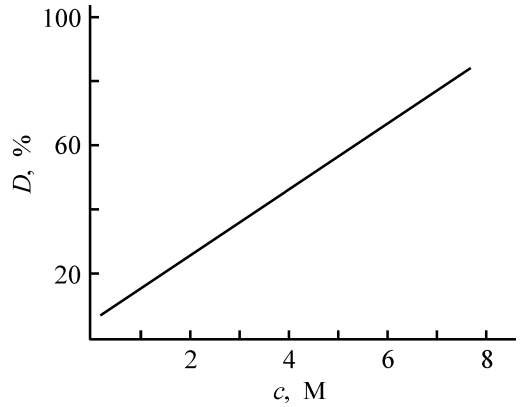

Fig. 3. Optical density D vs. titanium(III) oxide concentration c at 595 nm.

details of obtaining titanium(III) oxide by other methods, their advantages and disadvantages were also described in [16].

The reduced titanium was analyzed by spectrophotometry in the spectral range 340–850 nm on an SF-20 spectrophotometer and a pulsed tau-meter with an exponential sweep, fabricated by a standard technique. A series of glasses with varied concentration of trivalent titanium was prepared. The electronic absorption spectra show only a single broad band peaked at around 590 nm, with a pronounced shoulder at 660–800 nm, characteristic of trivalent titanium in condensed systems. It is necessary to note that the absorption peak in these glasses is shifted to longer wavelengths as compared with the spectra of sapphire crystals [1]. This indicates that the symmetry of the environment of Ti^{3+} ions changes, which is confirmed by the data of [16–18]. A spectrum of the glass series prepared is shown in Fig. 2. It differs from the other spectra of this series in that the intensity of absorption bands varies with the titanium concentration in the glass.

Table 1. Effect of titanium(III) concentration on physical and optical characteristics of $33.5\,K_2O$–$14.01\,Al_2O_3$–$38\,P_2O_5$ (mol %) glasses

$c_{Ti^{3+}}$, M	ρ, g cm^{-3}	n_D	ε, l mol^{-1} cm^{-1}
0.2	2.5165	1.51	15.4
0.33	2.4897	1.51	12.1
1	2.5129	1.51	16.1
2.6	2.5119	1.51	23
7.7	2.5175	1.51	12
$Al(PO_3)_3$–0.5%Ti^{3+}	2.66 [20]	1.497 [20]	
Al_2O_3–Ti^{3+}	3.5–4 [29]	1.765 [29]	

Further treatment of the spectra obtained confirms the results reported in [9, 10, 12, 13, 19–20] and leads to a conclusion that, in synthesis of a glass containing aluminum oxide as a component, Ti^{3+} isomorphously replaces aluminum in the unit cell of the glass, with the main Ti^{3+} term split.

The dependence of the optical density D on the titanium concentration (Fig. 3) is linear, which corresponds to Bouguer–Lambert–Beer law:

$$D = \varepsilon l c.$$

Here, ε is the extinction coefficient; l, glass thickness; and c, concentration of titanium(III) oxide in the glass.

This dependence can be used to calculate the average molar extinction coefficient ε_{av} (Table 1). The molar extinction coefficient ε is known to depend on the degree of covalence of the bond between metal ions and ligands. For example, the extinction coefficient of the Ti^{3+}-containing glass based only on sodium metaphosphate is 5 l mol^{-1} cm^{-1}. It increases to 8 l mol^{-1} cm^{-1} when chloride ions (in the form of NaCl) strongly depolymerizing the polymeric phosphate chains are introduced into the metaphosphate. For PASP glasses containing Ti^{3+}, the increase in the extinction coefficient 10 l mol^{-1} cm^{-1} is due to the presence of aluminum ions in the structural network. Their influence is expressed in a noticeable shortening of polymeric phosphate chains and in a decrease in the degree of Ti–O bond covalence [13]. It is seen from Table 1 that the deviation from this value is possibly associated with experimental and calculation errors. There is no need to obtain luminescence spectra, because the value of the extinction

coefficient fully confirms the presence of trivalent titanium in the glass.

It is necessary to note that the maximum luminescence intensity is observed for Ti^{3+} at a wavelength of 890 nm, with a clearly pronounced shoulder at 780–820 nm [20, 24–28]. Analysis of luminescence spectra was not among the goals of this study. Luminescence spectra for the given series of glasses will differ only in the intensity determined by the concentration of trivalent titanium in a glass.

The series of glasses under study was used to find the so-called concentration-induced quenching of luminescence, which is one of types of nonradiative transfer of the electronic excitation energy, with the help of luminescence decay curves.

By processing the luminescence decay curves (Fig. 4) by the method suggested in [30], we obtained the averaged coefficients of luminescence decay duration, τ_{av}, listed in Table 2.

As demonstrated by mathematical processing, the decay curves can be best described by the power function $\tau = 13.245c^{-0.0899}$, with an approximation reliability coefficient of about 0.8. This plot shows an approach to the titanium–titanium concentration quenching, which corresponds to the Ti^{3+} concentration range 4.6–7.7 M. Further increase in the activator (trivalent titanium) concentration does not improve significantly the optical and lasing properties. As demonstrated by the experiment, the physical properties of the glass are also impaired: the glass becomes more fragile and less completely melted because of the increasing viscosity. The latter requires that the temperature of glass melting should be raised because the melting point of titanium oxide is higher than 1500°C. An increase in the activator concentration by more than 7.7 M results in degradation of optical properties of glasses and leads to larger experimental errors.

Spectrophotometric studies of the glasses obtained confirmed the efficiency of the procedure suggested for trivalent titanium reduction. Plotting the dependence of the optical density on the titanium concentration in a glass can be used as a method for monitoring the completeness of reduction of trivalent titanium. Determination and study of the concentration range in glass, in which the concentration quenching is observed, enables control over lasing properties of other types of PASP glasses activated with Ti^{3+}. Hence follows that use of trivalent titanium as an activator in PASP is of current interest for fabrication of lasers with a wide range of emission wavelengths and good physical, optical, and lasing characteristics.

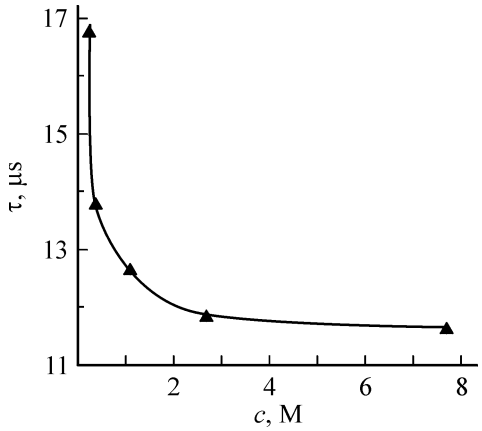

Fig. 4. Decay coefficient τ vs. titanium(III) concentration c in the glass at a luminescence wavelength of 890 nm.

CONCLUSIONS

(1) Several methods for $Ti^{4+} \rightarrow Ti^{3+}$ reduction were experimentally tested, their advantages and disadvantages were analyzed. The reduction with hydrogen was found to be the most promising procedure for this purpose.

(2) For the chosen procedure, an installation in which trivalent titanium is more easily obtained and the efficiency of this process is improved was created.

(3) The titanium(III) oxide obtained was used in making potassium-aluminum phosphate glasses. The optical properties of potassium-aluminum phosphate glasses activated with trivalent titanium were studied. The dependence of the optical and physical properties of the glass on the concentration of Ti^{3+} ions was revealed.

Table 2. Effect of Ti (III) concentration on the duration of luminescence decay in $33.5\,K_2O$–$14.01\,Al_2O_3$–$38\,P_2O_5$ (mol %) glass

$c_{Ti^{3+}}$, M	τ_{av}, μs	Absolute error in τ_{av}, μs	Total probability of spontaneous emission, A_{av}, μs^{-1}
0.2	16.7	5	0.06
0.33	13.8	6	0.072
1	12.6	3.2	0.08
2.6	11.8	7.1	0.085
2.7	11.6	4	0.086

REFERENCES

1. *Fizika i spektroskopiya lazernykh kristallov* (Physics and Spectroscopy of Laser Crystals), Kaminskii, A.A., Ed., Moscow: Nauka, 1986.
2. *Spravochnik po lazeram* (Handbook of Lasers), Prokhorov, A.M., Ed., Moscow: Sov. Radio, 1978, vols. 1 and 2.
3. Moulton, P.F., *Opt. News*, 1982, vol. 8, no. 6, p. 9.
4. Forster, Th., *Ann. Phys.*, 1948, vol. 2, no. 1, pp. 55–62.
5. Dexter, D.L., *J. Chem. Phys.*, 1953, vol. 21, p. 836.
6. Luchinskii, G.P., *Khimiya titana* (Chemistry of Titanium), Moscow: Khimiya, 1971.
7. Ivanova, R.V., *Khimiya i tekhnologiya titana* (Chemistry and Technology of Titanium), Moscow: Metallurgiya, 1973.
8. Dembovskii, S.A. and Chechetkina, E.A., *Stekloobrazovanie* (Glass Formation), Tananaev, I.V., Ed., Moscow: Nauka, 1990.
9. Demkina, L.I., *Fiziko-khimicheskie osnovy proizvodstva opticheskogo stekla* (Physicochemical Foundations of Optical Glass Production), Leningrad: Khimiya, 1976.
10. Kleshchinov, E.B., Nonradiative Transfer of Excitation Energy and Sensitization of Luminescence of Certain Triply Charged Rare-Earth Elements with Titanium(III) Ions in a Glassy System, *Cand. Sci. Dissertation*, St. Petersburg, 1997.
11. Gilles, P.W., Carlson, K.D., Frasen, H.F., and Walrlberk, P.G., *J. Chem. Phys.*, 1967, vol. 47, no. 7, pp. 2461–2465.
12. Tinus, A.M., Physicochemical and Spectral-Luminescent Properties of Potassium-Aluminum-Silico Phosphate Glass Activated by 3*d*-elements Ti(III), Cu(II), REE: Pr(III), Nd(III), Sm(III), Eu(III), *Cand. Sci. Dissertation*, St. Petersburg, 1999.
13. Batyaev, I.M. and Sukhanov, S.B., *Pis'ma Zh. Theor. Fiz.*, 1994, vol. 20, no. 10, pp. 38–42.
14. *Inorganic Syntheses*, New York: McGraw–Hill Book, 1946, vol. 3.
15. Nekrasov, B.V., *Osnovy obshchei khimii* (Fundamentals of General Chemistry), Moscow: Khimiya, 1967, vol. 2.
16. Leonov, A.V., Optical Properties of Condensed Glassy Lasing Materials Activated with Trivalent Titanium, *Cand. Sci. Dissertation*, St. Petersburg, 2005.
17. Bersuker, I.B., *Elektronnoe stroenie i svoistva koordinatsionnykh soedinenii: Vvedenie v teoriyu* (Electronic Structure and Properties of Coordination Compounds: Introduction to the Theory), Leningrad: Khimiya, 1986, 3rd ed.
18. Batyaev, I.M., *Zh. Obshch. Khim.*, 2001, vol. 71, no. 3, pp. 1–2.
19. Batyaev, I.M. and Kobezhikov, Yu.G., *Opt. Spektrosk.*, 1998, vol. 85, no. 1, pp. 68–70.
20. Batyaev, I.M. and Kobezhikov, Yu.G., *Pis'ma Zh. Theor. Fiz.*, 1996, vol. 22, no. 11, pp. 81–85.
21. Batyaev, I.M. and Sukhanov S.B., *Opt. Spektrosk.*, 1992, vol. 72, no. 6, pp. 67–70.
22. Sukhanov S.B., Spectral-Luminescent Properties of Phosphate Glass Activated with Titanium(III) and Neodymium(III), *Cand. Sci. Dissertation*, St. Petersburg, 1994.
23. Golodova, I.V., Spectral-Luminescent and Certain Physicochemical Properties of Gallium-Phosphate Glasses Activated with Ti^{3+} and Nd^{3+} Ions, *Cand. Sci. Dissertation*, St. Petersburg, 1972.
24. Batyaev, I.M. and Kleshchinov, E.B., *Opt. Spektrosk.*, 1996, vol. 81, no. 5, pp. 823–826.
25. Aristov, A.V., Kozlovskii, D.A., Batyaev, I.M., and Kobezhikov, Yu.G., *Opt. Zh.*, 2000, vol. 67, no. 3, pp. 8–15.
26. Batyaev, I.M. and Golodova, I.V., *Opt. Spektrosk.*, 1994, vol. 77, no. 1, pp. 54–56.
27. Kuznetsov, A.R., Lunter, S.G., Nikitina, S.I., et al., *Zh. Prikl. Spektrosk.*, 1992, vol. 56, no. 1, pp. 90–95.
28. Moultion, P.F., *Proc. IEEE*, 1992, vol. 80, no. 3, p. 348–364.
29. Privalova, T.A., Nonradiative Energy Transfer and Relaxation Spectroscopy Applied to a Study of Complexation of Ions of Rare-Earth Elements in Nonaqueous Solvents, *Cand. Sci. Dissertation*, St. Petersburg, 1972.
30. Ermolaev, V.L., Bodunov, E.N., Sveshnikova, E.B., and Shakhverdov, T.A., *Bezyzluchatel'nyi perenos energii elekrtronnogo vozbuzhdeniya* (Nonradiative Transfer of Electronic Excitation Energy, Leningrad: Nauka, 1977.

ISSN 1070-4272, Russian Journal of Applied Chemistry, 2007, Vol. 80, No. 8, pp. 1275–1280. © Pleiades Publishing, Ltd., 2007.
Original Russian Text © E.P. Lokshin, O.A. Tareeva, T.G. Kashulina, 2007, published in Zhurnal Prikladnoi Khimii, 2007, Vol. 80, No. 8, pp. 1237–1242.

INORGANIC SYNTHESIS AND INDUSTRIAL INORGANIC CHEMISTRY

A Study of the Solubility of Yttrium, Praseodymium, Neodymium, and Gadolinium Sulfates in the Presence of Sodium and Potassium in Sulfuric-Phosphoric Acid Solutions at 20°C

E. P. Lokshin, O. A. Tareeva, and T. G. Kashulina

Tananaev Institute of Chemistry and Technology of Rare Elements and Mineral Resources, Kola Scientific Center, Russian Academy of Sciences, Russian Academy of Sciences, Apatity, Murmansk oblast, Russia

Received February 28, 2007

Abstract—Solubility of yttrium, praseodymium, neodymium, and gadolinium sulfates in the presence of sodium and potassium ions and the composition of solid phases were studied at 20°C in relation to the concentration of acids in sulfuric acid, phosphoric acid, and sulfuric-phosphoric acid solutions containing up to 36 wt % H_2SO_4 and 33.12 g l^{-1} H_3PO_4.

DOI: 10.1134/S1070427207080022

A technique for recovery of lanthanides from phosphogypsum, based on sulfuric acid leaching and spontaneous crystallization of lanthanides from a sulfuric-phosphoric acid solution, has been suggested [1, 2]. To understand the fundamental aspects of crystallization of lanthanides from sulfuric-phosphoric acid leaching solutions containing admixtures of sodium and potassium ions, it is necessary to know the solubility of lanthanides in these solutions and the composition of the equilibrium solid phases.

Previously, the solubility of lanthanum and cerium sulfates, which are the main constituents of the sum of lanthanides of the Khibiny apatite, has been studied [3]. It was shown that, in the presence of stoichiometric amounts of sodium and potassium, the equilibrium solid phases are double sulfates of composition $LnM(SO_4)_2 \cdot H_2O$, where Ln = La, Ce and M = Na, K, and the solubility of the lanthanides in sulfuric-phosphoric acid solutions is determined by the solubility of these double sulfates.

The aim of this study was to complete the analysis of the solubility of double sulfates of the cerium-group lanthanides (praseodymium, neodymium) and to examine the solubility of yttrium and gadolinium sulfates.

It is known that, at 25°C and comparatively low Na_2SO_4 concentrations (≤2.39 wt %), $Y_2(SO_4)_3 \cdot 8H_2O$ crystallizes in the system $Y_2(SO_4)_3$–Na_2SO_4–H_2O, with the solubility of $Y_2(SO_4)_3$ being equal to 5.21–5.52 wt % and somewhat increasing with the Na_2SO_4 concentration. In the Na_2SO_4 concentration range 3.02–17.74 wt %, the solid phase is composed of $YNa(SO_4)_2 \cdot H_2O$ at a solubility of 5.20–2.15 wt % in terms of $Y_2(SO_4)_3$. As the Na_2SO_4 concentration increases further, $Na_2SO_4 \cdot 10H_2O$ is found in the solid phase. Although the solubility of $Y_2(SO_4)_3$ decreases as the content of Na_2SO_4 becomes higher (≥3.02 wt %), it still remains sufficiently high (about 4.2 g l^{-1} in terms of Y_2O_3) even at a Na_2SO_4 content of 21.88 wt % [4].

A similar behavior has been observed for the system $Y_2(SO_4)_3$–K_2SO_4–H_2O: at low K_2SO_4 contents (up to 4.93 wt %) only $Y_2(SO_4)_3 \cdot 8H_2O$ crystallizes [5]. The main distinction was the even higher maximum solubility of $Y_2(SO_4)_3$, up to 8.17 wt % at a K_2SO_4 content of the solution equal to 6.01 wt %.

The increase in the $Y_2(SO_4)_3 \cdot 8H_2O$ solubility on raising the concentration of alkali metal sulfates (at their low concentrations) indicates that associates, precursors of the corresponding double sulfates, exist in solutions.

The solubility in the systems $Ln_2(SO_4)_3$–M_2SO_4–H_2O (Ln = Pr, Nd, Gd) has not been studied, but the existence of double sulfates $LnM(SO_4)_2 \cdot H_2O$, and

also $2Nd_2(SO_4)_3 \cdot 3Na_2SO_4 \cdot 2H_2O$ and $2Ln_2(SO_4)_3 \cdot 3K_2SO_4 \cdot 4H_2O$, has been reported [6]. Data on the solubility of $Ln_2(SO_4)_3$ (Ln = Y, Pr, Nd, Gd) in sulfuric-phosphoric acid solutions containing sodium or potassium ions are unavailable.

EXPERIMENTAL

For the most part, the experimental procedure corresponded to that described previously [3]. The main distinction was that equimolar mixtures of a lanthanide and an alkaline metal, rather than preliminarily synthesized double sulfates, were introduced into the sulfuric-phosphoric acid solutions prepared.

The solubility of $Y_2(SO_4)_3$ was studied in sulfuric acid solutions with a concentration $c_{H_2SO_4}$ = 0–36 wt %, and that of $Ln_2(SO_4)_3$ (Ln = Pr, Nd, Gd), in sulfuric acid solutions with $c_{H_2SO_4}$ = 0–36 wt % and $c_{H_3PO_4}$ = 0–27.6 g l^{-1}. The experimental data obtained are listed in Tables 1–6.

Table 1. Equilibrium concentrations of Y_2O_3 (numerator) and Na_2O or K_2O (denominator) in sulfuric acid solutions at 20°C

$c_{H_2SO_4}$, wt %	Na_2O		K_2O	
	c, g l^{-1}	yttrium compound in the bottom phase	c, g l^{-1}	yttrium compound in the bottom phase
0	38.84 / 10.5	$YNa(SO_4)_2 \cdot H_2O$	26.6 / 11.3	$YK(SO_4)_2 \cdot H_2O$
4	35.5 / 9.37	$YNa(SO_4)_2 \cdot H_2O$	34.75 / 21.5	$Y_2(SO_4)_3 \cdot 8H_2O$
8	30.58 / 9.50	$Y_2(SO_4)_3 \cdot 8H_2O + YNa(SO_4)_2 \cdot H_2O$	29.8 / 15.6	$Y_2(SO_4)_3 \cdot 8H_2O$
12	23.78 / 9.55	$Y_2(SO_4)_3 \cdot 8H_2O + YNa(SO_4)_2 \cdot H_2O$	24.05 / 12.9	$Y_2(SO_4)_3 \cdot 8H_2O$
16	8.34 / 9.50	$Y_2(SO_4)_3 \cdot 8H_2O + YNa(SO_4)_2 \cdot H_2O$	14.38 / 8.64	$Y_2(SO_4)_3 \cdot 8H_2O$
20	12.0 / 6.37	$Y_2(SO_4)_3 \cdot 8H_2O + YNa(SO_4)_2 \cdot H_2O$	11.43 / 8.55	$Y_2(SO_4)_3 \cdot 8H_2O$
24	7.14 / 6.31	$Y_2(SO_4)_3 \cdot 8H_2O + YNa(SO_4)_2 \cdot H_2O$	5.80 / 4.48	$Y_2(SO_4)_3 \cdot 8H_2O$
28	4.92 / 6.15	$Y_2(SO_4)_3 \cdot 8H_2O + YNa(SO_4)_2 \cdot H_2O$	3.46 / 3.08	$Y_2(SO_4)_3 \cdot 8H_2O$
32	2.42 / 5.93	$Y_2(SO_4)_3 \cdot 8H_2O + YNa(SO_4)_2 \cdot H_2O$	2.04 / 3.62	$Y_2(SO_4)_3 \cdot 8H_2O$
36	1.6 / 5.72	$Y_2(SO_4)_3 \cdot 8H_2O + YNa(SO_4)_2 \cdot H_2O$	Undetermined	Undetermined

Table 2. Equilibrium concentrations of Pr_2O_3 and Na_2O in sulfuric acid and sulfuric-phosphoric acid solutions at 20°C

$c_{H_2SO_4}$, wt %	Content of Pr_2O_3 (numerator) and Na_2O (denominator) at indicated $c_{H_2SO_4}$, g l^{-1}				$c_{H_2SO_4}$, wt %	Content of Pr_2O_3 (numerator) and Na_2O (denominator) at indicated $c_{H_2SO_4}$, g l^{-1}			
	0	6.90	16.56	27.6		0	6.90	16.56	27.6
0	1.97 / 0.35	0.003 / 0.27	0.005 / 0.27	0.005 / 0.27	20	1.17 / 0.19	1.13 / 0.18	1.11 / 0.18	1.05 / 0.17
4	2.13 / 0.36	2.12 / 0.36	2.14 / 0.39	2.14 / 0.39	24	0.90 / 0.15	0.81 / 0.13	0.81 / 0.13	0.77 / 0.12
8	2.18 / 0.37	2.17 / 0.37	2.15 / 0.38	2.14 / 0.39	28	0.60 / 0.10	0.50 / 0.083	0.49 / 0.085	0.47 / 0.086
12	2.04 / 0.34	2.01 / 0.33	2.02 / 0.35	2.00 / 0.33	32	0.44 / 0.081	0.44 / 0.082	0.43 / 0.079	0.41 / 0.078
16	1.55 / 0.26	1.54 / 0.26	1.51 / 0.25	1.54 / 0.26	36	0.35 / 0.063	0.33 / 0.061	0.34 / 0.062	0.35 / 0.064

Table 3. Equilibrium concentrations of Pr_2O_3 and K_2O in sulfuric acid and sulfuric-phosphoric acid solutions at 20°C

$c_{H_2SO_4}$, wt %	Content of Pr_2O_3 (numerator) and K_2O (denominator) at indicated $c_{H_2SO_4}$, g l^{-1}				$c_{H_2SO_4}$, wt %	Content of Pr_2O_3 (numerator) and K_2O (denominator) at indicated $c_{H_2SO_4}$, g l^{-1}			
	0	6.90	16.56	27.6		0	6.90	16.56	27.6
0	5.0 / 1.35	0.008 / 0.41	0.007 / 0.28	0.014 / 0.22	20	5.1 / 1.36	5.0 / 1.30	4.9 / 1.28	4.2 / 1.14
4	6.5 / 1.78	6.4 / 1.76	6.6 / 1.85	6.5 / 1.70	24	3.8 / 1.00	3.6 / 0.98	3.5 / 1.00	3.3 / 0.94
8	7.1 / 1.91	7.0 / 1.86	6.8 / 1.75	6.7 / 1.72	28	3.10 / 0.88	3.02 / 0.85	3.03 / 0.86	3.00 / 0.80
12	6.6 / 1.84	6.6 / 1.83	6.7 / 1.84	6.6 / 1.78	32	2.29 / 0.61	2.26 / 0.59	2.29 / 0.61	2.27 / 0.60
16	5.9 / 1.54	6.0 / 1.55	5.8 / 1.51	5.6 / 1.47	36	1.81 / 0.49	1.79 / 0.48	1.77 / 0.47	1.72 / 0.46

Table 4. Equilibrium concentrations of Nd_2O_3 and Na_2O in sulfuric acid and sulfuric-phosphoric acid solutions at 20°C

$c_{H_2SO_4}$, wt %	Content of Nd_2O_3 (numerator) and Na_2O (denominator) at indicated $c_{H_2SO_4}$, g l^{-1}				$c_{H_2SO_4}$, wt %	Content of Nd_2O_3 (numerator) and Na_2O (denominator) at indicated $c_{H_2SO_4}$, g l^{-1}			
	0	6.90	16.56	27.6		0	6.90	16.56	27.6
0	2.03 / 0.36	0.033 / 0.41	0.040 / 0.47	0.040 / 0.47	20	1.25 / 0.22	1.27 / 0.23	1.27 / 0.23	1.25 / 0.22
4	2.22 / 0.38	2.21 / 0.38	2.42 / 0.42	2.39 / 0.41	24	0.94 / 0.17	0.90 / 0.16	0.90 / 0.16	0.89 / 0.16
8	2.30 / 0.40	2.26 / 0.39	2.24 / 0.38	2.24 / 0.38	28	0.68 / 0.12	0.63 / 0.11	0.64 / 0.11	0.60 / 0.10
12	1.95 / 0.35	1.93 / 0.34	1.94 / 0.35	1.95 / 0.35	32	0.46 / 0.084	0.46 / 0.084	0.45 / 0.083	0.44 / 0.081
16	1.65 / 0.28	1.65 / 0.28	1.64 / 0.27	1.65 / 0.28	36	0.32 / 0.057	0.32 / 0.057	0.31 / 0.056	0.30 / 0.055

Table 5. Equilibrium concentrations of Nd_2O_3 and K_2O in sulfuric acid and sulfuric-phosphoric acid solutions at 20°C

$c_{H_2SO_4}$, wt %	Content of Nd_2O_3 (numerator) and K_2O (denominator) at indicated $c_{H_2SO_4}$, g l^{-1}				$c_{H_2SO_4}$, wt %	Content of Nd_2O_3 (numerator) and K_2O (denominator) at indicated $c_{H_2SO_4}$, g l^{-1}			
	0	6.90	16.56	27.6		0	6.90	16.56	27.6
0	4.30 / 1.20	0.048 / 0.97	0.035 / 1.00	0.024 / 1.00	20	5.04 / 1.40	5.00 / 1.30	5.10 / 1.40	5.12 / 1.40
4	6.18 / 1.70	6.16 / 1.70	6.16 / 1.60	6.17 / 1.70	24	4.25 / 1.20	3.90 / 1.10	3.92 / 1.10	4.00 / 1.10
8	7.50 / 2.00	7.50 / 2.00	7.40 / 1.90	7.50 / 2.00	28	3.48 / 0.96	3.04 / 0.84	3.30 / 0.91	3.30 / 0.94
12	6.72 / 1.90	6.80 / 1.90	6.70 / 1.90	6.60 / 1.85	32	2.58 / 0.71	2.69 / 0.77	2.69 / 0.77	2.5 / 0.69
16	6.08 / 1.70	6.04 / 1.70	6.10 / 1.60	6.15 / 1.70	36	1.98 / 0.55	2.06 / 0.57	2.05 / 0.57	1.91 / 0.54

Table 6. Equilibrium concentrations of Gd_2O_3, Na_2O, and K_2O in sulfuric acid and sulfuric-phosphoric acid solutions at 20°C

$c_{H_2SO_4}$, wt %	Content of Gd_2O_3 (numerator) and $Na(K)_2O$ (denominator) at indicated $c_{H_2SO_4}$, g l^{-1}					$c_{H_2SO_4}$, wt %	Content of Gd_2O_3 (numerator) and $Na(K)_2O$ (denominator) at indicated $c_{H_2SO_4}$, g l^{-1}				
	Na_2O		K_2O				Na_2O		K_2O		
	0	27.6	0	6.9	27.6		0	27.6	0	6.9	27.6
0	5.6 / 0.88	0.80 / 0.89	16.6 / 11.2	0.27 / 5.2	U.d.*	20	4.10 / 0.66	4.47 / 0.70	8.7 / 6.4	8.6 / 5.7	9.2 / 6.5
4	9.0 / 1.44	9.5 / 1.53	19.1 / 8.05	21.2 / 7.7	24.5 / 9.2	24	2.82 / 0.43	2.84 / 0.44	5.46 / 11.1	5.81 / 5.7	5.88 / 5.4
8	8.71 / 1.36	8.9 / 1.37	17.5 / 7.7	18.6 / 8.2	20.6 / 8.5	28	1.79 / 0.27	1.80 / 0.28	3.10 / 8.7	3.22 / 7.7	3.48 / 5.7
12	7.30 / 1.16	7.53 / 1.19	15.1 / 8.0	15.8 / 7.8	16.8 / 6.3	32	1.30 / 0.20	1.32 / 0.21	1.70 / 8.0	2.19 / 5.4	2.16 / 5.9
16	5.50 / 0.88	5.68 / 0.89	12.4 / 7.4	11.6 / 6.5	12.7 / 5.8	36	0.90 / 0.14	1.00 / 0.15	U.d.	U.d.	U.d.

* Undetermined, the same for Table 7.

Table 7. $Ln_2O_3/Na(K)_2O$ molar ratio in equilibrium sulfuric acid solutions*

$c_{H_2SO_4}$, wt %	$Ln_2O_3/Na(K)_2O$ molar ratio in an indicated solution							
	I	II	III	IV	V	VI	VII	VIII
0	1.01	0.98	1.06	1.06	1.01	1.00	1.09	0.38
4	1.04	0.67	1.11	1.04	1.05	1.02	1.07	0.62
8	0.88	0.79	1.11	1.06	1.04	1.05	1.10	0.59
12	0.68	0.77	1.13	1.02	1.00	0.99	1.08	0.49
16	0.53	0.69	1.12	1.10	1.06	1.00	1.07	0.43
20	0.52	0.55	1.10	1.07	1.02	1.00	1.06	0.35
24	0.31	0.54	1.13	1.08	1.00	0.99	1.12	0.13
28	0.22	0.47	1.13	1.00	1.02	1.01	1.13	0.09
32	0.11	0.23	1.02	1.07	0.99	1.01	1.11	0.06
36	0.077	U.d.	1.04	1.05	1.01	1.00	1.10	0.04

* (I) $Y_2(SO_4)_3 + Na_2SO_4$, (II) $Y_2(SO_4)_3 + K_2SO_4$, (III) $Pr_2(SO_4)_3 + Na_2SO_4$, (IV) $Pr_2(SO_4)_3 + K_2SO_4$, (V) $Nd_2(SO_4)_3 + Na_2SO_4$, (VI) $Nd_2(SO_4)_3 + K_2SO_4$, (VII) $Gd_2(SO_4)_3 + Na_2SO_4$, (VIII) $Gd_2(SO_4)_3 + K_2SO_4$.

In sulfuric acid and sulfuric-phosphoric acid solutions, the molar ratio of cerium-group lanthanides (praseodymium, neodymium) and alkaline metals, as well as as that of gadolinium and sodium, varied within the range 0.99–1.13 (Table 7). This indicates that double sulfides with a 1 : 1 atomic ratio of a lanthanide and an alkaline metal are formed and congruently dissolve. This is confirmed by the results of an X-ray phase analysis of the equilibrium solid phases. Yttrium is present in the bottom phase in a sulfuric acid solution as $YNa(SO_4)_2 \cdot H_2O$ at $c_{H_2SO_4}$ = 0–4 wt % and as a mixture of $Y_2(SO_4)_3 \cdot 8H_2O$ and $YNa(SO_4)_2 \cdot H_2O$ at $c_{H_2SO_4}$ = 8–36 wt % (see figure). The double sulfate $YK(SO_4)_2 \cdot H_2O$ existed only in the aqueous medium. It dissolved congruently in sulfuric acid solutions with the concentrations studied. No double sulfates of gadolinium and potassium were found.

The manner in which the solubility of praseodymium and neodymium sulfates changes in sulfuric-phosphoric acid solutions containing sodium or potas-

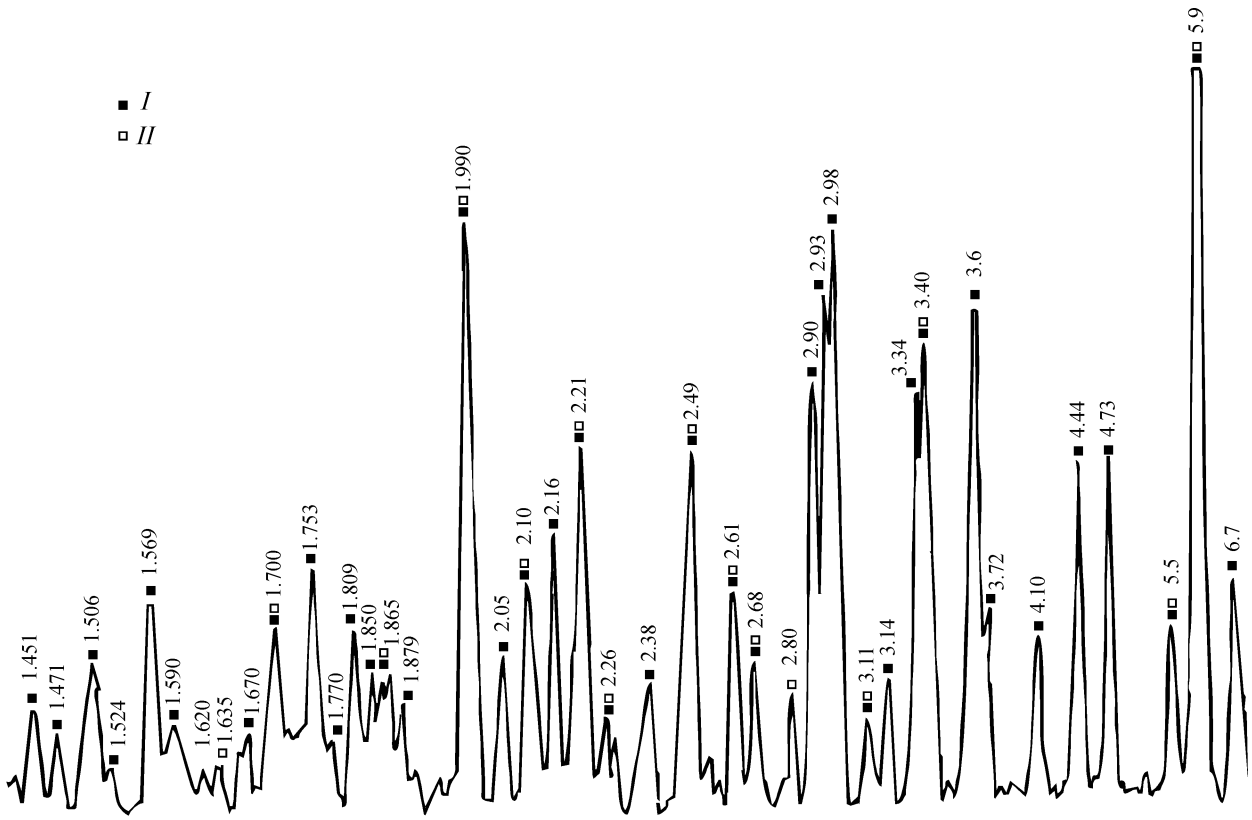

X-ray diffraction pattern of the bottom phase formed in the system $Y_2(SO_4)_3$–Na_2SO_4–H_2SO_4–H_2O at $c_{H_2SO_4}$ = 8–36 wt %. (*I*) $Y_2SO_4 \cdot 8H_2O$ and (*II*) $YNa(SO_4)_2 \cdot H_2O$.

sium ions is identical to that observed for lanthanum and cerium [3]. The solubilities of praseodymium, neodymium, and cerium sulfates in solutions of the same composition are virtually equal.

The solubility of yttrium sulfate in aqueous solutions containing Na_2SO_4 was found to be approximately 25% higher than that in [4]. The solubility of yttrium sulfate in aqueous solutions containing K_2SO_4 is close to that in [5].

At 20°C the solubility products in water for $PrNa(SO_4)_2 \cdot H_2O$, $NdNa(SO_4)_2 \cdot H_2O$, $GdNa(SO_4)_2 \cdot H_2O$, $PrK(SO_4)_2 \cdot H_2O$, and $NdK(SO_4)_2 \cdot H_2O$ are 7.28×10^{-8}, 7.84×10^{-8}, 3.09×10^{-6}, 3.02×10^{-6}, and 1.70×10^{-6}, respectively.

The data obtained previously [3] and in the present study do not confirm the data of [6], according to which the solubility of double sulfates dramatically increases in acid solutions.

For all the lanthanide sulfates studied, except yttrium, their solubility in solutions containing sodium ions is considerably lower than that in solutions with potassium ions. In sulfuric acid solutions, lanthanides forming poorly stable double sulfates (systems with sodium and potassium ions for yttrium) or forming no double sulfates (system with potassium ions for gadolinium) have a higher solubility. As, however, $c_{H_2SO_4}$ increases in the range 4–36 wt %, the relative decrease in the solubility of lanthanide sulfates exceeds that for double sulfates.

In an aqueous solution containing 27.6 g l^{-1} H_3PO_4, double sulfate of sodium and gadolinium decompose, as also do double sulfates of the rest of the lanthanides studied, to give, presumably, a poorly soluble gadolinium phosphate. However, in contrast to the cerium-group lanthanides, the solubility of gadolinium in sulfuric acid solutions containing minor amounts of phosphoric acid noticeably increases, especially in solutions containing ions of potassium, with which gadolinium forms no double sulfate.

Despite the high solubility of yttrium and gadolinium sulfates in sulfuric-phosphoric acid solutions containing sodium or potassium ions, which markedly exceeds their concentration in solutions for sulfuric acid leaching of lanthanides from phosphohemihydrate, it has been found that they are rather effectively transformed into a spontaneously crystallizing concentrate of lanthanides [7]. This suggests that there

occurs isomorphous co-crystallization of yttrium sulfate with the precipitating double sulfates of lanthanides, which is favored by the sufficient similarity of their crystal structures.

The data obtained confirm the previous assumption [3] that the low solubility of double sodium sulfates with cerium-group lanthanides is the reason for the limited accumulation of lanthanides in solutions in sulfuric acid leaching of phosphogypsum and phosphohemihydrate.

CONCLUSIONS

(1) The solubility of equimolar mixtures of yttrium, praseodymium, neodymium, or gadolinium sulfates with sodium or potassium sulfates in water, sulfuric acid, and sulfuric-phosphoric acid solutions containing 0–36 wt % H_2SO_4 and 0–27.6 g l^{-1} H_3PO_4 was determined.

(2) In water and sulfuric acid and sulfuric-phosphoric acid solutions, praseodymium and neodymium form with sodium and potassium ions, as also does gadolinium with sodium ions, incongruently soluble double sulfates with a 1 : 1 atomic ratio between the lanthanide and alkali metal ions. Double sulfates of yttrium are poorly stable in a sulfuric acid solution: $YK(SO_4)_2 \cdot H_2O$ is stable only in aqueous solutions, and $YNa(SO_4)_2 \cdot H_2O$, in solutions with a H_2SO_4 content of about 4 wt %.

(3) At 20°C, the solubility products in water for $PrNa(SO_4)_2 \cdot H_2O$, $NdNa(SO_4)_2 \cdot H_2O$, $GdNa(SO_4)_2 \cdot H_2O$, $PrK(SO_4)_2 \cdot H_2O$, and $NdK(SO_4)_2 \cdot H_2O$ are 7.28×10^{-8}, 7.84×10^{-8}, 3.09×10^{-6}, 3.02×10^{-6}, and 1.70×10^{-6}, respectively.

(4) In acid solutions of similar compositions, the solubilities of double sulfates of praseodymium, neodymium, and cerium in water and sulfuric acid solutions are virtually the same and lower than those of analogous double sulfates of lanthanum. The solubility of $GdNa(SO_4)_2 \cdot H_2O$ markedly exceeds that of the analogues studied. For all of the lanthanides studied, except yttrium, the solubility in sodium-containing solutions is substantially lower than that is solutions with potassium ions. As the concentration of sulfuric acid is raised, the solubility of the double sulfates studied first increases and then, after passing through a maximum, decreases. Raising the concentration of phosphoric acid, within the range studied, at a constant concentration of sulfuric acid affects the solubility of lanthanides in sulfuric acid solutions only slightly.

(5) The solubility of yttrium sulfate in sulfuric acid solutions containing sodium or potassium ions, and that of gadolinium sulfate in sulfuric acid and sulfuric-phosphoric acid solutions containing sodium or potassium ions, markedly exceeds their concentration in solutions formed in sulfuric acid leaching of lanthanides from phosphohemihydrate.

(6) The low solubility of double sulfates of sodium with cerium-group lanthanides is the key factor hindering the accumulation of lanthanides in solutions formed in sulfuric acid leaching of lanthanides from phosphohemihydrate.

ACKNOWLEDGMENTS

The study was financially supported by the Russian Foundation for Basic Research (project no. 06-08-00223-a).

REFERENCES

1. RF Patent 2225892.
2. Lokshin, E.P., Ivlev, K.G., and Tareeva, O.A., *Zh. Prikl. Khim.*, 2005, vol. 78, no. 12, pp. 1937–1945.
3. Lokshin, E.P., Tareeva, O.A., Ivlev, K.G., and Kashulina, T.G., *Zh. Prikl. Khim.*, 2005, vol. 78, no. 7, pp. 1080–1084.
4. Belousova, A.P., Shakhno, I.V., and Plyushchev, V.E., *Zh. Neorg. Khim.*, 1968, vol. 13, pp. 1998–2003.
5. Shakhno, I.V., Belousova, A.P., Pavkina, M.D., and Plyushchev, V.E., *Zh. Neorg. Khim.*, 1967, vol. 12, no. 9, pp. 2500–2504.
6. Komisarova, L.N., Pushkina, G.Ya., Shatskii, V.M., et al., *Soedineniya redkozemel'nykh elementov. Sul'faty, selenaty, telluraty, khromaty* (Compounds of Rare-Earth Elements: Sulfates, Selenates, Tellurates, Chromates), Moscow: Nauka, 1986.
7. Lokshin, E.P. and Kalinnikov, V.T., *Formirovanie osnov sovremennoi strategii prirodopol'zovaniya v EvroArkticheskom regione* (Development of Modern Strategy of Nature Management in the European-Arctic Region), Apatity: Kola Nauchn. Tsentr, Ross. Akad. Nauk, 2005, pp. 250–269.

ISSN 1070-4272, Russian Journal of Applied Chemistry, 2007, Vol. 80, No. 8, pp. 1281–1283. © Pleiades Publishing, Ltd., 2007.
Original Russian Text © A.K. Pyartman, V.A. Keskinov, V.V. Lishchuk, Ya.A. Reshetko, V.E. Skobochkin, 2007, published in Zhurnal Prikladnoi Khimii, 2007, Vol. 80, No. 8, pp. 1243–1245.

INORGANIC SYNTHESIS AND INDUSTRIAL INORGANIC CHEMISTRY

Stratification in a Ternary Liquid System $[Th(NO_3)_4(TBP)_2]$–$[UO_2(NO_3)_2(TBP)_2]$–Exide 100 Solvent at Various Temperatures

A. K. Pyartman, V. A. Keskinov, V. V. Lishchuk, Ya. A. Reshetko, and V. E. Skobochkin

St. Petersburg State Technological Institute, St. Petersburg, Russia

Received September 14, 2006; in final form, January 2007

Abstract—Phase diagram of a ternary liquid system $[Th(NO_3)_4(TBP)_2]$–$[UO_2(NO_3)_2(TBP)_2]$–Exide 100 solvent was studied at 298.15–333.15 K.

DOI: 10.1134/S1070427207080034

It has been found previously that the phase diagrams of ternary liquid systems (TLS) constituted by $[Ln(NO_3)_3(TBP)_3]$, (RED), and Exide-100 solvent (E-100) (Ln = Nd, Yb; TBP, tri-*n*-butyl phosphate; RED, extractive dearomitized diluent) comprise a region of homogeneous solutions and that of stratification into two liquid phases. To enable practical use of extractive systems based on mixtures of TBP, RED 1, and E-100 under complete saturation of the organic phase with nitrates of rare-earth metals(III) to give $[Ln(NO_3)_3(TBP)_3]$, it is necessary to partly replace paraffin solvents with hydrocarbon diluents containing up to 20% aromatic compounds for total homogenization of the systems at low temperatures.

In [2, 3], the phase diagrams of TLS constituted by $[Th(NO_3)_4(TBP)_2]$, $[UO_2(NO_3)_2(TBP)_2]$, and decane (tetradecane) were studied at 298.15–333.15 K. The ternary liquid system has a region of homogeneous solutions and that of two-phase liquid systems (systems with stratification), in which one phase (I) is enriched in $[Th(NO_3)_4(TBP)_2]$ and $[UO_2(NO_3)_2(TBP)_2]$, and the other (II), with hydrocarbon diluents.

This study is concerned with the effect of temperature on stratification processes in the system $[Th(NO_3)_4(TBP)_2]$–$[UO_2(NO_3)_2(TBP)_2]$–E-100, which is of practical interest in the technology for separation of uranium and thorium.

EXPERIMENTAL

Vacuum-distilled TBP (density $\rho_{298.15} = 0.9727$ g cm^{-3}) and E-100 solvent (saturated hydrocarbons with addition of 20 vol % aromatic hydrocarbons, $\rho_{298.15} = 0.8241$ g cm^{-3}) were used in the study. The solvates $[Th(NO_3)_4(TBP)_2]$ and $[UO_2(NO_3)_2(TBP)_2]$ were produced by 3–4-fold interaction of concentrated aqueous solutions of thorium(IV) and dioxo uranium(VI) with TBP. The concentrations and densities of the solvates were as follows: $[Th(NO_3)_4(TBP)_2]$, 1.80 ± 0.01 M, $\rho_{298.15} = 1.7022 \pm 0.0013$ g cm^{-3}; $[UO_2(NO_3)_2(TBP)_2]$, 1.82 ± 0.01 M, $\rho_{298.15} = 1.4215 \pm 0.015$ g cm^{-3}.

The binodal curves of the ternary systems were obtained using Alekseev's visual polythermic method, with account of the improvements reported in [1–4]. Solutions containing a mixture of thorium(IV) and dioxo uranium(VI) nitrate solvates were analyzed as follows. The content of dioxo uranium(VI) nitrate solvate in the organic phase was found directly by the Sakharov method [5, 6], and that of thorium(IV) nitrate solvate in the organic phase, by complexometry [7]. It was found in preliminary experiments that the change in the volume of the organic phase on mixing solutions of E-100 and thorium(IV) and dioxo uranium(VI) solvates did not exceed 0.3 vol %. The compositions of the coexisting phases (vol %) were recalculated to mass fractions with account of the solution densities. The bimodal

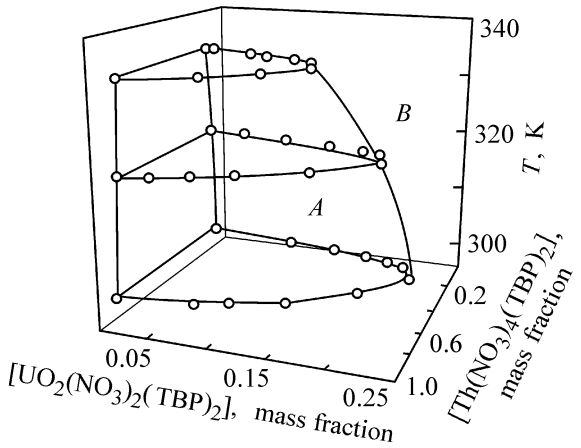

Fig. 1. Phase diagrams of the ternary system $[Th(NO_3)_4 \cdot (TBP)_2]$–$[UO_2(NO_3)_2(TBP)_2]$–E-100 at different temperatures. (*T*) Temperature. (*A*) Region of stratification into two liquid phases and (*B*) region of homogeneous solutions.

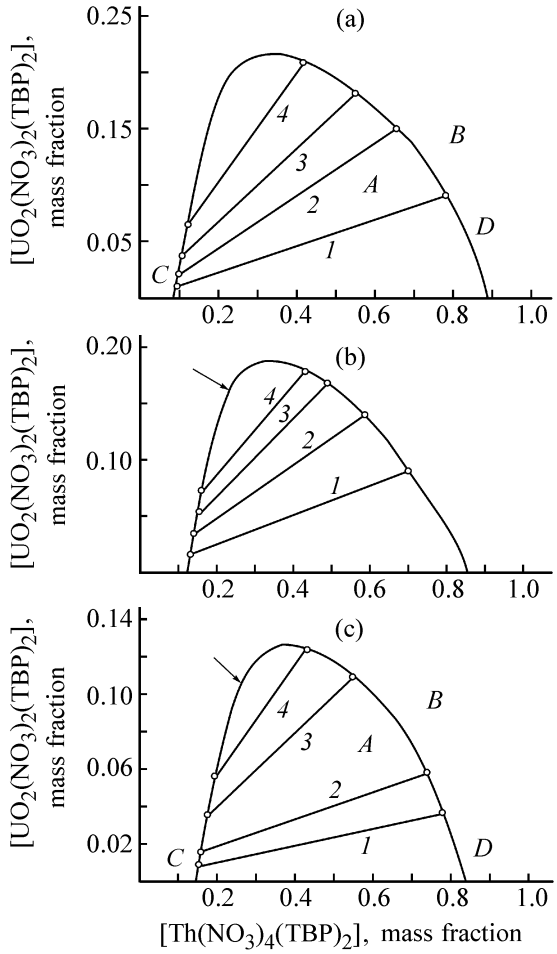

Fig. 2. Cross-sections of the phase diagram of the ternary system $[Th(NO_3)_4(TBP)_2]$–$[UO_2(NO_3)_2(TBP)_2]$–E-100. (*1–4*) Nodes; the critical composition is shown by the arrow. (*A*) Region of stratification into two liquid phases, (*B*) region of homogeneous solutions, and (*CD*) bimodal curve. Temperature (K): (a) 298.15, (b) 318.15, and (c) 333.15.

curves were approximated with a third- or fourth-order polynomial.

The phase diagrams of TLS in relation to temperature (Figs. 1, 2) are presented using the second Roseboom triangle: rectangular coordinates for two TLS components, with the mass fractions of the components (ω_1, ω_2, and ω_3; $\omega_3 = 1 - \omega_1 - \omega_2$). The errors in determining the mass fractions of the components did not exceed ± 0.001–0.002, and that in measuring the temperature, ± 0.2 K.

The binary system $[UO_2(NO_3)_2(TBP)_2]$–E-100 is a liquid single-phase system, and the binary system $[Th(NO_3)_4(TBP)_2]$–E-100, a liquid two-phase system in the entire range of temperatures studied (298.15–333.15 K) (Figs. 1, 2). Raising the temperature from 298.15 to 333.15 K leads to an only slight increase in the mutual solubility of the components of the system $[Th(NO_3)_4(TBP)_2]$–E-100 (Figs. 1, 2). It is impossible to determine the upper critical temperature for this system, because raising the temperature above 373.15 K leads to evaporation of E-100 and, in particular, of its aromatic components, rather than to homogenization of the system.

The ternary liquid system $[Th(NO_3)_4(TBP)_2]$–$[UO_2(NO_3)_2(TBP)_2]$–E-100 has a region of homogeneous liquid solutions (region *B*) and a two-phase region *A*, delimited by bimodal curves at different temperatures (Figs. 1, 2). An increase in temperature in the range 298.15–333.15 K makes narrower the region of stratification into two phases in three-component systems, which is particularly clearly manifested on going from 318.15 to 333.15 K (Fig. 1). Analysis of the nodes of TLS at different temperatures (Fig. 2) shows that, in the heterogeneous regions, two phases are typically formed, one of which is enriched in $[Th(NO_3)_4(TBP)_2]$ and $[UO_2(NO_3)_2(TBP)_2]$ (phase I), and the other, in E-100 (phase II).

As the temperature is elevated from 298.15 to 333.15 K, the mass fraction of $[Th(NO_3)_4(TBP)_2]$ at points of the critical TLS composition increases from 0.185 to 0.255 and that of $[UO_2(NO_3)_2(TBP)_2]$ decreases from 0.17 to 0.10 (Fig. 2), with the mass fraction of E-100 remaining virtually unchanged (~0.65).

Figure 3 shows the distribution diagrams of $[UO_2(NO_3)_2(TBP)_2]$, $[Th(NO_3)_4(TBP)_2]$, and E-100 among phases I and II. A characteristic feature is, according to Fig. 3, the preferential distribution of $[UO_2(NO_3)_2(TBP)_2]$ into phase I, despite that the binary system $[UO_2(NO_3)_2(TBP)_2]$–E-100 is single-phase at any of the temperatures studied. Probably, this is due to a dipole-dipole interaction between the

solvates $[Th(NO_3)_4(TBP)_2]$ and $[UO_2(NO_3)_2(TBP)_2]$. The preferential distribution of $[UO_2(NO_3)_2(TBP)_2]$ into phase I results in that, contrariwise, $[Th(NO_3)_4(TBP)_2]$ is redistributed into phase II (opposite runs of the isotherms for U and Th), and E-100 is redistributed from phase II into phase I (Fig. 3).

For practical use of extractive systems based on mixtures of TBP and E-100 under complete saturation of the organic phase with thorium(IV) and dioxo uranium(VI) nitrates to give $[UO_2(NO_3)_2(TBP)_2]$ and $[Th(NO_3)_4(TBP)_2]$ without stratification of the organic phase, it is necessary to use the extractive agent (TBP) in a diluent, with the mass fraction of the diluent not exceeding 0.6 (up to approximately 50 vol %). Further decrease in the TBP concentration is unadvisable because of the possible formation of three-phase liquid systems.

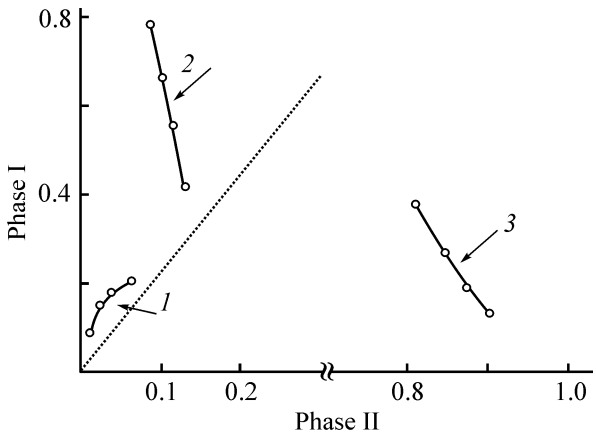

Fig. 3. Distribution diagram of (*1*) $[UO_2(NO_3)_2(TBP)_2]$, (*2*) $[Th(NO_3)_4(TBP)_2]$, and (*3*) E-100 among phases I and II at 318.15 K. Phase enriched: (I) in $[Th(NO_3)_4(TBP)_2]$ and $[UO_2(NO_3)_2(TBP)_2]$ and (II) in E-100.

CONCLUSIONS

(1) The binary system $[Th(NO_3)_4(TBP)_2]$–E-100 is limited in the mutual solubility of its components. Changing the temperature from 298.15 to 333.15 K has no significant effect on the mutual solubility of the components.

(2) The phase diagram of the ternary liquid system $[Th(NO_3)_4(TBP)_2]$–$[UO_2(NO_3)_2(TBP)_2]$–E-100 shows a region of homogeneous solutions and that of two-phase liquid systems (systems with stratification), in which one phase (I) is enriched in $[Th(NO_3)_4(TBP)_2]$ and $[UO_2(NO_3)_2(TBP)_2]$, and the other, in E-100 solvent. An increase in the temperature (298.15–333.15 K) makes narrower the region of stratification into two liquid phases in the ternary liquid system.

(3) To enable practical use of extractive systems based on mixtures of tri-*n*-butyl phosphate and E-100 under complete saturation of the organic phase with thorium(IV) and dioxo uranium(VI) nitrates to give $[UO_2(NO_3)_2(TBP)_2]$ and $[Th(NO_3)_4(TBP)_2]$ without stratification of the organic phase, it is necessary to use the extractive agent (tri-*n*-butyl phosphate) in a diluent, with the mass fraction of the diluent not exceeding 0.6 (up to approximately 50 vol %).

REFERENCES

1. Keskinov, V.A., Mishina, N.E., and Pyartman, A.K., *Radiokhimiya*, 2005, vol. 47, no. 5, pp. 520–522.
2. Keskinov, V.A., Lishchuk, V.V., and Pyartman, A.K., *Zh. Neorg. Khim.*, 2006, vol. 51, no. 6, pp. 1050–1052.
3. Treybal, R.E., *Liquid Extraction*, New York: McGraw–Hill, 1963.
4. Nikolaev, A.V. and Yakovlev, I.I., *Klatratoobrazovanie i fiziko-khimicheskii analiz ekstraktsionnykh sistem* (Clathrate Formation and Physicochemical Analysis of Extractive Systems), Novosibirsk.: Nauka, 1975.
5. Markov, V.K., Vinogradov, A.V., Elinson, V., et al., *Uran, metody ego opredeleniya* (Uranium and Methods for Its Determination), Moscow: Atomizdat, 1960.
6. Pyartman, A.K., Kopyrin, A.A., Berinskii, A.E., and Keskinov, V.A., *Radiokhimiya*, 2000, vol. 42, no. 2, pp. 128–130.
7. Pibil, R., *Analytical Applications of EDTA and Related Compounds*, Oxford: Pergamon, 1972.

ISSN 1070-4272, Russian Journal of Applied Chemistry, 2007, Vol. 80, No. 8, pp. 1284–1288. © Pleiades Publishing, Ltd., 2007.
Original Russian Text © I.I. Goncharik, F.F. Mozheiko, A.I. Voitenko, T.P. Kulikova, 2007, published in Zhurnal Prikladnoi Khimii, 2007, Vol. 80, No. 8, pp. 1246–1250.

INORGANIC SYNTHESIS AND INDUSTRIAL INORGANIC CHEMISTRY

Foaming Activity of Foam Compounds Based on Hexadecylammonium Chloride and Sodium Carboxylates

I. I. Goncharik, F. F. Mozheiko, A. I. Voitenko, and T. P. Kulikova

Institute of General and Inorganic Chemistry, National Academy of Sciences of Belarus, Minsk, Belarus

Received May 25, 2006; in final form, June 2007

Abstract—Formation of R_1R_2 associates between hexadecylammonium chloride and sodium carboxylates (octanoate, laurate, and palmitate) was studied by IR spectroscopy and chemical methods, and their foaming activity was characterized.

DOI: 10.1134/S1070427207080046

In flotation concentration of sylvinite ores, aqueous solutions of higher aliphatic amine salts (cationic surfactants) are currently used as collectors. As applied to flotation of high-clayey sylvinite ores, aliphatic amine salts have such disadvantages as high adsorption affinity for clay minerals, toxicity, and insufficient availability. Therefore, to replace higher aliphatic amines or reduce their a consumption, search for new efficient and more available flotation agents and modifiers for amines is a topical issue. In this relation, promising reagents are mixed solutions of cationic and anionic surfactants. In solutions of cationic (aliphatic amine salts $R_1^+X^-$) and anionic (sodium carboxylates $R_2^-Y^+$) surfactants, the presence of donor–acceptor centers in their molecules enable formation of associates of the type $R_1^+R_2^-$, whose surface activity is considerably higher than that of the initial components [1]:

$$R_1^+X^- + R_2^-Y^+ \rightleftarrows R_1^+R_2^- + Y^+X^-.$$

Previously [2] we have studied the adsorption and foaming activities of a mixture of hexadecylammonium chloride (HDAC, cationic surfactant) and sodium carboxylates C_4–C_{12} (Na-CAS) in flotation of potassium ores.

It was demonstrated that the amount of the amine adsorbed on KCl crystals depends on the chain length of a carboxylate and its concentration in solution. Even at a 1 : 1 ratio of these components, the amine is totally adsorbed (to 96–97%) in the presence of short-chain sodium carboxylates (butanoate, pentanoate, and hexanoate). In the case of octanoate and adipate, present in a mixture in concentrations of 15 and 25%, only 70% of the amine is adsorbed on KCl crystals. As the carboxylate concentration decreases to 50%, the adsorption of the amine falls to 20%. The experiments on sorption of the amine on KCl crystals were carried out according to the procedure described in [3].

The results obtained in studying the flotation dressing of sylvinite ore with mixed solutions of octadecylammonium chloride (BATZ grade) and sodium carboxylates also demonstrated a high flotation efficiency of these mixtures. Mixtures of the amine with short-chain carboxylates (butanoate, pentanoate, and hexanoate) appeared to be the most effective, which is consistent with the adsorption data. These results were interpreted in terms of formation in these mixtures of $R_1^+R_2^-$ associates, which are more efficient hydrophobizing agents for the particles to be floated as compared to the individual components.

Here we report chemical and IR spectroscopic data confirming the association of sodium carboxylates with hexadecylammonium chloride, and also data on the foamig activity of the resulting associates.

The R_1R_2 associates were prepared as follows. A stoichiometric amount of HDAC as a 0.5% solution was added to aqueous sodium carboxylate (octanoate, laurate, oxalate, and adipate) solutions of certain concentrations. The resulting precipitate was filtered off (Schott filter no. 4), washed with cold water (5°C), transferred into a Petri dish, and dried initially in air and then over P_2O_5.

The chemical composition of the precipitates was determined by the HDAC content in them [3]. It was demonstrated that 1 : 1 and 1 : 2 associates are

formed with monobasic (octanoic, lauric) and dibasic (oxalic, adipic) carboxylic acid salts, respectively.

The association was also confirmed by IR spectra recorded on a UR-20 spectrophotometer using KBr technique. Figure 1 shows the absorption spectra of the precipitates separated from the solutions containing HDAC and sodium laurate or adipate (curves *1*, *3*), and also of the mixtures of the solid components (curves *2*, *4*). The spectra of the mixtures show absorption bands at 1390–1620 cm^{-1} due to ionized carbonyls and NH groups of amines (in-plane bending vibrations). The spectra of the precipitated solids (curves *1*, *3*) show a slight low-frequency shift of the COO^- and NH bands and the appearance of a new strong band at 1500 cm^{-1}, which can be considered an indirect evidence in favor of the association.

Thus, the IR spectroscopic and chemical data suggest the formation of R_1R_2 associates in mixed solutions of hexadecylammonium chloride and sodium carboxylates.

Among factors controlling the performance of surfactants as flotation agents is their foaming activity. Therefore, we studied the foaming activity of mixtures of HDAC with sodium carboxylates. It was demonstrated that the foaming activity depends on the nature and concentration of carboxylates (Table 1).

Table 1 shows that the foaming activity of the mixtures increases with the carboxylate concentration. Individual solutions of sodium concentrates do not form foams at concentrations indicated in Table 1. At an HDAC concentration of 2.4×10^{-4} M (no carboxylate additive), the foam layer height is 22 mm. In the presence of 0.28×10^{-4} and 1.21×10^{-4} M sodium pentanoate, the foam layer height increases to 38 and 45 mm, and in the presence of 0.42×10^{-4} and 0.9×10^{-4} M sodium octanoate, to 57 and 45 mm, respectively. With long-chain carboxylates (laurate, palmitate), even at their concentrations of 0.15×10^{-4} and 0.12×10^{-4} M, the foam layer height decreases from the initial 22 mm to 12 and 6 mm, respectively. Thus, the dependence of the foaming activity of the mixtures on the chain length of the carboxylates passes through a maximum corresponding to sodium octanoate.

Furthermore, we found that the foams formed in the presence of sodium pentanoate and octanoate are more stable than those obtained with an individual amine. For example, a foam obtained with the individual amine was broken in 1 h, whereas that formed in the presence of the carboxylate additives retained 44.7–84.2% of its initial height even after 2 h. The opposite effect was exerted by the long-chain (C_{12}–C_{16}) carboxylates. On introduction of sodium palmitate into the amine solution, the foam was practically totally broken in several minutes. Evidently, soluble R_1R_2 associates are formed, in the mixed solutions of the amine with short-chain carboxylates, and these associates, being adsorbed on the gas–liquid interface,

Table 1. Effect of sodium carboxylate additives on the foaming activity of hexadecylammonium chloride (2.4×10^{-4} M)

Carboxylate	Carboxylate concentration $c \times 10^4$, M	Foam layer height, mm		Foam stability, %
		initial	2 h after	
Pentanoate	–	22	–	–
	0.28	38	17	44.7
	1.21	45	20	44.0
	3.20	38	33	86.8
	7.20	27	20	74.0
Octanoate	0.42	57	33	57.9
	0.90	45	32	71.1
	1.80	38	32	84.2
Laurate	0.15	12	9	75.0
	0.30	15	75	50.0
	0.75	9	4	44.4
	0.80	8	4	50.0
Palmitate	0.12	6	–	–
	0.24	4	–	–
	1.20	–	–	–

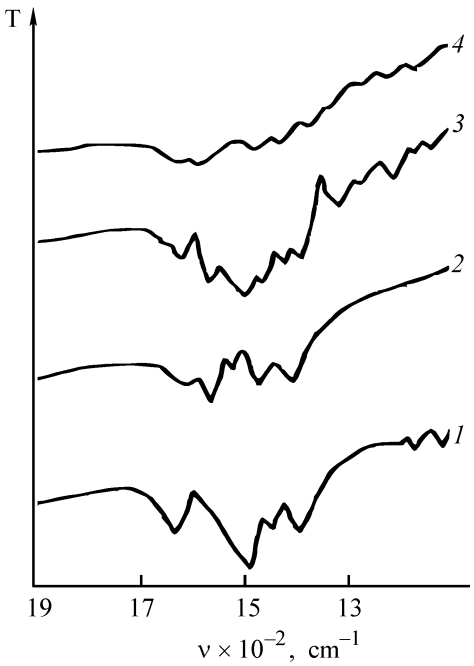

Fig. 1. IR spectra of precipitates separated from mixed solutions of HDAC with (*1*) sodium laurate and (*2*) sodium adipate, and of mechanical mixtures of the amine with (*3*) sodium laurate and (*4*) sodium adipate. (T) Transmission and (ν) wavenumber.

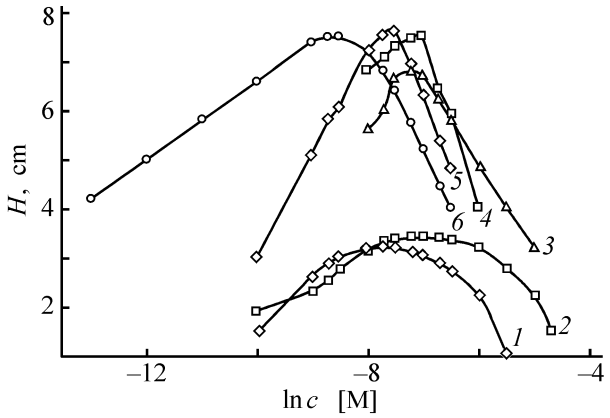

Fig. 2. Foaming activity H of mixtures of HDAC with (*1*, *2*) sodium laurate and (*3*, *6*) sodium pentanoate vs. the inorganic salt concentration c. Electrolyte: (*1*, *6*) $AlCl_3$, (*2*, *3*) KCl, (*4*) NaCl, and (*5*) $CaCl_2$.

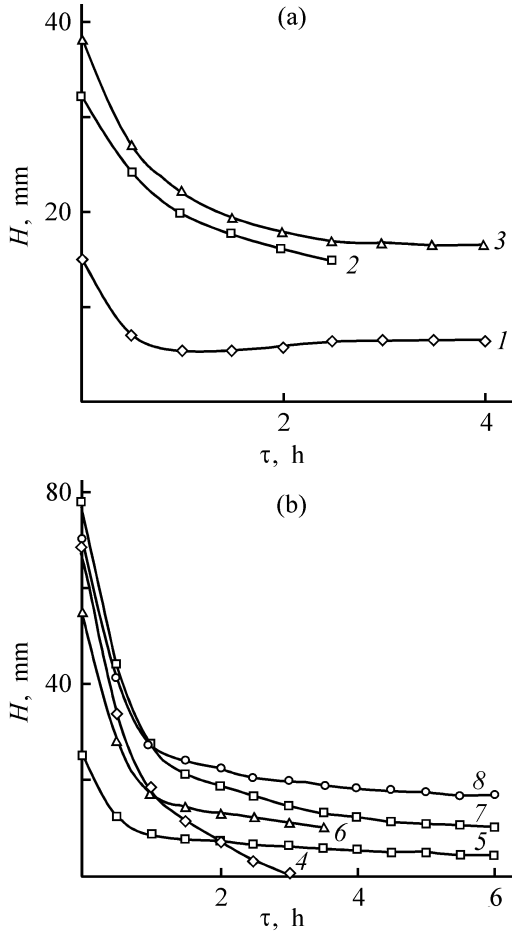

Fig. 3. Kinetic curves of break of foams formed by hexadecylammonium chloride in the presence of (a) sodium laurate and (b) sodium pentanoate (*1*, *5*) without and (*2–4*, *6–8*) with electrolyte additives. (H) Foam layer height and (τ) time. Salt concentrations (M): (*2*) 2.34×10^{-4} ($AlCl_3$), (*3*) 6.7×10^{-4} (KCl), (*4*) 4.7×10^{-5} ($AlCl_3$), (*6*) 2.25×10^{-4} ($CaCl_2$), (*7*) 6.7×10^{-4} (NaCl), and (*8*) 8.5×10^{-4} (KCl).

form saturated adsorption layer of increased mechanical strength, thus enhancing the foaming activity of the reagents. In the case of long-chain carboxylates, the associates are poorly soluble, and their precipitation decreases the surfactant concentration at the interface and thus diminishes the foaming. Therefore, long-chain carboxylates, such as sodium laurate and palmitate, serve as defoaming agents.

Since many industrial processes occur in the presence of inorganic salts, it was of interest to examine their effect on the foaming activity of solutions containing HDAC and sodium carboxylates. It is well known that the adsorption of ionic surfactants at the solution–air interface increases in the presence of electrolytes, which is due to partial dehydration of the polar groups, compaction of the diffusion part of the electrical double layer, caused by the transfer of a part of counterions to the Stern layer, and weakening of the electrostatic repulsion between the surfactant molecules. It is a common knowledge that properties of ionic surfactants are most strongly affected by counterions. Therefore, in studying the electrolyte effects, we used salts with cations of varied nature and charge, but with the same anion (KCl, NaCl, $CaCl_2$, and $AlCl_3$) (Fig. 2).

Figure 2 shows that addition of small amounts of the salts (0.23×10^{-5}–8.5×10^{-4} M) to the mixed HDAC–carboxylate solutions enhances the foaming. However, further increase in the electrolyte concentration decreases the foaming, depending on the nature and concentration of both carboxylates and electrolytes.

For example, in the system HDAC–sodium pentanoate, the inorganic additives have a stronger effect than in the system with sodium laurate (Fig. 2). In the former case, at a NaCl concentration of 6.7×10^{-4} M, the foam height was 77 mm, whereas in the latter case, it was only 30 mm, against 20 and 15 mm without electrolyte additive, respectively. A similar effect was also observed with the other salts. It should be pointed out that, with increasing charge of the cation, the maximal foam layer height was observed at a lower electrolyte concentration: 4.7×10^{-5}, 2.25×10^{-4}, 6.7×10^{-4}, and 8.5×10^{-4} M for $AlCl_3$, $CaCl_2$, NaCl, and KCl, respectively. Furthermore, electrolyte additives considerably increase the foam stability, depending on their nature (Fig. 3). In the system HDAC–sodium pentanoate, addition of NaCl, KCl, and $CaCl_2$ increased the foam layer height after 3 h from 7 mm to 25, 17, and 12 mm, respectively (Fig. 3a). In the presence of $AlCl_3$, the foam was broken virtually totally in this time (molar ratio HDAC : car-

Table 2. Effect of inorganic electrolyte concentration on W_0 and K_1 for foams obtained in HDAC–sodium carboxylate systems (HDAC : carboxylate = 0.9 : 0.1 at a total concentration of 2.24 M)

Carboxylate	NaCl			KCl			$AlCl_3$		
	$c_{NaCl} \times 10^4$, M	$W_0 \times 10^3$, m s^{-1}	K_1	$c_{KCl} \times 10^4$, M	$W_0 \times 10^3$, m s^{-1}	K_1	$c_{AlCl_3} \times 10^4$, M	$W_0 \times 10^3$, m s^{-1}	K_1
Pentanoate	–	20.0	0	–	20.0	0	–	20.0	0
	4.25	7.0	55.8	8.5	5.0	56.9	0.23	7.0	57.6
	6.7	5.0	57.6	16.8	8.0	56.9	0.94	7.0	57.6
	21.4	7.0	57.6	33.5	5.0	56.9	2.3	10.0	59.3
	42.7	14.0	57.6	100.7	5.0	57.1	23.0	8.0	59.8
	–	–	–	167.0	5.0	53.0	93.0	12.5	55.8
Caprylate	–	12.5	59.0	–	12.5	59.0	–	–	–
	0.85	10.0	57.3	6.7	9.0	64.4	–	–	–
	2.20	9.0	63.8	13.4	6.0	78.6	–	–	–
	8.5	8.0	59.8	20.1	8.0	65.2	–	–	–
	42.5	25.0	67.2	33.5	8.0	63.0	–	–	–
	–	–	–	67.0	25.0	56.8	–	–	–
Laurate	–	–	–	–	28.0	56.0	–	28.0	56.0
	–	–	–	0.45	25.0	57.4	0.067	6.0	67.2
	–	–	–	1.3	25.0	57.6	18.75	14.0	56.0
	–	–	–	3.35	16.0	58.4	–	–	–
	–	–	–	6.4	19.0	54.4	–	–	–
	–	–	–	33.5	17.0	60.8	–	–	–
	–	–	–	167.0	17.0	52.4	–	–	–

boxylate = 0.9 : 0.1 at a total concentration of 2.24 M). In the system HDAC–sodium laurate (Fig. 3b), inorganic electrolytes also improved the foam stability.

As can be seen, low electrolyte concentrations favor the formation of a denser adsorption layer of the surfactant at the gas–liquid interface, thus increasing the foaming activity of the solutions and foam stability. As the inorganic salt concentration is raised further, the surfactant is precipitated, and its concentration in the solution decreases. As a result, the foaming activity and foam stability decrease. The foam breakdown is also preceded leakage of the fluid from the foam (foam syneresis). The foam syneresis is characterized quantitatively by the increase in the volume of a liquid below the foam–solution interface in a fixed period. The time dependence of the fluid leakage rate from the foam can be described by an equation derived in [4]:

$$(K_1/2)\tau = \tau/V_1 - 1/W_0,$$

where K_1 is a constant; V_1, volume of the fluid leaked from the foam per unit cross section of a vessel (m); W_0, initial leakage rate (m s^{-1}); and τ, time (s).

The applicability of this equation to foams was confirmed in [4–6] and in this study. We examined the effect of the electrolyte (KCl, NaCl, $AlCl_3$) concentration on the leakage rate of a fluid from the foams in the systems amine–sodium pentanoate and amine–sodium laurate (HDAC:carboxylate = 0.9 : 0.1 at a total concentration of 2.24 M) (Table 2).

Table 2 shows that introduction of the electrolytes into the systems containing short-chain carboxylates (pentanoate, caprylate) decreases the leakage rate from 2×10^{-2} to 7×10^{-3} m s^{-1}. In the systems with long-chain carboxylates, this effect was insignificant (Table 2). These results are consistent with data presented in Fig. 3, i.e., the higher the foam layer height, the lower the leakage rate from the foam.

Finally, foam formation in HDAC solutions can be controlled by adding appropriate sodium carboxylates and inorganic electrolytes. The HDCA–sodium carboxylate systems can be used as foaming reagents in flotation dressing of potassium ores.

CONCLUSIONS

(1) IR spectroscopic and chemical data suggest that R_1R_2 associates are formed in aqueous solutions

containing hexadecylammonium chloride and sodium carboxylates.

(2) Addition of short-chain sodium carboxylates (pentanoate, octanoate) to hexadecylammonium chloride increases the foaming activity and foam stability.

(3) Introduction of inorganic electrolytes (KCl, NaCl, $CaCl_2$, and $AlCl_3$) into the amine–sodium carboxylate–water system decreases the initial rate of fluid leakage from the foam, which is consistent with data on the effect they exert on the foaming activity.

ACKNOWLEDGMENTS

The study was financially supported by the Belarusian Foundation for Basic Research (project Kh06-182).

REFERENCES

1. Lucasse-Reynders, E.H., *J. Colloid Interface Sci.*, 1982, vol. 85, no. 1, pp. 178–186.
2. Goncharik, I.I., Mitina, T.D., Dikhtievskaya, L.V., et al., *Zh. Prikl. Khim.*, 1998, vol. 71, no. 11, pp. 1803–1808.
3. Silverstein, R.M., *Anal. Chem.*, 1983, vol. 35, no. 2, pp. 154–167.
4. Kruglyakov, P.M. and Taube, P.R., *Zh. Prikl. Khim.*, 1965, vol. 38, no. 7, pp. 1514–1519.
5. Kruglyakov, P.M. and Taube, P.R., *Zh. Prikl. Khim.*, 1966, vol. 39, no. 7, pp. 1499–1504.
6. Kruglyakov, P.M. and Taube, P.R., in *Uspekhi kolloidnoi khimii* (Advances in Colloid Chemistry), Moscow: Nauka, 1973, pp. 304–308.

ISSN 1070-4272, Russian Journal of Applied Chemistry, 2007, Vol. 80, No. 8, pp. 1289–1294. © Pleiades Publishing, Ltd., 2007.
Original Russian Text © B.V. L'vov, V.L. Ugolkov, 2007, published in Zhurnal Prikladnoi Khimii, 2007, Vol. 80, No. 8, pp. 1251–1255.

PHYSICOCHEMICAL STUDIES OF SYSTEMS AND PROCESSES

Use of Potassium Permanganate as a Possible Kinetic Standard in Thermal Analysis

B. V. L'vov and V. L. Ugolkov

St. Petersburg State Polytechnic University, St. Petersburg, Russia
Institute of Silicate Chemistry, Russian Academy of Sciences, St. Petersburg, Russia

Received June 25, 2007

Abstract—Analysis of the mechanism of congruent dissociative evaporation of solid substances led to a suggestion that potassium permanganate can be used as a possible kinetic standard in thermal analysis.

DOI: 10.1134/S1070427207080058

A search for an appropriate kinetic standard for studies in thermal decomposition of solid substances and their melts is an interlaboratory scientific project initiated about 20 years ago by the Committee for kinetics at the International Confederation for Thermal Analysis and Calorimetry [1]. In experts' opinion [2], the main requirements to an ideal kinetic standard are the following.

(1) The reaction corresponding to thermal decomposition should be irreversible.

(2) The absolute value of the enthalpy of the reaction should be low to restrict the effects of self-cooling or self-heating of the reagent.

(3) The decomposition temperature should not be too high to preclude errors in maintaining this temperature.

(4) The reagent should not react with the ambient atmosphere and the decomposition rate is to be pressure-independent.

(5) The reaction should be independent from sample preparation techniques and particle size.

(6) Relative changes in mass in the course of decomposition should be sufficient for use of small samples.

As demonstrated by the results of interlaboratory tests, summarized by the Committee for kinetics in 1994 [2], the reaction of $Li_2SO_4 \cdot H_2O$ dehydration, chosen (rather arbitrarily) as a possible kinetic standard, proved to be absolutely unsuitable for this purpose. This primarily refers to the fulfillment of requirements 1 and 3–5. Depending on the conditions of thermal decomposition (in particular, presence of H_2O vapor), the parameter E in the Arrhenius equation varied within the range 57–220 kJ mol^{-1}. The negative outcome of these tests strongly diminished the interest in this problem. In the opinion of a participant of the project (D. Dollimor [2]), "the search for the kinetic standard may prove unfruitful because of the dependence of kinetic measurements on reaction pathways and on the effect of various factors on these pathways."

In contrast to the previously employed purely empirical search for a kinetic standard, a new thermochemical approach to the mechanism and kinetics of thermal decomposition processes, developed in the last decade and summarized in the monographs [3, 4], opens up an opportunity for its purposeful choice based on a preliminary theoretical analysis. Let us consider reactions suitable for this purpose. The most important of the above requirements to an ideal kinetic standard are conditions 1 and 4, which predetermine the irreversibility of the reaction and independence of the decomposition rate from the pressure and composition of the gaseous medium. These requirements can only be satisfied in those cases when all the primary products are in states that differ from their equilibrium states. To these cases belong, in particular, reactions of the general form

$$R(s) \rightleftarrows A(g)^* + B(g)^* \rightarrow A(s) + B(g), \qquad (1)$$

where $A(g)^*$ is a poorly volatile product condensed at the instant of decomposition, and $B(g)^*$ is a gaseous

product that is in a nonequilibrium state at the decomposition temperature, e.g., in the form of free O or N atoms which undergo association at the instant of decomposition to give equilibrium molecules O_2 and N_2.

Under these conditions, the partial pressures of the primary products $A(g)^*$ and $B(g)^*$ and, consequently, the decomposition rate of the reagent R(s), too, depend only on the stoichiometry and thermochemical characteristics of the reaction and should be independent of the composition and pressure of the gas in the reactor. An additional condition for constancy of the decomposition rate is the inertness of solid (equilibrium) decomposition products in the presence in the reactor of O_2, H_2, CO_2, H_2O vapor, etc.

Of particular interest among those classes of substances that have been studied so far and decompose to give oxygen and nitrogen in the atomic form [3, 4] are lead superoxide, which decomposes by the scheme

$$Pb_3O_4(s) \rightleftarrows 3PbO(g)\downarrow + O, \quad (2)$$

and, as first noted in the monograph [4], potassium, rubidium, and cesium permanganates. These permanganates have a crystal structure of barite ($BaSO_4$), which decomposes by the scheme [5, 6]

$$BaSO_4 \rightleftarrows BaO(g)\downarrow + SO_2 + O. \quad (3)$$

Taking into account that $BaSO_4$ and the permanganates mentioned above have the same crystal structure, we could expect that the primary stage of their decomposition also occurs with evolution of atomic oxygen:

$$2KMnO_4(s) \rightleftarrows K_2O(g) + 2MnO(g) + 5O \rightarrow K_2MnO_4(s) + MnO_2(s) + O_2. \quad (4)$$

All attempts of the authors of this study to use lead oxide as a kinetic standard failed. Experimental studies revealed that a reverse process, PbO oxidation by oxygen to Pb_3O_4, is superimposed on the process of Pb_3O_4 decomposition, which leads to a decrease in the decomposition rate in the presence of oxygen. A certain limitation on use of Pb_3O_4 is the only slight change (~2.3 wt %) in the mass of the reagent in reaction (2).

The thermal decomposition of potassium permanganate has been the subject of a huge number of studies. During 190 years after the appearance of the first publication in 1817 [7], the mechanism and kinetics of its decomposition have been analyzed by virtually all authoritative laboratories in the world and, in particular, by the authors of [8–16]. Beginning from [7], the equilibrium (resultant) reaction has been represented by the scheme

$$10KMnO_4(s) \rightleftarrows 5K_2MnO_4(s) + 5MnO_2(s) + 5O_2, \quad (5)$$

which is equivalent to the scheme of reaction (4), or by the scheme

$$10KMnO_4(s) \rightleftarrows 3K_2MnO_4(s) + 7MnO_2(s) + 2K_2O(s) + 5O_2, \quad (6)$$

suggested by Rüdorf more than 100 years ago [8]. The difference between these schemes is in the relative amounts of solid products and free oxygen, whose amount varies in the range 10–12 wt %.

EXPERIMENTAL

The main goal of our experiments was to verify the expected independence of the decomposition rate of $KMnO_4$ from the composition and pressure of the gas in the reactor. For this purpose, we measured by isothermal thermogravimetry the absolute decomposition rate of $KMnO_4$ in argon (1 bar) and air (at a pressure of 1 and 4×10^{-4} bar). These data were used to calculate the molar enthalpy of the reaction.

The change in the mass of a sample in unit time, $\Delta m/\Delta t$, and its temperature were measured with a Netzsch STA 429 thermal analyzer. A finely crystalline potassium permanganate (of analytically pure grade) was ground in an agate mortar and compacted into pellets 5.0 mm in diameter and about 0.5 mm thick. The mass of the pellets varied within the range 19.8–20.9 mg. A pellet was placed in a corundum crucible with an inner diameter of 5.7 mm and height of 4.0 mm and the crucible was closed with a small plug of glass wool (~10 mg) to prevent discharge of sample particles upon heating. The rate of sample heating from the ambient to a final temperature varied within the range 493–504 K was 10 deg min^{-1}. The measurements were made in argon (at a pressure of 1 bar) and air (1 and 4×10^{-4} bar) under isothermal conditions. Depending on the temperature of the experiment, the time of complete decomposition (with the stage of heating and the induction period disregarded) was 90 to 50 min. Table 1 lists as an example the results obtained in measuring the absolute decomposition rate of $KMnO_4$ in argon at 493.6 K and calculated values of the molar enthalpy of the reaction.

Let us explain the main stages of the calculation (the calculation scheme was described in detail in [3, 4]). The input parameters automatically recorded by the instrument in the thermogram are the relative loss of mass by a sample, $\Delta m/m$, in a chosen time interval Δt between signal measurements. In this study, Δt was chosen to be 5 min, or 300 s. Hence we found using the apparent formulas the quantities $\Delta m/\Delta t = m_0(\Delta m/m)/\Delta t$ and $\Delta\alpha = (\Delta m/m)/0.11$, where m_0 is the initial mass of a sample and 0.11 is the average, for reactions (5) and (6), fraction of the gaseous product (O_2) with respect to the mass of the reagent. The degree of decomposition at the instant of measurement, α_m, was calculated by summing values of $\Delta\alpha$ during the period of time preceding the measurement, with account of the loss during the time elapsed from the instant of furnace heating to the beginning of measurements. The absolute decomposition rate of powdered samples was calculated by the formula [3, 4]

$$J_p = \frac{\Delta m/\Delta t}{2.8S_m} = \frac{\Delta m/\Delta t}{2.8S_0(1 - \alpha_m)^{1/2}}, \quad (7)$$

where 2.8 is the empirical factor that accounts for the difference in the decomposition rates of the powder and the single crystal; and S_0 and S_m are the effective surface areas of a sample at the beginning of the experiment and at the instant of measurement, respectively.

In our calculations, we took into account that the surface area of a sample decreases as a result of its partial decomposition. It was found experimentally that the relative decrease in area, S_m/S_0, is $(1 - \alpha_m)^{1/2}$. This dependence can be interpreted as resulting from a decrease in the effective area of a compacted pellet with its diameter ("contracting disc" model).

The molar enthalpy of the decomposition reaction was calculated by the third-law method. The equilibrium pressure of atomic oxygen [primary product of reaction (4)] was found using the Hertz–Langmuir equation [3, 4]:

$$P_{eqp} = \frac{(2\pi MRT)^{1/2}}{\gamma M} J_p, \quad (8)$$

where M is the molar mass of oxygen atoms; R, gas constant (8.3145 J mol^{-1} K^{-1}); and γ, conversion factor for recalculating the pressure from pascals to bars (10^5 Pa bar^{-1}), in which units thermodynamic calculations are carried out.

Further, we calculated, taking into account the number ν of moles of the reaction products and the coefficient δ that accounts for the congruent nature of the decomposition [3, 4], the equilibrium constant of reaction (4)

$$K_p = (P_{eqp})^{\nu}/\delta. \quad (9)$$

It was shown in [4] that the congruence factor is determined by the molar masses and stoichiometric coefficients for the decomposition products. For reaction (4), which involves three products (A, B, and C), this factor is given by

$$\delta_C = (\beta_A^C)^a(\beta_B^C)^b, \quad (10)$$

where

$$\beta_A^C = \frac{c}{a}\left(\frac{M_C}{M_A}\right)^{1/2}, \quad (11)$$

$$\beta_B^C = \frac{c}{b}\left(\frac{M_C}{M_B}\right)^{1/2}. \quad (12)$$

Substituting tabulated values of the molar masses of the products of this reaction and the corresponding stoichiometric coefficients ($a = 1$, $b = 2$, $c = 5$), we obtain $\delta = 2.907$.

The enthalpy of the reaction was calculated by the equation

$$\Delta_r H_T^0 = T(\Delta_r S_T^0 - R\ln K_p), \quad (13)$$

where $\Delta_r S_T^0$ is the entropy of the reaction.

Because of the poor reliability of the tabulated values of entropy for some components of reaction (4), we used the averaged value of the molar entropy $\Delta_r S_T^0/\nu$, equal to 160 ± 9 J mol^{-1} K^{-1} in the case of decomposition of the reactants to metal products in the molecular form [3, 4, 17].

As can be seen in Table 1, J_p remains virtually constant (within ±10%) and equal to 7.0 ± 0.7 mg m^{-2} s^{-1} during 45 min of decomposition (with Δm increasing from 0.3 to 0.9). The scatter of $\Delta_r H_T^0/\nu$ from the average value (146.2 ± 0.4 kJ mol^{-1}) is even narrower, ±0.3%.

The method we described was used to determine the absolute decomposition rates and molar enthalpies of the reaction in $KMnO_4$ decomposition under the conditions of all the experiments (Table 2). Analysis of the data obtained suggests the following.

(1) The presence of O_2 in the reactor (0.21 bar) in decomposition of the permanganate in air has no effect on the decomposition rate, which indicates that

Table 1. Results of determination of the absolute rate and molar enthalpy of decomposition of a compacted $KMnO_4$ pellet in argon at 493.6 K (m_0 = 20.9 mg, S_0 47.1 mm^2)

Δt, min	$\Delta m/m$	$\Delta m/\Delta t$, μg s^{-1}	$\Delta\alpha$	α_m	$(1-\alpha_m)^{1/2}$	$J_p \times 10^6$, kg m^{-2} s^{-1}	P_{eqp}, bar	K_p, bar^8	$\ln K_p$	$\Delta_r H_T^0/\nu$, kJ mol^{-1}
0	0.0040	0.279	0.036	0.036	0.982	2.15	2.73×10^{-8}	1.06×10^{-61}	–140.4	151.0
5	0.0026	0.181	0.023	0.059	0.970	1.42	1.80×10^{-8}	3.74×10^{-63}	–143.7	152.7
10	0.0073	0.509	0.066	0.125	0.935	4.12	5.23×10^{-8}	1.93×10^{-59}	–135.2	148.3
15	0.0098	0.683	0.088	0.214	0.887	5.48	7.41×10^{-8}	3.11×10^{-58}	–132.4	146.9
20	0.0104	0.725	0.094	*0.307*[*]	0.832	*6.60*	*8.37 × 10^{-8}*	8.32×10^{-58}	–131.4	*146.4*
25	0.0098	0.683	0.088	*0.395*	0.777	*6.66*	*8.45 × 10^{-8}*	8.92×10^{-58}	–131.6	*146.4*
30	0.0089	0.620	0.080	*0.476*	0.724	*6.49*	*8.24 × 10^{-8}*	7.30×10^{-58}	–131.6	*146.5*
35	0.0086	0.599	0.077	*0.553*	0.668	*6.80*	*8.62 × 10^{-8}*	1.05×10^{-57}	–131.2	*146.3*
40	0.0087	0.606	0.078	*0.632*	0.607	*7.57*	*9.61 × 10^{-8}*	2.49×10^{-57}	–130.3	*145.8*
45	0.0084	0.585	0.076	*0.707*	0.541	*8.20*	*1.04 × 10^{-7}*	4.72×10^{-57}	–129.7	*145.5*
50	0.0073	0.509	0.066	*0.773*	0.476	*8.09*	*1.03 × 10^{-7}*	4.25×10^{-57}	–129.8	*145.6*
55	0.0058	0.404	0.052	*0.825*	0.418	*7.33*	*9.30 × 10^{-8}*	1.92×10^{-57}	–130.6	*146.0*
60	0.0044	0.307	0.040	*0.865*	0.368	*6.32*	*8.02 × 10^{-8}*	5.90×10^{-58}	–131.8	*146.6*
65	0.0038	0.265	0.034	*0.899*	0.318	*6.32*	*8.02 × 10^{-8}*	5.88×10^{-58}	–131.8	*146.6*
70	0.0028	0.195	0.025	0.924	0.275	5.38	6.82×10^{-8}	1.61×10^{-58}	–133.1	147.2

[*] Values of the parameters in the range of the steady decomposition of the sample are italicized.

Table 2. Results of determination of the absolute rate and molar enthalpy of the reaction in thermal decomposition of $KMnO_4$ in various media

Medium	P, bar	T, K	m_0, mg	$\Delta\alpha$	J_p, mg m^{-2} s^{-1}	P_{eqp}, bar	$\Delta_r H_T^0/\nu$, kJ mol^{-1}
Argon	1	493.2	20.1	0.29–0.81	5.6 ± 0.4	7.2×10^{-8}	146.9 ± 0.3
	1	493.6	20.9	0.31–0.90	7.0 ± 0.7	8.9×10^{-8}	146.2 ± 0.4
Air	1	494.3	20.5	0.31–0.86	8.5 ± 0.9	1.1×10^{-7}	145.6 ± 0.4
	1	499.0	20.3	0.30–0.75	8.8 ± 0.6	1.1×10^{-7}	146.8 ± 0.3
	1	504.0	19.8	0.36–0.85	12.1 ± 2	1.7×10^{-7}	145.3 ± 0.6
	4×10^{-4}	495.5	20.4	0.33–0.88	11.5 ± 2	1.5×10^{-7}	144.8 ± 0.9
	4×10^{-4}	500.3	20.1	0.36–0.95	18.2 ± 6	2.3×10^{-7}	144.3 ± 1.3

oxygen is released in the form of free atoms. This conclusion is confirmed by the results of [16].

(2) A decrease in the pressure of a foreign gas (air) in the reactor by more than three orders of magnitude has nearly no effect on the decomposition rate. A minor increase in the decomposition rate and a decrease in the molar enthalpy (by approximately 2 kJ mol^{-1}), made noticeable by the high precision of the third-law method, may be due to a decrease in the thermal conductivity of the medium, which accelerates the exothermic reaction.

(3) The steady-state decomposition mode is preserved as α varies from 0.3 to 0.9.

(4) An increase in temperature within the range 493–504 K is accompanied by a monotonic rise in the decomposition rate of $KMnO_4$ by approximately a factor of 2–3, but has virtually no effect on the molar enthalpy. The average value of $\Delta_r H_T^0/\nu$ over all the seven experiments is 145.7 ± 1.0 kJ mol^{-1}. The error characterizing the deviation of the results of separate experiments from the average exceeds by only a factor of 1.5–2 the error in determining these values in a single run.

(5) The average value of the molar enthalpy of the reaction (145.7 ± 1.0 kJ mol^{-1}), calculated by the third-law method, agrees with the results obtained in other studies by the method of Arrhenius plots (kJ mol^{-1}): 150 ± 12 [11], 142 ± 13 [13], 165 ± 10 [15], and 143 [16]. The value of the parameter E, found from our data (Table 2) by the sec-

ond-law method (see figure), is 151 kJ mol^{-1}. Because the temperature range of our measurements is narrow (only 10°), the ratio $T_{max}/\Delta T \approx 50$. This results in that the random determination error is 50 times that for the third-law method and reaches 50 kJ mol^{-1} [18].

An analysis of the data obtained in [12, 15, 16] led us to certain additional conclusions in favor of the choice of $KMnO_4$ as a kinetic standard. Erofeev and Smirnova convincingly demonstrated [12] that the kinetic decomposition curves are close for unground crystals and thoroughly ground powders. It was shown that "grinding of a preparation does not lead to any significant change in the kinetics of thermal decomposition of potassium permanganate" [12]. In particular, the maximum degree of decomposition is $\alpha = 0.47$ for the unground preparation (average over eight experiments) and $\alpha = 0.51$ for the ground sample (six runs). Thus, the effect of the particle size on the decomposition rate should not be strong (requirement 5 to the kinetic standard). These observations are confirmed by the data obtained by Brown and coworkers [15], who found no differences in the rates and molar enthalpies of the reactions for freshly prepared $KMnO_4$ crystals (grown from solution) and ground powders. The only distinction consisted in that the induction period decreased (by 10–15 min) for ground preparations. Another important result of [15] was the conclusion that the H_2O vapor does not affect (at pressures of up to 3.5 Torr) the kinetics of $KMnO_4$ decomposition.

Herbstein and co-authors demonstrated [16] by an exquisite experiment with a mixture of $KMnO_4$ crystals labeled with oxygen isotopes (O^{16} and O^{18}) that oxygen evolving as a result of decomposition (analyzed by mass-spectrometry) is composed of a 1 : 1 : 2 mixture of O_2^{32}, O_2^{36}, and O_2^{34}. The formation of O_2^{34} molecules indicates that oxygen is primarily released as free O^{16} and O^{18} atoms, which associate upon mutual collisions into O_2^{34} molecules. The same conclusion was made on the basis of a more complex decomposition mechanism by the authors of [16].

The present study should be regarded as only the beginning of a deeper research, which will be extended to single-crystal $KMnO_4$ samples, other media (in particular, H_2 and CO_2), various thermal analyzers, and measurement techniques (including those of nonisothermal nature). Of particular interest is interpretation of the by no means apparent exothermic nature of the $KMnO_4$ decomposition process, revealed by DTA and DSC [16].

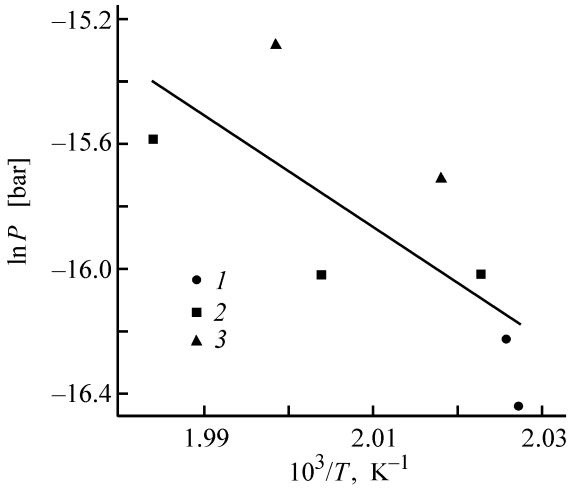

Logarithm of the equilibrium pressure P of atomic oxygen vs. inverse temperature for decomposition of a $KMnO_4$ pellet in various media. $y = -18.14x + 20.589$; $E = 150.8$ kJ mol^{-1}; $r^2 = 0.5571$. (*1*) Argon, (*2*) air (1 bar), and (*3*) air (4×10^{-4} bar).

CONCLUSIONS

(1) The assumption that the reaction of $KMnO_4$ decomposition can be used as a kinetic standard in thermal analytical measurements, made on the basis of a theoretical analysis of the mechanism of congruent dissociative evaporation of solid substances, was confirmed by the results of preliminary thermochemical measurements.

(2) It was shown that the molar enthalpy of the corresponding reaction, found by the third-law method, remains unchanged (145.7 ± 1.0 kJ mol^{-1}) irrespective of the composition (air, argon) and pressure (1 and 4×10^{-4} bar) of the medium.

ACKNOWLEDGMENTS

The authors are grateful to A.K. Galwey for the suggestion to use glass wool to preclude discharge of preparation particles from a crucible in the course of decomposition.

REFERENCES

1. Flynn, J.H., Brown, M.E., and Šestak, J., *Thermochim. Acta*, 1987, vol. 110, pp. 101–112.
2. Brown, M., Flynn, R.M., and Flynn, J.H., *Thermochim. Acta*, 2995, vol. 256, pp. 477–483.
3. L'vov, B.V., *Termorazlozhenie tverdykh i zhidkikh veshchestv* (Thermal Decomposition of Solid and Liquid Substances), St. Petersburg: Politekhn. Univ., 2006.

4. L'vov, B.V., *Thermal Decomposition of Solids and Melts*, Berlin: Springer, 2007.
5. L'vov, B.V. and Novichikhin, A.V., *Thermochim. Acta*, 1997, vol. 290, pp. 239–251.
6. L'vov, B.V. and Ugolkov, V.L., *Thermochim. Acta*, 2004, vol. 411, pp. 73–79.
7. Chevillot, P.E. and Edwards, W.E., *Ann. Chim. Phys.*, 1817, vol. 4, pp. 287–297.
8. Rüdorf, G., *Z. Anorg. Chem.*, 1901, vol. 27, pp. 58–61.
9. Hinshelwood, C.N. and Bowen, E.J., *Proc. Roy. Soc. A.*, 1921, vol. 99, pp. 203–212.
10. Roginskii, S.Z., *Zh. Fiz. Khim.*, 1938, vol. 12, pp. 427–444.
11. Prout, E.G. and Tompkins, F.C., *Trans. Faraday Soc.*, 1944, vol. 40, pp. 488–498.
12. Erofeev, B.V. and Smirnova, I.I., *Zh. Fiz. Khim.*, 1952, vol. 26, pp. 1233–1243.
13. Hill, R.A.W., Richardson, R.T., and Rodger, B.W., *Proc. Roy. Soc.*, London, 1966, vol. A291, pp. 208–211.
14. Boldyrev, V.V., Voronin, A.P., Nevolina, T.A., and Marusin, V.V., *Zh. Neorg. Khim.*, 1977, vol. 22, pp. 2179–2182.
15. Brown, M.E., Galwey, A.K., Mohamed, A.M., and Tanaka, H., *Thermochim. Acta*, 1994, vol. 235, pp. 255–270.
16. Herbstein, F.H., Kapon, M., and Weissman, A., *J. Therm. Anal.*, 1994, vol. 41, pp. 303–322.
17. L'vov, B.V., *Thermochim. Acta*, 2004, vol. 424, pp. 183–199.
18. L'vov, B.V., *J. Therm. Anal. Calorim.*, 2005, vol. 79, pp. 151–156.

ISSN 1070-4272, Russian Journal of Applied Chemistry, 2007, Vol. 80, No. 8, pp. 1295–1299. © Pleiades Publishing, Ltd., 2007.
Original Russian Text © I.V. Khoruzhii, G.F. Klyakin, V.A. Taranushich, V.I. Lachin, 2007, published in Zhurnal Prikladnoi Khimii, 2007, Vol. 80, No. 8, pp. 1256–1260.

PHYSICOCHEMICAL STUDIES OF SYSTEMS AND PROCESSES

A Study of the Electrothermal Method for Control over Combustion Velocity under Atmospheric Pressure of Energetic Condensed Systems Based on Ammonium Nitrate

I. V. Khoruzhii, G. F. Klyakin, V. A. Taranushich, and V. I. Lachin

South-Russian State Technical University, Novocherkassk, Rostov-on-Don oblast, Russia

Received January 11, 2007

Abstract—Experimental results obtained in the initial stage of studies of the electrothermal method for control over the combustion velocity under atmospheric pressure of energetic condensed systems based on an ammonium nitrate oxidizing agent for use in controllable solid-fuel power units are presented.

DOI: 10.1134/S107042720708006X

A topical field of research in aerospace technology still is, together with the development of new formulations for energetic condensed systems (ECS), a search for promising methods for physical control over working processes in solid-fuel gas-generating installations whose operation is independent of the hydrodynamic conditions in the combustion chamber and energy characteristics of the fuels used [1].

The method suggested in [2–4] is based on the fact that, under normal conditions, the composite solid fuel (CSF) is an insulator and the condensed phase (c-phase) of the reaction (combustion) zone has a high electrical conductivity because of the presence of components in the liquid phase, e.g., oxidizing agents (nitrates or perchlorates of alkali metals) or molten metals, or presence of free carbon on the ECS combustion surface with a negative oxygen balance. Passing an electric current through the reaction zone of the c-phase will lead to a rise in temperature and, in accordance with the Arrhenius law, to a change in the kinetics of the initial stages of oxidation reactions, and primarily to acceleration of rate-determining reactions or diffusion processes in heterogeneous systems, with the resulting increase in the combustion velocity.

To implement this method for control over the combustion velocity, a set of metallic electrodes is built in the solid-fuel charge in the combustion chamber. These electrodes provide a permanent contact between the conducting zone and a controllable power source, via which an electric current is passed through the reaction zone of ECS. All other conditions (chemical composition, initial temperature of the fuel, temperature and pressure in the chamber, etc.) being the same, the decomposition rate of the condensed phase will be a function of the current flowing through the electrically conducting layer. As the fuel combustion front moves and the electrodes in the form of thin metallic foil or a grid pass into the flame zone, they can burn out at the interface between the condensed and gaseous phases, i.e., can be involved in chemical reactions as a fuel.

EXPERIMENTAL

We used in our experiments model formulations (CSF) with edge burning, based on ammonium nitrate (AN) and ammonium perchlorate (APC) taken in various mass ratios. The fraction of the binder, ED-20 epoxy resin with urotropin as curing agent, was the same and equal to 10%. To prepare a charge, dried fractions of the oxidizing agents with 100–200-μm particles were mechanically mixed with the binder and then the fuel mass (20–25 g) was placed in special rectangular cassettes ($21 \times 15 \times 50$ mm) and compacted under a pressure of 8 ± 0.5 MPa. After that the binder was cured at 75–80°C for 18–20 h. The average combustion surface area of the samples was 3.2 cm^2.

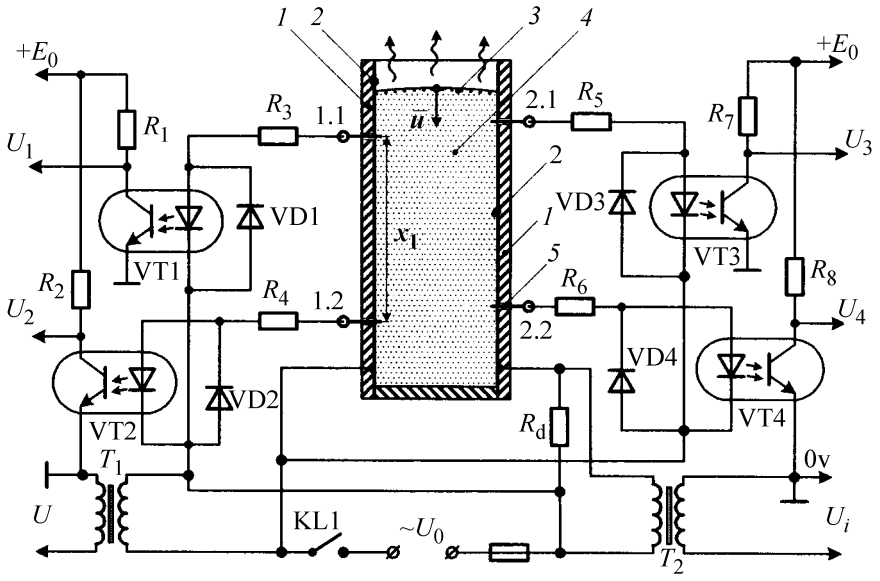

Fig. 1. Measuring unit of the experimental installation. (*1*) Charge case, (*2*) metallic foil, (*3*) combustion surface (front), (*4*) fuel mass, (*5*) electrodes (1.1, 1.2, 2.1, 2.2) of the combustion front position sensor; u is the motion velocity of the combustion front.

The procedure used to measure the charge combustion velocity [5] and the current and voltage in the reaction zone of ECS is schematically illustrated by Fig. 1. The two opposite sides of the dielectric case are made of plates of foil-clad textolite *1*, whose copper layers *2* face the fuel mass *4* and are connected to an electric voltage source ($\sim U_0$). The plates have apertures into which 0.4-mm-thick electrodes *5* are mounted so that they are insulated from the copper foil. The distances x_n between the electrodes were measured with an MBS-10 microscope. Thus, the chamber design is that of a flat capacitor. Under normal conditions, in the absence of adsorbed moisture on the open surface of the charges, the fuel masses have a resistance exceeding 20 MΩ (measured with V7-38 meter), which probably corresponds to a resistivity close to that of the binder.

In the course of combustion, the moving front of the heated electrically conducting reaction zone of the condensed phase of the fuel, having a thickness of about 0.1 mm, successively passes across the wire electrodes, which become connected to the voltage source ($\sim U_0$) at these instants of time, with the result that the optoelectronic switches VT1–VT4 are opened. When finding themselves in the flame zone, the electrodes melt and burn-out together with the case. The distances between the corresponding pairs of electrodes and the response instants of the switches VT are used to calculate the average combustion velocities on two sides of the charge. The choice of the number and positions of the electrodes is determined by the goals of an experiment.

Because the combustion of ECS may be rather fast, all the parameters being measured are recorded on-line with a computer connected via a multichannel analog data input interface (L-264 manufactured by L-card Co.), with the subsequent processing of the oscillograms with a special software [6]. The procedure used to determine the combustion velocity of ECS, which employs the electrical conductivity of the reaction zone, has a faster response as compared with the classical method of burning-out metallic threads, introduces the minimum perturbations into the combustion process, but is only applicable to measurements of comparatively steady-state processes along short control distances. Its application is reasonable in the absence of special acoustic (ultrasound) or optical measuring installations.

The velocity u of CSF combustion under the action of an electric current was measured at atmospheric pressure by the two-factor scheme: $u = F(\chi, U_x)$, where χ is the chemical composition of ECS, and U_x is the voltage applied to the charge. Five series of experiments with varied chemical composition (see table) were carried out, with 6–8 runs in each series at different effective ac (50 Hz) voltages in the range 2–235 V. All other factors affecting the combustion velocity were maintained constant. The calculation was made using the following for-

Sample composition and voltage ranges

Sample no.	Content of components χ^*, %	Density** $\rho \times 10^{-3}$, kg m^{-3}	ΔU_x, V
1	90 NA + 10 ED20	1.48	50–170
2	85 NA + 5 PBC + 10 ED20	1.51	2–235
3	90 [75 NA + 25 APC] + 10 ED20	1.52	30–200
4	90 [50 NA + 50 APC] + 10 ED20	1.56	50–235
5	90 [25 NA + 75 APC] + 10 ED20	1.60	2–200

* PBC is potassium bichromate.

** At a densification factor of 0.9.

mulas: $U_x = U_0 - U_{rd}$, voltage applied to the charge (V); $I = U_{rd}/R_d$, current in the reaction zone of the c-phase of ECS (R_d = const) (A); $R_x = U_x/I$, resistance of the reaction zone (Ω); $N = IU_x = I^2R_x = U_x^2/R_x$, electric power dissipated in the reaction zone (W); $Q = N/m''$, specific energy expenditure for control over the mass expenditure (kJ kg^{-1}); and $m'' = \rho Su$, mass (per-second) expenditure of the fuel (kg s^{-1}), where S is the combustion surface area; ρ, ECS density; and u, combustion velocity.

The experimental results we obtained are shown in Figs. 2–6. The approximating straight lines are plotted using the least-squares method. The measurement errors are mostly due to the scatter of physicochemical parameters of separate samples, which is due to their preparation technique.

Figures 2 and 3 show how the electric voltage and current affect the combustion velocity of composite solid fuels. The maximum increase in the combustion velocity (by a factor of 4.5) in the voltage range studied was observed for the [75 AN + 25 APC] fuel. The current and, accordingly, the thermal power released in the reaction zone is determined by its active resistance.

The numerical values of the resistances of the reaction zones, related to the geometric dimensions of the combustion surface (21 × 15 mm), can be found from the slopes of the straight lines in Fig. 4. It can be seen that the conductivity of the reaction zones decreases as the mass fraction of ammonium perchlorate in the CSF becomes higher. The linear run of the current–voltage (I–V) characteristics suggests that the electrical conductivity of the reaction zone is described by the Ohm's law in the ranges of steady combustion of the fuels studied.

It was found that the heating of the reaction zone by the electric current leads to accelerated ignition (from an external flame source) and stable combustion of CSF of all the compositions studied, under atmospheric pressure. At the same time, initial ignition and independent combustion in the absence of a voltage was only observed for [AN + PBC] and [25 AN + 75 APC] samples. Thus, the action of an electric current of a certain power can enable stable

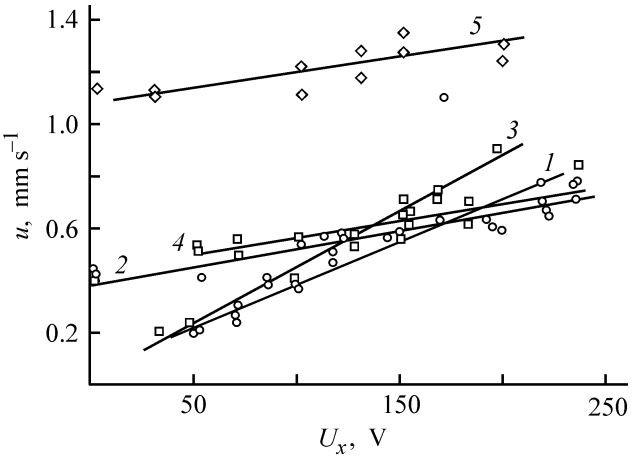

Fig. 2. ECS combustion velocity u vs. votage U_x. (*1*–*5*) sample nos.; the same for Figs. 3–6.

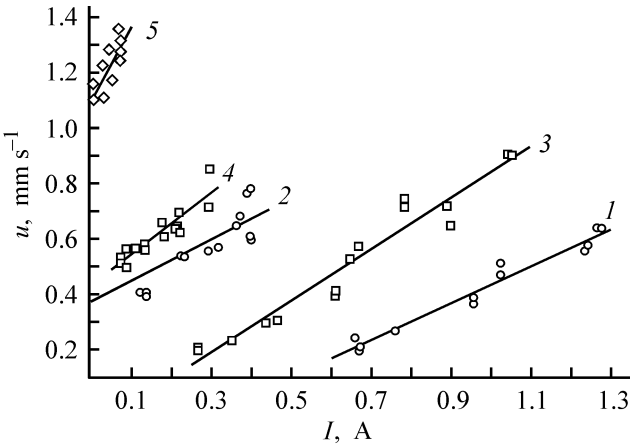

Fig. 3. Combustion rate u vs. current I.

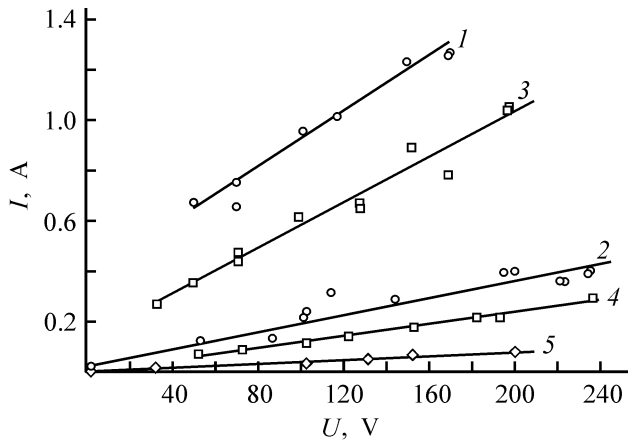

Fig. 4. *I–V* characteristics of the reaction zones of the c-phases of ECS. (*I*) Current and (*U*) voltage.

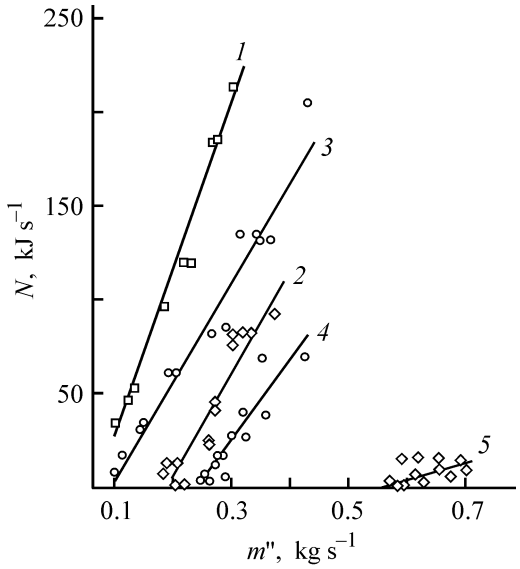

Fig. 5. Power *N* released by the electric current vs. mass expenditure *m*" of ECS.

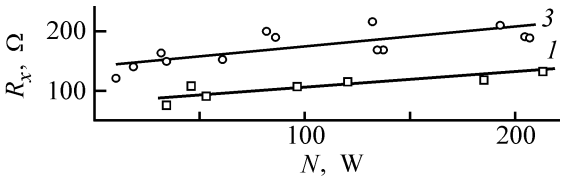

Fig. 6. Variation of the resistance R_x of the reaction zones with the power *N* released by the electric current.

combustion of solid fuels under pressures that are considerably lower than the critical threshold of the minimum pressure of the gas phase ($P_{cr} > 1$ MPa).

It follows from Fig. 5 that, under atmospheric pressure, the energy consumed for changing the mass expenditure of the fuel decreases for the samples studied by nearly an order of magnitude as the mass fraction of APC increases, i.e., the energy content of CSF becomes higher. The practical range of control over the mass expenditure by the gas-generating device can be primarily limited by the electric power of the current source used.

As the power released by the electric current grows, the resistances of the reaction zones become higher (Fig. 6), which can be attributed to an increase in the degree of their gasification and to a decrease in the resultant density of the liquid layer.

There exists an upper limit to the electrothermal acceleration of the combustion velocity of ECS, which depends on the chemical composition of the fuel. This is due to an increase in the degree of gasification of the liquid reaction zone and to discharge of molten fragments of CSF into the gas phase, which is reflected in a deviation of the forced combustion from the linear behavior.

For the CSF formulations [25 AN + 75 APC] and [85 AN + 5 PBC], which are capable of stable combustion under atmospheric pressure, we measured the amplitude-frequency dependences of the electrical conductivity of the reaction zones. For this purpose, we connected a G3-110 program-controlled sinusoidal voltage generator to the charge as a $\sim U_0$ voltage source (Fig. 2). During the ECS combustion, the frequency of the applied voltage $U_0 = 2$ V was discretely changed in a cyclic way every 0.8 s in the range from 50 Hz to 20 kHz. The generator output voltage $U_0(t)$ and the voltage $U_{rd}(t)$ across the resistor R_d were recorded by a computer with a sampling frequency dt = 10 kHz. In this frequency range, the voltage applied to the charge, $U_x(t) = U_0(t), - U_{rd}(t)$, remains constant and no phase shift between $U_0(t)$ and $U_x(t)$ is observed.

Similar results were obtained for CSF samples with potassium bichromate; however, the physical reasons for this similarity may be of some other nature. In this case, the formulation has a large negative oxygen balance and the combustion is accompanied by the formation on the surface of a considerable amount of a condensed carbon residue with electronic conduction. As a result, the AN melt in the reaction zone can be shunted by free carbon and the ionic type of conduction will not be manifested.

The results we obtained suggest that, in the cases studied, the electrical conductivity of the reaction zones has a predominantly electronic nature because the resistance of the combustion surface is frequency-independent in the frequency range specified. Thus, the reaction zone of the c-phase is an active load for

the current source. By contrast, pure melts of nitrates (NH_4NO_3, KNO_3) have ionic conductivity (NH_4^+, K^+, NO_3^-) and show a nonlinear frequency dependence of the conductivity.

Analysis of the effect of electrolysis on the kinetics of chemical reactions in the reaction zone requires a separate study. For example, electrochemical processes may be manifested in the case of a dc current in a difference between the ECS combustion velocities in the near-electrode regions of the cathode and anode.

We experimentally observed flame quenching and repeated ignition of (AN + APC) charges, with restoration of the combustion velocity, upon changes in the working voltage to, respectively, below and above a certain critical threshold (30–40 V). The repeated ignition occurred, if the reaction zone remained in the electrically conducting state, upon an increase in the effective power released by the flowing electric current. In fact, controlled combustion is a possible solution to the difficult problem of providing recurring short-time operation modes of solid-fuel installations by controlling the temperature of the reaction zone of the c-phase of ECS at the stable combustion threshold under the current thermodynamic conditions.

CONCLUSIONS

(1) An electrothermal method for control over the combustion velocity of energetic condensed systems was experimentally implemented.

(2) A stable combustion of samples of composite solid fuels (without catalysts) was obtained at atmospheric pressure under the action of electric current.

(3) The widest variation range of the combustion velocity (by a factor of up to 4.5) was observed for the formulation with 75% ammonium nitrate and 25% ammonium perchlorate. The specific energy consumption for control over the mass expenditure becomes lower as the energy content of the system increases (ammonium perchlorate concentration becomes higher).

(4) It was shown that the electronic conduction dominates in the reaction zones of the condensed phases of energetic condensed systems based on ammonium nitrate and ammonium perchlorate.

(5) It was concluded that the probable reason why the combustion velocity of the systems increases under the action of electric current is the occurrence of the electrothermic effect and the increase in the rate of chemical reactions in the condensed phase with temperature in accordance with the Van't Hoff rule and Arrhenius equation.

REFERENCES

1. Sokolovskii, M.I., Petrenko, V.I., Zykov, G.A., et al., *Upravlyaemye energeticheskie ustanovki na tverdom raketnom toplive* (Controllable Power Installations Operating on Solid Fuel), Sokolovskii, M.I. and Petrenko, V.I., Eds., Moscow: Mashinostroenie, 2003.
2. RF Patent 2 175 399.
3. RF Patent 2 208 694.
4. Khoruzhii, I.V., Taranushich, V.A., Klyakin, G.F., and Lachin, V.I., *Materialy 4-i Mezhdunarodnoi nauchno-prakticheskoi konferentsii "Komp'yuternye tekhnologii v nauke, proizvodstve, sotsial'nykh i ekonomicheskikh protsessakh," Novocherkassk, 14 noyabrya 2003 g.* (Proc. 4th Int. Sci.-Pract. Conf. "Computer Technologies in Science, Production, and Social and Economic Processes," Novocherkassk, November 14, 2003), Novocherkassk: YuRGTU(NPI), 2003, pp. 53–57.
5. Khoruzhii, I.V., *Materialy 6-i Mezhdunarodnoi nauchno-prakticheskoi konferentsii "Mikroprotsessornye, analogovye i tsifrovye sistemy: proektirovanie i skhemotekhnika, teoriya i voprosy primeneniya," Novocherkassk, 17 oktyabrya 2006 g.* (Proc. 6th Int. Sci.-Pract. Conf. "Microprocessor, Analog, and Digital Systems: Design and Circuitry, Theory and Application Issues," Novocherkassk, October 17, 2006), Novocherkassk: YuRGTU(NPI), 2006, pp. 40–43.
6. Khoruzhii, I.V. and Lachin, V.I., *Materialy 4-i Mezhdunarodnoi nauchno-prakticheskoi konferentsii "Mikroprotsessornye, analogovye i tsifrovye sistemy: proektirovanie i skhemotekhnika, teoriya i voprosy primeneniya," Novocherkassk, 27 fevralya 2004 g.* (Proc. 4th Int. Sci.-Pract. Conf. "Microprocessor, Analog, and Digital Systems: Design and Circuitry, Theory and Application Issues," Novocherkassk, February 27, 2004), Novocherkassk: YuRGTU(NPI), 2004, pp. 33–37.

ISSN 1070-4272, Russian Journal of Applied Chemistry, 2007, Vol. 80, No. 8, pp. 1300–1303. © Pleiades Publishing, Ltd., 2007.
Original Russian Text © A.G. Morachevskii, T.V. Butukhanova, 2007, published in Zhurnal Prikladnoi Khimii, 2007, Vol. 80, No. 8, pp. 1261–1263.

PHYSICOCHEMICAL STUDIES OF SYSTEMS AND PROCESSES

Application of the Zdanovskii Rule to Liquid Metal Systems with Strong Interaction of Components

A. G. Morachevskii and T. V. Butukhanova

St. Petersburg State Polytechnic University, St. Petersburg, Russia

Received June 27, 2007

Abstract—Applicability of the Zdanovskii rule to liquid metal systems with strong deviations from ideal behavior is discussed for the example of the lead–thallium–sodium system.

DOI: 10.1134/S1070427207080071

Seventy years ago Zdanovskii [1] established, based on a study of a large number of aqueous electrolyte solutions, a simple law, which became known as the Zdanovskii rule: the activity of water remains unchanged on mixing isopiestic solutions of different electrolytes that do not interact chemically with each other. In other words, there is a large number of ternary systems A(1)–B(2)–H_2O(3) in which lines of equal chemical potentials of water remain straight in a wide range of solution compositions. The main condition for this rule to be obeyed is the absence of a chemical interaction between the solutes. If we denote the molalities of components in the initial binary solutions by m_1^0 and m_2^0, and the molalities of the same components in the resulting mixed solution by m_1 and m_2, we can write down

$$m_1/m_1^0 + m_2/m_2^0 = 1, \quad (1)$$

$$m_2 = m_2^0 - m_1 m_2^0/m_1^0. \quad (2)$$

In a geometric representation of ternary systems described by the Zdanovskii rule, the plot of the $m_2 = f(m_1)$ dependence in the rectangular coordinate system (first Rosebome's method for representation of the composition of ternary systems [2]) is a straight line that intersects the coordinate axes at points corresponding to the component concentrations in binary mixtures with equal activities of the solvent (component 3, which is water in the case in question).

Later, the relationship under consideration was substantiated thermodynamically, which made it possible to distinguish among aqueous systems a special class of isoactive electrolytes described by the Zdanovskii rule [3–7]. Zdanovskii and other researchers also successfully applied the additivity principle to calculations of electrolyte properties, such as density, heat capacity, and heat of dissolution [8, 9].

The Zdanovskii rule can be used for a thermodynamic description of multicomponent electrolytes. Let us denote the molality of components in the initial binary solutions of a multicomponent system by m_i^0 (i = 1, 2, 3, ...), and the molality of the same components in the mixed system by m_i. Then, provided that the initial binary solutions are in an isopiestic equilibrium between each other and with the multicomponent solution formed, the mathematical form of the Zdanovskii rule for systems with n components will look like

$$\sum_{n}^{n-1} \frac{m_i}{m_i^0} = 1. \quad (3)$$

This rule is valid not only for solutions of salts with the same anion, as it was assumed originally, but for any mixed solution, irrespective of outward characteristics of systems. It was shown by Zhichang [10] that Eq. (3) retains its form irrespective of how the concentration is expressed, i.e.

$$\sum_{n}^{n-1} \frac{m_i}{m_i^0} = \sum_{n}^{n-1} \frac{x_i}{x_i^0} = \sum_{n}^{n-1} \frac{w_i}{w_i^0} = 1. \quad (4)$$

Here x_i and w_i are the respective mole and weight fractions of ith component in the initial binary solutions.

In this case, all the three expressions for the composition can be extended not only to the activity, but also to other partial molar functions.

Table 1. Mole fractions of components on sodium isoactivity lines

a_{Na}	x_i	Mole fraction of Pb (x_1), Tl (x_2), and Na (x_3) on sodium isoactivity lines along sections*				
		I	II	II	IV	V
0.005	x_1	0.775	0.642	0.408	0.172	0.0
	x_2	0.0	0.161	0.408	0.688	0.875
	x_3	0.225	0.197	0.184	0.140	0.125
0.010	x_1	0.710	0.584	0.381	0.160	0.0
	x_2	0.0	0.146	0.381	0.640	0.815
	x_3	0.290	0.270	0.238	0.200	0.185
0.050	x_1	0.548	0.450	0.296	0.129	0.0
	x_2	0.0	0.113	0.296	0.515	0.668
	x_3	0.452	0.437	0.408	0.356	0.332
0.100	x_1	0.475	0.391	0.263	0.114	0.0
	x_2	0.0	0.098	0.263	0.456	0.593
	x_3	0.525	0.511	0.474	0.430	0.407
0.200	x_1	0.386	0.323	0.217	0.097	0.0
	x_2	0.0	0.081	0.217	0.388	0.509
	x_3	0.614	0.596	0.566	0.515	0.491
0.400	x_1	0.275	0.236	0.166	0.075	0.0
	x_2	0.0	0.059	0.166	0.300	0.412
	x_3	0.725	0.705	0.668	0.625	0.588

* Section: I, Pb–Na; II, ($x_{Pb} : x_{Tl} = 4 : 1$)–Na; III, ($x_{Pb} : x_{Tl} = 1 : 1$)–Na; IV, ($x_{Pb} : x_{Tl} = 1 : 4$)–Na; V, Tl–Na.

In this study, we considered in detail the application of the Zdanovskii rule to liquid ternary metal systems including two boundary systems with a strong interaction between the components. The thermodynamic properties of the liquid systems Pb(1)–Tl(2)–Na(3) were studied by the electromotive-force method along sections with constant ratios of mole fractions of lead (x_1) and thallium (x_2) equal to 4 : 1, 1 : 1, and 1 : 4 at temperatures from the liquidus line up to 883 K [11]. The thermodynamic properties of the boundary systems Pb–Na and Tl–Na have also been studied in detail [12, 13]. In both systems, significant negative deviations from ideal behavior are observed (Fig. 1), whereas in the Pb–Tl system, both components are so close in properties that the system they form is nearly regular (Fig. 2) [14].

The compositions of liquid alloys of ternary system Pb–Tl–Na along the lines with constant sodium activ-

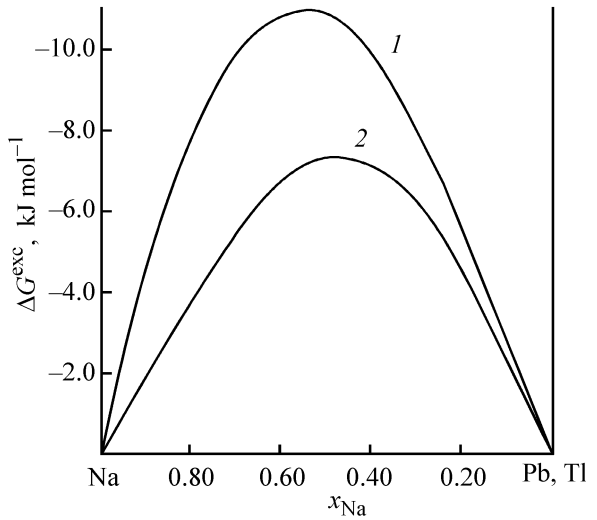

Fig. 1. Integral molar excess Gibbs energy ΔG^{exc} vs. the composition of the systems (*1*) Pb–Na and (*2*) Tl–Na at 850 K.

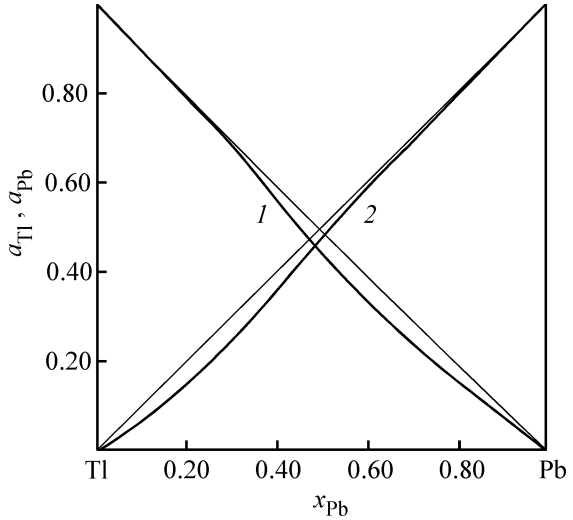

Fig. 2. Activity isotherms of (*1*) thallium a_{Tl} and (*2*) lead a_{Pb} in liquid alloys of the system Pb–Tl at 850 K.

Table 2. Sum $\Sigma = (x_1/x_1^0) + (x_2/x_2^0)$ for the compositions lying on sodium isoactivity lines along sections II–IV

Section	Sum Σ at a_{Na}					
	0.005	0.010	0.050	0.100	0.200	0.400
II	1.012	1.002	0.990	0.988	0.996	1.001
III	0.993	1.004	0.983	0.997	0.989	1.007
IV	1.008	1.011	1.006	1.009	1.014	1.001
Average absolute deviation from Eq. (5)	0.009	0.005	0.011	0.008	0.010	0.003

ity, found from experimental data (Fig. 3), are listed in Table 1. If the Zdanovskii rule is obeyed, the compositions along the sodium isoactivity lines should satisfy Eq. (4) written for the ternary system:

$$x_1/x_1^0 + x_2/x_2^0 = 1. \quad (5)$$

It is seen from Table 2 that deviations from the Zdanovskii rule for the compositions lying on sodium isoactivity lines do not exceed 1.5%, i.e., fall within the accuracy limits of the experimental method and the plotting procedures. Thus, as already noted [3], the Zdanovskii rule can be extended to ternary systems of varied nature, in which two components rather actively interact with a third component, conditionally regarded as a "solvent", and weekly interact (or virtually do not interact at all) with each other. From the thermodynamic standpoint, the systems described by the Zdanovskii rule belong to the class of systems in which isopotentials of one of the components (component 3, which is sodium in our case) are straight lines. The linearity of isopotentials of one of the components of a ternary system simplifies solution of quite a number of problems in a thermodynamic description of systems of this kind [3, 11].

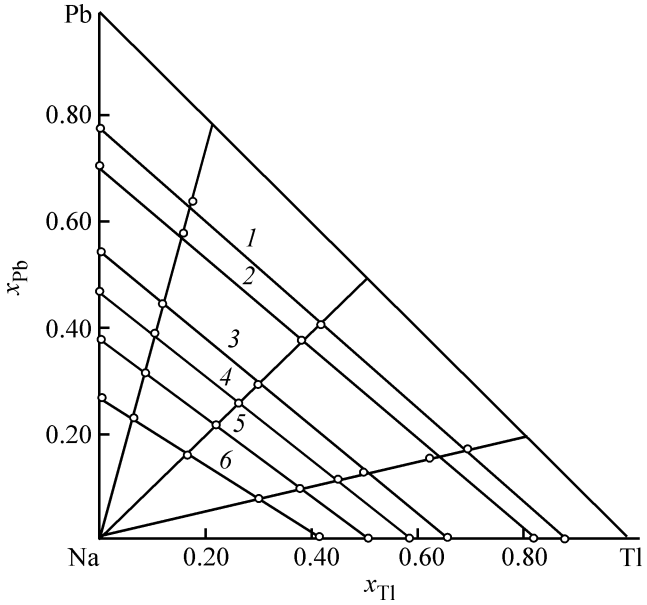

Fig. 3. Equal-sodium-activity lines in liquid alloys of the system Pb–Tl–Na (800 K). a_{Na}: (*1*) 0.005, (*2*) 0.010, (*3*) 0.050, (*4*) 0.100, (*5*) 0.200, and (*6*) 0.400.

CONCLUSIONS

It was shown that, during the seventy years of existence of the Zdanovskii rule, it has found application in description of the thermodynamic properties of ternary and more complex systems of substances of various classes. The applicability of the Zdanovskii rule to liquid alloys of the ternary system lead–thallium–sodium (850 K) was demonstrated.

REFERENCES

1. ZdanovskiI, A.B., *Zakonomernosti v izmeneniyakh svoistv smeshannykh rastvorov: Trudy solyanoi laboratorii* (Fundamental Aspects of Variation of Properties of Mixed Solutions: Works of Salt Laboratory), 1936, issue 6.
2. Anosov, V.J., Ozerova, M.I., and Fialkov, J.J., *Osnovy fiziko-khimicheskogo analiza* (Fundamentals of Physicochemical Analysis), Moscow: Nauka, 1978.
3. Filippov, V.K., *Khimiya i thermodinamika rastvorov* (Chemistry and Thermodynamics of Solutions), Leningrad: Leningr. Gos. Univ., 1973, issue 3, pp. 186–203.
4. Frolov, J.G., *Thermodinamika i stroenie rastvorov: Mezhvyzovskii sbornik* (Thermodynamics and Structure of Solutions: Intercollegiate Coll. of Works), Ivanovo, 1973, issue 1, pp. 28–36.
5. Ryazanov, M.A., *Zh. Fiz. Khim.*, 1987, vol. 61, no. 9, pp. 2397–2401.

6. Denisov, D.A. and Frolov, J.G., *Zh. Fiz. Khim.*, 1990, vol. 64, no. 1, pp. 222–224.
7. Vorob'ev, A.F., Nikolaev, V.P., and Zhdanova, T.A., *Koord. Khim.*, 1997, vol. 23, no. 11, pp. 831–834.
8. Zdanovskii, A.B., *Zh. Fiz. Khim.*, 1938, vol. 11, no. 6, pp. 858–860 and 861–863.
9. Denisov, D.A., *Trudy Moskovskogo khim.-tekhnol. inst.* (Coll. of Works of Moscow Chem.-Technol. Inst.), 1985, issue 136, pp. 129–136.
10. Zhichang, W., *Acta Met. Sinica*, 1980, vol. 16, no. 2, pp. 195–206.
11. Morachevskii, A.G., Statsenko, S.I., and Busse-Machukas, V.B., *Zh. Fiz. Khim.*, 1968, vol. 42, no. 1, pp. 40–45.
12. Morachevskii, A.G., *Zh. Prikl. Khim.*, 1997, vol. 70, no. 7, pp. 1057–1071.
13. Morachevskij, A.G. and Maiorova, E.A., *Zh. Prikl. Khim.*, 1999, vol. 72, no. 6, pp. 910–913.
14. Hultgren, R., Desai, P., Hawkins, D., et al., *Selected Values of Thermodynamic Properties of Binary Alloys*, Am. Soc. Met., 1973.

ISSN 1070-4272, Russian Journal of Applied Chemistry, 2007, Vol. 80, No. 8, pp. 1304–1308. © Pleiades Publishing, Ltd., 2007.
Original Russian Text © N.V. Shul'ga, I.L. Shashkova, N.V. Mil'vit, A.I. Rat'ko, 2007, published in Zhurnal Prikladnoi Khimii, 2007, Vol. 80, No. 8, pp. 1264–1268.

SORPTION AND ION-EXCHANGE PROCESSES

Specific Features of Absorption of Cu^{2+}, Zn^{2+}, Co^{2+}, and Pb^{2+} Cations from Aqueous Solutions by Calcium Phosphates

N. V. Shul'ga, I. L. Shashkova, N. V. Mil'vit, and A. I. Rat'ko

Institute of General and Inorganic Chemistry, National Academy of Sciences of Belarus, Minsk, Belarus

Received October 30, 2006; in final form, March 2007

Abstract—Kinetic characteristics of the interaction of trisubstituted calcium phosphate $Ca_3(PO_4)_2 \cdot xH_2O$ with Cu^{2+}, Zn^{2+}, Co^{2+}, and Pb^{2+} ions in aqueous solutions were studied.

DOI: 10.1134/S1070427207080083

Compared with the conventional sorbents and ion-exchange resins, calcium phosphates can absorb considerably larger amounts of heavy and nonferrous metals from aqueous solutions. The absorption proceeds by the chemisorption mechanism as a chemical reaction of substitution of calcium ions in the starting phosphate with ions of other metals and occurs in those cases when the forming product has a lower solubility than the starting phosphate.

It has been shown previously [1] that the reactivity of amorphous trisubstituted calcium phosphate $Ca_3(PO_4)_2 \cdot xH_2O$ in interaction with lead ions is largely determined by its porous structure. Macroporous calcium phosphates have high chemical activity and their theoretical sorption capacity is rapidly utilized when they are brought in contact with aqueous solutions containing Pb^{2+} ions. With calcium phosphate with a porous structure used as a sorbent, the stage of fast initial absorption is followed, depending on the reaction conditions, either by deceleration or by termination of the reaction. This occurs as a result of accumulation of chemisorption products and blocked access of Pb^{2+} ions to unreacted areas on the surface of the starting material. As the time of contact between the solid phase and the solution, which may occasionally be no less than 10–20 days, increases, chemisorption is resumed and proceeds to full completion. In this case, the theoretical sorption capacity of both meso- and macroporous samples for lead ions is utilized.

A study of this process by X-ray phase analysis and optical microscopy demonstrated that the resumption of the reaction between calcium phosphate and lead is due to crystallization of the final product, change in the volume of the substance, and dispersion of the starting phosphate particles into finer fragments.

The above pattern of interaction between calcium phosphates of varied porous structure and lead may be markedly different in absorption of other ions because of the differences in the chemical and phase composition of the final products, specific features of their crystallization, and physicochemical properties.

To elucidate the influence exerted by the nature of an ion being absorbed on the chemisorption activity of calcium phosphates, we studied the kinetics of absorption of copper, zinc, lead, and cobalt ions by macro- and mesoporous calcium phosphates.

EXPERIMENTAL

Phosphate samples of varied porous structure were obtained by chemical precipitation [1]. For this purpose, 5% solutions of calcium nitrate or ammonium hydrophosphate (both of (chemically pure grade) were alkalized with ammonia solutions to pH 10 and then were rapidly poured together. The volume ratio of the poured-together solutions was chosen so as to provide the required ratio Ca : P = 1.5 : 1.0. The gel-

Basic characteristics of macro- (B) and mesoporous (A) calcium phosphates

Series	Water content, wt %	Ca : P	S_{sp}, $m^2\ g^{-1}$	V_s	V	d, g cm^{-3}	
				$cm^3\ g^{-1}$		true	apparent
A	2.0 ± 0.1	1.56 : 1	115 ± 5	0.32 ± 0.01	0.30 ± 0.2	2.4 ± 0.01	1.4 ± 0.03
B	6.1 ± 0.1	1.57 : 1	56 ± 5	0.21 ± 0.01	2.8 ± 0.3	1.9 ± 0.01	0.3 ± 0.03

like precipitates obtained were washed on a Buchner funnel with a weak NH_4OH solution and dried in air, first at room temperature and then at 70°C. In one case (series A), the gel was not subjected to any additional treatment before drying. In the other (series B), the gel was preliminarily treated, when preparing coarsely porous phosphates, with ethanol in order to rapidly remove the main part of water from the humid precipitate and then was placed in a drying box. Calcium phosphate xerogels were ground in a mortar and the 125–160-μm fraction was screened out and further used in the study.

The samples obtained were dissolved in concentrated hydrochloric acid and analyzed for the content of calcium (complexometric titration with eriochrome black) and phosphorus (by photocolorimetry after formation of phosphor-molybdenum blue). The structural parameters, specific surface area S_{sp} ($m^2\ g^{-1}$) and sorption pore volume V_s ($cm^3\ g^{-1}$), were found from adsorption isotherms of carbon tetrachloride (measured on a weighing vacuum-adsorption installation with a spring balance), adsorption isotherms of nitrogen (obtained using a NOVA 2200 instrument), and low-temperature adsorption of nitrogen by the Klyachko–Gurvich method. The specific surface area was calculated by the BET method [2]. The residual content of water in the samples was found from the loss of mass upon calcination at 300°C for 1 h.

The absorption of ions of divalent metals from 0.01–0.05 M solutions of $M(NO_3)_2$ (analytically pure, M = Pb^{2+}, Co^{2+}, Zn^{2+}, Cu^{2+}) was studied under static conditions at room temperature. A 0.05-g portion of a substance from the screened-out 125–160-μm fraction was poured over with solutions of $M(NO_3)_2$ salts at a certain value of R characterizing the ratio between the liquid (ml) and solid (g) phases. When determining the chemisorption capacity for the metal ion M^{2+} and carrying out kinetic experiments, R was varied within the range from 200 to 1000 (10 to 50 ml of a solution per 0.05 g of the sorbent) so as to provide, irrespective of the concentration, a constant content of a metal in solution in an amount necessary for complete transformation of the starting sorbent into the final product. The thus obtained water–salt systems were kept, with periodic agitation, at a prescribed temperature (20°C) for various intervals of time (5 min to 60 h). Then, the precipitates were separated from the solution, washed with water, and dried for further study. The equilibrium liquid phase was analyzed for the content of M^{2+} by complexometric titration with methyl thymol blue as indicator in an acetate buffer solution at pH 5.

An X-ray phase analysis of the starting phosphates and reaction products was performed with a DRON-3 diffractometer with Cu_{K_α} radiation.

A MIN-8 microscope was used for visual inspection of processes occurring at the phase boundary.

The table lists the averaged results of chemical analyses of the samples synthesized and data on their specific surface area S_{sp} and sorption (V_s) and total (V) pore volumes calculated from the difference of the inverse apparent and true densities [22].

As can be seen from the table, the Ca : P ratio in the precipitated products is rather close to the stoichiometric value of 1.5 : 1.0, characteristic of tertiary calcium phosphate $Ca_3(PO_4)_2 \cdot xH_2O$, and, as demonstrated by experimental results [1], is independent of the phosphate preparation conditions.

Calcination of samples in air at 800°C yields anhydrous tertiary calcium phosphates, which is confirmed by the fact that tertiary salts containing no acid or basic impurities are obtained.

As follows from the results of an X-ray phase analysis, phosphates of series A are poorly crystalline products. Samples of series B are amorphous [1]. The ordering of the crystal structure of calcium phosphate probably creates more favorable conditions for removal of water, and, therefore, samples of series A contain a smaller amount of residual water (see table).

The results obtained in a study of the pore structure of the samples synthesized were reported in [1]. Figure 1 shows typical isotherms of carbon tetrachloride sorption by calcium phosphates of series A and B.

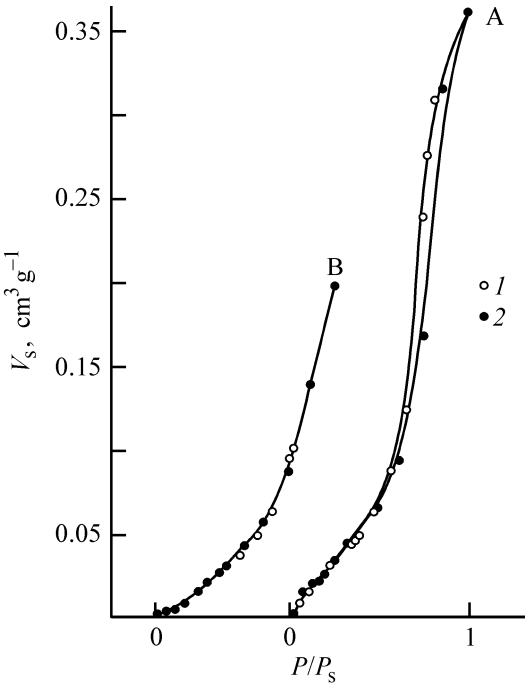

Fig. 1. Typical isotherms of CCl_4 sorption by calcium phosphates of series A and B. (V_s) Limiting sorption volume and (P/P_s) relative pressure. (*1*) Starting phosphate and (*2*) $Ca_3(PO_4)_2 \cdot 8H_2O$.

As follows from the data in the table and Fig. 1, the samples obtained markedly differ from each other in physical characteristics. For example, the sorption and total pore volumes found from the difference of the inverse apparent and total densities are virtually identical, whereas the total volume of pores in sample B markedly exceeds their sorption volume. This is a direct evidence that sample B contains macropores that are not filled by a liquefied vapor of the adsorbate in the course of adsorption.

Thus, sample A is a mesoporous sorbent according to the results of adsorption analysis (see table, Fig. 1). The absence of a hysteresis loop in the sorption isotherm, comparatively small specific surface area, and considerable difference between the sorption and total pore volumes of the phosphate sample B suggest that this sample is coarse-porous. In this case, the method of capillary condensation is unsuitable for determining the position at which the differential porosity and pore space volume are at a maximum because of the limited applicability of the Kelvin equation [2].

Figures 2a–2d show kinetic curves of absorption of Cu^{2+}, Zn^{2+}, Co^{2+}, and Pb^{2+} ions by calcium phosphate samples with macro- (B) and mesoporous (A) structure.

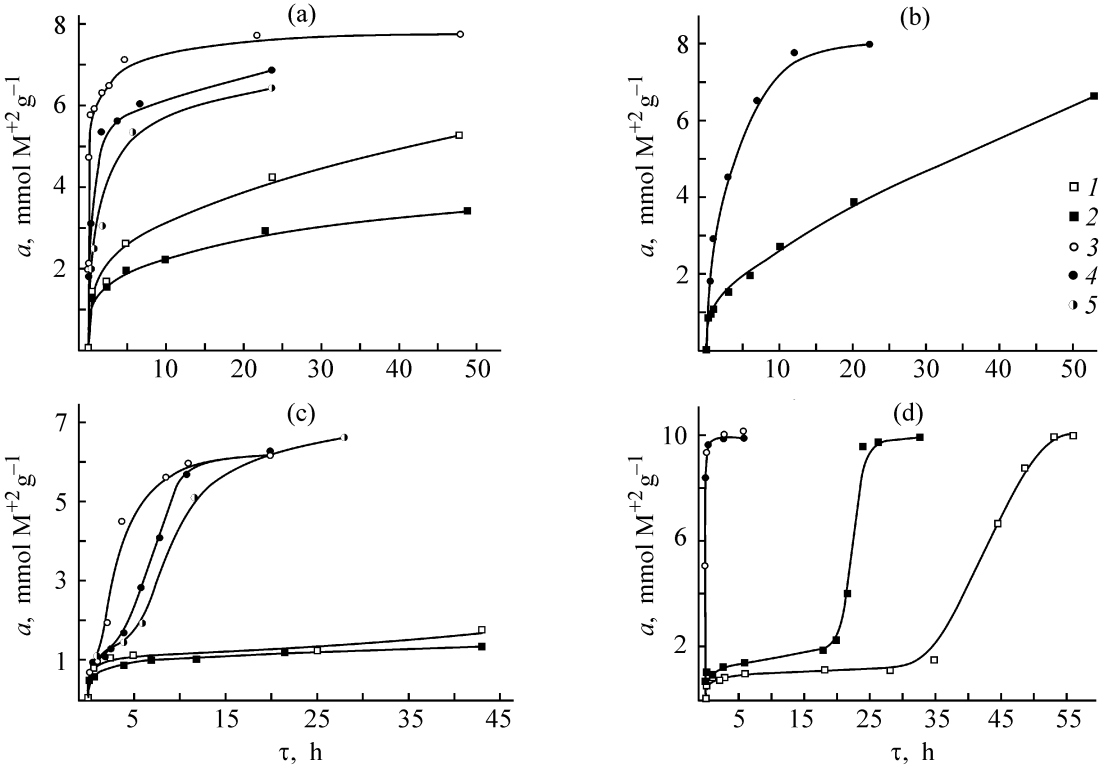

Fig. 2. Kinetic curves of absorption of (a) Cu^{2+}, (b) Zn^{2+}, (c) Co^{2+}, and (d) Pb^{2+} ions by calcium phosphate samples of series (*1*, *2*) A and (*3*–*5*) B from aqueous solutions at 20°C. (*a*) Amount of absorption and (τ) interaction time. M^{2+} concentration (mM): (*1*, *3*) 50, (*2*, *4*) 25, and (*5*) 10.

It follows from the results obtained (Fig. 2) that, in contrast to mesoporous phosphates, macroporous phosphates exhibit a higher activity in interaction with metal ions in aqueous solutions. In this case, the amount of absorption is as high as 10 (Pb^{2+}), 7–8 (Zn^{2+} and Co^{2+}), and 6.5 mmol (Cu^{2+}) per gram of the starting phosphate in a time $\tau \approx 5$–25 h, which constitutes 93, 72–83, and 67% of the theoretical value, respectively.

According to the results of an X-ray phase analysis, the final reaction products are the tertiary phosphates $Cu_3(PO_4)_2 \cdot 3H_2O$, $Zn_3(PO_4)_2 \cdot 4H_2O$, $Co_3(PO_4)_2 \cdot 8H_2O$, and in absorption of lead ions, pyromorphite $Pb_5(PO_4)_2OH$. In our case, all these reaction products, except copper phosphate, have a well-formed crystal lattice.

No indications that a new phase is formed are observed in the initial stage ($a < 1$ mmol g^{-1}) of absorption of Cu^{2+}, Zn^{2+}, Co^{2+}, and Pb^{2+} ions by calcium phosphate of series A. This is possibly due to a lag of crystallization processes behind the chemical stage of the reaction. For a macroporous sorbent of series B this lag becomes even more pronounced, as it is shown for the example of absorption of Co^{2+} ions by calcium phosphates (Fig. 3).

As the time of contact between the solid phase and an aqueous solution becomes longer, the degree of crystallization of the final product grows even in those cases (e.g., in sorption of lead) when the process of ion absorption virtually ceases. The reason for this effect is related to the crystallization mechanism of the reaction products. Specific features of this stage of the process are considered in detail in what follows.

X-ray phase analysis data are in good agreement with the results of a visual inspection with an optical microscope. For example, the initial absorption is characterized in all cases by absence of any indications of a chemical reaction, with the exception of a slight coloration of the surface of phosphate particles in their interaction with Co^{2+} or Cu^{2+} ions.

A specific feature of the chemical transformations that occur at the phase boundary is that the shape of kinetic curves, and their formal similarity or dissimilarity, give no way of making any unambiguous conclusions about the mechanism of a particular chemical process. This requires additional studies and, in particular, a phase analysis and visual monitoring of changes experienced by the starting solid phase and by the intermediate and final products formed in the course of the reaction.

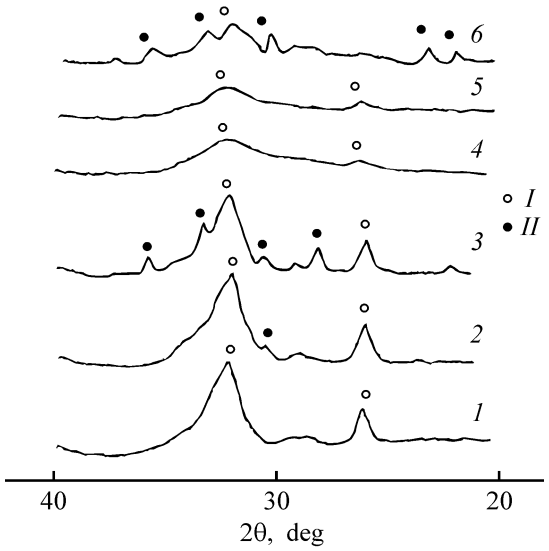

Fig. 3. X-ray diffraction patterns of calcium phosphates and products of their interaction with Co^{2+} ions in an aqueous solution. ($c_{Co^{2+}}$ = 25 mM). (2θ) Bragg angle. (*I*) Starting phosphate and (*II*) $Ca_3(PO_4)_2 \cdot 8H_2O$. (*1*) Starting $Ca_3(PO_4)_2$-A; (*2*) a = 1.0, τ = 18; (*3*) a = 2.1, τ = 0.96; (*4*) starting $Ca_3(PO_4)_2$-B; (*5*) a = 1.5, τ = 4; and (*6*) a = 2.8, τ = 6.

As shown previously [1], the reason for a dramatic decrease in the rate of absorption of Pb^{2+} ions by calcium phosphate of series A after the initial fast stage is the formation of a dense pseudo-amorphous layer of the reaction product, which hinders supply of metal ions to unreacted parts of the starting phosphate. The formation of the pseudmorphosis in the initial stage of the transformation does not change the outward appearance of a particle. The crystallization of the amorphous product is accompanied by a noticeable increase in the volume of a substance and its self-dispersion, followed by vigorous resumption of the reaction (Fig. 2d).

According to the results of a microscopic analysis, virtually no dissolution of the pseudomorphosis or reprecipitation of pyromorphite is observed in the course of the transformation near the surface of calcium phosphate A, and, therefore, the contribution of these processes to the subsequent self-acceleration of the reaction cannot be significant. Presumably, the resumption of the reaction and the avalanche rise in its rate are due to crystallization of pyromorphite within the pores of the starting phosphate and to disintegration of sorbent particles under the action of mechanical stresses, which surpass the ultimate strength of substance particles.

As demonstrated by the experimental data obtained, the absorption of Cu^{2+} ions by calcium phosphates

of series A and B occurs, untill full completion of the reaction, bypassing the stage of dissolution of pseudomorphosis. In this case, the reaction is not accelerated (Fig. 2b). After the absorption of Cu^{2+} ions is complete, phosphate particles retain their original dimensions and integrity, as it is observed in interaction of coarsely porous phosphate $Ca_3(PO_4)_2$ (B) with Pb^{2+} ions.

Despite the formal similarity of the sets of kinetic curves (Figs. 2a and 2b, and to a lesser extent Figs. 2c and 2d), noticeable differences are observed in absorption of Cu^{2+} and Zn^{2+} ions, and, respectively, Co^{2+} and Pb^{2+} ions, by calcium phosphates from aqueous solutions. For example, the final products of interaction of phosphates A and B with Co^{2+} and Zn^{2+} ions crystallize in all cases without exception via the stage of pseudomorphosis dissolution. The reprecipitation process occurs both at particle boundaries and in the near-surface layer of the solution. The certain discrepancies in the absorption rate of Zn^{2+} and Co^{2+} ions by phosphates A and B (Figs. 2b, 2c) and the appearance of inflections in the kinetic curves (Fig. 2c) can probably be attributed to the state of the starting substance (density, porosity, permeability) and to the properties of the intermediate pseudomorphoses obtained and, in particular, to their chemical composition and dissolution rate.

The results obtained are in good agreement with the known topochemical rule, according to which the physicochemical characteristics of the starting solid phase can strongly affect the properties of the forming product and the rate at which it passes through intermediate states. In our case, the wide diversity of the effects observed is due not only to the state of the starting calcium phosphate, but also to the different chemical compositions and properties of intermediate pseudomorphoses.

The experimental data were mathematically processed in terms of the known topokinetic equation $\alpha = 1 - e^{k\tau^n}$, where α is the degree of conversion of the starting substance; τ, time; and k and n, rate constant and kinetic parameter of the reaction [3], respectively. It was found that, in most cases, the absorption of Cu^{2+}, Zn^{2+}, Co^{2+}, and Pb^{2+} ions is limited, already in initial stages, by their diffusion to the unreacted surface of the phosphate across a layer of a poorly crystallized reaction product. The obtained values of the kinetic parameter n are 0.10–0.58, which is typical of diffusion processes. The permeability of the pseudomorphosis and the mechanism and rate of its crystallization predetermine the ability of calcium phosphate to absorb ions of heavy and nonferrous metals from aqueous solutions, as well as the rate and extent of the reaction.

CONCLUSIONS

(1) The chemisorption activity of tertiary calcium phosphates in interaction with ions of heavy and nonferrous metals in aqueous solutions is largely determined by their porous structure.

(2) The chemical composition and properties of chemisorption products and the rate and mechanism of crystallization of pseudomorphoses depend on the nature of a cation being absorbed.

(3) Specific features of the crystallization of the final reaction product are factors that can change the rate and extent of the chemisorption process.

REFERENCES

1. Shul'ga, N.V., Mil'vit, N.V., Shashkova, I.L., and Rat'ko, A.I., *Zh. Neorg. Khim.*, 2007, vol. 80, no. 5, pp. 731–738.
2. Gregg, S.J. and Sing, K.S.W., *Adsorption, Surface Area and Porosity*, London: Academic, 1982.
3. *Geterogennye khimicheskie reaktsii* (Heterogeneous Chemical Reactions), Pavlyuchenko, M.M. and Prodan, E.A., Eds., Minsk: Nauka i Tekhnika, 1965.

ISSN 1070-4272, Russian Journal of Applied Chemistry, 2007, Vol. 80, No. 8, pp. 1309–1315. © Pleiades Publishing, Ltd., 2007.
Original Russian Text © A.M. Akimbaeva, E.E. Ergozhin, 2007, published in Zhurnal Prikladnoi Khimii, 2007, Vol. 80, No. 8, pp. 1269–1275.

SORPTION AND ION-EXCHANGE PROCESSES

Anion Exchangers Based on Modified Shungites

A. M. Akimbaeva and E. E. Ergozhin

Bekturov Institute of Chemical Sciences, Almaty, Kazakhstan

Received September 26, 2006; in final form, January 2007

Abstract—Modification of shungite with polyamines, followed by cross-linking with epoxy compounds, yielded chemically and thermally stable polyfunctional anion exchangers. The effect of the nature of a polyamine and epoxy compounds and of the carbon content of shungites and the process conditions on the ion-exchange properties of the samples obtained was studied.

DOI: 10.1134/S1070427207080095

The intensive use of carbon sorbents in various fields of science and technology requires that the assortment of carbon materials should be made wider and scientifically substantiated methods should be developed for synthesis from these materials of ion exchangers with improved characteristics and high selectivity, whose application could solve numerous ecological problems. To sorbents of this kind belong varieties of shungites. It has been found that the organic substance of shungite is mainly represented by aliphatic saturated hydrocarbons and their oxygen-containing derivatives, ketones and esters, with a minor admixture of aromatic compounds [1], which favor compatibility of a filler with the polymeric matrix. A conclusion was made on this basis that the compositions of the organic substances contained in shungite rock and rocks with varied content of carbon are close. It is assumed that compounds of this kind are effective surfactants which combine into a single system fragments of the amorphous carbon phase and an inorganic phase, which thereby favor compatibility of the filler and the polymeric matrix. The importance of the practical use of these latter makes rather interesting the development of methods for their modification [2–4].

The authors suggest to chemically modify shungite with amino and epoxy compounds in order to obtain anion exchangers.

EXPERIMENTAL

The shungite rock (Sh) used in the study was natural shungite from Eastern-Kazakhstan oblast, with carbon content c_{sh} of about 20%. Demineralized samples were obtained from this rock by flotation and acid-alkaline dressing (c_{sh} 60 and 80%) [5].

Distilled glycidyl methacrylate (GMA) had the following properties: d_4^{20} = 1.03337 and n_D^{20} = 1.4480. Epychlorohydrin (ECH) of chemically pure grade was dried with calcium hydroxide and distilled to obtain a fraction boiling at 115–116°C/689 mm Hg, with n_D^{20} = 1.4380. Polyethylenamine (PEA) was kept over a granulated alkali for 5–6 days (MM = 30×10^3. The content of titrable nitrogen in an anhydrous sample was 29.3%. Poly-2-methyl-5-vinylpyridine (PMVP) had MM = 10×10^3 and content of titrable nitrogen equal to 8.6%.

Modification experiments were performed by treatment of natural shungite with polyamines (PEA, PMVP) in dioxane (100°C, 30 min), followed by cross-linking with epoxy compounds (GMA, ECH), with varied treatment duration τ (min), process temperature (°C), and mass ratio of the starting components. The samples were treated with hydrochloric acid to obtain an anion exchanger in the Cl^- form, washed to a neutral reaction of the washing water, and converted to the OH^- form by an appropriate treatment with an alkali.

The quality of the resulting ion-exchange material was evaluated by a set of parameters: static exchange capacity (SEC for Cl^-, mg-equiv g^{-1}), content of nitrogen and chlorine, and physicochemical parameters. The static exchange capacity and the physicochemical properties of the ion exchangers were determined in accordance with GOSTs (State Standards) 10 898.1–74 and 10 898.5–74.

The concentration of functional groups in the polymer phase, which corresponds to the SEC (mg-equiv g^{-1}) of the ion exchanger, was calculated by the procedure described in [6].

To determine the chemical and thermal resistance of an anion exchanger in the OH^- form, its weighed portions (each 1.0 g in terms of the dry product) were placed in 250-ml round-bottomed flasks. A 5 N solution of sulfuric acid was poured into one of these, a 5 N solution of sodium hydroxide into another, and distilled water into the third, with each liquid portion equal to 100 ml. The contents of the flasks were kept for 30 min (chemical resistance) and 24 h (thermal resistance) on a boiling water bath. Then the mixture was cooled in air to room temperature, the filtrate was separated from the ion exchanger, and the latter was converted into the hydrogen form, after which its SEC was determined.

The chemical and thermal resistance Y (%) was calculated by the formula

$$Y = 100E_1/E_0,$$

where E_0 and E_1 are the SEC (mg-equiv g^{-1}) before and after treatment of an ion exchanger.

The concentration of hydrogen ions was monitored with an I-130 ion meter with ESL-43-07 and ESL-63-07 glass electrodes calibrated against buffer solutions. The concentrations of the acid and alkali solutions used in the study were determined by titrimetry, with methyl orange and phenolphthalein as indicators.

Micrographs were taken on an S-6D Leica stereo microscope with a built-in DC300 video camera.

IR spectra of the samples were recorded with a NIKOLET-5700 Fourier spectrophotometer in pellets with KBr in the spectral range 400–4000 cm^{-1}. Spectra of solid samples (natural bentonite and organomineral ion exchangers) were measured for a powdered sample (0.5–1.0 mg) compacted into a pellet with optically pure KBr (200–250 mg). IR spectra of liquid samples (GMA) were measured with the samples placed between KRS plates.

Oxygen-containing functional groups present on the surface of carbon adsorbents are identical in chemical composition to the same groups contained in individual chemical compounds. Therefore, they can be identified and quantitatively determined by the methods commonly accepted for these purposes. Experiments were carried out on determining the presence and content of acid and base functional groups, and the static exchange capacity of a sample of natural shungite was calculated. The content of surface acid groups was found by neutralization with a 0.1 N KOH solution for 24 h and subsequent titration of the alkali residue in the filtrate with a 0.1 N solution of HCl. In a similar way was calculated the concentration of OH groups (mg-equiv g^{-1}) retained by anion-exchange centers on the shungite surface.

It was found that the concentration of the acid solution brought in contact with a sorbent changes only slightly upon completion of a run, whereas the alkali concentration changes significantly, compared with its initial value. Consequently, shungite possesses amphoteric properties with predominance of acid functional groups, compared with base groups. The SEC (mg-equiv g^{-1} shungite) for cations, determined by the commonly accepted method from data on KOH sorption from a 0.1 N aqueous solution, is 3.8 mg-equiv g^{-1}, and that found for a 0.1 N HCl solution, 1.5 mg-equiv g^{-1} (s : l = 1 : 100).

In the presence of chemically active oxygen-containing groups, modifier molecules can be attached to the external surface by chemisorption bonds. As shown above, the predominant acid properties of the shungite surface will probably favor formation of new chemical bonds in the case of its modification with amines.

After modification of the natural sorbent with PEA (100°C, 30 min), the absorption bands in the spectrum of the modified product, associated with the mineral fraction of shungite, remain virtually unchanged (Fig. 1a). The positions of the absorption bands associated with the organic component of the rock are somewhat changed. The frequency range 3426–3621 cm^{-1} belongs to stretching vibrations of the N–H bond and free NH, NH_2, and OH groups. The frequency 1597 cm^{-1} is related to terminal $–CH_2NH_2$ groups. An increase in the time of interaction of shungite with the polyamine (60 min, 100°C) shifts this band to higher frequencies (1626 cm^{-1}), which corresponds to deformation vibrations of amino groups. The frequency of 2955 cm^{-1} disappears, which is probably due to interaction of amino groups with OH groups on the surface of the mineral. The band at 1715 cm^{-1}, associated with vibrations of the C=O bonds of the carboxy group in aromatic and aliphatic acids, and that at 1261 cm^{-1}, related to stretching vibrations of the C=O bonds of the phenol and carboxy groups, are shifted. This indicates that the functional groups of shungite are involved in the formation of a modifying layer.

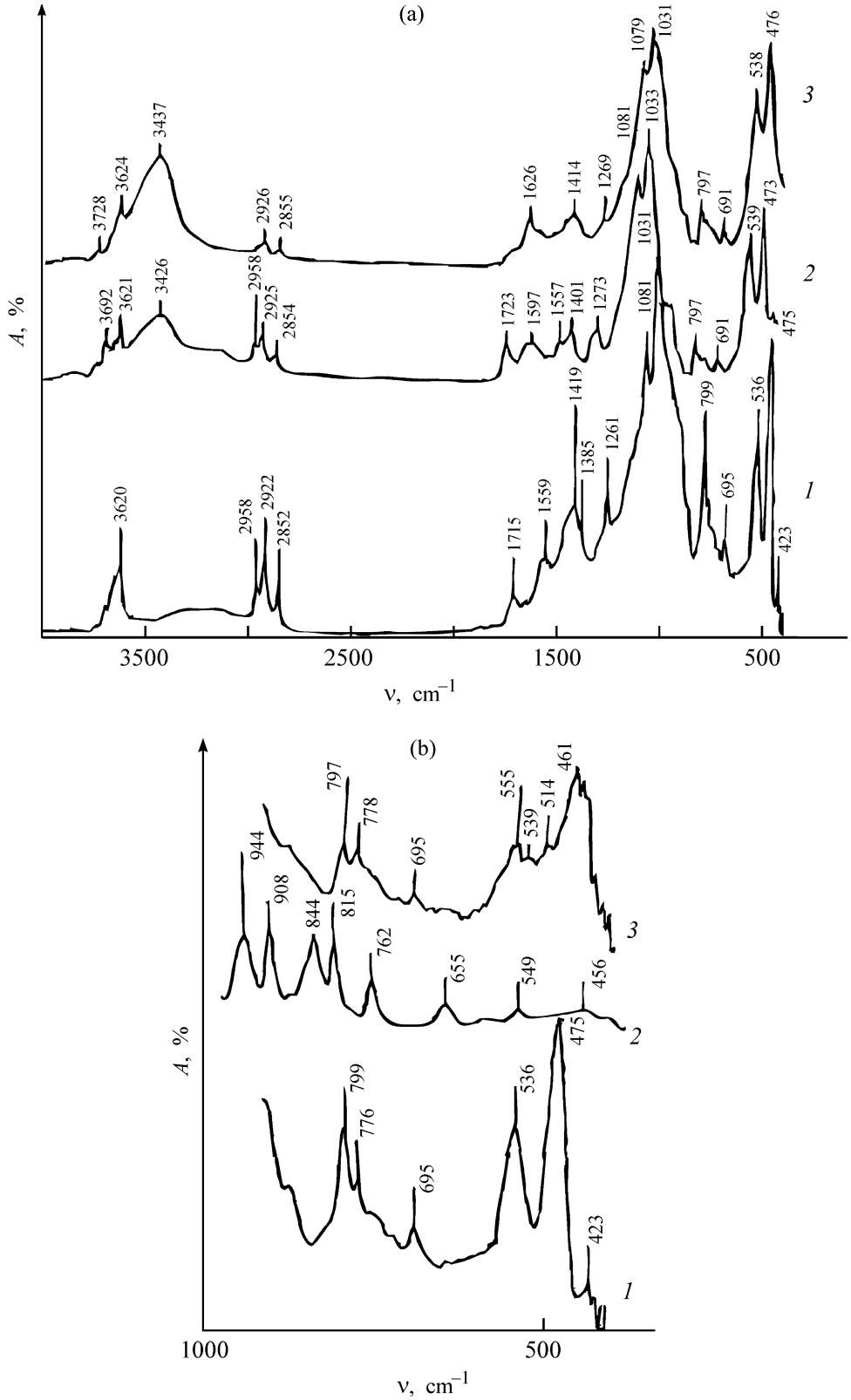

Fig. 1. IR spectra of (*1*) natural and (*2*, *3*) modified shungites. (*A*) Absorption and (ν) wave number. (a) Modification with PEA, 100°C, time of keeping (min): (*2*) 30 and (*3*) 60. (b) (*2*) Modification with PEA and (*3*) anion exchanger based on Sh–PEA–GMA.

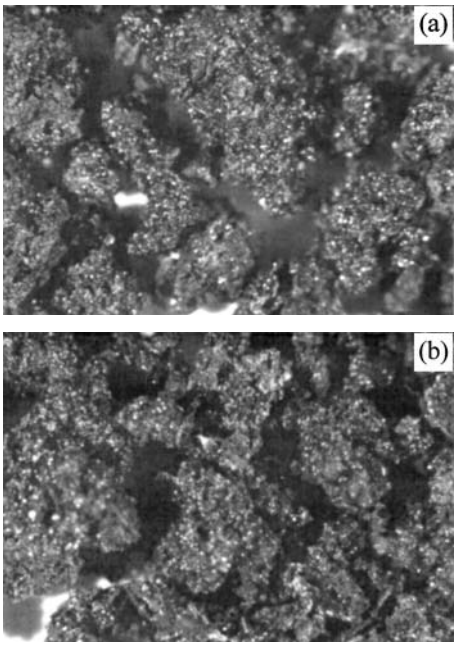

Fig. 2. Micrographs of anion exchangers (c_{sh} = 20%). (a) Sh–PEA–ECH and (b) Sh–PEA–GMA. (Magnification ×40).

Epoxy compounds, such as GMA and ECH, enable firm fixation of functional groups on the shungite surface. The reaction with polyamines involves both the epoxy group and the bound chlorine atom, which was not found in the products. The cleavage of the oxirane ring in interaction of GMA with amino groups is accompanied by heat release, which, in turn, leads to polymerization at the double bond. As a result of chemical modification under the conditions suggested, shungite acquires anion-exchange properties. No acid properties are found in this case. Probably, the surface-active groups of shungite interact with amino groups. As a result, the content of "inactive" nitrogen in the products increases.

Presumably, ECH and GMA interact with COOH and NH_2 groups on the surface of a dispersed carbon substance upon heating of the formulation by the mechanism of curing of epoxy compounds by organic acids, their anhydrides, and amines:

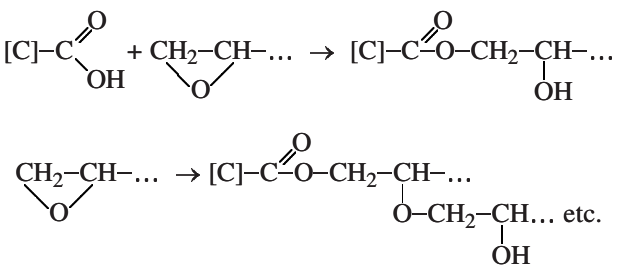

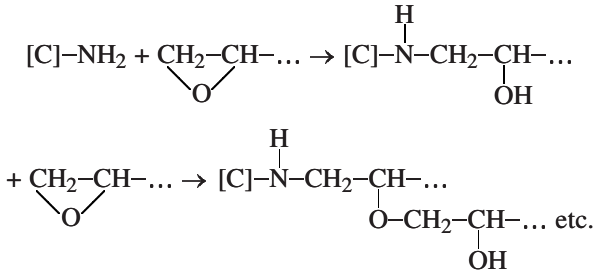

where [C] stands for shungite.

The heat released in chemical modification of the epoxy groups of GMA promotes polymerization of the monomer at the double bond:

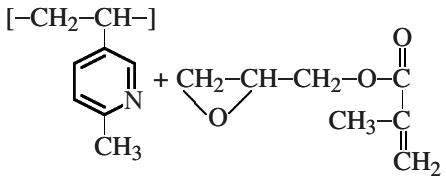

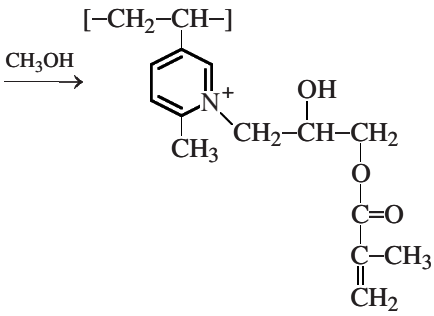

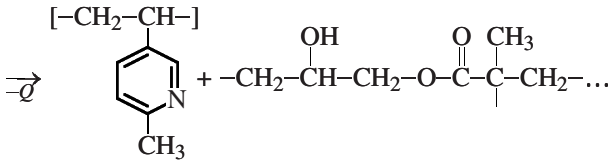

In the IR spectra of the anion exchangers, measured at 500–1000 cm^{-1} (Fig. 1b), the characteristic frequencies of deformation vibrations of epoxy groups at 762–944 cm^{-1} disappear, which points to their chemical transformation upon modification. In the final product, the absorption bands related to the mineral (461, 555 cm^{-1}) and organic (695–797 cm^{-1}) components of shungite have a lower intensity.

As can be seen in the micrographs in Fig. 2, the anion exchangers have the form of particles with a developed surface, whose shape and texture are identical to that of analogous organopolymer sorbents.

The modification was performed on shungites with varied content of carbon (20–80%). It was shown that an increase in the content of an aminating agent affects in different ways the exchange properties and

Table 1. SEC of anion exchangers at various mass ratios between the components of Sh–PEA–GMA (T = 100°C, τ = 5 h)

Sh : PEA : GMA (mass fraction)	SEC* for Cl^-, mg-equiv g^{-1} (c_{sh} = 20%)	N_{el}/N_{act}, %/%	SEC* for Cl^-, mg-equiv g^{-1} (c_{sh} = 60%)	N_{el}/N_{act}, %/%	SEC* for Cl^-, mg-equiv g^{-1} (c_{sh} = 80%)	N_{el}/N_{act}, %/%
1 : 1 : 1	1.99	6.96 / 2.79	3.50	9.32 / 4.90	1.99	6.33 / 4.52
1 : 2 : 1	3.99	10.59 / 5.59	4.98	8.5 / 6.97	2.00	10.07 / 7.19
1 : 3 : 1	4.98	14.69 / 6.97	4.00	8.65 / 5.6	2.49	10.35 / 7.39
1 : 4 : 1	2.98	14.30 / 5.57	3.90	13.87 / 5.46	3.96	11.56 / 8.25

* Titration with a 0.1 N solution of HCl.

Table 2. Effect of the content of polyamines on the SEC of Sh–PEA–GMA, Sh–PEA–ECH, and Sh–PMVP–GMA anion exchangers (c_{sh} = 20%)

PEA (mass fraction)	SEC* for Cl^-, mg-equiv g^{-1}, Sh : GMA = 1 : 1	N_{el}/N_{act}, %/%	SEC* for Cl^-, mg-equiv g^{-1}, Sh : ECH = 1 : 1	N_{el}/N_{act}, %/%	PMVP, (mass fraction)	SEC** for Cl^-, mg-equiv g^{-1}, Sh : GMA = 1 : 1	N_{el}/N_{act}, %/%
1	1.99	6.96 / 2.79	2.49	8.29 / 3.49	0.5	1.6	4.60 / 2.24
2	3.99	10.59 / 5.59	3.00	8.03 / 4.2	1	2.49	5.59 / 3.49
3	4.98	14.69 / 6.97	3.98	8.07 / 5.57	2	3.00	6.50 / 4.2
4	2.98	14.30 / 5.57	3.98	8.10 / 5.57	3	1.49	7.48 / 2.09

* Titration with a 0.1 N solution of HCl. ** Titration with a 0.1 N solution of NaCl.

Table 3. Effect of the amount of epoxy compounds on the SEC of anion exchangers (T = 100°C, τ = 5 h)

Sh : PEA : GMA (mass fraction)	SEC* for Cl^-, mg-equiv g^{-1}	Sh : PEA : ECH (mass fraction)	SEC* for Cl^-, mg-equiv g^{-1}	Sh : PMVP : GMA (mass fraction)	SEC** for Cl^-, mg-equiv g^{-1}
1 : 3 : 0.5	5.98	1 : 3 : 0.5	4.99	1 : 2 : 0.5	2.70
1 : 3 : 1.0	7.00	1 : 3 : 1.0	5.98	1 : 2 : 1	3.00
1 : 3 : 1.5	5.99	1 : 3 : 1.5	6.98	1 : 2 : 1.5	2.50
1 : 3 : 2.0	5.50	1 : 3 : 2.0	6.00	1 : 2 : 2	2.00

* Titration with a 0.1 N solution of HCl. ** Titration with a 0.1 N solution of NaCl.

the content of nitrogen in the products (Table 1). To exclude the stage of preliminary treatment of shungite and simplify the process, natural shungite (c_{sh} = 20%) was used in further studies.

One of the main parameters that enable control in a wide range over ion-exchange properties of adsorbents is the reagent ratio. A strong influence is exerted by the content of a polyamine in the reaction mixture. It was found that raising the amount of PEA and PMVP leads to an increase in the exchange capacity and in the nitrogen content, irrespective of the nature of the epoxy compound (Table 2). A further increase in the content of PEA to more than 3 mass fractions and in that of PMVP to more than 2 mass fractions impairs the ion-exchange properties of the anion-exchangers. This is due to the poorer curing conditions of the products. An analysis for the nitrogen content of the samples by the Kjeldahl method demonstrated that the total amount of nitrogen exceeds that in functional groups (exchange nitrogen).

At the optimal contents of PEA, found in this study, the influence exerted by the amount of the epoxy components on the exchange properties of the products obtained was analyzed (Table 3). An in-

Table 4. Effect of the process duration and temperature on the exchange capacity of anion exchangers with Sh : PEA : GMA = 1 : 3 : 1 (mass fraction) and Sh : PEA : ECH = 1 : 3 : 1.5 (mass fraction)

τ, h (100°C)	SEC* for Cl^-, mg-equiv g^{-1}		T, °C (5 h)	SEC* for Cl^-, mg-equiv g^{-1}	
	Sh–PEA–GMA	Sh–PEA–ECH		Sh–PEA–GMA	Sh–PEA–ECH
5	7.00	6.98	80	5.00	5.50
8	7.15	7.00	100	7.00	6.98
10	7.15	6.88	120	6.10	6.90
12	6.90	6.50	–	–	–

* Titration with a 0.1 N solution of HCl.

Table 5. Physicochemical parameters of the anion exchangers

Anion exchanger, mass fraction	SEC* for Cl^-, mg-equiv g^{-1}	Q	P_n	V_n	Chemical resistance, %		
		mg l^{-1}			5 N H_2SO_4	5 N NaOH	H_2O (100°C, 24 h)
Sh : PEA : GMA = 1 : 3 : 1	7.00	4.25	0.20	5.03	91	92.86	96.77
Sh : PEA : ECH = 1 : 3 : 1.5	6.98	3.20	0.24	4.21	95.98	93.83	95.84

* Titration with a 0.1 N solution of HCl.

crease in the concentrations of the epoxy components leads to a decrease in the SEC of the anion exchangers. It was shown that, after titration with a 0.1 N solution of HCl, the ion-exchange capacity for Cl^- becomes as high as 6.98–7.00 mg-equiv g^{-1} at mass ratios of 1 : 3 : 1 and 1 : 3 : 1.5 for the anion exchangers based on Sh–PEA–GMA and Sh–PEA–ECH, respectively.

For the anion exchanger based on the aromatic polyamine, SEC reaches a value of 3.00 mg-equiv g^{-1} under the experimental conditions upon titration with a 0.1 N solution of NaCl. The ion exchanger samples are composed of irregularly shaped gray-black particles ($d \leq 0.25–0.5$ mm).

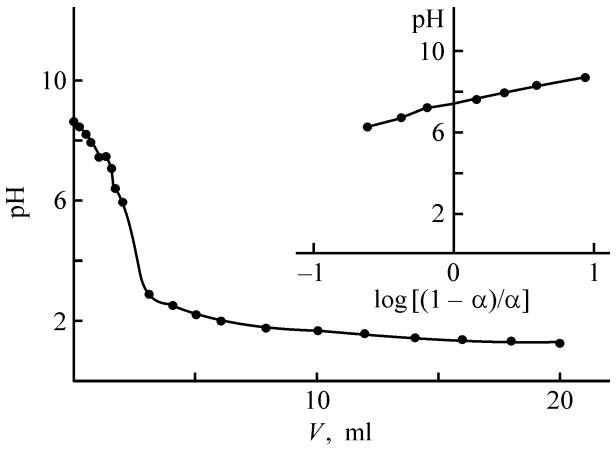

Fig. 3. Potentiometric titration curve for Sh–PEA–GMA anion exchanger (c_{sh} = 20%) and the dependence of the solution pH on $\log[(1 - \alpha)/\alpha]$. ($V$) Volume of the 0.1 N solution of HCl.

A study of the effect of the process duration and temperature demonstrated (Table 4) that the anion exchangers with Sh : PEA : GMA = 1 : 3 : 1 and Sh : PEA : ECVH = 1 : 3 : 1.5, which have high exchange parameters, are formed at a modification temperature of 100°C in 5–8 h. A decrease or increase in the process duration with respect to the range specified above leads to a decrease in SEC, which is presumably due to deterioration of the strength properties or to densification of the sorbent structure, respectively. The decrease in the ion-exchange properties of the products at high temperatures is due to an increase in the density of cross-linking bonds between macromolecules and the resulting hindered accessibility to ion exchange.

Under industrial conditions, ion exchangers may come in contact with solutions of acids and alkalis of various concentrations, as well as with water and aqueous solutions at elevated temperatures. This can cause chemical destruction leading to decomposition of ion exchangers and to a decrease in their capacity. As the resistance parameter was taken the change in capacity in relation to the time of contact between ion exchangers and corrosive solutions. Stability studies demonstrated that the chemical and thermal resistance of the anion exchangers synthesized is 91–97% (Table 5). Thus, the medium-basic anion exchangers can successfully work at elevated temperatures in various media. The bulk density of the anion exchangers is 0.20–0.24 g ml^{-1}, and the swelling capacity, 3.20–4.25 ml g^{-1}.

An important factor characterizing the functional groups of ion exchangers and determining the degree of their dissociation is the pH of the medium. The method of potentiometric titration was used to study the acid-base properties of the Sh–PEA–GMA anion exchanger. The acid dissociation constant p_{K_α} was found for the ionogenic groups of the ion exchanger from the potentiometric titration curves in Fig. 3. The dissociation constant of the anion exchanger under study, $p_{K_\alpha} = 7.35$, characterizes it as a medium-basic polyfunctional ion exchanger and falls within the limits reported in the literature for the known brands of anion exchangers.

CONCLUSIONS

(1) It was found that modification of shungite with various polyamines, followed by cross-linking with epoxy compounds, leads to formation of anion-exchange groups on the surface of the natural adsorbent.

(2) A method for synthesis of chemically and thermally resistant anion exchangers with a shungite matrix was developed on the basis of the results obtained.

(3) It was shown that the ion-exchange properties of the samples depend on the ratio between the reacting components, nature of modifiers, and parameters of modification of the starting material.

REFERENCES

1. Solov'eva, A.B., Rozhkova, N.N., Glagolev, N.N., et al., *Zh. Fiz. Khim.*, 1999, vol. 73, no. 2, pp. 299–303.
2. Akimbaeva, A.M., Ergozhin, E.E., and Sadvokasova, A.B., *Khim. Tverd. Tela*, 2005, no. 2, pp. 71–75.
3. Chmutin, I.A., Ryvkina, N.G., Solov'eva, A.B., et al., *Vysokomol. Soedin.*, 2004, vol. 46, no. 6, pp. 1061–1070.
4. Efremova, S.V., Korolev, Yu.M., Nauryzbaev, M.K., and Efremov, S.A., *Khim. Tverd. Tela*, 2003, no. 1, pp. 11–20.
5. Kolesnikov, B.Ya., Efremova, S.V., Balybin, Yu.F., and Efremov, S.A., Abstracts of Papers, *Mezhdunarodnaya konferentsiya po analiticheskoi khimii* (Int. Conf. on Analytical Chemistry), Almaty, 1998.
6. Toroptseva, A.M., *Laboratornyi praktikum po khimii i tekhnologii vysokomolekulyarnykh soedinenii* (Laboratory Course of Chemistry and Technology of Macromolecular Compounds), Leningrad: Khimiya, 1972.

ISSN 1070-4272, Russian Journal of Applied Chemistry, 2007, Vol. 80, No. 8, pp. 1316–1321. © Pleiades Publishing, Ltd., 2007.
Original Russian Text © G.I. Medvedev, N.A. Makrushin, V. Khamun'ela, 2007, published in Zhurnal Prikladnoi Khimii, 2007, Vol. 80, No. 8, pp. 1276–1281.

APPLIED ELECTROCHEMISTRY AND CORROSION PROTECTION OF METALS

Elecrodeposition of Lustrous Zinc Coatings from Sulfate Electrolyte

G. I. Medvedev, N. A. Makrushin, and V. Khamun'ela

Novomoskovsk Institute, Mendeleev Russian University of Chemical Engineering, Novomoskovsk, Tula oblast, Russia

Received December 19, 2006; in final form, March 2007

Abstract—Electrodeposition of lustrous zinc coatings from a sulfate electrolyte containing $ZnSO_4$, Na_2SO_4, buffer additives, and fixers (products of phenol-formaldehyde condensation) was studied.

DOI: 10.1134/S1070427207080101

Lustrous zinc coatings on articles of simple configuration are deposited from sulfate electrolytes containing various brightening additives (aldehydes, ketones, sulfo compounds, and various condensation products of complex composition [1–4]).

In this study, we examined the electrodeposition of zinc from a sulfate electrolyte containing a fixer, product of phenol-formaldehyde condensation with the structural formula

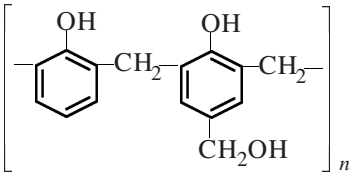

The study was performed in an electrolyte containing ($g\ l^{-1}$): $ZnSO_4 \cdot 7H_2O$ 200–250, $Na_2SO_4 \cdot 10H_2O$ 50–100, $Al_2(SO_4)_3 \cdot 18H_2O$, H_3BO_3, aminoacetic acid 25–30, and fixer 0.5–5, at 18–25°C and pH 2–5. Zinc plates served as anodes. A 6–15-μm-thick zinc layer was deposited onto unpolished St.3 steel. Polarization curves were recorded with a P-5828 potentiostat. The luster was measured on a FB-2 photoelectric luster meter. The leveling power P of the electrolytes was determined by a direct profile measurement of the sample surface with a sinusoidal microprofile. P was calculated by the formula [5]

$$P = 2.3a/2\pi h_{av} \log (H_0/H_i),$$

where a is the sine wave amplitude of the microprofile; h_{av}, average thickness of the coating (10 μm); H_0 and H_i, initial and final amplitudes of the sinusoidal microprofile, respectively.

The capacitance of the electric double layer was measured in the course of electrolysis with a P-5021 ac bridge at a frequency of 30 kHz in a series equivalent circuit. A zinc-coated platinum wire placed at the center of a platinum-coated cylinder served as the working electrode. The pH value in the near-electrode layer was measured by the method described in [6]. The degree of surface filling with organic additives, Q, was estimated using the polarization curves [7] by the formula

$$Q = 1 - \exp(\Delta E/b),$$

where ΔE is the potential shift in cathodic polarization, and b is the Tafel constant found from the polarization curves plotted in the semilog scale.

The internal stresses and microhardness of the coatings were determined as described in [8].

The results obtained in a study of the influence exerted by the fixer concentration, nature of the buffer additive, and current density on the outward appearance of the coatings show that dark gray coatings with a rough surface are formed from an electrolyte containing $Al_2(SO_4)_3$ buffer additive and a fixer at i_c = 1–11 A dm^{-2}. At the same time, lustrous coatings are formed from an electrolyte containing H_3BO_3

Table 1. Effect of buffer additives, fixer concentration, and current density on the outward appearance of zinc coatings [electrolyte composition (g l^{-1}): $ZnSO_4 \cdot 7H_2O$ 200 and $Na_2SO_4 \cdot 10H_2O$ 50; pH 3–4, T = 20°C]

Buffer additive, g l^{-1}	Fixer concentration, g l^{-1}	Current density, A dm^{-2}	Coating appearance
HBO_3, 30	0.5	1–5	Silvery
		6–11	Silvery with burn-on
	1–2	1	Silvery
		2–10	Lustrous
		11	Lustrous with burn-on
	3–4	1	Silvery
		2–5	Lustrous
		6–8	Semilustrous
		9–11	Semilustrous with burn-on
	5	1–3	Lustrous
		4–6	Semilustrous
		7–11	Semilustrous with burn-on
Aminoacetic acid 30	0.5	1–5	Silvery
		6–8	Silvery with burn-on
	1–2	1–8	Lustrous
		9–11	Lustrous with burn-on
	3–4	1–4	Lustrous
		5–8	Semilustrous
		9–11	Semilustrous with burn-on
	5	1–2	Lustrous
		3–5	Semilustrous
		6–8	Silvery
		9–11	Silvery with burn-on

and aminoacetic acid. As can be seen in Table 1, the outward appearance of the coatings varies in this case with the fixer concentration and with the cathode current density.

The widest range of current densities at which lustrous coatings are formed is observed at fixer concentrations of 1–2 g l^{-1}. In this case, the current densities vary in the range from 2 to 10 A dm^{-2} in an electrolyte containing H_3BO_3, and from 1 to 8 A dm^{-2} in an electrolyte containing aminoacetic acid. At higher fixer concentrations (c = 3–5 g l^{-1}), the range of current densities at which lustrous coatings are deposited is markedly narrower.

In the electrolytes studied, the pH value should be within the range 3–4. At pH < 3, the i_c range providing deposition of lustrous coatings and the current efficiency decrease. At pH > 4 lustrous coatings are deposited, but the electrolyte exhibits an unstable behavior. The current efficiency by zinc in the electrolytes yielding lustrous coatings varies from 85 to 97%. In the electrolyte containing aminoacetic acid, the current efficiency is the highest (Fig. 1, curves *1*, *2*).

Cathodic polarization curves were measured in the zinc-plating electrolytes. As can be seen in Fig. 2, the presence of a fixer enhances the cathodic polarization (Fig. 2, curves *1*, *2*). The inhibition effect of the fixer on the electrodeposition of zinc is due to its

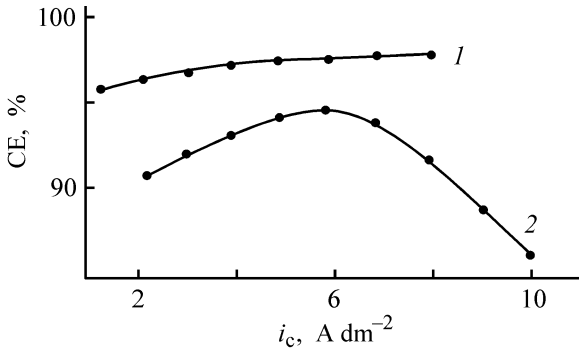

Fig. 1. Current efficiency CE by zinc vs. the current density i_c. Electrolyte composition (g l^{-1}): $ZnSO_4 \cdot 7H_2O$ 200, $Na_2SO_4 \cdot 10H_2O$ 50, fixer 1; pH 3.5. (*1*) Electrolyte + aminoacetic acid, 30 g l^{-1}; (*2*) electrolyte + H_3BO_3, 30 g l^{-1}.

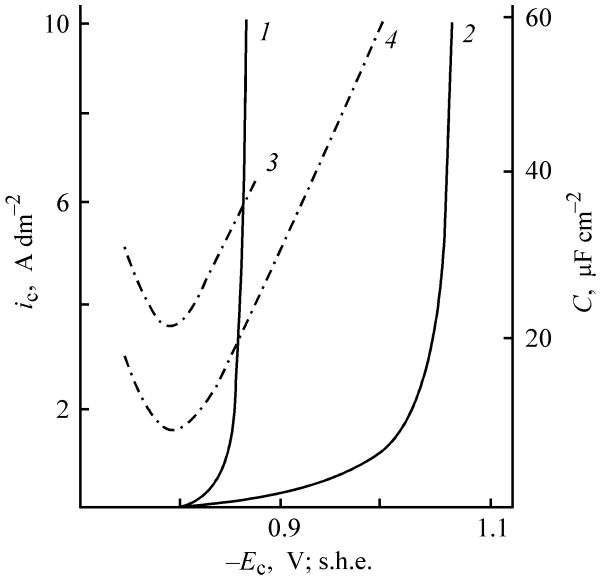

Fig. 2. Current density i_c and electric double layer capacitance C vs. the electrode potential E_c in a zinc-plating electrolyte. Electrolyte composition (g l^{-1}): $ZnSO_4 \cdot 7H_2O$ 200, $Na_2SO_4 \cdot 10H_2O$ 50, H_3BO_3 30, pH 3.5. (*1*), (*3*) Electrolyte, (*2*), (*4*) electrolyte + fixer, 1 g l^{-1}.

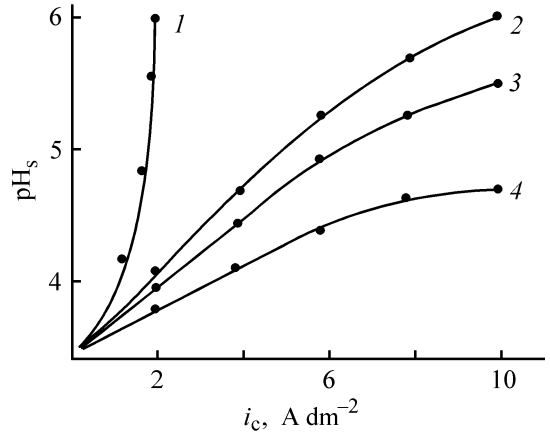

Fig. 3. Dependence of pH$_s$ in the near-cathode layer on the current density i_c in a zinc-plating electrolyte. Electrolyte composition (g l^{-1}): $ZnSO_4 \cdot 7H_2O$ 200, $Na_2SO_4 \cdot 10H_2O$ 50, fixer 1. (*1*) Electrolyte; (*2*) electrolyte + H_3BO_3, 30 g l^{-1}; (*3*) electrolyte + $Al_2(SO_4)_3 \cdot 18H_2O$, 30 g l^{-1}; (*4*) electrolyte + aminoacetic acid, 30 g l^{-1}.

adsorption on the cathode surface. This is confirmed by the results obtained in measuring the capacitance of the electric double layer. In the electrolyte containing no fixer, the capacity-vs.-potential dependence has a minimum (C = 20 μmF cm^{-2}) at a potential of –0.8 V (Fig. 2, curve *3*). Introduction of a fixer into the electrolyte lowers the double layer capacitance to 9 μmF cm^{-2} at E = –0.8 V (Fig. 2, curve *4*). An increase in the capacitance is observed at more negative potentials, which is due to partial desorption of the fixer from the electrode surface [9].

The electrolytes yielding lustrous zinc coatings exhibit the leveling effect. The leveling power varies from 0.2 to 0.4, depending on the cathode current density. The throwing power of the electrolytes is 8–12%. The microhardness of the zinc deposits varies within the range 80–100 kg mm^{-2}. The lustrous zinc coatings have small internal stresses (IS = 100–150 kg cm^{-2}).

As is known [3], the deposition of lustrous coatings is due to smoothing of the submicrometer surface roughness. For a dull coating to be formed, it suffices that an additive is adsorbed on the cathode surface and the electrocrystallization overpotential is raised, whereas formation of a lustrous coating, requires that an adsorption layer of a certain composition should be present on the cathode surface. Such layers can be formed from organic substances and products of secondary reactions in the near-cathode layer. In the case of a simultaneous metal deposition and hydrogen evolution, the adsorption layer may consist of hydroxides and other basic compounds [3].

The suggestion that zinc hydroxides are formed in the near-cathode space is confirmed by the results of pH measurements in the near-cathode layer (pH$_s$). As can be seen from Fig. 3, pH$_s$ varies at i_c = 1–10 A dm^{-2} from 4 to 6, depending on the nature of the buffer additive. In the electrolyte containing aminoacetic acid, the range of pH variation is the narrowest (curve *4*). It should be noted that the pH of hydrate formation in the zinc-plating electrolyte is 6.4. These results suggest that presence of zinc hydrates in the near-cathode layer is not necessary for lustrous coatings to be deposited. Apparently, lustrous coatings are deposited if a highly dispersed adsorption layer is formed on the surface [3].

Apparently, buffer additives control the dispersity of the adsorption layer. In their presence, the adsorption layer may change because of the formation of difficultly soluble zinc borates in the near-cathode space. It is not improbable that complex compounds of orthoboric and aminoacetic acids with zinc ions, as well as intracomplex (chelated) compounds of H_3BO_3 with the fixer, can be formed.

An important issue in elucidating the mechanism of formation of lustrous coatings, is determining the degree of filling of the cathode surface with the adsorbed additive. The dependences of the degrees of luster (curve *1*) and surface filling (curve *2*) on the cur-

rent density are shown in Fig. 4. It can be seen that, as the cathode current density increases, the degree of luster of the coatings passes through a maximum, whereas the degree of filling decreases. At the current densities studied, the degree of surface filling varies from 24 to 10%. This shows that lustrous coatings are formed at a well-defined degree of surface filling.

To elucidate the mechanism by which the fixer affects the electrodeposition of zinc, we carried out a quantum-chemical study of a system constituted by hydrated ions present in the electrolyte and fixer molecules. To find the degree of polymerization, n, of the fixer molecule, its molecular weight was determined by the cryoscopic method. The results of these measurements demonstrated that $n = 1$. Consequently, the electrolyte also contains a monomeric product of phenol-formaldehyde (F) condensation.

The quantum-chemical calculation was performed by the semiempirical PM3 method [11, 12]. Compared with other semiempirical methods and ab initio calculations with different basis sets [13], this method describes rather well the parameters of intermolecular interactions. The energy of interaction between the particles constituting the system under consideration was calculated as the difference between the total electronic energy of the system and the sum of the total electronic energies of its constituents. For example, we calculated for the system Zn_{49}–$[ZnF]^{2+}$, first, the energy of interaction between a complex-forming ion and the ligand in the complex $[ZnF]^{2+}$ ion

$$\Delta E_c = E_{[ZnF]^{2+}} - (E_{Zn^{2+}} + E_F),$$

and then the energy of interaction of the complex ion with the cluster

$$\Delta E_{cl} = E_{Zn_{49}-[ZnF]^{2+}} - (E_{[ZnF]^{2+}} + E_{Zn_{49}}).$$

The results of the calculation show that, similarly to the case of 2-butyne-1,4 diol [14], the interaction of Zn^{2+} ions with the formaldehyde molecules is more energetically favorable than the formation of a hydrated shell of the ion. In a sulfate zinc-plating electrolyte, complex ions of composition $[Zn(H_2O)_x(F)_y]^{2+}$, where $x = 1$–5, $y = 1$–3, are most likely to exist in the electrolyte bulk.

In the near-cathode layer, mixed aqua hydroxo complexes of various compositions with formaldehyde molecules can be formed via alkalization. In view of the fact that formaldehyde molecules displace water molecules from the Zn^{2+} aqua complexes (Fig. 5), the formation of $Zn(OH)_2$, $Zn(OH)^+$, and $[ZnF]^{2+}$–

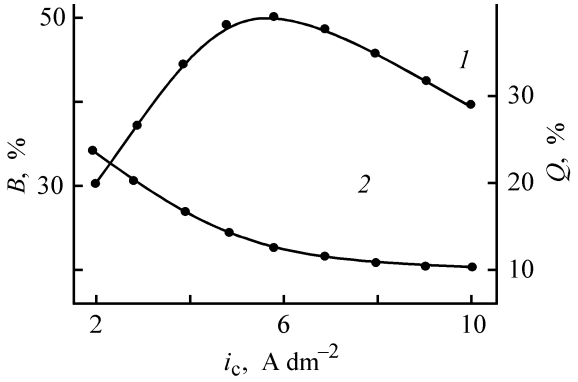

Fig. 4. Degree of luster B (*1*) and degree of the surface filling Q (*2*) vs. the current density i_c.

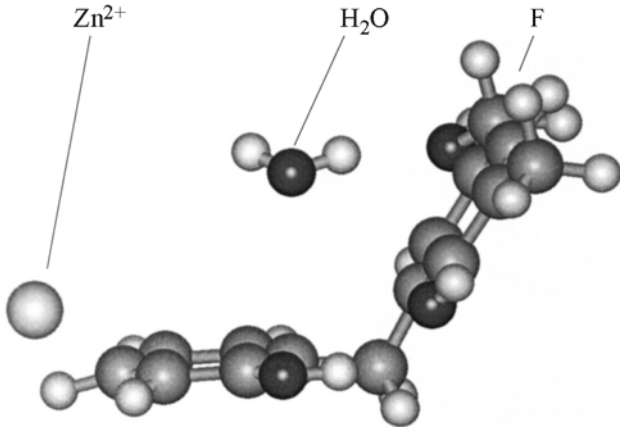

Fig. 5. Structure of a Zn^{2+} complex with a monomeric product of phenol-formaldehyde (F) condensation and a water molecule, according to the results of a quantum-chemical calculation Formaldehyde molecule: hydrogen atoms, white; carbon, gray; and oxygen, dark gray.

$[Zn(OH)F]^+$ species is most likely in the near-cathode layer. Less probable is the formation of $[Zn(OH)_2F]$ species.

In the next stage, we carried out a quantum-chemical study of the structure of complexes with formaldehyde molecules at the electrode–solution interface. In doing so, we modeled the surface of the zinc electrode with a cluster formed by 49 atoms arranged in two layers having the hexagonal form. The clusters were chosen as recommended in [15].

To simulate the reduction of Zn^{2+} on the surface of the zinc electrode, the zinc cluster system Zn_{49}–Zn^{2+}–F was calculated. It was shown that the highest interaction energy with the Zn_{49} cluster is observed for $Zn(OH)^+$ species. The formaldehyde molecules in the complex constitute, as they approach the cluster, a stable system at a distance of 418 pm from the cluster. In this case, the interaction energy is 437 kJ mol^{-1}, which considerably exceeds the value for interaction of the cluster with

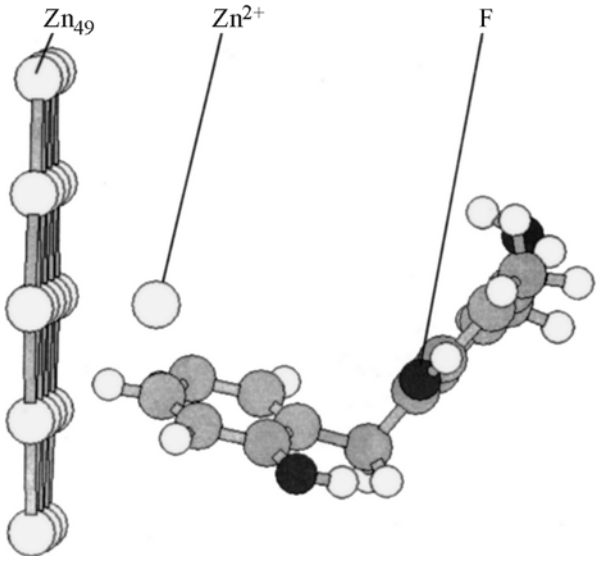

Fig. 6. Structure of a Zn^{2+} complex with a monomeric product of phenol-formaldehyde (F) condensation on the surface of the Zn_{49} cluster, according to the results of a quantum-chemical calculation.

a hydrated zinc ion (200 kJ mol^{-1}) and a $[Zn(OH)F]^+$ species. The presence of a formaldehyde molecule in the complex species makes distance between the zinc ion and the cluster surface considerably larger. This may result from the spatial structure of the forming complexes, which creates, owing to the large size of the formaldehyde molecule, steric hindrance to approach of zinc ions to the cluster (Fig. 6). It is noteworthy that, without Zn^{2+} ions, the formaldehyde molecule forms no stable system with the cluster.

The rather wide variety of complex species formed in the near-cathode layer suggest that their discharge can occur by different pathways. To assess the probabilities of these pathways, we calculated the change in the total energy of the reaction products (Table 2) in comparison with the total energy of the starting substances. In doing so, we took into account that the energy necessary for an electron to be involved in each of the above processes is constant. In the given case, the reactions involving and not involving formaldehyde molecules were considered.

Table 2. Changes in the total energy of the products in comparison with the total energy of starting substances

Reaction	Reaction equation	ΔE, kJ mol^{-1}
(1)	$Zn(OH)_2 + e = ZnOH + OH^-$	271
(2)	$ZnOH^+ + e = ZnOH$	–897
(3)	$[ZnF]^{2+} + e = Zn^+ + F$	–874
(4)	$[Zn(OH)F]^+ + e = ZnOH + F$	–662
(5)	$[Zn(OH)_2F] + e = ZnOH + OH^- + F$	173

It follows from the data in Table 2 that reactions (2)–(4) yielding ZnOH species and Zn^+ ions are the most probable from the energy standpoint. Presumably, of all three reactions, reaction (2) is the first to occur. The species forming in this case enter into the following electrochemical reactions:

$$ZnOH + e = Zn + OH^-,$$

$$Zn^+ + e \rightarrow Zn.$$

Thus, our quantum-chemical calculations demonstrated that, in a sulfate zinc-plating electrolyte containing formaldehyde molecules, the probability of existence of complex ions $[Zn(H_2O)_x(F)_y]^{2+}$ in the electrolyte bulk is the highest, whereas in the near-cathode space, $[Zn(OH)]^+$, $[ZnF]^{2+}$, and $[Zn(OH)F]^+$ are electrically active particles owing to alkalization.

The study we performed enabled us to develop a sulfate zinc-plating electrolyte of simple composition for deposition of lustrous coatings with smoothed surface. The electrolyte composition is as follows (g l^{-1}): $ZnSO_4 \cdot 7H_2O$ 200–250, $Na_2SO_4 \cdot 10H_2O$ 50–100, H_3BO_3 25–30, and fixer 1–2. The process is performed at i_c = 2–10 A dm^{-2}. The electrolyte temperature is 18–25°C, pH 3–4, and CE = 84–97%. The anodes are made of zinc. Aminoacetic acid (c = 25–30 g l^{-1}) can be taken instead of H_3BO_3. In this case, lustrous coatings are obtained at i_c = 1–8 A dm^{-2} with CE = 86–97%.

CONCLUSIONS

(1) A study of zinc electrodeposition from a sulfate electrolyte containing a fixer (product of phenol-formaldehyde condensation) and buffer additives demonstrated that the fixer taken together with H_3BO_3 or aminoacetic acid yields lustrous zinc coatings with smoothed surface at i_c = 1–10 A dm^{-2}.

(2) The system constituting hydrated zinc ions and fixer (formaldehyde) molecules was studied using the quantum-chemical method. It was shown that complexes of composition $[Zn(H_2O)_x(F)_y]^{2+}$ are most likely to be present in the electrolyte bulk. In the near-cathode layer, $[Zn(OH)]^+$, $[ZnF]^{2+}$, and $[Zn(OH)F]^+$ are electrically active species owing to alkalization.

(3) Sulfate electrolytes for deposition of lustrous zinc coatings with smoothed surface were developed.

REFERENCES

1. Kudryavtsev, N.G., *Elektroliticheskie pokrytiya metallami* (Metal Electroplating), Moscow: Khimiya, 1979.
2. Zhilienene, B.M., *Patentnaya literatura po elektroosazhdeniyu zinka iz netsianistykh rastvorov za 1960–1972 gody* (Patent Literature on Zinc Electrodeposition from Noncyanide Solutions, Published in 1960–1972), Vilnius: Inst. Khim. Khim. Tekhn., 1972.
3. *Blestyashchie elektroliticheskie pokrytiya* (Lustrous Electrolytic Coatings), Matulis, Yu.Yu., Ed., Vilnius: MINTIS, 1969.
4. Proskurin, E.V., Popovich, V.A., and Moroz, T.M., *Tsinkovanie: Spravochnoe izdanie* (Zinc Plating. Reference Book), Moscow: Metallurgiya, 1988.
5. Bakhchisarayunyan, N.G., Borisoglebskii, Yu.V., Burkat, G.K., et al., *Praktikum po prikladnoi elektrokhimii: Uchebnoe posobie dlya vuzov* (Laboratory Manual of Applied Electrochemistry: Textbook for Higher School Institutions), Voropaev, V.N. and Kudryavtsev, V.N., Eds., Leningrad: Khimiya, 1990, 3nd ed. revised.
6. Gershov, V.M., Purin, B.A., and Ozol'–Kalnin', G.A., *Elektrokhimiya*, 1972, vol. 8, no. 5, pp. 673–675.
7. Hangen, R., and Clampit, B., *J. Phys. Chem.*, 1954, vol. 58, no. 5, pp. 908–913.
8. Vyacheslavov, P.M., and Shmeleva, N.M., *Metody ispytanii elektroliticheskikh pokrytii* (Methods for Testing of Electrodeposited Coatings), Moscow: Mashinostroenie, 1977.
9. Damaskin, B.B., Petrii, O.A., and Batrakov, V.V., *Adsorbtsiya organicheskikh soedinenii na elektrodakh* (Adsorption of Organic Compounds on Electrodes), Moscow: Nauka, 1968.
10. Yakovlev, A.G., *Praktikum po fizicheskoi i kolloidnoi khimii* (Laboratory Manual of Physical and Colloid Chemistry), Moscow: Vysshaya Shkola, 1967.
11. Stewart, J.J.P., *J. Comput. Chem.*, 1989, vol. 10, no. 2, pp. 209–220.
12. Stewart, J.J.P., *J. Comput. Chem.*, 1991, vol. 12, no. 3, pp. 320–341.
13. Makrushin, N.A., Dubenkov, A.N., Ermakov, A.I., and Merkulov, A.E., *Izv. Tul'skogo Gos. Univ. Khimiya*, 2002, no. 3, pp. 24–31.
14. Larin, E.A., Makrushin, N.A., Dubenkov, A.N., et al., *Izv. Tul'skogo Gos. Univ., Khimiya*, 2004, no. 4, pp. 204–208.
15. Shapnik, M.S., *Elektrokhimiya*, 1994, vol. 30, no. 2, pp. 143–149.

ISSN 1070-4272, Russian Journal of Applied Chemistry, 2007, Vol. 80, No. 8, pp. 1322–1326. © Pleiades Publishing, Ltd., 2007.
Original Russian Text © G. Valyulene, A. Zhelene, V. Jasulaitene, B. Shimkunaite, 2007, published in Zhurnal Prikladnoi Khimii, 2007, Vol. 80, No. 8, pp. 1282–1286.

APPLIED ELECTROCHEMISTRY AND CORROSION PROTECTION OF METALS

Electrochemical Behavior and Composition of Bismuth Sulfide Coatings

G. Valyulene, A. Zhelene, V. Jasulaitene, and B. Shimkunaite

Institute of Chemistry, Vilnius, Lithuania

Received January 31, 2007

Abstract—Cyclic potentiodynamic voltammetry and X-ray photoelectron spectroscopy were used to study the electrochemical behavior and composition of bismuth sulfide coatings deposited by successive ionic layer adsorption and reaction on glassy carbon in a colloid solution of bismuth(III) compounds, with Na_2S as a sulfidizing agent.

DOI: 10.1134/S1070427207080113

In the last decade, semiconducting bismuth sulfide films have been intensely studied owing to their wide use in electronic industry. Close attention is paid to methods for synthesis of crystalline Bi_2S_3 and study of their semiconducting properties. Methods of vacuum deposition, anodic oxidation of bismuth in alkaline sodium sulfide solution, chemical, electrochemical, photochemical deposition in aqueous and nonaqueous solutions, etc. have been described [1–5]. The authors of [6] came to a conclusion that Bi_2S_3 films formed by chemical deposition from aqueous solutions are always amorphous and those electrodeposited are crystalline. Amorphous Bi_2S_3 is transformed to the crystalline state by thermal treatment [5]. Sulfide coatings of metals, including bismuth, used as current-conducting sublayers for decorative and functional metallization of insulators, are most frequently deposited by a simple and low-cost method of successive ionic layer adsorption and reaction (SILAR). The thus deposited layers of nonstoichiometric copper sulfide and Co_2S_3 are widely used in practice. The processes of their electrochemical reduction have been studied not only in supporting electrolytes, but also in nickel- and copper-plating electrolytes. It has been shown [7] that the electrodeposition of metals should be preceded by reduction of a sulfide to the metal. It is known that nickel can be electrochemically deposited onto Bi_2S_3 coatings [8]. However, the electrochemical behavior of Bi_2S_3 has been studied only in alkaline solutions containing sulfide ions. In these studies, the main attention was given to the kinetics and mechanism of formation of sulfide films in anodic oxidation of bismuth [1]. The run of the reduction curves depends on the Bi_2S_3 composition.

The aim of this study was to examine the electrochemical behavior in acid and alkaline solutions of Bi_2S_3 coatings deposited by SILAR onto glassy carbon from a colloid solution of Bi(III) compounds with the help of sodium sulfide and to determine the composition of these coatings.

EXPERIMENTAL

An electrically conducting Bi_2S_3 layer was deposited by the SILAR method, i.e., by successive treatment of the electrode in a 0.1 M BiO(OH) and(or) $Bi(OH)_3$ colloid solution, followed by washing with deionized water, sulfidation in 0.1 M Na_2S solution, and washing with water at room temperature [8]. The times of treatment in bismuth compound solutions and sulfidation were 1 min each, and the time of each washing with water, 30 s. The deposition cycle was repeated twice in electrochemical experiments and six times for a study of the coating composition by X-ray photoelectron spectroscopy (XPS). The colloid solution was prepared from $Bi(NO_3)_3 \cdot 5H_2O$, ammonia, and a special colloid-stabilizing ligand.

SU-1200 glassy carbon polished with 1-μm diamond particles served as a working electrode. Its working surface area was 1 cm^2. The inoperative area of the electrode was insulated with a PVC lacquer.

The electrochemical behavior of the Bi_2S_3 coatings was studied by cyclic potentiodynamic voltammetry

in solutions containing (M): NaOH 0.1, H_2SO_4 0.05, and Na_2S 0.001. The solutions were prepared from reagents of chemically pure grade and distilled water. The experiments were performed in a YaSE-2 cell at $20 \pm 1°C$. A platinum grid was used as auxiliary electrode, and a saturated silver chloride electrode, as reference. The potentials are given relative to a standard hydrogen electrode. Potentiodynamic voltammograms were measured with a PI-50-1 potentiostat and a PR-8 programming unit and recorded with an XY Recorder A3 potentiometer. The potential sweep rate was 5×10^{-2} and 5×10^{-3} V s^{-1}.

The composition of the Bi_2S_3 coatings was studied by XPS on a Vacuum Generator Scientific ESCALAB-MK II spectrometer (UK). A magnesium anode served as a source of soft X-ray radiation (1253.6 eV, 300 W). The pressure in the analytical chamber of the spectrometer was 1.33×10^{-8} Pa. Bi 4*f*, S 2*s*, and O 1*s* spectra were recorded. The empirical sensitivity factors for these elements were taken from the literature [9] and the spectra recorded were compared with reference spectra [10].

The voltammogram obtained in a 0.1 M NaOH solution on a glassy carbon electrode without a bismuth sulfide coating at the cathodic sweeping of the potential from its steady-state value E_{st} = +0.8 V to –1.8 V is shown in Fig. 1 (curve *1*). In this range of potentials, no current peaks associated with the side redox processes are observed. It can be seen that, up to $E = -1.3$ V, the cathode current does not exceed 5×10^{-4} A cm^{-2} and the anode current is even lower up to +0.8 V.

The run of the potentiodynamic curves significantly changes on treating the electrode in a colloid solution of trivalent bismuth and washing with water (Fig. 1, curve *2*). The cathodic branch of the curve shows a broad current peak K_1 at potentials in the range from –0.7 to –1.35 V. This peak is due to the reduction of Bi(III) hydrolysis products to metallic Bi. The hydrogen evolution occurs at $E < -1.5$ V. In a reverse sweep of the potential toward positive values, when $E > -0.3$ V, an anodic current peak A_1 is observed. In this range of potentials, metallic Bi can be oxidized to Bi_2O_3 by the reaction:

$$2Bi + 6OH^- - 6e \rightarrow Bi_2O_3 + 3H_2O. \quad (1)$$

Because the standard potential for reaction (1) is –0.46 V [1, 11] and the calculated equilibrium potential at pH 13 is –0.4 V, it may be suggested that the reaction proceeds under these conditions. However, the shape of the A_1 peak indicates that several anodic reactions occur in this range of potentials. It

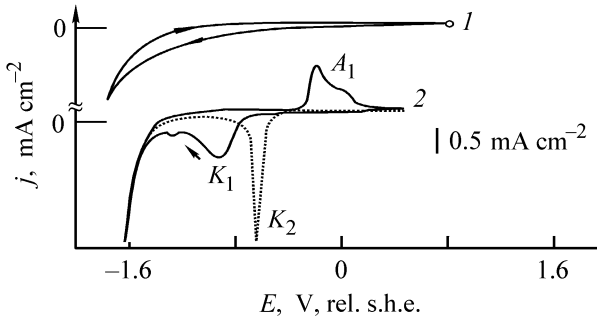

Fig. 1. Cyclic voltammetric curves obtained in a 0.1 M NaOH solution on (*1*) glassy carbon electrode and (*2*) glassy carbon electrode after a sixfold treatment in a colloid solution containing Bi(III) ions. Potential sweep rate $V = 5 \times 10^{-2}$ V s^{-1}, *Points* second cycle; the same for Figs. 2–5. (*j*) Current density and *E* potential (V, rel. s.h.e.); the same for Figs. 2–5.

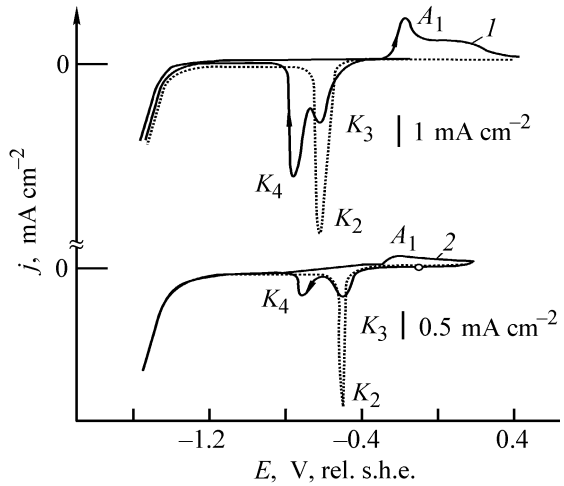

Fig. 2. Cyclic voltammetric curves obtained at different potential sweep rates in a 0.1 M NaOH solution on a glassy carbon electrode coated with bismuth sulfide. *V* (V s^{-1}): (*1*) 5×10^{-2} and (*2*) 5×10^{-3}.

was shown in [12] that electrochemical oxidation in a 1 M KOH solution of bismuth deposited on Pt can yield, along with $Bi(OH)_3$, also Bi(IV) compounds, which can be chemically oxidized to Bi(V). Cathodic current peaks corresponding to these oxidation processes were also observed. Only a single cathodic peak K_2 associated with the reduction of Bi(III) oxide compounds is observed in the second-cycle potentiodynamic curves at potentials of –0.5 to –1.0 V in potential sweep toward the anodic side after a cathodic cycle to –1.6 V. Therefore, we can suggest that no Bi(V) is formed.

Cyclic voltammograms obtained in alkaline solution in reduction of a Bi(III) sulfide coating deposited onto a glassy carbon electrode are shown in Fig. 2. These curves were recorded at different potential

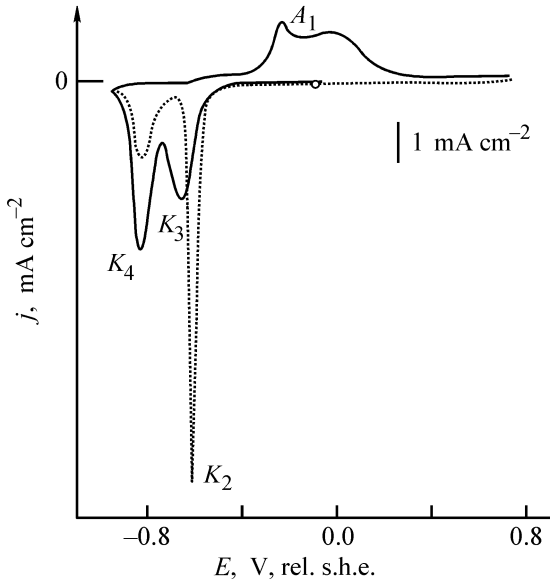

Fig. 3. Cyclic voltammetric curves obtained in a 0.1 M NaOH solution on a glassy carbon electrode coated with bismuth sulfide, with potential sweep from the steady-state value to –0.9 V.

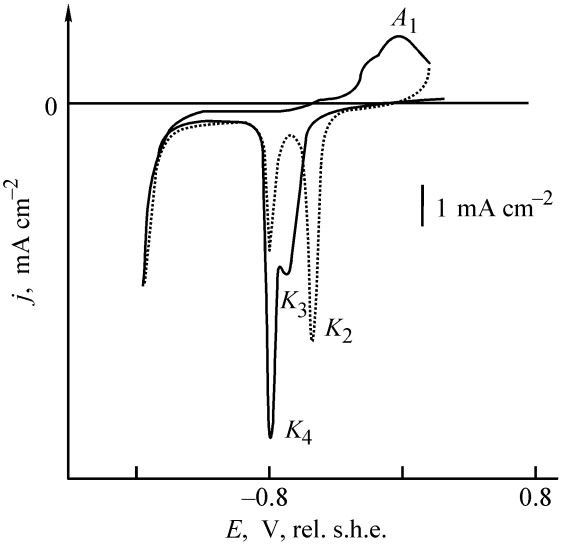

Fig. 4. Cyclic voltammetric curves obtained on a glassy carbon electrode coated with bismuth sulfide in a solution containing (M): NaOH 0.1 and Na_2S 0.001.

sweep rates V of 5×10^{-2} and 5×10^{-3} V s^{-1} (curves *1* and *2*, respectively). In a potential sweep from the steady-state value to –1.6 V, two current peaks, K_3 and K_4, are observed on each cathodic branch: at –0.64 and –0.77 V (curve *1*) and –0.51 and –0.72 V (curve *2*). With the potential sweep in the reverse direction, toward positive values, an anodic current peak A_1 appears (Fig. 2, curves *1*, *2*). Because the current peaks K_3 and K_4 are observed at both potential sweep rates, it can be suggested that they are due to reduction of different Bi(III) compounds [13]. On changing the potential sweep rate from 5×10^{-2} to 5×10^{-3} V s^{-1}, the K_3 and K_4 peaks shift toward positive potentials and their area markedly decreases. The cathodic peaks K_3 and K_4 are shifted by 0.13 V and 0.05 V, respectively.

It should be noted that, in reduction of the sulfide coating in a 0.1 M NaOH supporting electrolyte, with the potential swept from the steady-state value E_{st} (–0.054 V) to –0.45 V and then back in the anodic direction to +0.6 V, no current peak A_1 is observed in the anodic branch of the curve. This means that no redox processes occur in the bismuth sulfide coating in this range of potentials. The peak A_1 appears in the anodic curve of the voltammogram only after a potential of –0.9 V is reached in the cathodic cycle (Fig. 3). Undoubtedly, the anodic peak A_1 is due to oxidation of metallic Bi formed in reduction of the bismuth sulfide coating at potentials of –0.4 to –0.85 V (current peaks K_3, K_4). However, further studies demonstrated that the reduction of the sulfide coating in this range of the potentials is incomplete (Fig. 3). Two more current peaks, K_2 and K_4, appear in the cathodic branch of the curve after the first cycle in a potential sweep from –0.9 V toward the cathodic side (second cycle). It can be assumed that K_2 is due to reduction of Bi oxide compounds, and K_4, to reduction of Bi_2S_3. The current peak K_4 in the second cycle is not observed if a potential of –1.6 V, i.e., the potential of vigorous hydrogen evolution, is reached in the first cathodic cycle (Fig. 2, curve *1*).

The cyclic voltammogram obtained in reduction of a bismuth sulfide coating in a 0.1 M NaOH solution containing 0.001 M Na_2S is shown in Fig. 4. It is virtually identical to that obtained in a NaOH solution without addition of sulfide ions (Fig. 2, curve *1*). However, a difference between the curves in Figs. 2 and 4 is manifested in the second cathodic cycle: curve *1* (Fig. 2) has in the second cycle only a single current peak K_2 associated with the reduction of Bi(III) oxide compounds, whereas the cathodic portion of the second-cycle curve (Fig. 4) shows, alongside with the K_2 peak, also the peak K_4, in whose potential range probably occurs reduction of Bi_2S_3 formed in the anodic cycle owing to the presence of sulfide ions in the supporting electrolyte. Bi_2S_3 is reduced in an alkaline medium by the reaction

$$Bi_2S_3 + 6e \rightarrow 2Bi - 3S^{2-}. \quad (2)$$

The equilibrium potential, calculated for reaction (2) in a 0.1 M NaOH solution by taking into account that the standard potential is –0.818 V [14], is equal to

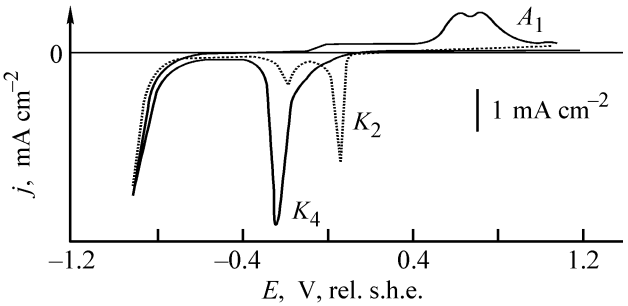

Fig. 5. Cyclic voltammetric curves obtained in 0.05 M H_2SO_4 solution on a glassy carbon electrode coated with bismuth sulfide.

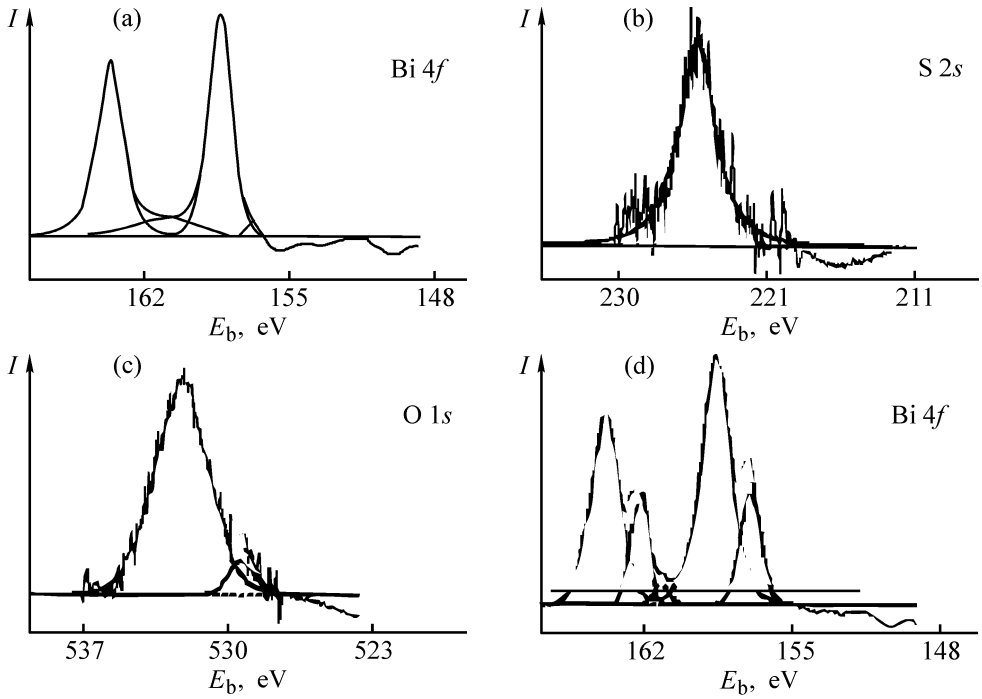

Fig. 6. XPS spectra of the surface of the bismuth sulfide coating. (I) Intensity and (E_b) binding energy. Spectrum: (a) Bi 4f, (b) S 2s, (c) O 1s, and (d) Bi 4f (after reduction of the coating in 0.1 M NaOH solution, with the potential swept from steady-state value to –0.9 V.

–0.73 V. These results demonstrate that reduction of Bi_2S_3 to metallic Bi is thermodynamically possible in the range of the current peak K_4.

The acidity of the supporting electrolyte strongly affects the run of the voltammograms. The current peak K_4 at $E = -0.24$ V and a slight increase in current in the range of the K_3 peak are observed in the cyclic voltammogram obtained in a 0.05 M H_2SO_4 solution on an electrode coated with bismuth sulfide, in a cathodic potential sweep from E_{st} to –1.0 V (Fig. 5). Probably, oxide or other compounds of Bi(III) dissolve in the acid, and the K_3 peak corresponding to their reduction of is not observed in the voltammogram.

Studies of the electrochemical behavior of sulfides of other metals deposited by adsorption demonstrated that elementary sulfur is also present in the composition of such coatings. Possibly, sulfur yielded in the formation of bismuth sulfide is reduced in the region of the K_3 current peak. However, this suggestion was not confirmed because a 10-min treatment of the coating at 80°C with sulfur solvents, such as tetrachloroethylene or toluene [15], had no effect on the character of the cyclic voltammogram obtained in a 0.1 M NaOH solution. The current peaks K_3 and K_4 were also observed in the cathodic portion of the curve after the treatment.

In an XPS study of the bismuth sulfide coating, primary attention was given to the distribution of Bi, S, and O elements. It was found that these elements are present on the surface in the following amounts (at, %): 10.34 Bi, 11.81 S, 18.08 O, 56.6 C, and 3.17 N.

The Bi4$f_{5/2}$ and Bi4$f_{7/2}$ spectra recorded show the range of binding energies, E_b = 163.7 and 158.4 eV, which corresponds to Bi_2S_3 (Fig. 6a). The Bi4*f* spectrum also shows a spectrum of S2*p* sulfur, peaked at E_b = 160.98 eV, which is characteristic of sulfide sulfur. Because of its being overlapped with the Bi4*f* spectrum, the spectrum of S2*s* (E_b = 225.38 eV) [10] was recorded separately (Fig. 6b).

The O1*s* spectrum in Fig. 6c shows two peaks: one, at E_b = 529.3 eV, is due to oxygen adsorption, and the other, at E_b = 523.31 eV, corresponds to the OH^- group [10] (Fig. 6c).

The theoretical Bi/S ratio in a sulfide coating is 0.66, and that found experimentally from XPS data, 0.88. For Bi_2S_3, the published value of the binding energy E_b is 158.9 eV [10], and that found experimentally, E_b = 158.4 eV. This difference suggests that other Bi(III) compounds are also deposited when Bi_2S_3 is formed from a colloid solution. These assumptions agree in part with the voltammetric data. As already shown, two current peaks, K_3 and K_4, are observed in the cathodic portion of the curve in reduction of a sulfide coating, and several Bi(III) compounds are reduced in their range of potentials (Fig. 2, curves *1*, *2*). Along with Bi_2S_3, oxide compounds, such as BiOOH or BiOHS [12, 13, 16], can be formed. However, the binding energies E_b of these compounds could not be found in the literature. It was noted in [17] that Co(III) compounds, CoOOH and CoOHS, are also deposited when CoS and Co_2S_3 are formed.

A study of the electrochemical behavior of metal sulfides demonstrated that some of them, e.g., Co_2S_3 cannot be reduced to metal in supporting electrolytes. Bismuth sulfide coatings are rather easily reduced both in alkalis and in dilute acid solutions. This is well seen in Fig. 6d, in which the Bi4*f* spectrum separates into the metallic and oxide components after reduction of a bismuth sulfide coating in a 0.1 M NaOH solution, with a potential sweep in the cathodic direction from E_{st} to –0.9 V. Comparison of the bismuth spectra in Figs. 6a and 6d shows that two peaks with binding energies of Bi_2S_3 (158.4 eV) and metallic Bi (156.8 eV) are observed in the Bi4*f* spectrum (Fig. 6d) after the reduction of the sulfide coating.

CONCLUSIONS

(1) It was shown that a bismuth sulfide coating is reduced in a 0.1 M NaOH supporting solution to metallic bismuth at potentials ranging from –0.4 to –0.85 V. The cathodic current peak at E = –0.64 V may be due to reduction of oxide compounds of Bi(III), and that at E = –0.77 V, to reduction of Bi_2S_3.

(2) X-ray photoelectron spectroscopy revealed the presence of the following elements on the surface of the sulfide coating (at %): about 10.34 Bi, 11.81 S, 18.08 O, 56.6 C, and 3.17 N. The experimentally measured ratio Bi/S is 0.88, which exceeds the theoretical value of 0.67. It was suggested that oxide compounds of Bi(III), BiOOH or BiOHS, are also deposited in the formation of Bi_2S_3.

REFERENCES

1. Grubač, Z., and Metikoš-Hukovič, M., *Electrochim. Acta*, 1999, vol. 44, no. 25, pp. 4559–4571.
2. Saitou, M., Yamaguchi, R., and Oshikawa, W., *Mater. Chem. Phys.*, 2002, vol. 73, pp. 306–309.
3. Grubač, Z., and Metikoš-Hukovič, M., *Thin Solid Films*, 2002, vol. 413, pp. 248–256.
4. Mane, R.S., Sankapal, B.R., and Lokhande, C.D., *Mater. Chem. Phys.*, 1999, vol. 60, pp. 196–203.
5. Sasaki, H., Shibayama, K., Ichimura, M., and Masui, K., *J. Crystal Growth*, 2002, no. 237–239, pp. 2115–2129.
6. Killedar, V.V., Katore, S.N., and Bhosale, C.H., *Mater. Chem. Phys.*, 2000, vol. 60, pp. 166–169.
7. Vinkyavichus, I., Mozhginskene, I., Zhieliene, A., and Pilite, S., *Zh. Prikl. Khim.*, 1997, vol. 70, no. 10, pp. 1987–1992.
8. EP Patent 1 174 530 (A2).
9. *Practical Surface Analysis by Auger and X-Ray Photoelectron Spectroscopy*, Briggs, D., and Seach, M.P., Eds., New York: Jon Wiley and Sons, 1983.
10. Wagner, C.D., Riggs, W.M., Davis, L.E., et al., *Handbook of X-Ray Photoelectron Spectroscopy*, Minnesota: Perkin–Elmer, 1978.
11. Rabinovich, V.A., and Khavin, Z.Ya., *Kratkii khimicheskii spravochnik* (Concise Chemical Reference Book), Leningrad: Khimiya, 1977.
12. Ismail, J., Ahmed, M.F., and Vishnu Kamath, P., *J. Electroanal. Chem.*, 1993, vol. 354, pp. 51–58.
13. Grubač, Z., and Metikoš-Hukovič, M., *J. Electroanal. Chem.*, 2004, vol. 565, pp. 85–94.
14. Licht, S., *J. Electrochem. Soc.*, 1988, vol. 135, no. 12, pp. 2971–2975.
15. Valiulienè, G., Žielienè, A., and Jasulaitienè, V., *Trans. IMF*, 2006, vol. 84, no. 3, pp. 162–167.
16. Wu, W.-T., Shi, L., Pang, W., et al., *Nanotechnology*, 2006, vol. 17, pp. 4999–5005.
17. Valiulienè, G., Žielienè, A., and Vinkevičius, J., *J. Solid State Electrochem.*, 2002, vol. 6, no. 6, pp. 396–402.

ISSN 1070-4272, Russian Journal of Applied Chemistry, 2007, Vol. 80, No. 8, pp. 1327–1330. © Pleiades Publishing, Ltd., 2007.
Original Russian Text © O.I. Kuntyi, E.V. Okhremchuk, V.T. Yavorskii, 2007, published in Zhurnal Prikladnoi Khimii, 2007, Vol. 80, No. 8, pp. 1287–1290.

APPLIED ELECTROCHEMISTRY AND CORROSION PROTECTION OF METALS

Electrochemical Deposition of Tellurium from $TeCl_4$ Solutions in Aprotic Solvents

O. I. Kuntyi, E. V. Okhremchuk, and V. T. Yavorskii

Lvivska Politekhnika National University, Lviv, Ukraine

Received November 30, 2006; in final form, June 2007

Abstract—Electrolysis of 0.01–0.1 M $TeCl_4$ solutions in dimethyl sulfoxide, dimethylformamide, and acetonitrile was studied in the temperature range 20–60°C. The microscopic structure of cathode deposits was analyzed.

DOI: 10.1134/S1070427207080125

The electrochemical deposition of tellurium has been studied in most detail in acid [1, 2] and alkaline [1, 3] aqueous solutions containing hydrated cations $[Te(H_2O)_n]^{4+}$ and oxo anions TeO_3^{2-}, respectively. The instability of water at elevated electrode potentials and the tendency of tellurium(IV) salts to undergo hydrolysis result in a number of side electrochemical and chemical reactions, which leads to difficulties in obtaining pure cathode deposits of tellurium.

Use of organic solvents makes it possible, in some cases, to eliminate these drawbacks and to obtain tellurium in a wide range of potentials from solutions of simple salts [4, 5].

This study, concerned with the electrochemical deposition of tellurium from organic aprotic solvents, continues the systems analysis of the electrochemical behavior of metals in the nonaqueous medium specified [6, 7].

EXPERIMENTAL

Electrode processes were studied in 0.01–0.1 M $TeCl_4$ solutions in dimethyl sulfoxide (DMSO), dimethylformamide (DMF), and acetonitrile (AN) in the temperature range 20–60°C. The organic solvents were of chemically pure grade, and $TeCl_4$ was synthesized by the procedure described in [8]. A PI-50-1.1 potentiostat with a standard electrochemical cell, platinum auxiliary electrode, and silver-chloride reference electrode was used.

Polarization curves were measured at a potential sweep rate of 2.0 mV s^{-1}. The cathode processes were studied using a graphite rod with a diameter of 6 mm and lateral surface insulated with a fluoroplastic tape. The anode processes were examined with tellurium press-fitted in a fluoroplastic cartridge. Before each experiment, graphite samples were trimmed with a fine-grained emery paper, polished with a velvet cloth, and washed with ethanol. To study the morphology of cathode deposits, the electrolysis was carried out with a soluble tellurium anode. Tellurium was deposited onto the edge surface of the graphite rod. The morphology of the anode surface was examined on a cleaved surface of metal lumps. In all cases, the electrolysis was carried out at a constant potential without stirring until a coating with an average thickness of 5 μm was obtained. The resulting cathode deposits remaining on a graphite sample, and anodically etched tellurium plates were washed with an appropriate aprotic solvent and acetone, dried in air at 60°C, and examined with a REMMA-102-02 scanning electron microscope.

A 200–300-mV plateau is observed in the cathodic polarization curves obtained in DMSO (Fig. 1a) and DMF (Fig. 1b) solutions, which points to a strong polarization of tellurium. In acetonitrile solutions (Fig. 1c), the polarization is less noticeable. In addition, the currents in AN considerably exceed those in DMSO and DMF at equal cathode potentials. This is primarily attributable to the fact that the donor numbers (DN) of DMSO and DMF markedly exceed the donor numbers of AN (DN_{SbCl_5} for DMSO, DMF, and AN are 29.8, 27.0, and 14.1, respectively [9]). Therefore, the stability of solvated tellurium(IV) cations in dimethyl sulfoxide and dimethylformamide

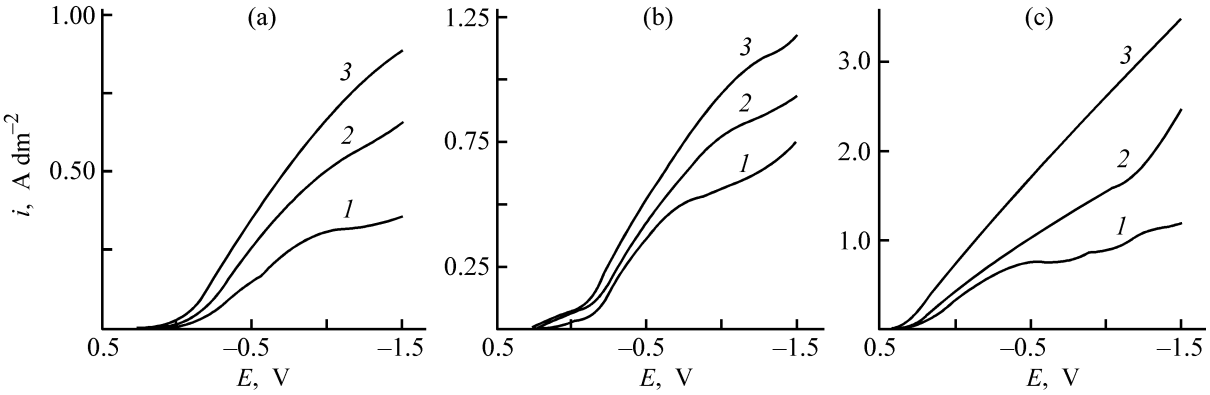

Fig. 1. Cathodic polarization curves obtained in $TeCl_4$ solutions in (a) dimethyl sulfoxide, (b) dimethylformamide, and (c) acetonitrile at different temperatures (c_{TeCl_4} = 0.05 M). (*i*) Current density and (*E*) potential; the same for Fig. 3. Temperature (°C): (*1*) 20, (*2*) 40, and (*3*) 60.

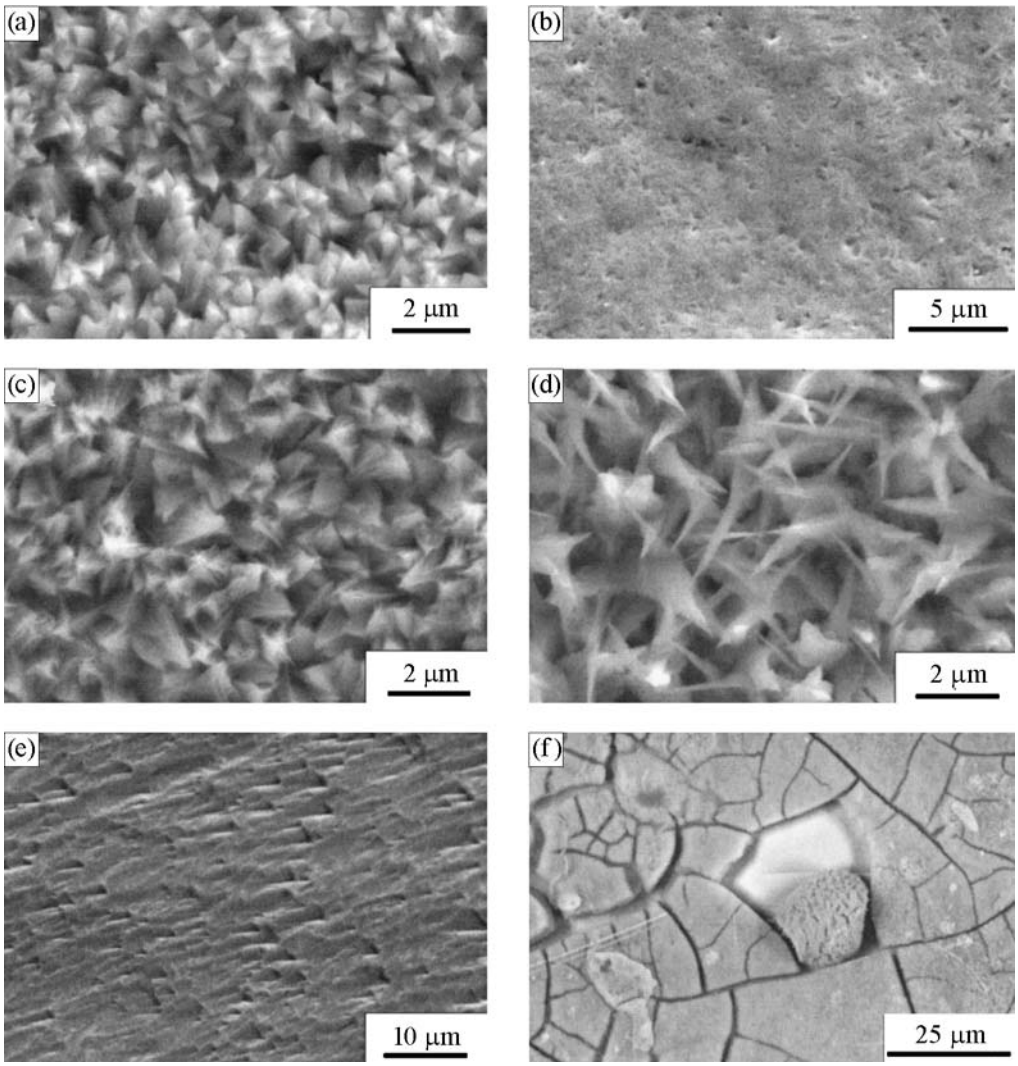

Fig. 2. Morphology of (a, d) tellurium cathode deposits on a graphite substrate and (e, f) tellurium surfaces after anodic dissolution in 0.005 M $TeCl_4$ solutions in (a, d, e) DMSO, (c, f) DMF, and (d) AN at different potentials. Potential (V): (a) –0.5; (b)–(d) –1.0; (e, f) 1.0. Magnification: (a, c, d) 10 000; (b) 5000; (f) (COMPO mode) 1200.

solutions is higher than that in acetonitrile solutions. Furthermore, the solvents specified strongly differ in viscosity: 2.003, 0.796, and 0.328 cP for DMSO, DMF, and AN, respectively [9], which is also an important factor of electrode polarization.

The increase in the cathode currents with temperature does not exceed 25% per 10° (Fig. 1). This indicates that the cathodic deposition of tellurium occurs under the diffusion control. As the concentration of $TeCl_4$ increases from 0.01 to 0.1 M, the cathode currents grow virtually proportionally.

In deposition of compact tellurium from DMSO, DMF, and AN solutions, comparatively solid and uniform coatings (Fig. 2) are formed. At low cathode potentials, crystallites with distinct configuration (Fig. 2a) are formed. As the potential (current density) increases in the DMSO medium, there occurs a kind of flattening and branching of the crystallites (Fig. 2b), which is manifested in that the coating becomes smoother and more lustrous. The tendency toward smoothing of the surface of a tellurium coating with increasing cathode potential (current density) is also observed in DMF solutions. However, this is mostly due to a decrease in the size of the crystallites and to an increase in their packing density (Fig. 2c). In AN, no smooth films are deposited (Fig. 2d). In this case, as the cathode potential increases, the crystallites decrease in size and coarsely crystalline dark gray coatings turn into finely crystalline black velvety crystals.

As demonstrated by the results of the study, the nature of a substrate chemically indifferent toward tellurium affects the morphology of a cathodic deposit only slightly. For example, the microscopic structure of the tellurium coating and the shape and sizes of crystallites on titanium and graphite samples differ only slightly in identical solvents at close cathode current densities (potentials).

The anodic dissolution of tellurium in DMSO and DMF solutions, as well as the cathodic deposition, occurs with polarization (Fig. 3, curves *1* and *2*). At potentials of 0.3–1.5 V, the anode currents depend virtually linearly on potentials, which points to an unhindered dissolution of tellurium.

Comparison of the initial surface tellurium with that after the anodic dissolution in DMSO solutions of $TeCl_4$ (Fig. 2e) shows that crystallites are etched-out in electrolysis. In this case, the surface becomes corrugated, but single-phase. In DMF solutions, a new phase appears in electrolysis on the tellurium surface

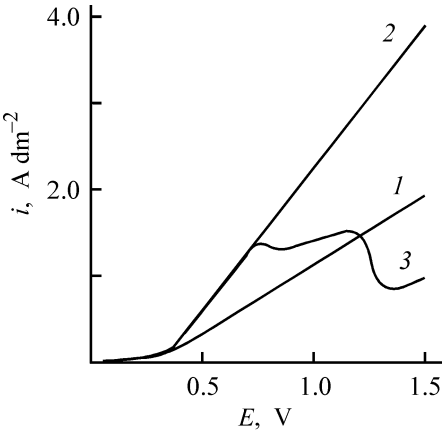

Fig. 3. Anodic polarization curves obtained on tellurium in 0.005 M $TeCl_4$ solutions in (*1*) DMSO, (*2*) DMF, and (*3*) AN at 40°C.

(Fig. 2f), as indicated by electron-microscopic studies in the COMPO. According to the energy-dispersion X-ray microanalysis, this phase contains chlorine. Thus, the anodic dissolution of tellurium in DMF occurs via formation of a solvated salt film. A similar pattern is observed in acetonitrile solutions. However, the film formation in DMF does not passivate the anode, as can be seen from the shape of the polarization curve (Fig. 3, curve *2*), whereas in AN, tellurium is passivated (Fig. 3, curve *3*).

CONCLUSIONS

(1) In dimethyl sulfoxide and dimethylformamide solutions of $TeCl_4$, the cathodic deposition of tellurium occurs with an appreciable polarization.

(2) Smooth films are formed on a graphite substrate in dimethylformamide, and smooth and lustrous coatings, in dimethyl sulfoxide. In acetonitrile, tellurium is deposited in the form of velvety coatings.

(3) In dimethyl sulfoxide solutions of $TeCl_4$, there occurs uniform electrochemical dissolution of tellurium, without accumulation of anodic products on the surface. This makes it possible to use soluble anodes in deposition of tellurium films in dimethyl sulfoxide.

REFERENCES

1. Baeshov, A., Zhurinov, M.Zh., and Zhdanov, S.I., *Elektrokhimiya selena, tellura i poloniya* (Electrochemistry of Selenium, Tellurium, and Polonium), Alma-Ata: Nauka, 1989.

2. Sahtos, M.C. and Machado, S.A.S., *Electrochim. Acta*, 2005, vol. 50, no. 11, pp. 2289–2295.
3. Ha, Y.-C., Sohn, H.-J., Jeong, G.-J., et al., *J. Appl. Electrochem.*, 2000, vol. 30, no. 11, pp. 315–322.
4. Fialkov, Yu.Ya. and Grishchenko, V.F., *Elektrovydelenie metallov iz nevodnykh rastvorov* (Electrowinning of Metals from Nonaqueous Solutions), Kiev: Naukova Dumka, 1985.
5. Liftman, Y., Albeck, M., Goldschmidt, J.M.E., and Yarnitsky, Ch., *Electrochim. Acta*, 1984, vol. 29, no. 12, pp. 1673–1678.
6. Kuntyi, O.I., Okhremchuk, E.V., and Khoma, M.S., *Fiz.-Khim. Mekhanika Materialov*, 2003, no. 6, pp. 103–105.
7. Kuntyi, O.I., *Voprosy Khim. Khim. Tekhnol.*, 2004, no. 2, pp. 160–162.
8. *Handbuch der Praparativen Anorganischen Chemie*, Brauer, G., Ed., Stuttgart: Ferdinand Enke, 1980.
9. Gutmann, V., *Coordination Chemistry in Nonaqueous Solutions*, New York: Springer, 1968.

ISSN 1070-4272, Russian Journal of Applied Chemistry, 2007, Vol. 80, No. 8, pp. 1331–1334. © Pleiades Publishing, Ltd., 2007.
Original Russian Text © P.E. Aleksandrov, A.I. Anurova, M.E. Petropavlovskii, V.S. Kotlyar, S.V. Zaitsev, 2007, published in Zhurnal Prikladnoi Khimii, 2007, Vol. 80, No. 8, pp. 1291–1295.

APPLIED ELECTROCHEMISTRY AND CORROSION PROTECTION OF METALS

Intrinsic Characteristics of Cathode and Anode Materials for Lithium-Ion Batteries

P. E. Aleksandrov, A. I. Anurova, M. E. Petropavlovskii, V. S. Kotlyar, and S. V. Zaitsev

OAO Istochnik Planning-and-Design and Technological Battery Research Institute, St. Petersburg, Russia

Received March 5, 2007

Abstract—Fundamental aspects of solving the problem of how the working capacity of lithium-ion batteries in prolonged cycling can be raised and the basic tendencies in the relationship between the intrinsic parameters of active materials of various brands and the electrochemical behavior of anodes and cathodes fabricated from these materials are considered.

DOI: 10.1134/S1070427207080137

The world industry of lithium-ion batteries (LIB) is characterized by a large number of manufacturers of various anode (based on graphite) and cathode ($LiCoO_2$, $LiNi_{1-x}Co_xO_2$, etc.) materials. Despite that materials from different manufacturers may strongly differ in their intrinsic characteristics (structural parameters, size and shape of particles, particle size distribution, specific surface area, surface morphology), they are all successfully used to create LIB competitive on the world market. Consequently, technological procedures and approaches adapted to a material of a particular type should be employed to enable effective use of active materials.

The study is devoted to a search for scientific criteria to be used in solving the problem of compatibility of certain intrinsic characteristics of the wide variety of the available materials with the rather large number of possible technological procedures employed in manufacture of LIB and with a certain electrochemical behavior of separate elements of LIB, including that in cycling.

EXPERIMENTAL

The samples studied had the form of finely dispersed powdered materials (SLA-1115, SLC-1520, SLC-1520P, and CZ-50 for anodes; $LiCoO_2$ manufactured by Merck and Baltiiskaya Manufaktura for cathodes). The samples were studied by electron microscopy and X-ray diffraction analysis. Histograms displaying the particle size distribution were plotted for the powder samples. Samples of anode and cathode materials, prepared by the standard technique commonly used in manufacture of LIB, were subjected to electrochemical testing in cells of C/Li and $LiCoO_2$/Li types, fabricated in CR-20 cases.

Of interest under the conditions of increasing demand for lithium-ion batteries that are capable of prolonged operation and can sustain a large number of cycles is a search for ways to choose the most preferable cathode material for LIB from those available, because practical electrochemical testing is time-and-labor consuming. The materials used as the active component of cathodes for lithium-ion batteries can be produced by various methods and, consequently, may have each its own individual impurity composition and homogeneity. The homogeneity and crystal perfection of an active material of the cathode largely determine the efficiency of an electrochemical system as a whole and its behavior in cycling. Without considering details of the preparation methods, we compared in this study cathode materials ($LiCoO_2$) purchased from two different manufacturers, Baltiiskaya Manufaktura and Merck, by means of X-ray diffraction analysis and electrochemical testing.

The starting $LiCoO_2$ powders were virtually identical in X-ray diffraction data. Minor differences in the interplanar spacings are due to their individual impurity compositions. Moreover, it is important to note that the structure identified for the samples under study belongs to the trigonal crystal system, which

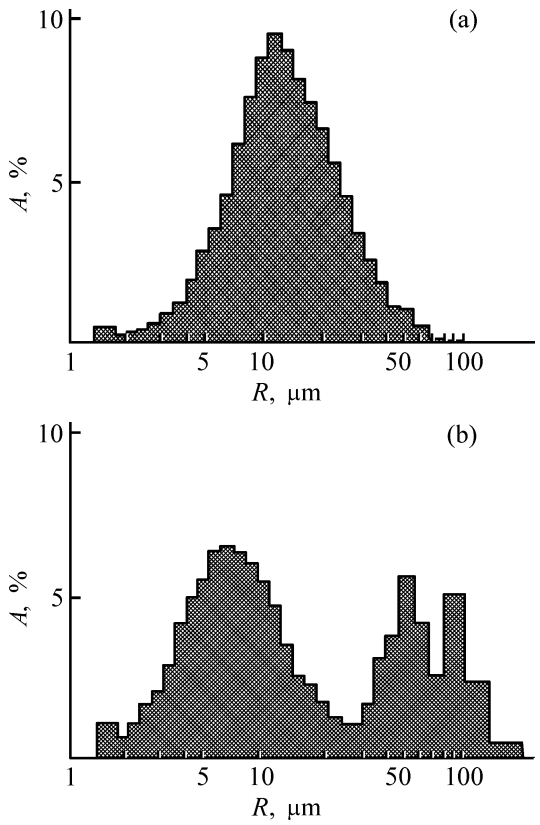

Fig. 1. Histograms of the distribution A of particles with respect to their size R in lithium cobaltate powders from (a) Merck and (b) Baltiiskaya Manufaktura Research-and-production company.

supplements published data indicating that there exist $LiCoO_2$ samples with a hexagonal structure [1]. This circumstance shows that conditions for an additional structural ordering in cobalt and lithium planes appear as $LiCoO_2$ is produced and the symmetry decreases to trigonal. Thus, the lithium and cobalt planes are mixed, which, in fact, makes it possible to distinguish one starting material from another by determining the "history" of a material in the course of lithium deintercalation.

The electrochemical behavior of cathodes fabricated from the powders under study was the same, at least in the first cycles (the testing was done at low current densities, $I = 0.3$ mA cm^{-2}). At the same time, reports have appeared recently, in which attempts were made to relate the identified properties of a sample to its behavior in cycling, with only the initial state of the sample considered. Probably, this way is not the best, because each sample acquires its "history" in the course of cycling, and, therefore, it is more appropriate to extrapolate to a large number of cycles some characteristics of a more changeable, farther from equilibrium, state of the structure than the initial state.

We identified $LiCoO_2$ phases which can or cannot restore their structural parameters in the course of lithium deintercalation. In particular, it was found that the initial $LiCoO_2$ phase in a sample with electrochemically deintercalated lithium, kept at 70°C for 30–35 days, turns into a mixture of spinel and trigonal phases. This process reflects the nonequilibrium and instability of the lithium-deintercalated state. Indeed, the nonequilibrium state of the structure is due to the presence of distortions and defects, and, because the process of lithium extraction is equivalent to a shift of the sequence of CoO_2 layers, it would be expected that the characteristic diffraction peak (003) will be broadened in the course of lithium deintercalation. X-ray diffraction patterns of samples with electrochemically lithium-deintercalated samples show a certain broadening of the peak, compared with its initial state, in the course of lithium deintercalation. In addition, the corresponding diffraction peaks for samples from different manufacturers should be dissimilar because of the different impurity compositions, "histories" of the materials, and particle size distribution histograms. Therefore, we suggest a semiquantitative criterion for determining the structural perfection of lithium-deintercalated $LiCoO_2$, the ratio between the halfwidth of the diffraction peak and its height, which can be used for extrapolation to a larger number of cycles and for evaluation of the quality of cathode materials in cycling.

It is also important to note that the samples of the powders studied have different histograms of particle size distributions (Fig. 1). The cathodes fabricated from the $LiCoO_2$ powders of the types under consideration exhibit virtually the same electrochemical behavior at low current densities in the first cycles. Nevertheless, the type of a distribution histogram is one of the most important intrinsic characteristics in the incoming control of the material, because it determines the efficiency of an electrochemical system in discharge and the intensity of degradation processes in charging. It can be assumed that the identical irreversible losses for the cathodes based on the powders under study at the current densities used are a consequence of the similar particle size distributions at small particle sizes in the histograms (left-hand parts of the histograms).

It is known that the main ways to improve cathode materials is their doping and development of mixed formulations [2]. However, there is no way of disregarding the way that relies upon the crystallochem-

ical aspect, i.e., analysis of a material, as such, from the standpoint of its crystal perfection and chemical composition. This way would enable a leap forward in the production technology of LIBs and yield batteries sustaining a larger number of cycles and operating for a longer time. For example, it would be preferable to obtain lithium cobaltate with a structure belonging to the hexagonal crystal system, because any structural ordering (trigonal in the case of lithium cobaltate) stabilizes the structure in the energetic regard, but impairs its reversibility with respect to the corresponding structural parameters in intercalation/deintercalation.

Carbon anode materials are finely dispersed powders whose particles have a structure of graphite. Studies aimed to synthesize new brands of graphite and change their intrinsic characteristics to lower the production cost and obtain higher-quality devices have been carried out during the entire history of development and improvement of the technology of LIB manufacture and are intensively carried out now [3].

In contrast to the case of cathode materials, it is unadvisable to impose particularly stringent requirements to the structural perfection of anode materials, both in their initial state and after being involved in an electrochemical process. The latter is due to the fact that the degradation process in graphite, i.e., its amorphization, is accompanied by loss of individual features by its structure and by a transition to a higher symmetry. This, in turn, points to an increase in the entropy of the system and to a higher thermodynamic stability of the newly formed phase, which can sustain intercalation and deintercalation during a rather large number of cycles. In addition, materials produced from natural graphite, which are successfully used in LIBs, contain a less thermodynamically stable rhombohedral β-modification, together with the hexagonal α-form. For example, natural graphite contains approximately 30% β-modification. In the fabrication technology of LIB, to compensate for the presence of the ordered β-form, and, consequently, to preclude its effect on the operation of LIB in prolonged cycling, it is advisable to use a certain excess of graphite (20–30%), compared with its amount used if only the equivalent amount of the cathode material and the amount of graphite consumed for formation of the passivating layer are taken into account. Therefore, we considered the intrinsic characteristics of graphite powders with the aim to develop LIB anodes exhibiting the nominal electrochemical behavior.

X-ray diffraction analysis was used to find the interplanar spacings d_{002} in the direction {002}, specific surface area of powdered active materials, and histograms of the distribution of particles over their size R_{av} (see table). The shapes and surface morphologies of particles were compared by electron microscopy.

Parameters of graphite powders and graphite anodes*

Graphite	d_{002}, Å	σ_{sp}, $m^2\ g^{-1}$	R_{av}, μm	ΔQ, %	Q, mA h g^{-1}
CZ-50	3.363	2.7	23	10	370
SLC-1520	3.347	0.95	29	35	250
SLC-1520P	3.367	1.1	27	40	270
SLA-1115	3.348	1.2	25	15	350

* Q is the specific discharge capacity, and ΔQ, irreversible loss.

It can be seen that the graphite structures somewhat differ in interplanar spacings. As a result, it would be expected that the diffusion characteristics of lithium in these materials and the electrochemical kinetics of interaction within the electric double layer will be also different. Indeed, it was shown in [4] that, on passing to graphites having an interplanar spacing different from a certain value (which is its own for each graphite brand), the irreversible loss of anodes fabricated from these graphites vary by the parabolic law with the structure parameter. This indicates that, not being an absolute physical constant, the interplanar spacing can be used, to a certain approximation, in incoming control of the active material for the anode.

An analysis of the polarization characteristics demonstrated that no noticeable differences are observed at high potential sweep rates providing that the electrochemical process of anodic polarization occurs in the kinetic mode. In addition, the differences in the specific surface areas of the powders did not reflect upon the on-off curves, i.e., these curves were virtually identical in the charging-discharge modes C/5 and C/10. Figure 2 shows discharge curves characterizing the nominal electrochemical behavior of anode made of graphites of (a) CZ50 and (b) SLA-1115 brands. Anodes fabricated from graphites of SLC-1520 and SLC-1520P brands show a high irreversible loss (35–40%) and lowered discharge capacity (see table). The decrease in the observed specific parameters of graphite, compared with the calculated values, are presumably due to specific features of the technological approach used. This is so because, as the content of binder is lowered from 10 to 8% and 3 to 5 wt % Ensaco carbon black is introduced, anodes made of SLC-1520 and SLC-1520P graphites exhibit, in electrochemical testing, specific parameters close to the calculated values. This is due

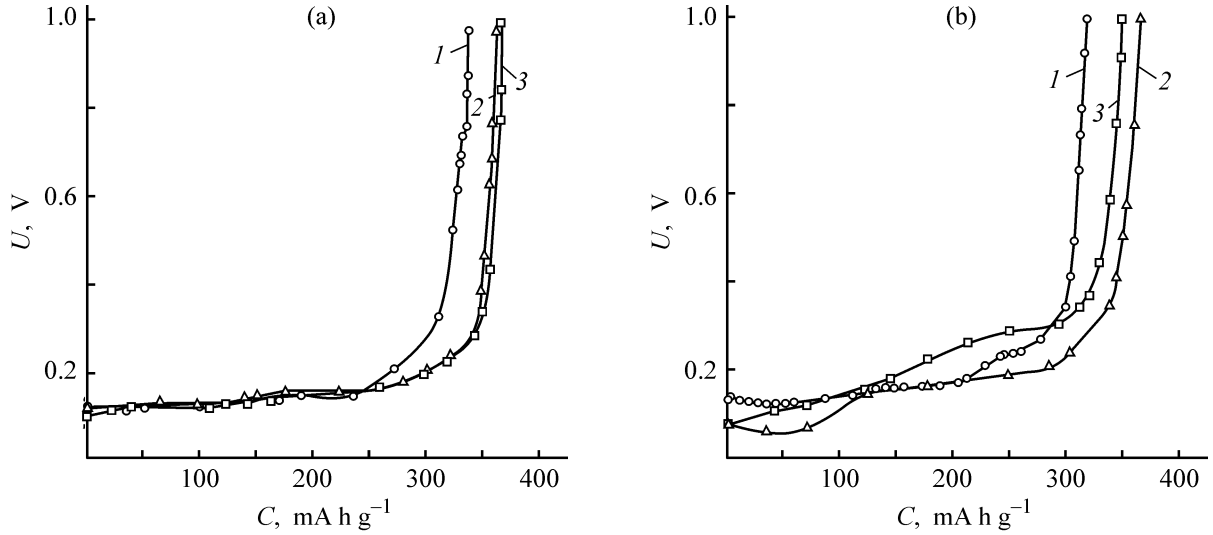

Fig. 2. Discharge curves for anodes made of graphites of (a) CZ-50 and (b) SLA-1115 brands. (*U*) Voltage and (*C*) capacity. Cycle: (a) (*1*) 1st, (*2*) 2nd and (*3*) 3rd; (b) (*1*) 1st, (*2*) 4th, and (*3*) 13th.

to specific features of the surface morphology of particles of the active material contained in the anode. Electron micrographs of particles of CZ-50 and SLC-1520 graphite powders show that the surface morphology of SLC-1520 graphite powder particles is more developed. In addition, the lack of any physical correlation between the polarization characteristics of the anodes and the intrinsic characteristics of the materials involved shows that not only the diffusion parameters of these materials, but also the true current densities, are close. Consequently, it should necessarily be taken into account that the binder material and its quality affect the mechanism of blocking of the active material.

CONCLUSIONS

(1) It was demonstrated that the structural features of active cathode materials are of key importance for solving the problem of raising the working capacity of lithium-ion batteries in prolonged cycling.

(2) It was found that the intrinsic parameters of the active materials, considered in the study, affect the electrochemical behavior of these materials. It was, in particular, shown that lithium cobaltate having a hexagonal symmetry is preferable to lithium cobaltate belonging to the trigonal crystal system.

(3) No physical correlation was observed between the polarization characteristics of the anodes and the intrinsic parameters of the active anode materials under study.

REFERENCES

1. Gummow, R., Thackeray, M.M., David, W.I.F., and Hull, S., *Mater. Res. Bull.*, 1992, vol. 27, pp. 32–33.
2. Skundin, A.M., *Elektrokhim. Energet.*, 2005, vol. 5, no. 2, pp. 65–73.
3. Kedrinskii, I.A. and Yakovlev, V.G., *Li-ionnye akkumulyatory* (Li-ion Batteries), Krasnoyarsk: IPK Platina, 2002.
4. Kinoshita, K., *New Trends in Electrochemical Technology: Energy Storage Systems for Electronics*, Osaka, T. and Datta, M., Eds., London: Gordon Breach Sci., UK, 2000, pp. 193–194.

ISSN 1070-4272, Russian Journal of Applied Chemistry, 2007, Vol. 80, No. 8, pp. 1335–1340. © Pleiades Publishing, Ltd., 2007.
Original Russian Text © R.V. Korzh, V.A. Bortyshevskii, T.V. Tkachenko, V.A. Evdokimenko, V.V. Boiko, 2007, published in Zhurnal Prikladnoi Khimii, 2007, Vol. 80, No. 8, pp. 1296–1301.

APPLIED ELECTROCHEMISTRY AND CORROSION PROTECTION OF METALS

Physicochemical Properties of Membranes Based on MSC-H and Purolite CT-275 Sulfocation-Exchange Resins

R. V. Korzh, V. A. Bortyshevskii, T. V. Tkachenko, V. A. Evdokimenko, and V. V. Boiko

Institute of Bioorganic and Oil Chemistry, National Academy of Sciences of Ukraine, Kiev, Ukraine

Received November 30, 2006; in final form, April 2007

Abstract—Various methods for synthesis of heterogeneous membranes based on MSC-H and Purolite CT-275 sulfocation-exchange resins were considered. The efficiency of a combined method for fabrication of membranes, based on casting followed by rolling, was analyzed.

DOI: 10.1134/S1070427207080149

Industrial membranes used in fuel cells and in purification and drying of alcohols are rather sensitive to the action of polar solvents. To make longer the service life of these membranes, manufactures of fuel cells operating on alcohols deposit onto the membrane surface a barrier layer of polybenzimidazole or sulfated polyvinyl alcohol, which leads to a dramatic increase in the production cost of the membranes. Coatings in the form of a protective alcohol-resistant film reduce the proton conductivity of membranes [1].

In contrast to linear polymers (Nation and its analogues), cross-linked polymers of the MK-40 type (Vladimir, Russia) are insoluble in alcohols and esters, and only somewhat swell in these solvents, which does not affect the physicochemical parameters [2] of membranes fabricated from these polymers. A disadvantage of these membranes is their poor thermal stability (up to 100°C), which restricts their use in medium- and high-temperature processes. Therefore, obtaining membranes that would combine high proton conductivity with chemical resistance and thermal stability up to 150°C is a rather topical task.

EXPERIMENTAL

It is known that an acceptable combination of the characteristics specified above is observed for heterogeneous membranes composed of an acid ion-exchange resin and a macromolecular polymeric binder [3, 4].

As an active component in fabrication of membranes were chosen granulated sulfocation-exchange resins based on copolymers of styrene and divinylbenzene: KU-2-8chS (Azot Research and Production Co., Cherkassy, Ukraine), MSC-H (Dow, USA), and Purolite CT-275 (Purolite Int. Ltd., UK) (Table 1). To form

Table 1. Parameters of the cation exchangers used

Parameter	KU-2-8chS	MSC-H	Purolite CT-275
Ionic form (commercial)	H^+	H^+	H^+
Density of functional groups per unit mass of dry substance, mg-equiv g^{-1}	4.8	4.9	5.4
Number of sulfo groups per benzene ring	1	1	>1
Mass fraction of moisture, wt %	48–58	53.0	50–60
Grain size, mm	0.4–1.25	0.3–1.2	0.3–1.2
Volume share of the working fraction, %	96.0	99.0	99.0
Bulk density, kg m^{-3}	760.0	760.0	760.0
Specific surface area, m^2 g^{-1}	–	30.0	30.0
Pore size, Å	–	200.0	200.0
Maximum working temperature, °C	100	160	150

Table 2. Physicochemical tests of heterogeneous membranes

Sample no.	Membrane			Content of the active component, wt %	Forming method	Membrane brand	Thickness of air-dry membrane, mm	Degree of swelling, K_{sw}	Total static exchange capacity, Π_m, mg-equiv g^{-1}
	active component	binder	support						
Laboratory-made membranes									
1	KU-2-8chS	KhSPE-20i	–	50	Rolling (T ~70°C)	–	0.8	1.25	1.8
2	KU-2-8chS	PEND	Lavsan	70	Compaction (T=100°C)	–	1.0	1.5	2.5
3	KU-2-8chS	KhSPE-20i	″	50	Casting	–	0.5	1.26	2.0
4	MSC-H	KhSPE-20i	″	50	Combined	ECM-1-0.5	0.5	1.24	2.0
5	MSC-H	KhSPE-20i	″	60	″	ECM-1-0.6	0.5	1.28	2.4
6	Purolite CT-275	KhSPE-20i	″	50	″	ECM-2-0.5	0.5	1.24	2.2
7	Purolite CT-275	KhSPE-20i	″	60	″	ECM-2-0.6	0.5	1.28	2.6
Commercial membranes									
8	KU-2-8	PEND	Lavsan	65	Rolling	MK-40L	0.3–0.4	1.25–1.35	2.3–2.9
9						MF-4-SK		1.18–1.2	0.83–0.93
10						Nafion-417		1.2	0.83–1.0

membranes, a cation-exchanger was ground on an electric mill at 5000 rpm and the 50-μm fraction of the resin was taken and dried at 100±5°C for 12 h, which provides drying to constant weight.

To improve the elasticity of a membrane, a binder compatible with ion-exchanger particles was introduced into its composition. Among a number of binders, we chose low-pressure polyethylene [PEND, TU (Technical Specification) U 20908-040] and chlorosulfonated polyethylene (KhSPE-20i) with a mass fraction of chlorine equal to 30 ± 4% (TU 6-55-9–90). KhSPE-20i polyethylene was used in the form of a 12.5–16% solution in toluene.

The membranes were formed by the conventional methods of polymer processing: compaction, rolling, casting, and combination of these [3, 4]. The membrane were reinforced with Lavsan (TU U 17-16 305 440.012–2002; thickness 0.3–0.5 mm, elongation to break 21–25%). Unreinforced membranes were also fabricated (Table 2, sample no. 1).

Membranes were formed by rolling on a FEB laboratory rolling machine in the temperature range 50–70°C. First, the polymeric matrix was rolled for 10–15 min and then, with rolls working, a powdered cation exchanger was gradually added. Filled films were further rolled for 10 min and then cooled to 20–30°C and removed. The mass ratio of the dry cation exchanger and the polymer was 1 : 1 (Table 2, sample no. 1).

In forming of membranes by compaction, the cation exchanger and PEND (≤50-μm fraction), taken in a mass ratio of 2.5 : 1, were thoroughly mixed and deposited onto an inert Lavsan support. The resulting material was kept in a mold at 135°C for 20 min and then cooled (sample no. 2).

In forming of membranes by casting, a dried cation exchanger was added to, and thoroughly mixed with a solution of KhSPE-20i in toluene. The resulting mixture was poured into a fluoroplastic mold. After it was uniformly spread over the mold, a Lavsan support was submerged in the mixture. The solvent was evaporated at room temperature in the course of 24 h. The mass ratio of the components was 1 : 1 (sample no. 3).

The forming of membranes by the combined method assumes that membranes are fabricated by joint use of casting and rolling. A weighed portion of a cation exchanger was kept to swelling in toluene and then a solution of KhSPE-20i in toluene was added. The mixture was thoroughly agitated and then deposited in five steps as a thin layer onto a Lavsan support until a uniform solid coating was obtained. After

each deposition step, the film was dried at 40–50°C. To smooth the surface of the film obtained, it was rolled at 100–110°C (sample nos. 4–7).

To remove organic solvents, the heterogeneous membranes fabricated by each method were boiled in a 30% aqueous solution of propanol-2 for 2–3 h and then washed six times with hot distilled water.

The chemical resistance of the membranes was evaluated by the time of keeping in ethanol and propanol-2 at temperatures of up to 145°C, necessary for a 10% loss of mass by the membranes.

The total static exchange capacity of the membranes was determined in accordance with GOST (State Standard) 17553–72 and 20255.1–89, and the moisture capacity, in accordance with GOST 17553–72 and 10898.1–84.

The degree of swelling of the membranes in water was calculated by the formula

$$K_{sw} = B_1/B_2, \quad (1)$$

where K_{sw} is the degree of swelling; B_1, thickness of a membrane kept in distilled water for 24 h (average over five measurements); and B_2, thickness of a membrane dried to constant weight.

The hydrodynamic permeability of the membranes was determined as the volume of a liquid (water or alcohol) transferred across the membrane via unit area in 1 h at the temperature of the experiment (as an average over 6 h) [5].

The methods used in determination of the gas permeability under atmospheric pressure and in gas-chromatographic analysis for hydrogen were described in [6].

The proton conduction was studied at a dc voltage of 12 V across the electrodes in the temperature range 25–95°C under atmospheric pressure [7]. The setup for measuring the proton conductivity had the form of a two-chamber steam-water cell with chambers separated by a membrane under study. Protons were generated in an electrolyte solution (distilled water) in the anode chamber, transferred across the membrane to the cathode chamber, and reduced in the latter to molecular hydrogen, with release of water. The anode was fabricated from compacted graphite, and the cathode, from nickel-plated stainless steel.

The proton transport number t_{H^+} was found by the formula

$$t_{H_2} = Fn_{H_2}/(I\tau), \quad (2)$$

where F is the Faraday number (C mol^{-1}); n_{H_2}, amount of hydrogen released at the cathode (mol); I, current strength (A); and τ, experiment duration (h) [8].

The proton conductivity of the membranes, σ (S cm^{-1}), was calculated using the formula [9]:

$$\sigma = (It_{H^+}l)/(US), \quad (3)$$

where l is the membrane thickness (cm); U, voltage across the electrodes (V); and S, cross-sectional area of the membrane (cm^2).

An analysis of the physicochemical parameters of the membranes obtained demonstrated that they surpass in exchange capacity the industrial membranes Nafion and MF-4-SK and are comparable in this regard with MK-40L (Table 2). All the four methods for membrane forming are applicable to their fabrication, but the most efficient is the combination of casting with rolling (sample nos. 4–7). The swelling coefficients of the membranes developed are 1.24–1.28 and satisfy the requirements of the standard. All the membranes studied sustained boiling in water for two hours.

A study of the permeability of the membranes to water and alcohols demonstrated that their permeability to water exceeds by two orders of magnitude that for industrial perfluorinated samples and is an order of magnitude lower than that for the analogue, MK-40 membrane (Table 3). The data obtained are accounted for by the high hydrophobicity of fluorine-containing polymers (Nafion and MF-4-SK). The decrease in the permeability of the membranes developed, compared with MK-40, is accounted for by densification of membranes and narrowing of their transport channel in forming with KhSPE, which does not occur in forming of KU-2-8ChS with polyethylene.

The permeability of the membranes based on sulfocation-exchange resin Purolite CT-275 (Table 2, sample nos. 6, 7) is twice that of MSC-H (sample nos. 4, 5). This is due to the difference in the total exchange capacities of both the starting cation exchangers and the resulting membranes, which is, in turn, determined by the degree of sulfonation of the active components. Because just the sulfo groups are responsible for the transport of water molecules across a membrane, it should be higher for membranes in which the concentration of these groups per benzene ring is higher (Purolite CT-275) and

Table 3. Permeability of membranes to liquids

Membrane	Water		Alcohol					
			methanol		ethanol		propanol-2	
	T, °C	permeability, $cm^3\,cm^{-2}\,s^{-1}\,atm^{-1}$	T, °C	permeability, $cm^3\,cm^{-2}\,s^{-1}\,atm^{-1}$	T, °C	permeability, $cm^3\,cm^{-2}\,s^{-1}\,atm^{-1}$	T, °C	permeability, $cm^3\,cm^{-2}\,s^{-1}\,atm^{-1}$
ECM-1-0.6	90	3.9×10^{-6}			55	2.3×10^{-6}	55	6.39×10^{-7}
ECM-2-0.5	90	2.9×10^{-6}			55	2.7×10^{-6}		
ECM-2-0.6	90	5.8×10^{-6}			55	3.5×10^{-6}	55	7.8×10^{-7}
MK-40L	90	1.8×10^{-5}			55	5.25×10^{-6}	55	5.3×10^{-6}
							68	8.77×10^{-6}
							90	6.3×10^{-6}
MF-4-SK	25	4×10^{-6} [10, 11]						
Nafion	25	3×10^{-8}–2×10^{-6}, [10, 11]	22	1.5×10^{-7}, [5]				
			60	3.4×10^{-6}, [5]				

should increase with the content of the active substance in the membrane (from 0.5 to 0.6).

An analysis of the concentration transport of an alcohol across the membranes demonstrated that it is considerably lower than that for water (Table 3). This fact is accounted for both by sorption factors and by steric and dynamic factors: the molecular volume of alcohols exceeds that of water, which causes a significant steric hindrance and makes lower the mobility of alcohol molecules. In contrast to water, the permeabilities to alcohols are close for all types of membranes, irrespective of the nature of an alcohol and origin of a membrane.

It was found that, as temperature increases, the diffusion rate of the alcohols passes through a maximum (Fig. 1). For propanol-2, the bending point is observed at T = 68–72°C. Further increase in temperatures leads to a decrease in the amount of diffusion.

In the narrow temperature range 68–72°C, in which the bend in the curve in Fig. 1 occurs, tetrameric associates of a liquid alcohol disintegrate to the mono- and dimeric state [12]. This effect builds up as an avalanche as temperature increases further. On heating to above 80°C, alcohol passes from the liquid state into the gaseous state and the diffusion rate decreases.

This is confirmed by the dependences shown in Fig. 2. It can be seen that the diffusion of liquid ethanol is two times faster than that of its vapor. Apparently, when the alcohol passes into the gaseous

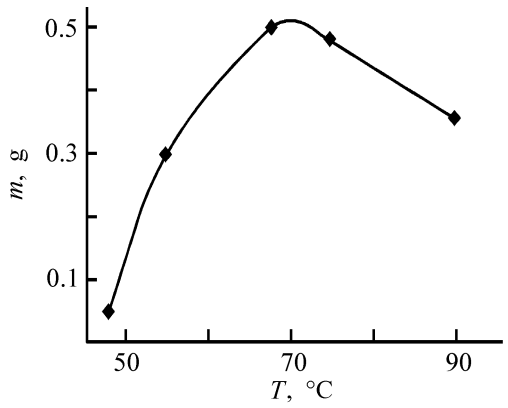

Fig. 1. Diffusion of propanol-2 across MK-40L membrane (P = 0.1 MPa) vs. temperature T. (m) Mass of propanol-2.

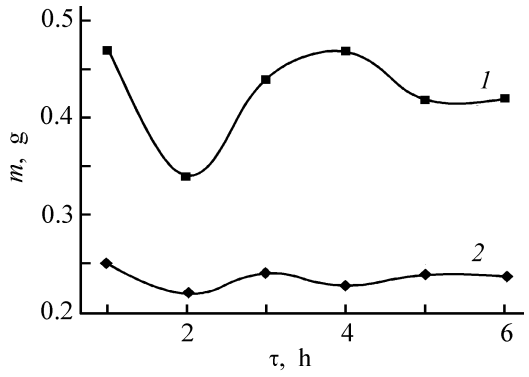

Fig. 2. Diffusion of ethanol across ECM-1-0.6 membrane working at 140°C. (m) Mass of ethanol and (τ) time. Alcohol: (*1*) in liquid state (P = 0.3 MPa) and (*2*) in gaseous state (P = 0.6 MPa).

Table 4. Permeability of the membranes to hydrogen

Membrane	Permeability, $cm^3\ cm^{-2}\ s^{-1}\ atm^{-1}$
ECM-1-0.6	3.11×10^{-4}
MK-40L	4.35×10^{-3}
Nafion	2×10^{-3} [10, 11]
Composite of polyamide and polyesters	1.8 [10]
Polyimide on Al_2O_3 (tubes)	2.26×10^{-2} [13]
Polyimide on tetrafluoroethylene	4.02×10^{-2} [13]

Table 5. Time of a 10% loss of mass by membranes

Membrane	Solvent	Working temperature, °C	Time till 10% loss of mass, h
MK-40L	Propanol-2	≤100	~720
MF-4-SK	Propanol-2	≤160	≤4
	Ethanol	≤160	≤6
ECM-1-0.6	Propanol-2	≤145	≥1440
	Ethanol	≤145	≥1440

state, the membrane is dried and the motion of diffusing molecules along pores becomes more difficult.

It was, in particular, shown that raising the temperature from 55 to 140°C (with a simultaneous increase in pressure to 0.6 MPa) leads to a decrease in the permeability of the ECM-1-0.6 membrane to ethanol by nearly an order of magnitude (from 2.3×10^{-6} to 3.62×10^{-7} $cm^3\ cm^{-2}\ s^{-1}\ atm^{-1}$). The decrease in the permeability of the membrane during the second hour, compared with that in the first hour of an experiment, observed in Fig. 2, is accounted for by a change in the moisture content of the membrane because of the dehydration of sulfo groups by the alcohol. Further minor increase in permeability occurs because of the equalization of the concentrations of the supplied alcohol and water contained in the membrane.

Comparison of the results obtained with the known published data indicates that the heterogeneous membranes fabricated under laboratory conditions from the sulfocation exchangers MSC-H and CT-275 show a satisfactory diffusion permeability to water and alcohols.

Comparison of the gas permeabilities of the membranes MK-40L and ECM-1-0.6 to molecular hydrogen at 80°C and atmospheric pressure shows that the diffusion of H_2 across the MK-40L membrane (4.35×10^{-3} $cm^3\ cm^{-2}\ s^{-1}\ atm^{-1}$) exceeds by an order of magnitude that for the laboratory sample (3.11×10^{-4} $cm^3\ cm^{-2}\ s^{-1}\ atm^{-1}$) (Table 4). In other words, the heterogeneous membranes fabricated under laboratory conditions are gas-impermeable and safe in operation.

It was shown that the chemical stability of the membranes against polar solvents (ethanol and propanol-2, in particular) exceeds 1440 h, in contrast to that of the MF-4-SK membrane (Table 5).

It was found in measurements of the current through the measuring cell with ECM-1-0.6 and ECM-2-0.6 membranes at 12 V that the absolute current strength across the ECM-2-0.6 membrane is higher (Fig. 3). This is accounted for by the higher specific exchange capacity of ECM-2-0.6, compared with ECM-1-0.6 (Table 1). The share of the proton component for the sample based on Purolite CT-275 is lower than that for MSC-H (t_{H^+} = 0.60-0.65 against 0.75–1.0, respectively).

The calculated proton conductivities σ at 85°C and atmospheric pressure for the ECM-1-0.6 and ECM-2-0.6 membranes (2.3×10^{-4} and 1.04×10^{-4} S cm^{-1}) are comparable with the values obtained under the same conditions for MF-4-SK and MK-40L (4.8×10^{-4} and 8.6×10^{-5} S cm^{-1}).

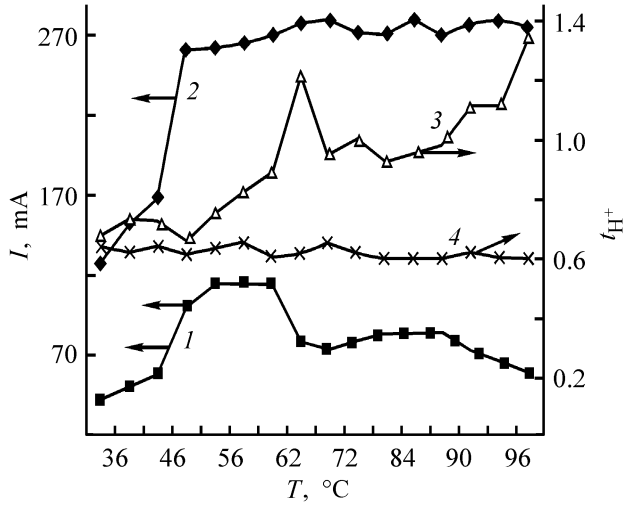

Fig. 3. (*1*, *2*) Total current strength *I* and (*3*, *4*) proton transport number t_{H^+} across membranes (*1*, *3*) ECM-1-0.6 and (*2*, *4*) ECM-2-0.6 vs. temperature *T*. *U* = 12 V, water as electrolyte.

CONCLUSIONS

(1) An analysis of various methods for fabrication of heterogeneous membranes based on the sulfocation exchangers MSC-H and Purolite CT-275 revealed that the most efficient of these is the combined method for membrane forming. The membranes produced using this method exhibit a unique resistance (>1440 h) to the action of polar solvents at a temperature of 145°C and pressure of 0.6 MPa.

(2) The membranes obtained are comparable in exchange capacity (2.0–3.0 mg-equiv g^{-1}) with MK-40L (2.3–2.9 mg-equiv g^{-1}). The swelling coefficients of the membranes are 1.24–1.28.

(3) The permeabilities of the membranes to polar liquids and molecular hydrogen are within $(2.3–8.7) \times 10^{-6}$ and 3.11×10^{-4} $cm^3\ cm^{-2}\ s^{-1}\ atm^{-1}$, respectively. At 90°C, the proton conductivity is as high as $(1–2.3) \times 10^{-4}$ S cm^{-1}, which is comparable with that of the known industrial membranes.

REFERENCES

1. Bagotskii, S.V., Osetrova, N.V., and Skundin, A.M., *Elektrokhimiya*, 2003, vol. 39, no. 9, pp. 1027–1045.
2. *TU* (Technical Specification) *6-06-205–91*; http:www.scitechlibrary.ru/rus.catalog.pages.3505.html.
3. Kesting, R.E., *Sintetic Polymeric Membranes. A Structural Perspective*, New York: J. Wiley and Sons, 1985.
4. Khuvink, R. and Staverman, A. *Khimiya i tekhnologiya polimerov* (Chemistry and Technology of Polymers), Moscow: Khimiya, 1965.
5. Bouchet, R., Miller, S., Duclot, M., et al., *Sol. State Ionics*, 2001, vol. 145, no. 41, pp. 69–78.
6. Bortyshevskii, V.A., Golovko, L.V., Shpak, A.P., et al., *Nanosist., Nanomater., Nanotekhnol.*, 2006, vol. 3, no. 4, pp. 957–966.
7. Tkachenko, T.V., Bortyshevskii, V.A., and Motornyi, V.G., *Katal. Neftekhim.*, 2003, no. 12, pp. 84–88.
8. Shel'deshov, N.V., Krupenko, O.N., Shadrina, M.V., and Zabolotskii, V.I., *Elektrokhimiya*, 2002, vol. 38, no. 8, pp. 989–993.
9. Antropov, L.G., *Teoretichna elektrokhimiya* (Theoretical Electrochemistry), Kiiv: Libid', 1993.
10. Tarasevich, M.R., Orlov, S.B., Shkol'nikov, E.I., et al., *Elektrokhimiya polimerov* (Electrochemistry of Polymers), Moscow: Khimiya, 1990.
11. La Conti, A.B., Fragala, A.R., and Boyack, J.R., *Proc. Symp. Electrode Materials and Processes for Energy Conversion and Storage*, McIntyre, J.D.E. et al., Eds., New York, 1977, vol. 77, no. 6, pp. 345–374.
12. *Vodorodnaya svyaz': Mezhmolekulyarnye vzaimodeistviya* (Hydrogen Bond: Intermolecular Interactions), Pogorelyi, V.K., Ed., Kiev: Naukova Dumka, 1993.
13. Alekseeva, O.K. and Amirkhanov, D.M., *Ross. Khim. Zh. (Zh. Ross. Khim. O–va im. D.I. Mendeleeva)*, 2004, vol. 48, no. 5, pp. 82–89.

ISSN 1070-4272, Russian Journal of Applied Chemistry, 2007, Vol. 80, No. 8, pp. 1341–1345. © Pleiades Publishing, Ltd., 2007.
Original Russian Text © G.A. Kolyagin, V.L. Kornienko, 2007, published in Zhurnal Prikladnoi Khimii, 2007, Vol. 80, No. 8, pp. 1302–1306.

APPLIED ELECTROCHEMISTRY AND CORROSION PROTECTION OF METALS

Double Layer Capacitance of Gas-Diffusion Electrodes Made of Acetylene Black and Expanded Natural Graphites and Evaluation of the Surface Area Wetted by the Electrolyte

G. A. Kolyagin and V. L. Kornienko

Institute of Chemistry and Chemical Technology, Siberian Division, Russian Academy of Sciences, Krasnoyarsk, Russia

Received December 26, 2006

Abstract—Cyclic voltammetry was used to determine the capacitance of the double layer in hydrophobized porous gas-diffusion electrodes made of acetylene black and expanded natural graphites. The average radius of pores by with an alkaline electrolyte, the area of these pores, and the true current density in electroreduction of oxygen were evaluated.

DOI: 10.1134/S1070427207080150

It is known that carbon-graphite materials and composites on their base are widely used as construction materials and electrodes [1] in various electrochemical devices employing aqueous electrolyte solutions: electrolyzers, power cells, electrochemical sensors [2], and capacitors [3–6]. In most cases, these materials have a pronounced porosity and highly developed internal surface. A knowledge of their structural characteristics and dynamics of their interaction with aqueous solutions is necessary for improvement of articles fabricated from these materials.

One of methods used to study and determine the structural characteristics of electrically conducting porous materials impregnated with an electrolyte solution is cyclic voltammetry (CVA) with linear potential sweep [7, 8–13]. This method is convenient in that, with a knowledge of the specific capacitance of materials under study, one can rapidly obtain necessary evidence concerning the interaction of porous bodies with a liquid medium under real operation conditions of electrodes without their disintegration or any change in their characteristics. If the specific capacitance of a material under study is unknown, the relative effects of various factors on the true working surface area of electrodes can be evaluated. For example, it was shown in [13] that the electric activity of carbon materials is proportional to the surface area evaluated by CVA, rather than to that given by BET. Recently, CVA has been frequently used to study expanded natural graphites (ENG) and fibers and articles made of these materials. For example, the possibility of using CVA to study articles made of ENG with a thickness of 2–6 mm and density of 160–470 g dm^{-3} at a potential sweep rate of 0.2–50 mV s^{-1} in order to determine the surface area, average pore radius, and porosity was demonstrated in [7].

It can be assumed that, under conditions of partial wetting of a porous body by water (porous hydrophobized gas-diffusion electrodes, electrically conducting composite materials, etc), CVA can be used to determine the surface area wetted by an aqueous solution. It is known that the activity of gas-diffusion electrodes strongly depends on the surface area wetted by the aqueous electrolyte; the knowledge of this parameter is necessary both for theoretical calculations and for applied studies, e.g., in finding the rate-determining stage of the process of current generation in the electrode.

This study continues research in the field of ENG-based hydrophobized gas-diffusion electrodes [1]. The aim of the study was to evaluate the surface area of hydrophobized gas-diffusion electrodes, wetted by an aqueous solution, by the CVA method and to correlate this surface area with the activity of electrodes in electroreduction of oxygen. To compare ENG with other carbon materials, electrodes fabricated from A-437E acetylene black with a specific surface area of 100 $m^2 g^{-1}$ were also studied.

Table 1. Parameters of electrodes fabricated from ENG of various brands and their activity in electroreduction of oxygen in 3 M KOH

Electrode no.	Graphite brand	ENG synthesis conditions		Density of electrodes, g dm^{-3}	Current density, mA cm^{-2}, at –0.9 V	
		acid, wt %	quantity of electricity, A h g^{-1}		?geometric	averaged true
1	A437E acetylene black	–	–	654	35*	0.0026*
2	GAK-3	HNO_3, 70	0.17	747	28	0.0175
3	GT-1	HNO_3, 70	0.22	724	25	0.0125
4	GAK-3	H_2SO_4, 92	0.15	773	11	0.018
5	GAK-3	HNO_3, 70	0.21	800	8	0.008
6	GT-1	HNO_3, 70	0.15	790	10	0.017

* Current densities at –0.3 V.

EXPERIMENTAL

Powders of expanded graphite were obtained by heating of intercalation compounds synthesized by the electrochemical method of intercalation with nitric and sulfuric acids. The electrolyzer for electrosynthesis of intercalation compounds, parameters of the graphites used, and procedures employed to obtain ENG and fabricate electrode pastes and electrodes were described in [1]. The graphite brands, acids, and quantities of electricity passed in electrosynthesis of intercalation compounds are listed in Table 1. The powders obtained were used to produce a hydrophobized electrode paste (with an aqueous suspension of fluoroplastic-4D as hydrophobizer), from which electrodes were fabricated by compaction in the form of discs with a thickness of 0.5 mm, mass of about 0.3 g, porosity of 60 vol %, and fluoroplastic-4D content of 10 wt %. Acetylene-black electrodes were fabricated with a thickness of 1 mm and porosity of 69 vol % from a paste containing 8 wt % fluoroplastic-4D. To enhance the mechanical strength and electrical conductivity, the acetylene-black electrodes were reinforced with a nickel grid of thickness 0.1 mm.

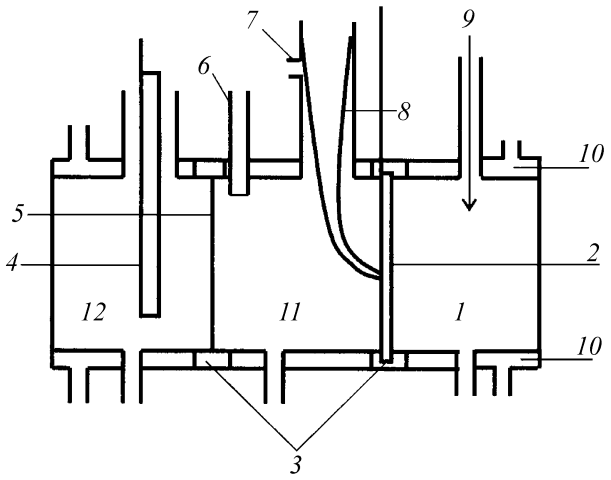

Fig. 1. Schematic of an electrolyzer cell with a hydrophobized gas-diffusion electrode: (*1*) gas chamber, (*2*) hydrophobized electrode, (*3*) fluoroplastic cartridges, (*4*) platinum counter electrode, (*5*) MF-4SK-100 ion-exchange membrane, (*6*) thermometer, (*7*) pipe for removal of gaseous products, (*8*) Luggin capillary, (*9*) supply of oxygen or inert gas, (*10*) thermostating jacket, and (*11, 12*) cathode and anode chambers filled with an aqueous electrolyte solution.

Electrochemical measurements were made at 20°C and atmospheric pressure in a 3 M KOH solution in a glass cell shown in Fig. 1. The catholyte volume was 0.023 l. A 1 M H_2SO_4 solution served as anolyte. The geometric current density was calculated per unit visible frontal surface area of the electrode (5 cm^2). The averaged true current density was calculated per unit electrolyte-wetted area, found in the study. The electrode potential was measured relative to a saturated silver chloride reference electrode. Oxygen was passed at atmospheric pressure via the gas chamber, wherefrom it was delivered into the electrode from its back side. Polarization curves were measured at a potential sweep rate of 4 mV s^{-1}. An inert gas was passed through the gas chamber when measuring the double layer capacitance. The charging current was determined at potentials of –0.14…0.0 V at rates of linear potential sweep ranging from 1 to 80 mV s^{-1}, with the electrode preliminarily kept at a zero potential. The charging current of the double layer was calculated at –0.075 V by dividing by two the absolute value of the current obtained by summation of the currents in the forward and reverse potential sweeps. Further, the slope of the dependence of the charging

current on the potential sweep rate was used to find the electrode capacitance and calculate the surface area [7] ($I = C_d S v$, where I is the charging current; C_d, specific capacitance per unit area; S, electrode surface area wetted by the electrolyte; and v, potential sweep rate). The calculations were made using published values of the specific capacitance of acetylene black and expanded graphite: 4.5 [9. 14] and 13.7 μF cm^{-2} [7], respectively. The average radius of pores wetted by the electrolyte was calculated by the formula [7] $r = 2V/S$, where V is the volume of electrolyte-wetted electrode pores, and S is the surface area wetted by the electrolyte. The volume of wetted pores was found by hydrostatic weighing of the electrodes [1] in 3 M KOH after experiments. The electrolyte porosity of the electrodes studied was 4–15 vol %. The characteristics of the electrodes and their activity in electroreduction of oxygen are listed in Table 1 and shown in Fig. 2.

Figure 3 shows typical examples of cyclic voltammograms obtained with expanded-graphite electrodes, which are similar to the dependences obtained for carbon materials [5], e.g., on graphite fabric [12], expanded-graphite fibers [4], or on carbon black and ultradispersed diamond [13]. It can be seen that the presence of polytetrafluoroethylene in a porous electrode does not affect the run of voltammograms.

Figure 4 shows dependences of the charging current on the potential at different potential sweep rates, obtained on the acetylene-black electrode. It can be seen that, in the potential range –0.05…–0.15 V, the charging current is directly proportional to the potential sweep rate and is independent of the electrode potential, which means that the ohmic loss is virtually zero [5]. Figure 5 shows dependences of the charging current on the potential sweep rate, obtained with different electrodes. The dependences obtained on electrode nos. 2 and 3 (Table 1) virtually coincide, and, therefore, Fig. 5a shows only the dependences obtained for one of these electrodes (no. 3). The nonlinearity of the dependences in Fig. 5b is due to ohmic loss in the electrodes. The larger the surface area and the higher the electrolyte porosity, the more linear the dependence of the charging current on the potential sweep rate and the smaller the error in determining the surface area by the CVA method, which means that higher potential sweep rates can be used [7]. To diminish the effect of the ohmic loss, the double layer capacitance of the electrodes was calculated from the slopes of the tangents to the cur-

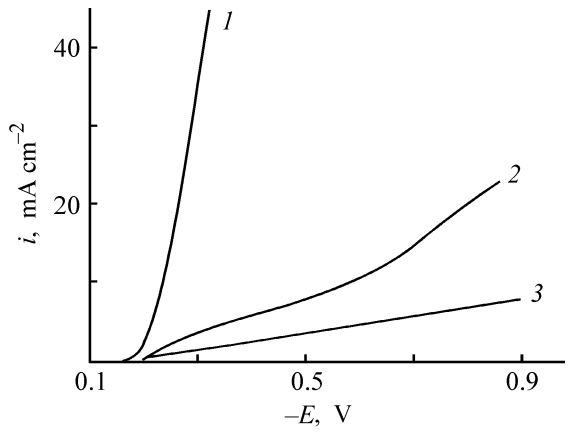

Fig. 2. Polarization curves of oxygen electroreduction, obtained in 3 M KOH on hydrophobized electrodes. (*i*) Geometric current density and (*E*) electrode potential; the same for Figs. 3, 4. Electrode (Table 1): (*1*) no. 1, (*2*) no. 3, and (*3*) no. 5.

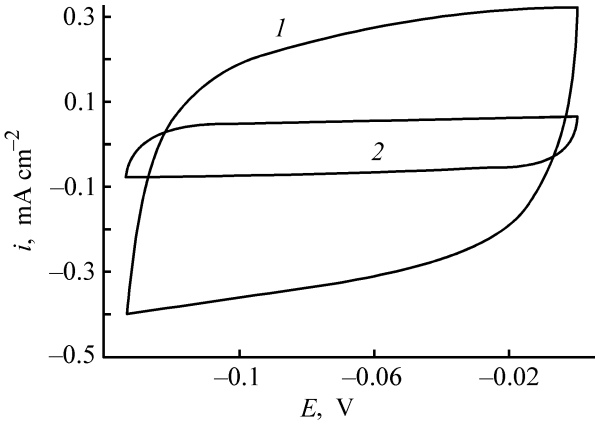

Fig. 3. Cyclic voltammograms obtained at a potential sweep rate of 10 mV s^{-1} on different ENG electrodes. Electrode (Table 1): (*1*) no. 3 and (*2*) no. 4.

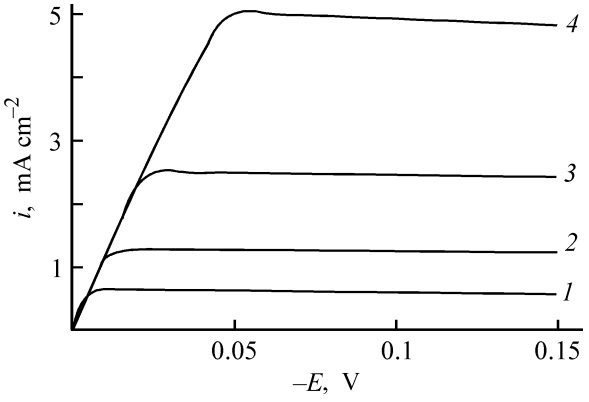

Fig. 4. Dependence of the charging current density on the potential, obtained on the acetylene-black electrode at different potential sweep rates. v (mV s^{-1}): (*1*) 10, (*2*) 20, (*3*) 40, and (*4*) 80.

Table 2. Double layer capacitance, average radius of electrolyte-wetted pores, and their surface area

Electrode no.	Graphite	Specific capacitance, F g^{-1}	Specific surface area, m^2 g^{-1}	Capacitance,* F cm^{-2}	Surface area,* m^2 cm^{-2}	Average radius of electrolyte-wetted pores, nm
1	A437E acetylene black	1.1	24.9	0.061	1.35	27
2	GAK-3	0.70	5.0	0.022	0.16	43
3	GT-1	0.91	6.5	0.029	0.2	130
4	GAK-3	0.25	1.8	0.008	0.06	210
5	GAK-3	0.41	3.0	0.014	0.1	240
6	GT-1	0.24	1.7	0.008	0.06	330

* Per unit visible electrode area.

ves at the origin of coordinates (Fig. 5b). The results of these calculations are listed in Table 2.

It follows from the data in Table 2 that the ENG surface area wetted by the electrolyte in the electrodes is smaller by a factor of 10 and more than that in the starting ENG powders (70–40 m^2 g^{-1} [1]). In the electrodes, the average radius of pores wetted by the electrolyte solution is an order of magnitude larger than the pore radius in ENG, found from the nitrogen adsorption (20–30 nm [1]). This can be attributed to blocking of graphite particles and narrow pores by fluoroplastic particles and to the impossibility of their wetting by the electrolyte solution. A similar effect of a polymer was described, e.g., in [6], where polyvinyl fluoride introduced in an amount of 20% reduced severalfold the original surface area of the carbon-graphite material because of the blocking of micropores. The decrease in the wetted area is also favored by working conditions of the electrode, because the back side of the electrode serves for delivery of a gaseous reagent into the electrode and is not in contact with the electrolyte. It is known that articles fabricated from expanded graphite exhibit hydrophobicity, closed porosity, and anisotropy of physical properties, which largely depend on their density [7, 15, 16]. This circumstance fundamentally distinguishes carbon blacks from ENG and leads to only a fourfold decrease in the surface area of the blacks and to a higher geometric current density on carbon-black electrodes, compared with those fabricated from ENG, at a lower true current density. The study failed to reveal the influence exerted by the nature of graphites and by the conditions of their processing on the wetted surface area and activity of hydrophobized electrodes. Only a slight effect of the amount of electricity passed in electrosynthesis of intercalation compounds on the true current density in electroreduction of O_2 was observed (Table 1). For example, the true current density is 0.0175 mA cm^{-2} on passing 0.15–0.17 A h g^{-1} and decreases to 0.0125–0.008 mA cm^{-2} at 0.21–0.22 A h g^{-1}. It is known [2, 4] that the method used to prepare ENG can affect its properties, e.g., the surface area and the capacitance of expanded carbon fibers. The following tendency is observed for all

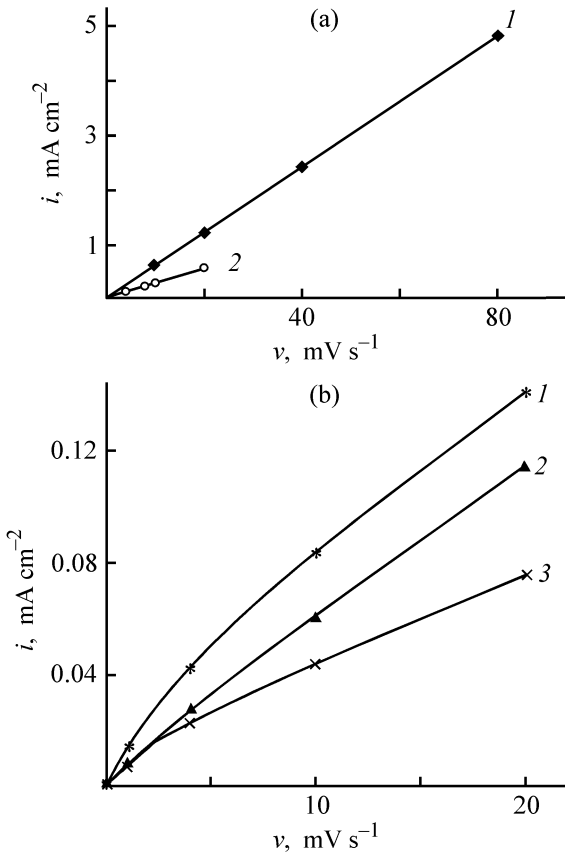

Fig. 5. Dependence of the charging current density i at –0.075 V on the potential sweep rate v, obtained on ENG electrodes. Electrode (Table 1): (a) (*1*) no. 1 and (*2*) no. 3; (b) (*1*) no. 5, (*2*) no. 4, and (*3*) no. 6.

the electrodes: as the density of the electrode increases, the capacitance, wetted surface area, and geometric current density decrease and the average diameter of hydrophilic pores grows, i.e., the fraction of pores with a smaller radius decreases. This is presumably due to the effect of fluoroplastic-4D particles, because, as the density of porous articles fabricated from the starting ENG increases, the average pore radius becomes smaller and the surface area decreases not so strongly [7, 15, 16].

As follows from the data in Table 2, all the electrodes can be divided into three groups with respect to their increasing density and decreasing capacitance and surface area. The highest capacitance and most developed surface is observed for the acetylene-black electrode, and then follow electrode nos. 2 and 3 and electrode nos. 4–6. In the same order varies the activity of the electrodes in electroreduction of oxygen (Fig. 2). It should be noted that the activities of electrode nos. 2, 3 and 4–6 virtually coincide, and, therefore, Fig. 2 shows as an example only a single curve for each group. Thus, it can be seen from the data obtained that there is a correlation between the wetted surface area and the geometric current density, despite that the wetted surface area is only roughly estimated.

No unambiguous dependence of the geometric current density on the surface area was found in the study, because the values of specific capacitance, used to calculate the area, were not for this particular material. It should also be noted that a direct dependence of the activity of electrodes on the electrolyte-wetted surface area takes place only in the kinetic mode with equal exchange currents, whereas in this study, the electrodes operate in the diffusion-kinetic mode.

CONCLUSIONS

(1) It was shown that cyclic voltammetry can be used to determine the double layer capacitance (1.1–0.24 F g^{-1}) and evaluate the wetted surface area (25–1.7 m^2 g^{-1}) of porous hydrophobized electrodes fabricated from carbon black and expanded natural graphites. The geometric current density in electroreduction of oxygen is proportional to this area. The averaged true current density decreases as the quantity of electricity expended for intercalation of acids into graphite grows. The larger the specific surface area determined and the smaller the ohmic loss, the more linear is the dependence of the charging current on the potential sweep rate.

(2) It was demonstrated that hydrophobized electrodes, the surface area accessible to the electrolyte sharply decreases, compared with that for the starting expanded natural graphite, from 70–40 to 6.5–1.7 m^2 g^{-1}, and the average radius of wetted pores increases from 20–30 to 43–330 nm. In contrast to graphites, the surface area of carbon black decreases by only a factor of 4, which is due to the significant difference between the properties of these materials.

(3) It was found that, as the density of the electrodes increases, their total capacitance, wetted surface area, and geometric current density in electroreduction of oxygen decrease and the average diameter of electrolyte pores becomes larger.

REFERENCES

1. Kolyagin, G.A., Kornienko, V.L., Kuznetsov, B.N., and Chesnokov, N.V., *Zh. Prikl. Khim.*, 2005, vol. 78, no. 10, pp. 1653–1658.
2. Ramesh, P., Suresh, G.S., and Sampath, S., *J. Electroanal. Chem.*, 2004, vol. 561, pp. 173–180.
3. Soneda, Y., Toyoda, M., Tani, Y., et al., *J. Phys. Chem. Solids*, 2004, vol. 65, nos. 2–3, pp. 219–222.
4. Masahiro Toyoda, Yuji Tani, and Yasusyi Soneda, *Carbon*, 2004, vol. 42, no. 14, pp. 2833–2837.
5. Frackowiak, E. and Beguin, F., *Carbon*, 2001, vol. 42, no. 6, pp. 937–950.
6. Hsisheng Teng, Yao-Jen Chang, and Chien-To Hsieh, *Carbon*, 2001, vol. 39, no. 13, pp. 1981–1987.
7. Calas-Blanchard, C., Comtat, M., Marty, J.-L., and Mauran, S., *Carbon*, 2003, vol. 41, no. 1, pp. 123–130.
8. Ramesh, P. and Sampath, S., *Anal. Chem.*, 2003, vol. 75, no. 24, pp. 6949–6957.
9. Tarasevich, M.R., Radyushkina, K.A., and Zhutaeva, G.V., *Elektrokhimiya*, 2004, vol. 40, no. 11, pp. 1369–1383.
10. Bagotskii, V.S., *Osnovy elektrokhimii* (Fundamentals of Electrochemistry), Moscow: Khimiya, 1988.
11. *Techniques of Electrochemistry*, Yeager, E. and Salkind, A.J., Eds., New York: Wiley-Interscience, 1972, vol. 1.
12. Oren, Y. and Soffer, A., *J. Electroanal. Chem.*, 1985, vol. 186, nos. 1–2, pp. 63–77.
13. Osina, M.A. and Bogdanovskaya, V.A., *Elektrokhimiya*, 2006, vol. 42, no. 8, pp. 987–992.
14. Tarasevich, M.R., Beketaeva, L.A., and Efremov, B.N., *Elektrokhimiya*, 2004, vol. 40, no. 5, pp. 621–622.
15. Biloe, S. and Mauran, S., *Carbon*, 2003, vol. 41, no. 3, pp. 525–527.
16. Mauran, S., Rigaud, L., and Coudevylle, O., *Transport in Porous Media*, 2001, vol. 43, pp. 355–376.

ISSN 1070-4272, Russian Journal of Applied Chemistry, 2007, Vol. 80, No. 8, pp. 1346–1352. © Pleiades Publishing, Ltd., 2007.
Original Russian Text © L.G. Shaidarova, A.V. Gedmina, I.A. Chelnokova, G.K. Budnikov, 2007, published in Zhurnal Prikladnoi Khimii, 2007, Vol. 80, No. 8, pp. 1307–1313.

APPLIED ELECTROCHEMISTRY AND CORROSION PROTECTION OF METALS

Electrocatalytic Oxidation and Voltammetric Determination of Dopamine on a Composite Film Electrode with an Iridium Deposit

L. G. Shaidarova, A. V. Gedmina, I. A. Chelnokova, and G. K. Budnikov

Kazan State University, Kazan, Tatarstan, Russia
Butlerov Chemical Institute, Kazan, Tatarstan, Russia

Received November 9, 2006; in final form, March 2007

Abstract—Electrochemical oxidation of dopamine on a composite glassy carbon electrode with an electrodeposited iridium layer coated with a Nafion film was studied. A procedure for voltammetric determination of dopamine on the composite film electrode was developed.

DOI: 10.1134/S1070427207080162

Dopamine [2-(3,4-dioxyphenyl)-ethylamine; DA] is one of the most important biogenic catecholamines and plays an important role of a neuromediator in the activities of the central and peripheral nerve systems. It is included in the list of prohibited preparations, energy stimulators, used by athletes in the form of nutritional additives and pharmaceutical preparations. Therefore, development of fast and simple methods for determining the content of this catecholamine in biological fluids is of indubitable interest not only for diagnostics of psychic diseases, but also for doping control of athletes.

Various physicochemical methods are used for quantitative determination of DA. These include titrimetry [1], spectrophotometry [2], chemiluminescence [3], potentiometry [4], and high-performance liquid chromatography (HPLC) [5]. In addition to advantages, these methods have certain limitations. A shortcoming of spectrophotometry, potentiometry, and titrimetry is their low concentration sensitivity, and HPLC requires a preliminary sample preparation, occasionally including preliminary derivatization. Direct voltammetry with unmodified electrodes also has a number of disadvantages associated both with the irreversible oxidation of DA at large potential shifts from equilibrium and with the lack of reproducibility of the electrochemical signal from a substratum under study. Use of chemically modified electrodes (CME) with mediator properties improves the reliability and makes it possible to lower the DA oxidation overvoltage and raise the sensitivity of determination of this compound. As CME mediators in voltammetric determination of DA are used gold, platinum metals, and electrically conducting polymeric-organic and inorganic films [6–9]. However, with CME used, the detection limit cannot be lowered to the level in which DA is present in physiological fluids and the effect of accompanying components of physiological fluids (e.g., ascorbic and uric acids) on its oxidation cannot be prevented.

This study was concerned with electrooxidation and voltammetric determination of DA on a composite electrode based on glassy carbon (GC) with an electrodeposited iridium layer coated with a Nafion (NF) film. This enabled development of a high-sensitivity voltammetric method for determination of DA, which combines concentration in a polymeric film and electrocatalysis.

EXPERIMENTAL

Cyclic voltammograms were recorded with a PI50-1.1 potentiostat in a three-electrode cell. A GC electrode with a working surface area of 0.096 cm^2 and Ir-GC, NF-GC, and NF-Ir-GC electrodes were used as a working electrode. A silver chloride electrode served as reference, and a platinum wire, as auxiliary electrode. Cyclic voltammograms were measured at a potential sweep rate of 20 mV s^{-1}.

The film electrode was fabricated using Nafion (5% solution in a mixture of aliphatic alcohols: 50% alcohols and 45% water) of pure grade, purchased from Aldrich. Polymer solutions of various concentrations were prepared by dilution of the starting commercial Nafion with ethanol in the range 2.5–0.25%. The polymer was deposited onto the GC surface by the method of drop evaporation, with the subsequent cyclic variation of the potential in the range from –0.1 to +1.0 V in a 0.1 M solution of H_2SO_4. Iridium was electrodeposited from an aqueous solution of its salt, prepared from $IrCl_3$ purchased from Aldrich. Prior to the modification of the electrode, the GC surface was subjected to a pretreatment: the electrode was polished on filter paper, washed with twice-distilled water, and activated by multiple potential sweeping in the range –0.5…+0.5 V, in 0.1 M H_2SO_4. The electrode surface was refreshed mechanically.

A 5% solution of DA served as the standard solution. Solutions of lower concentrations were obtained by successive dilution of the starting standard.

As supporting electrolytes served 0.1 M solutions of H_2SO_4 and Na_2SO_4. To obtain a certain pH value, NaOH was added to a solution. The pH values of the solutions under study were measured with pH-150 pH-meter.

Preliminarily, the electrochemical behavior of iridium deposited onto GC was studied. A voltammogram measured on GC with an electrically deposited iridium layer (Ir-GC) in 0.1 M H_2SO_4 is shown in Fig. 1. The first pair of peaks at potentials of about 0.0 V is associated with the sorption–desorption of weakly and firmly bound form of hydrogen H^+ and release of H_2 and confirms the presence of the metallic phase of iridium on the GC surface [10]. In addition, the anodic branch of the cyclic voltammogram obtained on GC with an electrodeposited iridium layer shows a wave at $E^{1/2}$ = 0.45 V, and the cathodic branch, a peak at E_p = 0.15 V.

The prewave observed at $E \approx +0.4$ V corresponds to the formation of a hydrated Ir(III) oxide (hydroxide) [10–12]:

$$2Ir + 6H_2O \rightleftarrows Ir_2O_3 \cdot H_2O + 6H^+ + 6e. \quad (1)$$

Hydrated Ir(III) oxide is stable only in alkaline and deaerated solutions. In acid solutions, the metal oxidizes to Ir(IV) via the stage of formation of an intermediate Ir_2O_3, which immediately oxidizes to $IrO_2 \cdot H_2O$:

$$Ir_2O_3 + H_2O \rightleftarrows 2IrO_2 + 2H^+ + 2e. \quad (2)$$

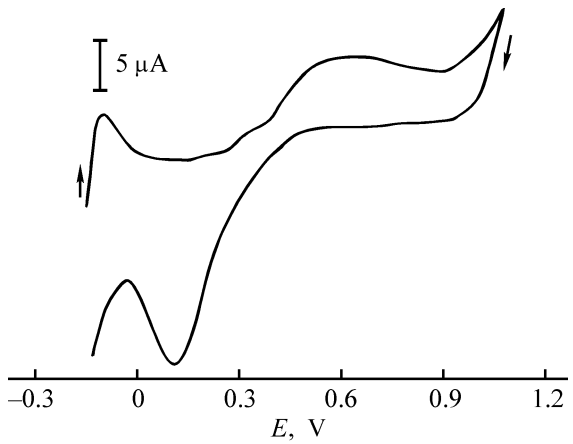

Fig. 1. Cyclic voltammogram obtained on Ir-GC in a 0.1 M H_2SO_4 solution. (*E*) Potential; the same for Figs. 2, 4, and 6.

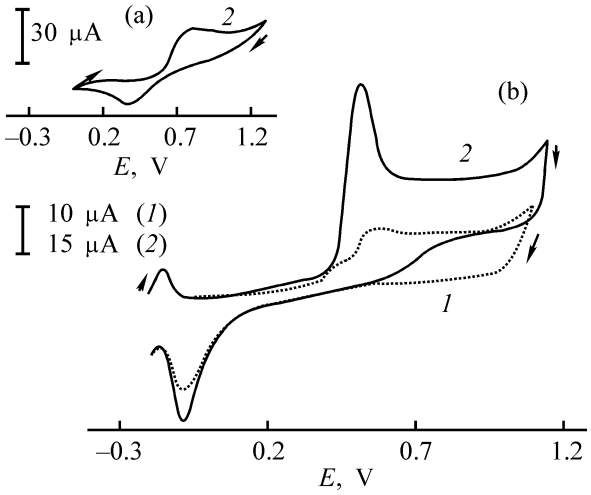

Fig. 2. Cyclic voltammogram obtained on (a) GC and (b) Ir-GC in a 0.1 M H_2SO_4 solution (*2*) with and (*1*) without dopamine. Dopamine concentration 5×10^{-3} M; the same for Figs. 4, 6.

In acid media, this process occurs at $E^{1/2}$ = 0.45 V. The cathodic peak at E_p = +0.15 V corresponds to reduction of hydrated Ir(IV) oxide to hydrated Ir(III) oxide. The overall cathodic and anodic processes at potentials more positive than +0.2 V can be described by the equation

$$Ir + (n + 2)H_2O \rightleftarrows IrO_2 \cdot nH_2O + 4H^+ + 4e. \quad (3)$$

Dopamin oxidizes on GC irreversibly and with an overvoltage at E_p = 0.80 V. In this case, the cyclic voltammogram shows a pair of anodic–cathodic peaks strongly extended along the potential axis (Fig. 2a).

Table 1. Catalytic effect in oxidation of dopamine on an Ir-GC electrode under various electrochemical conditions of iridium deposition

Potentiostatic deposition				Potentiodynamic deposition			
E, V	i_{cat}	i_{med}	i_{cat}/i_{med}	Potential range, V	i_{cat}	i_{med}	i_{cat}/i_{med}
	μA				μA		
0.00	37	6.5	5.6	+0.90…+1.10	–	1.5	–
–0.05	39	6.7	5.8	+0.60…+1.10	–	1.7	–
–0.10	41	7	5.8	+0.40…+1.10	17	3.8	4.3
–0.20	63	10	6.3	+0.20…+1.10	30	6.2	4.8
–0.30	70	16	4.3	+0.00…+1.10	40	7.5	5.3

The slope of the anodic wave of the cyclic voltammogram is 80 mV, which exceeds the value for the reversible process. The electrode reaction occurring at GC in a DA solution includes a two-electron process accompanied by transfer of two protons to give an *ortho*-quinoid fragment in the structure of the product formed in DA oxidation. In this case, the electrochemical process is described by the overall equation [13]:

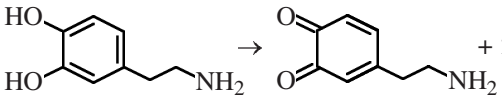

(4)

Figure 2b shows cyclic voltammograms obtained on an electrode with an electrodeposited iridium layer without (curve *1*) and with DA (curve *2*). The anodic branch of the cyclic voltammogram recorded on Ir-GC in the presence of DA (Fig. 2b, curve *2*) shows an increase in current up to a potential E = +0.50 V, with the background curve (Fig. 2b, curve *1*) exhibiting at the same potential a current peak characteristic of the redox pair Ir_2O_3/IrO_2. This means that DA is oxidized at mediator oxidation potentials. The current of the DA peak recorded on Ir-GC linearly depends on its concentration. The manyfold increase in current, decrease in the overvoltage potential of substratum oxidation (to 300 mV), and the value obtained for the Semerano coefficient [14] ($\Delta\log i_p/\Delta\log v$ = 0.3, where i_p is the peak current, and ν is the potential sweep rate) suggest that this process should be regarded as electrocatalytic. The catalytically active species are iridium(IV) oxo species, which oxidize the substratum diffusing toward the electrode surface and are regenerated in the process to iridium(III) oxo species. The mechanism of electrocatalysis can be represented as

$$Ir_2O_3 + H_2O \rightleftarrows 2IrO_2 + 2H^+ + 2e, \quad (5)$$

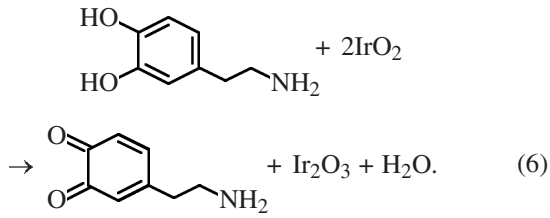

(6)

The dependence of the peak current of dopamine oxidation on the iridium electrodeposition conditions: duration and potential of electrolysis in the case of potentiostatic deposition, and the range of cyclic variation of the potential in potentiodynamic deposition. As can be seen from Table 1, higher mediator oxidation (i_{med}) and catalytic (i_{cat}) currents and a stronger catalytic effect in DA oxidation on CME (expressed as the i_{cat}/i_{med} ratio) are recorded if the electrode is formed by potentiostatic electrolysis. In this case, the increase in the catalytic current of DA oxidation is observed upon a shift of the iridium deposition potential into the cathodic region, in which the mediator is in the metallic form. A shift of the deposition potential into the anodic region leads to formation on the GC surface of a hydrated Ir(III) oxide unstable in an acid medium. The electrochemical characteristics of DA oxidation on Ir-GC, recorded under these conditions, differ little from those obtained on unmodified GC. Thus, the maximum catalytic effect is obtained at an iridium deposition potential of –0.20 V. The weaker catalytic effect in deposition of iridium at E < –0.30 V is probably due to release of H_2 in this range of potentials and to the resulting partial shielding of the catalytically active centers of the metal by hydrogen.

In addition, the catalytic effect depends on the metal deposition time. As can be seen in Fig. 3, a larger i_{cat}/i_{med} ratio is observed at a deposition time of 15 s, which is probably due to the formation of metallic iridium the nanoparticles having a higher mediator activity, compared with the catalytic activity of macroparticles.

Using the composite modified electrodes based on platinum metals coated with an NF film markedly improves the sensitivity of catecholamine determination because of the accumulation of the substratum in the polymeric matrix. Therefore, it was necessary to determine, when developing a composite electrode of this kind, the conditions in which an NF film is deposited and DA is accumulated in this film in order to record better electrochemical characteristics.

The cyclic voltammogram of DA oxidation on an electrode modified with an NF film (NF-GC) shows a current peak at E = +0.68 V (Fig. 4), whose amplitude is many times that of the peak of DA oxidation on GC without NF ($i_{NF\text{-}GC}/i_{GC} \approx 5.0$). The manyfold increase in the amplitude of the peak current of DA oxidation, recorded on NF-GC, is due to the accumulation of protonated DA molecules in hydrophilic channels of NF, which contain negatively charged $-SO_3H$ groups [15].

The polymer was deposited onto the GC surface by the method of drop evaporation from a solution prepared by successive 2-, 5-, 10-, 20-, and 50-fold dilutions of the starting 5% polymer solution with ethanol. As can be seen in Fig. 5 (curve *1*), the current of DA oxidation grows with the NF content. This is due to an increase in the number of ionogenic groups in the polymer film with the Nafion content of the solution deposited onto the GC surface. For example, the maximum current is recorded at a Nafion content of 5%. However, cracks appear on the electrode surface if the film is deposited from this solution. That is why a solution containing 2.5% Nafion was chosen for depositing the NF film. In addition, the current of DA oxidation differs only slightly in this case from the peak current obtained on the NF-GC electrode in the presence of the substratum under study. As the content of NF grows, the potential of DA oxidation shifts to more positive values (Fig. 5a, curve *2*), which is due to an increase in the thickness of the nonconducting polymeric film.

A study of the effect of the solution pH on the electrochemical characteristics of DA oxidation demonstrated that the current of DA oxidation increases as pH decreases (Fig. 5b, curve *1*). Because the NF film is a cation exchanger, its matrix will accumulate

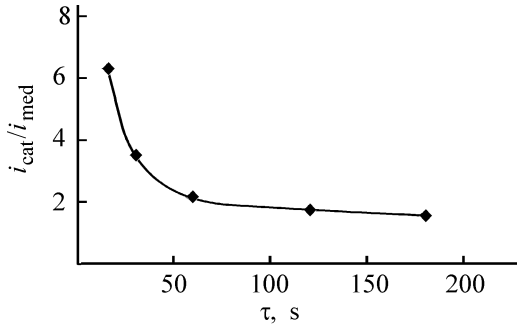

Fig. 3. Effect of the time τ of iridium deposition at E = –0.2 V on the catalytic effect (i_{cat}/i_{med} current ratio) in DA oxidation on Ir-GC.

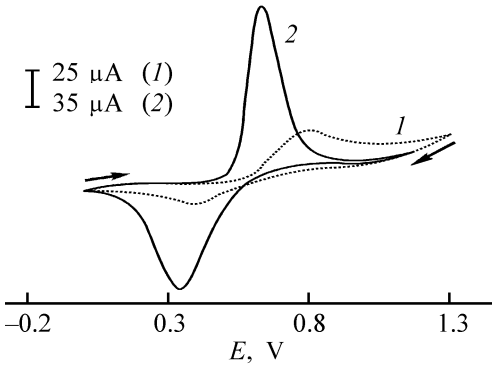

Fig. 4. Cyclic voltammograms obtained on (*1*) GC and (*2*) NF-GC in a 0.1 M solution of H_2SO_4 in the presence of DA.

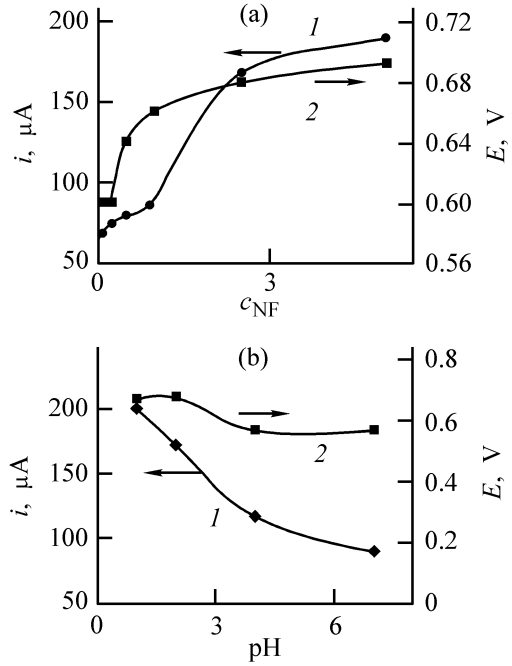

Fig. 5. Influence exerted by (a) content of Nafion in solution, c_{NF}, and (b) solution pH on (*1*) peak current i and (*2*) peak potential E of DA oxidation.

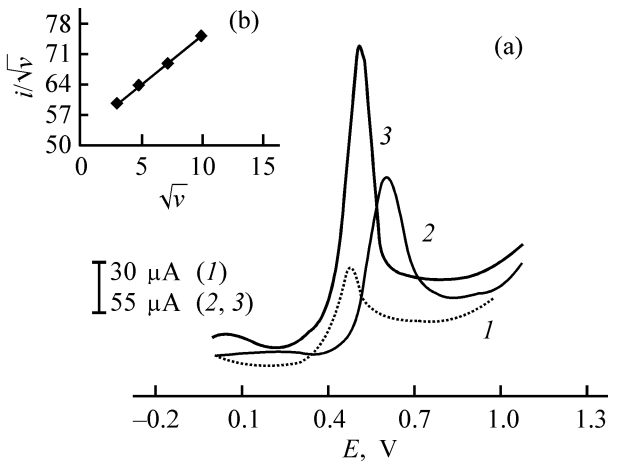

Fig. 6. (a) Voltammograms obtained on (*1*) Ir-GC, (*2*) NF-GC, and (*3*) NF-Ir-GC in the presence of DA and (b) dependence of the peak current of DA oxidation on the square root of the potential sweep rate.

only protonated molecules of catecholamine, and this is, indeed, observed at low pH values. The decrease in the current of DA oxidation in a neutral medium is due a decrease in the fraction of protonated DA species at pH > 5.13 ($pK_a = 14 - pK_b = 14 - 8.87 = 5.13$ [15]). As the solution pH increases, the potential of DA oxidation shifts into the cathodic region, which is typical of electrode processes that occur with release of protons (Fig. 5b, curve *2*).

In a repeated potential sweep, the peak current at $E_p = +0.68$ V increases. This suggests that protonated DA molecules are accumulated in the polymeric matrix of Nafion. Therefore, the dependence of the peak current on the time of DA accumulation, t_{acc}, was studied in an agitated solution. As can be seen in Table 2, the peak current of substratum oxidation grows as the accumulation time increases to t_{acc} = 1 min. As t_{acc} increases further, the peak current remains virtually unchanged, which is due to the saturation of the polymeric matrix.

Table 2. Peak current of dopamine oxidation at various accumulation times in the polymeric matrix of NF-GC and NF-Ir-GC electrodes and times of iridium electrodeposition at $E_d = -0.20$ V

NF-GC		NF-Ir-GC			
τ_{acc}, min	i, μA	τ_d, s	i, μA	τ_{acc}, min	i, μA
0	167	15	195	0	285
1	310	30	220	1	510
2	315	120	275	2	505
3	317	180	285	3	485

With a composite electrode based on GC with an iridium layer coated with an NF film (NF-Ir-GC), it was possible to lower the overvoltage of DA oxidation by 170 mV and raise the current of substratum oxidation by a factor of 2 and 4 relative to the current of oxidation on NF-GC and Ir-GC electrodes, respectively (Fig. 6a). DA oxidizes on the NF-Ir-GC electrode, as well as on the Ir-GC, at $E = +0.50$ V, i.e., at potentials characteristic of the IrO_2/Ir_2O_3 redox pair. In this case, too, Ir(IV) oxo species act as a mediator. The plot of the dependence of $i/\sqrt{v}$ on $\sqrt{v}$ has a positive slope (Fig. 6b). This indicates that the adsorption is the rate-determining stage of DA electrooxidation on the composite electrode. With account of the aforesaid, the following mechanism of DA electrooxidation on the composite electrode NF-Ir-GC can be suggested: the electrode process includes modifier electrooxidation to give iridium(IV) species, which further oxidize the substratum accumulated in the NF film. The electrocatalysis process can be schematically represented as

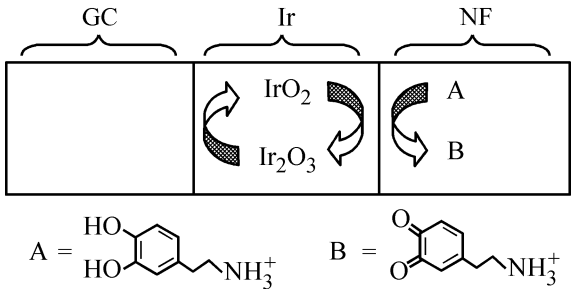

It was found that the extent to which the peak current of DA oxidation increases depends on the iridium deposition time (Table 2). As this time increases, the number of active centers on the GC surface, involved in the electrocatalytic oxidation of DA accumulated in the NF matrix, grows, which leads to a rise in the DA oxidation current. As already mentioned, the peak current of DA oxidation also increases in preliminary accumulation of the substratum on CME before recording a cyclic voltammogram. Table 2 lists the peak currents of DA oxidation in relation to the time τ_{acc} of DA accumulation in the polymeric matrix of the NF-Ir-GC electrode. The current of catecholamine oxidation on the NF-Ir-GC electrode first increases and then, at $\tau_{acc} > 1$ min, decreases, which is probably due to shielding of the catalytically active centers of the metal by the forming products of DA oxidation.

DA was determined on an electrode modified with a composite polymeric film with an iridium layer

as follows. A 10-ml volumetric flask was charged with a fixed volume of an analyte solution and 5 ml of a 0.2 M solution of H_2SO_4, and the solution was brought to the mark with distilled water. The solution was transferred to an electrochemical cell. Then the CME and the auxiliary and silver chloride electrodes were submerged in the solution under study. Before recording a cyclic voltammogram, catecholamines were preliminarily accumulated from the solutions under study for 1 min; the voltammogram was recorded in the potential range 0.00–1.20 V and used to find the peak current of oxidation at E_p = 0.50 V.

The peak current is proportional to the DA concentration in the range 1×10^{-6}–1×10^{-3} (for Ir-GC) and 1×10^{-8}–1×10^{-3} M (for NF–Ir-GC). These dependences are described by Eqs. (6), (8), respectively:

$$i_p = (6.4 \pm 0.4) + (1.0 \pm 0.3) \times 10^4 c, \quad r = 0.9999, \quad (7)$$

$$i_p = (10.05 \pm 0.5) + (0.11 \pm 0.02) \times 10^6 c, \quad r = 0.9998, \quad (8)$$

where i_p is the peak current (μA) and c is the concentration (M).

Thus, with a composite film electrode NF-Ir-GC, the range of determinable concentrations can be extended and the detection limit lowered by two orders of magnitude, compared with the Ir-GC electrode. This becomes possible because of the combination of concentration, provided by the ion-exchange properties of the polymeric film, and electrocatalysis associated with the mediator properties of the platinum-group metal.

The procedure was verified by the introduced-found method (Table 3). The reproducibility of the analytical signal increases on passing to the composite polymeric electrode. In this case, the relative standard deviation S_r does not exceed 5% in the whole range of concentrations studied.

CONCLUSIONS

(1) It was found that iridium species deposited onto a glassy-carbon electrode exhibit electrocatalytic activity in dopamine oxidation. A catalytic peak was observed at E_p = +0.50 V in the range of oxidation of Ir(III) oxo species. The optimal conditions of dopamine concentration on a glassy-carbon electrode coated with a Nafion film were determined.

(2) The conditions in which a composite electrode with an iridium deposit coated with a Nafion film can be obtained and the maximum catalytic effect can be recorded on this electrode in dopamine oxidation were determined. The use of the composite film electrode led to an increase in the oxidation current of the substratum being studied because of the combination of the electrocatalytic properties of iridium and ion-exchange properties of the polymeric matrix of Nafion.

(3) A chemically modified electrode with an electrodeposited iridium coated wit a Nafion film was used for voltammetric determination of dopamine. The dependence of the oxidation current of dopamine on its concentration is linear in the range 1×10^{-8}–1×10^{-3} M.

Table 3. Metrological characteristics of dopamine determination on CME (n = 6, P = 0.95)

Electrode	Dopamine concentration, μM		S_r
	introduced	found	
Ir-GC	5.0	4.8 ± 0.2	0.05
	10.0	9.9 ± 0.4	0.04
	100	101 ± 2	0.02
NF-Ir-GC	5.0	4.9 ± 0.2	0.04
	10.0	10.2 ± 0.3	0.03
	100	99 ± 1	0.01

ACKNOWLEDGMENTS

The study was supported by a joint grant from CRDF (U.S. Civilian Research & Development Foundation) and Ministry of Education and Science of the Russian Federation, BRHE (Basic Research and Higher Education Program), (REC-007).

REFERENCES

1. Amin, D., *Analyst*, 1986, vol. 111, no. 2, pp. 255–257.
2. Sastry, C.S., Das, V.G., and Rao, K.E., *Analyst*, 1985, vol. 110, no. 4, pp. 395–398.
3. Wang, S., Du, L., Wang, L., and Zhuang, H., *Anal. Sci.*, 2004, vol. 20, no. 2, pp. 315–317.
4. Lima, J.L.F.C. and Montenegro, M.C.B.S.M., *Mikrochim. Acta*, 1999, vol. 131, nos. 3–4, pp. 187–190.
5. Pastore, P., Favaro, G., Badocco, D., et al., *J. Chromatogr., Ser. A*, 2005, vol. 1098, nos. 1–2, pp. 111–115.
6. Raj, C.R., Okajima, T., and Ohsaka, T., *J. Electroanal. Chem.*, 2003, vol. 543, no. 2, pp. 127–133.
7. Gui, Z. and Dong, S., *Electroanalysis*, 2005, vol. 17, no. 7, pp. 607–611.

8. Xun, Z., Cai, Ch., Xing, W., and Lu, T., *J. Electroanal. Chem.*, 2003, vol. 545, pp. 19–27.
9. Mathiyarasu, J., Senthikumar, S., Phani, K.L.N., and Yegnaraman, V., *J. Appl. Electrochem.*, 2005, vol. 35, no. 5, pp. 513–519.
10. Juodkazyte, J., Sebeka, B., Valsiunas, I., and Juodkazis, K., *Electroanalysis*, 2005, vol. 17, no. 11, pp. 947–952.
11. Marshall, A., Borresen, B., Hagen, G., et al., *Electrochim. Acta*, 2006, vol. 51, no. 15, pp. 3161–3167.
12. Pauporte, T., Andolfatto, F., and Durand, R., *Electrochim. Acta*, 1999, vol. 45, no. 3, pp. 431–439.
13. Venton, B. J. and Wightman, R.M., *Anal. Chem.*, 2003, vol. 75, no. 3, pp. 414A–421A.
14. Budnikov, G.K., *Printsipy i primenenie vol'tampernoi ostsillograficheskoi polyarografii* (Principles and Application of Voltammetric Oscillographic Polarography), Kazan: Kazan. Gos. Univ., 1975.
15. *Elektrokhimiya polimerov* (Electrochemistry of Polymers), Tarasevich, M.R., Khanova, L.A., Shkol'nikov, E.I., et al., Eds., Moscow: Nauka, 1990.
16. Lur'e, Yu.Yu., *Spravochnik po analiticheskoi khimii* (Handbook of Analytical Chemistry), Moscow: Khimiya, 1971.

ISSN 1070-4272, Russian Journal of Applied Chemistry, 2007, Vol. 80, No. 8, pp. 1353–1359. © Pleiades Publishing, Ltd., 2007.
Original Russian Text © S.N. Tkachenko, E.Z. Golozman, V.V. Lunin, I.V. Kozlova, G.V. Egorova, E.A. Boevskaya, I.S. Tkachenko, A.I. Nechugovskii, M.P. Yaroshenko, 2007, published in Zhurnal Prikladnoi Khimii, 2007, Vol. 80, No. 8, pp. 1314–1320.

CATALYSIS

A Study of a Catalyst Based on Oxides of Base Transition Metals for Decomposition of Ozone and Oxidation of Toxic Organic Compounds

S. N. Tkachenko, E. Z. Golozman, V. V. Lunin, I. V. Kozlova, G. V. Egorova, E. A. Boevskaya, I. S. Tkachenko, A. I. Nechugovskii, and M. P. Yaroshenko[1]

Lomonosov State University, Moscow, Russia

Novomoskovsk Institute of Nitrogen Industry, Open Joint-Stock Company, Novomoskovsk, Tula oblast, Russia

TIMIS Research-and-Promotion Firm, Limited Liability Company, Moscow, Russia

Received August 29, 2006; in final form, March 2007

Abstract—Cement-containing GTT catalysts based on manganese, copper, and nickel oxides were developed and introduced into practice in processes employing ozone technologies and in oxidation of toxic organic compounds. Physicochemical methods were used to study the process of catalyst formation and the influence exerted by various brands of manganese salts and by preparation conditions and, in particular, calcination temperatures and grain molding technique on the characteristics of the catalytic systems obtained. Several commercial batches of GTT catalysts were manufactured.

DOI: 10.1134/S1070427207080174

At present, one of the most efficient and ecologically safe ways to purify drinking water, wastewater, and water in swimming pools is ozonation. The use of ozone is due to its oxidizing and bactericidal properties; however, the acrid smell and toxicity of ozone (MPC = 3.3 $\mu g\ m^{-3}$) makes topical the problem of destruction of residual ozone [1]. Photochemical, thermal, and catalytic methods of ozone decomposition are possible. The optimal in economical efficiency and simplicity of technological apparatus is the catalytic decomposition of ozone [2].

The industrially employed catalyst for ozone decomposition, hopcalite, is composed of 60% manganese oxide, 25% copper oxide, and 15% binder (bentonite clay). It has an important disadvantage, poor mechanical strength, to the point of grain disintegration under the action of moisture drops [3]. The known catalysts [4], distinguished by stability and operation efficiency under humid conditions, contain noble metals and, in particular, silver and are rather expensive.

Catalysts composed of oxides of nonprecious transition metals and exhibiting stable operation under various conditions have been created by developing cement-containing catalysts of GTT and GT brands, based on manganese, copper, and nickel oxides [5–9]. The activity of these catalysts in a dry flow is close to that of hopcalite and exceeds it by a factor of 1.5–2 in operation in a humid flow. These catalytic systems have high mechanical strength and water resistance, and their grains preserve shape when brought in contact with water. In a dry gas flow, the catalysts work at room temperature. In a humid flow, the working temperature range is 20–120°C. In case of a decrease in activity in a corrosive humid medium, the catalysts can be regenerated at 250–300°C in 2–3 h.

Tests demonstrated that GTT is efficient not only in ozone decomposition, but also in oxidation of carbon monoxide, methane, benzene, styrene, isopropylbenzene, butyl acetate, and other compounds. The GTT catalyst possesses the necessary developed surface, thermal stability, and resistance to coking in

[1] N.I. Murashov, Zh.V. Myasnikova, S.G. Dormidontova, and L.D. Kvasova took part in catalyst preparation on laboratory, pilot, and industrial installations, and also in catalytic activity tests and determination of other characteristics of catalysts.

Table 1. Basic characteristics of the cement-containing GTT catalyst (for extrudates)

Parameter	Grains of dark brown to black color
Bulk density, kg dm^{-3}, no more than	1.3
Mechanical strength, kg mm^{-1} grain diameter, no less than:	
average	1.1
minimum	0.6
Porosity Π, %, no less than	40
Specific surface area S_{sp}, $m^2\ g^{-1}$, no less than	100
Ozone decomposition factor* γ in a gas flow, no less than:	
dry gas flow	1.1×10^{-4}
humid gas flow	0.55×10^{-4}

* The quantity γ, the fraction of active, i.e., leading to decomposition, collisions of ozone molecules with the catalyst surface, is taken as a measure of the catalyst activity. The ozone decomposition factor is given by the Lunin–Popovich–Tkachenko formula [3] $\gamma = 4w[\ln(c_0/c)]V_tS$, where c_0 and c are the ozone concentrations at the reactor inlet and outlet, respectively; w, volumetric gas flow rate; V_t, thermal motion velocity of molecules; and S, total external surface area of catalyst grains. The parameter γ is proportional to the effective rate constant of the heterogeneous decomposition of ozone.

oxidation of the chemical products mentioned above. The basic technical characteristics of GTT are listed in Table 1.

The technology of GTT fabrication has been implemented at the catalyst shop of NIAP. The catalyst is manufactured as compacted pellets $d \times h = 6 \times 3$ (5×3) mm^2 and in the extruded form [extrudates with a diameter of 1.5 to 5 mm and length of 5 to 15 mm; pellets with $d \times h = 5 \times 3$ (4×3) mm^2].

The aim of this study was to examine, using a set of physicochemical techniques, the influence exerted by the preparation conditions and composition of the starting manganese-containing concentrate on the formation of the Mn–Cu–Ni–Al–Ca system and to determine the relationship between the phase composition of the catalyst and its catalytic activity in decomposition of ozone and oxidation of benzene.

EXPERIMENTAL

The catalyst was fabricated by the method of hydrothermal synthesis (HTS) [10, 11], which includes mixing of the starting components in the presence of aqueous ammonia and granulation of the resulting paste, followed by keeping of the grains first in a humid-air medium and then in hot water in the stage of hydrothermal treatment (HTT). After that the catalyst is dried and calcined.

An X-ray diffraction analysis was carried out on a DRON-3 diffractometer (graphite monochromator, Cu_{K_α} radiation, reflected beam). IR spectra were measured on a Specord 75-IR spectrophotometer, with samples prepared by compaction with KBr. The specific surface area of catalyst samples was determined by the low-temperature adsorption technique (BET). The total porosity was found from the true and apparent densities. The apparent density was calculated by dividing the mass of a sample by its geometric volume. The true density was determined by pycnometry, from the volume of toluene absorbed by a sample. The error in determining the total porosity was $\pm 5\%$.

An X-ray phase analysis (XPA) demonstrated that the synthesis of the catalyst involves, in stages of molding, humid-air treatment, HTT, and drying, the reaction of interaction (heterogeneous ion exchange) between hydroxocarbonates of copper (CHC) and nickel (NHC) and calcium aluminates (talum: CA, CA_2[2]) to give hydroxo aluminates (HA) of nickel and copper and calcite $CaCO_3$ [12]. XPA does not reveal any interaction of the starting $MnCO_3$ with the above components, whereas IR spectroscopy indicates [13] that a certain amount of manganese ions can be incorporated into the lattice of gibbsite formed as a result of talum hydration.

The temperature at which a catalyst is calcined strongly affects its formation and catalytic activity. For GTT samples calcined at 100–800°C, the phase composition and catalytic activity in ozone decomposition and benzene oxidation were determined. At low calcination temperatures (100–200°C), the starting

[2] CA, CA_2 are designations used in cement chemistry: CA = $CaO \cdot Al_2O_3$ and $CA_2 = CaO \cdot 2Al_2O_3$.

metal hydroxocarbonates and products of talum hydration and ion exchange are present. At higher temperatures, metal hydroxocarbonates decompose to the respective oxides. The starting manganese-containing component decomposes to oxides of various compositions. In the temperature range 300–350°C, a phase close in X-ray diffraction characteristics to MnO_2 appears in the sample composition, the intensity of Mn_2O_3-related peaks increases, and the Mn_3O_4 phase is weakly pronounced. At temperatures of 350–600°C, the content of Mn_3O_4 increases, that of Mn_2O_3 decreases, and MnO_2 disappears. At 700–800°C the main manganese containing phase in Mn_3O_4.

Samples calcined in the temperature range 300–600°C show an ozone decomposition factor γ of no less than 1.5×10^{-4} (Fig. 1). Samples calcined at 400–600°C exhibited the highest activity in ozone decomposition [$\gamma = (2.38–2.45) \times 10^{-4}$], and those calcined at 300–400°C, in benzene oxidation, with the temperature of benzene oxidation at 50% conversion equal to 230–240°C (Fig. 1). The decrease in the catalytic activity at calcination temperatures higher than 600°C is presumably due to recrystallization of the NiO and CuO phases. In accordance with this circumstance, the optimal temperature of catalyst calcination was chosen to be 350–400°C for ozone decomposition and 300–350°C for benzene oxidation.

The catalyst was prepared from different batches of a Mn-containing stock (Table 2) supplied under the brand Manganese hydroxocarbonate, which, according to XPA and IR spectral data, is anhydrous manganese carbonate, occasionally containing the Mn_2O_3 phase. For example, the IR spectrum of sample no. 1 contains, together with absorption bands at 1420–1440, 870, and 730 cm^{-1}, which characterize the carbonate anion in the composition of manganese carbonate, also strong absorption bands at 580–530 cm^{-1}, related to the presence of an oxide phase (Fig. 2). According to XPA data, this is Mn_2O_3. The study revealed that no $MnCO_3$ decomposition is observed up to 200°C; and at 300°C manganese oxides Mn_3O_4 and MnO_2 appear, together with $MnCO_3$ and Mn_2O_3, in stock sample nos. 1 and 2 and only Mn_3O_4 in sample no. 3. The MnO_2 phase was not found in any of the stock samples at 400°C, and in the range 400–800°C Mn_2O_3 is gradually converted to Mn_3O_4, which becomes the main manganese-containing phase at 800°C.

The above-mentioned brands of $MnCO_3$ were used to prepare GTT catalyst samples under laboratory conditions. XPA data for GTT catalyst samples calcined at 300–500°C are listed in Table 3. The decomposition of $MnCO_3$ in the catalyst occurs similarly to

Table 2. Phase composition of the manganese-containing stock at calcination temperatures of 200–800°C

T, °C	Phase composition		
	no. 1 $MnCO_3$ Sedema, supply from Belgium	no. 2 $MnCO_3$	no. 3 $MnCO_3$ (supply from Russia)
200	$MnCO_3$, Mn_2O_3	$MnCO_3$	$MnCO_3$
300	$MnCO_3$, Mn_2O_3, Mn_3O_4, MnO_2	$MnCO_3$, MnO_2, Mn_3O_4, Mn_2O_3	$MnCO_3$, Mn_3O_4
400	Mn_2O_3, Mn_3O_4	Mn_2O_3, Mn_3O_4	Mn_3O_4, $MnCO_3$
500	Mn_2O_3, Mn_3O_4	Mn_2O_3, Mn_3O_4	Mn_2O_3, Mn_3O_4
600	Mn_2O_3, Mn_3O_4	Mn_2O_3, Mn_3O_4	Mn_2O_3, Mn_3O_4
700	Mn_2O_3, Mn_3O_4	Mn_2O_3, Mn_3O_4	Mn_2O_3, Mn_3O_4
800	Mn_3O_4	Mn_3O_4	Mn_3O_4

that of the starting $MnCO_3$, although some distinctions are observed. At 300°C, the MnO_2 phase appears in all the three samples. This phase is more pronounced in sample no. 2; further, at 350–500°C,

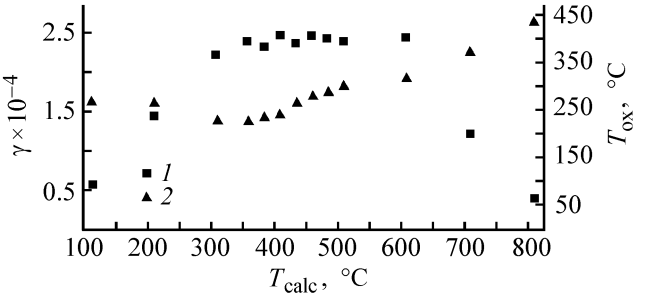

Fig. 1. Activity of the GTT catalyst in ozone decomposition and benzene oxidation vs. calcination temperature T_{calc}. (γ) Ozone decomposition temperature and (T_{ox}) temperature of 50% oxidation of benzene. (*1*) Ozone decomposition factor and (*2*) benzene oxidation temperature.

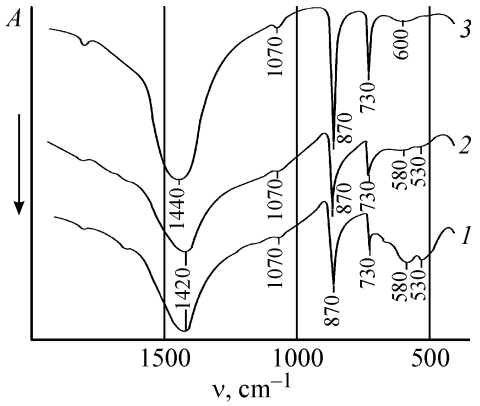

Fig. 2. IR spectra of uncalcined $MnCO_3$ samples. (*A*) Absorption and (ν) wave number. Supply source: (*1*) Sedema, Belgium; (*2*) Belgium; and (*3*) Russia.

Table 3. Phase composition of GTT samples (based on various brands of $MnCO_3$) calcined at 300–500°C

T, °C	Phase composition		
	no. 1 $MnCO_3$ Sedema supply from Belgium	no. 2 $MnCO_3$	no. 3 $MnCO_3$ (supply from Russia)
300	Mn_2O_3, MnO_2, CA_2, $CaCO_3$, $MnCO_3$, NiO, CuO	MnO_2, $CaCO_3$, CA_2, $MnCO_3$, NiO, CuO	$MnCO_3$, MnO_2, $CaCO_3$, CA_2, NiO, CuO
350	Mn_2O_3, Mn_3O_4, $CaCO_3$, CA_2, $MnCO_3$, NiO, CuO	Mn_3O_4, $CaCO_3$, Mn_2O_3, MnO_2, CA_2, $MnCO_3$, NiO, CuO	MnO_2, $MnCO_3$, $CaCO_3$, CA_2, Mn_2O_3, NiO, CuO
400	Mn_2O_3, Mn_3O_4, $CaCO_3$, CA_2	Mn_2O_3, Mn_3O_4, $CaCO_3$, MnO_2, CA_2, NiO, CuO	Mn_3O_4, $CaCO_3$, Mn_2O_3, CA_2, NiO, CuO
450	Mn_2O_3, $CaCO_3$, Mn_3O_4, CA_2, NiO, CuO	Mn_2O_3, Mn_3O_4, $CaCO_3$, CA_2, NiO, CuO	Mn_3O_4, Mn_2O_3, $CaCO_3$, CA_2, NiO, CuO
500	Mn_2O_3, Mn_3O_4, CA_2, $CaCO_3$, NiO, CuO	Mn_2O_3, Mn_3O_4, $CaCO_3$, CA_2, NiO, CuO	Mn_2O_3, Mn_3O_4, $CaCO_3$, CA_2, NiO, CuO

Table 4. Physicochemical characteristics and catalytic activity of GTT samples calcined at T = 400°C

GTT catalyst	Chemical composition: active components, %	γ	$T_{benz.ox}$, °C, at 50% conversion	S_{sp}, $m^2\ g^{-1}$	Π, %
no. 1 $MnCO_3$ Sedema, supplied from Belgium	Mn_3O_4, 29.3, CuO, 19.6, NiO, 10.1; Σ = 59	1.88×10^{-4}	250	100	70
no. 2 $MnCO_3$, supplied from Belgium	Mn_3O_4, 28.6, CuO, 21.2, NiO, 10.3; Σ = 60.1	1.85×10^{-4}	220	100	50
no. 3 $MnCO_3$, supplied from Russia	Mn_3O_4, 29.6, CuO, 20.6, NiO, 10.9; Σ = 61.1	1.85×10^{-4}	230	100	60

the content of this phase decreases and that of the oxides Mn_2O_3 and Mn_3O_4 increases, whereas in sample no. 3, mostly the content of the Mn_3O_4 phase grows. Also, the degree of crystallinity of the copper oxide phase is higher at these temperature than that of nickel oxide. This is due to the fact that mostly the nickel hydroxoaluminate phase is formed in the preceding stages, and especially in the HTT stage, and this leads to formation of a dispersed phase of nickel oxide in calcination.

Table 4 lists physicochemical parameters of samples calcined at T = 400°C. The total amount of the active component in samples of a finished catalyst is 59 to 61%. The specific surface areas of the samples are virtually the same (~100 $m^2\ g^{-1}$). The highest porosity (~70%) is observed for GTT sample no. 1.

Activity tests of samples prepared from different stock batches demonstrated that, at close compositions and surface areas, all the samples exhibit high activity in ozone decomposition, $\gamma = (1.81–1.88) \times 10^{-4}$. Consequently, presence of the Mn_2O_3 phase in the starting manganese-containing component does not exert any significant influence on the GTT activity in ozone decomposition. However, a minor decrease in activity is observed in benzene oxidation: the difference in benzene oxidation temperature at 50% conversion is 20–30°C.

Extrudates were prepared on a pilot apparatus from $MnCO_3$ of Sedema brand, supplied from Belgium, and $MnCO_3$ from Russia. The ozone decomposition factor for batch no. 1 (extrudates 1.5 mm in diameter), synthesized from $MnCO_3$ containing an admixture of Mn_2O_3 is 1.13–1.25 times lower than that for batch no. 2 (extrudates 1.5 mm in diameter), produced from $MnCO_3$ of domestic manufacture, in which the Mn_2O_3 phase is either absent or present in a minor amount. GTT no. 1 is inferior to GTT no. 2 in specific surface area, porosity, and total amount of the active com-

Table 5. Physicochemical characteristics and catalytic activity of laboratory-pilot batches of extrudates and molded GTT pellets calcined at $T = 415 \pm 15$°C

GTT catalyst	XPA data for finished catalyst, 415 ± 15°C	γ	$T_{benz.ox}$, °C at 50% conversion	S_{sp}, $m^2\ g^{-1}$	Π, %	Chemical composition: active components, %
No. 1, extrudates, d = 0.15 cm, based on $MnCO_3$ Sedema, supplied from Belgium	Mn_3O_4, NiO, $CaCO_3$, CuO, Mn_2O_3, CA_2	2.45×10^{-4}	240	110	40	Mn_3O_4, 28.9, CuO, 18.5, NiO, 11.3; Σ = 58.6
No. 2, extrudates, d = 0.15 cm, based on $MnCO_3$, supplied from Russia	Mn_3O_4, CaO_3, NiO, CuO, CA_2, boehmite	$(2.7–3) \times 10^{-4}$	250	120	10	Mn_3O_4, 29.2, CuO, 21.6, NiO, 10.7; Σ = 61.5
No. 3, extrudates, d = 0.25 cm, based on $MnCO_3$, supplied from Russia	Mn_2O_4, $CaCO_3$, NiO, CuO, CA_2	2.2×10^{-4}	260	120	60	Mn_3O_4, 30.2, CuO, 20.4, NiO, 11.3; Σ = 61.9
No. 4, extrudates, d = 0.30 cm, based on $MnCO_3$, supplied from Russia	Mn_3O_4, $CaCO_3$, CA_2, $MnCO_3$, NiO, CuO	$(2.1–2.2) \times 10^{-4}$	260	90	60	Mn_3O_4, 28.0, CuO, 22.7, NiO, 10.4; Σ = 61.1
No. 5, molded pellets, $d \times h$ = 5 × 3 mm, November 2004, based on $MnCO_3$, supplied from Belgium	CuO, MnO_2, Mn_3O_4, trace amounts CA_2, NiO, $CaCO_3$, aragonite, $MnCO_3$	1.58×10^{-4}	220	110	40	Mn_3O_4, 30.3, CuO, 20.2, NiO, 9.0; Σ = 59.5
No. 6, molded pellets, $d \times h$ = 5 × 3 mm, June 2005, based on $MnCO_3$, supplied from Belgium	CuO, MnO_2, $MnCO_3$, Mn_3O_4, CA_2, CA, NiO, $CaCO_3$, trace amounts	1.90×10^{-4}	220	100	60	Mn_3O_4, 26.5, CuO, 20.5, NiO, 9.5; Σ = 56.5
No. 7, molded pellets, $d \times h$ = 5 × 3 mm, June 2005, based on $MnCO_3$, supplied from Bulgaria	CuO, Mn_3O_4, MnO_2, $MnCO_3$, CA_2, $CaCO_3$, NiO, aragonite, trace amounts, CA	2.35×10^{-4}	230	110	70	Mn_3O_4, 27.1, CuO, 20.5, NiO, 9.0; Σ = 56.6

ponent (Table 5), which can also account for the decrease in γ. The catalytic activities of these batches in benzene oxidation do not differ significantly.

Molded pellets were produced on industrial equipment (FP-025 pellet-granulator, manufactured by Dzerzhinsk NIIkhimmash federal state unitary enterprise) from manganese carbonate from Belgium, which contains an insignificant amount of Mn_2O_3 (GTT catalyst batch nos. 5 and 6), and manganese carbonate manufactured in Bulgaria, which contains no Mn_2O_3 (catalyst batch no. 7) (Table 5). It was found that the ozone decomposition factor γ for GTT no. 7 is, on average, 1.4 times that for GTT nos. 5 and 6. It is, however, impossible to state unambiguously that the brand of $MnCO_3$ affects the catalytic activity of GTT in ozone decomposition in the case of industrial batches. It can be seen from the data presented that there is difference in porosities (by a factor of 1.17–1.5) even for batches prepared from the same brand of raw material, manganese carbonate manufactured in Belgium. The catalytic activities of these batches in benzene oxidation do not differ significantly.

A comparison of the basic characteristics of GTT batches produced under pilot-industrial conditions (extrudates of various diameters) and manufactured under industrial conditions (molded pellets) at the same calcination temperature demonstrated that that the activity of extrudates in ozone decomposition exceeds that of molded pellets by, on average, a factor

of 1.1–1.7 and that in benzene oxidation is lower (benzene oxidation temperature at 50% conversion is, on average, 30–40°C higher) (Table 5). These batches show insignificant differences in porosity, specific surface area, and amount of the active component. It can be assumed that the changes in activity are due to specific features of the decomposition of the starting manganese carbonates in the extrudates and pellets in the calcination stage. It has been found previously that the type of a manganese-containing phase formed is sensitive to the calcination temperature. In the range T = 300–350°C, the MnO_2 phase is formed in extrudates (Table 3), with the benzene oxidation temperature at 50% conversion equal to 230°C (Fig. 1) and $\gamma = (2.22–2.38) \times 10^{-4}$. In the range T = 400–450°C, Mn_3O_4 is the main manganese-containing phase, with $T_{benz.ox}$ = 240–280°C and $\gamma = 2.45 \times 10^{-4}$. In molded pellets, the MnO_2 phase is still present at T = 400–430°C, the benzene oxidation temperature at 50% conversion is 220–230°C, and $\gamma = (1.58–2.35) \times 10^{-4}$ (Table 5). Presumably, the predominance of the manganese-containing phase Mn_3O_4 in GTT samples (extrudates, pellets) at calcination temperatures in the range 300–450°C favors an increase in the activity of the catalyst in ozone decomposition, and the presence of the MnO_2 phase positively affects the activity in benzene oxidation.

According to the quality regulations for manganese-containing raw materials, the mass fraction of sulfur in terms of sulfates should not exceed 0.04%. The content of sulfur in the manganese-containing starting component, especially of domestic or Bulgarian manufacture, fails to satisfy these requirements. A number of test batches were prepared in the form of extrudates based on manganese carbonates containing 0.16 to 0.23% sulfates (SO_4^{2-}). In the finished catalyst, the content of sulfates varied from 0.08 to 0.11%. In this case, the ozone decomposition factor was $\gamma = (2.1–2.7) \times 10^{-4}$, which points to a high activity of the catalyst. Also, the benzene oxidation temperature at 50% conversion was found to be 240–260°C for this catalyst.

When preparing molded pellets, manganese carbonates containing 0.0076–0.026, 0.56–0.69, and 0.77–1.14% sulfates were used. The mass fractions of SO_4^{2-} in the finished catalysts were 0.0065–0.025, 0.032–0.15, and 0.197–0.36%, respectively. In this case, the ozone decomposition factors are $(1.35–1.85) \times 10^{-4}$, $(1.85–2.4) \times 10^{-4}$, and $(2.0–2.4) \times 10^{-4}$, respectively, which corresponds to a high catalytic activity in ozone decomposition. The catalytic activities of these batches in benzene oxidation were evaluated by the benzene oxidation temperature at 50% conversion: 210–230, 220–230, and 220–230°C, respectively.

Laboratory samples were produced with manganese carbonates containing 0.008 and 0.7% sulfates. The mass fraction of sulfates in the finished catalyst was 0.004 and 0.12%, respectively. The samples exhibited virtually the same activity in ozone decomposition: $\gamma = (1.9 \pm 0.2) \times 10^{-4}$. The benzene oxidation temperature at 50% conversion was 220 and 240°C.

It can be seen from these data that the mass fraction of sulfur in terms of sulfides in the starting manganese-containing component has no effect on the catalytic activity of the GTT catalyst in both ozone decomposition and benzene oxidation. It is known that a requirement to the purity of starting components affects their cost. Consequently, less expensive raw materials can be used in GTT manufacture. Industrial batches of the catalysts developed have been manufactured to order of TIMIS Research-and-Promotion Firm, Limited Liability Company at Novomoskovsk Institute of nitrogen industries and successfully work in ozonizer installations at more than 40 plants of Russia, Ukraine, Thailand, and Switzerland [14–16].

GTT catalysts are also effectively used in gas-convectors of the gas-discharge type, intended for purification of ventilation gases and recycled and influent air to remove toxic substances, such as butanol, styrene, toluene, phenol, benzene, formaldehyde, aniline, etc., formed in operation of motor transport, technological equipment, and public feeding facilities. Air is purified in a gas-convector under the action of an electric discharge on molecule of gases present in the discharge zone.

CONCLUSIONS

(1) An integrated study of the process in which catalysts for ozone decomposition are formed from copper and nickel hydroxocarbonates, manganese carbonate, and calcium aluminates (talum) demonstrated that a heterogeneous ion exchange occurs between the components in the course of preparation, to give precursors of the active phase.

(2) It was shown that presence of the manganese-containing phase Mn_3O_4 in GTT samples (extrudates, pellets) favors, at calcination temperatures of 300–450°C, an increase in the catalytic activity in ozone decomposition, and presence of the MnO_2 phase positively affects the activity in benzene oxidation. The optimal GTT calcination temperatures for ozone decomposition and benzene oxidation were determined.

(3) It was demonstrated that the catalytic activity of the GTT catalyst in both ozone decomposition and benzene oxidation is not affected to any significant extent by the composition of the manganese-containing raw material and by the amount of sulfur (in the concentration range studied) in the starting components.

(4) Extrudates with a diameter of 1.5–5 mm and length of 5–15 mm and molded pellets [($d \times h$ = 5×3 (4×3) mm^2] were produced. The catalyst obtained exhibits high activity and mechanical strength in operation in both dry and humid gases.

REFERENCES

1. Rodionov, A.I., Klushin, V.N., and Torocheshnikov, N.S., *Tekhnika zashchity okruzhayushchei sredy* (Environment Protection Technology), Moscow: Khimiya, 1989.
2. Tkachenko, S.N., Homogeneous and Heterogeneous Decomposition of Ozone, *Doctoral Dissertation*, Moscow, 2004.
3. Tkachenko, S.N., Golosman, E.Z., and Lunin, V.V., *Kataliz Prom–sti*, 2001, no. 2, p. 52.
4. Lunin, V.V., Popovich, M.P., and Tkachenko, S.N., *Fizicheskaya khimiya ozona* (Physical Chemistry of Ozone), Moscow: Mosk. Gos. Univ., 1998.
5. RF Patent 2077946.
6. USSR Inventor's Certificate, no. 1768274.
7. Makhov, E.A., Tkachenko, S.N., Golosman, E.Z., et al., *Khim. Prom–st. Segodnya*, 2003, no. 7, p. 11.
8. Yakerson, V.I. and Golosman, E.Z., *Katalizatory i tsementy* (Catalysts and Cements), Moscow: Khimiya, 1992.
9. Tkachenko, S.N., Lunin, V.V., Egorova, G.V., et al., *The Int. Ozone Association: 17th world congress* (IOA 17), Ozone and Related Oxidants, Innovative and Current Technologies, Strasbourg, France, August 22–25, 2005, p. 50.
10. Golosman, E.Z., *Kinet. Kataliz*, 2001, vol. 42, no. 3, pp. 383–393.
11. Golosman, E.Z. and Yakerson, V.I., *Proizvodstvo i ekspluatatsiya promyshlennykh tsementsoderzhashchikh katalizatorov* (Manufacture and Use of Industrial Cement-containing Catalysts), Available from NIITEKhIM, 1992, Cherkassy, no. 287-khp-92.
12. Nechugovskii, A.I., Grechenko, A.N., and Golosman, E.Z., *Zh. Prikl. Khim.*, 1990, vol. 63, no. 8, pp. 1747–1751.
13. Troshina, V.A., Mamaeva, I.A., Salomatin, G.I., et al., *Zh. Prikl. Khim.*, 2003, vol. 76, no. 3, pp. 430–436.
14. RF Patent 2163836.
15. Demidyuk, V.I., Tkachenko, S.N., Makhov, E.A., et al., *Kataliz Prom–sti*, 2003, no. 6, pp. 42–46.
16. Tkachenko, S.N., Demidyuk, V.I., Egorova, G.V., et al., *Khim. Prom–st.*, 1992, no. 10, p. 604.

ISSN 1070-4272, Russian Journal of Applied Chemistry, 2007, Vol. 80, No. 8, pp. 1360–1364. © Pleiades Publishing, Ltd., 2007.
Original Russian Text © V.F. Kurenkov, S.V. Snigirev, F.I. Lobanov, 2007, published in Zhurnal Prikladnoi Khimii, 2007, Vol. 80, No. 8, pp. 1321–1325.

ENVIRONMENTAL PROBLEMS OF CHEMISTRY AND TECHNOLOGY

Clarification of Kaolin Suspension and Turbid Natural Water in the Presence of Praestols and Aluminum Sulfate and Aluminosilicate Coagulants

V. F. Kurenkov, S. V. Snigirev, and F. I. Lobanov

Kazan State Technological University, Kazan, Tatarstan, Russia
Ashlend Eurasia Joint-Stock Company, Moscow, Russia

Received October 30, 2006; in final form, February 2007

Abstract—The kinetics of clarification of a kaolin suspension and turbid natural water in the presence of coagulants (aluminum sulfate and aluminosilicate) and flocculants (nonionic, cationic, and anionic Praestols) was studied in relation to the concentrations of coagulants and flocculants.

DOI: 10.1134/S1070427207080186

Polyacrylamide coagulants and flocculants are widely used for treatment of natural and waste waters and for concentration and dehydration of suspensions [1–3]. However, the relationship between the characteristics of the agents and their coagulation and flocculation properties is poorly understood. Previously, we have studied the influence exerted on treatment of natural water by a mixture of a coagulant and a flocculant {aluminum sulfate (AS) + partly hydrolyzed polyacrylamide (PAA) [4] or copolymer of acrylamide and sodium acrylate [5]; AS and aluminum polyoxychloride + anionic [6] and cationic [7] Praestols (coagulants widely used in Russia)}.

In this paper, we make a comparative analysis of the clarification kinetics of the kaolin suspension and turbid natural water in the presence of aluminum sulfate and aluminosilicate (ASC) coagulants and nonionic, cationic, and anionic Praestol flocculants.

EXPERIMENTAL

In our experimenrs, we used nonionic Praestol (PAA), anionic Praestols [copolymers of acrylamide (AA) with sodium acrylate (Na-AA)], and cationic Praestol [copolymers of acrylamide (AA) with *N*-acrylamidopropyl-*N*,*N*,*N*-trimethylammonium chloride (APTMAC)] produced by Moscow–Stockhausen–Perm Russian–German Joint-Stock Company. The properties of Praestol flocculants are listed in the table.

As coagulants we used technical-grade (purified) aluminum sulfate $Al_2(SO_4)_3 \cdot 18H_2O$ (AS) with

Properties of Praestol flocculants*

Sample	Praestol brand	$[\eta]$, $cm^3\,g^{-1}$	$\overline{M}_\eta \times 10^{-6}$	Content of units in copolymer, mol %		
				AA	Na-AA	APTMAC
A-1	2500	1550	8.7	97	3	–
A-2	2530	1800	4.4	80	20	–
K-1	650 VS	678	–	80		20

* Structure of units in macromolecule:

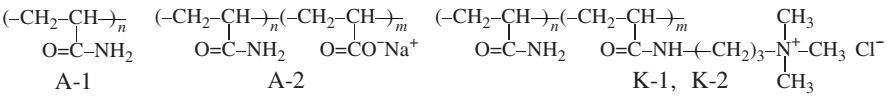

16.35 wt % content of Al_2O_3 and aluminosilicate $[(K,Na)_2SO_4 \cdot Al_2(SO_4)_3 \cdot mH_2O \cdot mH_2O + 2SiO_2 \cdot nH_2O]$ (ASC) [d_4^{20} 1.10 g cm^{-3}, 2.02 and 1.18% content of AlO and SiO groups, respectively], which was prepared by treatment of nepheline with sulfuric acid.

The experiments were performed with KE-1 brand kaolin [$Al_2O_3 \cdot 2SiO_2 \cdot 2H_2O$ with admixtures of Fe_2O_3, MnO, Na_2O, K_2O, and TiO_2] from the Eleninskoe deposit, which is characterized by high uniformity of the particle size distribution (average particle size 0.2×10^{-6} m). We also used turbid water (dispersed phase concentration c_d 0.23%) sampled from the water treatment system of the water supply point in the course of filter unloading.

All solutions were prepared using distilled water and chemicals of chemically pure grade.

The sedimentation kinetics was studied using 0.15% kaolin suspensions in turbid natural water in a cylinder with a VT-500 torsion balance. The sedimentation rate was determined from the weight of the precipitate accumulated on the balance dish in time t after tenfold mixing of the suspension by back-and-forth motion of a perforated disk.

The potentiometric measurements were carried out on a pH-121 pH-meter equipped with measuring (ESL 65-07) and auxiliary (silver chloride, EVL 1M3) electrodes.

First, we studied sedimentation of 0.15% kaolin suspensions using solely the coagulants. The experiments were performed at various coagulant concentrations c_c. Typical kinetic curves of accumulation of the precipitate on the balance dish, depending on the concentration of ASC coagulant, are shown as an example in Fig. 1. Similar dependences were obtained for SA coagulant. As can be seen from Fig. 1, the rate of precipitate accumulation P increases with c_c. This is due to the formation of positively charged aluminum hydroxide particles formed upon addition of the coagulant, which, being added to the suspension, is adsorbed on the oppositely charged kaolin particles (–4.2 mV ζ potential) and neutralizes them, causing aggregation and sedimentation of the system.

First, we calculated from the slopes of the initial portions of the kinetic curves the sedimentation rate v and then the flocculation parameter D_c, using the following equation:

$$D_c = (v - v_0)/v_0,$$

where v and v_0 are the rates of sedimentation of the kaolin suspension in the presence of coagulant and without it, respectively.

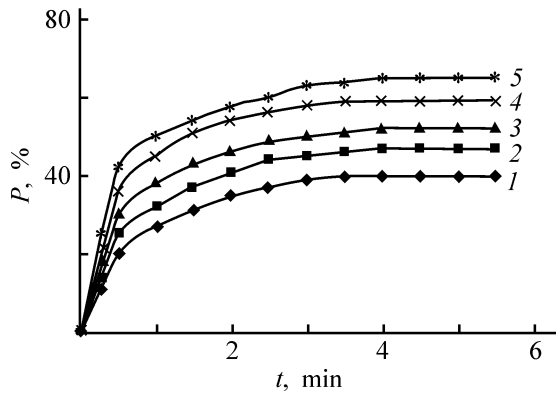

Fig. 1. Degree of kaolin sedimentation P vs. time t at various contents of Al_2O_3 in ASC. Al_2O_3 concentration, $c \times 10^4$, %: (*1*) 0.5, (*2*) 1.0, (*3*) 1.5, (*4*) 2.0, and (*5*) 2.5.

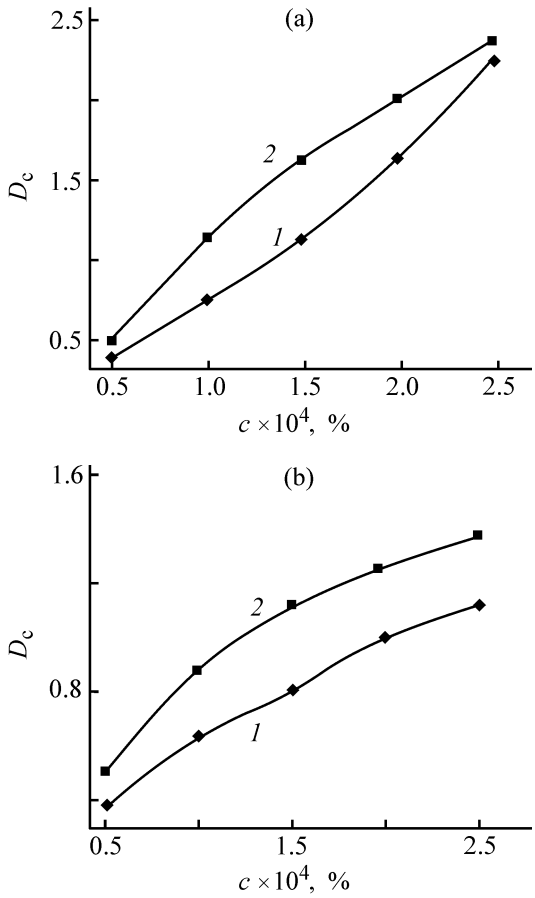

Fig. 2. Flocculation parameter D_c in clarification of (a) kaolin suspension and (b) natural water vs. the concentration of Al_2O_3 c in (*1*) AS and (*2*) ASC.

The effect of the Al_2O_3 content of the coagulant on D_c is illustrated in Fig. 2. As can be seen, the coagulation effect increases with the coagulant concentration, and at $c_{Al_2O_3}$ = const, D_c grows on passing from AS to ASC (from curve *1* to curve *2*, Fig. 2a).

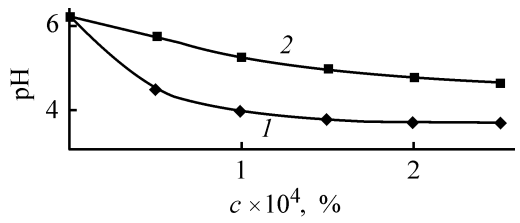

Fig. 3. pH of clarified water after kaolin sedimentation for 30 min vs. Al_2O_3 content c of (*1*) ASC and (*2*) AS.

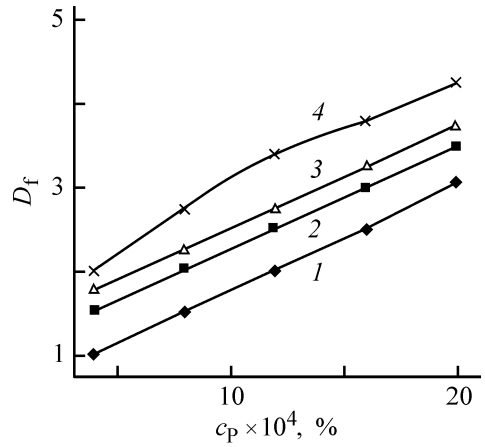

Fig. 4. Flocculation parameter D_f for kaolin sedimentation vs. the concentration c_P of cationic Praestol (K-1) at various concentrations of Al_2O_3 in (*1*, *2*) AS and (*3*, *4*) ASC at pH 7. Concentration of Al_2O_3 $c \times 10^4$, %: (*1*, *3*) 0.5 and (*2*, *4*) 2.0.

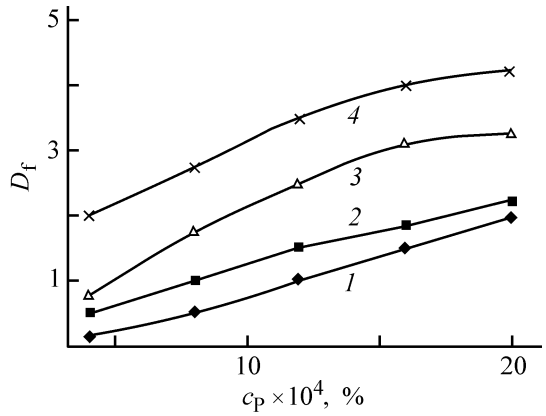

Fig. 5. Flocculation parameter D_f for kaolin sedimentation vs. the concentration of (*1*, *2*) anionic Praestol (A-2) and (*3*, *4*) cationic Praestol (K-1) at various concentrations of Al_2O_3 in AS. Concentration of Al_2O_3 $c \times 10^4$, %: (*1*, *3*) 0.45 and (*2*, *4*) 1.81.

It should be noted that the variation of pH with c_c in water can affect the coagulation; data on the effect of c_c on the solution pH are shown in Fig. 3. It can be seen that, as c_c increases, pH decreases owing to an increase in the concentration of H^+ ions in the course of coagulant hydrolysis. Apparently, hydrolysis of ASC is more pronounced, causing more significant changes in pH as compared to AS (at the same $c_{Al_2O_3}$). To eliminate the possible effect of pH on the coagulation and flocculation, all further tests were performed at pH 7 adjusted with NaOH (introduced 1 min after adding the flocculant).

To evaluate the dependence of sedimentation of the kaolin suspension on the concentration of the flocculant, flocculants were added to the suspension 1 min after adding the coagulant. The flocculation parameter D_f was calculated from the following expression:

$$D_f = (v - v_0)/v_0,$$

where v and v_0 are the rates of sedimentation of the kaolin suspension in the presence of flocculant and without it, respectively.

The $D_f = f(c_P)$ dependence for cationic Praestol (sample K-1), used together with AS and ASC, is shown in Fig. 4. As can be seen, D_f increases with c_P upon addition of the flocculant with AS (curves *1*, *2*) and with ASC (curves *3*, *4*). Moreover, D_f increases with the coagulant concentration (passing from curves *1*, *3* to curves *2*, *4*, respectively). These data indicate that the flocculation in the presence of cationic Praestol (K-1) in combination with ASC is more efficient than that with AS (Fig. 4, passing from curves *3*, *4* to curves *1*, *2*).

The dependences of the flocculation parameter D_f on the concentrations of anionic Praestol (A-2) (curves *1*, *2*) and cationic Praestol (K-1) (curves *3*, *4*), taken in combination with AS coagulant are shown in Fig. 5. As can be seen, D_f increases with c_P of both flocculants. This is due to the elevated adsorption of the flocculant macromolecules on the coagulated particles. The adsorbed cationic Praestol neutralizes the negative charge of the kaolin particles, and anionic Praestol neutralizes the positive charge of aluminum hydroxide particles formed by the coagulant hydrolysis. The resulting coarse particles lose their sedimentation stability and precipitate.

Figure 5 allow comparison of the flocculation activities of the anionic and cationic Praestols, because samples A-2 and K-1 have the same content of the ionic groups (see table). Comparison of the data at fixed c_P and similar concentrations of AS shows that D_f increases on passing from anionic to cationic Praestol (passing from curves *1*, *2* to curves *3*, *4*). Moreover, for both flocculants, D_f increases with c_c.

Similar dependences were obtained for ASC coagulant in the presence of both anionic and cationic Praestols.

We also compared the flocculation effect of nonionic Praestol (A-1) and anionic Praestol (A-2), as influenced by the presence of AS and ASC coagulants; the results are shown in Fig. 6. As can be seen from the comparison at c_P = const, D_f is higher when the above flocculants are used in combination with ASC, compared with AS (Fig. 6, curves *2*, *4* and *1*, *3*). Moreover, D_f increases on passing from anionic Praestol (A-2) to nonionic Praestol (A-1), which is probably due to the higher $\overline{M}_\eta$ of the nonionic Praestol (see table). With increasing molecular weight of the flocculant, the effective size of macromolecular globules $(\bar{r}^2)^{1/2}$ in solutions gorws, i.e., macromolecules can bind a larger number of kaolin particles. Therefore, formation of coarse floccules promoted their sedimentation and, thus, increased D_f. These experimental results agree well with well-known dependences of the flocculation effect of various water-soluble polymers on their molecular weight, which have been determined previously for natural water [2] and model kaolin suspensions [3].

Let us analyze the data on clarification of a turbid natural water containing 0.23% disperse phase under the effect of coagulants in the presence and absence of the flocculants. The effect of the Al_2O_3 content of the coagulants on D_f in the absence of flocculants is shown in Fig. 2b. As can be seen, D_f increases with the Al_2O_3 content of both coagulants, and this effect becomes more pronounced upon replacement of AS with ASC (Fig. 2b, passing from curve *1* to curve *2*). These data well agree with the results obtained for sedimentation of the kaolin suspension (Fig. 2a).

The dependences of D_f on c_P for cationic (K-1) and anionic (A-2) Praestols, used together with AS and ASC, are shown in Fig. 7. As can be seen, D_f increases with c_P in all the cases studied. Comparison of experimental data at $c_{Al_2O_3}$ = const and c_P = const shows that the efficiency of water treatment with cationic Praestol (K-1) is higher than that with anionic Praestol (A-2) (Fig. 7, passing from curves *1*, *3* to curves *2*, *4*), and ASC as the second component (coagulant) shows better performance than AS (passing from curves *3*, *4* to curves *1*, *2*). These results agree well with the data on sedimentation of kaolin suspensions, shown in Fig. 5. Our experimental data indicate that sedimentation of kaolin suspensions and clarification of natural water can be intensified by using cationic Praestol (K-1) in combination with ASC.

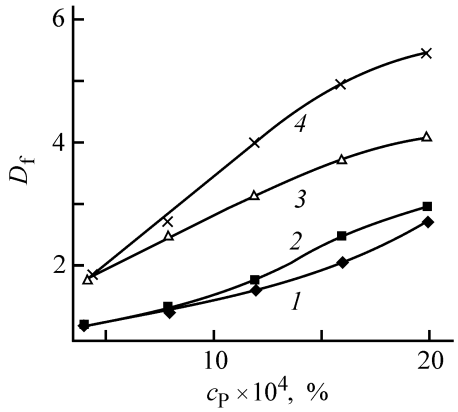

Fig. 6. Flocculation parameter D_f at kaolin sedimentation vs. the concentration c_P of (*1*, *2*) anionic Praestol (A-2) and (*3*, *4*) nonionic Praestol (A-1) in the presence of (*1*, *3*) AS and (*2*, *4*) ASC at pH 7. Concentration of Al_2O_3 1×10^{-4}%; the same for Fig. 7.

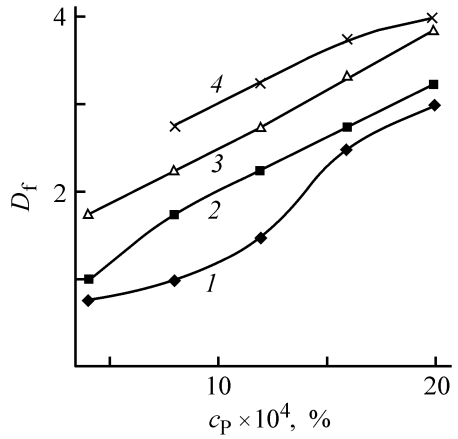

Fig. 7. Flocculation parameter D_f at water clarification vs. the concentration c_P of (*1*, *3*) anionic Praestol (A-2) and (*2*, *4*) cationic Praestol (K-1) in the presence of (*1*, *2*) AS and (*3*, *4*) ASC at pH 7.

CONCLUSIONS

(1) The dependences of sedimentation of kaolin suspensions and of clarification of natural water in the presence of aluminum sulfate and aluminosilicate (coagulants), used in combination with nonionic, cationic, and anionic Praestols (flocculants), show that the substitution of aluminosilicate for aluminum sulfate in the presence of flocculants and without them enhances the flocculating and coagulating effects, respectively.

(2) The flocculating effect increases with the concentration of aluminum sulfate and aluminosilicate and of nonionic, cationic, and anionic Praestols. In the case of flocculants, the flocculation effect in-

creases in the order cationic > anionic + nonionic > anionic. The strongest flocculation effect is attained when cationic Praestol is used in combination with aluminosilicate.

REFERENCES

1. Veitser, Yu.I. and Mints, D.M., *Vysokomolekulyarnye flokulanty v protsessakh ochistki prirodnykh i stochnykh vod* (Macromolecular Flocculants in Treatment of Natural and Waste Waters), Moscow: Stroiizdat, 1984.
2. Kurenkov, V.F., Hartan, H.-G., and Lobanov, F.I., *Khim. Komp'yut. Model. Butlerovsk. Soobshch.*, 2002, vol. 3, no. 11, pp. 31–40.
3. Myagchenkov, V.A., Baran, A.A., Bekturov, E.A., and Bulidarova, G.V., *Poliakrilamidnye flokulyanty* (Polyacrylamide Flocculants), Kazan: Kazan Gos. Tekhnol. Univ., 1998.
4. Kurenkov, V.F., Churikov, F.I., and Snigirev, S.V., *Zh. Prikl. Khim.*, 1999, vol. 72, no. 9, pp. 1485–1489.
5. Kurenkov, V.F., Churikov, F.I., and Snigirev, S.V., *Vest. Kazansk. Tekhnol. Univ.*, 1998, no. 2, pp. 104–108.
6. Kurenkov, V.F., Shatokhina, E.V., Hartan, H.-G., and Lobanov, F.I., *Zh. Prikl. Khim.*, 2005, vol. 78, no. 11, pp. 1903–1906.
7. Kurenkov, V.F., Nadezhdina, I.I., Hartan, H.-G., and Lobanov, F.I., *Khim. Tekhnol.*, 2006, no. 4, pp. 34–38.

ISSN 1070-4272, Russian Journal of Applied Chemistry, 2007, Vol. 80, No. 8, pp. 1369–1372. © Pleiades Publishing, Ltd., 2007.
Original Russian Text © I.A. Lyutarevich, V.A. Markov, 2007, published in Zhurnal Prikladnoi Khimii, 2007, Vol. 80, No. 8, pp. 1330–1333.

PROCESSES AND EQUIPMENT OF CHEMICAL INDUSTRY

Hydrodynamics and Mass Exchange in a Rotary Apparatus

I. A. Lyutarevich and V. A. Markov

Belarussian State Technological University, Minsk, Belarus

Received February 9, 2007

Abstract—Results of an experimental study of carbon dioxide desorption from water in a rotary apparatus are presented. The manner in which the volume mass-transfer coefficient in the fluid phase and the efficiency of mass transfer vary with a number of mode parameters was determined. Analytical dependences for calculating the hydraulic resistance and the rotor drive power were derived. These dependences will allow development of a procedure for engineering calculations of apparatus of this type.

DOI: 10.1134/S1070427207080204

The quality of products and the ecological parameters of a process (primarily, the content of impurities in fluid and gaseous industrial wastes) are important factors associated with improvement of technological processes. Of particular importance is carrying out effective mass exchange between flows at minimum energy expenditure.

A commonly accepted promising way to solve this problem is use of rotary apparatus with phase interaction in a swirling flow for mass-exchange processes.

Analysis of published evidence [1–3] shows that the efficiency of mass transfer in apparatus with external energy supply exceeds that for contact devices with the conventional types of phase interaction in gas–fluid systems. This favors a pronounced decrease in the apparatus dimensions.

Thus, rotary dispersion-film apparatus, in which the phase interaction occurs in the zone of intensive dispersion of a fluid by a spraying device and phases subsequently come in contact in the zone of a film-type flow of a fluid, should be distinguished among surface-type, spraying, bubbling, and rotary apparatus. In addition, use of a swirling flow in apparatus of this kind can intensify the processes performed and markedly raise the gas load at a comparatively low hydraulic resistance of an apparatus.

EXPERIMENTAL

We developed a two-stage design of a rotary dispersion-film apparatus for interaction of gas–fluid systems in a swirling flow (Fig. 1). It includes a cylindrical case *1*, tangential inlet *2* and outlet *3* for the gas, and fluid-dispersing devices *4* fixed on shaft *5* driven by electric motor *6*. The frequency control unit is used to set the required shaft rotation rate. The dispersing device has the form of a hollow perforated cylinder with flanges preventing fluid overflow.

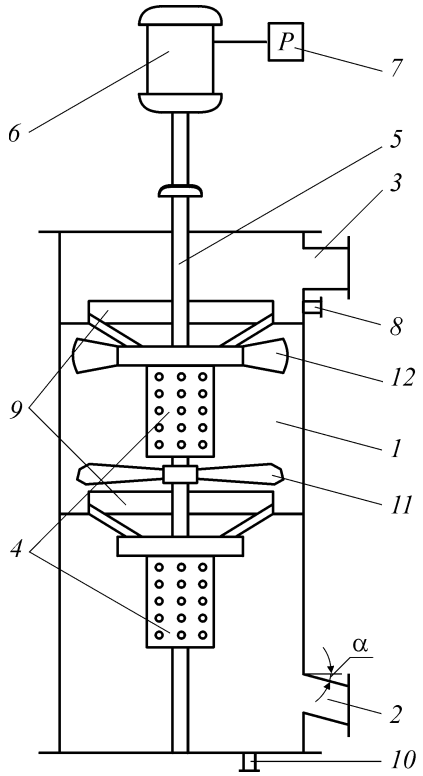

Fig. 1. Schematic of the experimental installation: (*1*) case, (*2*) inlet pipe, (*3*) outlet pipe, (*4*) dispersing unit, (*5*) shaft, (*6*) electric motor, (*7*) frequency control unit, (*8*) fluid supply pipe, (*9*) overflow unit, (*10*) fluid discharge pipe, (*11*) impeller, (*12*) blade swirler.

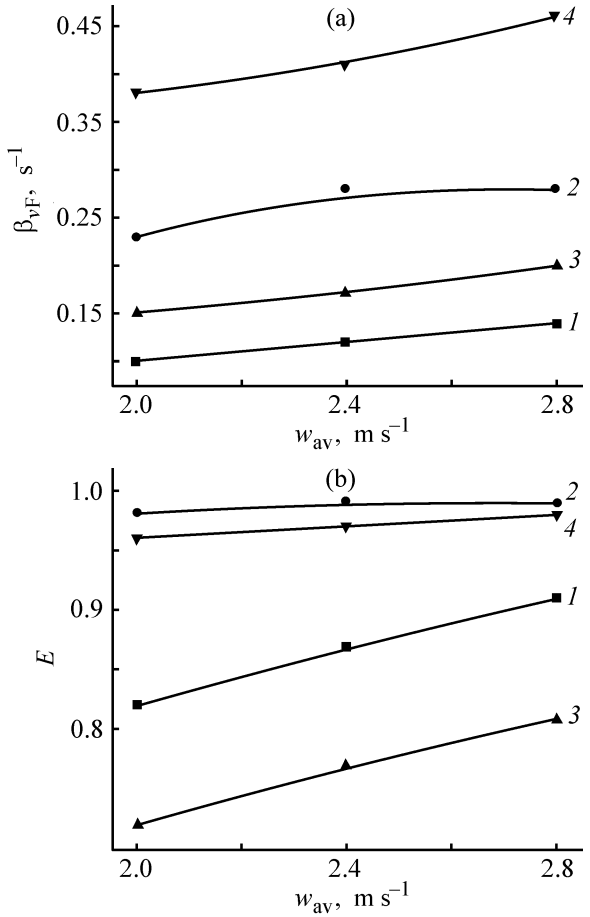

Fig. 2. (a) Volume-related mass-exchange coefficient β_{vf} and (b) mass-exchange efficiency E vs. gas flow velocity w_{av} at rotor rotation rate n = 23.3 rps. Spraying density q ($m^3\ m^{-2}\ h^{-1}$): (a) 3.266 and (b) 4.976. (*1*, *3*) Upper and (*2*, *4*) lower stages of the contact apparatus.

The diameters of the apparatus and dispersing unit are 0.195 and 0.054 cm, respectively; the inlet pipe is mounted at an angle of 7° to the horizontal.

The apparatus operates as follows: gas (air) is delivered into the apparatus from below and, on passing through the inlet pipe *2* tangential to the case, is swirled. The fluid (distilled water), saturated with CO_2, is delivered through pipe *8* via the overflow unit *9* into a rotating unit *4* and is dispersed into drops. Further, the fluid flows down the apparatus wall to a lower-lying contact stage, where the dispersion process is repeated, and is discharged via pipe *10*. The flow swirling in the upper stage is maintained by impeller *11* with helical blades, mounted on the shaft. The impeller also serves to separate fluid drops carried away from the lower stage of the contact apparatus. The gas flow cannot carry away fluid drops from the apparatus because an additional blade swirler *12* is mounted in the upper dispersing cylinder. Thus, the gas interacts with the fluid phase in both the dispersed and film modes.

The aim of our study was to examine the influence exerted by operation mode parameters of a rotary apparatus on the mass-exchange process and to obtain new experimental data and analytical dependences for calculation of the hydraulic resistance and power consumed by the rotor of the design we developed.

We studied mass exchange under laboratory conditions in desorption of CO_2 from water. Using the experimental data obtained, we calculated important parameters determining the number of stages and height of the apparatus, such as the efficiency of a stage of the contact apparatus and mass-transfer coefficient.

The content of CO_2 was found by measuring the acidity of the medium with a standard pH-meter. By processing the experimental data, we obtained a relation for determining the CO_2 concentration in water as a function of the solution acidity. At pH 5–7 this concentration was calculated by the formula [4]:

$$c = 2.69 \times 10^{5-\mathrm{pH}}. \quad (1)$$

In the course of our experiments, the initial solution acidity changed by no more than 0.03 pH units. The temperature of the gas and fluid was 15–18°C. The spraying density was varied in the range 3–8 $m^3\ m^{-2}\ h^{-1}$. The flow-rate average gas velocity in the apparatus was varied from 2 to 3.6 m s^{-1}.

For each operation mode parameter of the apparatus, we measured the initial and final CO_2 concentration in water and calculated the mass-transfer efficiency. In CO_2 desorption from water with air, it was calculated by the formula [5, 6]:

$$E_f = (c_{in} - c_{fin})/c_{in} = 1 - c_{fin}/c_{in}, \quad (2)$$

where c_{in} and c_{fin} are the initial and final CO_2 concentrations in water (%).

The mass-transfer coefficient in the liquid phase, related to the working volume of the apparatus, was found by the formula

$$\beta_{vf} = (L/V)\ln(c_{in}/c_{fin}), \quad (3)$$

where L is the flow rate of the fluid phase, and V is the working volume of the apparatus (m^3).

Having expressed the mass-exchange efficiency in terms of β_{vf}, we obtain

$$E_f = 1 - 1/\exp(\beta_{vf} V/L). \quad (4)$$

Figure 2a shows dependences of the volume-related mass-exchange coefficient in the fluid phase on

the gas flow velocity in the apparatus for different spraying densities. It can be seen that β_{vf} grows with the gas flow velocity and spraying density. This occurs because, as the spraying density increases, the volume of a mass-exchange apparatus contains at any instant of time a larger amount of a fluid, and, consequently, particles having about the same size as that at low spraying density are formed in a greater number. In this case, an increase in the gas flow velocity leads to turbulization of flows of the interacting phases.

The dependence of the efficiency of mass exchange on the gas flow velocity in an apparatus is shown in Fig. 2b for different spraying densities. It can be seen from the plot that the efficiency grows. This can be attributed to an increase in the tangential stresses at the phase boundary and to swirling of the fluid film on the apparatus wall upon an increase in the gas flow velocity in the apparatus. This leads to a longer residence of the fluid in the apparatus and, accordingly, to a rise in E. As the spraying density increases, the fluid film becomes thicker, which favors a faster flow of this film down the apparatus wall and, consequently, impairs the mass-exchange efficiency.

An important characteristic of mass-exchange apparatus, which determines the energy expenditure for the process, is their hydraulic resistance. It was found in our experiments that the spraying density and rotor rotation rate have no significant effect on the hydraulic resistance. Figure 3 shows how the hydraulic resistance depends on the gas flow velocity. The hydraulic resistance can be found using the relation obtained by processing of experimental data:

$$\Delta P = 94.984\, w_{av}^{2.205}. \quad (5)$$

The difference between the values calculated by Eq. (5) and found experimentally does not exceed 2.6%.

In addition to the hydraulic resistance, one more factor, power consumed for rotor rotation, will affect the specific energy expenditure. This effect is determined as the difference between the values of power N, consumed by the electric motor with and without the rotor mounted on the shaft (Fig. 4). The consumed power becomes lower as the gas flow velocity increases because the gas flow interacts with the impeller mounted on the shaft and thus promotes rotor rotation.

The dependence of the power consumed by the rotor on the rotor rotation rate and flow-rate average gas velocity in the apparatus was approximated with the following relation:

$$N = 13.42 + 24.32\, w_{av} - 0.994\, n - 0.215 w_{av} n\, w_{av}^2 + n^2. \quad (6)$$

The difference between the consumed power calculated by expression (6) and that found experimentally does not exceed 5.6%.

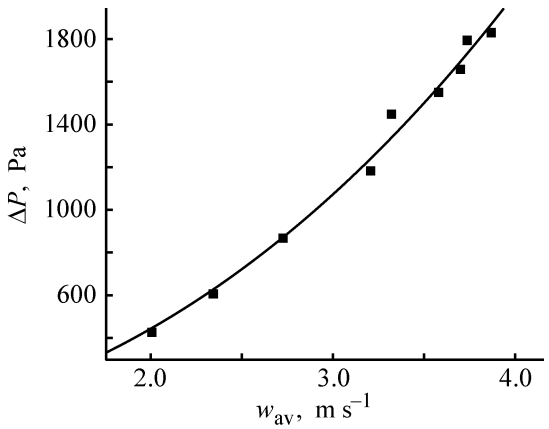

Fig. 3. Hydraulic resistance ΔP vs. gas flow velocity w_{av}.

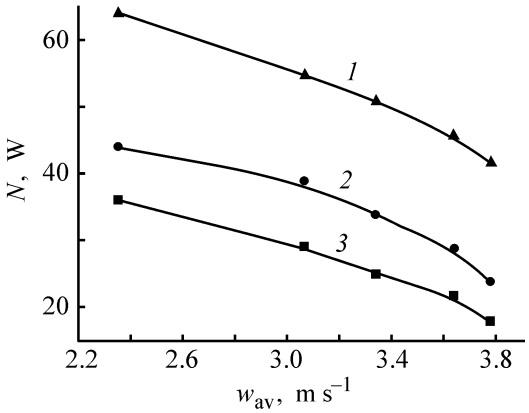

Fig. 4. Power N consumed by the rotor vs. gas flow velocity w_{av}. n (rps): (*1*) 23.3, (*2*) 16.7, and (*3*) 10.

CONCLUSIONS

(1) A study of specific features of mass exchange in CO_2 desorption by air in a rotary apparatus in interaction of phases in a swirling flow demonstrated the high efficiency of the design developed.

(2) Effect of operation mode parameters of the apparatus on the volume-related mass exchange coefficient in the fluid phase and on the efficiency of mass exchange was revealed.

(3) Equations for calculating the hydraulic resistance and power consumed by the rotor were suggested.

REFERENCES

1. Vasilinets, I.M. and Saburov, A.G., *Rotornye plenochnye apparaty v pishchevoi promyshlennosti* (Rotary Film Apparatus in Food Industry), Moscow: Agropromizdat, 1989.
2. Olevskii, V.M., Ruchinskii, V.R., Kashnikov, A.M., and Chernyshev, V.I., *Plenochnaya teplo- i massoobmennaya apparatura* (Film-type Heat-and-Mass-Exchange Apparatus), Moscow: Khimiya, 1988.
3. Kogan, V.B. and Kharisov, M.A., *Oborudovanie dlya razdeleniya smesei pod vakuumom* (Apparatus for Vacuum Separation of Mixtures), Leningrad: Mashinostroenie, 1976, pp. 286–312.
4. Vaitekhovich, P.E., Development and Study of Swirling Mass-Exchange Apparatus, *Cand. Sci. Dissertation*, Minsk, 1982.
5. Alekseevskii, G.V., Gol'ts, R.K., and Musakin, A.P., *Kolichestvennyi analiz* (Quantitative Analysis), Moscow: Khimiya, 1964, pp. 450–478.
6. Slobodnyak, I.P. and Grigor'ev, L.G., *Izv. Vyssh. Uchebn. Zaved., Pishch. Tekhnol.*, 1966, no. 3, pp. 151–157.

ISSN 1070-4272, Russian Journal of Applied Chemistry, 2007, Vol. 80, No. 8, pp. 1373–1375. © Pleiades Publishing, Ltd., 2007.
Original Russian Text © Xiaoping Zhao, Dzen Kwang Song, A.B. Radbil', B.A. Radbil', 2007, published in Zhurnal Prikladnoi Khimii, 2007, Vol. 80, No. 8, pp. 1334–1336.

ORGANIC SYNTHESIS AND INDUSTRIAL ORGANIC CHEMISTRY

Synthesis and Biological Activity of Schiff Bases Derived from Dehydroabietylamine and Benzaldehyde Derivatives

Xiaoping Zhao, Dzen Kwang Song, A. B. Radbil', and B. A. Radbil'

Institute of Chemical Processing of Wood Products, Academy of Wood of Chinese People's Republic, Nankin, China

Lesma Research and Promotion Firm, Limited Liability Company, Nizhni Novgorod, Russia

Received January 1, 2007

Abstract—Previously unknown Schiff bases were prepared from dehydroabietylamine and substituted benzaldehydes. Their physicochemical properties were determined, and the bactericidal activity toward some microorganisms was evaluated.

DOI: 10.1134/S1070427207080216

Schiff bases derived from primary amines and substituted benzaldehydes exhibit antibacterial, anticancer, and antitumor activity. Numerous studies have shown that such an activity of Schiff bases is caused by the presence of the >C=N– functional group. It is also known [1] that many amines derived from resin (diterpene) acids exhibit a wide spectrum of biological activity. In particular, Borglin has shown that dehydroabietylamine is an effective bactericidal and fungicidal agent [2]. It would be expected that Schiff bases derived from dehydroabietylamine will exhibit enhanced biological activity. However, data on the synthesis and properties of Schiff bases derived from dehydroabietylamine are lacking.

Here we report on the synthesis and biological activity of Schiff bases derived from dehydroabietylamine and substituted benzaldehydes. These Schiff bases were prepared in high yields (85–95%) by direct condensation in ethanol:

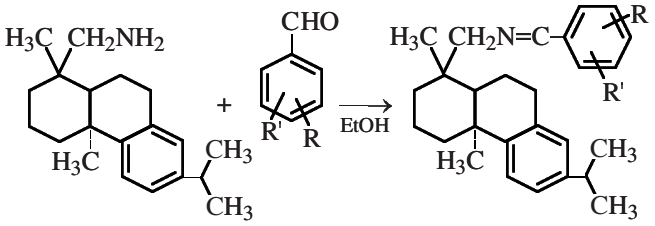

where R = R'= H (**a**); R = H, R' = *p*-OMe (**b**); R = H, R' = *p*-Cl (**c**); R = H, R' = *p*-F (**d**); R = H, R'= *o*-OH (**e**); R = *o*-OH, R' = *p*-NO_2 (**f**); R = *o*-OH, R' = *p*-Cl (**g**); R = *o*-OH, R' = *p*-OMe (**h**).

The rate of this reaction is fairly high. All the Schiff bases precipitate from the reaction mixture virtually immediately after the reactants solutions are mixed. They are insoluble in water and in ethanol at room temperature and soluble in dimethylformamide, chloroform, dimethyl sulfoxide, and some other solvents.

Table 1. Physicochemical properties of the Schiff bases

Compound	Empirical formula	Color	T_m, °C	Found, %			Calculated, %		
				C	H	N	C	H	N
a	$C_{27}H_{35}N$	White	104.5	86.22	9.49	3.61	86.86	9.39	3.75
b	$C_{28}H_{37}NO$	"	103.5	84.94	9.86	3.11	83.79	9.23	3.49
c	$C_{27}H_{34}NCl$	"	118.6	79.54	8.28	3.25	79.50	8.34	3.44
d	$C_{27}H_{34}NF$	"	106.5	82.78	9.40	3.19	82.86	8.69	3.58
e	$C_{27}H_{35}NO$	Yellow	153.2	82.84	9.51	3.75	82.86	8.95	3.58
f	$C_{27}H_{34}N_2O_3$	"	187.5	74.39	8.36	6.44	75.34	7.91	6.51
g	$C_{27}H_{34}NOCl$	"	177.8	76.11	8.50	3.17	75.96	7.97	3.28
h	$C_{28}H_{37}NO_2$	Red	105.2	79.84	9.23	3.36	79.43	8.75	3.31

The physicochemical parameters of the azomethines prepared are listed in Table 1.

The structures of the compounds were confirmed by IR and ^{1}H NMR spectroscopy (Table 2). The IR spectra of all the compounds contain a strong absorption band of the >C=N– group at 1660–1610 cm^{-1}. Its position only slightly depends on the structure of the compound and on substituents in the phenyl ring of the benzaldehyde moiety. The spectra of **e**–**h** also contrain a well-defined band of OH stretching vibrations at 3460–3410 cm^{-1}. In the spectra of the other compounds, this band is absent.

In the ^{1}H NMR spectra, the –N=C–H signal is observed at 8.2–8.4 ppm, and the OH signal, at 13.6–15.0 ppm.

The bactericidal activity of the compounds was studied with test cultures of *E. Coli*, *B. Subtilis*, and *S. Aureus*. The activity was evaluated by the diameter of the inhibition zone (cm) arising 48 h after introducing into the cultural medium 2×10^{-6} g ml^{-1}

Table 2. Spectroscopic characteristics of the Schiff bases

Compound	IR spectrum, ν, cm^{-1}	^{1}H NMR spectrum, δ, ppm
a	2931, 1644, 1040, 832	8.265 (1H, N=C*H*–); 7.765, 7.423, 7.2204, 7.024, 6.906 (8H, C=C*H*–); 3.536 (1H, N–CH_2–); 2.879 [1H, –C*H*(CH_3)$_2$]; 2.858, 2.303, 1.967, 1.794, 1.579 (10H, –CH_2–); 1.485 (1H, >C*H*–); 1.271, 1.258, 1.084 (9H, –CH_3)
b	2938, 1645, 1086, 823	8.224 (1H, N=C*H*–); 7.692, 7.391, 7.223, 7.032, 6.910 (7H, C=C*H*–); 3.527 (1H, N–CH_2–); 2.898 [1H, –C*H*(CH_3)$_2$]; 2.851, 2.319, 1.939, 1.790, 1.528 (10H, –CH_2–); 1.439 (1H, >C*H*–); 1.272, 1.265, 1.008 (9H, –CH_3)
c	2944, 1645, 1036, 825	8.207 (1H, N–CH_2–); 7.725, 7.246, 7.225, 7.026, 6.938 (7H, C=C*H*–); 3.884 (1H, N–CH_2–); 3.868 (3H, –OCH_3); 3.541 [1H, –C*H*(CH_3)$_2$]; 3.389, 2.902, 2.367, 1.743, 1.715 (10H, –CH_2–); 1.498 (1H, >C*H*–); 1.475, 1.298, 1.086 (9H, –CH_3)
d	2941, 1650, 1229, 831	8.249 (1H, N–CH_2–); 7.763, 7.282, 7.227, 7.091, 6.934 (7H, C=C*H*–); 3.547 (1H, N–CH_2–); 2.919 [1H, –C*H*(CH_3)$_2$]; 2.879, 2.315, 1.847, 1.724, 1.456 (10H, –CH_2–); 1.456 (1H, >C*H*–); 1.309, 1.281, 1.092 (9H, –CH_3)
e	3442, 2937, 1628, 1153, 759	13.619 (1H, –OH); 8.336 (1H, N–CH_2–); 7.349, 7.300, 7.209, 7.023, 6.879 (6H, C=C*H*–); 3.530 (1H, N–CH_2–); 2.864 [1H, –C*H*(CH_3)$_2$]; 2.313, 1.837, 1.806, 1.585, 1.503 (10H, –CH_2–); 1.412 (1H, >C*H*–); 1.281, 1.243, 1.079 (9H, –CH_3)
f	3423, 2935, 1618, 1330, 1098	14.982 (1H, –OH); 8.342 (1H, N–CH_2–); 7.282, 7.204, 7.031, 6.979, 6.914 (6H, C=C*H*–); 3.523 (1H, N–CH_2–); 2.843 [1H, –C*H*(CH_3)$_2$]; 2.325, 1.877, 1.854, 1.565, 1.421 (10H, –CH_2–); 1.410 (1H, >C*H*–); 1.279, 1.234, 1.099 (9H, –CH_3)
g	3459, 2935, 1639, 1991, 826	13.572 (1H, –OH); 8.268 (1H, N–CH_2–); 7.283, 7.234, 7.024, 7.004, 6.904 (6H, C=C*H*–); 3.538 (1H, N–CH_2–); 2.861 [1H, –C*H*(CH_3)$_2$]; 2.333, 1.835, 1.807, 1.579, 1.435 (10H, –CH_2–); 1.402 (1H, >C*H*–); 1.274, 1.257, 1.073 (9H, –CH_3)
h	3452, 2934, 1629, 1076, 832	14.167 (1H, –OH); 8.369 (1H, N–CH_2–); 7.282, 7.172, 7.011, 6.943, 6.799 (6H, C=C*H*–); 3.913 (3H, –OCH_3); 3.549 (1H, N–CH_2–); 2.842 [1H, –C*H*(CH_3)$_2$]; 2.308, 1.802, 1.630, 1.500, 1.448 (10H, –CH_2–); 1.414 (1H, >C*H*–); 1.273, 1.243, 1.073 (9H, –CH_3)

Table 3. Bactericidal activity of Schiff bases

Bacteria	Diameter of the inhibition zone, cm, for indicated compound							
	a	**b**	**c**	**d**	**e**	**f**	**g**	**h**
S. Aureus	1.05	0.95	1.20	1.65	0.90	1.25	1.10	1.10
B. Subtilis	0.95	1.20	1.72	1.32	0.85	0.90	1.20	0.90
E. Coli	1.15	1.01	1.12	0.90	0.90	0.80	0.85	0.92

solutions of the Schiff bases in dimethylformamide (Table 3).

All the compounds prepared exhibit bactericidal activity. Compound **c** derived from Cl-substituted benzaldehyde is the most active toward *B. Subtilis* (diameter of inhibition zone 1.72 cm), and compound **d** derived from fluorinated benzaldehyde, toward *S. Aureus* (diameter of inhibition zone 1.65 cm). It should be noted that the most active agent toward *E. Coli* is compound **a** derived from unsubstituted benzaldehyde (diameter of inhibition zone 1.15 cm); introduction of substituents into the benzaldehyde moiety does not enhance the bactericidal activity of the Schiff base.

Thus, introduction of substituents into the phenyl ring of the benzaldehyde moiety appreciably affects the bactericidal activity of Schiff bases. However, this effect is ambiguous and depends on numerous factors, primarily on the structure of the molecule, presence and nature of substituents in the dehydroabietylamine and benzaldehyde moieties, and particular microorganism.

EXPERIMENTAL

All the chemicals used for preparing Schiff bases (dehydroabietylamine; benzaldehyde and its derivatives) were of chemically pure or analytically pure grade and were used without additional purification.

Elemental analysis was performed with an RE-2400CHN device. The IR spectra were recorded on a Bio-Rad FTS-185 IR spectrophotometer using KBr cells. The ^{1}H NMR spectra were measured on a DPX-300 Bruker Avance 300 spectrometer (solvent $CDCl_3$, reference TMS). The melting points were determined with an XT-5 device.

Syntheses were performed in a vessel equipped with a stirrer, reflux condenser, and dosing unit. The vessel was charged with a solution of 10 mmol of dehydroabietylamine in 200 ml of ethanol, after which a solution of 10 mmol of benzaldehyde or its derivative in 100 ml of ethanol was slowly added from the dosing unit. The mixture was stirred for 3 h at 20°C. The crystals of the Schiff bases were filtered off, recrystallized three times from ethanol, and dried in a vacuum.

The bactericidal activity of each of the Schiff bases synthesized was evaluated by measuring the diameter of the inhibition zone [3, 4]. For this purpose, 0.5 ml of a suspension of spores of each test culture was added to a sterile agarized cultural medium just before its solidification, after which the mixture was poured into sterile Petri dishes (9 cm in diameter) and allowed to solidify. Solutions of the Schiff bases in dimethylformamide (2×10^{-6} g ml^{-1}) were prepared. Then sterile disks made of filter paper (7 mm in diameter) were wetted in a solution of appropriate Schiff base and placed into the Petri dishes. The Petri dishes were kept at 35°C for 48 h, after which the inhibition zones of bacterial growth were revealed and the diameter of each zone was measured. Three replicate experiments were performed with each Schiff base.

CONCLUSION

The Schiff bases synthesized from abietylamine and substituted benzaldehydes exhibit noticeable bactericidal activity toward certain microorganisms. The correlation between the molecular structure and biological activity is ambiguous.

REFERENCES

1. Sandermann, W., *Naturharze Terpentinöl-Tallöl. Chemie und Technologie*, Berlin: Springer, 1960. Translated under the title *Prirodnye smoly, skipidar, tallovoe maslo*, Moscow: Lesnaya Prom–st., 1964, pp. 303–310.
2. Borglin, S., *Soap Sanit. Chem.*, 1947, vol. 23, no. 12, pp. 147–149, 169.
3. Alzoreky, N.S. and Nakahara, K., *Int. J. Food Microbiol.*, 2003, vol. 80, pp. 223–230.
4. Sari, N., Arslan, S., Logoglu, E., and Sakiyan, I., *J. Sci.*, 2003, vol. 16, p. 283.

ISSN 1070-4272, Russian Journal of Applied Chemistry, 2007, Vol. 80, No. 8, pp. 1376–1378. © Pleiades Publishing, Ltd., 2007.
Original Russian Text © E.G. Mamedov, G.F. Mamedova, O.B. Gadzhieva, A.V. Nagiev, 2007, published in Zhurnal Prikladnoi Khimii, 2007, Vol. 80, No. 8, pp. 1337–1340.

ORGANIC SYNTHESIS AND INDUSTRIAL ORGANIC CHEMISTRY

Asymmetric Diene Synthesis of Bicyclo[2.2.2]octenes in the Presence of Lewis Acids

E. G. Mamedov, G. F. Mamedova, O. B. Gadzhieva, and A. V. Nagiev

Institute of Petrochemical Processes, National Academy of Sciences of Azerbaijan, Baku, Azerbaijan

Received August 2, 2006; in final form, May 2007

Abstract—Asymmetric diene synthesis of substituted bicyclo[2.2.2]octenes from (–)-menthyl acrylate and cyclohexa-1,3-diene in the presence of achiral Lewis acid catalysts ($TiCl_4$, $AlCl_3$, BBr_3, $AlCl_3 \cdot OEt_2$, $BBr_3 \cdot OEt_2$) was studied. The influence of various factors on the isomeric composition, yield, and enantiomeric purity of the compounds prepared was examined.

DOI: 10.1134/S1070427207080228

Many drugs, fragrant compounds, and chemicals for agriculture are produced today in the optically active form.

Bicyclo[2.2.2]octane and bicyclo[2.2.2]octene moieties are essential fragments of many important natural and synthetic biologically active compounds [1]. Therefore, synthesis of these compounds in the optically active form is of practical interest. A considerable researchers' interest is given today to optically active bicyclic amino acids important for organic and bioorganic chemistry, e.g., to 2-aminobicyclo[2.2.2]-octane-2-carboxylic acid:

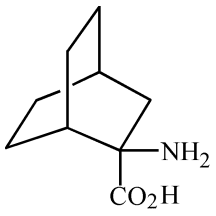

I

Synthesis of this acid in the optically active form by asymmetric diene synthesis (ADS) was described in [2].

Asymmetric diene synthesis from cyclohexa-1,3-diene (CHD) in the presence of catalysts is one of promising routes to chiral bicyclo[2.2.2]octane derivatives. The first asymmetric diene synthesis from CHD was performed by Cervinka and Kriz [3]. This reaction was carried our without a catalyst. After removal of the chiral reagent, the optical yield of the adducts was low (3.3%).

Here, we report on the synthesis of chiral bicyclo-[2.2.2]octenes by [4+2]-cycloaddition of (–)-menthyl acrylate to CHD in the presence of achiral Lewis acid catalysts ($TiCl_4$, $AlCl_3$, BBr_3, $AlCl_3 \cdot OEt_2$, $BBr_3 \cdot OEt_2$). The reaction was performed at temperatures from 0 to 80°C in various solvents (CH_2Cl_2, C_6H_6, $C_6H_5CH_3$, C_6H_5Cl). The reaction follows the scheme

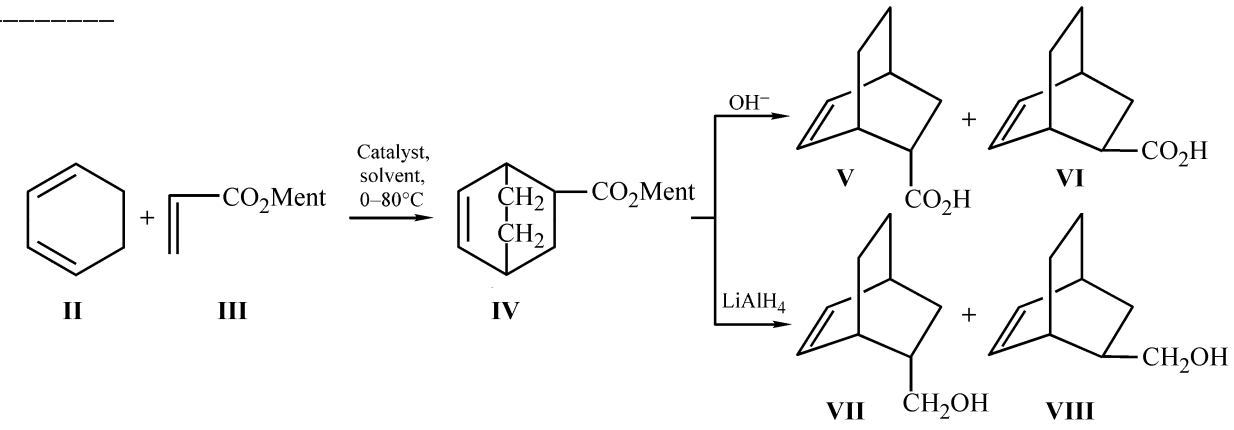

Table 1. Influence of the reaction conditions on the total and optical yields of **IV**, **V**, and **VII** in the reaction of CHD with (–)-menthyl acrylate in the presence of Lewis acids

T, °C	Solvent	Catalyst	Catalyst : dienophile molar ratio	Yield **IV**, %	Isomeric ratio for **IV**, %		Optical yield, %		$[\alpha]_D^{20}$, ethanol	
					endo	*exo*	**V**	**VII**	**V**	**VII**
0	CH_2Cl_2	BBr_3	0.25	33	99	1	86	87	+29.9	+4.6
10	CH_2Cl_2	BBr_3	0.25	38	98	2	80	81	+28.1	+4.3
20	CH_2Cl_2	BBr_3	0.25	41	96	4	72	74	+25.7	+3.9
40	CH_2Cl_2	BBr_3	0.25	48	94	6	53	55	+18.4	+2.9
60	C_6H_6	BBr_3	0.25	51	93	7	32	34	+11.8	+1.8
80	C_6H_6	BBr_3	0.25	58	92	8	28	29	+9.7	+1.5
40	CH_2Cl_2	$TiCl_4$	0.25	47	93	7	51	52	+17.7	+2.7
40	CH_2Cl_2	$AlCl_3$	0.25	46	93	7	50	51	+17.4	+2.7
40	CH_2Cl_2	$AlCl_3OEt_2$	0.25	44	92	8	49	50	+17	+2.7
40	CH_2Cl_2	BBr_3OEt_2	0.25	45	93	7	50	51	+17.4	+2.7
40	CH_2Cl_2	$AlCl_3$	0.5	47	94	6	51	52	+17.7	+2.7
40	CH_2Cl_2	$AlCl_3$	0.75	49	95	5	53	53	+18.2	+2.8
40	CH_2Cl_2	$AlCl_3$	1	52	96	4	54	53	+18.2	+2.8
40	C_6H_6	$AlCl_3$	0.25	45	93	7	50	51	+17.4	+2.7
40	$C_6H_5CH_3$	$AlCl_3$	0.25	46	94	6	50	51	+17.4	+2.7
40	C_6H_5Cl	$AlCl_3$	0.25	46	94	6	51	51	+17.7	+2.7

Table 2. Properties of the bicyclo[2.2.2]octenes synthesized

Compound	bp, °C/mm Hg, or mp (solvent)	Found, % / Calculated, %		Formula	IR spectrum, ν, cm^{-1}
		C	H		
IV	160–162/2	78.80 / 78.14	10.38 / 10.35	$C_{19}H_{36}O_2$	1730 (C=0), 1110 (C–O), 3030 (=C–H), 1625 (C=C)
V	56–57 (petroleum ether)	71.41 / 71.10	7.10 / 7.0	$C_9H_{12}O_2$	1735 (C=0), 1110 (C–O), 3031 (C=C–H), 1630 (C=C)
VII	75–76/10	77.91 / 78.30	10.31 / 10.4	$C_9H_{14}O$	3550 (O–H), 1625 (C=C), 3030 (=C–H)

The chiral auxiliary agent, menthyl (Ment) residue in adduct **IV**, was removed by base hydrolysis or reduction with $LiAlH_4$.

We examined the effect of the reaction conditions on the total yield, optical purity, and isomeric composition of the products.

Table 1 shows that the total yield of the product increases with temperature, reaching 58% at 80°C in the presence of BBr_3 (molar ratio to dienophile 0.25). At lower temperatures, the enantiomeric purity is higher: At 0°C in the presence of BBr_3 (molar ratio to dienophile 0.25) in CH_2Cl_2 the enantiomeric purity of **VII** reaches 87%. With increasing temperature, the endo selectivity decreases.

Table 1 also shows that the solvent effect on the total and optical yields is insignificant.

Under comparable conditions, different catalysts give similar results as regards the enantioselectivity, stereoselectivity, and total yield. In all the experiments, we obtained, after removing the chiral agent, dextrorotatory products **V**–**VIII**.

The isomeric composition of the adducts was determined by GLC analysis (7% polypropylene sebacate on Poravina). *Endo* and *exo* isomers of **V**–**VIII** were separated chromatographically (Merck Lirchromogorov [Silikat] Si–Go, eluent petroleum ether–ethyl acetate, 1 : 2). Only *endo* isomers **V** and **VII** were collected. The amount of the *exo* isomers was negligible, and they were not further studied in detail. The constants of the compounds prepared are listed in Table 2.

The composition and structure of the compounds were confirmed by elemental analysis and by IR (Table 2) and ^1H NMR spectroscopy.

The IR spectra of **V** and **VI** contain stretching vibration bands of C=O at 1730–1735, C–O at 1110, C=C at 1625–1630, and =C–H at 3030 cm^{-1}. The spectrum of **VII** contains stretching vibration bands of O–H at 3350, C=C at 1625, and =C–H at 3030 cm^{-1}.

In the ^1H NMR spectra of **IV**, **V**, and **VII**, the olefinic protons appear as a multiplet at 6.25–6.27 ppm (J 5.62 Hz); the OH proton in **VII** gives a singlet at 4.0 ppm, and the COOH proton in **V**, a singlet at 12.0 ppm.

The optical yield of **V** and **VII** (%) was determined by comparing their specific rotations with those of the enantiomerically pure samples of the same compounds [3]. THe correlation of the optical rotation sign for the compounds described in [3] allowed us to assign the 2R configuration to dextrorotatory isomers of **V** and **VII**.

EXPERIMENTAL

The IR spectra were measured on a UR-20 spectrophotometer in the range 4000–400 cm^{-1} from thin films or KBr pellets. The ^1H NMR spectra were recorded on a Tesla BS-487C spectrometer (80 MHz, CCl_4, internal reference HMDS). The optical rotation was measured with a Perkin–Elmer-141 polarimeter. Chromatographic analysis of the products and determination of their purity were done on an LKhM-8MD chromatograph equipped with a thermal conductivity detector (300 × 0.3-cm column, 7% polypropylene sebacate on Poravina, carrier gas He, flow rate 40 ml min^{-1}, column temperature 155°C, vaporizer temperature 250°C).

(–)-Menthyl acrylate III was prepared as described in [4]; $[\alpha]_D^{20}$ = –76° (c 4.4, EtOH).

(–)-Menthyl bicyclo[2.2.2]oct-5-ene-2-carboxylate IV. A solution of 1.25 g (0.005 mol) of BBr_3 in 10 ml of CH_2Cl_2 was added at –10°C to a solution of 4.2 g (0.02 mol) of (–)-menthyl acrylate **III** in 15 ml of CH_2Cl_2. Then the temperature was increased to 0°C, and a solution of 1.6 g (0.02 mol) of cyclohexa-1,3-diene **II** in 10 ml of CH_2Cl_2 was added dropwise. The mixture was stirred for 3 h at 0°C, after which it was treated successively with dilute HCl and 5% $NaHCO_3$, washed with distilled water, and dried over $MgSO_4$. The solvent was removed, and the residue was vacuum-distilled. Yield of adduct **IV** 1.914 g (33%), bp 160–162°C (2 mm Hg), $[\alpha]_D^{20}$ (c 0.5, EtOH).

The other experiments on synthesis of **IV** were performed similarly (for specific conditions and results, see Table 1).

(2R)-(+)-Bicyclo[2.2.2]oct-5-ene-5-carboxylic acid V was prepared by base hydrolysis of **IV**. Compound **IV** (5.8 g) was refluxed in 30 ml of a 5% solution of KOH in methanol for 2 h. After removing the solvent, the residue was dissolved in 30 ml of water, and the reaction products were extracted with ether. The aqueous layer was treated with dilute HCl, and the ether extraction was repeated. The extract was washed with water and dried over $MgSO_4$. After removing the solvent, compound **V** was obtained in a yield of 2.77 g, mp 56–57°C (from petroleum ether), $[\alpha]_D^{20}$ = +29.9° (c 0.2, EtOH).

(2R)-(+)-2-Hydroxymethylbicyclo[2.2.2]oct-5-ene VII. A solution of 5.8 g of adduct **IV** in 30 ml of absolute ether was added dropwise to a suspension of 4 g of $LiAlH_4$ in 200 ml of absolute ether. Excess $LiAlH_4$ was decomposed with water. Cooled dilute HCl was added to the resulting mixture, and the ether layer was separated, washed with 5% $NaHCO_3$ and water to neutral reaction, and dried over $MgSO_4$. The solvent was removed, and the residue was vacuum-distilled. Yield of **VII** 2.2 g (88%), bp 75–76°C (10 mm Hg), $[\alpha]_D^{20}$ = +4.6° (c 0.11, EtOH).

CONCLUSIONS

(1) Asymmetric diene synthesis from (–)-menthyl acrylate and cyclohexa-1,3-diene in the presence of achiral catalysts $TiCl_4$, $AlCl_3$, BBr_3, $AlCl_3 \cdot OEt_2$, and $BBr_3 \cdot OEt_2$ yields chiral bicyclo[2.2.2]octenes with the (2R)-(+) configuration.

(2) As temperature is lowered, the optical yield of bicyclo[2.2.2]octenes increases and reaches 87% at 0°C; as temperature is elevated, the total yield increases, and the *endo* selectivity decreases.

(3) The nature of the solvent and catalyst affects the optical and chemical yields of the products insignificantly. As the amount of the catalyst increases, the optical yield varies insignificantly, and the total yield grows.

REFERENCES

1. Potapov, V.M., *Stereokhimiya* (Stereochemistry), Moscow: Khimiya, 1988.
2. Chinchilla, R., Falvello, I.R., Gallindo, N., et al., *Tetrahedron. Asymmetry*, 1999, vol. 10, no. 6, pp. 821–825.
3. Cervinka, O. and Kriz, O., *Coll. Czech. Chem. Commun.*, 1968, vol. 33, pp. 2342–2345.
4. Williamson, K.L. and Li Hsu, Y., *J. Am. Chem. Soc.*, 1970, vol. 92, no. 16, pp. 7386–7389.

ISSN 1070-4272, Russian Journal of Applied Chemistry, 2007, Vol. 80, No. 8, pp. 1379–1383. © Pleiades Publishing, Ltd., 2007.
Original Russian Text © Yu.N. Sazanov, A.V. Gribanov, M.Ya. Goikhman, M.K. Abdulakhatov, S.A. Bartenev, S.A. Strelkov, N.G. Firsin, V.S. Gusel'nikov, 2007, published in Zhurnal Prikladnoi Khimii, 2007, Vol. 80, No. 8, pp. 1341–1345.

MACROMOLECULAR CHEMISTRY AND POLYMERIC MATERIALS

Thermochemical Aspects of Interaction of Polyimide Composites with Organic Sorbents

Yu. N. Sazanov, A. V. Gribanov, M. Ya. Goikhman, M. K. Abdulakhatov, S. A. Bartenev, S. A. Strelkov, N. G. Firsin, and V. S. Gusel'nikov

Institute of Macromolecular Compounds, Russian Academy of Sciences, St. Petersburg, Russia

Khlopin Radium Institute, Research and Production Association, Federal State Unitary Enterprise, St. Petersburg, Russia

Konstantinov Institute of Nuclear Physics, Russian Academy of Sciences, Gatchina, Leningrad oblast, Russia

Received June 7, 2007

Abstract—Interaction of ITA-31 polyimide binder with a series of industrial sorbents based on styrene and vinylpyridine derivatives was studied.

DOI: 10.1134/S107042720708023X

Utilization and disposal of wastes is among the most pressing technological problems. Some kinds of wastes and, in particular, wastes from nuclear power plants and chemical industry are a long-term environmental hazard because of their long half-life or slow degradation under natural conditions. There are many approaches to solving this problem, including immobilization of environmentally significant pollutants and radionuclides using sorbents and porous matrices. The experience gained in using various sorbents [1–6] reveals that among the problems on this way is low resistance of the basic industrial sorbents to many endo- and exogenic factors in long-term storage. In this context, the most important criteria of the applicability of sorbents are chemical and radiation resistance, and the heat resistance as well, stimulating the interest in development of composites based on carbonized heat-resistant polymers and carbonaceous materials [7]. Therefore, a new promising approach is to provide an additional thermal insulation of sorbents through use of heat-resistant binders. To our knowledge, such an approach has not been considered in the literature so far.

This study is a continuation of our previous works on polyimide binders [8] as insulating coatings for industrial sorbents for various pollutants, among them radionuclides.

EXPERIMENTAL

In the experiments, we mostly used VP-1AP anion-exchange resin, which is a modified copolymer of 2-methyl-5-vinylpyridine and divinylbenzene (DVB) as a cross-linking agent. The DVB content of the commercial sorbents ranges from 8 to 12%. Alkylation of this copolymer yields VP-1AP. The latter is a strongly basic resin with quaternary ammonium functional groups. Furthermore, we used in this study such anion-exchange resins as AV-17, ARA-8p, Amberlite IRA-400, and Dowex 1×4, which are also strongly basic resins. They are synthesized on the basis of styrene, trimethylamine, and DVB (4–8%).

As a test nuclide, we used iodine in the form of the iodide anion adsorbed on the resins in the static mode. As a binder, we used ITA-31, a fusible polyimide synthesized from 3,3',4,4'-benzophenonetetracarboxylic acid dianhydride and bis(4-acetylaminophenyl) ether [9].

Composite materials (CMs) were prepared as 2-mm-thick rigid plates on the basis of ELUR reinforcing additive and ITA-31 binder by hot pressing [10]. At a certain stage of molding, a sorbent was added, to make heat-resistance and compatibility tests.

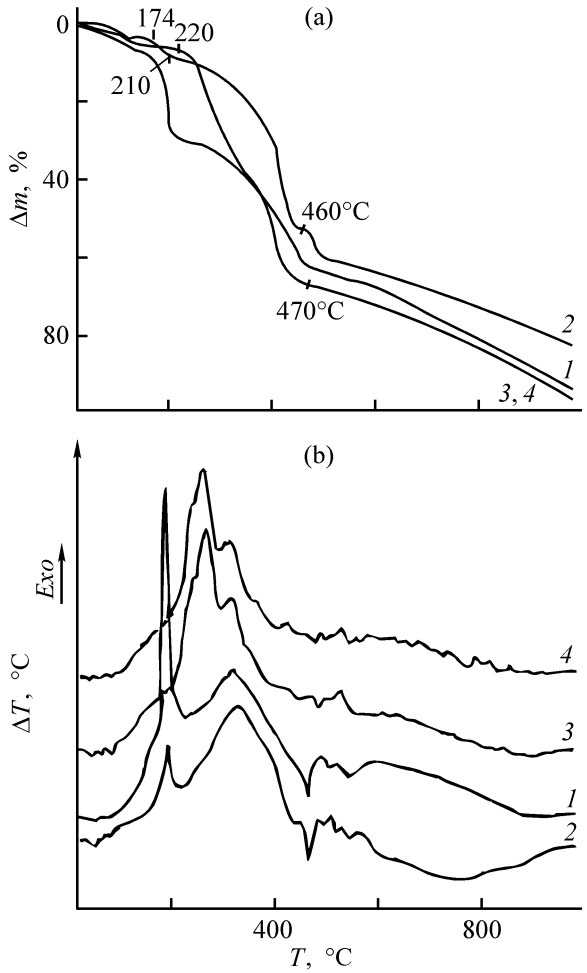

Fig. 1. (a) TG and (b) DTA curves of (*1*, *3*) initial and (*2*, *4*) isothermally heated (150°C, 3 h) sorbents: (*1*, *2*) VP-1AP and (*3*, *4*) AV-17. (Δ*m*) Weight loss and (*T*) temperature; the same for Figs. 2–5.

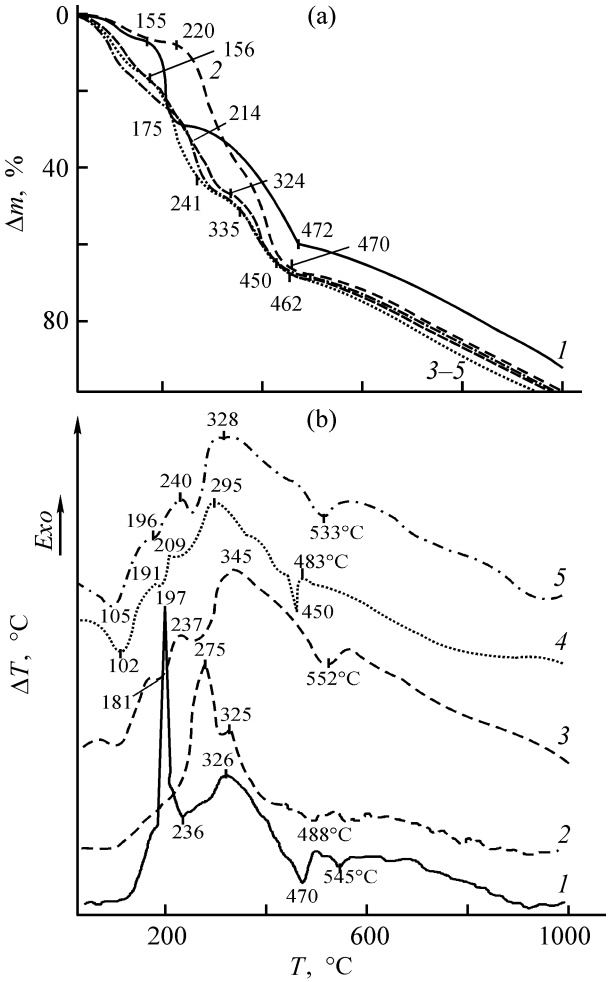

Fig. 2. (a) TG and (b) DTA curves of sorbents in the NO_3^- and OH^- forms: (*1*) VP-1AP (NO_3^-), (*2*) AV-17 (NO_3^-), (*3*) AV-17 (OH^-), (*4*) ANKB-2, and (*5*) Amberlite IRA-400 (OH^-).

We have analyzed the thermochemical transformation of ITA-31 in detail previously [8]. The focus of the present study is how this process is influenced by various anion exchangers added to fix iodine or other model nuclides. Our results demonstrated that, in the course of composite preparation, heating significantly alters the performance characteristics of the sorbents. Figure 1 shows as an example thermograms of the initial and isothermally heated VP-1AP and AV-17. The difference in thermal degradation kinetics between the two samples can be attributed to the cross-linking agent (DVB) content of the resins. For example, on heating to 250°C, VP-1AP decomposes in three stages, and AV-17, in two stages. A considerable difference between these samples was also observed when they were heated at 150°C for 3 h: VP-1AP gradually loses 24% of its weight, and AV-17, 12% of its weight, and this process ceased after 80 min. Comparison of thermal effects (Fig. 1b) accompanying the degradation of these samples shows that isothermal heating of AV-17 does not affect its thermal behavior, while for VP-1AP, thermal stability increases, especially in the initial stage of thermal degradation. Therefore, one may conclude that preliminary thermal analysis of sorbents in the temperature range of formation of the ITA-31-based prepreg allows prediction of the thermal behavior of the initial sorbents and adsorbed pollutants.

Similar experiments with the other sorbents studied showed that the thermal oxidative degradation occurs in several steps, depending on a particular resin. Characteristic features of this process are the effect of counterions and the weight loss dynamics in the course of heating from room temperature to 455–475°C. Over the indicated temperature range, degradation of

the sorbents in the OH form occurs in 3–4 overlapping steps with a weakly pronounced exothermic effect (Fig. 2). For VP-1AP and AV-17 in the nitrate form, there are two clearly pronounced regions of weight loss starting at 155 and 220°C, respectively, and also well distinguished exo effects corresponding to thermal oxidative degradation, which remarkably differs from the behavior of the same sorbents but in the OH form. Evidently, this is due to residual nitric acid, which acts as an additional oxidant for the sorbent at elevated temperatures. Another feature of the thermal behavior of the resins under study is the occurrence of the common to all of them final step in weight loss, which can be attributed to gradual carbonization, typical of carbon-chain polymers. On reaching the carbonization onset temperature, the samples lose about 66–68% of weight, except VP-1AP, for which this value is 58% and the coke number (CN) at 1000°C is 5.4%.

The preparation process of ITA-31 suggests that introduction of any of the anion exchangers studied into the melt involves a certain risk of thermal degradation of the sorbents and, therefore, of release of the compound adsorbed before solidification of the melt. To minimize these effects, it is necessary to optimize the time and concentration conditions of introduction of the sorbent into ITA-31 melt. In this case, the optimal conditions are those providing the required viscosity of the melt without impairing structural stability of the sorbent. Based on an analysis of the thermal characteristics of ITA-31 and sorbents under study, the optimized preparation conditions of ITA-31 melt are as follows: heating at 250–260°C for 10 min followed by introduction of the sorbent (1 : 1 w/w) in 1.5–2 min with stirring. Finally, the resulting mixture is cooled, powdered, and used to prepare a composite material with ELUR as a reinforcing additive [10]. Thermal analysis of CM containing anion exchangers suggests that interaction of VP-1AP with the matrix enhances the heat resistance of the composite. For example, addition of about 25% resin to CM decreases the weight loss by 1% at 300°C, 4.2% at 400°C, 10% at 500°C, 12.6% at 600°C, and 3% at 700°C against the reference sample containing no resin. The effect is leveled off only at 800°C, when the weight losses of both samples become equal (36.6%).

Thus, the resin interacts with the matrix to form a carbonizate, which differs in its heat resistance from the ITA-31 matrix. The TG and DTA curves of ITA-31 and its initial compounds with VP-1AP (Fig. 3), obtained under conditions similar to those in the first stage of composite preparation, suggest that, over

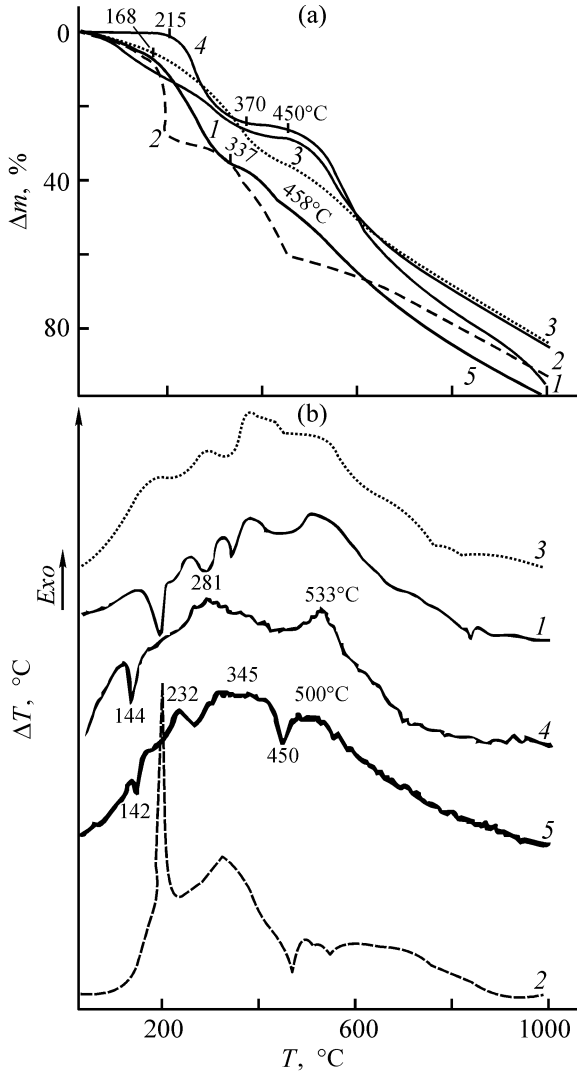

Fig. 3. (a) TG and (b) DTA curves of model mixtures of ITA-31 with various sorbents (1 : 1 w/w): (*1*) ITA-31, (*2*) VP-1AP, (*3*) ITA-31 + VP-1AP, (*4*) initial components of ITA-31, and (*5*) initial components of ITA-31 + VP-1AP.

the temperature range 200–260°C, a thermochemical reaction between ITA-31 and VP-1AP occurs to give a carbonizate differing in its characteristics from the starting components. For example, up to 340°C, the weight loss decreased by 5–12% relative to even ITA-31. At 340–600°C, ITA-31 demonstrates higher heat resistance. The increase in the weight loss can be attributed to the thermal degradation of VP-1AP (its weight loss is about 35% over the same temperature range). However, with further increase in the temperature to above 600°C, the heat resistance of the mixture of ITA-31 with the anion exchanger is higher. In this case, the composite is a new carbonized structure with a coke number of 19% at 1000°C (for ITA-31 CN = 5%). The DTA curves (Fig. 3b) give

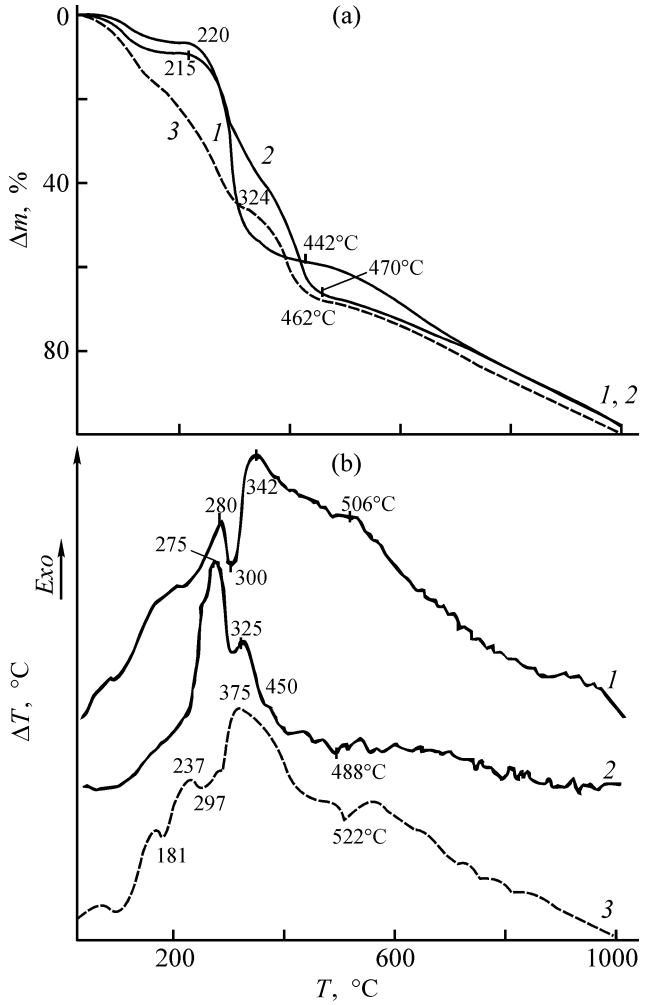

Fig. 4. (a) TG and (b) DTA curves of AV-17 resin in various ionic forms: (*1*) I^-, (*2*) NO_3^-, and (*3*) OH^-.

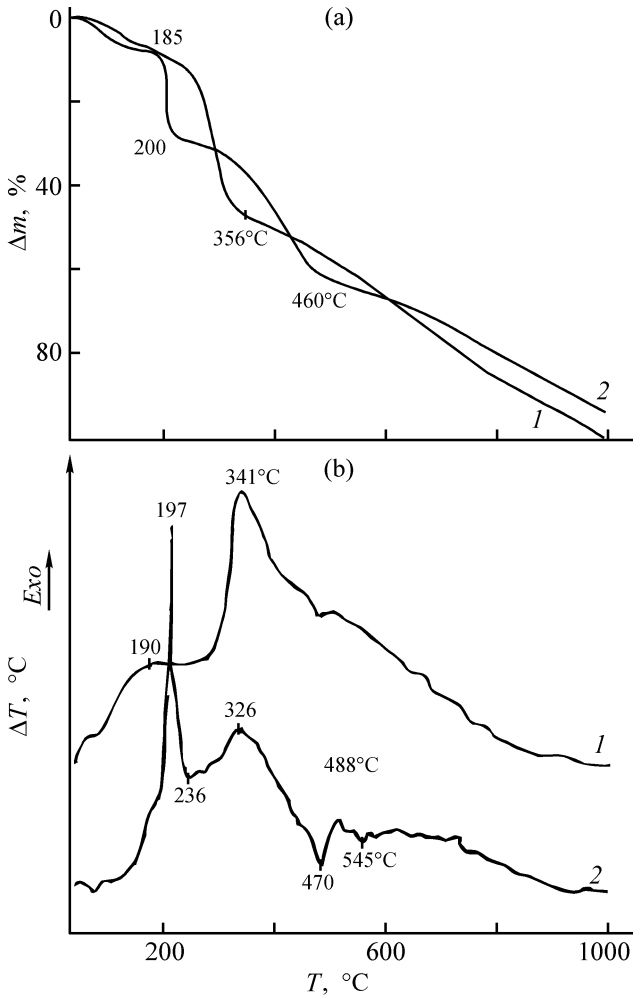

Fig. 5. (a) TG and (b) DTA curves of VP-1AP anion exchanger in various ionic forms: (*1*) I^- and (*2*) NO_3^-.

further evidence in favor of the above concept, by demonstrating thermal effects different from those of the starting components. Thus, thermal analysis of the mixtures of ITA-31 binder with the selected anion exchangers demonstrates the possibility of their use as sorbents working at elevated temperatures.

In further experiments, we examined the effect of a component sorbed on the resin over the temperature range typical of the working conditions of the composite. We selected aqueous potassium iodide as such a component. The procedure of introduction of iodine into the sorbent was designed so as to provide its final content (after all operations including sorption and washing) in the sorbent of about 50% relative to the initial weight of the sample. The thermograms of the resins (VP-1AP, AV-17, Amberlite IRA-400, and Dowex 1×4) containing sorbed iodine showed a remarkable difference from the straight sorbent in the kinetics of weight loss in dynamic heating in air. Comparison of the TG curves of these samples (Figs. 4a, 5a) shows two features. The first is that there is no longer a multistep weight loss over the temperature range (185–215)–(370–420)°C. The second feature is the increase in the weight of the residue, which undergoes 45–60% carbonization with simultaneous decrease in the onset temperature of this process. These features, as well as the thermal effects corresponding to these stages, depend on a particular sorbent.

Therefore, as also in the case of ITA-31, the mechanism of thermal degradation of the sorbents studied changes in the presence of a second component, iodine.

It remains to be understood in what stage of thermal degradation the sorbent releases iodine, in what chemical form iodine is released, and what is the onset temperature of iodine release. Analysis of the ther-

mograms suggests that the major part of iodine is liberated from the sorbent at 320–360°C, the minor part remaining in the carbonizate up to 700°C. More exact data could be obtained by identification and determination of volatile products of carbonization.

Our result that the sorbents studied may be involved in thermochemical reactions with a binder and sorbate allows conclusion about the possibility of modification of ITA-31-based polymeric composites with derivatives of polystyrene and its copolymers. The observed increase in the heat resistance of ITA-31 carbonizates through introduction of anion-exchange resins initiated a further thermochemical study of CMs based on ITA-31 and a reinforcing additive. As reported in [8], the interaction of ITA-31 with ELUR (carbonized PAN fiber) is characterized by the formation of a relatively weak chemical bond, which can be defined as π-electron interaction of the condensed units of ELUR fiber with separate aromatic fragments of carbonized ITA-31. As a result, the CN at 800°C of this composite did not exceed 60%, and the onset temperature of thermal degradation was in the range 280–300°C. Introduction of VP-1AP resin (25% by weight) raised CN to 78%, and the degradation onset temperature, to 420–430°C. Such an effect appeared to be possible due to the first principle of cocarbonization [11]: cocarbonization was carried out in the temperature range in which both ITA-31 and VP-1AP exhibit the highest thermal reactivity, thus providing a preferential cross-linking.

CONCLUSION

In cocarbonization of blends of industrial anion-exchange resins based on modified styrene and ITA-31 fusible polyimide binders, the heat resistance of the resins increases, and the resulting carbonizates are capable of retaining iodine.

ACKNOWLEDGMENTS

The study was financially supported by the International Science and Technology Center (ISTC Project no. 2391).

REFERENCES

1. *Ionnyi obmen v radiokhimii* (Ion Exchange in Radiochemistry), Laskorin, B.N., Ed., Moscow: Atomizdat, 1971.
2. Schaaf, R., *Kernenergie*, 1978, vol. 21, no. 2, pp. 53–56.
3. *Ionity v khimicheskoi technologii* (Ion-Exchange Resins in Chemical Technology), Nikol'skii, B.P. and Romankov, P.G., Eds., Leningrad: Khimiya, 1982.
4. Zemlyanukhin, V.I., Il'enko, E.I., et al., *Radiokhimicheskaya pererabotka yadernogo topliva AES* (Radiochemical Processing of Fuel of Nuclear Power Plants), Moscow: Energoatomizdat, 1983.
5. Bartenev, S.A., Lazarev, L.N., Romanovskii, V.N., et al., Selected Aspects of Safety of Sorption Processes in Nitric Acid Solutions, *Preprint of Khlopin Radium Institute*, 1996, no. 246.
6. Kulyukhin, S.A., Kulemin, V.V., et al., *Radiokhimiya*, 2004, vol. 46, no. 2, pp. 152–154.
7. Ohya, H., Kudryavtsev, V.V., and Semenova, S.I., *Polyimide Membranes: Application, Fabrication, and Properties*, Kodansha: Cordon & Breach., 1996.
8. Gribanov, A.V., Sazanov, Yu.N., Goikhman, M.Ya., et al., *Zh. Prikl. Khim.*, 2000, vol. 73, no. 12, pp. 2002–2006.
9. Goikhman, M.Ya., Svetlichnyi, V.M., Kudryavtsev, V.V., et al., *Zh. Prikl. Khim.*, 1990, vol. 63, no. 1, pp. 168–172.
10. Goykhman, M.Ya., Svetlichnyi, V.M., and Kudryavtsev, V.V., *Acta Montana* (Prague), Ser. B, 1997, no. 7 (105), pp. 9–19.
11. Sazanov, Yu.N. and Gribanov, A.V., *Zh. Prikl. Khim.*, 2006, vol. 79, no. 3, pp. 440–445.

ISSN 1070-4272, Russian Journal of Applied Chemistry, 2007, Vol. 80, No. 8, pp. 1384–1387. © Pleiades Publishing, Ltd., 2007.
Original Russian Text © Yu.N. Pozhidaev, N.S. Shaglaeva, O.V. Lebedeva, S.S. Bochkareva, A.P. Safronov, M.G. Voronkov, 2007, published in Zhurnal Prikladnoi Khimii, 2007, Vol. 80, No. 8, pp. 1346–1349.

MACROMOLECULAR CHEMISTRY AND POLYMERIC MATERIALS

Copolymers Based on Products of Base Hydrolysis of Tetraethoxysilane in the Presence of Poly-*N*-vinylazoles and Polyvinylpyridines

Yu. N. Pozhidaev, N. S. Shaglaeva, O. V. Lebedeva, S. S. Bochkareva, A. P. Safronov, and M. G. Voronkov

Irkutsk State Technical University, Irkutsk, Russia

Favorskii Institute of Chemistry, Siberian Division, Russian Academy of Sciences, Irkutsk, Russia

Received May 2, 2007

Abstract—The products of base hydrolysis of tetraethoxysilane in the presence of polymeric nitrogen bases poly-1-vinylpyrazole, poly-1-vinylimidazole, poly-4-vinylpyridine, and poly-2-methyl-5-vinylpyridine were isolated. The conditions of their formation, chemical composition, structural characteristics, and sorption properties with respect to noble metals (Ag, Au, Pt, and Pd) were studied. These products are highly dispersed thermally stable interpenetrating copolymers poorly soluble in water and organic solvents. Their composition and properties are governed by the kind of the polymeric nitrogen base.

DOI: 10.1134/S1070427207080241

Hybrid organic-inorganic composite materials containing an inorganic component (silicon, titanium, tin, zirconium, or aluminum oxide) chemically bound with an organic component are widely used in various field of science technology. The development of methods for preparing such materials and studies of their properties contribute to the development of chemistry and technology of nanomaterials [1–3].

An actively developing method for preparing hybrid organic-inorganic materials and coatings is based on a sol–gel process involving hydrolysis of alkoxysilanes in the presence of organic compounds [4, 5]. Currently the sol–gel technology is the main technique for purposeful synthesis of hybrid silicate and silica-carbonaceous materials (nanomaterials, coatings, membranes, sorbents, biologically active compounds, catalysts, etc).

It was reported in [6] that, in the first stage of hydrolysis of tetraethoxysilane in ethanol in the presence of polyvinylbutyral, poly-1-vinylimidazole, poly-4-vinylpyridine, or poly-1-vinyl-2-pyrrolidone, a homogeneous solution is formed. In further prolonged storage, these solutions become gelatinous and then solid compounds precipitate. It is believed that the supramolecular structure of these compounds is stabilized by numerous hydrogen bonds between the silanol groups and the electron-donor atoms (N, O) of the organic polymers. The sorption capacity of these materials for Cu^{2+} varies from 25 to 280 mg g^{-1}.

In this study, we isolated highly dispersed hybrid organic–inorganic composite materials by hydrolysis of tetraethoxysilane in the presence of poly-1-vinylazoles and polyvinylpyridines and examined their structural characteristics and thermal and chemical stability. These materials were also tested as sorbents for noble metal ions.

EXPERIMENTAL

1-Vinylpyrazole and 1-vinylimidazole were prepared by the reaction of pyrazole or imidazole with acetylene, as reported in [7, 8].

The commercial monomers 4-vinylpyridine and 2-methyl-5-vinylpyridine were purified by vacuum distillation.

Poly-1-vinylpyrazole (PVPz), poly-1-vinylimidazole (PVIm), poly-4-vinylpyridine (PVPy), and poly-2-methyl-5-vinylpyridine (PMVPy) were prepared by polymerization of the respective monomers by the methods reported in [9, 10].

Table 1. Elemental composition and properties of copolymers formed by hydrolysis of tetraethoxysilane in the presence of polymeric nitrogen bases

Copolymer	Elemental composition, %				Ratio of SiO_2 and nitrogen base units	Yield, %	S_{sp}, $m^2 g^{-1}$	T_{dec}, °C
	C	H	Si	N				
SiO_2 : PVPz	24.69	3.37	25.04	10.96	2.3 : 1	50.7	20.3	250
SiO_2 : PVIm	22.84	2.85	27.13	10.96	2.5 : 1	49.6	10.3	270
SiO_2 : PVPy	36.62	3.45	17.29	6.64	1.3 : 1	69.5	4.9	330
SiO_2 : PMVPy	55.49	6.00	12.81	8.45	0.8 : 1	68.3	33.7	314

The polycondensation of tetraethoxysilane (TES) was carried out in a solution of NaOH in an alcohol-water mixture.

The base hydrolysis of TES in the presence of a polymeric nitrogen base was carried out at room temperature as follows. TES (1.0 g) and 0.1 M aqueous NaOH (2.55 ml) were successively added to a polymeric nitrogen base (0.3 g) dissolved in ethanol (5 ml). On adding aqueous NaOH, the resulting mixture first became turbid and gel-like, and then an insoluble hybrid composite copolymer precipitated. This precipitate was repeatedly washed and then dried in a vacuum desiccator to constant weight.

The elemental analysis of the reaction products was carried out on a Thermo Finnigan gas analyser. The IR spectra (KBr pellets or mulls in mineral oil) were recorded on an IFS-25 spectrometer.

The surface structure of the organic-inorganic copolymers was examined on a Philips-525-M scanning electron microscope.

The specific surface area of these composite materials was measured by a method based on sorption of nitrogen on their surface at various pressures in a graduated high-vacuum unit.

The enthalpy of mixing was measured at 298 K on a Calvet calorimeter equipped with sensitive calorimetric cells (0.032 V W^{-1}). The experimental data were processed with a special software.

The thermogravimetric analysis was carried out on a Paulik–Paulik–Erdey derivatograph (MOM, Hungary) in air at a heating rate of 5 deg min^{-1}. The maximal temperature was 700°C, and the DTA sensitivity, 1/5 to 1/10.

The sorption properties of the composite materials were characterized with respect to Ag(I), Au(III), Pd(II), and Pt(IV) in model solutions of $AgNO_3$, $HAuCl_4 \cdot 4H_2O$, $PdCl_2$, and $H_2PtCl_6 \cdot 6H_2O$ (chemically pure grade) of concentration 0.2–5.0 (mg metal) l^{-1} in distilled water. The metal content of the aqueous phase was determined photometrically with a KFK-2 photocolorimeter [11, 12].

It is known that TES is hydrolyzed in alkaline media containing ethanol, and the hydrolysis products undergo polycondensation to form 3*D* cross-linked hydrated silicon dioxide $[SiO_2 \cdot nH_2O]_m$ of low molecular weight [13]. This product is isolated in the form of amorphous globular particles with the predominant diameter (>80%) of 37–74 nm and specific surface area of 175 $m^2 g^{-1}$.

A base hydrolysis of TES in the presence of poly-1-vinylazoles (PVPz, PVIm) and polyvinylpyridines (PVPy, PMVPy) for several minutes yields glass-like colorless hybrid copolymer precipitates. These products containing Si, N, C, O, and H atoms are thermally stable and poorly soluble in aqueous acids and organic solvents. Their main characteristics are listed in Table 1.

It has been reported [6] that the SiO_2 : nitrogen base units ratio in the composites precipitated in hydrolysis of TES (without base catalysis) in the presence of PVPy and poly-vinyl-2-pyrrolidone is close to 1 : 1, whereas that in the presence of PVIm this ratio is close to 2 : 1. It is believed [6] that this difference is caused by the difference in the basicities of the polymeric nitrogen bases.

In this study, we found no correlations between the hybrid copolymer composition and the basicity (pK^+_{BH}) of the nitrogen heterocycle (pK^+_{BH} of 1-vinylpyrazole, 1-vinylimidazole, 4-vinylpyridine, and 2-methyl-5-vinylpyridine is 1.7, 7.52, 5.62, and 5.67, respectively. In a copolymer prepared by base hydrolysis of TES in the presence of polyvinylpyridine, the ratio of SiO_2 to nitrogen base units is 0.8 : 1 for PVPy and 1.3 : 1 for PMVPy. In the case of copolymers based on TES and polyvinylazoles, this ratio is 2.3 : 1 for PVPz and 2.5 : 1 for PVIm (Table 1).

Table 2. Static sorption capacity SSC and limiting sorption capacity LSC of hybrid copolymers for noble metals and the distribution ratios D of noble metals between copolymers and aqueous solutions

Copolymer	SSC, mg g^{-1} / LSC, mg g^{-1}				D, cm^3 g^{-1}			
	Pd(II)	Pt(IV)	Au(III)	Ag(I)	Pd(II)	Pt(IV)	Au(III)	Ag(I)
SiO_2 : PVPz	139/457	582/840	115/849	273/465	1030	6150	500	28180
SiO_2 : PVIm	182/434	760/799	140/807	70/443	860	20500	1030	500
SiO_2 : PVPy	480/538	704/1010	302/1000	222/548	10660	89000	1430	2060
SiO_2 : PMVPy	370/635	420/1168	110/1180	47/647	1140	2500	980	420

In the system TES-PVPz containing no NaOH, the sol–gel process is complete only in two days, and the SiO_2 : nitrogen base units ratio in the resulting copolymers is close to 1 : 1. Thus, the composition of the hybrid copolymers significantly depends on the rate of base hydrolysis of TES and the latter, in turn, increases with pH [13].

The IR spectra of all the copolymers under consideration contain a strong absorption band (1200–1250 cm^{-1}) typical of the Si–O–Si stretching vibrations. The IR spectra of copolymers of SiO_2 with PVPy and PMVPy contain a shoulder at 1630 cm^{-1}. In the case of copolymers prepared in the presence of PVPz and PVIm, the copolymerization is manifested as a shift of the absorption bands of the azole rings from 1480 to 1520 cm^{-1}. We believe that these changes in the IR spectra of the copolymers obtained in the presence of polymeric nitrogen bases are caused by coordination of the "pyridine" nitrogen atom with the silicon-containing component.

The above hypothesis about chemical interactions between the silicon dioxide and organic components in the copolymers is consistent with the fact that the mixing of silicon dioxide and poly-1-vinylazoles is an exothermic process. The enthalpies of mixing in the systems SiO_2–PVPz and SiO_2–PVIm are –44.3 and –47.9 J g^{-1}, respectively.

The electron micrograph of the hybrid copolymers show that these compounds consist of globules of regular shape with a typical size of about 300 nm. Thus, the particles of hybrid copolymers are coarser than the particles of SiO_2 formed by hydrolysis of tetraethoxysilane in the absence of polymeric nitrogen bases. As can be seen from Table 1, this coarsening of particles causes a decrease in their specific surface area. The copolymers under consideration are multilayer nanoparticles consisting of a core (SiO_2) coated with an organic polymer.

The sorption properties of the copolymers based on PVPz, PVIm, and PVPy were examined for the example of sorption of Ag^+ from solutions of $AgNO_3$ in aqueous nitric acid and of Au(III), Pd(II), and Pt(IV) from their solutions in aqueous hydrochloric acid where these metals are present in the form of anionic complexes $[AuCl_4]^-$, $[PdCl_4]^{2-}$, and $[PtCl_6]^{2-}$ [14, 15]. We found that the degree of sorption recovery of these metals slightly decreases as the HNO_3 and HCl concentration increase from 0.1 to 5.0 M. We believe that this decrease in sorbability is caused by the competitive coordination of HNO_3 and HCl with the nitrogen atom in the pyridine ring of the copolymers. The static sorption capacity of the copolymers for noble metals (SSC) and the distribution ratios of these metals between the copolymers and 1 M aqueous HNO_3 and HCl (D) are listed in Table 2. These data show that the maximal sorbability is exhibited by Pt(IV), which is consistent with the known fact that anionic Pt(IV) chloride complexes are more strongly coordinated with the nitrogen-containing ligands than Ag^+ cations and anionic Au(III) and Pd(II) chloride complexes [14, 15]. It is known that similar correlations are typical of most of complexing sorbents containing nitrogen functional groups [16, 17], including silicon-containing sorbents [18].

In order to estimate the degree of saturation of the nitrogen functional groups of the copolymers with the noble metals in our sorption experiments,

Table 3. Degree of binding of nitrogen functional groups of copolymers with noble metal ions

Copolymer	Pd(II)	Pt(IV)	Au(III)	Ag(I)
	%			
SiO_2 : PVPz	30	69	14	59
SiO_2 : PVIm	42	95	17	16
SiO_2 : PVPy	89	70	30	40
SiO_2 : PMVPy	58	36	9	7

we calculated the limiting sorption capacity LSC of the copolymers for these metals, assuming that one nitrogen base unit of the copolymer coordinates one metal ion. The molecular weight of a structural unit of the copolymers containing one nitrogen functional group was calculated from the elemental composition of the copolymers (Table 1). As can be seen from Table 3, the ratio of SSC and LSC varies from 0.36 to 0.95 for Pt(IV) and from 0.30 to 0.89 for Pd(II). The degree of saturation of the copolymers with Ag(I) and Au(III) in our experiments appears to be appreciably lower.

In sorption of noble metals on the hybrid copolymers from acidic solutions, the protonated nitrogen atoms of the pyrazole, imidazole, and pyridine functional groups are coordinated with both Ag^+ cations and anionic Au(III), Pd(II), and Pt(IV) chloride complexes to form stable solid compounds [19]. The formation of the N–metal coordination bonds in the copolymers saturated with respect to the metals is manifested as new absorption bands (400–300 cm^{-1}).

CONCLUSIONS

(1) In base hydrolysis of tetraethoxysilane in the presence of poly-*N*-vinylazoles and polyvinylpyridine, mixed organic-inorganic copolymers are formed.

(2) The structure of mixed copolymers is built by interpenetration of the networks of hydrated silicon dioxide and polymeric nitrogen bases.

(3) The hybrid copolymers have high thermal and chemical stability, highly dispersed structure, and the developed surface area.

(4) The hybrid copolymers efficiently sorb noble metal ions from acidic solution.

ACKNOWLEDGMENTS

This study was financially supported by the Russian Foundation for Basic Research (project no. 06-08-00317).

REFERENCES

1. Hernandes-Pardon, G., Rojas, F, and Casta, V.M., *Nanotechnology*, 2004, vol. 15, no. 1, pp. 98–103.
2. Kwong, C.Y., Choy, W.C.H., Djurisic, A.B., et al., *Nanotechnology*, 2004, vol. 15, no, 9, pp. 1156–1161.
3. Wang Haitao, Xu Peng, Zhong Wei, et al., *Polym. Degrad. Stab.*, 2005, vol. 87, no. 2, pp. 319–327.
4. Apparicio, M., Lecoq, E., Castro, Y., and Duran, A., *J. Sol–Gel Sci. Technol.*, 2005, vol. 34, no. 3, pp. 233–239.
5. Gigant, K., Posser, U., Schottner, G., et al., *J. Sol–Gel Sci. Technol.*, 2003, vol. 26, no. 1, pp. 369–373.
6. Danilovtseva, E.I., Annenkov, V.V., Filina, E.A., and Trofimov, B.A. *Nauka Proizv.*, 2003, no. 6, p. 44–46.
7. Skvortsova, G.G., Domnina, E.S., Shestova, L.A., et al., *Khim. Geterotsikl. Soedin.*, 1976, no. 9, pp. 1247–1251.
8. Skushnikova, A.I., Domnina, E.S., Pavlova, A.L., and Korotaeva, I.M., *Vysokomol. Soedin., Ser. B*, 1988, vol. 30, no. 7, pp. 537–540.
9. Safronov, A.P., Tager, A.A., Voit, V.V., et al., *Vysokomol. Soedin., Ser. A*, 1988, vol. 30, no. 11, pp. 2360–2364.
10. Fuoss, R.M. and Strauss, V.P., *J. Polym. Sci.*, 1948, vol. 3, no. 1, pp. 246–253.
11. Marczenko, Z., *Kolorymetryczne oznaczanie pierwiastkow*, Warsaw: Naukowa-Techniczne, 1968.
12. *Probootbiranie i analiz blagorodnykh metallov* (Sampling and Analysis of Noble metals), Baryshnikov, I.F., Ed., Moscow: Metallurgiya, 1978.
13. Voronkov, M.G., Mileshkevich, V.P., and Yuzhelevskii, Yu.A., *Siloksanovaya svyaz'. Fizicheskie svoistva i khimicheskie prevrashcheniya* (Siloxane Bond. Physical Features and Chemical Transformations), Novosibirsk: Nauka, 1976.
14. Livingstone, C.E., *The Chemistry of Ruthenium, Rhodium, Palladium, Osmium, Iridium, and Platinum*, Oxford: Pergamon, 1978.
15. Paddephatt, R.I., *The Chemistry of Gold*, Amsterdam: Elsevier, 1982.
16. Myasoedova, G.V. and Savvin, S.B., *Khelatoobrazuyushchie sorbenty* (Chelating Sorbents), Moscow: Nauka, 1984.
17. *Korrelyatsiya i prognozirovanie analiticheskikh svoistv organicheskikh soedinenii* (Correlation and Prediction of Analytical Features of Organic Compounds), Basargin, N.N. and Isaev, E.I., Eds., Moscow: Nauka, 1986.
18. Voronkov, M., Vlasova, N., Pozhidaev, Yu., et al., *Polym. Adv. Technol.*, 2006, vol. 17, pp. 506–511.
19. Saladze, K.M. and Kopylova-Valova, V.D., *Kompleksuyushchie ionity (kompleksity)* (Complexing Ion Exchangers (Complexites)), Moscow: Khimiya, 1980.

ISSN 1070-4272, Russian Journal of Applied Chemistry, 2007, Vol. 80, No. 8, pp. 1388–1393. © Pleiades Publishing, Ltd., 2007.
Original Russian Text © V.F. Kurenkov, A.V. Kurenkov, H.-G. Hartan, F.I. Lobanov, 2007, published in Zhurnal Prikladnoi Khimii, 2007, Vol. 80, No. 8, pp. 1350–1354.

MACROMOLECULAR CHEMISTRY AND POLYMERIC MATERIALS

Copolymerization of Acrylamide with Sodium 2-Acrylamido-2-Methylpropanesulfonate in Aqueous-Alcoholic Solutions

V. F. Kurenkov, A. V. Kurenkov, H.-G. Hartan, and F. I. Lobanov

Kazan State Technological University, Kazan, Tatarstan, Russia
Ashlend Eurasia Joint-Stock Company, Moscow, Russia

Received February 6, 2007

Abstract—The effect of solvents on the kinetics of synthesis and molecular properties of copolymers formed by radical copolymerization of acrylamide with sodium 2-acrylamido-2-methylpropanesulfonate in water and in methanol–water (75 : 25, 50 : 50, 25 : 75), ethanol–water (50 : 50), and isopropanol–water (50 : 50) solutions in the presence of potassium persulfate initiating agent at pH 9 and 60°C was studied.

DOI: 10.1134/S1070427207080253

Water-soluble copolymers of acrylamide (AA) and sodium 2-acrylamido-2-methylpropanesulfonate (Na-AMS) can be used as effective flocculants for water treatment, thickening agents and emulsifiers for drilling, and stabilizing and antistatic agents for photomaterials [1, 2]. Because of a set of valuable properties of these polymers and scarcity of data on their preparation in various media, the development of procedures for direct synthesis of AA–Na-AMS copolymers with various characteristics is of particular importance. As is known [3–5], the reaction kinetics in radical polymerization of water-soluble monomers and properties of the resulting polymers strongly depend on the reaction medium. Hence, synthesis of water-soluble polymers can be efficiently controlled by changing the nature and composition of binary solvents. Previously we have studied copolymerization of AA and Na-AMS in aqueous–salt [5], aqueous–dimethyl sulfoxide [6], and aqueous–ethanol [7] solutions. In this study, we examined the dependences of copolymerization of acrylamide with sodium 2-acrylamido-2-methylpropanesulfonate in water–alcohol (methanol, ethanol, and isopropanol) mixtures, which exhibit different solvating and ionizing powers.

EXPERIMENTAL

2-Acrylamido-2-methylpropanesulfonic acid (H-AMS) was purchased from Lubrizol Corp. (UK) (mp 185°C). It sodium salt was prepared by potentiometric titration of aqueous H-AMS solutions with aqueous solution of NaOH to pH 9. Acrylamide was purchased from Mitsubishi Chem. Ind. Ltd. (Japan) (mp 84.5°C). Before experiments, potassium persulfate (PP) of chemically pure grade was twice recrystallized from aqueous solutions. The content of the main compound, determined by the redox method, was 97.8%. The working solutions were prepared using distilled water and other reagents of chemically pure grade.

Copolymerization was carried out to low conversions ($x < 2.5\%$) in glass dilatometers (8.4 cm^3 volume), and to high conversions in 50 cm^3 glass weighing bottles. Before copolymerization, Na-AMS was dissolved in water or water–alcohol mixture and neutralized with a 20% NaOH solution to pH 9. Then, the required amount of AA was added and the total volume of the reaction mixture was brought to 9.5 cm^3 with distilled water. The aqueous solution of PP (0.5 cm^3) was mixed with the resulting mixture, and finally, an appropriate alcohol (10 ml) was added. Then, the resulting solutions were transferred into a dilatometer or a weighing bottle with a long-needle syringe and heated at 60°C, using an EZE immersion thermostat (Germany). After copolymerization, the resulting polymers were precipitated from aqueous solutions with acetone, filtered off, washed with acetone, and dried to constant weight in a vacuum oven at 50°C.

The yield of the copolymers was determined gravimetrically. The content of ionic units Na-AMS in the copolymer was determined from the content of sulfur [8].

The molecular weight of a copolymer M was determined from the intrinsic viscosity [η], because, according to the Mark-Houwink equation, $[\eta] \approx M$. The intrinsic viscosity [η] of copolymer solutions was measured in a 0.5 M NaCl solution at 30°C, using a VPZh-3 viscometer (d_c = 0.56 mm). Because the kinetic energy correction did not exceed 2% it was disregarded in calculations of the reduced viscosities η_{sp}/c_p, where c_p is the copolymer concentration. The experimental dependence of the reduced viscosity on the copolymer concentration was plotted. Then, using the linear dependence $\eta_{sp}/c_p = f(c_p)$, we determined the intrinsic viscosity:

$$[\eta] = \lim(\eta_{sp}/c_p) \text{ at } c_p \to 0.$$

The kinetic measurements were performed by the dilatometric procedure, and the initial rates of copolymerization (v_0) at small conversions ($x < 3\%$) were calculated. The conversion (%) was calculated from the following expression:

$$x = (\Delta V/VK) \times 100,$$

where ΔV and V (cm^3) are the change in the volume and the initial volume of the reaction mixture at the copolymerization temperature, respectively, and K is the contraction factor at the experimental temperature, which was determined from the composition of the initial monomer mixture from the following equation:

$$K = K_{\text{Na-AMS}} W + K_{\text{AA}}(100 - W)$$

where $K_{\text{Na-AMS}}$ and K_{AA} are the contraction factors for homopolymerization of Na-AMS and AA, respectively, and W is the content of Na-AMS units in the initial monomer mixture.

The values of $K_{\text{Na-AMS}}$ and K_{AA} were calculated as follows:

$$K_{\text{Na-AMS}}(K_{\text{AA}}) = (\rho_p - \rho_m)/\rho_p,$$

where ρ_p and ρ_m are the densities ($g\,cm^{-3}$) of the polymer and monomer, respectively.

In our calculations, the following correction was introduced:

$$K' = K[1 + \alpha_m(T_1 - T_2)],$$

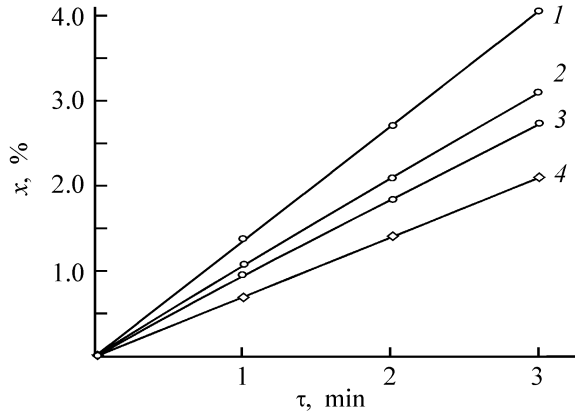

Fig. 1. Initial portions of kinetic curves of copolymerization of AA with Na-AMS v_0 in (*1*) water and (*2–4*) water–methanol mixtures. (x) Conversion and (τ) time. Water : methanol, vol%: (*2*) 75 : 25, (*3*) 50 : 50, and (*4*) 25 : 75; the same for Fig. 6.

where α_m is the volume expansion coefficient, and T_1 and T_2 are the temperatures of the experiment and monomer at filling of the dilatometer, respectively.

$$\alpha_m = (1/V)\,dV/dt,$$

where dV and V are the change in the volume and the initial volume of the reaction mixture, respectively.

The solution acidity was measured with a pH-121 pH-millivoltmeter equipped with an ESL-65-07 working glass electrode and an EVL 1M-3 silver chloride auxiliary electrode.

Copolymerization of AA (M_1) with Na-AMS salts (M_2) was carried out in 20% aqueous–alcoholic solutions of monomers at pH 9 and 60°C in the presence of potassium persulfate initiating agent ([PP] = 7.4×10^{-4} M). A constant pH 9 was maintained in the reaction mixture to provide high initiation efficiency [9] and its independence from the solution ionic strength [10] because of the change in the concentration of Na-AMS in the initial reaction mixture, and to preclude hydrolysis of AA in concentrated aqueous solutions. Copolymerization proceeds under the homogeneous conditions in aqueous–methanol and aqueous–ethanol solutions and under heterogeneous conditions in aqueous isopropanol. In all the cases no spontaneous polymerization was observed.

The reaction rate was monitored by the dilatometric procedure. Typical initial portions of the kinetic copolymerization curves are shown in Fig. 1. As can be seen, the initial portions of the kinetic curves are linear, and we determined from them the initial copolymerization rates v_0 at low conversions ($x < 4\%$).

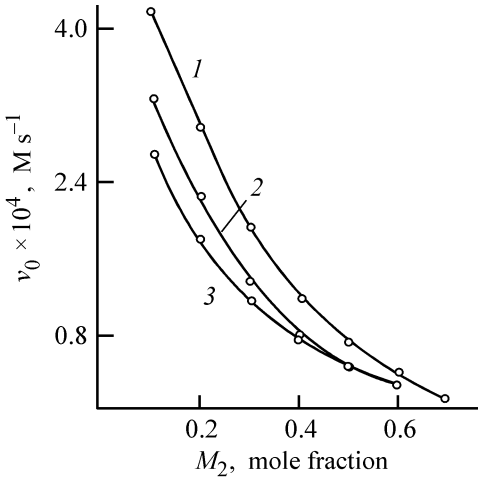

Fig. 2. Initial rate of copolymerization of AA with Na-AMS v_0 in aqueous–alcoholic (50 vol %) solutions vs. the mole fraction of Na-AMS in the initial monomer mixture M_2. Alcohol: (*1*) methanol, (*2*) ethanol, and (*3*) isopropanol; the same for Figs. 3 and 4.

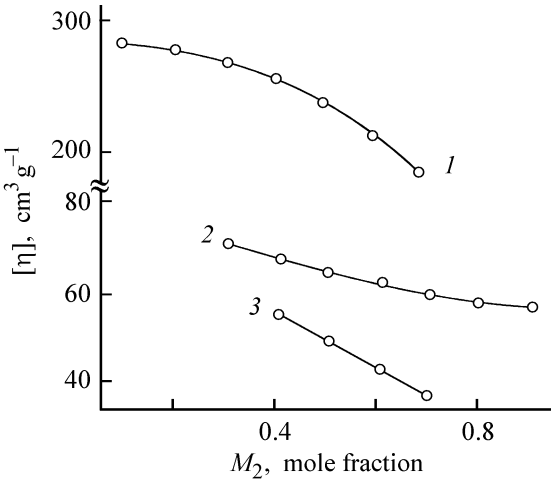

Fig. 3. Intrinsic viscosity of AA–Na-AMS copolymers [η] vs. the mole fraction of Na-AMS in the initial monomer mixture M_2 in copolymerization in aqueous–alcoholic (50 vol %) solutions.

To find out how the composition of the initial monomer mixture affects the features of copolymerization in aqueous-alcoholic solutions, we determined v_0 and [η] (Figs. 2, 3). As can be seen, both v_0 and [η] of the copolymers decrease as the content of Na-AMS in the initial monomer mixture increases, and these dependences are similar for all the binary solvents studied. These data suggest a higher activity of AA in copolymerization as compared to Na-AMS. As can be seen from Fig. 3, copolymers with the highest molecular weights are formed by copolymerization of AA with Na-AMS from the initial monomer mixtures enriched in AA.

Comparison of the above experimental data (Figs. 2, 3) at fixed M_2 shows that v_0 and [η] vary in the following order: water–methanol > water–ethanol > water–isopropanol.

The above-mentioned change in v_0 in the given solvents was promoted by the increase in the viscosity (Table 1) of the initial monomer mixture (at M_2 mole fraction of 0.2, c_p 0.2 g cm^{-3}, and 30°C), which makes weaker the reagent diffusion. Comparison of [η] at M_2 = const (Fig. 3) shows that the molecular weights of the copolymers prepared in water–methanol solutions are an order of magnitude higher than those of the copolymers prepared in water–ethanol and water–isopropanol solutions. This is apparently due to the higher activity of ethanol and isopropanol, compared to methanol, in chain-transfer reactions.

The yields of the copolymers are listed in Table 2. It can be seen that, in all of the systems studied, copolymerization proceeds to high conversions.

Changes in the instantaneous composition of AA–Na-AMS copolymer in the course of copolymerization

Table 1. Parameters of copolymerization of AA with Na-AMS in aqueous–alcoholic (50 vol%) solutions (viscosities of the monomer mixtures were measured at M_2 mole fraction of 0.2, c_p 0.2 g cm^{-3}, and 30°C)

Solvent	Viscosity of the monomer mixture (outflow time, s)	r_1	r_2	Analytical method
Water–methanol	25.2	1.06 ± 0.03	0.94 ± 0.05	Fineman–Ross
		1.08 ± 0.03	0.95 ± 0.05	Kelen–Tudos
Water–ethanol	33.3	1.42 ± 0.01	0.23 ± 0.01	Fineman–Ross
		1.43 ± 0.01	0.23 ± 0.01	Kelen–Tudos
Water–isopropanol	41.7	2.17 ± 0.05	0.01 ± 0.03	Fineman–Ross
		2.18 ± 0.03	0.01 ± 0.03	Kelen–Tudos

Table 2. Yield of AA–Na-AMS copolymers prepared in aqueous–alcoholic (50 vol %) solutions at various compositions of the initial monomer mixture

M_2, mole fraction	Yield, %			M_2, mole fraction	Yield, %		
	water–methanol	water–ethanol	water–isopropanol		water–methanol	water–ethanol	water–isopropanol
0.1	–	45	38	0.4	85	82	40
0.2	–	–	44	0.5	70	68	–
0.3	86	81	–	0.7	74	71	51

in various aqueous-alcoholic solutions (50 vol %) at low conversions ($x < 4$) in relation to the composition of the initial monomer mixture are shown in Fig. 4. It can be seen that, in a wide range of compositions of the initial monomer mixtures in all of the solvents studied, we obtained copolymers enriched in AA units. From the dependences $m_2 = f(M_2)$ (Fig. 4), we estimated the effective relative activities r_1 (AA) and r_2 (Na-AMS):

$$r_1 = k_{11}/k_{12} \text{ and } r_2 = k_{22}/k_{21}.$$

As can be seen from Table 1, the Fineman–Ross and Kelen–Tudos procedures gave consistent values of r_1 and r_2. In all the solutions, $r_1 > r_2$, which confirms the higher reactivity of AA in copolymerization as compared to Na-AMS. Comparison of experimental data in Fig. 4 at M_2 = const shows that the content of Na-AMS units in the copolymer increases in the order water–isopropanol < water–ethanol < water–methanol, which is due to an increase in r_2 and a decrease in r_1. At the same time, the effect of heterogeneity in the water–isopropanol solutions also cannot be ruled out.

In view of the highest v_0 and [η] for the copolymerization in water–methanol (50 vol %) solutions, compared to the other aqueous–alcoholic solutions (Figs. 2, and 3), we examined in more detail the influence exerted by the composition of the water–methanol mixtures on the copolymerization. Figures 1 and 5 show that v_0 and [η] increase with the content of water in water–methanol mixtures. These results agree well with published data on the copolymerization of AA in aqueous-organic solutions [11]. The dependences shown in Fig. 5 are due to an increase in the proton-donor power of the medium with the content of water in water–methanol binary mixtures, which makes higher the concentration of hydrogen bonds between the C=O groups of both monomers and the solvent. In this case, the polarity of the double bond increases, which is confirmed by the spectral

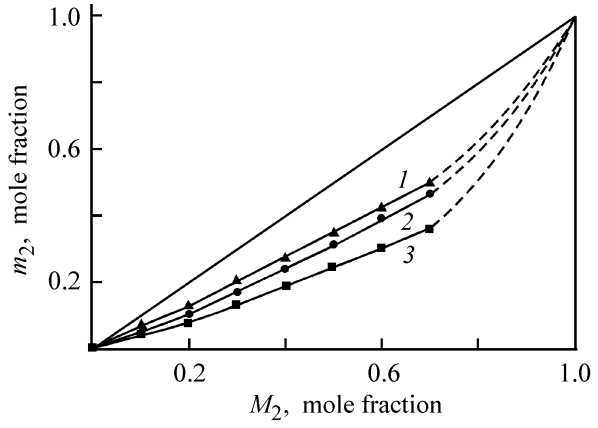

Fig. 4. Mole fraction of Na-AMS units m_2 in the copolymer at low conversions ($x < 4\%$) vs. the mole fraction of Na-AMS in the initial monomer mixture M_2 in copolymerization of AA with Na-AMS in aqueous–alcoholic (50 vol %) solutions.

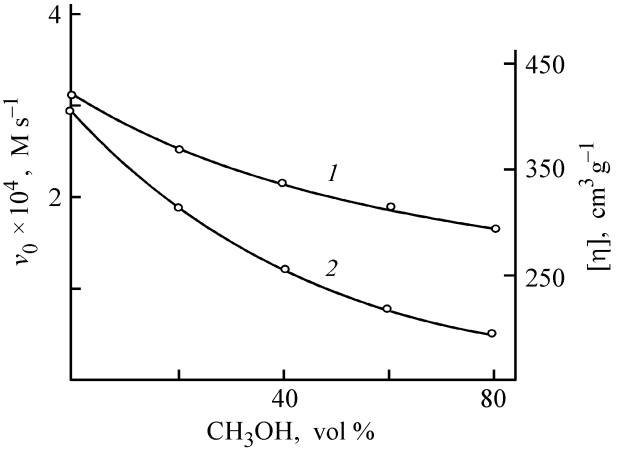

Fig. 5. (*1*) Initial rate of copolymerization v_0 of AA with Na-AMS and (*2*) intrinsic viscosity of copolymers [η] vs. the methanol content in the water–methanol mixture.

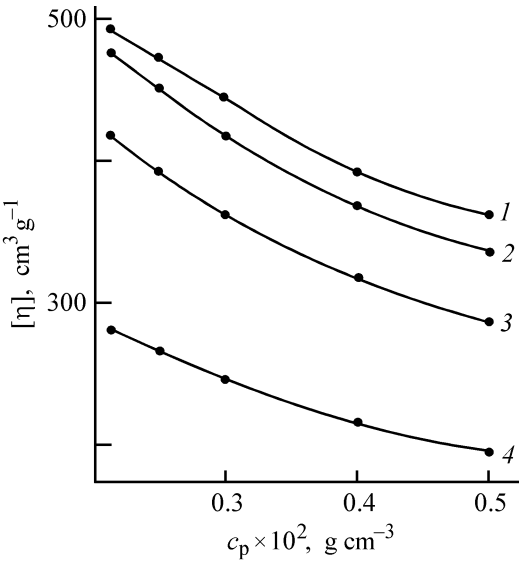

Fig. 6. Reduced viscosity of copolymers η_{sp}/c_p vs. the concentration c_p of copolymer of AA with Na-AMS ([η] 83 cm^3 g^{-1}, content of Na-AMS units 15.9 mol %) in (*1*) and (*2–4*) water–methanol mixtures at 30°C.

data for AA [11]. As a result, the monomer reactivity and v_0 increase.

The decrease in [η] (Fig. 5) with increasing methanol content in the water–methanol mixture can be due to enhanced chain transfer to the methanol molecule because of the presence of labile hydroxyl hydrogen atoms.

On addition of water to methanol, the solution polarity and the degree of ionization of the ionic Na-AMS groups and its units in the macroradicals increase. This alters the conformation state of the propagating chains, which is indirectly confirmed by viscometric data for AA–Na-AMS copolymer in water and in water–alcohol mixtures of various compositions (Fig. 6). As seen, the dependences of η_{sp}/c_p are typical of polyelectrolytes, which suggests a significant role of electrostatic interactions for AA–Na-AMS copolymers in the solvent systems studied. Analysis of experimental data at c_p = const shows that η_{sp}/c_p increases with the content of water in the solvent (Fig. 6, passing from curve *4* to curve *1*). This is due to an increase in the solvent polarity, which makes higher the degree of ionization of the Na-AMS units in the copolymer macromolecules. As a result, the electrostatic repulsion between the sulfate anions along the chain is enhanced, which causes unfolding of the polymer coils and an increase in η_{sp}/c_p. Under the copolymerization conditions studied, the electrostatic repulsion between the uniformly charged Na-AMS monomer and macroradical with the terminal Na-AMS unit increases with the solvent polarity. As a result, the reaction rate constant k_{22} and r_2 decrease in passing from water–methanol (50 vol %, r_2 0.94) to water (r_2 0.11) [6]. We believe that changes in the conformation state of macromolecules and in electrostatic interactions of the reacting units with increasing water content of the water–methanol mixtures also lead to a raised in v_0 in the systems studied.

CONCLUSIONS

(1) Water-soluble high-molecular-weight copolymers of acrylamide and sodium 2-acrylamido-2-methylpropanesulfonate with required properties can be prepared by radical copolymerization in aqueous–alcoholic (alcohol: methanol, ethanol, and isopropanol) solutions.

(2) The initial copolymerization rate and intrinsic viscosity of copolymers increase with the content of acrylamide in the initial monomer mixture and with the water content of the water–methanol mixtures; these quantities decrease in the order water–methanol > water–ethanol > water–isopropanol.

(3) The content of the ionic groups of sodium 2-acrylamido-2-methylpropanesulfonate in the copolymer increases with the content of this salt in the initial monomer mixture and decreases in the order water–methanol > water–ethanol > water–isopropanol, because of a decrease in r_2 (sodium 2-acrylamido-2-methylpropanesulfonate) and an increase in r_1 (acrylamide). In all the aqueous-alcoholic solutions, $r_1 > r_2$.

REFERENCES

1. Lisovtsev, V.V., Rostokin, G.A., and Kulikova, A.E., *Akrilaty i polivinilkhlorid: Obzornaya informatsiya* (Acrylates and Polyvinyl Chloride: Review), Moscow: NIITEKhIM, 1984, pp. 1–20.
2. *2-Acrylamido-2-Methylpropane Sulfonic Acid Monomer*, Wickliffe, Ohio: Lubrizol, 1994, pp. 1–18.
3. Kabanov, V.A. and Topchiev, D.A., *Polimerizatsiya ionizuyushchikhsya monomerov* (Polymerization of Ionizable Monomers), Moscow: Nauka, 1975.
4. Kabanov, V.A., Zubov, V.P., and Semchikov, Yu.D., *Kompleksno-radikal'naya polimerizatsiya* (Coordination Radical Polymerization), Moscow: Khimiya, 1987.
5. Kurenkov, V.F., Antonovich, O.A., and Khusainova, A.F., *Zh. Prikl. Khim.*, 2002, vol. 75, no. 10, pp. 1707–1711.

6. Kurenkov, V.F., Antonovich, O.A., Demina, T.A., and Selezneva, O.Yu., *Vysokomol. Soedin., Ser. A*, 2003, vol. 45, no. 8, pp. 1246–1252.
7. Kurenkov, V.F., Shchekonogova, E.S., Kurenkov, A.V., et al., *Zh. Prikl. Khim.*, 2006, vol. 79, no. 6, pp. 1002–1008.
8. Charlot, G., *Les methods de la chimie analytique. Analyse quantitative minerale*, Paris: Masson, 1961. Translated under the title *Metody analiticheskoi khimii*, Moscow: Khimiya, 1969, pp. 988–989.
9. Kholodnova, L.V., Pavlyuchenko, V.N., Alekseeva, Z.M., and Andreeva, A.I., in *Kataliticheskie i initsiiruyushchie sistemy dlya sinteza i modifikatsii polimerov* (Catalytic and Initiating Systems for Synthesis and Modification of Polymers), Leningrad: Plastpolimer, 1984, pp. 90–104.
10. Kolthoff, I.M. and Miller, I.K., *J. Am. Chem. Soc.*, 1951, vol. 73, no. 7, pp. 3055–3059.
11. Gromov, V.F., Bune, E.V., and Teleshov, E.P., *Usp. Khim.*, 1994, vol. 63, no. 6, p. 530–541.

ISSN 1070-4272, Russian Journal of Applied Chemistry, 2007, Vol. 80, No. 8, pp. 1394–1399. © Pleiades Publishing, Ltd., 2007.
Original Russian Text © A.P. Sivokhin, O.A. Kazantsev, K.V. Shirshin, 2007, published in Zhurnal Prikladnoi Khimii, 2007, Vol. 80, No. 8, pp. 1355–1360.

MACROMOLECULAR CHEMISTRY AND POLYMERIC MATERIALS

Spontaneous Copolymerization of 2-Acrylamido-2-Methylpropanesulfonic Acid with Acrylamide and Acrylonitrile in Concentrated Aqueous Solutions

A. P. Sivokhin, O. A. Kazantsev, and K. V. Shirshin

Nizhni Novgorod State Technical University, Nizhni Novgorod, Russia
Dzerzhinsk Polytechnic Institute, Dzerzhinsk, Nizhni Novgorod oblast, Russia

Received September 26, 2006; in final form, December 2006

Abstract—Spontaneous copolymerization of 2-acrylamido-2-methylpropanesulfonic acid with acrylamide and acrylonitrile in concentrated acidic aqueous solutions was studied.

DOI: 10.1134/S1070427207080265

Copolymers of salts of 2-acrylamido-2-methylpropanesulfo acid (AMPSA) with acrylamide (AA) and acrylonitrile (AN) are well known as promising drilling reagents [1, 2]. One of the procedures used for synthesis of these copolymers is radical polymerization in concentrated aqueous solutions. It has been shown recently that, under certain conditions, AMPSA [3] and AA [4] are capable of spontaneous homopolymerization in highly concentrated aqueous solutions. It was found that spontaneous polymerization of these monomers proceeds only in acidic medium, and, in the presence of sulfuric acid, the initial rate of spontaneous polymerization of AA linearly increases with acidity. For a series of other (meth)acrylic monomers, spontaneous polymerization can proceed in a neutral or weakly alkaline medium; in this case, addition of inhibitors of radical polymerization effectively prevents the process [5]. Based on a comprehensive study of the process [6], we suggested the mechanism of initiation of spontaneous polymerization in aqueous solutions, common to all (meth)acrylic monomers. We believe that, in concentrated aqueous solutions, monomers are associated to form intermediates having orientation of the C=C bonds favorable for polymerization. In these intermediates, radical initiating species are generated by a redox reaction involving anions present in the system and the C=C bonds.

Spontaneous polymerization in binary monomer systems is of interest from theoretical and practical standpoints, but remains poorly studied. There are published data on spontaneous polymerization that occurs in aqueous or alcoholic solutions containing *N*,*N*-dimethylaminoethyl metacrylate in combination with other vinyl monomers. For example, alternating copolymers of the above monomer with 2-methyl-5-vinylpyridine or AA have been prepared [7]. In acid-catalytic initiation in aqueous solution of the same amino ester and AMPSA, the homopolymer of the amino methacrylate is formed and AMPSA molecules only play the role of counterions. This fact is of particular interest since, when taken separately, AMPSA and *N*,*N*-dimethylaminoethyl methacrylate actively spontaneously polymerize in concentrated aqueous solutions under similar conditions [3, 9].

Polymerization in binary aqueous solutions of AMPSA and nonionic acrylic monomers in the absence of initiators has not been studied previously. In this study we examined the products and features of spontaneous copolymerization in the systems AMPSA–AA–H_2O and AMPSA–AN–H_2O.

EXPERIMENTAL

Before use, acrylonitrile was purified by distillation. AA was twice recrystallized from benzene. AMPSA was recrystallized from acetic acid. The copolymerization of AMPSA with AA or AN was performed in water at 50 ± 0.2°C in glass ampules. In all

experiments, including measurements of the solution viscosity, AMPSA was neutralized with sodium hydroxide to 50% (it has been found previously [3] that this degree of neutralization provides the highest rate of spontaneous polymerization of AMPSA). The total initial concentration of the monomers was 1.5–2.5 M. The individual concentrations of monomers in the reaction mixtures were estimated by liquid chromatography (AMPSA and AA) and gas–liquid chromatography (AN). For liquid chromatography, we used a Praha chromatograph equipped with a UV detector (λ = 254 nm) and a 150 × 4.6 mm steel column packed with modified silica gel Silasorb C_{18} (particle size 10 μm); acetonitrile was used as an eluent. The gas–liquid chromatographic measurements were performed on a Tsvet-500 device with flame-ionization detector and a column 2 m long and 3 mm in diameter, packed with 10% PEGA on Chromaton N-AW; the flow rate of carrier gas (nitrogen) was 2×10^{-3} $m^3\,h^{-1}$; vaporizer temperature 70°C, column temperature 40°C. The specific viscosity of aqueous solutions of the monomers was measured at 25 ± 0.1°C in an Ubbelohde viscometer with a capillary diameter of 0.56 mm.

It has been shown previously [3] that spontaneous polymerization of AMPSA and its salts proceeds in aqueous solutions only if the initial concentration of the monomer is no less than 1.0–1.2 M. For individual solutions of AA, polymerization starts in the presence of sulfuric acid (50 mol % relative to amide) at initial concentrations of no less than 2.0–2.2 M. Experiments performed with systems AMPSA–AA–H_2O showed that spontaneous (co)polymerization starts at a noticeable rate at the total concentration of the monomers exceeding 1.2 M (i.e., approximately as in solutions of the sulfonic acid taken separately).

The data on the kinetics of spontaneous homopolymerization of AMPSA and the total consumption of the monomers in the system AMPSA–AA–H_2O are compared in Fig. 1. As can be seen, the polymerization proceeds, upon substitution of AA for a small part of AMPSA at a rate close to the rate of AMPSA homopolymerization, and at a monomer ratio of 1 : 1, the total rate of the process somewhat decreases.

Data on the composition of copolymers prepared at various initial concentrations of the monomers by spontaneous copolymerization in the system AMPSA–AA–H_2O are listed in Table 1. At the concentration of the monomers of 1.5 and 1.75 M, the copolymer is enriched in AA units in the initial steps of the process. With more concentrated solutions, the composition of the copolymer abruptly changes: the content of AA units decreases from 60 to 16%. It should be noted that the trend toward enrichment of the copolymer in sulfonic acid comonomer (though considerably less pronounced) was observed in [10] in copolymerization of the above monomers in the presence of initiators.

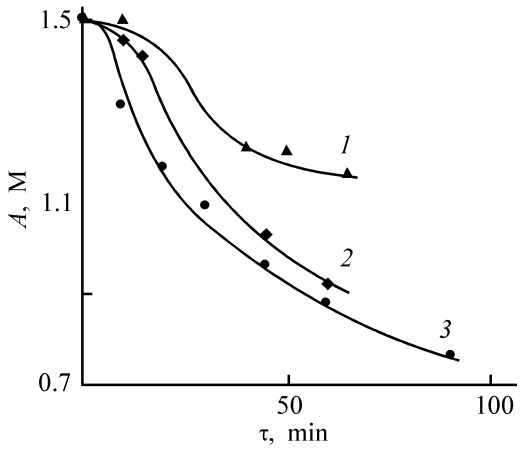

Fig. 1. Total consumption of monomers in the system AMPSA–AA–H_2O. ΣM_0 = 1.5 M, 50°C. (*A*) Total concentration of monomers and (τ) time; the same for Fig. 2. AMPSA : AA: (*1*) 50 : 50, (*2*) 86 : 14, and (*3*) 100 : 0.

Substitution of AN for AA leads to significant changes in the features of spontaneous polymerization. Preliminary experiments showed that, contrary to AA, AN does not polymerize spontaneously within the limits of its solubility. Spontaneous copolymerization in the system AMPSA–AN–H_2O starts only at the total concentration of the monomers exceeding 2.0 M and at a significant excess of the ionic monomer with respect to the nitrile. For example, as

Table 1. Influence of the total concentration of the monomers on the content of AA units in the copolymer ($[AMPSA]_0 : [AA]_0$ = 5 : 5)

Total concentration of monomers, M	Content of AA units in copolymer, mol %, at indicated conversion, %	
	10	20
1.5	60	59
1.75	60	50
2.0	26	42
2.5	16	20

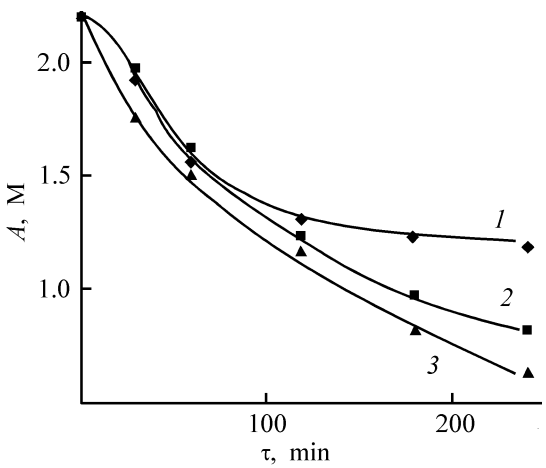

Fig. 2. Total consumption of monomers in the system AMPSA–AN–H_2O. ΣM_0 = 2.2 M, 50°C. AMPSA : AN: (*1*) 86 : 14, (*2*) 90 : 10, and (*3*) 95 : 5.

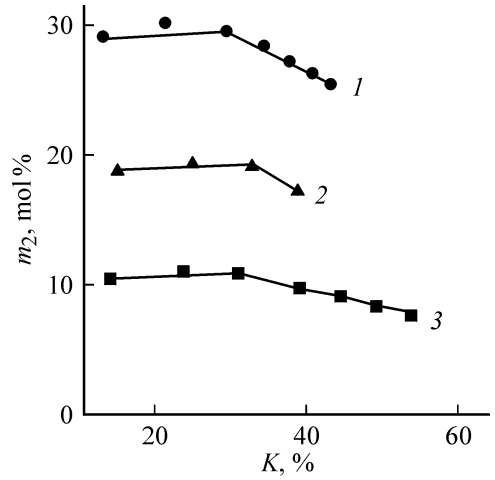

Fig. 3. Content of AN units, m_2, vs. degree of conversion, K in copolymerization of AMPSA with AN. ΣM_0 = 2.19 M, 50°C; the same for Fig. 4. AMPSA : AN: (*1*) 86 : 14, (*2*) 90 : 10, and (*3*) 95 : 5.

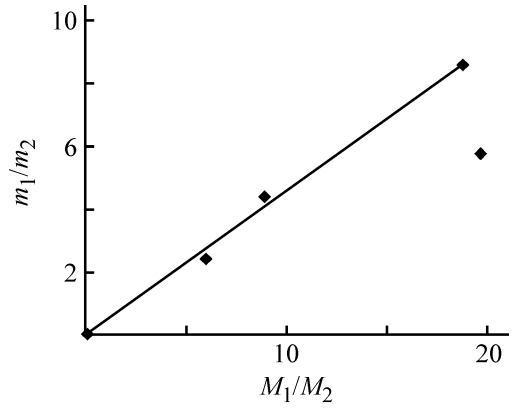

Fig. 4. Ratio of monomer units, m_1/m_2, in AMPSA–AN copolymer vs. the composition of the initial monomer mixture, M_1/M_2.

the content of nitrile increases to more than 15% (at a total concentration of 1.5 M) and to more than 20% (at a total concentration of 2.2 M), spontaneous polymerization does not proceed. Data on the total consumption of the monomers at their same total molar concentration and various ratios are presented in Fig. 2. As can be seen, addition of even a small amount of the nitrile to the AMPSA solution results in a decrease in the total copolymerization rate.

The composition of the AMPSA–AN copolymers obtained at various initial ratios of the monomers is plotted in Fig. 3. It should be noted that the copolymers are enriched in nitrile units and also that the compositions of the products do not vary up to an approximately 30% conversion. Figure 4 shows that the initial ratio of units in the polymers is in direct proportion to the ratio of monomers in the starting mixture; in this case, the coefficient of proportionality is close to 2. Summarizing the experimental results, we can emphasize the following regular trends in spontaneous polymerization in the systems AMPSA–AA–H_2O and AMPSA–AN–H_2O.

(1) Addition of AA to AMPSA solutions does not significantly affect the minimal monomer concentration at which spontaneous polymerization occurs; addition of AN raises this concentration.

(2) As the initial content of AA increases, the rate of the spontaneous process decreases insignificantly; with increasing fraction of the nitrile in the initial mixture, the decrease in the rate is more pronounced (to the point of complete suppression of the reaction).

(3) The degree of enrichment of the resulting polymers in the more active monomer strongly varies with both the total initial concentration of the monomers and their initial ratio.

Because spontaneous homopolymerization is caused by association of monomers [6], we studied, in order to account for the features of spontaneous copolymerization in the systems in hand, the features of intermolecular interactions of the reactants in aqueous solutions. Association processes are usually monitored by viscosimetry, measurements of electrical conductivity and surface tension, as well as by IR and ^{13}C and ^{1}H NMR spectroscopy. In particular, a certain run of the concentration dependences of the solution viscosity can confirm that association occurs in a solution [11].

The viscosity-concentration dependences (VCDs) of aqueous solutions of individual monomers and

their binary mixtures are shown in Figs. 5 and 6. In the range of its solubility in water, acrylonitrile does not tend toward association; this is suggested by the linear shape of curve *2* (Fig. 5a). In the case of acrylamide monomers (AMPSA and AA) capable of formation of stable hydrogen bonds, the specific viscosity of the solution increases with the concentration, which suggests aggregation of the monomers. As can be seen from the curves shown in Figs. 5a and 5b, AMPSA is a more actively associating agent than AA. In addition, the VCDs of these monomers, plotted on an enlarged scale show clearly pronounced bends between virtually linear portions. These inflections are observed for AA at concentrations of 6, 22, and 32% (Fig. 5a, curve *1*), and in the case of AMPSA, at 4, 10, 16, 22, and 26% (Fig. 5b). According to [12], the bends in the VCD curves are caused by transformation of the associates formed. Spontaneous polymerization of AA starts in the concentration range between the first and second bends, and, in the case of AMPSA, between the third and fifth bends. This is apparently caused by the fact that only definite structures of associates are favorable for spontaneous polymerization.

To study the binary association of the monomers, we recorded VCDs of aqueous solutions of monomer pairs. As can be seen from Fig. 6 (curves *1*, *2*), the viscosity increases more intensively on adding AN to an AMPSA solution; in this case, it starts at lower concentrations than that in the corresponding individual solution of sulfonic acid (although at the same total concentration of the monomers in the binary system the viscosities are somewhat lower, compared to the AMPSA solutions). Thus, AA molecules can be involved in AMPSA associates, laregly preserving their structuring. This fact, apparently, explains why addition of AA does not decrease the initial concentration of spontaneous polymerization.

By contrast, addition of even a small amount of AN to the AMPSA solution decreases the specific viscosity of the solution (Fig. 6, curves *2*, *3*), which is apparently caused by destabilization of sulfonic acid associates with nitrile molecules. Hydrophobic molecules of AN should tend to pass into fairly hydrophobic amide associates; however, in this case, nitrile molecules having no labile protons are not bound by strong bonds to amide molecules. This should result in a distortion of the ordered structure of AMPSA associates, causing difficulty in initiation of spontaneous polymerization (especially at a relatively high content of AN in the initial mixture).

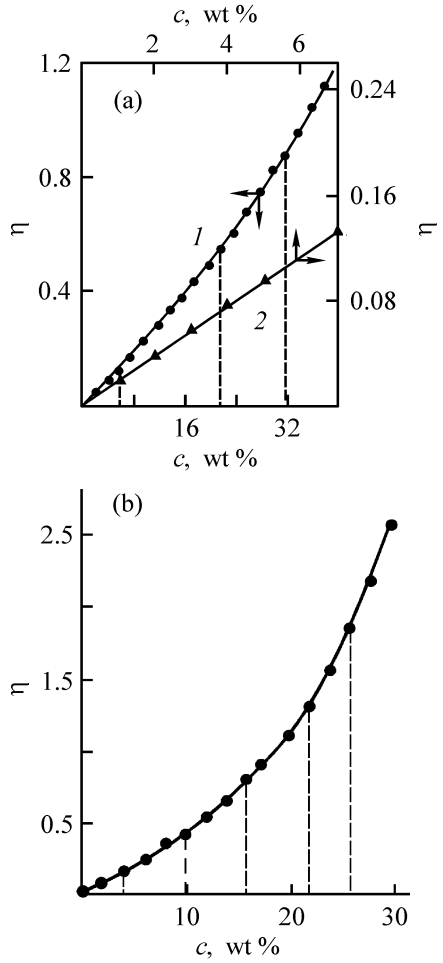

Fig. 5. Specific viscosity η of aqueous solutions of (a) (*1*) AA and (*2*) AN, and (b) Na-AMPSA vs. concentration of monomers *c* at 25°C.

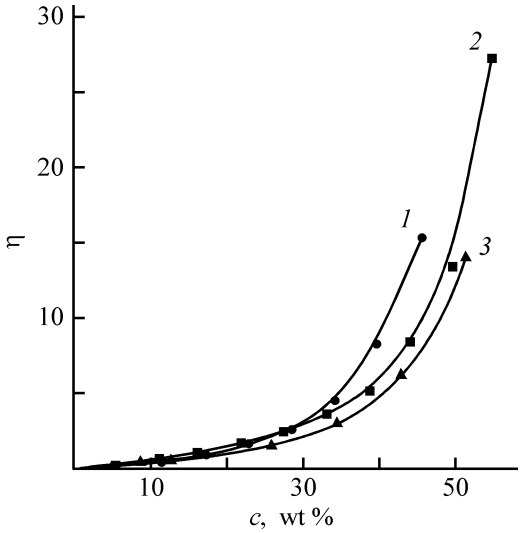

Fig. 6. Specific viscosity η of aqueous solutions of (*1*) Na-AMPSA : AA = 5 : 5, (*2*) Na-AMPSA, and (*3*) Na-AMPSA : AN = 7.5 : 2.5 vs. AMPSA concentration *c* at 25°C.

Table 2. Signals of the sulfonic monomer in the ^{1}H NMR spectrum of solutions of Na-AMPSA in D_2O

$\overset{1a-1f}{CH_2}=\overset{2a,b}{CH}CONH\overset{3}{C}(CH_3)_2\overset{4}{C}H_2SO_3^-Na^+$

Signal	[Na-AMPSA] = 11 wt %		[Na-AMPSA] = 30 wt %	
	δ, ppm	halfwidth, Hz	δ, ppm	halfwidth, Hz
1a	6.13	2.51	6.26	3.69
1b	6.10	3.15	6.23	4.59
1c	6.08	2.20	6.21	3.58
1d	6.04	2.26	6.17	3.57
1e	6.00	3.81	6.13	4.29
1f	5.94	3.81	6.07	4.71
2a	5.55	3.78	5.68	4.54
2b	5.52	3.88	5.65	4.36
3	1.35	2.57	1.48	3.79
4	3.28	2.40	3.39	3.65

Table 3. Signals in the ^{1}H NMR spectrum of solutions of Na-AMPSA and AN* in D_2O

$\overset{1a-1f}{CH_2}=\overset{2a,b}{CH}CONH\overset{3}{C}(CH_3)_2\overset{4}{C}H_2SO_3^-Na^+$

Signal	[Na-AMPSA] = 11 wt %		[Na-AMPSA] = 30 wt %	
	δ, ppm	halfwidth, Hz	δ, ppm	halfwidth, Hz
1a	6.19	2.58	6.28	2.31
1b	–	–	6.24	–
1c	6.13	2.66	6.23	2.15
1d	6.10	–	6.19	2.24
1e	6.06	3.97	6.15	3.67
1f	6.00	3.76	6.10	3.70
2a	5.61	3.77	5.70	3.75
2b	5.58	3.88	5.67	3.64
3	1.41	2.78	1.50	2.59
4	3.31	2.58	3.40	2.57

* [AN] = 2.65 wt %.

Similar conclusions can be made from the ^{1}H NMR spectra. According to the data in Table 2, the ^{1}H NMR signals of Na-AMPSA are shifted downfield and broadened as the concentration of the monomer increases. Previously [13], similar trends have been attributed to a decrease in the molecular mobility in a study of the influence of polymer additions on the association of surfactant monomers. The decrease in the mobility can be caused by packing of molecules in an associate, displacement of water molecules from it, and, the resulting increase in its hydrophobicity. It is of interest that, on adding AN to a dilute aqueous solution of Na-AMPSA, the position and halfwidth of the ^{1}H NMR signals of the sulfonic acid do not change noticeably, i.e., the nitrile does not exert under these conditions a significant effect on associates of sulfonic acid monomer (they are insufficiently hydrophobic, and AN molecules do not pass into the area of these hydrophilic associates).

In more concentrated solutions of Na-AMPSA, when, according to viscometric data, the viscosity of the monomer solution significantly increases (Fig. 5), addition of AN results in a significant decrease in the halfwidths of the ^{1}H NMR signals of Na-AMPSA; in this case, their values become close to those in dilute solutions of the sulfonic acid (Table 3). These data confirm the assumption that, in rather concentrated solutions, nitrile molecules can penetrate into associates of sulfonic acid and "loosen" them. In this case, introduction of AN into Na-AMPSA associates is accompanied by only insignificant variations of the characteristic signals of nitrile (small downfield shift of ^{1}H NMR signals and narrowing of these signals).

Thus, the results of a viscometric analysis and NMR study allow explanation of the experimental data on spontaneous polymerization in the systems AMPSA–AA–H_2O and AMPSA–AN–H_2O. First, the close correlation between spontaneous polymerization of the monomers and their association is confirmed. Second, the resulting polymers are enriched in that monomer which shows under these conditions a stronger tendency to be incorporated into associates. This tendency is caused by both the capability of the monomers for self-aggregation and their hydrophobicity (more hydrophobic monomers should show stronger tendency to pass into the arising associates).

In spontaneous copolymerization of AMPSA and AN in concentrated solutions, more hydrophobic molecules of AN actively pass into hydrophobic areas of associates formed by AMPSA molecules. As a result, the local concentration of nitrile in an associate becomes higher than its average concentration and exceeds the fraction of associated AMPSA molecules. Because polymerization occurs more readily in associates, the copolymer is enriched in AN units. In solutions of AA and AMPSA, binary associates are formed even in rather dilute solutions due to a strong tendency of both monomers toward association. However, they do not involve significant fraction of the initial comonomers; therefore, the polymer is enriched with more mobile and active AA molecules. In going to more concentrated solutions, the fraction of associated

molecules significantly increases; specifically, these molecules are predominantly incorporated into the copolymers at low and moderate degrees of conversion. Furthermore, in going to higher concentrations, the associates become more hydrophobic; therefore, the content of the more hydrophobic monomer (AMPSA) in the associates increases and, correspondingly, the fraction of its units in the polymer molecules grows.

CONCLUSIONS

(1) The possibility and rate of spontaneous polymerization, and also the composition of products formed in the systems 2-acrylamido-2-methylpropanesulfonic acid–acrylamide–water and 2-acrylamido-2-methylpropanesulfonic acid–acrylonitrile–water are governed by binary association of monomers.

(2) In the system 2-acrylamido-2-methylpropanesulfonic acid–acrylamide–water, polymerization proceeds at a concentration of monomers exceeding 1.2 M; in this case, the copolymer composition depends essentially on the total initial concentration of monomers: its increase results in a relative enrichment of the product in units of sulfonic acid monomer.

(3) In the system 2-acrylamido-2-methylpropanesulfonic acid–acrylonitrile–water, polymerization starts only at a low content of the nitrile and concentration of the monomers exceeding 2.0 M, and the resulting copolymers are enriched in acrylonitrile units.

REFERENCES

1. Lisovtsev, V.V., Rostokin, G.A., and Kulikova, A.E., in *Khimicheskaya promyshlennost': Akrilaty i polivinilkhlorid* (Chemical Industry: Acrylates and Polyvinyl Chloride), Moscow: NIITEKhim, 1984, pp. 1–20.
2. Maier, Zh.A., Synthesis and Characteristics of Copolymers of Sulfo Amido Acids with Acrylamide and Acrylonitrile as Versatile Stabilizing Agents of Bentonite Dispersions, *Cand. Sci. Dissertation*, Yaroslavl, 1998.
3. Kazantsev, O.A., Igolkin, A.V., Shirshin, K.V., et al., *Zh. Prikl. Khim.*, 2002, vol. 75, no. 3, pp. 476–480.
4. Kurlyankina, V.I., Ushakova, I.L., Molotkov, V.A., and Boldyreva, A.G., *Zh. Obshch. Khim.*, 1999, vol. 69, no. 1, pp. 97–100.
5. Kazantsev, O.A., Shirshin, K.V., Sivokhin, A.P., et al., *Zh. Prikl. Khim.*, 2004, vol. 77, no. 2, pp. 306–309.
6. Kazantsev, O.A. and Shirshin, K.V., *Polymer*, 2004, vol. 45, pp. 5021–5029.
7. Kaprielova, G.V. and Dzhalilov, A.T., *Izv. Vyssh. Uchebn. Zaved., Khim. Khim. Tekhnol.*, 1984, vol. 27, no. 12, pp. 1503–1505.
8. Valueva, S.V., Kipper, A.I., Rumyantseva, N.V., et al., *Zh. Prikl. Khim.*, 2000, vol. 73, no. 11, pp. 1883–1885.
9. Kazantsev, O.A., Kuznetsova, N.A., Shirshin, K.V., et al., *Vysokomol. Soedin., Ser. A*, 2003, vol. 45, no. 4, pp. 572–580.
10. Kurenkov, V.F. and Utikeeva, A.R., *Vysokomol. Soedin., Ser. A*, 2000, vol. 42, no. 4, pp. 587–593.
11. *Rastvoritel' kak sredstvo upravleniya khimicheskim protsessom* (Solvent as a Tool for Controlling a Chemical Process), Fialkov, Yu.Ya., Ed., Leningrad: Khimiya, 1990.
12. Batrakova, E.V., Orlov, Yu.N., Egorov, V.V., et al., *Vysokomol. Soedin., Ser. B*, 1985, vol. 27, no. 2, pp. 87–93.
13. Egorov, V.V., Ksenofontova, O.B., and Batrakova, E.V., *Kolloidn. Zh.*, 1991, vol. 53, no. 2, pp. 351–356.

ISSN 1070-4272, Russian Journal of Applied Chemistry, 2007, Vol. 80, No. 8, pp. 1400–1403. © Pleiades Publishing, Ltd., 2007.
Original Russian Text © E.N. Girfanova, S.E. Mitrofanova, E.N. Cherezova, 2007, published in Zhurnal Prikladnoi Khimii, 2007, Vol. 80, No. 8, pp. 1361–1364.

MACROMOLECULAR CHEMISTRY AND POLYMERIC MATERIALS

Performance of Polyfunctional Organic Additives Based on a Polyether

E. N. Girfanova, S. E. Mitrofanova, and E. N. Cherezova

Kazan State Technological University, Kazan, Tatarstan, Russia

Received November 27, 2006; in final form, February 2007

Abstract—The plasticizing and stabilizing power of new oligomeric additives containing sulfide, hydrosulfide, and sterically hindered phenolic groups was examined.

DOI: 10.1134/S1070427207080277

As a rule, polymers are not used without special additives increasing their storage and service life (stabilizers) and allowing processing under milder conditions (plasticizers).

In particular, polyvinyl chloride (PVC) cannot be molded without adding a plasticizer and is not used without stabilizers because of the poor resistance to oxygen and elevated temperatures [1].

The most widely used plasticizers for PVC are polyesters and, in particular, dioctyl phthalate (DOP) and dioctyl sebacate (DOS) [2]. However, low-molecular-weight additives show tendency toward volatilization and washout from the polymer. Polymeric stabilizers are free of these drawbacks, but, in this case, the effect of the functional groups is lower [3]. Apparently, use of oligomeric stabilizers would be the best solution.

To this end, we developed a procedure for preparing potential polyfunctional stabilizers based on an oligomeric sulfur-containing polyether [4]. The molecules of these additives contain sterically hindered phenolic (SHP) fragments scavenging peroxy radicals, which are primary products of polymer oxidation. Furthermore, they contain sulfide and hydrosulfide groups catalyzing the decomposition of hydroperoxides formed in the course of further oxidation. The polar ether bonds present in the additives may impart to them the plasticizing properties [5].

In this study, we examined the stabilizing and plasticizing performance of the new oligomeric additives with respect to PVC.

EXPERIMENTAL

In the experiments, we used suspension PVC of the S-7058-M brand and 4-dimethylaminomethyl-2,6-di-*tert*-butylphenol (Mannich's base, MB), mp 93–95°C.

Oligomeric additives were prepared from Laprol 373 commercial oligoether [TU (Technical Specification) 6-05-2042–87] [6]. Sulfur-containing Laprol with SH terminal groups (T-L-F) was prepared as follows: A flask equipped with a stirrer, reflux condenser, and thermometer was charged with chlorinated Laprol, prescribed amount of ethanol, sodium hydrogen sulfide, and formal. The mixture was stirred at 90–100°C for 4 h. The reaction progress was monitored by variation of the pH of the medium (≥9). After the reaction completion, the mixture was cooled to 30°C and excess NaSH was neutralized with orthophosphoric acid (to pH 5.5–6.5). A synthesis without formal (product T-L) was performed similarly. Polyfunctional additives with SHP fragments were prepared by reactions of T-L and T-L-F with MB. For this purpose, a flask equipped with a stirrer, reflux condenser, thermometer, and bubbler was charged with the sulfur-containing oligomers and with a calculated amount of MB (corresponding to the prescribed conversion of the SH groups of the oligomer). The mixture was stirred at 100–120°C in a nitrogen flow for 3–3.5 h. The reaction progress was monitored by the release of dimethylamine, which was absorbed by 0.1 N H_2SO_4 (with Methyl Orange as indicator). When the release of dimethylamine ceased, the reaction was considered to be complete.

The structures of the products can be schematically shown as follows:

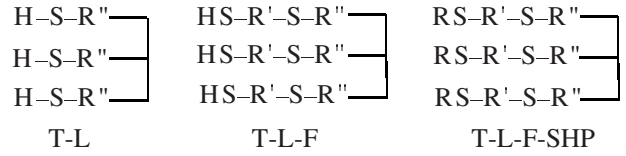

T-L T-L-F T-L-F-SHP

where R' = $CH_2CH_2OCH_2OCH_2CH_2$; R" = $[CH_2CH_2(CH_3)]_n$; R = H, 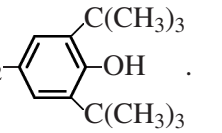 .

The physicochemical characteristics of the products are listed in Table 1.

The content (wt %) of SH groups was determined by a laboratory procedure according to GOST (State Standard) 12812–80, and the total sulfur content, according to [7].

The kinetics of the hydroperoxide (HP) decomposition in the presence of the synthesized sulfur-containing compounds was monitored by iodometric titration. The reaction was performed in isopropanol at 90–95°C, with ethylbenzene hydroperoxide (EBHP) as example [8]. The stoichiometry of HP consumption ν was determined at an HP concentration of 0.2–0.25 M and the additive concentration ranging from 1×10^{-3} to 1×10^{-4} M. The coefficient ν was calculated by the formula

$$\nu = ([ROOH]_0 - [ROOH]_\infty)/[InH]_0,$$

where $[ROOH]_0$ and $[ROOH]_\infty$ are the initial and final concentrations of EBHP, respectively, and $[InH]_0$ is the initial inhibitor concentration.

The resistance of PVC to thermal oxidation was evaluated as the time until the onset of the polymer dehydrohalogenation, according to GOST 14041–91 (ISO 182/1–90). PVC samples to be tested were prepared as 0.1–0.2-mm-thick films on a K-403 laboratory microroller at 160°C (rolling time 15 min).

The oxidation temperature and weight loss by the polymer were determined by differential thermal and thermal gravimetric analyses with an MOM derivatograph (Hungary) at a heating rate of 5 deg min^{-1}.

The glass transition point of the PVC material was determined thermomechanically with a Hoeppler consistometer at a heating rate of 2 deg min^{-1} and a cantilever load of 50 g. Samples were prepared as pellets 5 mm high and 5 mm in diameter, using an electrically heated hydraulic press (GOST 12019–66). The pressing was performed at 180°C for 20 min. The minimal press force was 1 MN, and the plate size, 600 × 600 × 36 mm. The mold was cooled under pressure.

Table 1. Characteristics of the oligomeric additives derived from Laprol 373 and containing sulfide (–S–), hydrosulfide (–SH), and sterically hindered phenolic fragments

Additive	Content, wt %			
	SH groups		sulfur	
	calculated	found	calculated	found
T-L	7.28	7.20	7.08	7.27
T-L-F	6.20	6.60	12.00	12.50
T-L-SHP^*_{25}	4.95	4.50	4.70	4.40
T-L-SHP^*_{100}	0.00	0.00	3.60	3.50
T-L-F-SHP^*_{25}	4.65	4.80	8.93	8.76
T-L-F-SHP^*_{100}	0.00	0.03	6.00	5.80

* Conversion of SH groups, 25 and 100%, respectively.

The oxidation of carrbon-chain polymers occurs as a chain reaction involving alkyl and peroxy radicals in the chain propagation steps [9]. The main agent branching the oxidation chain is HP; therefore, obtaining quantitative characteristics of the HP decomposition in the presence of an antioxidant is an important criterion in evaluating the stabilizing power of additives. As already noted, decomposition of HP can be catalyzed by compounds containing sulfur atoms [10]. The products prepared contain both sulfide and hydrosulfide groups.

Figure 1 shows the experimental data on the EBHP decomposition in the presence of the oligomeric addi-

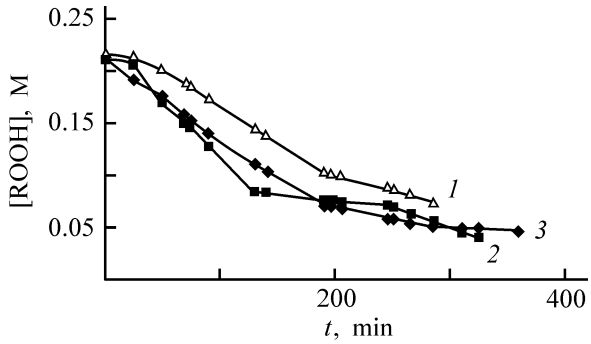

Fig. 1. Kinetic curves of EBHP decomposition in the presence of the additives prepared. 90–95°C, isopropanol. ([ROOH]) EBHP concentration and (*t*) time. Additive, M: (*1*) 5.62×10^{-3} T-L-F, (*2*) 5.64×10^{-3} T-L, and (*3*) 1.05×10^{-3} T-L-F-SHP_{100}.

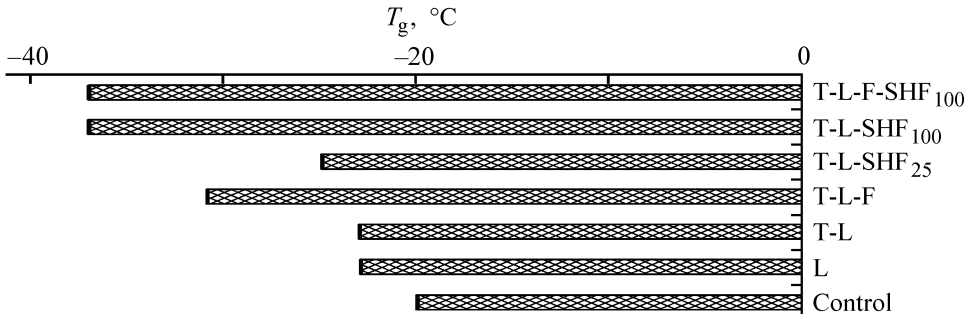

Fig. 2. Influence of the type of the additive on the glass transition point of PVC films, T_g.

Table 2. Stoichiometric coefficients of EBHP decomposition (90–95°C, isopropanol, [EBHP] = 2×10^{-2} M)

Additive	Stoichiometric coefficient	Concentration of additive, $c_{AO} \times 10^3$, M
T-L	30	5.64
T-L-F	67	5.62
T-L-F-SHP$_{100}$	154	1.05

Table 3. Time τ until the onset of dehydrochlorination of samples of PVC resin and PVC material stabilized with the additives synthesized (170°C, air)

Additive	τ, min	
	PVC resin*	PVC material**
L	6	60
T-L	8	84
T-L-F	13	100
T-L-SHP$_{25}$	8	68
T-L-SHP$_{100}$	9	70
T-L-F-SHP$_{25}$	10	73
T-L-F-SHP$_{100}$	12	84

* Formulation, wt proportion: PVC 100 and additive 10.

** Formulation, wt proportion: PVC 100, dioctyl phthalate (GOST 8728–88) 91.8, additive 8.2, calcium stearate (TU 6-09-17-317–96) 1, zinc stearate (TU 6-09-17-316–96) 1, and ED-20 epoxy resin (GOST 12844–74) 2.

Table 4. Effect of polyfunctional additives on the heat resistance of PVC compounds

Additive	Degradation parameters			
	T_o, °C	T of indicated weight loss, °C		
		5%	10%	50%
None (control)	243	243	257	289
T-L	257	257	260	287
T-L-F	263	263	264	292
T-L-SHP$_{25}$	262	262	265	293

* Formulation, wt proportion: PVC 100, DOP 91.8, and additive 8.2.

tives synthesized. The sulfur-containing oligomers without SHP fragment (T-L, T-L-F) show an induction period before the onset of EBHP decomposition. Introduction of the SHP fragment eliminates the induction period of the HP decomposition. The occurrence of an induction period suggests that a secondary catalyst is formed in the course of HP decomposition with the synthesized additives. The experimental data show that all the additives catalytically decompose the HP (Table 2).

According to the experimental data, introduction of the SHP fragment leads to a sharp increase in the stoichiometric coefficient. Presumablly, the catalytic center formed in this case exhibits a higher selectivity in the process.

The stabilizing performance of the oligomers was evaluated in accordance with the appropriate GOST as the time τ until the onset of PVC dehydrochlorination in the presence of the synthesized oligomeric additives without other additives (Table 3), and also as the time until the onset of release of acidic products from PVC films. The tests were performed in an oven in air at 170°C. They showed that the time until the onset of HCl release from PVC increases upon addition of the organoelement compounds synthesized.

The stabilizer performance was also evaluated by DTA from the temperatures of polymer oxidation T_o (°C) and of 5, 10, and 50% weight loss (Table 4). The results obtained show that the oligomeric sulfur-copntaining additives based on polyethers increase the oxidation temperature and the onset temperature of the weight loss, compared to the control sample without additives.

The plasticizing effect of the oligomeric sulfur-containing additives was evaluated by depression of the glass transition point T_g. All the additives synthesized decrease T_g to different extents (Fig. 2). The largest depression of T_g of PVC films is observed with the additives containing –S– bonds and SHP fragments.

CONCLUSIONS

(1) Polyvinyl chloride can be stabilized with additives based on a polyether and containing several centers inhibiting the polymer oxidation (sulfide and hydrosulfide groups, sterically hindered phenolic fragments).

(2) The synthesized products catalytically decompose hydroperoxides.

(3) Introduction of the new additives into polyvinyl chloride leads to the depression of the glass transition point of polyvinyl chloride films and increases the time until the onset of polymer oxidation and release of hydrogen chloride.

REFERENCES

1. Shtarkman, B.P., *Plastifikatsiya PVKh* (Plasticization of Polyvinyl Chloride), Moscow: Khimiya, 1981.
2. Kirilovich, V.I., *Plast. Massy*, 2003, no. 11, pp. 24–26.
3. Emanuel', N.M. and Buchachenko, A.L., *Khimicheskaya fizika molekulyarnogo razrusheniya i stabilizatsii polimerov* (Chemical Physics of Molecular Degradation and Stabilization of Polymers), Moscow: Nauka, 1988.
4. Mitrofanova, S.E., Girfanova, E.N., Averko-Antonovich, I.Yu., and Cherezova, E.N., *Zh. Prikl. Khim.*, 2006, vol. 79, no. 1, pp. 139–143.
5. Sedov, L.N. and Mikhailova, Z.V., *Nenasyshchennye poliefiry* (Unsaturated Polyethers and Polyesters), Moscow: Khimiya, 1977.
6. *Materialy konkursa studencheskikh nauchno-issledovatel'skikh rabot* (Proc. Competition of Students' Research Works), Kazan: Kazansk. Gos. Tekhnol. Univ., 2005.
7. Belyavskaya, T.A., *Prakticheskoe rukovodstvo po gravimetrii i titrimetrii: Uchebnoe posobie* (Manual on Gravimetry and Titrimetry: Textbook), Moscow: Mosk. Gos. Univ., 1986.
8. Antonovskii, V.L. and Buzlanova, M.M., *Analiticheskaya khimiya organicheskikh peroksidnykh soedinenii* (Analytical Chemistry of Organic Peroxy Compounds), Moscow: Khimiya, 1978.
9. Denisov, E.T. and Azatyan, V.V., *Ingibirovanie tsepnykh reaktsii* (Inhibition of Chain Reactions), Chernogolovka: Ross. Akad. Nauk, 1997.
10. Averko-Antonovich, I.Yu., Averko-Antonovich, L.A., Gonyukh, A.V., et al., Abstracts of Papers, *IV Vsesoyuznaya konferentsiya po khimii i fizikokhimii oligomerov* (IV All-Union Conf. on Chemistry and Physical Chemistry of Oligomers), Chernogolovka, 1990, p. 239.

ISSN 1070-4272, Russian Journal of Applied Chemistry, 2007, Vol. 80, No. 8, pp. 1404–1408. © Pleiades Publishing, Ltd., 2007.
Original Russian Text © K.V. Shirshin, O.A. Kazantsev, A.P. Sivokhin, T.A. Khokhlova, 2007, published in Zhurnal Prikladnoi Khimii, 2007, Vol. 80, No. 8, pp. 1365–1369.

MACROMOLECULAR CHEMISTRY AND POLYMERIC MATERIALS

Concentration Effects in Copolymerization of Sulfuric Acid Salt of *N*,*N*-Dimethylaminoethyl Methacrylate with Acrylonitrile and Acrylamide in Aqueous Solutions

K. V. Shirshin, O. A. Kazantsev, A. P. Sivokhin, and T. A. Khokhlova

Dzerzhinsk Polytechnic Institute, Nizhni Novgorod State Technical University Dzerzhinsk, Nizhni Novgorod oblast, Russia
Dzerzhinskoe Orgsteklo Open Joint-Stock Company, Dzerzhinsk, Nizhni Novgorod oblast, Russia

Received January 16, 2007; in final form, June 2007

Abstract—Copolymerization of sulfuric acid salt of *N*,*N*-dimethylaminoethyl methacrylate with acrylonitrile and acrylamide in aqueous solution was studied.

DOI: 10.1134/S1070427207080289

Polyelectrolytes based on *N*,*N*-dimethylaminoethyl methacrylate (DMAEM) salts and acrylamide (AA) are widely used for treatment of household and industrial wastewater [1]. The copolymerization of these monomers is often performed in relatively concentrated aqueous solutions. Studies of radical copolymerization of some vinyl monomers in water have revealed some interesting effects observed under certain conditions, e.g., effect of the initial concentration of the monomers on the chain propagation rate constant k_p [2, 3], abnormal acceleration of the process at high concentrations of the monomers [4], and constancy of the copolymer composition up to high conversions in copolymerization of monomers with essentially different relative activities [5]. Various authors attribute these effects to interaction of monomers and/or propagating macroradicals with the solvent [6], to variation of the ionic strength of solution in the course of copolymerization of ionic monomers [7], and to the influence exerted by association of the polymer chains [8]. More and more evidence is obtained that the polymerization of vinyl monomers in aqueous solutions is affected by association of the monomers. It has been shown that AA [9] and its *N*-substituted derivatives with ionic and nonionic substituents [10] form monomeric aggregates in concentrated aqueous solutions. Association of the monomers is mainly responsible for some abnormal phenomena observed in polymerization of acrylic acid [2, 3], AA [11], and *N*-isopropylacrylamide [12]. As shown in [13, 14], DMAEM and its salts also show increased tendency toward association in water.

In this study, we examined the influence exerted by the initial concentrations of the monomers and initiator on the composition of products in copolymerization of sulfuric acid salt of *N*,*N*-dimethylaminoethyl methacrylate (DMAEM · SA) with acrylonitrile (AN) and acrylamide in aqueous solutions.

EXPERIMENTAL

DMAEM and AN were distilled before use. AA was recrystallized from benzene. DMAEM · SA was prepared by adding an equivalent amount of a sulfuric acid solution to an aqueous solution of the monomer. The copolymerization of DMAEM · SA with AA and AN was performed in aqueous solution at 50°C in glass ampules. The total concentration of the monomers was 0.5–3.5 M. The initiator (potassium persulfate) concentration was varied in the range 0.075–2 mol % relative to the sum of the monomers. The concentrations of individual monomers were estimated by liquid (DMAEM · SA and AA) and gas–liquid (AN) chromatography.

Liquid chromatography was performed with a Praha chromatograph equipped with a UV detector (λ = 254 nm) and a 150 × 4.6-mm steel column packed with Silasorb C_{18} (particle size 10 μm). The eluent was acetonitrile. Gas–liquid chromatography was performed with a Tsvet-100 device equipped with a flame-ionization detector and a steel column, 2 m long and 3 mm in diameter, packed with 10% poly-(ethylene glycol adipate) on Chromaton N-AW. The carrier

gas was N_2 (flow rate 2×10^{-3} $m^3 h^{-1}$); vaporizer and column temperatures 70 and 40°C, respectively. The specific viscosity of aqueous solutions of the monomers was measured at 25 ± 0.1°C on an Ubbelohde viscometer (capillary diameter 0.34 mm); the relative error did not exceed 0.5%. The statistical processing of the data followed standard procedures [15, 16]. The specific viscosity was averaged over three measurements. The points were fitted with a straight line with a correlation coefficient exceeding 0.997. The adequacy of the regression equations to the experimental data was estimated with Fisher's test.

Figure 1 shows how the initial concentration of the monomers affects the composition of the forming copolymers in copolymerization of equimolar amounts of DMAEM · SA and AA in aqueous solutions. It can be seen that, for all the copolymers, there are portions in which the copolymer composition is independent of the conversion. The limiting conversion, at which the copolymer composition starts to change, largely depends on an initial concentration of the monomers. For example, in the experiment with the initial total monomer concentration of 1.2 M, the copolymer composition remains constant up to 30% conversion. At the total monomer concentration increased to 2.9 and 3.5 M, the copolymer composition does not change up to 45% and 50% conversion, respectively. Thus, appreciable changes in the running concentrations of the monomers with conversion do not lead to changes in the copolymer composition until a definite degree of conversion is reached. Also, an increase in the initial total monomer concentration from 1.2 to 3.5 M leads to a more than 10% decrease in the content of the DMAEM · SA units in the copolymers in the initial copolymerization steps.

In copolymerization of DMAEM · SA with AN, some features differ from those observed in copolymerization of DMAEM · SA with AA. Figure 2 shows that the copolymer of DMAEM · SA with AN is also enriched in the amino ester salt units, but the product composition steadily varies with the conversion (in experiments with the initial mole fration of AN exceeding 10%). To estimate the concentration effect, we performed experiments at different initial concentrations of the monomers (Fig. 3). In copolymerization of DMAEM · SA with AA (Fig. 1), an increase in the initial total monomer concentration led to a decrease in the content of the amino ester units, whereas in the copolymerization with AN, by contrast, the product was enriched with ionic monomer units.

The experiments show that the initial total monomer concentration strongly affects both the initial copolymer composition and the dynamics of its variation. The occurrence of the pronounced concentration effects and the available data on the capacity of (meth)acrylic monomers for self-association suggest that the association of the monomer plays an import-

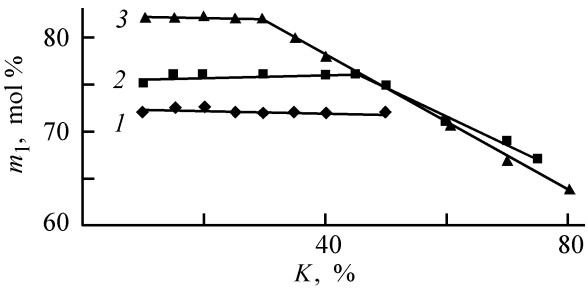

Fig. 1. Content m_1 of DMAEM · SA units in copolymers vs. conversion K in copolymerization of DMAEM · SA with AA. DMAEM · SA : AA ratio 5 : 5. $[DMAEM \cdot SA]_0$, M: (*1*) 1.75, (*2*) 1.45, and (*3*) 0.60.

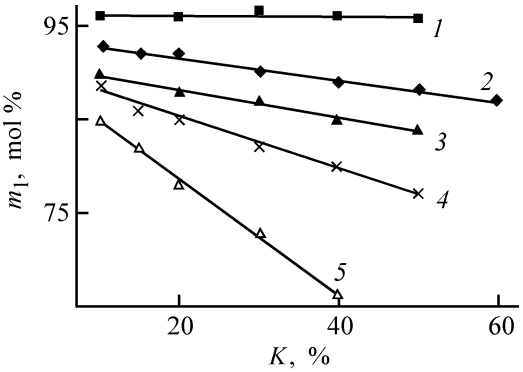

Fig. 2. Content m_1 of DMAEM · SA units in copolymers vs. conversion K in copolymerization of DMAEM · SA with AN. $[M_1 + M_2]_0 = 1.0$ M, $[K_2S_2O_8] = 0.8$ mol %. Composition of initial monomer mixture DMADM–SA : AN, mol %: (*1*) 90 : 10, (*2*) 80 : 20, (*3*) 70 : 30, (*4*) 50 : 50, and (*5*) 30 : 70.

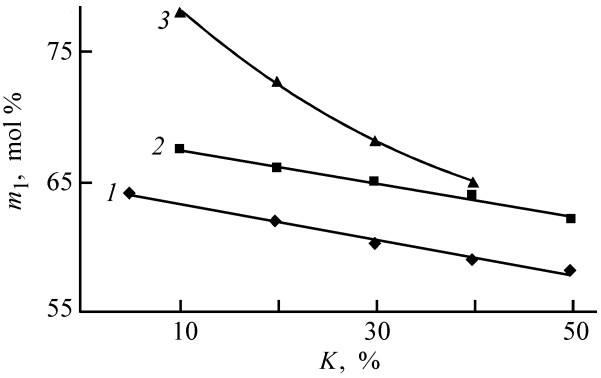

Fig. 3. Content m_1 of DMAEM · SA units in copolymers vs. conversion K in copolymerization of DMAEM · SA with AN. $[K_2S_2O_8] = 0.15$ mol %, DMAEM · SA : AN = 5 : 5. $[DMAEM \cdot SA]_0$, M: (*1*) 0.5, (*2*) 1.0, and (*3*) 1.5.

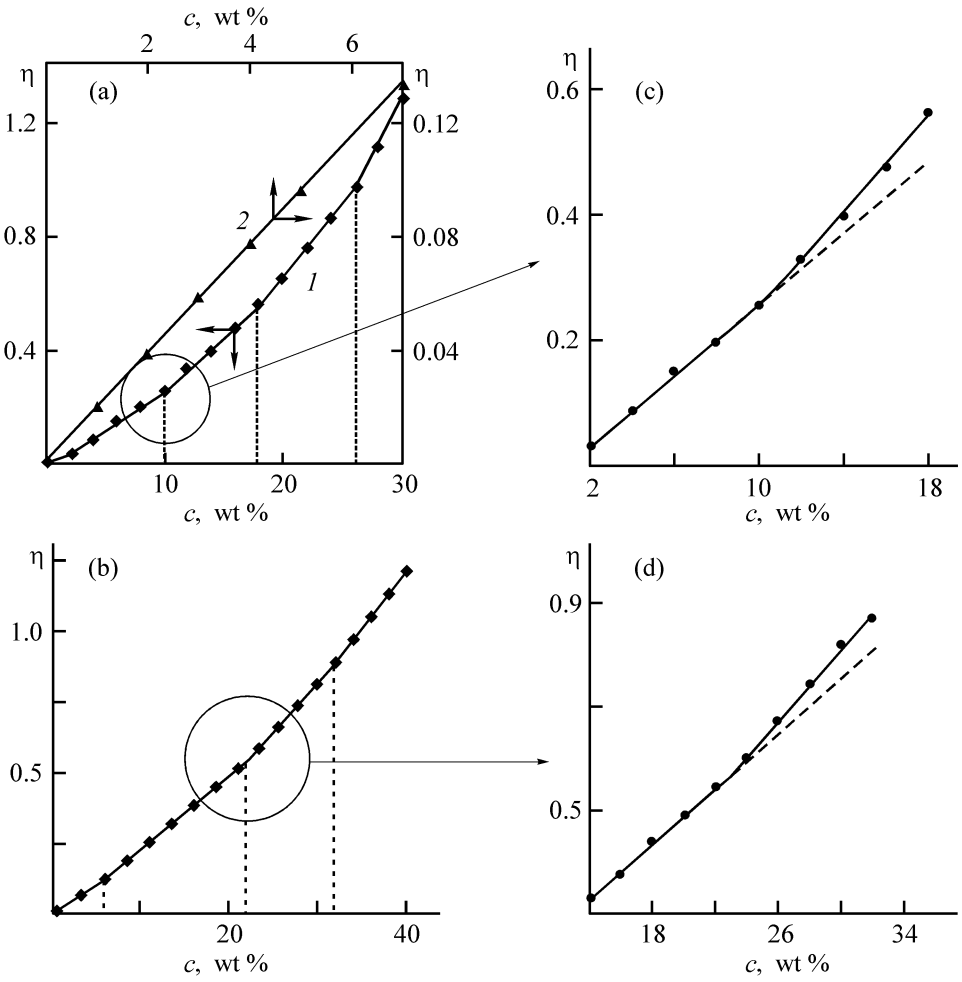

Fig. 4. Specific viscosity η of aqueous solutions of (a) (*1*) DMAEM · SA and (*2*) AN, and (b) AA at 25°C vs. the concentration *c*. (c, d) Regions of inflection points for DMAEM · SA and AA, respectively, plotted on the enlarged scale.

ant role in the process. Therefore, it was of interest to specially examine the association of the monomers in the systems under consideration.

To this end, we obtained the viscosity–concentration dependences (VCDs) for solutions of individual monomers DMAEM · SA, AA, and AN and of their binary mixtures. Figures 4a and 4b show that the specific viscosity of AN solutions is a linear function of the concentratiuon, whereas for the other two monomers, significant deviations from linearity are observed. As judged from the extent of these deviations and from the concentrations at which they are observed, the capacity of the monomers for self-organization decreases in the order DMAEM · SA > AA > AN.

The viscosity–concentration dependences for DMAEM · SA and AA indicate that the structures of the forming associates vary as the concentration of the monomer solution increases. This follows from the existence of several inflection points corresponding to the critical association concentrations (CACs): for AA, at concentrations of approximately 6, 22, and 32% (Fig. 4b); for DMAEM · SA, at concentrations of approximately 2, 10, 18, and 26% (Fig. 4a, curve *1*). On the enlarged scale (Figs. 4c, 4d), it is clearly seen that the VCDs consist of several linear portions separated by bends (the dashed line shows the continuation of the initial linear portion). It should be noted that, in aqueous solutions of (meth)acrylic monomers showing pronounced surface activity, the inflections in the concentration dependences of the physical properties are associated with transitions from spherical to anisotropic micelles and then to lamellas [17]. The existence of several CACs in DMAEM · SA and AA solutions is also attributable to transformations of the forming associates.

We also examined the viscosity–concentration dependences for the systems DMAEM · SA–AA–H_2O

and DMAEM · SA–AN–H_2O. Figure 5 shows that introduction of AA into a solution of the amino ester salt leads to a certain decrease in the CAC values corresponding to inflections in the viscosity–concentration dependence (to 4, 10, 14, and 20%). Furthermore, the presence of AA in a DMAEM · SA solution causes an increase in the viscosity as compared to solutions of the individual amino ester salt. The viscosity of individual AA solutions is lower than that of DMAEM · SA solutions (Figs. 4a, 4b), i.e., a synergic increase in the viscosity is observed in the binary systems. Hence, mixed associates DMAEM · SA–AA–H_2O are more stable than aggregates of each of the monomers taken separately. The existence of monomeric associates of different compositions should affect the copolymerization processes involving DMAEM · SA and AA, because the polymerization primarily occurs in the associates. At low concentrations, the monomeric associates and hence the copolymers are preferentially formed by DMAEM · SA molecules (more strongly tending to associate). With an increase in the total monomer concentration, the relative content of AA molecules in mixed associates becomes higher, which leads to an increase in the relative content of the amide in the copolymer.

Addition of AN to a solution of the amino ester salt, by contrast, makes the viscosity of the monomeric solution lower and CAC higher (to 5, 15, and 25%). This fact indicates that DMAEM · SA associates are more stable than binary associates with AN. As the concentration of the initial solutions is raised, the relative content of associated DMAEM · SA molecules grows, which leads to an increase in the fraction of DMAEM · SA units in the copolymer. Raising the initial fraction of DMAEM · SA units in the starting monomeric mixture also leads to an increase in the relative content of the associated molecules in the solution; as a result, the deviations of the copolymer composition from the linear trend with the conversion become less noticeable as the relative content of DMAEM · SA in the starting mixture increases. At a large excess of the amino ester salt relative to the nitrile (9 : 1), the copolymer composition does not change up to 50% conversion (Fig. 2).

Thus, the features of the copolymerization in the systems DMAEM · SA–AA and DMAEM · SA–AN are largely governed by the structure of the initial monomeric associates. With the progress of the polymerization, the monomeric associates become monomeric-polymeric. Incorporation of hydrophobic macromolecules should affect the structure of the associates and hence the further reaction course. According to the model taking into account selective solvation of

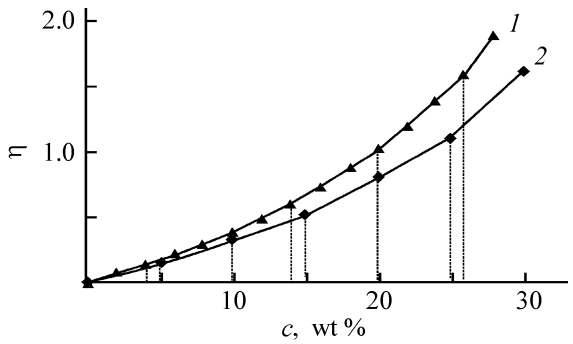

Fig. 5. Specific viscosity η of aqueous solutions of DMAEM · SA in the presence of (*1*) AA and (*2*) AN at 20°C vs. the DMAEM · SA concentration *c*. DMAEM · SA : M_2 ratio 5 : 5.

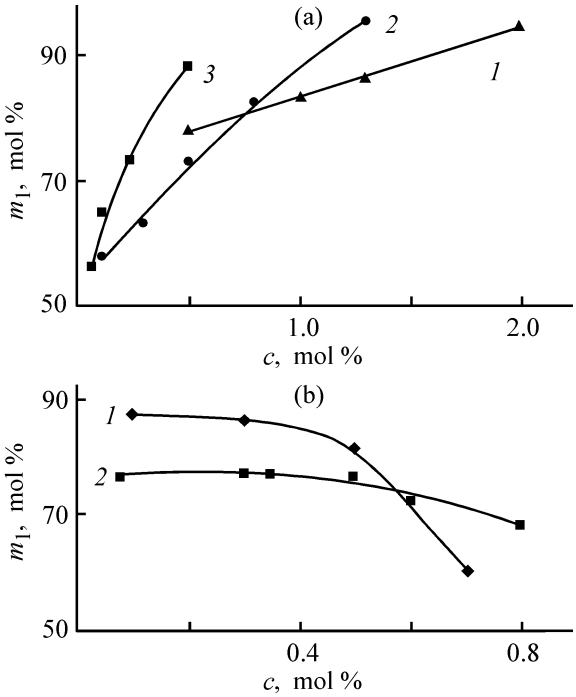

Fig. 6. Content m_1 of DMAEM · SA units in copolymers vs. initiator ($K_2S_2O_8$) concentration *c* in copolymerization of DMAEM · SA with (a) AN and (b) AA. Total monomer conversion 10%, DMAEM · SA : M_2 = 5 : 5. $[DMAEM \cdot SA]_0$, M: (a) (*1*) 0.25, (*2*) 0.50, and (*3*) 1.0; (b) (*1*) 0.50 and (*2*) 1.0.

macroradicals with monomers [18], the concentration of the hydrophobic monomer in polymeric associates increases owing to specific solvation, which leads to a rise in its content in the copolymer. This process should be favored by an increase in the molecular weight of the polymeric chains. In particular, this effect was attained with decreasing initiator concentration in experiments on copolymerization of styrene with methacrylic acid [19].

Figure 6a shows data on the influence of the initiator concentration on the composition of the DMAEM ·

SA–AN copolymer. It can be seen that as the initiator concentration in this system decreases, the copolymer gets enriched in units of the more hydrophobic monomer, AN. It should be noted that this effect is weakened as the initial concentration of the monomers decreases. This trend is consistent with the known fact that the role of monomeric solvation of polymerizing molecules in dilute solutions is weakened because of the competing effect of the solvent molecules [19].

A decrease in the initiator concentration in the DMAEM · SA–AA system (Fig. 6b) also leads to enrichment of the copolymers with units of the more hydrophobic monomer, amino ester salt. However, in contrast to the DMAEM · SA–AN system, the influence of the initiator concentration on the copolymer composition becomes considerably weaker as the initial concentration of the monomers increases. We attribute this difference to the fact that, as the solution concentration in the DMAEM · SA–AA system increases, both reagents are incorporated in monomeric associates to a greater extent; therefore, the formation of polymeric molecules only weakly affects the product composition (at least, at low conversions).

Thus, the experimental data obtained indicate that the composition of copolymers formed by copolymerization of DMAEM · SA with AN or AA in aqueous solutions is largely governed by association of the starting monomers and solvation of the propagating macroradicals by the monomers.

CONCLUSIONS

(1) The composition of copolymers formed in the systems *N*,*N*-dimethylaminoethyl methacrylate sulfuric acid salt–acrylamide and *N*,*N*-dimethylaminoethyl methacrylate sulfuric acid salt–acrylonitrile depends on the total initial concentration of the monomers.

(2) The concentration dependences of the specific viscosity of aqueous solutions of the monomers show that *N*,*N*-dimethylaminoethyl methacrylate sulfuric acid salt, acrylamide, and their mixtures are capable of association.

(3) The relative content of the hydrophobic monomer in the copolymer increases with the molecular weight of the products. This effect is partly eliminated off in copolymerization of *N*,*N*-dimethylaminoethyl methacrylate sulfuric acid salt with acrylonitrile in dilute solutions and with acrylamide in concentrated solutions.

(4) The decisive influence is exerted on the copolymer composition by association processes involving monomeric and polymeric molecules.

REFERENCES

1. Askarov, M.A., Mukhitdinova, N.A., and Nazarov, A., *Polimerizatsiya aminoalkilakrilatov* (Polymerization of Aminoalkyl Acrylates), Tashkent: Fan, 1977.
2. Lacik, I., Beuermann, S., and Buback, M., *Macromol. Chem. Phys.*, 2004, vol. 205, no. 8, pp. 1080–1087.
3. Lacik, I., Beuermann, S., and Buback, M., *Macromolecules*, 2003, vol. 36, no. 25, pp. 9355–9363.
4. Egorov, V.V., Zaitsev, S.Yu., and Zubov, V.P., *Vysokomol. Soedin., Ser. A*, 1991, vol. 33, no. 8, pp. 1587–1608.
5. Gromov, V.F., Bogachev, Yu.S., Bune, E.V., and Zhuravleva, I.L., *Vysokomol. Soedin., Ser. A*, 1993, vol. 35, no. 1, pp. 7–12.
6. Gromov, V.F., Bune, E.V., and Teleshov, E.N., *Usp. Khim.*, 1994, vol. 63, no. 6, pp. 507–518.
7. Kurenkov, V.F. and Utikeeva, A.R., *Vysokomol. Soedin., Ser. A*, 2000, vol. 42, no. 4, pp. 587–593.
8. Ringsdorf, H., Simon, J., and Winnik, F.M., *Macromolecules*, 1992, vol. 25, no. 21, pp. 5353–5357.
9. Chapiro, A. and Perec-Spritzer, L., *Eur. Polym. J.*, 1975, vol. 11, no. 1, pp. 59–69.
10. Kazantsev, O.A. and Shirshin, K.V., *Polymer*, 2004, vol. 45, no. 15, pp. 5021–5029.
11. Pascal, P., Winnik, M.A., Napper, D.H., and Gilbert, R.G., *Macromolecules*, 1993, vol. 26, no. 17, pp. 4572–4576.
12. Ganachaud, F., Balic, R., Monteiro, M.J., and Gilbert, R.G., *Macromolecules*, 2000, vol. 33, no. 23, pp. 8589–8596.
13. Kazantsev, O.A., Kuznetsova, N.A., Shirshin, K.V., et al., *Vysokomol. Soedin., Ser. A*, 2003, vol. 45, no. 4, pp. 572–580.
14. Shibalovich, V.G., Efimova, D.Yu., and Nikolaev, A.F., *Plast. Massy*, 2000, no. 3, pp. 25–27.
15. Kafarov, V.V., *Metody kibernetiki v khimii i khimicheskoi tekhnologii* (Cybernetic Methods in Chemistry and Chemical Technology), Moscow: Khimiya, 1985.
16. Batuner, L.M. and Pozin, M.E., *Matematicheskie metody v khimicheskoi tekhnike* (Mathematical Methods in Chemical Engineering), Leningrad: Khimiya, 1971.
17. Batrakova, E.V., Orlov, Yu.N., Egorov, V.V., et al., *Vysokomol. Soedin., Ser. B*, 1985, vol. 27, no. 2, pp. 87–93.
18. Harwood, H.J., *Macromol. Chem., Macromol. Symp.*, 1987, nos. 10/11, pp. 331–336.
19. Zaitseva, S.D., Knyazeva, T.E., Myasnikova, I.B., et al., *Vysokomol. Soedin., Ser. A*, 1998, vol. 40, no. 8, pp. 1271–1275.

ISSN 1070-4272, Russian Journal of Applied Chemistry, 2007, Vol. 80, No. 8, pp. 1409–1412. © Pleiades Publishing, Ltd., 2007.
Original Russian Text © V.D. Vasil'eva, V.E. Derbisher, I.Yu. Kovalets, T.P. Aleinikova, E.V. Derbisher, 2007, published in Zhurnal Prikladnoi Khimii, 2007, Vol. 80, No. 8, pp. 1370–1373.

MACROMOLECULAR CHEMISTRY AND POLYMERIC MATERIALS

Synthesis of Polymeric Peroxides and Their Use in Finishing Treatment of Textile Materials

V. D. Vasil'eva, V. E. Derbisher, I. Yu. Kovalets, T. P. Aleinikova, and E. V. Derbisher

Volgograd State Technical University, Volgograd, Russia

Received November 10, 2006; in final form, February 2007

Abstract—A polymeric peroxide was prepared by the reaction of α-chloroethyl *tert*-butyl peroxide with polyvinyl alcohol. Procedures for modification of wool and polycaproamide textile materials with this peroxide were suggested.

DOI: 10.1134/S1070427207080290

Peroxides accomplishing diverse functions are widely used in preparation and processing of polymers. For example, in treatment of textile materials, they play the role of oxidants in the bleaching and finishing processes [1]. At the same time, the majority of peroxides have serious drawbacks: low stability, toxicity, and strictly specific effect. Therefore, it becomes necessary to permanently expand the assortment of peroxides and comprehensively study their physicochemical properties. Preparation and application of new peroxides with improved properties is one of important problems of the modern chemical industry, including the chemical technology of textile materials.

One of the ways to solve this problem is to prepare polymeric peroxides by polymer-analogous transformations. It seems promising to prepare polyfunctional polymeric peroxides containing reactive hydroxy groups in the side chain.

Proceeding with studies in the field of synthesis of peroxides and their applications to chemical technology of textile materials in the finishing step [2, 3], we prepared a polymeric peroxide with –O–O– groups in pendant chains by the reaction of α-chloroethyl *tert*-butyl peroxide (α-CETBP) with polyvinyl alcohol (PVA), an agent widely used in finishing, in accordance with the scheme

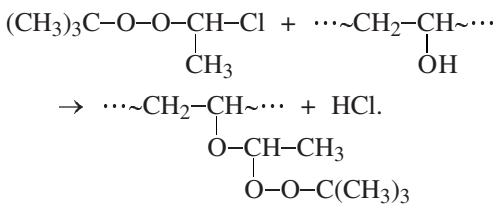

The starting α-CETBP was prepared by the reaction of acetaldehyde with *tert*-butyl peroxide according to the previously described procedure [2].

1-(*tert*-Butylperoxy)ethyl ether of polyvinyl alcohol (α-TBPE PVA) was prepared in chloroform.

From the structure and properties of the synthesized α-TBPE PVA, we made conclusions concerning its possible applications and, in particular, that for modification of textile materials with the aim to improve their properties. We proceeded from the fact that the textile finishing technology involves fairly wide use of textile modification processes based on interaction of reactive polymers with functional groups of the fiber, and also on graft copolymerization of vinyl monomers to the fiber by the radical mechanism in the presence of oxidants as initiators [1].

Therefore, we made laboratory trials of procedures for modification of textile materials using α-TBPE PVA both as reactive polymer and as initiator of graft copolymerization of a vinyl monomer (acrylamide) to the fiber. Trials were performed with specimens of polycaproamide and wood textile linen of various structures, and the initial and modified materials were compared.

The modification of polycaproamide textile linen was performed by treatment of the specimens with an aqueous 40–50 g l^{-1} solution of α-TBPE PVA, followed by washing and drying. The modification of wool textile materials was performed by treatment of the specimens with an aqueous acrylamide solution in the presence of α-TBPE PVA as initiator, at a total concentration of the components of 60–70 g l^{-1} and

Table 1. Properties of modified textile materials

Parameter	Polycaproamide woven fiber	Wool tricot fiber
Interweaving	Linen weave	Interlon
Surface density, g m^{-2}	110	185
Tensile strength, daN	55.4/63.6	43.5/49.4
Hygroscopicity, %	7.0/4.5	–
Electrifiability, Ω cm	$2.1 \times 10^9/4.2 \times 10^{10}$	–
Loss of strength, %, upon treatment with solutions:		
of sulfuric acid	7/12	–
of sodium hydroxide	0/3	–
Length shrinkage after five launderings, %	–	4.8/15.3
Wear resistance, cycles	–	1710/1235

* The parameters for the initial textile materials are given in the denominator.

acrylamide : initiator weight ratio of (1–5) : 1, followed by washing and drying.

The treatment parameters were optimized with the aim to provide a reproducible improvement of the processing and consumer's properties of the modified textile materials. The treatment temperature (95–100°C) was determined by the onset of thermal decomposition of α-TBPE PVA. The characteristics of the modified textile materials are listed in Table 1.

Table 1 shows that the processing and service properties of the modified textile materials are improved. For polycaproamide materials, the hygroscopicity increases by 50–60%, the material becomes more resistant to various chemicals, and the electrifiability decreases by an order of magnitude, compared with the unmodified specimens; for wool materials, the resistance to shrinkage and wear increase by 65–70 and 35–40%, respectively. The loss of strength by the modified textile materials is insignificant (12–13%), being close to the experimental error (7%).

The effect obtained upon the modification can presumably be understood as follows: the methyl and polymeric radicals formed by thermolysis of α-TBPE PVA at 95–100°C in the course of treatment of a textile material initiate the formation of polymeric macroradicals and their grafting to the fiber, and are also directly involved in these processes. This ensures formation and firm retention of a modifying polymer layer on the surface of a textile material. Taking this fact into account, we can describe the modification of polycaproamide and wool materials by the following reaction schemes.

(1) Polycaproamide + α-TBPE PVA → modified polycaproamide:

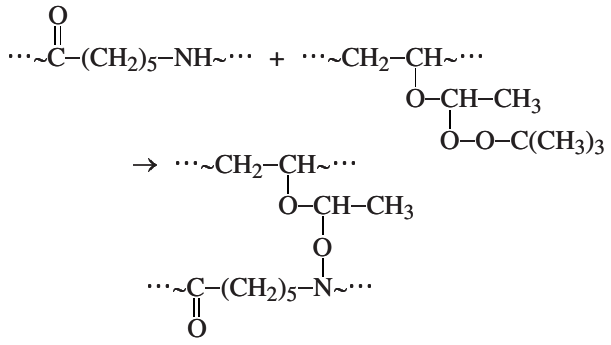

(2) Wool (keratin) + acrylamide + α-TBPE PVA → modified wool:

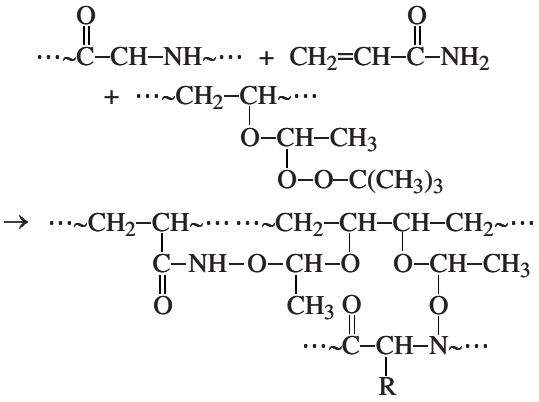

Thus, being an initiator of radical polymerization of the vinyl monomer (in modification of wool textile materials) and of the chemical reaction (grafting) of the polymer with a textile material, α-TBPE PVA simultaneously acts as a modifier of the fibrous substrate, incorporated in the forming modifying polymer layer. As a result, a firmly fixed thin polymer layer is formed on the material surface, imparting to the material increased hygroscopicity and resistance to various chemicals and making it less electrifiable.

EXPERIMENTAL

Chloroform used as solvent in the synthesis of 1-(*tert*-butylperoxy)ethyl ether of polyvinyl alcohol was purified by the standard procedure [4]. A reactor equipped with a stirrer, thermometer, and reflux condenser was charged with 100 ml of dried chloroform and 4.4 g (0.1 mol of monomer units) of polyvinyul alcohol. The mixture was heated at 60°C until the PVA dissolved completely. Then 15.2 g (0.1 mol) of α-CETBP was added. The mixture was vigorously stirred at 60°C for 3.5 h.

In the course of the synthesis, HCl was continuously removed from the reaction mixture by bubbling dry nitrogen and was absorbed in a NaOH solution. The reaction progress was monitored by titration of OH groups [5] in samples taken at regular intervals.

The optimal reaction parameters are 60°C, 3.5 h. A longer reaction does not lead to an increase in the product yield, and higher temperatures cause decomposition of the starting chlorinated peroxide.

After the synthesis, the mixture was washed first with 15% aqueous $NaHCO_3$ to neutral reaction and then with water, after which it was dried over anhydrous $MgSO_4$. Then the solvent was removed in a vacuum, and the product was analyzed.

The synthesized α-TBPE PVA is a yellowish odorless powder soluble in water at 60°C.

The structure of α-TBPE PVA was confirmed by IR spectroscopy, titration, and elemental analysis.

The IR spectra were taken on a Specord UV-VIS spectrophotometer in the range 500–4000 cm^{-1} from thin films. The IR data allowing identification of the corresponding structural fragments are listed in Table 2.

The content of the available oxygen was determined by iodometric titration [7]. A quantitative analysis of hydroxy groups and available oxygen showed that the degree of substitution of OH groups in the resulting polymeric peroxide, α-TBPE PVA, was 61.5%, and the available oxygen content, 6.15%. The results of elemental analysis are as follows:

Found, %: C 58.08, H 9.43.
Calculated, %: C 60.36, H 9.90.

A thermogravimetric analysis (TGA) was performed with an MOM derivatograph (Hungary), with heating from 10 to 500°C at a rate of 10 deg min^{-1}. The weight loss by the synthesized α-TBPE PVA on heating was

Table 2. IR characteristics of α-TBPE PVA

Group	IR spectrum, ν, cm^{-1}	
	experiment	[6]
–O–O–	860	890–820
C–H	2920	3600–2500
C–O–C	1150	1300–1000
–OH (bending)	1310	1300–1250
–OH (stretching)	3200	3600–2500

determined by TGA. The product shows insignificant weight loss in the range 20–95°C, followed by 65% weight loss at 96–290°C, apparently attributable to degradation of the pendant ether chains (including cleavage of –O–O– bonds) and further decomposition of the fragments. In the initial step, decomposition of α-TBPE PVA to give radicals is possible:

(1)

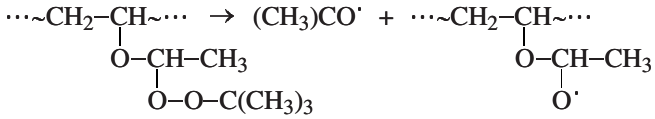

(2)

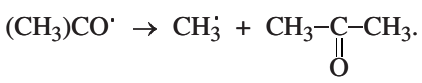

The weight loss in the range 300–400°C is insignificant. On further heating above 410°C, the sample undergoes complete degradation with a substantial weight loss.

The TGA data show that the α-TBPE PVA synthesized exhibits an enhanced heat resistance, compared to the most widely used commercial peroxides (decomposition temperature above 95°C). This expands its processing possibilities, making it no less valuable as an oxidant. Furthermore, the computational estimation of the ecological characteristics by pattern recognition methods [8] gives grounds to expect a low toxicity of the product (estimated hazard class III–IV).

In modification of polycaproamide textile materials, a specimen of polycaproamide fiber was immersed in an aqueous solution (50 g l^{-1}) of α-TBPE PVA prepared in an Erlenmeyer flask (solid : liquid = 1 : 30). The mixture was heated at 95–100°C for 30 min. The product was washed with water and dried to constant weight in an oven at 80°C.

The tensile strength of the specimens was determined in accordance with GOST (State Standard)

3813–72, and the hygroscopicity and electrifiability, in accordance with GOSTs 3816–81 and 19616–74. The resistance of specimens of polycaproamide textile materials to various chemicals was evaluated by the loss of strength after keeping in 40% H_2SO_4 and 40% NaOH solutions for 30 min at 50°C.

In modification of wool textile materials, a specimen of wool linen was immersed in an aqueous solution of α-TBPE PVA and acrylamide (total concentration 70 g l^{-1}, weight ratio acrylamide : α-TBPE PVA 1 : 1), prepared in an Erlenmeyer flask (solid : liquid = 1 : 30). The mixture was heated at 95–100°C for 60 min. The product was washed with water and dried to constant weight in an oven at 80°C.

The shrinkage and wear resistance were evaluated in accordance with GOSTs 8710–84 and 18976–73.

CONCLUSIONS

(1) A procedure was suggested for modification of polycaproamide textile materials with a formulation based on 1-(*tert*-butylperoxy)ethyl ether of polyvinyl alcohol. The properties of the modified material were studied.

(2) A procedure was suggested for modification of wool textile materials with a formulation based on a vinyl monomer and 1-(*tert*-butylperoxy)ethyl ether of polyvinyl alcohol. The properties of the modified material were studied.

REFERENCES

1. Krichevskii, G.E., *Khimicheskaya tekhnologiya tekstil'nykh materialov* (Chemical Technology of Textile Materials), Moscow: RSKhTK, 2000.
2. Kovalets, I.Yu., Aleinikova, T.P., and Derbisher, V.E., *Zh. Prikl. Khim.*, 2002, vol. 75, no. 8, pp. 1398–1400.
3. Kovalets, I.Yu., Aleinikova, T.P., and Derbisher, V.E., in *Sbornik materialov Mezhdunarodnoi nauchno-tekhnicheskoi konferentsii "Sovremennye naukoemkie tekhnologii i perspektivnye materialy tekstil'noi i legkoi promyshlennosti (Progress-2002)"* (Proc. Int. Scientific and Technical Conf. "Modern High Technologies and Promising Materials for Textile and Light Industry (Progress-2002)"), Ivanovo, 2002, pp. 138–139.
4. Gordon, A.J. and Ford, R.A., *The Chemist's Companion. A Handbook of Practical Data, Techniques, and References*, New York: Wiley, 1972.
5. *Praktikum po vysokomolekulyarnym soedineniyam* (Practical Course of Macromolecular Compounds), Kabanov, V.A., Ed., Moscow: Khimiya, 1985.
6. Bellamy, L.J., *Advances in Infrared Group Frequencies*, London: Methuen, 1968.
7. Antonovskii, V.L. and Buzlanova, M.M., *Analiticheskaya khimiya organicheskikh peroksidnykh soedinenii* (Analytical Chemistry of Organic Peroxy Compounds), Moscow: Khimiya, 1972.
8. Derbisher, E.V., Prediction of the Hazard Class of Substances on the Basis of Data Sample on Their Physicochemical and Medicobiological Properties, *Cand. Sci. Dissertation*, Volgograd, 2005.

ISSN 1070-4272, Russian Journal of Applied Chemistry, 2007, Vol. 80, No. 8, pp. 1419–1423. © Pleiades Publishing, Ltd., 2007.
Original Russian Text © V.S. Tkach, D.S. Suslov, G. Myagmarsuren, F.K. Shmidt, 2007, published in Zhurnal Prikladnoi Khimii, 2007, Vol. 80, No. 8, pp. 1380–1384.

MACROMOLECULAR CHEMISTRY AND POLYMERIC MATERIALS

Selective Trimerization of Ethylene in the Presence of a Catalytic System Based on Bis(acetylacetonato)palladium and Boron Trifluoride Etherate

V. S. Tkach, D. S. Suslov, G. Myagmarsuren, and F. K. Shmidt

Irkutsk State University, Irkutsk, Russia
National University of Mongolia, Ulan-Bator, Mongolia

Received September 26, 2006; in final form, April 2007

Abstract—Trimerization of ethylene was examined as a route to isohexenes [in particular, 3-methyl-2-pentene (*cis* + *trans*)] inaccessible by dimerization of propylene.

DOI: 10.1134/S1070427207080319

Oligomerization of ethylene is of considerable scientific and practical interest as a route to linear and branched monoolefins. Linear olefins are key intermediates in production of detergents, plasticizers, and other chemicals; branched olefins are of independent interest as high-octane additives to motor fuel [1]. The commercially implemented SHOP process (Shell) allows highly selective (selectivity up to 97%) synthesis on nickel catalysts of linear α-olefins with a broad molecular-weight distribution of the oligomeric products (from C_4 to C_{20}), but the relative content of the trimers is as low as 13% [2]. On chromium catalysts patented by BP Chemicals, ethylene oligomerizes with up to 91% selectivity with respect to linear trimers (1-hexene) [3]. Catalysts based on $(PPh_3)_2 \cdot NiBr_2$ in combination with methylalumoxane or CH_3AlCl_2 allow preparation with an up to 95% selectivity of ethylene trimers; their major components are isohexenes (total content up to 75%), with an up to 47% relative content of 3-methyl-2-pentene [4].

Catalysts based on bis(acetylacetonato)palladium and boron trifluoride etherate exhibit high potential in transformations of unsaturated hydrocarbons. They show high performance (high selectivity and high conversion of the starting substrates to the target products), in particular, in positional isomerization of α-alkenes [5, 6], dimerization of vinylaromatic hydrocarbons [7, 8], telomerization of dienes with secondary amines [9–11], and polymerization of norbornene and its derivatives [12, 13].

In this study, we examined the influence exerted by various factors, including the conditions of catalyst formation, solvent, and amount of acetylacetone as an astoichiometric modifying additive, on the catalytic properties of active complexes (ACs). The goal of this study was to gain additional information on the nature of the catalytic effect of systems based on bis(acetylacetonato)palladium and boron trifluoride etherate in transformations of unsaturated hydrocarbons, with the trimerization of ethylene as example.

EXPERIMENTAL

Oligomerization of ethylene was performed in a temperature-controlled glass vessel with continuous feeding of the substrate and shaking. A solution of $Pd(Acac)_2$ in an aromatic hydrocarbon was kept in an ethylene atmosphere at a chosen temperature for 10 min, BF_3OEt_2 was added, and the oligomerization was started. After the reaction completion, the catalyst was decomposed with 3% HCl, and the organic layer was separated and dried over $CaCl_2$. The products were separated by distillation.

The ethylene oligomerization products were analyzed by GLC on a Chrom-4 gas–liquid chromatograph equipped with a flame-ionization detector. A 100 m × 0.5 mm i.d. copper capillary column was coated with vacuum oil. The ^1H NMR spectra were recorded on a Varian VXR-500S spectrometer, and the IR spectra in the range 1800–400 cm^{-1}, on a Specord M-80 spectrophotometer. The cells and

Table 1. Variation of the composition of ethylene oligomers with time ($c_{Pd} = 8.33 \times 10^{-3}$ M, 398 K, solvent benzene, $V_0 = 30$ ml)

τ, min	Oligomeric components, wt %			Isomers of C_6H_{12}, wt %	
	C_4H_8	C_6H_{12}	C_8H_{16}	3-methyl-2-pentene, *cis* + *trans*	other hexenes
5	98.7	1.3	–	100.0	0.0
30	79.2	20.7	–	88.0	12.0
60	59.2	40.8	–	87.1	12.9
90	47.6	47.7	4.7	85.3	14.7
150	18.6	61.2	20.2	80.0	20.0

Table 2. Solvent effect on the conversion of ethylene into oligomers and composition of oligomers ($c_{Pd} = 8.33 \times 10^{-3}$ M, 303 K, $V_0 = 30$ ml, synthesis time 1.5 h)

Solvent	Oligomeric components, wt %			Isomers of C_6H_{12}, wt %		Conversion, (mol C_2) (g-at. Pd)$^{-1}$
	C_4H_8	C_6H_{12}	C_8H_{16}	3-methyl-2-pentene, *cis* + *trans*	other hexenes	
Benzene	34.3	65.7	–	86.5	13.5	1260
Toluene	72.5	26.9	0.6	87.4	12.6	1700
Isopropylbenzene	84.5	15.5	–	87.2	12.8	550

ampules were filled under argon. The solvents (benzene, toluene, isopropylbenzene) were dehydrated by the standard procedure and, just before use, were degassed on a vacuum installation and recondensed into an ampule over sodium mirror. The water content of the solvents was in the range 1×10^{-3}–3×10^{-3} M, as determined by Fischer titration [15]. Argon was thoroughly dried and deoxygenated [16]. Ethylene was of polymerization grade. Before use, boron trifluoride etherate was twice distilled in an argon atmosphere from calcium hydride. Acetylacetone was distilled in an argon atmosphere just before use; $Pd(Acac)_2$ was prepared according to [17], recrystallized from acetone, and vacuum-dried (1.333 Pa) at a temperature not exceeding 323 K.

In the experiments on ethylene oligomerization under the action of the catalytic system $Pd(Acac)_2$ + $30BF_3OEt_2$ (Table 1), we monitored how the ratio of ethylene dimers, trimers, and tetramers and the isomeric composition of ethylene trimers vary with time.

In the initial period, ethylene predominantly dimerizes into butenes, with 95–97% content of 2-butene (*cis* + *trans*), according to GLC. As butenes accumulate in the reaction volume, they start to codimerize with ethylene. In the next period (1.5 h after the start of the experiment), octenes (products of codimerization of hexenes with ethylene) appear in the reaction volume. Butenes, apparently, do not enter into homodimerization, otherwise octenes would appear in the reaction volume from the beginning of the experiment. The major components of ethylene oligomers by the end of the process are hexenes. Their content in the oligomer mixture reaches 61%. The isomeric composition of hexenes varies insignificantly in the course of ethylene oligomerization. The relative content of 2-methyl-2-pentene (*cis* + *trans*) by the end of the experiment is 80%.

We examined the influence exerted on the selectivity of ethylene trimerization into 3-methyl-2-pentene (*cis* + *trans*) by the solvent, B/Pd atomic ratio, catalyst concentration, and temperature.

The content of trimers in the oligomer mixture drastically decreases in the series of aromatic solvents benzene > toluene > isopropylbenzene (from 65.7 to 15.5%, Table 2). This trend may be due to competition between olefins and aromatic hydrocarbons for the vacancies in the AC coordination sphere. With an increase in the solvent polarity, secondary processes of ethylene oligomerization associated with the formation of hexenes and octenes are suppressed.

Table 3. Influence of the B/Pd atomic ratio on the conversion of ethylene into oligomers and composition of oligomers ($c_{Pd} = 8.33 \times 10^{-3}$ M, solvent benzene, $V_0 = 30$ ml, synthesis time 1.5 h)

B/Pd	Oligomeric components, wt %			Isomers of C_6H_{12}, wt %		Conversion, (mol C_2) (g-at. Pd)$^{-1}$
	C_4H_8	C_6H_{12}	C_8H_{16}	3-methyl-2-pentene, *cis* + *trans*	other hexenes	
3	53.1	46.9	–	86.2	13.8	821
5	32.8	64.3	2.9	86.1	13.9	970
10	26.6	65.2	6.2	86.9	13.1	985
20	34.3	65.7	–	86.5	13.5	1260
30	32.5	66.1	1.4	87.9	12.1	1214
40	27.8	70.3	1.9	86.7	13.3	1257

Table 4. Influence of the $Pd(Acac)_2$ concentration on the conversion of ethylene into oligomers and composition of oligomers (303 K, solvent benzene, $V_0 = 30$ ml, synthesis time 1.5 h)

$c_{Pd} \times 10^3$, M	Oligomeric components, wt %			Isomers of C_6H_{12}, wt %		Conversion, (mol C_2) (g-at. Pd)$^{-1}$
	C_4H_8	C_6H_{12}	C_8H_{16}	3-methyl-2-pentene, *cis* + *trans*	other hexenes	
1.67	74.1	25.9	–	86.3	13.7	3000
3.33	71.0	29.0	–	86.0	14.0	2000
8.33	34.3	65.7	–	86.5	13.5	1260
16.7	11.3	77.9	10.8	91.2	8.8	864

Table 5. Influence of temperature on the conversion of ethylene into oligomers and composition of oligomers ($c_{Pd} = 1.66 \times 10^{-3}$ M, solvent benzene, $V_0 = 30$ ml, synthesis time 1.5 h)

T, K	Oligomeric components, wt %			Isomers of C_6H_{12}, wt %		Conversion, (mol C_2) (g-at. Pd)$^{-1}$
	C_4H_8	C_6H_{12}	C_8H_{16}	3-methyl-2-pentene, *cis* + *trans*	other hexenes	
298	93.9	6.1	–	100	–	1600
303	74.1	25.9	–	86.3	13.7	3000
308	77.5	22.5	–	88.1	11.9	2900
313	71.0	29.0	–	88.6	14.4	2200
318	64.0	36.0	–	86.1	13.9	1800

Variation of the B/Pd atomic ratio in the range 5–40 (Table 3) does not lead to noticeable changes in the selectivity of ethylene oligomerization. The ethylene conversion grows as the B/Pd atomic ratio increases to 20, as in dimerization of propylene [18]. Further increase in the B/Pd atomic ratio to 40 does not noticeably affect the ethylene conversion.

The total conversion of ethylene into oligomers is strongly influenced by the catalyst concentration. At a relatively low catalyst concentration ($c_{Pd} = 1.67 \times 10^{-3}$ M), the conversion of ethylene into oligomers can reach 3000 mol of ethylene per 1 g-at. of Pd (Table 4).

With a decrease in the catalyst concentration from 16.7×10^{-3} to 1.67×10^{-3} M, the content of butenes in the oligomer mixture rapidly increases. The fraction of ethylene dimers in the oligomer mixture also grows with decreasing reaction temperature (Table 5). By contrast, the conversion of ethylene into oligomers passes through a maximum. This is due to the fact that, on the one hand, the stability of the catalytic system and the C_2H_4 : Pd ratio increase with decreasing catalyst concentration and temperature and, on the other hand, the catalyst becomes less active with decreasing temperature. The latter factor becomes decisive at temperatures below 303 K and is

Table 6. Influence of acetylacetone additions on the conversion of ethylene into oligomers and composition of oligomers ($c_{Pd} = 8.33 \times 10^{-3}$ M, 318 K, solvent benzene, $V_0 = 30$ ml, synthesis time 1.5 h)

AcacH : $Pd(Acac)_2$	Oligomeric components, wt %			Isomers of C_6H_{12}, wt %		Conversion, (mol C_2) (g-at. Pd)$^{-1}$
	C_4H_8	C_6H_{12}	C_8H_{16}	3-methyl-2-pentene, *cis* + *trans*	other hexenes	
–	31.8	68.2	–	83.5	16.5	630
6	15.9	71.3	12.7	85.9	14.1	900
8	4.3	81.2	15.5	87.5	12.5	1000
10	17.2	78.7	4.1	85.2	14.8	560

Table 7. Influence of the catalyst concentration on the conversion of ethylene into oligomers and composition of oligomers (328 K, solvent benzene, $V_0 = 30$ ml, synthesis time 1.5 h)

$c_{Pd} \times 10^3$, M	Oligomeric components, wt %			Isomers of C_6H_{12}, wt %		Conversion, (mol C_2) (g-at. Pd)$^{-1}$
	C_4H_8	C_6H_{12}	C_8H_{16}	3-methyl-2-pentene, *cis* + *trans*	other hexenes	
1.67	59.2	40.8	–	83.5	16.5	1750
3.33	2.7	84.2	13.1	87.5	12.7	1360
8.33	8.7	79.1	12.2	85.1	14.9	540
16.7	5.8	73.8	20.7	84.1	15.9	420

manifested in a decrease in the ethylene conversion from 3000 to 1600 mol of ethylene per 1 g-at. of Pd at 298 K. The major factor responsible for the decrease in the ethylene conversion at elevated temperatures is thermal decomposition of the catalyst to give a metallic mirror on the walls of the reaction vessel.

To raise the conversion of ethylene specifically into 3-methyl-2-pentene (*cis* + *trans*), we studied the oligomerization of ethylene in the presence of the catalytic system $Pd(Acac)_2/BF_3OEt_2$ modified with acetylacetone additions (Table 6). At the AcacH/Pd ratio of 8, the content of hexenes in the oligomer mixture reaches 81%.

Data on the oligomerization of ethylene on the catalytic system $Pd(Acac)_2$ + 5AcacH + $30BF_3OEt_2$ at 328 K are listed in Table 7. At a catalyst concentration $c_{Pd} = 3.33 \times 10^{-3}$ M, ethylene oligomerizes predominantly into 3-methyl-2-pentene (*cis* + *trans*). At the 3-methyl-2-pentene (*cis* + *trans*) content in the mixture of hexenes of up to 87.5%, and of hexenes in the oligomer mixture of up to 84.2%, the conversion of ethylene specifically into 3-methyl-2-pentene (*cis* + *trans*) is about 1000 mol of ethylene per 1 g-at. of Pd, or 74% of the total conversion of ethylene into oligomers (Table 7).

It is known that reactions of individual Pd(0) complexes of the type $Pd(PR_3)_2$ with Brønsted acids of the type HBF_4 or HBF_3OH [19–21] yield palladium hydride complexes, e.g., $HPd(PCy_3)_2BF_3X$, where X = F or OH, which can be regarded as models of complexes $HPd(L_2)BF_4$ active in transformations of alkenes.

To understand the modifying effect of acetylacetone on the catalytic system $Pd(Acac)_2$–BF_3OEt_2 in selective trimerization of ethylene, we studied the reaction of acetylacetone with boron trifluoride etherate by ^{1}H NMR and IR spectroscopy, at the ratio BF_3OEt_2 : AcacH = 2 : 1. The IR spectrum of the reaction products contains bands at 529 and 522 cm^{-1}, characteristic of the BF_4^- anion, and the ^{1}H NMR spectrum contains a signal at δ 9.7 ppm from the proton in HBF_4 apparently formed by the reaction

$$\text{AcacH} + 2BF_3OEt_2 \xrightarrow{-2OEt_2} HBF_4 + BF_2(\text{Acac}). \quad (1)$$

Thus, the modifying effect of acetylacetone can be accounted for by preliminary in situ formation of HBF_4 in the reaction mixture, followed by its involvement in the regeneration of AC by the reaction with Pd(0):

$$Pd(0) + HBF_4 + 2C_2H_4 \rightarrow [H\text{–}Pd(C_2H_4)_2]^+BF_4^-, \quad (2)$$

$$[H\text{–}Pd(C_2H_4)_2]^+BF_4^- \rightleftarrows H\text{–}Pd(C_2H_4)_2F \cdot BF_3. \quad (3)$$

CONCLUSIONS

(1) In modification of the catalytic system $Pd(Acac)_2/BF_3OEt_2$ with acetylacetone, the selectivity of formation of 3-methyl-2-pentene in low-molecular-weight oligomerization of ethylene reaches 87% relative to the sum of hexene, which, in turn, amounts to 84% of the sum of the oligomers.

(2) The modifying role of acetylacetone may consist in formation of HBF_4 in its reaction with $BF_3 \cdot OEt_2$.

REFERENCES

1. Keim, W., Behr, A., and Röper, M., *Alkene and Alkyne Oligomerization, Cooligomerization, and Telomerization Reactions, Comprehensive Organometallic Chemistry*, Oxford: Pergamon, 1982, vol. 8, pp. 371–462.
2. Al-Jarallah, A.M., Anabaisi, J.A., Siddiqui, M.A.B., et al., *Catal. Today*, 1992, vol. 14, pp. 1–124.
3. Patent Appl. WO 02/04 119, 2002.
4. Dixon, J.T., Green, M.J., Hess, F.M., and Morgan, D.H., *J. Organomet. Chem.*, 2004, vol. 689, pp. 3641–3668.
5. Myagmarsuren, G., Tkach, V.S., and Shmidt, F.K., *React. Kinet. Catal. Lett.*, 2004, vol. 83, no. 2, pp. 337–343.
6. Tkach, V.S., Suslov, D.S., *Myagmarsuren Gomboogiin, et al., Zh. Prikl. Khim.*, 2006, vol. 79, no. 1, pp. 88–91.
7. Tkach, V.S., Myagmarsuren, G., Mesyef, M., and Shmidt, F.K., *React. Kinet. Catal. Lett.*, 1999, vol. 66, no. 2, pp. 281–287.
8. Myagmarsuren, G., Tkach, V.S., Shmidt, F.K., et al., *J. Mol. Catal., A: Chem.*, 2005, vol. 235, pp. 154–160.
9. Chernyshev, M.L., Tkach, V.S., Dmitrieva, T.V., et al., *React. Kinet. Catal. Lett.*, 1992, vol. 66, no. 2, pp. 291–294.
10. Chernyshev, M.L., Tkach, V.S., Dmitrieva, T.V., et al., *Kinet. Katal.*, 1997, vol. 38, no. 4, pp. 575–580.
11. Keim, W., Röper, M., and Scheren, A., *J. Mol. Catal. A: Chem.*, 1983, vol. 20, p. 139.
12. Myagmarsuren, G., Ki-Soo Lee, O-Yong Jeong, and Son-Ki Ihm, *Catal. Commun.*, 2003, vol. 4, pp. 615–619.
13. Myagmarsuren, G., O-Yong Jeong, and Son-Ki Ihm, *Appl. Catal., A: General*, 2005, vol. 296, pp. 21–29.
14. Gordon, A.J. and Ford, R.A., *The Chemist's Companion. A Handbook of Practical Data, Techniques, and References*, New York: Wiley, 1972.
15. Kolthoff, I.M., Belcher, R., Stenger, V.A., and Matsuyama, G., *Volumetric Analysis, vol. 3: Titration Methods: Oxidation–Reduction Reactions*, New York: Interscience, 1957.
16. Rapoport, F.M. and Il'inskaya, A.A., *Laboratornye metody polucheniya chistykh gazov* (Laboratory Methods for Preparing Pure Gases), Moscow: GNTIKhL, 1963.
17. Grinberg, A.A. and Simonova, L.K., *Zh. Prikl. Khim.*, 1953, vol. 26, no. 8, pp. 880–882.
18. Myagmarsuren, G., Tkach, V.S., Suslov, D.S., and Shmidt, F.K., *React. Kinet. Catal. Lett.*, 2005, vol. 85, no. 1, pp. 197–203.
19. Sommovigo, M., Pasquali, M., Leoni, P., et al., *J. Organomet. Chem.*, 1991, vol. 418, p. 119.
20. Di Bugno, C., Leoni, P., and Pasquali, M., *Gazz. Chim. Ital.*, 1988, vol. 118, p. 861.
21. Leoni, P., Sommovigo, M., Pasquali, M., et al., *Organometallics*, 1991, vol. 10, p. 1038.

ISSN 1070-4272, Russian Journal of Applied Chemistry, 2007, Vol. 80, No. 8, pp. 1424–1428. © Pleiades Publishing, Ltd., 2007.
Original Russian Text © B.B. Troitskii, L.V. Khokhlova, V.N. Denisova, M.A. Novikova, D.A. Smirnov, M.A. Baten'kin, 2007, published in Zhurnal Prikladnoi Khimii, 2007, Vol. 80, No. 8, pp. 1385–1390.

MACROMOLECULAR CHEMISTRY AND POLYMERIC MATERIALS

Influence of the Synthesis Conditions of Emulsion Poly(Methyl Methacrylate) on the Surface Structure of the Specimens

B. B. Troitskii, L. V. Khokhlova, V. N. Denisova, M. A. Novikova, D. A. Smirnov, and M. A. Baten'kin

Razuvaev Institute of Organometallic Chemistry, Russian Academy of Sciences, Nizhni Novgorod, Russia

Received February 22, 2007

Abstract—The surface structure of poly(methyl methacrylate) specimens prepared by emulsifier-free emulsion polymerization of methyl methacrylate was examined in relation to the synthesis conditions (pH of the medium, initiator concentration, and addition of organosilicon compounds).

DOI: 10.1134/S1070427207080320

A considerable attention is received today by polymeric periodic nanosize structures, the so-called colloid crystals [1–10]. Research efforts in this field are aimed to prepare monodisperse colloid particles capable of strictly ordered stacking. A source of such particles can be found, e.g., in products of emulsion polymerization, such as polystyrene (PS) [1, 2], copolymers of styrene with methacrylic acid or glycidyl methacrylate [3, 4], poly(methyl methacrylate) (PMMA) [3, 5], poly-*tert*-butyl methacrylate [6], copolymers of methyl methacrylate (MMA) with styrene [7–9], and copolymers of 2-hydroxypropyl methacrylate with 4-vinylpyridine, obtained in the presence of organosilicon compounds [10].

The above-mentioned materials [1–10] have been synthesized by emulsifier-free emulsion polymerization yielding stable polymer dispersions with particles of identical size in water. Dispersions of this kind have been used for preparing photonic crystals [2–10]. It should be noted that the most extensively studied was the emulsifier-free polymerization of hydrophobic styrene monomer in water in the presence of a hydrophilic initiator, potassium (sodium, ammonium) persulfate [1].

The major task to be accomplished now is to find the best conditions for preparing strictly ordered colloid crystals. This makes it necessary to examine the crystal structure in relation to the preparation technique of colloid particles.

In this study, we examined the particle-size distribution of PMMA latexes as influenced by the conditions of emulsifier-free emulsion polymerization of MMA (pH of the medium, initiator concentration, and additions of alkoxysilanes). Also, we analyzed the suitability of these dispersions for preparation of colloid crystals.

EXPERIMENTAL

The PMMA specimens were prepared by emulsifier-free emulsion polymerizations of MMA in acid, neutral, and alkaline media (pH 3, 5, 7, 9, 10) with 0.07, 0.08, 0.35, and 1.00% potassium persulfate $K_2S_2O_8$ as initiator. The pH value was adjusted with 0.1 M HCl or 0.1 M NaOH, introduced into tvice-distilled water; it was measured on a Potential laboratory potentiometric titrometer. We did not introduce buffer additions to avoid further complication of the system. During polymerization, the pH of the system tends to decrease owing to decomposition of the initiator [1, 12]. In selected experiments, a prescribed amount (1, 3, 5, 7, 10, and 20 wt%) of tetraethoxysilane (TEOS) was added to the reaction mixture.

Water (10 ml) with a known pH of the medium was poured into a 50-ml three-necked flask equipped with a reflux condenser, stirrer, and capillary for argon supply, and heated to 80°C. When the desired temperature was achieved, 1.0 ml of the monomer, MMA, was added, and the mixture was stirred for 5 min. Next, 1.0 ml of a solution of the initiator, potassium persulfate (0.07, 0.08, 0.35, and 1.00% of the weight of the mixture) was added (in selected

Conditions of synthesis and properties of the specimens of emulsion PMMA

Run no.	pH	$K_2S_2O_8$	TEOS	Diameter, nm		rms deviation, %	Structure
		wt %		of particles	number-average		
1	3	0.07	–	233–385	315	18	Weakly ordered
2	7	0.07	–	205–294	250	9	Ordered
3	7	0.08	–	250–304	282	5	〃
4	7	0.35	–	258–352	303	6	〃
5	9	0.07	–	230–288	252	6	〃
6	10	0.35	–	170–260	209	11	Weakly ordered
7	5	0.07	20	140–329	218	21	Disordered
8	7	0.07	20	200–240	221	4	Ordered
9	10	1.00	1	252–380	300	12	Weakly ordered
10	10	1.00	3	250–810	617	24	Disordered
11	10	1.00	5	321–620	512	22	〃
12	10	1.00	10	260–700	485	24	〃

experiments, a prescribed amount of TEOS was also added). After that, the reaction mixture was stirred for 3–5 h at 80°C in an argon stream.

The resulting emulsion was poured onto a horizontal glass surface. After evaporation of the dispersion medium, the specimens were dried in a vacuum desiccator at 20 mm Hg and 60–80°C for 4–6 h. The dried specimens were ~400-μm-thick white opaque plates or scales, several millimeters in size (see table).

The surface of the specimens was examined by atomic-force microscopy (AFM) on Smena-A and Solver-P47 microscopes. The number-average diameter of the submicrometer particles was determined by AFM (no less than 100 measurements of the particle diameter in each case).

The emulsifier-free emulsion polymerization of MMA was carried out in the presence of potassium persulfate as initiator. Previous studies of the decomposition of potassium persulfate at 60°C in water with and without a monomer [1] have shown that the rate constant of initiator decomposition with styrene exceeds that without the monomer by an order of magnitude (8.6×10^{-5} against 5.02×10^{-6} s^{-1}). Presumably, a similar effect is also observed in the case of MMA. The initiation scheme can be represented by the equation

$$S_2O_8^{2-} + MMA \rightarrow \underset{\mathbf{A}}{SO_4^{-\cdot}} + \underset{\mathbf{B}}{{}^{-}O\text{–}\overset{\overset{O}{\|}}{\underset{\underset{O}{\|}}{S}}\text{–}O\text{–}MMA^{\cdot}}. \quad (1)$$

Free radical **B** in reaction (2) with the monomer is converted to a macroradical:

$$\begin{aligned} &{}^{-}O\text{–}\overset{\overset{O}{\|}}{\underset{\underset{O}{\|}}{S}}\text{–}O\text{–}MMA^{\cdot} + n\,MMA \\ &\rightarrow {}^{-}O\text{–}\overset{\overset{O}{\|}}{\underset{\underset{O}{\|}}{S}}\text{–}O\text{–}(MMA)_n\text{–}MMA^{\cdot}. \end{aligned} \quad (2)$$

Free radical **A** can be involved in reactions (3) and (4) with water and with the monomer:

$$SO_4^{-\cdot} + H_2O \rightarrow HSO_4^{-} + {}^{\cdot}OH, \quad (3)$$

$$SO_4^{-\cdot} + MMA \rightarrow {}^{-}O\text{–}\overset{\overset{O}{\|}}{\underset{\underset{O}{\|}}{S}}\text{–}O\text{–}MMA^{\cdot}. \quad (4)$$

Reactions (1), (2), and (4) yield macromolecular surfactants with a biphilic structure comprising an ionic hydrophilic group at the chain end and a hydrophobic part of the macrochain consisting of MMA units.

$$K^{+}\,{}^{-}O\text{–}\overset{\overset{O}{\|}}{\underset{\underset{O}{\|}}{S}}\text{–}O\text{–}\sim\!\sim$$

During polymerization in an aqueous medium, the biphilic macromolecules acting as surfactants become self-organized and form a colloid system of polymer-monomer particles. A major stabilization factor for the colloid system in emulsion-free polymeriza-

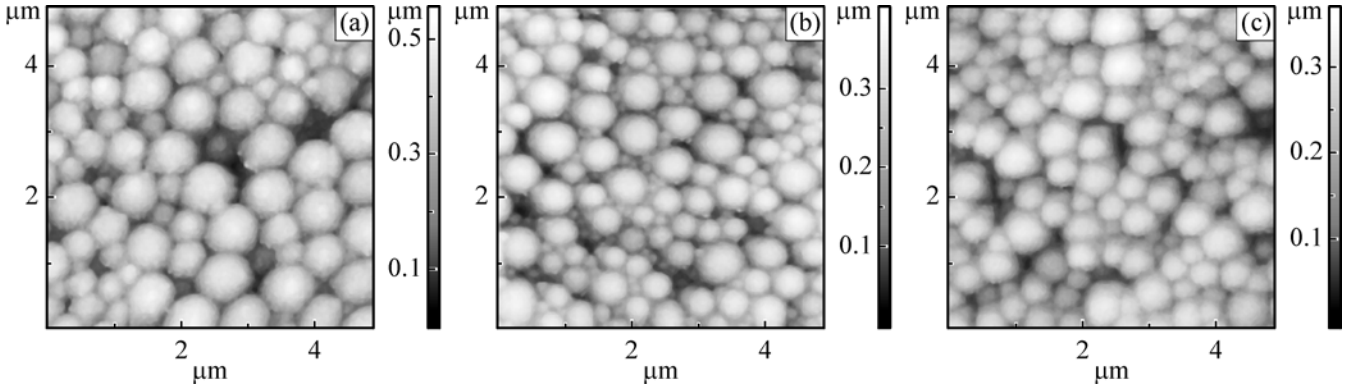

Fig. 1. Surface topographs of PMMA emulsions obtained at pH 10 at the $K_2S_2O_8$ concentration of 1.00 wt %. TEOS additive, wt %: (a) 3.0, (b) 5.0, and (c) 10.0.

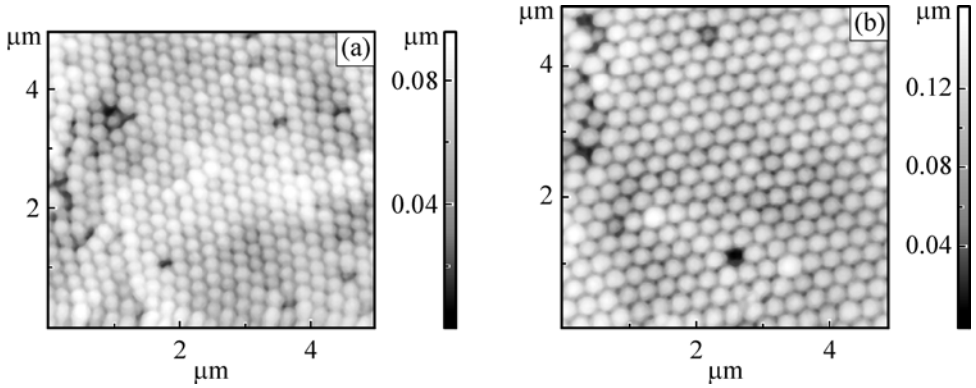

Fig. 2. Surface topographs of PMMA emulsion obtained at pH 7. Initiator concentration, wt %: (a) 0.08 and (b) 0.35.

tion of styrene or MMA in the presence of potassium persulfate is electrostatic repulsion of the particles having an electric double layer on the surface [1].

Let us analyze the experimental data in the context of the influence of various polymerization conditions on the stability of the colloid system and, hence, on the uniformity in shape and size of the resulting polymer particles. It is known [2] that uniformity in shape and size of the latex particles is one of the major preconditions for preparation of colloid crystals from these particles.

Figure 1 and the table (run nos. 9–12) show that the particle-size distribution is especially broad in the case of polymerization of MMA with the maximal concentration of the initiator, 1.0 wt %.

It is well known [12] that addition of inorganic salts (electrolytes) to a colloid system causes an increase in the ionic strength of the dispersion medium (water), compression of the electric double layer on the surface of the particles, and decrease in the stability of the dispersion. At a certain, relatively low, concentration of the salt (coagulation threshold), the colloid system breaks down (coagulates) [12]. Probably, potassium persulfate, which is an inorganic salt, impairs the stability of the polymer-monomer particles at a concentration of 1.0 wt %. This is responsible for the broad particle-size distribution (see table, run nos. 9–12). These latexes are unsuitable for preparation of colloid crystals (Fig. 1).

The latex obtained by polymerization of MMA at an initiator concentration lower by an order of magnitude (0.08 wt %) in the neutral medium gives a specimen whose surface consists of nanoparticles with identical sizes and shapes (see table, run no. 3; Fig. 2a). The specimen surface becomes iridiscent.

Polymerization of MMA at a low initiator concentration (0.07, 0.08 and 0.35 wt %) in a neutral (pH 7) or weakly alkaline (pH 9) medium (see table, run nos. 2–5) yields latexes that give a strictly ordered, densely packed structures (Figs. 2–4), with the regular stacking preserved up to 20 μm. An exam-

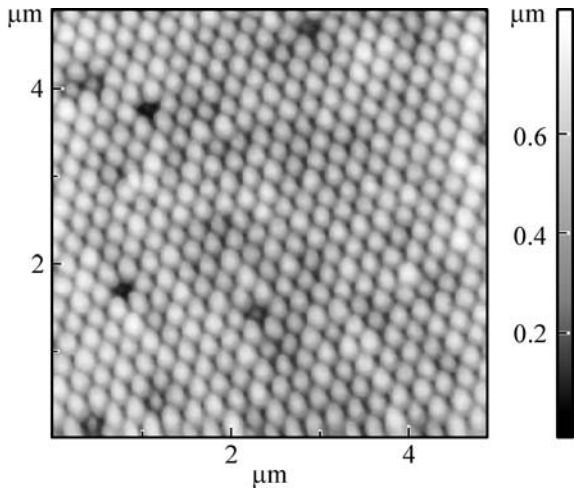

Fig. 3. Surface topograph of a PPMA emulsion obtained at pH 9 at the initiator concentration of 0.07 wt %.

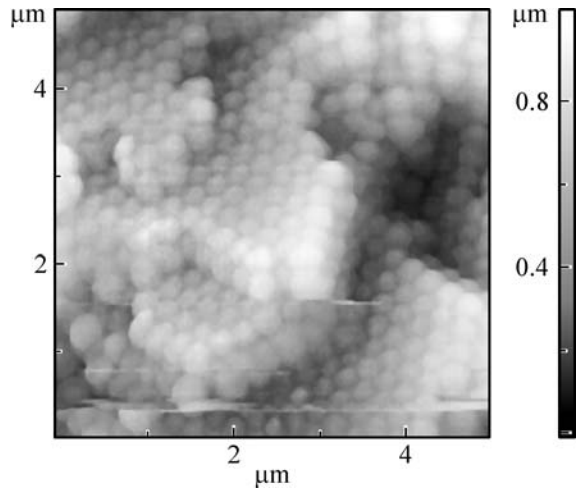

Fig. 4. End face topograph of PPMA emulsion obtained at pH 7 at the initiator concentration of 0.08 wt %.

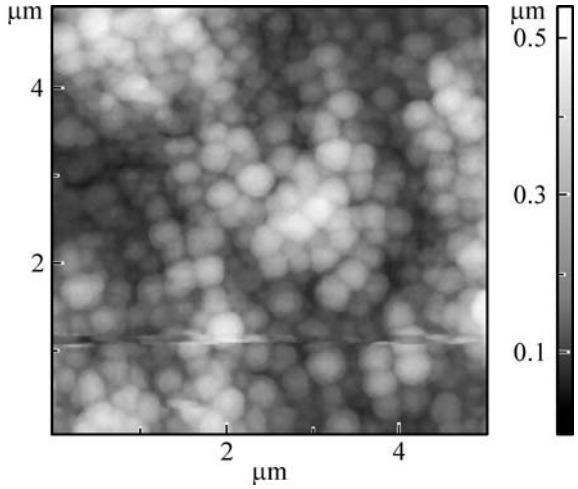

Fig. 5. Surface topograph of PMMA emulsion obtained at pH 3 at the initiator concentration of 0.07 wt %.

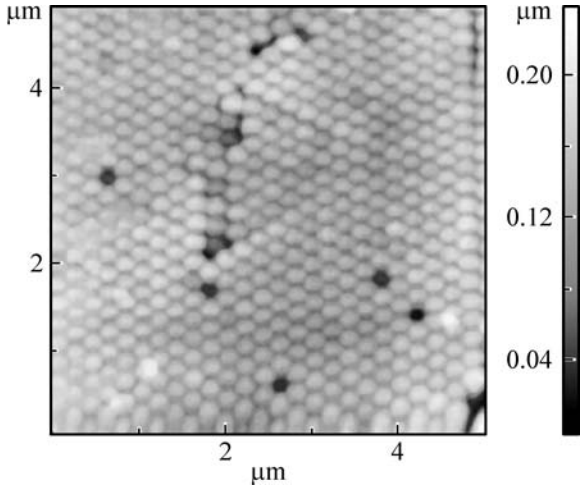

Fig. 6. Surface topograph of PMMA emulsion obtained at pH 7 at the initiator concentration of 0.07 wt %, with 20.0 wt % TEOS added.

ination of the topology of the end face of these specimens showed that, in the polymer bulk, particles of the same size are packed similarly (Fig. 4). Thus, these polymer specimens are 3*D* colloid crystals containing nearly a hundred of periods of submicrometer particles.

Acid medium (pH 3–5) in emulsifier-free emulsion polymerization of MMA causes, even at low initiator concentrations, the stability of the latex particles to decrease and their size distribution to broaden (see table, run nos. 1, 7). These latexes give specimens with a weakly ordered surface structure (Fig. 5).

As is known [11], hydrogen ions (acid medium) catalyze thermal decomposition of potassium persulfate in an aqueous medium. The activation energy of thermal decomposition of potassium persulfate in neutral and alkaline media (0.1 M NaOH) is 33.5 kcal mol^{-1}, and that in an acid medium (0.1 M $HClO_4$) is considerably lower, 26.0 kcal mol^{-1} [11]. Moreover, thermal decomposition of potassium persulfate proceeds by a different mechanism in an acid medium. The catalytic thermal decomposition of the initiator is described by the equations

$$S_2O_8^{2-} + H^+ \rightarrow HS_2O_8^- \rightarrow SO_4 + HSO_4^-, \quad (5)$$

$$SO_4 \rightarrow SO_3 + 1/2O_2. \quad (6)$$

There are no data on the kinetics and mechanism of catalytic decomposition of potassium persulfate

in an acid medium in the presence of monomers (styrene, MMA).

The data reported in [1, 11] suggest that reactions (5) and (6), characterized by a decreased activation energy, will compete with reaction (1), which is the basic reaction of synthesis of a biphilic surfactant stabilizing the colloid system. This will decrease both the surfactant concentration and the stability of the colloid system.

Interestingly, the emulsifier-free emulsion polymerization of MMA in a neutral medium with a low concentration of the initiator (0.07 wt %) and 20 wt % TEOS added yields a latex forming the most perfect colloid crystal (see table, run no. 8; Fig. 6). The same process with 1 wt % initiator yields latexes with the broadest particle-diameter distribution (see table, run nos. 9–12).

Upon drying in a vacuum desiccator at 60–80°C for several hours, the spherical particles in the specimens of the colloid crystals undergo minor deformations (Figs. 2–4). In the presence of TEOS, the MMA polymerization is paralleled by a sol-gel process yielding a thin layer of cross-linked silicon oxide on the surface of the latex particles. Probably, this layer prevents deformation of the latex particles, and their initial spherical shape is better preserved upon drying of the colloid crystal (Fig. 1).

Thus, formation of a strictly ordered surface structure of the colloid crystal from the latex prepared by emulsifier-free emulsion polymerization of MMA is most probable in the neutral medium with the minimal percentage (by weight) of the initiator and without alkoxysilane additions.

CONCLUSIONS

(1) Emulsifier-free emulsion polymerization of methyl methacrylate, initiated by potassium persulfate, yields colloid particles of identical shape and size at the lowest, within the range examined (0.07–0.35 wt %), concentration of the initiator in the reaction mixture.

(2) Formation from latex of a strictly ordered surface structure of the poly(methyl methacrylate) specimens suitable for preparation of colloid crystals is most probable when the emulsion polymerization of methyl methacrylate is performed in a neutral medium with the minimal percentage (by weight) of the initiator.

REFERENCES

1. Tauer, K., Deckwer, R., Kuhn, I., et al., *Colloid Polym. Sci.*, 1999, vol. 277, pp. 607–626.
2. Sinitskii, A.S., Khokhlov, P.E., Abramova, V.V., et al., *Mendeleev Commun.*, 2007, vol. 17, pp. 4–6.
3. Men'shikova, A.Yu., Shabsel's, B.M., Evseeva, T.G., et al., *Zh. Prikl. Khim.*, 2005, vol. 78, no. 1, pp. 161–167.
4. Men'shikova, A.Yu., Bilibin, A.Yu., Shevchenko, N.N., et al., *Vysokomol. Soedin., Ser. A*, 2006, vol. 48, no. 9, pp. 1579–1587.
5. Egen, M. and Zentel, R., *Macromol. Chem. Phys.*, 2004, vol. 205, pp. 1479–1488.
6. Zhong-Ze, Gu, Fujishima, Akira, and Sato, Osamu, *Chem. Mater.*, 2002, vol. 14, no. 2, pp. 760–765.
7. Lee, C.-F., *Colloid Polym. Sci.*, 2002, vol. 280, pp. 116–123.
8. Okudo, M., Izumi, J., and Takekoh, R., *Colloid Polym. Sci.*, 1999, vol. 277, pp. 875–880.
9. Okudo, M., Takekoh, R., and Sugano, H., *Colloid Polym. Sci.*, 2000, vol. 278, pp. 559–564.
10. Percy, M.J., Michailidou, V., Armes, S.P., et al., *Langmuir*, 2003, vol. 19, no. 6, pp. 2072–2079.
11. Kolthoff, I.M. and Miller, I.K., *J. Am. Chem. Soc.*, 1951, vol. 73, no. 7, pp. 3055–3059.
12. Voyutskii, S.S., *Kurs kolloidnoi khimii* (A Course of Colloid Chemistry), Moscow: Khimiya, 1976.

ISSN 1070-4272, Russian Journal of Applied Chemistry, 2007, Vol. 80, No. 8, pp. 1429–1431. © Pleiades Publishing, Ltd., 2007.
Original Russian Text © M.S. Masalovich, L.P. Ardasheva, G.A. Shagisultanova, 2007, published in Zhurnal Prikladnoi Khimii, 2007, Vol. 80, No. 8, pp. 1391–1393.

BRIEF COMMUNICATIONS

Thin-Film Conducting Polymers Based on Ni(II), Pd(II), and Pt(II) Complexes with 8-Quinolinol

M. S. Masalovich, L. P. Ardasheva, and G. A. Shagisultanova

Herzen Russian State Pedagogical University, St. Petersburg, Russia

Received May 16, 2007

Abstract—New thin polymeric films were prepared electrochemically on the basis of Ni(II), Pd(II), and Pt(II) complexes with 8-quinolinol, and conditions of synthesis were optimized. Basic characteristics of the films such as the thickness, charge transfer rate in the polymeric matrix, and photovoltaic effect were determined.

DOI: 10.1134/S1070427207080332

This study was aimed at solving fundamental problems related to synthesis and characterization of new thin-film organometallic polymers. Among basic characteristics of these materials are the electrical conductivity, electrochromism, photosensitivity, and luminescent properties. The necessity for improving electrochemical and photoelectrochemical characteristics, including the efficiency of charge transfer in the bulk of the polymer phase, stimulates a search for new organometallic polymers that can be used in devices for accumulation and conversion of solar energy (environmentally friendly solid-state voltaic cells and photosensors), and also as corrosion inhibitors, catalysts, materials for electrochromic devices, and chemical sensors. Studies in this field are actively pursued today.

Previously, a series of electroactive and photosensitive polymers have been synthesized by electrochemical oxidation on the basis of transition metal complexes with tetra- and bidentate Schiff bases containing such coordination cores as $N_2O_2^-$, N_4^-, and NO^- [1–5].

In this study, we examined transition metal complexes with another bidentate ligand, 8-quinolinol (qol), which, like Schiff bases, contains two functional groups with N and O heteroatoms involved in coordination to the central atom. In this case, the nitrogen atom is arranged in the pyridine ring of 8-quinolinol, in contrast to the previously studied ligand meSal [2], which coordinates to the metal via the nitrogen atom of the imino group.

Another distinctive feature of complexes with qol ligand, compared to complexes with Salen-like ligands, is their *trans* geometry. Therefore, one of the main goals of this study was to understand the effect of the qol ligand structure and coordination mode to the metal center on the electropolymerization of the complex.

Electropolymerization of complexes $[M(qol)_2]$, where M = Ni(II), Pd(II), and Pt(II),

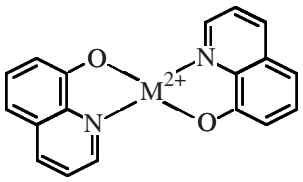

was carried out according to the procedure described in [2–5]. First, we optimized the synthetic conditions. The largest thickness of poly$[Ni(qol)_2]$ films (0.17 μm) was obtained by 15-fold cycling of the potential of a Pt wire electrode from 0.0 to 1.3 V in the acetonitrile solution of the complex (Fig. 1). As can be seen, potential cycling is accompanied by an increase in both the anodic and cathodic current peaks in the cyclic voltammograms and also by a gradual shift of peaks. As a result, by the 15th cycle, when the growth of the current peaks virtually ceases, there are one anodic peak at E_{pa} = 1.0 V and one cathodic peak at E_{pc} = 0.5 V. It has been demonstrated previously that an increase in the hight of the anodic and cathodic peaks is caused by the growth of the electroactive polymer film on the electrode, which can be observed visually. In this case, the transfer from the reduced form to the oxidized form is accompanied by an electrochromic effect (originally light green color becomes reddish yellow).

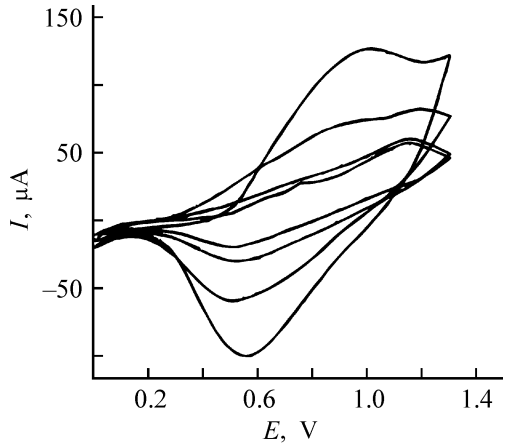

Fig. 1. Cyclic voltammograms after 1, 2, 5, and 15 potential sweep cycles (1 mM $[Ni(qol)_2]$ in 0.1 M Bu_4NClO_4/CH_3CN; v_s = 0.05 V s^{-1}). (*I*) Current and (*E*) potential.

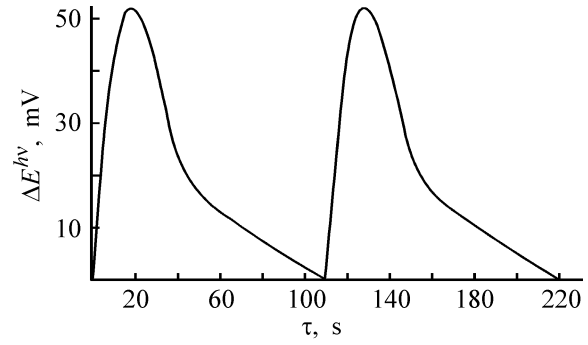

Fig. 2. Change in the potential $\Delta E^{h\nu}$ on the electrode with a deposited polymer film of $[Pd(qol)_2]$ (h_f = 0.07 μm) vs. the time τ of irradiation with polychromatic light in 0.1 M CH_3CN/Bu_4NClO_4.

Electrochemical synthesis of the polymer on the basis of the Pd complex under similar conditions gives a thinner (0.07 μm) and, therefore, less stable conducting layer. It was demonstrated in studying the possibility of oxidative polymerization of $[Ni(qol)_2]$ that an electroactive polymer is not formed in the potentiostatic mode at accumulation potentials *E* of +0.8, +0.9, +1.0, +1.1, and +1.2 V and fixed accumulation time of 10 min, suggesting that mechanisms of electropolymerization of the complexes in the dynamic and static accumulation modes are different.

A distinctive feature of $[Pt(qol)_2]$ is that it can be polymerized in the static mode at an accumulation potential E_{ac} = 1.0 and time τ_{ac} = 30–40 min in a dichloromethane solution of the supporting electrolyte. In this case. the thickness of the resulting films are even thicker (up to 2.2 μm) higher than that obtained with [PtSalen] [3].

The most important feature of poly$[M(qol)_2]$ is that they can occur in thin films in both oxidized and reduced forms. The IR spectra of poly$[Pt(qol)_2]$ confirmed the suggestion that the oxidized form is conducting, while the reduced form exhibits dielectric properties [1]. Poly$[Pt(qol)_2]$ in the oxidized form is characterized by a virtually full absorption ($T \sim 0$) in the near IR range (14000–4000 cm^{-1}), which confirms the presence of free charge carriers in the polymer matrix. At the same time, for the reduced form, the transmission increases, which suggests a decrease in the concentration of the radical cations [6] and loss of the conductivity.

Therefore, it is the ability of polymeric systems of this kind to undergo reversible electro- and photoinduced transitions from one form to another that is responsible for their conductivity, electrochromism, and photoelectrochemical activity. In this context, it was important to study features of charge transfer in the bulk of the polymer phase. Quantitatively, the charge transfer rate is characterized by the diffusion coefficient. The maximal diffusion coefficient of poly$[Ni(qol)_2]$ is 1.4×10^{-12} cm^2 s^{-1}, which is well consistent with that of Ni(II) complexes with Salen and MeSal in the films of similar thickness (~0.2 μm) [2, 4, 5]. The highest charge-transfer rate in the polymer matrix was observed for poly$[Pt(qol)_2]$ (D_{ct} = 8.0×10^{-11} cm^2 s^{-1}), which accounts for the high degree of reversibility of redox processes and for the resulting considerable electrochemical stability.

All the polymers investigated exhibit photoelectric activity. Photons excite some molecular fragments of the polymer, and oxidized fragments of the complex are accumulated by virtue of photoexcitation of the reduced form of the polymer and chain charge transfer, causing an abrupt change in the potential and the photovoltaic effect. The leveling off of the curve can be attributed to the attainment of a steady state in the system under irradiation, in which the rates of formation of excited fragments and of their deactivation are equal. In repeated photoexcitation of the electrode–polymer system, the photovoltaic effect is reproduced, which suggests the stability of the polymer to the action of light and reversibility of charge transfer in the bulk of the polymer phase.

In the supporting electrolyte solution continuously irradiated with polychromatic light, we observed an increase in the potential of the electrode with a deposited poly$[M(qol)_2]$ film in the reduced or partially oxidized state ($\Delta E^{h\nu}$). The maximal photovoltaic effect in 0.17-μm thick poly$[Ni(qol)_2]$ and 0.07-μm thick poly$[Pd(qol)_2]$, synthesized in the potentiodynamic mode in acetonitrile as a solvent, was 80 and 50 mV, respectively (Fig. 2). These values are well

comparable with the photovoltaic effect in poly-*trans*-[Ni(MeSal)$_2$] ($\Delta E^{h\nu}$ = 85 mV) [2]. However, for 1.6-μm thick film of poly[Pt(qol)$_2$], prepared in the static mode in the dichloromethane solution of the supporting electrolyte, we obtained $\Delta E^{h\nu}$ = 350 mV, which is among the highest values ever obtained for thin-film organometallic polymers, being well comparable with such classical photoelectroactive system as poly[PtSalen] ($\Delta E^{h\nu}$ = 370 mV) [3].

Finally, an important feature of [Pt(qol)$_2$] is that it can act (in contrast to other investigated monomeric complexes) as a monomeric unit in electrochemical synthesis of thin-film conducting polymers. Also, it can effectively form macromolecular ensembles via a photochemical reaction in the presence of atmospheric oxygen.

CONCLUSIONS

(1) Poly[Ni(qol)$_2$] and poly[Pd(qol)$_2$] films with the best characteristics (maximal thickness of the conducting layer and diffusion coefficient) are formed in the potentiodynamic mode with potential cycling from 0.0 to 1.3 V.

(2) [Pt(qol)$_2$] can be electrochemically polymerized in both static and dynamic modes. Under static conditions at E_{ac} = 1.0 V, the thickest and most electrochemically stable films are formed.

(3) Charge transfer in thin films of [M(qol)$_2$]-based polymers under the action of polychromatic light is characterized by high rate and high degree of redox reversibility ($\Delta E^{h\nu}$ = 50–370 mV).

REFERENCES

1. Shagisultanova, G.A., *Teor. Eksp. Khim.*, 1991, vol. 27, no. 3, pp. 330–338.
2. Shagisultanova, G.A. and Gubasova, T.N., *Zh. Prikl. Khim.*, 2000, vol. 73, no. 11, pp. 1826–1831.
3. Ardasheva, L.P., Luminescence Spectral, Photochemical, and Electrochemical Properties of Platinum(II) and Palladium(II) Complexes with Schiff Bases, *Cand. Sci. Dissertation*, Moscow, 1999.
4. Shagisultanova, G.A. and Ardasheva, L.P., *Zh. Prikl. Khim.*, 2003, vol. 76, no. 10, pp. 1669–1674.
5. Shagisultanova, G.A., Ardasheva, L.P., and Orlova, I.A., *Zh. Prikl. Khim.*, 2003, vol. 76, no. 10, pp. 1675–1681.
6. Ovsyannikova, E.V., Crosheva, M.Yu., and Alpatova, N.M., *Short Commun.*, 2004, vol. 40, no. 10, pp. 1089–1091.

ISSN 1070-4272, Russian Journal of Applied Chemistry, 2007, Vol. 80, No. 8, pp. 1432–1434. © Pleiades Publishing, Ltd., 2007.
Original Russian Text © K.I. Imanbekov, E.E. Ergozhin, E.R. Kendirzhanov, 2007, published in Zhurnal Prikladnoi Khimii, 2007, Vol. 80, No. 8, pp. 1394–1396.

BRIEF COMMUNICATIONS

Ion Exchangers Based on Vinyloxyethylamine and Epoxy-Phenol-Aldehyde Compounds

K. I. Imanbekov, E. E. Ergozhin, and E. R. Kendirzhanov

Bekturov Institute of Chemical Sciences, Ministry of Education and Science of the Republic of Kazakhstan, Almaty, Kazahstan

Received January 16, 2007

Abstract—A method for preparing highly permeable polyelectrolytes by the reaction of homo- and copolymers of vinyloxyethylamine with various glycidyl ethers of phenol-aldehyde compounds was developed. The physicochemical characteristics of these polyelectrolytes were studied.

DOI: 10.1134/S1070427207080344

In the development of ion-exchange polymeric mamerials based on various polymers of monoethanolamine vinyl ether, not only the composition and characteristics of functional groups but also the features of the structure of epoxy compounds as cross-linking agents are very significant. From this standpoint, nitrogen- and oxygen-containing aromatic epoxy compounds are of great interest for synthesis of polymers with high softening point and heat resistance. Ion-exchange polymers based on these compounds have a set of unique service characteristics. They are widely used for solving various chemical and technological problems, e.g., in recovery of ions of noble, rare, and nonferrous metals and purification of medical products [1–5]. Therefore, one of ways to improve physicochemical characteristics of ion exchangers of the polycondensation type is to introduce phenolic fragments into the structure of epoxy compounds. The homogeneity of functional groups of commercially available glycidyl ethers of phenol- and aniline-phenol-formaldehyde compounds and also the presence of alternating aromatic nuclei in their structure improves the chemical and thermal stability and also the regularity in the steric structure of the polyelectrolytes.

In this study, we prepared polyfunctional ion exchangers by polycondensation of homo- and copolymers of vinyloxyethylamine (VOEA) with glycidyl ethers of phenol-formaldehyde compounds and studied their physicochemical characteristics.

EXPERIMENTAL

Phenol epoxy compounds (PECs), namely, glycidyl ethers of phenol-formaldehyde (PFC), phenol-acetaldehyde (PAC), and aniline-phenol-formaldehyde (APFC) compounds, were synthesized by standard procedures [6]. Polymers based on VOEA, namely, homopolymer of VOEA (PVOEA) and copolymers of VOEA with *N*-vinylpyrrolidone (VOEA–NVP) and 2-methyl-5-vinylpyridine (VOEA–MVP), were synthesized at a 25 : 75 molar ratio of the monomers by the well-known procedure [7].

Highly permeable ion exchangers were synthesized by polycondensation of homo- and copolymers of VOEA with PECs in isobutanol at 60–120°C for 8–10 h [8]. The reaction mixture was poured off on a pan and the solvent was evaporated at 80°C. The final product was crushed, washed with ethanol to remove unchanged substances, dispersed, and a fraction with a grain size of 0.25 mm was taken [9, 10].

To evaluate the chemical resistance of ion exchangers to acid and alkaline solutions [9], two 1-g portions of ion exchanger were placed in 250-ml round-bottomed flasks. One portion was poured over with 100 ml of 5 N H_2SO_4, and the other, with 100 ml of 5 N NaOH. The mixtures were heated with a reflux condenser on a boiling water bath for 30 min. Then the mixtures were cooled to room temperature and the ion exchanger was separated by filtration. If necessary, the sorbent was converted to the OH form,

Table 1. Influence of the ratio and nature of the initial components on SEC of polymers

PEC	SEC for 0.1 N HCl, mg-equiv g^{-1}											
	PVOEA				VOEA–MVP				VOEA–NVP			
	1 : 1	1 : 2	1 : 3	1 : 4	1 : 1	1 : 2	1 : 3	1 : 4	1 : 1	1 : 2	1 : 3	1 : 4
PFC	4.0	5.7	6.8	7.6	6.4	7.4	7.9	8.1	1.5	1.8	1.9	2.0
PAC	3.6	5.5	6.7	7.4	6.2	7.3	7.7	8.1	1.4	1.8	1.9	2.1
APFC	4.2	7.1	9.2	10.9	5.9	6.9	7.4	7.8	2.4	2.3	2.3	2.2

Table 2. Influence of temperature T on SEC of anion exchangers

PEC	SEC for 0.1 N HCl, mg-equiv g^{-1}, at indicated temperature T, °C											
	PVOEA				VOEA–MVP				VOEA–NVP			
	60	80	100	120	60	80	100	120	60	80	100	120
PFC	6.5	7.6	7.6	7.1	5.9	7.9	8.1	8.0	1.3	1.9	2.0	1.8
PAC	6.9	7.4	7.3	7.0	7.0	7.8	8.1	7.9	1.3	1.9	2.1	1.9
APFC	6.7	10.9	10.6	10.1	6.3	7.4	7.8	7.6	1.7	2.0	2.4	2.3

Table 3. Influence of curing time τ on SEC of ion exchangers

PEC	SEC for 0.1 N HCl, mg-equiv g^{-1}, for indicated time τ, h											
	VOEA				VOEA–MVP				VOEA–NVP			
	4	6	8	10	4	6	8	10	4	6	8	10
PEC	6.6	7.2	7.4	7.3	7.3	7.8	8.1	8.1	1.5	1.9	2.1	2.1
APFC	9.2	10.4	10.9	10.6	6.9	7.2	7.8	7.7	1.6	2.0	2.4	2.4
PFC	6.5	7.3	7.6	7.6	7.2	7.8	8.1	8.0	1.4	1.7	2.0	2.0

washed with distilled water, and its static exchange capacity (SEC) was determined. The chemical resistance X (%) was determined by the formula

$$X = (\mathrm{SEC}/\mathrm{SEC}_0) \times 100,$$

where SEC and SEC_0 are the static exchange capacities before and after treatment with acid and alkaline solutions, respectively.

To determine the chemical resistance of ion exchangers to oxidant solutions, a weighed portion of ion exchanger (1 g) was poured over with 100 ml of 10% H_2O_2 and kept at room temperature for 48 h with intermittent stirring. The polymer was separated by filtration, converted to the OH form, washed with distilled water, and its SEC for HCl was determined.

A study of how the ratio of the initial components, time, and curing temperature affect SEC showed that, as the concentration of VOEA polymers is raised from 1 : 1 to 1 : 4 (Table 1), the SEC of ion exchangers increases. In the case of APFC : VOEA–NVP, as the SEC of the ion exchanger decreases, concentration of copolymer is raised, because *N*-vinylpyrrolidone units contain no ionic groups.

The conditions of prepolymer curing significantly affect the characteristics of the resulting ion exchangers. We found (Tables 2, 3) that the gels synthesized should be cured at 80–100°C, depending on the condensation temperature and nature of VOEA polymers, for 8–10 h.

The samples of the polyelectrolytes synthesized under optimal conditions have SEC for HCl (0.1 N)

within the range 1.3–10.9 mg-equiv g^{-1} and a limited specific swelling capacity. In treatment with concentrated 5 N H_2SO_4, 5 N NaOH, and 10% H_2O_2 solutions, the loss of the exchange capacity does not exceed 6%.

The resulting polyelectrolytes extract selectively gold ions from hydrochloric acid solutions in a wide concentration range. A study of the kinetics of sorption of gold ions by ion exchangers showed that the nature of epoxy compound does not affect the extraction rate. For example, for the ion exchangers based on FPC, the maximum degree of sorption is reached within 3 h, and in the first 0.5 h of contact, the sorbents absorb 50% of metal ions.

Thus, anion exchangers based on VOEA polymers and various PECs are highly efficient sorbents for recovery of gold ions from hydrochloric acid solutions. These anion exchangers extract 94.0–99.9% of gold ions; in so doing, they keep their sorption characteristics in a wide range of HCl concentration, which suggests their high chemical stability and selectivity.

CONCLUSIONS

(1) New ion exchangers were prepared by condensation of commercially available glycidyl ethers of phenol-aldehyde and aniline-phenol-formaldehyde compounds with homo- and copolymers of vinyloxyethylamine.

(2) The chemical stability of ion exchangers based on glycidyl ethers of phenol-aldehyde compounds and vinyloxyethylamine polymers in solutions of 5 N acids and alkalis and in 10% H_2O_2 is 95–99%.

(3) The polyelectrolytes synthesized selectively extract gold ions from hydrochloric acid solutions in a wide concentration range. The degree of sorption reaches 98–99%.

REFERENCES

1. Chalov. T.K., Highly Permeable Polyelectrolytes and Ion-Exchange Membranes Based on Some Oxygen- and Nitrogen-Containing Compounds, *Doctoral Dissertation*, Almaty, 2005.
2. Imanbekov, K.I., Quantum-Chemical Aspects of Synthesis of New Ion Exchangers Based on Epoxy Compounds and Pyridine Derivatives, *Doctoral Dissertation*, Almaty, 2006.
3. Nusipova, A.M., Quantum-Chemical Simulation of Intermediates and Final Products of the Reactions of Epichlorohydrin and Pyridine Derivatives, *Cand. Dissertation*, Almaty, 1999.
4. Ergozhin, E.E., Kenzhaliev, B.K., Chalov, T.K., et al., *Tsvet. Met.*, 2005, no. 2, pp. 43–46.
5. Imanbekov, K.I., Erkasov, R.Sh., and Nusipova, A.M., *Vestn. Kaz. Gos. Univ.*, 1998, no. 10, pp. 14–16.
6. Toroptseva, A.M., Belogorodskaya, K.V., and Bondarenko, V.M., *Laboratornyi praktikum po khimii i tekhnologii vysokomolekulyarnykh soedinenii*, (Laboratory Course of Chemistry and Technology of Macromolecules Compounds), Leningrad: Khimiya, 1972.
7. Nurkeeva, Z.S., Shaikhutdinova, E.M., and Seitov, A.Z., *Geterogennye protsessy v vodnykh i organicheskikh sredakh* (Heterogeneous Processes in Aqueous and Organic Media), Almaty: Kaz. Gos. Univ., 1984.
8. Kazakhstan Inventor's Certificate no. 17988.
9. Polyanskii, N.G., Gorbunov, G.V., and Polyanskaya, N.L., *Metody issledovaniya ionitov* (Methods of Studying Ion-Exchangers), Moscow: Khimiya, 1976.
10. *GOSTs* (State Standards) *10898–2.74, 10896–78, 10898–84, 10898–5.84, and 20255.1–89.*

ISSN 1070-4272, Russian Journal of Applied Chemistry, 2007, Vol. 80, No. 8, pp. 1435–1437. © Pleiades Publishing, Ltd., 2007.
Original Russian Text © K.V. Titova, V.P. Nikol'skaya, V.V. Buyanov, O.B. Pudova, G.P. Karzhavina, 2007, published in Zhurnal Prikladnoi Khimii, 2007, Vol. 80, No. 8, pp. 1397–1399.

BRIEF COMMUNICATIONS

Synthesis of $K_2[VO(O–O)_2F]$ and Solubility and Bactericidal Activity of Its Aqueous Solutions

K. V. Titova, V. P. Nikol'skaya, V. V. Buyanov, O. B. Pudova, and G. P. Karzhavina

Institute for Problems of Chemical Physics, Russian Academy of Sciences, Chernogolovka, Moscow oblast, Russia
State Research Institute of Biological Instrument Building, Federal State Unitary Enterprise, Moscow, Russia

Received January 11, 2007

Abstract—Low-expenditure method for synthesis of $K_2[VO(O–O)_2F]$ was developed. The solubility of this compound in water and the stability of its aqueous solutions were determined and its bactericidal activity, exceeding that of hydrogen peroxide by a factor of 1.5, was analyzed.

DOI: 10.1134/S1070427207080356

Peroxovanadates are widely used as catalysts for reactions of hydroxylation of aliphatic and aromatic hydrocarbons, epoxidation of olefins, and other processes [1]. However, they have not been used as carriers of active oxygen so far, although, e.g., $K_3[V(O–O)_4]$ contains 21.6% O_{act}, which corresponds to 45.9% H_2O_2.

Fully substituted peroxovanadates of alkali metals are poorly soluble in water. Until recently, partly substituted $M_3[VO_n(O–O)_{4-n}]$ have not been obtained in individual state. Synthesized $K_3[VO(O–O)_3]$ has also been found to be poorly soluble in water, which creates difficulties in attempts to find ways to use compounds of this group as sources of active oxygen in the field of, in particular, disinfection.

Fluorine-substituted peroxovanadates are soluble in water. Fluoroperoxovanadates of various compositions are known: $M_2[V(O–O)_3F]$, (M = NH_4, K, Na); $(NH_4)_3[V(O–O)_2F_4]$; $(NH_4)_3[VO(O–O)F_4]$; hydrated $M[VO(O–O)F(H_2O)_2]$, (M = K, Rb, Cs, NH_4); and hydroxylated forms $(NH_4)_2[VO(O–O)F_2OH]$ [1]. The most stable among fluoroperoxovanadates are the compounds $M_2[VO(O–O)_2F]$, (M = K, Rb, Cs, NH_4 [2–4].

In this study, a low-expenditure method for synthesis of $K_2[VO(O–O)_2F]$ was developed, its solubility in water was determined, stabilizers for its aqueous solutions were chosen, and the bactericidal activity of the vanadate was found to be 1.5 times that of hydrogen peroxide.

EXPERIMENTAL

According to published data, V_2O_5 or KVO_3, KF, and a solution of hydrogen peroxide serve as starting materials for synthesis of $K_2[VO(O–O)_2F]$. The fluoroperoxovanadate of this composition was first obtained in [2] by dissolution of V_2O_5 in water and addition to the resulting solution of potassium fluoride and a 30% solution of hydrogen peroxide. At –10°C, a precipitate was formed, which was filtered, washed with acetone, and dried.

In [2], the compound was synthesized by mixing solutions of H_2O_2, KF, and KVO_3. The product was precipitated with ethanol. To obtain salts of Na, K, Rb, Cs, and NH_4, a mixture of V_2O_5 and the respective fluoride was dissolved in dilute hydrogen peroxide, and a concentrated solution of the corresponding alkali was added with heating. The potassium salt was obtained in the form of crystals in [4] by dissolution of a dry mixture of V_2O_5 and KF in a 15% solution of hydrogen peroxide. Under the conditions of natural evaporation of water at 20°C, coarse yellow crystals precipitated.

Using the simplest method [4], the dependence of the composition of the forming fluoroperoxovanadate on the ratios KF : V_2O_5 and H_2O_2 : V_2O_5 between the starting components was studied.

Experiments were performed by dissolution of a ground mixture of V_2O_3 and $KF \cdot 2H_2O$ in hydrogen peroxide of various concentrations. The resulting transparent yellow solution was placed on a polymeric tray and water and an excess of H_2O_2 were removed

Table 1. Composition of potassium fluoroxodiperoxovanadate at various ratios between the starting components*

V_2O_5, g	KF, g	KF : V_2O_5, molar ratio	H_2O_2 concentration, %	H_2O_2 volume, ml	H_2O_2 : V_2O_5, molar ratio	Content in dry substance, %	
						H_2O_2	K
0.46	1.79	12.3 : 1	15.0	15.0	29.2 : 1	30.52	–
0.46	1.79	12.3 : 1	17.2	13.2	29.2 : 1	30.81	–
0.92	2.40	8.3 : 1	15.0	15.0	29.2 : 1	29.75	34.2
0.46	1.17	8.1 : 1	15.0	15.0	29.2 : 1	29.96	34.7
0.46	0.50	4.1 : 1	17.2	13.2	29.2 : 1	27.80	–
0.46	1.17	8.1 : 1	30.0	7.5	29.2 : 1	34.64	–
0.46	1.17	8.1 : 1	15.0	10.0	19.5 : 1	30.64	–
0.46	1.17	8.1 : 1	15.0	5.0	9.7 : 1	26.6	37.1

* Calculated for $K_2[VO(O–O)_2F]$ (%): H_2O_2 29.79, K 34.27.

Table 2. Stability of $K_2[VO(O–O)_2F]$ solutions in the presence of stabilizers

Stabilizer	Concentration, % relative to the mass of vanadate	τ, day	Content of H_2O_2 in solution, %	Loss of H_2O_2, %	Stabilizer	Concentration, % relative to the mass of vanadate	τ, day	Content of H_2O_2 in solution, %	Loss of H_2O_2, %
Oxalic acid	1.0	0	4.59	0	$Na_4P_2O_7$	1.0	0	3.85	0
		1	3.03	34.0			2	2.97	22.9
		5	0.19	74.1			3	2.49	35.3
	2.3	0	4.59	0			7	0.19	95.1
		1	2.40	47.7		2.0	0	3.85	0
		5	0.28	93.9			2	2.99	22.3
							3	2.54	35.3
							7	0.18	95.3
						3.9	0	3.88	0
Trilon B	1.0	0	4.05	0			2	3.04	21.8
		1	2.64	34.8			3	2.44	37.1
		2	0.24	94.1			7	0.10	97.4
	2.0	0	4.05	0		7.6	0	3.88	0
		1	2.90	28.4			2	3.15	18.8
		2	0.34	31.6			3	2.68	30.9
							7	0.21	94.6

at 20°C with a directed flow of air until a mixture half-composed of a solid phase was obtained. The precipitate was filtered off using a polymeric film with fine openings, washed with ethanol, and dried in a desiccator over sulfuric acid. The product was analyzed for the content of hydrogen peroxide by permanganatometry. Potassium was determined by the weighing method. The results obtained are listed in Table 1.

As can be seen in Table 1, the amount of potassium fluoride, sufficient for $K_2[VO(O–O)_2F]$ to be formed, corresponds to the molar ratio KF : V_2O_5 = (8.1–8.3) : 1. Apparently, there is little point in introducing potassium fluoride [2, 3] with a KF : V_2O_5 ratio of approximately 20 : 1. The amount of hydrogen peroxide can be reduced from H_2O_2 : V_2O_5 = 29 : 1 to 19 : 1.

Lowering the introduced amount of hydrogen peroxide further leads to a decrease in the content of active hydrogen in the solid product. In addition, hydrogen peroxide should not be used as a 30% solution, because it is difficult to remove its excess in such a concentrated form with ethanol. The yield of fluoroperoxovanadate is 56–60%.

According to [2], potassium fluoroxodiperoxovanadate is stable in storage in a closed state. Under polythermal conditions, the vanadate decomposes at 150°C. No quantitative data on the solubility of $K_2[VO(O–O)_2F]$ in water could be found in the literature. The study performed demonstrated that a saturated solution of the vanadate contains $4.9 \pm 0.2\%$ H_2O_2 at 20 ± 2°C. On the assumption that the dissolution process is not complicated by side reactions and occurs in accordance with the equation

$$K_2[VO(O–O)_2F] + 2H_2O = KVO_3 + K + 2H_2O_2,$$

the content of the peroxovanadate in the saturated solution is 16.4%.

Solutions of potassium fluoroxodiperoxovanadate in water are unstable. At H_2O_2 concentrations in the range 1.2–4.9%, they lose more than half of hydrogen peroxide in 24 h. In the presence of stabilizers, the loss of hydrogen peroxide decreases (Table 2).

As follows from Table 2, the most efficient stabilizer is sodium diphosphate; however, the decrease in the loss of hydrogen peroxide upon addition of this stabilizer in an amount of 4–8% is insufficient for the solutions to be stored for more than 24 h.

Measurements of the rate constant of inactivation of a suspension of *Bac. anthracoides* (strain 250, concentration $n \times 10^7$ cfu ml^{-1}) at 20±2°C [5] demonstrated that the constant K^{II} for $K_2[VO(O–O)_2F]$ is 0.1245, which is 1.5 times larger than the value of K^{II} for hydrogen peroxide (0.08±0.015) and 1.2 lower than K^{II} for $KF \cdot H_2O_2$ (0.1485±0.0124).

Apparently, potassium fluoroxodiperoxovanadate, stable in the solid state, can find use in disinfection with a limitation that its aqueous solutions should be used not later than 24 h after being prepared.

In view of the adaptation of microorganisms to permanently used disinfectants, development of new antibacterial preparations will ever be a topical task.

Potassium fluoroxodiperoxovanadate supplements the store of effective disinfectants in use.

It should be noted that solutions of fluoroxodiperoxovanadate contain, in addition to hydrogen peroxide, catalytically active vanadium compounds. It is known that peroxo complexes of vanadium are used as catalysts in oxidation of hydrocarbons with hydrogen peroxide. Oxidation of sulfides to sulfoxides is also carried out with compounds of vanadium(V) used as catalysts [7]. Probably, the increased, compared with hydrogen peroxide, bactericidal activity of the fluoroperoxovanadate solution is determined by the catalytic effect of vanadate. However, it is also possible that the decontaminating activity increases because the solution contains potassium fluoride, whose fluoride ions bind part of hydrogen peroxide into the complex anion $[F\ldots H–O–O–H]^-$ [8]. Hydrogen peroxide bound with the fluoride anion is deformed and more reactive than free or hydrated molecules of H_2O_2. It is these two factors that predetermine the increase in the decontamination constant of $K_2[VO(O–O)_2F]$ solutions, compared with hydrogen peroxide itself. Possibly, not only solutions of peroxovanadates, but also hydrogen peroxide solutions will exhibit an increased bactericidal activity upon introduction into the latter of a certain amount of fluoroperoxovanadates as catalysts.

CONCLUSION

The optimal synthesis conditions of potassium fluoroxodiperoxovanadate $K_2[VO(O–O)_2F]$ were found. The solubility of the vanadate in water at 20±2°C is 16.4 wt %, or 4.9±0.2% in terms of H_2O_2. The vanadate exhibits a bactericidal activity that is 1.5 times that of hydrogen peroxide.

REFERENCES

1. Vol'nov, I.I., *Peroksokompleksy vanadiya, niobiya i tantala* (Peroxo complexes of Vanadium, Niobium, and Tantalum), Moscow: Nauka, 1987.
2. Jere, G.V. and Kaushic, M.S., *Synth. Reactiv. Inorg. Metal-org. Chem.*, 1980, vol. 10, no. 2, pp. 255–259.
3. Stomberg, R., *Acta Shem. Scand.*, 1984, Ser. A, vol. 38, no. 2, pp. 223–228.
4. Chaudhuri, M.K. and Ghosh, S.K., *Polyhedron*, 1982, vol. 1, no. 2, pp. 533–535
5. Titova, K.V., Nikol'skaya, V.P., and Buyanov, V.V., *Koordinatsionnye soedineniya peroksida vodoroda* (Coordination Compounds of Hydrogen Peroxide), Chernogolovka: Inst. Probl. Khim. Fiz., Ross. Akad. Nauk, 2000.
6. EP Patent 0097551.
7. Di Furia, F. and Modena, G., *Rec. Trav. Chim.*, 1979, vol. 98, no. 1, pp. 181–187.
8. Titova, K.V., Nikol'skaya, V.P., Buyanov, V.V., and Pudova, O.B., *Zh. Neorg. Khim.*, 2005, vol. 50, no. 1, pp. 133–136.

ISSN 1070-4272, Russian Journal of Applied Chemistry, 2007, Vol. 80, No. 8, pp. 1438–1440. © Pleiades Publishing, Ltd., 2007.
Original Russian Text © B.M. Ginzburg, D.G. Tochil'nikov, A.K. Pugachev, V.M. Oichenko, Sh. Tuichiev, A.M. Leksovskii, 2007, published in Zhurnal Prikladnoi Khimii, 2007, Vol. 80, No. 8, pp. 1400–1402.

BRIEF COMMUNICATIONS

Tribological Properties of Fluoroplastics Modified with Fullerene Black in Sliding Friction with Water Lubrication

B. M. Ginzburg, D. G. Tochil'nikov, A. K. Pugachev, V. M. Oichenko, Sh. Tuichiev, and A. M. Leksovskii

Institute of Mechanical Engineering Problems, Russian Academy of Sciences, St. Petersburg, Russia

Plastpolimer Open Joint-Stock Company, St. Petersburg, Russia

Okhta Chemical Combine, St. Petersburg, Russia

Tadjik State National University, Dushanbe, Tadjikistan

Ioffe Physicotechnical Institute, Russian Academy of Sciences, St. Petersburg, Russia

Received March 21, 2007

Abstract—Effect of fullerene black additives on the antifriction properties and wear resistance of F-4 and F-4K20 fluoroplastics in sliding friction against steel with water lubrication was examined.

DOI: 10.1134/S1070427207080368

Polytetrafluoroethylene (PTFE) of F-4 brand [GOST (State Standard) 10007–80, Russia] possesses good antifriction properties and, at the same time, exhibits enhanced wear and cold flow under load. This makes is suitable as a structural material only under low loads. The wear resistance of F-4 can be improved by introduction of fillers [1, 2].

Most widely used materials based on F-4 fluoroplastic are the materials with various concentrations of carbon powder fillers. For the support surfaces of tribotechnical systems operating in water, the filler of choice is coke. The most widely used composition, F-4K20 [3], contains 80% F-4 and 20% coal coke. This composition exhibits a high wear resistance, low deformation under load, and low hygroscopicity. The major drawback of F-4K20 is the rather high friction coefficient (2–3 times that of F-4). To improve the wear resistance, the concentration of a carbon-containing filler is occasionally raised to 40–50%. However, introduction of over 20% filler into F-4 sharply decreases the strength of the composite.

In this study, we prepared and examined a fairly inexpensive antifriction polymeric material (APM) combining the low friction coefficient of F-4 and the high wear resistance of F-4K20.

EXPERIMENTAL

We used fullerene black (FB) produced by the Neo-Tek Research and Production Company, St. Petersburg [4]; it was introduced into F-4 in amounts of 1, 3, 5, or 10%. The fullerene black yielded by the initial extraction of fullerenes with toluene (FBE) was introduced into F-4 and F-4K20 in an amount of 1%. In all the cases, the soot introduction was in conforming with the technical specifications concerning F-4K20 preparation [3].

The tribological tests were run on a 2070 SMT-1 standard roller friction machine by the previously developed technique [5]. The samples tested were 10-mm-thick flat plates with rectangular cross sections. As a counterbody served a roller fabricated from 18Kh2N4MA steel [GOST (State Standard) 4543–71], rotating at 400 rpm, which corresponds to a sliding velocity of 1 m s^{-1}. The circularly polished working cylindrical surface of a roller with a width of 16 mm had the roughness R_a = 0.65 μm and was immersed by 6 mm into a water bath during the tests.

On the sample surface, a wear groove with an area of 30–50 mm^2 was preliminarily formed, so that the subsequent tests were made with conform counterbodies with a run-in friction contact. Successively

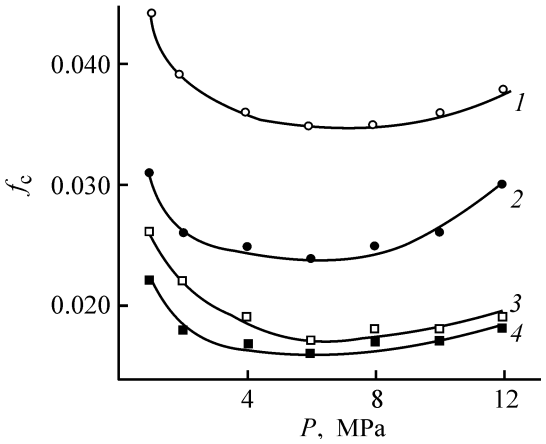

Fig. 1. Friction coefficient f_c vs. contact pressure P for sliding friction against steel with water lubrication: (*1*) F-4 and (*2*–*5*) F-4 + FB, %: (*2*) 1, (*3*) 3, and (*4*) 5.

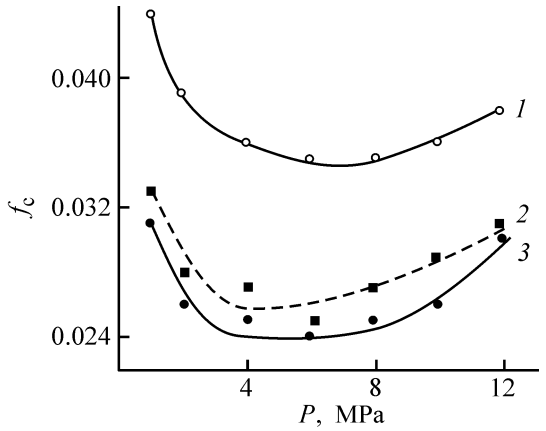

Fig. 3. Friction coefficient f_c vs. contact pressure P for friction against steel with water lubrication: (*1*) F-4, (*2*) F-4 + 1% FBE, and (3) F-4 + 1% FB.

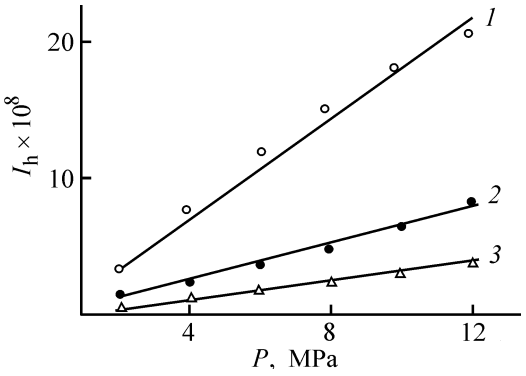

Fig. 2. Linear wear rate I_h vs. contact pressure P for sliding friction against steel with water lubrication: (*1*) F-4 and (*2*, *3*) F-4 + FB, %: (*2*) 1 and (*3*) 10.

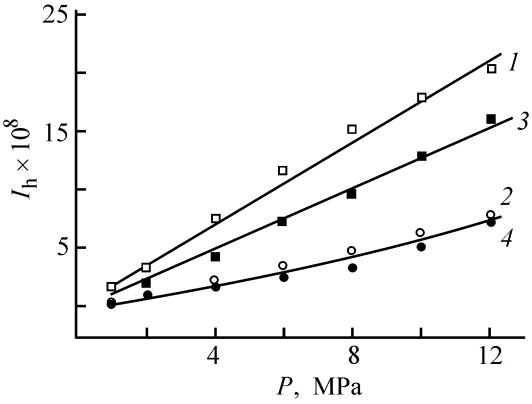

Fig. 4. Linear wear rate vs. contact pressure P for friction against steel with water lubrication: (*1*) F-4, (*2*) F-4 + 1% FB and F-4 + 1% FBE, (*3*) F-4K20, and (*4*) F-K420 + 1% FBE.

increasing normal loads F_N were applied to the sample. The time of tests at each load was 300 s. We determined the friction coefficients f_c and linear wear rates I_h, averaged over each test. Three to six tests were run for each load. The tribological parameters were determined as arithmetic means. The relative rms errors were within 5–10%.

At the working pressures within 1–10 MPa, addition FB causes the friction coefficient f_c to decrease to 0.015–0.021 (Fig. 1), and the linear wear rate I_h, to $(0.39–2.9) \times 10^{-8}$ (Fig. 2), i.e., f_c decreases by a factor of 1.5–2, and I_h, by a factor of 2–7.5.

Tests of samples of fluoroplastics F-4 and F-4K20 with addition of FBE revealed only minor deterioration of the characteristics relative to those FB (Figs. 3, 4). Both kinds of fullerene black produce virtually identical effects. It should be noted that adding only 1% of either fullerene black to F-4 leads to a significant reduction in I_h under water lubrication (in this parameter, F-4 is superior to F-4K20), and simultaneously, the friction coefficient tends to decrease (Figs. 3, 4). At contact pressures within 1–14 MPa, both the friction coefficient f and linear wear rate I_h decreased 2–3-fold.

In tests on friction against steel with water lubrication, as little as 1% FBE added to the F-4 and F-4K20 samples caused the permissible working pressure in friction contacts to increase by 25 and 20%, respectively.

It should also be noted that the efficiency of fullerene black additives may be insignificant at a small pressure on the contact but strongly grows with increasing pressure (Figs. 2, 4). Therefore, the efficiency of fullerene-containing additives can be conclusively judged only after testing the materials over a fairly wide pressure range.

As to mechanisms of the strengthening action of fullerene blacks in friction, the following conclusions can be made now. It is known that mechanical failure of polymers is accompanied by mechanical degradation of the polymer chains at the mouths of the cracks formed. Apparently, a similar process occurs at the mouths of the numerous cracks responsible for the formation of wear particles. Free radicals yielded by degradation can readily add to the fullerene molecules and form a fullerene-polymer network. Polymer radicals yielded by thermal degradation of many polymers [polystyrene, poly(methyl methacrylate), polyethylene glycol, poly-*N*-vinylpyrrolidone] have been shown to readily react with C_{60} [6, 7]. Thus, formation of a network from PTFE macromolecules and fullerenes is highly probable. Hence, the microcracks formed during tests are presumably closed (healed) on the fullerene molecules owing to their high electron-accepting power, instead of propagating around the fullerene-containing particles as common inclusions.

Our data show that fullerene black additives improve the antifriction properties and wear resistance of fluoroplastics. The efficiency of fullerene black additives should be evaluated by taking into account not only the technical potentialities of the new samples, but also the cost of their manufacture. Manufacturers report that adding 1 and 10% FB increases the cost of F-4 by 30% and more than 4-fold, respectively. Combined with the results of our tests, these data suggest that the best concentration of FB is 1%, because, with a further increase in its concentration, the tribological parameters are improved to a lesser extent than grows the cost of the materials.

FBE additives provide an even more substantial decrease in the cost of the new materials whose tribological properties remain virtually unaffected. These fullerene blacks are formed as waste in fullerene production and have no consumer value so far. However, it is necessary to take into account the cost of FBE drying (after extraction of fullerenes with toluene) and of its conversion into a commercial product. Therefore, drying could eliminate the gain from the low cost of FBE. Apparently, with all technical and economic factors taken into account, 1% FB should be recommended for commercial application.

The beneficial action on the antifriction properties and wear resistance of the PTFE-based fluoroplastics, exerted by addition of fullerene blacks, makes them candidates for use as APMs in sliding friction units against steel, operating both without [8] and with water lubrication.

The APMs suggested in this study can be manufactured on a large scale on existing plants by using the available processes for preparation of fluoroplastics and fullerene blacks.

CONCLUSIONS

(1) The antifriction properties and wear resistance of fluoroplastics F-4 and F-4K20 were examined as influenced by additions of fullerene blacks: the initial FB produced in the plasma electric discharge and FBE that remained after extraction of fullerenes with toluene from the initial fullerene black. The best concentration of the blacks was estimated at 1–3%.

(2) Both kinds of fullerene blacks are nearly equal in efficiency. However, the technical and economic analysis suggests that, for commercial application, 1% addition of FB to the fluoroplastics should be recommended.

ACKNOWLEDGMENTS

This study was financially supported by Basic Research Scientific Program no. 14, Division of Power Engineering, Machine Building, Mechanics, and Management Processes, Russian Academy of Sciences, as well as by the Russian Foundation for Basic Research (project no. 06-08-00910-a) and ISTC project T-1145.

REFERENCES

1. *Polimery v uzlakh treniya mashin i priborov: spravochnik* (Polymers in Friction Units of Machines and Instruments: Reference Book), Chichinadze, A.V., Ed., Moscow: Mashinostroenie, 1988.
2. *Primenenie poliolefinov, polistirolov, ftoroplastov i polivinilatsetatnykh plastikov: Katalog ONPO "Plastpolimer"* [Application of Polyolefins, Polystyrenes, Fluoroplastics, and Poly(Vinyl Acetate) Plastics: Catalog of Plastpolimer Okhta Research and Production Association], Cherkassy: Nauchno-Issled. Inst. Tekh.-Ekon. Issled., 1981.
3. *TU* (Technical Specifications) *6-05-1412–76: F-4K20 Material.*
4. RF Patent 2234457.
5. Tochil'nikov, D.G. and Ginzburg, B.M., *Vopr. Materialoved.*, 2002, no. 31 (3), pp. 39–48.
6. Ginzburg, B.M., Pozdnyakov, A.O., Zgonnik, V.N., et al., *Pis'ma Zh. Tekh. Fiz.*, 1996, vol. 22, no. 4, pp. 73–77.
7. Shibaev, L.A., Antonova, T.A., Vinogradova, L.V., et al., *Zh. Prikl. Khim.*, 1998, vol. 71, no. 5, pp. 835–841.
8. Ginzburg, B.M., Tochil'nikov, D.G., Shepelevskii, A.A., et al., *Zh. Prikl. Khim.*, 2006, vol. 79, no. 9, pp. 1534–1537.

ISSN 1070-4272, Russian Journal of Applied Chemistry, 2007, Vol. 80, No. 8, pp. 1441–1442. © Pleiades Publishing, Ltd., 2007.
Original Russian Text © A.I. Akhmedov, E.I. Gasanova, D.Sh. Gamidova, E.I. Isakov, 2007, published in Zhurnal Prikladnoi Khimii, 2007, Vol. 80, No. 8, pp. 1403–1404.

BRIEF COMMUNICATIONS

Viscosity Additives to Lubricating Oils, Based on Alkyl Methacrylates and Allyl Monomers

A. I. Akhmedov, E. I. Gasanova, D. Sh. Gamidova, and E. I. Isakov

Kuliev Institute of Chemistry of Additives, National Academy of Sciences of Azerbaijan, Baku, Azerbaijan

Received January 24, 2007

Abstract—New viscosity additives to oils, based on copolymers of alkyl methacrylates and allyl monomers, were developed.

DOI: 10.1134/S107042720708037X

The formulations of lubricating oils include additives of various functional actions and, in particular, viscosity additives (VAs). Various oil-soluble vinyl polymers have been studied as VAs. Viscosity additives of poly(alkyl methacrylate) type show advantages in that they are prepared by a simple and environmentally safe procedure (radical polymerization), are readily modified, and ensure better viscosity–temperature characteristics of oils, compared to oils modified with other additives. However, like other VAs, poly(alkyl methacrylates) exhibit poor resistance to degradation and do not meet the requirements of modern engineering in this respect. Therefore, the development of highly stable additives of the poly(alkyl methacrylate) type is a topical problem of modern petrochemistry.

It has been shown [1, 2] that one of simple procedures for preparing VAs resistant to degradation is copolymerization, i.e., chemical modification of the existing VAs.

This study deals with the copolymerization of alkyl methacrylates with allyl monomers.

EXPERIMENTAL

As alkyl methacrylates we used butyl methacrylate (BMA) (in synthesis of VAs to ester oils) and decyl methacrylate (DMA) (in synthesis of VAs to petroleum oils), and as allyl monomers, allyl alcohol (for the copolymerization with DMA) and *o*-allylphenol (for the copolymerization with BMA). The comonomers with the OH functional group were chosen with the aim of further transformations to obtain polyfunctional additives exhibiting also the thickening effect.

We used commercial monomers, except decyl methacrylate, which was synthesized in laboratory and had the following characteristics: M = 226, n_D^{20} = 1.4414, d_4^{20} = 0.8765, bp 290°C. All the monomers were distilled just before use and had 98–99% purity.

Copolymerization was performed in the presence of a freshly recrystallized radical polymerization initiator, azobis(isobutyronitrile) (AIBN), taken in an amount of 0.8–1 wt % relative to the sum of the monomers, at 65–70°C for 3–4 h. We examined the effect of various factors on the reaction results. We found that allyl monomers exert an inhibiting effect on the copolymerization, which is reflected in the yield and molecular weight of the products. Therefore, the molecular weight of the copolymers can be controlled by varying the content of allyl compounds in the starting monomer mixture, without using any additional means. After the copolymerization was complete, the mixture was kept in a vacuum to remove the unchanged monomers.

We prepared the copolymers of molecular weight $(8–14) \times 10^3$ in the case of copolymerization of DMA with allyl alcohol and $(12–17) \times 10^3$ in the case of copolymerization of BMA with *o*-allylphenol; the content of allyl monomer fragments was 5–10%.

The composition and structure of the copolymers were studied by elemental analysis and by IR and ^{1}H NMR spectroscopy. We found that allyl monomers form no homopolymers. We also revealed bonds between units of monomers taken for the copolymerization, which confirms the formation of a copolymer, rather than a mixture of homopolymers of the starting monomers. This result is consistent with the well-known fact that allyl monomers are used for preparing copolymers with regularly alternating monomeric units [3].

Influence of copolymer concentration on the viscosity–temperature characteristics of I-12A oil

Copolymer concentration, wt %	Kinematic viscosity at 100%, $mm^2 s^{-1}$	Viscosity index
0	3.90	90
1	4.1	125
3	6.70	150
3.5	7.30	150
4	8.20	152
5	10.60	152

Copolymers of DMA with allyl alcohol were tested as VAs to petroleum oils. With I-12A oil as an example, we examined how the copolymer concentration affects the viscosity–temperature characteristics of the oil (see table).

The table shows that the trend observed when the VA concentration is raised is typical of thickened oils: The viscosity index increases with the additive concentration to a certain level and then tends to a constant value. Dissolution of 4 wt % copolymer in I-12A oil yields a thickened oil meeting the existing requirements: viscosity at 100°C 8 ± 0.5 $mm^2 s^{-1}$, viscosity index no less than 125 units.

In addition, we studied the thermal degradation of the copolymers, in comparison with the DMA homopolymer of equal molecular weight (10 000), in a solution in turbine oil of L brand. The copolymer appeared to be more resistant to degradation (the solution viscosity decreased by 4%) than the DMA homopolymer (the viscosity decreased by 9.5%). Thus, the chemical structure of the copolymer ensures its higher stability, compared to the DMA homopolymer.

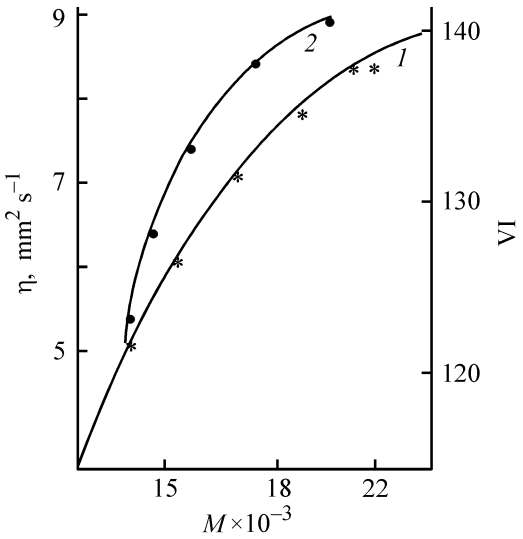

(*1*) Viscosity η and (*2*) viscosity index VI of pentaerythritol ester oil vs. the molecular weight of the copolymer *M*. Amount of allylphenol 10 wt %, copolymer concentration 1%.

The content of the allyl monomer does not noticeably affect the extent to which the copolymers improve the viscosity–temperature characteristics of the oils, i.e., introduction of allyl alcohol units into the DMA polymeric chain does not impair the viscosity–temperature properties of the thickened oils.

Copolymers of BMA with *o*-allylphenol were tested as VAs to a synthetic ester oil derived from pentaerythritol. Firstly, these copolymers do not dissolve in petroleum oils. Secondly, ester oils are used under more severe conditions than petroleum oils. Therefore, we chose a shorter-chain monomer, BMA, and copolymerized it with an aromatic compound (*o*-allylphenol) to make the macromolecules more resistant to thermal oxidation.

The figure shows how the molecular weight of the copolymer affects the viscosity characteristics of the pentaerythritol ester. An increase in the molecular weight of the copolymers leads to a rise in the viscosity index and kinematic viscosity at 100°C. However, an increase in the molecular weight of VAs makes them less resistant to thermal degradation. Therefore, the choice of the molecular weight and concentration of a VA is governed by specific requirements to a lubricating oil.

Thus, from alkyl methacrylates and allyl compounds we prepared VAs to petroleum and synthetic oils, exhibiting high resistance to degradation.

CONCLUSIONS

(1) Radical copolymerization of alkyl methacrylates with allyl monomers was performed.

(2) The copolymers obtained were tested as viscosity additives to lubricating oils. It was found that introduction of phenolic fragments into a polymeric chain makes the copolymers more heat-resistant.

REFERENCES

1. Kuliev, A.M., *Khimiya i tekhnologiya prisadok k maslam i toplivam* (Chemistry and Technology of Additives to Oils and Fuels), Leningrad: Khimiya, 1985.
2. Akhmedov, A.I., Farzaliev, V.M., and Aliguliev, R.M., *Polimernye prisadki i masla* (Polymeric Additives and Oils), Baku: Elm, 2000.
3. *Entsiklopediya polimerov* (Encyclopedia of Polymers), Moscow: Sov. Entsiklopediya, 1972.

ISSN 1070-4272, Russian Journal of Applied Chemistry, 2007, Vol. 80, No. 8, p. 1443. © Pleiades Publishing, Ltd., 2007.
Original Russian Text © Editorial board, 2007, published in Zhurnal Prikladnoi Khimii, 2007, Vol. 80, No. 8, p. 1405.

ANNIVERSARIES

Academician Vladimir Aleksandrovich Tartakovskii is 75

DOI: 10.1134/S1070427207080381

Academician Vladimir Aleksandrovich Tartakovskii is an outstanding specialist in organic chemistry and high-energy substances.

Vladimir Aleksandrovich Tartakovskii was born in Moscow on August 10, 1932. In 1955, he graduated from Lomonosov University in Moscow and went to work at Zelinskii Institute of Organic Chemistry, Academy of Sciences of the USSR. He successfully defended his candidate dissertation in 1959 and doctoral dissertation in 1966. Tartakovskii was elected a corresponding member of the Academy of Sciences of the USSR in 1987 and an academician of the Russian Academy of Sciences in 1992.

The main area of research by Academician Tartakovskii is chemistry of nitro compounds and their use in high-energy formulations. The variety of problems that have been solved under Tartakovskii's supervision and with his participation is extremely wide. These are nitration techniques, and new nitrating agents, and a broad spectrum of new nitro compounds. The results of his studies have been initiating, during many years, re- search in a number of specialized institutes and have opened-up many new issues in chemistry of nitro compounds.

Academician Tartakovskii and his co-workers have created a new area in chemistry of nitro compounds, which made it possible to extend the number of methods for synthesis of new heterocyclic systems. A Butlerov Prize was awarded to Tartakovskii for this series of works by the Academy of Sciences of the USSR in 1967.

The most prominent achievement of Academician Tartakovskii is the discovery of a new class of polynitrous compounds. The results of this study have been officially recognized as a discovery. The industrial implementation of this discovery and particular formulations acquired a State importance. Tartakovskii and his co-workers became Lenin Prize laureates in 1976. Tartakovskii's personal contribution to the practice of synthesis of these compounds and their use in various articles is tremendous. The broad erudition and outstanding talent enable Tartakovskii to solve equally thoroughly both theoretical and practical problems. Under his supervision, a system for engineering of structures with prescribed properties and a concept of prognostication of new polyheteroatomic organic compounds have been developed.

Academician Tartakovskii continues to be deeply involved in scientific and scientific-organizational activities. The laboratory headed by him is engaged in basic research in the field of high-energy compounds. He performs duties of the Academician-secretary of the Department of chemistry and materials science, Russian Academy of Sciences, and works in editorial boards of several journals published by the Russian Academy of Sciences.

The Editorial board and editorial staff of Zhurnal Prikladnoi Khimii (Russian Journal of Applied Chemistry) heartily congratulate Vladimir Aleksandrovich Tartakovskii on his jubilee and wish him sound health and every creative success.

ISSN 1070-4272, Russian Journal of Applied Chemistry, 2007, Vol. 80, No. 8, pp. 1444–1445. © Pleiades Publishing, Ltd., 2007.
Original Russian Text © Editorial board, 2007, published in Zhurnal Prikladnoi Khimii, 2007, Vol. 80, No. 8, p. 1406.

ANNIVERSARIES

Professor Mikhail Mikhailovich Vetyukov is 90

DOI: 10.1134/S1070427207080393

Mikhail Mikhailovich Vetyukov was born on August 1917 into a peasant's family at Shuiskoe village in Vologda province.

In 1935, Mikhail Mikhailovich finished with excelence a secondary school and went to work at the chair of electrometallurgy of nonferrous metals angrad Polytechnic Institute. Since that time, his life has been associated with this chair and this institute. Only in 1941, after graduating from the institute, he worked during a year at Ural aluminum plant (Sverdlovsk oblast) and after that served in the Soviet army till 1946.

Since demobilization in 1946 and until now, Mihail Mikhailovich has been working at Leningrad Polytechnic Institute (now St. Petersburg State Polyechnic University), at the chair of electropyrometallurgy of nonferrous metals (now Theoretical foundaions of the metallurgy of nonferrous metals,) as junior research worker, postgraduate student, docent, and professor. He defended his candidate dissertation in 1950 and doctoral dissertation in 1973. He headed the chair from 1975 till 1990.

The main field of Vetyukov's scientific and pedagogical activities is the theory and technology of electroytic manufacture of aluminum. He is acknowledged authority in this area not only in Russia, but in Europe as well.

He studied for the first time the thermodynamic properties of cryolite-alumina melts, obtained data on their density and viscosity, and determined kinetic characteristics of the electrode processes in manufacture of aluminum. He studied the behavior of sodium at the furnace bottom in order to proong the service life of aluminum electrolyzers. For the same purpose, he used new refractory compounds as electrolyzer lining.

During many years, Vetyukov had been a member of dissertation councils at Leningrad Polytechnic Intiute, Mining Institute, and VAMI (All-Russia Aluminum-Magnesium Institute). Twenty-six candidate disertations and 2 doctoral dissertations have been deended under his supervision. Vetyukov prepared and delivered a course of lectures on electrometallurgy of

nonferrous metals and created a laboratory course of metallurgy of light metals. He is the author of more than 150 scientific publications and inventions, monoraphs, and textbooks. His textbooks and monographs *Teoreticheskie osnovy metallurgii alyuminiya* (Theretical Foundations of the Metallurgy of Aluminum, 1953), Elektroliz rasplavlennykh solei (Electrolysis of Molten Salts, 1966), and *Elektrometallurgiya alyuminiya i magniya* (Electrometallurgy of Aluminum and Magnesium, 1987), written in co-authorship with Yu.V. Baimakov, G.A. Abramov, and others, still remain reference books of specialists in metallurgy. His theoretical papers devoted to kinetics of cathodic and anodic processes in electrolysis of aluminum, properties of cryolite-alumina and chloraluminate melts have been published in journals *Tsvetnye metally*, *Zhurnal Prikladnoi Khimii*, *Elektrokhimiya*, and others.

Numerous Vetyukov's students and postgraduate students have become prominent specialists, scientists, heads of institutes and ministries in Russia and other countries (Vietnam, Egypt, Hungary, Ghana, etc.).

Mikhail Mikhailovich Vetyukov has been awarded the title of Honored Professor of St. Petersburg State Polytechnic University.

At his age of 90, Vetyukov is deeply involved in the chair's activities and shares his scientific and life experience. He is still distinguished by interest in scientific and technological achievements of the electrometallurgy of aluminum as a whole and in works, achievements and success of his pupils, in particular.

Mikhail Mikhailovich is an open-hearted and well-wishing man. His house is always open for friends, pupils, friends, and all those who need his advice or friendly sympathy.

Staff members of the chair of theoretical foundations of metallurgy of nonferrous metals at St. Petersburg State Technical University and the Editorial board and editorial staff of Zhurnal Prikladnoi Khimii heartily congratulate Mikhail Mikhailovich on his jubilee and wish him sound health and further success in his scientific and pedagogical activities.

ISSN 1070-4272, Russian Journal of Applied Chemistry, 2007, Vol. 80, No. 9, pp. 1447–1452. © Pleiades Publishing, Ltd., 2007.
Original Russian Text © A.R. Kobeleva, V.Z. Poilov, 2007, published in Zhurnal Prikladnoi Khimii, 2007, Vol. 80, No. 9, pp. 1409–1415.

INORGANIC SYNTHESIS AND INDUSTRIAL INORGANIC CHEMISTRY

Technology for Production of Calcium Carbonate with Prescribed Properties

A. R. Kobeleva and V. Z. Poilov

Perm State Technical University, Perm, Russia

Received October 30, 2006; in final form, March 2007

Abstract—Physicochemical conditions for production of calcium carbonate with prescribed size and shape of particles and crystal structure by reaction of $CaCl_2$ and Na_2CO_3 solutions were studied. A technology for manufacture of calcium carbonate with prescribed properties was developed.

DOI: 10.1134/S1070427207090017

Calcium carbonate and products obtained from this compound are widely used in various fields of economy: in building, as a component of finishing materials; for manufacture of cement, glass, and ceramics; in pharmacology, to manufacture toothpastes and antacid preparations; in cosmetics, to produce creams; in water treatment, as filter materials; in paper industry, to manufacture cigarette, chalk-overlay, and tracing paper; in production of plastics and artificial leather; finely dispersed powdered chalk serves as a filler or pigment in cable, paint-and-varnish, polymer, rubber, and petrochemical industry; etc.

In all these fields, various requirements are imposed on calcium carbonate: on its chemical composition and size and shape of crystalline $CaCO_3$ particles, on which depend the commercial characteristics of calcium carbonate and fields of its use (Table 1).

Technologies for production of precipitated calcium carbonate from various raw materials: natural carbonates and solid carbonate wastes and solutions, have been and are being developed. Different processes are used, depending on a starting raw material and requirements to the final product. A technology widely used in Russia is that in which calcium carbonate is produced by carbonation of a $Ca(OH)_2$ suspension with carbon dioxide, with the subsequent separation of the precipitate from the solution and drying and calcination of the resulting product [1–4]. A disadvantage of this technology is that it is difficult to obtain the $CaCO_3$ product with prescribed properties.

Of practical interest is development of a technique based on $CaCO_3$ precipitation in a chemical reaction of technical soda Na_2CO_3 and a $CaCl_2$ solution produced from waste formed in manufacture of soda ash (distiller fluid) or by dissolution of natural chalk. The main development direction of this technology is production of calcium carbonate with prescribed physicochemical properties (definite particle size and shape, crystal structure, impurity content).

The process of calcium carbonate synthesis includes the chemical reaction

$$CaCl_2 + Na_2CO_3 = CaCO_3\downarrow + 2NaCl.$$

In this study, we examined conditions in which calcium carbonate is obtained in different reactant supply modes, ion concentration ratios $[Ca^{2+}]/[CO_3^{2-}]$, starting reactant concentrations, temperatures, and hydrodynamic modes of chemical precipitation of $CaCO_3$ in the presence of various modifiers.

In the batch mode of chemical precipitation of $CaCO_3$, a certain amount of a calcium chloride or soda solution was poured into the reactor and heated to a certain temperature, after which the second reactant was fed at a constant rate by a peristaltic pump. In the continuous mode of $CaCO_3$ synthesis, the reactants were permanently fed by pumps at a constant rate into the reactor filled to the stirrer blade level with distilled water. The process was performed with agitation during a certain time at a constant rate of rabble rotation. The resulting $CaCO_3$ precipitate was filtered off and washed on the filter with distilled water. The calcium carbonate paste was dried in a drying box at 100°C. The dried calcium carbonate was examined with a KS optical microscope at a $1500\times$ magnification in transmitted light. Photomicroscopic studies were performed by photographing $CaCO_3$ microcrystals with an Olympus C 500 digital

Table 1. Application fields of calcium carbonate with different characteristics and physicochemical properties

Crystal structure	Density, g cm^{-3}	Particle shape	Particle size, μm	$CaCO_3$ product characteristics	Main application fields
Calcite	2.71	Cubic	0.2–3.5	Developed surface	Paper industry
		Spindle-like	0.2–3.5	High mechanical strength	Plastics manufacture
		Barrel-like	0.2–3.5	Low caking	Rubber industry
Vaterite	2.64	Prismatic	2–5	High purity, low caking	Pharmaceuticals
		Spherical	0.5–0.1	Developed surface	Paper industry
		Platelike	2–5	High covering power	Paint-and-varnish materials
Aragonite	2.94	Needle-like	(2–7) × 0.5	High purity, high whiteness	Pharmaceuticals

Table 2. Parameters of particles of calcium carbonate obtained at various ion concentration ratios $[Ca^{2+}]/[CO_3^{2-}]$. Simultaneous supply of reactants, $T = 60°C$, $c_{CaCl_2} = 116$ g l^{-1}, $c_{Na_2CO_3} = 230$ g l^{-1}, feed rate: $v_{CaCl_2} = 0.8 \times 10^{-6}$ m^3 s^{-1}, $v_{Na_2CO_3} = 0.4 \times 10^{-6}$ m^3 s^{-1}, $\omega = 11$ rps

Ion concentration ratio $[Ca^{2+}]/[CO_3^{2-}]$ [g l^{-1}]	Shape of resulting particles	Particle size, μm			$CaCO_3$ content, wt %
		minimum	maximum	average	
0.21	Squared, spherical	1.5	8.0	3.5	99.11
0.26	Spherical	1.5	9.0	3.5	99.08
0.32	Squared, spherical	1.2	5.0	3.2	99.09
0.41	Spherical, rectangular	1.2	6.0	3.0	99.10
0.63	Cubic, spherical	1.2	6.0	3.0	99.07
0.73	Oblong, spherical, squared	1.2	5.2	2.5	99.08
0.98	Oblong, squared	1.0	4.0	2.0	99.09
1.22	Oblong	1.0	4.0	1.8	99.10

camera. The information obtained was processed on a computer, using Photoshop and Camedia software. The maximum, average, and minimum sizes of $CaCO_3$ crystals were measured and their shapes were determined. The particle sizes were found using a micrometer grid scale. The error in determining the particle sizes in the range 1–30 μm did not exceed 7%.

The laboratory studies revealed that the parameters of precipitate particles are strongly affected by the ion concentration ratio $[Ca^{2+}]/[CO_3^{2-}]$ (Table 2).

It was found that finely dispersed calcium carbonate particles of diameter $d \approx 1$–3 μm are formed in the stationary mode in the case of an excess of Ca^{2+} ions. If, however, CO_3^{2-} ions are in excess, coarsely dispersed particles of diameter $d \approx 2$–6 μm are obtained. At an excess of CO_3^{2-} anions, the solubility of calcium carbonate increases because of the formation of soluble complexes of the $[Ca_x(CO_3)_y]$ type, which makes lower the supersaturation and, accordingly, the primary nucleation rate [5]. The size of the forming $CaCO_3$ crystallites can also be controlled by varying the concentration of the reactants supplied (Table 3).

In the stationary precipitation mode, the crystallite size decreases as the concentration of the reactant solutions becomes higher. Because the reactant supply rate was maintained constant, an increase in the reagent concentrations results in higher flow rate of substances into the reactor.

The flow rate W_i was calculated by the formula

$$W_i = vc/V_r,$$

where v is the volumetric flow rate of a solution of ith substance (m^3 s^{-1}); c, concentration of ith substance (kg m^{-3}); and V_r, volume of the reaction medium in the reactor (m^3).

An increase in the flow rate of a substance into the reactor leads, in accordance with the mass action law, to a rise in the rate of the chemical reaction between Ca^{2+} and CO_3^{2-} ions. As a result, the supersaturation created in the solution becomes higher,

Table 3. Average diameter of $CaCO_3$ particles at various concentrations of reactants and modes of their supply

Run no.*	Concentration, g l^{-1}		Average diameter of $CaCO_3$ particles, μm, for indicated mode of reactant supply Q		
	Na_2CO_3	$CaCl_2$	simultaneous	$CaCl_2$ solution into a Na_2CO_3 solution	Na_2CO_3 solution into a $CaCl_2$ solution
1	110	55	10	11	6
2	150	75	8	9	3
3	230	116	5	2	1.5
4	90	116	3	3.5	3
5	110	116	3	3	3
6	150	116	4	3	2.5
7	180	116	4	2.5	2
8	230	45	11	4	3
9	230	55	8	3	2
10	230	75	6	2.5	2
11	230	90	6	2	1.5

* Mode: run nos. 1–3, stationary; nos. 4–11, nonstationary.

which accelerates the nucleation process and gives rise to a large number of fine crystalline particles.

In the nonstationary (batch) precipitation mode, the residence time of particles in the reactor exhibits a wide scatter and the concentration ratio of reagent ions, $[Ca^{2+}]/[CO_3^{2-}]$, permanently changes, which leads to size scatter and multitude of forms of calcium carbonate particles.

An increase in temperature markedly accelerates the chemical interaction between the ions, makes faster the primary nucleation (which results in the formation of finely dispersed precipitates), weakens the strength of binding between microblocks in the forming crystalline agglomerates (which favors their disintegration), and, to a lesser extent, leads to an increase in the face growth rate of crystalline particles (Fig. 1a).

The size of calcium carbonate particles is strongly affected by the hydrodynamic operation mode of the crystallizer (Fig. 1b). As the agitation rate increases from 3.3 to 11 rps, the crystallite size decreases by a factor of nearly 2. The reason is that both the primary nucleation rate and the disintegration rate of the forming unstable agglomerates of $CaCO_3$ particles increase.

The effect of organic and inorganic modifiers on the size of $CaCO_3$ crystalline particles was studied. For this purpose, a certain amount of an additive was introduced into a calcium chloride solution (Table 4).

Organic modifiers lead to a decrease in the size of $CaCO_3$ particles. In the presence of additives of this type, calcium carbonate crystals less than 1 μm in size can be obtained, which is predetermined by adsorption of molecules on the surface of nucleating crystals and by blocked growth of crystalline particles.

Inorganic modifiers favor an increase in the size of

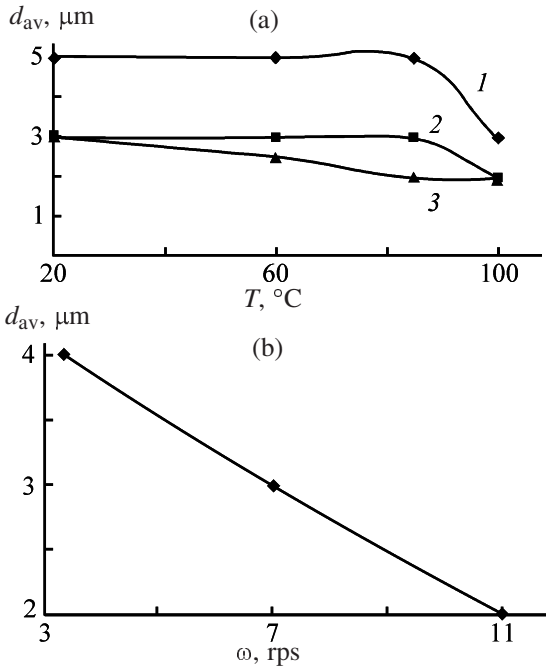

Fig. 1. Average diameter d_{av} of $CaCO_3$ particles vs. (a) process temperature T at different reactant sypply modes and stirrer rotation rate ω = 3 rps and (b) stirrer rotation rate ω at simultaneous delivery of reactants at T = 60°C. c_{CaCl_2} = 116 g l^{-1}, $c_{Na_2CO_3}$ = 230 g l^{-1}; v_{CaCl_2} = 0.8×10^{-6} m^3 s^{-1}, and $v_{Na_2CO_3}$ = 0.4×10^{-6} m^3 s^{-1}. (a) Mode of reactant supply: (*1*) simultaneous, (*2*) $CaCl_2$ solution into a Na_2CO_3 solution, and (*3*) Na_2CO_3 solution into a $CaCl_2$ solution.

Table 4. Effect of the type and concentration of modifies on the size and shape of $CaCO_3$ particles

Modifier type	Modifier	Content, wt %	Particle size, μm	Particle shape
Organic:				
anion-active	Carboxylic acids $C_nH_{2n+1}COOH$	0.09–13.04	1.3	Spherical
	Primary alcohols $C_nH_{2n+1}OH$	0.03–13.04	1.2	Oblong
cation-active	Aliphatic amines	0.09–13.04	1.0	Spherical
Inorganic	NH_4Cl	0.05–2.5	15.0	Hexagonal
	$PbCl_2$	0.07–1.25	5.0	Spherical, oblong

Table 5. Effect of modifiers on characteristics of washed $CaCO_3$ precipitates

Modifier, wt %	Diameter and shape of $CaCO_3$ particles after indicated stage							
	chemical precipitation		1st washing		2nd washing		3rd washing	
	d_{av}, μm	shape of crystals	d_{av}, μm	shape of crystals	d_{av}, μm	shape of crystals	d_{av}, μm	shape of crystals
–	5	Various	5	Various	3	Various	3	Various
NH_4Cl, 10	15	Hexagonal	10	Hexagonal	8	Hexagonal	10	Hexagonal
Soap, 2.5	4	Squared	3	Rectangular	3	Rectangular	3	Squared
Paraffins, 10	4	Polygonal	6	Squared	4	Polygonal	5	Squared
C_4H_9OH, 12×10^{-3}	5	Oblong	4	Various	3	Various	3	Various
SAA, 2×10^{-3}	4	Rounded	3	Rounded	4	Rounded	4	Oblong
Amines, 3×10^{-3}	3	Rounded	5	Rounded	4	Various	4	Various

$CaCO_3$ crystals by a factor of 1.5–2. This effect of inorganic modifiers is possibly due to selective adsorption of modifier ions and to a change in the charge on crystal faces (Table 4).

The shape of calcium carbonate particles (Fig. 2) is affected by the following parameters: ion concentration ratio $[Ca^{2+}]/[CO_3^{2-}]$, process temperature, and presence of a modifier.

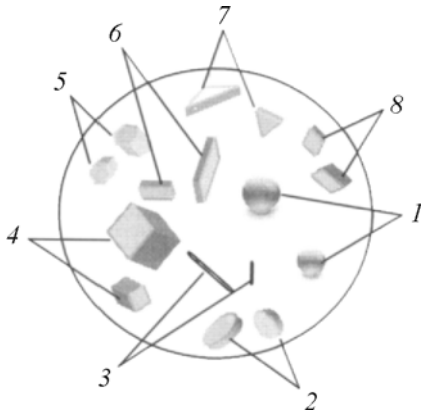

Fig. 2. Types of crystal habits: (*1*) spheres, (*2*) rounded plates, (*3*) needles, (*4*) cubes, (*5*) hexagons, (*6*) rectangular plates, (*7*) triangular plates, and (*8*) rhombic plates.

The effect of the ion concentration ratio $[Ca^{2+}]/[CO_3^{2-}]$ on the shape of $CaCO_3$ particles is presumably due to the sign and amount of charges of excess ions adsorbed on the surface of $CaCO_3$ particles being precipitated. For example, triangular, hexagonal, and rounded platelike particles are formed at a large excess of CO_3^{2-} anions. In this case, the triangular shape is the primary form, and the hexagonal and rounded forms are derivative products of disintegration and wear of triangular $CaCO_3$ particles upon their collisions with other particles, stirrer, and reactor walls. If the excess of CO_3^{2-} anions becomes less pronounced and the ion concentration ratio $[Ca^{2+}]/[CO_3^{2-}]$ approaches the stoichiometry, the platelike shape tends to pass to a three-dimensional, more compact shape of $CaCO_3$ particles: cubic and spherical [6].

A change in the precipitation temperature is reflected in the shape of the resulting calcium carbonate particles. At low temperatures, mostly particles of three-dimensional shape are formed, whereas at high temperatures (>90°C), $CaCO_3$ particles become needle-like, which points to an unequal acceleration of the growth of different faces of $CaCO_3$ particles (Fig. 3).

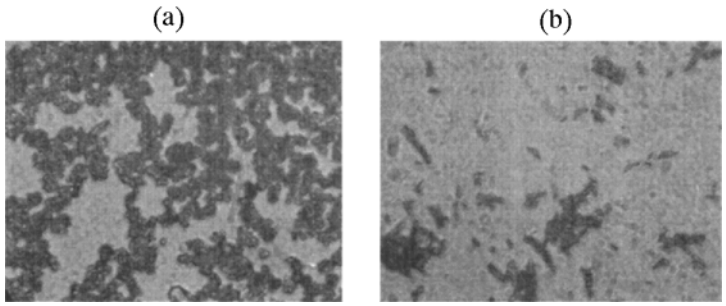

Fig. 3. Photographs of $CaCO_3$ particles obtained at (a) 23 and (b) 90°C. Magnification 1500×.

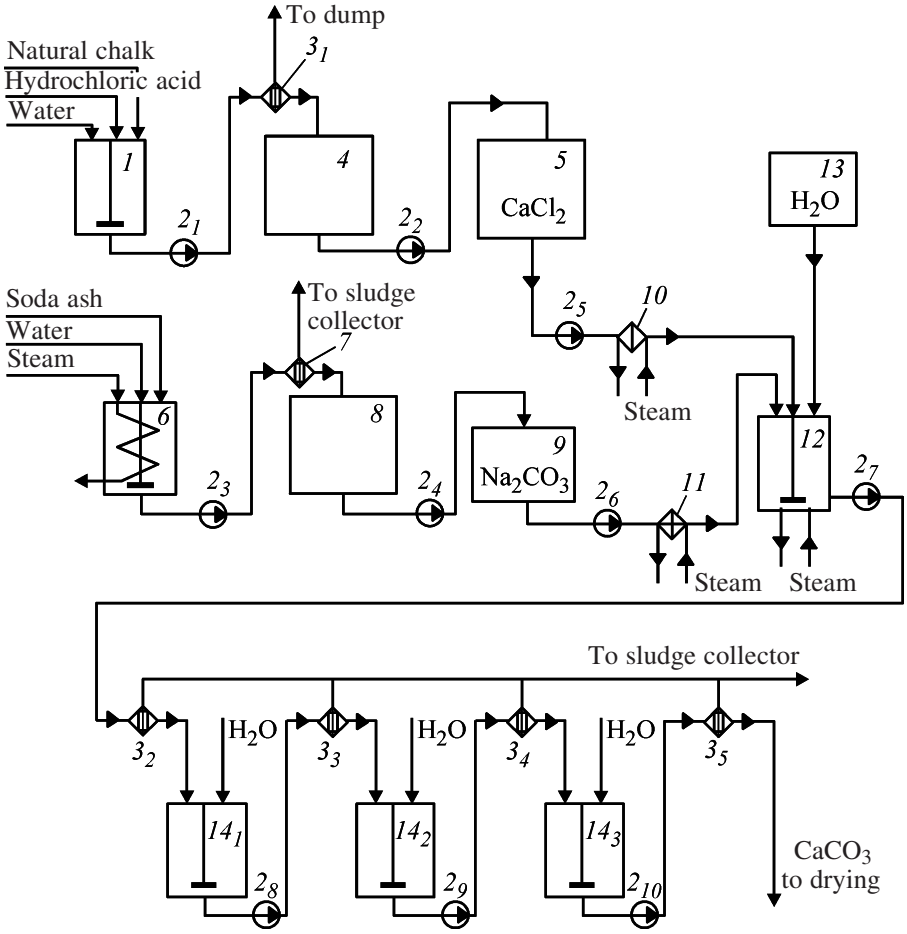

Fig. 4. Flowsheet for production of calcium carbonate. (*1*) Reactor for preparing a calcium chloride solution, ($2_{1–10}$) centrifugal pumps, ($3_{1–5}$) vacuum filters, (*4*) collector for the calcium chloride solution, (*5, 9*) receiving tanks, (*6*) reactor for preparing a soda solution, (*7*) plate-and-frame filter-press, (*8*) collector for the soda solution, (*10, 11*) heaters, (*12*) reactor for synthesis of calcium carbonate, (*13*) water supply tank, and ($14_{1–3}$) repulpers.

Adsorption of modifiers on active centers of the crystals can change the growth rate of their different faces to different extents, which leads to a change in the crystal habit. Inorganic modifiers (NH_4Cl, $PbCl_2$) favor an increase in the number of forms of $CaCO_3$ particles, with rounded, oblong, squared, and polygonal shapes obtained.

Also, ways to control the crystal structure of calcium carbonate and the possibility of obtaining products of different modifications were studied. The crystal structure of $CaCO_3$ was examined by X-ray diffraction analysis. Calcium carbonate with a phase composition of calcite can be obtained in continuous chemical precipitation from solutions containing cal-

cium and sodium ions in the presence of NH_4Cl, urea, and amine hydrochloride additives. Depending on an additive used, calcite crystals have different configurations: rhombic with NH_4Cl, cubic with urea, oval with the amine, and squared in the presence of surface-active anions (SAA).

Vaterite crystals are formed as spherulites or plates in the case of a continuous chemical precipitation from solutions containing calcium and sodium ions at 60°C and concentrations of the starting solutions equal to 116 and 180 g l^{-1}, respectively. In this case, $CaCO_3$ crystals become platelike.

Calcium carbonate with a phase composition of aragonite can be obtained in a continuous chemical precipitation from solutions containing calcium and sodium ions at 20°C and concentrations of starting solutions equal to 116 and 230 g l^{-1}, in the presence of a minor amount of sucrose.

Because $CaCO_3$ particles are formed in the presence of a NaCl solution, there is a stage of washing to obtain a purer product. The effect of washing on the size and shape of precipitated calcium carbonate particles was studied. A multistage washing can lead both to an increase and a decrease in the average diameter of product particles (Table 5). This change in the size and shape of the particles can be attributed to occurrence of ripening processes in the suspension (Ostwald phenomenon), with a simultaneous mechanical deformation of crystals and their disintegration as a result of agitation, which leads to a poorer uniformity of particles, and the crystal habit takes a characteristic shape with rounded corners and edges.

The results of the study were used to develop a process installation shown in Fig. 4. Calcium carbonate is produced in several stages: (1) preparation of a calcium chloride solution from natural chalk, (2) clarification of the calcium chloride solution, (3) preparation of a soda solution, (4) chemical precipitation and filtering-off of the calcium carbonate precipitate, (5) separation of the precipitate from the solution and desorption of impurities from the calcium carbonate precipitate, and (6) drying of the precipitate.

This procedure allows synthesis of $CaCO_3$ products with different properties on the same equipment unit.

CONCLUSIONS

(1) The technology developed enables control over the characteristics and consumer properties of the product in a wide range.

(2) The properties of the $CaCO_3$ product obtained upon precipitation can be controlled by changing the precipitation mode (temperature, rate at which supersaturation is created, and the rate and method of reactant supply), using complexing substances or modifier additives affecting the shape and size of $CaCO_3$ particles, and introducing a $CaCO_3$ seed.

(3) Finely dispersed and ultradispersed powders can be obtained in $CaCO_3$ precipitation by using not only aqueous, but also organic media and dispersing additives that prevent aggregation of $CaCO_3$ particles.

REFERENCES

1. GB Patent 9600488.
2. EP Patent 0812300.
3. GB Patent 441223.
4. FR Patent 2784371.
5. RF Patent 2218305.
6. RF Patent 2246445.

ISSN 1070-4272, Russian Journal of Applied Chemistry, 2007, Vol. 80, No. 9, pp. 1453–1456. © Pleiades Publishing, Ltd., 2007.
Original Russian Text © D.V. Cherednichenko, E.V. Vorob'eva, N.P. Krut'ko, I.I. Basalyga, Yu.V. Matrunchik, 2007, published in Zhurnal Prikladnoi Khimii, 2007, Vol. 80, No. 9, pp. 1416–1420.

INORGANIC SYNTHESIS AND INDUSTRIAL INORGANIC CHEMISTRY

Effect of Binder Reagents of Varied Nature on the Strength of Potassium Chloride Grains

D. V. Cherednichenko, E. V. Vorob'eva, N. P. Krut'ko, I. I. Basalyga, and Yu. V. Matrunchik

Institute of General and Inorganic Chemistry, National Academy of Sciences of Belarus, Minsk, Belarus

Received January 16, 2007; in final form, April 2007

Abstract—Specific features of structure formation in dispersed salt systems based on potassium chloride were studied from the standpoint of a relationship between the physicochemical properties of binder reagents, granulation conditions, and grain strength.

DOI: 10.1134/S1070427207090029

Granulated fertilizers have a number of advantages in agriculture over those finely grained: lower dusting and transportation loss, lower caking, higher agrochemical efficiency because of the decrease in washing-out of soluble salts from soil, etc. The compaction and pelletization are widely used for granulation of dispersed materials [1, 2]. In pelletization, the structure of a material is formed under dynamic conditions. The uninterrupted motion of a material being granulated, on the one hand, leads to formation and growth of grains and, on the other hand, causes disintegration of grains having the lowest strength. In the case of simultaneous occurrence of these counteractive processes, grains close in shape, size, and properties are formed. The pelletization efficiency can be improved by controlling the dispersity of particles and the state of their surface, which provides a compact "packing" of particles and a higher number of contact points [2, 3]. The pelletization has a number of advantages over compaction, the main of which is the lower specific energy consumption and better product quality because of the lower content of the dust fraction.

When using binder additives in order to raise the granulation efficiency and improve the grain quality, it is necessary to take into account the fact that the mechanisms of contact interaction in compaction and pelletization are different. Compaction at elevated pressures and temperatures of finely grained potassium chloride treated with binder reagents leads to formation of a three-dimensional structure from the particles and to bulk densification of the material. Pelletization yields, as a result of treatment of the material with binders or film-forming substances and the subsequent drying, a layered structure in which particle layers are attached to each other not only by crystallization–condensation contacts between particles, but also by the binding action of an additive. In the general case, use of additives in pelletization raises the grain strength by a factor of 3 and more, whereas in the case of compaction, this parameter can be only raised by 20–30% [4].

In granulation of KCl, the following features of dispersed salt systems should be taken into account: dissolution of the surface layer of KCl upon moistening with binder solutions; surface hydrophobicity of powdered fertilizers being granulated, caused by use of organic reagents in dressing of potassium ores; etc.

In view of the fact that pelletization has not been used as a method for potassium chloride granulation and approaches to use of binders in manufacture of granulated potassium fertilizers have been for the most part empirical, a study of the relationship between binder properties, conditions of structure formation in pelletization, and grain strength is topical.

EXPERIMENTAL

Powdered KCl of chemically pure grade with an average particle size of 0.5 mm was used in the study.

The following binders were used: polyethylene glycol, molecular weight $M = 12 \times 10^3$ (Loba Feinchemie, Germany) (P1); Na-carboxymethyl cellulose, $M = (4–5) \times 10^4$ (P2); and polyacrylamide (PAA) of Praestol brand (Degussa Eurasia Limited Liability Company, RF), $M \approx 14 \times 10^6$ (P3). Oligomeric products of urea polycondensation with formaldehyde [urea–formaldehyde resin (UFR), GOST (State Standard) 14231–88] (Kh1) were also used.

Potassium chloride was pelletized on a laboratory

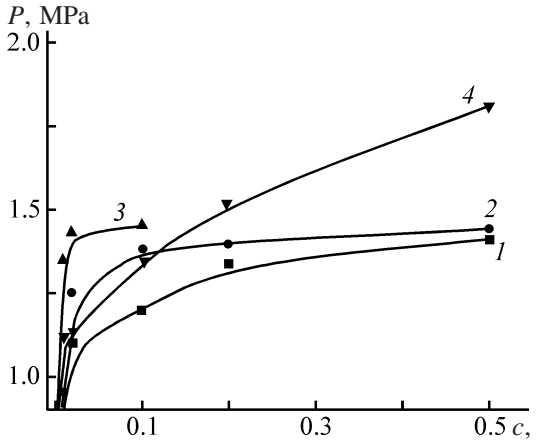

Fig. 1. Grain strength P vs. binder content c. (*1*) P1, (*2*) P2, (*3*) P3, and (*4*) Kh1.

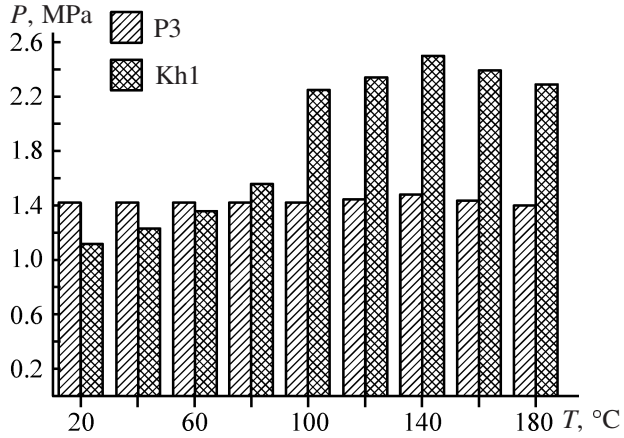

Fig. 2. Effect of temperature T on the strength P of grains treated with a polymer (P3) and oligomers (Kh1).

drum granulator under the same conditions (drum rotation rate, time and temperature of pelletization, weighed portion and moisture content of a material). After the pelletization was complete, grains were dried at different temperatures (40–180°C) for 12 h.

The static grain strength P (MPa) was used as an integral parameter characterizing the strength of contact interactions. The method for determining the static grain strength is based on measuring the mean breaking strength for 20 grains with an IPG instrument. The static strength was calculated by the equation

$$P = \sum_{i=1}^{20} F_i/20S_m,$$

where S_m is the mean area of the diameter cross section of a grain (mm^2), and F_i is the breaking strength (N).

Samples for IR measurements were prepared by deposition of aqueous solutions of polymers (in individual state and as a mixture of aqueous solutions taken in equimolar ratio) onto KCl, with the subsequent thermal treatment at 20, 40, 60, 80, 100, 120, 140, and 180°C for a certain time. Treated samples (mass 10 g) were reduced and the fraction with a particle size of less than 0.2 mm was taken for the measurements. The spectra of the thus prepared samples were recorded in the range 4000–400 cm^{-1} on an Avatar-330 Fourier spectrometer with a diffuse reflection attachment. Untreated KCl served as a reference.

The water-soluble polymers used in the study for treatment of KCl (P1–P3) can form films on the particle surface, which become denser in the course of heat treatment in the stage of grain stabilization [4]. The use of film-forming polymeric binders in pelletization enhances the grain strength (Fig. 1). As the amount of the polymer increases, the number of contacts between particles grows and, consequently, the strength of the structure is enhanced. Raising the polymer content at an invariable moisture content of the material impairs the reagent distribution over the particle surface and leads to a local increase in the thickness of the polymer films at places of contacts, which does not enhance the strength of the structure.

The efficiency of film-forming additives depends on the molecular weight of the polymer (Fig. 1): the higher the molecular weight, the smaller the amount of the polymer, necessary for grain strengthening. Use of polymers, especially those with high molecular weight, is hindered by the high viscosity of the solutions used, which precludes uniform distribution of the binder. Raising the dose at low polymer concentrations leads to excess moistening of the material.

The urea–formaldehyde resin (UFR) (Kh1) is a low-molecular-weight reactive oligomer capable of further chemical transformations under relatively mild conditions. Under the action of temperature, the functional groups of the resin react with each other to form a rigid and strong skeleton providing a high strength of the structured dispersed system.

The influence exerted by the grain treatment temperature on the strength of potassium chloride grains was studied. The results obtained (Fig. 2) indicate that an increase in temperature has virtually no effect on the physicomechanical properties of grains treated with a film-forming polymer additive (P3) and raises the grain strength by a factor of nearly 2 upon treatment with a reactive binder additive (Kh1).

Apparently, it is advisable to improve the granulation of KCl under dynamic conditions by using, on the one hand, the advantages of the high-molecular-weight binder as a film-forming reagent, which provides the required plasticity of a material being pelletized, and, on the other, the ability of the reactive oli-

gomers to form a strong structure in thermal treatment.

Use of a mixture of film-forming and reactive additives can markedly raise the grain strength, compared to the cases of individual components (Fig. 3).

The processes occurring in thermal treatment of a high-molecular-weight film-forming reagent (PAA), reactive oligomers (UFR), and mixtures of these were studied by IR spectroscopy.

The IR spectra of UFR samples contain absorption bands at 1550 (amide II) and 1660 cm^{-1} (amide I) due to vibrations of carbonyl and amide groups. The absorption bands at 1020 and 1250–1260 cm^{-1} can be attributed to vibrations of primary alcohol and ether groups [5, 6]. The intensities of the absorption bands at 1020, 1250, 1550, and 1660 cm^{-1} decrease as the temperature is elevated. This is due to interaction of alcohol, ether, and amide functional groups of the resin at elevated temperatures.

An increase in temperature had virtually no effect on the intensity of characteristic absorption bands in the PAA spectrum. And only elevating the temperature to above 120°C changes the spectrum and leads to a certain decrease in the intensity of the absorption band at 1660 cm^{-1}, associated with vibrations in the amide groups of the polymer, which points to imidization and appearance of cross-linked structures.

Special-purpose experiments demonstrated that thermal treatment of aqueous solutions of PAA at 120 and 140°C to complete removal of water yields a product that completely dissolves in 24 h, when brought in contact with water. Apparently, rare cross-links in the polymer chain containing amide groups cannot provide, in thermal treatment of the polymer, a strength of the three-dimensional structure, sufficient for making insoluble the heat-treated polymer.

IR spectroscopy was also employed to study samples of a mixture of UFR and PAA. The absorption bands associated with vibrations of carbonyl groups and N–H bonds in amide groups are close in the UFR and PAA spectra, which hinders their identification in a study of the component interaction. For this reason, spectra of a mixture prepared from aqueous solutions of the components (Fig. 4, spectrum *1*) and of their mechanical mixture (Fig. 4, spectrum *2*) not subjected to thermal treatment were compared. In view of the similar conditions of sample preparation, and equal contents of the polymers in the mechanical mixture and in the mixture of solutions, it can be stated that the difference in the spectra at 1450–1550 cm^{-1} is due to interaction of the components in the aqueous solution.

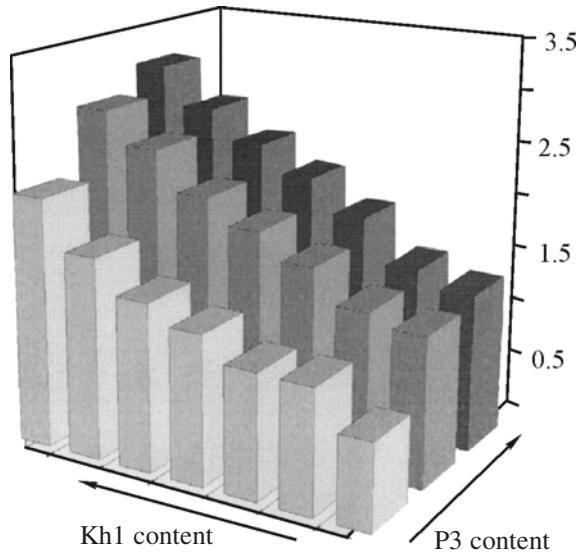

Fig. 3. Grain strength *P* of potassium chloride upon integrated treatment with binder reagents. Drying temperature 100°C.

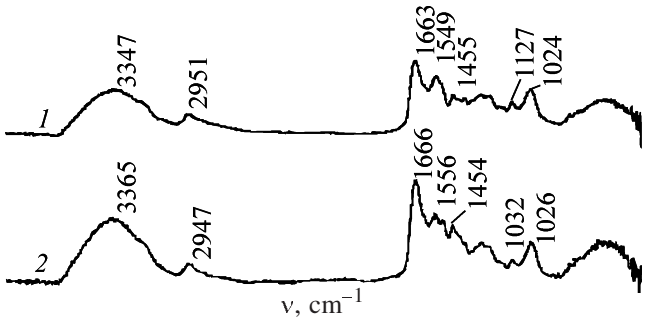

Fig. 4. IR spectra of (*1*) mixture prepared from aqueous solutions and (*2*) mechanical mixture of PAA and UFR.

In the case of a thermal treatment of the mixture of aqueous solutions, the intensity of the absorption bands at 1020, 1250, 1550, and 1660 cm^{-1} decreases, but the extents to which *D* changes on elevating the temperature are different for UFR in the individual state and in a mixture with PAA. Figure 5 shows values of *D*, which characterize the ratio between the intensity of an absorption band being analyzed in the spectrum of a sample thermally treated at temperatures of 40 to 180°C and the intensity of the same absorption band in the spectrum of a sample at 20°C, with data presented only for those absorption bands whose intensity changes on elevating the temperature. It can be seen that, as temperature increases, the intensity of the absorption bands at 1550 and 1020 cm^{-1} decreases to a greater extent for the UFR + PAA mixture, compared to UFR in the individual state. The extents to which the intensities of the band at 1250 cm^{-1} change are similar for UFR and the mixture. For the absorption band at 1660 cm^{-1}, the temperature dependences

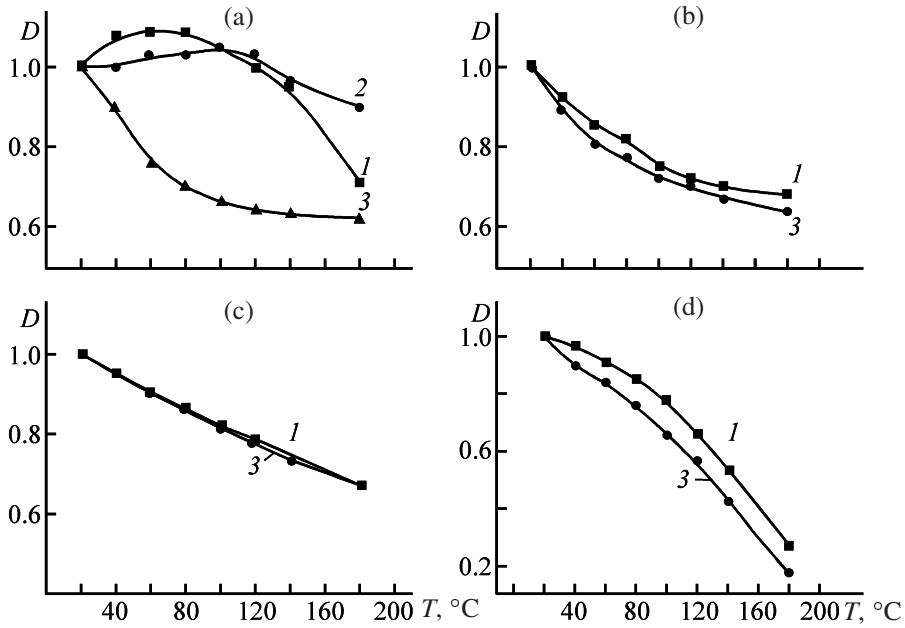

Fig. 5. *D* vs. thermal treatment temperature *T* for the absorption bands at (a) 1660, (b) 1550, (c) 1250, and (d) 1020 cm^{-1}. (*1*) UFR, (*2*) PAA, and (*3*) mixture of PAA and UFR.

of *D* are different for the individual components and their mixture.

The results obtained in the study suggest that, upon mixing of aqueous solutions of UFR and PAA and thermal treatment of the mixture, the functional groups of the components react with each other: there occur reactions between the carboxy groups formed in partial hydrolysis of PAA, amide groups of PAA, and alcohol and ether groups of UFR; also possible is the reaction of PAA with formaldehyde released upon heating of UFR. The observed quantitative difference between the changes in the intensities of the absorption bands indicates that the mechanisms by which the structural networks are formed in the cases of individual components and in their mixture are different.

CONCLUSIONS

(1) A study of the efficiency of the structure-forming action of polymers of the film-forming type and reactive oligomers in pelletization of potassium chloride demonstrated the advantage of a high-molecular-weight component in formation of a layered plastic shape of a grain and the ability of the oligomers to yield a firm structure in thermal treatment.

(2) Joint use of film-forming polymers and reactive oligomers enables control over the granulation process of potassium chloride in different stages: in the initial stage of pelletization under dynamic conditions, presence of a polymer (polyacrylamide) provides a high plasticity of the material and change in the shape of grains without their disintegration and improves the distribution of the binder additive over the potassium chloride surface. In the subsequent stages, structural formation occurs under the action of temperature, with the reactive oligomer (urea–formaldehyde resin) and a polymer involved. The strength of potassium chloride grains produced by pelletization can be markedly raised by taking into account the type of a binder additive (synergism of the action of the film-forming and reactive components), its physicochemical properties, and structure formation conditions.

REFERENCES

1. Vilesov, N.G., *Protsessy granulirovaniya v promyshlennosti* (Industrial Granulation Processes), Kiev: Tekhnika, 1976.
2. Klassen, P.V. and Grishaev, I.G., *Osnovnye protsessy tekhnologii mineral'nukh udobrenii* (Main Processes of Mineral Fertilizer Technology), Moscow: Khimiya, 1990.
3. Kochetkov, V.N., *Granulirovanie mineral'nykh udobrenii* (Granulation of Mineral Fertilizers), Moscow: Khimiya, 1975.
4. Wolfgang, P., *Agglomeration Processes: Phenomena, Technologies, Equipment*, Wiley, 2002.
5. Bellamy, L.J., *The Infra-Red Spectra of Complex Molecules*, New York: Wiley, 1957.
6. Banwell, C.N., *Fundamentals of Molecular Spectroscopy*, London: McCraw-Hill, 1983, 3rd.

ISSN 1070-4272, Russian Journal of Applied Chemistry, 2007, Vol. 80, No. 9, pp. 1457–1460. © Pleiades Publishing, Ltd., 2007.
Original Russian Text © K.V. Titova, V.P. Nikol'skaya, V.V. Buyanov, O.B. Pudova, Yu.G. Oboznaya, 2007, published in Zhurnal Prikladnoi Khimii, 2007, Vol. 80, No. 9, pp. 1421–1424.

INORGANIC SYNTHESIS AND INDUSTRIAL INORGANIC CHEMISTRY

Synthesis of $(NH_4)_2SO_4 \cdot H_2O_2$ and Methods of Its Stabilization and Storage

K. V. Titova, V. P. Nikol'skaya, V. V. Buyanov, O. B. Pudova, and Yu. G. Oboznaya

Institute of Chemical Physics Problems, Chernogolovka, Moscow oblast, Russia
State Research Institute of Biological Instrument Making, Federal State Unitary Enterprise, Moscow, Russia

Received January 11, 2007; in final form, April 2007

Abstract—Optimal conditions of the synthesis of ammonium sulfate peroxy solvate stabilized by carboxylic acids were developed.

DOI: 10.1134/S1070427207090030

The majority of peroxy solvates of salts of inorganic acids show low stability, which is caused by susceptibility of their component, hydrogen peroxide, to catalytic decomposition. However, hydrogen peroxide, both coordinated to salts and free, can be substantially stabilized by introducing various additives. For example, a wide set of stabilizers substantially enhancing the stability were found for potassium fluoride peroxy solvates $KF \cdot nH_2O_2$ (n = 1–3). The monoperoxy solvate $KF \cdot H_2O_2$ stabilized by potassium hydrofluoride decomposes within 7 years at an average rate of 0.47%/year, i.e., to 3.32% in this period of time [1]. Carboxylic acids are no less effective stabilizers for potassium fluoride monoperoxy solvate [2]. A new generation of disinfectants with a wide spectrum of antimicrobial action was developed on the basis of $KF \cdot H_2O_2$ [3].

The development of effective stabilizers for one group of peroxy solvates suggests that these or related compounds may exert a stabilizing effect also on less stable solvates of other salts. This would expand the range of solid forms of hydrogen peroxide for use in the fields of disinfection science and bleaching, and also in other fields depending on the properties of salts that are carriers of hydrogen peroxide. The ability of ammonium sulfate to solvate hydrogen peroxide was mentioned by Schumb et al. in [4]. The study of $(NH_4)_2SO_4$ solubility in anhydrous hydrogen peroxide has shown that the maximal amount of coordinated H_2O_2 corresponds to the composition $(NH_4)_2SO_4 \cdot H_2O_2$ [1].

In this study we found the optimal conditions of the synthesis, stabilization, and storage of $(NH_4)_2SO_4 \cdot H_2O_2$, providing the retention of available oxygen (observation time more than 100 days). Carboxylic acids were used as stabilizers.

EXPERIMENTAL

The peroxy solvate $(NH_4)_2SO_4 \cdot H_2O_2$ was synthesized by the reaction of chemically pure grade ammonium sulfate and hydrogen peroxide of various concentrations. Water and excess hydrogen peroxide were removed with a warm (50–55°C) air flow passed over a surface of the solution placed in a polymeric pan.

The experiments have shown that, at the molar ratio $H_2O_2 : (NH_4)_2SO_4$ = 1 : 1 and H_2O_2 concentration of 34 wt %, the solid product contains 13.7% hydrogen peroxide, which corresponds to the composition $(NH_4)_2SO_4 \cdot 0.65H_2O_2$. The increase in the amount of hydrogen peroxide up to the ratio $H_2O_2 : (NH_4)_2SO_4$ = 3 : 1 at the same its concentration slightly increases the content of H_2O_2 in the solid product. At a fivefold excess of hydrogen peroxide of the same concentration, the solid phase is the pure monoperoxy solvate $(NH_4)_2SO_4 \cdot H_2O_2$ (Table 1). Further increase in the H_2O_2 concentration to 60 wt % and an increase in its amount introduced into the reaction to 5 mol per mole of the salt does not lead to the formation of a solvate with a higher content of hydrogen peroxide. These results confirm the previous data that ammonium sulfate monoperoxy solvate is the compound with the maximum H_2O_2 content [4].

Ammonium sulfate peroxy solvate is a colorless crystalline product soluble in water. Its solutions are

Table 1. Synthesis conditions and characteristics of $(NH_4)_2SO_4 \cdot H_2O_2$. Content of H_2O_2 in the solvate 20.48%

Synthesis conditions		Characteristics of $(NH_4)_2SO_4 \cdot H_2O_2$	
initial concentration of H_2O_2 in solution, wt %	molar ratio $H_2O_2 : (NH_4)_2SO_4$	H_2O_2 content, wt %	solvate number
34.0	1 : 1	13.71	0.65
34.0	3 : 1	16.93	0.83
34.0	5 : 1	20.49	1.00
46.1	1 : 1	15.51	0.76
46.1	3 : 1	20.40	1.00
59.9	1 : 1	19.70	0.96
9.9	5 : 1	20.49	1.00

Table 2. X-ray diffraction pattern of $(NH_4)_2SO_4 \cdot H_2O_2$*

Line no.	*d*, nm	I_{rel}	Line no.	*d*, nm	I_{rel}	Line no.	*d*, nm	I_{rel}
1	5.216	4	10	2.936	100	19	2.078	3
2	4.955	81	11	2.884	9	20	2.025	4
3	4.635	34	12	2.618	15	21	1.895	11
4	4.311	11	13	2.567	3	22	1.755	7
5	4.086	5	14	2.491	12	23	1.642	6
6	3.778	69	15	2.426	3	24	1.479	5
7	3.446	3	16	2.318	4	25	1.221	10
8	3.278	23	17	2.279	3	26	1.161	1
9	3.084	4	18	2.151	8			

* *d* is interplanar spacing, and I_{rel}, relative intensity.

stable: the H_2O_2 content of a solution, 2.61% (pH 4.1), does not vary within the observation time longer than 7 days. The X-ray pattern of $(NH_4)_2SO_4 \cdot H_2O_2$ was recorded on an ADP-2-01 diffractometer (CuK_α radiation, Ni filter) using the program developed for DRON X-ray diffractometers and intended for automation of data acquisition, processing, and analysis. The thermograms were recorded on a Q-1500-D instrument with a Pt/Pt–Rh thermocouple and Al_2O_3 reference at a heating rate of 5 deg min^{-1}.

Table 3. Loss of H_2O_2 from ammonium sulfate peroxy solvate $[(NH_4)_2SO_4 \cdot H_2O_2]$ stabilized by carboxylic acids. Storage in a closed container, 20°C, 76 days

Stabilizer, wt %	Decomposition rate, % H_2O_2/day	H_2O_2 loss, % of initial content
Acid:		
succinic, 0.5	0.14	10.6
succinic, 1.0	0.28	21.1
fumaric, 0.5	0.25	19.1
fumaric, 1.0	0.10	7.4
No stabilizer	0.32	24.4

Interplanar spacings and relative intensities of the X-ray reflections of $(NH_4)_2SO_4 \cdot H_2O_2$ are given in Table 2. The comparison with the X-ray pattern of the starting $(NH_4)_2SO_4$ [5] shows that we synthesized a pure peroxy solvate, as the reflections of the starting ammonium sulfate were absent.

The solvate partially dissociates under polythermal conditions at 100°C with the release of hydrogen peroxide into the gas phase. The endothermic dissociation gives way to the exothermic irreversible decomposition of H_2O_2 at 110–125°C.

When the solvate is kept in an open container at room temperature (20±2°C) and a relative humidity of 50%, it loses hydrogen peroxide at an average rate of 4% per day. Carboxylic acids as stabilizers appeared inefficient under these conditions: the rate of the solvate decomposition in their presence did not decrease noticeably. The decomposition of $(NH_4)_2SO_4 \cdot H_2O_2$ stabilized by carboxylic acids on storage in closed polymeric containers occurs much more slowly (Table 3). Table 3 shows that the nonstabilized sample decomposes at an average rate of 0.32% in the course of 2.5 months and the total loss in this time is 24%. Succinic acid exerts an insignificant stabilizing effect,

Table 4. Stability of $(NH_4)_2SO_4 \cdot H_2O_2$ stabilized by carboxylic acids in storage in an open container over a desiccant (20±2°C)

τ, days	No stabilizer		Acid,* %			
			succinic, 0.5		fumaric, 1.0	
	H_2O_2, %, in solid product	H_2O_2 loss, % of initial content	H_2O_2, %, in solid product	H_2O_2 loss, % of initial content	H_2O_2, %, in solid product	H_2O_2 loss, % of initial content
0	19.73	0	18.85	0	20.36	0
5	19.87	0	19.16	0	20.44	0
12	19.41	1.62	18.83	0.02	20.16	0.20
19	18.93	4.05	18.55	0.30	20.26	0.10
26	19.42	1.57	18.92	0	20.27	0.09
35	20.10	0	19.79	0	20.40	0
42	19.75	0	18.46	0.39	20.42	0
49	19.83	0	18.86	0	20.60	0
56	19.69	0.2	19.08	0	20.54	0
69	19.56	0.86	19.11	0	20.48	0
76	20.02	0	19.01	0	20.41	0
90	19.67	0.30	19.14	0	20.37	0
106	19.29	2.23	19.01	0	20.37	0

* Similar results were obtained at the following content of acids (%): succinic 1.0, fumaric 0.5.

whereas fumaric acid in an amount of 1.0% reduces the decomposition rate by a factor of 3.

The stability of $(NH_4)_2SO_4 \cdot H_2O_2$ sharply increases on keeping in the presence of a desiccant. The experiments have shown that keeping the solvate in an open polymeric container in a desiccator over magnesium perchlorate or sulfuric acid for more than 100 days is accompanied by only insignificant loss of hydrogen peroxide (no more than 2.2% for a nonstabilized sample), and samples stabilized with carboxylic acids do not lose hydrogen peroxide at all (Table 4). Certain decrease in the H_2O_2 content in the initial stage of storage is due to adsorption of atmospheric moisture by samples during their preparation and loading into the desiccator. Then the adsorbed moisture is evaporated and absorbed by the desiccant.

Similar data on the essential effect of ambient air humidity on the stability of peroxy solvates were obtained previously for sodium carbonate peroxy solvate [6]. Keeping $Na_2CO_3 \cdot 1.5H_2O_2$ for 40 days in an open container in a desiccator without a desiccant gives a decomposition rate constant higher by an order of magnitude compared to keeping under the same conditions over a desiccant [$k_1 = 26.5 \times 10^{-3}$ and $k_2 = 2.6 \times 10^{-3}$ min^{-1} (100°C), respectively]. Obviously, water evolved in the initial stage of the solvate decomposition, or its vapor absorbed from a moist air, forms a microfilm of an alkaline or acid solution on the surface of solvate crystals, producing a catalytic effect on coordinated hydrogen peroxide. The adsorption of water vapor by a desiccant prevents the formation of such a film and makes the solvate more stable.

A desiccant for $(NH_4)_2SO_4 \cdot H_2O_2$ storage can be silica gel, aluminum oxide, or some other granular desiccant placed in a ready sample in a container with a surface permeable to water vapor. Such a technique is used in pharmacology and also in instrument making.

The results of this study indicate that, under the developed storage conditions, ammonium sulfate peroxy solvate along with other solid forms of hydrogen peroxide can be used both in disinfection science and in other fields. Advantages of ammonium sulfate peroxy solvate consist in availability and low price of the starting salt compared, e.g., to potassium fluoride. We believe that ammonium sulfate peroxy solvate shows promise for agriculture as a compact fertilizer with such additional valuable and environmentally safe disinfectant as hydrogen peroxide.

It should be noted that ammonium sulfate peroxy solvate is similar to sodium carbonate peroxy solvate in stability at a room temperature of 20±2°C and 50–

60% humidity. Numeorus effective stabilizers are used for stabilizing $Na_2CO_3 \cdot 1.5H_2O_2$; this problem is the subject of more than 300 patents. Although the mechanism of the stabilizing action is unknown in most cases, the attained stability of percarbonate was so high that it could be widely used in multicomponent detergents. In view of the possibility of using $(NH_4)_2SO_4 \cdot H_2O_2$ in various fields such as disinfection science, bleaching, and agricultural practice, the methods of its stabilization are not exhausted by this study, and their development should be continued using diverse stabilizers, their mixtures, and various application techniques.

CONCLUSIONS

(1) A method of the $(NH_4)_2SO_4 \cdot H_2O_2$ synthesis has been developed.

(2) Conditions for the stabilization and storage under which ammonium sulfate peroxy solvate does not lose available oxygen (observation time more than 100 days) have been found.

REFERENCES

1. Titova, K.V., Nikol'skaya, V.P., and Buyanov, V.V., *Koordinatsionnye soedineniya peroksida vodorova* (Coordination Compounds of Hydrogen Peroxide), Chernogolovka: Inst. Probl. Khim. Fiz. Ross. Akad. Nauk, 2000.
2. Titova, K.V., Nikol'skaya, V.P., Buyanov, V.V., Pudova, O.B., and Karzhavina, G.P., *Zh. Prikl. Khim.*, 2005, vol. 78, no. 2, pp. 287–291.
3. Buyanov, V.V., Nikol'skaya, V.P., Pudova, O.P., and Titova K.V., *Peroksosol'vaty v dezinfektologii* (Peroxo Solvates in Disinfection Science), Chernogolovka: Inst. Probl. Khim. Fiz. Ross. Akad. Nauk, 2000.
4. Schumb, W.C., Satterfield, Ch.N., and Wentworth, R.L., *Hydrogen Peroxide*, New York: Reinhold, 1955.
5. Titova, K.V., *Zh. Neorg. Khim.*, 2000, vol. 45, no. 2, pp. 320–326.
6. Titova, K.V., Kolmakova, E.I., and Rosolovskii, V.Ya., *Fiziko-khimicheskie svoistva i sposob stabilizatsii peroksogidrata karbonata natriya* $Na_2CO_3 \cdot 1.5H_2O_2$ (Physicochemical Properties and Ways of Stabilization of Sodium Carbonate Peroxohydrate $Na_2CO_3 \cdot 1.5H_2O_2$), Available from VINITI, Moscow, 1983, no. 1254-84 Dep.

ISSN 1070-4272, Russian Journal of Applied Chemistry, 2007, Vol. 80, No. 9, pp. 1461–1467. © Pleiades Publishing, Ltd., 2007.
Original Russian Text © M.A. Kruglova, M.P. Yaroshenko, 2007, published in Zhurnal Prikladnoi Khimii, 2007, Vol. 80, No. 9, pp. 1425–1431.

INORGANIC SYNTHESIS AND INDUSTRIAL INORGANIC CHEMISTRY

Preparation and Characteristics of Zirconium–Aluminum Oxide System

M. A. Kruglova and M. P. Yaroshenko

Novomoskovsk Institute of Nitrogen Industry, Novomoskovsk, Tula oblast, Russia

Received April 18, 2007

Abstract—The possibility of preparing highly dispersed mixed zirconium–aluminum oxides by precipitation of zirconium hydroxide on γ-Al_2O_3 was studied.

DOI: 10.1134/S1070427207090042

Zirconium dioxide and compositions based on it are important catalytic materials. ZrO_2 is used as a component of catalysts for various processes: dehydration, isomerization, alkylation, selective and full oxidation of hydrocarbons, Fischer–Tropsch synthesis, etc. [1–3]. Zirconium dioxide is also one of the most promising catalyst supports, as it is highly chemically and thermally stable in reducing media and has both acid and base centers on its surface [4]. However, application of zirconium dioxide is limited by the metastability of its low-temperature modifications (amorphous, cubic, and tetragonal) and ease of their transition into the stable monoclinic modification exhibiting, as a rule, high crystallinity and low specific surface area [5].

The interest in preparing nanocrystalline materials based on zirconium dioxide led to the development of approaches to stabilization of the ZrO_2 structure in low-temperature modifications. It is known [6] that addition of small amounts of compounds of rare-earth elements, e.g., yttrium, results in a stabilization of the low-temperature metastable tetragonal or cubic phase of zirconium dioxide. The addition to zirconium dioxide of oxides of Group II and III metals with the ionic radii close to that of zirconium makes it possible to prepare anion-deficient solid solutions $Zr_{1-x}(M^{2+})_xO_{2-x}$ or $Zr_{1-y}(M^{3+})_yO_{2-0.5y}$, where x, $y = 0.10-0.15$. Such solid solutions exist in the form of stabilized tetragonal or cubic modifications in a wide temperatures range [7]. Stabilization of metastable modifications of zirconium dioxide by doping with aluminum compounds was also reported [8, 9]; it is noted, however [10, 11], that ZrO_2–Al_2O_3 solid solutions decompose at relatively low temperatures because of appreciable oversaturation. Klimova et al. [5] note that the addition of even small amounts of Al_2O_3 strongly affects the structure of zirconium dioxide and hinders the conversion of the tetragonal ZrO_2 modification to the monoclinic modification, which is accounted for by the limited size of zirconium dioxide crystallites that can be incorporated in the matrix of aluminum oxide.

As a rule, zirconium-containing oxide systems are prepared by the coprecipitation of metal nitrates or chlorides from solutions or by a sol–gel method using metal alkoxides [5]. The precipitation of hydroxides involves serious problems with filtration and washing of gel precipitates [12].

In this study we attempted to obtain a zirconium–aluminum oxide system by precipitating hydrated zirconium oxide on γ-Al_2O_3, which is of interest for searching for a convenient industrial method ensuring, in particular, better filterability of the precipitate. Furthermore, the use of active aluminum oxide seemed to be helpful for further application of the material as catalyst support. The formation of the resulting zirconium–aluminum oxide systems and also the mutual influence of zirconium and aluminum oxides in such systems were examined in this study.

EXPERIMENTAL

Samples of ZrO_2–Al_2O_3 were prepared as follows: 1 M aqueous solution of zirconyl nitrate was mixed with a calculated amount of γ-Al_2O_3, and then NH_4OH_{conc} was added with continuous stirring. The precipitation was finished on reaching pH 9. The resulting precipitates were filtered off, washed with distilled water, and dried at a room temperature for 24 h and then at 120°C for 5 h. The samples were

Table 1. Phase composition and specific surface area of samples calcined at various temperatures

Sample	Al_2O_3, wt %	Phase composition* at indicated calcination temperature, °C								S_{sp}, $m^2\ g^{-1}$	
		120	300	400	500	600	700	800	1000	400	800
ZA0	0	A	A	m, t	m, t	m, t	m, t	m, t	m, t**	144	13
ZA25	25	A	A	A	t, A	t	t, m	t, m	m, t	136	35
ZA50	50	A, γ-Al_2O_3	A, γ-Al_2O_3	A, γ-Al_2O_3	A, γ-Al_2O_3	t, A, γ-Al_2O_3	t, γ-Al_2O_3	t, γ-Al_2O_3	t, γ-Al_2O_3, m, θ-Al_2O_3,** α-Al_2O_3**	225	131
ZA75	75	A, γ-Al_2O_3	A, γ-Al_2O_3	A, γ-Al_2O_3	A, γ-Al_2O_3	A, γ-Al_2O_3,	t, γ-Al_2O_3	t, γ-Al_2O_3	t, γ-Al_2O_3, θ-Al_2O_3, m, α-Al_2O_3**	258	138
ZA100	100	γ-Al_2O_3, gibbsite, bayerite	γ-Al_2O_3	γ-Al_2O_3	γ-Al_2O_3	γ-Al_2O_3	γ-Al_2O_3	γ-Al_2O_3	θ + γ-Al_2O_3, α-Al_2O_3	283	210
Mechanical mixture ZA0 + ZA100	50	A, gibbsite, bayerite	A, γ-Al_2O_3	t, m, γ-Al_2O_3	m, t, γ-Al_2O_3	m, t, γ-Al_2O_3	m, t, γ-Al_2O_3	m, t, γ-Al_2O_3	m, θ + γ-Al_2O_3, α-Al_2O_3, t**	–	–

* (A) Amorphous, (t) tetragonal, amd (m) monoclinic phases of ZrO_2.
** Traces.

calcined in air for 3 h at temperatures from 300 to 1000°C. Under the same conditions we prepared a sample of hydrated zirconium oxide (HZO) free of γ-Al_2O_3 additions. For comparison we prepared a sample of γ-Al_2O_3 treated with NH_4OH. The composition of the samples obtained is given in Table 1.

The X-ray experiments were carried out on DRON-3 and DRON-3M diffractometers (CuK_α radiation with a graphite monochromator on the reflected beam). To identify phases, we used a database of the Joint Committee on Powder Diffraction Standards (JCPDS). The average size of coherent scattering areas (CSAs) was determined from the broadening of diffraction peaks by the Selyakov–Scherrer formula. The content of the tetragonal phase of zirconium dioxide was determined from the relationship [13]

$$X_1 = \frac{I_t(111)}{I_m(111) + I_m(11\bar{1}) + I_t(111)},$$

where I_m and I_t are the integral intensities of the diffraction peaks of the monoclinic and tetragonal ZrO_2 phases, respectively.

The differential thermal analysis was carried out on a Q-1500D derivatograph. The heating rate was 5 deg min^{-1}. The specific surface area, pore volume, and pore size distribution were determined by low-temperature adsorption of nitrogen at 77 K on a Micrometrics ASAP 2010N instrument. The acidity of the surface of the samples calcined at 400°C was studied by temperature-programmed desorption of ammonia (TPD NH_3). After a pretreatment, saturation by ammonia mixed with nitrogen, and removal of excess ammonia the experiment was carried out in a He stream at a heating rate of 8 deg min^{-1}. The released ammonia was detected with a thermal conductivity detector.

The X-ray study has shown that a zirconium-containing phase in all noncalcined samples is in the X-ray amorphous state (Table 1). After calcination at 400°C and higher temperatures, essential changes are observed in the phase composition of the samples. The X-ray amorphous phase completely disappears from ZA0 sample above 400°C, and the crystalline metastable tetragonal (t-ZrO_2) and stable monoclinic (m-ZrO_2) phases of zirconium dioxide appear (Fig. 1). As the samples are highly dispersed, which results in considerable broadening of X-ray reflections, it is difficult to determine whether zirconium dioxide is in cubic or tetragonal modification; in what follows, the low-temperature metastable modification of ZrO_2 is referred to as tetragonal phase. Examination of the integral intensities of the t-ZrO_2 and m-ZrO_2 lines shows that after the calcination of the ZA0 sample in the temperature range 400–1000°C the tetragonal ZrO_2 phase is gradually converted to the monoclinic phase. The content of t-ZrO_2 in the sample varies from 45% at the calcination temperature of 400°C to 10–15% after calcination at 800°C, with complete

disappearance of this phase at 1000°C (Fig. 2). The same pattern is also observed on calcination of a mechanical mixture of the dried up ZA0 and ZA100 samples.

Unlike ZA0, in binary samples the X-ray amorphous phase is preserved up to high calcination temperatures. The crystallization of the metastable tetragonal ZrO_2 phase in the samples obtained by precipitation on γ-Al_2O_3 occurs in a wide temperature range (Table 1). For example, the t-ZrO_2 phase appears in the ZA25 sample after calcination at 500°C. In a certain temperature range, it coexists with the X-ray phase which disappears only above 600°C. In the ZA50 and ZA75 samples, the crystallization of t-ZrO_2 from the X-ray amorphous phase starts after calcination at 600 and comes to the end at 800°C (Table 1, Fig. 1). The monoclinic phase of zirconium dioxide is absent in ZA25 up to 700°C, and in the ZA50 and ZA75 samples, up to 1000°C. The t-ZrO_2 content (Fig. 2) of the samples decreases as the calcination temperature increases; however, after calcination at 1000°C this phase remains in the ZA25 sample (30% content), and in the ZA50 and ZA75 samples 95 and 85% of t-ZrO_2 is retained. It is seen from these data that the presence of γ-Al_2O_3 in the synthesized zirconium–aluminum oxide systems promotes an increase in the temperature of zirconium dioxide crystallization and the stabilization of its low-temperature tetragonal phase. The manifestation of this effect becomes stronger as the fraction of the added aluminum oxide increases.

It is known [6] that in binary mixtures containing ZrO_2 the crystallization temperature of a solid solution based on it increases as the concentration of a doping component increases. According to the DTA data, the crystallization of pure zirconium dioxide in the ZA0 sample was accompanied by an exothermic effect at 390°C (Fig. 3). In the case of the ZA25 sample, a weak exothermic effect corresponding to the crystallization of ZrO_2 has a maximum at 440°C. At a 50 wt % content of Al_2O_3 in the sample (ZA50), the pronounced exothermic effect is absent from the thermogram (Fig. 3), and we can speak only of the field of its probable appearance at temperatures above 550°C, corresponding to the temperature range of the onset of ZrO_2 crystallization detected by X-ray diffraction.

Such differences in the crystallization of the samples under discussion can serve as an evidence of a deep interaction in the Zr–Al–O system proceeding with the formation of solid solutions. This is also confirmed by the X-ray data which show that the position

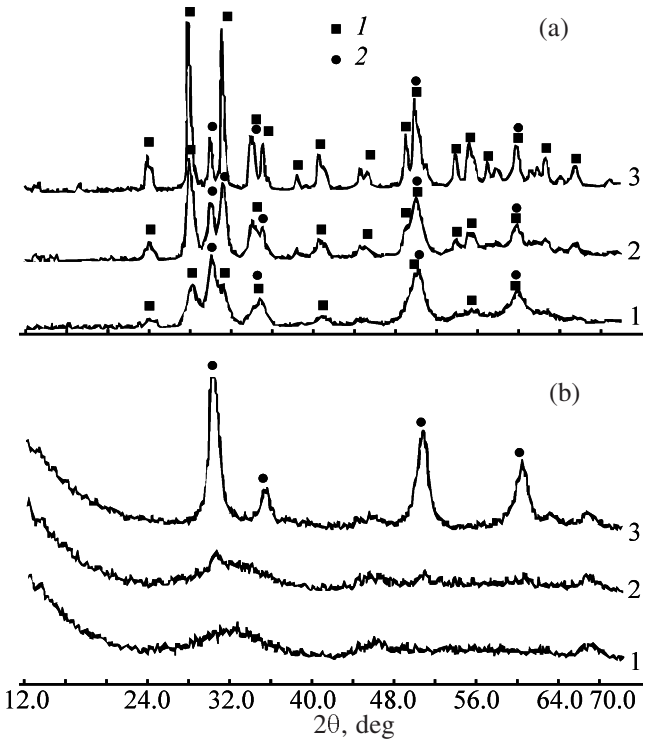

Fig. 1. X-ray diffraction patterns of samples (a) ZA0 and (b) ZA50 calcined at (*1*) 400, (*2*) 600, and (*3*) 800°C. (2θ) Bragg angle. (*1*) m-ZrO_2 and (*2*) t-ZrO_2.

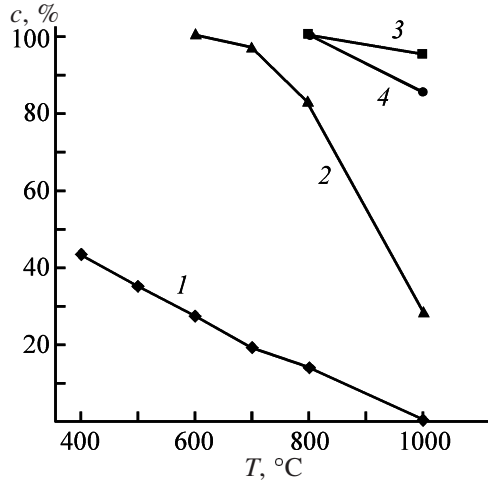

Fig. 2. Content of the tetragonal phase of zirconium dioxide *c* as a function of the calcination temperature *T* of samples (*1*) ZA0, (*2*) ZA25, (*3*) ZA50, and (*4*) ZA75.

of the (111) t-ZrO_2 line in all binary samples considerably differs from the positions of the corresponding line of the ZA0 sample and of a mechanical mixture of ZA0 and ZA100 (Table 2). In the series of these samples, the largest shift of the (111) line in the temperature range 600–800°C is observed with ZA50 sample with the chemical composition identical to that of the above-mentioned mechanical mixture.

Table 2. Interplanar spacings d_{111} of the tetragonal phase of zirconium dioxide

Sample no.	Interplanar spacing d_{111}, Å, in samples calcined at indicated temperature, °C					
	400	500	600	700	800	1000
ZA0	2.959	2.955	2.955	2.962	2.965	–
ZA25	–	–	2.938	2.940	2.946	2.951
ZA50	–	–	–	2.9346	2.9402	2.9592
ZA75	–	–	–	2.940	2.946	2.963
Mechanical mixture ZA0 + ZA100	2.960	2.960	2.962	2.962	2.965	–

The calcination of the binary samples ZA50 and ZA75 at 1000°C changes the position of the (111) line to values characteristic of pure ZrO_2. This fact is attributable to the separation of a solid solution into layers under the action of high temperature, with the isolation of pure zirconium dioxide. The largest difference in the interplanar spacing observed for the ZA50 sample seems to be due to the strongest effect of γ-Al_2O_3 on the formation of zirconium dioxide in the mixed oxide system of such composition.

Apparently, the effect of components in the synthesized zirconium–aluminum samples is mutual. Aluminum oxide in the structure of binary samples is represented by a single phase, γ-Al_2O_3. At the same time, the ZA100 sample contains after drying gibbsite and bayerite phases along with the γ-Al_2O_3 phase

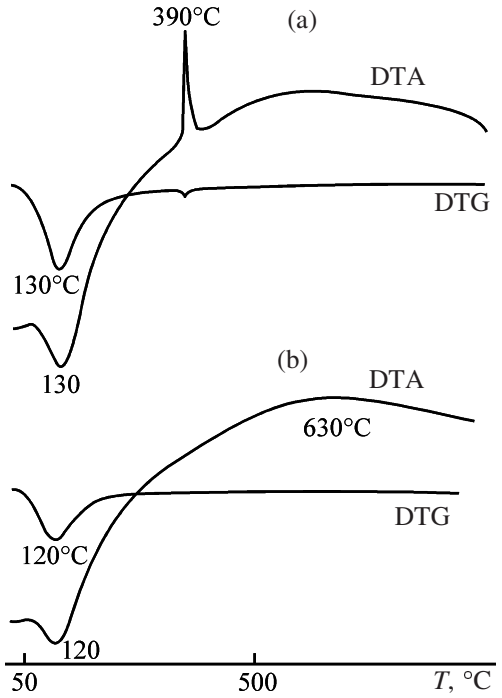

Fig. 3. Thermograms of samples (*1*) ZA0 and (*2*) ZA50. (*T*) Temperature.

(Table 1), suggesting partial hydration of aluminum oxide. Presumably, certain amount of these aluminum trihydroxides is formed also in binary samples but is not detected by X-ray diffraction. This assumption is supported by the presence of the corresponding endothermic effect in the thermogram of the ZA75 sample at 280°C. The simultaneous formation of zirconium and aluminum hydroxides under the synthesis conditions suggests that mixed hydroxides, precursors of Al_2O_3–ZrO_2 solid solutions, can appear.

One more specific feature of the formation of the zirconium–aluminum oxide systems is the presence of a significant amount of the low-temperature Al_2O_3 modification in samples calcined at 1000°C. It is known [14] that the high-temperature modifications θ- and α-Al_2O_3 are characteristic of aluminum oxide in this case, and just these modifications predominate in the ZA100 sample. The presence of foreign cations can hinder the rearrangement of Al_2O_3 into the corresponding forms [15]. Hence, we can assume that zirconium cations are also incorporated in the Al_2O_3 structure in binary samples, which caused stabilization of the low-temperature modification of aluminum oxide.

We have determined the average size of coherent scattering areas of the tetragonal ZrO_2 phase for the samples calcined at various temperatures. It is seen from the represented data (Fig. 4) that the sizes of t-ZrO_2 CSA for the ZA0 and ZA25 samples differ from each other not so strongly as in the case of samples with higher content of aluminum oxide, namely, ZA50 and ZA75. After calcination of these samples at 700–800°C, the size of t-ZrO_2 CSA remains on the level of 10 nm. As the calcination temperature increases to 1000°C, the size of t-ZrO_2 CSA increases sharply, to approximately 30 nm. This size is considered [7, 16] as a critical size of crystallites of the tetragonal phase, which is further converted to the monoclinic phase. However, in the ZA0 and ZA25 samples the conversion of t-ZrO_2 to m-ZrO_2 occurs at

sizes of crystallites much smaller than 30 nm; moreover, the formation of m-ZrO_2 with crystallite sizes of about 15 nm is observed. As the crystallization in one or another modification depends on the ratio of the surface and bulk free energy [4], it is influenced, in addition to the size of crystallites, by the presence of modifying anions and cations, the presence and the distribution of defects, and by other factors. As the above-listed factors differ depending on the composition and conditions of sample preparation, we can assume that in each case crystallites would have their own critical size.

The zirconium–aluminum system seems to be formed through the formation of ZrO_2–Al_2O_3 solid solutions. Their precursors are products of the reaction of zirconium hydroxide with the hydrated surface of aluminum oxide in the precipitation step. Under the conditions of the HZO precipitation, the addition of aluminum ions can terminate the chain of the polymerization of tetrameric complexes $[Zr_4(OH)_8(H_2O)_6]^{8+}$, thus yielding a defective structure of zirconium hydroxide. In turn, zirconium complex ions can be incorporated in the structure of the hydroxide layer of the Al_2O_3 surface on the phase boundary. Such mutually modified phases become precursors of ZrO_2–Al_2O_3 solid solutions with the composition and properties appreciably depending on the ratio of components in the system. The ZA25 sample is close to the ZA0 sample in the character of the structure formation [crystallization of t-ZrO_2 and m-ZrO_2, variation in the position of the (111) diffraction peak of t-ZrO_2, and CSA size]. Possibly, the addition of 25% Al_2O_3 leads to the formation of a solid solution based on zirconium dioxide, whereas the formation of the ZA75 sample seems to be substantially determined by the formation of a solid solution based on the Al_2O_3 structure. The presence of aluminum ions in the HZO structure favors preservation of the X-ray amorphous state of ZrO_2 up to a calcination temperature of 600°C. After crystallization of the ZrO_2–Al_2O_3 solid solution, aluminum oxide acts as a structural promoter hindering the growth of t-ZrO_2 particles beyond a critical size above which the low-temperature tetragonal phase of zirconium dioxide is converted to the stable monoclinic phase. Such promoting effect of aluminum oxide in the binary oxide system is observed within a wide range of ZrO_2/Al_2O_3 ratios. However, this effect is maximal in the case of the ZA50 sample, i.e., systems with a medium aluminum oxide content differ from individual oxides to the greatest extent.

We found that aluminum-containing samples have a larger surface area than the ZA0 sample obtained under similar conditions (Table 1) and preserve the developed surface up to high calcination temperatures (130–140 $m^2 g^{-1}$ at 800°C). The ZA25 sample is an exception, as its specific surface area considerably decreases (to 10–20 $m^2 g^{-1}$), which is also the case with ZrO_2 obtained from HZO. The drastic decrease in the surface area of the ZA25 sample makes it unsuitable as a support. The surface area successively increases in the series of other binary samples as the Al_2O_3 content increases and approaches a level characteristic for γ-Al_2O_3.

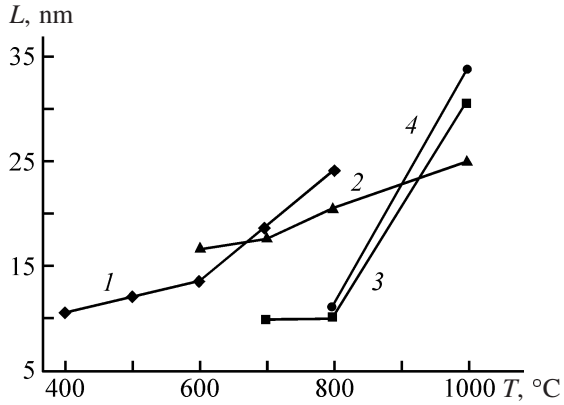

Fig. 4. CSA size in the tetragonal ZrO_2 phase L as a function of calcination temperature of samples T. Sample: (*1*) ZA0, (*2*) ZA25, (*3*) ZA50, and (*4*) ZA75.

The average pore size (Table 3) of γ-Al_2O_3 (5.39 nm) is noticeably larger than that for pure ZrO_2 (4.75 nm), and for the ZA50 sample the average pore size (5.84 nm) exceeds that of ZA100. The size distribution within a wide range characteristic for γ-Al_2O_3 was also preserved in the binary samples. The presence of ZrO_2 in the ZA75 sample shifts the maximum of the pore size distribution curve to the left (Fig. 5), which is caused by the disappearance of the widest pores. On the contrary, the pore size distribution for the ZA50 sample results in a shift of the distribution curve maximum toward wider pores. Thus, the ZA50 sample exhibits not only specific structural features but also specific features of the texture.

The results of the TPD NH_3 study of acid properties of sample surfaces are given in Fig. 6 and Table 3. It is seen that ZrO_2 exhibits two high-temperature desorption peaks with maxima at 490 and 580°C, corresponding to strong acid centers. It also contains certain amount of weak acid centers characterized by the ammonia desorption in the temperature range 100–400°C. Aluminum oxide has a considerable content of weak acid centers of two types, characterized by the desorption peaks at approximately 190 and 310°C. The shape of the thermal desorption curve

Table 3. Pore structure and acid properties of the surface of ZA samples calcined at 400°C

Sample	S_{BET}, $m^2\ g^{-1}$	Pore volume, $cm^3\ s^{-1}$	Average pore diameter, nm	Total number of acid centers, $\mu mol\ g^{-1}$	Density of acid centers, $10^{18}\ m^{-2}$
ZA0	144	0.19	4.75	86.9	0.36
ZA50	255	0.35	5.84	182.2	0.49
ZA75	258	0.30	4.68	54.1	0.13
ZA100	283	0.38	5.39	132.1	0.28

for the ZA75 sample suggests an appreciable mutual influence of components in the binary system, which results in the full disappearance of the weakest acid centers of γ-Al_2O_3 characterized by the desorption at temperatures below 200°C and in the formation of strong acid centers of ZrO_2 characterized by the maximum of NH_3 desorption at 640°C. The most strongly pronounced differences in acid properties

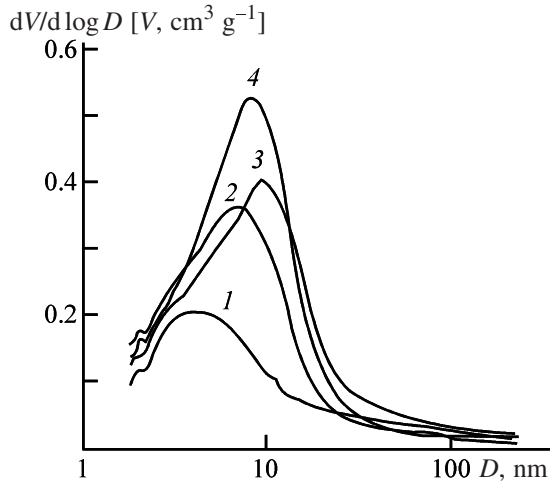

Fig. 5. Pore size distribution of samples calcined at 400°C. (*V*) Pore volume and (*D*) pore size. Sample: (*1*) ZA0, (*2*) ZA75, (*3*) ZA50, (*4*) ZA100.

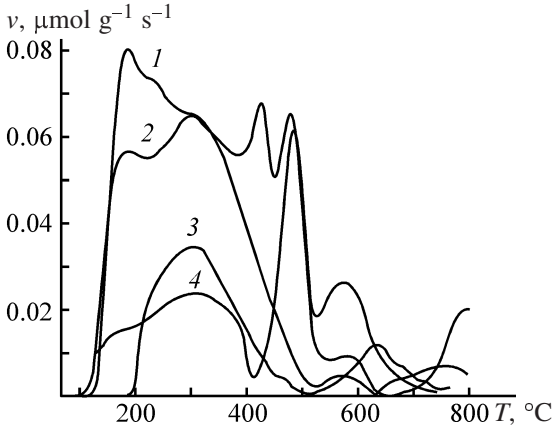

Fig. 6. TPD NH_3 data for samples calcined at 400°C. Sample: (*1*) ZA50, (*2*) ZA100, (*3*) ZA75, and (*4*) ZA0. (*v*) Rate of NH_3 desorption and (*T*) temperature.

of the surface of binary systems are observed for the ZA50 sample. Examination of the thermal desorption curve of this sample shows that, along with the preserved weak acid centers of γ-Al_2O_3 and strong acid centers of ZrO_2, the amount of the weakest centers on the surface (temperature of the maximum 180°C) increased and a significant amount of new acid centers represented by a well-defined peak with a maximum at 430°C appeared. Apparently, the formation of a new type of acid centers should be attributed to the manifestation of the properties arising during the formation of binary zirconium–aluminum oxide systems, namely, to the formation of Zr–O–Al bonds as believed by Li et al. [8].

Variation of the total amount of desorbed ammonia (Table 3) in the series of the samples under discussion also points to appreciable differences in properties of their surfaces. For example, the amount of desorbed ammonia for the ZA75 sample is much lower than that for any of pure oxides, and the greatest amount of desorbed ammonia caused by the highest density of acid centers was detected for the ZA50 sample. Thus, by varying the composition of binary zirconium–aluminum systems, we can adjust the structural and textural characteristics of the samples obtained.

Since the amount of acid centers is important for the practical use of oxide systems as supports, the ZA50 binary system with the maximal density of acid centers can be a promising support. The characteristic features connected with the appearance of new types of surface acid centers also suggest that this system can be used as a catalyst support for a number of processes.

CONCLUSIONS

(1) Binary zirconium–aluminum oxide systems with a developed surface and a high heat resistance can be synthesized by precipitating zirconium hydroxide onto γ-Al_2O_3. This technique ensures formation of well filterable precipitates.

(2) The stability of the highly dispersed ZrO_2

tetragonal phase in the synthesized binary mixtures is ensured in the range of calcination temperatures 600–1000°C, which is accounted for by the modifying effect of aluminum oxide arising from the formation of ZrO_2–Al_2O_3 solid solutions. Temperatures of the crystallization of the tetragonal ZrO_2 phase and of its conversion to the monoclinic phase depend on the composition of the systems obtained.

(3) The pore structure and acid properties of the surface of zirconium–aluminum oxide systems can be adjusted by varying the component ratio. The highest density of acid centers is observed for the samples containing 50 wt % ZrO_2.

(4) The binary systems obtained can be promising for use as sorbents, supports, or catalysts for various processes.

ACKNOWLEDGMENTS

The authors are grateful to V.V. Yushchenko for performing TPD NH_3 studies.

REFERENCES

1. Ivanova, A.S., *Kinet. Katal.*, 2001, vol. 42, no. 3, pp. 394–405.
2. Jung, K.T. and Bell, A.T., *Catal. Lett.*, 2002, vol. 80, nos. 1–2, pp. 63–68.
3. Caili, S., Dehua, H., Junrong, L., et al., *J. Mol. Catal. A: Chem.*, 2000, vol. 153, pp. 139–146.
4. Jung, K.T. and Bell, A.T., *J. Mol. Catal. A: Chem.*, 2000, vol. 163, pp. 27–42.
5. Klimova, T., Rojas, M.L., Castillo, P., et al., *Micropor. Mesopor. Mater.*, 1998, vol. 20, pp. 293–306.
6. Kharlanov, A.N., Turakulova, A.O., and Lunin, V.V., *Kinet. Katal.*, 2004, vol. 45, no. 2, pp. 278–283.
7. Murav'eva, G.P., Fionov, A.V., Lunina, E.V., et al., *Dokl. Ross. Akad. Nauk*, 2000, vol. 371, no. 1, pp. 52–55.
8. Li, G., Li, W., Zhang, M., et al., *Catal. Today*, 2004, vol. 93–95, pp. 595–601.
9. Li, G., Li, W., Zhang, M., and Tao, K., *Appl. Catal. A: Gen.*, 2004, vol. 273, pp. 233–238.
10. Moreau, S., Gervais, M., and Douy, A., *Solid State Ionics*, 1997, vols. 101–103, pp. 625–631.
11. Gao, L., Liu, Q., and Hong, J.S., *J. Mater. Sci.*, 1998, vol. 33, pp. 1399–1403.
12. Kon'kova, T.V., Liberman, E.Yu., Mikhailichenko, A.I., and Nefedova, N.V., *Khim. Prom–st. Segodnya*, 2004, no. 11, pp. 8–11.
13. Jakubus, P., Adamski, A., Kurzawa, M., and Sojka, Z., *J. Therm. Anal. Calorim.*, 2003, vol. 72, pp. 299–310.
14. *Physical and Chemical Aspects of Adsorbents and Catalysts*, Linsen, B.G., Ed., London: Academic, 1970.
15. Shkrabina, R.A., Ushakov, V.A., Koryabkina, N.A., and Ismagilov, Z.R., *Kinet. Katal.*, 2000, vol. 41, no. 3, pp. 433–438.
16. Chuah, G.K., Jaenicke, S., Cheong, S.A., and Chan, K.S., *Appl. Catal. A: Gen.*, 1996, vol. 145, pp. 267–284.

ISSN 1070-4272, Russian Journal of Applied Chemistry, 2007, Vol. 80, No. 9, pp. 1468–1471. © Pleiades Publishing, Ltd., 2007.
Original Russian Text © N.N. Gavrilova, O.V. Zhilina, V.V. Nazarov, 2007, published in Zhurnal Prikladnoi Khimii, 2007, Vol. 80, No. 9, pp. 1432–1435.

INORGANIC SYNTHESIS AND INDUSTRIAL INORGANIC CHEMISTRY

Synthesis of Mixed Cerium–Zirconium Oxides by the Sol–Gel Method

N. N. Gavrilova, O. V. Zhilina, and V. V. Nazarov

Mendeleev Russian University of Chemical Engineering, Moscow, Russia

Received January 16, 2007

Abstract—Mixed oxides CeO_2–ZrO_2 with the Ce/Zr molar ratios varying in a wide range were synthesized by the sol–gel method. The phase composition of the resulting particles was determined. The specific surface area of the mixed oxide calcined at various temperatures was found.

DOI: 10.1134/S1070427207090054

Mixed cerium–zirconium oxides are widely used in various fields of science and engineering [1]. Depending on composition, they can be employed in manufacture of solid-state oxide cells, gas sensors, and oxygen-conducting materials. Systems with high content of zirconium dioxide are used in production of ceramic materials and ionic conductors, and systems with predominance of cerium dioxide form a basis of various catalysts.

Mixed cerium–zirconium oxides catalyze numerous reactions [2, 3]. Owing to their specific structure, these systems are of particular interest in reactions of hydrocarbon oxidation, both full and selective [4–9].

The different conditions in which these reactions are carried out and the use of different types of supports result in that CeO_2–ZrO_2 are used both as highly dispersed powdered catalysts, coatings, materials with a required pore structure, and high-density materials.

The wide diversity of the properties of the final materials requires that the synthesis method should allow effective control over the properties of the products obtained and have high output capacity and low energy expenditure.

One of the most promising methods for synthesis of mixed oxides CeO_2–ZrO_2 and materials based on these oxides is the sol–gel technique. The possibility of varying the conditions in which separate stages of synthesis are performed allows control over the phase composition, size, and shape of the forming particles in a wide range. Different drying and thermal treatment modes can give products with a required pore structure.

The aim of this study was to obtain mixed hydrosols of CeO_2–ZrO_2 and to determine the basic parameters of CeO_2–ZrO_2 powders.

EXPERIMENTAL

The following chemicals of chemically pure grade were used in the study: cerium(III) nitrate; zirconium oxynitrate; sodium, potassium, and nickel nitrates; and aqueous solutions of ammonium hydroxide and nitric acid.

The concentration of the dispersed phase (in terms of the sum of cerium and zirconium oxides) was found by thermogravimetry, with the dry residue calcined at 650°C. An ultrasonic treatment was carried out in an ultrasonic bath with a working frequency of 25 kHz. The optical density was found turbidimetrically on a KFK-2 instrument at a wavelength of 440 nm (cell thickness 1–10 mm). The pH value was measured with a Schott CG 825 pH-meter with a glass electrode. The electrophoretic mobility was determined by the method of macroelectrophoresis with a mobile boundary. A dispersion medium produced by ultrafiltration of hydrosols served as a contact fluid. The particle size was found by the method of dynamic light scattering on an FK-22 installation including a He–Ne laser (wavelength 632.8 nm, power 5 mW), an F-221 photometer, and a UNICOR SP digital correlometer with 128 high-speed channel processors for on-line calculation of the correlation function (up to 100 ns). The specific surface area of the powders was found by the method of thermal desorption of nitrogen on a GKh-1 installation. The thermogravimetric measurements were made on an MOM Q-1500D derivatograph, with temperature elevated at a rate of

5 deg min^{-1}. The phase composition of the powders was studied by X-ray phase analysis on a DRON-3 diffractometer with CuK_α radiation.

Mixed hydrosols with various Ce/Zr molar ratios were produced by peptization. In this method, water-insoluble hydroxides are obtained from a salt solution and then are peptized in the presence of a strong acid. The OH/M molar ratio in the precipitation of hydroxides was 25. Ammonium hydroxide served as a precipitating agent. Then the precipitate obtained was washed with distilled water to pH 9 in order to remove residual electrolytes and then was peptized in the presence of nitric acid and treated with ultrasound for 2 min. As shown by these experiments, mixed hydrosols can be synthesized in a rather wide range of $[H^+]/[M]$ molar ratios.

The procedure developed can yield mixed CeO_2–ZrO_2 hydrosols with an initial concentration of 1.8 to 6.8 wt %, which can be then concentrated by evaporation or ultrafiltration to 13–43 wt %.

The resulting hydrosols are stable in acidic media at pH 1.0–4.5. Particles of the dispersed phase of the hydrosols are spherical, with an average hydrodynamic radius of 18 to 80 nm, depending on the CeO_2/ZrO_2 molar ratio.

An important factor in fabrication of supported catalysts is the adhesion of hydrosol particles to the support surface. This adhesion is largely determined by the charge on the surface of hydrosol particles. Measurements of the electrophoretic mobility demonstrated that hydrosol particles are positively charged and the ζ-potential, evaluated using the Helmholtz–Smoluchowski equation, is 11 to 32 mV at pH 1.0–4.5.

When sols are used as a basis of various formulations, it becomes necessary to introduce salts of various metals. The basic condition for a high-quality product to be obtained is the aggregative stability of the resulting formulation. To determine the maximum amount of an electrolyte, at which the hydrosols retain aggregative stability, their coagulation thresholds were measured in the presence of various electrolytes. It was found that mixed hydrosols are stable against 1–1 and 2–1 electrolytes. In the presence of $NaNO_3$, KNO_3, and $Ni(NO_3)_2$, coagulation is not observed even in high-concentration solutions of these electrolytes.

The stability of the hydrosols against electrolytes of the 1–1 and 2–1 types allows introduction of required amounts of metal nitrates into the hydrosols, which enables significant modification of the composition of catalytically active formulations.

It should be noted that xerogels produced by drying of concentrated hydrosols retain capacity for spontaneous dispersion in distilled water with pH adjusted to 1.0–4.5. The xerogels were produced by drying of hydrosols in air at 25°C.

A thermogravimetric analysis of these xerogels (Fig. 1) demonstrates that, for all the samples, a sharp weight loss is observed at 250°C, with the following two endothermic effects observed. Below 100°C, capillary and weakly bound water is removed, and the peak at 220–280°C is associated with the decomposition of nitrates. The exothermic effect associated with crystallization of zirconium dioxide is recorded at 380°C (below this temperature, zirconium dioxide is X-ray-amorphous) only for the $Ce_{0.2}Zr_{0.8}O_2$ sample. For other CeO_2/ZrO_2 molar ratios, a broad exothermic peak is observed in the temperature range 300–800°C. This is due to incorporation of Zr^{4+} into the crystal lattice of cerium dioxide.

The data obtained are in good agreement with the results of the X-ray phase analysis (Fig. 2). An analysis of the X-ray diffraction patterns of powders calcined at 600°C demonstrated that $CeZrO_2$ solid solutions are present in a wide range of CeO_2/ZrO_2 molar ratios. However, reflections characteristic of t-ZrO_2 are observed in some cases ($Ce_{0.9}Zr_{0.1}O_2$, $Ce_{0.8}Zr_{0.2}O_2$, $Ce_{0.2}Zr_{0.8}O_2$).

This may occur because the procedure suggested here for synthesis of hydrosols cannot provide full transition of ions into insoluble CeO_2–ZrO_2 compounds. Therefore, the hydrosols contain a certain amount of Ce and Zr in the ionic form, which can lead in further thermal treatment to formation of individual phases. This can be prevented by washing of xerogels with distilled water to complete removal of the ions.

To obtain information about the thermal stability of the mixed oxides synthesized, the specific surface areas of CeO_2–ZrO_2 powders calcined at various temperatures were found. Figure 3 shows the specific surface areas S_{sp} and particles sizes D as functions of calcination temperature and the ZrO_2 content of the system. The average particle size D was evaluated by the formula $D = 6/(\rho S_{sp})$, where ρ is the density of a powder, and S_{sp}, its specific surface area.

As can be seen from these dependences, the largest specific surface area (118 $m^2\ g^{-1}$) after calcination at 450°C is observed for the system $Ce_{0.9}Zr_{0.1}O_2$. However, it exhibits the strongest decrease in the specific surface area as the calcination temperature is raised. An insignificant decrease in the specific surface area

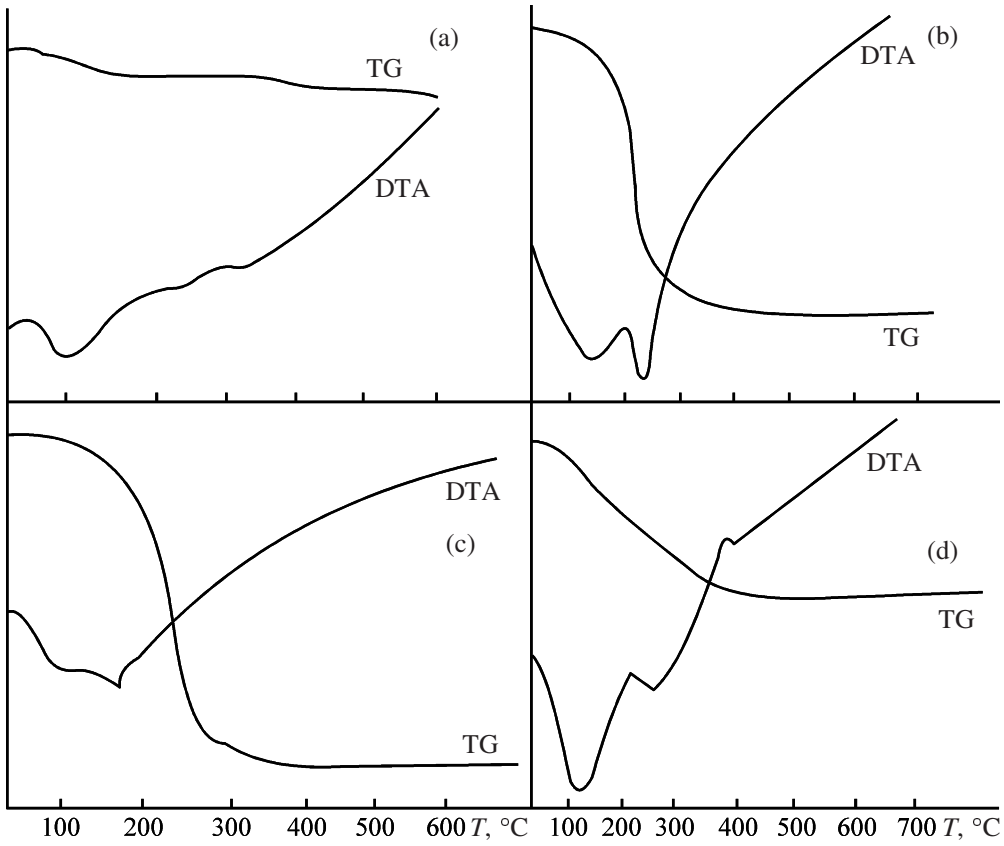

Fig. 1. Thermograms of CeO_2–ZrO_2 xerogels at various CeO_2/ZrO_2 molar ratios. (*T*) Temperature. (a) $Ce_{0.9}Zr_{0.1}O_2$, (b) $Ce_{0.8}Zr_{0.2}O_2$, (c) $Ce_{0.5}Zr_{0.5}O_2$, and (d) $Ce_{0.2}Zr_{0.8}O_2$.

is observed for the systems containing more than 50 mol % ZrO_2.

The hydrosols obtained using this procedure were used to produce various catalysts.

The method of impregnation of a commercial Al_2O_3-based support was used to obtain CeO_2–ZrO_2/Al_2O_3, CuO–CeO_2–ZrO_2/Al_2O_3, and Co_2O_3–CeO_2–ZrO_2/Al_2O_3 catalysts. The activity of these catalysts was studied in the oxidation of CO. The maximum conversion of carbon monoxide was 98%. It was observed in the temperature range 450–650°C, depending on the catalyst composition [10].

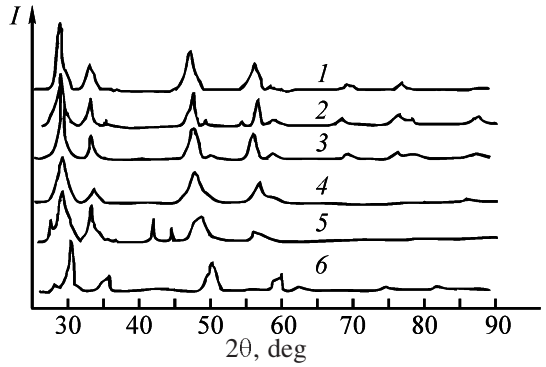

Fig. 2. X-ray diffraction patterns of mixed oxides CeO_2–ZrO_2 at various CeO_2/ZrO_2 molar ratios. (*I*) Intensity and (2θ) Bragg angle. Calcination temperature 600°C. (*1*) CeO_2, (*2*) $Ce_{0.9}Zr_{0.1}O_2$, (*3*) $Ce_{0.8}Zr_{0.2}O_2$, (*4*) $Ce_{0.5}Zr_{0.5}O_2$, (*5*) $Ce_{0.2}Zr_{0.8}O_2$, and (*6*) ZrO_2.

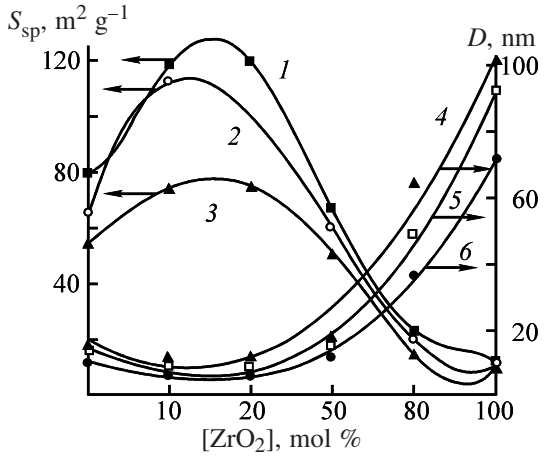

Fig. 3. (*1–3*) Specific surface area S_{sp} and (*4–6*) particle size *D* of mixed oxides CeO_2–ZrO_2 calcined at different temperatures vs. the ZrO_2 content of the system. Temperature, °C: (*1, 6*) 450, (*2, 5*) 600, and (*3, 4*) 750.

The selective oxidation of propane was carried out both on powdered CeO_2–ZrO_2–NiO catalysts and on ceramic membrane units with a catalytically active bed of the same composition. The reaction was studied in the temperature range 300–500°C. It was shown that higher selectivity and output capacity for propylene are achieved with membranes with a catalytically active bed [11].

CONCLUSIONS

(1) The peptization method can be used to obtain aggregatively stable mixed hydrosols of cerium and zirconium dioxides in a wide range of CeO_2/ZrO_2 molar ratios. The resulting hydrosols are stable against introduction of metal nitrates, which allows significant modification of the composition of catalytically active formulations. The hydrosols synthesized can be used for fabrication of both powdered and supported catalysts.

(2) The powders produced by calcination of xerogels have large specific surface area. Their phase composition is mainly represented by CeO_2–ZrO_2 solid solutions. The highest thermal stability is observed for systems with high content of zirconium dioxide.

REFERENCES

1. Trovarelli, A., *Catal. Rev*., 1996, vol. 38, no. 4, pp. 439–520.
2. Glinski, M. and Kijenski, J., *React. Kinet. Catal. Lett*., 2000, vol. 69, no. 1, p. 123.
3. *Fiziko-khimicheskie svoistva okislov* (Physicochemical Properties of Oxides), Samsonov, G.V., Ed., Moscow: Khimiya, 1978.
4. Jibril, B.Y., Al-Zahrani, S.M., and Abassed, A.E., *Catal. Lett*., 2001, vol. 74, nos. 3–4, p. 145.
5. Deshmukh, S.S., Zhang, S.M., Kovalchuk, ??, et al., *Appl. Catal*., 2003, vol. 45, pp. 135–145.
6. Sadykova, V.A., Kuznetsova, T.G., Veniaminov, S.A., et al., *React. Kinet. Catal. Lett*., 2002, vol. 76, pp. 83–92.
7. Passos, F.B., Oliveira, E.R. de, Mattos, L.V., et al., *Catal. Today*, 2005, vol. 101, pp. 23–30.
8. Breen, J.P., Burch, R., and Coleman, H.M., *Appl. Catal. B: Environ*., 2002, vol. 39, pp. 65–75.
9. Srinivas, D., Satyanarayana, C.V.V., Potdar, H.S., et al., *Appl. Catal. A: Gen*., 2003, vol. 246, pp. 323–334.
10. Kudinov, R.F., Liberman, E.Yu., Mikhailichenko, A.I., et al., Abstracts of Papers, *19-aya Mezhdunarodnaya konferentsiya molodykh uchenykh po khimii i khimicheskoi tekhnologii* (19th Int. Conf. of Young Scientists on Chemistry and Chemical Technology), Moscow, 2005, vol. 19, no. 10, p. 22.
11. Gavrilova, N.N., Zhilina, O.V., Nazarov, V.V., et al., *Nauchnye issledovaniya i ikh primenenie: Sovrenmennoe sostoyanie i puti razvitiya* (Scientific Studies and Application of Their Results: Modern State and Ways of Development), Odessa: Chernomor'e, 2005, p. 89.

ISSN 1070-4272, Russian Journal of Applied Chemistry, 2007, Vol. 80, No. 9, pp. 1472–1475. © Pleiades Publishing, Ltd., 2007.
Original Russian Text © V.D. Koshevar, V.G. Shkadretsova, 2007, published in Zhurnal Prikladnoi Khimii, 2007, Vol. 80, No. 9, pp. 1436–1439.

INORGANIC SYNTHESIS AND INDUSTRIAL INORGANIC CHEMISTRY

Low-Temperature Preparation and Properties of Shell Filler Pigments

V. D. Koshevar and V. G. Shkadretsova

Institute of General and Inorganic Chemistry, National Academy of Sciences of Belarus, Minsk, Belarus

Received November 30, 2006

Abstract—The effect of various factors (temperature of drying of the core substance, polymer concentration, concentration of coloring component, mechanical treatment procedures) on the preparation and properties of shell filler pigments was examined.

DOI: 10.1134/S1070427207090066

Much attention is given today in many countries to the development of nontraditional methods for production of pigments in the core, microencapsulated, and hollow forms. It is known that the main functions of pigments (ensuring the required optical density of a medium, color, etc.) are associated with optical phenomena: reflection, absorption, and scattering of light. These phenomena mainly occur in the surface layer. Therefore, to save raw materials (especially nonferrous metal compounds), it is appropriate to use a cheap material as a core and form on its surface a thin film (several tens of nanometers thick) of a more expensive coloring substance. Synthesis of core–shell particles attracts particular interest in materials science [1, 2], because such structures are potential building blocks for the preparation of composite materials with periodically modulated structure, composition, and functions.

Here we report experimental data on the preparation and properties of coloring shell powders. Their formation is based on controllable heterocoagulation followed by baking at temperatures not exceeding 200°C.

EXPERIMENTAL

As a modifying material we used SiO_2 particles of mean diameter 3–4 μm, prepared from phosphoric acid production waste [TU RB (Technical Specification of Belarus Republic) 00 203 714 006–94], and a shell-forming dispersion of polymers and coloring substances. As polymeric components we used latexes of butadiene–styrene, acrylic, and styrene–acrylate copolymers. As coloring agents we used aqueous dispersion of organic dyes, scarlet [TU (Technical Specification) 6-14-946–87] and blue (TU 2463-125-05-05 800 142–2003).

Before deposition of the shell, the surface of core particles was etched in 5% H_2SO_4, washed with water to pH 5–7 of wash waters, and dried at 0–200°C.

Shell powders were prepared from a mixed dispersion of a latex, a core-forming complex, and a coloring agent by various procedures: in a high-speed mechanical mixer, in a SAND ball planetary mill, and in a UZDI-1UCh.2 ultrasonic disperser.

The heterocoagulate was heat-treated in a thermostat at 50°C for 2 h. Then, to check the strength of adhesion of the shell to the core, the heterocoagulate was washed in water at 20°C for 24 h. After washing, the shell powders were dried in air at 20°C.

The stability of the color of the resulting coloring powder depends on the adhesion of the shell to the core and on the water permeability of the shell. These properties were estimated by turbidimetric measurement of the optical density of water from washing of the heterocoagulate. The higher the optical density of the wash water relative to the reference (distilled water), the lower the adhesion and the higher the water permeability of the shell. The optical density was measured with a KFK-3 photoelectric colorimeter at actinic wavelengths.

The sedimentation stability of the shell powders obtained was studied by the joint sedimentation method. For this purpose, 1% aqueous dispersions were placed in a graduated cylinder, and the shift of the dispersion medium–dispersed phase boundary was monitored up to complete clarification.

The formation of shell structures was studied by scanning electron microscopy (JSM-5610 microscope), IR spectroscopy, and derivatography. The IR absorption spectra in the range 400–4500 cm^{-1} were recorded on a GK-20 device using KBr prisms. Differential thermal analysis of the pigments was performed with an MOM derivatograph (Hungary) at a heating rate of 5 deg min^{-1}; the sample weight was 800 mg. Calcined aluminum oxide (chemically pure grade) was used as reference.

The optical density of the powders was measured with a DO-IM densitometer using appropriate color filters.

To examine the atmosphere resistance of the powders, they were treated with various chemical agents (hot distilled water for 2 h at 98°C; 2% NaOH; 4% CH_3COOH; 3% NaCl; 96% ethanol). The color stability was evaluated with an FMSh-56M device from the difference between the reflection coefficients of the specimens before and after reagent treatment.

Figures 1a, 1b, 2a, and 2b show how the core–shell adhesion strength depends on the chemical nature and concentration of latexes and on the temperature of predrying of the core component, SiO_2. It is seen that the dependence of the optical density of wash water on the latex concentration passes through a minimum. Apparently, the adhesion of the shell to the surface of the core SiO_2 particles stronglty depends on the shell thickness, which, in turn, is determined by the latex concentration. In particular, it is known [3] that the adhesion of a coating to a support can appreciably decrease with increasing coating thickness.

Figures 1a, 1b, 2a, and 2b also show that formation of a strong composite shell on the surface of SiO_2 particles, imparting to them an intense red color, depends on the temperature at which the core material was predried before treatment with the shell-forming dispersion. The drying temperature of 100°C appeared to be the best. At this temperature, apparently, physically adsorbed water is removed, which facilitates the access of a shell-forming agent to the SiO_2 surface, but the structural OH groups remain intact. Heating at a higher temperature (150°C) may cause partial dehydration of the OH groups specifically bound to the SiO_2 surface and making it hydrophilic. As a result, the wettability of the core decreases, which, apparently, results in worse adhesion of the shell (Figs. 1, 2, curves *3*: increase in the optical density).

As the concentration of the coloring agents in the shell-forming dispersion increases, a proportional increase in the intensity of the powder color is accompanied by an increase in the optical density of the wash water, with all the latex systems used. At coloring agent concentrations less than 2%, the optical density of wash water is close to that of the reference solution (Figs. 2a, 2b).

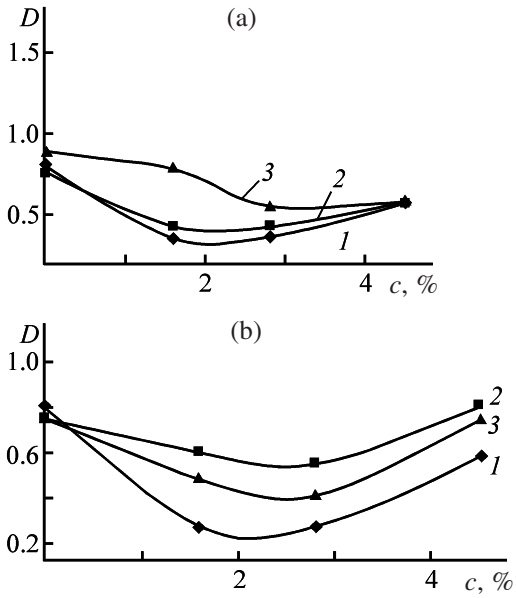

Fig. 1. Optical density D of wash water as a function of concentration c of latexes of (a) acrylic and (b) styrene–acrylate copolymers at various temperatures of predrying of silicon oxide. T, °C: (*1*) 120, (*2*) 20, and (*3*) 200; the same for Fig. 2.

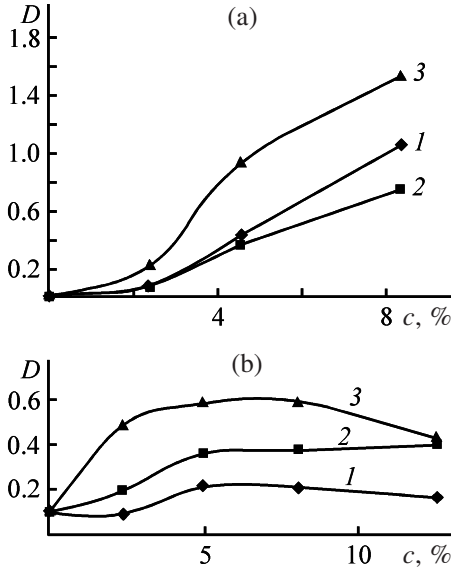

Fig. 2. Optical density D of wash water as a function of concentration c of coloring agent (scarlet) dispersed in latexes of (a) acrylic and (b) styrene–acrylate copolymers at various temperatures of predrying of silicon oxide. Latex concentration 2.38%.

Table 1. Influence of the procedure and time of mechanical treatment on the properties of shell powders

Treatment procedure	Dispersion no.	Dispersing time, min	Time of complete sedimentation, h	Optical density, GOST* units
High-speed mechanical mixer	1	15	2	1.05
	2	30	2	1.15
	3	60	2	1.15
SAND ball planetary mill	4	60	28	0.99
	5	120	30	0.95
	6	180	31	0.95
Ultrasonic disperser	7	2	4	1.2
	8	5	4	1.18
	9	10	4.5	1.14

* State Standard.

The dependences obtained allowed determination of the optimal conditions of efficient modification of the SiO_2 surface, at which washing of the ready powders is not required.

An appreciable effect on the properties and morphology of the SiO_2–shell-forming agent heterocoagulate is exerted by various mechanical treatment procedures used for preparing shell powders. Table 1 shows that the dispersions of shell powders prepared by mechanical treatment on a SAND planetary mill exhibit the highest sedimentation stability, and the heterocoagulate formed from dispersions subjected to ultrasonic treatment has the strongest color. Dispersion with a high-speed mixer, compared to the ultrasonic treatment, ensures somewhat lower color intensity. Prolonged treatment in a SAND mill, apparently, leads to certain damage of the shell, manifested as a decrease in the intensity of the powder color. The results obtained are confirmed by electron-microscopic examination. Powders obtained in a mill have, on the average, small particle size compared to the initial core-forming material.

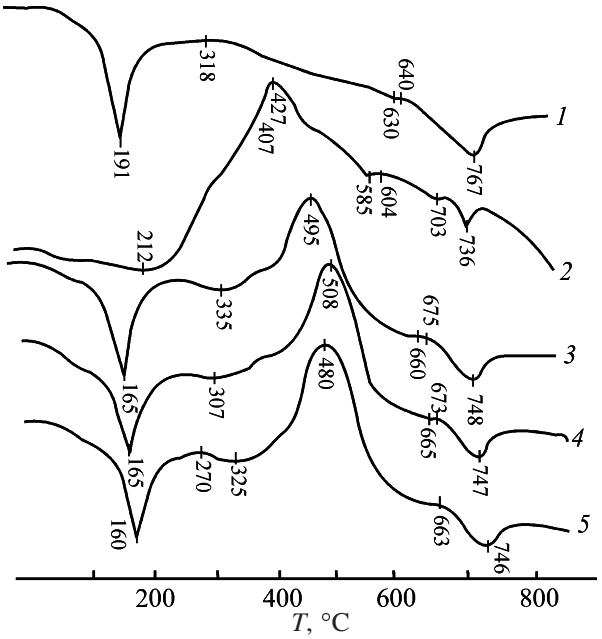

Fig. 3. Thermograms of (*1*) SiO_2, (*2*) blue coloring agent, and (*3*–*5*) powders prepared by various mechanical treatment procedures. (*T*) Temperature. Mechanical treatment with (*3*) high-speed mechanical mixer, (*4*) SAND mill, and (*5*) ultrasonic disperser; the same for Fig. 4.

To reveal the mechanism of formation of shell structures, let us analyze the DTA and IR data. The thermograms of straight SiO_2 and the heterocoagulate show medium-intensity endothermic effects in the range 160–168°C, caused by removal of adsorbed water and onset of the modifier thermolysis (Fig. 3). The relatively weak endoeffect in the range 307–325°C is observed only or the heterocoagulate, suggesting the formation of a relatively strong adsorption complex on the core–shell boundary. The formation of such complex is also indicated by a shift toward higher temperatures of the strong exothermic effect characteristic of the shell-forming substance and associated with its thermal decomposition and oxidation of the decomposition products.

Formation of a complex on the core–shell boundary is also confirmed by IR data (Fig. 4). For example, for the SiO_2–latex heterocoagulate, the coloring agent bands in the range 1520–1250 cm^{-1} almost completely disappeared, and the powder surface became more hydrophilic (especially for the powder prepared with SAND mill); the stretching and bending OH vibration bands of adsorbed water at 3000–3450 and 1750 cm^{-1} increased in intensity.

The core–shell adhesion strength in the powders was estimated, with the SiO_2–(styrene–acrylate

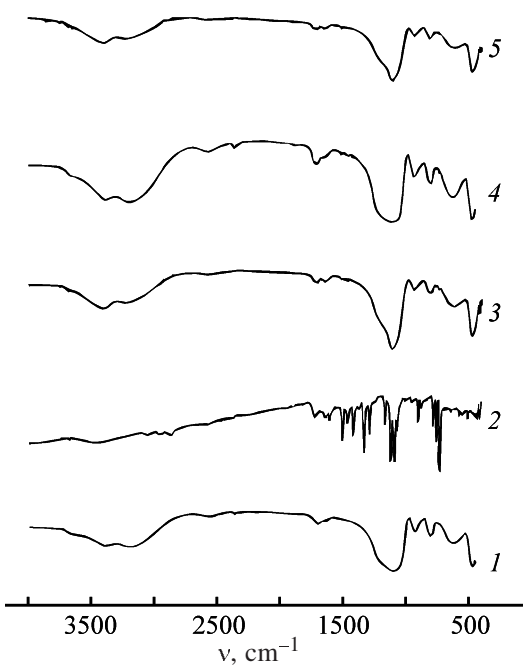

Fig. 4. IR absorption spectra of (*1*) SiO_2, (*2*) blue coloring agent, and (*3*–*5*) powders prepared by different mechanical treatment procedures. (ν) Wavenumber.

Table 2. Effect of the treatment procedure on optical properties of powders

Treatment procedure	Powder reflection coefficient, %, at indicated wavelength, nm		
	457	490	540
No treatment	37	28	9.5
NaCl, 3%; 20°C	37	28	9.5
C_2H_5OH, 96%; 20°C	37	28	9.5
CH_3COOH, 4%; 20°C	37	28	9.5
NaOH, 2%; 20°C	34	24	31
Distilled H_2O, 98°C	37	27	8

latex)–blue coloring agent composite as example, from the resistance of the powder to boiling water, dilute acids and alkalis, and a medium-polarity organic solvent (Table 2). It can be seen that the powders are resistant to all these reagents, showing no changes in the color intensity (reflection coefficient). That is, the core–shell adhesion is quite strong.

Shell powders of intense red and blue colors were successfully tested as filler pigments in production of water-dispersible paints and dry building mixes.

CONCLUSIONS

(1) Shell powders of intense red and blue colors, exhibiting high atmosphere resistance, were prepared by heterocoagulation of mixed dispersions of latexes and organic coloring agents on the surface of SiO_2 core particles.

(2) The major factors governing the properties of the powders are the temperature of SiO_2 predrying and the latex and coloring agent concentrations in their mixed aqueous dispersion.

(3) Derivatographic and IR studies showed that the required adhesion of the shell to the core is provided by specific interaction of the components on the core–shell interface.

REFERENCES

1. Raldugin, V.I., *Usp. Khim.*, 2004, vol. 73, no. 2, pp. 123–156.
2. Hong, L., Jeannie, Han., Panioukhine, A., and Kumacheva, E., *J. Colloid Interface Sci.*, 2002, vol. 255, pp. 119–128.
3. Prokopchuk, N.R. and Krut'ko, E.T., *Khimiya i tekhnologiya plenkoobrazuyushchikh veshchestv* (Chemistry and Technology of Film-Forming Substances), Minsk: Bel. Gos. Tekh. Univ., 2004.

ISSN 1070-4272, Russian Journal of Applied Chemistry, 2007, Vol. 80, No. 9, pp. 1476–1480. © Pleiades Publishing, Ltd., 2007.
Original Russian Text © O.I. Platonov, 2007, published in Zhurnal Prikladnoi Khimii, 2007, Vol. 80, No. 9, pp. 1440–1444.

INORGANIC SYNTHESIS AND INDUSTRIAL INORGANIC CHEMISTRY

Choice of a Scheme for Desulfurization of Rich Metallurgical Gases

O. I. Platonov

Gipronikel' Institute, Limited Liability Company, St. Petersburg, Russia

Received June 15, 2007

Abstract—Known schemes for production of sulfur from an oxygen-containing sulfurous gas are critically considered with account of the presence of sulfur trioxide in real metallurgical gases. An efficient technology for deep processing of metallurgical gases rich in sulfur dioxide was developed on the basis of a thermodynamic analysis and industrial "methane" technology for reduction of gases formed in autogenous smelting.

DOI: 10.1134/S1070427207090078

In view of the worldwide tendency toward excessive production of sulfuric acid [1] and the geographic separation of places of its manufacture and consumption, the requirements of the environment protection regulations revive interest in utilization of metallurgical sulfurous gases to obtain elemental sulfur, which is more suitable for transportation or prolonged storage than the acid. This is particularly topical for SO_2-rich gases formed in autogenous smelting, whose processing schemes are reviewed in [2]. However, most of these schemes, based on the rich experience of sulfur production from hydrogen sulfide [3], disregard the known specificity of metallurgical gases [4] and, therefore, require a critical analysis.

Flour Co. has developed a number of schemes for production of sulfur from the sulfurous gas. These schemes include stages of deoxygenation, hydrogenation and hydrolysis, Claus reaction, direct reduction, generation of a reducing gas, and purification. All the versions of the schemes suggested [5, 6] involve thermal or catalytic removal of oxygen from the gas, followed by the hydrogenation stage:

$$S + H_2 = H_2S, \quad (1)$$

$$SO_2 + 3H_2 = H_2S + 2H_2O, \quad (2)$$

performed at 200–450°C on a special catalyst. The necessary hydrogen is generated in substoichiometric burning of natural gas in a separate converter or directly in the deoxygenation reactor.

To remove steam, the gas discharged from the hydrogenation reactor is cooled in a boiler-utilizer and then in a contact heat exchanger (quencher) by circulating water, which also catches trace amounts of carbon black (fly ash). To limit the temperature in processing of a concentrated gas, part of the gas from the quencher is returned by a low-pressure blower into the hydrogenation reactor.

Hydrogen sulfide obtained in the hydrogenation reactor is further processed by the Claus method. In most of flowsheets [5, 6], about 1/3 of the initial amount of the sulfurous gas is delivered, bypassing the hydrogenation stage, directly into the Claus reactor, in which hydrogen dioxide reacts with hydrogen sulfide in accordance with the reaction equation

$$2H_2S + SO_2 = 2H_2O + 3/nS_n, \qquad n = 1–8. \quad (3)$$

The flow of the sulfurous gas is similarly divided in a 2 : 1 proportion in the scheme suggested by Worley Parsons [7]. To achieve the maximum yield of CO and H_2, natural gas is also burnt at a substoichiometric ($\alpha \approx 0.6$) air supply and steam feed. After that, the H_2S-rich process gas from the quenching column and the remaining 1/3 of the initial SO_2 are separately heated and after that combined in the first converter of the conventional Claus installation.

An original process for sulfur recovery from an SO_2 flow [7] is based on two known techniques. First, an endothermic reaction of natural gas and vapors of recycled sulfur is carried out in a catalytic reactor (reactors) on active aluminum oxide at 575–650°C:

$$CH_4 + 2S_2 = CS_2 + 2H_2S. \quad (4)$$

After cooling in a medium-pressure (4.2 MPa) boiler-utilizer and condensation of residual sulfur at

150°C, the gas containing H_2S and CS_2 is again heated in a heat exchanger to 210°C and delivered, together with concentrated (to 90 vol %) sulfur dioxide, into the first Claus reactor, in which reaction (3) between H_2S and SO_2 occurs in a fixed catalyst bed to give sulfur. Simultaneously, carbon disulfide is hydrolyzed to H_2S:

$$CS_2 + 2H_2O = CO_2 + 2H_2S. \quad (5)$$

In view of the exothermic nature of reactions (3) and (5), a considerable part of the gas is returned via the utilizing vessel and sulfur condenser into the first reactor of the sulfur recovery unit (SRU) in order to maintain the temperature mode of the Claus reactor. After cooling of the gas in the utilizing vessel to 340°C and condensation of sulfur at 150°C, the gas is delivered to the second and third stages of the Claus installation, with afterburning of the tail gas at 60°C and its discharge into the atmosphere.

Despite the wide variety of suggested schemes [2], the only acting industrial technology for recovery of sulfur from metallurgical gases is the "methane" method.[1]

In this technique [8], a sulfurous gas cleaned to a dust content of about 5 mg m^{-3} and cooled to 20–35°C is preliminarily enriched with oxygen to a concentration $[O_2]$ = 12–18 vol %. Further processing of the oxygen-containing sulfurous gas includes its heating by the heat released in the exothermic reaction of burning of natural gas

$$CH_4 + 2O_2 = 2H_2O + CO_2, \quad \Delta H = -802 \text{ kJ}; \quad (6)$$

thermal (1150–1200°C) reduction in a homogeneous reactor

$$CH_4 + 2SO_2 = 2H_2O + CO_2 + S_2; \quad (7)$$

catalytic conversion of the reduced gas in the target reaction (3); condensation of the resulting sulfur; and subsequent afterburning of the discharge gas. The reduction process is accompanied by decomposition of sulfur trioxide

$$2SO_3 \longrightarrow 2SO_2 + O_2, \quad (8)$$

present in the starting sulfurous gas [4]. The independence from the initial concentration of oxygen and presence of SO_3 predetermines the reliability of the methane method in processing of the real metallurgical gas.

A known disadvantage of this technique is the comparatively high specific expenditure of the reducing agent (natural gas), which is 800–1000 Sm^3 (m^3 under normal conditions) per ton of sulfur. This is commonly believed to be partly due to the high reduction temperature. However, as demonstrated by an analysis in [9], this is more likely associated with thermodynamic and kinetic features of the process. For example, at a stoichiometric expenditure of the reducing agent in reactions (6) and (7), the overall sulfur recovery coefficient does not exceed 65–70%, which is due to the insufficient extent of the single-stage catalytic conversion of the reduced gas [10]. Introduction of two catalytic stages and additional enrichment of the reduced gas with products formed in conversion of natural gas (CO and H_2) [11] raises the extent of sulfur recovery to 94% and lowers the specific expenditure of the reducing agent to approximately 750 Sm^3 per ton (at an initial concentration $[SO_2]_0$ in the sulfurous gas equal to 30 vol %). However, this expenditure of natural gas also seems to be excessive, which presents a problem of the methane method that has not been conclusively resolved.

To make lower the specific expenditure of the natural gas fuel in the methane method, it has been suggested to reduce the sulfurous gas at a lowered temperature (e.g., 750–950°C [12]) on a catalyst, which, as it is commonly believed, will markedly improve the economic efficiency of the methane technique. However, simplest quantitative estimates cast doubt on this "paradigm," because the contribution of the fuel expended for heating of the sulfurous gas to the reduction temperature is not the only factor predetermining the high specific expenditure of natural gas in the methane method.

For example, less than half of the reducing agent is consumed for oxygen binding and heating at common concentrations $[SO_2]_0 \geq 25$ vol % in the sulfurous gas in Vanyukov furnaces and maximum enrichment of the sulfurous gas to a concentration $[O_2]$ = 15% corresponding to the temperature of homogeneous reduction (~1200°C). With account of the afterburning of the discharge gas, the fraction of fuel expended for heating to the reduction temperature in the total expenditure of natural gas does not exceed 1/3. The difference between the minimum (for oxygen binding with heating to 600°C in catalytic processing) and maximum fuel consumption in thermal reduction does not exceed 1/4 of the total consumption of natural gas.

In addition, implementation of the catalytic proc-

[1] This method has been employed since 1987 for utilization of discharge gases from Vanyukov furnaces at the copper plant of the Norilsk Mining-and-Smelting Combine (presently, Norilsk Nickel Mining-and-Smelting Open Joint-Stock Company).

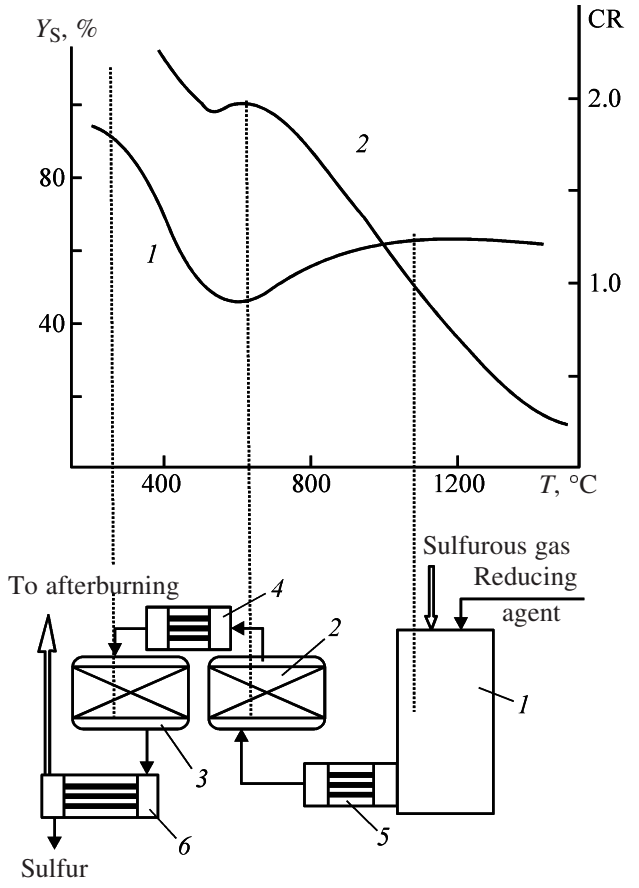

(*1*) Equilibrium yield of elemental sulfur and (*2*) Claus ratio CR vs. temperature *T*, and the flow chart of processing of the sulfurous gas. (*1*) Reducing reactor, (*2*) catalytic reactor, (*3*) Claus reactor, (*4, 5*) boiler-utilizers, and (*6*) sulfur condenser.

essing scheme involves additional operational expenditure (primarily of energy) for pumping of the process gas through the catalyst bed, which nullifies to an even greater extent the potential gain that can be obtained by lowering the process temperature. Therefore, there is no way of expecting a substantial saving of natural gas in the case of low-temperature catalytic processing of the sulfurous gas.

On the whole, qualitative analysis of the schemes suggested for processing of sulfurous gases [2] shows that, despite the scheme contrivances demonstrated by design companies, the substantially more intricate technique (including technologically dangerous processes, as in [7]) does not lead to any significant efficiency improvement. The reason is that, as noted in [13], the processing efficiency is determined in the end by the degree of conversion of sulfurous gases by the Claus reaction (3), which is common to all the known schemes of SO_2 processing.

Rameshni and Santo [7] believe that, compared with to existing methane method, their scheme requires a lower fuel consumption; however, this opinion is refuted by a quantitative analysis of this scheme with account of all heat loss channels. Indeed, the direct reduction process and the Worley Parsons scheme are similar in the overall stoichiometric balance of sulfur formation, which results in that they differ only in the fuel consumption for heating to the reduction temperature. Because the common efficiency of the furnace for flame heating in the scheme suggested by Worley Parsons for processing of the sulfurous gas is low, the total specific expenditure of natural gas will markedly exceed 1000 $Sm^3\ t^{-1}$, despite the apparent saving directly in the "technology" of sulfur recovery.

It should also be noted that all low-temperature techniques for processing of the sulfurous gas are exceedingly vulnerable to the action of sulfur trioxide present in the real metallurgical effluent gas. As assumed in [2], binding of this sulfur trioxide when concentrating the starting SO_2 involves additional capital and operational expenditure comparable with, or even exceeding that of sulfurous gas processing proper. In this case, the preliminary concentration of the gas being processed is not always justified, because it disturbs the temperature mode of the reactors and leads to their more intricate design and connection schemes (with introduction of recycles). This does not rule out the possibility of secondary formation of SO_2, which is especially favored by the temperature range of processing of the starting gas near 600°C. The sulfuric acid corrosion and catalyst poisoning can be eliminated by thermal decomposition of SO_3 by reaction (8), which is an additional positive argument in analysis of the potentialities of the "methane" method.

From the thermodynamic standpoint, the most energetically favorable reduction products in reaction (7), as well as in the Claus reaction (3), are H_2O and CO_2, with sulfur formed as a by-product. This is illustrated by the temperature dependences of the equilibrium yield of elemental sulfur (curve *1*) and of the Claus ratio in the upper part of the figure. These dependences were calculated for the stoichiometric [for reactions (6) and (7)] reduction with methane of the typical effluent gas from Vanyukov furnaces at the copper plant of Norilsk Nickel Mining-and-Smelting Open Joint-Stock Company, which contains (vol %): SO_2 39.65, SO_3 0.055, O_2 16.53, CO_2 0.88, H_2O 7.05, N_2 35.25, and Ar 0.6.

As can be seen from the figure, a Claus ratio CR $\equiv$ $[H_2S]/[SO_2] \geq 2$, acceptable for the subsequent

processing by reaction (3), is reached at catalytic reduction temperatures in the range 450–650°C, in which the equilibrium yield of elemental sulfur, Y_S, does not exceed 60 rel % (at 450°C). This gives no way of achieving a deep recovery of sulfur in a single stage of processing of the sulfurous gas. The kinetic limitations on the reduction process [9, 14] and on the subsequent catalytic conversion of the reduced gas [15] make deep processing of the sulfurous gas an even more complicated task.

Nevertheless, the results of a thermodynamic analysis, shown in the figure, make it possible to improve the technology of sulfur production from metallurgical gases: the flow chart with the main stages of processing of the sulfurous gas related to the working temperature scale is shown in the lower part of the figure.

The optimal scheme of processing of a washed sulfurous gas (see figure) includes enrichment with oxygen to a prescribed concentration and reduction with natural gas (methane) in a homogeneous reactor *1* at a temperature $T \approx 1100$°C. After that, SO_2 is additionally reduced in the catalytic reactor *2* at 400–550°C, elemental sulfur is condensed, conversion in the Claus reactor *3* is carried out, sulfur is condensed and separated, and toxic components of the waste gas are subjected to afterburning.

The stage of catalytic conversion at 400–650°C provides hydrolysis of carbon disulfide by reaction (5) and of carbonyl sulfide:

$$COS + H_2O \rightleftarrows H_2S + CO_2, \quad (9)$$

as well as additional reduction of sulfur dioxide by reactions (2), (3), and (7), and by the reactions

$$2COS + SO_2 \rightleftarrows 2CO_2 + 3/nS_n, \quad n = 1\text{–}8; \quad (10)$$

$$2CS_2 + SO_2 \rightleftarrows 2COS + 3/nS_n; \quad (11)$$

$$2CO + SO_2 \rightleftarrows 2CO_2 + 1/nS_n; \quad (12)$$

$$2H_2 + SO_2 \rightleftarrows 2H_2O + 1/nS_n. \quad (13)$$

Simultaneously, hydrogenation by the reaction

$$H_2 + 1/nS_n \rightleftarrows H_2S \quad (14)$$

and hydrolysis by a reaction reverse to (3) result in that elemental sulfur produced by reduction reaction (7) partly forms hydrogen sulfide. As a result, the Claus ratio at the outlet of the catalytic reactor (converter) *3* reaches at 500–550°C a value CR ≈ *2*. After cooling of the reduced sulfurous gas in the boiler-utilizer to 220–250°C (temperature controlled with a by-pass), its processing in the Claus reactor is identical to that in the conventional Claus process (3).

A specific feature of this flowsheet is that there is no sulfur condenser, mandatory in conventional Claus installations [3], before the first stage of catalytic conversion of the reduced gas. This is due to the insufficient content of hydrogen sulfide (CR ≤ 1) at the outlet of the reducing reactor and to the high temperature (400–550°C) in the first stage of catalytic conversion, which is necessary for effective hydrolysis of organosulfur components by reactions (8) and (9).

The elemental sulfur obtained in the homogeneous thermal reactor and hydrolyzed in the first catalytic stage to hydrogen sulfide reacts, in the subsequent catalytic processing by the Claus method, with sulfur dioxide, being again oxidized to elemental sulfur by the cycle $SO_2 \rightarrow 1/2S_2 \rightarrow H_2S \rightarrow 1/nS_n$. In accordance with the stoichiometry of the Claus reaction (3), processing of hydrogen sulfide yields elemental sulfur in an amount exceeding its content in hydrogen sulfide by a factor of 1.5. Therefore, hydrolysis of organosulfur compounds in the first catalytic stage to give hydrogen sulfide at an initial excess of SO_2 leads to an increase in the overall yield of sulfur.

The industrial experience confirms the fairly high efficiency of hydrogen sulfide generation at 350–450°C on typical aluminum oxide catalysts [15]. However, the high temperature in converter *2*, necessary in accordance with the chemical equilibrium (see figure), requires that a special catalyst stable against hydrothermal aging should be used in this case. Because ordinary aluminum oxide catalysts for the hydrolysis and hydrogenation reactions rapidly lose their activity in the Claus process, it is advisable to use industrial cobalt–molybdenum catalysts [2, 5, 7] or vanadium–titanium catalysts on an aluminum oxide support.

Use of by-passes for temperature control, instead of the conventional gas heaters, rules out any fuel expenditure for repeated heating of the process gas and is technologically justified because the efficiency of reaction (3) in the Claus reactor is independent of the presence or absence of elemental sulfur. Taken together with the lowered temperature of homogeneous reduction, this makes it possible to diminish the fuel expenditure and feeding water consumption and to bring down the capital investment at an increased throughput of the production line.

As applied to utilization of effluent gases from

Vanyukov furnaces, the three-stage processing provides 92–94% recovery of sulfur. In this case, the total (including that for afterburning) specific expenditure of natural gas is about 560 $Sm^3\ t^{-1}$, which is no worse than that in other schemes suggested for catalytic processing of the sulfurous gas [2]. The increase in other operational expense items (and primarily in electric power consumption) in implementation of any version of catalytic processing gives certain advantages to the improved scheme with the industrially mastered thermal reduction of the metallurgical sulfurous gas.

CONCLUSIONS

The analysis made in the study demonstrated that the known schemes of catalytic processing of sulfurous gases have no fundamental advantage over the already employed "methane" technology for sulfur recovery from effluent gases formed in autogenous smelting. At close sulfur recovery parameters (92–96%) and reducing agent consumptions, the key role is played by the extent to which a technology is developed, reliability, and safety, in which the improved technology of direct thermal reduction of a rich metallurgical sulfurous gas has obvious advantages.

REFERENCES

1. Searle, P. and Baker, C., *Sulphur 2005*, Moscow, October, 23–26, 2005, Conf. Papers, London: CRU, 2005, pp. 11–20.
2. Connock, L., *Sulphur*, 2006, no. 305, pp. 29–40.
3. Grunval'd, V.R., *Tekhnologiya gazovoi sery* (Technology of Sulfur Production from Gas), Moscow: Khimiya, 1992.
4. Platonov, O.I., Vasil'ev, Yu.V., Ryabko, A.G., et al., *Tsvetn. Met.*, 2004, no. 2, pp. 68–72.
5. Chow, T.K., Wong, V.W., Flood, T.M., and Gebur, J.A., *Sulphur 2005*, Moscow, October 23–26, 2005, Conf. Papers, London: CRU, 2005, pp. 53–61.
6. Cost Effective SO_x Removal, *Sulphur*, 2006, no. 302, pp. 31–38.
7. Rameshni, M. and Santo, S., *Sulphur 2005*, Moscow, October 23–26, 2005, Conf. Papers, London: CRU, 2005, pp. 83–98.
8. Ushakov, K.I., Eremin, O.G., Kalnin, E.I., et al., *Tsvetn. Met.*, 1980, no. 2, pp. 34–37.
9. Platonov, O.I., Severilov, A.V., and Isaenko, O.I., *Vestn. MANEB*, 1999, no. 8 (20), pp. 42–45.
10. Platonov, O.I. and Tsemekhman, L.Sh., *Tsvetn. Met.*, 2007, no. 2, pp. 63–68.
11. Vasil'ev, Yu.V., Knyazev, M.V., Platonov, O.I., et al., *Tsvetn. Met.* 2003, no. 7, pp. 75–79.
12. Tarasov, A.V. and Yeremin, O.G., *Sulphur 2005*, Moscow, October 23–26, 2005, Conf. Papers, London: CRU, 2005, pp. 63–69.
13. Vilesov, N.G. and Bol'shunov, V.G., *Zh. Prikl. Khim.*, 1988, vol. 77, no. 8, pp. 1894–1896.
14. Platonov, O.I., Ryabko, A.G., and Tsemekhman, L.Sh., *Proc. Eur. Metallurgical Conf. EMC-2005*, Dresden, 2005, vol. 3, pp. 1293–1299.
15. Egorov, V.N., Platonov, O.I., and Yatsenko, S.P., *Katal. Prom–sti.*, 2004, no. 4, pp. 41–44.
16. Platonov, O.I., Ryabko, A.G., and Tsemekhman, L.Sh., *Zh. Prikl. Khim.*, 2004, vol. 77, no. 8, pp. 1323–1326.

ISSN 1070-4272, Russian Journal of Applied Chemistry, 2007, Vol. 80, No. 9, pp. 1481–1485. © Pleiades Publishing, Ltd., 2007.
Original Russian Text © Yu.G. Khabarov, M.S. Yakovlev, 2007, published in Zhurnal Prikladnoi Khimii, 2007, Vol. 80, No. 9, pp. 1445–1449.

PHYSICOCHEMICAL STUDIES OF SYSTEMS AND PROCESSES

Enhancing the Sensitivity of Spectrophotometric Determination of Formic Acid with Mercury(II) Acetate

Yu. G. Khabarov and M. S. Yakovlev

Arkhangelsk State Technical University, Arkhangelsk, Russia

Received December 14, 2006

Abstract—A precise spectrophotometric method was developed for determination of formic acid. The method surpasses in sensitivity the method based on proper UV absorption of formic acid.

DOI: 10.1134/S107042720709008X

Formic acid is widely used in various branches of industry: as stain in dyeing, in textile and paper finishing, in leather treatment, in production of drugs and preservatives. It is often used as chromatographic eluent and as a reagent for organic synthesis, e.g., for preparing formamide, dimethylformamide, and oxalic acid [1–3].

There are diverse procedures for analytical determination of formic acid: alkalimetry, gas chromatography, UV and NMR spectroscopy, capillary electrophoresis, etc. [4–6]. The UV spectroscopic determination of formic acid is based on its absorption at 206 nm [7–9].

EXPERIMENTAL

The following chemicals were used: analytically pure grade mercury(II) acetate, chemically pure grade 85% formic acid, chemically pure grade glacial acetic acid, and chemically pure grade 37% Formalin. The formaldehyde solution was prepared by dilution of Formalin filtered through a paper filter.

The spectra were recorded on a Specord M40 spectrophotometer in the wavelength range 200–330 nm. The optical densities of solutions at 206 and 236 nm were measured with an SF-46 spectrophotometer. These measurements were performed in 1-cm quartz cells against distilled water.

Formic acid solutions were prepared by dilution of the acid. To prepare a solution of mercury(II) acetate, a 100-ml volumetric flask was charged with 1.165 g of the salt and 1.1 ml of glacial acetic acid (to prevent hydrolysis), and the solution was brought to the mark.

The photometric reaction was performed as follows. A 100-ml volumetric flask was charged with 80 ml of a formic acid solution (7.78–72.6 mg l^{-1}), the prescribed volume of the mercury(II) acetate solution was added, the mixture was brought to the mark with water and thoroughly mixed. The optical density of the solution at 236 nm, D_{236}, was measured 10, 20, 30, 60, and 120 min after adding the solution of mercury(II) acetate.

Determination of formic acid by proper absorption was performed by measuring the optical density of the solution at 206 nm, D_{206}.

To study the interfering effect of formaldehyde on the determination of formic acid, to a 100-ml volumetric flask we added in succession 80 ml of a formic acid solution (64.4 mg l^{-1}), the prescribed volume of the formaldehyde solution, and 1 ml of the mercury acetate solution. The mixture was brought to the mark with water. The optical density D_{236} was measured 10, 20, 30, and 60 min after adding mercury acetate.

The reaction of mercury(II) acetate with formic acid is accompanied by appearance of a strong absorption band at 236 nm (Fig. 1). In further experiments we determined the required amount of the mercury(II) acetate solution and examined the influence of the reaction time on the determination results. For this purpose, the photometric reaction was performed with 80 ml of a formic acid solution (51.5 mg l^{-1}) and varied amounts of the mercury(II) acetate solution: 0.2, 0.6, 1.0, 1.4, and 1.8 ml. The optical density of solutions D_{236} (minus the optical density in blank experiments without formic acid) is plotted in Fig. 2 against the amount of mercury(II) acetate added. It is seen that addition of the mercury(II) acetate solution in amounts over 1.0 ml does not lead to a further sig-

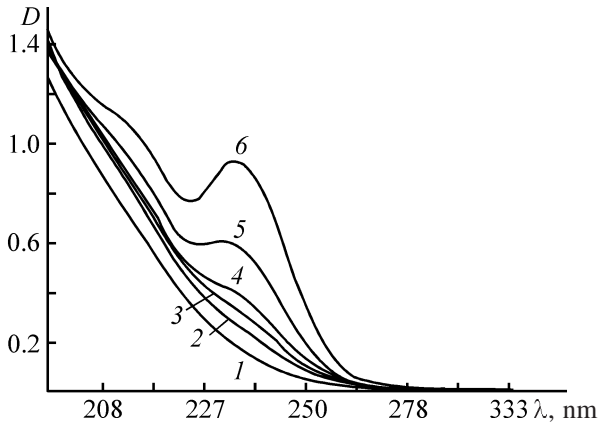

Fig. 1. Variation of the electronic absorption spectrum of the reaction product with the reaction time. (*D*) Optical density and (λ) wavelength. (*1*) Blank mercury(II) acetate solution and (*2–6*) reaction product. Reaction time, min: (*2*) 10, (*3*) 20, (*4*) 30, (*5*) 60, and (*6*) 120.

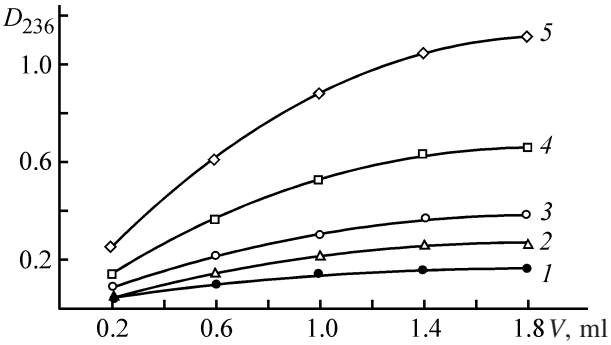

Fig. 2. Optical density of solutions D_{236} as a function of the volume *V* of the mercury(II) acetate solution added. Reaction time, min: (*1*) 10, (*2*) 20, (*3*) 30, (*4*) 60, and (*5*) 120.

nificant increase in the optical density. Therefore, further experiments were performed with addition of 1.0 ml of the mercury(II) acetate solution.

To construct calibration plots, the photometric reaction was performed with various preset concentrations of the formic acid solutions. Two replicate determinations were made for each point; the mean values of D_{236} are listed in Table 1.

Table 1. Mean values of D_{236} of formic acid solutions at various formic acid concentrations *c* and reaction times τ

c, mg l^{-1}	D_{236} at indicated τ, min				
	10	20	30	60	120
6.22	0.158	0.169	0.178	0.213	0.247
16.6	0.189	0.217	0.246	0.326	0.457
27.0	0.215	0.216	0.309	0.429	0.632
37.3	0.246	0.317	0.375	0.550	0.830
47.7	0.277	0.363	0.444	0.662	1.015
58.1	0.318	0.443	0.547	0.815	1.206

By the least-squares method, we calculated the coefficients of the calibration plots $D_{236} = a + bc$, where *c* is the formic acid concentration (mg l^{-1}), and the pair correlation coefficients (Table 2).

The concentration dependences of the optical density are linear, and the optical density of solutions of the photometric reaction product is described by the Bouguer–Lambert–Beer law.

Table 2 shows that the coefficients of the calibration equations strongly depend on the reaction time. Therefore, the calibration equation should include not only the formic acid concentration but also the reaction time. The best fitting of the experimental data was attained with a cubic logarithmic polynomial

$$c = 500 - 144\ln\tau + 8.01\ln^2\tau + 371\ln D_{236} + 62.8\ln^2 D_{236}$$
$$- 96.8\ln\tau\ln D_{236} + 0.494\ln^3\tau + 6.41\ln^2\tau\ln D_{236}$$
$$- 8.24\ln\tau\ln^2 D_{236} + 3.65\ln^3 D_{236},$$

The repeatability and accuracy of the determination were estimated in experiments with formic acid solutions of five different concentrations (four replicate measurements for each point). After performing the photometric reaction, we measured D_{236}, calculated from the three-dimensional calibration plot the formic acid concentrations, and compared them with the preset values (Tables 3, 4).

Tables 3 and 4 show that the suggested method exhibits good repeatability (coefficient of variation ≤3.6%) and accuracy (relative error about 3% on the average).

For comparison, we performed experiments on formic acid determination by proper absorption at 206 nm. For this purpose, we calculated the coeffi-

Table 2. Coefficients of equations of calibration plots and pair correlation coefficients R^2

τ, min	$D_{236} = a + bc$		R^2
	a	*b*	
10	0.136	0.00302	0.995
20	0.138	0.00471	0.999
30	0.139	0.00636	1.000
60	0.144	0.0108	1.000
120	0.141	0.0184	1.000

Table 3. Repeatability of D_{236} in the photometric reaction

τ, min	Introduced, mg l^{-1}	D_{236}					Root-mean-square deviation	Coefficient of variation, %
		D_1	D_2	D_3	D_4	D_{av}		
10	10.3	0.166	0.173	0.171	0.169	0.170	0.0030	1.8
20	10.3	0.189	0.189	0.195	0.184	0.189	0.0045	2.4
30	10.3	0.195	0.204	0.206	0.200	0.201	0.0048	2.4
60	10.3	0.237	0.255	0.254	0.255	0.250	0.0089	3.6
120	10.3	0.324	0.343	0.329	0.326	0.331	0.0086	2.6
10	20.6	0.189	0.196	0.194	0.196	0.194	0.0033	1.7
20	20.6	0.238	0.232	0.233	0.233	0.234	0.0027	1.1
30	20.6	0.267	0.279	0.263	0.283	0.273	0.0095	3.5
60	20.6	0.36	0.375	0.345	0.366	0.362	0.013	3.5
120	20.6	0.518	0.522	0.497	0.510	0.512	0.011	2.2
10	30.9	0.222	0.231	0.223	0.223	0.225	0.0042	1.9
20	30.9	0.28	0.278	0.288	0.285	0.283	0.0044	1.5
30	30.9	0.332	0.327	0.329	0.333	0.330	0.0028	0.8
60	30.9	0.472	0.486	0.456	0.471	0.471	0.012	2.6
120	30.9	0.698	0.708	0.691	0.700	0.699	0.0072	1.0
10	41.2	0.251	0.247	0.252	0.263	0.253	0.0071	2.8
20	41.2	0.337	0.329	0.332	0.341	0.335	0.0054	1.6
30	41.2	0.408	0.399	0.396	0.407	0.403	0.0059	1.5
60	41.2	0.59	0.602	0.566	0.602	0.590	0.017	2.9
120	41.2	0.879	0.891	0.856	0.881	0.877	0.01	1.7
10	51.5	0.289	0.284	0.282	0.278	0.283	0.0046	1.6
20	51.5	0.386	0.378	0.385	0.380	0.382	0.0039	1.0
30	51.5	0.477	0.477	0.462	0.469	0.471	0.0074	1.6
60	51.5	0.697	0.706	0.670	0.685	0.690	0.016	2.2
120	51.5	1.053	1.058	1.072	1.080	1.066	0.012	1.2

Table 4. Accuracy of formic acid determination with the photometric reaction

τ, min	D_{236}	c_{HCOOH}, mg l^{-1}		Mean error	
		introduced	found	absolute, mg l^{-1}	relative, %
10	0.170	10.3	10.6	0.3	2.6
20	0.189	10.3	10.9	0.6	5.8
30	0.201	10.3	9.7	–0.6	5.5
60	0.250	10.3	9.7	–0.6	6.1
120	0.331	10.3	10.3	0.0	0.5
10	0.194	20.6	19.1	–1.5	7.1
20	0.234	20.6	20.8	0.2	1.0
30	0.273	20.6	21.4	0.8	3.7
60	0.362	20.6	20.1	–0.5	2.5
120	0.512	20.6	19.9	–0.7	3.4
10	0.225	30.9	29.8	–1.1	3.5
20	0.283	30.9	31.2	0.3	1.1
30	0.330	30.9	30.6	–0.3	1.0
60	0.471	30.9	30.5	–0.4	1.4
120	0.699	30.9	30.3	–0.6	1.8
10	0.253	41.2	39.3	–1.9	4.5
20	0.335	41.2	42.1	0.9	2.2
30	0.403	41.2	41.8	0.7	1.6
60	0.590	41.2	41.6	0.4	1.0
120	0.877	41.2	40.2	–0.9	2.3

Table 4. (Contd.)

τ, min	D_{236}	c_{HCOOH}, mg l^{-1}		Mean error	
		introduced	found	absolute, mg l^{-1}	relative, %
10	0.283	51.5	48.8	–2.6	5.1
20	0.382	51.5	51.6	0.1	0.2
30	0.471	51.5	52.2	0.7	1.3
60	0.690	51.5	50.7	–0.8	1.5
120	1.066	51.5	50.6	–0.9	1.8

Table 5. Repeatability of D_{206} in formic acid determination by proper absorption

Introduced, mg l^{-1}	D_{236}					Root-mean-square deviation	Coefficient of variation, %
	D_1	D_2	D_3	D_4	D_{av}		
6.22	0.032	0.009	0.018	0.003	0.016	0.013	81.4
16.6	0.034	0.020	0.024	0.020	0.025	0.0066	27.0
27.0	0.024	0.034	0.030	0.014	0.026	0.0087	34.1
37.3	0.042	0.049	0.008	0.018	0.029	0.019	66.4
47.7	0.051	0.054	0.018	0.010	0.033	0.023	67.7
58.1	0.074	0.076	0.032	0.045	0.057	0.022	38.3

cients of the calibration plot and obtained the equation $D_{206} = 0.028 + 0.000892c$, where c is the formic acid concentration (mg l^{-1}), with the pair correlation coefficient $R^2 = 0.999$.

The repeatability and accuracy of determination were estimated with formic acid solutions of six different concentrations (four replicate measurements for each point); the results are given in Table 5.

Table 5 shows that the repeatability of D_{206} in the range of formic acid concentrations from 6 to 60 mg l^{-1} is very poor.

To evaluate the determination accuracy, photocolorimetric measurements were performed at 206 nm, and the formic acid concentrations were calculated from the calibration plots and compared with the preset values (Table 6).

Table 6. Accuracy of formic acid determination by proper absorption

D_{206}	c_{HCOOH}, mg l^{-1}		Mean error	
	introduced	found	absolute, mg l^{-1}	relative, %
0.016	6.22	0	–6.22	100
0.025	16.6	0	–16.6	100
0.026	27.0	0	–27.0	100
0.029	37.3	1.4	–35.9	96.2
0.033	47.7	5.9	–41.8	87.7
0.057	58.1	32.2	–25.9	44.5

Table 6 shows that the accuracy of formic acid determination by proper absorption in the examined concentration range is also very poor.

Thus, the new spectrophotometric method enhances the sensitivity of the determination (the lower determination limit decreases from 140 to 10 mg l^{-1}).

Since process solutions often contain formaldehyde along with formic acid, we examined the interfering

Table 7. Effect of formaldehyde (F) on formic acid (FA) determination with mercury(II) acetate. Formic acid concentration 51.5 mg l^{-1}

C_F, mg l^{-1}	F : FA weight ratio	D_{236} at indicated τ, min			
		10	20	30	60
0	0	0.286	0.382	0.477	0.702
32.6	0.6	0.286	0.383	0.474	0.706
65.1	1.3	0.282	0.378	0.469	0.696
130	2.5	0.282	0.381	0.467	0.698
651	13	0.288	0.394	0.485	0.712
2040	40	0.282	0.374	0.463	0.704
4070	79	0.277	0.373	0.464	0.694
20400	395	0.288	0.384	0.474	0.705
40700	790	0.293	0.387	0.469	0.688

effect of formaldehyde on the formic acid determination by the new method. The results are given in Table 7. It is seen that even a large excess of formaldehyde does not interfere with the determination of formic acid.

CONCLUSIONS

(1) A new spectrophotometric method was developed for determination of formic acid in solutions. The method is characterized by high accuracy and repeatability of the results at formic acid concentrations down to 10 mg l^{-1}.

(2) The method is more sensitive compared to the determination by proper absorption at 206 nm. Formaldehyde does not interfere with the determinations.

REFERENCES

1. Burridge, E., *Eur. Chem. News*, 2003, vol. 79, no. 2060, p. 15.
2. Jothilingam, S., *Synlett*., 2004, no. 5, pp. 910–911.
3. Pollarim I., *CLB Chem. Labor Biotech*., 2003, vol. 54, no. 10, pp. 380 –382.
4. Hog, M.F., Ernst, W.R., and Gelbaum, L.T., *TAPPI*, 1991, vol. 74, no. 8, pp. 217–220.
5. Kotel'nikova, T.S., Vdovenko, O.V., Voronina, S.G., and Perkel', A.L., *Zh. Anal. Khim.*, 2006, vol. 61, no. 4, pp. 338–342.
6. Castedo Peca, M. and Herrero, G.-M., *Int. J. Environ. Anal. Chem*., 2002, vol. 83, no. 3, pp. 247–253.
7. Korenman, I.M., *Fotometricheskii analiz: Metody opredeleniya organicheskikh soedinenii* (Photometric Analysis: Methods for Determination of Organic Compounds), Moscow: Khimiya, 1975, 2nd ed.
8. Gillam, A. and Stern, E.S., *An Introduction to Electronic Absorption Spectroscopy in Organic Chemistry*, London: Arnold, 1954.
9. *Spravochnik khimika* (Chemist's Handbook), Leningrad: Khimiya, 1965, vol. 4.

ISSN 1070-4272, Russian Journal of Applied Chemistry, 2007, Vol. 80, No. 9, pp. 1486–1490. © Pleiades Publishing, Ltd., 2007.
Original Russian Text © N.K. Luneva, L.I. Petrovskaya, 2007, published in Zhurnal Prikladnoi Khimii, 2007, Vol. 80, No. 9, pp. 1450–1454.

SORPTION AND ION-EXCHANGE PROCESSES

Microporous Carbons and Their Properties

N. K. Luneva and L. I. Petrovskaya

Institute of General and Inorganic Chemistry, State Scientific Institution, National Academy of Sciences of Belarus, Minsk, Belarus

Received December 26, 2006; in final form, April 2007

Abstract— Thermal degradation of saw dust impregnated with phosphorus- and nitrogen-containing solution with ammonium, lithium, and cesium additives in the 20–700°C range was studied by physicochemical methods. The conditions of preparing activated carbon were determined and its adsorption and structural characteristics were studied.

DOI: 10.1134/S1070427207090091

Activated carbons are used in chemical technology, in medicine, in food industry, as sorbents for treatment of gases and wastewater, etc. Wide use of ac tivated carbons is promoted by improvement of their preparation processes and quality and by utilization of cheap wastes from woodworking industry (wood chips, saw dust). Chemical composition and sorption properties of the resulting carbons depend on the nature of impregnation agent and temperature, time, and procedure of thermal treatment and on some other factors, whereas their use is hindered by high cost. As a rule, common procedures for preparing charcoal involve formation of the carbon precursor at 550°C and its further activation to improve the pore structure in the atmosphere of an oxidizing gas at 900–1000°C. A procedure is known for preparing charcoal by pyrolysis of wood impregnated with zinc chloride or phosphoric acid, which is carried out at 700°C for 4–6 h. All the procedures are power-, time-, and labor-consuming. Therefore, development of simple power-saving and environmentally safe procedures for preparing activated carbons is an urgent problem.

This paper concerns preparation of carbon sorbents by low-temperature pyrolysis of impregnated wood and properties of the resulting carbons.

EXPERIMENTAL

We examined the features of thermal degradation at 20–700°C of waste from woodworking industry (saw dust and chips with size from 3 to 30 mm) impregnated with phosphorus- and nitrogen-containing mixture [H_3PO_4–$CO(NH_2)_2$, mixture B] with lithium, cesium, and ammonium nitrate additives and the sorption properties of activated carbons prepared by thermal treatment of the impregnated wood. The weight gain related to the impregnation solution was 170% relative to the dry saw dust. The compositions of the phosphorus- and nitrogen-containing mixtures are listed in Table 1. In the course of thermal treatment at 20–550°C, the cellulose-containing material is carbonized with pore formation in the carbon residue. Impregnation solution catalyzes degradation of the carbohydrate–lignin wood complex. Therefore, dehydration and breakdown of both 1,4-anhydroglucose bonds and C–C and C–O bonds inside the glucopyranose rings occurs at low temperatures as compared to the initial wood. In this case, additives undergo chemical transformations and reorganization upon heating and act as supports in the combustible carbohydrate fraction of the material at shrinkage of the wood raw material, preventing closure of the pores and channels. After thermal treatment of the impregnated saw dust, the carbon residue was washed by multiple immersions in boiling water (liquid-to-solid ratio 20) followed by squeezing, until the wash water became neutral. Then, the residual water was removed by centrifugation and the residue was dried in air for 24 h at room temperature and for 2 h at 45°C. The content of nitrogen in the initial wood and activated carbon samples was

Table 1. Characteristics of phosphorus- and nitrogen-containing impregnation mixtures

Mixture no.	Impregnation mixture	N : P weight ratio*
1	B	1 : 2.1
2	B + NH_4NO_3	1 : 5.4
3	B + $LiNO_3$	1 : 9.3
4	B + $CsNO_3$	1 : 11.0

* Mixture nos. 2–4 contained nitrate additives.

determined by their wet combustion in concentrated H_2SO_4 by the Kjeldahl procedure [1], and the content of phosphorus, photocolorimetrically by formation of phosphomolybdic blue [2].

The specific surface areas of the resulting carbons were determined gravimetrically by sorption of CCl_4 vapor at 20°C using a vacuum installation with a quartz balance [3]. The activity of carbon to iodine was evaluated in accordance with GOST (State Standard) 17218–74, and the bulk density, in accordance with GOST 14922–77. The static ion-exchange capacity was measured by the procedure given elsewhere [4]. The crystallite size in the carbon residue was calculated from the X-ray diffraction (XRD) patterns using the standard procedure [5]. The XRD patterns of the heat-treated samples were recorded on a DRON-3 diffractometer (CuK_α, Ni filter) in the 2θ 2°–60° range. Thermal analysis of the impregnated saw dust samples was carried out in air on an MOM device (Hungary) at a heating rate of 20 deg min^{-1}. As seen from the experimental data, thermal degradation of the saw dust impregnated with nitrogen- and phosphorus-containing mixtures is most intensive in the temperature range from 80 to 360°C, and then the rate of thermal degradation decreases. The integral and differential dependences of the weight loss are shown in Fig. 1, and characteristics of thermal degradation of impregnated wood are listed in Table 2.

As seen from these data, the yield of the carbon product at 550°C depends on the composition of the impregnation mixture. For example, for mixtures B and B + NH_4NO_3 it amounts to 49.3 and 52.3%, respectively, whereas for $LiNO_3$ and $CsNO_3$ it is 45.5 and 47.0%, respectively. For samples impregnated with straight mixture B and with addition of ammonium nitrate, significant decrease in the degradation rate is observed above 300°C, and with mixtures containing cesium and lithium nitrates, above 360°C. Thermal degradation is the most intense in the 80–210°C range, where two processes occur (Fig. 1) rate and temperature depending on the impregnation mixture. The first process occurs at the maximal rate at 105–145°C, and the second, at 185–195°C. The first rate maximum is probably due to both decomposition of nitrogen- and phosphorus-containing complexes of cellulose and degradation of the polymer [6]. The second rate maximum is probably due to the thermal degradation of more stable condensed phosphate compounds and breakdown of the hydrocarbon structures of cellulose.

The observed features of degradation of impregnated saw dust are due to the differences in the mechanism of thermal degradation, which depends on the composition of the impregnation mixture. This is confirmed by the data of chemical and XRD analysis, namely, by different fractions of nitrogen and phosphorus, by differences in the phase composition, and by the yield of the carbon residue in the washed samples (Table 3). As seen from the data of chemical

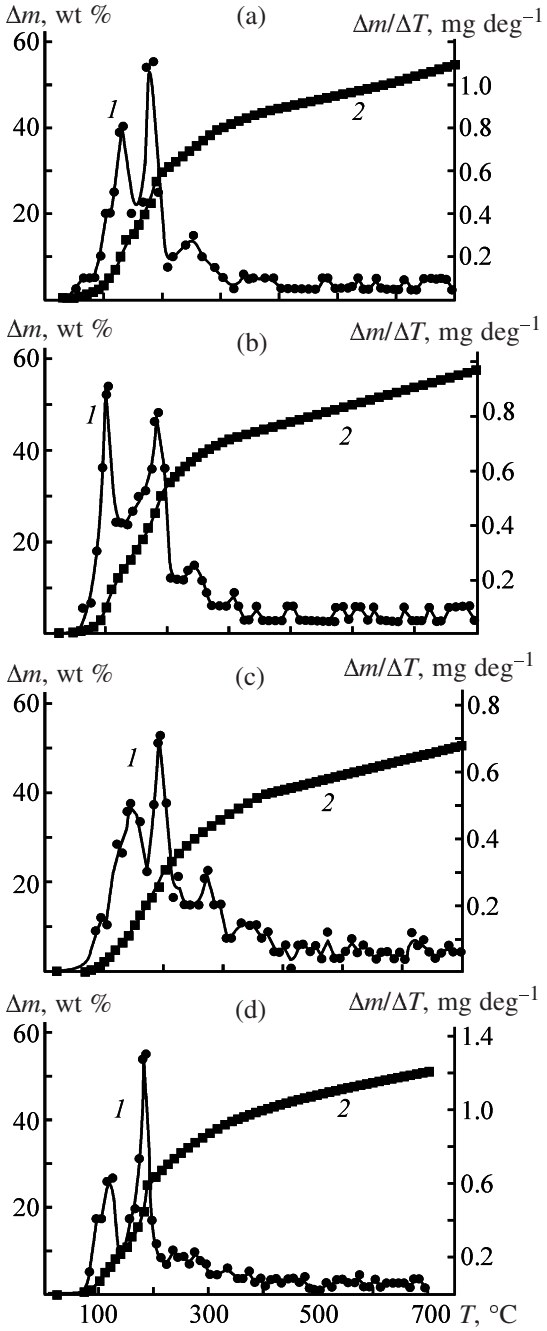

Fig. 1. (*1*) Integral and (*2*) differential thermogravimetric curves. (Δ*m*) Weight loss and (Δ*m*/Δ*T*) rate of the weight loss. (a) Mixture B, (b) B + NH_4NO_3, (c) B + $LiNO_3$, and (d) B + $CsNO_3$.

Table 2. Characteristics of thermal degradation of impregnated wood based on the data of differential thermal analysis

Impregnation agent	Characteristics of thermal degradation at indicated temperature, °C								
	process 1				process 2				
	105	125	135	145	185	195	245	255	275
	Rate,* mg deg^{-1}								
Mixture B	–	–	0.80	–	1.10	–	–	0.30	–
B + NH_4NO_3	0.90	–	–	–	0.80	–	0.25	–	–
B + $CsNO_3$	–	0.62	–	–	1.28	–	–	–	0.22
B + $LiNO_3$	–	–	–	0.50	–	0.70	–	–	0.30
	Weight loss, %								
Mixture B	–	–	12.0	–	24.7	–	–	35.5	
B + NH_4NO_3	7.8	–	–	–	28.0	–	38.0	–	–
B + $CsNO_3$	–	7.5	–	–	22.1	–	–	–	34.8
B + $LiNO_3$	–	–	–	9.3	–	20.7	–	–	32.3

* Maximal rate of thermal degradation of carbohydrate complexes.

Table 3. Results of chemical analysis and phase composition of washed samples after thermal degradation of wood impregnated with nitrogen- and phosphorus-containing mixtures

T, °C	Δm,* %	Content, wt %		Phase composition
		nitrogen	phosphorus	
		Mixture B		
20	0	3.60	10.96	–
180	25.0	5.11	2.12	–
260	37.5	5.25	5.30	–
460	54.5	6.15	3.44	X-ray amorphous phase
550	82.5	8.85	3.13	X-ray amorphous phase
		B + $LiNO_3$		
20	0	4.77	11.76	–
180	30.0	3.74	0.62	–
260	37.5	4.40	4.43	X-ray amorphous phase
460	54.1	6.03	4.23	X-ray amorphous phase
550	67.0	6.48	3.93	X-ray amorphous phase
		B + $CsNO_3$		
20	0	2.55	8.90	–
180	25.4	3.50	3.10	$(NH_4PO_3)_3$–AP** [7]
260	39.3	3.91	4.42	$(NH_4PO_3)_3$–AP [7]
460	49.2	5.22	4.54	AP–Kurrol salt + $CsPO_3$ [7, 8]
550	67.8	5.44	4.02	AP–Kurrol salt + $CsPO_3$ [7, 8]
		B + NH_4NO_3		
20	0	4.89	15.99	–
180	22.0	2.59	2.49	–
260	39.0	5.65	5.23	X-ray amorphous phase
460	54.5	8.10	3.72	X-ray amorphous phase
550	72.0	7.40	1.99	X-ray amorphous phase

* (Δm) Weight loss taking into account retention of the impregnation agent in the course of washing.
** (AP) Ammonium polyphosphate.

anallysis, the highest content of phosphorus and nitrogen is observed in the saw dust samples impregnated with the mixture containing $CsNO_3$ and treated at 180–550°C. To evaluate the effect of various impregnation agents on the carbonization, we used such conventional parameter as retention index, i.e., ratio of the actual content of the element in the sample taking into account the weight loss at given temperature to its initial content in the sample. Thermal treatment of the samples impregnated using mixtures with $LiNO_3$ or NH_4NO_3 additives yields the samples whose retention index is somewhat smaller (from 1.00 to 0.42 for nitrogen and from 0.30 to 0.04 for phosphorus). The retention index for nitrogen and phosphorus was 1.00–0.68 and 0.30–0.14, respectively (Table 4).

As seen from XRD data, only thermally treated and washed saw dust samples impregnated with mixture B + $CsNO_3$ contained crystalline phases of ammonium and cesium polyphosphates, whose d_α values agree with published data for these compounds [7, 8]. It should be noted that the samples treated at 180–260°C contained ammonium polyphosphate phase, and, with increasing temperature to 550°C, the phase of cesium polyphosphate crystallized along with ammonium polyphosphate (Kurrol salt) (Fig. 2). All the other samples prepared by thermal treatment of saw dust impregnated with straight mixture B and with addition of $LiNO_3$ and NH_4NO_3 were X-ray amorphous. The samples prepared using mixture B and mixture B + NH_4NO_3 or $LiNO_3$ contained crystallites of carbon material with a size of 8.7, 9.4, and 10.0 nm, respectively.

It is known that one of the best procedures to study the pore structure is physical sorption of vapors and gases. In accordance with BET method and IUPAC classification based on the hysteresis shape, the adsorption isotherms of carbon coke materials belong to type H_3 of the isotherms of physical sorption of the vapors, typical of microporous samples with pore size ≤1 nm. The apparent sorption volume varies from 0.40 to 0.67 $cm^3\ g^{-1}$ depending on the impregnation agent composition; it was calculated from the Dubinin equation in accordance with the theory of micropore volume filling [9]. Our data show that the largest apparent specific surface area (S_{sp} = 1100 $m^2\ g^{-1}$) is observed for carbon samples impregnated with mixture B + NH_4NO_3, and the smallest (S_{sp} = 690 $m^2\ g^{-1}$), with mixture B + $CsNO_3$. The adsorption and structural characteristics of the carbons prepared by pyrolysis (550°C) of wood impregnated with various mixtures are listed in Table 5.

Analysis of sorption properties (Table 5) shows that the adsorption activity to benzene and water is fairly high for all the activated carbons studied. The highest sorption capacity for benzene is observed for the samples impregnated with nitrogen- and phosphorus-containing mixtures with ammonium or cesi-

Table 4. Retention index for nitrogen and phosphorus in the washed samples after thermal degradation of impregnated wood samples

T, °C	Retention index	
	nitrogen	phosphorus
	Mixture B	
180	1.00	0.15
260	0.91	0.30
460	0.78	0.14
550	0.43	0.05
	Mixture B + $LiNO_3$	
180	0.55	0.04
260	0.58	0.24
460	0.58	0.16
550	0.45	0.11
	Mixture B + $CsNO_3$	
180	1.00	0.26
260	0.93	0.30
460	1.00	0.26
550	0.68	0.14
	Mixture B + NH_4NO_3	
180	0.41	0.12
260	0.71	0.20
460	0.75	0.11
550	0.42	0.04

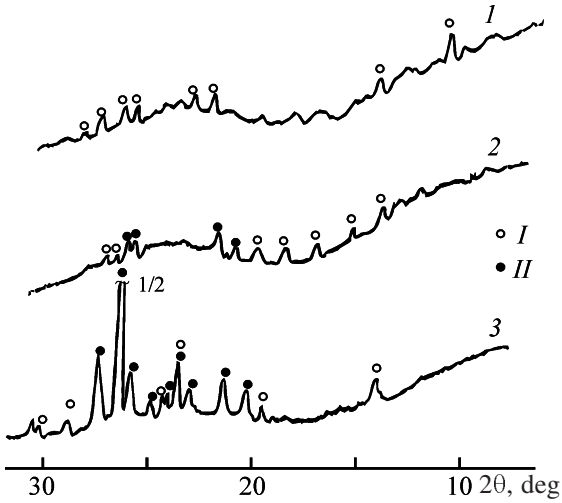

Fig. 2. XRD patterns of the impregnated and thermally treated saw dust samples. (2θ) Bragg angle. Washed samples, temperature, °C: (*1*) 180, (*2*) 460, and (*3*) 550, impregnation with mixture B + $CsNO_3$. (*I*) Ammonium polyphosphate NH_4PO_3 and (*II*) cesium polyphosphate $CsPO_3$.

Table 5. Adsorption and structural characteristics of carbons

Impregnation agent	Iodine number, %	Bulk density, g dm^{-3}	Sorption of benzene, %	Sorption of Methylene Blue, mg g^{-1}	Static ion-exchange capacity, mg-equiv g^{-1}	BET specific surface area S_{sp}, m^2 g^{-1}	BET sorption volume V_s, cm^3 g^{-1}
Mixture B	54.8	177	44	10	0.8	945	0.52
B + NH_4NO_3	41.1	225	60	10	0.4	1100	0.64
B + $LiNO_3$	48.9	210	60	12	0.3	895	0.67
B + $CsNO_3$	61.4	193	52	19	0.3	690	0.40

um nitrate additives; in both cases, the sorption capacity is 60%. The smallest sorption capacity for benzene (44%) is observed for the sample impregnated with mixture B. The activated carbons prepared exhibit fairly high sorption capacity for iodine (61.4–41.1%). For example, the iodine number for activated carbon impregnated with mixture B + NH_4NO_3 is 41.1%, and with mixture B + $CsNO_3$, 61.4%. As known, microporous sorbents are highly active with respect to small molecules such as benzene (size of C_6H_6 molecule 0.37 nm) and iodine (size of I_2 molecule ≤0.4 nm) and are less efficient in sorption of larger molecules, e.g., Methylene Blue (molecular size 34.9 nm). Our experimental results (Table 5) well agree with published data [10].

The sorption characteristics of some commercial carbons are listed in Table 6 for comparison. Tables 5 and 6 show that the activated carbons we prepared have the pore structure close to that of commercial sorbents produced by two-step procedure at high temperature.

It should be noted that the activated carbons prepared by our procedure also exhibit cation-exchange properties and their ion-exchange capacity for Na^+ is 0.3–0.8 mg-equiv g^{-1}.

Table 6. Adsorption characteristics of commercial carbons

Carbon brand	Sorption capacity, %		Sorption of Methylene Blue, mg g^{-1}	Bulk density, g dm^{-3}
	for iodine	for benzene		
OU-A, GOST 4453–74	–	–	225	–
BAU-A, GOST 6217–74	60	–	–	240
Busofit-T (0.40)	110	44*	250	–

* Our experimental data.

CONCLUSIONS

(1) Impregnation of saw dust with nitrogen- and phosphorus-containing mixtures containing NH_4NO_3, $LiNO_3$, and $CsNO_3$ additives, followed by pyrolysis at 20–550°C, yields activated carbons with the specific surface area of 690–1100 m^2 g^{-1} and sorption capacity for benzene and iodine of 44–60 and 41.1–61.4%, respectively.

(2) The resulting activated carbons are microporous sorbents which can be used for sorption of benzene and carbon tetrachloride vapors.

REFERENCES

1. Losev, I.P. and Fedotova, O.Ya., *Praktikum po khimii vysokomolekulyarnykh soedinenii* (Practical Course of Chemistry of Macromolecular Compounds), Moscow: Mir, 1962.
2. Brudz', V.G., Uskova, A.B., et al., *Sbornik tekhnicheskikh uslovii na khimicheskie reagenty* (Coll. of Technical Specifications for Chemical Reagents), Moscow: Khimiya, 1965.
3. Kiselev, A.V. and Dreving, V.P., *Eksperimental'nye metody v adsorbtsii i molekulyarnoi khromatographii* (Experimental Methods in Adsorption and Molecular Chromatography), Moscow: Mosk. Gos. Univ., 1973.
4. Ol'shanova, K.M., Potapova, M.A., Kopylova, V.D., and Morozova, N.M., *Rukovodstvo po ionoobmennoi, raspredelitel'noi i osadochnoi khromatografii* (Handbook of Ion-Exchange, Partition, and Sedimentation Chromatography), Moscow: Khimiya, 1965.
5. Martynov, M.A. and Vylegzhanina, K.A., *Rentgenografiya polimerov* (X-ray Diffraction Analysis of Polymers), Leningrad: Khimiya, 1972.
6. Luneva, N.K., Vorob'ev, V.K., and Petushok, I.A., *Zh. Prikl. Khim.*, 1997, vol. 70, no. 10, pp. 1729–1734.
7. Shen, C.Y., Stahlheber, and Dyroff, D.R., *J. Am. Chem. Soc.*, 1969, vol. 91, no. 1, pp. 62–66.
8. Chudinova, N.N., Borodina, L.A., Schulke, U., and Ishchet, K.Kh., *Izv. Akad. Nauk SSSR, Neorg. Mater.*, 1989, vol. 25, no. 3, pp. 459–465.
9. Dubinin, M.M., *Zh. Fiz. Khim.*, 1965, vol. 39, no. 6, pp. 1305–1318.
10. Mukhina, O.Yu., Piskunova, I.A., and Lysenko, A.A., *Zh. Prikl. Khim.*, 2003, vol. 76, no. 6, pp. 926–930.

ISSN 1070-4272, Russian Journal of Applied Chemistry, 2007, Vol. 80, No. 9, pp. 1491–1497. © Pleiades Publishing, Ltd., 2007.
Original Russian Text © V.A. Lebedev, V.I. Sal'nikov, M.V. Tarabaev, I.A. Sizikov, D.A. Rymkevich, 2007, published in Zhurnal Prikladnoi Khimii, 2007, Vol. 80, No. 9, pp. 1455–1461.

APPLIED ELECTROCHEMISTRY AND CORROSION PROTECTION OF METALS

Compatibility of TiO_2 with a CaO–$CaCl_2$ Melt

V. A. Lebedev, V. I. Sal'nikov, M. V. Tarabaev, I. A. Sizikov, and D. A. Rymkevich

Ural State Technical University, State Educational Institution for Higher Professional Education, Yekaterinburg, Russia
AVISMA Titanium and Magnesium Combine, Open Joint-Stock Company, Berezniki, Perm krai, Russia

Received September 16, 2006; in final form, February 2007

Abstract—Interaction of TiO_2 with a CaO–$CaCl_2$ melt was studied to determine whether electrolytic production of titanium from oxide raw materials is possible.

DOI: 10.1134/S1070427207090108

Titanium is among the most widely occurring metals and possesses a unique combination of properties. Its wide and efficient use in various fields of national economy is hindered by the high cost of the metal, which is due to the multistage and batch nature of the Kroll process employed in modern titanium industry. Numerous attempts to develop a continuous electrolytic technique for manufacture of titanium from titanium tetrachloride have failed to produce a widely used industrial technique because of the difficulties associated with the polyvalent nature of the metal, its high vapor pressure, and susceptibility of the tetrachloride to hydrolysis.

In recent years, a considerable interest has been observed in the possibility of electrolytic production of titanium from oxide raw materials. It has been found that understoichiometric titanium dioxide has high electrical conductivity and can serve as a cathode both in reduction of titanium oxides to the metal and in removal of dissolved oxygen from titanium.

It was suggested by Chen et al. [1, 2] to perform direct electrochemical reduction of TiO_2 to titanium in molten $CaCl_2$, which is the so-called FFC process. It was shown on laboratory scale that the reduction reaction occurs at 950°C on a cathode made of solid TiO_2, with oxygen anions oxidized on a graphite anode to give CO_2. Pure calcium chloride $CaCl_2$ was chosen as a molten salt electrode because of the high solubility of calcium oxide in this compound.

Ono and Suzuki [3] studied the high-temperature calcium reduction of TiO_2 and developed a process for continuous production of titanium. The electrolysis was performed at a voltage that was higher than the decomposition voltage of CaO, but lower than that of $CaCl_2$. Ca^{2+} ions were reduced at the cathode to Ca; oxygen evolved at the anode reacted with carbon to give CO and CO_2. A cell for continuous manufacture of titanium was developed and the possibility of using inert anode was discussed.

In [4], a TiO_2 powder or a preform was placed in a holder, and a Ca + 18 wt % Ni alloy, onto the electrolyzer bottom. The reduction was carried out without a current, with the electrochemical circuit formed between the TiO_2 cathode and the calcium alloy. In the process, TiO_2 was reduced and calcium ions were deposited at the anode. The alloy was replenished with calcium at regular intervals of time.

It seems that the FFC process is the best developed and ready for implementation [1, 2, 5, 6].

In view of the possible use of CaO as the main component in electrolytic reduction of TiO_2, it is necessary to substantiate the optimal CaO content and to analyze the oxidation kinetics of O^{2-} ions in relation to temperature and CaO concentration. It remains unclear whether TiO_2 is compatible with the $CaCl_2$–CaO melt.

The rich experience of the electrometallurgy of aluminum indicates that the main reason for a decrease in the current efficiency is the reverse reaction of the electrolysis products (aluminum and CO_2), which may lead to contamination of the metal by carbon via formation of carbides. This issue has not been studied for the materials under consideration. Possibly, it is necessary to choose a stable porous diaphragm for separating the cathode and anode spaces in electrolysis. The aim of this study was to elucidate these issues.

Table 1. Gibbs energy of formation of calcium and titanium oxides and chlorides

Substance	$-\Delta G^0$, cal mol^{-1}, at indicated T, K, according to indicated reference					
	[10]			[11]		
	1100	1200	1300	1100	1200	1300
CaO	124700	122400	119900	125348	122782	120218
$CaCl_2$	152800	150308	147700	153134	150416	147788
TiO	98900	96700	94500	109990	107824	105611
Ti_2O_3	290600	284350	278550	295847	289112	282433
Ti_3O_5	471050	460850	450500	–	–	–
TiO_2	178000	173890	169550	171410	167205	163011
$TiCl_2$	85100	81850	78650	–	–	–
$TiCl_3$	115600	110750	105900	–	–	–
$TiCl_4$	150050	147100	144150	141529	138763	136013

The previously published reports have virtually disregarded the mechanism, and presented no results of analysis, of the reaction between TiO_2 of varied origin with $CaCl_2$–CaO melts of various compositions. At the same time, the possible formation of $TiOCl_2$, $CaO \cdot TiO_2$, and $2CaO \cdot TiO_2$ can strongly affect the parameters and results of the electrolysis.

The solubility of TiO_2 in molten $CaCl_2$ is low, and that of metallic titanium reaches 0.5 wt % at 850°C [7].

The authors of [8] attributed the high residual currents in cathodic deoxidation of titanium in molten calcium chloride to the noticeable solubility of lower titanium oxides in $CaCl_2$.

It has been suggested [9], in an analysis of voltammetric data for oxidized titanium in a molten calcium chloride, that fast oxidation of oxygen ions from the oxide phase causes supersaturation of the $CaCl_2$ melt in CaO, which can react with partly reduced titanium oxide to give titanates of variable composition. The suggestions made in the studies mentioned above have not been directly confirmed.

To elucidate these issues, we made a thermodynamic assessment of the possibility of occurrence of various reactions in the system TiO_2–CaO–$CaCl_2$ and carried out chemical and X-ray phase analyses of the reaction products.

Table 1 lists the standard Gibbs energy of formation of calcium and titanium oxides and chlorides at 1100, 1200, and 1300 K according to [10, 11].

The values recommended by the authors are in reasonable agreement. To determine whether a reaction between titanium oxides and molten $CaCl_2$ is possible, we calculated, using the data in Table 1, the Gibbs energy of the corresponding reactions, ΔG^0_r. The results of these calculations for the temperatures of 1100, 1200, and 1300 K are listed in Table 2.

According to two references, the calculated results virtually coincide. The high positive values of ΔG^0_r indicate that there is no interaction in the systems under standard conditions. Judging from the decreasing value of ΔG^0_r, calculated per gram-atom of titanium, the probability of a reaction with the $CaCl_2$ melt increases in the order TiO_2, Ti_3O_5, Ti_2O_3, and TiO, in qualitative agreement with the suggestions made in [8].

In the system under consideration, perovskite $CaTiO_3$ can be formed in accordance with the equation

$$3TiO_2 + 2CaCl_2 = 2CaTiO_3 + TiCl_4. \quad (1)$$

Table 3 list thermodynamic parameters of the substances involved in reaction (1), according to the reference book [12].

The enthalpy of reaction (1) can be found using the equation

$$\Delta H^0_{r,298} = 2\Delta H^0_{CaTiO_3,298} + \Delta H^0_{TiCl_4,298} - 3\Delta H^0_{TiO_2,298} - 2\Delta H^0_{CaCl_2,298} = 2 \times 1661.7 - 805.96 + 3 \times 944 + 2 \times 797.17 = 297 \text{ kJ mol}^{-1}. \quad (2)$$

The value of ΔH^0_r at a temperature T is given by

$$\Delta H^0_T = \Delta H^0_{298} + \int_{298}^{T} \Delta C_p \, dT, \quad (3)$$

Table 2. Gibbs energy of reactions of titanium oxides with $CaCl_2$

Reaction	$-\Delta G_r^0$, cal mol^{-1} (cal at.$^{-1}$ Ti), at indicated T, K, according to indicated reference					
	[10]			[11]		
	1100	1200	1300	1100	1200	1300
$TiO_2 + 2CaCl_2 = 2CaO + TiCl_4$ (I)	84 150 (84 150)	82 600 (82 606)	81 000 (81 000)	85 453 (85 453)	83 710 (83 710)	82 138 (82 138)
$Ti_3O_5 + 5CaCl_2 = 5CaO + 2TiCl_4 + TiCl_2$ (II)	226 350 (73450)	224 340 (74780)	222 550 (74183)	–	–	–
$Ti_2O_3 + 3CaCl_2 = 3CaO + TiCl_4 + TiCl_2$ (III)	139 750 (69 879)	139 124 (69 562)	139 150 (69 575)	–	–	–
$Ti_2O_3 + 3CaCl_2 = 3CaO + 2TiCl_3$ (IV)	143 700 (71 850)	146 574 (73 287)	150 150 (75 075)	–	–	–
$TiO + CaCl_2 = CaO + TiCl_2$ (V)	41 900 (41 900)	42 758 (42 758)	43 650 (43 650)	–	–	–

Table 3. Thermodynamic parameters of substances involved in reaction (1)

Substance	$-\Delta H_{298}^0$, kJ mol^{-1}	S_{298}^0, J mol^{-1} K^{-1}	$C_p = a + b \times 10^{-3}T + c \times 10^5 T^{-2}$, J mol^{-1} K^{-1}		
			a	b	c
TiO_2	944.0	50.28	75.24	1.17	–18.21
$CaCl_2$	799.17	113.9	71.93	12.73	–2.51
$CaTiO_3$	1661.7	93.8	127.57	5.68	–28.01
$TiCl_4$	805.96	252.9	106.55	1.0	–9.88

where ΔC_p is the difference between the heat capaciteiss of the reaction products and starting substances, taken with their stoichiometric coefficients,

$$\Delta C_p = -7.89 - 16.61 \times 10^{-3}T - 6.25 \times 10^5 T^{-2}. \quad (4)$$

Integrating this equation, we obtain

$$\int_0^T \Delta C_p dT = -7.89T - 8.305 \times 10^{-3}T^2 + 6.25 \times 10^5 T^{-1}. \quad (5)$$

For 298, 100, 1100, and 1200 K, the values of the integral are –991, –15 570, –18 160, and –20 906 J mol^{-1}, respectively. The differences at 1000, 1100, and 1200 K are –14 580, –17 169, and –19 915 J mol^{-1}, respectively. Substituting these values and the enthalpy given by (2) into Eq. (3), we obtain $\Delta H_{1000}^0 = -282.42$, $\Delta H_{1100}^0 = -279.83$, and $\Delta H_{1200}^0 = -277.09$ kJ mol^{-1}.

We calculate the entropy of reaction (1) at 298 K by the equation

$$\Delta S_{298}^0 = 2S_{CaTiO_3,298}^0 + S_{TiCl_4,298}^0 - 3S_{TiO_2,298}^0 - S_{CaCl_2,298}^0$$
$$= 2 \times 93.8 + 252.9 - 3 \times 50.28 - 2 \times 113.9$$
$$= 61.86 \text{ J mol}^{-1} \text{ K}^{-1} \quad (6)$$

We find ΔS_T^0 as

$$\Delta S_T^0 = \Delta S_{298}^0 + \int_{298}^T (\Delta C_p/T) dT. \quad (7)$$

Taking into account Eq. (4), we can write

$$\int_0^T (\Delta C_p/T) dT = -7.89 \ln T - 16.61 \times 10^{-3}T + 3.125 \times 10^5 T^{-2}.$$

For 298, 1000, 1200, and 1300 K, we obtain –46.38, –70.80, –73.26, and –75.63 J mol^{-1} K^{-1}.

The differences of the integral at a temperature T and at 298 K give values of the integral $\int_{298}^T (\Delta C_p/T) dT$ at T(K), equal to –24.42, –26.88, and –29.25 J mol^{-1} K^{-1} for 1000, 1100, and 1200 K,

respectively. Substituting these values and the entropy given by (6) into Eq. (7), we obtain ΔS_T^0 equal to 37.44, 34.98, and 32.61 J mol^{-1} K^{-1} at 1000, 1100, and 1200 K, respectively.

We find the Gibbs energy of reaction (1) using the equation

$$\Delta G_T^0 = \Delta H_T^0 - T\Delta S_T^0. \quad (8)$$

At 1000, 1100, and 1200 K, the values of ΔG_T^0 are, respectively, 244 980, 241 352, and 237 958 J mol^{-1}, or 58 552, 57 689, and 56 873 cal mol^{-1}. It can be seen that these values are markedly (by a factor of nearly 2) lower than the respective values for reaction (I) in Table 2.

All the calculations were made for the standard conditions (component activities equal to unity, vapor pressure of 1 atm). The real activities and component concentrations, especially those of products of reaction (1), markedly differ from unity. According to experimental estimates, the concentrations of CaO and $TiCl_4$ in the final melt are lower than 0.01 mol %. Taking into account that the solubility limit of CaO in $CaCl_2$ at the temperature under consideration is close to 20 mol %, we can estimate the shift of ΔG_{CaO} to negative values by the equation

$$\Delta G_{CaO} = RT\ln(0.01/20) = 8.314T(-7.60) = -63.187T. \quad (9)$$

For 1000, 1100, and 1200 K, ΔG_T is –63 187, –69 513, and –75 833 J mol^{-1}, respectively.

The shift of ΔG_{TiCl_4} to negative values was estimated using the equation

$$\Delta G_{TiCl_4} = RT\ln(0.01/20) = 8.314T(-9.21) = -76.57T. \quad (10)$$

For 1000, 1100, and 1200 K, ΔG_{TiCl_4} is –76 570, –84 229, and –91 886 J mol^{-1}, respectively. The shift of the Gibbs energy of reaction (1) for 1000, 1100, and 1200 K is –202 944, –223 555, and –243 550 J mol^{-1}, respectively.

It can be seen that the values obtained become equal to, and even exceed in magnitude the positive standard values of ΔG_r^0, which indicates that, in principle, reaction (1) is possible.

For reaction (I) in Table 2, ΔG_r^0 is 352 084, 345 624, and 338 904 J mol^{-1} at 1100, 1200, and 1300 K, respectively, and the negative shift of the Gibbs energy, calculated by the equation

$$\Delta G_r = 2\Delta G_{CaO} + \Delta G_{TiCl_4}, \quad (11)$$

is obviously insufficient for compensating the positive values of ΔG_r^0. This means that this reaction is thermodynamically impossible.

Unfortunately, we could not find in reference literature any evidence about thermodynamic properties of the compound $TiOCl_2$. However, at temperatures above 300°C it can decompose to give TiO_2 and $TiCl_4$, and, with account of this circumstance, a thermodynamic analysis of reactions that involve this compound is similar to that of reactions involving $TiCl_4$.

EXPERIMENTAL

The aim of our experimental study was to examine the reaction of titanium dioxide TiO_2 with calcium chloride to elucidate the process mechanism and identify the products formed. We used as starting substances titanium dioxide and calcium chloride of chemically pure grade, subjected to preliminary dehydration.

Being an element of the secondary subgroup of Group IV, titanium is the most stable in the tetravalent state. All soluble compounds of Ti^{4+} are easily hydrolyzed, to TiO_2 upon complete hydrolysis, and to $TiOCl_2$ upon incomplete hydrolysis. According to Bol'shakov's data [13], $TiOCl_2$ decomposes at 300°C, whereas in an oxidizing atmosphere (O_2, H_2O) it can be formed at higher temperatures. Zelikman reported [14] that $TiOCl_2$ soluble in the chlorinator melt can be formed as an intermediate product of TiO_2 chlorination.

Titanium tends to form with alkali (M) and alkaline-earth metals (Me) titanates of the types M_2TiO_3, $M_2Ti_2O_5$, $MeTiO_3$, Me_2TiO_4, and Me_3TiO_5, which can be readily obtained by fusion of TiO_2 with carbonates of the respective metals. These properties of titanium suggest that the interaction of TiO_2 with $CaCl_2$ at temperatures above 800°C may involve reactions (I) (Table 2), (1), and

$$CaCl_2 + 2TiO_2 = CaTiO_3 + TiOCl_2. \quad (12)$$

Experiments were carried out in an electrically heated furnace, with the temperature controlled to within ±5°C. Portions of $CaCl_2$ and TiO_2, weighed with an accuracy as good as 1 mg, were placed in a beryllium oxide crucible and heated to 800°C, at which $CaCl_2$ was in the liquid state. The overheating of the melt over the melting point of $CaCl_2$ was 50°C. Preliminary experiments at a TiO_2 content of the stock equal to 25–30% demonstrated that the melting

Table 4. Conditions and results of interaction in the $CaCl_2–TiO_2$ system

Run no.	Initial weight, g (%)			Gain in TiO_2 weight, g	Weight and content of $TiOCl_2$ in the electrolyte, counting on TiO_2		Completeness of reaction (12) in terms of TiO_2, %
	$CaCl_2$	TiO_2	CaO		g	%	
1	18.731	3.268 (14.9)	–	0.156	0.224	1.30	13.3
2	14.582	2.610 (15.2)	–	0.198	0.285	1.93	21.6
3	14.008	1.920 (11.8)	0.283	0.147	0.211	1.70	22.0

of the components is accompanied by a substantial increase in the viscosity of the melt. This fact suggests a chemical reaction between the components to give low-mobile complex groups. Further, the content of TiO_2 in the stock was lowered to 12–15%. A melt of this composition had relatively low viscosity at 820°C.

The time of contact between $CaCl_2$ and TiO_2 after the melting was 1.5 h, after which the crucible was cooled, together with the melt, to room temperature and weighed. To evaluate the reaction completeness, the fusion cake was dissolved in water. The precipitate was filtered off on an ash-free paper filter. After washing, the precipitate was dried at 100–120°C, calcined to complete burning-out of the filter at 700°C, and weighed. The calcium chloride solution was analyzed for the presence of CaO and titanium ions.

Titanium was determined in the filtrate by photocolorimetry with diantipyrylmethane, which forms with titanium ions a soluble yellow compound with the light absorption maximum at 380 nm. Variation of acidity in the range 0.5–4 N HCl has no effect on the optical density of solutions. The detection limit of titanium is 0.01 $\mu g\ ml^{-1}$, and its molar extinction coefficient, 1.80×10^4. The coloration develops in 45 min and is stable during several months. The optical density of the solutions is proportional to the titanium concentration in a wide range of concentrations.

Titanium ions were not found in any of the samples we analyzed. The solutions exhibited a weakly acidic reaction, which confirms the occurrence of hydrolysis.

The mass of the precipitate exceeded that of the starting portion of TiO_2, which indicates that it reacts with $CaCl_2$ to give water-insoluble chemical compounds. The gain in the precipitate weight in run no. 1 (Table 4) was 156 mg (4.8%). Judging from the ratio of the molecular weights, the increase in the precipitate weight is possibly due to the occurrence of a reaction to give $TiCl_4$ and reaction (12) to give $TiOCl_2$. Reaction (I) (Table 2) leads to a decrease in the precipitate weight, because CaO is soluble in water and $TiCl_4$ volatilizes.

To experimentally verify the possibility of titanium tetrachloride formation, we carried out additional experiments (Table 4, run no. 2) in a hermetically sealed cell with a $TiCl_4$ condensation unit (see figure).

A beryllium oxide crucible with the starting substances, $CaCl_2$ and TiO_2, was placed in a hermetic steel cell closed with a rubber plug. After preliminary evacuation at 300–500°C to remove traces of moisture, the stock was heated to 840°C and kept at this temperature for 2.5 h. The condensation unit was cooled with flowing water having a temperature of 15°C.

The $TiCl_4$ vapor pressure is 5.5 mm Hg at 10°C and 10 mm Hg at 20°C. These conditions allow efficient condensation of $TiCl_4$. The end tube of the condensation unit was dipped into water to catch $TiCl_4$ in the case of its breakthrough. In the process, a gel-

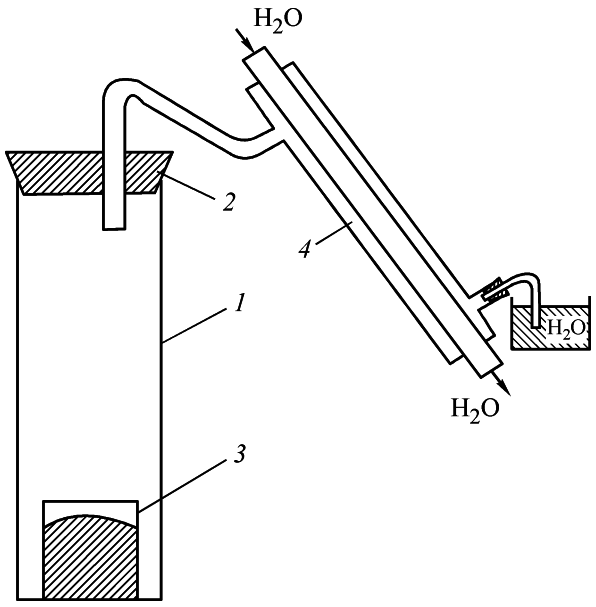

Schematic of the installation: (*1*) steel cell, (*2*) rubber plug, (*3*) crucible with a stock, and (*4*) vapor condenser.

like precipitate is to be formed. A visual monitoring of the cell demonstrated that $TiCl_4$ was not formed at all. This compound was found neither in the condensation unit, nor in the final aqueous solution. This indicates that reactions (1) and (I) (Table 2) do not occur. At the same time, the weight of the precipitate that was washed, filtered off, and calcined at 700°C increased by 0.198 g (7.6%). The increase in weight, compared with the first run, was 1.5 times larger. Calculation of the increase in the precipitate weight in terms of reaction (12) demonstrates that obtaining a weight gain equal to 0.198 g requires a TiO_2 expenditure of 0.287 g. The extent of reaction in terms of TiO_2 was 21.6%.

The increase in the precipitate weight is due to the formation of calcium titanate $CaTiO_3$, which can be yielded by two reactions, (1) and (12). Calculation in terms of reaction (1) shows that 1.134 g of TiO_2 should remain in the precipitate ($m^{in}_{TiO_2} - m^{react}_{TiO_2}$ = 2.61 – 1.476 = 1.134) and 1.674 g of $CaTiO_3$ and 1.169 g of $TiCl_4$ should be formed. In this case, the TiO_2 content of the precipitate will be 40.4% and that of $CaTiO_3$, 59.6%. An X-ray phase analysis of the precipitate demonstrated that the content of rutile (TiO_2) was 88.3%, and that of calcium titanate ($CaTiO_3$), 11.7%.[1] Such a significant discrepancy between the results obtained by the calculation of the composition of the precipitate and by its X-ray phase analysis, as well as the absence of a condensate, do not confirm the occurrence of reaction (1).

Calculation in terms of reaction (12) shows that 2.327 g of TiO_2 should remain in the precipitate and 0.481 g of $CaTiO_3$ should be formed. The content of TiO_2 will be 90.5%, and that of $CaTiO_3$, 9.5%. In this case, the calculated increase in the precipitate weight is very close to that furnished by X-ray phase analysis. This suggests that $CaCl_2$ interacts with TiO_2 by reaction (12) to give calcium titanate and titanium oxychloride, which dissolves in the molten salt.

In dissolution of the solidified fusion cake in water, $TiOCl_2$ is hydrolyzed by the reaction

$$TiOCl_2 + H_2O = TiO(OH)Cl + HCl \quad (13)$$

and precipitates. In calcination of the precipitate at 700–800°C, titanium oxychloride hydrate decomposes to TiO_2:

$$TiO(OH)Cl \rightarrow TiO_2 + HCl. \quad (14)$$

The results of run no. 3, performed at 860°C in the course of 3 h, show that a higher temperature and a longer keeping time favor more complete course of the reaction between $CaCl_2$ and TiO_2. The filtrate obtained on washing the precipitate was also analyzed for the content of free calcium oxide and titanium ions, and the calcined precipitate was weighed.

In run no. 3 (Table 4), we tested the effect of calcium oxide addition to the $CaCl_2$ melt on the reaction between TiO_2 and the salt melt. The content of CaO in the electrolyte was 2 wt % (about 4 mol %). The experiment was performed at a higher temperature (870°C), with stock keeping for 1 h. The increase in the weight of the precipitate after its washing to remove $CaCl_2$, filtration, and calcination was 0.147 g (7.7%), which virtually coincides in percentage with the results of run no. 2 (7.6%). This may indicate that the equilibrium state is attained by the system $CaCl_2$–TiO_2–$CaTiO_3$–$TiOCl_2$. The weight of $TiOCl_2$ in the electrolyte in run nos. 2 and 3 was, counting on TiO_2, 285 and 211 mg, respectively, and its content, about 1.9 and 1.7 wt %. The calculated extents of reaction between TiO_2 and $CaCl_2$ in run nos. 2 and 3 are virtually the same (21.6–22.0%).

To determine the content of CaO, the filtrate from run nos. 1–3, exhibiting an alkaline reaction, was titrated with solutions of hydrochloric and nitric acids in the presence of an indicator. The results of analysis of run nos. 1 and 2 point to the complete absence of free CaO in the filtrate. Consequently, the whole amount of calcium oxide formed in the reaction of $CaCl_2$ and TiO_2 passes into the precipitate as calcium titanates as a result of its reaction with excess titanium dioxide [reaction (12)]. In run no. 3, we found in solution 15 mg of CaO, which constituted 5.3% of the amount we charged. The incomplete conversion of calcium oxide to perovskite is presumably due to kinetic limitations.

CONCLUSIONS

(1) Thermodynamic calculations demonstrated that, in principle, titanium dioxide can react with a $CaCl_2$ melt to give perovskite $CaTiO_3$ and $TiCl_4$ or $TiOCl_2$.

(2) Experiments were performed to analyze the reaction of TiO_2 with molten $CaCl_2$ and $CaCl_2$–CaO at 820–870°C. The increase in the weight of the filtered-off and calcined precipitate and its quantitative X-ray phase analysis confirm that there occur reactions of TiO_2 with molten $CaCl_2$ to give perovskite. The extent of the reaction increases with temperature, keeping time, and CaO content of the starting melt.

[1] The X-ray phase analysis was made at the Institute of Solids, Ural Division, Russian Academy of Sciences.

The most probable pathway of the reaction of TiO_2 with the $CaCl_2$ melt is that described by Eq. (12).

(3) The binding of TiO_2 into calcium titanates markedly complicates the electrolytic production of titanium from oxide raw materials. This is so because the activity of TiO_2 in the titanates is substantially lower and it is difficult for CaO to pass from TiO_2 pellets into the $CaCl_2$ melt.

REFERENCES

1. Chen, G.Z. and Fray, D.J., *Progress in Molten Salt Chemistry 1: Prof. N.J. Bjerrum Special Volume*, Berg, R.W. and Hjuler, H.A., Eds., Elsevier, 2000, pp. 157–161.
2. Chen, G.Z., Fray, D.J., and Farthing, T.W., *Nature*, 2000, September, vol. 407, pp. 361–364.
3. Ono, K. and Suzuki, R.O., *J. Met*., 2002, February, pp. 59–61.
4. Abiko, T., Park, I., and Okabe, T.H., Abstracts of Papers, *10th World Conf. on Titanium*, Hamburg (Germany), July 15, 2003.
5. Stresov, L., Ratchev, I., et al., Patent WO 03/016 594 A1, February 27, 2003.
6. JPN Patent Appl. 2005-194 554 (P2005-194 554A).
7. Sibert, M.E., McKenna, Q.H., Steinberg, M.A., and Wainer, E., *J. Electrochem. Soc*., 1955, vol. 102, pp. 252–260.
8. Chen, G.Z., Fray, D.J., and Farthing, T.W., *Metall. Mater. Trans*., 2001, vol. 32B, pp. 1041–1051.
9. Chen, G.Z. and Fray, D.J., *J. Electrochem. Soc*., 2002, vol. 149, no. 11, pp. 455–467.
10. Wicks, C.E., and Block, F.E., *Thermodynamic Properties of 65 Elements, Their Oxides, Halides, Carbides, and Nitrides*, Washington: US Government, 1963.
11. Kubashevski, O. and Evans, E.L., *Metallurgical Thermochemistry*, London, 1951.
12. *Termodinamicheskie svoistva neorganicheskikh veshchestv: Spravochnik* (Thermodynamic Properties of Inorganic Substances: Reference Book), Zefirov, A.P., Ed., Moscow: Atomizdat, 1965, pp. 86, 118, 132.
13. *Khimiya i tekhnologiya redkikh i rasseyannykh elementov* (Chemistry and Technology of Rare and Trace Elements), Bol'shakov, K.A., Ed., Moscow: Vysshaya shkola, 1976, part 2.
14. Zelikman, A.N., *Metallurgiya tugoplavkikh redkikh metallov* (Metallurgy of Rare Refractory Metals), Moscow: Metallurgiya, 1986.

ISSN 1070-4272, Russian Journal of Applied Chemistry, 2007, Vol. 80, No. 9, pp. 1498–1502. © Pleiades Publishing, Ltd., 2007.
Original Russian Text © V.A. Lebedev, V.I. Sal'nikov, M.V. Tarabaev, I.A. Sizikov, D.A. Rymkevich, 2007, published in Zhurnal Prikladnoi Khimii, 2007, Vol. 80, No. 9, pp. 1462–1466.

APPLIED ELECTROCHEMISTRY AND CORROSION PROTECTION OF METALS

Kinetics and Mechanism of the Processes Occurring at Graphite Anode in a CaO–$CaCl_2$ Melt

V. A. Lebedev, V. I. Sal'nikov, M. V. Tarabaev, I. A. Sizikov, and D. A. Rymkevich

Ural State Technical University, State Educational Institution for Higher Professional Education, Yekaterinburg, Russia

AVISMA Titanium and Magnesium Combine, Open Joint-Stock Company, Berezniki, Perm krai, Russia

Received October 16, 2006; in final form, February 2007

Abstract—The polarization of a graphite anode in a $CaCl_2$–CaO melt in the temperature range 790–870°C at CaO concentrations of 1–8 mol % and current densities of 10^{-2}–10 A cm^{-2} was studied. The temperature and concentration dependences of the limiting current spent for the oxidation of oxygen ions were determined.

DOI: 10.1134/S107042720709011X

The electrode processes occurring at graphite anodes in oxide–halide melts are not yet interpreted unambiguously [1]. Commonly, the mechanism of electrode processes is determined by a simplified method based on using the decomposition potentials of calcium chloride (3.31 V) and calcium oxide (2.70 V) at 1100 K [2] under standard conditions (activity of calcium chloride and calcium oxide is unity, pressure of gaseous Cl_2, CO_2, and CO is 1 atm) instead of real conditions of the processes.

An interesting method for the description of anode processes that occur at the graphite anode in an oxide–halide melt was suggested by Antipin and Khudyakov [3]. They studied the composition of anode gases and the potentials of the graphite anode in electrolysis of cryolite–alumina melts at different current densities. The dependences obtained had characteristic inflections, due to changes in the CO_2 to CO pressure ratio in the anode gases. This result is confirmed by good coincidence of the experimental gas composition vs. anode potential curve with the dependence calculated by the equation of the gas electrode potential

$$E = E_0 - \frac{RT}{2F}\ln(P_{CO_2}/P_{CO}), \quad (1)$$

where R, T, and F have common meaning.

Equation (1) qualitatively describes the run of the whole polarization curves. In particular, the wave observed at the potentials more positive than 0.6 V may be explained by approximately constant composition of the anode gases (85% CO_2), which was found experimentally for the current densities higher than 0.32 A cm^{-2}.

However, Eq. (1) is, strictly speaking, approximate. Indeed, in accordance with the Nernst equation for the equilibrium potentials of the CO_2/C(graphite) and CO/C(graphite) systems, we can write

$$E_{CO_2/C} = E^0_{CO_2/C} + \frac{RT}{2F}\ln[(P_{CO_2})^{1/2}/(a_C)^{1/2}], \quad (2)$$

$$E_{CO/C} = E^0_{CO/C} + \frac{RT}{2F}\ln(P_{CO}/a_C), \quad (3)$$

where $E^0_{CO_2/C}$ and $E^0_{CO/C}$ are the standard potentials of the corresponding systems; P_{CO_2} and P_{CO} are partial pressures of CO_2 and CO, respectively; a_C is the graphite activity.

The shift ΔE of the anode potential to negative values with increasing CO_2 pressure in the gas phase may be presented by the difference in equilibrium potentials (2) and (3), by assuming that graphite activity is constant and equal to unity:

$$\Delta E = (E^0_{CO_2/C} - E^0_{CO/C}) + \frac{RT}{2F}\ln[(P_{CO_2})^{1/2}/P_{CO}]. \quad (4)$$

If a mixture of CO_2 and Cl_2 is evolved on the graphite electrode, then for the equilibrium potential

of the Cl_2/Cl^- system we can write

$$E_{Cl_2/Cl^-} = E^0_{Cl_2/Cl^-} + \frac{RT}{2F}\ln(P_{Cl_2}/a^2_{Cl^-}). \quad (5)$$

In this case, the shift of the anode potential will be determined by the difference between equilibrium potentials (5) and (2) and, on the assumption that the activity of chloride ions in the melts studied is close to unity, can be presented by the equation

$$\Delta E = (E^0_{Cl_2/Cl^-} - E^0_{CO_2/C}) + \frac{RT}{2F}\ln[P_{Cl_2}/(P_{CO_2})^{1/2}]. \quad (6)$$

Figure 1 demonstrates how the second terms in Eqs. (4) and (6), i.e., the ratio of CO_2, CO, CO_2, and Cl_2 partial pressures in the anode gases, affect ΔE. It is seen that the contributions to ΔE made by the CO_2/CO and Cl_2/CO_2 ratios are appreciably different. The characteristic change in the sign of the second derivative takes, however, place at equal partial pressures of the components, to which corresponds the potential ΔE^*. The shift of the anode potential from ΔE^* allows, using the curves presented in Fig. 1, quantitative interpretation of the electrode processes occurring at the graphite anode in oxide–halide melts.

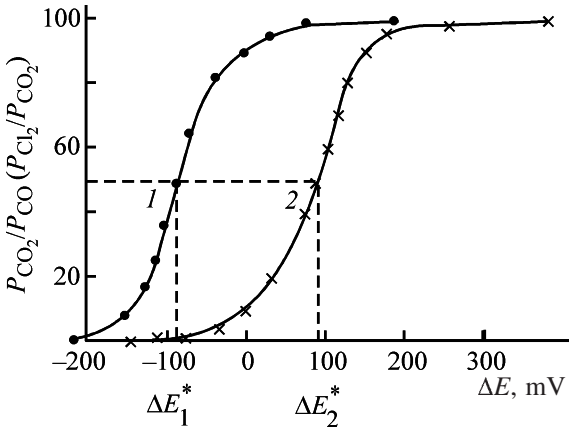

Fig. 1. Influence of partial pressure ratio of (*1*) P_{CO_2}/P_{CO} and (*2*) P_{Cl_2}/P_{CO_2} on the shift of the anode potential ΔE at 820°C.

EXPERIMENTAL

As electrolytic cell (Fig. 2) we used a metallic container closed from the top with a rubber stopper. Holes made in the stopper serve to evacuate air and feed argon and additional portions of CaO, with the latter fed through a quartz pipe. The electrolyte ($CaCl_2 + CaO$) was loaded in an alundum crucible. As anode we used graphite rod inserted into an alundum tube. A part of the graphite rod projecting outward had a constant surface area of 0.2 cm^2. As cathode served metallic lead on the bottom of the crucible. A lead electrode, $Pb/PbCl_2$ (5 wt %) + KCl–NaCl, in the form of an alundum pipe filled with a melt of salts and lead was a reference. Current was fed to the cathode and reference electrode through a molybdenum wire, and to the anode, through a steel wire threaded at the end to ensure contact with the graphite rod.

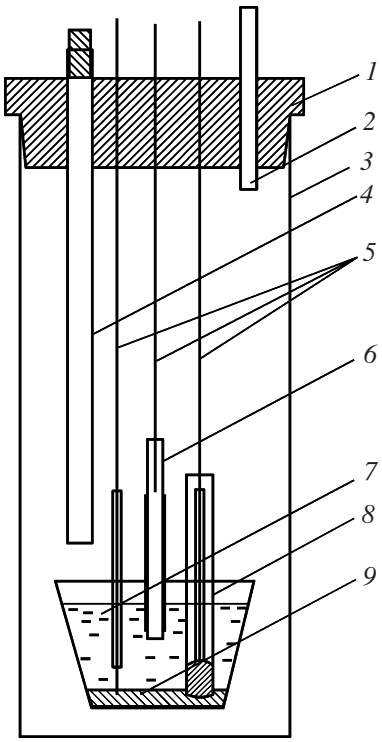

Fig. 2. Electrochemical cell: (*1*) rubber stopper, (*2*) tube for evacuating air and feeding argon, (*3*) metallic container, (*4*) tube for loading CaO, (*5*) current tips, (*6*) graphite anode, (*7*) electrolyte, (*8*) lead reference electrode, and (*9*) lead cathode.

The lead electrode was chosen because of the stability of its potential. At a lead chloride concentration in the electrolyte of 0.76 mol %, its potential relative to a chlorine reference electrode [3] can be calculated by the equation

$$E = 1.737 - 3.1 \times 10^{-4} T.$$

The required current strength was set by stabilized B5-49 power sources ensuring a preset current, irrespective of the electrochemical parameters of the cell. The current was measured with an M2015 ampere meter. The voltage applied to the electrochemical cell (between the anode and the cathode) and the anode potential relative to a lead electrode were meas-

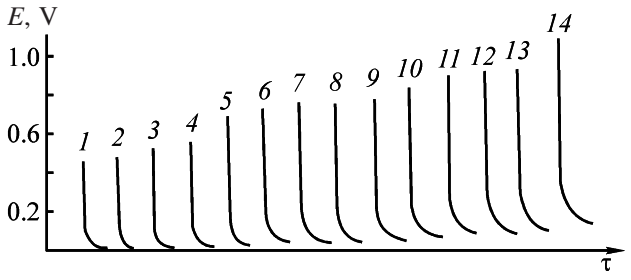

Fig. 3. Variations of the anode potential E with time τ in a $CaCl_2$ + 4.7 mol % CaO melt at 820°C after switching off polarizing current. Current density, A cm^{-2}: (*1*) 0.2, (*2*) 0.6, (*3*) 0.8, (*4*) 1.2, (*5*) 1.6, (*6*) 2.0, (*7*) 2.7, (*8*) 3.2, (*9*) 3.6, (*10*) 3.8, (*11*) 4.3, (*12*) 4.7, (*13*) 5.7, and (*14*) 7.3.

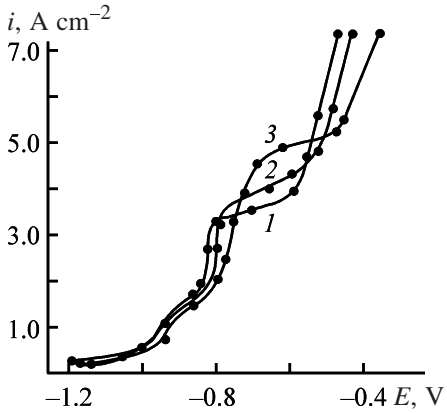

Fig. 4. Anodic polarization curves obtained on graphite in a $CaCl_2$+4.7 mol % CaO melt at different temperatures. (*i*) Current density and (*E*) potential vs. Cl_2/Cl^- reference electrode; the same for Fig. 5. Temperature, °C: (*1*) 790, (*2*) 820, and (*3*) 870.

ured with a digital voltmeter and recorded with a RECORDER two-coordinate recording potentiometer. The scheme of the electrical measuring installation made it possible to record the anode potential when the current is switched on and off. The heater was a shaft electrical furnace equipped with an electronic temperature controller. The temperature was maintained constant to within ±5° and measured with a Chromel–Alumel thermocouple.

The solubility of CaO in calcium chloride at 1173 K is 20 mol % [4]. The content of calcium oxide was varied within 1–8 mol %. The temperature range studied (790–870°C) was determined by the $CaCl_2$ melting point (772°C). The experiments were performed in dry argon.

The anode processes at the graphite electrode were studied by recording the polarization curves. The current density was raised stepwise from 0.03 to 3–6 A cm^{-2}. The anode potential relative to a lead electrode was measured, while switching off polarizing current, at each current density. The results obtained are presented in Fig. 3 as example. The values of the anode potential at the instant of switching off the current were used to construct the polarization curves.

The typical polarization curve has three characteristic portions at potentials of 0.47, 0.62, and 0.95 V relative to a lead reference electrode (Fig. 4, curve *2*). The potential of the lead reference electrode relative to a chlorine reference electrode at 820°C is –1.4 V [3]. Against the chlorine reference electrode, the potentials of these portions are –0.93, –0.78, and –0.45 V.

The characteristic waves in the polarization curves are due to several processes that proceed successively and simultaneously at the anode to form CO, CO_2, and Cl_2. In this case, the anode potential varies by more than 0.8 V.

The polarization curves were interpreted in terms of Eqs. (4), (6) for gas electrodes. Under the constant conditions of the electrolysis, the shift of the anode potential is determined solely by the ratio of the partial pressures of jointly evolving gases, and the calculated ΔE vs. $(P_{CO_2})^{1/2}/P_{CO}$ and ΔE vs. $P_{Cl_2}/(P_{CO_2})^{1/2}$ curves (Fig. 1) are suitable for quantitative interpretation of the results of the polarization measurements using the difference between the anode potential at a certain current density and ΔE^*.

CO is the major anode gas at low current densities. For example, at a current density of 0.1 A cm^{-2} the difference between E and ΔE^* is larger than –0.2 V, which corresponds to the relative concentration of CO in the anode gases of 98%. With increasing current density, the CO_2 concentration in the anode gases increases and at i_a = 0.9 A cm^{-2} becomes equal to the CO concentration. A further increase in the current density results in the growing shift of the anode potential toward positive values, which is due to predominance of CO_2 in the released gases. The stabilization of the anode potential at –0.75 V is associated with a nearly constant concentration of CO_2 (95%).

The limiting current i_{lim} for the oxidation of oxygen ions, at which the oxidation of chromium ions begins, is observed at a current density of 4.2 A cm^{-2}. Further run of the polarization curve is determined by change in the relative concentrations of Cl_2 and CO_2 in the anode gases, in accordance with Eq. (6).

The chlorine–oxygen molal ratio can be estimated by the equation

$$N_{Cl_2}/N_{O_2} = 2(i - i_{lim})/i_{lim},$$

where i and i_{lim} (A cm^{-2}) are the current density and the limiting current density for oxygen evolution, respectively.

At $2i_{lim}$, the chlorine to oxygen ratio is 2 and corresponds to the composition of phosgene $COCl_2$.

The potential shift at 1000 K ΔE_{1000} calculated from the Gibbs energy of formation of $COCl_2$ (–43 500 cal [2]) is –0.472 V, in good agreement with the potential of the last portion of the polarization curve.

Decreasing the temperature from 820 to 790°C shifts the anode potential to the negative region by approximately 10–15 mV, whereas increasing the temperature to 870°C shifts the anode potential to the positive region by 15–30 mV. With increasing temperature, the limiting current of oxygen evolution gradually increases, reaching 3.5, 4.2, and 5.2 A cm^{-2} at 790, 820, and 870°C, respectively (Fig. 4). The temperature dependence of i_{lim} is described by the equation

$$\log i_{lim} = 3.22 - 2860/T. \quad (7)$$

The extrapolation of i_{lim} to 960°C, a temperature of the electrolysis of a cryolite–alumina melt, yields a value of approximately 8 A cm^{-2} in the case of the electrolyte containing 4.7 mol % CaO. At the same content of Al_2O_3 in the cryolite–alumina melt, the limiting diffusion current spent for oxygen evolution at the carbon electrode is 4.5 A cm^{-2} [5]. This ratio of the limiting currents confirms the assumption that the degree of complex formation is lower in a $CaCl_2$–CaO melt than in a cryolite–alumina melt.

The anode polarization at other concentrations of CaO in the electrolyte was studied at 820°C (Fig. 5). It should be noted that the transition from the predominant evolution of CO to the predominant evolution of CO_2 is virtually temperature-independent and is mainly determined by the density of the polarizing current.

At a low concentration of CaO in the electrolyte (Fig. 5, curve *1*), the wave corresponding to the predominant evolution of carbon dioxide at a constant CO_2/CO ratio is not observed. Raising the CaO concentration in a calcium chloride melt increases the limiting currents of oxygen evolution.

The i_{lim} vs. CaO concentration curve (Fig. 6) is the linear dependence only up to CaO concentrations not exceeding 2 mol %:

$$i_{lim} = 1.43\, c_{CaO}.$$

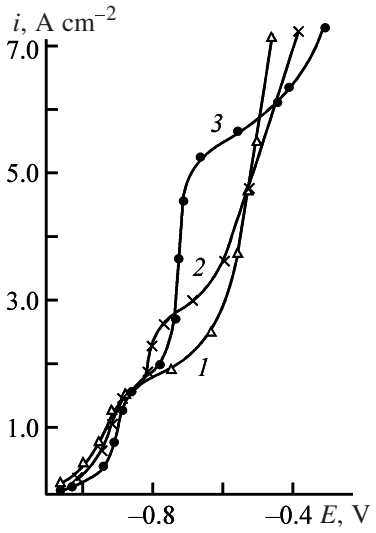

Fig. 5. Anodic polarization curves obtained on graphite at 820°C at various concentrations of CaO. CaO concentration, mol %: (*1*) 1.2, (*2*) 2.4, and (*3*) 8.4.

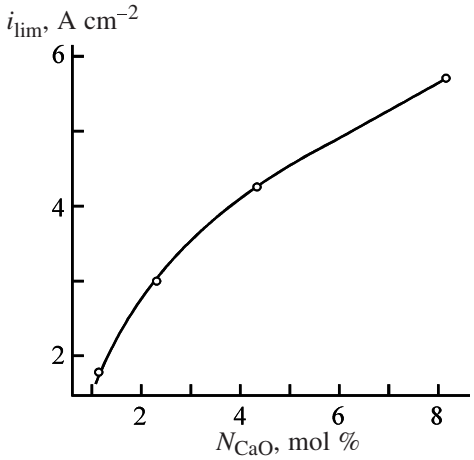

Fig. 6. Limiting current density i_{lim} of oxygen evolution at the graphite anode vs. CaO concentration N_{CaO} in the electrolyte.

The deviation of this dependence at larger CaO concentrations may be due to increase in the viscosity of a salt melt. In this case, adsorption equilibrium at the anode should also be taken into account [6].

The results of our study allow substantiated choice of the optimal concentration of CaO in the melt and of the optimal anode current densities.

CONCLUSIONS

(1) The results obtained in polarizing the graphite anode in a $CaCl_2$–CaO melt showed that the characteristic waves present in the polarization curves are

due to several processes that occur successively and simultaneously at the anode to form CO, CO_2, and Cl_2. The anode potential varies by more than 0.8 V. At high current densities, $COCl_2$, which decomposes in the electrolyte bulk, can also be a gaseous product.

(2) The temperature dependence of i_{lim} at a CaO concentration of 4.7 mol % is described by Eq. (7), whereas the dependence of i_{lim} on the CaO concentration is linear only to CaO concentrations not exceeding 2 mol %. At higher CaO concentrations, a deviation from this dependence is observed, which may be due to increased viscosity of the salt melt.

(3) The study performed allows substantiated choice of the optimal concentration of CaO in the melt and of the anode current densities.

REFERENCES

1. Abiko, T., Park, I., and Okabe, T.H., Abstracts of Papers, *The 10th World Conf. on Titanium*, Hamburg (Germany), July 15, 2003.
2. Wicks, C.E., and Block, F.E., *Thermodynamic Properties of 65 Elements, Their Oxides, Halides, Carbides, and Nitrides*, Washington: US Government, 1963.
3. Antipin, L.N., and Khudyakov, A.N., *Zh. Prikl. Khim.*, 1956, vol. 29, no. 6, pp. 908–914.
4. Ono, K., and Suzuki, R.O., *J. Met.*, 2002, February, pp. 59–61.
5. Baimakov, Yu.V., and Vetyukov, M.M., *Elektroliz rasplavlennykh solei* (Electrolysis of Molten Salts), Leningrad: Metallurgiya, 1966.
6. Ivanovskii, L.E., Lebedev, V.A., and Nekrasov, V.N., *Anodnye protsessy v rasplavlennykh galogenidakh* (Anode Processes in Molten Halides), Moscow: Nauka, 1983, pp. 58–72.

ISSN 1070-4272, Russian Journal of Applied Chemistry, 2007, Vol. 80, No. 9, pp. 1503–1508. © Pleiades Publishing, Ltd., 2007.
Original Russian Text © V.A. Lebedev, V.I. Sal'nikov, I.A. Sizikov, D.A. Rymkevich, 2007, published in Zhurnal Prikladnoi Khimii, 2007, Vol. 80, No. 9, pp. 1467–1472.

APPLIED ELECTROCHEMISTRY AND CORROSION PROTECTION OF METALS

Mechanism and Kinetics of Processes Occurring at TiO_2 Cathode in $CaCl_2$–CaO Melt

V. A. Lebedev, V. I. Sal'nikov, I. A. Sizikov, and D. A. Rymkevich

Ural State Technical University, State Educational Institution for Higher Professional Education, Yekaterinburg, Russia
AVISMA Titanium and Magnesium Combine, Open Joint-Stock Company, Berezniki, Perm krai, Russia

Received October 16, 2006; in final form, February 2007

Abstract—Preparation of titanium by the electrochemical reduction of titanium dioxide in a $CaCl_2$–CaO melt in a diaphragm electrolyzer using a graphite anode was studied.

DOI: 10.1134/S1070427207090121

Data on the kinetics and mechanism of the cathodic processes in electrochemical production of titanium from oxide raw materials within the framework of the FFC process [1] are limited:

$$TiO_x + 2xe = Ti + xO^{2-}. \quad (1)$$

The process kinetics is limited by electrical conductivity of the oxide phase [2]. As TiO_2 is reduced, the electrical conductivity of the oxide phase increases, which gives rise to an extremum in the current vs. time dependence.

Chen et al. [3] studied the mechanism of the cathodic deoxidation of oxidized titanium in molten $CaCl_2$ by cyclic voltammetry, with *IR* compensated by an external power source, along with pulsed ac measurements.

The potentials of various cathodic peaks observed in the *I–E* curves are given in Table 1 relative to a current peak potential of the reduction of Ca^{2+} ions to metallic calcium (c_1) [3].

The c_5 and c_6 peaks are due to the reduction of titanium dioxide to Ti_2O_3 and TiO; the c_3 peak, due to removal of dissolved oxygen from metallic titanium; and the c_2 peak, due to reduction to metallic titanium.

We used these data for interpreting the results of this study.

EXPERIMENTAL

Pigment-grade titanium dioxide with a micrometer grain size was used as the starting material for the electrochemical reduction. To fabricate electrodes, titanium dioxide was wetted in distilled water to paste and 1–2 cm^3 pellets were formed by pressing or modeling.

The pressing was performed with a mechanical screw press under a pressure of more than 1000 kg cm^{-2}. The pellets obtained were dried at 50–70°C in air and calcined at 800–850°C for 2–3 h, with the temperature raised at a rate of 300 deg h^{-1}. The mechanical strength of the calcined pellets was low. It was found that the strength of the pressed pellets is lower by an order of magnitude than that of the modeled pellets. After the calcination, the pressed pellets spontaneously separated into layers 2 mm and less thick in a direction transverse to application of the pressure, whereas the modeled pellets showed similar strength in all directions and therefore could be crushed mechanically to necessary pieces. The density of the titanium dioxide was 1.9–2.1 g cm^{-3} for pressed pellets and 1.7–1.9 g cm^{-3} for modeled pellets, and their porosity, evaluated from these values and the true density of TiO_2 (4.1–4.2 g cm^{-3}), was 49–54 and 54–59%, respectively.

An attempt to increase the mechanical strength of the pellets by impregnation with a saturated calcium

Table 1. Current peak potentials (V) elative to c_1 peak potential in the *I–E* curves

T, °C	c_3	c_6	c_5	c_2
800	0.15	0.53	0.90	1.6
900	0.20	0.50	0.954	1.5

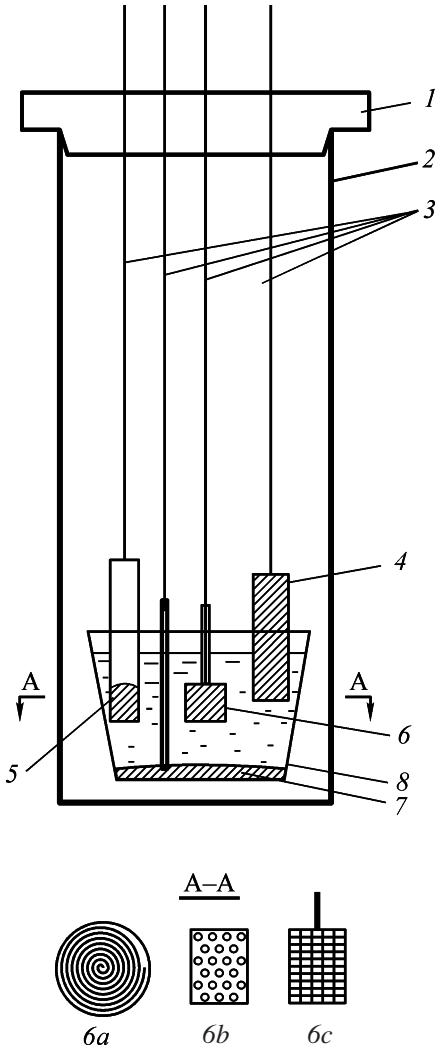

Fig. 1. Electrolytic reduction cell: (*1*) rubber stopper, (*2*) steel container, (*3*) current lead to electrodes, (*4*) graphite anode, (*5*) reference electrode (lead or titanium), (*6*) TiO_2 cathode (*6a*, coil; *6b*, perforated; *6c*, grid), (*7*) lead–calcium anode, and (*8*) alundum crucible.

chloride solution, followed by modeling or pressing and calcination, did not give positive results. The strength of the pellets decreased considerably. Therefore, the modeled pellets disintegrated to 2–5-mm pieces to avoid spontaneous breakdown were used for electrochemical reduction after the calcination.

Rutile was reduced in a cell (Fig. 1) at 840–960°C in argon. Melted calcium chloride was heated in a vacuum to 500°C to remove water. Current was fed to titanium oxide through a steel wire or perforated steel plate. In the first case, the wire was twisted in the form of a coil, with 0.5–1-mm separation between the turns (Fig. 1, section A–A). The upper part of the wire was enclosed in a ceramic straw to prevent deposition of calcium on it. The coil was placed in an alundum tube 1–1.5 cm in diameter. Onto the coil, a 1.5–2-cm layer of TiO_2 (2–3 g) was poured. In the second case, a layer of the wet paste 3–4 mm thick was deposited onto a perforated iron plate (area 2 cm^2) with the subsequent drying and calcination. A graphite rod served as anode. In some experiments, the same rod served as reference electrode for measuring the cathode potential after switching off the current. The current was set within 0.2–4.7 A with a stabilized power source. The voltage and potential were recorded with a RECORDER two-coordinate potentiometer. The amount of the passed electricity was varied within 60–300% of the theoretical value necessary for TiO_2 reduction.

First, the polarization measurements were performed with a polarizing current switched on for a short time (0.5–5 min), with raising its value from 0.2 to 4.7 A. The current density counting on the geometric surface area of the pellets was from 50 mA cm^{-2} to 2–3 A cm^{-2}. In the course of the main electrolysis, the cathode potential was recorded at the moments when the current was switched off for a short time and at the end of the experiment. After the experiment was complete, the electrodes were withdrawn from the electrolyte, transferred into the cold zone of the cell, and cooled to room temperature in argon. A visual examination of the crucible, electrolyte, and electrodes in the experiments with a carbon electrode revealed the formation of a finely divided carbon foam in an amount increasing with the amount of passed electricity, The amount of carbon foam in the electrolyte containing calcium oxide is the largest.

Presumably, calcium that has not reacted with TiO_2 dissolves in the electrolyte and reacts with gaseous carbon dioxide evolved on the anode to reduce it to amorphous carbon by the reaction

$$2Ca + CO_2 = 2CaO + C. \quad (2)$$

After the experiment was complete, the cathode was thoroughly washed to remove residual salts, dried, and classified with respect to the extent of darkening. It was noted that the parts of the cathode located directly on the iron current lead became dark from the surface and from the inside. The extent of darkening decreases with increasing distance from the current lead. When the excess amount of passed electricity is small, most of the cathode surface remains light, whereas when the excess is considerable (300–500%), virtually the whole bulk of the cathode becomes dark, which shows that the degree of TiO_2 reduction increases.

Table 2. Conditions and results of electrochemical reduction of TiO_2 with graphite anode

Run no.	Electrolyte	T, °C	TiO_2 weight, g	Q, A h (excess, %)	Fraction yield	
					dark	light
1	$CaCl_2$	860	3.2	7.1 (60)	30	70
2	$CaCl_2$+ 10 wt % CaO	880	3.06	10.6 (160)	80	20

The obtained fractions of the reduced product were ground in an agate mortar, their photographs at a magnification of 120 were taken, and X-ray phase analysis was done.[1] The results of the TiO_2 reduction with a graphite electrode are presented in Table 2.

All samples of the ground and reduced product had typical metallic luster and the structure of a titanium sponge (Fig. 2). The size of titanium grains was, however, small (several micrometers and less). In both experiments, the samples had light areas of unreduced rutile and formed perovskite; their amount was larger in the light fractions. An X-ray phase analysis (Table 3) revealed no titanium peaks but revealed peaks of unreduced phases (perovskite and rutile) in a ratio depending on the electrolysis conditions.

The perovskite content is higher at a large excess of the amount of passed electricity (run no. 2 compared to run no. 1). More complete conversion of unreduced rutile into perovskite is associated with the presence of the CaO additive in the electrolyte and with a larger amount of calcium oxide formed inside the cathode.

Finely dispersed metallic titanium was X-ray amorphous: only an increase in the total background intensity was observed in the X-ray diffraction patterns.

The electrolysis using calcium chloride occurred at a stable voltage at each polarizing current. After switching off the current, fast variation of the cathode potential relative to graphite anode was observed, without any phase transitions recorded. This is due to fast removal of chlorine on the anode in the reaction with dissolved calcium, making the anode potential unstable.

With 10 wt % CaO added, the mechanism of the anode process changed. The evolution of oxygen with the subsequent formation of CO and CO_2 were observed on the anode. At the moment of switching off the current, we recorded the reverse emf of the electrochemical cell relative to a graphite electrode, which regularly increased from 0.5 to 3.5 V as the current strength was increased from 1 to 4.7 A. The value of the reverse emf (3.5 V) confirms deposition of metallic calcium at the anode. Then, the cathode potential rapidly changed and stabilized at 1.4 V. The potential difference was 1.5–2.1 V and, according to the data of Table 1, the stabilization potential corresponded to metallic titanium. However, in this case also the anode as reference electrode is insufficiently reliable because of variations of its potential with time in the course of desorption of CO and CO_2 and their reaction with dissolved Ca and CaO.

The cell voltage in an electrolyte containing CaO was very unstable. This may be due to intense deposition of finely divided carbon, which was found after completing the experiment on the electrolyte surface under the anode and over the cathode.

Thus, the electrolysis in a diaphragmless cell using a graphite electrode involves a number of undesirable side processes: formation of $CaCO_3$ by reaction of CO and calcium oxide (Table 3, run no. 2); deposition of finely dispersed carbon leading to carbonization of the melt and formation of titanium carbide; oxidation of calcium dissolved in an electrolyte on the anode and by anode gases (Cl_2, CO_2), which considerably decreases the current efficiency.

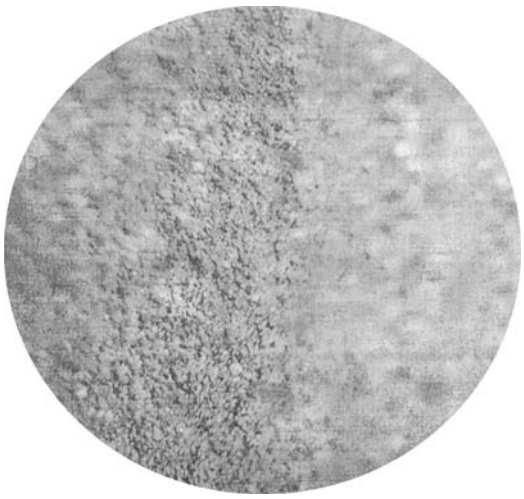

Fig. 2. Structure of the surface of finely divided reduction product (run no. 1). Magnification 120.

[1] X-ray phase analysis was performed at the Institute of Solid State Chemistry, Ural Division, Russian Academy of Sciences.

Table 3. Results of X-ray phase analysis of the TiO_2 reduction product

Run no. (sample no.)	Dark fraction, %		Light fraction, %		
	$CaTiO_3$	TiO_2	$CaTiO_3$	TiO_2	$CaCO_3$
1(1.4)	85	15	36.1	63.9	–
2(2.3)	100	–	79.2	–	20.8

Therefore, it was of interest to use a Pb–Ca melt containing 15–25 wt % Ca as anode and pure calcium chloride without calcium oxide additive as electrolyte. The study showed that the mechanism of the anode process principally changed. The dissolution of calcium from a lead alloy, instead of evolution of anode gases, occurred at the anode.

To make the TiO_2 reduction more complete, a smaller portion of TiO_2 (250–300 mg) was applied as paste to a perforated or grid cathode. As reference electrode (Table 4, run no. 3) we used a Pb–Ca alloy prepared directly in an electrochemical cell. To do this, calcium was deposited onto lead to 20 wt % content. In this case, the amount of calcium in lead was higher by an order of magnitude than that necessary for reduction of the TiO_2 portion and affected only slightly the composition of the Pb–Ca alloy in the course of the electrolysis. After the Pb–Ca alloy was formed, a graphite anode was withdrawn from the electrolyte, and evolved chlorine was evacuated. However, these precautions led only to a decreased amount of amorphous carbon. Therefore, in the further experiments a separate cell was used to form the Pb–Ca alloy, which made it possible to eliminate virtually completely the presence of carbon in the electrolyte upon electrochemical reduction of titanium dioxide. The conditions of the experiments are presented in Table 4.

The deposition potential of calcium (1.7 V) and two plateaus of the potential stabilization, at 0.8 and 0.34 V, were revealed by measuring the cathode potential relative to lead reference electrode after completing the electrolysis (run no. 4). The potential difference between the calcium deposition and the second plateau was 1.4 V, which, according to the data of Table 1, corresponds to metallic titanium. The first plateau with a potential difference of 0.9 V corresponds to formation of Ti_2O_3. One more plateau of the potential stabilization at 0.18 V, which corresponds to removal of dissolved oxygen from titanium, was found at short-time polarization of the cathode.

With titanium used as reference electrode (run no. 5), three plateaus of the potential stabilization were recorded after switching off polarization: 1.25 V is the potential of calcium deposition, and potentials pf 1.92 and 0.77 V correspond to c_3 and c_6 current peaks (Table 1). The potential of the TiO formation was not revealed.

The obtained products of the electrochemical reduction contained no light fraction and corresponded in the structure to dark fractions (run nos. 1, 2) with finely dispersed X-ray amorphous metallic titanium. Thus, the fineness of pigment-grade titanium dioxide predetermines the fineness of metallic titanium. Another factor is the formation of the intermediate oxide Ti_2O_3, which was revealed in the X-ray diffraction pattern.

When two-side metallic grid was used as current lead, a plate of precalcined titanium dioxide was placed inside the grid. The TiO_2 pellet was prepared by dry pressing with addition of 5% MgO to enhance its strength. The pressed pellet was dried at 50–80°C for 24 h and calcined for 5 h at 1050°C by raising the temperature at a rate of 300 deg h^{-1} to obtain coarser TiO_2 grains. The strength of the calcined pellet prepared by dry pressing was higher than that of the pellets modeled from a wet paste.

Calcium was deposited on the cathode at 920–930°C by raising the current density stepwise from 0.1 to 2.3 A cm^{-2}, using the Ca–Pb alloy as anode. The electricity was passed in 400% excess. A part of the electrochemical reduction product washed inside the metallic grid was in the form of grains whose size

Table 4. Conditions and results of electrochemical reduction of TiO_2 in $CaCl_2$ melt with Pb–Ca anode

Run no.	T, °C	TiO_2 weight, g	Current excess, %	Reference electrode	Graphite	Current lead to cathode	E,* V
3	880	300	200	Pb–Ca	Present	Perforated	2.0; 0.7; 0.4
4	910	250	200	Pb	Absent	Perforated	1.7; 0.8; 0.34
5	960	250	300	Ti	Absent	Grid	1.25; 1.02; 0.77

* Potential of the stabilization plateaus.

exceeded the size of the ground particles obtained in the previous experiments, and the remaining part was in the form of small metal-coated plates about 0.5 mm thick.

As seen from Fig. 3, the reduction product has a pronounced metal structure; grains are partially sintered and their size is substantially increased. By visual observation, most of the product is metallic titanium. However, despite large current excess, inclusions of incompletely reduced forms remained in the metal bulk.

The separation of the anode and cathode spaces with a ceramic diaphragm was necessary not only to make purity of the product higher but also to increase the current efficiency of the electrolysis. In a diaphragmless electrolyzer, most of the current is spent to compensate losses due to back reaction of the electrolysis products. The calcium evolving at the cathode can interact with the chloride and dissolve in it. The calcium solubility at 900°C is about 4 mol %. The dissolved calcium reacts with the anode products (gaseous chlorine or carbon dioxide) and transforms back into calcium chloride and oxide, or is anodically oxidized with the formation of bivalent ions. The occurrence of the side processes of calcium oxidation, first, results in the considerable overexpenditure of the electrical power for the electrochemical reduction of titanium from titanium oxide and, second, leads to a decrease in the efficiency or in the degree of titanium reduction owing to cathode depolarization. In the majority of the experiments performed, the cathode potential at the moment of switching off the current was lower than the deposition potential of metallic calcium, which, according to the results of X-ray phase analysis, mainly resulted in the reduction of titanium to intermediate products.

To decrease the influence of the side processes impeding deposition of metallic calcium on the cathode, the experiments were performed in an electrolyzer with its cathode and anode spaces separated by a diaphragm. As diaphragm we used porous magnesium oxide ceramics containing yttrium and cerium oxides as binders (60% porosity). The ceramics was produced at the Siberian Chemical Combine. The design of the cathode and anode compartments of the electrolyzer is shown in Fig. 4. Wet titanium dioxide for fabricating the cathode was modeled in a pellet 7–10 mm diameter and 1.5–2 cm high (mass 2.5–3 g) inside an alundum tube and was calcined at 950–1000°C to obtain coarser grains. After the calcination, a 1.5–2-mm hole was drilled in the center of the tube, into which a current lead made of iron wire and

Fig. 3. Structure of the surface of finely divided reduction product (run no. 5). Magnification 300.

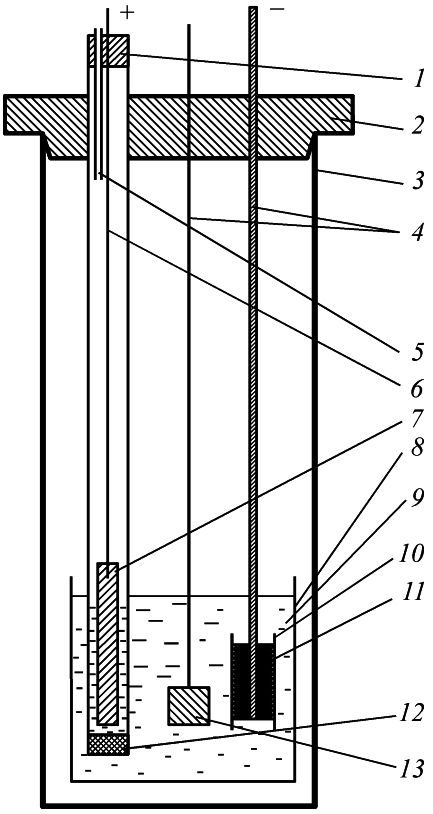

Fig. 4. Design of a diaphragm electrolyzer: (*1, 2*) rubber stoppers; (*3*) steel retort, (*4, 6*) current leads, (*5*) outlet of anode gases, (*7*) graphite anode, (*8*) alundum crucible, (*9*) electrolyte, (*10*) alundum tube, (*11*) rutile pellet, (*12*) diaphragm, and (*13*) titanium reference electrode.

covered with an alundum jacket to avoid contact with a salt melt was inserted.

A graphite rod inside a quartz tube was the anode. A ceramic diaphragm glued into the lower part of the tube impeded passage of dissolved anode gases into the catholyte and of dissolved calcium into the anolyte. A hole in the rubber stopper closing the cell allowed the upper part of the tube to be in contact with the atmosphere, which ensured outlet of the anode gases from the anode space and made their interaction with the catholyte minimal.

The electrolysis was performed in argon over the catholyte at 910–930°C in a calcium chloride melt with and without calcium oxide added. In this case, chlorine or carbon oxides were the anode products. The electrolyzer voltage, current, and the cathode potential relative to titanium reference electrode were recorded in the course of the experiments.

When the electrolysis was performed at low current densities (0.2–0.3 A cm^{-2}), the cathode potential did not reach the deposition potential of calcium, and TiO_2 was reduced with the formation of $CaTi_2O_4$ as major product. In contrast to the diaphragmless electrolysis, the reduction product contained no initial rutile phase. The pressed product showed small electrical conductivity, confirming the occurrence of reduction.

With the current density increased to 1.2 A cm^{-2}, the cathode potential increased to approximately 3.7–3.8 V in the chlorine scale, which corresponds to the deposition potential of metallic calcium. The amount of passed electricity was 450% of theoretical value to ensure higher degree of reduction of complex titanium oxides.

As previously, the washed powdered product was dark gray. As compared to the previous experiment, the amount of metallic fraction increased considerably. The powder did not conduct electrical current in the loose state but exhibited high electrical conductivity in the pressed state. The powder had pronounced pyrophoric properties. It was highly inflammable, which also confirms the presence of a finely divided metallic phase in it.

The reduction of rutile in a diaphragm electrolyzer made it possible to considerably increase the degree of reduction, with the same energy expenditure, and to shift the composition of the product toward formation of metallic titanium.

CONCLUSIONS

(1) The preparation of titanium by the electrochemical reduction of titanium dioxide in a $CaCl_2$–CaO melt using graphite anode is complicated by formation of CO_2 on the anode. CO_2 and CaO, present or formed by the electrolysis, react in the salt melt to give $CaCO_3$, and then the CO_3^{2-} ions are reduced to amorphous carbon with calcium dissolved in the electrolyte. This inevitably results in carbonization of the electrolyte and leads to the formation of titanium carbide. It seems impossible to produce quality metal under these conditions.

(2) Titanium dioxide pellets should be precalcined at 1050–1100°C, which allows considerable coarsening of the grains of the cathodic titanium deposit obtained.

(3) The possibility of the electrochemical reduction of titanium dioxide in a diaphragm electrolyzer was demonstrated. The obtained metallized product has a low concentration of oxygen and a high electrical conductivity and is pyrophoric. The electrolysis efficiency can be increased further by using the bulk reduction of finely divided titanium dioxide and further improving the reductive characteristics of the cathode process by raising its electronegative potential.

REFERENCES

1. Chen, G.Z., Fray, D.J., and Farthing, T.W., *Nature*, 2000, vol. 407, pp. 361–364.
2. Chen, G.Z., and Fray, D.J., *Progress in Molten Salt Chemistry 1: Prof. N.J. Bjerrum Special Volume*, Berg, R.W., and Hjuler, H.A., Eds., Elsevier, 2000, pp. 157–467.
3. Chen, G.Z., and Fray, D.J., *J. Electrochem. Soc.*, 2002, vol. 149, no. 11, pp. 455–467.

ISSN 1070-4272, Russian Journal of Applied Chemistry, 2007, Vol. 80, No. 9, pp. 1509–1514. © Pleiades Publishing, Ltd., 2007.
Original Russian Text © I.L. Baranov, L.V. Tabulina, L.S. Stanovaya, T.G. Rusal'skaya, Yu.A. Shostak, 2007, published in Zhurnal Prikladnoi Khimii, 2007, Vol. 80, No. 9, pp. 1473–1478.

APPLIED ELECTROCHEMISTRY AND CORROSION PROTECTION OF METALS

Specific Features of Synthesis, Chemical Composition, and Thermal Stability of Anodic Borosilicate Coatings on Silicon

I. L. Baranov, L. V. Tabulina, L. S. Stanovaya, T. G. Rusal'skaya, and Yu. A. Shostak

Belarussian State University of Informatics and Radioelectronics, Educational Institution, Minsk, Belarus

Received October 3, 2006; in final form, January 2007

Abstract—Thickness and resistivity of anodic borosilicate coatings synthesized on *n*-type silicon were studied in relation to the conditions in which the final forming potentials are reached and to the content of boric acid in an ethylene glycol solution. A method for synthesis of the coatings for use in nanoelectronics was suggested on the basis of data on the thermal stability of their chemical composition.

DOI: 10.1134/S1070427207090133

The development of the modern technology of integrated circuits (ICs) is based on use of nanosize intercomponent connections for their fabrication [1]. This brings up an urgent demand for diminishing the smearing of the structural profiles formed in ICs. A promising solution of this problem is use of electrochemical methods for obtaining layers with required properties on the surface of semiconducting silicon. In particular, oxide coatings doped with phosphorus- or boron-containing impurities can be synthesized by anodic oxidation of silicon in ethylene glycol solutions containing phosphoric or boric acid [2–5]. It has been suggested to use films of this kind in the IC technology as thin-film diffusion sources serving to form diode regions with improved switching characteristics in semiconducting silicon.

The advantages of the electrochemical method for synthesis of such diffusion sources, compared to the conventional high-temperature methods, consist in that it is performed at room temperature and the dopant content can be controlled by varying the composition of the electrolytic solution, and the film thickness in the course of growth, by changing the forming voltage [4, 5]. This method requires equipment that is simple in design and convenient in use. Because, in addition, the electrochemical method is based on passing electric current through the semiconductor silicon regions being treated, this provides a highly local transformation of their surface properties. For this reason, it has been suggested to perform selective anodic treatment of thermal silicon oxide layers in order to change their dielectric properties by varying the applied voltage [6, 7]. A particular advantage of the electrochemical method for synthesis of anodic silicon coatings is that it uses low-cost and environmentally safe reagents.

However, despite the indubitable process advantages, this method has not been used in the IC technology so far. The main reason is that the dopant distribution in the forming oxide coatings over the surface of semiconducting silicon is nonuniform. Removal of such coatings after diffusion doping of the starting silicon substrate gives rise to traces of erosion on the surface of the starting material. This adversely affects the electrical characteristics of *p*–*n* junctions. This effect is particularly pronounced in the case of diffusion sources based on anodic borosilicate coatings, whose structure shows increased friability [2, 4, 8].

To eliminate this effect, it has been suggested to use nitrate ethylene glycol solutions containing nitric acid as a current-conducting additive and a mixture of boric and arsenic acids ($H_3BO_3 : H_3AsO_4$ weight ratio 5 : 0.002) as dopant [9]. However, the electrolytic solution suggested is characterized by increased toxicity because of the use of arsenic acid, which is a noxious substance, and by the formation of explosive ethylene glycol nitrate in preparation of this solution from ethylene glycol and nitric acid [2].

This study is concerned with specific features of synthesis of anodic borosilicate (ABS) coatings on

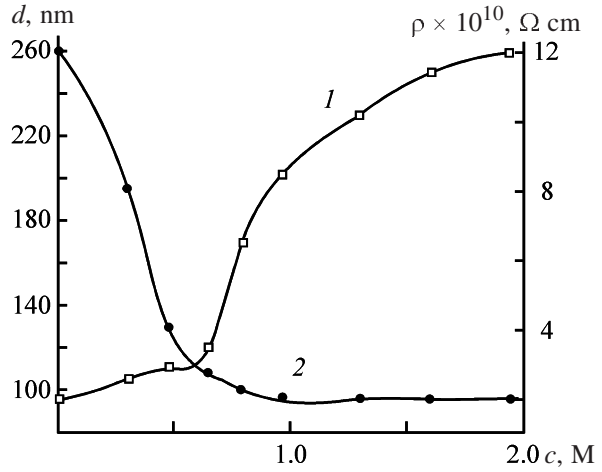

Fig. 1. Effect of the H_3BO_3 concentration c on (*1*) averaged thickness d and (*2*) resistivity ρ of anodic borosilicate coatings. Galvanostatic mode of anodic treatment (j = 6 mA cm^{-2}, U_{form} = 200 V).

the surface of semiconducting silicon in ethylene glycol solutions containing boric acid as dopant and ammonium nitrate as electrically conducting additive. In this case, the final forming potential was set either by a fixed current density (galvanostatic mode) or by current sweeping. The positive effect of the second method on the physicochemical properties of diffusion sources composed of ABS coatings was noted in [10]. Preliminary studies in [10] demonstrated that no *p–n* junctions are formed upon annealing in an inert atmosphere at 1100°C of ABS/Si structures whose oxide layers were synthesized in the current-sweeping mode. This circumstance made necessary a study of the chemical composition of these coatings both after synthesis and upon thermal treatment {at temperatures of 400–600°C at which silanol, Si–OH, and silanediol, Si–$(OH)_2$, bonds are actively dehydrated [11]}.

EXPERIMENTAL

The anodic oxidation was performed on polished, to finish class 14, Si (100) wafers doped with phosphorus to a resistivity of 4.5 Ω cm (KEF-4.5). ABS coatings were synthesized in the galvanostatic mode at current densities of 2–10 mA cm^{-2} [4] with current sweep rate of 0.4 mA cm^{-2} s^{-1} (current density amplitude 10 mA cm^{-2}) [12]. After a prescribed forming potential U_{form} was reached, the anodic treatment was continued in the potentiostatic mode for 60 min (to densify the structure of the ABS coatings). In the process, the initial current decreased by approximately a factor of 10–15. The synthesis was carried out in ethylene glycol solutions containing 0.01 M of ammonium nitrate and boric acid in a concentration varied within the range 0.3–2.0 M. The anodic treatment of silicon wafers with an area S of 5 cm^2 was performed in a cell with a graphite pressure contact. A molybdenum wire served as a cathode. The distance between the surface of the silicon anode and the cathode was 1 cm.

The thickness d of the ABS coatings formed was measured with an LEF-3M-1 laser ellipsometer (measurement error ±1.0 nm). Their breakdown voltage U_{br} was evaluated on a setup for measurement of capacitance voltage characteristics with an indium probe, based on an E-7-12 instrument [13]. The electrical characteristics of the ABS coatings were determined at five points on their surface (at the center and four points along the perimeter). The average values of the breakdown voltage, thicknesses of the oxide layers synthesized, and residual currents I_{res} upon completion of the synthesis process were used to calculate the averaged resistivity ρ by the formula

$$\rho = S U_{br}/dI_{res}.$$

The chemical composition and structure of the ABS coatings were studied by IR spectroscopy. The same method was applied to analyze structural specific features of the annealed coatings. The spectra were recorded on a Specord 75 IR spectrophotometer in the range 400–2200 cm^{-1}. Silicon wafers with coatings were annealed in a nitrogen flow at 400, 500, and 600°C for 10 min.

The variation of the averaged values of the thickness d of the ABS coatings and of the corresponding values of ρ with the concentration of boric acid in the electrolyte is illustrated by Fig. 1. These oxide coatings were synthesized in the galvanostatic mode at a current density of 6 mA cm^{-2} [4, 9] to U_{form} = 200 V. It follows from Fig. 1 that an increase in the concentration of boric acid in the electrolytic solution results in that substantially thicker coatings are formed. This effect is particularly pronounced when the H_3BO_3 concentration in the solution exceeds 0.5 M (Fig. 1, curve *1*). Simultaneously, the resistivity ρ of the coatings formed in electrolyte solutions in which the dopant concentration c varies from 0.2 to 1.0 M steadily decreases. An increase in c above 1.0 M has nearly no effect on the resistivity of the oxide layers (Fig. 1, curve *2*). These data are in agreement with the information about the properties of ABS coatings, reported in [2], where it was noted that these coatings are highly defective and their structure contains pores that extend to the outer surface. Prob-

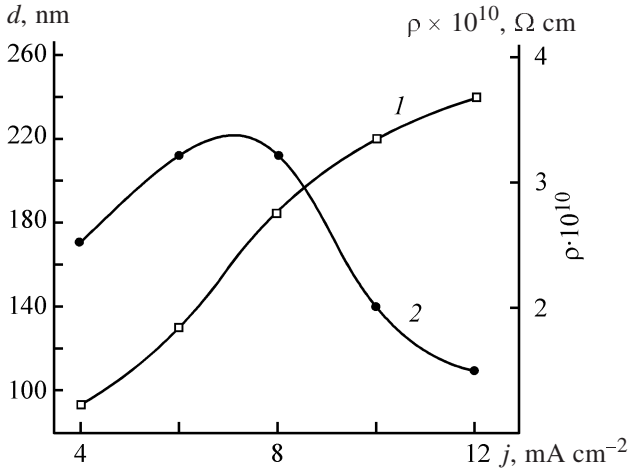

Fig. 2. Effect of the anode current density j on (*1*) averaged thickness d and (*2*) resistivity ρ of anodic borosilicate coatings. U_{form} = 200 V; H_3BO_3 concentration in solution 0.65 M.

ably, this intensifies exchange processes at the interface between the oxide layer and electrolyte solution, which makes higher the growth rate of ABS coatings. In this case, the presence of pores in their structure impairs their dielectric properties because of the adsorption of impurities from the electrolyte solution, including the doping additive, in pores. If ABS coatings are synthesized to U_{form} = 200 V in an electrolyte solution containing 0.65 M H_3BO_3, with the anode current density varied, an increase in this synthesis parameter leads to a steady and substantial rise in the average values of their thickness (Fig. 2, curve *1*). The corresponding ρ–j curve passes through a maximum at (6–8) mA cm^{-2} (Fig. 2, curve *2*). At higher current densities, the resistivity of the films synthesized markedly decreases. Thus, an increase in the dopant concentration in the electrolyte solution favors loosening of the structure of the resulting ABS coatings and leads to its enrichment in doping impurities. The same influence on the electrical state of the films being formed is exerted by the anode current density at its values exceeding 8 mA cm^{-2}. This predetermines the specificity of the choice of these parameters for synthesis of ABS coatings to be used as diffusion sources. It should be noted, however, that, at any concentration of boric acid in the electrolyte solution and current density used, these oxide films have a nonuniform thickness distribution over the silicon surface. This circumstance is illustrated by the data in Fig. 3. Their analysis shows that, depending on the H_3BO_3 concentration in the electrolyte solution and the anode current density, the scatter Δd of thicknesses of the ABS coatings on the surface of a silicon

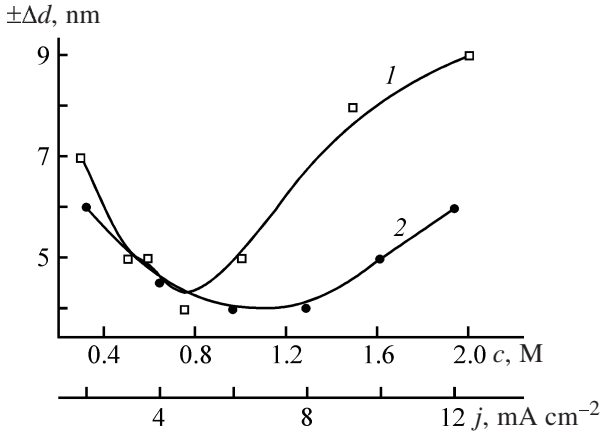

Fig. 3. Effect of (*1*) H_3BO_3 concentration c and (*2*) anode current density j on the thickness scatter $\pm\Delta d$ of anodic borosilicate coatings over the surface of a silicon substrate.

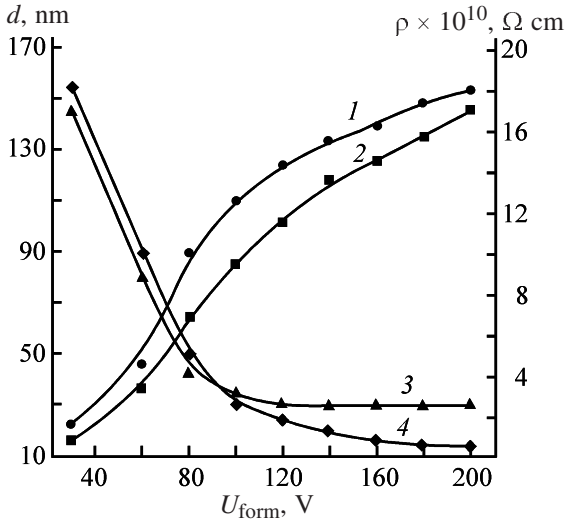

Fig. 4. Effect of the forming voltage U_{form} on (*1, 2*) averaged thickness d and (*3, 4*) resistivity ρ of anodic borosilicate coatings synthesized in (*1, 3*) galvanostatic mode and (*2, 4*) with current sweeping.

substrate is within ±(4–10) nm. The coatings synthesized in solutions containing 0.6–0.8 M H_3BO_3 at current densities of 4–10 mA cm^{-2} have Δd = ±(4–6) nm (Fig. 3; curves *1, 2*).

The averaged values of d and ρ of the oxide layers synthesized in an electrolyte solution containing 0.65 M H_3BO_3 at a current density of 10 mA cm^{-2} are shown in Fig. 4 (curves *1, 3*) as functions of U_{form}. The figure also presents similar dependences obtained for coatings formed in the same solution with current sweeping to the amplitude value corresponding to 10 mA cm^{-2} (Fig. 4; curves *2, 4*). Comparison of these data shows that the dependence d =

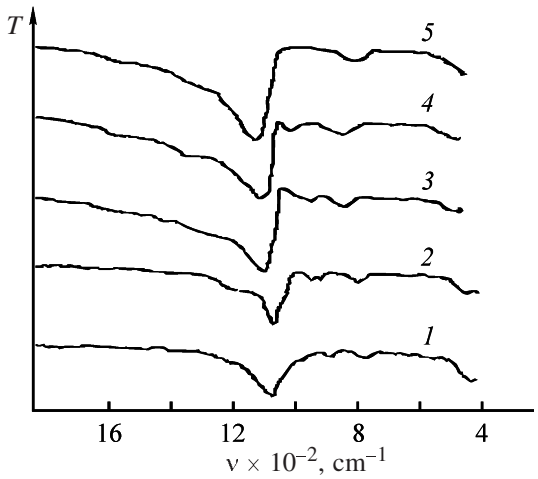

Fig. 5. IR spectra of anodic borosilicate coatings synthesized in electrolyte solution containing (*1*) 0.30 and (*2–5*) 0.65 M boric acid. (*A*) Absorption and (ν) wavenumber. State of the structure: (*1, 2*) initial and (*3–5*) that upon annealing at 400, 500, and 600°C, respectively.

$f(U_{form})$ for the ABS coatings synthesized with current sweeping is more linear and has a lower oxide layer growth coefficient than coatings formed in the galvanostatic mode (Fig. 4; curves *1, 3*). In the former case, the thickness scatter of the films synthesized over the surface of silicon substrates is always lower than the measurement error. In the galvanostatic mode, the scatter of *d* of the corresponding coatings is ±(5–8) nm (a wider thickness scatter is observed for the ABS coatings synthesized at U_{form} = 30–80 V).

Thus, use of current sweeping favors more uniform growth of ABS coatings on the surface of semiconducting silicon. Because this effect is manifested even at U_{form} = 30 V, it follows that the tendency toward such a behavior develops already in the initial stage of anodic oxidation of a silicon substrate. As a consequence, it can be suggested that use of current sweeping in synthesis of ABS coatings strongly affects the degree of structural ordering of the transition layer at the ABS/Si interface, which is characteristic of the crystalline state, as observed in [2].

Analysis of how ρ varies with U_{form} for coatings synthesized with U_{form} reached in different ways shows that, irrespective of specific features of their synthesis, the resistivity of the films steeply falls as U_{form} increases up to 100 V. At higher U_{form}, the dielectric properties of the coatings obtained in the galvanostatic mode remain virtually unchanged (Fig. 4, curve *3*), and those of the coatings synthesized with current sweeping in the initial stage steadily decrease (Fig. 4, curve *4*). The latter circumstance suggests that current sweeping allows a better control over the thickness of ABS coatings and their resistivity by varying the values reached by U_{form}. This is important when the coatings under study are used as diffusion sources in fabrication of *p–n* junctions of prescribed thickness in the nanosize IC technology. However, difficulties have been encountered in this case previously, and the reason for these difficulties can be accounted for by results of an IR spectral analysis.

IR spectral studies were performed on ABS coatings synthesized with current sweeping and U_{form} = 200 V in electrolyte solutions containing 0.30 and 0.65 M H_3BO_3. Their thicknesses were 1000 and 1250 nm, respectively. Their IR spectra (Fig. 5; curves *1, 2*) show strong absorption bands peaked at 1073 cm^{-1}, associated with stretching vibrations of Si–O bonds in silica tetrahedra. Medium-intensity bands at 750–850 cm^{-1} belong to stretching vibrations of Si–O–Si bonds in rings composed of SiO_4 tetrahedra, and those at 900–980 cm^{-1}, to stretching vibrations of Si–O–B bonds [14–16]. It should be noted that the absorption at 900–980 cm^{-1} may also be due to the defective state of the ABS coatings [15] and to superposition of stretching vibrations of Si–O–B and B–O bonds. The highly defective state of the structure of these films is evidenced by the abovementioned steep decrease in their resistivity upon an increase in their thickness (Fig. 4, curve *2*). The presence of Si–O–B bonds and B–O bonds in BO_3 groups is indicated by the appearance of a broad band with two weakly pronounced peaks at 925 and 945 cm^{-1} in the spectrum of a film synthesized in an electrolyte solution with 0.65 M H_3BO_3. The first of these is due to vibrations of Si–O–B bonds [16], and the second, to B–O bonds in which boron ions are not chemically bound to silicon ions [17] (Fig. 5, curve *2*). This indicates that boron ions may be present in the structure of ABS coatings both in a bound state and, probably, as boric acid molecules adsorbed within pores.

The IR spectra of coatings annealed at 400°C contain, in the 900–980 cm^{-1} region, a single band peaked at 925 cm^{-1}. For oxide layers annealed at 500°C, this band shifts to 950 cm^{-1} (Fig. 5, curves *3, 4*). This indicates that, after annealing at 400°C, boron ions in the structure of ABS coatings are mainly in the bound state and form Si–O–B bonds. Annealing at 500°C transforms these bonds to B–O bonds, i.e., boron ions are mainly present in ABS coatings in the form of BO_3 structural groups. Upon annealing at 600°C, the IR spectra of the coatings studied show no band at 900–980 cm^{-1}, which points to the absence of

boron-containing impurities (their amount is below the detection limit of IR spectroscopy) (Fig. 5, curve *5*).

In this context, it can be assumed that annealing at this temperature leads to intensive disintegration of Si–O–B bonds, followed by their transformation to BO_3 groups, with the oxide coating strongly depleted of boron-containing impurities. This probably occurs because of their volatilization from the structure of ABS films in the form of boric acid, which can sublime with water vapor [18].

Use of the coatings in question as diffusion sources in the IC technology involves a high-temperature treatment of the structure constituted by a borosilicate film and semiconducting silicon (1100–1200°C). Therefore, the IR data presented demonstrate that it is necessary to use protective layers on ABS coatings to prevent sublimation of boron-containing impurities from the coatings. In this study, anodic silicon films synthesized in an ethylene glycol electrolyte solution containing no boric acid served as protective layers. Composites of this kind (anodic silicon oxide/ABS coating) were first synthesized with current sweeping in an electrolyte solution containing 0.65 M H_3BO_3 to U_{form} = 160 V. Then, the ABS films obtained were additionally grown without densification to U_{form} = 200 V in an electrolyte containing no boric acid. After that, the films were densified. Fast annealing of the structures constituted by a composite ABS coating and semiconducting silicon at 1100°C for 3 min yielded *p–n* junctions of thickness 0.4 μm (the thickness was found by the method of staining of spherical polished sections [13, 14]). It was found that the corresponding current–voltage curves have no portions of a gradual transition to the breakdown state, which were observed in [4] when ABS coatings synthesized with U_{form} reached in the galvanostatic mode were used as diffusion sources. This suggests that ABS coatings formed with current sweeping in the initial stage of their synthesis can be used as diffusion sources for fabrication of nanosize intercomponent connections in the IC technology.

CONCLUSION

(1) The distribution of the thickness of anodic borosilicate coatings, synthesized with the use of the galvanostatic mode, over the surface of *n*-type silicon depends on the concentration of boric acid in an ethylene glycol solution and on the current density. The narrowest scatter of the coating thickness [~±(4–5) nm] is observed for coatings synthesized at current densities of 4–10 mA cm^{-2} in a solution containing 0.5–1.0 M boric acid.

(2) With current sweeping (sweep rate 0.4 mA cm^{-2} s^{-1}, current amplitude 10 mA cm^{-2}), thickness-uniform anodic borosilicate coatings are formed in an electrolyte solution containing 0.65 M boric acid, irrespective of the final value of the forming voltage. The resistivity of these coatings steadily decreases as the forming voltage is raised from 30 to 200 V. This enables control over the thickness and resistivity of anodic borosilicate coatings in the course of their synthesis.

(3) Borosilicate inclusions are incorporated into anodic borosilicate coatings because of the formation of Si–O–B bonds or in the form of boric acid molecules adsorbed within pores. Annealing at 500°C disintegrates Si–O–B bonds and transforms them into B–O bonds in BO_3 groups. Upon annealing at 600°C, no boron-containing inclusions are detected in the structure of anodic borosilicate coatings by IR spectroscopy. It is suggested that these inclusions sublime as boric acid molecules.

(4) Use of protective anodic layers of silicon oxide on anodic borosilicate coatings makes it possible to regard the electrochemical method for synthesis of these coatings as a promising technique for fabrication of low-temperature diffusion sources for nanoelectronics.

REFERENCES

1. Merkle, R.C., *IEEE Spectrum*, 2001, vol. 38, no. 1, pp. 19–21.
2. Mileshko, L.P., Avdeev, S.P., and Nestyurina, E.E., *Fiz. Khim. Obrab. Mater.*, 2003, no. 3, pp. 47–52.
3. Mileshko, L.P. and Varzaev, Yu.N., *Fiz. Khim. Obrab. Mater.*, 2002, no. 3, pp. 38–44.
4. Mileshko, L.P. and Chistyakov, Yu.D., *Elektronnaya tekhnika: Obzor Moskovskogo universiteta* (Electronics Technology: Review Publication by Moscow Univ.), Moscow: Mosk. Gos. Univ., 1977.
5. Mileshko, L.P., Sorokin, I.N., and Chistyakov, Yu.D., *Elektron. Tekh., Ser. 3: Mikroelektronika*, 1979, no. 3(8), pp. 99–101.
6. Paily, R., Das Gupta, A., and Das Gupta, N., *IEEE Electron Device Lett.*, 2002, vol. 23, no. 12, pp. 707–709.
7. Mileshko, L.P., *Fiz. Khim. Obrab. Mater.*, 2002, no. 6, pp. 55–59.
8. Mileshko, L.P. and Avdeev, S.P., *Fiz. Khim. Obrab. Mater.*, 2003, no. 6, pp. 67–72.

9. Mileshko, L.P. and Avdeev, S.P., *Fiz. Khim. Obrab. Mater.*, 2004, no. 2, pp. 84–86.
10. UK Patent 1000264.
11. Kiselev, V.F., *Poverkhnostnye yavleniya v poluprovodnikakh i dielektrikakh* (Surface Phenomena in Semiconductors and Insulators), Moscow: Nauka, 1970, pp. 115–117.
12. Baranov, I.L., Tabulina, L.V., Stanovaya, L.S., and Rusal'skaya, T.G., *Elektrokhimiya*, 2006, vol. 42, no. 4, pp. 320–325.
13. *Praktikum po khimii i tekhnologii poluprovodnikov* (Laboratory Course of Chemistry and Technology of Semiconductors), Ugai, Ya.A., Ed., Moscow: Vysshaya Shkola, 1978.
14. Borisenko, V.E., Gaponenko, N.V., Mileshko, L.P., and Sinilo, M.F., *Zh. Prikl. Spektrosk.*, 1991, vol. 54, no. 1, pp. 156–158.
15. Baranov, I.L., Stanovaya, L.S., Stepanishchev, S.D., and Litvinovich, G.V., *Izv. Akad. Nauk SSSR, Neorg. Mater.*, 1989, vol. 25, no. 3, pp. 406–409.
16. Tong, J.E., Schertenleib, K., and Carpio, R.A., *Solid State Technol.*, 1984, no. 1, pp. 161–170.
17. Plyusnina, I.N., *Infrakrasnye spektry mineralov* (Infrared Spectra of Minerals), Moscow: Mosk. Gos. Univ., 1977.
18. Glinka, N.L., *Obshchaya khimiya* (General Chemistry), Leningrad: Khimiya, 1984.

ISSN 1070-4272, Russian Journal of Applied Chemistry, 2007, Vol. 80, No. 9, pp. 1515–1522. © Pleiades Publishing, Ltd., 2007.
Original Russian Text © M.Yu. Malinskaya, N.I. Ivancheva, I.I. Oleinik, G.A. Tolstikov, S.S. Ivanchev, 2007, published in Zhurnal Prikladnoi Khimii, 2007, Vol. 80, No. 9, pp. 1479–1488.

CATALYSIS

Catalytic Activity of Systems Based on Titanium Bis(phenoxy Imine) Complexes: Effect of the Ligand Structure

M. Yu. Malinskaya, N. I. Ivancheva, I. I. Oleinik, G. A. Tolstikov, and S. S. Ivanchev

St. Petersburg Branch, Boreskov Institute of Catalysis, Siberian Division, Russian Academy of Sciences, St. Petersburg, Russia

Vorozhtsov Novosibirsk Institute of Organic Chemistry, Siberian Division, Russian Academy of Sciences, Novosibirsk, Russia

Received July 22, 2007

Abstract—Polymerization of ethylene at 30–70°C in the presence of catalytic systems based on titanium bis(phenoxy imine) complexes of various structures, activated with methylalumoxane, was studied. An attempt was made to systematize the effect of substituents in ligands, to find correlations, to account for the results obtained, and to reveal conditions under which the reaction occurs by the "living" polymerization mechanism. Some properties and structural features of the polyethylenes obtained were determined.

DOI: 10.1134/S1070427207090145

The recently discovered new class of postmetallocene catalysts of ethylene and α-olefin polymerization, based on transition metal phenoxy imine complexes, attracts attention of many research teams. Particularly active studies are performed by the team headed by T. Fujita (Mitsui Chem. Inc.), who published numerous papers on the synthesis of phenoxy imine complexes of zirconium, titanium, and other transition metals and examined their catalytic activity in polymerization of ethylene and α-olefins [1–3]. Somewhat later reviews written by other authors were published [4, 5].

The published studies revealed high capability of phenoxy imine catalytic systems for incorporation into the polymeric chain of α-olefins of various structures, including sterically hindered and even polar monomers. These studies demonstrated the possibility of controlling the formation of the macrochain forming in the course of polymerization and of expanding the assortment of the synthesized polymers by involving new monomers into the copolymerization. It was found that one of the factors responsible for the high catalytic activity of systems based on transition metal phenoxy imine complexes is the polydentate coordination mode, with intense electron exchange between the transition metal ion and unsymmetrical ligands. Therefore, the structure and electronic properties of the ligands exert a strong effect on the activity and selectivity of catalytic systems based on phenoxy imine complexes. Variation of the structure of phenoxy imine ligands is widely used in searching for new catalysts showing high activity and stability under the polymerization conditions.

Even in their first papers [6–8], Fujita et al. considered the dependence of the catalytic activity of phenoxy imine complexes (with methylalumoxane, MAO, as cocatalyst) on the kind of transition metal, with the complexes of Zr, Ti, Hf, and V as examples. They were also the first to analyze the influence exerted on the catalytic activity by the size of substituents in the imine and phenoxy moieties. The main conclusions made in these papers are as follows.

(1) The phenoxy imine catalytic systems containing an aldimine group show higher activity than their analogs with a ketimine group.

(2) Small substituents at the imine N atom do not prevent approach of the monomer to the active center of the propagating chain.

(3) A bulky substituent near the phenoxyl oxygen atom sterically protects it from the electrophilic attack of Lewis acids present in the polymerization medium and favors efficient separation of the cationic active species and anionic fragments of the cocatalyst.

(4) Fluorinated substituents at the imine nitrogen atom ensure the occurrence of the polymerization by the "living" mechanism.

These conclusions were based on the results of experimental studies of a relatively limited number of

zirconium phenoxy imine complexes, and accelerated experimental procedures were used.

In this study we examined a wide range of titanium phenoxy imine complexes and compared their activities. By so doing, we attempted to find a correlation between the structure of titanium phenoxy imine complexes and their catalytic activity in polymerization of ethylene. For this purpose, we tested titanium bis(phenoxy imine) complexes containing various ligands (Table 1) in polymerization of ethylene in the presence of MAO.

EXPERIMENTAL

Ultrapure grade toluene was dried for 24 h over calcined alumina, distilled from sodium metal in an argon flow, and stored over sodium metal in an inert gas atmosphere.

Isopropyl alcohol (chemically pure grade) was used without additional purification.

Ethylene (main substance content 99.5%) and Ar (extra grade) prior to feeding into the reactors were dried by passing through columns packed with calcined alumina, after which the moisture content of ethylene and argon did not exceed 10–20 and 10 ppm, respectively.

Methylalumoxane (Witko GmbH, commercial name Eurecen® Al 5 100/10 T) was used as 10% solution in toluene. According to the data of the company, the total aluminum content of MAO was 4.6–5.6 mol %, and the relative content of Al counting on trimethylaluminum was 32–36 mol %.

The catalysts were based on titanium bis(phenoxy imine) complexes synthesized at the Vorozhtsov Institute of Organic Chemistry, Siberian Division, Russian Academy of Sciences, Novosibirsk, by the following scheme:

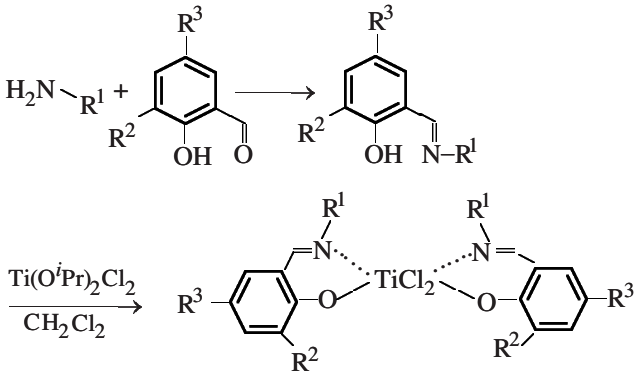

using the procedures described in [8–11].

The structures of the ligands and complexes were confirmed by elemental analysis and by ^{1}H NMR and IR spectroscopy.

Polymerization of ethylene was performed in a 150-ml stainless steel pressure vessel equipped with a detachable jacket and a magnetically driven propeller stirrer. Experiments were performed at a pressure of 0.6 MPa and temperatures from 30 to 80°C. The pressure in the vessel was maintained automatically, and the temperature was controlled by feeding water heated to the required temperature from an ultrathermostat to the jacket.

Before starting polymerization, the reactor was evacuated to a residual pressure of 1×10^{-1} mm Hg at 150–170°C for 1 h, after which it was filled with dry Ar and evacuated again. The procedure was repeated three times.

After cooling to room temperature, the calculated amount of toluene and components of the catalytic system were injected with a medical syringe through the loading tube in a counterflow of Ar. The mixture was saturated with ethylene and simultaneously brought to the required temperature and pressure. After the prescribed period, the reaction was stopped by adding isopropyl alcohol. The liquid phase was separated on a Büchner funnel, and the polymer obtained was washed with isopropyl alcohol and dried at 60°C in a vacuum to constant weight.

The molecular weight (MW) of the polymers obtained was determined from the viscosity data by the equation [12]

$$[\eta] = 6.2 \times 10^{-4} M^{0.70}.$$

The thermal characteristics of the polymers were determined by scanning calorimetry on a Shimadzu DSC-60 device. The specific heats of phase transitions and the characteristic temperatures were measured on the same differential scanning calorimeter at a heating rate of 10 deg min^{-1} and a sample weight of 5–10 mg.

The content of terminal groups in the polymers obtained was determined by IR Fourier spectroscopy on a Shimadzu FTIR-8300 spectrometer.

The catalytic systems under consideration were subdivided into three groups. In the first group, the complexes contained fixed *t*-Bu substituents in the *o*- and *p*-positions of the phenoxy group and varied substituents at the imine N atom. In the second group, the substituents in the phenoxy group were bulkier (cumyl), with varied substituents at the imine N atom. In the third group, the substituent at the imine N atom

Table 1. Titanium bis(phenoxy imine) complexes

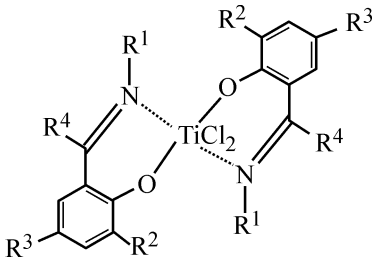

Catalyst	R^1	R^2	R^3	R^4
1	*n*-Bu	*t*-Bu	*t*-Bu	H
2		*t*-Bu	*t*-Bu	H
3		*t*-Bu	*t*-Bu	H
4	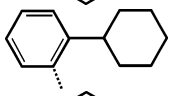	*t*-Bu	*t*-Bu	H
5	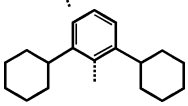	*t*-Bu	*t*-Bu	H
6	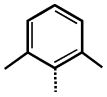	*t*-Bu	*t*-Bu	H
7		*t*-Bu	*t*-Bu	H
8	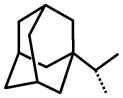	*t*-Bu	*t*-Bu	H
9		Cumyl	Me	H
10		Cumyl	Me	H
11		Cumyl	Me	Me
12		Cumyl	Cumyl	H
13	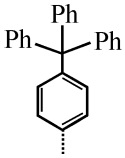	Cumyl	Cumyl	H
14		Cumyl	Cumyl	H
15	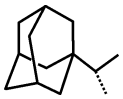	Cumyl	Cumyl	H

Table 1. (Contd.)

Catalyst	R^1	R^2	R^3	R^4
16		*t*-Bu	Me	H
17		Trityl	Me	H
18		*t*-Bu	Trityl	H
19		2-Isobornyl	Me	H
20		2-Isobornyl	H	H
21		1-Phenylethyl	H	H

Note: The dotted line denotes the site of substituent bonding to the ligand.

was fixed (cyclohexyl), and the substituents in the phenoxy group were varied.

The results of experiments on ethylene polymerization at various temperatrues with the first group of complexes (catalysts **1**–**8**) and the characteristics of the polyethylenes obtained are listed in Table 2.

Table 2 shows that the catalytic activity, molecular weight of polyethylenes obtained, and optimal temperature of catalyst operation are strongly influenced by a substituent at the imine N atom. For example, complex **1** containing an aliphatic substituent at the imine N atom shows moderate catalytic activity (1200–4700 $kg_{PE}\,(mol_{cat})^{-1}\,MPa^{-1}\,h^{-1}$) and the forming polyethylene has relatively low molecular weight (M_η = 220000–300000) with vinyl terminal groups at one or both ends of polymer chains.

Introduction of an alicyclic substituent at the imine N atom (complex **2**) leads to an increase in the catalytic activity. The molecular weight of the PE obtained is also higher. The electronic effects of *n*-Bu and cyclohexyl are similar. Both substituents exhibit donor properties and enhance the electrophilicity of the coordination core. Therefore, the difference between complexes **1** and **2** in the catalytic activity should be attributed to steric effects of *n*-Bu and cyclohexyl. It was shown recently [13] that the state of the active center bound to the transition metal strongly differs in the complexes containing different substituents at the imine N atom. This effect is attributed to differences in the distance between the Cl atom and its nearest neighboring C atom in substituents at the imine group. In the compound with the more "compact" cyclohexyl substituent, this distance is longer than in the complex with the *n*-Bu substituent, and hence the polymerization center can be less shielded, causing higher activity of complex **2** compared to **1**.

The catalytic activity of complex **3** containing an aromatic substituent, phenyl, at the imine group is slightly higher than that of **2**, but the molecular weight of the polyethylene obtained is lower. This difference may be due to different electronic effects of the alicyclic and aromatic substituents at the imine N atom, which can differently affect the titanium polymerization center.

Introduction of a bulky substituent (cyclohexyl) into the *o*-position of the phenyl group at the imine N atom (complex **4**) leads to a decrease in the catalytic activity by more than an order of magnitude. Apparently, the substituent in the *o*-position of the phenyl ring at the imine N atom, located in the vicinity of the polymerization center, prevents access of ethylene to the active center.

Complexes **5**–**8** are systems with further increased steric hindrance. As already noted, this factor prevents access of the monomer to the active center. As a result, the catalytic activity decreases.

It should be noted that substituents at the imine N atom, along with affecting the catalytic activity, can also shift the optimal temperature range of the catalyst functioning. As seen from Fig. 1a, with an increase in the temperature from 30 to 70°C, the curve of the catalytic activity of complexes **1** and **3** passes through a maximum; for complex **2**, the catalytic activity monotonically decreases, and for **4**, increases.

Table 2. Results of ethylene polymerization and properties of the polyethylenes obtained ($V_{toluene}$ = 50 ml, $P_{C_2H_4}$ = 3 atm)

Catalyst	T, °C	MAO/Ti	Amount of Ti, μmol	τ, min	Yield, g	A*	$M_\eta \times 10^{-3}$	IR, groups per 1000C		DSC	
								CH_3	C=C	mp, °C	$-\Delta H_m$, J g^{-1}
First group of complexes											
1	30	250	1.0	60	0.39	1200	300	0	0.07	138.1	223.2
	50	250	1.0	60	1.2	4700	248	–	–	–	–
	70	250	1.5	60	1.5	3200	220	–	–	–	–
2	30	250	1.25	60	10.2	17000	1761	–	–	141.6	250.3
	50	500	2.17	60	6.3	10800	800	–	–	144.2	245.8
	70	500	2.1	60	1.9	2940	494	–	–	142.8	235.6
3	30	500	2.01	60	8.8	14600	649	0	0.035	140.7	244.4
	50	500	1.94	60	14.1	24140	640	0	0.03	140.2	239.2
	70	500	2.07	60	5.05	8130	520	0	0.03	138.9	249.2
4	30	62.5	4.0	120	0.77	321	4400	0	0	144.5	270.5
	50	62.5	4.0	60	0.67	560	2500	0	0.015	145.5	263.5
	70	62.5	4.0	60	1.44	1200	2300	0.03	0.015	145.5	252.1
5	30	62.5	4.0	60	0.0096	8	–	–	–	–	–
	50	350	4.0	60	0.0084	7	–	–	–	–	–
6	30	62.5	4.0	60	0.04	25	–	0.05	0.21	139.6	199.2
	50	62.5	4.0	45	0.02	16.6	–	0	0.12	140.9	185.6
7	30	250	1.85	60	0.02	39.4	–	–	–	–	–
8	30	500	1.95	30	0.03	102	–	–	–	–	–
Second group of complexes											
9	30	500	1.1	60	20.9	64000	780	0	0.02	140.5	234.5
	50	500	1.1	60	10.1	30700	660	–	–	141.2	242.8
	70	500	0.9	60	5.9	21800	670	0	0.035	141.0	244.0
10	30	500	0.8	60	10.3	43100	650	0	0.04	139.3	237.1
	50	500	0.8	60	6.0	24960	1010	0	0.04	141.9	220.1
	70	500	0.8	60	1.9	8100	820	0	0.03	141.8	221.8
11	30	250	2.0	60	0.3	530	–	0	0.05	141.3	236.5
	50	250	2.1	30	0.2	640	–	–	–	–	–
12	30	500	2.0	60	7.8	16600	360	0	0.04	139.5	244.6
	50	500	2.0	60	11.6	20500	990	0	0.04	139.5	225.6
	70	500	2.0	60	4.4	7100	700	0	0.05	142.9	246.8
13	30	500	2.0	60	6.9	10400	720	0	0.04	140.3	236.1
	50	500	2.0	60	4.8	7700	1590	0	0.04	144.0	224.2
	70	500	2.0	60	1.8	3900	1140	0	0.03	139.3	257.0
14	30	500	2.3	30	0.2	580	–	–	–	–	–
15	30	500	4.8	30	0.07	95	–	–	–	–	–
Third group of complexes											
16	30	250	2.0	40	8.9	22250	1090	–	–	–	–
	50	250	2.2	60	8.2	12700	800	0	0.015	139.5	225.9
17	30	500	2.1	60	0.2	295	–	–	–	–	–
	50	500	1.7	60	0.3	522	–	–	–	–	–
18	30	500	2.0	30	Traces of polymer		–	–	–	–	–
19	30	250	1.9	60	0.9	1500	940	0	0.1	143.0	225.5
	50	250	1.9	60	0.6	1150	600	–	–	–	–
20	30	250	1.8	60	2.4	4490	1050	0	0.08	143.0	221.0

Table 2. (Contd.)

Catalyst	T, °C	MAO/Ti	Amount of Ti, μmol	τ, min	Yield, g	A*	$M_\eta \times 10^{-3}$	IR, groups per 1000C		DSC	
								CH_3	C=C	mp, °C	$-\Delta H_m$, J g^{-1}
20	50	250	1.8	60	1.4	2640	750	0	0.01	144.4	259.0
21	30	500	1.5	60	3.1	6890	920	–	–	–	–
	50	500	1.5	60	2.8	6300	780	0	0.03	140.3	228.7
	70	500	1.5	60	2.7	6100	480	0	0.05	141.1	212.7

* (*A*) Activity, $kg_{PE}\,(mol_{cat})^{-1}\,MPa^{-1}\,h^{-1}$

The results of studying the activity of the second group of phenoxy imine complexes (**9**–**15**) in ethylene polymerization are also given in Table 2. The most active is complex **9** containing an alicyclic substituent at the imine N atom in combination with a bulky substituent (cumyl) in the *o*-position of the phenoxy group. Comparison with the related complexes of the first group (**9** with **2**, **10** with **3**) shows that the catalytic activity increases by a factor of 3 and more. This fact shows that substituents at the imine N atom and in the phenoxy group exert a conjugated effect on the activity of the catalytic system.

Introduction of an aromatic substituent at the imine N atom (complex **10**) leads to a decrease in the catalytic activity by a factor of ~2 and to an increase in the molecular weight of the forming polyethylene.

Complex **11** containing the ketimine functional group exhibits low catalytic activity compared to the aldimine analog. This fact was already noted in [10].

Replacement of the *p*-methyl substituent in the phenoxy group (complex **10**) by the second bulky cumyl substituent (complex **12**) leads to a decrease in the catalytic activity and in the molecular weight of the forming polyethylenes. Apparently, two bulky substituents in the phenoxy group exert an effect decreasing the activity.

Comparison of the activity of the catalytic systems based on complexes **4**–**6** with that of the system with **13** shows that the position of substituents in the phenyl group bonded to imine nitrogen (Table 1) strongly affects the activity of the catalytic systems. In the *p*-position, even bulky substituents substituents (complex **13**) decrease the catalytic activity by a factor of only 1.5, whereas in the *o*-position even the methyl groups drastically (by more than two orders of magnitude) decrease the activity.

Complexes **14** and **15** containing bulky substituents at the imine N atom, 2-(isobornyl) and 1-(1-adamantyl) ethyl, exhibit virtually no catalytic activity.

Examination of the influence of temperature in the range 30–70°C on the activity of systems based on complexes **9**, **10**, **12**, and **13** showed that the activity of the systems based on **9**, **10**, and **13** decreases with increasing temperature, and that of the system based on **12** passes through a maximum at 50°C (Fig. 1b).

Data on the activity of catalytic complexes of the third group are also given in Table 2.

Complex **16** containing *t*-Bu in the *o*-position and Me in the *p*-position of the phenoxy group shows high activity, and the molecular weight of the resulting polyethylene is high. Replacement of the *o*-*t*-Bu group by a bulkier cumyl substituent (complex **9**) leads to an increase in the catalytic activity by a factor of 3, but the molecular weight of the forming polyethylenes decreases.

Introduction into the *o*- (complex **17**) or *p*-position (complex **18**) of very bulky trityl group drastically decreases the catalytic activity.

Complexes **19** and **20** containing a bulky isobornyl substituent in the *o*-position of the phenoxy group show moderate catalytic activity. The catalytic activity of complex **20** without *p*-substituents is higher.

Complex **21** containing 1-phenylethyl substituent in the *o*-position of the phenoxy group shows fairly high catalytic activity, which is only slightly dependent on temperature. Thus, by properly choosing substituents (and, in particular, their volume) in the phenoxy group, it is possible to ensure high activity of the complex at elevated temperatures.

Data on the effect of temperature on the activity of complexes **16** and **19**–**21** containing different substituents in the phenoxy group are shown in Fig. 1c. The catalytic activity of all the complexes decreases with increasing temperature from 30 to 50°C.

All the phenoxy imine complexes studied ensure formation of linear and highly crystalline polyethylenes, as indicated by the IR and DSC data (Table 2).

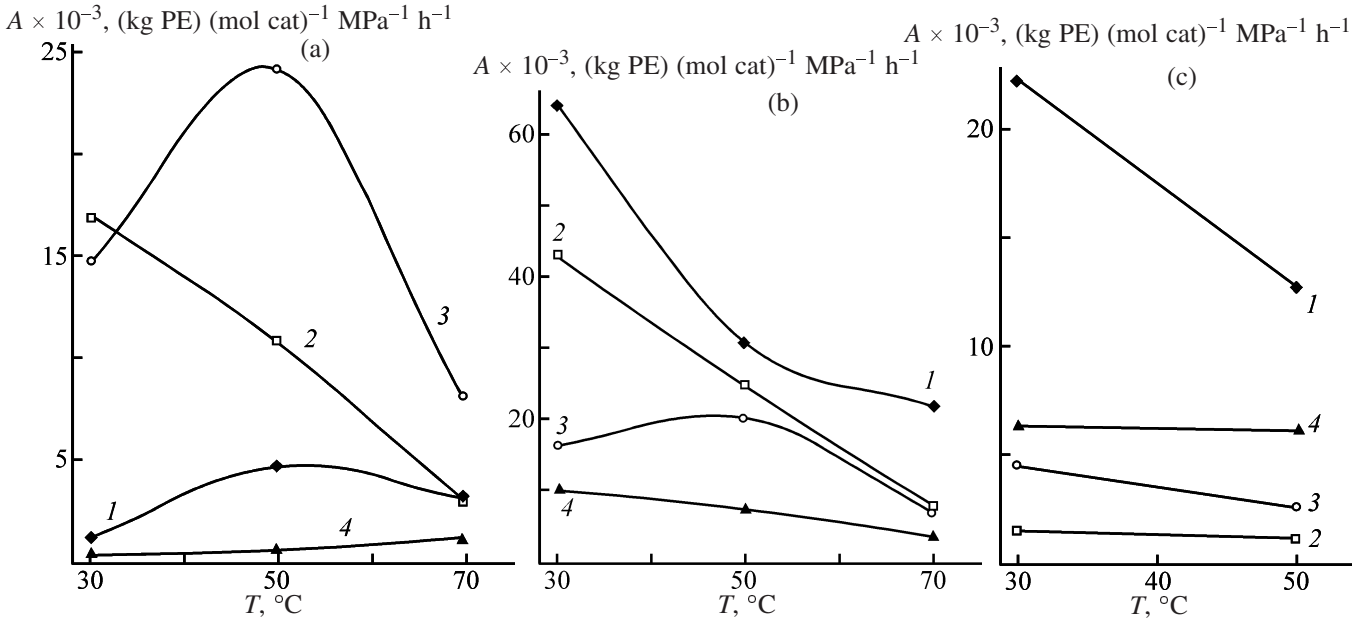

Fig. 1. Catalytic activity A of complexes as a function of polymerization temperature T. Polymerization conditions: $V_{toluene}$ = 50 ml, $P_{C_2H_4}$ = 3 atm. Complex: (a) (*1*) **1**, (*2*) **2**, (*3*) **3**, and (*4*) **4**; (b) (*1*) **9**, (*2*) **10**, (*3*) **12**, and (*4*) **13**; (c) (*1*) **6**, (*2*) **19**, (*3*) **20**, and (*4*) **21**.

With some phenoxy imine complexes, the "living" polymerization mechanism can be realized in the system. Initially this mechanism was established for structures containing perfluorinated aryl groups at the imine N atom [11, 14, 15]. Quantum-chemical MO calculations showed that the features of the living polymerization mechanism with these systems are associated with the electron-withdrawing effect of the F atoms, which can interact with the β-H atoms in the polymer chain, preventing the β-hydride transfer.

In later studies, the living polymerization was performed for the first time with nonfluorinated titanium phenoxy imine complexes [16, 17]. Similar results were noted in a recent review [5].

We attempted to find a correlation between the features of elementary reactions and the ligand structure. The influence of the structure of the complexes on the energy effects of formation of catalytically active species, of formation of a π complex of the catalyst with ethylene, of chain propagation and transfer, and of deactivation of the system was examined by the DFT method [18] for five phenoxy imine complexes of titanium and zirconium. The data obtained explained the differences in the behavior of the Ti and Zr complexes and the dependence of the activity of the catalytic system on the ligand structure. However, this is only the initial step in revealing correlations between the structures of the complexes and features of the elementary reactions in polymerization.

CONCLUSIONS

(1) Effect of substituents in ligands of phenoxy imine complexes on the activity of catalytic systems based on them in polymerization of ethylene depends on the structure of the substituents and their location in the imine or phenoxy moiety.

(2) Different substituents localized in the imine or phenoxy moiety of phenoxy imine complexes exert a conjugated effect on the activity of catalytic systems based on these complexes.

ACKNOWLEDGMENTS

The study was financially supported by the Presidium of the Siberian Division of the Russian Academy of Sciences within the framework of Integration Project no. 4.6 of the Siberian Division of the Russian Academy of Sciences.

The authors are grateful to S.Ya. Khaikin and E.V. Sviridova for the determination of structural and molecular characteristics of polymer samples and to M.G. Eremeeva and V.S. Misin for participation in the preparation of polymerization experiments.

REFERENCES

1. Mitani, M., Saito, J., Ishii, S.-J., et al., *Chem. Record.*, 2004, vol. 4, pp. 137–158.

2. Furuyama, R., Saito, J., Ishii, S., et al., *J. Mol. Catal. A: Chem.*, 2003, vol. 200, pp. 31–42.
3. Suzuki, J., Terao, H., and Fujita, T., *Bull. Chem. Soc. Jpn.*, 2003, vol. 76, no. 8, pp. 1493–1517.
4. Ivanchev, S.S., *Usp. Khim.*, 2007, vol. 76, no. 7, pp. 669–690.
5. Domski Gregory, J. and Brookhart, M., *Prog. Polym. Sci.*, 2007, vol. 32, pp. 30–92.
6. Matsui, S., Mitani, M., Saito, J., et al., *Chem. Lett.*, 1999, p. 1263.
7. Matsui, S., Mitani, M., Saito, J., et al., *Chem. Lett.*, 2000, p. 554.
8. Reinartz, S., Mason, A.F., Lobkovsky, E.B., and Coates, G.W., *Organometallics*, 2003, vol. 22, p. 2542.
9. Tohi, J., Nakano, T., Makio, H., et al., *Macromol. Chem. Phys.*, 2004, vol. 205, p. 1179.
10. Gagieva, S.Ch., Sukhova, T.A., Savinov, D.V., et al., *Izv. Ross. Akad. Nauk, Ser. Khim.*, 2003, no. 8, pp. 1605–1609.
11. Mitani, M., Mohri, J., Yoshida, Y., et al., *J. Am. Chem. Soc.*, 2002, vol. 124, no. 13, p. 3327.
12. Chiang, R., *J. Polym. Sci.*, 1959, vol. 36, pp. 91–102.
13. Terao, M., Ishii, S., Saito, J., et al., *Macromolecules*, 2006, vol. 39, pp. 8584–8593.
14. Saito, J., Mitani, M., Mohri, J., et al., *Chem. Lett.*, 2001, p. 576.
15. Ishii, S., Saito, J., Mitani, M., et al., *J. Mol. Catal. A: Chem.*, 2002, vol. 179, pp. 11–14.
16. Ivanchev, S.S., Trunov, V.A., Rybakov, V.B., et al., *Dokl. Ross. Akad. Nauk*, 2005, vol. 404, no. 1, pp. 57–67.
17. Ivanchev, S.S., Badaev, V.K., Ivancheva, N.I., et al., *Dokl. Ross. Akad. Nauk*, 2004, vol. 394, pp. 639–642.
18. Yakimanskii, A.V. and Ivanchev, S.S., *Dokl. Ross. Akad. Nauk*, 2006, vol. 410, no. 2, p. 1–3.

ISSN 1070-4272, Russian Journal of Applied Chemistry, 2007, Vol. 80, No. 9, pp. 1523–1528. © Pleiades Publishing, Ltd., 2007.
Original Russian Text © L.B. Belykh, N.I. Skripov, L.N. Belonogova, V.A. Umanets, F.K. Shmidt, 2007, published in Zhurnal Prikladnoi Khimii, 2007, Vol. 80, No. 9, pp. 1489–1494.

CATALYSIS

Preparation of High-Performance Nanosized Palladium Hydrogenation Catalysts Using White Phosphorus and Phosphine

L. B. Belykh, N. I. Skripov, L. N. Belonogova, V. A. Umanets, and F. K. Shmidt

Irkutsk State University, Irkutsk, Russia

Received November 20, 2006

Abstract—The nature and properties of nanosized palladium hydrogenation catalysts modified with elemental phosphorus and phosphine (PH_3) were studied.

DOI: 10.1134/S1070427207090157

Previously were studied the nature of particles active in hydrogenation that were formed by treatment with different reducing agents of palladium(II) complexes with organic phosphines [1–4]. Microheterogeneous nature of these catalysts was revealed, and the key steps of their formation was determined. In particular, the main reactions of palladium(II) phosphine complexes with hydrogen are reduction of Pd(II) to Pd(0) by hydrogenolysis of the Pd–X bonds (X is an acido ligand); degradation of phosphine ligands in the coordination sphere of Pd(0) by oxidative addition of organophosphorus ligands to Pd(0), followed by hydrogenolysis of the Pd–C bond with hydrogen and formation of polynuclear palladium phosphine and phosphinidene complexes (in the limiting case, palladium phosphides, Pd_6P and $Pd_{4.8}P$); and formation of Pd(0) clusters [2, 3]. Active in hydrogenation are Pd(0) clusters or cluster palladium hydrides [Pd_xH_y] immobilized on polynucliear palladium complexes with phosphide and posphinidene ligands or on palladium phosphides. Since formation of Pd(II) phosphine complexes involves stepwise degradation of organophosphorus ligands to form a heterophase system containing in the limiting case palladium phosphides of different composition and Pd(0) clusters, we suggested that phosphine (PH_3) and white phosphorus (P_4) can be used to modify the catalyst. This approach can simplify preparation of nanosized palladium hydrogenation catalysts. The aim of this study was to examine the nature and catalytic properties of the systems prepared by treatment with molecular hydrogen of mixtures of palladium bisacetylacetonate with white phosphorus or phosphine.

EXPERIMENTAL

The solvents and chemicals were purified by standard procedures used in handling of organometallic compounds [5]. Benzene was additionally dried by distillation from $LiAlH_4$ on a column and was stored in an argon atmosphere in sealed ampules over 4A molecular sieves.

To remove water and amine impurities, dimethylformamide was kept over anhydrous copper sulfate until a green solution was formed. Then the solvent was double-distilled in a vacuum (3 mm Hg) at temperature no higher than 42°C.

Palladium bisacetylacetonate was prepared by the procedure described in patent [6]. ^{1}H NMR: δ(CH) = 5.04 ppm (s, 1H), $\delta(CH_3)$ = 1.76 ppm (s, 6H).

To prepare phosphine, a solution of 25 g of KOH in 25 ml of water was added dropwise to a suspension of 10 g of red phosphorus in 30 ml of toluene, preheated to ~110°C [7]. The liberating gas was successively passed through a Tishchenko bottle filled with a 50% solution of an alkali in an H_2O + DMSO mixture to remove diphosphine impurities and then through columns packed with NaOH and P_2O_5 to remove water traces. Phosphine was collected by dissolution in benzene placed in a finger-like vessel. The phosphine concentration in the benzene solution was determined by ^{31}P NMR spectroscopy using 85% H_3PO_4 as external reference; ^{31}P NMR: δ_P = –238 ppm (q, J_{PH} = 188 Hz).

To remove surface oxidation products of white phosphorus, it was washed with anhydrous benzene. A benzene solution of white phosphorus was prepared

and stored under an inert atmosphere in a finger-like vessel. The design of this vessel allows evacuation and filling with argon. ^{31}P NMR: δ_P = 523 ppm.

Catalytic hydrogenation was performed in a duck-shaped vessel thermostated at 30°C at the initial hydrogen pressure of 1 atm in the presence of the catalytic system formed in situ. To a solution of $Pd(acac)_2$ (0.00304 g, 1×10^{-5} mol) in DMF (9 ml) placed in a duck-shaped vessel, a solution of phosphine (0.3×10^{-5} mol) in benzene (1 ml) was added dropwise in a hydrogen stream. The mixture was stirred for 5 min at room temperature. Then the system was heated to 80°C with stirring in a hydrogen stream. The resulting black-brown "solution" was cooled to 30°C. A substrate was injected with a syringe. It was hydrogenated with vigorous stirring to exclude the diffusion control of the reaction. The reaction course was monitored by GLC. The experiments at other P/Pd ratios and preparation of the palladium catalyst modified with white phosphorus were performed similarly. The optimal time required for preparing $Pd(acac)_2$–nP_4 catalytic system at 80°C was 25–30 min.

The palladium catalysts modified with white phosphorus were prepared in a temperature-controlled duck-shaped glass vessel in hydrogen at 80°C. To a solution of $Pd(acac)_2$ (0.761 g, 2.5×10^{-3} mol) in DMF (90 ml), a solution of phosphine (0.75×10^{-3} mol) (P/Pd = 0.3) in benzene (25 ml) was added drop-wise in a hydrogen stream. The mixture was stirred at a hydrogen pressure of 1 atm and 80°C for 15 min. The solution color changed to dark brown in 2–5 min. After reaction completion, the black suspension was cooled to room temperature and was transferred under an inert atmosphere into a finger-like vessel. Then the solvent was removed in a vacuum (2/3 of the volume). Ether was added until a precipitate was formed. The precipitate was washed with ether in an argon atmosphere and was dried in a vacuum (50°C/1 mm Hg). Yield 0.235 g. Elemental analysis, %: Pd 87.88; P 3.59; C 0.99; H 0.25. IR: no absorption in the range 4000–400 cm^{-1}.

Analysis for Pd and P was performed as follows. A weighed portion of the sample (about 0.01 g) was dissolved in 2 ml of boiling HNO_3. The resulting solution was diluted with water to 50 ml in a volumetric flask. The palladium concentration was determined by atomic absorption spectroscopy on a Perkin–Elmer 403 spectrometer in a propane–air flame. The phosphorus content was determined photocolorimetrically by the standard procedure [8].

The catalyst samples were studied by powder X-ray diffraction on a DRON-3M diffractometer using CuK_α radiation. The NMR spectra were recorded on a VXR-500S Varian pulse spectrometer. The ^{31}P chemical shifts are given relative to 85% phosphoric acid.

The samples were studied by transmission electron microscopy (TEM) on a BS-300 microscope (Czech Republic). A drop of the solution was applied onto a gauze coated with a carbon film and was dried in an argon atmosphere. The electron micrographs were taken under conditions excluding melting and degradation of the samples on exposure to an electron beam.

The procedure for determining Pd(0) is described in [9].

Previously we showed [1–4, 10] that palladium(II) β-diketonate–phosphine complexes became catalytically active in hydrogenation reactions only after their activation with a reducing agent, e.g., with molecular hydrogen. To compare the catalytic properties of the catalysts derived from palladium bisacetylacetonate [$Pd(acac)_2$] modified with white phosphorus and phosphine with those of palladium(II) complexes with organic phosphines (PPh_3, $PHPh_3$, PH_2Ph), these catalysts were prepared similarly in a hydrogen atmosphere at 80°C. It should be noted that at a lower temperature the rate of $Pd(acac)_2$ reduction is lower (Table 1). The properties of palladium catalysts modified with phosphine or white phosphorus were studied in relation to different parameters. It was found that the dependences of the specific activity in styrene hydrogenation on the P/Pd ratio passed through maxima. The most active catalysts are formed at similar ratio P/Pd = 0.3 (Fig. 1). We observed the similar dependence for the $Pd(acac)_2$–PH_2Ph system [10]. The influence of organophosphorus compounds on the catalytic activity of $Pd(acac)_2$ decreases in the following order: $P_4 \cong PH_2Ph$ [10] > PH_3 > $PHPh_2$ [11] > PPh_3 [3].

The most active promoters are white phosphorus and phenylphosphine, all catalytic reaction conditions being the same; the phosphine is slightly less effective; the palladium bisacetylacetonate + triphenylphosphine system exhibits the lowest catalytic activity in alkene hydrogenation (Fig. 2).

It should be noted that the specific activity of the palladium catalysts modified with phosphine (PH_3) increases with decreasing palladium concentration and reaches a maximum [330 (mol styrene) (g-at. Pd)$^{-1}$ min^{-1}] at $C_{Pd} = 5 \times 10^{-4}$ M. Nonlinear dependence of the reaction rate on the $Pd(acac)_2$ concentration in the case of the catalyst modification with both phosphine and phosphorus (Fig. 3) suggests associa-

Table 1. Hydrogenation of styrene in the presence of palladium catalysts modified with phosphine and white phosphorus. C_{Pd} = 1 mM, P/Pd = 0.3, [substrate]/Pd = 870, solvent DMF, T = 30°C, P_{H_2} = 1 atm

Conditions of catalyst preparation in hydrogen			W, (mol H_2) (mol Pd)$^{-1}$ min^{-1}	
T, °C	time, min		$Pd(acac)_2$–PH_3	$Pd(acac)_2$–P_4
	$Pd(acac)_2$–PH_3	$Pd(acac)_2$–P_4		
30	15	25	0	0
50	15	25	0	0
70	15	25	166	0
		40		181
80	15	25	190	280
90	15	25	56	137

Table 2. Specific hydrogenation activity of palladium catalysts modified with phosphorus and phosphine. C_{Pd} = 1 mM, solvent DMF, V_{DMF} = 10 ml, P/Pd = 0.3, T = 30°C, P_{H_2} = 1 atm

Substrate, mol	W, (mol H_2) (mol Pd)$^{-1}$ min^{-1}		Product yield, %	
	$Pd(acac)_2$–PH_3	$Pd(acac)_2$–P_4	$Pd(acac)_2$–PH_3	$Pd(acac)_2$–P_4
Styrene, 8.7	190	280	Ethylbenzene, 100	Ethylbenzene, 100
Phenylacetylene, 9.1	59	157	Ethylbenzene, 100	Ethylbenzene, 100
Nitrobenzene:				
4.9	21	64	Aniline, 100	Aniline, 100
2.4		128		Aniline, 100
Benzaldehyde, 9.8	1*	15*	Benzyl alcohol, 95; toluene, 5	Benzyl alcohol, 94; toluene (–)

* c_{Pd} = 5 mM.

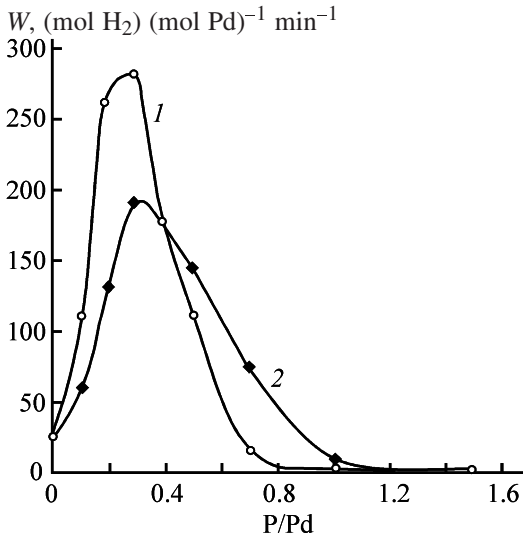

Fig. 1. Hydrogenation of styrene in the presence of palladium catalysts modified with (*1*) white phosphorus and (*2*) phosphine. C_{Pd} = 1 mM, [substrate]/Pd(acac)$_2$ = 870, solvent DMF, T = 30°C, P_{H_2} = 1 atm. (W) Specific activity; the same for Fig. 2.

tion of reactive palladium species in less active aggregates and microheterogeneity of the catalysts.

Palladium species modified with white phosphorus and phosphine are highly active and selective catalysts of hydrogenation of acetylene derivatives and nitro- and carbonyl groups (Table 2). For example, phenylacetylene is successively hydrogenated to styrene and ethylbenzene without its side di- or oligomerization.

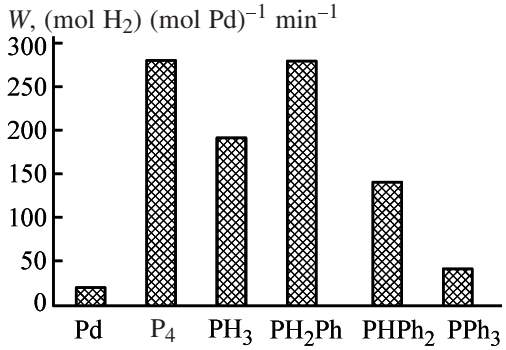

Fig. 2. Influence of the modifier on the specific activity of palladium hydrogenation catalysts.

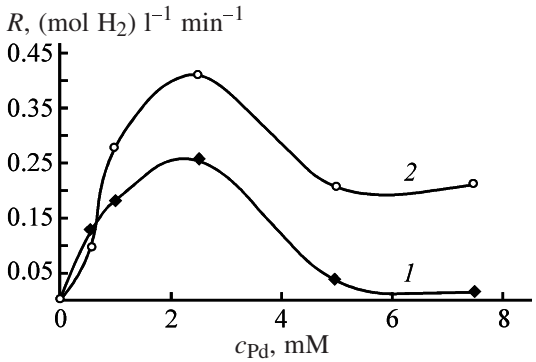

Fig. 3. Rate of styrene hydrogenation R in the presence of catalysts formed by reduction of (*1*) $Pd(acac)_2$–PH_3 and (*2*) $Pd(acac)_2$–P_4 systems as a function of palladium concentration. Solvent DMF, P/Pd = 0.3, T = 30°C, P_{H_2} = 1 atm, [substrate] = 8.7×10^{-3} mol.

At 96% conversion of phenylacetylene, the selectivity with respect to styrene is 94–95%. Nitrobenzene is selectively reduced to aniline.

Thus, the activity of the palladium catalysts modified with white phosphorus and phosphine (PH_3) is not only similar to, but in some cases even higher than that of the previously studied nanosized palladium catalysts prepared from palladium complexes with organic phosphines ($PHPh_2$, PPh_3).

The most active hydrogenation catalysts prepared by treatment of $Pd(acac)_2$ + $0.3PH_3$ (or P_4) system with molecular hydrogen were studied by X-ray diffraction and TEM.

As determined by TEM, the reaction of the $Pd(acac)_2$ + $0.3PH_3$ system with hydrogen yields a microheterogeneous system containing mainly high-contrast particles 7.2–7.8 nm in diameter (Fig. 4a). When the time of hydrogen treatment increases from 15 to 30 min, the system becomes more structured (Fig. 4b). The loose and dendritic structure observed in the micrographs is typical for fractal clusters [12]. These clusters are formed by self-aggregation of nanoparticales of similar size in the absence of stabilizing factors. It should be noted that, in the course of formation of microheterogeneous hydrogenation catalysts in the presence of phosphine ligands, fractal clusters were observed for the first time. Palladium particles formed by reduction of palladium(II) complexes in the presence of tertiary [3], secondary [11], or primary phosphines [10] are more stable to aggregation.

The composition of the black precipitate (sample I) isolated from $Pd(acac)_2$–$0.3PH_3$ system is described by the empirical formula $Pd_{7.5}P_{1.07}H_{2.1}$. As determined by X-ray diffraction, the precipitate is a heterophase mixture containing palladium phosphides of various compositions: Pd_6P (*d*/*n* 2.696, 2.583, 2.368, 2.291, 2.256, 2.232, 2.093, 1.998 Å), $Pd_{4.8}P$ (*d*/*n* 2.439, 2.327, 2.256, 2.232, 2.122, 1.998 Å), Pd_5P_2 (*d*/*n* 2.734, 2.696, 2.439, 2.291, 2.256, 2.232, 2.122, 1.993, 1.858, 1.432 Å) and crystalline palladium (*d*/*n* 2.256, 1.950, 1.375 Å) [13]. Palladium phosphides Pd_6P and $Pd_{4.8}P$ prevail in the sample. The fraction of reduced palladium determined by the chemical method is 31%. Knowing the total content of palladium and phosphorus, the fraction of reduced palladium, and the composition of palladium phosphides, we can describe the composition of sample I by the empirical formula

$$[\{Pd(0)\}_{2.33}\{Pd_6P\}_{0.40}\{Pd_{4.8}P\}_{0.55}\{Pd_5P_2\}_{0.026}].$$

The carbon and hydrogen in the sample most likely originate from the residual solvent (DMF). Hence, the composition will be described by the formula

$$[\{Pd(0)\}_{2.33}\{Pd_6P\}_{0.40}\{Pd_{4.8}P\}_{0.55}\{Pd_5P_2\}_{0.026}\{DMF\}_{0.3}].$$

X-ray diffraction analysis of the catalyst prepared in the presence of white phosphorus [$Pd(acac)_2$–0.3P] shows that the sample consists of palladium phosphide Pd_6P, crystalline palladium, and palladium hydride $PdH_{0.7}$ [13]. The fraction of reduced palladium, determined by the chemical procedure, is 25%. It should be noted that reduction of $Pd(acac)_2$ with hydrogen is an autocatalytic reaction, with the induction period in the presence of white phosphorus increasing from 7 to 18 min. This fact can be explained as follows. Palladium atoms formed in the first steps of hydrogen reduction react with white phosphorus to form palladium phosphides which are not capable to activate molecular hydrogen. After the phosphorus is completely bound into palladium phosphides, $Pd(acac)_2$ is autocatalytically reduced with hydrogen.

Thus, the general feature of formation of hydrogenation catalysts in the system in question is formation of palladium phosphides of different compositions and reduced palladium in the amount of about 25–30%. It should be noted that palladium phosphides as modifiers of organic phosphines, in particular phenyl- and triphenylphosphine, are formed after almost complete degradation of the organophosphorus ligand during treatment of the catalyst with molecular hydrogen at the molar ratio P/Pd ≤ 0.5 [3, 10, 14]. However, a long time required for reduction of $Pd(acac)_2$ with hydrogen in the presence of PH_3 and low stability of the resulting nanoparticles to aggrega-

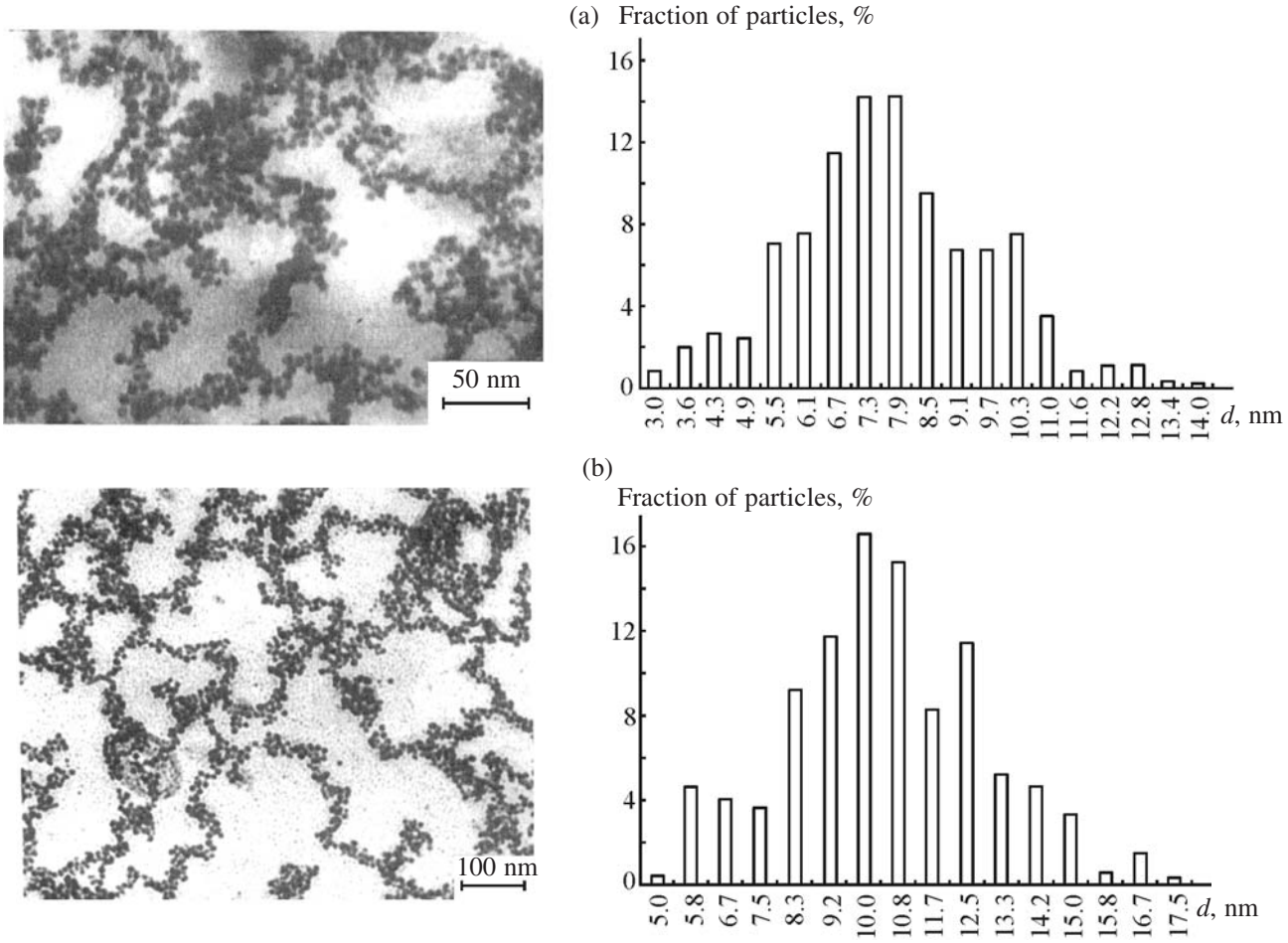

Fig. 4. Electron micrograph of the $Pd(acac)_2$–$0.3PH_3$ system treated with hydrogen at 80°C and particle size distribution. (*d*) Particle size. Treatment time, (a) 15 and (b) 30.

tion lead to a sharp decrease in the activity of the catalyst as compared to the catalysts prepared from $Pd(acac)_2$ and P_4, PH_3, and PH_2Ph.

To determine the mechanism of the promoting effect of the ogranophosphorus compounds on the catalytic properties of the palladium hydrogenation catalysts, we compared the fraction of the surface atoms for the $Pd(acac)_2$–$0.3PH_3$ catalytic system and that of Pd black formed under the similar conditions from $Pd(acac)_2$.

The size of Pd black particles determined by TEM is 25–30 nm, which is larger by a factor of almost 4 than that of particles formed in the $Pd(acac)_2$–$0.3PH_3$ system. It is known that the fraction of the surface atoms for metal particles 8–10 nm in diameter is 20–15%, and it decreases to 3–2% with increasing particle size to 25–30 nm [15]. The increase in the fraction of the surface atoms by a factor of 7 (on the average) correlates with the promoting effect of phosphine. Hence, formation of more finely dispersed system can be one of the reasons determining the promoting effect of phosphine. The assumption that the promoting effect of phosphine is due to an increase in the catalyst dispersity is well consistent with the experimental data for the case when Pd(0) atoms are located on the nanoparticle surface. Based on the results obtained, we suggest that microheterogeneous hydrogenation catalysts consist of nanoparticles whose cores are formed by palladium phosphides with Pd(0) clusters immobilized on the surface.

It should be noted that the high activity of nanosized palladium hydrogenation catalysts cannot be solely due to a small particle size. In particular, the particles of microheterogeneous palladium catalysts prepared from palladium complexes with organic phosphines are smaller (3–5 nm [3, 10]) than particles of the examined systems, but, as noted above, their catalytic activity is lower.

This is due to the fact that transformation of palladium phosphine complexes under the action of molecular hydrogen is a complex multistep process. The general feature of formation of hydrogenation catalysts from $Pd(acac)_2$ and different phosphines in hydrogen is not only formation of microheterogeneous systems but also oxidation of palladium particles after degradation of the phosphorus-containing ligands or reaction of Pd(0) with elemental phosphorus. The ratio of oxidized and reduced palladium changes depending on the ratio of the reduction rates of Pd(II) complexes, aggregation of reduced palladium particles, and degradation of phosphorus-containing fragments in the coordination sphere of Pd(0). In addition, the electron density on Pd(0) clusters can change after their immobilization on palladium phosphides. The structure and catalytic properties of the palladium nanoparticles depend on all of these factors. The particles formed after hydrogen treatment of $Pd(acac)_2$ modified with phosphine and elemental phosphorus have similar structure and a high content of reduced palladium, and hence their catalytic properties in hydrogenation are similar.

CONCLUSIONS

(1) White phosphorus and phosphine (PH_3) were used for the first time as modifiers in synthesis of effective palladium hydrogenation catalysts whose catalytic activity is not only similar to, but in some cases higher than that of nanosized palladium hydrogenation catalysts prepared from palladium complexes with organic phosphines.

(2) Reaction of $Pd(acac)_2$ with hydrogen in the presence of phosphine (PH_3) and white phosphorus yields Pd(0) and palladium phosphides of various compositions.

(3) The promoting effect of phosphine is caused, in particular, by smaller particle size of the catalysts prepared from $Pd(acac)_2$ as compared to Pd black.

ACKNOWLEDGMENTS

This study was financially supported by the Zamaraev International Charitable Foundation and Irkutsk State University grant no. III-020000/107.

REFERENCES

1. Shmidt, F.K., Belykh, L.B., Umanets, V.A., et al., *Kinet. Katal.*, 1999, vol. 40, no. 3, pp. 466–471.
2. Shmidt, F.K., Belykh, L.B., and Cherenkova, T.V., *Kinet. Katal.*, 2001, vol. 42, no. 2, pp. 182–194.
3. Shmidt, F.K., Belykh, L.B., and Goremyka, T.V., *Kinet. Katal.*, 2003, vol. 44, no. 5, pp. 683–691.
4. Belykh, L.B., Goremyka, T.V., Skripov, N.I., et al., *Kinet. Katal.*, 2006, vol. 47, no. 3, pp. 373–380.
5. Gordon, A.J. and Ford, R.A., *The Chemist's Companion. A Handbook of Practical Data, Techniques, and References*, New York: Wiley, 1972.
6. US Patent 3474464.
7. Osadchenko, I.M. and Tomilov, A.P., *Usp. Khim.*, 1969, vol. 37, no. 6, p. 1089.
8. *Metody kolichestvennogo organicheskogo elementnogo mikroanaliza* (Methods of Quantitative Organic Elemental Microanalysis), Gel'man, N.E., Ed., Moscow: Khimiya, 1987.
9. Shmidt, F.K. and Mametova, L.V., *Kinet. Katal.*, 1996, vol. 37, no. 3, p. 431.
10. Belykh, L.B., Goremyka, T.V., and Shmidt, F.K., *Zh. Prikl. Khim.*, 2004, vol. 77, no. 5, pp. 774–778.
11. Belykh, L.B., Goremyka, T.V., Rokhin, A.V., et al., *Kinet. Katal.*, 2004, vol. 45, no. 3, pp. 411–416.
12. Shmidt, F.K., *Fraktal'nyi analiz v fizikokhimii geterogennykh sistem i polimerov* (Fractal Analysis in Physical Chemistry of Heterogeneous Systems and Polymers), Irkutsk: Irkutsk. Gos. Univ., 2001.
13. *Powder Diffraction F.Q., Hanawalt Search Manual, Inorganic Phases*, JCDD, 1992, pp. 1–42.
14. Bakunina, T.I., Zinchenko, S.V., Khutoyarskii, V.A., et al., *Metallokompleksnyi kataliz* (Catalysis with Metal Complexes), Irkutsk: Irkutsk. Gos. Univ., 1989.
15. Gubin, S.P., *Khimiya klasterov* (Chemistry of Clusters), Moscow: Nauka, 1987.

ISSN 1070-4272, Russian Journal of Applied Chemistry, 2007, Vol. 80, No. 9, pp. 1529–1534. © Pleiades Publishing, Ltd., 2007.
Original Russian Text © E.V. Datskevich, V.I. Shutova, V.V. Goncharuk, 2007, published in Zhurnal Prikladnoi Khimii, 2007, Vol. 80, No. 9, pp. 1495–1500.

ENVIRONMENTAL PROBLEMS OF CHEMISTRY AND TECHNOLOGY

Determination of the Conditions of the Sol–Gel Synthesis of Biosorbents for Water Treatment

E. V. Datskevich, V. I. Shutova, and V. V. Goncharuk

Dumanskii Institute of Colloid Chemistry and Water Chemistry, National Academy of Sciences of Ukraine, Kiev, Ukraine

Received October 16, 2006; in final form, March 2007

Abstract—The feasibility of sol–gel synthesis of a series of biosorbents with encapsulated starches, intended for water treatment, was elucidated. The factors governing the morphology of the resulting materials were examined. The performance of the composites synthesized in sorption removal of polyvalent metal ions from water was estimated.

DOI: 10.1134/S1070427207090169

Water pollution with toxicants of different nature is a serious environmental and social problem. Metals have a special place among substances that pose health hazard, as they are, essentially, biotics that acquire toxicity with increasing concentrations [1]. Many countries enacted stringent environmental standards specifying the content of metal ions in water [2]. The principal methods to reduce their content in water include chemical precipitation, ion exchange, adsorption on active carbon, membrane processes, and electrodialysis. However, these methods have limitations like high operation costs or inability to fully satisfy the water quality standards.

Sound environmental protection is possible today only through introduction of advanced technologies and materials, including new sorption materials (adsorption was recognized as the best method for water treatment to remove pollutants) [3]. The most environment-friendly line in the development of materials for water treatment is waste-free production of hybrid nanocomposites [4–6], and the sol–gel method offers wide prospects for preparation of diverse functional materials [5]. For example, in "bionanocomposites," natural polymers encapsulated into an inorganic matrix preserve their activity and spectral properties [6]; bringing water in contact with such sorbents allows reduction of the content of hazardous pollutants virtually to zero [4].

Much research efforts were recently devoted to the development of new sorbents containing biopolymers [7–9]. Among natural polymers, special attention is deserved by polysaccharides because of their specific structure, physical and chemical characteristics, and excellent selectivity with respect to pollutants [8].

In this study, we examined the sol–gel synthesis of biosorbents (BSs) containing encapsulated starches with a view to intensify the removal of metal ions from water.

Starch, second to cellulose widespread biomolecule on the earth [10, 11], is chemically a mixture of two homopolysaccharides, linear amylose and branched amylopectin. Stable forms of starch in the solid state, below the gelation temperature (~60°C), are represented by coil structures; above this temperature in water they uncoil to a substantial extent, and more easily accessible hydroxy groups of the glucose units form hydrogen bonds with the solvent, yielding a gel. With time going, the starch gel slowly resumes its coil structure with formation of a precipitate. Incorporation of reactive functional groups into the starch framework yields products able of removing heavy metal ions from industrial wastewater [12]. However, starch products themselves are hardly suitable as sorbents, since they lack controllable particle size and certain wear resistance, hardness, and porosity. One of the methods to increase the stability of a biosorbent consists in incorporation of a natural polymer into an inorganic material [13]; the resulting hybrid nanocomposites typically exhibit synergism of the properties of the initial components. In this respect, the advantages offered by the silica matrix are chemical stability,

Table 1. Summary of the reagents used for synthesis of biosorbents

Biosorbent	Precursor solution composition (weight ratio)				Polysaccharide
BS-1.1	TEOS (5.3)	–	H_2O (4.35)	HCl (0.25)	Starch (1.0)
BS-1.2					Starch + urea
BS-1.3					Starch + thiourea
BS-2.1	TEOS (5.2)	Ethanol (4.35)	H_2O (0.5)	HCl (0.75)	Starch (1.0)
BS-2.2					Starch + urea
BS-2.3					Starch + thiourea
BS-3.1	TEOS (9.5)	Methanol (20)	H_2O (6.7)	–	Starch (1.0)
BS-3.2					Starch + urea
BS-3.3					Starch + thiourea
S-4	TEOS (9.5)	Methanol (20)	H_2O (6.7)	–	No polysaccharide
S-5	ECH (0.18)	–	H_2O (0.12)	NaOH (0.08)	Starch (1.0)

as well as large specific surface area, porosity, and mechanical strength [14]. Synthesis of silica gel matrix is underlain by polycondensation of silicic acid yielded by hydrolysis of silanes in an aqueous solution [6].

In this study, we examined immobilization of a series of starch products in a silica matrix by the sol–gel method and compared the degrees of sorption of Cu^{2+}, Fe^{3+}, and Al^{3+} on the resulting materials (to elucidate how the method of synthesis and the polysaccharide nature affect the performance of the biosorbent). Also, we compared the synthesized biosorbents with the known sorbents, silica [14] and starch cross-linked with epichlorohydrin [8].

EXPERIMENTAL

We used pure grade water-soluble starch [GOST (State Standard) 10 163–76]; chemically pure grade urea, thiourea, ethanol, sodium hydroxide, hydrochloric acid, and iron, aluminum, and copper chlorides; analytically pure grade tetraethoxysilane (TEOS) (Fluka) and epichlorohydrin (ECH) (Merck); and deionized water ($\chi < 1 \times 10^{-8}$ Ω^{-1} m^{-1}).

Samples of starch products were prepared using the technique from [15] (in part) at different urea : starch molar ratios (calculated from the glucose residue). Native starch was thoroughly mixed with the appropriate amount of the modifier (urea or thiourea) in an agate mortar. Next, the mixture was heated at atmospheric pressure and 100–105°C for 15–17 h and at 125–130°C for 7–8 h; the solid-state reaction was run to completion in a microwave oven (5 min at 900 VA). The resulting material was extracted in a Soxhlet apparatus with 70% aqueous ethanol and dried at 80–90°C.

The polysaccharide (starch or its derivatives) was suspended in an acidified water (pH ~4.0) and left for 1 day; after decantation, starch was washed successively with distilled water and ethanol, dried at 45–50°C, and mechanically activated before introduction of inorganic compounds (precursors) into the composition. The compositions of the precursors used for preparing a series of biosorbents (Table 1) were chosen according to [16].

The sol–gel synthesis procedures were as follows. Biosorbents 1 (BS-1.1–1.3) were synthesized by mixing the components for 5 h at room temperature (starch was added in the last hour), whereupon the resulting gel-like precipitate was dried for 2 days at 25°C and for 1 day at 90°C. The precursor components for biosorbents 2 (BS-2.1–2.3) after mixing were kept for 2 days in a refrigerator (–5°C), whereupon the polysaccharide was added. The resulting mixture was stirred for 30 min and dried for 1 day (90°C). The components of biosorbents 3 (BS-3.1–3.3) were mixed for 2 h; about 70% methanol was allowed to evaporate with exhaust ventilation at room temperature, whereupon starch was introduced into the precursor, and the resulting sample was dried (90°C).

For comparison, we also synthesized sorbent 4 (silica without starch) by the procedure identical to that in preparation of biosorbent 3, to estimate the sorption capacities of the silica matrices, and biosorbent 5 by the known technique [17] involving immobilization with epichlorohydrin. The dried precipitates of the sorbents were crushed and screened to collect 250–500-μm particles for sorption experiments.

To elucidate the role played by the polysaccharides in sol–gel processes, we examined the resulting mate-

rials with a scanning electron microscope (JSV-T20 JEOL). Figure 1 demonstrates the structure of biosorbent 3.1 (Table 1) with a three-dimensional network consisting of intersecting or branched fibers, dissimilar to that of solid nanoparticles in silica-based composite materials [5].

Linear polysaccharides are known to catalyze sol–gel transition in systems containing organosilicon precursors [18]. Catalysis is underlain by hydrogen bonding between the hydroxy groups of the carbohydrate and the silane hydrolysis products. Considering the structural features and chemical composition of starches [11], it can be presumed that the hydroxy groups of amylose enter into a condensation reaction with silanols (≡Si–OH). This results in nucleation of silica on the "fiber" macromolecules and formation of a matrix. The major portion of starch is encapsulated into the resulting silica gel matrix during its formation. It is believed that, in this case, the biomacromolecules preserve the ability for conformation transitions and, consequently, the individual sorption activity in the composite material [6]. The images obtained by atomic-force microscopy (AFM) (Fig. 2; Nanoscope IIIa Dimension 3000^{TM}) demonstrate "loose" island structures on the biosorbent surface, formed immediately after synthesis of the material (Fig. 2a). Within 5–7 days, these structures transformed into clear honeycomb structures with a wall height of about 200 nm (Fig. 2b). Such changes in the topography of the sample suggest that the end structure of the biosorbent was influenced by immobilized starch; retrogradation causes the polysaccharide macromolecules to rearrange into coil structures, thereby imparting a high rigidity to the material [19].

The structural organization of the material was little affected by replacement of starch by its derivatives in synthesis of the biosorbent. A possible reason is that the resulting starch products are neutral compounds, while the density and structure of the network are known to depend on the charge of the macromolecules [5].

Sorption of polyvalent metal ions was carried out as follows. A weighed portion of the biosorbent containing 0.1 g of starch and 100 ml of the appropriate aqueous solution ($FeCl_3$, $AlCl_3$, and $CuCl_2$) was placed into a reaction vessel. The initial concentration of the metal in solution was varied within 10–300 mg l^{-1}; pH of the initial solution (5.0–5.5) was adjusted with HCl and NaOH.

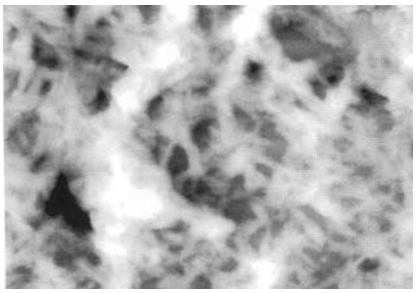

Fig. 1. Images of the biosorbent with immobilized starch. $\times 2 \times 10^5$ magnification, scanning mode.

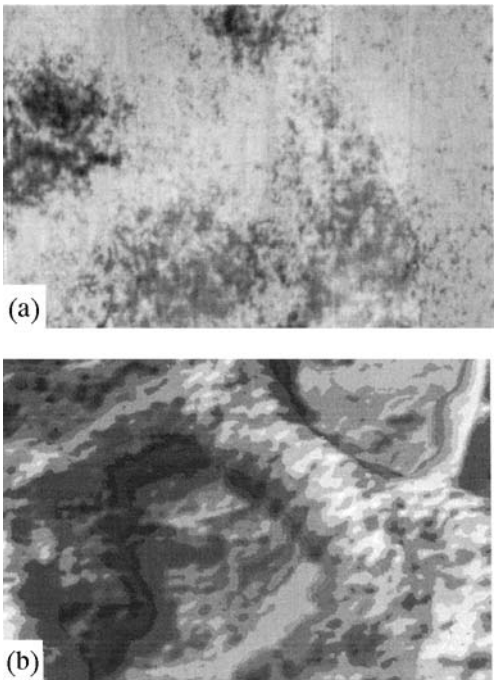

Fig. 2. Images of the biosorbent BS-2.1 surface (a) immediately after preparation of the composite and (b) after 7 days. $\times 5 \times 10^4$ magnification, AFM data.

The reaction mixture was left for 24 h under intermittent stirring at constant temperature (20°C) until the adsorption equilibrium was established. Next, the mixture was filtered, and the content of the cations in the filtrate was determined spectrophotometrically (SPEKOL 11, Carl Zeiss, Jena). The number of the sorbent-bonded ions was calculated by the formula

$$q = (c_0 - c)V/M,$$

where c_0 and c are, respectively, the initial and equilibrium concentrations of metal in the aqueous phase, mg l^{-1}; V, volume of the solution in the test flask, ml; and M, weight of immobilized starch or its derivatives, g.

Table 2. Absorption of metals with the biosorbents containing immobilized starch (c_0 = 50 mg l^{-1})

Biosorbent	q, mg g^{-1}		
	Cu^{2+}	Fe^{3+}	Al^{3+}
BS-1.1	14.05	10.20	7.80
BS-2.1	2.05	1.70	1.75
BS-3.1	25.20	18.25	14.00
S-4*	4.15	3.00	2.30
BS-5	20.00	14.80	11.65

* Calculations took into account the sorbent weight; the same for Table 3.

Table 3. Absorption q of the copper ions with biosorbents containing immobilized starch

Biosorbent	q, mg g^{-1}, at indicated c_0, mg l^{-1}		
	100	200	300
BS-1.1	20.02	24.10	28.90
BS-2.1	5.09	7.75	11.02
BS-3.1	43.63	49.05	52.00
S-4	8.00	10.60	13.25
BS-5	34.15	42.61	45.70

Taking into account the AFM data, the biosorbents were used no earlier than 7 days after synthesis.

For our experiments we chose composite materials, biosorbents with immobilized native starch (Table 2);

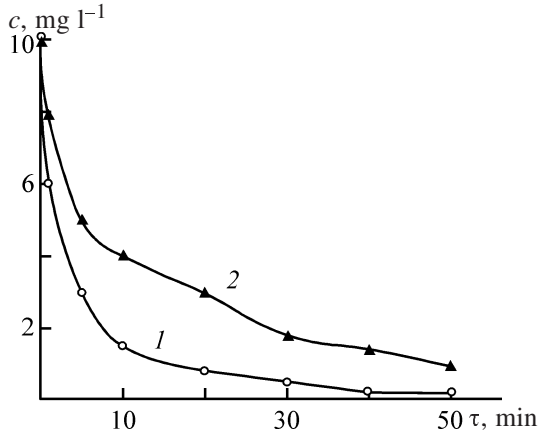

Fig. 3. Sorption of Fe^{3+} (c_0 = 10 mg l^{-1}) with biosorbents vs. time τ, min. (*c*) Concentration of the Fe ions. (*1*) BS-3.1 (starch immobilized in silica matrix) and (*2*) BS-5 (starch cross-linked with epichlorohydrin).

the initial concentration of the metal in water was 50 mg l^{-1}. The highest sorption capacity was exhibited by biosorbents BS-3.1 and BS-5; the weakest bonding of the metal ions was observed for biosorbent BS-2.1, which is a glassy nonporous material with the specific surface area of 3.2 ± 0.5 m^2 g^{-1}.

It should be noted that biosorbents BS-1.1 and BS-3.1 had a much larger specific surface area (210 and 290 m^2 g^{-1}, respectively) than the BS-5 material cross-linked with epichlorohydrin (S_{sp} = 45.0 m^2 g^{-1}). However, the difference in the degree of sorption cannot be attributed exclusively to that in the specific surface area of the sorbents. For example, the specific surface area of BS-3.1 sorbent with immobilized starch exceeds that of S-4 sorbent, silica free from starch (S_{sp} = 260 m^2 g^{-1}), by only 10%, but the sorption capacity of the biosorbent is appreciably larger. Therefore, the presence of immobilized polysaccharide in the structure of the material is essential in this case. The leading role of the polysaccharide is also suggested by the fact (Table 2) that the amount of bound Cu^{2+} is appreciably larger than those of Al^{3+} and Fe^{3+} because of a special affinity of carbohydrates for bivalent metals [20]. In experiments with high initial concentrations, the examined materials exhibited smaller differences in the sorption capacities (Table 3).

Figure 3 presents the kinetics of Fe^{3+} sorption by the biosorbents essentially differing in the method of synthesis, namely, for BS-3.1 (starch immobilized in a silica matrix) and BS-5 (starch cross-linked with epichlorohydrin). All the metals examined (similar curves were obtained for Cu^{2+} and Al^{3+}) were sorbed on BS-3.1 at a higher rate, with both biosorbents having close maximal sorption capacities. This can be explained by easier "accessibility" of the sorption centers of the materials formed from specific interaction of the silica matrix and starch, compared to the biosorbent with a high degree of cross-linking (BS-5), minimizing the metal sorption.

High rates of Cu^{2+}, Fe^{3+}, and Al^{3+} sorption on the biosorbents synthesized make these materials suitable for continuous removal from water of polyvalent metal ions at their low concentrations (≤ 50 mg l^{-1}).

The degree of sorption of the metal ions on the biosorbents containing starch derivatives is higher than that of the biosorbents containing native starch; it varies both with the nature of the modifier and with the valence of the metal sorbed (Fig. 4). The best sorption characteristics were exhibited by biosorbents BS-3.1–3.3, but the general trend is exhibited by all

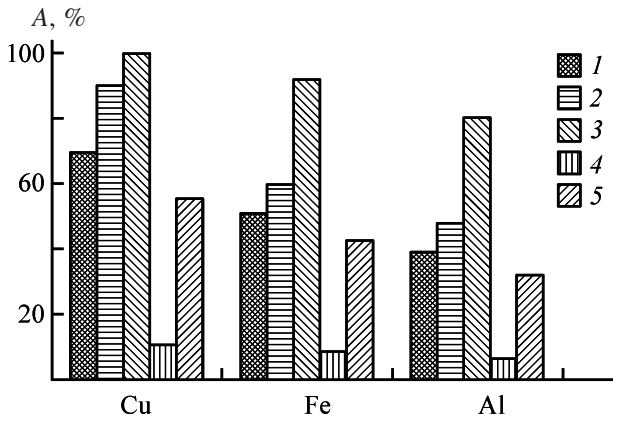

Fig. 4. Degree of sorption A of the cations from the aqueous solutions with various biosorbents. c_0 = 20 mg l^{-1}, M = 0.1 g, Z = 1. (*1*) BS-3.1, (*2*) BS-3.2, (*3*) BS-3.3, (*4*) S-4, and (*5*) BS-5.

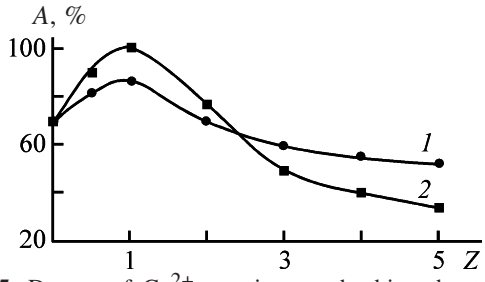

Fig. 5. Degree of Cu^{2+} sorption on the biosorbents containing starch derivatives. (*A*) Degree of sorption and (*Z*) urea/starch ratio. (*1*) Urea/starch and (*2*) thiourea/starch.

the materials synthesized. Even glassy materials with the minimal specific surface area (BS-2.1–2.3) differ in the sorption capacity [e.g., $q_{2.1}$ = 2.05, $q_{2.2}$ = 3.30, $q_{2.3}$ = 3.50 (mg Cu) g^{-1}]. This suggests above all that, under mild conditions of sol–gel synthesis of the composite material, the macromolecule preserves its "individual features," since the resulting biosorbents had virtually identical morphologies.

The difference in the sorption capacities of the starch products can be associated with the ability of the polysaccharides modified with ureas for chelation with metal ions. Reactions of starch with ureas during the solid-state synthesis yield a series of derivatives:

$$C_6H_9O_4(OH) + R^1{-}H \rightarrow C_6H_9O_4{-}R^1 + H_2O, \quad (1)$$

$$2C_6H_9O_4(OH) + H{-}R^2{-}H \rightarrow C_6H_9O_4{-}R^2{-}O_4H_9C_6 + 2H_2O, \quad (2)$$

where R^1 = $H_2N{-}\underset{\underset{O}{\|}}{C}{-}NH{-}$, $H_2N{-}\underset{\underset{S}{\|}}{C}{-}NH{-}$,

R^2 = $-HN{-}\underset{\underset{O}{\|}}{C}{-}NH{-}$, $-HN{-}\underset{\underset{S}{\|}}{C}{-}NH{-}$.

In metal–starch–urea chelates, the ligand is bonded to two metal atoms via the oxygen atom and (more weakly) via the nitrogen atom, and in the thiourea derivatives three metal atoms are bonded to the ligand via the sulfur atom and two nitrogen atoms [21]. Clearly, sorption on a material comprising a tridentate ligand will be larger than that on a biosorbent with a bidentate ligand (Fig. 4).

It should be noted that the degree of sorption on the biosorbents with immobilized starch derivatives varies with the urea : starch ratio (Fig. 5): Initially it tends to grow, attains a maximum, and then very sharply decreases. Starch is a polyoxy compound, and hydrogen bonding strongly affects the accessible surface area of the polysaccharide. Evidently, in the course of the solid-phase dextrinization reaction [11], the accessible starch surface area increases, and the degree of sorption increases due to a high probability of chelation. At the same time, at increased concentrations, ureas begin to act as cross-linking agents [12]. This is responsible for self-polymerization and a decrease in the accessible surface area of the starch product, which sharply decreases the degree of sorption of the metal ions from solutions on the biosorbent.

Thus, high-performance sol–gel-derived biosorbents of polyvalent metals should have the maximal porosity and contain immobilized starch derivatives. Such biosorbents have a good mechanical strength, and the nontoxic composition of the material makes it suitable for tap and potable water treatment.

CONCLUSIONS

(1) A series of biosorbents were synthesized from starch and its derivatives, immobilized in the silica matrix by the sol–gel method with various compositions of the precursors.

(2) The sorption capacity of the biosorbents synthesized varies with the conditions of synthesis; replacement of starch by its derivatives does not influence the morphology of the materials synthesized.

(3) The performance of the biosorbents synthesized in removal of polyvalent metal ions (Al^{3+}, Fe^{3+}, Cu^{2+}) from water varies with the composition of the polysaccharide as starch–thiourea > starch–urea > starch.

REFERENCES

1. Sitting, M., *Handbook of Toxic and Hazardous Chemicals*, Park Ridge, New York: Noyes, 1981.
2. *Ekologicheskie aspekty sovremennykh tekhnologii okhrany vodnoi sredy* (Environmental Aspects of Modern Water Environment Protection Technologies), Goncharuk, V.V., Ed., Kiev: Naukova Dumka, 2005.
3. Horacek, J., Soukupova, L., Puncochar, M., et al., *J. Hazard. Mater*., 1994, vol. 34, pp. 69–76.
4. *Nanotechnology Research Direction: IWGN Workshop Report: Vision for Nanotechnology R&D in the Next Decade*, Roco, M.C., Williams, K.S., and Alivisatos, P., Eds., Dordrecht: Kluwer, 2001.
5. Shchipunov, Y.A. and Karpenko, T.Y., *Langmuir*, 2004, vol. 20, pp. 3882–3887.
6. Pomogailo, A.D., *Usp. Khim*., 2000, vol. 69, no. 1, pp. 60–89.
7. Netpradit, S., Thiravetyan, P., and Towprayoon, S., *Water Res*., 2004, vol. 38, pp. 71–78.
8. Crini, G., *Prog. Polym. Sci*., 2005, vol. 30, pp. 38–70.
9. Reddad, Z., Gerente, C., Andres, Y., and Le Cloirec, M., *Environ. Sci. Technol*., 2002, vol. 36, pp. 2067–2073.
10. *Chemistry and Industry of Starch*, Kerr,, R.W.E., Ed., New York: Academic, 1950.
11. Whistler, R.L., BeMiller, J.N., and Paschall, E.F., *Starch Chemistry and Technology*, Orlando: Academic, 1984.
12. Holan, Z., Volesky, B., and Prasetyo, I., *Biotechnol. Bioeng*., 1993, vol. 41, pp. 819–824.
13. Iler, R.K., *The Chemistry of Silica*, New York: Wiley–Interscience, 1979.
14. Siemion, P., Kapusniak, J., and Koziol, J.J., Abstracts of Papers, *11th Int. Symp. on Starch Chemistry*, Moscow, June 17–19, 2003, p. 134.
15. Szilva, J., Kunsova, G., Patzak, M., and Dostalek, P., *J. Sol–Gel Sci. Technol*., 1997, no. 11, pp. 289–294.
16. Xiang Bo, Li Yijiu, and Ni Yaming, *Ind. Water Treat*., 2003, vol. 23, no. 8, pp. 26–29.
17. Han, B.H. and Antonietti, M., *Chem. Mater*., 2002, vol. 14, pp. 3477–3482.
18. Hancock, R.D. and Tarbet, B.J., *J. Chem. Educ*., 2000, vol. 77, no. 8, pp. 988–992.
19. Alekseev, Yu.E., Garnovskii, A.D., and Zhdanov, Yu.A., *Usp. Khim*., 1998, vol. 67, no. 8, pp. 723–744.
20. Khalil, M.I. and Abdel-Halim, M.G., *Carbohydrate Res*., 2000, no. 324, pp. 189–199.

ISSN 1070-4272, Russian Journal of Applied Chemistry, 2007, Vol. 80, No. 9, pp. 1535–1537. © Pleiades Publishing, Ltd., 2007.
Original Russian Text © V. Grazuleviciene, I. Grigalaviciene, J. Mikelaitis, J. Vedegyte, 2007, published in Zhurnal Prikladnoi Khimii, 2007, Vol. 80, No. 9, pp. 1501–1503.

ENVIRONMENTAL PROBLEMS OF CHEMISTRY AND TECHNOLOGY

Pollution of Environment with Products of Interaction of Stainless Steels with Fuel Combustion Products

V. Grazuleviciene, I. Grigalaviciene, J. Mikelaitis, and J. Vedegyte

Lithuanian Agricultural University, Kaunas region, Lithuania

Received October 20, 2006; in final form, June 2007

Abstract—Composition of condensates formed in flues equipped with stainless steel inserts was studied. Factors affecting corrosion of metallic sections of heating installations were determined.

DOI: 10.1134/S1070427207090170

Chromium and nickel are of particular importance among chemical pollutants of environment because of their high toxicity and carcinogenic action on the human health [1–3]. Corrosion occurring under the effect of atmospheric gases increases their concentration in the environment. Various metallic structures, roofs, house ironworks, and funnels undergo corrosion. The rate of corrosion depends on the season and on climatic and technogenic conditions. The concentration of heavy metals in the environment increases with the start of the heating season. This is due not only to an increase in the exhaust of heavy metals naturally present in the organic fuel and in the corrosion activity of the atmosphere owing to the increase in the concentration of such fuel combustion products as SO_2, NO_x, chlorine-containing compounds, and organic acids, but also due to additional emission of products formed by corrosion of metallic sections of heating installations such as flues, inserts, etc. This problem became topical after oil crises of 1973 and 1979 when production of high-efficiency boilers began. Because of lower temperature of combustion products outgoing from these boilers, a condensate is formed on the flue walls [4, 5]. Sometimes special systems to discharge accumulated condensate into the drainage system are developed. The condensate composition depends on the temperature and properties of the fuel combustion products, humidity, and some other factors. In combustion of natural gas, the condensate pH is 3–4 and for liquid fuel it varies from 1.8 to 3.7, which is due to sulfur contained in the fuel. In the course of combustion, sulfur yields SO_2 which is oxidized to SO_3 and then forms sulfuric acid with water vapor. The condensate destroys brick chimneys and primarily brick joints. To prevent the flue destruction, they are often equipped with inserts of stainless steel with a high content of chromium and nickel. Steel structures are used not only for modernization of the operating brick funnels but also as exhausters for fireplaces, furnaces, and boilers. However, stainless steels also undergo corrosion [6]. Therefore, condensate penetrating into the environment can also contain products of the stainless steel corrosion, including chromium and nickel compounds.

In this study we determined the composition and properties of condensates sampled from flues equipped with stainless steel inserts and evaluated the factors affecting the rate of corrosion of the metallic sections of heating installations.

EXPERIMENTAL

The condensates for studies were sampled from flues equipped with stainless steel inserts, and their pH, density, and contents of chloride ions, iron, nickel, and chromium were determined. To determine the total content of metals, the condensate was mineralized with a mixture of sulfuric and nitric acids [7]. The concentrations of chromium and nickel in the resulting solutions were determined by atomic absorption spectroscopy on an Analyst 100 device, and the iron concentration, by spectrophotometry with potassium thiocyanate [8]. The concentration of chloride ions was determined by titration of the condensates with a mercury nitrate solution. As seen from the results listed in Table 1, at similar pH the content of steel components in the condensates is different. The concentrations of chromium and nickel in the condensates vary from 0.4 to 46.8 and from 0.04 to

Table 1. Chemical composition and properties of the condensates

Condensate no.	Density, g cm^{-3}	pH	Content, mg l^{-1}			
			Cl^-	Cr	Ni	Fe
1	1.051	4	1092	1.68	0.62	5000
2	1.029	3.5	1773	0.40	1.74	122
3	1.031	3.4	1063	2.20	0.04	3030
4	Paste-like	3.0		46.8	123	59 800
5	1.018	3.0	563	–	–	5.2
6	1.010	2.8	612	–	–	11.5

Table 2. Chemical composition of stainless steels*

Steel no.	Content, mg l^{-1}										
	C	Si	Mn	Cu	Al	Cr	Mn	Ni	V	Ti	Nb
1	0.08	0.48	1.45	0.20	0.065	18.48	2.05	10.89	0.07	0.52	0.01
2	0.06	0.54	1.92	0.26	0.41	17.85	2.19	10.95	0.07	0.25	0.01
3	0.06	0.38	1.59	0.19	0.007	18.95	0.32	9.05	0.07	0.01	0.00

* Chemical composition of steels was determined on a Belec 2000 spectrum analyzer.

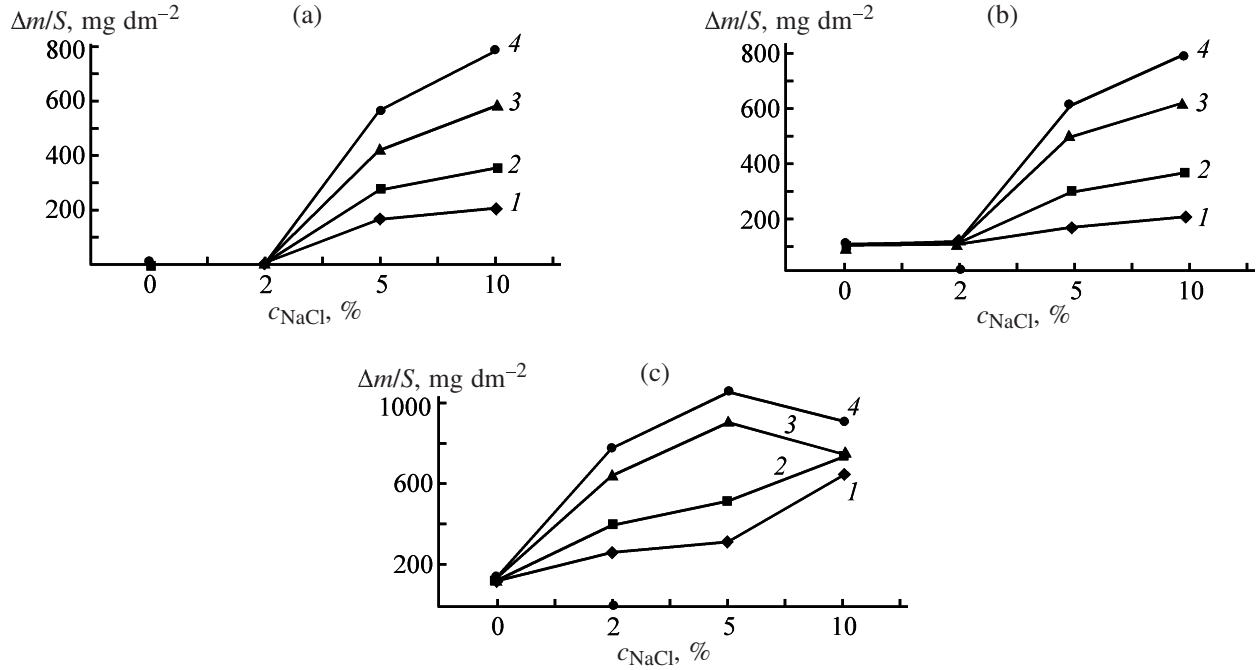

Fig. 1. Weight loss $\Delta m/S$ of stainless steel nos. 1–3 as a function of the content of chloride ions c_{NaCl} in 10% sulfuric acid solutions at various exposure times. Steel samples (Table 2): (a) no. 1, (b) no. 2, and (c) no. 3; the same for Fig. 2. Exposure time, days: (*1*) 5, (*2*) 10, (*3*) 20, and (*4*) 30.

123 mg l^{-1}, respectively. This is probably due to different chemical compositions of the steels, fuel type, composition of the fuel combustion products, design features of the boilers, and modes of their operation. The presence in the combustion area of chloride ions acting as corrosion activators [9] is an important factor accelerating corrosion of metallic parts of the heating systems.

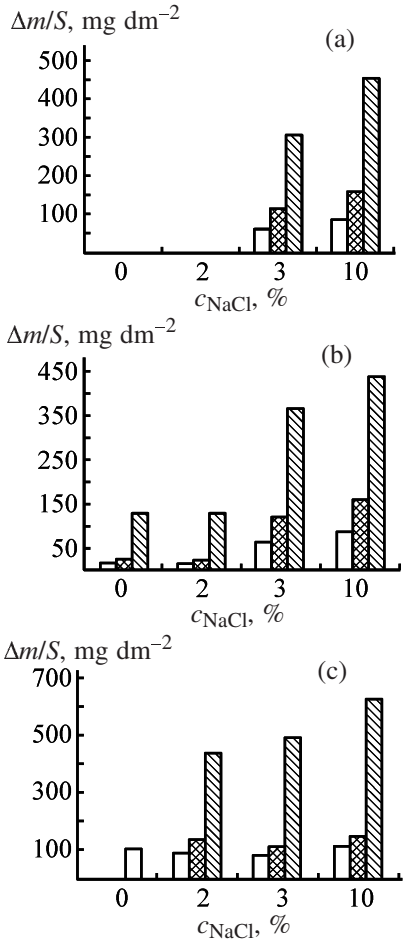

Fig. 2. Weight loss $\Delta m/S$ of components of stainless steel nos. 1–3 as a function of the content of chloride ions c_{NaCl} in 10% sulfuric acid solutions after exposure for 30 days. (a) Nickel, (b) chromium, and (c) iron.

It was of particular interest to compare corrosion resistance of stainless steels of various compositions in the acidic solutions similar to that of the condensate. The chemical composition of the steels is listed in Table 2. Sulfuric acid solutions (10%) with various contencentrations of sodium chloride were used as corrosive solutions. Steels with known composition (Table 2) were kept for a certain time in the above corrosive solutions, and the weight loss was evaluated. The results are shown in Fig. 1. As can be seen, the resistance of stainless steels in 10% sulfuric acid solutions is determined by their chemical composition. Steels containing titanium and molybdenum are the most resistant. After exposure for 30 days in corrosive solution, the weight loss for steel no. 1 (0.52% Ti and 2.05% Mo) was 1.97, and for steel no. 3 (0.01% Ti and 0.32% Mo), 135 mg dm^{-2}. Chloride ions present in solution decrease the corrosion resistance of stainless steel, and the protective effect of molybdenum and titanium is observed only when the concentration of sodium chloride in the sulfuric acid solution was no more than 2%. At higher concentrations of chloride ions, the weight loss of the stainless steels under consideration was similar.

After exposure for 30 days, the contents of iron, chromium, and nickel in the resulting acidic solutions were determined and the weight loss per surface unit was evaluated. The results are shown in Fig. 2. As can be seen, after exposure the solvents contained iron along with alloying components (chromium and nickel), and the weight loss of these elements was determined by both chemical composition of the steel and content of chloride ions in the solution.

CONCLUSIONS

(1) Condensates formed in flues equipped with stainless steel inserts contain the products of steel corrosion including chromium and nickel compounds hazardous for environment.

(2) Steels with elevated content of titanium and molybdenum are the most stable in the aggressive environment. Sound choice of steels for flue inserts being in contact with fuel combustion products not only makes longer the operation life of the installations but also decreases the environmental pollution.

(3) Chlorides present in the combustion atmosphere increase the content of chromium and nickel compounds in the corrosion products of stainless steel.

REFERENCES

1. Zakrzewski, S.F., *Podstawy toksykologii srodowiska*, Warsaw: Naukowe, 1997.
2. Alpoim, M.C., Geraldes, C.F., and Oliveira, C.R., *Biomed. Soc. Trans*., 1995, vol. 23, p. 241.
3. Davies, A.M., *J. Soc. Occup. Med*., 1986, vol. 36, p. 29.
4. Jarman, R.T. and Turville, C.M., *Atmosph. Environ*., 1983, vol. 17, no. 9, p. 1837.
5. Baltenenneck, S., *Rev. Metall.-Can. Inform. Tech*., 1994, vol. 91, no. 10, p. 1469.
6. Ryan, M.P., Williams, D.E., Chater, R.J., et al., *Nature*, 2002, vol. 415, p. 770.
7. *ISO 5515:1979 [E]: Fruits, Vegetables and Derived Products: Decomposition of Organic Matter Prior to Analysis Wet Method.*
8. *GOST* (State Standard) *4011–72: Potable Water. Methods for Determination of Total Iron Content*.
9. Podobaev, A.N., *Protect. Met*., 2005, vol. 41, no. 6, p. 548.

ISSN 1070-4272, Russian Journal of Applied Chemistry, 2007, Vol. 80, No. 9, pp. 1538–1543. © Pleiades Publishing, Ltd., 2007.
Original Russian Text © N.A. Samoilov, I.A. Mnushkin, O.A. Mnushkina, 2007, published in Zhurnal Prikladnoi Khimii, 2007, Vol. 80, No. 9, pp. 1504–1510.

PROCESSES AND EQUIPMENT OF CHEMICAL INDUSTRY

Specific Features of Operation of a Reaction–Rectification Column in Different Feed Modes

N. A. Samoilov, I. A. Mnushkin, and O. A. Mnushkina

Ufa State Technical University of Oil, Ufa, Bashkortostan, Russia
Peton Limited Liability Company, Ufa, Bashkortostan, Russia

Received April 13, 2006; in final form, January 2007

Abstract—Various feeding modes (discrete and distributed) into a reaction–rectification column for production of ethylene glycol are analyzed.

DOI: 10.1134/S1070427207090182

Interest in development of reaction–rectification apparatus [1] combining a chemical process with separation of the reaction products has markedly increased recently. Apparatus of this kind make it possible to simplify the process scheme, diminish the capital expenditure for construction of installations, and optimize the process as a whole [2–6]. Reaction–rectification columns can be used in such processes as esterification, hydrolysis, oxidation, alkylation, and isomerization, in which the chemical stage occurs in the boiling temperature range of components of the reaction mixture on several contact mass-exchange units of the column and, in particular, in synthesis of ethylene glycol.

The most widely employed method for production of ethylene glycol is direct hydration of ethylene oxide, accompanied by a number of side reactions of glycols with ethylene oxide to give diethylene glycol, triethylene glycol, and tetraethylene glycol. To suppress the side reactions, industrial synthesis of ethylene glycol is commonly performed in the liquid phase at elevated temperatures (~475 K) and pressures (1.5–2 MPa) in an excess of water [7].

Previously, a combined static-kinetic model of operation of the reaction–rectification column has been suggested [8]. This model includes calculation of the kinetics of the chemical process in the contact unit of a column with that of the statics of fractionation of the reaction mixture by the relaxation method.

A specific feature of the operation of the reaction–rectification column in synthesis of ethylene glycol is the possibility of recycling excess water within the column to suppress side reactions at virtually complete conversion of ethylene oxide and, accordingly, operation of the upper part of the column in the total reflux mode without distillate takeoff (Fig. 1a), which improves the fractionation efficiency [9]. In this case, the feed (water and ethylene glycol, taken in a 1 : 1 stoichiometric ratio) is introduced into one of the contact units (plates) in the middle of the column, mixed with the reflux composed of water with a minor content of impurities, and subjected to a chemical transformation to ethylene glycol with a minor admixture of higher glycols. Further, the reaction mixture is subjected to fractionation to give ethylene glycol with admixture of water and higher glycols in the bottom part of the column. Thus, the rectification process

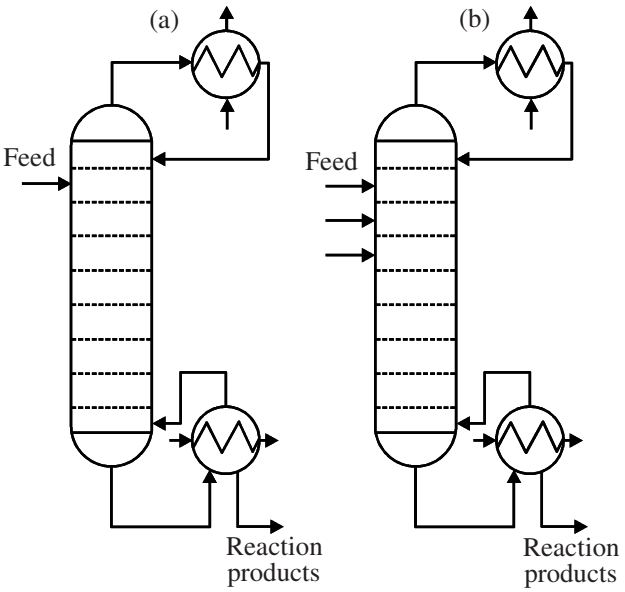

Fig. 1. Schematic of a reaction–rectification column operating in the total reflux mode, with feed in different ways. Feeding: (a) discrete and (b) distributed.

Table. 1. Compositions of counterflow nonequilibrium vapor and fluid on adjacent plates of a reaction–rectification column. Pressure in the column 0.5 MPa; reflux : ethylene oxide ratio at the input of 3rd plate 50 : 1

Component	Between 1st and 2nd plates		Between 7th and 8th plates	
	fluid	vapor	fluid	vapor
Ethylene oxide	2.53×10^{-6}	2.53×10^{-6}	1.46×10^{-11}	1.49×10^{-11}
Water	0.99	0.99	0.13	0.13
Ethylene glycol	3.60×10^{-5}	3.60×10^{-5}	0.86	0.86
Diethylene glycol	1.26×10^{-8}	1.26×10^{-8}	4.45×10^{-3}	4.21×10^{-3}
Triethylene glycol	1.35×10^{-11}	1.35×10^{-11}	2.06×10^{-5}	1.72×10^{-5}
Tetraethylene glycol	1.38×10^{-15}	1.38×10^{-15}	6.69×10^{-8}	4.03×10^{-8}

in the column consists, in fact, in separation of the reaction products from the recycled reflux.

In some cases, the operation of a reaction–rectification column can be improved by choosing the optimal place of feed input into the column, with discrete input onto a single plate or that distributed over several plates.

A calculation of the operation of a reaction–rectification column with discrete feeding onto a single reaction plate in a wide range of pressures (0.1–1.5 MPa) and reflux to starting ethylene oxide ratios (10 : 1 to 110 : 1) demonstrated that the compositions of nonequilibrium counterflows of vapor and fluid are rather close for adjacent plates (Table 1). This corresponds to apparatus operation in the total reflux mode.

The pressure in the column has virtually no effect on the separation quality and ratio of glycols in the reaction mixture formed. However, an increase in pressure accelerates the chemical reactions in the column and provides their fast completion within one or two plates in the feed zone, i.e., it can be assumed that the chemical process is complete on a single theoretical plate.

The purity of ethylene glycol discharged from the bottom part of the column is strongly affected by the ratio between the reflux and the starting ethylene oxide (Table 2). For example, at this ratio equal to 10 : 1, the content of ethylene glycol in the residue is 85.1 mol %, and at this ratio raised to 90 : 1, the content of ethylene glycol increases to 97.9 mol %. Of particular importance in this context becomes the high quality of mixing of raw materials delivered into the column with the reflux on the column plate. Because the chemical transformation is rather fast (0.5–1 min), the actual ratio between the reflux and the starting ethylene oxide becomes, in the case of a poor-quality mixing of the feed with the reflux, substantially lower than the calculated value, which leads to a higher intensity of side processes and a lower yield of the target product, ethylene glycol.

A possible way to provide high-quality mixing of the feed with the reflux is to replace the commonly used point input of raw materials into the column with its collector input into the liquid phase in the input part of a plate or even with supply of the feed directly into intensive-agitation zones near plate caps (Fig. 2). To preclude occurrence of side reactions directly in the collector for introduction of a feed with a water : ethylene oxide ratio of 1 : 1, it is necessary to

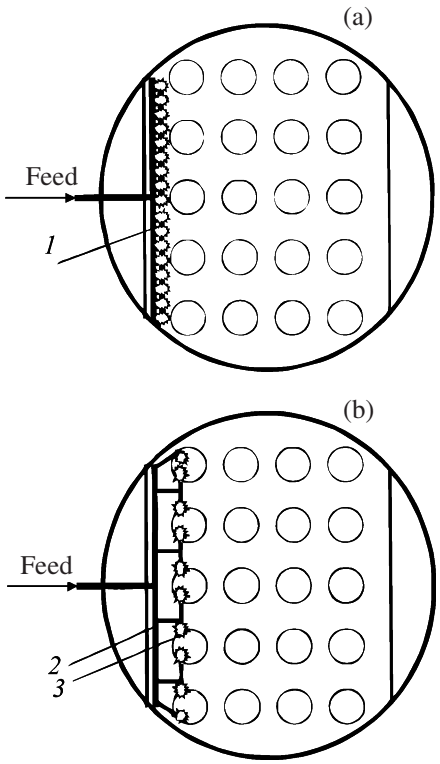

Fig. 2. Methods of feeding directly into a reaction plate. Feed: (a) distributed and (b) local to plate caps. (*1*) Perforated pressure collector, (*2*) pressure collector, and (*3*) nozzle.

Table 2. Effect of the molar ratio C between the reflux and ethylene oxide on the variation of the temperature T and equilibrium mole fractions of ethylene oxide (x_1), water (x_2), ethylene glycol (x_3), diethylene glycol (x_4), triethylene glycol (x_5), and tetraethylene glycol (x_6) in the liquid phase over theoretical plates of the reaction–rectification column

Plate no.	Parameter	C = 10 : 1	C = 30 : 1	C = 50 : 1	C = 70 : 1	C = 90 : 1	C = 110 : 1
1	x_2	0.99	0.99	0.99	0.99	0.99	0.99
	x_3	4.29×10^{-4}	1.62×10^{-4}	1.02×10^{-4}	7.73×10^{-5}	6.34×10^{-5}	5.50×10^{-5}
	T, K	470.3	470.3	470.3	470.3	470.3	470.3
2	x_2	0.99	0.99	0.99	0.99	0.99	0.99
	x_3	6.23×10^{-3}	2.36×10^{-3}	1.49×10^{-3}	1.12×10^{-3}	9.25×10^{-4}	8.02×10^{-4}
	T, K	470.5	470.4	470.3	470.3	470.3	470.3
3	x_2	0.91	0.96	0.97	0.98	0.98	0.98
	x_3	8.36×10^{-2}	3.33×10^{-2}	2.14×10^{-2}	1.61×10^{-2}	1.33×10^{-2}	1.15×10^{-2}
	T, K	473.2	471.4	471.0	470.8	470.7	470.7
4	x_2	0.90	0.95	0.96	0.96	0.96	0.96
	x_3	0.087	0.042	0.035	0.035	0.036	0.038
	T, K	473.3	471.7	471.4	471.4	471.4	471.5
5	x_2	0.85	0.84	0.79	0.75	0.71	0.68
	x_3	0.14	0.15	0.20	0.24	0.28	0.31
	T, K	475.0	475.6	477.3	478.9	480.4	481.7
6	x_2	0.69	0.51	0.40	0.34	0.29	0.26
	x_3	0.29	0.48	0.59	0.65	0.70	0.73
	T, K	511.0	519.9	526.7	531.4	534.9	537.8
7	x_2	0.324	0.155	0.100	0.077	0.064	0.055
	x_3	0.65	0.84	0.89	0.91	0.93	0.94
	T, K	533.0	550.8	558.2	562.0	564.4	566.1
8	x_1	7.53×10^{-10}	2.92×10^{-11}	6.52×10^{-12}	2.42×10^{-13}	1.13×10^{-13}	6.38×10^{-14}
	x_2	7.57×10^{-2}	1.76×10^{-2}	1.33×10^{-2}	1.09×10^{-2}	9.35×10^{-3}	
	x_3	0.85	0.94	0.96	0.97	0.97	0.98
	x_4	0.07	2.79×10^{-2}	1.75×10^{-2}	1.26×10^{-2}	9.99×10^{-3}	8.26×10^{-3}
	x_5	3.66×10^{-3}	5.43×10^{-4}	2.08×10^{-4}	1.05×10^{-4}	6.46×10^{-5}	4.36×10^{-5}
	x_6	1.30×10^{-4}	6.92×10^{-6}	1.62×10^{-6}	5.67×10^{-7}	2.68×10^{-7}	1.46×10^{-7}
	T, K	563.8	572.5	574.7	575.6	576.1	576.4

deliver a feed into the collector at a temperature lower than 50°C (323 K), at which the hydration of ethylene oxide virtually does not occur at all. The feed leaving the collector will be heated to the required temperature in the course of its mixing with the reflux and the hydration will occur at the required ratio between the reflux and the starting ethylene oxide.

Analysis shows that the purity of ethylene glycol obtained is virtually independent of the number of theoretical plates, beginning with five or six plates. This is so because an increase in the number of plates between the feed and residue discharge zones results in the formation on a number of theoretical plates of a kind of constant-concentration zone, in which the temperature and compositions of vapor and fluid flows remain virtually unchanged. As the number of theoretical plates is raised from 6 to 12, the content of ethylene glycol in the residue varies within a narrow range, 98.1–98.2 mol % (Table 3).

The positive effect of an increase in the ratio between the reflux and the starting ethylene oxide on the course of the process of ethylene glycol synthesis in a reaction–rectification column becomes largely negative because of the pronounced rise in the energy expenditure for heating of the bottom part of the column and heat removal from the condenser.

A possible way to diminish the energy expenditure for the process under consideration is to replace discrete feed into a single reaction plate with a distributed input into several plates in that zone of the column in which the quality of the reflux and vapor flows remains virtually unchanged (Table 3). Cardoso et al. believe [9] that this can provide a considerably lower expenditure at the same ratio between the reflux and starting ethylene oxide in the column. For example, discrete feed of 100 mol of ethylene oxide requires a reflux in an amount of 10 000 mol for providing a 100 : 1 ratio between the reflux and starting

Table 3. Effect of the number of theoretical plates n on the variation of the temperature T and mole fractions of water (x_2) and ethylene glycol (x_3) in the liquid phase flowing down from the plates of the reaction–rectification column. Pressure in the column 0.1 MPa; reflux : ethylene oxide ratio at the input of third plate 90 : 1

Plate no.	Parameter	$n = 6$	$n = 8$	$n = 10$	$n = 12$
1	x_2	0.99	0.99	0.99	0.99
	x_3	6.42×10^{-6}	4.98×10^{-6}	4.97×10^{-6}	4.97×10^{-6}
	T, K	372.2	372.2	372.2	372.2
2	x_2	0.99	0.99	0.99	0.99
	x_3	3.04×10^{-4}	2.35×10^{-4}	2.35×10^{-4}	2.35×10^{-4}
	T, K	372.2	372.2	372.2	372.2
3	x_2	0.98	0.98	0.98	0.98
	x_3	1.41×10^{-2}	1.10×10^{-2}	1.10×10^{-2}	1.10×10^{-2}
	T, K	372.5	372.4	372.4	372.4
4	x_2	0.85	0.98	0.98	0.98
	x_3	0.14	1.17×10^{-2}	1.10×10^{-2}	1.10×10^{-2}
	T, K	375.1	372.4	372.4	372.4
5	x_2	0.12	0.95	0.98	0.98
	x_3	0.87	4.56×10^{-2}	1.17×10^{-2}	1.15×10^{-2}
	T, K	415.5	373.1	372.4	372.4
6	x_2	9.45×10^{-3}	0.64	0.98	0.98
	x_3	0.98	0.34	1.40×10^{-2}	1.15×10^{-2}
	T, K	465.7	405.9	390.1	390.1
7	x_2		0.11	0.95	0.99
	x_3		0.88	4.58×10^{-2}	1.17×10^{-2}
	T, K		440.8	397.8	397.0
8	x_2		8.78×10^{-3}	0.64	0.98
	x_3		0.98	0.35	1.39
	T, K		466.0	405.0	397.1
9	x_2			0.11	0.95
	x_3	0.88	4.54×10^{-2}		
	T, K			440.9	397.8
10	x_2			7.73×10^{-2}	0.65
	x_3			0.98	0.34
	T, K			466.0	405.9
11	x_2				0.11
	x_3				0.88
	T, K				440.7
12	x_2				8.85×10^{-2}
	x_3				0.98
	T, K				465.9

ethylene oxide. At the same time, at distributed feeding of 100 mol into two plates, 50 mol for each plate, the expenditure of the reflux in the plates will decrease to 5000 mol at the same (100 : 1) ratio between the reflux and starting ethylene oxide, i.e., the energy expenditure will decrease by a factor of 2. However, the concepts reported in [9] were not substantiated by calculations or experimental data. Therefore, we considered a problem in which the results of operation of a reaction–rectification column with discrete and distributed feeding of the column are compared (Fig. 1b). Table 4 lists the results of calculation of the column for two alternative solutions of the problem.

In the first alternative, we compared the results of calculation of a column with eight theoretical plates and feeding in the following modes: (i) discrete input into third plate at a 30 : 1 ratio between the reflux and the starting ethylene oxide; (ii) uniform distribution of the feed over three plates (third–fifth), which actually provides a ratio of 90 : 1; and (iii) discrete input into third plate at a 90 : 1 ratio between the reflux and the starting ethylene oxide, as a control. Thus, a potential threefold energy saving would be expected in the first alternative of calculation. In the second alternative, we calculated a column with eight theoretical plates and feeding in the following modes: (i) discrete

Table 4. Effect of the feeding mode* on the variation of the temperature T and mole fractions of water (x_2) and ethylene glycol (x_3) in the liquid phase flowing down from the plates of the reaction–rectification column at a varied reflux : ethylene oxide ratio C in the feed plate. Pressure in the column 0.1 MPa

Plate no.	Parameter	First alternative			Second alternative		
		mode 1	mode 2	mode 3	mode 4	mode 5	mode 6
1	x_2	0.99	0.99	0.99	0.99	0.99	0.99
	x_3	0.000014	0.0002	0.0000045	0.000039	0.00042	0.088
	T, K	372.2	372.2	372.2	372.1	372.2	372.2
2	x_2	0.99	0.98	0.99	0.99	0.97	0.99
	x_3	0.00068	0.012	0.00023	0.0018	0.019	0.00041
	T, K	372.2	372.4	372.2	372.2	372.6	372.2
3	x_2	0.96	0.97	0.98	0.91	0.96	0.98
	x_3	0.031	0.021	0.011	0.080	0.037	0.019
	T, K	372.8	372.8	372.4	372.9	373.0	372.6
4	x_2	0.92	0.96	0.98	0.91	0.99	0.98
	x_3	0.031	0.031	0.017	0.080	0.53	0.019
	T, K	372.8	372.8	372.4	373.9	373.3	372.6
5	x_2	0.95	0.95	0.95	0.90	0.92	0.95
	x_3	0.044	0.45	0.045	0.80	0.75	0.039
	T, K	373.1	373.1	373.1	373.1	373.8	373.0
6	x_2	0.81	0.80	0.64	0.85	0.85	0.75
	x_3	0.17	0.18	0.34	0.13	0.13	0.24
	T, K	401.0	401.3	405.9	400.0	400.0	402.7
7	x_2	0.27	0.25	0.11	0.49	0.49	0.18
	x_3	0.72	0.73	0.88	0.49	0.49	0.81
	T, K	424.4	425.6	440.8	4113.7	411.8	431.8
8**	x_1	2.39×10^{-13}	1.99×10^{-13}	9.20×10^{-15}	6.30×10^{-12}	3.8×10^{-14}	5.2×10^{-14}
	x_2	0.025	0.23	0.008	0.069	0.068	0.015
	x_3	0.94	0.95	0.98	0.86	0.86	0.96
	x_4	0.025	0.025	0.09	0.064	0.070	0.015
	x_5	4.6×10^{-4}	5.05×10^{-4}	5.6×10^{-5}	3.21×10^{-3}	3.58×10^{-3}	1.77×10^{-4}
	x_6	5.50×10^{-6}	6.00×10^{-6}	2.28×10^{-7}	1.06×10^{-4}	1.52×10^{-4}	1.27×10^{-6}
	T, K	460.5	461.1	466.0	449.6	449.9	463.6

* Mode 1: discrete feeding into third plate, C = 30 : 1; mode 2: distributed feeding into third–fifth plates, C = 90 : 1; mode 3: discrete feeding into third plate, C = 90 : 1; mode 4: discrete feeding into third plate, C = 10 : 1; mode 5: distributed feeding into third–seventh plates, C = 50 : 1; mode 6: discrete feeding into third plate, C = 50 : 1.

** Mole fractions of other components: (x_1) ethylene oxide, (x_4) diethylene glycol, (x_5) triethylene glycol, and (x_6), tetraethylene glycol.

input into third plate at a 10 : 1 ratio between the reflux and the starting ethylene oxide; (ii) uniform distribution of the feed over five plates (third–seventh), which actually provides a ratio of 50 : 1; and (iii) discrete input into third plate at a 50 : 1 ratio between the reflux and the starting ethylene oxide, as a control. This had to provide a possibility of a fivefold energy saving in the second alternative of calculation.

The results of these calculations demonstrated (Table 4) that distributed feeding fails to provide the expected energy saving, because the purity of the residue in ethylene glycol is somewhat decreased, compared with the distributed input, at the same actual ratio between the reflux and the starting ethylene oxide. For example, the content of ethylene glycol in the residue is 98.20 mol % at an actual 90 : 1 ratio between the reflux and the starting ethylene oxide and 95.07 mol % in the case of a uniform feed distribution among third, fourth, and fifth plates, which only slightly exceeds the performance parameters at a discrete feed and a 30 : 1 ratio between the reflux and the starting ethylene oxide. In the case of a uniform feed distribution among third to seventh plates at a 50 : 1 ratio between the reflux and the starting ethylene oxide, the composition of the residue (86.1 mol %) was worse than not only that in the case of a discrete input and a 50 : 1 ratio (96.83 mol %), but also that with discrete input and a 10 : 1 ratio between the

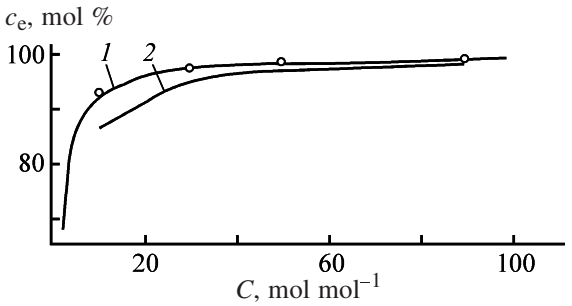

Fig. 3. Content of ethylene glycol in the residue, c_e, vs. the reflux : ethylene oxide ratio C at a pressure of 1.0 MPa. Content of ethylene oxide in the residue: (*1*) potential, according to the compositions of the reaction mixture on the discrete-feeding plate (C is water : ethylene oxide ratio); (*2*) calculated, upon fractionation of the reaction mixture on eight theoretical plates; points: potential, as a result of distinct fractionation of the reaction mixture for curve *2*.

reflux and the starting ethylene oxide. This occurs because, in the case of a distributed feed, ethylene oxide arriving at a next, except the first, plate of the feed zone (this is third plate according to the calculation) comes in contact with the reaction medium in this plate. This medium already contains a considerable amount of ethylene glycol, which enters into a reaction with ethylene oxide to give a diethylene glycol as by-product. This makes lower the yield of ethylene glycol in fourth, fifth, etc., plates. As follows from Table 4, the content of diethylene glycol in the residue is 2–4 times higher with distributed feeding as compared to the discrete input, all other conditions being the same. The potentially possible concentrations of ethylene glycol in the residue (i.e., in the case of a complete evaporation of water from the residue) coincide in evaluation of the residue composition by calculation of the process in the reaction–rectification column and by calculation from the composition of the reaction mixture in the reaction plate (Fig. 3).

Thus, the quality of the residue in fractionation of the reaction mixture primarily depends on the completeness and quality of the chemical process in the reaction zone of the apparatus.

CONCLUSIONS

(1) A study of various operation modes of a reaction–rectification column in a wide range of pressures and ratios between the reflux and starting ethylene oxide demonstrated that, if the column works in the total reflux mode, the quality of the resulting residue is virtually independent of the number of theoretical plates between the feeding and residue discharge zones, with a region of constant process concentrations formed in the middle part of the column.

(2) Alternatives of the point-like (discrete) and distributed feeding of the reaction–rectification column for synthesis of ethylene glycol were analyzed. The distributed feeding cannot provide energy saving because the residue quality in the fractionation of the reaction mixture primarily depends on the completeness and quality of the chemical process in the reaction zone of an apparatus, and the concentration of ethylene glycol in the residue is lower in distributed feeding, compared with the discrete input mode.

REFERENCES

1. Astarita, G., *Mass Transfer with Chemical Reaction*, Amsterdam: Elsevier, 1967.
2. Okasinski, M.J. and Doherty, M.F., *Ind. Eng. Chem. Res*., 1998, no. 7, pp. 2821–2836.
3. Buzad, G. and Doherty, M.F., *Comput. Chem. Eng*., 1995, no. 4, pp. 395–412.
4. Cardoso, M.F., Salcedo, R.L., and Feyo de Azevedo, S., *Comput. Chem. Eng*., 1996, no. 9, pp. 1065–1080.
5. Venkataraman, S., Chan, W.K., and Boston, J., *Chem. Eng. Prog*., 1990, no. 8, pp. 45–53.
6. Chang, Y.A. and Seader, J.D., *Comput. Chem. Eng*., 1988, no. 12, pp. 1243–1257.
7. Dyment, O.N., Kazanskii, K.S., and Miroshnikov, F.M., *Glikoli i drugie proizvodnye okisei etilena i propilena* (Glycols and Other Derivatives of Ethylene and Propylene Oxides), Moscow: Khimiya, 1976.
8. Samoilov, N.A., Mnushkin, I.A., and Mnushkina, O.A., *Zh. Prikl. Khim*., 2006, no. 12, pp. 1998–2006.
9. Cardoso, M.F., Salcedo, R.L., Feyo de Azevedo, S., et al., *Chem. Eng. Sci*., 2000, vol. 55, pp. 5059–5078.

ISSN 1070-4272, Russian Journal of Applied Chemistry, 2007, Vol. 80, No. 9, pp. 1544–1548. © Pleiades Publishing, Ltd., 2007.
Original Russian Text © A.A. Ryazantsev, A.S. Malikov, A.A. Batoeva, G.A. Faddeenkova, 2007, published in Zhurnal Prikladnoi Khimii, 2007, Vol. 80, No. 9, pp. 1511–1515.

PROCESSES AND EQUIPMENT OF CHEMICAL INDUSTRY

Liquid-Phase Oxidation of Hydrogen Sulfide in Centrifugal Bubbling Apparatus

A. A. Ryazantsev, A. S. Malikov, A. A. Batoeva, and G. A. Faddeenkova

Baikal Institute of Nature Management, Siberian Division, Russian Academy of Sciences, Ulan-Ude, Buryatia, Russia
Siberian State University of Means of Communication, Novosibirsk, Russia
Boreskov Institute of Catalysis, Siberian Division, Russian Academy of Sciences, Novosibirsk, Russia

Received August 3, 2006; in final form, January 2007

Abstract—Liquid-phase oxidation of H_2S in centrifugal-bubbling apparatus in the presence of catalysts [manganese(II) chloride, cobalt phthalocyanine disulfonic acid, and a catalytic system including cobalt phthalocyanine disulfonic acid and $MnCl_2$] was studied.

DOI: 10.1134/S1070427207090194

Sulfides, and hydrogen sulfide in particular, widely occur in nature, being present in water of many natural mineral springs and in volcanic gases, and are obtained in production of oil and natural gas and in mining of coal and ores of heavy and nonferrous metals. Sulfides (in particular, H_2S) are formed in anaerobic decomposition of natural sulfur-containing organic substances, fungicides, pesticides, and fertilizers and are discharged in large amounts into the natural environment with wastewater from plants of pulp-and-paper, oil-refining, chemical, and tanning industries.

The content of sulfides in wastewater formed in chrome tanning at tanneries may be as high as 1000 mg l^{-1}. One of methods for their detoxication is oxidation to nontoxic sulfur-containing compounds with atmospheric oxygen in aqueous–alkaline solutions, which is commonly performed in bubble columns. In this case, the oxidation of sulfides is rather slow even in the presence of highly active catalysts because of the low rate of oxygen dissolution in a solution. Mn(II) compounds are most frequently used as catalysts. For example, wastewater from tanneries, with an initial concentration of sulfides in the range 700–1400 mg l^{-1}, are oxidized to a residual content of 0.5–1.5 mg l^{-1} in bubble columns in the course of 6–12 h. In this case, the specific air expenditure is 30–35 $m^3\ m^{-3}$ [1]. The considerable expenditure of the catalyst (Mn^{2+}/HS^- mass ratio may be as high as 0.4–0.5) is due both to the high concentration of sulfides and to the presence in wastewater of a large amount of suspended and colloidal substances. These substances adsorb on their surface insoluble manganese compounds formed in oxidation of sulfides and thereby make lower the activity of the catalyst.

The oxidation of sulfides can be intensified and the expenditure of the catalyst can be lowered by changing the processing technology of spent solutions and wastewater.

Because more than a half of all the contaminants and more than 90% of sulfides (COD 15–35 g l^{-1}, HS^- 4–6 g l^{-1}, pH 8–12) is discharged into the wastewater disposal system from the liming process, it is advisable to collect and purify separately spent solutions and the most concentrated wastewater. The suspended and colloidal substances are removed by coagulation precipitation from a liming wastewater acidified to pH 4–4.5, and hydrogen sulfide formed in acidification is removed by bubbling of air through the solution. Then, H_2S-containing air is purified to remove H_2S in a centrifugal-bubbling apparatus (CBA) with a circulating aqueous–alkaline solution containing a dissolved catalyst, with simultaneous catalytic oxidation of the caught hydrogen sulfide to nontoxic products, sulfates and thiosulfates.

As catalysts were suggested Mn(II) salts [1], frequently used at tanneries, and also cobalt phthalocyanine disulfonic acid (CPDA) and a catalytic system constituted by a mixture of a Mn(II) salt and CPDA [2].

In an absorbing aqueous solution containing sodium carbonate, the CPDA catalyst is converted to a disodium cobalt phthalocyanine disulfonate, $\{CoPc(SO_3Na)_2\}$, a macrocyclic complex having the form of a planar symmetric 18-π-electron aromatic macroring with a cobalt atom situated in the central cavity and retained there by chemical bonds formed by unoccupied orbitals of the cobalt atom and lone-pair electrons of central nitrogen atoms [3]. In complexes of this kind, the metal plays the role of a redox center.

Previously, an attempt has been made to use CBA for oxidation with atmospheric oxygen of aqueous–alkaline solutions of sodium sulfide in the presence of a catalyst, tetrasodium cobalt phthalocyanine tetrasulfonate, $CoPc(SO_3Na)_4$ [4]. With CBA, a sharp increase in the oxidation rate of hydrosulfide ions by oxygen was observed, compared with oxidation of the same aqueous–alkaline solution in a rocking static "duck" reactor and in a bubbling reactor. According to [4], HS^- ions are oxidized by oxygen in both the "duck" and bubbling reactors under diffusion control. The product formed in CBA in oxidation of aqueous–alkaline solutions of hydrogen sulfide in the presence of $CoPc(SO_3Na)_4$ is sulfur. It should be noted that oxidation of sulfides in CBA to pure sulfur has a significant disadvantage: in prolonged operation, finely dispersed sulfur that accumulated in the absorbing solution settles on the walls of the swirling chamber of the reactor, altering the operation parameters of the apparatus and thus making its work impossible. Therefore, hydrogen sulfide removed from a spent liming solution was oxidized in CBA so as to prevent formation of elemental sulfur and obtain soluble salts, thiosulfates and sulfates, as a result of oxidation.

In weakly alkaline and alkaline aqueous solutions, oxidation of soluble sulfides by atmospheric oxygen may occur to give S^0, $S_2O_3^{2-}$, SO_3^{2-}, and SO_4^{2-}. The extent and rate of oxidation depend on the pH value, concentration ratio of HS^- ions and dissolved oxygen, temperature, and ionic strength of the solutions.

The oxidation of HS^- ions is strongly affected by the choice of a catalyst. The liquid-phase oxidation of H_2S by atmospheric oxygen in the presence of soluble salts of Mn(II) occurs at a high rate to give mainly $S_2O_3^{2-}$ and SO_4^{2-} ions. It should be noted that, at *Eh* of 0.3–0.4 V and pH 8–12, Mn(II) is rather easily oxidized to MnO_2 [5], whose activity in oxidation of sulfur compounds is substantially lower. In addition, it is to be taken into account that soluble salts of manganese are unstable in the presence of hydrosulfide ions and can coagulate to give manganese sulfides.

It has been found in an analysis of oxidation of HS^- ions with dissolved oxygen in the presence of cobalt phthalocyanine sulfonates $\{CoPc(SO_3Na)_n\}$ that there exist various redox forms of $CoPc(SO_3Na)_n$, containing cobalt in oxidation states I–III [6].

In a strongly alkaline medium (pH ≥ 11), hydrosulfide ions are oxidized with oxygen by the mechanism [7, 8] involving formation of a paramagnetic superoxocomplex $[Co(III)Pc(SO_3Na)_n \cdot O_2^-]$ and its subsequent interaction with the substrate:

$$[Co(III)Pc(SO_3Na)_n \cdot O_2^-] + HS^- \rightarrow [HS^- \cdot Co(III)Pc(SO_3Na)_n \cdot O_2^-]. \quad (1)$$

Further, this complex decomposes:

$$[HS^- \cdot Co(III)Pc(SO_3Na)_n \cdot O_2^-] \rightarrow Co(II)Pc(SO_3Na)_n + HSO_2^-, \quad (2)$$

and then HSO_2^- undergoes noncatalytic transformations to give thiosulfate, sulfite, and sulfate ions.

At pH 7.3–8.0, sulfides contained in a solution as hydrosulfide ions are oxidized with oxygen in the presence of $CoPc(SO_3Na)_n$ at a high rate mostly by the polysulfide mechanism [6]. The main oxidation product is elemental sulfur. HS^- ions are oxidized at the expense of redox transitions $Co(II)Pc(SO_3Na)_n \rightleftarrows Co(I)Pc(SO_3Na)_n$.

A transition from one oxidation mechanism of sulfides to another can occur upon a comparatively slight change in the reaction conditions (pH value; concentration ratio of hydrosulfides and dissolved O_2; catalyst concentration; presence in a solution of hydrosulfide oxidation products that favor or hinder accumulation of polysulfides in the reaction mixture [6, 9]). Changing the reaction conditions and choosing cobalt phthalocyanine disulfonate as the most appropriate catalyst make it possible to achieve the required hydrosulfide oxidation intensity and composition of the products obtained.

EXPERIMENTAL

Figure 1 schematically shows a laboratory rig for studying the kinetics of liquid-phase catalytic oxidation of easily volatile compounds, with hydrogen sulfide as example. A Na_2S solution or a spent liming solution is delivered by a pump from tank *1* to bubbling column *2*, to be acidified there by an H_2SO_4

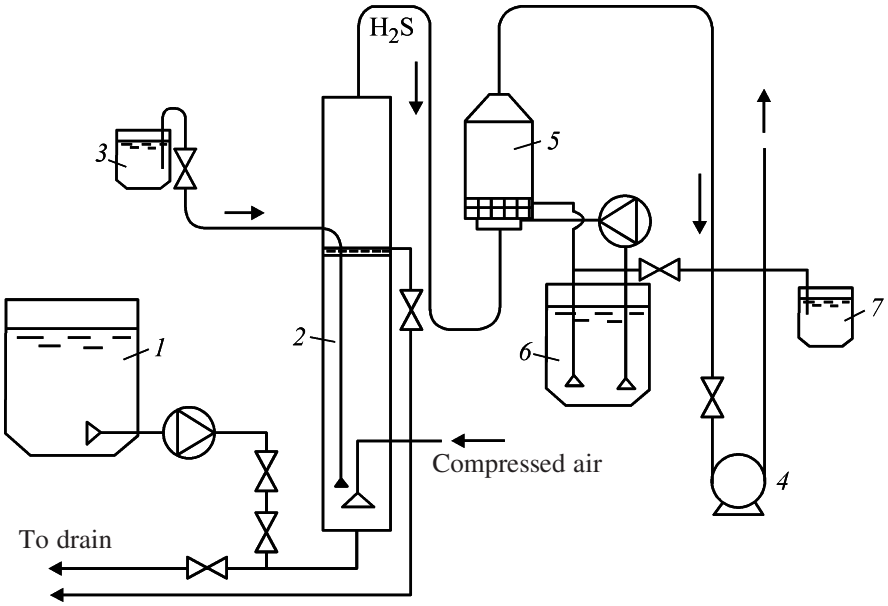

Fig. 1. Laboratory rig for liquid-phase oxidation of volatile compounds in CBA: (*1*) tank with an absorbing solution, (*2*) bubbling column, (*3*) vessel with H_2SO_4, (*4*) ventilator, (*5*) CBA, (*6*) vessel with an absorbing solution, and (*7*) vessel with a catalyst solution.

solution from vessel *3*. The forming hydrogen sulfide is removed from the column and is supplied, together with air, by sucking-in ventilator *4* into CBA *5* and is absorbed there by the circulating aqueous–alkaline solution *6* and rapidly oxidized upon delivery of the catalyst from vessel *7*.

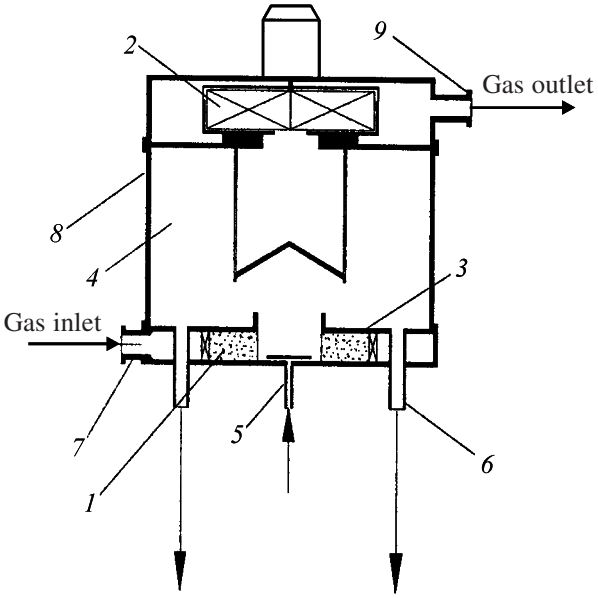

Fig. 2. Schematic of a centrifugal-bubbling apparatus: (*1*) rotating gas–liquid layer, (*2*) ventilator, (*3*) swirler, (*4*) separation zone, (*5, 6*) pipes for liquid delivery and discharge, (*7*) gas supply pipe, (*8*) cylindrical case, and (*9*) gas discharge pipe.

The operation principle of CBA (Fig. 2) is based on passing a gas through a rotating liquid layer *1*, which is retained within the swirling chamber by the gas flow. After ventilator *2* is switched on, gas passes through swirler slits, acquires a rotary motion, and involves the liquid in this motion. As a result, a gas–liquid layer with a developed and instantaneously renewed phase contact layer is formed within the apparatus. The gas and liquid are delivered from the swirling chamber into separator *4* and then discharged from the reactor. The air expenditure in the CBA is 100 $Sm^3\ h^{-1}$ (Sm^3 is m^3 under normal conditions). The circulation rate of the absorbing solution in the CBA is 50 $dm^3\ h^{-1}$.

In the stage of desorption, in contact of an acidified spent liming solution with air, hydrogen sulfide is virtually not oxidized at all. This occurs because the rate of noncatalytic oxidation of dissolved hydrogen sulfide is very low. The caught hydrogen sulfide is oxidized at a very high rate in CBA, because the absorbing solution contains catalysts that can diminish the time of oxidation of the forming hydrosulfide ions at room temperature and atmospheric pressure from several hours or even days to several seconds.

Hydrogen sulfide mixed with air was delivered into the CBA at rates of 2.8×10^{-2}, 5.3×10^{-2}, and 1×10^{-1} mol min^{-1} counting on H_2S. The presence of hydrosulfide ions in the solution discharged from the CBA and of hydrogen sulfide in the purified air at

Results of experiments on catching of hydrogen sulfide and its oxidation in CBA. Flow rate of the gas mixture 100 $Sm^3\ h^{-1}$; solution circulation rate 50 $l\ h^{-1}$; H_2S concentration in purified air less than 5 $mg\ m^{-3}$; no HS^- ions in the absorbing solution discharged from CBA. T = 25°C, P = 0.1 MPa

Run no.	Content of H_2S in gas mixture, vol %	Catalyst	$H_2S/MnCl_2$, mol/mol	Installation operation time,** min	pH of absorbing solution	Amount of caught H_2S, mol (g)
1	0.04	$MnCl_2$	86.83	72	11.5	2.16 (73.4)
2	0.07	$MnCl_2$	86.83	48	11.5	2.41 (81.9)
3	0.07	$MnCl_2$	17.36	78	11.5	3.96 (134.6)
4	0.14	$MnCl_2$	86.83	24	11.5	2.41 (81.9)
5	0.14	$MnCl_2$	17.36	43	11.5	4.41 (149.9)
6	0.15	$CoPc(SO_3Na)_2$		24	8.2–8.3	2.71 (92.1)
7	0.15	$MnCl_2$, $CoPc(SO_3Na)_2$		36	8.2–8.3	4.05 (137.7)
8	0.15	$MnCl_2$ $CoPc(SO_3Na)_2$	86.83	40	8.2–8.3	4.59 (156.1)

* Run no. 6: content of $CoPc(SO_3Na)_2$ in the absorbing solution 1.28×10^{-6} M (1.0 $mg\ dm^{-3}$); run no. 7: $MnCl_2$ content 1.28×10^{-6} M (0.16 $mg\ dm^{-3}$), $CoPc(SO_3Na)_2$ content 1.28×10^{-6} M (1.00 $mg\ dm^{-3}$); run no. 8: $CoPc(SO_3Na)_2$ content 1.28×10^{-6} M (1.00 $mg\ dm^{-3}$), $MnCl_2$ is batched into solution simultaneously with delivery of the gas mixture being purified.

** Operation time of the installation until appearance (breakthrough) of HS^- in the absorbing solution.

the CBA outlet was checked using lead indicator paper. The concentrations of hydrosulfide, thiosulfate, and sulfite ions were found by iodometric titration [10]. The concentration of sulfate ions in this absorbing solution was determined by complexometry [10] and gravimetry [11]. UV/Vis spectra of absorbing solutions containing CPDA and the catalytic system CPDA + $MnCl_2$ were recorded with an Agilent 8453 spectrophotometer.

An aqueous solution containing sodium carbonate, into which catalysts were introduced, served as an absorbing solution. In the case of a CPDA catalyst and a catalytic system containing CPDA and $MnCl_2$, a 0.001 M aqueous solution of Na_2CO_3 (pH 8.2–8.3) was used. With $MnCl_2$ serving as a catalyst, a 0.1 M Na_2CO_3 solution was used (pH 11.5).

The results of the experiments performed demonstrated (see table) that acidification of sulfide-containing wastewater to pH 4–4.5 and subsequent evaporation of H_2S in CBA enables virtually complete removal of sulfides from spent liming solutions. Hydrogen sulfide is completely caught by the absorbing solution and oxidized (oxidation of HS^- ions) in this apparatus at a high rate and low catalyst expenditure.

The main products formed in catalytic oxidation of hydrosulfide ions by atmospheric oxygen were sodium sulfate and thiosulfate.

The experiments demonstrated that the time during which the $MnCl_2$ catalyst remains in the working state (until appearance of HS^- ions) strongly depends on the method of its introduction into the absorbing solution. In the case of fractional batching of $MnCl_2$ into the reaction zone of the CBA, the amount of oxidized H_2S is 28–56% higher than that in a single-portion introduction of the same amount of $MnCl_2$ into the absorbing solution before the beginning of H_2S delivery into the CBA. Apparently, if the whole amount of the catalyst is introduced in a single portion, excess Mn^{2+} favors fast formation of a precipitate of low-active MnO_2.

The UV/Vis spectra of CPDA and Mn(II) solutions (Fig. 3) show that no chemical interaction occurs between these substances.

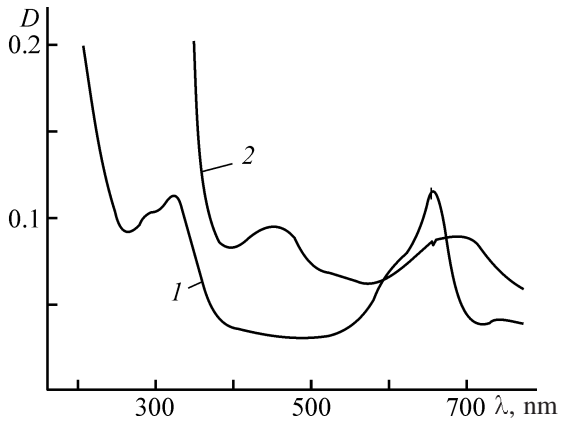

Fig. 3. UV/Vis spectra of CPDA. (*D*) Optical density and (λ) wavelength. Solution: (*1*) absorbing with CPDA + $MnCl_2$, 1.28×10^{-6} M each, after run no. 8 (see table); (*2*) Na_2S (0.45 M) with CPDA (0.86×10^{-6} M) after 60 min of oxidation in a bubbling column.

The spectrum of a CPDA solution obtained upon oxidation of H_2S in a CBA in run no. 8 contains two strong absorption bands at 655 and 320 nm, associated with π–π^* transitions from the ground state to the first excited singlet state. The additional bands appearing in the absorption spectrum of cobalt phthalocyanine disulfonate can be attributed to metal $\rightleftarrows$ ligand charge transfer or to appearance of weak π bonds between molecules of the complex to give dimers [12]. Oxidation of a sodium sulfide solution in the bubbling column in the presence of CPDA gives rise to a weak band at 450 nm in the absorption spectrum, associated with Co(I) $\rightleftarrows$ Co(II) transitions [6]. In oxidation of caught H_2S by atmospheric oxygen in a CBA under conditions of a developed phase contact area in a CPDA-containing absorbing solution both with and without $MnCl_2$, no absorption band at 450 nm is observed in the absorption spectrum of CPDA. In this case, the intensity of the absorption band at 320 nm, associated with Co(II) $\rightleftarrows$ Co(III) transitions, sharply increases.

CONCLUSIONS

(1) Liquid-phase oxidation of H_2S in centrifugal-bubbling apparatus in the presence of catalysts ($MnCl_2$, cobalt phthalocyanine disulfonic acid, and a catalytic system consisting of cobalt phthalocyanine disulfonic acid and $MnCl_2$) occurs at a high rate. The oxidation of hydrosulfide ions is not controlled by dissolution of oxygen in the contacting absorbing solution because of the large, and rapidly changing, area of the gas–liquid mass-exchange surface.

(2) Sulfates are the main oxidation products.

(3) It is recommended to use these catalysts in oxidation of hydrogen sulfide formed in acidified liming solutions from plants manufacturing half-finished leather articles by chrome tanning.

ACKNOWLEDGMENTS

The study was supported by the Russian Foundation for Basic Research (project nos. 05-08-50152 and 06-08-00761a).

REFERENCES

1. Laskov, Yu.M., Fedorovskaya, T.G., and Zhmakov, G.N., *Ochistka stochnykh vod predpriyatii kozhevennoi i mekhovoi promyshlennosti* (Purification of Wastewater from Plants of Tanning and Fur Industries), Moscow: Legkaya i Pishchevaya Prom–st., 1984.
2. Faddeenkova, G.A. and Kundo, N.N., *Zh. Prikl. Khim.*, 2003, vol. 76, no. 12, pp. 1995–1999.
3. Berezin, B.D., *Koordinatsionnye soedineniya porfirinov i ftalotsianinov* (Coordination Compounds of Porphyrins and Phthalocyanines), Moscow: Nauka, 1978.
4. Zavarukhin, S.G., Kuvshinov, G.G., Gogina, L.V., and Kundo, N.N., *Khim. Prom–st.*, 1999, no. 2, pp. 26–30.
5. Pourbaix, M., Zhang, H.M, and Yang, X.Z., *Atlas of Chemical and Electrochemical Equilibria in the Presence of a Gaseous Phase*, Brussels: CEBELCOR, 1996.
6. Kundo, N.N. and Keier, N.P., *Kinet. Katal.*, 1970, vol. 11, no. 1, pp. 91–99.
7. Hoffmann, M.R., *Environ. Sci. Technol.* 1991, vol. 25, pp. 1153–1162.
8. Abel, E.W., *Chem. Commun.*, 1971, no. 9, pp. 449–450.
9. Kundo, N.N. and Faddeenkova, G.A., *Khim. Inter. Ustoich. Razv.*, 2003, no. 11, pp. 619–625.
10. Lur'e, Yu.Yu., *Analiticheskaya khimiya promyshlennykh stochnykh vod* (Analytical Chemistry of Industrial Wastewater), Moscow: Khimiya, 1984.
11. Privalov, V.E., Khlopkova, L.I., and Popkov, G.I., *Analiz stochnykh vod koksokhimicheskikh zavodov* (Analysis of Wastewater from Coke-Chemical Plants), Moscow: Metallurgiya, 1976.
12. Hanack, M., Heckmann, H., and Polley, R., in *Methoden der Organischen Chemie* (Houben–Weyl), Stuttgart: Thieme, 1997, 4th ed., vol. E9d.

ISSN 1070-4272, Russian Journal of Applied Chemistry, 2007, Vol. 80, No. 9, pp. 1549–1557. © Pleiades Publishing, Ltd., 2007.
Original Russian Text © A.K. Khripunov, A.A. Tkachenko, Yu.G. Baklagina, L.N. Borovikova, V.K. Nilova, R.Yu. Smyslov, V.V. Klechkovskaya, N.A. Matveeva, A.Ya. Volkov, V.K. Lavrent'ev, M.E. Vylegzhanina, T.E. Sukhanova, V.V. Kopeikin, 2007, published in Zhurnal Prikladnoi Khimii, 2007, Vol. 80, No. 9, pp. 1516–1524.

NANOTECHNOLOGIES AND NANOMATERIALS

Formation of a Composite from Se^0 Nanoparticles Stabilized with Polyvinylpyrrolidone and *Acetobacter xylinum* Cellulose Gel Films

A. K. Khripunov, A. A. Tkachenko, Yu. G. Baklagina, L. N. Borovikova, V. K. Nilova, R. Yu. Smyslov, V. V. Klechkovskaya, N. A. Matveeva, A. Ya. Volkov, V. K. Lavrent'ev, M. E. Vylegzhanina, T. E. Sukhanova, and V. V. Kopeikin

Institute of Macromolecular Compounds, Russian Academy of Sciences, St. Petersburg, Russia
St. Petersburg State University, St. Petersburg, Russia
Institute of Cytology, Russian Academy of Sciences, St. Petersburg, Russia
Shubnikov Institute of Crystallography, Russian Academy of Sciences, Moscow, Russia

Received December 14, 2006; in final form, June 2007

Abstract—Formation of a composite from Se^0 nanoparticles stabilized with polyvinylpyrrolidone and *Acetobacter xylinum* cellulose gel films was studied. The optimal sorption parameters at which the amorphous form of the selenium complex is preserved in the composite were suggested.

DOI: 10.1134/S1070427207090200

Studies of physicochemical properties of bacterial cellulose synthesized by surface cultivation of *Acetobacter xylinum*, strain VKM V-880, showed that an *Acetobacter xylinum* cellulose gel film (AXC GF) fairly readily takes up from aqueous solutions (0.01–0.3 wt %) nanoparticles of zero-valent silver or selenium, stabilized with polyvinylpyrrolidone (PVP-nano-Ag^0 and PVP-nano-Se^0, respectively) [1, 2].

A study of the kinetics of this process shows that silver clusters of size 2–10 nm and larger selenium clusters (20–60 nm) penetrated into AXC GFs [2]. It was also noted that, when AXC GFs dried at 50°C were kept in 3% aqueous solutions of the nanocomplexes, large silver clusters (100–200 nm) or selenium crystals (up to 200–300 nm) were formed on the film surfaces [2]. Structural studies of such specimens allowed the crystalline formations of selenium observed in the electron micrographs to be assigned to trigonal [3] or α-monoclinic [4] modification.

It is well known that, owing to features of the electronic structure, selenium exists in numerous allotropic forms: amorphous, α- and β-monoclinic, trigonal, hexagonal, and others [3, 4]. The most stable is the hexagonal form built of helical selenium chains arranged parallel. These chains form a unit cell with the parameters $a = b = 0.436$ nm, $c = 0.495$ nm, and $\gamma = 120°$ [5].

Of particular interest are sorption and desorption interactions of PVP-stabilized amorphous selenium with AXC GF. The AXC GF structure is a network formed by highly crystalline fibrillar ribbons of nanometric size, surrounded by a large amount of water molecules [6, 7].

Data on sorption on, and desorption from AXC GFs of nanocomplexes PVP-nano-Ag^0 or PVP-nano-Se^0 are important for medical applications of these composite materials as a wound coating bearing PVP-stabilized clusters of Ag^0 or Se^0 [8]. Particular attention should be given to determination of the optimal modes of sorption of PVP-nano-Se^0 nanocomplexes on AXC GF and on their desorption from the film, which is necessary for evaluating the safe concentration of amorphous selenium in the medinicals to be used [9].

The goal of this study is determination of conditions for PVP-nano-Se^0 sorption taking into account structural features of AXC GF. Specimens of the composite materials AXC GF–PVP-nano-Se^0 were prepared by sorption for varied time from PVP-nano-Se^0 solutions of varied concentration on AXC gel films dehydrated at 20–50°C. The specimens were examined by X-ray and electron diffraction and by electron and atomic-force microscopy. Particular attention was given to study of structural changes that occur in

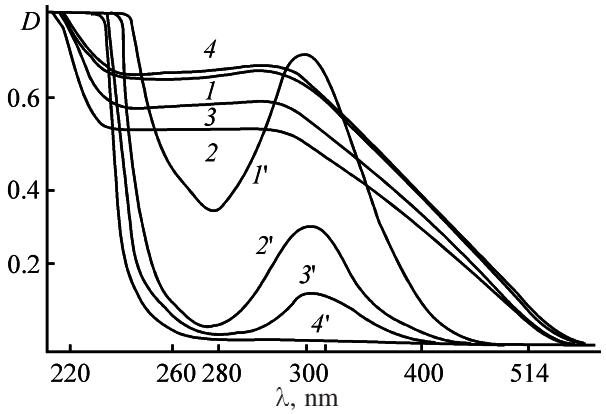

Fig. 1. Absorption spectra of 1% aqueous solution of PVP-nano-Se^0, the same solution in the course of sorption on AXC GF, and solutions obtained by desorption from dried AXC GF specimens. (*D*) Optical density and (λ) wavelength. (*1*) Before immersion of AXC GF into solution; sorption time, h: (*2*) 0.5, (*3*) 1.0, and (*4*) 24. Desorption time, h: (*1'–3'*) 0.5 and (*4'*) 24.

AXC specimens subjected after sorption and drying to desorption with water for 24 h.

EXPERIMENTAL

Biosynthesis of AXC GFs with VKM V-880 was described previously [1, 6]. After removing 80–90% of water by squeezing, film specimens were placed in aqueous solutions with different concentrations of PVP-stabilized selenium nanoparticles.

Selenium nanoparticles were prepared by chemical reduction of selenious acid with ascorbic acid in aqueous PVP solutions under conditions ensuring formation of PVP-nano-Se^0 nanocomposites with the weight ratio PVP : Se = 10 : 1 [10]. The amount of the complex sorbed in the AXC GF matrix was varied by varying the solution concentration (0.01–3 wt %) and the exposure time.

The variation of the PVP-nano-Se^0 concentration in aqueous solution in the course of contact with AXC GF was monitored with a Specord M40 spectrophotometer. The optical density *D* of 0.01% solutions was recorded in the range 200–600 nm.

The time of keeping the gel films in 0.01–3% aqueous solutions was varied from 15 min to 48 h. Then the specimens were dried at room temperature or at 50°C and immersed in a definite volume of distilled water for 0.5–24 h. The desorption kinetics was evaluated by measuring *D* of the solutions. The process was considered to be complete when the optical density decreased to zero.

X-ray studies of dry specimens of the starting AXC GFs and of gel films dried after sorption or desorption of nanoclusters were performed with DRON-2 (Russia) and XRD-3003 TT (Germany) diffractometers in the transmission and reflection modes, using Ni-filtered CuK_α radiation (λ = 1.54 Å). Electron-microscopic studies were performed with a JEM-7A microscope (Japan) at an accelerating voltage of 80 kV. Ultrathin sections of dry starting AXC GFs and of AXC GF–PVP-nano-Se^0 composites dried at 50°C and then cast into Araldite, or of speciments dried at 20°C and cast into Epon resin, were obtained with an LKB-III microtome (Sweden). The magnification was from 1500 to 21 000.

The surface topography of the AXC GFs dried after sorption or desorption of PVP-nano-Se^0 complexes with different content of Se nanoparticles was examined by atomic-force microscopy (AFM) in the tapping mode with a Nanotop NT-206 device (Mikrotestmashiny Limited Liability Company, Belarus). The AFM images were obtained in the constant amplitude mode.

The kinetics of the reaction occurring in the course of preparation of aqueous solutions of PVP-nano-Se (or -Ag^0) nanocomplexes and the morphological characteristics of these complexes were studied by light scattering and spectrophotometry [2, 10, 11]. According to data of static and dynamic light scattering, synthesis of selenium nanoparticles in aqueous PVP solutions at the ratio PVP : Se^0 = 10 : 1 yields aggregation-stable clusters of amorphous selenium with a hydrodynamic radius of about 57 nm. In these estimations, it is assumed that the hydrophobic interaction of PVP with Se^0 is the main driving force of PVP adsorption on selenium nanoparticles and that it leads to the formation of PVP-nano-Se^0 nanocomplexes of approximately spherical shape [2, 10, 11].

The optical density *D* of a 3% solution of the nanocomplexes in the range 245–260 nm noticeably decreases on keeping the gel film for 1 h, after which it increases to the initial value and remains constant for 48 h. On the contrary, with a 0.1% solution of the complex *D* increases during a period of 1 h. Thus, the most pronounced changes in the optical density of the PVP-nano-Se^0 solution on contact with AXC GF occur within the first 2 h.

To examine the sorption of the selenium nanocomplex on AXC GF, we also studied the desorption of this complex with water from the specimens dried at room temperature. The spectra of the solutions obtained (Fig. 1, curves *1'–3'*) differ essentially from the

spectra recorded in the course of sorption (curves *1*–*4*): A well-defined band with a maximum at 300 nm appears, and with increasing time of keeping the film in water its intensity decreases to zero. Presumably, the morphological characteristics of nanocomplexes released in the course of desorption with distilled water from dry films differ from those of the nanocomplexes in the solutions used for the sorption. Such changes in the initial characteristics of the nanocomplexes in the course of their intercalation into the gel film can be attributed to the appearance of new competing interactions of the cellulose matrix with fragments of the complex, i.e., of PVP with the matrix or of Se^0 with the matrix. Such interactions can alter not only the morphological characteristics of the complex, but also the structural parameters of the cellulose film.

Figure 2 shows the diffraction patterns of dried (20°C) specimens of the starting AXC GF (curves *1*, *3*) and the film kept in 1% solution of PVP-nano-Se^0 for 15 min (curves *2*, *4*) or 20 h (curve *5*), at perpendicular (Fig. 2a) or parallel (Fig. 2b) incidence of the X-ray beam relative to the film plane. It can be seen that the intensity of the reflections at 2θ 15°, 17°, and 35° from the ($\bar{1}$10), (110), and (004) planes, respectively, of the monoclinic lattice of cellulose I_β with interplanar spacings *d* 0.610, 0.523, and 0.256 ± 0.005 nm increases by a factor of 1.5–2.0, whereas the (200) reflection characteristic of the parallel-layer packing of hydrogen-bonded cellulose chains in crystallites (*d* = 0.389–0.392 nm; 2θ = 23°) undergoes no appreciable changes. With an increase in the time of sorption from the 1% solution (0.25, 0.5, 1, 4, 8, and 20 h), the most significant changes in the relative intensities of the (–100), (110), and (004) reflections were observed in the initial period (0.25–1 h), with no appreciable changes observed on further keeping the specimens in the initial solution (2–48 h). After 20-h exposure in 1% solution, along with appreciable increase in the intensity of the (110) and (004) reflections, an increase in the diffuse background in the range 2θ = 13°–25° was observed, attributable to the higher content of the complex sorbed in pores of the gel film or on its surface.

Using electron microscopy and X-ray diffraction, we examined how the concentration of aqueous PVP-nano-Se^0 solutions in the range 0.01–0.1 wt % affects the intercalation of nanostructures into AXC GFs at a constant sorption time of 0.5 h (see table; Fig. 3). Upon sorption from a very dilute solution (0.01 wt %), noticeable redistribution of the crystalline cellulose reflections was observed in the diffraction patterns of the dry specimens, similar to the trend observed in

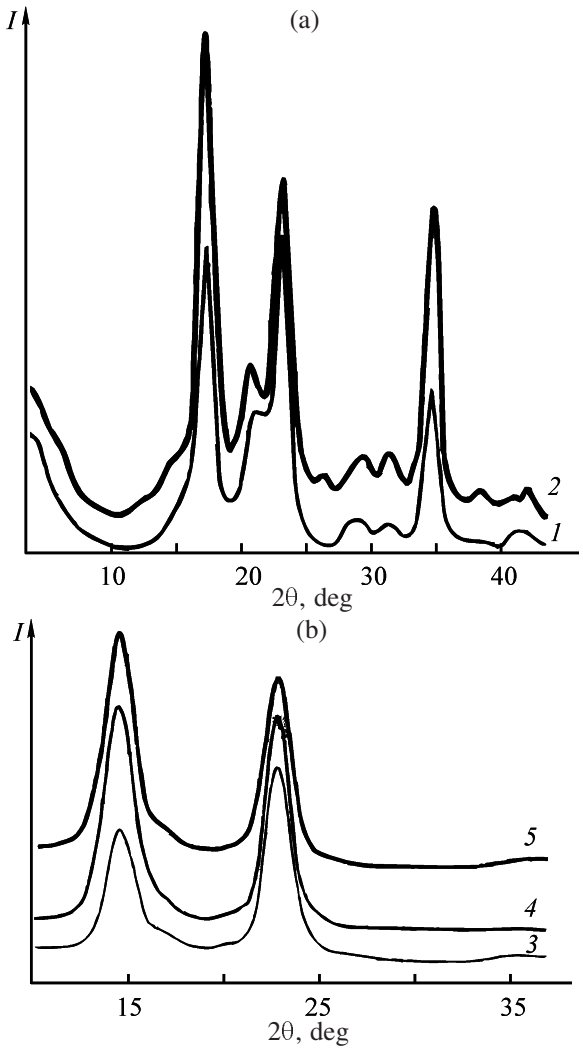

Fig. 2. Diffraction patterns obtained at (a) perpendicular and (b) parallel incidence of the X-ray beam relative to the plane of dried films: (*1*, *3*) starting AXC gel film, (*2*, *4*) AXC GF–PVP-nano-Se^0 composite after keeping in 1% aqueous PVP-nano-Se^0 solution for 15 min, and (*5*) the same, after keeping in this solution for 20 h. (*I*) Intensity and (2θ) Bragg angle; the same for Fig. 6.

going from curve *1* to curve *2* in Fig. 2: The intensities of the (110) and (004) reflections increased by a factor of 2, whereas the intensity of the (200) reflection did not change. The X-ray diffraction data for the specimens kept for 0.5 h in 0.01–1% solutions, dried at 20°C, and subjected to desorption with distilled water for 24 h are given in the table. It is seen that the desorption caused no significant changes in the relative intensities of the crystal reflections compared to the AXC GF–PVP-nano-Se^0 composites before desorption.

Figure 3 shows the electron micrographs of a transverse section of an AXC GF specimen modified in a

Relative changes in the intensity of reflections of the monoclinic lattice of dry AXC GF specimens after sorption (0.5 h) from PVP-nano-Se^0 solutions and subsequent desorption (24 h) with distilled water

Specimen no.	Concentration of aqueous PVP-nano-Se^0 solution, %	Reflection intensity					
		sorption			desorption		
		(110)	(200)	(004)	(110)	(200)	(004)
1	0	0.9	1	0.5	0.9	1	0.5
2	0.01	2.0	1	1.0	2.0	1	1.0
3	0.1	1.9	1	1.2	1.8	1	1.0
4	0.5	1.67	1	0.8	2.0	1	1.3
5	1.0	1.6	1	0.9	1.5	1	0.8

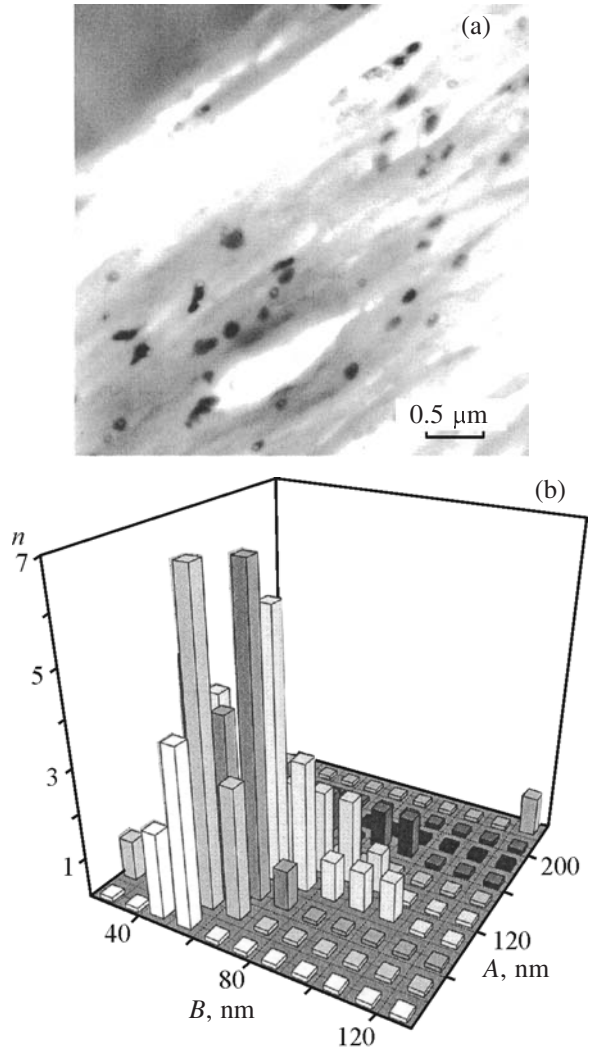

Fig. 3. (a) Electron micrograph and (b) histogram of sections of a dry AXC GF–PVP-nano-Se^0 specimen prepared by exposure of GF for 30 min in 0.01% solution of the complex, followed by drying at 20°C and desorption with water for 24 h. (*n*) Number of nanoparticles, (*B*) minor diameter, and (*A*) major diameter; the same for Fig. 4.

0.01% solution of PVP-nano-Se^0 for 30 min, dried at 20°C, subjected to desorption with water for 24 h, and finally dried at room temperature. The micrographs taken at different magnifications (5000–11 000) show that the distribution of selenium nanoparticles at the film surface is determined by the film arrangement in the course of the biosynthesis under the conditions of static cultivation of AXC: the upper surface contacting with air in the course of the biosynthesis and the lower surface immersed in the cultural medium are distinguished.

After the sorption from the 0.01% solution, ellipsoidal selenium nanoparticles with the major diameter ranging from 50 to 250 nm and the minor diameter, from 30 to 130 nm were detected in the bulk of the film. It can be clearly seen from the histogram that the majority of nanoparticles have an elliptical shape with major and minor diameters of approximately 80 and 60 nm, respectively.

Experiments on sorption on AXC GFs from more concentrated (0.1–1 or 3%) solutions (Fig. 4) showed that, along with nanoparticles detected in the bulk of the film, selenium crystals whose polymorphous modification and size depended on the dehydration temperature were formed on the specimen surface.

Figures 5a and 5c–5e show the AFM images of the upper surface, and Figs. 5b and 5f, those of the lower surface of dried AXC GF after intercalation with a 1% solution of the complex for (a, b) 15, (c) 30, and (d) 60 min, and (e, f) after intercalation for 30 min followed by desorption. It is seen that the lower and upper surfaces of the composite films after drying at 20°C essentially differ in the topography. On the upper surface of the composite, after the sorption for 15 min, there are numerous clusters of approximately spherical shape and size ranging from 50 to 290 nm, arranged on microfibrillar ribbons of AXC GF. On the

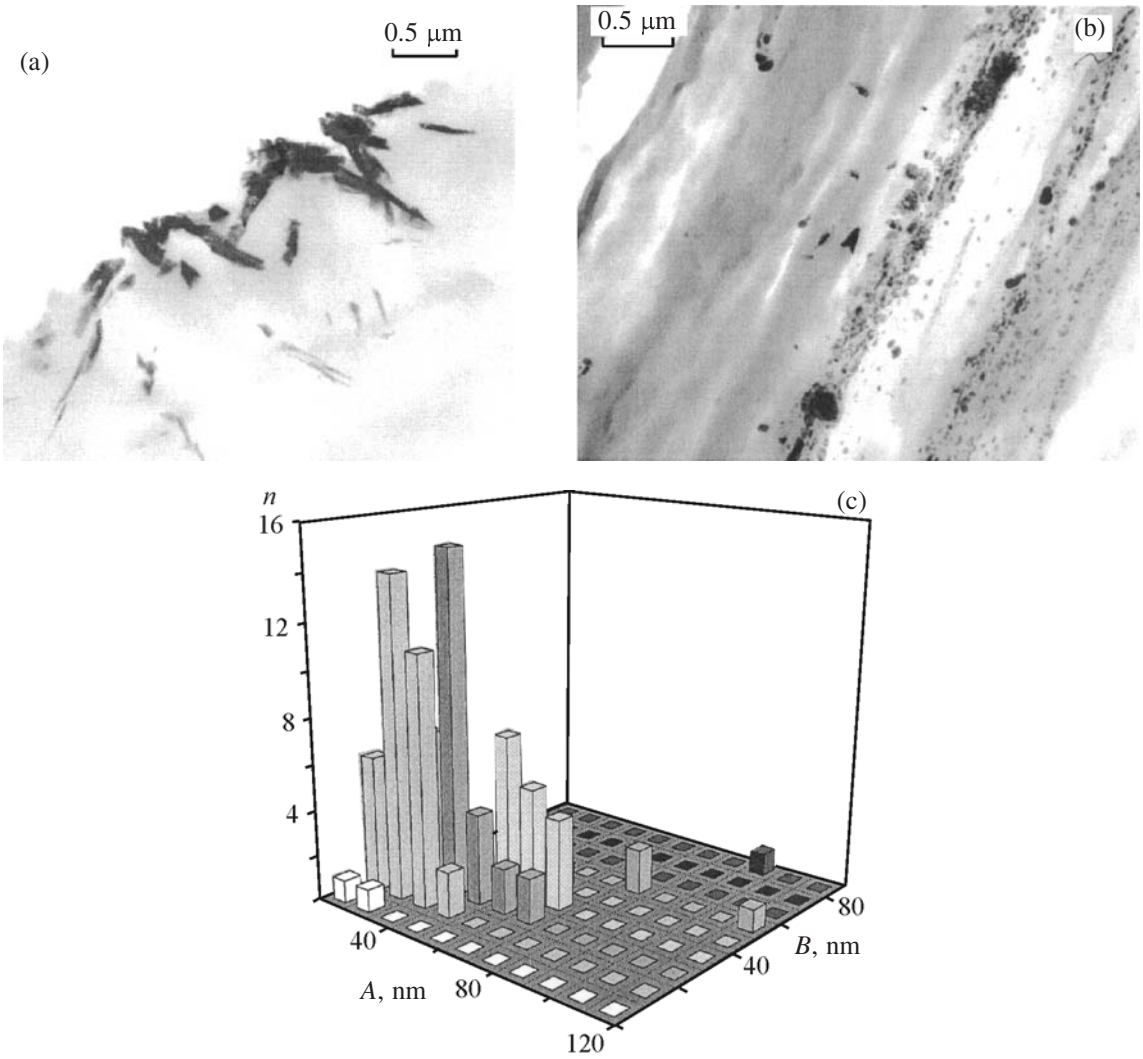

Fig. 4. (a, b) Electron micrographs and (c) histogram of sections of a dry AXC GF–PVP-nano-Se^0 specimen prepared by exposure of GF for 3 h in a 3% solution of the complex, followed by drying at 50°C. Distribution of (a) selenium crystals on the surface and (b) selenium particles in the bulk of the film.

lower surface of the same specimens, there are oval clusters with the minor diamter ranging from 100 to 420 nm, and the major diameter, from 150 to 800 nm.

After the sorption for 30 min (Fig. 5c), both spherical and strongly elongated oval particles were detected on the AXC GF surface. The size of the spherical particles varied in the same range as after the sorption for 15 min (from 55 to 290 nm). In this case, both surfaces of AXC GF have similar topography.

An increase in the sorption time to 60 min led to significant changes in the shape and size of the clusters: coarser aggregates up to 320 nm thick and up to 1000 nm long were observed. Apparently, at this sorption time separate clusters agglutinate to form elongated aggregates.

After the desorption for 24 h followed by drying, the topography of the upper surface changed insignificantly (Fig. 5e), whereas the other surface was "cleaned": microfibrillar ribbons were observed, with only a minor amount of clusters remaining in pores between them.

The AFM data indicate that, when an AXC GF is kept in a PVP-nano-Se^0 solution, the complex is irreversibly adsorbed on the upper surface already in the first 15 min of exposure. After the sorption for 30 min, both surfaces are virtually fully occupied by the clusters, and further increase in the sorption time (to 60 min and over) leads to the formation of microaggregates by agglutination of separate clusters.

In our previous study [12], on the surface of AXC

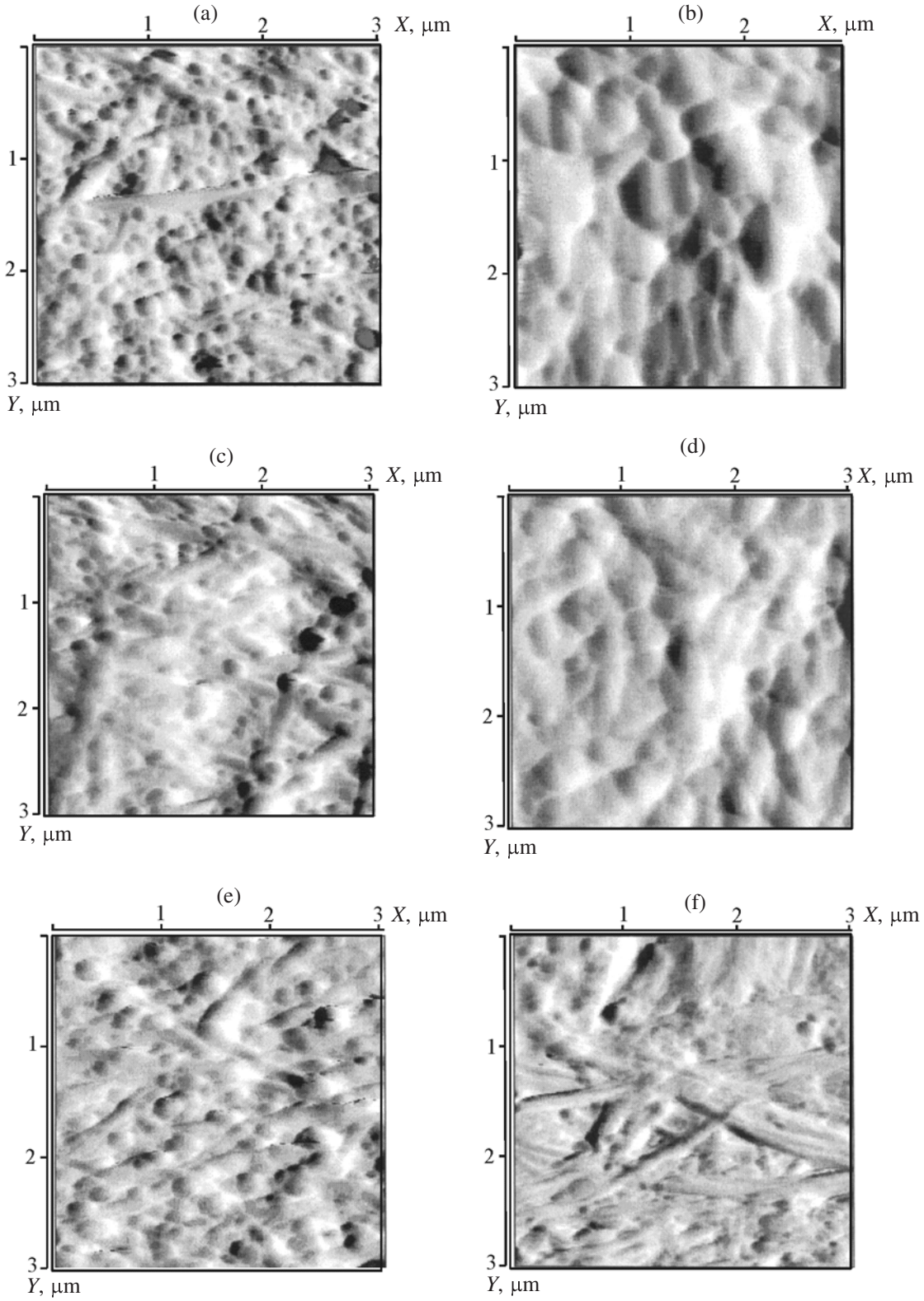

Fig. 5. AFM images, obtained in the constant amplitude mode, of regions of (a, c–e) upper and (b, f) lower surfaces of gel films after intercalation in a 1% aqueous solution of PVP-nano-Se^0 for (a, b) 15, (c, e, f) 30, and (d) 60 min, followed by (a–d) drying at 20°C and (e, f) desorption with water for 24 h and drying at 20°C. Scanning matrix size: (a, c–f) 256 × 256 and (b) 238 × 255. (*X*, *Y*) Coordinates.

GF–PVP-nano-Se^0 specimens prepared by sorption from a 3% aqueous solution of the complex and dehydrated at 40–50°C we detected two types of particles: spherical and rodlike. In the micrographs of sections of such a composite, one can see selenium crystals on the specimen surface (Fig. 4a) and elongated selenium particles with the ratio of major (*A*) and minor (*B*) diameters of 1.5–2 in the bulk of the film (Figs. 4b, 4c). The major diameter *A* varies from 20 to 60 nm, and the minor diameter *B*, from 10 to 40 nm.

In the diffraction pattern of such samples, there are reflections characteristic of trigonal selenium (Fig. 6, curve *1*). Figure 6 shows also the diffraction patterns of the samples dried at room temperature after sorption by the AXC matrix from a 1% solution of PVP-nano-Se^0 for 30 min (curve *2*). In this case, the selenium sorbed in AXC GF remains in the amorphous state. However, if such an AXC film after the sorption from a 1% PVP-nano-Se^0 solution for 30 min is immediately immersed in water for 24 h, additional reflections appear in the diffraction pattern of the specimen after drying at room temperature along with the reflections belonging to AXC GF. These additional reflections at 2θ 23°30′, 30°, 40°21′, 43°40′, and 45°20′ (Fig. 6, curve *3*) can be assigned, like the reflections in curve *1*, to the trigonal selenium cell with the parameters $a = b = 0.436$ nm, $c = 0.495$ nm, and $\gamma = 120°$ [4]. Figure 6 also shows the diffraction pattern of a dry powdered sample of PVP-nano-Se^0 (curve *4*), indicative of its amorphous structure. The presence of this complex in the composite will affect the diffuse background of the diffraction patterns.

It was shown previously [1, 6] that AXC GFs of VKM V-880 strain, dried at room temperature, exhibit axial-planar texture so that the crystallographic plane ($\bar{1}10$) of the monoclinic cellulose I_β cell ($d = 0.61$ nm) is arranged parallel to the specimen plane. In this case, the microfibrillar ribbons oriented in the gel film plane play the role not only of a reinforcing network but also of hydrophilic layers capable to sorb on their surface a large amount of water molecules, PVP, and water-soluble complexes PVP-nano-Ag^0 [1, 13].

According to Fink's model [7], nanofibrils or subunits from which AXC GF ribbons are formed in the course of biosynthesis have a rectangular cross section, 13×7 nm, and the crystallographic plane ($\bar{1}10$) is arranged parallel to the wide face. It was also noted in [14, 15] that the ($\bar{1}10$) face is highly hydrophilic because it incorporates primary hydroxy groups.

Based on the results of this study and previous data for AXC GF–VPV-nano-Ag^0 composites [1], using the Brown's [16] and Fink's models of the supramolecular structure of the intact (before drying) AXC film, we can suggest the scheme of intercalation of Se^0 nanoparticles in AXC GF shown in Fig. 7.

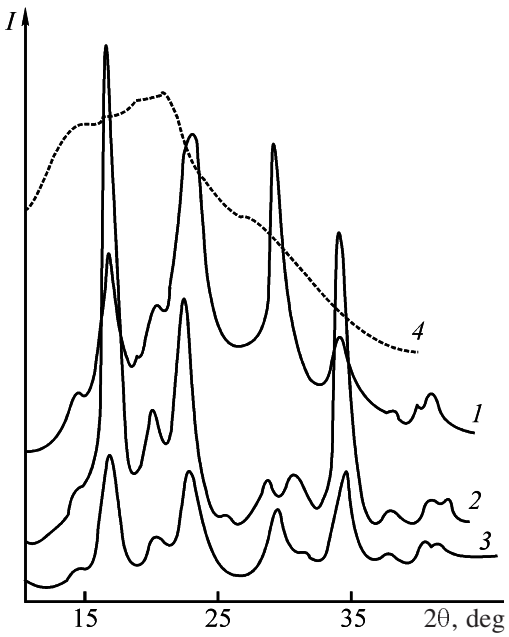

Fig. 6. Diffraction patterns of (*1*, *2*) AXC GF–PVP-nano-Se^0 composites prepared by sorption from 3 and 1% aqueous solution followed by drying at 50 and 20°C, respectively, (*3*) AXC GF specimen intercalated for 30 min in 1% PVP-nano-Se^0 solution with subsequent desorption for 24 h in water (without intermediate drying) followed by drying at 20°C, and (*4*) freeze-dried PVP-nano-Se^0 sample.

Examination of fine details of the biosynthesis and structure of AXC [2, 12] allows us to suggest that in the starting gel film the microfibrillar ribbon consists of numerous crystalline nanofibrils bounded by ($\bar{1}10$) and (110) faces (Fig. 7). The distances between these nanofibrils within the ribbon and between the adjacent ribbons are determined by the AXC strain used, synthesis conditions, and extent of squeezing of the gel film before sorption of water-soluble nanostructures. Nanochannels bounded by (110) faces of crystallites of adjacent nanofibrils build up a specific structure participating as a base in intercalation of nanocomplexes. Because of high surface energy of the ($\bar{1}10$) and (110) faces incorporating primary OH groups, nanosized selenium complexes can very rapidly (within 15–30 min) penetrate into the nanochannels or be accommodated on nanofibrils parallel to the wide face, without forming large clusters.

The deposition of selenium on these faces is proved by an appreciable (by a factor of 2) increase in the intensity of the ($\bar{1}10$) and (110) reflections in the dif-

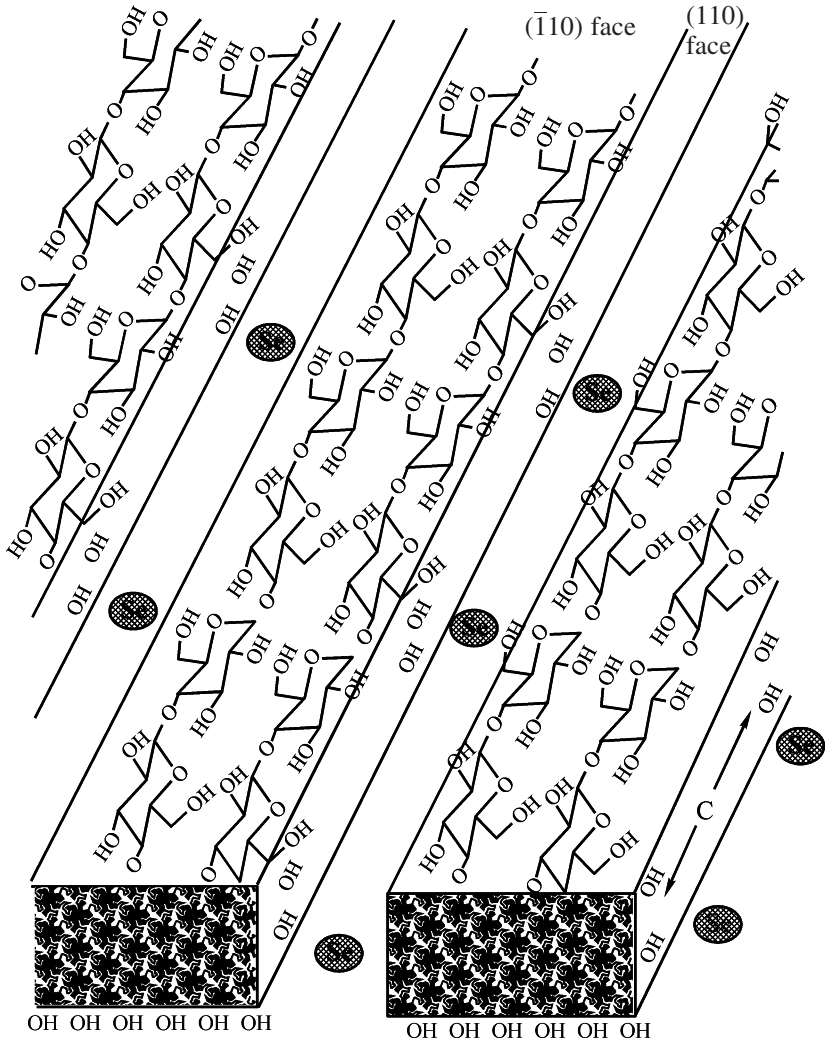

Fig. 7. Scheme of the sorption of PVP-nano-Se^0 by AXC gel film according to Fink's model [7].

fraction patterns of dry AXC GFs after their contact with aqueous PVP-nano-Se^0 solutions (see table; Fig. 2). The same trend is observed with the (004) reflections associated with the fixed periodicity of the deposition of Se^0 along the polymer chain (Fig. 7). Presumably, in this case enhancement of the intensity of the reflections is associated with an increase in the contrast from the ($\bar{1}$10), (110), and (004) planes. Indeed, the cellulose I_β reflections (200), (102), (012), and some other reflections do not change in intensity, because selenium nanocomplexes do not penetrate into nanofibril crystallites and do not alter the AXC structure, but only replace water molecules sorbed on primary OH groups of the crystallite walls.

Upon longer contact of AXC GFs with a 1% aqueous solution of PVP-nano-Se^0 (2–48 h) or with a more concentrated (e.g., 3%) solution, the relative intensities of the (110), (200), and (004) reflections do not change (Fig. 6). In this case, the observed noticeable increase in the total diffuse background and enhancement of the specimen color are due to localization on the specimen surface of coarse selenium clusters capable of crystallization (Figs. 5, 6). Presumably, both nanochannels and developed interribon internal and external surface of the gel films participate in the formation of the composite. Keeping such specimens in water for 24 h after drying at room temperature leads to no significant changes in the reflection intensities, and the specimen color and diffuse background in the diffraction patterns are preserved.

Thus, sorption of PVP-nano-Se^0 complexes from aqueous solutions on AXC GF having extremely developed internal surface can yield three types of composite materials with structure and properties depend-

ing on the concentration of the starting complex and on the sorption time.

(1) In AXC GF–PVP-nano-Se^0 specimens prepared at short sorption times (15–30 min) and low sorbate concentrations (0.01–0.1%), selenium particles are incorporated in the gel film in the amorphous state. Hence, the selenium sorption involves hydroxy groups of the nanochannels.

(2) In AXC GF–PVP-nano-Se^0 specimens prepared at short sorption times (15–30 min) but from more concentrated solutions (0.1–1%), both nanochannels and the developed interribbon surface with hydroxy groups located on the ($\bar{1}10$) faces of microfibrillar ribbons participate in the intercalation.

(3) In AXC GF–PVP-nano-Se^0 specimens prepared at long sorption times (2–48 h) and high sorbate concentrations (2–3% aqueous solutions of PVP-nano-Se^0), fairly large amount of clusters is sorbed on the surface of the gel film and in free volumes of the microfibrillar cellulose network. Specifically in these volumes heating to 30–50°C induces fairly easy crystallization of selenium.

CONCLUSIONS

(1) Differences in the distribution density and size of polyvinylpyrrolidone–nano-Se^0 clusters in their sorption in the bulk and on the surface of *Acetobacter xylinum* cellulose gel film were revealed. These differences may be due to orientation of microfibrillar ribbons and large number of channels between them, and also to high surface energy of the ($\bar{1}10$) and (110) crystal faces bearing primary OH groups.

(2) A scheme based on Fink's model was suggested for the predominant sorption of the polyvinylpyrrolidone–nano-Se^0 complex in channels between nanofibrils and microfibrillar ribbons at the ($\bar{1}10$) and (110) faces.

(3) Optimal conditions were suggested for stabilization of the amorphous form of selenium in a cellulose gel film: sorption from a 0.01–0.1% aqueous solution of the polyvinylpyrrolidone–nano-Se^0 complex in narrow ranges of temperature (20–25°C) and time (30–40 min).

ACKNOWLEDGMENTS

The study was financially supported by the Russian Foundation for Basic Research (project no. 05-03-32 842).

REFERENCES

1. Baklagina, Yu.G., Khripunov, A.K., Tkachenko, A.A., et al., *Zh. Prikl. Khim.*, 2005, vol. 78, no. 7, pp. 1197–1202.
2. Baklagina, Yu.G., Khripunov, A.K., Tkachenko, A.A., et al., *Kristallografiya*, 2006, vol. 5, no. 4, pp. 659–666.
3. Gates, B., Mayers, B., Cattle, B., and Xia, Y., *Adv. Funct. Mater.*, 2002, vol. 12, no. 3, pp. 219–227.
4. Cherin, P. and Unger, P., *Inorg. Chem.*, 1967, vol. 6, pp. 1589–1591.
5. Cherin, P. and Unger, P., *Acta Crystallogr., Sect. B*, 1972, vol. 28, pp. 313–317.
6. Baklagina, Yu.G., Khripunov, A.K., Tkachenko, A.A., et al., *Zh. Prikl. Khim.*, 2003, vol. 76, no. 6, pp. 1017–1024.
7. Fink, H.P., Puzz, H.J., Bohn, A., and Kunze, J., *Macromol. Symp.*, 1997, vol. 120, pp. 207–217.
8. Paramonov, B.A., Kopeikin, V.V., Tkachenko, A.A., et al., Abstracts of Papers, *1-ya Mezhdunarodnaya nauchno-prakticheskaya konferentsiya "Sovremennye polimernye materialy v meditsine i meditsinskoi tekhnike"* (1st Int. Scientific and Practical Conf. "Modern Polymeric Materials in Medicine and Medical Equipment"), St. Petersburg, 2005, pp. 203–205.
9. Baraboi, V.A., *Usp. Sovrem. Biol.*, 2004, vol. 124, no. 2, pp. 157–168.
10. Kopeikin, V.V., Valueva, S.V., Kipper, A.I., and Borovikova, L.N., *Vysokomol. Soedin., Ser. A*, 2003, vol. 45, no. 4, pp. 615–622.
11. Kopeikin, V.V. and Panarin, E.F., *Dokl. Ross. Akad. Nauk*, 2001, vol. 380, no. 4, pp. 497–500.
12. Sukhanova, T.E., Vylegzhanina, M.E., Kopeikin, V.V., et al., *Poverkhnost'*, 2006, no. 8, pp. 19–25.
13. Klechkovskaya, V.V., Baklagina, Yu.G., Stepina, R.D., et al., *Kristallografiya*, 2003, vol. 48, no. 5, pp. 813–820.
14. Ago, M., Shimizu, M., Moshizzuki, H., et al., *Senji Gakkaishi*, 2005, vol. 61, no. 5, pp. 119–123.
15. Kondo, T., Nojiri, M., Hishikawa, Y., et al., *PNAS*, October 29, 2002, vol. 99, no. 22, pp. 14 008–14 013.
16. Brown, R.M., Jr., *J. Mater. Sci., Pure Appl. Chem.*, 1998, vol. 33, no. 10, pp. 1345–1373.

ISSN 1070-4272, Russian Journal of Applied Chemistry, 2007, Vol. 80, No. 9, pp. 1558–1561. © Pleiades Publishing, Ltd., 2007.
Original Russian Text © Yu.A. Mirgorod, N.A. Efimova, 2007, published in Zhurnal Prikladnoi Khimii, 2007, Vol. 80, No. 9, pp. 1525–1528.

NANOTECHNOLOGIES AND NANOMATERIALS

Relationship between Size of Cadmium Sulfide Nanoparticles and Water Pool Diameter in Reverse Micelles

Yu. A. Mirgorod and N. A. Efimova

Kursk State University, Kursk, Russia

Received December 25, 2006; in final form, April 2007

Abstract—Preparation of CdS nanoparticles in water–sodium bis(2-ethylhexyl) sulfosuccinate–isooctane reverse micelles with various water contents is studied. A direct correlation between the water pool diameter in the reverse micelles and the mean size of CdS nanoparticles is found.

DOI: 10.1134/S1070427207090212

Recently a great interest has been attracted to preparation and characterization of nanomaterials [1]. Reverse micelles in hydrocarbon solvents proved to be appropriate systems for nucleation and growth of nanoparticles. Water droplets (pools) in surfactant-based micelles act not only as microreactors, but also as steric inhibitors of aggregation of atoms and molecules. Micellar synthesis was used to prepare various nanomaterials, among them CdS (see review [2]). Cadmium sulfide is a semiconductor used as a working medium in lasers and also as a material for fabrication of photoresistors, photodiodes, and solar batteries. The advantages of the synthesis of nanoparticles in reverse micelles are, first, in mild conditions of the process (no high temperature and pressure is required) and, second, in that the size and shape of nanoparticles can be controlled by the micelle structure and dynamics.

Presently, in this research field, the major focus is on preparation and characterization of nanoparticles, but not on properties of the dispersions. Particularly, it remains to be understood whether the properties of the micelles and microemulsions are different in the course of synthesis of nanoparticles.

Subdivision into micelles and microemulsions can be made by the microphase sizes in the system water–sodium bis(2-ethylhexyl) sulfosuccinate (AOT)–isooctane, as dependent on the temperature at various $[H_2O]/[AOT]$ ratios w [3]. At 50–60°C, these dependences are different: at $w = 15$ there is a descending curve, and at $w = 18$, an ascending one, suggesting formation of micelles and microemulsions at $w < 15$ and $w > 18$, respectively. According to [2, 3], over the range $0 < w < 15$–18, water occurs in the bound state, and with further increasing w, the structure of water is the same as in straight water. This hypothesis is supported by the trends in various physicochemical properties of water. For example, in the former case, the activity of emulsified water increases with increasing w, reaching saturation at $w = 15$. Similar trend is observed for the chemical shifts of protons of water, and the lifetime of hydrated electrons produced by radiolysis decreases, flattening out at $w = 15$ [2].

Here we report on synthesis of CdS nanoparticles in micelles and microemulsions at $w = 5$–18. Particularly, we analyzed the interrelation between the water pool diameter and nanoparticle size.

EXPERIMENTAL

In synthesis we used $CdCl_2$, Na_2S, $C_{20}H_{37}NaO_7S$ (AOT), and isooctane from Sigma–Aldrich. Water was distilled from potassium permanganate. The projected area of the AOT molecule was measured in a monomolecular layer. The surface tension of the aqueous AOT solution was determined by the plate method. The area of the AOT molecule in the adsorption layer was estimated from the surface tension isotherm obtained at 298 K (Fig. 1) at the water/air interface, assuming that the resulting area does not differ from that at the water/hydrocarbon interface. There are two features in the isotherm: one corresponding to the critical micelle concentration, and the second one, to the concentration at which the maximal adsorption G_m is attained. The quantity G_m was estimated by the Gibbs equation [4]:

$$G_m = -\frac{1}{RT}\frac{\partial\sigma}{\partial\log c}, \quad (1)$$

where σ is the surface tension of the solution

Table 1. Parameters* (nm) characterizing the microphases at various w, and standard deviations σ

w	d_m [3]	d_p [2]	d_p [5]	$d_m - 3.4$	$\overline{d}_p$	$\sigma_{\overline{d}_p}$	$\overline{d}_{CdS}$	$\sigma_{\overline{d}_{CdS}}$
5	6.1	1.8	2.7	2.7	2.4	0.5	2.2	0.2
9	7.0	2.7	4.1	3.6	3.5	0.7	2.9	0.3
15	8.0	4.5	6.3	4.6	4.8	1.1	3.4	0.5
18	9.4	5.4	7.4	6.0	6.3	0.9	4.5	0.5

* (d_m) Microphase diameter, (d_p) water pool diameter, ($\overline{d}_p$) mean diameter of water pools, and ($\overline{d}_{CdS}$) mean diameter of CdS nanoparticles; σ was estimated as $\sigma = \sum_{i=1}^{N}(d_i - \overline{d}_p)/(N-1)$, $N = 100$ for $\overline{d}_{CdS}$ and $N = 3$ for $\overline{d}_p$.

(mJ m^{-2}); R, gas constant (J mol^{-1} K^{-1}); T, temperature (K); and c, concentration (M).

The derivative was taken at the linear part of the curve. From G_m, the limiting area occupied by the AOT molecule on the water/hydrocarbon interface was estimated by Eq. (2):

$$S_0 = 1/(G_m N_A), \quad (2)$$

where N_A is the Avogadro number.

As a result, we obtain $G_m = 6.6 \times 10^{-6}$ mol m^{-2} and $S_0 = 0.25$ nm^2. The radius of the hydrophilic fragment of AOT was estimated from these values to be 0.28 nm.

The diameters of microphases at various w were taken from [2, 3, 5] (Table 1). According to data from [3], at $w = 0$, $d_m = 3.4$ nm. Therefore, this value corresponds to the size of "dry" micelles. Pileni [2] has demonstrated that the dependence of the water pool diameter of micelles d_p (nm) on w in the system water–AOT–isooctane is described by Eq. (3):

$$d_p = 0.3w. \quad (3)$$

As seen from Eq. (3), at $w = 0$, $d_p = 0$, which corresponds to such condition of the system when in the absence of water there is no apparent void volume in the pool. Bagwe and Khilar [5] suggested another equation for this dependence:

$$d_p = 0.36w + 0.9. \quad (4)$$

Subtraction of the micelle diameter (3.4 nm) from the microphase diameter gives us the water pool diameter of the micelle [2], whose value is well consistent with published data. By averaging data on the water pool diameters of micelles d_p, taken from three sources, we obtain the following correlation equation:

$$\overline{d}_p = 0.28w + 0.9. \quad (5)$$

It follows from Eq. (5) and Fig. 2 that, at $w = 0$, $d_p = 0.9$ nm, as in Eq. (4).

Determination of the relationship between d_p and d_{CdS} in the form similar to Eq. (5) should allow prediction of the size of CdS nanoparticles at a given w, which is practically significant.

CdS nanoparticles were prepared at room temperature as follows (Table 2). First, 1.3×10^{-4} M $CdCl_2$ and 1×10^{-4} M Na_2S solutions were prepared [6]. Then, to each solution, we added AOT to obtain w

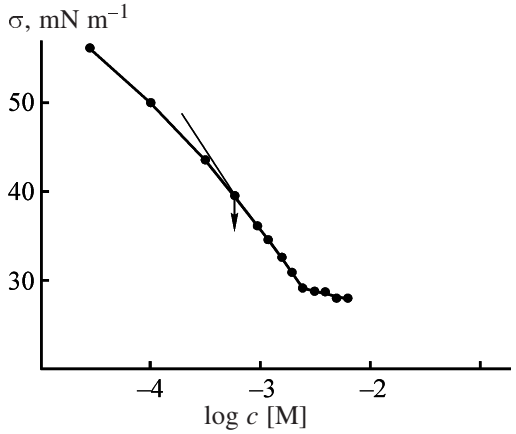

Fig. 1. Isotherm of the surface tension σ for aqueous AOT solution at 25°C. (c) Concentration.

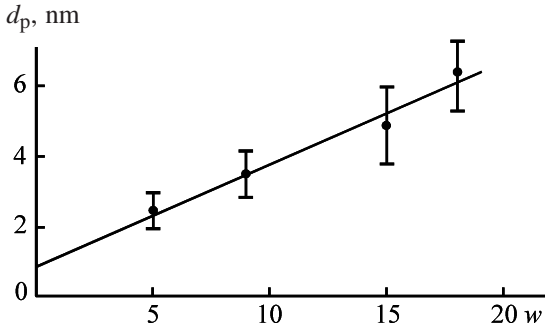

Fig. 2. Correlation between the water pool diameter d_p and $w = [H_2O]/[AOT]$.

Table 2. Compositions of systems used for preparing microemulsions of $CdCl_2$ and Na_2S

w	Component, g		
	H_2O	AOT	isooctane
5	5.00	24.86	299.60
9	5.00	13.76	187.60
15	5.00	8.44	134.40
18	5.00	7.10	121.00

ranging from 5 to 18 and isooctane (1 : 10). The systems were mixed with a low-frequency ultrasonic disperser until formation of dispersions. Finally, two dispersions with $CdCl_2$ and Na_2S were combined. In 0.5 h, CdS nanoparticles were formed in water pools of the micelles or microemulsions. The dispersion exhibited yellowish-orange opalescence. The nanoparticles were separated by adding DMF until yellow

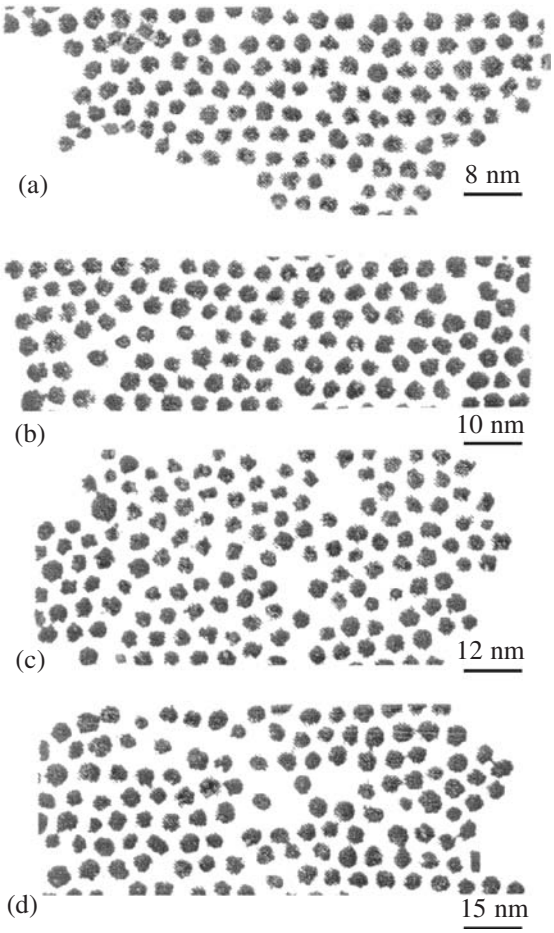

Fig. 3. TEM micrographs of CdS nanoparticles obtained at various w: (a) 5, (b) 9, (c) 15, and (d) 18; the same for Fig. 4.

floccules still remained at the interface between isooctane and aqueous DMF. Isooctane was then removed using a separating funnel. The CdS floccules were separated by centrifugation. The aqueous dispersion was removed by decanting. The precipitate was dispersed in distilled water; the nanoparticles were applied onto a carbon film, and their size was determined by TEM.

Carbon was sputtered onto a thin mica plate using an Edvards auto 306 vacuum evaporator. Along the edges of the plate, scratches were made to separate the carbon film from the mica film. Then one side of the mica film was immersed in water. The carbon film was detached by a needle from the mica film and remained to stand on the water surface. Then the carbon film was covered with a copper grid. Under this covered film, a sheet of waterproof paper was arranged, and after the grid and film were fastened onto the paper, it was withdrawn. The carbon film was cut along the perimeter of each grid, and a drop of the nanodispersion was applied onto it. After water was removed by evaporation, TEM micrographs were obtained with a Hitachi model H-600 transmission electron microscope. In determination of the size distribution of the nanoparticles, the diameters of each of 100 nanoparticles were averaged by the major and minor sizes. The averaged diameter of the particles at each w was determined as an arithmetic mean (Table 1). At $w = 9$, it was found to be 2.9 nm, which is in satisfactory agreement with that obtained in [7] at $w = 8$ for CdS nanoparticles containing adsorbed pyridine (3–4 nm). The micrographs of the nanoparticles are given in Fig. 3 for various w, and the size distribution, in Fig. 4. All the synthesized CdS particles are nearly spherical in shape. In the microphases, at $w = 5$, 81% of the clusters are from 2 to 2.5 nm in diameter; at $w = 9$, 89% of the clusters are from 2 to 3 nm in diameter; at $w = 15$, 71% of the clusters are from 2.5 to 3.5 nm in diameter; and at $w = 18$, 63% of the clusters are from 4 to 5 nm in diameter.

The dependence between the size of CdS nanoparticles and the mean water pool diameter (Fig. 5) is described by Eq. (6):

$$d_{CdS} = 0.74\bar{d}_p. \quad (6)$$

The water pool diameter in the microphases is approximately 26% larger than the size of CdS nanoparticles.

Let us then determine the minimal w at which CdS nanoparticles start to form in the micelles. As demonstrated above, at $w = 0$, $d_p = 0.9$. Let us in-

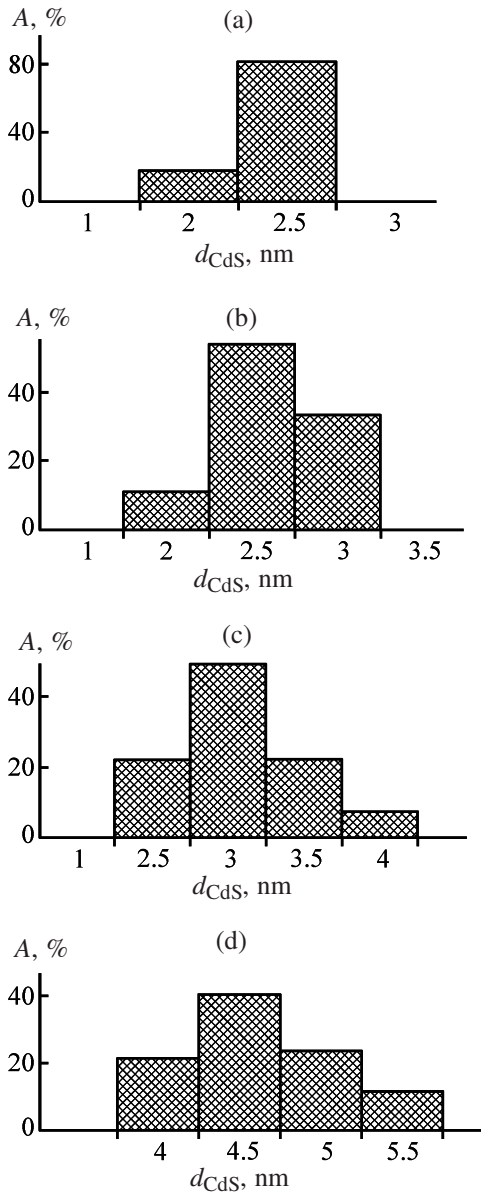

Fig. 4. CdS particle size distribution at various w. (A) Percentage and (d_{CdS}) diameter of CdS nanoparticles.

crease this diameter by 26% (this is the smallest diameter of water pools in which nanoparticles can be formed) to obtain d_p = 1.1 nm. The volume of a pool of such a diameter is 0.7 nm^3. Assuming the volume of the water molecule equal to 0.03 nm^3 [6], we obtain that the number of water molecules in the pool is about 23. The surface area of the water pool is 0.94 nm^2. On this area, four AOT molecules can be arranged, since, as demonstrated above, the projected area of the hydrophilic fragment of AOT is 0.28 nm^2. Hence, in this case, w = 6. Therefore, it is inadvisable to synthesize CdS nanoparticles at w < 6, despite

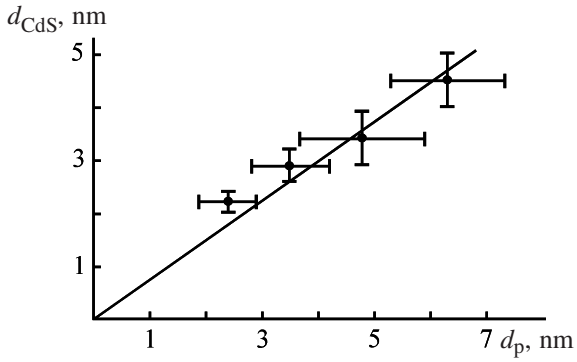

Fig. 5. Correlation between the diameter of CdS nanoparticles d_{CdS} and the water pool diameter d_p.

the fact that in this study we obtained them even at w = 5.

CONCLUSIONS

(1) CdS nanoparticles are synthesized at 25°C in microphases of the systems water–sodium bis(2-ethylhexyl) sulfosuccinate–isooctane at w 5, 9, 15, and 18. The surface tension isotherm of aqueous sodium bis(2-ethylhexyl) sulfosuccinate at 25°C and size distribution of the nanoparticles are determined.

(2) In the range of micelle formation at w = 15, there are linear relationships between w, the mean diameter of nanoparticles, and the mean water pool diameter, suggesting similar structures for reverse micelles and microemulsions in the investigated systems.

ACKNOWLEDGMENTS

The study was financially supported by the Ministry of Education and Science of the Russian Federation (project 1.1.07).

REFERENCES

1. Yadav, O.P., Palmqvist, A., Cruise, N., and Holmberg, K., *Colloids Surf. A: Eng. Aspects*, 2003, vol. 221, pp. 131–134.
2. Pileni, M.P., *Langmuir*, 1997, vol. 13, no. 13, pp. 3266–3276.
3. Eicke, H.F., *Chimia*, 1982, vol. 36, no. 1, pp. 6–15.
4. Frolov, Yu.G., *Kurs kolloidnoi khimii* (Course of Colloid Chemistry), Moscow: Khimiya, 1982.
5. Bagwe, R.P. and Khilar, K.C., *Langmuir*, 1997, vol. 13, no. 24, pp. 6432–6438.
6. Fu, D., Li, M., Wang, X., et al., *Supramol. Sci.*, 1998, vol. 5, nos. 5–6, pp. 495–498.
7. Jain, T.K., Cassin, G., Badiali, J.P., et al., *Langmuir*, 1996, vol. 12, no. 10, pp. 2408–2411.

ISSN 1070-4272, Russian Journal of Applied Chemistry, 2007, Vol. 80, No. 9, pp. 1562–1565. © Pleiades Publishing, Ltd., 2007.
Original Russian Text © S.M. Nurgalieva, T.A. Bispen, A.N. Il'in, D.D. Moldavskii, E.A. Rozhkova, 2007, published in Zhurnal Prikladnoi Khimii, 2007, Vol. 80, No. 9, pp. 1529–1532.

ORGANIC SYNTHESIS AND INDUSTRIAL ORGANIC CHEMISTRY

Perfluoroethanesulfonyl Fluoride: Preparation from Sultone

S. M. Nurgalieva, T. A. Bispen, A. N. Il'in, D. D. Moldavskii, and E. A. Rozhkova

Prikladnaya Khimiya Russian Scientific Center, St. Petersburg, Russia
Galogen Open Joint-Stock Company, Perm, Russia

Received November 21, 2006; in final form, March 2007

Abstract—A procedure was developed for preparing perfluoroethanesulfonyl fluoride by synthesis of hexafluoropropane-2-β-sultone from sulfuric anhydride and perfluoropropene, followed by hydrolysis of the sultone to α-tetrafluoroethanesulfonyl fluoride and fluorination of the latter with elemental fluorine.

DOI: 10.1134/S1070427207090224

Perfluoroalkanesulfonyl halides (PFASHs), including sulfonyl fluorides, are starting compounds for preparing perfluoroalkanesulfonic acids and their salts. They are also used as sources of perfluoroalkanesulfonyl groups in the synthesis of surfactants, dyes, antioxidants, UV stabilizers, and materials for chemical power cells [1–6]. Among PFASHs, of particular interest are lower homologs with 1–3 carbon atoms. However, application of PFASHs is limited by their high cost, caused by the lack of an efficient synthesis process. There are a number of procedures for preparing PFASHs, each having certain features and shortcomings. The best studied process is electrochemical fluorination (ECF), i.e., electrolysis of solutions of alkanesulfonyl halides in hydrogen fluoride [7, 8]:

$$RSO_2Hal \xrightarrow{HF,\ e} R_fSO_2F,$$

where Hal is F or Cl, R is alkyl, and R_f is perfluoroalkyl.

In Russia, the method is implemented at the Angarsk Electrochemical Plant for the production of trifluoromethanesulfonyl fluoride from methanesulfonyl chloride; the yield is 80–85%. Methanesulfonyl chloride, like other lower alkanesulfonyl chlorides, is not produced in Russia. Commercial electrochemical synthesis of perfluoroethanesulfonyl fluoride (PFESF) from ethanesulfonyl fluoride appeared to be unfeasible because of the low yield, which did not exceed 45%. The electrolysis is accompanied by formation of a large amount of impurities with boiling points close to that of PFESF; furthermore, a part of PFESF is mixed with hydrogen fluoride, and its significant fraction (up to 30%) remains dissolved in the electrolyte. Intermediate conversion of ethanesulfonyl chloride into ethanesulfonyl fluoride by the reaction with HF in the presence of a chromium–magnesium catalyst [9] allowed the PFESF yield to be increased to 70%, but its isolation appeared to be difficult. In electrolysis of higher alkanesulfonyl chlorides, the PFASH yields are as low as 25–30%. Another route to PFASHs is the reaction of perfluoroalkyl iodides or bromides with sodium dithionite, followed by chlorination of the resulting sodium perfluoroalkanesulfinate [10–12]:

$$R_fHal + Na_2S_2O_4 \rightarrow R_fSO_2Na,$$

$$R_fSO_2Na + Cl_2 \rightarrow R_fSO_2Cl + NaCl,$$

where R_f is perfluoroalkyl, and Hal is Br or I.

The reaction was performed in a water–acetonitrile mixture. The yield of perfluoroalkylsulfonyl chlorides reached 80%. We reproduced this procedure with perfluoroethyl iodide and obtained perfluoroethanesulfonyl chloride in 76% yield. Despite reasonable yield of PFASH, this procedure has significant drawbacks:

(1) use of expensive perfluoroalkyl iodides and bromides, which are in short supply, as starting compounds;

(2) use of sodium dithionite, which is not produced in Russia, and instability of this salt in storage, which gives rise to additional problems;

(3) strong corrosion of apparatus and pipelines, caused by chlorination of sodium perfluoroalkanesulfinates in aqueous solutions;

(4) overall complexity of the process: It involves steps of extraction, filtration, and regeneration of solvents. Implementation of the process requires a

large set of equipment, and many operations are performed manually;

(4) large amount of wastes: 1.5 t of solid and 2.5 t of liquid wastes are formed per ton of the finished product. The wastes mainly consist of toxic fluorinated compounds, and their regeneration and detoxication require additional chemicals, equipment, time, and energy.

Another procedure suggested for preparing PFASHs is based on the reaction of perfluoroolefins with sulfuryl fluoride or sulfuryl fluorochloride in the presence of cesium fluoride [13, 14]:

$$R_fCF{=}CF_2 + SO_2Hal_2 \xrightarrow{CsF} HalCF(R_f){-}CF_2SO_2Hal,$$

where Hal is Cl or F.

We checked this procedure and found that CsF, olefins, and solvents should be thoroughly dried. The water content should not exceed 0.001 wt %. However, even with such precautions the reaction mainly yielded a mixture of olefin oligomers and polymeric sulfonyl halides $Hal(R_fCF{-}CF_2)_nSO_2Hal$, $(R_fCF{-}CF_2)_n$, n = 1–50. The yield of monomeric PFASHs did not exceed 20%. It should be noted that polymeric sulfonyl halides are used as surfactants, lubricants, and components of impregnating formulations, ion-exchange membranes, and film materials.

The drawbacks of the above-considered procedures for preparing PFASHs make it necessary to search for a simple procedure for their synthesis involving chemicals commercially produced in Russia and to develop an efficient technology based on this procedure. Among possible routes to PFASHs, we chose conversion of sultones. In accordance with [15–17], polyfluorinated alkanesulfonyl fluorides are formed by hydrolysis of perfluorinated sultones which, in turn, are prepared by the reaction of sulfuric anhydride with perfluoroolefins. According to data reported by Knunyants [15, 16] and results of our experiments, the yield of hexafluoropropane-2-β-sultone is as high as 96–98%. The impurities (0.5–2%) are the linear isomer $CF_3{-}CF(SO_2F){-}COF$, six- and eight-membered sultones, and perfluoroallyl sulfate $CF_2{=}CF{-}CF_2O{\cdot}SO_2F$. Sultones are hydrolyzed to α-hydroperfluoroalkanesulfonyl fluorides (HPFSFs), which, as we expected, can be fluorinated to perfluoroalkanesulfonyl florides:

$$R_fCF{=}CF_2 + SO_3 \longrightarrow R_fCF(O_2S){-}CF_2{-}O$$

$$\xrightarrow{H_2O} R_fCFHSO_2F \xrightarrow{F_2} R_fCF_2SO_2F.$$

Experiments on optimization of the sultone synthesis showed that sulfuric anhydride should contain as low amounts of the monohydrate as possible: At 0.2% content of the monohydrate, the yield of the sultone is 98%. An increase in the monohydrate content leads to an increase in the content of impurities: monohydroperfluorocarboxylic acids $R_fCFH{-}COOH$, perfluoroalkenyl fluorosulfonates $R_fCF{=}CF{-}OSO_2F$, sulfuryl fluoride, and carbonyl fluoride. At 2% content of the monohydrate in sulfuric anhydride, the content of impurities reaches 15%.

The optimal temperature of sultone synthesis is 105°C. Above this temperature, the sultone starts to decompose, and its yield decreases. At temperatures below 100°C, the reaction becomes slower. At 50°C, the yield is 53%.

The monomer should be taken in 5–7% excess relative to the stoichiometry, to ensure complete binding of sulfuric anhydride. Free sulfuric anhydride promotes the subsequent acid hydrolysis of the sultone, with polyfluoroalkanoic and sulfonic acids becoming the major products.

Hydrolysis of hexafluoropropane-2-β-sultone involves two successive reactions: formation of (fluorosulfonyl)perfluoropropionic acid and its spontaneous decarboxylation with the formation of α-hydrotetrafluoroethanesulfonyl fluoride (TFESF):

$$CF_3{-}CF(O_2S){-}CF_2 + H_2O \longrightarrow CF_3{-}CF(SO_2F){-}COOH + HF,$$

$$CF_3{-}CF(SO_2F){-}COOH \longrightarrow CF_3CFH{-}SO_2F + CO_2.$$

The formation of hydrogen fluoride in the course of hydrolysis leads to the formation of tetrafluoropropionic acid:

$$CF_3{-}CF(SO_2F){-}COOH + H_2O \xrightarrow{HF} CF_3CFH{-}COOH + H_2SO_4 + HF.$$

The optimal hydrolysis temperature is 0–2°C. At this temperature, the yield of TFESF is 90%. TFESF contained up to 1% water. The content of other impurities did not exceed 0.03 wt %. After drying, the product was used for fluorination without additional purification.

Fluorination of polyfluorinated paraffins, ethers, tertiary amines, and their heterocyclic analogs by various procedures, including that with elemental fluorine, is a fairly well studied process, and high yields of the target products can be attained [18]. Fluorination of compounds containing an S–C bond is

much less studied. The energy of S–C bonds (about 270 kJ mol^{-1}) is appreciably lower than that of C–C (480 kJ mol^{-1}), C–O (360 kJ mol^{-1}), and even C–N (305 kJ mol^{-1}) bonds, which gives rise to certain problems in fluorination, because the cleavage of the C–S bond and formation of C–F and S–F bonds (energy 480 and 290 kJ mol^{-1}, respectively) is thermodynamically favorable. Kornilov et al. [19] studied fluorination of mercaptans with cobalt trifluoride. The major products were SF_6 and polyfluorinated paraffins. In our experiments on fluorination of TFESF with cobalt trifluoride, the yield of PFESF was 19%; the other products were SF_6, SO_2F_2, CF_4, and C_2F_6.

Fluorination of TFESF with elemental fluorine appeared to be more successful. Under static conditions, with slow supply of fluorine (0.5–0.7 ml s^{-1}) at 0–20°C into a reactor containing TFESF and packed with copper chips, the yield of PFESF was 92%. In dynamic experiments with a tubular reactor (nickel tube packed with copper chips), we sometimes observed plops when the rates of feeding the reactants changed or even without any apparent causes. In this case, SO_2F_2, SF_6, C_2F_6, CF_4, and carbon black became the major products. This result is attributable to inefficient removal of excess energy released in the course of fluorination. To remove this energy, it is recommended to use solvating solvents in combination with a heat-removing packing [20]. Among the examined compounds, the best results were obtained with HF and somewhat worse results, with TFESF and N_2. At the molar ratio F_2 : TFESF : HF = 1 : 1 : 1, 97% conversion and 95% selectivity were attained. If we consider the reactants as a donor–acceptor system [21] in which an electron is transferred from the donor (TFESF) to the acceptor (F_2)

$$CF_3CFHSO_2F + F_2 \longrightarrow CF_3\overset{\displaystyle CSO_2F}{\overset{\displaystyle |}{\underset{\displaystyle +\delta H\cdots}{\underset{\displaystyle |}{}}}}\ ,F^{-\delta}\!-\!F$$

$$\longrightarrow CF_3CFSO_2F + F + HF$$

with the formation of a radical pair, a diluent is required for stabilization of this pair and absorption of excess energy. This leads to temporary stabilization of the transition state, so that the radicals have time to recombine before escape into the reaction volume:

$$CF_3CFHSO_2F + F_2\cdots,HF \longrightarrow CF_3\overset{\displaystyle CFSO_2F}{\overset{\displaystyle |}{\underset{\displaystyle +\delta H\cdots}{\underset{\displaystyle |}{}}}}\ ,F^{-\delta}\!-\!F\cdots HF$$

$$\longrightarrow CF_3CFSO_2F + F\cdots HF + HF,$$

$$CF_3CFSO_2F + F\cdots HF \longrightarrow HF + CF_3CF_2SO_2F.$$

Apparently, the amount of HF correlates with the amount of supplied F_2. According to the theory of one-electron transfer, the optimal HF : F_2 ratio should be 1 : 1, i.e., the molar ratio of the components should correspond to the stoichiometric ratio. Indeed, as the HF concentration is decreased to 0.71 mol per mole of F_2, the selectivity decreases by 15–20%, and when it is increased to 1.5 mol per mole of F_2, the conversion of the starting reactants decreases, apparently due to the inhibiting effect of HF and a decrease in the fluorination rate.

Another major factor affecting the reaction is temperature. We found that 120–130°C is the optimal temperature of PFESF synthesis. Based on the results obtained, a pilot plant for PFESF synthesis was constructed at the Galogen Open Joint-Stock Company. The installation consists of units for distillation of sulfuric anhydride, synthesis of sultone, hydrolysis of sultone, fluorination of TFESF, neutralization of crude PFESF with alkalis, its drying with zeolites, and fractional distillation of PFESF to obtain the 99.9% pure products. The results of studies on fluorination of polyfluorinated alkanesulfonyl fluorides were protected with RF patents [22, 23].

EXPERIMENTAL

The reaction products were analyzed by gas chromatography [LKhM-80 chromatograph, thermal conductivity detector, 2-m column packed with Silokhrom + 20% 1,1,1-tris(β-cyanoethyl)acetophenone] and gas chromatography–mass spectrometry (Aligent-5973N, DB-5ms capillary column 60 m long).

Hexafluoropropane-2-β-sultone was prepared as described in [15]. Optimal conditions: hexafluoropropene : SO_3 ratio (1.05–1.08) : 1, 105–107°C, 12–14 h. α-Tetrafluoroethanesulfonyl fluoride was prepared by the procedure described in [15] with some modifications. Namely, the sultone was fed into water, which allowed us to increase the TFESF yield to 92%.

Fluorination of tetrafluoroethanesulfonyl fluoride with cobalt trifluoride. Into a nickel tube 800 mm long and 38 mm in diameter, packed with controllable heating, TFESF was fed from a batcher at a rate of 1–3 ml min^{-1}. The best results were obtained at 260–290°C. According to the gas-chromatographic analysis, the reaction mixture (after neutralization with aqueous NaOH) contained 23% SO_2F_2, 15% SF_6, 35% C_2F_6, 8% CF_4, and 19% $C_2F_5SO_2F$.

Fluorination with elemental fluorine under static conditions. A 2.0-l 12Cr18Ni10Ti stainless steel

vessel packed with copper chips and cooled to 0°C was charged with 18.5 g of TFESF, and fluorine was fed at a rate of 0.5–0.7 ml s^{-1} for 1 h (the procedure was performed in a steel box). After 24 h, the reaction mixture was condensed in a 12Cr18Ni10Ti stainless steel trap cooled with liquid nitrogen. After warming, it was neutralized with aqueous NaOH, dried over CaA zeolite, and collected in a trap cooled to –30°C. The product (yield 20 g) contained 95% PFESF and 5% impurities (CF_3SO_2F, SO_2F_2, C_2F_6, CF_4, SF_6).

Fluorination under dynamic conditions. A solution containing 92 g of TFESF and 10 g of HF was fed at a rate of 0.8–1.0 g min^{-1} from a batcher to a vaporizer (nickel tube 38 mm in diameter and 500 mm long, heated to 80–100°C). Fluorine was also fed to this tube at a rate of 120–130 ml min^{-1}. Then the mixture of the components came into a reactor (nickel tube 38 mm in diameter and 900 mm long, packed with copper chips and heated to 130–140°C). The reaction products were collected in a 12Cr18Ni10Ti stainless steel trap cooled to –120°C. After the reaction completion, the condensate was worked up as described above. The product (yield 90 g) contained 96.5% PFESF and 3.5% impurities (CF_3SO_2F, SO_2F_2, C_2F_6, CF_4, SF_6).

CONCLUSIONS

(1) A procedure was developed for preparing perfluoroethanesulfonyl fluoride by fluorination of tetrafluoroethanesulfonyl fluoride.

(2) The steps of perfluoroethanesulfonyl fluoride synthesis were optimized, and its pilot production was set up at the Galogen Open Joint-Stock Company.

ACKNOWLEDGMENTS

The authors are sincerely grateful to N.V. Baranov and G.G. Furin for the assistance in the work.

REFERENCES

1. Nikonorov, Yu.I. and Karelin, A.I., Abstracts of Papers, *IV Vsesoyuznaya konferentsiya po ftororganicheskim soedineniyam* (IV All-Union Conf. on Fluorinated Organic Compounds), Tashkent, September 9–12, 1982, Moscow, 1982, p. 12.
2. Eleev, A.F., Fetisov, V.I., and Sokol'skii, G.A., Abstracts of Papers, *IV Vsesoyuznaya konferentsiya po ftororganicheskim soedineniyam* (IV All-Union Conf. on Fluorinated Organic Compounds), Tashkent, September 9–12, 1982, Moscow, 1982, p. 172.
3. Yagupol'skii, Yu.L., Haas, A., and Savina, T.I., *Zh. Org. Khim.*, 1999, vol. 35, no. 12, pp. 1802–1804.
4. Kondratenko, N.V., Kolomeitsev, A.A., and Yagupol'skii, L.M., Abstracts of Papers, *IV Vsesoyuznaya konferentsiya po ftororganicheskim soedineniyam* (IV All-Union Conf. on Fluorinated Organic Compounds), Tashkent, September 9–12, 1982, Moscow, 1982, p. 7.
5. FRG Patent Appl. 10126929 A1.
6. Ukrainian Patent 27067.
7. Gramstad, T. and Haszeldine, R.N., *J. Chem. Soc.*, 1956, no. 1, pp. 173–180.
8. Gramstad, T. and Haszeldine, R.N., *J. Chem. Soc.*, 1957, no. 11, pp. 2640–2643.
9. Matalin, V.A., Shkul'tetskaya, L.V., and Moldavskii, D.D., Abstracts of Papers, *3-ya mezhdunarodnaya konferentsiya "Khimiya, tekhnologiya i primenenie ftorsoderzhashchikh soedinenii v promyshlennosti"* (3rd Int. Conf. "Chemistry, Technology, and Industrial Applications of Fluorinated Compounds"), St. Petersburg, June 3–6, 2001, pp. 21–22.
10. Furin, G.G., *Usp. Khim.*, 2000, vol. 69, no. 6, pp. 538–570.
11. Wei-Yuan Huang and Yian-Long Chen, *J. Fluorine Chem.*, 1987, vol. 35, no. 1, pp. 19–21.
12. Jin-Tao Liu, Guo-Dong Sui, and Wei-Yuan Huang, *J. Fluorine Chem.*, 1999, vol. 93, no. 1, pp. 49–51.
13. US Patent 2877267.
14. US Patent 3542864.
15. Knunyants, I.L. and Yakobson, G.G., *Sintezy ftororganicheskikh soedinenii* (Syntheses of Fluorinated Organic Compounds), Moscow: Khimiya, 1973.
16. Knuniants, I.L. and Sokolski, G.A., *Angew. Chem., Int. Ed. Engl.*, 1972, vol. 11, no. 7, pp. 583–595.
17. Dmitriev, M.A., Sokol'skii, G.A., and Knunyants, I.L., *Izv. Akad. Nauk SSSR, Ser. Khim.*, 1960, no. 6, pp. 1035–1038.
18. Bispen, T.A., Moldavskii, D.D., and Furin, G.G., *Zh. Prikl. Khim.*, 1998, vol. 71, no. 6, pp. 977–981.
19. Kornilov, V.V., Kostyaev, R.A., and Maksimov, B.N., *Zh. Prikl. Khim.*, 1995, vol. 68, no. 9, pp. 1409–1418.
20. Zakharov, V.Yu., Denisov, A.K., and Novikova, M.D., *Zh. Org. Khim.*, 1998, vol. 30, no. 12, pp. 1844–1846.
21. Mukhametshin, F.Kh., *Zh. Prikl. Khim.*, 1997, vol. 70, no. 1, pp. 127–134.
22. RF Patent 2237659.
23. RF Patent 2280030.

ISSN 1070-4272, Russian Journal of Applied Chemistry, 2007, Vol. 80, No. 9, pp. 1566–1569. © Pleiades Publishing, Ltd., 2007.
Original Russian Text © A.M. Kurdyukov, 2007, published in Zhurnal Prikladnoi Khimii, 2007, Vol. 80, No. 9, pp. 1533–1536.

ORGANIC SYNTHESIS AND INDUSTRIAL ORGANIC CHEMISTRY

In Situ Version of Radical-Chain Substitution Reactions

A. M. Kurdyukov

Volgograd State Technical University, Volgograd, Russia

Received April 27, 2007

Abstract—Peroxy acetals derived from an ether and a hydroperoxide can be prepared in situ and used without isolation to effect sulfochlorination of *n*-alkanes or chlorination of toluene to benzyl chloride.

DOI: 10.1134/S1070427207090236

The feasibility of initiated radical processes using activators prepared in situ in the reaction volume is obvious. The interest in such way of initiating chain reactions is particularly pronounced in production of polymers, e.g., of suspension PVC [1]. Acyl peroxides prepared in a polymerizer from a hydrogen peroxide salt and an acyl chloride in the monomer–water system are fairly effective. Peroxydicarbonates and sulfonyl peroxides are also used.

Common liquid-phase radical-chain reactions involving C–H substitution, such as chlorination and sulfochlorination of hydrocarbons, are performed in the bulk of a hydrocarbon or in a nonpolar solvent. The components of the chemical initiating system should be readily soluble or uniformly distributed in the hydrocarbon (RH). The majority of organic peroxides described in the literature are used in both polymerization and substitution reactions [2]. However, there are virtually no data in the literature on the use of a reaction mixture of initiator synthesis (without its isolation) for initiating a chain substitution reaction. In a sulfochlorinator or a chlorinator, the presence of oxygen and water, which are frequently used components in syntheses of peroxides, is inadmissible.

Here we consider a version of initiator synthesis in situ in the reaction volume, followed by an initiated substitution reaction. As investigation objects we chose well-known aldehyde derivatives, peroxy acetals.

Of particular practical value is the procedure for preparing mono- and diperoxy acetals from ethers and hydroperoxides in the presence of sulfuryl chloride SO_2Cl_2 or evaporated Cl_2 (taken separately or in a mixture with SO_2), described in [3]. It was demonstrated by numerous examples that aliphatic and cyclic (unstrained) ethers can be vigorously oxidized with *tert*-butyl hydroperoxide (TBHP) at the α-H atom relative to the ether bond. For example, 1,1-di-*tert*-butylperoxyethane (DTBPE) is rapidly formed in a good yield at the molar ratio Et_2O : TBHP : SO_2Cl_2 = (10–5) : (3–2.3) : 1 by the reaction

$$CH_3–CH_2–O–C_2H_5 + 2(CH_3)_3COOH + SO_2Cl_2 \xrightarrow{0\pm5^\circ C} (CH_3)_3COO–\underset{\displaystyle CH_3}{\underset{|}{CH}}–OOC(CH_3)_3 + C_2H_5OH + 2HCl + SO_2.$$

There is certain evidence that the reaction occurs via formation of the monoperoxy acetal, 1-ethoxy-1-*tert*-butylperoxyethane.

High yield was attained with a 1 : (1–0.2) mixture of Cl_2 and SO_2 taken instead of SO_2Cl_2. For example, 2-*tert*-butylperoxytetrahydrofuran (TBPTHF) is prepared in >90% yield on the standard equipment of chlorine plants [3] by passing Cl_2 and SO_2 evaporated from cylinders through a solution of TBHP in THF at 5–10°C for 20 min:

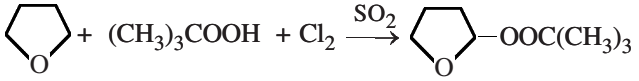

The procedure of synthesis of peroxy acetals fortunately matches the substitution reactions with respect to reagents, equipment, temperature, and reaction rate, which opens real prospects for simplifying the step of chemical initiation of chlorination and sulfochlorination of hydrocarbons. Indeed, under the conditions typical for the formation of an alkanesulfonyl chloride from a liquid alkane and a mixture of SO_2 and Cl_2 at 30–35°C,

$$R–H + SO_2 + Cl_2 \rightarrow RSO_2Cl + HCl,$$

it is absolutely unnecessary to prepare an initiator (e.g., TBPTHF, an effective sulfochlorination initiator [4]) in a separate step.

Before feeding the gases, it is sufficient to add a solution of TBHP in THF to the hydrocarbon and make sure that the initiator has formed in situ in the sulfochlorinator and affected the parameters of the reaction mixture.

The most important reaction parameter is the rate of accumulation of hydrolyzable chlorine Cl_h after Volhard. The figure shows the results of experiments under similar conditions with TBPTHF prepared beforehand (curve *3*) and in situ (curve *4*), and also with TBHP (curve *2*). These data show that the degree of sulfochlorination, and also the conversion of Cl_2 and RH (evaluated by various procedures) are higher when the initiator is prepared in situ, compared to the separate preparation of the initiator or UV initiation [4].

The idea put forward [4] was indirectly supported by experiments on revealing effective chemical initiators of toluene chlorination with sulfuryl chloride:

$$C_6H_5CH_3 + SO_2Cl_2 \longrightarrow C_6H_5CH_2Cl + SO_2 + HCl.$$

Benzyl chloride is obtained in a high yield only in the presence of benzoyl and lauryl peroxides and AIBN in amounts of 0.001–0.005 mol per mole of toluene, including experiments with 1 : 1 reactant ratio and heating for 20–30 min [5]. Without initiators, toluene does not react with SO_2Cl_2 even under refluxing for 6 h. In many books, this transformation is considered as a particular reaction: The reaction is selective owing to formation of the $^{\bullet}SO_2Cl$ radical in the initiation [2] and chain propagation steps. The reaction

$$Inc^{\bullet} + SO_2Cl_2 \longrightarrow IncCl + {}^{\bullet}SO_2Cl$$

is probable owing to fragmentation of the initially formed acyloxy radicals $R"COO^{\bullet}$ to $R"^{\bullet}$, followed by the reaction of $R"^{\bullet}$ with the reagent.

The results of experiments on preparation of benzyl chloride showed that in situ synthesis of peroxy acetals in the chlorinator ensures higher yield of the final product compared to the synthesis with the ready initiator (52±2°C, 30 min; see table). For comparison we used a protocol of the synthesis of benzyl chloride by the reaction of RH with SO_2Cl_2 at the molar ratio of the reactants of 1 : 0.5 in the presence of AIBN [5].

Under these conditions (run no. 1), the reaction is essentially incomplete. By distillation under reduced pressure, we isolated from the reaction mixture, along

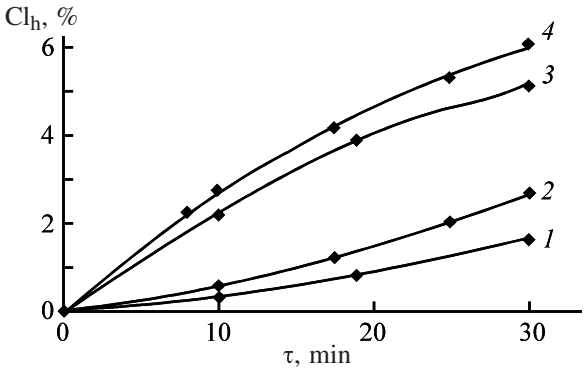

Accumulation of Cl_h with time τ in a dark vessel. (*1*) No initiator, (*2*) ~0.005 M TBHP, (*3*) ~0.005 M TBPTHF, and (*4*) 0.07 g of TBHP (72%) in 1.2 ml of THF (~0.005 M peroxide in reaction mixture). Gas supply rate 0.3 g min^{-1} each. RH weight, g: (*1*, *3*) 73 and (*2*, *4*) 72.

with benzyl chloride, also the unchanged reactants: toluene (63.4%) and SO_2Cl_2 (23.8%). Despite considerable differences in the boiling points of the mixture components, pure benzyl chloride cannot be isolated by single distillation; repeated distillation, desirably with a dephlegmator, is required.

When the peroxy acetal is prepared in the chlorinator in situ (run nos. 4–6), 98.7% pure (GLC data) benzyl chloride can be readily isolated by single distillation (run no. 4).

In the suggested procedure for preparing benzyl chloride [6], it is possible to attain almost quantitative conversion of the reactants with 85–90% product yield. The order of mixing the components exerts a noticeable influence. When a solution of TBHP in an ether is added to toluene before adding SO_2Cl_2, the

Yield of benzyl chloride with various initiators

Run no.	Initiator			Yield, %
	name	amount		
		g	mmol* × 10^3	
1	AIBN, mp 103°C	0.200	1.23	68.8
2	92% TBHP	0.118	1.25	Traces
3	96% TBPTHF	0.387	2.35	50.4
4	TBPTHF, in situ**	0.122	1.10	71.5
5	The same, from 92% TBHP	0.343	4.36	88.2
6	The same, from 92% TBHP	0.398	5.06	77.8

* Per mole toluene. Toluene amount: 92 g in run nos. 1–4, 74 g in run nos. 5 and 6.

** From 85% TBHP.

product yield is always 5–10% higher than when a solution of TBHP in an ether is added to the reactant mixture (run no. 6, as in run no. 1).

Thus, the mechanism of the effect of peroxides prepared in situ in the reaction vessel should not differ from the mechanism of the effect of pure peroxides (as sources of alkoxy radicals) on the system with predominance of RH:

$$0.5R''OOR'' + RH \longrightarrow R''OH + R^{\bullet}.$$

The dissociation of the O–O bond in mono- or diperoxy acetals should not be considered separately from the escape ot the resulting radicals into the bulk of solution. It is improbable, e.g., that the *tert*-butoxy radical would react with a chlorinating agent (including SO_2Cl_2) in the presence of RH (irrespective of whether RH is toluene or *n*-alkane).

The procedure suggested in [6] for preparing benzyl chloride is also very selective (the content of benzal chloride is as low as 0.25%), compared to chlorination of toluene with elemental Cl_2 in the presence of known initiators [2]. Presumably, the considerable differences between the results obtained with different chlorinating agents (Cl_2 or SO_2Cl_2) are associated with the structure and energy of the transition state in the chain propagation step involving these agents, at least provided that the benzyl radical $C_6H_5CH_2^{\bullet}$ is formed in the chain initiation step under the action of peroxides as generators of alkoxy radicals.

The initial component of the initiating system we suggest is TBHP, one of the most readily available organic peroxides whose commercial production is well mastered. At 30–50°C, the O–O bond in TBHP in hydrocarbon solutions does not noticeably dissociate. Experiments (figure, curve *2*; table, run no. 2) show that straight TBHP, irrespective of purity (chemically pure or technical grade), shows no promise for intensification of radical substitution reactions. The hydroxy derivative may react with SO_2Cl_2 as acid chloride or be reduced with SO_2. The latter process (at a high SO_2Cl_2 concentration) is, apparently, responsible for the low yield of the product when the chlorination is performed in the presence of TBPTHF (table, run no. 3) or when the initiating system is added to the reactants mixed beforehand (run no. 6).

Activation of the hydroperoxide with an ether or, more precisely, use of a mixture of TBHP with an ether for in situ preparation of a peroxy acetal (without its isolation) in the reaction volume is a simple way of effective initiation of substitution reactions.

EXPERIMENTAL

Freshly prepared peroxides with a high content of available oxygen (O_a; iodometric titration) were used. In all the cases the initiator was added into the hydrocarbon, after which the chlorinating agents were added. The initiator concentration is given counting on 100% purity.

Sulfochlorination of a liquid paraffin was performed in a round-bottomed vessel equipped with a bubbler for feeding gases, a stirrer, a reflux condenser, and a thermometer. The chlorinating mixture components, SO_2 and Cl_2, were evaporated from cylinders, dried, and fed in 1.1 : 1 ratio, using rheometers, to the reaction mixture at 30±2°C. As alkane we used synthine, TU (Technical Specification) 602-953–77, used in production of ionic surfactants, alkanesulfonates.

Synthine (synthetic paraffin) is a mixture of C_{12}–C_{18} *n*-alkanes with the mean molecular weight of 198; d_4^{20} 0.764–0.768, flash point 85°C, bp 290±65°C.

With TBPTHF prepared in situ from TBHP and THF in the sulfochlorinator, the reaction mixture parameters (figure, curve *4*) after blowing-off are as follows: d_4^{20} 0.8627, n_D^{20} 1.4458, Cl_h 5.65%, weight gain 1.15 g per gram of RH. The conversion evaluated from Cl_h is ~100% for Cl_2 and 34.89% for RH. In experiments described by curves *1–3*, the conversion and weight gain were lower.

Chlorination of Toluene with Sulfuryl Chloride in the Presence of Initiator Prepared in situ in the Chlorinator

Synthesis of benzyl chloride using TBPTHF prepared in situ from TBHP and THF (table, run no. 5). A reactor equipped with a stirrer, a reflux condenser, and a thermometer was charged with 74.0 g (0.8 mol) of toluene [analytically pure grade, GOST (State Standard) 5789–78], after which a solution of 0.343 g of TBHP (92% pure according to iodometric titration data) in 1.8 ml of THF was added. This amount corresponds to 0.004359 mol of TBPTHF per mole of toluene. Then 54.0 g (0.4 mol) of SO_2Cl_2 (bp 69°C, d_4^{20} 1.667) was added. The mixture warmed up to spontaneously to 37°C, and, before the temperature started to decrease, it was heated to 54±4°C and kept at this temperature for 30 min. The resulting mixture (89.0 g) was distilled from a Claisen flask. The following fractions were obtained: unchanged toluene (46.7 g, bp 54–56°C/100 mm Hg, n_D^{20} 1.4963, d_4^{20} 0.864) and benzyl chloride (33.1 g, bp 92–93°C/

43 mm Hg, n_D^{20} 1.5392, d_4^{20} 1.102, in agreement with reference data). According to GLC, the benzyl chloride was 99.35% pure (which is similar to the purity of a commercial sample after fractional distillation [6]). The residue was a dark tar (1.4 g). The yield of benzyl chloride was 88.24% (based on converted toluene, without taking into account the residue).

Synthesis of benzyl chloride with DTBPE prepared in situ from TBHP and diethyl ether. A stirred reactor was charged in succession with 46.1 g (0.5 mol) of toluene, a solution of 0.22 g of 85% TBHP in 1.5 ml of diethyl ether (which corresponds to 0.00206 mol of DTBPE per mole of toluene), and 27.1 g (0.2 mol) of sulfuryl chloride. The mixture warmed up virtually immediately, and vigorous gas evolution started. Although at 52 ± 2°C visually observed gas evolution practically ceased 15 min after the start of the reaction, the reaction was performed for 30 min. By simple distillation of the mixture (55.3 g), 29.0 g (33.5 ml) of unchanged toluene (bp 60–62°C/96 mm Hg) was obtained. Further distillation gave 20.1 g of a product with d_4^{20} 1.104, bp 71–74°C/17–18 mm Hg, n_D^{15} 1.5411, which agrees with the reference data for pure benzyl chloride. Yield of benzyl chloride 85% based on converted toluene or 79.5% based on converted sulfuryl chloride. This is good agreement taking into account possible loss of low-boiling SO_2Cl_2.

CONCLUSION

A mixture of *tert*-butyl hydroperoxide with an aliphatic or cyclic ether was suggested for in situ generation of peroxy acetals in a chlorinator or a sulfochlorinator with the aim of effective initiation of radical-chain C–H substitution reactions in hydrocarbons.

REFERENCES

1. Kronman, A.R., Semchikov, Yu.D., and Kanakov, A.E., *Plast. Massy*, 2002, no. 8, pp. 23–30.
2. Rakhimov, A.I., *Khimiya i tekhnologiya organicheskikh perekisnykh soedinenii* (Chemistry and Technology of Organic Peroxy Compounds), Moscow: Khimiya, 1979.
3. Kurdyukov, A.M., *Izv. Vyssh. Uchebn. Zaved., Khim. Khim. Tekhnol.*, 2004, vol. 47, no. 1, pp. 135–140.
4. RF Patent 2231524.
5. Weygand–Hilgetag, *Organisch-chemische Experimentierkunst*, Leipzig: Barth, 1964, 3rd ed.
6. RF Patent 2291144.

ISSN 1070-4272, Russian Journal of Applied Chemistry, 2007, Vol. 80, No. 9, pp. 1570–1574. © Pleiades Publishing, Ltd., 2007.
Original Russian Text © A.V. Kalinin, A.P. Voznyakovskii, 2007, published in Zhurnal Prikladnoi Khimii, 2007, Vol. 80, No. 9, pp. 1537–1542.

MACROMOLECULAR CHEMISTRY AND POLYMERIC MATERIALS

Application of Reverse Gas Chromatography to Studying the Microheterogeneous Structure of Block Copolymers

A. V. Kalinin and A. P. Voznyakovskii

Institute of Macromolecular Compounds, Russian Academy of Sciences, St. Petersburg, Russia
Lebedev Research Institute of Synthetic Rubber, St. Petersburg, Russia

Received December 25, 2006; in final form, May 2007

Abstract—The mechanism of processes occurring when a low-molecular-weight compound interacts with a block copolymer is considered. The anomalous results obtained with the butadiene–styrene stationary phase are accounted for. The effect of modifying additives on the sorption properties of the polymer is examined.

DOI: 10.1134/S1070427207090248

Previously we reported on a relationship between the nanoscopic structure of a polymer used as a stationary chromatoghraphic phase and the shape of the retention diagram, with a newly synthesized multiblock polyester–polysiloxane copolymer as example [1]. We demonstrated the potentialities of reverse gas chromatography (RGC) furnishing important information on the internal structure of a polymer and its solubility (or swellability) in various low-molecular-weight substances, using only small amounts of a polymer sample and simple and cheap equipment. This information allows a conclusion on whether the given polymer is suitable for preparing items contacting in the course of operation with a given solvent.

However, an attempt to confirm by RGC the existence of a complex domain nanostructure in a polymer (butadiene–styrene) failed. The retention diagrams of six different sorbates (*n*-alkanes C_5–C_9, chloroform, methylene chloride, carbon tetrachloride) were strictly linear, which, at first glance, contradicts the conlusions made in [1], because specifically for butadiene–styrene copolymer the existence of such structure was confirmed previously in numerous studies [2]. Here we attempt to rationalize this paradox.

EXPERIMENTAL

We used an installation based on an LKhM-8MD chromatograph, described in detail previously [1]. As the stationary phase we used multiblock copolymers of phenolphthalein terephthalate and polydimethylsiloxane with varied ratio of the rigid and flexible blocks, both straight and modified with low-molecular-weight compounds nonvolatile under the experimental conditions, as well as commercially available butadiene–styrene copolymers DST-20 and DSSK-20. The polyester–polysiloxane copolymers were prepared by the procedure described in [3], somewhat adapted to the available solvents. A photomicrograph of the synthesized block copolymer was obtained with a JEOL-S microscope.

To clarify the situation, we compared the retention diagrams of the same sorbate by stationary phases of the butadiene–styrene block copolymer and the random copolymer with the same ratio of the butadiene and styrene units (Fig. 1). It can be readily seen that both dependences are strictly linear, and at any temperature the retention volume for the random copolymer is larger than for the block copolymer.

To a first approximation, the sorption of a low-molecular-weight probe by block copolymers, which have a complex structure formed by nanosized domains of rigid blocks distributed in a continuous medium, can be represented as a sum of two independent processes occurring simultaneously: dissolution of a low-molecular-weight probe in the interdomain dispersion medium and its adsorption on the surface of domains of the "rigid" phase. Then the specific retention volume of a sorbate on the stationary phase V_g^0 ($cm^3\ g^{-1}$) is equal to [4]

$$V_g^0 = S + A, \quad (1)$$

where S is the contribution made by dissolution of sorbate molecules in the dispersion medium, and A, adsorption contribuition, $A = K_A S_A$, where K_A is the

constant of adsorption interaction of sorbate molecules with the surface of rigid vitrified domains, and S_A is the adsorption surface area.

However, Eq. (1) fails to fully explain some experimental results. For example, an assumption that the phases in polymers fully separate is inconsistent with the results of calculating partial contributions of the dissolution. The retention caused by this process is larger than it should be observed on the pure phase of the flexible block [1]. In addition, the fact that the nature of the flexible block strongly affects the chromatographic behavior of the polymer also contradicts the additive scheme [5]. This leads to a conclusion that the sorption of low-molecular-weight compounds is complicated by interaction of the components of the disperse polymer system with each other.

An important component of such interaction is adsorption of molecular segments of a flexible block on the surface of the rigid phase domain [6]. As a result, the mobility of the molecular chains of the flexible block is restricted not only by chemical bonds between the rigid and flexible segments of the macromolecule, but also by the adsorption interaction. Naturally, the adsorption of flexible chain segments on the surface of rigid block domains may affect the sorption properties of the copolymer with respect to low-molecular-weight sorbates.

When the surface of rigid phase domains is occupied by adsorbed segments of flexible block chains, low-molecular-weight sorbate molecules compete with the already adsorbed segments of the flexible phase, which can be represented as a quasi-chemical equation

$$A + MD \rightleftarrows AD + M, \qquad (2)$$

where M is a flexible block segment: D, adsorption center of a rigid block domain; and A, a low-molecular-weight sorbate.

The equilibrium constant of such a process, K_e, is

$$K_e = \frac{c_n^0[AD]}{[A][MD]} = \frac{(c_n^0 + x)x}{[A][N_0 - x]}, \qquad (3)$$

where c_n^0 is the concentration of flexible block segments in the interphase layer at the adsorption surface (mol cm^{-3}); x, concentration of sorbed molecules A (mol cm^{-2}): N_0, surface concentration of adsorbed flexible block segments (mol cm^{-2}); and [A], sorbate concentration in the dispersion medium (mol cm^{-3}).

Thus, the specific retention volume of a sorbate on a stationary phase consisting of a block copolymer is

$$V_g^0 = K_L\theta_L + (dq/dc)S, \qquad (4)$$

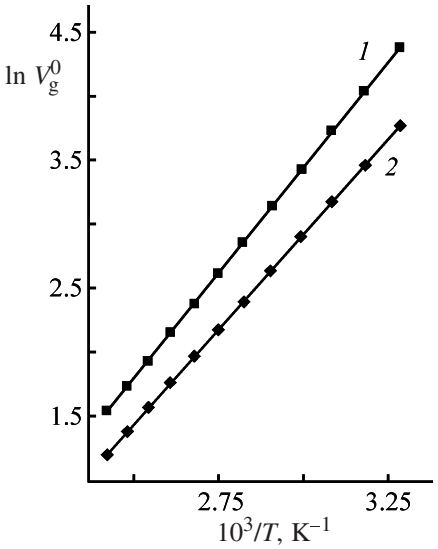

Fig. 1. Retention diagrams of *n*-pentane on (*1*) random and (*2*) block poly(butadiene–styrene). (*T*) Temperature; the same for Fig. 5.

where $K_L\theta_L$ is the contribution from sorbate dissolution in the dispersion medium; θ_L, specific volume of the dispersion medium; K_L, distribution coefficient of the sorbate, characterizing the dissolution process; $(dq/dc)S$, contribution from the adsorption interaction; S, surface area of rigid block domains in unit volume of the polymer; q, surface concentration of sorbate molecules (mol cm^{-2}); and c, concentration of sorbate molecules in the gas phase (mol cm^{-3}).

In our case, $q = [AD] = x$; therefore, solving Eq. (3) for x, we take into account that the contribution of the adsorption to the retention volume is

$$\frac{dq}{dx} = \frac{dx}{dc} = \frac{dx}{d[A]}\frac{d[A]}{dc} = K\frac{dx}{d[A]}. \qquad (5)$$

Then, substituting x in Eqs. (5) and (4), we obtain the following expression for calculating V_g^0:

$$V_g^0 = K_L\theta_L + K_L\{(-K_e/2) + (K_e/2)[1 + N_0(c_0^n + K_e k'h)] \times [1 + 4K_e k'hN_0/(c_n^0 + K_e k'h)^2]^{-1/2}\}S_A, \qquad (6)$$

where h is the peak area (mm); k', detector sensitivity (mol cm^{-2} mm^{-1}); and S_A, surface area of rigid phase domains in 1 cm^3 of the dispersion medium.

It can be readily seen that, with infinitely small samples ($h \to 0$), the expression for the specific retention volume takes the form

$$V_g^0 = K_L\theta_L + K_L K_e(N_0/c_n^0)S_A, \qquad (7)$$

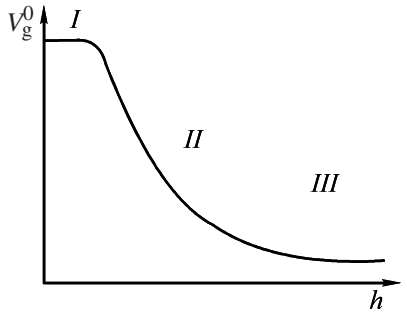

Fig. 2. Theoretical shape of the dependence of the retention volume V_g^0 on height h of the sample peak.

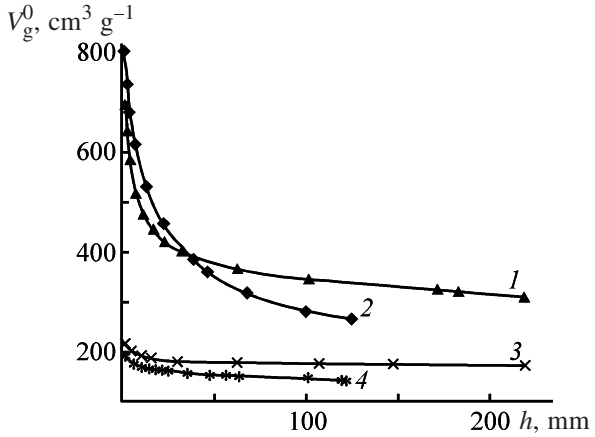

Fig. 3. Retention volume V_g^0 as a function of the height of the sample peak h at 30°C: (*1*) *n*-heptane on straight copolymer of phenolphthalein terephthalate with dimethylsiloxane; (*2*) methylene chloride on straight copolymer of phenolphthalein terephthalate with dimethylsiloxane: (*3*) *n*-heptane on butadiene–styrene block copolymer; and (*4*) methylene chloride on copolymer of phenolphthalein terephthalate with dimethylsiloxane, modified with 2 wt % dinonyl phthalate.

i.e., the retention volume becomes independent of the amount of the sample, and the shape of the chromatographic peak should be symmetrical. Comparing Eqs. (1) and (7), we obtain

$$K_A = K_L K_e (N_0/c_n^0). \quad (8)$$

Thus, K_A, adsorption interaction constant, depends on the ratio of the concentrations of flexible block segments adsorbed on the surface of rigid domains (N_0) and in the interphase layer (c_n^0). Hence, strictly speaking, the constants K_A for the block copolymer and homopolymer of the rigid block do not coincide.

For very large samples ($h \to \infty$), the retention volume described by Eq. (6) decreases, tending to $V_g^0 = K_L\theta_L$, i.e., to the contribution from dissolution of the sorbate in the dispersion medium.

Three portions can be distinguished in the plot of the retention volume vs. sample amount (Fig. 2, *I–III*). It is clear that the retention volume depends on the sample amount only in region *II*, and in regions *I* and *III*, as shown above, it is virtually constant.

It should be noted that actually attempts to construct the dependence $V_g^0 = f(h)$ do not always lead to a plot of the shape shown in Fig. 2. The experimental $V_g^0 = f(h)$ plots are largely determined by the apparatus parameters, primarily by the sensitivity of the chromatographic detector. A highly sensitive detector will give data for regions *I* ($V_{g,h\to 0}^0$), but even in region *II* the device response will become nonlinear.

On the other hand, with a low-sensitivity detector it will be impossible to detect a signal in region *I*.

The experimental dependences of the retention volumes on the sample amount for certain sorbates are shown in Fig. 3. Whereas for the polyester–polysiloxane stationary phase the dependence $V_g^0 = f(h)$ is well pronounced (curves *1*, *2*), for the butadiene–styrene copolymer the retention volume V_g^0 is almost constant, only slightly increasing at small h.

Another important feature of the chromatographic behavior of this polymer is virtually ideally symmetrical shape of the chromatographic peaks, whereas with the polyester–polysiloxane stationary phase the chromatographic peaks are essentially asymmetric (steep front and gently sloping rear wings). It follows from Eq. (6) that the $V_g^0 = f(h)$ dependence should be pronounced if c_n^0 is commensurable with $K_e K' h$. In our study we used the thermal conductivity detector of an LKhM-8MD chromatograph, for which $K' \approx 10^{-10}$ mol cm^{-3} mm^{-1}. Presumably, different block copolymer–sorbate pairs will have different K_e, and in the case of the poly(butadiene–styrene) stationary chromatographic pahse the equilibrium of the process described by Eq. (2) will be virtually fully shifted toward adsorption of flexible block segments on the surface of rigid block domains. In this case, the commensurability condition will not be fulfilled, and region *II* in the $V_g^0 = f(h)$ plot will become extremely narrow, degenerating into a jump, and in the retention diagram the dependence will be linear (because of the lack of the adsorption contribution).

To reveal the influence of the constant on the dependence $V_g^0 = f(h)$, this dependence was calculated by Eq. (6) at $c_n^0 = 5 \times 10^{-9}$ mol cm^{-3} and K_e 1.2, 0.7, 0.4, and 0.1 (Fig. 4). It seems possible to predict the extent of "shielding" of rigid block domains by flexible block chains in one or another copolymer by eval-

uating the compatibility of the homopolymers consisting of the same units as the blocks of the given copolymer. A convenient measure of the mutual compatibility of different polymers is the parameter Δ [7]: $\Delta = (\delta_1 - \delta_2)^2$, where δ_1 and δ_2 are the solubility parameters of the rigid and flexible blocks of the copolymer [(MJ m^{-3})$^{1/2}$]. The solubility parameters are related to the cohesion energy density as $\delta^2 = C$, where C is the cohesion energy density (MJ m^{-3}), $C = N_A w/V$, N_A is the Avogadro number, w is the potential energy of a single molecule, and V is the molar volume [8].

In this case, we proceeded from the assumption that the parameters δ for the rigid and flexible blocks of a copolymer differ from those of the corresponding homopolymer insignificantly. The smaller Δ, the more thermodynamically favorable is the mixing and the higher c_n^0. In particular, for phenolphthalein terephthalate, polydimethylsiloxane, polystyrene, and polybutadiene, δ = 21.4, 14.6, 18.2, and 16.9 (MJ m^{-3})$^{1/2}$, respectively.

It can be readily seen that Δ is the smallest in the polybutadiene–polystyrene pair. In view of this fact, the chromatographic behavior of butadiene–styrene copolymers can be accounted for as follows. As already noted, competing adsorption described by Eq. (2) occurs on the surface of polystyrene domains of the block copolymer. Because of small Δ, the equilibrium is virtually fully shifted toward adsorption of flexible polybutadiene segments rather than sorbate molecules. Actually, all the polystyrene fragments of the macromolecules, incorporated in rigid domains, do not take part in the chromatographic process. As for the random copolymer, it consists of macromolecules of averaged composition in which polystyrene units are uniformly distributed among polybutadiene units, and the formation of rigid nanosized domains is virtually impossible. Under the conditions of our chromatographic experiment (30–140°C), such copolymer is elastic, and the only operative mechanism of the sorbate retention is the dissolution, as in homopolybutadiene.

To finally confirm our hypothesis, we decided to simulate the effect of disappearance of the adsorption mechanism of retention on a polymer for which the occurrence of this mechanism was confirmed previously by RGC. For this purpose, we used the copolymer of phenolphthalein terephthalate and polydimethylsiloxane, whose chromatographic behavior was described in [1]. It was modified with an additive nonvolatile under the experimental conditions and was taken as a stationary chromatographic phase. The

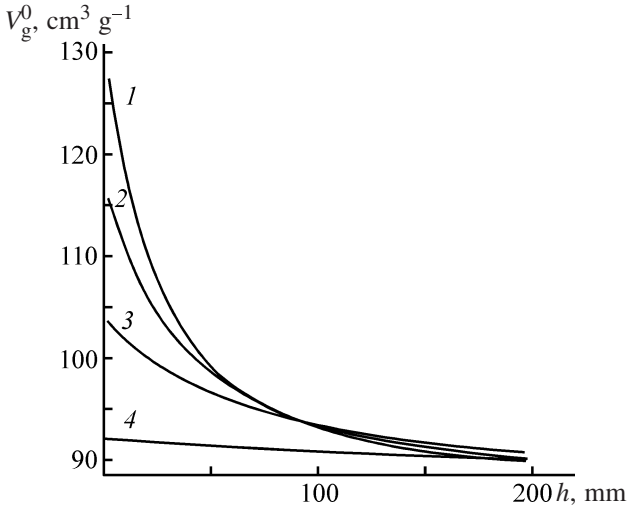

Fig. 4. Calculated dependences of the retention volume V_g^0 on the sample peak height h. $c_n^0 = 5 \times 10^{-9}$ mol cm^{-3}. K_e: (*1*) 1.2, (*2*) 0.7, (*3*) 0.4, and (*4*) 0.1.

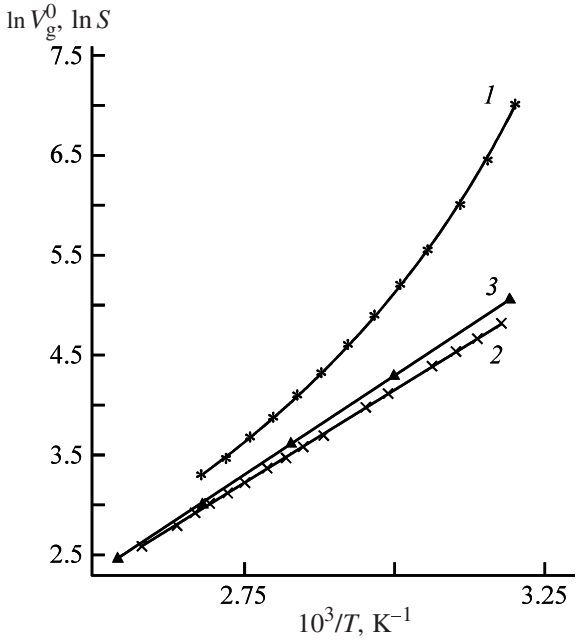

Fig. 5. Retention diagrams of *n*-pentane on (*1*) straight copolymer of phenolphthalein terephthalate with dimethylsiloxane and (*2*) the same copolymer modified with 2% squalene; (*3*) contribution from the dissolution of *n*-pentane in the straight copolymer as a function of reciprocal temperature.

results of the experiment are shown in Fig. 5. Linearization of the retention diagram after modification of the polyester–polysiloxane stationary phase with dinonyl phthalate or squalene indicates that in this case molecules of the additive, being sorbed on rigid block domains, fully shield them from the sorbate molecules, similarly to fragments of polybutadiene chains in butadiene–styrene block copolymer. Previously the

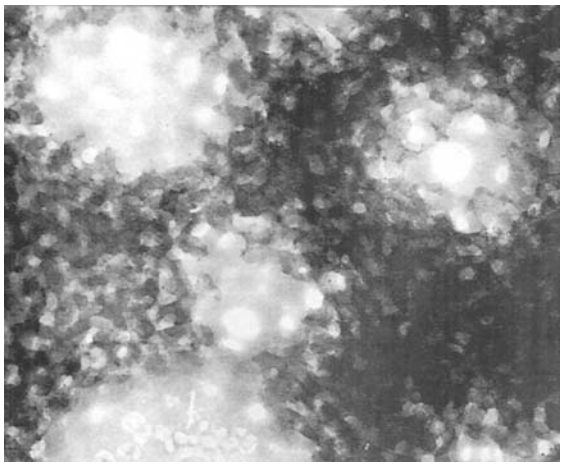

Fig. 6. Micrograph of a nanoscopic structure of a specimen of phenolphthalein terephthalate–dimethylsiloxane copolymer. Magnification 70×10^3.

dependence $\ln S = f(1/T)$ was obtained by calculation from the retention diagram [1]. This dependence almost coincides with the retention diagram for polyester–polysiloxane treated with dinonyl phthalate or squalene (Fig. 5). It should also be noted that modification of the block copolymer with these additives makes the chromatographic peaks less asymmetric.

Electron microscopy, a direct method for studying nanostructured objects, is used widely and for a long time for studying polymers [2]. However, often a minor difference between the optical densities of different blocks of a copolymer makes it impossible to obtain images of high quality with good resolution of details. The problem becomes much simpler if one of the components contains double bonds. High quality of micrographs of these speciments can be attained after their treatment with osmium tetroxide vapor [9, 10]. The OsO_4 molecules add across double bonds in macromolecules and thus increase the optical density of areas rich in an unsaturated component.

According to [11], it is possible to introduce low-molecular-weight unsaturated additives into the polymer, which allows the use of OsO_4 for staining a specimen for electron microscopy. As squalene is an unsaturated compound, this procedure appeared to be suitable for obtaining a micrograph of the phenolphthalein terephthalate copolymer (Fig. 6) demonstrating its nanoscopic structure.

CONCLUSIONS

(1) Factors responsible for the anomalous behavior of butadiene–styrene block copolymer as a stationary phase in a study of its structure by reverse gas chromatography were analyzed. The observed effect was accounted for in terms of the concept of competing adsorption.

(2) The effect of disappearance of the adsorption contribution, observed with butadiene–styrene block copolymer, was simulated with phenolphthalein terephthalate–polydimethylsiloxane copolymer by modification of this copolymer with low-molecular-weight additives.

(3) The conclusions concerning the structure of phenolphthalein terephthalate–polydimethylsiloxane copolymer, made in the previous paper, were confirmed by electron microscopy.

(4) The gas permeability of polymers can be controlled within wide limits by their modification with low-molecular-weight additives, which can be used in the development of membranes of selective gas permeability.

REFERENCES

1. Kalinin, A.V. and Voznyakovskii, A.P., *Zh. Prikl. Khim.*, 2006, vol. 79, no. 11, pp. 2022–2030.
2. Noshay, A. and McGrath, J.E., *Block Copolymers, Overview and Critical Survey*, New York: Academic, 1977.
3. Grigoryan, G.V., Polyester–Polysiloxane Block Co-Polymers, *Cand. Sci. Dissertation*, Leningrad, 1982.
4. Nesterov, A.E., *Obrashchennaya gazovaya khromatografiya polimerov* (Reverse Gas Chromatography of Polymers), Kiev: Naukova Dumka, 1988.
5. Voznyakovskii, A.P., Genkin, A.N., and Petrova, N.A., Abstracts of Papers, *Sed'maya Vsesoyuznaya konferentsiya "Khimiya i primenenie kremniiorganicheskikh soedinenii"* (Seventh All-Union Conf. "Chemistry and Applications of Organosilicon Compounds"), Tbilisi, November 20–23, 1990, vol. 2, p. 52.
6. Vakula, V.L. and Pritykin, L.M., *Fizicheskaya khimiya adgezii polimerov* (Physical Chemistry of Polymer Adhesion), Moscow: Khimiya, 1984.
7. Tager, A.A., *Fizikokhimiya polimerov* (Physical Chemistry of Polymers), Moscow: Khimiya, 1978.
8. *Entsiklopediya polimerov* (Polymer Encyclopedia), Kargin, V.A., Ed., Moscow: Sov. Entsiklopediya, 1972, vol. 1.
9. Kato, K., *Polym. Eng. Sci.*, 1967, vol. 7, no. 1, p. 38.
10. Livingstone, S.E., *The Chemistry of Ruthenium, Rhodium, Palladium, Osmium, Iridium and Platinum*, Oxford: Pergamon, 1973.
11. Voznyakovskii, A.P., Genkin, A.N., Plyushch, A.V., and Petrova, N.A., *Vysokomol. Soedin.*, 1986, vol. 28, no. 12, pp. 2621–2623.

ISSN 1070-4272, Russian Journal of Applied Chemistry, 2007, Vol. 80, No. 9, pp. 1575–1578. © Pleiades Publishing, Ltd., 2007.
Original Russian Text © B.B. Troitskii, L.V. Khokhlova, V.N. Denisova, M.A. Novikova, A.E. Golubev, A.V. Arapova, 2007, published in Zhurnal Prikladnoi Khimii, 2007, Vol. 80, No. 9, pp. 1543–1546.

MACROMOLECULAR CHEMISTRY AND POLYMERIC MATERIALS

Thermal Properties of Poly(Methyl Methacrylate) Prepared by Emulsifier-Free Emulsion Polymerization

B. B. Troitskii, L. V. Khokhlova, V. N. Denisova, M. A. Novikova, A. E. Golubev, and A. V. Arapova

Razuvaev Institute of Organometallic Chemistry, Russian Academy of Sciences, Nizhni Novgorod, Russia

Received January 22, 2007

Abstract—Emulsifier-free emulsion polymerization of methyl methacrylate in the presence of potassium persulfate initiator, taken in several different concentrations, at various pH values was studied with the aim to obtain colloidal crystals. The thermal properties of poly(methyl methacrylate) prepared by emulsifier-free emulsion polymerization, as the starting material for fabrication of photonic crystals, were examined in relation to the synthesis conditions.

DOI: 10.1134/S107042720709025X

An important feature of emulsifier-free emulsion polymerization is the possibility of preparing monodisperse polymeric particles with strictly ordered packing, which can serve as a basis for forming colloidal crystals [1, 2]. In turn, from colloidal crystals it is possible to prepare various kinds of photonic crystals opening wide prospects for the development of photonics [3] and showing promise for applications in medicine and optics, as materials for light guides and chemical sensors.

It appeared possible to control the properties of colloidal crystals by using various monomers. In particular, polymeric colloidal crystals based on poly(methyl methacrylate) (PMMA) were studied [2]. It was found [2] that the size of particles formed by emulsifier-free polymerization of methyl methacrylate (MMA) depends on the polymerization conditions and composition of the reaction medium.

At the same time, thermal properties of latex particle powders and of colloidal crystals prepared from these particles have been studied inadequately.

The degradation mechanism of poly(methyl methacrylate) at elevated temperatures has been studied in sufficient detail [4]. Thermal degradation of PMMA occurs by the mechanism of radical unbranched chain reactions. Thermal oxidative degradation of PMMA occurs by the mechanism of branched chain reactions with degenerate chain branching. The main degradation process is depolymerization. The monomer is virtually the only product of PMMA degradation (99% in thermal and 95% in thermal oxidative degradation) [5].

It was shown by mass spectrometry [6] that thermal degradation of atactic PMMA prepared by radical polymerization occurs in three steps. Shibaev et al. [6] assumed that the first degradation step occurring at 120–200°C involves a chain reaction initiated by the decomposition of head-to-head structures in macromolecules. In the second step, at 200–300°C, the degradation is initiated by decomposition of terminal double bonds. The major fraction of the polymer degrades at 300–420°C; the process is initiated by random scission of the macromolecule with the formation of macroradicals which subsequently undergo depolymerization.

It was interesting to examine the thermal properties of PMMA prepared by emulsifier-free emulsion polymerization, as this polymer is a raw material for preparing colloidal crystals. In this study, using DSC and TGA, we examined how the polymerization conditions (initiator concentration, pH) affect the thermal properties of emulsion PMMA.

EXPERIMENTAL

Emulsion polymerization of MMA was performed in an aqueous medium with vigorous stirring at a rate of 1200 rpm. The pH of the medium was adjusted using a pH meter, by adding to double-distilled water the required amount of 0.1 N NaOH or HCl. Water with the adjusted pH was heated to 80°C with continuous

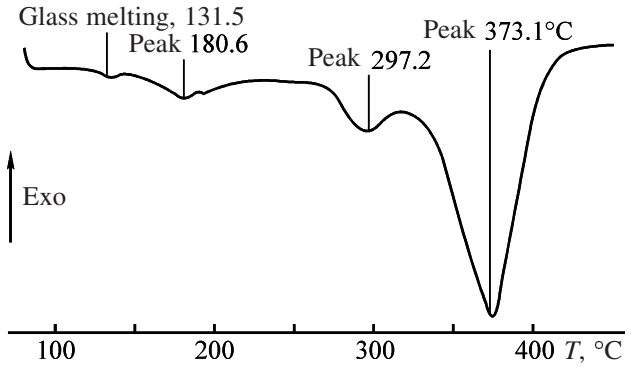

Fig. 1. DSC curve of emulsion PMMA prepared at an initiator concentration of 0.1% and pH 10 (run no. 3). (*T*) Temperature; the same for Fig. 2.

Table 1. Conditions of PMMA synthesis

Run no.	pH	Initiator concentration, %	Polymerization time, h
1	3	0.1	5
2	7	0.1	5
3	10	0.1	5
4	3	0.5	5
5	7	0.5	5
6	10	0.5	5
7	3	1.0	3
8	7	1.0	3
9	10	1.0	3

argon bubbling. Then the monomer purified by vacuum distillation was added in an amount of 10 wt % relative to the total weight of the mixture. The mixture was heated for 5 min, after which the required amount of potassium persulfate (analytically pure grade) dissolved in 1 ml of water was added. The reaction was performed at 80°C for 3–5 h depending on the initiator concentration. In the first 10 min the mixture was purged with argon, after which the argon supply was stopped to avoid foaming. The conditions of preparing polymer samples are given in Table 1.

The polymer obtained was filtered off on a membrane filter with a pore size of 0.2 μm under slightly reduced pressure (200–400 mm Hg) and dried in a vacuum oven to constant weight at 60–80°C.

The thermal properties of the samples obtained were studied by DSC and TGA. The DSC studies were performed with a DSK 204 F1 Phoenix differential scanning calorimeter (Netzsch, Germany) in an argon flow (flow rate 20 ml min^{-1}), with linear heating from 20 to 450°C at a rate of 2 or 10 deg min^{-1}. The sample (powder or film) weight was 2.4–6.5 mg. The onset temperatures of particular processes were determined with an accuracy of ±1°C. The glass transition point T_g was determined as an inflection point on the baseline in the region of glass transition (Fig. 1) and was averaged over three replicate measurements (repeatability ±1°C).

The rate of thermal oxidative degradation (TOD) at a constant temperature (302°C) was determined from

Table 2. Results of DSC study

Run no.	T_g, °C	Onset of decomposition, °C	Peaks in DSC curve					
			I		II		III	
			T, °C	*S*, %	*T*, °C	*S*, %	*T*, °C	*S*, %
1	130.6	154.4	184.0	0.7	293.5	8.4	368.3	90.9
2	129.3	154.6	169.0	11.0	297.4	4.5	370.2	84.5
3	131.5	156.0	180.6	6.0	297.2	6.8	373.1	87.2
4	127.6	144.6	178.3	25.7	292.3	13.5	377.7	60.8
5	126.9	145.4	179.5	18.9	293.6	10.1	376.7	71.0
6	125.6	136.7	177.6	22.9	291.6	9.3	379.7	67.8
7	129.4	162.2	183.1	22.4	291.1	15.2	381.4	62.4
8	128.8	148.2	176.2	27.3	294.0	7.3	385.7	65.4
9	126.2	147.8	173.3	26.0	294.8	6.0	384.5	68.0
7a*	66.0	–	176.7	20.4	293.6	8.0	381.8	71.6
8a*	69.2	–	176.9	25.2	291.0	9.3	380.8	65.5
9a*	90.5	–	173.5	5.3	295.8	17.9	380.8	76.8

* Films prepared from the corresponding powders.

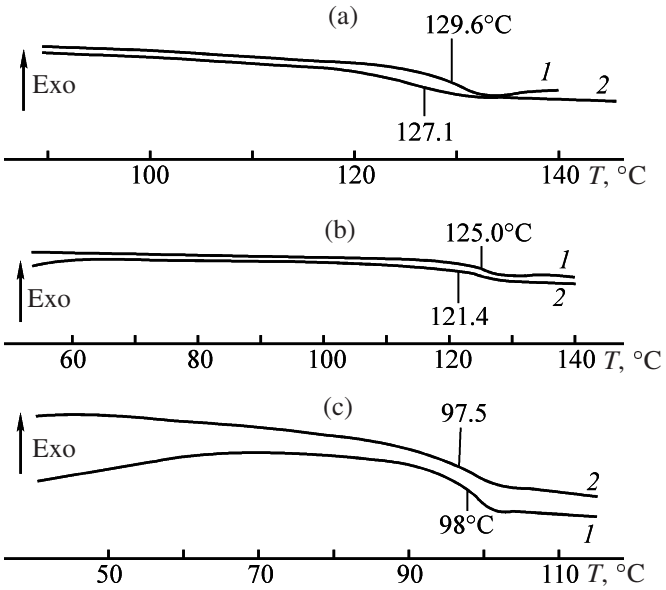

Fig. 2. DSC curves of emulsion PMMA in the form of (a, b) powder and (c) film. Heating rate, deg min^{-1}: (a) 10 and (b, c) 2. Heating run: (*1*) first and (*2*) second, after cooling to room temperature.

the weight loss in an atmosphere with oxygen partial pressure of 200 mm Hg. Samples in the form of ~100-μm-thick films were prepared from a 7–8 wt % solution of emulsion PMMA powder in methylene chloride by casting onto a glass surface followed by vacuum drying at 60–80°C.

The DSC curve (Fig. 1) exhibits the glass transition region and three endothermic peaks corresponding to the degradation of different structures in the PMMA macromolecule. The glass transition points are important characteristics of the emulsion PMMA samples. They appreciably exceed the glass transition points of films cast from powder solutions, and the highest glass transition point is exhibited by samples prepared at the lowest initiator content (Table 2, run nos. 1–3).

The glass transition points of the films are appreciably lower than those of the powders from which these films were prepared. Additional examination of the glass transition region (repeated heating after cooling of powder no. 1 from room temperature to 140°C at a rate of 10 deg min^{-1}) revealed a decrease in the temperature of the inflection point in the DSC curve from 129.6 to 127.1°C (Fig. 2a). The decrease is still more pronounced (from 125.0 to 121.4°C) at a heating rate of 2 deg min^{-1} (Fig. 2b). At the same time, in film sample no. 7a, on repeated heating at a rate of 2 deg min^{-1} after cooling, the glass transition point (97.5 and 98.0°C) remains essentially unchanged (Fig. 2c). This fact indicates that the high glass transition point of the powdered samples may be caused by the ordered structure of the emulsion PMMA in which the macromolecular motion is hindered. These structures are partially broken on heating. In the film samples, the polymer occurs in the glassy state and has no ordered structure, and therefore T_g of the films is considerably lower than that of the powders.

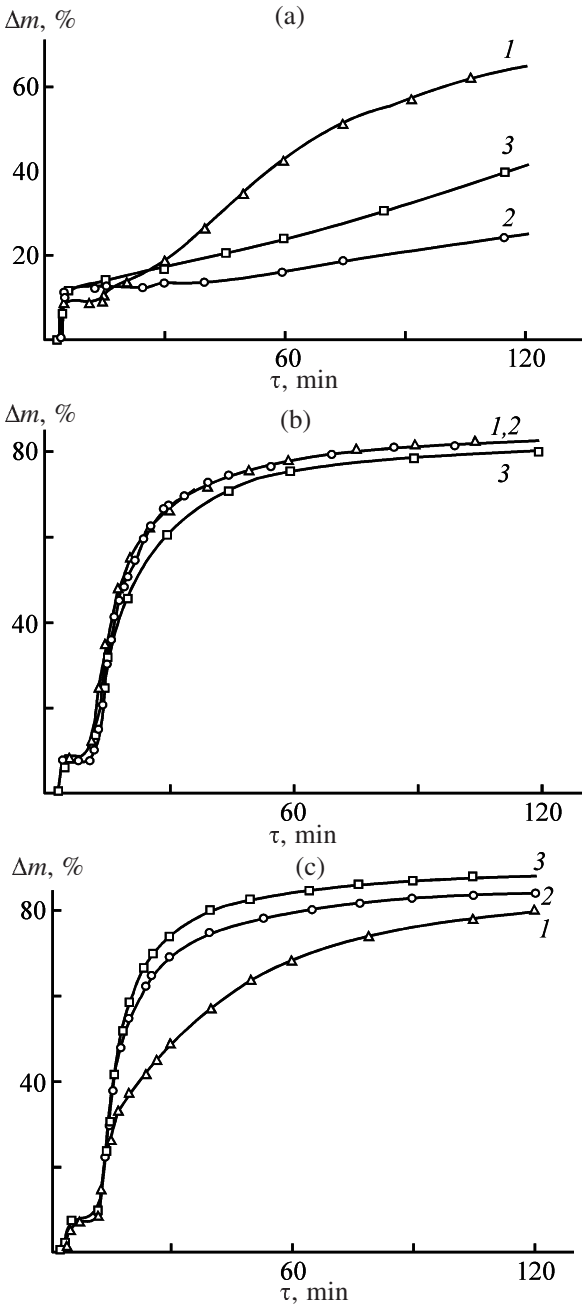

Fig. 3. Curves of weight loss Δm in the course of thermal oxidation degradation of PMMA film. 302°C, oxygen pressure 200 mm Hg. Samples prepared at initiator concentrations of (a) 1.0, (b) 0.5, and (c) 0.1%. (τ) Time. pH: (*1*) 3, (*2*) 7, and (*3*) 10.

As for the endothermic peaks, the temperature ranges of their occurrence suggest that they belong to three steps of thermal degradation of PMMA [6]. The peak areas *S* are proportional to the total thermal effects of the processes occurring in the polymer on heating.

The first DSC peak corresponds to the thermal effect of macromolecule degradation initiated by scission of weak bonds formed by head-to-head recombination of macroradicals. For the samples prepared in neutral medium, the peak area linearly grows with an increase in the initiator concentration. At the minimal initiator concentration (0.1%), the peak area is minimal at all pH values. This fact indicates that under these conditions the rate of macroradical recombination is low.

The second peak in the DSC curve corresponds to initiation of the degradation by cleavage of the terminal double bonds. For the samples prepared at the maximal initiator concentration (1.0%), the peak area grows with decreasing pH. Under these conditions of the polymerization, the disproportionation responsible for the formation of terminal double bonds plays a significant role.

The largest thermal effect is associated with the last step of the degradation, corresponding to random scission of the macromolecules. It is proportional to the area of the third peak. Its intensity grows with a decrease in the catalyst concentration.

A TGA study of thermal oxidative degradation of emulsion PMMA films showed (Figs. 3a–3c) that the polymer samples prepared at the highest initiator concentration (1%, Fig. 3a) were the most heat-resistant, with the highest degradation rate observed with the sample prepared at pH 3 (Fig. 3a, curve *1*). At 0.1% initiator concentration, the dependence of the PMMA heat resistance on pH of the polymerization medium is inverse.

CONCLUSIONS

(1) Increased glass transition points of poly(methyl methacrylate) samples prepared by emulsifier-free emulsion polymerization, compared to the film samples, are consistent with the ordered structure of the latex particles.

(2) Endothermic processes of degradation of emulsion poly(methyl methacrylate) in DSC analysis in an inert medium occur in three steps. Their temperature ranges correspond to the degradation of macromolecules initiated by terminal defective structures and random scission of the backbone.

(3) Thermal oxidative degradation of poly(methyl methacrylate) prepared by emulsifier-free emulsion polymerization occurs more slowly in samples prepared at a higher initiator concentration, which may be due to stabilization of the polymer by terminal sulfate groups of the macromolecules.

REFERENCES

1. Tauer, K., Deckwer, R., Kuhn, I., and Schellenberg, C., *Colloid Polym. Sci.*, 1999, vol. 277, pp. 607–626.
2. Egen, M. and Zentel, R., *Macromol. Chem. Phys.*, 2004, vol. 205, pp. 1479–1488.
3. *Photonic Crystal—Advances in Design, Fabrication, and Characterization*, Busch, K., Lolkes, S., Wehrspohn, R., and Foll, H., Eds., Wiley, 2004.
4. Grassie, N. and Scott, G., *Polymer Degradation and Stabilisation,* Cambridge: Cambridge Univ., 1985.
5. Song, J., Fischer, Ch.-H., and Schnabel, W., *Polym. Degrad. Stab.*, 1992, vol. 36, pp. 261–266.
6. Shibaev, L.A., Antonova, T.A. Vinogradova, L.V., et al., *Pis'ma Zh. Tekh. Fiz.*, 1997, vol. 23, no. 18, pp. 81–86.

ISSN 1070-4272, Russian Journal of Applied Chemistry, 2007, Vol. 80, No. 9, pp. 1579–1584. © Pleiades Publishing, Ltd., 2007.
Original Russian Text © S.V. Shilova, A.Ya. Tret'yakova, A.N. Bezrukov, V.A. Myagchenkov, V.P. Barabanov, 2007, published in Zhurnal Prikladnoi Khimii, 2007, Vol. 80, No. 9, pp. 1547–1552.

MACROMOLECULAR CHEMISTRY AND POLYMERIC MATERIALS

Effect of Molecular Weight of Poly-*N*-benzyl-*N*,*N*-dimethyl-*N*-methacryloyloxyethylammonium Chloride on Its Complexation with Sodium Dodecyl Sulfate

S. V. Shilova, A. Ya. Tret'yakova, A. N. Bezrukov, V. A. Myagchenkov, and V. P. Barabanov

Kazan State Technological University, Kazan, Tatarstan, Russia

Received February 28, 2007

Abstract—Complexation of a cationic polyelectrolyte, poly-*N*-benzyl-*N*,*N*-dimethyl-*N*-methacryloyloxyethylammonium chloride, with an anionic surfactant, sodium dodecyl sulfate, in aqueous solutions is studied. The effect of the molecular weight of the polymer on phase separation in the system and on the stability, conformation, and surface activity of the polyelectrolyte–surfactant complexes is examined.

DOI: 10.1134/S1070427207090261

Steadily increasing demand for polyelectrolyte-based materials for production of paints, electrophoretic coatings, cosmetics, and surfactants for oil production and transportation stimulate research in physical chemistry of polyelectrolytes [1–3]. Polyelectrolytes are of particular interest also as active components of drugs [4] and as models for studying the behavior of biopolymers in aqueous and aqueous salt solutions [5]. Practically significant are cationic polyelectrolytes, which are widely used as flocculants [6, 7], additives reducing the hydraulic resistance of turbulent flows of fluids [8], catalysts, ion-exchange resins, sorbents, emulsifiers, and stabilizers.

The presence of reactive functional groups in polyelectrolyte macromolecules is responsible for their ability to form complexes with various high- and low-molecular-weight compounds. Interaction of polyelectrolytes with oppositely charged ions of micelle-forming surfactants results in formation of new amphiphilic polymers with variable lyophilic–lyophobic balance, known as polymer–colloid complexes (PCCs) [9]. Wide use of sorption for recovery of surfactants from process solutions in solving different environmental tasks stimulates interest in studying complexing properties of polyelectrolytes. In the general problem of recovery of surfactants from mixed solutions, of particular significance is such aspect as effects of different factors on the formation, stability, and conformation of polyelectrolyte–surfactant complexes. Polymer–colloid complexes can also be used for synthesis of efficient flocculants selective with respect to some emulsified organic compounds [10].

The formation, structure, and properties of PCCs are strongly influenced by the molecular weight of the polyelectrolyte, the effect being ambiguous and hardly predictable [11–13].

In this study we examined the effect of molecular weight of a cationic polyelectrolyte (CPE), poly-*N*-benzyl-*N*,*N*-dimethyl-*N*-methacryloyloxyethylammonium chloride, on its complexation with an anionic surfactant, sodium dodecyl sulfate (SDS), in aqueous solutions.

EXPERIMENTAL

The CPE samples of various molecular weights MW were prepared from the starting polymer (MW 2.41×10^6) by the ultrasonic degradation (USD) method [14] using a UZDN-1 ultrasonic disintegrator (working frequency 22 kHz; power 4.4 W cm^{-2}) at varied exposure time.

Mild conditions that were selected for USD allowed broad variation of MW and elimination of depolymerization and interchain interactions of functional groups, the latter condition being critical for this study [15]. The molecular weights of the samples were estimated from the viscometric data by the Mark–Houwink equation: $[\eta] = KM^a$, where $[\eta]$ is the intrinsic viscosity (m^3 kg^{-1}), and K and a are con-

Table 1. Characteristics of poly-*N*-benzyl-*N,N*-dimethyl-*N*-methacryloyloxyethylammonium chloride (CPE) samples

Sample no.	Exposure time, min	$[\eta]$, $m^3\ kg^{-1}$	$M \times 10^{-6}$
1	0	0.375	2.41
2	1.5	0.270	1.60
3	3	0.172	0.91
4	20	0.036	0.13

stants (according to [10], $K = 2.94 \times 10^{-4}$ and $a = 0.8$; solvent 0.05 N KBr). The basic characteristics of the samples studied are given in Table 1.

Sodium dodecyl sulfate was purified by threefold recrystallization from ethanol. The purity of SDS was controlled by the critical micelle concentration (CMC) in water using conductometry and tensiometry; CMC was determined to be 8.4×10^{-3} M, which is consistent with the reference data [16].

Solutions were prepared with double-distilled water (conductivity 1×10^{-5} S cm^{-1}).

The phase separation conditions in mixed solutions of the polyelectrolyte and surfactant were studied turbidimetrically. The optical density D was measured on a Specol-10 instrument (Carl Zeiss, Jena, Germany) at $\lambda = 490$ nm against distilled water.

The PCC solutions were prepared by adding dropwise an SDS solution of a fixed concentration to a CPE solution with vigorous stirring. The critical aggregation concentration (CAC) of SDS in the presence of the polymer was determined from data on the solubilization of the organosoluble dye Sudan III. To 5 ml of mixed polymer–surfactant solutions of various compositions, 5 mg of the dye was added, and the system was allowed to stand for a week with intermittent shaking. Finally, excess of the dye was removed by centrifugation at 10000 rpm for 15 min, and the optical density of the solutions at 490 nm was measured. The critical aggregation concentration was determined from the concentration dependence of the optical density of the PCC solutions (as an inflection point of the curve).

The composition of the reaction mixture Z was expressed as the ratio of the molar surfactant concentration to the concentration of the polyelectrolyte units in the solution: $Z = c_{SUR}/c_{PE}$. The polyelectrolyte concentration c_{PE} was 1×10^{-3} (base mol) l^{-1} throughout the experiments with SDS. The surfactant concentration was varied from 1×10^{-6} to 1×10^{-2} M.

The equilibrium SDS concentration was determined potentiometrically with an EM-Br-01 modified commercial dodecyl sulfate selective heterogeneous membrane electrode and a CRYTUR Type 102 calomel reference electrode. The measurements were carried out in a temperature-controlled cell specially designed so to simultaneously obtain potentiometric (on a MICROTECHNA M-120 instrument to within 1 mV) and viscometric data. The electrode function was linear over a wide SDS concentration range. Performance characteristics of the electrodes and the analytical procedure were described in detail previously [17].

The degree of association of the polyelectrolyte with SDS θ was estimated by Eq. (1):

$$\theta = \frac{c_{SUR} - c_{SUR}^{eq}}{c_{PE}}, \quad (1)$$

where c_{SUR} and c_{SUR}^{eq} are the total and equilibrium concentrations of the surfactant in solution.

The stability of the PE–surfactant complexes was characterized by the apparent dissociation constant K_d:

$$K_d = \frac{c_{PE}(Z - \theta)(1 - \theta)}{\theta}. \quad (2)$$

Viscometric measurements were carried out at 25°C with a VPZh-1 Ubbelohde viscometer (capillary diameter 0.54 mm) to within 2%.

Polyelectrolytes bind oppositely charged ions of surfactants through both electrostatic interaction of charged groups and hydrophobic interaction of hydrocarbon radicals of surfactants with hydrophobic fragments of the polymer chain [3, 18]. The electrostatic mechanism may be represented by the following scheme:

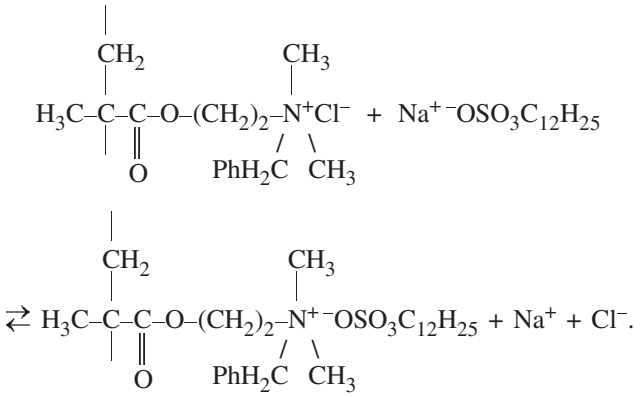

The use of surfactant-selective electrodes allows us to obtain SDS association isotherms (dependences of

the degree of association θ on the equilibrium SDS concentration) (Fig. 1). The initial section of the isotherm corresponds to the formation of intramolecular SDS micelles inside the macromolecular globule ("microreactor"). Figure 1 shows that, for all the curves, this section is S-shaped, which is typical of cooperative association. The CPE–SDS complex starts to form in an aqueous solution even at extremely low SDS concentrations. The critical aggregation concentration of SDS corresponding to the onset of cooperative association of the surfactant with the polyelectrolyte is near $c_{SUR} = 5 \times 10^{-5}$ M for all the CPE samples. This result is consistent with the published data [1], according to which surfactants start to bind to oppositely charged polyelectrolytes just at surfactant concentrations lower than CMC by 1–3 orders of magnitude. Saturation of the isotherms corresponds to the saturation of the polyelectrolyte macromolecules with the SDS ions. It should be pointed out that, with increasing molecular weight of the polymer, the limiting degree of association of the polyelectrolyte with SDS (θ_{max}) decreases (Table 2). Further increase in the SDS concentration results in degradation of the intramolecular micelles, i.e., in decreasing θ, and also in release of a considerable part of the SDS ions from the complex to the solution. The indicated structural transformation of the polyelectrolyte–surfactant complex was observed for the first time by Bilyalov et al. [19] in studying complexation of poly-4-vinyl-*N*-butylpyridinium bromide and attributed to collapse of the macrochains during coil–globule transition.

The change in the binding mode of SDS to cationic polyelectrolytes is more clearly demonstrated by the dependence of the degree of association θ on the composition of the reaction mixture *Z* (Fig. 2). Up to $Z = 0.7$, SDS is entirely associated with the polymer, which is reflected in a considerable increase in θ. As seen from Fig. 2, over the indicated range of *Z*, the run of the curves is practically independent of the molecular weight of the polyelectrolyte. However, the stability of the complexes increases with increasing molecular weight of the polymer samples, reaching a maximum at MW 2.41×10^6 (Table 2). At $Z > 0.8$, θ starts to abruptly decrease, which, as indicated above, is due to collapse of the macrochains during coil–globule conformation transition. For PCCs containing CPEs of lower molecular weights, the effect of dissociation of the complex is more clearly pronounced (Fig. 2, curves *3, 4*), being observed at lower θ.

To improve the efficiency of the use of polyelectrolyte–surfactant complexes as flocculants in waste-

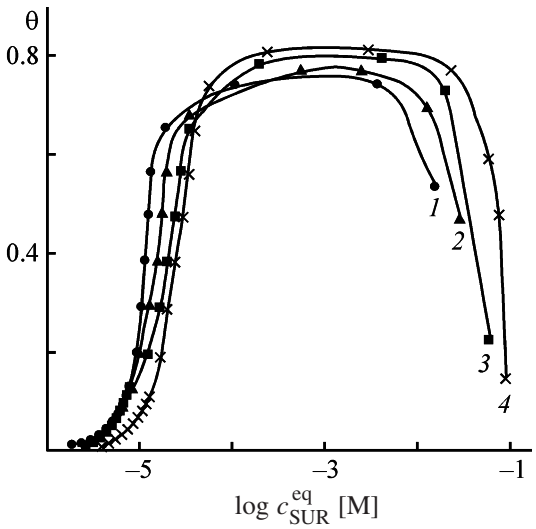

Fig. 1. Degree of CPE–SDS association θ as a function of the equilibrium SDS concentration c_{SUR}^{eq}. $c_{CPE} = 1 \times 10^{-1}$ monomol l^{-1}; the same for Figs. 2–5. Molecular weight of polyelectrolytes $M \times 10^{-6}$: (*1*) 2.41, (*2*) 1.60, (*3*) 0.91, and (*4*) 0.13; the same for Figs. 2–5.

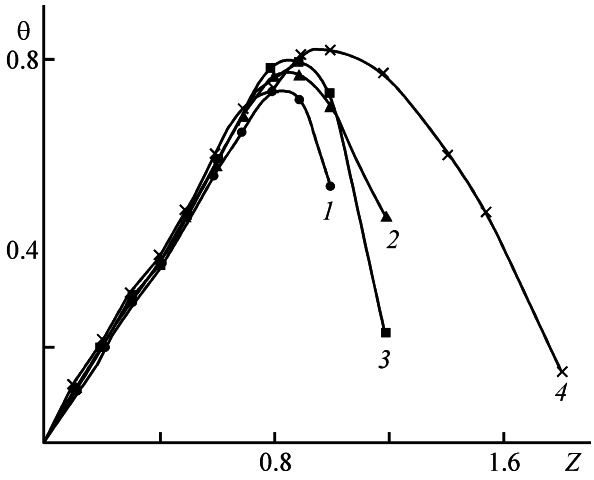

Fig. 2. Degree of association θ of SDS with CPE samples as a function of the composition of the reaction mixture *Z*.

Table 2. Characteristics of polymer–colloid complexes formed in aqueous solutions of CPE and SDS ($c_{CPE} = 1 \times 10^{-1}$ (base mol l^{-1}; $CAC_{SDS} = 5 \times 10^{-4}$ M)

CPE sample no.	$M \times 10^{-6}$	θ_{max}	$-\log K_d$ (θ = 0.03)	*Z*
1	2.41	0.74	6.06	0.70
2	1.60	0.77	5.98	0.70
3	0.91	0.79	5.86	0.70
4	0.13	0.81	5.80	0.70

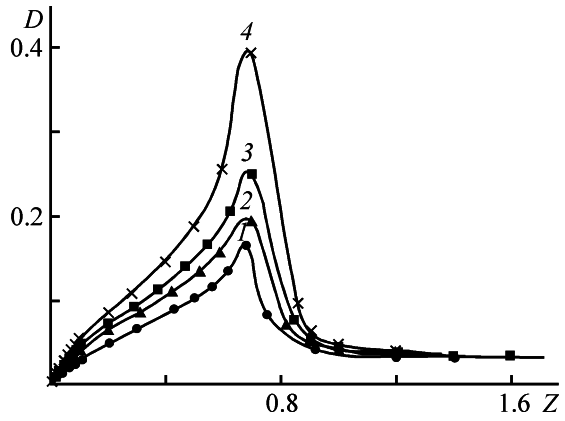

Fig. 3. Optical density D as a function of the composition of the reaction mixture Z.

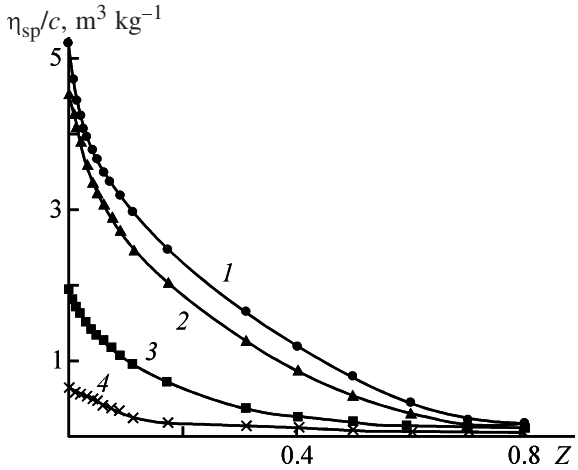

Fig. 4. Reduced viscosity η_{sp}/c of CPE–SDS solutions as a function of Z.

water treatment to remove surfactants, it is important to examine the effects of factors controlling the phase conditions of the complexes. Depending on the component ratio in mixed polyelectrolyte–surfactant solutions, both water-soluble nonstoichiometric and insoluble stoichiometric complexes can be formed. According to [20], three regions can be distinguished. The first one corresponds to $Z < Z_0$. In the zero solution, water-soluble PE–surfactant complexes are formed. In this case, free PE molecules coexist with PCC particles of the composition $\varphi = \varphi_0$. In the second region, at $Z_0 < Z < Z_1$, the zero solution contains only PCC particles whose composition φ practically coincides with the composition of the reaction mixture Z. Further hydrophobization of the complex ($Z \geq Z_1$) gives the third composition range, in which the remaining free fragments of the polymer chains cannot keep the complex particles in solution, and the system undergoes phase separation at the macroscopic level. In this case, practically stoichiometric complex ($\varphi \sim 1$) is separated as a precipitate.

To identify the existence ranges of the water-soluble and insoluble stoichiometric PCCs, we used turbidimetric titration. Figure 3 shows the concentration (by surfactant) dependences of the optical density of solutions of the cationic polyelectrolytes of various molecular weights. On adding relatively small amounts of SDS to the CPE solutions, we visually observed opalescence and an abrupt increase in the solution turbidity. No soluble polyelectrolyte–SDS complexes were formed. The PCC particles are strongly associated species forming colloid dispersions in aqueous solutions. At $Z = 0.7$, i.e., at the limiting Z_1, we observed the maximum of the optical density, which corresponds to the maximal hydrophobization of the macromolecular coil and to the highest degree of association in the isotherms $\theta = f(\log c^{eq}_{SUR})$. The position of the maximum in the turbidimetric titration curves is practically independent of the molecular weight of CPE. As the surfactant concentration in the reaction mixture increases, the optical density in the titration curves remarkably decreases as a result of precipitation of the stoichiometric complex. In the same composition range of the CPE–SDS mixtures, the degree of association of SDS decreases (Fig. 2). The height of the maximum in the turbidimetric titration curves strongly depends on the molecular weight of the polymer. With increasing MW, the optical density of the PCC solutions decreases, suggesting a decrease in the interaction strength in the CPE–SDS mixtures.

Based on the above experimental data, a preliminary finding is that the conformation and size of the macromolecular coils considerably affect the complexation between the cationic polyelectrolyte and SDS in aqueous solutions. The dependence of the reduced viscosity η_{sp}/c on Z (Fig. 4) provides additional evidence in favor of this suggestion, since a direct correlation occurs between the mean-square size of macromolecules $(\bar{R}^2)^{1.5}$ and η_{sp}/c [21–23]. The points on the ordinate ($Z = 0$) characterize the conformation state of the CPE samples in the aqueous solution without addition of SDS. According to the experimental data, with increasing MW, the hydrodynamic size of the macromolecular coils increases, and the maximal $(\bar{R}^2)^{1.5}$ was obtained for sample no. 1 with the maximal MW. Addition of SDS to solutions of all the polymer samples with various molecular weights results in regular decrease in the reduced viscosity, suggesting that the PE macromolecules become more compact as a result of screening of their charges by the SDS ions and hydrophobic interaction of the macroions with the alkyl radicals of SDS. Transformation to the globular conformation in

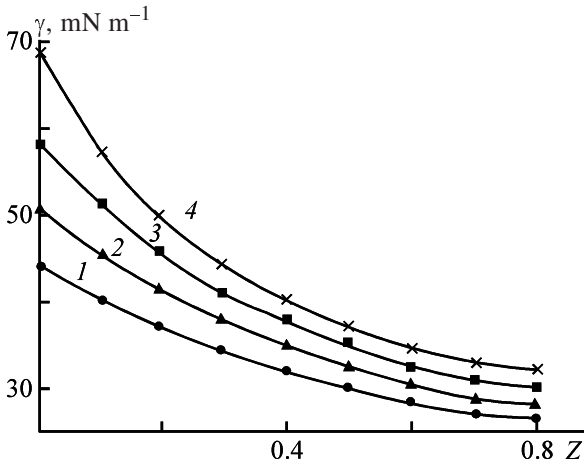

Fig. 5. Surface tension γ of CPE–SDS solutions at the solution/air interface as a function of *Z*.

the polymer macromolecules causes the maximal decrease in the solution viscosity to the value close to that of the pure solvent ($\eta_{sp} \to 0$). As seen from Fig. 4, the molecular weight of the polymer noticeably affects the dependence of the reduced viscosity on *Z*. First, the slope of the viscosity isotherms, characterizing the degree of compaction of the macromolecular coil, increases with increasing molecular weight of CPE. Second, the higher the molecular weight of the polymer, i.e., the larger the initial size of the macromolecular coil, the larger amount of SDS is required for the coil–globule conformation transition to occur. Sample nos. 1 and 2 (MW 2.41×10^6 and 1.60×10^6) take the globular conformation in the phase separation range ($Z = 0.7$); sample no. 3 (MW 0.91×10^6), at $Z = 0.5$; and sample no. 4 with the lowest MW, at $Z = 0.2$, i.e., just on introduction of very small amount of SDS.

Structure and properties of PCCs, as well as the prospects for their use as flocculants considerably depend on the component ratio. Particularly, the adsorption of PE–surfactant complexes is controlled by the ionization and conformation conditions of macromolecules in both the bulk of the phase and in the surface layers. Figure 5 shows the tensiometric titration curves of aqueous CPE solutions with an SDS solution at the solution/air interface. The surface tension of the PCC solutions decreases with increasing *Z*, i.e., as the SDS ions are associated, reaching a minimum for all the samples at $Z = 0.8$ corresponding to the phase separation with precipitation of the stoichiometric complex. With increasing MW, the slope of the surface tension isotherms of the cationic polyelectrolytes decreases, and the surface activity of PCC at the solution/air interface decreases as well. The highest surface activity is typical of the CPE–surfactant complex obtained with the lowest-molecular-weight polymer.

CONCLUSIONS

(1) The molecular weight of the cationic polyelectrolyte has a complex effect on its complexation with an anionic surfactant, sodium dodecyl sulfate, in aqueous solutions. Electrostatic interaction between anions of the surfactant and cationic groups of the polyelectrolyte starts at a surfactant concentration lower by two orders of magnitude than the critical micelle concentration, and the stability of the resulting complexes increases with increasing molecular weight of the polyelectrolyte.

(2) The effect of the molecular weight of the polyelectrolyte on structural transformations of polyelectrolyte–surfactant complexes was analyzed. The complexes exhibit high surface activity at the water/air interface, which decreases with increasing molecular weight of the polymer.

ACKNOWLEDGMENTS

The authors are grateful to A.V. Navrotskii (Volgograd State Technical University) for providing a CPE sample.

REFERENCES

1. Goddard, E.D., *Colloids Surf.*, 1986, vol. 19, no. 3, pp. 301–329.
2. Dubin, P.L., Stephens, S.T., Leong, M.G., and Chew, S.N., *Macromolecules*, 1990, vol. 23, no. 9, pp. 2500–2511.
3. Kabanov, V.A., Zezin, A.B., Kasaikin, V.A., et al., *Usp. Khim.*, 1991, vol. 60, no. 3, pp. 595–601.
4. Thunemann, A., *Langmuir*, 1997, vol. 13, pp. 6040–6051.
5. Kabanov, V.A., *Vysokomol. Soedin., Ser. A*, 2004, vol. 46, no. 5, pp. 759–782.
6. Myagchenkov, V.A., Baran, A.A., Bekturov, V.A., and Bulidorova, G.V., *Poliakrilamidnye flokulyanty* (Polyacrylamide Flocculants), Kazan: Kazan. Tekhnol. Univ., 1998.
7. Novakov, I.A., Navrotskii, A.V., Starovoitova, Ya.M., et al., *Zh. Prikl. Khim.*, 2003, vol. 76, no. 7, pp. 1200–1206.
8. Chichkanov, S.V., Shamsullin, A.I., and Myagchenkov, V.A., *Vestn. Kazan. Tekhnol. Univ.*, 2006, no. 1, pp. 175–181.

9. Goddard, E.D., *Interaction of Surfactants with Polymers and Proteins*, Goddard, E.D. and Ananthapadmanabhan, K.P., Eds., Londov: CRC, 1993, p. 171.
10. Shulevich, Yu.V., Formation and Properties of Water-Soluble Complexes of Supramolecular Cationic Polyelectrolytes and Sodium Alkyl Sulfates, *Cand. Sci. Dissertation*, Volgograd, 2005.
11. Tret'yakova, A.Ya., Barabanov, V.P., and Myagchenkov, V.A., *Kolloidn. Zh.*, 1990, vol. 52, no. 6, pp. 1211–1213.
12. Otdel'nova, M.V., Zakharova, Yu.A., Ivleva, E.M., et al., *Vysokomol. Soedin., Ser. A*, 2003, vol. 45, no. 9, pp. 1524–1532.
13. Bilalov, A.V., Babaev, A.A., Tret'yakova, A.Ya., et al., *Vysokomol. Soedin., Ser. A*, 2005, vol. 47, no. 11, pp. 1942–1955.
14. Myagchenkov, V.A. and Krikunenko, O.V., *Vysokomol. Soedin., Ser. A*, 1995, vol. 37, no. 1, pp. 44–49.
15. Myagchenkov, V.A., Krikunenko, O.V., and Churikov, F.I., *Ul'trazvukovaya destruktsiya vodorastvorimykh sopolimerov* (Ultrasonic Degradation of Water-Soluble Copolymers), Kazan: Kazan. Tekhnol. Univ., 1998.
16. *Poverkhnostno-aktivnye veshchestva: Spravochnik* (Surfactants: A Handbook), Abramzon, A.A. and Gaevoi, G.M., Eds., Leningrad: Khimiya, 1979.
17. Tret'yakova, A.Ya., Bilalov, A.V., and Barabanov, V.P., *Vysokomol. Soedin., Ser. A*, 1992, vol. 34, no. 5, pp. 86–90.
18. Okuzaki, H. and Osada, Y., *Macromolecules*, 1994, vol. 27, no. 2, pp. 505–512.
19. Bilalov, A.V., Manyurov, V.P., Tret'yakova, A.Ya., and Barabanov, V.P., *Vysokomol. Soedin., Ser. A*, 1996, vol. 38, no. 1, pp. 94–102.
20. Zakharova, Yu.A., Otdel'nova, M.V., Aliev, I.I., et al., *Kolloidn. Zh.*, 2002, vol. 64, no. 2, pp. 170–175.
21. Flory, P.I., *Principles of Polymer Chemistry*, Ithaca, New York: Cornell Univ., 1953.
22. Morawetz, H., *Chovani makromolekul v roztoku*, Praha: Academia, 1971.
23. Tsvetkov, V.N., Eskin, V.E., and Frenkel', S.Ya., *Struktura makromolekul v rastvorakh* (Structure of Macromolecules in Solutions), Moscow: Nauka, 1964.

ISSN 1070-4272, Russian Journal of Applied Chemistry, 2007, Vol. 80, No. 9, pp. 1585–1589. © Pleiades Publishing, Ltd., 2007.
Original Russian Text © R.Z. Khairullin, V.P. Arkhireev, A.M. Gafarov, 2007, published in Zhurnal Prikladnoi Khimii, 2007, Vol. 80, No. 9, pp. 1553–1557.

MACROMOLECULAR CHEMISTRY AND POLYMERIC MATERIALS

Viscosity of Melts and Solutions of Polyolefins Modified with Binary Mixtures of 2,4-Toluylene Diisocyanate and Lactams of Various Structrues

R. Z. Khairullin, V. P. Arkhireev, and A. M. Gafarov

Kazan State University of Technology, Kazan, Tatarstan, Russia

Received January 16, 2007

Abstract—The influence of binary mixtures of 2,4-toluylene diisocyanate and lactams of various structures on the viscosity of melts and solutions of polyolefin formulations was examined.

DOI: 10.1134/S1070427207090273

The progress of science and engineering requires the development of new types of polymeric materials with the properties that are not provided by the existing plastics. There are two ways to solve this problem: synthesis of new polymers with the required properties and modification of the existing polymers to impart to them the required characteristics. The second approach is more promising because of a wide set of commercially available polymers, among which polyolefins (POs) occupy a particular place because of availability of the raw materials and good performance [1].

Modification of polymers with individual compounds allows improvement of many processing and service characterustics. However, in many cases the use of binary mixtures gives an effect that considerably exceeds the effect of separate components (synergic effect), and the results attained with mixtures of modifying agents cannot be attained with individual compounds. From this viewpoint, modification with binary systems opens wide prospects for improving the properties of polymeric materials. On the other hand, it may be difficult to find components that enhance the effect of each other.

Of great interest is modification with binary mixtures of compounds that are capable of copolymerization under the conditions of PO processing. Among such compounds are isocyanates and lactams, which copolymerized under the conditions of anionic initiation at temperatures above 140°C to give copolymers whose macro- and supramolecular characteristics vary in a wide range depending on the composition of the starting monomer mixture and structure of the reactants.

In [2] we described chemical reactions occurring between components of the modifying mixture and between them and the modification substrate. The goal of this study was to find how the components of binary mixtures of 2,4-toluylene diisocyanate (TDI) with lactams of various structures affect the viscosity of melts and solutions of PO formulations, and also to reveal the relationship between the lactam structure and the rheological properties of the resulting polymeric compounds.

EXPERIMENTAL

The modification substrates were polypropylene (PP) of Balen 01 030 grade [TU (Technical Specification) 2211-020-00 203 521–96] produced by Polipropilen Private Company and high-density polyethylene (HDPE) of 277-73 grade [GOST (State Standard) 16 338–85] produced by the Kazan'orgsintez Open Joint-Stock Company.

As components of the binary mixture we used TDI, ε-caprolactam (ε-CLM), α-pyrrolidone (α-pyr), and laurolactam (LL). Their choice was governed by the following facts. Early studies of the influence exerted by the structure of isocyanates on the effect of PO modification showed that TDI as a PO modifier is more effective than 4,4'-diphenylmethane diisocyanate and SKU-PFL urethane prepolymer [3]. Therefore, it seems appropriate to use specifically this polymer as one of the components of the modifying mixture. As second component of the binary mixtures we used lac-

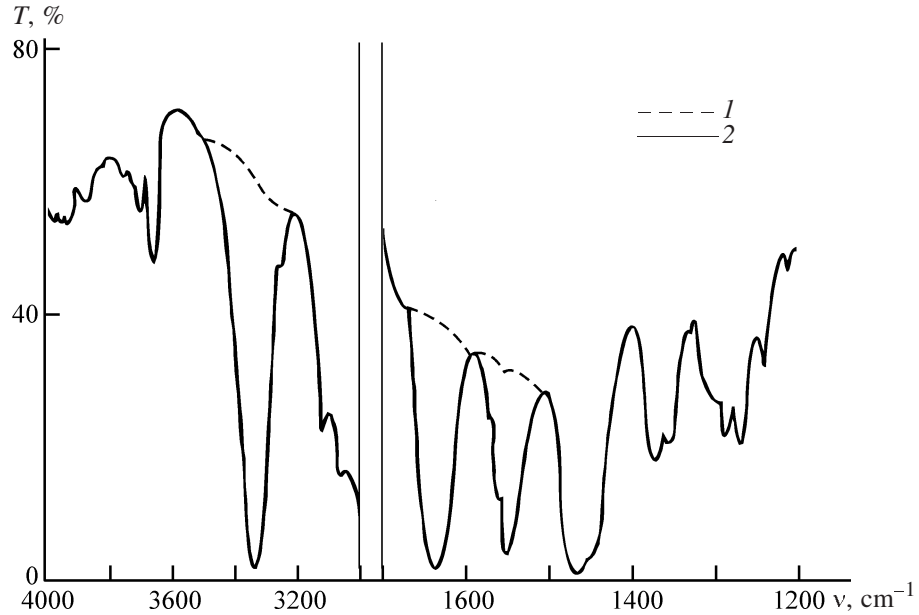

Fig. 1. IR spectra of (*1*) initial HDPE and (*2*) that modified with 12 wt % TDI + LL.

tams of various structures, differing in the ring strain and hence in the reactivity toward TDI.

To optimize the search for effective modifier formulations, we used the simplex–lattice experimental design [4]. As approximating polynomials we used third- and fourth-order Scheffe models.

The PO modification was performed in a melt on rollers for 5 min at 185°C for PP and 165°C for HDPE. The components of the modifying mixture were introduced simultaneously in the presence of 0.1 wt % catalyst, sodium caprolactamate.

The middle-IR spectra of the interaction products of the polyolefin and binary mixtures were taken on a Perkin–Elmer PC-16 spectrophotometer from the samples prepared as films. Quantitative IR analysis was performed with an internal reference [5].

The melt flow index (MFI) was determined according to GOST 11645–83 on an IIRT-type capillary viscometer at a capillary diameter of 0.2095 ± 0.0005 cm under the following conditions: 230°C, 2.16 kg load for PP; 190°C, 5 kg load for HDPE.

The intrinsic viscosity [η] in *o*-xylene at 25°C was determined with an Ubbelohde viscometer with a capillary diameter of 0.054 cm. The sample was preliminarily dissolved in an organic solvent. Then the solution was placed in a viscometer arranged in a thermostat (135°C for PP, 125°C for HDPE). After thermostating for 15 min, the outflow time was measured.

It should be noted that lactams added to PO are capable of copolymerization with TDI. In particular, in the IR spectrum of HDPE modified with a TDI : LL = 50 : 50 mixture (Fig. 1), there are new absorption bands at 1630–1680 and 1530–1550 cm^{-1}, corresponding to the C=O stretching, C–N stretching, and N–H bending vibrations in secondary amides, and at 3200–3400 cm^{-1}, corresponding to N–H stretching vibrations in secondary amides.

To examine changes that occur in PO on the macromolecular level, we measured the viscosities of melts and solutions of the compounds obtained.

The melt viscosities were evaluated by MFI, which is one of the most important processing characteristics determining the feasibility of polymer processing by plastic deformation methods.

We found that introduction into PP (MFI 2.6 g in 10 min) of 3 wt % LL or 3 wt % α-pyr increases MFI to 2.6 and 3.8 g/10 min, respectively (Figs. 2a, 2b).

Introduction of 3 wt % TDI into PP increases MFI to 3.5 g/10 min. The similar effect is attained on adding ε-CLM (Fig. 3a).

It should be noted that the highest MFI is attained when the components are taken in combination (Fig. 3a), which suggests that they interact not only with PP, but also with each other.

The composition–property diagrams for the ternary systems show that the optimum is shifted toward mixed formulations. Therefore, we performed chemical modification of PO with binary mixtures taken in an amount of up to 12 wt %. As the concentration

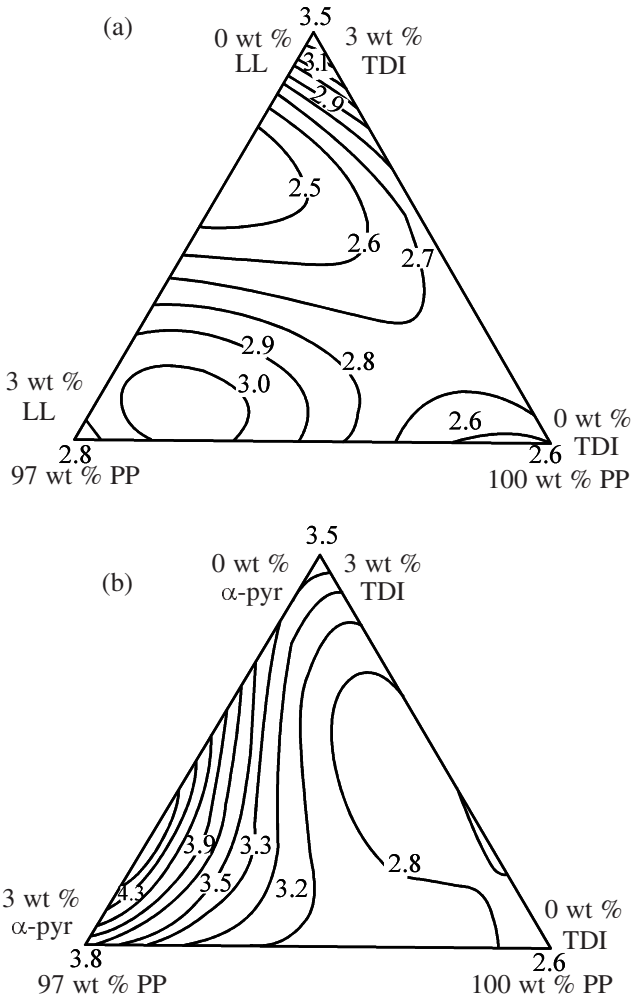

Fig. 2. Composition–property (MFI) diagrams of the systems (a) PP + TDI + LL and (b) PP + TDI + α-pyr.

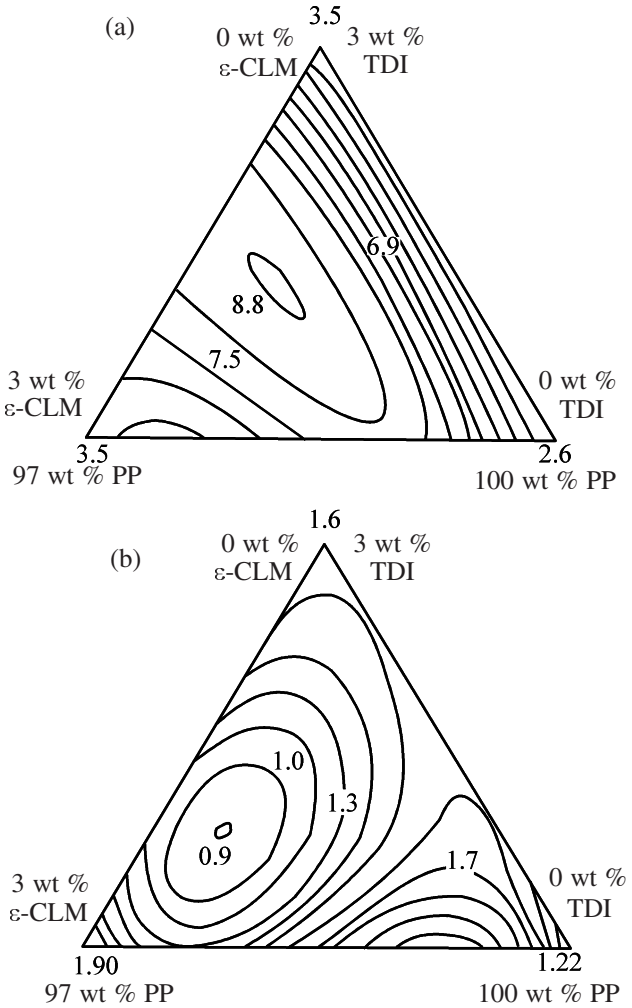

Fig. 3. Composition–property {(a) MFI, (b) [η]} diagrams of the system PP + TDI + ε-CLM.

interval is relatively wide, we used the fourth-order Scheffe model, which describes the real system more adequately because of the larger number of the experimental points. Data on the variation of MFI of PO formulations are given in Table 1.

Introduction of LL into PO does not noticeably alter MFI. Apparently, being capable of polymerization under the conditions of PO processing, LL forms

Table 1. MFI values for polyolefins modified with lactams of various structures

Lactam, wt %	MFI, g/10 min					
	HDPE			Balen PP		
	α-pyr	ε-CLM	LL	α-pyr	ε-CLM	LL
0		14.4			2.6	
3	15.2	15.2	14.8	3.8	3.5	2.8
6	16.3	14.2	14.2	6.2	16.0	2.7
9	18.8	24.2	14.6	12.0	18.0	2.9
12	19.0	20.6	19.4	14.3	19.2	3.3

Table 2. Melt flow index of HDPE modified with TDI and ε-CLM

Composition of binary mixture, wt %		MFI, g/10 min
TDI	ε-CLM	
6	–	15.5
9	–	14.0
12	–	14.8
3	3	16.2
6	3	12.6
–	3	15.2
–	6	14.2
–	12	20.6

Table 3. Physicomechanical properties of POs modified with lactams of various structures*

Lactam, wt %	HDPE						PP					
	α-pyr		ε-CLM		LL		α-pyr		ε-CLM		LL	
	σ, MPa	ε, %	σ, MPa	ε, %	σ, MPa	ε, %	σ, MPa	ε, %	σ, MPa	ε, %	σ, MPa	ε, %
0	30.3	52	30.3	52	30.3	52	34.0	10	34.0	10	34.0	10
1	26.2	200	28.0	30	26.6	173	34.9	60	33.2	15	33.5	6
3	26.7	448	31.1	35	26.1	252	34.2	87	33.2	20	38.5	8
6	28.7	585	33.2	40	27.5	335	35.7	96	35.8	36	36.0	8
9	27.9	620	31.5	165	28.3	305	34.0	95	34.3	32	33.9	8
12	28.3	685	31.7	110	26.6	280	33.8	93	33.9	34	33.0	5

* (σ) Breaking tensile stress and (ε) relative breaking elongation.

polyamide structures, with the effect being dependent on the processing temperature and more pronounced with PP. Presumably, under real conditions only the isocyanate component can react with PO in the presence of anionic catalysts.

On adding to PP other lactams, in particular, α-pyr, in a mixture with TDI, MFI reaches 5.8 g/10 min. With ε-CLM taken instead of α-pyr, MFI does not increase appreciably. However, ε-CLM added to PP without TDI increases MFI of PP considerably (to 19.2 g/10 min).

A different pattern is observed when binary mixtures of α-CLM and TDI are added to HDPE. In this case, the chemical structure of lactam affects MFI less significantly. The viscosity of HDPE decreases only at high (>9 wt %) concentrations of lactams, and the highest MFI is attained with ε-CLM as modifier (Table 2).

It should be noted that MFI regularly increases when mixtures of TDI and lactams, rather than the individual components, are used. Comparison of the effects of the additives on MFI of the polymeric compounds based on PP and HDPE shows that a decrease in the melt viscosity is observed in approximately the same concentration regions, i.e., the effect of the modifying mixture is only slightly dependent on the nature of the polyolefin.

Table 4. Intrinsic viscosities [η] of PP modified with TDI–lactam mixtures

Composition, wt %			[η], $cm^3\ g^{-1}$	
HDPE	TDI	lactam	α-pyr	LL
100	–	–	1.95	1.95
88	–	12	1.42	2.30
88	12	–	1.56	1.56
91	–	9	2.40	1.41
91	9	–	2.01	2.01
94	–	6	2.08	2.05
94	6	–	2.28	2.28
91	6	3	1.50	1.95
94	3	3	2.51	2.13

Introduction of lactams into POs alters the physicomechanical properties of the polymeric compounds. For example, introduction of α-pyr and ε-CLM into PO in most cases led to an increase in the relative elongation with increasing lactam content, especially with five-membered α-pyr (Table 3).

It is known [6] that the intrinsic viscosity [η] characterizes the behavior of an isolated macromolecule in an infinitely dilute solution. Therefore, a study of the behavior of macromolecules in a solution, where the distance to the adjacent macromolecule is long, is of certain interest.

Figure 3b shows that TDI and ε-CLM, when added to PP, exert effects of different signs. At low concentrations, there is a well-defined maximum of [η], apparently due to grafting of the copolyamide fragment to PO macromolecules, causing their branching. At high concentrations, formation of copolyamides may occur along with such interaction. Introduction of LL into PO does not appreciably affect [η]. This is apparently associated with the fact that the large length of the LL aliphatic radical levels off the difference in the sign of the effects exerted by the mixtures in different concentration ranges (Table 4).

CONCLUSION

The use of binary systems consisting of isocyanates and lactams allows significant improvement of the rheological properties of polyolefins. There are two

concentration ranges in which these effects are maximal. The first optimum, at small additions, is due to improvement of the structure of the polyolefins, caused by deactivation of the residual unsaturated bonds. The second optimum, at large additions, is apparently due to appearance of a copolyamide constituent, which is not chemicall bound to the polyolefin macromolecule and can form a separate phase.

REFERENCES

1. Kochnev, A.M., *Modifikatsiya polimerov: Monografiya* (Modification of Polymers: a Monograph), Kazan: Kazan. Gos. Tekhnol. Univ., 2002.
2. Gafarov, A.M., Galibeev, S.S., Kochnev, A.M., et al., *Zh. Prikl. Khim.*, 2004, vol. 77, no. 4, pp. 622–625.
3. Spiridonova, R.R., Galibeev, S.S., Kochnev, A.M., et al., *Zh. Prikl. Khim.*, 2003, vol. 76, no. 2, pp. 298–303.
4. Zergenidze, I.G., *Planirovanie eksperimenta dlya issledovaniya mnogokomponentnykh sistem* (Experimental Design for Studying Multicomponent Systems), Moscow: Nauka, 1976.
5. *Praktikum po khimii i fizike polimerov* (Practical Course of Polymer Chemistry and Physics), Kurenkov, V.F., Ed., Moscow: Khimiya, 1995.
6. Kochnev, A.M., Zaikin, A.E., Galibeev, S.S., and Arkhireev, V.P., *Fizikokhimiya polimerov* (Physical Chemistry of Polymers), Kazan: Fen, 2003.

ISSN 1070-4272, Russian Journal of Applied Chemistry, 2007, Vol. 80, No. 9, pp. 1590–1593. © Pleiades Publishing, Ltd., 2007.
Original Russian Text © L.N. Polyshchuk, E.S. Yanovskaya, V.V. Yanishpol'skii, V.A. Tertykh, K.M. Sukhoi, M.V. Burmistr, 2007, published in Zhurnal Prikladnoi Khimii, 2007, Vol. 80, No. 9, pp. 1558–1561.

MACROMOLECULAR CHEMISTRY AND POLYMERIC MATERIALS

Sorption of Mo(VI), W(VI), Cr(VI), and V(V) Anions on a Silica Gel Modified with Immobilized Polyionene

L. N. Polyshchuk, E. S. Yanovskaya, V. V. Yanishpol'skii, V. A. Tertykh, K. M. Sukhoi, and M. V. Burmistr

Institute of Surface Chemistry, National Academy of Sciences of Ukraine, Kiev, Ukraine
Shevchenko Kiev National University, Kiev, Ukraine
Ukrainian State University of Chemical Technology, Dnepropetrovsk, Ukraine

Received October 30, 2006

Abstract—The sorption of polyionene 1,4-MePh on the silica gel surface was studied. The silica gel modified with polyionene sorbed was used for sorption preconcentration of MoO_4^{2-}, WO_4^{2-}, $Cr_2O_7^{2-}$, and VO_3^- anions from aqueous solutions. The sorption isotherms of these anions on the initial and modified silica gels were obtained and analyzed.

DOI: 10.1134/S1070427207090285

Polymeric anion exchangers are widely used for sorption preconcentration and separation of Mo(VI) [1–3], Cr(VI) [4, 5], W(VI) [6], and V(V) [3, 5] anions. Although these polymeric sorbents are characterized by high sorption capacity, their drawbacks are large swelling and low sorption rate. In contrast to polymeric resins, modified silica gels and other inorganic sorbents do not swell and exhibit good kinetic characteristics. However, these sorbents have lower sorption capacity for oxoanions of polyvalent metals [7–10].

It is known [11, 12] that immobilization of polymers containing a quaternary nitrogen atom on the silica gel surface exhibiting weak cation-exchange properties allows preparation of inorganic anion exchangers. We can expect that such modified silica gels will combine useful properties of both an inorganic sorbent (no swelling) and anion-exchange resin (high sorption capaciity).

In this study silica gel was modified with a water-soluble polyionene containing a quaternary nitrogen atom in the polymer backbone. The most effective method for preparing such polymers is based on the Menshutkin reaction between substituted tertiary diamines and dihalides [13]. The reaction yields no low-molecular-weight products, and the backbone of the resulting polymer consists of regularly alternating quaternary ammonium groups in the backbone (onium polymerization). However, properties of silica gels modified with polyionenes have not yet been studied.

In this study we examined the sorption of Mo(VI), Cr(VI), W(VI), and V(V) from aqueous solutions on silica gels modified with polyionenes.

EXPERIMENTAL

The polyionene 1,4-MePh was prepared by the method reported in [14]. Its monomeric unit has the following structure:

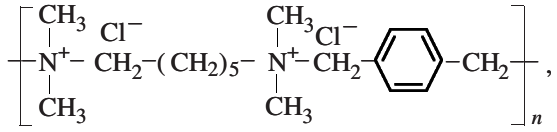

$n \leq 6$.

Silica gel (Merck, fraction 0.06 – 0.16 mm, specific surface area 256 $m^2\ g^{-1}$) was used as a support. The polyionene amount immobilized on the silica gel surface was determined spectrophotometrically from the light absorption of the polyionene–Bromophenol Blue complex at 600 nm.

The sorption of metals on the silica gel modified with immobilized polyionene was studied under static conditions. The sorption was carried out on the contact of the sorbent (0.1 g) with aqueous $(NH_4)_2MoO_4$, $(NH_4)_2Cr_2O_7$, Na_2WO_4, and $NaVO_3$ (25 ml). The equilibrium content of these anions before and after sorption was determined spectrophotometrically from the light absorption of their colored complexes:

molybdate anions, in the form of a red complex with SCN^- anions [15]; tungstate anions, in the form of tungstic–molybdic heteropoly blue formed in the presence of molybdenum salts [16]; bichromate anions, in the form of a violet complex with diphenylcarbazide in acidic solution [15]; and polyvanadate anions, in the form of a red-orange peroxide complex [17]. The spectrophotometric measurements were carried out on an SF-46 spectrophotometer (LOMO, Russia) in a 1-cm optical cell at the following wavelengths: molybdenum(VI) 470 nm, chromium(VI) 540 nm, tungsten(VI) 610 nm, and vanadium(V) 490 nm.

The degree of metal sorption was calculated by the formula

$$R = (m_{ads}/m_0) \times 100\% = (m_3 - m)/m_0 \times 100\%,$$

where m_0 is the metal content of the initial solution; m, metal content of the equilibrium solution after sorption ($m = cV$, where c is the equilibrium metal concentration in the solution, and V, solution volume).

It is known that, due to partial dissociation of the surface silanol groups, the silica gel surface is negatively charged. Therefore, polyionene can be immobilized on the silica gel surface by electrostatic intermolecular interactions according to the following scheme:

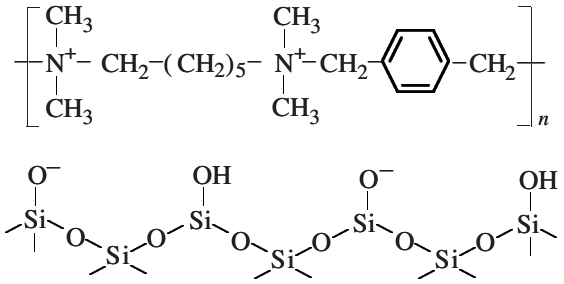

The sorption of polyionene on silica gel (Fig. 1) is described by the Langmuir sorption isotherm typical of chemisorption. The maximal sorption capacity of silica gel for polyionene is 100 mg g^{-1}.

The influence of pH on degree of sorption of aqueous Mo(VI), W(VI), Cr(VI), and V(V) anions on the silica gel modified with immobilized polyionene is illustrated by the table.

It is seen that W(VI) and Cr(VI) are sorbed most efficiently (to 95 and 65%, respectively) from acidic solutions (pH 2–4) where these metals are present in the form of polytungstate and polychromate anions [18]. The degree of sorption of polyvanadate anions is approximately 70–80% and is weakly dependent on

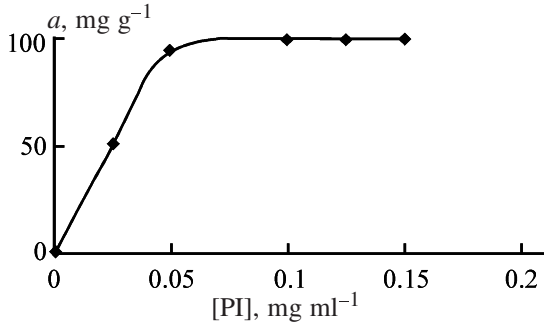

Fig. 1. Sorption isotherm of polyionene on silica gel: (a) polyionene sorption and [PI] equilibrium polyionene concentration in the solution.

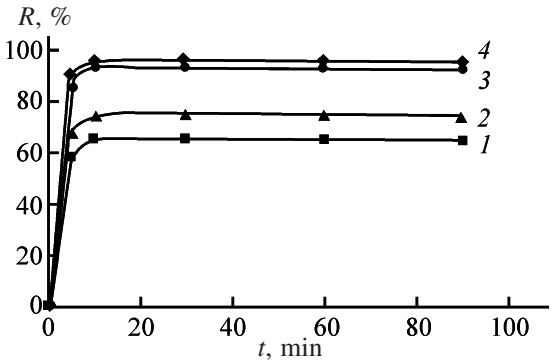

Fig. 2. Adsorption kinetics of (*1*) $Cr_2O_7^{2-}$, (*2*) VO_3^-, (*3*) WO_4^{2-}, and (*4*) MoO_4^{2-} on silica gel modified with immobilized polyionene. (*R*) Degree of sorption and (*t*) sorption time. pH: (*1, 4*) 2 and (*2, 3*) 4.

pH variations. This means that the sorption of V(V) on the modified silica gel is insensitive to the kind of its soluble species varying from $V_3O_9^{3-}$ in a strongly alkaline medium to $V_{10}O_{28}^{6-}$ at pH 1 [18]. The molybdate anions are efficiently sorbed (to 95%) from acidic solutions where they are present in the form of iso-

Degree of adsorption of molybdate, bichromate, tungstate, and vanadate anions on silica gel modified with polyionene at different pH values. Static sorption; sorbent weight 0.1 g, sorption time 10 min

pH	Degree of adsorption, %			
	Mo(VI)	W(VI)	Cr(VI)	V(V)
1.0	88.0	67.0	8.9	66.6
1.7	95.2	74.0	64.9	50.5
4.0	92.7	94.0	35.3	70.6
6.8	88.1	0	11.2	70.6
7.0	88.0	0	10.2	67.6
8.0	67.7	0	25.0	70.6
9.2	67.0	55.6	0	70.6

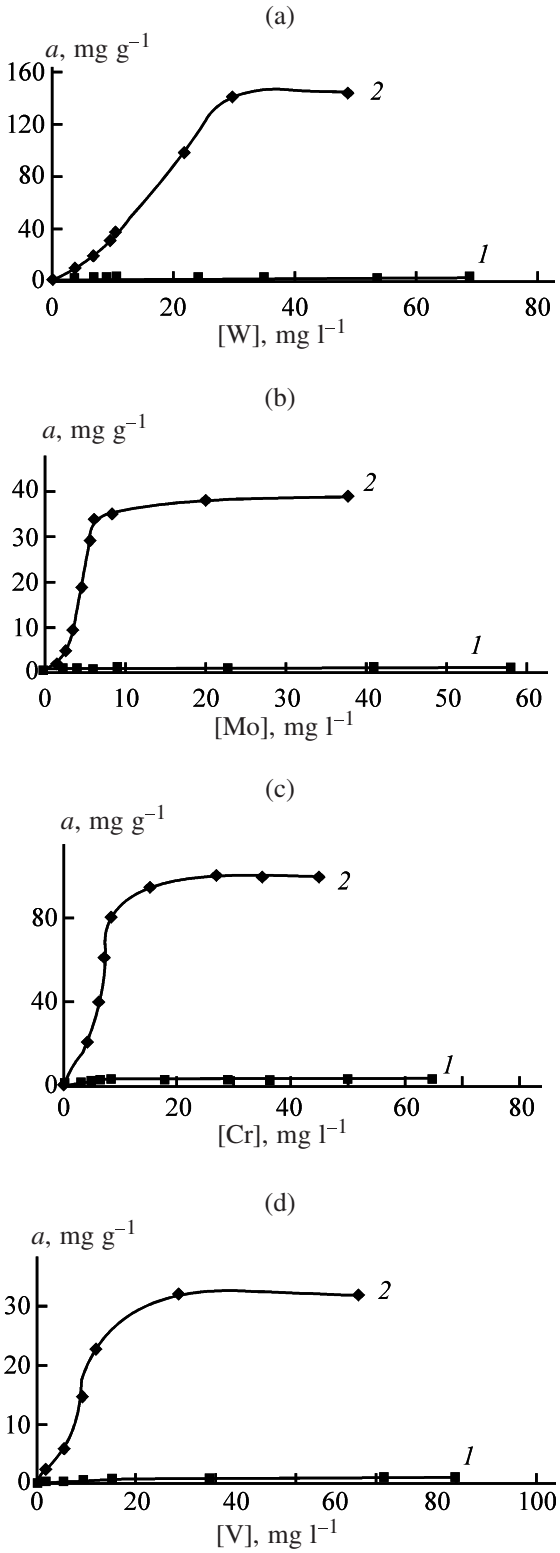

Fig. 3. Adsorption isotherms of (a) tungsten(VI), (b) molybdenum(VI), (c) chromium(VI), and (d) vanadium(V) on the (*1*) initial and (*2*) modified silica gel. (*a*) Adsorption; ([W], [Mo], [Cr], [V]) equilibrium metal concentrations in the solution. pH: (a, d) 4 and (b, c) 2.

poly acids. In going to alkaline media, where Mo(VI) occurs in the form of MoO_4^{2-}, its sorption decreases to 67% [18].

Figure 2 shows the adsorption kinetic curves for the metal-containing anions on silica gel modified with polyionene at optimal pH values for particular metals. It was found that the maximal sorption recovery of metals under consideration is attained within several minutes. Thus, silica gel modified with immobilized polyionene exhibits fairly fast sorption kinetics typical of the initial silica gel. Therefore, this modified sorbent can be used for recovering the metal concerned from aqueous solutions under dynamic conditions.

The comparison of the adsorption isotherms of molybdate, bichromate, tungstate, and vanadate anions (Figs. 3a–3d) on (*1*) initial silica gel and (*2*) initial silica gel modified with polyionene shows that the modified sorbent exhibits pronounced selectivity to these metal-containing anions. Their distribution ratios between modified silica gel and aqueous phase are as follows: Mo(VI), close to 2500; W(VI), 2800; Cr(VI), 4400; and V(V), 2500 ml g^{-1}. The limiting sorption of these metals (mg g^{-1}) calculated from their sorption isotherms is as follows: molybdenum, up to 38; chromium, up to 110; tungsten, up to 158; and vanadium, up to 32. These data show that the sorption power of the modified sorbent for the metal-containing anions exceeds that of the initial silica gel by a factor of 60–100. Thus, silica gel modified with polyionene can be used for efficient preconcentration of Mo(VI), Cr(VI), W(VI), and V(V) anions from aqueous solutions.

CONCLUSIONS

(1) Silica gel modified with immobilized polyionene efficiently sorbs MoO_4^{2-}, $Cr_2O_7^{2-}$, WO_4^{2-}, and VO_3^- anions from aqueous solutions. The sorption of molybdenum(VI) and chromium(VI) is the strongest in the pH range from 2 to 4 in which these metals are present in the form of polymolybdate and polychromate. The efficient sorption of tungsten(VI) and vanadium(V) is observed at pH > 4 favorable for formation of polytungstate(VI) and polyvanadate(V) anions.

(2) The characteristics of silica gel modified with polyionene combine useful properties of an inorganic sorbent (silica gel) and an anion-exchange resin (polyionene). This sorbent does not swell and has good kinetic characteristics and fairly high sorption capacity for Mo(VI), Cr(VI), Mo(VI), and V(V)

anions. Therefore, the modified silica gel can be used for recovery of these anions from wastewater and their preconcentration.

REFERENCES

1. Yamada, K., Kujirai, O., and Hasegawa, R., *Anal. Sci*., 1993, vol. 9, no 3, pp. 385–390.
2. Bruzzoniti, M.C., Mentasti, E., and Sarzanini, C., *Anal. Chim. Acta*, 1999, vol. 382, no. 3, pp. 291–299.
3. Shvoeva, O.P., Dedkova, V.P., and Savvin, S.B., *Zh. Anal. Khim*., 2000, vol. 55, no. 6, pp. 607–610.
4. Ososkov, V., Kebbekus, B., and Chesbro, D., *Anal. Lett*., 1996, vol. 29, no. 10, pp. 1829–1850.
5. Coedo, A.G., Lopez, T.D., and Alguacil, F., *Anal. Chim. Acta*, 1995, vol. 315, no. 3, pp. 331–338.
6. Luquegarcia, J.L. and Decastro, M.D., *Analyst*, 2002, vol. 127, no. 8, pp. 1115–1120.
7. Andreeva, I.Yu. and Drogobuzhskaya, S.V., *Zh. Anal. Khim*., 1990, vol. 45, no. 5, pp. 904–908.
8. Savvin, S.B., Trutneva, L.M., and Shvoeva, O.P., *Zh. Anal. Khim*., 1993, vol. 48, no. 3, pp. 502–507.
9. Savvin, S.B. and Mikhailova, A.V., *Zh. Anal. Khim*., 1996, vol. 51, no. 1, pp. 49–53.
10. Zaporozhets, O.A., Keda, T.E., and Seletskaya, L.E., *Zh. Anal. Khim*., 2000, vol. 55, no. 7, pp. 708–713.
11. Misaelides, P., Nikashina, V.A., Godelitsas, A., et al., *J. Radioanal. Nucl. Chem*., 1998, vol. 227, nos. 1–2, pp. 183–186.
12. Otruba, V., Pivnicka, J., and Kanicky, V., *Coll. Czech. Chem. Commun*., 2000, vol. 65, no. 12, pp. 1865–1874.
13. Razvodovskii, E.F., Nekrasov, A.V., and Ekinolopyan, N.S., *Vysokomol. Soedin*., 1971, vol. 13, no. 9, pp. 1980–1985.
14. Kravtsov, V.S., Burmistr, M.A., and Tyurina, T.G., *Ukr. Khim. Zh*., 1980, vol. 46, no. 4, pp. 397–399.
15. Marczenko, Z., *Kolorymetryczne oznaczanie pierwiastkow*, Warsaw: Naukowa-Techniczne, 1968.
16. Busev, A.I., Ivanov, V.I., and Sokolova, T.A., *Analiticheskaya khimiya vol'frama* (Analytical Chemistry of Tungsten), Moscow: Nauka, 1976.
17. Muzgin, V.N., Khalezina, L,V., Zolotavin, V.L., and Bezrukov, I.Ya., *Analiticheskaya khimiya vanadiya* (Analytical Chemistry of Vanadium), Moscow: Nauka, 1981.
18. Karapet'yants, M.Kh. and Drakin, S.I., *Obshchaya i neorganicheskaya khimiya* (General and Inorganic Chemistry), Moscow: Khimiya, 1981.

ISSN 1070-4272, Russian Journal of Applied Chemistry, 2007, Vol. 80, No. 9, pp. 1594–1597. © Pleiades Publishing, Ltd., 2007.
Original Russian Text © S.S. Glazkov, 2007, published in Zhurnal Prikladnoi Khimii, 2007, Vol. 80, No. 9, pp. 1562–1565.

MACROMOLECULAR CHEMISTRY AND POLYMERIC MATERIALS

A Model of Thermodynamic Compatibility of the Filler with the Polymeric Matrix in a Composite

S. S. Glazkov

Voronezh State Architecture and Building University, Voronezh, Russia

Received December 28, 2006; in final form, July 2007

Abstract—A thermodynamic approach to predicting the compatibility of the binder with the filler by calculating the nonpolar and acid–base parameters of the filler and polymeric matrix was considered. The calculated adhesion stabilities of the composite systems are consistent with the structural and functional features of their ingredients.

DOI: 10.1134/S1070427207090297

At present, the mutual compatibility of polymeric materials, in particular, ingredients of composites, is mostly estimated qualitatively and empirically. This approach does not adequately disclose the nature of interphase interactions of the binder with the filler, the main ingredients of composite materials (CMs). At the same time, specifically the interface is the main source of defects in CMs [1].

Bormotov et al. [2] believe that the binder in CMs provides simultaneous operation under load of all the filler particles via sticking them together into a conglomerate as a single whole. Therefore, a major role in strengthening of CMs belongs to adhesion at the polymer–filler interface. However, the nature of the polymer–filler interaction is very complicated and is not adequately understood [2].

As the starting point in elucidating the criteria of thermodynamic compatibility of the CM ingredients we will take the fundamental principle of thermodynamics postulating a negative free Gibbs energy, or the isobaric–isothermal potential, as the precondition to a spontaneous process [3].

Let us consider the expression suggested by van Oss [3] for the adhesion energy ΔG_{ij}^{a} (equal to the adhesion work W_{ij}^{a} with the opposite sign) of the ingredients i and j constituting the CM:

$$\Delta G_{ij}^{a} = \gamma_{ij} - \gamma_i - \gamma_j = -2[(\gamma_i^{LW}\gamma_i^{LW})^{1/2} + (\gamma_i^{+}\gamma_j^{-})^{1/2} + (\gamma_i^{-}\gamma_j^{+})^{1/2}]. \quad (1)$$

The free surface energy (FSE) of the CM ingredients is determined by the equation

$$\gamma = \gamma^{LW} + \gamma^{AB} = \gamma^{LW} + 2(\gamma_i^{+}\gamma_j^{-})^{1/2}, \quad (2)$$

where γ^{LW} are Livshits–van der Waals nonpolar terms, and γ^{AB}, acid–base interaction parameters (γ^{+} are parameters of Lewis acids, and γ^{-}, of Lewis bases).

Analysis of Eqs. (1) and (2) for highly compatible ingredients of CMs yields an expression determining the tendency of the system to a decrease in the free interphase adhesion energy:

$$\Delta G_{ij}^{a} = -2(\gamma_i^{+}\gamma_j^{-})^{1/2}. \quad (3)$$

Analysis of relationship (3) with account of Eqs. (1) and (2) gives preconditions for the tendency of the system to the maximal thermodynamic stability.

(1) $\Delta G_{ij}^{a} < 0$, if $\gamma_{ij} < (\gamma_i + \gamma_j)$ and $|\gamma_{ij}| \to 0$. Formal analysis of the first necessary and sufficient condition of thermodynamic compatibility suggests that, according to (3), the maximal decrease in the free interphase surface energy is always negative. However, the system will tend to the maximal thermodynamic stability via reduction of the interphase boundary until its disappearance at the maximal decrease of the interphase surface energy (tendency of its module to zero). The more prominent this tendency in interphase interaction, the more stable the composite.

(2) $\gamma_{ij}^{LW} \gg \gamma_{ij}^{AB}$. In this case, the surfaces of the interacting phases are mostly hydrophobic, and, being similar, they are well compatible. However, we will

demonstrate below that this applies mostly to the case of a hydrophobic nonpolar phase surface only. The ingredients are well compatible and form a stable composite.

(3) $\gamma_i^{LW} \gg \gamma_j^{AB}$, $\gamma_i^{AB} \ll \gamma_j^{AB}$. Composite materials in which the hydrophobic phase surface of one ingredient is poorly compatible with the hydrophilic phase surface of the other. The thermodynamic stability of such CMs is extremely low, and under exploitation the ingredient with a lower content migrates to the surface of the article. Technologists call this phenomenon the "sweating" of poorly compatible ingredients on the CM surface, accompanied by deterioration of its properties.

(4) $\gamma_{ij}^{LW} \ll \gamma_{ij}^{AB}$, $\gamma_i^{AB} \approx \gamma_j^{AB}$. The ingredients are hydrophilic and compatible, and the stability increases in the case when the acid component of one of the interacting phases is close in the parameter value to the base component of the other contacting phase, and vice versa, which can be expressed as follows:

$$\gamma_i^+ \approx \gamma_j^-,$$

$$\gamma_i^- \approx \gamma_j^+.$$

Thus, the best compatibility of the ingredients of a composite material is achieved in cases 2 and 4, provided that condition 1 is satisfied. For nonpolar, hydrophobic materials, characterized by the Livshits–van der Waals terms of FSE, the compatibility of the materials is obvious, while that for polar, hydrophilic materials is not unambiguous, as follows from condition 4. For these materials the compatibility tends to grow with leveling of the parameters of the acid and base components of the two contacting phases. In the simplified form, this can be formulated as the plus of one phase should be equal in magnitude to the minus of the other phase. This provides the maximal adhesion contact accompanied by the maximal decrease of the free interphase surface energy.

Methods for estimation of the surface tension of liquids are well known, while those for the free surface energy of solids are lacking. There exist several methods for indirect estimation of γ_s parameters. Based on the concept of additive contribution of the dispersion and polar terms, Owens and Wendt [4] and Good and van Oss [5] measured the contact wetting angle of a solid using a number of test liquids. The polar term is attributed [5] to short-range, basically donor–acceptor, interactions.

To determine the acid–base and nonpolar parameters, we measured the wettability of the examined surfaces of the materials with test liquids whose thermodynamic FSEs parameters can be found in reference books [nonpolar test (diiodomethane) and two polar (water and formamide) liquids]. We measured the contact wetting angles S on the solid surface being examined, substituted them in the system of Eqs. (4)–(6) with three variables, and obtained the acid–base (γ_s^+ and γ_s^-) and nonpolar (γ_s^{LW}) parameters of FSE of this solid:

Table 1. Surface energy terms of test liquids

Liquid	γ	γ^{LW}	γ^{AB}	γ^+	γ^-	γ^{AB}/γ, %
	mJ m^{-1}					
Water	72.80	21.80	51.00	25.50	25.50	70.06
Diiodomethane	50.80	50.80	0.00	0.00	0.00	0.00
Formamide	58.00	39.00	19.00	2.28	39.60	32.76

$$\gamma_s^{LW} = 0.25\gamma_{test}(1 + \cos\theta_{test})^2 + 0.25\gamma_{test}^{LW}(1 + \cos\theta_{test})^2, \quad (4)$$

$$\gamma_{11} = (1 + \cos\theta_1)^2 = (\gamma_s^{LW}\gamma_{11}^{LW})^{1/2} + 2(\gamma_s^+\gamma_{11}^-)^{1/2} + 2(\gamma_s^-\gamma_{11}^+)^{1/2}, \quad (5)$$

$$\gamma_{11} = (1 + \cos\theta_2)^2 = (\gamma_s^{LW}\gamma_{12}^{LW})^{1/2} + 2(\gamma_s^+\gamma_{12}^-)^{1/2} + 2(\gamma_s^-\gamma_{12}^+)^{1/2}, \quad (6)$$

where γ is FSE (for liquids, surface tension of liquids, mJ m^{-2}); superscript LW refers to physical nonpolar (Livshits–van der Waals) terms of FSE, mJ m^{-2}); θ is contact angle, deg, of wetting of the solid surface with the test liquid; subscript test characterizes the test nonpolar or inert liquid, i.e., diiodomethane; subscripts s and l refer to solid and liquid, respectively; subscripts 1 and 2 refer to the first and second of the two polar test liquids, respectively; and superscripts + and – refer to the Lewis acid and base terms of the surface tension, respectively.

For the liquids chosen, the values of the parameters γ, γ^{LW}, γ^{AB}, γ^+, and γ^- are known (Table 1).

EXPERIMENTAL

To combine nonpolar polyethylene waste with polar particles of a wood filler and improve the mechanical characteristics of the manufactured wood–polymeric materials (WPMs), we suggested treatment of the filler surface with modifiers based on synthetic

Table 2. Surface energy terms (mJ m^{-2}) of various solid materials

Material	γ [4]	γ^d [4]	γ^h [4]	γ [5]	γ^{LW} [5]	γ^{AB} [5]	γ^+ [5]	γ^- [5]
Natural wood (pine)	40.2	28.8	11.4	49.8	41.2	8.60	0.91	20.3
Recycled polyethylene	34.0	30.5	0.2	32.1	30.20	1.81	1.20	0.68
Wood modified with OBMA-6 copolymer	–	–	–	58.0	50.8	2.50	0.04	39.6
Wood modified with SKEPT copolymer	45.4	41.6	3.8	–	–	–	–	–

ethylene–propylene rubber, SKEPT-40TN [TU (Technical Specification) 2294-022-05766-801-014] and a solution of a copolymer of 4-vinylcyclohexene with maleic anhydride (OBMA-6). We used sawdust with particles having a thickness of 1.0–1.5 mm, width of 1.0–2.0 mm, and length of 5.0 mm and recycled polyethylene (RPE) with the particle size of 3.0 mm.

Specimens for measurements of FSE of the WPM components were prepared as follows. Recycled polymer specimens were prepared as plates. To this end, an agglomerate of recycled polymers was heated in a mold under pressure to a temperature exceeding by 10–20°C the melting point and then was cooled. To determine FSE of the sawdust, a block of pine from which it was obtained was cut at 20°C and 65% humidity into $1000 \times 100 \times 15$-mm cleats, whose tangential surfaces were planed. From the treated cleats we cut out ten specimens of a smaller size, $180 \times 12 \times 6$ mm. To prevent physicochemical modification of the wood surface, we used just prepared specimens to be tested only once. To determine FSE of the modified sawdust, the pine cleats of the same shape were treated with OBMA-6 by impregnation with a 80% aqueous solution of the copolymer (4% of the weight of the wood specimens). Next, the cleats were treated in an oven with programmed temperature rise from room temperature to 170°C.

Table 2 presents the calculated FSE, γ_s, of solids (standard absolute error ≤1%; correlation coefficient for graphic determination of FSE is ≥0.995), its three terms, γ^{LW}, γ^+, and γ^-, and the fraction of the polar term of FSE, γ^{AB}/γ.

Comparative analysis of the discussed approaches to assessment of the surface energy terms (Table 2) suggests that the van Oss method [5] has a number of advantages. In particular, it provides a better convergence of the experimental values of the surface energy terms and the wetting angles calculated therefrom.

The above-mentioned criteria of good compatibility of the CM ingredients imply either hydrophobic or monopolar ingredients, of which one should be a Lewis acid, and the other, a Lewis base. To combine hydrophilic sawdust with hydrophobic plastics, wood was treated with 6% OBMA-6 copolymer [6]. The fraction of the acid–base term of FSE of wood decreased from 17 to 3.6% (Table 2).

We found that a polymeric modifier with the structure of a surfactant modifies the surface by reducing its acid component, rather than simply reduces the interphase tension. A minor increase in basicity (Table 2) can be associated with an increase in the number of oxygen atoms in wood due to formation of ester bonds between the hydroxy groups in wood and carboxy groups in the copolymer and incorporation of the double bonds of the copolymer. Increase in the Livshits–van der Waals term is due both to a decrease in the acid–base term and appearance of a nonpolar hydrocarbon radical of the copolymer on the wood surface.

CONCLUSIONS

(1) The thermodynamic compatibility of filler, unmodified pine sawdust and that treated with the 4-vinylcyclohexene–maleic acid anhydride copolymer, with the binder based on recycled polyethylene was tentatively estimated from calculations and analysis of the experimental data.

(2) A low-molecular-weight polyelectrolyte is capable of directed modification of a wood-based filler.

(3) This fact reasonably agrees with the calculational and statistical data for the terms of the free surface energy, as well as with the compatibility criteria proposed on their basis and the structural and functional features of the ingredients of the composite materials.

REFERENCES

1. Solomatov, V.I., *Sinergetika kompozitsionnykh materialov* (Synergism of Composite Materials), Lipetsk: Orius, 1994.
2. Bormotov, A.N., Proshin, A.P., Bazhenov, Yu.M., et al., *Polimernye kompozitsionnye materialy dlya zashchity ot radiatsii: Monografiya* (Polymeric Composite Materials for Radiation Protection: a Monograph), Moscow: Paleotip, 2006.
3. Good, R.J. and Oss, C.J. van, *Modern Approaches to Wettability: Theory and Applications*, Schrader, M. and Loeb, G., Eds., New York: Plenum, 1992, pp. 1–27.
4. Owens, D.K. and Wendt, R.C., *J. Appl. Polym. Sci*., 1969, vol. 13, pp. 1741–1747.
5. Oss, C.J. van, Chaudhury, M.K., and Good, R.J., *Chem. Rev*., 1988, vol. 88, pp. 927–932.
6. Snycheva, E.V., Glazkov, S.S., Murzin, V.S., and Zobov, S.Yu., *Vestn. Voronezh. Gos. Univ*., 2005, no. 2, pp. 88–94.

ISSN 1070-4272, Russian Journal of Applied Chemistry, 2007, Vol. 80, No. 9, pp. 1598–1603. © Pleiades Publishing, Ltd., 2007.
Original Russian Text © N.P. Kuznetsova, R.N. Mishaeva, L.R. Gudkin, 2007, published in Zhurnal Prikladnoi Khimii, 2007, Vol. 80, No. 9, pp. 1566–1570.

MACROMOLECULAR CHEMISTRY AND POLYMERIC MATERIALS

Sorption Purification of Concentrated Hemoglobin Solutions

N. P. Kuznetsova, R. N. Mishaeva, and L. R. Gudkin

Institute of Macromolecular Compounds, Russian Academy of Sciences, St. Petersburg, Russia

Received October 26, 2005; in final form, March 2007

Abstract—A procedure was developed for purification of concentrated hemoglobin solutions from hemolyzate of human erythrocytes to remove soluble cellular impurities using a frontal chromatographic process on an anion exchanger under conditions of selective absorption of impurities and the absence of sorption of the target product, hemoglobin.

DOI: 10.1134/S1070427207090303

Hemoglobin (Hb), the main respiratory blood protein, is contained in specific cells, erythrocytes, serving the most important function of blood, reversible transfer of oxygen from lungs to tissues [1].

An Hb solution is obtained by breakdown of erythrocytes using the osmotic hemolysis with the subsequent removal of insoluble cellular fragments (stroma) by centrifugation. The resulting solution of hemolyzate contains Hb in a high concentration. Along with Hb, soluble components of erythrocyte membranes, the products of cellular metabolism, having no definite functional and molecular characteristics, pass into the solution. Typically, these are phospholipids and other phosphorus-containing components of a cell and also intracellular proteins and enzymes, the residues of plasma and membrane proteins.

One of serious problems arising in using Hb solutions as a basis for the development of blood substitutes, oxygen carriers [2], is the possibility of toxic reactions caused by the impurities, soluble stroma components. In this connection, it becomes necessary to develop procedures for hemolyzate purification to remove side cellular components. There are published data on procedures of Hb purification to remove impurities by affinity chromatography [3], displacement preparative HPLC [4], and ion-exchange chromatography using cationic and anionic systems [5]. The chromatographic methods suggested usually involved presorption of Hb from the hemolyzate solution with subsequent desorption in a gradient of pH or salt concentration in the eluting solution.

To be suitable as a base for a blood substitute (oxygen carrier), Hb (MW 64 500) should practically fully preserve the physiological activity, which poses stringent requirements upon operation with its solutions, such as narrow range of ionic strength, pH, temperature, and the shortest contact time with the sorbent. In this connection, as a method for purifying Hb from hemolyzate solutions containing Hb in high concentrations we suggested and studied the frontal version of anion-exchange liquid chromatography under such conditions when the main protein, Hb, is not sorbed but foreign soluble components are selectively absorbed from the hemolyzate.

EXPERIMENTAL

We used an EDE-10p anion exchanger (Plastics Plant, Nizhni Tagil, Sverdlovsk oblast, Russia). The sorption experiments were performed with the anion exchanger (grain size 0.1–0.2 mm) in the mixed OH–Cl form, prepared by titration of the OH form of the anion exchanger with 0.2 N HCl in 0.15 N NaCl to the corresponding equilibrium pH value.

Removal of impurities from the hemolyzate was studied in two modes: static (sorption with stirring for 2 h at 20°C) and dynamic (column size 6.5 × 1.2 cm, anion exchanger volume 6 ml, which corresponds to 2 g of dry sorbent, solution flow velocity 25 ml h^{-1} cm^{-2}). Approximately 80 ml of concentrated Hb solution (hemolyzate) was passed through the column; 5-ml fractions were collected and analyzed.

Hemoglobin was prepared from erythrocytes of human blood by osmotic hemolysis of cells. The erythrocytes were separated from blood serum by centrifugation (3000 rpm, 4°C, 20 min) and carefully

Table 1. Sorption of N- and P-containing components from hemolyzate on anion exchanger under dynamic conditions

Initial hemolyzate					Sorption			
Hb, mg ml^{-1}	pH	content, mg per gram of Hb		procedure of Hb precipitation	pH_{eq} of anion exchanger	sorbed, mg per gram of anion exchanger		% of initial
		N	P			N	P	
58	6.6	1.08	–	TCAA	7.4–7.6	0.92	–	29
50	6.8	3.30	–	$ZnSO_4$	6.8	1.25	–	25
50	6.8	2.20	–	$ZnSO_4$	7.9	1.10	–	20
50	6.8	–	1.04	TCAA	6.8	–	1.13	78
50	6.8	–	1.06	$ZnSO_4$	7.9	–	1.15	80

washed several times with 0.15 N NaCl solution. Washing solutions were removed by centrifugation. The osmotic hemolysis of the resulting erythrocyte mass was performed by addition of ice-cold distilled water in a volume ratio erythrocytes : water = 1 : 3 for 1 h in the cold with intermittent stirring. Then, insoluble degraded shells of erythrocytes (stroma) were separated by centrifugation (6000 rpm, 4°C, 20 min), the hemolyzate solution was withdrawn; pH was measured, and the concentration of Hb in the form of its stable cyano derivative was determined spectrophotometrically at a wavelength of 540 nm [6].

The presence of soluble stroma components in the hemolyzate and purified Hb solutions were determined visually from the turbidity of the solution (precipitation) appearing upon addition of a saturated ammonium sulfate solution in 1 : 1 volume ratio. The presence of soluble phospholipids was estimated qualitatively with hydroxylamine and iron chloride [7] from the appearance of a purple color of the samples applied to paper (against the background of Hb). The sensitivity of the procedure was 0.5 μg of phosphorus.

For quantitative determination of a low content of impurities, Hb was precipitated from the hemolyzate solution with 15% trichloroacetic acid (TCAA) to the final concentration of 3%. The mixture was thoroughly stirred, and the precipitate was separated by centrifugation and discarded.

In precipitation of Hb with zinc salts, pH 8.4 of the solution was adjusted with a saturated sodium tetraborate solution. An 0.03 M $ZnSO_4$ solution was added in a ratio $ZnSO_4$: Hb = 12 mol mol^{-1} with stirring. The precipitate of the resulting complex was separated by centrifugation. In transparent colorless solution, supernatant, the content of total nitrogen and phosphorus was determined.

Nitrogen-containing protein components were analyzed for total nitrogen by the modified Kjeldahl micromethod [8] by combustion of the sample in sulfuric acid with the catalyst (K_2SO_4 + $CuSO_4$). The ammonia formed was removed with water vapor and absorbed by 0.01 N H_2SO_4, after which the nitrogen content was determined by titration.

Phosphorus-containing components were determined by the Fiske–Subbarow method [9] using Eikonogen as a reducing agent. The phosphorus amount was determined spectrophotometrically using the calibration dependence at a wavelength of 720 nm.

The immunoassay of stroma impurities was based on the procedure of preparation of membrane specimens [10].

Hemoglobin is an extremely labile protein and in aqueous solutions with variation of pH it is readily subjected to autooxidation (irreversible oxidation of heme iron) to form biologically inactive methemoglobin. Therefore, outside erythrocyte Hb can occur in a solution in the functionally active state only in a narrow pH range from 6.3 to 7.8 in the vicinity of the isoelectric point of Hb (6.8–7.0) and in solutions with ionic strength close to the physiological value (approximately 0.15).

Since the content of impurity components in the hemolyzate is insignificant (from 0.5 to 2–3% of the content of the main protein, Hb), high concentrations of Hb (5–7%) hamper their quantitative estimation. The impurity phosphorus- and nitrogen-containing components were analyzed before and after sorption after precipitation of Hb from the solution with TCAA or $ZnSO_4$. The phosphorus amount in the supernatant did not depend on the procedure of Hb removal and was 1.0–1.1 mg of P per gram of Hb, and after precipitation of Hb with zinc sulfate the supernatant contained the largest amount of nitrogen-containing impurities, up to 3.3 mg of N per gram of Hb (Table 1).

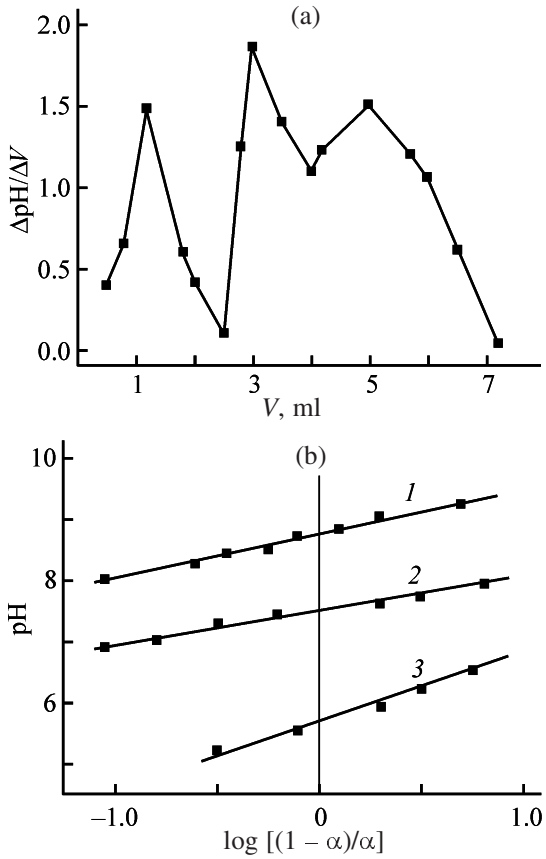

Fig. 1. Results of titration of EDE-10p anion exchanger plotted in (a) $\Delta pH/\Delta V$–V coordinates and (b) Henderson–Hasselbach coordinates. (a) Titrant 0.2 N solution of HCl in 0.15 N NaCl, weighed portion of anion exchanger 0.2 g, OH form. ($\Delta pH/\Delta V$) Variation of pH of the equilibrium solution as a result of addition of ΔV ml of titrant. (b) (*1*) Quaternary ammonium groups, (*2*) tertiary amino groups, and (*3*) secondary amino groups.

It is well known that many impurity proteins have isoelectric points in acidic medium [11], and phosphorus-containing components of cellular shells are mainly negatively charged. Therefore, for sorption of a wide set of impurity components from concentrated solutions of Hb we used polyfunctional anion exchanger EDE-10p, the product of polycondensation of polyethylenepolyamines with epichlorohydrin containing positively charged groups of various basicities.

Table 2. Characteristic of titrated groups of anion exchanger

Functional groups	TEC, mg-equiv per gram of anion exchanger	Titration pH	$pK_{\alpha=0.5}$
Quaternary ammonium	2.8	10.6–8.0	8.8
Tertiary amino	1.7	8.0–6.7	7.5
Secondary amino	1.7	6.7–4.3	5.7

To evaluate the basicity of the anion exchanger and its total exchange capacity (TEC), we performed potentiometric titration of functional groups by the method of individual weighed portions. For the polyfunctional anion exchanger, we considered the completion of titration of each type of functional groups from the differential titration curves plotted in the $\Delta pH/\Delta V$–V coordinates (V is the titrant volume, Fig. 1a). The basicity of three types of anion-exchange groups of the sorbent was determined by expressing the titration results in the Henderson–Hasselbach coordinates (Fig. 1b), pH vs. $\log[(1 - \alpha)/\alpha]$, where α is the degree of ionization. At $(1 - \alpha)/\alpha = 1$, the $pK_{\alpha=0.5}$ value corresponds to the pH value at which groups of a certain type are 50% ionized. The results are presented in Table 2. We determined that titration of the anion exchanger in the OH form is complete at pH 4.2–4.3, and for Cl form, at pH 10.5–10.6, i.e., the pH range of ionization of anion exchange groups of the sorbent is from 10.6 to 4.3. This range is suitable for sorption of soluble stroma components of uncertain nature from a hemolyzate solution.

In the vicinity of the isoelectric point of Hb, its molecule has zero total electric charge balanced with respect to positively and negatively charged functional groups. In this range, strongly basic groups of the anion exchanger are ionized completely, tertiary amino groups are half-ionized, and secondary amino groups able to form hydrogen bonds and participate in weaker interactions are very weakly ionized.

It should be noted that at pH > 8.5 Hb is significantly sorbed from the hemolyzate with the anion exchanger, since under these conditions Hb molecules have significant negative charge. It was shown in preliminary experiments that in the vicinity of the isoelectric point Hb is not sorbed on the anion exchanger, whereas stroma impurities are absorbed from the hemolyzate solution.

The optimum composition of the mixed OH–Cl form of the anion exchanger for absorption of stroma impurities was determined under static conditions. The anion exchanger was titrated until a certain pH of the equilibrium solution, pH_{eq}, was attained, after which the solution was removed by centrifugation. The impurities were sorbed from the hemolyzate under static conditions with stirring for 2 h at the weight ratio anion exchanger : Hb = 1 : 1. After re-

moval of the anion exchanger by centrifugation and precipitation of Hb, we determined the content of impurity phosphorus-containing components in the supernatant. The amount of impurities absorbed by the sorbent was estimated from the difference of the concentrations before and after sorption. The results are shown in Fig. 2.

The maximum absorption of phosphorus-containing impurities was observed for the anion-exchanger sample titrated to pH 5.5–5.7, when all three types of anion-exchange groups are ionized. However, we chose pH 6.5–7.7, which is the optimal range of equilibrium pH values of anion exchanger for preservation of the biological activity of Hb, when Hb undergoes autooxidation to a lesser extent and absorption of impurities remains significant even under static conditions of sorption.

The influence of the degree of ionization of functional groups in the range of pH_{eq} 6.8–7.9 on absorption of impurities from the hemolyzate is presented in Table 1. Absorption of phosphorus-containing impurity components in the dynamic frontal process reached 78–80% of the initial amount, and absorption of nitrogen-containing stroma impurities was 20–30% in the absence of Hb sorption.

The breakthrough curves of frontal chromatography of hemolyzate on anion exchanger (pH_{eq} 7.3) are shown in Fig. 3. The solution corresponding to the free column volume (6 ml) before appearance of colored solution at the outlet of the column was discarded, and in the subsequently collected fractions the hemoglobin and phosphorus concentrations c_{Hb} and c_P were determined. In the initial hemolyzate solution c_{Hb} = 58 mg ml^{-1} and c_P = 62 μg ml^{-1}. As follows from Fig. 3, in the first eight fractions (approximately 40 ml) phosphorus-containing components are practically absent, while Hb concentration remains essentially at the initial level. In this experiment 2.3 g of purified Hb was obtained.

Variation of pH of the initial hemolyzate solutions from 6.3 to 7.7 insignificantly affects the degree of chromatographic purification of Hb (with respect to absorption of phosphorus-containing components), but the absorption somewhat increased in the pH range equal to isoelectric point of Hb (pH 6.8) (Table 3).

In all sorption chromatographic experiments, the qualitative reactions for soluble stroma elements and for phospholipids gave negative results.

To make sure that the obtained degree of purification of concentrated Hb solutions is sufficient for

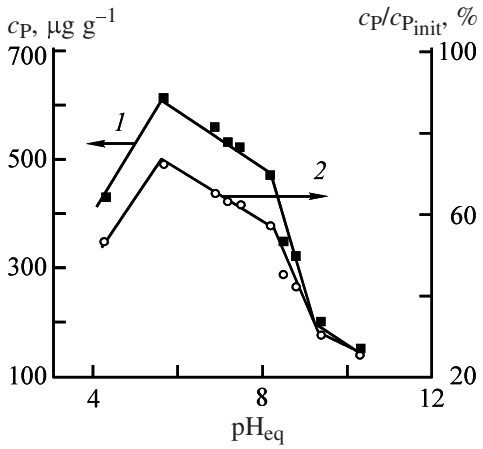

Fig. 2. Sorption of phosphorus-containing components from the hemolyzate of erythrocytes under static conditions as a function of pH_{eq} of the anion exchanger. Ratio anion exchanger : Hb = 1 g g^{-1}; phosphorus content in the supernatant was determined after removal of Hb by precipitation with TCAA. Amount of sorbed phosphorus: (*1*) absolute (c_P) and (*2*) relative to the initial content in hemolyzate ($c_P/c_{P_{init}}$).

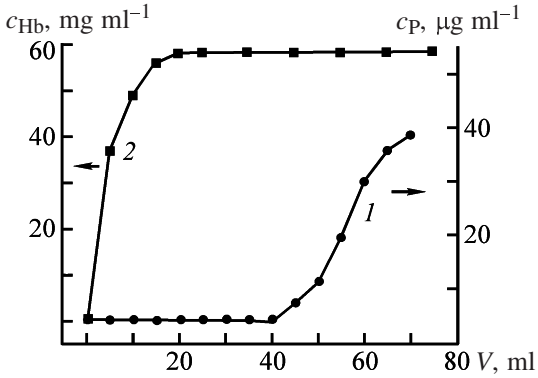

Fig. 3. Breakthrough curves of a frontal chromatographic process of hemolyzate purification. Column 6.5 × 1.2 cm containing 6 ml of EDE-10r; fraction volume 5 ml. (c_{Hb}) Hemoglobin concentration, (c_P) phosphorus concentration, and (V) titrant volume. (*1*) Sorption of phosphorus-containing components and (*2*) Hb content of fractions.

elimination of undesirable side reactions caused by stroma impurities in the hemolyzate, we used a highly sensitive immunological test for formation of antigen complex (in solutions of purified Hb and initial hemolyzate) with antibodies (in the antiserum). Formation of antigen–antibody complex was monitored from the ring precipitation reaction. For this purpose we used the solutions of the initial hemolyzate and purified 5% solution of Hb obtained after sorption of soluble stroma impurities under static conditions with variation of the Hb : anion exchanger weight ratio (Table 4).

Table 3. Sorption of phosphorus-containing components from hemolyzate solutions on anion exchanger (pH_{eq} 7.7) under dynamic conditions. c_{Hb} = 58 mg ml^{-1}

$pH_{hemolyzate}$	Phosphorus concentration in supernatant, mg per gram of Hb	After sorption on anion exchanger		
		pH of Hb solution in fractions	sorbed P*	
			mg per gram of anion exchanger	% of initial
6.3	1.09	7.7–7.0	2.1	60
6.7–6.8	1.05	7.9–7.4	1.8–2.0	66–70
7.4	1.05	8.0–7.8	1.6	57

* After precipitation of Hb with trichloroacetic acid.

Table 4. Results of immunoassay of the initial hemolyzate of erythrocytes and hemoglobin solution purified on anion exchanger under static conditions with stirring. 20°C, sorption duration 2 h, c_{Hb} 52 mg ml^{-1}, pH 6.8

Sample	Amount of anion exchanger in sorption, g	Anion exchanger : Hb, g g^{-1}	Value of immunological reaction, points*
Initial hemolyzate	–	–	2+
1	0.10	0.2	1+
2	0.50	1.0	0
3	0.75	1.5	0
4	1.00	2.0	0
5	1.50	3.0	0
6	2.00	4.0	0
Homogenate of erythrocyte membranes (stroma)	–	–	4+

* Points from 0 to 4+ at 1 : 2 dilution.

Immunoassay shows (Table 4) that solutions of Hb purified on anion exchanger under static conditions with variation of the anion exchanger : Hb weight ratio from 1.0 to 4.0 contain no stroma impurities. At the ratio of 0.2, the presence of impurities can be attributed to insufficient amount of the sorbent.

Thus, the possibility of selectively absorbing undesirable toxic impurities with an anion exchanger in the frontal chromatographic process without loss of the target protein, Hb, provided complete recovery of purified Hb and allowed us to find the conditions at which Hb molecules remain essentially intact and to scale the process.

The chromatographic purification of Hb to remove stroma impurities was scaled on a column containing 1.2 l of anion exchanger (420 g of dry sorbent). As a result of frontal chromatographic purification of the hemolyzate, approximately 9 l of a solution of purified Hb (approximately 5%) was obtained.

It should be emphasized that after purification Hb preserves its biological activity, first of all, the ability to reversibly bind oxygen. With respect to all functional parameters analyzed on the basis of the dissociation curves of oxyhemoglobin obtained on a Hem-O-Scan equipment (Aminco, the United States), the solutions of purified Hb were similar to Hb in the initial hemolyzate. The amount of methemoglobin in chromatographically purified HB was 2–4% of the total content of Hb at its initial content in the hemolyzate of 0.5–1.0%.

CONCLUSIONS

(1) The developed frontal chromatographic procedure of purification of concentrated hemoglobin solutions from hemolyzate of erythrocytes to remove soluble cell components on a polyfunctional anion exchanger provides complete recovery of hemoglobin with preservation of its biological activity and functional characteristics.

(2) The conditions of selective sorption of nitrogen- and phosphorus-containing stroma impurities, excluding sorption of the target protein, hemoglobin, were found.

ACKNOWLEDGMENTS

The authors are grateful to O.V. Berkos (Pavlov Institute of Physiology) for performing the immunoassay.

REFERENCES

1. Antonini, E. and Brunory, M., *Hemoglobin and Myoglobin in Their Reaction with Ligands*, Amsterdam: North-Holland, 1971.
2. *Artificial Cells, Blood Substitutes, and Immobilization Biotechnology*, Chang, T.M.S., Ed., Marcel Dekker, 1998, vol. 26, no. 2, pp. 173–180, 213–222.
3. US Patent 6 365 147.
4. Christensen, S.M., Midina, F., Winslow, R.W., et al., *J. Biochem. Biophys. Meth*., 1998, vol. 17, no. 2, pp. 143–154.
5. Williams, R.C., Jr. and Kuo-Yi Tsay, *Anal. Biochem*., 1973, vol. 54, no. 1, pp. 137–145.
6. Kushakovskii, M.S., *Klinicheskie formy povrezhdeniya gemoglobina* (Clinical Forms of Hemoglobin Damage), Leningrad: Meditsina, 1968.
7. Dawson, R., Elliot, D.C., Elliot, W.H., and Jones, K.M., *Data for Biochemical Research*, Oxford: Clarendon, 1986.
8. Petrun'kina, A.M., *Prakticheskaya biokhimiya* (Practical Biochemistry), Moscow: Medgiz, 1961.
9. Fiske, C.H. and Subbarow, Y., *J. Biol. Chem*., 1925, vol. 66, p. 375.
10. *Biochemical Analysis of Membranes*, Maddy, A.H., Ed., London: Chapman and Gall, 1976. Translated under the title *Biokhimicheskoe issledovanie membran*, Moscow: Mir, 1979, pp. 334–372.
11. Livshits, A.B., Berkovskii, A.A., Krylova, V.E., et al., *Gematol. Transfuziol*., 1992, no. 4, pp. 35–37.

ISSN 1070-4272, Russian Journal of Applied Chemistry, 2007, Vol. 80, No. 9, pp. 1604–1605. © Pleiades Publishing, Ltd., 2007.
Original Russian Text © V.V. Marakov, 2007, published in Zhurnal Prikladnoi Khimii, 2007, Vol. 80, No. 9, pp. 1571–1572.

BRIEF COMMUNICATIONS

Electromagnetic Method for Softening Natural Water

V. V. Marakov

Berezniki Branch, Perm State Technical University, State Educational Institution for Higher Professional Education, Berezniki, Perm krai, Russia

Received: October 9, 2006; in final form, March 2007

Abstract—A water softening method was saggested. The optimal parameters of the external electric field were determined and apparatus for the implementation of the suggested method was described. The mechanism of the coagulation of hardness salts was studied.

DOI: 10.1134/S1070427207090315

The hardness determined by the concentration of dissolved calcium and magnesium salts is one of important quantitative characteristics of quality of natural water. Thermal, chemical, and ion-exchange methods are used for water softening, i.e., for removal of hardness salts from it [1]. The thermal method of water softening does not remove magnesium salts and converts a half of dissolved calcium salts into insoluble compounds. The chemical and ion-exchange methods involve ion-exchange processes to substitute cations of dissolved calcium and magnesium salts by the cations of chemical reagents used for water softening. The above methods of water softening lead to secondary chemical contamination of water.

The known methods of electromagnetic softening do not provide the necessary technical result and require considerable energy expenditure per unit volume of treated water.

A softening method involving treatment of water with a pulsed electric field was developed [2]. In this method the energy expenditure per unit volume of treated water is minimal, with no chemical contamination of water.

In this study, the optimal parameters of the external electric field ensuring the necessary degree of softening of natural water were determined.

EXPERIMENTAL

It was found that the exposure of water, irrespective of its volume, to a low-frequency electric field causes hardness salts to convert into insoluble compounds which form a precipitate containing 75% calcium salts and 25% magnesium salts on the average. The necessary degree of water softening is obtained at a frequency of ac electric field varying from 1 to 5 Hz, intensity of the external electric field in the treatment zone of 2–2.5 units, and a treatment time of 10–15 s. As a result of this exposure, the hardness of natural water is half as large on the average. The second stage of the treatment performed under the same conditions (i.e., time and parameters of the external electric field are the same) causes the content of calcium and magnesium salts to decrease by 25% of their initial content on the average. The necessary content of hardness salts is obtained after multistage treatment. The choice of the parameters of the external electric field is determined by the technical result. When treatment is performed at a frequency of less than 0.5 Hz or more than 5 Hz, the hardness of natural water decreases by 10% on the average and the chemical contamination of water owing to the electrolysis takes place. The water softening method that we developed provides water treatment in both closed- and flow-type cells.

The developed method uses two flow-through electrolytic cells connected in series to decrease the energy expenditure per unit volume of treated water. Each cell has alternating ground and feeding electrodes. The number of the electrodes in the cells is determined by a water flow (average flow velocity in the interelectrode space $v \le 0.1$ m s^{-1}). This value of the flow velocity provides the necessary technical result on water softening. To the feeding electrodes of each cell, connected in a series, ac electric field with a frequency varying from 1 to 5 Hz was applied from one source.

The voltage diagram measured across the resistor (R = 5.86 Ω) connected in a series with the cell and used for the determination of the current strength passed through the treatment circuit was obtained for the natural water treated in a 13.5 cm^3 cell by ac elec-

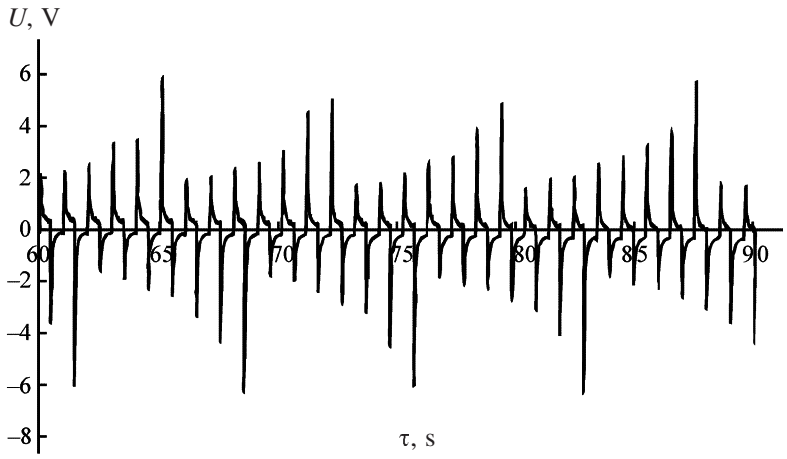

Fig. 1. Voltage U across the resistor measured under the exposure of natural water to ac electric field (frequency 1 Hz, voltage 3 V). (τ) Time; the same for Fig. 2.

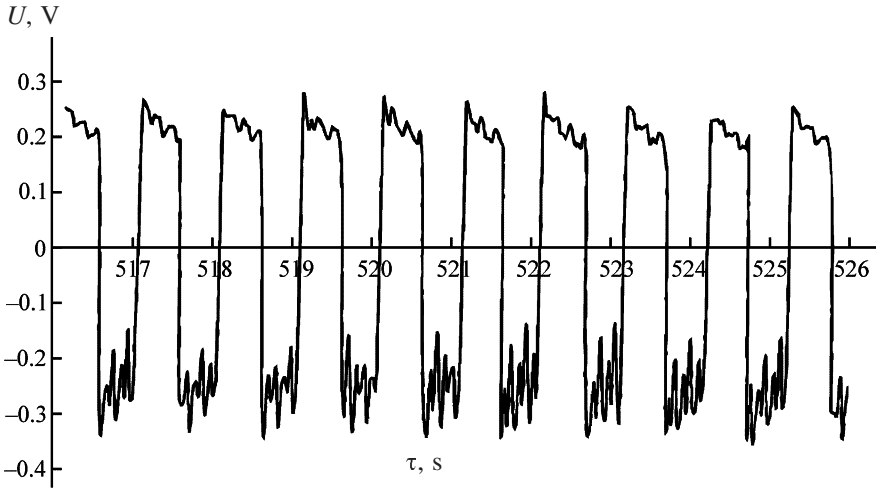

Fig. 2. Voltage U across the resistor measured under the exposure of distilled water to ac electric field.

tric field with a frequency of 1 Hz and a supply voltage of 3 V (Fig. 1). The voltage was measured using a Real Lab system for data collection and control, having an 8-channel analog collection unit with an interval of channel interrogation of 2 ms. A potential drop across the resistor was recorded by one channel of the measuring system. The analysis of the results showed that the potential drop and, consequently, the current passed through the resistor at any time of the measurements depend on the concentration of dissolved salts in the water [3].

We used distilled water to study the effect exerted by dissolved salts on the electrical properties of natural water. The voltage diagram measured across the resistor under the exposure of ac electric field (frequency 1 Hz, supply voltage 4.6 V) to distilled water ($V = 13.5$ cm^2) is presented in Fig. 2. The analysis of the results shows that, when the concentration of dissolved salts in distilled water is minimal, a voltage drop across the resistor remains virtually constant during the exposure time.

CONCLUSIONS

A pulsed method of water softening, causing no chemical contamination of water and ensuring minimum energy expenditure, was suggested.

REFERENCES

1. Kul'skii, L.A., Goronovskii, I.T., Koganovskii, A.M., and Shevchenko, M.A., *Spravochnik po svoistvam, metodam analiza i ochistke vody* (Reference Book on Properties, Analysis, and Treatment of Water), Kiev: Naukova Dumka, 1980.
2. RF Patent 2217384.
3. Sokol'skii, Yu.M., *Omagnichennaya voda: pravda i vymysel* (Magnetically Treated Water: Facts and Fiction), Leningrad: Khimiya, 1990.

ISSN 1070-4272, Russian Journal of Applied Chemistry, 2007, Vol. 80, No. 9, pp. 1606–1608. © Pleiades Publishing, Ltd., 2007.
Original Russian Text © A.F. Gogotov, A.V. Turova, O.I. Baranov, I.I. Batura, E.V. Puchenin, V.K. Stankevich, A.A. Levchuk, A.A. Gulyaeva, D.V. Gendin, 2007, published in Zhurnal Prikladnoi Khimii, 2007, Vol. 80, No. 9, pp. 1573–1574.

BRIEF COMMUNICATIONS

Use of By-Product Coke Phenols as Thermal Polymerization Inhibitors in Processing of Pyrolysis Intermediates

A. F. Gogotov, A. V. Turova, O. I. Baranov, I. I. Batura, E. V. Puchenin, V. K. Stankevich, A. A. Levchuk, A. A. Gulyaeva, and D. V. Gendin

Irkutsk State Technical University, Irkutsk, Russia
Angarsk Petrochemical Company, Open Joint-Stock Company, Angarsk, Irkutsk oblast, Russia
Angarsk Polymer Plant, Open Joint-Stock Company, Angarsk, Irkutsk oblast, Russia
Institute of Chemistry, Siberian Division, Russian Academy of Sciences, Irkutsk, Russia

Received January 31, 2007

Abstract—A new procedure was suggested for modification of by-product coke phenols with the aim to eliminate drawbacks revealed in the course of their long-term use as inhibitors of thermal polymerization of unsaturated pyrocondensate components, namely, low inhibiting activity, high water solubility, and unpleasant odor. These drawbacks are eliminated by phenol–formaldehyde polycondensation of total phenols, similar to Novolac production.

DOI: 10.1134/S1070427207090327

Inhibitors of undesirable polymerization are widely used at modern pyrolysis plants [1, 2]. In particular, a wide set of individual substances and formulations are used in ethylene–propylene and benzene production in the step of distillation of liquid pyrolysis intermediates. In Russia, the cheapest and the most available are phenolic fractions from thermal processing of coal and wood [3, 4]. Despite relatively high inhibiting effect of total by-product coke phenols, studies have been pursued in the past two decades with the aim to enhance the inhibiting efficiency by distillation recovery of the most active fractions, e.g., of the pyrocatechol fraction (PCF), which is the fraction of dihydric phenols [5–7]. The PCF composition (see table) determined with a Hewlett–Packard chromatograph–mass spectrometer using the available database [8] shows that the major components are pyrocatechols, resorcinols, and hydroquinones, with a low (about 5–6%) content of various monohydric phenols.

However, the fractionation of by-product coke phenols, solving the problem of enhancement of the inhibiting activity, fails to solve the environmental problem associated with the high water solubility of these compounds, namely, the hazard of ingress of these compounds into the industrial wastewater. Therefore, within the past 5–7 years this class of inhibitors was essentially displaced from the market by inhibitors of other classes.

Analysis of total phenols shows that they consist to ~60% of monohydric phenols and to ~30% of various dihydric phenols (see table), with the remainder being tar.

Attempts to use polymeric inhibitors of polymerization have been reported [9, 10], but prospects for their application were considered doubtful [4], because, along with certain advantages (high heat resistance, nonvolatility), they have significant drawbacks, being less effective and less soluble in the monomers. At the same time, various phenol–formaldehyde oligomers (PFRs) derived from monohydric alkyl(C_9–C_{20})-

Composition of pyrocatechol fraction

Components	Content, wt %
Phenol	2.5
Cresols	2.7
Xylenols + ethylphenols	0.9
Pyrocatechol	11.3
3-Methylpyrocatechol	7.6
4-Methylpyrocatechol	13.8
Resorcinol + hydroquinone	8.6
Dimethylhydroquinone isomers	4.3
Methylresorcinol isomers	14.8
Dimethyl- and ethylresorcinols	13.7

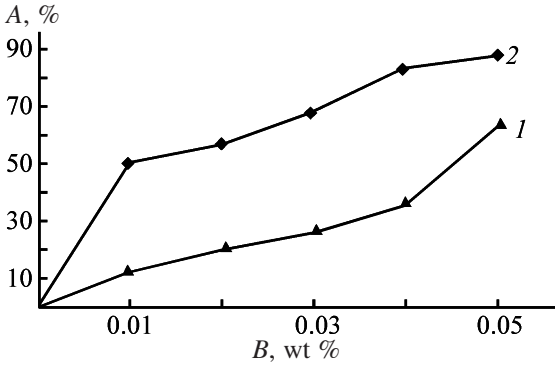

Inhibition efficiency *A* of (*1*) initial and (*2*) modified by-product coke phenols as a function of their concentration *B*.

phenols [11, 12] are widely used as components of so-called antifouling formulations and act as surfactants preventing deposition of polymeric products on the equipment surfaces.

It is well known [13] that the solubility of phenols can be suppressed by involving them in phenol–formaldehyde condensation as in Novolac production. The oligomer formed in the process remains soluble in organic solvents, e.g., in alcohols.

Indeed, standard Novolac PPR derived from monohydric phenol, when tested as a phenolic inhibitor in a concentration of 0.03 wt %, showed ~30% inhibiting effect. The Novolac polycondensate prepared from total by-product coke phenols showed in the same concentration 67% effect, and unmodified total by-product coke phenols showed 24% effect (see figure).

The inhibiting performance was determined as the per cent ratio of the difference between the polymer yields in the absence and in the presence of the inhibitor to the polymer yield without inhibitor. It should also be noted that PFRs synthesized from fractions of mono- or dihydric phenols recovered from total phenols showed appreciably lower inhibiting activity (30–35% at 0.03 wt % concentration) than PFR from the initial nonfractionated phenols. The optimal ratio of mono- and dihydric phenols in the starting mixture of by-product coke phenols taken for modification is (1–2) : 1. An increase in the content of monohydric phenols over the optimum leads to a decrease in the inhibitor performance.

Thus, the procedure suggested for modification of by-product coke phenols yields a product with enhanced inhibiting activity. The oligomeric product obtained is virtually fully soluble in butyl alcohols, which allows the inhibitor to be readily dosed to the reaction mixture. Butyl alcohols are among solvents permitted for use in petrochemical industry [14]. Phenol–formaldehyde oligomers derived from by-product coke phenols meet also other requirements to inhibitos, i.e., the inhibitor obtained does not precipitate from the solutionin the course of heat treatment of the pyrocondensates.

Furthermore, involving by-product coke phenols into phenol–formaldehyde polycondensation strongly reduces the intensity of specific odor of by-product coke phenols, making them more acceptable for industrial applications. The suggested procedure for chemical modification of by-product coke phenols was protected by an RF patent [15], and a project was developed for the production of the modified phenols in an amount of 5–10 t annually.

CONCLUSION

Chemical modification of by-product coke phenols, phenol–formaldehyde Novolac polycondensation, yields an inhibitor of thermal polymerization of unsaturated pyrocondensate components with improved performance and environmental characteristics.

ACKNOWLEDGMENTS

The study was financially supported by the Russian Foundation for Basic Research (project no. 05-08-50097).

REFERENCES

1. Mukhina, T.N., Barabanov, N.L., Babash, S.E., et al., *Piroliz uglevodorodnogo syr'ya* (Pyrolysis of Hydrocarbon Raw Materials), Moscow: Khimiya, 1987.
2. Kurbatov, V.A., Liakumovich, A.G., and Kirpichnikov, P.A., *Neftekhimiya*, 1983, vol. 23, no. 1, pp. 118–120.
3. Berents, A.D., Vol'-Epshtein, A.V., Mukhina, T.N., et al., *Pererabotka zhidkikh produktov piroliza* (Processing of Liquid Pyrolysis Products), Moscow: Khimiya, 1985, pp. 59–60.
4. Zav'yalov, A.N., Gol'dshmidt, Yu.M., Zav'yalova, Z.A., and Kasilova, L.V., *Drevesnosmolyanoi i drugie ingibitory tsepnykh protsessov* (Wood-Tar and Other Inhibitors of Chain Processes), Moscow: VNIPIEIlesprom, 1978.
5. Gusarov, S.V., Danilov, A.M., Kryukov, A.S., et al., *Neftepererab. Neftekhim.*, 1993, no. 3, pp. 20–22.
6. RF Patent 2127750, 1999.

7. Novichikhin, D.N., Zakazov, A.N., and Gogotov, A.F., *Khim. Prom–st.*, 1998, no. 1, pp. 20–21.
8. Gogotov, A.F., Novichikhin, D.N., Bobyleva, E.E., et al., *Neftepererab. Neftekhim.*, 1999, no. 10, pp. 23–27.
9. USSR Inventor's Cetficiate no. 899575.
10. USSR Inventor's Certificate no. 1073239.
11. US Patent 5985940.
12. US Patent 3375983.
13. *Entsiklopediya polimerov* (Polymer Encyclopedia), Kargin, V.A., Ed., Moscow: Sov. Entsiklopediya, 1977, vol. 3, pp. 710–719.
14. RF Patent 2154048, 2000.
15. RF Patent 2265005, 2005.

ISSN 1070-4272, Russian Journal of Applied Chemistry, 2007, Vol. 80, No. 9, pp. 1609–1610. © Pleiades Publishing, Ltd., 2007.
Original Russian Text © the Editorial Board, 2007, published in Zhurnal Prikladnoi Khimii, 2007, Vol. 80, No. 9, pp. 1575–1576.

OBITUARIES

Boris Veniaminovich Gidaspov (1933–2007)

DOI: 10.1134/S1070427207090339

On August 15, 2007, in Moscow suddenly died Boris Veniaminovich Gidaspov, a corresponding member of the Russian Academy of Sciences, doctor of chemical science, professor, laureate of Lenin Prize (1976) and State Prize (1981) in science and technology, an outstanding scientist in the field of technical chemistry and technology of highly energetic products, and founder and head of a world-renown scientific school.

B.V. Gidaspov was born on April 16, 1933, in Kuibyshev (now Samara). In 1955, he graduated from the Kuibyshev Industrial Institute and was left to work there as assistant at the chair of explosives. In 1959, he became a postgraduate student at Lensovet Institute of Technology in Leningrad and, having successfully defended his dissertation, made his way up from junior researcher to head of a chair and dean of a faculty. There, Boris Veniaminovich exhibited his remarkable talent of a pedagogue and scientist, combined with his outstanding organizational capacities. Under his supervision, both the chair and the faculty always demonstrated a high level of educational and research work, and the out-of-city research facilities of the chair became Tekhnolog (Technologist) Special Design Office and, headed by chief designer Gidaspov, occupied one of leading positions in the development of highly energetic formulations and special-purpose materials, most important for the country. For example, extensive studies aimed to develop original techniques for synthesis of nitro and polynitro compounds of aliphatic, aromatic, and heterocyclic series were carried out under Gidaspov's supervision and their structure, physicochemical properties, and reactivity were analyzed. The mechanism of the reactions of nitroaminoalkylation, transaminomethylation, N-nitration, and alkylation of tri- and tetrazoles was identified. For these and a number of other reactions, foundations of a quantitative theory were created and a general approach was developed, which enabled prediction of the chemical structure of the reaction products and the rate and equilibrium constants of reversible processes in relation to properties of the starting reactants and characteristics of the reaction medium.

Boris Veniaminovich's activities have been highly appraised; he was awarded Lenin and State Prizes and received a number of Government awards.

Boris Veniaminovich also exhibited his organizational capacity and scientist's talent when being the director general of the State Institute of Applied Chemistry, a most prominent scientific institution specialized in defense chemistry. His indefatigable nature manifested itself in a search for, and development of new methods for managing the chemical industry. On his initiative, a Tekhnokhim multibranch state association was created for the first time in the USSR to improve the working efficiency. Tekhnokhim included 16 institutes and pilot plants and shops, which were removed from the control of Lenneftekhim association and placed under control of the Council of Ministers of the USSR.

From 1989 till 1992, Gidaspov was the first secretary of the Leningrad Regional Committee of the Soviet Communist Party.

Gidaspov became chairman of the council of directors of Aviatsionnoe Vooruzhenie (Aircraft Armament) corporation in 1993 and chairman of the council of directors of Interkhimprom in 1996. From 2004 till 2006 he was director general of Prikladnaya Khimiya Russian Scientific Center, Federal State Unitary Enterprise, and in 2006, he became director general of SVL Proektnoe Upravlenie (SVL Design Control) Private Company and an advisor of the head of the Federal Agency for Science and Innovation.

Under the fundamentally changed economic conditions, Gidaspov organized reforms of the scientific and technological sphere in order to preserve and develop the scientific-industrial and defense potential of the country.

The rich legacy left by Boris Veniaminovich is in his scientific works, implemented technologies, practical recommendations, and the unique Russia's scientific school of broad-profile chemists-technologists.

Gidaspov has trained a large pleiad of specialists working in various fields of science and technology. Among his disciples are candidates and doctors of science and heads of enterprises, with all of whom he shared his ideas, professional experience, and knowledge.

We all sincerely grieve over the loss of a remarkable talented man and present our deep condolences to his relatives, colleagues, and friends. The memory of Boris Veniaminovich Gidaspov will forever remain in our hearts.

Staff members of Prikladnaya Khimiya Russian Scientific Center, Federal State Unitary Enterprise; St. Petersburg State Institute of Technolofy (Technical Univeristy); SKTB Tekhnolog Federal State Unitary Enterprise; Editorial Board and Editorial Staff of *Zhurnal Prikladnoi Khimii*

ISSN 1070-4272, Russian Journal of Applied Chemistry, 2007, Vol. 80, No. 9, pp. 1611–1612. © Pleiades Publishing, Ltd., 2007.
Original Russian Text © A.G. Morachevskii, 2007, published in Zhurnal Prikladnoi Khimii, 2007, Vol. 80, No. 9, pp. 1577–1578.

BOOK REVIEWS

Pogosyan, A.A., Besser, A.D., and Sorokina, V.S., *Pererabotka ispol'sovannykh akkumulyatorov – osnova retsiklinga svintsa* (Processing of Worked-out Batteries as a Basis for Lead Recycling)

Moscow: TsNIIATOMINFORM, 2005, 256 pp.

DOI: 10.1134/S1070427207090340

The monograph by A.A. Pogosyan and co-authors discusses evidence concerning the modern state of manufacture of secondary lead, based on utilization of worked-out lead batteries. According to the available statistical data, the share of refined lead smelted from secondary lead raw materials was 53.9% of the total world production of the metal. In some countries, the share of secondary lead in the total lead manufacture balance was 65–85%. All the evidence presented in the book is of technological nature. The authors analyze in ample detail the world's practice of collection, transportation, and processing of battery scrap and refining of secondary lead. Particular attention is paid to lead recycling in Russia.

The book comprises an introduction, seven chapters, conclusions and recommendations, and bibliographic list. The introduction (pp. 3–11) notes specific features of processing of secondary raw materials, which are primarily associated with the toxicity of lead and its compounds. In processing of secondary lead raw materials, it is necessary to monitor the environment contamination and minimize the amount of wastes formed. Chapter 1 (pp. 12–26) discusses the modern state of manufacture and consumption of lead, as well as lead recycling. At present, most part of lead output is consumed by the battery industry. In 2000, 74% of world's smelted lead was spent for manufacture of batteries, with this parameter markedly exceeding the average in some countries. In 2000, the fraction of lead used in the United Sates for battery fabrication was 86%. At present, there is no sound alternative to use of lead batteries in vehicles. The depletion of deposits of high-quality ores, decline in production of lead ore raw materials for environmental or economical reasons, necessity for utilization of all kinds of lead waste, and growing demand for lead, all lead to intensification of lead recycling and, in the first place, to utilization of lead battery scrap. In developed countries, more than 90% of worked-out batteries are subjected to processing.

Very brief chapter 2 (pp. 27–34) is devoted to the modern state of, and prospects for lead manufacture in Russia. Before the disintegration of the USSR, lead was mostly produced by processing of ore concentrates, and only 20% of lead was obtained from secondary raw materials and industrial waste. The main plants for manufacture of lead were situated in Kazakhstan and Ukraine. To provide lead for the seven battery plants on the territory of Russia and other consumers, it is necessary to primarily use secondary raw materials, with lead battery scrap collected and processed. Chapter 3 (pp. 35–48) discusses the situation with collection and transportation of worked-out lead batteries in other countries and in Russia. In quite a number of developed countries in the world (the United States, Germany, Japan, France, the United Kingdom, Sweden, Switzerland, etc.), the extent of lead recycling by processing of batteries is 80–100%, which is accounted for by a sufficiently perfect system for collection and utilization of the already accumulated and newly formed raw materials, existence of appropriate regulations, and state support of the activities of this kind. On the whole, present-day Russia's system for collection and transportation of worked-out lead batteries fails to satisfy modern world's standards. According to the available experts' estimates, the amount of battery scrap formed in Russia yearly increases by 150–200 thousand tons because of the rapidly increasing number of vehicles. The regulations of the Russian Federation, concerning the management of lead battery scrap, have become outdated and fail to satisfy modern environmental requirements.

Chapter 4 (pp. 49–77) considers the existing methods for preparation of worked-out batteries for metallurgical processing. In most countries (Russia not in-

cluded), worked-out batteries are included in the list of dangerous wastes because of their content of lead, sulfuric acid electrolyte, and lead-contaminated organic components. Hence follows the requirement that these dangerous kinds of waste should be processed to give the minimum amount of unutilizable materials. The regulations concerning the environment protection, storage of the solid waste, effluent gases, and industrial wastewater are steadily becoming increasingly stringent. The chapter discusses utilization of the electrolyte, battery cropping, desulfation of the active paste, and utilization of organic components.

Chapter 5 (pp. 78–183) analyzing modern methods for manufacture of secondary lead occupies the central place in the monograph. At present, worked-out lead batteries are processed exclusively by pyrometallurgical methods. According to the official statistical data for the year 2003, 68 plants in the world worked totally or partly on primary ores, and 190 plants processed only secondary raw materials. In Europe, plants with an annual output capacity of 30 to 50 thousand tons of lead are most widely used; in the United States, there are plants with an annual output capacity exceeding 100 thousand tons of lead; and in developing countries, the annual output capacity of many plants is less than 10 thousand tons.

The authors note that, recently, a tendency is observed in the world's practice of battery scrap processing toward separate smelting of the metallic fraction, desulfation, and subsequent reducing smelting of the active paste. Among the large number of flowsheets analyzed in the monograph, the authors should have been, in reviewer's opinion, more critical to use of electric furnaces in processing of secondary lead raw materials, the more so as the monograph considers it advisable to create, under the conditions of Russia, regional plants with low output capacity, up to 3–5 thousand tons of lead per year, depending on the amount of worked-out batteries collected in a region. This concept has been more than once substantiated by the reviewer. It should be kept in mind in this case that, for the toxic and comparatively volatile lead, the reducing process should be carried out at as low temperature as possible (720–740°C).

Chapter 6 (pp. 184–214) discusses processes of refining of secondary raw lead. The emphasis is on various pyrometalurgical procedures; any new or promising techniques are not considered by the authors. Chapter 7 (pp. 215–228) contains evidence about hydrometallurgical methods for processing of lead battery scrap. The true efficiency of these techniques cannot be estimated so far.

Of particular interest are the conclusions and recommendations in the final part of the monograph (pp. 229–240). The authors justly emphasize that, taking into account the vast territory of Russia, the problem of environment protection from contamination with various kinds of lead waste can be only solved by State policy on stimulation, by regional tax-reduction, of lead recycling, with heavy fines for discharge of lead-containing materials. It is necessary to bring the system for collection, transportation, and storage of worked-out batteries to the modern level to satisfy the requirements of international environmental regulations. Preliminary cropping of batteries before their metallurgical processing enables utilization of virtually all the battery components.

The bibliographic list (pp. 241–252) contains references to 217 publications of domestic and foreign authors, but, still, seems to be insufficient.

The monograph in question is undoubtedly useful and timely, and it is written by experienced specialists. Works by A.D. Besser and V.S. Sorokina on processing of secondary lead raw materials are widely known. The book makes quite a favorable impression and gives to a reader an exhaustive notion of the modern state of technologies for processing of worked-out lead batteries in Russia and other countries.

A. G. Morachevskii

ISSN 1070-4272, Russian Journal of Applied Chemistry, 2007, Vol. 80, No. 10, pp. 1613–1620. © Pleiades Publishing, Ltd., 2007.
Original Russian Text © A.M. Kalinkin, 2007, published in Zhurnal Prikladnoi Khimii, 2007, Vol. 80, No. 10, pp. 1585–1591.

INORGANIC SYNTHESIS AND INDUSTRIAL INORGANIC CHEMISTRY

Physicochemical Processes in Mechanical Activation of Titanium- and Calcium-containing Minerals

A. M. Kalinkin

Tananaev Institute of Chemistry and Technology of Rare Elements and Mineral Raw Materials, Kola Scientific Center, Russian Academy of Sciences, Apatity, Murmansk oblast, Russia

Received June 27, 2006; in final form, July 2007

Abstract—A comparative study of processes occurring in mechanical activation of perovskite, sphene, and vollastonite in air and in the atmosphere of carbon dioxide was made. Data on the effect of mechanical activation on the degree of perovskite and sphene decomposition by a 20% nitric acid solution under the standard conditions are presented.

DOI: 10.1134/S1070427207100011

A possible way to intensify processes in the technology of mineral raw materials is mechanical activation (MA) [1–4]. In [5–8], the effect of MA of natural and synthetic titanium-containing minerals, such as ilmenite, leucoxene, rutile, and anatase, on their reactivity toward sulfuric acid was studied. These minerals were mechanically activated with a vibrational grinder and centrifugal and ball mills. Commonly, titanium-containing raw materials are decomposed with concentrated sulfuric acid at temperatures higher than 180°C [9–11]. According to the data obtained in [5–7], the MA of the above-mentioned minerals raises their reactivity and makes it possible to achieve a high degree of titanium recovery under less "severe" decomposition conditions: with 75–85% H_2SO_4 at 140–180°C. A prolonged (for 100 h) grinding in a laboratory vertical ball mill enables a more than 80% dissolution of ilmenite with 50% H_2SO_4 at 120°C [8].

Natural minerals sphene (titanite) $CaTiSiO_5$ and perovskite $CaTiO_3$, which are promising sources of titanium dioxide in the Kola industrial region, are also difficult to decompose [9–11]. Sphene and perovskite differ from the titanium minerals studied in [5–8] in that they contain calcium. It was shown in [12] that preliminary MA of sphene in a centrifugal-planetary mill leads to virtually complete transfer of titanium into solution with a 20–25% solution of nitric acid at room temperature. No data on the effect of MA of perovskite on its acid decomposition could be found in the literature. The increase in the reactivity of titanium minerals difficultly decomposed in acids has been attributed to the higher crystal lattice defectiveness upon MA [5–8]. Apparently, changes in reactivity under MA depend, for different types of titanium-containing minerals, on the composition and structural features of a starting mineral. It should also be noted that the gas medium in which the grinding is carried out may be of particular importance [13]. It has been found that, when subjected to a strong mechanical treatment, a number of calcium- and magnesium-containing silicate minerals can absorb CO_2 from the ambient atmosphere in amounts comparable with the mass of a sample being ground [14, 15]. In the process, the physicochemical properties of activated substances may substantially change.

It was of interest to compare specific features of structural-chemical transformations and extents to which the reactivity of perovskite and sphene increase upon MA under identical conditions in air and atmosphere of CO_2. As an additional object of study was chosen a nonore silicate, vollastonite $CaSiO_3$. Perovskite, sphene, and vollastonite constitute a series: $CaTiO_3$ (calcium titanate), $CaTiSiO_5$ (calcium compound with a complex polyanion, titanosilicate), and $CaSiO_3$ (calcium silicate). It has been shown previously that the nature of a cation (Ca, Mg) and its share in the chemical formula of a mineral are of considerable importance in mechanochemical transformations of silicates [12, 14]. A study of processes occurring in the MA of the compounds that belong to the above series will provide a better understanding of the effect of the anion on their properties and reactivity toward carbon dioxide.

Table 1. Degree of carbonization of perovskite, sphene, and vollastonite after 30 min of MA in AGO-2 in the atmosphere of CO_2 and after 36 h of grinding in a mechanical mortar in air

Mineral	CaO content of a mineral, wt %	$\Delta_r G^0$ of reactions (1)–(3), kJ	Degree of carbonization, wt % CO_2	
			after 30 min of MA in AGO-2	after 36 h of MA in a mechanical mortar
Perovskite	41.3	–(48.0 ± 3.0)	11.6 ± 0.5	10.4 ± 0.5
Sphene	28.6	–(20.1 ± 4.8)	4.8 ± 0.2	6.9 ± 0.3
Vollastonite	48.3	–(41.1 ± 4.6)	11.8 ± 0.5	11.0 ± 0.5

EXPERIMENTAL

To exclude any influence of impurity minerals present in ore concentrates, the experiments were performed with synthetic minerals. The silicate $CaSiO_3$ in the form of a high-temperature pseudovollastonite was synthesized by sintering analytically pure $CaCO_3$ and amorphous SiO_2 of the same grade (calcined to remove water at 1000°C for 12 h), taken in the stoichiometric proportion. The sintering was done at 1200°C in the course of 10 h. Prior to sintering, the mixture was thoroughly ground and compacted into pellets. To provide the full extent of the reaction, the sintering with preliminary grinding and compaction was carried out three times. According to the results of chemical and X-ray phase (XPA) analyses, the substance obtained was a single-phase product, high-temperature pseudovollastonite. Perovskite and sphene were synthesized by the same scheme, with analytically pure $CaCO_3$, amorphous SiO_2 of the same grade, and chemically pure TiO_2 used as starting reagents.

The samples were mechanically activated in an AGO-2 planetary mill [2] in air and in the atmosphere of CO_2 and in a Fritsch mechanical agate mortar (model 2) in air at room temperature and relative air humidity of 30–40%. The weighed portion of a sample in the case of grinding in a mortar was 5 g. In the case of MA in the AGO-2 mill, the ratio between the mass of balls (5 mm in diameter) and samples was 20 : 1. Prior to activation in CO_2, the drum with balls and a sample was purged for 2–3 min with a weak jet of CO_2 from a cylinder to displace air, whose density is 1.5 times lower than that of CO_2. The filling of the drum with CO_2 was repeated after every 2 min of MA.

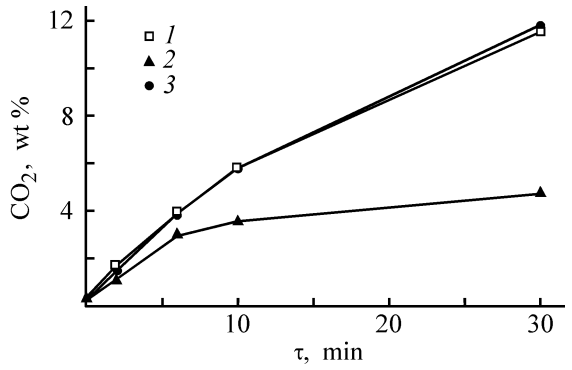

Fig. 1. Degree of carbonization with CO_2 of (*1*) perovskite, (*2*) sphene, and (*3*) vollastonite samples vs. MA duration τ in AGO-2 in the atmosphere of CO_2.

The XPA was carried out on a DRON-2 diffractometer (Cu_{K_α} radiation). IR spectra were measured in pellets with KBr on a UR-20 spectrometer. A thermal analysis was performed on an MOM derivatograph (Hungary). The weighed portion of a sample was 0.5 g, and the heating rate, 10 deg min^{-1}. The sensitivities of TG, DTA, and DTG were 200 mg, 1/5, and 1/10, respectively. The content of CO_2 in the samples was determined by the volumetric method [16] with an AN-7529 express analyzer. A weighed portion of a sample was calcined in a furnace at 1200°C, with the evolving CO_2 absorbed by a titrated solution of $Ba(OH)_2$. The amount of absorbed CO_2 was determined potentiometrically. The specific surface area of the samples was measured by the method of thermal desorption on a Flowsorb II 2300 installation (Micromeritics). Perovskite and sphene samples were decomposed with a 20% solution of HNO_3 at a temperature of 20 ± 2°C at s : l = 1 : 25 under continuous agitation in the course of 24 h.

As can be seen in Fig. 1, perovskite and vollastonite absorb CO_2 substantially more actively under mechanical activation, compared with sphene. In this case, the degrees of carbonization of perovskite and vollastonite virtually coincide (Table 1). On the whole, the result obtained confirms the previously observations [12, 14] according to which the capacity of a mineral for CO_2 absorption under MA increases with the CaO fraction in its chemical formula (Table 1). It

should be noted that, upon grinding of minerals in a mechanical agate mortar in air for 36 h, the degrees of their carbonization via absorption of atmospheric CO_2 are close to the values corresponding to 30 min of MA in pure CO_2 in a centrifugal-planetary mill (Table 1). It is noteworthy that, in the case of grinding in a mortar, the whole amount of CO_2 is absorbed by minerals directly from the atmosphere. Taking into account the amounts of the carbonate contained in the samples after 36 h of grinding, it can be stated that the selectivity of mechanically stimulated extraction of CO_2 from air, in which its content is as low as 0.03 vol %, is exceedingly high.

At the same time, it has been found previously that the degree of mechanically induced carbonization of Ca and Mg silicates is the higher, the more negative the change in the Gibbs energy of the reaction in which carbonates are formed from silicates [12]. For perovskite, sphene, and vollastonite, these reactions are written as

$$CaTiO_3 + CO_2 = CaCO_3(\text{calcite}) + TiO_2(\text{rutile}), \quad (1)$$

$$CaTiSiO_5 + CO_2 = CaCO_3 + TiO_2 + SiO_2(\alpha\text{-quartz}), \quad (2)$$

$$CaSiO_3 + CO_2 = CaCO_3 + SiO_2. \quad (3)$$

The changes in the Gibbs energy, $\Delta_r G^0$, under the standard conditions ($P^0 = 0.1$ MPa, $T = 298.15$ K), calculated for these reactions from reference data [17], are listed in Table 1. Comparison of the values of $\Delta_r G^0$ for reactions (1)–(3) with the other data in Table 1 shows that the previously found tendency is also observed for the series of minerals under consideration.

It is noteworthy that reactions (1)–(3) reflect the real process of CO_2 absorption by minerals under MA rather conditionally. It has been shown for the example of calcium- and magnesium-containing silicates that the mechanically induced sorption of CO_2 is accompanied by extensive incorporation of CO_2 molecules into the structurally disordered silicate matrix to give CO_3^{2-} groups and does not lead to formation of individual carbonate or other phases [12, 14, 15]. As shown below, XPA data demonstrate that the phases represented in the right-hand parts of Eqs. (1)–(3) are not formed, either, in the MA of perovskite, sphene, and vollastonite. Because the carbonate groups in MA minerals are supposedly associated with cations of doubly charged metals [14], the analogy between the mechanochemical processes under study and reactions similar to (1)–(3) is justified and can be used for modeling purposes. This conclusion is confirmed by the correlation between the Gibbs energies of the reactions and the extents of CO_2 absorption in the case of MA [12].

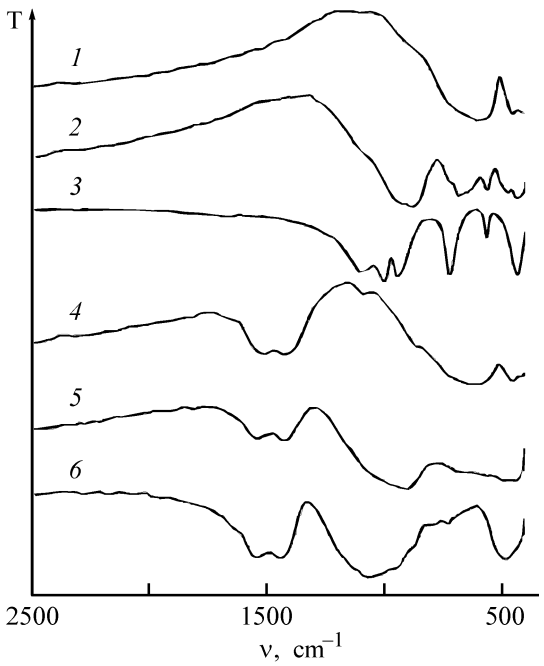

Fig. 2. IR spectra of (*1*, *4*) perovskite, (*2*, *5*) sphene, and (*3*, *6*) vollastonite samples. (T) Transmission and (ν) wave number. (*1*–*3*) Starting samples and (*4*–*6*) those after 30 min of MA in AGO-2 in the atmosphere of CO_2.

Thus, as regards the capacity of the compounds under study for CO_2 absorption under MA, two tendencies previously established for Ca and Mg silicates were confirmed. These tendencies are as follows: (i) the mechanically induced sorption capacity for CO_2 increases with the Ca(II) content and (ii) the degree of carbonization is related to the energy parameters of the reactions in which compounds are converted into carbonates. With account of the previously obtained results [12, 14], a conclusion can be made that the composition of a compound affects the amount of CO_2 absorbed by this compound under MA. The nature of the anion exerts a substantially weaker influence on the mechanochemical sorption of CO_2, compared with the nature of the cation, which is dependent on the position of a metal in the Periodic Table and on its content in the chemical formula of a mineral.

Carbon dioxide is present in activated samples in the form of carbonate ions with distorted configuration. This is indicated by the presence in the IR spectra of activated samples of a split band associated with stretching vibrations of the carbonate group at 1500 cm^{-1}, whose intensity grows with the activation time (Fig. 2). A similar band is present in the IR spec-

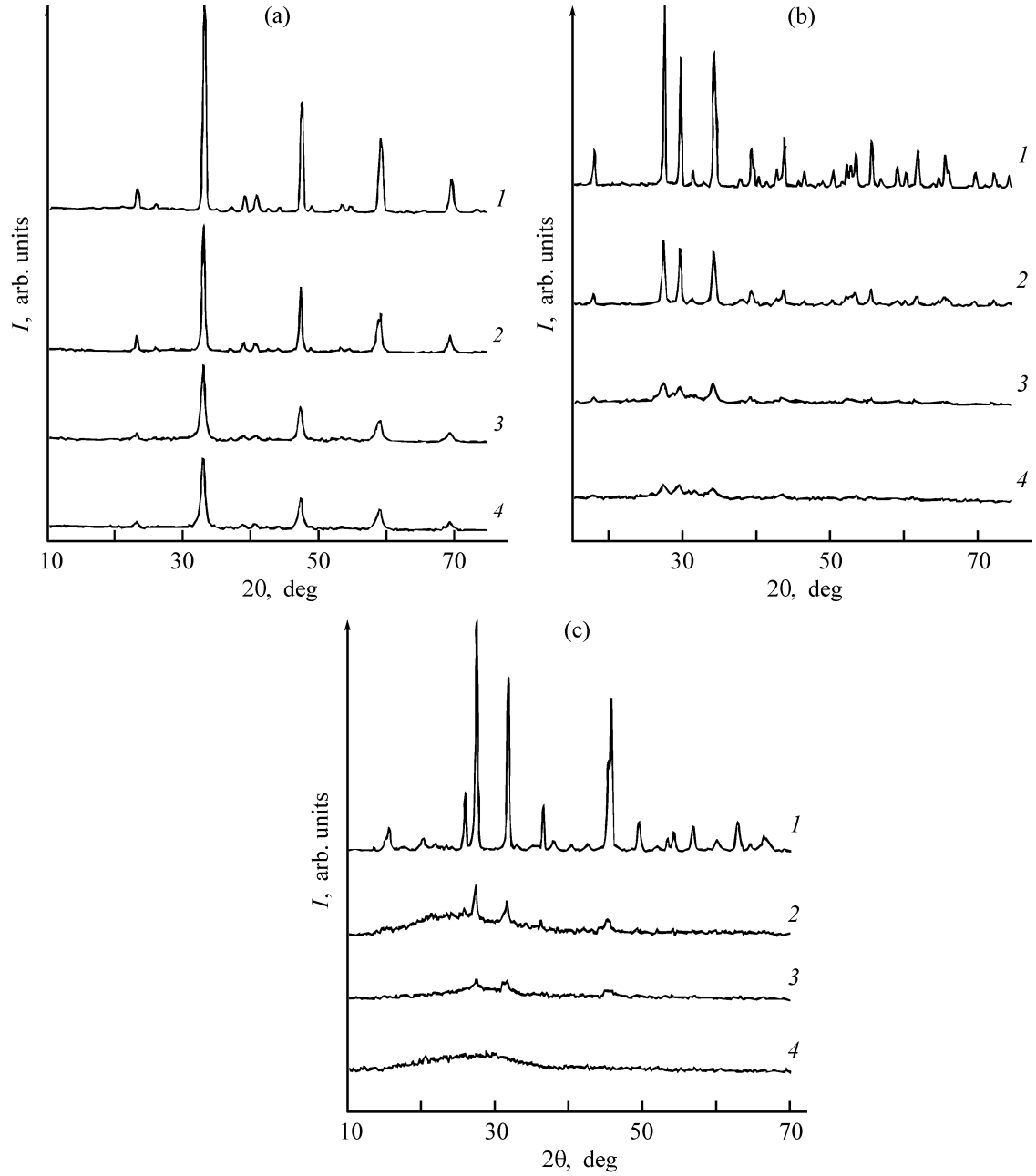

Fig. 3. X-ray diffraction patterns of (a) perovskite, (b) sphene, and (c) vollastonite samples. (*I*) Intensity and (2θ) Bragg angle. (*1*) Starting sample and (*2*, *3*, *4*) samples after MA in AGO-2 in air for 2, 10, and 30 min, respectively.

tra of MA samples of Ca and Mg silicates [12, 14, 15]. As already mentioned, the absorption of CO_2 under MA is accompanied by amorphization of a mineral and incorporation of CO_2 molecules into the disordered silicate matrix. The amorphous substance formed as a result of a mechanical treatment of the mineral in the presence of CO_2 is similar in nature to carbonate-containing glasses obtained by cooling of silicate melts of analogous composition, in which CO_2 is dissolved at high temperatures and pressures [14, 15, 18].

According to XPA data, mechanical activation of perovskite in a centrifugal-planetary mill in air for 30 min leads to a substantial decrease in the intensities of all the reflections, but no complete amorphization is observed (Fig. 3a). Structural changes in sphene and vollastonite in similar experiments are much more pronounced. After 30 min of MA in the centrifugal-planetary mill, vollastonite samples (Fig. 3c) and, to a lesser extent, those of sphene (Fig. 3b) become virtually X-ray-amorphous.

The changes occurring in minerals in the course of MA are presumably determined by specific features of their crystal chemistry. A distinctive feature of the atomic structure of perovskite is the 3D skeleton of vertex-bound Ti-octahedra, which corresponds to the $[TiO_3]^{2-}$ anion. The structure of perovskite is characterized by a cubic close-packed arrangement of oxygen atoms, with two kinds of voids, octahedral and tetrahedral. A cubooctahedral void is formed within each set of eight neighboring Ti-octahedra, in which cations may be situated [19]. A specific feature of the structure of titanium silicates, represented by sphene, consists in combinations of associations constituted by Ti-octahedra and silica tetrahedra. In the sphene structure, infinite associations of Ti-octahedra have SiO_4 orthotetrahedra as neighbors. This 3*D* structure constituted by Si-tetrahedra and Ti-octahedra with common vertices is very open-worked and contains a large number of voids and through channels. The volume of these voids is sufficiently large to accommodate big additional cations [19]. The vollastonite structure is based on an infinite narrow block constituted by three columns of Ca-octahedra. This block bears a "vollastonite" chain of Si-tetrahedra [20].

As is known, the Si–O bond in silicates is so strong that silicon and the nearest four oxygen atoms have virtually the same relative spatial arrangement in various types of structures and form a nearly regular tetrahedron. The bonds connecting structures formed by silica tetrahedra are less stable. As already noted, the perovskite structure is, in contrast to sphene and vollastonite, a very crystallochemically stable 3*D* skeleton of vertex-bound Ti-octahedra situated at sites of a cubic cell characterized by the densest packing of oxygen atoms. Presumably, it is these factors that are responsible for the noticeably higher stability of perovskite against disintegration under mechanical treatments. Under the same conditions, sphene and vollastonite exhibit substantial structural changes, with long-range order disrupted, but the primary structural unit (SiO_4 tetrahedron) remaining unchanged.

Comparison of X-ray diffraction patterns of perovskite samples activated in the AGO-2 mill in air (Fig. 3a) and in the atmosphere of CO_2 shows that the decrease in the intensity of reflections and their broadening as a result of MA in CO_2 are more pronounced, but no complete amorphization occurs under the experimental conditions. According to XPA data, the effect of the atmosphere in which grinding is performed on the degree of amorphization is not important for sphene and vollastonite. Being chemisorbed on a freshly formed surface and penetrating into the outer layers of particles to give carbonate ions, carbon dioxide can stabilize the defects forming in MA and prevent recrystallization by making faster the amorphization of a sample [21]. In the case of the perovskite lattice, which is more stable against mechanical impacts, this effect is rather clearly pronounced. Under the action of an energy-intensive mechanical treatment, the structures of sphene and vollastonite disintegrate to a very large extent and the contribution to defect stabilization via CO_2 absorption remains virtually unnoticeable for these minerals.

It should be noted that, according to XPA data, there are no reflections associated with calcium carbonates in X-ray diffraction patterns of samples of the minerals under study after MA in CO_2. At the same time, the content of the carbonate, in terms of $CaCO_3$, in perovskite and vollastonite samples subjected to 30 min of MA in a centrifugal-planetary mill in the atmosphere of CO_2 exceeds 25% according to the analytical data (Fig. 1, Table 1). Formation of amorphous calcium carbonate as a result of mechanically induced absorption of CO_2 by the minerals is hardly probable, because heating of amorphous $CaCO_3$ (produced by precipitation from aqueous solutions) is accompanied by a pronounced exothermic effect in the temperature range 200–350°C, associated with calcite crystallization [22]. According to the results of thermal (Fig. 4) and X-ray phase analyses, crystallization of calcite does not occur upon heating of mineral samples mechanically activated for 30 min in CO_2. This confirms the assumption that absorption of CO_2 molecules is accompanied by their introduction into the bulk of a structurally disordered mineral to give CO_3^{2-} ions and does not lead to formation of a carbonate as an independent phase [12, 14].

According to the thermal analysis data (Fig. 4) heating of samples subjected to 36 h of MA in a mechanical mortar first leads to removal of water present in the samples because of the absorption of atmospheric moisture in grinding. As temperature is raised further, the carbonate decomposes to give CO_2. For vollastonite and sphene, most part of CO_2 is removed in the interval 600–800°C (Figs. 4a, 4b). For perovskite, this interval is shifted by approximately 100°C to lower temperatures (Fig. 4c). The DTA curves of MA samples of vollastonite and sphene show exothermic peaks at 790 and 740°C, respectively, which correspond, according to XPA data, to crystallization of the starting material. To these temperatures also correspond, according to DTG, extrema in the rate of CO_2 removal (Figs. 4a, 4b). In contrast to sphene and vollastonite samples, the carbonate decomposes in the case of an MA perovskite a clearly

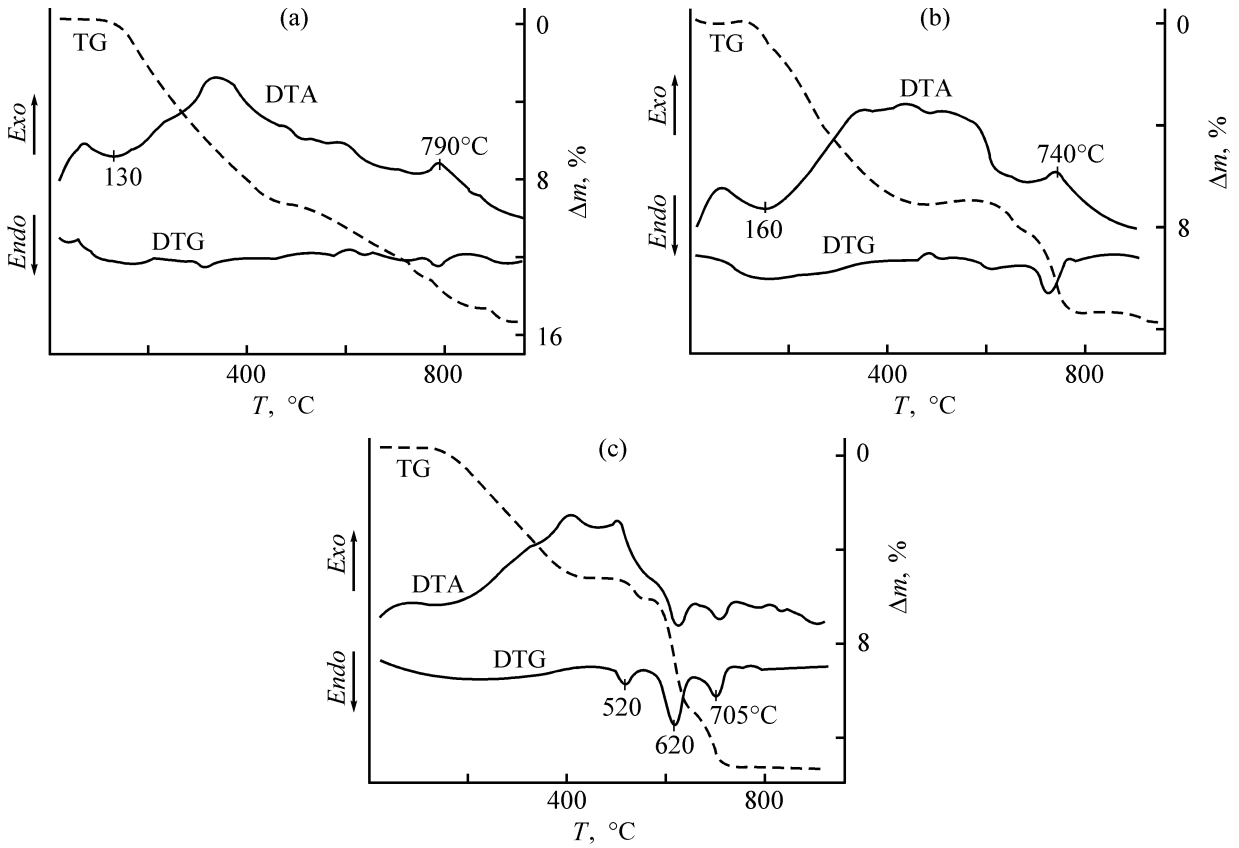

Fig. 4. Thermal analysis data for (a) vollastonite, (b) sphene, and (c) perovskite samples after 36 h of grinding in a mechanical mortar in air. (T) Temperature and (Δm) change in mass.

pronounced step-like nature. The position of the peaks and dips in the DTA and DTG curves indicates that the structure of the sample probably contains three types of CO_3^{2-} groups (Fig. 4c). According to the XPA data, heating of an MA perovskite sample in the temperature range 700–1000°C is accompanied by a gradual increase in the intensity of the reflections associated with the mineral and by a decrease in their halfwidth, but the reflection intensity is not restored completely.

Table 2. Specific surface area of perovskite, sphene, and vollastonite at different MA durations in AGO-2 in air (numerator) and in the atmosphere of CO_2 (denominator)

Mineral	S_{sp}, $m^2\ g^{-1}$, at indicated MA duration, min				
	0	2	6	10	30
Perovskite	0.4	4.9 / 4.9	5.8 / 4.8	7.7 / 5.0	16.0 / 3.4
Sphene	0.3	4.6 / 5.4	4.5 / 5.7	3.7 / 5.0	4.8 / 4.2
Vollastonite	0.3	4.9 / 5.5	4.4 / 5.1	2.2 / 2.5	2.8 / 3.2

The specific surface area of perovskite subjected to MA in air exceeds that obtained upon MA in CO_2, and this difference increases with the MA duration (Table 2). After 30 min of MA in air, S_{sp} of a perovskite sample exceeds a similar value after MA in CO_2 by a factor of 5. The dependence of the specific surface area on the MA duration for sphene and vollastonite (Table 2) is more complex, with the degree of dispersion less sensitive to the grinding atmosphere.

The physicochemical changes in perovskite and sphene upon MA are in agreement with the degree of decomposition of these minerals by a 20% solution of HNO_3 under ambient conditions. The degree of decomposition was defined as a percentage ratio of the amount of Ti(IV) that passed into solution to its content in the MA sample. It was found that the MA atmosphere does not exert any noticeable influence on the extent to which Ti(IV) passes into solution in acid treatment of mechanically activated perovskite and sphene. It is known that, at constant mass-transfer rate and temperature, the rate of heterogeneous chem-

ical processes depends both on the degree of structural distortions, which can markedly lower the activation energy, and on the phase boundary area. For sphene, both the parameters comparatively weakly depend on the type of MA atmosphere. In the case of perovskite, dispersion occurs more effectively in air (Table 2). At the same time, the degree of $CaTiO_3$ amorphization in MA in CO_2 exceeds that for MA in air. Thus, the dispersion and structural distortion factors neutralize each other in MA of perovskite in air and CO_2. As a result, the degree of acid decomposition of perovskite does not depend strongly on the MA medium.

As the time during which perovskite is activated in air increases, the degree of its acid decomposition grows from 1.6% for the starting mineral to 67% for a sample activated in a centrifugal-planetary mill for 30 min. Making the MA duration still longer (50 min) does not lead to any increase in the degree of decomposition. In the case of activation in CO_2, the situation is similar, although the degree of decomposition after 30 min of MA is somewhat lower (63%) than that after MA in air. Treatment of a sphene sample after 30 min of MA in AGO-2 with a nitric acid solution at room temperature provides a 95–98% recovery of Ti(IV) into solution. The solid residue formed upon interaction of a mechanically activated sphene with an HNO_3 solution is composed of virtually pure amorphous silica. These data are in agreement with the substantially stronger amorphization of sphene, compared with that of perovskite, in the course of MA (Figs. 3a, 3b).

CONCLUSIONS

(1) Among the minerals studied (titanate, titanosilicate, silicate), the nature of the anion exerts a considerably lesser influence on the pattern of CO_2 mechanosorption, compared with the nature of the cation, determined by the position of a metal in the Periodic Table and by its content in the chemical formula of the mineral.

(2) Structural distortions in sphene and vollastonite in mechanical activation are much more pronounced, compared with perovskite, which is due to crystallochemical features of the minerals. The medium in which the mechanical activation is performed (air or CO_2) has no effect on the degree of amorphization of sphene and vollastonite.

(3) The specific surface area of perovskite grows much faster in mechanical activation in air, compared with carbon dioxide. For sphene and vollastonite, S_{sp} is less sensitive to the dispersion atmosphere.

(4) The degree of decomposition of activated sphene and perovskite samples by nitric acid weakly depends on the type of the medium in mechanical activation. Treatment of a sphene sample after 30 min of activation in a centrifugal-planetary mill with a 20% solution of HNO_3 at room temperature provides a 95–98% recovery of Ti(IV) into solution. For a similar perovskite sample, the degree of recovery is 63–67%.

ACKNOWLEDGMENTS

The author thanks O.A. Zalkind and T.I. Makarova for help in preparation and analysis of samples.

The study was financially supported by the Russian Foundation for Basic Research (grant no. 06-03-32 198) and by the Program of Support for Leading Scientific Schools (grant no. NSh-4383.2006.3).

REFERENCES

1. Molchanov, V.I. and Yusupov, T.S., *Fizicheskie i khimicheskie svoistva tonkodispergirovannykh mineralov* (Physical and Chemical Properties of Finely Dispersed Minerals), Moscow: Nedra, 1981.
2. Avvakumov, E.G., *Mekhanicheskie metody aktivatsii khimicheskikh protsessov* (Mchanical Methods for Activation of Chemical Processes), Novosibirsk: Nauka, 1986.
3. Heinicke, G., *Tribochemistry*, Berlin: Akademie, 1984.
4. Balaz, P., *Extractive Metallurgy of Activated Minerals*, Amsterdam: Elsevier, 2000.
5. Vorobeichik, A.I., Pryakhina, T.A., Boldyrev, V.V., et al., *Izv. Sib. Otd. Akad. Nauk SSSR, Ser. Khim. Nauk*, 1979, issue 3, no. 7, pp. 37–45.
6. Vorobeichik, A.I., Pryakhina, T.A., Boldyrev, V.V., et al., *Izv. Sib. Otd. Akad. Nauk SSSR, Ser. Khim. Nauk*, 1983, issue 5, no. 12, pp. 119–125.
7. Vorobeichik, A.I., Pryakhina, T.A., and Boldyrev, V.V., *Izv. Sib. Otd. Akad. Nauk SSSR, Ser. Khim. Nauk*, 1983, issue 5, no. 12, pp. 125–130.
8. Welham, N.J. and Llewellyn, D.J., *Miner. Eng.*, 1998, vol. 11, no. 9, pp. 827–840.
9. Goroshchenko, Ya.G., *Khimiya titana* (Chemistry of Titanium), Kiev: Naukova Dumka, 1970.
10. Motov, D.L. and Maksimova, G.K., *Sfen i ego khimicheskaya pererabotka na titanovye pigmenty* (Sphene and Its Chemical Processing into Titanium Pigments), Leningrad: Nauka, 1983.
11. Kalinnikov, V.T., Nikolaev, A.I. and Zakharov, V.I., *Gidrometallurgicheskaya kompleksnaya pererabotka netraditsionnogo titano-redkometall'nogo i alyumo-*

silikatnogo syr'ya (Integrated Hydrometallurgical Processing of Unconventional Titanium–Rare-Metal and Aluminosilicate Raw Materials), Apatity: Kola Nauchn. Tsentr Ross. Akad. Nauk, 1999.

12. Kalinkin, A.M., Kalinkina, E.V., and Vasil'eva, T.N., *Kolloid. Zh.*, 2004, vol. 66, no. 2, pp. 190–197.
13. Khodakov, G.S., *Kolloid. Zh.*, 1994, vol. 56, no. 1, pp. 113–128.
14. Kalinkina, E.V., Kalinkin, A.M., Forsling, W., and Makarov, V.N., *Int. J. Miner. Process.*, 2001, vol. 61, no. 4, pp. 273–299.
15. Kalinkin, A.M., Politov, A.A., Boldyrev, V.V., et al., *Neorg. Mater.*, 2002, vol. 38, no. 2, pp. 215–220.
16. Dymov, A.M., *Tekhnicheskii analiz* (Technical Analysis), Moscow: Metallurgiya, 1964.
17. *Termicheskie konstanty veshchestv: Spravoschnik v 10-ti tomakh* (Thermal Constants of Substances: Reference Book in 10 vols.), Glushko, V.P., Ed., Moscow: VINITI, 1968–1979.
18. Kalinkin, A.M., Kalinkina, E.V., Zalkind, O.A., and Makarov, V.N., *Neorg. Mater.*, 2005, vol. 41, no. 5, pp. 566–572.
19. Pyatenko, Yu.A., Voronkov, A.A., and Pudovkina, Z.V., *Mineralogicheskaya kristallokhimiya titana* (Mineralogical Crystallochemistry of Titanium), Moscow: Nauka, 1976.
20. Deer, W.A., Howie, R.A., and Zussman, J., *Rockforming Minerals*, London: Longmans, 1962, vol. 2.
21. Politov, A.A., Kalinkin, A.M., Kalinkina, E.V., et al., *Fourth Int. Conf. on Mechanochemistry and Mechanical Alloying: Program and Abstracts*, Braunschweig, 2003, p. 125.
22. Koga, N., Nakagoe, Y., and Tanaka, H., *Thermochim. Acta*, 1998, vol. 318, no. 1–2, pp. 239–244.

ISSN 1070-4272, Russian Journal of Applied Chemistry, 2007, Vol. 80, No. 10, pp. 1621–1625. © Pleiades Publishing, Ltd., 2007.
Original Russian Text © I.P. Kremenetskaya, O.P. Korytnaya, T.N. Vasil'eva, A.T. Belyaevskii, 2007, published in Zhurnal Prikladnoi Khimii, 2007, Vol. 80, No. 10, pp. 1592–1596.

INORGANIC SYNTHESIS AND INDUSTRIAL INORGANIC CHEMISTRY

Reactions of Calcite and Dolomite with Iron(III) Sulfate Solutions

I. P. Kremenetskaya, O. P. Korytnaya, T. N. Vasil'eva, and A. T. Belyaevskii

Tananaev Institute of Chemistry and Technology of Rare Elements and Mineral Raw Materials, Kola Scientific Center, Russian Academy of Sciences, Apatity, Murmansk oblast, Russia

Received March 23, 2007

Abstract—Effect of the composition of carbonate minerals on the precipitation of iron from Fe(III) sulfate solutions under conditions of their partial neutralization with calcite and dolomite was studied.

DOI: 10.1134/S1070427207100023

Iron is the most important component of the geochemical migration of elements both in undisturbed geological systems and in regions of technologically induced abnormalities. Its sedimentary and originally sedimentary ores, as well as precipitates in the weathering crust, sedimentary rocks, and soils, are largely represented by oxide compounds. Processes of iron concentration, which formed its largest industrially important deposits, had occurred in the hypergenesis zone [1]. Data on the origin and transformation of hypergene iron oxides as possible collectors of heavy metals are of considerable interest for preventing contamination of natural water by heavy-metal compounds contained in acid drainage waters from tailing dumps, mines, and open pits by creating geochemical barriers from carbonate-containing materials [2].

Neutralization is the main method for water purification to remove metal cations forming insoluble hydroxo compounds from water. Among natural materials, calcite is the most widely used for water treatment. A large number of publications describe various methods for water treatment: multistage techniques [3], those with a solid reagent charged into a column, and a technique using a complex agent containing lime and chalk [4]. The high selectivity of calcite in removal of heavy metals has been noted [5]. Such a natural material as dolomite is used to prepare coagulants for surface water treatment. Acid wastewater can be neutralized by its filtration through a lime or dolomite filter or by addition of a finely ground reagent [6].

Because treatment of water from polluted sources and reactions of acid drainage solutions with neutralizing reagents are carried out in climatic conditions of rock weathering, the available data on the formation of iron-containing precipitates in the hypergenesis zone were analyzed. It has been noted [1] that ferrihydrite, which is a widespread hypergene mineral from the Fe(III) oxide group, plays an important part in the geochemical history of iron. It can be regarded as a typical product formed in oxidation of Fe^{2+} from underground water flowing-out at the surface, because the main condition for ferrihydryte formation is fast oxidation of Fe(II), which is rather characteristic of the Earth surface. For iron to be precipitated as ferrihydrite, a high rate of iron removal from a solution is required, and the appropriate conditions occur in reactions of dissolved Fe(III) salts with bases. The conversion of ferrihydrite to goethite in solutions of acids and alkalis consists in dissolution of an unstable phase, followed by precipitation of a substance stable under the same conditions from solution. In solutions with pH < 3, ferrihydrite is converted to goethite at room temperature.

Previously, a series of experiments on iron precipitation with calcite and dolomite from iron(II) sulfate solutions have been performed [7]. It was found that the composition and properties of iron oxohydroxides depend on numerous factors, the main of which are the reagent nature, final solution pH, and reaction duration.

Numerous studies have been devoted to the formation of Fe(III) hydrolytic precipitates. The publications earlier than 1990 were reviewed in the monograph [8]. It is commonly accepted that iron(III) exists in dilute strongly acidic solutions as $Fe(H_2O)_6^{3+}$.

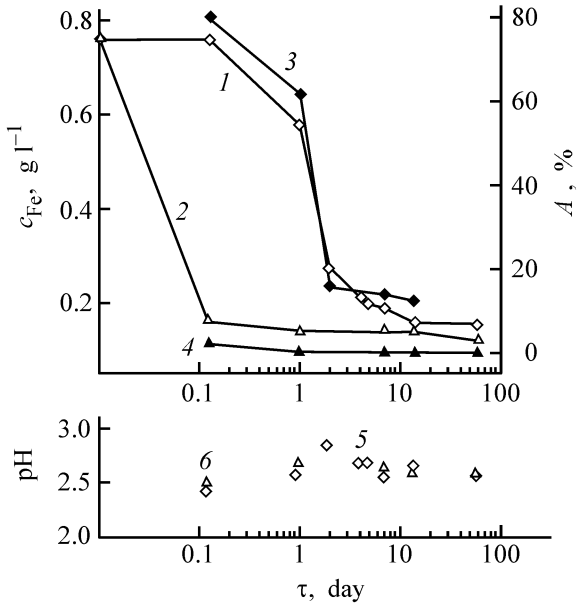

Fig. 1. (*1*, *2*) Iron concentration in solution c_{Fe}, (*3*, *4*) relative content of undissolved minerals *A*, and (*5*, *6*) pH of the suspension vs. the duration τ of reactions of (*1*, *3*, *5*) dolomite and (*2*, *4*, *6*) calcite with the $Fe_2(SO_4)_3$ solution.

The scheme of hydrolysis of Fe(III) hexaaqua complexes includes several stages: formation of equilibrium hydrolysis products, mono- and binuclear hydroxo complexes; formation of polynuclear hydrolysis products, aging of polymers with final conversion to oxide phases; and precipitation of oxide phases directly from equilibrium hydrolysis products. It is convenient to study these stages of hydrolysis in partly neutralized iron(III) solutions [9]. In the present study, we used the same methodological approach. The experiments were carried out using reagent/solution ratios smaller than necessary for complete transformation of iron aqua complexes to hydroxo species.

The aim of the study was to examine the effect of the composition of neutralizing minerals on the iron precipitation from iron(III) sulfate solutions. Such process is not observed in real conditions, but its experimental study will allow us to distinguish two parallel processes, Fe(II) → Fe(III) oxidation and formation of oxohydroxides.

EXPERIMENTAL

Marbled calcite $CaCO_3$ from the Koelga deposit (Chelyabinsk oblast) and dolomite $CaMg(CO_3)_2$ from the Titan deposit (Murmansk oblast) were used in the study. Rock samples were crushed in a porcelain mortar, and a fraction with particle size smaller than 70 μm was taken for the experiments. Source solutions with an iron concentration of 0.76 g l^{-1} were prepared from chemically pure $Fe_2(SO_4)_3 \cdot 7H_2O$ and distilled water. The experiments were carried out with agitation by a magnetic stirrer under conditions of easy air access.

Changes in the iron concentration in solution in reactions with neutralizing reagents were determined by the method of separate weighed samples. The dissolution of minerals was monitored by X-ray analysis of the precipitates composed of iron compounds and the undissolved part of a reagent. The extent of reagent dissolution was calculated from the results of a chemical analysis of the solutions. The properties of the precipitated phase were studied by crystal-optical, X-ray, and electron microscopic (SEM LEO 420 microscope) analyses.

The dependences of the iron concentration in solutions on the reaction duration in the systems with calcite and dolomite are shown in Fig. 1. Despite that the pH values of the suspensions formed are virtually equal, the kinetic curves of iron precipitation by various carbonate-containing reagents are strongly different. In the presence of calcite, the degree of solution purification in 3 h is 82% and changes only slightly as the precipitation duration increases, whereas an induction period is observed in the experiments with dolomite. After 14 days, the residual iron concentrations obtained in reactions of the source solution reactions with calcite and dolomite differ only slightly. The degree of iron precipitation varies in parallel with that of reagent dissolution.

The experimental data obtained demonstrate that the chemical composition of a reagent exerts strong influence on the formation of an iron-containing precipitate, with the main factor that affects the iron precipitation being the dissolution rate of minerals. Let us consider calcite and dolomite properties that are related to their reactivity.

First, it is necessary to note that calcite and dolomite have different crystal structures. As shown by morphological studies, calcite is characterized by a high polydispersity of samples, caused by the presence of small pebbles of the mineral, and a friable branched surface of particles (Figs. 2a and 2b), whereas dolomite particles are dense and smooth with a cleaved surface in the form of a conchoidal fracture (Figs. 2c and 2d). These features of the minerals should lead to a larger specific surface area and higher porosity of calcite, compared with dolomite, which is confirmed by the following data. The results obtained in determining the porosity of dolomite and calcite samples used in this study are presented in the mono-

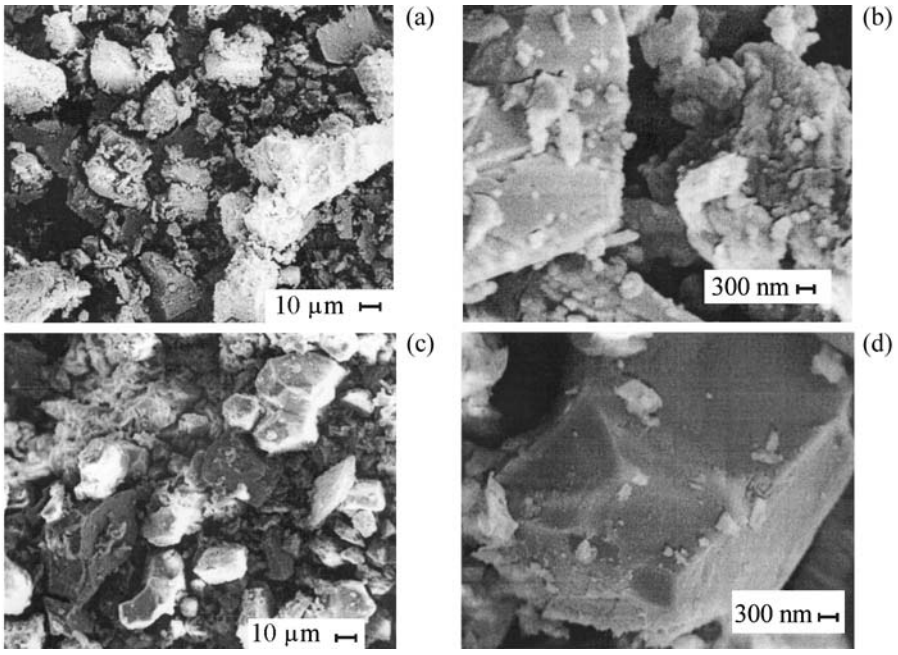

Fig. 2. Micrographs of the initial surface of (a, b) calcite and (c, d) dolomite particles.

graph [10]. The Koelga marble is distinguished by large average pore size (7.1 μm). The porosity of the dolomite marble is mainly associated with pores 0.01–0.03 μm in size. A high short-term water adsorption was also noted for calcite marble, which is due to its mesocrystalline structure. The specific surface area of mineral samples used in the study was determined by the method of low-temperature nitrogen adsorption. The specific surface area of calcite (1.57 $m^2 g^{-1}$) is almost five times that of dolomite (0.34 $m^2 g^{-1}$).

Thus, calcite is dissolved more rapidly, primarily because of its more developed surface area. It can be assumed that the difference in reactivity between the minerals may also be of certain importance. Dolomite is known to be less chemically active than calcite. In particular, dolomite is poorly dissolved in cold dilute acids and does not foam. In addition, when a solution of copper nitrate is used, calcite turns intense light blue due to azurite formation, whereas dolomite does not enter in the reaction, and its color remains unchanged [11].

To understand why the calcite and dolomite properties are strongly different, we examined the results of quantum-mechanical calculations reported in [12]. An estimation of the surface energy of crystal faces of minerals demonstrated that the energy characteristics of the $10\bar{1}1$, $10\bar{1}4$, and 0001 faces are comparable, whereas for the $10\bar{1}1$ and $11\bar{2}0$ faces, the surface energy of dolomite crystals is 5–9 times lower than that of calcite crystals. These specific features of the minerals result in that calcite has a higher reactivity than dolomite in chemical reactions accompanied by dissolution of the starting solid phase.

The data in Table 1 confirm that calcite is dissolved more rapidly than dolomite. It follows from these data that dolomite neutralizes the acid to markedly lesser extent than calcite does. It also follows from the experimental data that hydroxide ions formed in dissolution of minerals are almost completely bound in the $Fe_2(SO_4)_3$ solution to form hydroxo complexes of iron.

A calculation of the OH/Fe ratio in the experiments with calcite demonstrated that, for the systems under consideration, its value is substantially lower than 0.5. In this range of OH/Fe ratios, the time elapsed before precipitation onset rapidly decreases as this ratio increases [13]. Because the instant of time when minerals are added is characterized by a more intense neu-

Table 1. pH values of calcite and dolomite suspensions (reaction duration 10 min)

Source solution, pH value	pH value of mineral suspensions	
	calcite	dolomite
H_2SO_4, 2.2	5.7	2.5
$Fe_2(SO_4)_3$, 2.5	2.9	2.5

Table 2. Influence of magnesium on iron precipitation by calcite

Reaction duration, days	Calcite		Calcite + $MgSO_4$	
	pH	c_{Fe}, g l^{-1}	pH	c_{Fe}, g l^{-1}
0.01	2.75	0.206	2.78	0.204
0.125	2.75	0.170	2.79	0.181
1	2.92	0.293	3.00	0.280
2	2.77	0.231	2.86	0.246
4	2.84	0.162	2.86	0.165
5	2.71	0.140	2.81	0.165
7	2.68	0.126	2.73	0.146
14	2.62	0.117	2.70	0.138

tralization of the $Fe_2(SO_4)_3$ acid solution by calcite, compared with dolomite, this results in a shorter time before the beginning of iron precipitation in presence of calcite.

The data obtained can be explained by using the model of iron hydrolysis in partly neutralized solutions at OH/Fe < 0.5 [9, 13, 14]. A slow hydrolysis of the originally formed species occurs to give protons, whose neutralization shifts, owing to the dissolution of carbonates, the equilibrium toward the precipitate formation, and proceeds to complete dissolution of the active part of the reagents.

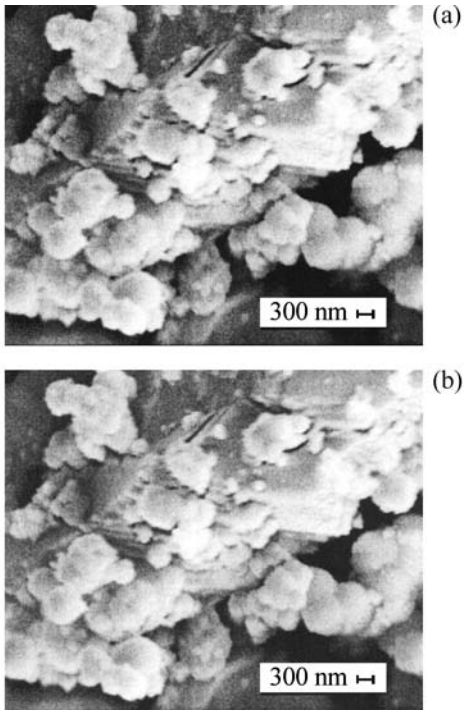

Fig. 3. Micrographs of particles of oxohydroxides precipitated from an iron(III) sulfate solution in the presence of dolomite at a reaction duration of (a) 24 h and (b) 5 days.

Dolomite contains magnesium, whose presence in solution can affect the formation of an iron-containing precipitate. Magnesium is known to have an inhibiting effect on crystallization of, e.g., calcite. As a rule, various mechanisms of the influence of magnesium are considered [15]. We can assume that magnesium cations can be adsorbed on faces of a calcite crystal thereby hindering its growth, or can be incorporated into the crystal lattice of calcite, which yields a more soluble magnesian calcite.

To elucidate the mechanism of the influence exerted by magnesium on the iron precipitation, we performed two series of experiments. In the first of these, calcite was added to a $Fe_2(SO_4)_3$ solution, and in the second, calcite and magnesium sulfate (Table 2). It can be seen from Table 2 shows that magnesium exerts significant influence neither on the rate of iron precipitation, nor on the dependence of the residual iron concentration on pH.

The morphologies of particles of the precipitates obtained in the reactions of iron(III) sulfate solution with calcite and dolomite do not differ from each other, being identical to that of ferrihydrite [1]. Micrographs of precipitates with particle size ranging from several hundred nanometers to 1–2 μm, obtained in the system with dolomite, are shown in Fig. 3. After a one-day reaction, ferrihydrite particles have a spherical shape with a smooth surface, being predominantly precipitated on active nonuniform areas of the mineral crystals. Unreacted dolomite particles with continuous and discontinuous fringes of a newly formed phase along their contour were detected by crystal-optical analysis. As the keeping duration increases to five days, very fine crystals are formed on the surface of the spheres, and elongated crystals are observed in the bulk of the precipitate.

A similar process was observed in [1], where it was found that ferrihydrite is slowly transformed to goethite in moderately acidic iron(II) solutions, and faster, in iron(III)-containing solutions at pH < 3, which is accounted for by the difference in the existence forms of iron. The conversion of ferrihydrite to goethite is a process in which the unstable phase formed upon incorporation of additional iron ions into the lattice of the starting ferrihydrite is dissolved, with the subsequent precipitation of a substance stable under the same conditions [1]. The transformation of the amorphous phase transformation becomes slower in solutions that contain no free iron cations [16]. Because free Fe(III) cations exist only in strongly

acidic solutions, the crystalline phase can be formed from ferrihydrite at pH < 3, which is also observed in partial neutralization of a $Fe_2(SO_4)_3$ solution with carbonate minerals.

CONCLUSIONS

(1) It was found that, upon addition of carbonate minerals to a $Fe_2(SO_4)_3$ solution, neutralization of the acid solution with calcite is faster than that with dolomite. This results in a shorter time before the onset of iron precipitation in the presence of calcite. The slow hydrolysis of the originally formed particles is accompanied by release of H^+ ions, whose neutralization due to the dissolution of carbonates shifts the equilibrium toward precipitate formation, and continues to complete dissolution of the active part of the reagents.

(2) The presence of magnesium in solutions exerts strong influence neither on the rate of iron precipitation, nor on the dependence of residual iron concentration on pH.

(3) Under the conditions of neutralization of $Fe_2(SO_4)_3$ solutions with carbonate minerals, iron precipitates in the form of amorphous compounds. As the reaction duration increases, a crystalline phase is formed in the systems studied.

REFERENCES

1. *Gipergennye oksidy zheleza v geologicheskikh protsessakh* (Hypergene Iron Oxides in Geological Processes), Petrovskaya, N.V., Ed., Moscow: Nauka, 1975.
2. Pestrikov, S.V., Isaeva, O.Yu., and Mustafin, A.G., *Inzhenernaya Ekologiya*, 2006, no. 2, p. 8.
3. *Tekhnika zashchity okruzhayushchei sredy* (Technology of Environment Protection), Torocheshnikov, N.S., Rodionov, A.I., Kel'tsev, N.V., and Klushin, V.N., Eds., Moscow: Khimiya, 1981.
4. Schilling, H. and Fischwasser, K., *Acta Hydrochim. Hydrobiol.*, 1989, vol. 17, no. 6, pp. 673–680.
5. Lupeiko, T.G., Gorbunova, M.O., and Bayan, E.M., *Zh. Prikl. Khim.*, 2004, vol. 77, no. 1, p. 83.
6. Godymchuk, A.J. and Il'in, A.P., *Khim. Tekhnol. Vody*, 2004, vol. 26, no. 3, p. 287.
7. Makarov, D.V., Makarov V.N., Kalinkina, E.V., et al., Available from VINITI, 2003, no. 2008-V2003.
8. Pechenyuk, S.I., *Sorbtsionno-gidroliticheskoe osazhdenie platinovykh metallov na poverkhnosti neorganicheskikh sorbentov* (Sorption-Hydrolytic Precipitation of Platinum Metals on the Surface of Inorganic Sorbents), Leningrad: Nauka, 1991.
9. Pykhteev, O.Yu. and Efimov, A.A., *Zh. Neorg. Khim.*, 1999, vol. 44, no. 4, p. 549.
10. Lashchuk, V.V., *Dolgovechnost' oblitsovochnogo kamnya Kol'skogo poluostrova* (Longevity of Facing Stone from Kola Peninsula), Apatity: Kola Nauchn. Tsentr, Ross. Akad. Nauk, 1996.
11. Deer, W.A., Howie, R.A., and Zussman, J., *Rock-Forming Minerals*, London: Longmans, 1962, vol. 5.
12. Titiloye, J.O., Leeuw, N.H., and Parker S.C., *Geochim. Cosmochim. Acta*, 1998, vol. 62, no. 15, p. 2637.
13. Kalyamin, A.V. and Bazalii, V.N., *Zh. Neorg. Khim.*, 1979, vol. 24, no. 4, p. 1117.
14. Pykhteev, O.Yu. and Efimov, A.A., *Zh. Neorg. Khim.*, 1998, vol. 43, no. 7, p. 1113.
15. *Carbonates: Mineralogy and Chemistry, Reviews in Mineralogy*, Reader, R.J., Ed., Washington, DC: Mineralogical Society of America, 1983.
16. Pechenyuk, S.I., Mikhailova, N.L., Kuz'mich, L.F., et al., *Zh. Neorg. Khim.*, 2003, vol. 48, no. 8, p. 1255.

ISSN 1070-4272, Russian Journal of Applied Chemistry, 2007, Vol. 80, No. 10, pp. 1626–1631. © Pleiades Publishing, Ltd., 2007.
Original Russian Text © Yu.I. Orlov, A.S. Brykov, 2007, published in Zhurnal Prikladnoi Khimii, 2007, Vol. 80, No. 10, pp. 1597–1602.

INORGANIC SYNTHESIS AND INDUSTRIAL INORGANIC CHEMISTRY

Dehydration of Aluminophosphate Solutions in a Microwave Field

Yu. I. Orlov and A. S. Brykov

Grebenshchikov Institute of Silicate Chemistry, Russian Academy of Sciences, St. Petersburg, Russia
St. Petersburg State Technological Institute, St. Petersburg, Russia

Received July 6, 2006

Abstract—Dehydration of solutions of aluminophosphate binders in a microwave field to obtain aluminophosphate powders of various compositions is considered. The effect of drying conditions and of the chemical composition of aluminophosphate binders on the phase composition and solubility of the products obtained is analyzed.

DOI: 10.1134/S1070427207100035

Aluminophosphate binders (APB) are aqueous solutions of aluminum phosphates with various degrees of substitution, being inorganic polymers in the systems Al_2O_3–P_2O_5–H_2O and Al_2O_3–M_2O_3–P_2O_5–H_2O (where M_2O_3 = Cr_2O_3, B_2O_3) [1, 2]. Aluminophosphate binders are produced by reacting H_3PO_4, $Al(OH)_3$, and modifying additives, Cr_2O_3 and B_2O_3, and used in manufacture of high-temperature materials (refractory and heat-resistant concretes, glues, and sealing compounds) and coatings [3] and electrically insulating formulations [4].

A disadvantage of APB is their low stability in storage. Development of crystallization processes entails a comparatively fast formation (in several months) of a precipitate of insoluble aluminum phosphates. This impairs the properties of materials produced with APB and occasionally makes their use impossible [1].

A possible way to improve the stability of APB is their manufacture in the form of water-soluble powders. For this purpose, it is necessary to dry the binder immediately after its synthesis, to obtain a product with moisture content providing a reversible dissolution. The partly dehydrated state of a binder can provide stability of its properties in the course of time [1].

Examples are known ob obtaining powdered APB by spraying drying [1, 5, 6]. However, use of a heat carrier with high temperature (up to 700°C) [7, 8] may change the properties of APB because of its excessive dehydration.

In this study, the method of microwave drying was employed to dry aluminophosphate solutions. The use of microwave electromagnetic radiation to heat a solution being dehydrated can create milder, compared with those in spraying drying, conditions of the process at comparatively low temperatures (up to 200–300°C) and minimum process duration. In particular, it has been shown that this method is efficient in production of hydrated sodium silicates by dehydration of liquid-glass binder solutions [9, 10].

EXPERIMENTAL

Aluminophosphate binders were produced by dissolution of $Al(OH)_3$ [analytically pure grade, GOST (State Standard) 11841–76] with heating and agitation in a 55–60% solution of H_3PO_4 (GOST 6552–80) in accordance with the recommendations made in [1, 11]. The resulting aluminophosphate solutions were modified by introduction of B_2O_3 in the form of H_3BO_3 [analytically pure grade, TU (Technical Specification) 6-09-17-263–89] and Cr_2O_3 in the form of CrO_3 (analytically pure grade, GOST 3776–78), with the subsequent reduction of CrO_3 with a stoichiometric amount of H_2O_2 (GOST 10929–76) in accordance with the equation

$$4CrO_3 + 8H_2O_2 + 12H^+ \rightarrow 4Cr^{3+} + 14H_2O + 7O_2\uparrow. \quad (1)$$

Chemical composition of aluminophosphate solutions

Run no.	Content of indicated components in a binder solution, wt %					$P_2O_5/(Al_2O_3+Me_2O_3)$, mol/mol	$Al_2O_3/(Al_2O_3+Me_2O_3)$, mol/mol
	P_2O_5	Al_2O_3	Cr_2O_3	B_2O_3	$P_2O_5 + Al_2O_3 + Me_2O_3$		
1	37.12	10.67	–	–	47.79	2.5	1.0
2	38.63	8.67	–	–	47.30	3.2	1.0
3	35.48	7.28	–	–	42.76	3.5	1.0
4	35.90	7.37	2.74	–	46.01	2.8	0.8
5	38.02	7.80	–	1.33	47.15	2.8	0.8

The parameters of the thus prepared aluminophosphate solutions are listed in the table.

A Sanyo household microwave oven operating at a frequency of 2450 MHz served as a source of microwave radiation. The solutions were dehydrated at a fixed output power of about 450 W.

A solution to be dried (weighed portion 100 h) in a $88 \times 62 \times 28$-mm fluoroplastic cuvette (solution layer thickness not exceeding 5 mm) was placed in the chamber of a microwave oven. The drying process was controlled by varying the duration of sample heating in the microwave field. Then, the cuvette with a sample was removed from the microwave oven and cooled in air at room temperature (20°C). The cooling rate was about 15–20 deg min^{-1}.

The residual moisture content of the drying products was found from the calcination loss at 800°C.

Because the aluminophosphate solutions synthesized contained different amounts of moisture, it was appropriate to consider, in order to compare the moisture removal rates, the dehydration curves in dimensionless variables: relative mass of removed water, w_{red}, and reduced drying time τ_{red} [10]:

$$w_{red} = \frac{w_\tau(H_2O)[1 - w(H_2O)_{in}]}{w(H_2O)_{in}[1 - w_\tau H_2O]}, \quad (2)$$

where $w_\tau(H_2O)$ is the moisture content of the product at instant of time τ (wt %) and $w(H_2O)_{in}$ is the moisture content of the starting solution (wt %).

The quantity w_{red} characterizes the amount of evaporated water relative to the initial amount of H_2O in the system.

$$\tau_{red} = \tau P/[mrw(H_2O)_{in}], \quad (3)$$

where τ is the drying time (s); m, solution mass (kg); r, specific heat of water evaporation (2256 kJ kg^{-1}); and P, microwave power (W).

For potentiometric measurements, 10% solutions were prepared from the dehydration products. The measurements were made with a laboratory pH-meter of the 673M type with a glass electrode at 20°C.

X-ray diffraction patterns of powder samples were recorded with a DRON-1 X-ray diffractometer (Cu_{K_α}). IR spectra were measured in KBr pellets on a UR-20 spectrophotometer.

A microwave treatment of aluminophosphate solutions for 4–5 min yielded a transparent melt that solidifies upon cooling as a brittle solid glassy mass. In some cases, a white nontransparent glassy mass was formed after a thermal treatment. If the drying duration was raised to more than 5–6 min, the mass swelled, with its volume becoming 2–3 times larger.

In the course of a microwave treatment of aluminophosphate solutions, the sample temperature increased to 250–280°C. This points to a strong absorption of the microwave radiation by aluminophosphate solutions, which is apparently due to the mostly orientational polarization of water molecules and to the ionic conduction by hydrated aluminum ions and phosphate ions, with the contribution of the ionic conductivity increasing as the system is dehydrated and its temperature increases [12].

Figures 1a and 1b show the kinetics of dehydration of aluminophosphate solutions in a microwave field. It follows from the data obtained that the dehydration curves have a rather typical shape: the rate is constant during the initial period; beginning with a certain value, the dehydration rate decreases and w_{red} tends to a constant value (~0.9).

The chemical composition of aluminophosphate solutions affects the dehydration process. For example, an increase in the content of aluminum oxide (a decrease in the P_2O_5/Al_2O_3 ratio) in a solution leads to a rise in the dehydration rate (Fig. 1a). The lowest dehydration rate is observed for a solution of H_3PO_4

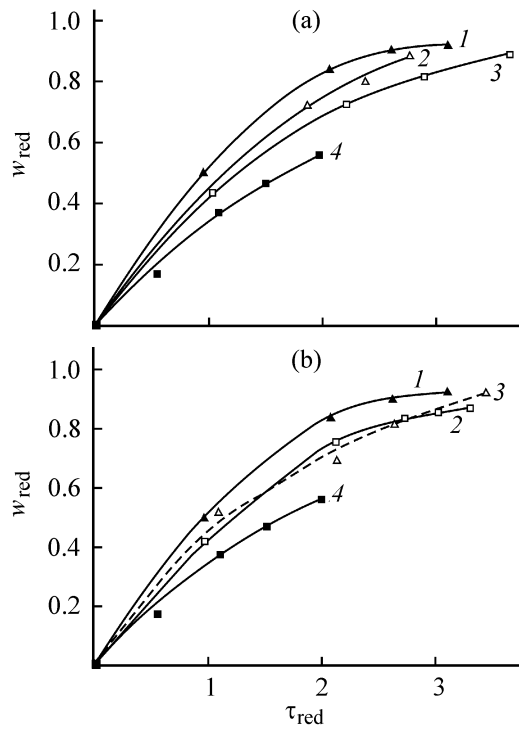

Fig. 1. Dehydration kinetics of solutions of aluminophosphate binders of various compositions and orthophosphoric acid, plotted in dimensionless variables. (w_{red}) Relative mass of removed water and (τ_{red}) reduced drying duration. (a) (*1*) $2.5P_2O_5 \cdot Al_2O_3$, (*2*) $3.2P_2O_5 \cdot Al_2O_3$, (*3*) $3.5P_2O_5 \cdot Al_2O_3$, and (*4*) 47% solution of H_3PO_4. (b) (*1*) $2.5P_2O_5 \cdot Al_2O_3$, (*2*) $2.8P_2O_5 \cdot 0.8Al_2O_3 \cdot 0.2B_2O_3$, (*3*) $2.8P_2O_5 \cdot 0.8Al_2O_3 \cdot 0.2Cr_2O_3$, and (*4*) 47% solution of H_3PO_4.

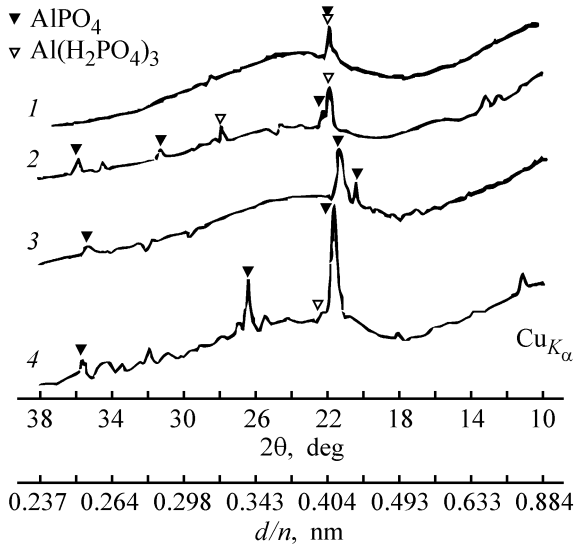

Fig. 2. X-ray diffraction patterns of powdered aluminophosphate binders. (2θ) Bragg angle and (*d*/*n*) interplanar spacing. Sample composition, w_{H_2O} (wt %), and drying time (min), respectively: (*1*) $3.5P_2O_5 \cdot Al_2O_3$, 21, 6; (*2*) $3.2P_2O_5 \cdot Al_2O_3$, 20.8, 5; (*3*) $3.2P_2O_5 \cdot Al_2O_3$, 10.5, 6.5; and (*4*) $2.5P_2O_5 \cdot Al_2O_3$, 7.0, 7.

(Fig. 1a, curve *4*). If Al_2O_3 is partly replaced with Cr_2O_3, the dehydration curve is virtually identical in its initial portion to that for an aluminophosphate solutions of a similar composition (Fig. 1b; curves *1*, *3*); further, the rate becomes somewhat lower. However, the final moisture contents of both products are virtually the same. Introduction of an equivalent amount B_2O_3 into the solution (aluminoborophosphate binder) makes the entire drying process slower (Fig. 1b, curve *2*).

This run of the dehydration curves can be attributed to differences in the acid-base properties of the oxides contained in APB. The presence of B_2O_3 in the system is equivalent to an increase in the P_2O_5 ratio and makes lower the basicity of the solution: the dehydration curve of a aluminophosphate solution modified with B_2O_3 (Fig. 1b, curve *2*) approaches the curve for orthophosphoric acid (curve *4*). Probably, a factor leading to the increase in the acidity of the system in this case is the possibility of formation of complex acids in a reaction between boric and phosphoric acids [13]. In addition, a stronger amorphization of the product formed in thermal treatment of aluminophosphates is observed in the presence of B_2O_3 [14], which may also make lower the rate of moisture removal from the solution.

The effect of chromium(III) oxide on the course of dehydration is comparable with that of aluminum oxide, because the rate of moisture removal from the aluminochromophosphate binder is rather high and approaches that for aluminophosphate solutions (Fig. 1b; curves *1*, *3*). Chromuim(III) oxide contained in an aluminophosphate binder manifests itself as a basic oxide and is analogous in this regard to aluminum oxide, whose higher content in a solution makes the dehydration faster.

Figure 2 shows the results of an X-ray phase analysis of the dehydration products, according to which the composition of all the samples is mostly represented by an amorphous phase, which follows from the clearly pronounced halo, characteristic of glassy materials. However, depending on the thermal treatment duration and chemical composition of the starting solution, samples contain different amounts of crystalline phases corresponding to aluminum phosphates with various degrees of substitution. As the drying duration increases and the P_2O_5/Al_2O_3 molar ratio decreases, the content of crystalline phases in the samples grows.

The X-ray diffraction patterns (Fig. 2) of products obtained at short drying duration (5 min) are dominated by lines corresponding to aluminum dihydro-

phosphates (0.408, 0.321 nm). As the drying duration increases, there appear or become markedly stronger lines characteristic of aluminum orthophosphate (0.428, 0.417, 0.402, 0.331, 0.251 nm) and the analytical lines in the X-ray diffraction patterns change their position. The intensities of the lines corresponding to aluminum dihydrophosphate decrease and they are gradually replaced by lines associated with various modifications of aluminum orthophosphate. This indicates that aluminum dihydrophosphate decomposes in the course of thermal treatment and the fraction of aluminum orthophosphate in the product being dried gradually increases, in agreement with the pattern of phase transformations of aluminophosphates, described in [4, 14, 15].

The change in the phase composition of the products formed in drying of aluminophosphate solutions affects the solubility in water of the products obtained. An increase in the drying duration, accompanied by crystallization processes in the bulk of the product being dried, impairs its solubility in water. This is presumably because, in contrast to aluminum dihydrophosphate readily soluble in water, aluminum orthophosphate is virtually water-insoluble. The powders obtained at drying durations of up to 5 min are rather easily and virtually completely soluble in water. As the drying duration increases, only partial solubility is observed and an insoluble crystalline precipitate is present in a solution even upon a prolonged heating.

In the experiments, the variation of the pH value of the liquid phase was recorded in the course of dissolution of the aluminophosphate powder in water. The deviation from the pH value corresponding to the starting solution of the binder and the kinetics of pH variation indicate a reversible solubility of the product in water [1] i.e., the regenerated binder solution (obtained by dissolution of an aluminophosphate powder) and the starting solution not subjected to dehydration are identical.

Figure 3 shows the kinetics of variation of the pH value in the course of dissolution of aluminophosphate powders in water. According to these data, the product obtained by drying an APB solution for 5 min, with a water content of 20.8 wt % (w_{red} = 0.72), rather rapidly passes into a solution. In the process, the intensive hydrolysis of the solid phase in the initial period results in that the pH value approaches (curve *1*) the pH of a H_3PO_4 solution of equivalent concentration (1.85, curve *4*). The complete dissolution of the product is only achieved on heating the solution, with the pH value of the regenerated aluminophosphate solution equal to 2.1 (curve *3*). In may be noted,

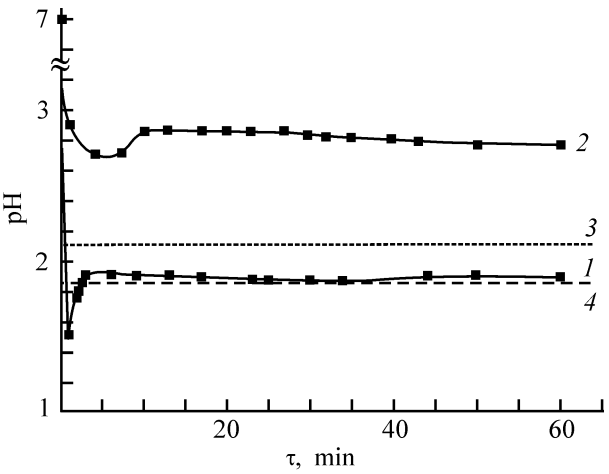

Fig. 3. Kinetics of pH variation in the course of dissolution of powder-like aluminophosphate binders (APB) in water. (τ) Time. APB composition, w_{H_2O} (wt %), and drying time (min), respectively: (*1*) $3.2P_2O_5 \cdot Al_2O_3$, 20.8, 5; (*2*) $3.2P_2O_5 \cdot Al_2O_3$, 10.5, 6.5. pH value: (*3*) ABP solution after complete dissolution of the $3.2P_2O_5 \cdot Al_2O_3$ powder, w_{H_2O} = 20.8 wt %, drying time 5 min; (*4*) 10% solution of orthophosphoric acid.

for comparison, that the pH of the starting binder solution of an equivalent concentration is 2.25.

The pH value of a solution of an aluminophosphate powder with a moisture content of 10.5 wt % (w_{red} = 0.88), produced by drying for 6.5 min, is substantially higher, 2.7–2.9, and shows a certain tendency to decrease (Fig. 3, curve *2*). However, complete dissolution is not achieved even upon prolonged drying and an insoluble precipitate is present in the solution.

These differences in solubility indicate that the dissolution of the products obtained is incongruent because of the hydrolysis of aluminophosphate in the initial stage of dissolution. The occurrence of this process is manifested in a clearly pronounced decrease in the pH value in the initial period (5–10 min) of contact between the liquid and solid phases (Fig. 3; curves *1*, *2*). In this case, a strong opalescence of the solution is visually observed, which disappears after several minutes of contact between the solution and the powder (the process is accelerated by heating and agitation.

The hydrolysis of aluminophosphates (analyzed for the example of aluminum dihydrophosphate) occurs in stages and is reversible:

$$Al(H_2PO_4)_3 + 6H_2O \rightleftarrows [Al(H_2O)_6]^{3+} + 3H_2PO_4^-, \quad (4)$$

$$[Al(H_2O)_6]^{3+} \rightleftarrows [AlOH(H_2O)_5]^{2+} + H^+, \quad (5)$$

$$[AlOH(H_2O)_5]^{2+} \rightleftarrows [Al(OH)_2(H_2O)_4]^+ + H^+. \quad (6)$$

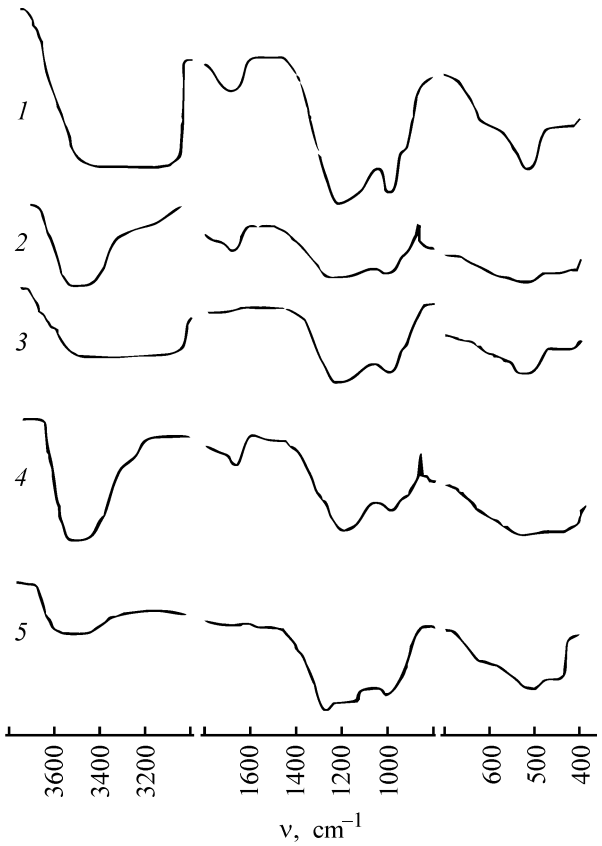

Fig. 4. IR transmission spectra of aluminophosphate solutions and powders. (ν) Wave number. APB: (*1*, *4*) starting solution, (*2*, *5*) powder, and (*3*) APB solution obtained by dissolution of the powder (sample no. 2). Composition: (*1*, *2*) $3.5P_2O_5 \cdot Al_2O_3$ and (*4*, *5*) $2.5P_2O_5 \cdot Al_2O_3$. w_{H_2O} (wt %): (*1*) 55; (*2*) 25.4, drying time 5 min; (*4*) 50; and (*5*) 7.0, drying time 7 min.

The occurrence of reactions (5) and (6) leads to a decrease in the solution pH, observed in the initial stage of dissolution of aluminophosphates. Subsequent keeping of a solution, and especially its heating, lead to occurrence of these reactions in the reverse direction, which is reflected in that the pH increases to values corresponding to the starting binder solution (Fig. 3).

When considering the influence exerted by the composition of aluminophosphates on their solubility, it should be noted that the solution formed in dissolution of products with a P_2O_5/Al_2O_3 ratio smaller than 3.5 is virtually always turbid and contains a crystalline precipitate. A decrease in the P_2O_5/Al_2O_3 molar ratio leads to an increase in the amount of the undissolved precipitate. The powders whose composition corresponds to a P_2O_5/Al_2O_3 ratio of 3.5 and more are completely dissolved to give transparent solutions without any precipitate.

This behavior is correlated with the dependence of the structure of the starting aluminophosphate solutions on their chemical composition, and primarily on the molar ratio between P_2O_5 and Al_2O_3. For example, it was noted in [16] that, at P_2O_5/Al_2O_3 molar ratios exceeding 3.4, aluminophosphate solutions are true solutions. At P_2O_5/Al_2O_3 smaller than 3.4, colloid formations appear in solutions.

If it is assumed that glass formation occurs in drying of an aluminophosphate binder because of the "freezing" of the structure of the starting solution [17], then dehydration of true aluminophosphate solutions ($P_2O_5/Al_2O_3 \geq 3.4$) will give glassy water-soluble products. Presence of colloid formations (at $P_2O_5/Al_2O_3 < 3.4$) that can serve as crystallization nuclei should enhance crystallization processes and favor an increase in the content of crystalline phases in the products formed in dehydration of binder solutions, just which is confirmed by the data obtained.

An IR spectroscopic study of the aluminophosphate products demonstrated (Fig. 4) that the IR spectra of both solutions and powders contain a number of broad bands in the region of stretching vibrations of hydroxyl groups (3580, 3300 cm^{-1}) and deformation vibrations of OH groups (1650, 1680 cm^{-1}), in agreement with the data of [4]. The positions of lines in the spectra of the starting solution (curve *1*) with a P_2O_5/Al_2O_3 ratio of 3.5 and a regenerated solution (curve *3*) are rather close (with the exception of the band at 1650 cm^{-1}, absent in the spectrum of the regenerated solution).

In the spectra of powdered aluminophosphates, the absorption intensity at 3000–3600 and 1650–1680 cm^{-1} decreases, compared with that in solutions, which is due to the removal of molecular water and hydroxyl groups in the course of dehydration (Fig. 4; curves *2*, *5*). Simultaneously, the region associated with absorption by hydroxyl groups and water becomes narrower (3000–3600 cm^{-1}) and lines in the region of stretching and deformation vibrations of P–O bonds (400–1400 cm^{-1}) are noticeably broadened.

In the spectrum of the aluminophosphate powder obtained upon drying of a solution with a P_2O_5/Al_2O_3 molar ratio of 2.5 (curve *4*), a diffuse broadening of the lines is observed, accompanied by their shift to higher frequencies. This points to noticeable structural changes occurring as a result of the intensive development of condensation and crystallization processes in thermal treatment of aluminophosphate solutions whose composition is characterized by P_2O_5/Al_2O_3 molar ratios smaller than 3.5.

CONCLUSIONS

(1) Kinetic dependences of moisture removal from aluminophosphate binder solutions in a microwave field were obtained. The influence exerted by their chemical composition and, in particular, by their modification with chromium and boron oxides on the dehydration process was considered. It was shown that the dehydration process is accelerated on raising the content of basic oxides (Al_2O_3, Cr_2O_3) in solution and decelerated in the case of acid oxides (P_2O_5, B_2O_3).

(2) An X-ray phase analysis demonstrated that mostly amorphous phases well soluble in water are formed in the initial stage of drying. As the drying is made longer, the content of crystalline products in the products obtained increases, which makes lower their solubility in water.

(3) The processes occurring in dissolution of aluminophosphates powders of various compositions in water were considered. The parameters of the chemical composition of powder-like aluminophosphate products that provide their complete solubility in water were suggested and substantiated: P_2O_5/Al_2O_3 ratio not lower than 3.5 and moisture content of no less than 18–20 wt %. The IR data obtained demonstrate that solutions prepared by dissolution of powders having the optimal chemical composition are identical to the starting aluminophosphate binders.

ACKNOWLEDGMENTS

The authors are grateful to A.I. Domanskii for assistance in X-ray phase analysis of samples.

REFERENCES

1. Kopeikin, V.A., Petrova, A.P., and Rashkovan, I.L., *Materialy na osnove metallofosfatov* (Materials Based on Metal Phosphates), Moscow: Khimiya, 1976.
2. Sychev, M.M., *Neorganicheskie klei* (Inorganic Glues), Leningrad: Khimiya, 1986, 2nd revised ed.
3. Kopeikin, V.A., Klement'eva, V.S., and Krasnyi, B.L., *Ogneupornye rastvory na fosfatnykh svyazuyushchikh* (Refractory Solutions Based on Phosphate Binders), Moscow: Metallurgiya, 1986.
4. Asnovich, E.Z. and Zabyrina, K.I., *Elektroizolyatsionnye materialy vysokoi nagrevostoikosti* (Electrically Insulating Materials with High Heating Resistance), Moscow: Energiya, 1973.
5. Kozlov, B.I., Rashkovan, I.L., Zolotavina, S.V., and Devyatovskaya, L.I., Abstracts of Papers, *Vsesoyuznyi seminar "Fosfatnye materially"* (All-Union Symp. "Phosphate Materials"), Apatity, 1990, part 2, p. 153.
6. Surkov, M.E., Krasnyi, B.L., Laguzina, A.I., et al., Abstracts of Papers, *VI Vsesoyuznaya konferentsiya po fosfatam "Fosfaty-84"* (VI All-Union Conf. on Phosphates "Phosphates-84"), Alma-Ata: KazNIINTI, 1984, part 3, pp. 469–470.
7. Kuz'menkov, M.I., Pechkovskii, V.V., and Plyshevskii, S.I., *Khimiya i tekhnologiya metafosfatov* (Chemistry and Technology of Metal Phosphates), Minsk: Universitetskoe, 1985.
8. Lykov, M.V., *Sushka raspyleniem* (Spraying Drying), Moscow: Pishchepromizdat, 1955.
9. Brykov, A.S., Danilov, V.V., and Korneev, V.I., *Zh. Prikl. Khim.*, 2000, vol. 73, no. 1, pp. 15–18.
10. Brykov, A. and Rikenglaz, L., *J. Microwave Power Electromagn. Energ.*, vol. 35, no. 3, 2000, pp. 191–196.
11. Tikavyi, V.F., Lapko, K.N., Zakharov, I.A., and Antonyuk, E.P., *Neorg. Mater.*, 1971, vol. 7, no. 9, pp. 1629–1632.
12. Knyazhevskaya, G.S., Firsova, M.G., and Kil'keev, R.Sh., *Vysokochastotnyi nagrev dielektricheskikh materialov* (High-Frequency Heating of Dielectric Materials), Leningrad: Mashinostroenie, 1989.
13. Molochnikov, L.S., Smirnov, S.V., Zolotavina, S.V., et al., Abstracts of Papers, *Vsesoyuznyi seminar "Fosfatnye materially"* (All-Union Symp. "Phosphate Materials"), Apatity, 1990, part 2, p. 145.
14. Tikavyi, V.F., Korpus', V.A., Chivenkov, A.N., and Lapko, K.N., *Neorg. Mater.*, 1973, vol. 9, no. 9, pp. 1608–1610.
15. Rashkovan, I.L., Kuz'minskaya, L.N., and Kopeikin, V.A., *Neorg. Mater.*, 1966, vol. 2, no. 3, pp. 541–549.
16. Chistyakova, A.A., Sivkina, V.A., and Sadkov, V.M., *Neorg. Mater.*, 1969, vol. 5, no. 10, pp. 1785–1792.
17. Orlov, Yu.I., *Fiz. Khim. Stekla*, 2002, vol. 28, no. 5, pp. 401–411.

ISSN 1070-4272, Russian Journal of Applied Chemistry, 2007, Vol. 80, No. 10, pp. 1632–1635. © Pleiades Publishing, Ltd., 2007.
Original Russian Text © A.M. Zhizhaev, E.N. Merkulova, I.V. Bragin, 2007, published in Zhurnal Prikladnoi Khimii, 2007, Vol. 80, No. 10, pp. 1603–1606.

INORGANIC SYNTHESIS AND INDUSTRIAL INORGANIC CHEMISTRY

Copper Precipitation from Sulfate Solutions with Calcium Carbonates

A. M. Zhizhaev, E. N. Merkulova, and I. V. Bragin

Institute of Chemistry and Chemical Engineering, Siberian Division, Russian Academy of Sciences, Krasnoyarsk, Russia

Received May 16, 2006; in final form, April 2007

Abstract—Mechanism of interaction of copper sulfate with natural calcium carbonates, responsible for low residual copper concentrations in solutions and for the behavior of open and closed systems in storage is considered.

DOI: 10.1134/S1070427207100047

Natural calcium carbonates (limestone, marble, and dolomite) are used in wastewater treatment mainly as neutralizing reagents included in formulations [1, 2]. The use of calcium carbonates for acidity neutralization is widely known and has been repeatedly implemented in practice. The possibility of fixing toxic admixtures, including copper(II) ions, has been reported [2–6]. The interaction of solutions with a solid phase is usually regarded in this case as exchange of calcium and magnesium ions for ions of heavy nonferrous metals in solution [5, 6] or as sorption of products of their hydrolysis by carbonates [3–5]. Accordingly, the sorption or exchange capacity of a precipitator should be in the range from one hundredth of a milligram to tens of milligrams per gram, which restricts the application field of natural calcium carbonates for treatment of wastewater with low concentrations of metals and complicates analysis of the resulting compounds [2, 3].

Hydrolytic purification of solutions to remove copper requires that they should be alkalized to pH 8–12 [7], whereas precipitation of copper on carbonates occurs at pH 4–7 and the pH rarely reaches a value of 7.5–8 in real flow-through systems [5, 8]. When cakes are subjected to X-ray and microscopic analyses, independent copper-containing mineral phases are occasionally identified (mostly poorly soluble basic salts) [3, 5, 8]. The capacity of a precipitator reaches 0.83 g g^{-1} [5], which corresponds to reagent (but not sorption) precipitation methods and is close in stoichiometry to complete decomposition of the carbonate matrix.

The precipitation of basic salts of heavy metals has been studied in sufficient detail for the case of crystallization from solutions [9]. The formation of basic salts in a heterogeneous system constituted by a sulfate solution and solid calcium carbonate has virtually not been considered, despite the discovery of a number of natural associates of the corresponding composition in deposits of oxidized copper ores [10, 11]. An attempts to synthesize their artificial analogues from malachite or in the $CuO–SO_3–H_2O$ system failed [12]. It was shown in [8] that a wide range of minerals of basic copper sulfates (brochantite, posnjakite, and devilline) can be formed, depending on conditions of precipitation on natural calcium carbonates (initial concentration, temperature, and precipitator grain size).

This study is devoted to analysis of the mechanism of copper sulfate interaction with natural calcium carbonates.

EXPERIMENTAL

In the experiments, we used model solutions of copper sulfate with copper concentrations of up to 1 g l^{-1}, prepared from pure-grade reactive copper sulfate pentahydrate. To 1 l of the solution was added 1, 2, or 5 g of a precipitator. The experiments were carried out in glass beakers under static and dynamic conditions at room temperature.

The pH of the pulp was measured at regular intervals of time and 5-ml liquid-phase samples were taken

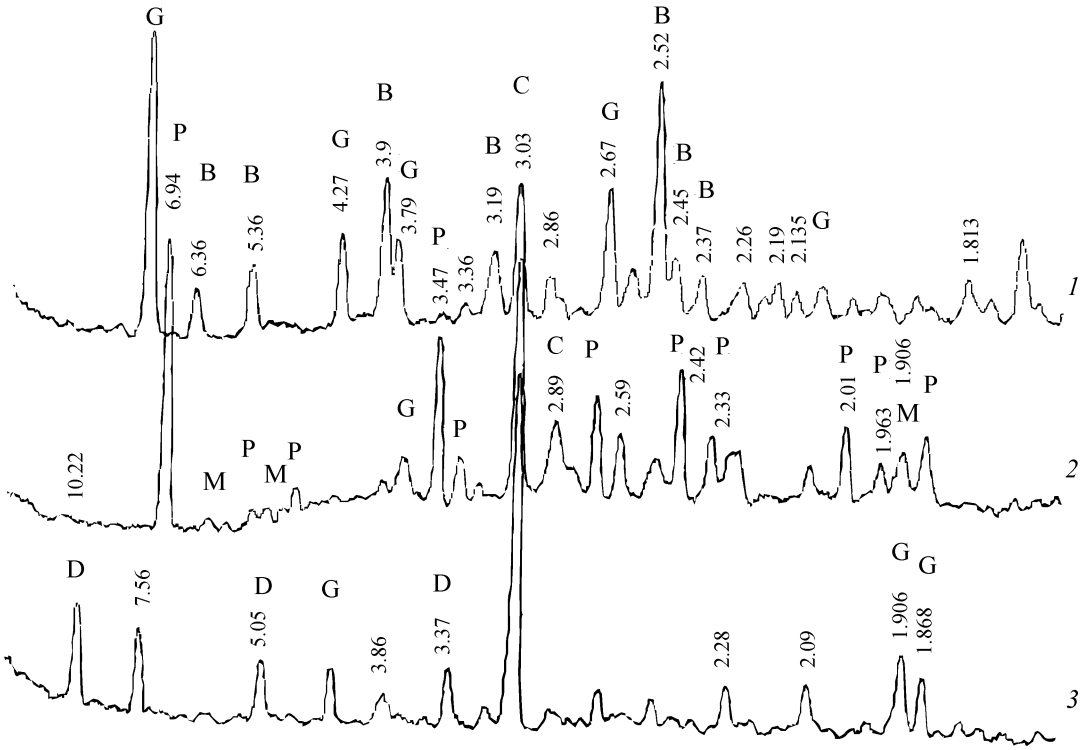

Fig. 1. X-ray diffraction patterns of the products of copper precipitation from sulfate solutions on (*1*) limestone, (*2*) marbled limestone, and (*3*) dolomite. Mineral phase: G, gypsum ($CaSO_4 \cdot 2H_2O$); B, brochantite [$CuSO_4 \cdot 3Cu(OH)_2$]; P, posnjakite [$CuSO_4 \cdot 3Cu(OH)_2 \cdot H_2O$]; C, calcite ($CaCO_3$); D, devilline [$CaCu_4(SO_4)_2(OH)_6 \cdot 2H_2O$]; and M, malachite [$Cu_2(OH)_2CO_3$].

for determining the copper content of a solution on an AAS-30 atomic absorption spectrometer (Carl Zeiss, Jena, Germany).

The X-ray phase analysis of the precipitates was carried out on a DRON-3 X-ray diffractometer (Cu_{K_α} radiation, scanning at 0.02° intervals, accumulation time at a point 1 s). The X-ray diffraction patterns obtained were interpreted by the standard method, using the JCPDS file of reference spectra.

Compact colored precipitates (cyan to light green) readily separable from the liquid phase in settling or filtration were obtained in all the experiments. According to published data, copper precipitation upon contact with natural carbonates proceeds by an exchange reaction to give basic copper carbonates: malachite or azurite [11], in accordance with the overall equation

$$2CaCO_3 + 2CuSO_4 + 3H_2O = CuCO_3 \cdot Cu(OH)_2 + 2CaSO_4 \cdot 2H_2O + CO_2. \quad (1)$$

The solubility product of malachite (1.7×10^{-34}) [13] is sufficiently low for deep purification of solutions; however, the calculation formula (2) for this open system contains equilibrium concentrations of carbonate and hydroxide ions, resulting from the solubility of poorly soluble calcium carbonate (SP = 3.8×10^{-9}) [13] and from partial hydrolysis of carbonate ions, respectively, which leads to a pronounced increase in the threshold concentration of copper precipitation.

$$SP_{malachite} < [OH^-]^2 [CO_3^{2-}] a_{Cu^{2+}}^2. \quad (2)$$

The appearance of gypsum in the system reduces the equilibrium concentrations to an even greater extent and raises the residual copper concentrations to tens of parts per million.

In the experiments on solution purification, we obtained well-crystallized copper minerals, which can be readily identified. The X-ray diffraction patterns of typical products of copper precipitation on natural calcium carbonates are shown in Fig. 1. The key factor in copper fixation is the content and form of calcite ($CaCO_3$, JCPDS, 47-1743, d = 3.03 Å). Gypsum ($CaSO_4 \cdot 2H_2O$, JCPDS, 6-46, d 7.56, 4.27, 3.79 Å) was crystallized in all the experiments, except those with the most dilute solutions. In all cases, the precipitates are a mixture of basic copper sulfates with

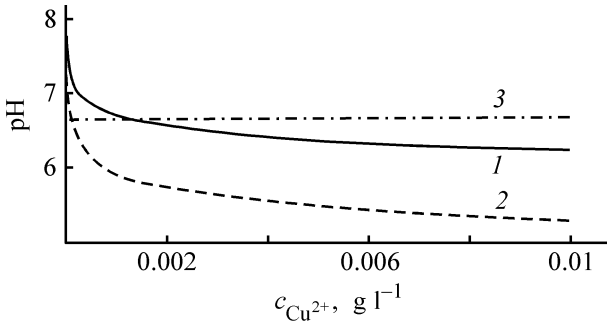

Fig. 2. Dependence of residual copper concentration $c_{Cu^{2+}}$ on the solution acidity. (*1*) Hydrolytic precipitation, (*2*) precipitation in the form of basic salts, and (*3*) pH of gypsum-carbonate buffer solution at 20°C.

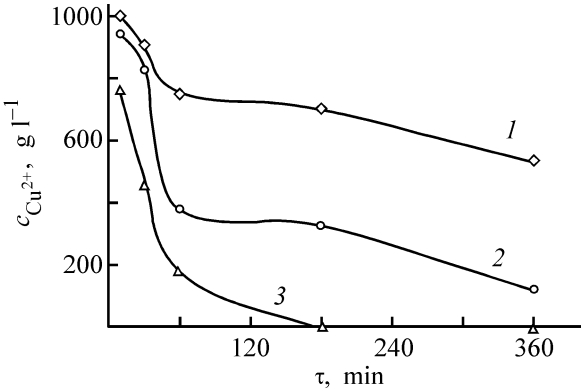

Fig. 3. Kinetics of copper precipitation on marbled limestone with 100% of particles less than 0.16 mm in size at various precipitator-to-copper ratios in solution. ($c_{Cu^{2+}}$) Concentration of copper in solution and (τ) time. Limestone-to-copper ratio (g : g): (*1*) 1 : 1, (*2*) 2 : 1, and (*3*) 5 : 1.

gypsum and residues of the starting calcium carbonate [brochantite, $Cu_4SO_4(OH)_6$, *d* 2.52, 6.38, 5.36 Å; posnjakite, $Cu_4SO_4(OH)_6 \cdot H_2O$, JCPDS, 20-364, *d* 6.94, 3.47, 2.70 Å; and devilline, $CaCu_4(SO_4)_2 \cdot (OH)_6 \cdot 3H_2O$, JCPDS, 13-285, *d* 10.22, 5.05, 3.37 Å]. Despite the diversity of mineral forms, the mechanism of copper precipitation on calcite reduces to the following scheme:

$$\underset{\text{Calcite}}{CuSO_4 + CaCO_3} \rightarrow Cu(OH)_2$$

$$\rightarrow \underset{\text{Brochantite}}{CuSO_4 \cdot 3Cu(OH)_2} + \underset{\text{Gypsum}}{CaSO_4 \cdot 2H_2O} + CO_2$$

$$\rightarrow \underset{\text{Posnjakite}}{CuSO_4 \cdot 3Cu(OH)_2 \cdot H_2O}$$

$$\rightarrow \underset{\text{Devilline}}{CaSO_3 \cdot CuSO_4 \cdot 3Cu(OH)_2 \cdot 3H_2O}$$

The results of our study and the existing theoretical concepts of formation of crystalline precipitates [9] suggest the following scheme for describing the interaction of aqueous copper sulfate solutions with calcium carbonate. First, copper hydroxide is formed when pH increases due to CO_3^{2-} hydrolysis in a solution layer close to the carbonate surface. This is a fast stage, but the given mineral phase is not identified by X-ray diffraction analysis, because it further coprecipitates with the excess of copper sulfate in the form of brochantite. The precipitates are formed with hexagonal lattices of the CdI_2 type in such a manner that each layer of metal ions is covered on both sides by similarly built layers of hydroxide groups. In sulfate solutions, the hydroxide groups of the intermediate disordered layers are replaced by sulfate anions, so that a SO_4^{2-} layer is situated between two OH^- layers. The formation of crystal hydrates in storage or in slow precipitate formation does not contradict the mechanism suggested and causes transfer from brochantite to posnjakite. In the case of a low concentration of sulfate ions (or a high gypsum concentration in the reaction zone), a layer of Ca^{2+} ions is further introduced via changed intermediate layers of SO_4^{2-} anions to give devilline.

If copper precipitates as a basic sulfate in contact of wastewater with calcium carbonate in accordance with the overall equation

$$3CaCO_3 + 4CuSO_4 + 5H_2O = Cu_4SO_4(OH)_6 + 3CaSO_4 \cdot 2H_2O + 3CO_2, \quad (3)$$

the threshold concentration of precipitation formation is determined mainly by the activity of sulfate anions

$$SP_{\text{Brochantite}} < [OH^-]^6 a_{SO_4^{2-}} a_{Cu^{2+}}^4$$

present in macroscopic concentrations in terms of hydroxide ions. On the whole, the resulting residual copper concentration is several orders of magnitude lower than that for the system corresponding to Eq. (2). In the case of univalent anions (Cl^- and NO_3^-), the dependence of the threshold concentration on the squared activity of the balance anion makes formation of malachite during the precipitation even less probable.

Furthermore, the formation of a large amount of gypsum and the presence of an excess of calcite result in that copper precipitates under the conditions of a gypsum-carbonate buffer solution maintaining pH at 6.3–6.5 [14]. A self-regulation of the fine precipitation mechanism takes place, because the concentration

of carbonate ions in solution is always lower than that of the salt-balance anions (in most cases, these are sulfates, but chlorides, nitrates, etc. are also possible) and there is no excess of hydroxide ions. In these conditions, no hydroxides and basic carbonates are formed, and heavy nonferrous metals precipitate in the form of basic salts. The described precipitation mechanism is made operative by the low solubility of calcium carbonates. Calculated dependences of the degree of copper precipitation as a hydroxide (curve *1*) and a basic salt (curve *2*) on the solution pH [15] are shown in Fig. 2. The straight line corresponds to the pH of the gypsum-carbonate buffer solution at 20°C. The precipitation of basic salts at this pH results in that the residual copper concentration in solution is nearly an order of magnitude lower than that for hydrolytic methods. The kinetics of copper precipitation on marbled limestone with 100% of particles smaller than 0.16 mm in size is shown in Fig. 3. With an excess of the precipitator (5 g of limestone per 1 g of copper in solution), the residual concentration of copper less than 0.1 ppm is reached in 3 h, with more than one day required at smaller ratios. The excess is necessary because calcite is partly consumed for neutralization of the starting weakly acid solution (as a result of Cu^{2+} hydrolysis, pH is ~5.5). In purification of solutions to remove copper, pH increased to 6.5–6.7, which indirectly confirms that the gypsum-carbonate buffer solution is formed. The pH level reached is apparently insufficient for deep hydrolytic precipitation [7] (Fig. 2).

Nevertheless, malachite can be formed under such conditions in view of (2) upon a sharp increase in the CO_3^{2-}-concentration, e.g., on adding concentrated Na_2CO_3 solutions, which is widely used in preparative syntheses of malachite and basic carbonates of other heavy nonferrous metals [9]. Alternatively, the process can be carried out in closed systems, which precludes fast removal of carbon dioxide (as it occurs under geological conditions). We also performed such a process in the study and obtained a well-crystallized malachite easily identified by X-ray diffraction analysis. However, the malachite formation is of clearly secondary nature, because brochantite is always formed in the first stage (which is readily indicated by the bright blue color of grains) and further reacts with carbon dioxide. This process also partly occurs as a result of saturation of solutions with atmospheric carbon dioxide in keeping, which causes the corresponding increase in the residual concentration of copper in the liquid phase in storage, as described in [3, 5].

CONCLUSIONS

(1) Copper precipitates from sulfate solutions on solid calcium carbonates in the form of basic sulfates. Basic carbonates can be formed in systems of this kind via secondary reactions of basic sulfates with carbon dioxide. The formation of a gypsum-carbonate buffer solution plays an essential role.

(2) The suggested scheme of formation and mutual transformations of basic sulfates can explain specific features of wastewater purification to remove copper and describe technological and geochemical processes in oxidized copper deposits.

REFERENCES

1. Robbins, E.I., Cravotta, C.A., Savela, C.E., and Nord, C.L., *Fuel*, 1999, vol. 78, no. 2, pp. 259–270.
2. RF Patent 2081839.
3. Makarov, V.N., Mazukhina, S.I., Vasil'eva, T.N., et al., *Zh. Prikl. Khim.*, 2001, vol. 74, no. 12, pp. 1985–1990.
4. US Patent 5098579.
5. Lupeiko, T.G., Ivleva, T.I., and Solov'ev, L.A., *Zh. Prikl. Khim.*, 2001, vol. 74, no. 4, pp. 567–570.
6. Lupeiko, T.G., Gorbunova, N.O., and Bayan, E.M., *Zh. Prikl. Khim.*, 2001, vol. 74, no. 10, pp. 1648–1651.
7. Svyatokhina, V.P., Isaeva, O.J., Pestrikov, S.V., and Krasnogorskaya, N.N., *Zh. Prikl. Khim.*, 2003, vol. 76, no. 2, pp. 330–332.
8. Zhizhaev, A.M., Bragin, V.I., and Mikhailov, A.G., *Obogashch. Rud*, 2001, no. 5, pp. 13–17.
9. Vasserman, I.M., *Khimicheskoe osazhdenie iz rastvorov* (Chemical Precipitation from Solutions), Leningrad: Khimiya, 1980.
10. Ptitsyn, A.B., Zamana, L.V., Yurgenson, G.A., et al., *Udokan: geologiya, rudogenez, usloviya osvoeniya* (Udokan: Geology, Ore Genesis, Conditions of Development), Novosibirsk: Nauka, 2003.
11. Perel'man, A.I. *Geokhimiya epigeneticheskikh protsessov* (Geochemistry of Epigenetic Processes), Moscow: Nedra, 1968.
12. Alekseev, L.S., *Khim. Tekhnol. Vody*, 1989, vol. 11, no. 11, pp. 1014–1018.
13. Rabinovich, V.A. and Khavin, Z.Ya., *Kratkii khimicheskii spravochnik* (Concise Chemical Reference Book), Leningrad: Khimiya, 1978.
14. Laptev, J.V., Sirkis, A.L., and Kolonin, G.R., *Sera i sul'fidoobrazovanie v gidrometallurgicheskikh protsessakh* (Sulfur and Sulfide Formation in Hydrometallurgical Processes), Novosibirsk: Nauka, 1987.
15. Zelikman, A.N., Vol'dman, G.M., and Belyavskaya, L.V., *Teoriya gidrometallurgicheskikh protsessov* (Theory of Hydrometallurgical Processes), Moscow: Metallurgiya, 1983.

ISSN 1070-4272, Russian Journal of Applied Chemistry, 2007, Vol. 80, No. 10, pp. 1636–1642. © Pleiades Publishing, Ltd., 2007.
Original Russian Text © V.I. Tikhomirova, T.A. Desyatova, V.A. Suvorova, 2007, published in Zhurnal Prikladnoi Khimii, 2007, Vol. 80, No. 10, pp. 1607–1612.

INORGANIC SYNTHESIS AND INDUSTRIAL INORGANIC CHEMISTRY

A Study of Palladium Recovery with Thiourea from Nitric Acid Solutions

V. I. Tikhomirova, T. A. Desyatova, and V. A. Suvorova

Institute of Experimental Mineralogy, Russian Academy of Sciences, Chernogolovka, Moscow oblast, Russia

Received September 22, 2006

Abstract—Interaction in the system Pd(II)–HNO_3–$SC(NH_2)_2$ was studied. It was shown that the precipitates formed, which have various compositions and solubilities, contain palladium(II) and thiourea conversion products. Elemental, X-ray diffraction, and atomic-adsorption analyses and IR and electronic absorption spectroscopies were applied to demonstrate the possibility of virtually quantitative precipitation of palladium(II) under certain conditions in the form of a poorly soluble precipitate $Pd_2(CN)_4 \cdot H_2O$.

DOI: 10.1134/S1070427207100059

The study was carried out in view of the necessity for development of a technology for utilization of spent nuclear fuel (SNF) temporarily stored in the form of 3–6 M nitric acid solutions. The problem of palladium(II) recovery from products of SNF processing was discussed in the review [1]. It was emphasized that it is necessary to isolate the fraction of noble metals, which create certain difficulties because of the formation of a metallic phase in SNF vitrification. It is important to adapt the recovery of the platinum group fraction to the existing processing technology. The difficulty is in that poorly soluble precipitates containing considerable amounts of platinum group metals, together with Mo, Zr, U, Pu, etc., are formed in different stages of the process. There exist various approaches to, and methods of, Pd recovery from a nitric acid medium: adsorption on anion-exchange resins or activated carbon; extraction with organic phosphates, macromolecular amines, and quaternary ammonium bases; electrochemical deposition of Pd onto electrodes; and precipitation with the use of complexation. However, none of the approaches and methods could be brought to the industrial level. Further search for effective reagents and studies of their interaction with SNF components in a nitric acid medium are necessary.

Previously, up to 10 mg of metallic Pd per gram of carbon could be precipitated in a study of Pd(II)on activated carbons treated first with a saturated NaOH solution and then with thiourea (Thio) [2]. It has been reported that poorly soluble Pd(II) compounds are formed in interaction of Thio with Pd(II) in a nitric acid medium [3]. However, their formation conditions and composition required further analysis.

The aim of this study was to analyze the conditions of Pd(II) recovery with thiourea from 3–6 M HNO_3 solutions, composition of the compounds obtained, and the process of interaction between Thio and HNO_3.

EXPERIMENTAL

UV-Vis spectrophotometry (Carl Zeiss UV-Vis instrument) was used in the study. X-ray phase, micro X-ray fluorescence (Camebax instrument), and classical elemental analyses served to examine solid compounds. IR spectra were measured with a Perkin-Elmer 983 instrument in the range 200–4000 cm^{-1}, with samples of the solids under study prepared in dispersed form in pellets with KBr or CsI.

Thiourea complexes of Pd(II) in solutions were studied by potentiometric titration in a cell with a platinum indicator electrode and silver chloride reference electrode with a salt bridge (1 M KNO_3) at 25°C. In the process, the solution was uninterruptedly agitated with a magnetic rabble.

Pd(II) solutions with an initial concentration of 1–2 mg ml^{-1} were prepared by dissolving the metal of special purity grade in nitric acid. Thiourea of the same grade was used both as a solid and when dissolved in 0.02–3.00 M HNO_3.

The concentration of Pd(II) in solutions over precipitates was determined by atomic-absorption ana-

lysis with flameless atomization (Shimadzu AA-670G instrument). The atomization procedure in a GFA-4A furnace consisted in stages of drying of a solution aliquot at 120°C, salt dissociation at 650°C, and atomization at 2600°C (λ_{Pd} = 244.8 nm). The sensitivity of the analytical procedure was 0.01 μg per 1 ml of a final-dilution solution in 2 M HNO_3.

Figure 1 shows how the potential of the platinum electrode varies in the processes that occur in a system containing 0.01 M of aqua nitrate Pd(II) complexes, 0.02 M of HNO_3, and thiourea. Previously, it has been demonstrated [3] by the method of isomolar series that, at Pd(II) : Thio molar ratios equal to 3 and 4, the compounds formed have UV absorptions peaks at 345 and 300 nm, respectively.

The initial potential of the system in the absence of thiourea is 0.84 V relative to the silver chloride electrode or 1.062 V relative to the standard hydrogen electrode (s.h.e.). According to the data of [4], the standard potential of the $[Pd(H_2O_4)_4]^{2+}$/Pd pair is 0.99 V, and, consequently, that for a Pf(II) solution with a concentration of 0.01 M would be 0.96 V (s.h.e.), which is lower than the observed value. Presumably, the complexes under consideration also contain acido ligands that make E higher.

Upon addition of first Thio aliquots to a Pd(II)/Thio molar ratio of 1.1 to 1.2, a brown precipitate is rapidly formed. In the process, the potential decreases to the minimum extent, because the interaction of Pd(II) with products formed in conversion of thiourea is fast, its adsorption on the electrode is insignificant, and the HNO_3 concentration remains virtually unchanged, which maintains a high electrode potential (curves *1–3*). Curve 4 [Pd(II) : Thio = 1 : 2.5] shows an abrupt decrease in the potential, which corresponds to its dependence on the concentration of free Thio in solution and its adsorption on the electrode surface in accordance with the equation [5]:

$$E = E^0 + \frac{RT}{2F} \ln [C_2S_2N_4H_6]/[SC(NH_2)_2]^2, \quad (1)$$

where $E^0 = 0.408 - 0.420$ V.

At a Pd(II) : Thio ratio of 1 : 3, the precipitate starts to dissolve and makes the solution bright orange. In this case, the fast decrease in E is replaced with its comparatively slow rise (curves *5–7*). This behavior of Pd(II) complexes is similar to the results of a study of the acid-base properties of Pt(II) aqua complexes, with coordinated water molecules replaced with thiourea in the $[Pt(H_2O)(Thio)_2]^{2+}$ aqua complex [6]. It can be assumed that, first, NO_3^- anions in *trans*-

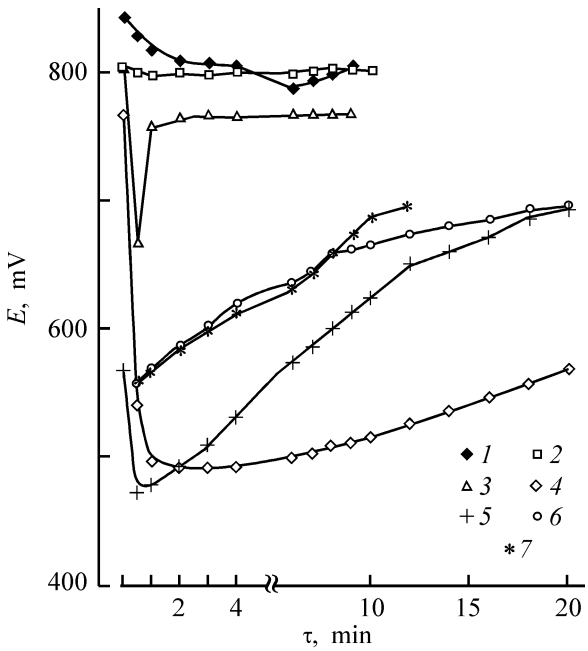

Fig. 1. Potential E of the platinum electrode in a solution of Pd(II) nitrate (10^{-2} M in terms of Pd) vs. time τ elapsed after addition of aliquots of a Thio solution (10^{-2} in a 0.02 M HNO_3 solution). Thio : Pd(II) molar ratio in solution: (*1*) 1.25, (*2*) 1.5, (*3*) 2.0, (*4*) 2.5, (*5*) 3.0, (*6*) 4.0, and (*7*) 4.5.

$[Pd(H_2O)_2(NO_3)_2]$ are substituted, and then water molecules themselves. At Pd(II) : Thio ratio of 1 : 4 (curve *6*), a stable yellow complex is formed (λ_{max} = 300 nm), which enables its use for analytical purposes [7].

As the Thio concentration is raised to Pd(II) : Thio = 1 : 6, the excess Thio is adsorbed on the electrode. This leads to a sharp decrease in the potential to 0.3 V for the Pt electrode and to 0.2 V for the Pd electrode relative to the Ag/AgCl reference electrode at a Thio concentration of 5×10^{-2} M. A calculation by Eq. (1) gives E = 0.25 V, which is close to the potentials obtained in [8] for acid sulfate solutions of Thio.

Further, precipitates formed in 3–6 M HNO_3 solutions with a Pd(II) concentration of 1×10^{-2} M were studied. Upon introduction of solid thiourea into the Pd(II) solutions, variously colored precipitates of Pd(II) compounds with Thio started to be formed. The precipitates were filtered off in 2 days, washed with distilled water to a neutral reaction, and dried in air. The residual content of Pd(II) in the filtrate was determined, and the Pd(II)/S ratio in the precipitates was found by the micro X-ray fluorescence technique (Table 1).

Table 1. Precipitate properties in relation to Pd(II) : Thio molar ratios in 3 and 6 M HNO_3 solutions upon addition of Thio

Pd(II) : Thio molar ratio	c_{HNO_3}, M	Thiourea	Precipitate color	Pd(II) : S in precipitate	Solubility $L \times 10^{-5}$, M, in 2 days
1.0 : 1.5	6	Solid	Brown	1.0 : 1.1	48.00
1.0 : 4.0	6	"	Red	2.1 : 1.0	4.55
1.0 : 6.5	6	"	Orange	1.6 : 1.0	0.13
1.0 : 10.0	6	"	Yellow	2.0 : 1.0	0.70
1.0 : 16.0	3	Dissolved with addition of solid	Yellow	2.1 : 1.0	1.30
1.0 : 4.0	3	Solid	Yellow	2.0 : 1.0	0.05

It can be seen from the data in Table 1 that, depending on the Pd(II) : Thio ratio and HNO_3 concentration, various poorly soluble compounds are formed. Raising the concentration of thiourea in the starting solution does not lead to any increase in the content of sulfur in the precipitates. In all probability, reactions involving products $SC(NH_2)_2$ of interaction with HNO_3 and HNO_2 are important under the experimental conditions. Therefore, accumulation of HNO_2 in the reaction of $SC(NH_2)_2$ with a 3–5 M solution of HNO_3 was studied.

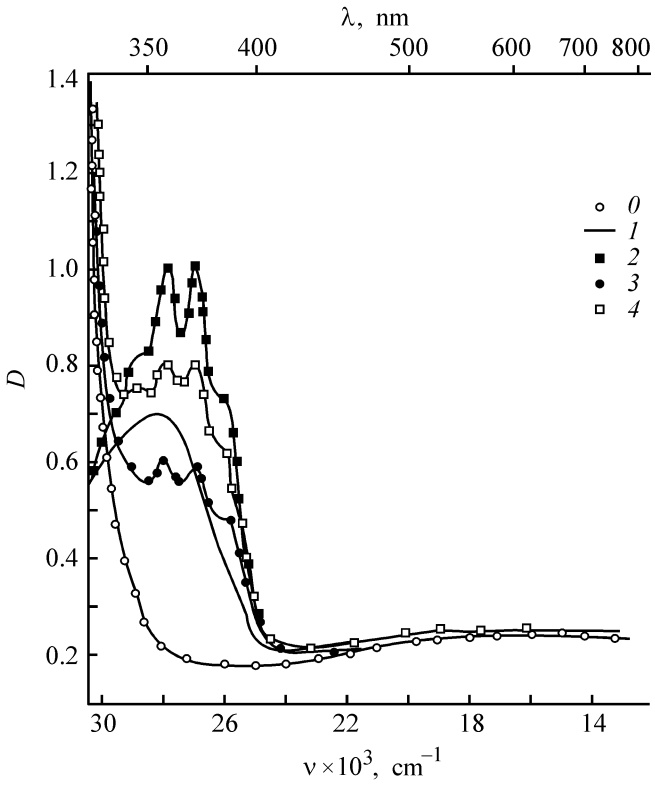

Fig. 2. Electronic absorption spectra of solutions of the starting HNO_3 and HNO_2 appearing as a result of reactions of HNO_3 with various reagents. (λ) Wavelength, (*D*) optical density, and (ν) wave number. Solution composition (M): (*0*) 4 HNO_3, (*1*) 0.05 $NaNO_2$, (*2*) 0.05 $NaNO_2$ + 0.5 HCl, (*3*) 4 HNO_3 + Thio (in 1 h), and (*4*) 4 HNO_3 + Thio (in 3 h).

In 3–6 M solutions of HNO_3, the potentials of the Pt electrode were fixed in the range 0.82–0.99 V (s.h.e.), which is determined by the equilibrium between HNO_3 and nitrogen oxides (for the $2HNO_3/N_2O_4$ pair, E^0 = 0.80 V) [9]. When $SC(NH_2)_2$ was mixed with HNO_3, the solution turned dark brown in 15–20 min and NO_2 was formed. However, the coloration rapidly disappeared, with gas evolution and the solution becoming turbid because of the release of elementary sulfur simultaneously observed. The formation of HNO_2 as a result of the reaction between Thio and a 4 M solution of HNO_3 was indicated by the absorption spectrum, which contained at 350–400 nm four equidistant bands (Fig. 2; curves *3*, *4*), absent in the spectrum of a pure HNO_3 solution (curve *0*). The thickness of the cuvette used was 0.5 cm. Because the same spectrum was observed for esters of HNO_2 [10], it was attributed to absorption by undissociated HNO_2, whose dissociation constant is 5×10^{-4}.

Figure 2 also shows absorption spectra of a 0.05 solution of $NaNO_2$ and of a mixture of 0.05 M of $NaNO_2$ with 0.5 M of HCl (curves *1*, *2*). It can be seen that, upon introduction of hydrogen ions in the form of HCl into the system, the absorption spectrum of NO_2^- ions takes the structure characteristic of HNO_2, which is attributed [11] to transitions in the –O–N=O group. According to the data obtained, the dependence of the absorption associated with HNO_2 on the concentration of NO_2^- ions in a 0.4 solution of HNO_3 is described by the Lambert–Beer law and can be used as a calibration dependence. The value

$\varepsilon = 20.4\ M^{-1}\ cm^{-1}$ obtained at $\lambda = 358$ nm coincides with that reported in [10].

Figure 3 shows dependences of the HNO_2 concentration in 3–5 M solutions of HNO_3 on the duration of their contact with thiourea. The initial concentration of thiourea in all the three sets of experiments was the same, 0.02 M. In the first, comparatively short, stage of HNO_2 accumulation, the rates of HNO_2 formation, found from the slopes of the initial portions of the curves, were 1.0×10^{-5}, 7.5×10^{-6}, and 5.0×10^{-6} mol l^{-1} s^{-1} in 5, 4, and 3 M solutions of HNO_3, respectively. This initial stage gives way to a rather long (22nd to 55th h) steady-state period, in which the rates of HNO_2 formation and expenditure are equal. In this case, the concentration of HNO_2 (0.032 M) is independent of the HNO_3 concentration and exceeds by approximately a factor of 1.6 the initial concentration of thiourea. As the HNO_3 concentration increases, the rates of HNO_2 formation and loss grow to the same extent and the steady-state period becomes shorter. The steady-state period is followed by the third stage, the HNO_2 concentration starts to decrease. This decrease corresponds to a first-order reaction in HNO_2 concentration, i.e., straight lines with slopes of -4.8×10^{-6}, -3.8×10^{-6}, and 2.4×10^{-6} are plotted in the $\ln c_{HNO_2}$–τ coordinates for 5, 4, and 3 M solutions of HNO_3, respectively. Thus, the rates of both expenditure and formation of HNO_2 are approximately proportional to the concentration of HNO_3.

The oxidation of thiourea is complex process; it depends on the solution acidity [6, 8, 12, 13] and occurs via intermediate formation of formamidine disulfide (FADS), which manifests itself in the UV part of the spectrum at 190–240 nm. In acid solutions, FADS is observed at potentials of 0.99–1.4 B (s.h.e.). The formation of FADS is preceded by protonation of Thio, which has been observed both in 1–3 M solutions of H_2SO_4 and in $HClO_4$ [8, 12, 14]. It has been shown, using X-ray photoelectron spectroscopy, that the protonation is associated with conversion of sulfur from the thion to thiol form, i.e., proton is added to a sulfur atom. In HNO_3 solutions with concentrations exceeding 2 M, FADS is also formed from thiourea [10]. Further transformations of FADS yield cyanamide, sulfur, thiocyanic acid, and HCN [15]. The main processes occurring when Thio is brought in contact with HNO_3 can be represented by the following reactions:

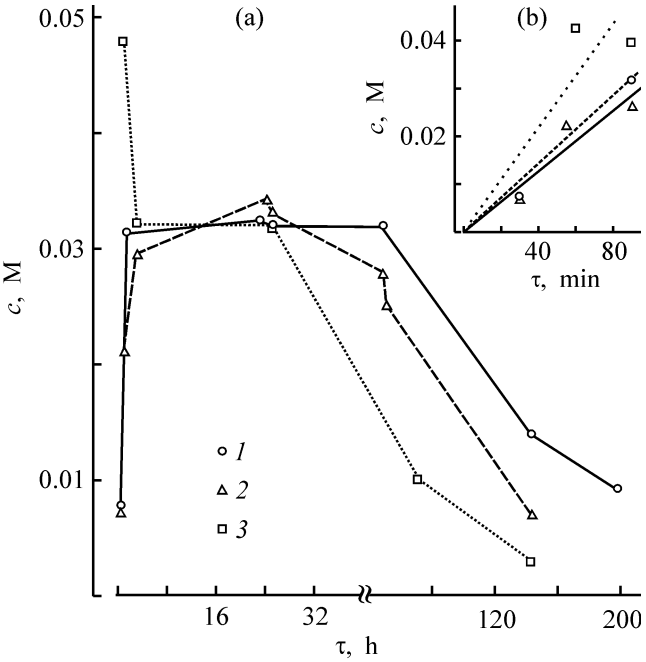

Fig. 3. (a) Dependences of the concentration c of nitrous acid on the time τ of contact between thiourea (2×10^{-2} M) and HNO_3 of various concentrations and (b) the same dependences in the initial 90 min. HNO_3 Concentration (M): (*1*) 3, (*2*) 4, (*3*) 5.

$$SC(NH_2)_2 + HNO_3 \rightleftarrows [H^+SC(NH_2)_2]NO_3, \quad (2)$$

$$2[H^+SC(NH_2)_2]NO_3 \rightarrow S_2C_2N_4H_6 + 2NO_2 + 2H_2O, \quad (3)$$

$$2NO_2 \rightarrow N_2O_4, \quad (4)$$

$$N_2O_4 + H_2O \rightarrow HNO_3 + HNO_2, \quad (5)$$

$$2[HSC(NH_2)_2]NO_3 + 2HNO_2 \rightarrow S_2C_2N_4H_6 + 2NO + 2H_2O + 2HNO_3, \quad (6)$$

$$2NO + HNO_3 + H_2O \rightarrow 3HNO_2 \quad (7)$$

$$S_2C_2N_4H_6 + HNO_2 \rightarrow S + NH_2CN + HNCS + N_2 + 2H_2O, \quad (8)$$

$$S + 2HNO_2 \rightarrow H_2SO_4 + N_2, \quad (9)$$

$$HNCS + 2HNO_3 \rightarrow HCN + H_2SO_4 + 2NO. \quad (10)$$

In the steady-state portion

$$[HNO_2] = \frac{K_2[HSC(NH_2)_2NO_3]^2}{K_7[S_2C_2N_4H_6]} = 3.2 \times 10^{-2}\ M. \quad (11)$$

It was shown in [16–18] that, in aqueous solutions of such acids as H_2SO_4, HCl, $HClO_4$, CF_3COOH,

Table 2. Formation conditions of Pd(II) compounds with RThio (white color) at an initial Pd(II) : Thio ratio of 1 : 6 in 3 and 4 M solutions of HNO_3

c_{HNO_3}, M	Duration of contact of Thio with HNO_3, h	Properties of precipitates		
		Pd(II) : S	duration of precipitate formation, days	solubility $L \times 10^{-5}$, M
3	90	45 : 1	3	1.40
			7	0.02
3	24	45 : 1	5	0.05
4	24	45 : 1	7	0.01

and in *n*-toluenesulfonic acid, the concentration of solvated protons is proportional to the acid concentration and independent of the nature of anions. According to [8], the protonation constant K_p of Thio in aqueous solutions of H_2SO_4 is 31.7, i.e., the basicity constant $K_b = 0.0315$. According to [19], the Hammett acidities $H_o = -\log h_o$ in 3, 4, and 5 M solutions of HNO_3 are –1.02, –1.32, and –1.57, respectively. In accordance with [20],

$$K_{eff} = K\alpha = \frac{K}{1 + 1/K_o h_o}. \quad (12)$$

where $\alpha = AH^+/c$, AH^+ is the concentration of protonated molecules, and $AH^+ + A = c$.

Thus, the concentration of $H^+SC(NH_2)_2NO_3$ in the initial stages is 5×10^{-3}, 7.9×10^{-3}, and 9.2×10^{-3} M in 3, 4, and 5 M solutions of HNO_3, respectively, and, accordingly, $K_2 \approx 1.4 \times 10^{-1}$ mol l^{-1} s^{-1} is obtained from the HNO_2 formation rates. After the steady-state portion, it follows from the slopes of the straight lines for the third stage that $K_7[S_2C_2N_4H_6] = 2.4 \times 10^{-6}$, 3.8×10^{-6}, and 4.8×10^{-6} s^{-1} in 3, 4, and 5 M nitric acid solutions. In the steady-state stage, the concentration $[H^+SC(NH_2)_2NO_3]$ is about 7.3×10^{-4}, 9.2×10^{-4}, and 1×10^{-3} M. According to estimates, approximately 25–30% of the initial amount of thiourea is converted by the beginning of the steady-state stage. While the ratio $[H^+SC(NH_2)_2NO_3]^2/[S_2C_2N_4H_6]$ retains a constant value, the concentration of HNO_2 remains at the level of 3.2×10^{-2} M. Lowering the $SC(NH_2)_2$ concentration to virtually zero leads to a decrease in the HNO_2 concentration via reactions (8) and (9). HCN is accumulated in solution.

Products of Thio oxidation in a nitric acid medium (RThio) form with Pd(II) white precipitates, some of whose properties are listed in Table 2.

It can be seen from Table 2 that the atomic content of Pd in the precipitates markedly exceeds that for S. The precipitates are completely formed after 5–7 days.

Taking into account the exceedingly low solubility of the practically important white precipitate, primary attention was given to its analysis. The following results were obtained in an elemental analysis of white precipitates (%): C 14.14 and 14.18, H 0.7 and 0.68, Cl not found, N 16.43 and 16.54, residue 62.55. The content of Pd in a precipitate dehydrated at 150°C is 67.84%. In accordance with the results of analyses, the formula of the compound can be represented as $[Pd_2(CN)_4] \cdot H_2O$. A precipitate with Ag^+, obtained under the same conditions, was identified by X-ray phase analysis (XPA) as AgCN. It can be assumed that a cyanide group is also present in the compound of Pd(II) with RThio. This was confirmed by the IR spectrum of the white precipitate (Fig. 4), which contains an absorption band with a frequency characteristic of the cyanide group (2213 cm^{-1}). Consequently, hydrocyanic acid, weakly dissociated in the acid medium ($K_{dis}HCN = 7.2 \times 10^{-10}$), is accumulated because of the complete destruction of thiourea.

The completeness of palladium precipitation in the form of $[Pd_2(CN)_4] \cdot H_2O$ with a solubility $L = 2 \times 10^{-7}$ M is reached in the course of time in interaction with HCN, which is gradually accumulated in the solution as a result of reaction (10). It was found that, in a solution with a M : Thio ratio of 1 : 10, the products of Thio conversion do not precipitate Fe(III), Ni(II), Mn(II), and Cr(III) ions.

The following results were obtained in an elemental analysis of red precipitates (%): C 12.74 and 12.38, H 1.13 and 1.12, Cl not found, N 20.78 and 20.73, S 7.91 and 8.72, Pd 49.71 and 49.08. The formula of the compound can be assumed to be $Pd_2(CMS) \times$

$(NH_2CN)(CN)_3 \cdot 2H_2O$. An XPA of white and red precipitates demonstrated that these compounds are amorphous. The white compound decomposes upon heating to 500–600°C to give a metallic Pd powder.

Figure 4 shows IR spectra of the white and red precipitates, together with the spectrum of the starting thiourea, which coincides with that reported in [21]. The absorption bands at 2213 cm^{-1} are associated with vibrations of the cyanide group –C=N [21–23]. A certain shift of these vibrations to higher frequencies suggests that bridging structures are formed [22]. The absorption bands peaked at 3421 and 1618 cm^{-1} are attributed to H_2O molecules [22]. The low-intensity bands at 544 and 464 cm^{-1} in the white substance and those at 548, 462, and 430 cm^{-1} in the red substance indicate that coordination bonds are formed between palladium(II) atoms and CN and CNS groups [22]. It was shown in [24] that simultaneous coordination of Pd(II) both with S atoms and with N atoms is possible. At the same time the band peaked at 1415 cm^{-1} for the red precipitate indicates that NH_2 groups are present in this compound, and the absorption band at 3428 cm^{-1} can be regarded as superposition of bands related to NH_2 and H_2O. The bands at 1380 and 730 cm^{-1} for thiourea and at 1340, 1225, and 780 cm^{-1} for the red precipitate are related to C=S vibrations [23].

CONCLUSIONS

(1) In principle, Pd(II) can be effectively recovered from nitric acid solutions as a $[Pd_2(CN)_4] \cdot H_2O$ complex formed in interaction of aqua acido complexes of palladium(II) with products of thiourea decomposition in solutions with an HNO_3 concentration of 3–6 M.

(2) The compound $[Pd_2(CN)_4] \cdot H_2O$ decomposes upon heating to 500–600°C to a pure metallic Pd powder.

ACKNOWLEDGMENTS

The authors are grateful to G.V. Bondarenko (Institute of Experimental Mineralogy, Russian Academy of Sciences) for measurements of IR spectra of the compounds obtained, to L.A. Tikhomirov (Chernogolovka branch of the Institute of Energy Problems of Chemical Physics, Russian Academy of Sciences) for making helpful suggestions in interpretation of the results obtained and for editing the manuscript, and to A.S. Astakhova (Institute of Problems of Chemical Physics, Russian Academy of Sciences) for elemental analyses of the compounds obtained.

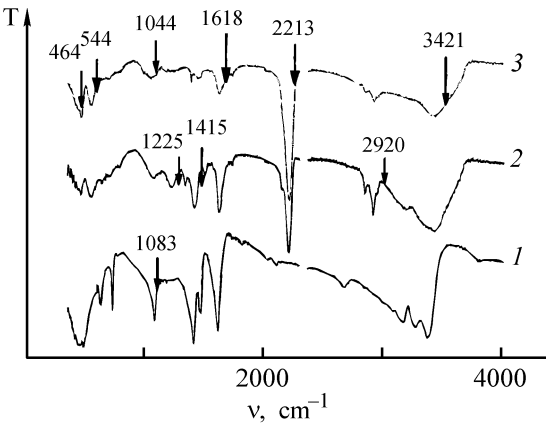

Fig. 4. IR spectra of thiourea and the resulting compounds of palladium(II) with Thio. (T) Transmission and (ν) wave number. Sample: (*1*) thiourea, (*2*) red compound, and (*3*) white compound.

REFERENCES

1. Pokhitonov, Yu.A. and Romanovskii, V.N., *Radiokhimiya*, 2005, vol. 47, no. 1, pp. 3–14.
2. Tikhomirova, V.I., Desyatova, T.A., and Akhmedzhanova, G.M., *Exp. GeoSci.*, 2000, vol. 9, no. 1, pp. 53–55.
3. Tikhomirova, V.I. and Bondarenko, G.V., *Elektron. Nauchinform. Zh. Vestn. Otd. Nauk Zemle Ross. Akad. Nauk*, no. 1(20), 2002; http://www.scgis.ru/russian/cp1251/h_dgggms/1-2002/informbul-1.htm#geoecol-6.
4. Sibirskaya, V.V. and Kukushkin, Yu.N., *Koordin. Khim.*, 1978, vol. 4, no. 7, pp. 963–991.
5. Kramareva, T.V., Shul'man, V.M., and Lavrenova, L.G., *Izv. Sib. Otd. Akad. Nauk SSSR, Ser. khim.*, 1964, no. 7, issue 2, pp. 101–105.
6. Kukushkin, Yu.H., Trusova, K.M., Sibirskaya, V.V., and Samuseva, V.M., *Zh. Neorg. Khim.*, 1977, vol. 22, no. 10, pp. 2781–2784.
7. Beamish, F.E., *The Analytical Chemistry of the Noble Metals*, Oxford: Pergamon, 1966.
8. Klimkovich, E.A., Nashivan'ko, L.V., and Usatenko, Yu.I., *Izv. Vyssh. Uchebn. Zaved., Khim. Khim. Tekhnol.*, 1973, vol. 16, no. 1, pp. 43–46.
9. *Spravochnik po elektrokhimii* (Handbook of Electrochemistry), Sukhotin, A.M., Ed., Leningrad: Khimiya, 1981.
10. *Obshchaya organicheskaya khimiya* (General Organic Chemistry), Kochetkov, N.K., Ed., Moscow: Khimiya, 1982, vol. 3.
11. Lever, A.B.P., *Inorganic Electronic Spectroscopy*, Amsterdam: Elsevier, 1984.
12. Prokof'eva, I.V., Ginzburg, S.I., Pichkov, V.N., et al., *Zh. Anal. Khim.*, 1971, vol. 26, no. 2, pp. 348–353.

13. Maslii, A.I. and Lupenko, G.K., *Izv. Sib. Otd. Akad. Nauk SSSR, Ser. Khim.*, 1974, no. 5, pp. 12–16.
14. Titova, K.V., Loginova, E.M., and Rosolovskii, V.Ya., *Zh. Neorg. Khim.*, 1977, vol. 22, no. 12, pp. 3225–3229.
15. *Khimicheskaya enciklopediya* (Chemical Encyclopedia), Zefirov, N.S., Ed., Moscow: Bol'shaya Ross. Enciklopediya, 1995, vol. 4.
16. Maiorov, V.D. and Librovich, N.B., *Zh. Phys. Khim.*, 1975, vol. 49, no. 11, pp. 2819–2823.
17. Librovich, N.B., Maiorov, V.D., and Vinnik, M.I., *Zh. Phys. Khim.*, 1977, vol. 51, no. 1, pp. 245–246.
18. Maiorov, V.D., Librovich, N.B., and Vinnik, M.I., *Zh. Phys. Khim.*, 1979, vol. 53, no. 4, pp. 1036–1038.
19. *Spravochnik khimika* (Chemist's Reference Book), Nikol'skii, B.P., Ed., Moscow: Khimiya, 1964, vol. 3.
20. Emmanuel', N.M. and Knorre, D.G., *Kurs khimicheskoi kinetiki* (A Course of Chemical Kinetics), Moscow: Vysshaya Shkola, 1962.
21. Yamaguchi, A., Penland, R.B., Mizushima, S., et al., *J. Am. Chem. Soc.*, 1958, vol. 80, no. 3, pp. 527–529.
22. Nakamoto, K., *Infrared Spectra of Inorganic and Coordination compounds*, New York: John Wiley, 1963.
23. Socrates, G., *Infrared Characteristic Group Frequencies: Tables and Charts*, Chichester: Wiley John & Sons, 1995, 2nd ed.
24. Simanova, S.A., Burmistrova, N.M., Panina, N.S., et al., *Zh. Prikl. Khim.*, 2000, vol. 73, no. 11, pp. 1813–1818.

ISSN 1070-4272, Russian Journal of Applied Chemistry, 2007, Vol. 80, No. 10, pp. 1643–1646. © Pleiades Publishing, Ltd., 2007.
Original Russian Text © I.V. Bachurina, M.A. Ilyushin, I.V. Tselinskii, Yu.A. Gruzdev, 2007, published in Zhurnal Prikladnoi Khimii, 2007, Vol. 80, No. 10, pp. 1613–1616.

INORGANIC SYNTHESIS AND INDUSTRIAL INORGANIC CHEMISTRY

High-Energy Complex Copper(II) Perchlorate with 1,5-Pentamethylenetetrasole as Ligand

I. V. Bachurina, M. A. Ilyushin, I. V. Tselinskii, and Yu. A. Gruzdev

St. Petersburg State Technological Institute, St. Petersburg, Russia

Received April 24, 2007

Abstract—Possibility of obtaining an energy-saturated metal complex, copper tetrakis[cyclopentamethylenetetrasol] perchlorate, was studied by reacting copper(II) perchlorate hexahydrate with cyclopentamethylenetetrazol. The composition and structure of the complex were confirmed by elemental analysis and UV, IR, ^{1}H NMR, and ESR spectroscopies. The thermal decomposition of the metal complex synthesized was analyzed and its explosive characteristics and combustion law, as well as the combustion law of a model formulation of a composite solid propellant with addition of the complex, were determined.

DOI: 10.1134/S1070427207100060

Modern tendencies in the development of rocket technology presume use of fuels with high energy-related characteristics. The specific momentum of the fuels is raised by introduction of energetic components with high heat of combustion, e.g., aluminum. However, this gives rise to the problem of a strong pressure dependence of the combustion velocity of fuels of this kind [1].

This problem can be solved by introduction into fuels of additives that intensify processes occurring in the condensed phase (C-phase).

It is known from the literature that copper complexes containing polynitrous compounds as a ligand can be used as modifiers of composite solid propellants (CSP) [2].

Modifiers based on complex copper perchlorates are use because they not only make weaker the pressure dependence of the combustion velocity of CSP, but also make faster the total combustion velocity of the fuels. In this case, the cation catalyzes the combustion velocity on the molecular level [3, 4].

We studied as a potential modifier of the combustion process of CSP the previously obtained complex copper(II) tetrakis-(1,5-pentamethylenetetrazol) perchlorate [complex (1)]:

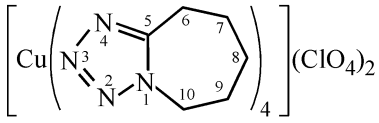

Complex (1)

Previously, complex (1) has been prepared in a solution of 2,2-dimethoxypropane in 96% yield [5].

Because of the high cost and deficiency of 2,2-dimethoxypropane, a search was carried out for alternative solvents and, in particular, the possibility of using water and isopropyl alcohol was analyzed.

1,5-Pentamethylenetetrazol (PMT) contains "pyridine nitrogen atoms" and has a high dipole moment (6.14 D). It exhibits both weak basic and weak acid properties [6, 7]. In the spectrochemical series of ligands, it occupies a place between water and ammonia [8]. In view of this circumstance, we can assume that it will replace water in the inner sphere of copper perchlorate hexahydrate, to form compounds with a neutral form of the ligand. The complex was synthesized by the following scheme:

$$Cu(ClO_4)_2 \cdot 6H_2O + 4PMT \rightarrow [Cu(PMT)_4](ClO_4)_2.$$

With water used as a solvent, the product yield is about 60%; with isopropyl alcohol (IPA), a minor amount of ethyl acetate (25% relative to the IPA volume) is to be added to the reaction mass for precipitating the target product. The yield of the product is about 80%.

IR spectra of the complexes synthesized contain absorption bands of all the fragments: coordinated pentamethylene and tetrazol rings, perchlorate anions.

Data furnished by ^{1}H NMR spectroscopy for a free ligand and the copper complex are listed in Table 1.

Table 1. Chemical shifts of protons in PMT and complex (1)

Compound	δ_1	δ_2	δ_3	δ_4	δ_5
	ppm				
PMT	1.68	1.80	1.91	3.07	4.51
$[Co(PMT)_4](ClO_4)_2$	1.57	1.70	1.81	2.92	4.41

As can be seen from Table 1, the methylene group bonded to the carbon atom of the tetrazol ring shows a stronger hypsochromic shift, compared with the methylene group bonded to N^1 nitrogen atom of the ring, which evidences in favor of the coordination of ligands at the N^4 nitrogen atom of the tetrazol ring.

An analysis of the UV spectrum of complex (1) demonstrated that PMT is a monodentate ligand. A single asymmetric absorption band lies in the range 670–800 nm and represents two *d–d* transitions, λ_{max} = 680 nm, ε = 61 (according to published data [9], λ_{max} = 670 nm, ε = 81).

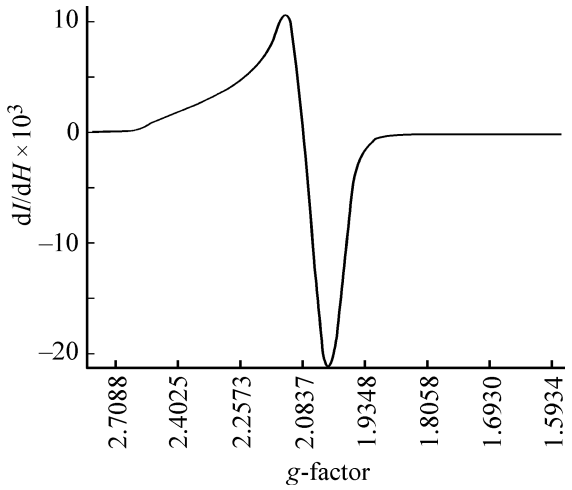

Fig. 1. ESR spectrum of a perchlorate copper complex.

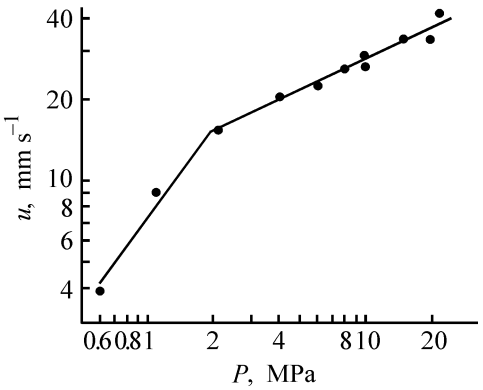

Fig. 2. Combustion velocity *u* of the perchlorate copper complex vs. pressure *P*.

The ESR data for complex (1) demonstrated that the compound obtained has a certain tetragonal symmetry with a distortion along the *Z* axis (Fig. 1).

The whole set of the physicochemical and spectral data we obtained indicates that complexes synthesized in various solvents are identical to the compound reported in the literature [5, 9].

A study of the thermal decomposition of complex (1) under nonisothermal conditions at a heating rate of 5 deg min^{-1} demonstrated its good thermal stability: the onset temperature of fast decomposition exceeds 230°C. In the first stage of decomposition, a 30% decrease in the sample mass is observed in the temperature range 185–235°C, accompanied by an exothermic effect. Probably, one PMT molecule is oxidized in this stage of thermal decomposition by one outer-sphere perchlorate anion. In the second stage of thermal decomposition, in the temperature range 240–305°C, a second PMT molecule is oxidized by the remaining perchlorate anion. The solid residue formed is a copper-containing product of unknown composition and structure.

To assess the possibility of using complex (1) as a catalyst of CSP combustion, we studied the combustion laws of both the complex itself and a model formulation with addition of this complex. A plot describing the pressure dependence of the combustion velocity (combustion law) is shown in Fig. 2.

The perchlorate copper complex we obtained shows two combustion portions with different slopes.

The lower combustion limit of the complex is 0.5 MPa. In the range from 0.5 to 2 MPa, the exponent ν in the combustion velocity law has a value of 1.089, i.e., the combustion process occurs exclusively in the gas phase. Above 2 MPa, the straight line describing the pressure dependence of the combustion velocity has another slope (ν = 0.383) because of the change of the limiting stage of the reaction. At high pressures, the processes occurring in the condensed phase become rate-determining.

The REAL software was used to calculate the combustion temperatures and theoretical composition of the combustion products. As an input parameter for the program we used the enthalpy of formation of the starting metal complex (ΔH_f^0 = 439 kJ kg^{-1}).

The calculated concentrations of the combustion products formed at 10 MPa are listed in Table 2.

The calculated combustion temperature of the complex is 1651 K.

Ballistic tests of model formulations composed of ammonium perchlorate, aluminum, copolymer of 2-methyl-5-vinyltetrazole with methacrylic acid (PMVT) [TU (Technical Specification) 38-403-208–88], and 2% addition of the complex demonstrated the following (Table 3). The exponent ν decreases from 0.71 for the base composition to 0.56, which confirms that the additive exerts positive influence on the processes occurring in the condensed phase.

EXPERIMENTAL

The IR spectra were recorded on a Shimadzu FTIR 8400 spectrophotometer in KBr pellets, and ^{1}H NMR spectra, on a Bruker AC radio spectrometer (working frequency 400 MHz), with DMSO-d_6 as internal standard. The UV spectra were measured with a Perkin–Elmer LAMBDA 40 spectrometer in quartz cuvettes (1 cm). The reaction course was monitored with TLC (UV-254 Silufol plates, 3% aqueous solution of sodium perchlorate as eluent).

A derivatographic analysis was performed on an MOM derivatograph (Hungary) at a heating rate of 5 deg min^{-1}.

The combustion velocity of the model formulation was measured in a BPD-25 bomb at constant pressures of 4 and 10 MPa.

PMT purchased from ACROS ORGANICS (98% purity, mp 58.5°C), copolymer of 2-methyl-5-vinyltetrazole with methacrylic acid (PMVT) (TU 38-403-208–88), and bis-(azidoethyl)-*N*-nitroamine plasticizer were used in the study.

The composition of the model fuel was as follows (%): ammonium perchlorate of C brand (<50 μm) 32, that of A brand (TU 84-942–82, S_{sp} = 12000 cm^2 g^{-1}) 32, aluminum of ASD-6 brand (S_{sp} = 6000 cm^2 g^{-1}) 6, binder and plasticizer 28, and complex (1) 2.

General procedure for synthesis of complex (1). Synthesis in an aqueous medium. To a solution of copper perchlorate (0.91 g) in 30 ml of water was added, under stirring at room temperature, a calculated amount of PMT (1.36 g), and the reaction mass was heated at 60°C for 2 h. The precipitate formed on cooling the mixture to 17°C was filtered off, washed with ethyl acetate (20 ml), and recrystallized from 30 ml of isopropyl alcohol, to give 0.61 g (60%) of a light blue product. IR spectrum, ν (cm^{-1}): 2860 (ν_s CH_2); 1925 (ν_{as} CH_2); 1454 (N=N); 1352, 1337 (C=N); 1282, 1268 (N–N); 1100–800 (Tz). ^{1}H NMR spectrum, δ (ppm): 4.41 (2H, s, CH_2–N), 2.92 (2H, s, CH_2–C), 1.81 (2H, s, C-7), 1.70 (2H, s, C-9), 1.57 (2H, s, C-8).

Found (%): C 34.99, H 5.1, N 27.49.

$C_{24}H_{40}Cl_2CuN_{16}O_8$.

Calculated (%): C 35.4, H 5.95, N 27.5.

Synthesis in isopropyl alcohol. To a solution of copper perchlorate (0.91 g) in 35 ml of isopropyl alcohol was added, under stirring at room temperature, a calculated amount of PMT (1.36 g), and the reaction mass was heated to 60°C and kept at this temperature for 1 h. On cooling the mixture to 17°C, a small amount of ethyl acetate (~5–10 ml) was added and the precipitate formed was filtered off, washed with ethyl acetate (20 ml), and recrystallized from 30 ml of isopropyl alcohol, to give 0.81 g (80%) of a light

Table 2. Calculated composition of the combustion products of complex (1)

Combustion product*	Concentration, mol kg^{-1}
C(c)	18.270
Cu(c)	1.218
HCl	2.444
N_2	9.788
H_2	17.459
CH_4	2.436
CO	8.534

* Trace amounts (mol kg^{-1}): CO_2 0.184, H_2O 0.910, HCN 0.013, and NH_3 0.040.

Table 3. Effect of complex (1) on the combustion of the model CSP

Formulation	Coefficients of the combustion velocity law $U = AP^{\nu}$		U^*_{10}	U^*_4
	A	ν	wt %	
Composition:				
base	11.1	0.71	47.2	26.6
with addition of 2%$[Cu(PMT)_4](ClO_4)_2$	16.1	0.56	58.4	35.0

* U_{10} is the combustion velocity at a pressure of 10 MPa, and U_4, that at 4 MPa.

blue product. IR spectrum, ν (cm^{-1}): 2860 (ν_s CH_2); 1925 (ν_{as} CH_2); 1454 (N=N); 1352, 1337 (C=N); 1282, 1268 (N–N); 1100–800 (Tz). ^1H NMR spectrum, δ (ppm): 4.41 (2H, s, CH_2–N); 2.92 (2H, s, CH_2–C); 1.81 (2H, s, C-7), 1.70 (2H, s, C-9), 1.57 (2H, s, C-8).

Found (%): C 35.2, H 5.2, N 27.26.

$C_{24}H_{40}Cl_2CuN_{16}O_8$.

Calculated (%): C 35.4, H 5.95, N 27.5.

CONCLUSIONS

(1) Copper(II) tetrakis-[1,5-pentamethylenetetrasol] perchlorate can be successfully obtained in an aqueous solution or in isopropyl alcohol.

(2) Copper(II) tetrakis-[1,5-pentamethylenetetrasol] perchlorate is a promising catalyst of combustion of solid propellants.

ACKNOWLEDGMENTS

The study was financially supported by the Ministry of Education and Science of the Russian Federation (Program "Development of the Scientific Potential of Higher School Institutions," subprogram II "Applied Research and Development in Priority Areas of Science and Technology") and by State contract no. 02.444.11.7051.

The authors are grateful to V.P. Sidnitskii (Mendeleev Russian University of Chemical Engineering) for assistance in determining the combustion velocity of the complex synthesized.

REFERENCES

1. Popenko, E.M., Cherepanov, S.S., and Sokolov, E.V., *Sbornik trudov Vserossiiskoi nauchno-tekhnicheskoi konferentsii "Uspekhi v special'noi khimii i khimicheskoi tekhnologii"* (Proc. All-Russia Sci.-Techn. Conf. "Advances in Special Chemistry and Chemical Technolofy"), Moscow, 2006, part 2, pp. 84–89.
2. Popenko, E.M., Cherepanov, S.S., and Sokolov, E.V., *Materialy mezhdunarodnoi nauchno-tekhnicheskoi i metodologicheskoi konferentsii "Sovremennye problemy spetsial'noi tekhnicheskoi khimii"* (Proc. Int. Sci.-Techn. and Methodol. Conf. "Modern Problems of Special Technical Chemistry"), Kazan, 2006, pp. 442–445.
3. Rogov, N.G. and Gruzdev, Yu.A., *Fiziko-khimicheskie svoistva porokhov i tverdykh raketnykh topliv* (Physicochemical Properties of Powders and Solid Propellants), St. Petersburg: SPb. Gos. Tekhn. Inst. (Tekhn. Univ.), 2005.
4. Sinditskii, V.P. and Fogel'zang, A.E., *Zh. Ross. Khim. O–va im. D.I. Mendeleeva*, 1997, vol. 41, no. 4, pp. 74–80.
5. Kuska, H.A., D'Itri, F.M., and Popov, A.I., *Inorg. Chem.*, 1966, vol. 5, no. 7, pp. 1272–1277.
6. Lavrenova, L.G., Larionov, S.V., and Ikorskii, V.N., *Zh. Neorg. Khim.*, 1985, vol. 30, pp. 946–967.
7. Ostrovskii, V.A. and Koldobskii, G.I., *Slabye organicheskie osnovaniya* (Weak Organic Bases), Leningrad: Len. Gos. Univ., 1990.
8. Moore, D.S. and Robinson, S.D., *Adv. Inorg. Chem.*, 1988, vol. 32, pp. 171–239.
9. D'Itri, F.M. and Popov, A.I., *Inorg. Chem.*, 1967, vol. 6, no. 3, pp. 597–600.

ISSN 1070-4272, Russian Journal of Applied Chemistry, 2007, Vol. 80, No. 10, pp. 1647–1650. © Pleiades Publishing, Ltd., 2007.
Original Russian Text © L.K. Altunina, V.N. Manzhai, L.A. Stas'eva, M.S. Fufaeva, 2007, published in Zhurnal Prikladnoi Khimii, 2007, Vol. 80, No. 10, pp. 1617–1621.

INORGANIC SYNTHESIS AND INDUSTRIAL INORGANIC CHEMISTRY

Production of Foamed Cryogels by Chemical Gas Generation in an Aqueous Solution of Poly(vinyl Alcohol)

L. K. Altunina, V. N. Manzhai, L. A. Stas'eva, and M. S. Fufaeva

Institute of Petrochemistry, Siberian Division, Russian Academy of Sciences, Tomsk, Russia

Received June 18, 2007

Abstract—Foamed cryogels were produced using the gas liberated in a redox reaction in an aqueous solution of poly(vinyl alcohol). The kinetics of the gas-generating reaction was studied. The mechanical and thermal characteristics of the foamed cryogels obtained were determined.

DOI: 10.1134/S1070427207100072

Cryogels formed from aqueous solutions of poly(vinyl alcohol) (PVA) in a freeze–thaw cycle and possessing properties of elastic bodies have found wide use in biotechnologies and medicine and are promising for technological processes used in extraction and transportation of oil [1]. Introduction of a gaseous phase into the solid cryogel matrix gives foamed cryogels, which can be used as heat-insulating materials and blocking screens of hydraulic works.

There exist various methods for formation of foamed cryogels by mechanical frothing of an aqueous solution of poly(vinyl alcohol) [2]. These are, for example, stirring and shaking of a polymer solution or bubbling of air through a Schott filter. Formation of foamed cryogels requires starting foams that are stable in the course of time. The stability of a foam increases with the polymer concentration in the solution. However, the foams formed by the mechanical method even from a concentrated solution (c_{PVA} = 100 kg m^{-3}) have a destruction time shorter than half an hour, which is obviously insufficient for full freezing of a frothed sample [3]. Any further increase in the polymer concentration in a solution is inadvisable because it leads to a sharp rise in the solution viscosity and makes impossible formation of a finely dispersed and stable foam from this solution. Therefore, it seems unlikely that the mechanical method for preparation of gas-saturated systems with large foam ratio could be used in practice. In addition, the foamed cryogels formed by the mechanical method have unstable and poorly reproducible properties. Therefore, to prepare a stable starting foam with a large volume ratio, we used the chemical gas-generation method in which the following reactions occurring in the acid medium were performed in the polymer solution:

$$NH_4Cl + NaNO_2 \rightarrow NaCl + 2H_2O + N_2\uparrow, \quad (1)$$
$$\Delta H = -309 \text{ kJ};$$

$$NH_4NO_3 + NaNO_2 \rightarrow NaNO_3 \cdot 2H_2O + N_2\uparrow, \quad (2)$$
$$\Delta H = -314 \text{ kJ};$$

$$NH_4CNS + 4NaNO_2 + 2H^+ \rightarrow Na_2SO_3 + 2Na^+ + 3H_2O + CO_2\uparrow + 3N_2\uparrow, \quad (3)$$
$$\Delta H = -1486 \text{ kJ};$$

$$(NH_4)_2CO_3 + NaNO_2 + 2H^+ \rightarrow NaNO_2 + 2NH_4^+ + H_2O + CO_2\uparrow, \quad (4)$$
$$\Delta H = -52 \text{ kJ}.$$

The advantage of the first three redox reactions is that they are accompanied by pronounced heat release and warming-up of the reaction mixture (Fig. 1). It

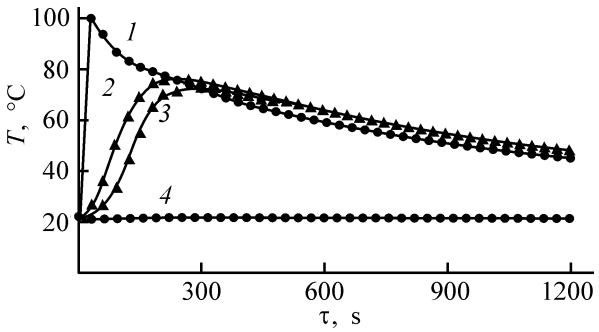

Fig. 1. Temperature T (°C) of aqueous solutions containing aluminum chloride vs. time τ. Reagents and concentrations (M), respectively: (*1*) $c_{NH_4CNS} = c_{NaNO_2} = 2.5$; (*2*) $c_{NH_4Cl} = c_{NaNO_2} = 2.5$; (*3*) $c_{NH_4NO_3} = c_{NaNO_2} = 2.5$; (*4*) $c_{NaNO_2} = 2.5$, $c_{(NH_4)_2CO_3} = 1.15$.

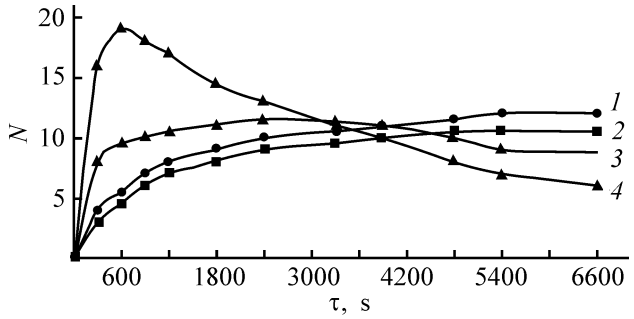

Fig. 2. Foam ratio N vs. the reaction time τ in poly(vinyl alcohol) solutions with a 50 g l^{-1} concentration in the presence of 1.25 M sodium nitrate and 0.05 M aluminum chloride. Additive: (*1*) NH_4Cl, (*2*) NH_4NO_3, (*3*) $(NH_4)_2CO_3$, and (*4*) NH_4CNS. Concentration of an additive (M): (*1*, *2*, *4*) 1.25 and (*3*) 1.15.

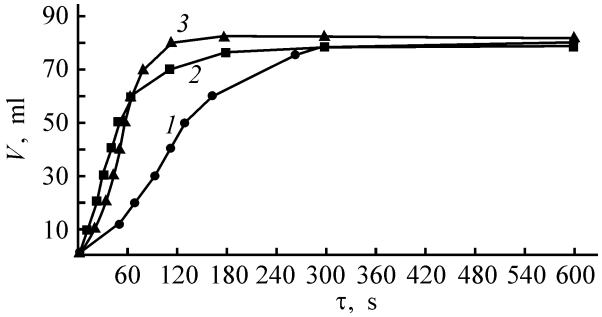

Fig. 3. Amount of evolved gas V vs. aluminum chloride concentration c_{AlCl_3} in interaction of equimolar solutions of sodium nitrite (c_{NaNO_2}) and ammonium chloride (c_{NH_4Cl}). $c_{NaNO_2} = c_{NH_4Cl} = 2.5$ M. (τ) Time. $AlCl_3$ concentration (M): (*1*) 0.116, (*2*) 0.35, and (*3*) 1.05.

is known that, in storage of a PVA solution at temperatures below 40°C, macromolecules associate and the polymer solution stratifies because of the sedimentation of supramolecular formations that have a somewhat higher density than the solvent [4].

These density fluctuations of the polymeric substance in the starting solution adversely affect the strength of foamed cryogels produced from this solution. The heat released in exothermic reactions homogenizes the starting poly(vinyl alcohol) solution.

The foams have low heat conductivity [5] and, therefore, a certain time is required to freeze them in production of a foamed cryogel. Therefore, only stable frothed systems can be used in practice. The variation of the foam ratio in reactions (1)–(4) in the polymer solutions in which competing processes of foam formation and destruction occur simultaneously is demonstrated in Fig. 2. The foam column increases or settles down, depending on which process dominates at a given instant of time. As follows from Fig. 2, the presence of carbon dioxide adversely affects the foam strength (Fig. 2, curves *3*, *4*); the foam already starts to disintegrate 1 hour after being formed. Consequently, it seems unpromising to use reactions (3) and (4) to produce foamed cryogels.

The most stable foam is formed in systems containing ammonium chloride or nitrate as a reducing agent. In the course of reactions (1) and (2), the volume of finely dispersed foam gradually increases, reaches a maximum in 2 h, and is preserved without any visually observed disintegration during several hours. Reaction (1) also yields, in addition to nitrogen, sodium chloride, whose presence makes the foamed cryogel stronger and improves its thermal stability [3]. Therefore, just the gas-generating reaction (1) was chosen as the optimal way to further formation of foamed cryogels after a freeze–thaw cycle of the frothed system. This reaction is catalyzed by weak acids.

The gaseous product formed by reaction (1) is nitrogen in a weakly acid medium (pH > 5) and nitrogen oxide oxidized to nitrogen dioxide in the presence of atmospheric oxygen at pH < 4 [reaction (1a)]. As a catalyst was chosen aluminum chloride, whose aqueous solutions have pH 3 to 7 at different concentrations of the hydrolyzed salt. Simultaneous reactions occur in these solutions. Depending on the acidity of the medium, the dominant reaction is (1) or disproportionation of the nitrite anion [reaction (1a)]:

$$3NaNO_2 + 2H^+ \rightarrow 2Na^+ + NaNO_3 + H_2O + 2NO, \quad (1a)$$

$$\Delta H = -167 \text{ kJ}.$$

The results obtained in determining the influence exerted by the concentration and catalyst on the volume and chemical nature of the evolving gas are shown in Fig. 3. It can be seen that, at the aluminum chloride concentration $c_{AlCl_3} = 0.3$ M, the rate of the redox reaction (1) is the highest At lower catalyst concentrations ($c_{AlCl_3} = 0.1$ M) the reaction rate is slower and the total amount of nitrogen evolved in a rather long period of time (more than 600 s) tends to a limiting value (curve *1*). At a catalyst concentration raised to 1 M, i.e., in a more acid medium, the reaction occurs in two directions to give both nitrogen and nitrogen oxide. In this case, reaction (1a) is dominant (curve *3*). The total volume of the gas evolved in this reaction is somewhat smaller because only 2/3 mol of nitrogen dioxide is formed in this reaction per mole of the oxidant. To preclude release of a chemically active "brown gas" in further experiments on frothing of a polymer solution, we used

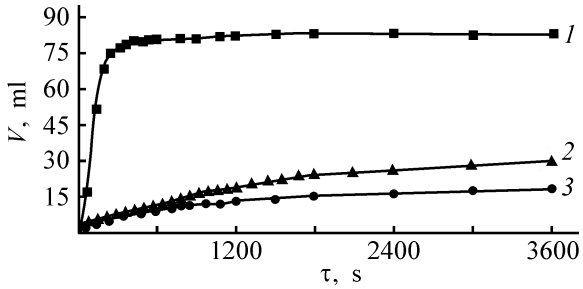

Fig. 4. Volume V of nitrogen evolved in oxidation of ammonium chloride with sodium nitrite vs. the reaction time τ. NH_4Cl, $NaNO_2$ concentration (M): (*1*) 2.5, in water; (*2*) 1.25, in water; (*3*) 1.25, in poly(vinyl alcohol) solution (c_{PVA}).

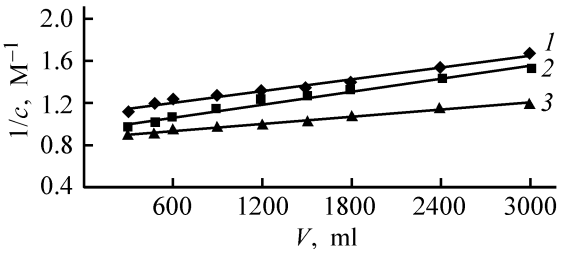

Fig. 5. Inverse concentration c of the reagents vs. the time τ of ammonium chloride oxidation with sodium nitrite in the presence of aluminum chloride. c_{AlCl_3} = 0.05 M. Solution (M): (*1*) aqueous, $c_{NH_4Cl} = c_{NaNO_2}$ = 1.25; (*2*) aqueous, $c_{NH_4Cl} = c_{NaNO_2}$ = 2.5; (*3*) polymer, c_{PVA} = 50, $c_{NH_4Cl} = c_{NaNO_2}$ = 1.25.

aluminum chloride in concentrations lower than 0.1 M, which results in that only nitrogen is released.

To form the foamed cryogel with prescribed foam ratio (gas saturation) at negative temperatures, it is necessary to know kinetic properties of the redox reaction (1) in a pure solvent (water) and in a polymer solution. The reaction of sodium nitrite and ammonium chloride was studied on a gas-meter installation. The concentrations of the reagents (oxidizing and reducing agents) in the solutions were varied, whereas the catalyst concentration was constant (0.05 M). The results of the experiments are shown in Fig. 4.

Based on the empirical data (Fig. 4), which are represented in Fig. 5 as a dependence of the inverse reagent concentrations on time, we found a second order for the reaction described by the kinetic equation

$$1/c = 1/c_0 + k\tau,$$

where τ is the reaction time; k, rate constant of the reaction; c_0, initial concentration of the reagents; and c, running concentration at instant of time τ.

The slopes of the straight lines *1* and *2* in Fig. 5 are the same [$k_w = 0.24 \times 10^{-3}$ l (s mol)$^{-1}$ at 25°C], i.e., the rate constant of reaction (1) in water is independent of the reagent concentrations. The decrease in the slope of the straight line *3* and, consequently, in the rate constant of the redox reaction in the polymer solution (c_{PVA} = 50 g l^{-1}) to a value $k_{PVA} = 0.14 \times 10^{-3}$ l (s mol)$^{-1}$ is due to the diffusion hindrance to motion of reagent molecules in the viscous polymeric medium. The experimentally determined rate constants of the reaction between sodium nitrite and ammonium chloride in water (k_w) and in polymer solution (k_{PVA}) at other temperatures are listed in Table 1. The activation energies of the reaction and the pre-exponential factors of the equation in water and polymer solution (E_w, A_w and E_{PVA}, A_{PVA}, respectively) were calculated using the Arrhenius equation from the empirical data in Table 1: $E_w \approx E_{PVA} \approx$ 60 kJ mol^{-1}, $A_w = 6.76 \times 10^6$ l (s mol)$^{-1}$ and $A_{PVA} = 4.14 \times 10^6$ l (s mol)$^{-1}$.

Using the kinetic pattern of chemical frothing of the polymer solution, elucidated in this study, i.e., varying the concentrations of the gas-generating components and the time of foam formation at positive temperatures (before the freeze stage), we obtained foamed cryogel samples with various compositions and viscosities. To form elastic foamed cryogels, viscous-flow polymer foams were frozen at –22°C for 20 h and thawed at 20°C in the course of 4 h.

Tests of the foam cryogels obtained demonstrated that they retain their stability when in contact with distilled and mineralized water, or with alkaline solutions and hydrocarbon liquids with various polarities. Samples of foamed cryogels are also stable in media with moderate acidity and disintegrate only in concentrated mineral acids.

Table 1. Rate constants of the reaction of sodium nitrite and ammonium chloride in water and a polymer solution at various temperatures

Run no.	T, °C	k_w	k_{PVA}
		l (s mol)$^{-1}$	
1	30	0.00028	0.00019
2	35	0.00044	0.00030
3	40	0.00076	0.00038
4	45	0.00090	0.00056

Table 2. Mechanical and thermal characteristics of foamed cryogels

Run no.	Composition	Concentration, g l^{-1}	Foam ratio	λ,* W (K m)$^{-1}$	G,* kPa	T_m, °C
1	PVA	50	1	0.34	5	73
	H_2O	950				
2	PVA	100	1	0.33	30	73
	H_2O	900				
3	PVA	50	2	0.26	6	110
	NaCl	100				
	Carbon black	30				
	H_2O	820				
4	PVA	100	5	0.14	7	85
	$NaNO_2$	70				
	NH_4Cl	60				
	H_2O	770				
5	PVA	50	10	0.12	2	85
	$NaNO_2$	70				
	NH_4Cl	60				
	H_2O	820				
6	PVA	50	5	0.14	3	85
	$NaNO_2$	70				
	NH_4Cl	60				
	H_2O	820				
7	PVA	50	5	0.14	5	80
	$NaNO_2$	70				
	NH_4Cl	60				
	Carbon black	30				
	H_2O	790				
8	PVA	50	5	0.14	4	110
	$NaNO_2$	70				
	NH_4Cl	60				
	NaCl	40				
	H_2O	780				
9	PVA	50	5	0.14	7	110
	$NaNO_2$	70				
	NH_4Cl	60				
	Carbon black	50				
	NaCl	40				
	H_2O	730				

* λ, heat conductivity coefficient; G, elastic modulus.

The results obtained in the study for the mechanical and thermal properties of the foamed cryogels of various compositions are presented in Table 2.

For run nos. 1 and 2, data for solid cryogels without a gas phase are presented. The foamed cryogel obtained by mechanical bubbling of a gas through a viscous polymer solution has a coarsely cellular structure and small foam ratio (run no. 3). The foamed cryogels formed by chemical frothing of the polymer solution (run nos. 4–9) have a finely dispersed structure and large foam ratio and, therefore, their heat conductivity coefficients are the lowest. To improve the rigidity (elastic modulus) and thermal stability (melting point), technical-grade carbon (carbon black) and sodium chloride were additionally introduced into some of foamed cryogel samples.

CONCLUSIONS

(1) The foam produced by the chemical method is stable and has finely dispersed structure and large foam ratio, which cannot be obtained in a highly viscous polymer solution by the mechanical method.

(2) The product of the reaction suggested for preparation of foamed cryogel is, in addition to nitrogen, sodium chloride, whose presence strengthens the foamed cryogel and makes higher the melting point of the gas-saturated material.

(3) The foamed cryogels formed by the chemical method do not lose elasticity at temperatures of up to –20°C, which enables their use as blocking or heat-insulating materials at negative temperatures without any threat of destruction of technological constructions.

REFERENCES

1. Lozinsky, V.I., *Usp. Khim.*, 2002, vol. 71, no. 6, pp. 559–585.
2. Lozinsky, V.I. and Damshkaln, L.G., *J. Appl. Polymer Sci.*, 2001, vol. 82, pp. 609–1619.
3. Altunina, L.K., Manzhai, V.N., and Fufaeva, V.I., *Zh. Prikl. Khim.*, 2006, vol. 79, no. 10, pp. 1689–1692.
4. Ushakov, S.N., *Polivinilovyi spirt i ego proizvodnye* (Polyvinyl Alcohol and Its Derivatives), Moscow: Akad. Nauk SSSR, 1960.
5. Tichomirov, V.K., *Peny: Teoriya i praktika ikh polucheniya i razrusheniya* (Foams: Theory and Practice of Their Formation and Disintegration), Moscow: Khimiya, 1983.

ISSN 1070-4272, Russian Journal of Applied Chemistry, 2007, Vol. 80, No. 10, pp. 1651–1655. © Pleiades Publishing, Ltd., 2007.
Original Russian Text © V.A. Kovalevich, A.L. Gulevich, E.M. Rakhman'ko, 2007, published in Zhurnal Prikladnoi Khimii, 2007, Vol. 80, No. 10, pp. 1622–1626.

PHYSICOCHEMICAL STUDIES OF SYSTEMS AND PROCESSES

Calculation of Equilibrium in Anion-Exchange Extractive Systems

V. A. Kovalevich, A. L. Gulevich, and E. M. Rakhman'ko

Belarussian State University, Minsk, Belarus

Received October 23, 2006; in final form, April 2007

Abstract—Anion-exchange extractive systems based on solutions of higher quaternary ammonium salts in the presence of solvating additives, derivatives of trifluoroacetophenone, were considered. A mathematical model of the extractive system was developed and average solvation numbers and constants of solvation of ClO_4^-, SCN^-, Br^-, and NO_3^- ions by variously structured derivatives of trifluoroacetophenone were calculated from experimental data.

DOI: 10.1134/S1070427207100084

At present, the most efficient way to enhance the extraction of anions by higher quaternary ammonium salts (QAS) is modification of the phase of the liquid anion exchanger with solvating additives, derivatives of trifluoroacetophenone [1]. The best-known solvating additive is hexyl ester of *n*-trifluoroacetyl-benzoic acid (HE) [2, 3]. Introduction of this substance into the organic phase can sharply enhance the anion-exchange extraction of doubly charged carbonate and oxalate anions [3–5], and of virtually all organic anions containing a –COOH group [1]. The magnitude of the effect is directly proportional to the HE content of the extractive agent, being equal to 1.5–2 orders of magnitude at its content of 0.01 M. In [1, 6], even more effective solvating additives, nitro and halo derivatives of trifluoroacetophenone, were described.

The main difficulty encountered when studying extractive systems of this kind consists in correct interpretation of the experimental data obtained, specifically, in calculating the stoichiometry of the solvates being formed and anion-exchange extraction constants and solvation constants.

In this communication, a mathematical model of an anion-exchange extractive system and an algorithm for calculation of constants, based on Mathematica 5.0 software, are suggested.

EXPERIMENTAL

Toluene solutions of a trinonyloctadecylammonium picrate salt $(C_9H_{19})_3C_{18}H_{37}N^+Dye^-$(TNODA) were used as an anion exchanger. The starting iodide salt of TNODA, which contained more than 99.7 wt % main substance, was converted to the picrate form by the extraction method [1]. The aqueous phase of the extractive systems was in the form of solutions of sodium perchlorate, rhodanide, bromide, and nitrate. Trifluoroacetophenone derivatives listed in Table 1 were used as solvating additives.

Table 1. Solvating additives used in the study

Solvating additive	Designation	Distribution constant in the toluene–water system, P_s
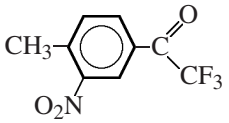	S13	102 ± 21
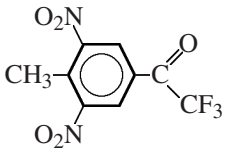	S14	2.6 ± 0.3
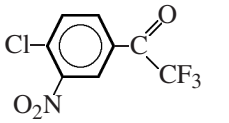	S17	11.1 ± 0.9
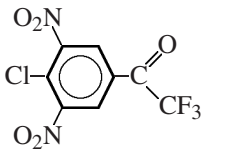	S18	2.5 ± 0.4

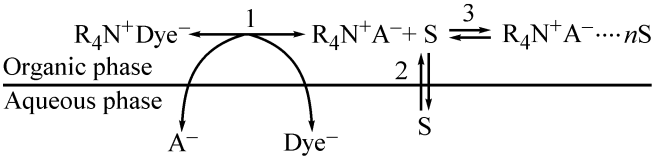

Fig. 1. Scheme of the anion-exchange extractive system. $R_4N^+Dye^-$, extractive agent in the form of a dye; A^-, anion being extracted; S, solvating agent; and *n*, average solvate number.

The extraction was carried out in test tubes with ground-in stoppers at a 1 : 1 phase volume ratio at a temperature of 293 ± 1 K. After the extraction, the aqueous phase was separated and filtered and the content of picrate ions in the aqueous phase was determined on an SF-26 spectrophotometer [7].

The set of equilibria in extractive systems of this kind can be represented by the scheme shown in Fig. 1. Three principal equilibria can be distinguished in this system: (1) anion-exchange equilibrium, (2) equilibrium of a solvating additive distribution among the aqueous and organic phases, and (3) equilibrium of solvate formation in the organic phase:

$$R_4N^+Dye^- + A^- \overset{K_{Dye^-}^{A^-}}{\rightleftarrows} R_4N^+A^- + Dye^-, \quad (1)$$

$$S_{aq} \overset{P_s}{\rightleftarrows} S_{org}, \quad (2)$$

$$R_4N^+A^- + nS_{org} \overset{K_s}{\rightleftarrows} R_4N^+A^-\ldots nS. \quad (3)$$

It has been experimentally confirmed that QAS in the form of a dye is virtually not solvated by S molecules. In addition, the scheme disregards QAS dissociation in the organic phase because of the very low dissociation constants (approximately 10^{-24} [9]).

Equilibria (1)–(3) are described by the exchange constant K_{Dye}^{A}, distribution constant P_s, and solvation constant K_s:

$$K_{Dye^-}^{A^-} = \frac{[R_4N^+A^-][Dye^-]}{[R_4N^+Due^-][A^-]}, \quad (4)$$

$$P_s = \frac{[S]_{org}}{[S]_{aq}}, \quad (5)$$

$$K_s = \frac{[R_4N^+A^-\cdots nS]}{[R_4N^+A^-][S]_{org}^n}. \quad (6)$$

Of the 11 parameters that appear in expressions (4)–(6), only four are known: the exchange constant K_{Dye}^{A} (determined in the absence of a solvating additive), distribution constant P_s (additionally found from experimental results), and equilibrium concentration of the dye in the aqueous phase $[Dye^-]$ (determined spectrophotometrically).

Because the initial concentrations of the extractive agent, anion being extracted, and solvating additive are known, we can write additional four independent equations that reflect the material balances for the anion being extracted (7), dye (8), QAS cation (9), and solvating additive (10):

$$c_{0,A^-} = [A] + [R_4N^+A^-] + [R_4N^+A^-\cdots nS], \quad (7)$$

$$c_{0,R_4Dye^-} = [R_4N^+Dye^-] + [Dye^-], \quad (8)$$

$$c_{0,R_4Dye^-} = [R_4N^+Dye^-] + [R_4N^+A^-] = [R_4N^+A^-\cdots nS], \quad (9)$$

$$c_{0,s} = [S]_{org} + [S]_{aq} + n[R_4N^+A^-\cdots nS]. \quad (10)$$

As a result, the total number of independent equations is seven at eight unknowns. For this reason, the system of equations cannot be directly solved by numerical methods.

To solve this system of nonlinear equations, we employed the linearization method with the use of iteration procedures. For this purpose, the system of equations (4)–(10) was reduced by a number of algebraic transformations to two equations, one of which can be represented as a linear graphical dependence whose slope rate can be used to judge about the average solvation number. Let us briefly consider this derivation.

Summing up expressions (7) and (8) and subtracting (9), we obtain expression (11), which reflects the principle of anion exchange equivalence:

$$c_{0,A^-} = [A^-] + [Kh]. \quad (11)$$

Equating (8) to (9), we obtain

$$[R_4N^+A^-] = [Dye] - [R_4N^+A^-\cdots nS]. \quad (12)$$

At the same time, it follows from (6) that

$$[R_4N^+A^-] = \frac{[R_4N^+A^-\cdots nS]}{K_s[S]_{org}^n}. \quad (13)$$

Then, we obtain from Eqs. (12) and (13)

$$[R_4N^+A^-\cdots nS] = \frac{[Dye^-]}{1 + \dfrac{1}{K_s[S]_{org}^n}}. \quad (14)$$

Now, substituting (14) into (13) we find $[R_4N^+A^-]$:

$$[R_4N^+A^-] = \frac{[Dye^-]}{1 + K_s[S]_{org}^n}. \quad (15)$$

From Eqs. (8) and (11), we have

$$[R_4N^+Dye^-] = c_{0,R_4N^+Dye^-} - [Dye]. \quad (16)$$

$$[A^-] = c_{0,A^-} - [Dye^-]. \quad (17)$$

Then we substitute (15)–(17) into Eq. (4) to obtain the final equation:

$$K_{Dye^-}^{A^-} = \frac{[Dye^-]^2}{(c_{0,R_4N^+Dye^-} - [Dye^-])(c_{0,A^-} - [Dye^-])} \times \frac{1}{1 + K_s[S]_{org}^n}, \quad (18)$$

which can be rewritten in a more compact form

$$K_{Dye^-}^{A^-} = \frac{\tilde{K}_{Dye^-}^{A^-}}{1 + K_s[S]_{org}^n}, \quad (19)$$

where $\tilde{K}_{Dye^-}^{A-}$ is the conditional exchange constant, which can be easily calculated from the known dye concentration in the aqueous phase:

$$K_{Dye^-}^{A^-} = \frac{[Dye^-]^2}{(c_{0,R_4N^+Dye^-} - [Dye^-])(c_{0,A^-} - [Dye^-])}. \quad (20)$$

Having taken logarithm of (19), we obtain a bilogarithmic equation (21), which is the equation of a straight line, whose slope can be used to determine the average solvation number, and the intercept on the ordinate axis, to find the numeric value of the solvation constant:

$$\log\left(\frac{\tilde{K}_{Dye^-}^{A^-}}{\tilde{K}_{Dye^-}^{A^-}} - 1\right) = \log K_s + n\log[S]_{org}. \quad (21)$$

The equilibrium concentration of a solvating additive, necessary for plotting this bilogarithmic straight line, will be determined by the extent of solvation processes and by the distribution of the solvating additive itself and can also be calculated using appropriate interrelation equations.

From Eq. (4), we find

$$[R_4N^+A^-] = K_{Dye^-}^{A^-}\frac{[R_4N^+Dye^-][A^-]}{[Dye]^-}. \quad (22)$$

The material balance equation (9) for the QAS cation gives

$$[R_4N^+A^-\cdots nS] = c_{0,R_4N^+Dye^-} - [R_4N^+Dye^-] - [R_4N^+A^-]. \quad (23)$$

Substituting (22) into (23), we obtain

$$[R_4N^+A^-\cdots nS] = c_{0,R_4N^+Dye^-} - [R_4N^+Dye^-] - K_{Dye^-}^{A^-}\frac{[R_4N^+Dye^-][A^-]}{[Dye^-]}. \quad (24)$$

With account of (16) and (17), expression (24) takes the form

$$[R_4N^+A^-\cdots nS] = [Dye^-] - K_{Dye^-}^{A^-}(c_{0,R_4N^+Dye^-} - [Dye^-]) \times \left(\frac{c_{0,A^-}}{[Dye^-]} - 1\right). \quad (25)$$

Using Eq. (5), we can express the equilibrium concentration of the solvating additive in the aqueous phase:

$$[S]_{aq} = [S]_{org}/P_s. \quad (26)$$

Further, we find from (10) and (26)

$$[S]_{org} = c_{0,s} - \frac{[S]_{org}}{P_s} - n[R_4N^+A^-\cdots nS] \quad (27)$$

and, after certain rearrangements, obtain

$$[S]_{org} = \frac{P_s}{P_s + 1}(c_{0,s} - n[R_4N^+A^-\cdots nS]). \quad (28)$$

Substituting Eq. (25) into 28), we obtain the final variant of the formula for calculating the equilibrium concentration $[S]_{org}$, which takes into account the distribution of a solvating additive among the aqueous and organic phases:

$$[S]_{org} = \frac{P_s}{P_s + 1}\left[c_{0,s} - n\left\{[Dye^-] - K_{Dye^-}^{A^-}(c_{0,R_4N^+Dye^-} - [Dye^-])\left(\frac{c_{0,A^-}}{[Dye^-]} - 1\right)\right\}\right]. \quad (29)$$

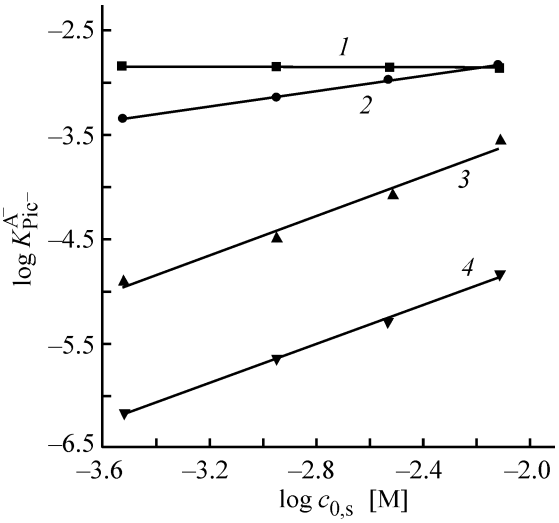

Fig. 2. Effect of the concentration $c_{0,s}$ of solvating additive S18 on the extractability of inorganic anions. ($K^{A^-}_{Pic^-}$) Exchange constant. Anion: (*1*) perchlorate, (*2*) rhodanide, (*3*) nitrate, and (*4*) bromide.

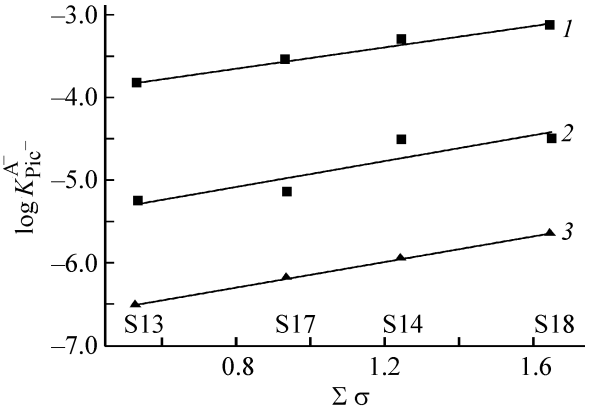

Fig. 3. Dependence of the constants of exchange of anions for the picrate ion, $K^{A^-}_{Pic^-}$, on the sum of the Hammett σ constants of substituents, plotted on the semilog scale. Concentration of solvating additives 1×10^{-4} M. Anion: (*1*) rhodanide, (*2*) nitrate, and (*3*) bromide. Equations of the straight lines: (*1*) $\log K = -4.17 + 0.65\Sigma\sigma$, $r = 0.992$; (*2*) $\log K = -5.72 + 0.79\Sigma\sigma$, $r = 0.922$; and (*3*) $\log K = -6.93 + 0.78\Sigma\sigma$, $r = 0.999$.

Equations (21) and (29) are solved as follows. A zeroth approximation $n_0 = 1$ is set and $[S]_i$ are calculated for each point. Then the log–log dependence (21) is plotted and its slope is used to calculate the first approximation n_1. Further, if the difference $n_1 - n_0$ exceeds a certain prescribed value (commonly 0.01), n_1 is set as zeroth approximation and the cycle is repeated. This procedure was performed using Mathematica 5.0 software.

As can be seen in Fig. 2, the modification of the organic phase with solvating additives differently affects the extraction of the inorganic anions under study. The extractability of bromide and nitrate anions, quantitatively expressed in terms of the conditional exchange constant $\tilde{K}^{A^-}_{Dye^-}$, sharply increases in the presence of solvating additives, with this dependence being directly proportional to the slope, which is close to unity. The effect of solvating additives on the extractability is substantially weaker for rhodanide anions and absent at all for perchlorate anions. This is also confirmed by the calculated values of the average solvation numbers and solvation constants (Table 2).

As can be seen in Table 2, the average solvation numbers for bromide and nitrate anions are close to unity, i.e., solvates of 1 : 1 composition, ($R_4N^+Br^-\cdots S$) and ($R_4N^+NO_3^-\cdots S$), are formed in the organic phase. The average solvation numbers for rhodanide anions are close to 0.5, and those for perchlorate anions could not be determined because the extractability of this anion is independent of the content of a solvating additive. Accordingly vary between these anions the numeric values of the solvation constants. For bromide and nitrate anions, they are substantially larger, compared with rhodanide anions.

Thus, the efficiency of any separate solvating additive is determined by its content in the organic phase. As for the efficiency of a particular anion, it is governed by the type of distribution of the negative charge over its surface. The higher the negative charge density on an anion, the stronger the influence of a solvating additive.

If the efficiency of additives is considered in relation to their structure, then, as can be seen in Fig. 3, there is a linear relationship between the log-

Table 2. Average solvation numbers and logarithms of solvation constants of some inorganic anions by trifluoroacetophenone derivatives

Anion	S13		S14		S17		S18	
	n	log K_s	*n*	log K_s	*n*	log K_s	*n*	log K_s
SCN^-	0.45 ± 0.09	1.43 ± 0.10	0.43 ± 0.03	2.03 ± 0.10	0.57 ± 0.08	2.16 ± 0.10	0.39 ± 0.01	2.16 ± 0.03
Br^-	1.49 ± 0.04	3.68 ± 0.11	0.86 ± 0.07	3.38 ± 0.19	0.99 ± 0.12	3.21 ± 0.10	1.01 ± 0.09	4.18 ± 0.28
NO_3^-	1.09 ± 0.09	3.55 ± 0.16	1.00 ± 0.06	4.33 ± 0.17	1.25 ± 0.19	4.24 ± 0.25	0.96 ± 0.08	4.36 ± 0.23

arithms of the conditional exchange constants and the sum of the Hammett σ constants of substituents in the structure of trifluoroacetophenone. Thus, the Hammett equation is observed for anion-exchange extractive systems:

$$\log K = \log K_0 + \rho\Sigma\sigma. \quad (30)$$

As expected, the maximum effect was obtained for the S18 structure, which has three electron-acceptor substituents: chlorine in the *para*-position and two nitro groups in *meta*-positions. The existence of relation (30) enables prognostication of the efficiency of solvating additives based on trifluoroacetophenone derivatives in relation to the nature and number of substituents.

CONCLUSIONS

(1) A mathematical model of the $R_4N^+Dye^-$ + S/A^- anion-exchange system was suggested and an algorithm for calculating the solvation constants and average solvation numbers was presented.

(2) The anion-exchange extraction of ClO_4^-, SCN^-, Br^-, and NO_3^- anions with toluene solutions of trinonyloctadecylammonium picrate was studied in the presence of solvating additives, trifluoroacetophenone derivatives of varied structure. The extractability of Br^-, NO_3^-, and SCN^- ions linearly increases with the concentration of solvating additives. The extractability of ClO_4^- is independent of the content of solvating additives in the phase of the quaternary ammonium salt.

(3) A linear correlation was found between $\log K_{Dye^-}^{A^-}$ and the sum of the Hammett σ constants, which enables prognostication of the extraction efficiency of solvating additives of varied structure.

REFERENCES

1. Gulevich, A.L., Anion-Exchange Extraction of Organic Anions with Higher Quaternary Ammonium Salts and Its analytical Application, *Doctoral Dissertation*, Minsk, 2002.
2. Pomelenok, E.V., Effect of the Steric Accessibility of the Exchange Center of Higher Quaternary Ammonium Salts on the Selectivity of Anion-Exchange Extraction, *Cand. Sci. Dissertation*, Minsk, 2004.
3. Gulevich, A.L., Rakhman'ko, E.M., and Podterob, A.P., *Zh. Phys. Khim.*, 1996, vol. 70, no. 12, pp. 2191–2193.
4. Bart, T.Ya., Karavan, V.S., Grekovich, A.L., et al., *Zh. Anal. Khim.*, 1990, vol. 45, no. 7, pp. 1364–1371.
5. Smirnova, A.L., Grekovich, A.L., and Materova, E.A., *Elektrokhimiya*, 1985, vol. 21, no. 10, pp. 1335.
6. Rakhman'ko, E.M., Gulevich, A.L., Kiiko, T.N., and Kovalevich, V.A., *Zh. Prikl. Khim.*, 2006, vol. 79, no. 1, pp. 71–76.
7. Starobinets, G.L., Rakhman'ko, E.M., and Soroka, Zh.S., *Zh. Neorg. Khim.*, 1978, vol. 23, no. 6, pp. 1628.
8. Podterob, A.P., Extraction of Substituted Benzoate Anions with Higher Quaternary Ammonium Salts and Its Analytical Application, *Cand. Sci. Dissertation*, Minsk, 1997.
9. Izmailov, N.A., *Elektrokhimiya rastvorov* (Electrochemistry of Solutions), Moscow: Khimiya, 1976, 3rd revised ed.

ISSN 1070-4272, Russian Journal of Applied Chemistry, 2007, Vol. 80, No. 10, pp. 1656–1660. © Pleiades Publishing, Ltd., 2007.
Original Russian Text © A.K. Pyartman, V.V. Lishchuk, V.A. Keskinov, 2007, published in Zhurnal Prikladnoi Khimii, 2007, Vol. 80, No. 10, pp. 1627–1631.

PHYSICOCHEMICAL STUDIES OF SYSTEMS AND PROCESSES

Kinetics of Thorium(IV) and Lanthanum(III) Extraction from Aqueous Salt Solutions with Composite Material Based on Trialkylamine and Polymeric Support at Various Temperatures

A. K. Pyartman, V. V. Lishchuk, and V. A. Keskinov

St. Petersburg State Institute of Technology (Technical University), St. Petersburg, Russia

Received January 29, 2007

Abstract—The kinetics of thorium(IV) and lanthanum(III) extraction from aqueous salt solutions with a composite material based on trialkylamine and a polymeric support at 293.15–333.15 K was studied. The mass transfer coefficients were found, and the apparent activation energy of the extraction reaction was estimated.

DOI: 10.1134/S1070427207100096

The thorium(IV) and lanthanum(III) extraction with a composite material based on trialkylamine (Alamin-336) and a polymeric support in the presence of 0–4 mol dm^{-3} sodium nitrate in the aqueous phase was studied in [1]. The extraction isotherms were described with regard to the formation of compounds $(R_3NH)_2[Th(NO_3)_6]$ and $(R_3NH)_3[La(NO_3)_6]$ in the phase of the composite material (CM).

To use CM in practice, data on both the equilibrium metal distribution [1] and the kinetic features of extraction at various temperatures are required.

In this study, we examined the kinetics of thorium(IV) and lanthanum(III) extraction from aqueous salt solutions with CM at 293.15–333.15 K.

The composite material is produced by Purolite Company in the form of spherical granules 0.5 mm in diameter, consisting of trialkylamine $[(C_7H_{17}–C_9H_{19})_3N]$ and a polymeric support (super-cross-linked polystyrene). The specific volume of CM is 2.50 ± 0.02 dm^3 kg^{-1}, and the extractant content of the CM phase, 0.97 ± 0.01 mol dm^{-3}. Before extraction, CM was treated with 4.0 mol dm^{-3} HNO_3 and then washed with water to obtain the $R_3NH^+NO_3^-$ form of the extractant [1]. Thorium(IV) and lanthanum(III) nitrates of analytically pure grade were used. The experiments were performed with 0.60 and 0.50 mol dm^{-3} Th^{4+} and La^{3+} solutions in the presence of 0.0, 1.0, 2.0, and 4.0 mol dm^{-3} $NaNO_3$. The thorium(IV) and lanthanum(III) concentrations in the aqueous phase were determined by the method described in [1, 2] with an error of ±1–2 rel %. In the kinetic experiments, the Th^{4+} and La^{3+} concentrations in the CM phase $c_{(o),t}$ (mol dm^{-3}) were found from the equation

$$c_{(o),t} = (c_{(aq),0}V_0 - c_{(aq),t}V_t)/(mV_{sp}), \quad (1)$$

where t is time; $c_{(aq),0}$, concentration (mol dm^{-3}) of Th^{4+} and La^{3+} nitrates in aqueous solution at $t = 0$, with the volume of the aqueous phase V_0 (dm^3); $c_{(aq),t}$, concentration (mol dm^{-3}) of Th^{4+} and La^{3+} nitrates in aqueous solution at the instant of time t, with the volume of the aqueous phase V_t (dm^3); m, weight (kg) of CM sample; and V_{sp}, specific volume (dm^3 kg^{-1}) of CM.

Two series of experiments were performed. In the first series, the kinetic experiments on absorption of Th^{4+} and La^{3+} nitrates were performed in a set of vessels from which samples were taken after different intervals of time. In the second series, sampling was performed successively from one vessel, provided that the change of the aqueous phase volume did not exceed 2–4%. The $c_{(o),t}$ values obtained in the two series of experiments agreed to within 2–5 rel %. In the kinetic experiments, aqueous solutions were thermostatically controlled for 60 min with an accuracy of ±0.2 K, and then a CM sample was introduced into the solution. Solutions with CM were stirred with a turbine stirrer with rotation speeds of 3.3, 5, and 6.7 s^{-1}. To determine the Th^{4+} and La^{3+} concentrations in the CM phase under equilibrium conditions, $c_{(o),eq}$ (mol dm^{-3}), aqueous solutions with CM were

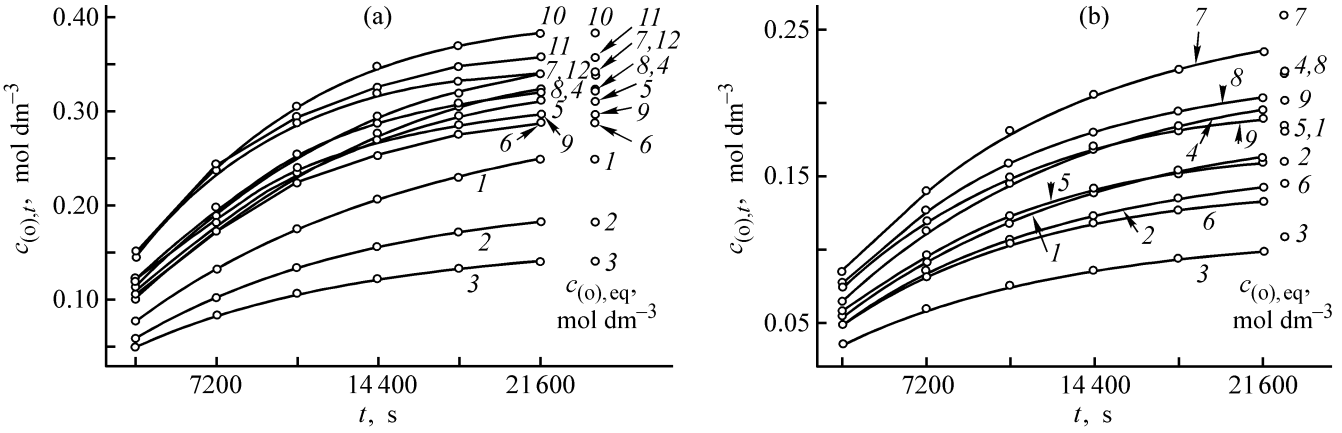

Fig. 1. Dependence of the concentration $c_{(o),t}$ of (a) thorium(IV) and (b) lanthanum(III) nitrates on time t and their equilibrium concentrations $c_{(o),eq}$ in the phase of the composite material. Speed of rotation 3.3 s^{-1}; the same for Fig. 3. $NaNO_3$ (mol dm^{-3}), T (K): (a) (*1*) without salting-out agent, 293.15; (*2*) without salting-out agent, 313.15; (*3*) without salting-out agent, 333.15; (*4*) 1, 293.15; (*5*) 1, 313.15; (*6*) 1, 333.15; (*7*) 2, 293.15; (*8*) 2, 313.15; (*9*) 2, 333.15; (*10*) 4, 293.15; (*11*) 4, 313.15; (*12*) 4, 333.15; (b) (*1*) 1, 293.15; (*2*) 1, 313.15; (*3*) 1, 333.15; (*4*) 2, 293.15; (*5*) 2, 313.15; (*6*) 2, 333.15; (*7*) 4, 293.15; (*8*) 4, 313.15; and (*9*) 4, 333.15; the same for Fig. 3.

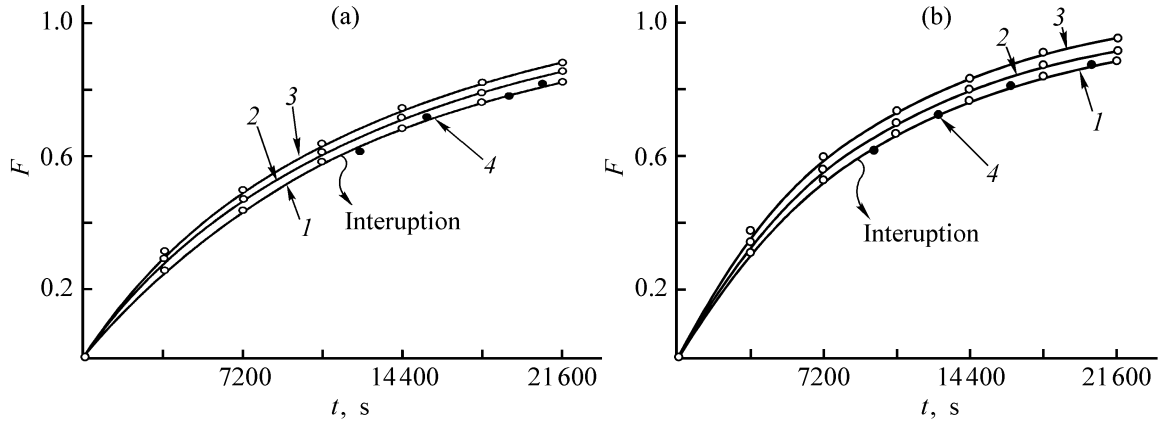

Fig. 2. Dependence of the degree of conversion, F, in extraction on time t at various rates of stirring of aqueous solution-composite material systems and experiments on interruption of metal absorption with the composite material. (a) $Th(NO_3)_4$ aqueous solution, 293.15 K; (b) $La(NO_3)_3$ aqueous solution, 293.15 K, 1 mol dm^{-3} $NaNO_3$, 293.15 K. Speed of rotation (s^{-1}): (*1*) 3.3, (*2*) 5, and (*3*) 6.7; (*4*) experiments with process interruption for 1.5 h.

stored at a given temperature for 3–4 days, then the composition of the aqueous phase was analyzed, and $c_{(o),eq}$ was calculated by Eq (1). In some experiments, absorption of Th^{4+} and La^{3+} nitrates with CM was interrupted on attaining a 40–50% conversion of CM, the CM was separated from the solution by decantation, allowed to stand for 1.5 h, and then the metal ion absorption with CM was resumed at the same temperature and stirring rate.

The dependences of the concentrations of Th^{4+} and La^{3+} nitrates in the CM phase on time at a rotation speed of 3.3 s^{-1} and the equilibrium metal ion concentrations in the CM phase in the absence and presence of sodium nitrate in the aqueous phase are shown in Fig. 1.

The equilibrium concentrations of Th^{4+} and La^{3+} nitrates in the CM phase decrease with increasing temperature at all sodium nitrate concentrations considered and, at a given temperature, increase with the sodium nitrate concentration in the aqueous phase (Fig. 1).

The dependences of the degree of conversion ($F = c_{(o),t}/c_{(o),eq}$) on time at a rotation speed of 3.3, 5, and 6.7 s^{-1} and 293.15 K are shown in Fig. 2. As can be seen, an increase in the rotation speed makes higher the F values at constant time and temperature, which is typical of the film kinetics, when the diffusion across the film at the interface between CM and the aqueous solution phase boundary is the rate-determining stage [3, 4]. Figure 2 also shows the data on

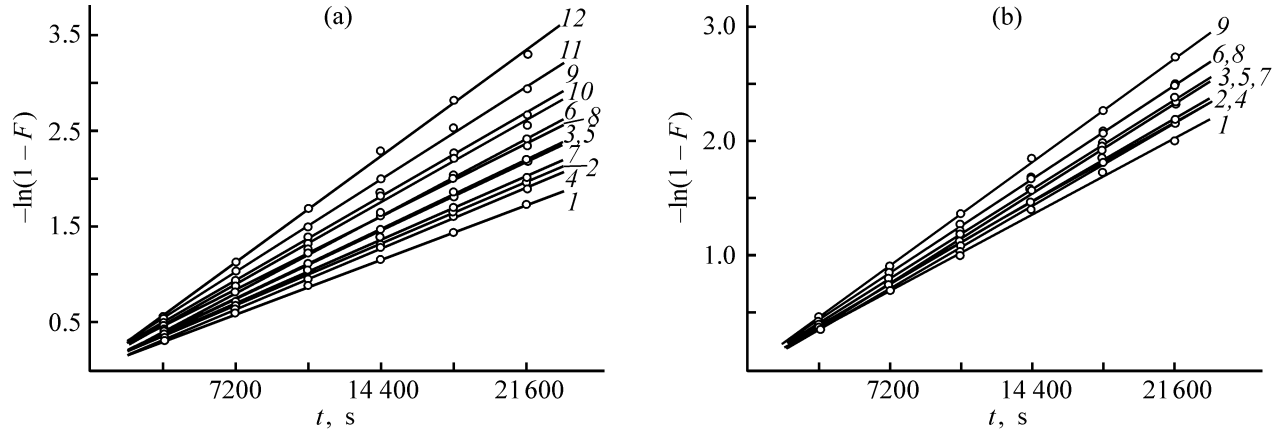

Fig. 3. Dependence of $-\ln(1-F)$ on time t for metal absorption by CM under various conditions.

extraction kinetics in the experiments with interrupted extraction. These data suggest that interruption of extraction for 1.5 h does not noticeably affect the shape of the kinetic curve, i.e., the stage of diffusion within the CM grain is not the rate-determining stage.

The extraction of thorium(IV) and lanthanum(III) nitrates with CM can be represented by the following equation of a heterogeneous reaction [1]:

$$Th^{4+} + 4NO^-_{3(aq)} + 2R_3NHNO_{3(o)} \rightleftarrows (R_3NH)_2[Th(NO_3)_6]_{(o)}, \quad (2)$$

$$La^{3+} + 3NO^-_{3(aq)} + 3R_3NHNO_{3(o)} \rightleftarrows (R_3NH)_3[La(NO_3)_6]_{(o)}, \quad (3)$$

where (aq) is aqueous phase, and (o), CM phase.

In this case, $c_{(o),eq}$ values approach $c_s/2$ and $c_s/3$, where c_s is the extractant concentration in the CM phase (Fig. 1).

To describe the kinetics of extraction of thorium(IV) and lanthanum(III) with CM, we can use the equation [3, 4]

$$dQ/dt = -jS, \quad (4)$$

where Q is the amount of the substance (mol) transferred into the CM phase [$Q = V_{(aq)}(c^0_{(aq)} - c_{(aq),t})$; $V_{(aq)}$, volume of the aqueous phase]; S, surface area (dm^2) involved in the extraction; j, extraction flow (mol s^{-1} dm^{-2}), or specific extraction rate, i.e., the amount of substance extracted in unit time and per unit surface area.

The Q value is numerically equal to the amount of substance in the CM phase at time t [$Q = V_{(o)}c_{(o),t}$; $V_{(o)}$ is CM volume (dm^3)].

The overall equation of the extraction flow, which takes into account the diffusion and chemical resistance [two-film model, presence of thin boundary layers of thickness δ_1 (exhaustive phase is aqueous) and δ_2, dm (extracting phase is CM) at the phase boundary], in the stationary mode is [3, 4]

$$J = \frac{c_{(aq),t} - c_{(aq),eq}}{\frac{\delta_1}{D_1} + \frac{\delta_2}{D_{ex}D_2} + \frac{1}{\vec{K}}}, \quad (5)$$

where D_1 and D_2 are the coefficients of mutual diffusion (dm^2 s^{-1}); $c_{(aq),eq}$, equilibrium concentration (mol dm^{-3}) of Th^{4+} and Ln^{3+} in the aqueous phase; D_{ex}, distribution coefficient, $D_{ex} = c_{(o),eq}/c_{(aq),eq}$; $\vec{K}$, rate constant of the first-order extraction reaction (dm s^{-1}).

Depending on the diffusion and chemical resistances, the extraction process can be controlled by the mass transfer or chemical reaction.

Equations (4) and (5) can be transformed into

$$dc_{(o),t}/dt = S(c_{(o),eq} - c_{(o),t})K/[V_{(o)}D_{ex}]. \quad (6)$$

were K is the mass-transfer constant (dm s^{-1}),

$$\frac{1}{K} = \left(\frac{\delta_1}{D_1} + \frac{\delta_2}{D_{ex}D_2} + \frac{1}{\vec{K}}\right). \quad (7)$$

The mass-transfer coefficient K' (s^{-1}) is equal to

$$K' = SK/[V_{(o)}D_{ex}]. \quad (8)$$

After transformation, Eq. (6) becomes

$$dc_{(o),t}/dt = K'[c_{(o),eq} - c_{(o),t}]. \quad (9)$$

In the semilog form, when $c_{(o),t} = 0$ at $t = 0$, Eq. (6) takes the form

$$\ln(1 - F) = -K't, \quad (10)$$

where F is the degree of conversion.

The dependences of $-\ln(1 - F)$ on t are shown in Fig. 3. In all cases, these dependences are linear at F

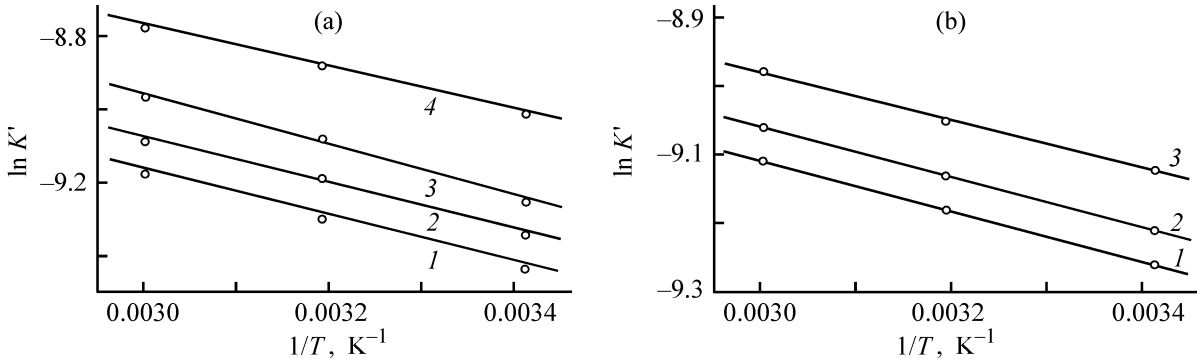

Fig. 4. Dependence of $\ln K'$ on reciprocal temperature T. (a) Thorium(IV) nitrate and (b) lanthanum(III) nitrate. (a) (*1*) Without salting-out agent; $NaNO_3$ (mol dm^{-3}): (*2*) 1, (*3*) 2, and (*4*) 4; (b) (*1*) 1, (*2*) 2, and (*3*) 4.

from 0.1 to 0.8–0.9. This fact indicates that the film kinetics controls the overall process. The calculated $\ln K'$ values under various conditions are shown in Fig. 4. As can be seen, the dependences of $\ln K'$ on reciprocal temperature are linear.

To estimate the apparent activation energy E_a, we used the equation

$$\ln K' = -\frac{E_a}{RT} + \text{const}, \qquad (11)$$

where R is the gas constant.

The E_a values are virtually independent of sodium nitrate concentration (Fig. 4) and amount, on the average, to 5.1 ± 0.3 (Th) and 2.8 ± 0.2 kJ mol^{-1} (La), which is characteristic of diffusion-controlled processes.

The mass transfer coefficients increase with temperature and sodium nitrate concentration in aqueous-salt solution. It follows from Eqs. (5) and (6) that an increase in the distribution coefficient after introducing a salting-out agent should decrease the mass-transfer coefficients. The increase in medium viscosity at increasing electrolyte concentration in the aqueous phase acts in the same direction. At the same time, at constant δ_1, δ_2, D_1, and D_2, the increase in the distribution coefficient decreases the diffusion resistance in the extracting phase and favors an increase in the mass-transfer constant. We believe that the decrease in the diffusion resistance in the extracting phase (decrease in $\delta_2/D_{ex}D_2$), caused by increasing distribution coefficient after introducing a salting-out agent into the aqueous phase, or the possible decrease in δ_1 because of the dehydrating effect of the electrolyte are the major factors causing an increase in the mass-transfer coefficients on raising sodium nitrate content of the aqueous phase (Figs. 3, 4). Differences in $\ln K'$ values between thorium(IV) and lanthanum(III) do not exceed 0.08–0.15 log units (Figs. 3, 4).

The dependence of the mass transfer coefficient on the sodium nitrate concentration in the aqueous phase is described by the equation

$$\ln K' = \ln K'(c_{NaNO_3} = 0) + \theta c_{NaNO_3}, \qquad (12)$$

where parameter θ is virtually independent of temperature and amounts to 0.10 ± 0.01 and 0.043 ± 0.005 for thorium and lanthanum, respectively, i.e., the effect of the supporting electrolyte is stronger for thorium(IV) than for lanthanum(III).

In practice, when using composite materials based on trialkylamine and a polymeric support for thorium(IV) and lanthanum(III) recovery from aqueous salt solutions, the extraction should be performed in the presence of a salting-out agent in the aqueous phase at elevated temperatures. By so doing, the time of the process can be decreased and the maximal equilibrium metal concentration in the CM phase can be attained.

CONCLUSIONS

(1) The diffusion across the phase boundary (film kinetics) is the rate-determining stage of sorption of thorium(IV) and lanthanum(III) nitrates from aqueous salt solutions with a composite material based on trialkylamine and a polymeric support.

(2) The coefficients of mass transfer increase with temperature and the sodium nitrate concentration in the aqueous phase. The E_a values are virtually independent of the sodium nitrate concentration and

amount to 5.1 ± 0.3 (Th) and 2.8 ± 0.2 kJ mol^{-1} (La), which is characteristic of diffusion-controlled processes.

(3) In practice, when using composite materials based on trialkylamine and polymeric support for thorium(IV) and lanthanum(III) recovery from aqueous salt solutions, the extraction should be performed in the presence of a salting-out agent in the aqueous phase at elevated temperatures. By so doing, the time of the process can be decreased and the maximal equilibrium metal concentration in the CM phase can be attained.

REFERENCES

1. Pyartman, A.K., Lishchuk, V.V., and Keskinov, V.A., *Zh. Prikl. Khim.*, 2006, vol. 79, no. 8, pp. 1280–1284.
2. Pyartman, A.K., Kopyrin, A.A., Berinskii, A.E., and Keskinov, V.A., *Radiokhimiya*, 2000, vol. 43, no. 2, pp. 128–130.
3. *Osnovy zhidkostnoi ekstraktsii* (Foundations of Liquid Extraction), Yagodin, G.A., Ed., Moscow: Khimiya, 1981.
4. Zelikman, A.I., Vol'dman, G.M., and Belyavskaya, L.V., *Teoriya gidrometallurgicheskikh protsessov* (Theory of Hydrometallurgical Processes), Moscow: Metallurgiya, 1975.

ISSN 1070-4272, Russian Journal of Applied Chemistry, 2007, Vol. 80, No. 10, pp. 1661–1666. © Pleiades Publishing, Ltd., 2007.
Original Russian Text © V.V. Smolenskii, A.V. Novoselova, A.L. Bove, 2007, published in Zhurnal Prikladnoi Khimii, 2007, Vol. 80, No. 10, pp. 1632–1637.

APPLIED ELECTROCHEMISTRY AND CORROSION PROTECTION OF METALS

Electrochemical Behavior of Ytterbium in an Equimolar Melt of Sodium and Potassium Chlorides

V. V. Smolenskii, A. V. Novoselova, and A. L. Bove

Institute of High-Temperature Electrochemistry, Ural Division, Russian Academy of Sciences, Yekaterinburg, Russia

Received July 30, 2007

Abstract—Electrochemical reduction of Yb(III) ions to Yb(II) was studied in an equimolar NaCl–KCl melt in the temperature range 973–1075 K. Linear, cyclic, and square-wave voltammetry, chronopotentiometry, and potentiostatic electrolysis with tungsten as the working electrode were used in the study.

DOI: 10.1134/S1070427207100102

At present, high-purity rare-earth elements are widely used in various fields of modern technology. Electrochemical recovery and electrorefining in salt melts form a compromise method for production of high-purity rare-earth elements [1–2].

Processing of spent nuclear fuel is another important field of use of salt melts for recovery of rare-earth elements [3]. Lanthanides are present in high-activity wastes as fission products, and, therefore, chemical and electrochemical information about their behavior in regeneration is very important. This is directly associated with calculations of conditional redox potentials of lanthanides and of their principal thermodynamic characteristics [4–14].

There is only scarce published evidence about the behavior of ytterbium compounds in chloride melts. In [15], the redox potential of the Yb(III)/Yb(II) pair in a eutectic LiCl–KCl melt was measured relative to a 1 M Pt(II)/Pt(0) reference electrode and its temperature dependence was presented. The electrochemical behavior of Yb(III) ions at an active electrode (Ni) in an equimolar NaCl–KCl melt was studied at 973 K [16]. It was found that the reaction goes in two stages: Yb(II) ions are formed in the first of these and electrochemical alloying occurs in the second. Transient techniques were used to study the electrochemistry of ytterbium(III) in molten chlorides of alkali metals [17]. The diffusion coefficients of Yb(III) and Yb(II) ions were calculated. Temperature dependences of the conditional standard redox potentials of Yb(III)/Yb(II) were presented and suggestions were made concerning the effect of the cationic composition of the solvent salt on the value of $E^{*}_{\mathrm{Yb(III)/Yb(II)}}$. In [18], the conditional standard redox potentials of Yb(III)/Yb(II) in molten chlorides of alkali metals were estimated using the correlation between aqueous solutions and chloride melts.

The aim of our study was to examine the electrochemical behavior of ytterbium, estimate the conditional standard redox potential of Yb(III)/Yb(II), and calculate the principal thermodynamic characteristics of $YbCl_3$.

EXPERIMENTAL

We paid particular attention to preparation of the starting reagents. Sodium and potassium chlorides of chemically pure grade were used in experiments as solvents. For this purpose, these compounds were dried in a vacuum for a long time, with temperature gradually raised, and then were melted in the atmosphere of an inert gas and after that purified by zone recrystallization [19]. Prior to being used, they were stored in glass ampules filled with argon.

Anhydrous ytterbium trichloride was prepared by chlorination of an appropriate crystal hydrate of the type $YbCl_3 \cdot nH_2O$ (n = 4.5–5.0) by heating in a carbon tetrachloride vapor [20]. The crystal hydrate was produced by dissolving Yb_2O_3 of IbO-L brand [TU (Technical Specification) 48-4-524–90] in hydrochloric acid to pH 1–1.5 and evaporating the solution on a water bath to dryness. The resulting ytterbium chloride had a metal-to-chlorine ratio of 1.0 : 3.01 and did not contain even trace amounts of the oxychloride. The thus prepared $YbCl_3$ was stored in ampules in a box filled with dry nitrogen. The con-

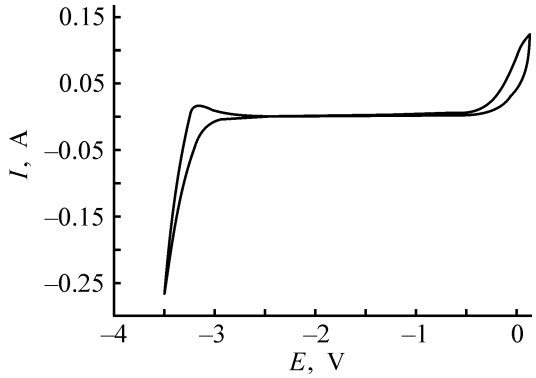

Fig. 1. Cyclic voltammogram of the NaCl–KCl melt at a potential sweep rate of 0.1 V s^{-1} on a W working electrode at 973 K. (*I*) Current strength and (*E*) potential; the same for Figs. 2, 3.

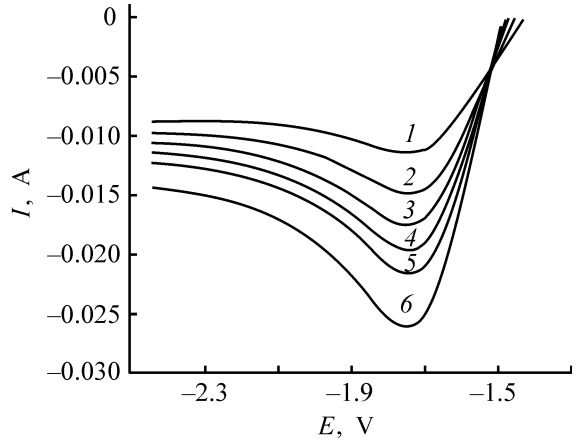

Fig. 2. Linear voltammograms of the NaCl–KCl–$YbCl_3$ melt (m_{YbCl_3} = 3.79×10^{-2} mol kg^{-1}), measured at different potential sweep rates for the reaction Yb(III) + e → Yb(II) on a W working electrode at 973 K. Potential sweep rate (V s^{-1}): (*1*) 0.1, (*2*) 0.2, (*3*) 0.3, (*4*) 0.4, (*5*) 0.6, and (*6*) 0.75.

centration of ytterbium trichloride was 3.9×10^{-2}–1.3×10^{-1} mol kg^{-1} in all the experiments.

We analyzed the electrochemical processes by the following techniques: cyclic, linear, and square-wave voltammetry and chronopotentiometry [21–23]. The measurements were made with an Eco-Chimie Autolab PGSTAT 30 potentiostat-galvanostat with v.4.9 software.

A three-electrode quartz cell with nickel shields was used in the experiments. A tungsten wire of TU 48-9-45–67 brand (diameter 1 mm) with a fixed surface area served as the working electrode. A SU-2000 glassy carbon rod (diameter 3 mm) was used as the counter electrode. The measurements were made relative to a chlorine reference electrode in crucibles made of SU-2000 glassy carbon. The cell was equipped with additional devices for changing the composition of the salt phase at a constant gas phase composition, chlorinating the melt, changing the gas phase composition, and taking samples.

After an experiment, we analyzed the solidified salt cake for the content of Yb^{3+} ions. As shown in [15], when a melt containing ytterbium dichloride is cooled in an inert atmosphere to room temperature, the disproportionation reaction does not occur:

$$3YbCl_2 \rightleftarrows 2YbCl_3 + Yb. \quad (1)$$

Ytterbium was determined in the solidified cake by the atomic-emission method with a Perkin–Elmer Optima 4200 DV optical spectrometer, with inductively coupled plasma as a source of atomization and spectrum excitation [24, 25]. The spectrometer was calibrated against solutions with know ytterbium concentration (100 mg l^{-1}), with a 100-mg l^{-1} chromium solution as internal standard. The concentration in solution samples were measured by determining the intensity ratios of Yb(II) lines at 328.937 or 369.419 nm to those of the internal standard Cr(II) at 267.716 nm. All the solutions used for calibrating the spectrophotometer had an acidity of no less than 2% in terms of hydrochloric acid. The relative measurement error in determining the content of ytterbium did not exceed 3%.

Figure 1 shows a cyclic voltammogram of a NaCl–KCl melt, measured on the tungsten working electrode relative to the chlorine reference electrode at a potential sweep rate of 0.1 V s^{-1} at 973 K. The electrochemical window for the solvent corresponds to reduction of sodium ions and oxidation of chlorine ions.

Upon introduction of ytterbium chloride into the melt, an additional wave appears in the voltammogram (Fig. 2). This wave can be attributed to reduction of trivalent ytterbium ions to the divalent state. Figure 2 shows linear voltammograms of reduction of ytterbium(III) ions, measured relative to the chlorine reference electrode on the tungsten working electrode at different potential sweep rates at 973 K.

A potentiostatic electrolysis at the potentials corresponding to the cathodic current peak did not yield any solid phase on the electrode surface, and the working electrode itself did not undergo any visually observable changes. This means that a soluble product is formed in this stage of the electrochemical process. The wave observed indicates that the electrode reaction occurs in the melt to give Yb(II) ions:

$$Yb(III) + e \rightarrow Yb(II). \quad (2)$$

It was found that the peak current is directly proportional to a square root of the polarization rate in the entire range studied and the potential of the current peak is independent of the logarithm of the potential sweep rate. According to the theory of linear and cyclic voltammetry, the electrode process of reduction of trivalent ytterbium ions to the divalent state is reversible and is controlled by mass transfer. The number n of electrons involved in the electrode reaction was determined by square-wave voltammetry (Fig. 3), by calculating the width of the half-peak ($W_{1/2}$, V) in the range in which the peak current is directly proportional to the square root of the frequency of the signal with the use of the equation [21–23]:

$$W_{1/2} = 3.52\frac{RT}{nF}. \quad (3)$$

Here, $W_{1/2}$ is the half-peak width (V); R, T, n, and F are commonly accepted designations.

Our calculations demonstrated that the number of electrons involved in the reduction of Yb(III) ions to Yb(II) is 0.98 ± 0.1.

To verify the results obtained, we used the method of cyclic voltammetry [21–23]. It was shown that the number of electrons, calculated using the equation

$$E_p^C - E_{p/2}^C = -2.2\frac{RT}{nF}, \quad (4)$$

for the reduction process, is 1.04 ± 0.2 [where E_p^C is the potential of the peak of the cathodic process (V), and $E_{p/2}^C$, the potential of the half-peak of the cathodic process].

It was demonstrated by cyclic voltammetry and chronopotentiometry that the reduction potential of divalent ytterbium ions to the metal in the NaCl–KCl melt is not recorded, because it lies in the range of more negative potentials than the background-decomposition potential.

It is known [26, 27] that tri- and divalent ytterbium ions exist in molten chlorides of alkali metals in the form of complex groups $[YbCl_6]^{3-}$ and $[YbCl_4]^{2-}$. The diffusion coefficients of $[YbCl_6]^{3-}$ ions in the NaCl–KCl melt were calculated by the Randles–Shevchik equation

$$I_p = 0.446(nF)^{3/2}c_0S(Dv/RT)^{1/2}, \quad (5)$$

where I_p is the peak current (A); S, cathode surface area (cm^2); c_0, concentration of electrically active species in the electrolyte bulk (mol cm^{-3}); D, diffusion coefficient (cm^2 s^{-1}); and ν, potential sweep rate (V s^{-1}).

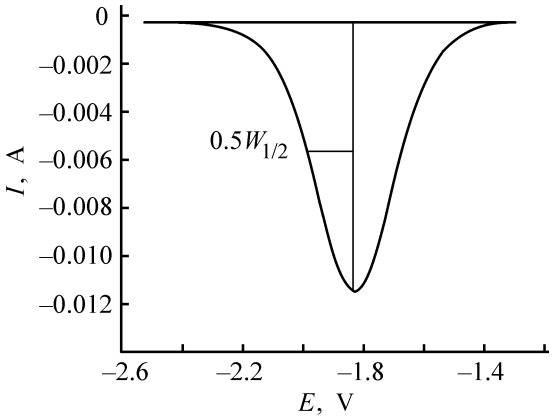

Fig. 3. Square-wave voltammogram of the NaCl–KCl–$YbCl_3$ melt ($m_{YbCl_3} = 3.79 \times 10^{-2}$ mol kg^{-1}) at $\nu = 20$ Hz on a W working electrode at 973 K.

The empirical temperature dependence of the diffusion coefficients of $[YbCl_6]^{3-}$ ions is described by the Arrhenius equation in the coordinates $\log D$–$1/T$:

$$\log D_{[YbCl)_6]^{3-}} = -2.18 - \frac{2377}{T} \pm 0.02. \quad (6)$$

The calculated diffusion coefficients of complex ytterbium(III) ions ($D_{[YbCl_6]^{3-}} = 2.77$ cm^2 s^{-1} at 1000 K) and the activation energies of diffusion (E_A = 45.4 kJ mol^{-1}) are in good agreement with the data obtained in [17] ($D_{[YbCl_6]^{3-}} = 2.34 \times 10^{-5}$ cm^2 s^{-1} at 1000 K and $E_A = 46.4$ kJ mol^{-1}).

According to the theory of voltammetry, the following relations are valid for the reversible electrochemical process between the cathodic (E_p^C) and anodic (E_p^A) potentials of the current peak and the half-wave potential $E_{1/2}$:

$$E_p^C = E_{1/2} - 1.11\frac{RT}{nF}, \quad (7)$$

$$E_p^A = E_{1/2} + 1.11\frac{RT}{nF}, \quad (8)$$

$$\frac{(E_p^C + E_p^A)}{2} = E_{1/2}, \quad (9)$$

$$E_{1/2} = E^0_{Yb(III)/Yb(II)} + \frac{RT}{F}\ln\left(\frac{D_{Yb(II)}}{D_{Yb(III)}}\right)^{1/2} + \frac{RT}{F}\ln\left(\frac{\gamma_{Yb(III)}}{\gamma_{Yb(II)}}\right). \quad (10)$$

For concentrations at which the mole fractions N of depolarizer ions do not exceed $(3–5) \times 10^{-2}$, we can assume that the activity coefficients in molten salts remain virtually constant. Introducing the conditional

Diffusion coefficients of $[YbCl_6]^{3-}$ ions, conditional standard redox potential of Yb(III)/Yb(II), and principal thermodynamic characteristics of $YbCl_3$ in NaCl–KCl and CsCl melts

T, K	$D_{[YbCl_6]^{3-}} \times 10^5$, $cm^2\ s^{-1}$	$E^*_{Yb(III)/Yb(II)}$, V	$-\Delta G^*_{YbCl_3}$	$-\Delta H^*_{YbCl_3}$	$-\Delta S^*_{YbCl_3}$	$K^* \times 10^8$
			kJ mol^{-1}			
			NaCl–KCl			
973	2.38	–1,671	160.93	195.96	0.036	4.39
1023	3.14	–1.652	159.13	195.96	0.036	1.34
1073	4.03	–1.634	157.33	195.96	0.036	0.46
			CsCl			
973	0.88	–1.853	178.36	218.25	0.041	37.84
1023	1.22	–1.832	176.31	218.25	0.041	10.14
1073	1.64	–1.811	174.26	218.25	0.041	3.06

standard potential $E^*_{Yb(III)/Yb(II)}$, we can write the following equation [28]:

$$E^*_{Yb(III)/Yb(II)} = E^0_{Yb(III)/Yb(II)} + \frac{RT}{F}\ln\left(\frac{\gamma_{Yb(III)}}{\gamma_{Yb(II)}}\right). \quad (11)$$

Assuming that the diffusion coefficients of tri- and bivalent ytterbium ions are close, $\frac{RT}{F}\ln\left(\frac{D_{Yb(II)}}{D_{Yb(III)}}\right)$ can be considered to be approximately zero.

In view of the aforesaid, we calculated the conditional standard redox potential $E^*_{Yb(III)/Yb(II)}$ by the equations

$$E^*_{Yb(III)/Y(II)} = E^C_p + 1.11\frac{RT}{F}, \quad (12)$$

$$E^*_{Yb(III)/Y(II)} = E^A_p + 1.11\frac{RT}{F}, \quad (13)$$

$$E^*_{Yb(III)/Y(II)} = \frac{(E^C_p + E^A_p)}{2}. \quad (14)$$

The overall temperature dependence of the conditional standard redox potential of the Yb(III)/Yb(II) pair in the NaCl–KCl melt is described by the empirical equation

$$E^*_{Yb(III)/Y(II)} = -(2.031 \pm 0.005) + (3.7 \pm 0.2) \times 10^{-4}T,\ V,\ [973\text{–}1075\ K]. \quad (15)$$

For example, the conditional standard redox potential of ytterbium in an equimolar melt of sodium and potassium chlorides ($E^*_{Yb(III)/Yb(II)} = -1.661$ V at 1000 K), obtained in this study, is in a quite satisfactory agreement with the data of Kuznetsov and Gaune-Escard ($E^*_{Yb(III)/Yb(II)} = -1.670$ V at 1000 K) [17].

The principal thermodynamic characteristics of ytterbium trichloride in the equimolar NaCl–KCl melt are listed in the table. It can be seen that ytterbium ions form stable complexes with chlorine ions in molten salts. A similar behavior has been observed for other polyvalent metals [4, 28–31].

The change in the conditional standard Gibbs energy of the redox reaction

$$YbCl_{2(s)} + 1/2Cl_{2(g)} \rightleftarrows YbCl_{3(s)} \quad (16)$$

is calculated by the formula

$$\Delta G^* = nFE^*. \quad (17)$$

Its temperature dependencies described by the equation

$$\Delta G^*_{YbCl_3} = \Delta H^*_{YbCl_3} - T\Delta S^*_{YbCl_3}. \quad (18)$$

For the molten equimolar mixture NaCl–KCl, this dependence has the following form:

$$\Delta G^*_{YbCl_3} = -195.96 + 0.036T \pm 2.46,\ kJ\ mol^{-1},\ [NaCl\text{–}KCl]. \quad (19)$$

Similar thermodynamic calculations can be made for ytterbium trichloride in a CsCl melt [32]:

$$\Delta G^*_{YbCl_3} = -218.25 + 0.041T \pm 2.46,\ kJ\ mol^{-1},\ [CsCl]. \quad (20)$$

The results of these calculations at different temperatures are listed in the table. It can be seen that the stability of complex ytterbium ions steadily decreases as the cation radius of the solvent salt becomes smaller, and temperature, higher.

The manner in which the thermodynamic parameters of the redox reaction (16) vary with the cation radius of the solvent salt indicates that the Yb–Cl bond in the complex groups $[YbCl_6]^{3-}$ and $[YbCl_4]^{2-}$ becomes stronger on passing to cesium chloride.

In dilute solutions, the stability of the complex species formed depends both on the ionic potential of the complexing agent ($\mu = z/r$, where z is the charge, and r, crystallochemical radius of the ion) [33] and on the cation size of the solvent salt. Based on the available published data on crystallochemical radii of triple- and double-charged ytterbium ions ($r_{Yb^{3+}} = 0.099$ nm and $r_{Yb^{2+}} = 0.102$ nm) [32, 34], we can state that the stability of $[YbCl_6]^{3-}$ complexes ($\mu = 30.30$) substantially exceeds that of $[YbCl_4]^{2+}$ groups ($\mu = 19.61$). At the same time, it is necessary to take into account the counterpolarizing effect of the cation of the solvent salt, which is the stronger, the smaller its radius. As a result, the relative stability of the complex species decreases on going from CsCl to NaCl–KCl. Elevating the temperature also makes weaker the interspecies bonds in the complex groups because of the more intense thermal motion of species in the melt.

Which of the complexes is preferable in a salt medium at a certain temperature can be judged from the conditional equilibrium constants of redox reactions and activity coefficients.

The conditional standard Gibbs energyq of the chemical reaction is related to the conditional equilibrium constant by

$$\Delta G^*_{YbCl_3} = -RT\ln K^*. \quad (21)$$

It follows from the data in the table that the equilibrium constant decreases as temperature becomes higher. Below are presented empirical equations describing the temperature dependence of the conditional equilibrium constants:

$$\log K^* = -1.88 + \frac{10\,239}{T} \pm 0.13, \text{ [NaCl–KCl]}, \quad (22)$$

$$\log K^* = -2.14 + \frac{11\,404}{T} \pm 0.13, \text{ [CsCl]}. \quad (23)$$

CONCLUSIONS

(1) The redox electrode reaction Yb(III) + e $\rightleftarrows$ Yb(II) in the equimolar melt NaCl–KCl was studied in the temperature range 973–1075 K by various electrochemical methods. It was shown that it is reversible and controlled by mass transfer. Its electrochemical parameters were determined and the diffusion coefficients of $[YbCl_6[^{3-}$ ions were calculated.

(2) The temperature dependence of the conditional standard redox potential of Yb(III)/Yb(II) in a molten equimolar mixture of sodium and potassium chlorides relative to a chlorine reference electrode was obtained.

(3) The principal thermodynamic characteristics of $YbCl_3$ in NaCl–KCl and CsCl melts were calculated.

(4) It was shown that the variation of the thermodynamic parameters of the redox reaction $YbCl_{2(s)} + 1/2Cl_{2(g)} \rightleftarrows YbCl_{3(s)}$ with the cation radius of the solvent salt indicates that the srength of the Yb–Cl bond in complex groups increases on passing to cesium chloride.

REFERENCES

1. Lebedev, V.A., *Izbiratel'nost' zhidkometallicheskikh elektrodov v rasplavlennykh galogenidakh* (Selectivity of Liquid-Metal Electrodes in Molten Halides), Chelyabinsk: Metallurgiya, 1993.
2. Iezowska-Trzebiatowska, B., Kopacz, S., Mikulski, T., *Pierwiastki Rzadkie*, Warszawa, 1976.
3. OCDE/NEA Report: Accelerator-Driven Systems (ADS) and Fast Reactors (FR) in Advanced Nuclear Fuel Cycles, A Comparative Study, 2002.
4. Cordoba, G. and Caravaca, C., *J. Electroanal. Chem.*, 2004, vol. 572, pp. 145–151.
5. Bermejo, R., Castrillejo, Y., Martinez, A., and Barrado, E., *Int. Conf. "Back-end of the Fuel Cycle, From Research to Solution,"* Paris, 2001, p. 272.
6. Castrillejo, Y., Bermejo, M.R., Diaz Arocas, P., et al., *J. Electroanal. Chem.*, 2005, vol. 579, pp. 343–358.
7. Kurata, M., Sakamura, Y., and Inoue, T., *Proc. 3rd Inform.-Exch. Meeting on Actinide and Fission Product Partitioning and Transmutation*, France, 1994, p. 407.
8. Serp, J., Allibert, M., Terrier, A.L., et al., *J. Electrochem. Soc.*, 2005, vol. 152, no. 3, pp. 167–172.
9. Serrano, K. Ph.D. Thesis, Université Paul Sabatier, 1998.
10. Lambertin, D., Ph.D. Thesis, Universite Pierre et Marie Curie, Paris VI, 2001.
11. Pernel, C., Ph.D. Thesis, Institute National Polytechnique de Grenoble, 2002.
12. Fusselman, S.P., Roy, J.J., Grimmett, L.F., et al., *J. Electrochem. Soc.*, 1999, vol. 146, pp. 2573–2580.
13. Mottot, Y., Ph.D. Thesis, Universite Pierre et Marie Curie, Paris VI, 1986.
14. Bermejo, M.R., Ph.D. Thesis, Universidad de Valladolid, 2003.
15. Johnson, K.E. and Mackenzie, J.R., *J. Electrochem. Soc.*, 1969, vol. 116, no. 12, pp. 1697–1703.
16. Guankun, L., Yexiang, T., Quichan, H., et al., *Trans.*

Nonferrous Met. Soc. China, 1998, vol. 8, no. 3, pp. 516–519.

17. Kuznetsov, S.A. and Gaune-Escard, M., *Proc. 7th Int. Symp. on Molten Salts Chemistry and Technology (MS 7)*, 2005, vol. 2, pp. 855–859.
18. Novoselova, A.V., Potapov, A.M., and Khokhlov, V.A., *Proc. EUCHEM Molten Salts Conference*, 2004, pp. 270–276.
19. Shishkin, V.Yu. and Mityaev, V.S., *Izv. Akad. Nauk SSSR, Neorg. Mater.*, 1982, vol. 18, no. 11, pp. 1917–1918.
20. Revzin, G.E., *Metody polucheniya khimicheskikh reaktivov i preparatov* (Methods for Synthesis of Chemical Reagents and Preparations), Moscow: IREA, 1967, issue 16, pp. 124–129.
21. Bard, A.J. and Faulkner, L.R., *Electrochemical Methods: Fundamentals and Applications*, New York: John Wiley & Sons, 1980.
22. Galus, Z., *Fundamentals of Electrochemical Analysis*, London: Ellis Horwood, 1994.
23. Bret, C.M.A. and Bret, A.M.O., *Electrochemistry: Principles, Methods and Applications*, Oxford: University, 1996.
24. Thompson, M. and Walsh, J.N., *A Handbook of Inductively Coupled Plasma Spectrometry*, Glasgow: Blackie, 1983.
25. Chudinov, E.G., *Itogi nauki i tekhniki, Ser. "Analiticheskaya khimiya"* (Advances of Science and Technology, Ser. "Analytical Chemistry"), Moscow: VINITI, 1990, vol. 2, pp. 122–147.
26. Anonymous, A. (Papatheodorou, G.N.), *Progress in Molten Salt Chemistry*, Paris: Elsevier, 2000, vol. 1, pp. 65–70.
27. Novikov, G.I., Polyachenok, O.G., and Frid, S.A., *Zh. Neorg. Khim.*, 1964, vol. 9, no. 2, pp. 472–475.
28. Smirnov, M.V., *Elektrodnye potentsialy v rasplavlennykh khloridakh* (Electrode Potentials in Molten Chlorides), Moscow: Nauka, 1973.
29. Martinot, L., *J. Inorg. Nucl. Chem.*, 1975, vol. 37, pp. 2525–2541.
30. Roy, J.J., *Mater. Sci. Technol.*, 1991, vol. 73–75, pp. 547–553.
31. Roy, J.J. and Grantham, L.F., *J. Electrochem. Soc.*, 1996, vol. 143, pp. 2487–2492.
32. Shannon, R.D., *Acta Crystallogr., Sect. A*, 1976, vol. 32, no. 5, pp. 751–767.
33. Smirnov, M.V., Stepanov, V.P., and Khokhlov, V.A., *Rasplavy*, 1987, vol. 1, no. 1, pp. 64–73.
34. Ryabukhin, A.G., *Vysokotemp. Rasplavy*, 1997, no. 1, pp. 58–63.

ISSN 1070-4272, Russian Journal of Applied Chemistry, 2007, Vol. 80, No. 10, pp. 1667–1669. © Pleiades Publishing, Ltd., 2007.
Original Russian Text © S.N. Vinogradov, O.K. Sinenkova, 2007, published in Zhurnal Prikladnoi Khimii, 2007, Vol. 80, No. 10, pp. 1638–1640.

APPLIED ELECTROCHEMISTRY AND CORROSION PROTECTION OF METALS

Electrodeposition and Physicomechanical Properties of Nickel–Chromium Coatings

S. N. Vinogradov and O. K. Sinenkova

Penza State University, Penza, Russia

Received December 25, 2006; in final form, March 2007

Abstract—Technique for deposition of wear- and corrosion-resistant lustrous coatings of a nickel–chromium alloy was developed.

DOI: 10.1134/S1070427207100114

Nickel–chromium coatings are rather hard and corrosion- and wear-resistant. Such coatings can find application in machine building instead of multilayer copper–nickel–chromium and chromium coatings.

A disadvantage is that the electrolyte is aggressive and ecologically unfriendly. Substitution of chromium(III) for chromium(VI) considerably reduces the ecological hazard of the galvanic process, but the electrolyte operation becomes unstable because of chromium oxidation at the anode during electrolysis. The oxidation of chromium not only changes the electrolyte composition, but also affects the coating quality and the process rate.

The main advantages of the technique suggested here are the stabilization of the electrolyte composition via elimination of chromium(III) oxidation to chromium(VI), deposition of lustrous coatings by introduction of brighteners into the electrolyte, improvement of the buffer properties of an electrolyte, and increase in the pH of formation of chromium(III) hydrates upon addition of ammonium sulfate.

The nickel–chromium alloy was electrodeposited from an electrolyte containing chromium sulfate, nickel sulfate, aminoacetic acid, ammonium sulfate, 1,4-butinediol, and saccharin. The electrolyte pH was maintained in the range 2.0–5.0 [1].

To prevent oxidation of chromium(III), an insoluble anode, e.g., made of lead, was placed in a complementary anode cell with a separating MA-40 anion-exchange membrane. The use of a complementary anode cell makes it possible to stabilize the compositions of the electrolyte and the alloy and to obtain lustrous alloy coatings.

The dependence of the chromium content of the alloy on the chromium(III) concentration in the electrolyte is described with a high correlation coefficient by the polynomial equation [2]:

$$[Cr]_{alloy} = 0.0708[Cr^{3+}]^2 + 2.4482[Cr^{3+}] + 0.5268;$$
$$R^2 = 0.9993$$

When the chromium(III) concentration in the electrolyte is raised from 10 to 45 g l^{-1} at current densities of 4 and 6 A dm^{-2}, the current efficiency by the alloy decreases from 22.6 to 10.5 and from 26.1 to 14%, respectively.

Lustrous coatings of the nickel–chromium alloy firmly adhering to the support are deposited on the cathode in the entire range of chromium(III) concentrations in the electrolyte at 40–60°C and current densities of 4 and 6 A dm^{-2}.

As the temperature of the electrolyte is elevated from 20 to 60°C at current densities of 4 or 6 A dm^{-2}, the chromium content of the alloy increases from 9.5 to 13 and from 10.2 to 15%, respectively.

The dependence of the chromium content of the alloys (%) on temperature (°C) is described by the polynomial equation

$$[Cr]_{alloy} = -0.2143[t]^2 + 2.4857[t] + 7.92;$$
$$R^2 = 0.9997.$$

When temperature is elevated from 20 to 60°C at a current density of 4 or 6 A dm^{-2}, the current efficiency by the alloy linearly grows from 10.5 to 16.5 and from 14 to 20%, respectively, i.e., the current

Table 1. Factors affecting the composition of the nickel–chromium alloy and the range of their variation

Design conditions	Factor			
	x_1, %	x_2, A dm^{-2}	x_3, °C	x_4
Main level	35	5.0	45	4.5
Variation range	5	1.0	5	0.5
Top level	40	6.0	50	5.0
Lower layer	30	4.0	40	4.0

efficiency increases with temperature and current density. This is due to the appreciable depolarization in alloy deposition.

Lustrous nickel–chromium coatings are formed at 40 and 60°C and current densities of 4 and 6 A dm^{-2}. At temperatures below 35°C, dull coatings are formed, which is due to deposition of nickel with brighteners.

When the electrolyte pH increases from 4.0 to 5.0, the chromium content of the alloy grows, which is due to a rise in the stability of the ammonia–glycocol complex of nickel. In this case, the chromium content of the alloy increases with the current density.

The dependence of the chromium content of alloys on the electrolyte pH is described by the polynomial equation

$$[Cr]_{alloy} = 0.1286[pH]^2 - 1.6114[pH] + 17.62;$$
$$R^2 = 0.9983.$$

The current efficiency by the alloy virtually linearly increases with the electrolyte pH. Similarly to the preceding dependences, the current efficiency by the alloy increases with the current density, which is due to the chromium behavior.

To optimize the technology of alloy electrodeposition, we derived a multifactorial regression equation that relates the optimization criterion and input parameters affecting the process.

The optimization criterion for the nickel–chromium alloy is the alloy composition, and the input data are the chromium(III) concentration in the electrolyte, current density, temperature, and pH of the electrolyte. As the mathematical model of the process serves the following regression equation, which relates the optimization criterion, alloy composition y, to the input parameters (factors): chromium(III) concentration in electrolyte, x^1; current density x_2; temperature x_3; and pH of the electrolyte, x_4.

$$y = b_0 + b_1x_1 + b_2x_2 + b_3x_3 + b_4x_4 + b_{12}x_1x_2 + b_{13}x_1x_3 + b_{14}x_1x_4 + b_{23}x_2x_3 + b_{24}x_2x_4 + b_{34}x_3x_4 + b_{123}x_1x_2x_3 + b_{134}x_1x_3x_4 + b_{124}x_1x_2x_4 + b_{234}x_2x_3x_4 + b_{1234}x_1x_2x_3x_4.$$

To optimize the electrolyte composition and the deposition mode in order to obtain a nickel–chromium alloy containing 12–13% chromium, we applied a four-factor method of experiment design. The factors affecting the alloy composition and the ranges of their variation are listed in Table 1.

The optimization parameter is the percentage content of chromium in the alloy, y, which should be in the range 12–13%. Data on the percentage content of chromium in the alloy, calculated from the results of a chemical analysis of the resulting alloys, are listed in Table 2, together with regression coefficients calculated on their basis.

On finding the coefficients in the regression equation, we verified their significance by Student's criterion. For this purpose, three parallel experiments were performed at the center of the design on the main level for all the factors. The chemical analyses of the thus prepared nickel–chromium alloys demonstrated that the alloy contains $y_1 = 11.9$, $y_2 = 12.3$, and $y_3 = 12.7$% chromium.

Table 2. Coefficients of the regression equation, calculated from data on the chromium content of an alloy

Chromium content of an alloy, %		Coefficients of the regression equation	
$y_1 = 6.5$	$y_9 = 8.4$	$b_0 = 10.72$	$b_{23} = -0.01$
$y_2 = 8.3$	$y_{10} = 11.6$	$b_1 = 1.48$	$b_{24} = 0.16$
$y_3 = 6.5$	$y_{11} = 10.3$	$b_2 = 0.72$	$b_{34} = 0.18$
$y_4 = 10.5$	$y_{12} = 13.3$	$b_3 = 1.29$	$b_{123} = -0.17$
$y_5 = 8.0$	$y_{13} = 11.5$	$b_4 = 1.66$	$b_{124} = -0.11$
$y_6 = 11.2$	$y_{14} = 14.5$	$b_{12} = 0.08$	$b_{134} = -0.01$
$y_7 = 9.5$	$y_{15} = 13.2$	$b_{13} = -0.02$	$b_{234} = -0.02$
$y_8 = 12.0$	$y_{16} = 16.2$	$b_{14} = 0.04$	$b_{1234} = 0.19$

As a result of the verification, insignificant coefficients b_{13}, b_{23}, b_{134}, and b_{234} of the regression equation were dropped, and the resulting model was tested for adequacy by Fisher's criterion.

The regression equation adequately describing the effect of technological factors on the composition of the nickel–chromium alloy has the form

$$y = 10.72 + 1.48x_1 + 0.72x_2 + 1.29x_3 + 1.66x_4 + 0.08x_1x_2 + 0.04x_1x_4 + 0.16x_2x_4 + 0.18x_3x_4 - 0.17x_1x_2x_3 - 0.11x_1x_2x_4 + 0.19x_1x_2x_3x_4.$$

It is seen from the equation that the alloy composition is strongly affected by the individual factors: chromium(III) concentration in the electrolyte, current density, temperature, and pH of the electrolyte. Less important are the interaction factors: [chromium(III) concentration in the electrolyte]–[current density], [temperature]–[electrolyte pH], and [chromium(III) concentration in the electrolyte]–[pF of the electrolyte]. This influence of the factors on the coating composition makes it possible to maintain the alloy composition within prescribed limits during electrodeposition by varying the deposition mode without adjusting the electrolyte with chromium(III) salts.

The derived single-factor polynomial equations relating the alloy composition to chromium(III) concentration in electrolyte, current density, temperature, and electrolyte pH, and also the four-factor regression equation serve for automatically maintaining and controlling the alloy composition and, hence, the properties of nickel–chromium coatings in their deposition on automated production lines.

Thus, the optimal electrolysis conditions providing lustrous nickel–chromium coatings are as follows: current density 4.0–6.0 A dm^{-2}, temperature 40–50°C, and pH 4.0–5.0.

The microhardness of the nickel–chromium coatings exceeds that of nickel coatings. For example, the microhardness for nickel and nickel–chromium alloy at a 50 g indentor load are 4.5 and 4.95 GPa, respectively. The increase in the microhardness is due to the incorporation of chromium atoms into the crystal lattice of nickel.

It is necessary to note that internal stresses in alloy coatings are considerably lower than those in pure nickel coatings [3]. This is due to the lower hydrogen pickup by nickel–chromium alloy coatings as compared with pure nickel. For example, the internal stresses for nickel and nickel–chromium alloy are 320 and 120 MPa, respectively, i.e., the fraction of hydrogen introduced into a coating and affecting the internal stresses is much greater for nickel as compared with the nickel–chromium alloy. The level of internal stresses arising in a coating during electrodeposition is one of the most important technological characteristics. Coatings with lower internal stresses are less susceptible to microcracking and peeling-off from a support, which should affect the wear resistance of a coating.

The wear resistance of coatings used in friction units is one of the most important characteristics governing the service life of an article. Our studies demonstrated that the wear resistance of nickel–chromium coatings is 30 times that of nickel coatings.

A study of the lattice microstructure demonstrated that the incorporation of chromium atoms into the crystal lattice of nickel results in its distortion and, as a consequence, in a higher coating hardness.

The corrosion tests carried out in the moist chamber for 56 days and in a salt-fog chamber for 7 days showed that the outward appearance of samples with a nickel–chromium alloy remained virtually unchanged after environmental tests, whereas the nickel coating somewhat lost its luster. After the test in the salt-fog chamber, minor corrosion centers were observed on a nickel coating, whereas a nickel–chromium coating remained unchanged.

CONCLUSIONS

(1) A technique for electrochemical deposition of corrosion- and wear-resistant nickel–chromium coatings was developed.

(2) An ecologically safe electrolyte was suggested for obtaining lustrous coatings. It has following composition (g l^{-1}): nickel sulfate (in terms of the metal) 83.47, nickel chloride (in terms of the metal) 20.38, chromium-potassium alum (in terms of the metal) 40, boric acid 30, 1,4-butinediol 0.5, saccharin 1.0, aminoacetic acid 220, and ammonium sulfate 200.

REFERENCES

1. RF Patent 2 199 369.
2. Akhnazarova, S.L. and Kafarov, V.V., *Optimizatsiya eksperimenta v khimii i khimicheskoi tekhnoplogii* (Optimization of the Experiment in Chemistry and Chemical Engineering), Moscow: Vysshaya Shkola, 1978.
3. Vagramyan, A.T. and Petrov, Yu.S., *Fiziko-mekhanicheskie svoistva elektroliticheskiklh osadkov* (Physicomechanical Properties of Electroplated Deposits), Moscow: Akad. Nauk SSSR, 1960.

ISSN 1070-4272, Russian Journal of Applied Chemistry, 2007, Vol. 80, No. 10, pp. 1670–1675. © Pleiades Publishing, Ltd., 2007.
Original Russian Text © E.A. Krainova, M.V. Avdeev, K.V. Merkushina, A.I. Rodionov, V.M. Garamus, R. Willumait, 2007, published in Zhurnal Prikladnoi Khimii, 2007, Vol. 80, No. 10, pp. 1641–1646.

ENVIRONMENTAL PROBLEMS OF CHEMISTRY AND TECHNOLOGY

Structural Studies of a Carbonizate Obtained from Solid Cellulose-containing Waste by Sulfuric Acid Carbonization

E. A. Krainova, M. V. Avdeev, K. V. Merkushina, A. I. Rodionov, V. M. Garamus, and R. Willumait

Joint Institute of Nuclear Research, Dubna, Moscow oblast, Russia
Mendeleev Russian University of Chemical Engineering, Moscow, Russia
GKSS Research Center, Geesthacht, Germany

Received November 10, 2006; in final form, April 2007

Abstract—Results of a study of a carbon material (carbonizate) obtained in processing of a solid cellulose-containing waste with concentrated sulfuric acid are presented. The mass fractions of water, water-soluble and -insoluble ash, and total pore volume for water were determined. Data furnished by electron microscopy and small-angle neutron scattering were used to analyze the structure of the material and identify factors affecting the cluster organization. Areas in which the carbonizate can be used are suggested.

DOI: 10.1134/S1070427207100126

The problem of processing of a municipal solid waste (MSW) remains topical. Waste of this kind is a large-tonnage heterogeneous mixture with morphological composition varying between different countries. A major part of MSW (up to 50%) is constituted by cellulose-containing components, such as paper, cardboard, and wood [1]. The methods most widely used for MSW utilization are burial (storage at dumping grounds), burning at incinerator plants for production of thermal and electric power, and classification and secondary processing at garbage processing plants. The results of an ecological-economical expertise indicate that all these techniques for MSW processing fail to satisfy the requirements of market economy, ecological safety, and resource saving. In some countries, the problem of MSW utilization is solved by preliminary classification aimed to recover components with consumers' value (metals, plastics, glass, paper, etc.). This approach markedly diminishes the specific expenditure for MSW utilization and improves ecological conditions.

In order to improve the MSW classification efficiency, a method has been suggested [2], which consists in that the whole mass of waste is preliminarily treated with concentrated sulfuric acid. Studies demonstrated that glass (cullet), polymeric materials (polyethylene, polypropylene, polyethylene terephthalate), rubber articles, and natural fancy leather are not subject to the action of the acid and are easily classified after this treatment, whereas perishable cellulose-containing components (paper, cardboard, textile, wood, food waste) are converted into biologically inert substances. The overall chemical reaction of the process can be represented by the equation

$$(C_6H_{10}O_5)_x + xH_2SO_{4(conc.)} = 6xC + xH_2SO_4 \cdot 5H_2O + Q, \quad (1)$$

where x is the number of structural fragments, and Q is the heat effect of the reaction.

The reaction yields a homogeneous black carbon-rich mass. The theoretical yield of pure carbon is about 35% relative to the total mass of the waste. Sulfonic acids are formed as by-products of the reaction.

Presently, products formed in interaction of concentrated sulfuric acid or oleum with carbon-containing materials are known. For example, interaction with coal anthracite) gives sulfo carbon [3, 4] (carbon in which sulfo groups $-SO_3H$ are fixed on the carbon matrix and provide the material with cation-exchange properties). Sulfo carbon is used in water treatment to remove organic substances, odor, and coloration [5, 6] and as a cation exchanger [7, 8]. Carbonization of var-

ious kinds of vegetable waste (including hydrolyzed lignin) with hot concentrated sulfuric acid yields activated carbon, Collactivit [9, 10]. This material is an active adsorbent used to purify syrups in hydrolysis industry. Spent Collactivit is added to polymer-concrete mixture for floors of stock farm buildings [11].

In order to use in various industrial applications the carbonizate obtained by sulfuric acid carbonization of cellulose-containing MSW, we obtained and analyzed its porosity-related structural characteristics. Based on electron-microscopic and small-angle neutron-scattering data, we distinguished structural-organization levels of pores and obtained their dependence on a method used for sulfuric acid removal.

To study the destruction of solid cellulose-containing waste under the action of concentrated sulfuric acid, we took representative samples of cellulose-containing MSW (sample no. 1) with the following component ratio (wt %): paper and cardboard 38.0, food waste[1] 40.0, wood 3.0, leather and rubber 2.5, textile 6.0, bones 2.0, polymeric materials 5.5, ferrous and nonferrous metals 3.0 [1]. The total mass of the representative sample was 427.0 ± 0.5 g, and its moisture content, ≤10%. The calculated content of cellulose did not exceed 75% of the total mass. After being weighed, sample no. 1 was placed in a 3-l glass vessel with a gas-outlet tube and poured over with 0.5 l of sulfuric acid (initial mass fraction of sulfuric acid 94%, density 1831.2 kg m^{-3}), and the mixture agitated for 5 min. At the initial instant of time, the temperature of the mixture increased to 120°C and the reaction proceeded with vigorous evolution of water vapor. In 30 min, the temperature decreased to 90°C and release of water vapor completely ceased. The resulting heterogeneous mixture (sample no. 2) was kept for 20.0 h prior to further studies.

The qualitative and quantitative composition of the heterogeneous mixture was determined by visual inspection of the residues of components and their weighing. The content of the components in sample no. 2 was as follows (wt %): undried carbon material with admixtures 89.5 (bulk density 1.5 g cm^{-3}, found by measuring the mass of a sample and its volume), leather and rubber 2.5, polymeric materials 5.5, rest 2.5; the pH value of the heterogeneous mixture was lower than 0.1 (final mass fraction of sulfuric acid 77%, density 1831.2 kg m^{-3}). The calculated moisture content did not exceed 25%.

[1] The averaged sample contained equal amounts of potato tuber skin, banana skin, bread, yellow corn grains, and white-cabbage stumps.

In the next stage, two methods were used to remove sulfuric acid from sample no. 2. In the first of these, sulfuric acid was extracted with distilled water to obtain the finished product (sample no. 3). The expenditure of distilled water until pH 6.5 of washing water was 1.21 m^3 kg^{-1}. In the second method, sulfuric acid was neutralized with $NaHCO_3$ (sodium hydrocarbonate) to give a carbon material with admixture of salts (sample no. 4). The chemical reaction occurring in the given process can be represented by equation [12]:

$$2NaHCO_3 + H_2SO_4 \cdot 1.7H_2O = Na_2SO_4 \cdot 2.7H_2O + 2CO_{2(gas)} + 1.4 \text{ kJ mol}^{-1}. \quad (2)$$

Most of carbon materials are used as raw materials for production of adsorbents. The size and volume of micropores are the most important parameters in description of adsorption of numerous substances from gaseous and liquid media by activated carbons. The limiting factor determining how the structure of carbon-containing raw materials changes is the treatment temperature of a carbon material [13]. Activated carbons are typically tested by the procedures described in [14–16].

Upon removal of sulfuric acid and drying in air, sample nos. 3 and 4 were analyzed for the content of water (moisture content) and ash and their total pore volume for water was determined.

A direct structural analysis of sample nos. 2–4 was made with a JEOL JSM-840 scanning electron microscope (SEM) at Laboratory of nuclear reactions (Joint Institute of Nuclear Research, Dubna).

Sample nos. 3 and 4 were studied by the method of small-angle scattering of thermal neutrons [17]. The experiments were carried out on a SANS-1 small-angle neutron scattering installation at a stationary reactor of the GKSS research center (Geesthacht, FRG). The samples were poured in a planar quartz cuvette of thickness 1.5 mm. In the experiments, the differential neutron scattering cross-section per unit volume (scattering intensity) was determined as a function of the scattering vector magnitude:

$$q = (4\pi/\lambda)\sin(\theta/2), \quad (3)$$

where λ is the wavelength of neutrons incident on a sample, and θ is the neutron scattering angle.

The wavelength of incident neutrons was 0.81 nm at a monochromatization $\Delta\lambda/\lambda = 10\%$. By varying the sample-to-detector distance within the range 0.7–

Table 1. Data for calculation of the heat effect of the reaction Initial temperature of the mixture 298.0 K

Parameter	Run no.				
	1	2	3	4	5
Specific heat of a substance at constant pressure [19]					
cellulose, J g^{-1} K^{-1}	2.3	2.3	2.3	2.3	2.3
H_2SO_4, J mol^{-1} K^{-1}	137.6	137.6	137.6	137.6	137.6
H_2O, J mol^{-1} K^{-1}	75.3	75.3	75.3	75.3	75.3
Cellulose mass, g	36.5	29.9	20.0	9.9	7.3
Amount of H_2SO_4, mol	1.23	0.92	0.62	0.31	0.22
Amount of H_2O, mol	0.89	0.68	0.45	0.23	0.16
Q_{in}, kJ	95.45	73.61	49.07	24.54	17.80
Final temperature of the mixture, K	393.0	418.0	409.0	398.0	378.0
Specific heat of a substance at constant pressure [19]					
carbon	13.14	13.9	13.64	13.3	12.61
H_2SO_4	137.6	137.6	137.6	137.6	137.6
H_2O	75.3	75.3	75.3	75.3	75.3
Amount of carbon, mol	1.35	1.11	0.74	0.37	0.27
Amount of H_2SO_4, mol	1.23	0.92	0.62	0.31	0.22
Amount of H_2O, mol	2.02	1.6	1.07	0.54	0.39
Q_{fin}, kJ	133.3	109.7	72.0	35.1	23.8
ΔQ, kJ	37.81	36.11	22.90	10.58	6.03
Amount of carbonized cellulose, mol	0.23	0.18	0.12	0.06	0.04
Specific amount of heat per 1 mol of cellulose, kJ mol^{-1}	164.41	200.61	190.87	176.37	150.79
Heat effect of the reaction at K_t = 0.75, kJ mol^{-1}	123.30	150.46	143.15	132.28	113.09

9.0 M, small-angle-scattering curves could be obtained in the q-range 0.04–2.7 nm^{-1}. The efficiency calibration of the detector was performed by the standard method of separate measurements of the incoherent scattering for water [18]. The scattering by an empty cuvette was subtracted as the background.

EXPERIMENTAL

According to the experimental data, the equation of reaction (1) has, under the optimal process conditions [moisture content of the representative sample (no. 1) not exceeding 10%; degree of carbonization of the cellulose-containing material, about 99%], the form

$$(C_6H_{10}O_5)\cdot H_2O + 5(H_2SO_4\cdot 0.5H_2O) = 6C + 5(H_2SO_4\cdot 1.7H_2O) + 127.67\ \text{kJ mol}^{-1}. \quad (4)$$

In the first stage of the process, the reaction mixture foams; this stage continues for 4–8 min. In the second stage, the volume of the mixture decreases by a factor of 2 to give a homogeneous black loose mass, the duration of this stage is 30–40 min. Consequently, the dehydration of cellulose and lignin is complete in this interval of time. In the case of a steady supply of the mixture into the reactor, the process temperature should be maintained at about 75°C. Under these conditions, no gases are evolved, including water vapor. The heat of the reaction (kJ) was calculated by the formula

$$Q = \Delta C_p \nu (T_{fin} - T_{in}) K_t, \quad (5)$$

where ΔC_p is the specific heat of a mole of the material (kJ mol^{-1} K^{-1}); ν, amount of mixture components (mol); T_{in} and T_{fin}, initial and final temperatures of the mixture, respectively (K); and K_t, coefficient of mixture heating in the reactor for the first hour of the process, K_t = 1 in the case of a steady supply of the mixture into the reactor during the working time.

The integral heat of dissolution of sulfuric acid (kJ) for Eq. (4) was calculated by the formula

$$\Delta H_r = \Delta H_i \nu_i (H_2SO_4), \quad (6)$$

where ΔH_r = [–41.26 – (–15.73)] × 5 = (–25.53) × 5 = –127.67 kJ [19].

The results of calculations, listed in Table 1, indicate that the released heat Q of the reaction in destruction of 1 mol of cellulose is numerically equal to the integral heat of dissolution of sulfuric acid, ΔH.

Table 2. Summary comparative characterization of carbon half-products and activated carbons [GOST (State Standard) 6217–74]

Parameter	Sample no. 3	Sample no. 4	ACC*
Bulk density, g cm^{-3}	0.9	0.8	–
Moisture content (GOST 12597–67), %	≥10.5	≥25.0	≥10.0
Total pore volume for water (GOST 17219–71), cm^3 g^{-1}	0.7–0.9	0.5–0.7	≤1.4
Mass fraction of ash (GOST 12596–67), %	≥1.5	≥30.0	7.0

* ACC, activated charcoal.

The data obtained in determining the moisture content, mass fraction of water-insoluble ash, and total pore volume for water are listed in Table 2.

Figure 1 shows SEM images of the surface of the carbon material. It can be clearly seen that the surface of the carbon material has concentration inhomogeneities. Sample no. 3 (Fig. 1a) has a developed nonuniform surface with spherical and spheroidal inclusions 100–1000 nm in size. In storage, the carbon material (sample no. 3) changes its structure: the developed external surface transforms into a densely packed layered surface (Fig. 1b). Sample no. 4 (Fig. 1c) has a layered surface with inclusions of crystal hydrates.

Figures 2 and 3 show small-angle neutron scattering curves and the results of their processing. It can be seen that there is a fundamental difference in the nature of scattering between sample nos. 3 and 4. Portions in which the intensity decreases by the power law as the scattering vector magnitude increases can be distinguished in the scattering curves [17]:

$$I(q) = B/q^P + C, \quad (7)$$

where B is the free parameter found from the data; the exponent P reflects the internal structure of the scattering units and characterizes the type of their 3D

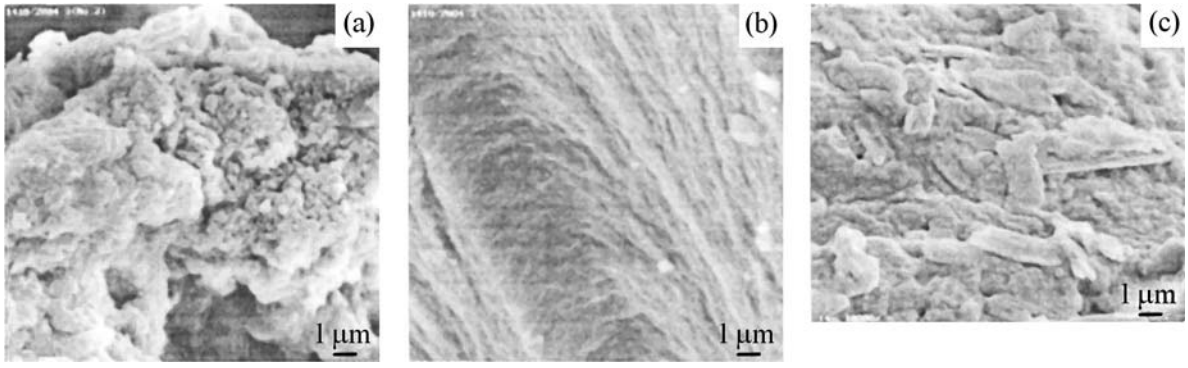

Fig. 1. SEM micrographs of samples. Scale 1 : 10000. Sample: (a) no. 3, freshly prepared; (b) no. 3, after storage for 1 year; and (c) no. 4.

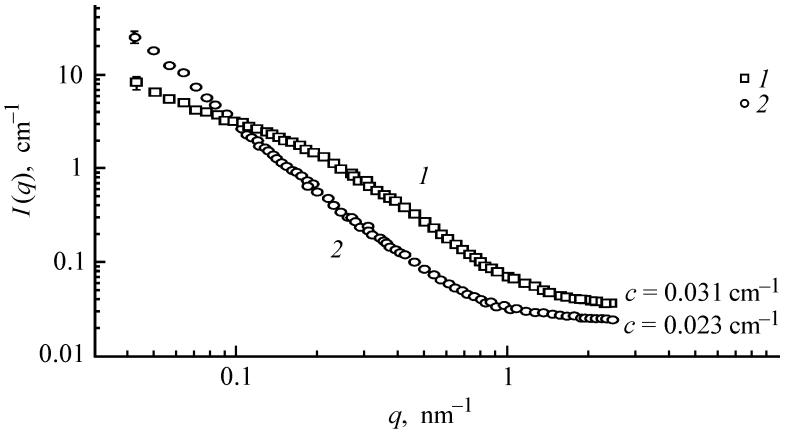

Fig. 2. Experimental small-angle neutron-scattering curves [scattering cross-section $I(q)$ per unit volume vs. the scattering vector magnitude q] reduced to the same bulk density, for sample nos. (*1*) 3 and (*2*) 4.

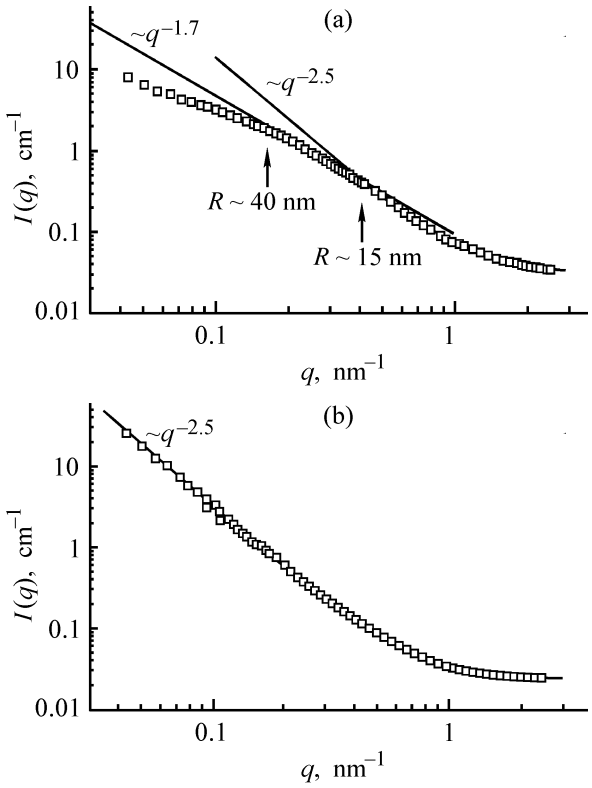

Fig. 3. Power-law portions and evaluation of characteristic radii on small-angle neutron-scattering curves $I(q)$–q for sample nos. (a) 3 and (b) 4.

or surface organization in accordance with the classification [20]:

$$I < P < 3, \tag{8}$$

a mass fractal with a fractal dimension $D = P$;

$$3 > P > 4, \tag{9}$$

a surface fractal with a fractal dimension $D_S = 6 - P$.

The case $P = 4$ corresponds to a smooth boundary surface (Porod's law), so that the dimension $D_S = 2$. Parameter C in Eq. (7) corresponds to the incoherent scattering background, which is proportional to the number of hydrogen atoms in a sample. Deviations from the law described by (7), observed as q decreases, corresponds to the characteristic radius of clusters

$$R \sim 2\pi/q. \tag{10}$$

The exponents and characteristic radii for sample nos. 3 and 4, estimated in accordance with Eqs. (7) and (10), are shown in Fig. 3. For sample no. 3, two scattering modes can be reliably distinguished, which correspond to fractal clusters with dimensions of 2.5 (characteristic radius 15 nm) and 1.7 (characteristic radius 40 nm). The radius of elementary pores constituting the clusters, equal to less than 1 nm, is below the sensitivity limit of the method for systems of this kind. The material has a multilevel organization structure. For sample no. 4, no effect of the final cluster size is observed. In this case, a lower estimate of the cluster radius, q, which is less than 100 nm, can be made by formula (10) from the minimum measured value. The material has a uniform, on this scale, fractal structure.

The method of small-angle neutron scattering confirms the existence of concentration inhomogeneities not only on the surface, but also in the internal structure of the carbon material. Analysis of the scattering curves reveals that the curves for samples nos. 3 and 4 coincide at large q to within a constant factor and the incoherent background, which suggests the common origin of these two materials. It should be noted, however, that the higher incoherent background of sample no. 3 indicates that it contains a larger amount of hydrogen, and consequently, of water as compared with sample no. 4. In addition, use of the neutralization method leads, in contrast to extraction with water, to a sharp increase in the size of the forming clusters and, consequently, makes smaller the total pore volume for water.

Thus, the structural parameters of the carbon material depend on the method used to remove sulfuric acid from sample no. 2.

CONCLUSIONS

(1) The carbon material obtained has, after preliminary treatment of the whole mass of cellulose-containing waste with concentrated sulfuric acid, a developed pore structure with a wide range of pore sizes, 1–1000 nm. Specific features of this structure depend on the method used to remove sulfuric acid from the heterogeneous mixture.

(2) Neutralization of sulfuric acid impairs, compared with the liquid extraction, the properties of the resulting half-product: the amount of impurities in the form of crystal hydrates increases (ash content ≤30%) and the total pore volume for water decreases to 0.5–0.7 cm^3 g^{-1}. At the same time, as also in the case of sulfuric acid extraction with water, the carbon material has an ash content not exceeding 1.5% and a total pore volume for water of up to 0.7–0.9 cm^3 g^{-1}.

(3) The final half-product exhibits good sorption properties and can be used as a sorbent or catalyst support.

REFERENCES

1. Rybal'skii, N.G., Malyarova, M.A., Gorbatovskii, V.V., et al., *Ekologiya i bezopasnost': Spravochnik, tom 2, Ekologicheskaya bezopasnost'* (Ecology and Safety: reference Book, vol. 2, Ecological Safety), Rybal'skii, N.G., Ed., Moscow: VNIIPI, 1993.
2. Krainova, E.A., *Usp. Khim. Khim. Tekhnol.*, 2003, vol. 17, no. 12, pp. 47–49.
3. *GOST* (State Standard) *5696–74, Sulfo Carbon, Technical Specification*, Moscow: Izd. Standartov, 1974.
4. *TU* (Technical Specification) *113-08-5015182-78–91, Sulfo Carbon for Water Purification at Boiler Houses*.
5. Kvitka, L.A., Development and Application of Modified Sulfo Carbon (SU-m) in Water Treatment, *Cand. Sci. Dissertation*, Moscow, 1993.
6. Ba Abdulai, Purification of Colored Natural and Waste Water with Modified Carbon Adsorbents, *Cand. Sci. Dissertation*, Moscow, 1997.
7. Ibragimov, K.D., Development and Study of an Efficient Method of Combined Production of Softened and Desalted Water, *Cand. Sci. Dissertation*, Moscow, 1992.
8. Pishenina, T.I., Ionizing of Water in Filters with Local Pseudofluidization of Sulfo Carbon, *Cand. Sci. Dissertation*, Kiev, 1994.
9. http://biochem.nm.ru/science/carbon.htm
10. http://www.sibpatent.ru
11. Narfont'eva, N.A. and Khol'kin, Yu.I., *Tekhnologiya i svoistva kollaktivita* (Technology and Properties of Collactivit), Moscow: Nauka, 1954.
12. Nikol'skii, B.P., Grigorov, O.N., and Pozin, M.E., *Spravochnik khimika* (Chemist's Handbook), Nikol'skii, B.P., Ed., Leningrad: Khimiya. 1965, vol. 3.
13. Mukhin, V.M., Tarasov, A.V., and Klushin, V.N., *Aktivnye ugli Rossii* (Activated Carbons of Russia), Moscow: Metallurgiya, 2000.
14. *GOST* (State Standard) *12597–67, Sorbents: Method for Determining the Mass Fraction of Water in Activated Carbons and Catalysts Based on Activated Carbons*, Moscow: Izd. Standartov, 1967.
15. *GOST* (State Standard) *12596–67, Activated Carbons: Method for Determining the Mass Fraction of Ash*, Moscow: Izd. Standartov, 1967.
16. *GOST* (State Standard) *17219–71, Activated Carbons: Method for Determining the Total Pore Volume for Water*, Moscow: Izd. Standartov. 1971.
17. Svergun, D.I. and Feigin, L.A., *Rentgenovskoe i neitronnoe malouglovoe rasseyanie* (X-ray and Small-Angle Neutron Scattering), Moscow: Nauka, 1986.
18. Jacrot, B., *Rep Prog Phys.*, 1976, no. 39, pp. 911–953.
19. Rabinovich, V.A. and Khavin, Z.Ya., *Kratkii spravochnik khimika* (Concise Chemist's Reference Book), Moscow: Khimiya, 1978.
20. Schmidt, P.W., in *Modern Aspects of Small-Angle Scattering*, Brumberger, H., Ed., Dordrecht: Kluwer Acad., 1995, pp. 1–56.

ISSN 1070-4272, Russian Journal of Applied Chemistry, 2007, Vol. 80, No. 10, pp. 1676–1679. © Pleiades Publishing, Ltd., 2007.
Original Russian Text © O.A. Abonosimov, S.I. Lazarev, S.V. Kovalev, 2007, published in Zhurnal Prikladnoi Khimii, 2007, Vol. 80, No. 10, pp. 1647–1650.

PROCESSES AND EQUIPMENT OF CHEMICAL INDUSTRY

A Study of the Longitudinal Agitation Coefficient in Roll Elements of Baromembrane Apparatus

O. A. Abonosimov, S. I. Lazarev, and S. V. Kovalev

Tambov State Technical University, Tambov, Russia

Received December 25, 2006

Abstract—Longitudinal agitation coefficient in industrial baromembrane roll apparatus was studied for two types of separating elements in relation to the motion velocity and pressure of the flow in the apparatus. Dependences of the longitudinal agitation coefficients on hydrodynamic parameters of baromembrane apparatus were analyzed and explained.

DOI: 10.1134/S1070427207100138

The aim of this study was to examine the effect of hydrodynamic parameters of industrial baromembrane apparatus with roll separating elements on the processes of substance transfer across membranes.

The hydrodynamic structure of the flow in a membrane unit strongly affects the mass transfer in baromembrane separation of solutions. In these units, fluid flows, as a rule, occupy an intermediate position in their structure between two idealized limiting cases, piston-flow and complete-mixing modes.

To evaluate the effect of longitudinal agitation on the separating characteristics of a baromembrane unit, it is necessary to have data on longitudinal agitation coefficients. For this purpose, the longitudinal agitation coefficient in baromembrane units was experimentally determined.

EXPERIMENTAL

To determine the longitudinal agitation coefficient, we used the known method of introducing a perturbation in a certain cross-section of the flow and recording the consequences (response of the system) in another cross-section. In experimental studies, we used the method of pulsed introduction of a tracer (20% aqueous solution of NaCl), with the elution curve subsequently recorded at the outlet of the membrane unit. The amount of the tracer introduced was varied, depending on the unit operation mode, and was chosen to use 60% of the scale of the measuring instrument (KSM-4). This was done because the variation of the solution concentration in the unit is small within this range and the displacement of the rheochord slide is proportional to changes in concentration.

The experimental installation used to determine the longitudinal agitation coefficient is shown schematically in Fig. 1.

The installation comprised the following elements: reverse-osmosis separating apparatus *1*; input-solution tank *2*; high-pressure pump *3*; choke *4*; rotameters *5* and *6* for retentate and permeate, respectively; gage *7*;

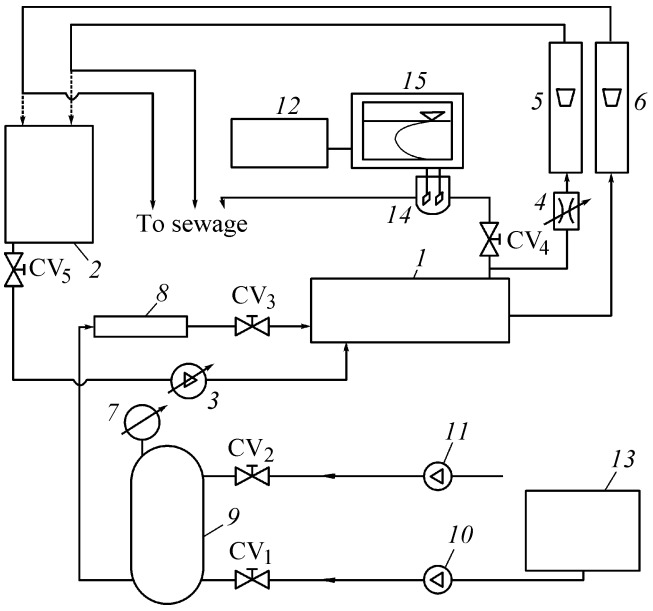

Fig. 1. Schematic of the experimental installation. For explanations, see text.

and tracer injection unit: batching cylinder with a piston, *8*; receiver *9*; high-pressure pump *10*; compressor *11*; resistance box *12*; vessel for solution, *13*; measuring cell *14*, automated bridge *15*; and control valves CV_1–CV_5.

The installation operated as follows. A solution (tap water) was delivered from the input tank by a high-pressure pump into the baromembrane unit, in which the necessary pressure was created. Two roll elements of the ERO-E-6.5/900A type or four of the ERO-K-92-475 type were mounted in the baromembrane unit. The necessary flow rate of the solution was set by adjusting the strokes of pump pistons. Before attaining the steady operation mode, the installation worked in the circulation mode, after which the permeate and retentate were discharged into sewage.

Because of the sufficiently high pressure in the unit (up to 4 MPa), we encountered the problem of fast and accurate introduction of the tracer into the system. It was solved by developing for this purpose an original design.

The tracer injection system operated as follows. The batching cylinder was filled with a required amount of the tracer. The air compressor and high-pressure pump created the required pressure in the receiver connected by a pipeline to the batching cylinder. By opening valve CV_3, the tracer was injected directly at the inlet of the reverse-osmosis unit. The pressure in the cylinder was always set to be somewhat higher than that in the baromembrane unit to provide a fast tracer injection into the unit. The time of tracer injection was 1–2 s.

The response curve was recorded with an electrically conducting cell mounted in parallel to the retentate flow at the unit outlet. The cell comprised two 4×8-mm rectangular parallel planar platinum electrodes spaced by 4 mm (Fig. 2). The cell volume being small, the solution portions between the electrodes rapidly changed.

The cell resistance was measured and recorded with a KSM-4 high-speed automated bridge. Because the electrical conductivity of tap water may somewhat vary, additional adjustment of the null position of the instrument scale was necessary. This adjustment was made by changing the resistance of the MSR-54 resistance box connected in series with the measuring cell. If the electrical conductivity of water increased or decreased, the resistance of the box was changed in the opposite direction, so that the total resistance of the cell and the resistance box remained approximately the same. The temperature of tap water was manually maintained constant because of the high sensitivity of the instrument to changes in its electrical conductivity with temperature.

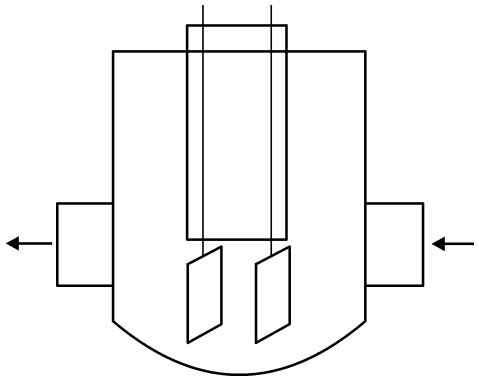

Fig. 2. Measuring cell.

The longitudinal agitation can be evaluated in terms of various theoretical models of the flow structure (cellular, recirculatory, combined, diffusion-type). The calculations were made using the diffusion model, the best applicable to the baromembrane unit under study, which can be classed with apparatus without any noticeably pronounced sectioning [1, 2].

The response C-curves were used to calculate the variance of the solution residence time in the apparatus.

The variance of the dimensionless C-curve was found using the equation [1]

$$\sigma^2 = \frac{1}{\tau_{av}^2}\left[\frac{\Sigma \tau_i^2 c_i}{\Sigma c_i} - \left(\frac{\Sigma \tau_i c_i}{\Sigma c_i}\right)^2\right], \quad (1)$$

where τ_{av} is the average residence time found in relation to the fluid velocity in the intermembrane channel by the formula

$$\tau_{av} = L/U, \quad (2)$$

L, unit length (m); and U, fluid velocity in the intermembrane channel (m s^{-1}).

The parameter of the diffusion model, modified Peclet number (Pe), was found using the known relationship [1] between the Peclet number and the variance of the distribution of the residence time, σ^2, for an infinitely long channel:

$$\sigma^2 = \frac{8}{Pe^2} + \frac{2}{Pe}. \quad (3)$$

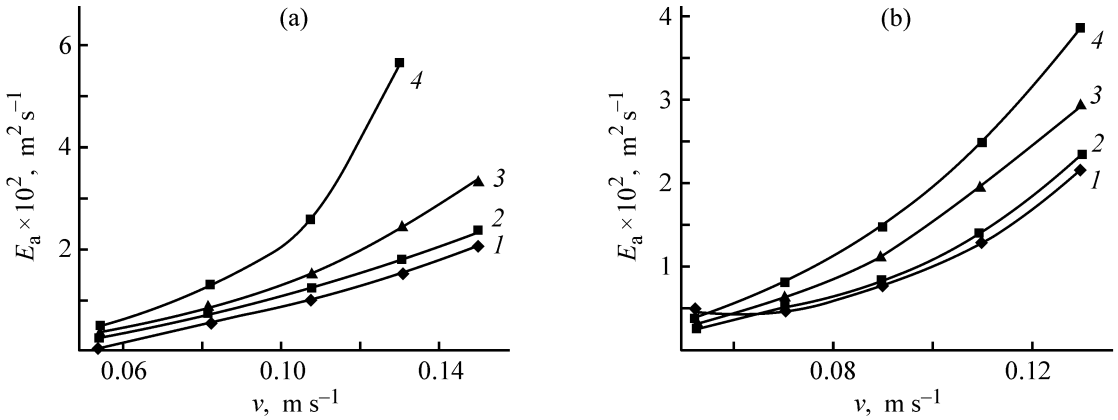

Fig. 3. Longitudinal agitation coefficient E_a vs. the fluid flow velocity v at different pressures in a unit with (a) ERO-E-6.5/900A and (b) ERO-K-92-475 roll elements. P (MPa): (*1*) 0.1, (*2*) 1.0, (*3*) 2.5, and (*4*) 4.0.

The resulting value of Pe was used to calculate the longitudinal agitation coefficient E_a by the formula

$$E_a = LU/\mathrm{Pe}, \quad (4)$$

where U is the solution flow velocity in the channel of the unit (m s^{-1}).

The longitudinal agitation in the baromembrane unit was studied at different solution flow velocities and pressures. The results obtained in experiments aimed to determine the dependence of the longitudinal agitation coefficient on the flow velocity and pressure of the fluid in the unit for both types of elements are shown graphically in Figs. 3a and 3b.

It can be seen that the longitudinal agitation coefficient substantially increases as the fluid flow velocity in the unit becomes higher. For a unit with ERO-K-92-475 elements, the longitudinal agitation coefficient is somewhat higher.

This can be attributed to enhancement of the turbulent agitation in the intermembrane channel of the element at higher fluid flow velocities, which is an important factor related to the intensity of longitudinal agitation. Moreover, additional mixing zones appear between the elements in the unit because of the specific design of element-to-element connections.

Empirical coefficients b, n, m in Eq. (5)

Membrane unit	$b \times 10^6$	n	m
ERO-E-6.5/900A	5.672	2.10	0.16
ERO-K-92-475	1.593	2.55	0.16

In these mixing zones, the flow is also strongly turbulized as the fluid flow velocity increases. The number of these zones is three for a unit with ERO-E-6.5/900A elements and five for that with ERO-K-92-475 elements. Therefore, a more complete agitation occurs in the latter unit, and just this circumstance accounts for the large values of the longitudinal agitation coefficient.

Analysis of the plots of the longitudinal agitation coefficient at different pressures in the unit also shows that the coefficient increases with the pressure in the unit.

The pressure in the unit is an additional factor affecting the longitudinal agitation coefficient. As the pressure in the unit increases, there appears an additional permeate flow, which gradually depletes the main flow along the unit length. The permeate flow is directed from the flow core in the intermembrane channel across the membrane, i.e., perpendicularly to the main flow. Therefore, the permeate flow gives rise to an additional agitation of the fluid flow in the membrane unit. At higher pressures, the permeate flow rate grows, which leads to an increase in the longitudinal agitation coefficient [3, 4]. ERO-K-92-475 membrane elements show a higher throughput in terms of the permeate than ERO-E-6.5/900A and, therefore, have somewhat larger values of the longitudinal agitation coefficient at equal pressures.

We used the experimental data obtained to construct approximation dependences of the longitudinal agitation coefficients on pressure and fluid flow velocity in the baromembrane unit for roll elements of the ERO-E-6.5/900A and ERO-K-92-475 types:

$$E_a = b\mathrm{Re}^n\left(\frac{P}{P_0}\right)^m, \quad (5)$$

where b, n, and m are empirical coefficients; and P and P_0 are the working pressure and pressure taken to be 0.1 MPa, respectively.

Values of the coefficients b, n, and m are listed in the table. The error of the calculated and experimental values of E_a did not exceed ±15%.

CONCLUSION

A strong longitudinal agitation occurs in baromembrane units. The magnitude of this agitation depends on the type of a membrane element, design features of the unit, hydrodynamic situation in the apparatus, and pressure difference.

REFERENCES

1. Gel'perin, N.I., Pebalk, V.L., and Kostanyan, A.E., *Struktura potokov i effektivnost' kolonnykh apparatov khimicheskoi promyshlennosti* (Structure of Flows and Efficiency of Column Apparatus in Chemical Industry), Moscow: Khimiya, 1977.
2. Levenspiel, O., *Chemical Reaction Engineering*, New York: John Wiley & Sons, 1965. Translated under the title Levenshpil', O., *Inzhenernoe oformlenie khimicheskikh protsessov*, Moscow: Khimiya, 1969.
3. Dytnerskii, Yu.I., *Membrannye processy razdeleniya zhidkikh smesei* (Membrane Processes for Separation of Fluid Mixtures), Moscow: Khimiya, 1975.
4. Hwang, S.-T. and Kammermeyer, K., *Membranes in Separations*, New York: John Wiley & Sons, 1975. Translated under the title *Khvang, S.-T., Kammermeier, K., Membrannye protsessy razdeleniya*, Dytnerskii, Yu.I., Ed., Moscow: Khimiya, 1981.

ISSN 1070-4272, Russian Journal of Applied Chemistry, 2007, Vol. 80, No. 10, pp. 1680–1682. © Pleiades Publishing, Ltd., 2007.
Original Russian Text © Yu.P. Osadchii, T.E. Nikiforova, 2007, published in Zhurnal Prikladnoi Khimii, 2007, Vol. 80, No. 10, pp. 1651–1653.

PROCESSES AND EQUIPMENT OF CHEMICAL INDUSTRY

A Model of Separation of Wastewater Containing Vat Dyes

Yu. P. Osadchii and T. E. Nikiforova

Ivanovo State University of Architecture and Building, Ivanovo, Russia
Ivanovo State University of Chemical Engineering, Ivanovo, Russia

Received November 14, 2006; in final form, April 2007

Abstract—Mechanism of fluid separation with capillary-porous polymeric membranes was studied and a mathematical model of separation by ultrafiltration of vat-dye-containing wastewater from finishing shops of textile plants was suggested. The model takes into account the effect of physical parameters on the mechanism and kinetics of the cross-membrane transfer of ingredients, in which a gel layer is formed.

DOI: 10.1134/S107042720710014X

The process of baromembrane separation of industrial wastewater containing dye vats, in which a gel layer is formed on the membrane, is nonstationary. The reason is that changes in the thickness of the gel layer affect the hydrodynamics and mass exchange because of the changing permeability and selectivity of this layer.

The objective in developing a mathematical model of separation of industrial wastewater containing vat dyes (Brilliant Green ZhD, Blue OD, Reddish 2ZhD) used in yarn dyeing in AKDU-6-02 apparatus is to describe the effect of physical parameters on the mechanism and kinetics of the cross-membrane transfer of ingredients, in which a gel layer is formed.

EXPERIMENTAL

The ultrafiltration process was performed under a pressure of 0.3–0.4 MPa, created within membranes by a centrifugal pump, flow velocity of 4–6 m^{-1}, pH 1–12, and temperature of the solution being separated in the range 15–90°C. The tubular membranes have the form of a multilayer tubular fiberglass frame covered from within with a semipermeable polymeric film. The input wastewater is concentrated via permanent circulation through BTU-0.5/2 membrane units comprising a set of tubular membranes [1], with continuous removal of the permeate. The resulting concentrate is delivered at regular intervals of time to a receiver tank for subsequent recirculation.

Apparatus with tubular membranes operate in the piston-flow mode. In the case in question, we have low concentrations of a vat dye (0.2–0.3 g l^{-1}) in water and weak effect of gelation on the permeability and selectivity of membrane durian a certain time. It is assumed that wastewater is separated at a constant pressure along the entire length of membrane units and constant temperature. A schematic of the baromembrane separation process is shown in Fig. 1.

The material balance equation for the flow rates of water and dye has the form

$$Q_1 = Q_2 + Q_3, \quad (1)$$

where Q_1 is the flow rate a substance (water and dye) before a cross-section under consideration (kg s^{-1});

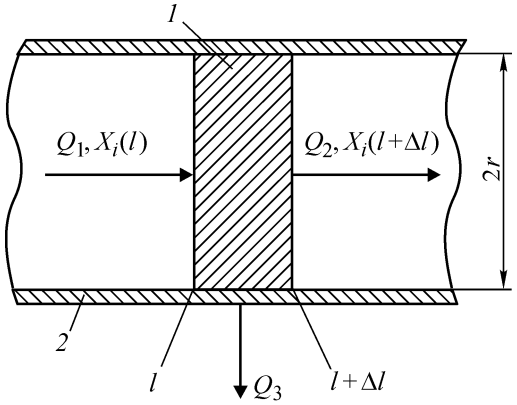

Fig. 1. Schematic of the ultrafiltration separation with a tubular membrane. (*1*) Arbitrary longitudinal cross-section of the flow being separated in the range from l to $l + \Delta l$, where l is an arbitrary coordinate along the tube length and (*2*) separating layer of a polymeric membrane, deposited onto the inner surface of the tube.

Q_2, flow rate of the substance after the cross-section (kg s^{-1}); and Q_3, flow rate of the substance across the membrane (kg s^{-1}).

In the general form, the flow rates are given for each of the components by

$$Q_1 = X_i(l)VS, \quad (2)$$

$$Q_2 = X_i(l + \Delta l)VS, \quad (3)$$

$$Q_3 = G_i \mathrm{d}F = 2G_i \pi r \mathrm{d}l, \quad (4)$$

where X_i is the mass fraction of a component in the flow (kg m^{-3}); V, flow velocity (m s^{-1}); l, coordinate along the apparatus (m); S, cross-section of a membrane tube (m^2); G_i, permeability to the substance (kg m^{-2} s^{-1}); F, separation surface area of the membrane (m^2); and r, membrane tube radius (m).

The mass fraction of the dye passing through the cross-section under consideration has the form

$$X_\mathrm{d}(l)VS = X_\mathrm{d}(l + \Delta l)VS + G_\mathrm{w}(1 - \varphi)2\pi r \mathrm{d}l, \quad (5)$$

$$G_\mathrm{d}\mathrm{d} = G_\mathrm{b}(1 - \varphi), \quad (6)$$

where X_d is the mass fraction of the dye (kg m^{-3}); G_d, membrane permeability to the dye (kg m^{-2} s^{-1}); G_w, membrane permeability to water (kg m^{-2} s^{-1}); and φ, degree of separation by the membrane or selectivity. After certain rearrangements, we obtain the integration constant from the initial conditions $l = 0$, $X_\mathrm{d} = X_{\mathrm{d}0}$ and expression (5) takes the form

$$X_\mathrm{k} = X_{\mathrm{k}0} - \frac{2G_\mathrm{b}(1 - \varphi)}{Vr} l. \quad (7)$$

The change in the mass fraction of the dye after putting wastewater through a single cycle ($l = L$) can be expressed as

$$2X_\mathrm{d} = \frac{GF}{V}[X_{\mathrm{d}0} - (1 - \varphi)]\,\mathrm{d}\tau, \quad (8)$$

where G is the overall permeability of the membrane (kg m^{-2} s^{-1}); V, volume of the permeate obtained in a given time (m^3); and τ, separation process duration (s).

According to the Darcy law [2], the change in the membrane permeability is given by

$$G = \frac{\Delta P \rho}{\mu(R_\mathrm{m} + R_\mathrm{g})}, \quad (9)$$

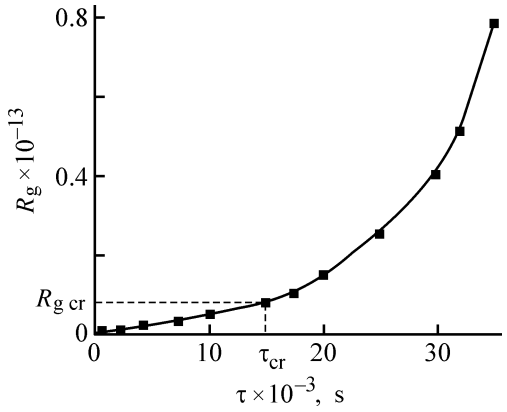

Fig. 2. Variation of the gel layer resistance R_g to the separation process with time τ. ΔP = 0.2 MPa, V = 2 m s^{-1}, T = 293 K.

where ΔP is the pressure difference over the membrane (N m^{-2}); ρ, density of wastewater being purified (kg m^{-3}); μ, dynamic viscosity for wastewater (N s m^{-2}); R_m, membrane resistance (m^{-1}); and R_g, gel layer resistance (m^{-1}).

The membrane resistance is found from the permeability equation for water and is taken to be constant. The gel layer resistance was found from experimental data, using Eq. (9). The plot describing the dependence of R_g on τ is shown in Fig. 2. It can be seen that this resistance starts to change after 7.5–8.5 h. This is the critical time τ_cr, to which corresponds the critical gel layer resistance. Further increase in τ leads to a pronounced rise in R_g and decrease in G.

A mathematical processing of the data yielded the following expression for the dependence of R_g on τ:

$$R_\mathrm{g} = b(e^{n\tau} - 1), \quad (10)$$

where $b = 2.06 \times 10^{10}$ m^{-1} and $n = 1.34 \times 10^{-4}$ s^{-1}.

We tested the adequacy of the calculation relation (10) with a satisfactory convergence at the previously obtained optimal separation process parameters [3]. Solving Eqs. (9) and (10), (8) and (11), we obtained

$$G = \frac{\Delta P \rho}{\mu[R_\mathrm{m} + b(e^{n\tau} - 1)]}, \quad (11)$$

$$\mathrm{d}X_\mathrm{d} = \frac{\Delta P \rho F[X_{\mathrm{d}0} - (1 - \varphi)]}{\mu V[R_\mathrm{m} + b(e^{n\tau} - 1)]}. \quad (12)$$

Having integrated Eq. (12) by the method of undetermined coefficients [4], we obtained an equation that can be used to calculate the mass fraction of a dye in an arbitrary cross-section of the apparatus:

Results of model adequacy tests

$\mu \times 10^3$, N s m^{-2}	$R_g \times 10^{-12}$	$R_m \times 10^{-1}$	$L \times 10^{-3}$, m	$\tau \times 10^{-3}$, s	X_d, kg m^{-3}		σ, %
	m^{-1}				calculation	experiment	
1.27	0.01	4.12	2.4	1.2	0.21	0.20	–0.35
1.27	0.01	4.12	4.8	2.4	0.36	0.35	–0.34
1.27	0.02	4.12	7.2	3.6	0.47	0.45	–0.31
1.27	0.07	4.12	14.4	7.2	0.79	0.75	–0.24
1.27	0.15	4.12	21.6	10.8	0.98	0.97	–0.21
1.29	0.31	4.12	36.0	14.4	1.45	1.49	+0.35
1.30	0.60	4.12	43.2	18.0	2.87	2.83	–0.21
1.31	1.15	4.12	50.4	21.8	5.67	5.32	–0.35
1.33	2.11	4.12	57.6	25.5	14.34	15.22	–0.45
1.35	3.99	4.12	64.8	28.3	17.23	17.01	–0.32
1.37	7.87	4.12	72.0	36.2	34.23	35.11	–0.56
1.39	14.34	4.12	82.6	38.4	64.35	68.45	+1.34

$$X_d = X_{d0} + \frac{\Delta P \rho F [X_{d0} - (1 - \varphi)]}{\mu V n [R_m - b]} \left[n\tau + \ln \frac{R_m}{R_m + b(e^{n\tau} - 1)} \right]. \quad (13)$$

Knowing how the mass fraction of the dye in an arbitrary cross-section varies with time, we found the optimal duration and degree of concentration of wastewater containing vat dyes, depending on changes in the resistance of the gel layer over the membrane.

To verify the adequacy of the model, we made a comparative analysis of the experimental and calculated values of X_d in certain intervals of time (see table).

CONCLUSIONS

(1) The model suggested makes it possible to calculate the concentration of vat dyes in a wastewater being separated, depending on the increase in the gel layer resistance.

(2) The calculated value $R_{g.\,cr} = 0.1R_m$ corresponds to a process duration of 8.3 h, which coincides with experimental data. The relative error in X_d is within 2.7–3.1%, which also confirms the validity of the relations used in the calculation. The satisfactory agreement between the experimental and calculated concentrations of vat dyes in wastewater being separated confirms the adequacy of the model suggested.

(3) The model can be used to find the optimal technological mode of the process, determine the main characteristics for both the nonstationary and steady modes, and choose the optimal degree of concentration of the components.

REFERENCES

1. *Membrany i membrannaya tekhnika: Katalog VNIISS i NIITEKHIM* (Membranes and Membrane Technology; Catalogue by VNIISS and NIITEKHIM), Cherkassy, 1999.
2. Nevskii, A.V., Meshalkin, V.P., and Sharnin, V.A., *Analiz i sintez vodnykh resursosberegayushchikh khimiko-tekhnologicheskikh system* (Analysis and Synthesis of Aqueous REsourse-saving Chemical-Technological Systems), Moscow: Nauka, 2004.
3. Beskov, V.S. and Safronov, V.S., *Obshchaya khimicheskaya tekhnologiya i osnovy promyshlennoi ekologii* (General Chemical Technology and Fundamentals of Industrial Ecology), Moscow: Khimiya, 1999.
4. Korn, G.A. and Korn, T.M., *Mathematical Handbook for Scientists and Engineers*, New York: McGraw–Hill, 1968.

ISSN 1070-4272, Russian Journal of Applied Chemistry, 2007, Vol. 80, No. 10, pp. 1683–1686. © Pleiades Publishing, Ltd., 2007.
Original Russian Text © S.V. Aleeva, O.A. Zabyvaeva, G.V. Chistyakova, S.A. Koksharov, 2007, published in Zhurnal Prikladnoi Khimii, 2007, Vol. 80, No. 10, pp. 1654–1657.

PROCESSES AND EQUIPMENT OF CHEMICAL INDUSTRY

Effect of Hydroxyethylated Alkyl Phenol and Triethanolamine on Absorption of Atmospheric Oxygen by Aqueous-Alkaline Solutions

S. V. Aleeva, O. A. Zabyvaeva, G. V. Chistyakova, and S. A. Koksharov

Institute of Solution Chemistry, Russian Academy of Sciences, Ivanovo, Russia

Received October 16, 2006; in final form, June 2007

Abstract—Changes in the driving force of the multistage interphase transfer of atmospheric oxygen in the presence of a nonionogenic wetting agent and triethanolamine were assessed by using analytical solutions of the film model of mass exchange at the phase boundary to describe the chemisorption uptake of oxygen by a sodium dithionite solution.

DOI: 10.1134/S1070427207100151

Alkaline treatments are an integral part of processes employed in purification of cellulose-containing materials to remove accompanying impurities in pulp-and-paper and textile industries and in initial processing of bast-fiber cultures to obtain cellulose and fibrous materials from annually renewable vegetable raw materials. In this case, the probability of damaging the main polymer is high because of the pronounced susceptibility of cellulose to oxidative destruction under the action of dissolved oxygen. This predetermines the topicality of studying the fundamental kinetic aspects of aerobic absorption of atmospheric oxygen and the influence exerted on this process by substances used to accelerate the wetting of cellulose materials and emulsify the impurities being removed. This is frequently done using nonionogenic surfactants based on products formed in hydroxyethylation of higher alcohols and alkyl phenols, and triethanolamine salts of their sulfo derivatives. Determining the effect of assistant substances on the chemisorption of oxygen is necessary for substantiating and developing cellulose-preserving techniques for processing of raw materials.

EXPERIMENTAL

In [1, 2], an approach to assessment of the driving force of the multistage process of interphase transfer of atmospheric oxygen into solution from experimental data on sodium dithionite (SDT) oxidation controlled by uptake of the oxidizing agent from the atmosphere was demonstrated. Previously, the adequacy of the method has been confirmed in description of chemisorption-induced oxidation of sodium hydroxymethane sulfinate (rongalite) [3]. Analysis of a concentration set of experimental curves describing the kinetics of dithionite oxidation by surface-absorbed oxygen and extrapolation of the dependences $W_S^{red} = f(c_{red})$ to $c_{red} = 0$ make it possible to characterize the state of an SDT-free solution, i.e., of the medium being analyzed, by analytical solutions obtained in terms of the film model of mass exchange at the phase boundary [4]. In this case, a differentiated assessment is possible of the influence exerted by assistant substances on the successive transfer of a gaseous oxidizing agent first to an adsorbed form and then to a solvated state, followed by its redistribution into the bulk via diffusion (absorption):

$$(O_2)_{atm} \xrightarrow{k_L^0} (O_2)_{ads} \xrightarrow{c_{ox(S)}} (O_2)_{solv} \xrightarrow{D_{ox}} (O_2)_{abs}. \quad (1)$$

As characteristics of stage-by-stage transformations can serve the following: mass-transfer coefficient k_L^0 at the interface (m s^{-1}), oxygen concentration in the surface layer of the solution, $c_{ox(S)}$ (M); and diffusion coefficient of oxygen, D_{ox} (m^2 s^{-1}). These coefficients are related in the model by the expressions

$$k_L^0 = W_S^0(c_{ox(S)} - c_{ox(V)}), \quad (2)$$

$$Y^0 = D_{ox}c_{ox(S)}(W_S^0)^{-1}, \quad (3)$$

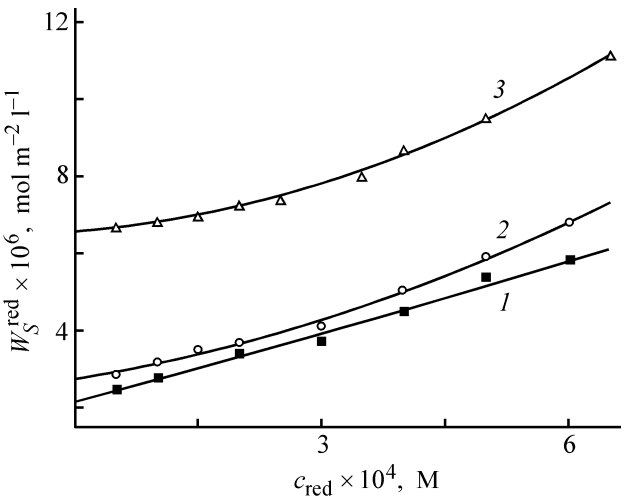

Fig. 1. Effect of the SDT concentration c_{red} on the rate of SDT oxidation by atmospheric oxygen, W_S^{red}, absorbed by aqueous-alkaline solutions (293 K, pH 12.5). (*1*) Without additives; additive (M): (*2*) OEAP (0.005) and (*3*) TEA (0.1).

where $c_{ox(V)}$ is the oxygen concentration in the solution bulk (M); $\{c_{ox(V)} = 0$, oxygen is absent in the solution bulk because of the fast chemical interaction between reagents [5]$\}$; Y^0, depth to which O_2 penetrates and thickness of the layer in which the reaction with SDT occurs (m); and W_S^0, rate of the surface uptake of oxygen by the solution in the absence of a chemical reaction (at $c_{red} = 0$) (mol m^{-2} s^{-1}).

The reaction of SDT with dissolved oxygen at 293 K and pH 12.5 was studied in thermostated (±0.1 K) test tubes with fixed solution volumes and areas of contact between the solution and the atmosphere. The loss of SDT was monitored spectrophotometrically by changes in the absorption associated with the dithionite ion $S_2O_4^{2-}$ (λ_{max} = 315.5 nm, $\varepsilon = 10^4$ l mol^{-1} cm^{-1}) [5]. The initial SDT concentration c_{red}^0 was varied within the range $(0.5–6) \times 10^{-4}$ M. The rate of surface oxygen uptake, W_S^{red} was calculated using the stationary portions of the kinetic curves of SDT oxidation, $c_{red} = f(\tau)$, with the condition $\Delta c_{red} << c_{red}^0$ satisfied.

The content of dissolved oxygen in solvents was determined using Winkler's iodometric method [6]. The diffusion coefficients of oxygen were found using the recommendations of [7] with account of the data on changes in the solvent viscosity, obtained in this study, from the relation

$$D_{ox} = [7.4 \times 10^{-8}(XM)^{0.5}T]/(V_0^{0.6}\eta), \quad (4)$$

where X is the solvent association parameter (for water, X = 2.6); M = 18, molecular weight of water; T, temperature (K); V_0 = 25.6 cm^3 mol^{-1}, molar volume of the solution at the normal boiling point [8]; and η, solvent viscosity (cP).

Viscometric studies were performed on an installation with an Ostwald capillary viscometer, equipped with systems for ultrathermostating and automated recording of the fluid effluence time, which provided viscosity measurements with an rms error not exceeding 0.1×10^{-5} m^2 s^{-1} for ten parallel runs.

The effect of wetting substances on the chemisorption uptake of atmospheric oxygen was studied for the example of two compounds belonging to the conventionally used assortment of textile-assistant substances (TAS); hydroxyethylated alkyl phenol [OEAP; $C_nH_{2n+1}C_6H_5(OCH_2CH_2)_mOH$, n = 10–13, m = 3] and triethanolamine [TEA; $N(CH_2CH_2OH)_3$ or $N(Et)_3$].

The concentration of the additives in the working solutions was 0.005 M for OEAP and 0.1 M for TEA.

Figure 1 shows how addition of the substances under consideration affects the concentration dependences of the calculated rates of SDT oxidation by the oxygen being absorbed. In accordance with the recommendations of [2], the accelerating effect of the chemical reaction on the rate of oxygen uptake upon an increase in the STD concentration can be described with a high reliability of approximation to experimental data (Fig. 1, *points*) by second-order polynomials (*lines*) for a system containing no surfactant (5) and systems with addition of OEAP (6) and TEA (7):

$$W_S^{red} = (2.1597 + 0.5627c_{red} + 0.0067c_{red}^2) \times 10^{-6}, \quad R^2 = 0.9941; \quad (5)$$

$$W_S^{red} = (2.7194 + 0.3541c_{red} + 0.0548c_{red}^2) \times 10^{-6}, \quad R^2 = 0.9990; \quad (6)$$

$$W_S^{red} = (6.5332 + 0.1683c_{red} + 0.0827c_{red}^2) \times 10^{-6}, \quad R^2 = 0.9965. \quad (7)$$

The first term in Eqs. (5)–(7) determines for each of the liquid-phase systems under study the rate of surface absorption of oxygen by a solution containing no sodium dithionite, W_S^0.

The content of oxygen in aqueous-alkaline solutions with addition of wetting substances was measured with account of the possible spatially nonuniform distribution of these latter. For this purpose, the averaged content of dissolved oxygen was first determined, in accordance with the method described in [1], for

Effect of TAS on the oxygen content and rheological properties of the surface layer of a NaOH solution (0.0315 M) and on kinetic characteristics of uptake of atmospheric oxygen

T, K	Additive, M	$c_{ox(S)}$, mol m^{-3}	$\eta_{(S)}$, cP	$W_S^0 \times 10^6$, mol m^{-2} s^{-1}	$k_L^0 \times 10^6$, m s^{-1}	$D_k \times 10^9$, m^2 s^{-1}	$\gamma^0 \times 10^4$, m
293	No additive	1.353	1.089	2.16	1.596	1.947	12.55
	TEA, 0.1	3.117	1.294	6.53	2.095	1.639	7.82
	OEAP, 0.005	1.388	0.986	2.72	1.960	2.150	10.97
333	No additive	0.823	0.477	6.49	7.886	5.049	6.40
	OEAP, 0.005	0.881	0.425	7.73	8.774	5.677	6.47

the concentration series of assistant substances being introduced, with slow agitation of a solution being analyzed after its equilibration under aerobic conditions. Then, an analysis for the content of oxygen in the surface layer separated from the rest of the liquid with a separatory funnel was made for solutions with TEA and OEAP concentrations of 0.1 and 0.005 M, respectively. The results obtained are shown in Fig. 2.

The increase in the equilibrium concentration of O_2 in the presence of TAS is presumably due to the more effective solvation of gas molecules via formation of hydrogen bonds between atoms of the nonpolar oxygen molecules and unionized alcoholic hydroxy groups of the compounds being introduced. In particular, the micellar state of surfactants, with the hydrophilic moiety of the molecules and alcoholic hydroxyl groups, accessible to interaction, oriented toward the outer shell of a micelle, is characteristic of OEAP solutions in the chosen concentration range. The more considerable increase in c_{ox} for the TEA additive, compared with OEAP, is due not only to the higher concentration of the former and, accordingly, to a large amount of hydroxyl groups involved in solvation processes. Presumably, the incorporation of TEA molecules into the network of hydrogen bonds between water molecules causes substantial changes in the state of the surface layer of the solution, which is manifested in an increase in the size of tetrahedral structures whose cells can retain an additional number of oxygen molecules without formation of H-bonds.

The virtually linear run of the concentration dependences $c_{ox} = f(c_{TAS})$ makes it possible to regard the experimentally recorded increase in the content of oxygen content in the surface layer of the working solution, $c_{ox(S)}$, by Δc_{ox} as a result of concentration of the assistant preparations. To the $c_{ox(S)}$ in Fig. 2 correspond the following concentrations of assistant substances (M): $c_{TEA(S)} = 0.626$ and $c_{OEAP(S)} = 0.0154$. To a first approximation, these values characterize the spatial redistribution of the assistant substances and their content in the surface layer of the aqueous-alcoholic solution.

The dynamic viscosities $\eta_{(S)}$ were determined for these concentrations of the substances subjected to analysis in systems being homogenized. Their values, listed in the table, reflect the rheological properties of the surface layer of the working solutions containing a specified amount of an additive. The table also summarizes the results of analyses of the influence

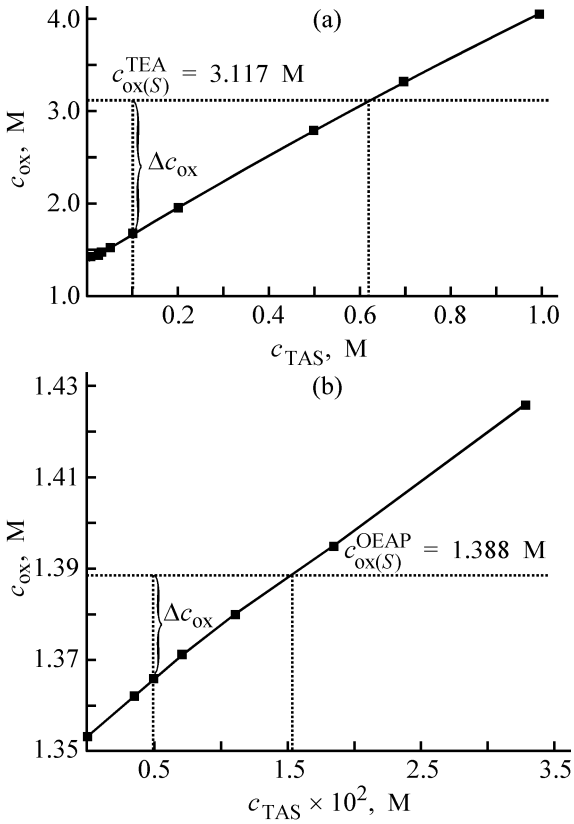

Fig. 2. Oxygen concentration c_{ox} in (a) TEA and (b) OEAP solutions at 293 K and pH 12.5. (c_{TAS}) Additive concentration.

exerted by assistant substances on the parameters of the interphase transfer of oxygen.

Analysis of the kinetic characteristics of the interphase transfer of oxygen into solution shows that the compounds compared intensify to virtually the same extent (by a factor of 1.23–1.31) the mass transfer at the phase boundary, k_L^0. In this case, the rate of surface oxygen uptake becomes more than three times higher owing to the 2.3-fold increase in the equilibrium concentration of oxygen on the surface of a solution with TEA additive, despite the slower inward diffusion. Upon introduction of OEAP into a solution, all stages of the chemisorption process are intensified, including the redistribution of O_2 into the solution bulk via diffusion. The joint effect of these factors provides a 1.26 times faster interphase transfer.

It is highly important in scientific and practical respects to assess the influence exerted by surfactants on the absorption of the oxidizing agent by heated aqueous-alkaline solutions under the real conditions of their application. In view of this circumstance, a set of studies described above was performed in order to determine kinetic parameters of the adsorption-diffusion process at 333 K.

As can be seen from the table, the presence of a wetting agent differently affects the characteristics of the successive stages of the interphase oxygen transfer. The rise in the mass-transfer coefficient at the phase boundary, k_L^0, decreases from 1.23 times at 293 K to 1.11 times at 333 K. At the same time, the temperature-induced decrease in $c_{ox(S)}$ is manifested to a lesser extent in a solution with OEAP additive, and the diffusion coefficient of oxygen, D_{ox} increases in this case more substantially, compared with that without an assistant substance. This manner of variation of the parameters of the adsorption-diffusion process indicates that the intensifying effect of the wetting agent on the rate of oxygen absorption by the solvent is preserved upon a change of the tendency of deviations of the surface layer depth Y^0 to which O_2 molecules penetrate before their complete interaction with sodium dithionite used in the experiment to determine the amount of absorbed oxygen. As applied to the conditions of alkaline treatment of cellulose materials, this means that solutions containing nonionogenic wetting agents based on hydroxyethylated fatty hydrocarbons and their triethanolamine derivatives are more rapidly saturated with oxygen, which makes more probable the oxidative destruction of cellulose.

CONCLUSIONS

(1) The concentration of triethanolamine and a wetting agent based on hydroxyethylated alkyl phenol in the surface layer of the aqueous-alkaline solution was experimentally confirmed. This process provides a steep increase in the solvating power of the liquid toward atmospheric oxygen being adsorbed.

(2) Addition of wetting agents makes lower the surface resistance of the solution and accelerates the mass transfer at the phase boundary by a factor of 1.2–1.3.

(3) Addition of triethanolamine decelerates the inward diffusion of dissolved oxygen, whereas wetting agents based on hydroxyethylated hydrocarbons intensify its diffusion redistribution, with the saturation of the solution with an oxidizing agent additionally accelerated on heating the solution.

(4) The joint effect of these factors intensifies the absorption of the oxidizing agent from the atmosphere 1.3-fold upon introduction of hydroxyethylated alkyl phenol and 3-fold in the presence of triethanolamine.

ACKNOWLEDGMENTS

The study was financially supported by grants of the President of the Russian Federation for young candidates of science (no. MK-8178.2006.3).

REFERENCES

1. Koksharov, S.A., Chistyakova, G.V., Aleeva, S.V., et al., *Izv. Vyssh. Uchebn. Zaved., Khim. Khim. Tekhnol.*, 2005, vol. 48, no. 3, pp. 50–53.
2. Aleeva, S.V., Koksharov, S.A., and Polenov, Yu.V., *Izv. Vyssh. Uchebn. Zaved., Khim. Khim. Tekhnol.*, 2005, vol. 48, no. 12, pp. 37–39.
3. Koksharov, S.A., Chistyakova, G.V., Murav'ev, O.N., et al., *Zh. Prikl. Khim.*, 1999, vol. 72, no. 7, pp. 1161–1164.
4. Sherwood, T.K., Pigford, R.L., and Wilke, C.R., *Mass Transfer*, New York, McGraw–Hill, 1975.
5. Ivanov, V.V., Koksharov, S.A., and Mel'nikov, B.N., *Kinet. Kataliz*, 1991, vol. 32, no. 33, pp. 3756–3759.
6. Lur'e, Yu.Yu., *Analiticheskaya khimiya promyshlennykh stochnykh vod* (Analytical Chemistry of Industrial Wastewater), Moscow: Khimiya, 1984, pp. 176–182.
7. *Chemical Engineer's Handbook*, Perry, J. H., Ed., New York: McGraw–Hill, 1963. Translation under the title *Spravochnik inzhenera-khimika*, Leningrad: Khimiya, 1969, vol. 1, pp. 403–410.
8. *Spravochnik khimika* (Chemist's Handbook), Nikol'skii, B.P., Ed., Moscow: Khimiya, 1964.

ISSN 1070-4272, Russian Journal of Applied Chemistry, 2007, Vol. 80, No. 10, pp. 1687–1690. © Pleiades Publishing, Ltd., 2007.
Original Russian Text © R.I. Khusnutdinov, A.R. Baiguzina, A.A. Smirnov, R.R. Mukminov, U.M. Dzhemilev, 2007, published in Zhurnal Prikladnoi Khimii, 2007, Vol. 80, No. 10, pp. 1658–1661.

ORGANIC SYNTHESIS AND INDUSTRIAL ORGANIC CHEMISTRY

Furfuryl Alcohol in Synthesis of Levulinic Acid Esters and Difurylmethane with Fe and Rh Complexes

R. I. Khusnutdinov, A. R. Baiguzina, A. A. Smirnov, R. R. Mukminov, and U. M. Dzhemilev

Institute of Petroleum Chemistry and Catalysis, Russian Academy of Sciences, Ufa, Bashkorkostan, Russia

Received October 3, 2006; in final form, July 2007

Abstract—The possibility of synthesis of levulinic acid esters by the reaction of furfuryl alcohol with aliphatic alcohols in the system CCl_4–$Fe(acac)_3$ was studied.

DOI: 10.1134/S1070427207100163

Levulinic, or 4-oxopentanoic, acid has many useful characteristics and has widespresd application [1]. For example, levulinic acid serves as a plant growth regulator and as a modifying additive for resins and Aerosils. Esters and salts of levulinic acid are used in food and pharmaceutical industries as preservatives, stabilizing agents, and odorants.

Levulinic acid is a product of cellulose processing. For example, in acid treatment of a plant material consisting of cellulose and hemicellulose, polysaccharides are first hydrolyzed to form simple sugars and then, under subsequent heating at 110°C for 28 h in the presence of 20% HCl, levulinic acid is formed is 40% yield [1, 2].

A more convenient procedure for production of levulinic acid is hydration and ring opening of furfuryl alcohol (**1**) in the presence of strong acids. When the reaction is carried out in water, the yield of levulinic acid is 80% [3], and in water-soluble ketones (acetone, 2-butanone), its yield reaches 93% [4].

A modification of this procedure is heating of furfuryl alcohol in the presence of water and HCl acting as a catalyst; in this case, furfuryl alcohol is gradually added to a mixture of concentrated HCl and levulinic acid. The main drawback of this procedure is the necessity for use of a significant amount of levulinic acid (up to 40%) as a solvent [5].

When furfuryl alcohol is involved in the reaction with alcohols under conditions of acid catalyst (concentrated HCl), the direction of its conversion changes to formation of levulinic acid esters. It should be noted that reaction of **1** with alcohols proceeds at a noticeable rate at a large (fourfold) excess of ROH and at slow addition of **1** to boiling alcohol so that its concentration does not exceed 2 vol%; in so doing, the water content should be less than 0.5%. However, even when the above conditions are met, the yields of levulinic acid esters are low, 52 and 67% for methyl and ethyl levulinate, respectively [6].

We found that levulinic acid esters can be synthesized by the reaction of furfuryl alcohol **1** with aliphatic alcohols in the presence of Fe-containing catalysts in CCl_4. Among the iron-containing catalysts [$FeBr_2$, $FeCl_3$, $Fe(OAc)_2$, $Fe(C_7H_{15}CO_2)$, and $Fe(acac)_3$] tested, iron(III) acetylacetonate showed the highest activity: with this catalyst, the yield of levulinic acid esters **2**–**5** was 80–90%. In the presence of other catalysts, the yield of **2**–**5** did not exceed 50%.

For example, the reaction of **1** with methanol occurs at 70°C and continuous stirring within 3.5–4 h with complete conversion of the starting furfuryl alcohol. The yield of methyl levulinate is quantitative (98%). The reaction of furfuryl alcohol with ethanol, propanol, and isopropanol occurs similarly. An attempt to make the yield of *i*-Pr (**4**) and *n*-Pr (**5**) levulinates quantitative by raising the reaction duration to 5 h failed, since a solid oligomeric product (molecular weight determined by the Rast's method 2114 Da) insoluble in water and in most of organic solvents is formed in this case:

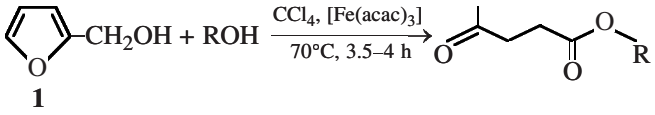

1

R = CH_3 (**2**, 98%), R = C_2H_5 (**3**, 95%), R = *i*-C_3H_7 (**4**, 85%), R = *n*-C_3H_7 (**5**, 80%).

With the aim to identify the actual catalytic species, iron salts or any other compounds, we analyzed the reaction mixture. Titration with NaOH and $AgNO_3$ solutions showed the presence of HCl in the solution in a concentration of 2–2.4 mg ml^{-1} throughout the process. It should be noted that the possibility of HCl formation in the system containing CCl_4, methanol, and iron salts at elevated temperature (140°C) has been found previously [7]. It was shown that generation of HCl from alcohols and CCl_4 under the action of iron compounds follows the scheme

$$RCH_2OH + CCl_4 \xrightarrow{[Fe]} [RCH_2OCl] \rightarrow HCl + RCHO.$$

In the experiments with furfuryl alcohol, carbonyl compounds (formaldehyde from CH_3OH, acetaldehyde from C_2H_5OH, propanal from n-C_3H_7OH, and acetone from *i*-C_3H_7OH) were formed along with HCl.

The presence of HCl in the reaction mixture suggests its possible involvement in the catalysis of formation of **2**–**5**, but in the form of a complex with $Fe(acac)_3$, rather than as free HCl, which causes the higher yield of esters **2**–**5** compared with unbound HCl.

Considering the possible involvement of HCl in the catalysis and taking into account published data [1, 8, 9], we can suggest the following mechanism of formation of esters **2**–**5**:

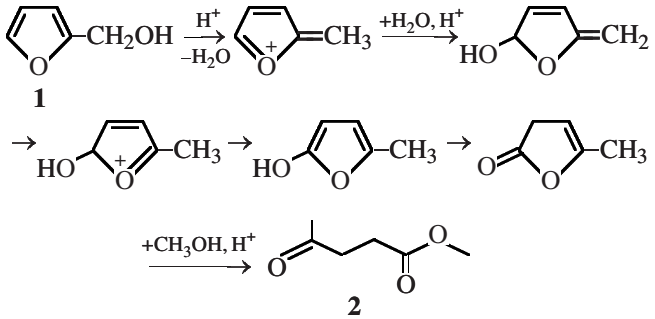

1

2

As further studies showed, the above reaction is also catalyzed by rhodium complexes and, in particular, by $Rh(PPh_3)_3Cl$: in its presence, the process duration decreases to 2–3 h.

The reaction of furfuryl alcohol with deuterated methanol (70°C, 4 h) yielded fully deuterated methyl levulinate, which is not unexpected considering the clearly pronounced capacity of levulinic acid for deuterium exchange in treatment with D_2O [2]:

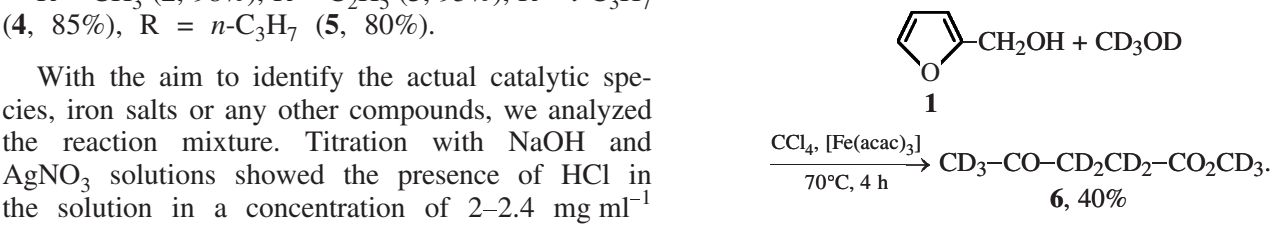

1

6, 40%

The following optimal ratios of the catalyst and reactants were found experimentally: $[Fe(acac)_3]$: [furfuryl alcohol] : [ROH] : $[CCl_4]$ = 1 : 100 : 400 : 200.

To direct the reaction toward formation of levulinic acid, we performed experiments with water instead of methanol. With iron compounds as catalysts, no noticeable conversion was observed, whereas in the presence of the catalyst $Rh(PPh_3)_3Cl$, furfuryl alcohol reacts with H_2O and CCl_4 to form 2,2'-difurylmethane **7** (yield 80%) and minor amount of difurfuryl ether **8**:

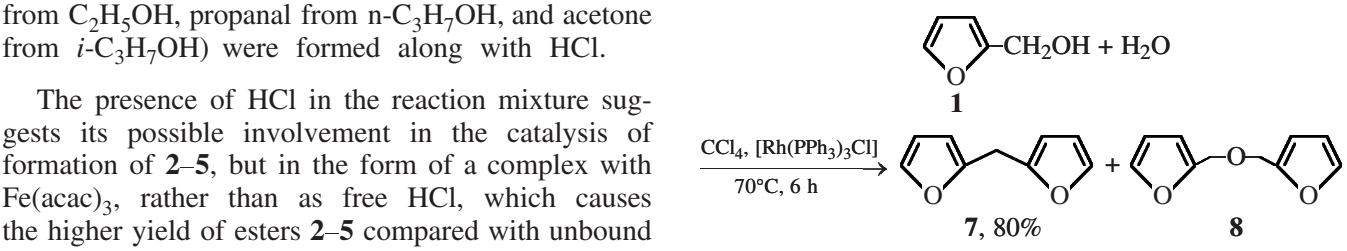

1

7, 80% **8**

It should be noted that the well-known procedures for synthesis of **7**, which is a valuable odorant and a monomer for preparation of sensors for ion-selective chromatography, are rather complicated [10]. For example, one of the widely used procedures for synthesis of **7** is decarboxylation of bis(5-carboxyfuryl)methane in the presence of powdered copper [11]. The procedure for synthesis of **7**, based on reduction of difuryl ketone with sodium in ethanol [12, 13], is still more complicated. As can be seen, the procedure we suggested for synthesis of **7** is simpler and requires more available starting compounds as compared to the other well-known procedures.

As regards the mechanism of formation of **7**, according to [2], 2,2'-difurfuryl ether is formed in the first stage, and then it decomposes to give formaldehyde and 2,2'-difurylmethane, which is promoted by the rhodium catalyst $Rh(PPh_3)_3Cl$ whose ability to form a complex with CH_2O is well known [14]:

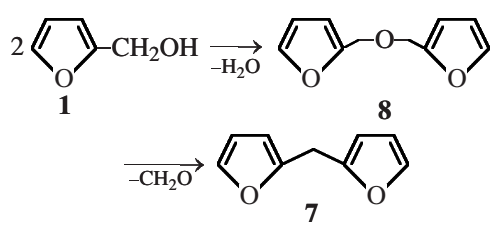

EXPERIMENTAL

The ^1H and ^{13}C NMR spectra of the compounds in $CDCl_3$ were recorded on a JEOL FX90Q spectrometer [90 MHz (^1H), 22.5 MHz (^{13}C)]; the chemical shifts δ (ppm) are given relative to TMS. The IR spectra were recorded on a UR-20 spectrophotometer in KBr pellets or in thin layer (film), and mass spectra, on a Finnigan MAT-112S chromatograph-mass spectrometer (EU, 70 eV). Chromatographic analysis was performed on a Chrom-5 device; 1.2 m × 3 mm column, stationary phase SE-30 (5%) on Chromaton N-AW-HMDS, heating from 50 to 250°C at a rate of 8 deg min^{-1}, carrier gas helium (47 ml min^{-1}). The hypochlorite concentration was determined by iodometric titration [15].

As the starting reactants we used commercially available alcohols: furfuryl alcohol, methanol, ethanol, propanol, and isopropanol, which were prepurified by distillation. Carbon tetrachloride was purified by the standard procedure.

Commercial iron acetylacetonate $Fe(acac)_3$ was recrystallized and dried in a vacuum desiccator before use; $Rh(PPh_3)_3Cl$ was synthesized by the procedure described previously and dried in a vacuum (20 h, 80°C) [16, 17].

The general procedure for synthesis of levulinic acid was as follows. A reactor (V = 100 ml) was charged with 0.1 mmol of $Fe(acac)_3$, 10 mmol of furfuryl alcohol, 40 mmol of aliphatic alcohol, and 20 mmol of CCl_4. The reaction was carried for 3.5–4 h at 70°C with continuous stirring. Then the reactor was cooled to room temperature and the reaction mixture was filtered through a silica gel bed (eluent hexane : ether = 1 : 1). The solvent was removed, and the residue was distilled.

The structure of the resulting compounds was confirmed by spectral data and also by comparison with authentic samples and reference data.

Methyl levulinate 2. Yield 98%, bp 76°C/10 mm Hg (bp 196°C [18]). ^1H NMR spectrum ($CDCl_3$; δ, ppm; J, Hz): 3.66 (3H, s, CH_3), 2.19 (3H, s, $COCH_3$), 2.56 (2H, t, CH_2, J 5.5), 2.70 (2H, t, CH_2, J 6.3), ^{13}C NMR (δ, ppm): 27.47 (C-2), 29.39 (CH_3), 37.65 (C-3), 51.37 (OCH_3), 173.03 (COO), 206.40 (CO). Mass spectrum, m/z (I_{rel}, %): 130 $[M]^+$ (10), 43 (96), 45 (7), 51 (1), 53 (3), 55 (57), 57 (38), 59 (40), 60 (4), 70 (2), 71 (32), 75 (6), 76 (1), 81 (4), 83 (1), 87 (25), 88 (45), 89 (3), 90 (0.5), 98 (44), 99 (100), 100 (10), 101 (2), 110 (0.5), 115 (98), 116 (6), 117 (2), 120 (0.5).

D_{10}-Methyl levulinate 6. Yield 40%. ^{13}C NMR ($CDCl_3$; δ, ppm): 27.09 (C-2, $^1J_{CD}$ 19.7 Hz), 37.15 (C-3, $^1J_{CD}$ 19.8 Hz), 29.00 (CH_3, $^1J_{CD}$ 19.1 Hz), 50.23 (OCH_3, $^1J_{CD}$ 19.3 Hz), 172.89 (COO), 206.40 (CH_3CO). Mass spectrum, m/z (I_{rel}, %): 140 $[M]^+$ (2), 44 (7), 45 (34), 46 (100), 57 (17), 61 (14), 62 (23), 76 (10), 77 (8), 92 (8), 93 (14), 95 (25), 96 (8), 102 (9), 103 (13), 104 (45), 105 (28), 106 (6), 119 (2), 120 (42), 121 (59), 122 (9), 129 (2), 130 (1), 138 (4), 139 (2), 140 (2).

Ethyl levulinate 3. Yield 95%, bp 73–74°C/6 mm Hg (bp 205–208 [18]). ^1H NMR spectrum ($CDCl_3$; δ, ppm; J, Hz): 1.25 (3H, t, CH_3, J 5.7), 2.17 (3H, s, $COCH_3$), 2.50 (2H, t, CH_2, J 5.5), 2.66 (2H, t, CH_2, J 6.3), 4.12 (2H, q, CH_2, J 6.1), ^{13}C NMR (δ, ppm): 28.32 (C-2), 36.95 (C-3), 29.52 (CH_3), 58.67 (OCH_2), 12.13 (CH_3), 171.52 (COO), 204.44 (CH_3CO). Mass spectrum, m/z (I_{rel}, %): 144 $[M]^+$ (5), 43 (100), 45 (7), 55 (8), 71 (10), 73 (15), 74 (20), 98 (13), 99 (80), 101 (24), 102 (22), 129 (30).

Isopropyl levulinate 4. Yield 85%, bp 86–87°C/10 mm Hg (bp 209–203 °C [18]). Mass spectrum, m/z (I_{rel}, %): 158 $[M]^+$ (0.3), 41 (12), 43 (93), 71 (8), 73 (7), 74 (29), 98 (5), 99 (100), 101 (19), 116 (13), 117 (15), 130 (3), 143 (7), 144 (0.2).

Propyl levulinate 5. Yield 80%, bp 95–96°C/10 mm Hg (bp 221–222°C [18]). ^1H NMR spectrum ($CDCl_3$; δ, ppm; J, Hz): 0.94 (3H, t, CH_3, J 5.2), 1.50–1.83 (2H, m, CH_2), 2.22 (3H, s, CH_3), 2.50–3.18 (4H, m, CH_2), 4.05 (2H, t, CH_2, J 5.5). ^{13}C NMR (δ, ppm): 29.59 (C-5, CH_3), 26.82 (C-2), 37.14 (C-3), 64.69 (OCH_2), 19.92 (CH_2), 8.59 (CH_3), 58.67 (OCH_2), 12.13 (CH_3), 170.68 (COO), 204.77 (CH_3CO). Mass spectrum, m/z (I_{rel}, %): 158 $[M]^+$ (0.3), 43 (99), 71 (12), 73 (14), 74 (21), 98 (18), 99 (100), 101 (31), 129 (39).

To synthesize difurylmethane, 0.1 mmol of Wilkinson complex $Rh(PPh_3)_3Cl$, 10 mmol of furfuryl alcohol, 40 mmol of water, and 20 mmol of CCl_4 were placed in a 100-ml reactor. The reaction mixture was heated with continuous stirring and kept for 6 h at 70°C. After cooling to room temperature, the reaction mixture was filtered through a silica gel

bed (eluent hexane : ester = 1 : 1), and the product was extracted with diethyl ether. The solvent was removed and the residue was distilled.

2,2'-Difurylmethane 7. Yield 80%, bp 88–89°C/10 mm Hg (bp 106–108°C/40 mm Hg, n_D 1.4865 [19]). ^{1}H NMR spectrum ($CDCl_3$, δ, ppm): 3.93 (2H, s, CH_2), 6.0–7.3 (6H, m, furyl). ^{13}C NMR spectrum ($CDCl_3$, δ, ppm): 150.52 (C-2, C-2'), 106.37 (C-3, C-3'), 107.21 (C-4, C-4'), 141.53 (C-5, C-5'). Mass spectrum, *m/z* (I_{rel}, %): 148 $[M]^+$ (87), 41 (2), 45 (3), 46 (4), 49 (1), 63 (8), 65 (19), 81 (12), 89 (6), 91 (100), 92 (14), 94 (15), 105 (3), 118 (2), 119 (20), 120 (29), 121 (4), 143 (7), 147 (15), 149 (10), 150 (1).

Difurfuryl ether 8. Yield 20 wt%, bp 100–101°C/2 mm Hg (bp 100–102°C/2 mm Hg [20]). ^{1}H NMR ($CDCl_3$, δ, ppm): 4.48 (4H, s, CH_2), 6.3–7.56 (6H, m, furyl). Mass spectrum, *m/z* (I_{rel}, %): 178 $[M]^+$ (6), 41 (6), 50 (2), 53 (22), 54 (6), 69 (6), 80 (3), 81 (100), 82 (50), 83 (4), 95 (7), 97 (11), 110 (5), 111 (1), 119 (0.5), 120 (0.5), 134 (0.5), 141 (0.2), 143 (7), 150 (0.5), 162 (1), 179 (1).

Oligomeric product. Yield 99%. Molecular weight *M* approximately 2144. Found (%): C 57.3, H 4.90, Cl 12.4. $(C_6H_8O_2)_x + (C_6H_9ClO_2)_y$, $x = 0.55$, $y = 0.45$. IR spectrum, cm^{-1}: 780, 1380, 1620, 1720.

CONCLUSIONS

(1) Synthesis of levulinic acid esters by the reaction of furfuryl alcohol with CCl_4 and alcohols under the action of $Fe(acac)_3$ and $Rh(PPh_3)_3Cl$ occurs with a high yield, 80–98%.

(2) In the reaction of furfuryl alcohol with a mixture of CCl_4 and water in the presence of Wilkinson complex $Rh(PPh_3)_3Cl$, 2,2'-difurylmethane is formed in 80% yield.

ACKNOWLEDGMENTS

This study was financially supported by the Ministry of Education and Science of the Russian Federation (grant no. NSh-7470.2006.3), Foundation for Assistance to Domestic Science, and grant of the President of Bashkorkostan Republic for young scientists and youth research teams (Contract no. 4).

REFERENCES

1. Timokhin, B.V., Baranskii, V.A., and Eliseeva, G.D., *Usp. Khim.*, 1999, vol. 68, no. 1, pp. 80–93.
2. Sunjic, V., Horvat, J., and Klaic, B., *Kem. Ind.*, 1984, vol. 33, pp. 599–606.
3. JPN Patent 62252742.
4. US Patent 3752849.
5. US Patent 5175358.
6. US Patent 2763665.
7. Khusnutdinov, R.I., Schadneva, N.A., Baiguzina, A.R., et al., *ARKIVOC*, 2004, no. 11, pp. 53–60.
8. Joule, J. and Smith, G., *Heterocyclic Chemistry*, London: Van Nostrand, 1972.
9. Horvat, J., Klaic, B., and Metelko, B., *Tetrahedron Lett.*, 1985, vol. 26, pp. 2111–2113.
10. Butin, A.V., Stroganova, T.A., Kul'nevich, V.G., *Khim. Geterotsikl. Soedin.*, 1999, no. 7, pp. 867–901.
11. Dinelli, D. and Morini, G.B., *Gazz. Chim. Ital.*, 1937, vol. 67, pp. 312–315.
12. Reichstein, T., Grussner, A., and Zschokke, H., *Helv. Chim. Acta*, 1932, vol. 15, pp. 1066–1069.
13. Gilman, H. and Wright, G.F., *J. Am. Chem. Soc.*, 1933, vol. 55, pp. 3302–3314.
14. Korneeva, G.A., Ezhova, N.N., Slivinskii, E.V., et al., *Izv. Akad. Nauk SSSR, Ser. Khim.*, 1989, no. 12, pp. 2670–2673.
15. Charlot, G., *Les Methods de la Chemie Analytique. Analyse quantitative Minerale, Quatrieme Edition*, Paris: Masson, 1961.
16. Gordon, A.J. and Ford, R.A., *The Chemist's Companion. A Handbook of Practical Data, Techniques and References*, New York: Interscience, 1972.
17. Becker, H., Berge, W., Domschke, G., et al., *Organicum. Organisch-chemisches Grundpractikum*, Schwentlick, Dr.K., Ed., Berlin: Wissenschaften, 1976.
18. *Dictionary of Organic Compounds*, Heilbron, I. and Bunbury, H.M., Eds., London: Eyre and Spottiswoode, 1946, vol. 2.
19. *Sintezy geterotsiklicheskikh soedinenii* (Syntheses of Heterocyclic Compounds), Mndzhoyan, A.L., Ed., Yerevan: Akad. Nauk Arm. SSR, 1958, issue 3.
20. Zanetti, J.E. and Bashour, J.T., *J. Am. Chem. Soc.*, 1939, vol. 61, no. 8, pp. 2249–2251.

ISSN 1070-4272, Russian Journal of Applied Chemistry, 2007, Vol. 80, No. 10, pp. 1691–1694. © Pleiades Publishing, Ltd., 2007.
Original Russian Text © V.M. Chernyshev, A.N. Sokolov, V.A. Taranushich, 2007, published in Zhurnal Prikladnoi Khimii, 2007, Vol. 80, No. 10, pp. 1662–1665.

ORGANIC SYNTHESIS AND INDUSTRIAL ORGANIC CHEMISTRY

A New Approach to Synthesis of 2-Sulfonylamino-1,2,4-Triazolo[1,5-*a*]pyrimidines

V. M. Chernyshev, A. N. Sokolov, and V. A. Taranushich

South-Russian State Technical University, Novocherkassk, Rostov oblast, Russia

Received January 22, 2007; in final form, April 2007

Abstract—A procedure for synthesis of 2-sulfonylamino-1,2,4-triazolo[1,5-*a*]pyrimidines by sulfonylation of 2-amino-4,7-dihydro-1,2,4-triazolo[1,5-*a*]pyrimidines, followed by oxidation of intermediate 2-sulfonylamino-4,7-dihydro-1,2,4-triazolo[1,5-*a*]pyrimidines, was suggested.

DOI: 10.1134/S1070427207100175

1,2,4-Triazolo[1,5-a]- and -[1,5-c]pyrimidines containing sulfonylamino group bonded to the triazole ring are of interest as new herbicides and plant growth regulators [1–7]. For example, 2-arylsulfonylamino-1,2,4-triazolo[1,5-a]pyrimidines has been suggested for weed removal from of wheat and soybean crops [4, 5], and 5,7-dimethoxy-2-(2-methoxy-4-trifluoromethylpyrid-3-yl)sulfonylamino-1,2,4-triazolo[1,5-*a*]-pyrimidine (Pyroxsulam^{R}) is intended for presprout protection of rice and corn crops [6, 7].

However, the existing procedures for synthesis of 2-sulfonylamino-1,2,4-triazolo[1,5-a]pyrimidines have certain drawbacks [4–7]. For example, cyclocondensation of 5-amino-3-sulfonylamono-1,2,4-triazoles with 1,3-dicarbonyl compounds can yield a mixture of isomers if unsymmetrically substituted dicarbonyl compounds are used. In addition, this procedure is limited by difficult synthesis of the initial compounds [8]. The procedures based on cyclization of *N*-hydroxy-*N*'-pyrimidinyl-*N*''-sulfonylguanidines by the Tisler reaction are multistage and require use of highly toxic chemicals [6, 7]. Sulfonylation of 2-amino-1,2,4-triazolo[1,5-*a*]pyrimidines usually proceeds with a low yield due to the low nucleophilicity of the amino group in these compounds [4–6]. A high yield of sulfonyl derivatives (92%) has been only reported for sulfonylation of 2-amino-5,7-dimethoxy-1,2,4-triazolo-[1,5-*a*]pyrimidine with 2,6-dichlorobenzenesulfonyl chloride [7]. However, acceptable yields of sulfonyl derivatives (55–75%) can be only obtained if sulfonylation of this substrate is catalyzed by sulfylimines [6]. Thus, a search for new routes to 2-sulfonylamino-1,2,4-triazolo[1,5-*a*]pyrimidines is an urgent task.

It can be assumed that the target 2-sulfonylamino-1,2,4-triazolo[1,5-*a*]pyrimidines can be synthesized by sulfonylation of more nucleophilic 2-amino-4,7-di-hydro-1,2,4-triazolo[1,5-*a*]pyrimidines, with subsequent oxidative heteroaromatization of intermediate 2-sulfonylamino-4,7-dihydro-1,2,4-triazolo[1,5-*a*]pyrimidines. A similar approach has been used previously in synthesis of acetylamino-1,2,4-triazolo[1,5-*a*]pyrimidines [9].

Here we studied the sulfonylation of 2-amino-4,7-dihydro-1,2,4-triazolo[1,5-*a*]pyrimidines (**I**–**VI**) and of 2-amino-6,6-dimethyl-9-phenyl-6,7-dihydro-1,2,4-triazolo[5,1-b]quinazolin-8(4H, 5H, 9H)-one (**VII**) containing a dihydropyrimidine fragment with sulfonyl chlorides and the oxidative heteroaromatization of the resulting sulfonyl derivatives:

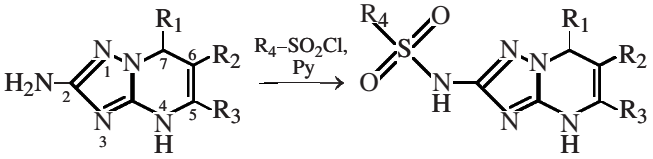

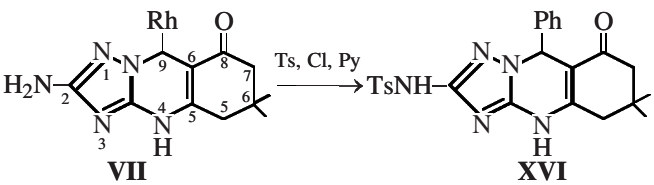

where R_1 Ph, R_2 H, R_3 Me (**I**, **X**, **XVII**); R_1, R_3 Ph, R_2 H (**II**, **XI**, **XVIII**); R_1 *p*-Me-C_6H_4, R_2 H, R_3 Ph (**III**, **XII**, **XIX**); R_1 Ph, R_2 H, R_3 *p*-Me-C_6H_4 (**IV**, **XIII**, **XX**); R_1 *p*-MeO-C_6H_4, R_2 H, R_3 Ph (**V**, **XIV**, **XXI**); R_1 Ph, R_2 COOEt, R_3 Me (**VI**, **XV**); R_4 *p*-Me-C_6H_4 (**X**, **XV**, **XVII**); R_4 *p*-Cl-C_6H_4 (**XI**, **XIV**, **XVIII**, **XXI**); Me (**XII**, **XIX**); Ph (**XIII**, **XX**).

The starting compounds **I**–**V** and 2-aminotriazoloquinazolinone **VII** were synthesized by condensation of 3,5-diamino-1,2,4-triazole **VIII** with unsaturated carbonyl compounds by the well-known procedures [10, 11], which are characterized by high regioselectivity and accessibility of the starting compounds and allow wide variation of substituents in the pyrimidine fragment [12–14]. 2-Amino-5-methyl-7-phenyl-6-ethoxycarbonyl-4,7-dihydro-1,2,4-triazolo[1,5-*a*]pyrimidine **VI** was synthesized by three-component condensation of diamine (**VIII**) with benzaldehyde and acetoacetic ester:

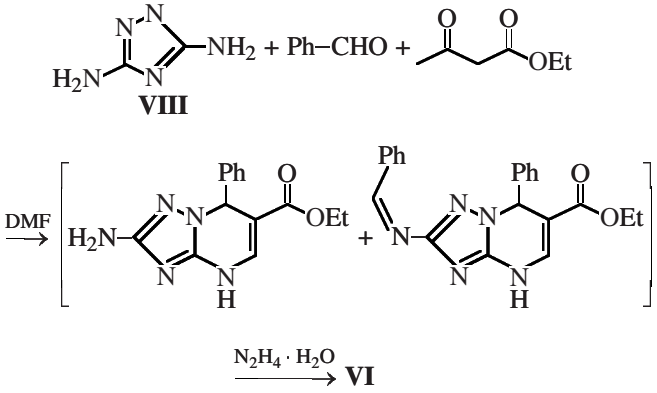

In the ^{1}H NMR spectrum of crude **VI**, there are signals of an impurity (its content is approximately 27%), which was assigned to azomethine **IX** (signals of aromatic protons in the range 7.5–7.9 ppm and of CH=N group, at 9.0 ppm). Compound **VI** was purified by refluxing in ethanol with hydrazine hydrate, followed by crystallization.

The reaction of **I**–**VII** with sulfonyl chlorides in dry refluxing pyridine gave 2-sulfonylamino-4,7-dihydro-1,2,4-triazolo[1,5-*a*]pyrimidines **X**–**XV** and 6,6-dimethyl-2-tosylamino-9-phenyl-6,7-dihydro-1,2,4-triazolo[5,1-b]quinolin-8(4H,5H,9H)-one **XVI** in a yield of 60–89%. Thus, the lower electron-acceptor power of dihydropyrimidine fragment in **I**–**VII** makes these compounds more reactive in sulfonylation in comparison with aromatic 2-amino-1,2,4-triazolo[1,5-*a*]pyrimidines. Compounds **X**–**XVI** have not been described previously; their structure was confirmed by elemental analysis and data of mass spectrometry and ^{1}H NMR spectroscopy (see table).

Oxidation of **X**–**XIV** with *N*-bromosuccinimide in ethanol at 50–60°C or with bromine in acetic acid at 10–20°C resulted in the formation of 2-sulfonylamino-1,2,4-triazolo[1,5-*a*]pyrimidines (**XVII**)–(**XXI**) in a yield of 90–94%. Their structure was confirmed by elemental analysis and spectral data (see table).

Attempts to perform heteroaromatization of **XV** and **XVI** failed. In treatment of **XV** with bromine in acetic acid, the only reaction product was bromine derivative **XXII**:

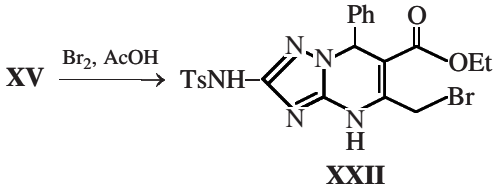

The reaction of quinazolinone **XVI** with bromine or *N*-bromosuccinimide yielded an inseparatable mixture of bromination products and the starting compounds. In an attempt to perform heteroaromatization of **XV** and **XVI** by refluxing in an alcoholic solution of alkali in air, following the procedure described in [15], only the starting substances were recovered. Apparently, the resistance of **XV** and **XVI** to the action of oxidants is caused by their stabilization due to the electron-acceptor effect of the carbonyl group.

EXPERIMENTAL

The ^{1}H NMR spectra were recorded on a Varian Unity-300 spectrometer (300 MHz, DMSO-d_6, the internal reference TMS). The mass spectra were recorded on a Finnigan MAT Incos 50 device with direct sample inlet at ionizing electron energy of 70 eV. The elemental analysis was performed on a Perkin–Elmer 2400 analyzer. The melting points were determined by the capillary method on a PTP unit.

2-Amino-5-methyl-7-phenyl-6-ethoxycarbonyl-4,7-dihydro-1,2,4-triazolo[1,5-*a*]pyrimidine VI. A mixture of 2 g (0.02 mol) of diamine (**VIII**), 2.12 g (0.02 mol) of benzaldehyde, 2.6 g (0.02 mol) of acetacetic ester, and 3 ml of DMF was refluxed for 30 min, then 10 ml of water was added and the mixture was cooled. The resulting precipitate was filtered off and mixed with 1 g (0.02 mole) of hydrazine hydrate, 1 ml of AcOH, and 5 ml of ethanol. The resulting mixture was refluxed for 30 min, cooled, and the precipitate of **VI** was filtered and crystallized from ethanol.

2-Sulfonylamino-4,7-dihydro-1,2,4-triazolo[1,5-*a*]pyrimidines X–XV. To a mixture of 0.0044 mol of appropriate 2-amino-4,7-dihydro-1,2,4-triazolo[1,5-*a*]-

Some physicochemical characteristics of **VI** and **X**–**XXII**

Compound	Yield, %	mp, °C	Formula*	^{1}H NMR spectrum, δ, ppm (*J*, Hz)
VI	44	228–230	$C_{15}H_{17}N_5O_2$	1.00 t (3H, CH_3, *J* = 7.1), 2.35 s (3H, CH_3), 3.91 q (2H, CH_2, *J* = 7.1), 5.19 s (2H, NH_2), 5.92 s (1H, CH), 7.08–7.38 m (5H, Ph), 10.42 s (1H, NH)
X	87	226–228	$C_{19}H_{19}N_5O_2S$	1.79 s (3H, CH_3), 2.34 s (3H, CH_3), 4.50 d (1H, CH, *J* = 3.7), 5.79 d (1H, CH, *J* = 3.7), 7.07 m (2H, arom), 7.24–7.30 m (5H, arom), 7.63 d (2H, arom, *J* = 8.1), 9.56 s (1H, NH), 10.71 s (1H, NH)
XI	69	274–276	$C_{23}H_{18}N_5ClO_2S$	5.16 m (1H, CH), 6.03 d (1H, CH, *J* = 3.7), 7.16 m (2H, arom), 7.31–7.38 m (6H, arom), 7.52 m (4H, arom), 7.76 d (2H, arom, *J* = 9.0), 10.02 c (1H, NH), 11.05 s (1H, NH)
XII	60	238–240	$C_{19}H_{19}N_5O_2S$	2.27 s (3H, CH_3), 3.19 s (3H, CH_3), 5.17 m (1H, CH), 6.04 d (1H, CH, *J* = 3.7), 7.14 m (4H, arom), 7.38 m (3H, arom), 7.57 m (2H, arom), 10.07 s (1H, NH), 10.48 s (1H, NH)
XIII	69	250–252	$C_{24}H_{21}N_5O_2S$	2.28 s (3H, CH_3), 5.10 m (1H, CH), 6.01 d (1H, CH, *J* = 3.7), 7.15 m (4H, arom), 7.28–7.62 m (8H, arom), 7.78 d (2H, arom, *J* = 7.3), 9.96 s (1H, NH), 10.92 s (1H, NH)
XIV	71	256–257	$C_{24}H_{20}N_5ClO_3S$	3.73 s (3H, CH_3æ), 5.12 m (1H, CH), 5.97 d (1H, CH, *J* = 3.7), 6.87 d (2H, arom, *J* = 8.6), 7.11 d (2H, arom, *J* = 8.6), 7.36– 7.56 m (7H, arom), 7.76 d (2H, arom, *J* = 8.6), 9.97 s (1H, NH), 10.37 s (1H, NH)
XV	64	220 (decomp)	$C_{22}H_{23}N_5O_4S$	1.00 t (3H, CH_3, *J* = 7.1), 2.37 s (6H, $2CH_3$), 3.94 q (2H, CH_2, *J* = 7.1), 6.08 s (1H, CH), 7.05–7.30 m (7H, arom), 7.62 d (2H, arom, *J* = 8.2), 10.75 s (1H, NH), 10.90 s (1H, NH)
XVI	73	314–315	$C_{24}H_{25}N_5O_3S$	0.96 s (3H, CH_3), 1.07 s (3H, CH_3), 2.10 m (2H, CH_2), 2.35 s (3H, CH_3), 2.43 m (2H, CH_2), 6.01 s (1H, CH), 7.10–7.26 m (7H, arom), 7.62 d (2H, arom, *J* = 8.2), 10.95 s (1H, NH), 11.10 s (1H, NH)
XVII	90(a)	284–285	$C_{19}H_{17}N_5O_2S$	2.36 s (3H, CH_3), 2.58 s (3H, CH_3), 7.39 m (3H, arom), 7.63 m (3H, arom), 7.86 d (2H, arom, *J* = 8.2), 8.00 m (2H, arom), 11.90 s (1H, NH)
XVIII	94(a)	276–277	$C_{23}H_{16}N_5ClO_2S$	7.55–7.72 m (8H, arom), 7.99 m (3H, arom), 8.10 m (2H, arom), 8.30 m (2H, arom), 12.23 s (1H, NH)
XIX	90(a)	288–289	$C_{19}H_{17}N_5O_2S$	2.44 s (3H, CH_3), 3.41 s (3H, CH_3), 7.44 d (2H, arom, *J* = 8.2), 7.59 m (3H, arom), 8.05 s (1H, CH), 8.19 d (2H, arom, *J* = 8.2), 8.35 m (2H, arom), 11.59 s (1H, NH)
XX	90(a), 92(b)	>320	$C_{24}H_{19}N_5O_2S$	2.37 s (3H, CH_3), 7.34 d (2H, arom, *J* = 8.0), 7.62 m (6H, arom), 7.97 m (5H, arom), 8.23 d (2H, arom, *J* = 8.0), 12.11 s (1H, NH)
XXI	93(a), 90(b)	280–282	$C_{24}H_{18}N_5ClO_3S$	3.90 s (3H, CH_3O), 6.87 d (2H, arom, *J* = 8.9), 7.54–7.71 m (5H, arom), 7.99 m (3H, arom), 8.19 d (2H, arom, *J* = 8.9), 8.31 m (2H, arom),12.27 s (1H, NH)
XXII	45	270–276 (decomp)	$C_{22}H_{22}N_5BrO_4S$	1.00 t (3H, CH_3, *J* = 7.1), 2.38 s (3H, CH_3), 3.96 q (2H, CH_2, *J* = 7.1), 4.63 s (2H, CH_2), 6.15 s (1H, CH), 7.10–7.32 m (7H, arom), 7.63 d (2H, arom, *J* = 8.2), 10.95 s (1H, NH), 11.19 s (1H, NH)

* The results of elemental analysis for C, H, and N agree with the calculated values to within ±0.34%; in the mass spectra of **VI**, **XX**–**XXI** there is a strong $[M]^+$ peak.

pyrimidine **I**–**VI** and 5 ml of dry pyridine, 0.0053 mol of the corresponding sulfonyl chloride was added with stirring. The reaction mixture was refluxed for 15–20 min, cooled, and diluted with 10 ml of water. The precipitate of **X**–**XV** was filtered and crystallized from a 1 : 3 DMF–ethanol mixture.

6,6-Dimethyl-2-tosylamino-9-phenyl-6,7-dihydro-1,2,4-triazolo[5,1-*b*]quinazolin-8(4H,5H)-one XVI was synthesized similarly to **X**–**XV** by tosylation of amine **VII**.

2-Sulfonylamino-1,2,4-triazolo[1,5-*a*]pyrimidines XVII–**XXI**. (a) To a stirred mixture of 0.0026 mol of dihydrotriazolopyrimidine **X**–**XIV** and 0.44 g (0.0052 mol) of sodium acetate in 10 ml of ethanol, 0.46 g (0.0026 mol) of *N*-bromosuccimidine was added in 0.1-g portions over of a period of 10 min at 50–60°C. Then the reaction mixture was refluxed for 15 min, diluted with 10 ml of water, and the precipitate of **XVII**–**XXI** was filtered off, washed with water (10 ml), and crystallized from a 1 : 3 DMF : ethanol mixture.

(b) To a stirred mixture of 0.0026 mole of dihydrotriazolopyrimidine **XIII**–**XIV** and 0.44 g (0.0052 mol) of sodium acetate in 2 ml of AcOH 0.42 g (0.0026 mol) of Br_2 was added dropwise over a period of 10 min. The reaction mixture was stirred for 30 min at 10–20°C and diluted with 10 ml of water, and the precipitate of **XX**–**XXI** was filtered off and crystallized from a 1 : 3 DMF-ethanol mixture.

5-Bromomethyl-2-tosylamino-7-phenyl-6-ethoxycarbonyl-1,2,4-triazolo[1,5-*a*]pyrimidine XXII. To a stirred mixture of 1.18 g (0.0026 mol) of dihydrotriazolopyrimidine **XV**, 0.44 g (0.0052) of sodium acetate, and 2 ml of AcOH, 0.42 g (0.0026 mol) of Br_2 was added dropwise over a period of 10 min. The reaction mixture was stirred for 30 min at 10–20°C and diluted with 10 ml of water; the precipitate of **XXII** was filtered off and crystallized from acetonitrile.

CONCLUSIONS

(1) Contrary to their aromatic analogs, 2-amino-4,7-dihydro-1,2,4-triazolo[1,5-*a*]pyrimidines are more reactive toward sulfonyl chlorides and form 2-sulfonylamino-4,7-dihydro-1,2,4-triazolo[1,5-*a*]pyrimidines in 60–89% yield.

(2) Oxidation of 2-sulfonylamino-4,7-dihydro-1,2,4-triazolo[1,5-*a*]pyrimidines with bromine or *N*-bromosuccinimide gives 2-sulfonylamino-1,2,4-triazolo[1,5-*a*]pyrimidines and can serve as an efficient procedure for their synthesis (yield 90–94%).

(3) 2-Sulfonylamino-4,7-dihydro-1,2,4-triazolo[1,5-*a*]pyrimidines containing carbonyl group in position 6 as a substituent are resistant to heteroaromatization.

REFERENCES

1. Parnell, J.S. and Hall, J.C., *J. Agric. Food Chem.*, 1998, vol. 46, no. 1, pp. 152–156.
2. Jabusch, T.W. and Tjeerdema, R.S., *J. Agric. Food Chem.*, 2005, vol. 53, no. 18, pp. 7179–7183.
3. Jabusch, T.W. and Tjeerdema, R.S., *J. Agric. Food Chem.*, 2006, vol. 54, no. 16, pp. 5962–5967.
4. US Patent 4638075.
5. US Patent 4822404.
6. Bell, B.M., Fanwick, P.E., Graupner, P.R., and Roth, G.A., *Org. Process Res. Dev.*, 2006, vol. 10, no. 6, pp. 1167–1171.
7. US Patent 6559101. *N*-(5,7-Diethoxy-[1,2,4]triazolo-[1,5-*a*]pyrimidin-2-yl)arylsulfonamide Compounds and Their Use as Herbicides.
8. Chibale, K., Dauvergne, J., and Wyatt, P.G., *Synthesis*, 2002, no. 2, pp. 185–190.
9. Chernyshev, V.M., Sokolov, A.N., and Taranushich, V.A., *Zh. Prikl. Khim.*, 2006, vol. 79, no. 7, pp. 1144–1147.
10. Desenko, S.M., Kolos, N.N., Tueni, M., and Orlov, V.D., *Khim. Geterotsikl. Soedin.*, 1990, no. 7, pp. 938–941.
11. Lipson, V.V., Desenko, S.M., Borodina, V.V., et al., *Zh. Org. Khim.*, 2005, vol. 41, no. 1, pp. 115–120.
12. Chebanov, V.A. and Desenko, S.M., *Curr. Org. Chem.*, 2006, vo. 10, no. 3, pp. 297–317.
13. Chebanov, V.A., Muravyova, E.A., Desenko, et al., *J. Comb. Chem.*, 2006, vol. 8, no. 3, pp. 427–434.
14. Fedorova, O.V., Zhidovinova, M.S., Rusinov, G.L., and Ovchinnikova, I.G., *Izv. Ross. Akad. Nauk, Ser. Khim.*, 2003, no. 8, pp. 1677–1678.
15. Lipson, V.V., Desenko, S.M., Ignatenko, I.V., et al., *Izv. Ross. Akad. Nauk, Ser. Khim.*, 2006, no. 2, pp. 335–340.

ISSN 1070-4272, Russian Journal of Applied Chemistry, 2007, Vol. 80, No. 10, pp. 1695–1698. © Pleiades Publishing, Ltd., 2007.
Original Russian Text © A.F. Shmidt, A.Al Halaiqa, V.V. Smirnov, 2007, published in Zhurnal Prikladnoi Khimii, 2007, Vol. 80, No. 10, pp. 1666–1669.

ORGANIC SYNTHESIS AND INDUSTRIAL ORGANIC CHEMISTRY

Enhancement of Catalyst Performance in Heck Reaction of Nonactivated Aryl Bromides in the Absence of Phosphine Ligands

A. F. Shmidt, A. Al Halaiqa, and V. V. Smirnov

Irkutsk State University, Irkutsk, Russia
Irkutsk State Technical University, Irkutsk, Russia

Received March 1, 2007

Abstract—Effective procedures for raising the yield of the Heck reaction, based on the reactants (bromobenzene, styrene), in the presence of the previously developed phosphine-free catalytic system ($PdCl_2$ + NaOOCH + NaOAc) were suggested.

DOI: 10.1134/S1070427207100187

The catalytic arylation of alkenes with aryl halides (I) [1, 2] has been extensively studied [3–7]:

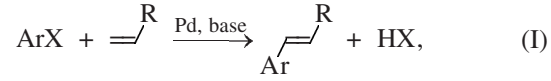

$$ArX + \text{alkene} \xrightarrow{\text{Pd, base}} \text{Ar-alkene} + HX, \quad (I)$$

X = I, Br, Cl.

A special attention is paid to development of new catalytic systems that can activate more readily available, but less reactive aryl bromides and chlorides. Use of these catalytic systems will allow industrial application of the Heck reaction [5–7]. Insufficient catalytic activity in reaction (I) is mainly due to the low reactivity of nonactivated aryl bromides and chlorides in the final step of the catalytic cycle, oxidative addition to Pd(0) complexes. As a result, the catalyst is removed from the main catalytic cycle owing to the competing Pd(0) aggregation.

The catalytic systems free of any ligands and, in particular, of the commonly used phosphines are of particular practical interest. Homogeneous phosphine-free catalytic systems containing simple palladium salts [$Pd(OAc)_2$, $PdCl_2$] and capable of activating nonreactive aryl bromides were developed in 2003 [8–10]. The reaction is accelerated with as the catalyst amount decreases [8, 9]. Introduction of small amounts of NaOOCH reducing Pd(II) to catalytically active Pd(0) and of an excess of aryl halides preventing aggregation of Pd(0) enabled not only quantitative arylation of an alkene [10], but also a larger turnover number of the catalyst [7, 11], including reactions with aryl chlorides [7]. Clearly, the use of an excess aryl halide substantially restricts the practical applicability of this method. Hence we suggest simple ways to raise the yield of the valuable product based on aryl bromide, taken in excess, with the high catalytic performance of the system developed in our previous studies [10, 11] preserved.

EXPERIMENTAL

The reactions were performed in a temperature-controlled reaction vessel equipped with a magnetic stirrer under aerobic conditions. The solvent was dimethylformamide (DMF). The samples taken at regular intervals were analyzed on a HP-4890 gas–liquid chromatograph with using a flame-ionization detector and a 15-m HP-5 capillary column (Hewlett–Packard). Naphthalene was used as the internal reference. The analysis was performed under programmed heating from 100 to 250°C. The solvents and chemicals were purified by the conventional methods. The model reaction of styrene with bromobenzene was performed by the previously developed procedure [11]. PhBr (60 mmol), styrene (10 mmol), NaOAc (11.2 mmol), NaOOCH (1.8 mmol), and naphthalene (2 mmol, internal reference for GLC) were dissolved in DMF (10 ml) in the reaction vessel. Then, a freshly prepared solution of $Pd(PhCN)_2Cl_2$ (2.5×10^{-2} in 25 ml of DMF, 0.1 ml) was added. The reaction vessel was placed in an oil bath preheated to 140°C. The reaction mixture was stirred with a magnetic stirrer. After the reaction was complete, the liquid phase was distil-

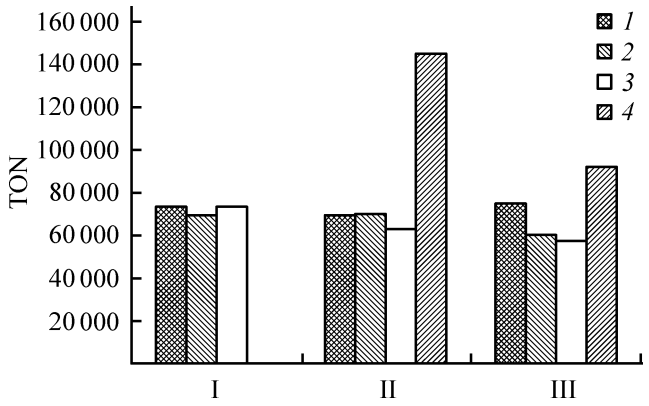

Fig. 1. Turnover number (TON) of the catalyst in successive cycles of reaction (II) with separation of liquid phase by (I) distillation and filtration through (II) glass filter and (III) aluminum oxide bed; the same for Fig. 2. In the fourth cycle, PhI was used instead of PhBr without addition of a fresh portion of the catalyst; the same for Fig. 2. (*1–4*) number of cycles; the same for Fig. 2.

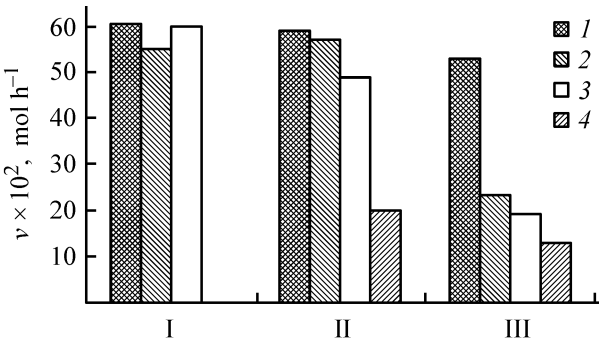

Fig. 2. Rate v of successive steps of reaction (II) with the use of different methods for separating the liquid phase.

led off (34–45°C, 3–5 mm Hg), or filtered through a finely porous glass filter, or passed through an Al_2O_3 bed. The composition of the liquid phase was analyzed. Prior to the next experiment, the required amounts of bromobenzene and styrene and fresh portions of $PdCl_2$, NaOAc, and NaOOCH were added to the resulting solution. In experiments without additional introduction of $PdCl_2$, iodobenzene was added in the amount equimolar to styrene, instead of bromobenzene, to the separated solution.

The turnover number of the simplest catalytic system containing $PdCl_2$ and sodium formate, without inert atmosphere or any ligands, at the bromobenzene : styrene ratio of 6 : 1 and 140°C is 0.74×10^5 in 70 min. It should be noted that, when the turnover number is equal to, or higher than 10^5, the catalyst content of the product is 10 ppm or lower and there is no need to separate the catalyst even in the case of a medical application of the product [5]. Since there is no alternative to use of excess aryl bromide to reach a high turnover number of the catalyst in the phosphine-free Heck reaction, the only way to raise the yield of the target product, based on the arylating agent, is recycling of aryl bromide remaining in the reaction mixture:

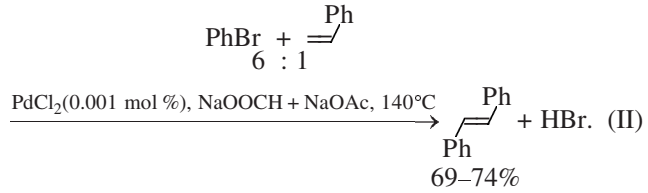

The yield of diphenylethylene based on styrene in this reaction at a low catalyst content (0.001 mol %) ranged from 69 to 74%. The yield of this product based on bromobenzene was lower by ~12% owing to a sixfold excess of bromobenzene. At a 70% yield based on styrene, the concentration of the reaction products and the initial reactants did not change on further heating of the reaction mixture, which suggested complete deactivation of the catalyst. The simplest way to raise the yield based on the initial reagents is to distill-off the liquid phase of the reaction mixture and reuse it in new catalytic cycles.

The results of three successive reactions with intermediate distillation of the liquid phase and addition of free portions of reactants (including palladium chloride) are shown in Fig. 1. The turnover number was calculated as the ratio of the total amount of the reaction products formed in the catalytic step examined to the total palladium amount used in this and all preceding steps. As can be seen from Fig. 1, the turnover number of the catalyst in all steps is about the same. To estimate the catalytic activity, the average reaction rate prior to the reaction completion can be used.

As can be seen from Fig. 2, the reaction rate did not substantially change after separation of the liquid phase by distillation. The yield of the target product increases upon addition of unchanged styrene and bromobenzene to the reaction mixture. The total stilbene yield based on styrene in the first, second, and third cycles is 74, 83, and 89%, respectively. Since the whole amount recycled bromobenzene is converted to the reaction product in the second and third cycles, the relative change in the yield based on bromobenzene present in a sixfold excess in the reaction mixture was more significant. The stilbene yield based on bromobenzene in the first, second, and third cycles was 12, 21, and 29%, respectively. Thus, the yield based on bromobenzene increased in three successive catalytic cycles by a factor of 2.4. Our experimental results show that distillation of the liquid phase prevents accumulation of compounds poisoning the cata-

lyst in the reaction mixture. Hence, the stilbene yield based on the initial reactants can be raised by making larger the number of catalytic cycles.

We also examined other methods for involving the reactants in repeated reaction cycles without additional heating of the reaction mixture and use of a reduced pressure. It is generally known [6, 7, 12] that the catalyst deactivation in the Heck reaction with nonactived aryl halides is caused by aggregation of catalytically active dissolved palladium. We found [7, 11] that the deactivation of a catalyst under these conditions was an autocatalytic process presumably catalyzed by the solid phase of the catalysts formed in the course of the reaction. Thus, introduction of additional portions of the catalyst after its deactivation cannot substantially raise the conversion. In addition, we suggested that filtration of the reaction mixture and addition of a fresh portion of the catalyst could raise the conversion without distillation of liquid reaction products, owing to the separation of the solid phase of the catalyst. As can be seen from Fig. 1, cold filtration of the reaction mixture through a glass filter did give the acceptable results. The turnover number of the catalyst after the third cycle was 63000. In going from the first to the third cycle, the reaction decelerated by no more than 17 % (Fig. 2).

According to the mechanism of the Heck reaction, palladium can exist in solution in the form of molecular complexes and colloidal particles [6–8, 10–12], which cannot be separated by filtration. To determine palladium in the filtrate, the fourth reaction cycle was performed without addition of the catalyst, but in the presence of reactive iodobenzene, instead of bromobenzene. In this case, the high conversion of the initial reactants and the high stilbene yield unambiguously suggest the presence of palladium in the filtrate in the form ineffective in the reaction with bromobenzene.

A fresh catalyst portion added to the solution containing colloidal palladium can initiate fast autocatalytic growth and subsequent coagulation of palladium particles, which can decrease the catalytic activity in the experiments with filtration through a glass filter. To make palladium separation from the reaction mixture make complete, the solution was filtered through an aluminum oxide bed. As can be seen from Fig. 1, the turnover number of the catalysts in the second cycle of these experiments significantly decreased. This tendency was more pronounced for the reaction rate. The decrease in conversion and the deceleration of the reaction with iodobenzene in the test for dissolved palladium indicated that the palladium concentration

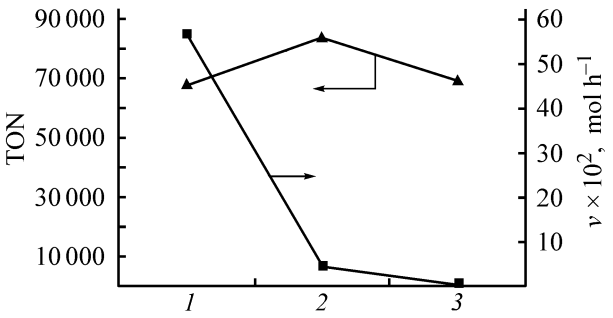

Fig. 3. TON of the catalyst and rate of reaction (II) catalyzed by (*1*) $PdCl_2$ and precipitate isolated after the first cycle of the reaction with (*2*) PhI and (*3*) PhBr.

in the solutions decreased, compared to the experiments with filtration through a finely porous glass filter. Thus, the presence of palladium in solution in experiments with filtration through a glass filter has a positive effect on the catalytic activity, whereas the decrease in the palladium concentration after filtration through an aluminum oxide bed impairs the catalyst performance.

We studied the catalytic activity of the precipitate isolated by filtration of the reaction mixture. The main components of the precipitate were NaBr and unchanged NaOAc. The precipitate was divided on the filter in two equal parts which were used as catalysts in the reactions with iodo- and bromobenzene without addition of fresh portions of the initial catalyst. As can be seen from Fig. 3, the turnover number of the catalyst in the reaction with iodobenzene slightly increases as compared to the first cycle, whereas the styrene conversion in the reaction with iodobenzene remains virtually the same. In both cases, the reaction is very slow. These experiments confirm that palladium irreversibly aggregates to form an agglomerate inert in arylation even with reactive aryl halides. As noted above, no appreciable conversion of the substrate is observed after introduction of a fresh portion of the catalyst without filtration of the reaction mixture. Thus, autocatalytic aggregation and deactivation of palladium in the Heck reaction are caused by palladium aggregates removed by filtration. These results are consistent with the mechanism of palladium deactivation in the phosphine-free catalytic systems [7, 8, 10–12]. In addition, the results of this study can be used to develop processes for indistrial arylation of alkenes, including continuous processes.

CONCLUSIONS

Methods were developed for raising the yield of the product based on the reactants with preservation of

high activity of the simplest phosphine-free catalytic systems in Heck reactions with nonactivated aryl bromides. Filtration of the reaction mixture, which, if necessary, can be supplemented with distillation of the liquid reaction components, allows repeated reaction cycles with preservation of a high turnover number of the catalyst and a high reaction rate.

ACKNOWLEDGMENTS

This study was financially supported by the Russian Foundation for Basic Research (project no. 05-03-32 222a).

REFERENCES

1. Heck, R.F. and Nolley, J.P., *J. Org. Chem.*, 1972, vol. 37, no. 14, p. 2320.
2. Mizoroki, T., Mori, K., and Ozaki, A., *Bull Chem. Soc. Jpn.*, 1971, vol. 44, no. 2, p. 581.
3. Beletskaya, I.P. and Chepracov, A.V., *Chem. Rev.*, 2000, vol. 100, no. 8, p. 3009.
4. Alonso, E., Beletskaya, I.P., and Yus, M., *Tetrahedron*, 2005, vol. 61, no. 50, p. 11771.
5. Farina, V., *Adv. Synth. Catal.*, 2004, vol. 346, nos. 13–15, p. 1553.
6. Phan, N.T.S., Van Der Sluys, M., and Jones, C.W., *Adv. Synth. Catal.*, 2006, vol. 348, no. 6, p. 609.
7. Schmidt, A.F., Al Halaiqa, A., and Smirnov, V.V., *Synlett.*, 2006, no. 18, p. 2861.
8. Vries, A.H.M. de, Mulders, J.M.C.A., Mommers, J.H.M., et al., *Org. Lett.*, 2003, vol. 5, no. 5, p. 3285.
9. Yao, Q., Kinney, E.P., and Yang, Z., *J. Org. Chem.*, 2003, vol. 68, no. 19, p. 7528.
10. Schmidt, A.F. and Smirnov, V.V., *J. Mol. Catal. A: Chem.*, 2003, vol. 203, nos. 1–2, p. 75.
11. Schmidt, A.F., Al Halaiqa, A., and Smirnov, V.V., *J. Mol. Catal. A. Chem.*, 2006, vol. 250, nos. 1–2, p. 131.
12. Vries, J.G. de, *J. Chem. Soc., Dalton Trans.*, 2006, p. 421.

ISSN 1070-4272, Russian Journal of Applied Chemistry, 2007, Vol. 80, No. 10, pp. 1699–1702. © Pleiades Publishing, Ltd., 2007.
Original Russian Text © E.E. Martsinko, I.I. Seifullina, A.G. Pesaroglo, T.V. Borovskaya, Yu.N. Anisimov, 2007, published in Zhurnal Prikladnoi Khimii, 2007, Vol. 80, No. 10, pp. 1670–1673.

ORGANIC SYNTHESIS AND INDUSTRIAL ORGANIC CHEMISTRY

Effect of Dicitrato- and Dimalatogermanic Acids on Polycondensation of Maleic Anhydride with Ethylene Glycol

E. E. Martsinko, I. I. Seifullina, A. G. Pesaroglo, T. V. Borovskaya, and Yu. N. Anisimov

Mechnikov National University, Odessa, Ukraine

Received April 26, 2007

Abstract—The catalytic activity of citric (H_4Citr) and malic (H_3Mal) acids, their coordination compounds with germanium(IV) $H_2[Ge(HCit)_2]$ and $H_2[Ge(Mal)_2]$, and germanium dioxide GeO_2 in polycondensation of maleic anhydride and ethylene glycol at various temperatures was studied (catalyst : ethylene glycol molar ratio 0.01 : 1). The process kinetics was evaluated and the time of its completion was determined. The copolymerization kinetics of some of the prepared oligoesters with triethylene glycol dimethacrylate was studied, and the copolymer properties were determined.

DOI: 10.1134/S1070427207100199

Polycondensation steadily attracts researcher's attention [1]. The problems of intensification of the condensation processes and, first of all, development and use of more effective catalysts are still topical. It is known that acids (including carboxylic acids) and their salts and a number of metal (magnesium, lead, thorium, uranium, etc.) [2] oxides are catalytically active in polycondensation of dicarboxylic acids with glycols. However, all these catalysts (even the most active) are toxic and deteriorate the physicochemical properties of the resulting oligoesters. It should be noted that in their presence, unsaturated polymeric resins (UPRs), should be synthesized from based dicarboxylic acid anhydrides and glycols at 180–200°C. No catalysts operate at lower temperatures. Thus, although UPRs are large-tonnage commercial products, there is no catalyst that would combine high activity with environmental safety and would allow resin preparation at lower temperatures.

In this regard, promise is shown by germanium complexes, which are successfully used as components of catalytic systems for preparing polymers based on styrene and other arylethylene monomers with high degree of syndiotacticity [3]. It is known that germanium compounds are effective polycondensation catalysts in synthesis of high-purity polyesters, polyethylene terephthalate, ethylene glycol, and bis-beta-hydroxyethyl terephthalates and in polymerization of α-olefins [4–6]. In this study, we examined the catalytic activity of new hydroxy acid complexes of germanium in polycondensation of maleic anhydride and ethylene glycol.

EXPERIMENTAL

Polyglycol maleinate (PGM) was prepared by polycondensation in a melt maleic anhydride and ethylene glycol (EG) of analytically pure grade [7]. This system was chosen as a model. The synthesis was carried out at 180°C until an acid number of about 45 was reached. The resulting oligomer was dried in a thermostat over calcined $CaCl_2$ at 200°C for 2 h.

The acid number was determined by titration of a sample taken directly from the reaction mixture and also found from the amount of water collected in a Dean-Stark trap.

Using a similar procedure [7], PGMs were prepared in the presence of several catalysts (catalyst : EG molar ratio 0.01 : 1) at 180 and 155°C. As catalysts we tested germanium dioxide GeO_2 (ultrapure grade), citric acid monohydrate $C_6H_8O_7 \cdot H_2O$ (H_4Cit) (chemically pure grade), malic acid $C_4H_7O_5$ (H_3Mal) (chemically pure grade), and complexes of germanium with these acids.

Complex dicitrato- and dismalatogermanic acids were prepared by the common procedure: Water (400 ml) was added to a mixture of GeO_2 (1.046 g, 0.01 mol) and H_4Citr (4.2 g, 0.02 mol) or H_3Mal (2.68 g, 0.02 mol). Then, the reaction mixture was boiled with

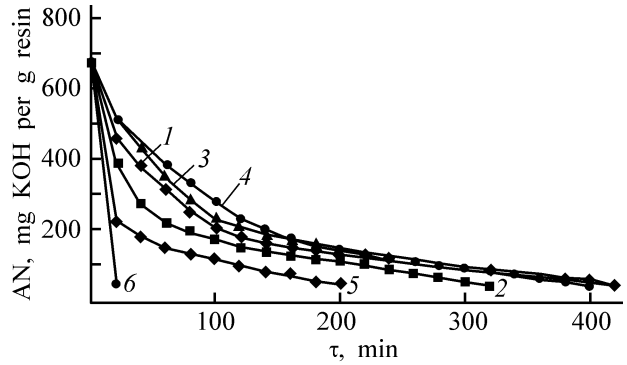

Fig. 1. Acid number AN of polyesters prepared at 180°C in the presence of a catalyst (1%) vs. the reaction time τ. (*1*) No catalyst, (*2*) GeO_2, (*3*) H_4Citr, (*4*) H_3Mal, (*5*) $H_2[Ge(HCitr)_2]$, and (*6*) $H_2[Ge(Mal)_2]$.

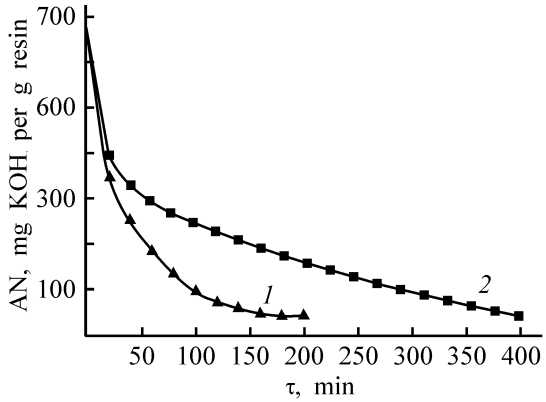

Fig. 2. Acid number AN of polyesters prepared at 155°C in the presence of a catalyst (1%) vs. the reaction time τ. (*1*) $H_2[Ge(Mal)_2]$ and (*2*) $H_2[Ge(HCitr)_2]$.

continuous stirring until the reactants completely dissolved and then was evaporated on a water bath until formation of white X-ray amorphous precipitates of Ge complexes (about 3 h). The resulting complexes were studied by chemical and X-ray diffraction analyses, thermogravimetry, and IR spectroscopy, and their formulas $H_2[Ge(HCit)_2]$ and $H_2[Ge(Mal)_2]$, were determined [8–10].

The effect of the procedure used to synthesize UPRs (with or without catalyst) on copolymerization was examined using 30% solutions of triethylene glycol methacrylate (TGM-3) in the UPRs prepared. The copolymerization constant was determined by dilatometry at 60°C, as using benzoyl peroxide (BP) initiator. The polymer densities were determined by hydrostatic weighing of standard bars ($120 \pm 2 \times 15 \pm 0.2 \times 10 \pm 0.2$ mm).

Kinetic characteristics of polycondensation of MA and EG in the presence of catalysts

Catalyst	$v_{pc} \times 10^3$, mol s^{-1} l^{-1}	Catalyst cycle	K_{pc}, $l\ s^{-1}\ mol^{-1}$	τ, min
Temperature 180°C				
–	2.3	–	0.3	420
GeO_2	4.1	1.8	0.7	330
H_4Citr	2.0	0.9	0.2	420
H_3Mal	2.0	0.9	0.3	400
$H_2[Ge(HCitr)_2]$	5.3	2.3	1.2	200
Temperature 155°C				
$H_2[Ge(HCitr)_2]$	3.7	1.6	0.6	200
$H_2[Ge(HCitr)_2]$	3.3	1.4	0.5	400

Analysis of experimental data shows that at 180°C citric and malic acids do not affect the polycondensation (Fig. 1, curves *1*, *3*, *4*), whereas germanium dioxide only slightly accelerates the process (Fig. 1, curve *2*). Complex germanium acids provide the highest reaction rate (Fig. 1, curves *5*, *6*). Moreover, the temperature of the process onset decreases in the presence of these acids and a significant fraction of the initial components is converted before the reaction temperature reaches 180°C. In the experiment with $H_2[Ge(Mal)_2]$, the reaction was so fast that only two points were obtained.

Therefore, complex germanium acid catalysts make it possible to perform polycondensation at lower temperatures and, thus, to diminish the energy consumption in synthesis of polyesters. Indeed, in the presence of these catalysts polycondensation was complete even at 155°C (Fig. 2) and $H_2[Ge(Mal)_2]$ strongly accelerated the process (Fig. 2, curve *1*).

Using data reported in [11], we calculated the rates of polycondensation in the initial stage at various temperatures and in the presence of various catalysts, determined the corresponding rate constants, and determined the catalyst cycle (see table).

From the experimental data at various temperatures, we calculated the activation energy of the process in the presence of complex catalysts $H_2[Ge(Mal)_2]$ (184.1 kJ mol^{-1}) and $H_2[Ge(HCitr)_2]$ (54.4 kJ mol^{-1}). The polycondensation is the second-order reaction, the activation energies are rather high, and the process is temperature-sensitive.

Based on published data for similar systems [12], we assumed that MA before esterification is protonated via dissociation of coordinated carboxy

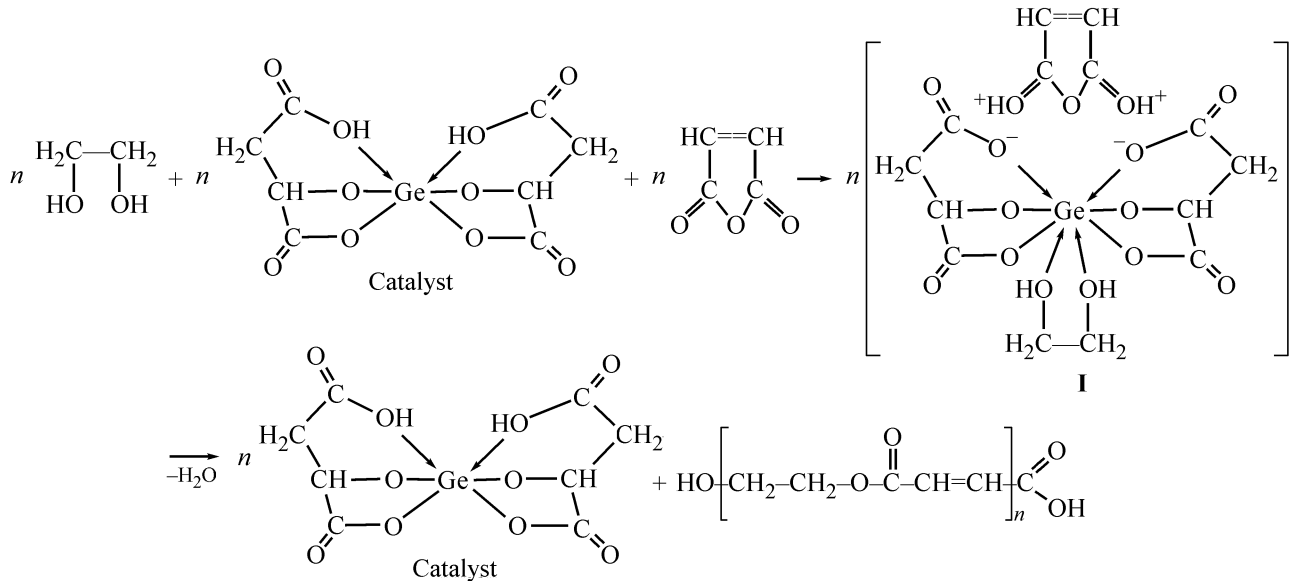

Fig. 3. Scheme of polycondensation of maleic anhydride with ethylene glycol in the presence of $H_2[Ge(Mal)_2]$.

groups of the complex germanic acid, in particular, $H_2[Ge(Mal)_2]$.

In the process, proton is attached to the carbonyl oxygen, making it more accessible to nucleophilic attack. Simultaneously EG is coordinated with germanium. Hence, intermediate **I** is formed in the first stage (Fig. 3), which accelerates the polycondensation. In the second stage, esterification with water removal and chain elongation occurs; simultaneously, the complex catalyst is regenerated.

Using the above scheme, we assumed that the catalytic activity of coordination compounds analyzed depends on the stability constant of the complex acid; the lower the stability, the higher the catalyst activity ($K_{y(H_2[Ge(HCitr)_2])}$ 100 and $K_{y(H_2[Ge(Mal)_2])}$ 4.13 [8, 9]).

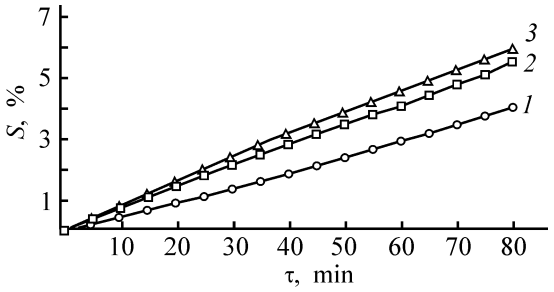

Fig. 4. Degree of S of UPR copolymerization with TMG-3 in the initial stages vs. time τ. BP concentration 0.02 M. (*1*) PGM, (*2*) PGM + 1% $H_2[Ge(HCitr)_2]$, and (*3*) PGM + 1% $H_2[Ge(Mal)_2]$. v_{cop}, mol l^{-1} s^{-1}: (*1*) 0.193, (*2*) 0.276, and (*3*) 0.285.

The copolymerization rate was determined as in [13]. It was found in a study of the copolymerization of UPRs (prepared by polycondensation in the absence of catalyst and in the presence of $H_2[Ge(Mal)_2]$ and $H_2[Ge(HCitr)_2]$) with TGM-3 (Fig. 4), the copolymerization rate is about the same in all the cases and independent of the presence of the catalyst. This fact additionally confirms that neither the metal nor the ligand are incorporated into the UPR molecule.

It was found that the physicomechanical properties of PGM copolymers with 30% TGM-3 cured in the presence of BP (1%) at 40°C and then heated at 80°C for 5 h, such as the hardness, impact resilience, electrical conductivity, and content of the gel fraction, are virtually independent of the catalyst. The properties of the copolymers were as follows: density 1.23–1.24 kg dm^{-3}, Brinell hardness 15–16 kgs mm^2, impact resilience 10–12 kJ m^{-2}, and electrical conductivity $(8–12) \times 10^{-9}$ Ω^{-1} m^{-1}.

CONCLUSIONS

(1) Complex dicitrato- and dimalatogermanic acids exhibit high catalytic acitivity in polycondensation of maleic anhydride and ethylene glycol.

(2) Complex catalysts lower the polycondensation temperature from 180 to 155°C; in addition, dimalatogermanic acid decreases the process time by a factor of 2.

(3) The mechanism of the catalytic reaction is

suggested. The less stable complex of germanium with malic acid is the most effective catalyst.

(4) The procedure for preparing unsaturated polymeric resins (with or without catalyst) noticeably affect neither the rate of their copolymerization with triethylene glycol methacrylate nor the physicomechanical properties of the resulting copolymers.

REFERENCES

1. Vinogradova, S.V. and Vasnev, V.A., *Usp. Khim.*, 2004, vol. 73, no. 5, pp. 526–541.
2. Vinogradova, S.V. and Vasnev, V.A., *Polikondensatsionnye protsessy i polimery* (Polycondensation Processes and Polymers), Moscow: Nauka, 2000.
3. Ukrainian Inventors Certificate no. 08/905620, 1997, *Ref. Zh. Khim.*, 2000, 10 S 379 P.
4. US Patent 6020421, 1998, *Ref. Zh. Khim.*, 2001, 3 S 382 P.
5. US Patent 6023608, 1998, *Ref. Zh. Khim.*, 2001, 11 19 S 373 P.
6. US Patent 6034192, 2000, *Ref. Zh. Khim.*, 2001, 13 19 S 383 P.
7. Toroptseva, A.N., Belogorodskaya, K.V., and Bondarenko, V.M., *Laboratornyi praktikum po khimii i tekhnologii vysokomolekulyarnykh soedinenii* (Laboratory Manual on Chemistry and Technology of Macromolecular Compounds), Leningrad: Khimiya, 1972.
8. Seifullina, I.I., Belousova, E.M., Pozharitskii, A.F., and Bobrovskaya, M.M., *Zh. Neorg. Khim.*, 1973, vol. 18, no. 10, pp. 2766–2771.
9. Seifullina, I.I., Belousova, E.M., and Pozharitskii, A.F., *Zh. Org. Khim.*, 1975, vol. 45, no. 7, pp. 1311–1314.
10. Seifullina, I.I., Martsinko, E.E., Aleksandrov, G.G., and Sergienko, V.S., *Zh. Neorg. Khim.*, 2004, vol. 49, no. 6, pp. 928–937.
11. Anisimov, Yu.N., Galibei, V.I., and Ivanchenko, P.A., *Protsessy polimerizatsii i fiziko-khimicheskie metody issledovaniya* (Polymerization Processes and Physicochemical Methods of Investigation), Kiev: Vishcha Shkola, 1987.
12. Morrison, R.T. and Boyd, R.N., *Organic Chemistry*, Boston: Allyn and Bacon, 1970
13. Anisimov, Yu.N. and Savin, S.N., *Zh. Prikl. Khim.*, 2001, vol. 74, no. 4, pp. 633–636.

ISSN 1070-4272, Russian Journal of Applied Chemistry, 2007, Vol. 80, No. 10, pp. 1703–1707. © Pleiades Publishing, Ltd., 2007.
Original Russian Text © M.V. Solovskii, M.Yu. Eropkin, E.M. Eropkina, A.V. Slita, M.Yu. Smirnova, E.N. Vlasova, E.B. Tarabukina, A.I. Amirova, 2007, published in Zhurnal Prikladnoi Khimii, 2007, Vol. 80, No. 10, pp. 1674–1678.

MACROMOLECULAR CHEMISTRY AND POLYMERIC MATERIALS

Synthesis and Properties of Low-Molecular-Weight Copolymers of Acrylamide with 2-Acrylamido-2-methylpropanesulfonic Acid, as Potential Drug Carriers

M. V. Solovskii, M. Yu. Eropkin, E. M. Eropkina, A. V. Slita, M. Yu. Smirnova, E. N. Vlasova, E. B. Tarabukina, and A. I. Amirova

Institute of Macromolecular Compounds, Russian Academy of Sciences, St. Petersburg, Russia
Research Institute for Influenza, Russian Academy of Medical Sciences, St. Petersburg, Russia

Received February 16, 2007; in final form, July 2007

Abstract—Nontoxic water-soluble low-molecular-weight (MW 14 000–36 000 Da) copolymers of acrylamide with 2-acrylamido-2-methylpropanesulfonic acid, containing from 17.3 to 37.6 mol % sulfonate-containing monomeric units, were synthesized by heterophase radical polymerization in isopropanol or ethanol at 50°C with azobis(isobutyronitrile) as an initiator.

DOI: 10.1134/S1070427207100205

Copolymerization of acrylamide (AA) with sulfonate-containing monomers has been extensively studied [1–7]. Synthesis of copolymers of AA with 2-acrylamido-2-methylpropanesulfonic acid (AAMPSA) was reported by Hollander et al. [1], whose aim was to examine the possibility of using such copolymers in oil production, since the performance of polyacrylamide itself somewhat deteriorates with time because of the partial degradation and sorption on porous mineral surfaces. A study of the behavior of polyacrylamide and AA/AAMPSA copolymer with respect to the sorbing substrate (sodium kaolinite) revealed a slightly lower adsorption, and, therefore, higher performance of the copolymer containing 6.8 mol % AAMPSA. Synthesis of random copolymers of AA with AAMPSA sodium salt and sodium 2-sulfoethyl methacrylate [MW $(5–20) \times 10^5$ Da] was reported in [2]. These copolymers can be used in well boring and also as flocculants.

High-molecular-weight copolymers of AA with AAMPSA (or its sodium salt) are generally synthesized by copolymerization in water [1–4] or aqueous-organic solvents [5–7] in the presence of potassium persulfate as an initiator. At the same time, despite that low-molecular-weight AA–AAMPSA copolymers are of significant practical interest as polymeric carriers for cationic bioactive compounds (according to [8], polyacrylamide is nontoxic), they are little studied yet.

Therefore, we synthesized in this study low-molecular-weight AA–AAMPSA copolymers and characterized their physicochemical and toxicological properties.

The target copolymers were synthesized by heterophase radical copolymerization of AA with AAMPSA in isopropanol or ethanol in the presence of azobis(isobutyronitrile) (AIBN) as an initiator. Taking into account the high polymerization activity and tendency of AA to form cross-linked structures, we carried out the process at 50°C and AIBN concentration of 3.0 or 4.5 wt %. The composition of the products was controlled by varying the initial monomer ratio. The results are presented in Table 1. As can be seen, the yield of AA–AAMPSA copolymers exceeds 95% under the optimal conditions. At such a high conversion, the composition of the resulting copolymers appears to be close to that of the initial monomer mixture. In accordance with the general trends in radical copolymerization, the molecular weight of the resulting copolymers increased with the concentration of the monomers in the starting mixture $[M_1^0 + M_2^0]$

Table 1. Copolymerization of AA (M_1) with AAMPSA (M_2) at 50°C

Run no.	Starting monomer mixture				AA–AAMPSA copolymers					
	$[M_2^0]$, mol %	$[M_1^0+M_2^0]$, wt %	[AIBN], wt %	solvent	sample no.	conversion in 24 h, %	S,* %	m_2, mol %	$[\eta]$, dl g^{-1}	$\overline{M}_w$, kDa
1	25	15	4.5	Ethanol	**I-1**	94.8	7.21	23.0	0.20	14
2	25	25	4.5	"	**I-2**	99.2	7.16	22.8	0.32	28
3	25	40	4.5	"	**I-3**	99.8	6.97	22.0	0.54	61
4	20	15	3.0	"	**I-4**	99.6	5.86	17.3	0.21	16
5	20	40	3.0	"	**I-5**	99.8	6.16	18.5	0.38	36
6	20	40	3.0	Isopropanol	**I-6**	99.8	6.18	19.1	0.25	19
7	20	50	3.0	"	**I-7**	98.8	6.07	18.2	0.28	23
8	40	20	4.5	Ethanol	**I-8**	95.0	9.13	33.1	0.17	–
9	40	40	4.5	"	**I-9**	99.7	9.42	37.6	0.25	–
10	100	30	1.0	"	**II**	59.7	15.8	100	0.10	40

* (S) Sulfur content of the copolymer.

(Table 1, run nos. 1–3; 4 and 5; 6 and 7; and 8 and 9). Another way to control the molecular weight of the copolymers is to change the chemical nature of the solvent. Passing from ethanol to isopropanol as a common chain-transfer agent is accompanied by a decrease in the weight-average molecular weight $\overline{M}_w$ of the resulting copolymer.

We found it incorrect to determine the relative activities of AA and AAMPSA in copolymerization, because the process occurs under heterophase conditions, which affects the reaction kinetics. The occlusion of the macroradicals, resulting in a considerable decrease in the chain termination rate, causes an increase in the overall rate of the heterogeneous copolymerization in alcohols as compared to the homogeneous copolymerization in DMSO. Therefore, the material balance equation cannot be derived correctly in the case of heterophase copolymerization.

The composition of copolymers **I-1**–**I-9** (sulfonic group content) was determined by microanalysis for sulfur. The structure of the copolymers was confirmed by the IR spectra. Figure 1 shows the IR spectra of polyacrylamide (PAA) and AA–AAMPSA copolymer no. **I-8**. As for PAA, the IR spectrum of the copolymer shows an absorption band at 1650 cm^{-1}, corresponding to stretching vibrations of the carbonyl group, and bands at 1565 and 3356 cm^{-1}, corresponding to bending and stretching vibrations of NH, respectively. Unlike PAA, the spectrum of the polymer additionally contains characteristic absorption bands of the $-SO_3H$ groups at 1227, 1040, and 624 cm^{-1} (Fig. 2).

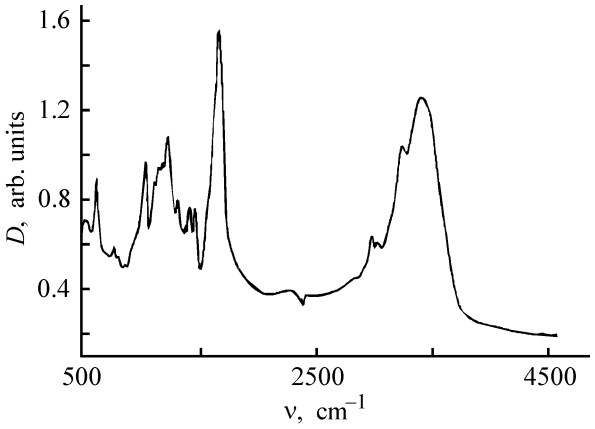

Fig. 1. IR spectrum of polyacrylamide in the range 400–4500 cm^{-1}. (D) Absorption and (ν) wavenumber; the same for Fig. 2.

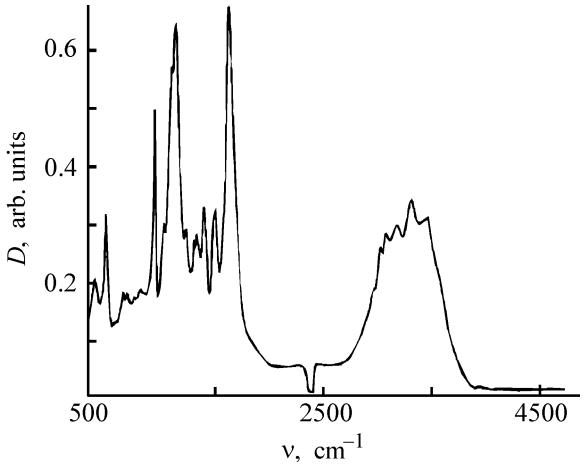

Fig. 2. IR spectrum of copolymer **I-8** in the range 400–4500 cm^{-1}.

Data of IR spectroscopy and elemental and functional analyses suggest the following structure for copolymers **I**:

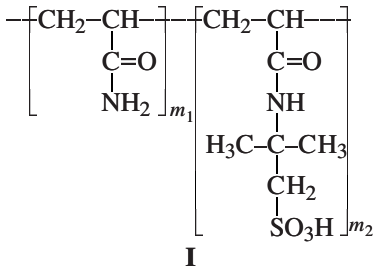

I

$m_1 + m_2 = 100$ mol %.

Copolymer nos. **I-1**–**I-9** are low-molecular-weight ($\bar{M}_w$ = 14000–37000 Da), containing 17.3 to 37.6 mol % $-SO_3H$ groups.

Copolymers **I** are strong polymeric acids, titratable with alkali solutions. Aqueous solutions of the copolymers are characterized by low pH, which decreases as the solution concentration increases (Fig. 3). At a fixed solution concentration, pH decreases with as the sulfonate group content of the copolymer grows (Fig. 4). Copolymers **I** are typical polyelectrolytes (polyanions), as demonstrated by the dependence of the reduced viscosity η_r of copolymer no. **I-2** on the NaCl concentration in solution (Fig. 5). The maximal η_r is observed in the absence of NaCl as a result of the strong repulsion between likely charged sulfonate groups of the copolymer. With increasing NaCl concentration, η_r decreases as a result of shielding of the sulfonate groups by the Na^+ counterions.

In run no. 10, AAMPSA homopolymer **II** was obtained in a yield of about 60% (Table 1). The sulfur content of the product is consistent with the theoretical value, and its molecular weight found from the diffusion and sedimentation data is 40000 Da.

It appeared significant to characterize the toxicity of the low-molecular-weight AA–AAMPSA copolymers obtained. The toxicity of copolymers **I**, homopolymer **II**, and such reference polymers as PAA, copolymer of AA with acrylic acid, and dextran sulfate was determined using the procedure described in [9]. As can be seen from Table 2, sulfonate-containing copolymer nos. **I-5** and **I-2** are less toxic than the copolymers of AA with acrylic acid of similar composition. Such a low toxicity of copolymer nos. **I-5** and **I-2** combined with the low molecular weight, solubility in water, and fairly high content of reactive sulfonate groups, makes these materials promising for use as polymeric carriers for lowmolecular-weight bioactive cationic compounds.

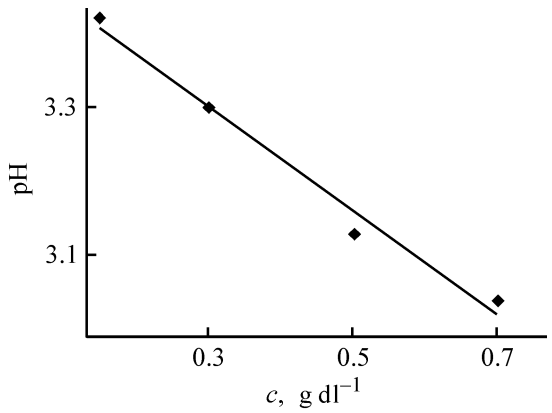

Fig. 3. pH of aqueous solution of copolymer no. **I-8** vs. the solution concentration c.

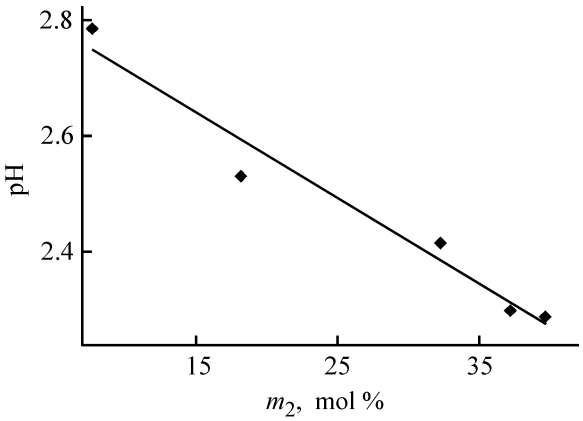

Fig. 4. pH of aqueous solution of copolymer **I** vs. the copolymer composition at c = 600 μg ml^{-1}. (m_2) Sulfonate group content of the copolymer.

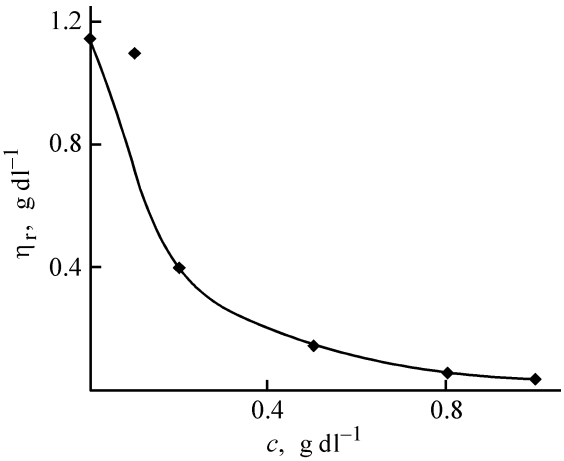

Fig. 5. Reduced viscosity η_r of aqueous solution of copolymer no. **I-2** vs. the NaCl concentration c.

As is known [10], certain polyanions demonstrate antiviral activity by themselves. In this context, it appeared interesting to test the investigated sulfonate-containing polymers for antiviral activity. As a reference served dextran sulfate, which, according to

Table 2. Cytotoxicity of sulfonate-containing and reference polymers

Polymer	m_2, mol %	M, Da	IC50, mg ml^{-1}
AA–acrylic acid	20.2	33 000	11.8 ± 0.30
AA–AAMPSA	18.5	36 000	18.0 ± 5.5
AA–AAMPSA	22.8	28 000	16.3 ± 4.3
Poly-AAMPSA	100	40 000	10.2 ± 1.6
PAA	0	28 000	18.8 ± 1.3
Dextran sulfate	100	70 000	29.1 ± 6.1

published data [10], demonstrates antiviral properties. Copolymer nos. **I-2** and **I-5** demonstrated no antiviral activity. By contrast, AAMPSA homopolymer **II** and dextran sulfate exhibit a well-defined antiviral effect [with respect to human herpes simplex virus type 1 (HSV1)], even when taken in a relatively low concentration (100 μg ml^{-1}). The indicated compounds exhibited antiviral activity in vitro against *Vero* cell culture, which was well comparable with such well-known antiherpes drug as Zovirax. As for the antiviral action mechanism of certain sulfur-containing polyanions, it has been suggested that they suppress the adhesion of virus species and their penetration to target cells by blocking the receptors on the cell surface [9]. The occurrence of antiherpes activity in homopolymer **II** opens the door for its medical use, at least when locally administered.

EXPERIMENTAL

Acrylamide (from Germany) was recrystallized twice from ethyl acetate; mp 84.5°C.

Found, %: C 50.48, H 7.15.
Calculated, %: C 50.65, H 7.03.

2-Acrylamido-2-methylpropanesulfonic acid was purified as follows. A 50-g portion of AAMPSA and 290 ml of 90% acetic acid were charged into a 500-ml three-necked flask equipped with a stirrer, reflux condenser, and thermometer. The mixture was heated on a water bath at 80–85°C with stirring for 15 min. The stirrer was turned off, and the mixture was slowly cooled to 15°C. Then the stirrer was turned on, and 65 ml of acetic anhydride was added in portions. The mixture was cooled with an ice–salt mixture to 15°C. The precipitated sulfonic acid was separated on a Buchner funnel, washed with two 50-ml portions of glacial acetic acid, and squeezed on the funnel. Crude AAMPSA was multiply treated with acetone (ultrapure grade) to remove acetic acid, separated on a Buchner funnel, and vacuum-dried to constant weight. Yield 39.6 g (79.2%). Found: S 15.74%, SO_3H groups 39.20 wt %; mp 185°C. Calculated: S 15.46%, SO_3H groups 39.13 wt %.

The reference polymers, low-molecular-weight polyacrylamide and copolymer of AA with acrylic acid, were prepared by the procedure described in [11]. Dextran sulfate (from Austria) with MW 100 000 Da was used.

AIBN was thrice recrystallized from a chloroform/ethanol (1 : 5) mixture. The yield of purified AIBN was 76.2%; mp 103°C. Dehydrated 2-propanol and rectified ethanol were used without additional purification.

Procedure of heterophase copolymerization of AA with AAMPSA (with an example of run no. 2). AIBN (0.08820 g), AA (1.5 g), AAMPSA (1.46 g), and 75 ml of ethanol were charged into a 100-ml ampule. After purging with Ar for 15 min, the ampule was sealed, and the reaction mass was allowed to stand for 24 h at 50 ± 0.5°C. The copolymer was precipitated by adding acetone, and then multiply treated with acetone to completely remove the monomer. Finally, the copolymer was filtered off and dried. Yield 1.94 g (99.2%).The resulting product was further treated by dialysis with water for 3 days and separated by freeze drying. Elemental analysis gives 7.16% for the sulfur content, which corresponds to 22.8 mol % AAMPSA units in the copolymer; [η] = 0.32 dl g^{-1}, MW = 28 000 Da.

The IR spectra of copolymer no. **I-8** and polyacrylamide were recorded on a Bruker IFS spectrometer using KBr technique (3 mg of the sample per 600 mg of KBr).

The weight-average molecular weights $\overline{M}_w$ of copolymers with m_2 = 17.3–22.8 mol % were calculated by the relation used for polyacrylamide [12]:

$$[\eta]^{30}_{1\ N\ NaNO_3} = 3.73 \times 10^{-4}\ M_w^{0.66}.$$

The molecular weight of AAMPSA homopolymer was determined by the diffusion-sedimentation method [13].

Toxicologic tests in vitro. As a test method for characterization of the condition of fibroblasts in the strain we used the Resazurin reduction method [9]. The IC50 values for the polymers under study were estimated by linear regression relationships, using MS Excel 2003 software.

The antiviral activity of the sulfur-containing polymers was determined by the procedure described in [14] with respect to human herpes simplex virus type 1 (HSV1) from the virus strain collection of the Ivanovskii Research Institute of Virology. The virus was grown in the *Vero* cell culture.

CONCLUSION

Conditions of radical polymerization of acrylamide with 2-acrylamido-2-methylpropanesulfonic acid were optimized to allow preparation of low-cytotoxic water-soluble low-molecular-weight copolymers with high (up to 37.6 mol %) content of sulfonate-containing units.

REFERENCES

1. Hollander, A., Somasandaran, P., and Gryte, C., *J. Appl. Polym. Sci.*, 1981, vol. 26, no. 7, pp. 2123–2139.
2. McCormic, C. and Chen, G., *J. Polym. Sci., Polym. Chem. Ed.*, 1982, vol. 20, no. 3, pp. 217–238.
3. McCormic, C., Chen, G., J., and Hutchinson, B., *J. Appl. Polym. Sci.*, 1982, vol. 27, no. 7, pp. 3103–3120.
4. Arai, K. and Ogiwara, Y., *Macromol. Chem. Rapid Commun.*, 1981, vol. 2, no. 5, pp. 363–367.
5. Kurenkov, V.F., Antonovich, O.A., Demina, T.A., and Selezneva, O.N., *Vysokomol. Soedin.*, 2003, vol. 79, no. 6, pp. 1242–1252.
6. Kurenkov, V.F., Shchelkonogova, E.S., Zigulyaeva, T.V., and Lobanov, F.I., *Izv. Vyssh. Uchebn. Zaved., Khim. Khim. Tekhnol.*, 2005, no. 7, pp. 14–19.
7. Kurenkov, V.F., Shchelkonogova, E.S., Kurenkov, A.V., et al., *Zh. Prikl. Khim.*, 2006, vol. 79, no. 6, pp. 1003–1006.
8. Savitskaya, M.N. and Kholodova, Yu.D., *Poliakrilamid* (Polyacrylamide), Kiev: Tekhnika, 1969.
9. Eropkin, M.Yu., Solovskii, M.V., Eropkina, E.M., and Shul'tseva, E.L., *Toksikolog. Vestn.*, 2006, no. 5, pp. 18–22.
10. Plate, N.A. and Vasil'ev, A.E., *Fiziologicheski aktivnye polimery* (Physiologically Active Polymers), Moscow: Khimiya, 1986.
11. Solovskii, M.V., Shul'tseva, E.L., Gavrilova, I.I., et al., *Plastmassy so spetsial'nymi svoistvami: Sbornik SPbGTI(TU)* [Specially Designed Plastics: Collection of Works of St. Petersburg State Technological Institute (Technical University)], St. Petersburg, 2006, pp. 77–80.
12. *Entsiklopediya polymers* (Encyclopedia of Polymers), Kargin, V.A., Ed., Moscow: Sov. Entsiklopediya, 1972, vol. 1.
13. Solovskii, M.V., Tarabukina, E.B., Shpyrkov, A.A., et al., *Zh. Prikl. Khim.*, 2005, vol. 78, no. 4, pp. 642–646.
14. Ershov, F.I., Narovlyanskii, A.N., Deryabin, P.G., et al., *Rukovodstvo po eksperimental'nomu (doklinicheskomu) izucheniyu novykh farmakologicheskikh veshchestv: Sbornik* [Guide on Experimental (Preclinical) Study of New Pharmaceutical Substances: Coll. of Works], Moscow: Meditsina, 2005, pp. 532–557.

ISSN 1070-4272, Russian Journal of Applied Chemistry, 2007, Vol. 80, No. 10, pp. 1708–1711. © Pleiades Publishing, Ltd., 2007.
Original Russian Text © E.V. Sivtsov, A.I. Gostev, N.A. Lavrov, 2007, published in Zhurnal Prikladnoi Khimii, 2007, Vol. 80, No. 10, pp. 1679–1682.

MACROMOLECULAR CHEMISTRY AND POLYMERIC MATERIALS

A ^{1}H NMR Study of Radical Copolymerization of *N*-Vinylsuccinimide with *n*-Butyl Acrylate in Dimethyl Sulfoxide

E. V. Sivtsov, A. I. Gostev, and N. A. Lavrov

St. Petersburg State Technological Institute (Technical University), St. Petersburg, Russia

Received April 12, 2007

Abstract—Kinetic features of radical copolymerization of *N*-vinylsuccinimide with *n*-butyl acrylate in dimethyl sulfoxide were studied by ^{1}H NMR spectroscopy. The dependences of the running concentrations of the monomers and of the "instant" and overall compositions of the copolymers on the reaction time were determined. The limiting conversions were established for correct analysis of the kinetic features of copolymerization at essentially different relative activities of the monomers. The copolymerization constants and the probability of alternation of the units in the copolymer chains were calculated.

DOI: 10.1134/S1070427207100217

Copolymers of *N*-vinylsuccinimide (VSI) and *n*-butyl acrylate (BA) have acquired importance in preparation of film materials for medical applications [1, 2]. Base hydrolysis of such copolymers involves opening of the succinimide ring to form *N*-vinylamidosuccinic acid (VASA) units containing a carboxy group at which low-molecular-weight physiologically active substances of basic nature can be added via formation of an ionic bond. The BA units act as an internal plasticizer.

Previously, we have studied the copolymerization of VSI with BA in dimethyl sulfoxide (DMSO) [3], acetic anhyride [4, 5], and pyridine [6]. The kinetic features of these reactions were examined by a combination of gravimetry (to estimate the conversion) with elemental analysis and IR spectroscopy (to determine the composition of the copolymer). Here, we employed a new technique for studying the copolymerization kinetics, which is based on monitoring the condition of the reaction mass by ^{1}H NMR spectroscopy at regular interval of time. For details of synthesis, see [3]. Samples were taken with a syringe via a rubber plug and immediately frozen. The ^{1}H NMR spectra were recorded in deuterated DMSO at 20°C, at a frequency of 400 MHz, with TMS as internal reference. This method for monitoring the copolymerization kinetics offers evident advantages.

(1) In examination of small amounts (tens of milligrams) of monomers, significant errors may originate from improperly performed additional operations (precipitation of the polymer; removal of residual monomers, initiator, and solvent; drying; and subsequent preparation for analysis of the copolymer composition). The results are strongly dependent on the thoroughness with which these manipulations are performed, which cannot be unified. The method that we suggest does not suffer from this drawback.

(2) Analysis of the spectra provides data on the running concentrations of both monomers. These data constitute a much more extensive body of information than those derived with the previously employed technique (elemental analysis or IR data provide information only about the overall composition of the coolymers obtained at different degrees of conversion). Using the running concentrations of the monomers, it is possible to determine the composition of individual fractions formed in a period between two successive measurements, in other words, to carry out a "virtual" fractionation of the copolymer, depending on its composition. It is especially important in the case of copolymerization of VSI, whose reactivity strongly differs from that of its comonomer, which result in that with copolymers nonuniform composition are formed. The extent of this nonuniformity should be taken into account when carrying out subsequent polymer-analogous transformations and immobilization of low-molecular-weight substances

(3) The new method can establish the limits within which the data on the conversion and composition

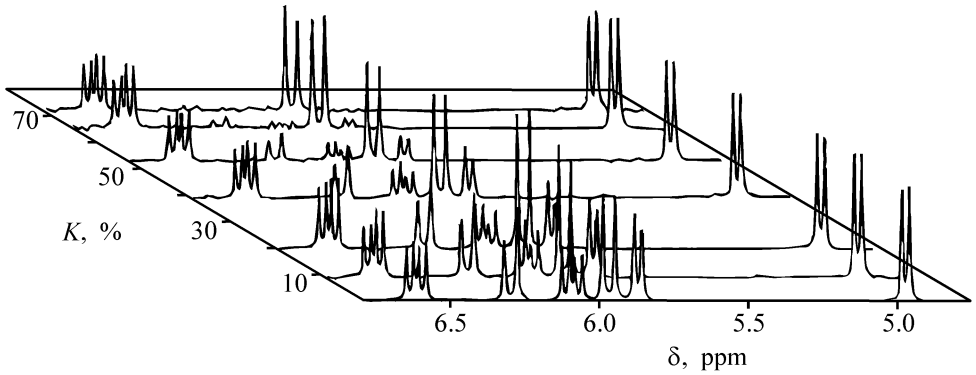

Fig. 1. Relative intensities of signals of the vinyl protons of VSI and BA vs. the conversion K in the ^{1}H NMR spectra of the VSI–BA copolymers. Content of VSI in the initial monomer mixture 50 mol %. (δ) Chemical shift.

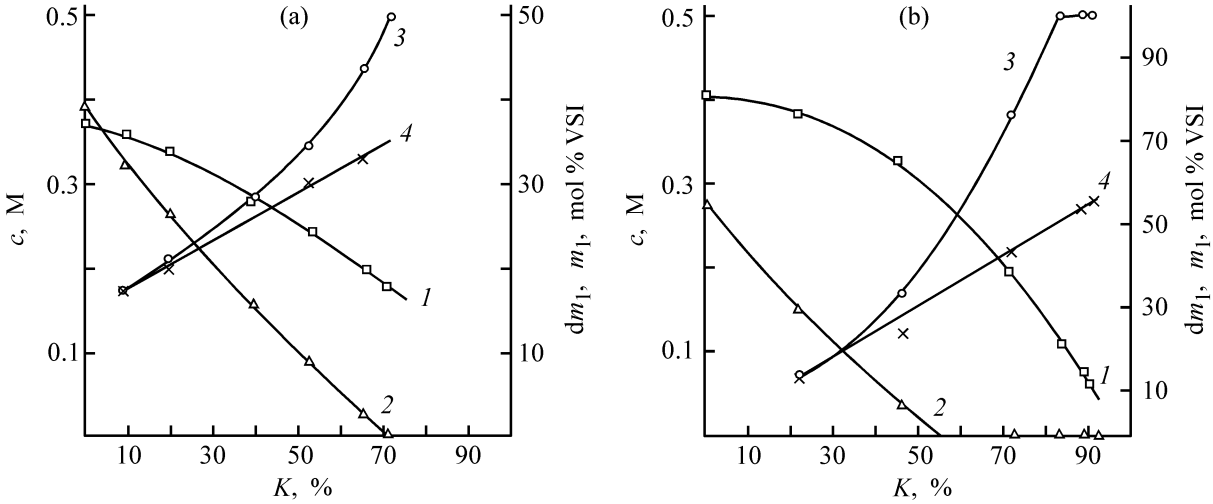

Fig. 2. (*1*, *2*) Concentration c of (*1*) VSI and (*2*) BA, (*3*) "instant" composition dm_1, and (*4*) empirical composition m_1 of the VSI–BA copolymers vs. the conversion K. Content of VSI in the initial monomer mixture, mol %: (a) 50 and (b) 60.

of the copolymers can be correctly used for calculation of the copolymerization constants. When the monomers differ substantially in relative activities, the overall composition at fairly high conversions may vary because of the homopolymerization of the unchanged less active monomer (after the more active monomer is completely spent). However, previous experiments did not answer the question as to whether this is really the case. In this situation, permanent monitoring of the concentrations of the monomers in the system can be helpful to avoid this error which is the more probable because of the use of new algorithms for calculational of copolymerization constants, based on the experimental data obtained at rather high conversions of up to 60%.

In this case the analysis of the composition of the reaction mixture is facilitated by the fact that the vinyl proton signals of the monomers that were used for calculations are clearly resolved in the spectra (Fig. 1). The following signals can be identified: for VSI, α-H appears as a doublet of doublets (6.63 ppm), and *cis*- and *trans*-β-H, as two doublets (5.96 and 4.99 ppm); α-H in butyl acrylate, as a doublet of doublets (6.11 ppm), and *cis*- and *trans*-β-H of BA, as two doublets (6.30 and 5.88 ppm). Figure 1 clearly demonstrates how the monomer ratio varies in the course of the reaction. In the beginning of the copolymerization reaction, the monomers are in the equimolar ratio; the intensities of the signals of their vinyl protons are equal. Because of the higher reactivity, BA is incorporated into the polymeric chain faster than VSI. This leads to depletion of the copolymer being formed in the VSI units relative to the running composition of the monoer mixture, which implies a faster expenditure of BA and a change of the concentration ratio of the monomers in favor of VSI. This is evident from the plots of the concentrations of the monomers and the composiion of the copolymer vs. the conversion (Fig. 2).

From the curves demonstrating how the concentrations of the monomers vary with the conversion

Table 1. VSI (M_1)–BA (M_2) copolymerization constants

Data for calculations obtained by indicated method	EBR		KT		Data for calculations obtained by indicated method	EBR		KT	
	r_1	r_2	r_1	r_2		r_1	r_2	r_1	r_2
Gravimetry and elemental analysis	0.18	3.68	0.20	3.79	^{1}H NMR spectroscopy	0.07	2.76	0.07	2.78

Table 2. Probability of formation of diads f and statistical average length Z of blocks of VSI units (M_1) and BA units (M_2) in the chains of the VSI–BA copolymers

VSI content of the initial monomer mixture, mol %	f_{11}	f_{22}	$f_{12} = f_{21}$	Z_1	Z_2
10	0.0003	0.9252	0.0372	1.01	25.8
20	0.0013	0.8455	0.0766	1.02	12.0
30	0.0035	0.7604	0.1181	1.03	7.44
40	0.0074	0.6693	0.1616	1.05	5.14
50	0.0143	0.5716	0.2071	1.07	3.76
60	0.0263	0.4666	0.2536	1.10	2.84
70	0.0482	0.3537	0.2990	1.16	2.18
80	0.0931	0.2326	0.3371	1.28	1.69
90	0.2123	0.1047	0.3415	1.62	1.31

(Fig. 2) we can derive the conversion corresponding to the onset of homopolymerization of the less active VSI after BA is completely spent. For the initial composition of the monomer mixture VSI : BA = 50 : 50, this conversion is 71%, and for VSI : BA = 60 : 40, 56%. After these conversions are reached, the empirical composition of the copolymers changes in favor of VSI exclusively via formation of the homopolymer PVSI, and the results obtained in this stage of the process are unsuitable for analyzing the kinetic relationships in copolymerization.

These data were used for calculating the constants of copolymerization of VSI (M1) with BA (M2) by the specially developed routine according to technique from [7]. The constants were determined by modified methods of Ezrielev–Brokhina–Roskin (EBR) [8] and Kelen–Tüdös (KT) [9] (Table 1).

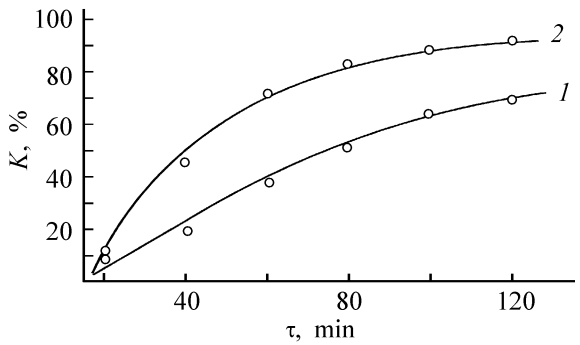

Fig. 3. Conversion of the monomers K vs. the reaction time τ. VSI content of the initial monomer mixture, mol %: (*1*) 50 and (*2*) 60.

Previously it has been shown by Lavrov and Krasil'nikova [7] and Ezrielev et al. [10] that the EBR method allows the most reliable determination of the copolymerization constants because the equations for the composition of the copolymer are symmetric with respect to r_1 and r_2. Therefore, just the values obtained by this method were used for calculating the effect of alternation of the units in the macromolecules of the copolymer [11], which is estimated by the probability of formation of various types of diads [M_1–M_1, M_1–M_2 (M_2–M_1), M_2–M_2] and by the statistical average length of blocks formed by units of each type in the polymer chains (Table 2).

Table 2 shows that formation of copolymers with alternating VSI and BA units (maximal values of f_{12} and f_{21}) is possible only in copolymerization of monomer mixtures containing VSI in a large excess (80–90 mol %). However, Fig. 2 suggests that, in this case, BA will be exhausted already at low conversions, and the subsequent process will consist in homopolymerization of VSI. Hence, a copolymer comparatively uniform in composition will be formed only in the initial stage of the reaction.

Copolymerization of VSI with BA is a homophase process; its pattern previously observed in [3] is confirmed by ^{1}H NMR in this study. The kinetic curves (Fig. 3) exhibit no gel effect; the reaction is

accelerated as the content of VSI in the initial monomer mixture is raised.

CONCLUSIONS

(1) ^{1}H NMR spectroscopy was applied for the first time to kinetic study of the radical copolymerization of *N*-vinylsuccinimide with *n*-butyl acrylate in dimethyl sulfoxide. This technique offers certain advantages over the previously used methods.

(2) An examination of the concentrations of the monomers and the "instant" and overall compositions of the *N*-vinylsuccinimide–*n*-butyl acrylate copolymers in the course of the reaction revealed the limiting conversions suitable for correct analysis of the kinetic relationships in copolymerization.

(3) Copolymerization constants were calculated with the use of a specially developed routine based on the Ezrielev–Brokhina–Roskin method, $r_{VSI} = 0.07$ and $r_{BA} = 2.76$, and Kelen–Tüdös method, $r_{VSI} = 0.07$ and $r_{BA} = 2.78$.

(4) It was shown that an *N*-vinylsuccinimide–*n*-butyl acrylate copolymer with a uniform composition can be obtained in dimethyl sulfoxide under the experimental conditions only at low conversions under a high excess of *N*-vinylsuccinimide in the initial monomer mixture (80–90 mol %).

REFERENCES

1. Shal'nova, L.I., Chudnova, V.M., and Trofimova, E.A., *Plast. Massy*, 1989, no. 11, pp. 29–34.
2. Lavrov, N.A., Shal'nova, L.I., and Nikolaev, A.F., *Zh. Prikl. Khim.*, 1997, vol. 70, no. 8, pp. 1356–1363.
3. Lavrov, N.A., Sivtsov, E.V., and Nikolaev, A.F., *Zh. Prikl. Khim.*, 1998, vol. 71, no. 12, pp. 2055–2058.
4. Lavrov, N.A., Sivtsov, E.V., and Nikolaev, A.F., *Zh. Prikl. Khim.*, 2000, vol. 73, no. 4, pp. 683–686.
5. Lavrov, N.A., Sivtsov, E.V., and Nikolaev, A.F., *Plast. Massy*, 2001, no. 10, pp. 43–45.
6. Lavrov, N.A., Sivtsov, E.V., and Pisarev A.G., *Zh. Prikl. Khin.*, 2003, vol. 76, no. 7, pp. 1154–1159.
7. Lavrov, A.N. and Krasil'nikova, Yu.O., *Khimicheskaya tekhnologiya, svoistva i primememie plastmass: Mezhvuzovskii sbornik nauchnykh trudov* (Chemical Technology, Properties, and Application of Plastics: Intercollegiate Coll. of Works), St. Petersburg: Sankt-Peterb. Tekhnol. Inst. (Tekh. Univ.), 1992, pp. 24–29.
8. Ezrielev, A.I., Brokhina, E.L. and Roskin, E.S., *Vysokomol. Soedin., Ser. A*, 1969, vol. 11, no. 8, pp. 1670–1680.
9. Tüdös, F., Kelen, T., Födes-Berezhnykh, T., Turcsänyi, B., *React. Kinet. Catal. Lett.*, 1975, vol. 2, no. 4, pp. 439–447.
10. *Metody rascheta otnositel'nykh aktivnostei monomerov pri sopolimerizatsii: uchebnoe posobie* (Methods of Calculation of the Relative Activities of Monomers in Copolymerization: A Manual), Sautin, S.N., Lavrov, N.A., Punin, A.E., and Hartman, K., Eds., Leningrad: Leningr. Tekhnol. Inst. im. Lensoveta, 1986.
11. Lavrov, N.A., *Raschet cheredovanii zven'ev v sopolimerakh: metodicheskie ukazaniya* (Calculation of Alternations of Units in Copolymers: Methodical Guide), Leningrad: Leningr. Tekhnol. Inst. im. Lensoveta, 1988.

ISSN 1070-4272, Russian Journal of Applied Chemistry, 2007, Vol. 80, No. 10, pp. 1712–1716. © Pleiades Publishing, Ltd., 2007.
Original Russian Text © A.I. Vorob'eva, M.N. Gorbunova, V.D. Surkov, R.R. Muslukhov, F.A. Sataeva, S.V. Kolesov, A.G. Tolstikov, Yu.B. Monakov, 2007, published in Zhurnal Prikladnoi Khimii, 2007, Vol. 80, No. 10, pp. 1683–1687.

MACROMOLECULAR CHEMISTRY AND POLYMERIC MATERIALS

Azanorbornenes in Radical Polymerization Reactions

A. I. Vorob'eva, M. N. Gorbunova, V. D. Surkov, R. R. Muslukhov, F. A. Sataeva, S. V. Kolesov, A. G. Tolstikov, and Yu. B. Monakov

Institute of Organic Chemistry, Ufa Scientific Center, Russian Academy of Sciences, Ufa, Bashkortostan, Russia

Institute of Technical Chemistry, Ural Division, Russian Academy of Sciences, Perm, Russia

Received April 19, 2007

Abstract—Activity of azanorbornenes: *N*-benzyl-2-azanorborn-5-ene, (2-azanorborn-5-en-2-yl)methyl acetate, and *N*-allyl-2-azanorborn-5-ene in radical homo- and copolymerization with vinyl monomers and sulfur dioxide was studied.

DOI: 10.1134/S1070427207100229

Polymers based on norbornenes have high elasticity and the ability to absorb mechanical energy [1–3]. Due to vibro- and sound-extinguishing properties, polynorbornenes are used in electronic, electrotechnical, motor-car, and packing industries [4, 5]. In addition, polynorbornenes are highly stable with respect to acids, alkali, fats, and oils, shows low shrinkage, and are environmentally harmless [5]. Polymerization with catalysts based on transition metals (metathesis catalysts), which allows preparation of polymers containing nonaromatic rings and double bonds in the backbone, is one of the main methods for synthesis of polynorbornenes. Spontaneous copolymerization of norbornene with sulfur dioxide by the radical mechanism at low temperatures (–40°C) to give alternating equimolar copolymers was reported in [6]. A search for novel polycyclenes and efficient methods of the synthesis of valuable macromolecular compounds from them is urgent because the polycyclene polymerization has high potential, but is poorly studied.

Heteroderivatives of norbornenes are of special interest. Much attention is focused on biologically active compounds in the series of azabicycloheptenes and heptanes [7–9]. In particular, derivatives of the above compounds demonstrate a highly selective activity with respect to various subspecies of nicotine and acetylcholine receptors and antagonists of muscarine receptors, used as an active ingredient of drugs for curing central nervous system [7], neurodegenerative and gastrointestine diseases [8], and in production of carbocyclic nucleosides used as antiviral preparations [9]. There are no data on radical polymerization of azanorbornenes (ANB). In this study, we examined the reactivity of *N*-benzyl-2-azanorborn-5-ene (BAN), (2-azanorborn-5-en-2-yl)methyl acetate (MAAN), and *N*-allyl-2-azanorborn-5-ene (AAN) in the radical copolymerization reactions and estimated the biological activity of the polymers synthesized.

EXPERIMENTAL

Azanorbornenes were prepared by the method described in [10]. The following fractions were used for polymerization: BAN, bp 99–102°C (66.6 Pa), n_D^{20} = 1.5489; MAAN bp 80–82°C (160.0 Pa), n_D^{20} = 1.4830; and AAN, bp 51–53°C (133.3 Pa), n_D^{20} = 1.4880. The chemical shifts and multiplicities of ^1H ^{13}C NMR signals are listed in Table 1.

Acrylonitrile (AN), methyl methacrylate (MMA), maleic anhydride (MA), styrene (ST), vinyl acetate (VA), azobis(isobutyronitrile) (AIBN), and benzoyl peroxide (BP) used for synthesis of copolymers, and also the solvents dimethyl sulfoxide (DMSO), methanol, and acetone had characteristics corresponding to reference data after purification by the standard methods. Sulfur dioxide was dried by passing through concentrated H_2SO_4 and freshly calcined $CaCl_2$.

The homo- and co-polymerization of azanorbornenes with vinyl monomers was performed in the bulk and in solution in the presence of AIBN (or BP) in

Table 1. ^{13}CNMR spectra of azanorbornenes **I**, **III**, **V** and their complexes with sulfur dioxide **II**, **IV**, and **VI** ($CDCl_3$, TMS, 25°C)

Compound*	Chemical shift and multiplicity of signals δ, ppm										
	C_1	C_3	C_4	C_5	C_6	C_7	C_8	C_9	C_{10}	C_{11}	C_{12}
I	65.40 d	53.09 t	44.92 d	130.21 d	136.33 d	46.53 t	60.03 t	139.89 s	129.55 d	130.53 d	126.17 d
II	65.94 d	43.13 t	42.39 d	142.97 d	162.31 d	56.30 t	50.71 t	132.30 s	128.41 d	131.42 d	128.32 d
III	64.32 d	52.20 t	43.61 d	130.78 d	136.63 d	48.12 t	58.06 t	136.16 d	116.23 t		
IV	65.41 d	46.12 t	42.59 d	142.10 d	161.40 d	55.66 t	50.06 t	129.84 d	121.39 t		
V	65.29 d	53.20 t	44.02 d	130.59 d	137.23 d	48.52 t	56.66 t	171.86 s	51.75 q		
VI	65.86 d	53.20 t	42.65 d	131.76 d	142.63 d	46.31 t	50.28 t	168.22 s	52.07 q		

* Structures of **I**–**VI**:

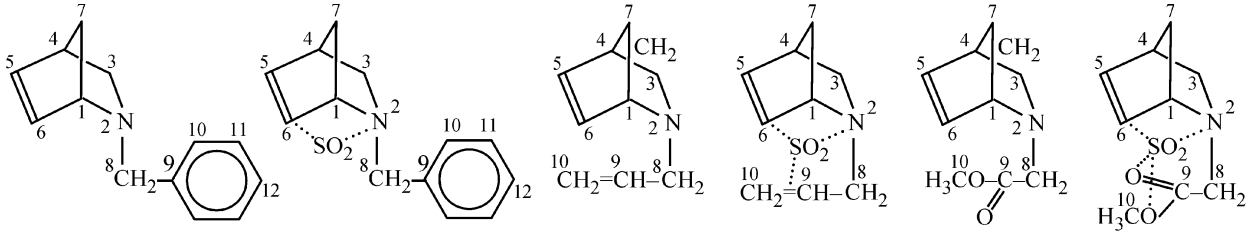

Table 2. Copolymerization of azanorbornenes (M_1) with vinyl monomers (M_2) in the bulk ($M_1 : M_2$ = 1 : 1, [AIBN] = 3 wt %)

M_1	M_2	*T*, °C	τ, h	Yield, %	Copolymer composition M_1/M_2	Copolymer solvent
BAN	AN	75	16	22.0	12.6/87.4	DMSO, DMF, chloroform
	MMA	70	6	35.3	12.6/87.4	DMSO, benzene, acetone,
	MMA*	70	6	23.1	21.3/78.7	chloroform
	MA**	75	9	10.0	26.8/73.2	DMSO, DMF
	ST	75	9	36.1	15.9/84.1	DMF, benzene, acetone,
	ST*	75	9	23.8	25.2/74.8	chloroform
	BA	80	18	8.0	70.6/29.4	DMSO, DMF, acetone
AAN	AN	80	3	9.5	15.6/84.4	DMSO, DMF, chloroform
	MMA	70	5	9.6	10.3/89.7	Benzene, acetone, chloroform
	ST	80	10	17.0	15.5/84.5	DMF, acetone, chloroform

* $M_1 : M_2$ ratio in the initial mixture 70 : 30 (mol %). ** Polymerization in acetone.

ampules in a vacuum, and copolymerization with SO_2, in a glass reactor [11]. The polymers obtained were purified by twofold reprecipitation from a solution in DMSO into a precipitant (acetone) and dried in a vacuum to constant weight at 50°C. The compositions of the polymers were calculated from the data of elemental analysis. The NMR spectra were recorded on a Bruker AM-300 spectrometer with a working frequency of 75.5 MHz (^{13}C). The spectra were recorded in the broad-band proton-decoupling mode and in the JMOD mode. DMSO-d_6 was used as solvent, and tetramethylsilane, as internal reference.

In the presence of radical initiators (AIBN, BP), ANBs are not noticeably involved in the homopolymerization. In particular, the yield of homopolymers in 10 h at 80°C does not exceed 0.5 wt % in the presence of 2.5 wt % AIBN. In copolymerization with vinyl monomers, ANBs are more active. The reaction conditions and results obtained are listed in Table 2. The copolymers formed (^{13}C NMR data) have a random distribution of comonomeric units in the macrochain. The data obtained show that ANB copolymerization with methyl methacrylate and styrene proceeds at higher rates. With respect to incorporation

Table 3. ^{13}CNMR spectra of copolymers BAN (**I**), MAAN (**II**), and AAN (**III**) with sulfur dioxide (DMSO-d_6, TMS, 25°C)

Compound*	Chemical shift and multiplicity of signals, δ, ppm, of atoms								
	C_1	C_3	C_4	C_5	C_6	C_7	C_8	C_9	C_{10}
VII**	54.62 d	61.46 t	36.37 d	74.90 d	85.50 d	51.42 t	68.90 t	138.42 s	130.07 d
VIII	57.38 d	64.14 t	38.42 d	77.16 d	84.50 d	49.97 t	70.16 t	171.68 s	51.13 q
IX	54.62 d	68.36 t	45.52 d	71.08 d	86.55 d	45.52 t	55.72 t	136.85 d	117.18 t

* Structures of **VII**–**IX**:

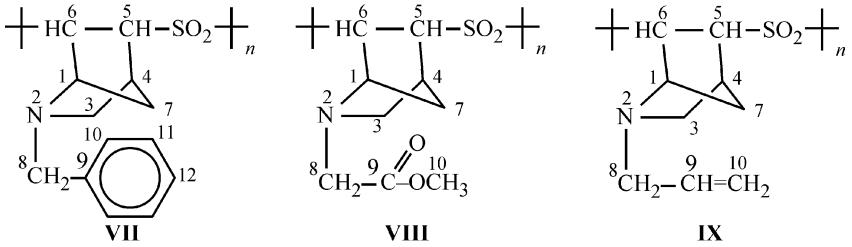

VII **VIII** **IX**

** In compound **VII**, C_{11} signal is doublet at 128.86 ppm and C_{12} signal, doublet at 126.77 ppm.

into the polymeric chain, ANBs are more active in copolymerization with vinyl acetate and maleic anhydride. In particular, the BAN content in the macrochain is about 70 mol % in copolymerization with VA at equimolar ratio of monomers in the initial mixture. In copolymerization with vinyl monomers, the copolymerization rates decrease with increasing ANB fraction in the reaction medium (Table 2).

In copolymerization with sulfur dioxide possessing a high electron-acceptor power, ANBs are substantially more active. This reaction proceeds at high rates to give alternating copolymers (data of spectral and elemental analysis) of equimolar composition, irrespective of the monomer ratio in the starting mixture, medium (in the bulk, in solvent), initiator (AIBN, BP), reaction temperature (60–90°C), and degree of conversion. The constancy of the copolymer composition at various monomer ratios in the reaction medium and known data on copolymerization of other unsaturated compounds with SO_2 [6, 13] suggest that the copolymerization proceeds through formation of donor–acceptor [ANB$\cdots$$SO_2$] complexes, which was confirmed by NMR studies.

Mixing of ANB with SO_2 gives black adducts. Comparison of ^{13}C NMR spectra of BAN, AAN, and products of their reaction with SO_2 (Table 3) shows substantial downfield shifts of signals of C_5 and C_6 atoms of the bicycle double bond. In particular, in the spectrum of BAN product with SO_2 (structure **II**), the C_5 and C_6 signals of bicycle double C bond are shifted downfield with respect to the monomer (structure **I**) by +12.76 and +25.98 ppm, respectively. The C_7 bridging atom in the reaction product is also noticeably (+9.77 ppm) deshielded. In addition, upfield shifts (–9.96 to –9.32 ppm) of signals of C_3 and C_8 atoms bonded with the nitrogen atom are observed. The above signal shifts indicate that the nitrogen atom, having a lone electron pair, is also involved in the complexation.

Similar shifts of the signals of the above carbon atoms are observed in the ^{13}C NMR spectra of the product of AAN reaction with SO_2. In the spectrum of the product (structure **IV**), the signals of the C_{10} atom in the double bond of the allyl group are shifted downfield, and those of C_9 atom, upfield by +5.16 and –6.32 ppm, respectively, as compared to the AAN spectrum (structure **III**). The shift and broadening of the signals of thedouble bonds of the allyl group in the AAN adduct show that these bonds are also involved in complexation. However, the signal shifts indicate that the double bond of norbornene ring makes the largest contribution to the formation of AAN complex with SO_2. The shifts of the signals of the corresponding carbon atoms in MAAN adducts with SO_2 are smaller (structures **V** and **VI**), which is probably due to redistribution of the electron density, with the acetate group involved.

The reaction conditions have no effect on the polymer composition, but strongly affect the reaction rate and copolymer yield. A study of the kinetic features of ANB copolymerization with SO_2 showed that dependences of the reaction rates on the ratio

of monomers pass through a maximum at their equimolar ratio (this is shown by the example of MAAN, Fig. 1). Both positive and negative deviations from the equimolar ratio lead to a decrease in the reaction rate, caused by a decrease in the concentration of the reactive complex in the system.

It is known that alternating copolymerization has pronounced specific features in comparison with random distribution [14], such as spontaneous initiation and insensitivity to the action of the majority of inhibitors. These features are manifested in copolymerization of ANB with SO_2. Copolymerization proceeds in the absence of initiators and also upon addition of inhibitors (diphenylpicrylhydrazyl or nitroxyl radical). However, the copolymerization rates in all the systems studied increase in the presence of the initiator. In particular, in BAN copolymerization with SO_2 in methanol at 75°C and 3.2 M concentration of monomers, the reaction rates in the absence of the initiator and at AIBN content of about 1 wt % are 0.5 and 0.9% per min, respectively. The reaction order with respect to initiator at AAD content within the range 0.55×10^{-1}–1.00×10^{-1} M is 0.45.

The solvent strongly affects ABN co-polymerization with SO_2. In DMSO, copolymerization of all ABNs proceeds at a substantially (approximately three times) higher rate as compared to methanol, which is probably due to different stabilities of the reaction complex in the above media.

As temperature is elevated, the reaction rate in the systems studied increases. The total activation energies of copolymerization of BAN and AAN with SO_2 in methanol, calculated from the Arrhenius equation within the 70–90°C range, are 76.4 and 79.6 ± 2.0 kJ mol^{-1}, respectively (Fig. 2). It is known [15] that the activation energy of alternating copolymerization is frequently lower than that for the majority of reactions of free-radical polymerization, whose apparent activation energy usually lies within the range 84–96 kJ mol^{-1}.

In the NMR spectra of the products of ANB reaction with SO_2 in the presence of initiator at 60–90°C, the signals of the C atoms of the double bond in the norbornene ring are absent. The products obtained contain up to 75% copolymers and about 15% exo- and endostereoisomeric dimers. The double bond of the AAN allyl group is not involved in copolymerization with SO_2, both at their equimolar ratio and at a twofold excess of SO_2.

Copolymers of ANBs with SO_2, which are black powders, are soluble in DMSO and methanol (in

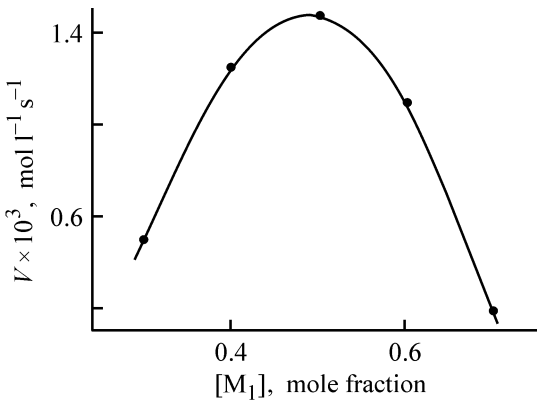

Fig. 1. Dependence of the initial rate V of MAAN (M_1) copolymerization with SO_2 (M_2) on the composition of the initial monomer mixture (mole fraction). $[M_1 + M_2] = 3.50$, $[AIBN] = 3.05 \times 10^{-2}$ M, $M_1 : M_2 = 1 : 1$, $T = 80$°C.

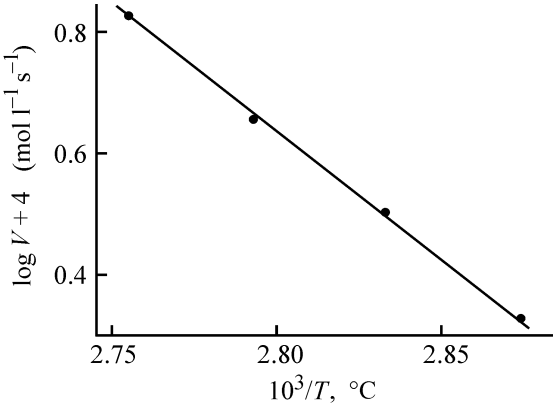

Fig. 2. Dependence of the initial rate V of MAAN (M_1) copolymerization with SO_2 (M_2) in methanol on temperature T. $[M_1 + M_2] = 3.15$, $[AIBN] = 5.47 \times 10^{-2}$ M, $M_1 : M_2 = 1 : 1$.

the initial steps of conversion) and insoluble in other commonly used solvents (acetone, methyl ethyl ketone, benzene, tetrahydrofuran, ethyl acetate, chlorinated hydrocarbons, etc.). The solubility of BAN copolymers with vinyl monomers depends of the nature of the second comonomer (Table 2).

Toxicological tests showed that copolymers of azanorbornenes with sulfur dioxide belong to hazard class 4 and can be used in medicine.

CONCLUSIONS

(1) Azanorbornenes, *N*-benzyl-2-azanorborn-5-ene, (2-azanorborn-5-en-2-yl)methyl acetate, and *N*-allyl-2-azanorborn-5-ene do not homopolymerize in the presence of radical initiators and are involved in copolymerization with vinyl monomers at low rates to give copolymers with a random distribution of comono-

meric units in the macromolecule and with a fairly high content of norbornene units in the macrochain. The copolymerization rate decreases as the azanorbornene fraction in the initial mixture becomes larger.

(2) Azanorbornenes demonstrate high activity in copolymerization with sulfur dioxide. Copolymerization proceeds at the double bond of the norbornene ring via formation of a donor–acceptor complex, to give alternating copolymers with equimolar composition, irrespective of the monomer ratio in the initial mixture and reaction conditions.

ACKNOWLEDGMENTS

The study was financially supported by the Russian Foundation for Basic Research (project no. 05-03-32097) and Foundation for Support of Leading Scientific Schools (grant NSh-9342.2006.3).

REFERENCES

1. Ivin, K.J., *Olefin Metathesis*, London: Academic, 1983.
2. Monakov, Yu.B., Dorogovets, T.E., Mudarisova, R.Kh., et al., *Dokl. Ross. Akad. Nauk*, 1995, vol. 340, no. 5, pp. 638–641.
3. Yakhina, E.Z., *Cand. Sci. Dissertation*, Ufa, 2000.
4. Ohm, R.F., *Chem. Technol.*, 1980, vol. 10, no. 3, pp. 183–187.
5. Egboh, S.H., *Eur. Polym. J.*, 1988, vol. 24, no. 10, pp. 1005–1007.
6. Zutty, N.L., Wilson, C.W., Potter, G.H., et al., *J. Polym. Sci. A*, 1965, vol. 3, pp. 2781–2799.
7. German Patent Appl. 10044905.
8. US Patent 6559171.
9. EPV Patent Appl. 1048650.
10. Surkov, V.D., in *Proc. All-Russian Conf. "Technical Chemistry: Progress and Prospects,"* Perm: Inst. Tekh. Khimii Ural'sk. Otd. Ross. Akad. Nauk, 2006, pp. 112–114.
11. Vorob'eva, A.I., Vasil'eva, E.V., Gaisina, Kh.A., and Leplyanin, G.V., *Vysokomol. Soedin., Ser. A*, 1996, vol. 38, no. 10, pp. 1663–1667.
12. Prozorovskii, V.B., Prozorovskaya, M.P., and Demchenko, V.M., *Farmakol. Toksikol.*, 1978, no. 4, pp. 497–502.
13. Vorob'eva, A.I., Gorbunova, M.N., Kuznetsov, S.I., et al. in *Order, Disorder in Polymer Reactivity*, Zaikov, G.E. and Howell, B.A., Eds., New York: Nova Science, 2006, pp. 125–135.
14. Semchikov, Yu.D., *Vysokomolekulyarnye soedineniya* (Macromolecular Compounds), Moscow: Akademiya, 2003.
15. Kabanov, V.A., Zubov, V.P., and Semchikov, Yu.D., *Komplexnoradikal'naya sopolimerizatsiya* (Complex-Radical Copolymerization), Moscow: Khimiya, 1987.

ISSN 1070-4272, Russian Journal of Applied Chemistry, 2007, Vol. 80, No. 10, pp. 1717–1720. © Pleiades Publishing, Ltd., 2007.
Original Russian Text © I.A. Opeida, M.A. Kompanets, O.V. Kushch, A.G. Matvienko, 2007, published in Zhurnal Prikladnoi Khimii, 2007, Vol. 80, No. 10, pp. 1688–1691.

MACROMOLECULAR CHEMISTRY AND POLYMERIC MATERIALS

N-Hydroxyphthalimide-Initiated Radical Polymerization of Vinyl Monomers

I. A. Opeida, M. A. Kompanets, O. V. Kushch, and A. G. Matvienko

Litvinenko Institute of Physicoorganic Chemistry and Coal Chemistry, National Academy of Sciences of Ukraine, Donetsk, Ukraine

Received May 2, 2007

Abstract—The initiating ability of *N*-hydroxyphthalimide in polymerization of methyl methacrylate and acrylonitrile was examined. For the polymerization of methyl methacrylate, the initial polymerization rates and activation energies were determined, and the dependences of the polymerization rates on the initiator and monomer concentrations were evaluated. An initiation mechanism was suggested.

DOI: 10.1134/S1070427207100230

In recent years, much attention has been received by *N*-hydroxyphthalimide (HPI), a catalyst for oxidation of organic substrates by molecular oxygen at C–H bonds, with a view to preparation of valuable oxygen-containing products [1]. In such processes, HPI acts as a radical catalyst of the chain propagation stage in which the *N*-oxyl radical of phthalimide, formed from the HPI molecule, exhibits high selectivity in abstraction of a hydrogen atom [2]. An examination of how it influences the oxidation of unsaturated compounds showed that *N*-hydroxyphthalimide is also efficient in initiation of radical polymerization of methyl methacrylate (MMA) and acrylonitrile (AN), i.e., it can enter into addition reactions at double bonds. Sato et al. [3] also mentioned the initiating effect of HPI in polymerization of vinyl compounds.

We examine here the kinetic relationships in *N*-hydroxyphthalimide-initiated radical-chain polymerization.

EXPERIMENTAL

N-Hydroxyphthalimide available from Fluka was used without additional purification. Benzoyl peroxide (BP) and azobis(isobutyronitrile) (AIBN) were recrystallized twice from ethanol. Acetonitrile was purified by the standard technique [4]. Methyl methacrylate was thrice washed with 10–15% aqueous alkali solution to exhaustively remove the inhibitor. Then it was thrice washed with distilled water, dried over anhydrous calcium chloride, and distilled in a nitrogen atmosphere at reduced pressure to isolate the (22 ± 0.2)°C/25 mm Hg fraction. We used freshly distilled methyl methacrylate.

Acrylonitrile was washed successively with dilute sulfuric acid, a 5% Na_2CO_3 solution, and water, whereupon it was dried over molecular sieves and distilled in a nitrogen stream.

The polymerization kinetics for methyl methacrylate and acrylonitrile was examined dilatometrically. The monomer content of the reaction mixture was 25 vol %. Polymerization of MMA and AN in the presence of HPI, BP, and AIBN was carried out in an acetonitrile solution at 339 K. The concentrations of AIBN and BP were 5×10^{-3} and 1×10^{-2}, respectively, and that of HPI, 1×10^{-3}–1×10^{-2} M.

The polymerization rates were estimated from the slope of the kinetic curve in the initial stage of the reaction (up to 5% conversion of the monomer), when it is virtually linear.

The table lists the initial rates of polymerization in acetonitrile for methyl methacrylate and acrylonitrile in the presence of BP, AIBN, and HPI, as well as of PB–HPI and AIBN–HPI systems.

It is seen that addition of *N*-hydroxyphthalimide to the monomer containing initiator (BP or AIBN) accelerates the polymerization of MMA. Importantly, HPI can by itself initiate the polymerization in the absence of classical initiators in the system. It should be noted that, under the actual conditions,

Rates of radical polymerization of MMA and AN in acetonitrile in the presence of initiating systems

Monomer	[HPI] × 10^{-3}	[BP] × 10^{-3}	[AIBN] × 10^{-3}	W_{pol}, mol l^{-1} s^{-1}
	M			
MMA	5.0			4.21 ± 0.04
		1.0		8.1 ± 0.1
			5.0	9.8 ± 0.1
	5.0	1.0		11.00 ± 0.02
	5.0		5.0	11.6 ± 0.1
AN	5.0			9.13 ± 0.03
	5.0		5.0	26.3 ± 0.04

MMA and AN do not polymerize without addition of initiators or HPI.

N-Hydroxyphthalimide is a very efficient radical catalyst in chain reactions of oxidation of organic compounds by molecular oxygen [5]. In the polymerization reactions (see table) it can act as initiator. Under steady-state conditions, the rate of initiated radical polymerization in the presence of two initiators is described by the equation

$$W_{0\Sigma} = k_p(k_t)^{-1/2}[RH](f_{HPI}k_d[In_1] + f_{AIBN}k_d[In_2])^{1/2} = (W_{0In_1}^2 + W_{0In_2}^2)^{1/2},$$

where k_d is the rate constant of decomposition of the initiator, In; f, initiation efficiency; k_p, chain propagation rate constant; and k_t, chain termination rate constant.

The experimental dependences of the polymerization rate on the concentrations of the initiators in reactions initiated by individual initiators and their mixture are consistent with the equation above. After substituting in it the polymerization rate of MMA in the presence of AIBN only (9.8×10^{-5} mol l^{-1} s^{-1}) or HPI (4.21×10^{-5} mol l^{-1} s^{-1}), we obtain the calculated rate of oxidation under the combined action of these initiators of 10.7×10^{-5} mol l^{-1} s^{-1} against the experimental $W_{0\Sigma} = 11.6 \times 10^{-5}$ mol l^{-1} s^{-1}. Similar results were obtained for benzoyl peroxide–*N*-hydroxyphthalimide mixtures. Thus, HPI acts in polymerization reactions as a typical initiator.

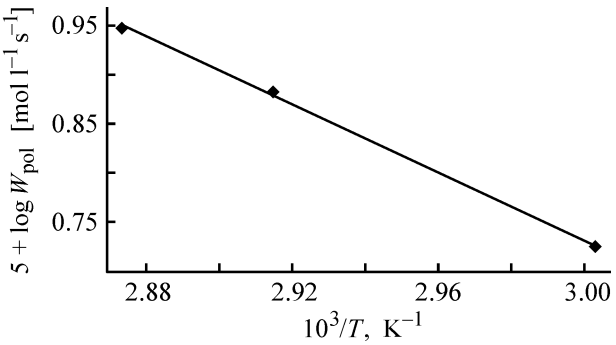

Fig. 1. Temperature dependence of the polymerization rate W_{pol} in the Arrhenius coordinates. Solvent acetonitrile, [MMA] = 2.24 M, and [HPI] = 0.005 M.

To elucidate the specific features of initiation with *N*-hydroxyphthalimide, we studied the kinetics of the MMA polymerization in the presence of this initiator.

Figure 1 shows the temperature dependence of the rate of *N*-hydroxyphthalimide-initiated polymerization of MMA. The activation energy of MMA polymerization is 32 ± 4 kJ mol^{-1} (Fig. 1); the activation energy of MMA polymerization initiated by AIBN was estimated at 84.3 ± 4 kJ mol^{-1}. These data suggest that the activation energy of the initiation reaction involving *N*-hydroxyphthalimide is much lower than that of the AIBN decomposition into radicals.

The activation energy of radical-chain polymerization can be represented as

$$E_a = 1/2E_{in} + E_p = E_t,$$

where E_{in} is the activation energy of initiation (in the case of AIBN, this is the activation energy of decomposition of the initiator); E_p, activation energy of chain propagation; and E_t, activation energy of chain termination.

Considering that the activation energy of AIBN decomposition is 125.4 kJ mol^{-1} [6]

$$E_{a.\,AIBN} - E_{a.\,HPI} = 1/2(E_{in.\,AIBN} + E_{in.\,HPI}),$$

$$E_{in.\,HPI} = 125.4 - 2(84.3 - 32) = 20.8 \text{ kJ mol}^{-1}.$$

we obtain 20.8 kJ mol^{-1} for the activation energy of initiation by *N*-hydroxyphthalimide, which cor-

responds to a bimolecular reaction. According to [7], the activation energy of monomolecular decomposition of the initiator molecules, accompanied by cleavage of covalent bonds, is within 115–130 kJ mol^{-1}.

We also found that, at a constant monomer concentration of 2.24 mol g^{-1}, the polymerization rate is proportional to the square root of the initiator concentration (Fig. 2). This suggests that, in the initiation stage, the reaction kinetics is described by the first-order equation with respect to *N*-hydroxyphthalimide concentration, since the radical-chain polymerization of MMA involves bimolecular termination of the poly(methyl methacrylate) radicals [8].

Figure 3 shows the plot of the polymerization rate vs. the monomer concentration. It is seen that the polymerization rate linearly varies with the methyl methacrylate concentration to power 3/2.

The IR spectrum of poly(methyl methacrylate) yielded by polymerization in the presence of *N*-hydroxyphthalimide is identical to that of the polymer obtained by thermal polymerization of methyl methacrylate. This supports the radical-chain mechanism of the polymerization.

These experimental dependences can be described by the following scheme:

$$M + HPI \rightarrow 2r_i^{\cdot}, \ k_i; \quad (1)$$

$$r_i^{\cdot} + M \rightarrow M^{\cdot}, \ k_p; \quad (2)$$

$$M^{\cdot} + M \rightarrow n_i M^{\cdot}, \ k_p; \quad (3)$$

$$n_i M^{\cdot} + n_j M^{\cdot} \rightarrow P, \ k_t, \quad (4)$$

where k_i, k_p, and k_t are the rate constants of the reactions of chain initiation, propagation, and termination, respectively; and M, methyl methacrylate monomer.

Under steady-state conditions and with long chains, the rate of *N*-hydroxyphthalimide-initiated polymerization of methyl methacrylate by reaction (1) is described by the equation

$$W_{pol} = k_p k_i^{1/2} (2k_t)^{-1/2} [M]^{3/2} [In]^{1/2}. \quad (5)$$

The initiation mechanism, i.e., the mechanism of reaction (1), still remains to be elucidated. In polymerization of vinyl compounds in the absence of oxygen and other initiation sources, chain initiation proceeds at a very low rate. Under the actual conditions, dissociation of the C–H, C–C, and C=C bonds into radicals is excluded (the strength of these bonds is within 260–500 kJ mol^{-1} [9]); the same is true for dissociation of the N–O and O–H bonds. More probable is formation of radicals from bi- and trimolecular reactions. As is known [3], polar vinyl monomers are able at temperatures below 100°C of complexing with organic compounds via hydrogen bonding or via π bonds. For example, the hydroperoxide and monomer molecules form an ROOH···M complex, which further yields radicals by the reaction ROOH + ⟩C=C⟨. This reaction is more competitive than the ROOH → RO· + ·OH reaction in the initiation stage.

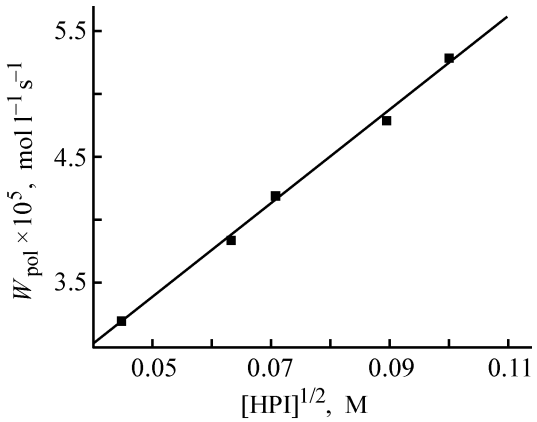

Fig. 2. Rate of MMA polymerization W_{pol} vs. initiator concentration [HPI]. Solvent acetonitrile, T = 339 K, and [MMA] = 2.24 M.

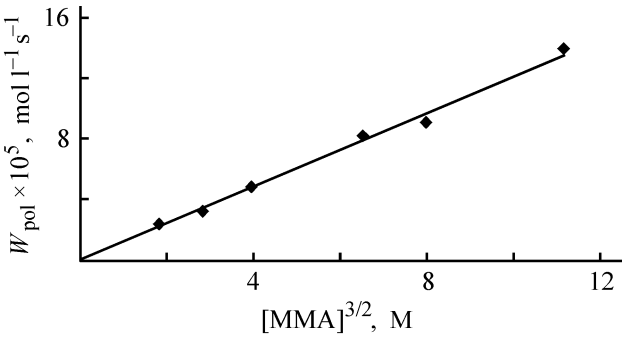

Fig. 3. Rate of polymerization of MMA W_{pol} vs. monomer concentration [MMA]. Solvent acetonitrile, T = 339 K, and [HPI] = 0.005 M.

Our experimental data suggest that *N*-hydroxyphthalimide is involved in the initiation stage. The following mechanism of radical formation in the methyl methacrylate polymerization in the presence of HPI can be presumed. In the first stage, *N*-hydroxyphthalimide and the monomer molecules form a complex, which further decomposes into radicals. In this case, two pathways of complexing are possible. The first pathway is via hydrogen bonding between the hydrogen of the hydroxy group in HPI and oxygen

of the carbonyl group in the methyl methacrylate molecule. Next, phthalimide-*N*-oxyl radical yielded by decomposition of the complex initiates polymerization:

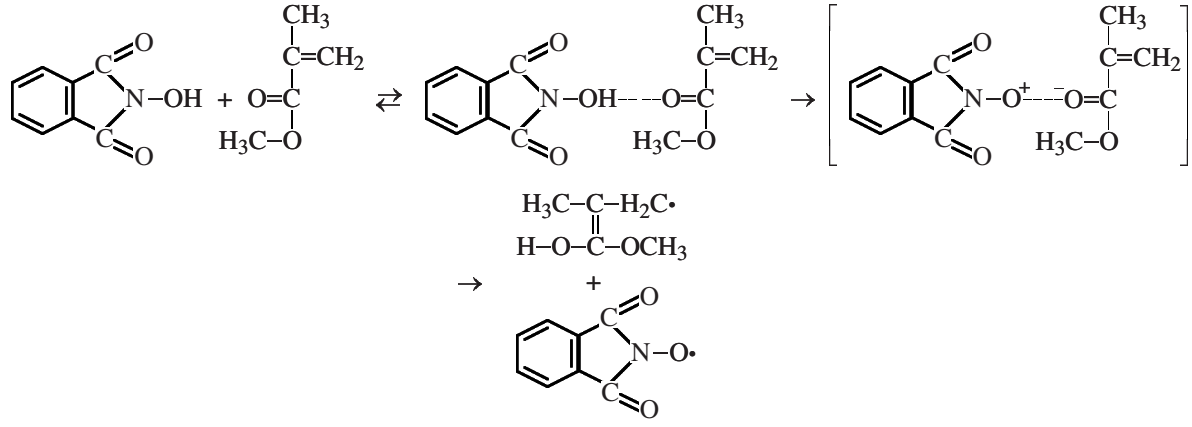

A similar mechanism has been suggested by Saito et al. [3] for the methyl methacrylate polymerization in the presence of *N*-hydroxysuccinimide. The second pathway of complexing involves the double bond of the monomer, similar to initiation by hydroperoxides. However, there are no experimental data to decide unambiguously between the first and second pathways of complexing in the initiation reaction.

The mechanism we suggested explains the experimentally established order of the polymerization reaction with respect to the monomer, namely, 3/2. At high MMA concentrations, the initiator is completely complexed with the monomer, and the polymerization rate is no longer dependent on the monomer concentration.

CONCLUSION

N-Hydroxyphthalimide efficiently initiates radical-chain polymerization of vinyl monomers in the bimolecular reaction of *N*-hydroxyphthalimide with the monomer. The low activation energy of this initiation reaction makes it promising for radical-chain polymerization reactions at temperatures lower than those for classical initiators.

REFERENCES

1. Ishii, Y., Nakayama, K., Takeno, M., et al., *J. Org. Chem.*, 1995, vol. 60, pp. 3934–3935.
2. Sheldon, R. and Arends, I.W.C.E., *Adv. Synth. Catal.*, 2004, vol. 346, pp. 1051–1071.
3. Sato, T., Metsugi, M., and Otsu, T., *Macromol. Chem.*, 1979, vol. 180, pp. 1175–1182.
4. Gordon, A.J. and Ford, R.A., *The Chemist's Companion. A Handbook of Practical Data, Techniques and References*, New York: Wiley–Interscience, 1972.
5. Aoki, Y., Sakaguchi, S., and Ishii, Y., *Tetrahedron*, 2006, vol. 62, pp. 1497–1500.
6. Bagdasar'yan, Kh.S., *Teoriya radikal'noi polimerizatsii* (Radical Polymerization Theory), Moscow: Nauka, 1966.
7. *Polymer Handbook*, Brandrup, J., Immergut, E.H., and Grulke, E.A., Eds., New York: Wiley 1999, p. 2250.
8. Mogilevich, M.M. and Pliss, E.M., *Okislenie i okislitel'naya polimerizatsiya nepredel'nykh soedinenii* (Oxidation and Oxidation Polymerization of Unsaturated Compound), Moscow: Khimiya, 1990.
9. *Energiya razryva khimicheskikh svyazei: potentsialy ionizatsii i srodstvo k elektronu* (Energy of Cleavage of Chemical Bonds: Ionization Potentials and Electron Affinities), Kondrat'ev, V.N., Ed. Moscow: Nauka, 1974.

ISSN 1070-4272, Russian Journal of Applied Chemistry, 2007, Vol. 80, No. 10, pp. 1721–1723. © Pleiades Publishing, Ltd., 2007.
Original Russian Text © N.I. Polezhaeva, A.A. Nefedov, 2007, published in Zhurnal Prikladnoi Khimii, 2007, Vol. 80, No. 10, pp. 1692–1694.

MACROMOLECULAR CHEMISTRY AND POLYMERIC MATERIALS

Kinetics of Thermal Oxidative Degradation of a Compound Based on a Polyester Resin and Dimethylethylphenylammonium Iodide

N. I. Polezhaeva and A. A. Nefedov

Siberian State University of Technology, Krasnoyarsk, Russia

Received October 30, 2006; in final form, January 2007

Abstract—The kinetics of thermal oxidative degradation of a compound based on a polyester resin and dimethylethylphenylammonium iodide was studied. The rate constants of thermal decomposition were determined. The degradation of the compound was studied by dynamic thermogravimetric analysis.

DOI: 10.1134/S1070427207100242

To develop various formulations of low-temperature solder creams, taking into account specific conditions of their application, it is necessary to know how materials used as an organic binder behave at working temperatures of solder cream fusion. In particular, the rate of their decomposition at working temperatures should be evaluated [1].

This paper reports on a further study of the developed formulations of low-temperature noncorrosive solder creams based on a polyester resin modified with rosin and on quaternary ammonium salts [2, 3].

EXPERIMENTAL

The parameters of thermal oxidative degradation of dimethylethylphenylammonium iodide (DMEPAI) and a compound based on a polyester resin and DMEPAI were determined by dynamic thermogravimetric analysis [4]. To determine more accurately the temperature at which the samples start to degrade, we recorded the DTG and DTA curves along with the TG curve (Figs. 1a, 1b). Measurements were performed with an MOM Q-1000 derivatograph (Hun-

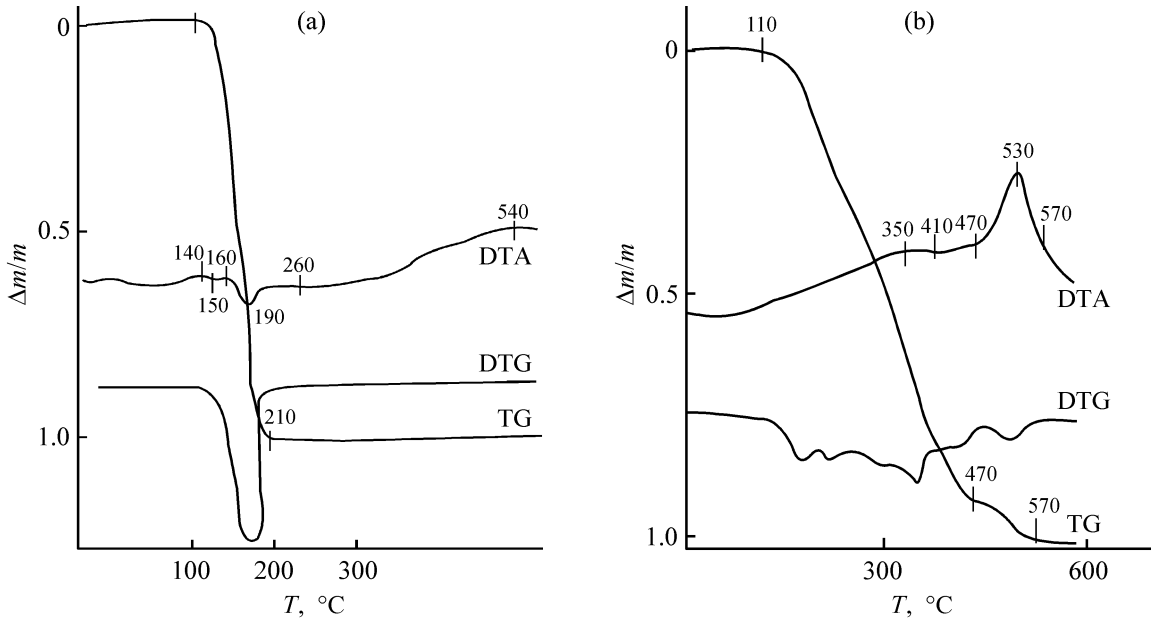

Fig. 1. Thermograms of (a) dimethylethylphenylammonium iodide and (b) compound based on a polyester resin and dimethylethylphenylammonium iodide. ($\Delta m/m$) Relative weight loss and (T) temperature.

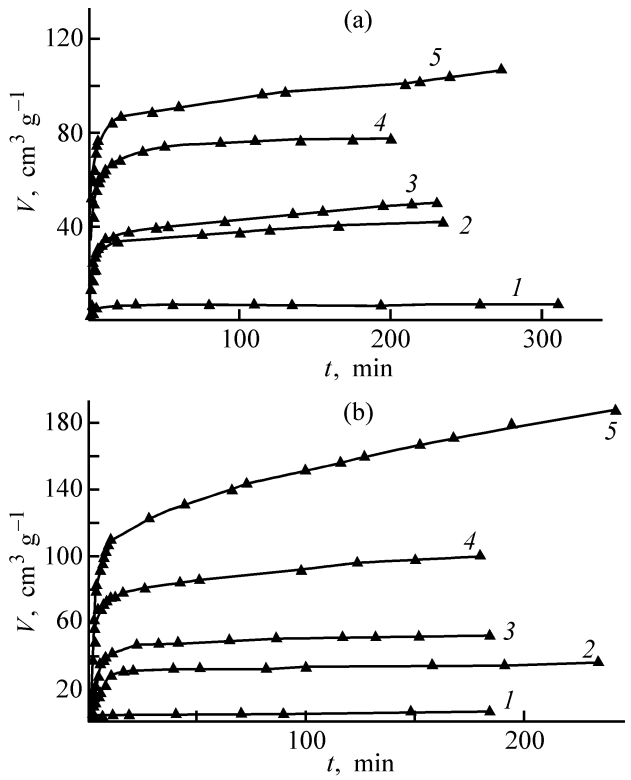

Fig. 2. Manometric curves of gas evolution from samples (a) 1 and (b) 2 at temperatures of up to 300°C. (V) Volume of the released gas and (t) time; the same for Figs. 3 and 4. Temperature, °C: (*1*) 100, (*2*) 150, (*3*) 180, (*4*) 250, and (*5*) 300.

gary) in the programmed-heating mode. Samples (0.05 g) were heated in a platinum crucible in air at a rate of 10 deg min^{-1}. The sensitivity parameters were as follows: balance, 100 mg; DTA, 1/3; and DTG, 1/10.

When heated in air, DMEPAI decomposes in the temperature range 140–200°C (Fig. 1a).

The compound, when heated in air, degrades in three steps in the temperature range 110–570°C (Fig. 1b). The first step (110–190°C) involves the weight loss due to removal of the residual solvent, free reaction water, alcohol, and unsaponifiable substances boiling in this temperature range. The second step (220–410°C) involves simultaneously occurring endothermic decomposition of DMEPAI and exothermic oxidation of a part of the released products [3, 5]. The third step is characterized by a complex exothermic effect with characteristic temperatures of 470 (onset of the exothermic peak in the DTA curve due to the onset of oxidation) and 530°C. The strong peak at 530°C corresponds to oxidation of gaseous products formed by thermal degradation of the polyster resin [2, 5].

The kinetics of thermal degradation under static conditions was studied by the manometric method using a glass Bourdon zero gage (hereinafter, manometer) at a residual pressure in the reaction volume of 10^{-1}–10^{-2} mm Hg in the temperature range 100–300°C. The temperature in the thermostat was maintained with an accuracy of ±(0.2–0.5)°C. The scheme of the installation and the experimental procedure were described in [6, 7].

To make the data comparable, the results of the manometric study of thermal degradation were converted to the normal volume of gaseous products per gram of the starting substance:

$$V_t = (T_0 V_r P_t)/(T P_0 m),$$

where V_r is the volume of the reaction space of the manometer (cm^3); P_t, pressure of decomposition products at time t (mm Hg); V_t, volume of gaseous decomposition products at time t (cm^3); T_0, temperature under normal conditions (273.15 K); T, experimental temperature (K); m, sample weight; and P_0, pressure under normal conditions (760 mm Hg).

Using experimental data, we plotted the time dependence of the volume of the released gases (per gram of starting substance). The character of the thermal degradation can be judged from the shape of the smoothed kinetic curve. When a substance degrades by a first-order rate law, the dependence $V_i = f(t_i)$ is described by a curve that levels-off (actually observed in our experiments). In this case, the rate constant of thermal degradation is calculated by the formula

$$k = (1/t)\ln[V_\infty/(V_\infty - V_t)],$$

where V_∞ is the total volume of gaseous decomposition products under normal conditions per gram of the starting substance (cm^3). The volume V_∞ was taken from the experimental manometric curves. It is specific too each temperature, because, as temperature increases, more and more components become volatile.

Because the working fusion temperature of low-temperature solder creams varies in the range 120–350°C, depending on composition, manometric studies of samples 1 and 2 were performed at 100, 120, 150, 180, 250, and 300°C [8].

Manometric studies of the polyester resin (sample 1) and its compound with DMEPAI (sample 2) showed that these substances are stable up to approximately 250°C (Figs. 2a, 2b). The gas evolution observed in the experiments was due to removal of the re-

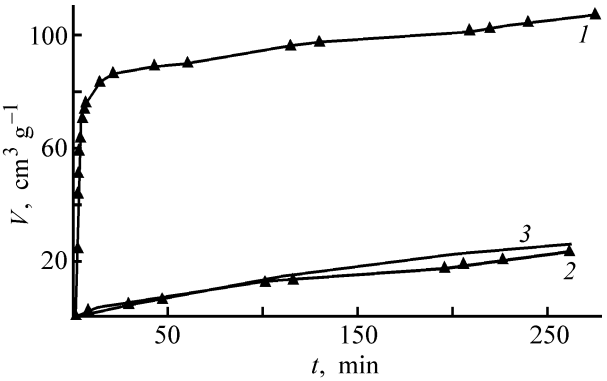

Fig. 3. Manometric curves of gas evolution from sample 1 at 300°C: (*1*) experimental curve, (*2*) curve after subtracting the volume of the initially released gases, and (*3*) fitting by a first-order rate equation.

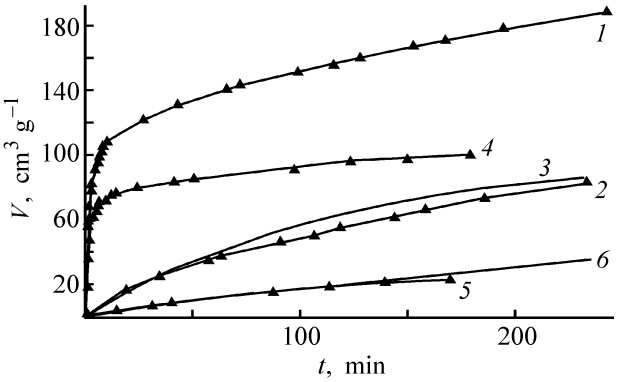

Fig. 4. Manometric curves of gas evolution from sample 2 at (*1–3*) 300 and (*4–6*) 250°C: (*1*, *4*) experimental curves, (*2*, *5*) after subtracting the volume of the initially released gases, and (*3*, *6*) fitting by first-order rate equations.

sidual solvent, free water, alcohol, and unsaponifiable substances. The initial gas evolution was up to 80 ml per gram of the sample (depending on temperature).

The thermal degradation of samples 1 and 2 starts at approximately 250°C. The initial portion of the manometric curve corresponds to removal of the solvent from the sample, and this is followed by degradation proper (Figs. 3, 4). Thermal degradation of the samples is described by first-order rate equations. The rate constant of thermal degradation (s^{-1}) of sample 1 is 6.9×10^{-5} at 300°C, and that of sample 2, 3.5×10^{-5} at 250 and 1.4×10^{-4} at 300°C, i.e., the substances are fairly heat-resistant. The higher resistance of sample 1, compared to sample 2, to thermal oxidative degradation may be due to acid catalysis of the degradation of the polyester resin by DMEPAI producing an acidic medium as a result of hydrolysis.

The results of the manometric studies are consistent with the data furnished by dynamic thermogravimetric analysis: Samples start to lose weight at approximately 100°C.

CONCLUSION

Thermal analysis of the polyester resin and its compound with dimethylethylphenylammonium iodide under isothermal and dynamic conditions shows that these substances are resistant to thermal oxidative degradation at temperatures of fusion of low-temperature solder creams.

REFERENCES

1. Pavlova, S.-S.A., Zhuravleva, I.V., and Tolchinskii, Yu.I., *Termicheskii analiz organicheskikh i vysokomolekulyarnykh soedinenii* (Thermal Analysis of Organic and Macromolecular Compounds), Moscow: Khimiya, 1983.
2. Polezhaeva, N.I., Polezhaeva, I.V., Levdanskii, V.A., et al., *Zh. Prikl. Khim.*, 2001, vol. 74, no. 4, pp. 684–685.
3. Polezhaeva, N.I., Polezhaeva, I.V., Levdanskii, V.A., and Kuznetsov, B.N., *Zh. Prikl. Khim.*, 2002, vol. 75, no. 4, pp. 689–690.
4. Wendlandt, W.Wm., *Thermal Methods of Analysis*, New York: Interscience, 1964.
5. Kovarskaya, B.M., Blyumenfel'd, A.B., and Levantovskaya, I.I., *Termicheskaya stabil'nost' geterotsepnykh polimerov* (Heat Resistance of Heterochain Polymers), Moscow: Khimiya, 1977.
6. Stepanov, R.S. and Kruglyakova, L.A., *Kinet. Katal.*, 1996, vol. 37, no. 3, pp. 316–317.
7. Gol'binder, A.I., *Laboratornye raboty po kursu vzryvchatykh veshchestv* (Laboratory Works for the Course of Explosives), Moscow: Rosvuzizdat, 1963.
8. Krasov, V.G., Petrauskas, G.B., and Chernozubov, Yu.S., *Tolstoplenochnaya tekhnologiya v SVCh mikroelektronike* (Thin-Film Technology in Microwave Microelectronics), Moscow: Radio i Svyaz', 1985.

ISSN 1070-4272, Russian Journal of Applied Chemistry, 2007, Vol. 80, No. 10, pp. 1724–1727. © Pleiades Publishing, Ltd., 2007.
Original Russian Text © N.I. Afanas'ev, G.F. Prokshin, T.F. Lichutina, M.A. Gusakova, A.P. Vishnyakova, D.A. Sukhov, O.Yu. Derkacheva, 2007, published in Zhurnal Prikladnoi Khimii, 2007, Vol. 80, No. 10, pp. 1695–1698.

MACROMOLECULAR CHEMISTRY AND POLYMERIC MATERIALS

Effect of Residual Lignin on the Supramolecular Structure of Sulfate Hardwood Cellulose: A Fourier IR Study

N. I. Afanas'ev, G. F. Prokshin, T. F. Lichutina, M. A. Gusakova, A. P. Vishnyakova, D. A. Sukhov, and O. Yu. Derkacheva

Institute of Environmental Problems of the North, Ural Division, Russian Academy of Sciences, Arkhangelsk, Russia
St. Petersburg State Technological University of Plant Polymers, St. Petersburg, Russia

Received February 6, 2007

Abstract—The effect of the content and structural features of residual lignin on the ordering of supramolecular structures in sulfate birch and aspen cellulose was studied by Fourier IR spectroscopy.

DOI: 10.1134/S1070427207100254

One of the advantages of molecular spectroscopy is the possibility of performing an integrated analysis of the main characteristics of lignocellulose materials. Among elements of the carbohydrate component, this nondestructive method can distinguish molecularly ordered (CI_{ord}) and molecularly disordered (CI_{dis}) regions of natural cellulose CI, and also structural regions of cellulose II (CII_{dis}) present in samples of wood origin. The simultaneously recorded IR spectra of the lignin component furnish information not only on the residual lignin content of fibers, but also on the relative amounts of lignin fragments in surface and bulk regions of fibers and on the relative content in lignin of aromatic structures of guaiacyl and syringyl type. The spectral data also allow estimation of the relative content of strongly bound water and of functional (carbonyl, carboxy) groups formed in lignin, depending on the procedure of lignin recovery from wood.

It has been shown previously [1, 2] that, in samples of sulfate softwood pulp containing less than 4% residual lignin, variations of the optical parameters of CI_{ord}, CI_{dis}, CII_{ord}, and CII_{dis} and the optical densities of residual lignin bands at 1600 and 1510 cm^{-1} closely correlate with each other and with the strength characteristics of cellulose fibers ($r = 0.80–0.90$).

The relative intensities of the lignin bands at 1600 and 1510 cm^{-1} are equal for birch and aspen wood. As the residual lignin content the intensity of the band at 1510 cm^{-1} of sulfate birch and aspen pulp becomes lower, by 20–30% [3], whereas in the pulp from the alkaline process this trend is not observed [4].

In this study, we examined by Fourier IR spectroscopy how the residual lignin content of sulfate birch and aspen cellulose affects the relative content of ordered and disordered supramolecular structures of cellulose.

EXPERIMENTAL

Pulping experiments were performed with manually prepared birch (*Betula pubesceus*) and aspen (*Populus tremula*) chips of length 25–30, width 20–25, and thickness 2–3 mm. The lignin content determined by the sulfuric acid method was 20.0% in birch wood and 20.4% in aspen wood; the cellulose content determined by the nitric acid–alcohol method was 45.6 and 50.6%, respectively.

Kraft pulpings were performed with white liquor (30% sulfidity, Na_2O amount 17% relative to aromatic structures of wood) with the same temperature schedule (uniform heating to 170°C over a period of 120 min, cooking at 170°C for 60 min) in a group of six autoclaves. Sulfate–ethanol and alkaline–ethanol pulpings were performed in the same mode in a liquor containing 50 vol % ethanol. After the pulping was complete, the pulp was squeezed, washed on the filter with hot water, and dried in air; then the yield and residual lignin content were determined. All the analyses were performed by the standard procedures [5].

To record the Fourier IR absorption spectra, pulp fiber samples were compacted in thin pellets 13 mm

Table 1. Yield and residual lignin content of cellulose samples

Sample no.	Characteristics of cellulose samples	Cellulose yield, %	Lignin content of cellulose, %	Amount of removed lignin, %
1	From kraft pulping of birch:			
	without additives	47.2	2.7	93.4
2	after extraction with methylene chloride	47.2	2.7	93.4
3	from pulping with addition of 3% DTO	45.7	1.80	95.9
4	From kraft pulping of aspen:			
	without additives	51.6	0.95	97.6
5	after extraction with methylene chloride	51.6	0.95	97.6
6	from pulping with addition of 3% DTO	51.7	1.0	97.5
7	From kraft pulping of 50 : 50 birch–aspen blend			
	without additives	52.0	1.80	95.3
8	after extraction with methylene chloride	52.0	1.80	95.3
9	from pulping with addition of 3% DTO	50.9	1.40	96.4
10	From sulfate–ethanol pulping of 50 : 50 birch–aspen blend	54.4	1.68	95.4
11	From alkaline–ethanol pulping of 50 : 50 birch–aspen blend	52.3	1.68	95.6

in diameter, weighing 2–4 mg, in a mold without adding KBr. Spectra were measured on an IFS-25 Fourier IR spectrometer (Bruker). Prior to measurements, samples were purged with air in the cell compartment of the device for 5 h to reduce the intensity of adsorption bands associated with atmospheric moisture and moisture adsorbed on the fiber surface. By so doing, the quality of the spectra was improved.

Addition of distilled tall oil (DTO) in the course of pulping allows the residual lignin content of hardwood cellulose to be decreased, with a simultaneous increase in the cellulose yield [6]. The specific effect of DTO additions on the residual lignin content and yield of cellulose in kraft pulping of birch and aspen wood may be caused by structural features of natural cellulose or by its changes in the course of pulping.

The characteristics of cellulose samples obtained by kraft pulping of birch (nos. 1–3) and aspen (nos. 4–6) wood and of a blend of birch and aspen chips (nos. 7–9), and also by sulfate–ethanol (no. 10) and alkaline–ethanol (no. 11) pulping of a 50 : 50 blend of birch and aspen chips are listed in Table 1.

Addition of 3% DTO (relative to aromatic structures of wood) in the course of pulping decreases the residual lignin content of birch cellulose but does not affect that of aspen cellulose. This additive somewhat decreases the cellulose yield in kraft pulping of birch wood and of birch–aspen blend. The highest cellulose yield is attained after sulfate–ethanol and alkaline–ethanol pulping of the blended chips.

The IR spectra of cellulose samples in the range 4000–400 cm^{-1} are shown in Fig. 1. The strong broad

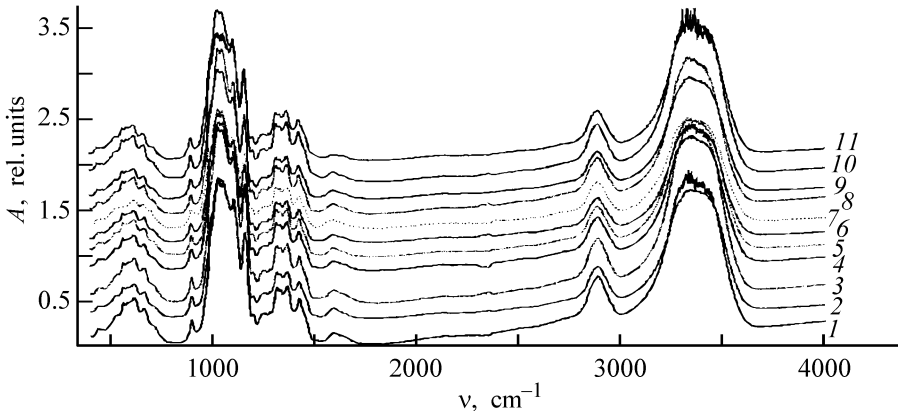

Fig. 1. Experimental IR absorption spectra of cellulose samples in the range 4000–400 cm^{-1}. (*A*) Absorption and (ν) wavenumber; the same for Fig. 2. *Figures at curves* are sample nos. in Table 1; the same for Fig. 2.

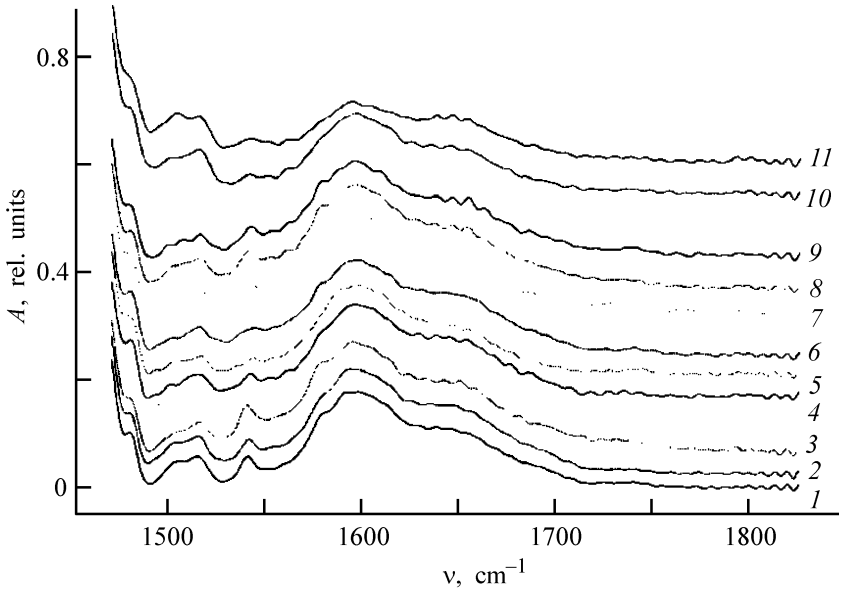

Fig. 2. Mathematically processed spectra of cellulose samples in the range 1450–1800 cm^{-1}.

absorption band at 3600–3000 cm^{-1} belongs to stretching vibrations of hydroxy groups involved in hydrogen bonding, and the band at about 2900 cm^{-1}, to stretching vibrations of the CH and CH_2 groups. For more detailed analysis of the experimental spectral curves, we used the method of Fourier self-deconvolution (Fig. 2) allowing improvement of their resolution and fairly accurate calculation of the intensities of some characteristic bands in the range 1450–1800 cm^{-1}.

The main components of the fibrous semifinished product absorb in this range. Along with complex bands of stretching vibrations of aromatic rings of residual lignin, peaked at 1600, 1540, 1515, 1510, and 1502 cm^{-1}, the spectrum also contains in this range an absorption band of strongly bound water at about 1650 cm^{-1} and a weak band of C=O stretching vibrations at 1740 cm^{-1}, belonging to the carbohydrate and lignin components. The relative intensities of the absorption bands at 1600 and 1510 cm^{-1} are listed in Table 2.

Table 2. Relative intensities *I* of absorption bands of lignin, strongly bound water, and functional groups, and parameters of supramolecular structure of the carbohydrate component

Cellulose sample no.	Lignin content, %	Lignin			Cellulose				
		I_{1600}	I_{1500}	G_{1515}/S_{1502}	I_{1650}	CI_{ord}	CI_{dis}	CII_{dis}	I_{1740}
1	2.7	2.00	0.53	1.2	0.27	0.18	0.26	0.56	0.07
2	2.7	2.15	0.56	1.3	0.23	0.14	0.26	0.61	0.03
3	1.8	1.90	0.16	1.5	0.31	0.17	0.25	0.58	0.13
4	0.95	1.75	0.38	1.7	0.26	0.19	0.26	0.55	0.06
5	0.95	1.90	0.40	1.6	0.20	0.21	0.25	0.55	0.15
6	1.00	1.70	0.26	1.6	0.23	0.20	0.26	0.54	0.16
7	1.80	2.00	0.28	1.3	0.18	0.19	0.24	0.57	0.09
8	1.80	1.90	0.26	1.6	0.26	0.17	0.28	0.55	0.07
9	1.40	1.85	0.20	1.5	0.26	0.18	0.25	0.58	0.14
10	1.68	1.55	1.05	1.9	0.20	0.17	0.27	0.56	0.02
11	1.68	0.90	1.04	1.2	0.24	0.19	0.22	0.60	0.11
Error		0.03	0.02	0.1	0.02	0.01	0.01	0.01	0.02

An accurate analysis showed that the latter band is a superposition of two bands peaked at 1515 and 1502 cm^{-1}, and their intensity ratio allows estimation of the relative content of rings of the guaiacyl (G) and syringyl (S) types in macromolecules of residual lignin of each sample. Also listed in Table 2 are the relative intensities of the absorption bands of bound water at 1650 cm^{-1} and quantitative data on the relative content of the main supramolecular structures of the carbohydrate component, determined by computer processing of the Fourier IR spectra.

In contrast to chemical analysis, the spectroscopic data show that addition of DTO decreases the residual lignin content of not only birch, but also aspen cellulose; the DTO addition appreciably alters the intensity of the bands at 1600 and 1510 cm^{-1}.

The results of our study show that the structural state of residual lignin can change in the process. For example, the relative content of guaiacyl- and syringyl-type rings in residual lignin macromolecules depends not only on the sample origin, but also on the delignification procedure. For example, the relative content of guaiacyl-type aromatic structures in residual lignin after kraft pulping of birch wood is somewhat lower, compared to aspen wood. It can be seen that macromolecules of residual lignin after sulfate–ethanol pulping contain a two times larger amount guaiacyl-type structures, compared to lignin after alkaline–ethanol pulping.

Table 2 shows that the modification–phase composition of the cellulose matrix varied insignificantly in the series of the examined samples. No appreciable effect of the pulping procedure on the cellulose structure was revealed. The level of crystallinity of aspen cellulose samples was somewhat higher than that of birch cellulose.

The content of strongly bound water does not significantly correlate with the lignin content of the cellulose and mainly depends on the sample pretreatment procedure. For example, the content of such water was somewhat lower in samples of birch and aspen deresined cellulose, which is apparently caused by their certain dehydration in the course of extraction.

A decrease in the intensity of the C=O band of carbonyl and carboxy groups, observed in cellulose samples after their extraction with methylene chloride, shows that a certain contribution to the intensity of the band at 1740 cm^{-1} is made by carbonyl and carboxy groups of resinous substances.

CONCLUSIONS

(1) The Fourier IR data show that addition of distilled tall oil makes lower the residual lignin content of both birch and aspen cellulose. Changes in the relative content of guaiacyl rings in residual lignin macromolecules and in the lignin content do not correlate with changes in the ordering of supramolecular structures.

(2) In the series of birch, aspen, and mixed cellulose samples prepared under similar conditions of kraft pulping with and without addition of distilled tall oil, the modification–phase composition of cellulose does not change, because it is determined by similar (and stronger) effects of white liquor, time, and temperature on the cellulose structure.

(3) The ratio of the ordered and disordered supramolecular structures in birch and aspen cellulose in the course of kraft pulping is not affected by tall oil addition either. The ordering of the supramolecular structures of cellulose is determined by the main parameters of kraft pulping.

REFERENCES

1. Sukhov, A.V., Derkacheva, O.Yu., Komarov, V.I., and Kazakov, Ya.V., *Lesn. Zh.*, 1994, no. 3, pp. 99–104.
2. Derkacheva, O.Yu., Sukhov, A.V., and Fedorov, A.V., in *Mezhdunarodnaya konferentsiya "Fizikokhimiya lignina"* (Int. Conf. "Physical Chemistry of Lignin"), Arkhangelsk, 2005, pp. 177–180.
3. Karklin', V.B., Treimanis, A.P., and Gromov, V.S., *Khim. Drev.*, 1975, no. 2, pp. 45–52.
4. Karklin', V.B., *Khim. Drev.*, 1981, no. 4, pp. 45–49.
5. Afanasjev, N., Prokshin, G., Vishnjakova, A., et al., Abstracts of Papers, *Eighth European Workshop on Lignocellulosics and Pulp*, Riga, 2004, pp. 465–468.
6. Obolenskaya, A.V., El'nitskaya, Z.P., and Leonovich, A.L., *Laboratornye raboty po khimii drevesiny i tsellyulozy* (Laboratory Works on Wood and Pulp Chemistry), Moscow: Ekologiya, 1991.

ISSN 1070-4272, Russian Journal of Applied Chemistry, 2007, Vol. 80, No. 10, pp. 1728–1731. © Pleiades Publishing, Ltd., 2007.
Original Russian Text © M.I. Abdullin, R.N. Asfandiyarov, A.B. Glazyrin, 2007, published in Zhurnal Prikladnoi Khimii, 2007, Vol. 80, No. 10, pp. 1699–1702.

MACROMOLECULAR CHEMISTRY AND POLYMERIC MATERIALS

Chlorinated Polymers Based on Low-Molecular-Weight 1,2-Polybutadiene

M. I. Abdullin, R. N. Asfandiyarov, and A. B. Glazyrin

Bashkir State University, Ufa, Bashkortostan, Russia

Received April 9, 2007

Abstract—Chlorinated polymeric products were synthesized from 1,2-polybutadiene by introduction of chlorine atoms into macromolecules at carbon–carbon double bonds.

DOI: 10.1134/S1070427207100266

Chlorinated polymers are widely used in production of materials having good mechanical and dielectric characteristics and resistant to acids, oils, and gasoline [1–3]. Among the general methods for synthesis of chlorinated polymers is chemical modification by introduction of chlorine atoms into macromolecules at reactive bonds of finished polymers. 1,2-Polybutadiene (1,2-PB) is a convenient polymer for chemical modification. The presence of the vinyl fragments in the side chains of the macromolecules enables addition of chlorine at unsaturated >C=C< bonds to give various chlorinated polymeric products.

In this study, we examined the functionalization of 1,2-PB by introduction of chlorine atoms at the unsaturated double bonds of the polydiene and properties of the resulting polymeric products.

For modification we used low-molecular-weight 1,2-PB (number-average molecular weight 8350; polydispersity 1.98) containing at least 70% 1,2-units, with 1,4-units the rest.

The microstructure of the initial and modified 1,2-PB was examined by ^{1}H NMR (Tesla BS-467 device) and ^{13}C NMR (Bruker AM-300). Infrared spectra were recorded on a Specord 75-IR spectrometer.

The dropping point of the test polymer, T_d, was recorded as a temperature at which the first drop of the polymer melt fell upon heating [4].

The viscosity of polymer solutions in chloroform was measured with an Ubbelohde viscometer at 25 ± 0.1°C. The intrinsic viscosity [η] was estimated by double extrapolation of the ratios η_{sp}/c and $\ln \eta_{rel}/c$ to $c \to 0$, where c is the solution concentration (g dl^{-1}) and η_{sp} and η_{rel} are the specific and relative viscosities [5].

The functionalization of 1,2-PB was carried out by addition of chlorine at carbon–carbon double bonds of the 1,2-PB macromolecules. Chlorine derivatives were synthesized at 10–20°C by bubbling chlorine gas through a solution of 1,2-PB in an organic solvent ($CHCl_3$ or CCl_4). After the completion of the synthesis, the reaction mixture was purged with nitrogen and treated with aqueous sodium hydrocarbonate. Finally, the polymer was precipitated from the organic phase by adding ethanol, separated from the solvent, and vacuum-dried.

The weight fraction of chlorine in the resulting polymeric products was determined by the Schoeniger combustion method [6]. The degree of functionalization of the polymer, α (%), was calculated as

$$\alpha = [w(\mathrm{Cl})/56.8] \times 100,$$

where w(Cl) is the actual chlorine content of the chlorinated polymer (wt %); 56.8, chlorine content (wt %) of the polymer estimated for the case of 100% functionalization at double bonds (this corresponds to addition of two chlorine atoms at the >C=C< bond of the polydiene in each monomeric unit of the macromolecule).

Properties of the adhesive composites used for fabrication adhesive PVC tapes, containing additives of the chlorinated 1,2-PBs, were characterized by (1) adhesion A to steel, by which is meant the detachment

(stripping) force related to 1 cm of the tape width; and (2) exfoliation time t_e [7]. The adhesion A of the adhesive PVC tape to steel was determined by uniform stripping at a peel angle of 180° to the steel surface for a length of 50–100 mm. The adhesion was calculated as

$$A = F/B,$$

where F is the peelling force (N) and B, width of the tape to be peeled (cm).

The exfoliation time t_e was determined for the adhesive tape by measuring the time of exfoliation of the tape folded up in half (adhesive layer inside) under a 100-g load. We synthesized chlorinated derivatives of 1,2-PB with a chlorine content of 5 to 56 wt %. The yield of the modified polymer was 87–95% (see table). The resulting products were characterized by IR and NMR spectra. The IR spectra of the chlorinated products show the bands characteristic of the ≡C–Cl bond in the range 710–770 cm^{-1}. In the ^1H NMR spectra there are signals (multiplets) of the $–CH_2Cl$ (3.6 ppm) and >CHCl groups (4.0 ppm). The ^{13}C NMR spectra of the modified polymer show the signals corresponding to $–CH_2Cl$ (62.6 ppm) and >CHCl groups (45.3 ppm). At the same time, the intensity of the signals of the olefinic carbon atoms at 115–143 ppm decreases upon chlorination. In the spectra of the chlorinated derivatives of 1,2-PM with a chlorine content above 30 wt %, the characteristic bands are broadened,, which is due to superposition of signals of different chlorine-containing structures formed in functionalization of the 1,2-polydiene.

Our results reveal that chlorine is quite readily added to the carbon–carbon double bonds of low-molecular-weight 1,2-PB, so it is possible to virtually totally chlorinate the olefinic bonds in both the backbone and side chains of the polydiene macromolecules. As a result, we synthesized polymeric products with a chlorine content of up to 56 wt %, which corresponds to degrees of functionalization of up to 99%.

Based on the IR and NMR data, we can suggest the following scheme for describing the chlorination of low-molecular-weight 1,2-PB:

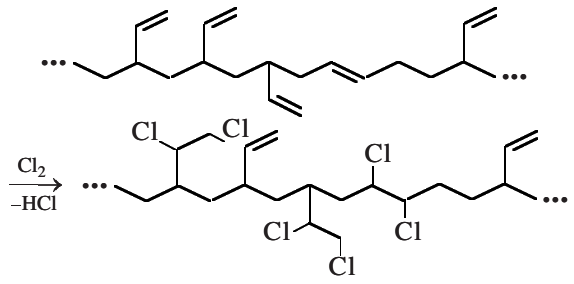

Intrinsic viscosity [η] and dropping point T_d of the modified polymer, as influenced by the degree of chlorination of 1,2-polybutadiene

Cl content in 1,2-PB, wt %	Degree of chlorination, %	[η],* dl g^{-1}	T_d, °C
0	0	0.34	54
5.2	9.2	0.29	60
16.3	28.7	0.26	67
23.7	41.7	0.23	73
35.4	62.3	0.21	80
42.4	74.6	0.18	84
50.3	88.6	0.13	127
56.4	99.3	0.11	Does not flow

* Temperature 25 ± 0.1°C; solvent chloroform.

The rheological study showed that solutions of chlorinated 1,2-PB in chloroform have a remarkably lower viscosity than those of the initial polymer (see table). As the degree of functionalization increases, the intrinsic viscosity [η] of 1,2-PB decreases, which can be attributed to changes in the thermodynamic affinity of the polymer for chloroform [8].

Among the parameters characterizing the flowability of polymeric products is the dropping point T_d. Our results show that T_d noticeably increases with the degree of chlorination of 1,2-PB (see table). Introduction of the polar chlorine atoms into the macromolecule strengthens the intermolecular interaction between the polymer chains and, as a result, raises T_d. This is confirmed by the fact that, at room temperature, samples of modified 1,2-PB with a chlorine content <25 wt % are viscous resinous compounds, while the polymers containing 30–56 wt % Cl are thermoplastic solids. It should be noted that modified 1,2-PB containing >56 wt % Cl does not flow under heating, which can be attributed not only to higher glass-transition point and T_d after chlorination, but also to degradation (primarily dehydrochlorination) of the chlorinated polydiene at elevated temperatures. The degradation is accompanied by cross-linking, which hinders the transition of the polymer into the viscous-flow state.

Introduction of the chlorine atoms into macromolecules generally improves the adhesion properties of polymeric products [9]. We examined the effect of chlorinated 1,2-PB with various Cl contents on the adhesive characteristics of the commercial adhesive composite intended for fabrication of an adhe-

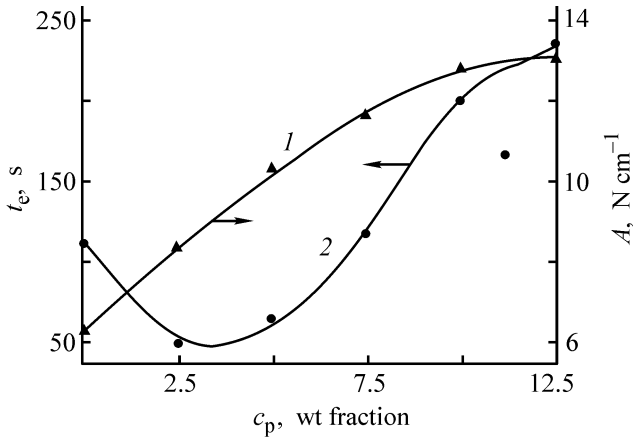

Fig. 1. (*1*) Adhesion to metal A and (*2*) exfoliation time t_e of an adhesive PVC tape as functions of the chlorinated 1,2-PB content c_p of the adhesive composite. Chlorine content of the modified polydiene 48 wt %.

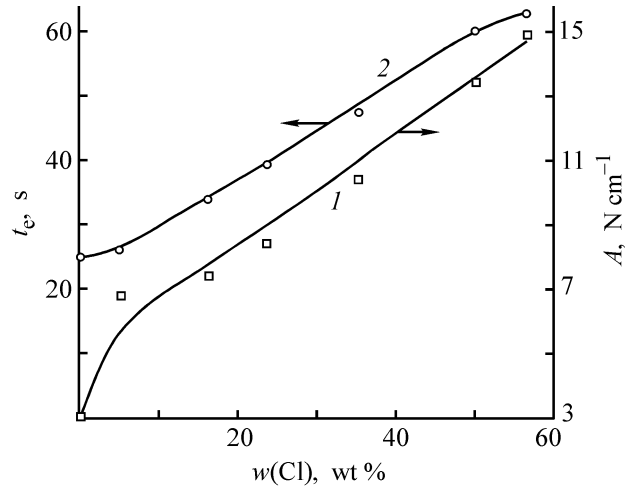

Fig. 2. (*1*) Adhesion to metal A and (*2*) exfoliation time t_e of an adhesive PVC tape with an adhesive composite modified with chlorinated 1,2-PB as functions of the chlorine content w(Cl) of chlorinated 1,2-PB. Chlorinated polymer content of the adhesive composite 5 wt %.

sive PVC tape for insulation of gas and oil pipelines. The adhesive composite includes perchlorovinyl resin (chlorinated PVC with a Cl content of 63 wt %), plasticizer [mixture of di(2-ethylhexyl) phthalate, di(2-ethylhexyl) sebacate, and KhP-470 chloroparaffin], adhesive agent (rosin), and filler (mixture of natural zeolite and calcium oxide). Into this composite, chlorinated 1,2-PB was additionally introduced in an amount of 2.5 to 12.5 wt %. The adhesive composite was applied to plasticized PVC film, and the adhesion A of the resulting adhesive tape to steel was determined.

Figure 1 shows that introduction of even a small amount (2.5 wt %) of chlorinated 1,2-PB [w(Cl) = 48 wt %] into the adhesive composite remarkably increases the adhesion of the PVC tape to the metal (Fig. 1, curve *1*). The adhesion steadily increases with the content of the chlorinated polydiene to at least 12.5 wt %. It should be noted that, by contrast, introduction of unmodified 1,2-PB into the adhesive composite leads to a decrease in A from 6 to 3 N cm^{-1}.

We also studied the effect of the degree of chlorination of 1,2-PB on the adhesion characteristics of the adhesive composite. The adhesion of the adhesive PVC film to steel considerably increases with the chlorine content of modified 1,2-PB (at fixed content of chlorinated 1,2-PB in the adhesive composite) (Fig. 2, curve *1*). The highest adhesion (A = 16.3 N cm^{-1}) was observed with modified 1,2-PB containing 56 wt % Cl, i.e., with 1,2-PB virtually totally chlorinated at double bonds (Fig. 2). Thus, addition of chlorinated low-molecular-weight 1,2-PB with high chlorine content may be recommended in production of adhesive PVC tape to improve the adhesion of the composite to metal.

Another significant parameter of adhesive composites for adhesive PVC films is the exfoliation time t_e characterizing the stickiness of the film [7]. This parameter quantifies the cohesion strength of the adhesive composite, because defoliation of adhesive PVC tape proceeds primarily across the adhesive layer.

The dependence of t_e on the content of chlorinated polydiene [w(Cl) = 48 wt %] in the adhesive composite passes through a minimum corresponding to a polymer content of the adhesive layer of about 3.0 wt % (Fig. 1, curve *2*). The exfoliation time of adhesive PVC film increases as the content of chlorinated 1,2-PB in the adhesive composite is raised further, and at the content >7.5 wt %, it starts to exceed t_e of the unmodified adhesive composite.

As the degree of chlorination of 1,2-PB increases (to a chlorine content of the polymer of at least 56 wt %), the stickiness of the adhesive layer grows (Fig. 2, curve *2*). This is evidently caused by an increase in the polarity of the chlorine-containing polydiene, which, in turn, makes hifher the energy of intermolecular interaction and, consequently, the cohesion strength of the adhesive composite.

CONCLUSIONS

(1) Chlorination of a 1,2-polydiene strongly changes the physicochemical characteristics of the polymer,

as the solution viscosity, dropping point, and adhesion properties.

(2) Chlorinated 1,2-polybutadiene can be recommended as an adhesion additive to adhesion mixtures based on chlorinated PVC to be used in production of variously purposed adhesive PVC films.

REFRENECES

1. Ronkin, G.M., *Plast. Massy*, 2003, no. 2, pp. 17–25.
2. RF Patent no. 2 252 226.
3. Ronkin, G.M., Mayanko, A.F., and Romashin, O.P., in *Nauchnye trudy Nauchno-issledovatel'skogo inst. "Sintez"* (Transactions of Sintez Research Inst.), Moscow, 1996, pp. 445–563.
4. *GOST* (State Standard) *6793–74: Petroleum Products: Determination of Dropping Point*.
5. Malkin, A.Ya. and Chalykh, A.E., *Diffuziya i vyazkost' polimerov: Metody izmereniya* (Diffusion and Viscosity of Polymers: Measuring Methods), Moscow: Khimiya, 1979.
6. Klimova, V.A., *Osnovnye mikrometody analiza organicheskikh soedinenii* (General Micromethods for Analysis of Organic Compounds), Moscow: Khimiya, 1975.
7. *TU* (Technical Specification) *2245-001-00 203 312 2003: Adhesive PVC Tape.*
8. Voyutskii, S.S., *Rastvory vysokomolekulyarnykh soedinenii* (Solutions of Macromolecular Compounds), Moscow: Goskhimizdat, 1960.
9. Berlin, A.A. and Basin, V.E., *Osnovy adgezii polimerov* (Principles of Adhesion of Polymers), Moscow: Khimiya, 1974.

ISSN 1070-4272, Russian Journal of Applied Chemistry, 2007, Vol. 80, No. 10, pp. 1732–1736. © Pleiades Publishing, Ltd., 2007.
Original Russian Text © A.M. Shul'pekov, G.V. Lyamina, N.I. Radishevskaya, T.V. Kal'yanova, 2007, published in Zhurnal Prikladnoi Khimii, 2007, Vol. 80, No. 10, pp. 1703–1707.

MACROMOLECULAR CHEMISTRY AND POLYMERIC MATERIALS

Structure and Properties of Nickel-Organosilicon Polymer Composites

A. M. Shul'pekov, G. V. Lyamina, N. I. Radishevskaya, and T. V. Kal'yanova

Department of Structural Macrokinetis, Tomsk Research Center, Siberian Division, Russian Academy of Sciences, Tomsk, Russia

Tomsk State University, Tomsk, Russia

Received November 30, 2006; in final form, March 2007

Abstract—Preparation of an electrically conducting heat-resistant composite from nickel powder (conducting component) and plasticized or unplasticized polymethylphenylsiloxane (binding matrix) was studied. The optimal preparation conditions and component ratio were determined. The phase composition, thermal resistance, and electrical conductivity of a coating based on this composite were studied in relation to the preparation temperature.

DOI: 10.1134/S1070427207100278

Composites based on organisilicon polymers and metal powders are widely used as conducting materials. These composites can be used for preparing flat heating elements [1]. The advantages of application of these materials as conducting coatings in heating elements are heat resistance, available raw materials, and simple preparation procedures. The electrical conductivity of a coating based on a polymer–metal system is provided by the electrical contact between particles of the conducting phase (metal). The electrical conductivity substantially depends both on the properties of the polymeric matrix, and type of the conducting particles and on the phase composition of the metal surface [2].

In this study, we examined the composite based on a nickel powder (conducting component) and plasticized or unplasticized polymethylphenylsiloxane (PMPS) (binding matrix). Nickel has a high electrical conductivity resistance to oxidation in air, and is, therefore, used in conducting composites to substitute silver.

The main requirement to materials used in heating elements is preservation of their conductivity at preparation and operation temperatures. The conductivity can decrease owing to structural rearrangements of the polymeric matrix on heating (as a consequence of local degradation of the conducting network) and to metal oxidation.

The aim of this study was to determine the influence of the composition and preparation temperature of PMPS/Ni composites on their electrical resistance and phase composition of the metal and to assess the possibility of preparing a film heating element.

The phase composition of nickel was determined in the course of heat treatment by the voltammetric procedure using a carbon-paste electroactive electrode (CPEE). The influence of the preparation temperature on the polymeric matrix was studied by IR spectroscopy.

EXPERIMENTAL

Model samples of conducting coatings were prepared from the following components: PNK-1L5 nickel as conducting powder (100–200 μm particles of almost spherical shape), 40% solution of PMPS in xylene, and 40% solution of plasticized PMPS (PlPMPS) of empirical formula $[C_6H_5Si_{1.5}]_m[C_6H_5Si(OH)_3]_{n-m} \cdot [(CH_3)_2SiO]_n \times 0.037$ in xylene. A pentaphthalic oligomer was used as the plasticizer.

A mixture of nickel powder and a polymer solution taken in different ratios (see table) was thoroughly mixed in a porcelain mortar for 5–10 min. Coatings were prepared by the following procedure. The mixture was cast onto glass supports and kept at room temperate to remove oxygen introduced in mixing. Then the samples were heated at different temperatures (up to 300°C). The electrical conductivity of the samples prepared at each temperature was measured, and their electrochemical behavior was studied.

To study the phase composition of nickel in the composite by voltammetry, a working CPEE was prepared from milled sample, carbon powder, and organic binder (paraffin) mixed in a 2 : 10 : 10 weight ratio. A saturated silver chloride electrode was used as an auxiliary electrode. The supporting electrolyte was 0.1 M KNO_3 in the 0.001 M HNO_3. Cyclovoltammograms (CV) were recorded on a PU-1 polarograph in differential mode of potential sweeping at a rate of 30 mV s^{-1} in the range from –0.2 to –1.4 V (cathodic current measurements) and from –1.4 to 0.8 V (anodic current measurements) [3–5].

The electrical resistance of the samples was measured with an F-400 ohmmeter. The current–voltage [$I(U)$] curves were measured on a unit consisting of a B5-43 DC source and an F4313 ammeter. A voltage of 0 to 10 V was applied to the sample. X-ray phase analysis was performed on a DRON-UM-1 diffractometer (ν = 4 deg min^{-1}, Co_{K_α}). The IR spectra were recorded on a Nicolet 5700 Spectrometer[1].

The temperature dependence of the resistance of the composites is shown in Fig. 1. The dependence passes through a maximum at 180°C. The increase in the resistivity of the composite in the first heating step is due to removal of the solvent and decrease in the mobility of macromolecules. On heating above 180°C, the resistivity decreases because of the densification of the composite structure and formation of a through-conducting network of nickel particles. The resistance of the composites containing plasticizer is, as a rule, higher than that of the composites with unplasticized polymer.

As the plasticizer content increases, the composite dries nonuniformly on heating, so that bubbles and cracks appear. As determined by CV, nickel in the composites with a high plasticizer content is oxidized significantly faster.

Nickel powder contained in the composite also changes during heat treatment. As determined by X-ray phase analysis, appreciable amounts of nickel oxide are formed only on heating above 300°C in air [6, 7]. However, nickel oxides were detected in the PlPMPS composite heated to only 100°C.

The influence of the composition and preparation temperature of the composites on their phase composition is seen from the CVs of the samples heated at 40, 100, and 150°C (Fig. 2). The increase in the current, observed when the content of the polymer binder decreases, is caused by the higher nickel content on the sample surface (Fig. 2b). However, the shapes of cyclovoltammograms of the samples treated at different temperatures and having different compositions are similar. The rise in the oxidation current (lower curves), observed as the heat treatment temperature is elevated, is due to an increase in the fraction of "accessible" nickel after removal of the solvent from the system. The cathodic current curve shows that the overvoltage of the electrolyte discharge typical of metals decreases along with an insignificant increase in the nickel oxide fraction. Therefore, nickel in mainly in the metallic form up to 150°C.

Composition of the composites

Sample no.	Nickel	PlPMPS	PMPS
	wt %		
1	35.0	65.0	0
2	34.8	48.5	16.7
3	34.6	32.1	33.2
4	51.9	48.1	0
5	51.7	36.0	12.4
6	51.4	23.9	24.7
7	68.3	31.7	0
8	68.1	23.7	8.2
9	67.9	15.8	16.3
10	87.8	12.2	0

The peaks on the cathodic curve suggest the presence of nickel oxide. Therefore, we used the reduction current peaks as an analytical signal to estimate

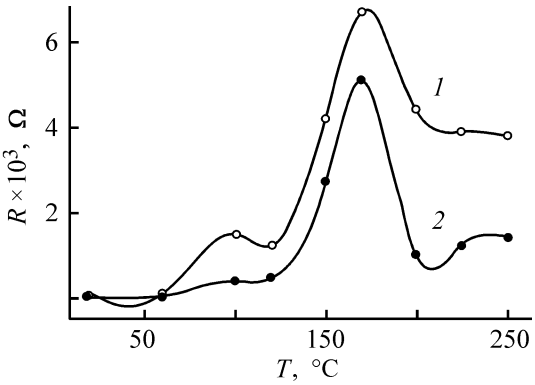

Fig. 1. Resistance of sample nos. (*1*) 4 and (*2*) 10 vs. temperature.

[1] IR spectra were recorded on a spectrometer of TPU Research Analytical Center.

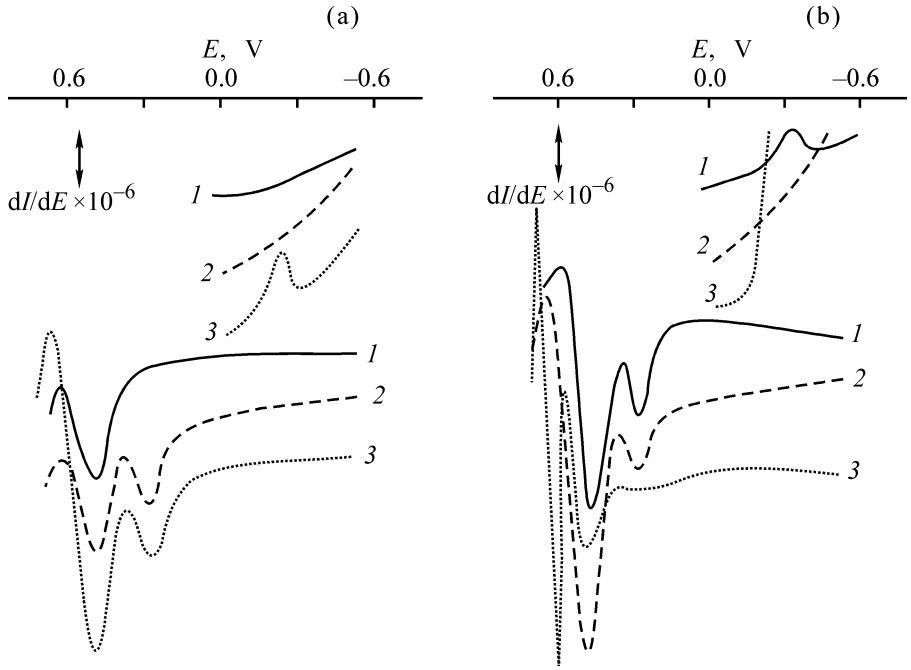

Fig. 2. Cyclovoltammograms of CPEE containing composite nos. (a) 2 and (b) 8 heated to (*1*) 40, (*2*) 100, (*3*) 150°C. (*E*) Voltage.

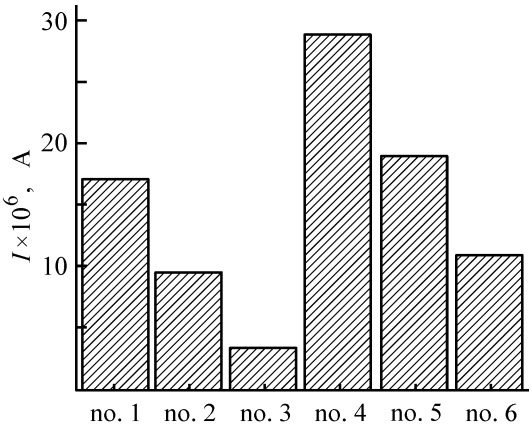

Fig. 3. Reduction current *I* of nickel ions on CPEE containing composite nos. 1–6 and heated at 150°C.

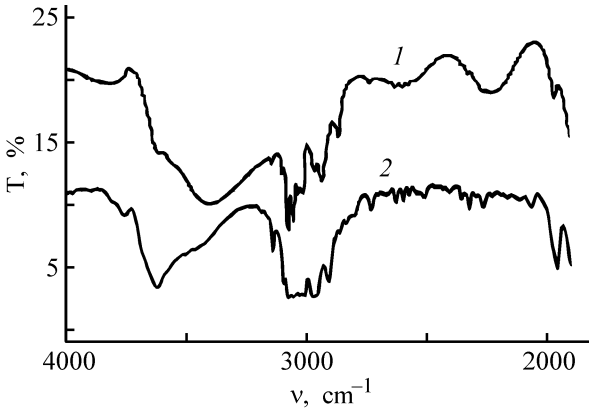

Fig. 4. Fragments of the IR spectra of (*1*) plasticized and (*2*) unplasticized PMPS. (T) Transmission and (ν) wavenumber.

the influence of the type of the polymer binder on the phase composition of nickel (Fig. 3). As can be seen from Fig. 3, the fraction of nickel oxide in the composite increases with the content of plasticized polymer.

Undoubtedly, the presence of OH groups in plasticizer molecules accelerates nickel oxidation. However, the chemical reaction of nickel particles with functional groups of the plasticizer is not the main reason. If this were the case, low-temperature oxidation would be faster since the mobility of accessible groups in the semiliquid composite is higher. The oxidation of nickel in the composite with a high plasticizer content is probably due to the fact that the spatial structure of PlPMPS differs from that of the unplasticized polymer. The OH groups of the plasticizer form strong hydrogen bonds with terminal OH groups of the polymer. This is clearly seen from the IR spectrum of the polymer (Fig. 4). The band at 2200 cm^{-1} is due to formation of strong intermolecular bonds. The intensity of this band in the spectrum of PlPMPS is significantly higher (Fig. 4, curve *1*) than that of PMPS (Fig. 4, curve *2*). In addition, a high water content of the polymer matrix is caused by the presence of the plasticizer. Water molecules are also

bound by hydrogen bonds to the functional groups of the polymer and plasticizer. The absorption in the range from 3200 to 3800 cm^{-1} is assigned to OH groups of the polymer, plasticizer, and water molecules. This band in the spectrum of PlPMPS is substantially broader owing to a higher content of bound OH groups.

The presence of the plasticizer and water molecules in the composite prevents cross-linking upon heating and, as consequence, the structure of the plasticized polymer is more porous. Nickel is oxidized in these systems by air penetrating into the pores.

It should be noted that introduction of the plasticizer in the system simplifies mixing of the polymer solution with the filler. As a result, the structure of these composites is more uniform. Hence, composites with minimal amount of the plasticizer should be used to prepare heating elements.

Fragments of $I(U)$ curves of sample no. 10 containing PlPMPS and prepared at different temperatures are shown in Fig. 5. These curves were constructed by measuring the current passing through a sample at a definite applied voltage. The curves consist of two linear portions at 0–(0.5–0.8) and (0.8–1)–10 V. The slope dI/dU corresponding to 1/R, of the first portion of the curve is smaller by a factor of approximately 2 than that of the second portion, which suggests a decrease in the resistance of the sample. At the same time, as the heat treatment temperature is raised, the slope decreases and the resistance accordingly increases. The voltage corresponding to the discontinuity in the curve increases with the heat treatment temperature.

To understand these results, it should be taken into account that the so-called "contact resistance" appearing when a charge carrier passes across the interface between two metal particles is the major factor determining the electrical conductivity [2]. Therefore, the state of the surface of metal particles plays in this case the critical role. It is known that the surface of metallic nickel exposed to air is coated with a 1–3 nm film consisting of oxide, hydroxide, and carbonate phases [8]. This film does not noticeably prevent transfer of electrons between particles. In this case, electrons can pass either directly between particles or via the tunneling effect. Hence, we suggest that the increase in the resistance with the heat treatment temperature is mainly due to growth of the surface film via oxidation of nickel by atmospheric oxygen. This is also consistent with an increase in the oxidation current observed on the voltammograms as the heat treatment temperature is raised. At a certain voltage (calculated field strength is 10^5–10^6 V m^{-1}) corresponding to the break in the $I(U)$ curve, electric break-down of the film is observed and the resistance decreases.

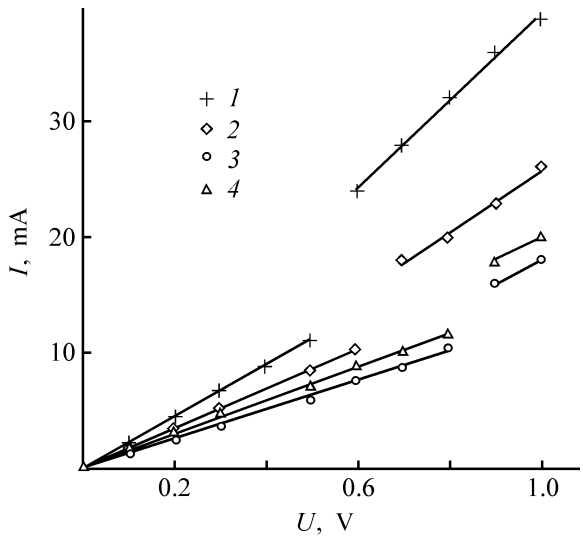

Fig. 5. $I(U)$ curves of sample no. 10 prepared at (*1*) 100, (*2*) 120, (*3*) 170, and (*4*) 250°C. (*I*) Current and (*U*) voltage.

CONCLUSIONS

(1) Introduction of the plasticizer into the polymethylphenylsiloxane–nickel composites promotes nickel oxidation.

(2) The recommended content of the filler in the matrix is no less than 50 wt%. The optimal preparation temperature of the composite is 200°C. The working eration temperature of the composites should not be higher than 300°C.

ACKNOWLEDGMENTS

This study was financially supported by Russian-American Program "Basic Research and Higher Education" (Ministry of Education and Science of Russian Federation, CRDF), project no Y2-P-16-16.

REFERENCES

1. Svechanskii A.D. and Malyshev, S.A., *Nizkotemperaturnye nagrevatel'nye elementy* (Low-Temperature Heating Elements), Moscow: Nauka, 1964.
2. Gul', V.E. and Shenfil', L.E., *Elektroprovodyashchie polimernye kompozitsii* (Elutrically Conducting Polymer Composites), Moscow: Khimiya, 1984.

3. Kuptsov, A.Kh. and Zhizhin, G.N., *Fur'e-spektry kombinatsionnogo rasseyaniya i infrakrasnogo pogloshcheniya polimerov: Spravochnik* (Fourier Raman and IR Absorption Spectra of Polymers: Handbook), Moscow: Fizmatlit, 2001.
4. Shul'pekov, A.M., Lyamina, G.V., Rybakov, A.N., et al., *Zh. Prikl. Khim.*, 2005, vol. 78, no. 4, pp. 595–598.
5. Vydra, F., tulik, K., and Julkova, E., *Rozpoutc Polarografic a Voltametrie*, Praha: Nakladatelstvi Technicke Literatury, 1977.
6. Zavin, B.G., *Organosilikatnye materialy* (Organosilicate Materials), Moscow: Znanie, 1986.
7. Shul'pekov, A.M., *Materialy II Vsesoyuznoi konferentsii "Fizika i khimiya vysokoenergeticheskikh system"* (Proc. II All Union Conf. "Physics and Chemistry of High-Energy Systems"), Tomsk May 4–6, 2006, pp. 489–492.
8. Holm, R., *Electric Contacts Handbook*, Berlin: Springer, 1958. Translated under the title *Elektricheskie kontakty*, Moscow: Inostrannaya Literatura, 1961.

ISSN 1070-4272, Russian Journal of Applied Chemistry, 2007, Vol. 80, No. 10, pp. 1737–1740. © Pleiades Publishing, Ltd., 2007.
Original Russian Text © G.N. Al'tshuler, N.V. Malyshenko, G.Yu. Shkurenko, 2007, published in Zhurnal Prikladnoi Khimii, 2007, Vol. 80, No. 10, pp. 1708–1711.

MACROMOLECULAR CHEMISTRY AND POLYMERIC MATERIALS

Kinetics of Cation Exchange on Sulfonic Polymer Based on Immobilized *cis*-Tetraphenylcalix[4]resorcinolarene

G. N. Al'tshuler, N. V. Malyshenko, and G. Yu. Shkurenko

Kemerovo Branch, Institute of Solid State Chemistry and Mechanochemistry, Siberian Division, Russian Academy of Sciences, Kemerovo, Russia

Received May 14, 2007

Abstract—Rates of cation exchange H^+–Li^+, H^+–Na^+, H^+–Ag^+, and H^+–Cu^{2+} on the sulfonic network polymer based on immobilized *cis*-tetraphenylcalix[4]resorcinolarene were studied, and the cation interdiffusion coefficients were estimated.

DOI: 10.1134/S107042720710028X

There is a steadily growing interest in calixarenes (macrocyclic polyphenols). The structure of *cis*-calix[4]resorcinolarenes (hydrophobic lower rim of benzene rings forming a cup-shaped structure and hydrophilic upper rim of hydroxy groups) makes them convenient matrices in design of molecular ensembles and supramolecules [1]. The progress in the calixarene chemistry is associated with functionalization which favors development of new types of highly organized reactive structures. Functionalized calixarenes show promise as new complexing agents, stabilizers for polymers, and extractants [2].

Immobilization of calixarenes in the polymer phase allows practical implementation of their unique properties. It is known that, in the polymer phase, immobilized calix[4]resorcinolarenes form supramolecular ensembles involving cations of alkali [3, 4] and transition [5, 6] metals and ammonium [7]. Previously, we have reported on synthesis and characterization of a network polymer based on *cis*-tetraphenylcalix[4]-resorcinolarene [3, 4]. This polymer, being a weakly acidic cation exchanger, can recover metal cations from alkaline solutions. The ion exchange rate in this polymer is controlled by slow diffusion of a substance in the polymer phase: the half-conversion time is longer than 500 s in sorption of cations from aqueous solutions [8].

Functionalization of immobilized calixarenes through introduction of the carboxy [5], furyl(hydroxy)methyl [3], or phosphoric acid [6] groups improves the cationic selectivity of the polymers. Previously [9, 10], we have synthesized a new sulfonic polymer based on *cis*-tetraphenylcalix[4]resorcinolarene. Thanks to the presence of the SO_3H groups dissociating with liberation of protons, this polymer is a strongly acidic sulfonic cation exchanger with enhanced performance as compared to the known calixarene-based cation exchangers. In particular, the sulfonic polymer based on immobilized *cis*-tetraphenylcalix[4]resorcinolarene behaves as a cation exchanger over a wide pH range [10]. The monomeric unit of the network sulfonic polymer contains (tetrasulfonatophenyl)calix[4]resorcinolarene cross-linked with the neighboring macrocycles via methylene groups:

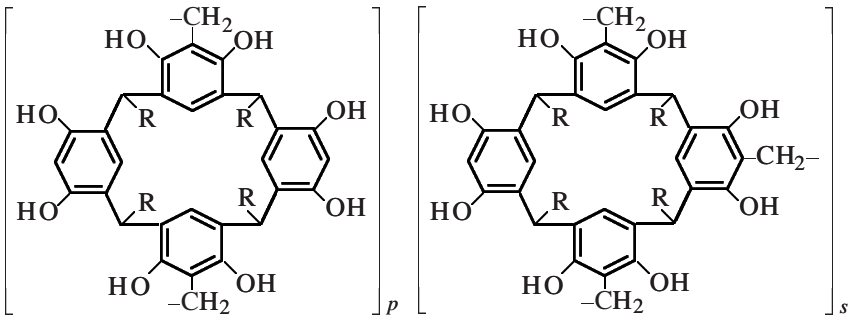

where R = Ph-SO_3H.

Compared to the existing *cis*-calixarene-based cation exchangers, the sulfonic polymer exhibits higher ion-exchange capacity [10]. In contrast to the commercial sulfonic cation exchangers, the monomeric unit of the sulfonic polymer has a highly organized 3*D* structure. According to the model views, the sulfur atoms of the sulfo groups of the monomeric unit are are situated vertices of a parallelogram with sides of 5 and 5.5 Å. As a result, the sulfonic polymer exhibits high selectivity with respect to polyvalent cations, and it can be used for separation of binary and multicomponent electrolyte mixtures [11].

The kinetics of ion exchange in the sulfonic polymer based on immobilized *cis*-tetraphenylcalix[4]resorcinolarene has not been studied yet. The highly organized 3*D* structure of the polymers generally causes a decrease in the interdiffusion rate of cations in the polymer phase. Therefore, a study of the kinetics of ion exchange on the new sulfonic polymer is theoretically and practically important.

In this study, we examined the kinetics of H^+–Cat^{z+} exchange on the sulfonic polymer based on immobilized *cis*-tetraphenylcalix[4]resorcinolarene from neutral solutions by the reaction:

$$\overline{R\text{–}SO_3H} + \frac{1}{z}Cat^{z+} = \frac{1}{z}\overline{R\text{–}SO_3Cat} + H^+, \qquad (1)$$

where the overscore designates the polymer phase, and $Cat^{z+} = Li^+$, Na^+, Ag^+, and Cu^{2+}.

EXPERIMENTAL

The polymer under study was prepared by sulfonation of the network polymer synthesized by resol polycondensation of *cis*-tetraphenylcalix[4]resorcinolarene with formaldehyde, as described in [3, 4]. The resulting product was obtained in the form of spherical granules 0.01–0.05 cm in diameter. The sulfur content of the polymer was determined according to [12] to be 7.8% (it has been shown previously [10] that the sulfo groups are situated in the lower (tetraphenyl) rim of the polymer). The size of the spherical granules was determined using an IMTs 100×50A microscope. The size distribution of the granules corresponded to the normal (Gaussian) distribution. The mean particle size was calculated as the arithmetic mean of the size of 1000 spherical granules to be $(1.02 \pm 0.53) \times 10^{-2}$ cm.

Interdiffusion coefficients $D_{H^+–Cat^{z+}}$ in network sulfonic polymer based on *cis*-tetraphenylcalix[4]resorcinolarene

Cation to be sorbed	$D_{H^+–Cat^{z+}} \times 10^7$, $cm^2\ s^{-1}$
Li^+	2.08 ± 0.08
Na^+	2.09 ± 0.35
Ag^+	1.91 ± 0.25
Cu^{2+}	1.99 ± 0.13

The dynamic ion-exchange capacity of the polymer (for sulfo groups) was determined in a column by passing 0.05 M NaCl through a bed of the polymer in the H form until saturation. The exchange capacity was related to 1 g of the polymer in the H form, dried at 105°C to constant weight. The resulting value is 2.25 mg-equiv g^{-1}.

The swellability was determined gravimetrically after separation of the sample in the H form from the equilibrium solution (isopiestic conditions) [13]. The moisture content was found to be 40 mol H_2O per 1 g-equiv of the exchange capacity of the polymer.

The sorption kinetics was studied at 298°C in the dynamic mode by the thin-layer method [14] from an infinite volume of solutions: 0.05 M LiCl, 0.1 and 0.01 M NaCl, 0.05 and 0.01 M $AgNO_3$, and 0.025 and 0.015 M $CuCl_2$. The degree of sorption was calculated as

$$F = g_t/g, \qquad (2)$$

where g_t is the current sorption of cations, and g, limiting sorption by the sulfo groups.

The interdiffusion coefficients for the pairs H^+–Li^+, H^+–Na^+, H^+–Ag^+, and H^+–Cu^{2+} were calculated by Eq. (3) [15]:

$$F = 1 - \frac{6}{\pi^2}\sum_{n=1}^{\infty}\exp\left(-\frac{Dn^2\pi^2 t}{r^2}\right), \qquad (3)$$

where r is the mean grain radius (cm); D, interdiffusion coefficient of cations in the polymer ($cm^2\ s^{-1}$); and t, time (s).

The kinetic curves of the sorption F plotted against $t^{0.5}$ are shown in Fig. 1.

The F-vs.-$t^{0.5}$ curves are linear ($r > 0.99$ at $F < 0.6$) and cross the origin (Fig. 1), suggesting that the interaction of the sulfonic polymer in the H form with aqueous LiCl, NaCl, $AgNO_3$, and $CuCl_2$ is controlled by diffusion of a substance in the polymer, being independent of the solution concentration [16]. Experimental data on the exchange of the protons of the SO_3H groups of the network sulfonic polymer with the metal cations are described by Eq. (3) over the entire range of the degrees of sorption, suggesting the gel kinetics of ion exchange [13].

The table lists the mean interdiffusion coefficients $D_{H^+–Cat^{z+}}$, calculated by Eq. (3) at a confi-

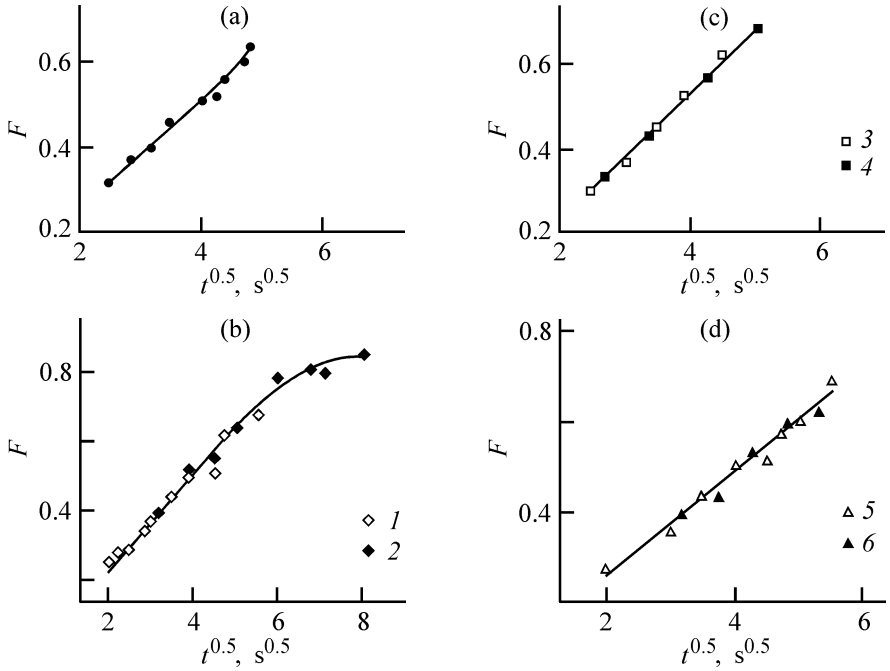

Fig. 1. Kinetic curves of sorption of metal cations on the sulfonic polymer based on *cis*-tetraphenylcalix[4]resorcinolarene in the H form from aqueous electrolyte solutions. (F) Degree of sorption and (t) time. Solutions (M): (a) LiCl 0.05; (b) NaCl: (*1*) 0.1 and (*2*) 0.01; (c) $AgNO_3$: (*3*) 0.05 and (*4*) 0.01; and (d) $CuCl_2$: (*5*) 0.025 and (*6*) 0.015.

dence level $p = 0.9$ from experimental data for the pairs H^+–Li^+, H^+–Na^+, H^+–Ag^+, and H^+–Cu^{2+}, in the sulfonic polymer. The interdiffusion coefficients are in the range $(1.9–2.1) \times 10^{-7}$ $cm^2\ s^{-1}$. Similar values are typical of commercial sulfonic cation exchangers, e.g., 1.1×10^{-7} $cm^2\ s^{-1}$ for Dowex 50×16 [17].

Figure 1 shows that the half-conversion time for all the cation pairs in the polymer under study is 16 ± 0.5 s, which is considerably shorter than that in the initial polymer (>500 s). Therefore, the ion exchange rate in the sulfonic polymer based on *cis*-tetraphenylcalix[4]resorcinolarene is considerably higher.

CONCLUSIONS

(1) The rate of ion exchange H^+–Cat^{z+} from aqueous solutions in a new sulfonic polymer based on *cis*-tetraphenylcalix[4]resorcinolarene is controlled by the gel kinetics, i.e., by the interdiffusion of cations in the polymer phase. The interdiffusion coefficients of protons and metal cations in the polymer phase are in the range $(1.9–2.1) \times 10^{-7}$ $cm^2\ s^{-1}$.

(2) Sulfonic polymer based on *cis*-tetraphenylcalix[4]resorcinolarene exhibits better kinetic characteristics of ion exchange than its nonsulfonated analog.

ACKNOWLEDGMENTS

The study was financially supported by the Russian Foundation for Basic Research (project 07-03-96030).

REFERENCES

1. MacGillary, L.R. and Atwood, J.L., *J. Am. Chem. Soc.*, 1997, vol. 119, p. 6931.
2. Popova, E.V., Volodina, Yu.M., Gazizov, A.S., et al., *Izv. Ross. Akad. Nauk, Ser. Khim.*, 2003, no. 10, pp. 2168–2169.
3. Altshuler, H., Ostapova, E., Fedyaeva, O., et al., *Macromol. Symp.*, 2002, vol. 181, pp. 1–4.
4. Al'tshuler, G.N., Abramova, L.P., Malyshenko, N.V., et al., *Izv. Ross. Akad. Nauk, Ser. Khim.*, 2005, no. 8, pp. 1919–1922.
5. Shinohara, T., Wakisaka, S., Ohto, K., and Inouc, K., *Chem. Lett.*, 2000, pp. 640–641.
6. Alexandratos, S.D. and Natesan, S., *Macromolecules*, 2001, vol. 34, pp. 206–210.
7. Ostapova, E.V., Al'tshuler, O.G., Sapozhnikova, L.A., and Al'tshuler, G.N., *Zh. Fiz. Khim.*, 2003, vol. 77, no. 5, pp. 909–913.

8. Al'tshuler, G.N. and Fedyaeva, O.N., *Zh. Fiz. Khim.*, 2001, vol. 75, no. 11, pp. 2088–2089.
9. RF Patent 2 291 171.
10. Al'tshuler, O.G., Sapozhnikova, L.A., and Al'tshuler, G.N., *Zh. Prikl. Khim.*, 2006, vol. 79, no. 8, pp. 1315–1319.
11. Al'tshuler, O.G., Sapozhnikova, L.A., and Al'tshuler, G.N., *Zh. Prikl. Khim.*, 2007 (in press).
12. Lebedeva, L.I. and Novozhilov, I.V., *Zh. Anal. Khim.*, 1961, vol. 16, p. 223.
13. Helfferich, F., *Ionenaustauscher*, Weinheim: Chemie, 1959, vol. 1.
14. Fedoseeva, O.N., Cherneva, E.P., and Tunitskii, N.N., *Zh. Fiz. Khim.*, 1959, vol. 33, p. 936.
15. Boyd, G.E., Adamson, A.W., and Myers, L.S., *J. Am. Chem. Soc.*, 1947, vol. 69, p. 2836.
16. Shataeva, L.K., Kuznetsova, N.N., and El'kin, G.E., *Karboksil'nye ionity v biologii* (Carboxylic Ion Exchangers in Biology), Leningrad: Nauka, 1979.
17. Boyd, G.E. and Soldano, V.A., *J. Am. Chem. Soc.*, 1953, vol. 75, p. 6091.

ISSN 1070-4272, Russian Journal of Applied Chemistry, 2007, Vol. 80, No. 10, pp. 1741–1744. © Pleiades Publishing, Ltd., 2007.
Original Russian Text © E.I. Galeeva, I.N. Bakirova, 2007, published in Zhurnal Prikladnoi Khimii, 2007, Vol. 80, No. 10, pp. 1712–1715.

MACROMOLECULAR CHEMISTRY AND POLYMERIC MATERIALS

Chemical Degradation of Elastic Foamed Polyurethanes under the Action of Thiodiglycol

E. I. Galeeva and I. N. Bakirova

Kazan State University of Technology, Kazan, Tatarstan, Russia

Received February 26, 2007

Abstract—Alcoholysis of elastic block foamed polyurethane under the action of thiodiglycol and its mixture with Laprol 3603 polyether was studied. The structure and physicochemical properties of alcoholysis products were determined.

DOI: 10.1134/S1070427207100291

Polyurethanes (PUs) are the most valuable and widely produced commercial polymers; their consumption increases by 4–5% annually [1]. The most demanded polyurethane-based materials are elastic block foamed polyurethanes (EFPUs). Thanks to a combination of low density, high air permeability, high concussion resistance, good heat and moisture exchange, physiological inertness, and feasibility of processing, these materials are widely used in production of soft furniture parts and bedding, in automobile production, textile industry, and other fields. Today the share of these materials in the total amount of PUs produced in the world is about 35% [2]. This rapid growth of the production and consumption inevitably involves the formation of waste whose utilization is an urgent problem.

Chemical degradation by alcoholysis seems to be the best way to utilize the EFPU waste. A number of hydroxyl-containing systems suitable for chemical cleavage of PUs have been reported. However, no data have been published on the use of organoelement polyols for this purpose. At the same time, it would be possible to prepare with such agents compounds containing atoms of S, P, and some other elements. Such products may be of interest for production of polymeric compounds with a set of special properties.

The goal of this study was to develop a procedure for chemical degradation of elastic block foamed polyurethanes under the action of thiodiglycol (TDG) and to prepare a thiourethane compound from the transformation product.

EXPERIMENTAL

As substrates we chose block EFPU samples, and as degradation agent (DA), TDG containing a sulfur atom along with two hydroxy groups and a mixture of DG with Laprol 3603 (L 3603) polyether. Laprol 3603 was added to decrease the concentration of OH groups in the degradation product. The EFPU : DA ratio was chosen empirically, so as to ensure reprocessing of the largest amount of waste and to minimize the DA consumption.

Alcoholysis was performed in a flask equipped with a stirrer, in the temperature range 180–200°C, by continuous supply of milled waste into DA at a stirring rate of 300 rpm. The time of addition of the EFPU crumb to the degradation agent was considered the start of degradation. Alcoholysis products were taken for analysis since the system homogenization.

The total content of hydroxy and amino grops, $c_{OH + NH_2}$, in alcoholysis products was determined by acetylation [GOST (State Standard) 25261–82).

The dynamic viscosity $\eta_{50°C}$ (Pa s) of alcoholysis products was determined with a Hoeppler rheoviscometer at 50 ± 0.1°C.

The chemical structures of DA and alcoholysis products were studied by IR spectroscopy with a Perkin–Elmer 16 spectrometer. Samples were prepared as thin liquid films between KBr plates.

The physicomechanical tests of the sealants were performed in accordance with the following standards: nominal tensile strength, relative elongation, and elongation set, with GOST 21751–76; adhesion

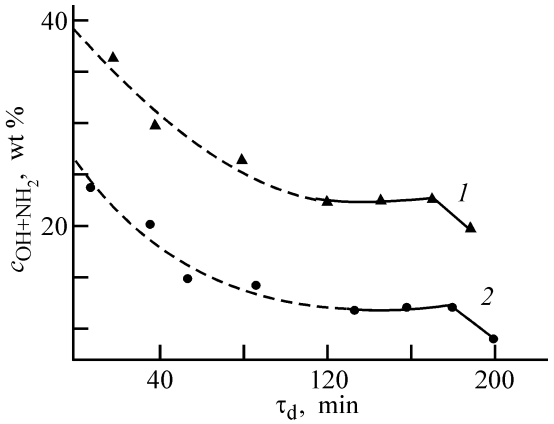

Fig. 1. Total concentration c_{OH+NH_2} in alcoholysis products vs. degradation time τ_d at 180°C. (*1*) EFPU + TDG and (*2*) EFPU + TDG + L 3603.

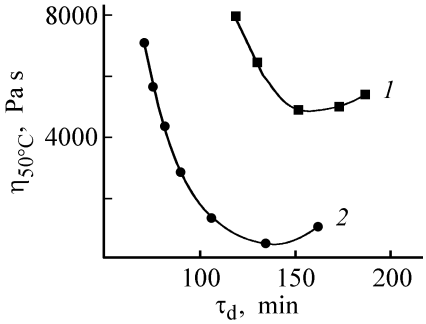

Fig. 3. Dynamic viscosity $\eta_{50°C}$ of alcoholysis products as a function of degradation time τ_d. System EFPU + TDG + L 3603.

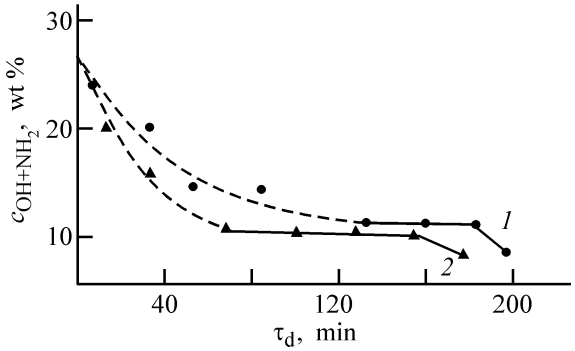

Fig. 2. Total concentration c_{OH+NH_2} in alcoholysis products vs. degradation time τ_d. System EFPU + TDG + L 3603. *T*, °C: (*1*) 180 and (*2*) 200; the same for Fig. 3.

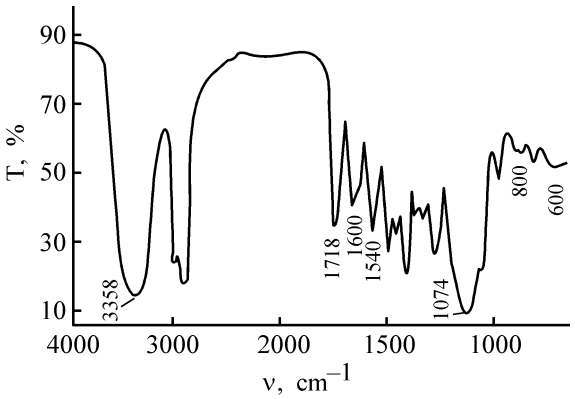

Fig. 4. IR spectrum of the alcoholysis product formed in the EFPU + TDG + L 3603 system. (T) Transmission and (ν) wavenumber.

strength to metal at exfoliation, with GOST 21981–76; and degree of swelling, with GOST 421–59.

The process parameter allowing monitoring of the degradation and use of the alcoholysis product as a secondary raw material is the total content of terminal hydroxy and amino groups. Figure 1 shows that, in the initial period of degradation, the c_{OH+NH_2} values show strong scatter because of the insufficient uniformity of the system, due to the presence of unchanged EFPU. This time interval is shown in Fig. 1 by dashed lines. With the progress of the degradation, the c_{OH+NH_2} values get stabilized at a level of 22.2 wt % for the EFPU + TDG system and 11.4 wt % for the EFPU + TDG + L 3603 system. Further treatment leads to a decrease in the content of OH and NH_2 groups via secondary cross-linking:

$$\sim R'\text{–}OH + HO\text{–}R''\text{–}OH + HO\text{–}R'''\sim \rightarrow \sim R'\text{–}O\text{–}R'\text{–}O\text{–}R'''\sim + 2H_2O, \quad (1)$$

where R', R'', and R''' are polyol fragments.

Elevating the temperature has virtually no effect on the equilibrium values but makes shorter the time required to attain them (Fig. 2).

The alcoholysis kinetics, monitored by the dynamic viscosity, is shown in Fig. 3. Initially the dynamic viscosity monotonically decreases owing to the progress of degradation and decrease in the molecular weight of the alcoholysis products. Then the viscosity gets stabilized, indicating that the system approaches the equilibrium state. However, longer heating leads to an increase in the viscosity of the degradation products, coinciding in time with a decrease in c_{OH+NH_2} (Fig. 2). It should be noted that an increase in the heat treatment temperature leads to a decrease in the absolute viscosity.

The chemical structure of alcoholysis products was studied by IR spectroscopy. The IR spectra of alcoholysis products of the EFPU + TDG + L 3603 system (Fig. 4) contain absorption bands characteristic of TDG and Laprol 3603: stretching vibrations of associated OH group (3360–3340 cm^{-1}), band of the ether

Main service and physicomechanical properties of sealants

Property	US_{EFPU}		U-30M	UT-30MES-5	Forsazh
	without solvent	with solvent			
Nominal tensile strength, MPa	6.2–7.3	3.5–4.6	2.5–4.0	2.5–4.0	1.5–2.5
Relative elongation, %	250–350	250–340	150–300	200–350	300–350
Relative residual strain after break, %	0–2	2–4	0–8	0–12	–
Rebound elasticity, %	24–28	25–32	–	–	–
Hardness, arb. units	60–65	55–65	50–65	40–60	–
Vitality, h	0.3–0.5	0.5–1.0	2–9	2–9	1–2
Adhesion strength to metal at exfoliation, kN m^{-1}	0.76 (with sublayer)		1.5 (with sublayer)		
	0.79 (without sublayer)	–	0–0.5 (without sublayer)	–	–
Swelling in 250 h, wt %:					
in distilled water	6	–	4–6	20	10
in hexane	7	–	No swelling	–	–
in transformer oil	10	–	″	–	30

C–O–C bond (about 1074 cm^{-1}), and a group of bands in the range 800–600 cm^{-1}, characteristic of the C–S bond. In the spectra of the reclaimed raw material, new peaks appear, assignable to vibrations of the aromatic fragment (1636–1600 cm^{-1}) and urethane group (1718 cm^{-1}, C=O stretching; 1540 cm^{-1}, NH bending). Interpretation of the amino group is complicated by the fact that its absorption range, 3500–3390 cm^{-1}, overlaps with the range of stretching vibration bands of associated OH groups; however, the presence of amino groups is quite probable [3].

Thus, analysis of the IR spectra of these groups shows that the degradation products are compounds with terminal hydroxy and amino groups, containing sulfide, urethane, and ether bonds in the backbone, which allows these compounds to be used in synthesis of thiourethane hermetic compounds as a hydroxyl-containing component. These polymers are prepared by the flowsheet shown in the scheme and ensuring chemical recycling of EFPU waste.

According to this scheme, the sealant is prepared by the reaction of an isocyanate component with the hydroxyl-containing component in 1 : 1 ratio.

The main service and physicomechanical properties of the thus prepared US_{EFPU} sealant are listed in the table in comparison with commercial compounds based on thiokols (U-30M, UT-30MES-5) and with Forsazh poly(ether–urethane) [4, 5]. It can be seen that the use of the reclaimed polymeric polyol allows preparation of a thiourethane sealant well competitive in its main properties with commercially produced thiokol vulcanizates and cured poly(ether–urethane) compounds.

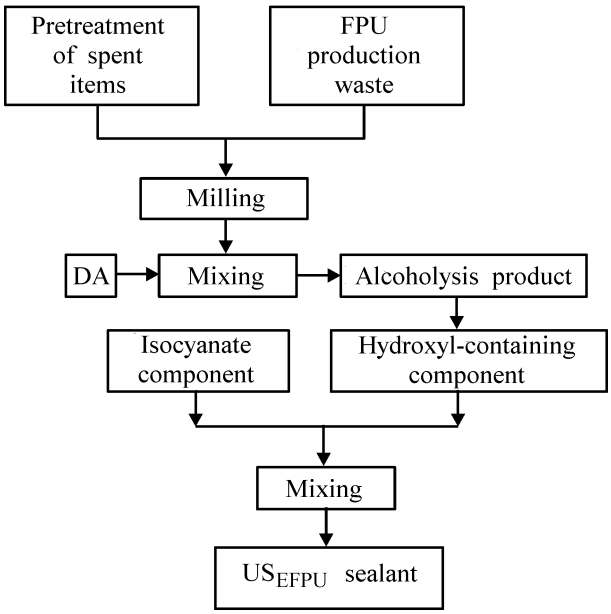

Scheme.

CONCLUSIONS

(1) A procedure was developed for chemical degradation of elastic block foamed polyurethanes under the action of thiodiglycol and its mixture with Laprol 3603 polyether.

(2) The degradation products are compounds with terminal hydroxy and amino groups, containing sulfide, urethane, and ether bonds in the backbone.

(3) Based on the reclaim obtained, a thiourethane sealing compound was developed, well competing in the main properties with commercial sealants.

REFERENCES

1. Kogelhik, H., *Kunststoffe*, 2001, vol. 91, no. 10, pp. 339–346.
2. Austiu, A., *Urethanes Technol.*, 1998, vol. 15, no. 4, pp. 53–54.
3. Kazitsyna, L.A. and Kupletskaya, N.B., *Primenenie UF, IK, YaMR i mass spektroskopii v organicheskoi khimii* (Applications of UV, IR, NMR, and Mass Spectroscopy to Organic Chemistry), Moscow: Mosk. Gos. Univ., 1979.
4. Labutin, A.L., *Antikorrozionnye i germetiziruyushchie materialy na osnove sinteticheskikh kauchukov* (Corrosion-Protecting and Sealing Materials Based on Synthetic Rubbers), Leningrad: Khimiya, 1982.

ISSN 1070-4272, Russian Journal of Applied Chemistry, 2007, Vol. 80, No. 10, pp. 1745–1749. © Pleiades Publishing, Ltd., 2007.
Original Russian Text © F.N. Kaputskii, V.I. Torgashov, T.L. Yurkshtovich, N.V. Golub, I.L. Ostrovskaya, V.A. Alinovskaya, 2007, published in Zhurnal Prikladnoi Khimii, 2007, Vol. 80, No. 10, pp. 1716–1720.

MACROMOLECULAR CHEMISTRY AND POLYMERIC MATERIALS

Sulfation of Polysaccharides with Sodium Pyrosulfate in Dimethyl Sulfoxide

F. N. Kaputskii, V. I. Torgashov, T. L. Yurkshtovich, N. V. Golub, I. L. Ostrovskaya, and V. A. Alinovskaya

Research Institute of Physicochemical Problems, Belarussian State University, Minsk, Belarus

Received February 8, 2007

Abstract—Sulfo esters of cellulose, dextran, starch, and amylopectin with a degree of substitution equal to 0.1–1.1 were prepared in the system constituted by sodium pyrosulfate and dimethyl sulfoxide. The intrinsic viscosity of aqueous solutions of sulfo polysaccharides was determined, and their anticoagulant activity was evaluated.

DOI: 10.1134/S1070427207100308

Polysaccharide derivatives with ionic groups are of interest as polymeric carriers for immobilization of enzymes and drugs. Among these derivatives, particular attention is attracted by sulfo esters exhibiting anticoagulant and antithrombotic activity [1, 2]. A combination of the intrinsic biological effect of a sulfated polysaccharide with the activity of an immobilized drug opens up prospects for development of a combined pharmaceutical preventing and curing a wider spectrum of complications of cardiovascular and other diseases.

This study continues our research on sulfation of polysaccharides. It is concerned with synthesis of water-soluble sulfo esters of starch, amylopectin, dextran, and cellulose in the sodium pyrosulfate–dimethyl sulfoxide (DMSO) system. The choice of this system was governed by its availability and suitability for medical applications, as sodium pyrosulfate $Na_2S_2O_7$ used as sulfating agent is nontoxic and DMSO is considerably less harmful than pyridine or dimethylformamide.

EXPERIMENTAL

As starting materials we used prehydrolyzed potato starch, amylopectin [TU (Technical Specification) 6-09-10-391–75], cellulose in the form of FN-15 chromatographic paper, and dextran with a molecular weight of 4×10^4.

Cellulose was hydrolyzed in refluxing 2 N HNO_3 (2 l of HNO_3 solution per 100 g of chromatographic paper) for 20–30 min to obtain a powder-like mass. The resulting microcrystalline cellulose (MCC) was washed with distilled water to neutral reaction of the wash water and was dried at room temperature to the air-dry state. The molecular weight of the MCC obtained was about 3×10^4.

The acid and enzymatic hydrolyses of starch and amylopectin were performed in accordance with [3]. A 20% suspension of polysaccharides in a 0.1 N sulfuric acid solution was prepared and kept for 6 h at 328 K with continuous stirring. Hydrolyzed starch and amylopectin were precipitated with acetone, washed with the water–acetone mixture (volume ratio 1 : 1), filtered, and dried at room temperature to the air-dry state.

For enzymatic hydrolysis of starch and amylopectin, we used pancreatin [3]. To 200 ml of a 14% polysaccharide paster, heated to 333 K, we gradually added with stirring 20 ml of a 1% pancreatin solution. The precipitation, washing, and drying of the hydrolyzed products were performed as described above for acid hydrolysis.

The sulfation of polysaccharides (PSs) in the $Na_2S_2O_7$–DMSO system was performed in accordance with [4]: 1–5 g of a polysaccharide dried to constant weight was placed in a flask with a ground-glass stopper, sodium pyrosulfate and dimethyl sulfoxide (pure grade) were added in succession with stirring, and the mixture was heated for the required time (no less than 6 h) on an oil bath at a definite temperature. After the lapse of the required time, the mixture was neutralized with a saturated sodium carbonate solution

Table 1. Influence of the conditions of polysaccharide pretreatment on the composition of sulfo esters* (sulfation temperature 333 K, time 6 h)

Polysaccharide	Hydrolysis conditions			DS_{SO_3H}	S, %	$[\eta]$, dl g^{-1}	Fraction yield, %	
	activating agent	τ, h	*T*, K				insoluble	water-soluble
Amylopectin (AP)	Initial	–	–	0.6	8.6	0.09	0	91
	0.1 N H_2SO_4,	6	323	0.3	4.4	–	70	17
	1% pancreatin	0.1	333	0.7	9.4	0.05	0	91
Starch (ST)	Initial	–	–	0	0	–	100	0
	0.1 N H_2SO_4,	6	323	0	0	–	100	0
	1% pancreatin	0.1	333	0.8	10.5	0.04	0	53
MCC	Initial	–	–	0	0	–	100	0
	2 N HNO_3	3	333	0.7	9.6	0.02	0	96

* Composition of the sulfating mixture, g g^{-1}: AP : $Na_2S_2O_7$: DMSO = 1.0 : 3.0 : 3.0; ST : $Na_2S_2O_7$: DMSO = 1.0 : 3.0 : 2.5; MCC : $Na_2S_2O_7$: :DMSO = 1.0 : 3.0 : 5.0; the same for Table 2.

to pH 8–10. After that, the sulfo esters were demineralized by dialysis on cellophane membranes until the qualitative reaction for sulfate ions in wash waters was negative. The solubility of polysaccharide sulfo esters was determined gravimetrically [5]. The purified solutions were freeze-dried. The sulfur content of polysaccharide sulfates was determined by potentiometric titration [6]. Prior to the analysis, the Na salt of the sulfo esters was converted to the H form by passing the solutions through a column packed with a KU-2 × 12 cation-exchange resin.

The sulfo esters synthesized were studied by IR spectroscopy with a Varian 3100 FT-IR spectrophotometer. Samples were prepared as KBr pellets.

The intrinsic viscosity of sulfo polysaccharides was measured in 0.5 N aqueous NaCl at 310 K in an Ubbelohde viscometer with a capillary diameter of 0.54 mm [7].

The effect of polysaccharide sulfo esters on the coagulation activity of plasma was evaluated by the change in the thrombin time [8].

The sulfation of polysaccharides with sodium pyrosulfate can be schematically described by the equation

$$R\text{–}OH + Na_2S_2O_7 \rightarrow R\text{–}OSO_3H + Na_2SO_4.$$

The process is accompanied by the side reaction

$$Na_2S_2O_7 + H_2O \rightarrow 2NaHSO_4,$$

i.e., the sulfating agent decomposes in the presence of water in PS or in the solvent, and the efficiency of its utilization in the target reaction with PS decreases. The simultaneous occurrence of the two concurrent reactions limits the degree of substitution (DS) of the sulfo derivatives. Their composition can be controlled by varying the reaction conditions.

As can be seen from Table 1, the polysaccharides studied differ considerably in the reactivity in sulfation with sodium pyrosulfate in DMSO. The initial cellulose and starch do not undergo modification in this system. At the same time, sulfation of amylopectin and dextran yields sulfo esters with a fairly high degree of substitution. To enhance the reactivity, the polysaccharides (cellulose, starch, amylopectin) were subjected to acid and enzymatic (starch, amylopectin) hydrolyses. As can be seen from Table 1, acid hydrolysis raises the reactivity of cellulose in sulfation, does not affect the reactivity of starch, and lowers the reactivity of amylopectin. The enzymatic hydrolysis considerably raises the reactivity of starch, and only slightly, that of amylopectin.

These features of the behavior of the polysaccharides are apparently caused by features of their structure (number and strength of hydrogen bonds, degree of polymerization). The acid hydrolysis of cellulose not only lowers the degree of polymerization, but also leads to cleavage of crystallites [9], thus making the cellulose structure more accessible to the sulfating agent.

The acid hydrolysis of starch and amylopectin also lowers the degree of polymerization, but is accompanied by accumulation of the linear component, which favors [3] an increase in the number of hydrogen bonds between the macromolecules, preventing the sulfation.

By contrast, the enzymatically hydrolyzed starch and amylopectin are sulfated considerably more readily, which may be due to weakening of intermolecular interactions. Indeed, it is known that, under the action

of the enzyme, polysaccharides are selectively hydrolyzed across α-1,4-glucoside bonds, and the degree of branching remains essentially unchanged. The process yields macromolecules of a critically small size, which cannot form ordered regions (crystallites) of the polysaccharides.

The sulfur content of the sulfo esters is a function of the composition of the sulfating mixture (Figs. 1, 2) and reaches a maximum at the weight ratios PS : $Na_2S_2O_7$: DMSO = 1.0 : (2.5–3.5) : (2.5–5.0), depending on a particular PS. The sulfo esters formed at the optimal component ratios not only have the highest DS, but are also more uniform in the composition, as suggested by their complete solubility in water. A decrease in the solvent amount relative to the optimum and further increase in the sodium pyrosulfate amount lead to worse swelling of PS in DMSO, which impairs the sulfation efficiency. At the same time, a decrease in the sodium pyrosulfate amount and an increase in the liquid to solid ratio lead to a decrease in the content of sulfo groups in the product in accordance with the law of mass action.

The trend in variation of the optimal liquid-to-solid ratio ensuring the highest DS along the series of PSs, seen from Fig. 2, is primarily determined by the degree of branching of the macromolecules, rather than by their size. An increase in the degree of branching of macromolecules in going from cellulose to dextran and amylopectin favors swelling and even dissolution of PS in DMSO, with the subsequent formation of more homogeneous partially substituted sulfo esters even at a low solvent content.

Table 2 shows that an increase in the temperature (except in the case of cellulose) and time of sulfation do not lead to an increase in DS of the sulfo esters. Similar results have been obtained in experiments on sulfation of PSs with other agents [1]. However, to obtain the most homogeneous partially substituted PS esters, it is advisable to perform sulfation in the $Na_2S_2O_7$–DMSO system at 333 K for no less than 5–6 h. Under these conditions, the PS swelling in the solvent is the strongest, and more homogeneous products are obtained. An increase in the homogeneity of PS sulfo esters with increasing time and temperature of the reaction can be judged from the fact that the turbidity of the sulfo ester solutions, caused by the presence of finely dispersed unsubstituted or low-substituted fractions, becomes weaker or even disappears at all.

The compositions of dextran, cellulose, starch, and amylopectin samples treated with the $Na_2S_2O_7$–DMSO system were monitored by IR spectroscopy (Fig. 3). It is known [2, 10] that the most significant changes in the absorption pattern upon introduction

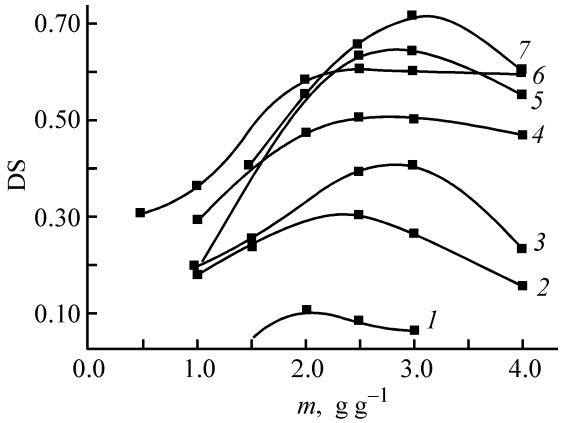

Fig. 1. DS vs. the weight ratio *m* between the sulfur-containing salt and PS for sulfo esters of (*1*, *4*, *5*) dextran, (*2*, *3*, *7*) cellulose, and (*6*) amylopectin. Reaction temperature 333 K, time 6 h; the same for Fig. 2. Liquid to solid ratio, g g^{-1}: (*1*, *2*) 2.5, (*3*, *6*) 3.0, (*4*, *7*) 5.0, and (*5*) 4.0.

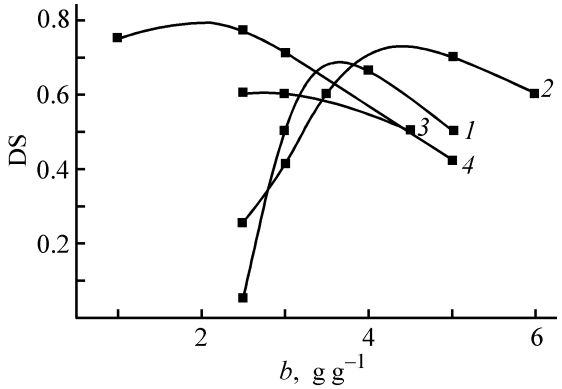

Fig. 2. DS of sulfo esters of (*1*) dextran, (*2*) cellulose, (*3*) amylopectin, and (*4*) starch, prepared by the reaction with sodium pyrosulfate (3 g g^{-1}), vs. the solvent (DMSO)/polysaccharide weight ratio *b*.

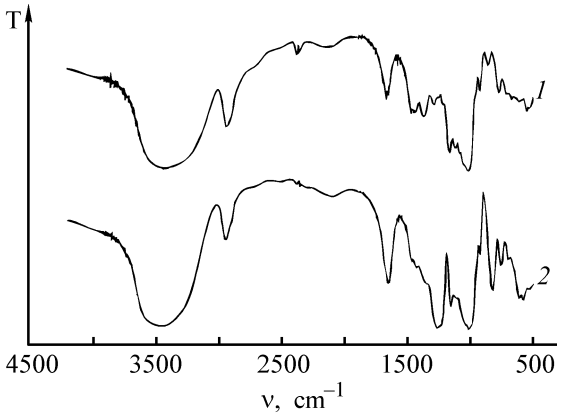

Fig. 3. IR spectra of (*1*) initial and (*2*) sulfated (DS 0.8) dextran: (T) transmission and (ν) wavenumber.

Table 2. Influence of the temperature and time of polysaccharide sulfation on the composition of sulfo esters

Polysaccharide	*T*, K	τ, h	DS_{SO_3H}	S, %	Yield, %	
					insoluble fraction	water-soluble sulfo ester
Amylopectin	303	6	0.7	9.1	0	93
	318	6	0.6	8.6	0	91
	333	0.5	0.6	8.6	0	90
	333	1	0.6	8.6	0	90
	333	6	0.6	8.6	0	91
Dextran*	303	6	0.8	10.5	0	92
	313	6	0.6	8.6	0	90
	323	6	0.6	8.6	0	83
	333	0.5	0.6	8.6	0	76
	333	1	0.6	8.6	0	80
	333	6	0.6	8.6	0	76
MCC	313	6	0.2	3.6	30	64
	323	6	0.3	4.4	25	69
	333	0.5	0.7	9.6	0	96
	333	1	0.7	9.6	0	95
	333	6	0.7	9.6	0	96
Starch**	303	6	0.8	10.5	0	62
	323	6	0.8	10.5	0	60
	333	0.5	0.8	10.5	0	55
	333	1	0.8	10.5	0	62
	333	6	0.8	10.5	0	60

* For dextran, the starting mixture had the following composition, g g^{-1}: D : Na_2S_2O7 : DMSO = 1.0 : 2.5 : 4.0.

** Sulfation experiments were performed with enzymatically hydrolyzed starch.

Table 3. Influence of sulfation conditions on some characteristics of polysaccharide sulfo esters*

Polysaccharide	Sulfating system	DS_{SO_3H}	S, %	Yield, %		[η], dl g^{-1}	Activity, units mg^{-1}
				insoluble fraction	water-soluble sulfo ester		
Amylopectin	$Na_2S_2O_7$–DMSO	0.6	8.6	0	90	0.09	3
Dextran		0.6	8.6	0	76	0.14	4
Starch		0.8	10.5	0	53	0.05	9
MCC		0.7	9.6	0	96	0.02	<2
Amylopectin	SO_3–DMF	0.9	11.0	0	91	0.08	<2
Dextran		0.03	0.80	0	69	0.14	0
Starch		0.8	10.5	36	40	0.08	4
MCC		1.1	13.1	0	92	0.01	2

* Prior to sulfation, starch was pretreated with the enzyme. For the composition of the sulfating mixture $Na_2S_2O_7$–DMSO and the time and temperature of the treatment, see notes to Tables 1 and 2. Sulfation with the SO_3–DMF complex [1] was performed at 293 K in the course of 24 h.

of sulfo groups into a polysaccharide are observed in the range 800–820 (C–O–S) and about 1240 cm^{-1} (S=O). Figure 3 shows the IR spectra of the initial and modified dextran. The appearance of strong absorption bands at 800 and 1240 cm^{-1} is consistent with the analytical data and indicative of the formation of polysaccharide sulfo esters.

Thus, sulfo esters with a fairly high degree of substitution and uniform composition can be prepared by treatment with sodium pyrosulfate in dimethyl sulfoxide. The dependences of the degree of substitution and the extent of homogeneity on the PS reactivity, PS : $Na_2S_2O_7$: DMSO weight ratio, and the temperature and time of the treatment were evaluated.

The results of a comparative in vitro evaluation of the anticoagulant activity of sulfo polysaccharides prepared with the $Na_2S_2O_7$–DMSO and SO_3–DMF systems are presented in Table 3. It can be seen that

the biological activity depends not only on the degree of substitution and structure of the polysaccharide, but also on the sulfating agent used. Sulfo polysaccharides prepared with the $Na_2S_2O_7$–DMSO system are more active anticoagulants than those prepared with the SO_3–DMF system, which may be due to the better homogeneity of the former substances.

CONCLUSIONS

(1) A comparative study of the reactivity of dextran, cellulose, starch, and amylopectin in sulfation with sodium pyrosulfate in the presence of dimethyl sulfoxide was made. The degree of substitution of the polysaccharides is primarily determined by the mixture composition and the procedure for polymer pretreatment prior to the reaction.

(2) With increasing temperature (from 298 to 333 K) and time (from 0.5 to 6 h) of the sulfation, more homogeneous sulfo polysaccharides fully soluble in water are obtained.

(3) Aqueous solutions of polysaccharide sulfo esters (degree of substitution 0.6–1.1) have the intrinsic viscosity in the range 0.01–0.14 dl g^{-1} and exhibit anticoagulant activity.

REFERENCES

1. Batura, L.I., Vikhoreva, G.A., Noreika, R.M., et al., *Cellulose Chem. Tehnol.*, 1981, vol. 15, no. 5, pp. 487–504.
2. Chaidedgumjorh, A., Toyoda, H., Woo, E.R., et al., *Carbohydr. Res.*, 2002, vol. 337, pp. 925–933.
3. *Khimiya i tekhnologiya krakhmala* (Chemistry and Technology of Starch), Tregubova, N.N., Ed., Moscow: Pishch. Prom–st., 1975.
4. USSR Inventor's Certificate, no. 1 244 151.
5. *Analiticheskii kontrol' proizvodstva iskusstvennykh volokon: Spravochnik* (Analytical Monitoring of Production of Artificial Fibers: Handbook), Dibrova, A.K. and Matveev, V.S., Eds., Moscow: Khimiya, 1986.
6. Polyanskii, N.G., Gorbunov, G.V., and Polyanskaya, N.L., *Metody issledovaniya ionitov* (Methods for Studying Ion Exchangers), Moscow: Khimiya, 1976.
7. Petropavlovskii, G.A., *Gidrofil'nye chastichno zameshchennye efiry tsellyulozy i ikh modifikatsiya putem khimicheskogo sshivaniya* (Hydrophilic Partially Substituted Cellulose Ethers and Esters and Their Modification by Chemical Cross-Linking), Leningrad: Nauka, 1988.
8. *Laboratornye metody issledovaniya v klinike: Spravochnik* (Laboratory Investigation Methods in a Clinic: Handbook), Men'shikov, V.V., Ed., Moscow: Meditsina, 1987.
9. *Recent Advances in the Chemistry of Cellulose and Starch*, Honeyman, J., Ed., London: Heywood, 1955.
10. Grant, D., Long, W.F., Moffat, C.F., and Williamson, F.B., *Biochem. J.*, 1991, vol. 275, pp. 193–197.

ISSN 1070-4272, Russian Journal of Applied Chemistry, 2007, Vol. 80, No. 10, pp. 1750–1752. © Pleiades Publishing, Ltd., 2007.
Original Russian Text © V.O. Kudyshkin, R.Yu. Milusheva, A.M. Futoryanskaya, M.Yu. Yunusov, S.Sh. Rashidova, 2007, published in Zhurnal Prikladnoi Khimii, 2007, Vol. 80, No. 10, pp. 1721–1723.

MACROMOLECULAR CHEMISTRY AND POLYMERIC MATERIALS

Synthesis of Graft Copolymers of *N*-Vinylcaprolactam on Chitosan

V. O. Kudyshkin, R. Yu. Milusheva, A. M. Futoryanskaya, M. Yu. Yunusov, and S. Sh. Rashidova

Institute of Polymer Chemistry and Physics, Academy of Sciences of Uzbekistan Republic, Tashkent, Uzbekistan

Received August 22, 2006; in final form, May 2007

Abstract—Graft copolymers of *N*-vinylcaprolactam on chitosan were prepared by the radical mechanism with potassium persulfate as initiator. The process characteristics were examined, and sorption of water vapor with the copolymers prepared was studied.

DOI: 10.1134/S107042720710031X

Chitosan (CS) shows much promise thanks to such valuable properties as biocompatibility, biogedradability, nontoxicity, etc. The development of chitosan compounds with synthetic polymers and, in particular, synthesis of graft and block copolymers based on two polymers differing in molecular structure and nature is of interest. The graft copolymerization of a number of monomers, including vinyl acetate and *N*-vinylpyrrolidone, on CS was studied by Nud'ga et al. [1, 2]. Here we report for the first time on graft radical copolymerization of *N*-vinylcaprolactam (VC) on CS in the presence of potassium persulfate (PPS). The influence of the synthesis conditions on the copolymer composition and moisture absorption is examined.

EXPERIMENTAL

Experiments were performed with crab CS. The molecular weight M = 750000 (±5%) was determined from the intrinsic viscosity of the initial CS, measured at 25°C in 0.25 M CH_3COOH + 0.25 M CH_3COONa buffer [3]. The degree of deacetylation was 63%. *N*-Vinylcaprolactam was purified by vacuum distillation. For synthesis under homogeneous conditions, we found an appropriate solvent: a mixture of water, acetic acid, and isopropyl alcohol (IPA), with 20% IPA content. Syntheses were performed in a flask equipped with a stirrer in a nitrogen stream, or in sealed glass ampules. In the latter case, the reaction mixture was purged with nitrogen for 15 min, after which the ampules were sealed. The synthesis temperature was 60°C. To isolate the synthesized copolymers, the mixture was poured into a Petri dish, and the solvent was allowed to evaporate at room temperature. To separate the homopolymer and unchanged VC monomer, the product was extracted with benzene, after which it was vacuum-dried to constant weight. The completeness of extraction was checked by adding a sample of the benzene extract to diethyl ether, which is a precipitant for PVC. If the extract contained PVC, the mixture became turbid. The nitrogen content of the copolymer was determined by the Dumas method. The IR spectra of the VC–CS copolymers were recorded on a Specord 75-IR spectrometer in the range 400–3800 cm^{-1}. Samples were prepared as KBr pellets. Sorption of water vapor by the copolymers was studied with a high-vacuum sorption installation with mercury seals and a MacBain quartz spring balance in the humidity range 0–100% at 25±0.5°C. Prior to measurements, the polymers and water were degassed at a residual pressure of 0.013 Pa to constant weight. The solvent was fed in successively increasing portions. The total relative error of the equilibrium amount of water sorbed by 1 g of the polymer did not exceed 3%, and the relative fixed error in measuring the vapor pressure, 0.1%.

The results of analysis of the copolymers for nitrogen are listed in the table. As can be seen, the weight

Copolymer composition at various concentrations of reaction mixture components (initial CS weight 0.25 and 0.1 g, IPS concentration 20%, synthesis time 5 h, total nitrogen content of the initial CS 7.45%)

CS, %	VC	PPS $c \times 10^3$	CH_3COOH	Copolymer weight, g	Nitrogen content of copolymer, %	VC content of copolymer, wt %
	M					
0.5	1.30	3.5	0.15	0.91	8.18	28
0.5	0.43	3.5	0.15	0.30	7.85	15
0.5	0.43	1.8	0.15	0.28	7.88	16
0.5	0.43	1.3	0.15	0.35	7.94	19
1.28	0.65	2.0	0.19	0.14*	7.81	14
0.93	0.65	2.0	0.16	0.14*	7.80	13
0.69	0.43	2.0	0.11	0.13*	7.72	10
0.63	0.43	2.0	0.10	0.13*	7.75	11

* Initial CS weight 0.12 g.

and total nitrogen content of the reaction product increase relative to the initial CS, which is one of the evidences in favor of the formation of the VC–CS copolymer. The copolymer composition was evaluated from the nitrogen content. Separation of VC homopolymer from the copolymer inevitably involves a certain loss of the copolymer in the course of extraction and decanting. Therefore, data on the weight gain and nitrogen content are not fully consistent, and the weight gain can be used only for confirming the fact of copolymer formation on the qualitative level.

We examined the synthesized copolymers by IR spectroscopy (Fig. 1). The spectrum of CS has a broad strong band peaked at 3450–3460 cm^{-1}, associated with stretching vibrations of –OH and –NH groups involved in hydrogen bonding. The band observed at 2940 cm^{-1} characterizes stretching vibrations of CH and CH_2 groups. A broad amide I absorption band of chitin units (1620 cm^{-1}) obscures the amide II absorption band at 1550 cm^{-1}. There are also several absorption bands in the ranges 1300–1450 and 1000–1260 cm^{-1}, mainly associated with CH, CO, and COC bending vibrations.

The PVC spectrum contains at 3450 cm^{-1} a strong absorption band of OH groups involved in hydrogen bonding; this band apparently originates from sorbed moisture. The stretching vibration bands of CH and CH_2 groups are observed at 2945 and 2875 cm^{-1}, and the C=O stretching vibration band, at 1620 cm^{-1}. The CH_2 bending vibration band is observed at 1400–1500 cm^{-1}. The range 1250–1350 cm^{-1} corresponds to bending vibrations of C–C and R–C=O bonds. The C–N bond gives absorption at 1225 and 1180 cm^{-1}. The band at 1140 cm^{-1} belongs to C–C stretching vibrations; that at 955 cm^{-1}, to CH bending vibrations; and that at 830 cm^{-1}, to CH_2 bending vibrations.

In the spectrum of the copolymer, the bands of hydroxy and amino groups of CS are shifted to lower frequencies, and a very strong and broad band at 1620 cm^{-1} is due to stretching vibrations of carbonyl groups of VC. The CS absorption band at 1000–1260 cm^{-1} is preserved but overlaps with the bands of VC units.

We monitored the variation of the reaction mixture viscosity in the course of the synthesis. For this purpose, the synthesis was performed in a VPZh-2 viscometer with a capillary diameter of 1.75 mm

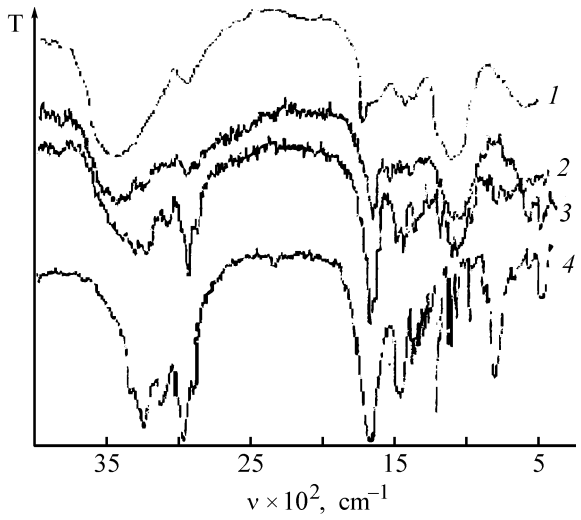

Fig. 1. IR spectra of (*1*) chitosan, (*2*, *3*) VC : chitosan graft copolymers, and (*4*) PVC. (T) Transmission and (ν) wavenumber.

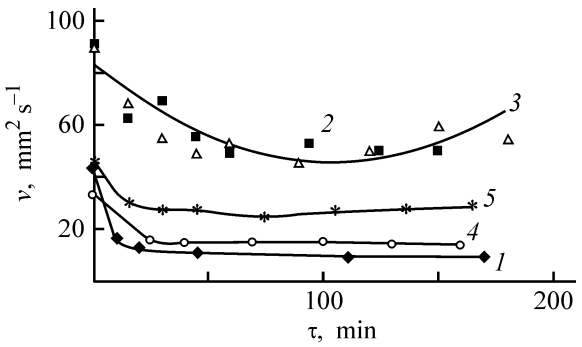

Fig. 2. Viscosity of the reaction mixture, ν, vs. synthesis time τ. PPS concentration *c*, mM: (*1*, *4*, *5*) 2 and (*2*, *3*) 1.8. CS concentration, M: (*1*) 0.53, (*2*) 1.23, (*3*) 0.93, (*4*) 0.69, and (*5*) 0.63. VC concentration, M: (*1*) 0, (*2–4*) 0.44, and (*5*) 1.0.

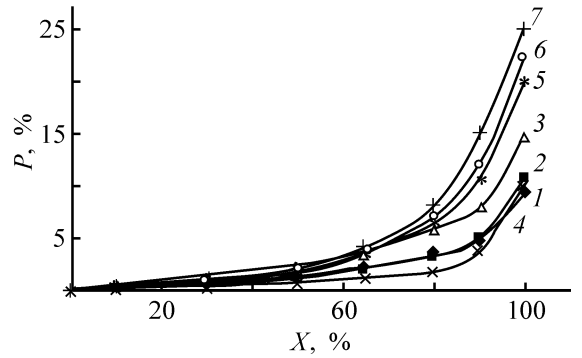

Fig. 3. Sorption *P* of water vapor by graft copolymers vs. relative humidity *X* of the medium. CS concentration 0.5%. PPS concentration, mM: (*1–4*) 3.5, (*5*) 1.8, (*6*) 1.3, and (*7*) 0.76. VC concentration, M: (*1*) 0.7, (*2*) 1.05, (*3*) 1.30, and (*4*) 0.43.

in a nitrogen atmosphere (Fig. 2). In all the cases, the viscosity of the reaction mixture decreased in the initial period after starting the synthesis. This fact suggests that the reaction of CS with PPS is accompanied by a decrease in the molecular weight of CS, presumably caused by cleavage of glycoside bonds in the macromolecules with PPS. Therefore, one of the possible mechanisms of copolymerization is growth of VC chains on active radicals generated by cleavage of glycoside bonds [2].

We studied the sorption of water vapor with the synthesized copolymers. Variation of the copolymer composition has virtually no effect on the sorption of water vapor. At the same time, the moisture absorption is strongly affected by the initiator concentration at which the copolymers were prepared. At high initiator concentrations, the resulting copolymers have a relatively dense 3*D* structure with low capacity for water absorption (Fig. 3). At decreased initiator concentrations, loosely cross-linked copolymers with higher water absorption are formed. With a further decrease in the initiator concentration, the copolymers become soluble.

It is known that PVC is a polymer with a lower critical temperature of solution. For VC–CS graft copolymers, this effect can be controlled by varying the copolymer composition and the size and distribution of comonomer blocks. This can be useful for various applications, e.g., in medicine, biology, and biotechnology.

Block and graft copolymers are also of interest from the viewpoint of the development of composite materials based on two polymers differing in molecular structure and nature. Of large interest is also the development of nanocomposite materials based on CS with synthetic polymers. Such materials can be used in food, cosmetic, and pharmacological industries, and also as carriers of drugs and biologically active substances. The presence in these composites of a block copolymer whose blocks exhibit affinity for each component of the material can favor formation and stabilization of the nanostructural organization.

CONCLUSIONS

(1) Graft radical copolymerization of vinylcaprolactam on chitosan in the presence of an initiator, potassium persulfate, was performed.

(2) Higher water absorption is observed with the copolymers synthesized at low initiator concentrations.

REFERENCES

1. Nud'ga, L.A., Petrova, V.A., Lebedeva, M.F., and Petropavlovskii, G.A., *Zh. Prikl. Khim.*, 1996, vol. 69, no. 7, pp. 1194–1199.
2. Nud'ga, L.A., Petrova, V.A., Litvinova, A.S., et al., *Zh. Prikl. Khim.*, 2002, vol. 75, no. 10, pp. 1712–1716.
3. Roberts, A.F., *Chitin Chemistry*, Haundmills: MacMillan, 1992, pp. 106–110.

ISSN 1070-4272, Russian Journal of Applied Chemistry, 2007, Vol. 80, No. 10, pp. 1753–1758. © Pleiades Publishing, Ltd., 2007.
Original Russian Text © E.N. Chebotok, V.Yu. Novikov, I.N. Konovalova, 2007, published in Zhurnal Prikladnoi Khimii, 2007, Vol. 80, No. 10, pp. 1724–1729.

MACROMOLECULAR CHEMISTRY AND POLYMERIC MATERIALS

Kinetics of Base Deacetylation of Chitin and Chitosan as Influenced by Their Crystallinity

E. N. Chebotok, V. Yu. Novikov, and I. N. Konovalova

Murmansk State Technical University, Murmansk, Russia
Knipovich Polar Research Institute of Marine Fisheries and Oceanography, Murmansk, Russia

Received December 25, 2006; in final form, April 2007

Abstract—Structural properties of the initial and reprecipitated chitin and chitosan samples in dry and wet states were studied.

DOI: 10.1134/S1070427207100321

Base hydrolysis of chitin (CTN) and chitosan (CSN) is one of the main procedures for deacetylation of these natural polysaccharides [1].

The kinetics of deacetylation of chitin and chitosan was analyzed in [2–4]. It was found that complete deacetylation of chitin and chitosan cannot be attained in a single-stage treatment of these polysaccharides with concentrated alkali. Several explanations were suggested for the decrease in the rate of chitin deacetylation in the alkaline solutions.

This paper is devoted to elucidation of the mechanism of chitin deacetylation on the basis of published data and our experimental results.

EXPERIMENTAL

Chitin and chitosan were prepared in laboratory by the known procedure [5] from shell-containing wastes from king crab processing.

Chitin and chitosan were deacetylated in a 50% NaOH solution at 100°C. Samples with various degrees of deacetylation were prepared from chitin and chitosan by repeated treatments with 50% NaOH solution at 100°C.

Prior to reprecipitation from NaOH, chitin was dissolved in alkali by the procedure described elsewhere [6]. A suspension of chitin (3 g) in a 40% aqueous solution of sodium hydroxide (75 g) was stored for 3 h at 25°C under reduced pressure. The resulting alkaline chitin was mixed with crushed ice (225 g) at approximately 0°C. The resulting chitin solution with a 10% alkali concentration was filtered through a Schott filter in a vacuum. Then, chitin was precipitated by gradual neutralization of this solution with HCl to pH 6.5. The precipitate was separated by centrifugation, and a part of the wet reprecipitated chitin was dried at 60°C.

Reprecipitation of chitin from acid solutions was performed as follows. Chitin (10 g) was mixed with cold concentrated HCl (200 ml), and the resulting mixture was stored for a day with intermittent stirring. Then, the chitin solution was filtered through a Schott filter in a vacuum. The resulting solution was diluted with cold distilled water (3 l) under stirring. The resulting suspension was kept until the precipitation was complete, and then the chitin precipitate was separated by centrifugatoin. The precipitate was washed with distilled water to pH 6.5, and a part of the resulting reprecipitated wet chitin was dried at 60°C.

Chitosan was precipitated from an acid solution. For this purpose, chitosan (2 g) was mixed with a 0.1 M HCl solution (200 ml), and the resulting mixture was kept for 18 h until the chitosan completely dissolved. The resulting solution was filtered through a Schott filter under reduced pressure and then was neutralized with stirring to pH 7.5 with a 0.5 M NaOH solution. The chitosan precipitate was separated by centrifugation and washed with distilled water. A part of the wet chitosan was dried at 60°C.

The degree of chitosan deacetylation was determined by potentiometric titration of the chitosan so-

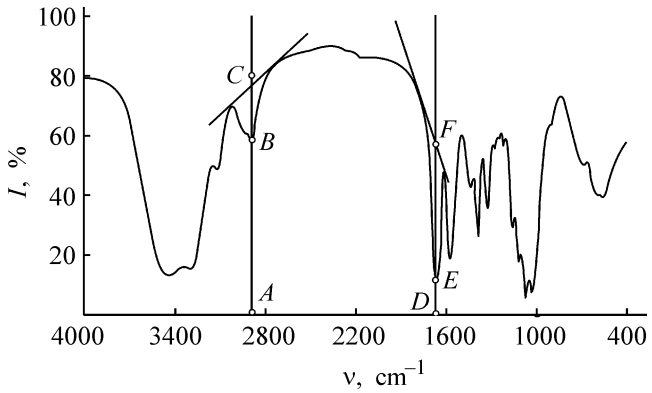

Fig. 1. IR absorption spectrum of a chitin sample. (*I*) Transmission and (ν) wavenumber. *Lines and points* illustrate the graphical processing of the data for DD calculation.

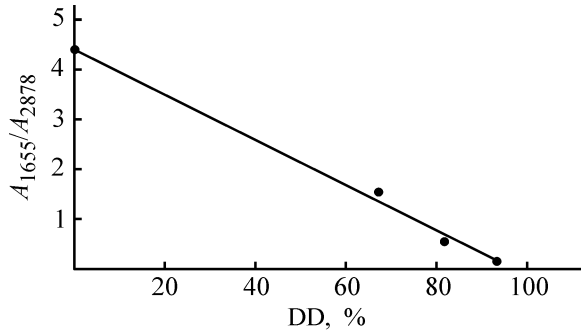

Fig. 2. Absorption of chitin in the IR spectra vs. the degree of deacetylation DD. (A_{1655}/A_{2878}) Ratio of the optical densities of the bands at 1655 and 2878 cm^{-1}.

lution with a 0.1 M HCl solution. The solution pH was measured on an Anion 4151 pH-meter (Infraspak-Analit Research and Production Enterprise, Russia). The absolute error in determining the degree of deacetylation was ±0.5%. The chitosan sample (0.2 g) weighed with an accuracy of ±0.0001g was dissolved in a 0.1 M HCl solution (20 ml), and the resulting solution was titrated with a 0.1 M NaOH solution with the resulting potentiometric titration curve plotted, pH = $f(V_{NaOH})$. Then, the points of the maxima of the first derivative, which correspond to the equivalence points in titration equivalence of excess HCl (V_1) and amino groups (V_2), were determined.

The degree of deacetylation DD (%) was calculated using the following expression:

$$DD = \frac{203.2}{42.0 + \dfrac{1000m}{c_{NaOH}(V_2 - V_1)}} \times 100,$$

where m is the content of chitosan in the sample, g; c_{NaOH}, concentration of the NaOH solution, M; $V_2 - V_1$, volume of the NaOH solution consumed in titration of the amino groups, cm^3; 203.2, molecular weight of the acetylated monomeric unit of the polysaccharide; 42.0, difference between the molecular weights of the acetylated and deacetylated monomeric units; 1000, factor of conversion of milliliters to liters; and 100, factor of conversion of DD to percents.

The degree of deacetylation of chitin and chitosan was also determined by IR spectroscopy [7, 8].

The IR spectra were recorded on an IR-420 Shimadzu spectrophotometer (Japan) in the 4000–400 cm^{-1} range using KBr pellets. The pellets were prepared using samples ground in a TI-100 mill (C.M.T. Co, Japan) for 10 min and dried to constant weight at 100°C. KBr was recrystallized from an aqueous solution and calcined at 600°C. The purity of KBr was checked by IR spectroscopy. The weight ratio of the sample and KBr in the pellet was 1 : 49. To prepare a pellet with diameter and thickness of 13 and 0.42 mm, respectively, the resulting mixture (120 mg) was compacted at a 650-kg cm^{-2} pressure for 1 min at room temperature on an SSP-1 hand press (Shimadzu, Japan).

The procedure for DD determination was improved for its use in a wide DD range. Using the samples with DD varying from 0 to 98%, we found that the IR absorption band at 2878 cm^{-1} is the most appropriate for measurements. This absorption band corresponds to the stretching vibrations of the C–H bond [8], and its optical density obeys Beer's law in the entire DD range studied. The bending vibrations of the amino group (amide I) are observed at 1655 cm^{-1}. The graphical processing of the IR spectrum is illustrated in Fig. 1.

The optical density was calculated as follows:

$$A_{2878} = \log(AC/AB),$$

$$A_{1655} = \log(DF/DE).$$

The degree of deacetylation was calculated from the calibration dependence obtained for samples with the known DD (Fig. 2). The resulting regression equation can be represented as

$$A_{1655}/A_{2878} = -0.04529DD + 4.4214,\ r^2 = 0.9946,$$

where r is the linear-regression coefficient.

The degree of crystallinity of the samples was determined by the known procedures [10, 11].

The structural properties of chitin and chitosan samples were studied at the Tananaev Institute of Chemistry and Technology of Rare Elements and Mineral Raw Materials (Kola Scientific Center, Russian Academy of Sciences) on a DRON-2 diffractom-

eter (Burevestnik Research and Production Association; Cu_{K_α}, Ni filter, 24 kV, 10 mA) in the range $2\theta = 6°–36°$. The X-ray diffraction (XRD) patterns were recorded from the initial wet samples and samples suspended in mineral oil deposited on sapphire supports. The reflections were identified using JCPDS tables [12] and published data [13].

The XRD patterns were mathematically processed using the Graph Digitizer Ver. 1.9 (Nick's Production), PeakFit Ver. 4.12 (SeaSolve Software Inc.), and Microsoft Excel 2002 program packages.

Kurita et al. [2] attributed the features of deacetylation to the crystal structure of natural chitin.

It is known that chitin is formed in nature in various crystal modifications. In most cases, it has a highly ordered structure, named α-chitin, which is typical of the majority of crustacea and insects [14].

Other modifications, such as β- and γ-chitin, are also known [15]; they differ in the mutual orientation of adjacent chitin macromolecules. Chitosan is also characterized by high crystallinity, but its structure differs from that of α-chitin [11].

As shown in [1, 4, 11], strong intermolecular hydrogen bonds should affect the rate of chemical reactions of the functional groups of macromolecules involved in formation of the crystal structure.

The degree of crystallinity, χ_{cr}, is frequently determined from the ratio of the integral intensity of the peak of the crystalline regions in the diffraction pattern to the total integral peak [10, 11].

To calculate the intensity of the peak originating from the crystalline regions in the samples, the total area under the diffraction curve S_{tot} and the area of the amorphous component S_{am} were determined graphically.

The degree of crystallinity, χ_{cr}, was calculated by the following expression:

$$\chi_{cr} = \frac{S_{tot} - S_{am}}{S_{tot}} \times 100,$$

where S_{tot} is the total area under the diffraction curve in the angle range $2\theta = 6°–36°$, and S_{am}, the area of the amorphous component in the same range.

The degrees of crystallinity evaluated by the above procedure are listed in the table.

It should be noted that the XRD patterns exhibit a series of peaks typical of the crystal structure of α-chitin, described in [12, 13].

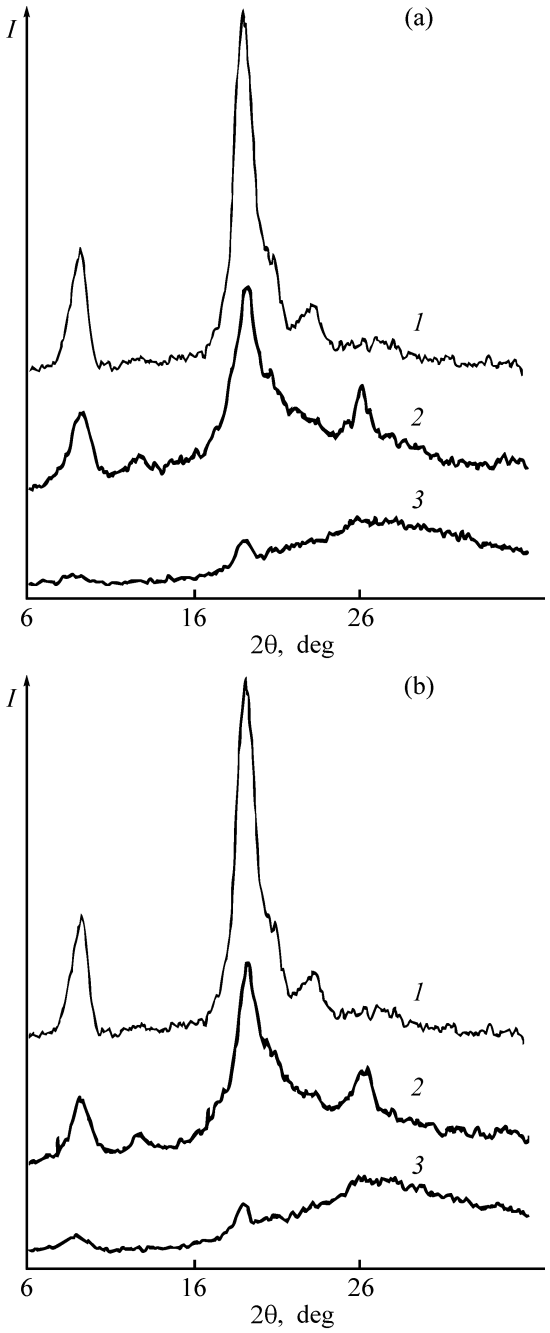

Fig. 3. XRD patterns of (*1*) initial chitin and (*2*) dry and (*3*) wet chitin reprecipitated from solutions of (a) NaOH and (b) HCl. (*I*) Peak intensity and (2θ) diffraction angle; the same for Fig. 4.

The results listed in the table show that reprecipitation virtually completely restores the crystal structures of chitin and chitosan. The diffraction peaks of the restored structures of the chitin samples recrystallized from solutions of NaOH (Fig. 3a) and HCl (Fig. 3b) are broader as compared to the initial chitin, but their positions in the XRD patterns are similar.

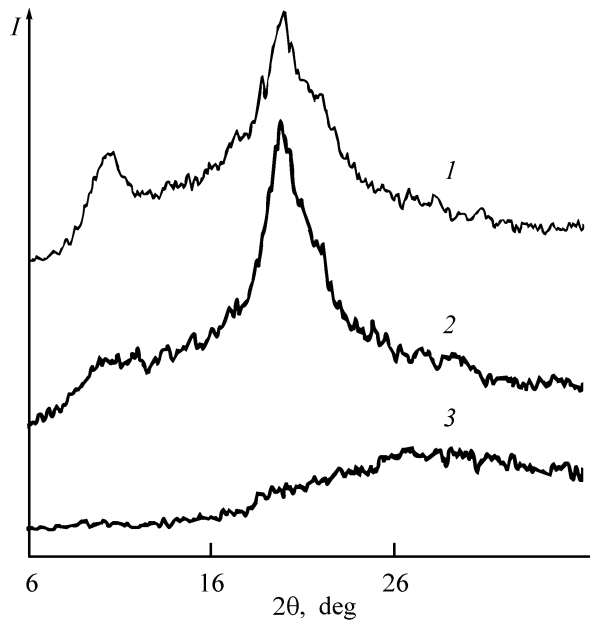

Fig. 4. XRD patterns of (*1*) initial chitosan and (*2*) dry and (*3*) wet chitosan reprecipitated from HCl solutions.

To compare the crystal structures of the chitin samples reprecipitated from acid and alkali, their XRD patterns were normalized as in [16]. It was found that dry chitin samples reprecipitated from NaOH and HCl exhibit similar XRD patterns, which suggests similarity of their structures.

Our results agree with experimental data reported in [2, 16].

It is assumed [2] that, in the course of recrystallization, the α-chitin structure is restored only partly, simultaneously with the formation of other crystal forms and amorphization.

Degree of crystallinity, χ_{cr}, of chitin and chitosan samples

Sample	χ_{cr}, %
Initial dry chitin	61.1
Chitin reprecipitated from NaOH, dry:	
from NaOH, dry	55.5
from HCl, dry	60.7
from NaOH, wet	8.8
from HCl, wet	8.5
Initial dry chitosan, DD 82%	35.8
Chitosan reprecipitated:	
from HCl, DD 82%, dry	37.5
from HCl, DD 82%, wet	3.8

As for chitosan samples, their crystal structure was also restored during reprecipitation (Fig. 4), with certain differences from the initial chitin structure. Two main peaks in the XRD pattern of chitosan are shifted as compared to α-chitin. In the XRD patterns of chitin with DD less than 71%, two peaks at 2θ 9.2° and 19.1° are observed. In the case of chitosan with DD 95%, these two peaks are shifted to 2θ 11.2° and 20.1°–20.4°, respectively. These experimental data do not contradict those reported in [2, 11, 16–18].

Partial restoration of the α-chitin structure after recrystallization and drying of the samples of α- and β-chitin was also confirmed by NMR, IR, and Raman spectroscopy [19].

On the whole, the above data suggest that the crystal structure of chitin and chitosan is restored after recrystallization of the initial sample from alkali and acid and their drying (see table).

The XRD patters of the wet chitin and chitosan samples show that they are virtually amorphous (Figs. 3 and 4, curves *3*).

It should be noted that the weak peaks observed in the XRD patterns of the wet recrystallized chitin (Figs. 3a, 3b) are absent in the XRD patterns of the wet recrystallized chitosan (Fig. 4).

It has been suggested previously [2, 20] that deacetylation of crystalline chitin proceeds more slowly than that of the amorphous compound.

Ottoy et al. [21] studied the DD distribution of various fractions of partly deacetylated chitosan exhibiting different solubilities in acid. Their experimental results suggest that deacetylation proceeds by the diffusion mechanism in which the deacetylation rate is controlled by the rate of alkali diffusion into the solid particles, rather than by the ratio of the crystalline and amorphous regions in the polysaccharide structure.

Chang et al. [22] showed that the deacetylation rate depends on the alkali concentration: as the NaOH concentration increases, the reaction rate constant becomes higher. Chang et al. suggested that the rate of heterogeneous deacetylation can be controlled by both the chemical reaction and the diffusion of the reactant and reaction products in the polysaccharide particle.

Thus, our experimental results and published data suggest that the kinetics of deacetylation of dry reprecipitated chitin and chitosan should be similar to that of the initial samples, whereas the rate of deacetylation of the wet recrystallized samples should be higher. However, our experimental kinetic de-

pendences of deacetylation do not fit in the model analyzing the effect of the degree of crystallinity of chitin on the degree of its deacetylation.

It is known that, as DD increases, the crystallinity of chitin decreases and, when DD reaches 90–95%, a new crystal structure typical of chitosan starts to form [2, 17]. In this case, the rate and degree of chitin deacetylation should increase with the initial DD owing to the rise in the content of amorphous regions. Previously, Novikov et al. have shown [23] that the rate of deacetylation of chitin and chitosan are independent of the initial degree of deacetylation of the corresponding polysaccharide. The shapes of the kinetic curves for chitin and chitosan with various initial DD (up to 95%) were similar [23, 24].

Yaghobi and Mirzadeh [25] explained the increase in the degree of deacetylation in the course of repeated alkaline treatments as follows. They suggested that the initial structure of chitin hinders penetration of NaOH molecules to all the polysaccharide molecules. When the alkaline treatment is performed continuously, the rate of deacetylation decreases at DD 75%. The authors assume that water-washing of chitin or partly deacetylated chitin after the first stage of deacetylation is of particular importance. Washing changes the chitin morphology, causing its swelling, and makes chitin macromolecules more accessible to NaOH molecules. At the same time, the authors attribute the decrease in the rate of continuous deacetylation to a decrease in the concentration of NaOH molecules from 50 to 43%, i.e., to a concentration at which, as they believe, deacetylation is terminated.

However, this explanation contradicts the experimental data. Novikov et al. have shown [26] that the NaOH concentration decreases insignificantly (from 50 to 49.4%). If the decrease in the rate of deacetylation were due to a decrease in the alkali concentration below some limit, then its increase would accelerate deacetylation. However, the rate of deacetylation does not increase in the presence of excess NaOH [26]. Probably, the deacetylation rate is determined by formation of solvated structures owing to interaction of polysaccharide macromolecules and low-molecular-weight electrolyte with the solvent.

For example, Percot et al. [27] suggested formation of NaOH hydrates, which are less active in chitin deacetylation than nonhydrated alkali molecules.

Previously, we suggested in [23, 24, 28] that OH^- complexes with chitin are formed and showed that deacetylation can be described by two parallel reactions of pseudo-first order: (1) deacetylation and (2) formation of chitin complex with hydroxide ions.

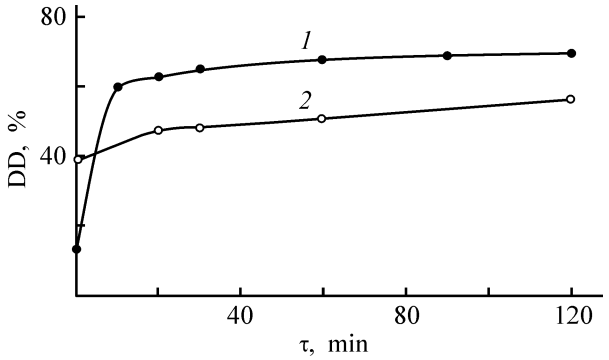

Fig. 5. Kinetic curves of deacetylation of (*1*) dry chitin and (*2*) wet chitin reprecipitated from 50% NaOH solution at 100°C. (DD) Degree of deacetylation and (τ) time.

Figure 5 shows the kinetic dependences of deacetylation of dry chitin (curve *1*) and wet chitin reprecipitated from NaOH solution (curve *2*). As can be seen, the rate of deacetylation of wet reprecipitated chitin (χ_{cr} 4.0%) is lower than that of the dry sample (χ_{cr} 59.0%). This fact suggests solvation (hydration) of polysaccharide molecules in NaOH solution. The water dipoles are located in a certain order near the acetamide and glycoside bonds of the chitin macromolecules. In accordance with the mechanism of deacetylation in the alkaline medium [29], hydrolysis of the acetamide bonds starts with a nucleophilic attack of the carbonyl carbon atom of the acetamide group by OH^- ions. The hydrate shell probably hinders this nucleophilic attack, causing a decrease in the deacetylation rate.

The above results suggest that the influence exerted by the degree of crystallinity of the samples studied on the deacetylation rate is significantly weaker than that exerted by the hydrate shell probably formed around the polysaccharide macromolecules, which hinders nucleophilic attack of the hydroxide ions and decreases the deacetylation rate.

CONCLUSIONS

(1) The IR spectrophotometric procedure for evaluating the degree of deacetylation of chitin and chitosan samples was improved.

(2) The possibility of formation of a hydrate shell around the macromolecules and its effect on the deacetylation rate were suggested.

(3) The influence exerted by the degree of crystallinity of the samples on the deacetylation rate is

weaker thanthat exerted by the hydrate shell formed around the polysaccharide macromolecules. This shell hinders nucleophilic attack of the hydroxide ions and decreases the deacetylation rate.

ACKNOWLEDGMENTS

The authors are grateful to staff members of the Tananaev Institute of Chemistry and Technology of Rare Elements and Mineral Raw Materials (Kola Scientific Center, Russian Academy of Sciences) L.D. Rogachev for X-ray diffraction analysis and to O.A. Zalkind for assistance in interpretation of the IR data.

REFERENCES

1. Kurita, K., *Prog. Polym. Sci.*, 2001, vol. 26, no. 9, pp. 1921–1971.
2. Kurita, K., Sannan, T., and Iwakura, Y., *Macromol. Chem.*, 1977, vol. 178, no. 12, pp. 3197–3202.
3. Mima, S., Miya, M., Iwamoto, R., and Yoshikawa, S., *J. Appl. Polym. Sci.*, 1983, vol. 28, no. 6, pp. 1909–1917.
4. Tsaih, M.L. and Chen, R.H., *J. Appl. Polym. Sci.*, 2003, vol. 88, no. 13, pp. 2917–2923.
5. No, H.K. and Meyers, S.P., *J. Aquatic Food Prod. Technol.*, 1955, vol. 4, no. 2, pp. 27–52.
6. Sannan, T., Kurita, K., and Iwakura, Y., *Macromol. Chem. Short Commun.*, 1975, vol. 176, no. 4, pp. 1191–1195.
7. Domszy, J.G. and Roberts, G.A.F., *Macromol. Chem.*, 1985, vol. 186, no. 8, pp. 1671–1677.
8. Wang, T., Turhan, M., and Gunasekaran, S., *Polym. Int.*, 2004, vol. 53, pp. 911–918.
9. Kazitsyna, L.A. and Kupletskaya, N.B., *Primenenie IK-, YaMR- i mass-spektroskopii v organicheskoi khimii* (Application of IR, NMR, and Mass Spectroscopy in Organic Chemistry), Moscow: Mosk. Gos. Univ., 1979.
10. Hein, S., Ng, C.-H., and Stevens, W.F., *Advances in Chitin Science*, Boucher, I., Jamieson, K., and Retnakaran, A., Eds., Montreal, 2004, vol. 7, pp. 13–18.
11. Gorbacheva, I.N., Ovchinnikov, Yu.K., Gal'braikh, L.S., et al., *Vysokomol. Soedin., Ser. A*, 1988, vol. 30, no. 12, pp. 2512–2515.
12. JCPDS—International Centre for Diffraction Data, PCPDFWIN, ver. 2.00, 1988.
13. Paralikar, K.M. and Balasubramanya, R.H., *J. Polym. Sci., Part C: Polym. Lett.*, 1984, vol. 22, no. 10, pp. 543–546.
14. Carlstrom, D., *J. Biophys. Biochem. Cytol.*, 1957, vol. 3, no. 5, pp. 669–683.
15. Cho, Y.-W., Jang, J., Park, C.R., and Ko, S.-W., *Biomacromolecules*, 2000, vol. 1, no. 4, pp. 609–614.
16. Rege, P.R. and Block, L.H., *Carbohydr. Res.*, 1999, vol. 321, nos. 3–4, pp. 235–245.
17. Focher, B. Naggi, A., Torri, G., et al., *Carbohydr. Polym.*, 1992, vol. 18, no. 1, pp. 43–49.
18. Nud'ga, L.A., Plisko, E.A., and Danilov, S.N., *Zh. Obshch. Khim.*, 1971, vol. 41, no. 11, pp. 2555–2559.
19. Focher, B., Naggi, A., Torri, G., et al., *Carbohydr. Polym.*, 1992, vol. 17, no. 2, pp. 97–102.
20. Gamzazadeh, A.I., *Khitin i khitozan: Poluchenie, svoistva i primenenie* (Chitin and Chitosan: Preparation, Properties, and Use), Skryabin, K.S., Vikhoreva, G.A., and Varlamov, V.P., Eds., Moscow: Nauka, 2002, pp. 112–118.
21. Ottoy, M.H., Varum, K.M., and Smidsrod, O., *Carbohydr. Polym.*, 1996, vol. 29, no. 1, pp. 17–24.
22. Chang, K.L.B., Tsai, G., Lee, J., and Fu, W.-R., *Carbohydr. Res.*, 1997, vol. 303, pp. 327–332.
23. Novikov, V.Yu., Orlova, T.A., and Voronina, I.E., *Izv. Vyshch. Uchebn. Zaved., Pishch. Tekhnol.*, 1990, no. 5, pp. 64–67.
24. Novikov, V.Yu., Extended Abstracts, *VII Mezhdunarodnaya konferentsiya "Sovremennye perspektivy v issledovanii khitin i khitozana"* (VII Int. Conf. "Modern Prospects in Study of Chitin and Chitosan"), St. Petersburg (Repino), September 15–18, 2003, Moscow: VNIRO, 2003, pp. 38–42.
25. Yaghobi, N. and Mirzadeh, H., *Iran. Polym. J.*, 2004, vol. 13, no. 2, pp. 131–136.
26. Novikov, V.Yu., Orlova, T.A., and Volkova, N.I., *Rybn. Khoz.*, 1988, no. 12, pp. 76–78.
27. Percot, A., Chaussard, G., Sorlier, P., et al., *Advances in Chitin Science*, Boucher, I., Jamieson, K., and Retnakaran, A., Eds., Montreal, 2004, vol. 7, pp. 1–6.
28. Novikov, V.Yu., Chebotok, E.N., Gizatulina, G.A., and Konovalova, I.N., *Vest. Mosk. Gos. Tekh. Univ.*, 2005, vol. 8, no. 1, pp. 179–182.
29. Shabarov, Yu.S., *Organicheskaya khimiya: Uchebnik dlya vuzov* (Organic Chemistry: Textbook for Higher School), part 1: Netsiklicheskie soedineniya (Acyclic Compounds), Moscow: Khimiya, 1994.

ISSN 1070-4272, Russian Journal of Applied Chemistry, 2007, Vol. 80, No. 10, pp. 1759–1763. © Pleiades Publishing, Ltd., 2007.
Original Russian Text © I.K. Ivanova, O.N. Chalaya, V.A. Kashirtsev, 2007, published in Zhurnal Prikladnoi Khimii, 2007, Vol. 80, No. 10, pp. 1730–1734.

CHEMISTRY OF FOSSIL FUEL

Normal Alkylbenzenes of the Composition $C_{12}H_{18}$–$C_{23}H_{40}$ in Oils from the Nepa–Botuoba Oil-and-Gas-Bearing Region and Possible Mechanism of *n*-Pentadecylbenzene Formation

I. K. Ivanova, O. N. Chalaya, and V. A. Kashirtsev

Institute of Problems of Oil and Gas, Siberian Division, Russian Academy of Sciences, Yakutsk, Sakha, Russia
Trofimuk Institute of Oil-and-Gas Geology and Geophysics, Novosibirsk, Russia

Received May 31, 2007

Abstract—Specific features of the distribution of high-molecular-weight normal alkylbenzenes in crude oils from the Nepa–Botuoba anteclise were studied by chromatography–mass spectrometry. The possible biochemical precursors and mechanisms of formation of normal alkylbenzenes with an odd number of carbon atoms in the molecule were determined.

DOI: 10.1134/S1070427207100333

Among precambrian crude oils of the Siberian platform, two independent families are distinguished. The first family is localized within the Baikit anteclise, and the second family fills traps of the Katanga saddle and Nepa–Botuoba anteclise. The main geochemical criteria for this classification are the results of studying the distribution of biomarker molecules, mainly of tricyclic cheilanthanes, tetracyclic steranes, and pentacyclic hopanes.

The GC–MS analysis[1] of aromatic hydrocarbons (ACs) in crude oil samples from the Nepa–Botuoba oil-and-gas-bearing region revealed the presence of a homologous series of alkylbenzenes with linear hydrocarbon substituents. Such substances have not been found previously in oils from this region.

The composition and distribution of alkylbenzenes C_{11}–C_{30} in oils, organic matter (OM) of rocks, and coals were examined in detail in numerous studies [1–12].

It was found that the content of high-boiling alkylbenzenes varies from 20 to 45 wt %. These hydrocarbons form several homologous series of different structures and can contain two or three methyl groups and one long linear or branched chain with up to 20 or even more carbon atoms. Among such compounds are *n*-alkylbenzenes, 1,2-, 1,3-, and 1,4-methylalkylbenzenes, 1,3- and 1,4-ethylalkylbenzenes, and C_{20} and C_{27} hydrocarbons with alkyl chains of the isoprenoid structure. The concentration of alkylbenzenes decreases with an increase in the molecular weight, and the concentration of *p*-substituted methylalkylbenzenes is considerably lower than that of the other disubstituted isomers.

Aromatic hydrocarbons are not synthesized by living organisms, but are formed from organic substances present in them by biochemical and thermochemical transformations. The aromatic structures found in nature are associated with lignins, pigments, and essential oils [1, 13, 14].

Unsaturated fatty acids of lipid components of the living matter are believed to be a biochemical source of high-molecular-weight alkylbenzenes with a linear chain. Presumably, the homologous series of *n*-alkylbenzenes is formed by dehydrative cyclization of these acids on natural catalysts, followed by degradation, addition of free radicals, and decarboxylation. The process follows the scheme acid–lactone–ketone–hydrocarbons [1, 6, 7]. The formation of alkylbenzenes and extension of the alkyl substituent can

[1] Performed at the Laboratory of Caustobiolith Geochemistry, Institute of Problems of Oil and Gas, Siberian Division, Russian Academy of Sciences.

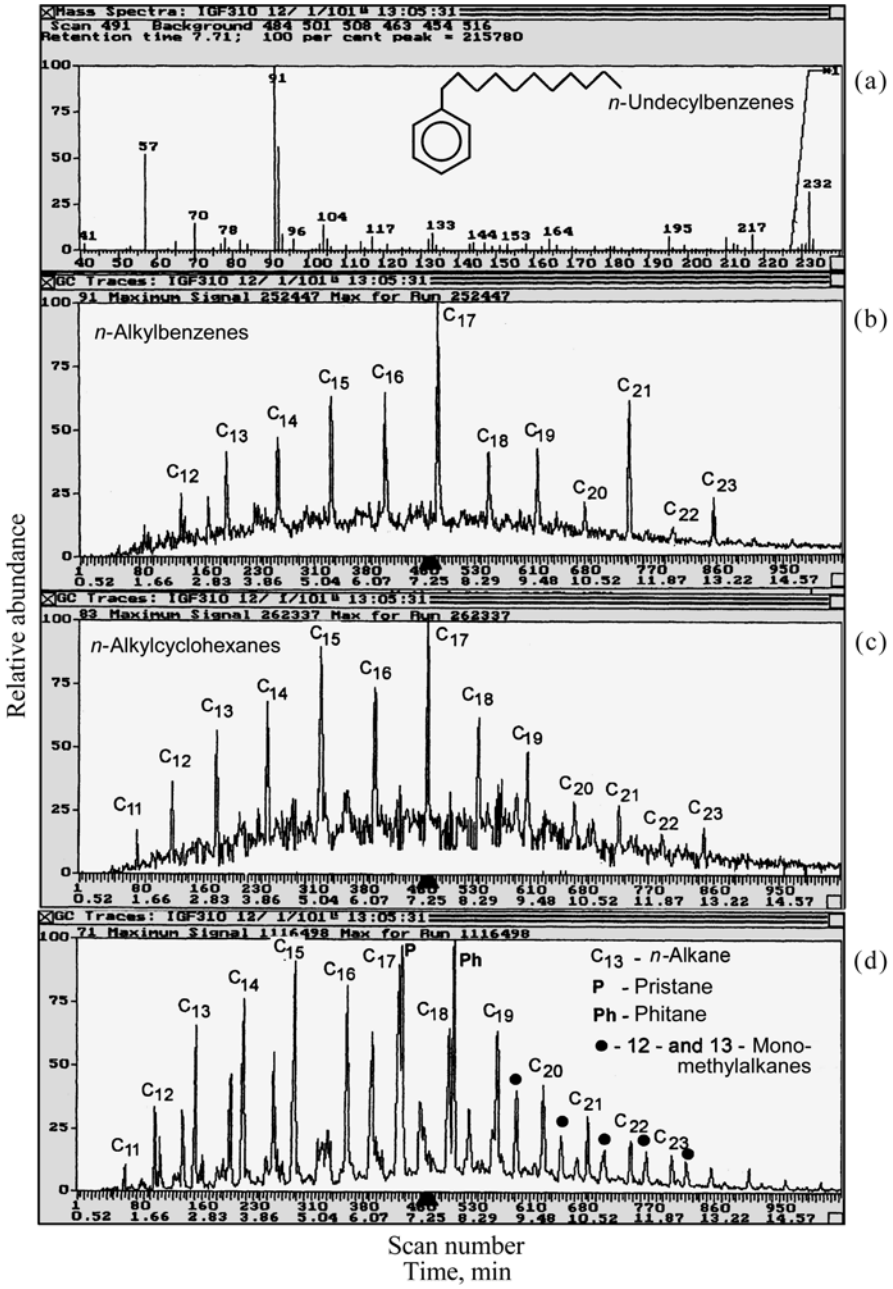

Fig. 1. (a) Mass spectrum of *n*-undecylbenzene and mass fragmentograms, recorded at *m*/*z* (b) 91 (*n*-alkylbenzenes), (c) 83 (*n*-alkylcyclohexanes), and (d) 71 (*n*-alkanes), of oils from the Talakan deposit.

occur under the conditions of catagenetic transformations of OM and oils.

Thus, analysis of the available data gives a fairly definite pattern of the composition and structure of monoaromatic petroleum hydrocarbons, their biological precursors, pathways of their transformations into petroleum hydrocarbons, and also transformations in deposits. Nevertheless, some problems related to their formation remain poorly understood.

In this paper, based on published and newly obtained data, we present our views on the formation of monoaromatic hydrocarbons (in particular, alkylbenzenes with linear alkyl chains) in the Earth's interior. The choice of *n*-alkylbenzenes was governed by the fact that they have no analogs in the living nature and hence their formation should reflect, to a certain extent, the pathways of transformation of bioorganic matter in the Earth's interior.

EXPERIMENTAL

Studies were performed with Vend-Cambrian crude oils from the Middle Botuoba, Irelyakh, and Talakan oil fields.

Crude oils from the Nepa–Botuoba oil-and-gas-bearing region are characterized by a broad range of physicochemical parameters: density 0.821–0.907 g cm^{-3}; paraffin content from trace amounts to 4.4%; sulfur content 0.1–2.0; naphtha yield 7–38%. The oils mainly differ in the methane composition (41–73% methane–naphthene hydrocarbons). Except Talakan oil, other oils have increased content of asphalt and resin substances: resin up to 43% and asphaltenes up to 11%.

Saturated and aromatic hydrocarbons of crude oils were analyzed by gas chromatorgaphy–mass spectrometry with a Q-mass-910-Autosystem quadrupole system (Perkin–Elmer). The chromatograph was equipped with a quartz capillary column (diameter 0.25 mm, length 90 m) coated with PE-5. The carrier gas was helium, flow rate 1 ml min^{-1}. The vaporizer temperature was 320°C. The column was heated from 40 to 300°C at a rate of 6 deg min^{-1}. The ionizing electron energy was 70 eV. Scanning of chromatograms at characteristic fragment peaks, *m*/*z* 71, 83, and 91, allowed identification of the homologous series of *n*-alkanes, *n*-alkylcyclohexanes, and *n*-alkylbenzenes in the crude oil samples.

The compounds were identified by comparing the individual mass spectra with those included in the library of the system and with published data [15].

The mass fragmentograms recorded at *m*/*z* 71, 83, and 91 are identical for all the three oil samples. For the subsequent discussion, we chose as an example the crude oil from the Talakan oil field.

As can seen be from Fig. 1 and the table, *n*-alkylbenzenes are mainly represented by the homologous series from $C_{12}H_{18}$ to $C_{23}H_{40}$, i.e., the linear alkyl substituent contains from 6 to 17 C atoms. Low-molecular-weight homologs prevail: $\Sigma(C_{12}–C_{16})$ 44.5, $\Sigma(C_{17}–C_{20})$ 37.9%. The relative content of high-molecular-weight homologs is 17.6%. The molecular-weight distribution of *n*-alkylbenzenes is bimodal with peaks at C_{17} and C_{21}. Among C_{17}–C_{23} *n*-alkylbenzenes, homologs with the odd number of C atoms prevail ($K_{odd/even}$ 1.90).

n-Alkanes are represented by the homologous series from C_{11} to C_{27}. The peaks of the *n*-alkane distribution are at C_{15} and C_{17}; the odd/even ratio is 1.11. The distribution of individual *n*-alkanes in the range C_{12}–C_{17} is similar to that of *n*-alkylbenzenes, but for higher-molecular-weight homologs the pattern is essentially different. Along with *n*-alkanes, we identified 12- and 13-monomethylalkanes, which are a "calling card" of a sort of East-Siberian crude oils.

Composition of *n*-alkylbenzenes, alkylcyclohexanes, and *n*-alkanes in crude oil from the Talakan deposit

Hydrocarbon	Relative content, %		
	n-alkylbenzenes	alkylcyclohexanes	*n*-alkanes
C_{11}		3.24	1.58
C_{12}	4.58	5.95	5.18
C_{13}	8.50	9.73	9.91
C_{14}	8.50	10.81	11.26
C_{15}	11.76	14.59	13.51
C_{16}	11.11	11.89	11.71
C_{17}	20.26	16.76	13.06
C_{18}	6.54	9.73	9.01
C_{19}	7.84	7.03	8.11
C_{20}	3.27	3.24	5.41
C_{21}	12.42	3.24	3.60
C_{22}	1.31	1.62	2.25
C_{23}	3.92	2.16	1.80
C_{24}	–	–	1.35
C_{25}	–	–	1.13
C_{26}	–	–	0.68
C_{27}	–	–	0.45
ΣC_{11}–C_{16}	44.45	56.21	53.15
ΣC_{17}–C_{20}	37.90	36.76	35.59
ΣC_{21}–C_{25}	17.65	7.02	10.13
ΣC_{26}–C_{27}	0.00	0.00	1.13
Maximum	C_{15}, C_{21}	C_{15}, C_{17}	C_{15}, C_{17}
$K_{odd/even}$	1.90	1.27	1.11

n-Alkylcyclohexanes are represented by the homologous series C_{11}–C_{23}. Low-molecular homologs prevail. The relative content (%) is as follows: C_{11}–C_{13} 56.2, C_{17}–C_{20} 36.8, and C_{21}–C_{23} 7.0. The peaks of the *n*-alkylcyclohexane distribution are observed at C_{15} and C_{17}. The odd/even ratio is 1.27. The distribution patterns of alkylcyclohexanes and *n*-alkanes are similar.

The differences in the ranges of the homologous series of *n*-alkylbenzenes and *n*-alkylcyclohexanes, compared to *n*-alkanes, can be attributed to specific features of oil catagenesis, which led to degradation of longer alkyl substituents, and the prevalence of low-molecular-weight homologs in the considered groups of petroleum compounds demonstrates the plankton–algal character of the initial organic matter.

As noted above, only the distribution of *n*-alkylbenzenes has a peak in the high-molecular-weight

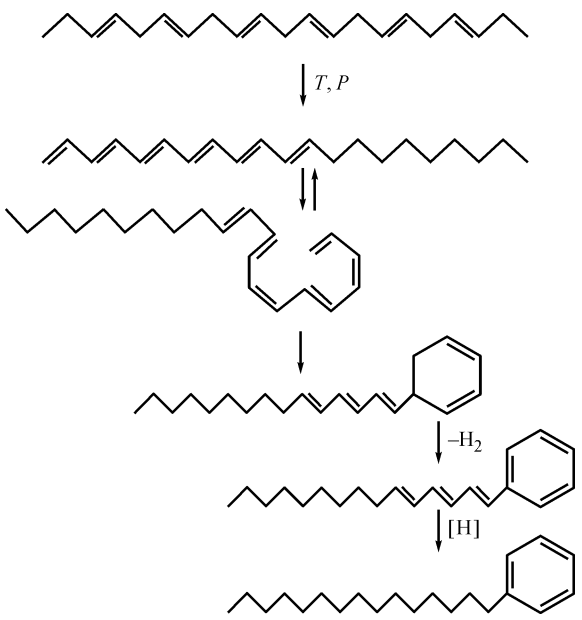

Fig. 2. Possible scheme of formation of *n*-pentadecylbenzene from polyene $C_{21}H_{32}$.

region, at C_{21}, and shows a pronounced prevalence of odd molecules over even molecules. Ostroukhov [16] attributed the prevalence of *n*-alkylbenzene C_{21} in oils to involvement of a definite organic compound of the composition C_{21} in the formation of this hydrocarbon.

The increased content of odd *n*-alkylbenzenes in the high-molecular-weight region may be due to a high content of odd linear polyenes C_{15}–C_{21} with one to six double bonds in marine plants [14]. The prevalence of the C_{21} hydrocarbon is attributable to the fact that some species of plankton algae contain only one hydrocarbon, polyene $C_{21}H_{32}$ with six double bonds: heneicosa-3,6,9,12,15,18-hexaene [17]. The suggested scheme of *n*-pentadecylbenzene formation from this hexaene is shown in Fig. 2. The other odd homologs are formed by cyclization and aromatization of other olefins.

The sequence of transformations leading to high-molecular-weight odd *n*-alkylbenzenes presumably consists of four steps.

The first step is isomerization of heneicosa-3,6,9,12,15,18-hexaene into conjugated thermodynamically stable heneicosa-1,3,5,7,9,11-hexaene. It is known that various conjugated polyenes are capable of concerted cyclization under the influence of light or heating. This reaction results in that a double bond disappears and the other double bonds are shifted, with the formation of a new single bond between two reactive ends of the conjugated system. Reactions of this type or reverse processes in which a cyclic product transforms into an acyclic polyene are termed electrocyclic reactions. As these reactions are reversible, their direction (direct or reverse) is governed by thermodynamic factors [18–25].

The second step is cyclization of the conjugated polyene to cyclohexadiene with an unsaturated hydrocarbon substituent.

The third step is dehydrogenation of the cyclohexadiene ring to benzene ring. The transformation product is 1-phenylpentadeca-1,3,5-triene.

The fourth step is reduction of the unsaturated substituent. Since ripening of the fossil organic matter had occurred under reducing conditions, hydrogenation of the unsaturated radical yielded *n*-pentadecylbenzene.

CONCLUSIONS

(1) A homologous series of *n*-alkylbenzenes with clearly pronounced prevalence of odd homologs in the range C_{17}–C_{23} was identified in crude oils from the main industrial oil fields of the Nepa–Botuoba anteclise.

(2) A possible model of the formation of an odd C_{21} *n*-alkylbenzene, *n*-pentadecylbenzene, from a polyene, heneicosa-3,6,9,12,15,18-hexaene (compound present in marine plankton algae), was suggested.

(3) The identified homologous series of *n*-alkylbenzenes, along with the known geochemical features of crude oils from this area, suggest that the genetic sources of the hydrocarbon fluids are similar or common.

ACKNOWLEDGMENTS

The study was financially supported by the Russian Foundation for Basic Research (project no. 06-05-96153).

REFERENCES

1. Petrov, Al.A., *Uglevodorody nefti* (Petroleum Hydrocarbons), Moscow: Nauka, 1984.
2. Ostroukhov, S.B., Aref'ev, O.A., Makushina, V.M., et al., *Neftekhimiya*, 1982, vol. 22, no. 6, pp. 723–728.
3. Ostroukhov, S.B., Aref'ev, O.A., Pustil'nikova, S.D., and Petrov, Al.A., *Neftekhimiya*, 1983, vol. 23, no. 1, pp. 20–30.
4. Ostroukhov, S.B., Aref'ev, O.A., and Zabrodina, M.N., in *Metody issledovaniya sostava organicheskikh soedinenii nefti i bitumoidov* (Methods for Examining

the Composition of Petroleum Organic Compounds and Bitumenoids), Moscow: Nauka, 1985, pp. 33–40.

5. Korzhov, Yu.V., Golovko, A.K., and Turov, Yu.P., *Izv. Sib. Otd. Akad. Nauk SSSR, Ser. Khim.*, 1989, no. 4, pp. 19–24.
6. Golovko, A.K., Petroleum Alkylaromatic Hydrocarbons, *Doctoral Dissertation*, Tomsk, 1997.
7. Golovko, A.K., Kontorovich, A.E., and Pevneva, G.S., Geokhimiya, 2000, no. 3, pp. 282–293.
8. Gallegos, E.J., *J. Chromatogr. Sci.*, 1981, vol. 19, pp. 177–182.
9. Seifert, W.K. and Moldovan, J.M., *Geochim. Cosmochim. Acta*, 1978, vol. 42, pp. 77–95.
10. Kissin, Y.V., *Org. Geochem.*, 1998, vol. 29, pp. 947–962.
11. Matisova, E., Kovacicova, E., Pham, T.H., et al., *J. Chromatogr.*, 1989, vol. 475, pp. 113–123.
12. Sinninghe Damste', J.C., Kock-Van Dallen, A.C., Albrecht, P.A., and De Leeuw, J.W., *Geochim. Cosmochim. Acta*, 1991, vol. 55, pp. 3677–3683.
13. Tissot, B.P. and Welte, D.H., *Petroleum Formation and Occurrence: A New Approach to Oil and Gas Exploration*, Berlin: Springer, 1978.
14. Hunt, J.M., *Geochemistry and Geology of Oil and Gas*, San Francisco: Freeman, 1979.
15. Petrov, Al.A., Golovkina, L.S., and Rusinova, G.V., *Mass-spektry neftyanykh uglevodorodov: Spravochnik (atlas)* (Mass Spectra of Petroleum Hydrocarbons: Handbook (Atlas)), Petrov, Al.A., Ed., Moscow: Nedra, 1986.
16. Ostroukhov, S.B., in *Materialy IV Mezhdunarodnoi konferentsii "Khimiya nefti i gaza"* (Proc. IV Int. Conf. "Chemistry of Oil and Gas"), Tomsk, 2000, vol. 1, pp. 349–354.
17. Blumer, M., Mullin, M.M., and Guillard, R.R.L., *Marine Biol.*, 1970, vol. 6, no. 3, pp. 226–235.
18. Kinney, R.E. and Clowley, D.J., *Ind. Eng. Chem.*, 1954, vol. 46, pp. 258–265.
19. Nohara, D. and Sakai, T., *Ind. Eng. Chem. Prod. Res. Develop.*, 1973, vol. 12, pp. 322–325.
20. Nohara, D. and Sakai, T., *Ind. Eng. Chem. Res.*, 1988, vol. 27, pp. 1925–1929.
21. Nohara, D. and Sakai, T., *Ind. Eng. Chem. Res.*, 1992, vol. 31, pp. 14–19.
22. Shabarov, Yu.S., *Organicheskaya khimiya* (Organic Chemistry), Moscow: Khimiya, 1996.
23. Turney, A., *Sovremennaya organicheskaya khimiya* (Modern Organic Chemistry), Moscow: Mir, 1981.
24. Berezin, B.D. and Berezin, D.B., *Kurs sovremennoi organicheskoi khimii: Uchebnoe posobie dlya vuzov* (Course of Modern Organic Chemistry: Textbook for Higher Schools), Moscow: Vysshaya Shkola, 1999.
25. Kim, A.M., *Organicheskaya khimiya* (Organic Chemistry), Novosibirsk: Sib. Univ., 2001.

ISSN 1070-4272, Russian Journal of Applied Chemistry, 2007, Vol. 80, No. 10, pp. 1764–1766. © Pleiades Publishing, Ltd., 2007.
Original Russian Text © M.V. Efanov A.I. Galochkin, 2007, published in Zhurnal Prikladnoi Khimii, 2007, Vol. 80, No. 10, pp. 1735–1737.

BRIEF COMMUNICATIONS

Mechanochemical Production of Nitrogen-containing Humic Fertilizers from Peat

M. V. Efanov and A. I. Galochkin

Research Institute of Wood Thermoplastics, Barnaul, Russia
Yugora State University, Khanty-Mansiisk, Khanty-Mansi aut. okrug, Russia

Received May 30, 2007

Abstract—Effect of the duration of mechanochemical synthesis (0.5–3 h) and amounts of hydrogen peroxide (0.1–0.5 g g^{-1} raw material) and ammonia (0.25–0.5 g g^{-1} raw material) on the content of nitrogen and humic and fulvic acids in products of oxidative ammonolysis of peat by the mechanochemical method was studied. The functional composition of fixed nitrogen was analyzed. Agrochemical tests of the preparations obtained as nitrogen-containing fertilizers were performed.

DOI: 10.1134/S1070427207100345

The agrochemical value of peat is largely determined by its organic component (humic and fulvic acids) and by its nitrogen content. However, the poor accessibility of the organic substance results in that the source peat only weakly manifests fertilizer properties. The organic component of peat can be activated with aqueous ammonia, which extracts humic substances as water-soluble ammonium humates [1].

A known method for production of a nitrogen-containing organic fertilizer, ammonified peat, consists in treating peat having certain moisture content with aqueous ammonia. The main disadvantages of the known method for peat ammonification are its long duration, which leads to loss of ammonia, and low content of fixed nitrogen in the ammonified peat [1].

Previously, a method has been developed for obtaining a plant-growth stimulant from peat by its treatment with hydrogen peroxide in aqueous ammonium in an autoclave at a hydromodulus of 9.5 : 1, ammonia content of 20–50%, and hydrogen peroxide content of 20–30% (both relative to absolutely dry peat mass) at 120°C for 4 h. This method has important technological disadvantages: high process temperature (120°C), duration of up to 4 h, and multistage nature [2].

A new mechanochemical technique has been suggested for production of nitrogen-containing organic fertilizers by oxidation of peat with hydrogen peroxide in an aqueous-ammonia medium to give humin-containing derivatives in quantitative yield [3].

The aim of the present study was to examine the effect of preparation conditions on the composition of products formed in oxyammonolysis of peat by the mechanochemical method.

EXPERIMENTAL

Raised-bog fuscum peat from the Vasyuganskoe deposit in Tomsk oblast was used as a raw material. It had the following parameters (%): degree of decomposition 10, ash content 2.6, and moisture content 60; and contained (%): total nitrogen 2.2, humic acids 13.8, and fulvic acids 18.5.

The mechanochemical synthesis of products of peat oxidation with hydrogen peroxide in an aqueous-ammonia medium was carried out in a vibration mill.

As shown by the results of the experiments performed (Table 1), the content of humic and fulvic

Table 1. Effect of the duration of mechanochemical vibration grinding on the composition of ammonified peat (moisture content of peat 60%, mass of absolutely dry peat 5.0 g, amount of hydrogen peroxide 0.1 g g^{-1} absolutely dry peat, amount of ammonia 0.25 g g^{-1} absolutely dry peat)

Sample	Grinding time, h	Content, %		
		total nitrogen	humic acids	fulvic acids
Starting peat	–	2.2	13.8	18.5
1	0.5	2.9	15.3	22.9
2	1.0	3.8	18.3	25.4
3	1.5	4.7	–	–
4	2.0	4.9	18.2	27.1
5	2.5	5.1	–	–
6	3.0	5.3	18.7	31.1

Table 2. Effect of the amount of hydrogen peroxide on the composition of ammonified peat (moisture content of peat 60%, mass of absolutely dry peat 5.0 g, duration of mechanochemical vibration grinding 1 h, amount of ammonia 0.25 g g^{-1} absolutely dry peat)

Sample	Amount of hydrogen peroxide, g g^{-1}*	Content, %		
		total nitrogen	humic acids	fulvic acids
Starting peat	–	2.2	13.8	18.5
2	0.1	3.8	18.3	25.4
7	0.2	4.2	19.2	26.7
8	0.3	5.0	20.3	28.1
9	0.4	5.1	21.5	29.6
10	0.5	5.2	22.9	30.2
11	0.6	5.3	23.2	30.5

* g g^{-1} absolutely dry peat.

Table 3. Effect of the amount of ammonia on the composition of ammonified peat (moisture content of peat 60%, mass of absolutely dry peat 5.0 g, duration of mechanochemical vibration grinding 1 h, amount of hydrogen peroxide 0.1 g g^{-1} absolutely dry peat)

Sample	Amount of ammonia, g g^{-1}*	Content, %		
		total nitrogen	humic acids	fulvic acids
Starting peat	–	2.2	13.8	18.5
2	0.25	3.8	18.3	25.4
12	0.35	4.8	20.4	28.8
13	0.4	4.9	21.6	29.5
14	0.45	5.0	22.3	30.6
15	0.5	5.3	23.0	30.9

* g g^{-1} absolutely dry peat.

acids in peat steadily increases as the duration of vibration grinding of peat in the presence of ammonia and an oxidizing agent (hydrogen peroxide) is made longer. The increase in the content of fixed nitrogen by a factor of 2.5 after 3 h of mechanochemical synthesis indicates that the organic substance of peat undergoes oxidative ammonolysis.

Raising the amount of hydrogen peroxide per gram of absolutely dry peat from 0.1 to 0.4 g leads to a steady rise in the amount of fixed nitrogen and humic and fulvic acids in the ammonified products obtained (Table 2). Further increase in the amount of the oxidizing agent to 0.6 g g^{-1} peat does not raise to any significant extent the content of fixed nitrogen and humic substances.

It can be seen from Table 3 that the amount of ammonia also affects the composition of nitrogen-containing fertilizers produced from peat. As can be seen from these data, raising the amount of ammonia by a factor of 2 leads to an increase in the content of fixed nitrogen by a factor of 1.4 and to a steady rise in the content of humic and fulvic acids in ammonified peat. It should be noted that, in all cases of mechanochemical oxidation (Tables 1–3), the content of fulvic acids increases to a greater extent than does that of humic acids, i.e., humic acids are converted into fulvic acids in oxidation.

The functional forms of fixed nitrogen were determined in the product of oxidative ammonolysis of peat, which contained (%): total nitrogen 5.3, humic acids 18.7, fulvic acids 31.1.

The content of ammonium nitrogen was determined after extraction of a weighed portion of ammonified peat with a 1 N KCl solution [4], and that of fixed nitrogen, by differentiated sulfuric acid hydrolysis with sulfuric acid solutions, with the concentration of these solutions raised from 0.5 to 5 N, by methods described in [5] and the content of residual nitrogen in hydrolyzed samples analyzed.

It was found that the products formed in oxyammonolysis of peat contain (%): ammonium nitrogen 24, amide nitrogen 15, ammine nitrogen 15, and heterocyclic nitrogen 43 of its total amount.

A product containing 5.3% fixed nitrogen was tested as a nitrogen-containing humic fertilizer for peas of Sakharnyi brand. It was shown that nitrogen-containing peat derivatives stimulate growth of peat plants by 26–34%, with the total biomass raised by 50–65%, and the chlorophyll content of the plants, by 66–120%.

CONCLUSIONS

(1) A method for synthesis of nitrogen-containing humic fertilizers from peat by its oxidative ammonolysis with hydrogen peroxide in an aqueous-ammonia medium by mechanochemical treatment was developed and products containing up to 5.3% organically fixed nitrogen and up to 23.2 and 31.1% humic and fulvic acids, respectively, were obtained.

(2) It was found that the products formed in oxyammonolysis of peat contain (%): ammonium nitrogen 24, amide nitrogen 18, ammine nitrogen 15, and heterocyclic nitrogen 43 of its total amount.

(3) It was shown that the products obtained exhibit high biological activity and can be used as nitrogen-containing humic fertilizers that improve the productivity of cereals by 26–34%.

REFERENCES

1. Tishkovich, A.V., *Teoriya i praktika ammonizacii torfa* (Theory and Practice of Peat Ammonification), Minsk: Nauka i Tekhnika, 1972.
2. RF Patent 2213452.
3. Efanov, M.V. and Galochkin, A.I., Abstracts of Papers, *4-yi Mezhdunarodnyi congress "Veist-Tek-2005"* (4th Int. Congr. "Waste-Tech-2005"), Moscow, 2005, pp. 155–156.
4. *Metodicheskie ukazaniya po analizu torfa* (Methodological Recommendations for Analysis of Peat), Moscow: VNIITP, 1973.
5. Efanov, M.V. and Dudkin, D.V., *Khim. Prirod. Soedin.*, 2004, no. 3, pp. 235–236.

ISSN 1070-4272, Russian Journal of Applied Chemistry, 2007, Vol. 80, No. 10, pp. 1767–1769. © Pleiades Publishing, Ltd., 2007.
Original Russian Text © A.Yu. Kuznetsov, V.V. Solov'eva, E.P. Buchikhin, A.M. Chekmarev, 2007, published in Zhurnal Prikladnoi Khimii, 2007, Vol. 80, No. 10, pp. 1738–1740.

BRIEF COMMUNICATIONS

Conversion of Rare-Earth Metal Oxides in Tributyl Phosphate

A. Yu. Kuznetsov, V. V. Solov'eva, E. P. Buchikhin, and A. M. Chekmarev

All-Russia Research Institute of Chemical Technology, Moscow, Russia
Mendeleev Russian University of Chemical Engineering, Moscow, Russia

Received May 2, 2007

Abstract—Dissolution of gadolinium, europium, neodymium, dysprosium, and samarium oxides to give nitrates of these metals was studied in a system constituted by tributyl phosphate (30 vol %), tetrachloroethylene (70 vol %), and NO_2. The activation energy of anhydrous dissolution of gadolinium oxide was calculated. The effect of water on the conversion efficiency of gadolinium oxide into nitrate was examined.

DOI: 10.1134/S1070427207100357

It is known that solvometallurgical methods for processing of ores and secondary raw materials [1] make it possible to intensify dissolution processes, improve the selectivity of the processing techniques, and substantially diminish, or even completely abandon use of water in technological processes [2].

Development of the solvometallurgical technologies for processing of mineral resources requires a study of the fundamental aspects of interaction between dissolved materials and nonaqueous systems. The authors of [3] studied the oxidative dissolution of rare-earth elements in tributyl phosphate (TBP). In [4], chlorination of yttrium oxide in the system constituted by dimethylformamide (DMFA) and Cl_2 was analyzed, with the kinetic properties of the interaction disregarded.

This study is concerned with the nonaqueous low-temperature nitration of gadolinium, europium, neodymium, dysprosium, and samarium oxides in the system constituted by TBP, tetrachloroethylene (TCE), and nitrogen dioxide.

EXPERIMENTAL

We used TBP of chemically pure grade, prepared by the method described in [5]. Tetrachloroethylene was purified by distillation [5].

The dissolution was studied in a temperature-controlled reactor (stirring rate 800–900 rpm). It was confirmed by preliminary experiments that these conditions correspond to the kinetic dissolution mode. Powders of gadolinium, europium, neodymium, dysprosium, and samarium oxides were prepared by calcination of their hydroxides under identical conditions at 800°C [6]. Gadolinium oxide used in the experiments had cubic structure.

Visible-range spectra of the organic solutions prepared were recorded on a Shimadzu UV-3000 instrument.

We studied the dissolution of gadolinium, europium, neodymium, dysprosium, and samarium oxides in the system constituted by tributyl phosphate (30 vol %), TCE (70 vol %), and NO_2 (1.5 M) at 40°C. The results of the experiments are shown in Fig. 1. The conversion of rare-earth element oxides proceeds without an induction period, with its rates in

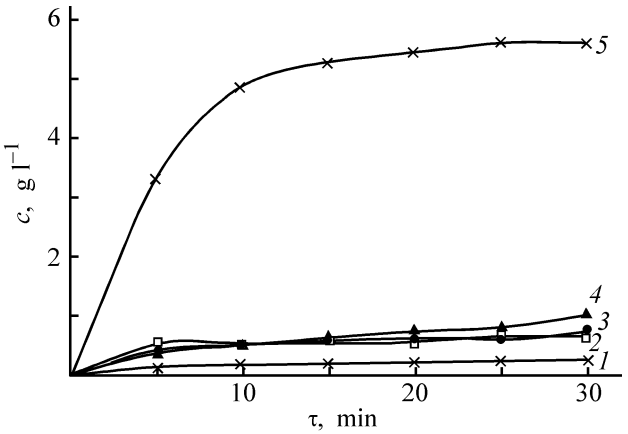

Fig. 1. Dissolution of REE oxides in the system TBP (30 vol %)–TCE (70 vol %)–NO_2 (1.5 M) at T = 40°C. (c) Concentration and (τ) time; the same for Figs. 2–4. REE: (*1*) Eu, (*2*) Sm, (*3*) Dy, (*4*) Nd, (*5*) Gd.

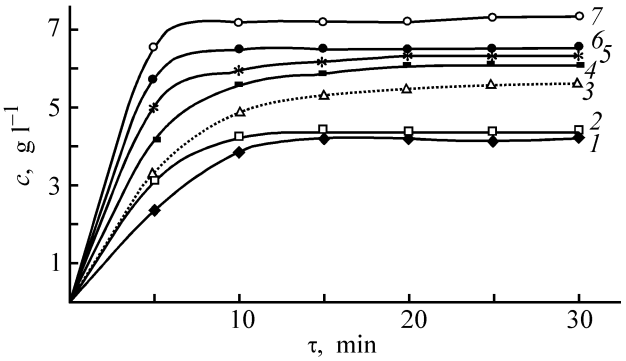

Fig. 2. Dissolution of Gd_2O_3 in the system TBP (30 vol %)–TCE (70 vol %)–NO_2 at different concentrations of NO_2 at T = 40°C. NO_2 concentration (M): (*1*) 0.5, (*2*) 1, (*3*) 1.5, (*4*) 2, (*5*) 2.5, (*6*) 3, and (*7*) 3.5.

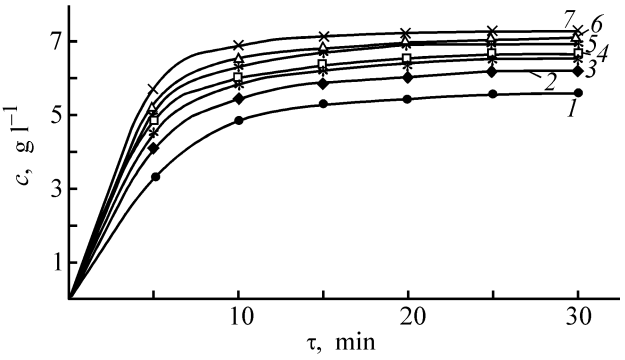

Fig. 4. Dissolution of Gd_2O_3 in the system TBP (30 vol %)–TCE (70 vol %)–NO_2 (1.5 M) with addition of small amounts of water at T = 40°C. H_2O content (vol %): (*1*) 0, (*2*) 0.3, (*3*) 2.5, (*4*) 0.5, (*5*) 2, (*6*) 0.76, and (*7*) 1.

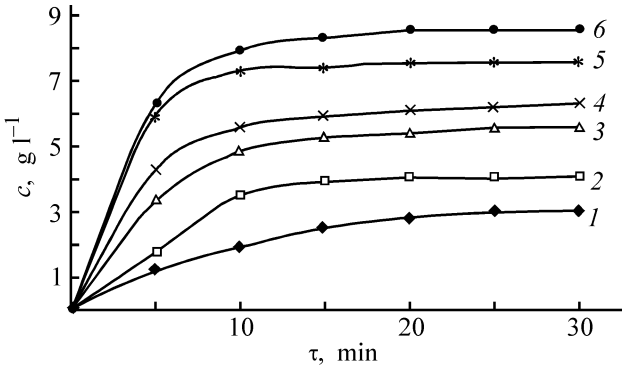

Fig. 3. Dissolution of Gd_2O_3 in the system TBP (30 vol %)–TCE (70 vol %)–NO_2 (1.5 M) at different temperatures. T (°C): (*1*) 20, (*2*) 30, (*3*) 40, (*4*) 50, (*5*) 60, and (*6*) 70.

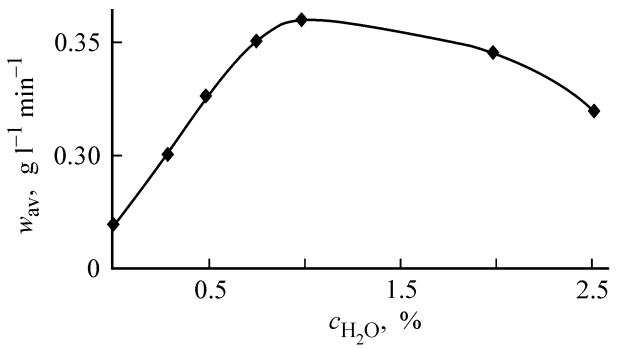

Fig. 5. Average gadolinium dissolution rates w_{av} at different contents of water c_{H_2O} in the course of 20 min.

the initial period increasing in the order Eu < Nd < Dy < Sm < Gd. In the spectrum, the characteristic absorption bands of Nd were observed at 422, 512, 526, 584, 678, 736, 743, 800, and 870 nm, which shows that the rare-earth metal is present in solution as Nd(III) [7]. The bands characteristic of the following elements in the following states were observed: Dy(III) at 449 nm [6], Sm(III) at 464 and 477 nm [8], and Eu(III) at 390 nm [6]. Thus, it was established that, upon nonaqueous low-temperature nitration of oxides of rare-earth elements (REE), they pass into the organic solution in the trivalent state.

The dissolution kinetics of gadolinium oxide in the system composed of TBP (30 vol %), TCE (70 vol %), and NO_2 was studied in relation to the oxidant concentration. The results of the experiments are shown in Fig. 2. The data obtained indicate that the dissolution rate increases with the NO_2 concentration in the solution. A calculation of the initial dissolution rates and processing of the experimental data by Microsoft Excel 97 software demonstrated that the conditional reaction order and the rate constant are n = 0.6 and K = 713.35 mg mol^{-1} min^{-1}, respectively.

The results obtained when studying the temperature dependence of the kinetics of gadolinium oxide dissolution in the range 20–70°C are presented in Fig. 3. The data obtained show that the dissolution rate increases with temperature. A calculation of the initial dissolution rates and processing of the experimental data by Microsoft Excel 97 software showed that the activation energy of the system is E_a = 30.6 kJ mol^{-1} and the constant $K = 7.515 \times 10^7$ mg l^{-1} min^{-1}.

It has been reported that water strongly affects the rate of interaction between metals and certain nonaqueous dissolving systems [9, 10].

We studied the dissolution kinetics of gadolinium oxide in the system constituted by TBP (30 vol %), TCE (70 vol %), and NO_2 (1.5 M), to which water was added. The results of the experiments are shown in Fig. 4. The data obtained were used to calculate the average dissolution rates of gadolinium oxide (Fig. 5).

As can be seen from Fig. 5, the given dependence has an extremum. It is known that nitrogen dioxide reacts with water to give nitric and nitrous acids. To study processes of anhydrous low-temperature dissolution, we used REE oxides, i.e., already oxidized substances. Thus, the oxidation process proper does not occur in the system, and, consequently, water must affect the conversion process only by making higher the acidity of the system. When the content of water is raised to more than 1.5 vol %, the whole amount of nitrogen dioxide is already reacted with water, and, further, the solution is diluted, i.e., the acidity of the system decreases.

CONCLUSIONS

(1) The results obtained in a study of the dissolution of gadolinium, europium, neodymium, dysprosium, and samarium oxides in the system composed of tributyl phosphate (30 vol %), tetrachloroethylene (70 vol %), and NO_2 with the formation of their nitrates demonstrate that gadolinium oxide is dissolved under the kinetic control and the activation energy of dissolution in this system is 30.6 kJ mol^{-1}.

(2) The relative reaction order with respect to NO_2 for the reaction of gadolinium oxide conversion is 0.6.

(3) The dissolution rate of gadolinium oxide is at a maximum at a water content of 1.0–2.0 vol %.

REFERENCES

1. Chekmarev, A.M., *Sol'vometallurgiya – prakticheskoe napravlenie metallurgii redkikh i tsvetnykh metallov* (Solvotometallurgy, Practically Feasible Field of the Metallurgy of Rare and Nonferrous Metals), Moscow: Atomenergoizdat, 2004.
2. Skorovarov, D.I., Shatalov, V.V., Buchikhin, E.P., et al., *Khim. Tekhnol.*, 2003, no. 1, pp. 29–34.
3. Morozov, A.E., Seleznev, V.P., and Sololov, I.P., *Zh. Neorg. Khim.*, 1993, vol. 38, no. 1, pp. 53–54.
4. Ulanov, A.V., Buchikhin, E.P., Kuznetsov, A.Yu., and Chekmarev, A.M., *Uspekhi v khimii i khimicheskoi tekhnologii: Tezisy dokladov 15 Mezhdunarodnoi konferentsii molodykh uchenykh po khimii i khimicheskoi tekhnologii "MKKhT–2001"* (Advances In Chemistry and Chemical Technology: Abstracts of Papers, 15th Int. Conf. of Young Scientists on Chemistry and Chemical Technology, "MKKhT–2001"), Moscow: Ross. Khim. Tekhn. Univ., 2001, vol. 15, issue 4.
5. Keil, B., Herout, V., Hudlicky, M., Ernest, I., Protiva, M., Gut, J., Komers, R., and Moravek, J., *Laboratorni Technica organicke Chemie*, Keil, B., Ed., Praha: Nakladatelstvi ceskoslovenske Akademie ved, 1963.
6. Ryabchikov, D.I., and Ryabukhin, V.A., *Analiticheskaya khimiya redkozemel'nykh elementov i ittriya* (Analytical Chemistry of Rare-Earth Elements and Yttrium), Moscow: Nauka, 1966.
7. Anagnostopoulos, A. and Sakellaridis, P.O., *J. Inorg. Nucl. Chem.*, 1970, vol. 32, pp. 1740–1742.
8. Gruen, D.M., *J. Inorg. Chem.*, 1957, vol. 4, no. 1, pp. 74–76.
9. Buchikhin, E.P., Kuznetsov, A.Yu., Vidanov, V.L., and Shatalov, V.V., *Radiokhimiya*, 2006, vol. 46, no. 5, pp. 409–411.
10. Buchikhin, E.P., Chekmarev, and Kuznetsov, A.Yu., *Izv. Vyssh. Uchebn. Zaved., Tsvetn. Metall.*, 2003, no. 2, pp. 13–16.

ISSN 1070-4272, Russian Journal of Applied Chemistry, 2007, Vol. 80, No. 10, pp. 1770–1772. © Pleiades Publishing, Ltd., 2007.
Original Russian Text © O.N. Chechina, S.V. Sokolov, V.V. Berenblit, V.A. Soshin, 2007, published in Zhurnal Prikladnoi Khimii, 2007, Vol. 80, No. 10, pp. 1741–1743.

BRIEF COMMUNICATIONS

Dissociation Constants of Polyfluorocarboxylic Acids

O. N. Chechina, S. V. Sokolov, V. V. Berenblit, and V. A. Soshin

Samara State Technical University, Samara, Russia
Lebedev Research Institute of Synthetic Rubber, Federal State Unitary Enterprise, St. Petersburg, Russia

Received March 23, 2007

Abstract—The effect of the structure and molecular weight of fluorocarboxylic acids on their dissociation constants in acetonitrile and its mixtures with water and methanol was studied.

DOI: 10.1134/S1070427207100369

It is known that, owing to the strong electron-acceptor properties of the trifluoromethyl radical, trifluoroacetic acid has a dissociation constant of 5.9×10^{-1} in water [1] and virtually does not differ from strong acids, such as hydrochloric acid. Its homologues, perfluorocarboxylic acids, are also rather strong acids. As, however, the length of the carbon chain increases, micelle formation leads to a decrease in the degree of ionization [2].

Electrochemical syntheses with anodic dimerization and cross-anodic combination of various fluorocarboxylic acids in acetonitrile mixed with water and methanol are of practical importance for preparation of new organofluoric compounds possessing various useful properties [3]. The specific role played by acetonitrile in electrolytic media, which primarily determines the efficiency of these processes, makes necessary a study of the electrochemical characteristics of fluorinated carboxylic acids in its mixtures with protonating electrolytes in order to choose the electrolysis conditions and prognosticate the results of electrosyntheses.

EXPERIMENTAL

The dissociation constants of fluorocarboxylic acids were determined by potentiometric titration [4] with a pH-673M millivoltmeter, using a glass working electrode and the standard calomel electrode. The solutions were agitated with a magnetic stirrer.

The dissociation constants of the acids were measured in individual solvents (acetonitrile, water, and methanol) and in their mixtures with relative solvent concentrations commonly used in electrochemical syntheses [3].

Depending on a medium, the following solutions were used as titrants: 0.1 M KOH for acetonitrile, 0.1M aqueous solution of NaOH for water and its mixtures with acetonitrile, and 0.1 M solution of sodium methylate in methanol for methanol and its mixture with acetonitrile.

The solvents were purified by the known procedures [5].

Titration was applied to 0.2 M solutions of the following polyfluorocarboxylic acids of reagent grade or those synthesized and purified by rectification: CF_3CF_2COOH (**I**) pentafluoropropionic acid; $CF_2ClCFClCOOH$ (**II**) 1,2-dichloroperfluoropropionic acid prepared by the method [6]; $CF_3CF_2CF_2COOH$ (**III**) heptafluoromaleic acid; $CF_3CF_2CF_2OCF(CF_3)$-COOH (**IV**) perfluoro-3-oxo-2-methylhexanoic acid; $CF_3OCF_2CF_2CF_2OCF(CF_3)COOH$ (**V**) perfluoro-3,7-dioxo-2-methyloctanoic acid [prepared by condensation of $CF_3OCF_2CF_2COF$ with hexafluoropropene oxide and subsequent hydrolysis of acylfluoride $CF_3OCF_2CF_2CF_2OCF(CF_3)COF$]; $CF_3CF_2CF_2OCF$-$(CF_3)CF_2OCF(CF_3)$C OOH (**VI**) perfluoro-3,6-dioxo-2,5-dimethylnonanoic acid; $F(CF_2CF_2O)CF_2COOH$ (**VII**) perfluoro-3,6,9,12-tetraoxotetradecenoic acid prepared by hydrolysis of the tetrafluoroethene oxide pentamer.

The equivalence point pH_{eq} was determined by differentiating the titration curve. The determination accuracy was ±2%.

The negative logarithm of the dissociation constant, pK_{HA}, was calculated by the equation [4]:

$$pK_{HA} = 2pH_{eq} - pK_{H_2O} + \log c_{HA} = 2pH_{eq} - 13.3010.$$

Calculated dissociation constants of polyfluorocarboxylic acids in various solvents

Acid	$K_{HA} \times 10^2$							
	CH_3CN	H_2O	CH_3OH	CH_3CN–H_2O, vol % CH_3CN				CH_3CN–CH_3OH, 10 vol % CH_3CN
				90	50	40	30	
CF_3CF_2COOH (**I**)	3.66	2.50	1.58	3.55	–	–	–	1.12
$CF_2ClCFClCOOH$ (**II**)	3.12	3.98	1.26	3.16	–	–	–	1.07
$CF_3CF_2CF_2COOH$ (**III**)	1.80	1.58	–	1.25	–	–	–	–
$CF_3CF_2CF_2OCFCOOH$ (**IV**) $\quad\quad\quad

pendant trifluoromethyl groups, also gives no way of observing this dependence.

CONCLUSIONS

(1) It was shown that the dissociation constants of fluorocarboxylic acids are lower by at least an order of magnitude than the dissociation constant of trifluoroacetic acid. Therefore, the above compounds cannot be classed with strong acids.

(2) In water and acetonitrile, the dissociation constants of fluorocarboxylic acids of various structures and molecular weights differ only slightly, although their dielectric constants are strongly different.

REFERENCES

1. Sheppard, W.A. and Sharts, C.M., *Organic Fluorine Chemistry*, New York: W.A. Benjamin, Inc., 1969.
2. Kauck, E.A. and Diesslin, A.R., *Ind. Eng. Chem.*, 1951, vol. 43, no. 10, p. 2.
3. Chechina, O.N. and Tomilov, A.P., *Elektrokhimiya*, 1999, vol. 35, no. 3, p. 149.
4. Khe'fets, V.L., Avdeev, D.K., and Reishakhrit, L.S., *Praktikum po teoreticheskoi elektrokhimii* (Practical Course of Theoretical Electrochemistry), Leningrad: Len. Gos. Univ., 1954.
5. Ptitsina, O.A., Kupletskaya, N.V., Timofeeva, V.N., et al., *Laboratornye raboty po organicheskomu sintezu* (Laboratory Works on Organic Synthesis), Moscow: Prosveshchenie, 1979.
6. Paleta, O., Havin, V., and Dedek, V., *Org. Chem. Technol.*, 1978, vol. 25, p. 105.
7. *Kratkii spravochnik fiziko-khimicheskikh velichin* (Concise Reference Book of Physicochemical Constants), Ravdel', A.A., Ed., Leningrad: Khimiya, 1983.
8. Radell, J., Brodman, B.W., Hirshfeld, A., and Bergmann, E.D., *J. Phys. Chem.*, 1965, vol. 69, p. 928.
9. Osipov, O.A. and Minkin, V.I., *Spravochnik po dipol'nym momentam* (Reference Book of Dipole Moments), Moscow: Vysshaya Shkola, 1965.

ISSN 1070-4272, Russian Journal of Applied Chemistry, 2007, Vol. 80, No. 10, pp. 1773–1775. © Pleiades Publishing, Ltd., 2007.
Original Russian Text © V.Yu. Gusev, E.V. Baigacheva, A.V. Radushev, T.D. Batueva, 2007, published in Zhurnal Prikladnoi Khimii, 2007, Vol. 80, No. 10, pp. 1744–1746.

BRIEF COMMUNICATIONS

Extraction of Copper(II) with *N*,*N*-Diethylbenzohydrazide

V. Yu. Gusev, E. V. Baigacheva, A. V. Radushev, and T. D. Batueva

Institute of Technical Chemistry, Ural Division, Russian Academy of Sciences, Perm, Russia

Received September 4, 2006; in final form, December 2006

Abstract—Extraction of Cu(II) with *N*,*N*-diethylbenzohydrazide and the effect of ammonium salts on this process were studied. The composition and structure of the complex being extracted was analyzed.

DOI: 10.1134/S1070427207100370

The exists a rather wide assortment of compounds that can be used for extraction of copper(II) from various media [1]. However, the extractive agents employed in industry have a number of disadvantages that limit their applicability and stimulate a search for new, more effective reagents. A promising class of compounds for Cu(II) extraction is constituted by hydrazides suggested for recovery of CuII) from acid solutions [2]. There have been no reports devoted to Cu(II) extraction with *N*,*N*-dialkyl derivatives of hydrazides. Meanwhile, introduction of two alkyl radicals into the hydrazide group can markedly change the extractive properties of the compounds obtained. This study is concerned with Cu(II) extraction with *N*,*N*-diethylbenzohydrazide (DEBH), $PhCONHN(Et)_2$.

EXPERIMENTAL

DEBH was synthesized as follows. Benzohydrazide [13.6 g (0.1 mol)] was dissolved in 100 ml of isopropanol, 19 ml (0.25 mol) of ethyl bromide was added, and a solution of 11.2 (0.2 mol) of KOH in 80 ml of isopropanol was introduced dropwise. The reaction mixture was heated to neutral reaction (2–3 h), filtered, and evaporated. To the residue was added 50 mol of chloroform and the mixture was filtered and evaporated. The residue was recrystallized from a 2 : 1 mixture of hexane and *n*-xylene. Yield 11.2 g (58%); mp = 121.5–123.0°C; R_f = 0.50 (*m*-xylene : BuOH = 2 : 1). IR spectrum, ν (cm^{-1}): 1572 (amide II); 1639, 1652 (amide I); 3195 (N–H). ^1H NMR spectrum, δ (ppm; *J*, Hz): 1.09 (t, 6H, Me, *J* = 6.9), 2.81 (q, 4H, CH_2, *J* = 6.9), 6.60 (s, 1H, NH), 7.3–7.5 (m, 3H, Ph), 7.69 (d, 2H, Ph, *J* = 7.2).

IR spectra were recorded on a Bruker JFS 66/S Fourier spectrometer in Vaseline oil, and ^1H NMR spectra on a MERCURY plus 300 spectrometer (300 MHz) in $CDCl_3$, with HMDS as internal standard. The pH values were measured with an I-160 M ion-meter with glass and silver chloride electrodes. UV spectra and the optical densities were measured with an SF-26 spectrophotometer. SILUFOL plates served as the chromatographic material. $CuSO_4$, $NiCl_2$, $CoCl_2$, and $K_2Cr_2O_7$ of analytically pure and chemically pure grades were used. The content of elements in standard solutions and in the aqueous phase was determined using the following methods: Co(II), Ni(II), and Cu(II) by complexonometry [3–5]; small amounts of copper(II), by the extractive-photometric technique with sodium diethyldithiocarbamate [6]; and Cr(VI), photometrically with diphenylcarbazide [7].

The solubility of the reagent, found gravimetrically, is 10.5 g l^{-1} in *m*-xylene and 1.6 g l^{-1} in hexane.

Figure 1 shows UV spectra of DEBH solutions in various media. It can be seen that, depending on pH, the reagent exists in different forms. The acid–base

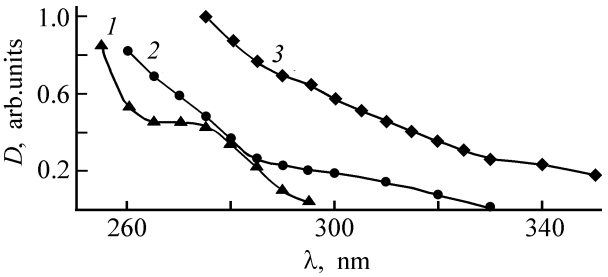

Fig. 1. UV spectra of DEBH solutions in various media. (*D*) Optical density and (λ) wavelength. *l* = 1 cm, H_2O : EtOH = 10 : 1, $c_{DEBH} = 4.9 \times 10^{-4}$ M. (*1*) pH 0.85, (*2*) pH 4.82, and (*3*) 7.3 M NaOH.

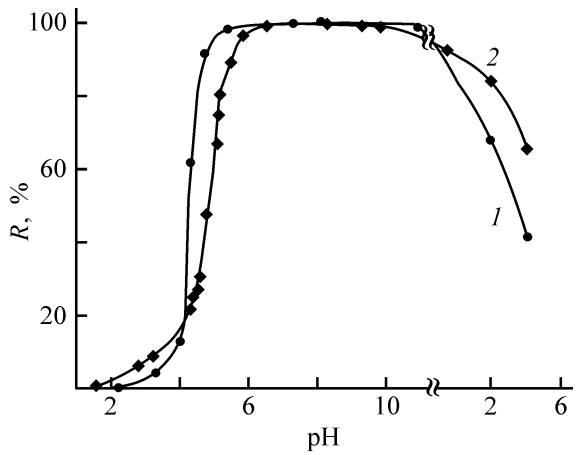

Fig. 2. Degree of copper(II) extraction, R, vs. the pH value of the aqueous phase. $V_{org} : V_{aq} = 1 : 10$, $c_{Cu(II)} = 0.001$ M, $\tau = 3$ min. 0.05 M DEBH solution: (*1*) in *m*-xylene and (*2*) in *i*-AmOH.

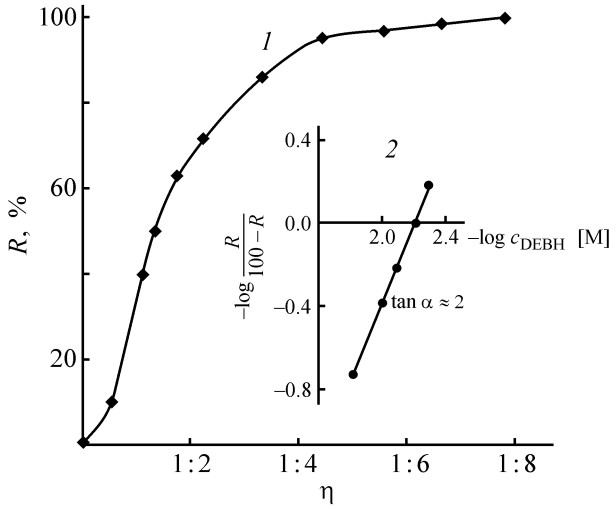

Fig. 3. Determination of the composition of the Cu(II) complex with DEBH. $c_{DEBH} = 0.05$ M, $c_{Cu(II)} = 0.004$ M, pH 9.0–10.5 (ammonia buffer solution), $I = 0.2$ (KCl). (R) Degree of Cu(II) extraction from solution and (h) [Cu(II)] : [DEBH] molar ratio. (*1*) Saturation curve and (*2*) processing of this curve by the equilibrium shift method.

equilibria in its solutions can be expressed in the general form as follows:

$$H_2L^+ \underset{-H^+}{\overset{pK_{a_1}}{\rightleftharpoons}} HL \underset{-H^+}{\overset{pK_{a_2}}{\rightleftharpoons}} L^-,$$

where HL is the DEBH molecule.

The pK_a values were determined spectrophotometrically in 10 : 1 H_2O : EtOH at $l = 1$ cm and $c_{DEBH} = 4.9 \times 10^{-4}$ M for pK_{a_1} at $\lambda = 260$ nm and $I = 0.1$ ($NaNO_3$) and for pK_{a_2} at λ 280 nm: $pK_{a_1} = 3.24 \pm 0.02$ ($n = 5$, $P = 0.95$) and $pK_{a_2} = 14.94 \pm 0.03$ ($n = 6$, $P = 0.95$) (at c_{NaOH} the Hammett function was used).

The extraction of Cu(II), Co(II), Ni(II), and Cr(VI) with a DEBH solution in *m*-xylene was studied. Co(II), Ni(II), and Cr(VI) ions are extracted from neither acid nor ammonium medium. The Cu(II) compound is extracted as a red complex; the dependence of the degree of extraction, R, on pH is shown in Fig. 2 (curve *1*). It can be seen that Cu(II) starts to be extracted at pH > 3; at pH 3.0–5.4, the degree of recovery steeply increases from 4 to 98% and then remains constant up to $c_{NH_3} = 1$ M. As the NH_3 concentration is raised further, to 4 M, R gradually decreases to 41%, which is presumably due to a competing formation of ammoniates.

The composition of the copper(II) complex was determined by the method of molar ratios. The curve obtained in an ammonia buffer solution had no pronounced inflections (Fig. 3). The method of the equilibrium shift revealed the formation of an extractable complex with a ratio [Cu(II)] : [DEBH] = 1 : 2.

When an extract of the complex, colored red brown, is passed through a KU-2-8 cation-exchange resin in the Na^+ form, the coloration of the extract is preserved, which indicates that the complex is not charged. This is only possible in the case when the complex contains hydrazide in a deprotonated form. The structure of the complex can reflected by the formula

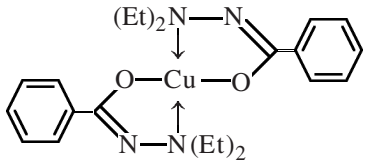

Because the deprotonated form of DEBH starts to be formed at pH > 13, which is not the case under the extraction conditions, it can be concluded that a reagent molecule already incorporated into the complex undergoes deprotonation.

By analogy with dimethylhydrazides [8], *N*,*N*-diethylbenzohydrazide forms a complex of the cation type with copper(II), with a blue-green coloration and $[Cu^{2+}]$: [DEBH] ratio of 1 : 2. The extraction of this complex was studied using a solution of DEBH in isoamyl alcohol. The curve obtained for the dependence of R on pH (Fig. 2, curve *2*) was found to be close to that obtained with the solution of the reagent in xylene. The extract was also red. This indicates that only an uncharged complex of the $[Cu(L–H)_2]$ type is extracted in both cases.

On shaking the blue-green solution of a charged complex of the cation type in isoamyl alcohol with

Effect of ammonium salts on the extraction of copper(II) from an ammonia solution [$c_{Cu(II)}$ = 0.005 M, V_{org} : V_{aq} = 1 : 2, c_{DEBH} = 0.05 M (*n*-xylene)]

$c_{(NH_4)_2SO_4}$, g l^{-1} / mol l^{-1}	$R_{Cu(II)}$, %	c_{NH_4Cl}, g l^{-1} / mol l^{-1}	$R_{Cu(II)}$, %	$c_{(NH_4)_2SO_4}$, g l^{-1} / mol l^{-1}	$R_{Cu(II)}$, %	c_{NH_4Cl}, g l^{-1} / mol l^{-1}	$R_{Cu(II)}$, %
0	97.5	0	97.5				
13.2 / 0.1	97.7	5.4 / 0.1	97.9	105.6 / 0.8	95.6	43.2 / 0.8	96.5
26.4 / 0.2	97.7	10.8 / 0.2	98.0	158.4 / 1.2	91.2	64.8 / 1.2	92.4
52.8 / 0.4	97.7	21.6 / 0.4	97.7	211.2 / 1.6	85.7	86.4 / 1.6	91.7

water, the coloration of the organic layer changes to red, which points to a transition of this complex to the neutral [Cu(L–H)$_2$]. The transition process can be represented as:

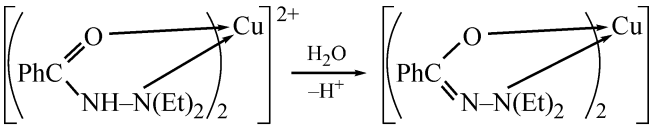

Industrial ammonia solutions of Cu(II) commonly contain ammonium salts, which can suppress the extraction. The results obtained in Cu(I) extraction from a solution containing 0.1 M NH_3 and varied amounts of $(NH_4)_2SO_4$ and NH_4Cl are listed in the table. It can be seen that presence of ammonium sulfate and chloride in amounts of up to 1 M has virtually no effect on the recovery of copper(II).

CONCLUSIONS

(1) *N*,*N*-Diethylbenzohydrazide effectively recovers Cu(II) from ammonia solutions with NH_3 concentrations of up to 1 M.

(2) Replacing *m*-xylene with isoamyl alcohol has virtually no effect on the dependence of the degree of Cu(II) recovery on pH. In both cases, the Cu(L–H)$_2$ complex is extracted.

(3) Presence of NH_4Cl and $(NH_4)_2SO_4$ in concentrations of up to 1 M has little effect on the degree of Cu(II) recovery.

REFERENCES

1. Radushev, A.V., Gusev, V.Yu., and Naboichenko, S.S., *Tsvetn. Met.*, 2002, no. 3, pp. 18–27.
2. Radushev, A.V., Gusev, V.Yu., Bogomazova, G.S., et al., *Zh. Prikl. Khim.*, 1996, vol. 69, no. 8, pp. 1283–1289.
3. Korostelev, P.P., *Fotometricheskii i kompleksonometricheskii analiz v metallurgii* (Photometric and Complexometric Analyses in Metallurgy),. Moscow: Metallurgiya, 1984.
4. Schwarzenbach, G. and Flaschka, H., *Die Komplexometrische Titration*, Stuttgart: Ferdinand Enke, 1965.
5. Lur'e, Yu.Yu. and Rybnikova, A.I., *Khimicheskii analiz proizvodstvennykh stochnykh vod* (Chemical Analysis of Industrial Wastewater), Moscow: Khimiya, 1974.
6. Podchainova, V.N. and Simonova, L.N., *Analiticheskaya khimiya elementov: Med'* (Analytical Chemistry of Elements: Copper). Moscow: Nauka, 1990.
7. Lavrukhina, A.K.and Yukina, L.V., *Analiticheskaya khimiya khroma* (Analytical Chemistry of Chromium), Moscow: Nauka, 1979, pp. 42, 43.
8. Zub, V.Ya., Bugaeva, P.V., Strizhakova, N.G., and Maletin, Yu.A., *Koordinats. Khim.*, 2004, vol. 30, no. 10, pp. 792–797.

ISSN 1070-4272, Russian Journal of Applied Chemistry, 2007, Vol. 80, No. 10, pp. 1776–1778. © Pleiades Publishing, Ltd., 2007.
Original Russian Text © V.N. Tseluikin, N.D. Solov'eva, O.G. Nevernaya, 2007, published in Zhurnal Prikladnoi Khimii, 2007, Vol. 80, No. 10, pp. 1747–1749.

BRIEF COMMUNICATIONS

Viscous Flow of Aqueous Solutions of Copper Sulfate in the Temperature Range 20–50°C

V. N. Tseluikin, N. D. Solov'eva, and O. G. Nevernaya

Engels Technological Institute, Saratov State Technical University, Engels, Saratov oblast, Russia

Received December 19, 2006; in final form, April 2007

Abstract—Apparent molar volume, enthalpy of activation, and Gibbs energy of viscous flow of aqueous copper sulfate solutions were calculated from experimental data. The concentration dependences of the above parameters were analyzed from the standpoint of structural transformations.

DOI: 10.1134/S1070427207100382

A solution is a complex equilibrium chemical system formed by a solvent, dissolved substance (solute), and products of their interaction. One of the most structurally sensitive properties of the solutions, which characterizes the internal friction of a liquid, is viscosity. As a rule, determining the viscosity under atmospheric pressure is rather simple. More severe difficulties arise when experimental data are discussed in order to identify structural changes in solution, associated with the component concentrations and temperature. There exist several approaches to interpretation of viscosity data as applied to structural transformations in electrolytes [1–3]. One of these is based on the Eyring theory [4], which allows calculation of activation characteristics of the viscous flow of dilute [3] and concentrated electrolyte solutions [5]. In the present study, this approach was used to analyze the viscous flow of aqueous copper sulfate solutions. The given salt is the main component of electrolytes used for plating of copper and its alloys.

EXPERIMENTAL

The solutions were prepared by gravimetric method from twice-distilled water and recrystallized reagents of chemically pure grade. Measurements were made in the temperature range 20–50°C. The kinematic viscosity was determined with a VPZh-4 viscometer with a capillary diameter of 0.56 mm [GOST (State Standard) 10028–81], and the density, by the pycnometric method. The measurement error was 0.2–0.4%. A calculation of the Cochran criterion [6] confirmed the reproducibility of the results.

The interaction of copper ions with water dipoles makes hydrogen bonds in the solvent structure weaker and, at higher concentrations, even leads to rupture of these bonds to give a hydrated ion $[Cu(H_2O)_n]^{2+}$. According to the data of [7], the Cu^{2+} ion in aqueous solution has a distorted octahedral environment of H_2O molecules. As shown in [8], the nearest environment of the Cu^{2+} ion is less ordered in copper sulfate solutions, compared with solutions containing other oxygen-containing anions. This phenomenon is accounted for by the effect of the sulfate ion, which competes with water molecules for the place in the first hydrate shell of the cation. It is known that SO_4^{2-} anions can occupy voids without any pronounced distortion of the water structure, with two water molecules in the lattice replaced by two oxygen atoms of the anionic tetrahedron, and two its other oxygen atoms occupy two adjacent voids. Being strongly hydrated, sulfate ions form with water molecules short hydrogen bonds and SO_4^{2-}–H_2O associates may appear in solutions containing these ions via transfer of a water molecule into a void [9].

The bulk properties of the solutions under study can be interpreted in terms of the approach suggested by Onori [10]. In this case, the solution is considered in the approximation of an ideal mixture of hydrated ions and molecules of "free" water, and the apparent molar volume V is determined by the relation

$$\Phi_V = (V - X_1V_1)/X_2, \quad (1)$$

where V is the average molar volume of the solution,

$$V = (X_1M_1 + X_2M_2)/\rho; \quad (2)$$

Gibbs energies of viscous flow, ΔG_η^*, of aqueous solutions of $CuSO_4$

T, °C	ΔG_η^*, kJ mol^{-1}, at indicated solution concentration, M								
	0.63	0.75	0.88	1.00	1.13	1.25	1.38	1.50	1.63
20	39.9	41.0	41.6	41.7	42.5	42.7	42.4	42.7	42.6
30	40.8	41.8	42.4	42.3	43.2	43.6	43.0	43.5	43.5
40	41.7	42.8	43.6	43.2	44.1	44.5	43.8	44.3	44.4
50	42.6	43.8	44.5	44.3	45.0	45.7	45.0	45.4	45.6

X_1, X_2, M_1, and M_2, mole fractions and molecular weights of the solvent and dissolved substance; ρ, solution density (g cm^{-3}); and V_1, volume of 1 mol of free water molecules, which can be calculated by the formula

$$V_1 = (1 - x)/V_s. \quad (3)$$

Here x is the mole fraction of water molecules in voids, and V_s is the molar volume of the skeleton.

The apparent molar volume of the ions grows with their concentration because of the decrease in the amount of water subjected to electrostriction and ceases to increase when no free water molecules remain in the solution outside the coordination sphere of the cations. Departure from linearity of the Φ_V–$c^{1/2}$ dependence for the solutions studied (see figure) may indicate that full hydration limit is reached. As is known [11], the molar volume of pure water increases with temperature. For copper sulfate solutions, the apparent molar volume Φ_V also increases as the temperature is raised from 20 to 50°C. This is probably due to deformation and rupture of hydrogen bonds in the solvent structure and to simultaneous binding of free water molecules into hydrated complexes.

Because water is an associated liquid, the viscous flow of aqueous solutions is accompanied by a structural deformation that involves energy expenditure [12]. The energy expenditure for the process of viscous flow can be estimated using the Eyring theory [4]. In terms of this theory, the Gibbs energy of the solutions studied was calculated by the formula

$$\Delta G_\eta^* = RT \ln \frac{\nu \overline{M}}{h N_A}, \quad (4)$$

where R is the universal gas constant; T, absolute temperature; η, kinematic viscosity (cm^2 s^{-1}); $\overline{M}$, average molecular weight ($\overline{M} = \Sigma M_i N_i$, M_i and N_i are molecular weights and mole fractions of the solution components); h, Planck constant; and N_A, Avogadro number.

Apparently, the change in the free Gibbs energy of viscous flow is due to the transformations occurring in the solution: destabilization of the structure is accompanied by a decrease in ΔG_η^*, whereas in the case of structuring, ΔG_η^* increases (see table).

The following equation [4]

$$\Delta H_\eta = R \frac{d \ln \nu}{d(1/T)} \quad (5)$$

was used to calculate the enthalpy of activation of the viscous flow, ΔH_η^*, for the solutions studied at t = 20–50°C:

c, M	0.63	0.75	0.88	1.00	1.13	1.25	1.38	1.50	1.63
ΔH_η^*, kJ mol^{-1}	4.7	4.6	4.5	7.6	6.9	5.4	6.2	5.7	5.5

The values of ΔH_η^* for the $CuSO_4$ solutions are lower than the enthalpies of activation of the viscous flow of water (ΔH_η^* of water is 16.26 kJ mol^{-1} [3]). This confirms that transition from one equilibrium

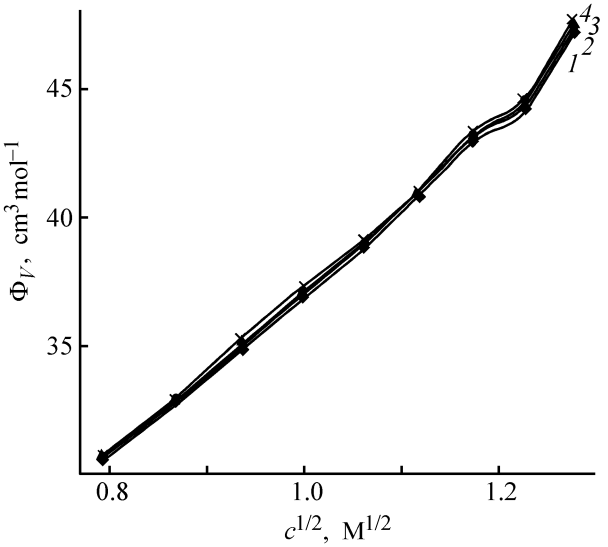

Φ_V–$c^{1/2}$ dependence for an aqueous $CuSO_4$ solution. (Φ_V) apparent molar volume and (c) concentration. Temperature, °C: (*1*) 20, (*2*) 30, (*3*) 40, and (*4*) 50.

to another is facilitated, and, consequently, the solution structure is disordered. The increase in ΔH_{η}^{*} on reaching $CuSO_4$ concentrations of 1.00 and 1.38 M is probably due to redistribution of water molecules in the hydrate spheres of the cations and anions and to formation of more stable hydrate complexes. Further decrease in the potential barrier with increasing viscosity can be understood on the assumption that a new polyionic structure consisting of hydrated ions and water molecules is formed in concentrated solutions. However, the forming structure is less stable than the water skeleton.

CONCLUSION

The manner in which in the activation characteristics of the viscous flow and the apparent molar volume of $CuSO_4$ aqueous solutions change with increasing concentration and temperature indicates that there occur complex structural transformations accompanied by destruction of the solvent structure, hydration of ions, and formation of a new polyionic structure in concentrated solutions.

REFERENCES

1. Krestov, G.A., *Termodinamika ionnykh protsessov v rastvorakh* (Thermodynamics of Ionic Processes in Solutions), Leningrad: Khimiya, 1984.
2. *Ionnaya sol'vatatsiya* (Ion Solvation), Krestov, G.A., Novoselov, I.P., Perelygin, I.S., et al., Eds., Moscow: Nauka, 1987.
3. Erdey Gruz, T., *Transport Phenomena in Aqueous Solutions*, London: Hilger, 1974.
4. Glasstone, S., Leider, K.J., and Eyring, H., *Theories of Chemical Reaction Rates*, New York: McGraw–Hill, 1941.
5. Solov'eva, N.D., Klinaev, Yu.V., and Tseluikin, V.N., *Zh. Fiz. Khim.*, 2003, vol. 77, no. 3, p. 459.
6. Tyurin, Yu.N., and Makarov, A.A., *Statisticheskii analiz dannykh na komp'yutere* (Computerized Statistical Data Analysis), Moscow: Infra-M, 1998.
7. Smirnov, P.R, and Trostin, V.N., *Struktura kontsentrirovannykh vodnykh rastvorov elektrolitov s kislorod-soderzhashchimi anionami* (Structure of Concentrated Aqueous Solutions of Electrolytes with Oxygen-containing Anions), Ivanovo: IKhNR, Ross. Akad. Nauk, 1994.
8. Fishkis, M.N. and Zhmak, V.A., *Zh. Strukt. Khim.*, 1974, vol. 15, no. 1, p. 3.
9. Lyashchenko, A.K., and Ivanov, A.A., *Zh. Strukt. Khim.*, 1981, vol. 22, no. 5, p. 69.
10. Onori, G., *J. Chem. Phys.*, 1988, vol. 89, p. 510.
11. Afanas'ev, V.N. and Tyunina, E.Yu., *Zh. Neorg. Khim.*, 2001, vol. 46, no. 12, p. 2095.
12. Grineva, O.V., and Korableva, E.Yu., *Zh. Fiz. Khim.*, 1998, vol. 72, no. 4, p. 657.

ISSN 1070-4272, Russian Journal of Applied Chemistry, 2007, Vol. 80, No. 10, p. 1779. © Pleiades Publishing, Ltd., 2007.
Original Russian Text © Editorial board, 2007, published in Zhurnal Prikladnoi Khimii, 2007, Vol. 80, No. 10, p. 1750.

OBITUARY

Georgii Gerogievich Furin (1939–2007)

DOI: 10.1134/S1070427207100394

On March 8, 2007, at the age of 69 passed away Georgii Georgievich Furin, a prominent Russia's fluoroorganic chemist, doctor of chemical science, professor. Georgii Georgievich was born on February 27, 1939, in Novorossiisk. Having early become an orphan (his father, G.I. Furin, was killed in action in December 1941, when defending Sevastopol), Georgii Georgievich got used to work already in his childhood; during years of education at Dnepropetrovsk University (1957–1962), he worked as loader, fireman, typography worker, and teacher of chemistry. Having graduated from the university in 1962, Georgii Georgievich became a staff member of Novosibirsk Institute of Organic Chemistry, where he worked during his whole life and made his way up from a senior laboratory assistant to deputy director for research activities. Georgii Georgievich was an exceedingly erudite chemist, closely acquainted with almost the entire body of chemical literature (he was the author of numerous articles in encyclopedias published by Springer, Guben-Weill, Harwood, and Elsevier publishing houses). G.G. Furin was an excellent experimenter-synthesist and a brilliant analyst.

The main area of Georgii Georgievich's scientific activities was study of fluorine-containing heterocyclic compounds; here, he was rightly considered a world-renown authority. G.G. Furin was the author of more than 400 papers, 30 reviews, and 8 monographs and holder of 40 patents. Georgii Georgievich was an excellent and attentive pedagogue. His pupils include 3 doctors and 9 candidates of science in Russia and 3 doctors of science in the Republic of Korea. Georgii Georgievich took care of his pupils during his whole life by helping in their employment, research, publication of papers and books, and, occasionally, financial problems. He was a member of scientific-technical councils at numerous chemical plants in our country and took part in the organization

of shops for manufacture of quite a number of fluoroorganic compounds.

Georgii Georgievich was a cultured person and a tactful, courteous and well-wishing, interesting and witty interlocutor, and a hospitable host. He was an honest man of principle who deeply loved his Motherland.

Respectful memory of Georgii Georgievich Furin will be forever preserved in hearts of all those who was acquainted with this excellent person.

Vorontsov Institute of Organic Chemistry, Siberian Division, Russian Academy of Sciences, Novosibirsk
Prikladnaya khimiya Russian Scientific Center Galogen Open Joint-Stock Company
Editorial board and editorial staff of Zhurnal Prikladnoi Khimii

ISSN 1070-4272, Russian Journal of Applied Chemistry, 2007, Vol. 80, No. 10, pp. 1780–1781. © Pleiades Publishing, Ltd., 2007.
Original Russian Text © A.G. Morachevskii, 2007, published in Zhurnal Prikladnoi Khimii, 2007, Vol. 80, No. 10, pp. 1751–1752.

BOOK REVIEWS

Fundamental'nye problemy preobrazovaniya energii v litievykh elektrokhimicheskikh sistemakh: Materialy IX Mezhdunarodnoi konferentsii (Fundamental Problems of Energy Conversion in Lithium Electrochemical Systems: Proc. IX Int. Conf.), Kolosnitsyn, V.S., Ed.,

Ufa: Reaktiv, 2006, 330 pp.

DOI: 10.1134/S1070427207100400

The proceedings of the International Conference on lithium power cells, held in Ufa on August 14–18, 2006, are published. The conference organizers included the Scientific Council for Electrochemistry (Section "General problems of chemical power cells") of the Russian Academy of Sciences, Academy of Sciences of Bashkortostan, Russian Foundation for Basic Research, and other institutions. The Proceedings volume reflects the results obtained in recent years in studies concerned with fundamental problems of energy conversion in lithium electrochemical systems. Particular attention is given to synthesis and properties of new materials for negative and positive electrodes of lithium power cells, mechanism of the processes occurring at the lithium electrode, thermodynamics of lithium intercalation into, and deintercalation from various electrode materials, and electrolyte properties.

The materials published in the collection of papers are grouped in six sections in accordance with the subjects covered. The first section (pp. 3–56, 20 papers) is devoted to the behavior, properties, and fabrication of the negative electrode in various lithium power cells. Problems associated with the behavior and cycling of metallic lithium in electrolytes based on aprotic organic solvents, behavior of the carbon electrode in charging of a lithium-ion battery, use of various brands of natural graphite and of modified oxide graphite as anode materials, and intercalation of lithium into various anodes are considered.

The second section (pp. 57–130, 27 papers) discusses a wide variety of issues associated with the behavior and choice of cathode materials for lithium power cells. Quite a number of papers consider synthesis of the $LiCoO_2$ compound and specific features of its use as a cathode material in lithium-ion batteries. Also discussed are cathode materials based on manganese compounds and more complex spinel formulations. One of the papers suggests that redox polymers with high content of sulfur should be used as an active cathode component for the lithium-sulfur battery. The possibility is discussed of employing natural pyrite FeS_2 and a thin-layer electrolytic FeS_2 composite as a cathode material for film-like lithium batteries.

The third section of the collection of works (pp. 131–221, 25 papers) presents new data on electrolyte systems. It should be noted that, despite the certain progress and extensive research in the field of polymeric electrolytes, solutions of lithium salts in aprotic media have been mostly used as liquid electrolytes in manufacture of lithium and lithium-ion batteries so far. On the whole, this circumstance is reflected in the subject field of the papers presented at the conference, which are mostly devoted to analysis and improvement of aprotic electrolytes. In particular, it is suggested to add polysulfides of various compositions to the electrolyte to improve the cycling capacity of batteries. The potentialities of polymeric gel-electrolytes in lithium and lithium-ion power cells are considered and the possibility of obtaining a solid polymeric electrolyte is discussed. An issue that remains topical is a search for various inorganic solid phases with high lithium-cationic conductivity.

The fourth section (pp. 222–255, 11 papers) contains evidence about the history of development and the modern state of manufacture of lithium-ion batteries. The lithium-ion technology can produce lithium-ion batteries with high specific energy and power, long service life, wide range of working temperatures, and high reliability. These advantages enable development of lithium-ion batteries for a wide range of purposes, including defense, space, and civilian applications. The positive electrode of industrially manufactured lithium-ion batteries is commonly fabricated

from lithium-intercalated cobalt oxide $LiCoO_2$, and the negative electrode, from various carbon materials, mostly graphite. The possibility of replacing graphite with thin-film hydrogenated silicon is considered. The choice of electrode materials and active paste formulations for a lithium-ion battery with increased capacity is discussed.

The fifth section of the collection of works (pp. 256–308, 11 papers) is devoted to lithium power cells. The problem of development of lithium–sulfur batteries with aprotic electrolytes, which has been attracting attention during many years, is discussed in detail. The theoretical specific energy of the Li–S system is 2600 W h kg^{-1}. This circumstance gives reason to believe that batteries with a specific energy as high as 500–700 W h kg^{-1} can be developed. The real specific energy of prototype lithium–sulfur batteries being developed by a number of companies is substantially lower, 250–350 W h kg^{-1}. Mechanisms of the possible corrosion processes in chemical power cells with a lithium anode are considered.

The small sixth section (pp. 309–318, 5 papers) discusses new devices and apparatus for studies of chemical power cells. These include an automated potentiostat-galvanostat, a stand and software for tests of chemical power cells in the prolonged-cycling and low-current mode, and a multifunctional automated stand for studies of electrode materials and power cell.

Analysis of the evidence presented in the collection of works suggests that lithium electrochemical systems are being most intensively studied in Russia at the following institutions: Istochnik Research Battery Institute (St. Petersburg); Siberian State Technological University (Krasnoyarsk); Frumkin Institute of Physical Chemistry and Electrochemistry (Moscow); Institute of Organic Chemistry, Ufa Scientific Center, Russian Academy of Sciences; Institute of High-Temperature Electrochemistry, Ural Division, Russian Academy of Sciences (Yekaterinburg); Favorskii Institute of Chemistry, Siberian Division, Russian Academy of Sciences (Irkutsk); Nikolaev Institute of Inorganic Chemistry, Siberian Division, Russian Academy of Sciences (Novosibirsk); and Chernyshevsky State University (Saratov).

A. G. Morachevskii

ISSN 1070-4272, Russian Journal of Applied Chemistry, 2007, Vol. 80, No. 10, p. 1782. © Pleiades Publishing, Ltd., 2007.
Original Russian Text © A.G. Morachevskii, 2007, published in Zhurnal Prikladnoi Khimii, 2007, Vol. 80, No. 10, pp. 1752–1753.

BOOK REVIEWS

Vakarin, S.V., *Orientirovannyi rost vol'framovykh bronz pri elektrolize rasplavov* (Oriented Growth of Tungsten Bronzes in Electrolysis of Melts),

Yekaterinburg: Ural. Otd. Ross. Akad. Nauk, 2005, 109 pp.

DOI: 10.1134/S1070427207100412

At the Institute of High-Temperature Electrochemistry, Ural Division, Russian Academy of Sciences, pupils of Academician A.N.Baraboshkin (1925–1995) continue systematic studies initiated by him in the field of the electrocrystallization of metals and various complex compounds from molten electrolytes. The research in this area, distinguished by original problem formulation and novelty, has already yielded theoretically and practically important results. The monograph by S.V.Vakarin is concerned with the oriented growth of crystals of tungsten bronzes in electrocrystallization from molten electrolytes. The book comprises an introduction, four chapters, conclusion, and bibliographic list.

The brief introduction (pp. 3, 4) notes advantages of the electrolytic method for growth of tungsten bronze crystals over other techniques. The aim is to find conditions under which crystals with a certain shape and spatial orientation can be obtained. The first chapter (pp. 5–36) analyzes some general evidence available in the scientific literature. It discusses the mechanism of crystal growth in various media under various conditions, morphological stability of crystals, and theory of formation of a preferential orientation of crystals. A separate section of the chapter is devoted to oxide tungsten bronzes, their nature, their synthesis by electrolysis of melts, and growth of single crystals.

The second chapter (pp. 37–46) includes description of methods for study of the oriented growth of single crystals directly in the course of electrolysis. The third chapter (pp. 47–89) considers the relationship between the growth rates of single crystals of bronzes with tetragonal and hexagonal structure and the overvoltage. The experiments performed with Baraboshkin's participation by the author of the monograph were aimed to measure the growth rates of crystals in different directions, analyze their faceting and the morphology of the crystal faces, and determine the chemical composition of the crystals and their lattice constants. Melts of the system K_2OWO_4–Na_2WO_4–WO_3 (700°C) served as the electrolyte in a study of the growth of single crystals of an oxide bronze with a tetragonal structure; single crystals of the oxide bronze with a hexagonal structure were obtained in electrolysis of a melt of the system K_2WO_4–Li_2WO_4–WO_3 (700°C).

The experimental results are illustrated by a large number of photographs. The author makes a comparative characterization of the morphological features of metals and oxide bronzes.

The small fourth chapter (pp. 90–98) discusses certain aspects of crystal structure formation. The conclusion (pp. 99, 100) summarizes the main concepts considered in the monograph. It is, in particular, noted that conclusions concerning the crystal growth types, made for oxide tungsten bronzes, can be extended to other substances. The bibliographic list (pp. 101–107) contains references to 148 domestic and foreign publications, with a prominent place occupied by works of Baraboshkin and co-workers, including the author of the monograph. As already noted, tungsten bronzes can be regarded as a model object in high-temperature studies of the electrocrystallization process.

The monograph by Vakarin may be of interest for a wide audience of specialists studying the crystallization process. The Institute of High-Temperature Electrochemistry (Ural Division, Russian Academy of Sciences), which celebrates its 50th foundation anniversary in 2007, is the only Russia's specialized institution engaged in broadscope studies of promising systems and processes associated with electrochemistry of molten and solid electrolytes. The research conducted at this institute is distinguished by a high experimental and theoretical level. The monograph is well written and accurately published, and makes quite a favorable impression.

A. G. Morachevskii

ISSN 1070-4272, Russian Journal of Applied Chemistry, 2007, Vol. 80, No. 10, p. 1783. © Pleiades Publishing, Ltd., 2007.
Original Russian Text © A.G. Morachevskii, M.S. Kokhatskaya, 2007, published in Zhurnal Prikladnoi Khimii, 2007, Vol. 80, No. 10, pp. 1753–1754.

BOOK REVIEWS

Tarantseva, K.R. and Pakhomov, V.S., *Pittingovaya korroziya nerzhaveyushchikh stalei: Teoriya i praktika zashchity* (Pitting Corrosion of Stainless Steels: Theory and Practice of Corrosion Protection),

Penza: Penz. Gos. Tekhnol. Akad., 2006, 134 pp.

DOI: 10.1134/S1070427207100424

As is known, pitting corrosion is one of the most dangerous and widely occurring types of local corrosion-induced disintegration of passivatable metals and alloys in media containing activator ions. A major contribution to studies of the pitting corrosion was made by Ya.M. Kolotyrkin (1910–1995), academician of the Russian Academy of Sciences, and his coworkers. It has been established that both pure metals (iron, zinc, aluminum, magnesium, nickel, cobalt chromium, titanium) and various alloys, including those in the amorphous state, may suffer from pitting corrosion. The set of anions, both causing the corrosion process and acting as inhibitors, has been outlined.

The small monograph by K.R. Tarantseva and V.S. Pakhomov presents modern concepts concerning the mechanism of pitting formation in stainless steels and considers factors affecting the resistance of steels to this kind of corrosion. Methods used to study the pitting corrosion, prognosticate pitting, and protect metals from pitting corrosion are discussed. The book comprises an introduction, five chapters, and bibliographic list including 455 references to publications by domestic and foreign authors.

The brief introduction (pp. 3, 4) notes that a number of issues in the theory of pitting corrosion and protection from this kind of corrosion require an additional analysis and there remains an important problem of prognostication of this kind of corrosion. The first chapter (pp. 5–12) discusses the mechanism of pitting corrosion of stainless steels. It shown that the following is necessary for this kind of corrosion to occur: a metal should be in the passive state; the amount of activator ions should exceed the critical concentration; and an oxidizing agent or external polarization, which shift the corrosion potential, should be present. Reasons for local disintegration of the passive film are discussed in detail and it is noted that the adsorption-electrochemical theory provides the presently most substantiated explanation of the passivity phenomenon.

The second chapter (pp. 13–34) considers factors that affect the pitting corrosion of steels. To these belong the composition of stainless steels, solution composition, temperature and heat-transfer conditions, and motion of the medium. The authors systematized the fundamentally important results obtained in studies of the pitting corrosion, including those carried out in the last 10–15 years. It is noted, in particular, that carbon, sulfur, and phosphorus adversely affect the resistance of steels to pitting corrosion. The low content of carbon in ferrite steels and their single-phase structure predetermine their high pitting resistance.

The third chapter (pp. 35–64) is devoted to methods for studying, modeling, and controlling the pitting corrosion. The fourth chapter (pp. 65–81) discusses the possibility of prognostication of the pitting corrosion. The final, fifth chapter (82–107) contains evidence about the principal ways of protection from this kind of corrosion. Of special interest is that section of this chapter in which practical recommendations for choice of pitting-resistant steels are given. The authors composed an algorithm for obtaining the necessary information when choosing corrosion-resistant materials in the stage of article design.

The monograph by Tarantseva and Pakhomov is well written, presents an analysis of a vast material, and is accessible to an exceedingly wide audience of specialists engaged in studies of corrosion processes and to engineers and technical workers of design bureaus and research institutes. The book may be of use for students and postgraduate students specialized in the field of corrosion and metal protection.

A.G. Morachevskii, M.S. Kokhatskaya

ISSN 1070-4272, Russian Journal of Applied Chemistry, 2007, Vol. 80, No. 10, p. 1784. © Pleiades Publishing, Ltd., 2007.

ERRATA

Erratum: "Synthesis and Biological Activity of Schiff Bases Derived from Dehydroabietylamine and Benzaldehyde Derivatives" [*Russian Journal of Applied Chemistry* 80 (8), 1373–1375 (2007)]

Xiaoping Zhao, Dzen Kwang Song, A. B. Radbil', and B. A. Radbil'

Institute of Chemical Processing of Wood Products, Academy of Wood of Chinese People's Republic, Nankin, China

Received September 14, 2007

DOI: 10.1134/S1070427207100436

The authors of this paper should be read as: Xiaoping Rao, Zhanqiang Song, which is commonly accepted English spelling.

The title of the institute the authors are affiliated with should read as: Institute of Chemical Industry of Forest Products, Chinese Academy of Forestry, Nanjing 210042, China

ISSN 1070-4272, Russian Journal of Applied Chemistry, 2007, Vol. 80, No. 11, pp. 1785–1792. © Pleiades Publishing, Ltd., 2007.
Original Russian Text © V.B. Aleskovskii, 2007, published in Zhurnal Prikladnoi Khimii, 2007, Vol. 80, No. 11, pp. 1761–1767.

INORGANIC SYNTHESIS AND INDUSTRIAL INORGANIC CHEMISTRY

Quantum Synthesis

V. B. Aleskovskii

St. Petersburg State University, St. Petersburg, Russia

Received February 21, 2007

DOI: 10.1134/S1070427207110018

All that exists is composed of comparatively not numerous "pure" individual substances and unimaginably enormous number of their extremely complex mixtures, substances of variable composition. When molecules, or individual substances, were discovered, chemistry naturally made them key objects of study and the XIX century became the century of its development. However, it was found in the XX century that most of substances are solid supramolecular substances that are not described by chemical laws, although these laws are based on the atomic-molecular theory whose reliability is beyond any doubt. Meanwhile, the physicochemical analysis was developed, which made it possible to determine the dependence of properties of a substance on its composition. And this was sufficient for the development of a technology for processing of solid substances into all kinds of materials. Because of this circumstance the chemical science accepted that, together with compounds of invariable composition, molecular compounds, there also exist individual solid compounds of variable composition, nonstoichiometric compounds. Despite that individual solid compounds were synthesized at the beginning of the second half of the XX century [1], it is still commonly believed that formation of stoichiometric solid compounds is prohibited by the nature.

One can readily imagine the huge loss inflicted on technologies by the necessity to "purify" starting substances to remove "impurities," or, in effect, to separate the solid solutions that surround us into components, i.e., chemical individuals. Also suffers the solid-state chemistry, which deprived itself of objects of study and degraded to an accessory of physics. The consequences are evident from the monograph [2], whose authors reported that "however, we are only beginning to understand the principles to be used in design and manufacture of nanostructures and nanodevices." And the reason is the lack of skill to synthesize "isolated nanostructures."

At the same time, studies of synthesis of solid chemical individuals, polyatomic compounds, demonstrated that their formation is exceedingly unlikely. To obtain these compounds, it is necessary to raise the probability of their formation to 100%; in other words, to collect and generalize the whole body of information about the nature of a compound and, primarily, to use it in the same way as genetic information is used in biosynthesis [3].

First of all, it was necessary to find out how an individual solid is built and what it is from the chemical standpoint. In the first half of the XX century, this problem was solved at the Lensovet Technological Institute in Leningrad. According to the "core theory" developed at this institute [4], the structure of a solid includes 0D, 1D, 2D, 3D, or coordination core composed of atoms bonded by covalent bonds. The surface of the core is constituted by functional groups. In contrast to the commonly accepted physical model, which only reflects the periodicity of the crystal structure, the core model reveals the atomic structure of a solid. A single glance at this model was sufficient for understanding that, by connecting all the peripheral atoms by functional groups, one can obtain a solid that is nothing other than a supramolecule of a stoichiometric solid compound, a polyatomic chemical individual.

Polyatomic individuals, including quantum bodies (nanostructures), have been synthesized as a result of the discovery of irreversible chemisorption, epitaxial method of atomically precise batching of reagents. Using this method, the surface of a solid with known area was treated with an excess of an adsorbate during a time required for 100% coverage of the substrate surface with a monolayer of the adsorbate. With one monolayer after another batched-out and bound together by chemical bonds, a number of simple, e.g., carbon-containing, substances have been synthesized by the above-mentioned molecular layering method,

and series of individual solids, by the chemical assembly technique. Apparently, these syntheses are controllable irreversible processes. At the same time, these are processes of batching-out of atomic portions (quanta) of a substance, i.e., quantum synthesis processes, and those of 3D writing with chemical symbols and the resulting materialization of information. Thus, it can be stated that, similarly to biosynthesis, synthesis of chemical individuals is based on production and materialization of information in quantum processes programmed to form solids in a stationary discrete nonequilibrium state, quanta of solid substances or solid bodies up to approximately 100 nm in size.

Similarly to biosynthesis, quantum synthesis occurs in an open system, with genetic information, energy, and reagents (and the related structural information) fed into the system; synthesis products and the information contained in these products extracted; and excess reagents, invaluable products, and degraded, low-temperature energy removed.

This process is initiated and controlled, similarly to biosynthesis, by the genetic information, which is "written" not in the DNA structure, but in the dynamic structure of flows of starting substances and, in part, in the structure of these substances themselves, but primarily in the program of synthesis, developed by its designers.

This synthesis is, similarly to biosynthesis, a process of transcription, translation, and production of information, although more primitive. Its additional characteristic feature is localization, isolation of the synthesis process from the ambient medium, which, however, does not preclude interaction with this medium. This suggested that, similarly to biosynthesis, quantum synthesis of polyatomic individuals is only possible in irreversible processes based on the same principles, including those of transcription and translation of the genetic information delivered by the corresponding mother structure (substrate, matrix).

Unfortunately, this remained unnoticed by nearly everyone. Meanwhile, as can be seen from what follows, all efforts of a large number of researchers struggling to solve the problem of synthesis of nanostructures, as well as the general problem of the nature of solid matter, have been in vain. However important the problems of modern chemistry may be, they fall far into the background now. In the light of the great discoveries of the XX century, there appeared an absurd, at first glance, concept of our world as a very rapidly expanding flow of waves, constituted by wave packets, which generates space and time in its motion. A wave packet is a quantum of mass–energy and action of certain value, which exchanges photons, quanta (quantity of action) of minimum value, with other packets. There is no way to know where a wave packet, i.e., an object, is situated at a given instant of time. However, the Schrödinger function ψ can be used to calculate the probability of its localization, and this can be found with 100% reliability by taking the square, ψ^2.

From this standpoint, atoms, molecules, and small bodies are nothing other than quantum particles, and chemistry is quantum chemistry obeying quantum probability laws.

Elements of quantum technology. Seeing no real reasons for accepting the impossibility of existence of solids of invariable composition, I started in mid-XX century, together with a group of co-workers, students, and postgraduate students, to study the problem of synthesis of polyatomic individuals, without realization of the opening-up prospects. It was found that the problem of synthesis of individuals consists in structuring of an appropriate substance in a certain stationary nonequilibrium discrete state, "quenching" of this substance in this state, and stabilization via modification. Thus, the individuals can be synthesized using any suitable irreversible process. This is demonstrated in the present paper for the example of flame quantum synthesis of benzene derivatives and nanodispersed activated carbon in combustion of methane.

In 1974, the Presidium of the Academy of Sciences of the USSR considered the report [5, 6] that solid substances of invariable composition, allegedly nonexistent according to modern concepts, were synthesized by molecular layering and chemical assembly. In that communication, we reported that this technique consists in multiple stages of alternating irreversible chemisorption of monolayers of the same or different compositions on a substrate prepared in an appropriate way and each stage is continued until 100% coverage of the substrate area. It was stated that the "chemical assembly method" can be used to obtain metastable modifications of solid substances. Their number is huge because it is due to the number of possible energy states constituting a whole band. Such a band lies between the formation energies E_{min} and E_{max} of a solid substance. To each discrete state of this energy spectrum corresponds a single chemical individual, a member of a homologous series of nanostructures, and to the continuum of degenerate states, the whole set of ordinary macroscopic solid bodies of the given composition. Thus, that communication

considered synthesis of chemical individuals for the first time as quantum synthesis, which can "synthesize materials, physical devices, and, in perspective, biological tissues and organs" [6].

Later, a number of syntheses of nanostructures and quantum devices were performed: e.g., chalcogenide superlattices, system of quantum wells. Also, diamond-like films, carbon nanostructures, and nanostructures of many other types were synthesized [6].

By the end of the XX century, it was found [7, 8] that, like biosynthesis, chemical assembly consists in replication, production, and materialization of information, its implementation in the structure of reaction products. Also, synthesis of individual chemical and biological products is only possible via batching of reagents on the atomic level. Thus, it was demonstrated that synthesis of chemical individuals is, in fact, quantum chemical synthesis. It was also found that chemical assembly is not the only possible method of quantum chemical synthesis. For example, the long-known, but used only by special branches of technology, chain chemical processes are true quantum processes, conversion of chemical energy, quantum after quantum, into heat and mechanical energy. And there is nothing that could prevent their reorganization on the basis of the principles underlying the chemical assembly technique into processes of quantum synthesis. Indeed, it is not so important that nanostructures are dwarfs among the known chemical structures. It is more important that they are, similarly to atoms, quanta of matter and obey laws of quantum theory and chemistry of highly organized substances [9]. Quantum processes play an important part not only in the microcosmos, they universally occur in nature in those cases when chemical and biological conversions of substance proceed. For example, they enable such oxidation processes as combustion and life. It is also essential that the corresponding individuals are formed in both cases. However, in the course of combustion, polyatomic individuals are converted into those with small number of atoms and their chemical energy degrades into heat, whereas in biosynthesis, by contrast, comparatively low-atomic individuals are converted into polyatomic and ultrapolyatomic ones and the chemical energy of the former is nearly entirely expended for creation of the structure of biosynthesis products. As shown in [10], chain reactions occur via relay transfer of electrons from starting substances to final products with a nearly 100% probability. The chemical energy is virtually not dissipated at all in these reactions. Synthesis proceeds at an exceedingly high rate, with release of the minimum amount of heat and by-products, being only slightly exceeded in efficiency by biosynthesis.

From combustion to quantum flame synthesis. Combustion was the first chemical process mastered by the humankind. Its heat and light enabled humans to survive and build first civilizations, and its working power, to approach the modern state of development. At present, the advances in knowledge open up prospects for use of the fire not only as the most accessible environmentally safe source of energy, but also as the most efficient generator of organic and inorganic products. And not only as a versatile chemical generator, but as a most potent source of information.

As a rule, ordinary chemical syntheses are comparatively slow probabilistic processes occurring near the equilibrium state. Their efficiency is low. To raise the rate of these processes, syntheses are performed at elevated temperatures. For example, technical-grade carbon, e.g., carbon black, is commonly synthesized at 1000–1300°C. The yield of the target product in this process commonly does not exceed 3–4%. Carbon black is obtained in a somewhat higher yield by combustion of a fuel, e.g. methane, in a narrow channel at a deficiency of oxygen. As carbon black is accumulated, it is discharged.

The flame freely burning in air, diffusion flame, is a self-organizing stationary process of oxidative degradation of a fuel to give the simplest inorganic compounds, H_2O and CO_2, as products. The combustion rate and, consequently, flame temperature are determined by the rates of oxygen supply and combustion product removal. At a deficiency of oxygen, as, e.g., in the above-mentioned synthesis of carbon black, an inseparable mixture of products of oxidative condensation of the fuel is formed in the flame, with the components of this mixture, such as individual polyatomic, including supramolecular, solid compounds condensed immediately after formation.

The flame combustion is known to be an instantaneously occurring multistage chain process of oxidation. Its products of a given composition, formed in a stage of this process, are instantaneously converted into products of another composition in the subsequent stage. In the case of an excess of oxygen, increasingly oxidized substances instantaneously appear from one stage to another. At the same time, at a deficiency of oxygen, the excess part of the fuel reacts with intermediates to give mixtures of highly condensed products, such as soot and carbon black.

It was shown in [11] how this exceedingly rapid process can be interrupted at one of stages so that

the product formed in this stage is preserved. Generalizing the data obtained in studies of chain processes, beginning with publications by N.N. Semenov and his school, Azatyan noted [12]: "branched-chain ignition, in contrast to the thermal ignition, is caused by avalanche multiplication of active intermediates, free atoms, radicals, and, occasionally, even excited species, in their fast reactions with starting reagents and with each other" and pointed to the efficiency of control over chain combustion by inhibitors. However, what is particularly important, he called attention to the fact that the chemical energy in branched-chain combustion is nearly totally accumulated as chemical energy of unpaired spins, rather than converted into heat and dissipated. This energy of free valences is "transferred by the relay mechanism to the newly formed atoms and radicals and is even expended for their multiplication." "Chain branching is a dominant factor" that determines the specific pattern of the given process.

It should, however, be noted that, from the standpoint of our theory of structural organization, the chain branching itself is controlled, as well as the entire combustion process, by genetic information introduced into it by the synthesis program. The oxidation processes occurring in living bodies, translating information and solar energy to molecules, feed the living world in the planet with these factors. At the same time, combustion processes devour that part of the living substance which cannot be eaten by living bodies themselves. Oxidation in cells is a complex process of electron transfer via chemical interaction of polyatomic complementary structures, programmed by the genetic (parental) information. Combustion is a process of instantaneous direct, "relay" transfer of electrons from one radical (free atom) to another. Both these processes, oxidation in a cell and combustion in a flame, are localized. However, combustion is a process of virtually instantaneous degradation of all reagents, with dissipation of most part of their chemical energy and synthesis of the simplest products at the expense of its remaining amount. At the same time, oxidation in cells is a process of successive conversions of nearly the whole oxidation energy into work of synthesis of highly organized products. Having analyzed the oxidation process from this standpoint, we decided to form a kind of a dynamic cell from the flame, in order to imitate biosynthesis by creating, based on such a modified combustion process, a new productive technology for synthesis of organic and inorganic products.

Combustion of gaseous substances is commonly initiated by a spark or a flame from any source. Free atoms and molecules flying from this auxiliary flame into the gas collide with gas molecules and enter into chain reactions, in which uncountable new radicals are vigorously formed, and the chain process encompasses the whole volume of the given gas and flame flares up. If the fuel and oxygen are replenished and delivered in such amounts that the heat expenditure is balanced by its inflow, with the combustion products continuously removed, and only CO_2 and H_2O are formed. However, the combustion process can also be directed to synthesis of an aliphatic or aromatic derivative, e.g., benzene, the intermediate product of the given process. According to the theory of structural organization, it is necessary to impart to the flame a certain shape and structure and to establish a synthesis mode in which products in a prescribed stationary nonequilibrium (e.g., discrete) state, i.e., nanostructures, can be obtained by instantaneously interrupting the process in an appropriate stage of the chain process.

Because chain processes occur at a great rate, an exceedingly large amount of products is formed in comparatively small flame volumes. And this makes unnecessary use of large-capacity reactors, pipes, and apparatus for gas-phase synthesis.

Construction of a compact flame. The spontaneous flame is a dynamic dissipative structure set by the genetic information inflowing from the outside. It can have a very peculiar shape, but this shape always provides the maximum dissipation of the combustion energy. Using the flame as a generator of certain intermediate combustion products, rather than a source of heat, we are, naturally, not interested in transformation of the chemical energy into heat and in dissipation of the latter. By contrast, our task is to use the maximum amount of the chemical energy released in the given process for formation of chemical bonds constituting the structure of the desired target product and to minimize the decomposition they experience when leaving the flame. For this purpose, we impart to the flame the form of a "dynamic cell," in which, as in cells of living bodies, degradation of reagent molecules precedes synthesis from their fragments of some programmed highly organized compounds.

As shown in the figure, the flame grows, in a literal sense, from flows of the oxidizing agent ($\downarrow\downarrow$) and fuel ($\uparrow\uparrow\uparrow$).

This flame was created by forming counterflows of reagents. Entering from two sides into the flame through the vapor–gas shell *3* heated to a temperature of about 350°C, counterflows of Cl_2 and CH_4 molecules are heated within the high-temperature zone *2* to

a temperature of dissociation, whose products, the corresponding atoms and radicals, enter into chain reactions. The heat of these reactions, released at the flame core, raises in this mode the combustion temperature in zone *1* to a certain value of about 10^3°C at which the given chemical system is in the equilibrium state. In the process, a plasma of clusters, corresponding "preproducts", is formed in zone *1*.

When flying into zone *2*, clusters react with each other and with products formed by dissociation of fuel and oxidant molecules, which move in the opposite direction, and lose most part of their excess energy on the periphery of this zone. Thus, when arriving into zone *3*, the clusters are in the stationary nonequilibrium discrete state and become target products upon "quenching." Because the flame lies at the axis of the reaction vessel whose walls are washed from the inside by water, the quenching of the reaction products occurs automatically: some are quenched when flying across shell *3* and others, upon collision with the surface of water flowing down over reactor walls.

Apparently, this method can be used to obtain from the flame of, e.g., methane any aliphatic or aromatic derivatives. Each of these derivatives is formed in its own synthesis mode, specifically, in the mode in which its clusters are in zone *1* in a prescribed "starting" state, i.e., in the next to last stage of the corresponding chain process. If we wish to obtain, e.g., hexachlorobenzene, we take chlorine as oxidizing agent and experimentally find the combustion mode in which this polychloride is formed. What is this mode? This is combustion, under other appropriate conditions, at a certain flow rate ratio of the fuel and chlorine, i.e., at the ratio for which the temperature in zone *1* of the flame reaches the above-mentioned maximum value. In this case, heat exchange occurs in shell *3* and "preliminary" structures of the target products, which are more complex and have higher energy content than those formed in the high-temperature mode, are formed in plasma *1*, and less complex, in zone *3* or outside this zone.

The principal specific feature of this synthesis consists in that it is quantum synthesis occurring via chain reactions localized in the dynamic cell, which is constituted by a flame formed in an appropriate way, and in that it is controlled by the natural or artificial genetic information coming from parents.

In a well-organized flame, the chemical energy of the fuel and oxidant is nearly completely converted into a higher-potential energy, as it also occurs in living cells, but without any enzymes, cofactors, or other intermediaries, and the amount of information

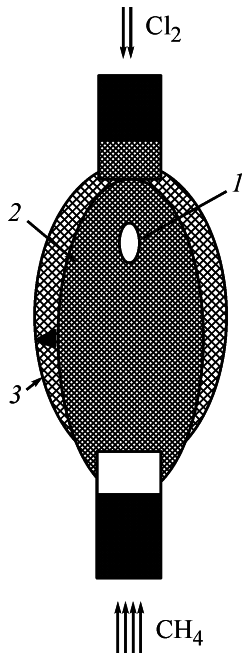

Schematic of the flame formed as a "dynamic cell." (*1*) Cluster plasma zone, (*2*) heat exchange and thermal dissociation zone, and (*3*) shell.

contained in them becomes many times larger and more valuable. In the process, both the energy and information are embodied in the structure of the synthesis products and thereby determine the level of the structural organization of the target products.

Being a branched-chain process, the quantum flame synthesis occurs via instantaneous transfer of electrons from donors to acceptors, i.e., by the quantum-chemical mechanism, without any significant dissipation of energy. Nearly the whole chemical energy of the reagents and the information they contain is converted into a high-potential energy of highly organized final products, rather than into heat or energy of bonding and structural information of CO_2, H_2O, and other simplest structures. The excess amount of the chemical energy is expended in the course of heat exchange for dissociation of molecules of the starting substances.

The fact that the flame is separated into temperature zones *1–3*, in which occurs effective heat exchange between products and reagents, the combustion products can lower, in the given synthesis mode, their energy state to a level prescribed by the program. In this flame, any desired target product can be, in principle, formed from the plasma of clusters-nuclei of intermediate products of oxidative condensation. Because virtually any, and not only organic, substance

can be burnt in a flow of an appropriate oxidizing agent, the flame quantum synthesis is a versatile synthesis technique, which is no less efficient than biosynthesis, but is considerably faster.

Pathway to life. The aforesaid leads to a working hypothesis according to which the pathway of evolution to the origination of life passed via flame, i.e., started from localization of a very tenacious, "energetically favorable" branched-chain process of oxidative condensation. However, because of its rapidity and excessive aggressiveness, this process did not become the process of life, but instead devoured its excessive and obsolete creatures and was subjected to evolutionary transformation. The genetic information programming the combustion process and incoming with heat fluxes from outer sources was substantially supplemented and, in the course of time, embodied in stationary structures of solid products. Chain reactions were replaced with a sequence of quantum reactions, along which the huge oxidation energy gradually, as over a staircase steps, descended to a moderate level and executed on its way a work of organism structuring. This gave rise to biosynthesis, the most perfect accomplishment of the evolution. In this way, the process of oxidative condensation formed a basis of two life phenomena: combustion, or complete destruction of a substance in a flame, and breathing and structuring of a substance in a living body. The flame quantum synthesis is a kind of symbiosis of these two phenomena, which is favorably distinguished from the known industrial processes by the very high utilization level of the energy of a fuel, exceedingly high rate, and full isolation from the ambient medium.

The atmosphere is not overheated and nothing is discharged into the environment except water. In this context, we can prognosticate with a quite substantiated confidence a transition from the existing technology to the quantum flame technology and, therefore, to the course of evolution, with all the resulting favorable consequences. As a prototype of the quantum flame technology can serve the process considered in what follows.

Synthesis of nanodispersed activated carbon. A study of the flame process of oxidative condensation of methane under the action of oxygen and chlorine [11, 13] demonstrated that a considerable part of methane burns in an oxygen flame in any combustion modes to give CO_2 and H_2O. At the same time, a chlorine process utilizes, in a certain range of conditions, the whole amount of methane carbon to give polyatomic aliphatic or aromatic chlorides, derivatives of benzene, naphthalene, anthracene, and hydrocarbons with numerous benzene rings. There also exists a combustion mode in which a predominantly nanodispersed carbon is formed. Having established these facts, we found the combustion parameters at which valuable products are formed and developed a synthesis program that makes it possible to pass from one combustion mode to another. This program contains a genetic information which directs the combustion process to disintegration of the structures of the starting products and formation of certain target products from these structural elements. Thus, the flame turns from a disintegrator of chemical products into a versatile generator of chemical compounds, and it is nearly as efficient as biosynthesis. The process of flame synthesis is localized (but not isolated from the medium) in the flame, where optimal conditions are created, as in living cells, for synthesis of individuals and premature contact with the medium of their not quite formed structures is precluded. Because chain processes occur at a very high rate, an exceedingly large amount of products is formed in a comparatively small volume of the flame. In many cases, e.g., in methane conversion, this makes unnecessary use of large-volume reactors, pipes, and apparatus for gas-phase synthesis.

At present, having accomplished under the author's supervision R&D work at Tekhnolog Special Design Office, State Unitary Enterprise in 2004–2005, the Scientific school of chemistry of highly organized substances, Aerotekhkosmos Private Company, and Nanomaterialy Limited Liability Company prepare to putting into operation a semicommercial model installation for flame synthesis of nanodispersed activated carbon and other individual products of conversion of natural gas in its combustion, e.g., hexachlorobenzene, which can be readily converted in a similar process into benzene. According to calculations, a finite set of large stationary and small mobile installations of this kind could provide the world with all that is necessary, at least until a demographic equilibrium is attained. Now, the task is, for the most part, to organize industrial implementation of this technology.

Theory. When trying to comprehend the knowledge accumulated by mid-XX century, I.R. Prigogine, one of the leading researchers of our time, outlined a scientific picture of the World, from which it can be seen that we live in a world of unique accidental events and irreversible processes, in a world in which all kinds of dissipative structures are accidentally formed under certain conditions far from equilibrium, among which "precursors" of life had once appeared. It is known from the thermodynamics of irreversible processes that the disorder governing a sys-

tem in equilibrium gives way to order relatively far from equilibrium: the system passes into a stationary discrete nonequilibrium state and takes on one of the wide variety of its possible structures. Which one? According to Prigogine [5], this occurs by chance. In what follows, we demonstrate that individual structures are formed under the action of an order factor, information, rather than by chance. For example, structures appear in the course of biosynthesis under the action of the genetic, parental information.

According to the quantum theory, there is neither a phenomenon, nor an event whose probability cannot be calculated. And if the square of the corresponding wave function, $\psi^2 = 1$, an event, e.g., formation of an individual solid compound, is not only possible, but undoubtedly occurs in nature.

At the end of the XX century, we found that, as expected, the probability of any event can, in principle, be raised in some way to 100% via expenditure of a certain amount of energy. What are the possible ways? As shown in [5, 6], these are synthesis procedures in the course of which a sufficiently large amount of information is produced. It was also suggested in these communications that the information and structure are inseparable: information is "inscribed" in the structure. Extending this working hypothesis, we take that substance consists of inseparable entities: mass, energy, and information. Bringing, in accordance with Prigogine's theory, a given system of interacting substances to the stationary state, we introduce into it, together with a flow of energy, a certain amount of information, specifically, that equal to the difference $(I - S_{min})$, where S_{min} is the minimum entropy corresponding to the stationary state of this system. The point is that, as is known, the sum $I + S = 1$.

If, however, this is so, then any chemical system, e.g., a system of interacting gases, say a reducing gas and an oxidizing gas, can be brought in an appropriate way to a stationary state in which individual products corresponding to the composition of the system are formed in it via a redox reaction. As shown above, the experiment confirms this working hypothesis.

CONCLUSION

The twentieth century was a century of great discoveries, which made clear that matter consists of exceedingly small quanta, "packets" of waves with a certain frequency, carrying mass and energy. Each of such clusters of mass–energy produces on all the other quanta an action proportional to a quantity on the order of 10^{-33} erg s, which changes to a certain extent their structure and causes an adequate counter effect (sets their program, i.e., programs their further existence). Our working hypothesis was the suggestion that substance is a mass intimately related not only to mass, but also to action and, consequently, to space and time. If it had no action, the quantity having dimension of energy multiplied by time, substance would be devoid of motion and its particles, quanta, could not interact by exchanging mass, energy, and action. Observing an action, we obtain information, a physical quantity of dimension nat J^{-1}. The quantum of action, Planck constant h, is a quantity on the order of 10^{-33}. The smallest quantum of matter, its elementary particles, has the same order of magnitude.

Constructing chemical processes as reproduction of natural processes, such as combustion (chain process) and biosynthesis (transcription, translation, and at the same time production and embodiment of information), we learned to create fast chemical synthesis processes.

ACKNOWLEDGMENTS

The author notes, with deep sincere gratitude, that he is fully obliged to his younger colleagues, many of whose names are mentioned in the book [14], and thanks foundation of Russian State for the financial support of the School.

REFERENCES

1. Aleskovskii, V.B., *Stekhiometriya i sintez tverdykh soedinenii* (Stoichiometry and Synthesis of Solid Compounds), Leningrad, 1976.
2. *Nanotechnology Research Directions: IWGN Workshop Report, Vision for Nanotechnology R&D in the Next Decade, On Behalf of NSTCCTIWGN*, Roco, M.C. (IWGN Chair), Williams, R.S., and Alivisatos, P., Eds., Boston, 2000.
3. *1–4-e Mezhdunarodnye konferentsii "Khimiya vysokoorganizovannykh veshchestv. Nauchnye osnovy nanotekhnologii"* (1st–4th Int. Conf. "Chemistry of Highly Organized Substances: Scientific Foundations of Nanotechnology"), St. Petersburg: Sankt-Peterb. Gos. Univ., 1996, 1998, 2001, 2004.
4. Aleskovskii, V.B., in *Voprosy khimicheskoi kinetiki, kataliza i reaktsionnoi sposobnosti: Sbornik* (Problems of Chemical Kinetics, Catalysis, and Reactivity: Coll. of Works), Moscow: Akad. Nauk SSSR, 1955, part 2, pp. 557–569.
5. Aleskovskii, V.B., *Vestn. Akad. Nauk SSSR*, 1975, June, pp. 48–51.

6. Aleskovskii, V.B., *Zh. Prikl. Khim.*, 1974, vol. 47, no. 9, pp. 2145–2157.
7. Aleskovskii, V.B., *Khimiya nadmolekulyarnykh soedinenii* (Chemistry of Supramolecular Compounds), St. Petersburg, 1996.
8. Aleskovskii, V.B., *Vestn. Sankt-Peterb. Gos. Univ.*, *Ser. 4*, 1992, pp. 75–76.
9. Aleskovskii, V.B., *Zh. Obshch. Khim.*, 2002, vol. 72, no. 4, pp. 611.
10. Aleskovskii, V., *Macromol. Symp.*, 1998, vol. 136, pp. 1–7.
11. Stadnyuk, N.P., in *Voprosy khimicheskoy kinetiki, kataliza i reaktsionnoi sposobnosti: Sbornik* (Problems of Chemical Kinetics, Catalysis, and Reactivity: Coll. of Works), Moscow: Akad. Nauk SSSR, 1955, part 2, p. 241.
12. Azatyan, V.V., *Usp. Khim.*, 1999, vol. 68, p. 1122.
13. Aleskovskii, V.B., Gorshkova, Yu.G., Romanenko, E.K., et al., *Vestn. Sankt-Peterb. Gos. Univ., Ser. 4*, 2001, no. 4, p. 145.
14. Aleskovskii, V.B., *Khimiko-informatsionnyi sintez: Nachatki teorii: Metody* (Chemical-Informational Synthesis: Elements of Theory: Methods), St. Petersburg: Sankt-Peterb. Gos. Univ., 1997.

ISSN 1070-4272, Russian Journal of Applied Chemistry, 2007, Vol. 80, No. 11, pp. 1793–1797. © Pleiades Publishing, Ltd., 2007.
Original Russian Text © L.N. Chukhlomina, 2007, published in Zhurnal Prikladnoi Khimii, 2007, Vol. 80, No. 11, pp. 1768–1772.

INORGANIC SYNTHESIS AND INDUSTRIAL INORGANIC CHEMISTRY

Fundamental Aspects of Silicon Nitride Synthesis by Combustion of an Iron–Silicon Alloy in Nitrogen

L. N. Chukhlomina

Tomsk Scientific Center, Siberian Division, Russian Academy of Sciences, Tomsk, Russia

Received January 12, 2007

Abstract—Synthesis of silicon nitride by reaction of a Fe–Si alloy with nitrogen gas in the mode of self-propagating high-temperature synthesis was studied.

DOI: 10.1134/S107042720711002X

Possessing a set of unique service properties (high mechanical strength, crack resistance, corrosion resistance in aggressive media, heat resistance), silicon nitride finds wide use in modern technology. The main industrial methods for synthesis of silicon nitride are furnace and plasmochemical syntheses. These methods are highly energy intensive and employ expensive equipment, which reflects on the production cost of silicon nitride powders obtained in these ways.

At present, silicon nitride is produced by the method of self-propagating high-temperature synthesis (SHS), which provides high output capacity at minimum energy expenditure. The SHS method for synthesis of silicon nitride is based on the reaction of silicon with nitrogen gas [1–3]. Alloys of a nitride-forming element with iron can serve as raw materials for synthesis of nitrides, instead of high-cost element powders [4, 5]. Iron and concomitant impurities contained in raw materials can be removed by acid enrichment.

In this study we examined the fundamental aspects of silicon nitride synthesis in combustion of a Fe–Si alloy in nitrogen gas and the acid enrichment of SHS products.

EXPERIMENTAL

We used as raw material the dust fraction of the Fe–Si alloy, formed in considerable amounts in crushing of industrial ferrosilicium. The material under study had the form of a polydispersed powder with a particle size less than 160 μm and silicon content of 82.0 wt %. According to the results of X-ray phase analysis (XPA), ferrosilicium is a two-phase material composed of silicon and high-temperature lebeauite ($FeSi_2$). The ferrosilicium powder was charged into cylindrical tube 50 mm in diameter, made of a metallic grid. Prior to synthesis, the starting ferrosilicium was dried in a vacuum oven at 150–200°C to remove moisture and volatile impurities. Samples were burnt in a constant-pressure installation in the atmosphere of gaseous nitrogen [GOST (State Standard) 9203–74] with a nitrogen content of 99.996 vol %. The nitrogen pressure was varied in the range 1–10 MPa. The samples were ignited using a powder-like igniting mixture, with a tungsten coil through which electric current was passed. After the combustion front passed, a sample was kept in the atmosphere of nitrogen to complete cooling; then, the pressure was relieved and the SHS product was removed from the installation for further studies. The XPA was performed on a DRON-2 diffractometer with Co radiation. The phase composition was evaluated using the standard calibration-curve method [6]. The calibration plot was constructed using artificial calibration mixtures with a known content of α- and β-Si_3N_4.

The content of nitrogen taken up in the course of combustion was preliminarily determined from the gain in mass, and more precisely, on a TN-114 (LECO) instrument by the standard procedure employing the hot-extraction method based on reductive fusion of samples being analyzed in the atmosphere of a chemically pure inert gas. The chemical composition of quenched combustion products was studied by X-ray fluorescence microanalysis (XRFMA) on a CAMEBAX-MICROBEAM instrument. The morphology of the starting and synthesized powders was examined with a JEM100CXII electron microscope with an ASID-4D scanning attachment (JEOL, Japan). The combustion temperature was measured with

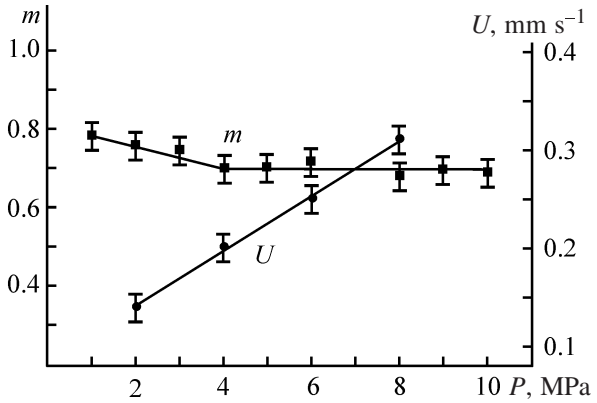

Fig. 1. Degree of nitriding, *m*, and the combustion velocity *U* of ferrosilicium vs. the nitrogen pressure *P*.

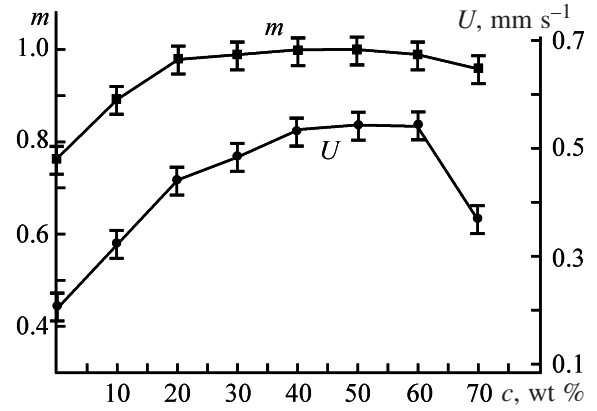

Fig. 2. Degree of nitriding, *m*, and the combustion velocity *U* of ferrosilicium vs. the dilution *c* of the starting alloy with ferrosilicium preliminarily nitrided at $P = 4$ MPa.

tungsten–rhenium thermocouples (VR5-VR20) 100 μm in diameter, introduced into samples to a depth of 10–15 mm.

The acid enrichment of the SHS products was performed in a special installation equipped with a thermostat and a stirrer. A weighed portion of a nitrided ferroalloy was placed into a reaction vessel with an acid and kept there for a certain time at a constant temperature under vigorous stirring. After a prescribed time elapsed, the content of iron and silicon that passed into solution was monitored. For this purpose, the undissolved precipitate was separated from the solution by filtration and the filtrate was subjected to chemical analysis. The residue that remained on the filter was washed, dried, and subjected to chemical analysis and XPA.

It was found experimentally that combustion of ferrosilicium in nitrogen occurs in the self-oscillating, rather than stationary mode. A burnt sample is composed of alternating layers with different colors. According to the results of chemical analysis, the light band is enriched in silicon nitride, and the dark band, in silicon and iron silicides. The presence of the components of the starting alloy (silicon and iron disilicide) in the combustion products points to the low degree of its nitriding. The degree of nitriding, *m*, was determined as the ratio of the amount of nitrogen taken up by a sample in the course of combustion to the amount of nitrogen necessary for complete conversion of silicon to silicon nitride. Characteristically, the degree of nitriding is smaller than unity in the entire pressure range studied (Fig. 1). The degree of nitriding equal to unity corresponds to formation in the course of combustion of a product composed of only silicon nitride and iron.

The pressure dependence of the combustion velocity of ferrosilicium is typical of silicon combustion in nitrogen [1]. As the pressure increases, the filtration rate in the reaction zone becomes higher, which accelerates the reaction at the interface between the condensed phase and the gas.

A study of the effect of synthesis parameters, such as the relative density of a sample, its diameter, particle size of the starting alloy, on the degree of nitriding demonstrated that the maximum degree of nitriding and stationary propagation mode of the combustion front cannot be achieved by varying these parameters.

An effective way to raise the degree of conversion is dilution of the starting stock with various additives.

To raise the degree of nitriding, the starting ferrosilicium was diluted with preliminarily nitrided ferrosilicium with the degree of nitriding equal to 0.76. The dependence in Fig. 2 shows that the degree of nitriding increases with the amount of an additive (the amount of nitrogen introduced with the additive was taken into account when calculating the degree of nitriding). Upon introduction of the additive in an amount of 40–60 wt %, the degree of nitriding becomes unity. Upon a 70% dilution, it somewhat decreases, and in the case of further dilution, the system becomes incombustible. The combustion velocity also increases from 0.2 to 0.5 mm s^{-1} upon introduction of nitrided ferrosilicium into the system.

A study of the microstructure of the starting alloy and quenched (by rapid discharge of nitrogen) samples demonstrated the following. In the case of combustion of undiluted ferrosilicium, a region is formed before the combustion front, characterized by the presence of molten particles, their coagulation, and formation of reaction cells whose size is several times the initial size of ferrosilicium particles (Fig. 3).

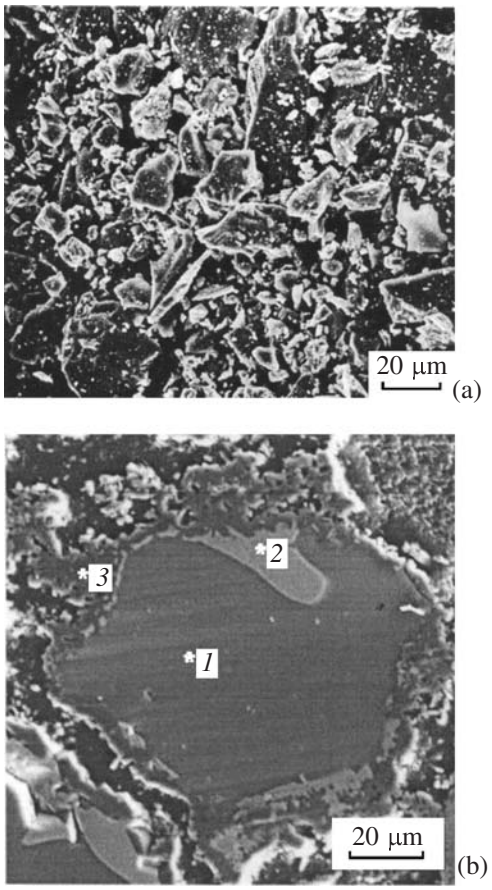

Fig. 3. Microscopic structure of (a) starting ferrosilicium and (b) quenched burnt sample. (*1*) Si, (*2*) $FeSi_2$, and (*3*) Si_3N_4.

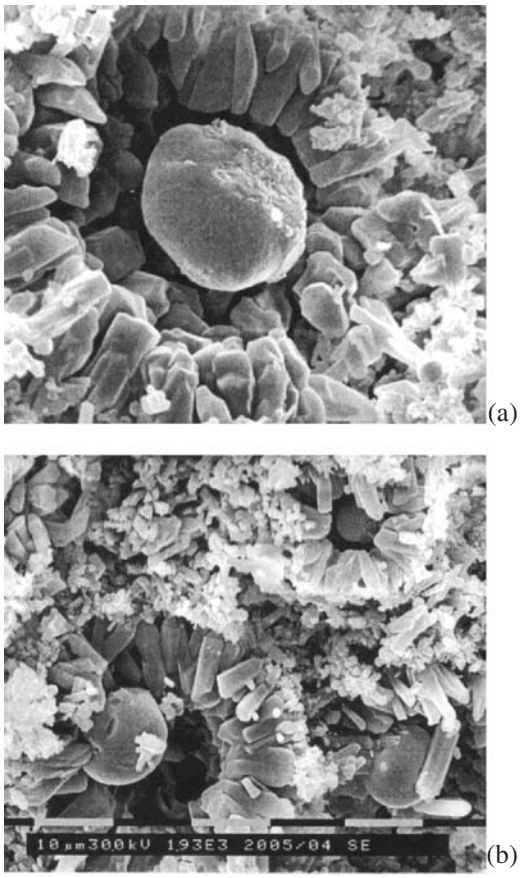

Fig. 4. Microscopic structure of quenched sample of nitrided ferrosilicium. Stock composition, %: ferrosilicium 40, nitrided ferrosilicium 60; P = 4 MPa. Magnification: (a) 1500 and (b) 1930.

Dilution with nitrided ferrosilicium precludes coagulation before the combustion front and favors preservation of the initial size of particles of the starting alloy, which leads to an increase in the combustion velocity and degree of conversion (Fig. 2, curve *2*).

Figure 4 shows microstructures of quenched samples burnt with addition of 60 wt % nitrided ferrosilicium to the starting alloy. The use of diluted samples made it possible to monitor the nitriding of separate ferrosilicium particles and formation of silicon nitride crystals. The microstructures shown are characterized by the presence of a spherical particle from which extend as rays columnar crystals, so that the structure resembles a "flower." An XRFMA of the spherical particle demonstrated that it is composed of silicon and iron, and the "petals of the flower" are crystals of silicon nitride. The "flowers" have different outer diameters, which is due to the polydispersity of the starting ferrosilicium. The results of electron-microscopic studies and XRFMA suggest the following growth mechanism of silicon nitride crystals.

In the course of SHS synthesis, when the combustion temperature exceeds the temperature at which the liquid phase appears (1206°C), particles of the starting ferrosilicium melt to give separate drops. The growth of silicon nitride crystals begins directly from the melt surface, at the place where particles of silicon nitride, "diluent," contact with the surface layer of the melt. In this case, silicon nitride particles serve as seed. As crystals grow and silicon evaporates from the melt, the diameter of a molten particle steadily decreases. In the growth process, silicon nitride crystals slowly extend from the melt until the entire amount of silicon in the melt is exhausted.

As additives were used ammonium halides and magnesium fluoride. Introduction of 1–10 wt % ammonium chloride and(or) fluoride results in that the maximum degree of nitriding is reached. Gasifiable additives intensify the synthesis of silicon nitride via formation of intermediates, such as silicon tetrachloride, tetrafluoride, and diimide. According to the data of [3], amorphous silicon nitride is formed in the

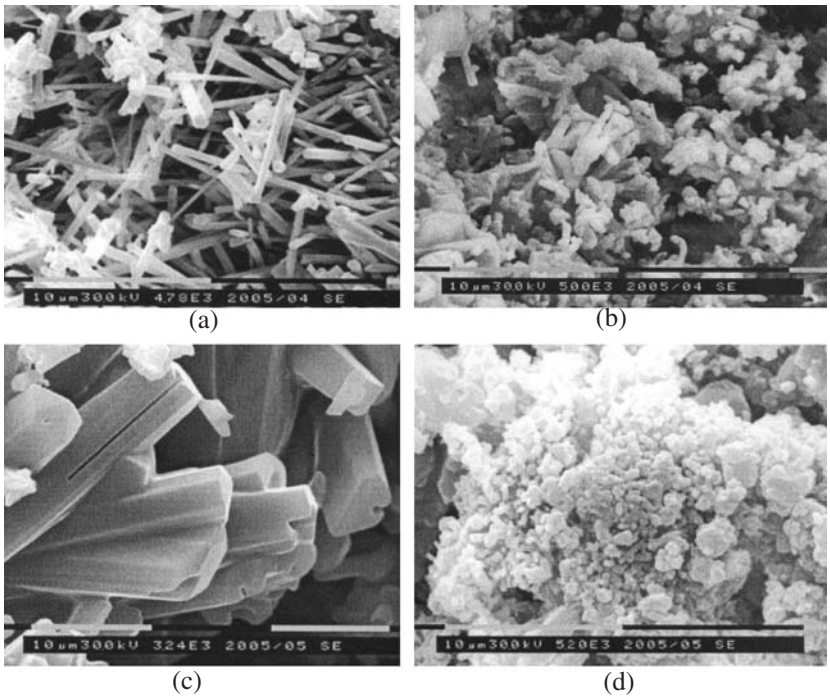

Fig. 5. Morphology of particles of silicon nitride formed in combustion of ferrosilicium in nitrogen in the presence of (a) magnesium fluoride and (b, d) ammonium chloride and (c) upon dilution with preliminarily nitrided ferrosilicium. Magnification: (a) 4780, (b) 5000, (c) 3240, and (d) 5200.

presence of ammonium salts even at 100°C, and it crystallizes at 1200°C to give α-Si_3N_4. Thus, the sample already contains synthesized silicon nitride before the onset of melting of the eutectic $FeSi_2$–Si (1206°C). The high-melting silicon nitride hinders coagulation of particles of the starting ferrosilicium, so that their initial size is preserved. Introduction of ammonium salts promotes reactions mostly in the gas phase, which, in the end, diminishes the filtration hindrance and raises the degree of nitriding.

Introduction of 1 wt % MgF_2 into the starting stock extends the ferrosilicium combustion range to 0.4 MPa (the minimum pressure at which combustion is observed without MgF_2 is 1 MPa). The activation of the nitriding process in this case is due to the high chemical activity of fluorides of alkaline-earth metals, which leads to removal of the oxide film from the surface of reacting particles.

Silicon nitride has two crystalline modifications: α- and β-Si_3N_4. Both modifications have hexagonal crystal lattices with unit cell parameters (nm) a = 0.776, c = 0.5662 and a = 0.7603, c = 0.2907, respectively [7].

According to the results of XPA, the products formed in the reaction of ferrosilicium with nitrogen are, as a rule, of predominantly the β-modification, with a minor amount (up to 20%) of α-Si_3N_4. Along with the main phases, the sample also contained silicon, iron, and iron silicides $FeSi_2$, FeSi, Fe_5Si_3, and Fe_3Si, whose presence indicates that the nitriding is incomplete.

Upon dilution of the starting alloy with preliminarily nitrided ferrosilicium, the combustion products always contained only the high-temperature β-modification. This occurred because the addition of the high-melting component eliminated the effect of coagulation hindrance to the reaction, the processes of nitrogen filtration to the reaction zone were improved, and, as a result, high synthesis temperatures were reached. The maximum temperature in the reaction zone was 2100°C, and the monotropic α → β transition occurs at substantially lower temperatures (1450–1500°C).

Magnesium fluoride intensifies nitriding of iron silicides, which ends in formation of silicon nitride and liberation of iron. The results of XPA of the combustion products indicate that β-Si_3N_4 is mostly formed (95%) in the presence of magnesium fluoride.

The introduction of ammonium chloride (1–10 wt %) into the starting ferrosilicium made it possible to obtain combustion products with various relative contents of α- and β-modifications of silicon

nitride. By varying the ratio between the initial nitrogen pressure and amount of ammonium chloride, one can obtain nitrided ferrosilicium both with 100% β-Si_3N_4 and with increased content of α-Si_3N_4 (up to 80 wt %).

Electron-microscopic studies of the morphology of silicon nitride particles demonstrated that their shape and size depend on the synthesis conditions. Upon dilution of the starting ferrosilicium with preliminarily nitrided ferrosilicium, coarse lamellar crystals of regular shape are formed (Fig. 5c). Upon introduction of ammonium chloride, the temperature and velocity of combustion become lower, which leads to a decrease in the particle size. In this case, silicon nitride particles are isometric shapeless formations (Figs. 5b, 5d). Introduction of magnesium fluorides into the starting ferrosilicium leads to the formation of whisker-like crystals of silicon nitride (Fig. 5a). Our study of the SHS process resulted in that a combustion product having the form of a formulation composed of silicon nitride and iron was obtained. It is known that iron well dissolves in mineral acids, whereas silicon nitride is, by contrast, stable in these acids. Therefore, we studied how iron passes into solutions of hydrochloric, sulfuric, and nitric acids. The dependences we obtained, which describe the accumulation of iron in acid solutions in the course of time, show that the rate at which iron passes into solution is virtually independent of the nature of an acid, with about 70 wt % of iron passing during the first 15 min. Further studies of the process of acid enrichment were carried out in hydrochloric acid solutions.

Using the data obtained, we found the optimal parameters of acid enrichment and produced pilot batches of silicon nitride powders. The residual content of iron in silicon nitride is 0.01–0.1 wt %, depending on the dispersity of the product formed in SHS synthesis.

CONCLUSIONS

(1) The combustion of the silicon–iron alloy in nitrogen occurs in the nonstationary mode. The combustion product is multiphase, heterogeneous, with low degree of nitriding (0.76). The maximum degree of nitriding (1.0) is achieved by introduction of nitrided ferrosilicium, ammonium halides, or magnesium fluoride into the starting ferrosilicium.

(2) Before the combustion front, the starting particles melt and coagulate to form reaction cells whose size is several times that of the starting particles. This makes smaller the reaction surface area, hinders filtration of nitrogen toward the reaction zone, and reflects on the kinetic characteristics of the process and on the degree of nitriding of synthesis products.

(3) Synthesis of silicon nitride with increased (up to 80 wt %) content of the low-temperature α-modification of silicon nitride is only possible in the presence of ammonium chloride. If other additives are used, β-Si_3N_4 predominates (>95 wt %) in the synthesis product.

(4) Acid enrichment of products formed in ferrosilicium combustion in nitrogen yielded silicon nitride with a residual iron content of less than 0.1 wt %.

REFERENCES

1. Mukas'yan, A.S., Martynenko, V.M., Merzhanov, A.G., et al., *Fiz. Goren. Vzryva*, 1986, no. 5, pp. 43–49.
2. Mukas'yan, A.S., Stepanov, B.V., Gal'chenko, Yu.A., and Borovinskaya, I.P., *Fiz. Goren. Vzryva*, 1990, no. 1, pp. 45–52.
3. Zakorzhevskii, V.V. and Borovinskaya, I.P., *Int. J. SHS*, 2000, vol. 9, no. 2, pp. 171–191.
4. Chukhlomina, L.N., Ziatdinov, M.Kh., and Maksimov, Yu.M., *Zh. Prikl. Khim.*, 2000, vol. 73, no. 9, pp. 1428–1432.
5. Chukhlomina, L.N., Ziatdinov, M.Kh., and Maksimov, Yu.M., *Int. J. SHS*, 2000, vol. 9, no. 1, pp. 65–73.
6. Zevin, L.S. and Zav'yalova, L.L., *Kolichestvennyi rentgenograficheskii fazovyi analiz* (Quantitative X-ray Phase Analysis), Moscow: Nedra, 1974.
7. Käll, P.-O., *Chem. Scripta*, 1988, vol. 28, pp. 439–446.

ISSN 1070-4272, Russian Journal of Applied Chemistry, 2007, Vol. 80, No. 11, pp. 1798–1803. © Pleiades Publishing, Ltd., 2007.
Original Russian Text © I.A. Farbun, I.V. Romanova, T.E. Terikovskaya, D.I. Dzanashvili, S.A. Kirillov, 2007, published in Zhurnal Prikladnoi Khimii, 2007, Vol. 80, No. 11, pp. 1773–1778.

INORGANIC SYNTHESIS AND INDUSTRIAL INORGANIC CHEMISTRY

Complex Formation in the Course of Synthesis of Zinc Oxide from Citrate Solutions

I. A. Farbun, I. V. Romanova, T. E. Terikovskaya, D. I. Dzanashvili, and S. A. Kirillov

Institute of Sorption and Problems of Endoecology, National Academy of Sciences of Ukraine, Kiev, Ukraine
Institute of Inorganic Chemistry and Electrochemistry, Tbilisi, Georgia

Received September 29, 2006; in final form, April 2007

Abstract—Complex formation of zinc(II) with citric acid in acidic medium was studied by pH-potentiometric titration at various metal to acid ratios. The speciation diagrams of the complexes in relation to pH were plotted, and the stability constants of the complexes were determined. Precursors of the synthesis of metal oxide materials were prepared at two reactant ratios. A scheme of the precursor thermal decomposition based on data of derivatography and IR spectroscopy was suggested, and the compositions of compounds formed during decomposition were determined.

DOI: 10.1134/S1070427207110031

Transition metal oxides and materials based on them attract researchers' interest for a long time due to a wide set of possibilities of their use as cathode masses for chemical power sources, catalysts and photocatalysts, highly selective sorbents, semiconductors, and magnetic materials [1–7]. Previously these materials were usually prepared by sintering of oxides or thermal decomposition of hydroxides or metal salts (nitrates, acetates, carbonates, oxalates). In the case of poorly soluble salts, their precipitation or coprecipitation preceded thermal decomposition.

A new step in the development of the synthesis of oxide materials is connected with the use of polybasic hydroxy carboxylic acids. Concentrated solutions containing metal salts and the above acids tend to form sols and then gels (or glasses). This procedure differs from traditional sol–gel methods in that the agent forming the polymeric matrix is polybasic hydroxy carboxylic acid and not hydrated silicon, titanium, zirconium, etc. species tending to form H-bond network, which significantly extends the range of objects that can be involved in the process. Precursors containing metal salts and excess acid are formed when the major fraction of water is removed from gels (glasses). Their further thermal treatment gives homogeneous oxide materials.

In [8], we suggested an optimized method for preparing oxide materials, which was tested with zinc, nickel, copper, manganese, and cerium salts. Many of the materials obtained showed high activity in catalytic oxidation of CO [9] and of volatile organic compounds: paraffin and aromatic hydrocarbons [10], alcohols, ethers, and esters [11].

Complex compounds are formed in the solution when the initial metal salts are mixed with the acid. Their composition and stability determine the composition of the precursor, pathway of its thermal decomposition, and parameters of the oxide material formed (crystal dimensions, specific surface area, porosity, etc.). These questions have not been adequately discussed in the literature [12].

In this study, with the Zn^{2+}–citric acid ($C_6H_8O_7$) system as example, we examined complex formation in solution at various pH values and metal to acid ratios, determined the compositions of complexes formed in solution, prepared the precursors, and analyzed pathways of their decomposition. Zinc was chosen because it does not undergo redox transformations which could complicate the precursor decomposition. In addition, zinc oxide has been actively studied recently for various applications [13, 14].

EXPERIMENTAL

All chemicals used were of chemically pure grade and were used without additional purification. The metal and acid concentrations were determined by complexometric and acid–base titration [15, 16].

The pH-potentiometric titration was performed on an I-160M device. The results were treated with CLINP 2.1 software for stability constant calculations [17]. The thermal decomposition of precursors was studied on a Q-1500D derivatograph. The composition of precursors and decomposition products was studied by IR spectroscopy on a Specord M-80 spectrophotometer within the 4000–400 cm^{-1} range using KBr pellets.

The metal ion to acid ratio in solutions was 1 : 1, 1 : 2, and 1 : 4, and the concentrations were varied within the 2.5×10^{-4}–1.0×10^{-3} M range. Low concentrations were taken to avoid introduction of additional chemicals for supporting the ionic strength, i.e., to ensure the conditions most similar to those of the actual synthesis.

The lower position of the titration curves of the mixtures with respect to those of citric acid suggests complex formation in the system (Fig. 1a). Similarity of the curves in the acid region shows that only acid carboxy groups participate in the process. This is confirmed by the curve inflection at addition of 3 equiv of alkali. In the alkaline region, the titration curves substantially diverge, probably due to formation of zinc(II) hydroxo complexes.

Based on these facts and data of [18–22], we can suggest that in the acid region at low concentrations 1 : 1 citrate complexes of zinc(II) are formed, and with increasing pH the degree of ligand deprotonation changes. The scheme of complex formation can be presented as follows:

$$M^{i+} + H_nL \rightarrow [MH_{n-m}L^{i-m}] + mH^+, \quad (1)$$

where $n = 4$ for citric acid.

The equilibrium constant of reaction (1) is

$$K = \frac{[MH_{n-m}L^{i-m}][H^+]^m}{[M^{i+}][H_nL]} = \frac{[MH_{n-m}L^{i-m}]}{[M^{i+}][H_{n-m}L^{m-}]}$$

$$= \frac{[H^+]^m[H_{n-m}L^{m-}]}{[M^{i+}][H_nL]} = \beta_i K_m, \quad (2)$$

where β_i is the stability (formation) constant of the protonated complex; K_m, total constant of acid ionization in step m, $K_m = k_1k_2k_3...k_m$, and k_i, ionization step constants.

The ionization constants of citric acid calculated from data obtained in this study ($pK_1 = 3.110 \pm 0.016$, $pK_2 = 4.450 \pm 0.015$, and $pK_3 = 5.810 \pm 0.017$) well coincide with the reference data [23–25].

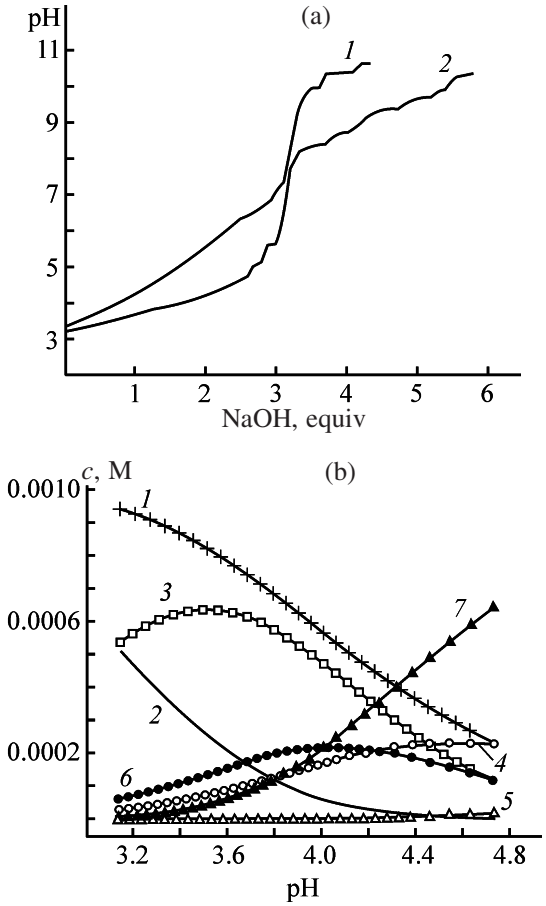

Fig. 1. (a) pH-potentiometric titration curves of (*1*) citric acid and (*2*) $Zn(NO_3)_2$–citric acid system; (b) speciation diagram of citric acid and metal citrate complexes in the system $Zn(NO_3)_2$–citric acid (H_4L)–NaOH at the molar ratio $Zn : H_4L$ 1 : 1. $c_a = 1 \times 10^{-3}$, $c_m = 1 \times 10^{-3}$ M; (*c*) concentration of components. (b) (*1*) Zn^{2+}, (*2*) H_4L, (*3*) H_3L^-, (*4*) H_2L^{2-}, (*5*) HL^{3-}, (*6*) ZnH_2L^0, and (*7*) $ZnHL^-$.

The calculated compositions of the complexes and their stability constants are listed in the table. From these data, the speciation diagrams of the acid and complexes in relation to pH at various component ratios were obtained. For example, in Fig. 1b, the diagram for system $Zn(NO_3)_2$–$C_6H_8O_7$ (H_4L)–NaOH is presented at equimolar ratio of the components.

At pH 3, zinc(II) exists in the solution almost entirely (95%) in the unbound state, irrespective of the citric acid concentration. With increasing pH, the acid dissociates (initially, at pH 3, half of the acid is dissociated), and two complexes with the metal ion to ligand ratio of 1 : 1 but with different degrees of the ligand protonation are formed.

At a metal ion to acid molar ratio of 1 : 1 and pH 4, 20% of zinc(II) ions are bound in ZnH_2L (**I**) and

Comparison of stability constants of zinc complexes with citric acid (H_4L), determined in this study, with published data

Molar ratio $Zn(NO_3)_2 : H_4L$	pK_i			
	this study		published data	
	MH_2L^0	MHL^-	MH_2L^0	MHL^-
1 : 1	3.35 ± 0.04	5.15 ± 0.015	2.42 [19], 2.98 [21]	4.36 [18], 4.83 [20], 4.98 [19, 21]
1 : 2	3.34 ± 0.08	4.6 ± 0.05		

20%, in the complex ZnHL (**II**). It follows from the speciation diagram that the second complex is more stable: at pH 4.5–4.75 65% of the initial metal exists in this form. The stability constants also show higher stability of complex **II** (see table).

The increase in the acid content of the solution does not change the composition of the complexes but increases their yield. The maximal amount of each complex at the acid excess is formed in more alkaline region than at the equimolar ratio. For example, at pH 4, 20% of metal ions (maximum) are bound in the complex at the metal ion to acid ratio of 1 : 1, whereas at the ratio of 1 : 2 their fraction is 36%. It should also be noted that, in spite of acid excess, 1 : 2 complexes in the systems studied are not formed, or their stability is low.

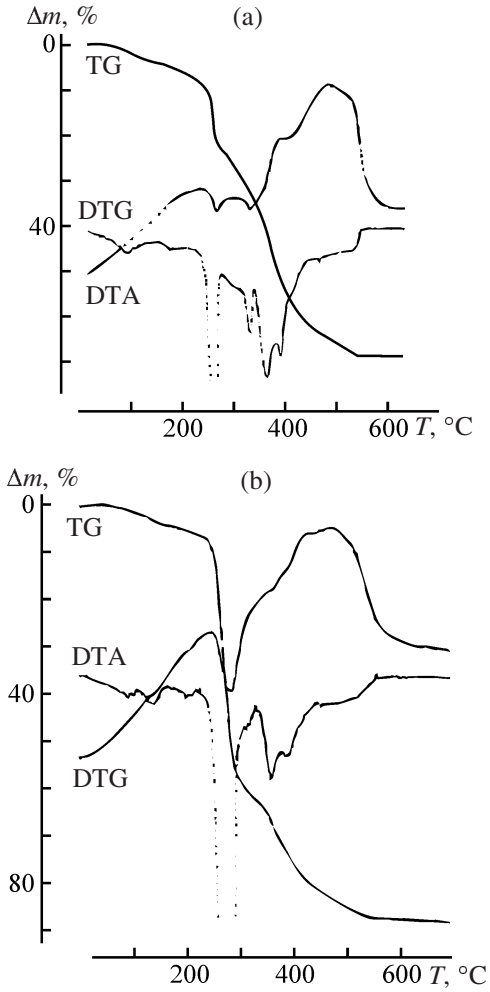

Fig. 2. DTA, DTG, and TG curves for the system $Zn(NO_3)_2$–citric acid. (Δm) Weight loss and (T) temperature. Molar ratio of components: (a) 1 : 1 and (b) 1 : 2; the same for Fig. 3.

To understand the structure of the precursors, they were studied by IR spectroscopy and derivatography. The samples were synthesized as in [8]. The concentrations of zinc nitrate and citric acid solutions were from 0.25 to 1 M, and the metal ion to acid ratios were 1 : 1 and 1 : 2. After mixing the components, keeping to attain the equilibrium, and removing water, a polymeric resin was obtained. The measurement of light scattering showed the absence of the Tyndall cone, which indicates that the samples obtained are glasses rather than gels. Drying of these glasses in an oven at 110–120°C leads to substantial (by a factor of up to 15) increase in the volume with formation of a porous product. In so doing, nitrogen oxides and physically bound water were removed.

The derivatogram of the precursor with the metal ion to acid ratio of 1 : 1 is shown in Fig. 2a. After water removal (~100°C), a strong endothermic effect accompanied by 20% weight loss was observed. Then, three small endothermic effects at 330, 360, and 400°C (weight loss 32, 43, and 51%, respectively) were observed against a background of an exothermic effect at 300–520°C. The process completes at 550°C; the total weight loss of 68.4% corresponds to the formation of ZnO.

The derivatogram of the precursor with the metal ion to acid ratio of 1 : 2 is characterized by similar effects, but with larger weight losses (figures in parentheses, %): 260 (33), 360 (66), and 390 (73). The process is complete at 550°C (87%); the calculated weight loss corresponding to the oxide formation is 82%.

The thermal decomposition products were studied by IR spectroscopy. It is known [26] that the thermal decomposition of citric acid (**1**) follows the scheme

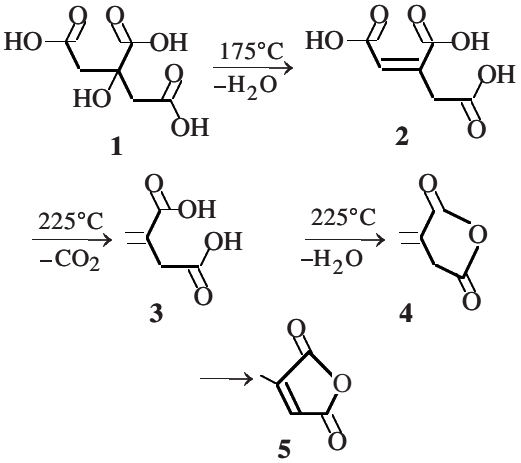

Initially, with removal of water molecule, aconitic acid (**2**) is formed. Then, CO_2 molecule is eliminated, and itaconic acid (**3**) is formed. On further heating, a mixture of two isomeric anhydrides [itaconic (**4**) and citraconic (**5**)] is evaporated. Presumably, a similar scheme should be realized in the thermal decomposition of metal citrates [26].

The most characteristic bands in the IR spectrum of citric acid are listed in [26]. The C–O bond of the α-hydroxy group gives a double band at 1075 cm^{-1}. Vibrations of the C=O bond in carboxy groups lie at 1700–1750 cm^{-1}. The O–H bonds of carboxy and α-hydoxy groups give a broad band at 3300–3100 cm^{-1} and a band at 3490 cm^{-1}. During gradual heating of citric acid, the following changes occur in the IR spectra. At 140°C, the band of the α-hydroxy group disappears as a result of dehydration of citric acid and formation of aconitic acid. At 160°C, the ν(C=O) bands characteristic for itaconic anhydride appear at 1780 and 1850 cm^{-1}. The appearance of a double band at 895, 1005 cm^{-1} is an additional evidence of the anhydride formation. At 180°C, citraconic anhydride is formed; in its IR spectrum, the above double band is shifted toward lower frequencies (to 700 and 980 cm^{-1}). Citraconic anhydride completely disappears at 210°C.

Deprotonation of citric acid and its coordination with *d*-metals are accompanied by the following changes in the IR spectrum [27, 28]. The strong ν(C=O) bands at 1700 cm^{-1} in the spectra of carboxylic acids are absent in the spectra of their salts. Instead of them, bands at 1300–1400 and 1550–1610 cm^{-1} assigned to symmetric and asymmetric stretching vibrations of ionized COO^- groups appear. If the compounds studied contain at least one undissociated –COOH group, the band at 1700 cm^{-1} is preserved.

If hydroxy groups do not participate in the complex formation, bands in the region of 3450 cm^{-1} (OH^- stretching vibrations) should be observed in the spectra. On detachment of protons from all hydroxy groups, these bands disappear. If undissociated hydroxy groups participate in the complex formation, low-frequency shift of ν(OH) should be observed [27].

The IR spectra of the 1 : 1 and 1 : 2 precursors and products of their thermal decomposition are shown in Fig. 3. As can be seen, the spectra of the initial compounds have certain differences. The spectra of the 1 : 1 precursor, recorded without heat treatment and after heating to temperatures of up to 120°C, contain the bands at 1410–1600 cm^{-1} assigned to coordinated carboxy groups, ν_s(C=O) and ν_{as}(C=O), but the band at 1700 cm^{-1} is also observed. This fact indicates that one carboxy group does not participate in the complex formation. The doublet at 1075 cm^{-1} corresponding to vibrations of α-hydroxy group of citric acid is preserved, i.e., this group does not participate in the complex formation either. Presumably, in this case the compound ZnH_2L is formed, in the which zinc ion is bound with two carboxy groups through oxygen atom.

The spectrum of the 1 : 2 precursor, recorded without heat treatment and after heating to temperatures of up to 120°C, in addition to the band of coordinated carboxy groups (1410–1600 cm^{-1}) and free carboxy group (1700 cm^{-1}), contained the double band of changed shape (1050–1110 cm^{-1}), which suggests participation of the α-hydroxy group in the complex formation. In this case, most likely, the zinc ion acts as a bridge between two acid molecules in the compound $Zn(H_3L)_2$.

For the further study of the decomposition of the 1 : 1 precursor, we compared the IR spectra of products of its thermal decomposition with the published data [26] and spectra of products of citric acid decomposition. Formation of zinc aconitate and itaconate was not observed, probably because of low stability of these compounds. The compound formed at 250°C, in accordance with the measured weight loss, is most likely zinc citraconate. Its further decomposition proceeds within the 300–350°C temperature range and is accompanied by evolution of CO_2 and H_2O (20 and 10% weight loss, respectively). The IR spectrum of the residue obtained contains a band at 450 cm^{-1} corresponding to vibrations of the Zn–O bond and weak

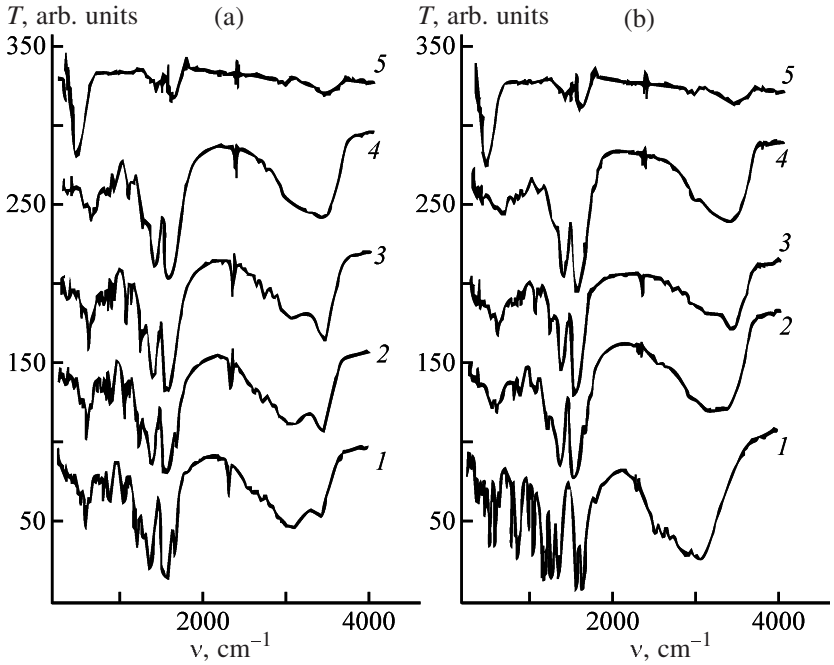

Fig. 3. IR spectra of precursors and products of their decomposition at various temperatures for the system $Zn(NO_3)_2$–citric acid. (*T*) Transmittance and (ν) wavenumber. Temperature of thermal decomposition, °C: (*1*) 120, (*2*) 220, (*3*) 250, (*4*) 300, and (*5*) 350. Zn : citric acid ratio: (a) 1 : 1 and (b) 1 : 2.

bands at 1360 and 1600 cm^{-1}, indicative of the presence of residual organic compounds. Their removal is complete after prolonged heat treatment of the residue at 700°C.

After heating to 250°C, the IR spectra of 1 : 1 and 1 : 2 precursors become identical (Fig. 3). Hence, the compound $Zn(H_3L)_2$ is unstable and decomposes to citric acid and ZnH_2L. This is confirmed by the presence in the spectrum of the 1 : 2 compound heat-treated at 220°C of two weak bands at 1770 and 1845 cm^{-1} (formation of cyclic anhydrides from free citric acid).

CONCLUSIONS

(1) In the $Zn(NO_3)_2$–citric acid (H_4L)–NaOH system, irrespective of the acid amount, complexes with the metal ion to ligand ratio of 1 : 1 with different degrees of ligand protonation, ZnH_2L (**I**) and ZnHL (**II**), are formed. At the metal ion to acid ratio of 1 : 1, the contents of **I** and **II** are equal. With increasing acid content of the solution, the yields of **I** and **II** increase; compound **II** is more stable than **I**.

(2) According to data of derivatography and IR spectroscopy, depending of the initial ratio of the components, the citrate precursors for preparing zinc oxide have different compositions and can contain the complexes ZnH_2L and $Zn(H_3L)_2$. On heating to 250°C, the second complex loses a citric acid molecule and transforms into the first complex. The subsequent decomposition pathways of both precursors are the same and are complete with the formation of zinc oxide at 350°C.

REFERENCES

1. Ookubo, A., Ooi, K., and Hayashi, H., *Langmuir*, 1993, vol. 9, no. 5, pp. 1418–1422.
2. *Materials for Lithium Ion Batteries*, Julien, C. and Stoynov, Z., Eds., *NATO Sci. Ser. 3, High Technology*, Dordrecht: Kluwer Academic, 2000, vol. 85.
3. Weidenkaff, A., Ebbinghaus, S.G., and Lippert, T., *J. Chem. Mater.*, 2002, vol. 14, no. 4, pp. 1797–1805.
4. Tas, A.C., Majewski, P.J., and Aldinger, F., *J. Am. Ceram. Soc.*, 2000, vol. 83, no. 12, pp. 2954–2960.
5. Alonso, J.A., Martinez-Lopez, M.J., Casais, M.T., et al., *J. Chem. Mater.*, 1999, vol. 11, no. 9, pp. 2463–2469.
6. US Patent 3 330 697.
7. Todorovsky, D.S., Dumanova, D.G., Todorovska, R.V., and Getsova, M.M., *Croat. Chem. Acta*, 2002, vol. 75, no. 1, pp. 155–164.
8. Farbun, I.A., Romanova, I.V., and Kirillov, S.A., Abstracts of Papers, *XVI Ukrains'ka konferentsiya po neorganichnoi khimii* (XVI Ukrainian Conf. on Inorganic Chemistry), Uzhgorod, 2004, pp. 32–33.

9. Romanova, I.V., Zazhigalov, V.A., and Kirillov, S.A., Abstracts of Papers, *Ukrainian-Polish Symp. "Theoretical and Experimental Studies of Interfacial Phenomena and Their Technological Applications,"* Sandomierz (Poland), September 5–9, 2005, pp. 239–240.
10. Zazhigalov, V.A., Stoch, J., Kowal, A., et al., Abstracts of Papers, *XXXVII Ogolnopolskie kolokwium katalityczne*, Krakow, 2005, pp. 154–155.
11. Delimaris, D., Kirillov, S.A., Romanova, I.V., et al., Abstracts of Papers, *7th European Congr. on Catalysis*, Sofia (Bulgaria), August 28–September 1, 2005, p. 272.
12. Kirillov, S.A., Romanova, I.V., and Farbun, I.A., *NATO–CARWC "New Carbon Based Materials for Electrochemical Energy Storage Systems"*, Dordrecht: Kluwer Academic, 2006, pp. 495–504.
13. Zhong Lin Wang, *J. Phys., Condens. Matter*, 2004, vol. 16, no. 25, pp. 829–858.
14. Ohta, H. and Hosono, H., *Mater. Today*, 2004, vol. 7, no. 6, pp. 42–51.
15. Schwarzenbach, G. and Flaschka, H., *Die komplexometrische Titration*, Stuttgart: Enke, 1965.
16. Alekseev, V.N., *Kolichestvennyi analiz* (Quantitative Analysis), Moscow: Khimiya, 1972.
17. Kholin, Yu.V., Konyaev, D.S., and Mernyi, S.A., *Vestn. Khar'k. Nats. Univ., Khim.*, 1999, no. 437, issue 3 (26), pp. 17–35.
18. Migal', P.K. and Sychev, A.Ya., *Zh. Neorg. Khim.*, 1958, vol. 3, no. 2, pp. 314–324.
19. Happe, J.A., *J. Am. Chem. Soc.*, 1973, vol. 95, no. 18, pp. 6232–6237.
20. Daniele, P. and Ostacoli, G., *Ann. Chim.* (Rome), 1977, vol. 67, no. 1, pp. 37–41.
21. Campi, E., Ostacoli, G., Meirone, M., and Saini, G., *J. Inorg. Nucl. Chem.*, 1964, vol. 26, no. 4, pp. 553–564.
22. Martin, R.B., *Antimicrob. Agents Chemother.*, 1988, vol. 32, no. 4, pp. 608–609.
23. Lur'e, Yu.Yu., *Spravochnik po analiticheskoi khimii* (Handbook on Analytical Chemistry), Moscow: Goskhimizdat, 1962.
24. Albert, A. and Serjeant, E., *Ionization Constants of Acids and Bases. A Laboratory Manual*, New York: Wiley, 1962.
25. Martell, A.E. and Calvin. M., *Chemistry of the Metal Chelate Compounds*, New York: Prentice-Hall, 1953.
26. Van Werde, K., Mondelaers, D., Vanhoyland, G., et al., *J. Mater. Sci.*, 2002, vol. 37, no. 1, pp. 81–88.
27. Kharitonov, Yu.Ya. and Alikhanova, Z.M., *Radiokhimiya*, 1964, vol. 6, no. 6, pp. 702–713.
28. Jung, C., *J. Mol. Recognit.*, 2000, vol. 13, no. 6, pp. 325–351.

ISSN 1070-4272, Russian Journal of Applied Chemistry, 2007, Vol. 80, No. 11, pp. 1804–1808. © Pleiades Publishing, Ltd., 2007.
Original Russian Text © N.Kh. Belous, V.D. Koshevar, T.E. Kreer, 2007, published in Zhurnal Prikladnoi Khimii, 2007, Vol. 80, No. 11, pp. 1779–1783.

INORGANIC SYNTHESIS AND INDUSTRIAL INORGANIC CHEMISTRY

Complex Plasticizing Additives for Cement Mortars

N. Kh. Belous, V. D. Koshevar, and T. E. Kreer

Institute of General and Inorganic Chemistry, National Academy of Sciences of Belarus, Minsk, Belarus

Received March 29, 2007

Abstract—New complex plasticizing additives for mortars based on Portland cement, increasing the mobility of the cement paste and improving some technological properties of the resulting materials, were prepared.

DOI: 10.1134/S1070427207110043

Wide use of various chemical modifying agents of various functional purpose is a typical feature of modern building technology. For example, corresponding plasticizers are widely used to provide the required properties of concretes and building mortars for the monolithic, composite, and composite-monolithic building constructions. These additives control the rheological properties of the cement paste, improve its mobility and placeability, and provide retention of its consistence, which, in turn, decreases the water consumption of mortars and enhances the strength parameters of the resulting objects [1]. Plasticizing additives optimize the setting time of the cement paste, providing transportation of the quality cement paste to the destination point and shorter time in which the formwork of concrete structures can be stripped [2].

Both domestic plasticizers of naphthalenesulfonic type (S-3, Russia), which have certain disadvantages, and new imported plasticizers (as a rule, polycarboxysilicate superplasticizers, such as Stachement-2000, Sika Visco Crete, Socolan [3]) are widely used in the monolithic building. Such additives decrease the water content by 35–40% and strongly increase the concrete strength [4]. Therefore, search for new types of domestic plasticizers and their adaptation to the cements produced in Belarus are urgent problems.

This study concerns preparation of new complex plasticizers, their addition to mortars based on the Portland cement, and properties of materials and mortars based on them.

EXPERIMENTAL

The complex plasticizers were prepared by mixing of an unsaturated fatty acid or its sodium salt with a modified tertiary amine in a wide range of the weight ratios. The process was carried out in a high-speed stirrer or ultrasonic dispersant (UZDN-1U, 15 kHz) providing high dispersity, uniformity, and stability of the resulting emulsions.

The complex additives (CAs) contain a hydrophilic microfoaming water-soluble component, namely, modified tertiary amine (MTA) and other components whose hydrophilic–lipophilic balance was varied in a wide range (from 1 to 18): unsaturated fatty acid (CA-1), a salt of fatty acid (CA-2), and the reaction product of the acid and alkanolamine (CA-3). We tested various procedures for preparing complex additives: addition of hydrophobic component (unsaturated fatty acid) into an organic solvent with subsequent mixing with a water-soluble component, mixing of acid with modified tertiary amine in the presence of emulsifier (CA-1), and mixing of the reaction product of the acid and alkanolamine with MTA (CA-3). The above procedures provide after mixing the formation of CAs exhibiting superadditive plasticizing effect, because, as was found, none of the individual components used in these systems provides effective thinning effect even at its high content in the mortar.

The complex plasticizers were added into the mortars in amounts from 0.5 to 0.8 wt %. The experiments were carried out using cement–sand blends based on domestic additive-free cement [M500 DO brand, GOST (State Standard) 10178–85, Belarus Cement Plant, Kostyukovichi, Belarus]. This cement is characterized by elevated content of aluminate component with high specific surface area. Before preparation of the cement–sand blends (cement : sand = 1 : 1.5), the sand was dried to constant weight and sieved; 0.16–2.00-mm fractions were used. The additives were introduced either directly at tempering of

the cement–sand mixture or into the hydrated mixture in certain time after mixing of the cement with water.

The mobility of the freshly prepared cement paste and changes in the mobility with time measured in 30-min intervals (time parameter of the mobility retention) were determined from the immersion of a minicone (100 mm in diameter, 60 mm high, GOST 10181.1).

From the mortar we prepared cubic samples ($2 \times 2 \times 2$ cm), which were hardened under the standard conditions (20–22°C, 80–90% humidity) and subjected to strength tests in accordance with GOST 10180.

Addition of the given plasticizers decreases the water consumption of the system and simultaneously increases the hydrophobicity of the pore walls, thus decreasing their water absorption capacity. Using the samples stored under the standard humidity conditions for 28 days, we determined their water absorption capacity and frost resistance grade in accordance with GOST 12730.3 and GOSTs 10060.1 and 10060.2, respectively.

The plasticizers prepared were identified by IR spectroscopy. The IR spectra of the initial components (unsaturated fatty acid, product of its reaction with alkanolamine) and of their mixtures with modified tertiary amine were recorded using silicon supports on a UR-20 spectrophotometer in the 650–4000 cm^{-1} range.

The crystalline products of hardening of the Portland cement mortars were identified by X-ray diffraction analysis on a DRF-2.0 diffractometer (CuK_α radiation).

The value and sign of the electrokinetic potential (ζ potential) of the electrical double layer on the surface of the cement articles were determined by electrophoresis on a Dzeta-90 apparatus (measurement range 5–80 mV, error 5%, resolution in the light background 3–50 μm, sample volume 5–50 ml).

The interaction of the hydrophobic and hydrophilic components of the complex additives was monitored by the IR spectra of fatty acid, product of its reaction with alkanolamine, and mixtures with modified tertiary amine. Unsaturated fatty acid was characterized by the stretching vibrations of the carbonyl group at 1711 cm^{-1}. New peak at 1550 cm^{-1} appears in the spectra of its mixtures with MTA (Fig. 1a). Simultaneously the intensity of the stretching vibrations of the carbonyl group decreases, which suggests interaction of the initial components to form a new compound with an ionic bond. The vibrations typical for modified tertiary amine at 967 cm^{-1} are observed in both individual compound and its mixture with acid. Their interaction is initiated by water and proceeds more actively in aqueous MTA solutions.

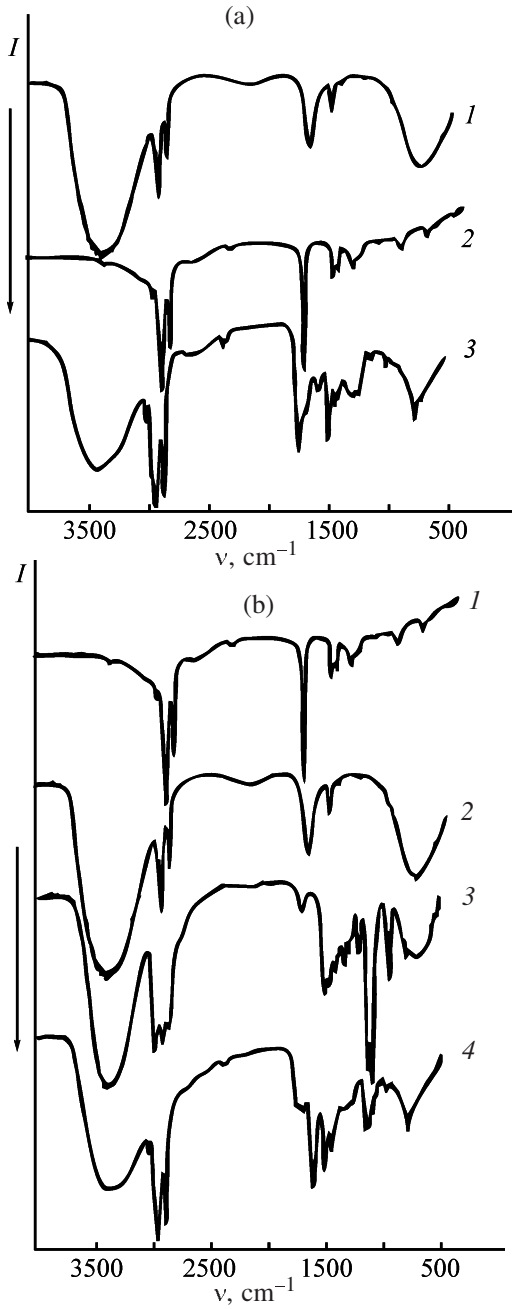

Fig. 1. IR spectra of the complex plasticizing additives. (*I*) Absorption and (ν) wavenumber. (a) (*1*) Modified tertiary amine, (*2*) unsaturated fatty acid, and (*3*) mixture of MTA and acid; (b) (*1*) unsaturated fatty acid, (*2*) modified tertiary amine, (*3*) alkanolamine, and (*4*) mixture of MTA, unsaturated fatty acid, and alkanolamine.

Upon addition of alkanolamine to unsaturated fatty

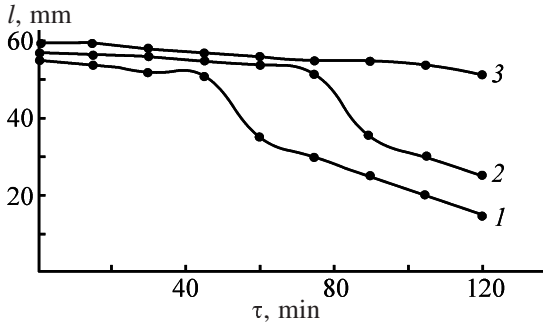

Fig. 2. Mobility *l* of mortars containing 0.5% CA-1 as a function of time τ; sand : cement weight ratio 1 : 1.5, the same for Fig. 3. (*1*) Mixing rate 60 rpm, time 5 min; (*2*) mixing rate 60 rpm, time 15 min; (*3*) mixing rate 90 rpm, time 5 min.

acid and MTA, the intensity of the carbonyl group at 1711 cm^{-1} decreases to a still greater extent than in the above-described system, simultaneously the intensity of the peak at 1560 cm^{-1} strongly increases, suggesting formation of the reaction product of the fatty acid and alkanolamine; tertiary amine interacts with this product.

The use of single-component additives for improving placeability of cement paste is hindered by the fact that most of them exhibit plasticizing power only at definite conditions of the concrete preparation, i.e., fixed conditions of mixing and preset content of cement in the mortar. As shown in [5], any attempt to attain strong plasticizing effect by mixing of organic surfactants of two types is not very promising. However, as shown in [1], the use in a complex additive of both hydrophilic and hydrophobic components differing in the surface tension provides intense air-entraining effect, which positively affects plasticizing of the cement paste. Therefore, the mobility and time parameter of the mobility retention of the building solutions are the functions not only of the plasticizer content but also of the time and intensity of mixing of the mortars.

The curves of the mobility loss by the mortars containing one of the additives prepared (CA-1) are shown in Fig. 2; the mortars were mixed on a mechanical stirrer at a rate of 60 rpm for 5 and 15 min (Fig. 2, curves *1, 2*) and 90 rpm for 5 min (Fig. 2, curve *3*). At relatively slow mixing of the building mortars (Fig. 2, curve *1*), the mobility of the mixtures is lower compared to mixing at higher rates (Fig. 2, curve *3*), which may be due to elevated air entrainment of the cement paste. The data on the density of the resulting materials measured by hydrostatic weighing confirms significant effect of air entrainment in the later case. With increasing mixing time to 15 min (Fig. 2, curve *2*), the mobility of the mixtures increases as compared to the above modes; simultaneously the air entrainment increases, the concrete density decreases, and the time parameter of the mobility retention also increases.

As shown in [6], floccules (coarse aggregates containing water) are formed in cement after addition of water. The effect of common plasticizers (deflocculating agents) is due to sorption of their molecules on the surface of cement particles and newly formed aggregates. These additives, being adsorbed, should provide formation of similar electrical charge on the particle surface and thus stabilize dispersions owing to the repulsion forces (electrostatic factor). Similar deflocculating effect can be caused by air inclusions which mechanically separate the cement particles and thus hinder their mutual approach to the distance of electrostatic attraction (structural-mechanical factor). To determine what factor provides the decisive effect on the plasticization of the mortars, we measured the electrokinetic potentials of the electrical double layer at the cement particle surface (ζ potential) in the absence of hydrophobic plasticizing additives and in their presence.

In the absence of plasticizers, the ζ potential of the particles of given concrete is negative (–9 mV) and after treatment of the cement surface with CA-1 the absolute value of the ζ potential increases (–11.3 mV). After treatment of the cement with CA-2, the ζ potential decreases to –7.7 mV. With increasing content of hydrophobic component in the complex additive CA-2, the negative value of the ζ potential decreases, and the electrical double layer undergoes recharging to +2.8 mV. Despite the above differences in the ζ potential, the plasticizing effects of these additives is similar, i.e., the effect of the electrokinetic potential on the mobility of the cement systems is not decisive. Hence, air inclusions presumably exert a stronger effect on the mobility of the mortars upon addition of the plasticizers. Moreover, unsaturated fatty acid present in the additive smoothes microroughness between the particles, decreases the internal friction, and forms a hydrophobic lubricating film on the cement particles plasticizing the cement paste.

The experiments with plasticizing additives introduced into preliminarily hydrated cements (postponed addition) were also performed. It was found that addition of chemical modifying agents in the preinduction period of the concrete hardening improves strength properties of the hardened materials; however, in this case the plasticizing effect decreases. These additives

Composition of the complex additives and properties of the resulting materials

Additive	Content, %		Decrease in water consumption, %	Time parameter of mobility retention	Compression strength after storage for 28 days, MPa	Water absorption, wt %	Frost resistance grade
	MTA in additive	additive in mortar					
CA-1	15	0.5	20	2.5	55	3.2	F 400
CA-1	5	0.8	22	2.7	50	3.0	F 400
CA-2	15	0.5	18	1.8	47	3.6	F 400
CA-2	5	0.8	21	2.3	45	3.3	F 400
CA-3	15	0.5	20	1.5	45	3.3	F 400
CA-3	5	0.8	25	2.0	42	3.6	F 400
Reference	–	–	–	1.0	50	5.5	F 300

also cause intensive thinning of the mortars with increasing mixing time.

We assumed that addition of the given hydrophobic-plasticizing agents into the mortars is accompanied by sorption of the oriented asymmetrically polar molecules on the hydrophilic surface of the cement particles, which is accompanied by a slight change in the ζ potential. The polar groups of diphilic molecules are bound with the cement particle surface, whereas the hydrophobic hydrocarbon radicals are oriented outwards. These radicals exhibit water-repellent properties, and polar sections of the adsorbed molecules can form water-insoluble salts of fatty acid with calcium and, thus, the hydrophobic section of the molecule is fixed of the solid surface, providing micromudding effect.

In accordance with Khigerovich's theory [7], sorption occurs not on the whole cement surface but only on its active centers, blocking them. Probably, plasticizer components form not continuous but cellular films on the cement surface, so that the cement can participate in hydration upon addition of water. Our complex plasticizing mixture also affects the morphology of the crystallization nuclei and growing crystals. Sorption hinders the crystal growth, and the structure of the concrete monolith becomes more disperse and poorly crystalline, which is confirmed by the data of XRD analysis: the content of calcium hydroxide decreases simultaneously with decreasing degree of crystallinity of the newly formed compounds, i.e., additives cause adsorption modification of the products of cement hydration.

The above results are confirmed by the kinetic data on the increase in the strength of the resulting materials (Fig. 3). Owing to the formation of adsorption layers on the cement surface, the mortars are characterized by slow strength increase as compared to those containing other polycarboxylate plasticizers (Fig. 3, curve *1*). However, owing to the growth of new formations and adsorption binding of the hydrophobic-plasticizing additives by their surfaces, the adsorption layers are broken, which causes an increase in the strength parameters of the resulting materials in the final stage of concrete hardening (28 days) (Fig. 3, curves *2, 3*).

With increasing content of the complex additive in the mortar over 0.8%, the mobility of the cement paste strongly increases and the time parameter of the mobility retention increases by a factor of 3.0–3.5. This is due to extremely small penetration of water through the layers of hydrophobic-plasticizing additive and causes noticeable deceleration of the cement hydration in the induction and accelerated periods of hardening. At a high content of the additive, the effect of air entrainment increases, which decreases the strength properties of the hardened materials, especially in earlier stages of hardening. As a rule, the strength of the materials even in the final stages of hardening is significantly lower than the strength of

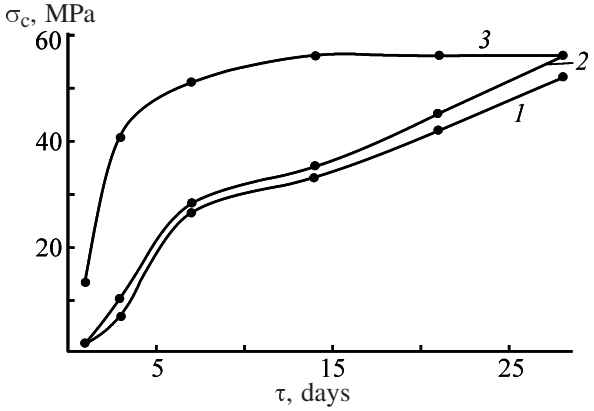

Fig. 3. Compression strength σ_c of hardened materials as a function of the hardening time τ. CA-3, %: (*1*) 0.8 and (*2*) 0.5; (*3*) 0.3% polycarboxylate plasticizer.

the material without additives, which hinders preparation of highly mobile mixtures and materials with satisfactory strength properties. The properties of materials prepared using hydrophobic-plasticizing additives CA-1, CA-2, and CA-3 are given in the table.

As seen from the experimental results, complex plasticizing additives improve some functional characteristics of the resulting materials, namely, decrease the water consumption of the cement paste, increase the time parameter of the mobility retention, decrease the water absorption, and improve the frost resistance of the hardened materials.

CONCLUSIONS

(1) New complex plasticizers containing unsaturated fatty acid and its salts or esters with modified tertiary amine increase the mobility and time parameter of the mobility retention of the cement mortars.

(2) New complex plasticizers containing components that differ in the hydrophilic–lipophilic balance and surface tension, when added to cement mortars, provide air entrainment, which positively affects the plasticization of the cement paste.

(3) Plasticizers added to Portland cements decrease the water consumption of the system, increase the hydrophobic properties of the pore walls, decrease the water sorption of the materials, and enhance their frost resistance.

REFERENCES

1. Batrakov, V.G., *Modifitsirovannye betony* (Modified Concretes), Moscow: Stroiizdat, 1998.
2. Bleshchik, N.P., *Stroit. Nauka Tekh.*, 2005, no. 1, pp. 53–60.
3. Vasilik, P.G. and Golubev, I.V., *Stroit. Mater.*, 2003, no. 9, pp. 24–26.
4. Ramachadran, V.S., Fel'dman, R.F., and Kallepardi, M., *Dobavki v beton* (Additives to Concrete), Boldyrev, A.S. and Ratinov, V.B., Eds., Moscow: Stroiizdat, 1988.
5. Ratinov, V.B. and Rozenberg, T.I., *Dobavki v beton* (Additives to Concrete), Moscow: Stroiizdat, 1978.
6. Teylor, H.F.W., *Cement Chemistry*, London: Academic, 1990.
7. Khigerovich, M.I. and Baier, V.E., *Gidrofobno-plastifitsiruyushchie dobavki dlya tsementov, rastvorov i betonov* (Hydrophobic-Plasticizing Additives to Cements, Mortars, and Concretes), Moscow: Stroiizdat, 1979.

ISSN 1070-4272, Russian Journal of Applied Chemistry, 2007, Vol. 80, No. 11, pp. 1809–1811. © Pleiades Publishing, Ltd., 2007.
Original Russian Text © V.G. Maiorov, A.I. Nikolaev, V.K. Kopkov, O.P. Adkina, 2007, published in Zhurnal Prikladnoi Khimii, 2007, Vol. 80, No. 11, pp. 1784–1786.

INORGANIC SYNTHESIS AND INDUSTRIAL INORGANIC CHEMISTRY

Influence of Fluoroelement Acids on Extraction of Group IV–VI Element Fluorides

V. G. Maiorov, A. I. Nikolaev, V. K. Kopkov, and O. P. Adkina

Tananaev Institute of Chemistry and Technology of Rare Elements and Mineral Raw Material, Kola Scientific Center, Russian Academy of Sciences, Apatity, Murmansk oblast, Russia

Received March 16, 2007

Abstract—Effect of titanium(IV) and silicon(IV) on extraction of Ti(IV), Nb(IV), Ta(V), and W(VI) with octanol and tributyl phosphate from fluoride solutions was studied.

DOI: 10.1134/S1070427207110055

The diversity of stable compounds of various elements recovered from fluoride solutions suggests the diversity of complexes formed in these media [1]. However, only some of them are well extracted as fluoride complexes. This is attributed to the fact that in fluoride systems metal ions are characterized by maximal coordination numbers and form fluoride complexes with a high negative charge. For example, Fe(III) forms the complex $FeCl_4^-$ in chloride solutions and FeF_6^{3-} in fluoride solutions. It is known that, the higher the charge of an ion, the worse it is extracted [2, 3].

In industry, fluoride systems are used most widely for extraction, separation, and purification of Ta(V) and Nb(V) [4, 5]. Usually, tantalite–columbite concentrates are used as the initial raw material. However, because of limited resources of rich niobium–tantalum raw material, growing attention is focused on recovery of tantalum and niobium from solutions in which the content of impurities substantially (by an order of magnitude) exceeds the content of the target metals. Such solutions are obtained by hydrometallurgical processing of unconventional mineral raw materials and artificial rare-metal concentrates. For example, Ti(IV), Si(IV), and Fe(III) in titanoniobates, Si(IV) and Zr(IV) in eudialyte, or Sn(IV) in tin dross are the major macroimpurities.

The efficiency of the extraction treatment of niobium–tantalum solutions with a high content of impurities is largely determined by the chemical state of metal ions in the fluoride solutions. The Ta(V) and Nb(V) ions are extracted from fluoride solutions as complex fluorometallic acids $HTa(Nb)F_6$. Published data [2–5] show that many extrinsic elements, similarly to Ta(V) and Nb(V), can form fluoroelement acids of types H_xMF_y, $H_xMO_zF_y$, etc. As a rule, these compounds are strong acids and readily dissociate, which increases the hydrogen ion concentration (i.e., solution acidity) and hence increases the Ta(V) and Nb(V) extraction. Using ^{19}F NMR, we found that Ti(IV) forms complex acids $HTiF_5 \cdot H_2O$ and H_2TiF_6 in 2 : 1 ratio. The compound H_2SiF_6 is stable in aqueous solution and behaves as a strong dibasic acid (stronger than sulfuric acid) [6]. The series of the stability of Group IV–VI element fluoride complexes is presented in [7]: $[ZrF_6]^{2-} \geq [MoO_2F_4]^{2-} \geq [HfF_6]^{2-} \geq [TiF_6]^{2-} > [VOF_4]^{2-} > [GeF_6]^{2-} > [SiF_6]^{2-} > [MoO_2F_3]^-$.

All the above facts provide a basis for the development of an extraction technology with the recovery of Ta(V) and Nb(V) from solutions containing only HF, without addition of other mineral acids (usually H_2SO_4 and less commonly HCl). The solution of this problem facilitates utilization of spent solutions with regeneration of HF.

Here we report preliminary data on the influence of fluorotitanic and fluorosilicic acids and (for comparison) H_2SO_4 on the Mo(VI) and W(VI) extraction. We also present some results from our previous papers [8–10] concerning the effect of the above acids on Ti(IV), Nb(V) and Ta(V) recovery.

Tributyl phosphate (TBP) and 1-octanol (OCL) were used as extractants. The chemicals were of analytically pure or chemically pure grade, and TBP and OCL were of pure grade. Extraction was performed at volume ratios $V_o : V_w$ equal to 1 : 1 for TBP and 2 : 1 for less basic OCL. To determine the

Extraction of Ti(IV), Nb(V), Ta(V), Mo(VI), and W(VI) from fluoride solutions

Concentration, M		Extractant	$V_o : V_w$	Recovery, %, from indicated solution						References
element	HF_{fr}			HF	HF + 2 M			HF + 4 M		
					H_2SO_4	Ti(IV)	Si(IV)	H_2SO_4	Si(IV)	
Ti(IV), 1.0	0.5	TBP	1 : 1	13.3	22.2	–	32.2	45.4	65.4	[10]
		OCL	2 : 1	3.3	10.0	–	16.7	26.1	66.0	
Nb(V), 0.075	3.0	TBP	1 : 10	<1	12.7	15.6	30.9	44.2	94.4	[8, 9]
		OCL	1 : 10	<1	2.7	–	17.6	21.2	64.2	
Ta(V), 0.0045	3.0	TBP	1 : 10	67.4	92.3	96.9	95.0	94.4	95.4	[8, 9]
		OCL	1 : 10	~1	17.1	–	35.6	39.1	80.8	
Mo(VI), 0.05	2.4	TBP	1 : 1	22.2	74.2	55.6	87.0	–	–	
		OCL	2 : 1	–	–	–	48.0	–	–	
W(VI), 0.03	2.4	TBP	1 : 1	0.6	17.7	30.0	39.1	–	–	
		OCL	2 : 1	–	–	–	21.6	–	–	

Mo(VI) or W(VI) concentrations in extracts, they were back-extracted with 4 M HF at $V_o : V_w = 1 : 2$, with subsequent colorimetric determination of Mo(VI) and W(VI) in the backwash. The extraction time was 30 min. The initial aqueous solutions for extraction were prepared from concentrated fluoride solutions containing (M): (1) 5.76 Mo(VI), 19.6 F^-; (2) 2.38 W(VI), 21.6 F^-; (3) 7.02 Ti(IV), 35.6 F^-; and (4) 4.75 Si(IV), 28.5 F^-. The other features of handling aggressive fluoride solutions and of analytical monitoring are described in [8].

The data on the influence of Ti(IV), Si(IV), and H_2SO_4 on the distribution of metal ions studied are listed in the table; HF_{fr} is the calculated HF content over the amount required for formation of the complexes H_2TiOF_4, H_2SiF_6, $HMoO_2F_3$, and $H_2WO_2F_4$ (in accordance with data of [3, 5, 7, 11], these complexes are dominating in the systems studied). Introduction of fluorotitanic and fluorosilicic acids sharply increases the Mo(VI) and W(VI) extraction. With respect to the influence of the acids considered on the Mo(VI) recovery, these acids can be ranked as follows: $H_2SiF_6 > H_2SO_4 > H_2TiOF_4 >> HF$. For the recovery of W(VI), the order is as follows: $H_2SiF_6 > H_2TiOF_4 > H_2SO_4 >> HF$. Under the conditions studied, Mo(VI) is extracted substantially better than W(VI). Probably, this is caused by the fact that Mo(VI) is predominantly recovered in the form of monobasic acid $HMoO_2F_3$, and W(VI), as worse extracted dibasic acid $H_2WO_2F_4$.

For the system with Ti(IV), the replacement of H_2SO_4 by H_2SiF_6 also substantially increases the Ti(IV) recovery. In extraction from the 0.5 M HF + 4 M Si(IV) solution, with $V_o : V_w = 2 : 1$ for TBP and 4 : 1 for OCL, the Ti(IV) recovery in one step of the extraction reaches 80% and more [10].

The effect of complex fluoroelement acids on the extraction decreases in the order $H_2SiF_6 > H_2TiOF_4 \geq H_2SO_4$ for Nb(V) and $H_2TiOF_4 \geq H_2SiF_6 \geq H_2SO_4$ for Ta(V). We also studied the influence exerted on the extraction by other elements capable to form fluoroelement acids: Al(III), Zr(IV), Sn(IV), and Fe(III). We found that Fe(III) affects the Nb(V) extraction more weakly than does Ti(IV). The influence of these elements on the Ta(V) recovery is close to the effect of Ti(IV), except Sn(IV) exerting a weaker effect. Coextraction of fluoroelement acids as macroimpurities with Nb(V) and Ta(V) at low $V_o : V_w$ is relatively small, and Nb(V) and Ta(V) can be readily separated from them by washing of the corresponding extracts.

It should be noted that fluosilicic acid affects the extraction of Ti(IV), Nb(V), Ta(V), Mo(VI), and W(VI) particularly strongly. For example, the recovery of Mo(VI) in extraction with TBP in the system with H_2SiF_6 in one step is more than 80%, which provides in the countercurrent extraction mode practically complete Mo(VI) extraction with separation from W(VI). In the presence of H_2SiF_6 at $V_o : V_w = 2 : 1$, the efficient recovery of Ti(IV) is also possible. At the same time, the complete Ti(IV) recovery from H_2SO_4 solutions is problematic under the conditions studied.

The data on extraction with OCL are also of interest. In the system with H_2SiF_6 in extraction from

2 M Si(IV), OCL is a weaker extractant than TBP, despite the fact that in some cases extraction with OCL is performed at large $V_o : V_w$ ratios (see table). However, at a Si(IV) content close to 4 M, the OCL extraction ability approaches that of TBP at similar $V_o : V_w$ ratios. We can expect that the same effect will also be observed for Mo(VI) and W(VI). This shows that the influence of fluoroelement acids (which generate H^+ ions) on the phase distribution of the metal ions studied depends not only on particular fluoroelement acid, but also on the organic extractant. The latter effect should be taken into the account when studying the influence of fluoroelement acids on extraction.

It should be noted that the use of OCL for extraction from acid fluoride solutions is preferable as compared to TBP, since TBP is hydrolyzed on contact with aqueous acid solutions [5]. In [12], we evaluated the extraction power of extractants by the degree of HF recovery depending on time of their contact with a solution of 4.25 M HF + 5 M H_2SO_4. In extraction with OCL, the HF recovery decreased in 160 days insignificantly, from 36 to 29%, whereas TBP completely decomposed in 70 days (a homogeneous solution was formed).

The results of our studies are of interest for the recovery of Ta(V) and Nb(V) from aqueous solutions of fluoroelement acids derived from macroimpurities, without addition of other mineral acids except HF. The implementation of this approach is urgent in connection with the observed tendency toward increased processing of lean niobium–tantalum raw materials with a high content of the impurities. From spent solutions [after Ta(V) and Nb(V) recovery], HF can be regenerated by dialysis or pyrolysis [13]. In so doing, so-called extrinsic elements in some cases can be obtained as marketable products, e.g., titanium (in one of procedures of loparite processing) in the form of titanium dioxide [13]. All the above-said provides a basis for the development of low-waste technology of processing of lean niobium–tantalum raw materials.

However, at a high content of impurities and hence at a high solution acidity, their extraction also increases. As a result, a strong competition arises between fluoroelement acids of Ta(V), Nb(V), and macroimpurities for the organic phase, which can deteriorate the separation and purification of Ta(V) and Nb(V). In this connection, further systematic study of the mutual influence of components in these complex extraction systems, including the influence of the extractant, is topical.

CONCLUSIONS

(1) Fluorotitanic and fluorosilicic acids affect the extraction of Group IV–VI element fluorides, Ti(IV), Nb(IV), Ta(IV), Mo(VI), and W(VI) to the same extent as does H_2SO_4, or even more strongly.

(2) Mutual influence of all metal ions capable to form fluoride complexes, which can dissociate by the acid type, should be taken into the consideration to efficiently use fluoride extraction systems.

REFERENCES

1. Davidovich, R.L., Kaidalova, T.A., Levshichina, T.F., and Sergienko, V.I., *Atlas infrakrasnykh spektrov pogloshcheniya i rentgenometricheskikh dannykh kompleksnykh ftoridov metallov IV i VI grupp* (Atlas of IR Absorption Spectra and X-ray Diffraction Data of Complex Fluorides of Group IV and V Metals), Moscow: Nauka, 1972.
2. Diamond R.M., and Tuck, D.G., *Extraction of Inorganic Compounds into Organic Solvents*, New York: Interscience, 1960.
3. Zolotov, Yu.A., Iofa, B.Z., and Chuchalin, L.K., *Ekstraktsiya galogenidnykh kompleksov metallov* (Extraction of Metal Halide Complexes), Moscow: Nauka, 1973.
4. Ritcey, G.M. and Ashbrook, A.W., *Solvent Extraction. Principles and Applications to Process Metallurgy*, Amsterdam: Elsevier, 1979.
5. Babkin, A.G., Maiorov, V.G., and Nikolaev, A.I., *Ekstraktsiya niobiya, tantala i drugikh elementov iz ftoridnykh rastvorov* (Extraction of Niobium, Tantalum, and Other Elements from Fluoride Solutions), Leningrad: Nauka, 1988.
6. Nekrasov, B.V., *Osnovy obshchei khimii* (Foundations of General Chemistry), Moscow: Khimiya, 1974, vol. 1.
7. Spivakov, B.Ya., Petrukhin, O.M., and Zolotov, Yu.A., *Zh. Anal. Khim.*, 1972, vol. 27, no. 8, pp. 1584–1597.
8. Maiorov, V.G., Nikolaev, A.I., and Kopkov, V.K., *Zh. Prikl. Khim.*, 1999, vol. 72, no. 6, pp. 929–932.
9. Maiorov, V.G., and Nikolaev, A.I., *Tsvetn. Metall.*, 2002, no. 11, pp. 24–28.
10. Maiorov, V.G., Nikolaev, A.I., Kopkov, V.K., and Korotkova, G.V., *Zh. Prikl. Khim.*, 2004, vol. 77, no. 4, pp. 683–684.
11. Ryss, I.G., *Khimiya ftora i ego neorganicheskikh soedinenii* (Chemistry of Fluorine and Its Inorganic Compounds), Moscow: Goskhimizdat, 1956.
12. Maiorov, V.G., Baklanova, I.V., Nikolaev, A.I., and Safonova, L.A., *Zh. Prikl. Khim.*, 2000, vol. 73, no. 10, pp. 1636–1640.
13. Sklokin, L.I., Zots, N.V., Shestakov, S.V., et al., *Tsvetn. Met.*, 2000, no. 10, pp. 48–53.

ISSN 1070-4272, Russian Journal of Applied Chemistry, 2007, Vol. 80, No. 11, pp. 1812–1815. © Pleiades Publishing, Ltd., 2007.
Original Russian Text © N.M. Panich, B.G. Ershov, A.F. Seliverstov, A.G. Basiev, 2007, published in Zhurnal Prikladnoi Khimii, 2007, Vol. 80, No. 11, pp. 1787–1790.

PHYSICOCHEMICAL STUDIES OF SYSTEMS AND PROCESSES

Ozone Solubility in Concentrated Aqueous Solutions of Salts

N. M. Panich, B. G. Ershov, A. F. Seliverstov, and A. G. Basiev

Frumkin Institute of Physical Chemistry and Electrochemistry, Russian Academy of Sciences, Moscow, Russia

Received April 19, 2007

Abstract—The effect exerted by the concentration of salts (NaCl, Na_2SO_4, and $NaNO_3$) on the ozone solubility in aqueous solution at 20, 30, and 40°C was studied. The solubility coefficients of ozone were calculated. The Henry constants and the Sechenov coefficients were determined.

DOI: 10.1134/S1070427207110067

The fields of ozone application have expanded considerably recently. Ozone is used for disinfection of drinking water and for oxidative decomposition of organic and inorganic impurities present in process waste and wastewater. At radiochemical and nuclear power plants, ozone is used, in particular, to decompose organic compounds in treatment of liquid radioactive waste containing high concentrations of dissolved salts (nitrates, chlorides, sulfates, and others) [1]. In the development of the optimal process conditions, the ozone solubility as a function of the salt concentration is an important parameter. The above parameter makes it possible to estimate the concentration of ozone in working solutions and predict the efficiency of oxidative processes and the rate of ozone removal from the reaction zone.

The effect of additives to the electrolyte on the solubility of ozone in aqueous solution was considered in [2–5]. These experiments were performed at a low concentration of salts under conditions minimizing the decomposition of dissolved ozone (in particular, at low pH).

This study is aimed to determine the ozone solubility in neutral aqueous solutions of certain salts in a wide range of concentrations typical of industrial processes.

EXPERIMENTAL

The objects of study were aqueous solutions of Na_2SO_4, NaCl, and $NaNO_3$ (all chemical purity grade). The concentrations of the salts were varied from 0.35 to 3.5 M. The solutions used had pH ~6.

The ozonation was performed in a temperature-controlled cell at 20, 30, and 40°C. The ozone was obtained in a Trinity ozonizer equipped with a capillary discharge chamber ensuring formation of the ozone–oxygen mixture (OOM) containing as much as 180 mg l^{-1} of ozone. The ozone–oxygen mixture passed through the solution being tested at a given temperature until a steady-state concentration of O_3 in the liquid phase was attained. The ozone concentration in the solution was continuously monitored by its absorption spectrum (λ_{max} = 258 nm and ε = 2900 l mol^{-1} cm^{-1} [6]), which allowed the time of attainment of the limiting solubility (about 10 min) to be established correctly. It was found by the special experiments that in the examined temperature range the position and shape of the absorption band of ozone in aqueous salt solutions remain constant.

It is known that the solubility of a gas depends on its concentration in the gas phase (Henry's law). As noted in [7], the Henry's law is fulfilled in a wide range of ozone concentrations. Therefore, the composition of the OOM was maintained constant. The concentration of O_3 in the OOM was 166 mg l^{-1}.

To estimate the O_3 solubility in the solution, we calculated a dimensionless parameter, the solubility coefficient α defined as a ratio of the O_3 concentration in the liquid to its concentration in the gas:

$$\alpha = c_l/c_g.$$

The data on the O_3 solubility in the solutions studied are listed in Tables 1–3 and Fig. 1. The coefficients α of the O_3 solubility in pure water, obtained by different authors at 293 K and a pressure of 0.1 MPa, lie within 0.23–0.41 [2, 4, 8, 9]. In our experiments α was equal to 0.3.

The data presented show that the ozone solubility

Table 1. Effect of salt concentration c_s on O_3 solubility in NaCl solutions at 20°C

c_s, M	α		K_s, l mol^{-1}		$H \times 10^{-3}$, MPa cm^3 mol^{-1}	
	no acidification	pH 2	no acidification	pH 2	no acidification	pH 2
0	0.3	0.27			7.5	8.2
0.51	0.19		0.39		11.9	
0.85	0.13	0.23	0.42	0.07	17.0	9.5
1.71	0.06	0.15	0.43	0.16	40.2	15.3
2.56	0.03	0.12	0.42	0.14	86.7	18.5

Table 2. Effect of salt concentration c_s on O_3 solubility in Na_2SO_4 solution

c_s, M	α		K_s, l mol^{-1}		$H \times 10^{-3}$, MPa cm^3 mol^{-1}	
	20°C	30°C	20°C	30°C	20°C	30°C
0	0.30	0.23	–	–	7.5	9.5
0.35	0.19	0.16	0.49	0.42	11.1	13.4
0.49	0.17	0.14	0.51	0.42	13.2	15.1
0.7	0.13	0.11	0.51	0.42	17.0	18.7
1.06	0.10	0.08	0.46	0.43	23.1	27.3

Table 3. Effect of salt concentration c_s on O_3 solubility in $NaNO_3$ solutions

c_s, M	α			K_s, l mol^{-1}			$H \times 10^{-3}$, MPa cm^3 mol^{-1}		
	20°C	30°C	40°C	20°C	30°C	40°C	20°C	30°C	40°C
0	0.30	0.23	0.16				7.5	9.4	13.3
0.59	0.26	0.19	0.14	0.10	0.14	0.07	8.5	11.3	14.6
1.18	0.22	0.17	0.14	0.11	0.11	0.05	10.2	12.5	15.3
1.76	0.18	0.15	0.11	0.12	0.10	0.08	12.1	14.1	18.4
2.35	0.15	0.14	0.10	0.13	0.10	0.08	15.4	15.6	20.1
3.50	0.12	0.10	0.08	0.11	0.11	0.08	17.3	22.7	25.0

decreases as the concentration of the salts in the solution and the temperature increase. The data for Na_2SO_4, NaCl, and $NaNO_3$ solutions are compared in Fig. 1. As seen, for $NaNO_3$, variations of the O_3 solubility with the molal concentration of the salt are the least pronounced. The Henry constant H was calculated as

$$H = P_{O_3}/M_{O_3},$$

where P_{O_3} is the partial pressure of ozone in the gas and M_{O_3}, molar concentration of ozone in the solution.

For water, $H_0 = 7.5 \times 10^3$ MPa cm^3 mol^{-1}, in good agreement with the value obtained by other authors [2, 4, 8] at 20°C. The Henry constant increases as the

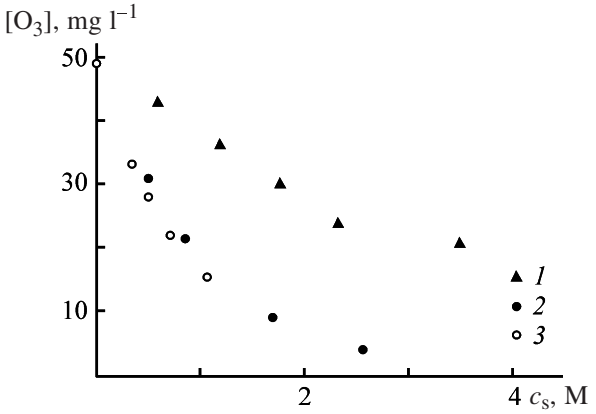

Fig. 1. Solubility of ozone $[O_3]$ in aqueous solution vs. salt concentration c_s at 20°C. (*1*) $NaNO_3$, (*2*) NaCl, and (*3*) Na_2SO_4.

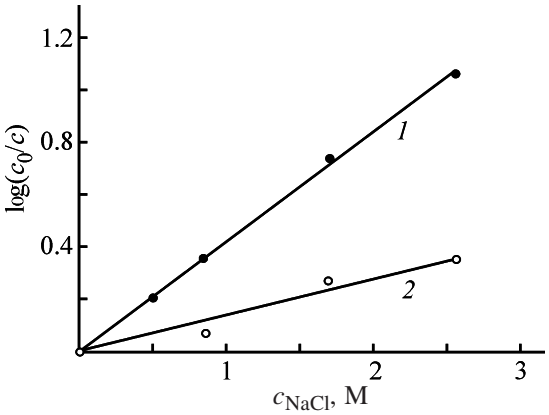

Fig. 2. $\log(c_0/c)$ for ozone vs. c_{NaCl} at 20°C. (*1*) Without acidification and (*2*) pH 2. Calculated K_s: (*1*) 0.4174 and (*2*) 0.1389.

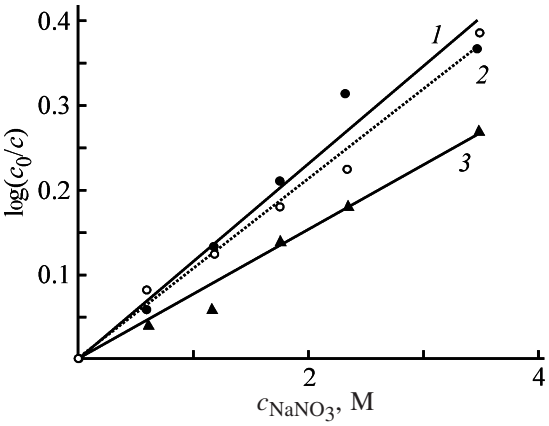

Fig. 3. $\log(c_0/c)$ for ozone vs. c_{NaNO_3}. Temperature, °C: (*1*) 20, (*2*) 30, and (*3*) 40. Calculated K_s: (*1*) 0.114, (*2*) 0.1051, and (*3*) 0.0756.

electrolyte concentration in the solution increases. For salt solutions at 20°C, the calculated H values are close to those obtained in [2]. Also, there is good agreement with the values measured for Na_2SO_4 solutions at 30°C in [3].

The effect of electrolyte concentration on the solubility of gases is described by the Sechenov equation [10]:

$$\log(c_0/c) = K_s c_s,$$

where c_0 is the solubility of the gas in pure water and c, its solubility in the salt solution; c_s is the salt concentration; and K_s is the salting-out coefficient or the Sechenov constant, a quantity characteristic of a given salt.

Thus, the Sechenov coefficients can be used for estimation of the solubility of a gas, and O_3 in particular, in aqueous solutions of electrolytes. As known [11], K_s depends on both the nature of the electrolyte and the temperature and pressure. Appreciable dependence of K_s on the electrolyte concentration is also possible in most cases [11]. It is rather important for practical purposes to establish the boundaries of applicability of this relationship.

The dependence of the ozone solubility in a solution on the NaCl concentration at 20°C is plotted in Fig. 2 in the coordinates of the Sechenov equation. As can be seen, the $\log(c_0/c)$ vs. c_s dependence is linear over the entire range of the salt concentrations studied. The K_s values for NaCl solutions in a wide range of the concentrations ranging from 0.5 to 2.56 M (see also Table 1) are approximately the same (0.42). The experimental procedure used here was checked in experiments on the dependences of ozone solubility for NaCl solutions acidified to pH 2.

It was found that the data obtained are in good agreement with the results of [2] for the same solutions. It is seen from Fig. 1 and Table 1 that the solubility coefficient α increases, whereas the Henry constant decreases on passing from neutral to acidic NaCl solution. In this case, the Sechenov equation is also well fulfilled over the entire range of the salt concentrations studied (Table 1). The K_s parameter decreases to 0.14.

It was also established for Na_2SO_4 solutions (Table 2) that the Sechenov equation is well fulfilled for two temperatures, 20 and 30°C, with K_s slightly decreasing with increasing temperature. As noted in [11], the Sechenov coefficients can noticeably depend on the electrolyte concentration at the concentrations of more than 0.5–1 m (molality) and decrease with increasing concentration at relatively high concentrations of the electrolyte. In our case, however, the Sechenov constants were virtually constant. According to the data of [2], the Sechenov equation may be fulfilled up to 1.5 M and only for KCl its fulfillment to 1.0 M may be expected.

No systematic studies was performed on the O_3 solubility in $NaNO_3$ solutions. The data of Table 3 demonstrate the change in the solubility coefficients of O_3, Henry constants, and Sechenov coefficients at the temperatures increased from 20 to 40°C at a salt concentration of up to 3.5 M. The values obtained may be useful when estimation of the ozone solubility in $NaNO_3$ solutions is necessary for technology. This electrolyte is the main salt formed when wastewater from nuclear power plants is concentrated by evaporation for the subsequent storage.

Raising the solution temperature from 20 to 40°C affects only slightly the salting-out coefficient, with K_s tending to slightly decrease. It should be noted that, for $NaNO_3$ solutions, the Sechenov equation is also fulfilled reasonably well. The $\log(c_0/c)$ vs. c_s dependence is satisfactorily fitted by a straight line with an average K_s value (Fig. 3). The plots for three temperatures and the K_s values calculated from the plots, averaged over the whole region of the salt concentrations, are presented in Fig. 3. The calculated values of H and K_s can be compared with the data of [2] for $Ca(NO_3)_2$ ($K_s = 0.182$ l mol^{-1}).

Thus, to estimate the ozone solubility in process solutions and wastewater, one should take into account the dependence of the salting-out coefficient K_s on the nature of the electrolytes contained in them and the effect of ambient temperature.

CONCLUSIONS

(1) Data on the ozone solubility in aqueous solutions of salts agree satisfactorily with the empirical model of salting-out of gases.

(2) The salting-out coefficient K_s for NaCl solutions at concentrations of 0.5–2.6 M is constant (about 0.42 at 20°C). For Na_2SO_4 solutions K_s is 0.48 (at 20°C), and for $NaNO_3$ K_s ~0.11 and remains constant up to 3.5 M. The coefficients decrease slightly with increasing temperature.

ACKNOWLEDGMENTS

The authors are grateful to the Russian Foundation for Basic Research (project no. 06-03-32682) for partial financial support.

REFERENCES

1. *Trudy 5-i Mezhdunarodnoi nauchno-tekhnicheskoi konferentsii "Obrashchenie s radioaktivnymi otkhodami"* (Proc. 5th Int. Scientific and Technical Conf. "Radioactive Waste Management"), Moscow: VNIIAES, November 22–24, 2005.
2. Rischbieter, E., Stein, H., and Schumpe, A., *J. Chem. Eng. Data*, 2000, vol. 45, no. 2, pp. 338–340.
3. Young Ku, Wei-Jeng Su, and Yung-Shuen Shen, *Ind. Eng. Chem. Res.*, 1996, vol. 35, no. 10, pp. 3369–3374.
4. Kosak-Channing, L.E., and Helz, G.R., *Environ. Sci. Technol.*, 1983, vol. 17, no. 3, pp. 145–149.
5. Raukas, M.M., Munter, R.R., and Siirde, E.K., *Zh. Prikl. Khim.*, 1984, vol. 57, no. 11, pp. 2597–2599.
6. Bader, H., and Holgne, J., *Ozone: Sci. Eng.*, 1982, vol. 4, no. 4, pp. 169–176.
7. Razumovskii, S.D., and Zaikov, G.E., *Ozon i ego reaktsii s organicheskimi soedineniyami* (Ozone and Its Reactions with Organic Compounds), Moscow: Nauka, 1974.
8. Matrozov, V.I., Kashtanov, S.A., Stepanov, A.M., and Tregubov, B.A., *Zh. Prikl. Khim.*, 1975, vol. 48, no. 8, pp. 1838–1841.
9. Aleksandrov, Yu.A., Tarunin, B.I., and Perepletchikov, M.L., *Zh. Fiz. Khim.*, 1983, vol. 57, no. 10, pp. 2385–2397.
10. Sechenov, M., *Z. Phys. Chem.*, 1889, vol. 4, pp. 117–125.
11. Namiot, A.Yu., *Rastvorimost' gazov v vode: Spravochnoe posobie* (Solubility of Gases in Water: Reference Book), Moscow: Nedra, 1991.

ISSN 1070-4272, Russian Journal of Applied Chemistry, 2007, Vol. 80, No. 11, pp. 1816–1821. © Pleiades Publishing, Ltd., 2007.
Original Russian Text © S.A. Semenova, Yu.F. Patrakov, 2007, published in Zhurnal Prikladnoi Khimii, 2007, Vol. 80, No. 11, pp. 1791–1796.

PHYSICOCHEMICAL STUDIES OF SYSTEMS AND PROCESSES

Liquid-Phase Ozonation of Fusainized Components of SS Coal

S. A. Semenova and Yu. F. Patrakov

Institute of Coal and Coal-Tar Chemistry, Siberian Division, Russian Academy of Sciences, Kemerovo, Russia

Received April 19, 1007

Abstract—Stepwise ozonation of leaning fusainized components of fossil coal of SS grade in acetic acid was studied. The dynamics of accumulation of oxygen-containing groups in the course of ozonation was examined, and the main pathways of the reaction of ozone with structural fragments of the coal substance were revealed.

DOI: 10.1134/S1070427207110079

Ozone is a powerful oxidant of the majority of organic compounds, which is due to low energy of detachment of an O atom from an O_3 molecule and high electron affinity of the ozone molecule [1]. Thanks to the reactivity of ozone toward hydrocarbons of various classes [2], ozonation finds wide use in coal chemistry in studies of structural features of solid fossil fuels and their processing productes (shales [3, 4], lignites [5, 6], coal tar [7, 8], humic acids [9], etc.). For example, analysis of the ozonation products of oil shale showed that kerogen has predominantly alicyclic structure [4]. Ozonation of polyfunctional humic acids [9] converts macromolecular substances forming their basis into low-molecular-weight water-soluble products. It is suggested [7, 8] to use ozonation of neutral oxygen-containing fractions and asphaltenes of coal tar for preparing aliphatic and aromatic dicarboxylic acids.

Previously [10–12] we considered the effect of ozonation in the gas phase and in chloroform on the organic matter of vitrinite components of coal with various degrees of metamorphism. We found that coals with the medium degree of metamorphism are the most reactive toward ozone, irrespective of the reaction medium (gas or liquid). In the liquid phase, the ozonation rate increased [12] with an increase in the ozone concentration in the solvent [1]. We also found that, in low-metamorphized coals, ozone primarily reacts with alkyl substituents of benzene rings by the radical mechanism, and with increasing degree of metamorphization the contribution of electrophilic addition of ozone across π bonds of condensed aromatic structures increases [10].

One of the problems of coal-mining industry is accumulation of large volumes of low-grade coal slacks enriched in mineral substances and in leaning petrographic components of the inertinite group. This problem is particularly acute for enterprises of the Prokop'evsk–Kiselevsk deposit where the coal mainly consists of fusainolites with the total content of leaning components as high as 50–70% [13]. At the same time, coal slacks depleted of baking compounds can be considered as raw materials for preparing organic oxygen-containing products by ozone treatment.

The goal of this study was to reveal specific features of liquid-phase ozonation of fusainized components of SS grade coal of the Kuznetsk coal fields and to examine the composition and properties of products soluble in acetic acid.

EXPERIMENTAL

As investigation object we used fusain petrographic coal lithotype (95–97 wt % content of microcomponent of inertinite group) recovered from SS coal slack (Ziminka mine, Prokop'evsk–Kiselevsk deposit, Kuznetsk coal fields). The recovery procedure was based on individual visual signs of the lithotype with additional fractionation of the recovered fusain varieties with respect to density under static conditions in the CCl_4–C_6H_6 mixture. The sample characteristics (%) are as follows: ash content A^d 10.0, moisture content W^a 1.3, reflection index of vitrinite $R_{0.r}$ 1.06; elemental composition, %: C 88.1, H 4.6, N + S 2.5, and O 4.8.

Ozonation was performed at 20°C in a temperature-controlled rotating reactor providing intense mixing of the reaction mixture, with continuous supply of an ozone–oxygen mixture (1.5 vol % ozone). As solvent we used glacial acetic acid (75 ml) in which the ozonation products are the most soluble. The coal sample (fraction 0–0.063 mm) was 2 g. After the process

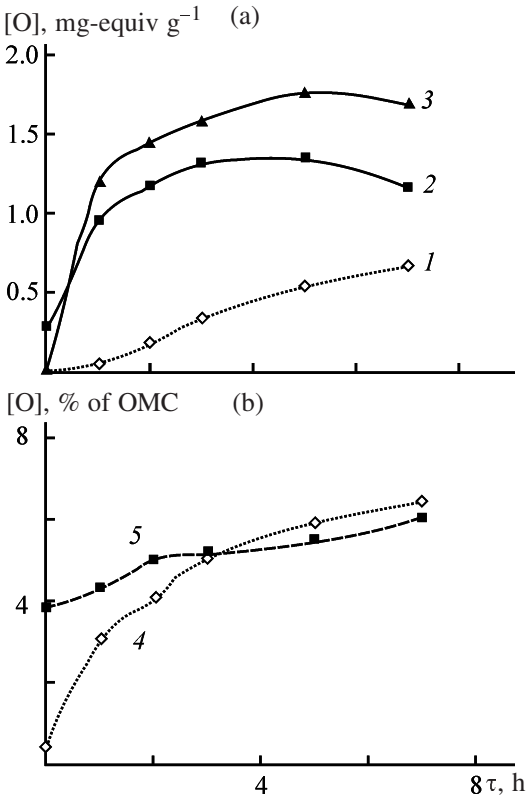

Fig. 1. (a) Amounts of (*1*) carboxy, (*2*) phenolic, and (*3*) carbonyl groups, and (b) oxygen content in (*4*) active and (*5*) inactive forms, as functions of ozonation time τ.

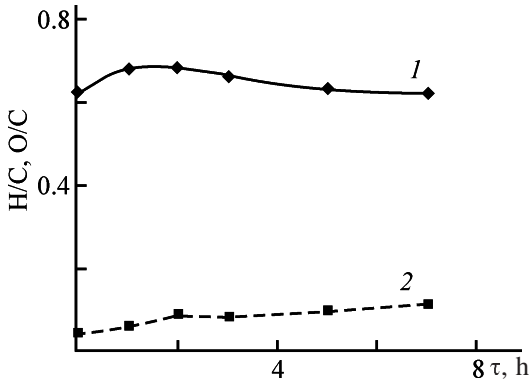

Fig. 2. Atomic ratios (*1*) H/C and (*2*) O/C in OMC as functions of ozonation time τ.

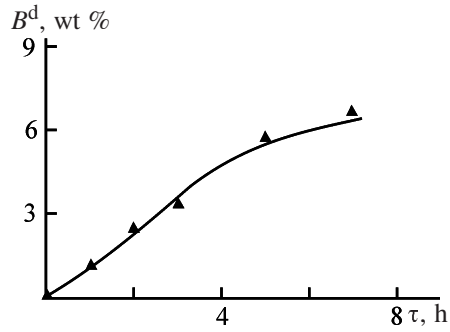

Fig. 3. Yield of ozonation products soluble in acetic acid B^d as a function of ozonation time τ.

completion, the coal was filtered off and the solvent was distilled off from the soluble products. The distillation residue was treated with 100 ml of distilled water, heated for 2 h on a water bath, and separated into water-soluble (WS) and water-insoluble (WI) products.

The samples were examined by elemental and chemical functional analysis, IR spectroscopy, thermal gravimetric analysis, and mass spectrometry.

The oxygen content in the "active" form was calculated by summation of its amounts in the form of phenolic, carbonyl, and carboxy groups, and in the "inactive" form, as the difference. The content of carbonyl groups was determined by the reaction with hydroxylamine hydrochloride; content of carboxy groups, by the acetate method; and total content of carboxy and hydroxy groups, by ion exchange with sodium hydroxide.

The IR diffuse reflection spectra were recorded on a Tensor-27 spectrometer (Bruker). Thermal analysis was performed with an STA 409 thermal analyzer (Netzsch); the sample (10–20 mg) was heated in a helium atmosphere to 500°C at a rate of 10 deg min^{-1}. The mass spectra of thermal degradation products were recorded on an Acolos mass-spectrometric unit, with ionization by electron impact (70 eV). Analysis by gas chromatography–mass spectrometry (GC–MS) was performed with a 19091S-433 device (Agilent) using an HP-5MS capillary column (5% diphenyl–95% dimethylsiloxane), 30 m × 0.25 mm × 0.25 μm; carrier gas helium. Prior to chromatographic analysis, the products were methylated with diazomethane in diethyl ether.

Ozonation of fusain in acetic acid leads to a considerable increase in the content of active oxygen-containing groups (Fig. 1). The carboxy, phenolic, and carbonyl groups are accumulated in the largest amount in the organic matter of coal (OMC) in 5 h of ozonation, after which their content varies insignificantly. The oxygen content in the inactive form (Fig. 1) and the O/C ratio (Fig. 2) monotonically increase throughout the process. A decrease in the rate of accumulation of active oxygen with an increase in the ozonation time may be due to saturation of the reaction surface of coal particles with oxidation products. In the process, the formation of products soluble in acetic acid decelerates also (Fig. 3).

Table 1. Characteristics of initial and residual coal and of ozonation products

Sample	Yield,* % based on OMC	Elemental composition, % based on OMC			Atomic ratio	
		C	H	O + N + S	H/C	O/C
Initial coal	100.0	88.1	4.6	7.3	0.62	0.04
Water-soluble products	75.0	48.8	4.2	47.0	1.03	0.72
Water-insoluble products	16.0	61.0	3.4	35.6	0.67	0.44
Residual coal	18.1	76.5	3.4	20.2	0.53	0.18

* Based on the initial (before ozonation) organic matter of coal.

Table 2. Results of functional and IR spectral analyses

Sample	Functional composition, mg-equiv g^{-1}			Oxygen in indicated groups, % based on OMC		IR parameters	
	–COOH	–OH	>C=O	active	inactive	A_{2920}/A_{1610}	A_{1690}/A_{3400}
Initial coal	–	0.28	–	0.50	3.81	–	–
Water-soluble products	8.36	1.50	4.24	32.54	14.46	0.22	1.38
Water-insoluble products	4.70	2.71	4.00	22.56	13.04	0.14	1.94
Residual coal	0.77	7.89	1.02	15.90	2.28	–	–

Therefore, we restricted the ozonation time to 5 h. To avoid further degradation of soluble products with ozone, in the subsequent experiments we performed ozonation in the stepwise mode, with intermittent removal of the soluble products from the reaction zone and washing of unchanged coal with fresh acetic acid. As a result of prolonged ozonation (12 cycles), the yield of soluble products exceeded 90% based on OMC. Among them, low-molecular-weight WS substances accounted for 75 wt % (Table 1).

The higher reactivity of fusain compared to vitrinite coals [11] is apparently due to specific structural features of this lithotype. Despite the common opinion that fusain exhibits higher aromaticity [14, 15], it is unlikely that its polynuclear fragments are highly condensed. The average statistical structural unit of this lithotype can be conventionally illustrated by the scheme

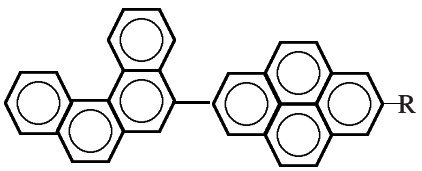

where R is an aryl, heteroatomic (O, N, S), or short-chain alkyl (–CH_2–) bridge between fragmentary units of OMC.

The dependence of the structure of fusains on metamorphic transformations of OMC [14–16] is weak, which is apparently responsible for the fact that the reaction with ozone is essentially independent of the degree of coal metamorphism.

Thus, whereas all the main reactions of ozone with organic matter of vitrinite coals of high degree of metamorphism can occur only in the peripheral region of condensed polyaromatic blocks of OMC [11], in the structure of fusains, according to the hypothetical model, there are considerably more sites for ozone attack. At the same time, the lack in fusain organic matter of a shell of peripheral alkyl and active oxygen-containing groups (Table 2) characteristic of low-metamorphized vitrinite coals may also be favorable for ozonation. As the most promising raw materials for preparing benzenecarboxylic acids are artificially carbonized coal formations with the smallest crystallite size (pyrolysis products of peat, lignite, wastes from hydrolysis and woodworking industry) [17], fusain can be considered as a natural material with the favorable structure of the carbon framework.

As the limiting factor of the process is the diffusion of an oxidant molecule to the reactive surface of coal, it is also necessary to take into account the specific features of the texture of this lithotype. For example, in contrast to other petrographic components, fusain

is characterized by the maximal total porosity, and coarse pores with the diameter of about 10^{-4} cm, formed in the course of thermal oxidative coal formation processes, account for 99% of the total pore volume [18, 19]. Thus, relatively large amount of macropores can also stimulate the ozonation owing to free diffusion of ozone into the interpore space of coal.

Based on the features of molecular and supramolecular structure of fusainized coal components [14–16, 18, 19], reactivity of ozone [2], and the occurring changes in the functional composition of OMC upon ozonation, the following pathways of the reaction of ozone with fusain organic matter can be outlined: (1) degradation of benzene ring via formation of ozonides and cleavage of interfragmentary alkyl links, leading to an increase in the amount of carboxy and carbonyl groups in OMC; (2) reaction of ozone with polyaromatic structures of OMC without ring cleavage, leading to an increase in the amount of phenolic groups; and (3) oxidation of anthracene-type fragments to anthraquinone and of ether links to carbonyl groups.

Presumably, π bonds of aromatic fragments undergo oxidative degradation first, with opening of condensed rings. This results in a decrease in the degree of aromaticity and in a certain increase in the H/C ratio (Fig. 2). In the next step, apparently, heteroatomic and "bridging" alkyl fragments of OMC are involved in the oxidation, with partial removal of hydrogen atoms from them into the gaseous or liquid medium; as a result, the H/C ratio returns to the level characteristic of the initial sample.

Analysis of the fusain ozonation products showed that the water-soluble substances are characterized by higher atomic ratios H/C and O/C (Table 1). This fact indicates that relatively low-molecular-weight oxygen-containing compounds prevail in their composition. The prevailing functional groups in WS and WI ozonation products are carboxy groups (Table 2). Whereas in the initial coal sample inactive oxygen (ether, heterocyclic [14]) prevailed, in ozonation products active oxygen-containing groups were predominant.

In the IR spectra of the WS and WI fractions (Fig. 4), the strongest bands belong to oxygen-containing groups [20]: 3100–3500 cm^{-1}, vibrations of OH groups of phenols and carboxylic acids, involved in hydrogen bonding; 2500–2700 cm^{-1}, stretching vibrations of OH groups involved in stronger intramolecular bonds (acid dimers). A strong ill-resolved peak at 1630–1780 cm^{-1} corresponds to vibrations of C=O groups in aromatic and aliphatic acids and in ketones. In the range 1100–1300 cm^{-1}, a broad strong band

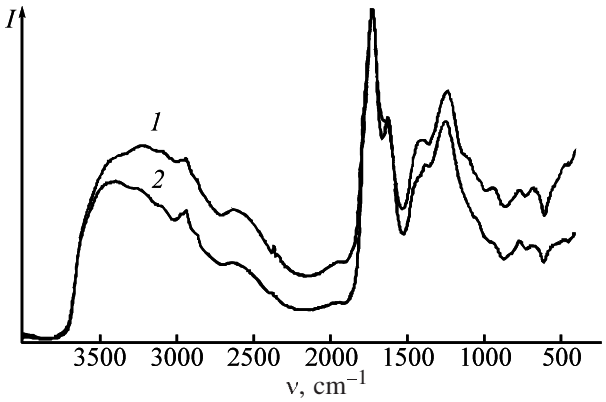

Fig. 4. IR spectra of (*1*) WS and (*2*) WI products of fusain ozonation. (*I*) Intensity and (ν) wavenumber.

with a maximum at 1260 cm^{-1} characterizes stretching vibrations of C–O groups of ethers, esters and phenols. The bands of all the O-containing groups are stronger in the spectra of water-soluble products. The intensities of the absorption bands of aliphatic CH_n (2920, 2850, 1440, 1380 cm^{-1}), aromatic C=C, and aromatic C–H (3040, 1600, 690–870 cm^{-1}) groups in the IR spectra of WS and WI substances differ insignificantly. More information can be gained from the ratios of the intensities of the absorption bands of aromatic C=C (1610 cm^{-1}), aliphatic CH_n (2920 cm^{-1}), carbonyl (1690 cm^{-1}), and phenolic and carboxyl OH groups (3400 cm^{-1}). For example, the parameter A_{2920}/A_{1610} (Table 2) correlates with the H/C atomic ratio (Table 1) and is lower for water-insoluble substances. The values of A_{1690}/A_{3400} are consistent with the results of functional analysis (Table 2), suggesting relatively higher content of acidic groups in WS products.

As thermal decomposition pathways of organic substances are largely determined by the content and chemical forms of oxygen in them, the results of thermal gravimetric analysis also bear certain information about the features of ozonation products. The shape of the temperature dependences of the weight loss rate indicates that oxygen-containing groups in the isolated products differ in the thermal stability (Fig. 5). The WS products in which the content of carboxy groups is the highest (Table 2) decompose in one step at low temperatures with a maximum at 152°C (weight loss rate 4.1 deg min^{-1}). The major volatile products of thermolysis of WS substances in the low-temperature range are water vapor (release of H_2O gives rise to peaks with *m*/*z* 17 and 18) and carbon oxides (*m*/*z* 28, 44) (Fig. 6a). Also detected are fragments of oxygen-containing (*m*/*z* 30, 46, 62), alkyl (*m*/*z* 14, 15, 38, 82), cyclic unsaturated (*m*/*z* 54, 80), and aromatic (*m*/*z* 76, 78, 92) hydrocarbons [20].

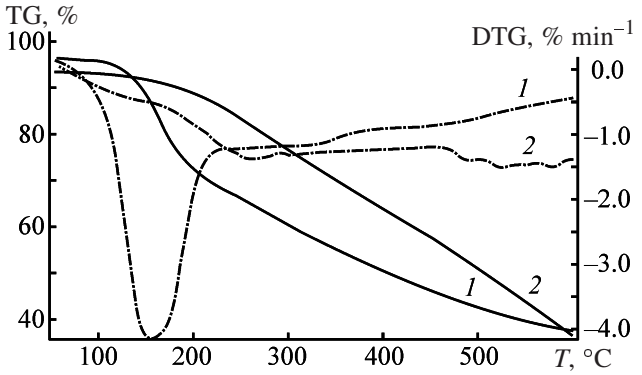

Fig. 5. TG and DTG curves for (*1*) WS and (*2*) WI products of coal ozonation. (*T*) Temperature.

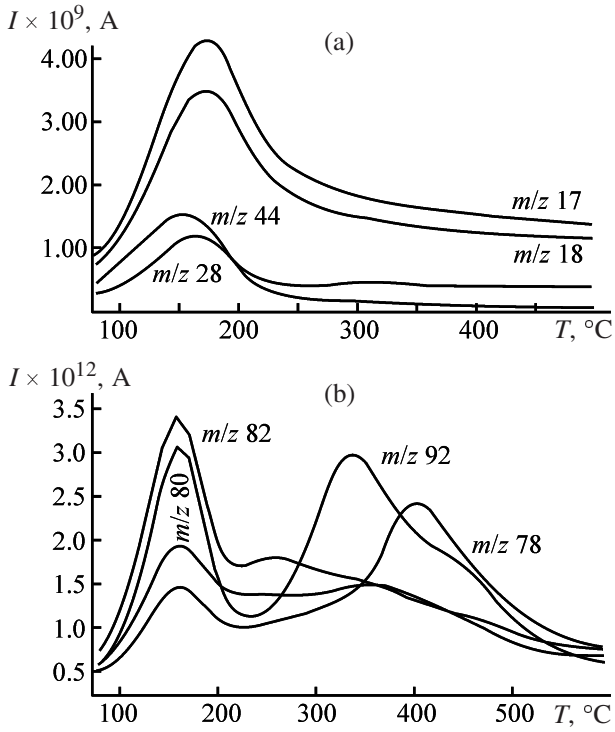

Fig. 6. Mass-spectroscopic patterns of release of (a) H_2O (*m*/*z* 17, 18) and CO_2 (*m*/*z* 28, 44), and (b) alkyl (*m*/*z* 82), unsaturtated (*m*/*z* 80), and aromatic (*m*/*z* 78, 92) volatile products of thermal degradation of WS compounds. (*I*) Ion current and (*T*) temperature.

The ion currents of the latter fragments increase with temperature (Fig. 6b).

The WI products, on the contrary, are characterized by a weak (1.4 deg min^{-1}) DTG peak, smeared over the whole temperature interval, which suggests the macromolecular polyfunctional structure of the WI compounds with close intervals of thermal decomposition of the components.

A GC–MS analysis of WS products of fusain ozonation revealed no aliphatic compounds. Phthalic acid (60.3%) and its isomers (19.5%) account for approximately 80% of aromatic compounds. Benzenetricarboxylic (trimellitic) and benzenetetracarboxylic (pyromellitic) acids account for 10.2 and 7.8% of the products, respectively, i.e., the major fraction of ozonation products of fusainized coal substance is a concentrate of benzenecarboxylic acids of relatively uniform composition. The content of oxy, hydroxy, and nitrogen-containing derivatives of aromatic compounds in water-soluble ozonation products is low.

From water-insoluble products esterified with diazomethane, we isolated an ether-soluble fraction containing esters of benzenedicarboxylic acids (43.5%) and higher linear aliphatic monocarboxylic acids (56.5%). The presence of palmitic (31.7%) and stearic (24.8%) acids in WI products suggests participation of natural fats in the genesis of fusainized coal [21].

CONCLUSIONS

(1) Experiments on stepwise ozonation of fusainized components of SS coal revealed the possibility of conversion of its organic matter into products soluble in acetic acid. The major components of the products obtained are low-molecular-weight water-soluble compounds: a concentrate of benzenecarboxylic acids with the prevalence of dicarboxylic acids.

(2) Thanks to high oxidation rate and to low cost and ready availability of reagents, ozonation of fusainized coal slacks can be considered as a route to valuable aromatic acids, alternative to classical oxidation of aromatic hydrocarbons.

REFERENCES

1. *Khimicheskaya entsiklopediya* (Chemical Encyclopedia), Knunyants, I.L., Ed., Moscow: Bol'shaya Ross. Entsiklopediya, 1992, vol. 3.
2. Razumovskii, S.D. and Zaikov, G.E., *Ozon i ego reaktsii s organicheskimi soedineniyami* (Ozone and Its Reactions with Organic Compounds), Moscow: Nauka, 1974.
3. Kutuev, R.Kh., Egudina, O.G., Yakovlev, V.I., and Proskuryakov, V.A., *Khim. Tverd. Topl.*, 1976, no. 2, pp. 108–113.
4. Egor'kov, A.N., Fekhervari, A., Barlai, I., et al., *Khim. Tverd. Topl.*, 1985, no. 1, pp. 30–33.
5. Perednikova, Z.M., Rumyantseva, Z.A., Gartsman, B.B., et al., *Khim. Tverd. Topl.*, 1986, no. 1, pp. 33–39.
6. Perednikova, Z.M., Rumyantseva, Z.A., Garts-

man, B.B., et al., *Khim. Tverd. Topl.*, 1992, no. 1, pp. 36–40.

7. Platonov, V.V., Klyavina, O.A., Vol'-Epshtein, A.B., et al., *Khim. Tverd. Topl.*, 1987, no. 1, pp. 88–92.
8. Platonov, V.V., Kudrya, A.N., and Proskuryakov, S.V., *Zh. Prikl. Khim.*, 2003, vol. 76, no. 1, pp. 154–158.
9. Verkhodanova, N.N., Myakina, I.A., Egor'kov, A.N., et al., *Khim. Tverd. Topl.*, 1981, no. 5, pp. 54–60.
10. Patrakov, Yu.F., Semenova, S.A., and Kam'yanov, V.F., *Khim. Tverd. Topl.*, 2002, no. 1, pp. 32–39.
11. Semenova, S.A., Patrakov, Yu.F., and Fedyaeva, O.N., *Khim. Inter. Ustoich. Razv.*, 2006, vol. 14, no. 1, pp. 47–52.
12. Semenova, S.A. and Patrakov, Yu.F., *Khim. Tverd. Topl.*, 2007, no. 1, pp. 18–22.
13. Ivanov, V.P., Stankevich, A.S., Shkoler, M.B., and Sivchikov, V.E., *Khim. Tverd. Topl.*, 2002, no. 4, pp. 3–19.
14. Eremin, I.V., Lebedev, V.V., and Tsikarev, D.A., *Petrografiya i fizicheskie svoistva uglya* (Petrography and Physical Properties of Coal), Moscow: Nedra, 1980.
15. Gagarin, S.G., Golovin, G.S., and Gyul'maliev, A.M., *Khim. Tverd. Topl.*, 2006, no. 1, pp. 12–39.
16. Gagarin, S.G. and Eremin, I.V., *Koks Khim.*, 1996, no. 8, pp. 11–18.
17. Sapunov, V.A., in *Destruktsiya i okislenie iskopaemykh uglei* (Degradation and Oxidation of Fossil Coals), Kiev: Naukova Dumka, 1979, pp. 56–85.
18. Markova, K., Radev, G., and Kostova, N., *Khim. Tverd. Topl.*, 1992, no. 3, pp. 20–22.
19. Ettinger, I.L., Eremin, I.V., Zimakova, B.M., and Bakaldina, A.P., *Dokl. Akad. Nauk SSSR*, 1964, no. 2, pp. 364–367.
20. Pretsch, D.P., Bühlmann, P., and Affolter, C., *Structure Determination of Organic Compounds*, Berlin: Springer, 2000.
21. Egor'kov, A.N., Kutuev, R.Kh., and Yakovlev, V.I., *Khim. Tverd. Topl.*, 1979, no. 4, pp. 122–127.

ISSN 1070-4272, Russian Journal of Applied Chemistry, 2007, Vol. 80, No. 11, pp. 1822–1825. © Pleiades Publishing, Ltd., 2007.
Original Russian Text © A.P. Pokutsa, A.B. Zaborovskii, D.S. Maksim, 2007, published in Zhurnal Prikladnoi Khimii, 2007, Vol. 80, No. 11, pp. 1797–1800.

PHYSICOCHEMICAL STUDIES OF SYSTEMS AND PROCESSES

Catalytic Decomposition of H_2O_2 in Hydrophilic Solvents: The Kinetic Aspect

A. P. Pokutsa, A. B. Zaborovskii, and D. S. Maksim

Department of Physical Chemistry of Fossil Fuels, Litvinenko Institute of Physical Organic Chemistry and Coal Fuel Chemistry, National Academy of Sciences of Ukraine, Lviv, Ukraine

Received May 16, 2007

Abstract—Decomposition of hydrogen peroxide in organic hydrophilic solvents, catalyzed by cobalt(II) palmitate [$Co(palm)_2$], was studied by the method of inhibitors.

DOI: 10.1134/S1070427207110080

Physicochemical characteristics of the medium affect the kinetics of homogeneous reactions, among them redox reactions, accelerating or inhibiting their elementary steps [1, 2]. Despite relatively low sensitivity of these processes to the solvent, variation of the rates of individual pathways can noticeably affect the yield of target products. Because the processes in hand, as a rule, involve the radical pathway of transformation, by which, in particular, the initiation reaction occurs, it is of interest and important to study this elementary stage. The most common initiators are peroxy compounds. It is commonly believed that the decomposition of peroxy compounds (including hydrogen peroxide) in solutions proceeds by two parallel pathways, molecular and induced [3]. The role of the solvent in these reactions is governed by its solvation characteristics [4] affecting molecular decomposition, and the induced decomposition is mainly governed by self-association of the solvent (cohesion energy density) [5]. An increase in the cohesion energy density accelerates the process, presumably due to strengthening of the effect of "cage" formed by solvent–solvent and solvent–peroxide hydrogen bonds [6], which results in decreased energy barrier of the reaction and increased rate of induced decomposition [7].

This work continues the study of catalytic decomposition of hydrogen peroxide in hydrophilic solvents [8]. The choice of H_2O_2 as a subject of the study is caused by the fact that its use as an oxidant of many organic substrates is promising from environmental, technological, and economical viewpoints. The kinetic data were obtained using the method of inhibitors as one of the most approved, accessible, and informative methods of studying radical reactions.

The decomposition of hydrogen peroxide was studied at 35°C in a temperature-controlled 25-ml glass cell with stirring by a Teflon-covered magnetic stirrer. The kinetics of H_2O_2 consumption in the solvents was studied by titration of the samples (1 ml), withdrawn from the reaction mixture, with a $KMnO_4$ solution. The electronic absorption spectra of the solutions placed in a quartz cell 1 cm thick were recorded on an SF-20 double-beam spectrophotometer. Quinone (InH) was synthesized from hydroquinone by the procedure described in [9] and purified by double recrystallization from ethanol. The solvents of analytically pure grade were purified by standard procedures and distilled just before experiments. Their characteristics are presented in [5, 7]. Cobalt(II) palmitate (Aldrich) was used without additional purification.

The experimental rates of pseudo-first-order decomposition of H_2O_2 catalyzed by Co^{2+} indicate that the solvent significantly affects this process (Fig. 1a, Table 1). In the solvents containing hydroxy groups (alcohols), the decomposition rate is very high ($W \sim 20 \times 10^{-5}$ mol s^{-1}), and within approximately 30 min after the beginning of the reaction the H_2O_2 concentration is close to zero. At the same time, in water and acetic acid the decomposition rate is significantly lower. The reaction rate in electron-donor dioxane and especially in morpholine is still lower. This experimental fact correlates well with the dependence of the decomposition rate of peroxides on the effect of specific (ability to form donor–acceptor complex) and nonspecific (electrostatic) solvation with the solvent [10]. Hence, the solvents containing hydroxy groups (alcohols) and, in a lesser extent, acids and water are favorable for decomposition of H_2O_2, whereas

electron-donor solvents (morpholine and dioxane) stabilize H_2O_2.

The presence of an inhibitor (quinone) significantly affects the pattern observed for the noninhibited process (Table 1). As known, in free-radical processes, species with free valence can induce decomposition of compounds with weakened O–O bond. Inhibitors of free radicals hinder this pathway of conversion of peroxy compounds [11], and thus it is possible to estimate quantitatively the contribution of individual decomposition pathways (molecular and induced) to the overall rate of hydrogen peroxide consumption. It was established experimentally (Fig. 1b) that an increase in the quinone concentration above 0.01 M does not further affect the rate of H_2O_2 consumption. Hence, it can be assumed that, at this concentration of the inhibitor, the decomposition of peroxide in the examined solvents proceeds by the molecular pathway.

The decomposition rate in solvents more prone to self-association is more sensitive to the presence of InH than in solvents containing no hydroxy groups (Table 1). For example, in alcohols and acetic acid the contribution of induced decomposition was approximately 90%. The next in this characteristic are acetonitrile and tetrahydrofuran (approximately 80%), and then go water, morpholine, and dioxane (40–70%). The special position of water in this series is apparently caused by a combination of electrochemical characteristics that distinguish water from alcohols and organic acids.

As follows from Table 1, the highest ratio of the overall rates of H_2O_2 decomposition in the examined solvents is approximately 16 ($W_{i\text{-PrOH}}/W_{\text{dioxane}}$). For molecular decomposition, this ratio is 3.6, and for induced decomposition, approximately 33. Hence, under the conditions studied, the medium affects the induced pathway of peroxide decomposition by almost an order of magnitude more significantly than the molecular pathway, which agrees with the published data [5].

With the aim of additional elucidation of the solvent effect on the conversion of Co^{2+} into Co^{3+}, we recorded the electronic absorption spectra of Co(II) palmitate solutions before and after their treatment with H_2O_2. The positions of absorption maxima corresponding to Co^{2+} and Co^{3+} (Table 2), similar to the rate of their transformations upon addition of hydrogen peroxide, depend on the physicochemical properties of the solvent. For example, in solvents capable of formation of strong hydrogen bonds (alcohols),

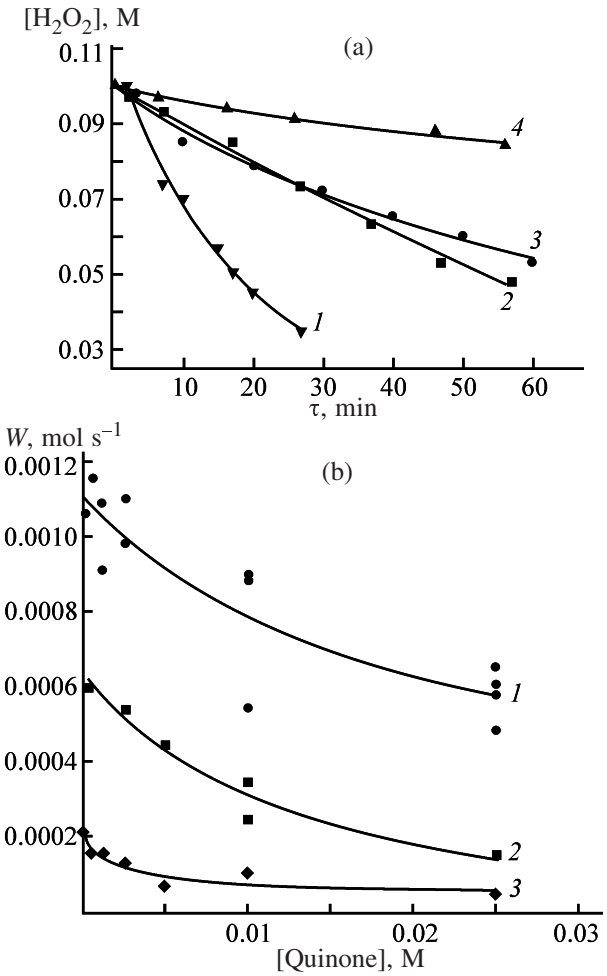

Fig. 1. (a) Kinetic curves of H_2O_2 decomposition catalyzed by $Co(palm)_2$ in solvents at 35°C and (b) rate of H_2O_2 consumption W in acetic acid as a function of quinone additions. (a) (*1*) THF, (*2*) MeCN, (*3*) acetic acid, and (*4*) morpholine. (b) $[H_2O_2] = 0.05$ M, 35°C. $[Co^{2+}]_0$, M: (*1*) 0.01, (*2*) 0.005, and (*3*) 0.0025.

Table 1. Total rate of hydrogen hydroxide consumption W and its molecular (W_{mol}) and induced (W_{ind}) components. $[H_2O_2] = 0.1$, $[Co(palm)_2] = 5 \times 10^{-3}$, [quinone] = 0.01 M, 35°C

Solvent	$W \times 10^5$	$W_{\text{mol}} \times 10^5$	$W_{\text{ind}} \times 10^5$	W_{ind}/W, %
	mol s^{-1}			
i-PrOH	19.0	2.5	16.5	87
t-BuOH	18.0	2.1	15.9	88
HOAc	6.2	0.8	5.4	87
H_2O	1.4	0.4	1.0	71
Dioxane	1.2	0.7	0.5	42
Morpholine	1.4	0.6	0.8	57
MeCN	5.5	0.8	4.7	75
THF	18.0	3.5	14.5	81

Table 2. Absorption maxima of Co^{2+} and Co^{3+} ions in various solvents, 20°C

Solvent	λ_{max}, nm	
	Co^{2+}	Co^{3+}
i-PrOH	490	605
HOAc	545	610
H_2O	530	610
Dioxane	520	610
Morpholine	550	570
MeCN	510	610
THF	525	610

the absorption maximum of Co^{2+} and Co^{3+} is observed at 490 and 605 nm, respectively (Fig. 2a, Table 2). The rate of transformation of Co^{2+} into Co^{3+} after addition of H_2O_2 in these solvents and also in MeCN is essentially diffusion-controlled. It is of interest that in acetic acid and in water, capable of formation of hydrogen bonds [7, 12] similarly to alcohols, a bathochromic shift of the absorption maxima of Co^{2+} is observed (Table 2). This may be due to the difference in the pK_a values of the two latter solvents.

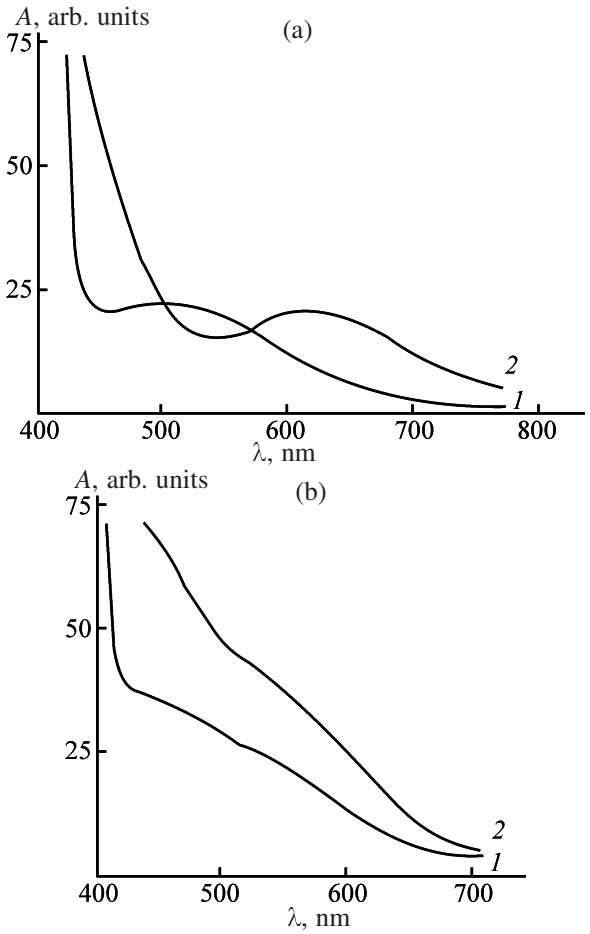

Fig. 2. Electronic absorption spectra of (a) $Co(palm)_2$ solution and (b) the same solution in the presence of 0.02 M of quinone (*1*) before and (*2*) after addition of H_2O_2. Solvent isopropanol, 20°C, $[Co^{2+}]_0 = 1 \times 10^{-3}$ M, $[H_2O_2]_0 = 5 \times 10^{-2}$ M.

In electron-donor solvents: morpholine, dioxane, and acetonitrile, the spectrum of Co^{2+} changes under the action of H_2O_2 within a short time (1 min). However, there is a discrepancy between the rate of formation of oxidized cobalt species and the rate of decomposition of hydrogen peroxide in these solvents. This fact is attributable to oxidation of the reduced Co^{2+} species in electron-donor solvents predominantly with $OH^{\bullet}$ radicals.

The absorption maxima of Co(II) in morpholine (550 nm), THF (525 nm), dioxane (520 nm), and acetone (510 nm) are shifted bathochromically in comparison with alcohols (Table 2). The absorption maximum of Co^{3+} in acetonitrile, THF, and dioxane (610 nm) coincides with that in the solvents capable of formation of hydrogen bonds (Table 2). As regards the electronic spectrum of Co^{3+} in morpholine, its absorption maximum (570 nm) is close to that of Co^{2+} (550 nm) in this solvent. This significant hypsochromic shift of the absorption for the more polar Co^{3+} ions in comparison with the other solvents is apparently caused by stronger electron-donor power and lower polarity of morpholine compared to MeCN [13].

Addition of hydrogen peroxide to a $Co(palm)_2$ solution in isopropanol containing 0.1 M quinone does not result in formation of oxidized cobalt species: The absorption peak corresponding to Co^{3+} is absent (Fig. 2b). The spectrum did not change in 1 h after mixing this solution with H_2O_2.

Thus, it was confirmed that the induced decomposition of hydrogen hydroxide makes a decisive contribution to the overall rate of hydrogen peroxide consumption and valence transformations of the catalyst in the solvents characterized by a high cohesion energy density and significant specific solvation. The influence of physicochemical characteristics of solvents on the rate of hydrogen peroxide decomposition is complicated and ambiguous. To a first approximation, we can assume that the decomposition rate is proportional to the solvent polarity (dielectric constant) and its electrophilicity (ability to be donor of hydrogen bonds). This fact suggests the combined contribution of several factors to the mechanism of hydrogen peroxide decomposition, as in the decomposition of per acids [14].

CONCLUSION

Physicochemical characteristics of solvents affect both the decomposition rate of hydrogen peroxide and formation of oxidized forms of the catalyst by affecting the ratio of the molecular and induced pathways of H_2O_2 decomposition.

REFERENCES

1. Hendry, D.G. and Russel, G.A., *J. Am. Chem. Soc*., 1964, vol. 86, pp. 368–381.
2. Howard, I.A. and Ingold, K.U., *Can. J. Chem*., 1964, vol. 42, pp. 1250–1264.
3. Bulgakova, G.M., Maizus, Z.K., and Skibida, I.P., *Kinet. Katal*., 1966, vol. 7, pp. 332–338.
4. Zaikov, G.E., Maizus, Z.K., and Emanuel', N.M., *Izv. Akad. Nauk SSSR, Ser. Khim*., 1968, vol. 2, pp. 256–260.
5. Emanuel', N.M., Zaikov, G.E., and Maizus, Z.K., in *Rol' sredy v radikal'no-tsepnykh reaktsiyakh okisleniya organicheskikh soedinenii* (Role of the Medium in Radical-Chain Oxidation of Organic Compounds), Moscow: Nauka, 1973.
6. Matienko, L.I., Goldina, L.A., Skibida, I.P., and Maizus, Z.K., *Izv. Akad. Nauk SSSR, Ser. Khim*., 1975, no. 2, pp. 287–292.
7. Buchachenko, A.L. and Sukhanova, O.P., *Usp. Khim*., 1967, vol. 36, no. 3, pp. 475–496.
8. Pocutsa, A., Makitra, R., and Maksim-Lutsik, D., Abstracts of Papers, *7th Eur. Symp. on Organic Reactivity*, Ulm, 1999, p. 185.
9. *Organic Syntheses*, Blatt, A.H., Ed., New York: Wiley, 1944, 2nd ed., coll. vol. 1.
10. Entelis, S.G., *Zh. Vses. Khim. O–va. im. D.I. Mendeleeva*, 1970, vol. 22, no. 3, pp. 324–333.
11. Denisov, E. and Khudyakov, I., *Chem. Rev*., 1987, vol. 87, pp. 1313–1357.
12. Kuz'mina, E.A., Shushunov, V.A., and Shchennikova, M.K., *Uspekhi khimii organicheskikh perekisnykh soedinenii i autookisleniya* (Progress in Chemistry of Organic Peroxy Compounds and Autooxidation), Emanuel', N.M., Ed., Moscow: Khimiya, 1969, pp. 294–300.
13. Barltrop, J.A. and Coyle, J.D., *Excited States in Organic Chemistry*, New York: Wiley, 1975.
14. Foster, W.R. and Williams, G.H., *J. Chem. Soc*., 1962, no. 8, pp. 2862–2873.

ISSN 1070-4272, Russian Journal of Applied Chemistry, 2007, Vol. 80, No. 11, pp. 1826–1831. © Pleiades Publishing, Ltd., 2007.
Original Russian Text © S.A. Shapovalov, 2007, published in Zhurnal Prikladnoi Khimii, 2007, Vol. 80, No. 11, pp. 1801–1806.

PHYSICOCHEMICAL STUDIES OF SYSTEMS AND PROCESSES

Formation of Ionic Associates by Phenol Red and Their Interaction with Ionic Surfactants in Aqueous Solutions

S. A. Shapovalov

Karazin Kharkov National University, Kharkov, Ukraine

Received January 16, 2007; in final form, June 2007

Abstract—Formation of associates between single- or double-charged anions of sulfophthalein dye Phenol Red and single-charged cations of cyanines in aqueous solutions was considered. The association constants were estimated from the spectral data. Geometric and energy characteristics of the associates were calculated. The suitability of the associates formed by Phenol Red for quantitative determination of cationic surfactants in aqueous solutions was examined.

DOI: 10.1134/S1070427207110092

Interaction of dye ions with organic counterions can substantially modify the optical properties of solutions because of formation of ionic associates [1]. Of special interest is association in aqueous solutions, since water is a medium in which protolytic and aggregated forms of dyes exhibit unique spectral-luminescent properties. Since recently, the focus of attention has been on association of ionic forms of sulfophthalein dyes [2], above all, of Phenol Red (PR). Under certain conditions, the dye associate can act as analytical reagent, color marker, and biological probe, which is essential for solving a number of applied problems. For example, Liu et al. [3] developed a highly sensitive method for detection of vitamin B_1, underlain by formation of an associate between the vitamin and PR. Phenol Red was successfully applied in the development of new pH sensors for cells and biological tissues [4] and of promising technologies for monitoring of the chemical composition of biological systems (e.g., determination of the acidity of cellular liquid [5] and monitoring of the liquid exchange via mucous membranes [6] and skin [7]).

We reported earlier [8] that the properties of PR associates can underlie development of new methods for analysis of surfactants in aqueous solutions. The associates prove to be more "sensitive" to the content of ionic surfactants than are dye ions proper. The reason is that, in associate + surfactant systems [1, 5, 9], spectral changes occur at much lower surfactant concentrations than in dye + surfactant systems [10]. Importantly, solving such practical problems implies elucidation of both the spectral properties of dyes and the equilibrium characteristics of the association processes. In this connection, we considered here in more detail the properties of single- and double-charged PR ions and the specific features of their association with cations of cyanine dyes, Pinacyanol (PNC) and Quinaldine Red (QR), as well as interaction of the associates of PR with ionic surfactants:

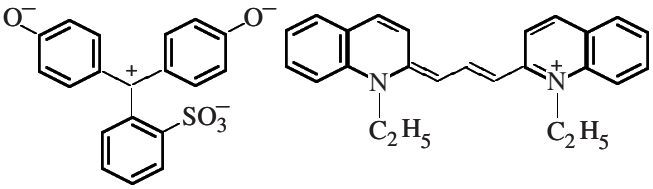

PR^{2-} anion

PNC^+ cation

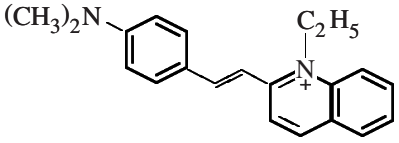

QR^+ cation

Owing to their physicochemical properties, many cyanines tend to form associates [1, 11]. Among them, PNC and QR cations proved to be suitable counterions for examination of the properties of ionic associates formed by dyes from different classes [1, 12, 13], in particular, sulfophthaleins [14].

EXPERIMENTAL

The procedures for spectral measurements and analysis of data obtained are basically identical to those in [9, 12, 15]. We used sodium salt of PR and chloride salts of PNC and QR. The degree of purity of

Table 1. Spectral and protolytic characteristics of dyes

Characteristic*	Ion			
	PR^- [18]	PR^{2-} [18]	PNC^+ [19]	QR^+
λ_{max}, nm (ν_{max}, cm^{-1})	430 (23250)	558 (17920)	600 (16660), α-band; 550 (18180), β-band; 510 (19610), γ-band	528 (18940)
ε_{max}, $l\,mol^{-1}\,cm^{-1}$	2.4×10^4	6.2×10^4	1.3×10^5	3.1×10^4
	Molecule			
	PR		PNC	QR
pK_{a1}	1.03 [20]		3.5 [21]	2.63 [18]
pK_{a2}	8.00 [18]		–	–

* The parameters λ_{max} were determined accurately to within 1 nm, and ε_{max}, to within 500 $l\,mol^{-1}\,cm^{-1}$.

the dyes was monitored spectrophotometrically using the known molar extinction coefficients ε_{max} of the protolytic forms at the absorption band maxima. The surfactants, anionic sodium dodecyl sulfate (SDDS) and cationic cetylpyridinium bromide (CPB), contained 98 ± 1% main substance. All other chemicals were of analytically pure grade; pH of medium was created by buffer solutions and monitored potentiometrically with a glass electrode. The absorption spectra were measured on Hitachi-U3210 and SF-46 spectrophotometers at room temperature.[1]

The equilibrium of PR in a solution can be represented by the scheme of stepwise dissociation of the tribasic acid

$$H_3An^+ \rightleftarrows H_2An^0 \rightleftarrows HAn^- \rightleftarrows An^{2-}.$$

The PR cation and molecule in aqueous media are weakly colored (the H_3An^+ species are manifested in anhydrous acetonitrile [16, 17]). By contrast, the anionic species HAn^- and An^{2-} have a high light absorption intensity (Table 1, ε_{max}), which facilitates spectral examination of ionic association at low concentrations of the species ($\geq 1 \times 10^{-6}$ M). The absorption bands of PR^- and PR^{2-} are well resolved. Owing to sufficient difference in the pK_{a1} and pK_{a2}, it is possible to achieve virtually absolute domination of the target anion in a solution. The cyanines examined exist as cation (Ct^+) over a wide pH range. Only in strongly acidic media Ct^+ is protonated into HCt^{2+}, and in alkaline media, carbinol CtOH is formed. Both processes result in decolorization of the solution.

[1] The spectral measurements were carried out with participation of Ya. Svishcheva and M. L'vovskaya.

There exist two essential prerequisites to examination of association: First, the basic light absorption law should be obeyed, and, second, the acidity of the medium should be maintained at the level providing the occurrence in solution of those ionic forms of dyes that form associates. We found that a satisfactory linear dependence of the optical density on the dye concentration (Bouguer–Beer law) is observed at PR concentrations within 1×10^{-6}–9×10^{-5} and QR concentrations of 1×10^{-6}–1×10^{-4} M. The linear regression equations (for three series of independent determinations with 8–9 concentrations in each series) have the form

$$PR^-: A_{430} = -0.0124_{(0.0083)} + 24345.6_{(277.51)}c_{PR},$$
$$R = 0.9981_{(0.018)},$$
$$PR^{2-}: A_{558} = 0.00944_{(0.0151)} + 675527.8_{(322.0)}c_{PR},$$
$$R = 0.9999_{(0.0054)},$$
$$QR^+: A_{528} = -0.0379_{(0.015)} + 33747.9_{(324.48)}c_{QR},$$
$$R = 0.9996_{(0.033)},$$

where A_{430} is the optical density at 430 nm (23250 cm^{-1}), A_{558}, at 558 nm (17920 cm^{-1}), and A_{528}, at 528 nm (18940 cm^{-1}); figures in parentheses are the rms deviations of the corresponding parameters; c, initial molar concentration of the dye; and R, correlation coefficient.

Since the absolute term of the regressions is close to zero, we took $A_i \approx kc$. To estimate the association constants, we created the PNC concentration of 5×10^{-7}–5×10^{-6} M, since higher concentrations favor undesirable self-association [15].

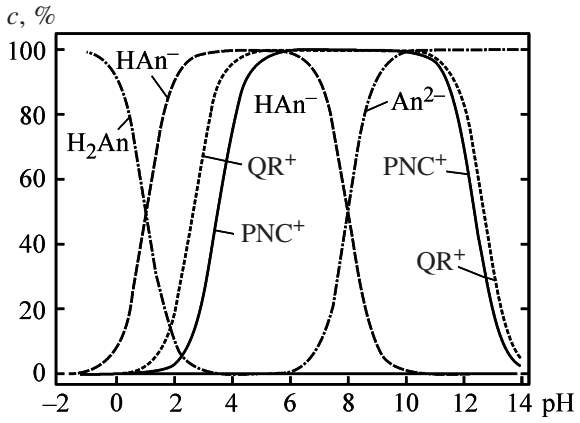

Fig. 1. Ranges of existence of protolytic forms of PR (H_2An, molecule; HAn^-, single-charged anion; and An^{2-}, double-charged anion) and single-charged cations of Pinacyanol (PNC^+) and Quinaldine Red (QR^+) in an aqueous solution. (*c*) Concentration, %.

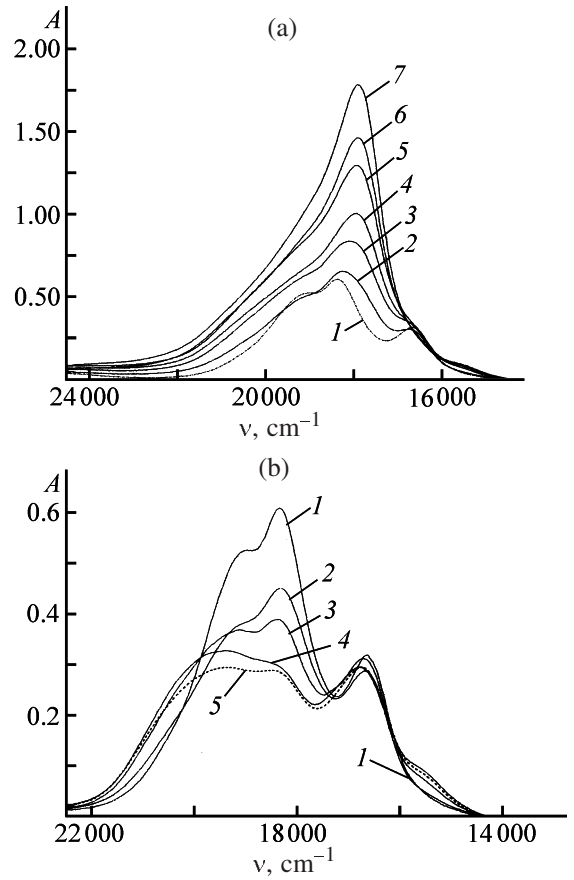

Fig. 2. Absorption spectra for the PNC + PR system. Reference solution: (a) water and (b) PR in indicated concentration. Absorption layer thickness 0.20 cm, pH 9.2, c_{PNC} 4.86×10^{-5} M. (*A*) Optical density and (ν) wavenumber; the same for Fig. 5. c_{PR}, M: (*1*) 0, (*2*) 2.5×10^{-5}, (*3*) 5.0×10^{-5}, (*4*) 7.5×10^{-5}, (*5*) 1.00×10^{-4}, (*6*) 1.25×10^{-4}, and (*7*) 1.50×10^{-4}.

To elucidate the optimal association conditions, we calculated (Fig. 1) the proportions of the species examined, taking into account the above-listed protolytic processes (Table 1, pK_a), occurring in aqueous solutions. Figure 1 suggests, in particular, that it is appropriate to observe interaction of QR^+ ions with HAn^- at pH 4.5–5.5, and that of PNC^+ with An^{2-}, at pH close to 10.

A characteristic feature of association of PR is a substantial decrease in absorption intensity, clearly observed upon adding ever growing amounts of one ion to the other ion whose content remains unchanged. For PNC^+ having a more developed vibronic structure (Table 1, α-, β-, and γ-bands), these changes are more distinct, but they are also observed in the case of QR^+. Analysis of the electronic spectra reveals nonadditivity of the optical density. The optical density of a mixture of dyes is systematically lower than the sum of the optical densities of individual dyes in the mixture. This fact is not always evident, especially when the absorption bands of the interacting dyes are located close to each other. In this case, changes of the optical density in individual portions of the spectrum can be "veiled" by absorption of one of the dyes, occurring in excess with respect to the counterion (Fig. 2a) (an excess is required for exhaustive association). Nevertheless, these changes can be revealed when a dye, rather than water, is used as the reference solution (Fig. 2b).

Analysis of the stoichiometric composition of the associates [2, 9, 12] showed that interaction of PR with cyanines can be represented by the scheme

$$Ct^+ + HAn^- \rightleftarrows Ct^+ \cdot HAn^-$$

$$2Ct^+ + An^{2-} \rightleftarrows (Ct^+)_2 \cdot An^{2-}.$$

The stability of these compounds is estimated from the equilibrium association constant K^t_{as} (thermodynamic parameter), determined from the mass action law. The K^t_{as} values obtained (by analogy with [15]) for associates of PR with PNC and QR differ from each other; the associates formed by PNC are more stable. For example, $\log K^t_{as}$ was estimated at 5.83 ± 0.10 for $PNC^+ \cdot PR^-$ and 11.81 ± 0.10 for $(PNC^+)_2 \cdot PR^{2-}$, and for $QR^+ \cdot PR^-$ and $(QR^+)_2 \cdot PR^{2-}$, at 5.13 ± 0.09 and 8.64 ± 0.09, respectively. One of the reasons for the difference in the stability of the associates is an increase in the proportion of hydrophobic interactions in the PNC-containing associates. The hydrophobic contribution from the quinolyl moiety in the PNC molecule exceeds that from the *N,N*-dimethylaniline moiety in the QR molecule. Also, association

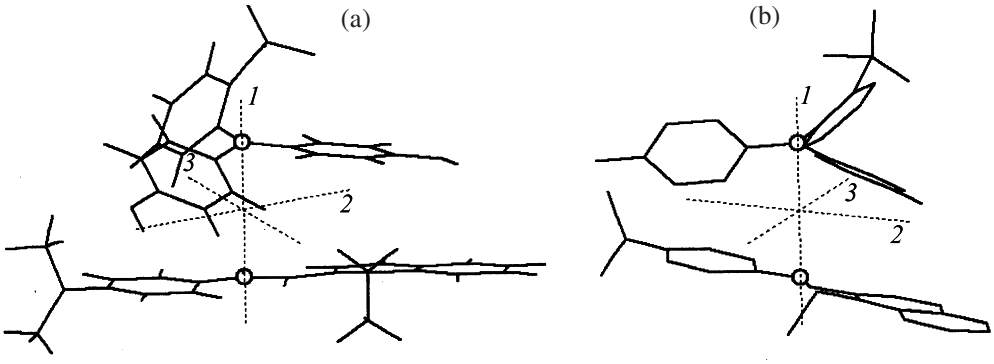

Fig. 3. Mutual location of the counterions in the $QR^+ \cdot PR^-$ associate (PR is on the top; projections (a) and (b) differ in the rotation about axis 1 by approximately 110°; the solvent molecules, as well as the hydrogen atoms, are not shown in projection (b)).

is enhanced by dispersion interactions prominent in developed π-electron systems [22, 23]. Because of specific structural features of PNC^+ and QR^+, they are more characteristic for the former.

Figure 3 shows the structure of the $QR^+ \cdot PR^-$ associate [from here on, calculations follow the MOPAC 2000 procedure [24, 25]: spatial optimization by AM1 method; convergence gradient for two consecutive iterations no larger than 1 kJ mol^{-1}; distance separating the marked atoms along axis *1*, 4.0 Å; and the dimension of the QR^+ cation (bottom) along axis *2*, approximately 13 Å]. The PNC + and QR^+ cations are planar (because of sp^3 hybridization, only ethyl groups in PNC^+ and QR^+ and the dimethylamino group of QR^+ are out of the chromophore plane). By contrast to cyanines, the PR anions have the benzene rings arranged like propeller blades, symmetrically about the central carbon atom. Therefore, the PR anions can be represented as spheres (radius of the sphere centered at the carbon atom marked in Fig. 3 is 5.6 Å; central angles with the carbon atom as apex, 119°–124°). However, despite the essentially different geometries, the counterions appreciably interact, as revealed not only by spectral measurements.

We carried out model calculation of the energies of the interacting species and the resulting associates (MOPAC 2000 procedure, vacuum as medium). Figure 4 presents the energy characteristics of interaction of PR^- with QR^+ (from here on, the dimensionality for all energy parameters is kJ mol^{-1}).

The initial states of QR^+ and PR^- are characterized by total energies of 65.2 and 274.2, respectively (Table 2; from here on, calculations are accurate to within 1.5 kJ mol^{-1}), and their algebraic sum, 339.4 (Fig. 4, energy level *1*), exceeds the energy of the associate, 276.7 (level *2*). Thus, the energy gain (ΔE) for the $QR^+ \cdot PR^-$ associate is 339.4 – 276.7 = 62.7 kJ mol^{-1}. It should be noted that ΔE for the interaction between PNC^+ and PR^- was estimated at 72.6, which exceeds that for the $QR^+ \cdot PR^-$ associate. The situation with the associates of the PR^{2-} anion is similar: ΔE = 149.1 [$(PNC^+)_2 \cdot PR^{2-}$ associate] and 122.5 [$(QR^+)_2 \cdot PR^{2-}$ associate]. For associates of PNC^+, ΔE systematically exceeds that of QR^+. This difference is due to stronger interaction with PR

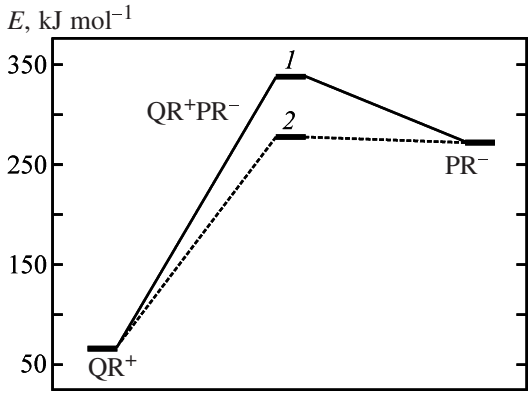

Fig. 4. Energy levels of the QR^+ and PR^- ions and of the $PNC^+ \cdot PR^-$ associate. (*E*) Energy: (*1*) sum of the total energies of PNC^+ and PR^- and (*2*) total energy of the associate.

Table 2. Energy characteristics of the interacting ions and associates*

Cation, Ct^+ (energy, kJ mol^{-1})	PR anions and associates (energy, kJ mol^{-1})	
	HAn^- (274.2)	An^{2-} (271.7)
QR^+ (65.2)	339.4**/276.7	402.1/279.6
PNC^+ (140.8)	415.0/342.4	553.3/404.2

* The data for the associates correspond to specific stoichiometric compositions, $Ct^+ HAn^-$ and $(Ct^+)_2 \cdot An^{2-}$.

** Numerator is the algebraic sum of total energies of the ions, and denominator, total energy of the associate.

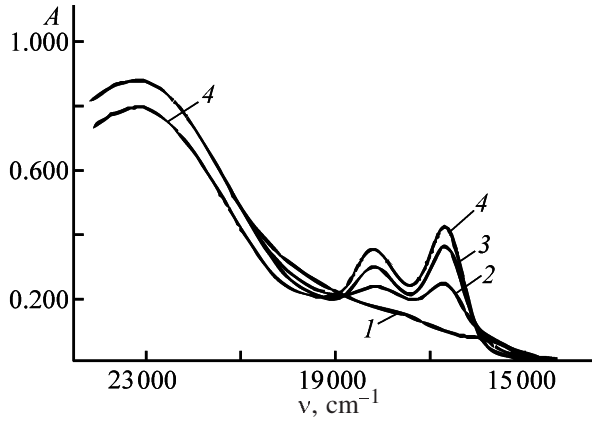

Fig. 5. Spectral changes in the PNC + PR system upon addition of CPB. Reference solution water; absorption layer thickness 1.00 cm; pH 4.6; $c_{PNC} = 4.9 \times 10^{-6}$, $c_{PR} = 7.1 \times 10^{-5}$ M; the same for Fig. 6. c_{CPB}, M: (*1*) 0, (*2*) 3.0×10^{-5}, (*3*) 6.0×10^{-5}, and (*4*) 8.0×10^{-5}.

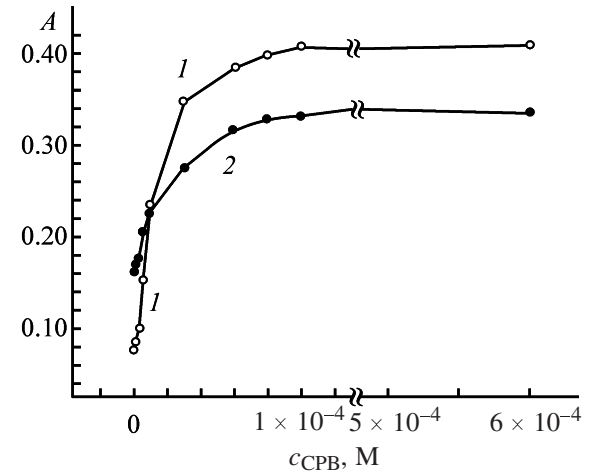

Fig. 6. Optical density of the solution vs. CPB concentration. λ, nm: (*1*) 600 and (*2*) 550.

anions for PNC^+ cation compared to the QR^+ cation because of van der Waals interactions (semiempirical calculations cannot take into account the hydrophobic interactions). The results presented agree with the calculated energy characteristics and association constants.

Addition of CPB or SDDS to the $Ct^+ \cdot HAn^-$ and $(Ct^+)_2 \cdot An^{2-}$ associates causes changes in the spectra of aqueous solutions, suggesting decomposition of the associates (Fig. 5; $PNC^+ \cdot PR^-$ associate as an example). In all cases, the shapes of the bands of each dye are restored in the absorption spectra [in Fig. 5, the short-wave absorption band with $\nu_{max} = 23\,250$–$22\,990$ cm^{-1} (430–435 nm) corresponds to the single-charged PR anion (with increasing content of the surfactant, the band slightly shifts), and bands with $\nu_{max} = 18\,180$ cm^{-1} (550 nm) and $\nu_{max} = 16\,660$ cm^{-1} (600 nm), to PNC]. Analysis of the experimental data suggests that, at low concentrations of the surfactants, the associate interacts with the dodecyl sulfate (DDS^-) anion or cetyl pyridinium bromide (CPB^+) cation according to the schemes

$$Ct^+ \cdot PR^- + DDS^- \rightleftarrows Ct^+ \cdot DDS^- + PR^-,$$

$$Ct^+ \cdot PR^- + CP^+ \rightleftarrows Ct^+ + CP^+ \cdot PR^-.$$

Thus, the corresponding ion of the surfactant exerts a competing effect on the ions of the dyes forming the associate.

Decomposition of the cyanine associates of PR upon addition of a surfactant is similar to that of the associate of the tetrabutylammonium cation with oxyxanthene dye tetrabromophenylfluorone which was examined earlier [26]. However, in our case, decomposition of the associates formed by PR is not evident. In view of its practical importance, we examined this aspect in more detail for the PNC + PR system and found that, under certain conditions, the parameter *A* at a fixed wavelength linearly increases with increasing content of CPB in the solution (Fig. 6, CPB concentration from 2×10^{-6} to 2×10^{-5} M). These changes are more profound for the long-wave band of PNC (curve *1*), since it has the highest absorption intensity. For the dye concentrations indicated in Fig. 6 and at 600 nm (16 660 cm^{-1}), *A* varies with the CPB content c_{CPB}, M, as $A_{600} = (0.032 \pm 0.010) + (2.31 \pm 0.09) \times 10^4 c_{CPB}$ (CPB concentration range 3×10^{-6}–2×10^{-5} M). Similar dependences can underlie the development of quantitative spectrophotometric and test methods for determination of cationic surfactants in solution. An advantage offered by such methods is that they combine a very high sensitivity (at a level of 1×10^{-6} M) and high contrast of the color reaction, provided by the presence in the solution of two dyes whose absorption bands are well separated in the spectrum (Table 1; cf. the λ_{max} values for the single-charged PR anion and PNC cation). The latter fact is of principal importance for the development of semiquantitative (test) methods for determination of surfactants, based on visual indication of the analytical signal.

CONCLUSIONS

(1) Interaction of single- (HAn^-) and double-charged (An^{2-}) anions of sulfophthalein dye Phenol Red with cations (Ct^+) of Pinacyanol or Quinaldine Red in an aqueous solution results in formation of

ionic associates with the stoichiometric composition $Ct^+ \cdot HAn^-$ and $(Ct^+)_2 \cdot An^{2-}$.

(2) The reasons for the decomposition of $Ct^+ \cdot HAn^-$ and $(Ct^+)_2 \cdot An^{2-}$ associates upon addition of cationic and anionic surfactants in low concentrations is the competing action of the surfactant ions on the ions forming the associate.

(3) The properties of the associates of Phenol Red, in particular, of $PNC^+ \cdot PR^-$, can be utilized in the development of new quantitative and test methods for the determination of the content of cationic surfactants (e.g., cetylpyridinium bromide) in aqueous solutions at concentrations $\geq 10^{-6}$–10^{-5} M. It was suggested that the quantitative determination be underlain by the direct proportionality between the optical density of the solution and the content of the cationic surfactant in it.

REFERENCES

1. Ishchenko, A.A. and Shapovalov, S.A., *Zh. Prikl. Spektrosk.*, 2004, vol. 71, no. 5, pp. 557–578.
2. Shapovalov, S.A., Koval, V.L., Chernaya, T.A., et al., *J. Braz. Chem. Soc.*, 2005, vol. 16, no. 2, pp. 232–240.
3. Liu, S., Zhang, Z., Liu, Q., et al., *J. Pharm. Biomed. Anal.*, 2002, vol. 30, no. 3, pp. 685–694.
4. Seki, A., Katakura, H., Kai, T., et al., *Anal. Chim. Acta*, 2007, vol. 582, no. 1, pp. 154–157.
5. Xia, X., Stanton, S., Jill, U., and Zhanfeng, C., *Med. Eng. Phys.*, 2006, vol. 28, no. 5, p. 468.
6. Dawes, C., *Archiv. Oral Biol.*, 2006, vol. 51, no. 2, pp. 111–116.
7. Balaguer, A., Salvador, A., Chisvert, A., et al., *Anal. Bioanal. Chem.*, 2006, vol. 385, no. 7, pp. 1225–1232.
8. Shapovalov, S.A., Chernaya, T.A., Samoilov, E.A., et al., *Mezhdunarodnaya konferentsiya "Sovremennye problemy fizicheskoi khimii"* (Int. Conf. "Modern Problems of Physical Chemistry"), Donetsk: Nord Komp'yuter, 2004, p. 15.
9. Shapovalov, S.A., Svishcheva, Ya.A., and Larin, V.I., *Izv. Vyssh. Uchebn. Zaved., Khim. Khim. Tekhnol.*, 2002, vol. 45, no. 4, pp. 37–42.
10. Savvin, S.B., Chernova, R.¤., and Shtykov, S.N., *Poverkhnostno-aktivnye veshchestva* (Surfactants), Moscow: Nauka, 1991.
11. Mishra, A., Behera, R.K., Behera, P.K., et al., *Chem. Rev.*, 2000, vol. 100, no. 6, pp. 1973–2012.
12. Shapovalov, S.A. and Svishcheva, Ya.A., *Vestn. Khar'k. Nats. Univ., Khim.*, 2003, no. 10 (33), pp. 142–146.
13. Shapovalov, S.A., *Ukr. Khim. Zh.*, 2004, vol. 70, no. 3, pp. 25–29.
14. Shapovalov, S.A., Koval', V.L., Mchedlov-Petrosyan, N.O., et al., *Dokl. Nats. Akad. Nauk Ukr.*, 1999, no. 2, pp. 156–161.
15. Shapovalov, S.A. and Svishcheva, Ya.A., *Vestn. Khar'kov. Nats. Univ., Khimiya*, 2000, vol. 477, no. 5 (28), pp. 112–116.
16. Kolthoff, I.M., Chantooni, M.K., and Browmik, S., *Anal. Chem.*, 1967, vol. 39, no. 3, pp. 315–320.
17. Kolthoff, I.M., Browmik, S., and Chantooni, M.K., *Proc. Nat. Acad. Sci. (USA)*, 1966, vol. 56, pp. 1370–1376.
18. *Indicators*, Bishop, E., Ed., Oxford: Pergamon, 1972.
19. Sheppard, S.E., *Rev. Modern Phys.*, 1942, vol. 14, April–July, pp. 303–340.
20. Gupta, D. and Read, J.B., *J. Pharm. Sci.*, 1970, vol. 11, pp. 1683.
21. Herz, A.H., *Photogr. Sci. Eng.*, 1974, vol. 18, no. 2, pp. 207–215.
22. Ishchenko, A.A., Derevyanko, N.A., Popov, S.V., et al., *Izv. Ross. Akad. Nauk*, 1997, no. 5, pp. 950–955.
23. Derevyanko, N.A., Ishchenko, A.A., Popov, S.V., et al., *Zh. Nauchn. Prikl. Fotogr. Kinematogr.*, 1997, vol. 42, no. 3, pp. 70–76.
24. Stewart, J.J.P., *J. Comput. Chem.*, 1989, vol. 10, no. 2, pp. 209–220.
25. Stewart, J.J.P., *MOPAC 2000: User's Manual*, New York: Fujitsu, 2000.
26. Shapovalov, S.A., Gladkov, E.S., and Chernaya, T.A., *Zh. Prikl. Khim.*, 2004, vol. 77, no. 6, pp. 981–984.

ISSN 1070-4272, Russian Journal of Applied Chemistry, 2007, Vol. 80, No. 11, pp. 1832–1835. © Pleiades Publishing, Ltd., 2007.
Original Russian Text © S.B. Selyanina, M.V. Trufanova, N.I. Afanas'ev, N.V. Selivanova, 2007, published in Zhurnal Prikladnoi Khimii, 2007, Vol. 80, No. 11, pp. 1807–1810.

PHYSICOCHEMICAL STUDIES OF SYSTEMS AND PROCESSES

Surfactant Properties of Kraft Lignins

S. B. Selyanina, M. V. Trufanova, N. I. Afanas'ev, and N. V. Selivanova

Institute of Environmental Problems in the North, Ural Division, Russian Academy of Sciences, Arkhangelsk, Russia

Received February 6, 2007; in final form, June 2007

Abstract—Formation of the adsorption layer at the solution–air interface is characterized by data on the surface tension in alkaline solutions of kraft lignins extracted from deresined spruce and birch wood. The effects of the lignin nature and solution concentration on intermolecular interaction in the surface layer are studied.

DOI: 10.1134/S1070427207110109

Many technologies for processing plant materials are based on heterogeneous reactions resulting in dissolution of lignin. Particularly, the removal of lignin from wood cell walls is one of the basic processes in cellulose production. The presence of a hydrophobic group and a lot of polar functional groups makes the lignin macromolecule diphilic. This, in turn, causes surface activity in lignin derivatives, which should be taken into account in pulping, regeneration of cooking liquor, and production of secondary products.

Surfactant properties of lignin derivatives obtained in sulfite delignification of spruce wood were studied in detail [1, 2]. However, sulfate lignins have not been studied from this standpoint. The kraft pulping allows production of cellulose not only from spruce wood, but also from other soft- and hardwood species. It is known that soft- and hardwood lignins differ from each other in their topological structure, molecular-weight distribution, hydrophilic–oleophilic properties, etc. [3–5].

In this study we examined the interfacial adsorption in aqueous alkaline solutions of lignins obtained from spruce and birch wood by sulfate delignification.

It should be taken into account that, generally, the solution obtained after alkaline delignification, in addition to lignin, contains also extractive substances, and that the major part of these substances (resin and fatty acids) in alkaline solutions form sodium salts exhibiting high surface activity. In the presence of such substances, it appears impossible to obtain reliable information on the surfactant properties of lignin itself. Therefore, to eliminate the effect of extractive substances on the surfactant properties of kraft lignins, lignin samples were prepared from wood preliminarily deresined by successive treatment with petroleum ether and 20% NaOH. Spruce and birch wood pulping was carried out using the standard procedure. The solution after delignification was concentrated by vacuum evaporation like that in the actual process, to remove volatiles. Lignin was precipitated from the solution by acidification to pH 2 with heating (80–85°C). The resulting flaky precipitate was settled, separated by decantation, and dried with water to neutral reaction. The spruce and birch lignin samples were different in the molecular weight (MW 9700 and 2800), elemental composition (C : H : O 63.1 : 5.8 : 31.1 and 66.0 : 7.8 : 26.2), and hydrophilic–oleophilic ratio (HOR 21.8 and 29.6, respectively).

Surfactant properties of kraft lignins were characterized by the surface tension of their solutions, measured by the Wilhelmy method. The lignin concentration was varied by successive dilution with 0.01 N NaOH of the initial lignin solution after neutralization with 1 N NaOH.

The specific feature of the formation of the interfacial adsorption layer in solutions of high-molecular-weight surfactants is that this process is kinetically controlled [6, 7]. It was demonstrated previously that, in lignosulfonate solutions, the adsorption equilibrium is established in 5–20 h.

Analysis of the $\sigma = f(\tau)$ curves (Fig. 1) revealed that, in the case of spruce lignin, the surface tension is decreased most rapidly in the first 10 min (initial portions of the curves). At low solution concentration (<1.5 g l^{-1}), the surface tension depression is in the range 1×10^{-3}–10×10^{-3} J m^{-2}. At higher concentra-

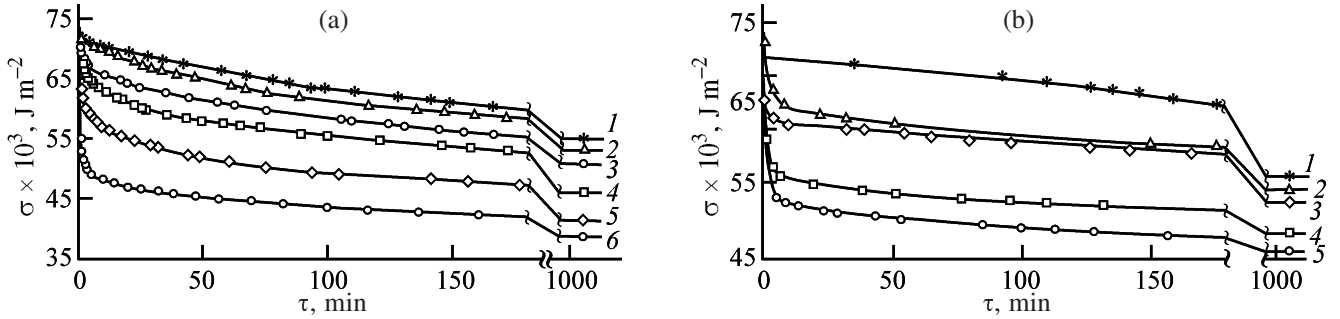

Fig. 1. Surface tension σ in alkaline solutions of (a) spruce and (b) birch lignins as a function of the time τ. Solution concentration, g l^{-1}: (a) (*1*) 0.044, (*2*) 0.22, (*3*) 0.52, (*4*) 1.54, (*5*) 7.70, and (*6*) 17.5; (b): (*1*) 0.02, (*2*) 0.17, (*3*) 0.56, (*4*) 1.4, and (*5*) 5.6.

tions (7–17.5 g l^{-1}), the decrease in the surface tension in the same time is more remarkable [(15–25) × 10^{-3} J m^{-2}]. In the next 10 min, as the adsorption layer is filled, the diffusion rate of the lignin macromolecules to the surface layer decreases, and the surface tension of the solution decreases to a lesser extent [$\Delta\sigma$ = (0.5–1.5) × 10^{-3} J m^{-2}]. In highly concentrated solutions, the adsorption equilibrium is established much more rapidly than in dilute solutions (Fig. 2a). In this case, with increasing solution concentration, the time required for the surface tension to acquire an equilibrium value increases from 4 to 20 h.

Similar trends were observed in the birch lignin solutions (Fig. 1b) with the difference that, in this case, the adsorption equilibrium is established more rapidly (Fig. 2a, curve *2*) because of the lower molecular weight and, therefore, higher mobility of the macromolecules. The lower the solution concentration, the more pronounced is the difference in the surface tension depression in the first 10 min after the beginning of the formation of the adsorption layer between the birch and spruce lignin solutions.

According to the recent data [8], native hardwood lignins are regularly branched star-like polymers with a tetrafunctional branching point, while native spruce lignin represents a randomly branched polymer. These structural features of the lignin macromolecules could affect their interfacial adsorption from aqueous alkaline solutions.

It was demonstrated in [7] that classical adsorption equations, derived for ideal processes, are inapplicable to the adsorption kinetics of high-molecular-weight surfactants. Therefore, we used modified equation (1) [2, 9] to describe the experimental curves $\sigma = f(\tau)$.

$$\sigma_\tau = (\sigma_0 - \sigma_{eq})\exp(-k_c\tau)^n + \sigma_{eq}, \qquad (1)$$

where σ_0 is the surface tension of the solvent; σ_τ and σ_{eq} are the current and equilibrium (static) surface tensions of the solution, respectively; k_c, rate constant of ideal adsorption; and n, exponent reflecting particle interaction in the adsorption layer, i.e., deviation of the system from ideality.

The difference $\sigma_0 - \sigma_{eq}$ is equivalent to the surface pressure π. For computation convenience sake, k_c^n can be expressed in terms of the rate constant of nonideal adsorption β.

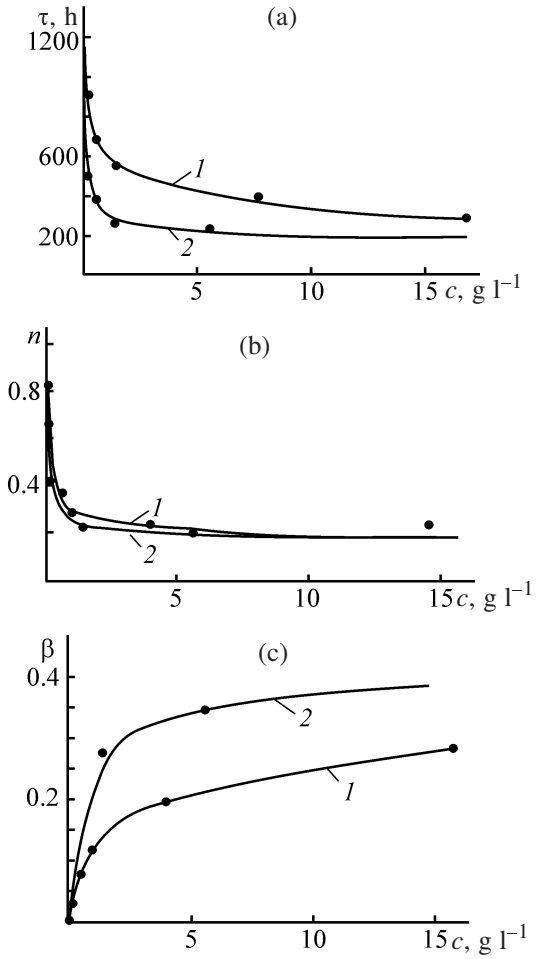

Fig. 2. (a) Time of establishment of equilibrium τ, (b) activity coefficient n, and (c) coefficient β as functions of the concentration c of (*1*) spruce and (*2*) birch lignins in solutions.

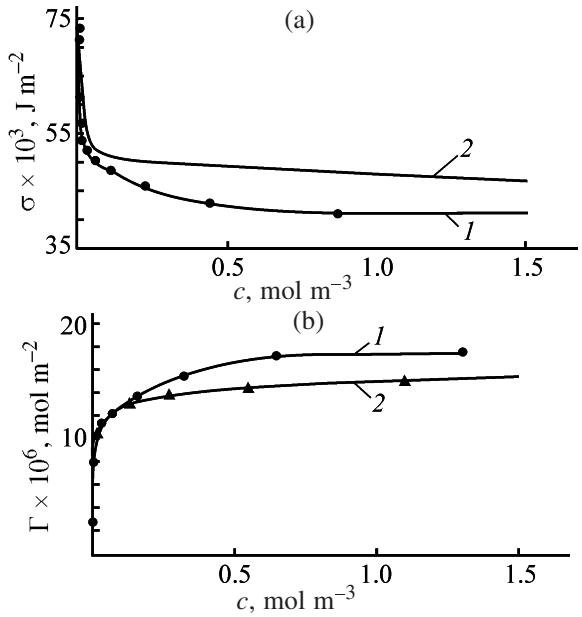

Fig. 3. (a) Surface tension σ and (b) adsorption Γ as functions of the concentration c of (*1*) spruce and (*2*) birch lignins in solutions.

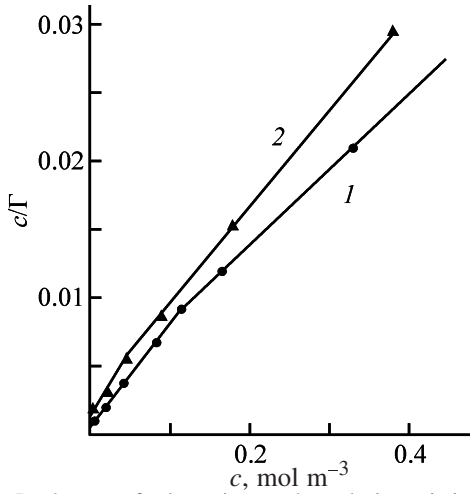

Fig. 4. Isotherms of adsorption at the solution–air interface in the Langmuir equation coordinates $c/\Gamma = f(c)$: (*1*) spruce and (*2*) birch lignins.

Theoretically, $n = 1$ corresponds to ideal adsorption layer (low degree of filling), i.e., Eq. (1) passes to a kinetic equation of the Langmuir type:

$$\sigma_\tau = (\sigma_0 - \sigma_{eq})\exp(-k_c\tau) + \sigma_{eq}. \quad (2)$$

In solutions of spruce and birch kraft lignins, n varies from 0.8 to 0.2, depending on the solution concentration (Fig. 2b), suggesting that intermolecular interaction in the adsorption layer increases with increasing degree of filling.

The time of establishment of the adsorption equilibrium is controlled by β. The higher β, the higher the rate of formation of the adsorption layer. It is seen from Fig. 2c that coefficient β increases with increasing solution concentration. This coefficient is slightly lower for spruce lignin than for birch lignin because of the lower mobility of the macromolecules (higher molecular weight).

The isotherms of the surface tension (Fig. 3a) and adsorption (Fig. 3b) of aqueous alkaline solutions of kraft lignins are classical curves typical of surfactants. For spruce lignin solution, the maximal surface tension depression, equivalent to the equilibrium surface pressure, is 30×10^{-3} J m^{-2}, which is well comparable with that of the solutions of such high-molecular-weight surfactants as lignosulfonates. For birch lignin, this value is slightly lower (25×10^{-3} J m^{-2}), suggesting higher surface activity of this more hydrophobic and higher-molecular-weight lignin. The surface activity of spruce and birch kraft lignins is 3100 and 830 J m mol^{-1}, respectively. For spruce lignin, saturation of the adsorption layer is observed at concentrations of 0.6–0.8 mol m^{-3} (6–8 g l^{-1}) (Fig. 3a), and for birch lignin, at lower concentrations [0.2–0.4 mol m^{-3} (0.7–1.4 g l^{-1})].

Analysis of the Langmuir isotherms $c/\Gamma = f(c)$ (Fig. 4) reveals that the interfacial adsorption of the lignin macromolecules from solutions corresponds to the model of monomolecular filling of the surface layer not in the entire concentration range, which is reflected in the deviation of the isotherms $c/\Gamma = f(c)$ from linearity by virtue of decreasing energy of interaction of the macromolecules with the gas phase, as a result of structural rearrangement in the surface layer. In the spruce lignin solution, the break in the isotherm is observed at a solution concentration of about 0.1 mol m^{-3} (1 g l^{-1}). For birch lignin, whose molecular weight is three times lower than that of spruce lignin, the isotherm deviates from linearity at higher solution concentration [0.64 mol m^{-3} (1.8 g l^{-1})]. As a result of changing adsorption mode, in the spruce lignin solution, the equilibrium adsorption constant K_{eq} decreases by an order of magnitude from 250 to 22. In the birch lignin solution, the rearrangement of the surface layer structure is accompanied by proportional decrease in K_{eq}, but at lower absolute values (from 71 to 7).

Another significant parameter characterizing the filling mechanism of adsorption layers is the area occupied by a macromolecule in the surface layer. We determined the areas occupied by molecules in an unfilled (S_m) and saturated (S_0) monomolecular layer using the Adamson procedure [6].

According to our estimates, the area occupied by

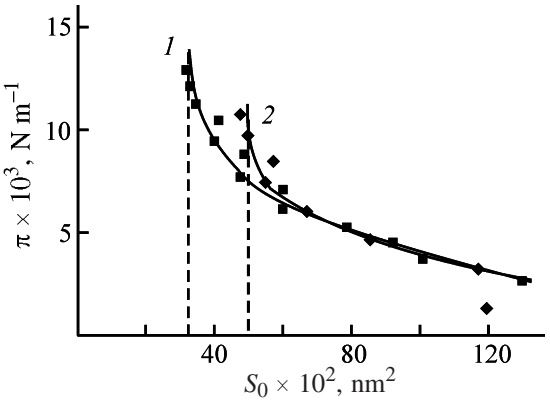

Fig. 5. Correlation between the surface area S_0 occupied by the lignin molecule at the solution–air interface (monomolecular filling) and a function of the surface pressure π: (*1*) spruce and (*2*) birch lignins.

spruce lignin molecules in the saturated monolayer (Fig. 5) is 49×10^{-2} nm^2. The birch lignin molecules occupy a smaller area (34×10^{-2} nm^2). These values are well comparable with those previously reported for lignosulfonates under condition of suppressed polyelectrolytic effect [2]. Finally, despite differences in the molecular weight and functional composition between spruce and birch lignosulfonates and kraft lignins, these compounds demonstrate similar trends in the surfactant properties and mechanisms of formation of adsorption layers at the solution–air interface.

CONCLUSIONS

(1) Kraft lignins can decrease the free energy at the solution–air interface, which allows considering them as surfactants.

(2) The time of establishment of the equilibrium at the solution–air interface in kraft lignin solutions is controlled by the solution concentration, ranging from 3 to 20 h, which should be taken into account in surface tension measurements. This time is longer in solutions of spruce lignin with higher molecular weight as compared to birch lignin.

(3) Formation of the adsorption layer in solutions of spruce and birch kraft lignins proceeds by the mechanism similar to that in lignosulfonate solutions, being controlled by the structure and functional composition of macromolecules.

REFERENCES

1. Telysheva, G.M. and Afanas'ev, N.I., *Khim. Drev*., 1990, no. 2, pp. 3–19.
2. Afanas'ev, N.I., Tel'tevskaya, S.E., Makarevich, N.A., and Parfenova, L.N., *Struktura i fiziko-khimicheskie svoistva lignosul'fonatov* (Structure and Physicochemical Properties of Lignosulfonates), Yekaterinburg: Ural. Otd. Ross. Akad. Nauk, 2005.
3. *Lignins: Occurrence, Formation, Structure, and Reactions*, Sarkanen, K.V. and Ludwig, C.H., Eds., New York: Wiley, 1971.
4. Maier, L.V., Macromolecular Properties of Hardwood Sulfate Lignin, *Cand. Sci. Dissertation*, Arkhangelsk, 1998.
5. Zakis, G.F., Mozheiko, L.N., and Telysheva, G.M., *Metody opredeleniya funktsional'nykh grupp lignina* (Methods for Determination of Functional Groups in Lignins), Riga, 1975.
6. Adamson, A.W., *Physical Chemistry of Surfaces*, New York: Wiley, 1976.
7. Verezhnikov, V.N., *Praktikum po kolloidnoi khimii poverkhnostno-aktivnykh veshchestv* (Practical Course of Colloid Chemistry of Surfactants), Voronezh: Voronezh. Gos. Univ., 1984.
8. Karmanov, A.P., *Samoorganizatsiya i strukturnaya organizatsiya lignina* (Self-Organization and Structural Organization of Lignin), Yekaterinburg: Ural. Otd. Ros. Akad. Nauk, 2004.
9. Makarevich, N.A. and Dikhtievskaya, L.V., *Zh. Fiz. Khim*., 1991, vol. 65, no. 2, pp. 453–457.

ISSN 1070-4272, Russian Journal of Applied Chemistry, 2007, Vol. 80, No. 11, pp. 1836–1840. © Pleiades Publishing, Ltd., 2007.
Original Russian Text © O.P. Zykova, T.A. Khodakovskaya, E.Ya. Markiv, V.S. Aleksandrova, S.A. Kirillov, 2007, published in Zhurnal Prikladnoi Khimii, 2007, Vol. 80, No. 11, pp. 1811–1814.

PHYSICOCHEMICAL STUDIES OF SYSTEMS AND PROCESSES

Sorption of Phosphate and Arsenate Ions from Solutions by Sorbents of the System TiO_2–Fe_2O_3–Al_2O_3–H_2O

O. P. Zykova, T. A. Khodakovskaya, E. Ya. Markiv, V. S. Aleksandrova, and S. A. Kirillov

Institute of Sorption and Endoecology, National Academy of Sciences of Ukraine, Kiev, Ukraine

Received November 21, 2006; in final form, April 2007

Abstract—Hydrated nanosize oxides of the system TiO_2–Fe_2O_3–Al_2O_3–H_2O were tested as sorbents for recovery of phosphate and arsenate ions from aqueous solutions in a wide range of pH values. The optimal compositions of the sorbents were found, their ion-exchange functions were studied, and limiting sorption capacities were determined.

DOI: 10.1134/S1070427207110110

Recently, researchers' attention has been focused on a search for efficient, nontoxic, and inexpensive sorbents for water treatment to remove phosphorus and arsenic [1]. These include hydrated oxides of Group II–IV metals having high affinity for phosphates, arsenates, and arsenites. In particular, the following sorption activity series have been established [2]: $Mg(OH)_2 < Zn(OH)_2 < Cu(OH)_2 < Co(OH)_2 < Ni(OH)_2 < Al(OH)_3 < Cr(OH)_3 < Fe(OH)_3$; $MnO_2 < Nb_2O_5 < ZrO_2 < TiO_2$. Moreover, it has been noted that the sorption of arsenates by soils correlates with their content of aluminum and iron oxides [3].

Because hydrated aluminum, iron, and titanium oxides are the most promising as absorbents of phosphates and arsenic, the sorption properties of their natural and synthetic varieties have been extensively studied [2, 4–11]. These substances retain high selectivity at low concentrations of the elements being absorbed (0.3–300 mg l^{-1}) and high concentrations of the salt background. They show an ion-exchange function toward phosphates, arsenates, and arsenites. Therefore, they can be repeatedly used, which makes them attractive for treatment of not only wastewater, but also drinking and mineral water.

An efficient method for control over the sorption-selective properties of inorganic ion exchangers is synthesis of mixed or modified sorbents [12, 13]. In addition, the cost of the thus obtained ion exchangers can be lowered by using intermediates and process waste from chemical and metallurgical industries as raw materials.

The aim of this study was to examine the sorption characteristics of new composite materials of the composition $TiO_2 \cdot xFe_2O_3 \cdot yAl_2O_3 \cdot zH_2O$, synthesized from a titanyl sulfate solution produced in the process cycle of breakdown of the ilmenite concentrate at Sumykhimprom Open Joint-Stock Company.

EXPERIMENTAL

A 3.184 M process solution of $TiOSO_4$ with iron and sulfate ion concentrations of 0.57 and 5.79 M, respectively, served as a titanium-containing raw material for synthesis of sorbents. The solution was diluted with water to a titanium concentration of 1 M and, when necessary, enriched with aluminum chloride. To this solution we added with vigorous stirring an equivalent, for complete precipitation of hydroxides, amount of a 3 M NH_4OH solution. The resulting gel was poured onto a filter paper and dried in air at room temperature to complete solidification. Further, it was washed for a long time with distilled water to remove sulfates, chlorides, and ammonium ions, with the presence of SO_4^{2-} and Cl^- ions in the filtrates monitored using qualitative reactions with barium and silver ions. Then it was dried in air at room temperature, ground, and sieved to select the 0.25–0.5-mm fraction.

The ion-exchange capacity and chemical resistance of the sorbents, as well as the sorption of phosphate and arsenate ions, were studied by the static method. To 20 ml of a solution we added 200 mg of a sorbent,

Table 1. Specific surface area of composites of the system TiO_2–Fe_2O_3–Al_2O_3–H_2O and their static sorption capacity for the phosphate ion

Ti : Fe : Al ratio	S_{sp}, $m^2\ g^{-1}$	pH_{in}	pH_{eq}	c_0, mM	A, mmol g^{-1}
1 : 0.18	–	3.2	3.6	50	1.4
1 : 0.18 : 0.25	422	9.3	8.3	50	2.0
		3.4	5.2	90	4.2
1 : 0.18 : 0.43	411	9.3	8.5	50	2.2
		3.4	5.5	90	2.8
1 : 0.18 : 0.67	476	9.3	8.6	50	2.5
		3.1	5.2	50	3.0
		7.1	7.5	80	4.5
		3.4	5.7	90	4.5

the system was equilibrated under shaking for 4 h, the precipitate formed after 72 h of sedimentation was filtered off, and the measurements were made. The pH-potentiometric studies were carried out on an I-160M device with NaOH and HNO_3 solutions, and a 0.1 M sodium nitrate as supporting electrolyte. Solutions of $Na_2HPO_4 \cdot 2H_2O$ and $Na_2HAsO_4 \cdot 7H_2O$ were used in sorption studies. When necessary, these solutions were acidified with phosphoric or hydrochloric acid. The sorption capacities A (mmol g^{-1}) were calculated by the formula

$$A = 10^{-3}(c_0 - c_{eq})V/m,$$

where c_0 and c_{eq} are the sorbate concentrations in the starting solution and equilibrium solution after sorption (mM); V, solution volume (ml); and m, sorbent mass (g).

All the analyses (iron as *o*-phenanthroline complex and aluminum as aluminon, phosphate as vanadium phosphomolybdate, and arsenate as molybdate complexes) were performed by photocolorimetry on a KFK-2 photocolorimeter. The maximum relative error of the A values presented does not exceed 15%. The sorbent density was found by pycnometry (with water as pycnometric liquid). The specific surface area of the sorbents and the pore radius distribution were determined with a Quantachrom NOVA 2200e instrument by the method of nitrogen and argon adsorption–desorption. IR spectra were obtained on a Specord M-80 spectrophotometer. Samples for the spectral range 4000–400 cm^{-1} were prepared as KBr pellets with a 1.9-mg portion of a substance under study, and those for the far-IR range (>200 cm^{-1}), as pellets with CsI and a 0.45-g portion of a substance.

An increase in the aluminum oxide content of the sorbents positively affects their absorbing capacity for phosphates and arsenates in both alkaline and acid media (Tables 1, 2). The sorption in the acid medium is accompanied by alkalization of a solution, and that in the alkaline medium, by its acidification. It can be seen that the values of A in the acid medium exceed those in the alkaline medium.

It is known that transition of substances to the nanosize state occurs when the size of their particles becomes 100 nm and less [14]. A calculation in accordance with [15] shows that crushing of particles of titanium, iron, and aluminum oxides to a size of 100 nm yields specific surface areas not exceeding 15 $m^2\ g^{-1}$. The oxides obtained in this study have specific surface areas exceeding 400 $m^2\ g^{-1}$. As the content of aluminum oxide increases, the specific surface area of the sorbents grows.

On the basis of these data, the sorbent with Ti : Fe : Al = 1 : 0.18 : 0.67 was chosen for a detailed study. It has a density of 1.901 g cm^{-3} and a porous structure with a minimum pore radius of about 18 Å, i.e., it is a mesoporous material (Fig. 1a). The main weight loss (40.1%) upon heating occurs at 200°C. The total weight loss is 42.3% (800°C). This corresponds to sorbent compositions $TiO_2 \cdot 0.09Fe_2O_3 \cdot 0.34Al_2O_3 \cdot 5.22H_2O$ (**1**) and $Ti(OH)_4 \cdot 0.18FeO(OH) \cdot 0.67AlO(OH) \cdot 2.79H_2O$ (**2**).

Table 2. Static sorption capacity of composites of the system TiO_2–Fe_2O_3–Al_2O_3–H_2O for the arsenate ion (c_0 = 50 mM)

Ti : Fe : Al ratio	pH_{in}	pH_{eq}	A, mmol g^{-1}
1 : 0.18 : 0.25	8.7	7.9	4.2
	2.8	4.0	4.4
1 : 0.18 : 0.67	8.7	8.4	4.2
	2.8	4.5	4.4

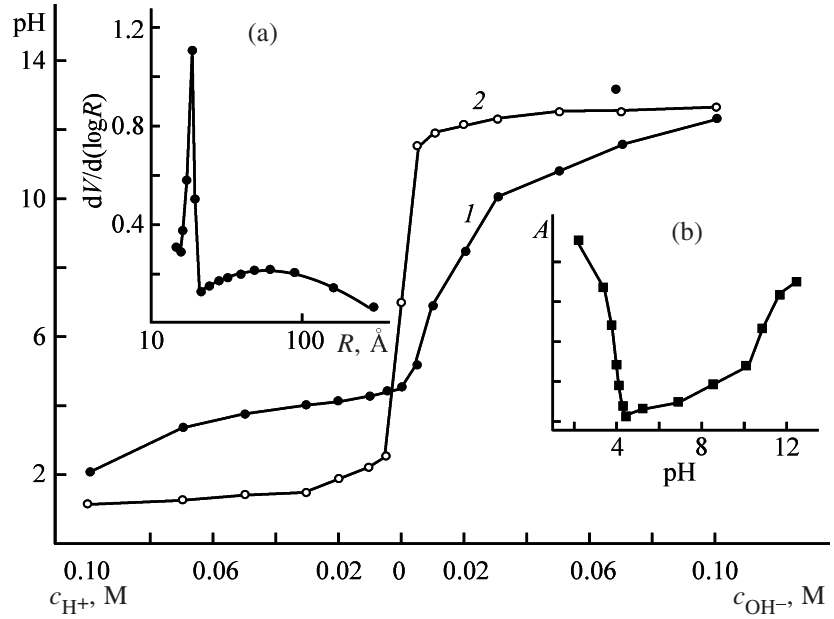

Fig. 1. (a) Pore distribution with respect to radii R for a sorbent of composition $Ti(OH)_4 \cdot 0.18FeO(OH) \cdot 0.67AlO(OH) \cdot 2.79H_2O$; variation of the pH of HNO_3 and NaOH solutions, with 0.1 N $NaNO_3$ as supporting electrolyte, (*1*) with and (*2*) without a sorbent; and (b) sorption capacity A vs. pH. [dV/d(log R)] Pore radius distribution, (c_{H^+}) concentration of H^+, and (c_{OH^-}) concentration of OH^-.

The results of a potentiometric titration suggest that the substance obtained is a typical ampholyte (Fig. 1b). Its ion-exchange capacity in acid and alkaline media is virtually the same, 7–9 mmol g^{-1} of exchangeable protons (Fig. 1c) or more than one third of OH groups contained in compound **2** (1.55–2 out of 4.85). The pH value of the sorbent suspension in distilled water (sorbent to water mass ratio 1 : 40) is 4.69. The sorbent shows a high hydrolytic stability in the entire pH range studied. Only in strongly acidic media (pH < 1.7), iron and aluminum start to be leached-out from the sorbent (0.0035 and 2.07%, respectively).

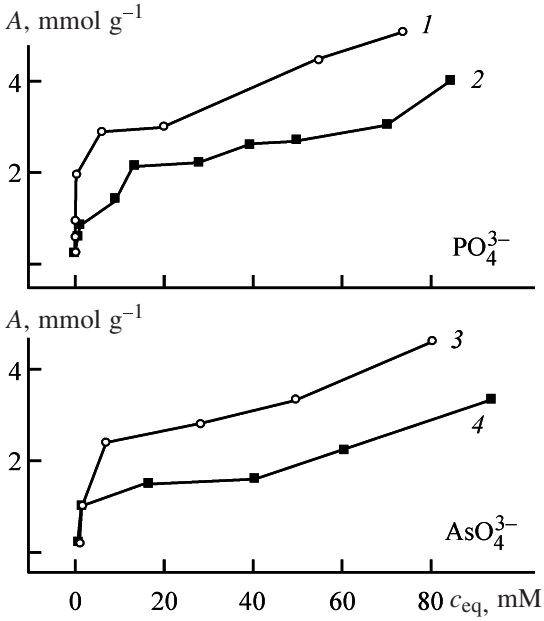

Fig. 2. Isotherms of sorption of phosphate and arsenate ions by a sorbent of composition $Ti(OH)_4 \cdot 0.18FeO(OH) \cdot 0.67AlO(OH) \cdot 2.79H_2O$. ($A$) Sorption capacity and (c_{eq}) sorbate concentration in the equilibrium solution after sorption. pH: (*1*) 2.2–3.4, (*2*) 8.2–9.0, (*3*) 2.5–3.6, and (*4*) 8.2–9.3.

Isotherms of sorption of phosphate and arsenate ions by the material under study from solutions with the maximum initial concentration of these ions equal to 125 mM are shown in Fig. 2. Depending on the pH of the medium, the maximum sorption capacities are 4.0–5.1 mmol g^{-1} for phosphate ions and 3.3–4.6 mmol g^{-1} for arsenate ions; in the concentration range 0.05–0.5 mM, phosphate ions are completely recovered from solutions. This circumstance places the material obtained among the best of the known sorbents for phosphate and arsenate ions [1]. Noteworthy is the fact that the sorption isotherms do not level-off. Presumably, this behavior is specific to materials with sorption centers of more than one type [13].

The understanding of the sorption process can be strongly aided by IR spectroscopy. For example, analysis of IR spectra in the range of vibrations of P–O bonds suggests that phosphate ions sorbed on oxides of iron [4, 10], titanium [8], and aluminum [7]

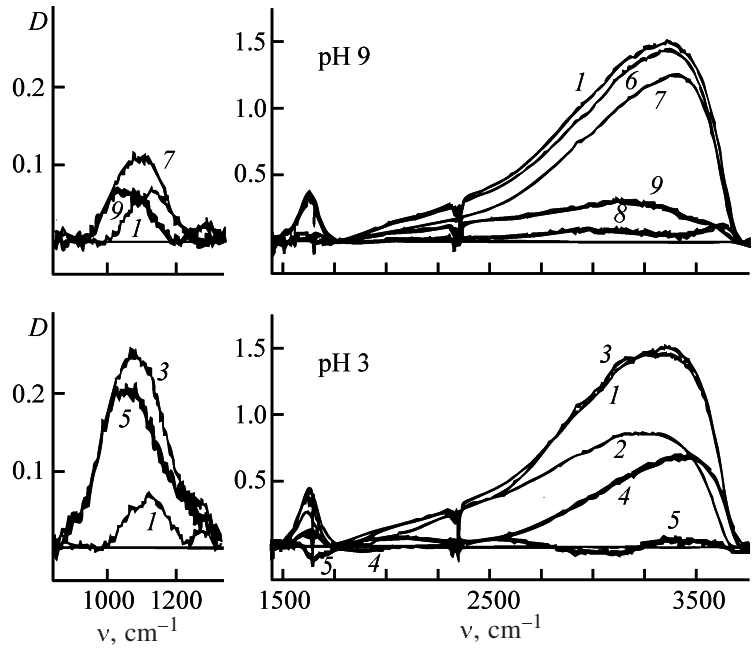

Fig. 3. IR absorption spectra of a sorbent of composition $Ti(OH)_4 \cdot 0.18FeO(OH) \cdot 0.67AlO(OH) \cdot 2.79H_2O$ (*1*) before sorption, (*2*) after treatment with an acid, (*3*) after sorption of the phosphate ion from an acid solution, (*6*) after treatment with an alkali, and (*7*) after sorption of the phosphate ion from an alkaline solution. (*D*) Optical density and (ν) wavenumber. Difference of the spectra: (*4*) 1 and 2, (*5*) 1 and 3, (*8*) 1 and 3, and (*9*) 1 and 7.

are bound to the surface in the mono- and bidentate fashion. As is known, in accordance with the dissociation equilibrium, phosphate ions are predominantly in the doubly charged form (HPO_4^{2-} content 97–98%) at pH ~9 and are singly charged (about 99% $H_2PO_4^-$) in an acid medium (pH ~3) [16]. Nevertheless, the spectra indicate that HPO_4^{2-} ions are present on the sorbent surface in acid media, and PO_4^{3-} ions, in alkaline media.

The data in Fig. 3 are consistent with these statements. The bands corresponding to the ν_3 vibration (F_2) of the PO_4^{3-} ion sorbed from acid (curve *5*) and alkaline solutions (curve *9*) are split, which shows that its symmetry is lowered via protonation and(or) coordination to the sorbent surface.

These conclusions can be refined by comparing the spectra in the range of stretching (ν_{OH}) and bending (δ_{OH}) vibration of the O–H bonds of the sorbent and water present on its surface before sorption, after treatment with an acid (alkali), and after sorption. The acid treatment leads to a substantial decrease in the absorption in the ν_3 and δ_{OH} ranges (curve *4*), which points to neutralization of OH groups of the sorbent and a considerable decease in the amount of surface water. In acid solutions, the absorption in the δ_{OH} range decreases after sorption of phosphate ions, whereas that in the ν_{OH} range remains virtually unchanged (curve *5*). This means that new OH groups appear on the surface through sorption of $H_2PO_4^-$ or HPO_4^{2-} ions (ν_{OH} bands of hydrophosphates have low intensity [17]). The alkaline treatment leads to a slight decrease in the absorption in the ν_{OH} and δ_{OH} range (curve *8*), which possibly indicates that the protons of OH groups are replaced with sodium ions. The sorption of the phosphate in alkaline solutions results in a considerably stronger decrease in the absorption in the ν_{OH} and δ_{OH} range (curve *9*) because of the substitution of OH groups of the sorbent by PO_4^{3-} ions containing no protons.

CONCLUSIONS

(1) Among hydrated oxides of the system TiO_2–Fe_2O_3–Al_2O_3–H_2O, the best absorbing capacity for phosphate and arsenate ions is exhibited by nanosize mesoporous ampholyte of the composition $Ti(OH)_4 \cdot 0.18FeO(OH) \cdot 0.67AlO(OH) \cdot 2.79H_2O$, which contains about 9 mmol g^{-1} of exchangeable protons.

(2) Depending on the pH of the medium, the maximum sorption capacities of the sorbents with the optimal composition are 4.0–5.1 mmol g^{-1} for phosphate ions and 3.3–4.6 mmol g^{-1} for arsenate ions, with complete recovery of phosphate ions from solutions in the concentration range 0.05–0.5 mM.

(3) Phosphates are sorbed on the sorbents under study as $H_2PO_4^-$ or HPO_4^{2-} ions from acidic solutions

and as PO_4^{3-} ions with lowered symmetry alkaline solutions.

REFERENCES

1. Strelko, V.V. and Chubar', N.I., *Khim. Tekhnol. Vody*, 2000, vol. 22, pp. 74–87.
2. Ookubo, A., Ooi, K., and Hayashi, H., *Langmuir*, 1993, vol. 9, pp. 1418–1422.
3. Goldberg, S., *Soil Sci. Soc. Am. J*., 2002, vol. 66, pp. 413–421.
4. Tejedor-Tejedor, M.I. and Anderson, M.A., *Langmuir*, 1990, vol. 6, pp. 602–612.
5. Waychunas, G.A., Rea, B.A., Fuler, C.C., and Davis, A., *Geochim. Cosmochim. Acta*, 1995, vol. 59, pp. 3655–3661.
6. Sun, X. and Doner, H.E., *Soil Sci*., 1996, vol. 161, pp. 865–872.
7. Laiti, E., Persson, P., and Oeman, L.-O., *Langmuir*, 1998, vol. 14, pp. 825–831.
8. Michelmore, A., Gong, W., Jenkins, P., and Ralston, J., *Phys. Chem. Chem. Phys*., 2000, vol. 2, pp. 2985–2992.
9. Goldberg, S. and Johnson, C.T., *J. Colloid Interface Sci*., 2001, vol. 234, pp. 204–216.
10. Arai, Y. and Sparks, D.L., *J. Colloid Interface Sci*., 2001, vol. 241, pp. 317–326.
11. Manna, B., Dasgupta, M., and Chosh, U.C., *J. Water Supply: Res. Technol.—AQUA*, 2004, vol. 53, pp. 483–495.
12. Pendelyuk, O.I., Lisnycha, T.V., Strelko, V.V., and Kirillov, S.A., *Adsorption*, 2005, vol. 11, pp. 784–799.
13. Pendelyuk, O.I., Lisnycha, T.V., and Kirillov, S.A., *Dopov. Nats. Akad. Nauk Ukr*., 2006, no. 10, pp. 195–200.
14. Chakravorty, D. and Giri, A.K., *Chemistry of Advanced Materials*, Rao, C.N.R., Ed., Oxford: Blackwell, 1993, pp. 217–236.
15. Voyutskii, S.S., *Kurs kolloidnoi khimii* (A Course of Colloid Chemistry), Moscow: Khimiya, 1975.
16. Lur'e, Yu.Yu., *Spravochnik po analiticheskoi khimii* (Handbook of Analytical Chemistry), Moscow: Khimiya, 1971.
17. Pechkovskii, V.V., Mel'nikova, R.Ya., Dzyuba, E.D., et al., *Atlas infrakrasnykh spektrov fosfatov* (Atlas of IR Spectra of Phosphates), Moscow: Nauka, 1981.

ISSN 1070-4272, Russian Journal of Applied Chemistry, 2007, Vol. 80, No. 11, pp. 1841–1844. © Pleiades Publishing, Ltd., 2007.
Original Russian Text © A.N. Khazipova, B.I. Kutepov, M.L. Pavlov, N.G. Grogor'eva, Ya.L. Shestopal, A.N. Pashkina, E.A. Travkin, 2007, published in Zhurnal Prikladnoi Khimii, 2007, Vol. 80, No. 11, pp. 1815–1818.

PHYSICOCHEMICAL STUDIES OF SYSTEMS AND PROCESSES

Synthesis of HNa Forms of High-Silica Faujasites

A. N. Khazipova, B. I. Kutepov, M. L. Pavlov, N. G. Grogor'eva, Ya. L. Shestopal, A. N. Pashkina, and E. A. Travkin

Institute of Petrochemistry and Catalysis, Russian Academy of Sciences, Ufa, Bashkortostan, Russia

Received May 2, 2007

Abstract—Synthesis conditions of HNa forms (with the residual content of Na_2O not exceeding 0.2 wt %) of high-silica (SiO_2/Al_2O_3 = 5.6–6.0) faujasites were found.

DOI: 10.1134/S1070427207110122

HNa forms of synthetic faujasites (zeolites of X and Y types) with different degrees of exchange of Na^+ cations for H^+ (α_{Na}) exhibit catalytic activity in acid–base reactions [1]. For example, the zeolite of the Y type with $\alpha_{Na} \geq 90\%$ is used as an active component of modern catalysts for cracking of hydrocarbons [2, 3]. The HNa forms of faujasites are most frequently synthesized by substitution of Na^+ cations with NH_4^+, with the subsequent thermal decomposition of NH_4Na forms in the temperature range 220–600°C [4–7]. The ion exchange of Na^+ for NH_4^+ in faujasites with the ratio $SiO_2/Al_2O_3 \leq 5$ was described in [4–11].

It was shown [6] that, upon a single ion-exchange treatment, the value of α_{Na} for the $Y_{0.5}$ zeolite (the subscript shows the silica ratio of the zeolite) does not exceed 65% and can be raised to 95% only upon nine successive treatments in a 0.1 M NH_4NO_3 solution. Raising the concentration of the ion-exchange solution of NH_4Cl from 1.0 to 1.5 M when performing five successive ion-exchange treatments [8] results in that α_{Na} increases from 73.1 to 93.0% and from 70.1 to 90.3% for $X_{2.53}$ and $Y_{4.25}$ zeolites, respectively.

It is known that, the higher the silica ratio, the lower the ion-exchange capacity of a faujasite. This is due to the lower charge of the crystalline skeleton of the zeolite. For Na^+ cations localized within small voids of the crystal lattice of faujasite to migrate into large voids, it is necessary to calcine the zeolite at 450–540°C between ion-exchange runs. However, a thermal treatment of this kind may lead to partial amorphization of the crystalline skeleton of the zeolite [6]. The thermal and high-temperature steam stability of the crystal structure of a zeolite are determined by its silica ratio, nature of the exchange cation, and presence of defects in the crystal structure. It has been found that the higher the silica ratio of a faujasite, the higher its thermal stability [4]. This ratio is commonly raised by special treatments. These treatments lead to partial dealumination of the crystal lattice of the faujasite, which may give rise to lattice defects [6, 12–16]. A method has been suggested for direct synthesis of high-silica zeolites of the Y type [17, 18]. This method yields faujasites in the sodium form, with a silica ratio of 5.6–7.2. The pattern of the deep exchange of Na^+ for NH_4^+ in these faujasites has not been described in the literature.

The aim of this study was to develop a technique for synthesis of HNa form of faujasites of this kind, with α_{Na} exceeding 98%, by ion exchange of Na^+ for NH_4^+ with intermediate thermal treatment and to examine the effect of the exchange conditions on the crystal structure of the zeolite.

EXPERIMENTAL

The study was performed with samples of $NaY_{5.6}$ and $NaY_{6.0}$ zeolites synthesized by the procedure described in [17, 18]. For comparison, industrial $NaY_{5.1}$ and $NaX_{2.5}$ zeolites manufactured by Salavatnefteorgsintez Open Joint-Stock Company were subjected to decationation. The ion exchange was carried out in a batch isothermal reactor, with vigorous agitation of a suspension of a powdered faujasite in an aqueous solution of NH_4NO_3. The use of highly dispersed zeolite samples and vigorous agitation minimized diffusion hindrance to exchange. The cation exchange at high temperatures was carried out in a stainless steel autoclave. Weighed portions of 20 g were used in all the experiments. The chemical composition of the starting zeolites is listed in Table 1.

Table 1. Chemical composition of zeolites with different silica ratios

Zeolite	Content, wt %		
	Na_2O	SiO_2	Al_2O_3
$NaX_{2.5}$	21.7	46.6	31.7
$NaY_{5.1}$	12.0	64.6	22.7
$NaY_{5.6}$	11.4	66.9	21.3
$NaY_{6.0}$	10.9	68.2	20.6

Table 2. Effect of temperature on α_{Na} in synthetic faujasites. G = 1.5, τ = 120 min

T, °C	α_{Na}, %			
	$X_{2.5}$	$Y_{5.1}$	$Y_{5.6}$	$Y_{6.0}$
20	60	52	50	50
40	65	56	55	55
70	75	65	65	65
180	78	70	65	65

The following parameters were varied in the course of the experiments: exchange temperature (T = 20–180°C), molar ratio between NH_4^+ cations in a solution to Na^+ in a zeolite (G = 0.25–20), pH of the medium (5.5–8.0), and exchange duration (τ = 0.4–1200 h). In some of the experiments, the exchange was performed with ultrasonic treatment (UT) of a zeolite suspension (frequency 22 kHz, power 30 W, temperature 45–70°C, duration 0.4–1 h).

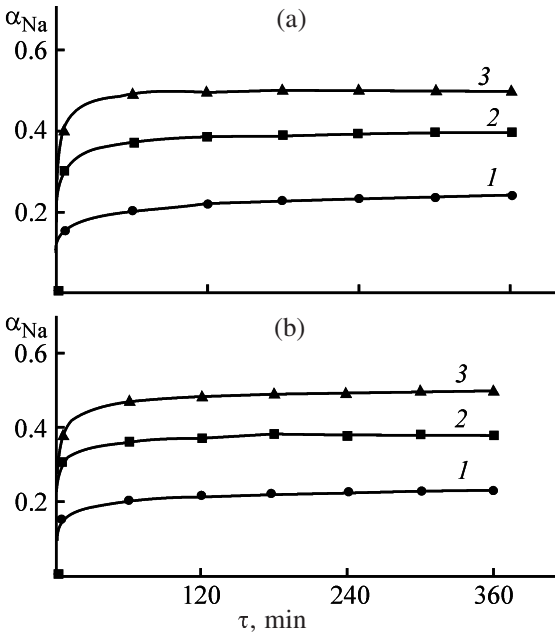

Fig. 1. Kinetic curves of ion exchange of Na^+ for NH_4^+ in powder-like NaY zeolites with various silica ratios M at 20°C. (α) Degree of ion exchange and (τ) time. M: (a) 5.1 and (b) 6.0. G: (*1*) 0.25, (*2*) 0.62, and (*3*) 1.5.

The exchange kinetics was studied by monitoring the variation of the chemical composition of the liquid and solid phases by flame photometry [19]. The phase composition of the zeolites was found by X-ray phase analysis (XPA) on a Philips PW 1800 automated diffractometer by the Debye–Scherrer (powder) method. The measurement conditions were as follows: $\theta/2\theta$ scanning; holder rotation at 1 rps; anode material, copper; scanning range 5°–55°/2θ; scanning step 0.05°; exposure in a step, 2 s; anode voltage and current, 40 kV and 30 mA, respectively. The X-ray diffraction patterns were identified using the known diffraction data [10].

The limiting adsorption capacity of the faujasites for water vapor was determined at 20°C and P/P_s = 0.5 by the desiccator method [20].

Figure 1 shows dependences of α_{Na} in samples of Y zeolites with different silica ratios on the duration of exchange at 20°C. It can be seen that the variation rate of α_{Na} is at a maximum in the first 15 min. During this period of time, the exchange of Na^+ in the zeolite for NH_4^+ from solution occurs at the highest rate, these concentrations rapidly decrease and, simultaneously, the concentrations of NH_4^+ in the zeolite and Na^+ in solution increase. After the initial period, the exchange rate markedly decreases and α_{Na} tends to a certain maximum value characteristic of specific exchange conditions (T, G, pH). This trend in variation of the concentrations of Na^+ and NH_4^+ indicates that the exchange reaction is reversible. Therefore, it is necessary to change the exchange conditions in order to raise α_{Na}.

It was found that, on raising G from 0.25 (deficiency of NH_4^+ cations) to 1.5 (excess of NH_4^+ cations), the degree of Na^+ exchange for NH_4^+ increases from 20 to 52% (Fig. 1, curves *1–3*). At the same time, raising G further, to 20, has no noticeable effect on α_{Na}. All other exchange conditions being the same, an increase in temperature from 45 to 180°C (Table 2) leads to an only slight rise in the degree of exchange, α_{Na}. In exchange of Na^+ for cations of rare-earth elements (REE) in Y zeolite, elevating the process temperature to 180°C leads to virtually complete replacement of Na^+ with REE cations [11]. However, raising the temperature from 70 to 80°C in exchange of Na^+ for NH_4^+ does not noticeably change α_{Na} (Table 2).

The authors of [6, 8] could raise α_{Na} in exchange of Na^+ for NH_4^+ in synthetic faujasite samples

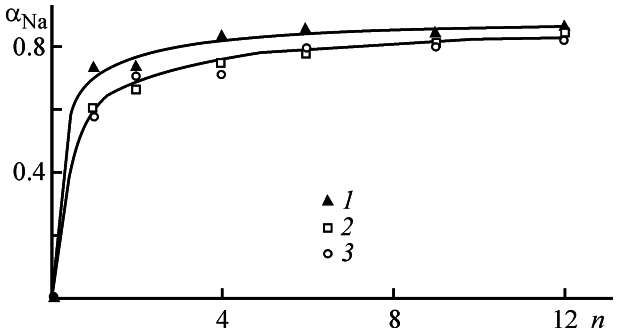

Fig. 2. Degree of ion exchange, α_{Na}, vs. the number n of treatments performed. G = 1.5, T = 70°C, τ = 120 min. (*1*) NaX (M = 2.5), (*2*) NaY (M = 5.1), and (*3*) NaY (M = 6.0).

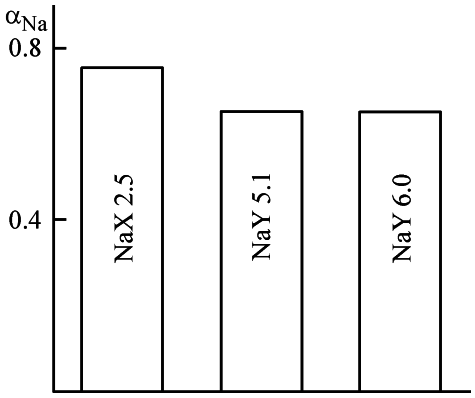

Fig. 3. Degree of ion exchange, α_{Na}, in faujasites after 1200 h of treatment. T = 20°C, G = 1.5.

by carrying out several exchanges and making these exchanges longer. Similar approaches were used in this study. For this purpose, the exchange solution containing Na^+ and NH_4^+ cations was discharged after a constant α_{Na} was reached and a repeated exchange was performed with the same amount of a NH_4NO_3 solution. It was found that even after 12 exchanges (Fig. 2) and total exchange duration of 50 days (Fig. 3), α_{Na} cannot be substantially raised. An ultrasonic treatment of a faujasite suspension in the exchange solution does not lead to any noticeable increase in α_{Na}, either (Table 3).

Thus, it was found that, under the conditions of Na^+ exchange for NH_4^+ in samples of synthetic faujasites with different silica ratios, α_{Na} can be raised only to values not exceeding 78 and 65% for X and Y zeolites, respectively. This is due to the fact that part of Na^+ cations (16 per unit cell), contained in hexagonal prisms, sodalite cells of the crystal lattice of faujasites, are difficultly accessible to exchange. The diameter of inlet windows leading to these cations is 2.5 Å and, consequently, they are inaccessible to NH_4^+ ions whose diameter is 2.86 Å [6]. In addition, as the zeolite silica ratio increases, repulsion between ammonium cations localized in the zeolite structure and present in the ion-exchange solutions becomes stronger, which hinders further migration of NH_4^+. A thermal treatment after an ion exchange is accompanied by thermal decomposition of the introduced NH_4^+ ions and migration of Na^+ cations from small into large voids, i.e., to places accessible to exchange. This allows Na^+ cations to enter into exchange in subsequent treatment of the zeolite with a NH_4NO_3 solution [6, 8], and, therefore, the experimental samples were subjected, before a repeated exchange, to thermal treatment at 540°C for 4 h, as described in [3]. The results obtained are listed in Table 4.

Table 3. Effect of ultrasonic treatment on α_{Na} in synthetic faujasites. G = 1.5, T = 70°C

τ, min	α_{Na}, %			
	$X_{2.5}$	$Y_{5.1}$	$Y_{5.6}$	$Y_{6.0}$
15	72	62	62	61
30	74	65	63	63
45	78	65	64	62
45*	73	60	59	58

* Without ultrasonic treatment.

Table 4. Effect of the number n of ion-exchange runs with intermediate calcination on α_{Na} in faujasites, content β of the amorphous phase, and adsorption capacity γ

n	$X_{2.5}$			$Y_{5.1}$			$Y_{5.6}$			$Y_{6.0}$		
	α_{Na}, %	β, %	γ, cm^3 g^{-1}	α_{Na}, %	β, %	γ, cm^3 g^{-1}	α_{Na}, %	β, %	γ, cm^3 g^{-1}	α_{Na}, %	β, %	γ, cm^3 g^{-1}
0	0	0	0.29	0	0	0.29	0	0	0.29	0	0	0.29
1	74	15	0.26	65	6	0.29	65	0	0.29	65	0	0.29
2	97	42	0.20	95	12	0.26	94	0	0.28	93	0	0.29
3	99	70	0.11	99	60	0.14	98	0	0.28	98	0	0.29

A triple ion exchange with two intermediate calcinations yielded HNa forms of faujasites with α_{Na} not lower than 98.0%. A study of the phase composition of the faujasite samples obtained demonstrated that, as α_{Na} increases from 74 to 99% for $X_{2.5}$ zeolite, there occurs partial amorphization from 15 to 70% of the crystalline skeleton. As α_{Na} increases from 65 to 99% for $Y_{5.1}$ zeolite, the degree of amorphization increases from 6 to 60%. The crystal structure of high-silica $Y_{5.6}$ and $Y_{6.0}$ zeolites is stable and does not disintegrate even when α_{Na} increases from 65 to 98% (Table 4). The results obtained using the XPA method were later confirmed by adsorption measurements (Table 4).

CONCLUSIONS

(1) On varying temperature, concentration ratio of the exchange cations in the zeolite and in solution, and duration of ion-exchange treatments, the replacement of Na^+ with NH_4^+ in zeolites of the Y type with a silica ratio of 5.1–6.0 is possible to an extent not exceeding 70%.

(2) To obtain HNa forms of faujasites with a residual content of Na_2O not exceeding 0.1 wt %, it is necessary to perform a triple ion exchange of Na^+ for NH_4^+ with two intermediate thermal treatments at 540°C for 4 h.

(3) Ion exchange with an intermediate thermal treatment at 540°C leads to partial amorphization of faujasites with a silica ratio of 5.1 and lower, which increases to 70% for $X_{2.5}$ zeolite and 60% for $Y_{5.1}$. In zeolites of the Y type with a silica ratio of 5.6 and more, the crystalline skeleton does not disintegrate.

REFERENCES

1. Isakov, Ya.I., *Neftekhimiya*, 1998, vol. 38, pp. 404–438.
2. Khadzhiev, S.N., Suvorov, Yu.P., et al., *Kreking neftyanykh fraktsii na tseolitsoderzhashchikh katalizatorakh* (Cracking of Oil Fractions on Zeolite-Containing Catalysts), Moscow: Khimiya, 1982.
3. Nefedov, B.K., Radchenko, E.D., and Aliev, R.R., *Katalizatory protsessov glubokoi pererabotki nefti* (Catalysts for Deep Processing of Oil), Moscow: Khimiya, 1992.
4. *Zeolite Chemistry and Cayalysis*, Rabo, J.A., Ed., Washington: Am. Chem. Soc., 1976.
5. Mishin, I.V., Klyachko, A.L., Brueva, T.R., et al., *Kinet. Katal.*, 1993, vol. 34, no. 5, p. 929.
6. Mishin, I.V. and Baier, G.K., *Kinet. Katal*., 1997, vol. 38, no. 3, p. 484.
7. Chukin, G.D. and Serikov, P.Yu., *Kinet. Katal*., 1999, vol. 40, no. 4, pp. 628–635.
8. Fletcher, R. and Townsend, R., *J. Chem. Soc., Faraday Trans. 1*, 1982, vol. 78, no. 6, p. 1741.
9. Sato, K., et al., *Microporous Mesoporous Mater*., 2003, vol. 59, no. 2, pp. 133–136.
10. Breck, D.W., *Zeolite Molecular Sieves*, New York: Wiley, 1974.
11. Nesmeyanova, T.S., Mirskii, Ya.V., Kaliko, M.A., and Cherednichenko, V.T.. in *Tseolity i tseolitsoderzhashchie katalizatory* (Zeolites and Zeolite-Containing Catalysts), Groznyi, 1974, issue 27, pp. 77–86.
12. Kerr, G., *J. Phys. Chem*., 1968, vol. 72, p. 2594.
13. Beanmont, R. and Barthomeuf, D., *J. Catal*., 1972, vol. 27, p. 45.
14. Mishin, I.V., Baier, G.K., Klyachko, A.L., et al., *Kinet. Katal*., 1987, vol. 28, no. 3, p. 706.
15. Scherzer, J. and McArthur, D.P., *Katalistik's 7th Annual Fluid Catalytic Cracking Symp*., Venice (Italy), 1986, p. 10.
16. Jacoquinot, E., Mendes, A., Raatz, F., and Marcilly, C., *Appl. Catal*., 1990, vol. 60, pp. 101–117.
17. RF Patent 2151739.
18. Pavlov, M.L., New Methods for Synthesis of Low- and High-Silica Zeolites and Their Use for Production of Catalysts and Adsorbents, *Doctoral Dissertation*, Ufa, 2002.
19. *OST* (Branch Standard) *38.01161–78: Catalysts for Cracking: Microspherical and Ground: Testing Methods*, 1973.
20. Kel'tsev, N.V., *Osnovy adsorbtsionnoi tekhniki* (Fundamentals of Adsorption Technology), Moscow: Khimiya, 1984.

ISSN 1070-4272, Russian Journal of Applied Chemistry, 2007, Vol. 80, No. 11, pp. 1845–1851. © Pleiades Publishing, Ltd., 2007.
Original Russian Text © N.V. Mil'vit, I.L. Shashkova, A.I. Rat'ko, V.A. Vecher, 2007, published in Zhurnal Prikladnoi Khimii, 2007, Vol. 80, No. 11, pp. 1819–1825.

PHYSICOCHEMICAL STUDIES OF SYSTEMS AND PROCESSES

Sorption Properties of Carbonate-Containing Tripolites

N. V. Mil'vit, I. L. Shashkova, A. I. Rat'ko, and V. A. Vecher

Institute of General and Inorganic Chemistry, National Academy of Sciences of Belarus, Minsk, Belarus
Belarussian Geological Exploration Research Institute, Minsk, Belarus

Received January 22, 2007; in final form, September 2007

Abstract—Adsorption-structural and chemisorption properties of carbonate tripolites were studied in relation to their chemical and mineral composition and conditions of sorption of heavy and nonferrous metal ions. Prospects for application of carbonate tripolites as chemisorbents were considered.

DOI: 10.1134/S1070427207110134

The innovation policy of the state in the field of rational nature management is aimed to involve new, presently unused local types of mineral resources into material production. The most promising in this regard are carbonate-siliceous and siliceous deposits of the Coniacian stage of the Cretaceous system, tripolite and opoka, which widely occur in the eastern part of Mogilev oblast. These siliceous rock with sand-clayey or carbonate clayey admixtures are valuable raw materials whose main application area is manufacture of cement. In addition, they are used as binders, abrasives, filtering materials, and sorbents [1].

Studies of specific features of the mineral composition and physicochemical properties of carbonate tripolites from the Stal'noe deposit (Republic of Belarus), carried out at the Institute of General and Inorganic Chemistry, National Academy of Sciences of Belarus, and Belarussian Geological Exploration Research Institute, Republican Unitary Enterprise, indicate that there are serious prospects for use of carbonate tripolites as adsorption raw materials. Carbonate tripolites have favorable sanitary-hygienic parameters and exhibit high biological activity; they contain no toxic impurities. The polycomponent phase composition of the rock is represented by a finely dispersed mixture of amorphous silica, zeolite, montmorillonite clay, and calcium carbonate, with each of the mineral components having individual sorption properties.

This paper summarizes the results of studies of the chemisorption capacity of carbonate tripolites for ions of heavy and nonferrous metals Pb(II), Cr(III), Cu(II), Zn(II), and Fe(III) and considers prospects for use of carbonate tripolites.

EXPERIMENTAL

As demonstrated by the results of detailed surveys, the tripolite resources of the Stal'noe deposit are characterized by rather strong variability of the composition of the main rock-forming components (Table 1).

On the basis of statistical processing of data on the chemical composition of 60 group samples taken from wells rather uniformly distributed over the deposit area, four representative laboratory samples of tripolite were prepared. These samples reflect the main types (classes) of ores of the deposit, their chemical composition is represented in Table 2.

The mineral composition of tripolites was determined by quantitative X-ray phase analysis (XPA) on a DRF-2 diffractometer (CuK_α radiation), and the

Table 1. Chemical composition of tripolites from the Stal'noe deposit

Component	Content, %
$SiO_{2(tot)}$	34.35–66.26
Al_2O_3	5.06–9.22
Fe_2O_3 + FeO	1.13–2.60
TiO_2	0.15–0.32
MnO	0.01–0.02
P_2O_5	0.01–0.12
SO_3	0.04–0.32
CaO	15.78–34.14
MgO	0.87–2.83
Na_2O	0.30–1.80
K_2O	0.96–1.59
CO_2	12.40–26.82

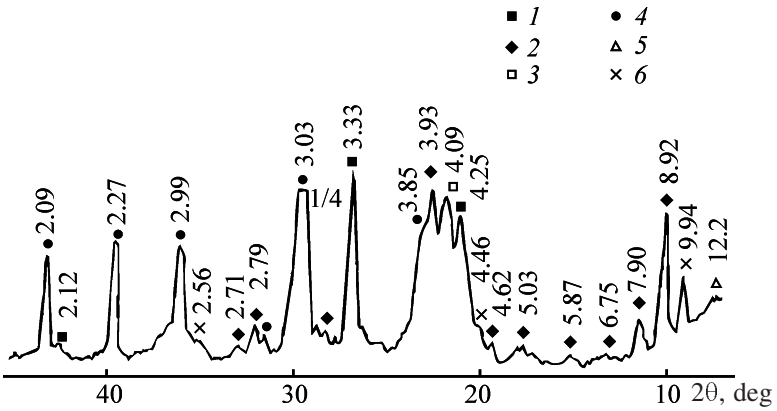

Fig. 1. X-ray diffraction pattern of carbonate tripolite. (2θ) Bragg angle. Mineral composition: (*1*) quartz, (*2*) clinoptilolite, (*3*) opal, (*4*) $CaCO_3$ (calcite), (*5*) montmorillonite, and (*6*) mica.

chemical composition, by X-ray fluorescence analysis on an SRF instrument. An analysis for carbon was made on a CHN analyzer.

The adsorption-structural parameters of the samples were calculated from adsorption isotherms of benzene and carbon tetrachloride, measured in a vacuum adsorption installation with a McBain–Bakr spring balance at 20°C.

The chemisorption properties of tripolites with varied content of $CaCO_3$ for Pb(II), Cr(III), Cu(II), Zn(II), and Fe(III) ions were determined under static conditions at 15–20°C from 0.001–0.1 N nitrate solutions. The sorbent (0.2 g, 0.09–0.25-mm fraction) was poured over with 25 ml of a metal salt solution, and the mixture was kept for 24 h with intermittent agitation. Then, the solution was separated from the solid phase. In the filtered solution, the residual content of metal ions being adsorbed was determined by complexometric titration or atomic-absorption spectroscopy (AAS-3 spectrometer). In order to obtain information about the mechanism of absorption of metal ions by tripolites, the solid phase was subjected to XPA after the sorption.

The X-ray diffraction patterns of the tripolites under study, obtained from various wells at the Stal'noe deposit, are qualitatively identical and show the same reflections, with only the relative intensities of peaks varying in accordance with quantitative changes in the mineral composition of a rock being studied. A typical X-ray diffraction pattern of a carbonate tripolite is shown in Fig. 1.

Table 2. Chemical composition of carbonate tripolite samples from the Stal'noe deposit

Sample no.	Content of indicated oxides, %				
	$SiO_{2(tot)}$	CaO	Al_2O_3	$Fe_2O_3 + FeO$	CO_2
1	44.60	24.22	7.02	2.32	15.65
2	49.12	21.72	6.81	2.18	18.74
3	57.40	17.93	6.10	1.91	16.31
4	73.66	9.55	5.29	1.78	5.48

As can be seen in Fig. 1, the phase composition of the tripolites is represented by four basic rock-forming minerals: opal–cristobalite, clinoptilolite, montmorillonite, and calcite, and the aleurite material, by quartz, chlorite, and mica.

The adsorption-structural parameters of tripolites directly depend on their mineralogical and chemical composition.

The total content of SiO_2 is the main parameter reflecting and determining the quality of natural adsorbent raw materials. The amount of SiO_2 in tripolites is determined by the total contribution of weakly crystallized free silica of opal–cristobalite, X-ray amorphous biogenic silica, silica of a finely dispersed material (quartz, feldspar, mica, clay), and silica of zeolites.

The adsorption isotherms of benzene and carbon tetrachloride by tripolites with varied content of silica and calcite are shown in Fig. 2, and the specific surface areas S_{sp} and limiting sorption volumes V_s of the samples under study are listed in Table 3.

All the adsorption isotherms are S-shaped and show capillary-condensation hysteresis, which indicates that the tripolites are structurally inhomogeneous. Under pressures close to saturation, the sorption branches of the isotherms steeply ascend, whence follows that the main amount of the adsorbate is absorbed in intermediate pores. The higher the SiO_2

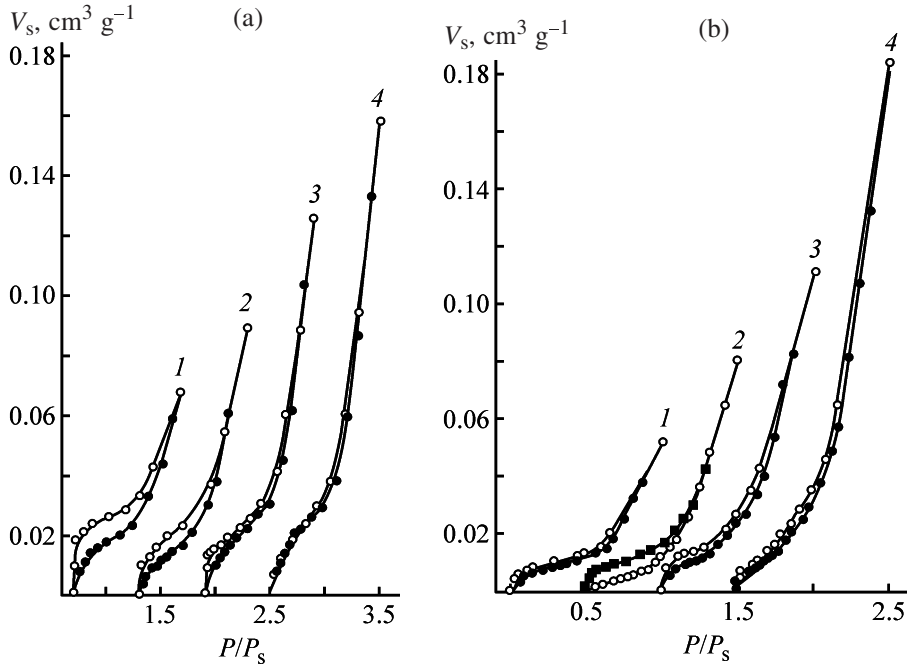

Fig. 2. Adsorption isotherms of (a) benzene and (b) carbon tetrachloride vapors by tripolites with varied silica content. (V_s) Limiting sorption volume and (P/P_s) relative pressure. Silica content, wt %: (*1*) 1, (*2*) 2, (*3*) 3, and (*4*) 4.

content of a tripolite, the larger its adsorption-structural parameters: specific surface area and limiting sorption pore volume.

As the carbonate component of the samples increases, the adsorption-structural parameters of the tripolites become worse, and the carbonate tripolites are markedly inferior to "pure" tripolites and opokas as porous sorbents. However, it has been shown [2–5] that carbonate tripolites show a substantial chemisorption capacity for ions of heavy and nonferrous metals, with the chemisorption capacity of a rock the higher, the larger the $CaCO_3$ content of the tripolite.

Figure 3 shows absorption curves of Pb(II), Cr(III), Cu(II), Zn(II), and Fe(III) ions by tripolites with varied content of calcium carbonate. The maximum absorption of lead ions for tripolites containing 37 and 43% $CaCO_3$ is 5.5 and 9.01 mg-equiv g^{-1}, respectively; for the sample containing no $CaCO_3$, this value does not exceed 1 mg-equiv g^{-1}.

A study of chemisorption products by XPA and chemical analysis demonstrated that absorption of ions of heavy and nonferrous metals is accompanied by formation of amorphous or crystalline carbonates, hydroxo carbonates, and, only in some cases, metal hydroxides.

The absorption of metal ions by carbonate-containing tripolites can be represented as a set of main reactions occurring in the system constituted by $CaCO_{3(cryst)}$ and a $M(NO_3)_n$ solution.

(1) Reactions at the surface of a solid calcium carbonate to give less soluble M(II) carbonates:

$$CaCO_{3(cryst)} + M^{n+} \longrightarrow MCO_{3(s)} + Ca^{2+}.$$

(2) Formation at the surface or nearby of poorly soluble hydroxo carbonates and hydroxides of polycharged metals:

$$CaCO_{3(cryst)} + M^{n+} + HOH \rightarrow [M(OH)_{n(s)}$$
$$\text{and/or } M_x(CO_3)_y(OH)_{z(s)}] + Ca^{2+} + H^+,$$

where n is the degree of M oxidation, $nx = 2y + z$.

Table 3. Adsorption-structural parameters of tripolites with varied content of calcium carbonates and silica

Sample no.	Adsorbate			
	C_6H_6		CCl_4	
	S_{sp}, m^2 g^{-1}	V_{sp}, cm^3 g^{-1}	S_{sp}, m^2 g^{-1}	V_{sp}, cm^3 g^{-1}
1	39	0.074	14	0.052
2	37	0.090	10	0.080
3	47	0.126	20	0.112
4	62	0.158	20	0.134

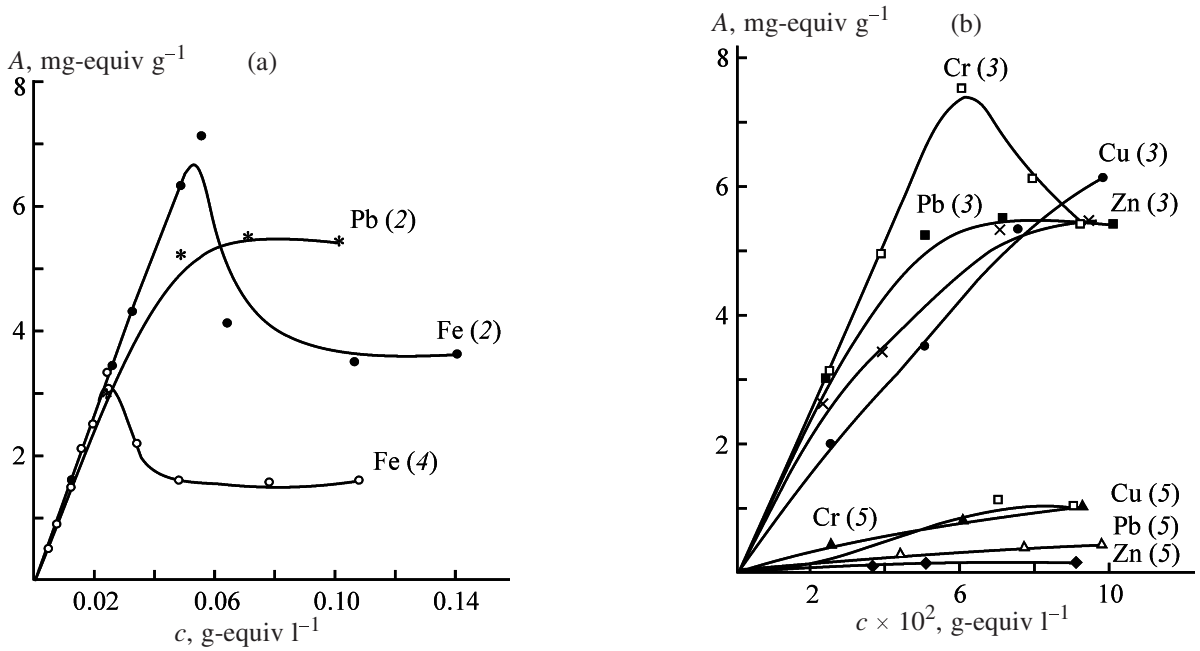

Fig. 3. Curves of absorption A of Pb(II), Cr(III), Cu(II), Zn(II), and Fe(III) ions by natural carbonate-containing tripolites. (c) Initial concentration of $M(NO_3)_n$ solutions. $CaCO_3$ content of tripolite sample, wt %: (*2*) 43, (*3*) 37, (*4*) 13, and (*5*) 0.

Depending on the conditions, the chemisorption process can occur by different mechanism to give different products. The anomalous shape of the chemisorption curves in Fig. 3 indicates that the chemical processes occurring in the system change.

Analysis of the previously obtained results [2–5] suggests that the most complete removal of metal ions from solutions can be only achieved in those case when the equilibrium solution has pH values necessary for complete precipitation of multiply charged metal ions in the form of carbonates, hydroxo carbonates, or hydroxides.

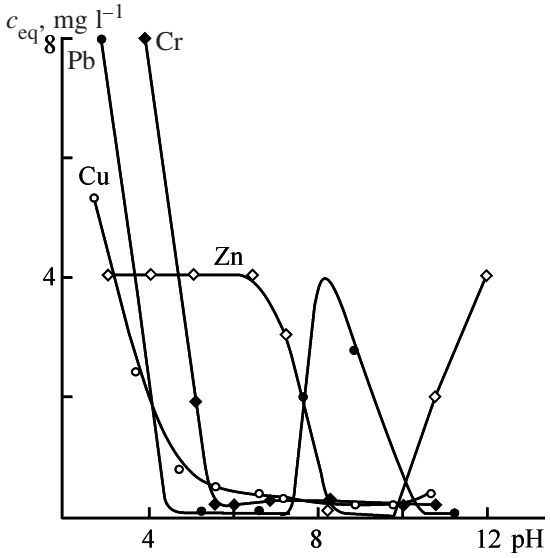

Fig. 4. Equilibrium concentration of Pb(II), Cu(II), Zn(II) and Cr(III) in solution after absorption c_{eq} as a function of equilibrium pH.

The maximum recovery of copper, chromium, and zinc ions is observed at pH 7–10, >5.5, and 8.5–9.5, respectively. At these pH values, the equilibrium concentration (concentration after sorption) of Cu^{2+}, Zn^{2+}, and Cr^{3+} ions does not exceed 0.2–0.3 mg l^{-1}. The dependence of the equilibrium concentration of metal ions on the solution pH is shown in Fig. 4.

It can be seen that the $c_{eq}^{M^{n+}}$–pH curve has for lead ions, in contrast to other ions, two minima, at pH 5–7 and pH > 10.5. The existence of two minima in the $c_{eq}^{Pb^{2+}}$–pH dependence indicates that, in absorption of Pb^{2+} ions by tripolite, compounds (or their modifications) with different solubilities are formed at different pH values.

As demonstrated by the XPA results, the forming products are X-ray amorphous substances in the pH range 7.0–10.5, i.e., near the peak in the $c_{eq}^{Pb^{2+}}$–pH curve. At pH > 10.5, the X-ray diffraction pattern shows that crystalline products are formed: a mixture of cerussite and lead(II) hydroxo carbonate of the composition $Pb_3(OH)_2(CO_3)_2$. Amorphous substances are, as a rule, more soluble than crystalline substances.

According to the XPA data, zinc ions are absorbed

by tripolite from solution as $Zn_2(OH)_2CO_3$ up to pH ~7, whereas at pH > 7, the amorphous phase, $Zn(OH)_2$, is formed.

After sorption of Cu^{2+}, the X-ray diffraction pattern of carbonate tripolite starts to show reflections of copper hydroxo nitrate of composition $Cu_2(OH)_3NO_3$. Its formation in interaction of calcium carbonate with Cu^{2+} ions indicates that the interaction of metal ions with solid carbonates is governed not only by the nature of a cation, its concentration, and solution pH, but also by the nature of anions present in solution.

A particular place among ions of nonferrous metals is occupied by iron(III). Underground natural sources of drinking and technical water contain admixtures of mineral substances, of which iron(III) is the most widely occurring. Its presence in water gives rise to problems in operation of various kinds of equipment for housing, public utilities, and industries, and, therefore, preliminary measures should be taken for its removal in conformity with the existing regulations. As can be seen from the data obtained, carbonate tripolites can be successfully used for these purposes. However, as shown by the study, the degree of purification to remove iron(III) approaches 100% only in those cases when the pH of a solution after its contact with tripolite exceeds 7 [4].

The absorption efficiency of multiply charged metal ions from aqueous solutions by natural carbonate-containing tripolites is determined by acid–base equilibria in the system under consideration and, in particular, by the equilibrium pH value. This value is, in turn, a function of the pH of the starting solution and of the ratio between the tripolite mass and the solution volume, i.e., bath ratio M.

To find the relationship between these parameters, acid–base equilibria were studied in the tripolite–water system under static conditions in a wide range of pH values and s : l ratios. In doing so, the experimental procedure was similar to that in a study of the absorption of metal ions, with the only difference that the weighed portion of a sample was poured over by distilled water with different pH values adjusted with HNO_3 or NaOH solutions, rather than by a solution of a metal salt. The results obtained are shown in Fig. 5 as a set of pH_{eq}–$1/M$ curves for solutions with different pH_0 values.

A mathematical processing of a set of five equations determining the pH_{eq}–$1/M$ dependence at different pH values, described in detail in [4], revealed a relationship between pH_{eq}, pH_0, and bath ratio M = s : l, which has the form of a linear equation

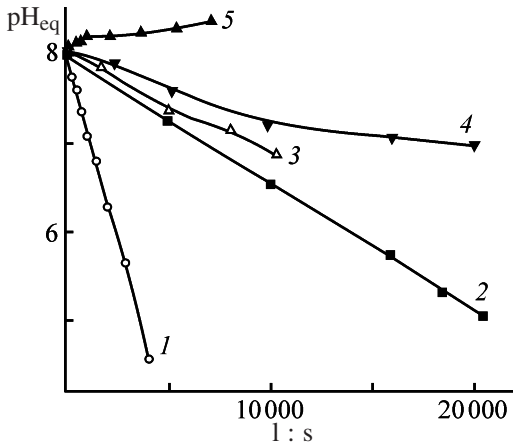

Fig. 5. pH of the equilibrium solution vs. the l : s ratio. (pH_{eq}) Equilibrium value in the solution after absorption and (l : s) ratio between the tripolite mass and volume of the starting aqueous solution. pH of the starting solution: (*1*) 2.6, (*2*) 3.5, (*3*) 4.6, (*4*) 6.5, and (*5*) 7.5.

$$pH_{eq} = 7.98 - (31.372 - 4.1627\,pH_0) \times 10^{-5}M. \quad (1)$$

This linear dependence is observed for solutions with pH_0 in the range 3.5–7.5 and can be used for rapid evaluation of the efficiency of carbonate-containing materials in purification of real solutions. For example, at a 1-kg weighed portion of tripolite and a prescribed pH_0 value of 6, the solution volume V_l (l) that can be neutralized to pH 7 can be readily found using the equation

$$V_{eq} = \frac{(31.37 - 4.16\,pH_0) \times 10^{-5}T}{7.98 - pH_{eq}} = 6.5 \times 10^5. \quad (2)$$

At present, dilute solutions of nonferrous metal ions are concentrated using nonselective and selective ion-exchange materials. In the former case, all ions present in a solution are absorbed, and in the latter, only the group of nonferrous metal ions. The nature of selectivity in chemisorption processes is quite different. In contrast to ion-exchange materials, selective chemisorbents can be used not only for group concentration of nonferrous metal ions, but also for their separation. Poorly soluble carbonates of bivalent metals and, in particular, alkaline-earth metals show chemisorption activity toward ions of heavy and nonferrous metals, because, in the process, compounds less soluble than the starting compounds are formed. The efficiency of chemisorption depends on a number of factors, the main of which is ΔSP, difference of the solubility products (SP) of the starting sorbent and the compound formed in chemisorption.

Table 4. Results of determination of the concentration and pH of $Fe(NO_3)_3$–$Ni(NO_3)_2$ solutions before and after sorption

Ion concentration in solution, mg l^{-1}				Sorbed, mg-equiv g^{-1}		Degree of Fe(III) recovery from solution, %	Solution pH	
Ni(II)		Fe(III)		Fe(III)	or recovered Ni(II)		before sorption	after sorption
in initial solution	after sorption	in initial solution	after sorption					
Sorbent $CaCO_3$								
14	12	10	0	0.1	0.02	100	3.19	7.40
82	67	60	0	0.8	0.2	100	2.85	7.32
165	135	121	0	1.6	0.4	100	2.74	7.10
330	223	242	0.5	3.2	0.7	99.8	2.55	7.58
666	547	488	0.6	6.5	1.0	99.9	2.41	7.34
Sorbent carbonate tripolite								
14	11	10	0	0.1	0.04	100	3.19	7.60
82	60	60	0	0.8	0.3	100	2.85	7.46
165	135	121	0	1.6	0.4	100	2.74	7.24
330	244	242	0.6	3.2	0.7	99.8	2.55	7.10
666	556	488	0.9	6.5	1.0	99.8	2.41	5.62

A sorbent suitable for absorption of certain ions from the mixture can be chosen using the solubility series of carbonates of doubly and triply charged metals.

A possible promising area is application of chemisorption processes for selective recovery of nonferrous metal ions from two- and multicomponent solutions.

Previous studies [5] confirmed that natural carbonates can be used as selective sorbents for recovery of iron(III) ions from binary solutions containing Fe(III)–Ni(II). Two-component (Fe^{3+}–Ni^{2+}) dilute aqueous solutions are formed in processing of worked-out nickel–iron battery electrodes [6] and in processing of electrolytic baths for nickel-plating of iron articles.

The solubility products of $CaCO_3$ and $NiCO_3$ are virtually equal (4.8×10^{-9} and 6.6×10^{-9}, respectively). The SP of iron hydroxide, which is formed, according to published data, in contact of Fe(III) ions with calcium carbonate, is many orders of magnitude lower. Thus, calcium carbonate should selectively absorb iron(III) ions from a two-component Fe^{3+}–Ni^{2+} solution. The experimental data obtained confirmed this assumption.

Table 4 lists the concentrations of iron(III) and nickel(II) ions in two-component Fe^{3+}–Ni^{2+} solutions before and after sorption and pH values of the starting and equilibrium solutions. It also lists the following parameters calculated from the solution concentrations before and after sorption: amounts of absorbed ions and those released into solution (mg-equiv g^{-1}) and degrees of recovery of iron(III) ions from solutions with various concentrations (%).

In the case of two-component solutions with initial iron(III) concentrations exceeding 240 mg l^{-1}, the solutions obtained after sorption contain small amounts of iron, 0.5–0.9 mg l^{-1}.

In three-component and more complex systems, the course of chemisorption processes will be primarily determined by the ratio between the sorbent mass and solution volume. It is quite apparent that the chemisorption technique can be used for successive selective recovery of ions forming the least soluble compound from more complex, multicomponent mixtures. In doing so, the weighed portion of a sorbent should be calculated with account of the amount of ions of the metal forming the least soluble compound with the precipitating anion.

With account of the fact that chemical reactions proceed rather efficiently in concentrated solutions, the chemisorption techniques can be used for successive recovery of ions from relatively concentrated solutions and for processing of an electroplating waste.

Practical implementations of chemisorption techniques for selective absorption of metal ions may be widely diverse. In addition to the cases described above, the "reverse selectivity" mode is possible. The solubility products of carbonates, basic carbo-

nates, and hydroxides of virtually all heavy and nonferrous metals, except nickel, are substantially lower than that of calcium carbonate.

Thus, carbonate materials can be used to purify nickel solutions to remove admixtures of other metals, under both static and dynamic conditions. It is interesting to note that, according to experimental data, calcium carbonate does not adsorb from solutions cobalt ions, either, although reference values of SP for cobalt carbonate and hydroxide are several orders of magnitude lower than the SP of calcium carbonate. Apparently, the conditions in this heterogeneous system (pH, concentration, ratio between masses of the sorbent and the solution, temperature, etc.) are unfavorable for formation of these compounds. For example, a strong absorption of cobalt ions in the form of hydroxide in contact with shell rock was observed in [7] only at elevated temperatures.

CONCLUSIONS

(1) Tripolites from the Stal'noe deposit are a natural composite whose sorption properties are determined by the relative contents of the principal rock-forming phases: opal–cristobalite (silica) and calcite (calcium carbonate).

(2) The limiting sorption volume and specific surface area vary similarly to the content of silica in tripolite.

(3) The adsorption-structural parameters of tripolites become worse as the content of calcite in the mineral increases; however, this improves the chemisorption properties of tripolites.

(4) Carbonate tripolites containing 20–30% calcite and more are highly efficient sorbents for ions of heavy and nonferrous metals. They show promise for solution of a number of technological and environmental problems: treatment of technical and drinking water, processing of electroplating wastes, selective recovery and concentration of nonferrous metals, and deironing of water.

REFERENCES

1. Distanov, U.G., Mikhailov, A.S., Konyukhova, T.P., et al., *Prirodnye sorbenty SSSR* (Natural Sorbents of the USSR), Moscow: Nedra, 1990.
2. Rat'ko, A.I., Shashkova, I.L., Vecher, V.A., et al., *Vestsi Akad. Navuk Bel., Ser. Khim. Navuk*, 1997, no. 1, pp. 32–37.
3. Shashkova, I.L., Rat'ko, A.I., Mil'vit, N.V., et al., *Zh. Prikl. Khim.*, 2000, vol. 73, no. 6, pp. 914–919.
4. Shashkova, I.L., Rat'ko, A.I., Panasyugin, V.S., et al., *Zh. Prikl. Khim.*, 2001, vol. 74, no. 2, pp. 249–254.
5. Shashkova, I.L., Mil'vit, N.V., and Rat'ko, A.I., *Zh. Prikl. Khim.*, 2005, vol. 78, no. 11, pp. 1859–1863.
6. Demidov, A.I. and Krasovitskaya, O.A., *Zh. Prikl. Khim.*, 2000, vol. 73, no. 10, pp. 1656–1660.
7. Batalova, Sh.B., Likerova, A.A., Tabanova, Kh.G., et al., *Kompleksn. Ispol'z. Miner. Syr'ya*, 1984, no. 12, pp. 58–60.

ISSN 1070-4272, Russian Journal of Applied Chemistry, 2007, Vol. 80, No. 11, pp. 1852–1855. © Pleiades Publishing, Ltd., 2007.
Original Russian Text © N.A. Shvab, V.D. Litovchenko, L.M. Rudkovskaya, 2007, published in Zhurnal Prikladnoi Khimii, 2007, Vol. 80, No. 11, pp. 1826–1829.

APPLIED ELECTROCHEMISTRY AND CORROSION PROTECTION OF METALS

Mechanism of Reduction of Thiosulfate Ions on the Cathode

N. A. Shvab, V. D. Litovchenko, and L. M. Rudkovskaya

Vernadsky Institute of General and Inorganic Chemistry, Ukrainian National Academy of Sciences, Kiev, Ukraine

Received December 26, 2006; in final form, May 2007

Abstract—The effect exerted by current density, cathode material (platinum, palladium, nickel, silver, copper, and cadmium), and temperature on the rate of the reduction of sodium thiosulfate was studied.

DOI: 10.1134/S1070427207110146

Previous studies [1–5] of the cathodic reduction of anions showed that the reduction rate is determined by the zero-charge potential. The reduction starts at potentials corresponding to positive charges on the metal surface, then the current reaches limiting value, and at potentials close to the zero-charge potential it starts to decrease. After passing a minimum, the current increases again with increasing negative potential. Since the cathode surface acquires a negative charge with increasing negative potential, the anions are repelled from the cathode and the current increase is due to the reduction of hydrogen ions. In this case, the reaction rate is limited by the concentration of hydrogen ions and by the overvoltage of hydrogen evolution. Presumably, in the region of hydrogen evolution the thiosulfate anions may be reduced on the cathode. It was shown that pure silver, a mixture of silver with silver sulfide, or pure silver sulfide is formed on the cathode, depending on current density [6]. In this case, as seen from Fig. 1, the amount of silver sulfide and, consequently, sulfide anions is directly proportional to the cathodic current density. At less negative potentials, the reduction rate of the thiosulfate ions is determined by the zero-charge potential and is low [7].

In the region of the potentials of hydrogen evolution, the thiosulfate ions are reduced with atomic hydrogen. In this case, the reaction rate is determined by the surface concentration of atomic hydrogen on the cathode. The hydrogen concentration depends on both the overvoltage of hydrogen evolution and the current density [8–10]. Increasing the current and using the cathodes with a large overvoltage of hydrogen evolution results in the increase in the concentration of atomic hydrogen.

The dependence of the reduction rate of thiosulfate ions on the current density and cathode material can be predicted from the above results. For example, platinum and palladium have a low overvoltage of hydrogen evolution, and nickel, silver, copper, and cadmium, higher overvoltage. The higher the overvoltage, the higher the concentration of atomic hydrogen on the cathode surface [8]. Therefore, it was of interest to study the rate of reduction of thiosulfate ions to sulfide ions on metals with various potentials of hydrogen evolution as a function of current density.

Reduction of thiosulfate ions with atomic hydrogen can be proved using an electrochemical cell equipped with a membrane cathode made of a thin palladium foil. The polarization of the cathode membrane causes atomic hydrogen to evolve on its back side. The amount of the evolved hydrogen on the surface is de-

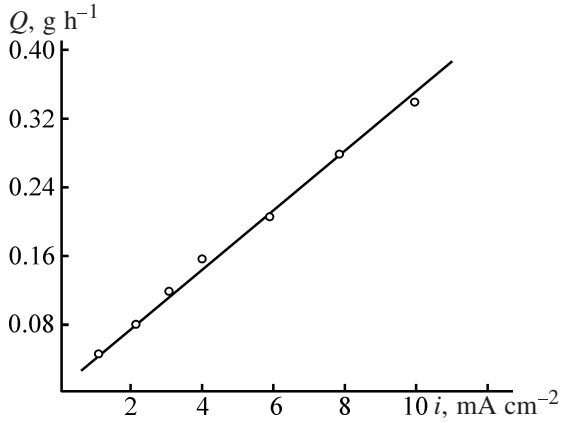

Fig. 1. Effect of current density i on the rate of silver sulfide deposition on the cathode Q. Electrolyte: 0.5 g l^{-1} silver and 0.5 M sodium thiosulfate; stainless steel cathode (11 cm^2).

termined by the recombination or electrochemical desorption of hydrogen atoms to form the molecules [11]. As established in [12, 13], the rate of diffusion of atomic hydrogen through a palladium cathode membrane is inversely proportional to the membrane thickness, i.e., the thinner the membrane, the higher the diffusion rate. Therefore, this study is concerned with the effect exerted by the current density on the amount of sulfide ions obtained by reduction of thiosulfate ions with atomic hydrogen on a membrane cathode 80 μm thick.

The effect of the cathode material on the rate of reduction of thiosulfate ions was studied in a U-shaped glass cell. The cathode and anode compartments of the cell were separated with a glass filter no. 1. The volume of the cathode space was 60 cm^3. Cathodes 3×4 cm in size were made of a thin sheet of different metals, and their nonworking side was insulated with epoxy resin. Reduction of thiosulfate ions with atomic hydrogen was studied in a rectangular Plexiglas cell. The cathode and anode compartments of the cell were separated with a membrane made of a tightened Khlorin fabric, and its diffusion space was separated from the cathode compartment with a palladium membrane, with no electric and liquid contact between the cathode and diffusion spaces. The thickness of the membrane was 80 μm and its area, 10 cm^2. In each of three compartments, the electrolyte volume was 40 cm^3. A 0.5 M solution of sodium thiosulfate was poured into the diffusion space in all experiments. In the course of the experiments, the palladium membrane deformed owing to absorption of atomic hydrogen. Therefore, it was annealed at 800°C for 1 h and then cooled in a muffle furnace to room temperature. After that, it was flattened between two thin nickel sheets, mounted between the cathode and diffusion spaces, and fixed there with bolts. Hermetic gaskets made of acid-resistant rubber were arranged on each side of the palladium membrane. As anode we used platinum. A 0.5 M sodium hydroxide solution was poured into all the three compartments and the electrolysis was performed at a current density of 20 mA cm^{-2} for 1 h until saturation of the palladium cathode with atomic hydrogen. In the process, hydrogen in the form of bubbles started to evolve on the opposite side of the palladium cathode after 30–35 min. Experiments were performed with chemically pure grade chemicals. Prior to the experiment, cathodes were polished, degreased with Vienna lime, and washed in distilled water. The amount of sulfide and sulfite ions formed in the solutions in the course of the experiments was determined titrimetrically [14].

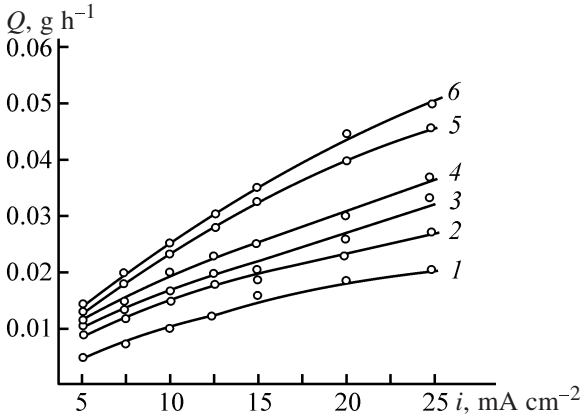

Fig. 2. Effect of cathode material and current density i on the rate of generation of sulfide ions Q in the cathode space. Catholyte: 0.5 M solution of sodium thiosulfate, volume 60 cm^3, cathode area 8 cm^2. Cathode material: (*1*) Pt, (*2*) Pd, (*3*) Ni, (*4*) Ag, (*5*) Cu, and (*6*) Cd.

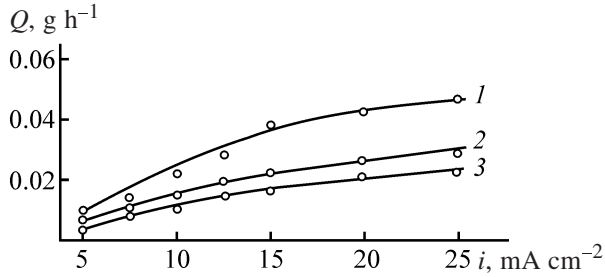

Fig. 3. Effect of current density i and temperature on the rate of generation of sulfide ions Q in the cathode space. Cathode material cadmium; catholyte: 0.5 M solution of sodium thiosulfate. Temperature, °C: (*1*) 20, (*2*) 50, and (*3*) 75.

The study performed showed that, for all the cathodes studied, the reduction rate of the thiosulfate ions increases by a factor of 5 on passing from platinum to cadmium cathode and with increasing current density, i.e., it increases with the overvoltage of hydrogen evolution (Fig. 2). The overvoltage of hydrogen evolution decreases with increasing temperature [11]. As a result, the rate of recombination of atomic hydrogen into the molecule increases, whereas the reduction rate of the thiosulfate ions decreases (Fig. 3, curves *1–3*).

We also studied the reduction of thiosulfate ions with atomic hydrogen in the diffusion compartment of the electrochemical cell. When cathodic current is applied to the polarization side of the cathode membrane and the potential is shifted to the negative side, the evolution of hydrogen occurs initially only on the polarization side and then, after 0.5 h, hydrogen in the form of bubbles evolves on the diffusion side. The results obtained in reduction of thiosulfate ions

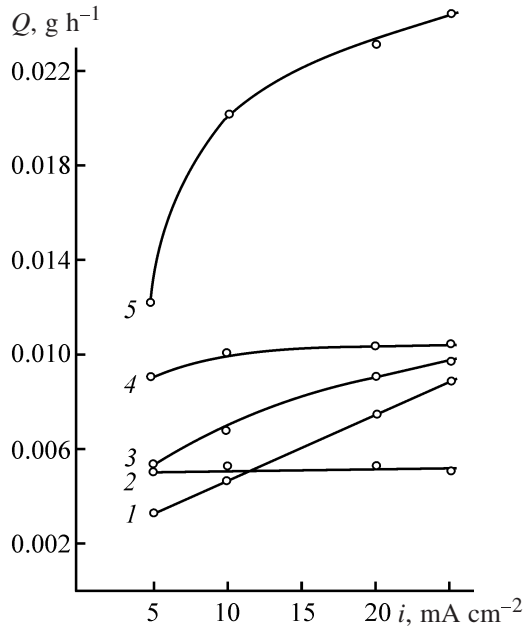

Fig. 4. Effect of cathodic current density i on the rate of generation of sulfide ions Q in the (*1–3*) diffusion space and (*4, 5*) catholyte. Electrolyte: (*1*) 0.5 M solution of sodium hydroxide; (*2*) 0.5 M solution of sodium thiosulfate; (*3, 4*) 0.5 M solution of sodium hydroxide + 1 g l^{-1} sodium thiosulfate; and (*5*) 0.5 M solution of sodium thiosulfate.

with atomic hydrogen in the diffusion compartment are presented in Fig. 4. In the presence of pure sodium hydroxide in the cathode compartment, the amount of sulfide ions in the diffusion space (curve *1*) increases with increasing current on the cathode side of the membrane. This is because the amount of atomic hydrogen on the cathode surface increases with the cathodic current density [8] and the rate of diffusion through the palladium membrane toward the diffusion compartment of the cell increases. When 1 g l^{-1} of sodium thiosulfate, which is reduced on the cathode to the sulfide ion and increases the overvoltage of hydrogen evolution [11], is introduced into the cathode space, the concentration of atomic hydrogen on the surface of the cathode membrane increases. The increase in the amount of atomic hydrogen on the cathode increases the rate of its diffusion through the cathode membrane toward the diffusion space, with the rate of the reduction of thiosulfate ions to sulfide ions increasing (curve *3*). If a 0.5 M sodium thiosulfate solution is used in the cathode space, then the rate of its reduction to sulfide ions sharply increases (curve *5*), thus decreasing the amount of atomic hydrogen on the cathode. In the process, the rate of diffusion of atomic hydrogen through the membrane cathode toward the diffusion space decreases, thus decreasing the reduction rate of the thiosulfate ions (curve *2*).

The analysis of the electrolysis products in the cathode and diffusion compartments showed that, along with sulfide ions, the sulfite ions in equimolar amount are also present in the solution. Reduction of thiosulfate ions with atomic hydrogen proceeds in the near-cathode layer, and the process rate is determined by the concentration of atomic hydrogen rather than by the electrode potential, i.e., the reduction proceeds by the chemical mechanism. The standard potential of the reaction $H = H^+ + e$ is –2.106 V [15], which confirms the high reductive ability of atomic hydrogen. The reduction of thiosulfate ions is described by the equation

$$S_2O_3^{2-} + H + OH^- = S^{2-} + SO_3^{2-} + H_2O. \quad (1)$$

At electrode potentials not exceeding the potential of hydrogen evolution, the thiosulfate ions are reduced to sulfide and sulfite ions by the equation [16]

$$S_2O_3^{2-} + 2e = S^{2-} + SO_3^{2-}. \quad (2)$$

In this case, the reduction rate of the thiosulfate ions, as established in [7], is determined by the zero-charge potential.

Our study allowed us to establish the following mechanism of the reduction of thiosulfate ions on the cathode. At cathode potentials not exceeding the potential of hydrogen evolution, the reduction rate of the thiosulfate ions is determined by the zero-charge potential. At electrode potentials closer to the potentials of hydrogen evolution, a part of hydrogen atoms reduces the thiosulfate ions to sulfide and sulfite ions owing to the retardation of the recombination of hydrogen atoms into the molecules. In this case, the reduction rate is determined by the cathode material, i.e., by the overvoltage of hydrogen evolution or by the amount of atomic hydrogen on the cathode surface.

Our results allow us to suggest the conditions of the electrochemical neutralization of spent fixing solutions of sodium thiosulfate [17]. On storage, the above solutions absorb oxygen and undergo chemical transformations resulting in the formation of toxic compounds with unpleasant odor. Upon electrolysis of sodium thiosulfate solutions containing iron sulfate, the final products of the electrolysis are an insoluble iron sulfide deposit and sodium sulfite in a solution, i.e., less toxic products are formed.

CONCLUSIONS

(1) The study of the effect exerted by the current density, cathode material (platinum, palladium, nickel, silver, copper, and cadmium), and temperature on the rate of the reduction of thiosulfate ions showed that the process rate increases with the overvoltage of hydrogen evolution on the metals and decreases with increasing temperature of the solution. The electrolysis proceeds with the formation of equivalent amounts of sulfide and sulfite ions.

(2) The reduction of thiosulfate ions with atomic hydrogen diffusing through a palladium membrane cathode is determined by the rate of hydrogen diffusion. The amount of atomic hydrogen is determined by the current density on the membrane cathode and by the overvoltage of hydrogen evolution.

(3) The mechanism of the reduction of the thiosulfate ions on the cathode was determined.

REFERENCES

1. Nikolaeva-Fedorovich, N.V., Rybakov, B.N., and Radyushkina, K.A., *Elektrokhimiya*, 1967, vol. 3, no. 9, pp. 1086–1093.
2. Fedorovich, N.V., Frumkin, A.N., and Keis, Kh.E., *Coll. Czech. Chem. Commun*., 1971, vol. 36, no. 2, pp. 722–729.
3. Nikolaeva, N.V., and Grosman, A.A., *Dokl. Akad. Nauk SSSR*, 1954, vol. 45, no. 5, pp. 760–762.
4. Frumkin, A.N., Fedorovich, N.V., and Kulakovskaya, S.I., *Elektrokhimiya*, 1974, vol. 10, no. 2, pp. 330–334.
5. Frumkin, N.A., Fedorovich, N.V., and Kulakovskaya, S.I., *Elektrokhimiya*, 1974, vol. 10, no. 1, pp. 130–134.
6. Shvab, N.A., Gur'yanova, I.A., and Omel'chuk, A.A., *Zh. Prikl. Khim*., 2005, vol. 78, no. 1, pp. 86–89.
7. Gur'yanova, I.A., Omel'chuk, A.A., and Shvab, N.A., *Vestn. Nats. Khar'k. Univ*., 2005, no. 648, issue 12 (35), pp. 264–267.
8. Vetter, K.J., *Elektrochemische Kinetik*, Berlin: Springer, 1961.
9. Frumkin, A.N., *Elektrodnye protsessy: Izbrannye trudy* (Electrode Processes: Selected Works), Moscow: Nauka, 1987.
10. Frumkin, A.N., *Perenapryazhenie vodoroda: Izbrannye trudy* (Hydrogen Overvoltage: Selected Works), Moscow: Nauka, 1988.
11. Antropov, L.I., *Teoreticheskaya elektrokhimiya* (Theoretical Electrochemistry), Moscow: Vysshaya Shkola, 1984.
12. Schuldiner, S. and Hoare, J.P., *J. Electrochem. Soc*., 1956, vol. 103, no. 3, pp. 178–181.
13. Hoare, J.P. and Schuldiner, S., *J. Electrochem. Soc*., 1956, vol. 103, no. 4, pp. 237–241.
14. Busev, A.I., and Semenova, P.N., *Analiticheskaya khimiya elementov* (Analytical Chemistry of Elements), Moscow: Nauka, 1975, pp. 65–72.
15. *Spravochnik po elektrokhimii* (Handbook on Electrochemistry), Sukhotin, A.M., Ed., Leningrad: Khimiya, 1981.
16. Konpic, N, and Holzinger, F., *Monatsh. Chem*., 1954, vol. 85, no. 3, pp. 140–153.
17. Shvab, N.A., and Litovchenko, V.D., *Ekotekhnol. Resursosberezh*., 2005, no. 6, pp. 59–61.

ISSN 1070-4272, Russian Journal of Applied Chemistry, 2007, Vol. 80, No. 11, pp. 1856–1859. © Pleiades Publishing, Ltd., 2007.
Original Russian Text © O.I. Kuntyi, V.R. Ivashkin, V.T. Yavorskii, G.I. Zozulya, 2007, published in Zhurnal Prikladnoi Khimii, 2007, Vol. 80, No. 11, pp. 1830–1833.

APPLIED ELECTROCHEMISTRY AND CORROSION PROTECTION OF METALS

Electrochemical Processing of WC–Ni Pseudoalloys in Sulfuric Acid Solutions to Ammonium Paratungstate and Nickel(II) Sulfate

O. I. Kuntyi, V. R. Ivashkin, V. T. Yavorskii, and G. I. Zozulya

L'vivs'ka Politekhnika National University, Lviv, Ukraine

Received February 26, 2007; in final form, May 2007

Abstract—Electrolysis of a WC–Ni pseudoalloy in aqueous sulfuric acid solutions was studied. A flowsheet for production of ammonium paratungstate and nickel(II) sulfate is suggested, in which the process solutions are recycled. The principal electrolysis parameters are presented.

DOI: 10.1134/S1070427207110158

Tungsten is a high-melting metal whose natural resources are close to exhaustion. Therefore, secondary tungsten becomes the principal source of this metal and its compounds. One of the most promising, in technological, energetic, and environmental regards, methods for processing of secondary tungsten is electrolysis of aqueous solutions [1–6]. The variety of products of the electrochemical transformation depends on the form of tungsten in secondary raw materials and on the electrolyte composition. For example, tungsten is anodically oxidized in alkaline and alkaline–ammonia electrolytes to the tungstate ion WO_4^{2-} from alloys, including those containing tungsten carbide (WC) [1, 2]. In acid electrolytes, WC–Co is converted to the oxide WO_3 [1, 3–5]. Tungsten carbides are contained in hard alloys widely used to fabricate special tools, drills, and military equipment. Therefore, integrated processing of worked-out and obsolete articles of this kind is a topical area of the electrochemistry of tungsten.

This study proceeds with an integrated analysis of the utilization of secondary tungsten with the use of electrochemical processes [7, 8] and is aimed to develop process aspects of electrolysis of a poorly studied WC–Ni system in order to obtain commercial products, ammonium paratungstate and nickel(II) sulfate.

EXPERIMENTAL

Cores of armor-piercing shells 18 and 30 mm in diameter and 70 mm high, fabricated from a WC–Ni alloy of compositions (wt %): W 86.4, C 5.8, Ni 7.2, were used in the study.

The electrolysis was performed in a laboratory electrolyzer of capacity 5 dm^3, schematically shown in Fig. 1. A 1 M H_2SO_4 solution served as the starting electrolyte. The cores were placed in a titanium basket *1*. During the electrolysis, the basket was shaken every 15 min with a vibrator *2*, and the electrolyte (H_2SO_4 + $NiSO_4$) was filtered at regular intervals. After the electrolysis was terminated, the cores were cleaned to completely remove tungsten oxides and

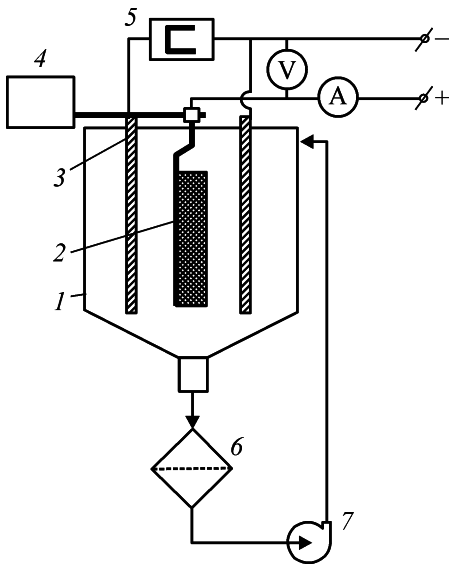

Fig. 1. Schematic of the laboratory installation. (*1*) Titanium basket, (*2*) vibrator, (*3*) aluminum cathodes, (*4*) electrolyzer case, (*5*) coulometer, (*6*) filter, and (*7*) pump.

weighed. The loss of mass by the cores and the mass gain of the coulometer cathodes were used to calculate the anode current efficiency CE_a. The precipitate of tungsten oxides was washed with water, centrifuged, and dissolved using ammonia water or gaseous ammonia. The ammonium tungstate solution formed was filtered and evaporated on a water bath. After cooling, the resulting crystals of ammonium paratungstate $(NH_4)_{10}[H_2W_{12}O_{42}]\cdot 4H_2O$ (APT) were filtered off, washed with water, and thermally analyzed for the content of tungsten(VI) oxide. To study the surface morphology of the samples, electrolysis was performed at E = const with a PI-50-1.1 potentiostat and a silver chloride reference electrode. The morphology of the core samples was examined with a REMMA-102-02 scanning electron microscope (SEM),[1] with the outward appearance of the surface with tungsten oxides photographed using a digital camera.

The anodic behavior of the WC–Co [3] and WC–Ni [8] systems in acid solutions is characterized by selective dissolution of the binder, cobalt or nickel, respectively, with the subsequent conversion of the carbide to WO_3 and CO_2.

$$Ni \rightarrow Ni^{2+} + 2e, \quad (1)$$

$$WC + 5H_2O \rightarrow WO_3 + CO_2 + 10H^+ + 10e. \quad (2)$$

The potential of nickel oxidation by reaction (1) is 0.5–0.7 V lower than the conversion potential of tungsten carbide by reaction (2) [8]. Therefore, anodic dissolution of the nickel binder is the leading stage of electrolysis of the WC–Ni system, causing a change in the surface profile (Fig. 2). It becomes more developed, which intensifies the conversion of tungsten carbide.

The occurrence of anodic reaction (2) favors formation of a film composed of hydrated stoichiometric oxide WO_3 and hydrated nonstoichiometric oxides WO_x (including the "tungsten blue" $WO_{2.8}$). Its growth is accompanied by cracking (Fig. 3) and periodic detachment of the conversion deposit from the substrate. This behavior is accounted for by the very large Pilling–Bedworth ratio (3.45 for the W–WO_3 system), which is defined as the ratio V_{WO_3}/V_W, where V_{WO_3} and V_W are the molar volumes of tungsten(VI) oxide and metallic tungsten, respectively [9].

Under the conditions of electrolysis with a bulk anode, i.e., with baskets, spontaneous removal of

[1] The SEM studies were carried out at the Scientific, Technical, and Educational Center for Low-Temperature Studies, Franko National University (Lviv, Ukraine).

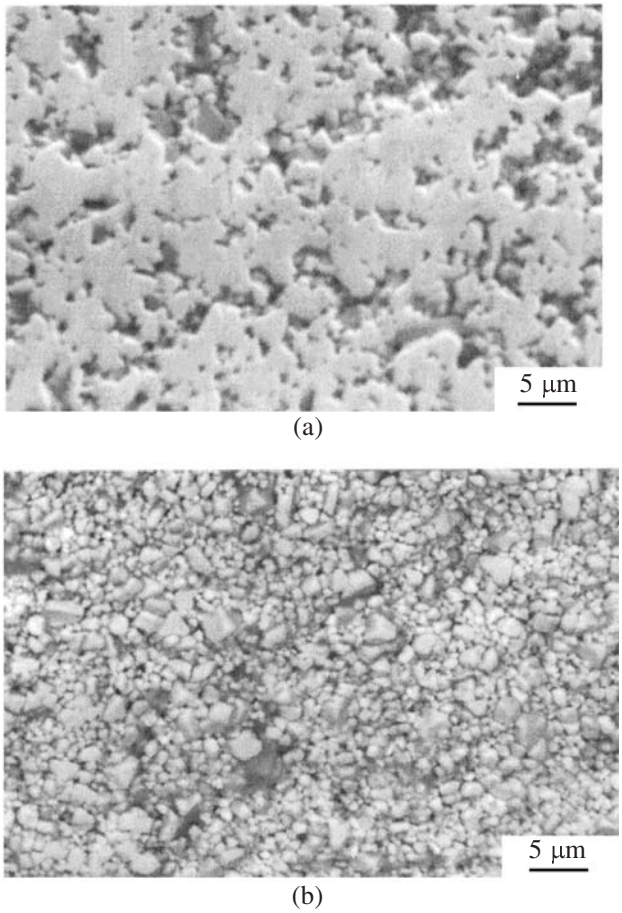

Fig. 2. Surface morphology of cores made of a WC–Ni pseudoalloy (a) before and (b) after selective anodic dissolution of the nickel binder in 1 M H_2SO_4 at 20°C and E = 0.2 V.

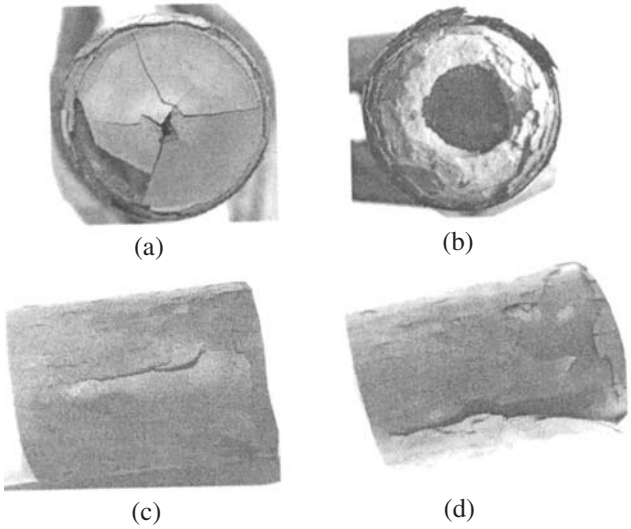

Fig. 3. Fragments of (a, b) edge and (c, d) lateral core surfaces made of a WC–Ni pseudoalloy after anodic forming of a film of tungsten oxides in 1.0 M H_2SO_4 at T = 20°C and E = 1.7 V.

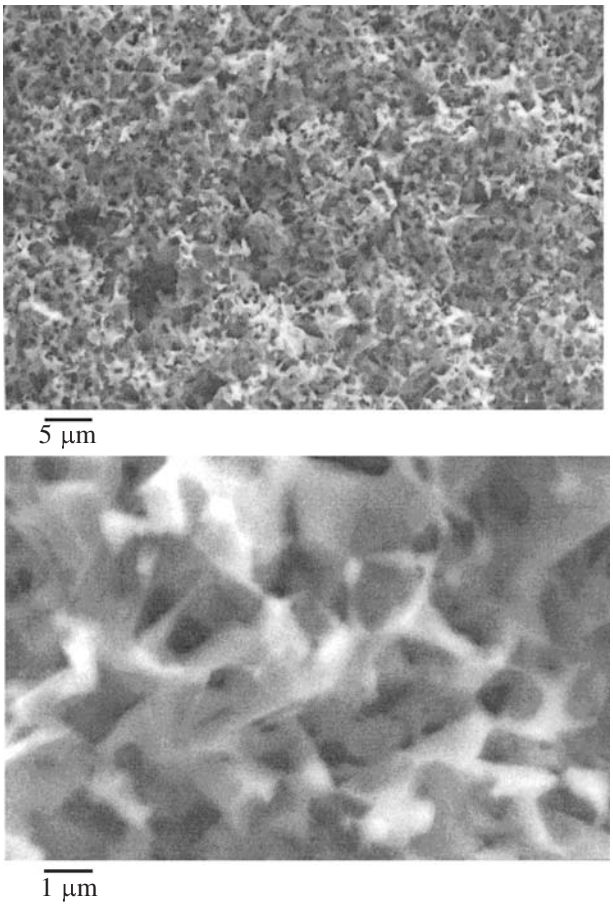

Fig. 4. Nickel skeleton after selective anodic dissolution of the carbide WC from the WC–Ni pseudoalloy in 1.5 M NaOH at T = 20°C and E = 1.3 V at different magnifications.

the forming deposit of tungsten oxides becomes more complicated. As a result, the core surface is blocked, which leads to a decrease in the anode currents. It was found on the laboratory electrolyzer (Fig. 1) that periodic shaking of the basket in solution circulation favors removal of the anode deposit from the core surface into the electrolyte bulk and restoration of the anode currents to their initial values.

Principal parameters of electrochemical processing of the WC–Ni system in 1.0 M H_2SO_4

U, V	i_r,* A dm^{-2}	CE_a, %
3.5	5	103.00
4.0	6	104.58
4.5	7.6	105.00
5.0	9	102.25
6.0	13	105.35

* i_r is the reduced current density (ratio between the current strength and cross-sectional area of the bulk anode).

As shown by the study, tungsten carbide is completely converted into the oxide in prolonged electrolysis. Thus, all WC particles are provided with an electric contact until their complete anodic conversion. This is due to the structure of the cores, because a strongly branched nickel skeleton is formed in the course of compaction of a powder formulation composed of tungsten carbide and nickel (Fig. 4). With account of the comparatively high nickel content (7–10 wt %) of the WC–Ni system, it, in fact, envelops each tungsten carbide particle and thereby acts as a rigid current lead.

The main part of the deposit formed in the course of electrolysis is composed of the oxide WO_3 and nonstoichiometric oxides ("tungsten blue") embedded in this deposit. This is due to the fact that the conversion occurs with a stage-by-stage formation of oxides. For example, lower tungsten oxides are converted into higher oxides in the direction away from the metal surface and into the oxide WO_3 at the interface between the solid phase and the electrolyte [10]. In detachment of the conversion product from the anode surface, especially under vibration conditions, incompletely oxidized oxides are incorporated into the deposit. Therefore, the current efficiency in terms of tungsten(VI) oxide exceeds 100% (see table).

The reduced current density reaches values (see table) that are acceptable to industrial processing of cores by electrolysis. As the voltage is raised, the current density i_r increases to 15 A dm^{-2} and more. However, under these conditions, not only the specific electric power expenditure increases, but also the electrolyte is rapidly heated and hydrogen vigorously evolves at the cathode. The first, energetic, factor can affect the production cost, whereas the last two complicate the electrolysis technology. Therefore, the optimal current density can be only found on an industrial electrolyzer.

One of the most frequently used tungsten compounds is ammonium paratungstate, which, taken in large amounts, can serve as a raw material for manufacture of a tungsten powder [1]. Therefore, it is electrochemically appropriate to process alloys of the system WC–Ni into APT.

On the basis of the experimental data obtained, a flowsheet for processing of secondary alloys of the system WC–Ni was suggested for the example of cores of armor-piercing shells. The flowsheet comprises three principal stages: electrolysis, synthesis of

Flowsheet for electrochemical processing of the WC–Ni pseudoalloy in sulfuric acid solutions

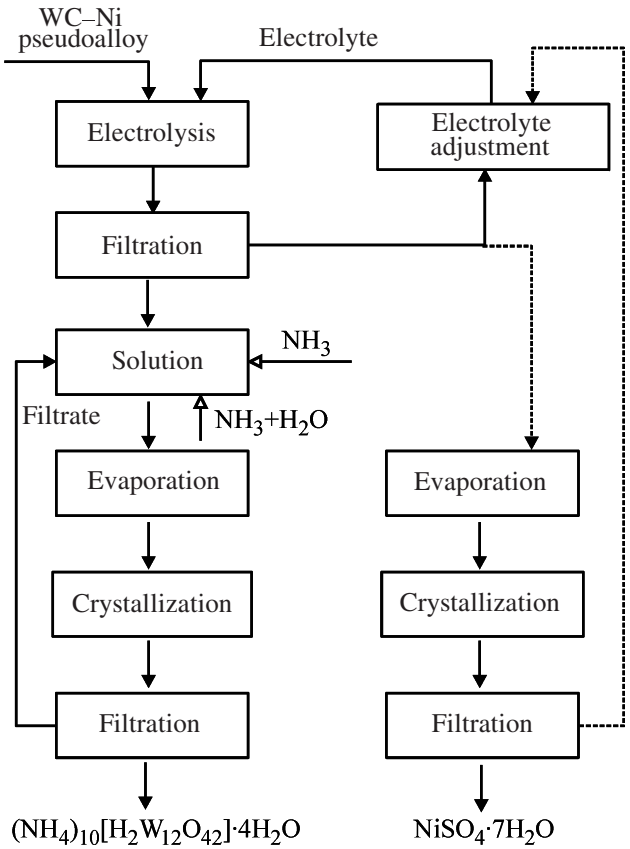

ammonium paratungstate, and recovery of nickel(II) sulfate. The central stage of the process is electrolysis, whereas the remaining stages are typical processes of chemical technology.

The electrolysis yields a suspension from which tungsten oxides are recovered by filtration. After being washed, the tungsten oxides are delivered in the form of slurry to dissolution with gaseous ammonia. The solid residue (~0.5 wt %) is mostly composed of graphite not oxidized by reaction (2). The solution formed is evaporated to remove the excess amount of ammonia and convert ammonium tungstate into poorly soluble ammonium paratungstate.

The solution filtered off after the electrolysis is delivered, as nickel sulfate is accumulated, to recovery of the salt in the form of a crystal hydrate. The electrolyte is adjusted with sulfuric acid in an amount equivalent to the recovered product, $NiSO_4 \cdot 7H_2O$.

Thus, the suggested technique for processing of an alloy of the system WC–Ni, which provides the environmental safety of the process, can yield two commercial products, ammonium paratungstate and nickel sulfate crystal hydrate. The products are of pure grade. Their purity is improved, i.e., their conditioning is carried out, by the known methods.

CONCLUSIONS

(1) Anodic treatment of a WC–Ni pseudoalloy in sulfuric acid solutions causes nickel dissolution and tungsten conversion into the oxide WO_3 at a specific electric energy expenditure of 4.0–7.5 kW h kg^{-1} of the starting product.

(2) Shaking and circulation of the electrolyte enable use of bulk anodes and electrolysis at current densities of 5–13 A dm^{-2}.

(3) The degree of electrochemical conversion of tungsten into oxide and of nickel dissolution reaches 100%, which enables processing of a WC–Ni pseudoalloy to give pure commercial products, ammonium paratungstate and nickel sulfate. The technique provides full recycling of process solutions and environmental safety of the processes performed.

REFERENCES

1. Zelikman, A.N. and Nikitina, L.S., *Vol'fram* (Tungsten), Moscow: Metallurgiya, 1978.
2. Palant, A.A. and Pavlovskii, V.A., *Tekhnol. Met.*, 2003, no. 11, pp. 3–7.
3. Chernogorenko, V.B., Davidyan, K.G., and Zaichenko, V.N., *Zh. Prikl. Khim.*, 1999, vol. 72, no. 6, pp. 958–960.
4. Palant, A.A., Levin, A.M., and Bryukvin, V.A., *Tsvetn. Met.*, 1999, no. 8, pp. 42–45.
5. Madhavi Latha, T. and Venkatachalam, S., *Hydrometallurgy*, 1989, vol. 22, no. 3, pp. 353–361.
6. Jing-Chie Lin, Jain-Yuan Lin, and Shie-Peir Jou, *Hydrometallurgy*, 1996, vol. 43, nos. 1–3, pp. 47–61.
7. Kuntyi, O.I., Minakova, R.V., Kozak, S.I., et al., *Fiz.-Khim. Mekh. Mater.*, 2004, no. 1, pp. 123–125.
8. Kuntyi, O.I., Yavorskii, V.T., Ivashkiv, V.R., and Kozibroda, Ya.I., *Vopr. Khim. Khim. Tekhnol.*, 2005, no. 5, pp. 169–172.
9. Uhlig, H.H. and Revie, R.W., *Corrosion and Corrosion Control. An Introduction to Corrosion Science and Engineering*, New York: Wiley, 1985, 3rd ed.
10. Vas'ko, A.T. and Kovach, S.K., *Elektrokhimiya tugoplavkikh metallov* (Electrochemistry of High-Melting Metals), Kiev: Tekhnika, 1983.

ISSN 1070-4272, Russian Journal of Applied Chemistry, 2007, Vol. 80, No. 11, pp. 1860–1864. © Pleiades Publishing, Ltd., 2007.
Original Russian Text © A. Timinskas, A. Češuniene, M. Kurtinaitiene, 2007, published in Zhurnal Prikladnoi Khimii, 2007, Vol. 80, No. 11, pp. 1834–1838.

APPLIED ELECTROCHEMISTRY AND CORROSION PROTECTION OF METALS

Electrodeposition of Acicular Metals in Pores of Anodic Aluminum Oxide

A. Timinskas, A. Češuniene, and M. Kurtinaitiene

Institute of Chemistry, Vilnius, Lithuania

Received February 12, 2007

Abstract—Electrodeposition of the Co–Cu system in pores of anodic aluminum oxide was studied.

DOI: 10.1134/S107042720711016X

The electrodeposition of metals and semiconductors in pores of various membranes is an urgent problem of the past decade, which is stimulated by the demand for nanosized regular structures in various scientific and technical areas. The above membranes can be obtained by different methods. One of them is bombardment in a cyclotron of polymeric, mostly polycarbonate, film with high-energy heavy ions [1, 2]. These membranes have a nonequilibrium and random pore distribution. A porous layer of oxide formed on the surface of aluminum and its alloys by anodizing in aqueous solutions of di- and tribasic acids is essentially free of this drawback. The pore distribution in an anodic oxide layer is reasonably uniform, and manufacture of porous membranes of a cellular structure with a porosity from 10^9 to 10^{11} pores per 1 cm^2 is fairly facile. The pore diameter in such membranes varies from several to 300 nm, and their thickness can reach 250 μm [3–6].

Nonetheless, studies concerning the direct electrodeposition of metals in pores of anodic aluminum oxide are relatively few. We have in view only dc electrodeposition, because the processes of ac deposition are used for a long time. Among classic studies of the deposition of silver and copper in pores of anodic oxide are those by Gileadi et al. [7, 8]. They showed that contact with a support is realized owing to "invasion" of a barrier part of anodic oxide. The same conclusion was made in studying the behavior of anodic oxide in an acid electrolyte of tin salts in [9]. In addition, the optical properties of a gold deposit and the magnetic properties of ferroelectric metals deposited in pores of anodic oxide were studied in [10, 11] and [12, 13], respectively. Also, studies are available on the filling of pores of anodic aluminum oxide with nanoparticles of zinc and antimony oxides and sulfides [14, 15]. The comparatively small number of studies concerning processes that occur upon direct filling of anodic oxide with metallic nanoneedles is apparently caused by difficultes arising from a breakdown of a semiconductor barrier layer on the pore bottom under the conditions of dc electrolysis.

As shown previously [16], a two-stage chemical treatment of anodized aluminum ensures virtually complete removal of the barrier layer formed at the pore bottom of anodic oxide film. The first stage involves treatment with a 0.08 M solution of phosphoric acid, and the second, with a fluoroborate immersion solution, which is commonly used for pretreating the surface of aluminum and its alloys prior to electroplating [17]. The two-stage treatment results in the formation of a porous membrane on the aluminum surface. With the above membrane, the electrodeposition of metals in pores using dc current can be performed.

This study is concerned with the deposition of the Co–Cu system. We used differences in the deposition of copper and cobalt to reveal certain details of the electrodeposition of the above metals in a limited space inside pores and the specific features of diffusion of the discharging metals. This study is necessary to understand the conditions at which various metallic nanosystems, including multilayer magnetic systems, are formed in pores of anodic aluminum oxide and polycarbonate membranes.

EXPERIMENTAL

We used in the study aluminum (ultrapure and ADOM grades) and AMg-2 alloy [18]. Prior to anodizing, their surfaces were etched in a 1 M solution of

sodium hydroxide at a solution temperature of 40°C for 2 min, washed with distilled water, treated in a 1 : 1 solution of nitric acid at 20°C for 30 s, and washed again with distilled water. Aluminum was anodized in a 0.045 M solution of oxalic acid at a voltage of 90 V and a solution temperature of 15°C for 80 min, and then the voltage was lowered stepwise by 10 V every 5 min. The anodizing process was terminated on reaching a voltage of 0.1 V. Then the electrodes were treated with 0.08 M phosphoric acid at 20°C. The duration of the treatment is indicated below in the text. After washing with distilled water, a barrier layer of anodic oxide was formed by etching in a fluoroborate immersion solution containing (M) $Ni(BF_4)_2$ 0.87, NH_4BF_4 0.38 (pH 4±1), and $Zn(BF_4)_2$ 0.17 [17].

Cobalt needles and layered needles of cobalt and copper (Co–Cu system) were deposited from a solution containing (M) $CoSO_4$ 0.5, $CuSO_4$ 0.01, and H_3BO_3 0.65. The electrodeposition was carried out by alternation of two potentiostatic pulses. Copper was deposited during the first pulse (0 to –0.6 V, 20 s) and cobalt, during the second pulse (–0.9 to –1.1 V, 2 s). The current values during the pulses were recorded wiht a computer using appropriate programs and devices. The potentials are given relative to a silver chloride electrode (EVL-1M3-100).

The atomic force microimages of the surface of anodized aluminum were obtained on an Explorer TM atomic force microscope. We also used in the study a Model XL 30 scanning (Philips) and PEM-100 transmission electron microscopes.

The electrolyte chosen for the electrodeposition of a multilayer Co–Cu system had a high concentration of Co^{2+} ions and a low concentration of Cu^{2+} ions. Layers of pure copper and the cobalt layers with only minor amount of copper impurity can be obtained from the above electrolyte by varying the deposition potential. The deposition of multilayer systems should be performed in the potentiostatic mode to maintain the composition of the single layers constant. The voltammetric study showed that the copper deposition occurs at the potentials from 0 to –0.6 V employed at the limiting current, and the cobalt deposition, at the potentials from –0.9 V to –1.1 V on the ascending branch of the polarization curve. Hence, variation of the potential in the above intervals does not noticeably affect the current of the copper deposition, but affects considerably the current of the copper deposition. These features of the electrodeposition of copper and cobalt were taken into account in studying the different polarizations in pores of anodic oxide and

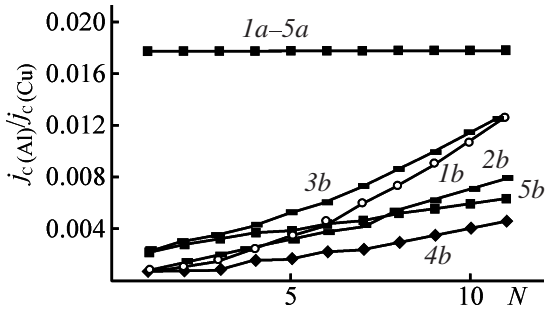

Fig. 1. Ratio of the current on the anodized surface of ultrapure aluminum to the current on a copper electrode $j_{c(Al)}/j_{c(Cu)}$ vs. the number of pulses N applied for deposition of (*a*) copper and (*b*) cobalt. Time of treatment of anodized surface in 0.08 M phosphoric acid, h: (*1*) 0, (*2*) 0.5, (*3*) 1, (*4*) 2, and (*5*) 5; subsequent treatment in an immersion solution for 10 min; the same for Fig. 3.

on metallic electrodes. Therefore, it was reasonable to calculate for copper and cobalt the ratios of the deposition currents in pores of anodic aluminum oxide and on a copper electrode $j_{Cu(Al)}/j_{Cu(Cu)}$ and $j_{Co(Al)}/j_{Co(Cu)}$.

Apparently, the efficiency of the pretreatment of anodized aluminum for electrodeposition of metals in pores of the oxide can be evaluated to a certain extent from the current ratios. For example, the relative increase or decrease in the total pore area of the oxide where the metal electrodeposition can occur can be estimated in relation to the brand of aluminum and probably to the method of pretreatment of its surface. It should be emphasized that, in the given case, the true active pore area cannot be determined because of differences in the diffusion processes occurring in pores of aluminum oxide and on a metallic electrode, which, in turn, determines the differences in the current densities.

The study showed that the $j_{Cu(Al)}/j_{Cu(Cu)}$ and $j_{Co(Al)}/j_{Co(Cu)}$ ratios depend on the purity of the applied aluminum, which determines the size of pores in anodic oxide. The lowest values of the $j_{Cu(Al)}/j_{Cu(Cu)}$ and $j_{Co(Al)}/j_{Co(Cu)}$ ratios are observed on ultrapure grade aluminum (Fig. 1), in which the total pore area is small (Fig. 2). For aluminum of lower purity the ratios increase (Figs. 3, 4). This may be accounted for by accumulation of lattice defects in the bulk of the metal and on its surface with increasing impurity concentration in aluminum. In the defective zones, the anodizing process is faster and the anodic oxide film has a more branched structure. As compared to aluminum, the intermetallic Al–Mg compounds on aluminum alloys with magnesium are anodized more readi-

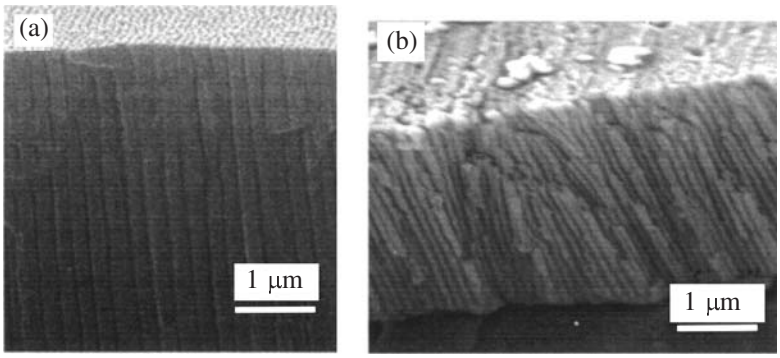

Fig. 2. Electron micrographs of the surface of anodic oxide on the surface of (a) ultrapure grade and (b) ADOM aluminum after anodizing in 0.045 M oxalic acid at a voltage of 90 V, which was then lowered stepwise by 10 V every 5 min to a value of 0.1 V, and treatment in 0.08 M phosphoric acid for 5 h.

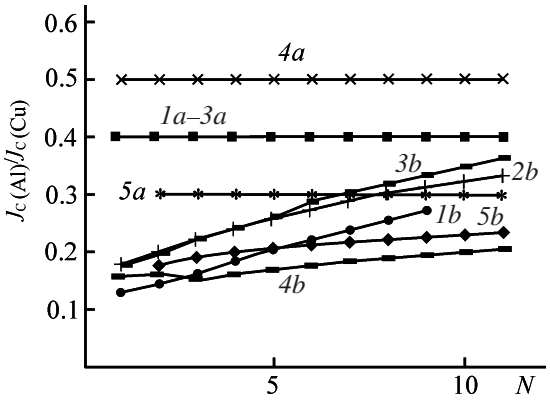

Fig. 3. Ratio of the current on anodized surface of ADOM aluminum to the current on a copper electrode $j_{c(Al)}/j_{c(Cu)}$ vs. the number of pulses N applied for deposition of (*a*) copper and (*b*) cobalt.

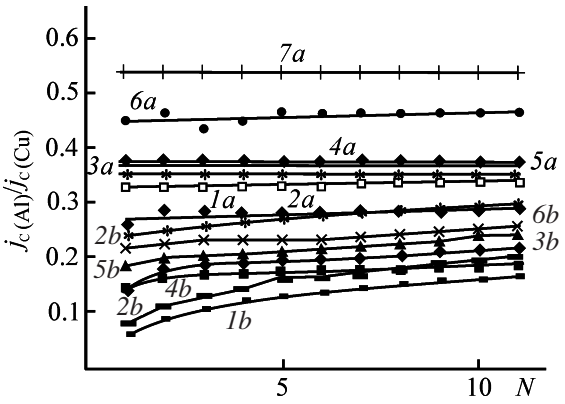

Fig. 4. Ratio of the current on anodized surface of AMg-2 alloy to that on a copper electrode $j_{c(Al)}/j_{c(Cu)}$ vs. the number of pulses N applied for deposition of (*a*) copper and (*b*) cobalt. Time of treatment of the anodized surface in 0.08 M phosphoric acid, h: (*1, 2*) 0, (*3*) 0.5, (*4*) 1, (*5*) 2, (*6*) 3, and (*7*) 5; (*1*) without stepwise lowering of the voltage after anodizing for 80 min; subsequent treatment in an immersion solution for 10 min.

ly and are dissolved in anodizing electrolytes many times faster [19, 20]. Therefore, the total pore area should be larger on the surface of anodized aluminum alloys or on the surface of aluminum with higher concentration of impurities. Moreover, the $j_{Cu(Al)}/j_{Cu(Cu)}$ and $j_{Co(Al)}/j_{Co(Cu)}$ ratios for each type of aluminum are different (Figs. 1, 3, 4). In the initial stages of the deposition of a multilayer Co–Cu system, the $j_{Co(Al)}/j_{Co(Cu)}$ ratios are considerably lower than the corresponding $j_{Cu(Al)}/j_{Cu(Cu)}$ values. With increasing the number of pulses, the current ratios approach each other (Figs 1, 3, 4). However, the $j_{Co(Al)}/j_{Co(Cu)}$ values rarely, if ever, reach the $j_{Cu(Al)}/j_{Cu(Cu)}$ values. Apparently, the $j_{Co(Al)}/j_{Co(Cu)}$ ratios are also affected by the conditions of the pretreatment of the anodized aluminum surface, because the increase in the $j_{Co(Al)}/j_{Co(Cu)}$ ratios upon cobalt deposition can also be due to the specific shape of pores of anodic aluminum oxide. Presumably, after the appropriate procedure such as, e.g., treatment in an immersion solution, pores, and their tops in particular, become to a certain extent funnel or conic in shape. This suggestion is satisfactorily illustrated by the atomic force topographic images of the surface of the anodized aluminum after the treatment in an immersion solution (Fig. 5a). The above suggestion is also consistent with the shape of acicular cobalt formations separated from the pores after treating the anodic aluminum oxide in a 1.25 M sodium hydroxide solution (Fig. 5b). This causes the surface area on which the Co–Cu system is deposited to increase also with increasing number of pulses, i.e., the electrolysis conditions become nearly identical to those on a metallic, e.g., copper electrode.

In the limiting case, as shown previously [16], the electrolytic deposition of metals gets out from a pore

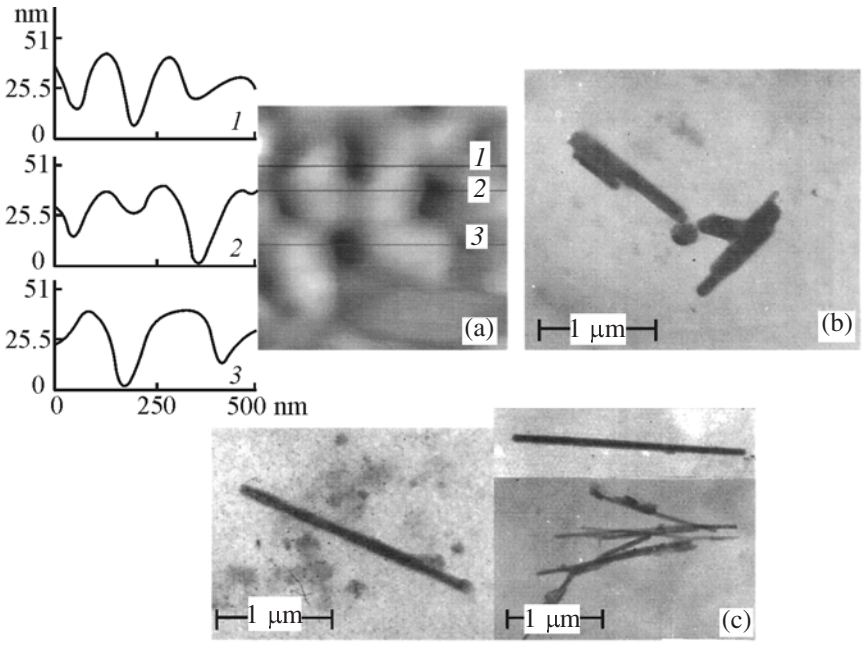

Fig. 5. (a) Atomic force image (scan area 500 × 500 nm) and roughness of the anodized surface of ADOM aluminum after treatment in immersion solution for 10 min and (b, c) acicular cobalt formations separated from pores of anodic aluminum oxide (ADOM brand). Time of treatment in 0.08 M phosphoric acid, h: (a, c) 5 and (b) 3.

space onto the aluminum surface to form a so-called "cap." At the same time, attention should be drawn to the fact that the $j_{Cu(Al)}/j_{Cu(Cu)}$ ratio is independent of the number of pulses, which is, in all probability, due to the fact that the copper deposition at the potentials employed occurs at the limiting current. However, the fact that the $j_{Co(Al)}/j_{Co(Cu)}$ ratios are lower than the $j_{Cu(Al)}/j_{Cu(Cu)}$ ratios suggests that the electrodeposition of metals in pores is hindered. The additional studies showed that the $j_{Co(Al)}/j_{Co(Cu)}$ values can be made closer to the $j_{Cu(Al)}/j_{Cu(Cu)}$ ratios by increasing the cathodic polarization in the course of cobalt electrodeposition to –50 mV. Presumably, at the very beginning of the electrodeposition the polarization increase is due to the retardation of cobalt deposition owing to passivation. This is assisted by the well-known physicochemical properties of aluminum and its oxide [20, 21]. Then, apparently, an increase in the concentration polarization caused by the specific features of metal deposition in pores is predominant. Owing to the small diameter of the pores and a comparatively large spacing between them, some of pores start acting as microelectrodes, described previously in [22, 23].

The behavior of microelectrodes can be accounted for by the features of diffusion of the ions involved in the reactions in the oxide pores and in the solution near the electrode surface. One of such features is an appreciable decrease in the concentration restrictions. Under these conditions, the overall concentration gradient and the thickness of the diffusion layer are equal to the thickness of the anodic oxide layer (approximately 5–6 μm in the given case). The thickness of the diffusion layer in electrodeposition of metals on metallic electrodes can reach 500 μm in an electrolyte without stirring and up to 10 μm in a stirred electrolyte [24]. Hence, the current density in pores should be higher than on the surface of a metallic electrode. This is due to the increased concentration polarization. The above suggestion is confirmed by a simple calculation based on size, and, consequently,

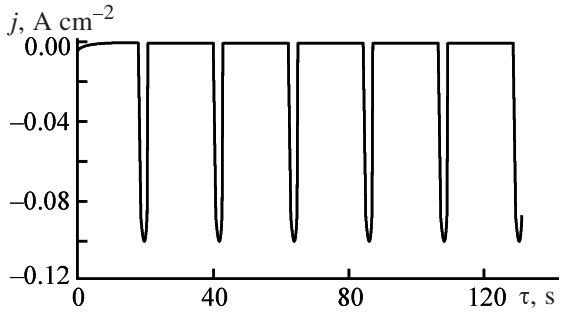

Fig. 6. Current density j of the pulsed deposition of the Co–Cu system vs. time τ, obtained on a copper electrode. Pulse duration, s: Cu 20 and Co 2. Potential amplitude, V: Cu –0.4 and Co –1.1.

mass of acicular cobalt deposits (Fig. 5c). According to the above calculation, the current density in pores is $(1.5–2.3) \times 10^{-1}$ A cm^{-2}, i.e., twice larger on the average than the current of the cobalt deposition on a copper electrode in both pulse and continuous modes at a potential of –1.1 V (1×10^{-1} A cm^2) (Fig. 6).

CONCLUSIONS

(1) The current densities of the electrodeposition of metals in pores of anodic aluminum oxide are no less than twice higher than in the case when the electrodeposition occurs on a copper electrode at the same potential. This is apparently due to the fact that the anodized aluminum behaves in the process like a combination of microelectrodes. The most acceptable method for determining current densities in pores of anodic aluminum oxide involves calculations based on size, and, consequently, mass of acicular metallic deposits.

(2) For copper and cobalt, the ratios of deposition currents in pores of anodic aluminum oxide and on a copper electrode ($j_{Cu(Al)}/j_{Cu(Cu)}$ and $j_{Co(Al)}/j_{Co(Cu)}$) show the relative increase or decrease in the total pore area of the oxide depending on aluminum purity and, in part, on the conditions of pretreatment of the anodized aluminum surface.

ACKNOWLEDGMENTS

The authors thank A. Jagminas for the assistance in SEM studies.

REFERENCES

1. Wang, L., Yu-Zhang, K., Metrot, A., et al., *Thin Solid Films*, 1996, vol. 288, pp. 86–89.
2. Valizadeh, S., George, J.M., Leisner, P., and Hultman, L., *Thin Solid Films*, 2002, vol. 402, no, 1–2, pp. 262–271.
3. Diggle, J., Downie, F., and Goulding, C., *Chem. Rev*., 1969, vol. 69, pp. 365–384.
4. Takahashi, T., and Nagayma, M., *J. Chem. Soc. Jpn*., 1968, vol. 36, pp. 34–39.
5. Li, A.P., Müller, F., Birner, A., et al., *J. Appl. Phys*., 1998, vol. 84, pp. 6023–6026.
6. Jagminas, A., Bigelienė, D., Mikulskas, J., and Tamosiūnas, R., *J. Cryst. Growth*, 2001, vol. 233, pp. 591–598.
7. Gruberger, J., and Gileadi, E., *Electrochim. Acta*, 1986, vol. 31, no. 12, pp. 1531–1540.
8. Zagiel, A., Natinhan, P., and Gileadi, E., *Electrochim. Acta*, 1990, vol. 35, no. 6, pp. 1019–1030.
9. Jagminas, A., Lichusina, S., Kurtinaitiene, M., and Matulionis, E., *Chemija*, 2003, vol. 14, no. 1, pp. 22–28.
10. Hornyak, G., Kröll, M., Pugin, R., et al., *Chem. Eur. J*., 1997, vol. 3, no. 12, pp. 1951–1956.
11. Foss, C.A., Hornyak, G.L., Stockert, J.A., and Martin, C.R., *J. Phys. Chem*., 1994, vol. 98, no. 11, pp. 2963–2971.
12. Lyberatos, A., Chantrell, R.W., Sterringa, E.R., and Lodder, J.C., *J. Appl. Phys*., 1991, vol. 70, no. 8, pp. 4431–4437.
13. Hoch, H., Raub, Chr., Rauscher, G., et al., *Galvanotechnik*, 1995, vol. 86, no. 3. pp. 734–745.
14. Gao, T., Meng, G., Tian, Y., et al., *J. Phys.: Condens. Matter*, 2002, vol. 14, pp. 12651–12656.
15. Zhang, Y., Li, G., Wu, Y., et al., *Adv. Mater*., 2002, vol. 14, no. 17, pp. 1227–1230.
16. Timinskas, A., Češuniene, A., Kurtinaitiene, M., and Skominas, V., *Zh. Prikl. Khim*., 2002, vol. 75, no. 6, pp. 929–932.
17. Timinskas, A., and Kaušpedas, Z., *Chemija*, 1993, no. 3, pp. 44–57.
18. *GOST* (State Standard) *4784–74. Alyuminii i splavy alyuminievye deformiruemye: Marki* (Aluminum and Aluminum Alloys Deformable: Brands), Moscow: Izd. Standartov, 1979.
19. Jagminas, A.I., Syrus, V.P., and Skominas, V.J., *Tr. Akad. Nauk Lit. SSR, Ser. B*, 1979, vol. 3, no. 112, pp. 55–64.
20. *Anodnye oksidnye pokrytiya na metallakh i anodnaya zashchita* (Anodic Oxide Coatings on Metals and Anodic Protection), Frantsevich, I.N., Ed., Kiev: Naukova Dumka, 1985.
21. Hatch, J., *Aluminum: Properties and Physical Metallurgy*, Cleveland: Am. Soc. of Metals, 1984.
22. Stasiukaitis, P.V., and Skominas, V., *J. Electroanal. Chem*., 1998, vol. 459, pp. 121–133.
23. Zagidulin, D., Timinskas, A., and Skominas, V., *Chemija*, 2001, vol. 12, no. 1, pp. 71–75.
24. *Spravochnoe rukovodstvo po gal'vanotekhnike* (Reference Manual on Electroplating), Lainer, V.I., Ed., Moscow: Metallurgiya, 1969.

ISSN 1070-4272, Russian Journal of Applied Chemistry, 2007, Vol. 80, No. 11, pp. 1865–1870. © Pleiades Publishing, Ltd., 2007.
Original Russian Text © T.Zh. Sadyrbaeva, 2007, published in Zhurnal Prikladnoi Khimii, 2007, Vol. 80, No. 11, pp. 1839–1844.

APPLIED ELECTROCHEMISTRY AND CORROSION PROTECTION OF METALS

Membrane Extraction and Electrodeposition of Silver(I) in Systems with Di(2-ethylhexyl) Hydrogen Phosphate

T. Zh. Sadyrbaeva

Institute of Inorganic Chemistry, Riga Technical University, Salaspils, Latvia

Received March 23, 2007

Abstract—Extraction of silver(I) from nitric acid solution by electrodialysis with liquid membranes containing di(2-ethylhexyl) hydrogen phosphate with addition of tri-*n*-octylamine in 1,2-dichloroethane is studied. The effects of the composition of aqueous solutions and liquid membranes as well as of the basic parameters of electrodialysis on the Ag(I) transport and electrodeposition rates are examined, and the process conditions are optimized.

DOI: 10.1134/S1070427207110171

Acid organophosphorus reagents are widely used for extraction of metal cations from neutral and weakly acidic solutions [1]. Particularly, di(2-ethylhexyl) hydrogen phosphate (HDEHP) was used as a cation exchanger for Ag(I) in systems with emulsion and impregnated liquid membranes [2–4]. In these cases, membrane extraction proceeds by the mechanism of countercurrent transport of Ag(I) and hydrogen ions:

$$Ag^{+}_{(w)} + HR_{(o)} \rightarrow AgR_{(o)} + H^{+}_{(w)}, \quad (1)$$

where HR = HDEHP; and (w) and (o) stand for the aqueous and organic phases, respectively.

Back extraction of Ag(I) is performed with highly acidic solutions, since the driving force of the process is the pH gradient between the feeding and receiving solutions.

On applying an electric field to the membrane extraction system, the transport of metal cations occurs in the same direction as that of hydrogen ions. In this case, the transport of ions across the liquid membrane is intensified, and back extraction of metals into dilute mineral acids becomes possible [5]. Previously, we reported on recovery of copper(II) from sulfuric acid solutions [6] by electrodialysis with HDEHP-based liquid membranes, and also on separation of Cu(II) and platinum metals in their recovery from hydrochloric acid solutions [7, 8]. It was shown that, after introduction of a tri-*n*-octylamine (TOA) additive to increase the conductivity, liquid membranes containing crude HDEHP provide efficient recovery and thorough separation of copper(II) from palladium(II) and platinum(IV).

Silver is widely used in various branches of industry, as a corrosion inhibitor, antifriction additive, as a material improving the conductivity and reflectance, and also in manufacturing surgical armaments and for decorative finishing. In silver plating, highly toxic cyanide-containing electrolytes are generally used [9]. To replace them, a number of cyanide-free electrolytes (iodide-, thiocyanate-, sulfite-, and pyrophosphate-based) are developed [10]. However, they are not widely used, and, therefore, developments in silver electroplating are of a significant practical interest.

In this study, we examined recovery of Ag(1) by galvanostatic electrodialysis with crude HDEHP-based liquid membranes modified with TOA. Also the silver electroplating conditions from the receiving solution were optimized.

EXPERIMENTAL

The transport of Ag(I) was studied using an assembled fluoroplastic cell with a liquid membrane confined between vertical cellophane films. Silver electroplating was examined using a four-compartment cell with a cathode placed in the receiving solution:

(+) Pt, HNO_3	$AgNO_3$ HNO_3	HDEHP TOA	$HClO_4$, Pt (–)
	MK 1	2	

In a series of experiments, we also used a five-compartment cell with a separate cathodic chamber:

(+) Pt, anodic solution	$AgNO_3$ HNO_3	HDEHP TOA	Receiving solution	Receiving solution, Pt (–)
	1		2	

A dc current was passed across flat platinum electrodes in the galvanostatic mode. The volume of the liquid membrane was 2 cm^3, its thickness, 0.2 cm, and the phase contact area, 7.1 cm^2. The cellophane films confining the liquid membrane were preliminarily soaked in water. The electrode compartments 17 cm^3 in volume were separated from the feeding and receiving solution chambers (both 13 cm^3 in volume) with solid MK-40 cation-exchange or MA-40 anion-exchange membranes. Generally, 0.1 M HNO_3 was used as an anodic electrolyte and 0.05 M $HClO_4$, as a cathodic electrolyte in the four-compartment cell (or 0.1 M HNO_3 in the five-compartment cell).

As liquid membranes, we used 1,2-dichloroethane solutions of crude HDEHP (about 63% main product) with addition of TOA (pure grade). Generally, we used 20 vol % HDEHP containing 0.1 M TOA. The feeding solution was prepared by dissolving $AgNO_3$ (analytically pure grade) in 0.01 M HNO_3. The initial Ag(I) concentration was generally 0.01 M. The Ag(I) concentration in the aqueous solutions was determined spectrophotometrically with rubeanic acid [11]. The optical density was measured on an SF-46 spectrophotometer.

In organic solutions, HDEHP forms an ion pair with TOA, i.e., a binary extractant [12]:

$$Oct_3N + HR \rightleftarrows Oct_3NH^+R^-, \quad (2)$$

where Oct_3N = TOA and HR = HDEHP.

Silver(I) is extracted into the organic phase via the cation-exchange mechanism:

$$Ag^+_{(w)} + NO^-_{3(w)} + Oct_3NHR_{(o)} \rightleftarrows AgR_{(o)} + Oct_3NHNO_{3(o)}, \quad (3)$$

where (w) and (o) stand for the aqueous and organic phases, respectively.

In a polar solvent, the extracted complex dissociates [13]:

$$AgR \rightleftarrows Ag^+ + R^-. \quad (4)$$

The Ag(I) ions are transferred by diffusion to the feeding solution/liquid membrane phase boundary (boundary 1) and interact with the carrier. Under the electric field, the resulting complex is transported across the organic layer, to be decomposed at the liquid membrane/receiving solution phase boundary (boundary 2) by the reaction reverse to (3). The carrier molecules diffuse back to boundary 1, which is driven by the concentration gradient. The hydrogen ions are transferred across the liquid membrane in the same direction as Ag(I). The X^- anions from the receiving solution are transferred across the liquid membrane in the opposite direction, interacting with the amine salt via the anion-exchange mechanism, and passing to the feeding solution:

$$H^+_{(w)} + NO^-_{3(w)} + R_3N_{(o)} \rightleftarrows R_3NHNO_{3(o)}, \quad (5)$$

$$X^-_{(w)} + R_3NHNO_{3(o)} \rightleftarrows R_3NHX_{(o)} + NO^-_{3(w)}, \quad (6)$$

where $X^- = ClO^-_4$, OH^-, or NO^-_3.

In the preliminary electrodialysis experiments, the transport of Ag(I) was studied using a five-compartment cell with a separated cathodic solution. It was demonstrated that applying electrical field induces Ag(I) transfer across the liquid membrane to the receiving nitric acid or ammonia solution, but the process is commonly accompanied by precipitation in the aqueous solutions or on the cellophane film at boundary 2 (Table 1). In the case of nitric acid solutions, a precipitate is formed in the receiving solution, and when dilute ammonia solutions were used, white precipitates were formed at the liquid membrane/receiving solution phase boundary. Electrodialysis is strongly affected by the nature of the solid ion-exchange membranes confining the electrode compartments. With the MA membrane in the anodic chamber and ammonia receiving solution, precipitates are formed in the initial Ag(I) solution and on the membrane surface, and the length of electrodialysis decreases because of desalting of the initial solution and abrupt increase of the potential. When the anode compartment is confined with the MK membrane, a precipitate is formed on the cellophane film at the liquid membrane/receiving solution phase boundary. With the cation-exchange (MK) membranes in both electrode compartments, the Ag(I) ions are transferred across the receiving solution and solid membrane to the cathodic solution, to be deposited on the platinum cathode. This explains the observed decrease in the Ag(I) concentration in the receiving solution with increasing current density (Table 1). In the further experiments, the transmembrane transport followed by silver electrodeposition was studied in a four-compart-

Table 1. Influence of the electrodialysis conditions on Ag(I) recovery into the liquid membrane E and into the receiving solution R (five-compartment cell; c_{HDEHP} = 20 vol %, c_{TOA} = 0.1 M, and c_{Ag} = 0.01 M)

i, mA cm^{-2}	τ, min	Anodic solution	Solid membranes	Receiving solution	E, %	R, %	Precipitation
6.3	43	H_2SO_4	MA	0.1 M HNO_3	100	5.6	+
6.3	60	H_2SO_4	MA	1.0 M HNO_3	31	1.1	+
4.2	46	H_2SO_4	MA	0.1 M NH_4OH	99.6	15.2	+
4.2	60	H_2SO_4	MA	1.0 M NH_4OH	100	34.4	–
4.2*	20	H_2SO_4	MA	1.0 M NH_4OH	99.2	6.7	+
4.2*	60	HNO_3	MK	1.0 M NH_4OH	77.4	16.5	–
4.2	60	HNO_3	MK	1.0 M NH_4OH	89.7	18	–
8.5	60	HNO_3	MK	1.0 M NH_4OH	92.5	4	–
4.2	60	HNO_3	MK, MA	1.0 M NH_4OH	80.3	20	+
8.5	60	HNO_3	MK, MA	1.0 M NH_4OH	97.6	20	+

* c_{HDEHP} = 10 vol %.

ment cell with the only cation-exchange membrane MK-40 in the anode compartment.

As a cathodic solution for silver electroplating, we used ammonia, nitric acid, and perchloric acid solutions. The composition of the receiving solution has a considerable effect on the adhesion of the resulting silver deposits to the platinum cathode (Table 2). In the case of ammonia solutions, the resulting loose Ag precipitates demonstrate poor adhesion to the electrode. In the course of electrodialysis, white precipitates are formed on the cellophane film confining the ammonia solution. In the case of nitric acid receiving solution, we also observed partial peeling of the deposited metal from the cathode. It was found that the densest finely crystalline silver deposits, demonstrating good adhesion to the electrode, are separated from perchloric acid solutions. A decrease in the $HClO_4$ concentration to 0.05 M increases the Ag(I) recovery, and further decrease results in silver precipitation from the receiving solution (Table 2). Therefore, the effects of the basic parameters of membrane extraction on the Ag(I) transport and electrodeposition rates were examined at an $HClO_4$ concentration of 0.05 M.

An increase in the current density results in proportional increase in the Ag(I) recovery and electrodeposition over the current density range 0–8 MA cm^{-2} (Fig. 1). Further increase in the current density has no effect on the Ag(I) transport rate, and at i = 12 mA cm^{-2}, silver precipitation occurs in the receiving solution. In 1 h of electrodialysis at i = 10 mA cm^{-2}, about 90% of Ag(I) is extracted from the initial solution with c_{Ag} = 0.01 M into the liquid

Table 2. Influence of the receiving solution composition on Ag(I) recovery into liquid membrane E and into receiving solution R (four-compartment cell; i = 6.4 mA cm^{-2}; τ = 60 min; c_{HDEHP} = 20 vol % and c_{TOA} = 0.1 M)

Receiving solution	i, mA cm^{-2}	E, %	R*, %	Precipitation
0.1 M NH_4OH	6.4	52.9	–	+
0.1 M HNO_3	6.4	–	5.6	+
1.0 M HNO_3	6.4	27.7	9.6	+
0.1 M $HClO_4$	6.4	–	1.15	–
0.1 M $HClO_4$	9.9	59.7	9.9	–
0.05 M $HClO_4$	9.9	73.9	10.3	–
0.03 M $HClO_4$	9.9	80.2	0.2	+

* Not taking electrodeposition into account.

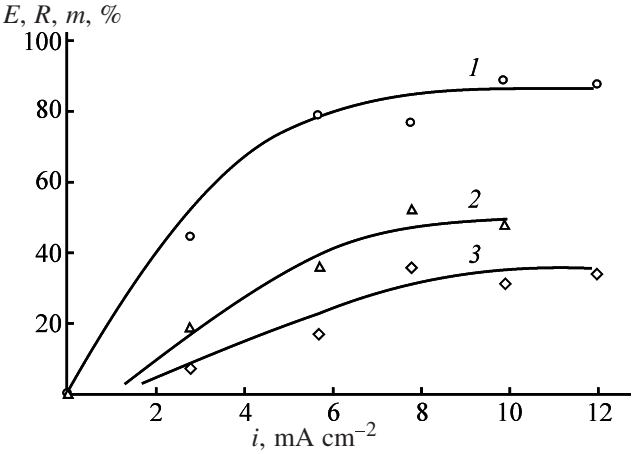

Fig. 1. Ag(I) recovery into (*1*) liquid membrane (E) and (*2*) receiving solution (R), and (*3*) electrodeposition efficiency m as functions of the current density i. τ = 60 min; c_{HDEHP} = 20 vol % and c_{TOA} = 0.1 M.

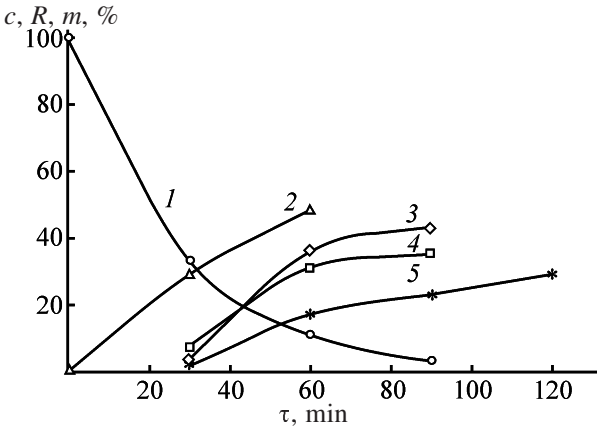

Fig. 2. (*1*) Ag(I) concentration in the initial solution *c*, (*2, 3*) recovery into the receiving solution *R*, and (*4, 5*) electrodeposition efficiency *m* as functions of the time τ. *i*, mA cm^{-2}: (*1, 2, 4*) 9.9 and (*3, 5*) 5.7.

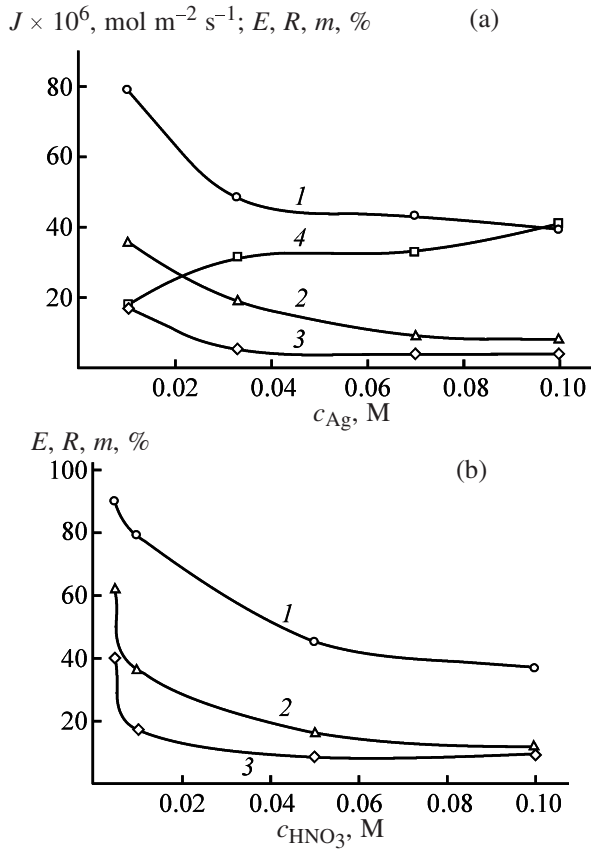

Fig. 3. Ag(I) recovery into (*1*) liquid membrane (*E*) and (*2*) receiving solution (*R*), (*3*) electrodeposition efficiency *m*, and (*4*) transport rate *J* as functions of (a) c_{Ag} and (b) c_{HNO_3} in the initial solution. i = 5.7 mA cm^{-2}; receiving solution 0.05 M $HClO_4$; and τ = 60 min.

membrane; about 50% of silver passes to the receiving solution; and about 35% of silver is deposited on the cathode. The current efficiency of Ag(I) in the transmembrane transport, estimated from the liquid membrane surface area, is below 10% under the experimental conditions. With supporting electrolyte taken in excess, the current across the liquid membrane is passed by essentially hydrogen ions from the initial solution and perchlorate ions from the receiving solution.

The kinetic dependences of Ag(I) transport and electrodeposition in the galvanostatic electrodialysis mode at various current densities are presented in Fig. 2. At a high current density (i = 10 mA cm^{-1}), Ag(I) is practically totally recovered from the initial solution in 1.5 h. The Ag(I) recovery into the receiving solution reaches about 50% in 1–1.5 h, depending on the current density. It should be pointed out that, at low current density, the recovery of Ag(I) into the receiving solution is late by about 30 min, and, correspondingly, the electrodeposition starts later than at i = 10 mA cm^{-2}. The length of electrodialysis is confined by the precipitation from the receiving solution and then from the initial solution, which starts 1.5–2 h after the beginning of the process.

With increasing Ag(I) concentration from 0.01 to 0.1 M, the Ag(I) flux across the liquid membrane and the cathodic deposit weight increase, but the recovery and electrodeposition efficiencies decrease (Fig. 3a). The current efficiency with respect to Ag(I) slightly increases with increasing starting Ag(I) concentration, remaining, however, rather low (about 7%). Within the experimental Ag concentration range, the current across the membrane is passed by essentially supporting electrolyte ions.

Increasing nitric acid concentration in the initial solution from 5×10^{-3} to 1×10^{-1} M considerably decreases the rates of transmembrane transport and electrodeposition of Ag(I) (Fig. 3b), which is caused by the decrease in the extracting power of HDEHP with increasing acidity of the aqueous phase [14]. The optimal HNO_3 concentration in the initial Ag(I) solution is 5×10^{-3} M. At this concentration and at a moderate current density, in 1 h of electrodialysis, the Ag(I) recovery from the initial solution is 90%, back extraction into the receiving $HClO_4$ solution is 60%, and about 40% of Ag(I) is deposited on the cathode.

With increasing $HClO_4$ concentration in the receiving solution from 0.05 to 1.0 M, the Ag(I) recovery and electrodeposition efficiencies decrease (Fig. 4). Such an effect of pH of the cathodic solution is typical of the electrodialysis transport, in contrast to the traditional membrane extraction with HDEHP, which requires high acidity of the stripping solution. An increase in the $HClO_4$ concentration results in increas-

Table 3. Influence of the composition of the liquid membrane on the Ag(I) recovery into the liquid membrane E and receiving solution R, electrodeposition efficiency m, and flux J (i = 5.7 mA cm^{-2}; receiving solution 0.05 M $HClO_4$; τ = 60 min)

c_{HDEHP}, vol %	c_{TOA}, M	E	R	m	J, mol m^{-2} s^{-1}
		%			
10	0.1	61.2	38.2	18.9	1.95×10^{-5}
20	0.1	78.7	35.7	16.8	1.82×10^{-5}
30	0.1	82.4	46.2	25.7	2.36×10^{-5}
40	0.1	74	34.4	15	1.76×10^{-5}
20	0.05	91.6	40.7	18.9	2.08×10^{-5}
20	0.2	64.9	36.5	18.9	1.86×10^{-5}
20	0.3	71.2	31.1	13.6	1.59×10^{-5}

ing flux of the ClO_4^- anions across the liquid membrane, which, in turn, decreases the current efficiency with respect to Ag(I).

Table 3 illustrates the influence of the HDEHP and TOA concentrations in the liquid membrane on the rates of Ag(I) transport and electrodeposition. An increase in the carrier concentration from 10 to 40 vol % at a fixed amine content increases the recovery of Ag(I) into the organic phase, only slightly influencing the transmembrane transport rate. The observed slight decrease in the Ag(I) recovery and electrodeposition efficiencies in the system with 40 vol % HDEHP can be attributed to an increase in the viscosity of the organic phase.

Solutions of crude HDEHP demonstrate low conductivity because of the presence of large amount of strongly associated monoalkylphosphoric acid [1]. To employ these solutions in electrodialysis with liquid membranes, it is necessary to use additives enhancing the conductivity. It was demonstrated that changing TOA concentration in the liquid membrane from 0.05 to 0.3 M slightly decreases the Ag(I) recovery into the organic phase and receiving solution (Table 3), which is probably due to an increase in the ClO_4^- flux with increasing concentration of the anion-exchange carrier.

An increase in the TOA concentration in the liquid membrane results in increasing conductivity and decreasing potential in the system. On the contrary, an increase in the carrier (HDEHP) concentration decreases the conductivity of liquid membranes (Fig. 5). In the course of electrodialysis, generally, the potential gradually decreases as a result of increasing total concentration of ions in the liquid membrane upon HDEHP extraction of Ag(I) and amine extraction of acids, and also because of accumulation of water in the organic phase. With increasing $HClO_4$ concentra-

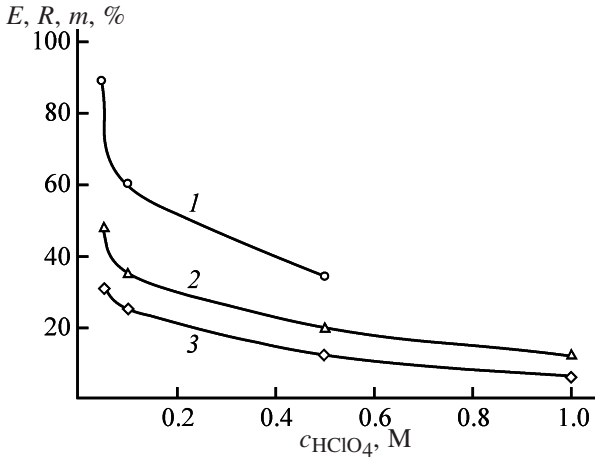

Fig. 4. Ag(I) recovery into (*1*) liquid membrane (E) and (*2*) receiving solution (R), and (3) electrodeposition efficiency m as functions of c_{HClO_4} in the receiving solution. i = 9.9 mA cm^{-2} and τ = 60 min.

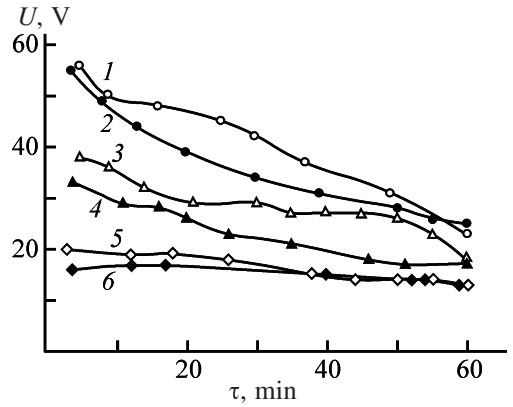

Fig. 5. Influence of the HDEHP and TOA concentrations on the dynamics of the potential U. i = 5.7 mA cm^{-2}, receiving solution 0.05 M $HClO_4$. (τ) Time. c_{HDEHP}, vol %: (*1*) 40, (*2, 4–6*) 20, and (*3*) 30. c_{TOA}, M: (*1, 3, 4*) 0.1, (*2*) 0.05, (*5*) 0.2, and (*6*) 0.3.

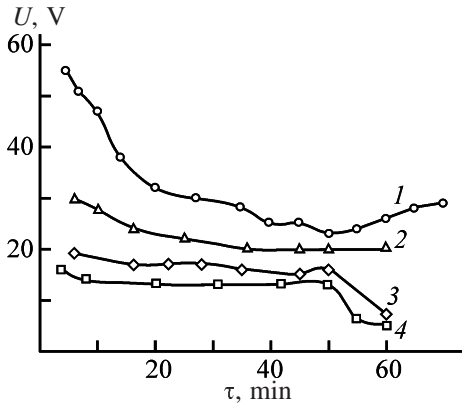

Fig. 6. Influence of the $HClO_4$ concentration in the receiving solution on the dynamics of the potential U. i = 9.9 mA cm^{-2}. (τ) Time. c_{HClO_4}, M: (*1*) 0.05, (*2*) 0.1, (*3*) 0.5, and (*4*) 1.0.

tion in the receiving solution, the conductivity of the membrane system considerably increases (Fig. 6). In some cases, after 50–55 min of electrodialysis, an abrupt drop of the potential was observed, which can be attributed to the transfer of water to the organic phase (so-called electrical breakdown) (Fig. 6, curves *3, 4*). Water is transferred into the liquid membrane as a component of the ionic hydration–solvation shells and also via electroosmotic transport [15]. The observed increase in the potential in the system with the lowest $HClO_4$ concentration (curve *1*) is probably due to desalting of the receiving solution as a result of the transfer of the perchlorate ions across the liquid membrane into the feeding solution and also of the cathodic reduction of the hydrogen ions.

CONCLUSIONS

(1) In galvanostatic electrodialysis, liquid membranes containing crude HDEHP and TOA additive in 1,2-dichloroethane provide Ag(I) transport from nitric acid solutions into dilute ammonia, perchloric acid, and nitric acid solutions.

(2) The densest Ag(I) deposits with the highest adhesion to the electrode were obtained in electrodeposition from perchloric acid solutions. The optimal $HClO_4$ concentration in the receiving solution is 0.05 M.

(3) The Ag(I) transmembrane transport and electrodeposition rates increase with increasing current density, electrodialysis duration, and starting metal concentration in the initial solution. The HDEHP concentration in the organic phase only slightly influences the transport of Ag(I).

(4) An increase in the nitric acid concentration in the initial solution and in the perchloric acid concentration in the receiving solution, and also in the TOA concentration in the liquid membrane has a negative effect on the Ag(I) recovery and electrodeposition rates.

REFERENCES

1. Yagodin, G.A., Kagan, S.Z., Tarasov, V.V., et al., *Osnovy zhidkostnoi ekstraktsii* (Principles of Solvent Extraction), Yagodin, G.A., Ed., Moscow: Khimiya, 1981.
2. Lee, S.C., Mok, Y.S., and Lee, W.K., *J. Ind. Eng. Chem.*, 1996, vol. 2, no. 2, pp. 130–136.
3. Taoualit, N. and Hadj-Boussaad, D.E., *Desalination*, 2002, vol. 144, pp. 273–277.
4. Gherrou, A., Kerdjoudj, H., Molinari, R., and Drioli, E., *Sep. Purif. Technol.*, 2002, vol. 28, no. 3, pp. 235–244.
5. Purin, B.A., *Proc. Int. Symp. on Solvent Extraction*, Moscow, 1998, pp. 234–241.
6. Sadyrbaeva, T.Zh. and Purin, B.A., *Khim. Tekhnol.*, 2000, no. 11, pp. 23–27.
7. Sadyrbaeva, T.Zh., *Zh. Prikl. Khim.*, 2005, vol. 78, no. 4, pp. 581–585.
8. Sadyrbaeva, T.Zh., *J. Membr. Sci.*, 2006, vol. 275, nos. 1–2, pp. 195–201.
9. Belen'kii, M.A. and Ivanov, A.F., *Elektroosazhdenie metallicheskikh pokrytii* (Metal Electrodeposition), Moscow: Metallurgiya, 1985.
10. Bor, P., Vrobel, L., Tsera, V., and Purin, B., *Elektroliticheskoe osazhdenie serebryanykh pokrytii s zadannymi funktsional'nymi svoistvami* (Electrodeposition of Silver Coatings with Preset Performance), Riga: LatNIINTI, 1988.
11. Levitman, X.Ya. and Gorskaya, E.V., *Sb. Nauchn. Tr. Belorus. Politekh. Inst.*, 1959, issue 87, pp. 55–65.
12. Khol'kin, A.I., Belova, V.V., Pashkov, G.L., et al., in *Sovremennye problemy khimii i tekhnologii ekstraktsii* (Present-Day Problems of Extraction Chemistry and Technology), Moscow, 1999, vol. 1, pp. 112–135.
13. Gindin, L.M., *Ekstraktsionnye protsessy i ikh primenenie* (Extraction Processes and Their Application), Moscow: Nauka, 1984.
14. Martynov, B.V., *Ekstraktsiya organicheskimi kislotami i ikh solyami* (Extraction with Organic Acids and Their Salts), Moscow: Atomizdat, 1978.
15. Golubev, V.N. and Purin, B.A., *Dokl. Akad. Nauk SSSR*, 1977, vol. 232, no. 6, pp. 1340–1342.

ISSN 1070-4272, Russian Journal of Applied Chemistry, 2007, Vol. 80, No. 11, pp. 1871–1877. © Pleiades Publishing, Ltd., 2007.
Original Russian Text © A.V. Artemov, E.A. Veretennikov, I.V. Tselinskii, 2007, published in Zhurnal Prikladnoi Khimii, 2007, Vol. 80, No. 11, pp. 1845–1852.

ORGANIC SYNTHESIS AND INDUSTRIAL ORGANIC CHEMISTRY

Heterophase Nitration of *o*-Nitrotoluene with Sulfuric–Nitric Acid Mixtures of Low Nitrating Activity in Gas-Containing Emulsions

A. V. Artemov, E. A. Veretennikov, and I. V. Tselinskii

St. Petersburg State Institute of Technology (Technical University), St. Petersburg, Russia

Received July 12, 2007

Abstract—Heterophase nitration of *o*-nitrotoluene, in which an increase in the contribution of the reaction in the boundary adsorption monolayer under conditions of surface aeration leads to a higher yield of 2,4-dinitrotoluene and larger 2,4-/2,6-dinitrotoluene isomer ratio, was studied.

DOI: 10.1134/S1070427207110183

It is known that, in a two-phase reaction system formed in nitration of aromatic hydrocarbons with mixtures of sulfuric and nitric acids, nitration commonly occurs in a rather narrow region of the acid phase, adjacent to the phase boundary. At least two zones in which the nitration reaction occurs can be distinguished in this region: (i) bulk of the acid phase and (ii) boundary adsorption monolayer adjacent to the phase boundary on the acid phase side, in which the reaction proceeds between adsorbed molecules of the nitrating agent (nitronium cation) and an aromatic compound [1]. The kinetics and mechanisms of these reactions are different [1, 2].

The overall reaction rate v_n can be written as a sum of the nitration rate in the bulk (bulk nitration), v_{bl} (mol s^{-1}), and the rate of boundary nitration, related to the volume taking into account the adsorption monolayer thickness, v_{bn} (mol s^{-1}):

$$v_n = v_{bl} + v_{bn}. \quad (1)$$

Despite the attempts made [1], rigorous evaluation of the contribution of the boundary reaction to the overall rate and regioselectivity of the process has been impossible so far. As evidence that the reaction occurs just in the boundary region can serve the change in the isomeric composition of products formed in nitration of toluene and its *o*-nitro derivative (*o*-NT), compared with nitration in the bulk of the acid phase, because the reaction occurs with spatially oriented molecules of the aromatic hydrocarbon (Fig. 1) [1–3].

The nitration of *o*-NT in the boundary layer can occur when the rate of the chemical reaction in the boundary layer is comparable with, or higher than, the rate of *o*-NT diffusion across the phase boundary into the boundary layer of the acid phase. If this condition is satisfied, the reaction zone can contract to the thickness of the boundary layer.

EXPERIMENTAL

o-NT was nitrated with sulfuric–nitric acid mixtures of low nitrating activity (nitrating activity factor Φ = 70%) at 1-, 2.5-, 5-, and 10-fold molar excess of nitric acid in a 30 cm^3 glass reactor equipped with a thermostating jacket, four-blade turbine stirrer, vertical deflecting partitions, and thermocouple for measuring the reaction mass temperature.

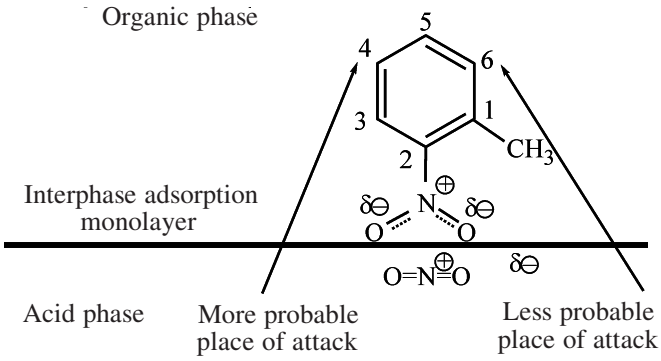

Fig. 1. Orientation of *o*-NT molecules at the phase boundary [1].

Table 1. Compositions of the acid mixtures

Mixture no.	Content, wt %		
	HNO_3	H_2SO_4	H_2O
1	35.0	52.5	12.5
2	27.0	56.5	16.5
3	20.0	60.0	20.0
4	10.0	65.0	25.0
5	5.0	67.5	27.5

Table 2. Gas content Γ of sulfuric–nitric acid mixtures at different temperatures*

Stirrer rotation rate, rpm	Gas content of acid mixture, vol %, at indicated temperature, °C		
	25 ± 1	50 ± 1	75 ± 1
5000	65.2	70.8	76.1
3000	39.5	46.5	48.8
2000	29.7	34.4	36.1
1500	12.9	14.9	15.6
1000	4.9	5.6	5.9
700	–	<1	<1

* Averaged gas contents are given for the acid mixtures used (as shown by the study, Γ varies only slightly within the composition range of the acid mixtures).

The deflecting partitions were mounted at a 90° angle with respect to each other in order to prevent formation of a whirlpool and projected by 5 mm over the reaction mixture to raise the air content of the foamed acid mixture. The agitation intensity was varied in the range 700–5000 rpm.

Nitric and sulfuric acids of pure grade were used in the experiments. The concentrations of the acid mixtures were determined by titration to within 0.02%. The acid mixtures were prepared by successive mixing of concentrated acids at 0°C with double-distilled water to reach a prescribed concentration. *o*-NT of chromatographic purity was used. The compositions of the acid mixtures used are listed in Table 1.

As the molar concentration of HNO_3 decreases in the series of acids in Table 1 (and, simultaneously, the molar concentration of water increases), the equilibrium concentration of the nitronium ion falls (1.0, and 0.3, and 0.1 mol % for mixture nos. 1, 2, 3, respectively [4]).

The isomeric composition of products and the yield of dinitrotoluenes (DNT) were determined on a Laboratorni Pristroje liquid chromatograph with an LCD 2563 UV double-beam detector at a wavelength of 254 nm. A 250 × 46-mm DuPont chromatographic column with a ZorbaxR Sil direct stationary phase with particle size of 5 μm was used. Eluent, 400 : 8 : 2 mixture of *n*-hexane, dichloromethane, and 2-propanol; elution rate, 0.4 ml min^{-1}; relative error in the yield of nitrotoluene and DNT isomers, ±0.2%.

In nitration of *o*-nitrotoluene, a calculated amount of this compound was introduced with a syringe into a reactor charged with an acid mixture, under agitation at a prescribed reaction temperature. After the lapse of the prescribed time, the agitation was switched off and the reaction mixture was poured into a fivefold amount of cold water (10–15°C). The nitro products were twice extracted with chloroform, with 6 ml of the solvent taken per gram of toluene subjected to nitration. Combined extracts were washed with an equal amount of water, the solvent was removed, and the nitro products were analyzed for the content of mono- and dinitro derivatives.

The gas content of the acid mixture was found from the increase in the volume of an agitated acid mixture with respect to that without agitation. The acid mixture was poured into the reactor to the lower overflow level of the apparatus. The temperature was raised to a prescribed level by supply of a heat-carrying agent into the apparatus jacket, and the reaction mixture was kept without agitation for 10 min. The volume of the acid mixture remaining in the apparatus (V_1) accounted for the thermal-expansion loss of the acid mixture. Similarly was measured the volume of the acid mixture remaining in the reactor after agitation for 5 min (V_2).

The gas content of the acid mixture at fixed parameters, Γ (vol %), was calculated by the formula

$$\Gamma = \frac{V_1 - V_2}{V_1} \times 100. \quad (2)$$

The values obtained for the gas content of the acid mixture at different temperatures are listed in Table 2.

The aim of this study was to examine the effect of *o*-NT nitration parameters on the isomeric composition of DNT.

The boundary mechanism in *o*-NT nitration includes the following stages [1]: (1) *o*-NT diffusion from the bulk of the dispersed organic phase toward the phase boundary, (2) diffusion of nitronium ions from the bulk of the acid phase to the phase boundary, (3) adsorption of nitronium ions and *o*-NT at the

phase boundary, (4) reaction between adsorbed nitronium ions and *o*-NT at the phase boundary, and (5) desorption of the product (dinitrotoluene) and its removal from the phase boundary.

Toluene is nitrated by sulfuric–nitric acid mixtures to mononitrotoluene in the diffusion mode at all the agitation modes studied. By contrast, the contribution of the kinetic component (chemical reaction proper) in nitrotoluene nitration to the overall process rate increases because of the decrease in the substrate reactivity [2, 5], whereas in *o*-NT nitration with sulfuric–nitric acid mixtures of low nitrating activity, this contribution may be even more significant.

Stages 1 and 2 cannot be rate-determining, because the acid mixtures used in mononitrotoluene nitration in this study have low nitrating activity. The adsorption/desorption stages (stages 3 and 5) involve small-size molecules [2] and are expected to be very fast. Consequently, it can be assumed that stage 4, i.e., the chemical reaction, can be rate-determining stage.

If the model [1] of heterogeneous nitrobenzene nitration is used, the overall nitration rate v_n (mol s^{-1}) can be expressed by the equation

$$v_n = -dm_n/dt = v_{bl} + v_{bn}, \quad (3)$$

where m_n is the nitric acid content of the system (mol %);

$$v_n = k'_{bl}[ArNO_2]_a^{sol}[NO_2^+]_a V_a + k'_{bn} S[ArNO_2]_{bn}^{sol}[NO_2^+]_{bn}, \quad (4)$$

where k'_{bl} and k'_{bn} are second-order rate constants for the bulk (m^3 mol^{-1} s^{-1}) and boundary (m s^{-1}) types of nitration, respectively; V_a, volume of the acid phase (m^3); $[ArNO_2]_a^{sol}$, concentration of *o*-NT dissolved in the acid mixture (mol m^{-3}); $[NO_2^+]_a$, concentration of nitronium cations in the mineral phase (mol m^{-3}); S, surface area of the phase boundary (m^2); $[ArNO_2]_{bn}^{sol}$ and $[NO_2^+]_{bn}$, boundary concentrations of *o*-NT and nitronium cations, respectively (mol m^{-2}).

It is important that hydrated protons in the acid phase compete with nitronium cations for the adsorption sites at the phase boundary. Consequently, the concentration of NO_2^+ ions at the phase boundary will depend on the ratio between the concentrations of NO_2^+ and protons in the bulk of the acid phase. This ratio increases with the sulfuric acid concentration. This fact was confirmed in [1], where the effective rate constant k_{bn} of the boundary reaction increased with the H_2SO_4 concentration.

It is known that, at a stirrer rotation rate exceeding a certain value, agitation is accompanied by spontaneous capture of air from the surface of a liquid being agitated (surface aeration) and gas bubbles are dispersed in the bulk of the reaction mass to give a gas-containing emulsion [6]. Under these conditions, the air content of the reaction mass increased from 0 to 65% (Table 2) as the agitation intensity was raised within the limits specified above.

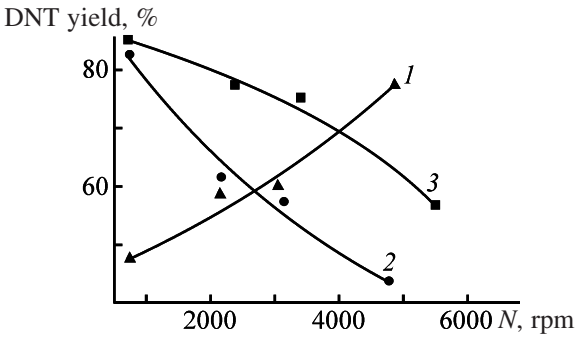

Fig. 2. DNT yield vs. the agitation intensity N in *o*-NT nitration with sulfuric–nitric acid mixtures (Φ = 70). (*1*) 7.2% HNO_3, 30.0% H_2SO_4, 62.8% H_2O, *o*-NT : HNO_3 = 1 : 10; (*2*) 15.5% HNO_3, 30.0% H_2SO_4, 54.5% H_2O, *o*-NT : HNO_3 = 1 : 10; (*3*) 22.3% HNO_3, 30.0% H_2SO_4, 47.7% H_2O, *o*-NT : HNO_3 = 1 : 5. T, °C: (*1*) 50 and (*2, 3*) 25. τ, min: (*1, 2*) 60 and (*3*) 30.

A study of the *o*-NT nitration yielded results that have not been obtained previously in analysis of the nitration macrokinetics of aromatic nitro compounds. First, raising the stirrer rotation rate, and accordingly the gas content of the reaction mass, in acid mixtures containing 22.3 and 15.5 mol % HNO_3 leads to a decrease, rather than an increase, in the nitration rate of *o*-NT (Fig. 2, Table 3, run nos. 1–8). For example, the yield of DNT in 30 min in *o*-NT nitration with a mixture containing 22.3 mol % HNO_3 is 85% at 700 rpm and 57.7% at 5000 rpm. Second, raising the agitation intensity changes the isomeric composition of the forming DNT: the content of 2,4-DNT grows, with the 2,4-/2,6-DNT ratio increasing to 2.50–2.68, compared with that obtained (1.85 [7]) under the standard nitration conditions (sulfuric–nitric acid mixture; Φ = 80.2; excess of nitric acid over the theoretical value 20%; zero or low gas content).

The experimental data obtained contradict the assumption that increase in the phase boundary area should lead to a higher formation rate of dinitrotoluene (because of the increase in the overall rate of the chemical reaction and mass-exchange processes). Consequently, the observed decrease in the overall nitration rate is due only to the gas content of the reaction mass, because it is known that an increase in the gas content of the reaction mass leads to a decrease in its density and viscosity and, accordingly, to

Table 3. Effect of the agitation rate on the nitration of *o*-NT

Run no.	*N*, rpm	Gas content, vol %	DNT yield, %	Isomeric composition, %		2,4-/2,6-DNT ratio	*T*, °C	τ, min
				2,4-DNT	2,6-DNT			
	22.3 mol % HNO_3, 30.0 mol % H_2SO_4, 47.7 mol % H_2O; *o*-NT/HNO_3 = 1 : 5 mol/mol							
1	5000	65.2	57.7	71.43	28.57	2.50	25	30
2	3000	39.5	75.5	69.88	30.12	2.32	25	30
3	2000	29.7	77.7	68.15	31.85	2.14	25	30
4	700	–	85.0	67.21	32.79	2.05	25	30
	15.5 mol % HNO_3, 30.0 mol % H_2SO_4, 54.5 mol % H_2O; *o*-NT/HNO_3 = 1 : 10 mol/mol							
5	5000	65.2	48.8	72.83	27.17	2.68	25	60
6	3000	39.5	61.4	71.26	28.74	2.48	25	60
7	2000	29.7	57.6	69.14	30.86	2.24	25	60
8	700	–	82.5	67.85	32.15	.2.11	25	60
	7.2 mol % HNO_3, 30.0 mol % H_2SO_4, 62.8 mol % H_2O; *o*-NT/HNO_3 = 1 : 10 mol/mol							
9	5000	70.8	77.7	68.35	31.65	2.16	50	60
10	3000	46.5	60.0	68.35	31.65	2.16	50	60
11	2000	34.4	59.1	68.15	31.85	2.14	50	60
12	700	–	48.6	67.74	32.26	2.10	50	60
	3.5 mol % HNO_3, 30.0 mol % H_2SO_4, 66.5 mol % H_2O; *o*-NT/HNO_3 = 1 : 10 mol/mol							
13	5000	76.1	71.0	65.75	34.25	1.92	95	30
14	5000	76.1	83.7	65.28	34.72	1.88	95	60
15	3000	49	69.4	65.52	34.48	1.90	95	60
16	2000	36	65.8	65.64	34.36	1.91	95	60
17	700	–	52.8	65.40	34.60	1.89	95	60

lower rates of mass transfer between the immiscible phases [6]. Thus, the nitration rate in the bulk of the acid phase, governed by mass-transfer processes, will decrease, which will make larger the contribution of the boundary reaction to the overall process rate.

The mass-transfer processes between phases are presumably also decelerated because, at high agitation intensity, the interaction between drops of the dispersed organic phase is largely suppressed and drops behave as solid spheres within which the mass transfer is hindered [8].

At a slow stirrer rotation rate (700–1500 rpm) and insignificant gas content (0–15 vol %), the contribution of the reaction in the boundary zone to the overall rate is presumably low as compared with the reaction in the bulk of the acid phase. Under these conditions, the highest dinitrotoluene yields are observed (Fig. 2, Table 3; run nos. 4, 8). However, the contribution of the boundary reaction increases as the gas content grows and rate of mass-exchange processes decreases, with the nitration rate in the bulk of the acid phase accordingly becoming lower.

As an additional evidence in favor of the possibility of the reaction in the boundary layer can serve the isomeric composition of the forming dinitrotoluene, which is distinguished by high content of 2,4-DNT (Table 3, run nos. 1–8).

By contrast, raising the stirrer rotation rate in *o*-NT nitration with weaker acid mixtures from 700 to 5000 rpm leads to an increase in the nitration rate, rather than to its decrease, and makes larger the DNT yield despite the higher gas content of the reaction mass (Fig. 2, Table 3, run nos. 9–17). For example, the yield of DNT in nitration with a mixture containing 7.2 mol % HNO_3 for 60 min is 48.6% at 700 rpm and 77.7% at 5000 rpm. In the given case, in which the rate of the chemical reaction is substantially lower than the diffusion rate, the reaction zone shifts, as the agitation intensity increases, from the surface layer into the bulk of the acid phase, and just there the reaction between the dissolved *o*-NT and the nitrating agent occurs. However, the decrease in the rate of mass-exchange processes in gas-containing systems results in that the overall reaction rate is mostly affected under the conditions specified by diffusion of

Table 4. Effect of the agitation rate on the nitration of *o*-NT. Reaction duration 30 min, *o*-NT/NHO_3 molar ratio 1 : 2.5, T = 50°C

Run no.	N, rpm	Gas content, vol %	DNT yield, %	DNT yield, %		2,4-/2,6-DNT ratio
				2,4-DNT	2,6-DNT	
		31.1 mol % HNO_3, 30.0 mol % H_2SO_4, 38.9 mol % H_2O				
1	700	–	87.8	64.29	35.71	1.80
2	2000	34.4	94.7	65.16	34.84	1.87
3	3000	46.5	95.6	66.10	33.90	1.95
4	5000	70.8	95.5	67.00	33.00	2.03
		22.3 mol % HNO_3, 30.0 mol % H_2SO_4, 47.7 mol % H_2O				
5	700	–	88.8	65.99	34.01	1.94
6	2000	34.4	94.2	66.78	33.22	2.01
7	3000	46.5	90.7	67.74	32.26	2.10
8	5000	70.8	79.5	68.65	31.35	2.19
		15.5 mol % HNO_3, 30.0 mol % H_2SO_4, 54.5 mol % H_2O				
9	700	–	76.0	65.40	34.60	1.89
10	2000	34.4	83.0	66.10	33.90	1.95
11	3000	46.5	73.3	67.11	32.89	2.04
12	5000	70.8	70.7	67.85	32.15	2.11
		7.2 mol % HNO_3, 30.0 mol % H_2SO_4, 62.8 mol % H_2O				
13*	700	–	93.4	64.54	35.46	1.82
14*	2000	34.4	92.9	65.16	34.84	1.87
15*	3000	46.5	89.3	65.52	34.48	1.90
16*	5000	70.8	90.5	66.22	33.78	1.96

* *o*-NT/HNO_3 molar ratio 1 : 10.

the reacting components into the reaction zone.

As evidence in favor of the occurrence of the reaction under kinetic control in the bulk of the acid phase in *o*-NT nitration with acid mixtures containing 7.2 and 3.5 mol % nitric acid can serve the isomeric composition of the forming dinitrotoluene: the content of 2,4-DNT decreases as the agitation intensity is raised from 700 to 5000 rpm and the 2,4-/2,6-DNT ratio is smaller (1.89–2.16) than that in nitration with mixtures containing 22.3 and 15.5 mol % HNO_3.

Further studies were concerned with the effect of temperature, agitation intensity, and composition of the sulfuric–nitric acid nitrating mixture (with the excess of nitric acid reduced to 1- and 2.5-fold) on the relative contributions of the kinetic and diffusion components of the *o*-NT nitration process on the overall process rate at different gas contents of the reaction mixture. The decrease in the *o*-NT/HNO_3 molar ratio made it possible to diminish the expenditure of the acids to bring the process closer to preparative conditions.

The dependence of the 2,4-/2,6-DNT ratio on the nitric acid content of the acid mixture passes through a maximum at 22.3 mol % HNO_3 at any of the agitation intensities studied (Table 4, Fig. 3).

As evidence in favor of the occurrence of the reaction under kinetic control in the bulk of the acid phase in *o*-NT nitration with acid mixtures containing 7.2

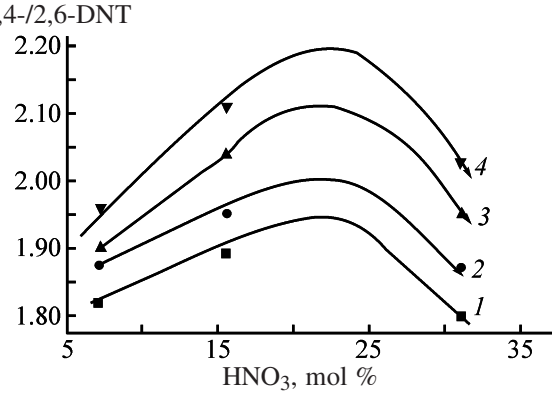

Fig. 3. 2,4-/2,6-DNT isomer ratio vs. the HNO_3 content of the acid mixture at different agitation intensities. 30.0 mol % H_2SO_4, T = 50°C, reaction duration 30 min, *o*-NT/HNO_3 molar ratio 1 : 2.5. Agitation intensity, rpm: (*1*) 700, (*2*) 2000, (*3*) 3000, and (*4*) 5000.

Table 5. Effect of temperature on the nitration of *o*-NT at the highest gas content of the reaction mass. Reaction time 30 min, stirrer rotation rate 5000 rpm

Run no.	*o*-NT/HNO_3 molar ratio	Temperature, °C	DNT yield, %	Isomeric composition, %		2,4-/2,6-DNT ratio
				2,4-DNT	2,6-DNT	
		31.1 mol % HNO_3, 30.0 mol % H_2SO_4, 38.9 mol % H_2O				
1	1 : 1	25	45.5	68.55	31.45	2.18
2*		25	46.2	67.95	32.05	2.12
3		50	54.4	67.85	32.15	2.11
4*		50	61.2	67.11	32.89	2.04
5		75	65.0	65.99	34.01	1.94
6*		75	67.5	64.91	35.09	1.85
7	1 : 2.5	25	94.2	68.65	31.35	2.19
8		50	95.5	65.87	34.13	2.03
9		75	96.2	65.52	34.48	1.90
		22.3 mol % HNO_3, 30.0 mol % H_2SO_4, 47.7 mol % H_2O				
10	1 : 2.5	25	78.3	67.85	32.15	2.31
11		50	79.5	66.67	33.33	2.19
12		75	96.6	65.52	34.48	1.90
		15.5 mol % HNO_3, 30.0 mol % H_2SO_4, 54.5 mol % H_2O				
13	1 : 2.5	25	43.6	68.85	31.15	2.21
14		50	70.7	66.22	33.78	2.11
15		75	94.5	64.29	35.71	1.80

* Reaction time 60 min.

and 3.5 mol % nitric acid can serve the isomeric composition of the forming dinitrotoluene: the content of 2,4-DNT decreases as the agitation intensity is raised from 700 to 5000 rpm and the 2,4-/2,6-DNT ratio is smaller (1.89–2.16) than that in nitration with mixtures containing 22.3 and 15.5 mol % HNO_3.

Further studies were concerned with the effect of temperature, agitation intensity, and composition of the sulfuric–nitric acid nitrating mixture (with the excess of nitric acid reduced to 1- and 2.5-fold) on the relative contributions of the kinetic and diffusion components of the *o*-NT nitration process to the overall process rate at different gas contents of the reaction mixture. The decrease in the *o*-NT/HNO_3 molar ratio made it possible to diminish the expenditure of the acids to bring the process closer to preparative conditions.

The dependence of the 2,4-/2,6-DNT ratio on the nitric acid content of the acid mixture passes through a maximum at 22.3 mol % HNO_3 at any of the agitation intensities studied (Table 4, Fig. 3).

It is known that raising the concentration of nitric acid in the acid mixture at the expense of the H_2O content in heterogeneous nitration leads both to an increase in the solubility of aromatic compounds in the bulk of the acid phase [9] and to a rise in the activity of the nitronium cation [4]. Presumably, as the content of nitric acid is raised from 7.2 to 22.3%, the contribution from the rise in the activity of the nitronium cation prevails over that of the increase in the solubility of *o*-NT in the acid mixture, which leads to contraction of the reaction zone, larger contribution of the reaction in the boundary layer, and increase in the 2,4-/2,6-DNT ratio from 1.96 to 2.19.

Possibly, further increase in the HNO_3 content of the acid mixture causes the rise in the substrate solubility and in the equilibrium concentration of *o*-NT in the bulk of the mineral phase, which can lead to a larger contribution of the reaction in the bulk of the acid phase, which is a function of the reactant concentrations, to the overall process rate [1].

The experimental data obtained confirm the assumption that underlies this study: specifically, that raising the molar concentration of HNO_3 in the nitrating mixture at a constant molar content of H_2SO_4 leads to an increase in the nitration rate and decrease in the 2,4-/2,6-DNT ratio. This indicates that the contribution of the kinetic component to the overall process rate becomes more pronounced. This fact was additionally confirmed in a study of how the reaction

rate and isomeric composition of DNT depend on the agitation intensity (Table 4; run nos. 1–4, 5–8, etc.). The increase in the 2,4-/2,6-DNT ratio from 1.80 to 2.03 on raising the stirrer rotation rate from 700 to 5000 rpm (Table 3) confirms the increasing contribution of the nitration in the boundary region and is well consistent with the previously obtained data [1].

The noticeable increase in the contribution of *o*-NT in the boundary layer in the entire range of compositions of acid mixtures studied at an agitation intensity of 5000 rpm can be further confirmed by the effect of temperature on the yield and relative contents of isomers in the forming DNT. It would be expected that, as the reaction temperature is raised, the solubility of *o*-NT in the mineral phase should increase and the interaction between drops should be enhanced, with their size increasing and the rate of mass-exchange within drops becoming slower [8]. Consequently, the contribution of the boundary reaction in the adsorption layer to the overall kinetic component of the process will decrease.

In the range of acid mixtures studied, the content of 2,4-DNT falls as the nitration temperature is raised. For example, the 2,4-/2,6-DNT isomer ratio in nitration with an acid mixture containing 15.5 mol % HNO_3 falls from 2.21 to 1.80 as temperature is elevated from 25 to 75°C (Table 5, run nos. 13–15). This dependence is observed at 5000 rpm, i.e., under high gas content conditions (Table 5).

At the same time, a slight increase in the total yield in 60 min of the reaction was observed at nitric acid contents in the range 22.3–31.1 mol % as temperature was elevated (e.g., from 61.2 to 67.5% on raising the temperature by 25°C) (Table 5, run nos. 4 and 6). An insignificant increase in the reaction rate is observed when the rate-determining stage of nitration is diffusion of components into the reaction zone at a high rate of the chemical reaction itself. This behavior can be understood if the temperature coefficients of the rates of the chemical reaction and diffusion are compared. For example, raising the temperature by 10°C leads to a 3–4-fold increase in the rate constant of the chemical reaction of nitration, whereas the diffusion rate of aromatic compounds increases by only a factor of 1.1–1.5 [7]. In nitration with a weaker acid mixture containing 15.5 mol % HNO_3, the increase in the product yield with temperature is more pronounced (Table 5, run nos. 13–15), which indicates that the contribution of the chemical reaction stage to the overall process rate increases.

CONCLUSIONS

(1) The heterophase nitration of *o*-nitrotoluene can be performed with weak sulfuric–nitric acid mixtures of various compositions and a nitrating activity factor Φ equal to 70.

(2) Raising the gas content of the reaction mixture by high-intensity agitation (>2000 rpm) results in that the contribution of the reaction in boundary adsorption monolayer to the overall process rate increases, the yield of 2,4-dinitrotoluene grows, and the 2,4-/2,6-DNT isomer ratio becomes larger.

(3) The rise in the contribution of nitration in the bulk of the acid phase as a result of a decrease in the reaction temperature and an increase in the molar concentration of nitric acid in the acid mixture is accompanied by an increase in the yield of 2,6-dinitrotoluene.

(4) The deceleration of the mass exchange between phases, observed as the gas content of the reaction mass increases, occurs because, at high agitation intensity, the interaction between drops of the dispersed organic phase is largely suppressed and the drops behave as solid spheres within which mass exchange is hindered.

REFERENCES

1. Modak, S.Y. and Juvekar, V.A., *Ind. Eng. Chem. Res.*, 1995, vol. 34, pp. 4297–4309.
2. Milligan, B., *Ind. Eng. Chem. Fundam.*, 1986, vol. 25, pp. 783–789.
3. Kasarekar, R.B., Ramakrishna, M., and Juvekar, V.A., *Chem. Eng. Technol.*, 1997, vol. 20, pp. 282–284.
4. Edwards, H.G.M. and Fawcett, V., *J. Mol. Struct.*, 1994, vol. 326, pp. 131–143.
5. Kobe, K.A. and Fortman, J.T., *Ind. Eng. Chem.*, 1961, vol. 53, pp. 269–274.
6. Braginskii, L.N., Begachev, V.I., and Barabash, V.M., *Peremeshivanie v zhidkikh sredakh* (Agitation in Liquid Media), Leningrad: Khimiya, 1984, pp. 212–213.
7. Orlova, E.Yu., *Khimiya i tekhnologiya vzryvchatykh veshchestv* (Chemistry and Technology of Explosives), Leningrad: Khimiya, 1973.
8. Giles, J., Hanson, C., and Ismail, A.M., *Industrial and Laboratory Nitrations, ACS Symp. Ser. 22*, Washington, DC: Am. Chem. Soc., 1976, pp. 190–209.
9. Schieferle, D.F., Hanson, C., and Albright, L.F., *Industrial and Laboratory Nitrations, ACS Symp. Ser. 22*, Washington, DC: Am. Chem. Soc., 1976, pp. 176–182.

ISSN 1070-4272, Russian Journal of Applied Chemistry, 2007, Vol. 80, No. 11, pp. 1878–1882. © Pleiades Publishing, Ltd., 2007.
Original Russian Text © V.N. Chupis, O.Yu. Rastegaev, V.I. Mar'in, I.M. Skvortsov, 2007, published in Zhurnal Prikladnoi Khimii, 2007, Vol. 80, No. 11, pp. 1853–1857.

ORGANIC SYNTHESIS AND INDUSTRIAL ORGANIC CHEMISTRY

Composition of Reaction Mixtures Formed by Ethanolamine Detoxication of Yperite

V. N. Chupis, O. Yu. Rastegaev, V. I. Mar'in, and I. M. Skvortsov

State Research Institute of Industrial Ecology, Federal State Institution, Saratov, Russia

Received December 19, 2006; in final form, April 2007

Abstract—The reaction mixture from detoxication of technical-grade yperite with monoethanolamine was fractionated, and its composition was determined. The structures of the free thiomorpholine bases formed in the process were determined by gas chromatography–mass spectrometry.

DOI: 10.1134/S1070427207110195

In accordance with the Convention on the Prohibition of the Development, Production, Stockpiling and Use of Chemical Weapons and on Their Destruction, various war gases, in particular, yperite **1**, accumulated in Russia, are subjected to detoxication. The detoxication is based on the reaction with ethanolamine **3** with the formation of 2-(thiomorpholin-4-yl)ethanol **4**, similar to the reaction described as early as 1934 for the bromine analog of yperite **2** [1–5]:

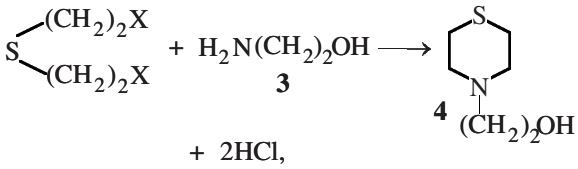

where X = Cl (**1**), Br (**2**).

The released hydrogen chloride is absorbed by a base: excess **3** [1], sodium carbonate [2], or reaction product **4** [3–5]. The reaction of pure yperite **1** with **3** can yield either free compound **4** or its hydrochloride **5** depending on the amount of the bases taken:

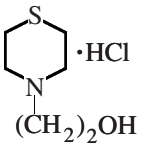

5

Technical-grade yperite intended for use as a war gas is a mixture of substances. Its composition depends on the synthesis procedure, purity of the starting compounds, and storage conditions. According to published data [6], technical-grade yperite contains as impurities homologs **6**–**10**, 1,2-bis(2-chloroethylthio)-ethane (sesquiyperite) **11**, small amounts of 1,4-dithiane **12** and 2-methyl-1,4-dithiane **13**, and other polysulfurous compounds:

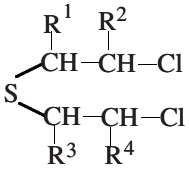

1, **6**–**10**

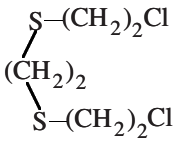

11

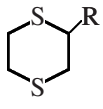

12, **13**

where $R^1 = R^2 = R^3 = R^4 = H$ (**1**); $R^1 = CH_3$, $R^2 = R^3 = R^4 = H$ (**6**); $R^1 = R^3 = R^4 = H$, $R^2 = CH_3$ (**7**); $R^1 = R^3 = CH_3$, $R^2 = R^4 = H$ (**8**); $R^1 = R^4 = CH_3$, $R^2 = R^3 = H$ (**9**); $R^1 = R^3 = H$, $R^2 = R^4 = CH_3$ (**10**); R = H (**12**); R = CH_3 (**13**).

The presence of homologs **6**–**10** in technical-grade yperite may be due to the presence of a propylene impurity in ethylene taken for the synthesis of yperite [6]. In detoxication of technical-grade yperite, the products of reaction with base **3** will be rather diverse, and the composition of the reaction mixture will depend on the composition of technical-grade yperite. This can be readily seen from comparison of data of [6–8].

According to the process sheet accepted in Russia, 2.4–2.6 mol of ethanolamine **3** as aqueous solution is taken per mole of technical-grade yperite. Therefore, the reaction mixture is alkaline (pH 9–10). In such a medium, the corresponding free bases should be inevitably present along with the hydrochlorides described in the literature [3, 9]. Among such bases are compound **4**, methyl derivatives of 2-(thiomorpholin-4-yl)ethanol **14**–**21**, 6-thia-3,9-diazaundecane-1,11-diol

22, 6,9-dithia-3,12-diazatetradecane-1,14-diol **23**, and their derivatives:

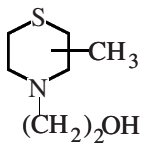

14, **15**

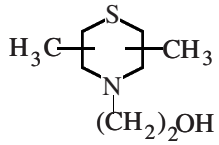

16–**21**

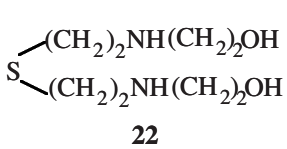

22

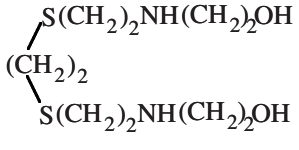

23

The formation of free base **4** by the reaction of **1** with aqueous ethanolamine **3** was described in [4].

The presence of free bases in the reaction mixture was proved by extraction of an aqueous solution of the reaction mixture with hexane, ether, or chloroform, followed by analysis by gas chromatography–mass spectrometry (GC–MS). The analysis revealed the presence of 1,4-dithiane **12**, 2-methyl-1,4-dithiane **13**, 2-(thiomorpholin-4-yl)ethanol **4**, isomeric 2-(2-methylthiomorpholin-4-yl)ethanol **14** and 2-(3-methylthiomorpholin-4-yl)ethanol **15**, and six isomeric (including *cis* and *trans* isomers) dimethyl derivatives of 2-(thiomorpholin-4-yl)ethanol **16**–**21**. Compounds **4** and **12** were identified by comparison of their mass spectra with those from the MAINLIB NIST library.

Compounds **4**, **12**, **13**, and their methyl derivatives **14**–**21** were detected by GC–MS in gases released from bitumen–salt masses incorporating products of yperite detoxication by its reaction with base **3** [8]. The positions of methyl groups were not indicated.

The structures of amino alcohols **14** and **15** (without assignment within this pair) and of six isomeric dimethyl derivatives **16**–**21** (each of which can exist as *cis* and *trans* isomers) were determined by comparison of their mass spectra with that of base **4**. The *m*/*z* values for the molecular ions (162 for **14** and **15**, 176 for six isomers **16**–**21**) correspond to their molecular weights, and the number of the observed isomers agrees with that expected theoretically. The strongest peaks in the mass spectra, *m*/*z* 130 (100) and 131 (100) for two monomethyl derivatives **14** and **15**, and 144 (100) for six dimethyl derivatives **16**–**21**, correlate with the strongest peak in the mass spectrum of **4**, *m*/*z* 116 (100), differing from the latter peak by the weight of one and two CH_2 groups, respectively. The structure of cyclic disulfide **13** was determined by comparison of its mass spectrum with that of 1,4-dithiane **12**. The GC–MS data for reaction mixtures are given in the table. The presence of hydrochlorides was proved by alkali treatment of the solution after the extraction of free bases, followed by extraction of the released bases with chloroform. Compounds **12** and **13** were absent in the extract, and the qualitative composition of the bases (compounds **4**, **14**–**21**) repeated the composition of the mixture of bases in extracts from the initial aqueous solution of the reaction mixture.

Thus, within the framework of the accepted process for detoxication of technical-grade yperite, the formation of thiomorpholine derivatives can be described by the following scheme:

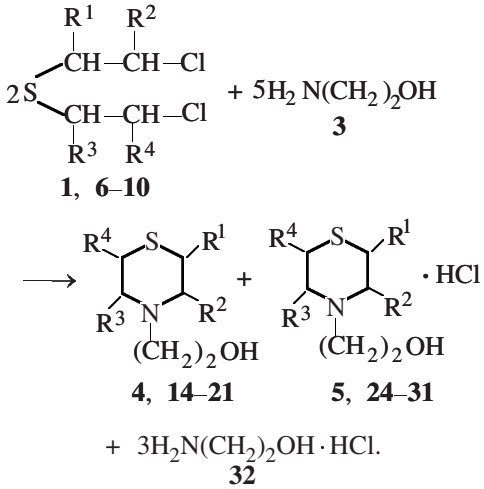

1, **6**–**10** **3** **4**, **14**–**21** **5**, **24**–**31**

32

where $R^1 = R^2 = R^3 = R^4 = H$ (**1**, **4**, **5**); $R^1 = CH_3$, $R^2 = R^3 = R^4 = H$ (**6**, **14**, **24**); $R^1 = R^3 = R^4 = H$, $R^2 = CH_3$ (**7**, **15**, **25**); $R^1 = R^3 = CH_3$, $R^2 = R^4 = H$ (**8**, **16**, **17**, **26**, **27**); $R^1 = R^4 = CH_3$, $R^2 = R^3 = H$ (**9**, **18**, **19**, **28**, **29**); $R^1 = R^3 = H$, $R^2 = R^4 = CH_3$ (**10**, **20**, **21**, **30**, **31**).[1]

Open-chain free bases of types **22** and **23**, as well as their derivatives, were not studied.

EXPERIMENTAL

The reaction mixture was taken from a plant for elimination of chemical weapons near Gornyi urban village, Saratov oblast, Russia.

Gas–liquid chromatography (GLC) was performed on a Kristall-2000 M device equipped with a CP-

[1] There are no data in the literature on the stereoisomerism of **6**–**10**. Therefore, their isomerism is assumed but is not considered in detail. We did not assign the peaks of two isomeric methyl derivatives of 2-(thiomorpholin-4-yl)ethanol to particular compound **14** or **15**. Six peaks of dimethyl derivatives of 2-(thiomorpholin-4-yl)ethanol were not assigned to particular isomers either.

Results of GC–MS analysis of reaction mixture components: 1,4-dithianes and 2-(thiomorpholin-4-yl)ethanols

Compound no.	*M*	Retention time, min	*m/z* (intensity, % of the strongest peak of given compound)*
12	120.22	5.3	***120(100)***, 105(20), 87(5), 73(2), 59(10), 45(3)
13	134.25	5.8	***134(100)***, 119(35), 106(6), 75(8), 59(12), 45(1)
4	147.78	7.6	**148(51)**, 146(7), 130(3), *116(100)*, 102(3), 88(40), 70(5), 56(3), 42(10)
14 or **15**:			
first isomer	161.81	8.1	**162(60)**, 146(7), *130(100)*, 114(2), 100(10), 88(22), 70(2), 56(20), 42(3)
second isomer	161.81	8.9	**162(97)**, 144(7), *131(100)*, 116(3), 102(18), 84(15), 72(6),56(3), 42(4)
16–**21**:			
first isomer	175.83	9.2	**176(18)**, 160(5), *144(100)*, 130(5), 115(3), 102(30), 70(7), 56(22), 42(10)
second isomer	175.83	9.3	**176(21)**, 160(6), *144(100)*, 130(3), 115(4), 102(30), 70(6), 56(24), 42(10)
third isomer	175.83	9.6	**176(5)**, 160(1), *144(100)*, 130(8), 115(5), 101(40), 88(17), 70(7), 56(15), 42(23)
fourth isomer	175.83	9.8	**176(5)**, 160(3), *144(100)*, 130(12), 115(5), 100(16), 88(36), 74(25), 56(77), 42(17)
fifth isomer	175.83	10.2	**176(3)**, 160(6), *144(100)*, 130(10), 114(8), 102(32), 88(8), 70(20), 56(42), 42(15)
sixth isomer	175.83	10.6	**176(3)**, 160(3), *144(100)*, 130(8), 118(10), 102(32), 85(10), 73(20), 56(32), 42(15)

* The *m/z* values and intensities for the molecular peaks are printed bold, and those for the strongest peaks of the given compound are printed italic.

WAX-58 (FFAP) capillary column (length 30 m, inside diameter 0.32 mm, thickness of liquid phase coating 0.25 μm) and a flame ionization detector. The carrier gas was helium (flow rate 1.0 ml min^{-1}). The vaporizer and detector temperatures were 280 and 300°C, respectively. The temperature was elevated from 80 to 160°C at a rate of 8 deg min^{-1}.

The GC–MS studies were performed with a Saturn 2200 gas chromatograph–mass spectrometer (Varian) equipped with an ion trap detector and a CP-SIL 8CB LOW BLEED/MS capillary column (length 30 m, inside diameter 0.25 mm, thickness of liquid phase 0.25 μm). The flow rate of the carrier gas (helium) was 0.9 ml min^{-1}. Experiments were performed with a typical sample of the reaction mixtrue obtained by detoxication of technical-grade yperite with 80% aqueous ethanolamine.

The compounds that do not exhibit basic properties, dithianes **12** and **13**, were studied as follows: 15.11 g of the reaction mixture and 25 ml of distilled water were shaken up in a 250-ml Erlenmeyer flask for 5 min. The resulting dark brown solution of the reaction mixture with a small amount of undissolved fine black particles had pH 9–10 according to universal test-paper. The mixture was acidified with ~20% HCl to pH 1–2 and extracted with three portions of ether (20, 10, and 10 ml). The combined extracts were analyzed by GLC. Dithiane **12** was eluted first (identification with an authentic sample). Its structure and the structure of its homolog **13** were confirmed by GC–MS. The ratio of the GLC peak areas of **12** and **13** was 2.2 : 1.

The quantitative determination of the sum of dithianes **12** and **13** was performed as follows: Combined light yellow ether extracts were dried over anhydrous sodium sulfate, and the ether extract was carefully decanted from the desiccant to a preliminarily weighed 250-ml flat-bottom flask. The solvent was evaporated, and the remaining oil gradually crystallized to form light yellow needle-like crystals. The weight of the neutral fraction thus obtained (mixture of dithianes **12** and **13**) was 0.30 g.

To confirm the structure of substances present in the reaction mixture, we examined by GC–MS the *n*-hexane extract from the reaction mixture diluted by a factor of 2 with distilled water. The extract (1 μl)

was introduced into the injector of the gas chromatograph–mass spectrometer. The injector temperature was 250°C. The temperature schedule of the column was as follows: 100°C, 3 min; heating to 150°C, 10 deg min^{-1}; 150°C, 3 min; heating to 250°C, 5 deg min^{-1}; 250°C, up to the end of the run. The total analysis time was 30 min. The ion trap was not switched on in the first 10 min, and then the analysis was performed in the El Auto mode. As a result, we identified dithianes **12** and **13**.

To examine the components present in the reaction mixture in the form of hydrochlorides, the reaction mixture was diluted with a fivefold volume of distilled water, filtered through silica gel, and repeatedly extracted with chloroform. The chloroform extracts were discarded, and the aqueous solution was alkalized with 20% aqueous NaOH to pH 11–12 and again extracted with chloroform to recover components that were initially present in the reaction mixture as hydrochlorides. A 1-μl portion of the extract was introduced into the GC–MS injector. The injector temperature was 250°C. The temperature schedule of the column was as follows: heating from 50 to 250°C at a rate of 15 deg min^{-1}. The total analysis time was 20 min. The ion trap was not switched on in the first 5 min, and then the analysis was performed in the El Auto mode. Among bases **4**, **14**, and **15**, 2-(thiomorpholin-4-yl)ethanol **4** was eluted first, which was followed by elution of **14** and **15** (the order of their elution was not determined). The ratio of the areas of the three peaks (in the order of their elution) was 6 : 2.3 : 1. Six isomeric dimethyl-2-(thiomorpholin-4-yl)ethanols **16**–**21** were also detected in small amounts.

We determined the weight fractions of basic products formed by the reaction of yperite with ethanolamine and present in the reaction mixture in the form of both hydrochlorides and free bases.

For the quantitative determination of components present in the reaction mixture in the form of free bases and tars, the reaction mixture (23.92 g) was placed in a flask and diluted with 120 ml of distilled water. The contents were shaken up for 5 min. By so doing, we obtained a dark brown aqueous solution of the reaction mixture with a small amount of undissolved fine black tarry particles. The solution pH was 9–10 by the universal test-paper.

A wool filter was placed in a tip of a chemical funnel, after which the funnel was charged with 25 g of silica gel. The aqueous solution of the reaction mixture was filtered through this filtering unit to separate tars and fine particles. The filtrate was a transparent yellow-brown solution, which became turbid within several hours.

The silica gel with the deposited tars was dried for 24 h at 45–50°C. The weight of the tars was estimated from the difference between the weights of the initial silica gel and silica gel with the deposited tars; it was 1.59 g.

From the aqueous solution of the reaction mixture, we recovered by extraction with chloroform (nine 15-ml portions) both neutral substances (1,4-dithiane, 2-methyl-1,4-dithiane, unidentified polysulfides) and basic compounds [mixture of homologs of 2-(thiomorpholin-4-yl)ethanol and 6-thia-3,9-diazaundecane-1,11-diol] in the form of free bases. In so doing, ethanol did not pass into the chloroform phase, which was confirmed by TLC (Silufol plate, eluent acetone).

When the extraction was performed in a separating funnel, three layers formed. The upper layer was an aqueous solution of the reaction mixture; the lower layer was the chloroform extract; and the middle layer was a stable emulsion consisting of the aqueous reaction mixture and chloroform. In each extraction run, only the chloroform extract was taken. The chloroform extracts were combined.

After the extraction completion, the remaining emulsion and reaction mixture were left to settle for 2 days. The chloroform extract thus obtained was separated and combined with the other chloroform extracts.

The chloroform and aqueous solutions were filtered prior to the next extraction runs, and an additional 0.74 g of tars insoluble in water and chloroform was obtained. Thus, the total content of tars in the given portion of the reaction mixture was 2.33 g. After the chloroform evaporation, a mixture of neutral and basic (in the form of free bases) substances was obtained (total amount 2.87 g).

It was shown above that 1,4-dithianes were present in the reaction mixture in an amount of 2.0%. Thus, in the given portion of the reaction mixture (23.92 g) the weight of basic compounds present in the form of free bases was 2.39 g. The remaining aqueous solution of the reaction mixture was used for further recovery of basic compounds present in the reaction mixture as hydrochlorides.

For quantitative determination of basic components present in the reaction mixture as hydrochlorides, an aqueous solution of the reaction mixture after the recovery of free bases and 1,4-dithianes was alkalized with 10% aqueous NaOH to pH 11–12, which was

followed by repeated extraction with chloroform (eight 10-ml portions). A transparent light yellow extract was obtained; after the solvent evaporation, 1.74 g of basic compounds was recovered.

The total content of water, ethanolamine, and other unidentified water-soluble organic compounds that were not recovered by extraction was determined as the difference between the initial weight of the reaction mixture and total weight of all the recovered components. For the given reaction mixture sample, it amounted to 16.98 g.

CONCLUSIONS

(1) The major components of the reaction mixture obtained by detoxication of yperite with ethanolamine are mixtures of free bases, 2-(thiomorpholin-4-yl)ethanols and the corresponding salts (hydrochlorides). The ratio between the bases and their salts is 1.37 : 1. 1,4-Dithianes are detected as minor impurities.

(2) A fractionation procedure was developed, allowing separation of free 2-(thiomorpholin-4-yl)ethanols, their salts, and 1,4-dithianes.

REFERENCES

1. Burrows, L.A. and Reid, E.E., *J. Am. Chem. Soc.*, 1934, vol. 56, no. 8, pp. 1720–1724.
2. Tcherkerzoff, N., *Rev. Inst. Franc. Petrole Ann. Combust. Liq.*, 1963, vol. 18, no. 3, pp. 438–470.
3. Luganskii, I.N., Sheluchenko, V.V., Krotovich, I.N., et al., *Ross. Khim. Zh.*, 1994, vol. 38, no. 2, pp. 34–36.
4. Procell, L.R., Wagner, G.W., Sorrick, D.C., et al., *Proc. ER–Dec Sci. Conf. Chem. Biol. Def. Res.*, 1998 (Published 1999), pp. 659–665.
5. Guzikhin, V.A., Zayats, M.Ya., Lyamkin, D.I., et al., *Kauchuk Rezina*, 2001, no. 4, pp. 2–6.
6. Trofimov, B.A., Gusarova, N.K., Dorofeev, I.A., et al., *Zh. Prikl. Khim.*, 1994, vol. 67, no. 1, pp. 161–166.
7. Ermakova, I.T., Safrina, N.S., Starovoitov, I.I., et al., *Mikrobiologiya*, 2004, vol. 73, no. 3, pp. 358–363.
8. Savel'eva, E.I., Radilov, A.S., Kuznetsova, T.A., and Apraksin, V.F., *Zh. Prikl. Khim.*, 1999, vol. 72, no. 9, pp. 1501–1506.
9. Kapashin, V.P., Sevost'yanov, V.P., Shebanov, N.P., and Tolstykh, A.V., *Khimicheskoe razoruzhenie: Tekhnologii unichtozheniya otravlyayushchikh veshchestv* (Chemical Disarmament: Processes for Elimination of War Gases), Saratov: Kolledzh, 2000.

ISSN 1070-4272, Russian Journal of Applied Chemistry, 2007, Vol. 80, No. 11, pp. 1883–1887. © Pleiades Publishing, Ltd., 2007.
Original Russian Text © S.A. Solov'ev, R.N. Zatelepa, E.V. Gubaren, P.E. Strizhak, and E.M. Moroz, 2007, published in Zhurnal Prikladnoi Khimii, 2007, Vol. 80, No. 11, pp. 1858–1863.

ORGANIC SYNTHESIS AND INDUSTRIAL ORGANIC CHEMISTRY

Activity and Stability of Ni/Al_2O_3 Catalysts in Carbon Dioxide Conversion of Methane as Influenced by Alkali Metal Oxide Additives (K_2O, Na_2O, Li_2O)

S. A. Solov'ev, R. N. Zatelepa, E. V. Gubaren, P. E. Strizhak, and E. M. Moroz

Pisarzhevskii Institute of Physical Chemistry, National Academy of Sciences of Ukraine, Kiev, Ukraine
Boreskov Institute of Catalysis, Siberian Division, Russian Academy of Science, Novosibirsk, Russia

Received June 26, 2007

Abstract—Properties of Ni/Al_2O_3 composites supported by synthetic cordierite ceramic block matrices of honeycomb structure in carbon dioxide conversion of methane in the presence of alkali metal oxides (K_2O, Na_2O, Li_2O) were studied in comparison with those of GIAP-18 granulated catalyst.

DOI: 10.1134/S1070427207110201

Production processes of ammonia, alcohols, and other compounds are based on oxidative conversion of methane into synthesis gas. Only steam and steam–air conversion is used in modern industry. Carbon dioxide conversion of methane (CDCM) attracts growing researchers' attention. This reaction can be used for processing greenhouse and flue gases [1] and for preparing synthesis gas in production of dimethyl ether (high-performance additive to gasoline) [2]. In addition, activation of fairly inert molecules of CH_4 and CO_2 is of great scientific interest.

Highly active and cheap nickel-containing catalysts (NiO/Al_2O_3, NiO/ZrO_2) are most frequently used in oxidative conversion of methane. High positive enthalpy of the reaction $CH_4 + CO_2 \rightleftarrows 2CO + 2H_2$ ($\Delta H^0 = +247$ kJ mol^{-1}) and deactivation of all the known catalysts owing to their carbonization [3] complicate industrial implementation of CDCM. Nickel-containing catalysts are fairly active in CDCM, but they are rapidly deactivated owing to formation of elemental carbon on their surface.

These are several approaches to solve the problem of carbonization of CDCM catalysts. One of them is adjustment of the structural properties of catalysts. The operation stability of the catalysts in CDCM increases with a decrease in the particle size of metallic nickel [1, 4]. The catalysts containing 10–20-nm nickel particles have the highest stability [4]. This is due to the fact that the nanocomposite catalysts provide the required balance between the rates of degradation of CH_4 on metallic nickel and of dissociation of CO_2 at the metal–oxide interface [5]. In this connection, NiO/Al_2O_3 composites can be promising catalysts for CDCM. Preparation of the catalysts from these components involves formation of spinel $NiAl_2O_4$ during the heat treatment and reduction of spinel to form finely divided metallic nickel stabilized in the Al_2O_3 matrix. The other way to improve the catalyst stability in CDCM is to enhance the surface basicity, which is usually accomplished by introducing alkali and alkaline-earth metal oxides as promoters [6].

Thermodynamics of oxidative conversion of methane (steam, carbon dioxide) requires high temperatures to reach high methane conversion. This reaction is controlled, as a rule, by diffusion. Catalytic oxidation of methane penetrates into a catalyst granule to a depth of no larger than 0.25 mm. Therefore, ceramic block matrices with honeycomb structure and small wall thickness show promise as the catalyst supports. We expect that these catalysts will not only increase the process productivity but also decrease carbonization of the internal surface of the catalyst owing to facilitation of oxidant diffusion into the reaction zone.

The aim of this study was to examine the influence of alkali metal oxides (K_2O, Na_2O, Li_2O) on the activity and operation stability in CDCM of Ni/Al_2O_3 catalysts supported by ceramic block matrices of honeycomb structure.

Ceramic block matrices of honeycomb structure made from synthetic cordierite ($2Al_2O_3 \cdot 2MgO \cdot$

Table 1. Activity and performance of the catalysts in CDCM. Concentrations of CH_4 and CO_2 are 5.5 and 7.0%, respectively

Sample no.	Catalyst, %	Temperature of 80% conversion, °C	Performance	
			$A \times 10^6$, mol s^{-1} g_{cat}^{-1-1}	$B \times 10^6$, mol s^{-1} g_{NiO}^{-1}
1	GIAP-18	485	12.96	1.62
2	(8.2NiO + 11.2Al_2O_3)/cordierite	480	38.3	4.8
3	(3.8NiO + 11.2Al_2O_3)/cordierite	492	30.0	7.8
4	(1.0NiO + 2.0Al_2O_3)/cordierite	533	27.6	27.6

$5SiO_2$)[1] were used as supports. The cell size was 1.0 × 1.0 mm, and the wall thickness was 0.2 mm. The support is stable up to 1250°C.

The catalysts were prepared by impregnation of block matrices with a solution of nickel and aluminum nitrates, followed by calcination in a muffle furnace at 600°C for 3 h in air. The salt ratio in the solution provided the required composition of the catalysts. To modify Ni/Al_2O_3 catalysts with alkali metal oxides (K_2O, Na_2O, Li_2O), the samples were impregnated with aqueous solutions of the corresponding alkali metal carbonates, dried, and calcined.

To determine the catalytic activity, a cylindrical 0.25-g fragment 7 mm in diameter and 12 mm long was cut from a sample of the block catalyst. The catalyst fragment was placed in a flow reactor so as to prevent breakthrough of the gaseous reaction mixture without contacting the catalyst. Comparative study of GIAP-18 catalyst was performed with a 1.0-g weighed portion of the 1–2-mm fraction. Prior to the experiment, the catalyst was reduced in the reactor with 2% H_2 in He at 700°C for 2 h. Then, the sample was cooled to the temperature of CDCM in a flow of the reducing gas mixture. To determine the catalytic activity, the methane conversion at different temperatures was measured. The flow rate of the gas mixture was 100 ml min^{-1}. The space velocity of the reaction mixture in the experiment with block catalysts and GIAP-18 was 6000 and 3000 h^{-1}, respectively. We used a mixture of He with 5.5 vol % CH_4 and 7.0 vol % CO_2. The composition of the reaction mixture was analyzed chromatographically with a thermal conductivity detector.

The strength of the Ni–O bond in the catalysts was determined by temperature-programmed hydrogen reduction (TPHR). The experiments were performed on a flow unit with chromatographic determination of hydrogen consumed for reduction of the catalyst. The unit was heated from 20 to 850°C at a rate of 10 deg min^{-1}. The reaction products (water vapor) were collected at –50°C in a trap packed with 5 Å molecular sieves. A mixture of 10% hydrogen with argon was used as the reducing agent.

The activity and performance of the block catalysts with different compositions and honeycomb structure (samples nos. 2–4) are presented in Table 1 in comparison with those of GIAP-18 catalyst (sample no. 1). It is seen that the activities of granulated (sample no. 1) and block (sample no. 2) catalyst with similar content of the reactive component (8% NiO) are similar. However, the performance of the block catalyst per unit weight of the catalyst is higher than that of granulated GIAP-18 catalyst by a factor of approximately 4. The difference in performance of the granulated and block catalyst per unit weight of nickel oxide is still higher. This is due to the fact that the wall thickness of a block in the catalysts with honeycomb structure is commensurable with the depth of the working layer. As a result, the performance of the reactive component in the catalytic reaction increases.

To estimate the operation stability of the catalyst in CDCM, the $x = f(T)$ dependences are successively measured for the sample catalyst sample. The temperature dependence of the methane conversion $x = f(T)$ in the presence of (1.0%NiO + 2.0%Al_2O_3)/cordierite catalyst repeatedly measured after keeping the sample at each temperature to the constant conversion are shown in Fig. 1. It is seen that the methane conversion is incomplete in the second experiment (curve *2*). The conversion decreases on heating above 700°C. The strongest decrease in the methane conversion is observed in the third experiment (curve *3*), and then the catalyst is deactivated owing to carbonization. Some decrease in the reaction onset temperature in the third experiment may be due to reduction of the catalyst with the reaction gas mixture.

[1] The ceramic block supports were developed and prepared at Frantsevich Institute of Materials Science Problems, National Academy of Science of Ukraine.

Coke can be formed on the catalyst by the following reactions [3]:

$$CH_4 = C + 2H_2, \quad \Delta H^0 = +74.8 \text{ kJ mol}^{-1}, \quad (1)$$

$$2CO = C + CO_2, \quad \Delta H^0 = -172.5 \text{ kJ mol}^{-1}. \quad (2)$$

The reaction enthalpy shows that an increase in the temperature is favorable for reaction (1) and a decrease in the temperature, for reaction (2). The most pronounced decrease in the catalytic activity is observed at high temperatures (Fig. 2). Hence, the most probable pathway of catalyst carbonization is reaction (1).

The mechanism of CDCM on the nickel catalyst can be described by the following steps [3, 7]:

$$CH_4 + Z \rightleftarrows \{CH_x\}\text{–}Z + (4 - x)H_{ads} \rightleftarrows ZC + 2H_2, \quad (3)$$

$$CO_2 + Z \rightleftarrows Z\text{–}O + CO, \quad (4)$$

$$Z\text{–}C + Z\text{–}O \rightleftarrows Z\text{–}CO + Z, \quad (5)$$

$$Z\text{–}CO \rightleftarrows Z + CO, \quad (6)$$

where Z is an active center of the catalyst.

Activation of methane and its dissociation to form molecular hydrogen and carbon occur on the acid centers of the catalyst surface. The rate-determining step is oxidation of carbon with surface oxygen [reaction (5)].

High surface acidity accelerates methane activation [reaction (3)] but promotes coke accumulation, thus deactivating the catalyst. Carbonization of the catalyst can be decreased by adjustment of the acid–base properties of the catalyst surface. However, this can slightly decrease the catalytic activity. The activity of the Ni/Al_2O_3 catalyst is maximal in the first reaction steps. The nickel catalysts on base supports Ni/MgO, Ni/CaO, Ni/MnO, and Ni/ZrO_2 show higher performances than does Ni/Al_2O_3, and these catalysts are stable to carbonization [8].

The temperature dependences of methane conversion in the presence of the catalysts modified with alkali metal oxides are shown in Fig. 2. The most active is the catalyst modified with K_2O (curve *1*), and the least active is the catalyst containing Li_2O (curve *3*). In addition, the latter catalyst is characterized by unstable operation. At high temperature providing high methane conversion, the activity of this catalyst decreases with time. This is probably due to the fact that lithium oxide exerts a corroding effect on the majority of metals at high temperatures [9].

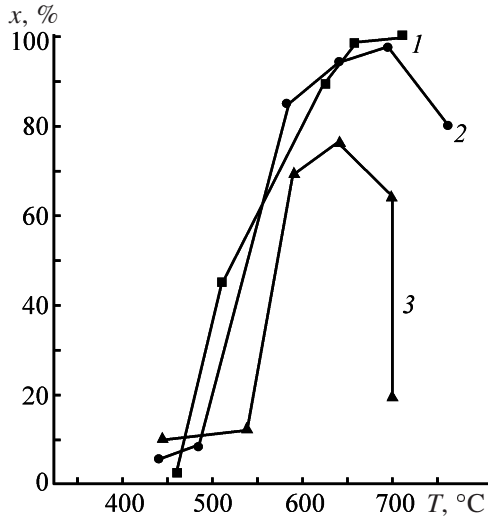

Fig. 1. Variation of the activity of (1.0% NiO + 2.0% Al_2O_3)/cordierite catalyst in repeated experiments on CDCM. (*x*) Conversion and (*T*) temperature; the same for Figs. 2 and 3. (*1–3*) Run nos.

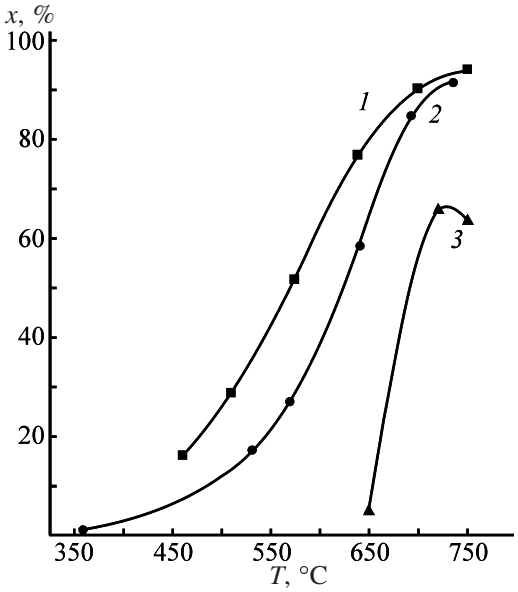

Fig. 2. Temperature dependence of methane conversion in the presence of catalysts with alkali additives: (*1*) 1.0% NiO + 2.0% Al_2O_3 + 0.6% K_2O, (*2*) 1.0% NiO + 2.0% Al_2O_3 + 0.9% Na_2O, and (*3*) 1.0% NiO + 2.0% Al_2O_3 + 0.7% Li_2O.

It reacts with metallic nickel to form nickel oxide inert in CDCM [10]. The catalytic activity slightly decreases with increasing potassium oxide content from 0 to 1.3% (Fig. 3), which can be caused by formation of inactive alkali metal aluminates. In this case, however, the operation stability of the catalyst increases.

Thus, alkali metal oxides (K_2O, Na_2O) decrease carbonization of the nickel–aluminum catalyst in

Table 2. Influence of CO_2 concentration on CDCM at 700°C and CH_4 concentration of 5.5 vol %

Catalyst, %	Methane conversion, %, at indicated CO_2/CH_4 ratio			
	1.3	1.6	1.8	2.2
1.0NiO + 2.0Al_2O_3 + 0.6K_2O	98	90	85	78
1.0NiO + 2.0Al_2O_3 + 1.3K_2O	95	88	77	63

CDCM, thus increasing their operation stability. The activity of nickel–aluminum catalyst significantly decreases after its modification with lithium oxide.

To prevent carbonization of a catalyst in steam conversion of methane, excess oxidizing agent (H_2O) is introduced into the reaction mixture [11]. Usually, the H_2O/CH_4 ratio is 2.0–2.5. We studied the influence of the CO_2 concentration on CDCM. In these experiments we used the catalysts modified with potassium oxide (1.0% NiO + 2.0% Al_2O_3 + 1.3% K_2O and 1.0% NiO + 2.0% Al_2O_3 + 0.6% K_2O), which show stable operation in this reaction. The methane conversion at 700°C with increasing CO_2/CH_4 ratio from 1.3 to 2.0 was measured. The results are summarized in Table 2.

As seen from Table 2, the methane conversion decreases with increasing CO_2 concentration. The negative effect of the oxidizing agent increases with increasing the K_2O content of the catalyst from 0.6 to 1.3%. This is probably caused by reaction of CO_2 with K_2O to form low-active surface carbonates [12]. This data confirm the assumption that reverse Boudoir reaction of CO_2 with carbon [13] is not the main pathway of CDCM in the presence of the catalysts in question.

The activity of oxide catalysts in redox reactions can be estimated from the oxygen–catalyst bond energy, which, in turn, can be estimated form the reduction onset temperature and peak temperatures in the TPHR curves. The TPHR curves of unmodified nickel–aluminum catalyst (curve *1*) and the catalyst modified with alkali metals (curves *2–4*) are shown in Fig. 4. It can be seen that the reduction rate of the catalysts with hydrogen decreases in the following order: NiO + Al_2O_3 > NiO + Al_2O_3 + Na_2O > NiO + Al_2O_3 + K_2O > NiO + Al_2O_3 + Li_2O. The activity of these catalysts in CDCM varies similarly (Fig. 2).

The results of these experiments agree with the above mechanism of CDCM. According to this scheme, the surface carbon formed by dissociation of adsorbed methane is oxidized with oxygen of

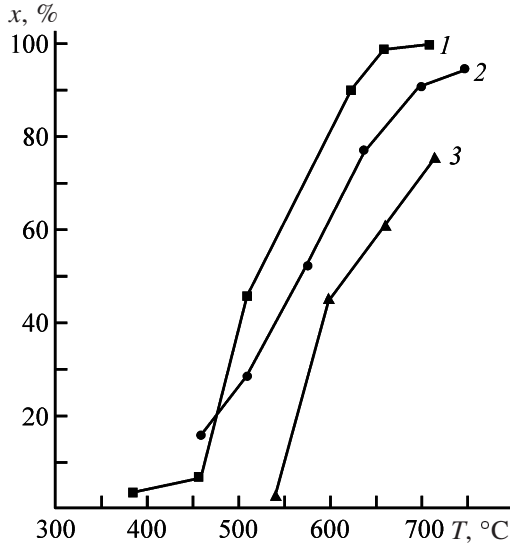

Fig. 3. Conversion of methane in CDCM on (*1*) 1.0% NiO + 2.0% Al_2O_3, (*2*) 1.0% NiO + 2.0% Al_2O_3 + 0.6% K_2O, and (*3*) 1.0% NiO + 2.0% Al_2O_3 + 1.3% K_2O.

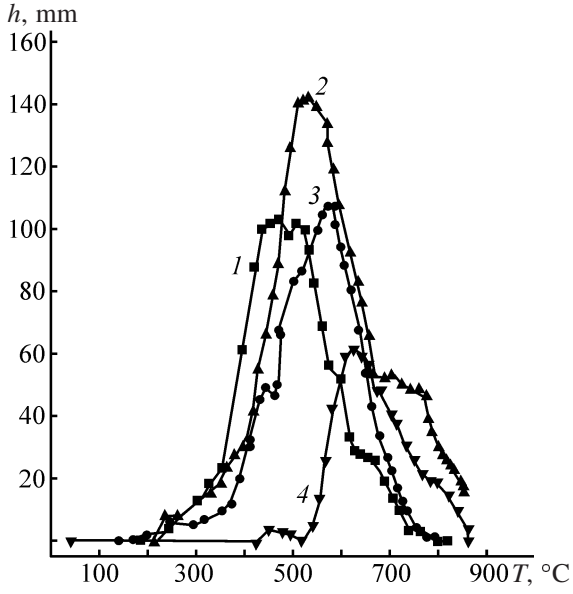

Fig. 4. TPHR curves of (*1*) 1.0% NiO + 2.0% Al_2O_3, (*2*) 1.0% NiO + 2.0% Al_2O_3 + 0.6% K_2O, (*3*) 1.0% NiO + 2.0% Al_2O_3 + 0.9% Na_2O, and (*4*) 1.0% NiO + 2.0% Al_2O_3 + 0.7% Li_2O. (*h*) Peak height and (*T*) temperature.

the catalyst surface. The surface oxygen formed by partial reoxidation of the reactive component rapidly reacts with surface carbon. This process not only accelerates the methane decomposition, but also decelerates the reaction $CO_2 + Ni–C \rightarrow 2CO + Ni$, which, as suggested in [13], can be the rate-determining step of CDCM. The promoting effect of an alkali metal is caused by formation of finely divided nickel particles which cannot be detected by X-ray diffraction [6, 14, 15].

In addition, alkali metals decrease the acidity of the catalyst surface, thus suppressing methane dissociation to form coke. The presence of potassium additive in the catalyst decreases not only the carbonization but also the methane conversion.

CONCLUSIONS

(1) Ni/Al_2O_3 composites supported by synthetic cordierite ceramic block matrices of honeycomb structure are effective catalysts of carbon dioxide conversion of methane. The performance of these catalysts is significantly higher than that of conventional granulated catalysts. The use of structured catalysts with thin walls eliminates the diffusion problems in carbon dioxide conversion of methane, thus decreasing coke formation.

(2) Introduction of alkali metal oxides increases the operation stability of the catalysts by controlling the acid–base properties of the catalyst surface. The decrease in the carbonization of the surface of the catalysts modified with alkali metal oxides improves the stability of the catalyst operation.

(3) Alkali metal oxide additives slightly decrease the catalytic activity owing to alteration of the crystal structure of nickel and formation of thermodynamically stable and low-reactive alkali metal aluminates. As a result, the strength of the nickel–oxygen bond increases, which is manifested in deceleration of the reduction of nickel–aluminum catalysts modified with alkali metals.

REFERENCES

1. Chunshan Song and Wei Pan, *Catal. Today*, 2004, vol. 98, pp. 463–484.
2. Seung-Ho Lee, Wonihl Cho, Woo-Sung Ju, et al., *Catal. Today*, 2003, vol. 87, pp. 133–137.
3. Krylov, O.V., *Ross. Khim. Zh.*, 2000, vol. 44, no. 1, pp. 19–33.
4. Bo-Oing Xu, Jun-Mei Wei, Ying-Tao Yu, et al., *J. Phys. Chem. B*, 2003, vol. 107, pp. 5203–5207.
5. Buchkov, V.Yu., Tyulenin, Yu.P., Krylov, O.V., and Korchak, V.N., *Kinet. Katal.*, 2002, vol. 41, no. 5, pp. 775–782.
6. Tochihiko, O. and Toshiaki, M., *J. Catal.*, 2001, vol. 204, no. 1, pp. 89–97.
7. Bychkov, V.Yu., Krylov, O.V., and Korchak, V.N., *Kinet. Katal.*, 2002, vol. 43, no. 1, pp. 94–103.
8. Kim., J.-H., Suh, D.J., Park, T.-J., and Kim, K.-L., *Proc. V Int. Natural Gas Conversion Symp.* (Giardini-Naxos, Sicily, 1998), Amsterdam: Elsevier, 1998, pp. 771–776.
9. *Kratkaya khimicheskaya entsiklopediya* (Brief Chemical Encyclopedia), Moscow: Sov. Entsiklopediya, 1963, vol. 2, p. 990.
10. Kapran, A.Yu. and Orlik, S.N., *Teor. Eksp. Khim.*, 2005, vol. 41, no. 6, pp. 360–363.
11. Ketov, A.A., Saulin, D.V., Puzanov, I.S., et al., *Zh. Prikl. Khim.*, 1997, vol. 70, no. 3, pp. 446–450.
12. Bychkov, V.Yu., Korchak, V.N., Krylov, O.V., et al., *Kinet. Katal.*, 2002, vol. 42, no. 4, pp. 618–631.
13. Bychkov, V.Yu., Tyulenin, Yu.P., Krylov, O.V., and Korchak, V.N., Abstracts of Papers, *VI Rossiiskaya konferentsiya "Mekhanizmy kataliticheskikh reaktsii"* (VI Russian Conf. "Mechanisms of Catalytic Reactions") (Moscow, October 1–5, 2002), Novosibirsk, 2002, vol. 1, report OP-I-35, pp. 110–112.
14. Osaki, T. and Mori, T., *J. Catal.*, 2001, vol. 204, no. 1, pp. 89–97.
15. Artyunov, V.S. and Krylov, O.V., *Usp. Khim.*, 2005, vol. 74, no. 12, pp. 1216–1244.

ISSN 1070-4272, Russian Journal of Applied Chemistry, 2007, Vol. 80, No. 11, pp. 1888–1893. © Pleiades Publishing, Ltd., 2007.
Original Russian Text © V.I. Gerasimov, G.V. Kalinin, Yu.A. Nikonov, Yu.F. Titovets, A.E. Kalabushkin, O.S. Alekhin, K.V. Nekrasov, S.N. Rusetskaya, O.V. Arapov, N.I. Alekseev, E.V. Kustova, V.V. Lishchuk, M.A. Pleshkov, K.N. Semenov, V.A. Keskinov, N.A. Charykov, 2007, published in Zhurnal Prikladnoi Khimii, 2007, Vol. 80, No. 11, pp. 1864–1869.

ORGANIC SYNTHESIS AND INDUSTRIAL ORGANIC CHEMISTRY

Single-Stage Plasma-Arc Synthesis of Metallo-Endofullerenes

V. I. Gerasimov, G. V. Kalinin, Yu. A. Nikonov, Yu. F. Titovets, A. E. Kalabushkin, O. S. Alekhin, K. V. Nekrasov, S. N. Rusetskaya, O. V. Arapov, N. I. Alekseev, E. V. Kustova, V. V. Lishchuk, M. A. Pleshkov, K. N. Semenov, V. A. Keskinov, and N. A. Charykov

Innovation at Leningrad Institutes and Enterprises, Private Company, St. Petersburg, Russia
Ioffe Physicotechnical Institute, Russian Academy of Sciences, St. Petersburg, Russia
St. Petersburg State University, St. Petersburg, Russia
St. Petersburg State Institute of Technology (Technical University), St. Petersburg, Russia

Received July 6, 2007; in final form, September 2007

Abstract—Single-stage plasma-arc synthesis of metallo-endofullerenes of the types $C_{60}Pd$, $C_{60}Ni$, and $C_{60}Cr$, whose content in a mixture of extracted fullerenes was 0.05 to 0.15 wt %, was performed. The effect of introduction of these metals into the reaction plasma on the total yield of fullerenes and on the fraction composition of the fullerene mixture was studied. The fullerene mixtures were analyzed by mass spectrometry and liquid chromatography.

DOI: 10.1134/S1070427207110213

As is known [1], endofullerenes is the commonly accepted name for derivatives of light (C_{60}, C_{70}) or heavy (C_n, $n \geq 72$) fullerenes with one or several noncarbon atoms (X) incorporated within the hollow skeleton of fullerenes. To our knowledge, stable endofullerenes based on the so-called ultralight fullerenes or "subfullerenes" (C_n, $n \leq 58$) have not been described, although part of these can have a hollow structure (C_{36}–C_{58}). The role of a heteroatom X can be played both by atoms of metals: alkali, alkaline-earth, transition, heavy, lanthanide, and actinide (X = Li, Na, K, Cs, Ca, Mg, Hf, Ti, Zr, Y, Sc, La, Ce, Sm, Gd, Tb, U, Pu, and some others) [2, 3], and by atoms of some nonmetals and, primarily, noble gases (X = He, Ne, Ar, Kr, Xe, N), as well as by some diatomic molecules (X = CO, CN) [1, 4]. Typically, a single heteroatom is incorporated in fullerenes (C_nX compounds), although endofullerenes have been described with two (C_nX_2 compounds) and even three heteroatoms (C_nX_3), which may be identical ($C_{60}La_2$ [2]) or different ($C_{60}Cs_2Rb$ [5]).

The main methods for synthesis of metallo-endofullerenes are the same as those for ordinary fullerenes [1]: namely, laser evaporation of graphite in the atmosphere of inert gases, resistive and high-frequency heating of graphite in an inert gas, evaporation of graphite in focused solar light, burning of graphite electrodes in an electric arc in an inert gas (plasma-arc method), evaporation of graphite microparticles in a thermal plasma under atmospheric pressure, combustion of hydrocarbons in a laminar of volume flame [6–13]. The basic issue is the way in which metal ions (or atoms) are introduced into the carbon-containing reaction plasma generated in synthesis of "ordinary" fullerenes.

Several methods have been described in the literature: impregnation of graphite articles (rods, discs) with solutions of well-soluble salts of the type $LaCl_3$ [1, 2] in laser or flame-arc synthesis of fullerenes; introduction of high-purity metal compounds, commonly oxides, directly into the material of a graphite rod (anode) being evaporated, by compaction followed by preliminary annealing, e.g., of La_2O_3, in plasma-arc synthesis of a lanthanum-endofullerene $C_{60}La$ [14]; implantation of metal ions (e.g., Li^+) into the carbon plasma or, vice versa, implantation of fullerene ions (e.g., C_{60}^-) into a metal-containing plasma [3]; also possible is synthesis of endofullerenes by direct introduction of some heteroatoms [He, Ne, Ar, Kr, Xe, N (N_2)] into already synthesized fullerene voids from the gas phase at comparatively high temperatures (600–1000°C) and pressures (100–1000 atm) [4].

Metallo-endofullerenes can be used as high-tem-

perature superconductors [5, 15–17], ferromagnetic materials [18], heterogeneous catalysts in organic synthesis and, in particular, in (de)hydrogenation [19], medicine, pharmacology, etc.

The aim of this study was to develop a simple technologically convenient single-stage method for synthesis of metallo-endofullerenes and an analytical method for their identification.

Metallo-endofullerenes were synthesized by the plasma-arc method [12] on an installation described in [13]. The electrode being evaporated, anode, had the form of a rod (ultrapure graphite, 99.999 wt % carbon) 12 mm in diameter. An orifice 1 mm in diameter was drilled in the electrode and a metallic wire of the same diameter was pressed into this orifice. The wire was composed of individual metals: Ni, Cr, Pd (99 wt %), or Nichrome alloy (with 40 wt % Cr). No metals were introduced into the cathode (12-mm graphite rod). The synthesis was performed in the atmosphere of ultrapure He (99.9995 vol %) at a pressure of about 300 mm Hg.

This synthesis method proved suitable only for sufficiently high-melting metals with melting points not lower than 1400°C. With lower-melting metals (e.g., Cu), microdrops of metals spattered and metal ions were not delivered in sufficient amounts to the plasma reaction zone, with the result that metallo-endofullerenes were not formed in noticeable amounts.

Samples were prepared for analysis as follows: the carbon black accumulated in the carbon-black receiver and in the reaction chamber after synthesis was collected and sieved on a sieve with a 40-μm mesh; the ordinary fullerenes and metallo-endofullerenes formed were extracted with *o*-xylene (analytically pure grade) at room temperature under vigorous stirring (magnetic stirrer) in the course of 60 min. The phase ratio in the extraction was 1 mg of carbon black per 1 ml of *o*-xylene (the solvent was taken in manyfold excess).

The solution of fullerenes was allowed to settle for 30 min and then twice filtered through a blue-band paper filter. The filtrate was evaporated to a humid paste on a rotary evaporator at 80±5°C. The paste was evaporated to constant weight in a vacuum oven for 150 min at 220–230°C and a residual pressure of 0.01–0.1 mm Hg (dynamic vacuum).

The expected forms of fullerenes in the resulting mixtures are the following: light (C_{60}, C_{70}) and heavy fullerenes (C_n, $n \geq 72$); subfullerenes (C_n, $n \leq 58$); fullerene oxides, the so-called epoxites (C_nO_m) formed because of the presence of oxygen or water vapor admixtures (the most probable is formation of monoxides of light fullerenes: $C_{60}O$ and, possibly, $C_{70}O$); metallo-endofullerenes C_nX_m (in this case, too, formation of mono derivatives of light fullerenes, $C_{60}X$ and, possibly, C_{70}, is the most probable).

Fullerene mixtures are commonly analyzed by the following methods: spectrophotometry (for proximate analysis), high-resolution liquid chromatography, mass spectrometry, and liquid chromatogeaphy–mass spectrometry (the latter technique is a combination of the second and third methods).

The spectrophotometric analysis [20] is suitable only for rough determination of the composition of a fullerene mixture in terms of light fullerenes and approximate estimation of the total content of fullerenes in the mixture and, therefore, cannot be used for our purposes.

Liquid chromatography was used in the mode described in [21]: Lumachrom chromatograph (manufactured by Lumex Co., St. Petersburg), with UV detection at a wavelength λ = 254 nm. A characteristic example of the chromatograms obtained is shown in Fig. 1. As can be seen from the chromatogram, all the fullerene groups mentioned above can be qualitatively identified. However, two groups of subfullerenes, "C_{60} companions," and the group C_{62}–C_{84}, "C_{70} companions," are eluted as two broad unresolved peaks. Even after a 10-fold increase in the device sensitivity, two well-resolved peaks of heavy fullerenes of the C_{76}–C_{84} group were followed by difficultly identifiable and poorly resolved broad peaks of mixed origin, associated with heavier fullerene groups C_{86}–C_{116} and, possibly, with some metallo-endofullerenes of uncertain composition. Thus, this method is equally unsuitable for precise quantitative determination of the fullerene composition of the mixtures obtained (including metallo-endofullerenes).

A mass-spectrometric method was developed for analysis of fullerene mixtures. This method enables quantitative determination of the concentrations of all the fullerene components of interest. For this purpose, we dissolved fullerene mixtures without a residue in *o*-xylene (analytically pure grade), with a solution containing 0.1 mg of a sum of fullerenes per 1 ml of solution. Then, a 1-ml sample of this solution was taken and transferred to a quartz cell. After that, the solvent was evaporated at 100°C, with the fullerenes (about 100 μg) forming in the process a thin yellowish film on the quartz surface. The mass-spectrometric analysis was made on an MKh-1320 instrument at a pressure of 10^{-7} mm Hg, sublimation temperature of

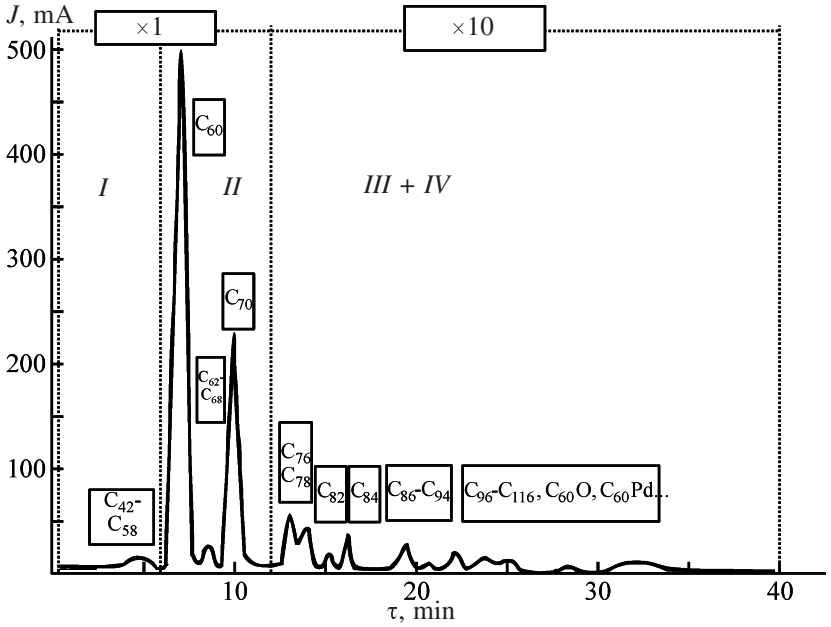

Fig. 1. Chromatogram of a fullerene extract containing subfullerenes, light and heavy fullerenes, monoxides of light fullerenes, and PdC_{60}. (*J*) Current strength and (τ) elution time. (*I*) Subfluuerenes, (*II*) light fullerenes, (*III*) heavy fullerenes, and (*IV*) fullerene derivatives; the same for Fig. 3.

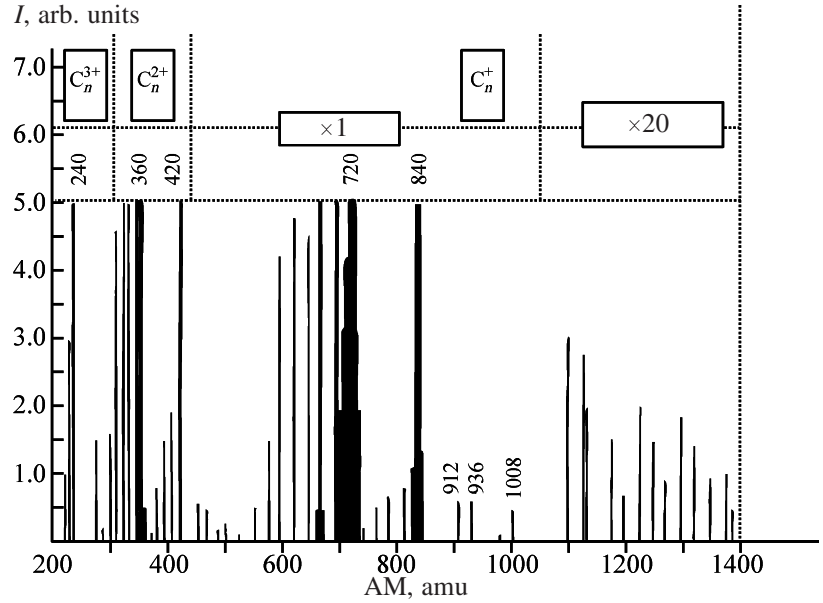

Fig. 2. Mass spectrogram of a fullerene extract containing subfullerenes, light and heavy fullerenes, monoxides of light fullerenes, and PdC_{60}. (*I*) Ion current and (AM) atomic mass.

250–480°C, and ionization by electron impact (ionization energy 10–100 eV). In the course of the analysis, all the fullerene components were nearly completely evaporated from the surface of the quartz cell (analysis for the residual content of fullerenes on the cell of the KU brand was made spectrophotometrically by the light absorption at a wavelength λ = 335.67 nm, common to the absorption by light fullerenes [20]).

As a result, we obtained mass spectra whose typical shape is schematically shown in Fig. 2 (chromatogram of a Pd-containing fullerene extract). Figures 3a–3c show the same mass spectrograms on the more convenient semilog scale. Similar mass spectrograms were obtained for fullerene extracts containing individual Ni and Cr. However, these spectra exhibited no specific features, compared with those in Fig. 3c, and, therefore, are not presented here.

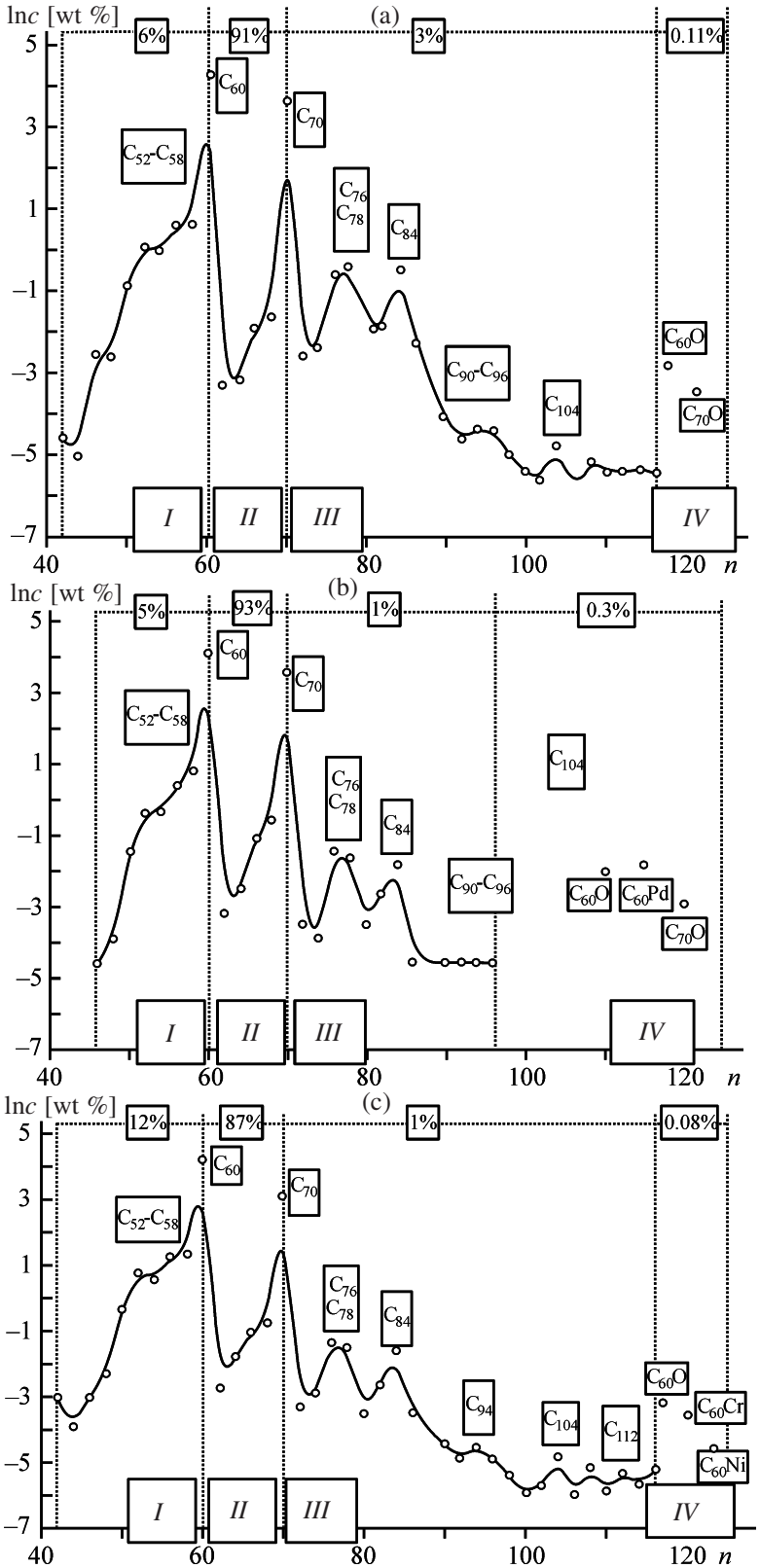

Fig. 3. Mass spectrograms of fullerene extracts containing (a) subfullerenes, light and heavy fullerenes, and monoxides $C_{60}O$ ($C_{70}O$), (b) PdC_{60}, and (c) NiC_{60} + CrC_{60}. (*c*) Content of a fullerene in the mixture and (*n*) number of carbon atoms in C_n fullerene. (a) Standard nonmetallized extract from a mixture of fullerenes for comparison, (b) Pd-containing fullerene extract, and (c) (Ni + Cr)-containing fullerene extract.

Figure 2 shows sets of peaks corresponding to different extents of nondestructive ionization of fullerenes, which increase in the series $C_n^{3+} \rightarrow C_n^{2+} \rightarrow C_n^+$ (in Fig. 3, these intensities corresponding to a single fullerene form are summed up).

When recording the mass spectrogram shown in Fig. 2, we raised the instrument sensitivity by a factor of 20, beginning with fullerene atomic masses exceeding 1050 amu.

It can be seen from Figs. 2 and 3 that this analytical technique enabled quantitative determination of the concentrations of all forms of fullerenes, including fullerene derivatives: metallo-endofullerenes and epoxides.

The results obtained in extraction and mass-spectrometric measurements demonstrate the following: (i) the total content of all the fullerene components contained in the fullerene black is virtually independent of whether or not metallic phases are present in the anode and equal to 12 ± 1 wt % (typical value for the installation described in [13]); (ii) the ratio of the main fullerene components, light fullerenes C_{60} and C_{70}, is also nearly insensitive to presence of metallic phases and equal to about 2.5/1.0; (iii) the content of metallo-endofullerenes of the types $C_{60}Pd$, $C_{60}Ni$, and $C_{60}Cr$ in a mixture of extracted fullerenes is in the range from 0.05 wt % (for $C_{60}Pd$ and $C_{60}Ni$, irrespective of whether Ni or Cr are introduced into the anode, or both these metals simultaneously) to 0.15 wt % (for $C_{60}Pd$); (iv) upon introduction of Ni and/or Cr, the content of subfullerenes in the fullerene black substantially increases; and (v) no metallo-endofullerenes are found in the fullerene black upon introduction of a lower-melting metal (Cu) into the anode.

In the context of discussion of the results obtained, we note some additional fundamental issues.

(1) The paper describes syntheses of just endo forms of light-fullerene derivatives, i.e., metal atoms are situated in these compounds within the carbon skeleton of fullerenes. It is clear that direct mass-spectrometric measurements cannot answer the question as to what form, endo or exo (with a metal atom outside the fullerene carbon skeleton), of metallofullerenes is formed in a synthesis. Although we did not carry out additional labor-consuming spectral studies capable of tackling with this issue in a direct experimental way, the answer seems to be quite obvious because, on the one hand, no metallo-exofullerene of the type $C_{60}Me_n$ or $C_{70}Me_n$ has been synthesized so far (whereas the tens of metallo-endofullerenes have been synthesized and identified) and, on the other hand, even rough quantum-mechanical calculations demonstrate that, just for metallofullerenes, formation of endo forms is strongly preferential, compared with exo forms.

(2) Despite that the content of the synthesized metallo-endofullerenes in the samples obtained is comparatively low, up to 0.15 wt % in the sum of fullerene products, their preparative recovery even in comparatively large amounts (grams) is not difficult because (according to the results of a preliminary study) the solubility of metallo-endofullerenes in some heterocyclic compounds, e.g., pyridine, markedly exceeds that of their nonmetallized analogues, C_{60} and C_{70}, which, in turn, are considerably better soluble in ordinary aromatic solvents, e.g., *o*-xylene. Thus, rather pure materials (<90 wt %) can be produced in a rather simple way by the method of recrystallization recovery of metallo-endofullerenes at a comparatively low recovery loss. Micro- and milligram amounts of metallo-endofullerenes can, naturally, be extracted by liquid chromatography.

(3) The output capacity of the method we develop can be improved (or, in other words, the fraction of metallo-endofullerenes in the sum of fullerene products can be made larger), with its operation principle [12, 13] preserved, by raising, based on general considerations, the mass fraction of metals in the metal–carbon–helium plasma in the zone of preferential formation of metallo-endofullerenes (1500–4000 K). A probably good solution in this case would be removal of heat from metals in the reactor plasma by heavier molecules of inert gases (with He possibly replaced with Ne or Ar). However, in addition to the expected rise in the fraction of metallo-endofullerenes in the sum of fullerenes, such a replacement might lead to a simultaneous decrease in the total content of fullerenes in the fullerene black, so that such a technological modification would require a rather prolonged optimization.

CONCLUSIONS

A comparatively simple and low-cost direct single-stage plasma-arc method for synthesis of metallo-endofullerenes and a proximate technique for their identification in the fullerene black were developed.

The synthesis was performed for the example of metallo-endo derivatives of light fullerenes, C_{60} and C_{70}, with Ni, Cr, and Pd used as metals.

ACKNOWLEDGMENTS

The study was supported by the Federal Target Research Program "Research and Development in Priority Areas of Science and Technology" for 2002–2006 (State contract no. 02.467.11.7005 of May 23, 2005).

REFERENCES

1. Sidorov, L.N., Yurovskaya, M.A., Borshchevskii, A.Ya., et al., *Fullereny* (Fullerenes), Moscow: Ekzamen, 2005.
2. Heath, J.R., O'Brien, S.C., Zhang, Q., et al., *J. Am. Chem. Soc*., 1985, vol. 107, pp. 7779–7793.
3. Shinohara, H., *Rep. Prog. Phys*., 2000, vol. 63, pp. 843–851.
4. Trefilov, V.I., Shchur, D.V., Tarasov, B.P., et al., *Fullereny – osnovy materialov budushchego* (Fullerenes as a Basis for Materials of the Future), Kiev: ADEF-Ukraina, 2001.
5. Prassides, K., Kroto, H.W., Taylor, R., et al., *Carbon*, 1992, vol. 30, no. 8, pp. 1277–1286.
6. JPN Patent 05 238 717.
7. JPN Patent 5 004 810.
8. FR Patent 2 710 049.
9. EP Patent 568 918.
10. EP Patent 646 644.
11. US Patent 5 273 729.
12. WO Patent 2005/070 826.
13. WO Patent 2005/087 662.
14. Guo, T., Diener, M.D., Chai, J., et al., *Science*, 1992, vol. 257, pp. 1661–1693.
15. Haddon, R.C., *Acc. Chem. Res*., 1992, vol. 25, pp. 127–133.
16. JPN Patent 05 238 885.
17. US Patent 5 380 703.
18. JPN Patent 6 102 547.
19. EP Patent 635 515.
20. Ponomarev, A.N., Yudovich, M.E., Nikitin, V.A., et al., *Opt. Spectrosc*., 2000, vol. 88, no. 2, pp. 195–197.
21. *GOST* (State Standard) *8.563–96, Certification of MVI no. 242/81–2004.*

ISSN 1070-4272, Russian Journal of Applied Chemistry, 2007, Vol. 80, No. 11, pp. 1894–1897. © Pleiades Publishing, Ltd., 2007.
Original Russian Text © Yu.N. Sazanov, L.I. Kutsenko, D.M. Kostycheva, A.M. Bochek, 2007, published in Zhurnal Prikladnoi Khimii, 2007, Vol. 80, No. 11, pp. 1870–1873.

MACROMOLECULAR CHEMISTRY AND POLYMERIC MATERIALS

Thermochemical Reactions of Flax Lignocarbohydrate Complexes and Their Cyanoethylated Derivatives

Yu. N. Sazanov, L. I. Kutsenko, D. M. Kostycheva, and A. M. Bochek

Institute of Macromolecular Compounds, Russian Academy of Sciences, St. Petersburg, Russia

Received April 5, 2007

Abstract—A thermochemical study of short flax fibers and boon and of their cyanoethylated derivatives was made with the aim to examine the possibility of preparing carbonized materials.

DOI: 10.1134/S1070427207110225

The development of technologies for production of carbon materials by industrial processing of cheap plant wastes whose volumes are very large is a topical problem. This problem is closely associated with utilization of wastes from production of linen articles and with the development of a wasteless technology of flax processing. The studies pursued today concern utilization of wastes from production of flax fibers [lignocarbohydrate complex including short flax fibers (SFFs) and ligneous part of flax stems (boon)] as cellulose raw materials to replace cotton linter and wood cellulose.

It is known that various cellulose derivatives [1–4], carbon adsorbents [5, 6], and building materials [7] can be prepared from SFFs and boon [1–4]. Gribanov and Sazanov [8, 9] showed that nitrogen atoms play an important role in formation of structures of carbon materials in the course of carbonization of heteropolymers. This phenomenon was also noted in studies of carbonization of some cellulose ethers and esters [10, 11] and of cocarbonization of polyacrylonitrile with chitin and chitosan [12, 13].

In this study we examined thermochemical reactions of lignocarbohydrate complexes of SFFs and boon and of their cyanoethylated derivatives (CEFFs, CEB) with the aim to assess prospects for carbonization of these products.

EXPERIMENTAL

As starting materials we used SFFs (degree of polymerization of cellulose 3350) and boon (degree of polymerization of cellulose 2600). The degree of polymerization of cellulose in the starting samples was determined according to [14]. The cellulose materials used in the study were examined by the methods described in [15–17] to determine the chemical composition (see table). To prepare cellulose ethers, SFFs and boon were purified to remove waxes, fats, and resins by treatment with an alcohol–benzene (1 : 1 by volume) mixture in a Soxhlet apparatus, and pectins were removed by treatment with an aqueous solution of ammonium citrate. Boon was finely divided in a knife mill. Cyanoethyl ethers of cellulose were prepared as follows:

$$C_6H_7O_2(OH)_3 + xCH_2{=}CH{-}CN \xrightarrow{NaOH} C_6H_7O_2(OCH_2{-}CH_2CN)_x(OH)_{3-x}.$$

Prior to cyanoethylation, SFFs and boon were allowed to swell in an excess of a mixture of 7% aqueous NaOH and dimethyl sulfoxide (volume ratio 1.5 : 1) at 20°C for 2 h. After sqeezing to triple initial weight, the cellulose material was treated with excess

Chemical composition of flax fibers and boon used

Component	Content, wt %	
	boon	fibers
Ash	2.1	1.3
Fats, waxes	2.0	1.2
Lignin	31.6	4.9
Cellulose	47.2	72.1
Pectin	2.5	1.2
Hemicelluloses	7.8	13.8
Moisture	6.4	5.2

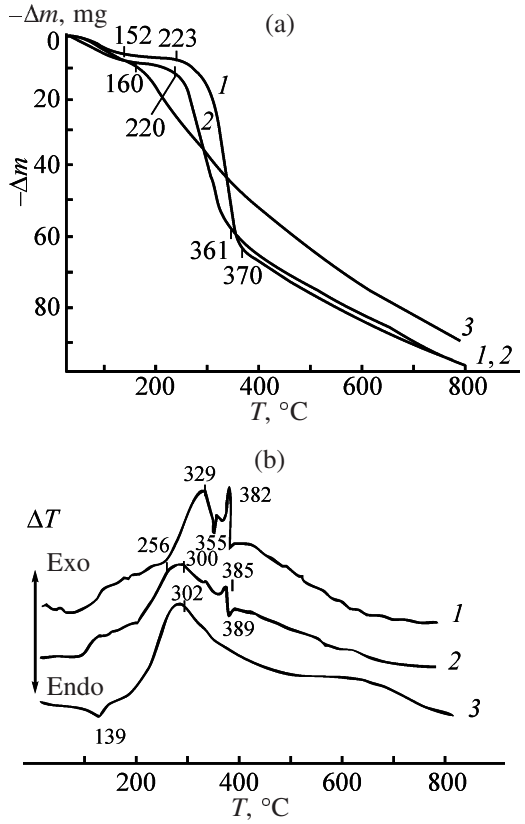

Fig. 1. (a) TG and (b) DTA curves of samples of (*1*) SFFs, (*2*) boon, and (*3*) lignin. (Δ*m*) Weight loss on heating in air at a rate of 10 deg min^{-1} and (*T*) temperature; the same for Fig. 2.

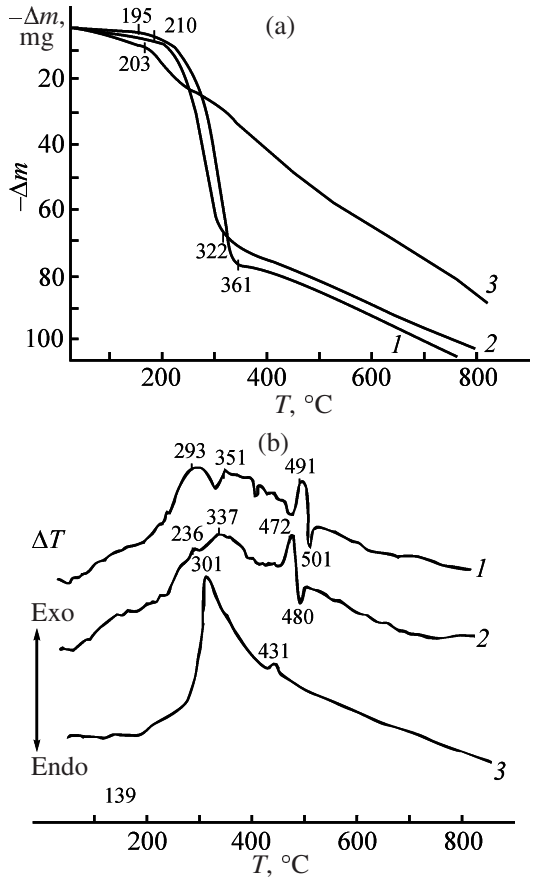

Fig. 2. (a) TG and (b) DTA durves of samples of (*1*) CEFFs, (*2*) CEB, and (*3*) LG + PAN blend (3 : 1 by weight).

acrylonitrile at 20°C for 24 h. After the reaction completion, excess NaOH was neutralized with an aqueous solution of acetic acid, after which excess acrylonitrile was removed by extraction with ethanol. The washed samples were dried at room temperature. The nitrogen content of the samples was determined by the Kjeldahl method. It amounted to 12 wt % in flax fibers and 10.9 wt % in boon. It should be noted that, in contrast to cyanoethylated flax fibers, samples of chemically modified boon retain a certain fraction of lignin. This fact is confirmed by the presence of the lignin absorption band at 1512 cm^{-1} [4] in the IR spectra of the initial and cyanoethylated boon.

Thermal analysis of samples (50 mg) was performed on a C derivatograph (MOM) in air under conditions of dynamic heating (10 deg min^{-1}).

Thermal analysis shows (Figs. 1, 2) that SFFs and boon, as well as their cyanoethylated derivatives, degrade on heating to 800°C in three steps. The temperature limits of these steps are close for all the samples; nevertheless, there are certain specific features. For example, for SFFs, the weight loss due to removal of residual volatiles (solvents, washing, etc.), observed on heating to 152°C, is about 5%, whereas for boon it is about 8% of the initial weight. The second step of degradation of SFFs and boon, with a major weight loss (48–55%), starts at 220–223°C and involves thermal oxidative degradation of cellulose macromolecules. In this step, a certain difference is observed between SFFs and boon, attibutable to the presence of residual lignin in boon. Thus, before the onset of carbonization (third step), SFFs lose about 65% of their weight, and the weight loss of boon is approximately 10% smaller. Carbonization occurs in the typical mode of uniform weight loss starting from 360–370°C and is complete at 800°C when the residue fully burns out. In this step, there are no sharp changes in the weight loss rate; however, thermal effects with maxima at 355, 382°C for SFFs and 385, 389°C for boon (Fig. 1b, curves *1*, *2*) should be noted. These effects can be assigned to the formation of oriented phases in the initial step of carbonization of both samples.

Thus, SFFs and boon are promising raw materials for preparing carbon materials with carbon residues

exceeding those of cotton cellulose. This is seen from comparison of data on carbonization of these natural compounds under the conditions of dynamic heating to temperatures in the range from 400 to 800°C. The carbon residues of cotton linter at 400, 500, 600, 700, and 800°C, according to [28], are 20, 17, 8.5, 1.5, and 0%, respectively, whereas for SFFs and boon (in parentheses) the carbon residues are 30 (37), 24 (29), 16 (18), 8 (11), and 2% (2), respectively.

As for cyanoethylated samples of SFFs and boon (Fig. 2), their behavior is essentially similar to that of the initial samples. The effect of cyanoethyl groups is noticeable in the first step of thermal degradation: The initial weight loss tends to zero, apparently because the samples are more hydrophobic. The weight loss in the second step of thermal degradation increases by 12–18 wt % compared to SFFs and boon. This fact is apparently associated with loosening of the structure of the starting compounds due to introduction of bulky cyanoethyl substituents and to a decrease in the relative content of hydroxy groups responsible for intermolecular bonds in SFFs and boon. The above-noted differences in the thermal stability, caused by significant amount of lignin in the boon, are also preserved in the cyanoethylated samples, which is clearly seen from the carbonization parameters (third step, from 322 to 800°C, Fig. 2a, curve *2*). The role of nitrogen atoms in the formation of carbonized structures via cyanoethylation of SFFs and boon cannot be unambiguously interpreted on the basis of only one series of thermal measurements. For example, no effect of nitrogen can be noticed from the parameters of thermal stability derived from TG curves at a constant heating rate (Fig. 2a). However, in the third step of degradation, internal changes in the carbonization products can be revealed from the shape of the DTA curves (Fig. 2b). The above-noted exo- and endothermic effects associated with probable formation of partially ordered structures shifted toward higher temperatures by approximately 100°C. The exothermic peaks with maxima at 491 and 472°C (curves *1*, *2*) can be characterized as effects of crystallization, similar to those noted in [11] for samples of cyanoethyl cellulose and its blends with polyacrylonitrile. Apparently, the participation of nitrile groups in carbonization of SFFs and boon provides the conditions for the formation of intermediate nitrogen-containing cyclic compounds giving rise to exo- and endothermic effects in the DTA curves. It should also be noted that increased heat resistance of CEB compared to CEFFs, observed also for the corresponding noncyanoethylated samples (Fig. 1a) and attributed to the presence of lignin in boon, gives grounds to consider thermochemical reactions of lignin and its blends with polyacrylonitrile (PAN) by analogy with [10–12]. The assumption that lignin (LG) enhances the heat resistance of boon is confirmed by the thermograms of LG and LG + PAN (Figs. 1 and 2, curves *3*). The results of these measurements show that, starting from 300°C and up to 800°C, the thermal degradation of LG is accompanied by smaller weight loss compared to SFFs and boon. Introduction of 25% polyacrylonitrile into an LG sample by blending the powdered components did not noticeably affect the course of thermal degradation of lignin. Hence, for the nitrile nitrogen to act as initiator of thermochemical synthesis of a new carbonizate derived from LG, the conditions of heat treatment should be changed essentially, in accordance with principles of cocarbonization [19].

CONCLUSIONS

(1) Carbonized products of flax processing: short flax fibers, flax, and ligneous part of stems (boon), are promising carbon materials for preparing sorbents.

(2) The presence of residual lignin in flax enhances the heat resistance of carbonization products and increases the carbon residue.

(2) The nitrogen atoms of nitrile groups of cyanoethylated derivatives of flax and boon affect the formation of carbonized residues.

REFERENCES

1. Bazarnova, N.T., Tokareva, N.V., and Galochkin, A.I., Abstracts of Papers, *III Vserossiiskoe soveshchanie "Lesokhimiya i organicheskii sintez"* (III All-Russian Meet. "Wood Chemistry and Organic Synthesis"), Syktyvkar, 1998, p. 55.
2. Kutsenko, L.I., Karetnikova, E.B., Bochek, A.M., and Petropavlovskii, G.A., Abstracts of Papers, *Vserossiiskaya konferentsiya "Khimiya i tekhnologiya rastitel'nykh veshchestv"* (All-Russian Conf. "Chemistry and Technology of Plant Substances"), Syktyvkar, September 25–30, 2000, p. 110.
3. Kutsenko, L.I., Bochek, A.M., and Vlasova, E.N., *Resursy, Tekhnol., Ekon.*, 2004, no. 6, pp. 31–33.
4. Kutsenko, L.I., Bochek, A.M., Vlasova, E.N., and Volchek, B.Z., *Zh. Prikl. Khim.*, 2005, vol. 78, no. 12, pp. 2075–2079.
5. Abramov, M.V., Gal'braikh, L.A., Tyulina, R.M., and Yaroslavtsev, V.G., *Izv. Vyssh. Uchebn. Zaved., Tekhnol. Tekstil'n. Prom–sti.*, 1994, no. 5, pp. 18–20.
6. Elets, L.V., Levit, R.M., Strukova, I.M., et al., *Khim. Volokna*, 1996, no. 6, pp. 20–22.

7. Vasil'ev, V.V. and Komarov, E.E., in *Tekhnologiya drevesnykh plit i plastikov* (Technology of Wood Boards and Plastics), Yekaterinburg: Ural. Gos. Lesotekh. Akad., 1994, pp. 51–55.
8. Gribanov, A.V. and Sazanov, Yu.N., *Zh. Prikl. Khim.*, 2000, vol. 73, no. 3, pp. 465–469.
9. Gribanov, A.V. and Sazanov, Yu.N., *Zh. Prikl. Khim.*, 1997, vol. 70, no. 6, pp. 897–901.
10. Sazanov, Yu.N., Nud'ga, L.A., Petrova, V.A., et al., *Zh. Prikl. Khim.*, 2004, vol. 77, no. 8, pp. 1366–1369.
11. Sazanov, Yu.N., Kutsenko, L.I., and Novoselova, A.V., *Zh. Prikl. Khim.*, 2005, vol. 78, no. 4, pp. 652–654.
12. Sazanov, Yu.N., Novoselova, A.V., Nud'ga, L.A., et al., *Zh. Prikl. Khim.*, 2005, vol. 78, no. 8, pp. 1344–1348.
13. Sidorovich, A.V., Sazanov, Yu.N., Praslova, O.E., et al., *Zh. Prikl. Khim.*, 2006, vol. 79, no. 8, pp. 1341–1344.
14. Nikitin, N.I., *Khimiya drevesiny i tsellyulozy* (Chemistry of Wood and Cellulose), Moscow: Akad. Nauk SSSR, 1962.
15. Bochek, A.M., Shevchuk, I.L., and Lavrent'ev, V.N., *Zh. Prikl. Khim.*, 2003, vol. 76, no. 10, pp. 1725–1728.
16. *Spravochnik khimicheskoi tekhnologii obrabotki l'nyanykh tkanei* (Handbook of Chemical Technology of Treatment of Linen Fabrics), Fridlyand, I.G., Ed., Moscow: Legkaya Industriya, 1973.
17. Bochek, A.M., Zabivalova, N.M., Shamolina, I.I., et al., *Zh. Prikl. Khim.*, 2002, vol. 75, no. 9, pp. 1549–1554.
18. Sazanov, Yu.N., Larina, E.I., and Petropavlovskii, G.A., Abstracts of Papes, *VII konferentsiya po stareniyu i stabilizatsii polimerov* (VII Conf. on Aging and Stabilization of Polymers) (Dushanbe, 1988), Chernogolovka, 1989, pp. 47–48.
19. Sazanov, Yu.N. and Gribanov, A.V., *Zh. Prikl. Khim.*, 2006, vol. 79, no. 3, pp. 440–445.

ISSN 1070-4272, Russian Journal of Applied Chemistry, 2007, Vol. 80, No. 11, pp. 1898–1901. © Pleiades Publishing, Ltd., 2007.
Original Russian Text © E.O. Kazyuka, A.P. Polikarpov, I.G. Poplevka, Yu.I. Matusevich, L.B. Yakimtsova, L.P. Krul', 2007, published in Zhurnal Prikladnoi Khimii, 2007, Vol. 80, No. 11, pp. 1874–1877.

MACROMOLECULAR CHEMISTRY AND POLYMERIC MATERIALS

Thermal Properties of Copolymerization Products of Methyl Methacrylate with Methacrylamide

E. O. Kazyuka, A. P. Polikarpov, I. G. Poplevka, Yu. I. Matusevich, L. B. Yakimtsova, and L. P. Krul'

Belarussian State University, Minsk, Belarus
Research Institute of Physicochemical Problems, Belarussian State University, Minsk, Belarus
Institute of Physical Organic Chemistry, National Academy of Sciences of Belarus, Minsk, Belarus

Received April 10, 2007

Abstract—Radical copolymerization of methyl methacrylate and methacrylamide was studied. For polymer films prepared from acetic acid solutions, the heat resistance and thermomechanical behavior were evaluated, and adhesion to silicate glass was determined.

DOI: 10.1134/S1070427207110237

Much attention is given today to the development and improvement of optical information technologies, because their capabilities with respect to the information transfer rate and information content and to the performance of separate components are significantly higher as compared to microelectronics [1]. Among the materials for recording and treatment of optical information, exhibiting high optical transparency in the visible region and relative stability of the recorded information in a wide temperature range, various polymers, e.g. polymethyl methacrylate (PMMA), are of particular importance [2–4]. However, low thermal and adhesion properties hindering their use in optical recorders operating in contact with silicate glass at elevated temperatures are the main disadvantages of the materials based on PMMA.

Modification of PMMA by copolymerization of methyl methacrylate (MMA) with polar monomers, yielding polymers with a higher softening point [5, 6], is one of solutions of this problem. Methacrylamide (MAA) [5] and acrylic acid [6] were studied as such polar monomers. Kuo et al. [5] examined in detail the composition of the copolymerization products of MMA and MAA and the dependence of the glass transition point (DSC data) on the content of methacrylamide units in the copolymer. However, there are no data on changes in the other thermal properties of PMMA on passing to the copolymerization products of MMA and MAA and on the adhesion properties of the resulting copolymers.

In this study we examined the heat resistance and the thermomechanical and adhesion properties of the products of MMA and MAA copolymerization.

EXPERIMENTAL

The radical copolymerization of MMA and MAA was performed in a 40% solution of the monomer mixture in acetone at 57°C for 5 h in the presence of 2,2'-azobis(isobutyronitrile) (AIBN) initiator taken in an amount of 0.2% with respect to the monomer weight. The MAA : MMA molar ratio was varied from 1 : 4 to 3 : 2, i.e., the mole fraction of MAA in the monomer mixture α was varied from 0.2 to 0.6.

The synthesis was carried out in a three-necked flask equipped with a mechanical stirrer with a hydraulic lock and a reflux condenser. A weighed portion of MAA was dissolved in acetone at 40°C with continuous stirring, and then freshly distilled MMA was added. The mixture was heated to 55°C, and the required amount of the initiator was added. The reaction began in 10–15 min, which was confirmed by formation of a precipitate after addition of an aliquot of the reaction mixture into ethanol. Simultaneously, the viscosity of the reaction mixture increased. After heating for 5 h, the reaction mixture was cooled and the reaction products were reprecipitated from acetone with water and additionally washed with acetone.

The homopolymerization of MMA and MAA was also performed in a 40% monomer solution in acetone

at 57°C using AIBN initiator (0.2% with respect to the monomer weight), the synthesis time was 5 h. PMMA was soluble in acetone, and it was separated by precipitation with water. Polymethacrylamide (PMAA) precipitated from the acetone solution in the course of the synthesis, and the residual monomer was washed out with acetone.

The compositions of the resulting samples were determined by IR spectroscopy. As analytical bands for the products of copolymerization of MMA and MAA we chose strong absorption bands at 1730 and 1650 cm^{-1}, belonging to the vibration of the carbonyl group in the ester and amide side functional groups. The calibration dependences of the optical densities of the absorption bands at 1730 and 1650 cm^{-1} on the mole fraction of the MAA units were plotted using the IR data for the mixtures of MMA and MAA homopolymers. The content MAA units in copolymer β was expressed in mole fractions.

The heat resistance and the glass transition and flow points of the copolymerization products of MAA and MMA were studied by the methods of combined thermal and thermomechanical analysis. The combined thermal analysis was performed on an MOM OD-103 derivatograph (Hungary) in air at a heating rate of 5 deg min^{-1} using 100-mg samples. The thermomechanical analysis was carried out on a UIP-70 apparatus (TsKB UP, USSR Academy of Sciences) in air at the same heating rate; the pressure applied to the sample was 0.59 MPa. The glass transition and flow points were evaluated using the dependences of the relative yield-point strain ε (%) on temperature T (°C).

The polymer samples for thermal and thermomechanical tests were prepared from 6% acetic acid solutions. These solutions were cast onto glass or polypropylene plates and dried at 90°C to remove the solvent. The completeness of solvent removal from the films (~50 μm thick) was controlled by the absence in the IR spectrum of the absorption band in the 1690–1700 cm^{-1} region typical for the vibrations of the carbonyl group in the carboxy group of acetic acid. The spectra of the PMMA films prepared from acetic acid solutions and water are identical. This suggests that, owing to high volatility, acetic acid completely evaporated from the films upon drying and did not affect the results of thermal analysis. The adhesion properties were evaluated from the strength of their adhesion to silicate glass support.

Along with radical copolymerization of MMA and MAA, homopolymerization of these monomers could also take place. Since polymerization occurs in an acetone solution of the monomers and among three possible products (namely, copolymer of MAA and MAA, MMA homopolymer, and MAA homopolymer) only two compounds are soluble in acetone, the resulting product can contain not only the copolymer but also MMA homopolymer. The monomers were completely removed by precipitation of the product from acetone solution with water, followed by washing with acetone, because MAA and MMA are readily soluble in water and acetone, respectively. The yield of the polymerization products was higher than 80%, and the MMA : MAA molar ratio depended on the mole fraction of MAA in the initial monomer mixture. For example, α 0.3 corresponded to β 0.35, and α 0.4, 0.5, and 0.6, to β 0.65, 0.67, and 0.78, respectively. At a low content of MAA in the monomer mixture (α 0.2), the composition of the monomer mixture coincided with the copolymer composition. At a higher content of MAA in the monomer mixture, the product was enriched in MAA units.

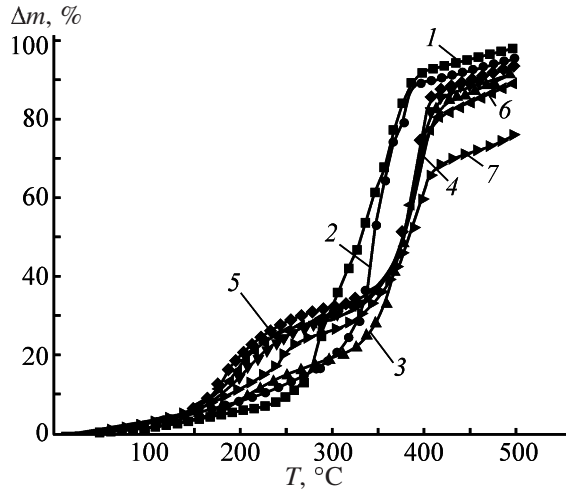

Fig. 1. Weight loss Δm of (*1*) PMMA, (*2–6*) products of MMA and MAA copolymerization, and (*7*) PMAA as a function of temperature T. β: (*2*) 0.2, (*3*) 0.35, (*4*) 0.65, (*5*) 0.67, and (*6*) 0.78.

Casting of the solutions of the copolymerization products of MAA and MMA onto supports led to the formation of optically transparent films, except the sample with β 0.78 when an opaque milk-white film was obtained.

The results of thermal analysis of the products of MAA and MMA copolymerization are illustrated in Fig. 1. In the 20–170°C range, the weight loss Δm for all the samples is similar. In the 170–270°C range corresponding to intensive degradation of the samples, Δm of the copolymerization products with β 0.65–0.78 (Fig. 1, curves *4–6*) is higher than that of the homopolymers (Fig. 1, curves *1* and *7*); Δm for co-

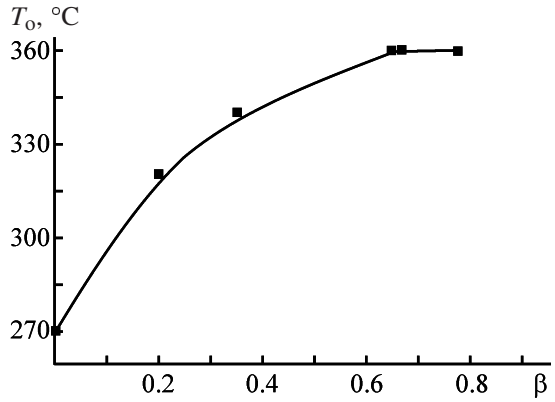

Fig. 2. Onset temperature T_o of intensive degradation of the products of MMA and MAA copolymerization as a function of the content of MAA units β.

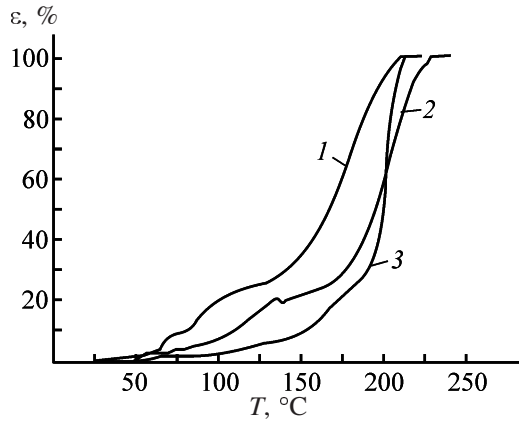

Fig. 3. Relative yield-point strain of (*1*) PMMA and (*2, 3*) products of MMA and MAA copolymerization as a function of temperature *T*. β: (*2*) 0.2 and (*3*) 0.78.

polymers with β 0.2–0.35 is intermediate between the weight losses of PMMA and PMAA, i.e., the heat resistance of PMMA in the given temperature range is higher. However, at temperatures higher than 300°C, Δm for copolymerization products is smaller than that for PMAA, which indicates that their thermal stability increases as compared to PMMA, and the smallest weight loss is observed for PMAA. Probably, thermal oxidative stability depends on both the composition of the products of MAA and MMA copolymerization and on the experimental temperature. With increasing β from 0.2 to 0.78, the onset temperature of intensive degradation T_d of the copolymerization products increases from 320 to 360°C (Fig. 2). Probably, in the initial stage of degradation the MMA–MAA copolymer exhibits higher thermal stability compared to PMAA and PMMA. The thermomechanical curves of the initial PMMA and products of MMA and MAA copolymerization are shown in Fig. 3. As can be seen, the thermomechanical curve for PMMA is typical for amorphous polymer, and we can determine the temperature ranges corresponding to glassy, hyperelastic, and viscous-flow states. The transition points from glassy to hyperelastic state (glass transition point T_g) and from hyperelastic to viscous-flow state (flow point T_f) for PMMA are 63 and 155°C, respectively. The thermomechanical curve for the copolymer with β 0.2 is principally similar to that of PMMA except higher glass transition and flow points (T_g 82°C, T_f 183°C). For both samples, the deformations corresponding to the hyperelastic state are similar. With increasing β to 0.78, the glass transition and flow points increase to 150 and 193°C, respectively. Owing to small difference between T_g and T_f, the region of hyperelastic state is poorly pronounced.

Thus, copolymerization of MMA and MAA yields the products with higher softening temperatures as compared to PMMA. Copolymerization increases not only the glass transition point (as shown previously [5]), but also the flow point. Moreover, on passing from PMMA to the products of MMA and MAA copolymerization, the adhesion of the polymer film to the glass support increased according to qualitative estimates.

CONCLUSIONS

(1) Copolymerization of methyl methacrylate and methacrylamide increases the glass transition and flow points and the heat resistance of the polymer and enhances its adhesion to silicate glass supports.

(2) The effect of increase in the glass transition and flow points and in the heat resistance on passing from polymethyl methacrylate to the copolymerization products of methyl methacrylate and methacrylamide increases with increasing content of methacrylamide units in the polymer, but at a high content of these units (β 0.78) the film losses its transparency.

(3) The films prepared from the copolymerization products of methyl methacrylate and methacrylamide at $\beta < 0.78$ show promise as a polymer support for design of optical recorders operating in contact with silicate glass at elevated temperatures.

REFERENCES

1. Kar Ajoi, K., *Polym. Adv. Technol.*, 2000, vol. 11, nos. 8–12, pp. 553–559.
2. Veniaminov, A.V. and Sedunov, Yu.Yu., *Vysokomol. Soedin., Ser. A*, 1996, vol. 38, no. 1, pp. 71–76.

3. Steckman, G.J., Solomatine, I.O., Zhou, G., and Psaltis, D., *Opt. Lett*., 1998, vol. 23, no. 16, pp. 1310–1312.

4. Andreeva, O.V., in *Problemy kogerentnoi i nelineinoi optiki: Sbornik statei* (Problems of Coherent and Nonlinear Optics: Coll. of Papers), St. Petersburg: Sankt-Peterb. Gos. Univ. Tochnoi Mekhaniki i Optiki, 2004, pp. 58–90.

5. Kuo, S.-W., Kao, H.-C., and Chang, F.-C., *Polymer*, 2003, vol. 44, p. 6873–6882.

6. Krul', L.P., Matusevich, Yu.I., Matusevich, V.Yu., et al., Abstracts of Papers, *Mezdunarodnaya konferentsiya po organicheskoi khimii "Organicheskaya khimiya ot Butlerova i Beil'shteina do sovremennosti"* (Int. Conf. on Organic Chemistry "Organic Chemistry from Butlerov and Beilstein to the Present Time"), St. Petersburg, 2006, pp. 192–193.

ISSN 1070-4272, Russian Journal of Applied Chemistry, 2007, Vol. 80, No. 11, pp. 1902–1905. © Pleiades Publishing, Ltd., 2007.
Original Russian Text © T.K. Chalov, E.E. Ergozhin, A.I. Nikitina, T.V. Kovrigina, K.Kh. Khakimbolatova, 2007, published in Zhurnal Prikladnoi Khimii, 2007, Vol. 80, No. 11, pp. 1878–1881.

MACROMOLECULAR CHEMISTRY AND POLYMERIC MATERIALS

Mechanism of Polycondensation of Allyl Bromide, Epichlorohydrin Oligomer, and Polyethylenimine

T. K. Chalov, E. E. Ergozhin, A. I. Nikitina, T. V. Kovrigina, and K. Kh. Khakimbolatova

Bekturov Institute of Chemical Sciences, Ministry of Education and Science of the Kazakhstan Republic, Almaty, Kazakhstan

Received January 31, 2007; in final form, September 2007

Abstract—The kinetics of polycondensation of allyl bromide, epichlorohydrin oligomer, and polyethylenimine was studied. The rate constants and activation energies were determined.

DOI: 10.1134/S1070427207110249

The kinetic parameters and relationships of chemical reactions are the main quantitative characteristics necessary for providing a basis for efficient control of chemical processes [1]. In studying kinetic characteristics of practically all reactions, one of the most important experimental problems is determination of how the concentrations of the reaction participants vary in time. A very promising and convenient method for studying kinetics and mechanism of chemical reactions, among them polymerization and polycondensation in solutions, is classic polarography, in which the error in determination of the monomer concentration is 2–3 rel %.

Previously [2] we developed procedures of synthesis of anion exchangers based on allyl bromide, epichlorohydrin oligomer, and polyethylenimine, and studied their main physicochemical characteristics [2].

Here we report on a polarographic study of the kinetics of polycondensation of the above compounds.

EXPERIMENTAL

Dimethylformamide (DMF) of pure grade was dried over calcium hydride and distilled at 44–45°C/15 mm Hg; n_D^{20} 1.4300 (bp 153°C/1013 hPa [3]).

Epichlorohydrin (ECH) of chemically pure grade was dried over calcium hydride and distilled; the fraction boiling at 115–116°C/918 kPa was collected; n_D^{20} 1.4380 (bp 161.1°C; n_D^{20} 1.4381).

Epichlorohydrin oligomer (ECHO) was synthesized in the presence of the M-14 catalyst, activated aluminosilicate ($H^+ + Al^{3+}$), taken in an amount of 1% of the monomer weight. The reaction mixture was heated for 2 h at 30–50°C and for 5–6 h at 60–80°C with stirring at a constant rate and then cooled. The reaction product was dissolved in benzene, precipitated with water–ethanol mixture (2 : 1), and filtered off. The resulting viscous brown product was dried at room temperature in a vacuum to constant weight.

Allyl bromide (AB) was of chemically pure grade, n_D^{20} 1.4690 (bp 71.3°C/1013 hPa).

Polyethylenimine (PEI) (MW 1×10^4) was used in the form of 50% aqueous solution. The content of titratable nitrogen in anhydrous sample was 29.3%.

Polycondensation of ECHO with AB and PEI in a weight ratio of 1 : 1 : 1 was performed in DMF at 40–70°C for 4 h. Samples were withdrawn from the reaction mixture at certain intervals and diluted with a large excess of DMF to completely stop the reaction. Then, the content of the monomer, allyl bromide, in the samples was determined polarographically.

The polarographic study was performed in a temperature-controlled cell at 25 ± 0.2°C on a PU-1 polarograph with a capillary characteristic at an open circuit $m^{2/3}t^{1/6} = 4.38$ mg$^{2/3}$ s$^{-1/2}$. Saturated calomel electrode was used as a reference electrode. Oxygen was removed from the solution by argon bubbling for 5 min. The polarography was performed using an 0.02 M solution of $(C_2H_5)_4NI$ in 50% DMF as a supporting electrolyte.

It should be noted that, among three reactants (AB, ECHO, and PEI), only allyl bromide is polarographic-

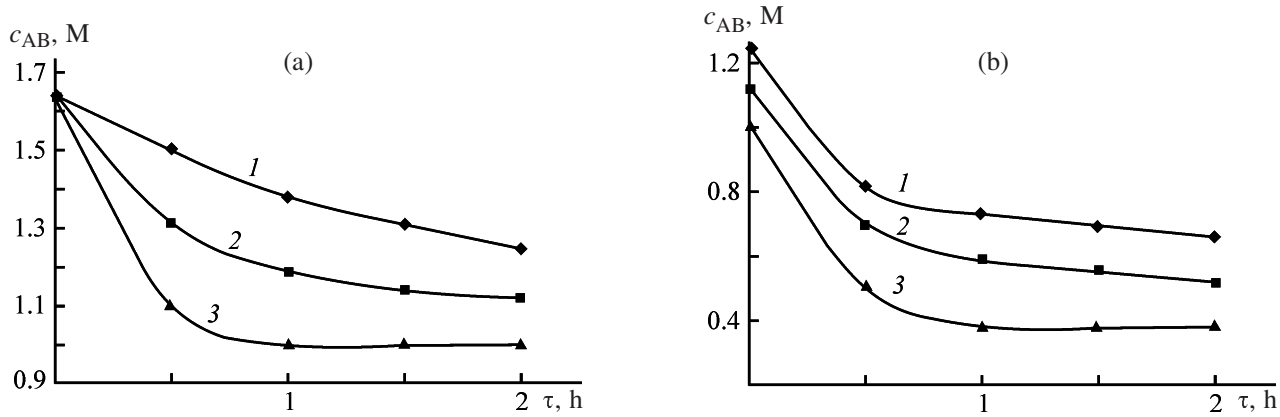

Fig. 1. Kinetic curves of allyl bromide consumption in the reaction of (a) AB with ECHO and (b) AB, ECHO, and PEI. (c_{AB}) Concentration of allyl bromide and (τ) time. Temperature, °C: (*1*) 43, (*2*) 50, and (*3*) 57.

ally active. It is reduced on a mercury dropping electrode with 0.05 M $(C_2H_5)_4NI$ in 90% DMF as a supporting electrolyte at $E_{1/2}$ = –1.82 V; therefore, the reaction order was determined only with respect to AB.

The rate constants were evaluated by the first-order reaction equation [1]:

$$k = 2.303\frac{\log h_1 - \log h_2}{t_1 - t_2},$$

where h_1 is the wave height at time t_1 and h_2, the wave height at time t_2.

The activation energy was found graphically from the Arrhenius plot.

The polarographic analysis of the reaction mixture for the content of allyl bromide, performed at certain intervals, showed that allyl bromide is consumed both in the first and in the second stages. The kinetic curves of AB consumption, obtained for the reaction of AB with ECHO, are presented in Fig. 1a. Two hours after the start of the reaction, PEI was added to the reaction mixture and the process was continued at the same temperature for an additional 2 h. The kinetic curves of AB consumption in the second stage are presented in Fig. 1b.

To determine the reaction order of the first stage, i.e., the reaction of AB with OEBH, we used the integral method [4]. For this purpose, we plotted the dependence of $\ln(c/c_0)$ on time, where c_0 is the initial concentration of AB and c is the current concentration. The resulting linear dependence passing through the origin of the coordinates suggests the first reaction order (Fig. 2a).

The plot of $\log k$ vs. $1/T$ for the reaction of AB with ECHO shows (Fig. 3a) that the points fall on a straight line, following the Arrhenius equation. The apparent activation energy of the reaction of AB with ECHO, evaluated from the Arrhenius plot, is 108.35 kJ mol^{-1} (see table).

Previously [5] polycondensation of AB, diglycidyl resorcinol ether (DGRE), and polyethylenepolyamine (PEPA: MW 265; n_D^{20} 1.4546, total nitrogen content 22%, content of titratable nitrogen 19.1%) was studied and the activation energy of the reaction of AB with DGRE was found to be 32.15 kJ mol^{-1}. Comparing the results obtained with published data [5], we can

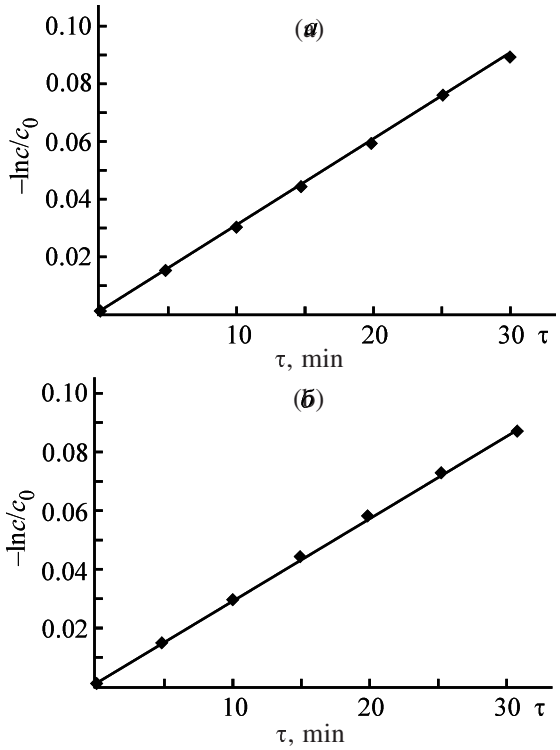

Fig. 2. $\ln(c/c_0)$ as a function of the reaction time τ. Reaction of (a) AB with ECHO and (b) AB, ECHO, and PEI.

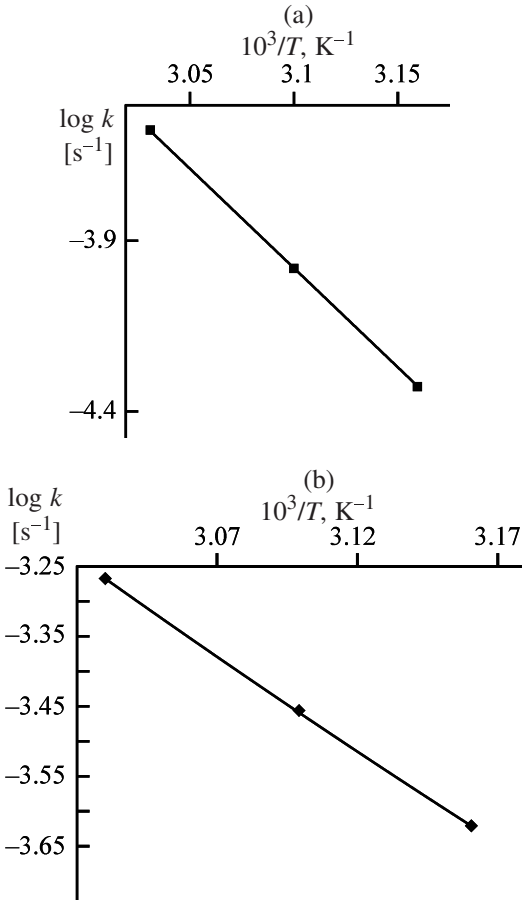

Fig. 3. Rate constant k of the reaction of (a) AB with ECHO and (b) AB, ECHO, and PEI as a function of temperature T in the Arrhenius coordinates.

conclude that ECHO is significantly less active in the reaction with AB than DGRE, which reacts with AB at room temperature. This is apparently caused by the oligomeric nature of ECHO. It was also shown [6] that the reaction of AB with DGRE is a first-order reaction with respect to allyl bromide. Thus, the results obtained in this study are in good agreement with published data.

Kinetic characteristics of the reaction of AB with ECHO and of AB, ECHO, and PEI

T, K	$k \times 10^5$, s^{-1}	E_a, kJ mol^{-1}
	AB–ECHO	
316	4.76	108.35
323	11.73	
330	27.18	
	AB–ECHO–PEI	
316	24.01	45.02
323	32.81	
330	53.25	

Figure 2b shows that the second stage of the reaction of AB, ECHO, and PI in the initial period is also the first-order reaction with respect to allyl bromide concentration. The rate constants of polycondensation of AB, ECHO, and PEI, evaluated from the first-order kinetic equation, and the apparent activation energy found from the Arrhenius plot (Fig. 3b) are presented in the table.

It is seen that the second stage of the process is significantly faster than the first stage. The similar relationship was also found for the polycondensation of AB, DGRE, and PEPA [7]. This is not in conflict with published data [4], where it was noted that in multistage reactions one of the stages is usually significantly slower than the other stages.

A conductometric study of the kinetics of the reaction of ECH oligomers and some di- and polyamines in DMF at various temperatures [5] showed that the apparent activation energy of amination of ECH oligomer with polyethylenimine is 24.24 kJ mol^{-1}. As seen from our data, addition of the third component, AB, into the system hampers the reaction and for the reaction of AB with ECHO and PEI a higher energy is required.

A study of polycondensation of AB, DGRE, and PEPA [8] showed that in the first stage the reaction between AB and DGRE involves opening of the epoxy ring of the ether and the cleavage of the C–Br bond in allyl bromide. In the second stage, on adding PEPA into the reaction mixture, a cross-linked anion exchanger is formed owing both to rupture of the C–Br bond in the intermediate and of the N–H bond in the amino group, and to cleavage of the double bond of the allyl group.

The first stage of the reaction between AB and ECHO apparently involves the reaction of terminal OH groups of ECHO and AB with the release of HBr and, which is less likely, the opening of a small amount of residual epoxy groups, similar to the reaction between AB and DGRE:

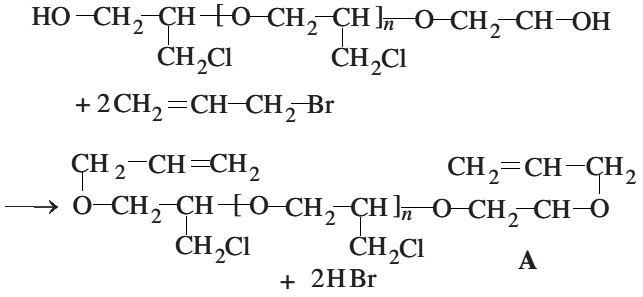

In the second stage, after addition of PEI into the reaction mixture, an anion exchanger of the following structure is formed via abstraction of proton of PEI amino group with chlorine atoms of the product of the first reaction stage (**A**) and, simultaneously, via attack of NH groups by allyl bromide with elimination of HBr, and also, apparently, via cleavage of the double bond of the allyl group:

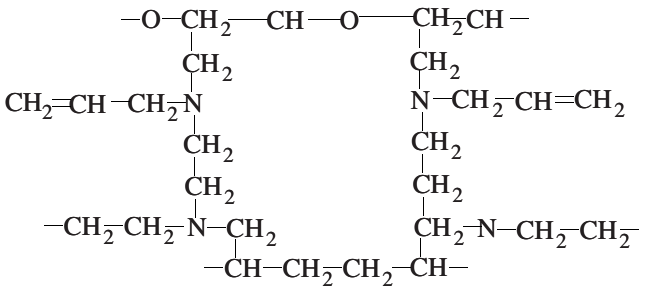

CONCLUSIONS

(1) A kinetic study of polycondensation of allyl bromide, epichlorohydrin oligomer, and polyethylenimine showed that the process occurs in two stages, each of which is a first-order reaction with respect to the concentration of allyl bromide.

(2) The activation energies show that the reaction of allyl bromide with epichlorohydrin oligomer proceeds at a lower rate than the second stage.

REFERENCES

1. Bezuglyi, V.D., *Polyarographiya v khimii i tekhnologii polimerov* (Polarography in Chemistry and Technology of Polymers), Leningrad: Khimiya, 1968.
2. Ergozhin, E.E., Chalov, T.K., Rozhkova, A.G., and Iskakova, R.A., *Zh. Prikl. Khim.*, 2005, vol. 78, no. 10, pp. 1620–1633.
3. *Organic Solvents. Physical Properties and Methods of Purification*, Weissberger, A., Proskauer, E.S., Riddick, J.A., and Toops, E.E., Eds., New York: Interscience, 1955.
4. Berlin, A.A., Volf'son, S.A., and Enikolopyan, N.S., *Kinetika polimerizatsionnykh protsessov* (Kinetics of Polymerization Processes), Moscow: Khimiya, 1978.
5. Iskakova, R.A., Polyfunctional Anion Exchangers Based on Epoxy and Allyl Compounds and Some Polyamines, *Cand. Sci. Dissertation*, Almaty, 2001.
6. Chalov, A.K., Ergozhin, E.E., Iskakova, R.A., and Nikitina, A.I., *Izv. Min. Obr. Nauki Resp. Kaz., Nats. Akad. Nauk Resp. Kaz., Ser. Khim.*, 2001, no. 1, pp. 15–18.
7. Ergozhin, E.E., Tastanov, K.Kh., and Menligaziev, E.Zh., *Izv. Akad. Nauk Kaz. SSR, Ser. Khim.*, 1983, no. 3, pp. 69–78.
8. Chalov, A.K., Ergozhin, E.E., Iskakova, R.A., and Nikitina, A.I., *Izv. Min. Obr. Nauki Resp. Kaz., Nats. Akad. Nauk Resp. Kaz., Ser. Khim.*, 2000, no. 5, pp. 3–8.

ISSN 1070-4272, Russian Journal of Applied Chemistry, 2007, Vol. 80, No. 11, pp. 1906–1909. © Pleiades Publishing, Ltd., 2007.
Original Russian Text © I.A. Novakov, S.S. Radchenko, A.S. Pastukhov, F.S. Radchenko, 2007, published in Zhurnal Prikladnoi Khimii, 2007, Vol. 80, No. 11, pp. 1882–1885.

MACROMOLECULAR CHEMISTRY AND POLYMERIC MATERIALS

Properties of Aqueous Solutions of Polymer–Colloid Complexes of Polyethylenimine with Aluminum Hydroxychloride

I. A. Novakov, S. S. Radchenko, A. S. Pastukhov, and F. S. Radchenko

Volgograd State Technical University, Volgograd, Russia

Received April 9, 2007

Abstract—Turbidimetry and gel-permeation chromatography were applied to examine the composition of the polymer–colloid complexes of polyethylenimine with aluminum hydroxychloride. The size-distribution characteristics of the macromolecules of the polymer–colloid complexes were determined by photon correlation spectroscopy.

DOI: 10.1134/S1070427207110250

Polyelectrolytes belong to reactive polymers; they enter, in particular, into reactions in which their ionic groups interact with inorganic colloid particles, yielding in aqueous solutions polymer–colloid complexes (PCCs) [1, 2].

The chemistry and physical chemistry of these complexes attracts ever increasing interest because of the widening scope of their application as high-performance flocculants, structure-formation agents, and stabilizers of colloid dispersions. Previously [3] we demonstrated that PCCs based on polyethylenimine (PEI) and aluminum hydroxychloride (AHC) exhibit high performance characteristics in separation of model and real oil- and fat-containing dispersions. A specific feature of such PCCs is high reactivity in acid media, associated with the conformational behavior of the macromolecules. The relationships in formation and physicochemical properties of PCCs are examined inadequately.

We examined here the composition and size-distribution characteristics of PCCs of PEI with AHC.

EXPERIMENTAL

We used AHC prepared by the procedure from [4] (Al^{3+} content 12.8 wt %, atomic ratio Cl^-/Al^{3+} = 0.48, pH 4.5, ρ = 1330 kg m^{-3}, dry residue 46.5 wt %) and PEI with the molecular weight of 30000–40000, available from Serva, the United States. Polycomplexes were prepared by mixing an aqueous solution of PEI (1 wt %) with an aqueous solution of AHC at room temperature; the molar ratio of the reactants, calculated for Al^{3+} : PEI unit, varied from 0.25 to 4. Prior to measurements, the solutions were kept for 1 day.

The viscosity of PEI and PCCs was measured on an Ubbelohde viscometer (Cannon, d_{cap} = 0.25 mm) at 30 ± 0.1°C; pH of solutions was adjusted within 3.5–6.0 using a pH-300 pH-meter (HANNA Instruments, the United States) with an HI 1131 glass electrode.

The optical density was determined on a Specol-10 (PGH Radio Fernsehen Elektro Marienbery) spectrophotometer at λ = 460 nm in a cell with a layer thickness of 5 cm. The PCCs were precipitated from aqueous solutions by adding sodium sulfate available from Reakhim. The precipitated PCCs were separated from water with a Hermle-Z200A (Hermle Labortechnik GmbH) centrifuge at a rotation rate of 5000 rpm and the centrifugation time of 10 min. The precipitates were dried to constant weight in a desiccator at 110°C.

The gel-permeation chromatographic analysis was carried out in a KNAUER (Advanced Scientific Instruments) chromatographic system. The column was packed with PolySep-SEC 1000 (Phenomenex) gel with the fractionation range of 1000–100000 for dextrans.

The PCC particle size was determined by photon correlation spectroscopy with a He–Ne laser (λ = 633 nm, 15 mW) as the light source; the temperature in the measurement cell was maintained accurately to within 0.1°C. The autocorrelation functions (ACFs) of fluctuations of the scattered light intensity were meas-

ured using a FotoCor-SP 288-channel correlator with a logarithmic time scale extending from 2.5×10^{-8} to 6800 s. The signal accumulation time was 600 s. The ACFs were analyzed using the DynaLS program by the regularization method (to obtain the size distribution of the scattered particles).

Prior to measurements, all the solutions were filtered through Millipore membrane filters (pore diameter 0.8 μm) directly into the measurement cell to remove dust.

In [5] we showed that PEI can occur in three states: totally charged (pH < 3.4), partially charged (3.4 < pH < 9.8), and totally uncharged (pH > 9.8). Evidently, under these conditions, the complexing ability of PEI with respect to AHC can be manifested in different ways. However, Pilipenko et al. [6] showed that, at pH > 6, AHC is hydrolyzed and forms an insoluble precipitate $Al(OH)_3$, and in this pH range PEI can be complexed with these aluminum hydroxide partciles rather than with aluminum polycations. Hence, examination of the complexing between AHC and PEI at pH > 6 seems unreasonable.

We examined how the specific viscosity of a mixture of aqueous solutions of PEI and AHC with the molar ratio Al^{3+} : PEI unit = 1 : 1 is influenced by pH of the medium and compared this dependence with that for an aqueous solution of PEI (Fig. 1). It is seen that, at pH < 3.5, the mixture of the components and PEI have virtually identical viscosities. The reason is that, at low pH values, AHC is depolymerized, and aluminum occurs in aqueous solutions as hydrated Al^{3+} ions [6]. Thus, we further examined complexing at pH 4.5, at which the PEI macromolecules assume the most extended conformation.

In this contest, the composition of PCCs, i.e., the number of particles bound to one polymer macromolecule, is one of the essential issues.

We carried out a turbidimetric study of the aqueous solutions of PCCs with different compositions under varied ionic strength of solution (Fig. 2). At the molar ratios Al^{3+} : PEI unit under 1.25, salting-out of the complexes was observed only at high ionic strengths of the solution, exceeding fourfold those at which individual AHC is precipitated. A probable reason is that the number of hydrophobic units of the PEI macromolecules bound to different AHC particles is insignificant, i.e., the particles are uniformly distributed among the PEI macromolecules. When the molar ratio Al^{3+} : PEI unit increases beyond 1.25 and the AHC concentration grows, the tubridimetric curves are shifted to lower ionic strengths. This effect

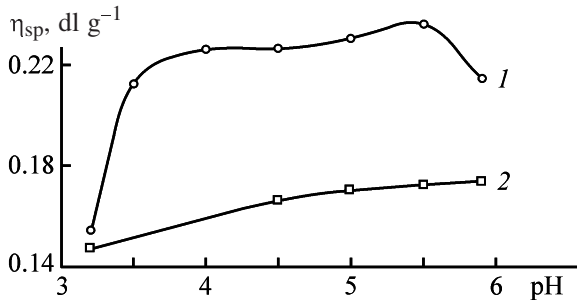

Fig. 1. Specific viscosity η_{sp} of (*1*) PEI and (*2*) PEI–AHC mixture with the molar ratio Al^{3+} : PEI unit = 1 : 1 vs. pH of the aqueous solution. PEI concentration 0.5 g dl^{-1}, T = 30°C.

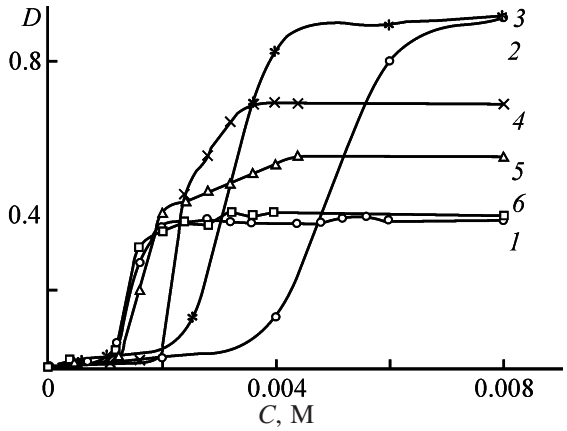

Fig. 2. Optical density D of aqueous solutions of PCCs with different compositions vs. the ionic strength of solution C, created by sodium sulfate. Al^{3+} concentration 0.02 g dl^{-1}, T = 30°C. Molar ratio Al^{3+} : PEI unit: (*1*) 0, (*2*) 1.25, (*3*) 2, (*4*) 3, (*5*) 4, and (*6*) 10.

is not associated with an increase in the ionic strength of solution due to increase in the AHC concentration, since AHS is a weak electrolyte. A probable reason is an increase in the number of the hydrophobic PEI units, bound to several different AHC particles, with increasing PCC content.

The precipitates formed during PCC salting-out with sodium sulfate were analyzed for the nitrogen content by elemental analysis (see table).

Our data suggest that the nitrogen content of the PCCs increases with increasing molar ratio Al^{3+} : PEI unit in the initial mixture and attains a maximum at the ratio of 1.25. This suggests an increase in the number of PEI macromolecules complexed with AHC particles. With a further increase in the ratio of the reactants, the content of nitrogen in the precipitate decreases, since the latter contains both complexed AHC and AHC unbound to the macromolecules of the polymer as the AHC amount is increased. This fact

Aluminum content of aqueous solutions of PCCs and nitrogen content of the precipitate in relation to the molar ratio of the reactants. c(PEI) = 0.5 g dl^{-1}, c(Na_2SO_4) = 1 M

Molar ratio Al^{3+} : PEI unit in initial mixture	Al^{3+} content of initial mixture, g	Nitrogen content of PCC, wt %
0.25	0.02	6.60
0.50	0.04	6.85
0.75	0.06	8.06
1.25	0.10	9.13
1.50	0.12	6.60
2.00	0.16	5.96
3.00	0.24	3.90
4.00	0.32	3.65

suggests that, at the molar ratios of interest, PEI is exhaustively complexed.

To elucidate how complexation is influenced by the molar ratio of the reactants, we used gel-permeation chromatography. This method provides information about the molecular-weight distribution of the particles of the PCC formed. We found that the chromatograms of individual AHC (Fig. 3) are characterized by unimodal distribution at Al^{3+} concentrations under 0.3 g dl^{-1}. With increasing aluminum concentration, the distribution becomes bimodal, with the second mode corresponding to particles with a higher molecular weight. This fact, combined with the results reported by Radchenko et al. [7] and Zakharchenko et al. [8], suggests that aqueous solutions of AHC consist to 95% of small particles, and large particles are present only in insignificant amounts; their number increases only at high AHC concentrations. Also, we showed (Fig. 4) that, when the molar ratio of reactants (Al^{3+} : PEI unit) is increased to 1.25, the gel chromatogram contains one well-defined maximum with the retention time corresponding to individual AHC and a less-defined maximum with the retention time of PEI. This suggests that, above all, a complex with small AHC particles is formed in which the number of the polymer macromolecules corresponds to that of the PCC particles. With further increase in the molar ratio, the retention time of the PCC particles decreases; the maximum in the chromatogram becomes well-defined and is enhanced, which suggests increases in the molecular weight of the PCC particles and in their concentration.

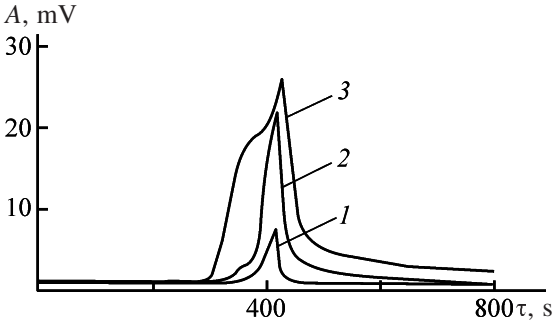

Fig. 3. Gel chromatograms of aqueous solutions of AHC (T = 30°C). Al^{3+} concentration, g dl^{-1}: (*1*) 0.08, (*2*) 0.31, and (*3*) 0.94. (*A*) Signal intensity and (τ) elution time; the same for Fig. 4.

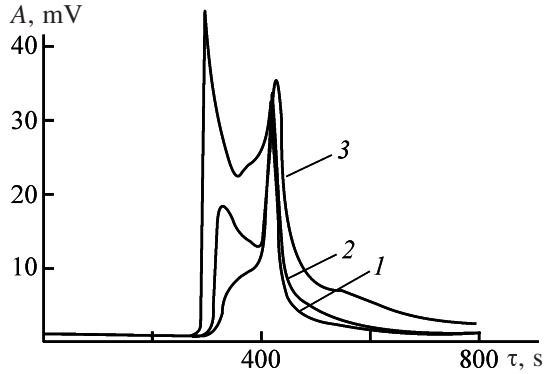

Fig. 4. Gel chromatograms of aqueous solutions of PCCs. Molar ratio of reactants (Al^{3+} : PEI unit): (*1*) 0.25, (*2*) 1.25, and (*3*) 3.00. PEI concentration 0.5 g dl^{-1}, T = 30°C.

To determine the size-distribution characteristics of PCCs, these complexes were examined in detail by photon correlation spectroscopy. We found that, with increasing molar ratio of the reactants, the correlation time increases. This suggests interaction of the polymer macromolecules with aluminum polycations and formation of strongly associated particles of the complex. To determine the hydrodynamic radii of the particles, we calculated the size distributions reconstructed from the corresponding ACFs (Fig. 5). We showed that, for individual components, the presence of particles 10 nm in size (for PEI) and 2 and 40 nm in size (for AHC) is typical. A mixture of these components with the molar ratio under 1.25 is characterized by three peaks in the histogram, which suggests complexation of PEI both with "small" and "large" AHC particles; also, the system contains free polymer macromolecules. Up to the molar ratio of the components of 1.25, an increase in the AHC concentration is responsible for an increase in the relative intensity of the peak corresponding to large particles, which suggests their significant contribution to the light scattering. We showed in [3] that, at the molar ratio Al^{3+} : PEI unit of 1.25, all the PEI macromolecules are complexed, and a PCC with this composition is characterized by the largest number of bonds between the reactants. Further increase in the molar ratio is accompanied by disappearance of the mode corresponding to free PEI, and a new peak appears which

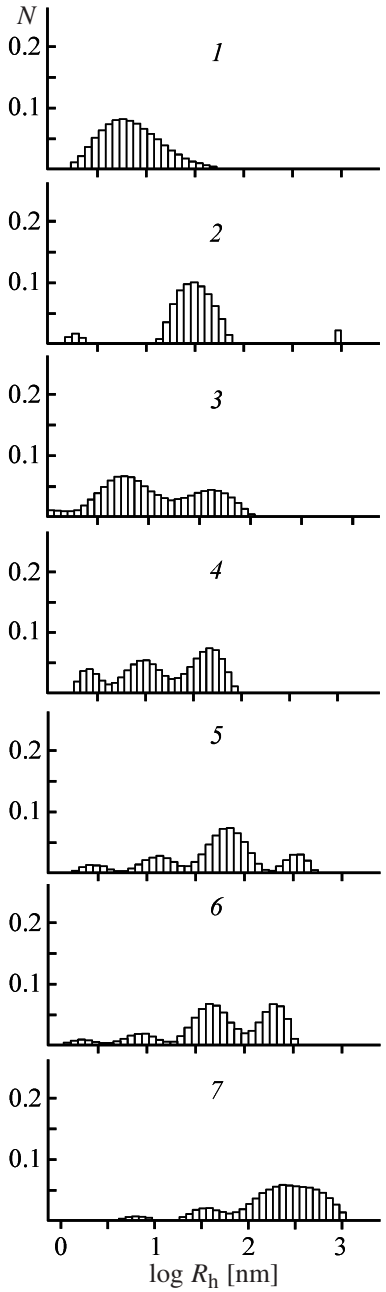

Fig. 5. Particle-size distribution for (*1*) unbound PEI, (*2*) unbound AHC, and (*3*–*7*) PEI–AHC complexes at molar ratios Al^{3+} : PEI unit of (*3*) 0.50, (*4*) 1.25, (*5*) 2.00, (*6*) 3.00, and (*7*) 4.00. Scattering angle 90°, T = 30°C. (*N*) Reduced light scattering intensity, and (R_h) hydrodynamic radius of the particle.

corresponds to strongly associated PCC particles with the size of 100–300 nm. This is accompanied by a smooth growth of the total intensity of the scattered light. The latter fact suggests that, throughout the examined range of the mixture compositions, an increase in the average molecular weight of the light-scattering particles is associated with formation of a complex comprising at least one PEI macromolecule and several AHC particles, both small and large.

CONCLUSIONS

(1) In aqueous solutions, polyethylenimine macromolecules and aluminum hydroxychloride particles form a polymer–colloid complex whose composition varies in the range of the molar ratios of reactants, Al^{3+} : polyethylenimine unit, of 1.25–4.

(2) At molar ratios of the components under 1.25, the system contains two types of particles of the complex, formed with small (2 nm) and large (40 nm) aluminum hydroxychloride particles occurring in the system.

(3) Further increase in the Al^{3+} : polyethylenimine unit ratio results in formation of associated particles of the polymer–colloid complex, whose size differs from that of the initial particles by approximately an order of magnitude.

REFERENCES

1. Kabanov, V.A., Zezin, A.B., Kasaikin, V.A., et al., *Usp. Khim.*, 1991, vol. 60, no. 3, pp. 595–601.
2. Kabanov, V.A., *Usp. Khim.*, 2005, vol. 74, no. 1, pp. 5–23.
3. Novakov, I.A., Radchenko, S.S., Pastukhov, A.S., and Radchenko, F.S., *Zh. Prikl. Khim.*, 2006, vol. 79, no. 3, pp. 472–477.
4. RF Patent 2280615.
5. Pastukhov, A.S. and Radchenko, F.S., *Izv. Volgograd. Gos. Tekh. Univ., Ser.: Khim. Tekhnol. Elementoorg. Monom. Polim. Mater., Mezhvuz. Sb. Nauchn. Stat.*, 2006, issue 3, no. 1 (16), pp. 120–122.
6. Pilipenko, A.T., Falendysh, N.F., and Parkhomenko, E.P., *Khim. Tekhnol. Vody*, 1982, vol. 4, no. 2, pp. 136–150.
7. Radchenko, F.S. and Ozerin, A.S., *Izv. Volgograd. Gos. Tekh. Univ., Ser.: Khim. Tekhnol. Elementoorg. Monom. Polim. Mater., Mezhvuz. Sb. Nauchn. Stat.*, 2006, issue 3, no. 1 (16), pp. 124–127.
8. Zakharchenko, S.O., Litmanovich, E.A., Radchenko, F.S., et al., *Kolloidn. Zh.*, 2006, vol. 68, no. 4, pp. 467–471.

ISSN 1070-4272, Russian Journal of Applied Chemistry, 2007, Vol. 80, No. 11, pp. 1910–1913. © Pleiades Publishing, Ltd., 2007.
Original Russian Text © V.M. Misin, N.N. Glagolev, M.V. Misin, 2007, published in Zhurnal Prikladnoi Khimii, 2007, Vol. 80, No. 11, pp. 1886–1889.

MACROMOLECULAR CHEMISTRY AND POLYMERIC MATERIALS

Structure and Properties of Polymeric Ethyne–Hexacarbonyldicobalt π Complexes

V. M. Misin, N. N. Glagolev, and M. V. Misin

Emanuel' Institute of Biochemical Physics, Russian Academy of Sciences, Moscow, Russia

Received March 16, 2007

Abstract—A polymeric ethyne–hexacarbonyldicobalt π complex was prepared by the reaction of poly-*p*-diethynylbenzene with $Co_2(CO)_8$. The conformations in which the polymer chains can exist and the conformations in which the –C≡CH and –Ph– groups can form π complexes with $Co_2(CO)_8$ were revealed by analysis of Stuart–Briegleb molecular models. The IR spectra of the polymeric complexes were analyzed, and their thermal degradation in air was examined.

DOI: 10.1134/S1070427207110262

Interest in polymers containing metal atoms π-coordinated to organic macromolecules is due to the possibility of preparing catalytically active systems based on such polymers. Catalytic systems in which a transition metal is π-coordinated to a polymeric support acting as a macroligand are well known [1]. Of particular interest are π complexes with polyconjugated polymers, because of their specific physicochemical, electrophysical, and catalytic properties. In particular, some of these complexes are organometallic ferromagnetics, i.e., materials absorbing or scattering electromagnetic fields. Sergeev et al. [2] prepared π-arene–tricarbonylmetal complexes derived from carbonyls of molybdenum, chromium, vanadium, and various polyphenylenes. At the same time, numerous π-acetylene–hexacarbonyldicobalt complexes with various mono- and disubstituted acetylenes as ligands are known [3].

Therefore, it seemed interesting to synthesize π complexes of metal carbonyls with polysubstituted polymers containing ethynyl groups –C≡CH.

Previously [4] we described preparation and molecular structure of poly-*p*-diethynylbenzene (PDEB), a polyconjugated polyene polymer containing ethynyl groups in pendant chains, $–[HC{=}C(p\text{-}C_6H_4{–}C{\equiv}CH)]_n–$ [4]. The polymer was prepared by selective polymerization of *p*-diethynylbenzene HC≡C–(*p*-C_6H_4)–C≡CH via one of the –C≡CH groups in the presence of an anionic initiator. The use of such polymers opens prospects for preparing diverse complexes whose structure will be preset by both the polymeric chain and the complexing metal fragment. By properly choosing the type and amount of the complexing metal species, it may be possible to prepare in a polymeric matrix both small organometallic fragments and relatively lengthy metal clusters.

This study deals with the synthesis of π-acetylene complexes with a metal carbonyl, based on PDEB. As metal carbonyl we took octacarbonyldicobalt, $Co_2(CO)_8$.

EXPERIMENTAL

The starting PDEB is an X-ray amorphous brown polymer soluble in aromatic and polar solvents. To prepare polymeric complexes, we used polymers with a number-average molecular weight of 3500, containing 0.62 ethynyl group per monomeric unit of the macromolecule [4].

Ethyne–hexacarbonyldicobalt π complex with PDEB (PDEBC). A reactor preliminarily purged with argon was charged with 0.3 g of PDEB in 30 ml of benzene, and a solution of 0.19 g of $Co_2(CO)_8$ in 6 ml of benzene was added dropwise. The reaction was performed at room temperature until the CO evolution ceased. The presence of unchanged $Co_2(CO)_8$ was monitored by TLC on Silufol, eluent hexane. After 3 h, the solution was filtered and the product was precipitated into hexane at the solvent : precipitant ratio of 1 : 10. Yield of PDEBC 0.31 g (68%).

The IR spectra were recorded on a UR-20 spectrophotometer from KBr pellets (1%) or from 5% benzene solutions. The ESR spectra were taken on an

EPR-20 spectrometer (Institute of Chemical Physics, Russian Academy of Sciences; HF modulation, 100 kHz, HI_{max} = 0.6 G). The TGA/DTA curves in air were recorded with an OD-2 derivatograph (MOM, Hungary, continuous heating at a rate of 5 deg min^{-1}).

The molecular weights and molecular-weight distributions of polymers were determined with a GPC-200 liquid gel permeation chromatograph (Waters) using Styrogel columns. The solvent, THF, was fed at a rate of 1 ml min^{-1}; temperature 25°C.

It seemed necessary first to consider the intramolecular structure of the initial poly-*p*-diethynylbenzene with the aim to examine he possibility of formation of metal π complexes with one or several unsaturated groups of the polymer: –C=C– bonds in the polyene chain, *p*-phenylene groups $–C_6H_4–$, and ethynyl groups –C≡CH. To this end, using Stuart–Briegleb molecular models, we considered four different conformations of the poly-*p*-diethynylbenzene chains: *trans-S-cis*, *cis-S-trans*, *cis-S-cis*, and *trans-S-trans*. In so doing, we took into account two possible modes of coupling of unsymmetrical monomer R–C≡C–H (R = $HC≡C–C_6H_4–$): head-to-tail or head-to-head:

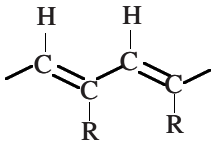

trans-S-trans-Form, "heat-to-tail"

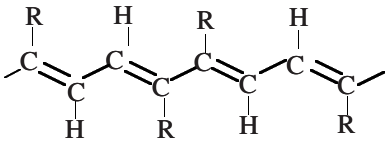

trans-S-trans-Form, "heat-to-head"

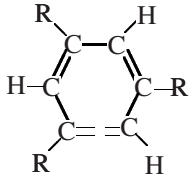

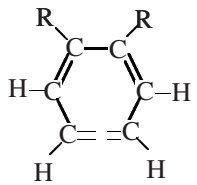

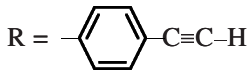

cis-S-cis-Form, "heat-to-tail"

cis-S-cis-Form, "heat-to-head"

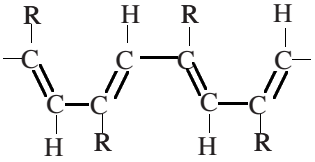

trans-S-cis-Form, "heat-to-tail"

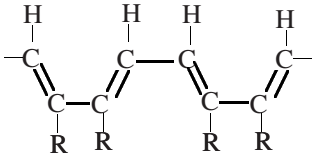

trans-S-cis-Form, "heat-to-head"

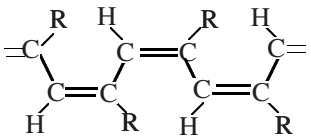

cis-S-trans-Form, "heat-to-tail"

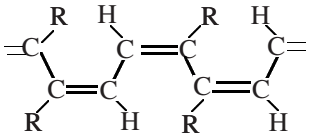

cis-S-trans-Form, "heat-to-head"

In earlier papers [5], we admitted the possibility of existence of all these coupling modes in chains of substituted polyacetylenes. However, we found that only assembling of no less than six to eight units could give an adequate estimate of steric hindrance in one or another conformation. If only three units are assembled, any of the eight possible conformations is possible.

We found that the poly-*p*-diethynylbenzene molecule cannot exist because of steric hindrance in the following three forms: *trans-S-cis*, head-to-head; *cis-S-trans*, head-to-tail; and *cis-S-trans*, head-to-head.

For all the other five forms, we considered the possibility of formation of metal π complexes with both –C≡CH and $–C_6H_4–$ groups. We found that π complexes of cobalt carbonyl with the –C≡CH group can be formed with four out of five forms (except *trans-S-trans*, head-to-tail).

The complexation of $Co_2(CO)_8$ with Ph groups is possible in only two forms: in the linear *trans-S-cis*, head-to-tail structure and helicoidal *cis-S-cis*, head-to-head structure. The complexation with –C=C– units of the polyene chain is possible in none of the conformations.

However, as will be shown below, under the reaction conditions the π electrons of the phenyl ring did not react with $Co_2(CO)_8$. Cobalt carbonyl reacted only with the π electrons of the –C≡CH triple bond:

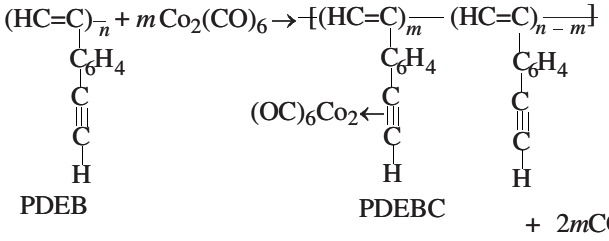

PDEB PDEBC

The reaction yielded ethyne–hexacarboyldicobalt π complex in which the –C≡CH bond of the acetylenic ligand is perpendicular to, and noncoplanar with the Co–Co axis [3].

The PDEBC samples prepared were brown powders insoluble in organic solvents. It should be emphasized that the complex, as a rule, lost the solubility

Composition of polymeric complexes

Sample	Initial molar ratio $[C{\equiv}CH] : [Co_2(CO)_8]$	Reaction time, h	Molar ratio of fragments $[C{\equiv}CH] : [\overset{C}{\underset{C}{\|\|}}{\rightarrow}Co_2(CO)_6]$ in polymeric complex	Co content by elemental analysis, %	
				calculated	found
PDEBC-1	3 : 1	3	2.45 : 1	14.50	12.55
PDEBC-2	2 : 1	8	1.28 : 1	17.32	15.19
PDEBC-3	1.5 : 1	15	0.65 : 1	21.50	19.55
PDEBC-4	1 : 1	20	0.04 : 1	25.61	24.59

only after precipitation. At the maximal $Co_2(CO)_8$: –C≡CH ratio, 1 : 1 (see table), the insoluble product formed directly in the course of the synthesis. It was shown previously that, under the mild conditions used in our experiments (room temperature), the –C≡C– bond in disubstituted acetylenic monomers is not opened, and the corresponding macromolecules are not formed [6]. Therefore, the loss of the solubility in the course of complexation with the polymer cannot be attributed to the cross-linking of the macromolecules via the same –C≡CH bonds in PDEB units. More likely, the insolubility of the product is due to more complex physicochemical factors preventing the penetration of solvent molecules between macromolecules of the polymeric complex in the course of its attempted repeated dissolution.

To determine the extent of transformation of the –C≡CH group, we performed the elemental analysis of the complexes. The results are given in the table. It can be seen that $Co_2(CO)_8$ reacts with the triple bond of PDEB within the reaction time virtually quantitatively.

The formation of the fragments $\overset{C}{\underset{C}{\|\|}}{\rightarrow}Co_2(CO)_6$ is confirmed by IR spectroscopy (Fig. 1). The IR spectrum of a benzene solution of the polymeric complex [the reaction mixture containing no $Co_2(CO)_8$ according to TLC] contains, along with bands of the starting polymer, also four characteristic strong bands of CO stretching vibrations in the range 2100–2000 cm^{-1} [7]. Preservation of these bands after the isolation of the polymeric complexes from the solution shows that the complexes do not decompose in the course of precipitation. According to [7], the stretching band of a coordinated monosubstituted triple bond –C≡CH is observed at 1550 cm^{-1}. Unfortunately, this band cannot be recorded, because it is obscured by strong stretching vibration bands of PDEB benzene rings. In the range 480–550 cm^{-1}, there are a number of bands corresponding to bending vibrations of carbonyl groups and stretching vibrations of Co–C bonds.

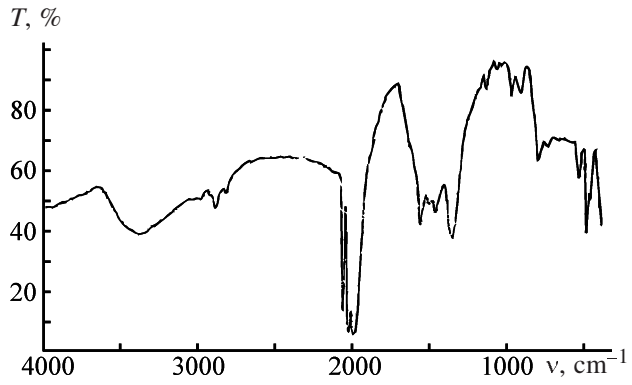

Fig. 1. IR spectrum of the π complex of hexacarbonyldicobalt with poly-*p*-diethynylbenzene. (*T*) Transmission and (ν) wavenumber.

In addition, in the IR spectra of complexes with a low content of $\overset{C}{\underset{C}{\|\|}}{\rightarrow}Co_2(CO)_6$ fragments (PDEBC-1), there is a well-defined band at 3300 cm^{-1}, corresponding to ≡C–H stretching vibrations in unchanged ethynyl groups –C≡CH [8]. This band decreases in intensity with an increase in the content of the above fragments in the polymeric complexes, and in PDEBC-4 it is lacking at all. Simultaneously, in the IR spectra of the complexes with a high content of $\overset{C}{\underset{C}{\|\|}}{\rightarrow}Co_2(CO)_6$ fragments (PDEBC-3, -4), the band at 2100 cm^{-1}, characteristic of stretching vibrations of the monosubstituted triple bond RC≡CH in PDEB, disappears. No changes in the bands characteristic of aromatic groups were observed in the spectra, suggesting the absence of complexation between the phenyl groups and cobalt carbonyls.

The polymeric complexes prepared were studied by TGA/DTA (Fig. 2). The TG curves show that the thermal oxidative stability of polymeric complexes PDEBC is considerably lower than that of the starting PDEB polymers. In the DTA curves of the polymeric complexes, there are exothermic peaks at 120 and

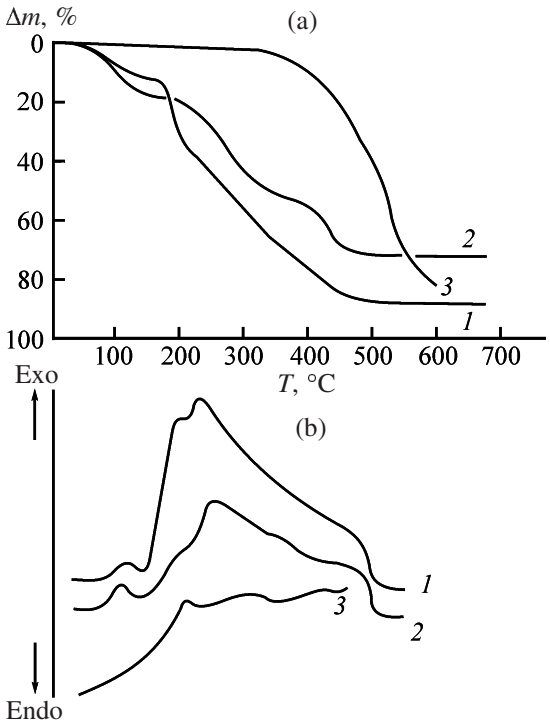

Fig. 2. Thermal oxidative degradation of polymeric π complexes. (Δ*m*) Weight loss and (*T*) temperature. (a) TGA and (b) DTA. (*1*) PDEBC-1, (*2*) PDEBC-4, and (*3*) partially cross-linked PDEB (thermolysis in a vacuum, 100°C, 6 h).

205°C. The former peak, corresponding to significant weight loss, is attributable to elimination of two CO groups from the $\begin{matrix}C\\ \|\\ C\end{matrix}\!\!\rightarrow Co_2(CO)_6$ fragments. This assumption is confirmed by the fact that the weight loss at 120°C, according to TGA data (8% for PDEBC-1 and 12% for PDEBC-4), is approximately equal to the weight fraction of two CO groups in the polymeric complex, calculated from the analytical data (7.37% for PDEBC-1 and 11.67% for PDEBC-4). The exothermic peak at 205°C corresponds to opening of the –C≡CH triple bond. A peak in this region was also observed in DTA studies of partially cross-linked PDEB [4] and polydiphenylacetylene [6].

The polymers studied, as well as their complexes with cobalt carbonyl, exhibit paramagnetism. The concentration of paramagnetic species in the starting polymer is about 10^{17} spins g^{-1}, and it does not noticeably change upon formation of the polymeric complex. Then the polymeric complexes obtained were subjected to additional treatment with the aim to obtain the corresponding ferromagnetic material. As a result, the first laboratory samples of a new radio-absorbing material with improved properties was obtained. The material decreased the Q-factor in an ESR spectrometer waveguide ($\lambda = 3 \pm 1.2$ cm) by $(5–13) \pm 10\%$ dB mg^{-1}, instead of 0.6–0.8 for ferrite-containing materials taken for comparison. Thus, we prepared a substance ensuring by a factor of 2.3 lower material consumption (down to 2.8 kg m^{-2}).

CONCLUSIONS

(1) π-Acetylenic complexes of poly-*p*-diethynylbenzene with octacarbonyldicobalt, $Co_2(CO)_8$, were prepared.

(2) The formation of π complexes of cobalt carbonyl with the –C≡CH group of the side substituent of the polymer is possible in four types of intramolecular conformations. No complexation of cobalt carbonyl with phenyl rings or polyene chain is observed.

(3) Samples of a radio-absorbing material were prepared from the synthesized complexes.

REFERENCES

1. Yuffa, A.F. and Lisichkin, G.V., *Usp. Khim.*, 1978, vol. 47, no. 8, p. 1414.
2. Sergeev, V.A., Vdovina, L.I., and Kononenko, N.E., *Vysokomol. Soedin., Ser. A*, 1982, vol. 24, no. 6, p. 1304.
3. Greenfield, H., Stenberg, H.W., Friedel, R.A., et al., *J. Am. Chem. Soc.*, 1956, vol. 78, no. 1, p. 120.
4. Glagolev, N.N., Misin, V.M., Zaichenko, N.L., et al., *Khim. Fiz.*, 1986, vol. 5, no. 7, p. 972.
5. Chauser, M.G., Rodionov, Yu.M., Misin, V.M., et al., *Usp. Khim.*, 1976, vol. 45, no. 4, p. 695.
6. Glagolev, N.N., Misin, V.M., Zaichenko, N.L., et al., *Vysokomol. Soedin.*, 1986, vol. 28, no. 10, p. 2123.
7. Iwashita, Y., Ishikava, A., and Kainosho, M., *Spectrochim. Acta (A)*, 1971, vol. 27, no. 2, p. 271.
8. Dyer, J.R., *Applications of Absorption Spectroscopy of Organic Compounds*, Englewood Cliffs, New Jersey: Prentice-Hall, 1965.

ISSN 1070-4272, Russian Journal of Applied Chemistry, 2007, Vol. 80, No. 11, pp. 1914–1917. © Pleiades Publishing, Ltd., 2007.
Original Russian Text © G.R. Timerbaeva, Yu.S. Zimin, I.M. Borisov, I.A. Bondareva, Yu.B. Monakov, 2007, published in Zhurnal Prikladnoi Khimii, 2007, Vol. 80, No. 11, pp. 1890–1893.

MACROMOLECULAR CHEMISTRY AND POLYMERIC MATERIALS

Radical Mechanism of Pectin Oxidation in Aqueous Solution

G. R. Timerbaeva, Yu. S. Zimin, I. M. Borisov, I. A. Bondareva, and Yu. B. Monakov

Bashkir State University, Ufa, Bashkortostan, Russia
St. Petersburg State Academy of Veterinary Medicine, St. Petersburg, Russia
Branch of Moscow State University of Technologies and Management, Meleuz, Bashkortostan, Russia

Received March 16, 2007

Abstract—The kinetic features of functionalization of natural polysacharide, pectin, by liquid-phase oxidation were studied.

DOI: 10.1134/S1070427207110274

Water-soluble oligomers of natural polysaccharides (chitosan, arabinogalactan, and pectin) are promising environmentally clean raw materials for preparing prolonged-action pharmaceuticals and additives for food and cosmetic industry [1–3]. It is interesting to examine the possibility of preparing pharmaceuticals from modified (additionally functinalized) low-molecular-weight natural polymers (oligomers) in which the polymeric carrier is a transporter of the pharmaceutical through cell membranes. It is known that natural polysaccharide pectin is a radioprotector and detoxicant [4]. Combination of these properties with therapeutic action of a pharmaceutical in the form of a pectin complex results in effective positive effect on an organism. Pectin can be readily functionalized by oxidation in an aqueous solution. Preparation of a water-soluble oxidized polysaccharide using nontoxic and readily separable oxidizing agents is an urgent problem. To determine the optimal preparation conditions of the oxidation product with required properties, the kinetic features of oxidation of the biopolymer in an aqueous solution should be studied.

EXPERIMENTAL

We used citrus pectin with molecular weight of 132000 ([η] = 2.4 dl g^{-1}, 25°C). Hydrogen peroxide (H_2O_2), iron(II) sulfate, ethylenediaminetetraacetic acid disodium salt (Na_2EDTA), and potassium iodide were of chemically pure grade; crystalline iodine was of pure grade. An ozone–oxygen mixture was prepared with the aid of an ozonizer of the known design [5]. We used freshly prepared double-distilled water as the solvent. Oxidation of aqueous pectin solutions was performed in a glass temperature-controlled bubbling reactor. Samples of the reaction mixture were taken at regular intervals. The total concentration of the carboxy groups was determined by titration with NaOH.

A chemiluminescence unit consisted of a lightproof chamber in which a glass temperature-controlled reactor equipped with a reflux condenser, a stirrer, and a syringe for injection of reactants was placed. The experiments were performed by the following procedure. An aqueous solution with a known pectin concentration was placed in the reactor and the reactor was controlled thermostatically for 15 min. Hydrogen peroxide was then rapidly injected with the syringe, or an ozone–oxygen mixture was bubbled with stirring. A change in the chemiluminescence intensity measured in arbitrary units proportional to the signal height was recorded. The UV spectra of 0.2% aqueous solution were recorded on a Specord M-40 spectrophotometer.

Pectins are macromolecular compounds whose chemical structure is close to that of hemicelluloses (colloidal polysaccharides) or plant glucopolysaccharides. Pectins are composed of *D*-galacturonic acid residues bound by α-(1→4)-glycoside bonds into a straight-chain macromolecule of polygalacturonic (pectic) acid [6]. No thermal degradation and oxidation of pectin are observed in an aqueous solution at 50–80°C. Under these conditions, pectin is not oxidized even when air is bubbled through the solution. The content of carboxy groups of pectin increases after addition of H_2O_2 to an aqueous pectin (P) solution or bubbling of an ozone–oxygen mixture through the solution (Fig. 1).

Since accumulation of carboxy groups in the examined reaction systems decelerates with time (Fig. 1), we used the initial rate of accumulation of carboxy groups V_{COOH} as the quantitative parameter of the process.

Previously we showed [7, 8] that oxidation of natural polysaccharide arabinogalactan and poly(vinyl alcohol) in an aqueous solution, initiated by hydrogen peroxide or an ozone–oxygen mixture, was a radical reaction. To determine the oxidation mechanism in the system in question, we determined the initial rate of accumulation of carboxy groups in the presence of phenol (Fig. 2).

Phenol is a conventional inhibitor of radical-chain oxidation of organic compounds [9]. As seen from Fig. 2, phenol inhibits pectin oxidation, which suggests the radical mechanism of polysaccharide oxidation.

Variable-valence metal cations (M^{n+}) catalyze radical decomposition of hydrogen peroxide [10]:

$$H_2O_2 + M^{n+} \rightarrow HO^- + HO^\bullet + M^{(n+1)+}, \qquad (1)$$

and hence this reaction may initiate radical processes. Therefore, variable-valence metal salts should catalyze pectin oxidation with hydrogen peroxide, which is the case.

The dependence of the initial rate of accumulation of carboxy groups on the concentration of iron(II) sulfate at $T = 70°C$, $[P]_0 = 0.2$ wt %, $[H_2O_2]_0 = 1$ M is presented below.

$[FeSO_4] \times 10^4$, M	$V_{COOH} \times 10^4$, mol l^{-1} min^{-1}
0	0.76
1	1.35
3	2.94
5	4.61
7	5.84
10	8.88

It is seen that the rate of initiation by reaction (1) increases with increasing content of Fe^{2+} ions in the solution. As a result, accumulation of carboxy groups accelerates. Trace amounts of variable-valence metal ions can be introduced into the reaction mixture with distilled water which was not subjected to special treatment to remove M^{n+} impurities [11]. Therefore, pectin oxidation can be weakly initiated in P + H_2O_2 + O_2 + H_2O system by reaction (1) even in the absence of $FeSO_4$.

To confirm the radical mechanism of pectin oxidation, we added disodium salt of ethylenediaminetetra-

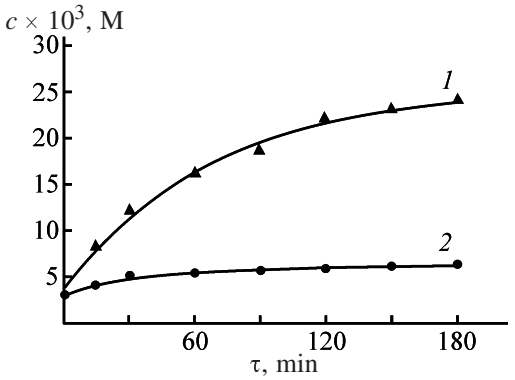

Fig. 1. Kinetic curves of accumulation of carboxy groups in (*1*) P + O_3 + O_2 + H_2O and (*2*) P + H_2O_2 + O_2 + H_2O systems at 70°C. $[P]_0 = 0.2$ wt %, $V_{O_3+O_2} = 6.3$ l h^{-1}, $[H_2O_2]_0 = 1$ M. (*c*) Concentration of –COOH groups and (τ) time.

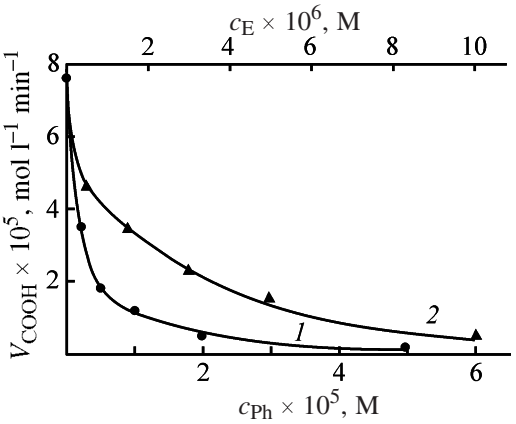

Fig. 2. Initial rate of accumulation of carboxy groups V_{COOH} as a function of the initial concentration of (*1*) phenol c_{ph} and (*2*) Na_2EDTA c_E at 70°C. $[P]_0 = 0.2$ wt %, $[H_2O_2]_0 = 1$ M.

acetic acid. It is known that Na_2EDTA is a strong complexing agent forming complexes with variable-valence metal cations [12, 13]. These complexes do not catalyze decomposition of hydrogen peroxide by reaction (1) [14]. Introduction of Na_2EDTA into the system decreases the concentration of free variable-valence metal cations and decreases the rate of initiation by reaction (1), thus decreasing V_{COOH} (Fig. 2).

Oxidation of pectin in aqueous solutions at 70°C with hydrogen peroxide or with an ozone–oxygen mixture bubbled through the solution is accompanied by chemiluminescence (CL) in the visible range. It is known [15] that CL is observed, as a rule, in systems in which species having a free valence are generated. For example, in the absence of an initiator in the P + O_2 + H_2O system, no free radicals are formed and CL

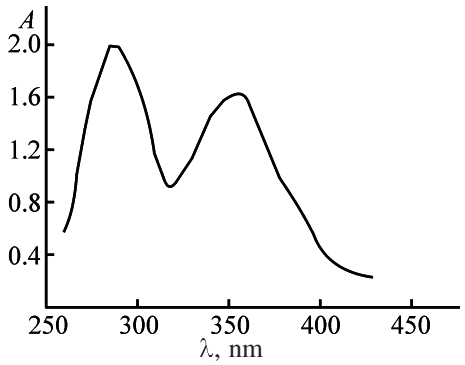

Fig. 3. UV spectrum of a solution of mixture I at 25°C. $[P]_0$ = 0.2 wt %, $[I_2]_0 = 10^{-4}$ M, $[KI]_0 = 6\times10^{-4}$ M. (*A*) Optical density and (λ) wavelength.

is not observed. CL signals in P + O_3 + O_2 + H_2O and P + H_2O_2 + O_2 + H_2O systems are observed in the first reaction steps (~30–200°C), with CL intensity decreasing exponentially. It should be noted that CL in the examined systems can be due to oxidation of not only pectin but also readily oxidizable impurities [16] present in the polysaccharide in trace amounts.

A great attention is paid to the study of different biologically active additives prepared from food fibers. Biologically active compounds can be readily prepared by treatment of pectin with molecular iodine [17]. These compounds are probably formed by electron donor–acceptor interactions of pectin functional groups and I_3^- formed in an aqueous solution of I_2 + KI mixture. We studied how oxidative functionalization of the biopolymer affects the bonding in these complexes.

The electronic absorption spectrum of an aqueous solution of a mixture containing 10^{-4} M I_2 and 6×10^{-4} M KI has two bands at 285 and 355 nm (Fig. 3), typical for I_3^- anion [18]. These bands are absent in the spectrum of an aqueous solution of pectin.

These bands are also present in the spectrum of a P + I_2 + KI mixture (I) with commensurable concentrations of the components. The intensities of these bands increase by a factor of approximately 1.3–1.6, which suggests formation of pectin complexes with triiodide ions. Formation of this complex is also confirmed by a change in the color of the solution from dark brown to intense yellow [19]. The intensity of these bands increases to a lesser extent after complexation of oxidized pectin with I_3^-. Probably, functional groups of pectin responsible for complexation of I_3^- are oxidized.

CONCLUSIONS

(1) Oxidation of pectin with molecular oxygen in an aqueous solution in the presence of hydrogen peroxide or ozone occurs by the radical mechanism.

(2) Variable-valence metal ions initiate radical oxidation in the presence of H_2O_2. Phenol and Na_2EDTA inhibit peroxide oxidation of the biopolymer.

ACKNOWLEDGMENTS

This study was partially financially supported by the state scientific and technical program of Bashkortostan Republic "New Materials, Chemical Technologies for Industry, Medicine, and Agriculture on the Basis of Petrochemical, Mineral, and Recyclable Raw Materials of Bashkortostan Republic" for the year 2007.

REFERENCES

1. Arifkhodzhaev, A.O., *Khim. Prirodn. Soedin.*, 2000, no. 3, pp. 185–197.
2. Ovodov, Yu.S., *Bioorg. Khim.*, 1998, vol. 24, no. 7, pp. 483–501.
3. Suzuki, K., Mikami, T., and Okawa, Y., *Carbohydr. Res.*, 1986, vol. 151, pp. 403–408.
4. Golubev, V.N. and Shelukhina, V.P., *Pektin: Khimiya, tekhnologiya, primenenie: Uchebnoe posobie* (Pectin: Chemistry, Technology, Applications: Textbook), Moscow: RATN IECh, 1995.
5. Vendillo, V.G., Emel'yanov, Yu.M., and Filippov, Yu.V., *Zavod. Lab.*, 1959, vol. 25, no. 11, p. 1401.
6. Degtyarev, A.S., Kupchik, M.P., Donchenko, L.V., et al., *Izv. Vyssh. Uchebn. Zaved., Pishch. Tekhnol.*, 2002, no. 4, pp. 15–18.
7. Borisov, I.M., Zimin, Yu.S., Shirokova, E.N., et al., *Teor. Osn. Khim. Tekhnol.*, 2004, vol. 45, no. 4, pp. 514–518.
8. Zimin, Yu.S., Ageeva, A.F., Borisov, I.M., et al., *Izv. Vyssh. Uchebn. Zaved., Khim. Khim. Tekhnol.*, 2006, vol. 49, no. 1, pp. 52–57.
9. Roginskii, V.A., *Fenol'nye antioksidanty: Reaktsionnya sposobnost' i effektivnost'* (Phenolic Antioxidants: Reactivity and Performance), Moscow: Nauka, 1988.
10. Sychev, S.Yu. and Isaak, V.G., *Usp. Khim.*, 1995, vol. 64, no. 12, pp. 1183–1209.
11. Zimin, Yu.S., Ageeva, A.F., Borisov, I.M., et al., *Izv. Vyssh. Uchebn. Zaved. Khim. Khim. Tekhnol.*, 2006, vol. 49, no. 2, pp. 58–62.

12. Glinka, N.L., *Obshchaya khimiya* (General Chemistry), Leningrad: Khimiya, 1984.
13. Kharitonov, Yu.Ya., *Analiticheskaya khimiya* (Analytical Chemistry), Moscow: Vysshaya Shkola, 2001.
14. Shirokova, E.N., Oxidation of Arabinogalactan with Hydrogen Peroxide and Potassium Persulfate in Aqueous Solution, *Cand. Sci. Dissertation*, Ufa, 2003.
15. Shlyapintokh, V.Ya., Karpukhin, O.N., Postnikov, L.M., et al., *Khemilyuminestsentnye metody issledovaniya medlennykh khimicheskikh protsessov* (Chemiluminescence Methods for Studying Slow Chemical Reactions), Moscow: Nauka, 1966.
16. Khalikov, S.S., Pominova, T.Yu., Pereverzeva, E.I., et al., *Khim. Prirodn. Soedin.*, 1995, no. 6, pp. 896–902.
17. RU Patent 2 265 377.
18. Mokhnach, V.O. and Rusakova, N.M., *Dokl. Akad. Nauk SSSR*, 1980, vol. 135, no. 5, pp. 1143–1146.
19. Kutepov, A.M., *Biologicheski aktivnye veshchestva v rastvorakh: Struktura, termodinamika, reaktsionnaya sposobnost'* (Biologically Active Compounds in Solutions: Structure, Thermodynamics, Reactivity), Moscow: Mir, 2001.

ISSN 1070-4272, Russian Journal of Applied Chemistry, 2007, Vol. 80, No. 11, pp. 1918–1922. © Pleiades Publishing, Ltd., 2007.
Original Russian Text © Yu.V. Bondar', S.W. Lee, 2007, published in Zhurnal Prikladnoi Khimii, 2007, Vol. 80, No. 11, pp. 1894–1898.

MACROMOLECULAR CHEMISTRY AND POLYMERIC MATERIALS

Synthesis of Chemically Active Polymeric Fibers Bearing Sulfo and Carboxy Groups

Yu. V. Bondar' and S. W. Lee

Institute of Environmental Geochemistry, Kiev, Ukraine
Yeungnam University, Yeungnam, Korea

Received May 2, 2007

Abstract—A chemically active material bearing two types of acid groups, strongly acidic sulfo groups and weakly acidic carboxy groups, was prepared by radiation-induced graft copolymerization of two kinds of monomers, acrylic acid and sodium styrenesulfonate, onto polypropylene fibers. The main parameters affecting the graft copolymerization are considered.

DOI: 10.1134/S1070427207110286

The development and improvement of chemical procedures for the synthesis of functional polymeric materials participating as active components in various chemical processes is of large scientific and applied interest. The majority of developments in this field concern preparation of functional polymers in the granulated form for the use in traditional ion-exchange processes. However, synthesis of chemically active polymeric materials in the form of fibers would substantially expand possible applications of functional polymers. This is due to the fact that fibers have a developed surface and show high kinetic and adsorption parameters; they can be readily molded into articles of any size and shape; they show high performance when used in closed-loop processes.

Passing from traditional functional polymers to their new physical forms (fibrous and bulk-porous) requires new approaches to the synthesis and modification of polymers. One of such modern methods is radiation-induced polymerization. This method allows grafting of a nano- or microchain of a monomer with a desired functional group onto the surface of an inert polymeric matrix, ensuring control over the length and density of the grafted chains. The method can be used for modification of the surface, bulk, or a local section of a material or ready article [1–3]. The method is environmentally clean and economical, and it is widely used for preparing chemically active polymeric materials (based on diverse polymeric matrices) for industry, medicine, biotechnology, and environmental protection [2–9].

The range of vinyl monomers with functional groups, used in radiation-chemical technologies, is narrow. Grafting of a monomeric precursor followed by polymer-analogous transformations, or copolymerization of several monomers with different functional groups expands the possibilities for the synthesis of functional polymeric materials.

From the practical viewpoint, it is extremely interesting to prepare chemically active polymeric fibers with sulfo groups. The common route to such materials is sulfonation of grafted polystyrene chains [10–12].

Direct introduction of sulfo groups by radiation-induced graft polymerization with sodium styrenesulfonate as vinyl monomer failed [13]. Only postradiation copolymerization of acrylic acid (AA) and sodium styrenesulfonate (SSS) onto the surface of a polyethylene film led to a positive result: A cation-exchange membrane with an ion-exchange capacity of 25 mg-equiv g^{-1} was obtained. However, in that paper the specific features of radiation-induced copolymerization of two monomers were not considered, and the content of sulfo groups in the synthesized cation exchanger was not reported. Therefore, a study of the radiation-induced copolymerization of two monomers and evaluation of the ion-exchange properties of the product remains a topical problem.

EXPERIMENTAL

As a polymeric base for performing radiation-induced graft copolymerization of a mixture of monomers, acrylic acid (CH_2=CHCOOH, Junsei Chemical Co. Ltd) and sodium styrenesulfonate [CH_2=CHC_6H_4·

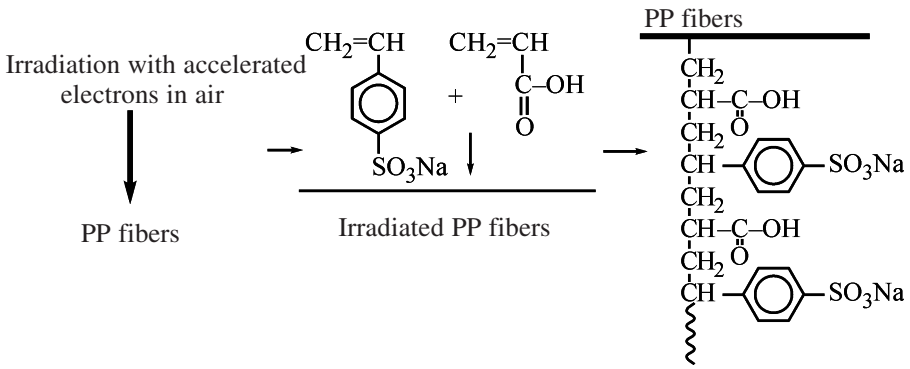

Fig. 1. Scheme of the experiment on copolymerization of acrylic acid and sodium styrenesulfonate monomers on the surface of polypropylene fibers.

SO_3Na, Tokyo Kasei Kogyo Co. Ltd (Japan)], we used a nonwoven material of polypropylene (PP) fibers with a density of 120 g m^{-2} and degree of crystallinity of 65% (Toray-Saehan Co. Ltd, Korea). Irradiation was performed on an ELV-04 accelerator by accelerated electrons (1 MeV) in air (preirradiation procedure). After the irradiation, the sample was stored in a desiccator at room temperature, and the copolymerization was performed within 1–5 days after the irradiation.

The preliminarily weighed irradiated sample was placed in a flask containing an aqueous solution of monomers [0.1 mol (20.6 g) of SSS + 0.1 mol (7.2 g) of AA in 100 ml of H_2O] and Mohr's salt [$(NH_4)_2 \cdot Fe(SO_4)_2 \cdot 6H_2O$, Merck, Germany]; the solution was saturated with nitrogen, the flask was tightly stoppered and thermostated at 50°C, and the graft copolymerization was performed with continuous stirring.

After the reaction completion, the product was thoroughly washed in a Soxhlet apparatus for 12 h with water and methanol to remove the adsorbed homopolymers and unchanged monomers, dried in a vacuum oven at 50°C to constant weight, and weighed.

The degree of graft copolymerization of the two monomers, Q_{gr} (%), was calculated from the results of gravimetric analysis, namely, from the weight gain after the reaction:

$$Q_{gr} = \frac{m_{gr} - m_0}{m_0} \times 100,$$

where m_0 and m_{gr} are the sample weights before and after grafting, respectively.

The functional groups were detected with a Perkin–Elmer Golden Gate Single Reflection ATR System IR spectrophotometer.

The total exchange capacity of the product, E_{ex} (mg-equiv g^{-1}), reflecting the total number of acid groups introduced into the PP material, was calculated from the results of back-titration [14]. The content of sulfo groups was estimated from the results of static sorption of Cu(II) and Co(II) ions from acidic solutions of their salts.

The amount of metal ions adsorbed on unit weight of dry modified fibers, S_M (mmol g^{-1}), was calculated by the formula

$$S_M = \frac{c_0 - c}{m} V,$$

where c_0 and c are the concentrations of metal ions in the solution (mmol mg^{-1}) before and after adsorption, respectively; V, volume of the solution being analyzed (ml); and m, weight of the modified sample (g).

The concentration of M(II) ions in aqueous solution was measured on a UNICAM 989 atomic absorption spectrometer (the United Kingdom).

The scheme of the experiment is shown in Fig. 1.

This paper deals with the effect of various process parameters on the copolymerization of SSS and AA monomers on polypropylene fibers as support. Three sets of parameters related to the irradiation, graft copolymerization proper, and nature of the support affect the degree of radiation grafting. We examined the effect exerted by the main parameters: absorbed dose, temperature, reaction time, and inhibitor concentration.

In the course of irradiation of a polymeric matrix with accelerated electrons in the presence of atmospheric oxygen, the major products formed on its surface and in the bulk are hydroperoxides, which are stable at ambient temperature but decompose on heat-

Influence of the Mohr's salt content on the degree of graft copolymerization of SSS and AA monomers

Mohr's salt content	Degree of grafting, %	
	SSS + AA monomer mixture	7% AA
0	18.6	57.7
5×10^{-5}		61.7
10^{-4}	29.3	113.0
5×10^{-4}	86.5	150.4
10^{-3}	110.0	164.6
5×10^{-3}	82.2	108.3
10^{-2}	79.7	101.4
10^{-1}	19.9	34

ing above 60°C with the generation of macroradicals ($PPO^{\bullet}$) and hydroxyl radicals ($^{\bullet}OH$). In the macroradicals, there is a site for monomer (M) grafting, and hydroxyl radicals can initiate the homopolymerization of the monomers. The reaction mechanism is discussed in numerous papers (see, e.g., [15]) and can be presented as follows:

$$PP \xrightarrow{\text{Irradiation}} PPH^{\bullet} \xrightarrow{O_2} PP\text{–}OOH \xrightarrow{\text{Heating}} PPO^{\bullet} + {}^{\bullet}OH,$$

$$M + {}^{\bullet}OH \rightarrow {}^{\bullet}M\text{–}OH \xrightarrow{n\text{M}} {}^{\bullet}M\text{–}(M)_n\text{–}OH,$$

$$PPO^{\bullet} + M \rightarrow PPO\text{–}M^{\bullet} \xrightarrow{k\text{M}} PPO\text{–}(M)_k\text{–}M^{\bullet},$$

$$PPO^{\bullet} + {}^{\bullet}M\text{–}(M)_n\text{–}OH \longrightarrow PPO\text{–}M\text{–}(M)_n\text{–}OH,$$

$$PPO\text{–}(M)_k\text{–}M^{\bullet} + {}^{\bullet}OH \longrightarrow PPO\text{–}(M)_k\text{–}M\text{–}OH,$$

$$PPO\text{–}(M)_k\text{–}M^{\bullet} + {}^{\bullet}M\text{–}(M)_n\text{–}OH \longrightarrow PPO\text{–}(M)_{k+n+2}\text{–}OH.$$

The homopolymerization can be suppressed by adding transition metal salts [16, 17]:

$$^{\bullet}OH + Fe^{2+} \longrightarrow OH^{-} + Fe^{3+}.$$

If the grafting is performed at temperatures lower than 60°C, the degree of radiation grafting can also be increased by adding transition metal salts, as in their presence hydroperoxides decompose more efficiently:

$$PP\text{–}OOH + Fe^{2+} \longrightarrow PPO^{\bullet} + OH^{-} + Fe^{3+}.$$

At the same time, an excess of such salts can deactivate the system and lead to a decrease in the degree of polymerization:

$$PPO^{\bullet} + Fe^{2+} \longrightarrow PPO^{-} + Fe^{3+}.$$

The influence of the content of Fe^{2+} ions (Mohr's salt) on the degree of graft copolymerization of SSS and AA onto irradiated (absorbed dose 70.5 kGy) samples of PP fibers, performed at 50°C for 12 h, is illustrated by the table. It can be seen that, on adding Fe(II) ions into the reaction medium, the degree of grafting increases and reaches a maximum on adding 10^{-3} wt % Mohr's salt.

We examined how the degree of graft copolymerization of SSS and AA from aqueous solution of these monomers onto PP fibers depends on the absorbed dose (Fig. 2).

In contrast to Chen et al. [16], who reported on a linear increase in the degree of radiation-induced grafting of AA onto a polypropylene material with an increase in the absorbed dose to 120 kGy, we obtained a more complex dependence of the degree of radiation-induced graft copolymerization of the two monomers on the absorbed dose. Figure 2 shows that the degree of radiation-induced graft copolymerization first slowly increases with an increase in the absorbed dose to 40.3 kGy and then rapidly increases with a further increase in the absorbed dose to 70.5 kGy.

To reveal the specific features of graft copolymerization of SSS and AA monomers, we examined the copolymerization kinetics at 50°C and analyzed the IR spectra of the corresponding samples. The kinetic curve shown in Fig. 3 consists of several portions (0–9, 9–12, 12–33 h), apparently reflecting the stepwise course of the copolymerization at this temperature. In the first step of the process (0–9 h), smooth ascent of the kinetic curve suggets slow development of the copolymerization; in the second step (9–12 h), the copolymerization rate sharply increases, and in the third step (12–30 h) it increases more slowly, reaching saturation in 28–32 h.

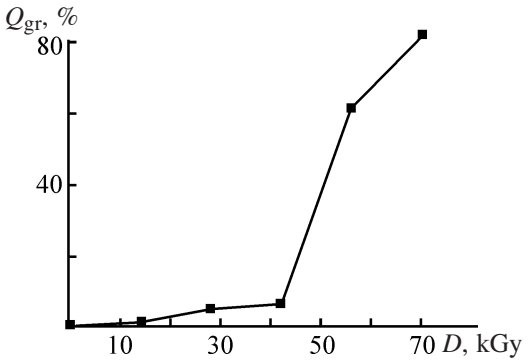

Fig. 2. Degree of graft copolymerization of two monomers, Q_{gr}, onto PP fibers as a function the absorbed dose D.

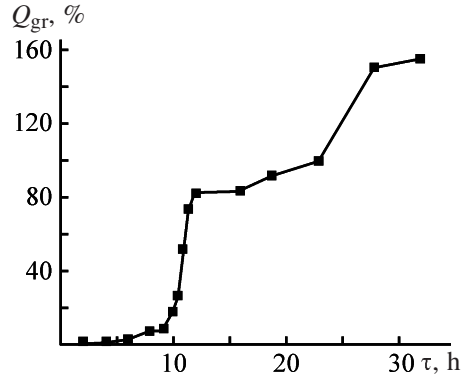

Fig. 3. Degree of graft copolymerization of SSS and AA, Q_{gr}, as a function of the copolymerization time τ.

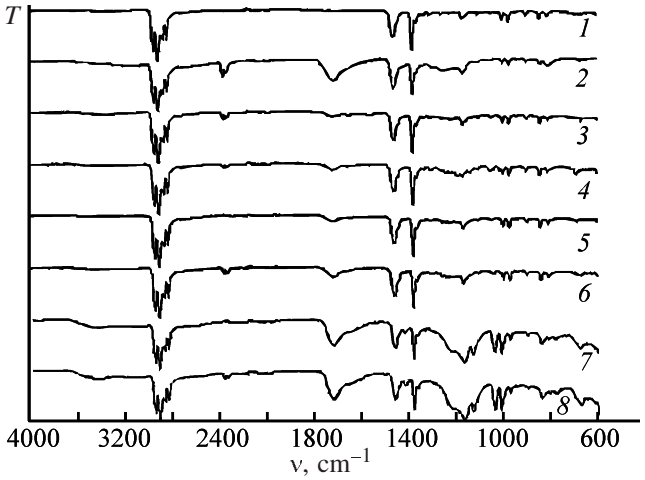

Fig. 4. IR spectra of (*1*) initial PP fiber, (*2*) PP fiber with grafted polyacrylic acid (Q_{gr} = 95%), and (*3*–*8*) PP fibers modified with SSS + AA, with different degrees of grafting. (*T*) Absorption and (ν) wavenumber. Q_{gr}, %: (*3*) 2.9, (*4*) 7.7, (*5*) 8.8, (*6*) 17.8, (*7*) 73.0, and (*8*) 98.6.

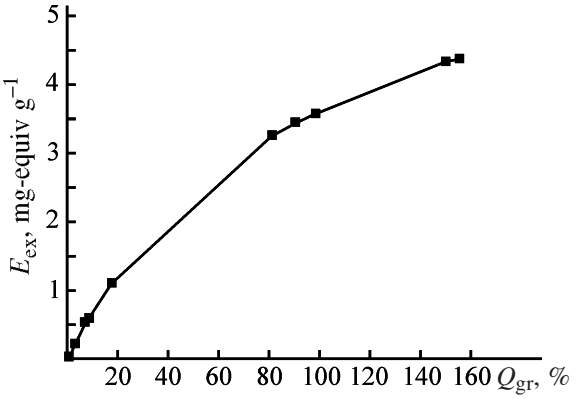

Fig. 5. Total exchange capacity E_{ex} of chemically active PP fibers as a function of Q_{gr}.

Figure 4 shows the IR spectra of the initial unmodified PP fibers, PP fibers with grafted polyacrylic acid chains (Q_{gr} = 95%), and samples of PP fibers with different degrees of graft copolymerization.

In the IR spectra *3*–*6* of the samples corresponding to the first step of the copolymerization (Q_{gr} 2.9, 7.3, 8.6, and 17.8%, respectively), there is an absorption band at 1715 cm^{-1}, assigned to the C=O vibrations in acrylic acid. The intensity of this band grows with an increase in the degree of grafting. The characteristic absorption bands of the sulfonate group (1150, 1030, 670 cm^{-1}) appear in the IR spectra in the second and third steps of the copolymerization (spectra *7* and *8*, Q_{gr} 73.0 and 98.6%, respectively). Their intensity, like that of the above-noted absorption band of acrylic acid, grows with an increase in the degree of polymerization.

Comparison of the kinetic curve of the copolymerization of SSS and AA monomers with the IR spectra of the corresponding samples shows that the copolymerization of the monomers starts with grafting of acrylic acid monomers (in the first step), and sodium styrenesulfonate monomers are incorporated in the propagating chains in the subsequent steps.

This can also be confirmed by the results of a blank grafting experiment in which the irradiated fiber samples were placed for 9–12 h in a nitrogen-saturated aqueous solution containing 10^{-2} wt % Mohr's salt and heated to 50°C, after which AA was added and the mixture was kept at 50°C for an additional 5–9 h. The absence of characteristic absorption bands of AA in the IR spectra of the resulting samples indicated that, under these conditions, virtually all the active centers capable to initiate the graft copolymerization were deactivated. Thus, we can conclude with confidence that SSS monomers are incorporated in the propagating polyacrylic acid chains, rather than grafted directly to PP fibers.

By the radiation-induced copolymerization of sodium styrenesulfonate and acrylic acid monomers, we prepared chemically active PP fibers bearing two types of functional groups: strongly acidic sulfo groups and weakly acidic carboxy groups. As the synthesized fibers can be considered as a bifunctional adsorbent (cation exchanger), it is very interesting to evaluate its ion-exchange parameters. For several samples, we determined by back-titration the total exchange capacity reflecting the actual number of acid groups. Figure 5 shows the dependence of the total exchange capacity of the samples on the degree of graft copolymerization of SSS + AA.

The maximal total exchange capacity (acid groups), 4.37 mg-equiv g^{-1}, was obtained for the sample with 155% degree of grafting.

To single out the contribution of sulfo groups to the total exchange capacity, we performed a series of

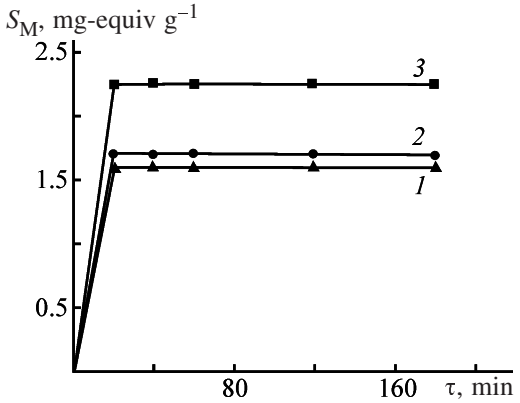

Fig. 6. Adsorption S_M of Cu(II) and Co(II) ions acidic solutions of their salts (pH 4) with the synthesized PP fibers as a function of time τ. Curve nos. are sample nos.

experiments on the adsorption of Cu(II) and Co(II) ions from acidic solutions of their salts (pH 4). As in acidic solutions (at pH < 5) the carboxy groups of AA are only weakly ionized and do not take part in the ion exchange to a noticeable extent, the sorption occurs only via strongly ionized sulfo groups.

Three synthesized samples in the H^+ form with the total exchange capacity of 3.2 (sample 1), 3.4 (sample 2), and 4.3 mg-equiv g^{-1} (sample 3) were chosen for the experiments.

The kinetic curves of adsorption of Cu(II) and Co(II) ions with the synthesized PP fibers from acidic solutions of their salts are given in Fig. 6.

It can be seen that the equilibrium adsorption values (1.55, 1.68, 2.55 mg-equiv g^{-1}) are almost two times lower than the total exchange capacities of the samples. This fact suggests that chemically active PP fibers synthesized by radiation-induced graft copolymerization of SSS and AA monomers contain groups of a strong acid (sulfonate groups). In the examined samples, the amount of these groups is large and comparable with the amount of carboxy groups.

CONCLUSIONS

(1) A chemically active polymeric material bearing two types of acidic groups, strongly acidic sulfonate and weakly acidic carboxy groups, was prepared by radiation-induced graft copolymerization of two types of monomers, acrylic acid and sodium styrenesulfonate, onto polypropylene fibers.

(2) The main parameters affecting the graft copolymerization are the absorbed dose, reaction temperature and time, and inhibitor concentration.

(3) The kinetics of the copolymerization of acrylic acid monomers and sodium styrenesulfonate at 50°C was studied. The copolymerization starts with the grafting of acrylic acid monomers, and sodium styrenesulfonate monomers are subsequently incorporated in propagating monomer chains.

REFERENCES

1. Ivanov, V.S., *Radiatsionnaya khimiya polimerov* (Radiation Chemistry of Polymers), Leningrad: Khimiya, 1988.
2. Bhattacharya, A. and Misra, B.N., *Prog. Polym. Sci.*, 2004, vol. 29, pp. 767–814.
3. Bhattacharya, A., *Prog. Polym. Sci.*, 2000, vol. 25, pp. 371–401.
4. Nasef, M.M. and Hegazy, E.A., *Prog. Polym. Sci.*, 2004, vol. 29, pp. 499–561.
5. Kato, K., Uchida, E., Kang, E., et al., *Prog. Polym. Sci.*, 2003, vol. 28, no. 2, pp. 209–259.
6. Saito, K., Tsuneda, S., Kim, M., et al., *Radiat. Phys. Chem.*, 1999, vol. 54, pp. 517–525.
7. Dargaville, T.R., George, G.A., Hill, D.J.T., et al., *Prog. Polym. Sci.*, 2003, vol. 28, no. 9, pp. 1355–1376.
8. Tamada, M., Seko, N., and Yoshii, F., *Radiat. Phys. Chem.*, 2004, vol. 71, nos. 1–2, pp. 223–227.
9. Kumar, V., Bhardwaj, Y.K., Rawat, K.P., and Sabharwal, S., *Radiat. Phys. Chem.*, 2005, vol. 73, no. 3, pp. 175–182.
10. Nasef, M.M., Saidi, H.A., Nor, H.M., and Foo, O.M., *J. Appl. Polym. Sci.*, 2000, vol. 76, pp. 1–11.
11. Yamaki, T., Asano, M., Maekawa, Y., et al., *Radiat. Phys. Chem.*, 2003, vol. 67, pp. 403–407.
12. Pirogov, A.V., Chernova, M.V., Nemtseva, D.S., and Shpigun, O.A., *Vestn. Mosk. Univ., Ser. 2: Khim.*, 2002, vol. 172, no. 3, pp. 172–177.
13. Tsuneda, S., Saito, K., Mitsuhara, H., and Sugo, T., *J. Electrochem. Soc.*, 1995, vol. 142, pp. 3659–3663.
14. Kreshkov, A.P., *Osnovy analiticheskoi khimii* (Principles of Analytical Chemistry), Moscow: Khimiya, 1970, vol. 2.
15. Kaur, I., Kumar, S., Misra, B.N., and Chauhan, G.S., *Mater. Sci. Eng.*, 1999, vol. 270A, pp. 137–144.
16. Chen, J., Nho, Y.Ch., and Park, J.Sh., *Radiat. Phys. Chem.*, 1998, vol. 52, nos. 1–6, pp. 201–206.
17. Viengkhou, V., Ng, L.T., and Garnett, G.L., *Radiat. Phys. Chem.*, 1997, vol. 49, no. 5, pp. 595–602.

ISSN 1070-4272, Russian Journal of Applied Chemistry, 2007, Vol. 80, No. 11, pp. 1923–1927. © Pleiades Publishing, Ltd., 2007.
Original Russian Text © N.K. Luneva, L.I. Petrovskaya, T.I. Ezovitova, 2007, published in Zhurnal Prikladnoi Khimii, 2007, Vol. 80, No. 11, pp. 1899–1903.

MACROMOLECULAR CHEMISTRY AND POLYMERIC MATERIALS

Synthesis and Properties of Cellulose Phosphates

N. K. Luneva, L. I. Petrovskaya, and T. I. Ezovitova

Institute of General and Inorganic Chemistry, State Scientific Institution, National Academy of Sciences of Belarus, Minsk, Belarus

Received January 12, 2007

Abstract—Conditions for modification of cellulose under laboratory and industrial conditions with A-1 and A-2 fire retardants as P,N-containing modifiers were examined with the aim to prepare difficultly inflammable materials. The degrees of crystallinity of the products, crystallite size, and features of their thermal decomposition in air in the range 20–500°C were examined.

DOI: 10.1134/S1070427207110298

Wide use of cellulose-containing materials in private life gives rise to permanent fire hazard in case of violation of fire safety requirements. Therefore, the amount of goods produced in fire-safe modifications in developed countries is doubled every year. In CIS contries, fireproof cellulose-containing materials for domestic purposes virtually are not produced, whereas the demand of offices, hotels, boarding schools, hostels, and transport for these materials steadily grows. Studies on preparation of phosphorus-containing cellulose esters made it possible to formulate the requirements to esterifying fire-retardant agents for cellulose and to technologies for production of phosphorus-containing materials of decreased combustibility.

The goal of this study was to develop the conditions for treatment of fabrics with P,N-containing fire retardants and to examine the properties of the resulting materials.

EXPERIMENTAL

In our study we used P,N-containing fire retardants (A-1 and A-2) differing in the anionic form of the phosphates taken for the modification [1, 2]. Treatment of fabrics differing in the thickness and density (markings 134, 142, 1672, 3154) was performed both under laboratory conditions and in pad equipment of a textile finishing shop; heat treatment was performed both an an SNOL laboratory oven (130–170°C) and in a Textima-140 tenter drier (175–200°C) at a fabric feeding rate of 6 m min^{-1}. After the heat treatment, the samples were washed in a bath (bath ratio 15) with water under laboratory conditions or in an Eliteks-4580 dye-rolling machine to negative reaction for phosphorus in wash waters [3]. The phosphorus content of fabrics heat-treated in different chambers of the Textima-140 apparatus is given in Table 1.

The wash waters from laboratory samples heat-treated at 130–170°C were subjected to chromatographic analysis for the content of condensed phosphates. The results are given in Table 2.

The composition of the ester groups of cellulose phosphates prepared at different temperatures was determined by their enzymatic hydrolysis followed by evaluation of the degree of condensation of phos-

Table 1. Phosphorus content of fabric treated with fire retardants, after heat treatment in Textima-140 apparatus

Fire retardant	Marking of fabric	pH of fire retardant	Drying temperature, °C					Phosphorus content,* wt %
A-1	263	1.3	130	140	150	160	170	2.0
A-2		2.4	130	140	150	160	170	2.7
A-1	1672	1.3	130	150	170	180	170	3.4
A-2		2.4	130	150	170	180	175	4.4
A-1	3154	1.3	160	165	165	185	210	5.0
A-2		2.4	160	165	165	185	210	5.7

* Coarse calico washed to negative reaction of wash water for phosphorus.

Table 2. Content of condensed phosphates in wash waters from modified fabric heat-treated at different temperatures

Fire retardant	Phosphorus content, wt %, at indicated temperature, °C					
	20	130	140	150	160	170
A-1	–	10.6	18.4	26.8	29.4	32.3
A-2	20	27.4	32.3	40.2	53.0	67.0

phates after their chromatographic separation [4]. The results are given in Table 3.

The above data show that the ester groups of the samples prepared by treatment of the fabric with A-1 fire retardant mainly consist of orthophosphoric acid residues. Treatment of the fabric with A-2 fire retardant yields an ester containing up to 48 wt % phosphates with the degree of condensation $n \geq 2$ (mainly pyrophosphate) [5]. Presumably, in the course of treatment with A-1 and A-2 fire retardants, acidic salts of orthophosphoric acid react with cellulose by the scheme shown below.

Scheme of reaction of acidic salts with cellulose

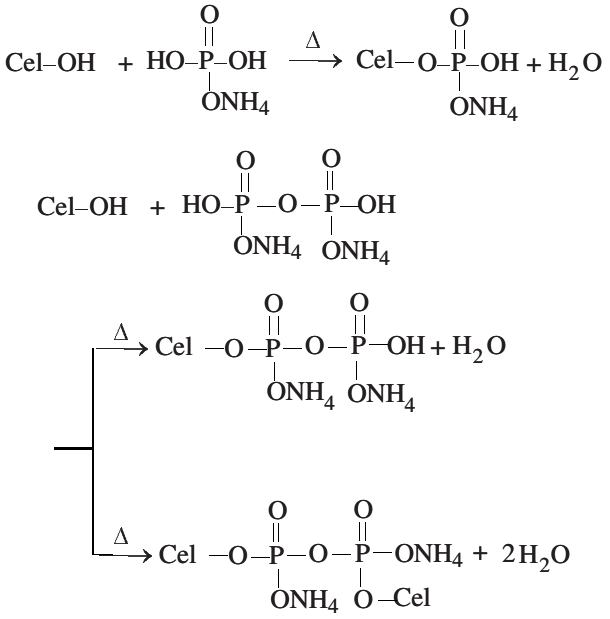

The structural changes occurring in cellulose crystallites upon phosphorylation were monitored by X-ray phase analysis. The X-ray diffraction patterns of the samples were taken with a URS-50M device (copper cathode, Ni-filtered CuK_α radiation, λ 1.5405 Å) using the POWDER X program. As seen from the diffraction patterns (Figs. 1a, 1b), the crystalline cell

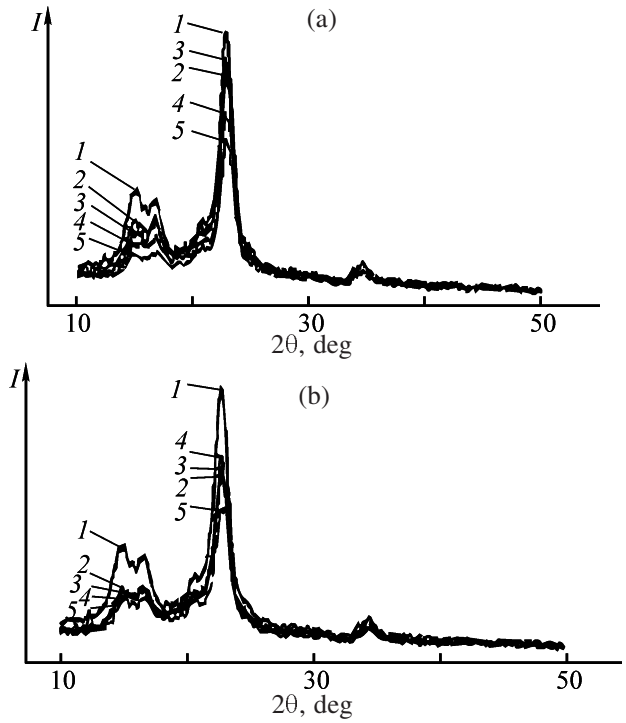

Fig. 1. X-ray diffraction patterns of celluloses modified with (a) A-1 and (b) A-2 fire retardants. (*I*) Intensity and (2θ) Bragg angle. (*1*) Initial cellulose; phosphorus content, wt %: (a) (*2*) 2.0, (*3*) 3.2, (*4*) 4.2, and (*5*) 5.1; (b) (*2*) 2.2, (*3*) 3.8, (*4*) 4.9, and (*5*) 5.9.

of cellulose does not undergo significant structural changes, as indicated by preservation of the (101), (10$\bar{1}$), and (002) reflections at 2θ 14.5°, 16.5°, and 22.3°, respectively.

The degree of crystallinity and composition of the modified fabrics were calculated according to [6]. The crystallite size was estimated by the Scherrer formula [7, 8]. The structural chaarcteristics of cellulose phosphates differing in the phosphorus content are given in Table 4.

As seen from Tables 1 and 4, the phosphorus content of fabrics increases with an increase in the temperature of treatment with A-1 and A-2 fire retardants. The degree of crystallinity of the samples tends to decrease, which is apparently due to the occurring amorphization of cellulose and to increasing defectiveness of the crystallites as a result of distortion of the chain arrangement in the polymer, which leads to a decrease in the crystallite size. The strength characteristics of cellulose phosphates prepared under the industrial conditions are given in Table 5.

Upon treatment with fire retardants, washing, and drying, the strength of the modified fabrics (markings 742, 1672, 3154) somewhat decreases (by 7–40%) but

Table 3. Composition of ester groups of cellulose phosphates in relation to the fire retardants used and to the temperature and time of the heat treatment

Fire retardant	Treatment conditions		Phosphorus content, wt %	Content of ester groups, wt %		
	T, °C	τ, min		ortho-	pyro-	tripoly-
A-1	130	40	2.8	98	2	–
	140	40	3.2	96	4	–
	150	40	4.2	90	10	–
	160	30	5.1	84	16	–
A-2	130	40	2.0	77	22	1.0
	140	40	3.8	71	26	3.0
	150	40	4.9	65	33	2.0
	160	10	5.9	52	40	8.0

Table 4. Comparative characteristics of the supramolecular structure of the initial and modified cellulose in relation to the preparation conditions and kind of fire retardant

Modifier	Phosphorus content, wt %	Degree of crystallinity, %	Cellulose crystallite size, nm
–	–	88.5	10.1
A-1	2.0	77.3	8.4
	3.2	76.4	8.4
	4.2	76.7	8.1
	5.1	77.0	8.1
A-2	2.2	76.7	8.1
	3.8	74.3	8.1
	4.9	72.1	8.3
	5.9	67.3	8.1

remains sufficient and still meets the standard requirements to these kinds of fabrics.

The heat resistance of the fabrics on heating in air was evaluated with an MOM derivatograph (Hungary) at a heating rate of 10 deg min^{-1}. The results obtained are given in Table 6. We found that the modified cellulose materials started to degrade at temperatures 60–90°C lower compared to the temperature of the major degradation of the unmodified cellulose. The degradation rate reached a maximum at 180–200°C for the fabrics treated with A-1 and at 200–215°C for those treated with A-2. It should be noted that the degradation rate of the modified cellulose decreased in the low-temperature step from 1.25 to 1.0, and in the major degradation step, from 15.5 to 10.0 mg min^{-1}. The degradation intensity for the modified fabrics was also appreciably lower (2.0 against 3.1 mg deg^{-1}). In the course of thermal degradation of the modified fabrics, the amount of evaporated phosphorus-containing volatiles decreases. The yield of the condensed residue (CR) at 500°C is 13 wt % for the initial fabric, 22–32 wt % for the fabric treated with A-1, and 28–40 wt % for the fabric treated with A-2. Exothermic effects in the DTA curves in thermal decomposition of phosphorus-containing cellulose are 30–40% weaker than those observed with the initial cellulose.

The efficiency of fire protection of the fabrics, characterized by the combustibility coefficient K, is plotted in Fig. 2 vs. phosphorus content. The combus-

Table 5. Tensile strength of the initial and modified fabrics

Marking of fabric	Tensile strength, N			
	before treatment		after treatment	
	warp	weft	warp	weft
134	32.4/44.2*	27.0/41.2	31.6	20.2
742	35.0/86.6	20.0/41.2	64.2	26.4
1672	30.0/18.0	33.1	30.2	34.3
3154	97.0/104.0	45.0/56.7	97.0	45.0

* Numerator: GOST (State Standard) requirements; denominator: strength of fiber taken for treatment.

Table 6. Characteristics of thermal degradation of fabrics

Sample	Phosphorus content, wt %	Cellulose dehydration (20–200°C)			Polymer degradation (200–500°C)		
		maximal weight loss rate, mg min^{-1}	degradation intensity, mg deg^{-1}	weight loss, %	maximal weight loss rate, mg min^{-1}	degradation intensity, mg deg^{-1}	CR yield, %, at 500°C
Initial fabric	–	1.25	0.30	7	15.5	3.1	13
Fabric + A-1	2.0	1.00	0.20	30	15.5	3.1	22
	3.2	1.00	0.20	25	14.5	2.9	29
	5.1	1.20	0.25	30	13.5	2.7	32
Fabric + A-2	2.2	1.00	0.20	22	12.0	2.4	28
	3.8	1.00	0.20	17	12.0	2.2	37
	5.9	1.00	0.20	35	10.0	2.0	42

tibility coefficient was determined by the formula $K = S_{test}/S_{inc} - 1$, where S_{test} is the area enclosed by the temperature curve of the release of gaseous combustion products and the straight line drawn through the initial temperature point and the temperature point after testing for 20 min; S_{inc} is the analogous quantity for an asbestos cement plate taken as incombustible reference. If $K > 2.5$, the material is combustible; if $K < 1$, it is difficultly combustible; and if $1 \le K \le 2.5$, it is combustible but difficultly inflammable.

The results obtained show that the fire protection efficiency for cellulose polyphosphates containing 2.1 wt % phosphorus ($K = 1$) virtually coincides with that determined for cellulose orthophosphate containing 5.0 wt % phosphorus. Thus, the fire protection efficiency depends not only on the phosphorus content, growing with its increase, but also on the anionic organization of the phosphorus chain in the ester.

The fire protection tests were performed by the procedure described in [9], from the length of the carbonized section of the specimens (in accordance with the standard, the limit is 150 mm for difficultly inflammable fabrics).

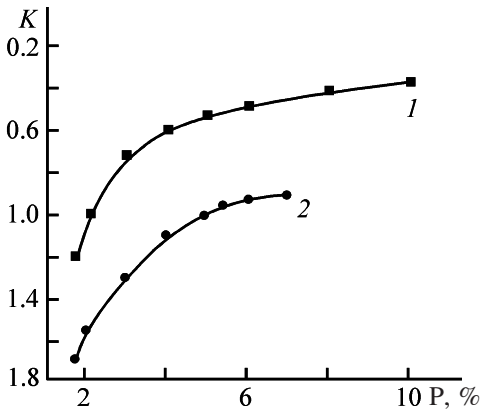

Fig. 2. Combustibility coefficient K of phosphorus-containing materials as a function of phosphorus content. Cellulose modified with (*1*) A-2 and (*2*) A-1.

The results of the fire protection tests show that treatment of cellulose materials with any of the two fire retardants ensures preparation of a flame-retarded (difficultly inflammable) fabric whose combustion or smoldering do not continue after withdrawing the specimen from the flame. For the modified fabrics, the length of the carbonized section of the fabric varied from 90–111 mm depending on the phosphorus content and the fire retardant used, which meets the requirements to fire-retarded fabrics.

It should be noted that the flame-resistant properties of the phosphorus-containing fabrics obtained is preserved to high extent after launderings, which is a very valuable property. For example, the combustibility coefficient of the tested samples treated with A-1 and A-2 did not increase after ten alkaline launderings under the conditions described in [10].

We also examined the possibility of preparing fire-protected blend fabrics (cotton or viscose 30–86%, polyester 14–70%) of density 254–293 g cm^{-2} (markings 5S 35KV, 6S 35KV, 7S 12KV, 7S 44KV, 6S 15KV, 6S 21KV), produced by the MOGOTEKS Open Joint-Stock Company. We found that, after modification with A-2 fire retardant, the mixed fabrics containing no less than 50 wt % cellulose fibers (cotton or viscose) exhibit high flame resistance, are stable in laundrings, and only slightly (by up to 10%) lose the mechanical strength.

CONCLUSIONS

(1) The conditions for the synthesis of cellulose phosphates involving modifiers based on ortho- and polyphosphates were optimized. The resulting prod-

ucts contain 2–5.9 wt % phosphorus. The polymer modification leads to a decrease in the degree of crystallinity and crystallite size.

(2) The dehydration of modified cellulose in the temperature range 20–500°C in air starts at 90–130°C lower temperature compared to the initial polymer, and the rate of degradation of the carbohydrate moiety decreases considerably.

(3) The phosphorus-containing fabrics modified with A-1 and A-2 fire retardants are difficutly inflammable fabrics. The fire protection efficiency is preserved after alkaline launderings. The fire-retarded fabrics can be produced at finishing shops of weaving-mills, and their strength is sufficient for use as clothes.

(4) Fabrics of decreased combustibility can be produced from 100% cotton fabric or cotton (viscose)–polyester blend fabrics containing no less than 50 wt % cotton or viscose.

REFERENCES

1. RF Patent 2028399.
2. Luneva, N.K. and Oputina, A.G., *Polym. Eng. Sci.*, 1997, vol. 37, no. 6, pp. 940–944.
3. Feigl, F. and Anger, V., *Spot Tests in Inorganic Analysis*, Amsterdam: Elsevier, 1972.
4. Karl-Kroupa, E., *Anal. Chem.*, 1956, vol. 28, no. 7, pp. 1091–1097.
5. Luneva, N.K., Petushok, I.A., Trofimova, I.V., et al., *Zh. Prikl. Khim.*, 1992, vol. 65, no. 6, pp. 1433–1436.
6. Ant-Wuorinen, O. and Visapaa, A., *Pap. Ruu*, 1965, vol. 47, no. 5, pp. 477–483, 485–487.
7. Bokii, G.B. and Porai-Koshits, M.A., *Prakticheskii kurs rentgenostrukturnogo analiza* (Practical Course of X-ray Structural Analysis), Moscow: Mosk. Gos. Univ., 1951, vol. 1; 1960, vol. 2.
8. Martynov, M.A. and Vylegzhanina, K.A., *Rentgenografiya polimerov* (X-ray Diffraction Analysis of Polymers), Leningrad: Khimiya, 1972.
9. *NPB* (Belarussian Regulations) *80–2003: Textile Materials: Procedures for Inflammability Tests: Classification*.
10. Simigin, P.A., Zusman, M.N., and Raikhlin, F.I., *Zashchitnye propitki tekstil'nykh materialov* (Protective Impregnations of Textile Materials), Moscow: Ministerstvo Legkoi Promyshlennosti SSSR, 1957.

ISSN 1070-4272, Russian Journal of Applied Chemistry, 2007, Vol. 80, No. 11, pp. 1928–1930. © Pleiades Publishing, Ltd., 2007.
Original Russian Text © V. Grazuleviciene, L. Augulis, J.V. Grazulevicius, P. Kapitanovas, J. Vedegyte, 2007, published in Zhurnal Prikladnoi Khimii, 2007, Vol. 80, No. 11, pp. 1904–1907.

MACROMOLECULAR CHEMISTRY AND POLYMERIC MATERIALS

Biodegradable Starch, PVA, and Peat Composites for Agricultural Use

V. Grazuleviciene, L. Augulis, J. V. Grazulevicius, P. Kapitanovas, and J. Vedegyte

Lithuanian University of Agriculture, Kaunas Region, Lithuania
Kaunas University of Technology, Kaunas, Lithuania

Received July 16, 2007

Abstract—Mechanical and sorption properties of starch-, PVA-, and peat-based composites for fabricating planting containers are studied.

DOI: 10.1134/S1070427207110304

Because of their lightness, good mechanical properties, and low cost, polymeric materials are widely used in agriculture. Diverse polypropylene, polyethylene, or polystyrene containers are used in hothouse and lawn-and-garden farming for plant seeding, prickling-out, and growing. However, in contrast to other materials, synthetic polymers are not biodegradable under natural conditions [1, 2]. Recycling of plastics is cost expensive, and the essential part of plastic wastes is fired or dumped, thus deteriorating the environmental situation [3, 4]. The problem of utilization of plastic wastes may be eliminated, if using containers fabricated from biodegradable materials, such as peat- or cellulose-based composites.

It is known [5, 6] that biodegradable polymers combine good mechanical properties of synthetic polymers with easy biodegradability of natural polymers. Among such materials are hydroxy carboxylic acid based polymers, polyvinyl alcohol (PVA), commercial polymers (polyethylene and polypropylene) functionalized to make them biodegradable, and also composites of the indicated polymers with biodegradable additives [7, 8]. However, the cost of these materials is much higher as compared to large-tonnage commercial synthetic polymers, thus reducing the potentiality of their agricultural applications.

Composite materials based on renewable natural polymers (starch, cellulose, proteins) with various additives are used in agriculture [9–12], most well-known among them are starch-based composites [13]. Presently, the primary issue is the problem of compatibility of components, which is critical not only for performance characteristics of the resulting materials, but also from the technological standpoint.

In this study, we examined mechanical and sorption properties of polymeric composite materials based on starch, PVA, and peat.

EXPERIMENTAL

For fabrication of biodegradable composites we used potato starch (Lach-Ner, Czech Republic), polyvinyl alcohol Mowiol 23-88 (Kuraray Specialities Europe), glycerol (Barta a Cihlar, Czech Republic), and peat pots (Floryn, Poland).

Test samples were prepared as follows. A solution containing starch and PVA (see table for the solution composition) was stirred at 80°C for 60 min until gelation, and glycerol (4%) was added. From the resulting mixture, films were formed (10-ml portions were cast into Petri dishes 10 cm in diameter and dried at 40°C). Peat-based composites were prepared by impregnation of plates cut from peat pots in the resulting mixture at 80°C for 5 min, followed by dry-

Composition of polymers

Sample no.	Concentration in solution, %	
	starch	PVA
1	10	0
2	8	2
3	6	4
4	4	6
5	2	8
6	0	10

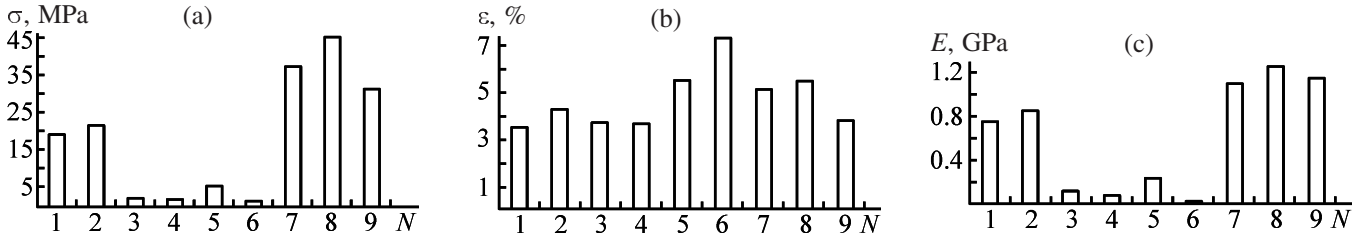

Fig. 1. Mechanical characteristics of films: (σ) tensile strength, (ε) elongation, and (*E*) Young modulus. (*N*) Sample no.; (7, 8) polypropylene and (9) polystyrene films.

ing at 40°C. As a result, we obtained samples whose total starch and PVA content was as follows (% of the dry weight): sample no. 1, 43; nos. 2–4, 30; no. 5, 26; and no. 6, 18.

Mechanical characteristics of the films were tested with a device specially designed for uniaxial microtension tests [14]. From the experimental dependences of the mechanical stress on the elongation $\alpha = f(\varepsilon)$, we determined the Young modulus, tensile strength, and elongation under maximal load.

The moisture absorption was determined gravimetrically after keeping the sample in a desiccator at 100% relative humidity and 20°C. The vapor permeability was determined as follows. The film was tightly fixed on the top of a beaker filled with water and allowed to stand in a desiccator at 0% relative humidity and 20°C. After a certain time, the sample was weighed, and the vapor permeability VP (g m^{-2} day^{-1}) was estimated. pH of the samples was measured on an IQ140 pH meter with a CER711 electrode.

The principal criteria in selecting materials for fabricating planting pots are sufficient mechanical strength and high moisture retention and vapor permeability.

Figure 1 shows the experimental mechanical characteristics of the starch and PVA. For comparison, data for commercial polypropylene (sample nos. 7, 8) and polystyrene (sample no. 9) films, used for fabricating planting pots, are presented. Among the biodegradable films studied, starch and starch–PVA (8 : 2) films exhibited the highest strength. However, their strength is about half that of the synthetic polymer films. The highest relative elongation at maximal load was shown by PVA and PVA–starch (8 : 2) films. The Young modulus, characterizing the resistance of the films to tensile stress, was estimated at a 2% strain of the samples. The highest Young modulus was obtained for the synthetic films and for starch and starch–PVA (8 : 2) films.

Data on the water absorption of the films and composites are shown in Fig. 2. The sorption capacity of the samples depends on their composition. As can be seen, the water absorption is different for the polymers (Fig. 2a) and their composites with peat (Fig. 2b). The water absorption of straight peat plates (sample no. 0) is much lower than in the polymer-containing composites.

Data on the vapor permeability of the composites after 20-day testing are presented in Fig. 3. The high-

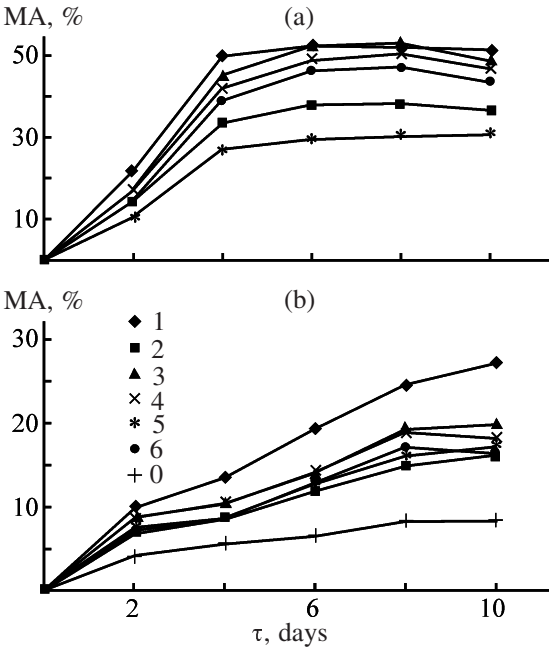

Fig. 2. Moisture absorption MA of (a) films and (b) composites as a function of the time τ. (1–6) Sample no.

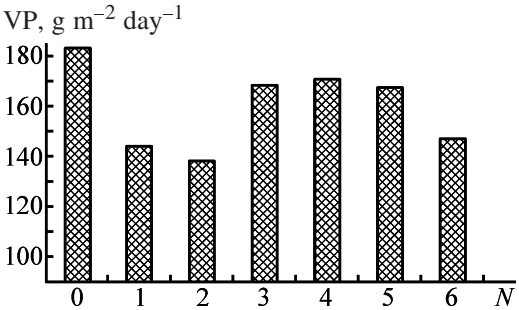

Fig. 3. Vapor permeability VP of composites. (*N*) Sample no.; the same for Fig. 4.

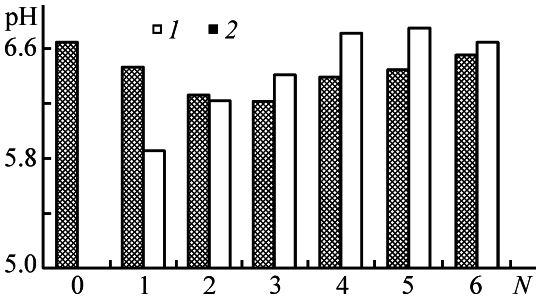

Fig. 4. pH in (*1*) films and (*2*) composites.

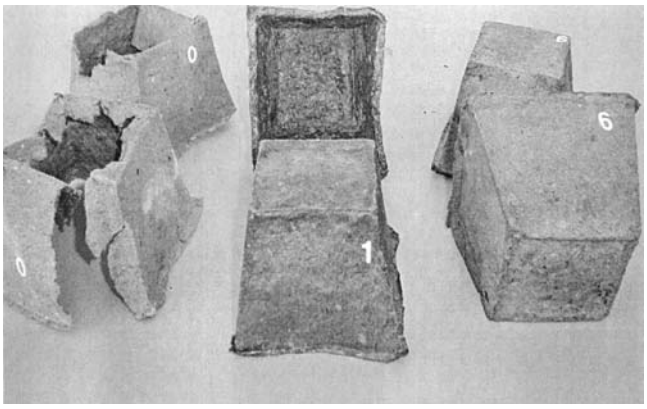

Fig. 5. Appearance of the spent planting pots: (0) peat, (1) starch + peat, and (6) PVA + peat.

est water permeability was observed in peat plates (sample no. 0). Addition of polymers decreases this parameter.

In plant growing, among the most significant parameters is pH of the soil. The most favorable is pH 6–7. In contrast to the inert polypropylene or polyethylene, the materials of biodegradable planting pots are components of the nutrition medium, participating also in ion-exchange processes. Therefore, a material for fabricating planting pots should not significantly disturb the soil nutrition system and pH. Figure 4 shows that, with increasing PVA content, pH of the films increases. Modification of the peat plates with the polymer solution only slightly changes pH.

The changes in the mechanical characteristics in the containers after use for a month under the natural conditions were evaluated visually. The used containers after washing and drying are shown in Fig. 5. As can be seen, the peat pots are totally destroyed, while starch–peat and PVA–peat pots could be reused.

CONCLUSION

Biodegradable polymeric composites, based on starch, polyvinyl alcohol, and peat, are suitable materials for fabricating planting pots. They exhibit better (compared to peat pots) mechanical properties: higher moisture absorption and lower vapor permeability, which is needed to keep steady moisture–temperature regime in the soil.

REFERENCES

1. Zheng, Y., Yanful, E.K., and Bassi, A.S., *Crit. Rev. Biotechnol.*, 2005, no. 25, p. 243.
2. Orhan, Y., Hrenovic, J., and Buyukgungor, H., *Acta Chim. Slov.*, 2004, no. 51, p. 579.
3. Bledzki, A., Pawlacryk, K., and Nawacrek, W., *Recycling materialow polymerowych*, Warsaw: Naykowo-Techniczne, 1997.
4. *Plastics and the Environment*, Andrady, A.I., Ed., Hoboken, NJ: Wiley, 2003.
5. Chandra, R. and Rustgi, R., *Prog. Polym. Sci.*, 1998, vol. 23, p. 1273.
6. Chiellini, E., Cinelli, P., D'Antone, S., and Ilieva, V.I., *Polimery*, 2002, vol. 47, nos. 7–8, p. 538.
7. Okada, M., *Prog. Polym. Sci.*, 2002, vol. 27, p. 87.
8. Kountny, M., Lemaire, J., and Delort, A.M., *Chemosphere*, 2006, vol. 64, p. 1243.
9. Ban, W., Song, J., Argyropoulos, D.S., and Lucia, L.A., *Ind. Eng. Chem. Res.*, 2006, vol. 45, no. 2, p. 627.
10. Grega, T., Najgebauer, D., Sady, M., et al., *J. Polym. Environ.*, 2003, vol. 11, no. 2, p. 75.
11. Franko, C.R., Cyras, V.P., Busalmen, J.P., et al., *Polym. Degrad. Stabil.*, 2004, vol. 86, p. 95.
12. Gaspar, M., Benko, Zs., Dogossy, G., et al., *Polym. Degrad. Stabil.*, 2005, vol. 90, no. 3, p. 563.
13. Jayasekara, R., Harding, I., Bowater, I., et al., *J. Polym. Environ.*, 2003, vol. 11, no. 2, p. 49.
14. Augulis, L., Tamulevicius, S., Augulis, R., et al., *Opt. Laser. Eng.*, 2004, vol. 42, p. 1.

ISSN 1070-4272, Russian Journal of Applied Chemistry, 2007, Vol. 80, No. 11, pp. 1931–1935. © Pleiades Publishing, Ltd., 2007.
Original Russian Text © V.G. Korsakov, S.A. Alekseev, M.M. Sychev, M.N. Tsvetkova, E.V. Komarov, B. Lee, S.V. Myakin, I.V. Vasil'eva, 2007, published in Zhurnal Prikladnoi Khimii, 2007, Vol. 80, No. 11, pp. 1908–1912.

MACROMOLECULAR CHEMISTRY AND POLYMERIC MATERIALS

Estimation of the Permittivity of Polymeric Composite Dielectrics from the Surface Characteristics of the Filler Using a Thermodynamic Model

V. G. Korsakov, S. A. Alekseev, M. M. Sychev, M. N. Tsvetkova, E. V. Komarov, B. Lee, S. V. Myakin, and I. V. Vasil'eva

St. Petersburg State Institute of Technology (Technical University), St. Petersburg, Russia
School of Materials Science and Technology, Clemson University, Clemson, the United States
Radiant Technological Center, St. Petersburg, Russia

Received April 11, 2007; in final form, June 2007

Abstract—A linear correlation between the permittivity of a composite dielectric based on polyvinyl alcohol cyanate and the content of active surface sites in its filler (dispersed barium titanate) was established. This correlation, in combination with a thermodynamic model of composite dielectrics, allows estimation of their permittivity from the surface characteristics of the filler.

DOI: 10.1134/S1070427207110316

Electrophysical characteristics of functional composites containing micro- and nanodispersed fillers are controlled by the energy of the interfacial interactions between the composite components, which depends on the filler dispersity and the kind of filler functional groups. Therefore, to elucidate how the chemical or physical modification of fillers affects the composite permittivity, the surface features of fillers should be taken into account. In the thermodynamic model of the composite dielectrics developed in [1, 2], the local and cooperative filler–polymer interactions were evaluated taking into account the polymer–filler interface structure [3]. This model allowed estimation of the physicochemical features of vulcanized siloxane rubber filled with titanium dioxide of different crystalline modifications and brands [2]. With this model, the dielectric properties of polyvinyl alcohol cyanate (PVAC) filled with modified barium titanate were also analyzed on the basis of characteristics of active sites on the filler surface, determined from the sorption of Hammett indicators [4–7]. In these experiments, along with the initial barium titanate, its samples modified by hydration and thermal treatment were also examined. This modification was found to change the particle size, specific surface area, and chemical composition of barium titanate particles. In this study, dispersed barium titanate was modified without thermal treatment or chemical impact. For this purpose, the initial barium titanate was irradiated with accelerated electrons [8] ensuring selective modification of its surface layer without changes in the specific surface area and chemical composition [9].

Since the filler permittivity ε exceeds that of the polymer by two orders of magnitude, the composite dielectric features are mainly determined by changes in the polymer characteristic at the polymer–filler interface, caused by interactions between functional groups of the filler and polymer. Taking into account that a solution is an equilibrium multicomponent system, the surface layers of filler particles uniformly distributed over the polymer bulk can be considered as their solution in the polymer [10]. It was shown [2] that, in accordance with the thermodynamic theory of curved surfaces [11], the change in the free energy of polymer molecules arranged on the surface of monodispersed filler ΔG_k is proportional to the specific surface area of filler S_s squared and the surface energy at the polymer–filler interface σ_s^0, which depends on the character of the polymer–filler interactions. ΔG_k is also dependent on the shape of distribution of the potential field of the filler in the bulk of the polymer. In the case of the exponential distribution,

$$\Delta G_k = \frac{8R_m c_f \sigma_s^0}{2R^2 k R_m} = \frac{4c_f \sigma_s^0}{R^2 k} = \text{const}\frac{\sigma_s^0 S_s^2}{k}, \quad (1)$$

where k is the exponent index.

This thermodynamic model allows evaluation of the critical size and surface energy of filler particles at which ΔG_k starts to noticeably affect the composite characteristics [4]. The correlations between physicochemical and electrophysical characteristics of polymeric composites, on the one hand, and the surface features of the natural mineral fillers [12] and luminophores [13], on the other hand, were established. However, the experimental measurement of the surface energy σ_s^0 is rather difficult. Therefore, to estimate the filler–polymer interaction, instead of σ_s^0 we determined the concentration of sorption sites on the filler surface q_{pK_a} capable of binding the polar functional groups of the polymer. It is evident that the filler–polymer interface interaction is dependent on the active site concentration. Therefore, with a knowledge of this concentration, the permittivity of composite dielectrics can be estimated from analysis of the ε–$S_s^2 q_{pK_a}$ correlation.

In this study the factors influencing the permittivity of polymeric dielectric composites were analyzed, and the possibility of estimating the permittivity of composite dielectrics based on their thermodynamic model was demonstrated. The problems under consideration were examined by the example of a dielectric composite based on polyvinyl alcohol cyanate (PVAC) containing large amount of polar functional groups. Dispersed $BaTiO_3$ modified by irradiation with accelerated electrons was used as filler.

EXPERIMENTAL

Dispersed barium titanate [TU (Technical Specification) 027.800.FGO] with an average particle size of 5.4 μm and the permittivity of 1600 was used as filler. The specific surface of barium titanate was determined by low-temperature adsorption of air. The electron-beam treatment of $BaTiO_3$ was carried out on an RTE-V transformer-resonance electron accelerator [9] (electron beam energy 900 keV, current 1 μA, absorbed dose from 25 to 200 kGy). To prevent air access, a thin layer of $BaTiO_3$ powder to be irradiated was placed into a polyethylene container. The absorbed dose was monitored by the optical density of standard dosimetric films CDP-F2 based on polycarbonate containing a phenazine dye.

The surface concentrations of active centers in the initial and modified barium titanate were determined by sorption of the acid–base Hammett indicators with pK_a from –5 to 14 [6–8, 12, 13]. The optical densities of solutions of the indicators before and after sorption were recorded on an SF-46 spectrophotometer (LOMO) in the 200–640 nm range. The content of particular sorption centers q_{pK_a} was assumed to be equal to the amount of sorbed indicator with a certain pK_a. The changes in the filler surface state caused by its modification are manifested either as the changes in q_{pK_a} or as the shift of pK_a of the indicator adsorbed on a certain sorption site. The acidity function of the filler surface was determined by the formula $H_0 = \Sigma pK_a q_{pK_a} / \Sigma q_{pK_a}$, where Σq_{pK_a} is the total amount of the sorption sites of all the kinds.

The indicators with the lowest (as a rule, negative) pK_a are selectively adsorbed on the sorption sites of Lewis base type containing unshared electron pairs. The water molecules fixed on these sites dissociate to liberate the hydroxide anions. With increasing pK_a of indicators, they start to be selectively adsorbed on sites of the Brønsted acid type (pK_a 0–7). These water molecules dissociate to liberate protons. The active surface sites of the Brønsted base type (the surface hydroxide anions capable of dissociation) have pK_a in the range 7–14. The sorption sites of the Lewis acid type (atoms with free orbitals) binding the hydroxide anions have $pK_a > 14$. The sorption of water molecules on these sites is accompanied by liberation of protons.

In preparing film polymeric composites based on PVAC, both the initial and modified barium titanate powders were used as fillers [14]. The PVAC samples were prepared at the Plastpolimer Joint-Stock Company (Laboratory of Polyvinyl Acetate Polymers and Vibration-Absorbing Materials). Dielectric film composites 30–35 μm thick, based on the initial and modified barium titanate, were prepared by the screen printing technique. The initial paste-like reaction mixture was prepared by dispersing a barium titanate powder in a solution of PVAC in dimethylformamide–ethylene glycol monomethyl ether mixture. The optimal concentration of barium titanate in these films was found to be 40%. At higher filler content, the physicomechanical characteristics of films became worse and their permittivity decreased. The composite film permittivity was measured on an R5010 ac bridge in accordance with GOST (State Standard) 6433.4–71.

Figure 1 shows the distribution of the sorption sites of different kinds for the initial and irradiated barium titanate. It can be seen that the initial barium titanate surface is enriched in the sorption sites of the Lewis base type (pK_a –4.4 and –0.3). These sites are apparently the Ba–O groups formed during thermal treatment of barium titanate in the course of its synthesis. The Brønsted acid sorption sites can be as-

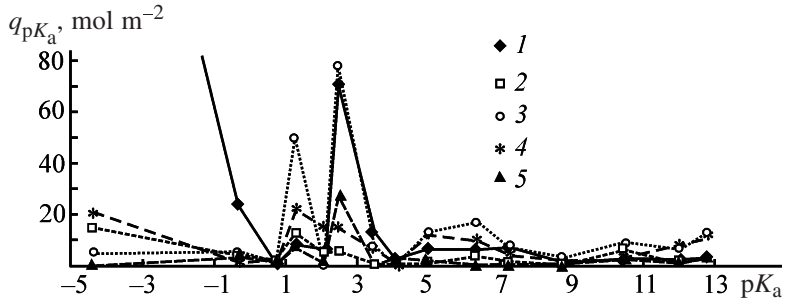

Fig. 1. Distribution of active sites of different kinds on the surface of (*1*) initial $BaTiO_3$ and (*2–5*) $BaTiO_3$ irradiated with accelerated electrons. (q_{pK_a}) Active site content and (pK_a) negative logarithm of the indicator ionization constant. Absorbed dose, kGy: (*2*) 100, (*3*) 25, (*4*) 200, and (*5*) 50.

signed to the Ti–OH groups formed by the hydrolytic sorption of water [7].

After irradiation of barium titanate to the absorbed dose of 25 kGy, the Lewis base sorption sites virtually completely disappear. At the same time, the content of Brønsted acid (pK_a 1.3–6.4) and base (pK_a 8.2–12.8) sorption sites increases. We believe that these changes in the distribution of the surface sorption sites are caused by hydroxylation of barium titanate surface by the reaction of the lattice oxygen atoms with H and OH radicals formed in radiolytic decomposition of adsorbed water by the scheme

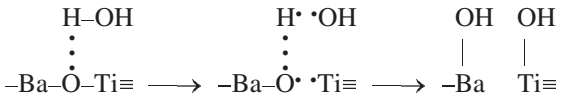

Since the barium cation charge is smaller than that of Ti^{4+} and its size is larger, the Ba–O bonds in Ba–OH groups are weakened and the formation of the Brønsted base sorption sites prevails. Therefore, for example, after electron-beam treatment of barium titanate to an absorbed dose of 25 kGy, the surface acidity function H_0 changed from –1.6 to 3.9, and the total concentration of the active sites decreased from 410 to 215 μmol m^{-2}.

With increasing absorbed dose to 50 kGy, the content of all kinds of active sites decreases. This effect was assigned to dehydroxylation of barium titanate surface caused by the radiation heating [9]. With a further increase in the absorbed dose to 100–200 kGy, the active site content increases again, which is apparently due to formation of radiation defects (deterioration of barium titanate surface structure, rupture of surface metal–oxygen bonds followed by partial surface hydroxylation). At the same time, the irradiation does not affect the particle size and their specific surface area.

The table shows that, as the absorbed dose changes, the amount of the particular active sites and their total content change differently. In particular, the permittivity of composites based on irradiated $BaTiO_3$ well correlates (linear correlation factor of 0.99) with the content of the Brønsted base sites only.

This correlation and also the fact that both the permittivity and the content of the Brønsted base active sites depend on absorbed dose similarly (Fig. 2) indicate that the permittivity of the composite is controlled by the interfacial interactions between $BaTiO_3$ particles and the polymer. With increasing content of the Brønsted surface sites (after irradiation to the absorbed dose of 25 kGy), the surface interactions of $BaTiO_3$ with the functional groups of the polymer (nitrile, hydroxy) are enhanced, and the macromolecules and supramolecular structures transform into the ordered state. As a result, the free energy of the system decreases, whereas the permittivity increases. On the contrary, with decreasing concentration of the Brønsted base sites (after irradiation to the absorbed dose of 50 kGy), the polymer–filler interactions weaken, and, as a result, the permittivity decreases.

Since the irradiation of barium titanate with accelerated electrons causes insignificant changes in the specific surface area, the knowledge of content of the Brønsted sorption sites determined by the indicator technique is sufficient for predicting the permittivity of polymeric dielectric composites based on barium titanate treated with accelerated electrons. However, along with this case, it was of interest to examine whether the thermodynamic model is applicable to predicting the permittivity of polymeric composites based on barium titanate modified by other techniques (chemical treatment, thermal treatment).

Figure 3 shows that, in accordance with Eq. (1), the experimental permittivity of composites based on the initial barium titanate and that modified by various techniques linearly depends on the term $S_s^2 \Sigma q_{pK(BB)}$,

Linear correlation factors between the permittivity of polymeric composites and content of sorption sites of different types on the surface of irradiated $BaTiO_3$

q_{pK_a}, μmol m^{-2}	Type of sorption center	Absorbed dose, kGy					Correlation factor ε–q_{pK_a}
		0	25	50	100	200	
$q_{-5–0}$	Lewis base	280	10	3	18	22	–0.23
$q_{0–7.5}$	Brønsted base	121	175	43	32	88	0.77
$q_{7.5–13}$	Brønsted acid	10	31	6	12	25	0.99
$\sum_{-5}^{13} q_{pK_a}$	–	410	215	51	62	134	0.19

where $\Sigma q_{pK(BB)}$ is the total content of the Brønsted base sites. Composite samples corresponding to curves *3* and *4* were modified by keeping barium titanate in water and calcining it in air, respectively [5].

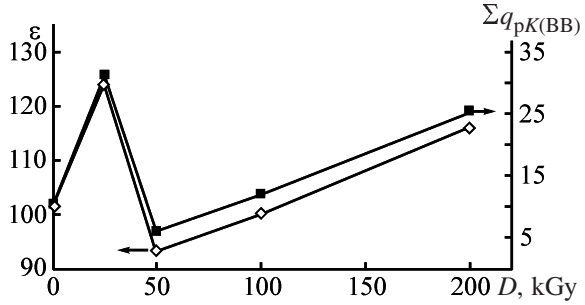

Fig. 2. Dependence of the permittivity of the composite dielectric ε and content of the Brønsted base sites $\Sigma q_{pK(BB)}$ on the absorbed dose *D* in barium titanate irradiated with accelerated electrons.

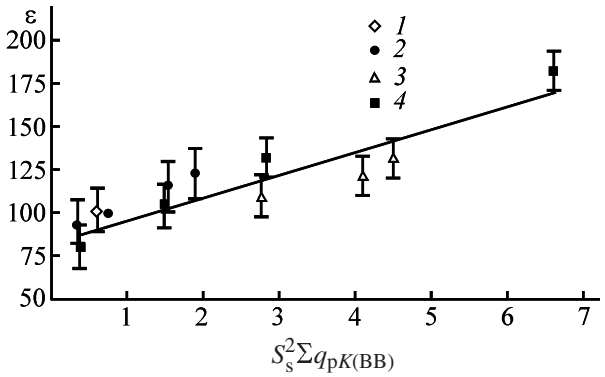

Fig. 3. Plot of the composite permittivity ε vs. the term of the thermodynamic model $S_s^2\Sigma q_{pK(BB)}$ characterizing both the content of the Brønsted base sites and the particle size of modified barium titanate. $\varepsilon = 13.4S_s^2\Sigma q_{pK(BB)} + 81.4$; $R = 0.92$. Barium titanate: (*1*) initial, (*2*) irradiated with accelerated electrons, (*3*) treated by hydration, and (*4*) thermally treated.

The ε–$S_s^2\Sigma q_{pK(BB)}$ correlation curve given in Fig. 3 shows that, although the averaged correlation factor is equal to 0.92, the separate groups of samples modified by identical techniques are characterized by the correlation factor close to unity. We believe that this difference is caused by the fact that the set of indicators used in our experiments is insufficient to determine all the active sites present on the modified $BaTiO_3$ surface. Apparently, more detailed evaluation of the distribution of the active surface sites by thermal desorption or potentiometric techniques [1] may allow more accurate estimation of the permittivity of composites based on modified fillers.

It should be noted that our results are consistent with the qualitative correlations between donor–acceptor characteristics of the filler surface and features of suspensions and polymeric composites reported in [15–17]. It was found [18] that PVA adsorption on Aerosil involves its nondissociated acid–base centers.

Thus, the concentration of sorption sites on the surface of a filler, determined by an indicator technique, allows quantitative estimation of the permittivity of polymeric film composites using their thermodynamic model taking into account both the chemical and geometric factors influencing the interfacial polymer–filler interactions.

CONCLUSIONS

(1) The model based on the thermodynamics of curved surfaces can be used for predicting the permittivity of film composites based on polyvinyl alcohol cyanate and modified $BaTiO_3$ as filler.

(2) The permittivity of polymeric composites based on polyvinyl alcohol cyanate and dispersed ferroelectric $BaTiO_3$ as filler is controlled by interactions between the polar functional groups of the polymer

and the Brønsted base surface sites of $BaTiO_3$ particles.

(3) The changes in composition of the active surface sites of dispersed $BaTiO_3$ irradiated with accelerated electrons correlate with the absorbed dose. The irradiation of $BaTiO_3$ with accelerated electrons under optimal conditions allows the permittivity of composite dielectrics to be increased owing to an increase in the concentration of the Brønsted base surface sites.

REFERENCES

1. Aleskovskii, V.B. and Korsakov, V.G., *Fiziko-khimicheskie osnovy ratsional'nogo vybora aktivnykh materialov* (Physicochemical Fundamentals for Appropriate Chose of Active Materials), Leningrad: Leningr. Gos. Univ., 1980.
2. Korsakov, V.G., Yartsev, I.K., and Razin, A.A., in *Formirovanie i svoistva vysokodispersnykh sistem* (Formation and Properties of Highly Dispersed Systems), Leningrad: Leningr. Tekhnol. Inst., 1989, pp. 118–127.
3. Todda, M.G. and Shi, F.G., *J. Appl. Phys*., 2003, vol. 94, no. 7, pp. 4551–4557.
4. Korsakov, V.G., Sychov, M.M., Mjakin, S.V., et al., in *Proc. II Int. Conf. on Physics and Control*, St. Petersburg, August 24–26, 2006, pp. 52–55.
5. Alekseev, S.A., Korsakov, V.G., Sychev, M.M., et al., *Zh. Fiz. Khim*., 2006, vol. 80, no. 4, pp. 700–703.
6. Nechiporenko, A.P., Burenina, T.A., and Kol'tsov, S.I., *Zh. Obshch. Khim*., 1984, vol. 55, no. 9, pp. 1907–1912.
7. Cheremisina, O.A., Sychev, M.M., Myakin, S.V., et al., *Zh. Fiz. Khim*., 2002, vol. 76, no. 9, pp. 1625–1628.
8. Myakin, S.V., Vasil'eva, I.V., Korsakov, V.G., and Rylova, E.V., *Zh. Fiz. Khim*., 2002, vol. 76, no. 1, pp. 92–97.
9. *Elektronno-luchevoe modifitsirovanie funktsional'nykh materialov* (Electron-Beam Modification of Functional Materials), Myakin, S.V., Sychev, M.M., and Vasil'eva, I.V., Eds., St. Petersburg: PGUPS, 2006.
10. Karapet'yants, M.Kh., *Vvedenie v teoriyu khimicheskikh protsessov* (Introduction to Theory of Chemical Processes), Moscow: Khimiya, 1975.
11. *The Solid–Gas Interface*, Flood, F.A., Ed., New York: Dekker, 1967.
12. Iordanova, E.N., Korsakov, V.G., and Tsvetkova, M.N., *Zh. Prikl. Khim*., 2003, vol. 76, no. 3, pp. 393–397.
13. Sychov, M.M., Mjakin, S.V., Nakanishi, Y., et al., *Appl. Surf. Sci*., 2005, vol. 244, nos. 1–4, pp. 461–464.
14. Rodionov, G., Ejenkova, L.L., Sychov, M.M., et al., in *Proc. Advanced Display Technologies Symp*., Korolev, August 2003, pp. 75–77.
15. Sychev, M.M., Control of Properties of Composite Macrostructures for Electroluminescent Light Sources, *Cand. Sci. Dissertation*, St. Petersburg, 1998.
16. Sychov, M.M., Cheremisina, O.A., Korsakov, V.G., et al., Abstracts of Papers, *103rd Am. Ceram. Soc. Annual Meet*., Indianapolis: ACerS, 2001.
17. Kol'tsov, Yu.S. and Kol'tsov, S.I., in *Aktual'nye problemy khimii tverdykh veshchestv: Mezhvuzovzkii sbornik nauchnykh trudov* (Topical Problems of Chemistry of Solids: Intercollegiate Coll. of Scientific Works), St. Petersburg: Sankt-Peterb. Gos. Tekhnol. Inst. (Tekh. Univ.), 1992, pp. 196–199.
18. Platonov, B.E., Bratunets, A.G., and Polishchuk, T.A., *Kolloidn. Zh*., 1979, vol. 41, no. 3, pp. 585–588.

ISSN 1070-4272, Russian Journal of Applied Chemistry, 2007, Vol. 80, No. 11, pp. 1936–1939. © Pleiades Publishing, Ltd., 2007.
Original Russian Text © M.I. Abdullin, A.B. Glazyrin, A.V. Sheludchenko, A.M. Samoilov, V.N. Zaboristov, 2007, published in Zhurnal Prikladnoi Khimii, 2007, Vol. 80, No. 11, pp. 1913–1917.

MACROMOLECULAR CHEMISTRY AND POLYMERIC MATERIALS

Viscoelastic and Rheological Properties of Syndiotactic 1,2-Polybutadiene

M. I. Abdullin, A. B. Glazyrin, A. V. Sheludchenko, A. M. Samoilov, and V. N. Zaboristov

Bashkir State University, Ufa, Bashkortostan, Russia
Efremov Synthetic Rubber Plant, Open Joint-Stock Company, Efremov, Tula oblast, Russia

Received November 27, 2006; in final form, April 2007

Abstract—The physicomechanical, viscoelastic, and rheological characteristics of syndiotactic 1,2-polybutadiene were studied and compared with those of the analogs produced in other countries.

DOI: 10.1134/S1070427207110328

Thermoelastoplastics, i.e., polymers combining the elasticity of vulcanized rubbers with the capability to pass into the viscous-flow state at elevated temperatures and to be processed like thermoplastic polymers, find growing use today. Among such thermoelastoplastics is syndiotactic 1,2-polybutadiene (1,2-SPB) prepared by stereospecific polymerization of butadiene in solution [1–4].

In this study we examined the physicomechanical, viscoelastic, and rheological properties of 1,2-SPB prepared by polymerization of 1,3-butadiene in the presence of a cobalt catalytic system [4]. As references we used syndiotactic polydienes of the JSR RB-820 and JSR RB-830 brands (Japan Synthetic Rubber Co.).

EXPERIMENTAL

Polymer samples for physicomechanical tests were prepared by pressing (150°C, 11 MPa, 10 min). The ultimate strength and relative elongation at break were determined according to GOST (State Standard) 270–75, and the Shore hardness, according to GOST 263–75. The brittle point was determined according to GOST 7912–74. The glass transition and melting points of the polymers were determined on a thermomechanical installation at a load of 9 kg mm^{-2} and heating rate of 3 deg min^{-1}. The molecular weight of the polymeric products was determined with a Waters Breeze gel permeation chromatograph using high-resolution columns (effective range of molecular weights $500-4\times10^6$) packed with divinylbenzene gel. The content of 1,2-polymerization units was determined by IR spectroscopy. The spectra were recorded with a Specord M-82 spectrophotometer. The viscoelastic properties of the polymers at shear were measured with an RPA-200 device (Alpha Technologies) at a frequency of 1 Hz and strain amplitude of 10% (~0.7°) in the temperature range 40–180°C. The rheological properties of polymers were studied by capillary viscometry with an IIRT device in the temperature range 120–180°C at a load of 11.8–158.9 N (capillary length 8 mm, diameter 2.09 mm).

We used syndiotactic 1,2-polydiene samples SPB-1, SPB-2, and SPB-3 and polymers of the JSR RB series, differing in the molecular weight, polydispersity, degree of crystallinity, and syndiotacticity (Table 1), and also polydiene of SKD-SR brand, which is amorphous atactic 1,2-polybutadiene (M_n = 76×10^3, 71.8% 1,2-units).

The experimental results show that the synthesized polymeric products are similar to JSR RB polymers in the molecular weight ($M_w\times10^{-3}$ = 115–128) and microstructure (content of 1,2-units 86–89%, Table 1). SPB-1 and SPB-2 are simlar in the degree of crystallinity to JSR RB-820, and SPB-3, to JSR RB-830. As for the physicomechanical parameters, 1,2-polydienes SPB-1 and SPB-3 are the most similar to the Japanese analogs (Table 2). It should be noted that the density and hardness of the synthesized syndiotactic 1,2-polybutadienes are somewhat lower than those of the JSR polymers (Table 2).

Figures 1 and 2 show the temperature dependences of the elastic modulus G' and mechanical loss modulus G'' for the synthesized 1,2-polydienes. As seen

Table 1. Characteristics of syndiotactic 1,2-polybutadiene

Parameter	SPB-1	SPB-2	SPB-3	JSR RB-820	JSR RB-830
Content of 1,2-units, %	85.6	85.5	88.6	89.0	93.0
Molecular weight:					
$M_w \times 10^{-3}$	115	117	128	128	115
$M_n \times 10^{-3}$	57.3	52.6	71.6	62.8	65
M_w/M_n	2.01	2.22	1.79	2.04	1.77
Degree of crystallinity, %	14	18	22.5	17	26
Syndiotacticity, %	40	53	60	53	68

Table 2. Physicomechanical properties of 1,2-polybutadienes

Parameter	SPB-1	SPB-2	SPB-3	JSR RB-820	JSR RB-830
Density, g cm^{-3}	0.85	0.88	0.89	0.91	0.91
Tensile strength, MPa	8.5	5.6	12.4	10.3	12.7
Relative elongation, %	695	420	520	700	670
Shore hardness *A*, arb. units	80	85	85	95	99
Melting point, °C	92	–	105	95	110
Glass transition point, °C	–18(33)	–	–12(47)	–25	–
Brittle point, °C	–37	–36	–35	–37	–36

from Fig. 1, the elastic modulus of syndiotactic polydiene G' (curves *1–4*) quantitatively characterizing the resistance of the polymer to the development of elastic strain varies with temperature more strongly than does G' of the atactic polymer, for which the dependence $\log G' = f(T)$ is approximately linear. For syndiotactic 1,2-polydiene, in the temperature range 40–100°C, a correlation is observed between the elastic modulus and degree of crystallinity of the polymer: An increase in the degree of crystallinity is accompanied by an increase in the elastic modulus G' of the polymer (Table 1, Fig. 1). For the syndiotactic polymer samples with different initial degrees of crystallinity, the G' values at temperatures exceeding 100°C differ insignificantly (Fig. 1). Apparently, variations of G' in the range 40–100°C are mainly determined by elastic deformation of the crystalline phase, and at higher temperatures, exceeding the melting point of the crystalline phase, they are determined by rheological properties of the polymer melt.

The temperature dependences of the mechanical loss modulus G'' of 1,2-polydiene, characterizing the amount of energy scattered in unit time in the course of dynamic deformation of the polymer, have characteristic inflections (Fig. 2) corresponding to significant changes in G'': at 75°C for SPB-2, at 90°C for SPB-1, at 110°C for SPB-3, and at 115°C for JSR RB-830 (curves *1–4*). These temperatures are close to the melting points of the polymers, found from the ther-

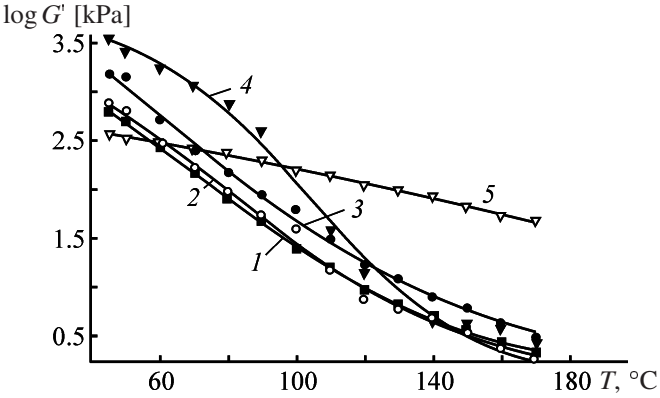

Fig. 1. Elastic modulus G' of polymers as a function of temperature T: (*1*) SPB-2, (*2*) SPB-1, (*3*) JSR RB-830, (*4*) SPB-3, and (*5*) SKD-SR; the same for Fig. 2.

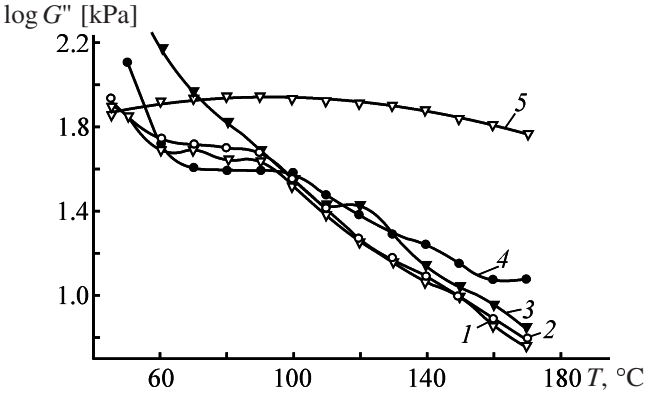

Fig. 2. Mechanical loss modulus G'' as a function of temperature T.

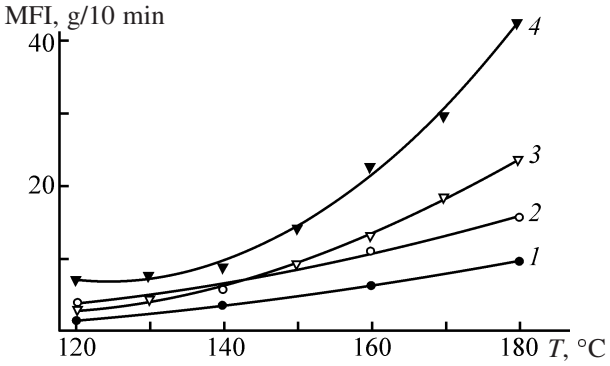

Fig. 3. Influence of temperature T on the melt flow index (MFI) of (*1*) SPB-3, (*2*) SPB-1, (*3*) JSR RB-820, and (*4*) SPB-2 at a load of 49 N.

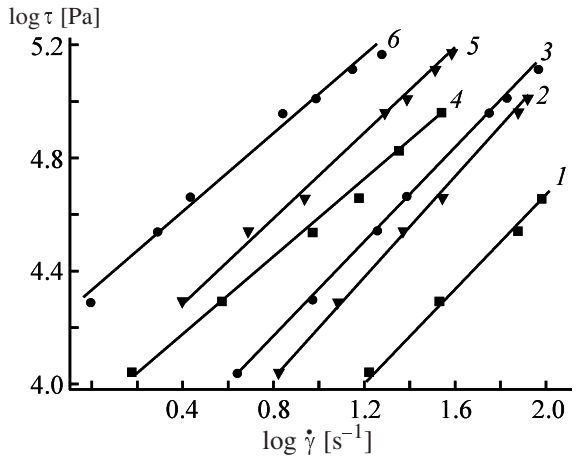

Fig. 4. A log–log plot of the shear stress τ vs. shear rate $\dot{\gamma}$ for (*1*, *4*) SPB-3, (*2*, *5*) SPB-1, and (*3*, *6*) SPB-2. T, °C: (*1–3*) 120 and (*4–6*) 180; the same for Fig. 5.

momechanical curves (Table 2). The characteristic changes of G'' are apparently associated with the destruction (melting) of the crystalline phase and transition of the polymer into the viscous-flow state.

A different pattern is observed with atactic 1,2-polydiene. In the $\log G'' = f(T)$ plot for SKD-SR, there are no bends characteristic of syndiotactic polydienes (Fig. 2, curve *5*). Also, atactic SKD-SR is characterized by higher values of G' and G'' in the range 110–180°C, compared to syndiotactic 1,2-polydiene (Figs. 1, 2). The experimental results show that atactic 1,2-polydiene preserves the hyperelastic properties in the above temperature range and therefore cannot be processed by converting it into the viscous-flow state, in contrast to thermoplastic syndiotactic 1,2-polydienes.

Analysis of the thermomechanical properties of 1,2-SPB revealed two glass transition points: in the ranges from –12 to –18°C (T_1) and from 33 to 47°C (T_2) (Table 2). The presence of two glass transition points of 1,2-SPB is apparently due to the existence in 1,2-polydiene of two phases. Namely, the macromolecules of the thermoelastoplastic contain, along with syndiotactic 1,2-structures forming ordered crystalline regions [5], also sequences of units formed by 1,4-polymerization of the monomer (10–15% content), which are highly flexible and form an amorhous phase. Fragments consisting of 1,4-polymerization units apparently act as flexible links between macrochain blocks consisting of syndiotactic 1,2-polymerization units.

The rheological characteristics of polydiene melts were studied in the temperature range 120–180°C at a load of 11.8–158.9 N. The flow of the polymers was evaluated by the melt flow index (MFI).

We found that melts of SPB-2 characterized by relatively low number-average molecular weight and broad molecular-weight distribution (Table 1) show higher flowability compared to the other analogs (Fig. 3). At the same time, the flowability of JSR RB-820 changes with temperature more strongly than that of SPB-1, although SPB-1 has a somewhat lower molecular weight.

From the experimental MFI values, we determined according to [6, 7] the parameters of the viscous flow of the polymers: shear rate $\dot{\gamma}$, shear stress τ, and effective viscosity of the polymer melt η_{eff}.

The log–log plot of the shear stress τ of polymer melts vs. shear rate $\dot{\gamma}$ in the examined range of $\dot{\gamma}$ and τ is linear (Fig. 4). For SPB-1, SPB-2, and SPB-3, the flow index n [8, 9] found from the slope of the experimental straight lines $\log\tau = f(\log\dot{\gamma})$ (Fig. 4) is essentially the same, 0.7 ± 0.03 (in the temperature range 120–180°C).

As seen from the plot of $\log\lambda_{eff} = f(\log\tau)$ (Fig. 5), the effective viscosity η_{eff} of the SPB-2 melt, under equal other conditions, is appreciably lower than that of the SPB-1 and SPB-3 melts, which should be attributed to differences in the molecular characteristics of these polymers.

The $\log\eta_{eff}$–$1/T$ dependences obtained at different temperatures for the examined 1,2-polydienes are linear (Fig. 6). The apparent activation energy of viscous flow E_a for SPB-1, SPB-2, and SPB-3, calculated from this dependence, is 53 ± 1 kJ mol^{-1}, and the load applied does not appreciably affect E_a. For JSR RB-820 polymer, E_a is similar (58 ± 1 kJ mol^{-1}). As the activation energy of viscous flow is almost independent of the molecular weight of the polymer and is mainly determined by the size of the polymer chain segment [8], the experimental results suggest

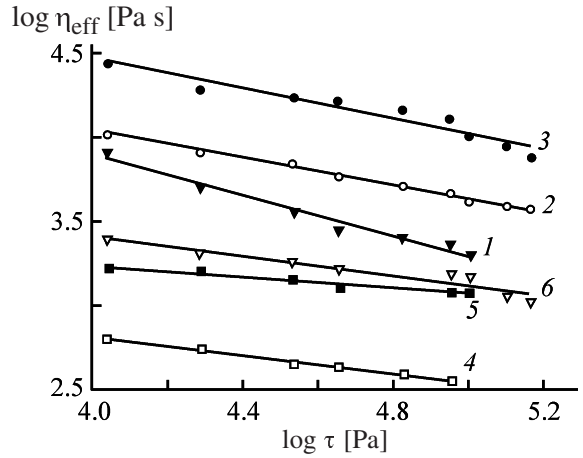

Fig. 5. Effective viscosity η_{eff} of melts of (*1*, *4*) SPB-2, (*2*, *5*) SPB-1, and (*3*, *6*) SPB-3 as a function of the shear stress τ (log–log plots).

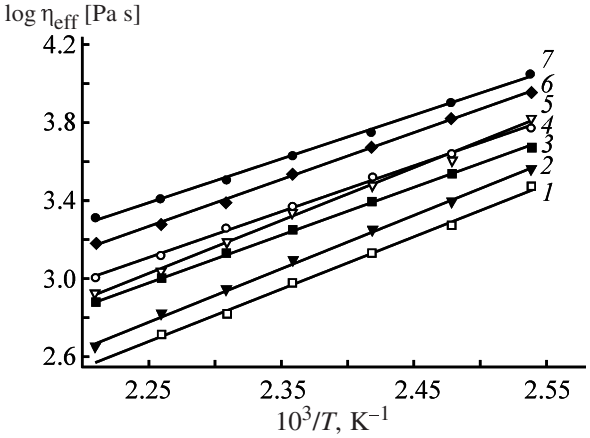

Fig. 6. Effective viscosity η_{eff} of polymer melts as a function of reciprocal temperature. Polymer: (*1*, *2*) SPB-2, (*3*, *4*) SPB-1, (*5*) JSR RB-820, and (*6*, *7*) SPB-3. Load, N: (*2*, *4*, *5*, *7*) 49 and (*1*, *3*, *6*) 98.

similar molecular structures of the 1,2-polydienes under consideration.

It should be noted that the activation energies of viscous flow E_a obtained for the polydiene thermoelastoplastics are appreciably lower than E_a of a commercial thermoelastoplastic, divinyl–styrene block copolymer (77–118 kJ mol^{-1}) [5]. Hence, 1,2-SPB melts can be processed at lower temperatures and loads than divinyl–styrene thermoelastoplastics.

CONCLUSIONS

(1) The synthesized syndiotactic 1,2-polybutadienes are similar to JSR RB commercial polymers in the molecular, physicomechanical, and rheological parameters. The viscoelastic properties of syndiotactic 1,2-polybutadiene are mainly determined by the degree of crystallinity of the polymer, and the rheological properties, by the molecular characteristics of 1,2-polydiene.

(2) By controlling the molecular characteristics and degree of crystallinity of syndiotactic 1,2-polybutadienes in the synthesis step, it is possible to prepare 1,2-polybutadienes with variable properties.

(3) The manifestation of thermoelastoplastic properties by syndiotactic 1,2-polybutadiene is due to the two-phase character of its structure, namely, to the presence in the polymer of a rigid crystalline phase formed by 1,2-polymerization units and an amorphous phase formed by 1,4-polymerization units.

(4) Syndiotactic 1,2-polybutadiene exhibits good physicomechanical properties and is of interest for the production of materials requiring a balance of properties of an elastomer and a thermoplastic polymer (packaging and electric-insulation materials, shoe sole parts, blow articles, etc.). This substance can also be used as a polymeric modifier for improving the processing conditions and properties of composites based on thermoplastics and elastomers.

REFERENCES

1. US Patent 6545107.
2. US Patent 6620760.
3. US Patent 4051308.
4. RF Patent 2177008.
5. *Termoelastoplasty* (Thermoelastoplastics), Moiseev, V.V., Ed., Moscow: Khimiya, 1985.
6. Laput'ko, B.N. and Savel'ev, A.P., *Plast. Massy*, 1994, no. 3, pp. 31–34.
7. Kalinchev, E.L. and Sakovtseva, M.B., *Svoistva i pererabotka termoplastov* (Properties and Processing of Thermoplastics), Leningrad: Khimiya, 1983.
8. Schramm, G., *A Practical Approach to Rheology and Rheometry*, Karlsruhe: Gebrueder Haake, 1994.
9. Bartenev, G.M. and Zelenev, Yu.V., *Fizika i mekhanika polimerov: Uchebnoe posobie dlya vtuzov* (Physics and Mechanics of Polymers: Textbook for Higher Technical Schools), Moscow: Vysshaya Shkola, 1983.

ISSN 1070-4272, Russian Journal of Applied Chemistry, 2007, Vol. 80, No. 11, pp. 1940–1944. © Pleiades Publishing, Ltd., 2007.
Original Russian Text © A.A. Grishchuk, Ya.I. Estrin, 2007, published in Zhurnal Prikladnoi Khimii, 2007, Vol. 80, No. 11, pp. 1918–1922.

MACROMOLECULAR CHEMISTRY AND POLYMERIC MATERIALS

Viscosity of Concentrated Solutions of Polystyrene and Poly(Vinyl Acetate) (Empirical Equations)

A. A. Grishchuk and Ya. I. Estrin

Institute of Problems of Chemical Physics, Russian Academy of Sciences, Chernogolovka, Moscow oblast, Russia

Received January 16, 2007; in final form, June 2007

Abstract—The viscosity of solutions of polystyrene with M_w from 2.8×10^4 to 7.8×10^5 in toluene and of poly(vinyl acetate) with M_w from 2×10^4 to 1.4×10^5 in butyl acetate at 30–80°C is measured. The dependence of the activation energy of the viscous flow of the solutions on the molecular weight of the polymers and solution concentration is examined. This dependence is approximated by a cubic polynomial for polystyrene solutions and by a quadratic polynomial for poly(vinyl acetate) solutions. The dependences of the solution viscosity on the concentration, molecular weight, and temperature are approximated by exponential equations in which the exponents are sums of polynomials. The coefficients of the polynomials are determined.

DOI: 10.1134/S107042720711033X

Many polymers, in particular, polystyrene, are produced in batch reactors with stirrers, in which the polymerization is performed in the bulk to high conversions of the monomer. An advantage of such technology is that the afterpolymerization performed in continuous reactors at high temperatures yields a ready polymer, with no need in special recovery procedures required for polymerization in solutions or emulsions (suspensions) and no contamination of the polymer with auxiliary substances used in dispersion polymerization. At the same time, in bulk polymerization, the temperature is considerably more difficult to control than in polymerization in solutions or dispersions. One of the major factors complicating the temperature control is inevitable increase in the viscosity of the reaction mixture by several orders of magnitude with the progress of bulk polymerization, making the heat exchange considerably less efficient.

Usually the dependence of the coefficient of heat transfer to the inner wall of the reactor on the liquid viscosity is described by criterial equations of the form [1]

$$\mathrm{Nu} = C\mathrm{Re}_c^{a1}\mathrm{Pr}^{a2}(\mu/\mu_w)^{a3}\Gamma_1^{a4}\Gamma_2^{a5}..., \quad (1)$$

where $\mathrm{Nu} = \alpha D/\lambda$; D is the apparatus diameter; α, heat transfer coefficient, λ, thermal conductivity of the liquid; $\mathrm{Re}_c = nd^2\rho/\mu$, centrifugal Reynolds criterion; n and d, rotation frequency and diameter of the stirrer; $\mathrm{Pr} = \mu c\rho/\lambda$; c, heat capacity; Γ_1, Γ_2, etc., geometric simplexes determined by the sizes and shapes of system elements.

The ratio of the liquid viscosity in the bulk to that at the wall temperature, μ/μ_w, takes into account the effect exerted by the heat flow direction on the heat transfer coefficient. According to experimental data, $a2 \approx 0.33$ and $a3 \approx 0.14$. The quantity $a1$ can vary from 0.4 to 0.92 depending on the stirring mode; at the turbulent mode, $a1 \approx 0.67$. The quantity C depends on the type and number of stirrer blades, presence of reflecting partitions, interval of Reynolds numbers, and other parameters. According to [1], C varies from 0.35 to 0.76. If we assume all the quantities except viscosity to be constant and take $(\mu/\mu_w)^{a6} \sim 1$, then for the dependence of α on viscosity we obtain

$$\alpha = C_1/\mu^b, \quad (2)$$

where b can vary from 0.07 to 0.6.

At a turbulent mode, b should be approximately equal to 0.34. This means that, when the viscosity varies from the value characteristic of the monomer (<1 cP) to the value of several hundreds of poises, characteristic of concentrated polymer solutions, i.e., by more than five orders of magnitude, α can decrease by a factor of more than 100 (provided that the turbulent mode will be preserved; otherwise the heat transfer intensity will decrease to a considerably greater extent).

Apparently, variation of the intensity of heat transfer by several orders of magnitude will inevitably affect the thermal conditions in the reactor. Such conditions were considered in [2] for the initiated radical and "living" anionic polymerization of styrene. In both cases, a transition to the high-temperature mode of reaction completion is possible, when already after 50% conversion of the monomer the reaction mixture temperature decreases by several tens of degrees as compared to the temperature of the heat carrier in the reactor jacket.

With an increase in the viscosity of the reaction mixture, the power consumption for stirring increases considerably, giving rise to an additional heat source which noticeably affects the temperature conditions. However, the calculations made in [2, 3] were based on the dependences of the polymer solution viscosity on the concentration C and molecular weight M, taken from the literature:

$$\mu(C) = AC^a, \quad \mu(M) = BM^b, \tag{3}$$

where $a \sim 4.8–5$, $b \sim 3.4–3.5$ [4].

Equations (3) are quite suitable for qualitative consideration, but are a very rough approximation for quantitative simulation of the reactor. Available specific data on the dependences of the viscosity of concentrated polymer solutions on the concentration, M, and temperature, covering wide ranges of these parameters, are few. In most cases, such studies are aimed to refine one or another model of the theory of viscosity of polymer solutions and/or melts and to compare the expressions obtained with the experimental data. For example, Pogrebnyak and Toryanik [5] substantiate an equation of type (3) on the basis of the theory of viscosity of polymer melts. For the dependences of the viscosity of aqueous poly(ethylene oxide) solutions on M, the calculated viscosities reasonably agree with the experimental data up to $M \sim 10^5$ and solution concentration of 40%; however, the concentration dependence of the viscosity is not analyzed in detail. Some parameters of the equations are fitted to attain agreement with the experiment.

The concentration dependences of the viscosity of concentrated solutions of some polymers (e.g., polystyrene, vinyl acetate) are described by Irzhak et al. [6]. They showed that analytical description of these dependences, based on the model of compressible coils, is possible only up to concentrations not exceeding 20–30 wt % (for polyisobutylene, up to 50%). Exceptions are solutions of polydimethylsiloxane in siloxane pentamer, for which the model is valid up to 100% concentration in a wide range of M. The dependences of the viscosity on the concentration and M are well described by equations of type (3), with the parameters a and b equal to 8 and ~4.5, respectively. It should be noted that the numerical values of the main parameters in the equation for this model are chosen empirically, on the basis of the "best linearization" criterion. Deviations from this equation are also observed for dilute solutions.

In recent Sadeghi's paper [7], the modified nonrandom factor model (NRF) is compared with the measurement results for poly(ethylene oxide) solutions with M from 192 to 6000 at 25–55°C in several solvents over a wide concentration range, up to the neat polymer melt. In the latter case, the dependence of the viscosity on M is described by an equation of type (3) with $b \approx 6$.

Wang et al. [8] described a model of a reactor for styrene polymerization in the bulk, using the nonlinear adaptive control of the temperature conditions of the process taking into account the influence exerted on the heat exchange intensity by the viscosity of the reaction mixture. However, in that paper, the equation used for the dependence of the viscosity on the conversion (polymer concentration), M, and temperature gave the viscosity values that differed from the experimental data by several orders of magnitude.

Thus, data available in the literature are rather contradictory, and for polystyrene and poly(vinyl acetate) they are apprently insufficient for constructing an adequate thermal model of a reactor for bulk polymerization.

In this connection, it seemed appropriate to measure experimentally the dependences of the viscosity of polymer solutions on the concentration, M, and temperature in as wide ranges of these parameters as possible and to describe these dependences by an approximating function suitable for computer models of reactors. The goal of this study was to obtain such dependences for solutions of polystyrene and poly(vinyl acetate) (PVA).

EXPERIMENTAL

The viscosity of dilute solutions was measured with a glass capillary Ubbelohde viscometer with suspended level. For solutions with intermediate viscosities (up to 10^3 P), we used a Höppler falling-ball rheoviscometer, and for more viscous solutions, a Höppler consistometer (VEB MLW Prüfgeräte-Werk Medingen). For each solutions, measurements were performed at temperatures from 30 to 60°C (for some

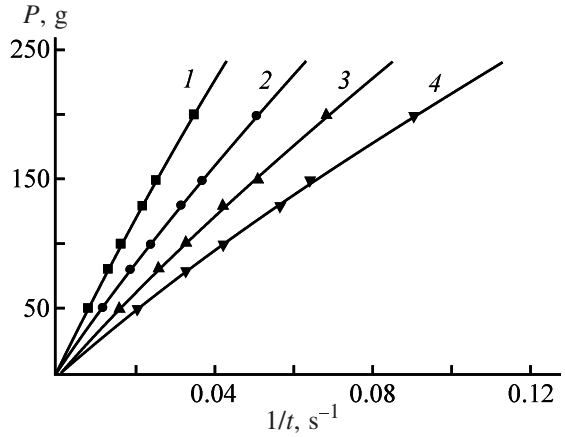

Fig. 1. Load P vs. shear rate $1/t$ for a 52% solution of polystyrene ($M_n = 9.6 \times 10^4$, $M_w = 2.8 \times 10^5$) in toluene. Temperature, °C: (*1*) 30, (*2*) 40, (*3*) 50, and (*4*) 60. Points: experimental data; solid lines: fitting by quadratic polynomials.

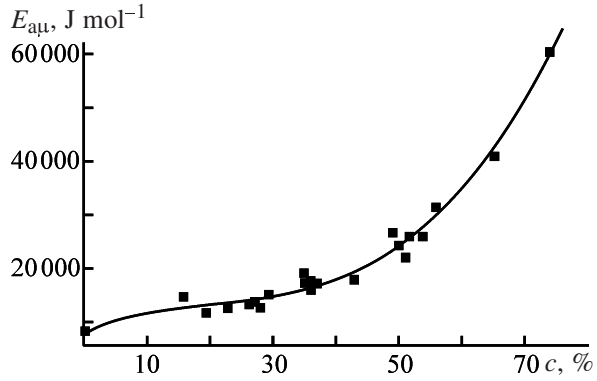

Fig. 2. Activation energy of viscous flow $E_{a\mu}$ of solutions of polystyrene ($M = 2.8 \times 10^4$–7.8×10^5) in toluene as a function of solution concentration c.

solutions, up to 80°C). For polystyrenes, the range of M (M_w) was 28×10^3–780×10^3; the concentration range, 0–56 wt %; and the temperature range, 30–80°C (for the lowest-molecular-weight sample, the maximal concentration was 74 wt %). For PVA, the range of M_w was 2×10^4–1.4×10^5; the concentration range, 0–50 wt %; and the temperature range, 30–70°C.

Because for viscous solutions the measurements take a long time, to avoid changes in the solution concentration in the course of measurements due to uncontrollable polymerization of the monomer, we used toluene as a solvent for polystyrene and butyl acetate as a solvent for poly(vinyl acetate), as these solvents are similar to the corresponding monomers in the thermodynamic, viscometric, and thermophysical parameters. The choice of butyl acetate instead of ethyl acetate, a closer analog of vinyl acetate, is governed by the high volatility of ethyl acetate, which also leads to appreciable changes in the solution concentration at elevated temperatures.

Concentrated solutions of polystyrenes that were prepared by radical polymerization and have the polydispersity index exceeding 2 behave as non-Newtonian fluids. Figure 1 shows the plot of the stress vs. shear rate for one of the solutions. These dependences are well approximated by second-order polynomials. Therefore, in these cases we used as a viscometric characteristic of solutions the maximal Newtonian viscosity obtained by extrapolation of the derivatives of the polynomials to zero shear rate (μ_0).

Solutions with the concentration less than 20% behave as Newtonian fluids, as also do solutions of polystyrene with $M = 3 \times 10^5$ and narrow MWD (polydispersity index 1.2) up to ~40% concentration; in what follows, this sample is denoted as ND.

Figure 2 shows the concentration dependence of the effective activation energy of viscous flow $E_{a\mu}$ found from the Arrhenius dependences of the viscosity. We found that $E_{a\mu}$ is essentially independent of M of polystyrene but strongly depends on the solution concentration at a polymer content exceeding 30%. The dependence obtained is satisfactorily described by a third-degree polynomial

$$E_{a\mu} = 8280 + 458c - 15.55c^2 + 0.255c^3, \qquad (4)$$

where $E_{a\mu}$ is the activation energy (J mol^{-1}) of the viscous flow of the polystyrene solution in toluene, and c is the solution concentration (wt %).

The point for the zero concentration corresponds to $E_{a\mu}$ for toluene [9]. The rms deviation is 1.6 kJ mol^{-1}.

Figure 3 shows the semilog plots of the viscosity of polystyrene solutions in toluene vs. concentration at 30°C. Similar dependences were obtained at other temperatures. It can be seen that all the dependences are well fitted by third-order polynomials:

$$\ln \mu_0 = -5.26 + B_1c + B_2c^2 + B_3c^3. \qquad (5)$$

(with the viscosity measured in P, and concentration, in wt %).

The dependences of the coefficients B_1, B_2, and B_3 of Eq. (5) on M are shown in Fig. 4. For B_1, the dependence is well described by a linear function. The dependences for B_2 and B_3 can also be approximated by linear functions, but the scatter is larger than for B_1. It is noteworthy that the coefficients B_2 and N_3 for

the sample with a narrow MWD do not fit in the linear dependences for the other polymers with a broad MWD. Apparently, the coefficients B_2 and B_3 depend on the MWD width considerably more strongly than does B_1 and reflect the influence exerted on the solution viscosity by the polymer polydispersity.

Hence follows that the dependences of the viscosity of polystyrene solutions on M are exponential rather than power, and the concentration dependences of the viscosity cannot be described by simple equations at all. Apparently, power equations of type (3) can be used in relatively narrow ranges of variation of the parameters, and the exponents will depend on the interval of M chosen and on the kind of the polymer.

Summing up the dependences obtained, we can write the following empirical equation for calculating the viscosity of polystyrene solutions:

$$\ln\mu_0 = -5.26 + (6.51\times10^{-2} + 1.326\times10^{-6}M)c + (1.52\times10^{-3} - 3.497\times10^{-8}M)c^2 - (4.309\times10^{-6} - 3.022\times10^{-10}M)c^3 + (8280 + 458c - 15.55c^2 + 0.255c^3)(1/T - 0.0033)/8.31, \quad (6)$$

where μ_0 is the viscosity at zero shear rate (P); M, weight-average M of polystyrene (M_w); c, solution concentration (wt %): and T, temperature (K).

The viscosities calculated using Eq. (6) in most cases closely coincide with the experimental data. Noticeable deviations (the calculated values exceed the experimental values) are observed only with the lowest-molecular-weight sample ($M_w = 2.8\times10^4$, deviations by up to an order of magnitude) and with concentrated (>30%) solutions of the highest-molecular-weight sample ($M_w = 7.8\times10^5$; deviations by a factor of 3–4, which corresponds to the error in calculation of the heat transfer coefficient by a factor of no more than 1.4–1.5). It should be noted, however, that both these samples have the polydispersity index exceeding 3.5, in contrast to the other samples whose polydispersity index is 2.2–2.7. Apparently, it would be more correct to use for the approximations the viscosity-average values of M, which may significantly differ from M_w in the case of a broad MWD. However, when simulating polymerization processes, it is possible to calculate and use in further calculations only the statistical moments of MWD (M_n, M_w, M_z, etc.). Consideration of the effect of MWD on the viscosity characteristics of solutions would apparently allow refinement of the model.

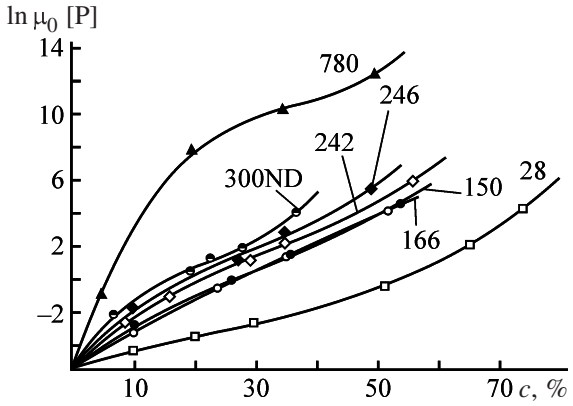

Fig. 3. Viscosity μ_0 of solutions of polystyrene in toluene at 30°C as a function of solution concentration c. Figures at curves are the values of $M_w\times10^{-3}$; points: experimental data; solid lines: approximation by cubic polynomials. Curve denoted by 300ND corresponds to a sample with a narrow MWD ($M_w/M_n = 1.2$); the polydispersity indices for the other samples range from 2.2 to 2.6.

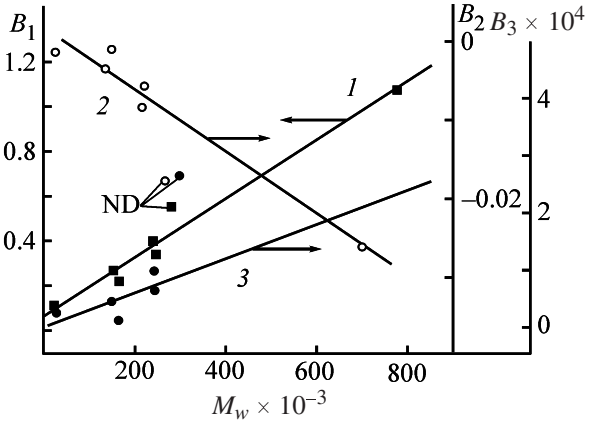

Fig. 4. Coefficients of Eq. (5): (*1*) B_1, (*2*) B_2, and (*3*) B_3, as functions of M of polystyrene. Points denoted by ND refer to the sample with a narrow MWD. These points were not taken into account when constructing linear approximations for B_2 and B_3.

Similar measurements showed that solutions of PVA in butyl acetate (ranges: concentration 0–50 wt %, M 2×10^4–1.4×10^5, M_w/M_n 3.1–5.6), in contrast to polystyrene solutions, behave as Newtonian fluids. The concentration dependences of the viscosity are well described by an exponential function in which the exponent, in turn, is a function of M and concentration. The concentration dependence of the logarithm of viscosity is well approximated by second-order polynomials (Fig. 5).

The activation energy of viscous flow $E_{a\mu}$ of PVA solutions in the temperature range 30–70°C, similarly to polystyrene solutions, increases with the concentration, and this dependence is well described by a sec-

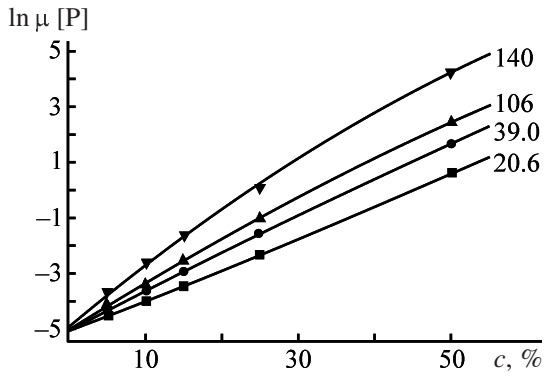

Fig. 5. Viscosity μ of solutions of poly(vinyl acetate) in butyl acetate at 30°C as a function of concentration *c*. Points: measured values; solid lines: approximation by second-order polynomials. Figures at curves denote the values of $M_w \times 10^{-3}$ of PVA samples.

ond-order polynomial. In the above-indicated ranges of parameters, the viscosity of PVA solutions can be calculated from the following equation:

$$\ln \mu = -5.0 + (0.0916 + 9.015 \times 10^{-7}M)c + (2.93 \times 10^{-4} - 7.949 \times 10^{-9}M)c^2 + (7910 + 410c + 1.65c^2)(1/T - 0.0033)/8.31, \quad (7)$$

where μ is the viscosity (P); *M*, weight-average molecular weight of poly(vinyl acetate); *c*, solution concentration (wt %); and *T*, temperature (K).

Empirical equations (6) and (7) can be actually applied only to the parameter intervals that were used in the approximations, with only short extrapolations admissible. However, these intervals, especially for polystyrene, correspond to those realized most frequently in batch polymerization reactors [10]. Therefore, when simulating reactors, these equations can provide considerably higher level of adequacy of the models compared to equations of type (3) and thus can enhance the reliability of predicting the thermal modes of polymerization.

CONCLUSIONS

(1) The dependences of the viscosity of concentrated solutions of polymers on *M* and concentration in the case of polystyrene and poly(vinyl acetate) are more complex than simple power functions. These dependences are described considerably more accurately by exponential functions whose exponents, in turn, are complex functions of both the solution concentration and the molecular weight of the polymer.

(2) The features of the molecular-weight distribution of polymers also make certain contribution to these dependences. Simpler dependences obtained with poly(vinyl acetate) are most likely due to the fact that the measurements were performed in a relatively narrow range of *M* and were restricted to relatively low solution viscosities (≤50 P). Extension of the ranges of *M* and concentration in the case of poly(vinyl acetate) may make it necessary to use approximating polynomials of the order higher than 2.

(3) The activation energy of the viscous flow dramatically increases at solution concentrations exceeding 40% but is essentially independent of *M* of the polymers.

ACKNOWLEDGMENTS

The study was financially supported by ISTC, project no. 1529.

REFERENCES

1. Romankov, P.G. and Frolov, V.F., *Teploobmennye protsessy khimicheskoi tekhnologii* (Heat-Exchange Processes of Chemical Technology), Leningrad: Khimiya, 1982.
2. Zhirkov, P.V. and Estrin, Ya.I., *Polym. Process Eng.*, 1984, vol. 2, nos. 2–3, p. 219.
3. Zhirkov, P.V. and Estrin, Ya.I., *Vysokomol. Soedin., Ser. A*, 1988, vol. 30, no. 6, p. 1169.
4. *Entsiklopediya polimerov* (Polymer Encyclopedia), Moscow: Sov. Entsiklopediya, 1974, vol. 2, p. 894.
5. Pogrebnyak, V.G. and Toryanik, A.B., *Vysokomol. Soedin., Ser. A*, 1979, vol. 21, no. 4, p. 902.
6. Irzhak, V.I., Rozenberg, B.A., and Enikolopyan, N.S., in *Setchatye polimery: Sintez, struktura, svoistva* (Network Polymers: Synthesis, Structure, Properties), Moscow: Nauka, 1979, pp. 169–182.
7. Sadeghi, R., *Fluid Phase Equil.*, 2005, vol. 232, nos. 1–2, p. 70.
8. Wang, Z.L., Pla, F., and Corriou, J.P., *Chem. Eng. Sci.*, 1995, vol. 50, no. 13, p. 2081.
9. Weissberger, A. and Proskauer, E.S., *Organic Solvents. Physical Properties and Methods of Purification*, Riddick, J.A. and Toops, E.E., Eds., New York: Interscience, 1955.
10. Beisenberger, J.A. and Sebastian, D.H., *Principles of Polymerization Engineering*, New York: Wiley, 1983.

ISSN 1070-4272, Russian Journal of Applied Chemistry, 2007, Vol. 80, No. 11, pp. 1945–1946. © Pleiades Publishing, Ltd., 2007.
Original Russian Text © the Editorial Board, 2007, published in Zhurnal Prikladnoi Khimii, 2007, Vol. 80, No. 11, pp. 1923–1924.

ANNIVERSARIES

Sergei Stepanovich Ivanchev (to His 75th Birthday)

DOI: 10.1134/S1070427207110341

On December 1, 2007, Sergei Stepanovich Ivanchev, Deputy Editor-in-Chief of *Zhurnal Prikladnoi Khimii* (Russian Journal of Applied Chemistry), corresponding member of the Russian Academy of Sciences, professor, doctor of chemical science, Honored scientist and technologist of the Russian Federation, director of the St. Petersburg Branch of Boreskov Institute of Catalysis (Siberian Division, Russian Academy of Sciences), is 75.

S.S. Ivanchev was born in Mukachevo, Transcarpathia. In 1954, he graduated with excellence from the chemical faculty of Uzhgorod State University, and in 1957, finished his postgraduate education at the Chair of Physical Chemistry at Franko State University, Lvov. He early started his working life, combining education at the university with work as teacher of physics in an evening school. Having finished his postgraduate education, he remained as a lecturer at the Chair of Physical Chemistry, and, after his supervisor was transferred to Odessa, worked at the newly organized Chair of Physical Chemistry of Polymers at Mechnikov State University in Odessa as assistant professor, professor, and dean of the chemical faculty.

Since 1970, the development of Ivanchev as a scientist and researcher continued in Leningrad, where he was invited to head the research laboratory created at Plastpolimer Okhta Research and Production Association (ORPA). Soon the laboratory became a research department and Sergei Stepanovich was appointed, first, deputy director, and then, director of the Research Institute of Polymerization Plastics at the Association. In 1981, he became the first deputy director of Plastpolimer ORPA. In this position, he exhibited capacity for research organization in the whole subbranch of polymerization plastics, became engaged in the development and implementation of new technological solutions and in creation of the pilot experimental facilities of the subbranch at the Tomsk Petrochemical Combine being constructed. He supervised and coordinated research work in COMECON countries in the field of polymerization plastics as head of the corresponding Scientific Council and member of the Scientific Council at the Ministry of Chemical Industries.

As a scientist, Ivanchev made a major contribution to solution of a number of basic problems of polymer syntheses. He scientifically substantiated and implemented pathways for synthesis of new classes of polyfunctional components used in manufacture of reactive oligomers, polymers, block-grafted oligomers, and filled polymer formulations. He suggested and confirmed the polymerization–recombination mechanism of macromolecule formation in the case when polyfunctional initiators are used. He made an important contribution to the improvement of the technology of emulsion polymerization and development of technologies for production of latexes with hollow particles and vibration-absorbing polymeric coatings for ship-building industry. In the past decade, he has been actively engaged in the development of new catalytic systems for polymerization and polymeric membrane systems for various purposes, including polymeric proton-conducting membranes for fuel cells.

In view of the change of the situation in the field of polymerization plastics and liquidation of the Ministry of Chemical Industries, Ivanchev, already a corresponding member of the Russian Academy of Sciences, went to work in the Academy and organized the St. Petersburg Branch of the Boreskov Institute of Catalysis and has been successfully heading the branch ever since.

Ivanchev is the author and co-author of more than 600 publications, including 4 monographs, more than 40 reviews, and more than 250 patents and inventor's certificates in Russia, the United States, Germany, Japan, and France. He is the founder of an acknowledged scientific school in the field of synthesis and modification of polymers, represented by 9 doctors of science and more than 40 candidates of science.

Ivanchev was a member of the Expert council of the Higher Attestation Commission for three decades and a member of the Editorial Board of *Vysokomolekulyarnye Soedineniya* (Macromolecular Compounds) journal for more than two decades. At present, he is a member of the Editorial Board of *Uspekhi Khimii* (Russian Chemical Reviews) journal and Deputy Editor-in-Chief of *Zhurnal Prikladnoi Khimii*.

Professor Ivanchev is a laureate of the Award of the Council of Ministers of the USSR (1989), laureate of the Academician Kargin Prize of the Russian Academy of Sciences (1993), Honorary Chemist of the Russian Federation (1995). He was awarded Tsiolkovsky gold medal (2002) and Academician Zhukov gold medal (2004). He is Honored Engineer of St. Petersburg (2002), Honorary Doctor of the Belyi Institute of Mechanics of Metal–Polymer Systems (National Academy of Sciences of Belarus) (2005), and bearer of the gold sign of the Mendeleev Russian Chemical Society (2006).

Sergei Stepanovich is full of creative energy and optimism and continues active work.

Friends, co-workers, Editorial board and editorial staff of *Zhurnal Prikladnoi Khimii.*

ISSN 1070-4272, Russian Journal of Applied Chemistry, 2007, Vol. 80, No. 11, pp. 1947–1950. © Pleiades Publishing, Ltd., 2007.
Original Russian Text © A.G. Morachevskii, 2007, published in Zhurnal Prikladnoi Khimii, 2007, Vol. 80, No. 11, pp. 1925–1928.

HISTORY OF CHEMISTRY AND CHEMICAL TECHNOLOGY

To Centennial Anniversary of the First Mendeleev Congress on General and Applied Chemistry

DOI: 10.1134/S1070427207110353

In January 1907, the Russian Physicochemical Society (RFKhO), Russia's science, and the world's scientific community suffered severe losses. On January 20, 1907 (hear and hereinafter dates are given in Julian calendar), died Honorary chair of the Department of chemistry of RFKhO, Honored Professor Dmitrii Ivanovich Mendeleev (1834–1907). On January 23, 1907, deceased president of RFKhO, one of its founders, Honored Professor Nikolai Aleksandrovich Menshutkin (1842–1907).

Already on February 1, 1907, was held, in commemoration of the scientists, joint meeting of the departments of physics and chemistry of RFKhO. After detailed information about the funeral was provided, a decision was made to hold, in commemoration of D.I. Mendeleev, a memorial meeting during the Christmas vacations of 1907. It was decided to hold a special meeting in commemoration of N.A. Menshutkin by agreement with the Council of the Polytechnic Institute [1]. In conformity with these decisions, the question of organizing the Mendeleev Congress on General and Applied Chemistry was considered on May 3, 1907, at a meeting of the Council of the Department of Chemistry of RFKhO [2]. It was decided to hold the Congress in St. Petersburg on December 20–30, 1907. It was recommended to have three types of meetings at the Congress:

(1) Memorial meetings devoted directly to Mendeleev (biography, scientific works, and recollections of the scientist).

(2) Joint meetings devoted to general issues of interest for all the participants.

(3) Meetings in separate specialties.

The statute of the Congress read that the Mendeleev Congress on General and Applied Chemistry is aimed to promote advances in chemistry and its applications in Russia, on the one hand, and understanding between those dealing with chemistry. All persons interested in the advances in chemistry in Russia can be participants of the Congress. The Congress is held by the Russian Physicochemical Society affiliated with the Imperial St. Petersburg University and is under the authority of the Minister for Public Education. The program of the Congress includes problems of general chemistry, all branches of chemical technology, and applications of chemistry in other fields. Particular attention is to be given to the following topics:

Dmitrii Ivanovich Mendeleev.

(1) General chemistry (inorganic, organic, analytical, physical).

(2) Methods for technical analysis.

(3) Fuels, oil.

(4) Chemistry of metallurgical processes. Metallography.

(5) Electrometallurgy. Applied electrochemistry.

(6) Glass. Ceramics. Cements.

(7) Biological chemistry. Hygiene. Pharmaceutical chemistry. Forensic chemistry. Chemistry of nutrients.

(8) Agronomic chemistry.

On its meeting on May 8, 1907, the Department of physics of RFKhO supported the suggestion to convene the Mendeleev Congress on General and Applied Chemistry [2]. The final name of the Congress was as follows: "Mendeleev Congress on General and Applied Chemistry, held by the Russian Physicochemical Society." The Congress was held in St. Petersburg on schedule, on December 20–30, 1907.

The oldest Russian chemist, N.N. Beketov (1827–1911), was elected the chair of the first Mendeleev Congress. Because of the death of F.F. Beilstein (1838–1906), Beketov was at that time the only chemist among full members of the Imperial St. Petersburg Academy of Sciences. Known scientists, chemists and physicists representing various regions of Russia, were elected deputy chairpersons: F.M. Flavinskii (Kazan), N.E. Zhukovskii (Moscow), P.N. Lebedev (Moscow), P.I. Walden (Riga), I.A. Kablukov (Moscow), S.N. Reformatskii (Kiev), and D.N. Pryanishnikov (Moscow). Among the foreign participants was elected S. Arrhenius, director of the Nobel Institute in Stockholm, 1903 Nobel Prize laureate, foreign corresponding member of St. Petersburg Academy of Sciences.

Participants of the Congress headed its special departments. This work was done by St. Petersburg scientists representing various higher-school institutions of the city, who supervised the following departments of the Congress: N.S. Kurnakov, Department of Chemistry of Metallurgical Processes and Metallography; A.A. Krakau, Department of Electrometallurgy and Applied Electrochemistry; A.A. Baikov, Department of Cements; A.M. Sokolov, Department of Glass, Ceramics, and Technology of Mineral Substances; S.A. Przhibytek, Department of Pharmaceutical Chemistry, Forensic Chemistry, and Chemistry of Nutrients; V.I. Palladin and S.S. Salazkin, Department of Biological Chemistry; G.V. Khlopin, Department of Hygiene; P.S. Kossovich, Department of Agronomic Chemistry; and O.D. Khvol'son, Department of Physics.

Prior to the opening of the Congress, a memorial board was opened on the building of the Central Board of Weights and Measures, where Mendeleev had worked beginning in 1892. The first memorial meeting devoted to Mendeleev was commenced on December 20, 1907, at 2 p.m. in the central building of the University. V.E. Tishchenko, one of the oldest members of RFKhO and Mendeleev's and Butlerov's disciple, delivered a report "D.I. Mendeleev: Brief Biography." The final part of a rather detailed report noted that the scientific achievements of Mendeleev were acknowledged and highly appreciated not only in Russia, but also in a large number of other countries. The scientist had been elected honorary member of all Russian universities and many other higher-school institutions of Russia, a corresponding member of the Imperial Academy of Sciences, and honorary member of the Russian Physicochemical Society and many other Russian scientific societies. Mendeleev had a *honoris causa* degree from Edinburgh, Oxford, Cambridge, Göttingen, and Princeton universities and was a member of the Royal Society (Great Britain) and of quite a number of academies of France, Germany, Italy, and other countries. He was recipient of most honored scientific awards, including Davy and Faraday medals.

A brief report "Importance of D.I. Mendeleev's Periodic System" was delivered by Academician Beketov. The report "General Review of D.I. Mendeleev's Scientific Activities" was presented by a young scientist, lecturer of St. Petersburg Technological Institute, V.Ya. Kurbatov.

At the second (December 26, 1907) and final third (December 30, 1907) memorial meeting of the Congress, devoted to Mendeleev, 14 more reports were presented, in which the achievements of the great Russian scientist in widely diverse areas of science, technology, and public life were analyzed. In addition to works in chemistry and physics, Mendeleev's studies in aeronautics, manufacture of explosives, and oil industry were discussed. Separate reports were devoted to scientist's works on industrial-economical, educational, and metrological issues.

In addition to the reports presented at three memorial meetings devoted to Mendeleev, 147 reports were made at meetings of Departments (sections) of Chemistry, Physics, Agrochemistry, Biology, Hygiene and at joint meetings of the Departments of Chemistry and Physics. These reports included:

68 at the Department of Chemistry;

13 reports at the Department of Physics;

23 reports at the Department of Agrochemistry;

13 reports at the Department of Biology;

ТРУДЫ

ПЕРВАГО

МЕНДЕЛѢЕВСКАГО СЪѢЗДА

ПО

ОБЩЕЙ И ПРИКЛАДНОЙ ХИМІИ,

состоявшагося въ С.-Петербургѣ съ 20-го по 30-е декабря 1907 г.

ИЗДАНЫ

Распорядительнымъ Комитетомъ Съѣзда

ПОДЪ РЕДАКЦІЕЙ

дѣлопроизводителя Съѣзда ***В. Е. Тищенко.***

С.-ПЕТЕРБУРГЪ.
Типо-литографія М. П. Фролевой. Галерная, 6.
1909.

Title page of the Proceedings of the first Mendeleev Congress on General and Applied Chemistry. Printed: Proceedings of the first Mendeleev Congress on General and Applied Chemistry, which took place in St. Petersburg, December 30–30, 1907. Published by the Administrative Committee of the Congress, edited by Congress secretary V.I. Tishchenko. St. Petersburg: M.P. Frolova's Typolithography, Galernaya 6, 1909.

4 reports at the Department of Hygiene.

Twenty-six reports were presented at joint meetings of the Departments of Chemistry and Physics. Detailed information on the reports made at meetings of the Departments and their work can be found in Proceedings of the first Mendeleev Congress on General and Applied Chemistry [3], with brief evidence included in the collection of works [4].

The Congress attracted considerable interest of a wide audience of specialists and students. The Congress gathered 1008 delegates from 80 cities of Russia. The full list of delegates, with places of their work and positions occupied, can be found in the proceedings of the Congress [3].

The Congress approved the statute of periodically convened Mendeleev Congresses on General and Applied Chemistry.

The congresses were originally organized by the Russian Physicochemical Society, and later, by the Academy of Sciences of the USSR. The second Mendeleev Congress on General and Applied Chemistry was held also in St. Petersburg on December 21–28, 1911. During the Congress, Mendeleev's study-museum, organized by the Russian Physicochemical Society at the building of St. Petersburg University and situated there until now, was opened for visitors.

REFERENCES

1. *Zh. Russk. Fiz.-Khim. O–va., Khim.*, 1907, vol. 39, no. 2, pp. 241–314.
2. *Zh. Russk. Fiz.-Khim. O–va., Khim.*, 1907, vol. 39, no. 5, pp. 636–647.
3. *Trudy Pervogo Mendeleevskogo s''ezda po obshchei i prikladnoi khimii* (Proc. First Mendeleev Congr. on General and Applied Chemistry), St. Petersburg, 1909.
4. Kozlov, V.V., *Ocherki istorii khimicheskikh obshchestv SSSR* (Essays on History of the Chemical Societies of the USSR), Moscow: Akad. Nauk SSSR, 1958.

A. G. Morachevskii

ISSN 1070-4272, Russian Journal of Applied Chemistry, 2007, Vol. 80, No. 11, pp. 1951–1952. © Pleiades Publishing, Ltd., 2007.
Original Russian Text © A.G. Morachevskii, 2007, published in Zhurnal Prikladnoi Khimii, 2007, Vol. 80, No. 11, pp. 1929–1930.

BOOK REVIEWS

Kozin, L.F. and Volkov, S.V., *Sovremennaya energetika i ekologiya. Problemy i perspektivy* (Modern Power Engineering and Ecology: Problems and Prospects)

Kiev: Naukova Dumka, 2006, 773 pp.

DOI: 10.1134/S1070427207110365

The monograph devoted to topical problems of modern power engineering was written by known Ukrainian chemists, staff members of the Vernadsky Institute of General and Inorganic Chemistry (National Academy of Sciences of Ukraine), Prof. L.F. Kozin and Academician S.V. Volkov (academician of the National Academy of Sciences of Ukraine). In the monograph, the extent to which leading countries in the world are provided with energy carriers is analyzed and prospects for use of renewable power sources and development of hydrogen energetics are discussed. The book comprises an introduction, nine chapters, conclusion, bibliographic list, and subject index.

In the introduction (pp. 5–10), the authors note that their purpose is to familiarize the reader with the state of modern problems of power engineering in the world and in Ukraine, with particular attention given to hydrogen energetics and renewable power sources. Chapter 1, entitled "Energy, Technological Progress, Hydrogen, and Ecology" (pp. 11–32), analyzes the general world's energetic and environmental problems and their interrelationship. Special attention is paid to the situation with power resources in Ukraine. At present, 47–50% of the consumed electric power is provided in this country by nuclear power plants, whereas the resources of oil and natural gas are exceedingly scarce.

Chapter 2 (pp. 33–66) discusses the consumption scale of various kinds of energy carriers in industrially developed and developing countries. The energy balance takes into account the consumption of basic kinds of organic fuel: coal, oil, and natural gas, as well as the contribution of renewable energy sources and nuclear power plants. Chapter 3 (pp. 67–127) discusses the world's resources of combustible fossil fuels (coal, oil, natural gas) and their distribution over regions and countries. A separate section of the chapter is devoted to hypotheses of the origin of the hydrocarbon fuel on the Earth; in particular, the authors substantiate their own approach to this problem. The final part of the chapter analyzes the relationship between the most important parameters characterizing the standard of living in a country (energy consumption per capita, gross domestic product, life duration, population, etc.).

Chapter 4 (pp. 128–209) is devoted to nuclear power engineering, its origination, development, and prospects. The basic evidence concerning the present-day state of nuclear power engineering is summarized in the first section of the chapter. The authors cover a wide variety of problems, which necessarily leads to brevity of presentation and separate disputable issues. The small second, third, and fourth sections deal with promising designs: possibility of developing high-temperature liquid-salt reactors, prospects for combination of nuclear and hydrogen energetics, and controlled fusion. The final, fifth section of Chapter 4 considers the environmental safety of the nuclear power engineering, based on two aspects: safe operation of nuclear power plants and reliable disposal of nuclear waste. The authors analyze in detail the reasons for the largest technological disaster of the late XX century, accident at the fourth unit of Chernobyl nuclear power plant. The whole contents of the nuclear reactor was melted and discharged by explosion into the environment.

Chapter 5 (pp. 210–252) discusses power production in the United States, Germany, Russia, and Ukraine. The energy balance of Ukraine is considered in most detail. As already noted, in this balance, 47.75% of power is produced by nuclear power plants; 45.66%, by thermal power plants and other hydrocarbon fuel consumers; 6.53%, by hydroelectric power plants; and 0.66%, by other renewable energy sources. According to the data presented by the authors, in the last 25 years, the electric power production in Ukraine was at a maximum (298.4 billion kW h^{-1}) in 1990 and

at a minimum in 2000 (171.4 billion kW h^{-1}).

Chapters 6 (pp. 253–438) and 7 (pp. 439–533) are devoted to production of hydrogen and prospects for development of hydrogen energetics. The authors consider in detail the basic technological parameters of ten most promising methods for hydrogen production, which include both already existing techniques and those possible in the future. Prospects for use of hydrogen as an environmentally clean and unique energy carrier in industry, vehicles, and energy conversion (fuel cells of various deigns) are discussed in detail. Special attention is given to problems associated with hydrogen storage and transportation.

In Chapter 8 (pp. 534–662), the authors consider global environmental problems that alarm the modern society: the so-called greenhouse effect, its causes and the related illusory climatic changes, "ozone holes," and "acid rains." The book substantiates the standpoint according to which the human technological activities do not exert, for the time being, any detrimental influence on the thickness of the ozone layer over our planet. It is also emphasized that the greenhouse gases (CO_2, CH_4, H_2O, etc.) produced by human activities cannot affect the climatic changes.

Chapter 9 (pp. 663–703) prognosticates the components of the world's energy balance in the XXI century and third millennium. The main concepts the authors elaborate upon are summarized in the brief conclusion presented in Russian (pp. 704–710) and English (pp. 711–717). The bibliographic list at the end of the book (pp. 718–760) is compiled separately for each of the chapters and contains 1068 references in all. The book is provided with a subject index (pp. 761–769). The table of contents is given in Russian and English. The polygraphic design of the book deserves a high appreciation.

On the whole, the book analyzes a vast and diverse material, with an important contribution to the problems discussed made by many years' research by the authors themselves. Although the book has an official status of a monograph, the numerous publicistic digressions do not arouse any discord and are interesting and justified. Kozin and Volkov have written a book of interest and use and discussed a wide variety of problems affecting the development of modern civilization. Thanks to the understandable manner of presentation, the book can attract the attention of an extremely wide audience of readers.

A. G. Morachevskii

ISSN 1070-4272, Russian Journal of Applied Chemistry, 2007, Vol. 80, No. 11, p. 1953. © Pleiades Publishing, Ltd., 2007.
Original Russian Text © I.N. Beloglazov, A.G. Morachevskii, 2007, published in Zhurnal Prikladnoi Khimii, 2007, Vol. 80, No. 11, pp. 1930–1931.

BOOK REVIEWS

Davenport, W.G., Jones, D.M., King, M.J., and Partelpoeg, E.H., *Flash Smelting: Analysis, Control, and Optimization*

Warrendale: TMS, 2001

Translated under the title *Vzveshennaya plavka: kontrol', analiz i optimizatsiya,* Starykh, R.V., Ed.

Moscow: MISIS, 2006, 400 pp.

DOI: 10.1134/S1070427207110377

At present, flash smelting is widely used in manufacture of copper and nickel all over the world. The book by W.G. Davenport and co-authors presents in chronological order modern achievements and understanding of the process of flash smelting. The descriptive and mathematical sections of the book reflect the level of industrial use of smelting as of 2000. Microsoft Excel software was used in mathematical calculations.

The book comprises twenty-three chapters and a supplement. The first three chapters (pp. 5–14, 15–59, 60–76) present general evidence about furnaces for flash smelting and their purpose and discusses in detail the smelting processes used by Outokumpu and INKO companies. The flash smelting is mostly used to produce matte with high copper content from a fine flotation Cu–Fe–S concentrate. Further, the matte is subjected to conversion to give raw copper. The flash smelting is the most important process in recovery of copper from sulfide ores.

Chapter 4 (pp. 78–94) considers the basic equations describing the mass and heat balances for a steady-state flash smelting process. In the following several brief chapters, from 5 to 14 inclusive (pp. 95–175), the mass-and-heat balance equations are applied to analysis of various particular processes: flash smelting of compound concentrates, effect of nitrogen on the smelting process, production of mattes with prescribed composition (65% Cu) in autogenous smelting of concentrates, and other processes are discussed. Chapter 15 (pp. 176–191) pays main attention to the expenditure of technical oxygen and fuel in smelting of pure $CuFeS_2$. Chapter 16 (pp. 192–202) discusses the behavior of moisture in flash smelting. Various issues of the smelting technology are discussed in Chapters 17 to 21 (pp. 203–312). Chapter 22 (pp. 313–333) is devoted to methods for control over flash smelting furnaces; Chapter 23 (pp. 334–353) presents results of optimization calculations. Reference data, thermodynamic parameters, and results of process calculations are summarized in the supplement (pp. 354–385).

Each chapter of the book ends with a brief conclusion and problems to be solved without assistance. Most of chapters include lists of recommended literature. The book by Davenport and co-authors has original structure, contains a vast body of technological evidence, and can be of use for research and design-office workers and senior students specialized in metallurgy of heavy nonferrous metals.

I. N. Beloglazov and A. G. Morachevskii

ISSN 1070-4272, Russian Journal of Applied Chemistry, 2007, Vol. 80, No. 11, p. 1954. © Pleiades Publishing, Ltd., 2007.
Original Russian Text © A.G. Morachevskii, I.N. Beloglazov, 2007, published in Zhurnal Prikladnoi Khimii, 2007, Vol. 80, No. 11, p. 1931.

BOOK REVIEWS

Boiko, V.I., Vlasov, V.A., Zherin, I.I., Maslov, A.A., and Shamanin, I.V., *Torii v yadernom toplivnom tsikle* (Thorium in a Nuclear Fuel Cycle)

Moscow: Ruda i Metally, 2006, 360 pp.

DOI: 10.1134/S1070427207110389

The book generalizes and systematizes the results of studies concerned with the place of thorium in the nuclear fuel cycle, carried out at Tomsk Polytechnic Institute and at a number of other leading Russian and foreign scientific centers. It discusses the chemical properties of thorium and its most important compounds, describes the technology of production of thorium compounds and the metal for nuclear power engineering, and considers nuclear and physical properties of thorium and its compounds. The monograph compares the advantages and disadvantages of the uranium–plutonium and thorium–uranium nuclear fuel cycles.

The book comprises a foreword, ten chapters, and conclusion. Bibliographic lists with references to domestic and foreign publications are contained at the end of each chapter. Chapter 1 (pp. 6–15) presents brief evidence about basic stages of nuclear fuel cycles, materials used, and methods for uranium fuel enrichment. Chapters 2 (pp. 16–33), 3 (pp. 34–48), 4 (pp. 49–97) and 5 (pp. 99–118) contain data on the occurrence of thorium in nature, chemical properties of thorium and its compounds, processing technology of thorium-containing ores, production of the main thorium compounds (thorium dioxide, tetrafluoride, and tetrachloride), production of metallic thorium by thermal reduction and electrolysis, iodide refining, and production of a compact metal.

Chapter 6 (pp. 119–163) considers nuclear, physical, and thermal properties of thorium, its alloys, and ceramic compounds of thorium. Chapter 7 (pp. 164–209) includes general evidence about operation of a nuclear power installation. Chapter 8 (pp. 210–251) compares the nuclear and physical properties of the thorium and uranium cycles.

Chapter 9 (pp. 252–314) summarizes the experience gained in use of ex-warhead plutonium in nuclear power installations and discusses the possibility of organizing the thorium–plutonium nuclear cycle. The problem discussed is associated with the release of warhead plutonium in nuclear warfare reduction. Chapter 10 (pp. 315–353) is devoted to processing of irradiated nuclear fuel in various kinds of cycles. The brief conclusion emphasizes that thorium actually remains undemanded by the world's technological practice, although its use has certain positive aspects.

The book is of indubitable interest for specialists engaged in design and research work in the field of nuclear technologies and may be of use in training of masters and postgraduate students specialized in certain scientific areas.

A. G. Morachevskii and I. N. Beloglazov

ISSN 1070-4280, Russian Journal of Applied Chemistry, 2007, Vol. 80, No. 11, pp. 1955–1958. © Pleiades Publishing, Ltd., 2007.
Original Russian Text © B.B. Sadykov, N.V. Volynskova, Sh.S. Namazov, B.M. Beglov, 2007, published in Khimicheskaya Promyshlennost', 2007, Vol. 84, No. 3, pp. 122–126.

TECHNOLOGY OF ORGANIC AND INORGANIC CHEMISTRY

Ammonium Sulfatophosphate Producing from the Phosphorites of Central Kyzylkum

B. B. Sadykov, N. V. Volynskova, Sh. S. Namazov, and B. M. Beglov

Institute of General and Inorganic Chemistry, Academy of Sciences of Republic Uzbekistan, Uzbekistan
Ammofos Co., Almalyk, Uzbekistan

Received March 22, 2007

Abstract—The necessity of using sulfur-containig fertilizers in agricultural production is evidenced. By neutralizaation with gaseous ammonia of a mixture of extractive phosphoric and sulfuric acids the ammonium sulfatophosphates are produced, containing nitrogen, phosphorus and sulfur in various ratio. The regimes for producing them are described and material flows in the industrial manufacturing are given.

DOI: 10.1134/S1070427207110390

Our target was development of technology for production of a complex fertilizer containing sulfur, besides nitrogen and phosphorus. D.N. Pryanisnikov has pointed that sulfur as an element for feeding plants occupy position in the same row as nitrogen, phosphorus and potassium [1]. However, till the recent years this element attracted little attention. In part this is explained by the fact that with the development of industry a great amount of sulfur attained the fields providing enough feeding of plants at that level of development of agiculture. But since recently in many countries, including Uzbekistan, the content of sulfur was found deficient.

Sulfur is supplied to the soil from atmosphere with rainfalls and from mineral fertilizers. Amount of sulfur in the atmosphere becomes lower because industrial plants are equipped with apparatus for trapping sulfur dioxide from exhaust gases. Production of sulfur-containing fertilizers (ordinary superphosphate and ammonium sulfate) is insufficient. In 2004, the plants of Uzbekistan have produced 157.7 thousands tons of nitrogen as carbamide, 509.6 thousands tons as ammonium nitrate and only 27.8 thousands tons as ammonium sulfate; phosphorus has produced as 108.6 thousands tons of P_2O_5 in ammophos (ammonium phosphate) and 24 thousands tons only as ordinary superphosphate.

The importance of sulfur for agriculture was considered in [2–6]. Sulfur is a component of aminoacids cystine and methionine, it is importatn for the protein metabolism and oxidation-reduction processes. Sulfur shows positive effect on the formation of chlorophyll, promotes formation of nodules at the roots of legumes and of rhizobiums responsible for binding atmospheric nitrogen. Deficiency of sulfur in plants destroys metabolism and synthesis of protein and causes chlorosis leading to decrease in productivity and quality of plant production [2]. At growing cotton plant, sulfur shows positive effect of the process of growing, yield, technological properties of cotton fiber and the quality of seeds for sowing, at low dozes of fertilizers in particular. It promotes increase in effect of nitrogen fertilizers and increases mobility of soil phosphates. Yield of cotton plant increases in the range from 2.1 to 16.3%, the oil content in the seeds up to 3.8%. Optimal norm for sulfur content in the soil is 20 to 40 kg per hectare [5].

The total content of sulfur in the layer form 0 to 20 cm of Uzbekistan's gray desert soil is 300 [5], while power black soil contains 1506 kg per hectare, turfy-podzilic soil contains 756 kg per hectare [7]. The main part of sulfur (up to 90%) constitutes organic substance of a soil. Humus contains sulfur and nitrogen in a certain ratio, commonly N : S = (8–12) : 1. Acessibility of organic sulfur in a great extent is defined by the rate of its transformation into sulfate form. The process of sulfur mineralization proceeds slowly. Its intensity is affected by the composition and activity of the soil microflora, humidity and temperature.

Many of farm cultures consume as much sulfur as phosphorus or even more. The S : P consuming ratio more than unity is characteristic for lucerne, cabbage, onion, weat, barely, sunflower and rape. The most

demanding toward sulfur as an element of food are the plants form the families of Cruciferae, Legumes and Hemorocallis. Cramineaes require less sulfur. Much sulfur consuming from soil is characteristic of cabbage, sugar beet, turnip, onion and lucerne; clower and cotton plant also consume much enough sulfur; potato, cereals and food grains are less demanding toward this element. The sulfur consuming can be estimated from the following data:

Yield, centner per hectare	Culture	Sulfur consuming, kg per hectare
26–38	Cereals	5–15
60	Corn	8–10
170–250	Potato	11–12
520–540	Table beet	14–15
250–350	Cabbage	30–60
150–350	Onion	18–22
200–300	Turnip	25–55
50–100	Lucerne	20–30
40–100	Clower	15–30
40–100	Cereal herbs	8–15
350–400	Sweet beet	31–35
24	Cotton plant	36–51

The sulfur consuming from soil depends directly from the plant yield. Therefore additional placement it to the soil is particularly important for the countries with highly productive agriculture [4].

A diagnostic index of the sulfur demand of cotton plant is the N : S ratio in its leafs. The optimal N : S ratio showing sufficient providing the cotton plant with sulfur is 20 : 1 in the initial phase and 15.0–13.5 : 1 in the further phases of its growing [5].

We suggest that the best way of making sulfur-containing complex fertilizer is ammonization of a mixture of phosphoric and sulfuric acids. This method is protected by several patents [8–10]. According to the patent [8] to the neutralized by ammonia mixture of the acids should be added KCl and carbamide. The acids should me mixed in a proportion providing P_2O_5 : SO_3 ratio (0.5–0.9): 1, and the pulp after ammonization the ratio (N + SO_3) : P_2O_5 should fall to the range (1.6–1.9): 1. In the patent [9], sulfuric acid amount is 0.2–0.5 ton per 1 ton of P_2O_5, ammonium for neutralization should be added in amount sufficient for achieving in the final product the molar ratio NH_3 : H_3PO_4 = 1 : 1.5 and the obtained phosphate pulp should be mixed with KCl or K_2SO_4 and then passed to granulation and drying. By the patent [10], the method for producing sulfoammophos includes neutralization of phosphoric and sulfuric acids with ammonia for obtaining phosphoric–sulfuric acid pulp with pH 4.6–5.8, the phosphoric acid should preliminary be neutralized with ammonia maintaining it in the zone of neutralization, pH 6.2–9, in the presence of magnesium salts in amount 7–28% MgO relatively to content of P_2O_5 in the phosphoric acid.

Publication [11] is denoted to production of fertilizers containing phosphates and ammonium sulfate. It claims that increase in amount of ammonium sulfate in the solution of ammonium phosphate leads to increase in total solubility of the salts with simultaneous decrease in content of ammonium phosphates in such solutions, viscosity of the saturated sulfate–phosphate solutions falls and pressure of ammonium over these solution diminishes. Varying the ratio of ammonium sulfate and ammonium phosphates in solution allows controlling over their contents in the produced salt.

We also obtained a preliminary patent on the method of producing ammonium sulfatophosphate [12], that defines technology realized on the facility of ammofos production in Almalyk enterprise "Ammofos". The raw material is:

– extractive phosphoric acid produced by the dehydrat method from the thermoconcentrate of the phosphorites of Central Kyzylkum, containing 21.5% or more P_2O_5 and 3.0 g/100 cm^3 or less SO_3;

– Sulfuric acid with weight fraction of H_2SO_4 monohydrate 92.5% or higher;

– Crude liquid ammonia with weight fraction of NH_3 99.6% or higher;

– Acidic effluences with density 1.1–1.15 g cm^{-3}.

The essence of technology consists in mixing acids, their neutralization with ammonia, granulation and drying of the pulp in the presence of returning product in a drum type granulator – dryer, classifying the product and cooling. The ratio of acids at mixing is defined by the required composition of the product. Neutralization of the acid mixture is carried out by introducing gaseous ammonia at 80–100°C to pH 4.2–4.5. At the higher temperature ammonia is evolved to gas phase, at lower temperature the salts can crystallize from the saturated solution. The acidic effluents consist of the absorbing liquid (a weak solution of ammonium sulfatophosphate) formed after absorption of vapor–air mixture from the saturator where the neutralization is carried out, BGS and the dust from the sanitary equipment returning to the saturator for neutralization. Temperature of the gas flow at the inlet of the BGS apparatus is 500–800°C, at the outlet 100–120°C.

Regimes for producing ammonium sulfatophosphate of six sorts are developed. According to the Technical Requirments TSh 6-12-96 they should satisfy the following conditions:

Condition	Norm for sort A		Norm for sort B		Norm for sort C	
	high quality	first quality	high quality	first quality	high quality	first quality
1. Weight fraction of general phosphates,%	23±1	20 ±1	17±1	15±1	7±1	4±1
2. P_2O_5 hydrogen / P_2O_5 total, %	50	50	50	50	50	50
3. Weight fraction of general nitrogen, %	15±1	16±1	17±1	18±1	18±1	19±1
4. Weight fraction of water, less than, %	2.0	2.0	2.0	2.0	2.0	2.0
5. Content of granules with size:						
1–4 mm, no less than, %	80	80	80	80	80	80
more than 6 mm, %	-	-	-	-		
6. Strength of granules, kg/cm^2	30	30	30	30	30	30
7. Friability, %	100	100	100	100	100	100

Note: Contents of sulfur in these products is: Sort A high quality 12%, first quality 13.2%; Sort B high quality 15.3%, first quality 16.8%; Sort C high quality 21.0%, first quality 21.6%.

In 2006 was produced 14,600 ton of ammonium sulfatophosphate recalculated on the 100% P_2O_5 .

Figure shows the scheme of material flows at the production of ammonium sulfatophosphate of A sort.

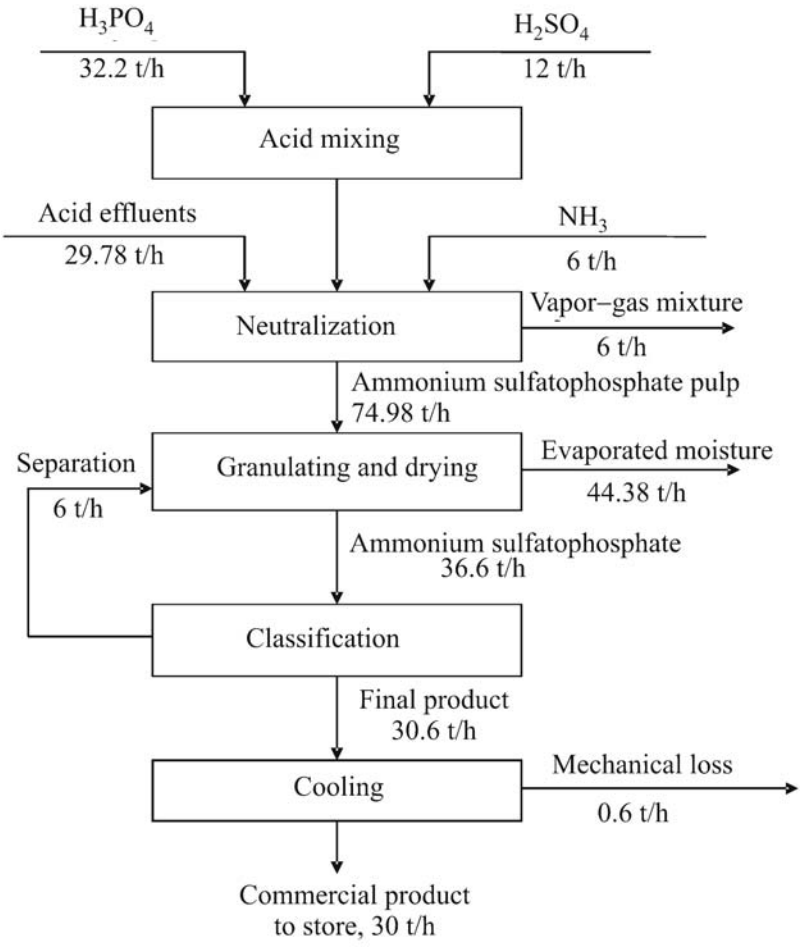

REFERENCES

1. Pryanishnikov, D.N., *Agrokhimiya. Izbrannye sochineniya* (Agrochemistry. Assays), Vol. 1, Moscow: Sel'khozgiz, 1952 g, 692 str.
2. Sokolovskii, A.A. and Unanyants, T.P., *Kratkii spravochnik po mineral'nym udobreniyam* (Brief Handbook on Mineral Fertilizers), Moscow: Khimiya, 1977.
3. *Sernoe pitanie i produktivnost' rastenii* (Sulfur feeding and plants productivity), Kiev: Naukova Dumka, 1953.
4. Slutskaya, L.D., *Agrokhimiya*, 1972, no. 1, p. 130–148.
5. Taddese Roble Girma, C*and. Sci. (Chem.) Dissertation*, Tashkent, 1988.
6. Zakirov, T., *Sel'skoe Khozyaistvo Uzbekistana*, 2000, no. 4, p. 35.
7. Aidinyan, R.Kh., *Agrokhimiya*, 1964, no. 10, p. 3–16.
8. Kalmykov, V.V., Nikulin, D.O., Dmitriev, V.E., Karpovich, E.O., Zarechenii, V.G., Vorobiova, I.P. and Silich, G.V., Patent Ukraine 63680, MPK7 SO5 V 11/00, *Ref. Zh. Khim.*, 2004, no. 21, L 122.
9. Brodskii, A.A., Grinevich, V.A., Kopakov, Yu.A., Grishaev, I.G. and Lobacheva, M.P., Russian Patent 2230051, MPK7 SO5 G 1/06, SO5 V 7/00., *Ref. Zh. Khim*., 2004, no. 21, L 124.
10. Dmitrevskii, B.A., Treushchenko, N.N., Yur'eva, V.I., Nikolenko, T.V. and Ryazanova, V.V., Russian Patent 2202522, MPK7 SO5 V 7/00, SO5 D 5/00; *Ref. Zh. Khim,* 2003, no. 16, L 111.
11. Yushina, V.S., Kharlampovich, G.D. and Skoropupova, T.G., *Koks Khimiya*, 1968, mo. 12, p. 20–24.
12. Ibragimov, G.I., Shaimardanov, Sh.S., Marinov, G.S., Sadykov, B.B., Volynskova, N.V., Kononov, A.I., Ergashev, Zh.A., Yakubov, R.Ya., Namazov, Sh.S. and Rakhimov, M.I.,Uzbekistan Patent no. IAP 02633; *Byull. Izobr.*, 2005, no. 2.

ISSN 1070-4280, Russian Journal of Applied Chemistry, 2007, Vol. 80, No. 11, pp. 1959–1963. © Pleiades Publishing, Ltd., 2007.
Original Russian Text © O.N. Filimonova, N.S. Nikulina, S.S. Nikulin, V.A. Sedykh, 2007, published in Khimicheskaya Promyshlennost', 2007, Vol. 84, No. 3, pp. 131–136.

TECHNOLOGY OF ORGANIC AND INORGANIC CHEMISTRY

Application of Polymerized Bottoms from Styrene Rectification to Producing Polybutadiene

O. N. Filimonova, N. S. Nikulina, S. S. Nikulin, and V. A. Sedykh

Voronezh State Forestry Engineering Academy, Voronezh, Russia

Received February 28, 2007

Abstract—Polymeric materials are obtained by high-temperature copolymerization of bottoms from styrene rectification with maleic acid, which can be used for preparation of antioxidant solutions for further adding at the polybutadiene processing before passing the latter to the step of isolation.

DOI: 10.1134/S1070427207110407

Vinylaromatic hydrocarbons are the most widespread monomers for producing plymeric materials of wide application. However, their production is accompanied by the formation and accumulation of great amount of wastes (about 20-25 kg per one ton of commercial styrene), basically the bottoms forming at the isolation and purification of the main product [1]. The bottoms are composed of many various organic compounds including styrene, which cannot be isolated completely at the current industrial technology. The composition of bottoms at the styrene rectification (styrene bottoms) in a great extent is defined by the method of styrene producing, the used inhibitors and technological features of the processing. Depending on the conditions of its isolation, the styrene content in styrene bottoms can vary from 10 to 50 %, the content of polystyrene can fall to the range from 15 to 70% [2]. A problem for effective using the styrene bottoms consists in the fact that its qualitative and quantitative composition varies in a wide range. Despite this fact, research works on their processing and application are in progress. A series of work has been published in this respect [3–5]. The proposed method of styrene bottoms processing are mainly directed to the obtaining on their base of polymer materials, and this has been applied in commercial scale. The polymers based on the styrene bottoms were widely used at manufacturing of painting materials. In some publications [6, 7] was shown performance of application the polymeric materials from styrene bottoms for impregnating compositions for protection and improving commercial quality of wooden materials and for similar purposes. Nevertheless, up to now the prospecting research on processing and application of styrene bottoms are continued. Exploring the most progressive methods for processing the sturene bottoms are important in scientific and applied sense because this could decrease loses of valuable hydrocarbon raw material, obtain materials with a complex of new properties and improve ecological situation. Development of new technologies and processes of recovering based on secondary products still remains an important industrial challenge toward increase productivity of technological processes and economical consumption of chemical raw materials.

The aim of this work is producing low molecular weight polymeric material from the styrene bottoms for the further consideration of its application in polybutadiene manufacturing.

The low molecular weight polymeric material from styrene bottoms can be introduced into polybutadiene resin by the following methods:

- Direct mixing of solution of polybutadiene with a solution of low molecular weight polymeric material based on the styrene bottoms;

- Dissolving in the obtained low molecular weight polymeric material of antioxidants before its passing to the mixing with polybutadiene solution;

- Dissolving antioxidants in the low molecular weight polymeric material followed by emulsifying the obtained polymer-antioxidant mixture in water phase containing surfactants and mixing this emulsion with the polybutadiene solution.

The two last methods are preferable because adding the polymeric material from styrene bottoms to the polybutadiene allows rather complete consuming the expensive raw material.

For isolation of the rubber from solution we used method of aqueous degassing. The water removing was achieved by drying in a drier at 80–85°C. Further the polybutadiene thus obtained was used for preparation of rubber mixtures and vulcanized products.

In the present work we studied synthesis of polymers based on the styrene bottoms from the join production of styrene and propylene oxide, containing, by the data of chromatography, the following compounds, %: styrene 28.08, acetophenone 35.45, methylphenylcarbinol 10.96, ethylbenzene 0.96, α-methylstyrene 1.65, diphenyldiethyl ether 4.49, benzaldehyde 1.58, not identified components 3.93, heavy residue 12.9.

To the styrene bottoms was added maleic acid in amount up to 5.0 %. Use of maleic acid in this process gives rise to solving the problem of its application, because maleic acid is a by-product which did not find quality application [8].

The following procedure was used for the synthesis:

To a reactor equipped with a stirring unity were loaded styrene bottoms and added precalculated amounts of maleic acid and hydroperoxide. The reactor was hermetically closed and the reaction mixture was heated at 110, 130 and 150±2°C and kept a given time at continuous stirring. The process was monitored by periodical taking samples from the reactor and distilling from them off the unreacted compounds.

Experimental data on the influence of temperature and the process duration on the yield of polymeric materials from the styrene bottoms are shown in Table 1.

The study showed that polymerization of styrene and other unsaturated compounds composing the styrene bottoms requires elevated temperature and long process duration. Additional introducing pinane or ethylbenzene hydroperoxides (5% calculated on unsaturated, the process duration 50 h) to the reaction mixture showed that their absence in the reaction mixture does not affect significantly the yield of polymeric materials based on styrene bottoms (Table 2). Study of application in the process of hydroperoxides, the ethylbenzene hydroperoxide in particular, was stipulated by the fact that this compound is formed intermediately and hence its formation in this step of the process is not excluded.

Table 1. Effect of process duration and reaction mixture temperature on the yield of polymeric materials based on styrene bottoms and maleic acid

Process temperature, °C	Yield of polymeric materials (wt.%) at the process duration, h:					
	3	6	9	16	30	50
110	38.8	42.6	52.7	58.3	61.2	67.9
130	43.9	47.1	55.1	66.6	75.4	84.7
150	48.3	53.6	59.2	69.8	77.3	86.5

$$C_6H_5–CH_2–CH_3 + O_2 \rightarrow C_6H_5–\underset{\displaystyle OOH}{\underset{|}{CH}}–CH_3$$

Therefore consideration of a possibility of its application in the same technological process is reasonable. This would allow solving the problem of application the side product of the manufacturing and increase yield on polymeric materials from styrene bottoms. However, as our study showed, adding more hydroperoxides during the process do not increases yield. On the other hand, this results in the increase of content of low molecular weight fraction due to decomposition of the initiator and probably owing to destruction and oxidation processes under action of peroxide.

Mathematical treatment of experimental results gave equations reflecting the effect of the polymerization processes duration (x, h) on the yield of polymeric materials based on styrene bottoms (Y, %) at various temperatures (110, 130 and 150°C).

$$Y_{110} = 36.78 + 1.439x - 1.671 \times 10^{-2}x^2$$
$$Y_{130} = 38.49 + 1.897x - 1.968 \times 10^{-2}x^2$$
$$Y_{150} = 44.55 + 1.690x - 1.725 \times 10^{-2}x^2$$

It is significant to note that the process of producing polymeric material based on styrene bottoms in this case includes various processes and joins polymerization, dehydration of methylphenylcarbinol, reaction with maleic acid and others, leading not only to polymeric material but also to ethers and esters. The esters (ethers) formed can play the role of plasticizer in the polymeric material based on styrene bottoms. The esters (ethers) should be compatible with the polymer composition based on the styrene bottoms, containing many polar functional groups in the chain. Presence of such components in the reaction products poits to formation of rather complex multicomponent system possessing a complex of new versatile properties. Structure of the obtained polymeric material can be represented as follows:

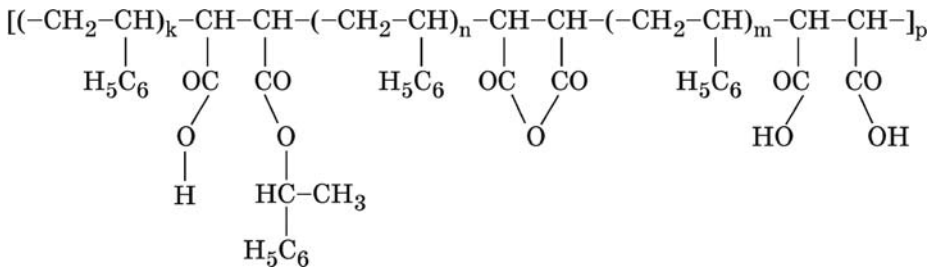

In some publications [9–11] has been shown a possibility of application low molecular weight copolymers from the wastes and side products of petroleum chemistry for making rubber mixtures. Adding the polymeric materials from side products of petroleum technology to butadiene resin, which is characterized by low plasticity, allows to increase the plasticity and decrease viscosity of the resin. By their action such additives approaches to the plasticizer PN-6.

An important aspect is the method of introducing the polymeric material to the rubber and estimation of its effect on the properties of the obtained resin, resin mixtures and vulcanized rubber. Introducing the of low molecular weight polymeric materials based on wastes and side products of petroleum chemistry to the resin by means of rolling in the process of producing rubber mixtures does not provide fast and homogenous distribution of the material in the rubber matrix bulk. The most prospective is using a solution of the polymeric material in toluene for preparation of solution of an antioxidant followed by adding it to the solution of polybutadiene before degassing the latter. Even more prospective is preliminary emulsification of the obtained toluene solution of the styrene bottoms polymer and antioxidant before passing the mixture to mixing with polybutadiene solution. The polymeric material based on styrene bottoms possess many active oxygen-containing functional groups enhancing its affinity to aqueous phase, and this should provide formation of stable emulsion practically without adding surfactants. However, emulsification requires use of water phase which contains alkali. The latter reacts with anhydride and carbonyl functional groups to form salts which provide formation of stable emulsion.

Table 2. Effect of hydroperoxide nature and process temperature on the yield of plymeric materials based on styrene bottoms

Hydroperoxide	Yield of polymeric material (wt %) at the temperature, °C :		
	110	130	150
Pinane hydroperoxide	68.4	85.2	87.2
Ethylbenzene hydroperoxide	68.2	84.9	78.1

Table 3. Properties of butadiene rubber, rubber mixtures and vulcanizates

Characteristics	Content of styrene bottoms copolymer in the polybutadiene, wt%				Oil PN-6, 5.0 wt%	Check sample
	0.5	1.5	3.0	5.0		
Viscosity by Mooney μ_b 1+4(100°C)	45	44	43	41	40	46
Weight loss at drying, %	0.10	0.12	0.14	0.15	0.13	0.13
Ash weight fraction %	0.13	0.15	0.16	0.18	0.16	0.17
Stress at 300 % elongation, MPa	8.5	8.4	7.8	7.5	7.1	8.7
Tensile strength, MPa	19.5	19.1	18.7	18.0	17.3	19.8
Tear elongation, %	610	610	600	570	630	590
Tear residual deformation, %	6	6	7	6	8	6
Aging coefficient (100°C, 72 h) :						
- by strength	0.42	0.44	0.50	0.49	0.35	0.42
- by relative elongation	0.54	0.55	0.59	0.57	0.49	0.52

Note: Vulcanization temperature 143 °C, vulcanization duration 40 min, agidol-2 content 0.6 wt%

The molecular mass of the polymeric materials from styrene bottoms determined by the method of viscosimetry falls to the range 20000 to 30000.

To the obtained from styrene bottoms polymeric material was added additional toluene to decrease its viscosity and for obtaining solution with the concentration 40–60 wt.%. Then was added an antioxidant (agidol-1, agidol-2, BTC-150, BC-30 or other) used at the polybutadiene producing. The polybutadiene with polymeric material from styrene bottoms and antioxidant emulsified in the aqueous solution containing 2.0 % of sodium hydroxide was then isolated from the solution by means of aqueous degassing and dried in a dryer at 80–85°C. From the obtained samples of polybutadiene the rubber mixtures were prepared alongside the common prescriptions and vulcanized. The resins and vulcanizates obtained were examined by commonly used methods. The results obtained are shown in Table 3.

Consideration of the obtained results shows that introducing the polymeric material based on styrene bottoms to polybutadiene provides mild plasticizing action and leads to small decrease in elastic-strength characteristics of the vulcanizates. This is seen particularly when content of the polymeric material from styrene bottoms in the polybutadiene is enhanced. Estimation of the effect of PN-6 oil on the polybutadiene properties in comparison with the effect of the synthesized polymeric material shows advantage of the latter expressed as lesser decrease in strength characteristics of vulcanizates. This can be explained by strengthening of polymer matrix by polystyrene fragments which are known to possess higher physico-mechanical properties than polydienes.

It should also be noted that adding antioxidant together with polymeric material provides less loses of the former in the process of degassing (isolation of rubber from solution)consisting in removing not polymerized monomers and solvent from the polymerizate. This can result from the fact that at the preparation of solution the phenol or amine type antioxidant can form hydrogen bonds with the molecules of polymeric material based on the styrene bottoms. As a result, occurs decrease in the loses of the antioxidant in the step of degassing. Probably a "depo" of antioxidant is formed which provides more rational use of the latter, decrease in loses and admitting greater protecting properties of the commodity. The possibility of formation of antioxidant's "depo" has been shown in [12]. This should enhance the rubber and based on it vulcanizates quality.

CONCLUSIONS

1. By copolymerization of styrene bottoms with maleic acid can be obtained polymeric materials.

2. Additional introducing of radical initiators does not lead to increase in the polymeric material yield.

3. A solution of the synthesized polymeric material can be used in the polybutadiene technology for preparation of antioxidant solution or emulsion.

4. It is reasonable to provide content of the polymeric material in the polybutadiene matrix on the level below 3.0 wt.%.

5. The polymeric material based on the styrene bottoms shows milder plasticizing effect on the properties of the forming rubber than the PN-6 oil.

6. Introducing the antioxidant together with the polymeric material based on styrene bottoms allows to enhance stability of vulcanizates toward thermo-oxidative aging.

REFERENCES

1. Kirpichnikov, P.A., Beresnev, V.V. and Popova, L.M. *Al'bom tekhnologicheskikh skhem osnovnykh proizvodstv promyshlennosti sinteticheskogo kauchuka* (Album of technological schemes of the main technologies for producing synthetic rubber), Leningrad: Khimiya, 1986.
2. Fomenko, A.I. and Terekhin, R.M., *Promyshlennost' Sinteticheskogo Kauchuka*, 1983, No. 1, p. 15–16.
3. Nikulin, S.S., Shein, V.S., Zlotskii S.S. *et al., Otkhody and pobochnye produkty neftekhimicheskikh proizvodstv – syr'e dlya organicheskogo sinteza* (Wastes and side products of petrochemical technology as raw material for organic synthesis), Moscow: Khimiya, 1989.
4. Petykhin, Yu.M. and Kontsova, L.V. *Otkhody neftekhimicheskikh proizvodstv – syr'e dlya sinteticheskikh produktov* (By-products of petrochemical technology as a raw material for synthetic products), Moscow: TsNIITEneftekhim. 1991.
5. Nikulin, S.S., Butenko, T.R., Ryl'kov, A.A., Fazliakhmetov, R.G. and Furer, S.M., *Perspektiva ispol'zovaniya kubovykh ostatkov proizvodstva vinilaromaticheskikh monomerov* (Prospects of using bottoms from the technology of vinylaromatic monomers), Moscow: TsNIITEneftekhim. 1996.
6. Nikulin, S.S., Khokhlova, O.A., Filimonova, O.N. *et al.*, *Izv. Vuzov. Stroitel'stvo*, 1998, no. 10, pp. 56–60.

7. Nikulin, S.S., Sakhokiya, I.A., Dmitrenkov, A.I. *et al*., *Izv. Vuzov*. *Stroitel'stvo*, 2001, no. 1, pp. 39–45.
8. Moldavskii, B.L. and Kerno, Yu.D., *Maleinovyi angidrid and maleinovaya kislota* (Maleic anhydride and maleic acid), Moscow: Khimiya, 1976.
9. Nikulin, S.S., Smirnov, V.S., Shein, V.S. *et al*., *Promyshlennost' Sinteticheskogo Kauchuka, Shin i RTI*, 1989, no. 2, pp. 16–18.
10. Zaboristov, V.N., Anosov, V.I., Antonova, N.G. and Domogatskaya, M.I., *Kauchuk i Rezina*, 1983, no. 6, pp. 23–25.
11. Filimonova, O.N., Nikulin, S.S. and Ososhnik, I.A., *Proizvodstvo i Ispol'zovanie Elastomerov*, 1998, no. 2, pp. 6–9.
12. Legotski, P. and Kavun, S.M., Abstracts of Papers, *VI Rossiiskaya nauch.-prakt. konf. "Syr'e and materialy dlya rezinovoi promyshlennosti. Ot materiala – k izdeliyam"* (VIth Russian Scientific and Practical Conference "Raw materials for Rubber Industry. From Material to Commodity"), Moscow: 1999, pp. 141–143.

ISSN 1070-4280, Russian Journal of Applied Chemistry, 2007, Vol. 80, No. 11, pp. 1964–1968. © Pleiades Publishing, Ltd., 2007.
Original Russian Text © Yu.V. Pokonova, 2007, published in Khimicheskaya Promyshlennost', 2007, Vol. 84, No. 4, pp. 178–185.

TECHNOLOGY OF ORGANIC AND INORGANIC CHEMISTRY

Technology for Producing Adsorbents from Petroleum Residues

Yu. V. Pokonova

St. Petersburg State Technological Institute (Technical University)

Received February 28, 2007

Abstract—Advantage of use residue from thermal cracking and products of its condensation as components of the mixture for manufacturing mechanically rigid (93%) granulated and ground carbon sorbents with extended volume of micropores (up to 0.27 cm^3/cm^3), showing enhanced sorption activity (E is up to 25.6 kJ mol^{-1}) and high ability of separation various gas mixtures is demonstrated. As a carrier for medicine preparations these adsorbents show higher performance as compared with industrial samples. Solutions of the cracking residue can be used for impregnation of worked out zeolites for petroleum technology and for production of organomineral adsorbents with high adsorption capacity on extraction mercury from sewages.

DOI: 10.1134/S1070427207110419

Currently in Russia is mined and treated up to 80% of petroleum with high an extra high content of sulfur which also contain up to 20% of petroleum residues which, as our study showed [1–4], are appropriate as raw material for obtaining many practically important products with higher exploitation properties as compared with the analogs produced by industry. Profound treatment of petroleum for enhance yield of light petroleum products and improving their quality is achieved by means of secondary thermal technological processes. This results in formation of cracking residues. Taking into account low cost of these residues, great enough resources of this raw material and high exploitation properties of the products based on them, use of the cracking residues can be considered as reasonable practically and economically. The prospective products that can be used as binders and as components of mixtures at producing adsorbents are the multifunctional compounds in the cracking residues. Their molecules consist of condensed aromatic structures with some of heterocycles and alkyl substituents. The cracking residues contain very reactive double bonds capable of entering to polymerization reactions for three-dimensional structuring. Therefore the cracking residues are cross-linking (structuring) agents like divinylbenzene, butadiene and glycol dimethacrylates.

In the present publication we summarize the methods for application cracking residues as components of a mixture for obtaining carbon adsorbents for organo-mineral adsorbents.

1. APPLICATION OF CRACKING RESIDUES AS COMPONENTS OF MIXTURES

As a raw material for the investigation we used residue of thermal cracking with the following characteristics: density kg/m^3, coking capacity 39.4%; temperature of softening by ring and ball 82°C, iodine number 93; content, wt%: asphaltenes 34.5; carbenes and carboids 6.6; sulfur 2.3. Sludge at benzene purification contained, wt%: tar-asphaltene substances 34, sulfuric acid 26. Also was used coil dust from Kuznetsk field (the mine Central) of the following composition, wt%: volatile substances 13.7; ash 8.1; carbon 90.2, hydrogen 3.9.

Adsorption and selectivity properties were estimated from the values of specific capacity on low-boiling gases. The conditions of developing chromatographic analysis were taken as follows: column height 1 m, internal diameter 4 mm, temperature of column 28, 110 and 160°C; carrier gas helium (rate 41 ± 0.1 ml/min), the adsorbate doze volume 1.0 cm^3; the sample loaded to the column 12 cm^3; adsorbent particle size 0.25–0.5 mm.

The cracking residue being not modified can not be used directly as a component of mixture due to its low softening temperature: in the beginning of the process it can be melted out from the mixture. On the other side, owing to its high reactivity it can react with aldehydes, and the polycondensates thus obtained can be used directly (after carbonization and activation) or can be included into the mixture composition. An example of

such polycondensate is furanoformolyte which has been obtained from cracking residue, technical furfurol and acidic sludge. Inclusion of the latter allows to use its asphaltene tars as additional source of raw material and sulfuric acid as a catalyst [5]. At mixing occurs vigorous exothermic reaction and appears a frothed block with low mechanical strength and therefore easily crumbling. The reaction is completed in 15–20 min, and then the block should be kept in a thermostat at 100°C for 2 h for solidification, then it is ground and used in composition of the mixture for producing adsorbents by industrial scheme. For producing the polycondensate (furanoformolyte) the ratio of the components cracking residue : furfural : acidic sludge equals 33 : 25 : 42, and the mixture for the adsorbents consists of, respectively, 39 : 39 : 22 wt% of coal dust, furanoformolyte and wood tar. The adsorbents produced alongside the industrial scheme [6–7] (Table 1) show high C:H ratio, that is, they are highly condensed, contain low ash, contain 10-fold more oxygen and twofold more sulfur than industrial carbon AR-3 (recuperation carbon) providing high polarity of surface. The performed investigations (Table 1) attest presence of molecular size pores in the adsorbents with less than 10% combustion loss; they sorb methane, carbon dioxide and xenon better than industrial adsorbents.

The high content of heteroatoms that provide surface polarity give rise to ability of intensive sorption of polar gases. Thus, ratio of retained volumes of xenon and methane (that differ by polarity almost by 21.5 times at approximately equal sizes) is 1.8 times higher for the cracking residues as compared with AG-2 gas carbon. Hence, these adsorbents can be used for fine purification of hardly sorbed and polar gases.

A possibility to change properties of adsorbent is using the cracking residues copolycondensates of different nature. For this purpose can be used the compounds with reactivity similar to that of the cracking residues, in part, schist phenols and tars. By industrial technology the copolycondensates with the schist tars and phenols (Table 2) are produced with the high mechanical strength and can be used as ground adsorbents [8]. For this purpose the copolycondensate prils were exposed to thermo-oxidation (180°C) and carbonization in rotating drum oven in two steps (450 and 800°C) under the CO_2 atmosphere and activated with steam at 820°C. As seen from the data in Table 3 the difference in recipe and in content of gel fraction affect the carbonizates properties. The highest yield of carbon residue is found in the case of copolycondensate 1 and the product was the most dense and rigid. Arter two steps of carbonization it has

Table 1. Characteristics of the adsorbents produced from furanoformolytes

Characteristics	Combustion loss, %			
	0	3.6	6.9	19.7
Density, g/cm^3				
bulk	0.55	0.53	0.52	0.50
apparent	0.88	0.85	0.83	0.80
Total volume of pores, cm^3/cm^3,				
on methanol	0.56	0.50	0.59	0.61
on benzene	0.48	0.54	0.57	0.61
on carbon tetrachloride	0.41	0.48	054	0.61
Atomic ratio C:H	6.49	7.00	7.33	8.27
Ash content, %	6.9	7.3	7.7	8.3
Content of heteroatoms, %	-	6.81	7.52	12.25
Strength, %	90	88	74	6.8
Volume of pores, cm^3/cm^3:				
micro	–	0.10	0.12	0.17
meso	–	0.01	0.02	0.04
macro	–	0.20	0.23	0.37
Specific retained volume*, cm^3/cm^3				
on methane	5.7	10.9	14.5	13.6
on carbon dioxide	100.5	82.7	79.0	73.2
on xenon	11.4	138.0	162.0	248.2

* For AG-2 the retained volumes on methane, carbon dioxide and xenon are 16.2; 53.0; 158.2 cm^3/cm^3, respectively.

Table 2. Characteristics of copolycondensates and produced from them ground carbonizates

Characteristics	Sample		
	1	2	3
Ratio of components in the mixture for producing copolycondensates, wt%:			
cracking residue	20	20	22
furfural	50	65	50
schist tars	27	13	25
sulfuric acid (conc.)	3	2	3
Properties of copolycondensates:			
yield, %	96	89	94
content of gel fraction, wt%	76	89	82
Atomic ratio C:H	1.6	1.3	1.4
Properties of carbonizates:			
yield, g/cm^3	79	69	77
density, g/cm^3	0.64	0.43	0.58
bulk	1.05	0.75	1.03
apparent	87	73	80
Total vaolume of pores on benzene, cm^3/cm^3	0.19	0.23	0.21

Table 3. Characteristics of porous structure of ground adsorbents with low combustion loss

Characteristics	Number of sample		
	1	2	3
Density, g/cm^3			
bulk	0.61	0.42	0.54
apparent	1.02	0.67	0.96
Combustion loss, %	4	11	7
Strength, %	83	74	77
Total volume, cm^3/cm^3			
on methanol	0.42	0.96	0.41
on benzene	0.33	0.36	0.33
on carbon tetrachloride	0.31	0.42	0.24
Volume of po res, cm^3/cm^3 on benzene:			
micro	0.18	0.13	0.13
meso	0.02	0.01	0.01
macro	0.11	0.23	0.19
Adsorption energy, kJ mol^{-1}	31.5	30.66	25.80
Oxygen content, %	5.23	5.03	5.06
Ash content, %	0.25	0.15	0.50

the lowest volume of pores. The most extended volume of pores on benzene (0.28 cm^3/cm^3) has the carbonizate from the product 2 (Table 3), containing maximal gel fraction and schist phenols content.

The values of total volume of pores of the carbonizates with low combustion loss (Table 3) on various pycnometric liquids point to presence in the adsorbents of the properties of molecular sieves. The maximum strength inherent in the adsorbent 1 obtained from the copolycondensate with the lowest content of gel fraction (76%), that is, with the lowest cross-linking.

Earlier was shown [9] that the adsorbents by their sorption and retaining capability toward γ-globulin can be recommended as a base for hemo-sorbents. Characteristics of the above described adsorbents show that they also can be used for this purpose. To confirm this viewpoint the ground adsorbent 2 containing minimum ash was treated by 6N solution of HC1 followed by washing with diluted 0.5N solution of HC1 to iron for reducing ash content. Then the ground adsorbent was heated under vacuum and washed in a column with 2.6% NaC1 solution. After 10 times washing with equilibrium with the adsorbent 2.5% solution of sodium chloride it was examined on mechanical strength. The loss due to mechanical damaging was 5–6%. For estimation efficiency of application the ground adsorbent as a carrier for medicine preparations it was saturated

Table 4. Characteristics of porous structure of adsorbents with moderate combustion loss

Sample	Combustion loss, %	Mechanical rigity, %	Volume of pores, cm^3/cm^3			*E*, kJ mol^{-1}	Oxygen content, %
			micro	*meso*	*macro*		
1	26	79	0.30	0.04	0.26	21.0	5.73
	29	74	0.32	0.05	0.27	20.0	5.98
2	24	66	0.13	0.01	0.44	25.6	5.62
	35	51	0.13	0.02	0.50	25.1	5.98
3	26	72	0.23	0.03	0.32	20.8	5.17
	34	69	0.28	0.04	0.33	18.4.	5.20

Table 5. Characteristics of sorption and separation properties of sorbents

Sample	T, °C	Specific retained volume of a gas, cm^3/cm^3				Criterion of separation of air mixture with a gas		
		air	methane	CO_2	Xe	CH_4	CO_2	Xe
1	28	7.5	30.5	350	35	4.6	–	–
	110	3.1	6.5	13.6	46.2	2.9	5.1	5.0
	160		4.1	6.50	17.8	2.3	3.5	4.8
2	28	7.3	36.6	152.1	350.0	3.2	3.2	–
	110	3.2	7.2	15.9	51.9	2.3	3.4	3.2
	160	2.6	4.3	7.41	3.4	1.4	2.6	0.5
3	28	10.2	26.4	85.3	303.2	4.1	29.2	42.1
	110	2.7	3.8	6.0	14.4	1.7	3.6	5.6
	160	2.3	3.1	3.8	7.7	1.5	2.3	3.9
AG-2	28	–	–	27.1	120	–	3.2	5.0
	160	–	–	3.4	10.4	–	0.6	3.2

Table 5a. Characteristics of sorption of cyanide complexes of metals by ground adsorbent 1 (from Table 2)

Experiment duration	Sorption capacity, mg/g							Selectivity factor on Au, %
	Au	Ag	Cu	Zn	Ni	CO	Sum	
4	0.7	0.1	4.3	2.2	0.3	0	7.6	9
12	0.8	0.2	4.3	2.2	0.3	0	7.8	11
24	1.2	0.2	8.7.	11.9	0.3	0.1	22.4	5
48	1.3	0.3	16.2	12.9	0.3.	0.1	31.1	4
72	1.5	0.5	36.8	12.9	0.3	0.1	52.1	3
96	1.8	0.5	46.6	14.0	0.3	0.1	63.3	3
120	2.3	0.6	46.6	14.0	0.3.	0.1	63.9	4
			Combustion loss 26%					
8	3.0	0.7	8.2.	0	0.2	0.5.	12.6	23.0
12	3.5	0.8	15.5	2.1	0.4.	0.5	22.8	14.5
24	4.0	0.9	18.5	11.3	0.4	0.5	35.6	11.5
48	5.0	1.1	25.9	14.3	0.4	0.5	47.2	10.5
72	5.8	1.3	45.1	15.5	0.4	0.5	68.6	8.5
96	6.0	1.3	54.3	20.5	0.4	0.5	83.0	7.5
120	6.8	1.4	54.3	20.5	0.5	0.5	84.0	8.0
			Combustion loss 29%					
4	2.0	0.5	16.3	8.7	0.7	0	28.2	7.5
8	3.0	0.7	16.3	8.7.	0.8	0	29.5	10
12	3.5	0.9	16.3	5.5	0.8	0	27.0	13
24	4.5	1.1	25.0	14.1	0.8	0	45.5	10
48	5.6	1.8	25.0	14.1	0.8	0	47.3	12
72	6.5	2.0	25.0	14.1	1.1	0	48.7	13
96	7.2	2.0	59.6	24.0	1.5	0.4	94.7	7.5
120	7.8	2.0	67.2	26.0	1.5	0.4	104.9	7.5
	Industrial adsorbents							
		SKT						
120	5.5	1.4	37.5	29.5	2.0	0.3	76.2	7.5
		KAD-iodine						
120	3.6	0.8	27.2	27.5	1.5	0.3	60.9	6.5
			Anionite AM-2B					
120	3.7	0.3	34.2	53.2	0.6	0.4	92.4	4.0

with caffeine – sodium benzoate. Through a column with the adsorbent was passed a solution of caffeine – sodium benzoate (concentration 40 g/l) with the rate 1.3 ml/min. Adsorption was conducted till complete saturation of the adsorbent, then with the same rate the column was washed with 0.85% NaC1 solution [5]. Then was measured the amount of sodium benzoate retained in the sorbent after washing. The adsorption ability on caffeine–sodium benzoate was determined under isothermal conditions at keeping for 7 days, change in concentration was measured spectrphotometrically. For estimation we calculated selectivity factor ($K_{selectivity}$), characterizing partition coefficient for caffeine–sodium benzoate between the adsorbent and solution (Table 5): $K_{selectivity} = \alpha/C_{equilibrium}$, α is the adsorbent capacity on the caffeine – sodium benzoate at equilibrium concentration.

These data show that retaining ability of the adsorbent on caffeine – sodium benzoate is satisfactorily in comparison with the carbons applied for extraction compounds from solutions: it is lower compared with SKT but higher than BAU shows.

2. APPLICATION OF CRACKING RESIDUE AS IMPREGNATOR

In the oil refinement technology are used zeolites, mostly for deparaffinization. The zeiolites extract

paraffines from petroleum fractions and then desorbed with ammonia, calcinated and passed for recirculation. Zeolite can work for 4–5 years and then should be renewed. They are the side products of oil refinement appearing in multitons amounts. But they can be utilized for producing practically important products, inpart, organomineral adsorbents. In this publication we propose a technplogy fro impregnation the used zeolites with a solution of cracking residue in furfural. The binder is prepared by the following procedure: crude furfural is mixed with cracking residue and sludge, then sludge is added to the mixture in portions.The mixture is used for impregnation of zeolite in an installation consisting of column 30 cm height and 10 cm diameter with porous glass membrane at bottom. To the column bottom is attached a receiver for collection of unused impregnating mixture and a cock on side wall below the glass membrane, attached through throttle bottle to vacuum pipe. The column is filled by half with worked out zeolite and impregnator is passed through it. After coplete impregnation, when the liquid is passed the zeolite layer, the column is sealed and evacuated for 15 min. Then fresh portion of impregnant is loaded and operation is continued till the impregnant is no more consumed and is passed through the zeolite layer almost without delay. The impregned zeolite is left in the column to formation of three-dimensional polycondensate, then is unloaded into flat metallic pan, covered with metallic sheet and left for 24 h in air to complete solidification. Then stick particles are separated in a shaker. The impregnated zeolites are carbonized in a rotating oven at 800 ± 10°C under carbon dioxide and activated in the same oven at 82010°C with steam to combustion loss 30–35%. The obtained organo-mineral zeolite was used for extraction mercury from waste water of the following composition: pH 8.12, content of sulfate ion 480 mg/l, chloride ion 124.1 mg/l, mercury as nitrate 1.24 mg/l.

The adsorption ability on mercury was measured by atomic absorption spectroscopy on a Perkin-Elmer instrument, model 503. Kinetic characteristics were determined by the method of constant concentrations of the targeted component and salt composition (with change of solution under static conditions). Sorption capacity of the impregnated zeolite at combustion loss 30–33% was 15.8–16.6 mg/g at 120 h sorption. Under the same condition the sorption capacity of KAD-iodine was 5.6–6 mg/l.

REFERENCES

1. Pokonova, Yu.V., *Khimiya vysokomolekulyarnykh soedinenii nefti* (Chemistry of High-Molecular Compounds of Oil), Leningrad: LGU, 1980.
2. Pokonova, Yu.V., *Neftyanye ostatki* (Petroleum Residues), St. Petersburg: Sintez, 2004.
3. Pokonova, Yu.V. and Speit, J., I*spol'zovanie neftyanykh ostatkov* (Utilization of Oil Residues), St. Petersburg: Sintez, 1992.
4. Pokonova, Yu.V., *Neft' i nefteproducty* (Oil and petroleum products), St. Petersburg: Professiya, 2003.
5. Pokonova Yu.V., *Fuel Sci. Tecnol. Intern*., 1991, vol. 9, no. 10, p. 1245.
6. Pokonova Yu.V., *Fuel Sci. Tecnol. Intern.*, 1993, vol. 11, no. 7, p. 875.
7. Pokonova, Yu.V., *J. Advan. Material*, 2000, vol. 5, no. 2, pp. 95–98.
8. Pokonova, Yu.V. and Potashov, V.A., *Khimiya Tverd. Topliva*, 2001, no. 3, pp. 38–48.
9. Pokonova, Yu.V., Carbon, 1998, vol. 36, no. 4, pp. 95–98.
10. Pokonova, Yu.V. and Grabovskii, A.I., *Tsvetnye Metally*, 1995, no. 5, pp. 26–28.

ISSN 1070-4280, Russian Journal of Applied Chemistry, 2007, Vol. 80, No. 11, pp. 1969–1972. © Pleiades Publishing, Ltd., 2007.
Original Russian Text © A.V. Zaichuk, V.V. Koleda, Ya.I. Belyi, 2007, published in Khimicheskaya Promyshlennost', 2007, Vol. 84, No. 4, pp. 186–191.

TECHNOLOGY OF ORGANIC AND INORGANIC CHEMISTRY

On the Synthesis of Glass and Glass-Crystalline Black-Blue Facing on Thin Ceramic

A. V. Zaichuk, V. V. Koleda, and Ya. I. Belyi

Ukrainian State Chemical Technological University, Dnepropetrovsk, Ukraine

Received June 28, 2007

Abstract—By x-ray phase analysis the optimal temperature is established for the spinel formation in the oxide system Co_2O_3–Fe_2O_3 at the producing ceramic black-blue pigment and the phases playing the role of basic chromophores. The synthesized pigments provide the glass facing with black-blue color and strong flashing (up to 86%) and with semi-dull fine crystalline facture based on the developed unfritted glaze characterized by strong and stable color in a wide range of roasting temperature.

DOI: 10.1134/S1070427207110420

The consumers' demand of ceramic products, those of everyday use in particular, is defined in much by their appearance which in turn depends on the color and quality of glaze facing. Producing the exclusive strong drinks induces necessity in development of special ceramic bottles with high aesthetic and decorative characteristics. Therewith significant is the process of glazing, that is, formation on surface of glass layer either flashing or of semi-dull fine-crystalline facture. Developing research in this direction is very actual. Therefore the purpose of this work is development of compositions and investigation of pigment-containing black-blue glaze covers.

The blue and black pigments, as is known [1], should be synthesized as a rule at high temperature (up to 1300°C), predominantly from the cobalt, iron, manganese and chromium oxides.

Earlier investigations [2] showed that it is reasonable to use two-component oxide system CoO–Fe_2O_3 for the synthesis of black ceramic pigments, in part, for high melting unfritted glazes. The basic chromophores in this system providing formation of required color of glass layer are cobalt ferrite ($CoFe_2O_4$) and free cobalt oxide.

Taking above into account, at the synthesis of such pigments we studied the compositions that include cobalt and iron oxides with Co_2O_3/Fe_2O_3 ratio in the range from 1.40 to 2.38. Their thermal treatment initially was carried out in laboratory roasting furnace at maximal temperature 1000°C with isothermal 1 h exposure.

From the data of x-ray phase analysis (Fig. 1) follows that the experimental pigments besides cobalt ferrite also contain cobalt oxide, the latter in much bigger amount than necessary for stoichiometric spinel $CoFe_2O_4$. At higher values of Co_2O_3/Fe_2O_3 ratio the intensity of diffraction maxima corresponding to cobalt oxide (Co_3O_4, d = 2.43; 2.86; 1.43) increases considerably. The phase composition of the pigment also includes gematite (α-Fe_2O_3), appearing due to incomplete spinel formation.

The studied pigments were ground in a ball mill to the particle size 5–10 m and were added in amount up to 8 wt. fraction above 100 wt % into unfritted transpaent glaze containing pegmatite, sand, chalk, kaolin and microvollastonite. The obtained dross with 38% moisture was applied by pulverization on the ceramic samples that after drying were roasted at maximum temperature 1200°C for 2 h. Properties of the glazes obtained are listed in the table.

The data obtained show that including the synthesized by us ceramic pigmets into the mixture for producing unfritted transparent glaze allows obtaining after roasting the glass layer of strong black-blue color, as seen visually and as follows from spectral wavelength of the cover which is related to purple region (575–579 nm), as well as from low values of color purity (1–2%) and CDR (coefficient of diffuse reflection) in the range 3.20–3.69% inherent in black color. The most intense black-blue color has the glaze containing pigment n-8 with maximum Co_2O_3/Fe_2O_3 rate. The CDR of such glass coating material is minimal, being equal to 3.20%, and flash is 87%.

Formation of cobalt ferrite at the thermal treatment of the pigment mixture leads to black colorization of glaze cover. Appearance of blue color is stipulated by

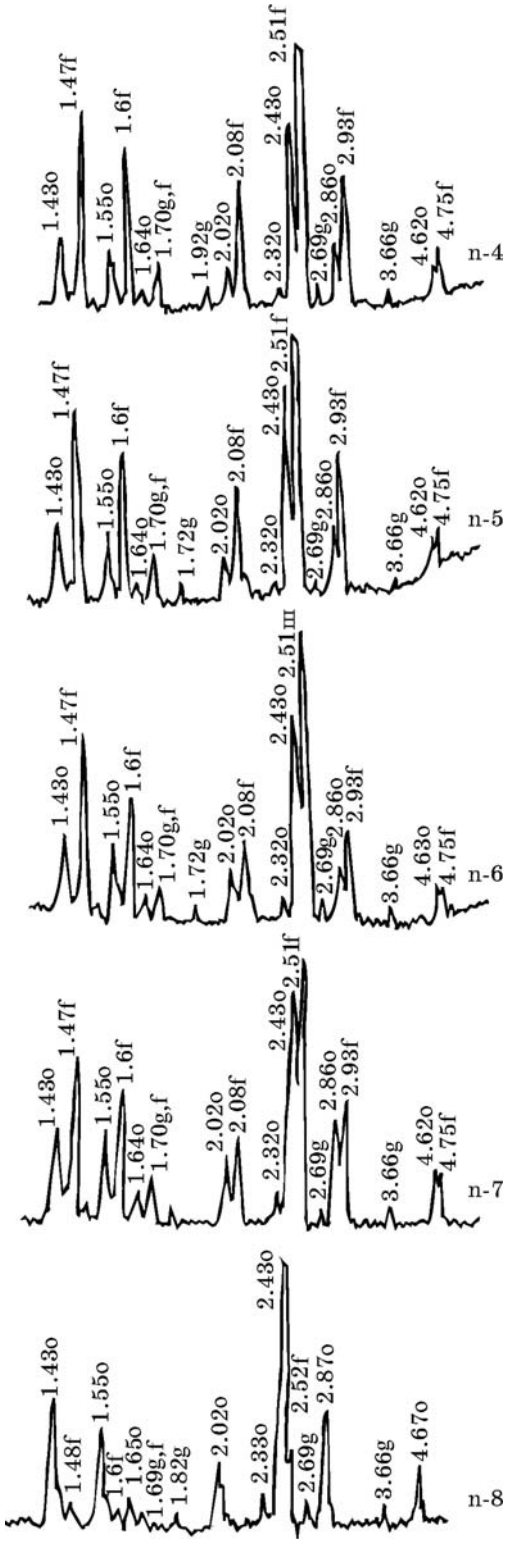

Fig. 1. Difractograms of experimental ceramic pigments synthesized at 1000°C (numbers correspond to the table): (f) cobalt ferrite ($CoFe_2O_4$); (g) gematite (α-Fe_2O_3); (o) cobalt oxide (Co_3O_4).

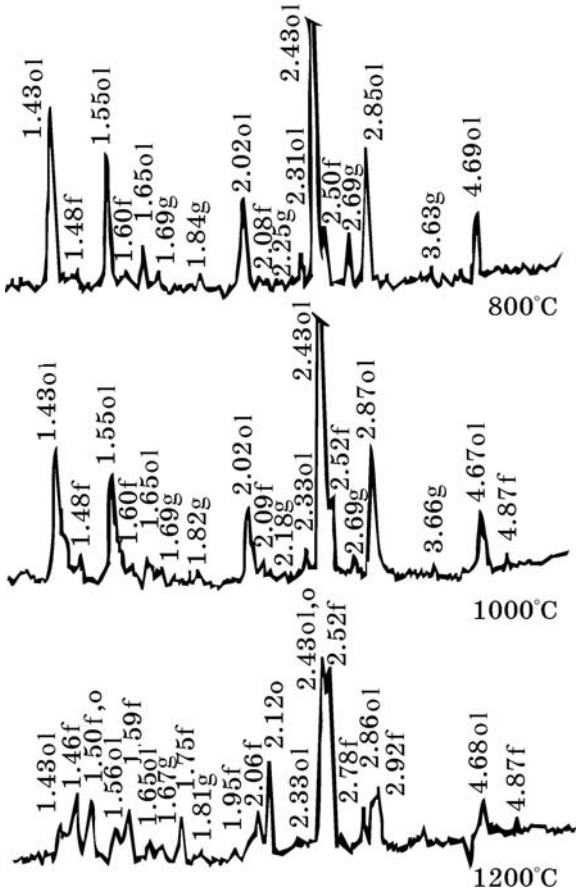

Fig. 2. X-ray diagrams of experimental ceramic pigment n–8 synthesized at various temperatures: (f) cobalt ferrite ($CoFe_2O_4$); (g) gematit (α-Fe_2O_3); (o1) cobalt oxide Co_3O_4; (o) cobalt oxide CoO.

the presence in the glass layer of tetracoordinated ions of bivalent cobalt arising due to dissolution in the glaze melt of the not bound into spinel cobalt oxide in the composition of experimental pigment mixture. As showed investigations, increase in the fraction of Co_3O_4 in the pigment leads to increase in the fraction of blue color in the resulting glass layer.

Thus, at roasting the studied not fritted glaze its color appears via two mechanisms: pigmental – by formation of cobalt ferrite, and ionic, due to dissolving cobalt oxide in melted glaze and formation in the glass coating of stable complexes consisting of tetracoordinated Co^{2+} ions.

A disadvantage of experimental pigment-containing glaze covers is appearance on the surface so-called "metallization" due probably to the incomplete proceeding of the processes of phase formation in the studied pigment mixtures roasted at 1000°C.

Characteristics of glaze coverings roasted at 1200°C

Rate Co_2O_3/Fe_2O_3 in pigment mixtures	Number of pigment				
	n–4	n–5	n–6	n–7	n–8
	1.40	1.59	1.81	2.07	2.38
Properties of glaze coverings					
Color (visual estimation)	Black with blue background		Black, tinged with blue	Black-blue	Saturated black-blue
Color tint, nm	577	575	575	575	579
Color purity, %	2	2	2	2	1
CMR*, %	80	82	86	86	87
CDR**, %	3.69	3.59	3.40	3.35	3.20

* Coefficient of mirror reflection.
** Coefficient of diffuse reflection.

For elucidating optimal temperature of the synthesis of pigment n-8 whose composition provides best color characteristics, its initial mixture was roasted in the temperature range from 800 to 1200°C.

As seen from x-ray diagrams (Fig. 2), the phase composition of pigment n–8 powder obtained at 800–1200°C consists mainly of cobalt oxide Co_3O_4 and includes cobalt ferrite ($CoFe_2O_4$) and gematite (b-Fe_2O_3).

Phase composition of the pigment n-8 synthesized at 800°C is characterized by high content of Co_3O_4 (d = 2.43; 2.86; 1.43) and α-Fe_2O_3 (d = 2.69; 1.84; 1.69), as confirmed by intensity of diffraction maxima, and this fact points to incomplete spinel formation.

Roasting at 1000°C also not allows complete binding iron oxide at spinel formation, as confirmed by the presence of low intensity peaks characteristic of gematit (Fig. 2b). The maximum possible formation of spinel in the pigment appears at roasting temperature 1200°C, as seen from high intensity of main diffraction maxima (d = 2.52; 1.50; 1.46) related to cobalt ferrite. Intensity of the peaks inherent in cobalt oxide and b-Fe_2O_3, on the contrary, falls down. Besides, partial transfer of Co_3O_4 into CoO (d = 2.43; 2.12; 1.50) is noted, Fig. 2c.

At higher temperature the synthesis of these pigments leads to less "metallization" of glaze cover, and roasting of the ceramic pigment at 1200°C results in its complete absence. This fact says in favor of the statement that this temperature provides the most complete interaction of components of pigment mixture, cobalt and iron oxides, promoting decrease in content of free cobalt oxide and not bound iron oxide in the composition of the synthesized pigments providing their rather high stability toward aggressive glaze melt. The glass cover formed in this case are characterized by saturated black-blue color which is confirmed by the low CDR value and color purity, 3.05% and 1% respectively, and by high flashing, 86%.

Using these developed pigment-containing glaze covers we investigated ways for achieving lusterless surface. We proceeded from the fact that known methods of synthesis the covers with low dull are differ principally from each other by the mechanism of the process of their preparation. Our method consists in the adding to the glaze composition of mineral or synthetic material providing function of high-melting filler. This method is the simplest and most economical one.

Therefore for producing glass black-blue covers with semi-dull fine crystalline structure with high decoration characteristics of the fine ceramic goods in the process of their exploitation, we studied introducing into ground mixture of not fritted pigment-containing glaze of high disperse fire resistant fillers as alumosilicate chamotte (ShK-38) and crude alumina (G-00) in amounts 8–14 and 1–4 wt. fraction respectively.

Dependence of optical and color characteristics of glass cover on the content of experimental additives in the composition of not fritted glaze is shown in Fig. 3.

From the graphic plots follows that increase in amount of alumosilicate chamotte in the composition of experimental pigment-containing glaze from 8 to 14 wt.

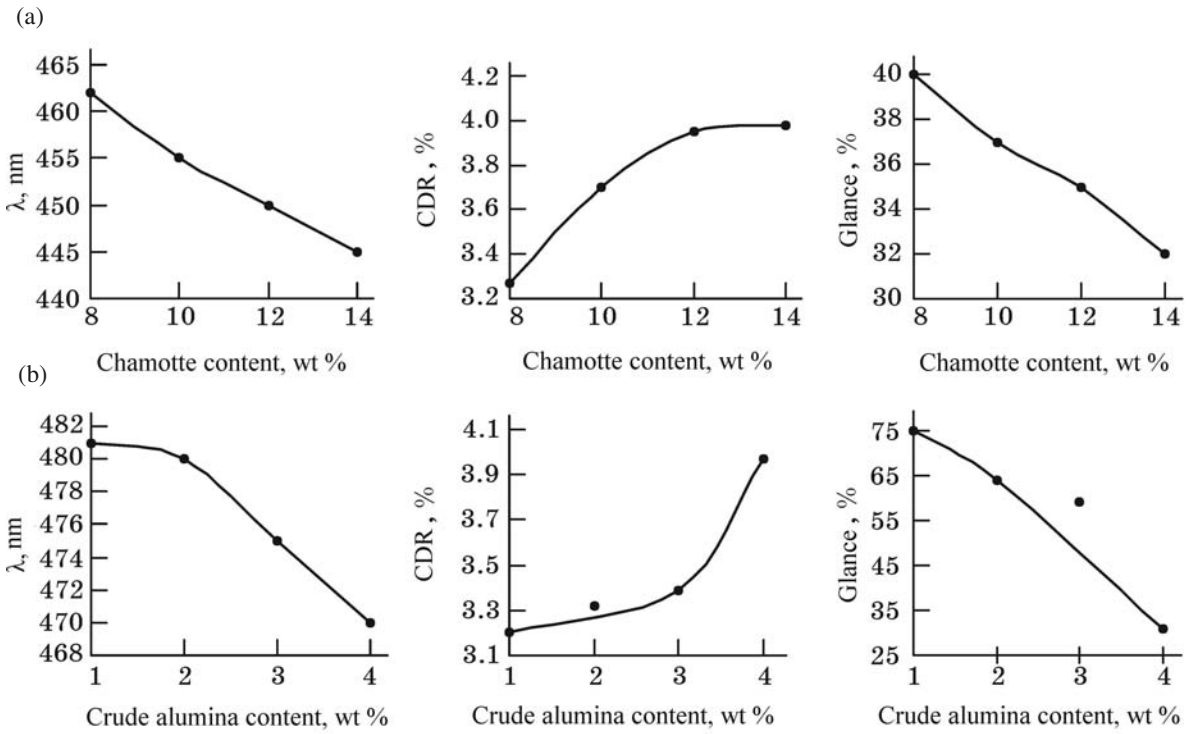

Fig. 3. Effect of flame resistant fillers on optical and color characteristics of experimental glaze covers. (a) Chamotte, (b) crude alumina.

fraction leads to stepwise decrease in flashing of glass cover to 32%. Simultaneously was registered certain decrease in strength of black-blue color, as seen from increase in CDR from 3.27 to 3.98% and by shift of wavelength value from 462 nm to shorter wavelengths in blue part of spectrum, 445 nm.

Increase in the composition of experimental glaze of crude alumina up to 4 wt. fraction results in formation in the process of roasting of semi-dull surface with reduce in flashing from 75 to 31%. However, simultaneously grows CDR, from 3.20 to 3.97%, due to decrease in saturation with black-blue color. The main wavelength of glaze cover falls to the range 470–481 nm.

The characteristics of the glass cover prepared by roasting at 1200°C shows that shamotte and crude alumina being homogenously distributed in the glaze melt practically are not dissolved in it within this temperature range and remains as fine disperse particles thus providing micro-heterogeneity of the system and at cooling of the ceramic product glass layer is formed with fine crystalline inclusions differ by refraction index from the bulk glass mass. Finally this leads to appearance of unusual decorative effect of semi-dull surface. Optimal concentration of the flame resistant additives for obtaining semi-dull glaze covers is: chamotte 8–10 wt. fraction, crude alumina 3 wt. fractions [3].

Thus, as a result of performed investigations we synthesized ceramic pigments based on the iron-cobalt oxide system at the temperature 1200°C, which provide formation of glass cover on fine ceramic goods with saturated black-blue color with either high (up to 87%), or low (37–59%) flashing, formation temperature is 1180–1220°C, using not fritted glazes not containing deficient and very expensive raw material (barium carbonate, zinc oxide and talk). The developed glazes are successfully used in technological processes at "Dneprokeramika" enterprise (town Pologi, Zaporozh'e area) for external covering ceramic bottles used for exclusive alcohol beverages.

REFERENCES

1. Pishch, I.V. and Maslennikova, G.N., *Keramicheskie pigmenty* (Ceramic pigments), Minsk: Vysshaya Shkola, 1987.
2. Belyi, Ya.I. and Zaichuk, A.V., *Steklo i Keramika*, 2005, no. 9, p. 28–30.
3. Zaichuk, A.V., Koleda, V.V., Belyi, Ya.I. and Furleta, E.D., Abstracts of Papers, *Scientific and Technology Conference*, Dnepropetrivsk, September 27-29, 2006, p. 97–98.

ISSN 1070-4280, Russian Journal of Applied Chemistry, 2007, Vol. 80, No. 11, pp. 1973–1976. © Pleiades Publishing, Ltd., 2007.
Original Russian Text © A.R. Seitnazarov, S.A. Musaeva, Sh.S. Namazov, B.M. Beglov, 2007, published in Khimicheskaya Promyshlennost', 2007, Vol. 84, No. 4, pp. 192–196.

TECHNOLOGY OF ORGANIC AND INORGANIC CHEMISTRY

Mechanochemical Activation of Ordinary Phosphorite Powder of Central Kyzylkum Mixed with Urea Nitrate and Ammobium Carbonate Salts

A. R. Seitnazarov, S. A. Musaeva, Sh. S. Namazov and B. M. Beglov

Institute of General and Inorganic Chemistry, Academy of Sciences of Republic , Uzbekistan

Received April 24, 2007

Abstract—Grinding of ordinary phosphorite powder of Central Kyzylkum with urea nitrate and ammonium carbonate salt to the particles size less than 0.16 mm is shown leading to significant increase in content of consumable by plants form of P_2O_5 in the products.

DOI: 10.1134/S1070427207110432

In 21 century the world food problem increased sharply owing to higher growing of population as compared with the increase in production of food and due to decrease in such basic resources as arable land, fresh water basin and energy sources necessary for agricultural production [1]. The population growing on the planet can be judged form the following data. To the beginning of 20-th century the whole population was 1.62 billion. In the following 60 years the population increased twice and in the next 25 years it triplicated. In 2000 the world community consisted of 6.1 billion of inhabitants. According to calculations, at the current rate of growing population to the year 2050 the planet will have 8.9 to 10 billion people. At the same time the land area under food grains fall from 0.24 to 0.12 hectare per capita. By calculations, to 2050 it will be contracted to 0.08 hectare per capita.

The processes of arable land contracting per capita stipulate the necessity of wide application of industrial technology in agriculture. The second half of 20th century becomes "era of chemization" due to wide application of mineral fertilizers and pesticides. The world consumption of mineral fertilizers within 40 years period (1951–1990) increased ten-fold, from 14 million to 140 million ton. Many countries were able to solve the food problem in part due to chemization. A bright sample is China: in 10 years of reformation of agriculture (1975–1984) at the practically the same area of arable land consumption of mineral fertilizers increased from 6 to 19 million ton on active component, that is, 3.2-fold. This led to increase in grain production to 365 million ton providing absolute increase 120 million ton.

In 21-th century the exclusively important factors for solving world food problem become chemization and irrigation. In Uzbekistan there is 25 736 000 hectare of agricultural land, but 3 730 000 hectare is irrigated [2]. But the irrigated land gives 97 % of all agricultural production of the Republic. Due to insufficient water resources, Uzbekistan has no possibility of significant extension of the area of irrigated arable land. Therefore priority belongs here to the problem of chemization of agricultural production.

Demand of nitrogen, phosphorus and potassium fertilizers in the Republic is 761 820 ton of nitrogen, 518 270 ton of P_2O_5 and 278 120 ton of K_2O as 100% active substance. The industry produces 740,000 ton of nitrogen and 137,000 ton of P_2O_5. Potassium fertilizers 25,000 ton of K_2O purchased from Russia. While providing agriculture with nitrogen fertilizers is more or less satisfactory, the problem with phosphorus and potassium is hard. The Republic Government makes all possible for improving this situation. It was decided to built Dekhkanbad plant of potassium fertilizers based on Tyubegatan birthplace of potassium salts in Kashkadarine region, to increase facility of Kyzylkum phosphorite mill, on reconstruction of Almalyk "Ammofos" and of "Samarkandkimye" join stocks. Despite, the plants producing phosphorus-containing

fertilizers exert problems. The plant of Republic began treatment of local raw material, the phosphorite of Central Kyzylkum. This ore is poor in respect of phosphorus, contains much carbonates and chlorine and is difficultly enriching. In the world such raw material is used for production of ordinary superphosphate. Such low quality product is manufactured by Kokand plant, it contains 11% of P_2O_5 and 1.5% of N. To produce high quality phosphorus-containing fertilizer from such ore enrichment is requiring. The multistep enrichment is carried out in Kyzylkum mill, it includes grinding, dry enrichment giving ordinary phosphorite powder, washing out of chlorine and roasting for removing CO_2. In fourth quarter of 2006 in this plant were brought into use the facility for producing 400 000 ton/year of washed and roasted phosphorus concentrate containing up to 30% of P_2O_5, 200 000 ton/year of washed and dried phosporus concentrate (18–19% P_2O_5) and 200 000 ton/year of ordinary phosphorite powder (16-18% P_2O_5).

Washed and roasted phosphorite concentrate will be used in Almalyk "Ammofos" for producing concentrated phosphorus-containing fertilizers: ammophos, superphos and ammonium sulfate-phosphate. From washed and dried phosphorite concentrate in Kokand plant will be produced ordinary ammonized superphosphate and from the ordinary phosphorite powder in Samarkamd plant will be produced nitrocalcium phosphate [3]. In summary, industry will produce in the year 2010 169 000 ton of 100% P_2O_5, but this amount is still far from agriculture demand of phosphorus fertilizers.

Enriching the Central Kyzylkum phosphorites in Kyzylkum phosphorite mill leads to formation of wastes in a great amount. At the dry enriching at producing ordinary phosphorite powder the dust fraction (18–19% P_2O_5) and mineralized mass (12–14% P_2O_5) are pushed aside. At the washing out chlorine the 30% of P_2O_5 in the ore is washing off with washing water into sludge receiver. The P_2O_5 content in the phosphorite from dried sludge is 8–10%. These wastes in our opinion form a reserve for increasing production of phosphorus-containing fertilizers. But acid methods are not acceptable for their treatment. For these materials would be appropriate so-called mechanochemical activation: transfer of not plant feeding form of P_2O_5 in the raw material into acceptable form by mechanical treatmet in the presence of certain chemical reagents [4–6].

We studied mechanochemical activation of various sorts of Central Kyzylkum phosphorites with ammonium nitrate and sulfate [7–10]. Both ammonium nitrate and ammonium sulfate increased sharply the content of acceptable form of P_2O_5 in the phosphate raw material after mechanical activation. The product of phosphorite mechanochemical activation has one defect: it has dust-like form not convenient for introducing into soil. However, this defect can be overcame, because the product can be easily granulated by pressing [11].

In this work we used for mechanochemical activation the ordinary phosphorite powder of Central Kyzylkum with the composition (wt %): P_2O_{5total} 18.33; relative content of $P_2O_{5acceptable}$ with Trilon B 12.1; CaO 47.48; CO_2 15.20, in a mixture with ammonium carbonates produced by Chirichik join stock company "Elektro-khimpribor" and urea nitrate of "pure" grade. The ammonium carbonates contained 23.12% N and showed pH 8.19 (10% water solution). The urea nitrate contained 33.97% N, its 10% solution showed pH 0.81. The mixtures were prepared with different nitrogen – phosphorus ratio. The ammonium carbonate salts are also interesting as they themselves are effective nitrogen fertilizers and simultaneously they capable to convert hardly soluble soil phosphates into the form acceptable by plants [12, 13]. As to ammonium nitrate, it attracts attention of Indian scientists as a reagent promoting mechanochemical activation of phosphate raw material [14–16].

The grinding was carried out using laboratory porcelain stamp to the particle size below 0.16 mm. Grinding of phosphorite powder only resulted in increase of relative content of $P_2O_{5acceptable}$ with Trilon B to 23.8%, that is, twice. Analysis of the products of the fertilizer grinding was conducted alongside the known procedures [17]. The acceptable form of P_2O_5 was determined with Trilon B. The experimental results are listed in Tables 1 and 2.

As seen from Table 1, the ammonium carbonate salts promote activation of phosphate raw material. The relative content of P_2O_5 acceptable form in the product varies from 56.97% at the N:P_2O_5 ratio in the mixture 1 : 0.75, to 80.39% at N: P_2O_5 = 1 : 0.15. The higher amount of ammonium carbonate salts n the mixture, the higher value of relative content of acceptable form of P_2O_5. The products with even this ratio of acceptable P_2O_5 form to its overall content are prospective nitrogen-phosphorus fertilizers. They include nitrogen in a varied amount in the range of 11.54 to 18.71%, and P_2O_{5total} from 3.11 to 9.25%. By composition they are advantageous over simple ammonized superphosphate. At the activation of the mixture, in the product appears also the water-soluble

Table 1. Composition of mixtures of phosphorite powder with ammonium carbonate salts after mechanical activation

Ratio of $N:P_2O_5$ in the mixture	Amount of ammoniumcarbonate salts, g	Amount of phosphorite powder, g	Amount of product, g	Chemical composition of the product, wt %						Nitrogen loss, %
				N	P_2O_{5total}	$P_2O_{5acceptable}$	$P_2O_{5water\text{-}soluble}$	$\frac{P_2O_{5acceptable}}{P_2O_{5total}}$	$\frac{P_2O_{5water\text{-}soluble}}{P_2O_{5\ total}}$	
1:0.150	25.0	4.71	28.41	18.71	3.11	2.50	0.18	80.39	5.79	8.05
1:0.224	25.0	7.07	30.76	17.30	4.31	3.32	0.20	77.03	4.64	7.92
1:0.300	25.0	9.43	33.18	16.08	5.33	3.87	0.18	72.61	3.38	7.68
1:0.375	25.0	11.78	35.6	15.11	6.20	3.98	0.18	64.19	2.90	6.93
1:0.450	25.0	14.14	38.03	14.20	6.97	4.32	0.17	61.98	2.44	6.56
1:0.525	25.0	16.49	40.45	13.37	7.65	4.64	0.17	60.65	2.22	6.43
1:0.600	25.0	18.85	42.92	12.68	8.25	4.94	0.17	59.88	2.06	5.84
1:0.750	25.0	23.56	47.8	11.54	9.25	5.27	0.16	56.97	1.73	4.57

Table 2. Composition of mixtures of phosphorite powder with urea nitrate after mechanical activation

Weight ratio $N:P_2O_5$	Prduct pH	Product chemical composition, wt. %											Degree of decarbonization, %
		N	$P_2O_{5\ total}$	CaO_{total}	$P_2O_{5acceptable}$	$P_2O_{5water\text{-}soluble}$	$CaO_{acceptable}$	$CaO_{water\text{-}soluble}$	$\frac{P_2O_{5\ aceptable}}{P_2O_{5total}}$	$\frac{P_2O_{5\ water\text{-}soluble}}{P_2O_{5\ total}}$	$\frac{CaO_{acceptable}}{CaO_{total}}$	$\frac{CaO_{water\text{-}soluble}}{CaO_{total}}$	
1:0.3	2.01	21.19	6.51	17.49	6.42	4.70	17.33	13.38	98.62	72.20	99.09	76.50	98.12
1:0.5	3.01	17.03	9.43	25.34	6.40	0.70	19.42	10.73	67.87	7.42	76.63	42.34	83.19
1:0.7	6.90	13.88	11.08	29.77	6.31	0.19	21.56	2.91	56.95	1.71	72.42	29.93	75.63
1:1	7.30	12.70	12.46	33.48	5.66	0.19	22.08	6.98	45.43	1.52	65.95	20.85	49.24

form of P_2O_5 (0.16–0.20 absolute %), attesting the fact that the solid phase reaction between the phosphorite and ammonium carbonate salts leads to formation of either $Ca(H_2PO_4)_2$, or $NH_4H_2PO_4$. A disadvantage of the process is nitrogen loss into gas phase. At grinding the mixture is heated, and thermally instable ammonium carbonates partially decompose with escape nitrogen into gas phase. In our case the nitrogen loss falls to the range 4.57 to 8.05%. The loss value was determined from the mixture weight loss at the grinding and from the nitrogen content in the initial mixture and the product.

Table 2 shows results of mechanochemical activation of phosphorite powder with urea nitrate. Changing N: P_2O_5 ratio in the mixture from 1 : 0.3 to 1 : 1 leads to appearance of acceptable P_2O_5 in amount 98.62 to 45.43% of total P_2O_5. Presence in the product of water-suluble form of CaO in a significant amount shows that the solid phase reaction of phosphorite powder with urea nitrate first of all results in decomposition of carbonates with formation of calcium nitrate. This conclusion is attested also by the data on the changes in the degree of decarbonization of the mixture. Simultaneously proceeds partial decomposition of mineral phosphate with formation of acceptable and water-soluble forms of P_2O_5. At the N : P_2O_5 ratio in the initial mixtureequal to 1 : 0.5 we obtain the fertilizer containing (wt. %): N_{total} 17.03; P_2O_{5total} 9.43; $P_2O_{5acceptable}$ 6.40; $P_2O_{5water\text{-}soluble}$ 0.70; CaO_{total} 25.34; $CaO_{acceptable}$ 19.42; $CaO_{water\text{-}soluble}$ 10.73, the content of acceptable form of P_2O_5 is 67.87% of the total one. By its composition, this is a good nitrogen-phosphorus fertilizer. But high content of calcium nitrate leads to high hygroscopicity and necessity of conditioning.

REFERENCES

1. Gordeev, A. and Chernyakov, B., *Voprosy Ekonomiki*, 2001, no. 6, pp. 50–59.
2. Kurbanov, E. and Kuziev, R., *Gornyi Vestnik Uzbekistana*, 2001, no. 1, pp. 94–96.
3. Radzhabov, R.R., *Khim. Tekhnologiya. Kontrol' Upravlenie*, 2006, no. 3, pp. 5–11.
4. Beglov, B.M. Namazov, Sh.S., Mirzakulov, Kh.Ch. and Umarov, T.Zh., *Aktivatsiya prirodnogo fosfatnogo syr'ya* (Activation of natural phosphate raw material), Tashkent: Khorezm, 1999.
5. Chaikina, M.V., *Nauka-Proizvodstvu*, 2002, no. 2, pp. 29–32.
6. Chaikina, M.V., *Khim. Tekhnologiya*, 2000, no. 6, pp. 5–12.
7. Seitnazarov, A.R., Namazov, Sh.S. and Beglov, B.M., Abstracts of Papers, *Proceedings of int. scientific-practical conference "Problems of chemical technology of inorganic, organic, silicate and building materials and teaching of specialists"*, Shymkent, October 28–30, vol. 1, pp. 222–225.
8. Seitnazarov, A.R., Namazov, Sh.S., Salimov, Z.S., Mirzakulov, Kh.Ch. and Beglov, B.M., Khimicheskaya promyshlennost' segodnya, 2003, No. 4, p. 42–44.
9. Seitnazarov, A.R., Namazov, Sh.S., Mirzakulov, Kh.Ch. and Beglov, B.M., Doklady Akad. Nauk Rep. Uzbekistan, 2003, No. 2, p. 40–43.
10. Seitnazarov, A.R., Namazov, Sh.S., Mirzakulov, Kh.Ch. and Beglov, B.M., Doklady Akad. Nauk Rep. Uzbekistan, 2005, No. 4, p. 56–58.
11. Namazov, Sh.S., Yakubov, R.Ya., Seitnazarov, A.R., Musaeva, S.A. and Beglov, B.M., *Khimicheskaya promyshlennost'*, 2005, no. 4, pp. 163–168.
12. Nosko, B.S., Maksimova, V.P. and Khristenko, A.A., In: *Elementi regulyatsii v roslinnitstvi* (Elements of regulation of growing), Kiev: Kompas, 1998, pp. 116–124.
13. Davydova, O.E, Veshitskii, V.A. and Mal'tseva, N.N., *Novye elementy bioregulyatsii dlya ustoichivogo razvitiya v agroekosistemak*h (New elements of bioregulation for stable development of agroecological systems), Kiev: Naukova Dumka, 2004.
14. Narayanan, K.T.R. and Vasudeva, M.A.R., *Indian J. Technol.*, 1972, vol. 10, no. 11, pp. 408–412.
15. Narayanan, K.T.R. and Vasudeva, M.A.R., *Indian J. Technol*., 1974, vol. 12, no. 10, pp. 447–450.
16. Pathak D.N., *Technology* (India), 1974, vol. 11, no. 4, pp. 432–433.
17. Vinnik, M.M., Erbanova, L.N. and Zaitsev, P.M., *Metody analiza fosfatnogo syr'ya, fosfornykh i kompleksnykh udobrenii, kormovykh fosfatov* (Methods of analysis of phosphate raw material, phosphoric and complex fertilizers and food phosphates), Moscow: Khimiya, 1975.

ISSN 1070-4280, Russian Journal of Applied Chemistry, 2007, Vol. 80, No. 11, pp. 1977–1983. © Pleiades Publishing, Ltd., 2007.
Original Russian Text © O.E. Khotyanovich, M.I.Kuz'menkov, 2007, published in Khimicheskaya Promyshlennost', 2007, Vol. 84, No. 5, pp. 233–241.

TECHNOLOGY OF ORGANIC AND INORGANIC CHEMISTRY

Technology of Magnesium Hexafluorosilicate Production

O. E. Khotyanovich and M. I. Kuz'menkov

Belarussian State Technical University, Minsk, Belarus

Received July 11, 2007

Abstract—Systematic study of parameters of the techological process for producing crystalline magnesium hexafluorosilicate from hexafluorosilic acid and caustic magnesite: reagents concentrations and ratio, temperature of the synthesis and evaporation, order of pouring the reagents (caustic magnesite suspension and hexafluorosilic acid), intensity of the solution stiring at its crystallization. Optimal values providing maximal yield of the targeted product are elucidated.

DOI: 10.1134/S1070427207110444

Currently in the Republic Belarus' increased demand on the magnesium hexafluorosilicate, the main component for producing the impregnating compositions for the increase endurance limit of concrete and ferroconcrete constructions. However, in the countries of former Soviet Union including Republic Belarus' this product did not produce on the industrial scale. The current demand is covered by import from USA, Germany, Italy and other countries.

Reviewing published sources and patent data showed that in distinct to other fluorine-containing salts the bivalent metal hexafluorosilicates, those of magnesium, calcium and zinc in particular, are the poorly studied compounds. Publications [1–8] are not complete and often contradict one another, up to now there is no general opinion concerning optimal technological parameters for producing the bivalent metal hexafluorosilicates. Therefore the aim of this research is development of technological process for producing magnesium hexafluorosilicate from crude raw material.

In this study we used hexafluorosilic acid of the company "Gomel' Chemical Plant", the side product of the production of extractive phosphoric acid. The authors [1–5] have used for the synthesis of magnesium hexafluorosilicate the hexafluorosilic acid of 8–15 wt % concentration; the solution obtained then should be evaporated for isolation of $MgSiF_6 \cdot 6H_2O$. In this sense, it would be preferable to use concentrated acid (up to 33 wt % H_2SiF_6) [6], to obtain in the process of the synthesis a suspension of magnesium hexafluorosilicate in its saturated solution. However, in the "Gomel' Chemical Plant" at the producing extractive phosphoric acid, in the process of absorption of fluorine gases with water is formed hexafluorosilic acid with concentration 12–14 wt%. It is technologically difficult to increase its concentration, because it would lead to sharp increase in aggressive action on the material of evaporating unit. Therefore in the study we used hexafluorosilic acid of 14% concentartion. As a neutralizing agent was used caustic magnesit PMK-75 (State standard GOST 1216-87) with the composition, wt%: MgO 75–80, CaO 2.5–3.0, SiO_2 2.0–2.5.

For the development of the magnesium hexafluorosilicate regime of synthesis the following technological parameters were varied: concentration of each reagent and their ratio, temperature of the synthesis and evaporation of solution, order of pouring the reagent, caustic magnesite and solution of hexafluorosilic acid, intensity of stirring the solution in the process of crystallization.

For the synthesis of magnesium hexafluorosilicate we used a three-neck flask placed into a thermostate unit, to provide stability of chosen temperature. The following order of operations was applied: To the reaction vessel was loaded given precalculated amount of hexafluorosilc acid taken with excess against stoichometry. At the permanent stirring to the acid was poured caustic magnesit in one portion. The suspension obtained was filtered and the filtrate was evaporated on a water bath. The crystalline product obtained was dried in a drier to constant weight.

For identification of the targeted product were applied chemical method (complexometry) and X-ray phase analysis (difractometer DRON-3 with CuK illumination) and IR spectroscopy (SPECORD-751R).

In the first step we studied effect of the order of pouring the initial reagent on the yield of magnesium hexafruorosilicate. The synthesis temperature was maintained at 50°C, hexafluorosilic acid concentration 14 wt%, its excess 2 wt% over stoiciometry. The magnesit suspension concentration was varied. This reagent was loaded to the reactor in one portion. The results obtained are shown in Table 1. As seen, at the same other parameters of the synthesis the order of pouring when hexafluorosilic acid is added to the suspension of caustic magnesit in the most cases leads to decrease in the yield of $MgSiF_6 \cdot 6H_2O$. This obviously is connected with two-step formation of magnesium hexafluorosilicate: In the initial step the solution is oversaturated with Mg^{2+} ions relatively to SiF_6^{2-} resulted in formation of magnesium fluoride [9]. In the further process the solution is oversaturated with SiF_6^{2-} ions leading to dissolution of magnesium fluoride and formation of magnesium hexafluorosilicate. However, up to 4% of magnesium fluoride remains in the precipitate, which leads to decrease in the yield of crystalline magnesium hexafluorosilicate and its contamination with the products of the synthesis. At the alternative order of pouring, the magnesium hexafluorosilicate is formed in one step alongside the reaction:

$$MgO + H_2SiF_6 = MgSiF_6 + H_2O \quad (1)$$

Reverse order of pouring reagents, namely, adding of caustic magnesit suspension to the solution of the acid restrict its homogenous dozing. Therefore further research on the regime of synthesis of magnesium hexafluorosilicate was carried out at mixing initial components by adding caustic magnesit as a powder to the solution of hexafluorosilic acid, to provide maximum yield of the targeted product and simplify the technological process by excluding the step of preparation of water suspension of caustic magnesit.

The next step of research was denoted to the problem of effect of the reagents ratio on the yield of the final product. For this purpose was varied the hexafluorosilic acid excess relatively to stochiometric amount from 0 to 14 wt%.

The dependence of magnesium hexafluorosilicate yield on the excess of hexafluorosilic acid over stoichiometry is shown in Table 2

It is seen that increase in the acid excess to 7–10 wt% leads to increase in the yield. This can be explained by decrease of magnesium hexafluorosilicate solubility in the $MgSiF_6 \cdot H_2SiF_6 \cdot H_2O$ system at the increase of free hexafluorosilic acid content in the mother liqueur [6] affecting positively the yield of $MgSiF_6 \cdot 6H_2O$.

Excess of hexafluorosilic acid over 10 wt% does not affect significantly the magnesium hexafluorosilicate yield. On the basis of the data obtained on the influence of reaction product yield on the ratio of the components we conclude that hexafluorosilic acid excess should be applied, because this leads, all other conditions are the same, to more complete proceeding of the reaction and practical absence of amorphous silicon oxide in the crystalline reaction product.

Table 1. Effect of the order of pouring reagents on the yield of magnesium hexafluorosilicate

Magnesite suspension concentration, wt%	Magnesium hehafluorosilicate yeld depending on the pouring order, wt%	
	direct hexafluorosilic acid to caustic magnesite suspension	reverse suspension of caustic magnesite to hehafluorosilic acid
5	93.6	97.0
10	95.5	97.4
20	96.9	98.1

Table 2. Effect of technological parameters on the yield of magnesium hexafluorosilicate

Excess of hexafluorosilic acid over stoichiometry, wt%	Magnesium hexafluorosilicate yield(%) at the temperature of synthesis,°C			
	20	40	60	70
0	92.1	93.8	88.7	87.0
2	92.9	95.5	89.5	87.2
5	92.8	97.2	90.0	87.3
7	93.2	97.9	90.0	87.5
10	93.1	98.1	90.4	87.0
14	93.7	98.0	90.4	88.1

X-ray diffraction analysis of a sample obtained with optimal regime showed that the main phase consists of magnesium hexafluorosilicate, which contains as admixed phase calcium hexafluorosilicate. IR spectrum contans the bands characteristic of both $MgSiF_6 \cdot 6H_2O$ and $CaSiF_6 \cdot 2H_2O$. These obtained experimental data well conform to the published ones [10]. According to chemical analysis the product obtained has a composition, wt%: $MgSiF_6 \cdot 6H_2O$ 96–98, $CaSiF_6 \cdot 2H_2O$ 2.0–2.5, other is admixture of amorphous silica. The content of main product obtained experimentally well conform to the calculated value.

At the study of the effect of temperature on the yield of magnesium hexafluorosilicate crystals we varied the temperature in the range from 20 to 70°C. At the temperature above 70°C the synthesis was not performed due to beginning of hydrolysis of magnesium hexafluorosilicate leading to formation of magnesium fluoride and silic acid [1, 2].

As seen from thr data in Table 2, increase in temperature of reaction mixture to 30-40°C while all other parameters remain unchanged leads to increase in nagnesium hexafluorosilicate yield, while at further increase in temperature occurs the yield falls down. The temperature factor in the range is known important at the synthesis of well soluble substances because rate of formation is proportional to $e^{-1/T}$, while the rate of formation of poorly soluble substances is proportional to e^{-T} [11]. From the x-ray diffraction data of the sample obtained at 30°C is seen that the main phase is magnesium hexafluorosilicate, and the admixed phase is calcium hexafluorosilicate.

At further increase in temperature to 50°C and over despite the decrease in viscosity and diminished deceleration at the penetration of acid into the magnesit particles the yield of magnesium hexafluorosilicate falls. It is explainable by hydrolytic decomposition of magnesium hexafluorosilicate at the temperature above 50°C with formation of amorphous silicon oxide and magnesium fluoride, the latter is registered by x-ray diffraction. Besides, the SiF_6^{2-} ions existing in the solution are also unstable and inclined to hydrolysis alongside the reaction equation: $SiF_6^{2-} + 2H_2O \rightarrow SiO_2 + 4H^+ + 6F^-$. Our experimental data correlate with data in [10].

Thus, the optimal temperature for the synthesis of magnesium mhexafluorosilicate falls to the range 30–40°C, which provides maximum yield of the product (up to 98 wt%), all other conditions are the same.

In respect of isolation crystalline magnesium hehafluorosilicate from its solution, we studied effect of the crystallization temperature on the yield. The magnesium hexafluorosilicate solubility changes by ~10% only when the slution temperature is varied in the range from 0°C to 60°C, therefore crystallization under cooling in this case is not effective. Therefore oversaturation in the system was created by partial removing the solvent by evaporqation.

As noted above, at the temperature over 50°C magnesium hexafluorosilicate exerts hydrolytic decomposition, therefore for its isolation in crystalline form the process of evaporation was carried out at the lower temperature. While studying the effect of evaporation temperature on the yield of magnesium hexafluorosoilicate crystals the temperature was varied in the range from 20°C to 50°C (see Fig. 1).

As seen, increase in the temperature affords crystalline magnesium hexafluorosilicate in higher yield. It can be assumed that at higher temperature the rate of formation of the crystal nuclei grows not only due to diminishing of their critical size but also because the ions are less hydrated and their joining into the nucleus is easier. Besides, at the elevated temperature falls the surface tension on the board between the solution and forming

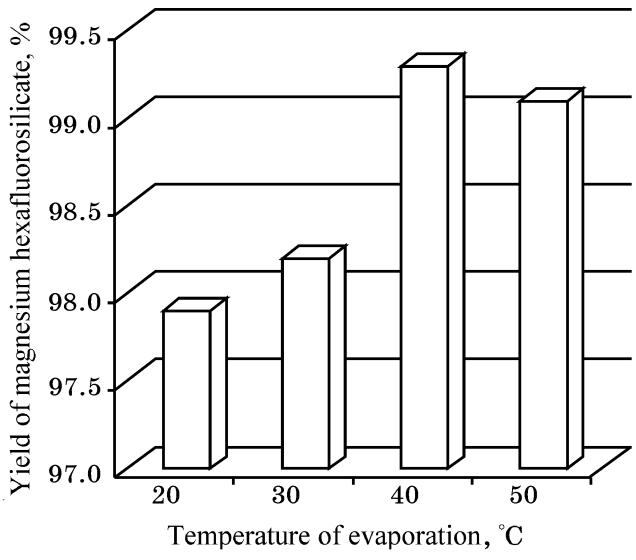

Fig. 1. Dependence of the yield of crystalline magnesium hexafluorosilicate on the temperature of evaporation of its solution.

Table 3. Dependence of magnesium hexafluorosilicate crystals size on the excess over stoichiomettry of water and evaporation temperature

Excess of hexafluorosilicate acid over stoichiomettry, wt%	Size of the crystals $MgSiF_6 \cdot 6H_2O$ at evaporation temperature, °C			
	20	30	40	50
5	2.4	2.4	2.3	1.9
7	2.5	2.6	2.5	1.9
10	3.8	3.8	3.6	2.1
14	3.7	3.8	3.7	2.2

nucleus and hence degreases the work function of their formation 11].

In the process of the experiment was found that not only the yield, but also the size of the $MgSiF_6 \cdot 6H_2O$ crystals grows with increase in the temperature (Table 3).

Obviously crystallization in the region of higher temperatures promotes increase in the size of crystals of the targeted product. This fact can probably be explained by decrease in the hydration of ions thus making much easier their transfer from the structurized in a certain degree laminar layer of the solution on the crystal surface to the crystal lattice, thus promoting faster grow of the crystals. A certain role probably plays also decrease in the solution viscosity, thus diffusion of the substance to the growing crystal edges accelerates.

As seen from Table 3, the crystal size depends substantially on the presence in the solution of hexafluorosilic acid excess. Studying the effect of silic acid excess in the system on the size of depositing crystals of magnesium hexafluorosilicate we found that decrease in the hexafluorosilic acid concentration leads to decrease in the average size of the crystals $MgSiF_6 \cdot 6H_2O$. This can be explained as follows. On one side, the magnesium hexafluorosilicate hexahydrate solubility falls with increase in hexafluorosilic acid content in the solution, that is, the solution becomes oversaturated by SiF_6^{2-} ions relatively to the ions of Mg^{2+}. Thus, when oversaturation of the solution increases, also increases concentration of submicro nuclei and becomes easier their joining together. On the other hand, the rate of appearance of the nuclei also grows, but not all them form further a crystal. Some of them join together or combine with a macrocrystal accelerating grow of the latter. By this

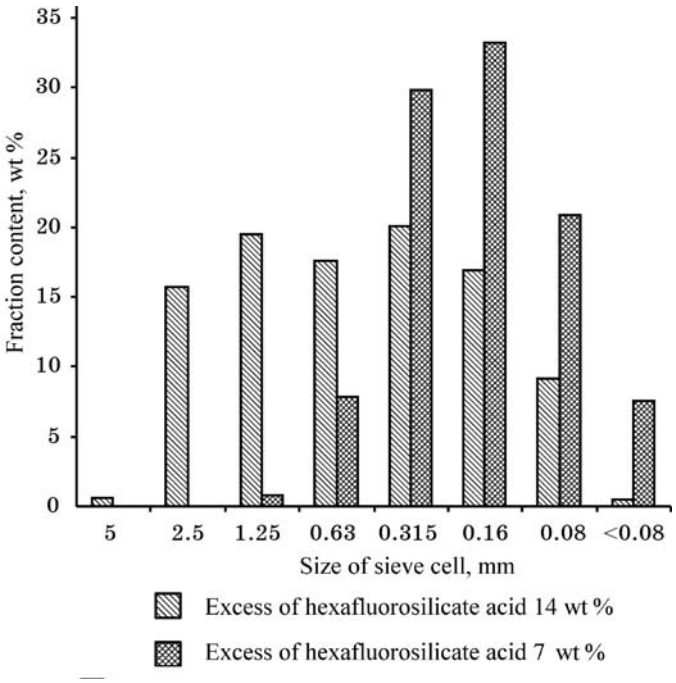

Fig. 2. Size distribution of magnesium hexafluorosilicate particles.

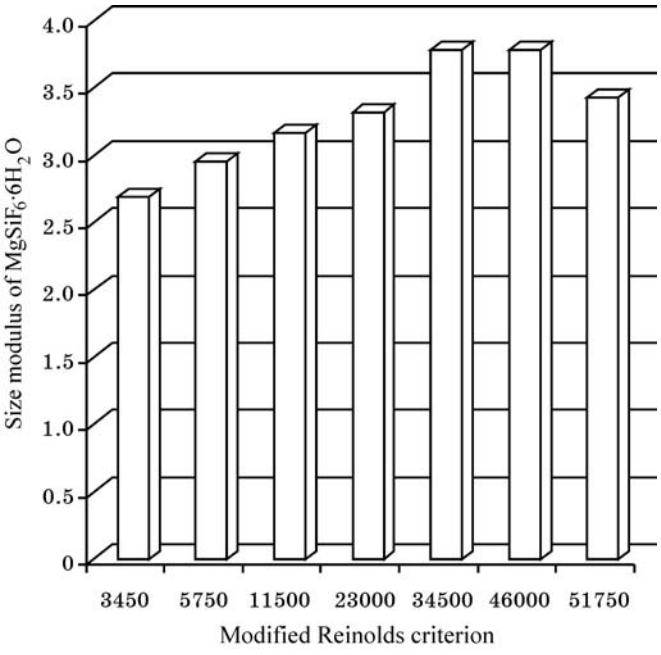

Fig. 3. Influence of hydrodynamic situation in the reaction vessel on the size modulus of $MgSiF_6 \cdot 6H_2O$ crystals.

reason, the higher oversaturating due to higher evaporation temperature and presence of hexafluorosilic acid excess, the less a number of appearing nuclei that then form separate crystals. The increase in crystal size with increase in oversaturation in a system at the sedimentation of soluble salt has been noted in literature [11, 12].

At the applied oversaturations while other synthesis parameters remains the same (synthesis temperature 30–40°C, hexafluorosilic acid concentration 14 %, excess of hexafluorosilic acid over stoichiometry 10 %, evaporation temperature 40°C) the magnesium hexafluorosilicate crystals precipitate with the size modulus in the range 3.6 to 3.8.

The precipitates obtained are polydisperse ones, due to non-simultaneous formation of critical nuclei and difference in the rate of grow of small and large particles [13]. Fig. 2 shows a histogram of distribution of magnesium hexafluorosilicate particles by the size.

As seen from the histogram, crystalline magnesium hexafluorosilicate consists of the particles with the size within a certain range of dispersion. Decrease in the excess of hexafluorosilic acid in the system leads to narrowing of this range and shifting it to the side of formation of the finely divided crystalline product.

Among the many factors affecting the rate of crystals growing in the mother liqueur, a significant one is intensity of supplying of the "building material" to the growing crystal edges. The growing of crystals is known depending in a great extent on the concentration fluctuations appearing in the process of stirring or sometimes due to changes in density in the reaction process or due to changes in temperature due to the exothermic reaction. Direction and intensity of the concentration fluctuations affect the rate of the crystal growing. Therefore it is significant to study effect of the intensity of stirring at the evaporation the magnesium hexafluorosilicate on its crystallochemical parameters..

For the description of the stirring process we used the modified Reynolds criterion (Re_M) [14, 15]. In the investigation we varied rotation frequency of the propeller-type agitator in the range from 30 rpm (Re_M = 3450) to 450 rpm (Re_M = 51750). Diminishing in the rotation frequency below 30 rpm (Re_M < 3450) leads to restrictions in stirring the crystalline magnesium hexafluorosilicate suspension in its saturated solution and the process is not homogenous.

Influence of hydrodynamic situation in the reaction vessel on the size of the formed crystals of magnesium hexafluorosilicate is shown in Fig. 3. It is seen that increase in modified Reynolds criterion from 3450 (rotation frequency 30 rpm) to 34500 (rotation frequency 300 rpm), all other conditions of the synthesis and evaporation are the same, leads to increase in average size of $MgSiF_6 \cdot 6H_2O$ crystals. But further increase in the rotation rate either leads to some decrease in the average size, or does not affect the crystals size.

Thus, from the data obtained we can conclude that increase in the intensity of stirring of the solution at its evaporation to a certain value (Re_M = 34500) makes easier access of "building material" to the face of growing crystal and the rate of the crystal growing increases resulting in the increase of its average sizes. However, at the increase in the modified Reynolds criterion above this value the rate of dissolving of surface layers of the growing crystal becomes higher than the positive effect of acceleration of diffuse supply of the substance and the rate of crystal growing falls [11]. Besides, there is an opinion [12] that under such conditions of crystallization can occur acceleration in the growing of big crystals and deceleration in the growing of the crystals of small size. This all leads to decrease in the average size of the magnesium hexafluorosilicate crystals at the increase in modified Reynolds criterion over 34500. Therefore we accept this intensity of stirring the solution at its evaporation as the optimal.

On the basis of this research we optimized regime of the sybthesis of magnesium hexafluorosilicate from caustic magnesit and hexafluorosilic acid. We established that the optimal parameters are: hexafluorosilic acid concentration 14 wt%, excess of hexafluorosilic acid over stoichoiometric amount is 7–10 wt%; temperature of the synthesis 35–45°C; temperature of evaporation 40–50°C [16].

These optimized conditions of the synthesis are taken as a basis for the technology of industrial scale producing magnesium hexafluorosilicate hexahydrate (Fig. 4).

The developed technological regime of the synthesis of magnesium hecxafluorosilicate allowed to produce this material with the quality some as imported analogs. Experimental bathes produced in the plant "Gomel' Chemical Plant" showed a possibility of organization of industrial producing of magnesium hexafluorosilicate.

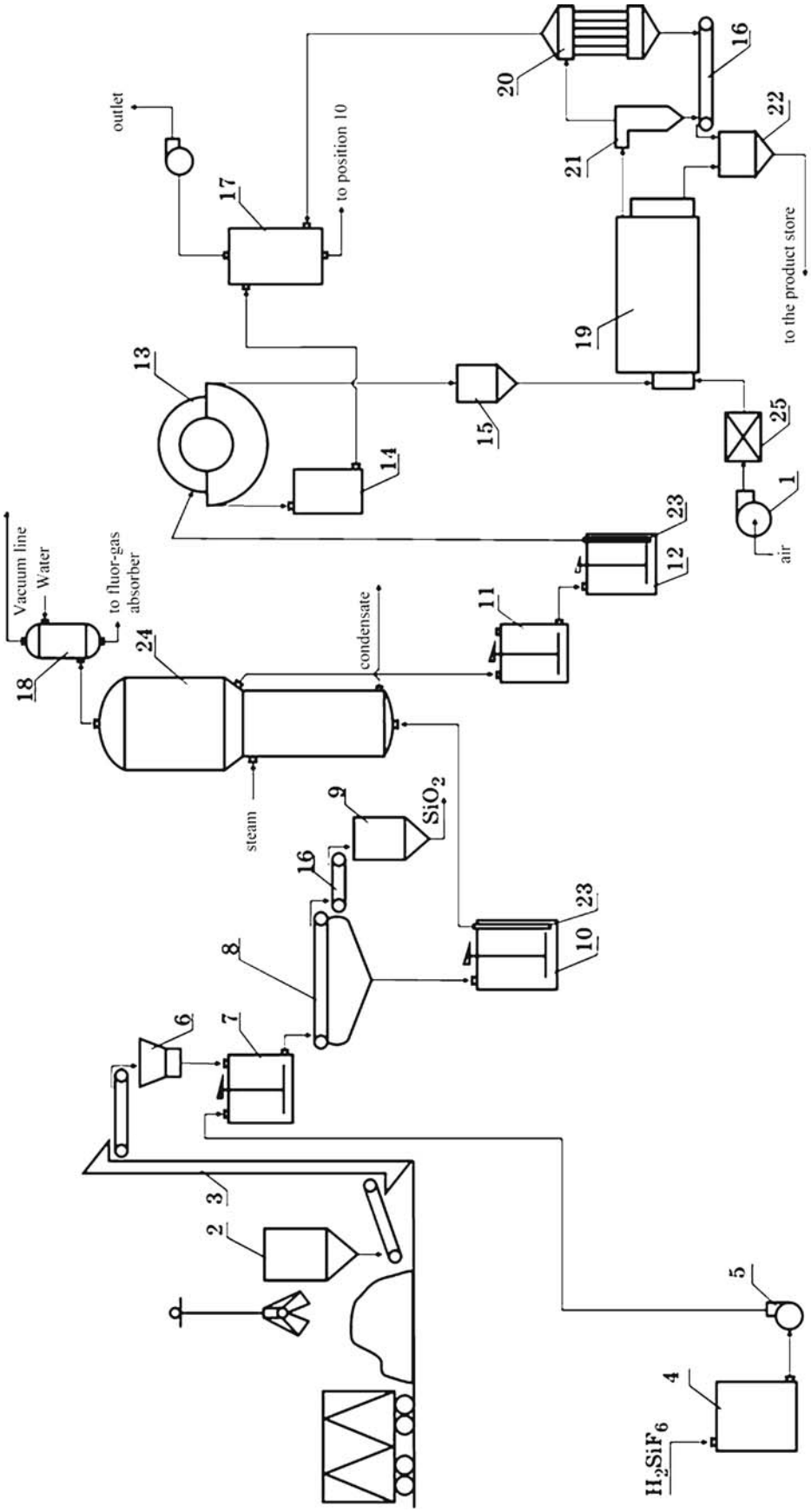

Fig. 4. Influence of hydrodynamic situation in the reaction vessel on the size modulus of $MgSiF_6 \cdot 6H_2O$ crystals. (1) blower, (2) receiver for caustic magnesite, (3) elevator, (4) receiver for hehafluorosilic acid, (5) pump, (6) weight dosing unit, (7) reactor, (8) tape vacuum filter, (9) receiver for silicate gel, (10, 12) intermediate receivers, (11) crystallizer, (13) drum vacuum filter (14) collector for mover liquor, (15) receiver, (16) conveyer, (17) absorber, (18) barometric condenser, (19) drier, (20) electric filter, (21) cyclone, (22) buncer for final product, (23) immersion pump, (24) evaporator, (25) heater. .

REFERENCES

1. Ryss, I.G., *Khimiya ftora i ego neorganicheskikh soedinenii* (The Chemistry of Fluorine and Its Compounds), Moscow: Gos. Nauchno-Tekhnicheskoe Izd. Khimicheskoi Literatury, 1956.
2. Pozin, M.E., *Tekhnologiya mineral'nykh solei* (Technology of Mineral Salts), Leningrad: Khimiya, 1961.
3. Zaitsev, V.A., Novikov, A.A. and Rodin, V.I., *Proizvodstvo ftoristykh soedinenii pri pererabotke fosfatnogo syr'ya* (Producing of Fluorine Compounds at the Treatment of Phosphate Row Material), Moscow: Khimiya, 1982.
4. Gabrielova, M.G., *Kremneftoridy magniya, kal'tsiya i tsinka. Issledovaniya po prikladnoi khimii* (Silicofluorides of Magnesium, Calcium and Zinc. Investigations on Applied Chemistry), Collection of papers, Moscow: Izdatel'stvo Akademii Nauk SSSR, 1955, pp. 244-248.
5. Lopatkina, G.A. and Kolosova, T.N., *Zh. Prikl. Khim*., 1969, No. 3, pp. 684–686.
6. Lopatkina, G.A., Kolosova, T.N. and Groznykh, M.A., *Zh. Prikl. Khim*., 1968, No. 7, pp. 1608–1611.
7. Lopatkina, G.A., Kolosova, T.N., Groznykh, T.A. and Vandysheva, P.V., *USSR Inventory Certificate 224496*, MKI5 S 01b 33/10; *Sposob polucheniya kremneftoridov magniya i tsinka* (Method of producing magnesium and zinc silicofluorides), no. 1096893/23-26; presented 11.08.66; published 12.08.68, *Byull. Izobr.,* no. 26.
8. Kalach, V.S., Bogdanova, N.S. and Mikhaleva, T.K., *USSR Inventory Certificate 538983*, MKI5 S 01b 9/08, 33/10. *Sposob polucheniya ftoristykh i kremneftoristykh solei* (Metod of producing fluorine and silicofluorine salts), no. 2029805/26; prezented 03.06.74; published 15.12.76, *Byull. Izobr*., no. 46.
9. Murashkevich, A.N., Kunitskaya, O.M. and Zharskii, I.M., *Vestsi NAN Belarusi, Ser. Khim. Navuk*, 2001, no. 1, pp. 5–11.
10. Davidovich, R.L., Kaidalova, T.A., Levchishina, T.F. and Sergienko, V.I., *Atlas infrakras-nykh spektrov pogloshcheniya i rentgenometricheskikh dannykh kompleksnykh ftoridov metallov IV i V grupp* (Collection of IR Absorption Spectra and X-ray Data of the Complexes of IV and V Grops Metals), Moscow: Nauka, 1972.
11. Matusevich, L.N., *Kristallizatsiya iz rastvorov v khimicheskoi promyshlennosti* (Crystallization from Solutions in Chemical Industry), Moscow: Khimiya, 1968.
12. Khamskii, E.V., Podozerskaya, E.A., and Freidn, B.M., *Kristallizatsiya i fiziko-khimicheskie svoistva kristalliziruemykh veshchestv* (Crystallization and Physico-chemical Properties of the Crystallizing Compounds), Lenigrad: Nauka, 1969.
13. Melikhov, I.V. and Pechnikov, V.G., *Dokl. Akad. Nauk SSSR*, 1969, vol. 185, no. 5, pp. 1083-1086.
14. Kasatkin, A.G., *Osnovnye protsessy i apparaty khimicheskoi tekhnologii* (Basic Processes and Apparatuses of Chemical Technology), Moscow: Al'yans, 2004.
15. Timonin, A.S., *Osnovy konstruirovaniya i rascheta khimiko-tekhnologicheskogo i priro-dookhrannogo oborudovaniya* (Basicity for Construction and Calculation of Chemico-Technological and Environment-Safing Equipment), Kaluga: Izd. N. Bochkarevoi, 2002.
16. Kuz'menkov, M.I., Trakhimchik, O.E., Lyudkov, A.A. *et al*., Republic Belarus Patent 7658 C1 BY, MPK7 S 01V 33/10, no. a 20030011, 2003; *Byull. Izobr.*, no. 2, 2005.

ISSN 1070-4280, Russian Journal of Applied Chemistry, 2007, Vol. 80, No. 11, pp. 1984–1988. © Pleiades Publishing, Ltd., 2007.
Original Russian Text © R.K. Kurbaniyazov, A.M. Reimov, A.T. Dadakhodzhaev, Sh.S. Namazov, B.M. Beglov, 2007, published in Khimicheskaya Promyshlennost', 2007, Vol. 84, No. 5, pp. 242–248.

TECHNOLOGY OF ORGANIC AND INORGANIC CHEMISTRY

Nitrogen-Phosphoric Fertilizers Produced by Introduction of Central Kyzylkum Phosphate Raw Material into Ammonium Nitrate Melt

R. K. Kurbaniyazov, A. M. Reimov, A. T. Dadakhodzhaev, Sh. S. Namazov, and B. M. Beglov

Institute of General and Inorganic Chemistry, Academy of Sciences of Republic Uzbekistan, Uzbekistan

Received April 24, 2007

Abstract—Composition of nitrogen-phosphoric fertilizers produced by introduction into ammonium nitrate melt of ordinary phosphorite powder, dust fraction and mineralized mass of Central Kyzylkum phosphorites in the amount necessary for providing final product with 0.5 to 5% of P_2O_5 is described.

DOI: 10.1134/S1070427207110456

Currently in various countries in the world is produced and circulated ammonium nitrate in a huge amount (ca. 33 000 000 ton in 2002) for covering agriculture demand. A significant part of world production (6 400 000 ton) is used as low cost and safe raw material for producing industrial explosives at the places of their application instead of expensive and dangerous for application explosives produced in plants [1]. The most powerful facilities for producing ammonium nitrate belong to USA and Russia, the world fraction of each country is estimated slightly over 13% (in USA these facilities include carbamide – ammonium nitrate solutions and other ammonium nitrate solutions 60%, products of industrial use 28%; in Russia these facilities include mainly granulated product for agriculture) [2]. In Uzbekistan three plants produce ammonium nitrate for agriculture, their total product is above one million ton per year.

Ammonium nitrate has two significant disadvantages: deterioration in storage and explosion risk [3, 4]. While one can avoid aggregation by means of various additives, the problem of explosion risk does not surmount completely. To avoid caking, sulfate, sulfate-phosphate or sulfato-phosphato-borate additives as well as caustic magnesite and other compounds are used [5]. Caustic magnesite is found the best one. Since 1949, "Elektrokhimprom" company in Chirik and since 1952 "Azot" corporation in Severodinetsk have produced caking-resistant ammonium nitrate by mixing with the product of apatite decomposition (RAP) with nitric acid as an additive introduced in the amount providing 0.7–1.6% P_2O_5 in the ammonium nitrate [6]. But to the end of 70th this additive was refused owing to depositing insoluble components in the heat exchange units and clogging granulators. The plants turned to use a technology with caustic magnesite. Nevertheless, adding RAP in amount much larger than necessary to avoid caking seems to be prospective also for diminishing explosiveness of ammonium nitrate. However, hopefully the problem of ammonium nitrate explosion risk can be resolved using phosphorus-containing additives. In publications [7–9] was described technology for producing complex nitrogen-phosphate fertilizer containing 32.3% of N and 5.2% of P_2O_5 by introducing to the ammonium nitrate melt of liquid complex fertilizer containing 11% of N and 37% of P_2O_5, based on the superphosphoric acid. This additive increased initial temperature of the ammonium nitrate decomposition by 22–24°C, reduced rate of its thermal decomposition, increased strength of granules, decreased the product porosity, increased resistance of the product to repeated phase transformations and, that is the most important, decreased its ability to detonation. The "Cherepovets Azot" plant applied this technology in 2002 to produce 1000 ton per a day, in a great extent owing to the fact that required liquid fertilizer was produced at a neighboring plant. The plant technologists noted that explosiveness of the product is less than that of pure

Table1. Material composition of phosphate raw material

Raw material	Content of components, wt%							$P_2O_{5\ acceptable}/\ P_2O_{5total}$
	P_2O_5	CaO	Al_2O_3	Fe_2O_3	MgO	F	CO_2	
Ordinary phosphorite powder	17.20	46.22	1.24	1.05	1.75	2.00	16.00	18.49
Dust fraction	18.54	44.72	0.95	0.80	0.80	2.22	14.80	20.71
Mineralized mass	14.68	40.80	1.17	1.37	0.53	1.85	12.84	16.41

Table 2. Dispersion composition of raw material

Size class, mm	Yield of fraction, %		
	Ordinary phosphorite powder	Dust fraction	Mineralized mass
2 – 0.5	–	–	4.4
0.5 – 0.315	1.5	1.5	10.2
0.315 – 0.16	6.3	5.6	34.1
0.16 – 0.1	20.3	5.7	14.5
0.1 – 0.063	38.3	15.0	16.3
0.063 – 0.05	17.2	9.8	4.7
> 0.05	16.4	62.4	15.8
Total mass	100	100	100

ammonium nitrate, but mixing of ammonium nitrate and liquid complex fertilizer solutions is accompanied by formation of precipitates causing troubles in the steps of evaporation and granulation [9].

The authors' certificates [10, 11] also propose methods of producing complex fertilizers by introduction of superphosphoric acid into ammonium nitrate melt, in [10] with additional loading apatite.

The Russian plants "Azot" in Kemerovo, join stock company "Kirovo-Chepetskii Khimkombinat," join stock company "Minudobreniya" in town Rossosh and Novgorod join stock company "Akron" decided to produce stabilized ammonium nitrate by adding phosphorus-containing materials. The first enterprises that realized in 2001 industrial producing the nitrogen-phosphorus fertilizer based on ammonium nitrate used as the phosphorus-containing raw material the extraxtion phosphoric acid or ammonium dihydrogen phosphate solution produced from this acid [12–14]. The problem that appeared were: (1) strong corrosion on the liquid – gas interphase board due to fluorine containing in the phosphoric acid, (2) Sedimintation of Fe, Al, Mg and Ca salts on the equipment walls leading even to sealing. The system productivity felt down more than twice as compared with the work on pure ammonium nitrate.

In 2003 started industrial producing the nitrogen phosphorus fertilizers (32% of N and 6% of P_2O_5) with the preliminary purified nitro-phosphoric acid extract from the azofoska production [15, 16]. This led to the same problems as at the use of extraction phosphoric acid.

Therefore searching for appropriate phosphorus-containing material for stabilization of ammonium nitrate is continued. In the Kirovo-Chepetsk chemical mill was proposed to load mixed extraction phosphoric and sulfuric acids into the nitric acid prior to ammonizarion [17]. But at evaporation of the solution formed and granulation here also will be occurring the equipment stoppage.

We decided to produce stabilized ammonium nitrate by introducing phosphate raw material from Central Kyzylkum, namely, ordinary phosphorite powder, dust fraction and mineralized mass, either. The two latter materials are side products at producing the phosphorite powder by dry enrichment of phosphorite ore. Of course, granulation of ammonium nitrate should be carried out in a drum-type granulator-drier or in plate or drum granulator, as proposed, e.g., in the patent [18], rather than in a tower granulator. The initial raw material composition is shown in Table 1.

The ordinary powder contains fluoroapatite $Ca_5F(PO_4)_3$ 40.6% and calcium carbonate $CaCO_3$ 36.4%. The dust fraction contains these components,respectively, 43.9 and 33.70%, mineralized mass 34.70 and 29.2%.

The aim of this work is studying composition of the products obtained at introducing phosphate raw material from Central Kyzylkum into the ammonium nitrate melt. The ammonium nitrate produced at Chirik join stock company "Elektrokhimprom" was melted in a metallic cup heated by electric heater. To the melt obtained was introduced phosphate raw material in amount corresponding to the final product P_2O_5 content 0.5 to 5%. At 180°C the mixture was stirred for 30 min. Cooled product was grinded and analyzed alongside the known procedures [19]. The acceptable forms of P_2O_5 and CaO were determined from solubility of the product in citric acid. The loss to gas phase was measured by weighting

Table 3. Chemical composition of fertilizer obtained at introduction of ordinary phosphorite powder into ammonium nitrate melt

No	Amount of phosphorite raw material, g	Amount of melt, g	pH of 10 % solution in water	N, %	P_2O_{5total}, %	$P_2O_{5acceptable}$, %	CaO_{total}, %	$CaO_{acceptable}$, %	$CaO_{water\text{-}soluble}$, %	CO_2, %	$\frac{P_2O_{5acceptable}}{P_2O_{5total}}$, %	$\frac{CaO_{acceptable}}{CaO_{total}}$, %	$\frac{CaO_{water\text{-}soluble}}{CaO_{total}}$, %	Decarbonization, %	Loss to gas phase, g
1	1.5	50	6.825	33.70	0.51	0.50	1.35	1.28	0.57	0.23	98.04	94.81	42.22	48.65	0.6
2	3.5	50	6.890	32.25	1.05	1.03	2.70	2.44	0.94	0.53	98.09	90.37	34.81	47.49	0.8
3	5.0	50	6.957	31.10	1.52	1.48	4.31	3.74	1.70	0.75	97.36	86.77	30.16	46.80	1.1
4	6.5	50	6.980	30.75	2.01	1.95	5.69	4.79	1.45	0.97	97.01	84.18	25.48	45.70	1.2
5	9.0	50	6.991	29.30	2.61	2.51	7.30	5.88	1.40	1.29	96.16	80.54	19.17	45.49	1.2
6	10.0	50	7.010	29.15	3.00	2.87	8.35	6.60	1.52	1.45	95.66	79.04	18.20	44.09	1.4
7	12.0	50	7.050	28.09	3.52	3.33	9.60	7.38	1.54	1.72	94.60	76.87	16.04	42.85	1.4
8	15.0	50	7.090	27.10	4.10	3.83	11.01	8.05	1.57	2.10	93.41	73.11	14.25	41.42	1.5
9	16.7	50	7.110	26.01	4.56	4.20	12.10	8.66	1.60	2.36	92.10	71.57	13.22	39.27	1.6
10	20.0	50	7.148	25.24	5.04	4.45	13.12	9.02	1.61	2.85	88.29	68.75	12.27	35.96	1.7

Table 4. Chemical composition of fertilizer obtained at introduction of dust fraction into ammonium nitrate melt

No.	Amount of phosphorite raw material, g	Amount of melt, g	pH of 10 % solution in water	N, %	P_2O_{5total}, %	$P_2O_{5acceptable}$, %	CaO_{5total}, %	$CaO_{acceptable}$, %	$CaO_{water\text{-}soluble}$, %	CO_2, %	$\frac{P_2O_{5acceptable}}{P_2O_{5total}}$, %	$\frac{CaO_{acceptable}}{CaO_{total}}$, %	$\frac{CaO_{water\text{-}soluble}}{CaO_{total}}$, %	Decarbonization, %	Loss to gas phase, g
1	1.5	50	6.761	33.80	0.55	0.54	1.32	1.26	0.57	0.22	98.18	95.45	43.18	49.55	0.7
2	2.5	50	6.852	32.81	0.90	0.88	2.18	1.96	0.78	0.37	97.78	89.90	35.78	48.25	0.8
3	4.5	50	6.900	31.77	1.52	1.48	3.66	3.18	1.10	0.66	97.36	86.88	30.05	46.98	1.0
4	6.0	50	6.948	30.70	2.01	1.95	4.84	4.08	1.21	0.86	97.01	84.29	25.00	46.54	1.1
5	7.5	50	6.951	29.90	2.46	2.37	5.92	4.88	1.26	1.06	96.34	82.43	21.28	45.94	1.2
6	10.0	50	6.965	29.24	3.15	3.03	7.60	6.18	1.31	1.39	96.19	81.31	17.23	44.86	1.3
7	11.5	50	6.980	28.28	3.52	3.34	8.50	6.68	1.34	1.61	94.88	78.58	15.76	43.14	1.4
8	13.5	50	6.991	27.41	4.10	3.83	9.67	7.06	1.36	1.86	93.41	73.01	14.06	41.90	1.6
9	16.0	50	6.995	26.90	4.67	4.25	11.20	8.12	1.38	2.23	91.01	72.50	12.32	39.82	1.6
10	18.5	50	7.002	26.01	5.17	4.56	12.51	8.63	1.40	2.63	88.20	68.98	11.19	36.31	1.8

Table 5. Chemical composition of fertilizer obtained at introduction of mineralized mass into ammonium nitrate melt

No.	Amount of phosphorite raw material, g	Amount of melt, g	pH of 10% solution in water	N, %	P_2O_{5total}, %	$P_2O_{5acceptable}$, %	CaO_{total}, %	$CaO_{acceptable}$, %	$CaO_{water\text{-}soluble}$, %	CO_2, %	$P_2O_{5acceptable}$ P_2O_{5total}, %	$CaO_{acceptable}$ CaO_{total}, %	$CaO_{water\text{-}soluble}$ CaO_{total} %	Decarbonization, %	Loss to gas phase, g
1	1.9	50	6.711	32.98	0.46	0.37	1.57	1.29	0.65	0.34	80.43	82.16	41.40	38.47	0.5
2	4.0	50	6.756	31.71	1.02	0.79	3.23	2.53	1.07	0.75	77.45	78.32	33.12	33.24	0.7
3	6.0	50	6.809	30.49	1.45	1.08	4.58	3.35	1.33	1.12	74.48	73.14	29.04	28.35	0.8
4	8.0	50	6.837	29.49	2.01	1.43	5.86	4.08	1.41	1.53	71.14	69.62	24.06	24.41	0.9
5	10.0	50	6.852	28.35	2.38	1.63	6.92	4.71	1.32	1.92	68.48	68.06	19.07	21.38	1.0
6	13.0	50	6.866	27.83	2.96	1.96	8.17	5.42	1.47	2.47	66.21	66.34	17.99	18.64	1.3
7	15.0	50	6.877	26.67	3.47	2.17	9.29	6.03	1.49	2.83	62.53	64.90	16.03	16.99	1.6
8	18.0	50	6.886	25.58	4.14	2.48	10.86	6.88	1.61	3.36	59.30	63.35	14.82	13.98	1.6
9	21.0	50	6.895	24.75	4.48	2.58	12.02	7.50	1.63	3.84	57.58	62.39	13.56	12.01	1.8
10	24.0	50	6.903	23.94	4.95	2.76	13.47	8.24	1.71	4.28	55.75	61.17	12.69	10.64	1.8

the cup with the initial mixture and with the final product. The results are listed in Tables 3 – 5.

From the tables is seen that the ammonium nitrate melt activates phosphate raw material, that is, transfers the non-acceptable form of P_2O_5 into the form acceptable by plants. The product containing 5% P_2O_5 from ordibary phosphorite powder contains 25.24% of N and 88.29% of acceptable form of P_2O_5 to the total P_2O_5. The product from dust fraction with 5% of P_2O_5 contains 26.01% of N and 88.20% of acceptable P_2O_5 to the total one. The values for the product containing 5% of P_2O_5 from mineralized mass are: 23.94% of N and55.75% acceptable P_2O_5 to total P_2O_5. More phosphate raw material is introduced, less content of acceptable forms of P_2O_5 and CaO and less phosphorite decarbonization. Presence in the product of water-soluble form of CaO and loss to gas phase indicate that at 180°C occurs reaction between ammonium nitrate and calcium carbonate in the phosphate raw material leading to formation of calcium nitrate:

$$2NH_4NO_3 + CaO \rightarrow Ca(NO_3)_2 + 2NH_3 + H_2O$$

Thus, introduction of phosphate raw material into nitrate ammonium melt allows obtaining effective nitrogenphosphorus fertilizers.

REFERENCES

1. Chernyshev, A.K., Levin, B.V., and Konvisar, L.V., *Ammiachnaya selitra i udobreniya na ee osnove* (Ammonium Nitrate and Fertelizers Based on It), Moscow: 2003.
2. Zhmai, L. and Khristianova, E., *Mir Sery, Azota, Fosfora i Kaliya*, 2004, no. 2, pp. 8–12.
3. Levin, B.V. and Sokolov, A.N., *Mir Sery, Azota, Fosfora i Kaliya*, 2004, no. 2, pp. 13–21.
4. Lavrov, V.V. and Shvedov, K.K., *Nauchno-Tekhnicheskie Novosti*: *INFOKhIM*, Special Issue, 2004, no. 2, pp. 44–49.
5. *Tekhnologiya ammiachnoi selitry* (Technology of Ammonium Nitrate), Ed. V.M. Olevskii, Moscow: Khimiya, 1978.
6. Nabiev, M.N., *Azotnokislotnaya pererabotka fosfatov* (Nitric Acid Treatment of Phosphates), vol. 2, Tashkent: FAN, 1976.
7. Il'in, V.A., *Cand. Sci. (Chem.) Dissertation,* Ivanovo, 2006.
8. Il'in, V.A., Patokhin, O.I., Glagolev, O.L., Selin, E.N., Levin, B.V., Sokolov, A.N., Sokolov, A.Yu., Samsonov, V.P., Rezen'kov, M.I., Ansheles, V.R., Simbireva, Z.P.,

Zhavoronkova, N.E. and Vasil'kova, O.E., RF Patent no. 2223932, Kl. SO5 V 7/00, SO5S 1/00, 2004.02.20.
9. Glagolev, O.L., *Mir Sery, Azota, Fosfora i Kaliya*, 2004, no. 2, pp. 21–23.
10. Shipyatskaya, R.I., Chulanova, G.A., Kozlova, T.G., Fomina, E.A. and Syrkin, L.N., USSR Inventor's Certificate, no. 455077, Kl. SO5 v 7/00; *SSSR Byull. Izobr.*,1974, no. 48.
11. Kozlova, T.G., Shipyatskaya, R.I., Chulanova, G.A., Syrkin, L.N. and Fomina, E.A., USSR Inventor's Certificate, no. 471351, Kl. S05 v 13/06; *SSSR Byull. Izobr.,* 1975, no. 19.
12. Il'in, V.A., Aleshkin, N.P., Selin, E.N., Zhavoronkova, N.E., Simbireva, Z.P., Vasil'kova, O.E., Glagolev, O.L., Soko-lov, A.Yu. and Samsonov, V.P., RF Patent no. 2169720, Kl. SO5V 7/00, SO5 G 1/06, 2001.06.27.
13. Il'in, V.A., Pakhotin, O.I., Selin, E.N., Zhavoronkova, N.E., Simbireva, Z.P., Vasil'kova, O.E., Glagolev, O.L., Sokolov, A.Yu., Samsonov, V.P. and Ansheles, V.R., RF Patent no. 2171795, Kl. SO5 V 7/00, SO5 S 1/00, 2001.08.10.
14. Avramenko, A.N., Kononov, S.M., Shirobokov, O.A., Gromotkov, V.N., Sundiev, S.A., Kostyuchenko, S.S., Kontareva, E.N. and Dmitrieva O.A., Patent of Russia no. 2263652, Kl. SO5 G 1/06, SO5 S 1/02, 2005; *Byull. Izobr*., no.31.
15. Spakhova, L.V., Grosheva, L.P., Gorshkova, N.V., Maklashina, E.A., Samsonov, Yu.K., Lysenko, E.V., Milovanov, V.A., Balagurov, A.V., Pestov, A.E., and Uvarov, S.P., RF Russia no. 2228322, Kl. SO5 G 1/06, SO5 V 11/06, 2003.03.17.
16. Sezemin, V.A. and Abramov., O.B., RF Patent no. 2253639, Kl. SO5 V 7/00, SO5 G 1/06, SO5 S 1/02, 2005; *Byull. Izobr.,* no. 16.
17. Drozhdin, B.I. Dedov, A.S. Zub, V.V. Machekhin, G.N., Utkin, V.V. Abramov, O.B. Tereshchenko, O.L., Loginov, N.D., Sezemin, V.A., Kiselevich, P.V., Yuzhanin, G.A., Such-kov, V.A., Krashunskii, L.M., Guterman, M.D., Vulis, F. and Tel'kina, A.V., RF Patent no. 2174970, Kl. SO5 S 1/00, SO5 G 1/06, 2001.10.20.
18. Avramenko, A.N., Kononov, S.M., Shirobokov, O.A., Gromotkov, V.N., Perepechko, V.F., Kostyuchenko, S.S., Kontareva, E.N., Tsarevskii, V.A., Mitsak, I.A., Zorov, V.G., and Ovchinnikov, V.M., RF Patent no. 2265001, Kl. SO5 G 1/08, SO5 D 3/02, 2005; *Byull. Izobr.,* no. 33.
19. Vinnik, M.M., Erbanova, L.N. and Zaitsev, P.M., *Metody analiza fosfatnogo syr'ya, fosfornykh i kompleksnykh udobrenii, kormovykh fosfatov* (Methods of Analysis of Phosphate Raw Material, Phosphoric and Complex Fertilizers and Food Phosphates), Moscow: Khimiya, 1975.

ISSN 1070-4280, Russian Journal of Applied Chemistry, 2007, Vol. 80, No. 11, pp. 1989–1992. © Pleiades Publishing, Ltd., 2007.
Original Russian Text © A.B. Golovanchikov, A.A. Shagarova, N.A. Dul'kina, I.M. Shandybina, 2007, published in Khimicheskaya Promyshlennost', 2007, Vol. 84, No. 3, pp. 137–140.

MODELLING AND CALCULATION OF TECHNOLOGICAL PROCESSES

Modelling a Flow of a Highly Viscous Liquid with the Boundary Layer of Low Viscosity in an Extruder

A. B. Golovanchikov, A. A. Shagarova, N. A. Dul'kina, and I. M. Shandybina

Volgograd State Technical University, Volgograd, Russia
e-mail: dnataly@mail.ru

Received June 1, 2007

Abstract—Features of the flow of a highly viscous liquid in an extruder with boundary layer of low viscosity liquid at the cylinder wall and at the endless screw surface are considered. The liquid flow is modeled under conditions of isothermal simple shift using cylindrical model of a screw canal. The profiles of rates for the stream of a highly viscous liquid with the ring boundary layer of low-viscous liquid at the cylinder wall and at screw in the both presence and absence of a counter pressure are calculated. Consideration of computer calculations shows that increase in the flow rate is possible when the counter pressure tends to zero and the low-viscous liquid forms a ring boundary layer at the cylinder wall.

DOI: 10.1134/S1070427207110468

A great amount of polymeric materials in the industry is treated by the method of extrusion. Intensity of this method can be increased by different ways, one is creation of a lubricant layer between the processed material and the canal wall.

A construction of extruder is known where the screw wall is porous or perforated, and through the holes to it surface is supplied a gas or low-viscous liquid [1]. Another variant is also possible, with the lubricant layer near the wall of cylindrical case.

In this work we consider features of the flow of a highly viscous liquid in an extruder with a low-viscous boundary layer at the cylinder wall and on a screw surface. A physical model of such flow is shown in Fig. 1. It is represented by a cylindrical canal with the radius R and length l, containing inside a rod with the radius $R_1<R$ moving symmetrically relative the axis with angular rate ω and rate along the axis u. The main stream of highly viscous liquid μ_1 moves in the ring gap $R–R_2$, the stream of low-viscous liquid μ moves in a ring layer $R_2 –R_1$ near the rod wall.

The differential equation in the tensions for axial moving along the z axis is represented by [2, 3]:

$$-\frac{\partial p}{\partial z}+\frac{1}{r}\frac{\partial\left(r\,\tau_{rz}\right)}{\partial z}=0 \qquad (1)$$

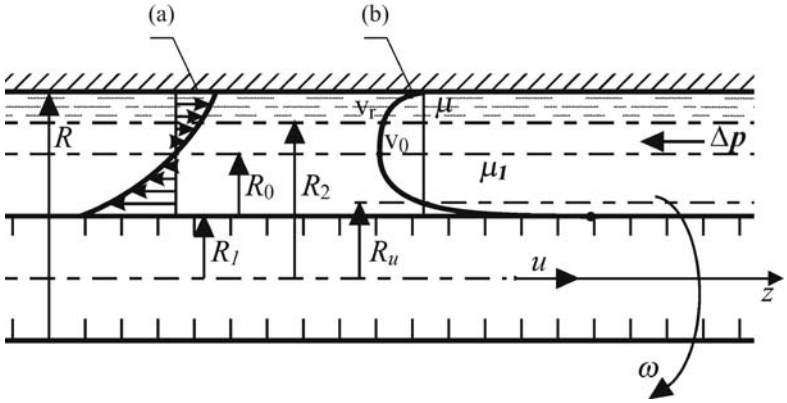

Fig. 1. Scheme of moving liquid with low-viscous boundary layer near vthe wall: (a) epure of tangent tensions, (b) profile of rates (R_2 is ring board of two liquids, R_0 is a radius coreesponding to the maximal rate, $\tau=0$; R_u is a board where the flow rate changes sign from plus to minus).

Let $\Delta p/\Delta z = \Delta p/l$: pressure increases along the axis, because the screw works like a pump, then:

$$\tau_{rz} = \frac{\Delta p}{2l} r + \frac{c_1}{r} \tag{2}$$

For the highly viscous liquid moving in the ring gap ($R_2 - R_1$):

$$\tau_{rz} = \mu_1 \frac{dv_z}{dr} \tag{3}$$

Join solving the equations (2) and (3) leads to the expression:

$$v_1 = -\frac{\Delta p}{2l\mu_1} r^2 + \frac{c_1}{\mu_1} \ln r + c_2 \tag{4}$$

At a $r = R_1$, v_1 = boundary conditions u we obtain:

$$v_1 = u + \frac{\Delta p}{4l\mu_1}\left(r^2 - R_1^2\right) + \frac{c_1}{\mu_1} \ln \frac{r}{R_1} \qquad R_1 \le r \le R_2 \tag{5}$$

Similarly, for low-viscous liquid moving in the ring gap ($R–R_2$):

$$\tau_{rz} = \mu \frac{dv_z}{dr} \tag{6}$$

$$v = \frac{\Delta p}{4l\mu} r^2 + \frac{c_3 \ln r}{\mu} + c_4 \tag{7}$$

Accounting for the boundary conditions $r = R$, $v = 0$, the expression is transformed into:

$$v = -\frac{\Delta p}{4l\mu}\left(R^2 - r^2\right) + \frac{c_3}{\mu} \ln \frac{r}{R} \qquad R_2 \le r \le R \tag{8}$$

The integration constants c_1 and c_3 are found from the equality of tangent tensions and rates at $r=R_2$:

$$c = c_1 = c_3 = -\frac{u + \frac{\Delta p}{4l}\left(\frac{R^2 - R_2^2}{\mu} + \frac{R_2^2 - R_1^2}{\mu_1}\right)}{\frac{1}{\mu} \ln \frac{R}{R_2} + \frac{1}{\mu_1} \ln \frac{R_2}{R_1}} \tag{9}$$

Finally we obtain formulas for calculation of rate profile for both the liquids:

$$\begin{cases} v_1 = u + \dfrac{\Delta p}{4l\mu_1}\left(r^2 - R_1^2\right) + \dfrac{c}{\mu_1} \ln \dfrac{r}{R_1}; \quad R_1 \le r \le R_2 \\ v = -\dfrac{\Delta p}{4l\mu}\left(R^2 - r^2\right) + \dfrac{c}{\mu} \ln \dfrac{r}{R}; \quad R_2 \le r \le R \end{cases} \tag{10}$$

Integrating equations for elementary flows

$$\begin{cases} q_1 = 2\pi \int_{R_1}^{R_2} v_1 r dr \\ q = 2\pi \int_{R_2}^{R} v r dr \end{cases} \tag{11}$$

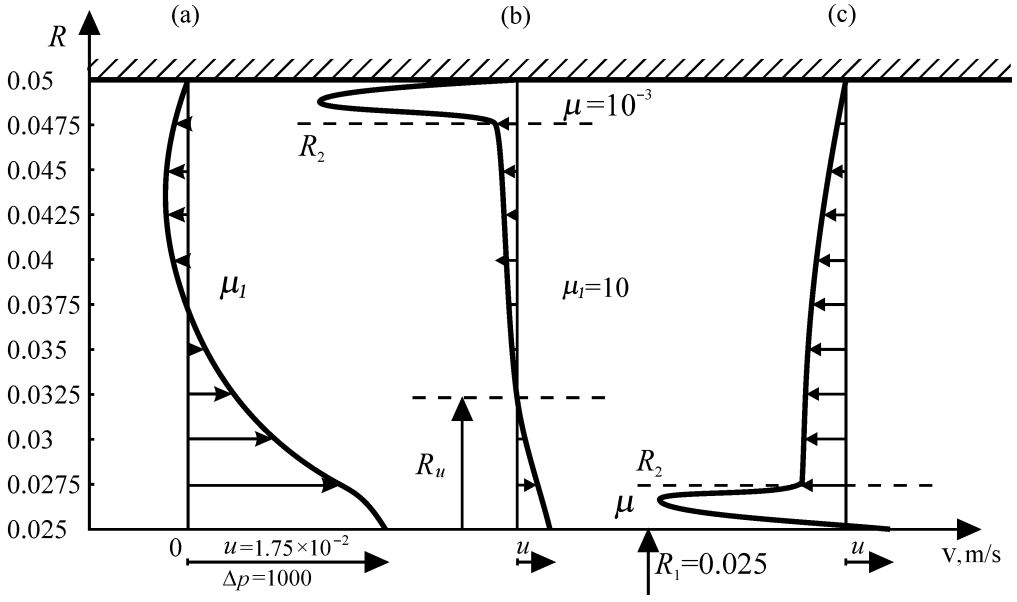

Fig. 2. Dependence of model profiles of the flow rate of highly viscous liquid μ_1 = 10 Pa sec in a screw extruder at $\Delta p/l$ = 1000 Pa m^{-1}, R_1 = 0.025 m, R = 0.05 m: (a) Flow of highly viscous liquid only, (b) Flow in the case of boundary ring layer of low-viscous liquid (water) μ=10^{-3} Pa sec at the cylinder wall, δ = 0.0025 m; (c) Flow with boundary ring layer of low-viscous liquid at the screw, $\ddot{a}$ = 0.0025 m.

we obtain:

$$\begin{cases} q_1 = \pi\left\{u\left(R_2^2 - R_1^2\right) + \dfrac{\Delta p}{8l\mu_1}\left(R_2^2 - R_1^2\right)^2 + \dfrac{c}{\mu_1}\left[R_2^2 \ln\dfrac{R_2}{R_1} - \dfrac{\left(R_2^2 - R_1^2\right)}{2}\right]\right\} \\ q = \pi\left\{-\dfrac{\Delta p}{8l\mu}\left(R^2 - R_2^2\right)^2 + \dfrac{c}{\mu}\left[R_2^2 \ln\dfrac{R}{R_2} - \dfrac{\left(R^2 - R_2^2\right)}{2}\right]\right\} \end{cases} \quad (12)$$

Fig. 2 shows rate profiles according to equations of the system (10) accounting for the integration constant (9). As seen from the figure, at $u = 1.75 \times 10^{-2}$ m s^{-1} and $\Delta p/l$ = 1000 Pa m^{-1} at the geometric sizes R_1 = 0.025 m, R = 0.05 m and viscosity μ_1 = 10 Pa sec and $\mu = 10^{-3}$ Pa sec (water) at the boundary layer of low-viscous liquid near the cylinder wall (Fig. 2b) with thickness 0.0025 m or at the screw with the same thickness (Fig. 2c) there is no gain in flow rate of the main stream of the highly viscous liquid (Fig. 2a) as compared with ordinary working endless screw when it flows over all the section.

Analysis of the results obtained using cokputer calculations shows that such a gain is possible in the case when counter pressure is near the zero and low-viscous liquid forms ring shape boundary layer near the cylinder wall (Fig. 3b).

For this case when $\Delta p/l = 0$ (no counter pressure, all energy of the screw dissipates) we obtain at R_2 = 0.0475 m: q=6.5 × 10^{-6} m^3 s^{-1} c; q_1=8.9 × 10^{-5} m^3 s^{-1} (Fig. 3b).

When R_2=R, when the bounder layer of low-viscous liquid (water) near the cylinder wall is absent $R_2 = R$ = 0.05 m; R_1=0.025 m; $q = 0$; $q_1 = 4 \times 10^{-5}$ m^3 s^{-1}, that is,

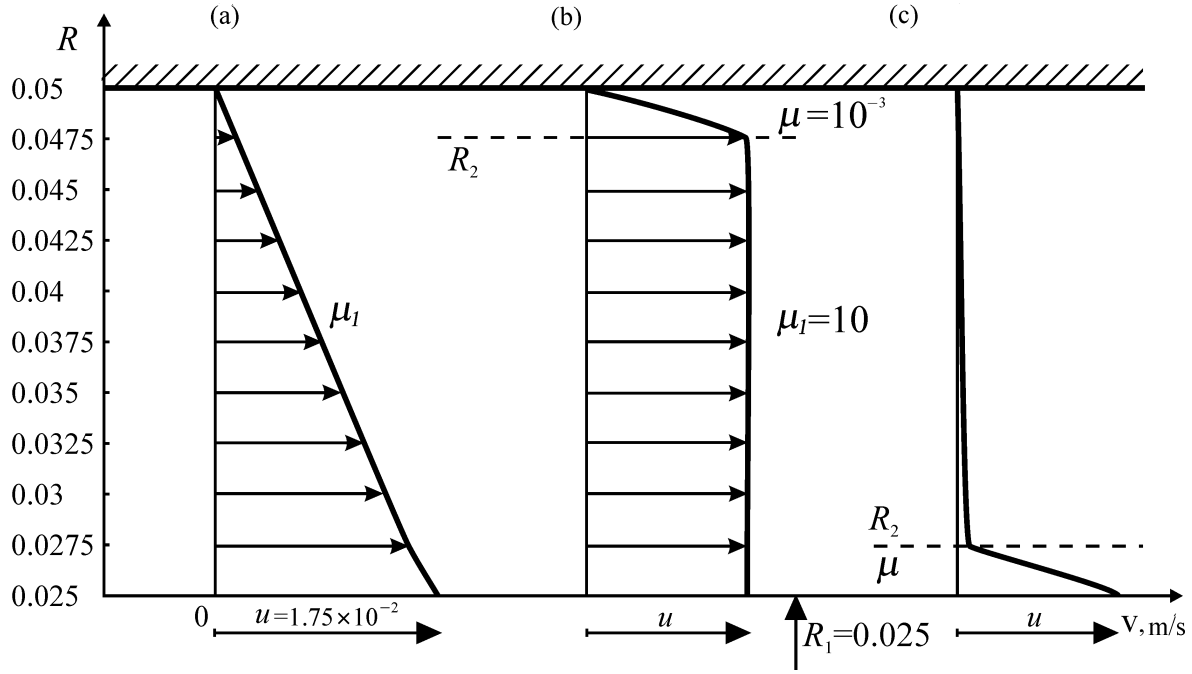

Fig. 3. Dependence of the model rate profile of a highly viscous liquid μ_1 = 10 Pa sec in an endless screw extruder at $\Delta p/l$ = 0 Pa m^{-1} R_1 = 0.025 m, R = 0.05 m: (a) Flow of highly viscous liquid only, (b) Flow in the case of boundary ring layer of low-viscous liquid (water) $\mu = 10^{-3}$ Pa sec at the cylinder wall, δ = 0.0025 m; (c) Flow with boundary ring layer of low-viscous liquid at the screw, δ = 0.0025 m.

if the flow rate of low-viscous liquid (water) at the cylinder wall equals 7.3 % of the main stream of highly viscous liquid, the flow rate of the latter ecreases by 2.22 times (Fig. 3a). When the ring boundary layer of low-viscous liquid is near the screw, the flow rate of the main stream of highly viscous liquid falls, $q_1 = 3.5 \times 10^{-6}$ m^3 s^{-1} (Fig. 3b).

Thus, it is reasonable to feed the low-viscous liquid as ring boundary shape to the cylinder wall and when there is no counter pressure.

REFERENCES

1. RF Patent no. 069149, MKI B 29 S 47/38, Endless screw extruder.
2. Middleman, S., *Polymer Processing,* McGraw-Hill Book Company, 1977.
3. Thorner, R.V., *Osnovnye protsessy pererabotki polimerov. Teoriya i metody rascheta* (Basic Processes in the Working up Polymers. Theory and Methods of Calculations), Moscow: Khimiya, 1972.

ISSN 1070-4280, Russian Journal of Applied Chemistry, 2007, Vol. 80, No. 11, pp. 1993–1996. © Pleiades Publishing, Ltd., 2007.
Original Russian Text © D.Yu. Morozov, M.V. Shulaev, I.A. Khramova, L.I. Khabibullina, 2007, published in Khimicheskaya Promyshlennost', 2007, Vol. 84, No. 3, pp. 141–144.

INDUSTRIAL ECOLOGY

Investigation of Adsorption Purification of the Effluences Containing Heavy Metal Ions

D. Yu. Morozov, M. V. Shulaev, I. A. Khramova, and L. I. Khabibullina

Kazan State Ubiversity, Kazan, Russia

Received April 24, 2007

Abstract—Kinetics of adsorption purification of effluences containing heavy metal ions and adsorption of the metal ions under dynamic conditions using various adsorbents, including the products from industrial wastes are studied.

DOI: 10.1134/S107042720711047X

We investigated and considered adsorption characteristics of various adsorbents at the adsorption of the ions Cr(VI), Mn(VII), Fe(II), Cd(II), Cu(II) and Zn(II). As the adsorbents, we used granulated active carbon SKT-3, the zeolite-containing rock diatomite from he birth place in Ul'yanovsk region and precipiates which could form at local coagulation purification of effluences at producing polysulfide resins (thiocols) with 30% iron(III) chloride and aluminum chloride solutions, the iron-containing precipitate (ICP) and aluminum-containing precipitate (ACP), respectively. The precipitates are solid disperse materials with hydrogen sulfide odor.

The results of studying kinetics of adsorption of the ions Cd(II), Zn(II), Cu(II), Cr(VI), Mn(VII) and Fe(II) are shown in Figs. 1–6 and table 1.

Consideration of the data obtained leads to conclusion that in the initial step all the curves are similar: for the

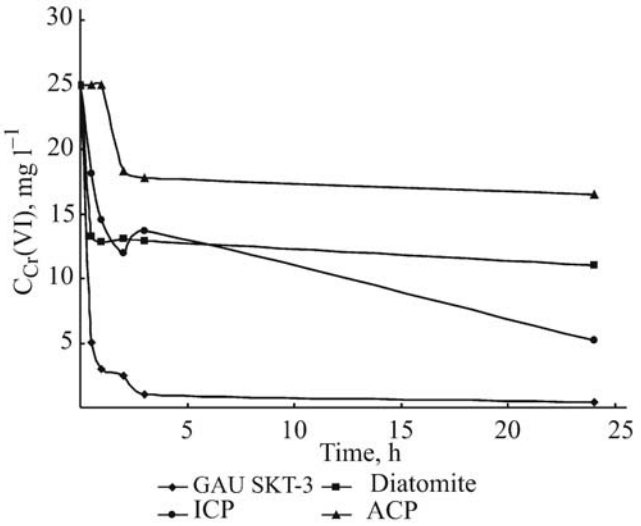

Fig. 1. Kinetic curves of adsorption Cr(VI) ions.

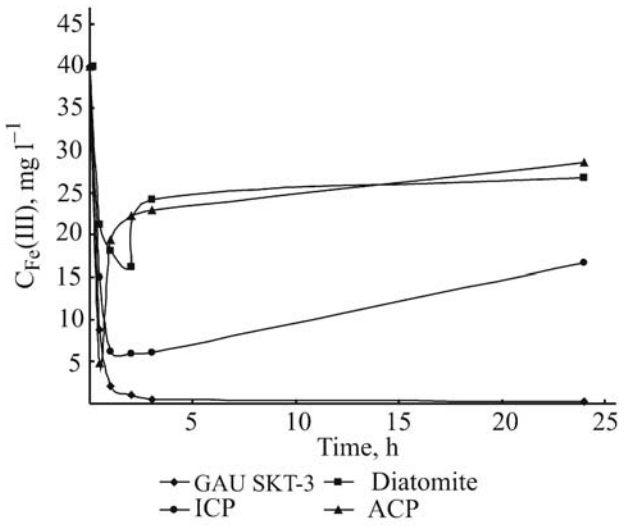

Fig. 2. Kinetic curves of adsorption Fe(III) ions.

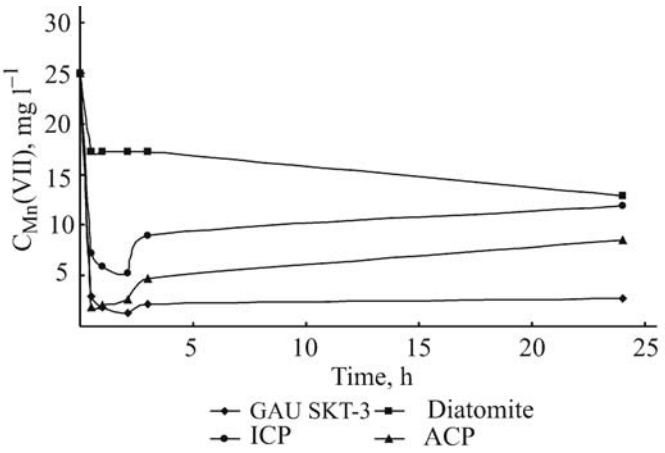

Fig. 3. Kinetic curves of adsorption Mn(VII) ions.

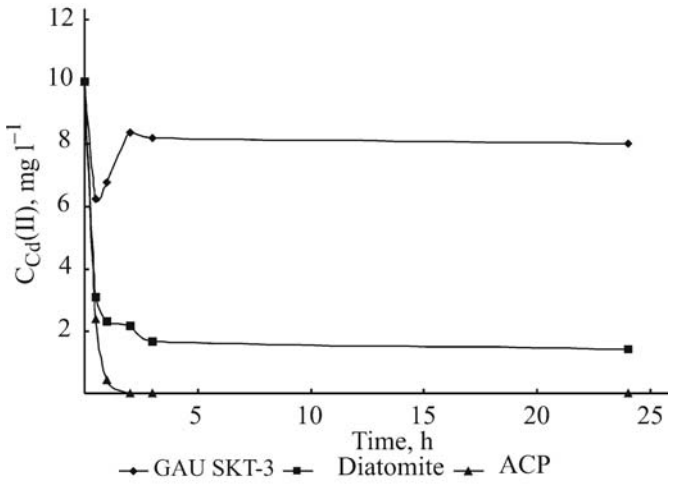

Fig. 4. Kinetic curves of adsorption Cd(II) ions.

first 1 to 2 h of each experiment the concentration of heavy metal ions in the model effluences falls down sharply. Then the curves run differently, and we could select 5 main types of the kinetic curves by the mode of changes of the heavy metal ion concentration during experiment:

(1) After sharp fall in the initial period, the system is stabilized and concentration of heavy metal ion remains practically unchanged during whole experiment. Thus, static adsorption equilibrium is achieved. The such type curve is characteristic of Zn(II) ion adsorption with all the studied adsorbents, ions Fe(II) and Cr(VI) with granulated active carbon SKT-3, ions Cd(II), Cu(II) and Cr(VI) with ACP and Cd(II) ions with diatomite.

(2) Sharp fall of heavy metal ion concentration in the initial step of experiment is replaced by stepwise decrease up to the end of experiment. Here adsorption equilibrium is not achieved. Such curve reflects adsorption of Mn(VII) ions on diatomite.

(3) Sharp fall of heavy metal ion concentration in the initial step of experiment is replaced by stepwise growing concentration. Equilibrium in the system is also not achieved. The curve of such type occurs for Fe(II) ions adsorption on iron-containing precipitate (ICP).

(4) After sharp fall occurs fast growing in concentration of heavy metal ion at 1 to 3 h after the experiment beginning, and then concentration decreases smoothly up to the end. Such variantions can be explained by different adsorption affinity of various heavy metal ions toward asorbent, leading to substitution of one ion by another during the experiment. This leads to

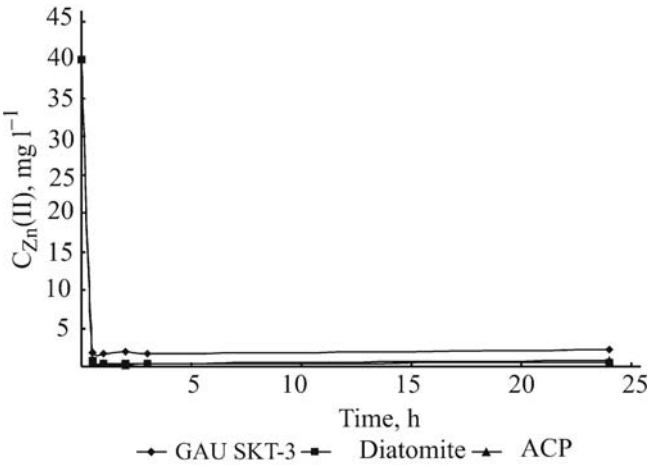

Fig. 5. Kinetic curves of adsorption Zn(II) ions.

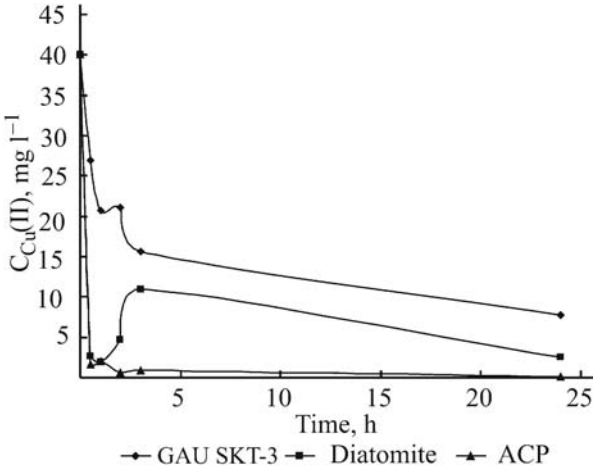

Fig. 6. Kinetic curves of adsorption Cu(II) ions.

Table 1. Kinetics of adsorption of heavy metal ions from solution

Adsorbents	Heavy metal ions								
	Cr(VI)			Mn(VII)			Fe(II)		
	Initial concentration, mg/ml	Final concentration, mg/ml	Purification, %	Initial concentration, mg/ml	Final concentration, mg/ml	Purification, %	Initial concentration, mg/ml	Final concentration, mg/ml	Purification, %
Granulated active carbon SKT-3	25	0.440	98.24	25	2.753	88.99	40	0.168	99.58
Diatomite	25	11.035	55.86	25	12.820	48.72	40	26.9	32.75
Iron-containing precipitate	25	5.215	79.14	25	11.863	52.55	40	13.336	66.66
Granulated active carbon SKT-3	10	8.003	19.97	40	2.260	94.35	40	7.756	80.61
Diatomite	10	1.439	85.61	40	0.492	98.77	40	2.584	93.54
Aluminum-containing precipitate	10	-	99.99	40	0.752	98.12	40	0.068	99.83
Aluminum-containing precipitate	25	16.458	34.17	25	8.550	65.80	40	28.5	28.75

appearance of concentration gradient between phases resulting in change of concentrations of the heavy metal ions in a model effluence, that is, no equilibrium ocurs in the system. Such kinetic curve is characteristic of adsorption Cr(VI) ions with iron-containing ptecipitate (ICP) and Cu(II) ions on the active carbon and diatomite.

(5) After sharp changes in the heavy ion concentrations during the first 3 h of the experiment, the concentration grows stepwise till the experiment end. Such curve type reflects adsorption of Mn(VII) ions with granulated active carbon SKT-3, ACP and ICP, of Fe(II) ions on diatomite and ACP and of Cd(II) ions with carbon.

The data obtained show that the most effective adsorbents are activated carbon, aluminum-containing precipitate (ACP) and diatomite. The iron-containing precipitate (ICP) shows stable satisfactory results.

ISSN 1070-4280, Russian Journal of Applied Chemistry, 2007, Vol. 80, No. 11, pp. 1997–2000. © Pleiades Publishing, Ltd., 2007.
Original Russian Text © A.V. Zheranin, 2007, published in Khimicheskaya Promyshlennost', 2007, Vol. 84, No. 3, pp. 151–155.

PROCESSES AND DEVICES OF CHEMICAL MANUFACTURES

Parameters of Heterogenic Liquid Phase Process and Temperature Profile in a Displacement-Type Reactor

A. V. Zheranin

Biisk Technological Institute (Filial) of Polzunov Altai State Technical University, Biisk, Russia

Received January 23, 2007

Abstract—The results are presented of mathematical modeling the processes of heat and mass transfer in a displacement-type reactor.

DOI: 10.1134/S1070427207110481

Our earlier calculations [1] showed a possibility of application a displacement-type reactor [2] for the carrying out exothermic heterogenic liquid phase process complicated by heat and mass transfer due to extended heat transferring surface of specific configuration with rational mutual location of heat transferring elements (Fig. 1). In the calculations was presumed that the disperse phase drops are parting (fusing) instantly and their size (diameter) is changed and following homogenous distribution of parent component and reaction product over the drop volume proceeds instantly.

However, actual distribution of parent component and reaction product over the volume of a newly forming disperse phase drop in the beginning of sections n2, n3, n4 at the top of canal and n3, n2, n1 at its bottom (Fig. 1) is not homogenous and is close to that occurring in the bulk of drops in the end of preceding section. The sections are defined in correspondence with the accepted in [1] scheme of moving (and parting) the drops of disperse phase in the continuous medium flow along the canal changing with its height. Therefore now let us define the parameters of heterogenic liquid phase processwith fast chemical transformation on the interphase surface [3] and the temperature profile in th canals of the reactor [2] taking into account the non-homogenous distribution of parent component and reaction product in the bulk of newly forming disperse phase drops. We will use the model in [4] and accept the same as in [1] scheme of moving (and parting) the disperse phase drops in the flow of continuous medium along the canal changing with its height. For all five variants of the reactor construction (see the table) the accept changing of canal along height like in [1], alongside the formula: $h_i = aR_i^{-b}$. The disperse phase and continuous medium are feeding into the canal in the amounts 0.35 and 1.3 kg/s, respectively.

Distribution of weight fractions of the initial component C(r, t) and reaction product Cm(r, t) over the volume of a newly forming drop of dispersion phase in the beginning of the sections n2, n3, n4 in top part and n3, n2, n1 in the bottom part of the canal initially is taken the same as in the bulk of the parent drops at the end of preceding section. For example, distribution of weight fraction C(r, t) of the parent component is shown in Fig. 4. Then we define the extent of conversion SP_n of the parent component in the bulk of newly forming drops at the beginning of the sections n2, n3, n4 in top part and n3, n2, n1 in the bottom part of the canal (at the initial moment of passing these sections).

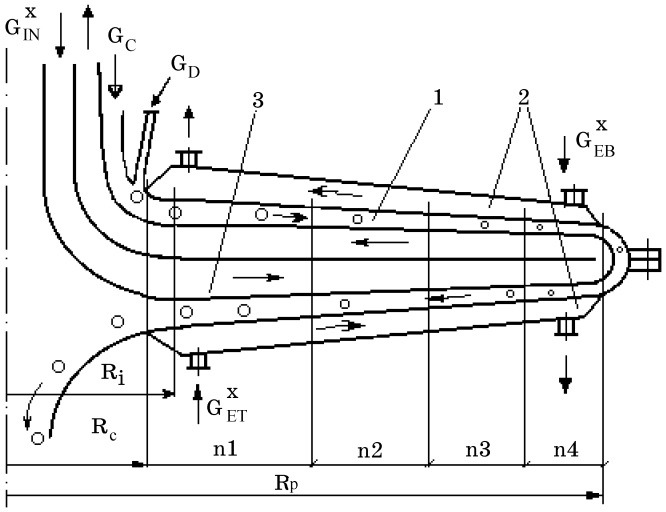

Fig. 1. Scheme of a displacement-type reactor. (1) canal with medium (disperse G_D and continuous G_C phases); (2) external top and bottom canals with cooling agent (G_{ET}^{X}, G_{EB}^{X}); (3) internal canal with cooling agent (G_{IN}^{X}).

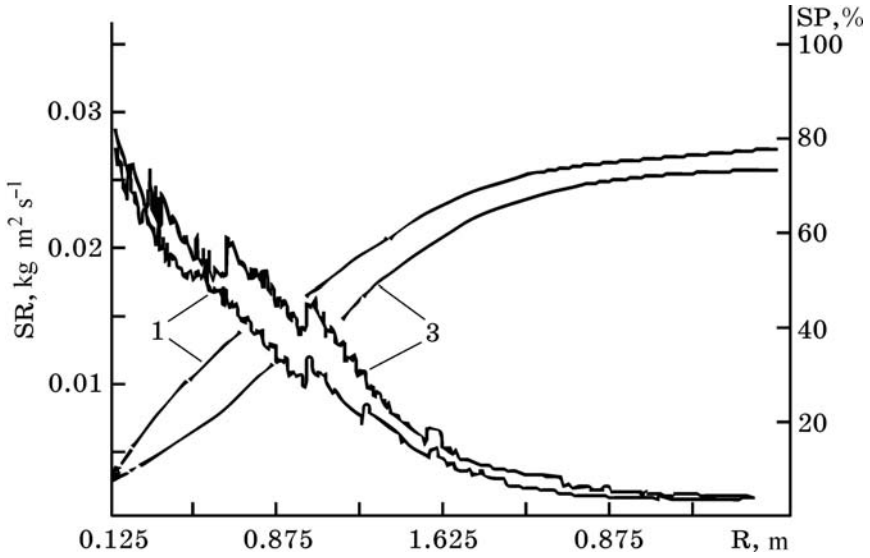

Fig. 2. Change in the process rate SR and extent of conversion SP along the canal for the variants 1 and 3 of reactor construction.

The extent of conversion SP_n we calculate using the formula: $SP_n=((TL-TLj)/TL)\times100\%$, where TL is a quantity of initial component in one parent drop of disperse phase that did not enter to the reaction in the time period when it was located in a preceding section, per one newly formed drop; TLj s a quantity of the parent component in one newly forming drop of disperse phase that did not enter to the reaction in the period of location the disperse phase drops in the beginning of next section.

Then we begin correction of distribution of weight fractions C(*r, t*) and Cm(*r, t*) continuing it till the extent of conversion SP_n approaches zero. The correction is needed because the quantity of initial component in two newly forming drops (from one parent), which did not enter to the reaction, should necessarily be equal to the same quantity in one parent drop in the end of preceding section.

The extent of conversion SP*(t)* (Fig. 2) of initial component during its time of location of the disperse phase drops in the reactor we calculate, same as in [1], alongside the formula: $SP(t) = SP = ((\rho_T V_T - T(t)dh)/(\rho_T V_T))\times100\%$, where ρ_T and V_T are respectively density and volume of the "parent" drop of disperse phase, *dh = 1, 2, 4, 8* is the number of "new" drops forming from one "parent" drop in the sections, respectively, n1, n2, n3 and n4, *T(t)* is the quantity of parent component in a drop in each actual time moment of location the disperse phase in the reactor. The smoothness of the curves *SP(t)* = SP = *f(R)* in Fig. 2 obviously better corresponds to real character in varying of extent of conversion SP*(t)* of the parent component in time (SP is change along the canal) than their step-like form obtained in [1] where inhomo-genity of distribution of the parent component and reaction product over the volume of a newly forming drop was not taken into account.

Systematic small fluctuations (Fig. 2) of the process rate *SR* defined in the model of [4] as a mass flow [3] of parent component to the drop surface are stipulated, like in [1], by the variations in the coefficients of mutual molecular diffusion of the parent component, D(*r, t*), and the reaction product, Dm(*r, t*). The diffusion coefficients were varied in each step of realization of the differential schemes [4] for providing balance of mass flows of the diffusing components. More significant splashes on the curves SR=*f(R)* are stipulated by the significant changes in the gradient of mass fraction of the initial component near the interphase surface. This is connected with parting (fusing) of the drops and redistribution of the fraction of parent component and the reaction product over their volumes.

The temperature profile in the reaction canals we determine by solving, similarly to [1], the boundary Cauchy problem for each of four sections n1, n2, n3, n4 in the top and bottom parts of the reactor. Solving this problem allowed to find the temperature profiles of medium and cooling agent for all five variants (see the table) of the reactor construction (e.g., see Fig. 3) and to find required cool consumption (cooling agent flow rate) and cooling agent temperature at the canals inlet.

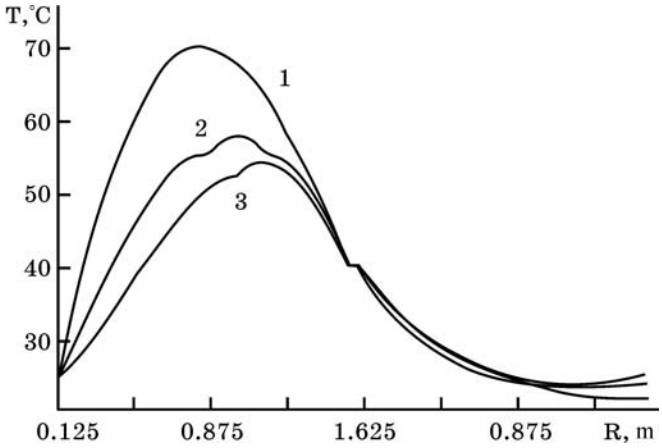

Fig. 3. Variation in the medium temperature T along the canal for the reactor construction variants 1, 2 and 3.

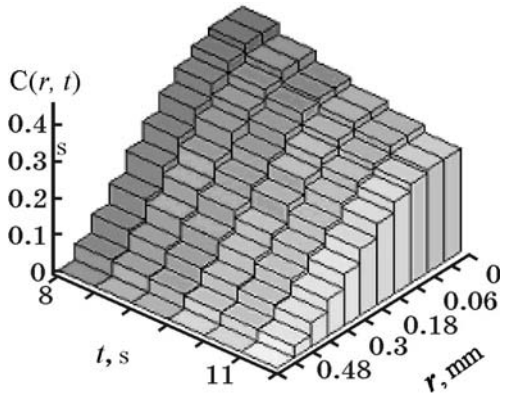

Fig. 4. Distribution of weight fraction C(*r, t*) of the parent component along the radius r of a drop of disperse phase in time t for the 4th section n4 of the canal bottom part for the variant 3 of the reactor construction.

The results obtained in turn confirm:

– capability of application reactor [2] for carrying out the process of exothermic heterogenic liquid phase process complicated by heat and mass transfer at the enough high extent of conversion of the parent component at the values (see note under the table) of the coefficient of mutual molecular diffusion inherent [5] in organic not viscous binary mixtures;

Parameters		Number of the variant of construction				
		1	2	3	4	5
Koefficients of the canal height	$A \times 10^3$	1.63	1.44	1.28	1.17	1.13
	b	1	0.75	0.5	0.33	0.25
Canal height, h,mm	In the center	13	6.8	3.6	2.3	1.9
	On the periphery	1	1	1	1	1
Diration of location[1], s		27	22	19	17	16
The process rate maximal[2] $SR \times 10^3$, kg m^{-2} s^{-1}		28/**42**/54	29/**42**/55	29/**42**/52	29/**43**/53	35/**45**/55
The process rate minimal[3] $SR \times 10^3$, kg m^{-2} s^{-1}		1.4/**1**/0.6	1.7/**1.3**/1	1.6/**1.3**/1	1.5/**1.3**/1	1.6/**1.3**/1.1
Extent of conversion[4] maximal *SP*, %		78 /**91**/98	74/**87**/94	73/**85**/93	74/**86**/93	74/**85**/92
Medium temperature[5], °C maximal		71/**86**/99	59/7**0**/76	55/**64**/70	55/**65**/71	54/**63**/68
Medium temperature[6], °C at the outlet		25/**23**/21	25/**23**/21	23/**21**/20	22/**20**/19	21/**20**/19
Cooling agent temperature[7], °C at the inlet to canals	Top external	11/**12**/10	13/**11**/12	12/**11**/11	12/**11**/11	11/**11**/12
	Bottom external	10/**10**/11	11/**12**/10	11/**11**/11	11/**10**/11	12/**12**/12
	Internal	12/**12**/12	13/**11**/12	12/**11**/12	13/**11**/12	13/**12**/12
Cooling agent consumption[8], kg s^{-1} in the canals:	Top external	3.8/**4.6**/4.6	3.5/3.**8**/4.6	3.3/3.**8**/4.6	3.2/3.**8**/4.5	3.1/3.**8**/4.5
	Bottom external	1.1/**1.1**/1.1	1.4/1.**4**/1.1	1.4/1.**4**/1.3	1.6/1.**4**/1.4	1.6/1.**5**/1.4
	Internal	5.8/**6.4**/6.4	5.5/5.**3**/6.4	5.3/5.**3**/6.3	5.1/5.**3**/6.3	5.0/5.**3**/6.2

[1–8]The values of parameters 1 to 8 are determined at the temperature values: medium at the canal inlet 25°C, cooling agent at the canals outl 20°C. The values of the parameters 2 to 8 written with slashes ../../.. are determined at the values of diffusion coefficient at 25°C) equal to 0.0013 **/ 0.0019 /** 0.0025 mm^2 s^{-1}, respectively.

– reasonability of using water as a cooling agent, which at moderate feeding it to the reactor cooling canal allow maintaining in the reactor the temperature appropriate for the technological process, owing to, in part, the extended heat transferring surface (area 33 m^2).

REFERENCES

1. Zheranin, A.V., and Ovcharenko, A.G., *Khimicheskoe i Neftegazovoe Mashinostroenie*, 2006, no. 7, pp. 6–7.
2. *USSR Inventor's Sertificate*, 324322, MKI B01J 19/28.
3. Frank-Kamenetskii, D.A., *Diffuziya i teploperedacha v khimicheskoi kinetike* (Diffusion and Heat Transfer in Chemical Kinetics), Moscow: Nauka, 1967..
4. Zheranin, A.V. and Ovcharenko, A.G., *Izv. Vuzov, Ser. Khim. Khim. Technologiya*, 2005, vol. 48, no. 12. pp. 89–91.
5. Sherwood, T., Pigfird, R., and Wilkey, C., *Mass Transfer* (Russian translation), Moscow: Khimiya, 1982.

ISSN 1070-4280, Russian Journal of Applied Chemistry, 2007, Vol. 80, No. 11, pp. 2001–2004. © Pleiades Publishing, Ltd., 2007.
Original Russian Text © K.V. Zubov, A.V. Zubov, V.A. Zubov, 2007, published in Khimicheskaya Promyshlennost', 2007, Vol. 84, No. 4, pp. 206–210.

PROCESSES AND DEVICES OF CHEMICAL MANUFACTURES

Phenomenon of Influence of Natural Disasters (Hurricanes and Earthquakes) on Long-Range Order in Liquids. Risks and Chances

K. V. Zubov[a], A. V. Zubov[b], and V. A. Zubov[a]

[a]*"A IST H&C" Co., Design Section, PF 520253, D-12592 Berlin, Germany; Phone: 004930 5625323*
e-mail: aist@zubow.de
[b]*Informatics Institute, Computer Science Faculty, Gumbold University, D-12489 Berlin, Rudovershoss 25, Germany*
e-mail: zubow@informatik.hu-berlin.de

Received April 24, 2007

Abstract—The work showed a phenomenon of influence of seismic and resonance shock waves on the long-range order in a liquid. On examples of damage of ion pair solvated clusters in aqueous solutions of NaCl (3.5 wt%), HCl (2 wt%), $AgNO_3$ (1.7 wt%) and molecular bunches (clusters) in distilled water placed to laboratory chemical reactor far distant from the epicenters of earthquakes the relations between incoming shock and seismic waves and instability of cluster and supracluster long range organization (molecular bunches assocoates) in a liquid is demonstrated. Understanding of risks for chemical industry both in respect of quality and chemical processes instability, and in respect of loose control over chemical technology is considered. Examples of changes in internal organization of solutions in the period of strong hurricane in Europe at February 17, 2007, strong earthquake in Japan at March 25, 2007 and a series of earthquakes at April 4 to 9, 2007 are given and the phenomenon is explained. The risks for chemical industry and the chances of practical using the phenomenon are considered. The clusters in liquids show different responses to the processes in the disaster epicenter, and their responses can be used for understanding chemical processes in Earth crust and in the centers of hurricanes and for strategy of disposing and protecting chemical facilities.

DOI: 10.1134/S1070427207110493

INTRODUCTION

For long time was noted that natural disasters influence state of health of animals, which even have been used by people in the regions of frequent earthquakes for advance informing about their forthcoming. At the moment there is no clear understanding of reasons for these effects. It is only clear that behavior of animals and forthcoming earthquake are connected.

Japan seismologists found that prior to an earthquake, liquids exert sharp changes in their properties. For example, viscosity of olive oil grows anomalously [1]. The authors do not explain these phenomena, but intuitively point to certain interconnection between natural disaster and structure of liquid. Another group of Japanese investigators [2] describes anomalous effects in the properties of water in the area of forthcoming earthquakes. These effects could not be omitted by specialists on chemical technology and safety of chemical plants.

Let us attempt to find sources of this interconnection basing on the known low-energy changes in structure of liquids described by us earlier [3, 4]. The aim of this work is finding a connection between long-range order in a liquid and natural disasters.

MATERIALS AND METHODS

As the objects of investigation were taken: distilled water, agarose hydrogel (0.7 wt. %), solutions of salts and acid [NaCl (3.5 wt%), HCl (2 wt%), $AgNO_3$ (1.7 wt. %)]. The experimental procedure has been described in details in [3–6]. The works on the study of long-range order in liquids in the North part of Germany were carried out in the period from February to May 2007. Comparison of the data on the long-range order in liquids and natural disasters is made using the principle of "coincidence" in the time of events in the cell of measurements (53.08° north latitude and 12.75° east

longitude) and time of a disaster that has not been predicted to the moment (except the hurricane at February 17, 2007 over North Sea and territory of Germany). All event times are by Greenwich.

RESULTS AND DISCUSSION

Study of long-range order in the agarose hydrogel commonly used for modeling biological matrices showed effects of instability of long-range structure appearing as a sharp increase in average value of f parameter that characterizes interaction of clusters with environment [3, 4] (Fig. 1).

Average scattering of f parameter thus reflects "nervousness" of the system of supracluster structure in the hydrogel long-range order. The agarose hyrogel contains up to 99.3 wt.% of water, therefore increase in the cluster vibrations can be with a great probability assigned to strengthening in oscillation of water clusters. The water clusters, as is known, affect conformations of biomolecules [7], hence, influence direction and rate of certain biochemical processes in living organisms and, further, affect their biological reactions, that is, behavior. Thus we can trace indirect influence of the impact of the earthquake seismic waves on the organism biomatrix and fix connection between behavior of people and animals and natural disasters. Damage of long-range order in cluster structure of water in a biomatrix can influence health state of the operators in chemical plants and this can introduce the factor of human risks, which should be taken into account.

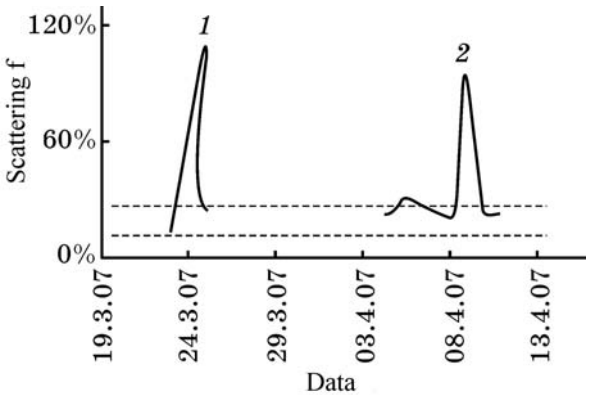

Fig. 1.

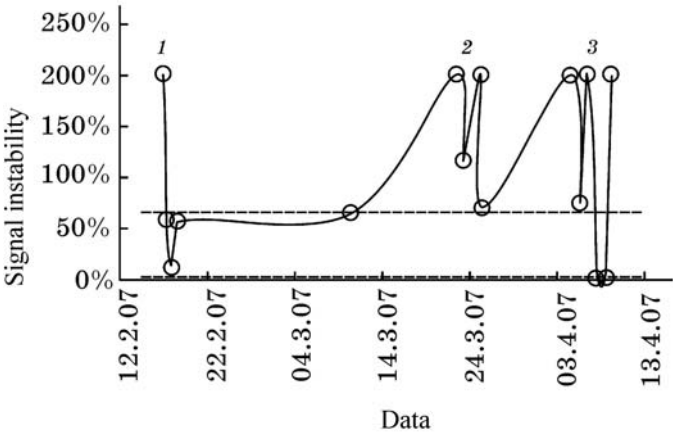

Fig. 2.

It should be noted that in the period of April 4 to 9, 2007 occurred many earthquakes, and we succeeded to register events shown in Fig. 1, proceeding from the time of achieving cells of flicker noise spectrometer (FNS) in Germany by seismic waves (4-7 km/sec) and the time of experiment carrying out. At other events the time of registering FN spectra and that of coming earthquake shock wave did not coincide. We found that coming shock wave activates FNS sensor differently and strongly depends on the chemical composition of liquid. In some liquids the long-range order reaction on the shock wave impact can continue for several hours and is selective in respect of mode of the molecular bunch. On the other hand, chemical processes in the earthquake epicenter can be understood by means of analysis of this selectivity which reflects resonance interaction of such oscillators in the measuring cell and in the earthquake epicenter. Therefore for chemical plants working in continuous regime can be used the possibility of monitoring events in the Earth interior for understanding the whole wide spectrum of chemical processes of earthquake.

Fig. 2 shows variations in average value of f parameter for ion pair solvated clusters of NaCl and water in 3.5 wt. % solution modeling sea water. From the figure is seen that these NaCl clusters response to damage of long-range order in sea water. Therewith, it is not significant whether this is a damage due to hurricane (1) or due to compression in the epicenter of a earthquake in ocean (2, 3). The long-range damage in the salt solution can be represented by the scheme (I):

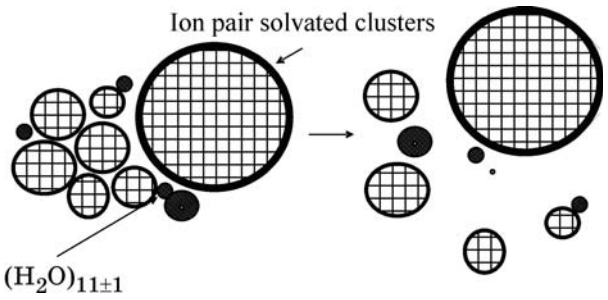

Such a scheme assumes dispersing the salt ion pair solvated cluster nanosuspension under the action of shock wave of the earthquake or resonance wave from the ion pair solvated cluster damaged due to hurricane in the North Sea. This process is not stable one, and the system quickly returns into the state close to the initial even in a few hours. However, for some of large NaCl ion pair solvated clusters the process of achieving equilibrium of its interaction with environment can get a few days. We found that integral characteristics of solutions, including such as average molecular weight of all clusters ($M_{FNS}= m \cdot |f|$) "fill" appearance of earthquake in two-three days, as probably a result of strong pressure in the earthquake zone prior to the collapse and the sea water long-range order damage in the zone of epicenter.

Understanding the Scheme I of developing the process of disintegration of ion pair solvated clusters in salt solutions should be taken into account in chemical technology, because this can lead to sharp increase in the rate of chemical reaction and distortion of stability of chemical plants. On the other hand, one can expect that architecture of displacement of chemical reactors with forced dissolving and forced stirring near the reactors of fine synthesis can lead, according to the Scheme I, to induced or continuous action on the long-range order in the reactor for the synthesis, or on psychological stability of staff.

Some difference occurs in the response of hydrochloric acid solution to the natural disasters. Fig. 3 presents change in average molecular weight of clusters in 0.6 M HCl solution. As seen from the figure, increase in M_{FNS} at approaching earthquake in ocean can be registered even in a few days (shown by arrows). Thus, the integral characteristics of long-range order can be used to predict earthquakes. According to view of Japanese seismologists [1] that in the region of earthquake in Japan Sea occurs dehydration of mineral pores under the action of very high pressure of moving layers, we can assume that such dehydration affects strongly the structure of solvated ion pairs in sea water due to forced shift of equilibrium to the side of formation of HCl ion pair solvated clusters with the size less than the size of solvated clusters of NaCl ion pair [5, 8, 9].

$$NaCl{\cdot}aq + H_2O \rightarrow HCl{\cdot}aq + NaOH{\cdot}aq$$

Thus, principally appears a possibility of obtaining distant information on the chemical processes in the zone of earthquake and on their influence on technological processes with solutions.

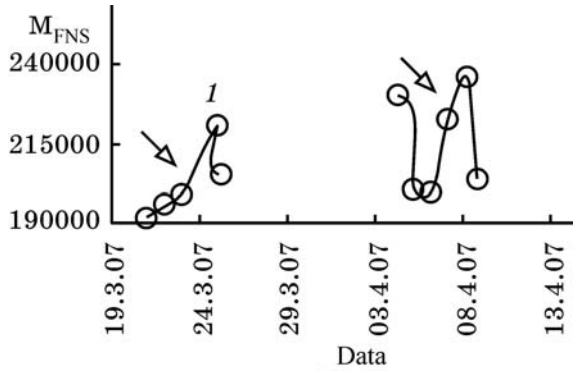

Fig. 3.

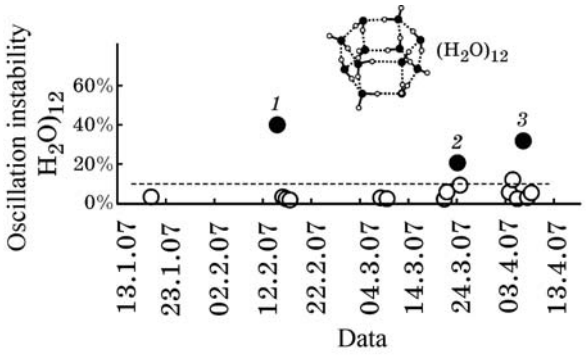

Fig. 4.

Fig. 4 presents dynamics of variations in instability of *f* signal of water cluster $(H_2O)_{12}$ [10] in 0.1N $AgNO_3$ solution. This cluster also is found to be distant sensitive toward weak energy streams of oscillation of its analogs in sea water affected by hurricane or earthquake. In the series of earthquakes in the period April 4 to 9, 2007, it showed selectivity in respect of shock waves attaining the place of measuring. Hence, seismic waves are the superpositions of a series of waves, and the clusters response actively to those defined by signals from their damaged analogs in the epicenter of hurricane or earthquake. For chemical technology this means a necessity to select technology and equipment appropriate for the zone of frequent natural disasters.

CONCLUSION

Liquids are unique natural sensors of energetically weak processes in nature. Natural disasters affect distantly long-range order in liquid. Changes in long-range order in a liquid under the influence of seismic waves or resonance fields of oscillation of molecular bunches (clusters) can result in destabilization of technological process and even lead to failure. These

changes can be used for early information on forthcoming disasters by continuous monitoring of structure of the liquids applied in technological processes. Risks of chemical processes due to this phenomenon lie in the quality of products, stability of technological processes and in the area of human factor: fatigue and overstrain. In our opinion the situation can be improved by means of inclusion to technology of the systems for monitoring distant influence on the long-range order in liquids and distribution of early information.

ACKNOWLEDGMENTS

We are grateful to "Aist Handels- und Consulting" GmbH (FNS project) for financial support of the work in the area of flicker noise spectroscopy.

REFERENCES

1. Soichi, O., Tetsuya, K.and Shigenori, M., *Dehydration Event and Earthquake in the Subductig Stab*, Frontiers Science Series, 2004, p. 44; *Physicochemistry of water in geological and biological systems,* pp. 241–257, Univarsal Academy Press, Inc.
2. Tsukuda, T, Gotoh, K and Sato, O., *Bull. Earthq. Res. Inst*., Univ. Tokyo, 2005, vol. 80, pp. 105–131.
3. Zubov A.C. Zubova K.C., Zubov C.A., *Khimicheskaya Promyshlennost'*, 2006, vol. 83**.** pp. 300–306.
4. Zubov, A.V., Zubov , K.V. and Zubov, V.A., *Khimicheskaya Promyshlennost'*, 2007, vol. 84, no. 1, pp. 40–48.
5. Zubova , K.V., Zubov , A.V. and Zubov, V.A., *Zh. Prikladnoi Spektroskopii*, 2005, vol. 72, no. 6, pp. 766–772.
6. Zubova , K.V., Zubov , A.V. and Zubov, V.A., *Zh. Prikladnoi Spektroskopii*, 2005, vol. 72, no. 3, p. 305–312.
7. Shiryayev, A., Pagan, D.L., Gunton, J.D., Rhen, D.S., Saxena, A. and Lookman, T.*, J. Chem. Physics*, 2005, vol. 122, p. 234911.
8. Heyrovska, R., *Chem. Phys. Letters,* 2007, vol. 436, pp. 287–293.
9. Yokogawa, D., Sato, H. and Sakaki, S., *Chem. Phys. Letters*, 2006, vol. 432, pp. 595–599.
10. Lenz, A., and Ojamäe, L., *Chem. Phys. Letters*, 2006, vol. 418, pp. 361–367.

ISSN 1070-4280, Russian Journal of Applied Chemistry, 2007, Vol. 80, No. 11, pp. 2005–2007. © Pleiades Publishing, Ltd., 2007.
Original Russian Text © A.S. Pushnov, M.G. Berengarten, A.M. Kagan, A.S. Ryabushenko, 2007, published in Khimicheskaya Promyshlennost', 2007, Vol. 84, No. 5, pp. 249–251.

PROCESSES AND DEVICES OF CHEMICAL MANUFACTURES

Helicoid-Structural Packing with Varied Stacking Geometry

A. S. Pushnov, M. G. Berengarten, A. M. Kagan, and A. S. Ryabushenko

Mendeleev Chemical Society, Moscow Division, Moscow, Russia
Vedeneev Research Institute of Hydraulic Engineering, Moscow, Russia

Received April 24, 2007

Abstract—Due to obsolescence of basic technological equipment of fan-type cooling towers in the enterprises of chemical complex built in 1980 and earlier the actual problem is their reconstruction using new technological solutions and developments aimed at the increase in efficiency of the process of evaporation cooling.

DOI: 10.1134/S107042720711050X

Due to obsolescence of basic technological equipment of fan-type cooling towers in the enterprises of chemical complex built in 1980 and earlier the actual problem is their reconstruction using new technological solutions and developments aimed at the increase efficiency of the process of evaporation cooling.

In [1] has been proposed a regular polymer packing constructed of four-blade helicoid elements turbulizing gas and liquid flow. The blades were stacked in horizontal rows turned by right angle in neighboring rows. Further development of this approach was shown in [2] publishing the results of examination of modernized constructions of helicoid-structural packing of PN-2D type made of polymer material.

Construction of helicoid-structural packing with varied geometry of stacking the individual blades in a block allows to recommend such packing for providing a given profile of the air flow rate along the transverse section of trickling space of cooling tower [3]. Programming the profile of rates in a cooling tower using the proposed prospective construction consisting of horizontal helicoids is performed keeping unchanged block height only by varying geometry of stacking and distance between the helicoid blades. This results in changing living section and hence in hydraulic resistance of the packing blocks [3]. The packing PN-2D allows varying the stacking pitch in the range from 1 to 3 diameters of the helicoid.

General view of the packing of PN-2D type with different modes of stacking geometry is shown in Fig. 1. The following modes of stacking geometry are possible:

- PN-2D kd – unstaggered (corridor) stacking,
- PN-2D ch – staggered (chess type) stacking,
- PN-2D kk – slant canal.

In this work we present results of air-thermal examination of helicoid-structural packing PN-2D with a predetermined stacking geometry of elements in a block.

The experiments were carried out under identical conditions, on the installations in the Vedeneev Research Institute of Hydraulic Engineering and Moscow State University of Engineering Ecology according to the procedure described in [4].

Plots in Figs. 2–4 show experimental data on the dependence of degree of cooling water in cooling tower, Δt, on the value of specific liquid rate, q_L, obtained on

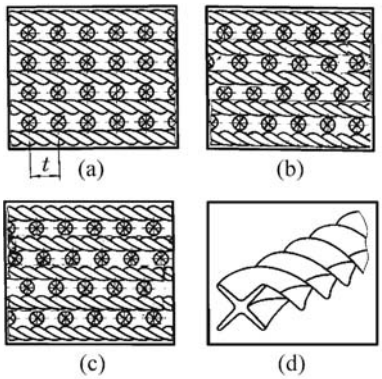

Fig. 1. General view of blocks of PN-2D packing with different modes of stacking of its elements, the helicoids: (a) PN-2D kd – unstaggered (corridor) stacking, (b) PN-2D ch – staggered (chess type) stacking, (c) PN-2D kk – slant canal, (d) general view of separate packing element.

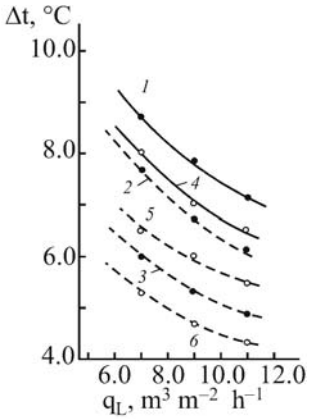

Fig. 2. Effect of the mode of stacking helicoids PN-2D ch and PN-2D kd on the character of the plot $\Delta t = f(q_L)$ at $X_t = 2$, block height H = 0.86 m, W_o = Var (*1, 3*) packing PN-2D ch, W_o = 2.0 m/s; PN-2D kd, W_o = 2.0 m/s; (*2, 4*) packing PN-2D ch, W_o = 1.5 m/s; PN-2D kd, W_o = 1.5 m/s; (*3, 6*) packing PN-2D ch, W_o = 1.0 m/s; PN-2D kd, W_o = 1.0 m/s.

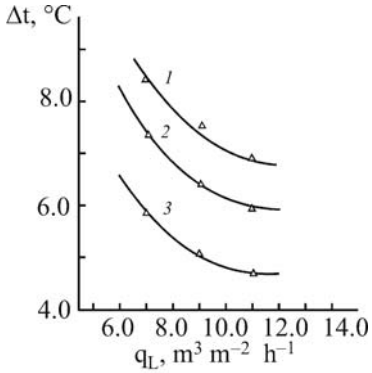

Fig. 3. Plot $\Delta t = f(q_L)$ for the mode of packing geometry PN-2D kk at varied air flow rate W_o: (*1*) W_o = 2.0 m/s; (*2*) W_o = 1.5 m/s; (*3*) W_o =1.0 m/s.

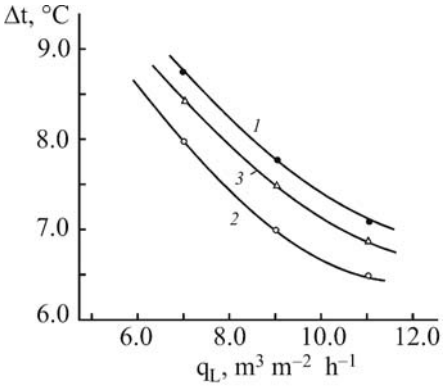

Fig. 4. Plot $\Delta t = f(q_L)$ at W_o = 2.0 m/s. (*1*) packing PN-2D ch, (*2*) packing PN-2D kd; (*3*) packing PN-2D kk.

the installation at various geometry of stacking helicoids in the packing. As seen, in the studied range of liquid rate (q_L from 0 to 12.0 m^3 m^{-2} h^{-1}) and gas rate (W_0 from 0 to 2.5 m/sec, the air flow rate calculated on the full section of empty tower), increase in amount of cooled water the cooling degree Δt regularly falls. This is seen particularly at increase in q_L from 6.0 to 10.0 m^3 m^{-2} h^{-1}.

The experimental data for the process of evaporation cooling in cooling tower are given as a dependence of evaporation number K_{vap} on the relative air consuming λ [4]:

$$K_{vap} = A\,\lambda^m, \quad (1)$$

where A and m are coefficients, $\lambda = q_G/q_L$, (q_G and q_L are specific gas and liquid consuming values, respectively).

Dependence of the A coefficients as A/H plots against geometry parameter X_t for the packing of PN-2D kd type is shown in Fig. 5.

The X_t parameter equals:

$$X_t = \frac{t}{d}, \quad (2)$$

where d is external diameter of a helicoid, mm; t is distance between central axes of neighboring helicoids, mm (see Fig. 1).

The hydraulic resistance coefficient of the packing, ξ, was calculated according to the known Weisbach formula, which in mixed units system (MKGCS-SI) looks as [4]:

$$\xi = \frac{\Delta P 2g}{\gamma_{air} W_o^2}, \quad (3)$$

where ΔP is pressure loss (difference in the air pressure) in the packing [kg m^{-2}] or [mm Hg]; γ_{air} is air

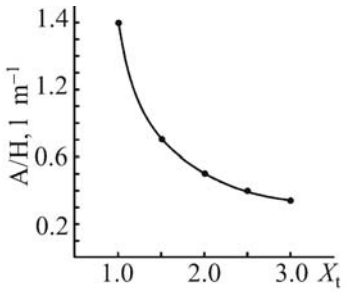

Fig. 5. Dependence of A/H simplex on the geometry parameter X_t from the experiments with spryer block PN-2D

Table 1. Values of A and ξ coefficients for the packing differ by geometry

Packing type	PN-2D kd	PN-2D ch	PN-2D kk
A_0=A/H [1/m]	0.65	0.67	0.665
Hydraulic resistance coefficient ξ	25	26	25.2

Table 2. Characteristics of PN-2D kd packing

Geometry parameter X_t	2
Porosity, ε, m^3/m^3	0.907
Equivalent diameter, d_{eq}, m	0.052
Specific surface, S, m^2/m^3	70

specific gravity [kg/m^{-3}]; g is acceleration by gravity pull [m s^{-2}]; W_o is average air flow rate calculated on the full section of empty tower [m s^{-1}].

The values of obtained A and ξ values for PN-2D packing with different stacking geometry are listed in Table 1. Here X_t = 2.

The values of hydraulic resistance ξ of the blocks of examined packing at the block height H = 0.86 m in Table 1 are given at liquid flow rate q_L = 10 m^3 m^{-2} h^{-1} and air flow rate W_o = 1.5 m/s.

Geometry characteristics of the most widely used packing PN-2D kd are shown in Table 2. The principal chatracteristics of PN-2D type packing are considered in [2].

From the data in Table 1 is seen that the value of hydraulic resistance coefficient ξ for the blocks of PN-2D kk packing is practically the same as for PN-2D kd. Among the studied three modes of packing the PN-2D kk is the most prospective because it provides higher efficiency at the lower hydraulic resistance.

REFERENCES

1. Kagan, A.M., Pushnov, A.S., Myzenkov, G.B., Osipov, P.M., and Buravlev, V.M., *Khimicheskaya Tekhnika*, 2004, no. 7, pp. 28–31.
2. Pushnov, A.S., Kagan, A.M., Berengarten, M.G., Ryabushenko, A.S., and Shishov, V.I., *Khimicheskaya Promyshlennost' Segodnya*, 2007, no. 3, pp. 33–40.
3. Pushnov, A.S., Berengarten, M.G., and Ryabushenko, A.S., *Proceedings of Litovian Academy of Applied Sciences* (Litva, Kaunas), 2007, no. 4, pp. 1–16.
4. Sukhov, E.A. and Gel'fand, R.E., *Izvestiya VNIIG Vedeneeva*, 1971, vol. 96, pp. 256–262.

ISSN 1070-4280, Russian Journal of Applied Chemistry, 2007, Vol. 80, No. 11, pp. 2008–2013. © Pleiades Publishing, Ltd., 2007.
Original Russian Text © V.I. Kel'bas, A.F. Kazankina, Yu.I. Kartashev, V.V. Fomenko, 2007, published in Khimicheskaya Promyshlennost', 2007, Vol. 84, No. 5, pp. 262–269.

MANUFACTURING SAFETY

Mass Transfer Flame Resistant Working Fluids for Hydraulic Systems

V. I. Kel'bas, A. F. Kazankina, Yu. I. Kartashev, and V. V. Fomenko

Russian Scientific Center "Applied Chemistry", St. Petersburg, Russia

Received February 28, 2007

Abstract—The experience in running mineral oils in hydraulic system allows us to conclude that basically their properties obey requirements: they provide reliability and durability of work of a hydraulic transmission, but have unavoidable disadvantage: flammability.

DOI: 10.1134/S1070427207110511

Modern hydraulic transmissions as a rule contain many actuating mechanisms with many connectors and oil seals. The working fluid exerts a pressure tenths and hundreds over atmospheric one. Even minor disturbance in the system tightness can lead to spraying the oil, formation of aerosols (oil fogs) prone to inflammation or even explosion due to presence of hot surfaces or from electric spark and other sources of ignition. World practice knows many cases of conflagration caused by such sources.

In the last decade in the world practice found wide application the working fluids with diminished flammability. A series of fluids differ by their chemical nature and not equal from the viewpoint of fire resistance, toxicity, performance, cost and other characteristics was developed.

According to international classification, the flame resistant liquids for hydraulic systems fall to four classes:

HFA – aqueous emulsions of "oil in water" type consisting of 97–98 % of water and 2–3 % of mineral oil with additives. Low viscosity (2–4 mm^2/sec at 50°C), not high enough lubricant properties and low stability restrict their application in the hydrosystems designed for working on mineral oil.

HFC – inverted emulsions of "water in oil" type containing 40 % of oil and 60 % of water and additives (the most important additive is emulsifier which allows comprising smallest particles of water by oil). By lubricant properties these fluids are second to mineral oils, with low stability and disposed to separation, but rather inexpensive.

HFC – water–glycol liquids containing 30–50% of water, 45–60% and polymer tickening agent, together with antirust, antiwear, fireproofing and other additives. Such fluids are compatible with practically all classes of metallic construction materials, plastics, the materials based on gum, are nontoxic, possess good lubricant properties, are stable and can be used in the hydraulic systems designed for mineral oil without significant construction improvement. They can be used at moderate power regimes, at the temperature up to 60°C. Their disadvantage is evaporation of water, especialy at elevated temperature and in not enough hermetic systems.

HFD – synthetic fluids not containing water. They comprise organic silicon, chlorine and fluorine compounds and the compounds based on phosphoric esters.

The fluids of HFD class are expensive, toxic, not compatible with oil seals based on nitrile gums that commonly are used in the hydrosystems on petroleum oils, but they possess high lubricant characteristics and can be used at rigid regimes of strength and work temperature.

The most widespread in world practice are fire safe and ecologically safe water–glycol fluids of HFC class.

In the Russian scientific center "Applied Chemistry" during 30 years period has been developed a big set of flame safe working fluids of water–glycol class with viscosity form 1 to 40 mm^2/sec at 50°C [1–8]. Some of them are shown in Table 1.

For determination the name of water–glycol fluid appropriate for application in a certain hydraulic transmission should be considered its physico-chemical, antiwear, antirust and other properties in comparison with mineral oil recommended for the same hydraulic transmission [9].

The physico-chemical properties of fluids are listed in Table 2.

Table 1. Physico-chemical characteristics of fire safe working fluids

Fluid name	Number of technical requirments	Analog	Density at 20°C, kg/m^3	Viscosity at 50°C mm^2/s	Solidification point, °C
Thermosol-17	6-02-2904-87	–	1050	1	–17
VLP-10	6-02-2-940-87	VMG3	1055	10	–50
Polus	6-02-2-1337-86	AMG-10 MGE-10	1090	10	–60
PGV	GOST 25821-83	AU, AUP	1152	13	–50
Promhydrol P2OM1	6-02-1140-78	I-20	1130	20	–18
Promhydrol P2OM3	6-02-2781-84	IGP-30, VNIIP-403, T_p-22, T-30	1055	30	–30
Promhydrol P-40	301-02-166-91	IGP-36	1055	40	–30
UZhTG-46	6-02-2-787-84	T-46	1055	46	–40

Table 2. Comparative physico-chemical properties of water–glycol fluids and mineral oils

Fluid	Viscosity, mm^2/s		Density at 20°C, kg/m^3	Solidification point, not higher, °C	Ignition temperature, not higher, °C	Flammability at spraying at the pressure 25 atm to the flame of acetylene burner
	50°C	20°C				
Promhydrol P2OM1 TU6-02-1140-78	18–24	59?77	1125–1140	–18	no	
Promhydrol P2OM3 TU6-02-2-781-84	24–30	85?110	1050–1058	–30	no	Do not burn and do not propagate flame along the spray steram
PGV GOST25821-83	12–16	42-60	1152–1158	–50	no	
VLP-10 TU6-02-2-940-87	9–13	31	1040–1055	–50	no	
Oil AU (spindel) GOST1642-75	12–14	47–49	0.888–0.896	–45	163	
Oil (turbine) Tp22 GOST32-74	20–22	85–90	0.890	–15	180	
Oil VNIINP-403 GOST16-728-78	25–35	120	0.850	?10	190	Burning, the flame propagates along the stream of spraying oil
Oil IGP-18 GOST38-101-413-78	16.5–20.5	–	0.880	–15	170	
Oil (transformers) GOST982-68	9.6	30	–	–45	135	
Oil VMGZ TU38-1-196-68	10	–	0.805	–60	135	

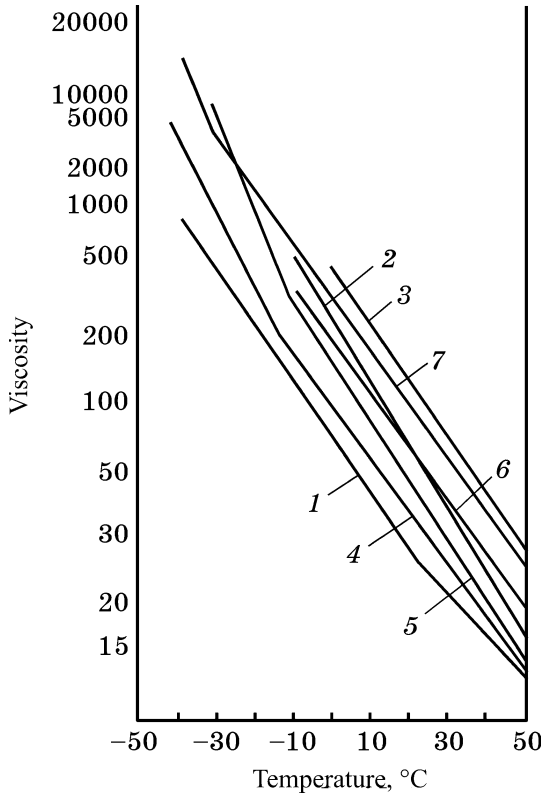

Fig. 1. Viscosity-temperature characteristics of water–glycol fluids and mineral oils. (*1*) Oil VMGZ; (*2*) Oil IGP-18; (*3*) Oil VNIINP-403; (*4*) Fluid VLP-10; (*5*) Fluid PGV; (*6*) Promhydrol P-2OM1; (*7*) Promhydrol P–2OM3.

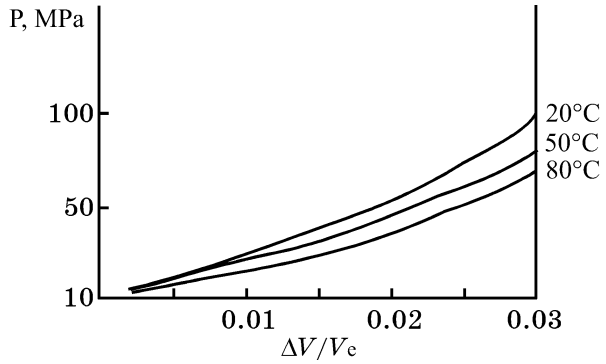

Fig. 2. Compressibility of the fluid Promhydrol.

Table 3. Thermophysical characteristics of water–glycol fluids and mineral oil

Fluid	Specific temperature cal g^{-1} deg^{-1}	Heat conductivity kcal m^{-1} g^{-1} deg^{-1}
Promhydrol	0.71–0.75	0.305
oil	0.45–0.50	0.139

An important property of working fluid is its viscosity. For the correct operations of the hydraulic transmission is providing required viscosity-temperature characteristics of working fluid.

Viscosity defines the possibility of formation of liquid layer on the surfaces of rubbing pair and the rate of flow, heating of liquid and parameters of work for all mechanisms.

For effective operations of a hydraulic system the fluid viscosity should fall to a certain range responding to the types of used mechanisms.

Viscosity of a liquid varies with its temperature. Fig. 1 shows comparison of dependence of viscosity on the temperature for water–glycol fluids PGV, Promhydrol P-2OM1, Promhydrol P-2OM3 and VLP-10, and the mineral oils in hydraulic transmissions.

The plots shows that by viscosity-temperature characteristics in the temperature range from +50 to +10°C to the mineral oil IGP-18 best fits the fluid Promhydrol P-2OM1, and in the range from +10 to "10°C the fluid Promhydrol P-2OM3; to mineral oil Tp-22 and VNIINP-403 corresponds fluid Promhydrol P-2OM3, to transformer oil and to spindle oil AU the best corresponds by these characteristics the fluid PGV; to the mineral oil VMG3 which is recommended for use in winter period best fits by viscosity-tmperature characteristics the fluid VLP-10.

Study of baric dependence of viscosity and density of water–glycol fluids showed their low compressibility. The data for Promhydrol are shown in Fig. 2.

By their toxic properties the water–glycol fluids relate to low hazard or moderate hazard substances (III-IU class according to the classification GOST 12.I.007-76).

Ecological safety at the exploitation of water–glycol fluids is provided by their property of fast biochemical degradation at the accidental spilling or at purification of sewages in regional biochemical stations. For example, the fluid Promhydrol P-2OM3 áhas the following biochemical charatcteistics: (a) Chemical absorption of oxygen (CAO) 1.09 mg/mg, (b) Biochemical absorption of oxygen BAO_5 0.69, BAO_{20} 0.99 mg/mg.

Thus, biochemical index BAO_{20}/CAO is enough high, being equal to 0.90. This characterizes the product as appropriate for biological decomposition.

At the same time, stability of water–glycol fluids

toward biological damage in the process of exploitation is provided by special additives.

A doubtless advantage of water–glycol fluids at their exploitation from the viewpoint of industrial culture and requirements on technological safety is their easy washing off from surface at the occasional pouring.

Fire resistance of water–glycol fluids is stipulated by the presence of water in them. Testing the water–glycol fluids on several characteristics that are recommended by Russian Institute of Fire Guard (VNIIPO) showed their high fire resistance. At spraying under high pressure (up to 25 MPa) on the flame of acetylene burner the water–glycol liquids, in distinct to mineral oil, are inflammable, do not burn and do not propagate flame along the spray stream.

In distinct to mineral oil that shows high electric resistance, that is, are insulators for electric current, the water–glycol fluids are conductors. Their specific resistance at 20°C is $(3–6) \times 10^5$ Ohm m. The dielectric permeability at the frequency 500 kHz is ca. 49.0, hence they are unsatisfactory dielectrics.

Such fluids can not be used in the systems with immersed to liquid electroelements with unprotected contacts.

By their thermophysical characteristics, the water–glycol fluids are much advantageous over mineral oil and provide effective heat transfer from the friction nodes making the regime of exploitation much milder. The comparative characteristics for the fluid Promhydrol and oil are shown in Table 3.

A significant requirement to the fluids for hydraulic systems is their ability to liberate air without frothing. Strong frothing leads to lose of the fluid and can cause damage of elements of the hydraulic system.

Practically, liquids always contain some dissolved air, more at higher pressure. The presence of air at constant pressure is commonly imperceptible. However, reducing in pressure leads to liberating dissolved air, and this probably results in fuming.

Due to higher density of water–glycol fluids as compared with oil, their ability to deaeration is lower and gas liberation proceeds slower.

The acceptable frothing of water–glycol fluids is defined by the standard GOST 25821-83: it should be below 100 ml. Antifrothing property of water–glycol fluids is provided by introducing antifrothing additives to their compositions.

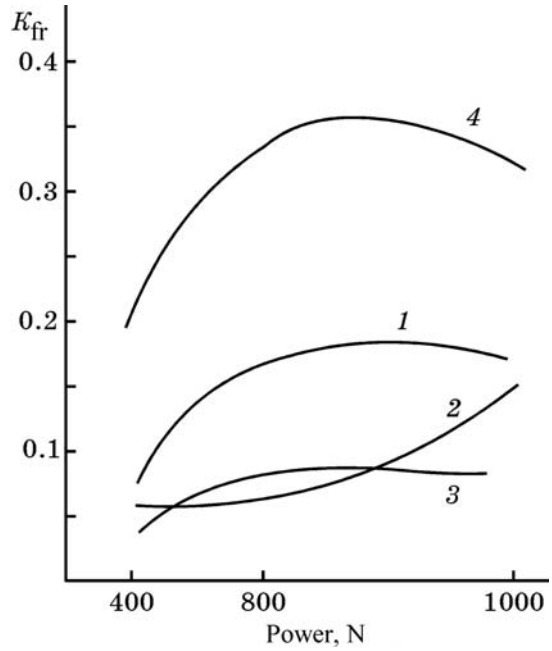

Fig. 3. Dependence of friction coefficient onn the strength at the examination on an IST-MT/5 friction machine (*1*) Promhydrol P-2OM1; (*2*) Promhydrol P-2OM3; (*3*) PGV; (*4*) Oil IGP-18;

The working fluid in a hydraulic system should possess high lubricant property, which is characterized by a scope of antiscuff, antiwear and antifriction factors.

This property defines intensity of wearing the friction nodes and reliability of the hydraulic transmission as a whole.

The standard method for estimation antiwear property is examination of the hydraulic fluid on a 4-balls friction machine (GOST 9490-75) which contain friction node as a pyramid of four bearing balls. Three balls in the base of the pyramid are fixed in the cup with the tested liquid and are unmovable; the upper

Table 4. Estimated antiwear property of water–glycol fluids and mineral oil, by GOST 9490-75

Working fluid	Characteristics		
	I_s	P_c, kg	P_w, kg
Oil IGP-18	23,6	40	141
Promhydrol P-2OM1	50–60	63	282
Promhydrol P-2OM3	45–55	89	251
PGV	30–40	63	168
VLP-10	28	50	141

Table 5. Rate of corrosion of metallic construction materials in the fluid Promhydrol P-2OM-3, in comparison with mineral oil IGP-18

Material	Rate of corrosion, mm per year	
	Promhydrol P-2OM3	Oil IGP-18
Steel ST-3	0.0001	0.0001
Steel 30KhGSA	0.0001	0.0001
Aluminum D16AT	0.0002	0.0003
Bronze BrAZh9-4	0.0003	0.0015
Copper M-3	0.0009	0.0031
Brass L-63	0.0003	0.0008

Note: Test duration 720 h, temperature 50°C

Table 6. Examination of nonmetallic materials in the fluid Promhydrol P-2OM3

Material	Swelling wt.%
Fiber construction	+9.2
Fiber laying	+19.00
Glass plastic	+0.98
Textolite A	+3.69
Fluoroplast 3	0.0
Paronit UV-10	+10.8
Polyamide 68	+1.18
Polyethylene	+0.078
Capron B	+3.52
Asbestos cotton	+19.9

Note. Test duration 30 days, at 50°C.

Table 7. Results of testing of various gums in the fluid Promhydrol P-2OM3

Gum	Basic rubber	Swelling, wt.%
V-14	Nitrile	1.6
V-14-1	Nitrile	1.1
No-68-1	Nitrile –chloropren	0.3
2542-N	Chloropren	1.3
IRR-1136	Fluorinated	0.3

Note: Test duration 30 days, at 50°C.

ball is fixed in a rotating spindle. The bottom balls are held up to the top one with a given power. The lubricant property of the fluid is characterized by:

- Scuff index (I_s) defines effect of the fluid on the wearing of the rubbing surfaces;

- Critical pressure (P_c), kg is the power just before sharp increase the wearing spot on the balls;

- Welding pressure (P_w), kg is the power leading to welding of the balls.

The higher I_s, P_c and P_w values, the better antiwear property. The results of examination are listed in Table 4.

The table shows that by all antiscuff characteristics the water–glycol fluids have better characteristics than the mineral oil IGP-18.

At the estimation of lubricating ability of working fluids and prognosis of their working capacity is significant the dependence of friction coefficient on the power and temperature which characterize antifriction property of the fluid.

Examination of dependence of friction coefficient on the force was performed on an ITS-MT/5 machine with top boll rotating at the constant rate. Axial pressing was varied stepwise within 1000 Newton.

The friction coefficients for the water–glycol fluids in the force range from 400 to 1000 N is by 2.5–3 times lower than for the mineral oil IGP-18 (Fig.3).

The dependence of friction coefficient on temperature was exaqmined by thermal method according to GOST 17604-72 on a 4-boll machine KT-2. The method is based on an external heationg of samples and surrounding layer of a lubricant at the constant pressing in the contact of friction, with low rate of sliding, to avoid heating due to friction and appearing of liquid-type lubricating. The examination was carried out in the temperature range 20 to 200°C, the

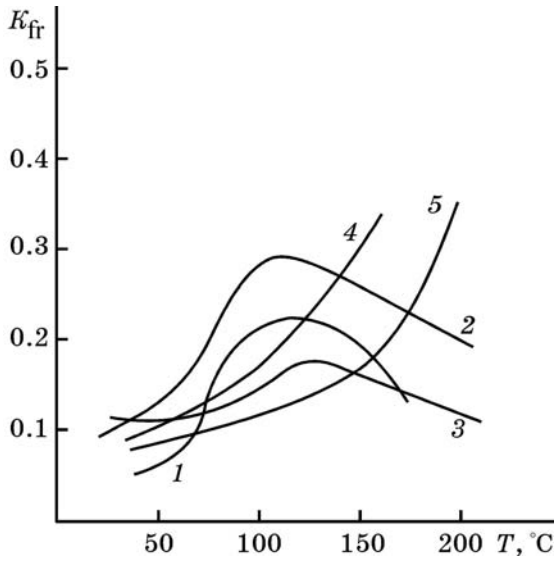

Fig. 4. Dependence of friction coefficient on the temperature of working fluids. (*1*) Promhydrol P-2OM1; (*2*) Promhydrol P-2OM3; (*3*) PGV; (*4*) Oil IGP-18; (*5*) Transformer oil.

sliding rate was 0.2 mm s^{-1} , pressing 110 N, which provides contact pressure 0.21 MPa.

The friction coefficients of water–glycol fluids and mineral oil IGP-18 in the temperature range from 20 to 120°C are comparable by value, however, at the temperature above 120°C those of the former show tendency to decrease when temperature grows (Fig. 4).

The working fluid should be compatible with the material of hydrosystem. This means that metal, cover and various construction materials contacting or under certain conditions could contact with the fluid should be mutually inert.

Our study showed that the water–glycol fluids owing to antirust additives show high antirust properties toward basic classes of construction materials (Table 5).

From Table 5 follows that the corrosion rate of construction materials in the fluid Promhydrol P-2OM-3 is comparable with that in mineral oil IGP-18.

A very important property is chemical resistance of gum and other non-metallic laying, thickening and covering materials. As a rule, gum swelling should not exceed 3%. The results of examination of thickening materials are listed in Table 6.

Among the examined nonmetallic materials in the Promhydrol P-2OM3 fluid the unstable ones are fiber and asbestos, and they are not recommended for use. Paronit is moderately stable material.

The results of examination of gum of various types on the swelling in the fluid Promhydrol P-2OM3 are listed in Table 7.

To conclusion, we note that in the RSC "Applied Chemistry" is accumulated prolonged experience on continuous expluatation of water-glycol fluids in hydraulic systems including the system of screw, axial-plunger, plate, gear and other types of pump.

REFERENCES

1. Shpak, V.S., Sukhotin, A.M., Kelbas, V.I., Kazankina, A.F., et al., *USSR Inventor's Sertificate*, no. 591493 (1975).
2. Sukhotin, A.M., Kelbas, V.I., et al., *USSR Inventor's Sertificate*, no. 615125, 1977.
3. Kazankina, A.F., Kelbas, V.I., et al., *USSR Inventor's Sertificate*, no. 772208, 1979.
4. Kazankina, A.F., Kelbas, V.I., et al., *USSR Inventor's Sertificate*, no. 986097, 1981.
5. Kazankina, A.F., Kelbas, V.I., et al., *USSR Inventor's Sertificate*, no. 1271056, 1986.
6. Kazankina, A.F., Kelbas, V.I., et al., *USSR Inventor's Sertificate,* no. 266229, 1987.
7. Kazankina, A.F., Kelbas, V.I., et al., *USSR Inventor's Sertificate,* no. 1782026, 1990.
8. Kelbas, V.I., Kazankina, A.F. et al., *USSR Inventor's Sertificate*, no. 1483925, 1987.
9. *Negoryuchie teplonositeli i gidravlicheskie zhidkosti* (Nonflammable heat carriers and hydraulic fluids), Sukhotin, A.M., Ed., Leningrad: Khimiya, 1979.

ISSN 1070-4272, Russian Journal of Applied Chemistry, 2007, Vol. 80, No. 12, pp. 2015–2019. © Pleiades Publishing, Ltd., 2007.
Original Russian Text © M.N. Novokreshchenova, T.V. Daminova, Yu.M. Yukhin, 2007, published in Zhurnal Prikladnoi Khimii, 2007, Vol. 80, No. 12, pp. 1937–1941.

INORGANIC SYNTHESIS AND INDUSTRIAL INORGANIC CHEMISTRY

Precipitation of Bismuth(III) Oxobromide from Bromide Media

M. N. Novokreshchenova, T. V. Daminova, and Yu. M. Yukhin

Institute of Solid-State Chemistry and Mechanochemistry, Siberian Division, Russian Academy of Sciences, Novosibirsk, Russia

Received August 27, 2007

Abstract—Abstract—X-ray phase analysis, thermogravimetry, IR spectroscopy, and chemical analysis were used to study bismuth(III) precipitation from nitrate solutions upon addition of aqueous solutions of hydrobromic acid or ammonium bromide, and from bismuth-containing hydrobromic acid solutions. The conditions in which bismuth(III) oxobromide of BiOBr composition is formed were determined and the possibility of obtaining a high-purity product was assessed.

DOI: 10.1134/S1070427207120017

Bismuth oxobromide is used in veterinary medicine [1], in technology for manufacture of piezo-, pyro-, and ferroelectric materials, and in physical development of silver-containing photographic materials [2, 3]. This compound is obtained by dissolving bismuth oxide of reagent-grade purity in hydrobromic acid, with the subsequent dilution of the resulting solution with hot water [4, 5]. A method is known for preparation of bismuth oxobromide, in which a mannitol-containing aqueous solution of bismuth nitrate is reacted with an alkali metal bromide at pH 5.0–5.2 in the presence of a buffer mixture based on urotropin and hydrobromic acid [6].

Bismuth compounds are commonly synthesized from a metal of Vi1 brand (mass fraction of Bi ≥98%) by dissolution of its grains in 9 M nitric acid, followed by hydrolytic purification of bismuth to remove impurity metals at pH 1.5–2.0 [7]. A disadvantage of this method is in that toxic nitrogen oxides are released into the gas phase in the stage of preparation of bismuth nitrate solutions, because the dissolution process occurs in accordance with the equation

$$Bi + 6HNO_3 = Bi(NO_3)_3 + 3NO_2\uparrow + 3H_2O. \quad (1)$$

It has been shown [8] that preliminary oxidation of metallic bismuth with atmospheric oxygen to give a technical-grade oxide makes it possible to reduce the expenditure of nitric acid by a factor of 2 and to eliminate release of nitrogen oxides into the atmosphere in the stage of preparation of bismuth nitrate solutions. This is so because the dissolution process is described in this case by the equation

$$Bi_2O_3 + 6HNO_3 = 2Bi(NO_3)_3 + 3H_2O. \quad (2)$$

Hydrobromic acid well dissolves bismuth oxide, as also does nitric acid, and the dissolution reaction has the form

$$Bi_2O_3 + 6HBr = 2BiBr_3 + 3H_2O. \quad (3)$$

It is of practical interest in this context to study synthesis of bismuth(III) oxobromide directly from solutions produced by dissolution of technical-grade bismuth oxide in nitric or hydrobromic acid.

This communication reports on a study of the influence exerted by the concentration of bromide ions and the process temperature on the purity and degree of bismuth(III) oxobromide precipitation from nitrate and bromide solutions. The metal was oxidized in a stainless steel reactor equipped with a screw for melt agitation. A single batch charged into the oxidation reactor was 150–160 kg. The metal was melted at a temperature of 350°C and bismuth oxide from the preceding stage of oxidation of metallic bismuth was introduced in an amount of 20% into the melt under agitation. The temperature was raised to 600°C and the powder was agitated for 6 h. The technical-grade oxide contained 88.4% bismuth.

Hydrolytic processing of technical-grade bismuth oxide I to give oxobromides II–IV

Product	Content, %					
	Pb	Cu	Ag	Fe	Zn	Cd
I	1.08	8.7×10^{-3}	5.0×10^{-2}	5.6×10^{-3}	5.8×10^{-4}	27×10^{-3}
II	6.2×10^{-2}	7.5×10^{-4}	3.0×10^{-3}	1.0×10^{-3}	2.0×10^{-5}	5.0×10^{-5}
III	0.22	7.8×10^{-4}	9.0×10^{-3}	5.2×10^{-4}	1.2×10^{-5}	3.6×10^{-5}
IV	4.8×10^{-5}	1.0×10^{-6}	2.0×10^{-6}	$<1.0 \times 10^{-4}$	1.0×10^{-5}	5.0×10^{-6}

Its composition (I) in terms of impurity metals is presented in the table.

A bismuth(III) nitrate solution containing 380 and 110 g l^{-1} of Bi(III) and free nitric acid, respectively, was prepared by dissolving technical-grade oxide in 6 M nitric acid. The composition corresponded to that of solutions commonly used in the technology of bismuth compounds. A bismuth(III) bromide solution containing 385 g l^{-1} of bismuth and 70 g l^{-1} of free hydrobromic acid was obtained by dissolving technical-grade bismuth(III) oxide in 7 M hydrobromic acid. The volume ratio between the starting and final bismuth-containing solutions was 1 : 10. Upon addition of hydrobromic acid or an ammonium bromide solution to the bismuth nitrate solution, it was adjusted by addition of distilled water.

The bismuth-containing bromide solution was processed by its dilution with distilled water (1 : 9). This was done in glass vessels with the use of stirrers. The mixture was agitated for 20 min. After settling for 0.5 h, the precipitate was filtered off with the use of a vacuum, washed on the filter with distilled water, and dried in air. An X-ray phase analysis (XPA) of the precipitation products was made on a DRON-3 diffractometer with Cu_{K_α} radiation, counter rotation rate of 0.5 deg min^{-1}, and I = 4000. Curves of differential thermal analysis (DTA) and thermogravimetry (TG) were measured for the samples under study on an MOM derivatograph (Hungary) at a heating rate of 10 deg min^{-1}. Electron microscopic images of the products were obtained using a JSMT-20 scanning electron microscope with a resolution of 200 Å. The specific surface area of the samples obtained was measured by the chromatographic method of thermal desorption of argon. Macroscopic amounts of bismuth(III) in the liquid and solid phases were determined by titration with a solution of Complexon III, with Xylenol Orange as indicator, and microscopic amounts, by photocolorimetry in the presence of KI. The concentrations of metals (Pb, Ag, Cu, Fe, Zn) were determined by the atomic-absorption method on a Saturn 2M spectrophotometer. The precipitation products were preliminarily dissolved in nitric acid (1 : 1). The concentration of nitrate ions was found by voltammetry on a renewable copper electrode [9], and that of bromide ions, on a silver electrode, after being transferred to solution by preliminary treatment with a sodium hydroxide solution (2 M) at 70–90°C.

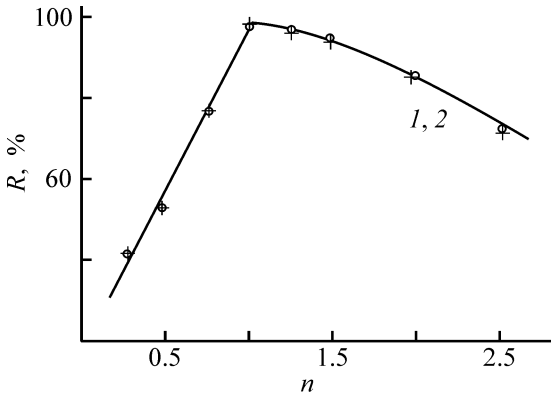

Fig. 1. Degree R of bismuth(III) precipitation from a nitrate solution vs. the molar ratio n between bromide ions and bismuth(III) in the system. Process temperature (°C): (*1*) 22 and (*2*) 90.

The study of the hydrolytic processing of bismuth-containing bromide solutions demonstrated that, upon their dilution with distilled water (1 : 9), the degree of bismuth(III) recovery into oxobromide at 25 and 65°C is 97.9 and 96.5%, respectively. In precipitation of bismuth(III) from nitrate solutions by addition of a hydrobromic acid solution, the dependence of the degree R of metal precipitation on the molar ratio n between bromide ions and bismuth in solution passes through a maximum at 1.0–1.1 (Fig. 1). In this case, the degree of bismuth(III) precipitation is 99.4%. The decrease in the degree of bismuth(III) precipitation at $n > 1$ is due to the formation of bromide complexes of the type $BiBr_x^{3-x}$ in solution [11], which hinders bismuth precipitation in the form of oxobromide. It can also be seen in Fig. 1 that raising the process temperature has virtually no effect on

the degree of bismuth(III) recovery into a precipitate. It should be noted that solutions of both hydrobromic acid and ammonium bromide can be used for quantitative precipitation of bismuth(III). With ammonium bromide used as a donor of bromide ions, the degree of bismuth recovery into the precipitate somewhat increases to become 99.6% at $n = 1.0$.

Bismuth oxobromide has clearly pronounced diffraction peaks at d 8.10, 4.05, 3.52, 2.82, 2.77, 1.96, and 1.61 Å (Fig. 2) [12]. It follows from the results of X-ray studies that, in bismuth precipitation from nitrate solutions to which bromide ions were added, the positions of these peaks remain virtually unchanged, irrespective of the nature of the solutions used (Fig. 2, curve *1*). This confirms that bismuth precipitates from these solutions as the oxobromide BiOBr in the pH range under study (0–3). X-ray studies also demonstrate that bismuth(III) precipitation from bromide solutions upon addition of water to these solutions depends both on the process temperature and on the order in which reagents are introduced. At a process temperature of 22°C and addition of a bismuth bromide solution to water, the X-ray pattern of the product corresponds to bismuth oxobromide (Fig. 2, curve *2*). If, however, water is added to a bismuth bromide solution (Fig. 2, curve *3*) or the process is performed at an elevated temperature (90°C) (Fig. 2, curve *4*), an additional reflection appears in the X-ray diffraction patterns at $d = 6.32$ Å. As a result of washing of these products with water, this reflection disappears. An analysis demonstrated that the washing solution contains hydrogen ions and bromide ions. This indicates that, in bismuth precipitation from bromide solutions (ratio between bromide ions and bismuth equal to 3.8), the product can capture hydrobromic acid, which can be removed in the stage of product washing with water.

DTA and TG data for bismuth oxobromide samples obtained by processing of nitrate solutions (Fig. 3a) indicate that the product is stable in a wide temperature range. On heating of bismuth oxobromide, the loss of mass begins at temperatures higher than 600°C, which is due to sublimation of bismuth in the form of bromide to give oxobromides with a Bi : Br molar ratio exceeding unity [13]. In the case of samples obtained by bismuth precipitation from bromide solutions (Fig. 3b), the loss of mass begins at 250°C and is complete at 300°C. In this case, the loss of mass is 6.3% for a product obtained upon addition of water to a bismuth-containing solution at a process temperature of 22°C and 2.7% in the case of a reverse order of addition of the reagents. When synthesis is performed at 90°C, the loss of mass by the product upon

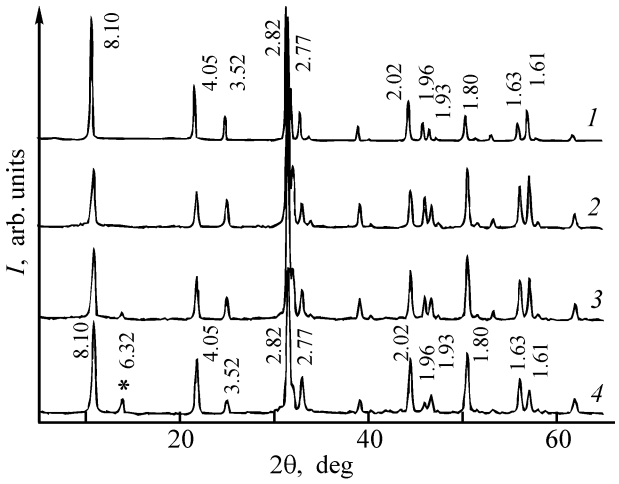

Fig. 2. X-ray diffraction patterns of bismuth oxobromides obtained by precipitation from (*1*) nitrate solutions and (*2*–*4*) bromide solutions, with (*2*, *4*) a bismuth solution added to water and (*3*) water added to a bismuth solution. (*I*) Intensity and (2θ) Bragg angle. Temperature (°C): (*1*) 65, (*2*) 22, and (*4*) 90.

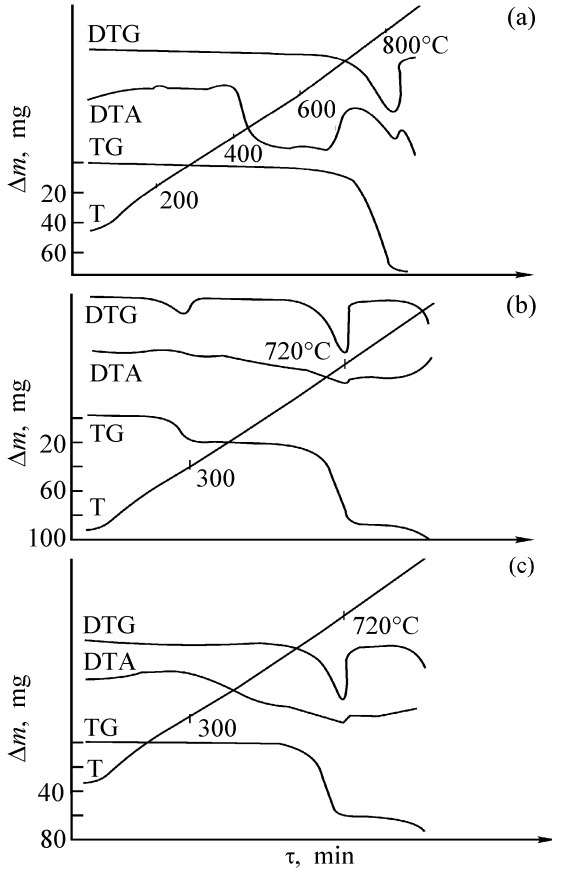

Fig. 3. Thermograms of bismuth oxobromides obtained by precipitation from (a) nitrate and (b) bromide solutions and (c) of bismuth oxobromide formed by thermal treatment of the product at 300°C. Sample mass 300 mg. (Δm) Loss of mass and (τ) time.

calcination is 6.7% in both cases. A chemical analysis of a product calcined at 300°C and kept in air for 10 days demonstrated that this product is pure bismuth oxobromide (its thermogram is shown in Fig. 3c). It should be noted here that the product obtained from bromide solutions has a yellowish tint, which disappears upon washing with water or calcination at 300°C.

Analysis of IR absorption spectra of bismuth oxobromides obtained by precipitation from both nitrate and bromide solutions, and of the same oxobromides calcined at 300°C, shows that all these spectra contain in the spectral range under study (400–4000 cm^{-1}) only a single band associated with symmetric stretching vibrations of the Bi–O bond (510 cm^{-1}) of the A_{2u} type.

According to the results of electron-microscopic studies of hydrolysis products, bismuth oxobromide produced by precipitation from nitrate and bromide solutions has in all cases, irrespective of the order in which reagents are poured-in, the form of aggregates composed of thin-lamellar oval microcrystals with a size of 0.3–3 μm in the basal plane and a thickness of about 0.1 μm. On washing with water, the morphology of the initial microcrystals remains virtually unchanged. The specific surface areas of bismuth(III) oxobromides obtained at 22 and 65°C from nitrate solutions are 1.7 and 1.3 $m^2 g^{-1}$, respectively, and of those formed at 22 and 90°C from bromide solutions, 1.9 and 1.2 $m^2 g^{-1}$. The order of introduction of the reagents has virtually no effect on the specific surface area of the product. In the case of washing with water of a bismuth oxobromide having a specific surface area of 1.2 $m^2 g^{-1}$, it increases to 3.0 $m^2 g^{-1}$, and upon calcination at 300°C, decreases to 1.0 $m^2 g^{-1}$. A product with a specific surface area of 23 $m^2 g^{-1}$ was obtained by bismuth precipitation from dilute [20 $g l^{-1}$ Bi(III)] bromide solutions.

In order to synthesize bismuth(III) oxobromide of increased purity, the possibility of its purification to remove basic impurity metals in precipitation from bromide media was assessed. A processing of bismuth-containing bromide solutions diluted with water (1 : 9) at a process temperature of 65°C, with the subsequent washing of the precipitate with water at 65 ± 5°C and drying of the product at 100°C, yielded bismuth(III) oxobromide whose composition (II) is listed in the table. The results of an analysis of the product obtained indicate that processing of bismuth-containing bromide solutions does not involve effective purification of bismuth to remove lead, silver, and iron. In this context, the possibility of obtaining bismuth oxobromide from nitrate solutions commonly used in synthesis of bismuth compounds was analyzed. Precipitation of bismuth(III) from nitrate solutions in the form of an oxobromide at a molar ratio between bromide ions and bismuth equal to 1.05, as well as its precipitation from bromide solutions, fails to provide effective purification of bismuth to remove lead and silver [see table, composition (III)].

Precipitation of bismuth from nitrate solution in the form of a compound of composition $[Bi_6O_5(OH)_3](NO_3)_5 \cdot 3H_2O$ enables its effective purification to remove impurity metals. This process is used to synthesize special-purity bismuth(III) oxide [14]. Therefore, in order to obtain high-purity bismuth oxobromide, it is advisable to preliminarily purify bismuth nitrate solutions to remove associated metals by precipitation of bismuth in the form of an oxo hydroxonitrate, followed by its dissolution in nitric acid.

In view of the aforesaid, the variant of bismuth oxobromide synthesis by precipitation from nitrate solutions was chosen for larger-scale tests. An additional advantage of this process is that it yields solutions more concentrated in terms of bismuth in the stage of dissolution of the technical-grade oxide and enables use of stainless steel apparatus employed in synthesis of other bismuth compounds. Metallic bismuth of the Vi1 brand was used in the tests.

High-purity bismuth(III) oxobromide was synthesized by its precipitation from a bismuth nitrate solution upon addition of a hydrobromic acid solution at a molar ratio between bromide ions and bismuth equal to 1.05 and a process temperature of 65°C. The precipitate was twice washed with distilled water at 65°C and dried at 100°C. The tests yielded bismuth(III) oxobromide containing (%) 68.54 bismuth, 26.21 bromide ions, and less than 1×10^{-3} nitrate ions. The contents of impurity metals in product (IV) are listed in the table. The degree of bismuth recovery from the technical-grade oxide into oxobromide is 90.3%.

CONCLUSIONS

(1) Bismuth(III) is virtually completely precipitated as an oxobromide of composition BiOBr from bromide solutions upon their dilution with water and from nitrate solutions upon addition of bromide ions.

(2) The product obtained in processing of bromide solutions may contain hydrobromic acid, which is removed by washing of the product with water or its calcination at 300°C.

(3) To obtain high-purity bismuth oxobromide from technical-grade products, it is necessary to preliminarily purify bismuth to remove associated metals by its precipitation from nitrate solutions in the form of a compound of composition $[Bi_6O_5(OH)_3](NO_3)_5 \cdot 3H_2O$.

REFERENCES

1. Polyvyannyi, I.R., Ablanov, A.D., and Batyrbekova, S.A., *Vismut (Bismuth)*, Alma-Ata: Nauka, 1989.
2. Yukhin, Yu.M. and Mikhailov, Yu.I., *Khimiya vismutovykh soedinenii i materialov* (Chemistry of Bismuth Compounds and Materials), Novosibirsk: Sib. Otd. Ross. Akad. Nauk, 2001.
3. Dolgikh, V.A., Kholodkovskaya, L.N., and Popovkin, B.A., *Zh. Neorg. Khim.*, 1996, vol. 41, no. 6, pp. 970–975.
4. *Handbuch der praparativen anorganischen Chemie*, Bd. 3, von Brauer, G., Huber, F. et al., Eds., Stuttgart: Ferdinand, 1981.
5. *Gmelins Handbuch der anorganischen Chemie, 8 Auflage, Wismut*, Weinheim Bergstr: Chemie, 1964.
6. USSR Inventor's Certificate, no. 1116011.
7. Karyakin, Yu.V. and Angelov, I.I., *Chistye khimicheskie veshchestva* (Pure Chemical Substances), Moscow: Khimiya, 1974.
8. Yukhin, Yu.M., Daminova, T.V., and Smirnov, V.I., *Khim. Interesakh Ustoich. Razv.*, 1999, vol. 7, pp. 745–749.
9. Aleksandrova, T.P. and Kletenik, Yu.B., *Zh. Anal. Khim.*, 1994, vol. 49, pp. 615–619.
10. Kletenik, Yu.B., Tarasova, V.A., and Bek, R.Yu., *Zh. Anal. Khim.*, 1987, vol. 42, pp. 891–896.
11. Fedorov, V.A., Kalosh, T.N., Shmyd'ko, L.I., and Mironov, V.E., *Zh. Neorg. Khim.*, 1972, vol. 17, no. 8, pp. 2089–2095.
12. JCPDS-International Center for Diffraction Data, 1995.
13. Nurgaliev, B.Z., Popovkin, B.A., and Stefanovich, S.Yu., *Zh. Neorg. Khim.*, 1983, vol. 28, pp. 2207–2211.
14. Yukhin, Yu.M., Mikhailov, Yu.I., Afonina, L.I., and Podkopaev, O.A., *Vysokochist. Veshch.*, 1996, no. 4, pp. 62–71.

ISSN 1070-4272, Russian Journal of Applied Chemistry, 2007, Vol. 80, No. 12, pp. 2020–2023. © Pleiades Publishing, Ltd., 2007.
Original Russian Text © V.G. Mayorov, A.I. Nikolaev, V.K. Kopkov, L.A. Safonova, N.V. Serba, 2007, published in Zhurnal Prikladnoi Khimii, 2007, Vol. 80, No. 12, pp. 1942–1945.

INORGANIC SYNTHESIS AND INDUSTRIAL INORGANIC CHEMISTRY

Study of Conditions of Vanadium(IV, V) Leaching from Ash

V. G. Mayorov, A. I. Nikolaev, V. K. Kopkov, L. A. Safonova, and N. V. Serba

Tananaev Institute of Chemistry and Technology of Rare Elements and Mineral Resources, Kola Scientific Center, Russian Academy of Sciences, Apatity, Murmansk oblast, Russia

Received May 2, 2007

Abstract—Leaching of vanadium(IV, V) with water and a NaOH solution from ash produced in black oil combustion was studied.

DOI: 10.1134/S1070427207120029

The world production and consumption of vanadium has been steadily growing, especially in recent years. Vanadium is one of the most promising alloying elements. Vanadium has acquired particular importance as an element that can considerably improve, even when present in low concentrations (0.03–0.15%), the physicochemical, technological, and service characteristics of steels. For example, introduction of vanadium in amounts of hundredths to tenths of a percent (0.06–0.12%) into steels of various brands raises their hardness by 15–30%. These properties of vanadium and its low cost in comparison with other alloying metals, such as tungsten, molybdenum, and niobium, make it the most preferable additive in manufacture of low-alloy steels, the extent of whose industrial application has become an important indication of advances in technology. There is steadily growing demand for low-alloy steels for industrial and civil engineering, construction of natural gas and oil pipelines, and automotive industry. Vanadium and its compounds are also widely used in many other industries.

Vanadium is widely abundant in nature. Its content in the earth crust is higher than of, e.g., copper, zinc, and lead. At the same time, vanadium is a considerably more scattered element and industrial deposits of vanadium ores proper are scarce. Therefore, recovery of compounds with this element from various half-products, such as, e.g., ashes formed in black oil combustion, is a topical issue. The vanadium content of high-sulfur oils is as high as 300 g per ton, and that of ash, up to 10–20 wt % V_2O_5. The extraction of vanadium is also necessitated by ecological regulations, because vanadium compounds are highly toxic. The maximum permissible concentration (MPC) of V_2O_5 in air is 0.0001 mg l^{-1} [1–8].

This communication reports on a study of recovery of vanadium compounds from ash formed in black oil combustion (Kirov Heat and Power Plant, Apatity, Murmansk oblast). The ash was ground in a ball mill and sieved, with the <0.2-mm fraction used in the experiments (yield of this fraction, 76%). The ash composition is listed in Table 1. The results of X-ray

Table 1. Chemical composition of ash and mass loss Δm upon heating

Ash	Content, wt %							Δm, %, (T,* °C)
	V_2O_5	Ni	Fe	S	C	SiO_2	P	
Initial**	9.67	1.6	15.6	12.9	6.81	1.13	0.065	2.2 (100) 9.6 (400)
Calcined at T, °C:								
600	16.6	–	–	3.62	0.016	–	–	20.8 (600)
900	18.9	–	–	0.02	0.013	–	0.10	49.4 (900)

* Heating temperature is given in parentheses.

** According to emission spectral analysis, ash calcined at 400°C contains (wt %): Mg ~0.1, Ti, Cr ~0.2; Ca, Mn ~0.3, and Al 0.3–1.

Table 2. Leaching of vanadium(IV, V) with water at 20°C

Experiment no.	s : l	τ, h	Concentration of V_2O_5 in the liquid phase, g l^{-1}	Mass of residue after leaching and calcination at 400°C, g	Degree of V(IV–V) recovery into solution, %
1	1 : 3	12	17.0	–	61.5
2	1 : 3	20	23.0	2.6	87.6
3	1 : 5	~100	12.5	2.7	71.1
4	1 : 10*	6	7.1	–	89.6

* Leaching with a 200 g l^{-1} H_2SO_4 solution at 50°C.

Table 3. Leaching of vanadium(IV, V) with a 100-g l^{-1} NaOH solution (agitation time 6 h)

Experiment no.	s : l	*T*, °C	Concentration of V_2O_5 in the liquid phase, g l^{-1}	Mass of residue after leaching and calcination at 400°C, g	Degree of V(IV–V) recovery into solution, %
1	1 : 5	20	7.5	5.45	38.7
2	1 : 3	50	15.0	–	57.4
3	1 : 3*	20	17.0	5.77	62.3
4**	1 : 10	50	8.5	4.40	75.6
5	1 : 10	100	8.5	–	70.3***
6	1 : 5	50	7.1	–	48.5****

* Leaching time 20 h.

** Calcination at 600°C before leaching;

*** After additional treatment with a 150-g l^{-1} solution of Na_2CO_3 (s : l = 1 : 10, temperature 100°C), the total degree of extraction was 83.7%.

**** After calcination of the residue at 800°C and second leaching with a 100-g l^{-1} NaOH solution (s : l = 1 : 5, 50°C) the total degree of extraction was 94.2%.

phase and other physicochemical analyses tentatively suggest that the ash contains Fe(II) and Fe(III) hydroxides, Fe(II) and Fe(III) sulfates, $VOSO_4$, and V(III)-iron and Ni(II)-iron spinels. Preliminary experiments demonstrated that, upon treatment of ash with water and acid and alkaline solutions, a major part of vanadium compounds easily pass into the liquid phase. This shows that vanadium is present in ash mainly as V(IV) and V(V), and only partly, as V(III). V(IV) compounds are more stable in acid solutions, and V(V) compounds, in alkaline solutions. Vanadium(III) is present in the ash in form of spinels, which are known to be difficult to decompose. Therefore, to make the overall recovery of vanadium compounds higher, the ash was subjected to oxidative calcination in some experiments, as in the case of processing of vanadium slag, in order to convert V(III) to V(IV) and V(V) [1–4, 9].

Tables 2 and 3 present results obtained in recovery of vanadium(IV, V) from the ash. The weighed portion was 10 g. Leaching was performed under agitation. The precipitate formed upon treatment with the reagent was filtered and washed with water, and the wash water was combined with the main filtrate. The ash was calcined for 8 h, with NaCl and $NaNO_3$ preliminarily added in amounts of 25 and 2%, respectively, relative to the mass of the product. Vanadium was determined by atomic emission spectroscopy with inductively coupled plasma.

Because of the hydrolysis of iron sulfates, water treatment of ash results (Table 2) in a decrease in the pH of the liquid phase to approximately 2 (at s : l = 1 : 3), i.e., leaching is, in fact, performed with a dilute H_2SO_4 solution. With the leaching time τ raised from 12 to 20 h (run nos. 1 and 2), the degree of vanadium(IV, V) recovery increases to 87.6%. However, iron sulfates pass into the liquid phase together with vanadium(IV, V), which is indicated by the small mass of the precipitate formed upon the treatment of the ash with water.

Raising the solid-to-liquid ratio (run no. 3) makes lower the degree of V(IV, V) recovery. A possible reason is that an increase in water expenditure diminishes the solution acidity, and, as consequence, impairs leaching of vanadium compounds. This is con-

firmed by the results of run no. 4, in which the degree of the V(IV, V) recovery from the ash by treatment with a H_2SO_4 solution (200 g l^{-1}) was 89.6%. It can be tentatively concluded that acid leaching provides a 90% transfer of vanadium into the liquid phase. Presumably, more complete recovery is only possible upon introduction of a stage of oxidative calcination.

The leaching of ash with alkaline solutions was studied in more detail (Table 3), because, in this case, transfer of Fe(II) and Fe(III) to the liquid phase is impossible. At the same time, the degree of V(IV, V) recovery in the case of leaching with NaOH solution at s : l = 1 : 5 and room temperature was only 38.7% (run no. 1). Intensification of the leaching by raising the process temperature (Table 3, run no. 2), making longer the treatment time (run no. 3), or introducing a calcination stage and making larger the solid-to-liquid ratio and elevating temperature (run no. 4) essentially improved the transfer of V(IV, V) to the solution. An even better recovery of vanadium compounds was achieved in a two-stage leaching (Table 3, run no. 5) and a two-stage treatment with an intermediate calcination (run no. 6), with the total degree of V(IV, V) transfer to the liquid phase as high as 83.7 and 94.2%, respectively. However, the alkali leaching of ash is, on the whole, less efficient than acid leaching, and acceptable results were only obtained by introducing additional procedures, which makes the technology more expensive.

Other modes of ash treatment with joint use of calcination, acid leaching, and alkali leaching were also tested in the study. In successive leaching with a solution of 100 g l^{-1} HCl (s : l = 1 : 10), calcination at 800°C, and leaching with a NaOH solution (100 g l^{-1}, s : l = 1 : 10), the total degree of recovery was 97.2%. In the case of a preliminary calcination at 900°C, followed by leaching, first, with a NaOH solution (100 g l^{-1}, s : l = 1 : 5, 50°C) and then, with a H_2SO_4 solution (75 g l^{-1}, s : l = 1 : 5), the total degree of V(IV, V) transfer into solution was as high as 99.25%. In these experiments, the V(IV, V) recovery is close to 100%; however, the mass of the residue obtained after the joint treatment is small, which shows that V(IV, V) and Fe(II, III) are not separated. Moreover, these modes are labor consuming and expensive.

Analysis of the experimental data leads to a tentative conclusion that the leaching conditions in which V(IV, V) virtually completely passes into the solution and Fe(II, III) remains in the solid phase have not been found so far. The optimal leaching conditions are as follows: (1) treatment with water and (2) double leaching with alkaline solutions.

Naturally, leaching with water is attractive because of its simplicity. The solution obtained in this mode contained about 20 g l^{-1} V_2O_5. With this solution, two ways to separate V(IV, V) from Fe(II, III) were tested. The first of these consisted in hydrolysis and precipitation of NH_4VO_3 by addition of a NH_4Cl solution [1, 2, 9]. In the course of the hydrolysis (pH 1–2, 80–90°C, 2 h), separation was not achieved because the above components precipitated in nearly equal amounts.

In the second variant, Fe(II, III) hydroxides were preliminarily recovered from solution by neutralization with a NaOH solution to pH ~9, after which NH_4VO_3 was precipitated by addition of a NH_4Cl solution (270 g l^{-1}). To raise the degree of extraction, the precipitate of Fe(II, III) hydroxides was treated with a NaOH solution and NH_4VO_3 was also precipitated from the liquid phase after filtration. The NH_4VO_3 precipitate was washed with a NH_4Cl solution (20 g l^{-1}) and calcined at 500°C to obtain V_2O_5. The total direct yield of V_2O_5 from the ash into the final product was about 50%. An emission spectral analysis of V_2O_5 revealed the following impurities (wt %): 0.1–0.3 Al, 0.03–0.1 Si, 0.01–0.03 Fe, and ~0.01 Ni. With account of the possible recycling, the yield of V_2O_5 can be raised to 75% and higher.

A promising avenue of research is direct use of ash as an alloying additive in steel melting. In this case, it is unnecessary to separate V(IV, V) and Fe(II, III). The mass of ash decreases two-fold upon calcination at 900°C, with the content of carbon and, especially, sulfur sharply decreasing (Table 1). It is known that high-quality steels should contain less than 0.01% phosphorus and sulfur [5, 6, 8]. In widely used steels, the content of vanadium does not exceed 0.2%. The calcined ash contains 18.9% V_2O_5 or 10.6% V (Table 1), which exceeds that in steels by approximately a factor of 50. Accordingly, in the case when calcined ash is used as an alloying additive, the content of P and S introduced into the steels with the ash will be considerably lower than the value specified above (0.01%). The presence of nickel in ash is also a positive factor.

CONCLUSIONS

(1) It was found that, under the optimal conditions, the degree of vanadium(IV, V) recovery into solution is 87.6% in the case of leaching with water, 83.7% in two-stage leaching with alkaline solutions, and more than 97% in the case of joint use of calcination, acid leaching, and alkaline leaching.

(2) It was demonstrated that calcined ash containing 19 wt % V_2O_5 can be used as an alloying additive to steels.

REFERENCES

1. Kieffer, R. and Braun, H., *Vanadin, Niob und Tantal*, Berlin: Springer, 1963.
2. Muzgin, V.N., Khamzina, L.B., Zolotavin, V.L., and Bezrukov, I.Ya., *Analiticheskaya khimiya vanadiya* (Analytical Chemistry of Vanadium), Moscow: Nauka, 1981.
3. Leont'ev, L.I., Zhuchkov, V.I., Sheshukov, O.Yu., and Zaiko, V.P., *Resursy. Tekhnol. Ekonom.*, 2006, no. 1, pp. 8–14.
4. Anufrieva, S.I., Sladkova, G.A., Losev, Yu.N., and Tigunov, L.P., *Materialy 7-oi vserossiiskoi nauchno-prakticheskoi konferentsii "Ekologicheskie problemy promyshlennykh raionov"* (Proc. 7th All-Russian Sci.-Pract. Conf. "Ecological Problems in Industrial Regions"), Yekaterinburg: AMB, 2006, pp. 162–163.
5. Sorokin, V.G., Volosnikova, A.V., Vyatkin, S.A., et al., *Marochnik stalei i splavov* (Reference Book of Steels and Alloys), Sorokin, V.G., Ed., Moscow: Mashinostroenie, 1989.
6. Filippenkov, A.A., *Vanadiisoderzhashchie stali dlya otlivok* (Vanadium-containing Steels for Casting), Yekaterinburg: Sib. Otd. Ross. Akad. Nauk, 2001.
7. Smirnov, L.A., Deryabin, Yu. A., and Shavrin, S.V., *Metallurgicheskaya pererabotka vanadiisoderzhashchikh titanomagnetitov* (Metallurgical Processing of Vanadium-containing Titanomagnetites), Chelyabinsk: Metallurgiya, 1990.
8. Nesterov, D.K., Fomin, N.A., Gordienko, M.S., et al., *Stal' dlya vysokokachestvennykh rel'sov* (High-Quality Rail Steels), Kharkov: Ukr. Nauchno-Issled. Inst. Metallurgii, 1995.
9. Cotton, F.A. and Wilkinson, G., *Advanced Inorganic Chemistry*, New York: Wiley, 1962.

ISSN 1070-4272, Russian Journal of Applied Chemistry, 2007, Vol. 80, No. 12, pp. 2024–2027. © Pleiades Publishing, Ltd., 2007.
Original Russian Text © I.V. Goshu, Yu.V. Tsarev, V.V. Kostrov, 2007, published in Zhurnal Prikladnoi Khimii, 2007, Vol. 80, No. 12, pp. 1946–1949.

INORGANIC SYNTHESIS AND INDUSTRIAL INORGANIC CHEMISTRY

Study of Chromium(VI) Reduction in the Presence of Metal Salt Additives

I. V. Goshu, Yu. V. Tsarev, and V. V. Kostrov

Ivanovo State University of Chemical Engineering, Ivanovo, Russia

Received May 10, 2006; in final form July, 2007

Abstract—Reduction of Cr(VI) to Cr(III) in a model wastewater in the presence of copper, iron, and nickel nitrates, sulfates, and chlorides was studied. The effect of the process temperature on the final pH values of the solutions was examined.

DOI: 10.1134/S1070427207120030

Chromium is a hazardous impurity in the environment, with the form Cr(VI) being the most toxic. To prevent discharge of this form of chromium into the environment, it is necessary to reduce Cr(VI) to Cr(III) and to remove it from wastewater. Beukes and co-workers studied reduction of Cr(VI) with sulfites in wastewater [1]. The experiments were carried out in an aqueous solution of $Na_2Cr_2O_7 \cdot 2H_2O$ at various pH values and contact durations. It was shown that the rate of Cr(VI) reaction with sulfites strongly depends on the pH of the reaction mixture. As pH increases from 2.0 to 5.0, the rate of Cr(VI) reduction decreases. This process is in many respects analogous to Cr(VI) reduction in neutral aqueous media by Fe(II) ions; however, Fe(II) is effective in a wider pH range.

The catalytic analytical methods used to determine components in redox reactions and the mechanism of catalytic action were considered in [2]. This mechanism consists in that the oxidized form of the catalyst vigorously reacts with a reducing agent, and the resulting product is rapidly oxidized under the action of the oxidizing agent. The reaction of Fe^{3+} ions with thiosulfate, which is catalyzed only by copper(II) ions, was considered as an example.

According to the data of Smirnov and co-workers [3], metal-organosiloxanes containing a transition metal (including copper) that is used in traditional catalysts, can be chosen for homogeneous catalysis. It was shown that the activity of copper-containing compounds is rather high.

The reduction of iron(III) to iron(II) with sodium sulfite was studied in [4]. It was found that the maximum yield of iron(II) is observed in the pH range 2.8–3.0, with the yield of iron(II) decreasing as pH increases.

It was of interest to study the Cr(VI) reduction in aqueous solutions containing copper, iron, and nickel nitrates additives. The reason why these additives are used is due to the necessity for acceleration of the process of Cr(VI) reduction, because it is rather slow in neutral media [1].

The aim of this study was to examine the effect of the process temperature T and duration τ on the Cr(VI) reduction to Cr(III) in the presence of $Cu(NO_3)_2$, $Fe(NO_3)_3$, and $Ni(NO_3)_2$ additives.

EXPERIMENTAL

We carried out experiments were carried out with a model wastewater solution based on chromic anhydride (CrO_3) with a Cr(VI) concentration of 100 mg l^{-1}. A 5% Na_2SO_3 solution was used as a reducing agent. The reduction was carried out in the presence of 10% aqueous solutions of $Cu(NO_3)_2$, $Fe(NO_3)_3$, and $Ni(NO_3)_2$ introduced into 100 ml of the model solution in amounts of 2 mg.

The content of Cr(VI) in the presence of Cr(III) in the model wastewater was determined by photometry [1].

The technique used in the kinetic experiments was described in [5]. The duration of the Cr(VI) reduction process was 60 min.

Previously, it has been found that the degree of Cr(VI) reduction in the model chromic acid solution

under study exceeds that in solutions of its salts [5]. It was noted that the higher degrees of Cr(VI) reduction are due to lower pH values of the reaction medium. Because the rate of chromium(VI) reduction in a neutral medium is extremely low, the reduction was accelerated with metal salts as catalysts: aqueous solutions of copper(II), iron(III), nickel(II), and sodium nitrates, and also solutions of copper and sodium sulfates and chlorides. Based on the data on the redox power of the substances present in the model solution, we made a thermodynamic analysis of the possibility of occurrence of various redox reactions. The standard reduction potentials of the systems under study [6, 7] are listed in the table.

Based on the results of the thermodynamic analysis and on the fundamental concepts of the theory of homogeneous catalysis [2, 7], we suggested a mechanism of the chromium(VI) reduction involving copper, iron, and nitrate ions.

Let us consider the reaction of Cr(VI) reduction

$$2H_2CrO_4 + 3SO_3^{2-} + H_2O \xrightarrow{[Cat]} 2Cr(OH)_3\downarrow + 3SO_4^{2-}. \quad (1)$$

Based on the data in the table and using the "Z" rule for determining the pathways of redox processes, we can assume that the following reactions can occur in the presence of copper(II) ions:

$$SO_4^{2-} + H_2O + 2e \rightarrow SO_3^{2-} + 2OH^-, \; E^0 = -0.93 \text{ V};$$

$$Cu^{2+} + e \rightarrow Cu^+, \qquad E^0 = +0.153 \text{ V};$$

$$2Cu^{2+} + SO_3^{2-} + 2OH^- \rightarrow 2Cu^+ + SO_4^{2-} + H_2O; \quad (2)$$

$$Cu^{2+} + e \rightarrow Cu^+, \qquad E^0 = +0.153 \text{ V};$$

$$CrO_4^{2-} + 8H^+ + 3e \rightarrow Cr^{3+} + 4H_2O, \; E^0 = 1.477 \text{ V};$$

$$3Cu^+ + CrO_4^{2-} + 8H^+ \rightarrow 3Cu^{2+} + Cr^{3+} + 4H_2O. \quad (3)$$

The difference of the standard potentials for reactions (2) and (3), $\Delta E^0 > 0$, is positive and, consequently, $G_p^0 > 0$, which points to a high thermodynamic probability of their occurrence. Based on the properties of Cu^{2+} ions in solution [2, 3], we can assume that the mechanism of the Cr(VI) reaction

Standard potentials of a number of redox systems present in the model solution

Reaction	E^0, V
$SO_4^{2-} + H_2O + 2e \rightarrow SO_3^{2-} + 2OH^-$	–0.93
$Cu^{2+} + e \rightarrow Cu^+$	+0.153
$CrO_4^{2-} + 8H^+ + 3e \rightarrow Cr^{3+} + 4H_2O$	+1.477
$NO^{3-} + 3H^+ + 2e \rightarrow HNO_2 + H_2O$	+0.94
$Fe^{3+} + e \rightarrow Fe^{2+}$	+0.771

with sodium sulfite is described by Eqs. (2) and (3). We estimated in a similar way the effect of iron(III) nitrate and confirmed the possibility of involvement of iron(III) ions in the reduction of Cr(VI) by sodium sulfite. It would be expected that nickel(II) nitrate can affect the Cr(IV) reduction only at temperatures exceeding 200°C.

The temperature dependences of the final pH value and of the degree of chromium(VI) reduction in the presence of various metal salt additives are shown in Figs. 1 and 2. It was shown in [5] that the solution pH changes because of the nonbuffer nature of the model solution under study. The temperature dependence of pH of the model wastewater solution after the reduction of chromium(VI) to chromium(III) in this wastewater at a $Na_2SO_3 : H_2CrO_4$ ratio of 3 : 1 is shown in Fig. 1. It is seen that the final pH values of the model wastewater differ from the initial values. For example, the initial pH value of the model wastewater is 5.3–5.5. In the course of the reduction of chromium(VI) to chromium(III) upon addition of

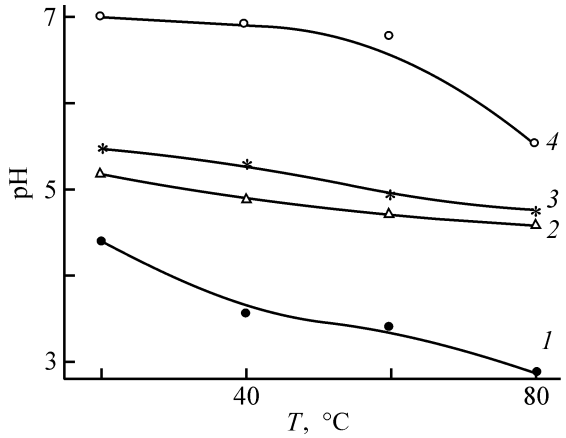

Fig. 1. Final pH value vs. temperature T of the model solution in the presence of various salts. $H_2CrO_4 : Na_2SO_4$ = 1 : 3; the same for Fig. 2. Additive: (*1*) $Fe(NO_3)_3$, (*2*) $Ni(NO_3)_2$, (*3*) $Cu(NO_3)_2$, and (*4*) none.

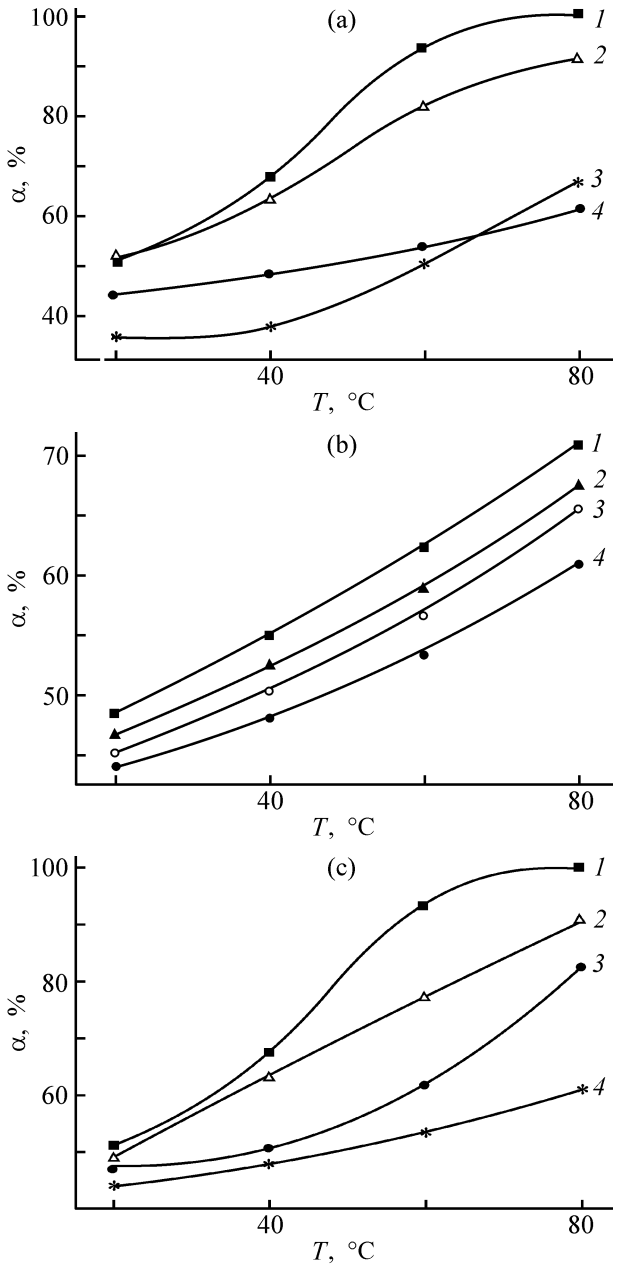

Fig. 2. Degree α of Cr(VI) reduction vs. temperature *T* in model solutions (*1*–*3*) containing various additives and (*4*) free of additives. Addition: (a) (*1*) $Cu(NO_3)_2$, (*2*) $Fe(NO_3)_2$, (*3*) $Ni(NO_3)_2$; (b) (*1*) $NaNO_3$, (*2*) NaCl, (*3*) Na_2SO_4; (c) (*1*) $Cr(NO_3)_2$, (*2*) $CuCl_2$, (*3*) $CuSO_4$.

Na_2SO_3, the final pH value of the model solution increases. The system constituted by sodium sulfite and chromic acid free of metal nitrates is characterized by higher final pH values (up to 6.5–7.0). This is due to the presence of an excess amount of sodium sulfite in the solution, which favors an increase in the solution pH. Thus, the degree of chromium(VI) reduction correlates with the change in pH during the reduction, which may be due to the completeness of sodium sulfite consumption in the course of the reaction.

For the systems constituted by sodium sulfite and chromic acid with copper and nickel nitrate additives, the pH values virtually do not vary with the reduction temperature, whereas for the system with iron nitrate, pH decreases from 4.5 to 3.0. Similarly to the case of the system without metal nitrate additives, the final value of the solution pH is determined by the degree of chromium reduction and, hence, by the completeness of sodium sulfite consumption in the reduction reaction.

The temperature dependence of the degree α (%) of chromium(VI) reduction in the presence of Cu^{2+}, Fe^{3+}, and Ni^{2+} cations and nitrate anions at H_2CrO_4 : Na_2SO_3 = 1 : 3 is shown in Fig. 2. It is seen that addition of metal nitrates raises the degree of chromium(VI) reduction to 95–99% for Cu(II) and 82–90% for Fe(III) at 60–80°C. The only exception is the system with nickel nitrate, for which the degree of chromium reduction (30%) at 20–40°C is even somewhat lower than that for the system without an additive.

Such a behavior of the system constituted by chromic acid, sodium sulfite, and nickel nitrate results from the fact that the reaction of sodium sulfite with chromium(VI) is rather slow because of the high pH value of the solution. At 60–80°C, the degree of reduction increases to 60%, which can be attributed to involvement of nitrate ions. This is confirmed by the experimental data in Fig. 2b, which demonstrate the effect of anions (nitrate, chloride, and sulfate) on the chromium(VI) reduction. It was found that higher degrees of chromium(VI) reduction are observed in model solutions containing nitrate ions.

Because nickel has a stable oxidation state +2, its ions are not involved in the chromium(VI) reduction, which is confirmed by experimental data (Fig. 2a).

Under the experimental conditions, the temperature of the model aqueous solution of chromium(VI) did not exceed 80°C, and, therefore, formation of high positive oxidation states of nickel is unlikely [8].

At the same time, nickel ions can inhibit the chromium(VI) reduction via formation of nickel chromates by the scheme [8, 9]:

$$[Ni(H_2O)_6]^{2+} \rightarrow Ni^{2+} + 6H_2O, \quad (4)$$

$$Ni^{2+} + CrO_4^{2-} \rightarrow NiCrO_4. \quad (5)$$

The efficiency of the influence exerted by cations on the degree of Cr(VI) reduction to Cr(III) in

the systems under consideration decreases in the order $Cu^{2+} > Fe^{3+} > Ni^{2+}$.

To evaluate the contributions of anions and cations to the reduction process, we measured the temperature dependences of the degree α of chromium reduction in the presence of NO_3^-, Cl^-, and SO_4^{2-} anions and copper(II) and sodium cations at $H_2CrO_4 : Na_2SO_3 = 1 : 3$. The experimental results obtained are presented in Figs. 2b and 2c.

It can be seen from Fig. 2b that nitrate ions make the greatest contribution to the increase (by 5–12%) in the degree of chromium(VI) reduction. The effect of sulfate and chloride ions is considerably less pronounced. The effect of anions on the degree of Cr(VI) reduction to Cr(III) in the systems under consideration can be described by the series $NO^{3-} > Cl^- > SO_4^{2-}$.

The temperature dependence of the degree of chromium reduction in the presence of NO_3^-, Cl^-, and SO_4^{2-} anions and copper cations at $H_2CrO_4 : Na_2SO_3 = 1 : 3$ is shown in Fig. 2c. The system with a copper(II) nitrate additive is characterized by a high degree of reduction. The degree of Cr(VI) reduction upon addition of $Cu(NO_3)_2$ and $Fe(NO_3)_3$ is 60% in the temperature range 20–40°C and as high as 99.7% at temperatures of up to 80°C. Because the contribution of anions to the chromium(VI) reduction does not exceed 5–12%, we can conclude that, for the salts under study, Cu^{2+} and Fe^{3+} cations make the main contribution to the increase in the degree of chromium(VI) reduction. In the case of nickel(II) nitrate, the experimental data suggest that the increase in the degree of chromium(VI) reduction is caused by the presence of nitrate ions.

CONCLUSIONS

(1) The reduction of chromium(VI) by sodium sulfite in the presence of $Cu(NO_3)_2$, $Fe(NO_3)_3$, and $Ni(NO_3)_2$ solution additives was studied in model solutions of chromic acid with pH ~7. A thermodynamic analysis of the reactions that can proceed in the model solution was made, and a mechanism of the process of chromium(VI) reduction by sodium sulfite, with copper(II) and iron(III) ions involved, was suggested.

(2) Is was shown that the final values of the solution pH characterize the completeness of chromium(VI) reduction by sodium sulfite.

(3) It was found that Cu^{2+} and Fe^{3+} ions make the greatest contribution to the increase in the degree of chromium(VI) reduction, whereas nickel ions do not affect the chromium(VI) reduction. The effect of the anions under study on the degree of reduction is insignificant and the strongest in the presence of nitrate ions.

REFERENCES

1. Beukes, J.P., Pienaar, J.J., Lachmann, G., and Giesekke, E.W., *Water, S. Afr.*, 1999, vol. 25, no. 3, pp. 363–370.
2. Pilipenko, A.T., and Pyatnitskii, I.V., *Analiticheskaya khimiya* (Analytical Chemistry), Moscow: Khimiya, 1990.
3. Smirnov, V.V., Levitskii, M.M., Nevskaya, S.M., and Golubeva, E.N., *Kinet. Katal.*, 1999, vol. 40, no. 1, pp. 86–89.
4. Vasekha, M.V. and Motov, D.L., *Zh. Prikl. Khim.*, 2005, vol. 78, no. 1, pp. 41–44.
5. Goshu, I.V., Tsarev, J.V., and Kostrov, V.V., *Izv. Vyssh. Uchebn. Zaved., Khim. Khim. Tekhnol.*, 2007, vol. 50, no. 2, pp. 33–36.
6. Suvorov A.V. and Nikol'skii, A.B., *Obshchaya khimiya* (General Chemistry), St. Petersburg: Khimizdat, 2007, 5th ed.
7. Nakamura, A. and Tsutsui, M., *Principles and Applications of Homogeneous Catalysis*, Ontario: John Wiley, 1993.
8. Ugai, Ya.A., *Neorganicheskaya khimiya* (Inorganic Chemistry), Moscow: Vysshaya Shkola, 1989.
9. Perel'man, F.M. and Zvorykina, A.J., *Kobal't i Nikel'* (Cobalt and Nickel), Moscow: Nauka, 1975.

ISSN 1070-4272, Russian Journal of Applied Chemistry, 2007, Vol. 80, No. 12, pp. 2028–2030. © Pleiades Publishing, Ltd., 2007.
Original Russian Text © L.D. Kurbatova, D.I. Kurbatov, 2007, published in Zhurnal Prikladnoi Khimii, 2007, Vol. 80, No. 12, pp. 1950–1952.

INORGANIC SYNTHESIS AND INDUSTRIAL INORGANIC CHEMISTRY

Extractable Oxo Complexes of Vanadium(V) with Di(2-ethylhexyl) Hydrogen Phosphate

L. D. Kurbatova and D. I. Kurbatov

Institute of Solid State Chemistry, Ural Division, Russian Academy of Sciences, Yekaterinburg, Russia

Received January 31, 2007

Abstract—Extraction of vanadium(V) with di(2-ethylhexyl) hydrogen phosphate from 1.0–8.0 M aqueous sulfuric acid solutions was studied. The optimal conditions for the extraction were found. The composition of the extractable complex was determined, and the reaction equation for the extraction of V(V) was established. The extraction constant was determined.

DOI: 10.1134/S1070427207120042

It is known that di(2-ethylhexyl) hydrogen phosphate (HDEHP) is an efficient extractant for V(IV). It has also been reported [1] that HDEHP poorly extracts V(V) present in solutions in the form of dioxocations VO_2^+. At the same time, it was shown earlier that HDEHP effectively extracts V(V) from weakly acidic solutions. In this study, we examined extraction of V(V) with HDEHP from moderately concentrated aqueous sulfuric acid.

EXPERIMENTAL

Before use, di(2-ethylhexyl) hydrogen phosphate was purified to remove mono(2-ethylhexyl) dihydrogen phosphate [3]. The extraction of V(V) with HDEHP was studied at 25.0 ± 0.5°C by multistage contact of neat HDEHP with a solution of V(V) in aqueous sulfuric acid for 4 min. The V(V)-containing solutions were prepared by dissolving potassium metavanadate in aqueous sulfuric acid (chemically pure grade). The V(V) concentration was determined by the atomic-absorption method. The electronic absorption spectra of both the solutions of V(V) in aqueous sulfuric acid and V(V)–HDEHP extracts were recorded in the range 13000–30000 cm^{-1} in a 1-cm quartz cell (Specord UV-VIS spectrophotometer). The IR spectra of V(V)–HDEHP extracts (thin layer between KRS-6 plates) were recorded in the range 400–4000 cm^{-1} on a Specord 75 IR spectrometer.

In this study we examined the extraction of V(V) from both straight moderately concentrated aqueous sulfuric acid solutions ($c_{H_2SO_4}$ = 1.0–8.0 M) and those containing cationic and anionic additives. We found that the extraction of V(V) with HDEHP starts at a sulfuric acid concentration higher than 5.0 M, when extractable ionic species of V(V) are formed. The electronic absorption spectra of a solution of V(V) in aqueous sulfuric acid of concentration 1.0–3.0 M contains the absorption bands at 48000, 44000, and 36000 cm^{-1}, which belong to mononuclear complexes of V(V) with the dioxocationic VO_2^+ coordination center [4]. An increase in the sulfuric acid concentration over 5 M results in that the optical density grows and the shape of the spectrum noticeably changes. These spectroscopic effects suggest that a new kind of extractable ionic V(V) species is formed under these conditions.

To identify ionic species of V(V) extracted with HDEHP, the IR and electronic absorption spectra of V(V)–HDEHP extracts were examined. It can be seen from Fig. 1 that, in going from HDEHP–H_2SO_4

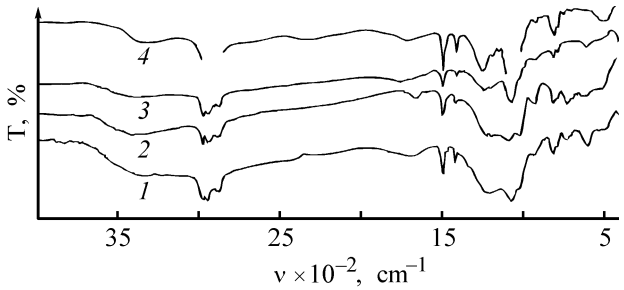

Fig. 1. IR spectra of HDEHP–H_2SO_4 and HDEHP–V(V) extracts. (T) Transmission and (ν) wavenumber. (*1*) HDEHP–V(V) extract (c_V^{init} = 0.1053 M), (*2*) HDEHP-V(V) extract after compensation of HDEHP absorption, (*3*) HDEHP–H_2SO_4 extract, and (*4*) HDEHP.

extract to HDEHP–V(V) extract, the component (1680 cm^{-1}) of the absorption band of P–OH groups shifts to 1630 cm^{-1}.

Two other components of the absorption bands ν_{P-OH} of HDEHP (2260, 2660 cm^{-1}) are lacking in the IR spectrum of the V(V)–HDEHP extract. This fact suggests that V(V) is extracted by the ion-exchange mechanism involving coordination of the P–OH groups with V(V) [5]. The IR spectrum of the V(V)–HDEHP extract also contains absorption bands at 1170 and 1050 cm^{-1}, assigned to ν_s(POO) and ν_{as}(POO) vibrations, respectively [5]. The low-frequency shift of the absorption bands of the ν_{as}(POO) vibrations in the spectrum of the HDEHP–V(V) extract, compared to that of the HDEHP–H_2SO_4 extract, shows that the POO groups are also coordinated with V(V) [6]. This IR spectrum also contains a doublet band (980–990 cm^{-1}) against the background of absorption bands of HDEHP and sulfate anions. The compensation of the absorption of HDEHP in the IR spectrum of the V(V)–HDEHP extract reveals an absorption band of medium intensity at 985 cm^{-1}. By analogy with [7], this absorption band can be assigned to ν_1 vibrations of the dimeric oxovanadium(V) cation. We found no absorption band at 750 cm^{-1}, apparently because it is obscured by the stronger absorption band of HDEHP. These spectroscopic data show that HDEHP extracts V(V) from 8 M aqueous sulfuric acid in the form of a complex of HDEHP with dimeric oxovanadium(V) cation by the cation-exchange mechanism.

It has been reported previously [8] that V(V) is extracted with HDEHP from 12 M aqueous sulfuric acid by the cation-exchange mechanism. Under these conditions, dimeric oxovanadium(V) hydrosulfate cations are extracted. We found that the electronic absorption spectra of extracts of V(V) from 8 and 12 M H_2SO_4 are identical. In both cases, the electronic spectra of V(V)–HDEHP extracts contain the absorption band at 25 000–26 000 cm^{-1}. Thus, the composition of the V(V)–HDEHP extractable complex remains unchanged upon dilution of sulfuric acid.

Sulfate anions and water molecules present in the V(V)–HDEHP extractable complexes formed in extraction of V(V) from 12 M and 8 M aqueous sulfuric acid are manifested as the absorption bands at 660 (sh), 580, and 3400 cm^{-1} [9]. To determine the composition of V(V)–HDEHP extractable complexes formed in extraction of vanadium from moderately concentrated solutions of sulfuric acid, the interaction between V(V) and HDEHP was examined. Using the molar ratio technique, we found

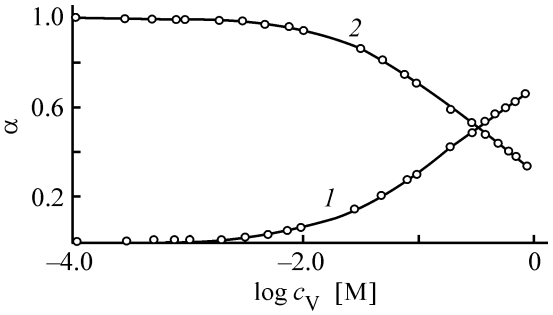

Fig. 2. Speciation of V(V) in 8 M aqueous H_2SO_4 vs. V(V) concentration. (α) Degree of formation of V(V) species and (c_V) V(V) concentration. (*1*) VO_2^+ and (*2*) $V_2O_3^{4+}$.

that the V(V) to HDEHP molar ratio in the extractable complex is 1 : 2 and its stoichiometry can be expressed by the formula $V_2O_3 \cdot (H_2O)_{6-n} \cdot (HSO_4)_n \cdot (HR_2)_2^{(2-n)+}$. The extraction of V(V) with dimeric HDEHP from 8 M aqueous sulfuric acid can be described by the equation of the following heterogeneous reaction:

$$V_2O_3 \cdot (H_2O)_{8-n} \cdot (HSO_4)_n^{(4-n)+} + 2H_2R_2 \rightleftarrows V_2O_3 \cdot (H_2O)_{6-n} \cdot (HSO_4)_n \cdot (HR_2)_2^{(2-n)+} + 2H_3O^+.$$

The extraction constant of V(V) with HDEHP was determined taking into account the data on V(V) polymerization reported in [10]. Figure 2 shows the distribution of V(V) species (VO_2^+ and $V_2O_3^{4+}$) in 8 M aqueous H_2SO_4 vs. the V(V) concentration.

The V(V) speciation in aqueous sulfuric acid was calculated using the dimerization constant of V(V) in 8 M H_2SO_4, reported in [7]. Figure 2 shows that a solution of V(V) in 8 M H_2SO_4 is an equilibrium mixture of its monomeric and dimeric species. At low V(V) concentrations ($c_V < 1 \times 10^{-3}$ M), the monomeric V(V) dioxocations prevail. A noticeable amount of dimeric species appears only at $c_V > 5 \times 10^{-3}$ M. Taking into account that the extractable species of V(V) is dimeric V(V) oxocation, the constant of extraction of V(V) with HDEHP was determined using V(V) solutions in moderately concentrated H_2SO_4, with the V(V) concentration ranging from 6×10^{-3} to 1.4×10^{-2} M. The equilibrium concentration of dimeric oxovanadium(V) cations was calculated taking into account the dimerization of V(V) in aqueous sulfuric acid [10]. We found that, at sulfuric acid concentration of 8.0 M and $\alpha = 0.95$, the extraction constant of V(V) $K = (3.47 \pm 0.02) \times 10^{-1}$.

CONCLUSIONS

(1) Di(2-ethylhexyl) hydrogen phosphate extracts V(V) within a wide range of sulfuric acid concentrations (5.0–12.0 M).

(2) V(V) is extracted with HDEHP by the cation-exchange mechanism in the form of mixed-ligand extractable complexes of dimeric oxovanadium cations with hydrosulfate and alkyl phosphate anions.

REFERENCES

1. Laskorin, B.N., Ul'yanov, V.S., and Sviridov, R.A., *Zh. Neorg. Khim.*, 1965, vol. 38, no. 5, pp. 1133–1135.
2. Kurbatov, L.D., Medvedeva, N.I., and Kodess, M.I., *Zh. Neorg. Khim.*, 1997, vol. 42, no. 11, pp. 1927–1929.
3. Tserkovnitskaya, I.A. and Kaukhova, L.V., *Primenenie organicheskikh reagentov* (Application of Organic Reagents), Leningrad: Leningr. Gos. Univ., 1969.
4. Bonchev, P.R. and Nikolov, G.S., *J. Inorg. Nucl. Chem.*, 1966, vol. 28, no. 11, pp. 2609–2614.
5. Stoyanov, E.S., Popov, V.M., and Mikhailov, V.A., *Zh. Prikl. Spektrosk.*, 1984, vol. 40 no. 1, pp. 77–81.
6. Stoyanov, E.S., *Zh. Strukt. Khim.*, 1994, vol. 35, no. 6, pp. 60–65.
7. Madic, C., Begun, G.M., Hahn, R.L., et al., *Inorg. Chem.*, 1984, vol. 23, no. 4, pp. 469–476.
8. Kurbatova, L.D., Kurbatov, D.I., and Medvedeva, N.I., *Zh. Prikl. Khim.*, 2004, vol. 77, no. 4, pp. 680–682.
9. Nakamoto, K., *Infrared Spectra of Inorganic and Coordination Compounds*, New York: Wiley, 1963.
10. Kurbatova, L.D. and Kurbatov, D.I., *Zh. Neorg. Khim.*, 2006, vol. 51, no. 5, pp. 908–910.

ISSN 1070-4272, Russian Journal of Applied Chemistry, 2007, Vol. 80, No. 12, pp. 2031–2035. © Pleiades Publishing, Ltd., 2007.
Original Russian Text © O.I. Platonov, L.Sh. Tsemekhman, P.N. Kalinkin, O.N. Kovalenko, 2007, published in Zhurnal Prikladnoi Khimii, 2007, Vol. 80, No. 12, pp. 1953–1957.

INORGANIC SYNTHESIS AND INDUSTRIAL INORGANIC CHEMISTRY

Analysis of the Activity of an Aluminum Oxide Claus Catalyst in Commercial Operation

O. I. Platonov, L. Sh. Tsemekhman, P. N. Kalinkin, and O. N. Kovalenko

Institut Gipronikel' Limited Liability Company, St. Petersburg, Russia
Institute of Catalysis, Siberian Branch, Russian Academy of Sciences, Novosibirsk, Russia
Novosibirsk State University, Novosibirsk, Russia

Received July 11, 2007

Abstract—Activity dynamics of an AO-MK-2 aluminum oxide catalyst in conversion of hydrogen sulfide and carbonyl sulfide during four years of service in an industrial Claus reactor was analyzed. The rate constants of the Claus reaction were determined and changes in the active surface area of the catalyst were examined.

DOI: 10.1134/S1070427207120054

The efficiency of manufacture of elementary sulfur by the Claus method primarily depends on the activity of the catalysts used [1], which necessitates their current diagnostics and prognostication of their remaining life.

The known methods for laboratory monitoring with accelerated catalyst aging procedures [2, 3] fail to reproduce industrial conditions and, therefore, are inadequate to real working conditions. Catalyst sampling from an industrial reactor, followed by standard testing, requires regular shutdowns of the reactor, which is, apparently, not always possible under the conditions of an operating plant.

A widely used way to monitor the current activity of a catalyst is to examine industrial reactors in the on-line mode, which is, however, not quite versatile. For example, a criterion of equilibration of an effluent gas, developed for a gas-processing plant [4], is virtually inapplicable in the case when the source of an acid gas and its oxidation mode are unstable. This situation is typical of Claus installations that process gases of, e.g., by-product coking origin [5], with low content (<8 vol %) of hydrogen sulfide. This predetermines the topicality of a current diagnostics of catalysts for the Claus process, irrespective of the composition of a gas being processed.

In this communication, we present a procedure for catalyst diagnostics and results of an analysis of how the activity of an AO-NKZ-2 catalyst (original name AO-MK-2 [5, 6]) varied during four years of operation in a Claus reactor in the line for desulfurization of the coke gas at a by-product coke shop (BCP) of Magnitogorsk metallurgical combine (MMC) at a temperature of 230–260°C and volume load W = 2000 h^{-1}. A specific feature of the acid gas being processed is the considerable variability of the concentration at its low value: the content of hydrogen sulfide is 6–8 vol % at the inlet of the Claus furnace and ≤1.5 vol % at the inlet of catalytic units. In addition to the chromatographically determinable gas components (concentrations of N_2, O_2, H_2, CH_4, CO_2, CO, H_2S, COS, and SO_2 are determined in dried samples), the gas being processed contains 10–30 g m^{-3} of elementary sulfur and about 120 g m^{-3} of H_2O.

The activity of the AO-NKZ-2 catalyst in the passive-experiment mode in operation of a technological Claus line at MMC was evaluated by the degrees of conversion of the main sulfur-containing components (H_2S, COS, and SO_2), found by the commonly accepted technique [5] in the Claus reactor unit being tested.

Taking into account that the conversion of the sulfur-containing components depends on composition, we determined the catalyst activity at a ratio between the initial concentrations of components in the gas equal to $\gamma \equiv ([H_2S]_0 + [COS]_0)/([SO_2]_0 \approx 2$, which corresponds to the stoichiometry of the target reac-

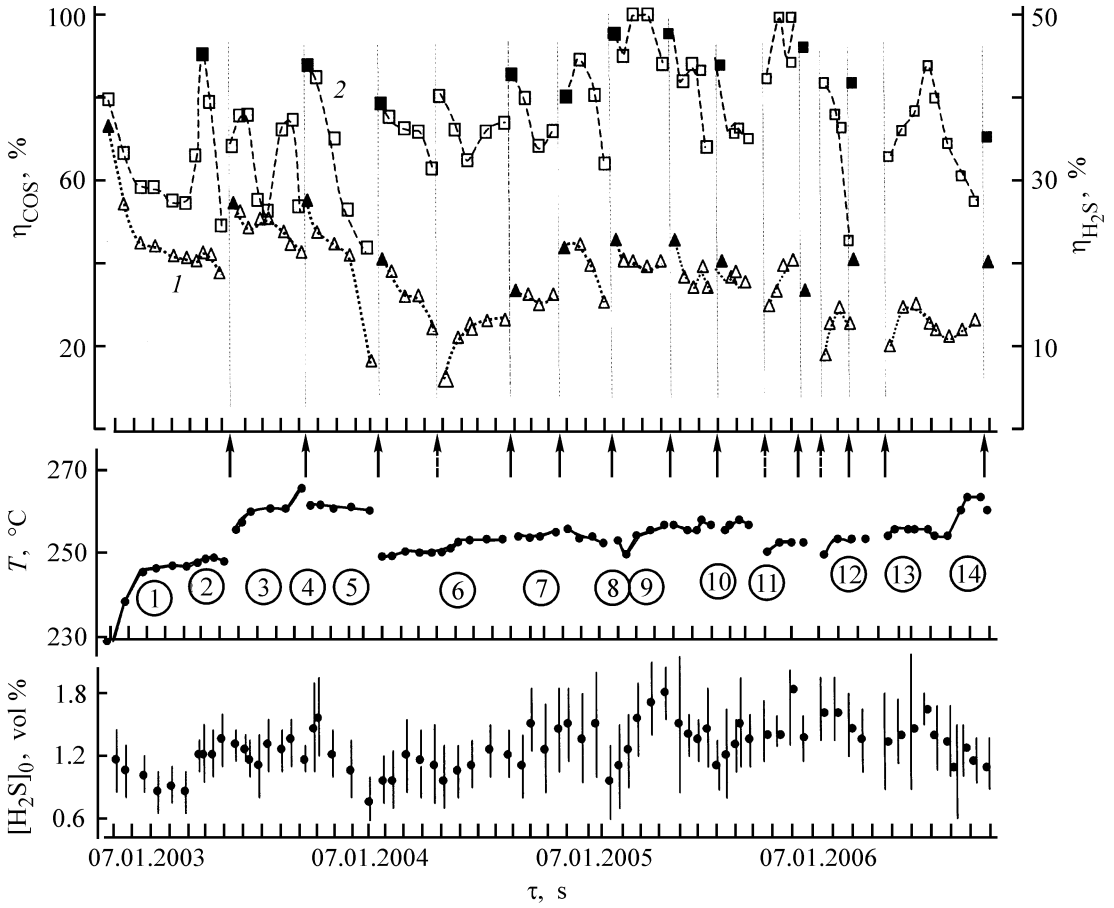

Variation of the observable conversion η of (*1*) carbonyl sulfide and (*2*) hydrogen sulfide on an AO-NK3-2 catalyst at $W = 2200\ h^{-1}$ and $T = 253 \pm 13°C$ during the period from 04.02.2003 to 03.25.2007. For explanations, see text. *The arrows* show instants of catalyst regeneration, and *black points*, values of conversion on a fresh (regenerated) catalyst; *digits in circles* are the numbers of events being analyzed.

tions of the Claus conversion, (1) and (2), and hydrolysis (3):

$$2H_2S + SO_2 = 2H_2O + 3/nS_n; \quad (1)$$

$$2COS + SO_2 = 2CO_2 + 3/nS_n, \quad n = 1–8; \quad (2)$$

$$COS + H_2O = H_2S + CO_2. \quad (3)$$

Quantitatively, the catalyst activity in the kinetic equation describing the hydrogen sulfide consumption on a aluminum oxide catalyst

$$-d[H_2S]/dt = k[H_2S][SO_2]^{0.5} \quad (4)$$

was estimated with account of the process factors, taking into account the definition of the rate constant k [7]

$$k = (1 - c^{1/2}/c_0^{1/2})/(\tau c^{1/2}) = (c_0^{1/2}/c^{1/2} - 1)/(\tau c_0^{1/2}), \quad (5)$$

from the initial ($c_0 \equiv [H_2S]_0$) and final ($c \equiv [H_2S]$) hydrogen sulfide concentrations reached during a contact time τ at stoichiometric initial concentrations of the reagents, $[H_2S]_0 = 2[SO_2]_0 = 2c_0$.

Independent laboratory tests were performed in a flow-through quartz reactor with a fixed catalyst bed. A catalyst of the 6–8-mm fraction was tested at 255°C on model gas mixtures containing (vol %): 1–7 H_2S, 0.5–3.5 SO_2, 30 H_2O, and He the rest. The flow rate of the dry gas mixture was 10 $l\ h^{-1}$ at a volumetric flow rate (for the working conditions) of about 3500 h^{-1}.

The specific surface area and content of sulfates in a catalyst sample taken from the Claus reactor were determined by the methods described in [3].

The activity dynamics of a catalyst in its operation in a Claus reactor at MMC during the period from 04.02.2003 to 03.25.2007 is shown in the figure.

Table 1. Activity parameters of the AO-NKZ-2 catalyst during different periods of operation in a Claus reactor at BCP MMC from 04.02.2003 to 03.25.2007

Averaging period	$[H_2S]$, vol %	T, K	τ,* s	η_{H_2S}, rel %	k,* s^{-1} $atm^{-1/2}$
09.15–10.15.2003	1.26	522	1.73	45	2.0
03.19–03.30.2004	1.53	535	1.68	44	1.8
07.23–08.02.2004	1.04	522	1.73	38	1.7
10.27–11.18.2004**	1.11	525	1.70	46.6	2.3
02.27–03.14.2005	1.17	527	1.71	47.7	2.3
05.22–06.08.2005	1.53	527	1.71	39.8	1.5
08.12–09.01.2005	1.13	526	1.71	47.6	2.3
09.12–09.28.2005	1.75	529	1.70	51**	2.1
11.14–11.30.2005	1.56	530	1.70	47.4	1.9
02.04–02.15.2006	1.27	529	1.70	44	1.9
06.11–06.26.2006	1.50	527	1.71	46	1.9
07.10–07.19.2006**	1.47	526	1.70	38	1.8
08.24–09.03.2006	1.31	527	1.71	42	1.8
11.10–11.22.2006**	1.41	527	1.71	44	1.9
10.12.2006	1.11	500	1.80	46.6	2.2
03.22–03.25.2007	1.05	532	1.68	35	1.6

* Fictitious values. ** After shutdowns without thermal regeneration.

Table 2. Parameters of the AO-NK3-2 aluminum oxide catalyst in the initial state and after three years of commercial operation in a Claus reactor at 245–265°C

Catalyst	S_{BET}, m^2 g^{-1}	Pore volume,* cm^3 g^{-1}	Average size, Å	SO_4^{2-} content, wt %
Starting	249.3	0.291	49.7	–
Used	147.7	0.348	92.0	1.1

* Volume of pores in the range 17–3000 Å.

The upper part of the figure presents average conversions of hydrogen sulfide (η_{H_2S}) and carbon oxysulfide (η_{COS}). The lower panels show the corresponding variations of the principal conversion factors: average temperature of the catalyst bed and initial concentration of hydrogen sulfide at the inlet of the Claus reactor, $[H_2S]_0$. The vertical portions correspond to variance of the average hydrogen sulfide concentrations $[H_2S]_0$ in the corresponding intervals of time.

The arrows on the time scale show "instants" of catalyst regeneration: 11.13–14.2003, 03.17–18.2004, 07.22.2004, 02.25–26.2005, 05.20–21.2005, 08.10–11.2005, 11.12–13.2005, 02.02–03.2006, 06.09–10.2006, 08.20–21.2006, and 03.21.2007, which consisted in raising the catalyst bed temperature to 280–300°C without changes in the inlet-gas composition (we used the built-in bypass of the exhaust-heat boiler of the Claus furnace). Dashed lines shows cases of restarting the Claus line after shutdowns (idle periods): 10.22–26.2004, 03.25–04.24.2006, 06.27–07.09.2006, and 09.04–10.11.2006, when the catalyst was heated to working temperatures after line shutdown with flue gas (α ~1.07) in the absence of hydrogen sulfide.

The activity parameters of the AO-NKZ-2 catalyst in a Claus reactor at BCP MMC [hydrogen sulfide conversion and rate constant of the reaction, calculated by Eq. (5)] in relation to the process parameters are listed for the period of time from 04.02.2003 to 03.25.2007 in Table 1.

The texture parameters of the AO-NKZ-2 aluminum oxide catalyst in the initial state and after tree years of operation and the content of surface sulfates are listed in Table 2.

Analysis of the data presented in the figure shows the following specific features of the conversion dynamics of hydrogen sulfide and carbonyl sulfide.

Dynamics of hydrogen sulfide conversion. Even minor (within 3–5°C) temperature increments (these events are indicated on the time scale by digits) in the course of operation are accompanied by a considerable increase in the observable hydrogen sulfide conversion. This effect is manifested to the greatest extent at the leading edge of the temperature rise at average catalytic bed temperatures of 245–250°C (events 1, 2, 6, 7). A monotonic lowering of the catalyst bed temperature is accompanied by a fast and strong decrease in the hydrogen sulfide conversion (period from 03.19.2004 to 07.20.2004, event 5). Regeneration of the catalyst in a flow of the reaction mixture at 280–300°C and treatment of the catalyst with oxygen-containing flue gases (α ~1.07) at temperatures equal to, or lower than 250°C leads to a virtually full restoration of the hydrogen sulfide conversion.

Thus, the deactivation of the catalyst in the Claus reaction is reversible and the activity of the AO-NKZ-2 catalyst in hydrogen sulfide conversion is virtually preserved during four years of operation. Therefore, it can be assumed that the main reason for the catalyst deactivation in the Claus reaction (1) is closure (blocking) of the active surface because of sulfur deposition in pores of the catalyst. Evaporation of sulfur upon each rise in temperature and(or) during an idle run opens the active surface, with the catalyst thereby regenerated.

The rate constants of the Claus reaction (1), calculated by Eq. (5) for the corresponding conversions $\eta^0_{H_2S}$ during the post-regeneration periods (Table 1), show that the rate of irreversible aging of the AO-NK3-2 catalyst in hydrogen sulfide conversion does not exceed 3–5% per year, which provides its service life of no less than 7–10 years.

Dynamics of carbonyl sulfide conversion. The data presented in the figure demonstrate that the conversion of carbonyl sulfide irreversibly decreases by 50% from the initial value two months after the beginning of operation (40 and 73%, respectively). Treatment of the catalyst with oxygen-containing flue gases (α ~1.07) leads to a sharp decrease in COS conversion (to ≤20%) (see figure, events 6, 11, 12, and 13). Subsequent delivery of a flow of a technological gas containing H_2S results in that η_{COS} starts to grow immediately after the reactor startup. This means that, in contrast to the case of the Claus reaction, the catalyst deactivation is reversible only partly in reactions (2) and (3) of carbonyl sulfide conversion, and the sulfation of the catalyst surface under the action of a dry weakly oxidizing gas mixture results in strong, but reversible deactivation of the catalyst. It can be assumed that the irreversible deactivation of the AO-NK3-2 aluminum oxide catalyst in carbonyl sulfide conversion is primarily due to loss of the active surface via hydrothermal aging. The specific surface area S_{BET} of the catalyst in its sample taken on 04.03.2006 during a shutdown of the Claus line from the upper (back) part of the catalyst bed after its complete cooling was 148 $m^2 g^{-1}$ at an initial surface area of a fresh AO-NKZ-2 catalyst equal to about 270 $m^2 g^{-1}$ (Table 2). To this decrease in the active surface area of the catalyst in three years of operation corresponds a relative decrease in the conversion η^0_{COS}.

As shown previously [8, 9], the sharp decrease in the specific surface area of the catalyst occurs already during first hours of its operation. The results obtained in an industrial examination, presented here, suggest the specific surface area of the AO-NKZ-2 catalyst also occurs during first two months of operation, which leads to a rapid fall of the carbonyl sulfide conversion.

Conversion of organosulfur compounds under the working conditions (temperature 240–260°C, volumetric flow rate ~2000 h^{-1}) is virtually fully governed by the hydrolysis reaction [10]. Hydrolysis of COS under typical industrial conditions (volumetric flow rate ~1000 h^{-1}) on an aluminum oxide catalyst rater completely occurs at temperatures exceeding 330°C [11]. In the conditions of AO-NKZ-2 catalyst operation in the MMC reactor, the Claus reaction (1) occurs under the diffusion control, when the decrease in the specific surface area is compensated for by an increase in the pore size, and the slower reaction (3) of carbonyl sulfide hydrolysis proceeds under the kinetic control, with the activity of the catalyst directly proportional to its specific surface area. In other words, η_{COS} depends on the specific surface area of the catalyst to a greater extent than η_{H_2S} does. Because the AO-NKZ-2 catalyst has a considerable reserve of a surface area for the Claus reaction [3], hydrothermal aging should not noticeably limit the H_2S conversion.

One more factor affecting both the reversible and irreversible deactivation of the catalyst in the reaction of COS conversion is the sulfation of the catalyst. It is known that the hydrolysis reaction is more sensitive to the content of sulfates on the catalyst surface than the Claus reaction [12].

A study of a catalyst sample taken on 04.03.2006 demonstrated that the amount of sulfates present on the catalyst surface is 1.1 wt % (Table 2) and should

not exert any significant influence on the hydrogen sulfide conversion [12].

The comparative independence of the activity of the catalyst in the Claus reaction (1) from sulfation of its active surface can be understood in terms of the mechanism of the Claus reaction, suggested in [8]. Sulfur is formed on the catalyst surface via formation of thiosalts (thiosulfate, polythionates), and the sulfate is a by-product of the reaction. This means that, even when the H_2S/SO_2 molar ratio is nearly stoichiometric and the gas mixture contains no oxygen, a stationary concentration of oxygen sulfurous salts adsorbed on both Lewis and Brønsted basic centers is present at the catalyst surface in the reaction medium. These centers are responsible, as shown in [13], for the catalyst activity in the hydrolysis reaction, and their blocking results in that the hydrolysis rate decreases not only on Al_2O_3, but on TiO_2 and ZrO_2 as well.

The industrial experiment we performed demonstrated that, with the H_2S/SO_2 molar ratio maintained close to stoichiometry and no oxygen present in the gas mixture, the activity of the aluminum oxide catalyst in the Claus reaction weakly depends of the sulfation of the catalyst, which directly determines its activity in hydrolysis of organosulfur compounds. It can be assumed that (i) the differences revealed are typical of catalysts used in processing of sulfur-containing gases and (ii) individual selection of catalysts is necessary for hydrolysis of organosulfur compounds (the catalysts should be sulfation-resistant) and Claus conversion of hydrogen sulfide (the best for this purpose are comparatively low-cost aluminum oxide catalysts). Therefore, it is advisable to use different types of catalysts in preliminary stages of hydrolysis of sulfur-containing compounds and in low-temperature Claus conversion in installations for sulfur recovery.

The differences between the aging rates of the AO-NKZ-2 aluminum oxide catalyst in conversion of carbonyl sulfide and hydrogen sulfide mean that the frequently used determination of the activity of Claus catalysts in hydrolysis of sulfur-containing compounds (carbon disulfide [2]) for monitoring the operation of catalysts for the Claus process is incorrect.

CONCLUSION

A study of how the activity of the AO-NKZ-2 (AO-MK-2) aluminum oxide catalyst varies in the course of four years of operation in a Claus reactor of the line for purification of the coke oven gas at Magnitogorsk metallurgical combine at an average temperature of 245–260°C and a volumetric flow rate of about 2000 h^{-1} revealed fundamental differences in the conversion dynamics of hydrogen sulfide and carbonyl sulfide. It was shown that it is advisable to use specialized catalysts in the stages of hydrolysis of organosulfur compounds and low-temperature Claus conversion.

REFERENCES

1. Pearson, M.J., *Khim. Pererab. Uglevodorodov*, 1978, no. 4, pp. 19–24.
2. Kijlstra, W.S., Clark, P.D., Dowling, N.I., and Huang, M., *Sulphur*, 2001, no. 276, pp. 71–79.
3. Kovalenko, O.N., Kalinkin, P.N., Platonov, O.I., et al., *Kataliz Prom–sti*, 2005, no. 4, pp. 23–28.
4. Makhoshvili, Yu.A., Filatova, O.E., Krennikov, S.V., and Kislenko, N.N., *Gaz. prom–st.*, 2001, no. 12, pp. 49–51.
5. Platonov, O.I., Ryabko, A.G., and Tsemekhman, L.Sh., *Zh. Prikl. Khim.*, 2004, vol. 77, no. 8, pp. 1323–1326.
6. Kataev, M.P., Babkin, M.V., Avramov, V.V., et al., *Kataliz Prom–sti*, 2004, no. 3, pp. 49–56.
7. Egorov, V.N., Platonov, O.I., Tarasov, N.A., and Chistyakov, N.P., *Kataliz Prom–sti*, 2002, no. 1, pp. 17–22.
8. Clark, P.D., Dowling, N.I., Huang, M., et al., *Appl. Catal., Ser. A, General*, 2002, no. 235, pp. 61–69.
9. Legendre, O. and Jaeger, Ph., *React. Kinet. Catal. Lett.*, 1995, vol. 55, no. 2, pp. 501–511.
10. Clark, P.D., Dowling, N.I., and Huang, M., *Appl. Catal., Ser. B, Environmental*, 2001, vol. 31, pp. 107–112.
11. Grunval'd, V.R., *Tekhnologiya gazovoi sery* (Technology of Gaseous Sulfur), Moscow: Khimiya, 1992.
12. Pearson, M.J., *Hydrocarbon Proc.*, 1978, vol. 57, no. 4, pp. 99–103.
13. Bachelier, J., Aboulayt, A., Lavalley, J.C., et al., *Catal. Today*, 1993, vol. 17, pp. 55–62.

ISSN 1070-4272, Russian Journal of Applied Chemistry, 2007, Vol. 80, No. 12, pp. 2036–2039. © Pleiades Publishing, Ltd., 2007.
Original Russian Text © G.F. Klyakin, V.A. Taranushich, 2007, published in Zhurnal Prikladnoi Khimii, 2007, Vol. 80, No. 12, pp. 1958–1961.

INORGANIC SYNTHESIS AND INDUSTRIAL INORGANIC CHEMISTRY

Phase Stability in the System Constituted by Ammonium Nitrate, Potassium Dichromate, and Alkaline-Earth Metal Nitrates

G. F. Klyakin and V. A. Taranushich

South-Russian State Technical University, Novocherkassk, Rostov-on-Don oblast, Russia

Received April 10, 2007

Abstract—Methods for modification of ammonium nitrate as an oxidizing agent for ecologically safe solid propellants were sought for and the influence exerted on phase transitions in ammonium nitrate by three-component inorganic additives in which a synergic effect lowering the transition energy is manifested was determined.

DOI: 10.1134/S1070427207120066

A promising approach that can be employed to make lower the cost of solid propellants and diminish the amount of chlorine-containing discharges is to use ammonium nitrate (AN) as an oxidizing agent partly or completely replacing ammonium perchlorate (APC). The cost of ammonium nitrate is an order of magnitude lower and it forms no ecologically dangerous products in combustion. The most important difficulties associated with the development of AN-based fuels consist in that AN undergoes polymorphic transformations at working temperatures of the fuel, which are accompanied by an increase in volume, and its combustion velocity is low.

The existing technical solution [1] based on cocrystallization of AN with a binary additive (ammonium nitrate + calcium nitrate) eliminates only the phase stability problem. Additional use of catalysts making higher the thermal decomposition rate and combustion velocity in a phase-stabilizing additive to AN will allow an integrated solution of the problem of its suitability as an oxidizing agent for ecologically safe solid propellants.

EXPERIMENTAL

One of the most effective and readily available compounds, potassium dichromate (PDC), was used as a catalyst. It was introduced into a binary additive composed of potassium nitrate (PN) and nitrates of alkaline-earth metals, such as magnesium nitrate (MN), calcium nitrate (CN) and strontium nitrate (SN). In some systems, potassium nitrate was replaced with potassium perchlorate. The total content of the additive in modified AN was 4%.

Experiments were carried out using Scheffe's design [2], which makes it possible to evaluate nonlinear effects in binary and ternary additive mixtures. The experiments were replicated and their results were used to construct polynomial models whose adequacy was estimated by Fisher's criterion. The models were constructed with exclusion of nonsignificant (according to Student's criterion) coefficients, followed by recalculation [3], which yielded adequate models with the smallest number of terms.

The additives were introduced into AN by isothermal crystallization from aqueous solutions. The solid phase was additionally dried and subjected to differential-thermal analysis (DTA). After the drying, all procedures were performed in a chamber with a relative air humidity not exceeding 50%.

The DTA of a powder of the <400-μm fraction was made in the temperature range from –50°C to the melting point. The weight of a sample for analysis was about 0.1 g, and the heating rate, 3 deg min^{-1}. DTA curves were recorded in the coordinates of the sample temperature and the temperature difference between a sample and the reference. The phase transition energy (J g^{-1}) was evaluated by the area under the corresponding peaks in the DTA diagram, with the use of a calibration plot.

The experiments demonstrated that the V → IV phase transition in AN is not manifested in the whole range of additive compositions studied. The dependences of the energy of the IV → III phase transition in AN on the composition of the ternary additives: (i) potassium nitrate, potassium dichromate, and magnesium nitrate, J_{Mg}; (ii) potassium nitrate, potassium dichromate, and calcium nitrate, J_{Ca}; and (iii) potassium nitrate, potassium dichromate, and strontium nitrate, J_{Sr}; are described by the equations

$$J_{Mg} = 6.3c_{MN} + 20.5c_{PN} + 14.8c_{PDC} - 37.3c_{MN}c_{PN} - 25.4c_{MN}c_{PDC} - 178.7c_{MN}c_{PN}c_{PDC}, \quad (1)$$

$$J_{Ca} = 10.0c_{CN} + 20.9c_{PN} + 15.0c_{PDC} - 38.0c_{CN}c_{PN} - 26.7c_{CN}c_{PDC} - 196.9c_{CN}c_{PN}c_{PDC}, \quad (2)$$

$$J_{Sr} = 15.9c_{SN} + 21.4c_{PN} + 15.3c_{PDC} - 18.9c_{SN}c_{PN} - 34.0c_{SN}c_{PDC} + 688.6c_{SN}c_{PN}c_{PDC}, \quad (3)$$

where c_{MN}, c_{CN}, c_{SN}, c_{PN}, and c_{PDC} are the mass fractions of, respectively, magnesium, calcium, strontium, and potassium nitrates and potassium dichromate.

The general form of Eqs. (1)–(3) demonstrates that the energy of the phase transition in AN is constituted by parts associated both with the effect of individual components (equation terms containing the mass fraction of only a single component) and with that of their binary mixtures (equation terms named binary interaction terms, which contain a product of the mass fractions of two components) and ternary mixtures (equation terms named ternary interaction terms, which contain a product of the mass fractions of three components).

As follows from an analysis of the coefficients at those terms in Eqs. (1)–(3) which contain only individual components, introduction of alkaline-earth metal nitrates improves the phase stability of AN, because these coefficients are smaller than the energy of the IV → III phase transition in AN (19.8 J g^{-1}, according to reference data [4]). Introduction of potassium nitrate in the amount studied has virtually no effect on the transition energy, whereas potassium dichromate has a phase-stabilizing power close to that of strontium nitrate. The coefficients at the terms of the individual components increase in the order: magnesium nitrate, calcium nitrate, strontium nitrate,

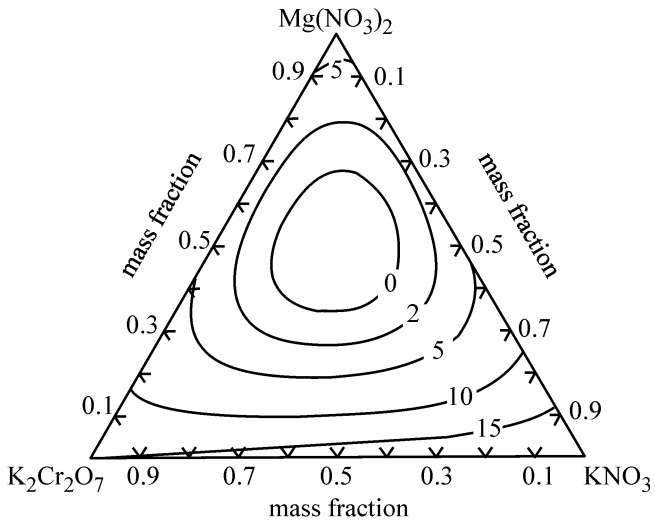

Fig. 1. Diagram relating the composition to the energy of the IV → III phase transition in ammonium nitrate for the additive KNO_3–$K_2Cr_2O_7$–$Mg(NO_3)_2$. *Curves*, lines of equal phase transition energies; the same for Figs. 2–5.

which corresponds to a decrease in the phase-stabilizing power in the same order.

The negative sign of the coefficients at all binary interaction terms in Eqs. (1)–(3) indicates that there is a synergic effect making lower the phase transition energy in the presence of binary mixtures of alkaline-earth metal nitrates with potassium nitrate or potassium dichromate. The absence of the interaction term $c_{PN}c_{PDC}$ in Eqs. (1)–(3) demonstrates that the mixture of potassium nitrate and potassium dichromate virtually does not make any additional contribution to *J*.

The ternary additives containing magnesium and calcium nitrates [Eqs. (1) and (2)] cause a decrease in the phase transition energy (negative sign of the corresponding ternary interaction term), and that with strontium nitrate [Eq. (3)] makes *J* larger.

If the absolute values of the coefficients at the binary-interaction terms in Eqs. (1)–(3) are considered, it can be seen that virtually the same contributions to the overall estimate of *J* come from the binary additives (magnesium nitrate + potassium nitrate) and (calcium nitrate + potassium nitrate), whereas the binary additive composed of potassium and strontium nitrates has a considerably weaker effect. If potassium nitrate is replaced with potassium dichromate, the binary additive containing strontium nitrate as the second component improves the phase stability of AN to a considerably greater extent, compared with other nitrates of alkaline-earth metals.

The graphical interpretation of Eqs. (1)–(3) is shown in Figs. 1–3.

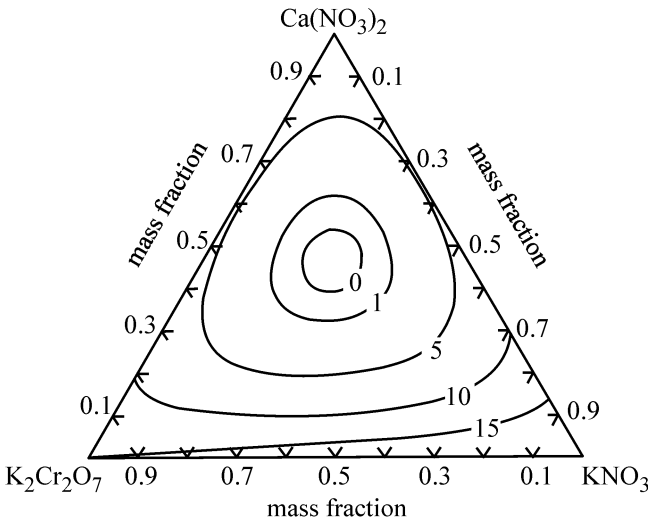

Fig. 2. Diagram relating the composition to the energy of the IV → III phase transition in ammonium nitrate for the additive KNO_3–$K_2Cr_2O_7$–$Ca(NO_3)_2$.

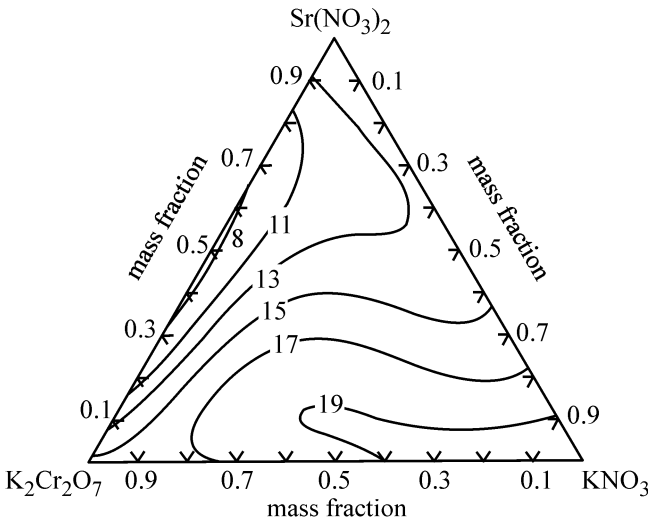

Fig. 3. Diagram relating the composition to the energy of the IV → III phase transition in ammonium nitrate for the additive KNO_3–$K_2Cr_2O_7$–$Sr(NO_3)_2$.

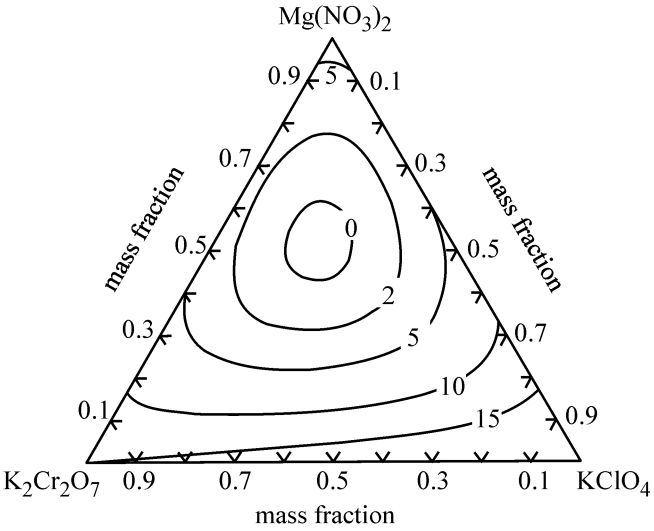

Fig. 4. Diagram relating the composition to the energy of the IV → III phase transition in ammonium nitrate for the additive $KClO_4$–$K_2Cr_2O_7$–$Mg(NO_3)_2$.

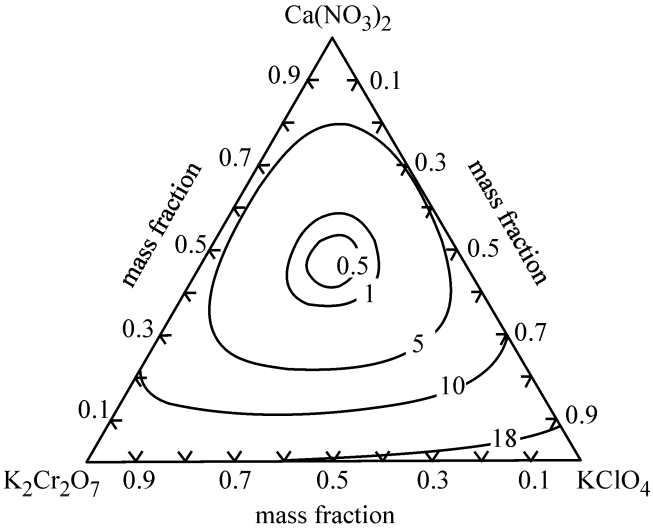

Fig. 5. Diagram relating the composition to the energy of the IV → III phase transition in ammonium nitrate for the additive $KClO_4$–$K_2Cr_2O_7$–$Ca(NO_3)_2$.

For the ternary additives containing magnesium and calcium nitrates (Figs. 1, 2), there are ranges of minimum energies of the phase transition in AN (zero energies according to the models), which lie within the composition–property diagram.

Comparison of the diagrams in Figs. 1 and 2 shows that the region of minimum phase transition energies becomes narrower for the additive containing calcium nitrate at the invariable position of this region in the diagram. Replacement of magnesium and calcium nitrates with strontium nitrate leads to a substantial general deterioration of the phase stability and to a shift of the region of minimum energies to the tie line between the components of the binary additive composed of strontium nitrate and potassium dichromate (Fig. 3). This is accounted for by the large positive value of the coefficient at the ternary-interaction term in Eq. (3), which, in turn, may result from appearance in the ternary mixture of an intermolecular complex formed because of the substantial increase in the radius of the strontium ion, compared with the magnesium ion.

Also, a ternary additive containing potassium perchlorate (PPC) instead of potassium nitrate was stud-

ied. The dependences of the energy of the IV → III phase transition in AN on the composition of the ternary additives: (i) potassium perchlorate, potassium dichromate, and magnesium nitrate, J_{Mg}; and (ii) potassium perchlorate, potassium dichromate, and calcium nitrate, J_{Ca}; are described by the equations

$$J_{Mg} = 6.3c_{MN} + 22.1c_{PPC} + 15.0c_{PDC} - 31.8c_{MN}c_{PPC} - 26.8c_{MN}c_{PDC} - 170.4c_{MN}c_{PPC}c_{PDC}, \quad (4)$$

$$J_{Ca} = 10.2c_{CN} + 21.9c_{PPC} + 15.2c_{PDC} - 40.7c_{CN}c_{PPC} - 25.4c_{CN}c_{PDC} - 186.2c_{CN}c_{PPC}c_{PDC}. \quad (5)$$

Diagrams relating the composition to the energy of the phase transition in ammonium nitrate, plotted using Eqs. (1)–(3), are shown in Figs. 4, 5. It can be seen that the replacement of potassium nitrate with potassium perchlorate has virtually no effect on the position of the region of minimum phase transition energies, but makes somewhat smaller its diameter for the additive containing magnesium nitrate and lowers the minimum depth (according to the model, the energy does not reach the zero value) for calcium nitrate. The experiments demonstrated that an increase in the total content of the ternary additive KNO_3–$K_2Cr_2O_7$–$Mg(NO_3)_2$ to 5% makes the region of zero phase transition energies substantially broader.

Thus, introduction of additives containing potassium, calcium, and magnesium nitrates, potassium perchlorate, and potassium dichromate into ammonium nitrate yields phase-stabilized ammonium nitrate with an increased thermal decomposition rate, which can be used as an oxidizing agent for ecologically safe solid propellants.

CONCLUSIONS

(1) Under the conditions of a differential-thermal analysis, ternary additives (potassium nitrate + potassium dichromate + magnesium nitrate and potassium nitrate + potassium dichromate + calcium nitrate) to ammonium nitrate suppress the V → IV phase transition and lead to a synergic decrease in the energy of the IV → III phase transition in ammonium nitrate to values smaller than the experimental error.

(2) Replacement of magnesium and calcium nitrates with strontium nitrate gives rise to an antagonism, which markedly impairs the phase stability of ammonium nitrate.

(3) Replacement of potassium nitrate in a ternary additive with potassium perchlorate does not change fundamentally the pattern of interactions in the system, but somewhat diminishes the range of zero transition energies.

(4) Additional introduction of a potassium dichromate additive does not impair the phase stability of ammonium nitrate and, as a result, an oxidizing agent for solid propellants with a substantially higher thermal decomposition rate can be obtained.

REFERENCES

1. RF Patent 2240283.
2. *Primenenie matematicheskikh metodov dlya issledovaniya mnogokomponentnykh sistem* (Use of Mathematical Methods for Analysis of Multicomponent Systems), Moscow: Metallurgiya, 1974.
3. Ruzinov, L.P., *Statisticheskie metody optimizatsii khimicheskikh protsessov* (Statistical Methods for Optimization of Chemical Processes), Moscow: Khimiya, 1972.
4. *Spravochnik khimika* (Chemist's Reference Book), Nikol'skii, B.P., Ed., Leningrad: Khimiya, 1971, vol. 1.

ISSN 1070-4272, Russian Journal of Applied Chemistry, 2007, Vol. 80, No. 12, pp. 2040–2044. © Pleiades Publishing, Ltd., 2007.
Original Russian Text © E.A. Maiorov, Yu.G. Dobryakov, 2007, published in Zhurnal Prikladnoi Khimii, 2007, Vol. 80, No. 12, pp. 1962–1966.

PHYSICOCHEMICAL STUDIES OF SYSTEMS AND PROCESSES

Limiting Activity Coefficients of Hydrocarbons in Phenol

E. A. Maiorov and Yu. G. Dobryakov

St. Petersburg State University, St. Petersburg, Russia

Received August 10, 2007

Abstract—Temperature dependence of the limiting activity coefficients of saturated (*n*-hexane, *n*-heptane, *n*-octane, and cyclohexane) and aromatic (benzene, toluene, ethylbenzene, *o*-xylene) hydrocarbons in phenol was studied in the temperature range 308–348 K by the headspace analysis method.

DOI: 10.1134/S1070427207120078

Among the thermodynamic characteristics of solutions, to be known in development of processes for substance separation and impurity extraction, are the limiting activity coefficients γ^{∞} of solutes. Values of γ^{∞} for various substances in the same solvent furnish information about the solvent selectivity toward this series of substances and enables evaluation of the extraction properties of the solvent [1]. Finally, values of γ^{∞} are related to parameters of the correlation equations widely used at present for description and calculation of liquid–vapor equilibria in binary and multicomponent systems, which makes it possible to calculate and prognosticate liquid–vapor equilibria at any concentration of the components of the system [2].

Studies of phenol-containing systems are initiated by the practical and theoretical interest in strongly associated solutions in which the effect of hydrogen bonds is manifested and, as a result, deviations of solution properties from the ideal behavior are observed. It is difficult to describe systems of this kind in terms of the existing models, because reliable experimental data necessary for estimating the base energy parameters of the interaction are occasionally lacking.

Huge amounts of phenols are necessary for production of lacquers, synthetic resins, and plastics, for development of a number of new types of polymeric materials, synthetic rubber, pesticides, and surfactants, and for preparation of plastifiers, drugs, and many other products [3]. The amounts of consumption of phenols are significant and steadily grow every year. Nevertheless, published data on the properties of dilute solutions with phenol as a solvent are comparatively scarce. The limiting activity coefficients in systems of this kind have been mainly investigated by the dynamic method of gas–liquid chromatography (on the basis of the retention time) [1, 4], with significant discrepancies between experimental data obtained by different authors.

The aim of this study was to apply the static vapor-phase analysis as an alternative experimental method for determining γ^{∞} at low temperatures and to measure the limiting distribution and activity coefficients of a number of organic substances in phenol in order to refine and supplement the available published data. Hydrocarbons of various homologous series: alkanes (*n*-hexane, *n*-heptane, *n*-octane, and cyclohexane) and arenes (benzene, toluene, ethylbenzene, and *o*-xylene), were chosen as solutes.

EXPERIMENTAL

The limiting activity coefficients of hydrocarbons in phenol were determined experimentally by the headspace analysis, with the vapor phase calibrated against an exterior standard [5, 6], using a Perkin Elmer Multifract F-45 Headspace analyzer. This method is well suitable for measurements in systems with a volatile dissolved component. The chromatograms were obtained and interpreted using a Multichrom hardware-and-software complex of version 1.47. The chromatographic analysis was carried out on a 300 × 0.3 mm steel column with an SE-30 (20%) packing on 60–80 mesh celite. The analysis conditions were as follows: column temperature 100–180°C, carrier-gas flow rate 20 ml min^{-1}, flow divider 1 : 20. Gas samples were taken automatically from glass vials with solutions under study by a pneumatically operated Headspace injector equipped with an internal liquid ther-

Table 1. Constants of the Antoine equation for calculation of the saturated vapor pressure of the hydrocarbons under study

Substance	*A*	*B*	*C*	Temperature range T_{min}–T_{max}, K
n-Hexane	15.8366	2697.55	–48.78	245–370
n-Heptane	15.8737	2911.32	–56.51	270–400
n-Octane	15.9426	3120.29	–63.63	292–425
Cyclohexane	15.7527	2766.63	–50.50	280–380
Benzene	15.9008	2788.51	–52.36	280–377
Toluene	16.0137	3096.52	–53.67	280–410
Ethylbenzene	16.0195	3279.47	–59.95	300–450
o-Xylene	16.1156	3395.57	–59.46	305–445

mostat and additional heater for the upper space to avoid condensation of substance vapors on the vial covers. The purity of all the reagents was checked by the chromatographic method; in case of unsatisfactory results, the substances were rectified on a rotary rectifying column with an efficiency of 20 theoretical plates. Phenol (purchased from Merck), with the main product content of no less than 99.5%, was not subjected to additional purification because it contained no admixtures that could hinder determination of a dissolved component.

Equal amounts (3 ml) of liquid phenol (mp 41°C) were poured into 22.3-ml glass vials of the same type with an automatic dispenser. The solvent mass was determined by weighing on an electronic analytical balance (Ohaus Explorer, USA) to within 0.1 mg. Then, the second component was introduced in an amount of 1 to 5 μl with a microsyringe into each vial with phenol. A series of solutions with mole fractions x_2 of the solute in the range 0.0002–0.001 was prepared. The same volumes of the second component were introduced into empty vials to prepare reference samples. The vials were hermetically sealed and thermostated for 1 h, after which the vapor phase was automatically sampled and analyzed by chromatography. At least three parallel samples were prepared for each concentration.

We assumed in calculations that the partial pressure and the number of moles of the second component in the gas phase are proportional to the area of its chromatographic peak. As a result of an experiment, we directly determined the distribution coefficient of a solute (index 2) between a vapor and a liquid by the relation

$$K_2^{l-v} = \frac{c_2^l}{c_2^v} = 1 + \frac{V^0}{V^l}\left(\frac{S_2^0}{S_2} - 1\right). \quad (1)$$

Here, K_2^{l-v} is the distribution coefficient of component 2 between the liquid and vapor phases; c_2^l and c_2^v, molar concentrations of component 2 in the liquid and vapor phases, respectively; S_2^0 and S_2, areas of the peaks corresponding to component 2 in a reference vial and over the solution; V^0 and V^l, total volumes of a vial and the volume of the liquid in it.

To determine the limiting distribution coefficient K_2^∞, we extrapolated the data obtained for a series of solutions to zero concentration and then calculated the limiting activity coefficient γ_2^∞ by the formula

$$\gamma_2^\infty = \frac{\rho_l RT}{p_2^0 K_2^\infty M_l}. \quad (2)$$

Here, p_2^0 is the vapor pressure of pure component 2 at the temperature of experiment, T; ρ_l and M_l, density (g cm^{-3}) and molecular weight (94.13 g mol^{-1}) of the solvent; R, universal gas constant; and T, thermodynamic temperature (K).

Formula (2) was derived on the assumption of an ideal vapor phase, which is fully justified at low pressures and temperatures.

The phenol density ρ_l (g ml^{-1}) at the experimental temperatures was calculated using the relation obtained on the basis of the reference data [7] on the molar volume of phenol at various temperatures:

$$\rho = \frac{94.13}{7.63 \times 10^{-5}T^2 + 2.40 \times 10^{-2}T + 73.9}, \quad (3)$$

where T is temperature (K).

In the temperature range under study, polynomial (3) better reproduces the experimental dependence of phenol density on temperature than the Francis equation [7]. The vapor pressures of the pure solutes, p_2^0 (mm Hg), were calculated by Antoine's equation [8]

$$\ln p_i^0 = A - \frac{B}{C + T}. \quad (4)$$

The values of constants A, B, and C for the substances under study are listed in Table 1.

Table 2. Experimental values of the limiting distribution coefficients K_2^∞ in liquid–vapor systems and the limiting activity coefficients of hydrocarbons in phenol, γ_2^∞

Solute	K_2^∞, (γ_2^∞), at indicated temperature, °C			
	35	45	60	75
n-Hexane	–	49 ± 3	33 ± 2	22 ± 1
	–	(13.3 ± 0.9)	(12.3 ± 0.9)	(11.6 ± 0.8)
n-Heptane	179 ± 9	122 ± 6	73 ± 4	46 ± 2
	(16.4 ± 1.1)	(15.9 ± 1.1)	(15.2 ± 1.1)	(14.3 ± 1.0)
n-Octane	–	310 ± 16	167 ± 8	101 ± 5
	–	(18.0 ± 1.3)	(17.5 ± 1.2)	(15.9 ± 1.1)
Cyclohexane	–	135 ± 7	90 ± 5	60 ± 3
	–	(7.3 ± 0.5)	(6.7 ± 0.5)	(6.2 ± 0.4)
Benzene	420 ± 20	319 ± 16	224 ± 11	160 ± 8
	(3.5 ± 0.2)	(3.1 ± 0.2)	(2.6 ± 0.2)	(2.3 ± 0.2)
Toluene	1145 ± 57	815 ± 41	538 ± 27	345 ± 17
	(4.0 ± 0.3)	(3.7 ± 0.3)	(3.1 ± 0.2)	(2.8 ± 0.2)
Ethylbenzene	–	1950 ± 100	1110 ± 60	690 ± 35
	–	(4.1 ± 0.3)	(3.7 ± 0.3)	(3.3 ± 0.2)
o-Xylene	–	2170 ± 110	1260 ± 60	780 ± 40
	–	(5.1 ± 0.4)	(4.5 ± 0.3)	(3.9 ± 0.3)

The limiting distribution and activity coefficients of hydrocarbons (hexane, heptane, octane, cyclohexane, benzene, toluene, ethylbenzene, and *o*-xylene) in phenol were measured in the temperature range 308–348 K (Table 2). The distribution coefficients fall within the range from 23 to ~2200, the extreme values being somewhat beyond the optimal applicability range of the static Headspace method [9]. Nevertheless, the resulting values of γ_2^∞ agree (especially at low temperatures) with published data obtained by different methods [10–16]. As temperature increases, a certain divergence of the results (with the maximum value of about 15%) is observed. This is probably due to the possible, in the case of the dynamic GLC method, decrease in the mass of the liquid phase in a column via its uncontrollable vaporization and removal by the gas-carrier, and also to adsorption of the dissolved substances at the phase boundaries between the fixed liquid phase and the solid support.

Positive deviations from Raoult's law are observed in all of the binary systems studied. Values of γ_2^∞ fall within the range 2.3–5.1 for aromatic hydrocarbons and 6.2–18 for alkanes. The data are described by linear dependences on inverse temperature within the experimental error (5–7%) (Figs. 1a–1e).

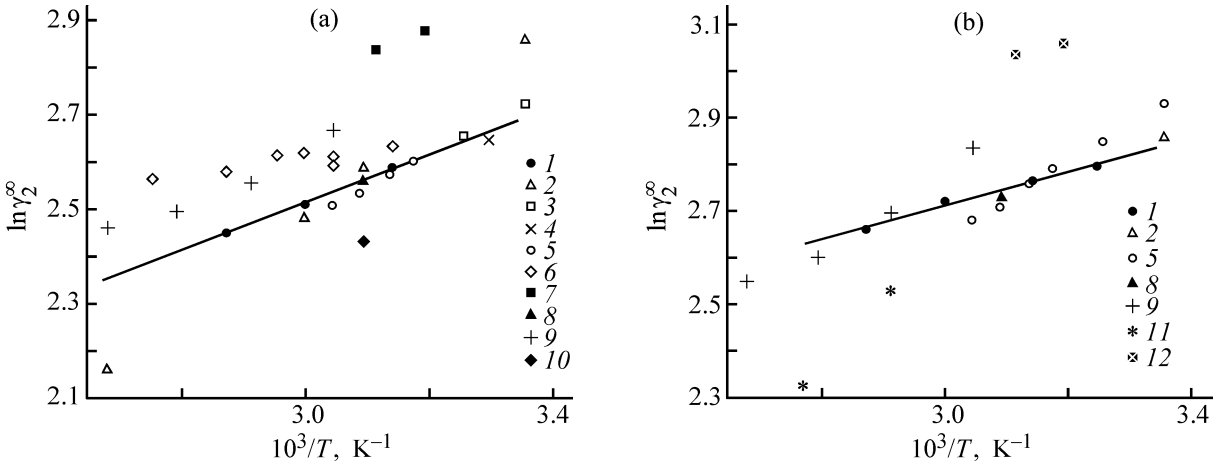

Fig. 1. Limiting activity coefficients γ_2^∞ of (a) hexane, (b) *n*-heptane, (c) cyclohexane, (d) benzene, and (e) toluene in phenol vs. inverse temperature 1/*T*. (*1*) results of this study; (*2–12*) published data [1, 4] obtained by dynamic gas-liquid chromatography methods: (*2*) [10], (*3*) [11], (*4*) [12], (*5*) [13], (*6*) [14], (*7*) [15], (*8*) [16], (*9*) [17], (*12*) [19]; by continuous gas extraction method: (*10*) [14]; by other methods: (*11*) [18].

The limiting activity coefficients for ethylbenzene and *o*-xylene in phenol were measured for the first time. For some hydrocarbons, the values of γ_2^∞ in supercooled liquid phenol were found experimentally at 35°C, which is 5°C below the melting point of phenol. Despite that phenol can be supercooled to room temperature, we did not carry out further measurements because the design of the Headspace analyzer used in the study does not allow thermostating of samples being analyzed below +30°C. Nevertheless, the experimental study of thermodynamic properties of such systems at low temperatures is of particular interest for examining the effect of hydrogen bonds, on which the extractive properties and dissolving power of numerous organic substances depend. The data on γ_2^∞ obtained at 35°C well agree with the values found by extrapolation of the $\ln\gamma_2^\infty$–$1/T$ straight lines to this temperature range (Figs. 1b, 1d, 1e). Thus, the extrapolation of experimental data to the range of metastable equilibria is well justified; however, it is necessary to take into consideration that the error in the thus obtained results can considerably increase. The temperature dependence of the limiting activity coefficients can be used to calculate the partial molar excess enthalpy at infinite dilution, $H_i^{E\infty}$, by the Gibbs–Helmholtz differential equation

$$\left(\frac{\partial \ln \gamma_i^\infty}{\partial (1/T)}\right)_{P, x_i} = \frac{H_i^{E\infty}}{R}. \qquad (5)$$

The dependences $\ln\gamma_2^\infty$–$1/T$ for normal alkanes in phenol (Fig. 2) in the C_6–C_8 homologous series have virtually the same slope, with the value of $H_i^{E\infty}$ equal to 3700 ± 450 (12%) J mol^{-1}. The calculation of the excess thermodynamic functions at infinite dilution from the temperature dependence of limiting activity coefficients can be considered fully reliable.

CONCLUSIONS

(1) Static vapor-phase analysis is a sufficiently simple, rather fast, and reliable method for study of thermodynamic functions at infinite dilution for systems with solute distribution coefficients between the liquid and the vapor of up to 2000. In this method, there are no sources of errors difficult to estimate, which are associated with interphase adsorption and uncontrolled removal of a phase, as in the case of the dynamic GLC based on the retention time.

(2) In contrast to the dynamic variant and continuous gas extraction, the static Headspace analysis

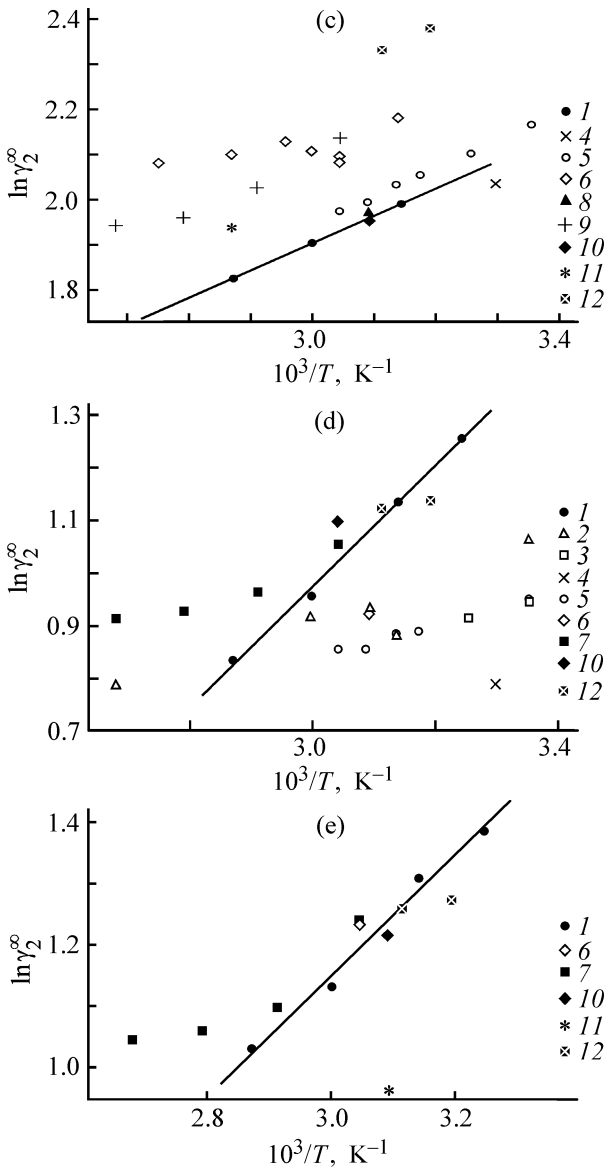

Fig. 1. (Contd.)

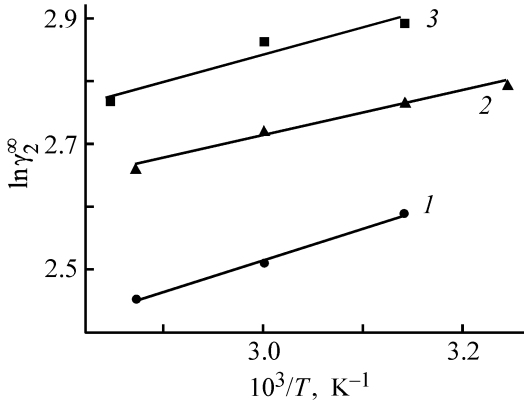

Fig. 2. Limiting activity coefficients γ_2^∞ for alkanes in phenol vs. inverse temperature $1/T$. (*1*) *n*-Hexane, (*2*) *n*-heptane, and (*3*) *n*-octane.

method makes it possible to study liquid–vapor equilibria in supercooled (metastable) solutions.

ACKNOWLEDGMENTS

The authors are grateful to professor N.A. Smirnova for helpful discussions and useful remarks. The study was financially supported by the Federal Program "Leading Scientific Schools" (project no. NSh-676.2003.3).

REFERENCES

1. MorachevskiI, A.G., Smirnova, N.A., Balashova, I.M., and Pukinskii, I.B., *Termodinamika razbavlennykh rastvorov neelektrolitov* (Thermodynamics of Dilute Solutions of Nonelectrolytes), Leningrad: Khimiya, 1982.
2. Prausnitz, J., Andersen, T., Grens, E., et al., *Computer Calculation for Multicomponent Vapor–Liguid Equilibria*, New York, 1980.
3. Kharlampovich, G.D., and Churkin, Yu.V., *Fenoly* (Phenols), Moscow: Khimiya, 1974.
4. Gmehling, J., Menke, J., and Schiller, M., *Activity Coefficients at Infinite Dilution: Dechema Data Series*, Frankfurt am Main: Dechema, 1994, vol. 9, part 3.
5. Kolb, B., Welter, C., and Bichler, C., *Chromatograph.*, 1992, vol. 34, nos. 5–8, pp. 235–240.
6. Dobriyakov, Yu.G., Asprion, N., Hasse, G., et al., *Teor. Osn. Khim. Tekhnol.*, 1997, vol. 31, no. 6, pp. 605–612.
7. Smith, B.D. and Srivastava, R., *Thermodynamic Data for Pure Compounds, Phys. Sciences Data 25, part A + B*, Amsterdam: Elsevier, 1986.
8. Reid, R.G., Prausnitz, J.M., and Sherwood, T.K., *The Properties of Gases and Liquids*, New York: McGraw–Hill, 1977.
9. Vitenberg, A.G. and Ioffe, B.V., *Gazovaya ekstraktsiya v khromatograficheskom analize: Parofaznyi analiz i rodstvennye metody* (Gas Extraction in Chromatographic Analysis: Vapor-Phase Analysis and Related Methods), Leningrad: Khimiya, 1982.
10. Deal, C.H. and Derr, E.L., *Ind. Eng. Chem., Process Des. Dev.*, 1964, vol. 3, no. 4, pp. 394–399.
11. Vernier, Ph., Raimbault, C., and Renon, J., *J. Chim. Phys. et Chim.–Phys. Biol.*, 1969, vol. 66, no. 3, pp. 429–436.
12. Pul'tsin, M.N., Gaile, A.A., and Proskuryakov, V.A., *Zh. Fiz. Khim.*, 1973, vol. 47, no. 3, pp. 751–752.
13. Vernier, Ph., *These, Universite de Paris*, 1967.
14. Santacesaria, E., Berlendis, D., and Carra, S., *Liquid Phase Equilibria*, 1979, vol. 3, no. 2, pp. 167–176.
15. Leitman, Y.I., Gaile, A.A., and Proskuryakov, V.A., *Zh. Fis. Khim.*, 1973. vol. 47, p. 751.
16. Thomas, E.R., Newman, B.A., Long, T.C., et al., *J. Chem. Eng. Data*, 1982, vol. 27, pp. 399–405.
17. Liu, Y., Greenkorn, R.A., and Chao, K.C., *J. Chem. Eng. Data*, 1981, vol. 26, pp. 386–388.
18. Tassios, D.P., *Ind. Eng. Chem., Process Des. Dev.*, 1972, vol. 11, pp. 43–46.
19. Leitman, Y.I. and Gaile, A.A., *Zh. Fis. Khim.*, 1971, vol. 45, p. 2113.

ISSN 1070-4272, Russian Journal of Applied Chemistry, 2007, Vol. 80, No. 12, pp. 2045–2048. © Pleiades Publishing, Ltd., 2007.
Original Russian Text © O.V. Surov, M.I. Voronova, 2007, published in Zhurnal Prikladnoi Khimii, 2007, Vol. 80, No. 12, pp. 1967–1269.

PHYSICOCHEMICAL STUDIES OF SYSTEMS AND PROCESSES

Determination of Partial Pressures of Components of the Water–Dimethylsulfoxide System with a Double Effusion Chamber

O. V. Surov and M. I. Voronova

Institute of Solution Chemistry, Russian Academy of Sciences, Ivanovo, Russia

Received September 17, 2007

Abstract—Knudsen's method with a double effusion chamber was used to determine the partial pressures of water and dimethylsulfoxide over their solutions and over the water–dimethylsulfoxide–cellulose system.

DOI: 10.1134/S107042720712008X

Knudsen's effusion method is widely and successfully used to study substances with low saturated vapor pressure. However, it has, despite advantages, certain limitations: the upper applicability level of Knudsen's method does not exceed a pressure of 10 Pa, and the radius of the effusion orifice, 1 mm. This is due to the fact that the conditions of molecular outflow of a vapor from the effusion orifice are only satisfied in the case when the mean free path of molecules within the cavity of the effusion chamber substantially exceeds the diameter of the effusion orifice. When pressures substantially exceeding 10 Pa are measured, various corrections are commonly introduced to take into account deviations of the vapor outflow mode from the molecular conditions [1]. Provided that an appropriate calibration is carried out, the effusion method can be successfully used to determine the equilibrium water vapor pressure and calculate the thermodynamic characteristics of the desorption process [2].

The aim of our study was to develop a technique for determining the partial vapor pressures of components of a binary mixture with the use of a double effusion chamber. This method markedly extends the number of systems accessible to study and enables analysis of real technological processes that commonly occur at pressures exceeding the Knudsen limit (10 Pa).

EXPERIMENTAL

The experimental effusion installation and the method for determining the equilibrium water vapor pressure were described in detail in [2]. We chose as object of study the system water–dimethylsulfoxide (DMSO) previously examined with an MI-1201 mass spectrometer [3]. We used a double effusion chamber schematically shown in Fig. 1. Under our experimental conditions, changes in the mixture composition during measurements were negligible. Thus, the whole body of the data obtained can be related to the state of the system, which is characterized by the starting composition.

A solution to be analyzed was placed in chamber *I* (evaporation chamber). After the solution was heated to a temperature T, vapors of its components passed through a connecting channel into chamber *II* (effusion chamber), where the effusion occurred. With this design of the effusion unit, the pressure in the effusion chamber $\sum_{i=1}^{n} p_{2i}$ at a given temperature T will be determined by the vapor pressure in the evaporation chamber, $\sum_{i=1}^{n} p_{1i}$, and by the relative throughputs of

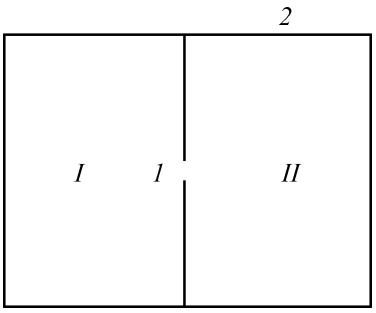

Fig. 1. Schematic of a double effusion chamber. Chamber: (*I*) evaporation and (*II*) effusion; (*1*) connecting channel and (*2*) effusion orifice.

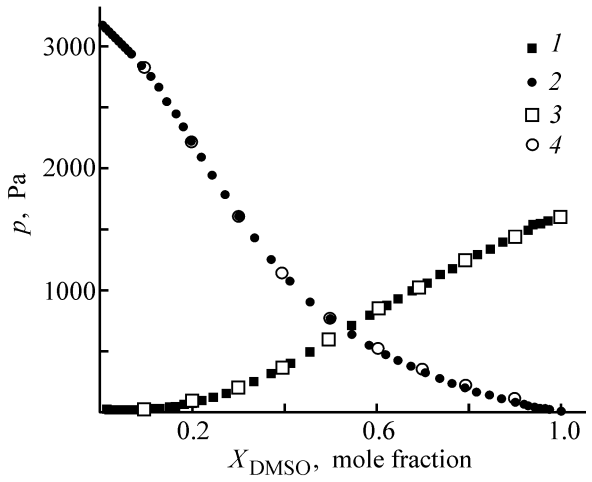

Fig. 2. Partial saturated vapor pressures p of (*1*, *3*) DMSO and (*2*, *4*) water over solutions of various compositions at 298 K. (X_{DMSO}) DMSO concentration in the mixture; the same for Fig. 3. (*1*, *2*) Data of [4]; (*3*, *4*) results of experiments performed in this study. The partial pressures of DMSO are multiplied by 20.

the connecting channel (S_1L_1) and effusion orifice ($S_{ef}L_{ef}$). The flux ρ_1 arriving into the effusion chamber is given by

$$\rho_1 = S_1L_1\Sigma A_i\Sigma p_{1i}, \quad A_i = (2\pi M_iRT)^{-1/2}, \qquad (1)$$

where ρ_1 is the flux of a mixture of n gases leaving the evaporation chamber in unit time (mol m^{-2} s^{-1}); S_1, cross-sectional area of the connecting channel (m^2); L_1, Clausing coefficient characterizing the resistance of the connecting channel to a vapor flow; M_i, molecular mass of ith component of the mixture (kg mol^{-1}); R = 8.314 J mol^{-1} K^{-1}, universal gas constant; T, absolute temperature (K) $\sum_{i=1}^{n} p_{1i}$; total pressure of a mixture of n gases in the evaporation chamber (Pa); and p_{1i}, partial pressure of ith component of the mixture in the evaporation chamber (Pa).

The flux ρ_2 leaving the effusion chamber is given by

$$-\rho_1 = S_1L_1\sum_{i=1}^{n} A_i\sum_{i=1}^{n} p_{2i} + S_{ef}L_{ef}\sum_{i=1}^{n} A_i\sum_{i=1}^{n} p_{2i}, \qquad (2)$$

where S_{ef} and L_{ef} are the cross-sectional area of the effusion orifice and the Clausing coefficient, respectively, and p_{2i} is the partial pressure of ith component of the mixture in the effusion chamber (Pa).

In the steady-state mode, the fluxes are equal ($\rho_1 = \rho_2$) and we have

$$\sum_{i=1}^{n} p_{2i} = [S_1L_1/(S_1L_1 + S_{ef}L_{ef})]\sum_{i=1}^{n} p_{1i}. \qquad (3)$$

The experiment can be performed in two ways. In the first case, a water–DMSO solution with a known concentration of the components is placed in chamber *I*, and water, in chamber *II*. If chamber *II* contains pure water, analysis of Eqs. (1)–(3) shows that, in this case, the water vapor pressures in chambers *I* and *II* will be the same and equal to the saturated water vapor pressure at the temperature of the experiment. This situation will be preserved while pure water is in chamber *II*. In this case, DMSO will evaporate from chamber *I*, and water will only evaporate from chamber *II* and will act as a seal that prevents evaporation from chamber *I*. In the second variant, pure DMSO is in the effusion chamber, and a two-component water–DMSO solution of known concentration, in the evaporation chamber. In this case, the role of a seal is played by DMSO, which prevents evaporation of DMSO from chamber *I*, so that only water evaporates from chamber *I*. Generally speaking, it is necessary, when recording the fluxes ρ_1 and ρ_2, to make a correction for the transfer of a component from a chamber with a lower partial pressure into that with a lower partial pressure, because the concentrations of the solutions vary in the closed isolated space in such a way that the vapor pressures over the solutions tend to equalize. However, it is shown below that this correction can be neglected under the conditions of a not-too-long effusion experiment. The dismountable design of the effusion unit makes it possible to record the loss of mass by a solution in each chamber during the experiment and to vary the throughput capacities of the connecting channel and effusion orifice to achieve the optimal conditions of the experiment. The loss of mass by the solution, temperature of the effusion unit, and evaporation time were used to calculate the vapor pressure in the effusion and evaporation chambers by the Knudsen equation. The vapor pressure of ith component in the effusion chamber, p_{2i} (Pa), is given by

$$p_{2i} = (\Delta m_i/\alpha\tau S_{ef}L_{ef})(2\pi M_iRT)^{1/2}, \qquad (4)$$

where Δm_i is the mass of substance effused from the effusion unit (kg); τ, evaporation time (s); and α, condensation coefficient.

Then, with account of Eq. (3), we can express the vapor pressure of ith component in the evaporation chamber as

$$p_{1i} = (\Delta m_i/\alpha\tau S_{ef}L_{ef})[(S_1L_1 + S_{ef}L_{ef})/S_1L_1](2\pi M_iRT)^{1/2}. \qquad (5)$$

Thus, measuring the loss of mass by a solution in the evaporation chamber in two variants of the exper-

iment, we can obtain the partial pressures of the solution components in relation to concentration. We used in the experiment an effusion orifice with a throughput $S_{ef}L_{ef}$ of 8.206×10^{-10} m^2. The throughput of the connecting channel S_1L_1 was varied as follows: 6.6×10^{-11}, 5.66×10^{-10}, and 1.09×10^{-9}. The procedure described in detail in [2] was used to construct a calibration plot relating the water vapor pressure calculated by the Knudsen equation (5) to the true pressure. It was also found that the condensation coefficient α in Eq. (5) is 0.63 for pure DMSO. Further, we used this value to calculate partial pressures of DMSO in water–DMSO solutions.

Figure 2 shows the partial pressures of water and DMSO, obtained at 298 K using the procedure described above, in comparison with published data [4]. It can be seen that the agreement is very good.

In addition, we determined the equilibrium partial pressures of water and DMSO over the cellulose–water–DMSO system. The procedure used to measure the water vapor pressure over cellulose samples was described in detail in [2]. With account of the specific features of analysis of a two-component water–DMSO solution, the method consists in the following. A preliminarily dried cellulose sample is wetted with a minor amount of the water–DMSO solution and an effusion experiment is carried out using a double effusion chamber. In the experiment, the partial pressures of water and DMSO vapors were determined at 298 K over a cellulose sample wetted with water–DMSO solutions of various concentrations. The content of a component in cellulose, α_i, at which the equilibrium vapor pressure p_i of the component starts to deviate from its saturated vapor pressure p_{i0} at the temperature of the experiment (298 K), i.e., the ratio pD_i/p_{i0} starts to deviate from unity, corresponds to the maximum sorption of the component by cellulose at a given concentration of the solution [2]. In this way, we obtained individual isotherms of water and DMSO sorption by cellulose from a water–DMSO mixture at 298 K.

Figure 3 shows individual isotherms of water and DMSO sorption by cellulose from a water–DMSO mixture at 298 K, obtained in three different ways: (1) by determining the total absorption of the solution by cellulose (cellulose swelling) [5], (2) by calculated from an experimental isotherm of composition variation [6], and (3) by the method described in the present study.

The method for calculating individual sorption isotherms of components from the isotherm of variation of the mixture composition has been described in detail in the literature [7], whereas the method for

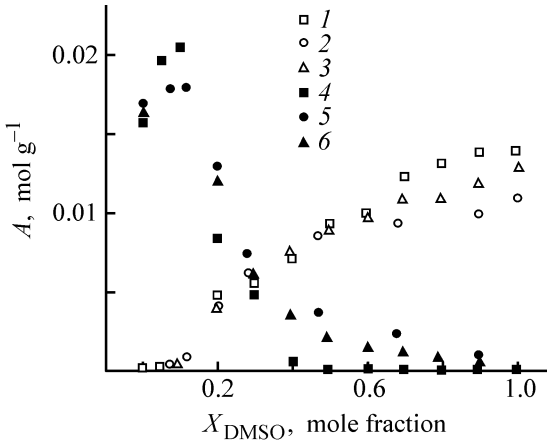

Fig. 3. Individual isotherms of (*1–3*) DMSO and (*4–6*) water sorption *A* from a water–DMSO mixture on cellulose at 298 K. (*1*, *4*) Obtained by determining the total absorption of the solution by cellulose; (*2*, *5*) calculated from an experimental isotherm of composition variation (data of [6]); (*3*, *6*) obtained using the method described in the present study.

determining the total absorption of a solution by cellulose requires a more detailed description. A sample of cellulose wetted with a water–DMSO solution was centrifuged at 8000 rpm for 15 min. These conditions make it possible to remove the solution mechanically bound to cellulose and obtain a cellulose sample with the content of components equal to the physical sorption on cellulose [5]. The content of DMSO in the cellulose sample was determined by extraction of DMSO into a fixed volume of water. The concentration of the resulting solution was found by refractometry. The water content of the sample was calculated from the total mass of the solution sorbed by cellulose (after the centrifugation) and the DMSO content of the sample.

It can be seen from Fig. 3 that the dependence of water sorption by cellulose from a binary water–DMSO solution has an extremum: the maximum sorption of water is observed at DMSO concentrations X_{DMSO} = 0.05–0.1 mol fraction. The possible reasons for the appearance of an extremum in the water sorption curve for the water–DMSO system was discussed in detail in [6]. It is important to note here that three independent methods for obtaining individual sorption isotherms of components in the water–DMSO–cellulose system give well-consistent results. This confirms the adequacy of these methods.

CONCLUSIONS

The method for determining the partial pressures of the components of a two-component mixture with

the use of a double effusion chamber shows good agreement with the results of other independent methods and can be used as a proximate technique for determining the partial pressures of two-component mixtures with vapor pressures considerably exceeding the common upper applicability limit of Knudsen's method (10 Pa).

REFERENCES

1. Sidorov, L.N., Korobov, M.V., and Zhuravleva, L.V., *Mass-spektral'nye termodinamicheskie issledovaniya* (Mass-Spectral Thermodynamic Studies), Moscow: Mosk. Gos. Univ., 1985.
2. Surov, O.V., Voronova, M.I., and Zakharov, A.G., *Zh. Prikl. Khim.*, 2007, vol. 80, no. 1, pp. 43–48.
3. Zakharov, A.G., Pelipets, O.V., Voronova, M.I., et al., *Zh. Fiz. Khim.*, 2005, vol. 79, no. 7, pp. 1216–1219.
4. Lai, J.T.W., Lau, F.W., Robb, D., et al., *J. Sol. Chem.*, 1995, vol. 24, no. 1, pp. 89–102.
5. Jayme, G. and Roffael, E., *Papier.*, 1970, vol. 24, no. 4, pp. 181–186.
6. Zakharov, A.G., Voronova, M.I., Prusov, A.N., et al., *Zh. Fiz. Khim.*, 2006, vol. 80, no. 8, pp. 1472–1476.
7. Adamson, A.W., *Physical Chemistry of Surfaces*, New York: John Wiley & Sons, 1976.

ISSN 1070-4272, Russian Journal of Applied Chemistry, 2007, Vol. 80, No. 12, pp. 2049–2050. © Pleiades Publishing, Ltd., 2007.
Original Russian Text © A.V. Kurzin, A.N. Evdokimov, V.B. Antipina, O.S. Pavlova, 2007, published in Zhurnal Prikladnoi Khimii, 2007, Vol. 80, No. 12, pp. 1970–1971.

PHYSICOCHEMICAL STUDIES OF SYSTEMS AND PROCESSES

Liquid–Vapor Equilibrium in the System Acetone–Methanol–*N*-Butylpyridinium Hexafluorophosphate

A. V. Kurzin, A. N. Evdokimov, V. B. Antipina, and O. S. Pavlova

St. Petersburg State Technological University of Plant Polymers, St. Petersburg, Russia

Received July 24, 2007

Abstract—The liquid–vapor equilibrium in the system acetone–methanol-*N*-butylpyridinium hexafluorophosphate was studied at 313.15 K.

DOI: 10.1134/S1070427207120091

Azeotropic mixtures can be separated either by varying the pressure in the course of distillation or by using selective methods such as, e.g., frequently used salt distillation [1]. In this method, the relative volatility of components of an azeotropic mixture is changed by adding an appropriate salt until complete disappearance of the azeotrope. In the modern versions of salt distillation, both organic salts with bulky ions and ionic liquids readily soluble in organic solvents are used.

In this study, we examined, using the headspace gas-chromatographic analysis, the effect of *N*-butylpyridinium hexafluorophosphate on the liquid–vapor equilibrium in the system acetone–methanol-*N*-butylpyridinium hexafluorophosphate at 313.15 K. There are published isothermal and isobaric data on the vapor–liquid equilibrium in the binary system acetone–methanol [2] and in certain ternary systems acetone–methanol–electrolyte (including an ionic liquid) [3].

Our experimental data on the liquid–vapor equilibrium in the system acetone–methanol–*N*-butylpyridinium hexafluorophosphate are listed in Table 1.

Table 1 shows that the minimal concentration of *N*-butylpyridinium hexafluorophosphate required for elimination of the azeotrope in the system acetone–methanol–*N*-butylpyridinium hexafluorophosphate is 0.1 mol kg^{-1}. The phase equilibria in ternary systems containing a binary solvent and an electrolyte are frequently analyzed in terms of the following models of solutions: NRTL, UNIFAC, UNIQUAC, and LIQUAC [4, 5]. In this study, we used the NRTL elec-

Table 1. Liquid–vapor equilibrium in the system acetone (1)–methanol (2)–*N*-butylpyridinium hexafluorophosphate (3) at 313.15 K

x_1	y_1	x_1	y_1	x_1	y_1	x_1	y_1	x_1	y_1
at indicated m_3, mol kg^{-1}									
0.000		0.100		0.300		0.500		1.000	
0.1005	0.2351	0.1005	0.2402	0.1005	0.2602	0.1005	0.2697	0.1005	0.2835
0.2003	0.3652	0.2003	0.3784	0.2003	0.4076	0.2003	0.4302	0.2003	0.4593
0.3007	0.4583	0.3007	0.4896	0.3007	0.5123	0.3007	0.5497	0.3007	0.5804
0.5000	0.6086	0.5000	0.6365	0.5000	0.6604	0.5000	0.7083	0.5000	0.7403
0.6000	0.6591	0.6000	0.6899	0.6000	0.7325	0.6000	0.7785	0.6000	0.8096
0.7001	0.7311	0.7001	0.7701	0.7001	0.7896	0.7001	0.8396	0.7001	0.8603
0.8006	0.8069	0.8006	0.8322	0.8006	0.8578	0.8006	0.8952	0.8006	0.9114
0.8472	0.8471	0.8472	0.8713	0.8472	0.8972	0.8472	0.9217	0.8472	0.9142
0.8903	0.8856	0.8903	0.8999	0.8903	0.9208	0.8903	0.9440	0.8903	0.9393

Table 2. Parameters of interactions between components in the ternary system acetone–methanol–*N*-butylpyridinium hexafluorophosphate, used in the NRTL model

Component		α_{ij}	Δg_{ij}	Δg_{ji}
i	*j*		J mol^{-1}	
Acetone	Methanol	0.300	924.2	863.1
Methanol	Salt	0.359	9865.7	–5322.4
Acetone	Salt	0.422	13442.6	–4756.1

trolytic model [6]. This model has been previously used for describing liquid–vapor equilibria in ternary systems containing organic salts with bulky ions [7–9]. The energies of interactions of components in mixed solvents were taken from [3], and the parameters of the salt–solvent interaction were calculated from experimental data on the liquid–vapor equilibria in the corresponding binary systems. The vapor pressures of pure acetone and methanol, used in our calculations, were 54.2 and 34.2 kPa, respectively. The parameters used in our model calculations are listed in Table 2.

The characteristics of liquid–vapor equilibrium in the system acetone–methanol–*N*-butylpyridinium hexafluorophosphate, calculated using the NRTL model, reasonably agree with the experimental values. The mean absolute deviation between the calculated and experimental $|y_i|$ values was 0.007.

EXPERIMENTAL

Acetone and methanol (analytically pure grade) were distilled and dried by standard procedures [10]. The content of main substances in these solvents, determined by gas chromatography, exceeded 99.8%. *N*-Butylpyridinium hexafluorophosphate (Acros), mp 76°C, was used without additional purification.

Ternary mixtures metanol–acetone–*N*-butylpyridinium hexafluorophosphate were prepared gravimetrically. The individual components were weighed with an error not exceeding 0.1 mg. An 8-ml sample of a ternary mixture to be studied was weighed and placed in a preheated hermetically sealed 30-ml vessel. This vessel was kept in a temperature-controlled cell at a prescribed temperature (±0.05°C) with continuous stirring for 6 h. The temperature was measured with an accuracy of 0.1 K. The content of the individual components in the gas phase, y_i, was determined by gaschromatography [5, 11]. In analysis, 0.2-ml samples of gas phase were taken with a syringe. The gas phase was assumed to be ideal. To prevent partial condensation of vapor in the syringe and a shift of the liquid–gas equilibrium in the vessel, both the syringe and vessel were maintained at equal temperatures. The sampled gas phase was analyzed on a Chrom-5 (former Czechoslovakia) gas–liquid chromatograph (glass column, 2.5 m × 3 mm; stationary phase OV-17, 5% on Chromaton N-Super, 0.125–0.160 mm; vaporizer and column temperature 160 and 120°C, respectively; carrier gas argon, 99.9% purity, flow rate 0.5 ml s^{-1}).

CONCLUSIONS

(1) The liquid–vapor equilibrium in the system acetone–methanol–*N*-butylpyridinium hexafluorophosphate at 313.15 K was studied by gas chromatography and adequately described in terms of NRTL electrolytic model.

(2) The minimal concentration of *N*-butylpyridinium hexafluorophosphate for eliminating the azeotrope in the system acetone–methanol–*N*-butylpyridinium hexafluorophosphate is 0.1 mol kg^{-1}.

REFERENCES

1. Tsiparis, I.N., Dobroserdov, L.L., and Kogan, V.B., *Solevaya rektifikatsiya* (Salt Distillation), Leningrad: Khimiya, 1969.
2. Kogan, V.B., Fridman, V.M., and Kafarov, V.V., *Ravnovesie mezhdu zhidkost'yu i parom* (Liquid–Vapor Equilibrium), Moscow: Nauka, 1966, vol. 1.
3. Orchilles, O.V., Miguel, P.J., Vercher, E., and Martinez-Andreu, A., *J. Chem. Eng. Data*, 2007, vol. 52, no. 1, pp. 141–147.
4. Smirnova, N.A., *Molekulyarnye teorii rastvorov* (Molecular Theories of Solutions), Leningrad: Khimiya, 1987.
5. *Termodinamika ravnovesiya zhidkost'–par* (Thermodynamics of Liquid–Vapor Equilibria), Morachevskii, A.G., Ed., Leningrad: Khimiya, 1989.
6. Mock, B., Evans, L.B., and Chen, C.-C., *Am. Inst. Chem. Eng. J.*, 1986, vol. 32, no. 10, pp. 1655–1664.
7. Kurzin, A.V., Evdokimov, A.N., Poltoratskiy, G.M., et al., *J. Chem. Eng. Data*, 2004, vol. 49, no. 2, pp. 208–211.
8. Kurzin, A.V., Evdokimov, A.N., Antipina, V.A., and Gusev, V.E., *J. Chem. Eng. Data*, 2005, vol. 50, no. 6, pp. 1861–1863.
9. Kurzin, A.V., Evdokimov, A.N., Antipina, V.A., and Pavlova, O.S., *J. Chem. Eng. Data*, 2006, vol. 51, no. 4, pp. 1361–1363.
10. Gordon, A.J. and Ford, R.A., *The Chemist's Companion. A Handbook of Practical Data, Techniques, and References*, New York: Wiley, 1972.
11. Takamatsu, H. and Ohe, S., *J. Chem. Eng. Data*, 2003, vol. 48, no. 2, pp. 277–279.

ISSN 1070-4272, Russian Journal of Applied Chemistry, 2007, Vol. 80, No. 12, pp. 2051–2056. © Pleiades Publishing, Ltd., 2007.
Original Russian Text © L.A. Zemnukhova, S.V. Sukhoverkhov, E.D. Shkorina, A.V. Kovekhova, S.V. Tomshich, 2007, published in Zhurnal Prikladnoi Khimii, 2007, Vol. 80, No. 12, pp. 1972–1977.

PHYSICOCHEMICAL STUDIES OF SYSTEMS AND PROCESSES

Use of High-Performance Exclusion Chromatography for Analysis of the Molecular Mass of Polysaccharides Produced from Buckwheat and Sunflower Wastes

L. A. Zemnukhova, S. V. Sukhoverkhov, E. D. Shkorina, A. V. Kovekhova, and S. V. Tomshich

Institute of Chemistry, Far-Eastern Division, Russian Academy of Sciences, Vladivostok, Russia

Far-Eastern State University, Vladivostok, Russia

Pacific Institute of Bioorganic Chemistry, Far-Eastern Division, Russian Academy of Sciences, Vladivostok, Russia

Received April 18, 2007

Abstract—High-performance exclusion chromatography was used to study polysaccharide samples obtained by successive extraction with water, ammonium oxalate, and alkali from waste produced in buckwheat and sunflower processing. The molecular-mass distribution of fractions (protein–polysaccharide complex, polysaccharides, and low-molecular-weight compounds) was analyzed in relation to sources of carbohydrates and methods of their production.

DOI: 10.1134/S1070427207120108

Vegetable polysaccharides constitute a large and rather important group of natural compounds, carbohydrates, and form rapidly replenishable resources of organic substances with unique physicochemical and biological properties, which attract attention of chemists, pharmacists, toxicologists, and other specialists. The properties of polysaccharides are determined by their monosaccharide composition, structure, and molecular mass. The best studied polysaccharides are those produced from sea weeds [1] and higher medicinal plants [2–5] exhibiting a wide spectrum of pharmacological effects. It should be noted that, as a rule, biological activity is exhibited by carbohydrates with medium and low degree of polymerization [3]. In addition, composite materials including various polysaccharides that make a material compatible with a living organism are widely used at present in medicine and allied sciences [6, 7].

Large-tonnage wastes of crops, and primarily of those formed at factories in shelling of seeds (e.g., of buckwheat, rice, sunflower) can serve as raw materials for industrial production of vegetable polysaccharides. However, published evidence about properties of carbohydrates of this origin is scarce. Previously, polysaccharides have been recovered by successive extraction with water, ammonium oxalate, and alkali from wastes formed in processing of rice [8], buckwheat [9], and sunflower [10] grown on the territory of Primorski, Krasnoyarsk, Altai, and Krasnodar krais and their monosaccharide composition has been determined in relation to a botanic species of a plant. It has also been found that carbohydrates produced from rice husk hinder growth of human tumor cells of K562 strain [11], and aqueous, oxalate, and alkaline extracts from rice and buckwheat husk inhibit steel corrosion [12].

The present study, which continues analysis of polysaccharides produced from buckwheat and sunflower wastes [9, 10], is devoted to examination of the molecular-mass distribution (MMD) of their fractions [protein–polysaccharide complex (PPC), polysaccharides (PS), and low-molecular-weight compounds (LC)] by high-performance exclusion chromatography (HPEC).

EXPERIMENTAL

Polysaccharide samples obtained by successive extraction with water, ammonium oxalate, and alkali by procedures described in [9, 10] from buckwheat

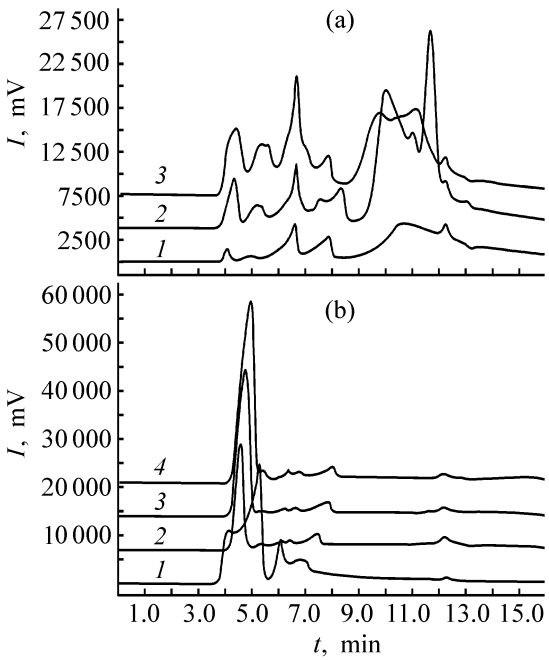

Fig. 1. Chromatograms of polysaccharides recovered from oxalate extracts from (a) buckwheat husk and (b) sunflower husk. (*I*) Intensity and (*t*) time. (a) (*1*) GSh-6, (*2*) GSh-8, and (*3*) GSh-10; (b) (*1*) PSh-1, (*2*) PSh-2, (*3*) PSh-3, and (*4*) PSh-4.

husks GSh-6 (Primorski krai, Izumrud breed), GSh-8 (Primorski krai, Pri-7 breed), and GSh-10 (Minusinsk), buckwheat straws GS-4 (Primorski krai, Izumrud breed) and GS-7 (Primorski krai,Natasha breed), and sunflower husks PSh-1 (Rostov-onDon), PSh-2 (Altai krai), PSh-3 (Kuban), and PSh-4 (Uryupinsk, Volgograd oblast).

The MMD of the polysaccharides was determined by HPEC [13] on a Shimadzu LC-20A Prominence chromatograph (Japan) with an RID-10A refractometric detector and an SPD-M20A diode array detector. The separation was performed on a Shodex Asahipak GS520 HQ column (Showa Denko, Japan),with twice-distilled water as eluent and flow rate of the mobile phase equal to 1 ml min^{-1}. Calibration curves for determining the molecular mass *M* were plotted using pullulan standards manufactured by Showa Denko (Japan) in the molecular mass range 5.9–788 kDa [13]. Chromatograms were recorded and processed using an LCsolution ver. 1.21 hardware-and software complex (Shimadzu, Japan).

To analyze the polysaccharides under study, a precisely weighed portion of a sample (10 mg) was dissolved in 10 ml of distilled water at room temperature. The resulting solution was filtered through a Kurabo 25A membrane filter with a pore size of 0.45 μm and analyzed by HPEC.

It was found in [9] that PS obtained by aqueous or oxalate extraction of all GSh and GS-4 samples are distinguished by increased content of glucose and, in the case of alkaline extraction, have a more complex monosaccharide composition and contain residual amounts of rhamnose, arabinose, xylose, mannose, glucose, and galactose. Aqueous PS from straw (GS-4 and GS-7) contain considerable amounts of inositol (17 and 31 mol %, respectively), whereas in other polysaccharides studied, this compound was observed in trace amounts. Uronic acids are represented in PS from buckwheat wastes mainly by galacturonic acid (GalA). Glucuronic acid (GlcA) was found only in trace amounts and not in all PS samples. All the PS produced by aqueous extraction, from both buckwheat husk and straw, have low content of uronic acids, with the exception of PS from GS-7, in which the amount of uronic acids is comparable with that of hexoses. By contrast, oxalate PS have a high content of uronic acids, with the content of GalA in polysaccharides from GSh-6, GS-4, and GS-7 exceeding by a factor of 2–4 the total content of hexoses. Similarly to aqueous PS, soluble PS produced by alkaline extraction contain a smaller amount of uronic acids (GalA and GlaA, with the former clearly predominant) than the corresponding oxalate PS. Similarly to oxalate PS, insoluble oxalate PS contain a considerable amount of galacturonic acid, especially PS from straw.

Polysaccharides from sunflower husk differ from the buckwheat polysaccharides in a wider diversity of the monosaccharide composition, which depends on a plant variety and extraction method and contain considerable amounts of GalA [10]. For example, xylose is present in PS of aqueous and oxalate extraction in trace amounts, whereas in PS of alkaline extraction, its content occasionally exceeds 50% (PSh-3 and PSh-4). Mannose and inositol are found in minor amounts only in aqueous PS. Residual rhamnose, arabinose, glucose, and galactose are contained in al PS in various relative amounts. Uronic acids are represented only by GalA and are contained in considerable amounts in all of the polysaccharides obtained, with their content being at a maximum in PS of oxalate extraction (55–71 mol %). Their amount is 2–3 times that of arabinose in aqueous PS (or 40–47 mol %), and is the smallest in PS of alkaline extraction (8–12 mol %).

An HPEC study of polysaccharide solutions obtained from buckwheat and sunflower wastes demonstrated that they contain, in addition to the polysaccharide fraction, protein admixtures and low-molecular-weight substances. The molecular-mass distributions of all the fractions are represented in the table, and Figs. 1a and 1b show typical chromatograms of

aqueous solutions of PS recovered from buckwheat and sunflower husks by oxalate extraction of the raw material.

Polysaccharides from buckwheat waste. In analysis of polysaccharides from aqueous extracts from buckwheat husk, the first eluted peak in chromatograms is that of a macromolecular PPC with $M > 300$ kDa. This peak is detected by both refractometric and spectrophotometric (at 280 nm) detectors. The precise molecular mass of this PPC cannot be determined because the exclusion limit of the Shodex Asahipak GS-520 HQ column is 300 kDa. Its content is within the range from 0.6 to 9.6%, depending on a sample (see table). The second eluted peak is that of a polysaccharide with M > 300 kDa, which is detected only by the refractometric detector and shows no absorption at 280 nm. The content of this polysaccharide varies from 6.7 to 7.4%, depending on a sample (see table). This peak is followed by three peaks of pro-

Molecular-mass distribution of fractions in polysaccharides from various extracts from buckwheat and sunflower husks

Raw material	Protein-polysaccharide complexes		Polysaccharide fraction		Low-molecular-weight impurities	
	M, kDa	content, %	*M*, kDa	content, %	*M*, kDa	content, %
			Aqueous extract			
GSh-6	>300	0.6	>300	6.7	3.2	25.1
	212.4	20.7			0.6	4.2
	50.4	10.9			0.3	21.0
	25.9	5.9			0.1	4.8
GSh-8	>300	5.7	>300	7.4	2.6	20.0
	172.4	14.8			0.6	5.5
	48.6	7.6			0.3	31.2
	24.5	5.7			0.1	2.1
GSh-10	>300	9.6	>300	7.3	5.8	11.0
	147.3	22.4			1.3	9.6
	50.1	8.8			0.3	19.0
	27.8	8.3			0.1	4.0
			Oxalate extract			
GSh-6	>300	3.1	>300	2.6	1.2	49.0
	155.8	18.9			0.2	10.3
	51.2	12.5			0.1	3.5
GSh-8	>300	6.0	>300	4.0	2.2	36.4
	169.0	9.2			0.6	8.7
	56.3	3.7			0.3	24.3
	28.5	5.5			0.1	2.0
GSh-10	>300	11.9	>300	11.1	5.1	19.4
	125.1	20.1			1.3	9.1
	43.2	5.3			0.5	19.6
					0.1	3.4
			Alkaline extract			
GSh-6	>300	30.8	>300	10.6	0.3	4.4
	43.9	47.0			0.1	6.6
GSh-8	251.1	40.0	>300	19.6	0.3	9.2
	53.2	26.0			0.1	3.7
GSh-10	129.3	20.0	>300	34.9	0.2	2.2
	81.8	8.0				
	39.6	29.0			0.1	3.0
	15.8	18.0				

Table. (Contd.)

Raw material	Protein-polysaccharide complexes		Polysaccharide fraction		Low-molecular-weight impurities	
	M, kDa	content, %	*M*, kDa	content, %	*M*, kDa	content, %
			Aqueous extract			
PSh-1	>300	9.9				
	193.7	22.0				
	85.9	11.0	>300	25.0	0.2	2.6
	48.1	14.4				
	7.2	15.1				
PSh-2	>300	0.9				
	290.0	14.3				
	123.8	16.7	>300	8.9	0.2	13.3
	67.6	24.5				
	15.2	21.3				
PSh-3	>300	10.3				
	277.4	12.3				
	110.7	17.5	>300	9.2	0.2	4.0
	56.7	29.3				
	15.9	17.4				
PSh-4	>300	17.3				
	163.5	15.0				
	80.6	20.7	>300	14.8	0.2	2.1
	38.7	18.0				
	10.4	12.2				
			Oxalate extract			
PSh-1	>300	74.3				
	279.1	11.7	–	–	0.1	0.3
	85.1	13.6				
PSh-2	>300	68.8				
	290.0	4.3	>300	2.9	0.1	9.2
	143.5	3.5				
	70.7	11.2				
PSh-3	>300	82.5				
	294.0	2.6	>300	1.9	0.1	2.7
	117.9	2.6				
	53.7	7.6				
PSh-4	>300	84.2				
	215.6	2.9	>300	2.5	0.1	2.0
	103.0	2.7				
	47.3	5.7				
			Alkaline extract			
PSh-1	215.1	18.4	>300	39.5	0.2	18.0
	69.9	24.0				
PSh-2	>300	6.2				
	161.2	23.8	>300	45.0	0.1	1.9
	52.7	18.1				
PSh-3	>300	15.5				
	138.5	19.5	>300	52.8	0.1	2.3
	48.3	9.8				
PSh-4	>300	23.8				
	127.1	21.0	>300	40.2	0.1	2.1
	35.6	13.0				

tein-polysaccharide complexes with M of 24.5 to 212.4 kDa. These peaks are not only detected by the refractometric detector, but also show a strong absorption at 280 nm. The content of these complexes varies in the range from 5.7 to 22.4%, depending on the raw material and molecular mass of the fraction. The last to be eluted are low-molecular-weight impurities with $M < 10$ kDa, which are detected only by the refractometric detector.

Analysis of polysaccharides obtained from oxalate extracts from buckwheat husk shows that, in their chromatograms (see Fig. 1a), as also in chromatograms of PS from aqueous extracts, the first eluted peak is that of macromolecular PPC. After this peak, a peak of the polysaccharide fraction is eluted, followed by peaks of protein–polysaccharide complexes, and the last to appear are peaks of low-molecular-weight fractions. The molecular-mass distribution of fractions in the PS from oxalate extracts from buckwheat husk somewhat differs from the distribution for PS from aqueous extracts (see table). The main difference is in that the content of low-molecular-weight impurities in PS from oxalate extracts from buckwheat husk substantially exceeds that in PS from aqueous extracts and show strong absorption at 280 nm.

In analysis of PS from alkaline extracts from buckwheat husk, the first chromatographic peak to be eluted is that of the polysaccharide fraction, followed first by peaks of protein–polysaccharide complexes and then by peaks of low-molecular-weight impurities. The molecular-mass distribution of fractions in PS from alkaline extracts from buckwheat husk markedly differs from the distributions in PS from aqueous and oxalate extracts (see table). The difference is due to the absence of macromolecular PC in PS from GSh-8 and GSh-10. In addition, the PS from the alkaline extracts contains a considerably larger amount of the polysaccharide fraction, whose content is 10.6 to 34.9%.

Polysaccharides from sunflower husk. In the chromatograms of PS recovered from aqueous extracts from sunflower husk, the first eluted peak is that of macromolecular PPC. This peak is followed, first, by a peak of the polysaccharide fraction, then, by peaks of protein–polysaccharide complexes, and finally, by a peak of low-molecular-weight impurities. Their content is shown in the table. However, in contrast to similar PS from aqueous extracts from buckwheat husk, sunflower husk contains a considerably smaller amount of low-molecular-weight impurities. Different PS from aqueous extracts from sunflower husk rather strongly differ in the PPC composition and content of the polysaccharide fraction, which is presumably due both to breed characteristics of plants and to climatic features of places in which the raw material grows.

A chromatographic analysis of PS from oxalate extracts from sunflower husk demonstrated (see Fig. 1b) that they noticeably differ in fractional composition from the PS from aqueous extracts: the content of a macromolecular PPC in the former is as high as 68.8–84.2%, depending on the plant breed (see table).

The eluted peaks of fractions of the PS from alkaline extracts from sunflower husk indicate that the main component of these carbohydrates is the polysaccharide fraction (see table). Its content is high as 39.5 to 52.8%, which considerably exceeds that in PS recovered from other extracts from sunflower husk or in a similar PS from buckwheat husk.

CONCLUSIONS

(1) It was found using high-performance exclusion chromatography that polysaccharides obtained by successive extraction with water, ammonium oxalate, and sodium hydroxide from buckwheat and sunflower husks contain not only polysaccharide fractions, but also protein–polysaccharide complexes and low-molecular-weight compounds.

(2) It was shown that the composition of the polysaccharide fraction, protein–polysaccharide complex, and low-molecular-weight compounds depends on the plant species and breed and on extraction conditions.

REFERENCES

1. Loenko, Yu.N., Artyukov, A.A., Kozlovskaya, E.P., et al., *Zosterin* (Zosterin), Vladivostok: Dal'nauka, 1997.
2. Popov, S.V., *Vzaimodeistvie fagotsitov mlekopitayushchikh s polisakharidami rastenii* (Interaction of Mammal Phagocytes with Plant Polysaccharides), Syktyvkar: Komi Nauchn. Tsentr, Ural. Otd. Ross. Akad. Nauk, 2002.
3. Ovodov, Yu.S., *Bioorgan. Khim.*, 1998, vol. 24, no. 7, pp. 483–501.
4. Sgrebneva, M.N., Tyupeleev, P.A., and Khasina, E.I., *Mikroelementy Meditsine*, 2004, vol. 5, no. 4, pp. 124–126.
5. Krishtanova, N.A., Safonova, M.Yu., Bolotova, V.Ts., et al., *Vestn. Vladivost. Gos. Univ., Ser. Khim. Biol. Farmats.*, 2005, no. 1, pp. 212–221.
6. Felix, G. and Zhang, T., *J. Chromatogr.*, 1993, vol. 639, no. 2, pp. 141–149.

7. Ivanov, A.E., Saburov, V.V., and Zubov, V.P., *Adv. Polym. Sci.*, 1992, vol. 104, pp. 135–175.
8. Zemnukhova, L.A., Tomshich, S.V., Mamontova, V.A., et al., *Zh. Prikl. Khim.*, 2004, vol. 77, no. 11, pp. 1901–1904.
9. Zemnukhova, L.A., Tomshich, S.V., Shkorina, E.D., and Klykov, A.G., *Zh. Prikl. Khim.*, 2004, vol. 77, no. 7, pp. 1192–1196.
10. Zemnukhova, L.A., Tomshich, S.V., Kovekhova, A.V., and Greben', L.Yu., *Zh. Prikl. Khim.*, 2007, vol. 80, no. 7, pp. 1200–1205.
11. Mamontova, V.A., Tomshich, S.V., Komandrova, N.A., and Zemnukhova, L.A., *Materialy III Mezhdunarodnoi konferentsii "Mediko-sotsial'naya ekologiya lichnosti: sostoyanie i perspektivy"* (Proc. III Int. Conf. "Medical-Social Ecology of Personality: State and Prospects"), Minsk, 2005, part 2, pp. 132–135.
12. Zemnukhova, L.A., Chernov, B.B., Shkorina, E.D., and Shchetinina, G.P., *Transport. Delo Rossii, Special issue*, no. 7, Moscow, 2006, pp. 149–152.
13. Sukhoverkhov, S.V., *Zh. Anal. Khim.*, 2002, vol. 57, no. 8, pp. 1–8.

ISSN 1070-4272, Russian Journal of Applied Chemistry, 2007, Vol. 80, No. 12, pp. 2057–2062. © Pleiades Publishing, Ltd., 2007.
Original Russian Text © E.A. Sosnov, A.A. Malkov, A.A. Malygin, 2007, published in Zhurnal Prikladnoi Khimii, 2007, Vol. 80, No. 12, pp. 1978–1983.

PHYSICOCHEMICAL STUDIES OF SYSTEMS AND PROCESSES

Structure of Products Formed in Chemisorption of Titanium Tetrachloride by Porous Silicas

E. A. Sosnov, A. A. Malkov, and A. A. Malygin

St. Petersburg State Technological Institute, St. Petersburg, Russia

Received March 15, 2007; in final form, September 2007

Abstract—IR and diffuse-reflectance spectroscopies were used to study the effect of the porous structures of the starting silica and temperature conditions of thermal pretreatment of the matrix and $TiCl_4$ chemisorption on the structure of titanium oxochloride complexes formed on the silica gel surface.

DOI: 10.1134/S107042720712011X

The chemisorption of $TiCl_4$ on various kinds of silicas (silica gels of varied origin and aerosils) has been extensively studied [1–14]. However, mostly the chemical aspects of transformations occurring in an interaction of the matrix with a low-molecular-weight reagent have been considered. At the same time, the structure of new functional groups being formed on the surface can largely determine the reactivity, catalytic activity, and selectivity of modified silicas. A rather important influence is exerted on the structure of the surface groups formed in $TiCl_4$ chemisorption by the origin and thermal pretreatment of the support, which determine the composition and topography of the hydroxo groups of the starting silica [6, 9, 15].

The present study is concerned with the effect of the pore size of silica and arrangement of hydroxo groups on its surface on the structure of the titanium oxochloride complex formed on the support surface via $TiCl_4$ chemisorption.

The methodological aspects of synthesis and analysis of products formed in interaction of a $TiCl_4$ vapor with the surface of porous silica have been considered in detail [16]. To compare the chemical composition of the surface groups formed on various matrices, their titanium content was related to 1 g of anhydrous silica (g_0) [1, 17]. IR spectral studies were performed in the in situ mode on an IKS-29 spectrometer in a flow-through quartz cuvette combined with a reactor [18]. Diffusion-reflection spectroscopy (DRS) was performed on an SF-26 spectrophotometer with a PDO-5 attachment, which enabled analyses without contact with the atmosphere in the spectral range 300–1000 nm [19]. A-300 aerosil calcined at 600°C was used as optical reference.

It has been shown previously [15] that, after treatment of wide-porous silica (ShSKG) in the temperature range of pretreatment of the starting silica (T_0) and chemisorption (T_{cs}) (200–600°C) with a titanium tetrachloride vapor, hydroxyls unreacted with $TiCl_4$ remain on the silica surface. Their amount is, depending on T_0, 25–45% relative to the total amount of OH groups in the starting silica gel. The amount of unused hydroxo groups may be so large for several reasons. First, these hydroxyls can be inaccessible to $TiCl_4$, e.g., because of their position in long narrow pores or at places of contact between globules [20]. Second, they can be shielded by chemisorbed titanium oxochloride groups [4, 21], including those cases in which coordination bonds are formed between grafted surface groups and closely situated silanols [22, 23].

Let us consider the possible contributions of each of these factors. To determine the influence exerted by the porous structure of the starting silica at $T_{cs} = T_0 = 200$°C, we studied the chemical composition of silica gels with an effective pore size in the range 2.3–15.6 nm and changes in their specific surface area after chemisorption of $TiCl_4$ (Table 1). The amount of chemisorbed titanium per unit mass grows for the silicas under consideration, as the specific surface area of the starting matrix increases, from 1.08 mmol g_0^{-1} (ShSKG) to 2.48 mmol g_0^{-1} (KSM-5) (with the exception of the KSM-6S sample). The decrease in the content of titanium on the KSM-6S silica gel is presumably due to partial inaccessibility of the micropore space (d_p = 2.3 nm) to new portions of $TiCl_4$ molecules. However, the amount of chemisorbed titanium per 1 m^2 of the surface of the starting silicas is smaller than that for the coarse-porous silica gel ShSKG and the specific surface area of the samples after chemi-

Table 1. Structural and chemical characteristics* of various silicas and products of their interaction with $TiCl_4$ at $T_{cs} = T_0 = 200°C$

Silica	Starting silica					Titanium-containing silica					
	structural characteristics			concentration and characteristic of OH groups		[Ti]		ω_{Ti}, nm^2	$\frac{[OH_{res}]}{[OH_{in}]}$, % (calculation)	S_{sp}	ΔS_{sp}
	S_{sp}, $m^2\ g^{-1}$	V_p, $cm^3\ g^{-1}$	d_p, nm	$[OH_{in}]$, mmol g^{-1}	ω_{OH}, nm^2	mmol g_0^{-1}	μmol m^{-2}			$m^2\ g^{-1}$	
ShSKG	246	0.96	15.6	3.46	0.118	1.08	3.94	0.421	44.0	226	20
KSS-2.5	376	0.97	10.3	3.51	0.178	1.69	3.86	0.431	17.4	259	117
KSS-3	522	0.93	7.3	5.68	0.153	2.33	3.60	0.461	33.8	367	155
KSS-4	650	0.76	4.7	4.68	0.231	2.25	2.83	0.587	21.4	377	273
KSM-5	715	0.58	3.2	5.35	0.222	2.48	2.78	0.597	25.6	374	341
KSM-6S	624	0.36	2.3	7.08	0.146	0.87	1.23	1.346	78.2	509	115

* Error in determining the structural characteristics of the silicas was 3–4%, and that for the chemical composition of grafted groups, ≤2.6% [16].

sorption of the halide is significantly smaller ($\Delta S > 100\ m^2\ g^{-1}$). This indicates that micropores are also blocked for silica gels of the KSS and KSM brands, which should lead to appearance of structurally inaccessible silanols.

At 200°C, 3.94 μmol of Ti per square meter is chemisorbed on the surface of the ShSKG silica gel (one titanium oxochloride group per 0.421 nm^2), which is in good agreement with the results obtained in [1, 8, 9] under the same conditions on various coarse-porous silicas (3.8–4.25 μmol m^{-2} and 0.413 ± 0.016 nm^2, respectively). Thus, it can be concluded that the contribution of structurally inaccessible silanols to the total number of unreacted hydroxyls is insignificant for coarse-porous silica gels.

Let us consider the possibility of hydroxo group shielding by chemisorbed groups without formation of coordination bonds, as it was observed in $TiCl_4$ chemisorption on aerosils with strong surface curvature in [4]. In this case, the frequency of stretching vibrations of a shielded OH group of silica gel (3750 cm^{-1}) should remain unchanged after chemisorption of $TiCl_4$. However, comparison of the IR spectra of samples, obtained before and after chemisorption of $TiCl_4$ at different T_{cs} (Fig. 1), shows that the clearly pronounced absorption band of single hy-

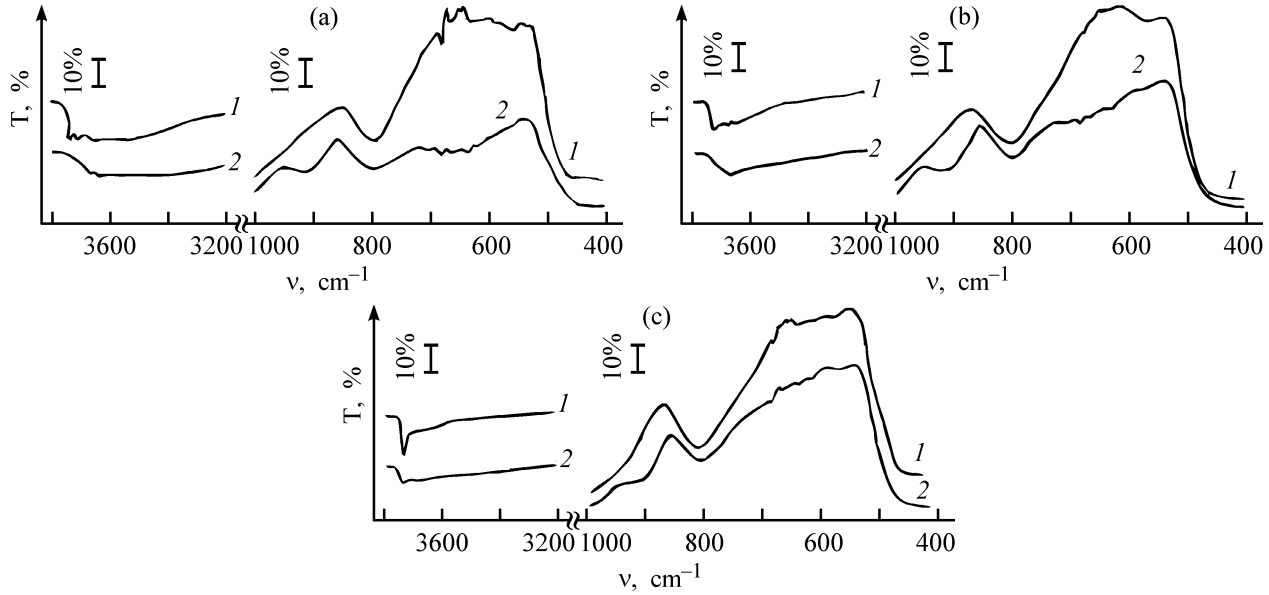

Fig. 1. IR spectra of samples synthesized on the ShSKG silica gel at temperatures $T_{cs} = T_0$ of (a) 200, (b) 400, and (c) 600°C. (T) Transmission and (ν) wave number. Silica: (*1*) starting and (*2*) that after $TiCl_4$ chemisorption.

Table 2. Chemical composition of groups on the surface of the ShSKG silica gel after $TiCl_4$ chemisorption and the results of band resolution in DRS spectra

$T_{cs} = T_0$, °C	Titanium oxochloride groups		$[OH]_{res}$,* mmol g_0^{-1}	Characteristics of bands in DRS spectra*					
				1st band			2nd band		
	[Ti], mmol g_0^{-1}	[Cl]/[Ti]		λ_1, nm	E_1, eV	I_1, %	λ_2, nm	E_2, eV	I_2, %
200	1.08	2.17	1.58	344	3.61	9	387	3.20	91
400	0.79	1.70	0.69	346	3.58	18	405	3.06	82
600	0.49	1.65	0.51	362	3.43	34	402	3.08	66
800	0.28	2.29	0.38	369	3.36	27	403	3.08	73

* Calculated.

droxyls in the spectral range of stretching vibrations of OH groups disappears after interaction with the halide, although the amount of hydroxo groups that did not enter into the chemical reaction is 44, 28, and 31% at $T_{cs} = T_0 = 200$, 400, and 600°C, respectively [15]. Thus, the IR spectral data obtained suggest that "pure" shielding of OH groups, similar to that observed for A-300 and A-380 aerosils [4], is untypical of silica gels. The disappearance of the band at 3750 cm^{-1} from IR spectra after chemisorption of $TiCl_4$, with the broad absorption band in the range of stretching vibrations of OH groups bound by hydrogen bonds (3300–3700 cm^{-1}) simultaneously preserved, may be due to partial involvement of hydroxyls in fixation of titanium oxochloride structures on the silica gel surface, probably as various coordination complexes.

To examine the coordination state of titanium in titanium oxochloride structures formed on the surface of porous silica in the temperature range 200–800°C, we synthesized products whose chemical composition is presented in Table 2. A DRS study of modified silica demonstrated (Fig. 2a) that the DRS spectra have an intricate shape, which is probably due to simultaneous presence on the silica surface of several types of titanium oxochloride structures with different electron transition energies. To determine characteristics of electron transition ranges, we resolved the spectra obtained into components on the assumption that the electron transitions are described by the Fermi–Dirac distribution [24]. An example of such a resolution is shown in Fig. 2b. The results of a mathematical processing of the spectra (Table 2) enable suggestions concerning the fundamental aspects of formation of element oxochloride groups on the silica gel surface.

As T_0 is raised, samples of modified silica gel show an increase in the reflectance (R_D) in the longer-wavelength part of the spectrum ($\lambda > 450$ nm), which reaches its maximum value at $T_0 \geq 600$°C (Fig. 2a) and is virtually independent of the amount and chemical composition of surface titanium oxochloride groups. The reflectance of these samples apparently changes because trace amounts of organic impurities, which are carbonized in an oxygen-free medium during chemisorption of $TiCl_4$ (a known active carbonization catalyst) and serve as a "gray filter" absorbing light in the whole spectral range under consideration, are removed from the surface of the starting silica [25]. At the same time, an insignificant amount of organic impurities does not affect reactions on

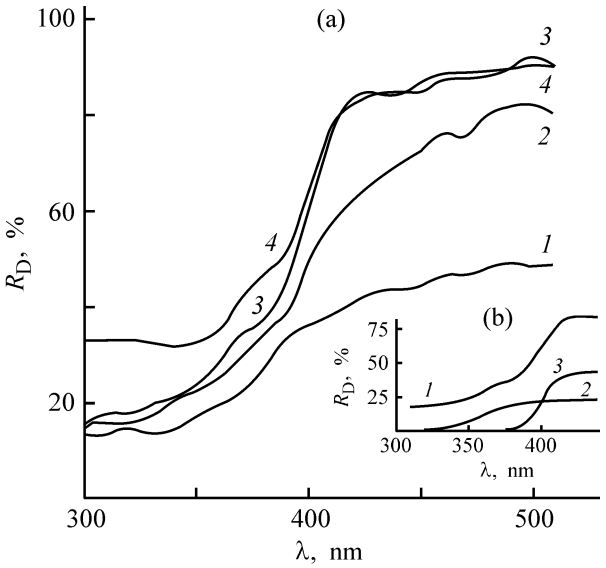

Fig. 2. (a) DRS spectra of samples synthesized on the ShSKG silica gel at $T_{cs} = T_0$ of (*1*) 200, (*2*) 400, (*3*) 600, and (*4*) 800°C and (b) an example of a mathematical resolution of a DRS spectrum into two components. (R_D) Diffuse reflectance and (λ) wavelength. (b) (*1*) Initial spectrum and (*2*, *3*) components of the DRS spectrum.

the surface of the matrix and the chemical composition of the forming titanium oxochloride structures [15, 16].

A mathematical processing of DRS spectra (Fig. 2) demonstrated that two electron transitions characteristic of groups with different coordination environments of the titanium atom are simultaneously present in all the spectra (Table 2). The electron transitions centered at 345–370 nm (E = 3.4–3.6 eV) are characteristic of tetrahedrally coordinated titanium (coordination number CN_{Ti} = 4), and those centered at 385–405 nm (E = 3.0–3.2 eV) are observed for octahedrally coordinated titanium (CN_{Ti} = 6) [19].

As T_{cs} is raised, the middle of the electron transition corresponding to the presence of a titanium oxochloride with CN_{Ti} = 4 on the surface steadily shifts from 344 to 369 nm (which corresponds to a decrease in the activation energy of the electron transition from 3.61 to 3.36 eV). This effect may be due to a certain decrease in the degree of distortion of titanium oxochloride groups via equalization of the angles and lengths of interatomic bonds in the surface group, which presumably occurs because of an increase in the mobility of near-surface silicon-oxygen tetrahedra of the silica matrix at higher T_{cs} [26].

It should be noted, when analyzing the region of electron transitions for groups with CN_{Ti} = 6, that the group formed on the surface at T_{cs} = 200°C has a transition energy of 3.21 eV. This is rather close to the energy gap of TiO_2 in the anatase modification, whereas at $T_{cs} \geq 400$°C, the electron transition energy of the complex (3.06–3.08 eV) is close to the energy gap of the high-temperature modification of TiO_2, rutile [27].

An IR spectral study of samples synthesized at different T_{cs} (Fig. 1) demonstrated that Si–O–Ti bonds between the substrate and titanium oxochloride groups are formed as a result of $TiCl_4$ chemisorption on silica gel. This is manifested in the appearance of an absorption band peaked at 910–920 cm^{-1} (Fig. 1, curves *2*). Published data on the peak of absorption by the Si–O–Ti bond are rather contradictory [7, 12, 28–34]. For example, an absorption band at 959 cm^{-1} is attributed to the structural fragment Si–O–Ti–Cl with CN_{Ti} = 4 [28]. Close values (950–960 cm^{-1}) have been observed in numerous studies in pyrogenic titanosilica [29] or that synthesized by cohydrolysis of alkoxy compounds and then calcined [30]. However, some researchers have also observed lower absorption peak positions: 935–945 [31, 32], 930 [33], 924 [12], 919–925 [34], 920 [7], and even 900 cm^{-1}, with the appearance of the absorption band at 900 cm^{-1} attributed by Shalumov and co-workers to an increase in CN_{Ti} to 5 [30].

Thus, we can conclude, based on the above published data, that the absorption band peaked at 910–920 cm^{-1}, observed in our case, is presumably due to the formation on the silica surface of a Si–O–Ti bond with titanium atoms whose degree of coordination increases because of the formation of additional coordination bonds with oxygen atoms from adjacent siloxane bridges or from silanols unused in the course of $TiCl_4$ chemisorption. However, there is no absorption band of single hydroxyls at 3750 cm^{-1} in the IR spectra of samples treated with a $TiCl_4$ vapor (Fig. 1, curves *2*). This may indicate that, despite the only partial utilization of silanols in the chemisorption reaction (Table 2), OH groups are involved in the formation on the silica gel surface of titanium-containing structures in which titanium has a coordination higher than that in $TiCl_4$. At the same time, as T_0 is raised, the DRS spectra show (Fig. 2a) a considerable amount of a tetrahedrally coordinated titanium, despite the increasing number of strained siloxane bridges. This may indicate that the oxygen from the siloxane bridges contributes to a considerably lesser extent to an increase in the coordination of titanium atoms. Thus, in chemisorption of $TiCl_4$, part of silanols form with surface titanium oxochloride groups coordination compounds of the type

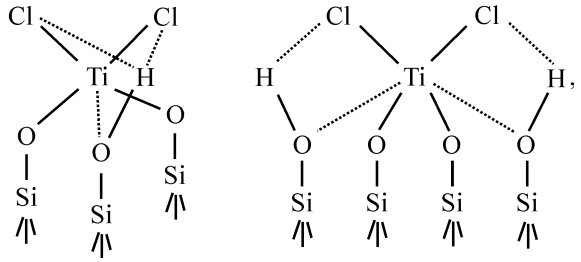

in which the CN of titanium increases to 5–6, rather than entering into a chemical reaction with the tetrachloride.

The possible formation of coordination bonds between the titanium oxochloride group and silanols is also indicated by quantum-chemical calculations of the structure of a cluster formed in $TiCl_4$ chemisorption, performed for the (111) and (110) surfaces of β-cristobalite [35]. As follows from Fig. 3, the CN_{Ti} increases on the surface because of the coordination interaction with adjacent silanols, despite the distortions appearing in the crystal lattice of the matrix. It is noteworthy that, for the (111) face, coordination bonds can only be formed for $TiCl_3$ groups, whereas

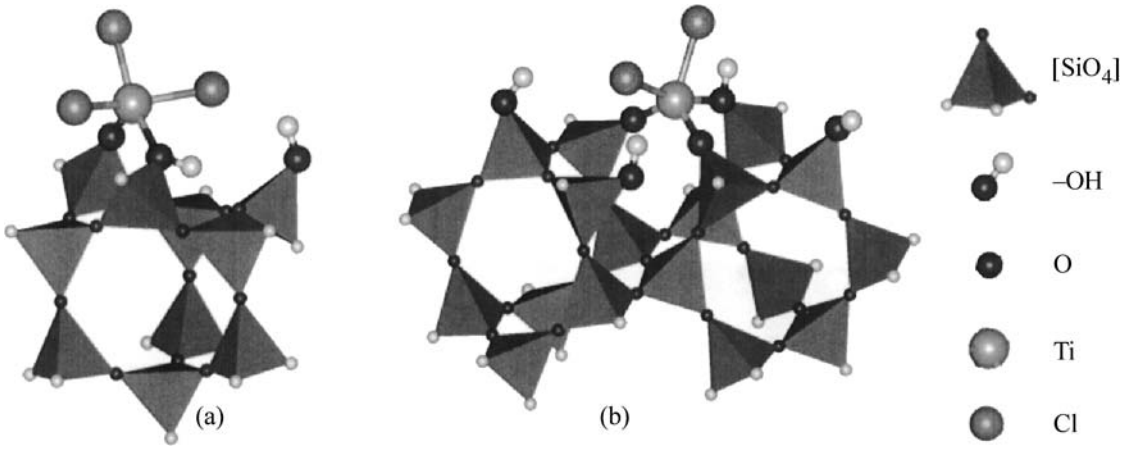

Fig. 3. Model structures of products of $TiCl_4$ chemisorption on (a) (111) and (b) (110) faces of β-cristobalite.

at the (110) face, an increase in CN_{Ti} is also possible for double-bonded ($=TiCl_2$) groups (Fig. 3b).

CONCLUSIONS

(1) Products formed in $TiCl_4$ chemisorption on porous silicas were subjected to an integrated study with the use of results of chemical analyses, IR spectroscopy, and DRS, which are in agreement with quantum-chemical calculations of clusters formed on the (111) and (110) faces of β-cristobalite. A conclusion was made that, in addition to the formation of Si–O–Ti chemical bonds via an electrophilic substitution of protons of silanol groups by titanium oxochloride structures, coordination bonds are formed between chemisorbed groups and used silanols, which is accompanied by an increase in the coordination number of titanium atoms to 5–6.

(2) It was shown that the siloxane bonds present on the silica surface are virtually not involved in the formation of coordination complexes, which is manifested in the preferential formation of titanium oxochloride structures with $CN_{Ti} = 4$.

ACKNOWLEDGMENTS

The authors thank S.D. Dubrovenskii for assistance in the visualization of the structure of titanium oxochloride complexes.

The study was financially supported in part by the Russian Foundation for Basic Research (grant nos. 06-03-81010 and 07-03-12038).

REFERENCES

1. Kol'tsov, S.I. and Aleskovskii, V.B., *Zh. Fiz. Khim.*, 1968, vol. 42, no. 5, pp. 1210–1214.
2. Kohlschutter H.W. and Bogel, U., *Fortschr. Koll. Polym.*, 1971, vol. 55, no. 1, pp. 29–33.
3. Hair, M.L. and Hertl, W., *J. Phys. Chem.*, 1973, vol. 77, no. 17, pp. 2070–2075.
4. Koval'kov, V.I., Malygin, A.A., Kol'tsov, S.I., and Aleskovskii, V.B., *A Study of the Interaction of Titanium Tetrachloride with Aerosils*, Available from VINITI, 1976, Leningrad, no. 1747-76Dep.
5. Ermakov, Yu.I., Zakharov, I.A., and Kuznetsov, B.N., *Zakreplennye kompleksy na okisnykh nositelyakh v katalize* (Fixed Complexes on Oxide Supports in Catalysis), Novosibirsk: Nauka, 1980.
6. Riis, T., Dahl, I.M., and Ellestad, O.H., *J. Mol. Catal.*, 1983, vol. 18, no. 2, pp. 203–214.
7. Kinney, J.B. and Staley, R.H., *J. Phys. Chem.*, 1983, vol. 87, no. 19, pp. 3755–3740.
8. Ellestad, O.H. and Blindheim, U., *J. Mol. Catal.*, 1985, vol. 33, pp. 275–287.
9. Damyanov, D., Velikova, M., Ivanov, Iv., and Vlaev, L., *J. Non-Cryst. Solids*, 1988, vol. 105, no. 1, pp. 107–113.
10. Morrow, B.A. and McFarlan, A.J., *J. Non-Cryst. Solids*, 1990, vol. 120, pp. 61–71.
11. Haukka, S., Lakomaa, E.-L., and Root, A., *J. Phys. Chem.*, 1993, vol. 97, no. 19, pp. 5085–5094.
12. Schrijnemakers, K., Impens, N.R.E.N., and Vansant, E.F., *Langmuir*, 1999, vol. 15, pp. 5807–5813.
13. Aarik, J., Aidle, A., Mandar, H., and Uustare, T., *Appl. Surf. Sci.*, 2001, vol. 172, pp. 148–158.
14. *Khimiya poverkhnosti kremnezema* (Chemistry of Silica Surface), vol. 1, part 1, *Sintez kremnezema i svoistva ego poverkhnosti* (Synthesis of Silica and Properties of Its Surface), Chuiko, A.A., Ed., Kiev: IKhP Nats. Akad. Nauk Ukr., 2001.
15. Sosnov, E.A., Malkov, A.A., and Malygin, A.A., *Zh. Prikl. Khim.*, 1988, vol. 61, no. 1, pp. 29–34.
16. Sosnov, E.A., Malkov, A.A., and Malygin, A.A., *Zh. Prikl. Khim.*, 2000, vol. 73, no. 7, pp. 1074–1079.

17. Sosnov, E.A., Malkov, A.A., and Malygin, A.A., *Zh. Prikl. Khim.*, 2005, vol. 78, no. 3, pp. 373–379.
18. Khabibova, S.V., Tolstoi, V.P., Malkov, A.A., and Malygin, A.A., *Zh. Prikl. Khim.*, 1989, vol. 62, no. 2, pp. 341–344.
19. Pak, V.N. and Ventov, N.G., *Zh. Fiz. Khim.*, 1975, vol. 49, no. 10, pp. 2535–2537.
20. Strelko, V.V., Burushkina, T.N., and Kartel', N.T., *Adsorbts. Adsorbenty*, 1996, no. 4, pp. 38–43.
21. Malygin, A.A., *Zh. Obshch. Khim.*, 2002, vol. 72, no. 4, pp. 617–632.
22. Kiselev, A.V. and Lygin, V.V., *Infrakrasnye spektry poverkhnostnykh soedinenii* (Infrared Spectra of Surface Compounds), Moscow: Nauka, 1972.
23. Nakamoto, K., *Infrared Spectra of Inorganic and Coordination Compounds*, New York: John Wiley & Sons, 1963.
24. Yavorskii, B.M. and Detlaf, A.A., *Spravochnik po fizike* (Handbook of Physics), Moscow: Nauka, 1979.
25. Petsev, N., Kotsev, N., *Nar''chnik po gazova khromatografiya* (Handbook of Gas Chromatography), Sofiya: Nauka i Izkustvo, 1984.
26. Lygin, V.I., *Ross. Khim. Zh. (Zh. Ross. Khim. O–va im. D.I. Mendeleeva)*, 2002, vol. 46, no. 3, pp. 12–18.
27. Goroshchenko, Ya.G., *Khimiya titana* (Chemistry of Titanium), Kiev: Naukova Dumka, 1970, part 1.
28. Kriegsmann, H. and Licht, K., *Z. Elektrochem.*, 1958, vol. 62, no. 10, pp. 1163–1174.
29. Pakhlov, E.M., Voronin, E.F., and Sushko, R.V., *Zh. Prikl. Spektrosk.*, 1987, vol. 47, no. 2, pp. 311–313.
30. Shalumov, B.Z., Zhukova, L.A., Ryabenko, E.A., et al., *Izv. Akad. Nauk SSSR, Neorg. Mater.*, 1986, vol. 22, no. 2, pp. 254–257.
31. Chuiko, A.A., Voronin, E.F., Tertykh, V.A., et al., *Adsorbts. Adsorbenty*, 1983, no. 11, pp. 22–23.
32. Smith, C.F., Condrate, R.A., and Votava, W.E., *Appl. Spectrosc.*, 1975, vol. 29, no. 1, pp. 79–81.
33. Varshal, B.G., Denisov, V.N., Mavrin, B.N., et al., *Opt. Spektrosk.*, 1973, vol. 47, no. 3, pp. 619–622.
34. Shevyakov, A.M., Kuznetsova, G.N., and Aleskovskii, V.B., *Khimiya vysokotemperaturnykh materialov* (Chemistry of High-Temperature Materials), Leningrad: Nauka, 1967, pp. 149–155.
35. Dubrovenskii, S.D., *Materialy 2-i Vserossiskoi konferetntsii "Khimiya poverkhnosti i nanotekhnologiya," SPb–Khilovo, 23–28 sentyabrya 2002 g.* (Proc. 2nd All-Russia Conf. "Surface Chemistry and Nanotechnology," St. Petersburg–Khilovo, September 23–28, 2002), St. Petersburg: RIO SPb GTI (TU), 2002, pp. 63–64.

ISSN 1070-4272, Russian Journal of Applied Chemistry, 2007, Vol. 80, No. 12, pp. 2063–2072. © Pleiades Publishing, Ltd., 2007.
Original Russian Text © A.V. Artemov, I.V. Tselinskii, S.A. Kukushkin, E.V. Filatova, V.V. Ashikhin, 2007, published in Zhurnal Prikladnoi Khimii, 2007, Vol. 80, No. 12, pp. 1984–1993.

ORGANIC SYNTHESIS AND INDUSTRIAL ORGANIC CHEMISTRY

Control over *m*-Nitrotoluene Concentration in Products of Heterogeneous Mononitration of Toluene

A. V. Artemov, I. V. Tselinskii, S. A. Kukushkin, E. V. Filatova, and V. V. Ashikhin

St. Petersburg State Institute of Technology (Technical University), St. Petersburg, Russia

Received July 12, 2007

Abstract—Heterogeneous mononitration of toluene with sulfuric–nitric acid mixtures, occurring in the charged interfacial monolayer with high *para* selectivity, was studied. Ways to suppress the *meta* substitution in the toluene mononitration stage by controlling the nitrating mixture composition, process parameters, and catalytic additives were found.

DOI: 10.1134/S1070427207120121

The isomeric distribution of dinitrotoluenes (DNT) in the second stage of toluene nitration (2,4-/2,6-DNT ratio and concentration of *ortho* isomers) is significant in production of toluylene diisocyanate (TDI), whose world-wide annual output is about 1 million tons [1]. The DNT isomer ratio in the second nitration stage is controlled by largely the yield ratio of mononitrotoluene isomers in the first stage.

The problem of control over the nitrotoluene (NT) isomer ratio can be subdivided into two main tasks: (1) to change the *o*-/*p*-NT ratio and (2) to decrease the concentration of *m*-nitrotoluene (*m*-NT), which is an undesirable by-product in production of di- and trinitrotoluene [2].

Table 1 summarizes the published data [2–4] on the *m*-NT content of NT isomer mixtures obtained in titration of toluene with nitric acid and sulfuric–nitric acid mixtures at various temperatures. As can be seen, the *m*-NT content changes moderately (by no more than a factor of 2) over a wide temperature range from –30 to +60°C. Nevertheless, the *m*-NT content increased with temperature in all the cases.

It is known that the activation energy of toluene nitration at the *meta* position is higher than that at the *para* position by 1.1 kcal mol^{-1} [5] (1.62 [3]). Therefore, an increase in temperature accelerates nitration at the *meta* position to a greater extent. Evidently, as temperature increases, the competition of these reactions results that the *m*-NT content grows, which is consistent with the available experimental data.

Another factor having a considerable effect on the yield of *m*-NT is the nitrating power of the acid mixture. For example, Orlova [2] reported that, in toluene nitration with sulfuric–nitric acid mixtures containing 10 wt % HNO_3 at 55°C, an increase in the H_2SO_4 concentration in the acid mixture from 28 to 47 mol %, which corresponds to rise in the nitrating acid efficiency factor from 68 to 82%, lowers the yield

Table 1. Influence of the temperature and acid mixture composition on the *m*-NT content of the NT isomer mixture [2–4]

T, °C	*m*-NT percentage in isomer mixture*							
	1	2	3	4	5	6	7	8
–30	3.5	–	–	–	3.0	–	–	–
0	3.9	2.5	4.5	3.3	5.7	–	–	–
20	–	4.3	4.5	3.9	–	–	–	–
25	–	–	–	–	–		2.2	–
30	4.4	–	–	–	4.4	3.9		1.9
35	–	–	–	–	–	–	1.1	–
40	–	–	4.2	–	–	–		–
50	–	–	4.3	–	–	4.5	8.6	1.6
60	5.1	–	–	–	4.9	4.9	–	–

* (1) 55–61% HNO_3, (2) 94% HNO_3, (3) 23.8% HNO_3 + 58.7% H_2SO_4, (4) 13.7% HNO_3 + 64.4% H_2SO_4, (5) 5.5% HNO_3 + 71.4% H_2SO_4 + 1.75% HNO_2, (6) 0.5% HNO_3 + 71.7% H_2SO_4; (7) HNO_3 in the system CF_3COOH–H_2O (95.0% CF_3COOH); and (8) $HNO_3 : H_2SO_4 : (CH_3CO)_2O$ = 1 : 1 : 30.

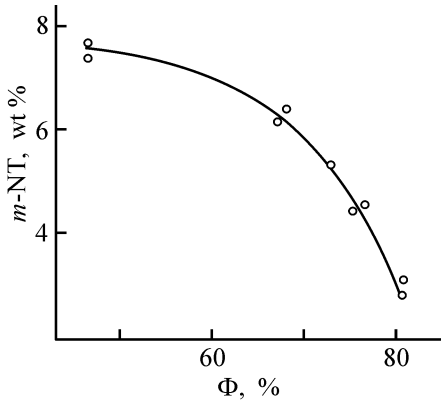

Fig. 1. Yield of *m*-NT vs. the nitrating acid efficiency factor Φ in heterogeneous nitration of toluene with sulfuric–nitric acid mixtures (10 wt % HNO_3) at constant temperature [3].

of the *meta* isomer by a factor of 2.4 (Fig. 1). Because toluene nitration with the indicated acid mixtures is accompanied by the formation of di- and trinitrotoluenes, data presented in Fig. 1 were obtained by recalculation of the amounts of *o*-dinitrotoluenes (3,4-, 2,3-, and 2,5-DNT) and asymmetrical isomers of TNT, contained in trotyl, to the *m*-NT content of the mononitration product. Similar results were obtained in heterogeneous nitration of toluene diluted with *n*-heptane, thus confirming the generality of this trend (Table 2) [3].

Thus, in nitration of toluene with acid mixtures commonly used in industrial processes, the yield of *m*-NT, and, therefore, of the so-called *ortho* isomers of DNT, formed in the second nitration step, can be reduced by carrying out nitration at low temperatures and, probably, by using more concentrated nitrating mixtures [2, 3]. Unfortunately, the technically feasible temperature variation range is rather narrow, and the composition range of the industrial acid mixtures used in the mononitration step is limited for a number of reasons as well.

Table 2. Influence of the sulfuric acid content on the *m*-NT percentage in the isomer mixture [3] (35 mol % HNO_3, 30°C, mineral to organic phase volume ratio 100 : 1, 5% toluene in heptane)

m-NT, %	H_2SO_4	
	mol %	wt %
4.04	32.0	71.7
2.70	46.0	82.0
1.49*	62.0	89.88

* *m*-NT content was estimated taking into account the 2,5-, 3,4-, and 2,3-DNT concentrations in the second stage [2].

The yield of the *meta* isomer can be influenced by various additives. Addition of sodium nitrite allows reduction of the yield of the *meta* isomer [2]. However, it should be pointed out that addition of $NaNO_2$ in amounts above 6% produces remarkable amounts of side products:

Yield of *m*-NT in toluene nitration in the presence of $NaNO_2$ [2] (Φ 73%, HNO_3 content of the acid mixture 10 wt %)

$NaNO_2$, wt %	0	1.5	3.0	4.5	5.9	8.6	11.0
m-NT, wt %	5.4	4.3	4.1	3.5	2.8	2.7	2.6

Hanson et al. [6] reported the effects of the solvent and external electric field on the isomer ratio in the continuous mononitration of toluene. Since the temperature was constant, and the amount of *m*-NT remained unchanged throughout the experiment, primarily the *ortho*/*para* isomer ratio was considered, which ranged from 1.20 to 1.97. In the cited paper, an empirical model was suggested, which allows prediction of the *ortho*/*para* isomer ratio from the electrical and physical properties of the solvent and field-induced dipole moment.

A low (1.6%) *m*-NT yield can be achieved in toluene nitration in the system $HNO_3 : H_2SO_4 : (CH_3CO)_2O$ = 1 : 1 : 30 at 50°C [7]. A zero yield of *m*-NT has been reported for toluene nitration with a mixture of 32% HNO_3 and 68% $(CH_3CO)_2O$ at 10°C [3]. However, in these cases, an abnormal *ortho*/*para* isomer ration was obtained (88 and 12%, respectively), which is unsuitable in the common TDI production process.

The mass-exchange effect on the regioselectivity of nitration of toluene and other aromatic hydrocarbons is an important aspect of the problem of two-phase heterogeneous nitration. This aspect was discussed in [8, 9] in terms of the mechanism of nitration in the interfacial adsorption monolayer, which is suggested to be operative along with the ordinary nitration mechanism (in the bulk of the acid phase). Modak and Juvekar [8] examined the nitration of mononitrobenzene and suggested that the approach they used is applicable primarily to nitration of polar molecules, such as mononitro derivatives of aromatic hydrocarbons.

The key point of the interfacial nitration mechanism is that nitroaromatic molecules adsorbed at the interfacial monolayer react with the nitronium cations from the acid phase. Evidently, the electric field formed at the interface as a result of the adsorption of polar molecules affects the nitration regioselectivi-

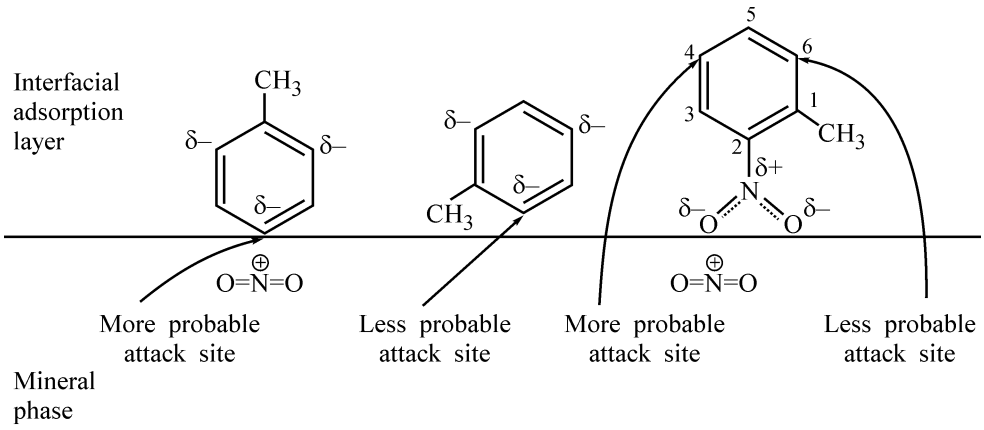

Fig. 2. Orientation of toluene and mononitrotoluene molecules at the interface.

ty in this region. The total nitration selectivity with respect to a given isomer is a weighted average of the bulk and interfacial selectivities. When passing across the interface, nitrotoluene molecules are oriented in the interfacial layer so that the hydrophobic methyl groups are directed toward the organic phase as a result of repulsive action of the hydrophilic mineral layer (Fig. 2) [8].

The contribution of the interfacial mechanism is controlled by the interface area, i.e., by the stirring rate. It should be expected that the above statements are valid for a relatively slow nitration of nitrobenzene and other mono- and dinitro derivatives of aromatic hydrocarbons, i.e., for the cases when diffusion of the substrate to the bulk of the acid phase is not a rate-determining stage under common process conditions, in contrast to the nitration of the starting hydrocarbons.

Since the starting aromatic hydrocarbons are low-polar, one may expect that the adsorption of NO_2^+ at the interface is insignificant if the organic phase contains no nitration products. At the same time, if the organic phase contains nitro derivatives, the negative charge of the interfacial layer facilitates adsorption of the NO_2^+ cation, thus favoring interfacial nitration.

Based on the common knowledge, it can be suggested that the contribution of the interfacial mechanism to the nitration of aromatic hydrocarbons, such as toluene and benzene, can be raised in three cases: (1) when the reaction rate in the interfacial layer is higher or well-comparable with the rate of substrate diffusion across the interface to the interfacial layer, as it occurs in nitration of aromatic hydrocarbons with acid mixtures with high sulfuric acid content (above 35 mol %); (2) when the reaction proceeds in an intermediate mode between the diffusion and kinetic control, which occurs in nitration of aromatic hydrocarbons with sulfuric–nitric acid mixtures of low nitrating efficiency at high stirring rate (>3000 rpm); and (3) in continuous nitration of aromatic hydrocarbons, i.e., at a sufficiently high concentration of a nitro derivative in the organic phase.

Previously [8–10], it has been demonstrated that the selectivity of the interfacial nitration differs from that in the bulk of the acid phase, and the *ortho*/*para* isomer ratio can be altered by changing the contribution of any of the two principal nitration mechanisms.

EXPERIMENTAL

Toluene nitration was carried out in a 30-ml glass reactor equipped with a temperature-control jacket, four-blade turbine stirrer, vertical baffle walls, and thermocouple for measuring the temperature of the reaction mass. The baffle walls were arranged at right angles relative to each other to avoid formation of a whirlpool and projected by 5 cm over the reaction mass to improve the aeration of the acid mixture. In the experiments, the stirring rate was varied from 200 to 5000 rpm.

The gas content of the acid mixture was determined from the increase in the reaction mass volume under given conditions with or without stirring. The mixture was poured into the reactor up to the lower overflow level. The temperature was raised to a desired value by circulating water in the jacket, and the reaction mass was allowed to stand for 10 min without stirring. The volume of the acid mixture remaining in the reactor, V_1, corresponded to the loss for thermal expansion. Similarly we determined the mixture volume V_2 after stirring for 5 min. The gas content

Γ (vol %) of the mixture under given conditions was estimated as

$$\Gamma = \frac{V_1 - V_2}{V_1} \times 100.$$

The results are listed in Table 3 for various temperatures and stirring rates.

In the experiments, we used nitric and sulfuric acids of pure grade and chromatographically pure toluene. The composition of the acid mixtures was determined titrimetrically to within 0.02%. The acid mixtures were prepared by successive mixing of the concentrated acids with double-distilled water at 0°C. The compositions of the acid mixtures are specified in the tables.

The isomeric composition of the products and residual toluene content were determined by gas chromatography on a KhROMOS 1000.1 instrument with a flame ionization detector (SUPELCO column, 30 m × 0.32 mm; stationary phase 5% polydiphenyl + 95% polydimethylsiloxane; carrier gas helium, flow rate 30 ml min^{-1}). The relative error of determination of NT isomers and DNT was ±5%.

In toluene nitration, a calculated amount of toluene was introduced with a syringe into the reactor with an acid mixture at a fixed temperature with stirring. After a fixed time, stirring was switched off, and the reaction mass was poured into a fivefold volume of cold water (10–15°C). The nitration products were extracted twice with chloroform taken in an amount of 6 ml per gram of toluene used for nitration. The combined extracts were washed with the equal volume of water. Finally, the products were analyzed for mono- and dinitro derivatives.

The main focus of this study was to characterize parameters controlling the reaction zones in which particular NT isomers are preferentially formed and to elucidate factors that could decrease the formation rate and yield of *meta*-nitrotoluene.

Our results show that, in toluene nitration with sulfuric–nitric acid mixtures with low molar concentration of sulfuric acid (acid mixtures were prepared from 50% H_2SO_4) and high content of HNO_3 and water, an increase in the temperature remarkably changes the *o*- and *m*-NT contents, but only slightly, the *p*-NT content (Fig. 3, Table 4).

As a hypothesis we suggested that the *para* selectivity of nitration is higher in the charged interfacial monolayer in which the nitrating agent reacts with the spatially oriented substrate molecules, and

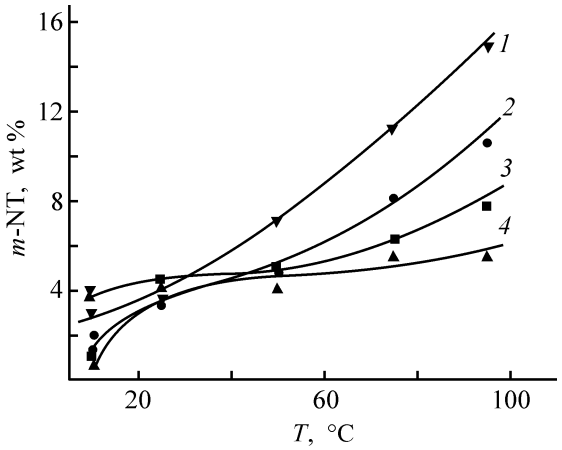

Fig. 3. Yield of *m*-NT vs. the temperature *T* in heterogeneous nitration of toluene with sulfuric–nitric acid mixtures. HNO_3 : toluene molar ratio 1.5. Acid mixture composition, mol %: (*1*) HNO_3 42.54, (*2*, *3*) H_2SO_4 10.2, and (*4*) H_2SO_4 7.60. N, rpm: (*1*, *2*, *4*) 300 and (*3*) 800.

ortho- and *meta*-nitrotoluenes are predominantly formed in the bulk of the acid phase.

Indeed, the observed decrease in the *m*-NT yield with increasing nitration efficiency factor of the acid mixture, accompanied by a decrease in the *o*-/*p*-NT ratio (Fig. 1) [2, 3], also suggests that an increase in the H_2SO_4 molar concentration promotes the interfacial nitration, whose rate grows with the H_2SO_4 concentration much more strongly than does the rate of the reaction in the bulk of the acid phase [8]. It follows from the aforesaid that, in the interfacial monolayer, the nitronium cation attacks essentially the *para* position, thus reducing the relative content of *o*- and *m*-isomers in the product.

To check this hypothesis for consistency, we carried out a series of experiments on toluene nitration under conditions similar to those indicated above with sulfuric–nitric acid mixtures containing various contents of sulfuric acid (14.07, 35.70, and 52.62 mol %). We

Table 3. Gas content Γ (vol %) of sulfuric–nitric acid mixture at various temperatures

Stirring rate *N*, rpm	Γ, vol %, at indicated $T \pm 1$°C		
	25	50	75
5000	65.2	70.8	76.1
3000	39.5	46.5	48.8
2000	29.7	34.4	36.1
1500	12.9	14.9	15.6
1000	4.9	5.6	5.9
700	–	<1	<1

Table 4. Temperature effect on the isomeric composition* of nitrotoluenes in toluene nitration with sulfuric–nitric acid mixtures of low nitrating efficiency (reaction time 60 min, HNO_3/toluene molar ratio 1.5)

Run no.	*T*, °C	*N*, rpm	Toluene, %	NT isomeric composition, %			*ortho*/*para*-NT
				o-NT	*m*-NT	*p*-NT	
Φ = 38.2; 10.20 mol % H_2SO_4, 30.41 HNO_3, 59.37 H_2O (25.1% H_2SO_4, 48.08 HNO_3, 26.82 H_2O)							
1	10	800	68.60	59.17	3.68	37.15	1.59
2	25		56.04	58.38	4.50	37.12	1.57
3	50		41.66	57.73	5.08	37.19	1.55
4	75		26.22	56.11	6.40	37.49	1.50
5	95		14.23	55.24	7.85	36.90	1.49
6	10	300	93.89	60.46	1.45	38.09	1.59
7	25		69.11	58.83	3.40	37.78	1.56
8	50		39.60	57.32	4.86	37.82	1.52
9	75		35.90	54.84	8.21	36.95	1.48
10	95		14.89	53.32	10.67	36.01	1.48
Φ = 30.9; 7.60 mol % H_2SO_4, 45.32 HNO_3, 47.07 H_2O (16.76% H_2SO_4, 64.19 HNO_3, 19.05 H_2O)							
11	10	800	42.82	59.77	0.73	39.50	1.51
12	25		21.98	56.87	4.07	39.06	1.46
13	50		20.69	57.01	4.10	38.90	1.47
14	75		15.01	55.91	5.55	38.54	1.45
15	95		8.73	55.83	5.64	38.51	1.45
42.54 mol % HNO_3, 57.45 H_2O							
16	10	300	93.61	59.27	2.95	37.78	1.57
17	25		84.77	58.64	3.72	37.64	1.55
18	50		64.30	55.42	7.17	37.41	1.48
19	75		54.47	52.01	11.39	36.60	1.42
20	95		45.72	49.75	15.07	35.18	1.41

* By isomeric composition is meant the percentage of mononitrotoluene isomers in the three-component mixture.

Table 5. Influence of the stirring rate on the NT isomer ratio in toluene nitration with sulfuric–nitric acid mixture with Φ = 48 at various temperatures [reaction time 60 min, HNO_3/toluene = 1.5; HNO_3 15.98%, H_2SO_4 41.72, and H_2O 42.29 (HNO_3 8.39, H_2SO_4 14.07, and H_2O 77.54 mol %)]

Run no.	*T*, °C	*N*, rpm	Toluene, %	NT isomeric composition, %			*ortho*/*para*-NT
				o-NT	*m*-NT	*p*-NT	
21*	25	400	68.31	58.73	35.77	5.50	1.64
22*	50		55.75	59.03	34.46	6.51	1.71
23	75		2.99	55.29	37.98	6.73	1.46
24	95		0	55.85	29.4	5.12	1.90
25*	10	2000	99.4	0	0	0	0
26*	25		61.45	57.94	37.83	4.24	1.53
27*	50		59.40	58.12	38.08	3.80	1.53
28	75		32.63	60.22	37.27	2.52	1.62
29	95		1.47	58.51	37.93	3.57	1.54
30*	25	3000	99.21	0	0	0	0
31*	50		96.8	65.15	32.09	2.76	2.03
32	75		85.26	61.78	35.46	2.77	2.34
33	95		4.12	58.85	38.05	3.10	1.74
34	10	5000	92.69	62.50	35.10	2.40	1.78
35	25		38.75	68.40	29.16	2.44	2.35
36	50		17.57	61.82	35.48	2.70	1.74
37	95		3.90	54.97	42.16	2.87	1.30

* In run nos. 21, 22, 25–27, 30, and 31, the reaction time was 100 min.

Table 6. Influence of the reaction time and stirring rate on the NT isomer ratio in toluene nitration with sulfuric–nitric acid mixture with Φ 75.1 and 85.8 (HNO_3/toluene molar ratio 1.04, T = 50°C)

Run no.	τ, min	N, rpm	Γ, vol %	Toluene, %	NT isomeric composition, %			*ortho*/*para*-NT	DNT, %
					o-NT	*m*-NT	*p*-NT		
Φ = 75.1; 74.55% H_2SO_4, 1.11 HNO_3, 24.34 H_2O (35.70 mol % H_2SO_4, 0.83 HNO_3, 63.47 H_2O)									
38	15	200	0	66.59	57.39	5.40	37.21	1.54	3.10
39		600	<0	17.02	59.72	4.14	36.13	165	1.57
40		800	5	2.11	58.96	3.74	37.30	1.58	7.36
		5000							
41		2000	34.4	2.35	57.84	4.01	38.16	1.52	0.84
42		3000	46.5	12.69	59.15	4.04	36.81	1.61	0.75
43		5000	70.8	12.31	60.11	3.60	36.29	1.66	0
Φ = 85.8; 85.42% H_2SO_4, 0.63 HNO_3, 13.95 H_2O (52.62 mol % H_2SO_4, 0.61 HNO_3, 46.77 H_2O)									
44	7	200	0	58.82	65.40	3.01	33.92	1.93	35.6
45		600	<1	23.28	58.91	3.20	37.90	1.55	65.6
46		800	5	22.33	54.96	4.07	40.97	1.34	53.3
47		1500	14.9	11.45	58.64	4.073	37.28	1.30	67.3
48		2000	34.4	7.31	58.64	4.07	27.28	1.13	54.8
49		3000	46.5	0.99	48.45	5.77	45.78	1.06	65.4
50		5000	70.8	0.00	47.67	5.39	46.94	1.02	58.5

believed that it is sulfuric acid that controls the acidity of the nitrating mixture, and, therefore, the reaction rate, depending on the stirring rate, gas content, and temperature (Tables 5, 6).

Our results show that the effects of the stirring rate, gas content, and temperature on the *m*-NT yield are more clearly pronounced in toluene nitration with an acid mixture of low nitration activity (14.07 mol % H_2SO_4, Φ 48). At low stirring rate (400 rpm), the *m*-NT yield is higher than ordinary, 3–4%, and tends to increase with temperature (Table 5, run nos. 1–4). With increasing stirring rate, the temperature dependence of the *m*-NT yield becomes more complex (Table 5, run nos. 25–29, 34–37). At a constant temperature, the *m*-NT yield steadily decreased in most of the experiments from 6.5 to 2.5–2.7 at 3000 rpm with increasing stirring rate and gas content of the reaction mass. This additionally confirmed our concept that an increase in the contribution of the interfacial nitration mechanism can reduce the *o*- and *m*-NT content of the isomer mixture (Fig. 4).

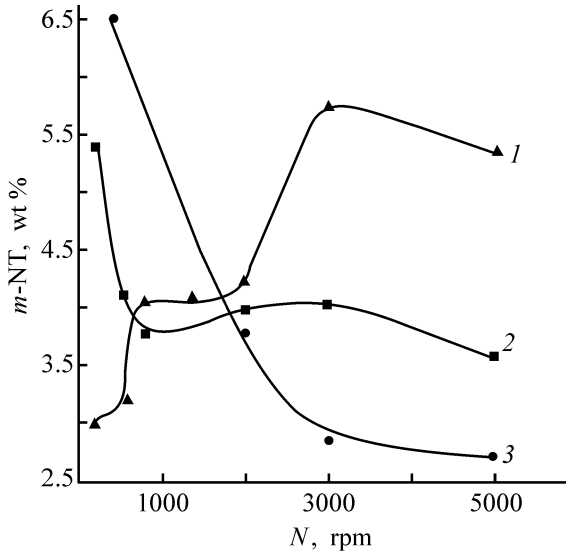

Fig. 4. *m*-NT content of toluene nitration products vs. the stirring rate N at 50°C. H_2SO_4 concentration in the mixed acid, mol %) (*1*) 52.62, (*2*) 35.70, and (*3*) 14.07.

In toluene nitration with an acid mixture with an initial sulfuric acid content of 35.70 mol % at a 4% molar excess of nitric acid, the *m*-NT yield also tends to decrease from 5.4 to 3.6% with increasing stirring rate. Note that this tendency is considerably less pronounced than that in nitration with the low-activity acid mixture containing 14.07 mol % H_2SO_4 (Fig. 4; Table 6, run nos. 38–43).

However, in toluene nitration with a high-activity acid mixture (initial sulfuric acid concentration 52.62 mol %, 4% molar excess of nitric acid), the *m*-NT yield increases with the stirring rate. In this case, the *m*-NT yield significantly increases at a stirring rate exceeding 2000 rpm, when the reaction mass is saturated with air bubbles. The increase in

the contribution of the interfacial nitration is also evidenced by the decrease in the *ortho*/*para* ratio approximately by half as the stirring rate is raised from 400 to 5000 rpm (Table 6, run nos. 44–50).

The observed increase in the *m*-NT yield with the H_2SO_4 concentration can be attributed to specific solvation of the toluene molecules with sulfuric acid. The solubility of toluene in sulfuric acid is more than doubled as the H_2SO_4 content is raised from 35.70 to 52.62 mol % [2]. This suggests that association occurs via formation of hydrogen bonds with the π-electron system of toluene, the hydrogen bonding being the strongest in the areas with the maximal electron density, i.e., at the *ortho* and *para* positions of the aromatic ring. In such associates, the hydrogen bonds partially block the *ortho* and *para* positions, while the meta position of the ring remains accessible to the attack by the nitronium ion [11].

This suggestion is confirmed by low *m*-NT content of the products of toluene mononitration with nitration agents of low acidity, e.g., with mixtures of nitric acid with acetic anhydride, trifluoroacetic acid, or nitronium salts [2, 11].

The hydrogen bonding in toluene–H_2SO_4 associates is accompanied by at significant loss of entropy, which is particularly pronounced for the reaction in the bulk of the mineral phase. At the same time, the entropy loss caused by the formation of hydrogen bonds should be less significant in the case of the interfacial nitration, when the toluene molecules are spatially oriented. Therefore, the effect of specific solvation of toluene is more pronounced at the highest stirring rates, when the contribution of the interfacial nitration dominates.

Our experiments show that, in toluene nitration with low-activity acid mixtures with a sulfuric acid content of 7.60–14.07 mol %, at low stirring rate (below 1000 rpm), i.e., when the effect of specific solvation of toluene is insignificant, an increase in the H_2SO_4 concentration at a fixed temperature results in a decrease in the *m*-NT yield (Fig. 3; Table 4, run nos. 1–10 and others).

To study the possibility of controlling the *m*-NT yield by changing the diffusion and kinetic contributions to the total nitration rate, we carried out experiments on toluene nitration with acid mixtures containing various concentrations of sulfuric acid and various molar excesses (25, 50, and 75%) of nitric acid, as influenced by the temperature. Selected results are presented in Figs. 5 and 6.

At the minimal (4%) molar excess of nitric acid, the dependence of the *m*-NT yield on the sulfuric acid content is rather complex with a distinct minimum at an H_2SO_4 content of 28–35 mol % (Fig. 5). In this case, the temperature effect is not the least important of the factors.

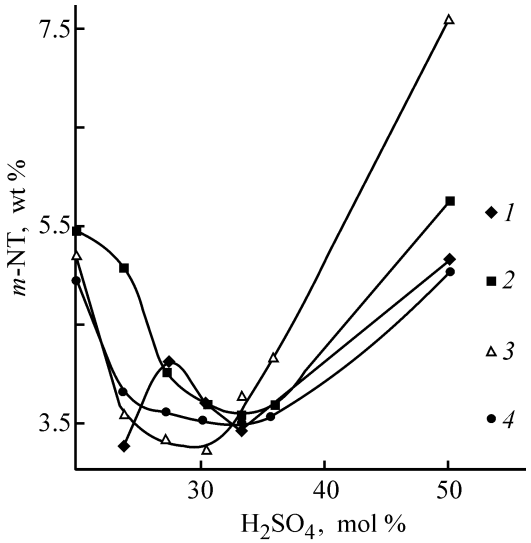

Fig. 5. *m*-NT yield vs. the H_2SO_4 concentration in the acid mixture. HNO_3/toluene molar ratio 1.04, N = 800 rpm. T, °C: (*1*) 10, (*2*) 50, (*3*) 75, and (*4*) 95.

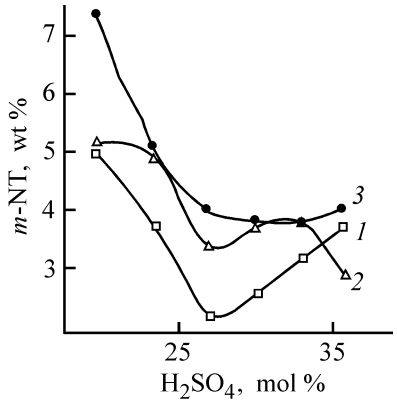

Fig. 6. *m*-NT yield vs. the H_2SO_4 concentration in the acid mixture. N = 800 rpm, T = 50°C. HNO_3/toluene molar ratio: (*1*) 1.25, (*2*) 1.5, and (*3*) 1.75.

At a high molar excess of nitric acid (see Fig. 6, HNO_3/toluene 1.25, 1.50, and 1.75) and at fixed temperature (50°C), the *m*-NT yield tends to decrease the H_2SO_4 content is raised to 27–30%. With a further increase in the H_2SO_4 content, the *m*-NT yield remains unchanged or only slightly increases. Evidently, the reaction zone shifts toward the bulk of the acid phase by virtue of the increase in the toluene solubility with the HNO_3 content os the sulfuric–nitric acid mixtures. As the H_2SO_4 content increases, and, therefore, the nitration rate grows, the rate of sub-

Table 7. Influence of alkali metal nitrates on the NT isomer ratio [Φ = 75.1; HNO_3/toluene molar ratio 1.04, T = 50°C, nitration time 15 min; H_2SO_4 74.55, HNO_3 1.11, and H_2O 24.34% (H_2SO_4 35.70, HNO_3 0.83, and H_2O 63.47 mol %)]

Run no.	Γ, vol %	N, rpm	Salt concentration, M	Toluene, %	NT isomeric composition, %			*ortho*/*para*-NT	2,4-/2,6-DNT	DNT, %
					o-NT	*m*-NT	*p*-NT			
				KNO_3 additive						
51	<1	800	1.58	1.16	57.71	3.68	38.61	1.49	2.07	12.12
52			0.79	0.38	56.86	3.97	39.18	1.45	2.49	17.51
53			0.40	0.41	55.96	3.98	40.05	1.40	2.39	21.43
54			0	2.11	53.37	3.38	33.77	1.58	2.43	7.36
				$NaNO_3$ additive						
55	70	5000	1.58	0	34.0	5.89	58.1	0.585	2.46	59.70
56	30	2000	1.58	0	48.96	5.23	45.81	1.07	2.44	43.25
56	<1	800	1.58	0	35.14	7.78	57.09	0.62	2.48	75.95
57			0.79	0	42.55	6.05	51.39	0.83	2.07	56.56
58			0.40	0	49.24	5.00	45.75	1.08	2.43	43.83
59			0	2.11	53.37	3.38	33.77	1.59	2.43	7.36
				$LiNO_3$ additive						
60	70	5000	1.58	0	39.10	5.76	55.15	0.71	2.40	66.51
61	30	2000	1.58	0	40.14	7.10	52.76	0.76	2.74	67.84
62	<1	800	1.58	0	40.96	6.38	52.66	0.78	2.23	58.41
63			0.79	0	44.67	5.88	49.46	0.90	2.31	51.19
64			0.40	0	52.34	4.37	43.29	1.21	1.88	28.15
65			0	2.11	53.37	3.38	33.77	1.58	2.43	7.36

strate diffusion from the organic phase to the acid phase becomes insufficient for the acid phase to be saturated with toluene, and the reaction zone shifts toward the interface, where, as demonstrated above, the nitration proceeds with a higher *para* selectivity. At the same time, raising the H_2SO_4 content to above 30 mol % provides a slight increase in the *m*-NT yield as a result of an enhanced specific solvation of toluene.

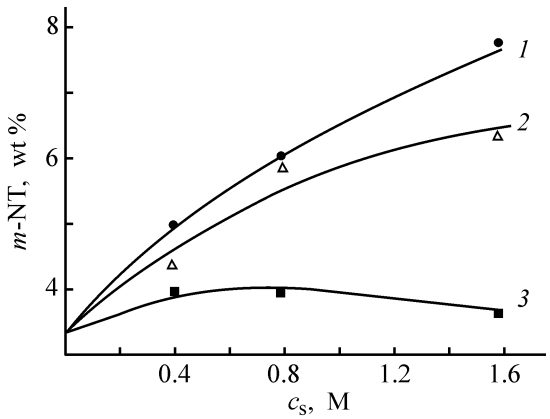

Fig. 7. *m*-NT yield vs. the inorganic salt concentration c_s in the acid mixture of the composition (mol %): H_2SO_4 35.70, HNO_3 0.83, and H_2O 63.47. HNO_3/toluene molar ratio 1.04, 50°C, N = 800 rpm. (*1*) $NaNO_3$, (*2*) $LiNO_3$, and (*3*) KNO_3.

To study the effect of inorganic salt additives on the formation of *m*-NT and on the *ortho*/*para* ratio, we performed a series of experiments on toluene nitration with an acid mixture containing 35.70 mol % H_2SO_4 and 4% molar excess of HNO_3 in the presence of Li, K, and Na nitrates. All the salts were calcined and added to the mixed acid just prior to use.

The salt concentrations were chosen taking into account the data from [4, 7]. Some of the results obtained are listed in Table 7 and presented in Figs. 7 and 8.

Our results show that the salt additives promote the formation of the *meta* and *para* isomers, and the *ortho*/*para* ratio decreases (Table 7). In the presence of the inorganic nitrates, the *m*-NT yield is more than twice that in the experiments without salt additives (Table 7, run nos. 51–65; Fig. 7). It is known [11] that the dipole moment of the nitrotoluene mol-

ecules and, therefore, of the π complexes with the nitronium ion, increases in the order *o*-NT < *m*-NT < *p*-NT. Therefore, addition of the electrolytes should primarily affect the *meta* and *para* selectivity, which is confirmed by the experimental data (Fig. 8; Table 7, run nos. 56–59, 62–65, and others).

The effect of the salt additives on the regioselectivity of toluene nitration decreases in the order $Na^+ > Li^+ > K^+$. The maximal increase in the *m*-NT yield and the maximal decrease in the *ortho*/*para* ratio were observed as the concentration of sodium nitrate in the acid mixture increased, but not with increasing concentration of lithium nitrate, as would be expected, i.e., this trend is inconsistent with the order in which the cation charge density grows (Fig. 7). Evidently, the lithium cation is considerably more strongly solvated in the acid mixture than the sodium cation. As a result, the effective radius of the lithium solvate is higher, and, therefore, it is more weakly adsorbed at the interface and increases the charge of the electric double layer to a lesser extent, compared to the sodium solvate. Thus, the increase in the contribution of the interfacial nitration is more clearly pronounced in the presence of the sodium cation.

Upon addition of $LiNO_3$, which has a higher affinity for water and exists as a crystal hydrate under ambient conditions, the *m*-NT yield increases against the reference experiment, and the dependence of the *m*-NT yield on the stirring rate passes through a maximum (Fig. 8). As the stirring rate is raised above 2000 rpm, i.e., when the gas content of the reaction mass starts to be an important factor, the *m*-NT yield decreases, probably due to a rise in the contribution of the interfacial nitration, as demonstrated by an increase in the *p*-NT yield and a decrease in the *ortho*/*para* ratio (Table 7, run nos. 62–65 and others).

Presumably, these salts bound water to form stable hydrates, thus making higher the nitration activity of the acid mixture and shifting the reaction zone toward the interface, i.e., promoting the interfacial nitration and raising the para selectivity.

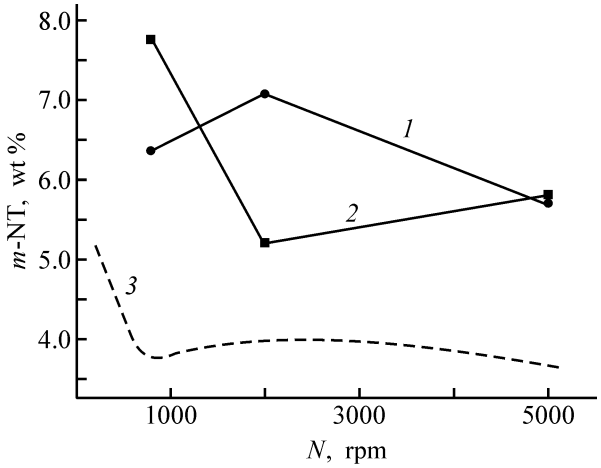

Fig. 8. *m*-NT yield vs. the stirring rate *N* (rpm) in heterogeneous nitration of toluene with the acid mixture of composition (mol %): H_2SO_4 35.70, HNO_3 0.83, and H_2O 63.47 in the presence of alkali metal nitrate additives (1.58 M): (*1*) $LiNO_3$, (*2*) $NaNO_3$, and (*3*) KNO_3. HNO_3/toluene molar ratio 1.04, 50°C.

CONCLUSIONS

(1) *Para*-selective two-phase toluene nitration with sulfuric–nitric acid mixtures proceeds in the charged interfacial monolayer, in which the nitrating agent reacts with the spatially oriented toluene molecules, while the formation of *ortho*- and *meta*-nitrotoluenes occurs essentially in the bulk of the acid phase.

(2) To reduce the *meta*-substitution rate in toluene nitration, it is necessary to diminish the mass-transfer effect on the total reaction rate and to raise the contribution of the interfacial reactions. This can be done lowering the reaction temperature, raising the sulfuric acid concentration in the acid mixture, and raising the stirring rate to 3000–5000 rpm, when a gas-filled emulsion is formed the reaction mass is saturated with air bubbles).

(3) Addition of alkali metal nitrates affects the rates of both the interfacial and bulk nitration. The former effect is caused by an increase in the positive charge in the electric double layer at the interface, and the latter effect, by a decrease in the steady-state toluene concentration in the bulk of the acid phase (salting-out effect).

(4) Introduction of alkali metal nitrates raises the yields of *meta*- and *para*-nitrotoluenes by promoting the nitration at the *para* and *meta* positions of the aromatic ring, since the corresponding reaction intermediates have a higher dipole moment, compared to *ortho*-nitrotoluene.

REFERENCES

1. Hermann, H. and Gebauer, J., *Nitration: Recent Laboratory and Industrial Development*, Albright, L.F., Carr, R.V.C., and Schmitt, R.J., Eds., ACS Symp. Ser. 623, Washington, DC: Am. Chem. Soc., 1996, pp. 234–249.
2. Orlova, E.Yu., *Khimiya i tekhnologiya brizantnykh vzryvchatykh veshchestv* (Chemistry and Technology of High Explosives), Lenningrad: Khimiya, 1973.

3. Milligan, B., *Ind. Eng. Chem. Fundam.*, 1986, vol. 25, p. 783.
4. Librovich, N.B., Medvetskaya, I.M., Voloshenko, G.I., et al., *Izv. Akad. Nauk SSSR, Ser. Khim.*, 1988, pp. 2793–2796.
5. Roberts, R.A., Heiberger, P., Watkins, J.D., et al., *J. Am. Chem. Soc.*, 1958, vol. 80, pp. 4285–4287.
6. Hanson, C., Michael, W.T.P., Sorabi, T., et al., *J. Appl. Chem. Biotechnol.*, 1975, vol. 25, p. 727.
7. Krylov, E.N. and Khromova, I.N., *Zh. Obshch. Khim.*, 1988, vol. 19, no. 11, pp. 2382–2389.
8. Modak, S.Y. and Juvekar, V.A., *Ind. Eng. Chem. Res.*, 1995, vol. 34, pp. 4297–4309.
9. Kasarekar, R.B., Ramakrishna, M., and Juvekar, V.A., *Chem. Eng. Technol.*, 1997, vol. 20, pp. 282–284.
10. Schieferle, D.F., Hanson, C., and Albright, L.F., *Industrial and Laboratory Nitrations*, Albraight, L.F. and Hanson, C., Eds., ACS Symp. Ser. 22, Washington, DC: Am. Chem. Soc., 1976, pp. 176–182.
11. Zbarskii, V.L. and Zhilin, V.F., *Toluol i ego nitroproizvodnye* (Toluene and Its Nitro Derivatives), Moscow: URSS, 2000.

ISSN 1070-4272, Russian Journal of Applied Chemistry, 2007, Vol. 80, No. 12, pp. 2073–2076. © Pleiades Publishing, Ltd., 2007.
Original Russian Text © E.I. Grushova, A.V. Kuchuk, 2007, published in Zhurnal Prikladnoi Khimii, 2007, Vol. 80, No. 12, pp. 1994–1997.

ORGANIC SYNTHESIS AND INDUSTRIAL ORGANIC CHEMISTRY

Intermolecular Interactions and Properties of Mixtures of Triethylene Glycol with Ethanol and Isopropyl Alcohol

E. I. Grushova and A. V. Kuchuk

Belarussian State Technological University, Minsk, Republic of Belarus

Received January 12, 2007

Abstract—Density and viscosity of solutions formed in the systems triethylene glycol–ethanol and triethylene glycol–isopropyl alcohol were studied in the full concentration range at 20, 40, 50, and 60°C. The thermodynamic activation functions of viscous flow were calculated. The contribution of specific interactions to these functions was determined.

DOI: 10.1134/S1070427207120133

Although numerous studies aimed to develop efficient methods for recovery of aromatic hydrocarbons from oil fractions have been carried out [1–3], liquid extraction with triethylene glycol (TEG) as separating agent remains important. To improve the extractive properties of TEG, it has been suggested to use additives of polar compounds, coextractants [4–6]. However, wide application of coextractants requires that the mechanism of their effect on the main solvent should be known.

In this study, solvents of compositions TEG–ethanol and TEG–isopropyl alcohol were objects of analysis. Methods described in [7, 8] were used to study in the temperature range 20–60°C their viscosity ν^{60} and density ρ_4^{60} and to determine the thermodynamic functions of activation of viscous flow ($\Delta G_\nu^\#$ is the activation energy of viscous flow; $\Delta S_\nu^\#$, enthalpy; and $\Delta H_\nu^\#$, entropy) and the average degree of association of the solvents, f_{60}, in the flowing state. The experimental data obtained and the results of calculation are listed in Table 1. The relative error in viscosity measurements did not exceed 0.02%. The error in determining the activation parameters was ±2.5–5%. The reliability of these results is confirmed by comparison of the value of f for ethanol at 20°C (Table 1) with published data [9].

According to the data in Table 1, an increase in the alcohol concentration leads to a steady decrease in the density, kinematic viscosity, and free activation energy of the viscous flow, which points to destabilization of the liquid-phase structure. In this case, an increase in the concentration of the second component causes a decrease in the entropy of activation of viscous flow for the TEG–ethanol system, whereas for the system TEG–isopropyl alcohol, $\Delta S_\nu^\#$ slightly increases. This may be due to the ability of isopropyl alcohol molecules introduced into the solution to fill free cavities in the solution structure.

In general, the concentration dependences of the enthalpy of activation of viscous flow for both the systems are similar, i.e., $\Delta H_\nu^\#$ decreases as the alcohol concentration increases, and this behavior is more pronounced for the TEG–ethanol system. Moreover, the $\Delta H_\nu^\#$ and $\Delta S_\nu^\#$ dependences pass through a minimum at low ethanol concentrations. The average degree of association of the solutions in the flowing state also steadily decreases as the alcohol concentration in both systems increases.

The concentration dependences of the specific activation energy of viscous flow [8] and of the density of the enthalpy of activation of viscous flow [5] are shown in Figs. 1a and 1b. According to the graphical data, only small ethanol additives cause deviations of the above parameters from the corresponding values calculated using the additivity rule.

Because hydrogen bonds can be formed between molecules of the solutions under study, it was of interest to determine the contribution of specific and nonspecific interactions to the enthalpy of activation

Table 1. Density, viscosity, thermodynamic functions of activation of viscous flow, and average degree of association of solvents

Alcohol concentration, mole fraction	ρ_4^{60}	$\nu^{60} \times 10^6$, $m^2\ s^{-1}$	$\Delta G_\nu^\#$, kJ mol^{-1}, at 40–60°C	$\Delta S_\nu^\#$, kJ $mol^{-1}\ K^{-1}$	$\Delta H_\nu^\#$, kJ mol^{-1}	f_{60}
TEG	1.1110	9.015	31.01	0.14	78.32	21.8
TEG–ethanol system						
0.05	1.0897	7.262	32.72	0.09	59.20	51.73
0.10	1.0827	6.516	30.19	0.08	58.12	23.98
0.15	1.0732	6.379	28.11	0.12	69.43	18.50
0.22	1.0593	5.375	26.69	0.11	64.78	9.01
0.26	1.0501	4.831	25.79	0.11	62.78	7.48
0.28	1.0455	4.601	25.37	0.10	60.92	6.37
0.37	1.0276	3.828	23.83	0.10	56.15	5.13
0.58	0.8981	2.308	19.58	0.07	43.07	4.44
0.77	0.8356	1.507	16.02	0.05	31.93	1.42
0.83	0.8132	1.293	14.75	0.04	28.08	1.04
0.88	0.7950	1.142	12.80	0.06	31.12	0.68
0.97	0.7665	0.940	12.10	0.02	19.26	0.73
1.00	0.7553	0.773	15.40	0.09	44.00	4.33
1.00*	0.7893	1.590	–	0.09	44.00	12.44; 13.1 [9]
TEG–isopropyl alcohol system						
0.07	1.0833	7.790	30.03	0.14	78.01	18.54
0.12	1.0743	7.137	29.50	0.14	77.47	17.11
0.18	1.0608	6.304	28.70	0.14	77.01	15.11
0.22	1.0523	5.826	28.17	0.15	76.82	13.91
0.30	1.0302	4.884	27.04	0.15	76.02	11.65
0.51	0.9285	3.214	24.32	0.15	74.68	7.81
0.70	0.8632	2.157	21.75	0.15	73.06	5.50
0.79	0.8390	1.861	20.70	0.15	72.07	5.05
0.85	0.8479	1.636	19.94	0.16	71.92	5.42
0.95	0.7842	1.332	18.16	0.16	71.27	6.17
1.00	0.7701	1.222	18.04	0.16	71.02	6.60

* Parameters were determined at 20°C.

of viscous flow, $\Delta H_\nu^\#$ [8]. For this purpose, we determined the kinematic viscosity of dilute solutions of TEG–ethanol solvents in carbon tetrachloride. In these systems, specific interactions between molecules of the solvents under study are virtually nonexistent. Further, the linear part of the $\nu = f(x)$ dependences, where x is the molal concentration of the solvent studied, was extrapolated to $x = 1$ to obtain the viscosity

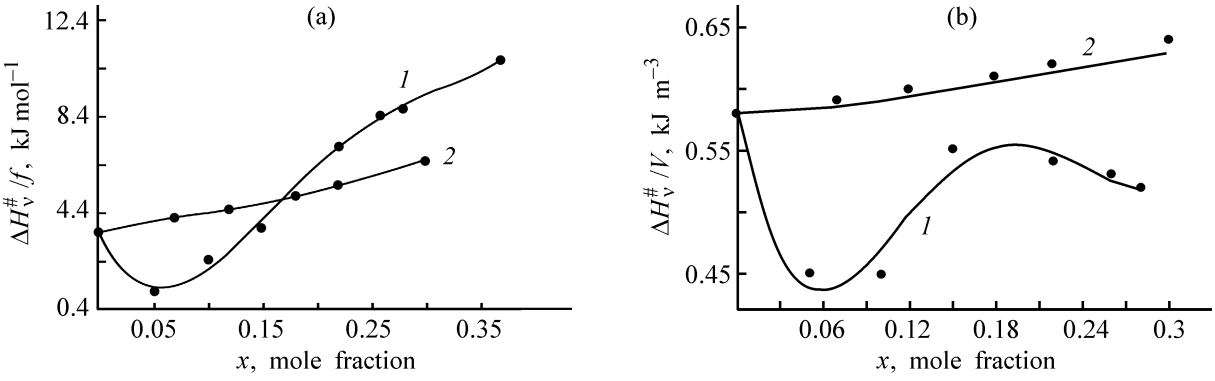

Fig. 1. (a) Specific enthalpy of activation of viscous flow ($\Delta H_\nu^\#/f$) and (b) density of the enthalpy of viscous flow ($\Delta H_\nu^\#/V$) at 60°C vs. the alcohol concentration x. System: (*1*) TEG–ethanol, (*2*) TEG–isopropyl alcohol.

Table 2. Properties of hypothetical solvents

Solvent	$\nu^{50h} \times 10^6$, $m^2\ s^{-1}$	$\Delta G_\nu^{\#h}$, kJ mol^{-1}	$\Delta S_\nu^{\#h}$, kJ $mol^{-1}\ K^{-1}$	$\Delta H_{\nu\,60}^{\#h}$, kJ mol^{-1}	f_{60}^{h}
TEG	1.339	21.89	0.14	69.9	5.41
TEG + 5 mol % ethanol	0.908	15.79	0.18	44.0	0.91
TEG + 10 mol % ethanol	0.804	12.48	0.14	34.9	0.36
Ethanol	0.749	2.82	0.05	20.1	0.032

Table 3. Specific enthalpies of activation of viscous flow ($\Delta H_\nu^{\#}/f$) and densities of enthalpies of viscous flow ($\Delta H_\nu^{\#}/V$) of real and hypothetical solvents at 60°C*

Solvent	$\Delta H_\nu^{\#}/f$, kJ mol^{-1}	$\Delta H_\nu^{\#}/V \times 10^{-3}$, kJ m^{-3}	$(\Delta H_\nu^{\#} - \Delta H_\nu^{\#h}) : \Delta H_\nu^{\#}$
TEG	3.59	0.58	0.11
TEG + 5 mol % ethanol	1.14	0.45	0.26
TEG + 10 mol % ethanol	2.42	0.45	0.40
Ethanol	10.16	0.70	0.54

* V, molar volume of the solvent at 60°C.

of hypothetical solvents and calculate the thermodynamic activation functions of the viscous flow. The results obtained are listed in Tables 2, 3.

As can be seen, the viscosity parameters and thermodynamic characteristics of the hypothetical solvents strongly differ from the corresponding parameters of real systems (Table 1). Presumably, the higher values of $\Delta S_\nu^{\#}$ indicate that the hypothetical solvents containing 5 and 10 mol % ethanol have a more ordered structure.

However, the enthalpy of activation of viscous flow, $\Delta H_\nu^{\#}$, for these solutions is considerably lower than that for real systems. It can be seen from the data in Table 3 that the contribution of the specific interaction to $\Delta H_\nu^{\#}$ increases upon addition of small amounts of ethyl alcohol to TEG. At the same time, the parameter $\Delta H_\nu^{\#}/V$, suggested in [5] for characterizing the density of the attraction energy in a flowing liquid, decreases. This parameter linearly correlates with the solvent capacity, which, according to [1], is estimated by the reciprocal limiting activity coefficient of benzene in the separating agent. Consequently, the dissolving capacity of the solvent increases upon addition of minor amounts of ethanol to TEG, but the contribution of specific interactions to the enthalpy of activation of viscous flow grows, too.

The results obtained were compared with the parameters of extraction of the benzene–hexane model system with the solvents under study at 20°C. The benzene : hexane : solvent volume ratio was 1 : 1 : 2. As can be seen from Fig. 2, additions of ethanol and isopropyl alcohol differently affect the selective and dissolving properties of TEG. At small concentrations, isopropyl alcohol affects only slightly the distribution coefficient of benzene and the separation selectivity. If, however, ethanol is added to TEG, the dissolving power of the extractant and the separation selectivity are improved. These data are in agreement with the results of a viscometric study of TEG–alcohol systems.

Thus, it follows from the aforesaid that a viscometric study and comparative analysis of the properties of real solvents and of the corresponding hypothetical solvents can be used to gain better insight into the mechanism of formation of extractive properties in development of new solvents and coextractants.

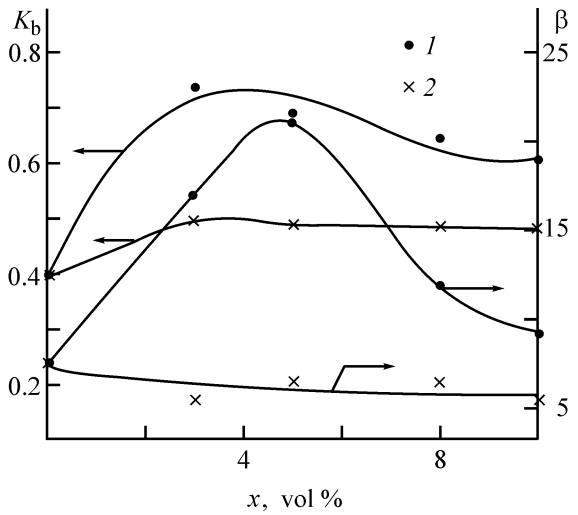

Fig. 2. Distribution coefficient of benzene, K_b, and separation selectivity β vs. the concentration x of (*1*) ethanol and (*2*) isopropyl alcohol in TEG.

CONCLUSION

The extractive properties of the systems triethylene glycol–ethanol and triethylene glycol–isopropyl alcohol are determined by the density of enthalpy and by the activation energy of viscous flow per structural unit of the associate.

REFERENCES

1. Gaile, A.A., Somov, V.E., and Varshavskii, O.M., *Aromaticheskie uglevodorody: Vydelenie, primenenie, rynok: Spravochnik* (Aromatic Hydrocarbons: Separation, Application, and Market: Reference Book), St. Petersburg: Khimizdat, 2000.
2. Gaile, A.A., Zalishchevskii, G.D., Gafur, N.N., et al., *Khim. Tekhn. Topl. Masel*, 2004, no. 4, pp. 11–14.
3. Zalishchevskii, G.D., Gaile, A.A., Yakovlev, A.A., et al., *Neftekhim. Neftepererab.*, 2004, no. 9, pp. 31–34.
4. RF Patent 2 202 529.
5. Grushova, E.I., Catalogue of Papers, *3-ya Mezhdunarodnaya Konferentsiya "Ekstraktsiya organicheskikh soedinenii"* (3rd Int. Conf. "Extraction of Organic Compounds"), Voronezh, October 17–21, 2005, p. 227.
6. Grushova, E.I., Kurozhko, M.V., and Korshak, V.V., *Trudy Bel. Gos. Tekhn. Univ., Ser. IV, Khim. Tekhnol. Organ. Veshch.*, Minsk, 2001, issue 9, pp. 76–78.
7. Kuchuk, A.V. and Grushova, E.I., *Vestsi Nats. Akad. Navuk Bel., Ser. Khim. Navuk*, 1999, no. 3, p. 42–45.
8. Grushova, E.I. and Yusevich, A.I., *Russ. J. Phys. Chem.*, 2006, vol. 80, suppl. 1, pp. S189–S192.
9. Obraztsov, V.I. and Khrustalev, A.A., *Zh. Fiz. Khim.*, 1973, vol. 47, no. 4, pp. 812–814.

ISSN 1070-4272, Russian Journal of Applied Chemistry, 2007, Vol. 80, No. 12, pp. 2077–2084. © Pleiades Publishing, Ltd., 2007.
Original Russian Text © M.S. Masalovich, L.P. Ardasheva, G.A. Shagisultanova, 2007, published in Zhurnal Prikladnoi Khimii, 2007, Vol. 80, No. 12, pp. 1998–2006.

ORGANIC SYNTHESIS AND INDUSTRIAL ORGANIC CHEMISTRY

Photochemical Reactions in Solutions of the Platinum(II) Complex with 8-Quinolinol

M. S. Masalovich, L. P. Ardasheva, and G. A. Shagisultanova

Herzen Russian State Pedagogical University, St. Petersburg, Russia

Received May 29, 2007; in final form, October 2007

Abstract—The rate of photochemical reaction in solutions of luminescent platinum(II) complex with 8-quinolinol was studied in relation to the type of solvent, irradiation time, photon energy and intensity of a luminous flux, concentration of the complex, and presence of oxygen. The structure of the photochemical reaction product was studied by X-ray photoelectron, IR, and electronic absorption spectroscopy. The quantitative kinetic parameters and quantum yield of the photochemical reaction performed under various irradiation conditions are reported.

DOI: 10.1134/S1070427207120145

Platinum(II) complexes exhibit a unique combination of optical, catalytic, and luminescence spectral properties [1–13]. An important feature is that platinum(II) complexes can aggregate or polymerize to give photosensitive and luminescent supramolecular ensembles [1–4].

Among these compounds are platinum(II) complexes with Schiff bases like [PtSalen], which exhibit photochemical activity and can electrochemically polymerize. The study of photo- and electrochemical reactions of platinum complexes with Schiff bases can provide an insight into the mechanism of formation of dimers and polymers [2–4]. In this study, we examined photochemical reactions of the platinum(II) complex with 8-quinolinol, a bidentate ligand coordinated to platinum via oxygen and nitrogen atoms. The structure of $[Pt(qol)_2]$, where qol is 8-quinolinol, is as follows:

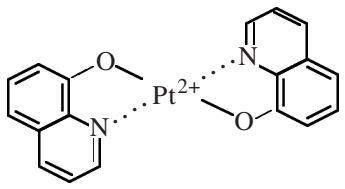

The electronically excited states (EESs) of $[Pt(qol)_2]$ were characterized by luminescence spectral methods [8, 13–16]. However, the possibility of deactivation of EESs by a photochemical reaction and structural rearrangement of the complex are still poorly understood. These data are of practical importance since $[Pt(qol)_2]$ can be used as monomer in electrochemical synthesis of thin-layer conducting polymers [17].

The aim of this study was to analyze photostimulated aggregation of $[Pt(qol)_2]$ to form new molecular structures.

EXPERIMENTAL

The complex $[Pt(qol)_2]$ was prepared by the modified procedure [14] from potassium tetrachloroplatinate(II) K_2PtCl_4 and 8-quinolinol C_9H_7ON (Merck) recrystallized from ethanol.

Since the platinum complex is a photochemically labile compound in the presence of atmospheric oxygen dissolved in the solution [10, 14], its synthesis and preparation of its solutions for photochemical experiments and recording of absorption and luminescence spectra were performed in the dark.

8-Quinolinol and its platinum complex were identified by electronic absorption spectroscopy and X-ray photoelectron spectroscopy (XPS). The UV-Vis absorption spectra of $[Pt(qol)_2]$ were recorded on SF2000 and Shimadzu UV-2401 PC spectrophotometers.

The X-ray photoelectron spectra were measured on an Axis Ultra electron spectrometer (Kratos Analytical, UK) using monochromatic Al_{K_α} radiation

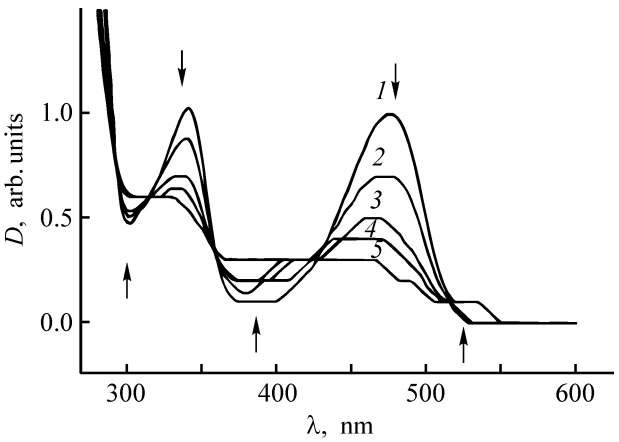

Fig. 1. Absorption spectrum of 1×10^{-4} M air-saturated solution of $[Pt(qol)_2]$ in CH_2Cl_2 irradiated with unfiltered light for τ_{irr} (min): (*1*) 0, (*2*) 1, (*3*) 3, (*4*) 5, and (*5*) 7. (*D*) Optical density and (λ) wavelength; the same for Figs. 2 and 3.

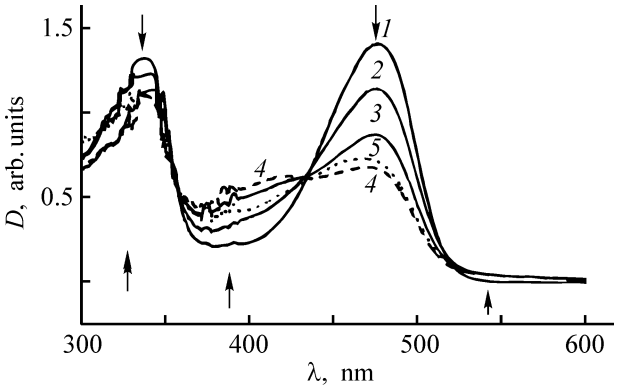

Fig. 2. Absorption spectrum of 2×10^{-4} M air-saturated solution of $[Pt(qol)_2]$ in DMF irradiated with unfiltered light for τ_{irr} (min): (*1*) 0, (*2*) 5, (*3*) 10, (*4*) 25, and (*5*) 60.

(1486.6 eV). The working residual pressure in the spectrometer was 5×10^{-7} Pa. The spectra were processed using Vision2 software (Kratos Analytical, UK). The binding energy scale was calibrated against the C1*s* line of aromatic carbon (E_b = 285.0 eV). The atomic concentration was determined with an accuracy of 10%.

The photochemical experiments were performed in quartz cells (l = 1 cm) under continuous exposure of the solution to light from a DRSh-1000 lamp for a required time. The IR light was cut-off with a water filter. THe light with wavelengths λ 315–320, 436, and 480 nm was obtained with the aid of a set of glass filters. The light intensity was determined with a ferrioxalate actinometer [18, 19]. The experiments were performed in a solution saturated with air or oxygen or deaerated with argon. We used dimethylformamide (DMF), dichloromethane, and acetonitrile (ultrapure grade) as solvents.

The quantum yields of the photochemical reactions were determined from the experiments performed in dichloromethane. We showed that luminescence in the dichlorometahne solutions exposed to monochromatic light was the most intense and the equilibrium in these solutions was rapidly attained.

The IR spectra of a dry photolyte sample (KBr pellets) were recorded on an IFS-88 IR Fourier spectrometer in the range 500–16000 cm^{-1}. The phosphorescence and excitation spectra in deaerated solution in DMF and dichloromethane at T = 298 K were measured on a Flyuorat-02-Panorama spectrofluorimeter (Lyumeks Joint-Stock Company). The excitation was performed with a high-pressure xenon lamp. The excitation wavelength was adjusted with a monochromator. Prior to each experiment, the solutions were deaerated by bubbling of high-purity argon for 20 min.

The phosphorescence in frozen DMF : toluene (1 : 1) solutions at T = 77 K was recorded on a KSVU-1 unit; the spectra were excited with an LGI-21 nitrogen laser (λ = 337 nm, τ_{pulse} = 10 ns).

The quantum yield was measured with fluorescein (Φ = 0.85) and $[Ru(bipy)_3]Cl_2$ (Φ = 0.0284) as references [18, 19].

The electronic absorption spectra of $[Pt(qol)_2]$ in dichloromethane are consistent with published data [8, 16] and contain two strong bands with vibronic structure (Fig. 1, curve *1*). The high-energy band at λ_{max} = 345 nm (ε = 8000) is due to intraligand π–π^* transitions, and the low-energy band at λ_{max} = 475 nm (ε = 6900) is assigned to intraligand charge transfer from oxygen atom of the phenol moiety to the nitrogen atom of the pyridine ring (ILCT band) [8]. It is known that the spectra of most of transition metal complexes with organic ligands contain in this range metal-to-ligand charge-transfer (MLCT) bands with extinction coefficients not higher than 2000–3000 $l\,mol^{-1}\,cm^{-1}$ [3, 4]. Therefore, this band may be a superposition of ILCT with a less intense MLCT band.

As can be seen from Figs. 1–3, with an increase in the irradiation time of a solution, the intensity of both bands decreases, i.e., the $[Pt(qol)_2]$ concentration decreases. At the same time, the absorption in the range in which the $[Pt(qol)_2]$ absorption is minimal or absent increases. The appearance of new weak bands and the presence of isobestic points in the spectrum suggest that a product being in the equilibrium with the initial complex is accumulated in the course of the photochemical reaction. The most intense new band is observed at λ_{max} = 425 nm (shoulder) in the spectrum of a DMF solution irradiated for 25 min (Fig. 2). The intensity of this band decreases, and

the isobestic points caused by the presence of two or more absorbing species being in the equilibrium are disturbed after irradiation of the solution for 60 min.

It should also be noted that the appearance of new poorly resolved bands in the ranges 350–425 and 520–600 nm, red-sifted with respect to the bands of the initial complex, suggests that molecular associates are formed in the course of the photochemical reaction. A strong bathochromic shift of the absorption bands of the photochemical reaction product with respect to the spectrum of the initial monomer complex is typical [1–3] of electro- or photostimulated dimerization or polymerization.

As the irradiation time increases, the color of the solution of the platinum complex changes from orange to green-yellow. It is significant that the transformations in the solution determined visually and spectroscopically are preserved for indefinitely long time after irradiation completion. A dark brown compound was isolated by evaporation of the irradiated solution. The absorption and emission spectra of a solution of this compound in various solvents are similar to the corresponding spectra recorded immediately after the irradiation completion. Thus, the product of the photochemical reaction is stable and does not transform into the initial complex in the dark.

We found that the solvent affects the reaction kinetics and does not affect the spectrum transformations. The maximal concentration of the reaction product in a dichloromethane solution is observed after its exposure to polychromatic light for 5–6 min. A similar result in acetonitrile and DMF was obtained in 20–30 min. Probably, the viscosity and dielectric constant of the solvent ($\eta = 0.411 \times 10^3$ Pa s and $\varepsilon = 8.93$ for dichloromethane, $\eta = 0.340 \times 10^3$ Pa s and $\varepsilon = 36.02$ for acetonitrile, and $\eta = 0.796 \times 10^3$ Pa s and $\varepsilon = 36.7$ for DMF) have the most significant effect on the photoreaction kinetics. The high rate of the photochemical reaction in dichloromethane is due to its low viscosity and dielectric constant. Hence, the viscosity of the solvent affects the rate of diffusion and recombination of primary photolysis products, which is typically observed in formation of dimers or oligomers.

It is known that the quantum yield and the accumulation rate of the products of photochemical reactions whose order differs from unity depend on the reagent concentrations. We found that the accumulation rate of the product formed by irradiation of $[Pt(qol)_2]$ in DMF depends on the concentration of the initial complex. This dependence is extremal. The concentration of the initial monomer was 0.05, 0.1, 0.2, 0.4, and 0.8 mM. The rate of the photochemical reaction was maximal at a $[Pt(qol)_2]$ concentration of 0.2 mM.

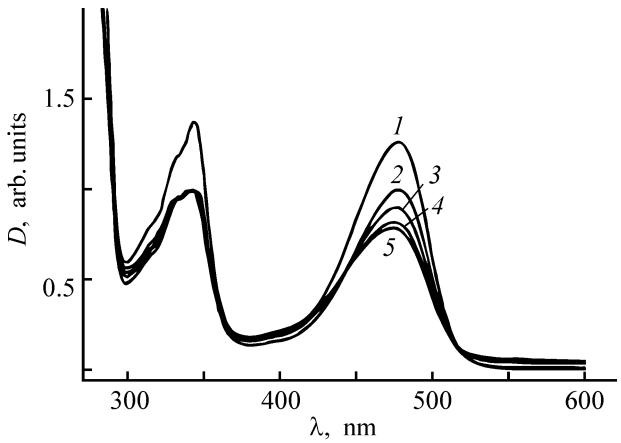

Fig. 3. Absorption spectrum of 1×10^{-4} M air-saturated solution of $[Pt(qol)_2]$ in CH_2Cl_2 irradiated for τ_{irr} (min): (*1*) 0, (*2*) 5, (*3*) 30, (*4*) 60, and (*5*) 90. $\lambda_{irr} = 480$ nm, $I_{luminous\ flux} = 9 \times 10^{-9}$ einstein s^{-1}.

To reveal the kinetic features of the photochemical reactions, we studied the influence of the intensity and wavelength of the irradiation on the spectral transformations of the examined solutions. It should be noted that the rate of the photochemical reaction decreases and the time required for formation of the reaction product increases when a solution is irradiated with monochromatic light (λ = 315–320, 436, and 480 nm) instead of unfiltered light. For example, when a dichloromethane solution was irradiated with a monochromatic light (λ = 480 nm), the time required for formation of the reaction product in the maximal yield was as long as 90 min (Fig. 3), whereas on exposure of the solution to unfiltered light the product was formed within 7 min. The shape of the spectrum of $[Pt(qol)_2]$ solution recorded in the final steps of irradiation with monochromatic light (Fig. 3, curve *5*) was similar to that of the solution exposed to unfiltered radiation for 2–3 min (Fig. 1, curve *3*). Thus, the composition of the reaction products prepared under different irradiation conditions is similar but their yields depend to a greater extent on the intensity of luminous flux.

To determine the type of the electronically excited state formed in the course of photochemical transformation of the complex, we performed several experiments with different wavelengths of the exciting light. Exposure to 436- and 480-nm light whose wavelength is close to the peak of the low-energy band in the absorption spectrum of CH_2Cl_2 significantly decreases the optical density of this band, whereas

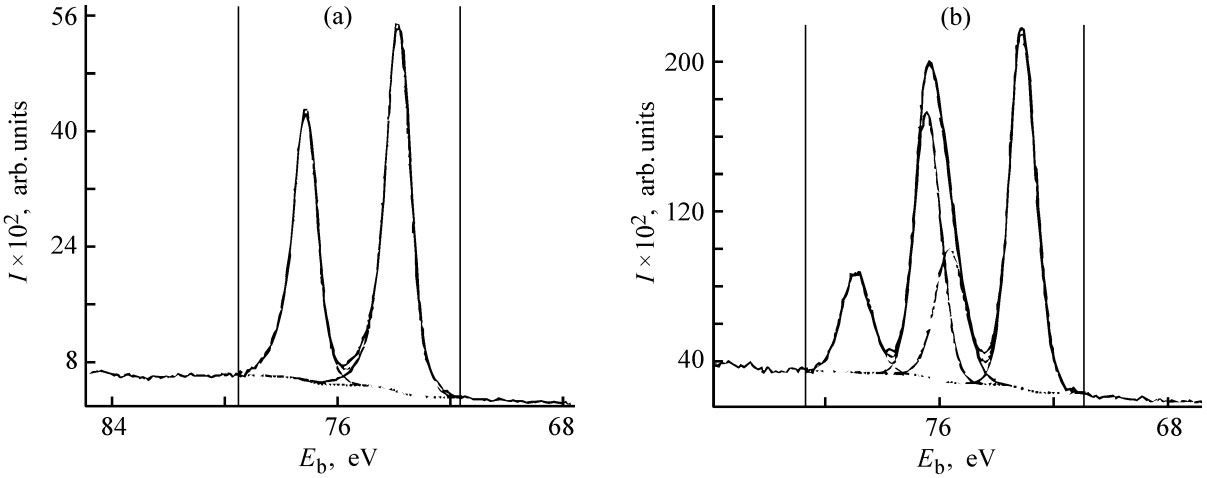

Fig. 4. Pt 4*f* XPS spectra of (a) initial $[Pt(qol)_2]$ and (b) reaction products formed on exposure of an air-saturated solution of $[Pt(qol)_2]$ in CH_2Cl_2 to unfiltered light for 7 min. (*I*) Intensity and (E_b) binding energy.

the intensity of this band only slightly changes on exposure to UV light (315–320 nm).

Thus, the products of photochemical reactions initiated with light of different wavelengths and intensities are formed at different rates. Therefore, the efficiencies of deactivation of a Franck–Condon electronically excited state into a photochemically active EES differ. It is most likely that specifically the electrons involved in the intraligand charge transition from the oxygen atom of the phenol moiety to the nitrogen atom of the pyridine ring of 8-quinolinol [8] and in MLCT mainly take part in the formation of the photochemically active state.

Table 1. XPS data for $[Pt(qol)_2]$ and its photolysis product

Line	Initial $[Pt(qol)_2]$		Product*	
	E_b, eV	concentration, at. %	E_b, eV	concentration, at. %
C 1*s*	285.0	17.3	285.0	65.52
	285.9	53.44	286.4	14.98
	286.8	7.57	288.1	1.26
			289.2	2.79
O 1*s*	531.9	6.62	532.2	7.74
	532.9	1.66	533.7	3.17
	534.2	0.84		
N 1*s*	400.9	6.59	400.6	2.95
	401.7	1.47	402.4	0.21
	402.8	0.44		
Pt 4*f*	73.7	4.07	73.1	0.97
			75.6	0.41

* Samples obtained by irradiation of a $[Pt(qol)_2]$ solution in CH_2Cl_2 for 10 min.

To estimate the influence of atmospheric molecular oxygen on the photochemical reactions, we studied the photoreaction kinetics and the photolysis products in solutions deaerated with argon and aerated with pure oxygen.

We found that the rate of photochemical reactions in oxygen-free solvents is lower. The rate of the photochemical reaction in deaerated dichloromethane solutions is lower by a factor of 2 than that in the air-saturated solutions. The isobestic points in the spectrum of $[Pt(qol)_2]$ solutions saturated with pure oxygen are distorted after exposure to 480-nm light for 15 min. Hence, it can be concluded that atmospheric oxygen affects the mechanism of photolysis.

To determine the composition and structure of the photolysis product, solid samples obtained by evaporation of the reaction mixture were studied by XPS and IR spectroscopy. The spectrum of the photolysis product contains, unlike the spectrum of the initial complex, a new line with E_b = 75.6 eV (Fig. 4), which suggests partial oxidation of Pt(II) to Pt(IV) during photolysis. These data confirm our assumption that the electronically excited $[Pt(qol)_2]$ formed by metal-to-ligand charge transfer is involved in the photochemical reaction.

The XPS spectrum of the photolysis product contain strong oxygen lines. A quantitative analysis of XPS data (Table 1) showed that the concentration of oxygen atoms in the product is higher by a factor of 4 than that of nitrogen atoms. The concentration ratio of these heteroatoms in the initial complex is 1 : 1.

Resoluting the XPS spectrum into the Gaussian components showed the presence of new carbon lines

with binding energies of inner electrons of 288.1 and 289.2 eV typical of –C=O and $-COO^-$ (–COOR) groups, respectively (R is a hydrocarbon radical). The content of carboxyl (ester) oxygen is higher by a factor of two than that of carbonyl oxygen.

The IR absorption spectrum of the solid photolysis product is shown in Fig. 5. The spectrum in the range of stretching vibrations of the C=C, C=N, and C–H bonds of the aromatic ring (1500–600 cm^{-1}) is similar to that of the initial complex. However, the spectrum of the photolysis product contains new stretching bands. The band at 1726 cm^{-1} can be assigned to unsaturated esters whose absorption is observed in the range 1730–1710 cm^{-1}. The bands in the range 2960–2850 cm^{-1} are due to the presence of methylene groups $-CH_2-$, which can be formed by partial saturation of the –CH=CH– bonds via cleavage of the phenol rings and loss of aromaticity.

The absence of absorption in the range typical of conducting polymers (14000–4000 cm^{-1}) [20–24] confirms the degradation of the conjugated chain in the course of trimerization and conductivity loss.

To study the properties of the photolysis product and the type of the electronically excited intermediate, we compared the luminescence spectral parameters of the initial complex $[Pt(qol)_2]$ [10, 14–16] and its photolysis product isolated in different irradiation steps.

The luminescence spectrum of $[Pt(qol)_2]$ strongly depends on temperature and the type of solvent [8, 16]. Emission at $\lambda_{max} = 650$ nm with the lifetime $\tau = 3.5$ μs was observed in a DMF solution of this complex at 293 K [15]. Donges et al. [8] showed that the emission was caused by ^{3}ILCT from the single lowest EES.

The luminescence spectrum of an unirradiated solution of the platinum complex in dichloromethane ($c = 1 \times 10^{-4}$ M) at 298 K is shown in Fig. 6 (curve *1*). The maximal emission is observed at $\lambda_{max} = 645$ nm.

An analysis of the EES in $[Pt(qol)_2]$ [15] showed that luminescence from low long-lived triplet state can be quenched with atmospheric oxygen. However, a series of experiments showed that the rate of the photochemical reactions in the presence of oxygen was noticeable. We suggest that the photochemical reaction and radiative deactivation involve ^{3}ILCT EES and are competing processes. Formation of mixed (^{3}ILCT + ^{3}MLCT) EES is possible, which is conformed by the presence of Pt(IV) in the photolysis product (XPS data). The relaxation of electronically excited $[Pt(qol)_2]^*$ in a dichloromethane solution can be described by the following scheme:

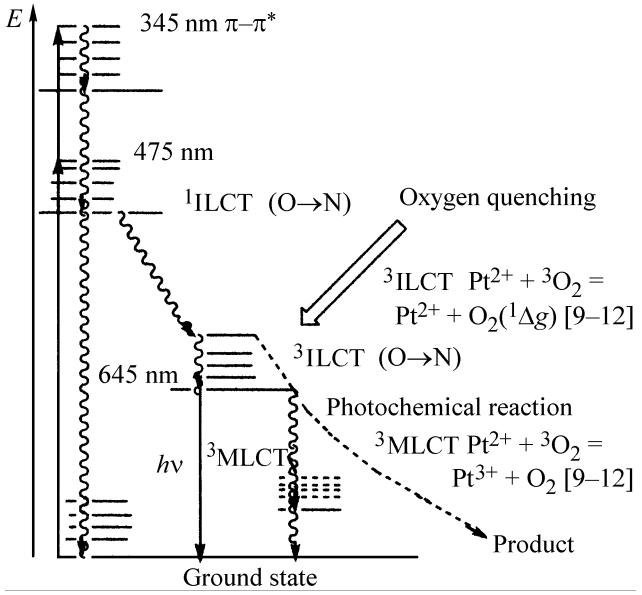

As can be seen from Fig. 6, the luminescence intensity of $[Pt(qol)_2]$ solutions decreases as the irradiation time increases, with the emission maximum (λ_{max} = 645 nm), quantum yield, and lifetime of phosphorescence remaining the same. The shape and intensity of the luminescence spectra are independent

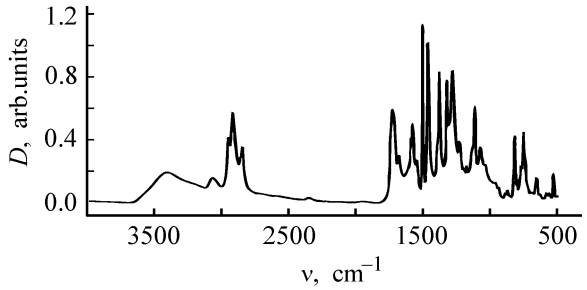

Fig. 5. IR absorption spectrum of the product formed upon exposure of an air-saturated $[Pt(qol)_2]$ solution in CH_2Cl_2 to unfiltered light for 7 min. (*D*) Optical density and (ν) wavenumber.

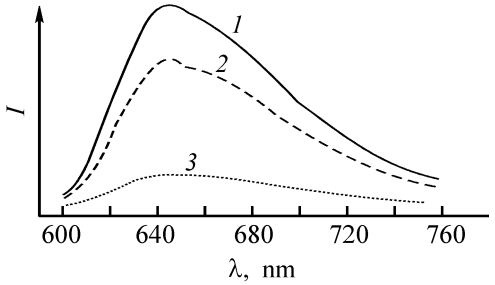

Fig. 6. Luminescence spectrum of 1×10^{-4} M solution of $[Pt(qol)_2]$ in CH_2Cl_2 preliminarily irradiated with unfiltered light for $\tau_{prelim.\,irrad}$ (min): (*1*) 0, (*2*) 5, and (*3*) 10. T = 298 K and λ_{ex} = 485 nm. (*I*) Intensity and (λ) wavelength; the same for Fig. 7.

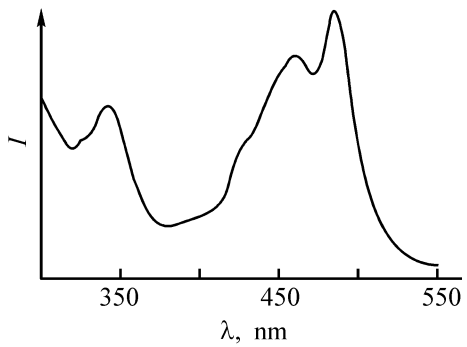

Fig. 7. Excitation spectra of irradiated 1×10^{-4} M solution of $[Pt(qol)_2]$ in CH_2Cl_2. T = 298 K, λ_{rec} = 645 nm.

of the wavelength of the preliminary irradiation (λ 337, 345, 436, and 475 nm). Therefore, phosphorescence of the photolyte in the solution occurs from triplet ILCT EES.

Since the photochemical reaction occurs in a homogeneous solution in which the initial complex is in equilibrium with its photolysis product, it is unclear what complex is the luminescent species. To determine the luminescent species, we compared the excitation and absorption spectra of irradiated and unirradiated solutions of $[Pt(qol)_2]$. The excitation spectra were measured at a wavelength equal to the maximum of the band in the spectrum of the peak solutions examined (λ = 645 nm). The excitation spectra of both solutions are similar (Fig. 7). This spectrum is similar to the absorption spectrum of monomeric $[Pt(qol)_2]$ and differs from that of the photolysis product (Fig. 1). Thus, the photolysis product does not luminesce, and its emission is due to the presence of unchanged $[Pt(qol)_2]$.

The structure of the photolysis product was suggested on the basis of an analysis of the electronic absorption and emission spectra and of the XPS and IR data. As can be seen from Table 1, the atomic concentration ratio of Pt(II) and Pt(IV) in the photolysis products is 2 : 1. Therefore, the primary product of this composition is presumably a trimer in which platinum(IV) atoms are covalently bonded with two axial oxidized fragments of the initial palladium(II) complex. The ratio of the carbonyl and ester groups determined in dry samples of the photolysis product by IR spectroscopy and XPS, is 1.26 : 2.79 (~1 : 2). These groups are probably formed by oxidation of the phenol moieties of $[Pt(qol)_2]$ with atmospheric oxygen. As demonstrated previously [25–27] for the example of photocatalytic oxidation of phenol, the aromatic ring can open under the attack by a cation of dissolved oxygen to form mono- and dibasic acids and(or) aldehydes. In addition, in the course of quenching of $[Pt(qol)_2]$ phosphorescence with molecular oxygen, electronically excited complexes can sensitize formation of singlet oxygen and(or) superoxide ion which can enter into reaction with the sensitizer in the ground state (see scheme) [9–12].

As noted above, the strong batochromic shift of the absorption in the spectrum of the photolysis product with respect to the spectrum of the monomer suggests that a trimer is formed. It is known that the energy gap between the lowest unoccupied and highest occupied molecular orbitals decreases upon molecular association, which simplifies the LUMO-HOMO transition and results in the bathochromic shift of the absorption band. In addition, the bathochromic shift can be due to the presence of platinum(IV) compounds which absorb in a longer-wavelength range as compared to platinum(II) complexes.

Thus, successive photooxidation steps of the ligand and platinum yield the following compound:

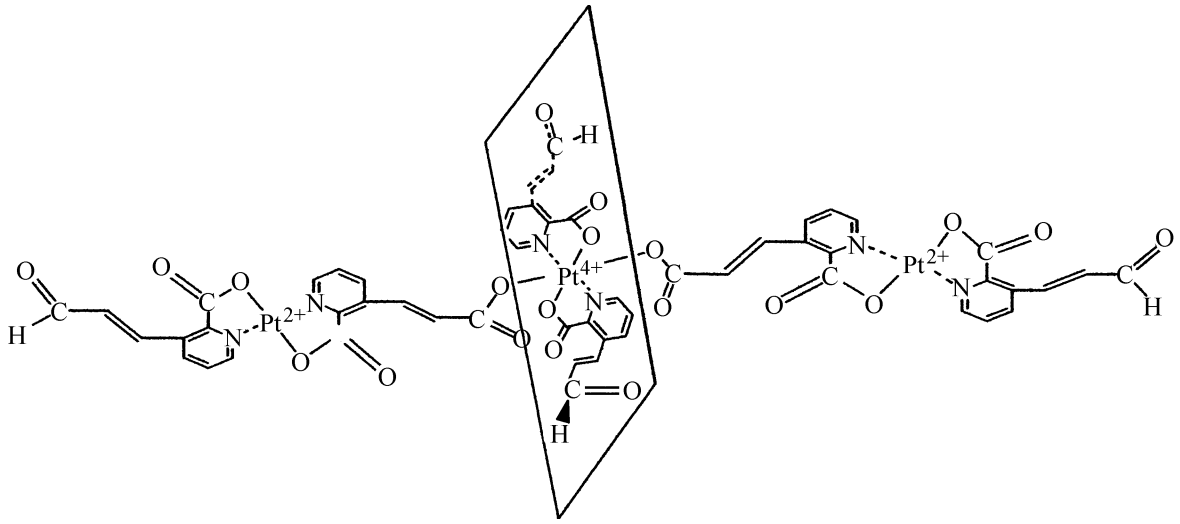

Table 2. Rate of formation and quantum yield of the photolysis product under various irradiation conditions

Irradiation conditions	Formation rate of photolysis product V, ml min^{-1} l^{-1}	Quantum yield of photoreaction Φ, mol $einstein^{-1}$
Unfiltered light:		
air-saturated solution	2.7×10^{-6}	
deaerated solution	1.6×10^{-6}	
Monochromatic light:		
λ = 480 nm, air-saturated solution	0.8×10^{-6}	1.1×10^{-2}
λ = 315–320 nm, deaerated solution	0.4×10^{-6}	0.5×10^{-2}

The overall photochemical reaction can be described by the equation

$$3[Pt(C_9H_6NO)_2] + 7O_2 \rightleftarrows [Pt_3C_{54}H_{34}O_{20}] + H_2.$$

The rate of accumulation of the photolysis product in different irradiation steps was quantitatively determined on the assumption that the reaction product is a trimer and the concentration quenching is absent in the solutions of the initial complex. The rates were calculated from the change in the residual concentration of the initial complex, which, in turn, was determined from a decrease in the luminescence of the reaction mixture (Fig. 8). The rates of accumulation of the trimer and the quantum yields of the product are listed in Table 2.

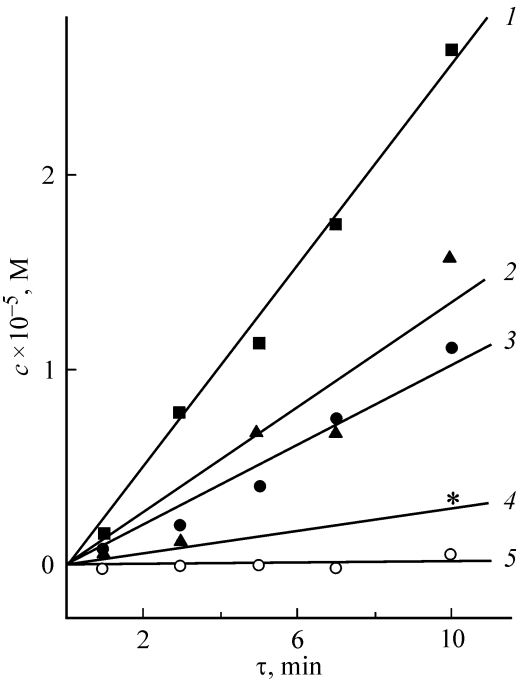

Fig. 8. Concentration c of the photolysis product vs. irradiation time τ. Irradiation of: (*1*) air-saturated and (*2*) deaerated solutions with unfiltered light; (*3*) air-saturated and (*5*) deaerated solutions with monochromatic light (λ_{irr} = 480 nm); (*4*) air-saturated solution with monochromatic light (λ_{irr} = 315–320 nm).

CONCLUSIONS

(1) Complex $[Pt(qol)_2]$ can undergo photostimulated oxidative aggregation in solution.

(2) The electronically excited state of the complex responsible for photochemical processes involves ^{3}ILCT and ^{3}MLCT.

(3) The XPS, IR, and electronic spectroscopy data suggest that the photolysis product has a trimeric structure.

(4) The product of the photochemical reaction does not luminesce.

(5) The rate and quantum yield of the photoreaction are maximal on exposure of an air-saturated solution of the complex to unfiltered light and are minimal on exposure of deaerated solutions to monochromatic light (λ = 315–320 nm).

ACKNOWLEDGMENTS

The authors are grateful to A.V. Shchukarev (St. Petersburg State University) for assistance in XPS analysis and to M.V. Puzyk (Herzen Russian State Pedagogical University) for assistance in the luminescence-spectroscopic study.

REFERENCES

1. Blinova, I.A., Vasil'ev, V.V., and Shagisultanova, G.A., *Zh. Neorg. Khim.*, 1994, vol. 39, no. 2, pp. 266–269.
2. Ardasheva, L.P., Luminescence Spectral, Photochemical, and Electrochemical Properties of Platinum(II)

and Palladium(II) Complexes with Schiff Bases, *Cand. Sci. Dissertation*, Moscow, 1999.

3. Shagisultanova, G.A. and Ardasheva, L.P., *Koord. Khim.*, 1999, vol. 25, no. 11, pp. 843–849.
4. Gubasova, T.N., Synthesis and Study of Polymers Derived from Nickel(II), Palldium(II), Platinum(II), and Copper(II) Complexes with Schiff bases, *Cand. Sci. Dissertation*, St. Petersburg, 2002.
5. Chernyaev, I.I., *Kompleksnye soedineniya platiny: Izbrannye trudy* (Platinum Complexes: Selected Papers), Moscow: Nauka, 1973.
6. Vinogradov, S.A., Balashev, K.P., and Shagisultanova, G.A., *Koord. Khim.*, 1987, vol. 13, no. 9, pp. 1272–1275.
7. Balashev, K.P., Vasil'ev, V.V., and Shagisultanova, G.A., *Elektrokhimiya*, 1989, vol. 25, no. 2, pp. 722–725.
8. Donges, D., Nagle, J.K., and Yersin, H., *Inorg. Chem.*, 1997, vol. 36, no. 14, pp. 3040–3048.
9. Shavaleev, N.M., Adams, H., Best, J., et al., *Inorg. Chem.*, 2006, vol. 45, no. 23, pp. 9410–9415.
10. Dungey, K.E., Thompson, B.D., Kane-Maguire, N.A.P., and Wright, L.L., *Inorg. Chem.*, 2000, vol. 39, no. 23, pp. 5192–5196.
11. Anbalagan, V.J., *J. Coord. Chem.*, 2003, vol. 56, no. 3, pp. 161–172.
12. Connick, W.B. and Gray, H.B., *J. Am. Chem. Soc.*, 1997, vol. 119, no. 48, pp. 11 620–11 627.
13. Borgarello, E., Pelizzetti, E., Ballardini, R., and Scandola, F., *Nouv. J. Chim.*, 1984, vol. 8, no. 10, pp. 567–569.
14. Balardini, R. Varani, G., Indelli, M.T., and Scandola, F., *Inorg. Chem.*, 1986, vol. 25, no. 22, pp. 3858–3865.
15. Ballardini, R., Indelli, M.T., Varani, G., et al., *Inorg. Chim. Acta*, 1978, vol. 31, p. L423–L424.
16. Bartocci, C., Sostero, S., and Traverso, O., *J. Chem. Soc. Faraday Trans.*, 1980, vol. 76, p. 797–803.
17. Shagisultanova, G.A., Masalovich, M.S., and Ardasheva, L.P., *Zh. Prikl. Khim.*, 2007, vol. 80, no. 6, pp. 994–1001.
18. Kryukov, A.I. and Kumchii, S.Ya., *Osnovy fotokhimii koordinatsionnykh soedinenii* (Principles of Photochemistry of Coordination Compounds), Kiev: Naukova Dumka, 1990.
19. *Ekspeimental'nye metody khimicheskoi kinetiki: Uchebnoe posobie* (Experimental Methods of Chemical Kinetics: Textbook), Emanuel', N.M. and Kuz'min, M.G., Eds., Moscow: Mosk. Gos. Univ., 1985.
20. Goldsby, K.A., *J. Coord. Chem.*, 1988, vol. 19, no. 3, pp. 83–90.
21. Tourillon G. and Ganler, F., *J. Phys. Chem.*, 1983, vol. 87, no. 13, pp. 2289–2292.
22. Patil, A.O., Heeger, A.J., and Wudl, F., *Chem. Rev.*, 1988, vol. 88, no. 1, pp. 183–200.
23. Geskin, V.M. and Letuchii, Ya.A., *Elektrokhimiya polimerov* (Electrochemistry of Polymers), Moscow: Nauka, 1990, pp. 121–145.
24. Ovsyannikova, E.V., Crosheva, M.Yu., and Alpatova, N.M., *Short Commun.*, 2004, vol. 40, no. 10, pp. 1089–1091.
25. Pak, V.N. and Kharangi, S., *Zh. Fiz. Khim.*, 1996, vol. 70, no. 9, pp. 1696–1701.
26. Okamoto, K., Yamamoto, Y., and Tanaka, H., *Bull. Chem. Soc. Jpn.*, 1985, vol. 58, no. 7, pp. 2015–2022.
27. Okamoto, K., Yamamoto, Y., Tanaka, H., and Itava, A., *Bull. Chem. Soc. Jpn.*, 1985, vol. 58, no. 7, pp. 2023–2028.

ISSN 1070-4272, Russian Journal of Applied Chemistry, 2007, Vol. 80, No. 12, pp. 2085–2089. © Pleiades Publishing, Ltd., 2007.
Original Russian Text © M.K. Mamedov, A.G. Piraliev, R.A. Rasulova, 2007, published in Zhurnal Prikladnoi Khimii, 2007, Vol. 80, No. 12, pp. 2007–2011.

ORGANIC SYNTHESIS AND INDUSTRIAL ORGANIC CHEMISTRY

Synthesis of Bicyclo[2.2.1]hept-2-yloxyethyl Acrylates and Saturated Acid Esters Derived from Them

M. K. Mamedov, A. G. Piraliev, and R. A. Rasulova

Institute of Petrochemical Processes, National Academy of Sciences of Azerbaijan, Baku, Azerbaijan

Received February 15, 2007; in final form, July 2007

Abstract—New reactive monomers, bicyclo[2.2.1]hept-2-yloxyethyl acrylates, were prepared by esterification of monoethers derived from ethylene glycol and bicyclic alcohols with acrylic acid, using naphthalene-1,5-disulfonic acid as a new effective catalyst. The related propionates and isobutyrates were prepared by hydrogenation of these acrylates.

DOI: 10.1134/S1070427207120157

Esters of alicyclic alcohols and acrylic acids are widely used as reactive monomers for preparing plastics [1, 2], superadhesives [3], printer's inks [4], and lenses for protection from UV radiation [5]. Previously, we have developed procedures for preparing acrylic and methacrylic acid esters of bi- and tricyclic alcohols [6–8] and showed that these compounds can be used as monomers for preparing valuable macromolecular compounds [9].

In this study, we performed esterification of monoethers derived from ethylene glycol and bicyclic alcohols with acrylic acidwith the aim to prepare new reactive alicyclic functional monomers. We found that the reaction mainly follows the pathway of formation of bicyclo[2.2.1]hept-2-yloxyethyl acrylates:

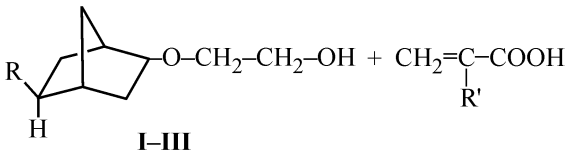

I–III

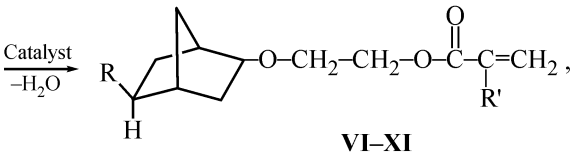

VI–XI

where R = H (**I**, **VI**, **IX**), CH_3 (**II**, **VII**, **X**), CH_3CH_2 (**III**, **VIII**, **XI**); R' = H (**VI**–**VIII**), CH_3 (**IX**–**XI**).

To choose an effective esterification catalyst, and study its catalytic activity for the example of the reaction of bicyclo[2.2.1]hept-2-yloxyethanol (BEL) with acrylic acid (AA), we tested sulfuric acid, naphthalenesulfonic acid (NSA), KU-2 and KU-2-8 ion-exchange resins, *p*-toluenesulfonic acid (TSA), and naphthalene-1,5-disulfonic acid (NDSA), which were taken in an amount of 2.5 wt % (in terms of sulfo groups) relative to the starting compounds. The reaction was performed until the water evolution ceased. The results are listed in Table 1.

We found (Table 1) that, among the catalysts tested in synthesis of bicyclo[2.2.1]hept-2-yloxyethyl acrylate, NDSA is the most effective, because it provides a product yield as high as 91.2%, whereas with the other esterification catalysts the yield is 52–74%.

Therefore, experiments on the synthesis of other related monomers by esterification of bicyclo[2.2.1]-hept-2-yloxyethanol and its alkyl derivatives with acrylic and methacrylic acids were performed with NDSA as catalyst. The results are listed in Table 2.

The results obtained show (Table 2) that, with NDSA as catalyst, the yield of acrylates and methacrylates reaches 50.2–55.0 g (87–94%)

It should be noted that, with alkyl-substituted bicycloheptyl monoether of ethylene glycol as starting compound, the yield of acrylates and methacrylates tends to decrease with increasing molecular weight. This is caused by steric hindrance and a certain decrease in the activity of the OH group.

We determined the physicochemical constants and elemental composition of the synthesized 2-(bicyclo-

Table 1. Effect of the catalyst on the esterification of BEL with AA

Catalyst	BEL	AA	Reaction conditions		Acrylate yield*	
	g		*T*, °C	τ, h	g	%
NSA, 2.10	39.0	18.0	78–82	4	27.5	52.4
KU-2, 1.70	39.0	18.0	78–82	4	32.8	62.5
TSA, 1.73	39.0	18.0	78–82	3	35.9	68.4
H_2SO_4, 1.00	39.0	18.0	78–82	3	37.3	71.0
KU-2-8, 1.32	39.0	18.0	78–82	4	38.8	74.0
NDSA, 1.42	39.0	18.0	78–82	3	47.9	91.2

* The remainder is unchanged starting compound and tars.

Table 2. Conditions of formation of alkylbicyclo[2.2.1]hept-2-yloxyethyl acrylates and methacrylates (MAA) from the corresponding ethylene glycol monoethers (EGM)

Compound	AA	MAA	NDSA catalyst	Reaction conditions		Obtained	
	g			*T*, °C	τ, h	compound	g
II, 42.5	18.0	–	1.56	78–82	3	**VII**	52.4
III, 46.0	18.0	–	1.60	78–82	3	**VIII**	55.0
I, 39.0	–	21.5	1.56	78–82	3	**IX**	50.2
II, 42.5	–	21.5	1.60	78–82	3	**X**	52.8
III, 46.0	–	21.5	1.68	78–82	3	**XI**	54.8

Table 3. Yields, physicochemical constants, and elemental compositions of the synthesized 2-(bicyclo[2.2.1]hept-*exo*-2-yloxy)ethyl acrylates and methacrylates

Compound	Yield, %	bp, °C/10 mm Hg	n_D^{20}	d_4^{20}	Calculated, %		Formula	Found, %	
					C	H		C	H
VI	91.2	126–127	1.4710	1.0428	68.56	8.62	$C_{12}H_{18}O_3$	68.29	8.51
VII	93.6	138–139	1.4756	1.0201	69.61	8.99	$C_{13}H_{20}O_3$	69.41	8.81
VIII	92.5	150–151	1.4785	1.0190	70.55	9.30	$C_{14}H_{22}O_3$	70.44	9.00
IX	89.6	140–141	1.4805	1.0025	69.61	8.99	$C_{13}H_{20}O_3$	69.49	8.89
X	88.8	152–153	1.4821	1.0015	70.55	9.30	$C_{14}H_{22}O_3$	70.41	9.24
XI	87.0	165–166	1.4852	0.9987	71.40	9.57	$C_{15}H_{24}O_3$	71.30	9.47

[2.2.1]hept-*exo*-2-yloxy)ethyl acrylates and methacrylates and their 5-*exo*-alkyl-substituted derivatives (Table 3). Their structures were confirmed by independent syntheses. Hydrogenation of the acrylates on Ni/kieselguhr yielded bicyclo[2.2.1]hept-2-yloxyethyl esters of the corresponding saturated acids:

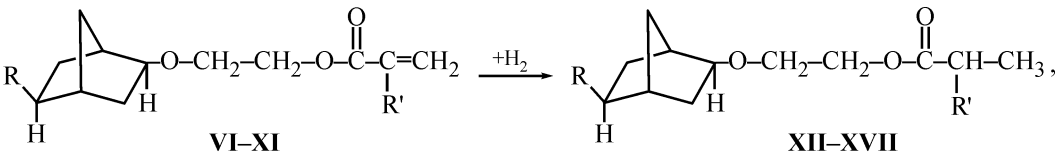

VI–XI **XII–XVII**

where R = H (**VI**, **IX**, **XII**, **XV**), CH_3 (**VII**, **X**, **XIII**, **XVI**), C_2H_5 (**VIII**, **XI**, **XIV**, **XVII**); R' = H (**VI**–**VIII**, **XII**–**XIV**), CH_3 (**IX**–**XI**, **XV**–**XVII**).

Table 4. Conditions of hydrogenation of acrylates and methacrylates to propionates and isobutyrates

Taken into reaction				Experimental conditions		Obtained		
compound	weight, g	Ni on kieselguhr, g	H_2, atm	T, °C	τ, h	compound	weight, g	%
VI	210.0	21.0	80	100	3	**XII**	205.8	97.1
VII	224.0	22.4	80	100	3	**XIII**	216.0	95.6
VIII	238.0	23.8	80	100	3	**XIV**	227.7	94.9
IX	224.0	22.4	80	100	3	**XV**	209.0	92.5
X	238.0	23.8	80	100	3	**XVI**	222.7	92.8
XI	252.0	25.2	80	100	3	**XVII**	230.1	90.6

Table 5. Physicochemical constants and elemental composition of the synthesized bicyclo[2.2.1]hept-2-yloxyethyl propionates and isobutyrates

Compound	bp, °C/10 mm Hg	n_D^{20}	d_4^{20}	Calculated, %		Formula	Found, %	
				C	H		C	H
XII	127–128	1.4775	1.0615	67.92	9.43	$C_{12}H_{20}O_3$	60.80	9.30
XIII	140–141	1.4788	1.0311	69.02	9.73	$C_{13}H_{22}O_3$	69.00	9.53
XIV	152–153	1.4795	1.0101	70.00	10.00	$C_{14}H_{24}O_3$	70.00	9.99
XV	142–143	1.4799	1.0012	69.02	9.73	$C_{13}H_{22}O_3$	68.93	9.59
XVI	154–155	1.4842	1.0011	70.00	10.00	$C_{14}H_{24}O_3$	69.87	9.87
XVII	167–168	1.4865	0.9998	70.86	10.23	$C_{15}H_{26}O_3$	70.56	10.13

Table 6. ^1H and ^{13}C NMR chemical shifts of the esters synthesized

Ester structure	Chemical shift δ, ppm	
	^1H NMR	^{13}C NMR
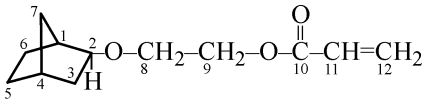	6.23 (H^{11}), 5.75 (H^{12}), 4.62 (H^2), 3.71 (H^8), 3.65 (H^9), 2.22 (H^4), 2.20 (H^1), 1.42 (H^3), 1.25 (H^6), 1.13 (H^7), 1.11 (H^5)	168.6 (C^{10}), 137.0 (C^{11}), 135.6 (C^{12}), 85.2 (C^2), 70.3 (C^9), 70.0 (C^8), 42.0 (C^1), 39.5 (C^4), 36.2 (C^3), 32.1 (C^7)
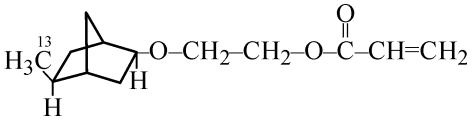	6.23 (H^{11}), 5.75 (H^{12}), 4.62 (H^2), 3.71 (H^8), 3.65 (H^9), 2.22 (H^4), 2,20 (H^1), 1.42 (H^3), 1.25 (H^6), 1.13 (H^7), 1.11 (H^5), 1.00 (H^{13})	168.5 (C^{10}), 137.0 (C^{11}), 135.4 (C^{12}), 85.1 (C^2), 70.2 (C^9), 70.0 (C^8), 42.0 (C^1), 39.5 (C^4), 36.2 (C^3), 32.1 (C^7), 27.0 (C^{13})
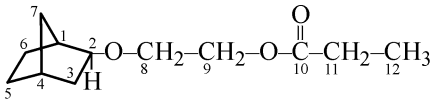	4.51 (H^2), 3.80 (H^9), 3.01 (H^8), 2.20 (H^4), 2.18 (H^1), 1.40 (H^3), 1.24 (H^6), 1.12 (H^7), 1.10 (H^5), 1.05 (H^{11}), 1.00 (H^{12})	166.7 (C^{10}), 85.5 (C^2), 70.1 (C^9), 70.0 (C^8), 41.2 (C^1), 39.3 (C^4), 36.5 (C^3), 28.2 (C^6), 27.6 (C^{11}), 27.2 (C^7), 24.9 (C^5), 18.8 (C^{12})
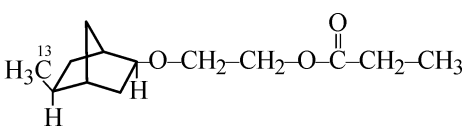	4.51 (H^2), 3.80 (H^9), 3.01 (H^8), 2.20 (H^4), 2.18 (H^1), 1.40 (H^3), 1.24 (H^6), 1.12 (H^7), 1.10 (H^5), 1.05 (H^{11}), 1.00 (H^{12}) 0.91 (H^{13})	166.8 (C^{10}), 85.4 (C^2), 70.3 (C^9), 70.1 (C^8), 42.0 (C^1), 39.5 (C^4), 36.2 (C^3), 32.1 (C^7). 28.2 (C^6) 26.6 (C^{11}), 19.9 (C^{12}), 17.2 (C^{13})

The experimental conditions and yields of the synthesized unsaturated esters are listed in Table 4. The physicochemical constants and elemental composition of the synthesized 2-bicyclo[2.2.1]hept-2-yloxyethyl propionates and isobutyrates and of the corresponding alkyl derivatives are listed in Table 5.

The composition and purity of the synthesized compounds were determined by GLC analysis, and their structure was confirmed by IR and ^1H and ^{13}C NMR spectroscopy. The synthesized ethylene glycol monoether monoesters were 99.0–99.5% pure.

The IR spectra of all the synthesized acrylic acid esters contain strong absorption bands of C–C and C–H bonds in three regions: 3000–2800, 1400–1300, and about 700 cm^{-1}. The C=C stretching vibrations in the ester molecules are manifested at 1645 cm^{-1}, and the C=C bending vibrations in *exo*-5-alkylbicyclo-[2.2.1]hept-*exo*-2-yloxyethyl esters, at about 980 cm^{-1}. The bands at 1725 and 1190 cm^{-1} are indicative of the presence of the ester (C=O) group, the bands at 810 and 890 cm^{-1} belong to the vinyl group, and the band at 1380 cm^{-1}, to the methyl group.

The ^1H and ^{13}C NMR spectra of some of the synthesized esters of unsaturated and saturated acids are given in Table 6. The compounds prepared are transparent liquids, some of which exhibit a pleasant odor with fruit tints. As analogs of bicyclo[2.2.1]hept-2-yloxyethyl esters of saturated acids, they can also be used as components of perfume formulations. Acrylates and methacrylates readily polymerize to form transparent polymers, which are of scientific and practical interest for preparation of new macromolecular compounds containing a bicyclo[2.2.1]hept-2-yloxy group.

EXPERIMENTAL

The composition and purity of the synthesized ethylene glycol monoether monoesters were determined by GLC on an LKhM-8 MD chromatograph [column length 1.5 m, liquid phase 10% poly(ethylene glycol succinate) on Sferokhrom, temperatures of the column, detector, and vaporizer 140–150, 200–220, and 250–270°C, respectively; detector current 120 mA; carrier gas flow rate 45 ml min^{-1}].

The IR spectra were recorded on a UR-20 spectrophotometer, and the ^1H and ^{13}C NMR spectra, on a Varian FT-80 spectrometer (USA) at a working frequency (^1H) of 80 MHz from CCl_4 solutions, with HMDS as internal reference.

The esterification of the monoether of bicyclic alcohols and ethylene glycol with acrylic acids in the presence of NDSA catalyst was performed in benzene with azeotropic distillation of water using a Dean–Stark trap. To prevent polymerization of the starting acrylic acids, an inhibitor (hydroquinone) was added in an amount of 0.01 wt %. After the reaction completion, NDSA was neutralized with an equimolar amount of $Ca(OH)_2$, the liquid phase was separated from the precipitate, and the target product was isolated by vacuum distillation.

The catalyst and the starting compounds had the following characteristics: NDSA, mp 240–245°C [10]; 2-(bicyclo[2.2.1]hept-*exo*-2-yloxy)ethanol, bp 71°C/5 mm Hg, d_4^{20} 1.0152, n_D^{20} 1.4718; 2-(*exo*-5-methylbicyclo[2.2.1]hept-*exo*-2-yloxy)ethanol, bp 95–96°C/5 mm Hg, d_4^{20} 1.0040, n_D^{20} 1.4726; 2-(*exo*-5-ethylbicyclo[2.2.1]hept-*exo*-2-yloxy)ethanol, bp 110–111°C/5 mm Hg, d_4^{20} 1.0002, n_D^{20} 1.4738.

Bicyclo[2.2.1]hept-2-yloxyethanols were prepared by addition of ethylene glycol to the corresponding bicyclic olefins in the presence of a catalyst. The physicochemical properties of these monoethers and of the acrylic acids used agreed with reference data [11, 12].

The hydrogenation of the synthesized bicyclo-[2.2.1]hept-2-yloxyethyl acrylates was performed in a 1-l stainless steel rotating autoclave. The catalyst, Ni on kieselguhr, was taken in an amount of 10 wt % relative to the acrylate. The reaction was performed under a hydrogen pressure of 80 atm at 100°C until the hydrogen uptake ceased (3 h). After the reaction completion, the mixture was filtered, and the target products, bicyclo[2.2.1]hept-2-yloxyethyl propionates and isobutyrates, were isolated by vacuum distillation.

CONCLUSIONS

(1) Bicyclo[2.2.1]hept-2-yloxyethyl acrylates, which are new reactive monomers, were prepared in 87–93% yield by esterification of bicycloheptyloxyethanol with acrylic acids in the presence of an effective catalyst, naphthalene-1,5-disulfonic acid.

(2) Bicyclo[2.2.1]hept-2-yloxyethyl propionates and isobutyrates were prepared by hydrogenation of the synthesized bicyclo[2.2.1]hept-2-yloxyethyl acrylates in the presence of Ni on kieselguhr. These compounds can be used as components of synthetic perfumes.

REFERENCES

1. *Entsiklopediya polimerov* (Polymer Encyclopedia), Moscow: Sov. Entsiklopediya, 1974, vol. 2, p. 504.
2. Yamada, B., Azukizama, M., and Yamazoe, H., *Polymer*, 2000, vol. 41, no. 15, p. 5611.
3. Marek, O. and Tomka, M., *Akrilové polymery*, Prague: SNTL, 1963.
4. Golding, B., *Polymers and Resins—Their Chemistry*

and Chemical Engineering, New Jersey: Van Nostrand, 1959. Translated under the title *Khimiya i tekhnologiya polimernykh materialov*, Leningrad: Khimiya, 1963, p. 422.

5. JPN Appl. 61-53242, *Ref. Zh. Khim.*, 1986, 9N66P.
6. Mamedov, M.K., Nabieva, E.K., and Dzhafarova, E.N., *Zh. Org. Khim.*, 2001, vol. 37, no. 12, p. 1781.
7. Mamedov, M.K., Dzhafarova, E.N., and Rasulova, R.A., *Azerb. Khim. Zh.*, 2005, no. 2, pp. 116–122.
8. Mamedov, M.K. and Nabieva, E.K., *Protsessy Neftekhim. Neftepererab.*, 2005, no. 3 (22), pp. 57–64.
9. Mamedov, M.K., Azizov, A.G., and Nabieva, E.K., *Protsessy Neftekhim. Neftepererab.*, 2001, no. 4(7), pp. 46–50.
10. *Spravochnik khimika* (Chemist's Handbook), Nikol'skii, B.P., Ed., Moscow: Khimiya, 1964, vol. II, p. 820.
11. Gasanov, A.G. and Nagiev, A.V., *Zh. Org. Khim.*, 1994, vol. 30, no. 5, pp. 707–709.
12. Goronovskii, I.T., Nazarenko, Yu.G., and Nekryach, E.F., *Kratkii spravochnik po khimii* (Concise Chemical Handbook), Kiev: Naukova Dumka, 1974.

ISSN 1070-4272, Russian Journal of Applied Chemistry, 2007, Vol. 80, No. 12, pp. 2090–2092. © Pleiades Publishing, Ltd., 2007.
Original Russian Text © V.A. Matalin, G.I. Kaurova, V.V. Berenblit, V.I. Gribel', 2007, published in Zhurnal Prikladnoi Khimii, 2007, Vol. 80, No. 12, pp. 2012–2014.

ORGANIC SYNTHESIS AND INDUSTRIAL ORGANIC CHEMISTRY

Electrochemical Fluorination of Toluene and Benzotrifluoride in the Presence of Triallylamine

V. A. Matalin, G. I. Kaurova, V. V. Berenblit, and V. I. Gribel'

Prikladnaya Khimiya Russian Scientific Center, Federal State Unitary Enterprise, St. Petersburg, Russia

Lebedev Research Institute of Synthetic Rubber, Federal State Institution, St. Petersburg, Russia

Received Decemver 25, 2006; in final form, October 2007

Abstract—Electrochemical fluorination of benzotrifluoride in the presence of triallylamine as depolarizer was studied. The possibility of preparing perfluoromethylcyclohexane and its isomers with high current efficiency and substance yield in combination with perfluorinated tertiary amines was examined.

DOI: 10.1134/S1070427207120169

Electrochemical fluorination (ECF) in anhydrous HF on nickel anodes is one of frequently used methods for conversion of hydrocarbons and partially fluorinated organic compounds into their perfluorinated analogs, with the preservation of the functional group or structure of the starting compound containing a heteroatom. This method was described for the first time in the late 1940s by Simons and then was developed by many researchers [1] who used it for fluorination of organic compounds containing C–O, C–N, C–S, or C–P bonds.

Perfluorocycloalkanes are not usually mentioned among numerous functional perfluorinated compounds that have found practical use after they became accessible by ECF, because attempts to prepare these compounds by electrolysis of their hydrocarbon analogs, which are insoluble in the electrolyte, have been not very successful.

However, the development of a method for preparing these compounds remains an important practical problem, because they exhibit unusual combinations of physicochemical properties: low boiling points, critical temperatures, and critical pressures at high molecular weights, densities in the liquid state, and coefficients of expansion and compressibility. The last two provide a very low speed of sound in these media. These compounds have considerably lower, compared to other liquids, surface tension and refractive index. They have excellent electric-insulation properties and unique chemical and biochemical stability, making them "virtually nontoxic."

Nyberg [2–4] has reported on a synthesis of perfluoromethylcyclohexane (PFMCH) in poor yield by ECF of toluene. With benzotrifluoride as starting compound, the yield is 47%, but the electrolysis cannot be performed in the continuous mode because of the electrolyte tarring [5].

As shown in [6], these effects can be restricted by adding a depolarizer fixing the steady-state electrolysis mode. This is particularly important when the ECF substrate is insoluble in HF and nonconducting, because this additive provides both the conductivity of the electrolyte and the solubility of the substrate in it.

In this study, we made an attempt to use ECF for preparing perfluorinated cyclic paraffins using an electrolytic additive whose electrolysis occurs without tarring and yields products that are of practical interest.

In this context, we performed a comparative study of the dependence of the PFMCH yield in ECF of toluene and benzotrifluoride in the presence of a depolarizing additive, triallylamine $(CH_2{=}CHCH_2)_3N$ (TAA), whose ECF occurs in the steady-state mode under conditions of continuous electrolysis and gives in high yield a mixture of perfluorotripropylamine with nitrogen-containing heterocycles, in particular, perfluoro-*N*-(*n*-propyl)-*cis*-3,4-dimethyl- and perfluoro-*N*-(*n*-propyl)-*trans*-3,4-dimethylpyrrolidines and perfluoro-*N*-(*n*-propyl)-3-methylpiperidine [7].

Table 1. Signals in the ^{19}F NMR spectra of isomers present in the target fraction

Signal no.	$CFCl_3$, ppm	Multiplet	J_{F-F}, Hz	Number of F	Structure
			Perfluoro-1,1-dimethylcyclopentane		
1	–59.6	q.q.(m)	$^{1}F–^{9}F$ 12; $^{1}F–^{x}F$, 7	6	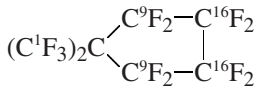
9	–114.6	septet	$^{9}F–^{1}F$, 12	4	
16	–123.3	m		4	
			Perfluoro-*cis*-1,2-dimethylcyclopentane and perfluoro-*trans*-1,2-dimethylcyclopentane		
3	–70.6	t		6	
4	–70.8	m		6	
12	–119.4	d	$^{12}F–^{3}F$, 277	4	
15	–123.3	d.m	$^{15}F–^{12}F$, 277	4	
18	–124.2	d	$^{18}F–^{19}F$, 274	2	*cis-trans* 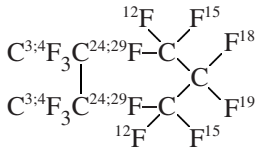
19	–128.2	d	$^{19}F–^{18}F$, 274	2	
24	–183.0	s		2	
24	–183.0	s		2	
			Perfluoro-*cis*-1,3-dimethylcyclopentane and perfluoro-*trans*-1,3-dimethylcyclopentane		
5	–71.4	t	$^{5}F–^{x}F$, 15	6	
6	–71.6	sextet	$^{6}F–^{x}F$, 7, 6	6	
16	–122.4	d.m	$^{16}F–^{x}F$, 271	4	
17	–124.0	d	$^{16}F–^{x}F$, 271	4	*cis-trans* 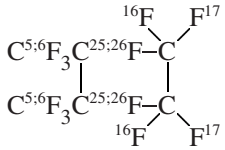
25	–183.3	s		2	
26	–184.0	s		2	
			Perfluoroethylcyclopentane		
7	–90.0	t	$^{7}F–^{x}F$, 11	3	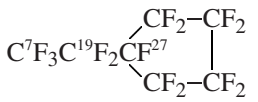

EXPERIMENTAL

As starting products for preparing perfluoromethylcyclohexane by ECF we used compounds formed in electrolysis of mixtures of benzotrifluoride or toluene with triallylamine as electrolytic additive.

The electrochemical fluorination was performed in a 660-ml carbon steel Simons electrolyzer equipped with a water-cooled coil and a stack of nickel electrodes with the surface area of the anodes of 500 cm^2. The electrolyzer was also equipped with a reflux condenser for condensing HF entrained by electrolysis gases and returning it into the electrolyte. The current during the experiments was constant, 15 A, and the current density was 0.034 A cm^{-2}.

As an electrolyte we used a solution of 5 wt % benzotrifluoride or toluene and 5 wt % triethylamine in liquid anhydrous HF. The concentration of the organic substrate in the electrolyte was maintained constant by feeding a mixture of the starting organic compounds once or twice an hour in amounts corresponding to their consumption coefficients. In ECF of a mixture of toluene with triallylamine, the excess amount of the consumed electricity (Q) (over the calculated value) was considerably larger than that in ECF of benzotrifluoride.

The ECF products, whose density was higher than that of the electrolyte, were collected in the lower part of the electrolyzer and drained at equal intervals. The crude product was discharged beneath a water layer and neutralized with sodium carbonate. After that, the crude product was purified by treatment with aqueous-alcoholic alkali to remove incompletely fluorinated products and dried over silica gel. The dried crude product was distilled on a column to obtain three fractions: head fraction (bp 53–54°C), target fraction (bp 76–78°C), and heavy fraction (bp 129–131°C).

The products in the fractions were identified by ^{19}F NMR on a Bruker Spectrospin AM-500 spectrometer (operating frequency 470.572 MHz) in C_6F_6 as solvent and internal reference. The products were also analyzed by GLC on a Tsvet-100 device equipped with a thermal conductivity detector, using a column

Table 2. Electrochemical fluorination of mixtures of toluene and benzotrifluoride with triallylamine

Loaded, g (mol)		*Q*, A h	Obtained in fractions, g (mol)			Yield, mol % [g (A h)$^{-1}$]	
$CH_3C_6H_5$	$N(CH_2CHCH_2)_3$		head cyclo-C_6F_{12}	target cyclo-C_7F_{14}	heavy $C_9F_{21}N$ + cyclo-$C_9F_{19}N$	cyclo-C_6F_{12} + cyclo-C_6F_{12}	$C_9F_{21}N$ + cyclo-$C_9F_{19}N$
62.0(0.68)	75.0(0.55)	788	2.5(0.013)	5.0(0.021)	32.2(0.081)	5.1(0.017)	8.1(0.073)
$CF_3C_6H_5$	$N(CH_2CHCH_2)_3$		C_6F_{12}	C_7F_{14}	$C_9F_{21}N$ + $C_9F_{21}N$	cyclo-C_6F_{12} + cyclo-C_6F_{12}	$C_9F_{21}N$ + cyclo-$C_9F_{19}N$
127.4(0.87)	121.0(0.89)	440	41.4(0.14)	236(0.67)	82.2(0.21)	93(0.35)	24(0.105)

with 20% α,α,α-tricyanoacetophenone on Silokhrom-80 as stationary phase. The composition determined by GLC is well consistent with the signal intensities in the ^{19}F NMR spectra.

In the head fraction with the empirical formula cyclo-C_6F_{12}, we identified two compounds: perfluorocyclohexane and the product of ring contraction, perfluoromethylcyclopentane.

The target fraction with the empirical formula cyclo-C_7F_{14}, boiling at 76–78°C, contained up to 80% perfluoromethylcyclohexane CF_3-cyclo-C_6F_{11}, whose ^{19}F NMR spectrum agrees with that described in [7], and its isomers, products of ring contraction: perfluoro-1,1-dimethylcyclopentane, perfluoroethylcyclopentane, and stereoisomeric perfluoro-1,2-dimethyl- and perfluoro-1,3-dimethylcyclopentanes. The characteristic signals in the ^{19}F NMR spectra of the isomers present in the target fraction are listed in Table 1.

The heavy fraction was a mixture containing perfluorotri(*n*-propyl)amine (20.3 wt %) and cyclic products of the empirical formula $C_9F_{19}N$, in particular, perfluoro-*N*-(*n*-propyl)-*cis*-3,4-dimethylpyrrolidine (41.2 wt %), perfluoro-*N*-(*n*-propyl)-*trans*-3,4-dimethylpyrrolidine (18.7 wt %), and perfluoro-*N*-(*n*-propyl)-3-methylpiperidine (19.3 wt %). Their spectra were described in [7].

The conditions and results of ECF of mixtures of toluene and benzotrifluoride with triallylamine are listed in Table 2.

The observed substance yields and current efficiencies do not contradict the published data [2–5], and the use of *n*-triallylamine as an electrolytic additive allows the yield of useful fluorination products to be raised to 78%.

The target fraction from ECF contains up to 20% products of contraction of the cyclohexane ring. These isomers, forming a eutectic with PFMCH, depress the freezing point of the mixture down to –65°C, i.e., by 30°C relative to PFMCH.

Because the electrolysis process is stable in time, our study opens up prospects for producing in a common process a series of organofluorine products for medicine and engineering in high yields by ECF of benzotrifluoride in a mixture with triallylamine.

CONCLUSIONS

(1) The possibility of preparing perfluoromethylcyclohexane by electrochemical fluorination in the presence of triallylamine as electrolytic additive was demonstrated. The process occurs with a good current efficiency and is stable in time and practically feasible.

(2) The electrolysis additionally yields perfluorinated tertiary amines, which are widely used in industry, medicine, and defense technology.

REFERENCES

1. Abe, T. and Nagase, S., *Preparation, Properties and Industrial Application of Organofluorine Compounds*, ch. 1: *Electrochemical Fluorination (Simons Process) as a Route to Perfluorinated Organic Compounds of Industrial Interest*, Banks, R.E., Ed., Horwood: Chichester, 1982, pp. 19–43.
2. Nyberg, K., *Acta Chem. Scand.*, 1970, vol. 24, pp. 1609–1618.
3. Nyberg, K., *Acta Chem. Scand.*, 1971, vol. 25, pp. 534–537, 2499–2503, 2983–2985.
4. Nyberg, K., *Acta Chem. Scand.*, 1973, vol. 27, pp. 530–509.
5. Yonekura, M., Nagase, S., Baba, H., et al., *Bull. Chem. Soc. Jpn.*, 1976, vol. 49, pp. 1113–1122.
6. Berenblit, V.V., Grachev, V.I., Dolgopol'skii, I.M., and Davydov, G.A., *Zh. Prikl. Khim.*, 1974, vol. 47, no. 3, p. 590.
7. Jolley, K.W., Satcliffe, L.H., and Walker, S.M., *Trans. Faraday Soc.*, 1968, vol. 64, pp. 269–277.

ISSN 1070-4272, Russian Journal of Applied Chemistry, 2007, Vol. 80, No. 12, pp. 2093–2096. © Pleiades Publishing, Ltd., 2007.
Original Russian Text © A.Ya. Samuilov, E.I. Galeeva, A.V. Kulikov, I.N. Bakirova, Ya.D. Samuilov, 2007, published in Zhurnal Prikladnoi Khimii, 2007, Vol. 80, No. 12, pp. 2015–2018.

ORGANIC SYNTHESIS AND INDUSTRIAL ORGANIC CHEMISTRY

Thiodiglycol-Based Oligomers

A. Ya. Samuilov, E. I. Galeeva, A. V. Kulikov, I. N. Bakirova, and Ya. D. Samuilov

Kazan State Technological University, Kazan, Tatarstan, Russia

Received March 23, 2007

Abstract—Sulfur-containing oligoethers were prepared by polycondensation of thiodiglycol in the presence of acid catalysts. These oligoethers are oligomers with terminal hydroxy groups, comprised of oxyalkyl sulfide units.

DOI: 10.1134/S1070427207120170

Development of oil- and gas-resistant materials is an urgent task faced by modern polymer chemistry. One of the ways to accomplish this task consists in incorporation of sulfur atoms into the polymer matrix. For example, vulcanizates of Thiokols are well known to be resistant to fuels and oils [1]. Their large-scale production is hindered, however, by imperfect technology of production of polysulfide oligomers, yielding abundant wastewater. Wastewater utilization entails large costs, which increases the price of Thiokols. Also, materials based on polysulfide oligomers have poor strength characteristics. A high strength is exhibited by SKU-PFL commercial polyurethane based on oligo(oxytetramethylene) glycol (OOTMG). This is currently the most demanded castable polyurethane, but its oil and gas resistance is low.

In this context, it was of interest to replace OOTMG in synthesis of SKU-PFL polyurethane with a sulfur-containing oligoether diol and compare the properties of the new material with those of the OOTMG-based material. It could be expected that the new material would combine the properties of Thiokols and polyurethanes.

EXPERIMENTAL

As the initial compound for preparation of the oligoether with sulfur atoms in the backbone served thiodiglycol (TDG) synthesized by the reaction between ethylene chlorohydrin and sodium sulfide [2, 3]:

$$2HO–CH_2–CH_2–Cl + Na_2S \rightarrow HO–CH_2–CH_2–S–CH_2–CH_2–OH.$$

Oligothiodiglycols (OTDGs) with a molecular weight of 800–1200 were prepared by TDG polycondensation [4]:

$$n HO–CH_2–CH_2–S–CH_2–CH_2–OH \rightarrow HO–[–CH_2–CH_2–S–CH_2–CH_2–O–]_nH + (n – 1)H_2O.$$

For synthesis, we used both "crude" TDG (TDG-C) and that freed from impurities by distillation. The process was run at 110–115°C in a toluene medium with azeotropic distillation of water; sulfuric acid served as the catalyst.

The content of the hydroxy groups in the oligoethers was determined by acetylation with acetic anhydride in the presence of pyridine according to GOST (State Standard) 252–61. The concentration of isocyanate groups was determined by the "amine equivalent" method [5]. The IR spectra were recorded for oligoether films on a PE FTIR 1720 Perkin–Elmer (UK) spectrophotometer, and the ^{1}NMR spectra, in a perdeuteroacetonitrile solution on a Bruker MSL-400 (Germany) device at 400 MHz.

Quantum chemical calculations were carried out by B3LYP ab initio hybrid method in the STO 3-21G basis set with the use of the GAUSSIAN 03 software package [6]. The calculations involved full optimization of the configuration of the compounds. The initial optimization of the configuration was carried out by RM3 semiempirical method, and the resulting data were used for further calculations.

Polyurethanes were prepared via synthesis of a prepolymer by the reaction between OOTMG or

Table 1. Properties of oligoether diols

Oligoether diol	Structural formula	State of aggregation	Content of OH groups, wt %	$\overline{M}_n$	Sulfur content, wt %		Viscosity, Pa s (25°C)
					calculation	experiment	
OOTMG	H–[–O–CH_2–CH_2–CH_2–CH_2–]$_n$–OH	Viscous liquid	3.30	1100	0	0	0.5786
OTDG	H–[–O–CH_2–CH_2–S–CH_2–CH_2–]$_n$–OH from refined TDG	Light brown viscous liquid	2.98	1140	30.88	29.95	1.2734
OTDG-C	H–[–O–CH_2–CH_2–S–CH_2–CH_2–]$_n$–OH from crude TDG	Dark brown viscous liquid	4.29	790	28.35	29.30	–

Table 2. Enthalpies ΔH_f^0, entropies ΔS_f^0, and Gibbs free energies ΔG_f^0 of formation of butanediol, thiodiglycol, and the products of their reactions with methyl isocyanate at 298 K

Compound	ΔH_f^0, kcal mol^{-1}	ΔS_f^0, cal mol^{-1} K^{-1}	ΔG_f^0, kcal mol^{-1}
HO–CH_2–CH_2–CH_2–CH_2–OH	–48.15	99.12	–16.36
HO–CH_2–CH_2–S–CH_2–CH_2–OH	–24.45	107.65	–49.96
CH_3–N=C=O	4.60	76.15	10.04
CH_3–NHCOO–$(CH_2)_4$–OH	–68.51	132.86	–18.63
CH_3–NHCOO–$(CH_2)_2$–S–$(CH_2)_2$–OH	–50.23	143.13	–58.16

OTDG and 2,4-toluylene diisocyanate (TDI), followed by curing with 4,4'-methylenebis(*o*-chloroaniline). The molar ratio of the reactants was 1 : 2 : 0.8.

The physicomechanical properties of the polyurethanes were determined by conventional techniques. The thermomechanical curves were measured on an automatic recording setup with a sample exposed to a permanent load of 0.64 MPa. The heating rate was 2 deg min^{-1}. The height of the samples was 2 mm, and diameter, 4 mm.

Table 1 compares the characteristics of OTDG and OOTMG. The theoretical sulfur content of OTDG reasonably agrees with that determined experimentally. The viscosity of OTDG is higher than that of OOTMG at comparable molecular weights. The increased viscosity of OTDG is consistent with the fact that vacant *d* orbitals of the sulfur atoms in it can interact with the occupied *p* orbitals of the oxygen atoms. This should result in the formation of intermolecular donor–acceptor bonds. This phenomenon cannot be observed in the case of OOTMG.

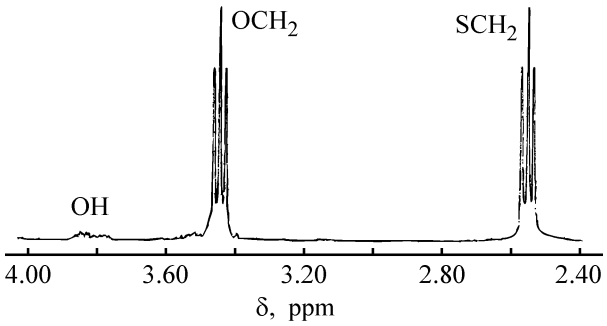

Fig. 1. NMR spectrum of OTDG. (δ) Chemical shift.

The IR spectra of the OTDG samples contain absorption bands at, cm^{-1}, 3400 (stretching vibrations of the HO groups), 2860 (stretching vibrations of the CH_2 group), and 1105 (stretching vibrations of the C–O–C moiety). A group of bands at 600–800 cm^{-1} belongs to the C–S bond.

In the ^{1}NMR spectra (Fig. 1), the protons of the methylene groups at the sulfur atom appear as a triplet at 2.60–2.40 ppm, and the protons of the methylene groups at the oxygen atom, as a triplet at 3.5–3.4 ppm. The protons of the hydroxy groups give a broadened signal at 3.80–3.90 ppm.

These data suggest that the TDG polycondensation product is indeed an oligomer with terminal hydroxy groups, containing sulfide and ether bonds in the chain.

To elucidate the difference between the pathways of the reactions of isocyanates with OOTMG and OTDG, we carried out quantum-chemical calculations of the thermodynamic parameters of the model reactions of TDG and 1,4-butanediol with methyl isocyanate. Table 2 lists the thermodynamic param-

Table 3. Enthalpies ΔH_r^0, entropies ΔS_r^0, and Gibbs free energies ΔG_r^0 of the reactions of butanediol and TDG with methyl isocyanate at 298 K and the equilibrium reaction constants K_e at 298 and 473 K

Compound	ΔH_r^0, kcal mol^{-1}	ΔS_r^0, cal mol^{-1} K^{-1}	ΔG_r^0, kcal mol^{-1}	$K_{e\,298}$	$K_{e\,473}$
HO–CH_2–CH_2–CH_2–CH_2–OH + CH_3–NCO → CH_3–NHCOO–$(CH_2)_4$–OH	–24.96	–42.41	–12.31	1.15×10^9	1.87×10^2
HO–CH_2–CH_2–S–CH_2–CH_2–OH + CH_3–NCO → CH_3–NHCOO–$(CH_2)_2$–S–$(CH_2)_2$–OH	–30.38	–40.67	–18.24	2.66×10^{13}	1.47×10^5

eters of formation of the compounds examined, and Table 3, the thermodynamic parameters of the transformations discussed.

The reactions examined are characterized by large negative entropies and enthalpies. The enthalpy of the reaction between isocyanic acid and methanol in the gas phase, calculated from the enthalpies of formation of isocyanic acid (–24.3 kcal mol^{-1} [7]), methanol (–48.07 kcal mol^{-1} [8]), and methyl urethane (–101.6 kcal mol^{-1} [9]), is –29.23 kcal mol^{-1}. The enthalpy of the reaction between phenyl isocyanate and 1-butanol was estimated at –20.1 in [10] and at –25.1 kcal mol^{-1} in [11]. These enthalpies of the reactions are close to the experimental data.

The reaction of methyl isocyanate with TDG is much more exothermic than that with 1,4-butanediol. Accordingly, the equilibrium constants of formation of urethane from TDG strongly exceed those in the case of 1,4-butanediol. Our data suggest that incorporation of the thiodiglycol moiety into the polyurethane structure should increase the stability of the urethane group.

A kinetic study of the reaction of OTDG and OOTMG with TDI showed that the time corresponding to 50% conversion of the isocyanate groups is 45 and 60 min, respectively (Fig. 2, curves *1*, *2*), which suggests a slightly higher activity of OTDG. Thus, introduction of the sulfur atom into the glycol moiety not only improves the thermodynamic stability of the urethanes but also accelerates their formation.

A different situation is observed when OTDG is replaced with OTDG-C (Fig. 2, curve *3*). In this case, the isocyanate groups are fully consumed already in 15 min. Such a fast decrease in their concentration is evidently due to the presence in the system of impurity metal compounds introduced with the oligoether because of the use for its synthesis of "crude" TDG (the TDG preparation technique involves the use of sodium sulfide containing an impurity iron sulfide). These impurities accelerate not only the formation of urethanes, but also the formation of allophanates and isocyanurates, undesirable for the prepolymer preparation [12]. This made OTDG-C unsuitable for synthesis of polyurethanes via the prepolymer stage.

Then we identified the temperature areas of serviceability of the polyurethanes synthesized. Figure 3 shows the thermomechanical curves (TMCs) for the polyurethane elastomer whose flexible segment is formed by OTDG, in comparison with SKU-PFL. It is seen that the profile of the TMCs depends on

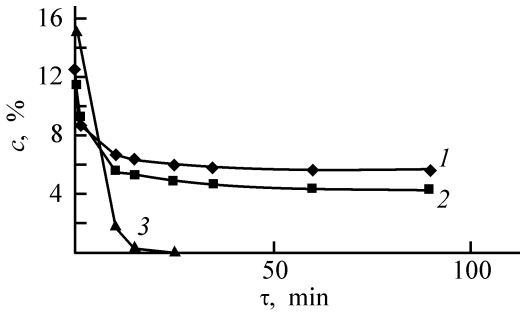

Fig. 2. Kinetic curves of the loss of NCO groups in the reaction between oligoether diols and TDI at 60°C. (*c*) Content of NCO and (τ) time. (*1*) OOTMG, (*2*) OTDG, and (*3*) OTDG-C.

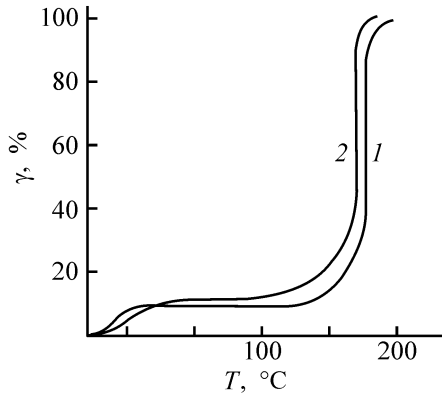

Fig. 3. Thermomechanical curves of the polyurethanes based on (*1*) OOTMG and (*2*) OTDG. (γ) Strain and (*T*) temperature.

Table 4. Properties of the cast polyurethanes based on OTDG and OOTMG

Parameter	Oligoether	
	OTDG	OOTMG
Nominal tensile strength, MPa	8.4	36.2
Relative elongation at break, %	80	380
Relative elongation set, %	4.0	0
Rebound elasticity, %	29.0	38.0
TM-2 hardness, arb. units	90.0	94.0
Degree of equilibrium swelling, %:		
in transformer oil	1.0	9.2
in toluene	10.2	48.4
Glass transition point, °C	–24	–38
Flow point, °C	190	200

the nature of the oligoether component. In going from OOTMG to OTDG, the glass transition point increases, whereas the flow point, by contrast, decreases (Table 4). This is accompanied by narrowing of the hyperelasticity area.

These data suggest that, upon introduction of sulfur atoms into the flexible segment of the polymer, the kinetic section of the material increases and the density of its physical network decreases. In the polymers examined, the formation of the 3*D* network is mainly due to hydrogen bonding. This is associated with taking a minor excess of isocyanate for synthesis.

The physicomechanical properties of the polymers (Table 4) suggest that the sulfur-containing polyurethanes unfavorably compare with those based on OOTMG in the tensile strength, relative elongation, and elasticity, but considerably exceed them in the resistance to solvents. For example, the equilibrium degree of swelling in transformer oil is by an order of magnitude, and that in toluene, by a factor of 5, higher.

Thus, polyurethanes based on oligoether diol comprised of oxoalkyl sulfide units are of interest for manufacture of articles contacting with oils and hydrocarbon solvents during exploitation.

CONCLUSIONS

(1) Polyurethanes based on oligothiodiglycol are characterized by high resistance to swelling in hydrocarbons, but lower level of physicomechanical properties.

(2) Introduction of the sulfur atom into the glycol moiety increases the thermodynamic stability of the urethanes and accelerates their formation.

REFERENCES

1. Smyslova, R.A., *Germetiki na osnove zhidkogo tiokola* (Sealants Based on Liquid Thiokol), Moscow: TsNIITEneftekhim, 1974.
2. *Organic Synthesis*, Blatt, A.H., Ed., New York: Wiley, 1946, 2nd ed., coll. vol. 2.
3. Idson, B. and Spoerri, P., *J. Am. Chem. Soc.*, 1954, vol. 76, p. 2902.
4. Woodward, F.N., *J. Polym. Sci.*, 1959, vol. 41, p. 219.
5. Siggia, S. and Hanna, J.G., *Quantitative Organic Analysis via Functional Groups*, New York: Wiley–Interscience, 1979.
6. Frisch, V.J. et al., *Gaussian 03, Revision A.1.*, Pittsburgh, PA: Gaussian, 2003.
7. Chase, M.W., *J. Phys. Chem. Ref. Data*, 1998, monograph 9.
8. Stull, D.R., Westrum, E.F., and Sinke, G.C., *The Chemical Thermodynamics of Organic Compounds*, New York: Wiley, 1969.
9. Bernard, M.A. et al., *Thermochim. Acta*, 1976, vol. 16, no. 2, pp. 267–275.
10. Pannone, M.C. and Macosko, C.W., *J. Appl. Polym. Sci.*, 1987, vol. 34, no. 7, pp. 2409–2432.
11. Lovering, E.G. and Laidler, K.J., *Canad. J. Chem.*, 1962, vol. 40, no. 1, pp. 26–30.
12. Saunders, J.H. and Frish, K.C., *Polyurethanes. Chemistry and Technology*, part 1: *Chemistry*, New York: Interscience, 1962.

ISSN 1070-4272, Russian Journal of Applied Chemistry, 2007, Vol. 80, No. 12, pp. 2097–2099. © Pleiades Publishing, Ltd., 2007.
Original Russian Text © L.M. Popova, S.V. Vershilov, 2007, published in Zhurnal Prikladnoi Khimii, 2007, Vol. 80, No. 12, pp. 2019–2021.

ORGANIC SYNTHESIS AND INDUSTRIAL ORGANIC CHEMISTRY

Oxidation of Perfluoro-Substituted Derivatives of 1,3-Diazines and 1,2,4-Triazoles

L. M. Popova and S. V. Vershilov

St. Petersburg State Technological University of Plant Polymers, St. Petersburg, Russia

Received May 30, 2007

Abstract—Oxidation of 6-perfluoro-substituted 2-amino-4-methylpyrimidines and 5-amino-3-perfluoro(1,4-dimethyl-2,5-dioxaoctyl)-1,2,4-triazole with potassium permanganate and of 3-perfluoro-substituted 5-mercapto- and 5-amino-1,2,4-triazoles with hydrogen peroxide in alkaline solution was studied.

DOI: 10.1134/S1070427207120182

In the development of new composite materials containing fluorinated surfactants, it is important to understand chemical transformation of these compounds under the action of oxidants. Proceeding with studies of fluorinated azine [1] and azole [2, 3] derivatives, we examined oxidation of 6-perfluoro-substituted 2-amino-4-methylpyrimidines **I**–**V** and 5-amino-3-perfluoro(1,4-dimethyl-2,5-dioxaoctyl)-1,2,4-triazole **XI** with potassium permanganate in alkaline solutions to the corresponding azobis(diazine) derivatives **VI**–**X** and 5,5'-azobis[3-perfluoro(1,4-dimethyl-2,5-dioxaoctyl)-1,2,4-triazole] **XII**.

In addition, we performed oxidation of 3-perfluoro-substituted 5-mercapto- (**XIII**, **XIV**) and 5-amino-1,2,4-triazoles (**XI**) with hydrogen peroxide in alkaline solution and obtained 5-hydroxy derivatives **XV** and **XVI**.

The strarting 2-aminopyrimidines **I**–**V** were prepared by intermolecular cyclocondensation of unsymmetrical fluorinated β-diketones with guanidine [4], and 5-amino-3-perfluoro(1,4-dimethyl-2,5-dioxaoctyl)-1,2,4-triazole **XI** and 3-perfluoro-substituted 5-mercapto-1,2,4-triazoles **XIII** and **XIV**, by intramolecular condensation of perfluoro(1,4-dimethyl-2,5-dioxaoctyl)aminoguanidine and base cyclization of perfluoroacylthiosemicarbazides [2].

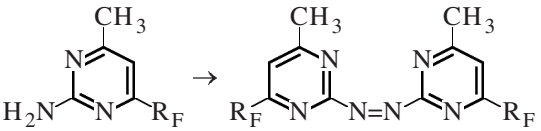

I–**V** → **VI**–**X**

R_F = C_6F_{13} (**I**, **VI**); C_8F_{17} (**II**, **VII**); $CF(CF_3)OC_3F_7$ (**III**, **VIII**); $CF(CF_3)OCF_2CF(CF_3)OC_3F_7$ (**IV**, **IX**); $CF(CF_3)[OCF_2CF(CF_3)]_2OC_3F_7$ (**V**, **X**).

4,4'-Dimethyl-6,6'-bis(perfluoro)-substituted 2,2'-azobispyrimidines **VI**–**X** were prepared by oxidation of the corresponding 2-aminodiazines **I**–**V** with a 10% aqueous-alcoholic solution of potassium permanganate in alkaline medium at room temperature for 6 h. Azo coupling products **VI**–**X** were isolated after treatment of the reaction mixture with 5% HCl to pH 4–5 followed by extraction with Freon 113. After distilling off the solvent and drying, the yield of **VI**–**X** reached 60–70%. Perfluoro-substituted azobispyrimidines were viscous oils with a specific odor.

The IR spectra of 6,6'-bis(perfluoro)-substituted azobispyrimidine derivatives **VI**–**X** contained stretching vibration bands of methyl groups at 3392–2850 cm^{-1}, skeleton vibration bands of the heteroring at 1770–1405 cm^{-1}, and C–F stretching vibration bands at 1350–890 cm^{-1}.

It was also interesting to evaluate the resistance of perfluoro-substituted 5-aminotriazoles to oxidants. For example, oxidation of 3-perfluoro-substituted 5-amino-1,2,4-triazole **XI** with $KMnO_4$ in 10% aqueous KOH at room temperature for 6 h gave 5,5'-azobis derivative **XII** in 65% yield:

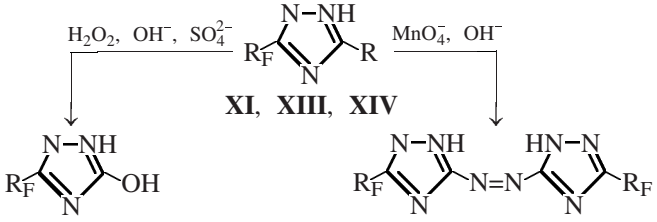

XI, **XIII**, **XIV** → **XV**, **XVI**; **XII**

R = NH_2, R_F = $CF(CF_3)OCF_2CF(CF_3)OC_3F_7$ (**XI**), (**XII**); R = SH, R_F = C_6F_{13} (**XIII**), (**XV**); $CF(CF_3)\cdot OCF_2CF(CF_3)OC_3F_7$ (**XIV**), (**XVI**).

The action of alkali without an oxidant caused no changes in the structure of 3-perfluoro-substituted 5-amino-1,2,4-triazole **XI** but merely converted it into the corresponding salt.

The composition and structure of **XII** were confirmed by elemental analysis and spectroscopic data. For example, in the IR spectrum of 5,5'-azobis[3-perfluoro(1,4-dimethyl-2,5-dioxaoctyl)-1,2,4-triazole] **XII** there are NH stretching vibration bands at 2995–3505 cm^{-1}, skeleton vibration bands of the heteroring at 1459–1734 cm^{-1}, and C–F stretching vibration bands at 1350–890 cm^{-1}.

It is known that 5-mercapto-1,2,4-thiazole derivatives can undergo desulfurization under the action of both oxidants and reductants [5]. In particular, treatment of 5-mercapto-1,2,4-triazole derivatives with hydrogen peroxide in acid solution on heating [6] and with concentrated nitric acid [7] resulted in replacement of the thiol group by hydrogen.

By treatment of 3-perfluoro-substituted 5-mercapto-1,2,4-triazoles **XIII** and **XIV** with 50% hydrogen peroxide in alkaline solution at room temperature for 2 h, we prepared the corresponding 5-hydroxy derivatives **XV** and **XVI**, which were isolated in 66–75% yield after testing the reaction mixture for the absence of residual peroxide and acidifying with 10% HCl to pH 3–4.

Compound **XVI** was also prepared in 66% yield by oxidation of 3-perfluoro-substituted 5-amino-1,2,4-triazole **XI** with 30% hydrogen peroxide under reflux for 3 h. The IR spectra of 3-perfluoro-substituted 5-hydroxy-1,2,4-triazoles **XV** and **XVI** contain stretching vibration bands of the OH group at 3500 cm^{-1} and of the NH group at 3000–3300 cm^{-1}, heteroring vibration bands at 1435–1735 cm^{-1}, and a mixed vibration band of the C–F and C–O bonds at 1100–1400 cm^{-1}.

EXPERIMENTAL

The IR spectra were recorded on a Shimadzu IR-470 spectrophotometer (Japan) from thin films. The UV spectra were measured on an SF-48 spectrophotometer from 10^{-4} M aqueous-alcoholic solutions; the layer thickness was 1 cm. The reaction progress and product purity were monitored by TLC on Silufol UV-254 plates. The starting 6-perfluoro-substituted 2-amino-4-methylpyrimidines **I**–**V** were prepared according to [4], and 5-amino- (**XI**) and 5-mercapto-1,2,4-triazoles (**XIII**, **XIV**), according to [2].

2,2'-Azobis(4-methyl-6-perfluorohexylpyrimidine) VI. A solution of 0.9 g (0.014 mol) of KOH in 20 ml of water was added dropwise to a solution of 1.2 g (0.0028 mol) of 2-amino-4-methyl-6-perfluorohexylpyrimidine **I** in 10 ml of ethanol. Then a solution of 0.44 g (0.0028 mol) of $KMnO_4$ in 15 ml of water was added, and the mixture was allowed to stand for 6 h. After that the mixture was acidified with 5% HCl to pH 4–5, extracted with Freon 113, washed with water, and dried, after which the solvent was distilled off. Yield 0.7 g (60%), yellow oil. IR spectrum (thin film), ν, cm^{-1}: 3280, 3180 (C–H); 1740, 1680, 1610, 1580 (heteroring); 1350, 1145 (C–F).

Found, %: C 30.85, F 57.90, N 9.62.
$C_{22}H_{68}F_{26}N_6$.
Calculated, %: C 31.08, F 58.09, N 9.88.

2,2'-Azobis(4-methyl-6-perfluorooctylpyrimidine) VII was prepared similarly to **VI** from 2.1 g (0.004 mol) of 2-amino-4-methyl-6-perfluorohexylpyrimidine **II**. Yield 1.3 g (63%), yellow oil. IR spectrum (thin film), ν, cm^{-1}: 3392, 2915, 2870 (C–H); 1770, 1685, 1550, 1460 (heteroring); 1390–890 (C–F).

Found, %: C 29.45, F 61.19, N 7.88.
$C_{26}H_8F_{34}N_6$.
Calculated, %: C 29.73; F 61.50; N 8.00.

2,2'-Azobis[4-methyl-6-perfluoro(1-methyl-2-oxapentyl)pyrimidine] VIII was prepared similarly to **VI** from 2.0 g (0.005 mol) of 2-amino-4-methyl-6-perfluoro(1-methyl-2-oxapentyl)pyrimidine **III**. Yield 1.4 g (70%), yellow oil. IR spectrum (thin film), ν, cm^{-1}: 3200, 3180 (C–H); 1680, 1620, 1540, 1440 (heteroring); 1300–1280 (C–F).

Found, %: C 30.29, F 53.13, N 10.39.
$C_{20}H_8F_{22}N_6O_2$.
Calculated, %: C 30.71, F 53.43, N 10.74.

2,2'-Azobis[4-methyl-6-perfluoro(1,4-dimethyl-2,5-dioxaoctyl)pyrimidine] IX was prepared similarly to **VI** from 2.2 g (0.004 mol) of 2-amino-4-methyl-6-perfluoro(1,4-dimethyl-2,5-dioxaoctyl)pyrimidine **IV**. YIeld 1.4 g (65%), light yellow oil. IR spectrum (thin film), ν, cm^{-1}: 3480, 3390, 3120, 2910, 2850 (C–H); 1680, 1620, 1590, 1440 (heteroring); 1340–980 (C–F).

Found, %: C 27.89, F 58.17, N 7.34.
$C_{26}H_8F_{34}N_6O_4$.
Calculated, %: C 28.03, F 57.97, N 7.54.

2,2'-Azobis[4-methyl-6-perfluoro(1,4,7-trimethyl-2,5,8-trioxaundecanyl)pyrimidine] X was prepared similarly to **VI** from 7.23 g (0.005 mol) of 2-amino-4-methyl-6-perfluoro(1,4,7-trimethyl-2,5,8-trioxaundecyl)pyrimidine **V**. Yield 4.4 g (60%), light brown oil.

IR spectrum (thin film), ν, cm^{-1}: 3392, 3110, 2900 (C–H); 1769, 1683, 1405 (heteroring); 1309–995 (C–F).

Found, %: C 26.14, F 60.05, N 5.33.
$C_{32}H_8F_{46}N_3O_6$.
Calculated, %: C 26.57, F 60.42, N 5.81.

5,5'-Azobis[3-perfluoro(1,4-dimethyl-2,5-dioxaoctyl)-1,2,4-triazole XII. A solution of 5.6 g (0.1 mol) of KOH in 20 ml of water was added dropwise to a solution of 12.0 g (0.025 mol) of 5-amino-3-perfluoro(1,4-dimethyl-2,5-dioxaoctyl)-1,2,4-triazole **XI** in 10 ml of ethanol. Then a solution of 0.63 g (0.025 mol) $KMnO_4$ in 30 ml of water was added with vigorous stirring, and the mixture was allowed to stand for 4 h. After acidification of the mixture with 5% HCl to pH 4–5, the product was extracted with Freon 113, washed with water, and dried; the solvent was distilled off. Yield 7.8 g (65%), colorless crystals, mp 89–91°C. IR spectrum (Freon 113, 5%), ν, cm^{-1}: 3505, 3225, 3125, 2995 (N–H); 1734, 1670, 1647, 1600, 1540, 1459 (heteroring); 1340, 1100–980 (C–F). UV spectrum (*i*-PrOH), λ_{max}, nm (log ε): 198 (3.88), 245 (3.68). TLC (acetone–water, 1 : 1): R_f 0.37.

Found, %: C 22.46, H 0.28, F 60.59, N 10.38.
$C_{20}H_2F_{34}N_8O_4$.
Calculated, %: C 22.58, H 0.18, F 60.70, N 10.53.

5-Hydroxy-3-perfluorohexyl-1,2,4-triazole XV. To 21 g (0.05 mol) of 5-mercapto-3-perfluorohexyl-1,2,4-triazole **XIII** in 100 ml of 10% aqueous KOH, 12 ml of 50% H_2O_2 (d^{20} 1.2) was added dropwise, and the mixture was left for 2 h. After testing for the absence of residual peroxide, the mixture was acidified with 10% HCl to pH 3–4. The precipitate was filtered off and washed with water to neutral reaction. The product was dissolved in alcohol, the solution was filtered, the solvent was distilled off, and the residue was dried. Yield 15.1 g (75%), mp 112–113°C. IR spectrum (Freon 113, 5%), ν, cm^{-1}: 3500 (O–H); 3280, 3180 (N–H); 1735, 1680, 1610, 1580 (heteroring); 1350, 1140 (C–F, C–O).

Found, %: C 23.97, F 61.14, N 10.35.
$C_8H_2F_{13}N_3O$.
Calculated, %: C 23.84, F 61.27, N 10.42.

5-Hydroxy-3-perfluoro(1,4-dimethyl-2,5-dioxaoctyl)-1,2,4-triazole XVI was prepared similarly to **XV** from 16.5 g (0.03 mol) of 5-mercapto-3-perfluoro(1,4-dimethyl-2,5-dioxaoctyl)-1,2,4-triazole **XIII**. The product was extracted with ethyl acetate, the extract was filtered, the solvent was distilled off, and the residue was dried. Yield 10.6 g (66%), amorphous substance. IR spectrum (thin film), ν, cm^{-1}: 3500 (O–H); 3300, 3120, 3000 (N–H); 2850, 1735, 1620, 1590, 1435 (heteroring); 1340, 1100 (C–F, C–O).

Found, %: C 22.57, F 60.31, N 7.72.
$C_{10}H_2F_{17}N_3O_3$.
Calculated, %: C 22.45, F 60.36, N 7.85.

5-Hydroxy-3-perfluoro(1,4-dimethyl-2,5-dioxaoctyl)-1,2,4-triazole XVI. To a solution of 4.2 g (0.008 mol) of 5-amino-1,2,4-triazole **XI** in 20 ml of 5% KOH, 2.5 ml of 30% hydrogen peroxide was added dropwise. The mixture was acidified with acetic acid and extracted with diethyl ether. The extract was dried over $MgSO_4$, and the solvent was distilled off. Yield 2.5 g (60%).

Found, %: C 22.68, H 0.50, F 60.29, N 8.06.
$C_{10}H_2F_{17}N_3O_3$.
Calculated, %: C 22.45, H 0.38, F 60.36, N 7.85.

CONCLUSIONS

(1) Oxidation of perfluoro-substituted derivatives of 1,3-diazines and 1,2,4-triazoles with 10% aqueous-alcoholic solution of potassium permanganate in alkaline solution at room temperature yields azobispyrimidine derivatives and 5,5'-azobis[3-perfluoro(1,4-dimethyl-2,5-dioxaoctyl)-1,2,4-triazole].

(2) Treatment of 3-perfluoro-substituted 5-mercapto- (at room temperature) and 5-amino-1,2,4-triazole (under reflux) with an aqueous-alkaline solution of hydrogen peroxide yields the corresponding 5-hydroxy derivatives.

REFERENCES

1. Popova, L.M., Trishina, A.U., Vershilov, S.V., et al., *J. Fluorine Chem.*, 1999, vol. 96, pp. 51–56.
2. Vershilov, S.V., Popova, L.M., Mungalov, V.E., and Ryabinin, N.A., *Zh. Prikl. Khim.*, 1994, vol. 67, no. 7, pp. 1124–1126.
3. Vershilov, S.V., Popova, L.M., Mungalov, V.E., and Ryabinin, N.A., *Zh. Org. Khim.*, 1994, vol. 30, no. 8, pp. 1241–1244.
4. Popova, L.M., Trishina, A.Yu., Vershilov, S.V., et al., Abstracts of Papers, *Mezhinstitutskii kollokvium "Khimiya azotistykh geterotsiklov"* (Interinstitutional Colloquium "Chemistry of Nitrogen-Containing Heterocycles"), Chernogolovka, October 18, 1995, p. 96.
5. *Fluorine Compounds: Modern Technology and Applications*, Ishikawa, N., Ed., Tokyo: CMC, 1987.
6. Chipen, G.I., Duka, D.E., and Grinshtein, V.Ya., *Khim. Geterotsikl. Soedin.*, 1966, no. 1, pp. 117–121.
7. Chipen, G.I., Bokalder, R.P., and Grinshtein, V.Ya., *Khim. Geterotsikl. Soedin.*, 1966, no. 1, pp. 110–116.

ISSN 1070-4272, Russian Journal of Applied Chemistry, 2007, Vol. 80, No. 12, pp. 2100–2103. © Pleiades Publishing, Ltd., 2007.
Original Russian Text © Z.P. Pai, P.V. Berdnikova, A.A. Nosikov, 2007, published in Zhurnal Prikladnoi Khimii, 2007, Vol. 80, No. 12, pp. 2022–2025.

ORGANIC SYNTHESIS AND INDUSTRIAL ORGANIC CHEMISTRY

Catalytic Epoxidation of α,β- and β,γ-Unsaturated Bicyclic Ketones with Hydrogen Peroxide

Z. P. Pai, P. V. Berdnikova, and A. A. Nosikov

Boreskov Institute of Catalysis, Siberian Division, Russian Academy of Sciences, Novosibirsk, Russia
Tomsk Polytechnic University, Tomsk, Russia

Received July 5, 2007

Abstract—The possibility of preparing epoxides from α,β- and β,γ-unsaturated bicyclic ketones formed as by-products in liquid-phase oxidation of cyclohexane with atmospheric oxygen (a stage in production of caprolactam, adipic acid, and other products) was examined. The reaction products were analyzed by gel chromatography and mass spectrometry.

DOI: 10.1134/S1070427207120194

Epoxy compounds are valuable and demanded intermediates for both basic and fine organic synthesis. They are used as effective modifiers, stabilizers, and thinners of polymeric masses with the aim to obtain polymeric materials with required properties. Many heterocyclic epoxides are biologically active compounds or their precursors.

It is known that liquid-phase oxidation of cyclohexane **I** with atmospheric oxygen, performed in industry with the aim to obtain cyclohexanone **II**, is accompanied by side reactions yielding α,β- and β,γ-unsaturated cyclic ketones: 2-cyclohexylidenecyclohexanone **III** and 2-(1-cyclohexenyl)cyclohexanone **IV**, forming the "light fraction" of X-oils:

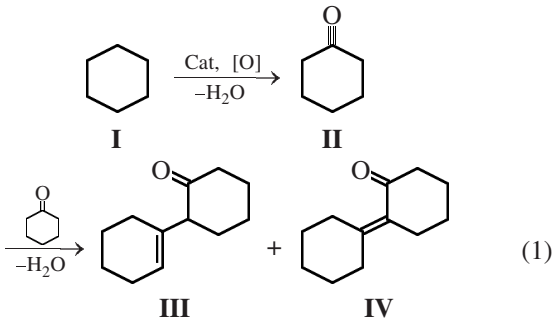

(1)

According to the estimates based on data of [1–3], the amount of such by-products is 80–100 kg per ton of converted **I**. It is known [4] that compound **III** is thermodynamically unstable and isomerizes into **IV** at 150°C. The isomerization is reversible, and an equilibrium mixture obtained under common conditions consists of **III** and **IV** in an approximately 9 : 1 ratio. This mixture can be separated by low-temperature crystallization.

One of promising ways to perform epoxidation of various organic substrates is phase-transfer catalysis in combination with the use of bifunctional homogeneous nanostructured catalysts based on peroxopolyoxotungstates [5–14]. Studies using various physicochemical methods (NMR, IR, Raman, UV spectroscopy, etc.) have shown that the peroxo complexes formed in the systems H_2O_2–H_3PO_4–Na_2WO_4 and $H_3PW_{12}O_{40}$–H_2O_2 are fairly stable, and the most active in oxidation is the $\{PO_4[WO(O_2)_2]_4\}^{3-}$ anion (Fig. 1) [7, 8, 10, 11]. The use of phase-transfer catalysts, quaternary ammonium cations Q^+, in combination with the oxidation catalyst, peroxopolyoxo anion, allows the oxidation to be performed as a one-pot process in two-phase solutions.

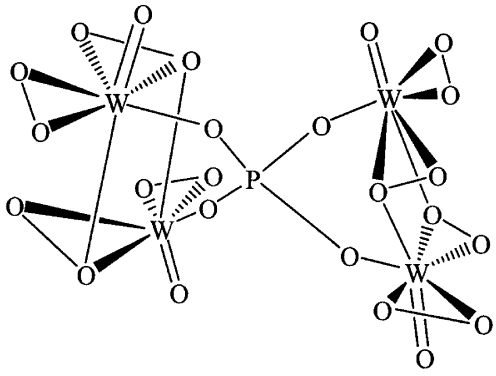

Fig. 1. Structure of the peroxo anion $\{PO_4[WO(O_2)_2]_4\}^{3-}$.

In this study, we examined the possibility of preparing epoxides from α,β- and β,γ-unsaturated cyclic ketones, by-products from oxidation of cyclohexane with atmospheric oxygen.

The expected products of catalytic oxidation of cyclic ketones **III** and **IV** containing C=C bonds with hydrogen peroxide are 2-(7-oxabicyclo[4.1.0]hept-1-yl)cyclohexanone **V** and 13-oxadispiro[5.0.5.1]tridecan-1-one **VI** [15]:

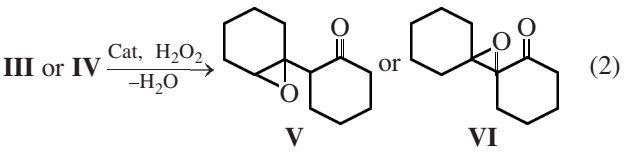

(2)

EXPERIMENTAL

As substrate we used a mixture isolated by vacuum distillation from the "light" fraction of X-oil from cyclohexanone production (Azot Joint-Stock Company, Kemerovo). It was a light yellow oily liquid (density 1.1 g cm^{-3}).

As catalyst we used a quaternary ammonium salt of tetra(oxodiperoxotungstato)phosphate, $Q_3\{PO_4 \cdot [WO(O_2)_2]_4\}$, where Q is the cation of tetra-*n*-butylammonium chloride $[(C_4H_9)_4N]Cl$ (95%) or *N*-hexadecylpyridinium chloride $[1\text{-}C_5H_5N(CH_2)_{15}CH_3]Cl$ (Acros). The catalytic systems were prepared by the procedure described in [11].

The epoxidation was performed in a duck-shaped catalytic vessel shaken at a rate of 300–400 double rockings per minute and equipped with a reflux condenser and a temperature-control jacket. The reaction temperature (55–65°C) was maintained with a water thermostat with an accuracy of ±1.0°C.

The reaction mixture was analyzed by gel chromatography–mass spectrometry (GC–MS) (Saturn 2000 device, USA; quartz capillary column 30 m long, stationary phase CP-SIL 8 CB; ionizing electron energy 70 eV. Quantitative processing of the chromatographic data was performed using normalization [16].

First we analyzed by GC–MS the substrate (light fraction of X-oil) with the aim to determine its composition. We detected (Fig. 2) residual amounts of **I**, ketones **III** and **IV**, and also 1,2,3,4,6,7,8,9-octahydrodibenzo[*b*, *d*]furan **VII** and compounds giving a molecular ion at *m*/*z* 258, which corresponds to the molecular weight of tricyclic ketones, 2,6-dicyclohexylydenecyclohexanone **VIII** and 2,6-di(1-cyclohexenyl)cyclohexanone **IX**. It should be noted that the tricyclic ketones formed by condensation of three cyclohexanone molecules, like bicyclic ketones, form isomers:

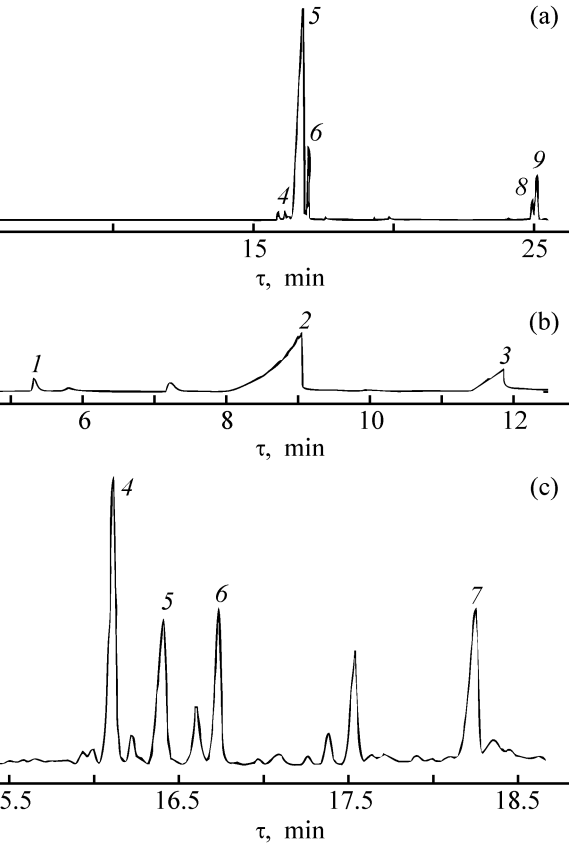

Fig. 2. Chromatograms of the organic phase of the reaction mixture. (τ) Retention time. (a) Substrate; (b, c) fragments of the chromatogram of the reaction mixture after the oxidation. (*1*) Cyclohexanone **I**, (*2*, *3*) carboxylic acids, (*4*) dibenzofuran **VII**, (*5*, *6*) ketones **IV** and **III**, (7) epoxide **VI**, and (*8*, *9*) tricyclic ketones **VIII** and **IX**.

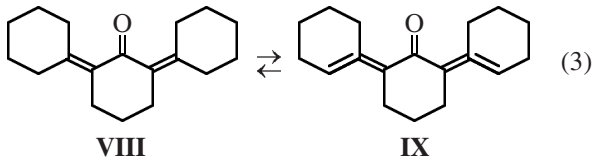

(3)

On the whole, the results of the GC–MS analysis (see table) were consistent with the composition of the light fraction of X-oil given in [2].

We performed a series of experiments on catalytic oxidation of the substrate containing a mixture of ketones **III** and **IV**. In these experiments, we varied the catalyst and the reaction temperature. We revealed a difference in the catalytic activity of peroxopolyoxotungstate complexes, depending on the structure of the phase-transfer catalyst. The most active catalytic

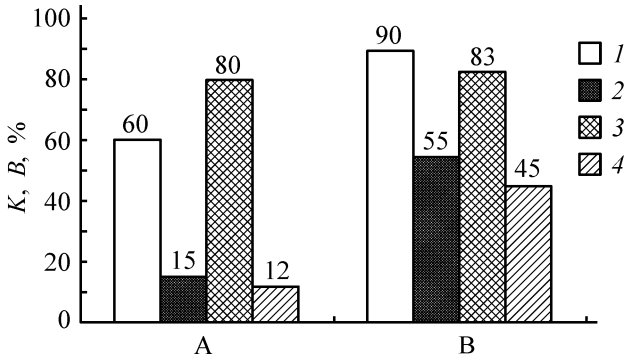

Fig. 3. Effect of catalyst cation on the conversion *K* of ketones and epoxide yield *B*. Reaction conditions: $[H_2O_2]$/[substrate] = 3, [substrate]/[catalyst] = 200, solvent dichloroethane, 65°C, 3 h. Catalytic complex: (A) $[(C_4H_9)_4N]_3 \cdot \{PO_4[W(O)(O_2)_2]_4\}$, and (B) $[C_5H_5N(CH_2)_{15}CH_3]_3 \cdot \{PO_4[W(O)(O_2)_2]_4\}$. (*1*) Conversion of **III**, (*2*) conversion of **IV**, (*3*) selectivity with respect to epoxide **VI**, and (*4*) yield of **VI**.

system (Fig. 3) is *N*-hexadecylpyridinium tetra(oxodiperoxotungstato)phosphate. In the presence of this catalytic system, 13-oxadispiro[5.0.5.1]tridecan-1-one **VI** is obtained in 45% yield at 90% conversion of **III** and 55% conversion of **IV**. The weaker catalytic activity of $[(C_4H_9)_4N]_3\{PO_4[W(O)(O_2)_2]_4\}$ is consistent with the lower lipophilicity of the phase-transfer agent, $[(C_4H_9)_4N]^+$, compared to *N*-hexadecylpyridinium.

A decrease in the temperature of the catalytic oxidation from 65 to 55°C, with *N*-hexadecylpyridinium tetra(oxodiperoxotungstato)phosphate as catalyst, does not appreciably affect, under equal other conditions, the yield of epoxide **VI**. However, we detected an untypical of these conditions increase in the concentration of cyclopentanecarboxylic acid as epoxidation by-product (Fig. 2b): from 8 to 12% in the product mixture.

Composition of the light fraction of X-oil

Compound	Content of components	
	mol %*	wt % [2]
Cyclohexanone **I**	0.2	3.6**
2-(1-Cyclohexenyl)cyclohexanone **IV**	78.5	90.6
2-Cyclohexylidenecyclohexanone **III**	7.8	
Tricyclic ketones **VIII** and **IX** (cyclohexanone trimerization products)	8.6	
1,2,3,4,6,7,8,9-Octahydrodibenzo[*b*,*d*]furan **VII**	1.0	5.8
Unidentified products	3.9	

* Results of GC–MS analysis.
** Content of cyclohexanone and cyclohexanol.

The presence of carboxylic acids in the reaction products raises the acidity of the reaction mixture, which may promote opening of the oxirane ring. To lower the acidity, we added AV-17-8 anion-exchange resin in the OH form to the reaction mixture. A GC–MS analysis of the mixture after the oxidation showed the absence of carboxylic acids in the organic layer of the reaction mixture. However, addition of the anion exchanger had a strong effect on the conversion of the starting compounds, and it cannot be recommended for synthesis of the epoxides as target products.

Comparison of our results with published data [17–19] reveals certain analogies. The following most probable mechanism of the oxidation of the starting α,β- and β,γ-unsaturated cyclic ketones **III** and **IV** can be suggested.

Formation of epoxide **VI** from ketone **IV** with involvement of the oxygen atom of the peroxy group of the catalyst occurs in the organic phase:

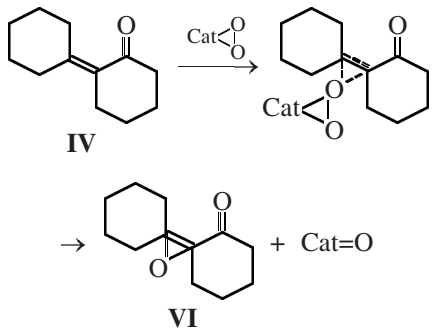

(4)

Regeneration of the catalyst with hydrogen peroxide occurs at the phase boundary.

Identification of the other components of the reaction mixture is complicated by the presence of a large amount of background fragment peaks in the mass spectra of the products. Nevertheless, comparison of the results of our mass-spectrometric analysis with published data [17–20] suggests that one of the reaction products is 1,2,3,4,6,7,8,9-octahydrodibenzo[*b*,*d*]-furan **VII**, whose concentration in the organic layer after the reaction completion was about 11% against 1% in the starting substrate (see table). A comparison of the reference mass spectrum of pure **VII** with the mass spectrum of component 5 (Fig. 2c) revealed a full coincidence of the peak positions and a 62% coincidence of the peak intensities.

The formation of compounds containing a furan ring was described in [18]. Namely, 2-cyclohexylidenecyclohexanone **III** transformed in a very acidic medium into **VII**. Creese and Smissman [17] described the mechanism of cyclic dehydration of 2-(1-cyclohexenyl)cyclohexanone epoxide **V** to give of octahydrodibenzofuran **VII**. Therefore, we can assume that the precursors of 1,2,3,4,6,7,8,9-octahydrodibenzo[*b*, *d*]furan **VII** are ketone **III** and also cyclohexanone **I** and tricyclic ketones present in the reaction mixture.

CONCLUSIONS

(1) Epoxides of bicyclic ketones, and also dibenzofuran derivatives and carboxylic acids are formed from the light fraction of X-oils (by-product from caprolactam production) under the conditions of phase-transfer catalysis in two-phase solutions. Oxidation with hydrogen peroxide occurs under mild conditions: atmospheric pressure, temperature ≤65°C, low catalyst concentrations ([substrate] : [catalyst] = 200).

(2) Oxidation of 2-cyclohexylidenecyclohexanone with hydrogen peroxide in the presence of a homogeneous bifunctional catalyst, *N*-hexadecylpyridinium tetra(oxodiperoxotungstato)phosphate, gives an epoxide, 13-oxadispiro[5.0.5.1]tridecan-1-one, with 83% selectivity at 55% conversion of the starting ketone.

(3) Oxidation of 2-(1-cyclohexenyl)cyclohexanone with hydrogen peroxide in the presence of *N*-hexadecylpyridinium tetra(oxodiperoxotungstato)phosphate mainly yields 1,2,3,4,6,7,8,9-octahydrodibenzo[*b*, *d*]-furan and cyclopentanedicarboxylic acid.

ACKNOWLEDGMENTS

The authors are grateful to A.S. Noskov for support of our studies and to V.A. Utkin for performing the GC–MS analysis.

The study was financially supported by the Federal Target Scientific and Technical Program "Research and Development in Priority Fields of the Scientific and Technological Complex of Russia in 2007–2012" (State Contract no. 02.515.11.5009) and by the Division of Chemistry and Materials Science of the Russian Academy of Sciences (project no. 5.6.3).

REFERENCES

1. Furman, M.S. and Gol'dman, A.M., *Proizvodstvo tsiklogeksanona i adipinovoi kisloty* (Production of Cyclohexanone and Adipic Acid), Moscow: Khimiya, 1967.
2. Krasnykh, E.L., Glazko, I.L., Sokolov, A.B., et al., *Khim. Prom–st.*, 2002, no. 6, pp. 53–54.
3. *Proizvodstvo kaprolaktama* (Production of Caprolactam), Ovchinnikov, V.I., Ed., Moscow: Khimiya, 1977.
4. RF Patent 2 233 852.
5. Venturello, C., D'Aloisio, R., Bart, J.C.J., and Ricci, M., *J. Mol. Catal.*, 1985, vol. 32, p. 107.
6. Sheldon, R.A., *Stud. Sci. Catal.*, 1990, vol. 55, p. 1.
7. Venturello, C. and Ricci, M., *J. Org. Chem.*, 1986, vol. 51, no. 9, p. 1599.
8. Ishii, Y., Yamawaki, K., Ura, T., et al., *J. Org. Chem.*, 1988, vol. 53, no. 15, p. 3587.
9. Pai, Z.P., Berdnikova, P.V., Tolstikov, A.G., et al., *Katal. Prom–sti.*, 2006, no. 5, pp. 12–23.
10. Matoba, Y., Inoue, H., Akagi, Jun-ichi, et al., *Synth. Commun.*, 1984, vol. 14, no. 9, p. 865.
11. Pai, Z.P., Tolstikov, A.G., Berdnikova, P.V., et al., *Izv. Ross. Akad. Nauk, Ser. Khim.*, 2005, no. 8, pp. 1794–1801.
12. Timofeeva, M.N., Pai, Z.P., Tolstikov, A.G., et al., *Izv. Ross. Akad. Nauk, Ser. Khim.*, 2003, no. 2, pp. 458–463.
13. Kozhevnikov, I., *Catalysis for Fine Chemical Synthesis, vol. 2: Catalysis by Polyoxometalates*, Chichester: Wiley, 2002.
14. Noyori, R., Aoki, M., and Sato, K., *Chem. Commun.*, 2003, no. 16, pp. 1977–1986.
15. Reese, J., *Ber.*, 1942, vol 75, p. 384.
16. Vinarskii, V.A., *Khromatografiya* (Chromatography), Minsk: Bel. Gos. Univ., 2002, part 1.
17. Creese, M.W. and Smissman, E.E., *J. Org. Chem.*, 1976, vol. 41, no. 1, p. 41.
18. Svetozarskii, S.V., Feller, K.L., Samitov, Yu.Yu., et al., *Izv. Akad. Nauk SSSR, Ser. Khim.*, 1964, no. 1, pp. 121–127.
19. Kataev, V.E., *Issledovaniya B.A. Arbuzova v oblasti izomerizatsii i stereokhimii bitsiklicheskikh monoterpenov* (B.A. Arbuzov's Studies in the Field of Isomerization and Stereochemistry of Bicyclic Monoterpenes), Kazan: Kazan. Gos. Univ., 2003, pp. 205–237.
20. US Patent 4 065 469.

ISSN 1070-4272, Russian Journal of Applied Chemistry, 2007, Vol. 80, No. 12, pp. 2104–2106. © Pleiades Publishing, Ltd., 2007.
Original Russian Text © E.V. Churilina, Ya.I. Korenman, P.T. Sukhanov, V.M. Bolotov, G.V. Shatalov, 2007, published in Zhurnal Prikladnoi Khimii, 2007, Vol. 80, No. 12, pp. 2026–2028.

ORGANIC SYNTHESIS AND INDUSTRIAL ORGANIC CHEMISTRY

Recovery of Anthocyan Dye from Aqueous-Salt Solutions with Polyethylene Glycol PEG-5000

E. V. Churilina, Ya. I. Korenman, P. T. Sukhanov, V. M. Bolotov, and G. V. Shatalov

Voronezh State Technological Academy, Voronezh, Russia
Voronezh State University, Voronezh, Russia

Received February 9, 2007

Abstract—Extraction with PEG-5000 was studied as a method for recovering and concentrating a natural anthocyan dye from sodium and ammonium sulfate solutions. The effects of the type of salt cation, pH, and addition of aliphatic alcohols on the dye recovery were examined.

DOI: 10.1134/S1070427207120200

The involvement of synthetic dyes in carcinogenesis makes natural dyes, which are harmless and, what is more, useful, preferable for food and pharmaceutical industries [1, 2]. Among these natural dyes are red pigments (anthocyans) causing coloration of red wines and fruit juices. Anthocyans belong to the group of phenolic flavonoid compounds [3]:

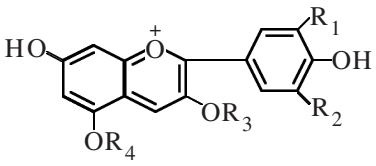

where R^1, R^2 are H, OH, or OCH_3, and R^3, R^4 are H atoms or carbohydrate residues.

Anthocyan extracts contain biologically active components (vitamins, microelements, organic acids) and aliphatic alcohols, added to aqueous solutions to facilitate dye extraction from the vegetable raw material [4].

For recovery and concentration of the natural dyes from aqueous solutions, the extraction with water-soluble high-molecular-weight compounds forming a separate aqueous-organic phase in the presence of salting-out agents shows promise. Polyethylene glycols (PEGs), which are nontoxic compounds used as thickeners and binders in pharmaceutical industry and cosmetology [5], belong to such polymers. Two-phase aqueous systems based on PEG are successfully used in extraction recovery and separation of organic and inorganic substances of various classes [6–8].

The goal of this study was to optimize the conditions of the recovery and concentration of the anthocyan dye from aqueous solutions, using dye extraction with PEG-5000 from aqueous-salt solutions.

EXPERIMENTAL

THe anthocyan dye was recovered from black-currant berries with ethanol at 50–55°C by the known method [9]. The dye distribution was studied in systems constituted by an aqueous solution and solution of sodium or ammonium sulfate. The polymer manufactured by Loba Chemie Co. with a molecular weight of 5000 and salting-out agents and aliphatic alcohols of chemically pure grade were used.

A 15-ml portion of an anthocyan dye solution containing $(NH_4)_2SO_4$ (40 wt %) or Na_2SO_4 (15 wt %) was placed in a flask with a ground-glass stopper, 3 ml of PEG solution (0.1–20 wt %) was added, and extraction was performed on a vibromixer for 3–5 min (time in which the phase equilibrium is attained).

The efficiency of the extractive recovery of the dye was evaluated by the degree of dye recovery, R (%):

$$R = (A_0 - A)/A_0 \times 100,$$

where A_0 and A are the optical densities of the aqueous solutions before and after extraction.

The optical densities of the solutions were measured on a KFK-2MP photocolorimeter at 490 nm using optical cells of thickness 1 and 3 cm. The content of the red pigment in the anthocyan dye was determined

by the known method, using a standard solution of $CoSO_4 \cdot 7H_2O$ [10]. Aliphatic alcohols were introduced into aqueous-salt solutions in experiments aimed to study the hydrotropic effect on the dye extraction.

Two-phase aqueous–polymeric systems were prepared by salting-out of the polymer from its aqueous solutions with certain salts [6]. Polyethylene glycols form such systems in the presence of sulfates of alkali metals and ammonium. The most efficient salting-out agents are $(NH_4)_2SO_4$ and Na_2SO_4. To attain the maximal volume of the aqueous-organic phase of the polymer, salt solutions close to saturation are used.

The degree of the anthocyan dye recovery from aqueous-salt solution depends on the polymer concentration and salt cation (Fig. 1).

Water in the phase containing ammonium sulfate is almost completely incorporated in the solvation spheres of ammonium ion; sodium ions are hydrated to a lesser extent [11]. Therefore, irrespective of the PEG concentration, systems with $(NH_4)_2SO_4$ are more effective. For example, on adding 0.3 wt % PEG to the aqueous solution, more than 75% of the dye is extracted from the saturated $(NH_4)_2SO_4$ solution, whereas in the presence of Na_2SO_4 only about 40% of the dye is recovered under similar conditions. Differences in the R values become less pronounced as the polymer content of the aqueous solution increases. In a single extraction, the maximal degree of dye recovery (97%) is attained in salting-out from ammonium sulfate solutions.

The high efficiency of extraction systems containing PEG is associated with the formation of PEG complexes with the dye via hydrophobic interactions of ethylene groups of the polymer with aromatic groups of the dye and formation of hydrogen bonds between OH groups of the polymer and dye.

We studied the influence of aqueous solution pH on the anthocyan dye recovery of the (Fig. 2). As can be seen, the efficiency of recovery is virtually constant within the pH range from 1 to 4. At a PEG content of 1.67 wt %, 94 and 97% of the dye is recovered from solutions with pH 1 and 4, respectively. The insignificant influence of pH on the dye recovery is caused by the large contribution of hydrophobic interactions in the extraction systems studied. In alkaline media, the extraction was not studied because the dye is unstable at pH > 7 [12].

To recover the anthocyan dye from vegetable raw materials, various organic solvents, including aliphatic alcohols, are used [4, 9]. Therefore, we studied the effect of ethanol, 1-propanol, 1-butanol, and 3-methyl-1-butanol added to the aqueous phase on the extractive recovery of the anthocyan dye and on the formation of the two-phase system (see table).

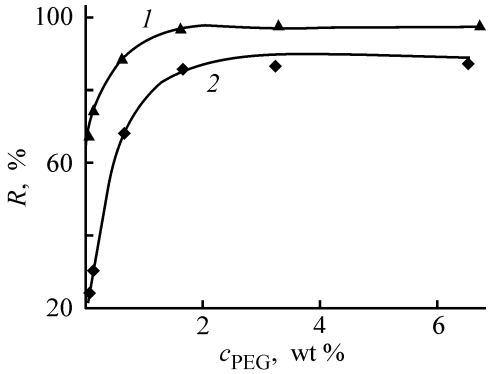

Fig. 1. Degree R of anthocyan dye recovery vs. PEG-5000 content c_{PEG} of the aqueous solution in the presence of a salting-out agent. (*1*) $(NH_4)_2SO_4$ and (*2*) Na_2SO_4.

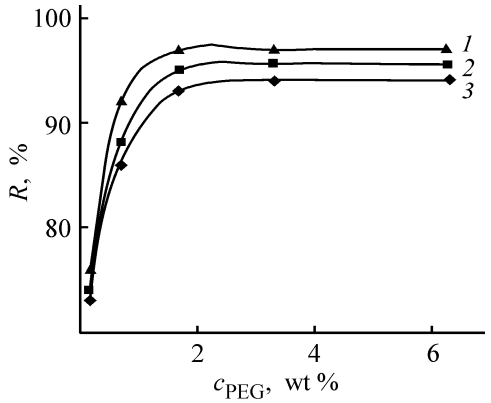

Fig. 2. Influence of pH on the degree of recovery of the anthocyan dye R in the presence of $(NH_4)_2SO_4$. (c_{PEG}) Polyethylene glycol content. pH: (*1*) 4, (*2*) 3, and (*3*) 1.

Correlation of equilibrium volumes of aqueous and organic phases and degree of recovery of the anthocyan dye with polyethylene glycol from aqueous ammonium sulfate solutions in the presence of alcohols

Alcohol	c_{PEG} = 1.67 wt %		c_{PEG} = 0.67 wt %	
	$V_w : V_o$	R, %	$V_w : V_o$	R, %
None	15 : 0.4	97	15 : 0.2	91
Ethanol	15 : 0.5	89	15 : 0.4	84
1-Propanol	15 : 1.4	86	15 : 0.9	76
1-Butanol	15 : 2.0	88	15 : 1.5	86
3-Methyl-1-butanol	15 : 1.5	73	15 : 1.5	67

The following competing processes occur when alcohols are introduced into the aqueous solution: low-molecular-weight alcohols increase an dye solubility in water (hydrotropic effect); alcohols are extracted by the polymer phase; and hydrophilic alcohols are salted-out, with the organic phase containing PEG and alcohol formed.

In the presence of ammonium sulfate, irrespective of the PEG content, the dye recovery is maximal in the absence of alcohols and in the systems with ethanol. Introduction of highly hydrated ethanol decreases the dye recovery from 97 to 89% (c_{PEG} = 1.67 wt %) and from 82 to 57 % (c_{PEG} = 0.67 wt %), i.e., the hydrotropic effect of ethanol is observed. The volume of the equilibrium organic phase, V_o, changes insignificantly. An increase in V_o in the systems PEG-1-propanol and PEG-1-butanol is caused by the different solubilities of alcohols in aqueous-salt solution. The degree of dye recovery and the volume V_o are maximal in the presence of 1-butanol, probably because of the optimal relationship between the competing processes as compared to the extraction in the presence of 1-propanol and 3-methyl-1-butanol.

In the series of the alcohols studied, 3-methyl-1-butanol is the most hydrophobic and hence is recovered by the forming polymer phase to a greater extent, but coordination-active PEG groups are shielded by the alcohol, and, as a result, the degree of dye recovery decreases.

CONCLUSIONS

(1) For virtually complete (97%) recovery of anthocyan dye from aqueous solutions, systems with 1.67 wt % PEG-5000 and 40 wt % ammonium sulfate, pH 1–4, can be used.

(2) The presence of hydrophilic alcohols in the aqueous phase decreases the dye recovery by 10–14%.

REFERENCES

1. *IARC Monographs on the Evaluation of the Carcinogenic Risk of Chemicals to Humans*, Lyon (France): IARC, 1972–1985.
2. Sarafanova, L.A., *Pishchevye dobavki: Entsiklopediya* (Food Supplements: Encyclopedia), St. Petersburg: GIORD, 2003.
3. Tanchev, S.S., *Antotsiany v plodakh i ovoshchakh* (Anthocyans in Fruits and Vegetables), Moscow: Pishchevaya Prom–st., 1980.
4. Bolotov, V.M. and Nechaev, A.P., *Pishch. Ingred.: Syr'e Dobavki*, 2001, no. 1, pp. 4–10.
5. *Khimicheskaya entsiklopediya* (Chemical Encyclopedia), Knunyants, I.L., Ed., Moscow: Bol'shaya Ross. Enstiklopediya, 1998, vol. 1.
6. Nifant'eva, T.I., Matoushova, V., Adamcova, Z., and Shkinev, V.M., *Vysokomol. Soedin., Ser. A*, 1989, vol. 31, no. 8, pp. 2131–2135.
7. Molochnikova, N.P., Shkinev, V.M., and Myasoedov, B.F., *Radiokhimiya*, 1995, vol. 37, no. 5, pp. 385–397.
8. Nifant'eva, T.I., Shkinev, V.M., Zavarzina, A.G., and Demin, V.V., *Zh. Anal. Khim.*, 2000, vol. 55, no. 10, pp. 1030–1032.
9. RF Patent 2228344.
10. Kharlamova, O.A., and Kafka, B.V., *Natural'nye pishchevye krasiteli* (Natural Edible Dyes), Moscow: Pishchevaya Prom–st., 1979.
11. Korenman, I.M., *Ekstraktsiya v analize organicheskikh veshchestv* (Extraction in Analysis of Organic Substances), Moscow: Khimiya, 1977.
12. Goto, T., *Prog. Chem. Org. Nat. Prod.*, 1987, vol. 52, pp. 113–158.

ISSN 1070-4272, Russian Journal of Applied Chemistry, 2007, Vol. 80, No. 12, pp. 2107–2110. © Pleiades Publishing, Ltd., 2007.
Original Russian Text © A.B. Shishmakov, Yu.V. Mikushina, M.S. Valova, O.V. Koryakova, L.A. Petrov, 2007, published in Zhurnal Prikladnoi Khimii, 2007, Vol. 80, No. 12, pp. 2029–2032.

ORGANIC SYNTHESIS AND INDUSTRIAL ORGANIC CHEMISTRY

Titanium Dioxide Xerogel Modified with Powder Cellulose in Oxidation of Trimethylhydroquinone

A. B. Shishmakov, Yu. V. Mikushina, M. S. Valova, O. V. Koryakova, and L. A. Petrov

Institute of Organic Synthesis, Ural Division, Russian Academy of Sciences, Yekaterinburg, Russia

Received May 2, 2007

Abstract—A procedure was developed for modification of titanium dioxide xerogel by addition of powder cellulose in the stage preceding hydrolysis of tetramethoxytitanium. The resulting catalytic systems based on the new material were studied in a model liquid-phase catalytic process of oxidative dehydrogenation of trimethylhydroquinone with atmospheric oxygen.

DOI: 10.1134/S1070427207120212

Titanium dioxide is widely used as a sorbent and a catalyst support. The efficiency of its application is mainly governed by the structural and texture characteristics, development of the surface, and accessibility of its active centers throughout the entire volume.

Synthesis of xerogels of element oxides by any method is accompanied by their shrinkage and, as a result, by a decrease in the specific surface area on drying. There are several ways to eliminate this phenomenon: variation of the composition of dispersion medium, drying for longer time, and the use of special additives [1–9].

The aim of this study was modify titanium dioxide with powder cellulose (PC) and to study the resulting materials in a model catalytic process of oxidative dehydrogenation of trimethylhydroquinone (TMHQ) with atmospheric oxygen.

EXPERIMENTAL

Powder cellulose was prepared by hydrolysis of kraft cellulose produced at the Baikal Paper and Pulp Plant (Technical Specification OP 13-027 94 88-08–91) in 2.5 N hydrochloric acid at 100°C. Hydrolysis was performed for 2 h. The resulting product was washed with distilled water on a filter until neutral pH of the aqueous extract. The product was dried at 100°C.

Three samples of titanium dioxide xerogels K1, K2, and K3 were prepared as follows: 1.5, 3, and 9 ml of tetrabutoxytitanium (TBT), respectively, was dissolved in 20 ml of methanol. Hydrolysis was performed with 500 ml of water at 20°C. The precipitate was washed on a filter until the absence of butanol in the wash water and dried at 100°C.

To prepare modified xerogels (MXs) with the TiO_2 : PC ratios of 0.45 : 0.55, 0.26 : 0.74, and 0.06 : 0.94, 9-, 3-, and 1.5-ml portions of TBT, respectively, were dissolved in 20 ml of methanol. To each of these solutions, 1 g of PC was added. Hydrolysis was performed at 20°C in 500 ml of water with stirring. The solutions were kept for 10 min and by this time the major fraction of the precipitate settled. The aqueous phase was decanted from the modified TiO_2. The precipitate was treated as described above.

The TiO_2 and TiO_2 : PC gels of compositions 0.31 : 0.69, 0.62 : 0.38, and 0.81 : 019 were prepared from a solution of 9 ml of TBT in 20 ml of methanol. Modification was performed by addition of 2, 1, and 0.5 g of PC, respectively, to the solution. Hydrolysis was performed in 500 ml of water. The precipitate was separated on a filter without preliminary decantation and washed. After completion of washing, the paste was placed in a flask filled with 50 ml of water.

The IR spectra of the samples in the form of solid powders were recorded on a Perkin-Elmer Spectrum One IR Fourier spectrophotometer in the range 4000–370 cm^{-1} using diffuse reflection attachment (DRA). The sorption of 1,4-hydroquinone (HQ) was performed by addition of a solution of HQ in methanol into MX [weight ratio HQ : MX = 1 : (0.25–8)], followed by

drying of the sample at room temperature for 3 days. The bands were assigned on the basis of reference data [10]. The intensities of the spectra were processed using the spectrometer software.

The kinetic experiments were carried out in a temperature-controlled reactor equipped with a reflux condenser, with stirring of the aqueous-methanol solution (volume ratio water : methanol = 1 : 1) by air bubbling. The air flow rate was 3.1 $1\,h^{-1}$.

TMHQ was oxidized at 50 ± 0.2°C. The concentration of the substrate was 66, and that of $CuCl_2 \cdot 2H_2O$, 6 mM.

The kinetic measurements were performed by stopping the reaction and determining the content of the starting substance. The resulting functions of concentrations were subjected to polynomial approximation. The initial reaction rates were found by numerical differentiation and interpolation. The error in their determination was no more than 10%. The TMHQ content was determined by gas-liquid chromatography on a Chrom-4 chromatograph [11].

The resulting cellulose-inorganic materials were studied by IR spectroscopy. The IR spectrum of titanium dioxide xerogel contains a strong absorption band peaked at 340 and 560 cm^{-1}, which can be regarded as a superposition of vibrations of the Ti–O bonds and water librations. In the range 1000–1200 cm^{-1}, there are three extremely weak peaks, which can be assigned to bending modes of the Ti–OH groups (1192, 1168, and 1090 cm^{-1}). For modified samples of TiO_2, there are no changes in the range of vibrations of the Ti–O bonds. Weak peaks corresponding to the Ti–OH groups are not observed on the background of the bands of PC. The IR spectrum of cellulose is mainly determined by absorption of three hydroxy groups incorporated in a glucopyranose unit. In the spectrum of PC there are the following absorption bands: 3348 cm^{-1}, stretching modes of hydroxy groups; in the range 3000–2800 cm^{-1}, stretching modes of methylene and methine groups of cellulose; 1640 cm^{-1}, δ_{HOH}, bending modes of water of crystallization. The band at 1451 cm^{-1} corresponds to δ(OH); 1427, to $\delta(CH_2)$ + δ(CH); 1369, to δ(CH); 1335, to δ(OH) (in-plane); 1315, to $\delta(CH_2)$ (wagging vibrations); 1281, 1248, 1235, and 1203, to δ(OH) + δ(CH) [12]. According to published data [13], the band at 1159 cm^{-1} corresponds to asymmetric stretching modes of the C–O–C bridge; however, in some publications [14] this band is assigned to the C–O stretching or O–H bending modes of the C–OH group. The band at 1054 cm^{-1} is assigned to the stretching modes of the C–O bond in the C^3H–OH group, and the band at 1035 cm^{-1}, to the stretching modes of the primary alcoholic group in various conformations. In the spectrum of PC in the range 860–400 cm^{-1}, there is a broad diffuse absorption on whose background a series of ill-defined bands characterizing various vibrations of the pyranose ring and bending modes of hydroxy groups are observed. The interaction of PC with hydrated titanium dioxide in the modified samples results in variation of the intensities of the absorption bands corresponding to hydroxy groups (the band ν_{as} at 2900 cm^{-1} was used as an internal reference). The most significant increase in the intensity (by a factor of 1.2–2) is observed for the bands at 1159, 1054, and 1035 cm^{-1}. Variations in the spectrum of PC increase with the fraction of the inorganic component in the sample. Thus, variation of the spectral characteristics of PC suggests that its hydroxy groups are involved in interparticle interaction with TiO_2 via hydrogen bonds.

Previously, [15] we have studied the model catalytic liquid-phase oxidation of TMHQ with atmospheric oxygen in the medium of TiO_2 gel:

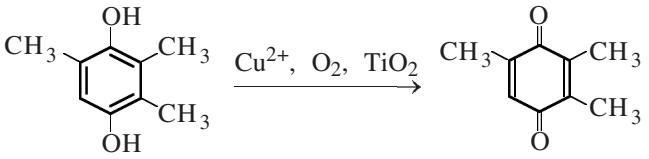

It has been established by ESR spectroscopy [16] that, depending on the Cu(II)/TiO_2 ratio, several types of Cu(II) compounds are formed in the titanium dioxide phase: mono complexes, associates of mono complexes, copper(II) hydroxide, and polynuclear bridged compounds. The last kind of compounds was the most reactive.

Addition of powder cellulose does not affect the course and parameters of the catalytic process. Apparently, Cu(II) does not react with PC under the reaction conditions.

The dependences of the initial rate of TMHQ oxidation on the Cu(II) content of the MX phase for the samples of various compositions are shown in Fig. 1. The dependences are nonlinear because of the formation of various Cu(II) compounds and also because of limitations imposed by the sorption capacity of xerogel for Cu^{2+} ions. The maximum observed in the dependences is caused by the formation of the most catalytically active Cu(II) species on the surface of titanium dioxide. The number of these compounds increases with the fraction of PC in the sample. The sample of the composition of TiO_2 : PC = 0.06 : 0.94 did not affect the reaction due to the small

amount of TiO_2 in the weighed portion, whose increase hampers stirring of the reaction mixture.

One of the ways to produce gels of element oxides with various specific surface areas is to vary the concentrations of substances being hydrolyzed [17]. However, these distinctions are lost in the course of drying to the xerogel state (Fig. 1, curve *1*). Modification of PC allows us to prevent to a certain extent these undesirable changes.

To elucidate the interactions occurring in the system MX–substrate, we studied the sorption of hydroquinone on MX by IR spectroscopy. The choice of HQ is caused by its resistance to air, minimal overlapping of the spectra of HQ and MX, fairly simple spectrum of HQ, and higher intensity of its bands, allowing detection of HQ in the analytical range of optical densities even at its low content in the system. The absorption bands of the aromatic ring, ν 1515 and 1470 cm^{-1}, are manifested fairly clearly in the IR spectra, and analysis using these bands presents no problems.

The absorption bands of hydroquinone were assigned on the basis of published data [10]. The absorption bands corresponding to the skeleton vibrations of aromatic rings are manifested at 517, 1009, 1470, and 1515 cm^{-1}. The stretching absorption bands of OH groups appear at 3255 cm^{-1}; the absorption bands of C–OH group appear at 1240 (C–O stretching modes) and 1210 cm^{-1} (bending modes).

In the spectrum of HQ sorbed on TiO_2 : PC = 0.45 : 0.55 at the ratio HQ : MX = 1 : 0.5, we observed redistribution of the intensities of the absorption bands corresponding to the skeleton vibrations of the aromatic ring of HQ, ν 1515 and 1470 cm^{-1}. At the ratio HQ : MX = 1 : 1, a shoulder at 1500 cm^{-1} appears in the band at 1514 cm^{-1}; at the ratio HQ : MX = 1 : 4 the band at 1515 cm^{-1} is shifted to 1500 cm^{-1} and the intensity of the band at 1470 cm^{-1} decreases. The apparent variation of the intensities of the bands corresponding to vibrations of the C–C bonds of HQ suggests that the MX surface interacts with the π-electron system of the ring. Analysis of the other bands of HQ is difficult because of super-position of the spectra of HQ and PC.

The spectral changes observed are in good agreement with data on sorption of HQ on previously obtained TiO_2 gels [15]. Based on this fact and also on the insensitivity of the homogeneous catalytic reaction to addition of PC, we can conclude that the sorption-active component in MX is its inorganic component.

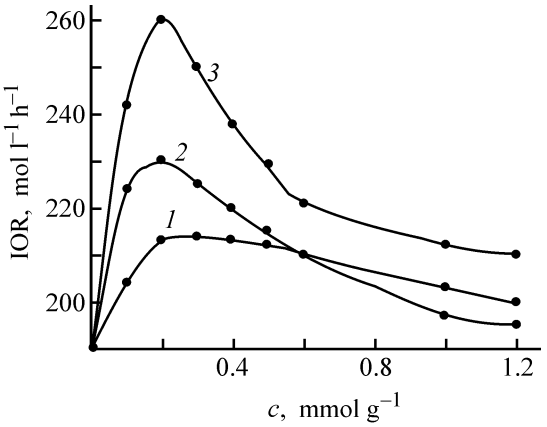

Fig. 1. Initial rate of TMHQ oxidation (IOR) vs. the Cu(II)/MX ratio c in the reaction area. Concentration of Cu(II) 6 mM; the same for Fig. 3. (*1*) K1-K3, (*2*) PC : TiO_2 = 0.35 : 0.45, and (*3*) PC : TiO_2 = 0.74 : 26; the same for Fig. 3.

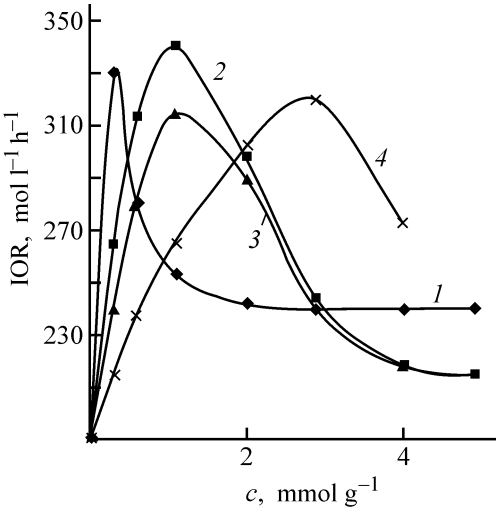

Fig. 2. Initial rate of TMHQ HCO oxidation (IOR) vs. the Cu(II)/TiO_2 ratio c in the reaction area. Gel: (*1*) TiO_2, (*2*) TiO_2 : PC = 0.81 : 0.19, (*3*) TiO_2 : PC = 0.62 : 0.38, and (*4*) TiO_2 : PC = 0.31 : 69.

The kinetic data recalculated to TiO_2 are presented in Fig. 2. For the samples of MX, the maximum of copper activity is shifted to higher Cu(II)/TiO_2 ratios as the PC fraction increases, i.e., the most catalytically active polynuclear Cu(II) compounds in the material phase are formed at a lower amount of TiO_2. This fact is caused by an increase in the specific surface area of titanium dioxide in MX with increasing PC/TBT ratio in the stage of hydrolysis.

To elucidate which stage of xerogel formation is influenced by the modifying additive, it was of interest

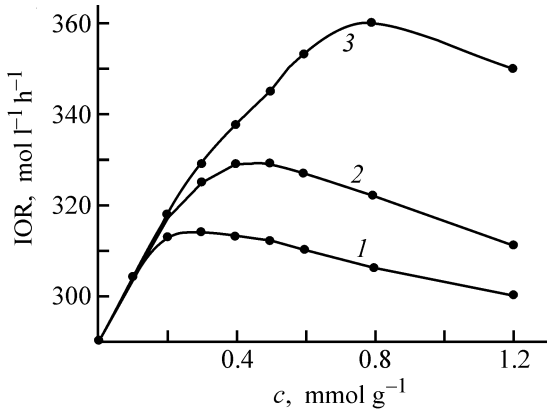

Fig. 3. Initial rate of TMHQ HCO oxidation (IOR) vs. the Cu(II)/TiO_2 ratio c in the reaction area.

to perform the model reaction with the modified TiO_2 gels. The data obtained are presented in Fig. 3.

For the modified gels, the effect similar to that for xerogels is observed, i.e., the maximum of the activity is shifted to higher Cu^{2+}/TiO_2 ratios. Thus, the influence of PC goes beyond the stage of drying, but is manifested even in the stage of gel formation and results in the formation of more sorption-active TiO_2 particles of a smaller size.

CONCLUSIONS

(1) Samples of titanium dioxide xerogels modified with powder cellulose with various ratios of TiO_2 to the modifying additive were prepared.

(2) The activity of Cu(II) in the matrix of modified samples in catalysis of oxidative dehydrogenation of trimethylhydroquinone is higher than that in the process occurring in the presence of unmodified titanium dioxide xerogel.

REFERENCES

1. *Physical and Chemical Aspects of Adsorbents and Catalysts*, Linsen, B.G., Ed., London: Academic, 1970.
2. Neimark, I.E., *Sinteticheskie mineral'nye adsorbenty i nositeli katalizatorov* (Synthetic Mineral Adsorbents and Catalyst Supports), Kiev: Naukova Dumka, 1982.
3. Ermolenko, V.F. and Efros, M.D., *Regulirovanie poristoi struktury okisnykh adsorbentov i katalizatorov* (Control of the Pore Structure of Oxide Adsorbents and Catalysts), Minsk: Nauka i Tekhnika, 1971.
4. Iler, R.K., *The Chemistry of Silica*, New York: Wiley-Interscience, 1979.
5. Dobruskin, V.Kh., Belotserkovskii, G.M., Karel'skaya, V.F., and Plachenov, T.G., *Zh. Prikl. Khim.*, 1968, vol. 41, no. 11, pp. 2443–2448.
6. Airapetyan, S.S. and Khachatryan, A.G., *Zh. Prikl. Khim.*, 2003, vol. 76, no. 6, pp. 918–921.
7. Khimich, N.N., Venzel', B.I., Drozdova, I.A., and Koptelova, L.A., *Zh. Prikl. Khim.*, 2002, vol. 75, no. 7, pp. 1125–1130.
8. Fenelonov, V.B., Tarasova, D.V., and Gavrilov, V.Yu., *Izv. Sib. Otd. Akad. Nauk SSSR, Ser. Khim. Nauk*, 1978, no. 9, issue 4, pp. 116–129.
9. Ur'ev, N.B. and Potanin, A.A., *Tekuchest' suspenzii i poroshkov* (Fluidity of Suspensions and Powders), Moscow: Khimiya, 1992.
10. Bellamy, L.J., *The Infra-Red Spectra of Complex Molecules*, London: Methuen, 1954.
11. Kharchuk, V.G., Kolenko, I.P., Petrov, L.A., and Gus'kova, L.M., *Zh. Org. Khim.*, 1986, vol. 22, no. 11, pp. 2306–2315.
12. Mam, I. and Marrian, H., *Trans. Faraday Soc.*, 1956, vol. 52, p. 492.
13. Liang, C.Y. and Marchesssault, R.H., *J. Polym. Sci.*, 1959, vol. 37, pp. 385–395.
14. Nelson, M.L. and O'Connor, R.T., *J. Appl. Polym. Sci.*, 1964, vol. 8, pp. 1311–1324.
15. Kharchuk, V.G., Buldakova, L.Yu., Shishmakov, A.B., et al., *Zh. Obshch. Khim.*, 2004, vol. 74, no. 1, pp. 110–113.
16. Shishmakov, A.B., Kharchuk, V.G., and Kuznetsova, O.V., *Zh. Fiz. Khim.*, 2003, vol. 77, no. 4, pp. 623–628.
17. Shishmakov, A.B., Liquid-Phase Oxidation of Trimethylhydroquinone in the Presence of Hydrogels of Silicon, Titanium, and Tin Dioxides, *Cand. Sci. Dissertation*, Yekaterinburg, 2006.

ISSN 1070-4272, Russian Journal of Applied Chemistry, 2007, Vol. 80, No. 12, pp. 2111–2112. © Pleiades Publishing, Ltd., 2007.
Original Russian Text © S.M. Danov, A.V. Sulimov, A.E. Fedosov, 2007, published in Zhurnal Prikladnoi Khimii, 2007, Vol. 80, No. 12, pp. 2033–2034.

ORGANIC SYNTHESIS AND INDUSTRIAL ORGANIC CHEMISTRY

Kinetics of Butanol-2 Oxidation on Titanium Silicalite

S. M. Danov, A. V. Sulimov, and A. E. Fedosov

Dzerzhinsk Polytechnic Institute, Nizhni Novgorod State Technical University, Dzerzhinsk, Nizhni Novgorod oblast, Russia

Received January 16, 2007

Abstract—Kinetics of butanol-2 oxidation by hydrogen peroxide on titanium silicalite was studied. The experimental data obtained were used to calculate parameters of the kinetic model suggested.

DOI: 10.1134/S1070427207120224

A priority avenue of the modern technological progress consists in development of efficient, technologically convenient, and ecologically safe processes for synthesis of a number of chemical products and, in particular, methyl ethyl ketone. The most promising method for industrial synthesis of methyl ethyl ketone is liquid-phase heterogeneous-catalytic oxidation of *n*-butane with hydrogen peroxide on titanium silicalite (TS-1) to give butanol-2 and methyl ethyl ketone in the first and second stages, respectively. However, there is no published evidence about the kinetic aspects of the reaction of *n*-butane oxidation by hydrogen peroxide. This communication presents the results of a study of the fundamental kinetic aspects of *n*-butane oxidation by hydrogen peroxide on titanium silicalite TS-1.

EXPERIMENTAL

The following reagents were used in the study: butanol-2 of pure grade, TU (Technical Specification) 6-09-4620-784, preliminarily distilled and dehydrated; methyl ethyl ketone of pure grade, TU 38.10243–80; hydrogen peroxide of technical grade, GOST (State Standard) 177–88; the catalyst TS-1 was produced using the method described in [1].

The experiments were performed in the temperature range 30–80°C at the following concentrations of the reagents (M): butanol-2 0.1–10, hydrogen peroxide 0.1–0.9, water 3–8, methyl ethyl ketone 0.1–1; the content of TS-1 remained constant (5 wt %) in all the experiments. The reaction of butanol-2 oxidation was performed in a glass reactor equipped with a reflux and thermometer. The reaction mass was agitated with a magnetic stirrer. Required amounts of butanol-2 and TS-1 were charged into the reactor, the magnetic stirrer was switched on, and the reactor was thermostated at a prescribed temperature. The instant at which hydrogen peroxide was charged into the reactor was regarded as the reaction onset time.

The components of the reaction mixture were analyzed by GLC on a Tsvet 500 chromatograph (3 m × 3 mm) glass column; 15 wt % Carbowax supported by Chromaton-N-AW as a sorbent; flame-ionization detector; carrier-gas nitrogen; flow rate of nitrogen through the column, 30 ml min^{-1}). The temperatures of the evaporator and column thermostat were maintained at 150 and 80°C, respectively. Hydrogen peroxide was determined by iodometric titration.

In the opinion of many authors [2, 3], the reaction of alcohol oxidation can proceed via an intermediate having the form of a complex of hydrogen peroxide with active Ti-centers and a molecule of an alcohol. It was shown in [4] that the total energy of the system decreases upon the formation of a five-membered complex involving hydrogen peroxide, active Ti-centers, and an alcohol molecule, and this decrease accounts for the high oxidation rate of alcohols even at a low concentration of titanium silicalite. The mechanism of the oxidation reaction is the following:

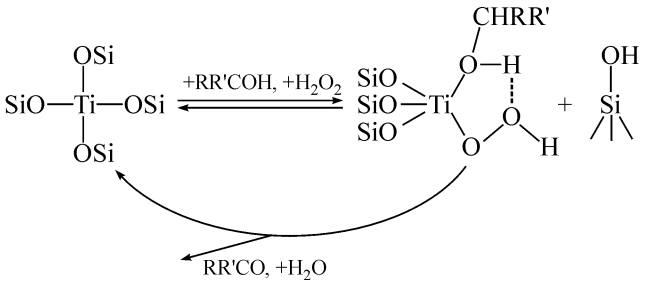

Results of the calculation and the statistical parameters of the regression*

Constant	E, J mol^{-1}	log A	R^2	S
k_1	22 660 ± 1699	15.6 ± 1.2		
K_1	13 480 ± 850	2.1 ± 0.2	0.92	0.144
K_2	11 200 ± 300	17.3 ± 1.7		

* R^2, Pearson's multiple correlation coefficient; S, root-mean-square deviation; E, activation heat of the oxidation kinetics; and log A, pre-exponential factor in the kinetic equation.

The oxidation reaction occurs in several stages: (1, 2) adsorption of hydrogen peroxide and butanol-2 on the surface of titanium silicalite to give a five-membered complex, (3) chemical reaction, and (4) desorption of methyl ethyl ketone:

$$\text{S–ROH} + \text{H}_2\text{O}_2 \overset{K_1}{\rightleftharpoons} \text{S–ROH–H}_2\text{O}_2, \quad (1)$$

$$\text{S} + \text{ROH} \rightleftarrows \text{S–ROH}, \quad (2)$$

$$\text{S–ROH} \cdot \text{H}_2\text{O}_2 \xrightarrow{k_1} \text{S–M} + \text{H}_2\text{O}, \quad (3)$$

$$\text{S–M} \overset{K_2}{\rightleftharpoons} \text{S} + \text{M}. \quad (4)$$

The experiments demonstrated that the rate of the oxidation reaction increases with the hydrogen peroxide concentration. This suggests that the surface reaction, rather than the adsorption of hydrogen peroxide, is the rate-determining stage of the process. Methyl ethyl ketone, butanol-2, and hydrogen peroxide can compete for adsorption on active Ti-centers. Because of this circumstance, the adsorption of methyl ethyl ketone can affect the process kinetics.

The kinetic model based on the Langmuir–Hinshelwood model was constructed on the assumption that the chemical reaction is the rate-determining stage of the process and all the adsorption processes are equally important.

On the basis of the assumptions made and the suggested reaction scheme, the kinetic model of the process of butanol-2 oxidation can be represented as

$$r_{\text{MEK}} = \frac{k_1 K_1 c_{\text{H}_2\text{O}_2}}{1 + K_1 c_{\text{H}_2\text{O}_2} + K_2 c_{\text{MEK}}}, \quad (5)$$

where k_1 is the rate constant of the surface reaction (M s^{-1}); K_1, constant of the adsorption equilibrium for hydrogen peroxide (M^{-1}); K_2, constant of the adsorption equilibrium for methyl ethyl ketone (M^{-1}); $c_{\text{H}_2\text{O}_2}$ and c_{MEK}, concentrations of hydrogen peroxide and methyl ethyl ketone, respectively (M).

The effect of temperature on the rate constants of the chemical reaction and adsorption equilibria is described by the Arrhenius and Van't Hoff equations, respectively.

The kinetic equation was integrated by the modified Euler method with a variable integration step, and the constants of the kinetic equation were found by the nonlinear Newton method from the condition of the minimum sum of squared deviations between the calculated and experimentally found concentrations:

$$S = \sum_{m=1}^{L} (c_m^{\text{calc}} - c_m^{\text{exp}})^2,$$

where c_m^{calc} and c_m^{exp} are the calculated and experimentally found concentrations of methyl ethyl ketone (M).

The calculation results and the statistical parameters of the regression equation are listed in the table.

It can be seen in the table that the suggested mechanism is adequately described by the Langmuir–Hinshelwood equation. The multiple correlation coefficient is 0.92, and the root-mean-square deviation $S = 0.144$.

Analysis of the kinetic model obtained shows that the reaction rate increases with the hydrogen peroxide concentration. Because methyl ethyl ketone and hydrogen peroxide compete for adsorption on active Ti-centers, an increase in the concentration of methyl ethyl ketone markedly decelerates the oxidation reaction.

CONCLUSIONS

(1) A kinetic model of butanol-2 oxidation, which can be represented as Eq. (5), was suggested on the basis of the presumed reaction scheme with account of the assumptions made.

(2) The parameters of the kinetic model were calculated using experimental data. It was shown that the butanol-2 oxidation is described by the Langmuir–Hinshelwood model and the reaction proceeds via formation of an intermediate complex of hydrogen peroxide and an active Ti-center, stabilized by butanol-2.

REFERENCES

1. US Patent 4 410 501.
2. Maspero, F. and Romano, U., *J. Catal.*, 1994, vol. 146, pp. 476–482.
3. Khouw, C.B., Dartt, C.B., Labinger, J.A., et al., *J. Catal.*, 1994, vol. 149, pp. 195–205.
4. Clerici, M., Bellussi, G., and Romano, U., *J. Catal.*, 1991, vol. 129, pp. 159–163.

ISSN 1070-4272, Russian Journal of Applied Chemistry, 2007, Vol. 80, No. 12, pp. 2113–2118. © Pleiades Publishing, Ltd., 2007.
Original Russian Text © S.F. Grebennikov, A.T. Kynin, E.I. Zaitseva, Yu.S. Chulkova, 2007, published in Zhurnal Prikladnoi Khimii, 2007, Vol. 80, No. 12, pp. 2035–2040.

MACROMOLECULAR CHEMISTRY AND POLYMERIC MATERIALS

Molecular Structure of Polymeric Materials and Sorption of Water Vapor

S. F. Grebennikov, A. T. Kynin, E. I. Zaitseva, and Yu. S. Chulkova

St. Petersburg University of Technology and Design, St. Petersburg, Russia

Received March 28, 2007; in final form, July 2007

Abstract—Methods for calculating the coefficients of the thermal equation of water vapor sorption by polymeric materials were developed. These methods enable calculation of the equilibrium amounts of sorption in a wide temperature range from the cohesion energy of a polymer.

DOI: 10.1134/S1070427207120236

Under working conditions, polymeric materials are in contact with water vapor (humid air), and drying is the final technological operation for most of them. To calculate the drying, it is necessary to know equilibrium data on the water vapor sorption in a wide temperature range and the sorption heat. "Inert" sorbates are absorbed in accordance with the adsorption laws, i.e., with layer-by-layer coverage of the surface and the bulk polymer properties remaining unchanged. Noninert sorbates are distributed throughout the polymer volume, change the energy of intermolecular interaction, and cause a change in the volume of the system (swelling). Just this process, in which sorbed moisture substantially lowers the glass-forming point [1] and strongly affects the mechanical properties of the polymeric material, was the subject of the present study. These factors predetermine the topicality of a search for new methods for calculating the water vapor sorption in a wide temperature range, which is an important applied problem in physical chemistry of polymers.

The first generalizations of mechanisms of sorption processes in polymers have been made and the formalism of their description has been suggested in fundamental studies by a number of authors [2–4]. The general conclusion made in these studies is that the sorption by polymers should be classed with adsorption phenomena. This has been confirmed by a comprehensive examination of polymer systems with the use of a wide variety of instrumental techniques [5]. The physical meaning of the constants of the classical adsorption equations (BET, Langmuir, Henry) was analyzed, as applied to swelling polymer systems, in [6, 7].

A new approach to analysis of the state of a polymer and a sorbate was suggested in [8], where a structural-mechanical model of water vapor adsorption by polymers was developed. New concepts enabled the authors to explain a number of phenomena in polymeric systems, including the mechanism of sorbate clustering and sorption hysteresis. The physicochemical formalism was used to demonstrate the high efficiency of the equation following from the theory of volume filling of micropores (TVFM) for various polymer–water systems.

It was also shown in [9–11] that the TVFM equation can describe the sorption of various vapors by numerous swelling polymeric materials. However, the shape of the isotherm, the adsorption mechanism [12], and the state of the microporous adsorbent sharply differ from those for swelling polymeric systems [6, 8]. Therefore, the parameter n (rank) of Weibull's equation, which is a basis for the TVFM equation, is 2 or 3 for microporous bodies and $n < 1$ for polymeric systems. For this reason, the equation describing the vapor sorption by polymers is named, for swelling polymeric systems, the equation of the theoretical-probabilistic model (TPM). It is of interest to consider the possibility of an a priori (based on reference data or on a minimum amount of experimental data) evaluation of the coefficients of this equation.

The TVM equation of sorption has the form [9, 10]

$$a = a_0 \exp[-(-\Delta\mu_1/E)^n + \alpha(T - T_0)], \qquad (1)$$

where a is the amount of sorption at a partial vapor pressure P and temperature T; a_0, limiting amount of sorption at a saturated vapor pressure P_0 and tem-

perature T_0; $\Delta\mu_1 = RT \ln P/P_0$, change in the chemical potential of water vapor upon sorption; E, characteristic sorption energy; and α, thermal coefficient of sorption:

$$\alpha = \left(\frac{\partial \ln a}{\partial T}\right)_{\Delta\mu_1}. \quad (2)$$

As a rule, sorption occurs only in amorphous regions of a polymer [13], and, therefore,

$$a_0 = a_0^a(1 - x_c), \quad (3)$$

where a_0^a is the limiting amount of sorption in amorphous regions of the polymer, and x_c is the degree of crystallinity of the polymer.

From Eq. (1) follow relations for calculating the thermodynamic functions [10] of the sorption process: partial molar entropy of the sorbate

$$\Delta\overline{S}_1 = -\left(\frac{\partial\Delta\mu_1}{\partial T}\right) = \frac{\alpha E}{n}\left(\ln\frac{a_0}{a}\right)^{1/n-1}, \quad (4)$$

partial molar enthalpy of the sorbate

$$\Delta H_1 = \Delta\mu_1 + T\Delta\overline{S}_1 = E\left[-\left(\ln\frac{a_0}{a}\right)^{1/n} + \frac{\alpha T}{n}\left(\ln\frac{a_0}{a}\right)^{1/n-1}\right], \quad (5)$$

and integral heat of sorption

$$q_i = \frac{Ea_0}{n}(1 - \alpha T)\Gamma(1/n), \quad (6)$$

where $\Gamma(1/n)$ is the gamma function: $\Gamma = 0.8861$ at $n = 0.7$ and 1 at $n = 0.5$.

These relations make it possible to analyze the sorption mechanism for new polymeric materials and calculate heat fluxes in drying of materials [14]. For this purpose, it is necessary to know the coefficients a_0, n, E, and α. At present, there are no theoretical methods for calculation of these coefficients, and, therefore, the aim of our study was to seek relationships between their values, on the one hand, and structural characteristics of polymeric materials, on the other.

EXPERIMENTAL

Polymeric materials (produced on industrial and semi-industrial installations and washed to remove brightening formulations) in the form of fibers and films served as objects of study. The constants of Eq. (1) were analyzed using sorption isotherms measured by the authors and those reported in [15–17].

Water sorption isotherms were measured on a thermostated McBain–Bakr balance with quartz coil constants of 2–4 mg mm^{-1} and a KM-4 cathetometer with a measurement accuracy of ±0.005 mm. Picein was used as a lubricant for ground joints at high temperatures. The time of equilibration at a given water vapor pressure and temperature of 293–303 K was 4–5 days.

The sorption by hydrophobic and moderately hydrophobic [8] materials was measured using the isopiestic (desiccator) method in which large weighed portions of samples can be used and, consequently, the measurement accuracy can be substantially improved. The partial vapor pressures were created with saturated solutions of salt crystal hydrates [18]. The equilibration time at 298 K was 30–40 days. The McBain–Bakr balance and desiccators were placed in air thermostats with a water jacket, with temperature maintained to within ±0.3°C.

The relaxation state of a polymer determines the value of the parameter (rank) n in Eq. (1). It was shown in [9] that the average value of n can be taken to be 0.7 for glassy polymers and 0.5 for elastomers. The data reported in [8] are in agreement with this value and, consequently, the parameter n is a priori known for the object of study.

The limiting sorption a_0 is an extensive quantity dependent on the number of active sorption centers, and, because only amorphous regions of the polymer are accessible to water molecules [10, 13], there appears a relationship between a_0 and the degree of crystallinity. Having analyzed isotherms of water sorption by a number of polymers with known degrees of crystallinity, Van Krevelen suggested an additive method for calculating the amount of sorption a_0 (g g^{-1}) in amorphous regions of polymers, based on the molecular structure of the polymer unit:

$$a_a = \frac{M_{H_2O}\Sigma a_i}{M_{un}}, \quad (7)$$

where a_i is sorption by ith atom or group of atoms in the polymer chain (mol H_2O/mol units); M_{H_2O} and M_{un} are the molecular masses of water and structural unit of the polymer macromolecule.

Values of a_i were reported in [13] for $T = 298$ K and relative pressures $P/P_0 = 0.3$, 0.5, 0.7, 0.9, and 1.0.

Thus, the van Krevelen method can be used to calculate the isotherm of water sorption by a hypothetical amorphous polymer. The sorption isotherm obtained can be further plotted in the linear coordinates of Eq. (1) at $T = T_0 = 298$ K

$$\ln a_a = \ln a_0^a - \frac{1}{E^n}(-RT \ln P/P_0)^n, \quad (8)$$

with the constants of the equations calculated: a_0^a (portion intercepted by the straight line on the ordinate axis, $\ln a_0^a$) and E (slope of the line is $1/E^n$).

Table 1. Constants of Eq. (1) for water vapor sorption by glassy polymers (n = 0.7)

Polymer	Composition of the elementary unit	Scheme for calculation* of ΔE^*	ΔE^*, J g^{-1}	E, J mol^{-1}	$-\alpha \times 10^3$, K^{-1}
Anid (cord)	$(CH_2)_5NHCO$	$\Sigma\Delta E_a + \Delta E_d + \Delta E_h$	397	1510	3.5
PA 12	$(CH_2)_{11}NHCO$	$\Sigma\Delta E_a + \Delta E_d + \Delta E_h$	310	1460	-
PA 6	$(CH_2)_5NHCO$	$\Sigma\Delta E_a + \Delta E_d + \Delta E_h$	397	1700	3.5
PA 548	$(CH_2)_5NHCO$	$\Sigma\Delta E_a + \Delta E_d + \Delta E_h$	397	1580	3.5
PA 4	$(CH_2)_3NHCO$	$\Sigma\Delta E_a + \Delta E_d + \Delta E_h$	464	1470	3.5
SVM	$-NHC_6H_3NNHCC_6H_4OC_6H_4CO$	$\Sigma\Delta E_a + 2\Delta E_h + 3\Delta E_d + 3\Delta E_r$	406	1910	3.1
PABI	$-NHC_6H_3NNHCC_6H_4OC_6H_4CO$	$\Sigma\Delta E_a + 2\Delta E_h + 3\Delta E_d + 3\Delta E_r$	406	1900	3.4
Capron (cord)	$(CH_2)_5NHCO$	$\Sigma\Delta E_a + \Delta E_d + \Delta E_h$	397	1530	3.4
Viscose rayon (cord)	$C_6H_{10}O_5$	$\Sigma\Delta E_a + \Delta E_d + \Delta E_h$	454	1900	4.6
Cotton	$C_6H_{10}O_5$	$\Sigma\Delta E_a + \Delta E_d + \Delta E_h$	454	2000	4.4
Acetate fiber	$C_6H_7O_2(OCOCH_3)_2$	$\Sigma\Delta E_a + \Delta E_d + \Delta E_h$	270	1200–1400	1.9
PVA (thermally stabilized)	$CH_2(CHOH)$	$\Sigma\Delta E_a + \Delta E_h$	510	1500–1600	5.4
Lavsan	$OCC_6H_4OCO(CH_2)_2O$	$\Sigma\Delta E_a + 2\Delta E_d + \Delta E_r$	227	1400	1.6
PGA (polyglycolide)	CH_2OCOCH_2OCO	$\Sigma\Delta E_a + 2\Delta E_d$	224	1040	–
HFPEM [15]	$Ph-C(CF_3)_2-Ph$	$\Sigma\Delta E_a + 2\Delta E_h + 2\Delta E_r$	229	910	–
PDMS [16]	$(CH_3)_2SiO$	$\Sigma\Delta E_a + \Delta E_d$	209	1070	–
Wool fabric* [17]	$(OCNH-CHR_1-OCNHCHR_2)$	$\Sigma\Delta E_a + 1.3\Delta E_h + 1.4\Delta E_d$	500	3480	3.4–4
Terlon	C_6H_4NHCO	$\Sigma\Delta E_a + \Delta E_h + \Delta E_d + \Delta E_r$	437	2500	3.5–3.7
Gelatin*	$OCNH-CHR_1-OCNHCHR_2$	$\Sigma\Delta E_a + 1.3\Delta E_h + 1.4\Delta E_d$	496	2590	3.9

* ΔE^* calculated for the average elemental composition.

Further, we pass at a known degree of crystallinity to the true sorption isotherm. Experience shows that using the published data [13] or direct determination of a_0^a at $P/P_0 = 1$ occasionally leads to a gross error, because the Schreder effect is observed for a number of polymers (especially those with a linear amorphous structure) in this transition region between the saturated vapor and the liquid phase ($\mu_{vap} = \mu_{liq}$ at $P/P_0 = 1$). In an analysis of a new object, its degree of crystallinity can be estimated if sorption is measured at one or several partial pressures of water vapor, e.g., by the desiccator method, and then the sorption obtained is compared with that calculated by the van Krevelen technique:

$$a/a_a = 1 - x_c. \quad (9)$$

The rather high reliability of this method was demonstrated in the monograph [3] for a number of aliphatic polyamides. The following degrees of crystallinity were obtained for fibers of an aromatic polyamide, Kevlar (polyparaphenyleneterephthalamide), by the van Krevelen method at above-mentioned relative pressures: 66, 62, 63, 73, 74% ($x_{av} = 68 \pm 5\%$). According to published data, the X-ray degree of crystallinity is about 70%.

As can be seen from Eqs. (5) and (6), the characteristic sorption energy E and the thermal coefficient of sorption are energy-related parameters of sorption. For example, at $a/a_0 = 1/e$, the enthalpy of sorption is determined only by these parameters: $\Delta\bar{H}_1 = E(-1 + \alpha T/n)$.

The enthalpy of sorption is proportional to the difference between the energy of bonds between macromolecules, which are ruptured in sorption, and the energy of formation of new polymer–sorbate bonds, with account of the change in the volume of the system ($\Delta H = \Delta U + P\Delta V$). Of these terms, only the first, frequently named the cohesion energy, can be rather easily calculated. It was shown in [20] that the cohesion energy taking into account the molecular packing of macromolecules, ΔE^*, can be calculated as an additive quantity $\Delta E^* = \Sigma\Delta E_i$ on the basis of the chemical structure of the polymer unit and energy contributions of separate atoms (ΔE_a) and types of molecular interactions (ΔE_d, ΔE_h, ΔE_r for the dipole–dipole interaction, hydrogen bond, and energy of the six-membered ring, respectively) to the cohesion energy. Equilibrium sorption data are commonly related to the mass of the polymer, rather than to a mole of polymer units. Therefore, we sought a correlation between α and E, on the one hand, and the specific cohesion energy (J g^{-1}), on the other, calculated from the contributions ΔE_i reported in [20]

$$\Delta E^* = \Sigma\Delta E_i/M_{un}. \quad (10)$$

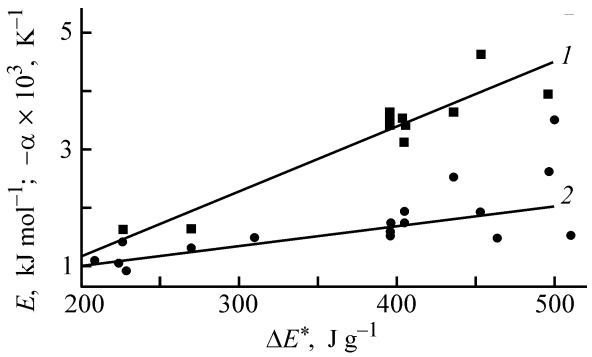

Fig. 1. (*1*) Thermal coefficient of sorption, α, and (*2*) characteristic energy E of water vapor sorption vs. the cohesion energy ΔE^* of glassy polymers.

Table 1 lists values of E and α, calculated from sorption isotherms, and schemes for calculation of ΔE^* on the basis of the molecular structures of units for a number of glassy polymers.

The characteristic sorption energy E is independent of temperature and degree of crystallinity of a polymer [10], but strongly depends on the method used to produce (synthesize) a polymer, drying conditions (i.e., extent to which the structure is not in equilibrium), and other technological factors. Therefore, E may vary rather widely even for the same polymer. For example, E has the following values for cellulose hydrate fibers (kJ mol^{-1}): 2.79 for Siblon, 1.9–2 for rayon cord, and 2.53 for chatelaine. Because of this circumstance, our and published (Table 1) data presented in Fig. 1 show a certain scatter near the linear dependence of the characteristic sorption energy E (J mol^{-1}) on the cohesion energy ΔE^* (J g^{-1}):

$$E = 350 + 3.3\Delta E^* \ (\pm 7.1\%). \quad (11)$$

In most cases, elastomers are low-polar or nonpolar polymers, and, therefore, their interaction with water is accompanied by weak sorption. Table 2 lists certain data on the characteristic sorption energy in relation to the polymer solubility parameter δ, which is proportional to the cohesion energy [13, 20]. No dependence of E on δ is observed in a rather wide range of δ values, and it can be taken, in a rough approximation, that the characteristic sorption energy is independent of the nature of a polymer: $E_{av} = 300 \pm 80$ J mol^{-1}. A similar behavior has been observed previously for sorption of other vapors by elastomers [9]. Probably, this is so because the heats of sorption are small in this case and the decrease in the Gibbs energy is mostly due to an increase in the entropy of sorption ($\Delta S > 0$) and, accordingly, to the rise in the amount of sorption with temperature ($\alpha > 0$). This has been observed in, e.g., sorption of vapors by polyurethanes [21].

Table 2. Characteristic energy of water vapor sorption by elastomers ($n = 0.5$)

Polymer	δ, MPa	E, J mol^{-1}
Spandex	29.9	400
PEM copolymer [15]	26	240
HCPEM copolymer [15]	24	290
Methyl polynorbornene [23]	20.2	440
Butyl polynorbornene [23]	19	230
Hexyl polynorbornene [23]	18.5	150
Decyl polynorbornene [23]	18	330
Copolymer of PA-12 and polytetrahydrofuran [24]	15–16	400–500

The thermal coefficient α characterizes the effect of temperature on the amount of sorption, its sign and magnitude are determined by the energy of interaction of water molecules with the elementary unit of a polymer. For polar polymers, the enthalpy and entropy of sorption $\Delta H < 0$ and $\Delta S < 0$ and, consequently, $\alpha < 0$ in the overwhelming majority of cases [22]. These interactions of water with a macromolecular compound are reflected to the greatest extent by the contributions ΔE_d and ΔE_h (dipole–dipole interactions and energy of the hydrogen bond) to the cohesion energy. The data of Table 1 are generalized in Fig. 1:

$$\alpha = 1.17 \times 10^{-3} - 1.12 \times 10^{-5}\Delta E^* \ (\pm 9.4\%). \quad (12)$$

Here, strong deviations are observed at a sufficiently high degree of linear correlation. Probably, this occurs because the value of α is mostly determined by the contributions ΔH_h and ΔH_d to the cohesion energy, i.e., by the presence of only polar groups in a polymer. For example, for cellulose materials and polyvinyl alcohol (PVA, main contribution from OH groups), the thermal coefficient $\alpha_{av} = -(5.1 \pm 0.3) \times 10^{-3}$ K^{-1}, and for aliphatic, aromatic, and natural polyamides containing OCNH groups, $\alpha = -(3.5 \pm 0.2) \times 10^{-3}$ K^{-1}.

The relations obtained enable calculation of the isotherm of water vapor sorption from a known degree of crystallinity of a polymer sample. Otherwise, it is necessary to measure at least a single point in the sorption isotherm.

Let us demonstrate this for the example of a thermally stabilized PVA fiber in which crystallization begins already in the stage of drying and continues in the course of thermal stabilization ($T = 487$ K).

To find the degree of crystallinity, we measure the amount of sorption at $P/P_0 = 0.7$ and $\alpha = 0.093$ g g^{-1}. Based on the chemical structure of the PVA unit, –CH_2–CHOH– ($M_{un} = 44$), and data of [13], we calculate using Eq. (7) the amount of sorption by amorphous PVA:

$$a_a = \frac{(2 \times 3.3 \times 10^{-5} + 0.75) \times 18}{44} = 0.307 \text{ g g}^{-1}.$$

Then the degree of crystallinity is found from $1 - x_c = 0.093 : 0.307 = 0.30$ to be $x_c = 0.70$.

Using Eqs. (10), (11), and (12), we calculate, respectively, the cohesion energy, characteristic sorption energy, and thermal coefficient of sorption:

$$\Delta E^* = \frac{2\Delta E_C + 4\Delta E_H + \Delta E_O + \Delta E_h}{M_{un}}$$

$$= \frac{2 \times 2305 + 4 \times 200 + 597 + 16\,447}{44} = 510 \text{ J g}^{-1},$$

$$E = 350 + 3.3\Delta E^* = 2030 \text{ J mol}^{-1},$$

$$\alpha = 1.1 \times 10^{-3} - 1.12 \times 10^{-5} \times 510 = -4.6 \times 10^{-3} \text{ K}^{-1}.$$

Using Eq. (1) with $T = T_0 = 298$ K, $a = 0.093$ g g^{-1}, and $P/P_0 = 0.7$, we calculate a_0:

$$\ln a_0 = \ln a + \left(-\frac{8.314 \times 298 \ln 0.7}{2030}\right)^{0.7} = -1.82,$$

$$a_0 = 0.163 \text{ g g}^{-1}.$$

Thus, we found all the constants of Eq. (1), i.e., we know the thermal equation of sorption

$$a = 0.163\exp\left[-\left(\frac{RT \ln P/P_0}{2030}\right)^{0.7} - 4.6 \times 10^{-3}(T - T_0)\right]. \quad (13)$$

Figure 2 shows experimental data on water vapor sorption by a thermally stabilized PVA fiber at 293 and 375 K (temperature close to that in drying) and results of calculations by Eq. (13). The information obtained makes it possible to calculate the integral heat of sorption by Eq. (6), e.g., at a drying temperature of 373 K:

$$q_i = \frac{2030 \times 0.163}{0.7 \times 18}(1 + 4.6 \times 10^{-3} \times 373) \times 0.8861$$

$$= 63.2 \text{ J g}^{-1}.$$

CONCLUSIONS

(1) It was shown that the thermal equation of sorption [Eq. (1)] can be used to calculate the amounts of water vapor sorption by polymeric materials in a wide temperature range.

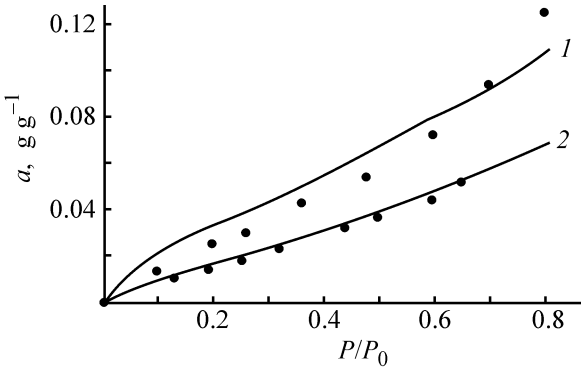

Fig. 2. Isotherms of water sorption a by thermally stabilized polyvinyl alcohol fiber at temperatures of (*1*) 293 and (*2*) 395 K.

(2) Equations relating the characteristic sorption energy and thermal coefficient of sorption to the cohesion energy of a polymer were obtained.

(3) An example calculation of the isotherms of water vapor sorption and heat of sorption was performed on the basis of the molecular structure of the polymer unit.

REFERENCES

1. Klyuev, L.E., Kynin, A.T, and Grebennikov, S.F., *Zh. Prikl. Khim.*, 1989, vol. 62, no. 10, pp. 2299–2303.
2. Papkov, S.P. and Fainberg, E.Z., *Vzaimodeistvie tsellyulozy i tsellyuloznykh materialov s vodoi* (Interaction of Cellulose and Cellulose Materials with Water), Moscow: Khimiya, 1976.
3. Chalykh, A.E., *Diffuziya v polimernykh sistemakh* (Diffusion in Polymeric Systems), Moscow: Khimiya, 1987.
4. Zaikov, G.E., Iordanskii, A.A., and Markin, V.A., *Diffuziya elektrolitov v polimerakh* (Diffusion of Electrolytes in Polymers), Moscow: Khimiya, 1984.
5. *Water in Polymers*, Rowland, S.P., Ed., Washington, D.C.: American Chemical Society, 1980.
6. Laatikainen, M. and Lindstrom, M., *Acta Polytechn. Scand. Chem. Technol. Met. Ser.*, 1987, no. 178, pp. 105–116.
7. Klyuev, L.E. and Grebennikov, S.F., *Zh. Fiz. Khim.*, 1996, vol. 70, no. 11, pp. 2053–2058.
8. Mikheev, Yu.A. and Zaikov, G.E., *Vysokomol. Soedin., Ser. A*, 1999, vol. 41, no. 5, pp. 852–863.
9. Grebennikov, S.F. and Kynin, A.T., *Zh. Prikl. Khim.*, 1982, vol. 55, no. 10, pp. 2299–2303.
10. Grebennikov, S.F., Perepelkin, K.E., and Kynin, A.T., *Gigroskopicheskie svoistva khimicheskikh volokon:*

Obzornaya informatsiya, Ser. "Prom–st. Khim. volokon" (Hygroscopic Properties of Chemical Fibers: Review Information, Series "Industry of Chemical Fibers"), Moscow: NIITEKhIM, 1989.

11. Kynin, A.T., Grebennikov, S.F., and Zaitseva, E.I., *Vestn. SpB. Gos. Uiniv. Tekhnol. Dizain.*, 2006, no. 12, pp. 106–110.
12. Grebennikov, S.F., Serpinskii, V.V., Pakhomov, Yu.I., and Yakubov, T.S., *Izv. Akad. Nauk SSSR, Ser. Khim.*, 1983, no. 3, pp. 498–503.
13. Van Krevelen, D.W., *Properties of Polymers*, Amsterdam: Elsevier, 1997.
14. Grebennikov, S.F., Kynin, A.T., and Serkov, A.T., *Khim. Volokna*, 1988, no. 5, pp. 48–49.
15. Dubey, V., Kuthe, S., Saxena, C., and Jaiswal, D., *J. Appl. Polym. Sci.*, 2003, vol. 88, no. 10, pp. 1760–1767.
16. Rezas, M., John, T., and Peromm, P., *J. Appl. Polym. Sci.*, 1997, no. 10, pp. 1983–1990.
17. Nikitina, L.M., *Termodinamicheskie parametry i koeffitsienty massoperenosa vo vlazhnykh materialakh* (Thermodynamic Parameters and Mass-Transfer Coefficients for Humid Materials), Moscow: Energiya, 1968.
18. *Spravochnik khimika* (Chemist's Handbook), Nikol'skii, B.P., Ed., Leningrad: Khimiya, 1971, pp. 1057–1058.
19. Grebennikov, S.F. and Gracheva, N.N., *Zh. Fiz. Khim.*, 1989, vol. 63, pp. 1988–1989.
20. Askadskii, A.A. and Matveev, Yu.I., *Khimicheskoe stroenie i fizicheskie svoistva polimerov* (Chemical Structure and Physical Properties of Polymers), Moscow: Khimiya, 1983.
21. Lipatov, Yu.S., Kercha, Yu.Yu., and Sergeeva, L.M., *Struktura i svoistva poliuretanov* (Structure and Properties of Polyurethanes), Kiev: Naukova Dumka, 1970.
22. Grebennikov, S.F., *Izv. Vyssh. Uchebn. Zaved., Khim. Khim. Tekhnol.*, 1984, vol. 27, no. 10, pp. 1185–1187.
23. Stasye, R. and Rezac, T., *Polymer*, 2004, vol. 45, no. 8, pp. 2641–2649.
24. *Polymer Data Handbook*, Mark, J.E., Ed., Oxford: Univ., 1999.

ISSN 1070-4272, Russian Journal of Applied Chemistry, 2007, Vol. 80, No. 12, pp. 2119–2123. © Pleiades Publishing, Ltd., 2007.
Original Russian Text © S.A. Trifonov, A.A. Malygin, A.K. D'yakova, J.-M. Lopez-Cuesta, N. Cinausero, 2007, published in Zhurnal Prikladnoi Khimii, 2007, Vol. 80, No. 12, pp. 2041–2045.

MACROMOLECULAR CHEMISTRY AND POLYMERIC MATERIALS

Thermal Transformations of a Polymeric Composite Consisting of Poly(Methyl Methacrylate) and Phosphorus-containing Nanodispersed Aluminum Oxide

S. A. Trifonov, A. A. Malygin, A. K. D'yakova, J.-M. Lopez-Cuesta, and N. Cinausero

St. Petersburg State Institute of Technology (Technical University), St. Petersburg, Russia
Centre des Materiaux de Grande Diffusion, Ecole des Mines d'Ales, France

Received May 31, 2007

Abstract—Thermal-oxidative properties of polymeric composites based on poly(methyl methacrylate), containing surface-modified nanosized aluminum oxide as filler, were examined. The possibility of chemical grafting to the Al_2O_3 surface of phosphorus-containing groups to decrease the combustibility of filled polymeric composites was examined by IR spectroscopy.

DOI: 10.1134/S1070427207120248

Inorganic fillers are widely used to improve the performance characteristics of polymeric composite materials [1]; they bring about a wide spectrum of interactions at the polymer–filler interface, thereby substantially affecting the mechanical and physicochemical, in particular, thermal-oxidative, properties of filled polymer system as a whole. The nature of these interactions is governed to a significant extent by the chemical composition of the filler surface [2].

Since recently, the focus of the special attention of researchers has been on highly dispersed (nanosized) fillers. They have a large specific surface area and exhibit enhanced reactivity toward polymer matrix, thereby promoting formation of chemical bonds limiting the mobility of various kinetic units of the polymer. Introduction of highly disperse fillers can change the packing density of the polymer chains, as well as the conformation and orientation of the segments occurring at the polymer–filler interface [3, 4].

Of special interest is chemical modification of fillers, considerably expanding the spectrum of their functions in composite materials. Directed modification of the filler surface aimed to produce groups capable of forming strong chemical bonds with macromolecules or increasing the resistance of polymers to thermal and thermal-oxidative degradation appreciably enhances the stability of filled composite materials [2, 5]. However, various chemical techniques applied to this end should not substantially affect the particle size of highly dispersed fillers and cause agglomeration of nanosize particles.

Among the promising ways of chemical modification of solid surfaces is molecular layer deposition (MLD) [6, 7]. With MLD method, the entire surface being activated is uniformly coated with the additives introduced, which form strong chemical bonds with the surface; the composition can be precisely set at the molecular level, and multicomponent structures with prescribed ratio and mutual position of elements can be formed.

We examined here the thermochemical transformations of a polymeric composite material based on poly(methyl methacrylate) (PMMA), filled with nanodispersed aluminum oxide and products of its surface modification with phosphorus-containing groups by the MLD method.

EXPERIMENTAL

As filler for PMMA served Aeroxide AluC (Degussa) nanodispersed aluminum oxide. Its specific surface area estimated from low-temperature nitrogen adsorption on a SORBI® N.4.1 instrument was 100 ± 3 $m^2 g^{-1}$; the average particle size was 13 nm. Samples of the composite materials were prepared by mixing crushed granules of Altuglas V 825T PMMA

Chemical composition and specific surface area of the fillers

Number of cycles of treatment with PCl_3 and H_2O vapors	Sample	Phosphorus content, mmol g^{-1}	Specific surface area, $m^2\ g^{-1}$
0	Al_2O_3	0	100
1	Al_2O_3-P	0.37	98
2	Al_2O_3-PP	0.55	100

with the initial or modified nanodispersed aluminum oxide on a Haake PolyLab installation at 225°C. The degree of filling for all the composites was 5%, and the mixing time, 10 min.

The filler surface was modified by the MLD method on a flow-type setup, comprised of a system for drying the carrier gas (air), reservoirs containing low-molecular-weight agents, an indirect heating glass reactor, and a system of adsorbers for sorption of gaseous reaction products [5]. As the low-molecular-weight agent served phosphorus trichloride PCl_3 (phosphorus compounds rank among the best flame retardants) [8]. The element oxide groups on the aluminum oxide surface were synthesized at 200 ± 10°C; the dew point of the carrier gas was not higher than –50°C. The chemical reaction occurring on the filler surface can be represented by the following scheme [7]:

$$n(\text{–AlOH}) + PCl_3 \rightarrow (\text{–Al–O–})_nPCl_{3-n} + n\text{HCl}. \quad (1)$$

To replace the chloride ions with OH groups in the composition of the surface structures of aluminum oxide, its surface was treated with water vapor:

$$(\text{–Al–O–})_nPCl_{3-n} + (3 - n)H_2O \rightarrow (\text{–Al–O–})_nP(OH)_{3-n} + (3 - n)\text{HCl}. \quad (2)$$

The phosphorus concentration was raised by repeated alternate treatment of aluminum oxide with

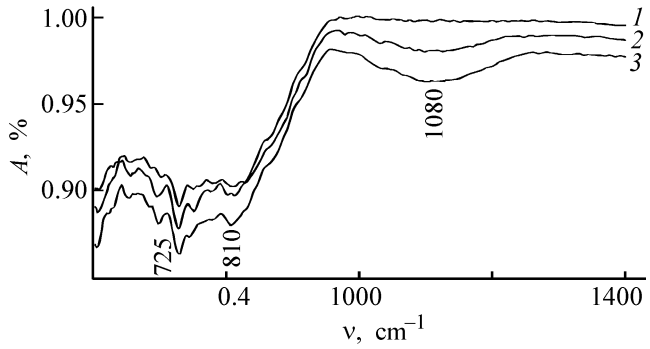

Fig. 1. IR Fourier spectra of the initial and modified aluminum oxide. (*A*) Absorption, and (ν) wavenumber; the same for Fig. 5. (*1*) Al_2O_3, (*2*) Al_2O_3-P, and (*3*) Al_2O_3-PP; the same for Fig. 5.

PCl_3 and water vapor. The flame retardant content of the filler was estimated by chemical analysis according to the known photocolorimetric procedure [9], accurately to less than 10%.

The thermal-oxidative properties of the resulting composite materials were determined by thermogravimetric analysis on a TGA 92 16.18 SETARAM installation in air under dynamic conditions at a constant heating rate of 5 deg min^{-1} and temperatures within 30–700°C. The weighed portion was 10–20 mg. The initial PMMA and PMMA-based composites were tested for combustibility by the cone calorimeter method [10]: samples (100 × 100 × 4-mm plates) were kept under constant external thermal flux of 35 kW m^{-2} and temperature near 650°C. This method allows determination of the maximal heat release Q_{max} and total heat release Q_{tot} for a polymeric material in combustion.

The IR spectra of the initial and phosphorus-containing samples of aluminum oxide, and also of the coke residues for the filled polymer composites after keeping at 650°C, were recorded on a Bruker IFS66 IR Fourier spectrometer equipped with a "golden gate" attachment at 400–4000 cm^{-1} with a resolution of 1 cm^{-1} [11].

To obtain filled polymer composites, we prepared samples of nanodispersed aluminum oxide by treatment with phosphorus chloride and water vapor in one and two cycles. The table lists the chemical compositions and specific surface areas of the initial and modified fillers.

The data in the table show that, as the number of the treatment cycles increases, the phosphorus concentration in the samples grows by nearly a factor of 1.5. It should be noted that synthesis of the phosphorus-containing structures by the MLD method on the Al_2O_3 surface does not substantially raise the size of the nanoparticles, as suggested by the close specific surface areas of the initial and modified samples (see table).

Figure 1 shows the IR Fourier spectra of the initial and modified Al_2O_3. The spectrum of the initial

filler contains absorption bands at 725 and 810 cm^{-1} corresponding to stretching vibrations of the Al–O bond (Fig. 1, curve *1*) [12]. Treatment of nanodispersed aluminum oxide with PCl_3 vapor gives rise a broad absorption band near 1080 cm^{-1}, associated, according to [12], with stretching vibrations of the P–O bond in aluminum phosphate, which suggests that element oxide groups are chemically grafted to the surface [scheme (1)]. This peak grows in intensity with as the modifier concentration increases (Fig. 1, curves *2*, *3*).

Thermogravimetric measurements showed that thermal-oxidative degradation of PMMA proceeds in two stages within the 250–340 and 340–425°C ranges (Fig. 2, curve *1*). Introduction of both the initial and modified fillers does not affect the two-stage character of the degradation of the polymeric composite. Figure 3 shows the temperature dependences of the mass loss for the initial and filled PMMA samples. The heat resistance of the polymer slightly increases upon introduction of aluminum oxide into the composition. The temperature corresponding to a 50% mass loss shifts by 20°C to higher temperatures relative to the initial material (Fig. 3, curve *2*). Also, the temperature corresponding to the maximal degradation rate in both stages increases by 10–20°C (Fig. 2, curve *2*). These changes are, evidently, due to adsorption and chemisorption interactions of the nanodispersed aluminum oxide surface with the polymer molecules, resulting in structure formation in the filled system [2]. The heat resistance of the polymer composite is virtually unaffected by synthesis of phosphorus-containing structures on the filler surface; it corresponds to that of the polymer with nanodispersed aluminum oxide. A probable reason is that the phosphorus concentration in the filled composites is very low, specifically, 0.05 and 0.09%, depending on the number of the cycles of treatment of aluminum oxide with PCl_3 vapor (Fig. 3, curves *3*, *4*).

The influence of chemical modification of the aluminum oxide surface with PCl_3 vapor is manifested most clearly in evaluation of the combustibility of the resulting composite materials. Figure 4 shows the time dependences of the heat release for the samples of the composites. The maximal heat release is 550 kW m^{-2} (Fig. 4, curve *1*). Upon introduction of unmodified oxide and a filler with the phosphorus concentration of 0.37 mmol g^{-1}, this combustibility parameter decreases to 500 kW m^{-2} (Fig. 4, curves *2*, *3*).

The combustibility of the composite tends to further decrease with increasing concentration of the flame retardant in aluminum oxide; the maximal heat release decreases by a factor of 1.35 (Fig. 4, curve *4*), compared to unfilled PMMA. Also, the total heat release, as estimated from the area enclosed by the curves in Fig. 4, significantly decreases, specifically, from 199.8 (initial polymer) to 96.4 MW m^{-2} upon introduction of aluminum oxide with the phosphorus concentration of 0.55 mmol g^{-1}.

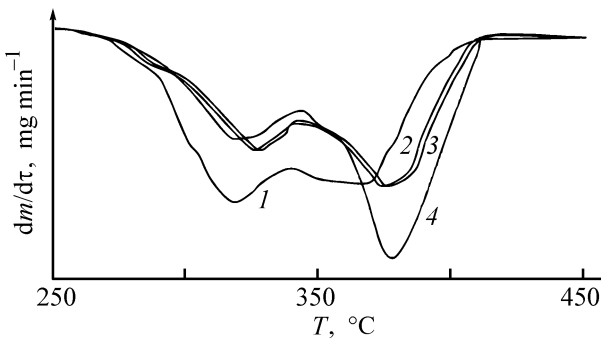

Fig. 2. DTG curves of the initial and filled PMMA samples. (d*m*/dτ) Mass change rate and (*T*) temperature. (*1*) Initial PMMA, (*2*) PMMA + Al_2O_3, (*3*) PMMA + Al_2O_3-P, and (*4*) PMMA + Al_2O_3-PP; the same for Figs. 3, 4.

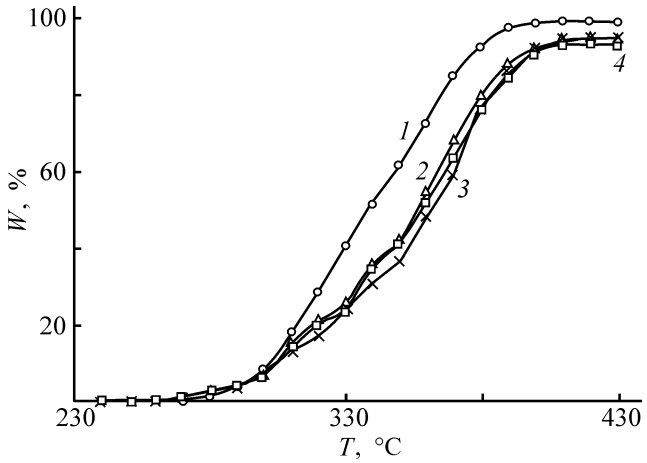

Fig. 3. Variation of the mass loss *W* of the initial and filled PMMA samples with temperature.

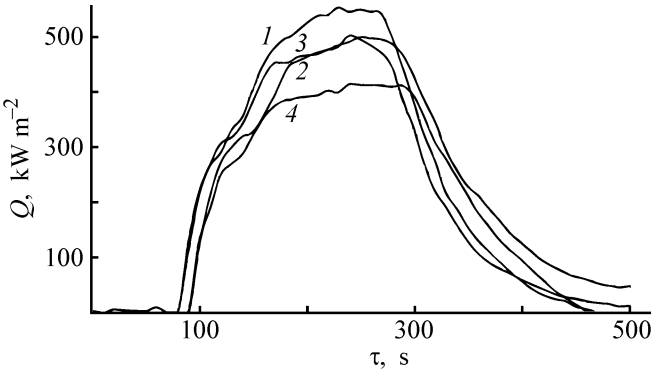

Fig. 4. Heat release *Q* for the composites based on PMMA and aluminum oxide. (τ) time.

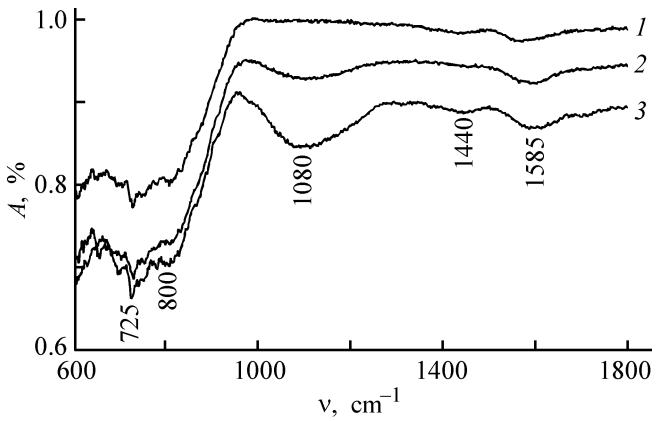

Fig. 5. IR Fourier spectra of the coke residues of the filled composites.

A decrease in the combustibility of the filled samples of the polymer material can be explained as follows. Degradation of PMMA starts with cleavage of weak bonds in the oxygen-containing functional groups. This is followed by cleavage of the bonds in the polymer backbone, accompanied by elimination of low-molecular-weight volatile products. The polymer degrades virtually exhaustively and yields a minor amount of a nonvolatile residue (coke) [2]. Introduction of aluminum oxide into the composite can promote adsorption of the PMMA degradation products on the nanodispersed filler surface [13], which is specifically responsible for a decrease in the heat release parameters in combustion of the composite. According to [8], the inhibiting effect of phosphorus compounds is manifested primarily in the condensed phase and is associated with their catalytic action on the coke formation in polymer materials. The presence of a flame retardant in the filled PMMA, evidently, exerts an additional influence on degradation of the polymer, due to involvement of the volatile pyrolysis products into structure formation in the nonvolatile residue. Stable organophosphorus compounds can be formed [14], which are involved in the coke formation, thereby decreasing further the combustibility of PMMA.

The above assumptions were confirmed by the results of an IR study of the coke residues from the filled samples. The mass loss of the initial PMMA at 650°C was close to 100%. The IR spectrum of the solid phase of the composite containing aluminum oxide contains absorption bands at 725 and 800 cm^{-1}, associated with stretching vibrations of the Al–O bond (Fig. 5). The phosphorus-containing structures in the coke residue are characterized by a band near 1080 cm^{-1}, associated with the stretching vibrations of the P–O bond (Fig. 5, curves *2*, *3*). The appearance of an absorption band at 1585 cm^{-1} and, upon increase in the phosphorus content, of a band near 1440 cm^{-1} (Fig. 5, curve *3*) can be associated with the presence [15] of heat-resistant aromatic compounds involved in formation of the solid phase.

Thermogravimetric data obtained upon heating of the residues formed in calorimetric tests to 1000°C agree with the IR data. The mass loss for the PMMA filled with aluminum oxide was 7.4%. In the presence of the flame retardant, the mass loss increases upon high-temperature treatment, specifically to 9.4 and 14.2% for one and two cycles of treatment of the filler with PCl_3 and H_2O vapors, respectively (see table). Thus, upon introduction of nanodispersed aluminum oxide into a PMMA-based composite, the organic component increases in size, and the phosphorus-containing groups make an additional contribution to the formation of a solid residue owing to heat-resistant aromatic fragments yielded by heat treatment.

CONCLUSIONS

(1) The combustibility and heat resistance of polymer composites can be controlled by chemical modification of the filler surface, as demonstrated for poly(methyl methacrylate)–nanodispersed aluminum oxide system as an example.

(2) Chemical grafting of phosphorus-containing groups to the aluminum oxide surface causes the total heat release of the filled poly(methyl methacrylate) samples to decrease by a factor of 1.5–2.0, depending on the content of the flame retardant in the composite.

(3) Phosphorus-containing structures, presumably, affect the degradation of poly(methyl methacrylate) in combustion; they are involved in the structure formation and coke formation in filled composite materials, as demonstrated by IR studies and combustibility tests.

ACKNOWLEDGMENTS

This study was financially supported in part by the Russian Foundation for Basic Research (project no. 06-03-81010).

REFERENCES

1. *Napolniteli dlya polimernykh kompozitsionnykh materialov* (Fillers for Polymeric Composite Materials), Kats, G.S. and Milevski, D.V., Eds., Moscow: Khimiya, 1981.
2. Bryk, M.T., *Destruktsiya napolnennykh polimerov*

(Degradation of Filled Polymers), Moscow: Khimiya, 1989.

3. Du, J., Zhu, J., Wilkie, C.A., and Wang, J., *Polym. Degrad. Stab.*, 2002, vol. 77, pp. 377–381.
4. Laachachi, A., Leroy, E., Cochez, M., et al., *Polym. Degrad. Stab.*, 2005, vol. 89, pp. 344–352.
5. Trifonov, S.A., Malkov, A.A., and Malygin, A.A., *Zh. Prikl. Khim.*, 2000, vol. 73, no. 4, pp. 659–664.
6. Malygin, A.A., *Zh. Prikl. Khim.*, 1996, vol. 69, no. 10, pp. 1585–1593.
7. Malygin, A.A., Malkov, A.A., and Dubrovenskii, S.D., *Adsorption on New and Modified Inorganic Sorbents*, vol. 99 of *Studies in Surface Science and Catalysis*, Dabrowsky, A. and Tertykh, V.A., Eds., Amsterdam: Elsevier, 1996, p. 213.
8. Kodolov, V.I., *Zamedliteli goreniya polimernykh materialov* (Flame Retardants for Polymer Materials), Moscow: Khimiya, 1980.
9. Charlot, G., *Les methods de la chimie analytique. Analyse quantitative minerale*, Paris: Masson, 1961, 4th ed.
10. *ISO 5660-1:2002: Reaction-to-Fire Tests: Heat Release, Smoke Production, and Mass Loss Rate*, part 1: *Heat Release Rate (Cone Calorimeter Method)*.
11. Walls, D.J., *Appl. Spectrosc.*, 1991, vol. 45, no. 7, pp. 1193–1198.
12. Yurchenko, E.N., Kustova, G.N., and Batsanov, S.S., *Kolebatel'nye spektry neorganicheskikh soedinenii* (Vibrational Spectra of Inorganic Compounds), Novosibirsk: Nauka, 1981.
13. Aseeva, R.M. and Zaikov, G.E., *Gorenie polimernykh materialov* (Combustion of Polymer Materials), Moscow: Nauka, 1981.
14. Trifonov, S.A. and Malygin, A.A., *Plast. Massy*, 1997, no. 5, pp. 37–39.
15. Kazitsyna, L.A. and Kupletskaya, N.B., *Primenenie UF-, IK- i YaMR spektroskopii v organicheskoi khimii: uchebnoe posobie dlay vuzov* (Application of UV, IR, and NMR Spectroscopy to Organic Chemistry: Handbook for Higher Schools), Moscow: Vysshaya Shkola, 1971.

ISSN 1070-4272, Russian Journal of Applied Chemistry, 2007, Vol. 80, No. 12, pp. 2124–2128. © Pleiades Publishing, Ltd., 2007.
Original Russian Text © Yu.N. Sazanov, A.V. Novoselova, G.N. Fedorova, E.M. Kulikova, A.V. Gribanov, 2007, published in Zhurnal Prikladnoi Khimii, 2007, Vol. 80, No. 12, pp. 2046–2050.

MACROMOLECULAR CHEMISTRY AND POLYMERIC MATERIALS

Mechanism of Low-Temperature Carbonization of Polyacrylonitrile

Yu. N. Sazanov, A. V. Novoselova, G. N. Fedorova, E. M. Kulikova, and A. V. Gribanov

Institute of Macromolecular Compounds, Russian Academy of Sciences, St. Petersburg, Russia

Received May 28, 2007

Abstract—Low-temperature carbonization of polyacrylonitrile was studied in relation to the synthesis procedure, heat treatment conditions, and presence of natural polymers as cocarbonization participants.

DOI: 10.1134/S107042720712025X

Carbonization of polyacrylonitrile (PAN) and specific features of thermochemical transformations of this unique polymer have been the subject of numerous studies summarized in monographs and reviews [1–6]. Certain attention was given in these studies to elucidation of the mechanism of PAN transformation into carbon structures in a wide temperature range. However, the mechanism of this transformation and of its particular steps has not been analyzed in detail. Data on simulation (theoretical and experimental) of thermochemical reactions of PAN on the fundamental level, and not under the specific conditions dictated by practical requirements (feasibility, cost efficiency, environmental safety), are virtually lacking.

The majority of studies have been performed with poorly characterized commercial PAN samples. In this study, we examined thermochemical transformations occurring in the range 20–600°C in various PAN samples prepared in a laboratory.

EXPERIMENTAL

Three types of PAN were examined. The first of these was PAN prepared by anionic polymerization (A-PAN) in the presence of butyllithium by the procedure described in [7]; this polymer has a high molecular weight (MW) and narrow molecular-weight distribution (MWD), it does not contain low-molecular-weight fractions and branchings and has an increased stereoblock structure parameter [8], because it is most similar to the ideal polymer in the molecular structure. The second was PAN prepared by radical polymerization in the presence of a widely used catalytic redox system (R-PAN) [9]; in contrast to A-PAN, R-PAN samples are characterized by high polydispersity, presence of branchings in polymer chains, noticeable content of low-molecular-weight fractions, and presence of oxygen-containing terminal groups. The third was A-PAN partially cyclized in the course of the synthesis (C-PAN). We also used a series of PAN-containing composite systems with addition of 75% chitin, chitosan, cyanoethyl cellulose, allyloxyethyl cellulose, and kraft cellulose.

Let us consider the results of a calorimetric analysis of a series of PAN samples differing in the procedure of polymer synthesis (Fig. 1). The analysis revealed thermophysical processes occurring in the range 400–600°C. A simultaneous TGA of the same samples showed no sharp changes in the weight loss rate. The thermograms of all the three PAN samples demonstrate exo- and endothermic effects. As judged from the peak shape, they reflect melting and crystallization processes. Comparison of the peak temperatures, peak areas, and order in which thermal effects appear shows that the thermal effects are the most pronounced in A-PAN and the least pronounced in R-PAN. This difference is apparently associated with the molecular-weight characteristics of the objects. It is known that thermal cyclization of R-PAN involves release of low-molecular-weight products of thermal degradation [10]. This is associated with a broad MWD and with branchings in R-PAN chains. Therefore, the density of macromolecular packing in R-PAN precipitated from solution is low, and samples undergo more intense oxidation, which is reflected in the temperature and area of the exothermic peak. In contrast to R-PAN, A-PAN samples have a narrow MWD, with no low-molecular-weight fractions and branchings, which, combined with the stereoblock structure, predetermines

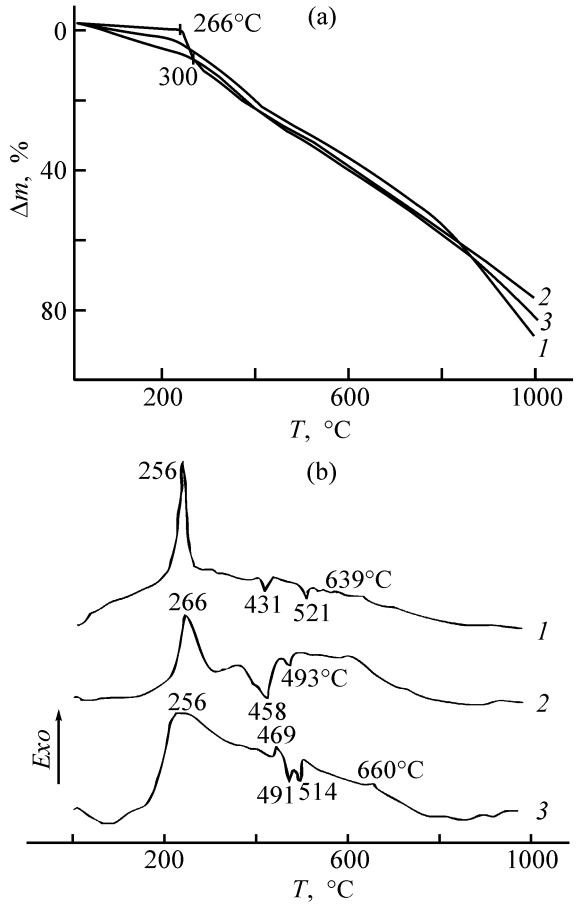

Fig. 1. (a) TG and (b) DTA curves of various PAN samples in air. MOM derivatograph, model C; sample weight 50 mg; heating rate 10 deg min^{-1}. (Δm) Weight loss and (T) temperature. (*1*) R-PAN, (*2*) A-PAN, and (*3*) C-PAN.

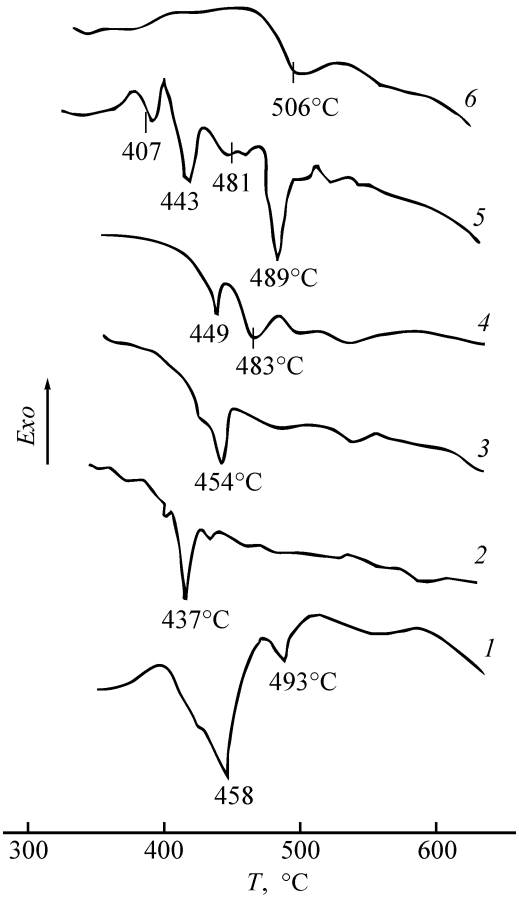

Fig. 2. DTA curves of powdered A-PAN samples annealed in nitrogen at (*2*) 250, (*3*) 270, (*4*, *5*) 350, and (*6*) 400°C for (*2–4*, *6*) 4 and (*5*) 10 h; (*1*) unannealed sample. (T) Temperature; the same for Figs. 3 and 4.

the high density of A-PAN and the corresponding changes in the characteristics of its thermal effects. An additional factor determining the high packing density is the steric ordering of A-PAN macromolecules.

In solution, A-PAN macromolecules form a double-helix structure whose constituent chains are linked by weak bonds between cyano groups and α-H atoms, between cyano groups, and, occasionally, between naphthyridine rings [4, 5, 11]. These structural features of A-PAN result in the preferable cyclization, compared to thermal degradation, and this is reflected in the TG and DTA curves. Furthermore, the stereoblock structure of A-PAN is apparently responsible for the presence of two endothermic effects in the temperature range 400–600°C, each of which reflects melting of an *iso*- or *syndio*tactic block. Ordered blocks may also be present in R-PAN, but their size and relative content are considerably lower than in A-PAN. As for the DTA curve of the C-PAN sample, the shift of the temperatures of its two endothermic effects (491 and 514°C) reflects the increased heat resistance of cyclic stereoblocks formed in the course of the synthesis.

When considering the pattern of low-temperature carbonization of PAN, we should note that, to obtain new condensed structures by transformation of macromolecular compounds, one should take into account the "diffusion factor." This phenomenon, typical of coal fuel chemistry, is associated with control over the release of low-molecular-weight thermal degradation products from the area of thermochemical reactions. As a result, the balance between the degradation and cross-linking is shifted toward cross-linking. The simplest way to reduce the release of low-molecular-weight products is to raise the sample weight and density and to perform an isothermal heat treatment for a longer time. By so doing, it will be possible to follow more clearly the thermophysical phase transformations in the PAN samples.

Figure 2 shows the DTA curves of A-PAN samples annealed in nitrogen at temperatures of the max-

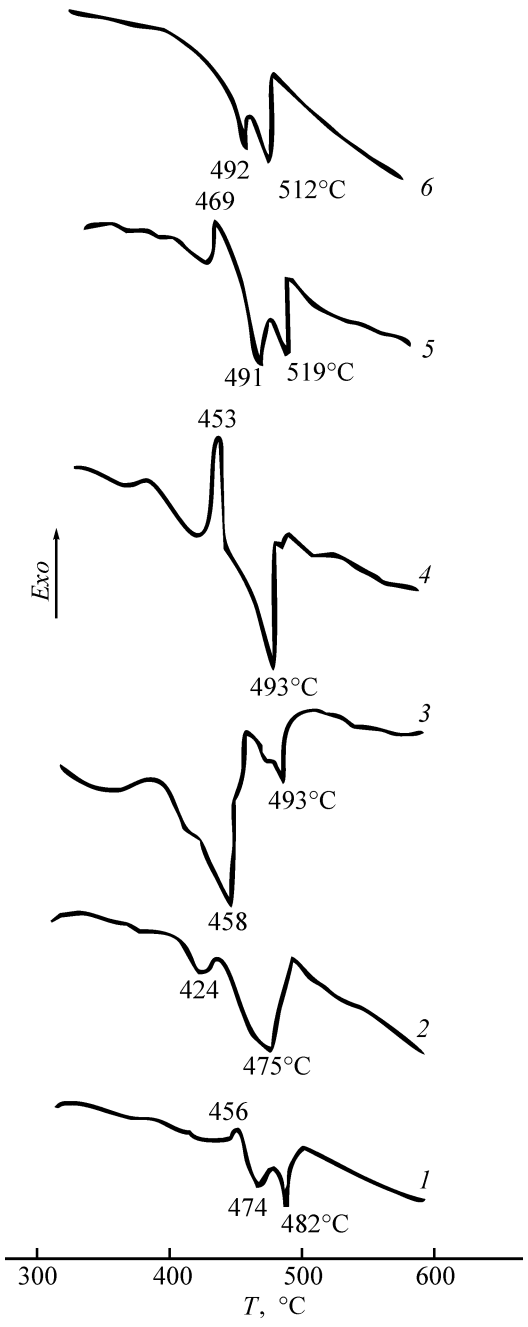

Fig. 3. DTA curves of powdered PAN samples compacted in a closed crucible: (*2*) R-PAN, (*4*) A-PAN, and (*6*) C-PAN; (*1*, *3*, *5*) the same samples in open crucibles.

imal thermal activity of PAN (250–400°C), when the linear structure of PAN transforms into a cyclic structure. As for the thermal effects related to phase transitions and assignable to crystallization and melting of new structural modifications, the clearest pattern is observed on heating an A-PAN sample for 10 h at 350°C. At this temperature, the exothermic process of A-PAN cyclization to give the most oriented stereoblocks of the syndiotactic structure is complete [8]. Because this process is characterized by the lowest activation energy, compared to the corresponding processes in isotactic A-PAN and R-PAN, prolonged heating at 350°C results in the gradual formation of segments of the turbostratic structure, which melt at 407, 443, and 489°C and are characterized by different steric orientations of cyclic blocks formed in the polymer. At lower annealing temperatures, the formation of the block structure is incomplete, and at higher temperatures, degradation of strained cyclic blocks starts, with an increase in the degree of carbonization.

The effect of the diffusion factor is demonstrated in Fig. 3. It is seen that, irrespective of the procedure of PAN synthesis, compaction of the sample and its isolation from the oxidizing medium essentially change the pattern of thermophysical effects in the samples. For some of them, we observe not only an increase in the energy of endothermic effects related to ordered areas, but also appearance of exothermic effects (curves *4*, *5*) assignable to the crystallization of the labile structure of the precarbonizate. Note that, with compaction of the sample, the coke residue increases as compared to powder samples of small weight.

It is interesting to use the phenomena of fractal orientation of PAN macromolecules, discovered when fractal-matrix structurizers (FMS) produced by Airis company were used [12]. In that study, we demonstrated for the examples of A- and R-PAN samples in solution that, on prolonged keeping of R-PAN solutions in the presence of FMS, solutions become more heterogeneous but remain isotropic. Under the same conditions, A-PAN solutions undergo self-orientation with a change in the structural parameters. On prolonged interaction with FMS, anisotropic structures are formed. This phenomenon allows control over the structural orientation of A-PAN and thus enables simulation of the precursors of turbostratic structures before the onset of carbonization.

Proceeding with these studies, we performed experiments in which the time of the action of FMS on the similar solutions of R- and A-PAN was made more than ten times longer. An analysis of the viscous characteristics of the polymer solutions stored for 4 and 10 months, in combination with two methods of polymer isolation (precipitation and solvent evaporation), showed that the fractional separation of the low-molecular-weight fraction occurs in the R-PAN solution, whereas in A-PAN this fraction is not detected. Furthermore, the viscosity of R-PAN solution decreased in the course of keeping with the structurizer

by almost a factor of 3 (without FMS, by a factor of 1.7). Under the same conditions, the A-PAN solution showed no response to the presence of FMS. Thus, longer keeping of PAN solutions both with FMS and without it allows the polydispersity and degree of branching of R-PAN to be decreased. This phenomenon positively affects the mechanical characteristics of films cast from R-PAN solutions. By raising their elasticity, tensile strength, and Young's modulus. As for A-PAN films, their strength and elasticity somewhat decrease because of the increased heterogeneity of the system and of its tendency toward self-organization, which leads to gelation and negatively affects the mechanical properties of the films.

The effect of FMS treatment on the subsequent carbonization of A-PAN cannot be revealed unambiguously. On the one hand, the more pronounced heterogeneity of the structure allows better separation of the thermal effects related to fragments of the A-PAN macromolecule with different stereoblock structures because of the increased mobility of segments with atactic units. On the other hand, there is no direct evidence that the structural organization of these samples remains unchanged after the removal of the solvent.

One more indirect evidence that a structural rearrangement occurs in PAN in the temperature range 400–600°C to give ordered fragments of the turbostratic type is furnished by interpretation of the structural polymorphism of coals in the same temperature interval. According to an X-ray diffraction analysis [13–15], the maximum of the internetwork ordering is observed at 450–525°C, i.e., in the range of the plastic state of coals and formation of a semicoke. As the temperature is raised to 700°C, the mutual ordering of networks that formed carbon structures is distorted, they are disoriented, and then, at temperatures above 1000°C, repeated orientation on the level of graphitizing structures is observed. A decrease in the internetwork ordering at temperatures above 700°C is due to the "wedging" effect of the growing carbon networks, with preservation of strong valence bonds between them through the irregular part of the structure preventing mutual orientation of the networks [16]. Thus, even in such a complex system as coking coals, there is a temperature interval of increased molecular mobility, in which ordered carbon structures with clear orientation parameters are formed. The coincidence of this temperature interval with that of the endo- and exothermic thermophysical effects observed in our case allows us to draw a certain analogy between these processes.

The above-noted similarity in the low-temperature carbonization of PAN and formation of a semicoke

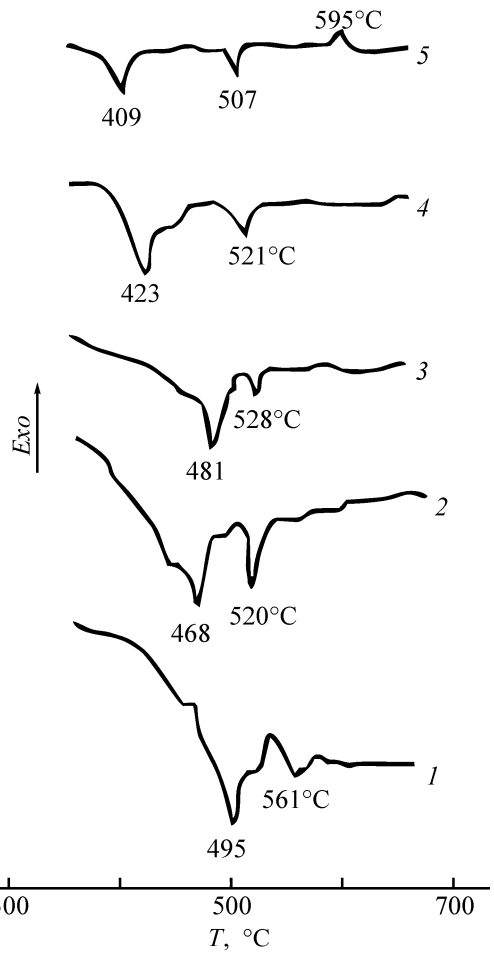

Fig. 4. DTA curves of composite samples of R-PAN with additions of polymers (75 wt %): (*1*) chitosan, (*2*) chitin, (*3*) cyanoethyl cellulose, (*4*) allyloxyethyl cellulose, and (*5*) kraft cellulose.

in the interval of the plastic state of coals confirms the concept of polymer cocarbonization [17], according to which the process occurs as thermochemical reactions of two polymers to give carbon structures whose thermophysical characteristics differ from those produced by the polymers taken separately. Indeed, our experiments revealed the formation of new structures with specific thermal characteristics in the temperature range 400–600°C. Figure 4 shows as an example the DTA curves of PAN cocarbonizates with a series of natural compounds. It is seen that introduction into PAN of 75 wt % of a second polymer (chitin, chitosan, cyanoethyl cellulose, allyloxyethyl cellulose, kraft cellulose, etc. [18–20]) does not decrease the thermal effects of structural organization in this temperature range. This fact confirms the significant influence exerted by the chemical nature of the second component on the formation of the base

structure of oriented carbon products. The role of PAN consists in the formation of nitrogen-containing polyheterocycles favorable for carbonization of the composites and their transformation into carbon structures at lower temperatures, compared to carbon-chain polymers.

CONCLUSIONS

(1) It was shown that polyacrylonitrile prepared by anionic polymerization is the most suitable compound for studies of low-temperature carbonization.

(2) The role of isothermal heat treatment and diffusion factor in the formation of oriented carbonized structures of polyacrylonitrile was elucidated.

(3) The optimal conditions were determined for thermal reactions of polyacrylonitrile with a series of natural polymers with the aim to obtain ordered cocarbonizates.

REFERENCES

1. Konkin, A.A., *Uglerodnye i drugie zharostoikie voloknistye materialy* (Carbon-Based and Other Heat-Resistant Fibrous Materials), Moscow: Khimiya, 1974.
2. Fialkov, A.S., *Uglerod, mezhsloevye soedineniya i kompozity na ego osnove* (Carbon and Intercalation Compounds and Composites Based on It), Moscow: Aspekt, 1997.
3. Varshavskii, V.Ya., *Uglerodnye volokna* (Carbon Fibers), Moscow: Varshavskii, 2006.
4. Beeveres, R.B., *Macromol. Rev.*, 1968, vol. 3, pp. 113–175.
5. Henrici-Olivie, G. and Olivie, S., *Adv. Polym. Sci.*, 1979, vol. 32, pp. 125–152.
6. Sazanov, Yu.N. and Gribanov, A.V., *Zh. Prikl. Khim.*, 1997, vol. 70, no. 6, pp. 881–902.
7. Novoselova, A.V., Erusalimskii, B.L., Krasulina, V.N., and Zashcherinskii, E.V., *Vysokomol. Soedin., Ser. A*, 1971, vol. 13, no. 1, pp. 87–90.
8. Sazanov, Yu.N., Novoselova, A.V., Amsharov, K.Yu., et al., *Zh. Prikl. Khim.*, 2005, vol. 78, no. 3, pp. 810–813.
9. Sazanov, Yu.N., Shirokov, N.A., and Goltsin, B.E., *Thermochim. Acta*, 1979, vol. 32, pp. 73–79.
10. Sazanov, Yu.N., Kutsenko, L.I., and Novoselova, A.V., *Zh. Prikl. Khim.*, 2005, vol. 78, no. 4, pp. 652–654.
11. Rumynskaya, I.G., Agranova, S.Ya., Novoselova, A.V., et al., *Vysokomol. Soedin., Ser. A*, 1999, vol. 41, no. 6, pp. 1–6.
12. Silinskaya, I.G., Novoselova, A.V., Sazanov, Yu.N., et al., *Zh. Prikl. Khim.*, 2006, vol. 79, no. 8, pp. 1391–1393.
13. Kasatochkin, V.I. and Larina, N.K., *Stroenie i svoistva prirodnykh uglei* (Structure and Properties of Natural Coals), Moscow: Nedra, 1975.
14. Chernousov, Ya.M., *Protsessy i zakonomernosti ugleobrazovaniya* (Processes and Relationships of Coal Formation), Kiev: Vishcha Shkola, 1978.
15. Artem'ev, V.B., Eremin, I.V., Lisurenko, A.V., and Gagarin, S.G., *Usloviya obrazovaniya i kharakternye priznaki dinamicheski aktivnykh uglei* (Conditions of Formation and Characteristic Features of Dynamically Active Coals), Moscow: Nedra, 1999.
16. *Strukturnaya khimiya ugleroda i uglei* (Structural Chemistry of Carbon and Coals), Kasatochkin, V.I., Ed., Moscow: Nauka, 1968.
17. Sazanov, Yu.N. and Gribanov, A.V., *Zh. Prikl. Khim.*, 2006, vol. 79, no. 3, pp. 440–445.
18. Sazanov, Yu.N., Nud'ga, L.A., Petrova, V.A., et al., *Zh. Prikl. Khim.*, 2004, vol. 77, no. 8, pp. 1366–1369.
19. Sazanov, Yu.N., Nud'ga, L.A., Petrova, V.A., et al., *Zh. Prikl. Khim.*, 2004, vol. 77, no. 4, pp. 643–648.
20. Sazanov, Yu.N., Kutsenko, L.I., and Novoselova, A.V., *Zh. Prikl. Khim.*, 2005, vol. 78, no. 4, pp. 652–654.

ISSN 1070-4272, Russian Journal of Applied Chemistry, 2007, Vol. 80, No. 12, pp. 2129–2131. © Pleiades Publishing, Ltd., 2007.
Original Russian Text © N.A. Nesterova, I.I. Gavrilova, E.F. Panarin, 2007, published in Zhurnal Prikladnoi Khimii, 2007, Vol. 80, No. 12, pp. 2051–2053.

MACROMOLECULAR CHEMISTRY AND POLYMERIC MATERIALS

Enzymatic Polymerization of Vinyl Monomers

N. A. Nesterova, I. I. Gavrilova, and E. F. Panarin

Institute of Macromolecular Compounds, Russian Academy of Sciences, St. Petersburg, Russia

Received July 5, 2007

Abstract—The possibility of using horse radish peroxidase as a catalyst for polymerization of monomers (vinylformamide and sodium vinylsulfonate) in the presence of hydrogen peroxide and 2,4-pentanedione in aqueous medium at room temperature was studied.

DOI: 10.1134/S1070427207120261

The use of horse radish peroxidase (HRP) and other oxidases for catalysis of radical polymerization of vinyl monomers was first reported in [1]. Horse radish peroxidase is recovered from horse radish roots. It belongs to the group of isoenzymes with the molecular weight of $(38-42) \times 10^3$ and the isoelectric point of 7.2; it is stable in the pH range 4.5–12. Peroxidase consists of colorless glycoprotein and brown-red ferriporphyrin bound to it [2]. Peroxidase catalyzes oxidation of chemical compounds with oxygen of hydrogen peroxide via a series of intermediate complexes [3]:

$$\text{–Fe(III)–} \rightarrow (H_2O_2 \rightarrow H_2O) \rightarrow \text{–Fe(O)(IV)}^{\cdot+}, \quad \textbf{I}$$

$$\text{–Fe(O)(IV)}^{\cdot+} \rightarrow (RH \rightarrow R^{\cdot} + H^+) \rightarrow \text{–Fe(O)(IV)–}, \quad \textbf{II}$$

$$\text{–Fe(O)(IV)–} \rightarrow (RH + H^+ \rightarrow H_2O + R^{\cdot}) \rightarrow \text{–Fe(III)–}. \quad \textbf{III}$$

In a series of publications [3–5] devoted to enzymatic polymerization, β-diketones were used as proton donors, along with HRP, as an initiating system for polymerization of acrylamide, methyl methacrylate, and styrene. Based on these publications, we used in this study HRP, 2,4-pentanedione (PD), and H_2O_2 as an initiating system.

The scheme of the stage of polymerization initiation can be represented as:

$$H_2O_2 + 2RH \rightarrow (HRP) \rightarrow 2H_2O + 2R^{\cdot},$$

$$2R^{\cdot} + M \rightarrow RM^{\cdot},$$

where M is monomer and RH is 2,4-pentanedione:

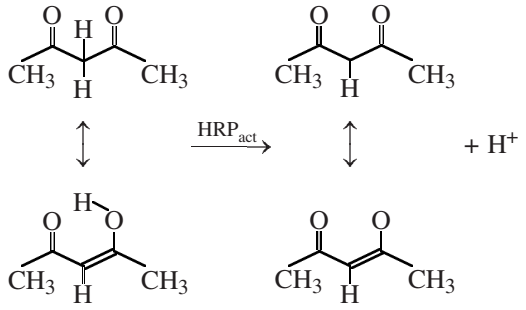

One H_2O_2 molecule produces two catalytically active forms of HRP, each of which oxidizes the initiator (RH) producing free radical ($R^{\cdot}$). Then the radical initiator reacts with monomers (M) to form monomer radicals ($RM^{\cdot}$), which react with other monomers to form a polymer [6].

The use of HRP in the composition of a system initiating the polymerization of monomers by the radical mechanism allows the process to be performed under mild conditions, i.e., in an aqueous medium and at low temperatures, which is extremely important in production of polymers for medical and biological purposes.

The aim of this study was to examine the possibility of polymerization of *N*-vinylformamide (VFA) and sodium vinylsulfonate (NaVS) in the presence of HRP:

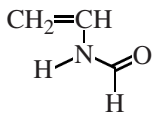

VFA

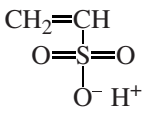

NaVS

Table 1. ^{1}H and ^{13}C NMR chemical shifts of polyvinylformamide and sodium polyvinylsulfonate

Polymer	Chemical shift δ, ppm						
	$-C_{\alpha}H-$		$-CH_2-$		$-C(=O)H$		–NH–
	^{1}H	^{13}C	^{1}H	^{13}C	^{1}H	^{13}C	^{1}H
PVFA	3.936	42.434	1.707	39.482	8.045	163.554	7.708
NaPVS	3.739		2.392				
	3.562		2.073				
	3.155		1.843				

EXPERIMENTAL

We used HRP (Reanal, Hungary) with an activity of 350–500 units per milligram (*o*-diazidine method) and spectral index of purity *RZ* = 0.24. The *RZ* factor was determined on a Specord M-40 spectrophotometer as the ratio of the intensity of UV absorption of an HRP solution in acetate buffer solution (pH 5) at 410 nm to the intensity of the absorption at 275 nm [7]. The H_2O_2 concentration was 3.4% (Krasnodar Pharmaceutical Factory) and was checked by permanganatometric titration [8]. 2,4-Pentanedione (PD) was purchased from the München Co. (Germany), bp 108°C. *N*-Vinylformamide (Aldrich) was purified by vacuum distillation, bp 71°C (3 mm Hg). Sodium vinylsulfonate (Aldrich) was freeze-dried from 25% aqueous solution.

Polymerization was performed in an inert atmosphere (argon) in water at 20, 25, and 37°C in glass ampules. Initially, the monomer was charged into ampules and then HRP dissolved in water (0.4 mg ml^{-1}), H_2O_2 (0.224 mmol), PD (0.082 mmol), and water were added.

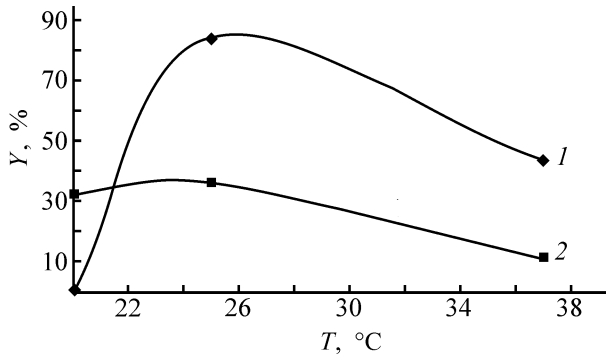

Influence of the polymerization temperature *T* on the polymer yield *Y*. Polymerization time 48 h for PVFA and 24 h for NaPVSN, concentration of monomers in water 26 wt %, concentration of HRP 0.4 mg ml^{-1}, H_2O_2 : PD = 0.224 : 0.082 (mmol). (*1*) PVFA and (*2*) NaPVS.

Polyvinylformamide (PVFA) was isolated by precipitation from an aqueous solution into acetone; sodium polyvinylsulfonate (NaPVS) and low-molecular-weight PVFA were isolated by freeze-drying after purification by dialysis.

The molecular weights of the polymers were determined by the viscometric method [9] at 25°C in 1 M aqueous KCl and in 0.2 M aqueous NaCl for PVFA and in 0.5 M aqueous NaCl for NaPVS. The viscometric measurements were performed with an Ostwald viscometer. The molecular weight was evaluated using the Mark–Kuhn–Houwink relationship. For PVFA,

$$[\eta] = 10.7 \times 10^{-3} M^{0.76},\ [\eta] = 8.44 \times 10^{-3} M^{0.78},\ [10];$$

for NaPVS,

$$[\eta] = 2.15 \times 10^{-4} M^{0.65}\ [11].$$

The structure of NaPVS and PVFA was determined by ^{1}H and ^{13}C NMR spectroscopy. The NMR spectra of solutions in D_2O were recorded on an AVANCE 400 spectrometer (Bruker, Germany). The chemical shifts of the resulting polymers are listed in Table 1. The results of experiments on polymerization of VFA and NaVS are presented in Table 2.

The influence of the polymerization temperature *T* (°C) on the yield of PVFA and NaPVS is shown in the figure. For this catalytic system, the optimum reaction temperature is 25°C, at which the yield of the polymers is the highest.

Polymerization of VFA was performed in 8, 26, and 59% solutions of the monomer. Irrespective of the polymerization time, the yield of the polymer did not exceed 16% at 20°C and a monomer concentration of 26 wt %. At 25 and 37°C, the maximal yield reached 84 and 44%, respectively (in both cases, polymerization for 48 h, monomer concentration in aqueous solution 26 wt %). The molecular weight

Table 2. Results of enzymatic polymerization of vinylformamide and sodium vinylsulfonate with horse radish peroxidase as a catalyst [concentration of horse radish peroxidase 0.4 mg ml^{-1}, H_2O_2 : PD = 0.224 : 0.082 (mmol)]

Sample no.	Monomer	Polymerization conditions			Yield, wt %	$[\eta]^{25}$,* dl g^{-1}	$M_\eta \times 10^3$
		monomer concentration in water, wt %	T, °C	τ, h			
1	VFA	59	20	72	6	0.24	27
2	VFA	26	20	72	12	0.30	36
3	VFA	8	20	72	6	0.31	36
4	VFA	8	25	72	56	0.28	31
5	VFA	26	20	48	1	–	–
6	VFA	26	25	48	84	0.24	27
7	VFA	26	37	48	44	0.26	28
8	VFA	8	20	48	0	–	–
9	VFA	8	25	48	18	0.34	40
10	NaVS	26	20	24	32	0.03	2.4
11	NaVS	26	20	48	36	0.03	2.4
12	NaVS	26	25	24	36	0.04	2.9
13	NaVS	26	37	24	12	0.02	1.1
14	NaVS	10	20	24	36	0.02	1.1
15	NaVS	10	20	48	26	0.02	1.1
16	NaVS	52	37	24	14	0.01	0.2

* At 25°C in 1 M aqueous KCl for sample no. 6; in 0.2 M aqueous NaCl for sample nos. 1–5 and 7–9; in 0.5 M aqueous NaCl for sample nos. 10–16.

of PVFA prepared under the above conditions is in the range from 27000 to 40000. Thus, the optimal conditions for polymerization of VFA are as follows: monomer concentration in water 26%, 25°C, 48 h.

Polymerization of NaVS was performed in 10, 26, and 52% aqueous solutions of the monomer at 20, 25, and 37°C. Irrespective of the other conditions of polymerization, the yield of the polymer at 37°C does not exceed 14%. At 20 and 25°C, the yield reaches 40% (polymerization at 20°C for 93 h, monomer concentration in water 26 wt %). All the obtained samples of NaPVS have low molecular weight, up to 2400.

CONCLUSION

Horse radish peroxidase is suitable for polymerization of water-soluble monomers vinylformamide and sodium vinylsulfonate.

REFERENCES

1. Derango, R.A., Chiang, L., Dowbenko, R., and Lasch, J.G., *Biotechnol. Tech.*, 1992, vol. 6, no. 6, pp. 523–526.
2. Andreeva, V.A., *Ferment peroksidaza* (Peroxidase Enzyme), Moscow: Nauka, 1988.
3. Teixeira, D., Lalot, T., Brigodiot, M., and Marechal, E., *Macromolecules*, 1999, vol. 32, no. 1, pp. 70–72.
4. Kalra, B. and Gross, R.A., *Biomacromolecules*, 2000, no. 1, pp. 501–505.
5. Singh, A., Ma, D., and Kaplan, D.L., *Biomacromolecules*, 2000, no. 1, pp. 592–596.
6. Singh, A., Roy, S., Samuelson, L., et al., *Macromol. Sci. Pure Appl. Chem., Ser. A*, 2001, vol. 38, no. 12, pp. 1219–1230.
7. Shannon, L.M., Kay, E., and Lew, J.Y., *J. Biol. Chem.*, 1966, vol. 241, no. 9, pp. 2166–2172.
8. Korostelev, P.P., *Prigotovlenie rastvorov dlya khimiko-analiticheskikh rabot* (Preparation of Solutions for Chemical Analytical Works), Moscow: Nauka, 1964.
9. Tsvetkov, V.N., Eskin, S.Ya., and Frenkel', S.Ya., *Struktura makromolekul v rastvorakh* (Structure of Macromolecules in Solutions), Moscow: Nauka, 1964.
10. Pavlov, G.M., Korneeva, E.V., Ebel, C., et al., *Vysokomol. Soedin., Ser. A*, 2004, vol. 46, no. 10, pp. 1732–1736.
11. Dialer, K. and Kerber, R., *Makromol. Chem.*, 1955, vol. 17, no. 56, pp. 955–957.

ISSN 1070-4272, Russian Journal of Applied Chemistry, 2007, Vol. 80, No. 12, pp. 2132–2135. © Pleiades Publishing, Ltd., 2007.
Original Russian Text © V.D. Pautov, T.D. Anan'eva, I.I. Gavrilova, 2007, published in Zhurnal Prikladnoi Khimii, 2007, Vol. 80, No. 12, pp. 2054–2057.

MACROMOLECULAR CHEMISTRY AND POLYMERIC MATERIALS

Stability of Transition Metal Complexes with Sulfonated Polymers

V. D. Pautov, T. D. Anan'eva, and I. I. Gavrilova

Institute of Macromolecular Compounds, Russian Academy of Sciences, St. Petersburg, Russia

Received May 23, 2007; in final form, July 2007

Abstract—Stability constants of macromolecular metallocomplexes of transition metal ions (Ag^+, Cu^{2+}, Ni^{2+}, Fe^{3+}) with sulfonated polymers in water and aqueous HCl and NaCl solutions were determined from quenching by transition metal ions of the luminescence of macromolecules labeled with luminescent groups.

DOI: 10.1134/S1070427207120273

In modern technologies involving combinations of polymers and transition metal ions [1–4], it is frequently necessary to prepare macromolecular metallocomplexes (MMCs) which can be formed in aqueous solutions only in acidic media, as dictated by the solubility of metal salts. Polymers containing weakly acidic (e.g., carboxy) groups at pH < 3 are not noticeably ionized and cannot bind transition metal ions [5]. In an acid medium, only polymers containing strong acid groups and in particular, sulfo groups retain their charge. The complexing ability of such polymers toward transition metal ions in solutions at low concentrations of both metal ($<10^{-4}$ M) and complexing groups of the polymer can be evaluated by the procedure we have developed previously [5]. It is based on quenching of the luminescence of labeled polymers by transition metal ions upon complexation.

This paper deals with evaluation of the stability of MMCs formed by sulfonated polymers with transition metal ions (Ag^+, Cu^{2+}, Ni^{2+}, Fe^{3+}) in aqueous solutions at low concentrations of both metal and polymer and with elucidation of the influence exerted by the metal ion, pH, and ionic strength on the MMC stability.

EXPERIMENTAL

Macromolecular metallocomplexes of water-soluble solfonated polymers were the objects of the study. Water-soluble sodium polyarylenamidosulfonate (**I**) with $M = 7.0 \times 10^3$ prepared from isophthalic acid [6] was taken as a sulfonated polymer:

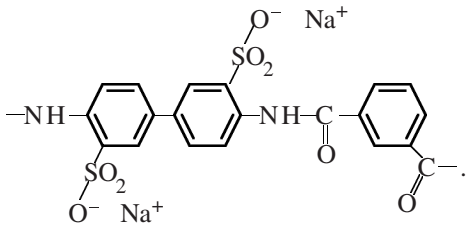

I

It contains in each monomeric unit two sulfo groups capable of forming electrovalent contacts with metal ions. The luminescence-labeled polymer **I** with 9-alkylanthracene groups as luminescence markers at the ends of the polymer chains was prepared by the reaction of the terminal amino groups of the polymer with 9-anthrylmethyl isocyanate [7].

Copolymer of *N*-vinylpyrrolidone with sodium vinylsulfonate (NaVS) **II** containing 29 mol % NaVS units:

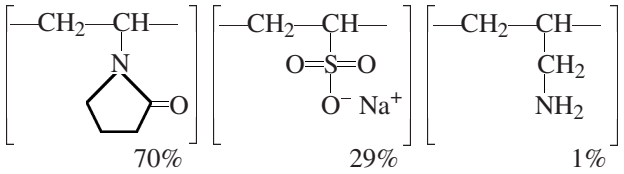

70% 29% 1%

was taken as a polymer in which only a part of units bear sulfo groups.

In polymer **II**, a small (1 mol %) amount of allylamine units was introduced. Polymer **II** labeled with 9-alkylanthracene luminescent marker was prepared by the reaction between amino groups of allylamine units with 9-anthrylmethyl isocyanate [7].

Stability constants K_{st} of MMCs of transition metal ions with sulfonated polymers and the energy of interaction of metal ions with sulfo groups ΔG in solutions at 25°C

Run, no.	Polymer	Ion	Solvent	K_{st}	ΔG, kJ mol^{-1}
1	**I**	Ag^+	H_2O	$(9.9 \pm 0.5) \times 10^1$	11
2		Cu^{2+}	H_2O	$(2.5 \pm 0.3) \times 10^6$	36
3			0.01 M HCl	$(4.3 \pm 0.3) \times 10^5$	32
4		Ni^{2+}	H_2O	$(4.1 \pm 0.4) \times 10^6$	38
5			0.01 M HCl	$(2.6 \pm 0.6) \times 10^6$	37
6		Fe^{3+}	0.01 M HCl	$(3.7 \pm 0.4) \times 10^{10}$	60
7	**II**	Cu^{2+}	H_2O	$(2.2 \pm 0.3) \times 10^7$	42
8			0.01 M HCl	$(1.4 \pm 0.2) \times 10^6$	35
9			0.01 M NaCl	$(1.1 \pm 0.2) \times 10^6$	34
10			0.1 M NaCl	$(1.5 \pm 0.7) \times 10^5$	30
11		Ni^{2+}	H_2O	$(1.2 \pm 0.3) \times 10^7$	40
12			0.01 M HCl	$(8 \pm 2) \times 10^6$	39
13			0.01 M NaCl	$(6 \pm 2) \times 10^6$	39
14			0.1 M NaCl	$(9 \pm 3) \times 10^4$	28
15		Fe^{3+}	0.01 M HCl	$(2.6 \pm 0.4) \times 10^{11}$	65
16			0.1 M HCl	$(1.1 \pm 0.4) \times 10^{11}$	63
17			0.01 M HCl + 0.09 M NaCl	$(2.3 \pm 0.8) \times 10^{11}$	65

N-Vinylpirrolidone and allylamine monomers were purified by distillation. In copolymerization, we used a 25% aqueous solution of sodium vinylsulfonate (Aldrich). The copolymerization was performed in a sealed ampule in an inert gas atmosphere. The concentration of monomers in the aqueous solution was 45 wt %; azobis(isobutyronitrile) (1% of monomer weight) was an initiator. The reaction was performed at 65°C for 24 h. The polymer obtained was cooled with acetone and dried in a vacuum. The copolymer composition was determined by analysis for the sulfur content and titration of sulfo groups. The content of allylamine units was determined spectrophotometrically from the light absorption of the complex of allylamine units with trinitrobenzenesulfonic acid at λ_{max} = 420 nm. The molecular weight of the copolymer was roughly estimated from the intrinsic viscosity in ethanol at 25°C by the formula

$$[\eta] = 2.3 \times 10^{-4} M^{0.65},$$

reported in [8] for *N*-vinylpyrrolidone homopolymers. The molecular weight of polymer **II** was 1.2×10^4.

To form MMCs, we took aqueous solutions of $AgNO_3$, $CuCl_2$, $NiSO_4$, and $FeCl_3$. This set of cations allowed us to follow the effect of the metal and its valence on the MMC stability.

The MMC stability constants were estimated according to [5] from data on the quenching by transition metal ions at 25°C of the luminescence of polymers labeled with luminescence markers.

The luminescence spectra were recorded on an LS-100 luminescence spectrometer (PTI Company). The luminescence quenching was estimated from the change in the intensity of the maximum of the luminescence band of the anthracene group (~390, 413, and 440 nm) and from the change in the integral intensity of light emission within the 380–500 nm range. The polymer concentration was varied from 1.5 to 0.05 mg ml^{-1}. The ratio of the molar concentrations of metal ions and sulfonated monomeric units, β, was varied from 0 to 5 for M^+, from 1 to 2 for M^{2+}, and from 0.6 to 1 for M^{3+}.

The effect of metal ion on the structural organization of molecules of sulfonated polymer **II** at MMC formation was estimated by the intramolecular mobility of the metal ion. The relaxation time τ_{IMR} characterizing the intramolecular mobility of the polymeric chains of macromolecules with luminescence markers was determined by the method of polarized luminescence [9]. The luminescence duration was measured on an LS-100 luminescence spectrophotometer.

We found that, in the aqueous solutions with a concentration of units bearing sulfo groups ranging from 10^{-2} to 10^{-4} M, the molecules of sulfonated polymers form MMCs with polyvalent metal ions in both neutral and acidic solutions. The metal valence has the strongest effect on the stability of such complexes. In going from univalent (Ag^+) to bivalent (Cu^{2+}, Ni^{2+}) and then trivalent (Fe^{3+}) metal ions, the MMC stability constants K_{st} and the free energies of interaction between metal ions and polymer sulfo groups ΔG, calculated from these quantities, sharply increase under similar experimental conditions (see table, run nos. 1, 2, and 4; 3, 5, and 6; 8, 12,

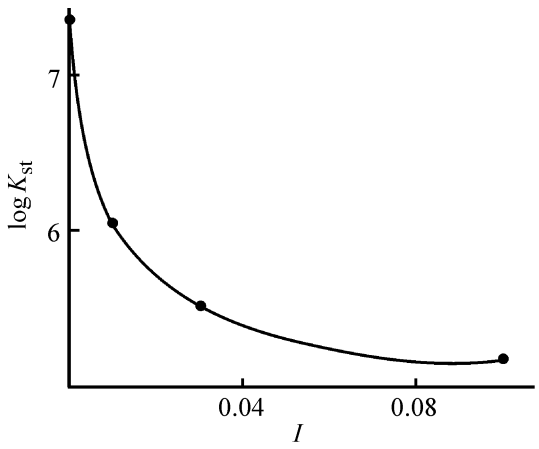

Stability constant K_{st} of MMC of polymer **II** with Cu^{2+} vs. the ionic strength I produced by NaCl addition (25°C).

and 15). This means that electrovalent contacts between metal ions and sulfo groups play the decisive role in the formation of MMCs. The contribution of coordination bonds to MMC stabilization is insignificant, in contrast to the interaction of transition metal ions with carboxy groups of carboxyl-containing polymers [5]. This is indicated by the fact that the ΔG values divided by the number of electrovalent bonds of the ion for MMCs formed under the same experimental conditions by ions with different coordination capacities (Cu^{2+}, Ni^{2+}, and Fe^{3+}) [1, 4] are close.

The influence of a polyvalent metal ion on the energy of a single electrovalent bond with sulfo groups depends on the ion size. For Ag^+, whose radius is substantially larger than those of Cu^{2+}, Ni^{2+}, and Fe^{3+} ions (0.126 nm for Ag^+, 0.072 for Cu^{2+}, 0.069 for Ni^{2+}, and 0.064 nm for Fe^{3+} [10]), it is almost two times lower than for the other metal ions studied (see table).

The data obtained show that the influence of the ionic strength on the MMC stability strongly depends on the metal valence. The destabilizing effect of the ionic strength on MMCs of the sulfonated polymer with Ag^+ ions is so strong that the MMC completely decomposes at a solution ionic strength of 0.01. As compared to aqueous solutions, the stability of MMCs with bivalent metals substantially decreases in 0.01 M HCl (see table, run nos. 2 and 3, 7 and 8, 11 and 12). These changes are associated with variation of the ionic strength, rather than lowering of pH. Indeed, an increase in the solution ionic strength to 0.01 upon addition of a neutral salt (NaCl) has a similar effect on K_{st} (see table, run nos. 7, 8, and 9; 11, 12, and 13). The strongest (by almost two orders of magnitude) decrease in K_{st} of MMCs of a sulfonated polymer with ions of bivalent transition metals is observed in the region of low ionic strengths ($\leq$0.03). With a further increase in the ionic strength (to 0.1), K_{st} decreases by only a factor of 2–3 (see figure). The stability of MMC with trivalent Fe^{3+} does not noticeably change within the solution ionic strength range from 0.01 to 0.1 on addition of HCl or NaCl (see table, run nos. 15–17).

The data obtained show that the MMC stability with all the polyvalent ions studied increases (K_{st} increases by a factor of 3–8) in going from polymer **I** (containing two sulfo groups in each unit) to polymer **II** (in which only a part of units contain sulfo groups), i.e., upon replacement of an aryl group as a bearer of sulfo groups with an alkyl support, both in water and in aqueous solutions of HCl or NaCl (see table).

A study of the influence of Cu^{2+} and Ni^{2+} on the intramolecular mobility (IMM) of the polymeric chains of polymer **II** upon MMC formation showed that IMM does not noticeably change upon coordination of metal ions with the polymer. The relaxation time τ_{IMM} characterizing the mobility of the polymeric chains remains on the level of 9–10 ns upon a ~50% substitution of protons with metal ions in sulfo groups of the polymer. This means that the sulfo groups closely situated in the chain are involved in the formation of electrovalent contacts of sulfonic acid groups with a metal ion, and the MMC formation is not accompanied by compaction of macromolecules. In the formation of MMC, the change in the luminescence intensity is relatively small (1.5–3-fold intensity changes), which also indicates that the initial compactness of the macromolecules does not change. If the MMC formation is accompanied by compaction of macromolecules, the luminescence intensity can change by 1–2 orders of magnitude [5].

CONCLUSIONS

(1) Sulfonated macromolecules can be used to form of stable macromolecular metallocomplexes with polyvalent (in contrast to monovalent) transition metal ions in the acid region (pH < 3).

(2) For macromolecular metallocomplexes with bivalent metal ions, the decrease in the complex stability with decreasing pH should be taken into account. This effect is due to a rise in the ionic strength, rather than to an increase in acidity.

REFERENCES

1. Pomogailo, A.D. and Uflyand, I.E., *Makromolekulyarnye metallokhelaty* (Macromolecular Metal Chelates), Moscow: Khimiya, 1991.
2. Pomogailo, A.D., Uflyand, I.E., and Vainshtein, E.F., *Usp. Khim.*, 1995, vol. 64, no. 9, pp. 913–933.
3. Pomogailo, A.D. *Polimernye immobilizovannye metallokompleksnye katalizatory* (Polymeric Immobilized Metal Complex Catalysts), Moscow: Nauka, 1988.
4. Saldadze, K.M. and Kopylova-Valova, V.D., *Kompleksoobrazuyushchie ionity* (kompleksity) [Complexing Ion Exchangers (Complexites)], Moscow: Khimiya, 1980.
5. Pautov, V.D., Anufrieva, E.V., Anan'eva, T.D., et al., *Vysokomol. Soedin., Ser. A*, 2006, vol. 48 no. 2, pp. 299–308.
6. Anufrieva, E.V., Nekrasova, T.N., Lushchik, V.B., et al., *Vysokomol. Soedin., Ser. B*, 1992, vol. 34, no. 1, pp. 31–34.
7. Krakovyak, M.G., Lushchik, V.B., Sycheva, E.A., and Anufrieva, E.V., *Vysokomol. Soedin., Ser. B*, 1986, vol. 28, no. 4, pp. 289–294.
8. Levy, G.B. and Frank, H.P., *J. Plym. Sci.*, 1955, vol. 17, pp. 247–254.
9. Anufrieva, E.V. and Gotlib, Yu.Ya., *Adv. Polym. Sci.*, 1981, vol. 40, pp. 1–69.
10. *Handbook of Chemistry and Physics*, Weast, R.C., Ed., Florida: Boca Raton, 1983–1984, 64th ed., p. F–170.

ISSN 1070-4272, Russian Journal of Applied Chemistry, 2007, Vol. 80, No. 12, pp. 2136–2141. © Pleiades Publishing, Ltd., 2007.
Original Russian Text © A.Yu. Vasil'kov, B.A. Zachernyuk, Z.N. Karpikov, I.O. Volkov, Ya.V. Zubavichus, A.A. Veligzhanin, A.A. Chernyshov, M.I. Buzin, L.N. Nikitin, V.I. Nedel'kin, 2007, published in Zhurnal Prikladnoi Khimii, 2007, Vol. 80, No. 12, pp. 2058–2063.

MACROMOLECULAR CHEMISTRY AND POLYMERIC MATERIALS

Magnetodielectric Composites Based on Functionalized Polyphenylene Sulfides Containing Iron Nanoparticles

A. Yu. Vasil'kov, B. A. Zachernyuk, Z. N. Karpikov, I. O. Volkov, Ya. V. Zubavichus, A. A. Veligzhanin, A. A. Chernyshov, M. I. Buzin, L. N. Nikitin, and V. I. Nedel'kin

Nesmeyanov Institute of Organoelement Compounds, Russian Academy of Sciences, Moscow, Russia
Russian Research Centre Kurchatov Institute, Moscow, Russia

Received April 27, 2007

Abstract—Preparation of iron-filled polyaminophenylene sulfides and polyhydroxyaminophenylene sulfides by the metal vapor procedure was studied. Nanocomposites based on these metal-containing polymers and epoxy–isopropylidenediphenol oligomers (ED-20) were prepared and their composition, properties, and structure were studied by X-ray diffraction and thermogravimetric analyses, and thermomechanical methods. The magnetic and dielectric properties of the materials were determined.

DOI: 10.1134/S1070427207120285

The preparation of magnetic dielectric materials with valuable properties is extensively studied owing to particular interest in the magnetic information carriers, magnetically connected parts of special devices, and other materials. Magnetodielectrics consist of a polymeric matrix and a filler with a magnetic function. However, common magnetodielectrics have certain disadvantages, such as low strength, low thermal stability, and poor dielectric characteristics, because of the high concentration of the filler (metal and its compounds) [1]. Filling of polymers with nanoparticles causes sharp changes in the physicochemical properties of the particles and materials based on them, which can be useful for preparing nanocomposites with required electrical, magnetic, and catalytic properties [2–5].

Previously, low-melting polyaminophenylene sulfoxides (PAPSs) (**1**) and polyhydroxyaminophenylene sulfides (PHAPSs) (**2**) were prepared by direct polycondensation of elementary sulfur with aniline and phenol [6, 7]; these polymers are soluble in THF, dioxane, *N*-methylpyrrolidone, and other solvents.

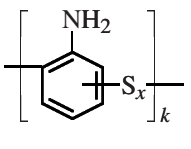

1

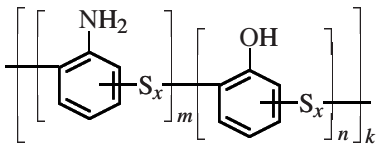

2

Later, network polyepoxides with good thermal characteristics were prepared from these polymers and epoxy–isopropylidenediphenol oligomers (ED-20) [8]. Taking into account the valuable characteristics of the resulting network polyepoxides, it was of particular interest to study the possibility of using polyamino- and polyhydroxyaminophenylene sulfides containing iron nanoparticles as fillers for ED-20 epoxy resin to obtain magnetodielectric materials with improved properties. It was expected that the resulting composites would possess high magnetic and dielectric properties, combined with the inherited thermal and chemical stability of polyphenylene sulfide matrices.

EXPERIMENTAL

In this study we used polyaminophenylene sulfide (**1**) and polyhydroxyaminophenylene sulfide (**2**) prepared and characterized in accordance with [6, 7]. Iron-filled PAPS (**3**) and PHAPS (**4**) were prepared by metal vapor synthesis (MVS) [2–4]. Iron was evaporated by resistive heating from a tungsten at a residual pressure not exceeding 10^{-2} Pa. The vapors of metal and THF were trapped on the reactor walls cooled with liquid nitrogen at the metal : ligand molar ratio of about 1 : 300. Then this cocondensate was heated to melt and the resulting organosol was added to THF solutions of polymers **1** and **2**. After that, the solvent was evaporated, and the result-

ing metal-containing polymers **3** and **4** were dried in a vacuum (residual pressure 1 Pa) at 373 K. The metal-filled composites **5**–**8** (Table 1) based on functionalized polyphenylene sulfide and epoxy–isopropylidenediphenol oligomer ED-20 were prepared by the procedure described elsewhere [8]. To eliminate the possible internal stresses, the composites based on ED-20 filled with PAPS and PHAPS containing iron nanoparticles were cured by the stepwise procedure: 343 K, 1 h; 358 K, 1 h; 373 K, 4 h; 413 K, 4 h; 433 K, 1 h; and 453 K, 1 h. The content of the sol fraction was determined under the conditions described previously [9]. The IR spectra of the samples were recorded on a UR-20 spectrometer using KBr pellets.

The thermomechanical compression curves were recorded at a constant load of 8.8 MPa and a heating rate of 70–80 deg h^{-1}. The thermogravimetric analysis (TGA) and differential thermal analysis (DTA) were performed on an MOM K derivatograph (Hungary) in air at a heating rate of 5 deg min^{-1}.

The magnetic and dielectric properties of the composites were determined in accordance with the procedure described in [10].[1] The powder X-ray diffraction patterns were recorded on a DRON-3 diffractometer in the Bragg–Brentano configuration using Cu_{K_α} radiation (λ 1.5418 Å), a graphite monochromator in the secondary beam, 36 kW × 20 mA generator mode, continuous θ/2θ scanning with a 0.05° step, and scanning rate of 1 deg min^{-1}.

The X-ray absorption spectra and of small-angle scattering curves were measured using synchrotron X-ray radiation [11]. The incident beam energy was selected using a Si(III) monoblock monochromator. The XANES and EXAFS spectra were measured with a scintillation detector as fluorescence yields.

The time of signal accumulation was 15–20 min and 6–8 h for XANES and EXAFS spectra, respectively. The preliminary processing of the EXAFS spectra was carried out using the IFEFFIT software package [12]. The intensity of the small-angle X-ray scattering was measured with a FujiFilm Imaging Plate coordinate detector (sample-to-detector distance 1 m; wavelength of incident X-ray radiation, λ 0.95 Å; 10-min exposure). The curves were processed using the GNOM software [13].

The photoelectron spectra were recorded on an XSAM-800 spectrometer (Kratos, UK). The excitation source was a magnesium anode with a characteristic radiation energy of 1253.6 eV. The power released at the anode in the course of the measurements did not exceed 90 W (15 kV, 6 mA); the pressure in the working chamber was 10^{-8} Pa. A quantitative analysis was performed by the procedure described in [14].

[1] In collaboration with staff members of Kharkov Aviation Institute (Ukraine).

Table 1. Composition of materials **5**–**8** based on ED-20 and PHAPS filled with iron nanoparticles

Component	Nanocomposite composition, wt fraction			
	5	**6**	**7**	**8**
ED-20	100	100	100	100
PHAPS filled with iron nanoparticles*	32.0	33.2	33.6	35.0

* Nanocomposites **5** and **6** contain 6.0 wt % Fe, and **7** and **8**, 8.2 wt % Fe.

The development of magnetodielectric materials involves two main stages: filling of functionalized polyphenylene sulfides **1** and **2** with iron nanoparticles and subsequent curing of ED-20 oligomer with the above products. The filling of PAPS and PHAPS with iron nanoparticles is illustrated by the scheme below.

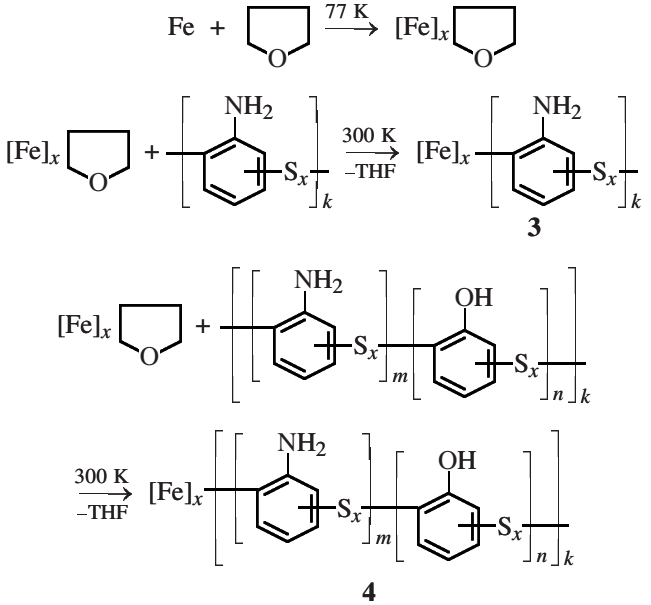

Scheme of nanoparticle introduction into PAPS and PHAPS matrices.

The iron nanoparticles were prepared by the reaction of the iron and THF vapors at 77 K. The organosol of Fe in THF, obtained after defrosting, was added to solutions of functionalized polyphenyl-

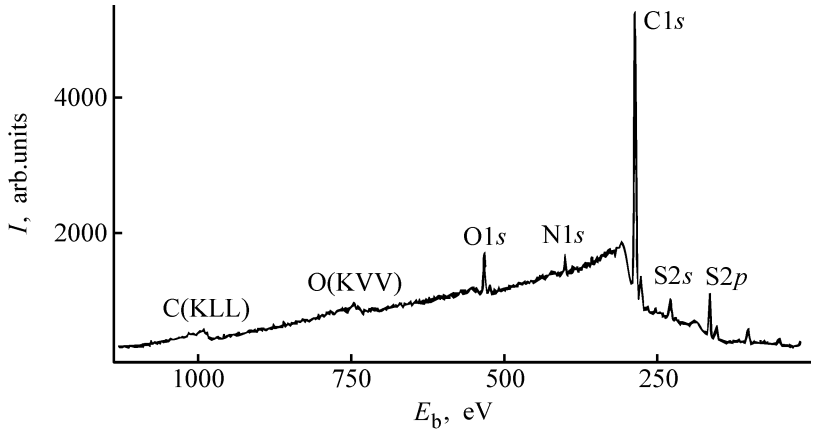

Fig. 1. Survey XPS spectrum of composite **4** containing 8.2 wt % Fe. (*I*) Intensity and (E_b) binding energy.

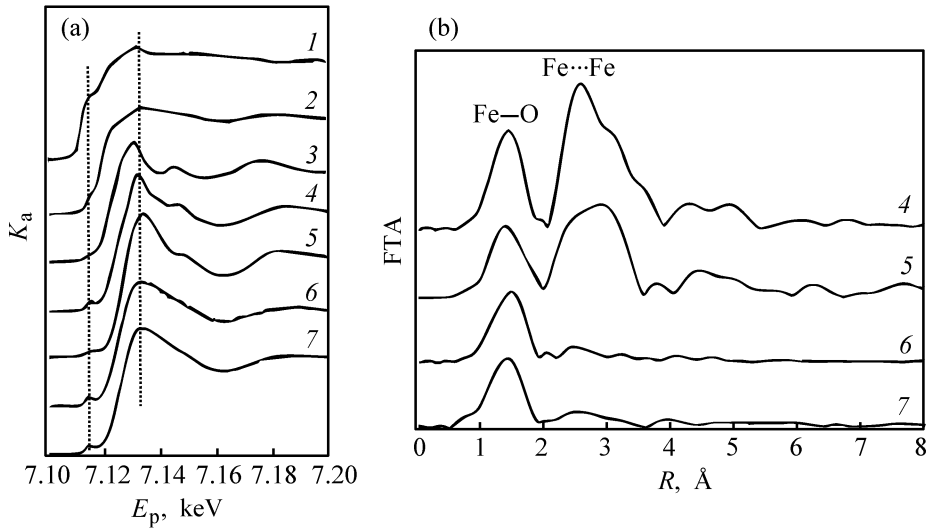

Fig. 2. (a) Fe *K*-edge XANES spectra and (b) Fourier-transformed EXAFS spectra of samples **4**–**7**. (K_a) Absorption coefficient, (FTA) Fourier transform amplitude, (E_p) photon energy, and (*R*) radius. (*1*) Carbonyl iron-PAPS, (*2*) FeS, (*3*) FeO, (*4*) Fe_3O_4, (*5*) Fe_2O_3, (*6*) Fe nanoparticles–PAPS, and (*7*) Fe nanoparticles–PHAPS.

ene sulfoxides in the same solvent. The resulting iron-containing composites **3** and **4** were studied by various physicochemical methods. According to the results of an elemental analysis, the content of iron in the filled samples was 11.4 wt % for polymer **3** and 6.0 and 8.2 wt % for polymer **4**. Data on the chemical state of iron in the filled composites were obtained by X-ray diagnostics including XANES (X-ray Adsorption Near-Edge Structure) and EXAFS (Extended X-ray Absorption Fine Structure), X-ray diffraction, small-angle X-ray scattering, and X-ray photoelectron spectroscopy (XPS).

The XPS spectrum of compound **4** (Fig. 1) indicates that there is no iron in the surface layer (up to 50 Å) of the filled polymeric nanocomposites. No degradation of the samples in the course of measurements was observed. Probably, the active metal particles are effectively encapsulated by the polymer and, as a result, the surface layers contain almost no iron as compared to its total content in the polymer.

Along with the data of elemental analysis, the presence of iron in the polymer samples is confirmed by XANES and EXAFS spectra recorded using the synchrotron radiation. These spectra also furnished data on the chemical state and environment of iron atoms in filled polymers **3** and **4**.

The XANES spectra at the Fe *K*-edge for samples **3** and **4** are shown in Fig. 2 (curves *6* and *7*) in comparison with the standard spectra recorded under similar conditions (curves *1*–*5*). As references we used FeS, FeO, Fe_3O_4, Fe_2O_3, and PAPS sample filled with commercial carbonyl iron (~1-μm average particle size). Comparison of these experimental spectra

shows that the state of iron in the filled polymeric samples strongly differs from that of metallic iron (polymeric sample filled with carbonyl iron) or FeS and is close to that in iron oxides. The profile and position of the absorption edge in the samples are the closest to those in the spectrum of Fe_3O_4 with account of the pronounced shoulder associated with the $1s \rightarrow 3d$ electronic transition. This conclusion was additionally confirmed by the shape of the Fourier-transformed EXAFS spectra (Fig. 2b). The Fourier-transformed spectra of the filled samples exhibit a single pronounced peak corresponding to the Fe–O bond, with no other features belonging to the Fe–S and Fe–Fe bonds observed. Such a pattern is typical of disordered oxide nanoparticles.

The powder diffraction patterns of the initial sample and iron-filled PHAPS composite are shown in Fig. 3. The polymeric matrix is virtually X-ray amorphous. The diffraction pattern exhibits only a broad halo at about 20° and a diffuse maximum at 42°. Nevertheless, some differences between the diffraction curves of these materials are observed; the difference curve is shown in the inset (Fig. 3). As can be seen, two broad diffraction peaks are observed at 35° and 63°; their position is close to that of the two strongest reflections (311) and (400) in the diffraction pattern of crystalline magnetite Fe_3O_4 (marked by arrows in Fig. 3). These data agree with the assumption that iron in the polymeric matrix forms nanoparticles of an oxide close in composition and structure to Fe_3O_4. The size of these oxide nanoparticles can be reliably evaluated from small-angle X-ray scattering data. The experimental curves for the sample of polyaminophenylene sulfide **3** filled with iron nanoparticles and similar sample containing metallic (carbonyl iron) microparticles are shown in Fig. 4.

Both curves show a broad peak at s = 0.35–0.40 Å^{-1}, apparently associated with structural features of the polymeric matrix, and level out at $s >$ 0.6 Å^{-1}. The plateau is determined by the scattering on the polymeric matrix and by the isotropic background of X-ray fluorescence from iron atoms present in the samples (the small-angle X-ray scattering curves were measured using radiation with energy higher than the K edge of iron absorption). Nevertheless, the scattering curve for sample **3** contains a pronounced region of strong scattering in the range s = 0.1–0.2 Å^{-1} which can be reliably attributed to scattering on nanosize iron oxide particles present in the sample. The differential curve, mainly determined by this contribution, was processed using the GNOM software. In the approximation of a polydisperse distribution of

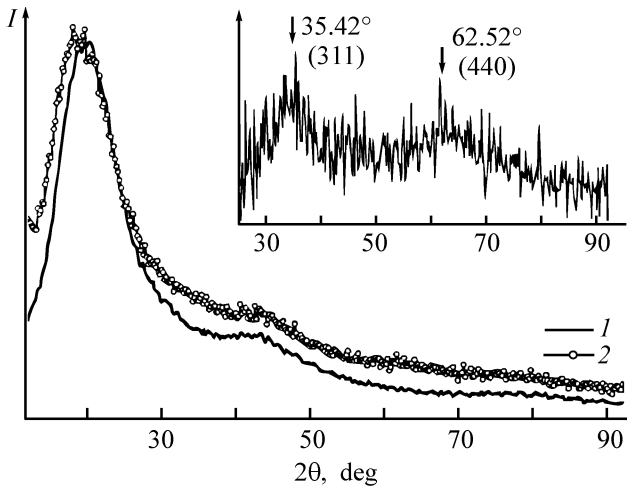

Fig. 3. X-ray diffraction pattern of (*1*) unfilled polymeric matrix **2** and (*2*) composite **4**; the difference spectrum is shown in the inset. The positions of the two strongest peaks in the diffraction pattern of crystalline magnetite Fe_3O_4 are marked by arrows. (*I*) Scattering intensity and (2θ) Bragg angle.

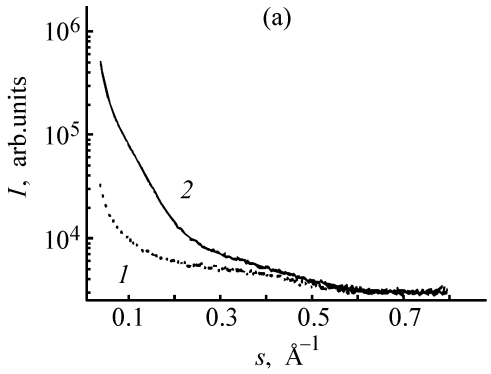

Fig. 4. (a) Curves of small-angle X-ray scattering of the samples (*1*) carbonyl iron–PAPS and (*2*) iron nanoparticles–PAPS, (b) difference curve (*solid line*) and theoretical curve of model distribution of rigid spheres, and (c) size distribution of rigid spheres, corresponding to the theoretical curve. (*I*) Scattering intensity and (*R*) radius.

Table 2. Characteristics of magnetodielectric composites **5**–**8** based on ED-20 and PHAPS filled with iron nanoparticles

Parameter	Nanocomposite			
	5	**6**	**7**	**8**
Bulk electrical resistivity at 293 K, $\Omega\,cm^{-1}$	10^{12}	10^{12}	10^{11}	10^{11}
Breakdown voltage, kV	8.7	8.0	9.1	8.8
Relative magnetic permittivity, $V\,N^{-1}$	2.47	2.52	2.67	2.60

rigid spheres, the scattering curve corresponds to a relatively narrow unimodal distribution of spherical particles, centered at approximately 15 Å (particle radius).

The second step in the development of magnetodielectric materials involved curing of ED-20 oligomer with iron-filled composites **3** and **4** prepared and examined in the first step of this study. The temperature mode of curing of ED-20 with PAPS and PHAPS containing iron nanoparticles was similar to that used for preparing network polyepoxides based on ED-20 and unfilled phenylene sulfide oligomers [8] it should be noted that curing of ED-20 oligomer with iron-filled nanocomposites **3** and **4**, and with unfilled polymers **1** and **2**, goes virtually to completion. This is confirmed by the low content of the sol fraction in the resulting samples (0.1–0.35%) and by the absence of the absorption bands at 930 and 960 cm^{-1}, characteristic of free epoxy rings, in the IR spectra of the cured samples [8]. The compositions of composites **5**–**8** based on ED-20 and composite **4** are listed in Table 1.

Analysis of the electrical properties of composites **5**–**8** (Table 2) shows that these composites containing iron nanoparticles exhibit better dielectric properties in the temperature range from 363 to 453 K as compared to iron-containing materials based on ED-20

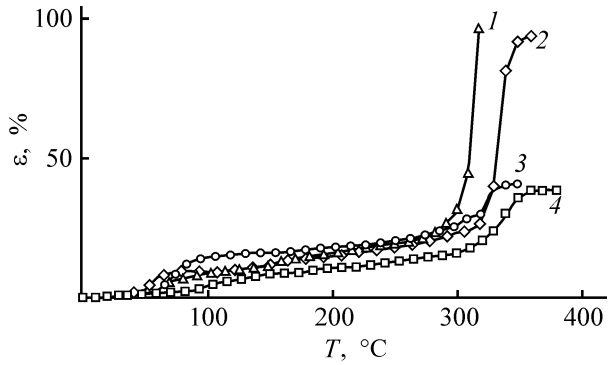

Fig. 5. Thermomechanical curves of ED-20 samples cured with (*1*) PAPS, (*2*) PHAPS, (*3*) PAPS + Fe, and (*4*) PHAPS + Fe. (ε) Strain and (*T*) temperature.

and functionalized polyphenylene sulfides filled with carbonyl iron microparticles. Moreover, use of composites **3** and **4** as curing agents for ED-20 improves the chemical stability of the resulting magnetodielectric materials as compared to the materials based on polymers **1** and **2**.

It should be noted that changes in the metal concentration in composites **5**–**8** do not noticeably affect the magnetic permittivity.

Under similar conditions, magnetodielectric composite **9** based on PAPS was prepared by curing of oligomer ED-20 with composite **3**. At an iron content of 11.4%, the magnetic permittivity of composite **9** was 2.2 $V\,N^{-1}$.

The thermal characteristics of materials prepared previously by curing oligomer ED-20 with polymers **1** and **2** allow us to trace changes in the softening point and heat resistance of composites on passing from unfilled curing agents to iron-filled composites **3** and **4**. The thermal characteristics of the resulting magnetodielectric composites were studied by thermomechanical and thermogravimetric methods. Comparison of the thermomechanical curves of the iron-free and iron-filled samples (Fig. 5) shows that, at 300°C, the samples based on PAPS, PHAPS, and ED-20 are nearly completely deformed under the stress, whereas the strain in the materials based iron-filled composites **3** and **4** and ED-20 does not exceed 20–25% under the similar experimental conditions. It should be noted that the system based on composites **3** is better cross-linked on heating than that based on composite **4**.

In accordance with TGA data, differences in the composition of polymers PAPS and PHAPS do not affect the heat resistance of materials prepared from them and ED-20. A similar pattern is observed with the materials based on ED-20 and iron-filled polymers PAPS and PHAPS. The TGA and DTA curves for composites **2** and **4** with ED-20 are shown in Fig. 6. The heat resistance of composites **2** and **4** with ED-20 in air is similar. The temperature of de-

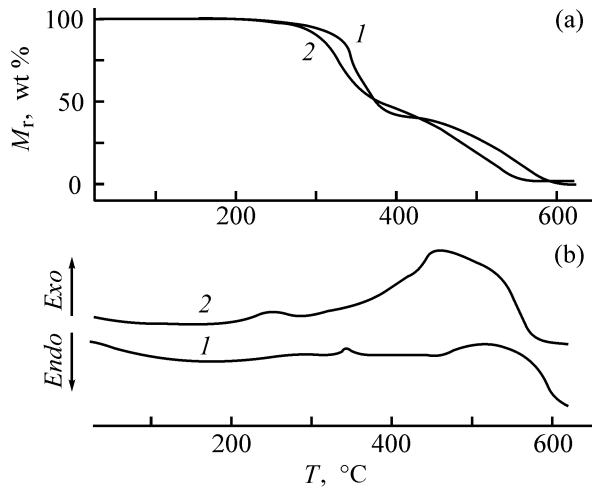

Fig. 6. (a) TGA and (b) DTA curves recorded in air for (*1*) unfilled and (*2*) iron-filled composites based on ED-20 and polyhydroxyaminophenylene sulfide. (M_r) Residual weight and (T) temperature.

gradation onset, i.e., the temperature corresponding to a 5% weight loss by the sample, $T_{5\%}$, for composite **2** with ED-20 is 295°C. Introduction of iron nanoparticles into the composite lowers $T_{5\%}$ to 276°C. As can be seen from TGA (Fig. 6a) and DTA (Fig. 6b) curves, the onset of the weight loss by the composite with iron nanoparticles is preceded by an exothermic peak at 248°C, which is not observed for the initial composite **2** with ED-20. This is probably due to thermal oxidative processes occurring in the composite filled with iron. The low relative deformation of the metal-filled composites noted above may be due to the formation of internal cross-links appearing in the course of thermal oxidation.

CONCLUSION

Combination of thermosetting epoxy matrices with polyamino- and polyhydroxyaminophenylene sulfides filled with iron nanoparticles improves the properties of common materials and allows development of nanocomposites with required magnetic, dielectric, and thermal properties.

ACKNOWLEDGMENTS

The authors are grateful to V.V. Luk'yanchenko (Kharkov Aircraft Institute) for assistance in evaluation of the magnetic and dielectric properties of the composites.

The study was financially supported by the Russian Foundation for Basic Research (project nos. 05-03-32871 and 07-03-91584-ASP_a).

REFERENCES

1. Buchachenko, A.L., *Usp. Khim.*, 2003, vol. 72, p. 419.
2. Vasil'kov, A.Yu., Olenin, A.Yu., Titova, E.F., and Sergeev, V.A., *J. Colloid Interface Sci.*, 1995, vol. 169, p. 369.
3. Solodovnikov, S.P., Vasil'kov, A.Yu., Olenin, A.Yu., and Sergeenko, V.A., *J. Magn. Magn. Mater.*, 1994, vol. 129, p. 317.
4. Nikolaev, S.A., Vasil'kov, A.Yu., Smirnov, V.V., and Tyurina, L.A., *Kinet. Katal.*, 2005, vol. 46, p. 915.
5. Jasti, R.K., Kanjilal, A., and Sehgal, H.K., *Nanotechnology*, 2003, vol. 14, p. 809.
6. Sergeev, V.A., Nedel'kin, V.I., Timofeeva, G.A., et al., *Vysokomol. Soedin., Ser. B*, 1985, vol. 27, no. 10, p. 740.
7. USSR Inventor's Certificate, no. 1206383, *Byull. Izobret.*, 1986, no. 3, p. 96.
8. Sergeev, V.A., Nedel'kin, V.I., Timofeeva, G.A., et al., *Vysokomol. Soedin., Ser. B*, 1986, vol. 28, no. 11, p. 863.
9. Sergeev, V.A., Nedel'kin, V.I., and Novikov, V.U., *Vysokomol. Soedin., Ser. B*, 1983, vol. 25, no. 6, p. 1311.
10. Trotskii, V.A., Rolik, A.I., and Yakovlev, A.I., *Magnitnye dielektriki v silovoi elektrotekhnike* (Magnetic Dielectrics in Power Electrical Engineering), Kiev: Tekhnika, 1983.
11. Amarantov, S.V., Veligzhanin, A.A., Guseva, E.V., at al., Structural Materials Science Station at the Kurchatov Source of Synchrotron Radiation, *Preprint of the Russian Research Centre Kurchatov Inst.*, 2004, no. IAE-6335.
12. Ravel, B. and Newville, M., *J. Synchrotron Radiat.*, 2005, vol. 12, p. 537.
13. Semenyuk, A.V. and Svergin, D.I., *J. Appl. Crystallogr.*, 1991, vol. 24, p. 537.
14. Naumkin, A.V., Vasil'kov, A.Yu., Volkov, I.Yu., et al., *Neorg. Mater.*, 2007., vol. 43, no. 4., pp. 445–449.

ISSN 1070-4272, Russian Journal of Applied Chemistry, 2007, Vol. 80, No. 12, pp. 2142–2148. © Pleiades Publishing, Ltd., 2007.
Original Russian Text © S.V. Kononova, E.N. Korytkova, K.A. Romashkova, Yu.P. Kuznetsov, I.V. Gofman, V.M. Svetlichnyi, V.V. Gusarov, 2007, published in Zhurnal Prikladnoi Khimii, 2007, Vol. 80, No. 12, pp. 2064–2070.

MACROMOLECULAR CHEMISTRY AND POLYMERIC MATERIALS

Nanocomposite Based on Polyamidoimide with Hydrosilicate Nanoparticles of Varied Morphology

S. V. Kononova, E. N. Korytkova, K. A. Romashkova, Yu. P. Kuznetsov, I. V. Gofman, V. M. Svetlichnyi, and V. V. Gusarov

Institute of Macromolecular Compounds, Russian Academy of Sciences, St. Petersburg, Russia
Grebenshchikov Institute of Silicate Chemistry, Russian Academy of Sciences, St. Petersburg, Russia

Received April 26, 2007

Abstract—Polymeric nanocomposites based on aromatic polyamidoimide and nanotubes of magnesium hydrosilicate $Mg_3Si_2O_5(OH)_4$ with a chrysotile structure were obtained and studied for the first time. The morphology and mechanical and transport properties of the composites formed were analyzed, which enabled optimization of their synthesis conditions.

DOI: 10.1134/S1070427207120297

Studies of hybrid nanocomposite materials combining an organic matrix and inorganic fillers arouse considerable interest because of the potential opportunity for synthesis of composites with improved properties. Hybrid systems with physicomechanical characteristics different from those typical of the starting substances have been reported [1, 2]. These differences are the most pronounced in synthesis of materials that belong to the group of filled polymers. This is due to processes of distribution of nanosize inorganic particles in a polymeric matrix and is primarily determined by the following factors: number and nature of reactive groups, hydrophilic–lipophilic balance for each of the components combined, presence in the polymer structure of fragments ("potential ligands") for the chosen filler, and also its size and structure. Filled polymers are used not only in development of new construction materials [3, 4], but also in design of industrial polymeric membranes stable under severe conditions of a separation process [5]. Use of polymeric nanocomposites is appropriate in solution of complicated tasks, such as development of membranes with required transport properties on the basis of materials with improved mechanical characteristics. The reason is in the morphological features of nanocomposites, which are manifested not only in the mechanical properties, but also in permeability and selectivity parameters of nonporous membranes. The structure and transport properties of polyimide-based composites containing zeolite 4A or carbon molecular sieves have been studied [6, 7]. It was shown that, in the case of a good compatibility of components, the ordered structure of the inorganic component is responsible for the gas separation efficiency [6–8]. Widely known are studies in which inorganic additives having in most cases a crystalline structure are introduced into the polymeric matrix in order to enhance the barrier properties with respect to gases and liquids [9]. The decrease in the free volume, which accompanies the formation of composites of the given type, diminishes the region of molecular transport of the permeate because of the insolubility of its molecules in the crystalline regions of the matrix. The transport mainly occurs in the amorphous part of the polymer.

In recent years, publications have appeared concerning the application of carbon nanotubes in membrane materials [10–12]. This is primarily due to the high specific surface area of the material of the nanotubes and to the resulting formation of a considerable number of nanosize voids and hollows. It was demonstrated that carbon-based nanotubes have diffusion and sorption parameters that favorably distinguish them from the known materials. The parameters of N_2 and CO_2 diffusion and sorption in single-wall carbon nanotubes, measured at room temperature, depend on the diameter of the nanotubes [13].

The appearance of studies devoted to synthesis of noncarbon (most frequently oxide and oxyhydroxide)

tubular structures with varied morphology and surface activity [14–16] opens up opportunities for formation of composite membrane materials intended for catalytic and pervaporation purposes. It is known that structural characteristics of nanotubes, their shape, length, and ratio between the inner and outer diameters can predetermine the morphological features [17] of composites. However, general principles of component compatibility and fundamental aspects of gas and liquid transport across membranes of the polymer–nanotubes type have not been studied so far.

Of particular interest in this context is development of new composite materials based on aromatic polyamidoimide, with inorganic nanotubes and, in particular, those composed of $Mg_3Si_2O_5(OH)_4$ with a chrysotile structure as fillers. Also important are studies of the morphological features of the composites obtained and of their mechanical and transport properties. The choice of the filler is governed by the knowledge of the physicochemical foundations of directed hydrothermal synthesis of nanotubes composed of $(Mg, Fe, Ni, Co)_3Si_2O_5(OH)_4$ hydrosilicates, by the existence of routine methods for control over their structure, morphology, and size [18], and by the available data on introduction of hydrosilicate nanotubes into polyimide films, which results in that the mechanical properties of the material substantially improved [3, 17].

EXPERIMENTAL

Poly(diphenyloxyamido-*N*-phenylphthalimide) (PAI) with a molecular mass of 57 000, synthesized by the known procedure, was used as a matrix for synthesis of a hybrid composite material [19].

The following inorganic fillers were used in the composites: natural montmorillonite intercalated with quaternary aliphatic amine; commercial product Cloisite 15A (Southern Clay Products, Inc., USA); and nanotubes (NT) of $Mg_3Si_2O_5(OH)_4$ composition with a chrysotile structure. These NT were produced by hydrothermal treatment of various precursors: magnesium oxide, silicon dioxide, and $MgSiO_3$ with NaOH solutions with NaOH content of up to 3 wt % at temperatures of 250–450°C and pressures of 30–100 MPa by the procedure described in [14, 16]. Nanotubes of composition $Mg_3Si_2O_5(OH)_4$ were used, with a cylindrical morphology and various dimensions: (a) outer diameter d_o = 10–15 nm, inner diameter d_i = 2–3 nm, and length L = 100–250 nm (NT I); (b) d_o = 20–25 nm, d_i = 4 nm, and L = 500–1000 nm (NT II); and (c) d_o = 50–110 nm, d_i = 5–6 nm, and L = 300–700 nm (NT III).

The composites were prepared in *N*-methyl-2-pyrrolidone (N-MP) under ultrasonic agitation of 8-wt % solutions of PAI in air at room temperature. The duration of agitation of the dispersions obtained (up to 20 h) was determined by the required degree of homogeneity of the resulting composites. The content of the inorganic components was varied from 2 to 10 wt %.

The dispersions were applied by casting onto the smooth surface of glass plates, on which thin nonporous films with thicknesses of 20 and 40 μm were formed after removal of the solvent by thermal treatment at temperatures of up to 150°C.

Mechanical tests of the films were performed on a UTS-10 versatile installation (UTStestsysteme, Germany) in the uniaxial tension mode at a tensile load of 0.5 MPa. In the tests, the modulus of elasticity E, plastic limit σ_p, tensile strength σ_t, and breaking strain ε_b.

The membrane morphology was studied by scanning electron microscopy (SEM) with Jeol JSM-35C and FE-SEM JSM 6400-F instruments (Japan).

The pervaporation parameters of solid film membranes were determined for water and in separation of ethanol–water mixtures (50 wt % ethanol) at 40°C on a pervaporation installation with a working area of the membrane equal to 12.4 cm^2. The pressure under the dry membrane (before the pervaporation process) was about 1×10^{-2} Pa. The compositions of the starting solution and of the permeate were determined by refractometry. The membrane selectivity was characterized by the separation factor $F_{i/j}$ calculated for components i and j of the mixture being separated by the formula

$$F_{i/j} = [c_i/c_j]_{per}/[c_i/c_j]_{st},$$

where $[c_i/c_j]_{per}$ is the concentration ratio of the components being separated in the permeate, and $[c_i/c_j]_{st}$, that in the starting (to be separated) mixture.

If the working area of the membrane and the amount of the permeate passed across the membrane are known, the permeate flux Π (kg m^{-2} h^{-1}) can be estimated.

It has been shown in our previous studies that, depending on hydrothermal synthesis conditions, inorganic nanotubes of varied composition, size, and morphology ("cylinder in cylinder," "cone in cone," and "sockets") can be obtained [14, 16, 18]. These results enabled us to consider in this study the morphological parameters of nanotubes as factors that

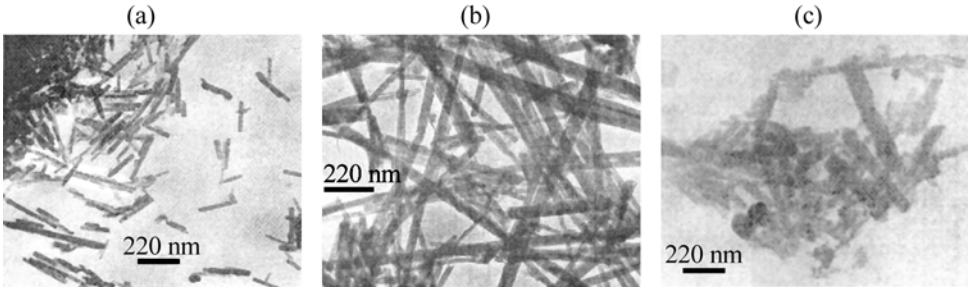

Fig. 1. SEM micrographs of $Mg_3Si_2O_5(OH)_4$ nanotubes. (a) NTI, (b) NTII, and (c) NTIII.

can be used in structural optimization of the PAI–NT composite. This approach is justified by the necessity for obtaining the composite material without introduction of additional organic substances or preliminary treatment of NT with surfactants. Until now, it has been for the most part possible to achieve the best compatibility of the inorganic and polymeric phases via introduction of additional organic components into the polymer–NT medium [20]. However, introduction of even minor amounts of additional substances in synthesis of membrane materials in which liquid or gaseous mixtures are separated by the diffusion–sorption mechanism may lead to a fundamental change in their transport properties. For this reason, the combining conditions of the components were optimized in this study without introduction of organic additives, by varying the structural and concentration parameter and conditions of the distribution process.

As in most of the known cases [21], composites constituted by a polymer and an inorganic filler were formed by vigorous and prolonged agitation of the components in solution. After 10 h of agitation, visually homogeneous PAI–NT I–III dispersions were obtained, of which PAI–NTI and PAI–NTII stratified in the course of 1 h, and PASI–NTIII remained visually homogeneous. This effect can be attributed primarily to different synthesis conditions of nanotubular hydrosilicates. NTI samples were synthesized by hydrothermal treatment of a mixture of oxides, MgO + SiO_2, with aqueous NaOH solutions (1 wt %) at 350°C and a pressure of 70 MPa for 1 h. As a result, the treatment product contained, in addition to the nanotubular hydrosilicate $Mg_3Si_2O_5(OH)_4$, an admixture of magnesium hydroxide and nanotubes had small dimensions and were partly composed of such defective morphological forms as "cylinder in cylinder," "sockets," and tubes with rough surface (Fig. 1a). NTII samples were synthesized from the MgO + SiO_2 mixture in a 1-wt % NaOH solution under the conditions optimal for production of morphologically homogeneous nanotubes (temperature 350°C, pressure 50–70 MPa, duration 24 h). These samples contained no impurities and were composed of cylindrical nanotubes of the hydrosilicate $Mg_3Si_2O_5(OH)_4$, which are free of morphological defects and have virtually the same diameters (Fig. 1b). NTIII samples were obtained by hydrothermal treatment of a $MgSiO_3$ + MgO mixture in a 2-wt % NaOH solution at 300°C and 70 MPa for 48 h. The synthesis product is composed of nanotubes of the hydrosilicate $Mg_3Si_2O_5(OH)_4$, with an admixture of a layered hydrosilicate $Mg_3Si_4O_{10}(OH)_4 \cdot nH_2O$ having a structure of montmorillonite, an intermediate in synthesis of $Mg_3Si_2O_5(OH)_4$ from the $MgSiO_3$ + MgO mixture. The NTIII nanotubes are considerably thicker than NTII and have a rough surface (Fig. 1c). Consequently the stratification of the PAI–NTI and PAI–NTII dispersions can be attributed to a chemical and morphological inhomogeneity of the inorganic components introduced into the polymer solution.

Casting of a visually homogeneous stable dispersion PAI–NTII onto the smooth surface of a glass plate yielded nonporous PAI–NTII(10) films of thicknesses 20 and 40 μm. Figure 2 shows SEM micrographs of the upper (Figs. 2a, 2b) and lower (Figs. 2c, 2d; formed on the glass side) surfaces of the 20-μm-thick film. As can be seen in Fig. 2, the nonporous PAI–NTII(10) films contain fragments with absolutely different morphologies, with the structural inhomogeneities observed across the entire thickness of the film being due to the poor compatibility of the polymeric and inorganic components. The presence of more homogeneous regions near the upper surface led to a conclusion that a homogeneous film can be obtained by making longer the time during which the components are agitated. This was done and Fig. 2 also shows micrographs of the upper (Fig. 2e) and lower (Fig. 2f) surfaces of a film produced by casting of a PAI–NTII(20) dispersion formed as a result of 20-h agitation of the components in solution. These data indicate that a homogeneous dispersion is formed and a uniform composite film is ob-

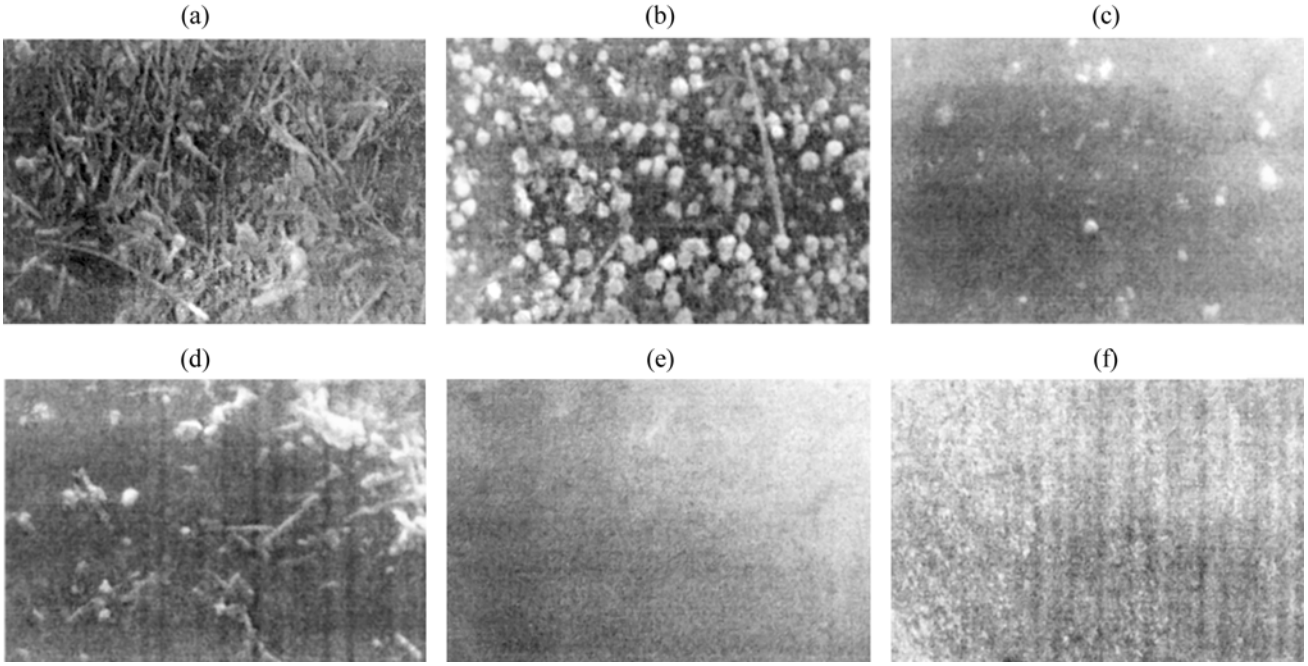

Fig. 2. SEM micrographs of (a, b, e) upper and (c, d, f) lower surfaces of (a–d) PAI–NTII(10) and (e, f) PAI–NTII(20) of thickness 20 μm.

tained, whose surface profiles are similar to the respective profiles of a homogeneous film of the basis PAI polymer.

Introduction of hydrosilicate nanoparticles (nanotube and intercalated montmorillonite MMT-15A) into the PAI matrix resulted in pronounced changes in the mechanical properties of the films obtained from these composites, compared with the films of an unmodified PAI (Table 1). It has been shown [3, 22] that changes in the mechanical behavior of films of heterocyclochain polymers, caused by introduction of nanoadditives into the polymer, are primarily manifested in an increased rigidity of the material: its modulus of elasticity, tensile strength, and, in some cases, strength are higher. Simultaneously with these changes, the failure strain of the films becomes substantially lower, to the point of synthesis of brittle samples.

The first of these tendencies is manifested in full measure in films of nanocomposites obtained in this study. Indeed, introduction of nanotubes and MMT even in small amounts (2 wt %, which corresponds to a volume content of nanoparticles slightly exceeding 1%) leads to a pronounced increase in the modulus of elasticity and tensile limit of the material. It is noteworthy that the results obtained clearly demonstrate the fundamental importance of achieving a high homogeneity of nanoparticle distribution in the poly-

Table 1. Mechanical characteristics of films at different compositions of the corresponding nanocomposites and durations τ of homogenization of their solutions

Type of nanoparticles	c,* wt %	τ, h	E, GPa	σ_p, MPa	σ_t, MPa	ε_b, %
–	0 (PAI_{st})	10	4.02 ± 0.07	102 ± 3	127 ± 4	45 ± 3
Nanotubes	2	10	4.36 ± 0.19	107 ± 3	126 ± 4	35 ± 4
	2	20	4.94 ± 0.14	122 ± 3	141 ± 3	31 ± 3
	10	20	4.18 ± 0.08	106 ± 6	104 ± 6	Up to 29
MMT-15A	2	10	4.80 ± 0.13	119 ± 3	118 ± 4	5.0 ± 0.5

* c is the concentration of the inorganic component; the same for Tables 2, 3.

Fig. 3. SEM micrograph of the region of low-temperature disintegration of a PAI–NT II(20) film.

mer volume for effective modification of the matrix material. Indeed, the rigidity of the material starts to increase considerably only after a prolonged (20 h) mechanical homogenization of a dispersion of the PAI–NT nanocomposite in a solvent, whereas 10 h of homogenization under the same conditions fails to provide a pronounced change in rigidity. These data are in good agreement with the results of the electron-microscopic study of the films (Fig. 2).

The same is indicated by the results of introduction into PAI of increased (10 wt %) amounts of nanotubes (Table 1). In this case, a film only slightly different from the starting PAI in both the modulus of plasticity and tensile limit. Presumably, this occurs because of the aggregation of nanoparticles in solution, observed on raising their concentration [23, 24].

The mechanical test results demonstrate a significant difference in the behavior of materials containing hydrosilicate nanotubes and MMT nanolayers. On the one hand, MMT-15A is a commercial intercalated product prepared for dispersion in polymeric matrixes. Therefore, it is easier to provide a high quality of its distribution in PAI, compared with introduction of nanotubes: already a 10-h homogenization of a nanodispersion yields films with higher modulus of plasticity and tensile limit, comparable with those obtained after 20 h of homogenization of suspensions with nanotubes. On the other hand, films of nanotube-containing nanocomposites strongly surpass the material modified with MMT in their deformation characteristics.

Indeed, PAI–MMT, as well as quite a number of nanocomposites described in the literature, disintegrates under uniaxial tension already near the tensile limit (breaking strain 5%), which strongly hinders practical use of these films. Introduction into PAI of the same amount (2 wt %) of nanotubes does not lead to any noticeable decrease in the deformability, compared with the starting material: extension of nanocomposite films of this kind leads (as also in the case of PAI films) to formation of a neck, its spreading across a sample, and the subsequent transition to the strain strengthening region, in which the sample disintegrates. Thus, use of hydrosilicate nanotubes for PAI modification can yield films that combine an enhanced rigidity with good deformation properties.

An additional specific feature of the mechanical behavior of PAI–NT II(20) nanocomposite films is associated with the manner in which the material disintegrates at low temperatures. A PAI film shows brittle disintegration at liquid-nitrogen temperature, whereas with films of PAI–NT II(20) nanocomposites, brittle cleavages could not be obtained under the same conditions: the deformation behavior of the material remains plastic at these temperatures. The pattern of plastic disintegration of a film of PAI–NT II(20) nanocomposite at liquid-nitrogen temperature is shown in Fig. 3.

A study of the transport properties of the corresponding films (homogeneous membranes) in pervaporation demonstrated the following. Introduction into the polymeric matrix of porous inorganic particles with tubular structure (nanotubes of the NT I–III types) without their additional treatment (chemical or orienting) leads to an increase in the flux of water across the corresponding film membrane (Table 2,

Table 2. Permeability to water of nonporous films of PAI–NT I–III composites in comparison with a nonporous PAI film in pervaporation at 40°C

Sample no.	Sample	c, wt %	l,* μm	Π, kg m^{-2} h^{-1}	Πl,* kg m^{-2} h^{-1} μm
1	PAI	0	15	0.043	0.645
2	PAI–NT I	2	15	0.044	0.660
3	PAI–NT II	10	15	0.084	1.260
4	PAI–NT III	2	12	0.056	0.672

* l is the sample thickness, and Πl, sample permeability normalized to thickness.

Table 3. Permeate flux ∏ and separation factor for water, F_w, for nonporous composite films (sample nos. 5, 6) in comparison with a nonporous PAI film (sample no. 1) in pervaporation separation (40°C) of an aqueous solution containing 48 wt % ethanol

Sample no.	Sample	c, wt %	l,* μm	∏, kg m^{-2} h^{-1}	F_w
1	PAI	0	15	3.20	5.5
5	PAI–NT II	2	15	3.75	7.9
6	PAI–MMT-15A	2	15	2.35	5.8

* PAI characteristics well correlate with those previously reported in [25].

sample nos. 2–4), which is the most pronounced for NT II in the case of a good compatibility of components of the composite material (Table 2, sample no. 3). Table 3 compares the results of tests of PAI and PAI–NT II(20) (2 wt %) films, and of a composite PAI–MMT-15A (2 wt %) film obtained under the conditions in which PAI–NT II(20) was formed, in dehydration of an aqueous solution of ethanol (48 wt % ethanol) in the course of pervaporation at 40°C. As the content of nanotubes in the composite increases from 2 to 10 wt % (Table 3, sample no. 5 and Table 2, sample no. 3, respectively), the permeability of the material to polar liquids, such as water and ethanol, grows. A possible explanation of this effect is that the permeability is affected by the probable, in principle, appearance of microscopic inhomogeneities or defects (on the nanosize level or coarser) in the nonporous matrix of the composite film upon introduction of the inorganic component. However, this assumption is easily refuted by analysis of the data in Table 3, because introduction of 2 wt % NT II into a PAI film yields a composite for which the separation factor of the water/ethanol mixture not only does not decrease, but even somewhat increases as compared with that for the homogeneous PAI film.

In this property (an increase in permeability to liquids upon introduction of inorganic nanotubular additives), the PAI–NT II(20) composite material obtained strongly differs from typical composites constituted by a polymer and an inorganic filler. As a rule, introduction of inorganic particles into a polymeric matrix results in that an inorganic phase impermeable to gases and liquids is formed in the matrix and the mass-transfer zone becomes narrower. As a result, the permeability on nonporous films falls [26]. For this reason, introduction into the PAI matrix of 2 wt % MMT-15A particles under the same conditions yields a composite material with lowered permeability, as shown in Table 3. Because inorganic MMT-15A particles and hydrosilicate nanotubes are close in chemical composition, no other components are present in the systems under consideration, and the formation conditions remain unchanged, it can be assumed that the nanosize structural features of the films exert a decisive influence on their transport properties.

CONCLUSION

A new nanocomposite material with improved physicomechanical properties and higher permeability in pervaporation to polar liquids and, in particular, aqueous–alcoholic mixtures than the starting polymer was obtained on the basis of poly(diphenyloxyamido-*N*-phenylphthalimide) and layered magnesium hydrosilicate $Mg_3Si_2O_5(OH)_4$ with tubular structure.

ACKNOWLEDGMENTS

The study was financially supported by the Russian Foundation for Basic Research (grant no. 04-03-81005-Bel).

The authors are grateful to I.A. Drozdova and I.L. Potokin for electron-microscopic studies.

REFERENCES

1. Sreekumar, T.V., Liu, T., Min, B.G., et al., *Adv. Mat.*, 2004, vol. 16, no. 1, pp. 58–61.
2. Korytkova, E.N., Pivovarova, L.N., Dobrodumov, A.V., et al., Abstracts of Papers, *V Mezhdunarodnaya nauchnaya konferentsiya "Khimiya tverdogo tela i sovremennye mikro- i nanotekhnologii"* (V Int. Sci. Conf. "Solid State Chemistry and Modern Micro- and Nanotechnologies"), 2005, pp. 22–24.
3. Yudin, V.E., Otaigbe, J.U., Gladchenko, S., et al., *Polymer*, 2007, vol. 48, pp. 1306–1315.
4. Neverov, V.M., Chvalun, S.N., J.Blackwell, et al., *Vysokomol. Soedin., Ser. A*, 2000, vol. 42, no. 3, pp. 450–461.
5. US Patent 5932361.
6. Vu De, Q., Koros, W.J., and Miller, S.J., *Ind. Eng. Chem. Res.*, 2002, vol. 41, no. 3, pp. 367–380.

7. Moaddeb, M. and Koros, W.J., *J. Membr. Sci.*, 1997, vol. 136, no. 1, pp. 273–277.
8. Singh-Ghosal Anshu and Koros, W.J., *Ind. Eng. Chem. Res.*, 1999, vol. 38, pp. 3647–3654.
9. Nunes, S.P., Peinemann, K.V., Ohlrogge, K., et al., *J. Membr. Sci.*, 1999, vol. 157, p. 219.
10. Potschke, P., Fornes, T.D., and Paul, D.R., *Polymer*, 2000, vol. 41, p. 3861.
11. Baughman, R.H., Zakhidov, A.A., and Heer, W.A., *Science*, 2002, vol. 297, pp. 787–792.
12. Sholl, D.S. and Johnson, J.K., *Science*, 2006, vol. 312, no. 5776, pp. 1003–1004.
13. Skoulidas, A. and Sholl, D.S., *Am. Inst. Chem. Eng. Ann. Meeting*, Cincinnati, OH, November 2005.
14. Korytkova, E.N., Maslov, A.V., and Gusarov, V.V., *Sbornik trudov "Khimiya poverkhnosti i sintez nizkorazmernykh sistem"* (Coll. of Works "Surface Chemistry and Synthesis of Low-Dimension Systems"), St. Petersburg: RIO SPbGTI (TU), 2002, pp. 54–59.
15. Korytkova, E.N., Maslov, A.V., and Gusarov, V.V., *Temperaturnye funktsional'nye pokrytiya: Trudy XIX Vserossiiskogo soveshchaniya* (High-Temperature Functional Coatings, Proc. XIX All-Russia Symp.), St. Petersburg, 2003, vol. 1, pp. 186–189.
16. Korytkova, E.N., Maslov, A.V., Pivovarova, L.N., et al., *Fiz. Khim. Stekla*, 2004, vol. 30, no. 1, pp. 72–78.
17. Gofman, I., Svetlichniy, V., Yudin, V., et al., *Bull. Czech. Composite Carbon Mater. Soc.*, 2006, no. 1, pp. 33–37.
18. Korytkova, E.N., Pivovarova, L.N., Drozdova, I.A., and Gusarov, V.V., *Fiz. Khim. Stekla*, 2005, vol. 31, no. 6, pp. 1099–1106.
19. Gusinskaya, V.A., Koton, M.M., Batrakova, T.V., and Romashkova, K.A., *Vysokomol. Soedin. Ser. A*, 1976, vol. 18, no. 12, pp. 2681.
20. Dobrodumov, A.V., Gofman, I.V., Korytkova, E.N., et al., Abstracts of Papers, *III Vserossiiskaya konferentsya "Khimiya poverkhnosti i nanotekhnologiya"* (III All-Russia Conf. "Surface Chemistry and Nanotechnology"), St. Petersburg, 2006, pp. 239–240.
21. Wise, K.E., Park, C., Siochi, E.J., et al., *Chem. Phys. Lett.*, 2004, no. 391, p. 207.
22. Delozier, D.M., Orwoll, R.A., Cahoon, J.F., et al., *Polymer*, 2002, vol. 43, no. 3, p. 813.
23. Zhang Yi-He, Wu Jun-Tao, Fu Shao-Yun, et al., *Polymer*, 2004, vol. 45, no. 22, p. 7579.
24. Jiang Xiaowen, Bin Yuezhen, and Matsuo Masaru, *Polymer*, 2005, vol. 46, no. 18, p. 7418.
25. Kononova, S.V., Kuznetsov, Yu.P., Romashkova, K.A., et al., *Zh. Prikl. Khim.*, 1995, vol. 68, no. 8, pp. 1361–1366.
26. Yamaguchi, T., Miyazaki, Y., Nakao, S., et al., *Ind. Eng. Chem. Res.*, 1998, vol. 37, pp. 177–184.

ISSN 1070-4272, Russian Journal of Applied Chemistry, 2007, Vol. 80, No. 12, pp. 2149–2150. © Pleiades Publishing, Ltd., 2007.
Original Russian Text © Editorial board, 2007, published in Zhurnal Prikladnoi Khimii, 2007, Vol. 80, No. 12, pp. 2071–2072.

ANNIVERSARIES

Evgenii Fedorovich Panarin (to His 70th Birthday)

DOI: 10.1134/S1070427207120303

January 17, 2008 is the 70th birthday of Professor, Corresponding Member of the Russian Academy of Sciences, Director of the Institute of Macromolecular Compounds (Russian Academy of Sciences), Evgenii Fedorovich Panarin.

E.F. Panarin graduated from the Lensovet Technological Institute (St. Petersburg) in 1960. After completion of his postgraduate course (1963), he entered the Institute of Macromolecular Compounds, Russian Academy of Sciences (IVS RAS). Since 1987 E.F. Panarin has been working as the director of IVS RAS.

E.F. Panarin is an outstanding scientist who contributed significantly to the progress of chemistry of macromolecular compounds. His scientific activities are associated with applied research in hydrophilic polymers and polymers for biomedical use and with basic research in synthesis of polymeric drugs.

E.F. Panarin has developed foundations for directed modification and correction of the bioactivity of drug preparations with polymers, and methods for synthesis of multipurpose water-soluble polymer carriers bearing diverse functional groups that provide addition of bioactive compounds to a target site of the macromolecule. Such polymers were offered as a model for certain biopolymers, and also as carriers for transportation of bioactive compounds (hormones, antibiotics, enzymes, antiseptics, DNA, etc.) to target organs.

Of great importance are studies of mechanisms of chemical reactions used in synthesis and modification of polymers, including chemical and enzymatic synthesis of vinylsaccharides, preparation of water-soluble polymers from *N*-vinylamides and functionalized vinyl and allyl monomers, and also studies of the reactivity of functional groups of polymers. E.F. Panarin was the first who established the relationship between the chemical structure and intrinsic bioactivity of water-soluble polymers. As a result of this research, a new class of polymers exhibiting antimicrobial, antiviral, antitumor, immunomodulating, growth-promoting, and other kinds of activities has been discovered.

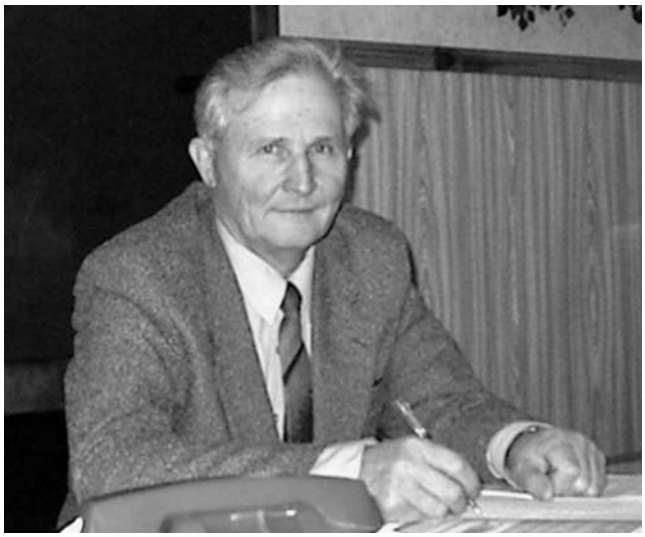

E.F. Panarin has developed foundations and methods for designing polymeric polyfunctional bioactive nanostructured materials. As a result, polymeric nanodrugs Poviargol and Katapol were developed on the basis of biogenic elements and diphilic ions of bioactive compounds.

E.F. Panarin applies basic research results to various practical problems of industry, medicine, agriculture, and environmental protection. Under his guidance, processes for production of novel domestic water-soluble polymers and polymer-based drug preparations have been developed. E.F Panarin contributes significantly to the development of domestic blood substitute Gelenpol (approved for medical use) based on polymeric hemoglobin, and also to the development of novel plant protectors based on bioactive polymers.

E.F. Panarin is a Honored Inventor of the Russian Federation. He is a coauthor of the monographs *Antimikrobnye polimery* (Antimicrobial Polymers) and *Vozbuzhdennye sostoyaniya v khimii polimerov* (Excited States in Polymer Chemistry), of a handbook *Polimery v meditsine i farmatsii* (Polymers in Medicine and Farmacy), and of more than 500 scientific publications and inventions. E.F. Panarin pays great

attention to the problems of organization of science and pedagogical activities. He is at the head of the experimental base of the Department of Medical Biotechnology of the St. Petersburg Polytechnic University at the Institute of Macromolecular Compounds, Russian Academy of Sciences. Ten candidates and six doctors of science were brought up under his guidance.

E.F. Panarin is the Deputy Editor-in-Chief of *Zhurnal Prikladnoi Khimii* (Russian Journal of Applied Chemistry) and a member of Editorial Boards of other scientific journals. His multidisciplinary and very fruitful activities were commended with government awards and prizes.

The Editorial Board and Staff of *Zhurnal Prikladnoi Khimii*, E.F. Panarin's friends and colleagues cordially congratulate him on this jubilee and wish him splendid health and creative longevity in scientific and pedagogical activities.

ISSN 1070-4272, Russian Journal of Applied Chemistry, 2007, Vol. 80, No. 12, pp. 2151–2156. © Pleiades Publishing, Ltd., 2007.
Original Russian Text © S.L. Buyantuev, I.V. Starinskii, 2007, published in Khimicheskaya Promyshlennost', 2007, Vol. 84, No. 6, pp. 296–302.

TECHNOLOGY OF ORGANIC AND INORGANIC SUBSTANCES

Investigation of Sorption Properties of Carbon Treated with Low-Temperature Plasma

S. L. Buyantuev and I. V. Starinskii

East-Siberian State Technological University, Russia

Received February 12, 2007

Abstract—Plasma based technology for producing active carbon is proposed.

DOI: 10.1134/S1070427207120312

In the modern world there is clear tendency to organization of ecologically pure industrial production. This is connected with the general view that catastrophic and practically throughout environment pollution is a real fact [1]. The main sources of pollution are industrial and domestic effluences containing petroleum products, oil, phenols, pesticides, herbicides, heavy metals and a scope of organic chemicals. All these substances are potential hazards for people and live nature. A significant amount of pollutions is produced by energetic enterprises, the power station using coil in particular. The more and more rigid restrictions concerning various hazardous effluences are issued, and they require development and application of new and more effective materials and technologies providing ecological safety of operation of power stations.

Among the known methods of purification water, its deep purification to any degree of purity provides sorption purification only. This method is based on the application of sorbents, active carbon predominantly [2].

The principal restriction to application of carbons sorbents for energetic ecology is high cost and deficient due to disadvantage of currently used technology. The known technologies of producing carbon sorbents (from coil, wood, nut crust and other) use energy of fuel combustion or electric heating [3, 4]. Alternatively, for producing active carbon by existing methods can be applied energy of low temperature plasma. The low temperature plasma increases considerably efficiency of processing solid fuel and intensifies the process of production of active carbon owing to presence in the plasma of active radicals, ions, electrons, and due to its significant temperature and high specific power [5].

Thus, investigations directed to the study and development of plasma technology for producing sorbents are actual and can result in development of technology for producing active carbon of any type with lower energy consuming.

For the studying processes of plasma pyrolysis and gasification of carbon using electric arc reactor as a generator of low temperature plasma we created an experimental installation (Fig. 1), consisting of the following principal nodes: system of electric feeding, combined type electric arc reactor, direct current electromagnetic coil, vapor generator, system of feeding with carbon and air, system for gas output, cooling and purification, control console, muffle chambers with connecting pipes for gas reagents, separation chambers and chambers for pyrolysis and activation.

During the experiment the active carbon samples from pyrolysis and activation chamber are investigated on sorption activity on iodine, benzene, methylene blue and iron and compared with currently used sorbents (birch active carbon BAC).

In the process of experiments material and heat flows were registered in all nodes of installation. In part, were registered consuming of carbon, vapor, air, graphite electrodes, active carbon, dust and sublimates, and electric power of reactor, heat power, heat loss in plasma reactorm muffle chambers and gas outlet.

Initially, the experiment was conducted in the absence of air and vapor. In the course of experiment the grinded

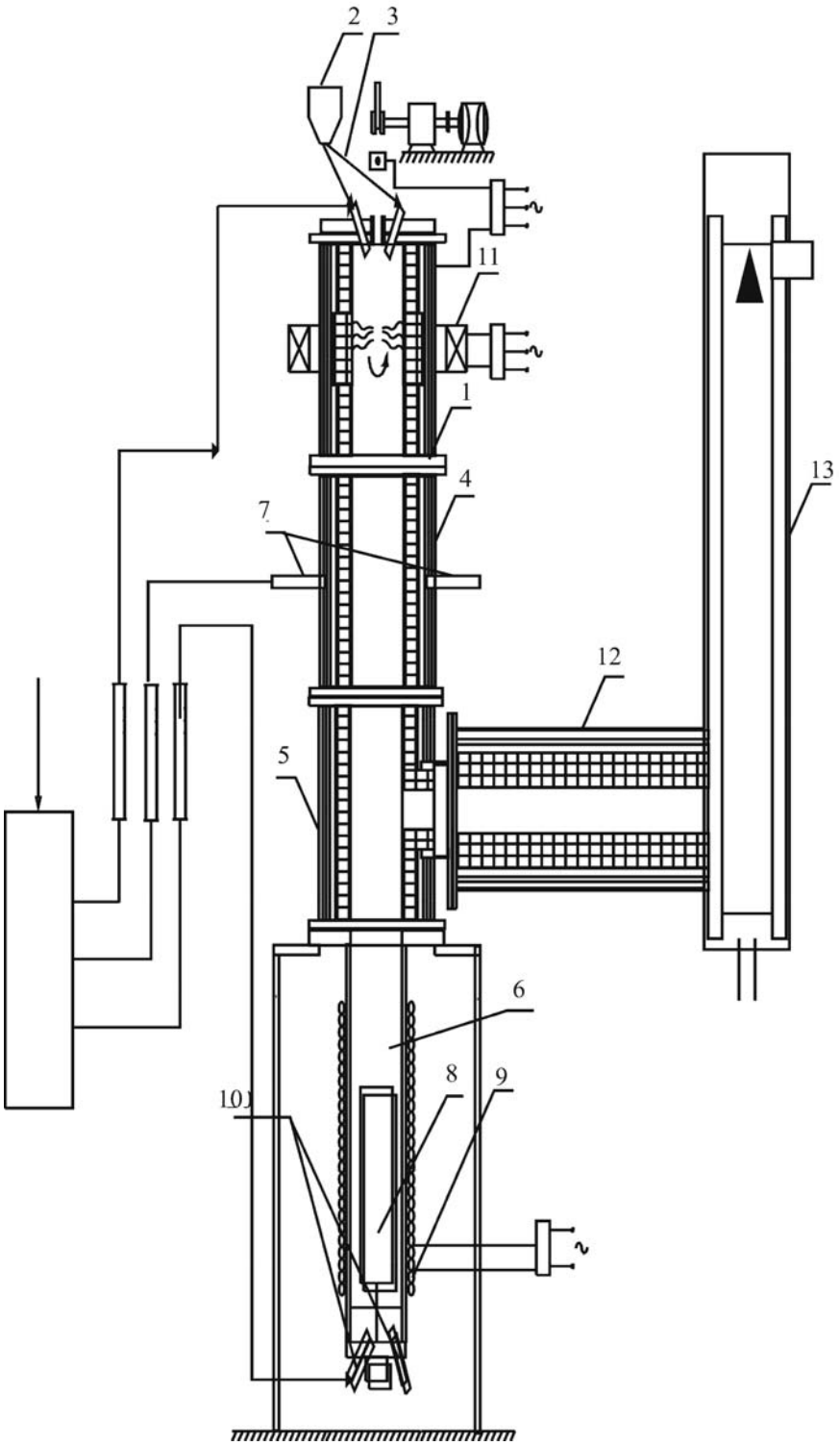

Fig. 1. Module of one-step plasma installation for complex treatment of carbon. (1) plasma reactor, (2) dust feeder, (3) dust pipe, (4) muffle chamber, (5) separation chamber, (6) pyrolysis and activation chamber, (7) gas outlet, (8) stirring unit, (9) heating elements, (10) gas inlet of pyrolysis and activation chamber, (11) electromagnetic coil, (12) chamber of gas outlet, (13) gas purification system.

carbon is passed through plasma reactor where it is heated in electric arc using energy of combustion of finely dispersed component of carbon. To the end of the experiment was measured carbon combustion loss and were performed analyses of its sorption activity. In the second step were conducted experiments at feeding with vapor for maximum developing porous structure [2]. The results of analyses are listed in Table 1.

In the process of analyses it was found that pouring the carbon treated with low temperature plasma and vapor into water (common water-pipe water was used) results in separation of carbon into two fraction: heavy fraction with is collected at the bottom (Table 1, line 7), and light fraction (line 6), floating up to surface. An insignificant part of carbon particles floated in bulk water.

Light fraction constituted a significant part (76.5%) of the carbon and featured by a very bad wettability and good magnetic properties.

Analysis of sorption properties of the fractions showed that heavy fraction shows high ash content (88.0%) and good chemosorption property (sorption activity on iron is 14.52 mg/g), the light (floated up) fraction shows moderate ash content (32.4%) and good oil sorption property.

The chemosorption properties on iron are not unambiguous. Iron ions are known to have small size even as compared with ultra-micro pores. Therefore binding of iron ions should be connected wuth the presence in the sorbent of mineral fraction inducing cation-exchange processes, that is, chemosorption [6]. Ions of potassium, sodium and calcium can be washed out from the minerals by the ions with higher oxidation number, including Fe^{3+}. Therefore the high sorption capacity of the heavy fraction is well explainable: this fraction contains 88% of mineral part. High sorption capacity of this fraction allows us to suggest that so-called *iron removing* sorbent is obtained, which can be applied to purification effluences and drinking water from iron admixtures. This sorbent acts as cation exchanger and provides high degree of water purification. The light fraction has not high sorption activity on iron, the same as that of parent carbon (see Table 1). Besides, the light fraction shows excellent magnetic properties, that allows to judge that it initially contains much iron. Appears the state of chemical equilibrium, and additional amount of iron can not be absorbed. For heavy fraction no magnetic property was registered. Despite the fact that by 88% it consists of mineral part, it does not practically contains iron. This is why it well consumes iron at the treatment with the solution containing Fe^{3+} ions.

Considering the data on the sorption of benzene vapor One can see that sorption capacity of carbon increases after treatment in all cases (see Table 1). This fact indicates significant increase in number of meso pores in the sorbent structure. The light fraction shows high capacity on benzene: it increases twice as compared with the parent carbon. Low capacity of heavy fraction (Table 1, line 7) is due to insufficient development of meso-porous structure and low content of organic part. Owing to high sorption capacity on benzene and unique hydrophobic properties of light fraction we studied it in more details.

We measured oil capacity of this sorbent. The value of oil capacity (0.48 g/g) is excellent for the sorbents of oil removing type [6]. This sorbent can collect petroleum 4-5 times more than modern industrial solvents allow. Besides, this sorbent shows hydrophobic property, hence, it would not disturb ecology of water layer. The sorbent used for oil consumption can be easily collected. Further, the sorbent impregnated with oil or petroleum products can be used in various directions: as a high-calorie low-ash solid fuel, at stacking asphalt and so on.

Below are given the results of studying microporous structure of carbon before and after treatment with low temperature plasma. The microanalysis was conducted with metallography measuring microscope NEOPHOT-21 at different zoom.

Fig. 2 shows the presence of closed micro pores (1, 2, 3, 4) indicating not developed structure of the parent carbon.

In Fig. 3 many micro pores can be seen: 1–15 nm diameter, combined with other micro pores, joining with 5 nm micropores 2 and 3 is seen clearly. The micro pore 2 is combined with 4 through the transfer micro pore 5.

It is these connections appearing as a fracture (passage) that allow suggest about good sorption ability of the carbon, which is confirmed by chemical analyses of the sorption activity of the carbon on methylene blue, benzene, iodine and iron, and of oil capacity (Table 1).

Fig. 4 shows smaller pores as fractals (canals) 0.1–3 nm width, as confirmed by chemical analyses of sorption activity on iron. The micro pores 1–3 being connected form a pass through whole section of the carbon particle. The micro pore 3 in the right area has 1 nm diameter and in left area achieves 3 nm. The micro

Results of analysis of the carbon after treatment with low temperature plasma

No.	Carbon combustion loss, %	Sorption activity on iodine, cm^3/g	Sorption activity on benzene. cm^3/g	Sorption activity on iron. mg/g	Sorption activity on methylene blue, mg/g	Fraction compositions			Notes
						below 0.2 mm	from 0.2 to 1 mm	above 1 mm	
1		12.3	0.082	—	21.1	25	63	12	Parent carbon
2		15.6			50				Experiment without air pass to the reactor
3	72	17.8	0.085	3.10	123.85	8	78	16	Experiment with passing overheated steam to the reactor, less than 5 kg/h
4	72	20.3	0.133	2.60	123.89	12	74	16	Experiment with passing overheated steam to the reactor, less than 10 kg/h
5	72	19.4	0.157	2.24	123.9	13	81	6	Experiment at carbon gasification
6	72	19.1	0.192	2.54	133.5	11	57	32	Light fraction
7		15.6	0.046	14.52	58.3	38	61	1	Heavy fraction
8		30.5	0.22		38–40				Common sorbent (BAU)

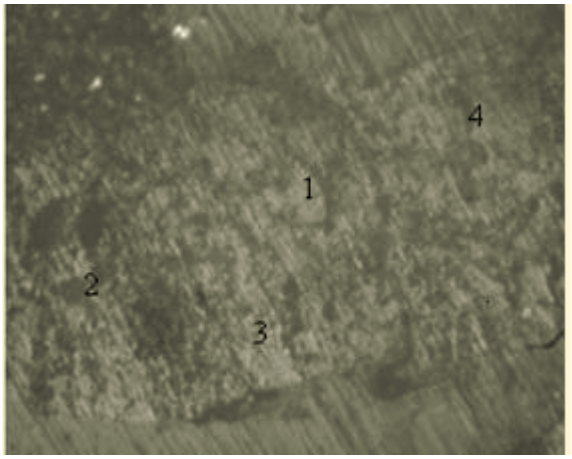

Fig. 2. Structure of carbon particles before and after treatment with low temperature plasma (zoom 400:1).

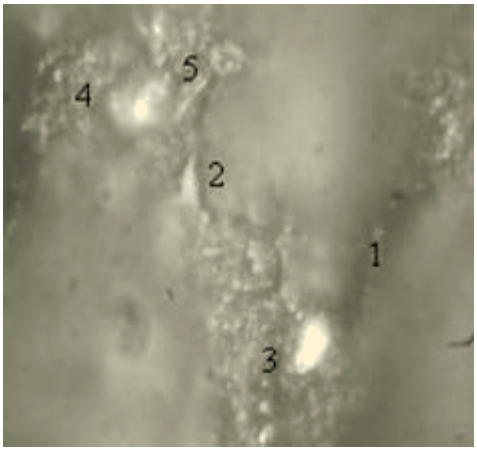

Fig. 3. Structure of carbon particle after treatment in the plasma reactor (zoom 1000:1).

pores 4 and 5 form pass to the sample particle inside and their diameters are approximately 2 and 1 nm, respectively. Calculation shows that the micro pores of this range of the canal width constitute up to 60% of all visible pores on the sample section.

In Fig. 5 is seen many micro fractals passing through the active carbon particle on the whole section area. Two micro pores are clearly seen: 1 passes through whole particle, and its canal structure is well seen. Besides, it goes into the particle body. The micro pore 2 is of less size but also is well seen. In Fig. 5b also are seen canals across the pores 1–3, mostly going into the particle body. Presence of many pores makes the particle density less than that of water, allowing collecting wastes as oil spots from water surface.

The sorbent produced can be used as filling of the filters for purification effluences from petroleum products and other nonpolar (organic) liquids. The

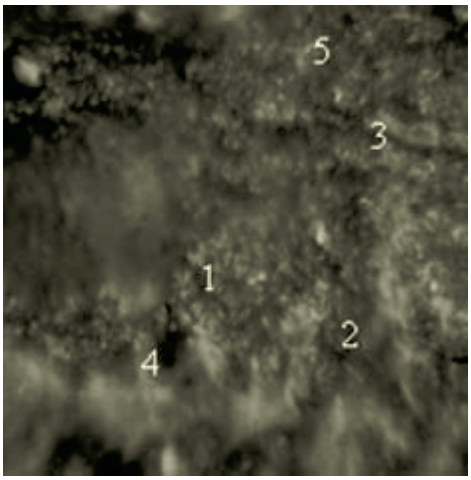

Fig. 4. Structure of a particle of iron removing sorbent (zoom 1000:1).

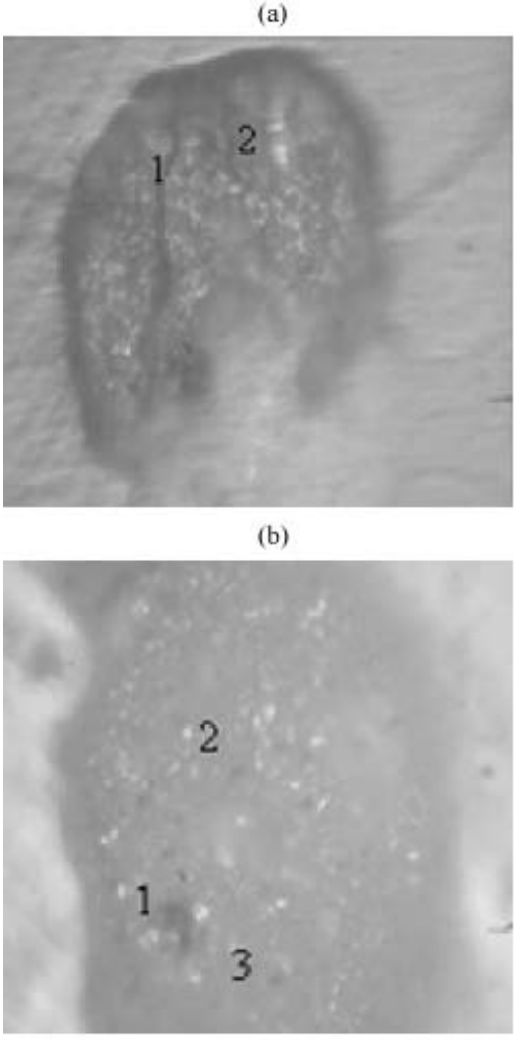

Fig. 5. Structure of the particles of oil removing sorbent (zoom 1000:1).

Fig. 6a. Oil spot on water surface.

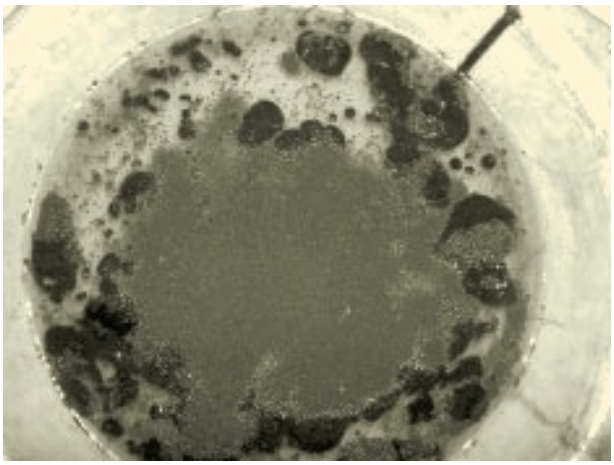

Fig. 6b. Oil spot covered with active carbon.

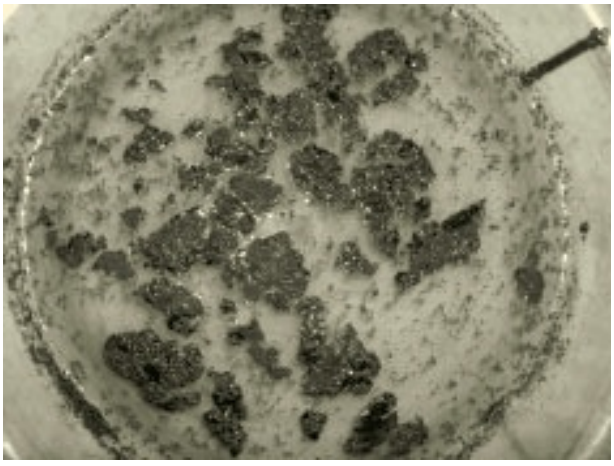

Fig. 6c. Oil spot absorbed with active carbon.

sorption technology based on this sorbent can be used for narrowing propagation and for collection of petroleum wastes in water basins, soil, ground, snow and other surfaces.

Note that in the process of the active carbon production is formed the synthes-gas consisting of: CO_2 1.1%, O_2 0.8%, CO 40.2%, H_2 46.7%; caloricity 3710 kcal/kg.

Comparison of characteristics of active carbon before and after treatment in the plasma reactor shows increase in sorption activity on all tests. The most significant is increase activity on methylene blue, from 21.1 to 133.3 mg/g, evidencing existence of micro pores with diameter over than 1.5 nm. Comparison with birch active carbon (BAC, table, line 8) prepared by traditional procedure shows 4-fold higher characteristic of the sorbent obtained by the plasma technology. The data on benzene and iodine are not so high; this is a result of ohysical structure of the parent raw material [2].

Thus, the proposed plasma technology for producing active carbon is advantageous, as compared with traditional technology, by the following [7]:

– liquid and gaseous fuel is not consumed;

– Potential heat of the initial carbon is consumed completely;

– large size granules of carbon can be quickly heated to high temperature in the zone of gas formation in account of heat of combustion of dust fraction;

– simplicity of the process technology;

– flexible technological parameters in a wide range;

– compactness of the equipment used.

REFERENCES

1. Volkov, E., Blokhin, A., and Keneman, F., *Vestnik elektroenergetiki*, 1996, no. 3, pp. 35–44.
2. Kolyshkin, D.A. and Mikhailova, K.K., *Aktivirovannye ugli* (Active Carbons), Handbook, Moscoow: Khimiya, 1972, p. 270.
3. Kostomarov, M.A., Perederii, M.A., and Suriniva, V.I., *Poluchenie adsorbentov iz iskopaemykh uglei* (Sorbents Producing from Coil), Moscow, 1976, pp. 5–15.
4. Sevryugov, L.B., Lepilin, V.N., and Buravtseva, M.I., *Preparation, Structure and Properties of Sorbents* (Collection of Publications), Leningrad: LTI, 1985, p. 13–22.
5. Zhukov, M.F., Kalinenko, R.A., and Levitskii, A.A., *Plasmokhimicheskaya pererabotka uglya* (Plasma Chemical Processing of Carbon), Moscow: Nauka, 1990, p. 201
6. Reznik, Ya.E., *Promyshlennaya Energetika*, 1981, no. 6, pp. 9–20 .
7. Buyantuev, S.L. and Starinskii, I.V., Patent application 14.05.2007, no. 2006124168/15(026207). Decision on issuing the patent.

ISSN 1070-4272, Russian Journal of Applied Chemistry, 2007, Vol. 80, No. 12, pp. 2157–2162. © Pleiades Publishing, Ltd., 2007.
Original Russian Text © M.B. Generalov, 2007, published in Khimicheskaya Promyshlennost', 2007, Vol. 84, No. 7, pp. 325–331.

TECHNOLOGY OF ORGANIC AND INORGANIC SUBSTANCES

Formation of Charges of Plastic Industrial Explosives by Extrusion

M. B. Generalov

Moscow State University of Engineeric Ecology, Moscow, Russia

Received May 25, 2007

Abstract—Principles of application of extrusion technology for the formation of charges of industrial plastic explosives are considered, including analysis of extruder operation and modeling of extrusion process.

DOI: 10.1134/S1070427207120324

Extrusion. For the hardware forming at the manufacturing plastic composite industrial explosives, extrusion technology is ordinary applied.

Extrusion is a technological process consisting essentially of admitting to the material of required form in the cross-section by pressing it through a profiling unit (the matrix).

By the extrusion technology the plastic composition of an explosive can be transformed into a final product having a certain form: sheet, profile band, cord, rod, pipe, etc.

The principal instruments for working up plastic compositions are single- or multi-screw *syringe machines* or *extruders*. Detailed description of extruder design can be found in [1–3]. One- and two-worm extruders are used not only at producing hardware but also in other technological processes at the manufacturing plastic explosives, as mixer, plasticizer and granulator [4].

Modern extruder is a machine that provide simultaneous heating of polymer material in account energy formed at of internal friction and its homogenization owing to large shift deformations, as well as creating hydrostatic pressure necessary for continuous pressing the material through the profiling unit. Therefore it i possible to define the modern extruder as a pump completely free of pulsation that passes thermally homogenous polymer composition with constant productivity and at the constant pressure.

The most wide application in the industry of polymers workup have found the single-screw extruders. Correspondently, the most developed area of theory of treatment concerns the extrusion process on the single-worm extruders. Therefore let us consider the processes occurring at the extrusion on such single-worm machine (Fig. 1). It consists of: cylindrical body (4) with loading hopper (5) for feeding with granules or pieces of plastic explosive, worm (auger) (3) located in the thrust bearing

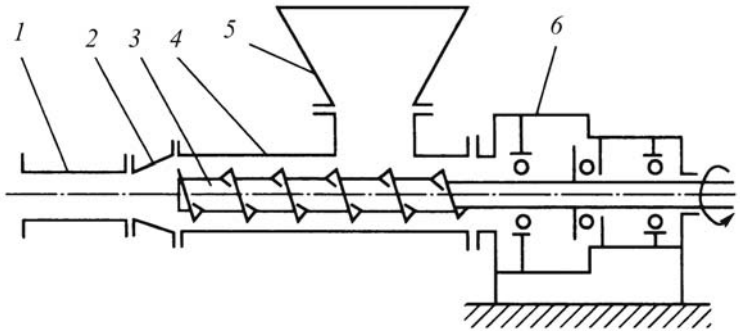

Fig. 1. Extruder: general scheme. See the text.

node (6), press-node consisting of cone tube (2) and forming matrix (1), and a drive. In some types of the extruder the internal surfaces of body and forming matrix are equipped with controlled heating.

The auger is essential working element of extruder. It takes granules of the material from hopper feedthroat hole and passes it uniformly as a homogenous viscous flowing mass to the forming unit.

By the character of the processes in each part of the auger, the latter can be separated along its length into three principal zones: the *feeding* or *loading zone* where the treated material is in solid state, the *compressing zone*, where proceed almost completely its homogenization, and *dozing zone*, where the material becomes viscous-flowing, or plastic.

Qualitative analysis of extruder operation. Commonly the extruders differ by the treated material: for processing elastomers and for thermoplasts. In the first case extruder is feeded by plasticized material, e.g., as pieces of tapes from rolls; in the second case, granulated material is processed.

To the feeding zone the granulated material commonly is passed at the room temperature. After filling the canal, material is moved like hard rod. In the course of moving, the rod is tightening, and owing to friction retarding the moving is compressed in volume. In some cases the pressure in the end of this zone achieves value uo to 10 MPa.

Rate of motion of the block of granules along the auger canal depends on the ratio of friction coefficients between the granules and granules with the surface of the auger and body. Lower the friction coefficient between the body surface and the polymer, higher the rate of the block motion.

For diminishing the friction coefficient, the screw surface is abraded and polished. On the contrary, finishing of internal surface of the body is defined by the reasons of convenience at cleaning of the machine. Often the body internal surface has longitudinal grooves (riffles).

The most significant is thermal regime of operation in the *feeding zone*. Commonly, the temperature of internal surface of body falls to the range 50-80°C, to provide anchncing in plastic properties of the processed material.

The *feeding zone* length is commonly from 4 to 6 diameters of screw.

In the *compression zone* the material transforms from the solid state into viscous flow under the action of heating evolved as a result of shift deformation of the material. The solid block of granules while moves along the auger screw canal exerts circular compression (autohesion) effect due to increasing pressure and cohesion (shifting) effect. As a result, the porous structure of the compressed granules gets properties of monolithic poreless homogenous mass in viscous-flow state.

In the *dozing zone* the screw canal of auger is filled with the polymer in viscous-flow state. From this moment, the polymer moving is similar to the moving of viscous liquid along the canal of a screw pump. Actually the polymer moves in the dozing zone by screw trajectory. Such motion commonly is represented as a sum of two independent motions.

The first one is forward motion (translation) along the axis of the screw canal. The volume flow rate of this motion defines eventually volume productivity of the extruder and hence defines the upper limit of the rate of granular block movement within the feeding and melting zones.

The second one is circular movement of the polymer in the direction at the right angle to the screw canal axis. Moving crosswise in the canal the flow meets the canal wall and turns back. The circular movement provides homogenization of the polymer composition, averages distribution by temperature and allows to use extruder as a mixer.

A part of the material that achieves the canal wall does not turn back but passes ring gap between the wall and the screw. This is a *leaking flow*. Thus the productivity of the dozing zone is defined by the difference between the productivity of compelled and leaking flows.

Interconnection of all the steps of extrusion shows that analysis of the process requires considering all the phases together. The main factor controlling interaction of all phases of the process is constancy of material consuming of the polymer in any section of the auger.

So far as the auger productivity is defined by the *dozing zone*, let us consider the method of mathematical description of operating of this zone.

Mathematical model of extrusion process. By the principle of its operation, the dozing zone of mono-screw extruder is a type of screw pump. Due to high viscosity of the pumped liquid, flow in such screw pump is always

laminar, with the Reynolds number close to unity (so-called *creeping flow*).

The mathematical model of the screw pump can be obtained by join solving a system of equations that express the laws of mass retention, and pulse transfer at laminar flow with the equations describing rheological properties of the pumped liquid.

This problem has been many times considered in the works of both domestic and foreign scientists. The most systematically the mathematic model of screw isothermal flow of a Newtonian fluid has been considered in a series of publications by Charley, Malluk and McKelvey who thus were the parents of hydrodynamic approach to description of the extrusion process.

Let us consider basic equations of the polymer motion in the dozing zone of auger. At the rotation of screw the material becomes located inside a mechanical system which is restricted by moving surfaces of screw (cylindrical base and sides of screw canal) and immovable surface of the auger body. As a result, forced flow becomes established. The material is moved exclusively due to existence of this forced flow. The necessary condition of existence of the forced flow is certain viscosity of the material. A hypothetical material with zero viscosity can not be transported by screw pump, and hence forced flow can not appear.

Figure 2 shows symbols defining the screw geometry and used for denoting its details. For the complete analysis we consider a multiple-thread screw with two parallel channels. The cylinder internal diameter is $D_1 = 2R_1$ defines the distance between internal auger diameter $D_0 = 2R_0$ and the cylinder surface. Radial gap between the external diameter of screw and cylinder surface is c. The step of screw is connected with the angle α of screw line measured at external diameter of screw by the equation:

$$E = \pi(D - 2e)\tan\alpha, \quad (1)$$

where E is screw step.

If W is the canal width, then the screw having m threads the following eqation can be obtained:

$$m(W + e) = E\cos\alpha, \quad (2)$$

where e is thickness of the screw loop.

The screw pump operating occurs when screw is rotated and cylinder remains fixed, although opposite situation is also possible: rotating cylinder and fixed screw. In both the cases the material will be moving in the same direction and with the same characteristics of the process. The design with rotating screw is simpler and such type machines are the most useful.

For hydrodynamic analysis of a screw pump should be considered in details the trajectory of a particle of material (in phenomenological sense, the particle means a material dot of continuous medium moving in the auger canal) in the screw canal relatively to the fixed coordinates. There are two possibilities of defining position of the material particle: relatively to the cylinder or relatively to the screw. Further we consider position of material particle relatively to the screw. We consider the screw as a fixed part, while the cylinder is considered as rotating, that is, we use the principle of inverted motion.

Let us apply a simplification very useful in hydrodynamic analysis: we consider the screw canal as two parallel planes. Conventionally, we uncoil the screw canal and consider it as unmoved rectangular groove with the movable upper plane, the internal surface of cylinder (Fig. 3). The z axis corresponds to the axis of the screw canal, its positive direction is taken the direction of movement of material to the canal outlet; the canal length equals Z.

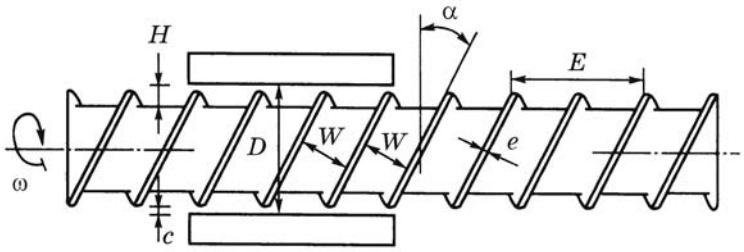

Fig. 2. Sizes of the details of the auger screw canal at vibration thickening.

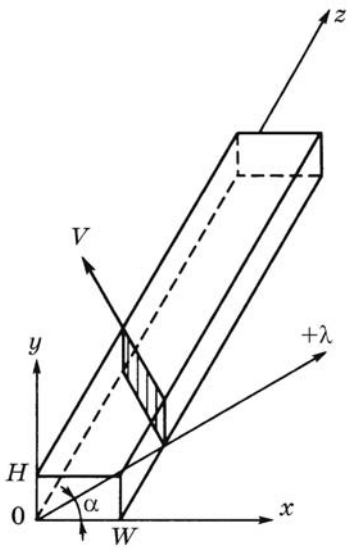

Fig. 3. Scheme for calculations of the extruder dozing zone.

The canal cross section width (the screw pitch width) at right angle to z axis is denoted as W, its height as H. The λ axis directed in parallel with the longitude axis of the auger has total length L and inclined by angle α (that corresponds to the screw ascent) to the x axis. The cross-hatched section is located in the plane at right angle to the λ axis. For the material moving from loading hopper to the auger outlet this section moves to +λ direction.

The rate vector of the material movement in any point of the screw canal can be decomposed into the components v_x, v_y and v_z, acting to te directions in parallel to the corresponding axes of the orthogonal coordinate system.

The upper plane of the canal in which the material is moving is the surface of cylinder of radius R_1, which moves with constant rate in parallel with the $x - y$ plane at the distance H from it. Motion of this plane is described by rate vector V directed at right angle to the λ axis. This vector modulo equals to linear rate of rotation of the cylinder surface

$$V = \omega R_1, \tag{3}$$

where ù is angular rate of the screw rotation.

The transfer rate vector V can be decomposed into two components, V_1 and V_2, directed along z and x axes, respectively, as shown in Fig. 4. Their values are:

$$V_1 = \omega R_1 \sin\alpha \quad V_2 = \omega R_1 \cos\alpha. \tag{4}$$

The rate V_1 defines forced (straight) flow of the material in the screw canal, the rate V_2 defines circular motion of the material in the canal cross section.

The proposed planar-parallel model of cylindrical screw pump operation commonly is used when $(H/D)_1$ ratio is small enough, because in this case the introduced error is small. Theoretical analysis in [11] and experimental study of the screw pump operation confirm this conclusion for many cases.

Thus, any material particle at its motion (starting at the loading hole at $z = 0$) along the screw canal passes enough complicated way. It is difficult to describe its mothion mathematically. Meanwhile, such complete mathematical description is not necessary for calculation pf productivity of auger unit.

The volume productivity can be obtained at integration of equation (5):

$$Q = \int_0^H \int_0^W v_z \, dxdy. \tag{5}$$

For the steady isothermal motion of an incompressible liquid the flow indissolubility equation gets the following form:

$$\frac{\partial v_x}{\partial x} + \frac{\partial v_y}{\partial y} + \frac{\partial v_z}{\partial z} = 0. \tag{6}$$

We suggest that at the motion of the polymer along z axis $v_x = v_y \equiv 0$, because $v_x << v_z$ and $v_y << v_z$. Then from Eq. (6) follows that vz can be a function of the coordinates x and y only, $v_z(x, y)$.

Using the Navier–Stokes equation, motion of material along flat canal can be written as:

$$v_x \frac{\partial v_z}{\partial x} + v_y \frac{\partial v_z}{\partial y} + v_z \frac{\partial v_z}{\partial z} = -\frac{1}{\rho} \frac{\partial p}{\partial z} \nu \left(\frac{\partial^2 v_z}{\partial x^2} + \frac{\partial^2 v_z}{\partial x^2} + \frac{\partial^2 v_z}{\partial z^2} \right). \tag{7}$$

The terms in the left part of Eq. (7) reflect acceleration which can be omitted in the case of slow motion. Moreover, at low H/W ratio of the auger (strictly speaking, $H/W << 1$), then v_2 little depends on x, and $\frac{\partial^2 v_z}{\partial x^2}$ derivative can be omitted as compared with $\frac{\partial_x^2 v_z}{\partial y^2}$. Then

Eq. (7) can be rewritten as:

$$\frac{1}{\mu}\left(\frac{\partial p}{\partial z}\right) = \frac{\partial^2 v_z^2}{\partial y^2}. \quad (8)$$

Suppose that there is no gap between external diameter of the screw and internal surface of cylinder, then boundary conditions for single-thread screw (m = 1) are: $v_z = V_1$ (at $y = H$) and $v_z = 0$ (at $y = 0$).

Assuming that pressure within a canal section is varying insignificantly, the solution of Eq. (8) obeying above boundary conditions can be written as:

$$v_z = V_1 \frac{y}{H} - \frac{y(H-y)}{2\mu}\left(\frac{\partial p}{\partial z}\right). \quad (9)$$

Join solving of Eqs. (8) and (9) gives for the volume productivity:

$$Q = V_1 \frac{WH}{2} - \frac{WH^3}{12\mu}\left(\frac{\partial p}{\partial z}\right). \quad (10)$$

The first term in (10) characterizes forced flow Q_1 due to screw rotation. The second term gives reverse flow Q_2 due to the pressure generated by the forming press-unit.

Effect of radial gap. Most extruders have although small but defined gap between the screw outer diameter and internal surface of cylinder. Due to this radial gap, leakage of some amount of the material to the direction opposite of transporting is possible, that finally reduces productivity of the auger unit.

The forced flow formula should include a coefficient $(1 - c/H)^2$ accounting for the loss in the forced flow due to the presence of the gap. The area of forced flow is extended not to the cylinder internal surface but from the screw internal diameter to the point $H - c$. Hence, volume productivity of forced flow is:

$$Q_V = Q_1\left(1 - \frac{c^2}{H}\right). \quad (11)$$

The correction factor for productivity of the flow under pressure with the gap is:

$$Q_{corr} = Q_2\left[1 + \left(\frac{c}{H}\right)^3 \left(\frac{W}{e}\right)\left(\frac{1}{\sin\alpha\cos\alpha}\right)^2\right]. \quad (12)$$

Hydrodynamic characteristic of auger. Accounting for eqs. (11) and (12) and resuming the result in the form

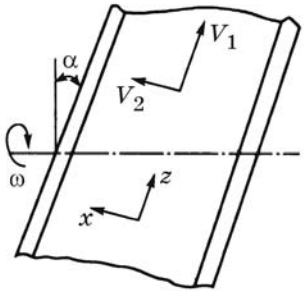

Fig. 4. Velocity diagram.

applicable for an auger with a multi-thread screw (m > 1) and accounting for the fact that for incompressible material Q does not depend on z we obtain from Eq. (10):

$$Q = a N - \frac{b}{\mu}\Delta p, \quad (13)$$

where N is the screw rotation rate, Δp is pressure difference along the screw canal of Z length.

Here:

$$a = \frac{\pi^2 D^2 H \sin\alpha\cos\alpha}{2} \times \left[1 - \frac{2c}{D_1} - \frac{me}{\pi D_1 \sin\alpha}\right]\left[1 - \frac{c}{H}\right]^2$$

$$b = \frac{\pi D_1 H^3 \sin^2\alpha}{12Z}\left(1 - \frac{2c}{D_1} - \frac{me}{\pi D_1 \sin\alpha}\right) \times \left[1 + 2\left(\frac{c}{H}\right)^3\left(\frac{W}{e}\right)\frac{1}{\sin 2\alpha}\right].$$

Equation (13) is hydrodynamic characteristic of auger.

Hydrodynamic characteristic of forming press-unit. At the auger outlet the material is passed through a forming unit (press-unit). If the material retains the properties of Newton fluid, then its volume consuming and pressure drop are connected by the following relation (Eq. 14):

$$Q = \frac{K}{\mu}\Delta p, \quad (14)$$

where K is a constant depending on the geometry of the press-unit of the extruder.

The pressure drop Δp in Eq. (14) means the same as in Eq. (13) if the pressure at the auger inlet is the same as at the outlet.

Volume productivity of extruder. Join solving eqs. (13) and (14) characterizing auger and forming unit, respectively, relatively Δp gives the following expression for volume productivity of extruder on the worked up material:

$$Q = \frac{aK}{b + K} N. \quad (15)$$

Eq. (15) shows that volume productivity is directly proportional to the screw rotation rate. But do not forget that this conclusion is true for a specific case only when reological properties of worked up material are the same as for the flow of Newton fluid under isothermal conditions.

Calculation of technological parameters of extruders accounting for the non-Newtonian reological properties of the worked up polymers and for non-isothermal processes of heat transfer requres much more complicated mathematical solutions.

REFERENCES

1. Shenkel, G., *Shnekovye processy for plastmass* (Auger Processes for Plastics), Leningrad: Gos. Nauchno-Tekhnich. Izd. Khim. Lit., 1962.
2. McKelvi, D.M., *Pererabotka polimerov* (Treatment of Polymers), Moscow: Khimiya, 1965.
3. Torner, R.V., *Osnovnye processy pererabotki polimerov* (Basic Processes for Treatment of Polymers), Moscow: Khimiya, 1965.
4. *Vzryvchatye veshchestva, pirotekhnika, sredstva initsiirovaniya v poslevoennyi period* (Explosives, Pyrotechnics and Initiators in the Period after the Second World War), Puzyrev, N.G., Ed., St. Petersburg: Gumanistik, 2001.

ISSN 1070-4272, Russian Journal of Applied Chemistry, 2007, Vol. 80, No. 12, pp. 2163–2164. © Pleiades Publishing, Ltd., 2007.
Original Russian Text © Yu.V. Pokonova, 2007, published in Khimicheskaya Promyshlennost', 2007, Vol. 84, No. 7, pp. 332–334.

TECHNOLOGY OF ORGANIC AND INORGANIC SUBSTANCES

Carbon Adsorbents for the Sorpting and Concentrating Nobel Metals

Yu. V. Pokonova

St. Petersburg State Technological Institute, St. Petersburg, Russia

Received March 19, 2007

Abstract—Kinetic, sorption and selectivity properties of commercial adsorbents are improved by adding petroleum residues (tar asphaltene concentrates) 13% of whole mass. Obtained adsorbents can be used for selective extraction of nobel metals from multicomponent polymetallic solutions of heavy metals and fro sewages purification for removing arsenic.

DOI: 10.1134/S1070427207120336

In this communication we describe data on modification of commercial carbon adsorbents by addin tar-asphaltene petroleum concentrates (TAC). This does not change industrial technology of manufactiring adsorbents. The improving is achieved using a simple procedure that is reasonable from economic and technology viewpoints. In preceeding publication [1] was shown that oxidative-reductive interaction of sludge with asphalt from propane and gasoline deasphalting the products are formed in 65–92% yield containing consisting of concentrated tar-asphaltene components of sludge, asphalt and asphaltite. These products (residues from residues) were named tentatively as secondary petroleum residues. They costitute a new resource of petroleum raw material with a high reactivity and exclusively low cost. Their utilization can solve an ecological problem of petroleum processing and petrochemical plants that uses sulfuric acid technology for purification of oil and paraffin and processes of sulfonation. As is know, more than 70% of wasted sulfuric acid are collected in ponds where they penetrate soil and escapes to water basins.

For producing tar-asphaltene concentrates we used sludge after purification of transformer and motor oils containing 36.3% of organic mass (including 21.2% of sulfonic acids) and 55.4% of sulfuric acid. A s a reducing component was taken asphaltite from gasoline deasphalting. Properties of the used gasoline asphaltite are listed in Table 1. Carbon adsorbents were formed alongside industrial technology [2,3]. It was impossible to introduce more than 15% of secondary petroleum residue to the mixture because this led to sticking granules together in the process of carbonization, owing to their low softening temperature not appropriate for the technology of sorbent manufacturing.

The porous structure was characterized by benzene vapor adsorption at 20°C using vacuum microbalances [4]. The pres volume was calculated proceeding from the total value of pores obtained from the value of real dencity relatively to water and apparent density determined by mercury procedure. Sorption properties were studied using the method of constant concentration of the targeted component and salt composition by changing

Table 1. Technology for manufacturing sorbents

Characteristics	Adsorbent with 13% petroleum residue
Mixture composition, %	
secondary petroleum residie	13
wood tar	28
coal dust	59
Conditions of producing:	
formation pressure, MPa	25
Yield, %	
at carbonization	72
at activation	62.2
total	41.4
Strength, %	90
Bulk density, kg/m^3	537

Table 2. Characteristics of sorption and selective properties of adsorbents

Characteristics	Degree of activation, %			Commersial adsorbent SKT
	20.8	33.2	45.5	
Pores volume, cm^3/cm^3:				
micro	0.21	0.25	0.12	
macro	0.28	0.31	0.33	
meso	0.04	0.06	0.08	
Static activity, g/l:				
on benzene	125	159	83	
on toluene	123	154	79	
Gold sorbed, mg/g, during the period, h:				
24	3.36	4.34	2.67	3.78
96	5.57	6.30	4.20	5.75
120	6.10	6.89	4.82	6.33
Selectivity coefficient on gold, %:	9.1	12.0	7.6	10.2
Silver sorbed, mg/g, during the period, h:				
24	0.18	0.60	0.55	0.67
96	0.48	0.63	0.84	1.04
120	0.53	0.68	0.97	1.14
Selectivity coefficient on silver, %:	1.01	1.56	1.41	1.83

solution alongside the earlier described procedure [5]. Concentration of metal ions in solution after the contact with the adsorbent was measured using atomic adsorption spectrophotometry on a Percin–Elmer model 503 instrument. Selectivity coefficients toward nobel metals were determined from weight fractions of adsorbed silver and gold relatively to the total sum of all metals. Sorption properties toward noble metals was measured from two solutions of which one contained the following elements at the concentrations (mg/g): Au 1.03; Ag 0.83; Nu 93.4; Zn 29.40; Ni 1.02; Co 0.46. Due to faster saturation of the adsorbents with dicyanurates as compared with dicyanoregenerates, for determination of adsorption ability and selectivity toward silver were used solutions with minimum concentration of gold ions. Therefore the second solution had the following composition (mg/g): Au 0.1; Ag 0.9; Cu 63.2; Zn 55.8; Ni 0.48; Co 0.20.

The data obtained showed that using the petroleum residue allows obtaining the sorbent with high capacity factor (micro pores volume expressed in cubic centimeters per 1 cm3 of adsorbent layer) and good transport porosity. Development of the pores of all types is provided by the fact that the secondary petroleum residue contains various tar-asphaltene substances varied by the length of alkyl substituents which are dealkylated in a certain time period.

From the data in Table 2 is obviously that the adsorbent containing 13% of tar-asphaltene substances possess micropores in good enough volume and maximal sorption and selectivity properties can be achieved at conbustion loss 33.2%.

Thus we found that a simple procedure consisting in adding secondary petroleum residue without changing industrial technology the adsorbents with improved sorption and selectivity characteristics as compared with the perfect domestic adsorbent SKT could be obtained. Good selectivity of the obtained adsorbents gives a way for saturation them with metal containing by-products in a high concentration, which makes reasonable to use the latter as secondary raw material.

REFERENCES

1. Pokonova, Yu.V., *Khim. Tekhnologiya Topliv Masel*, 2004, no. 3, pp. 48–49.
2. Pokonova, Yu.V., *Neft' i nefteprodukty* (Petroleum and Petroleum Products), St. Petersburg: Sintez, 2002.
3. Pokonova, Yu.V., *Prakticheskii spravochnik po nefteproduktam* (Practical Handbooc on Petroleum Products) St. Petersburg: Sintez, 2005.
4. Greg, S. and Sing, K., Adsorption Specific Surface and Porosity, Moscow: Mir, 1970.
5. Grabovskii, A.I., *Zh. Prikl. Khim*., 1978, vol. 57, no. 7, pp. 1515–1517.

ISSN 1070-4272, Russian Journal of Applied Chemistry, 2007, Vol. 80, No. 12, pp. 2165–2168. © Pleiades Publishing, Ltd., 2007.
Original Russian Text © S.A. Malin, B.M. Laskin, A.S. Malin, 2007, published in Khimicheskaya Promyshlennost', 2007, Vol. 84, No. 7, pp. 335–339.

TECHNOLOGY OF ORGANIC AND INORGANIC SUBSTANCES

Reaction of α-Bromocarboxylic Acids with Hydrazine and Dimethylhydrazine

S. A. Malin, B. M. Laskin and A. S. Malin

Russian Scientific center "Applied Chemistry," St. Petersburg, Russia

Received March 13, 2007

Abstract—Nucleofilic reaction of a series of α-bromocarboxylic acids with hydrazine and dimethylhydrazine is studied. High reactivity of α-bromocarboxylic acids is revealed and a series of α-hydrazinoarboxylic acids and *N*-(1-carboxyalkyl)-*N*,*N*-dimethylhydrazinium bromides are synthesized.

DOI: 10.1134/S1070427207120348

α-Bromocarboxylic acids are known as parent compounds for the synthesis of potentially biologically active compounds, α-hydrazino- and α-dimethylhydrazinocarboxylic acids, the analogs of aminoacids. These latter compounds show antiviral and antitumor activity and can serve as a basis for producing antibiotics, peptidomimetics and related substances [1–3].

Methods for the synthesis of α-hydrazinocarboxylic acids have not been sufficiently studied and the known data are mutually very contradicting in respect both conditions of carrying out the process and product yields [4–6]. Therefore we performed search of appropriate methods for the synthesis of α-hydrazinocarboxylic acids and study of main regularities of the process.

As the model targeted compounds we choose the following α-bromocarboxylic acids: α-bromopropanoic (**Ia**), α-bromobutyric (**Ib**), α-bromo-isovaleric (**Ic**) and α-bromophenylacetic (**Id**). These α-bromoacids were involved to the reaction of nucleophilic substitution with hydrazine and dimethylhydrazine according to the scheme:

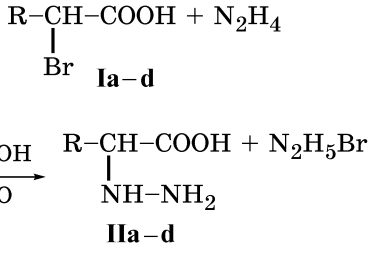

where R is Me (**a**), Et (**b**), *i*-Pr (**c**) and Ph (**d**).

We studied influence of the reagents ratio, parameters of duration and temperature and solvent (medium) nature on the reaction proceeding and results. We found that reaction of compounds **Ia–d** with hydrazine proceeds smoothly enough at carrying out the process in the medium of aqueous ethanol at the molar ratio I : hydrazine = 1: 4–6, temperature 70–80°C and reaction dura-tion 6–8 h with high yield (50–70%) of compounds **IIa–d**. Reaction conditions of **IIa–d** are listed in Table 1.

The most smooth process occurs with 40–60% hydrazine hydrate which provides necessary solvation of removing anion in the process of nucleophilic substitution.

Isolation of α-hydrazinocarboxylic acids was carried out by concentrating the reaction solution (by 40 –50%) under vacuum followed by diluting with water and filtrating the product. The crystals formed were filtered off and recrystallized from 40% ethanol (α-hydrazinopropanoic acid or hydrazoalanine), from isopropyl alcohol (α-hydrazinobutyric acid), water (α-hydrazinoisovaleric acid) or ethyl acetate (α-hydrazinophenylacetic acid or hydrazinophenylalanine). The α-hydrazinocarboxylic acids obtained were characterized by means of elemental analysus, IR and ^{1}H NMR spectroscopy.

IR and NMR spectroscopy data (Table 2) and elemental analyses (Table 3) confirmed structure and composition of the obtained compounds.

The high reactivity of the bromine atom in α-bromocarboxylic acids in the reactions of nucleophilic sub-

Table 1. Reaction conditions for the synthesis of compoinds **IIa–d**

No.	α-Bromocarboxylic acids	Mole ratio I : hydrazine	Reaction duration, h	Temperature, °C	Yield, %	mp, °C
1	**I a**	1 : 4	6	80	62	188–189
2	**I b**	1 : 5	7	77	67	201–203
3	**I c**	1 : 6	8	75	71	239–241
4	**I d**	1 : 3	12	70	58	195–200

Table 2. Spectral characteristics of compounds **IIa–d**

No.	Compound	IR spectrum, cm^{-1}	^1H NMR spectrum, δ, ppm (DMSO-d_6)
1	**IIa**	3120 (NH_3^+); 1680 (C= O)	1.45 d (3H, CH_3); 3.5 q (1H, CH); 6.22 s (4H, NH, NH_2,OH)
2	**IIb**	3115 (NH_3^+); 1690 (C=O)	1.1 t (3H, CH_3); 1.7 m (2H, CH_2); 3.28 q (1H, CH); 5.98 s (4H, NH, NH_2,OH)
3	**IIc**	3130 NH_3^+); 1685 (C=O)	1.01 d (3H, CH_3); 1.9 d (3H, CH_3); 2.28 m (1H, CH); 3.1 d (1H); 6.1 C(4H, NH, NH_2, OH)
4	**IId**	3110 (NH_3^+); 1700 (C=O)	4.48 s (1H, CH); 6.6 s (4H, NH, NH_2,OH); 7.33–7.6 ($5H_{arom}$)

Table 3. Elemental analysis data for compounds **IIa–d**

No.	Compound	Formula	Elemental analysis data					
			found, %			calculated, %		
			C	H	N	C	H	N
1	**IIa**	$C_3H_8N_2O_2$	34.45	**7.8**	**27**	34.61	7.75	26.91
2	**IIb**	$C_4H_{10}N_2O_2$	41.0	8.7	22.8	40.67	8.53	23.71
3	**IIc**	$C_5H_{12}N_2O_2$	44.98	9.22	21.7	45.44	9.15	21.2
4	**IId**	$C_8H_{10}N_2O_2$	58.0	6.11	16.4	57.82	6.07	16.86

Table 4. Reaction conditions for the synthesis of *N*-(1-carboxyalkyl)-*N*,*N*-hydrazinium bromides **IIIa–c**

No.	Compound	Reaction duration, h	Temperature, °C	Yield, %	mp, °C
1	**IIIa**	8	60	62	244
2	**IIIb**	8.5	65	65	239
3	**IIIc**	9	70	68	232
4	**IIId**	12–15	65	73	203

stitution with hydrazine hydrate allowed us to expect that dimethylhydrazine can also be involved in this process. The latter compound is known possessing highr enucleophilicity and basicity as compared with the unsubstituted hydrazine, and this should promote bromine substitution in the α-bromocarboxylic acids and should lead to practically unstudied α-dimethylhydrazinocarboxylic acids. We studied reaction of dimethylhydrazine with compounds **Ia–d**. As might be expected, dimethylhydrazine reacts with compounds **Ia–d** in absolute alcohol or acetonitrile medium smoothly. Small excess of dimethylhydrazine (1.05 to 1.1 mol per 1 mol of α-bromocarboxylic acid) was used and reaction was carried out at 40–60°C during 5–10 h leading to formation of *N*-(1-carboxyalkyl)-*N*,*N*-hydrazinium bromides **IIIa–c** in 60–70% yield according to equation:

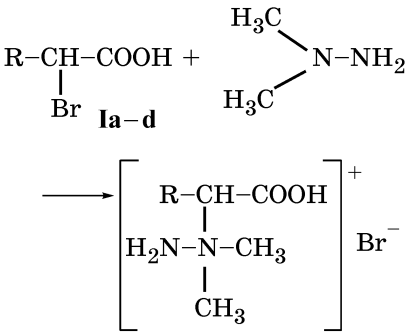

Ia–d **IIIa–d**

where R is Me (**a**), Et (**b**), *i*-Pr (**c**) and Ph (**d**).

The data on the synthesis conditions of hydrazonium salts **IIIa–d** are comprised in Table 4.

Isolation of the reaction products included concentrating the reaction solutions under vacuum, cooling from –5 to –10°C, filtrating the crystals formed and recrystallizing them from 2:1 isopropyl alcohol–dioxane mixture. It is noteworthy that the compounds obtained are hygroscopic ones and require use of absolute solvents both in the steps of synthesis and recrystallization.

Nature of the obtained compounds is confirmed by the data of IR and ^{1}H NMR spectroscopy (Table 5) and the data of elemental analysis (Table 6). Presence in the IR spectra of characteristic absorption bands in the region of 3220–3240 cm^{-1}characteristic adsorption attests presence of protonated NH_3^+ group and points probably to zwitter-ionic structure of α-dimethylhydrazinocarboxylic acids. This also is confirmed by ^{1}H NMR spectra where occur signals (multiplet) in the range 3.1–3.5 ppm depending on substituent R (500 MHz, DMSO-d_6) of α-methine fragment; presence of clearly defined signal at 5.6 ppm (4H) and absence of signals of OH and NH_2 groups points probably to zwitter-ionic structure of the compounds.

Like with hydrazinocarboxylic acids, the dimethylhydrazinium salts are characterized by signal of methine group at 3.05–4.3 ppm (multiplet), by signal of methyl groups at 3.5–3.6 ppm (singlet), while the signal at 5.35–5.67 ppm (singlet) is probably in correspondence with the existence of compounds **IIIa–d** as internal salts.

EXPERIMENTAL

^{1}H NMR spectra are registered on a Bruker AM 500 spectrometer (internal reference TMS) in DMSO-d_6. IR spectra are obtained on a IKS-29 spectrmeter from the pastes with Vaseline oil.

General procedure for preparation of α-hydrazinocarboxylic acids IIa–Id. To a three-necks flask equipped with mechanical stirrer, reflux condenser and

Table 5. Spectral characteristics of compounds **IIIa–d**

No.	Compound	IR spectrum, cm^{-1}	^{1}H NMR spectrum, δ, ppm (DMSO-d_6)
1	**IIIa**	3220 (NH_3^+); 1610 (C= O)	1.55 d (3H, CH_3); 3.15 q (1H, CH); 3.52 s (6H, $2CH_3$), 5.36 s (3H, NH_2, OH)
2	**IIIb**	3250 (NH_3^+); 1590 (C=O)	0.94 t (3H, CH_3); 2.2 m (2H, CH_2); 3.05 q (1H, CH); 3.52 d (6H, $2CH_3$), 5.4 s (3H, NH_2, OH)
3	**IIIc**	3300 NH_3^+); 1595 (C=O)	0.91 d (3H, CH_3); 0.94 d (3H, CH_3); 2.98 m (1H, CH); 3.6 d (6H, $2CH_3$), 4.28 m (1H, CH); 5.66 s (3H, NH_2, OH)
4	**IIId**	3320 (NH_3^+); 1620 (C=O)	3.58 d (6H, $2CH_3$), 4.12 C (1H, CH); 5.67 s (3H, NH2,OH); 7.64–8.03 ($5H_{arom}$)

Table 6. Elemental analysis data for compounds **IIa–d**

No.	Compound	Formula	Elemental analysis data							
			found, %				calculated, %			
			C	H	N	Br*	C	H	N	Br
1	**IIIa**	$C_5H_{13}N_2O_2$ Br	26.2	6.2	13.18	38.0	26.18	6.15	13.15	37.5
2	**IIIb**	$C_6H_{15}N_2O_2$ Br	31.6	6.7	12.4	35.22	31.73	6.66	12.34	35.18
3	**IIIc**	$C_7H_{17}N_2O_2$ Br	34.9	7.13	11.59	33.07	34.87	7.11	11.62	33.14
4	**IIId**	$C_{10}H_{15}N_2O_2$ Br	43.8	5.7	10.21	29.1	43.65	5.5	10.18	29.04

Note: Content of bromine ion in compounds **IIIa–d** was analysed by the mercurymetric method.

thermometer was placed 20–30% solution of α-bromocarboxylic acid in 60–80% aqueous ethanol and precalculated amount of 80% hydrzine hydrate (bromocarboxylic acid to hydrazine hydrate mole ratio is 1 : 4–5) was added dropwise. The reasction mixture was heated to slow boiling, kept at this temperature for 4–8 h and then left for 12 h at 0–5°C. The crystals formed were filtered off and recrystallized from water or alcohol, and dried. Yield of α-hydrazinocarboxylic acids 60–70%.

Procedure for preparation of *N*-(1-carboxyalkyl)-*N*,*N*-hydrazinium bromides IIIa–c. To a three-necks flask equipped with mechanical stirrer, reflux condenser and thermometer was placed 20–30% solution of α-bromocarboxylic acid in anhydrous acetonitrile. The solution was cooled to 10–15°C and to it was slowly dozed precalculated amount of 40–50% solution of dimethylhydrazine in acetonitrile (bromocarboxylic acid to dimethylhydrazine mole ratio is 1 : 2–2.5) at the temperature not below 20°C. The reaction mixture was then slowly heated to 40–50°C, kept at this temperature for 3–5 h monitoring continuously formation of mineral bromine (mercurymetry). After completing the process, the reaction mixture was cooled to 0–5°C, the crystals dropped were filtered off, washed with isopropyl alcohol and dried in a vacuum dessicator. Yield of hydrazonium salts **IIIa–d** is 60–75%.

CONCLUSION

The α-hydrazino- and α-dimethylhydrazino-derivatives of a series of carboxylic acids are synthesized, the process of synthesis regularities are revealed, some of physico-chemical properties of the compounds obtained are measured and nature and assumed salt structure of these compounds are established.

REFERENCES

1. Carmi, A., Pollak, G., et al., *J. Org. Chem.,* 1960, vol. 25, no. 1, pp. 44–46.
2. de Luca, L., Falorni, M., et al., *Tetrahedron Lett.,* 1999, vol. 40, pp. 8701–8704.
3. Oguz, U., McLaughlin, M., et al., *Tetrahedron Lett*., 2002, vol. 43, pp. 2873–2875.
4. Carmi, A., Pollak, G., et al., *J. Org. Chem.,* 1964, vol. 7, pp. 220–224.
5. Gustafsson, H., *Acta Chem. Scand*., 1975B, vol. 29, no. 1, pp. 93–98.
6. Darapsky, A., *J. Prakt. Chem.*, 1936, vol. 146, pp. 268–288.

ISSN 1070-4272, Russian Journal of Applied Chemistry, 2007, Vol. 80, No. 12, pp. 2169–2173. © Pleiades Publishing, Ltd., 2007.
Original Russian Text © A.N. Chernaya, O.N. Filimonova, S.S. Nikulin, 2007, published in Khimicheskaya Promyshlennost', 2007, Vol. 84, No. 7, pp. 340–346.

TECHNOLOGY OF ORGANIC AND INORGANIC SUBSTANCES

Modification of Petroleum Polymer Resin from C9 Fraction with Maleic Acid and its Application to Protecting Treatment of Wood

A. N. Chernaya, O. N. Filimonova, and S. S. Nikulin

Voronezh State Forest Academy, Voronezh, Russia

Received June 2, 2007

Abstract—Modification of petroleum polymer resin with maleic acid is studied and changes in acid number, molecular weight and bromine number of the forming product in time are determined. The modified petroleum polymer resin is shown useful for enhancing hydrophobic properties of wood.

DOI: 10.1134/S107042720712035X

Wastes and by-products formed and accumulated in the enterprises of chemical and petrochemical profiles are numerous and various both in quality and quantity aspects. Solution of the problem of treatment and use of the formed by-products of industrial and social origin is closely connected with environment saving against pollutions and complex consumption of sources of raw materials whose reserves fall down. Development of new technologies and solutions of treatment of secondary sources increases performance of processes, promotes complete and economical consumption of expensive raw materials and allows to increase assortment of products.

One of such side products is hydrocarbon C_9 fraction. On the basis of this fraction now is produced on commercial scale the petroleum polymer resin used as a film-forming component in paint and varnish compositions [1]. A significant advantage of this material is low color depth (less than 100 units in iodine color scale) which allows applying it in transparent paint and varnish materials. In [1] was described modification of petroleum polymer materials with maleic anhydride and acrylic monomers and esters which allow increasing their resistance to oxidation. The petroleum polymer materials are recommended for application at producing paper, cardboard, plates, etc.

An interesting pathway in this respect is considering a possibility of modification of petroleum polymer resin from C_9 fraction with maleic acid by their join high temperature treating. This process should afford material of complex composition with inclusion of destruction products, the products of reaction of maleic acid with petroleum polymer resin and others. It can be assumed that the macromolecules containing anhydride and acid groups in the chain are interesting for creation of polymer film-forming materials, complexing agents, biologically active substances and other valuable materials [2].

Introducing maleic acid into the petroleum resin composition allows admitting to the latter some useful properties. Appearance of functional groups in the molecules of the polymer increases its polarity. This is significant in particular at the application of these products for protecting wooden materials which contain as a main components cellulose, gemicellulose and lignin bearing many various functional groups. This will promote interaction of the modifying agent and wooden components functional groups with formation of hydrogen bonds and polymer carcass. Such disadvantages of the modifying agent as its washing out from the products and similar at their exploitation decrease. The wooden material density grows and it acquires enhanced strength and water repelling properties. Besides, wood of low value species acquires light-brown to dark-brown tone and by properties approaches to the wood of valuable species.

In the first step we carried out modification of petroleum resin based on C_9 fraction produced on commercial scale. The resin main components are: 1,3-cyclopentadiene, styrene, α-methylstyrene, vinyltoluene

and dicyclopentadiene. The following modification procedure was appied:

To reactor was loaded the peroleum resin based on C_9 fraction and introduced maleic acid in amount 2 to 9% of the resin. Reactor was hermetically closed and the process was carried out at 110, 150 or 190°C for 2 to 8 h.

The process was monitored by measuring the system viscosity, molecular weight, acid and bromine numbers, taking samples from the reactor periodically. The results of investigations are listed in Tables 1–3.

Analysis of experimental observations leads to conclusion that increase in content of maleic acid in the polymer resin based on C_9 fraction leads to increase in acid number and molecular weight with simultaneous decrease in bromine number showing its unsaturation. Decrease in unsaturation, that is, in the number of double bonds, can result from the fact that high temperature treatment of the composite leads to grafting maleic acid

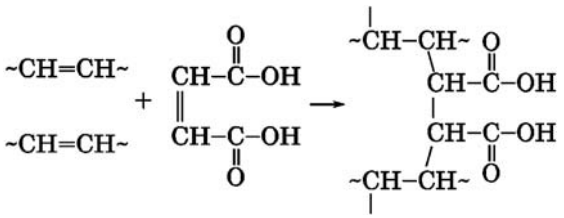

to tar components in polymer resin and to cross-linking of oligomer molecules. This is confirmed by increasing in molecular weight of the obtained products. Necessary to note that increase in the process duration to 8 h leads to increase in molecular weight and acid number and decrease in bromine number.

Further increase in duration of the modification process leads to decrease in acid number. This can be connected with maleic acid loss and its transforming into maleic anhydride. Proceeding of decarboxylation reaction is also possible [2]. Molecular weight of the products thus obtained continues to increase, while bromine number falls down. The system viscosity grows.

Study of temperature dependence of the modification process showed that rather high temperature should be maintained, 150°C or higher. Decrease in temperature to 110°C leads to decrease in the rate of molecular weight and acid number and growing and to bromine number falling.

Analysis of experimental data leads to conclusion that modified polymers thus obtained have not high molecular weigh and can be classified as oligomers. Due to low molecular weight and hence small size of the molecules they can relatively easy penetrate porous materials filling up processing defects, increasing strength characteristics and water repelling properties of a hardware. A special interest is application of oligomeric products in wood

Table 1. Dependence of acid number, bromine number and molecular weight on the duration of interaction at 110°C

Products	Interaction duration, h	Acid number, mg KOH/kg	Bromine number, mg Br_2/100 g	Molecular weight
Initial petroleum resin based on C_9 fraction	–	0.6	140	1020
Petroleum resin based on C_9 fraction with 2% of maleic acid	2	1.4	136	1190
	4	1.7	132	1300
	5	2.2	126	1470
	6	5.9	121	1710
	8	4.2	118	1830
Petroleum resin based on C_9 fraction with 6% of maleic acid	2	6.7	130	1390
	4	7.0	110	1420
	5	8.7	106	1450
	6	15.7	103	1500
	8	12.9	97	1530
Petroleum resin based on C_9 fraction with 10% of maleic acid	2	8.4	122	1430
	4	9.6	108	1470
	5	12.6	101	1610
	6	48.8	96	1740
	8	37.6	90	1860

Table 2. Dependence of acid number, bromine number and molecular weight on the duration of interaction at 150°C

Products	Interaction duration, h	Acid number, mg KOH/kg	Bromine number, mg Br_2/100 g	Molecular weight
Petroleum resin based on C_9 fraction with 2% of maleic acid	2	1.9	134	1350
	4	2.2	127	1470
	5	2.5	122	1530
	6	3.1	117	1540
	8	2.8	112	1870
Petroleum resin based on C_9 fraction with 6% of maleic acid	2	9.0	124	1860
	4	9.5	107	1940
	5	9.7	102	1970
	6	11.2	97	2010
	8	10.7	92	2220
Petroleum resin based on C_9 fraction with 10% of maleic acid	2	15.7	118	1900
	4	16.3	101	2090
	5	17.4	86	2190
	6	18.0	79	2340
	8	12.3	72	2490

Table 3. Dependence of acid number, bromine number and molecular weight on the duration of interaction at 190°C

Products	Interaction duration, h	Acid number, mg KOH/kg	Bromine number, mg Br_2/100 g	Molecular weight
Petroleum resin based on C_9 fraction with 2% of maleic acid	2	1.4	132	1240
	4	1.7	124	1330
	5	2.2	121	1520
	6	2.5	114	1710
	8	2.0	107	1810
Petroleum resin based on C_9 fraction with 6% of maleic acid	2	5.3	115	1780
	4	5.6	104	1820
	5	6.2	99	1830
	6	8.4	96	1980
	8	4.2	90	2060
Petroleum resin based on C_9 fraction with 10% of maleic acid	2	6.2	109	1690
	4	7.0	98	1740
	5	7.3	90	2130
	6	9.0	86	2010
	8	4.5	80	2460

treatment industry because wood and materials based on it are particularly sensitive toward various aggressive media.

Next step of this study is revealing effect of the product obtained from petroleum resin C_9 fraction and maleic acid as impregnating material for increase hydrophobic properties of wood.

For the study was used a product obtained with maleic acid content 6%; treatment was carried out for 6 h at 150°C. The product had the following characteristics:

(a) Content of product in solution 50%,
(b) Acid number 11.2 mg of KOH per 1 g,
(c) Bromine number 97 mg of Br_2 per 100 g,
(d) Molecular weight ~ 2000.

We studied the process of modification of birch wood using the method of experiment planning. Effect of such factors as temperature and duration of impregnation, temperature and duration of thermal treating were studied using fourth order Greek-Latin squire plan [3]. For each factor were taken four leves of varying: temperature of

Table 4. Plan and results of testing impregnated birch wood samples (after 24 h)

A	B			
	b_1 = 1 h	b_2 = 3 h	b_3 = 5 h	b_4 = 7 h
a_1 =40°C	c_1 = 110°C d_1 = 1 h y_1 = 31.8 y_1' = 9.9 y_1'' = 12.9	c_2 = 130°C d_2 = 3 h y_2 = 26.4 y_2' = 6.2 y_2'' = 9.8	c_3 = 150°C d_3 = 5 h y_3 = 23.8 y_3' =5.1 y_3'' = 9.0	c_4 = 170°C d_4 = 7 h y_4 = 20.7 y_4' = 3.4 y_4'' = 7.2
a_2 =70°C	c_2 = 130°C d_3 = 5 h y_5 = 21.4 y_5' = 4.4 y_5'' = 8.0	c_1 = 110°C d_4 =7 h y_6 = 19.2 y_6' = 3.2 y_6'' = 6.9	c_4 = 170°C d_1 = 1 h y_7 = 18.8 y_7' = 2.6 y_7'' = 6.1	c_3 = 150°C d_2 = 3 h y_8 = 18.8 y_8' = 3.1 y_8'' = 7.0
a_3 = 100°C	c_3 = 150°C d_4 = 7 h y_9 = 18.5 y_9' = 2.8 y_9'' = 6.2	c_4 = 170°C d_3 = 5 h y_{10} = 16.8 y_{10}' = 2.3 y_{10}'' =5.8	c_1 = 110°C d_2 = 3 h y_{11} = 17.7 y_{11}' = 2.6 y_{11}'' = 6.1	c_2 = 130 °C d_1 = 1 h y_{12} = 16.0 y_{12}' = 2.4 y_{12}'' = 6.0
a_4 = 130°C	c_4 = 170°C d_4 = 3 h y_{13} = 15.7 y_{13}' = 2.4 y_{13}'' = 5.5	c3 = 150°C d_1 = 1 h y_{14} = 14.6 y_{14}' = 2.2 y_{14}'' = 5 .3	c_2 = 130°C d_4 = 7 h y_{15} = 13.2 y_{15}' = 1.8 y_{15}'' = 4.7	c_1 = 110°C d_3 = 5 h y_{16} = 11.8 y_{16}' = 1.5 y_{16}'' = 4.1

Note: y_i is water absorption, %, y_i' is radial swelling, %, y_i'' is tangential swelling, %.

Table 5. Plan and results of testing impregnated birch wood samples (after 30 h)

A	B			
	b_1 = 1 h	b_2 = 3 h	b_3 = 5 h	b_4 = 7 h
a_1 = 40°C	c_1 = 110°C d_1 = 1 h y_1 = 99.2 y_1' = 13.9 y_1'' = 16.5	c_2 = 130°C d_2 = 3 h y_2 = 84.7 y_2' = 8.7 y_2'' = 12.8	c_3 = 150°C d_3 = 5 h y_3 = 70.6 y_3' = 6.3 y_3'' = 10.1	c_4 = 170°C d_4 =7 h y_4 = 74.5 y_4' =7.3 y_4'' = 11.1
a_2 = 70°C	c_2 = 130°C d_3 = 5 h y_5 = 96.8 y_5' = 8.3 y_5'' = 10.8	c_1 = 110°C d_4 = 7 h y_6 = 76.2 y_6' =6.9 y_6'' = 10.1	c_4 = 170 °C d_1 =1 h y_7 = 70.6 y_7' = 6.3 y_7'' = 10.1	c_3 = 150°C d_2 = 3 h y_8 = 70.5 y_8' = 6.6 y_8'' = 9.8
a_3 = 100°C	c_3 = 150°C d_4 = 7 h y_9 = 76.5 y_9' = 7.0 y_9'' = 9.4	c_4 = 170 °C d_3 = 5 h y_{10} = 80.5 y_{10}' = 7.6 y_{10}'' =9.0	c_1 = 110°C d_2 = 3 h y_{11} = 70.0 y_{11}' = 6.5 y_{11}'' = 11.1	c_2 = 130 °C d_1 = 1 h y_{12} = 61.6 y_{12}' = 6.5 y_{12}'' = 9.3
a_4 = 130°C	c_4 = 170°C d_4 = 3 h y_{13} = 81.1 y_{13}' = 6.2 y_{13}'' = 9.0	c3 = 150°C d_1 = 1 h y_{14} = 67.9 y_{14}' = 6.9 y_{14}'' = 9.1	c_2 = 130°C d_4 = 7 h y_{15} = 54.5 y_{15}' = 6.4 y_{15}'' = 7.8	c_1 = 110°C d_3 = 5 h y_{16} = 48.4 y_{16}' = 6.0 y_{16}'' = 7.5

Note: y_i is water absorption, %, y_i' is radial swelling, %, y_i'' is tangential swelling, %.

impregnating composition (Factor A) 40, 70, 100 and 130°C, impregnating duration (Factor B) 1, 3, 5 and 7 h, temperature of thermal treatment (Factor C) 110, 130, 150 and 170°C, duration of thermal treatment (Factor D) 1, 3, 5 and 7 h.

Properties of the birch samples after modifying impregnation were revealed by measuring such characteristics as absorption of water, radial and tangential swelling after one and thirty days. The matrix of experiment planning is shown in Tables 4 and 5,

The treatment was conducted as follows: A preliminary dried sample after weighting and size measuring was poured into impregnating bath with petroleum resin based on C_9 fraction modified with 6% of maleic acid and kept for as given period at a given temperature. Impregnated sample was taken out of the bath, dried and treated thermally. After thermal treatment the sample was cooled to room temperature, weighed, and its size was registered. Then the sample was poured to water. Water adsorption was measured by gravimetric method registering change in the wood weight. Content of modified tar-like substance in the wood achieved 50%, depending on the conditions defined by above considered factors. Swelling was determined by measuring cross section of each sample in radial and tangential directions.

After computational treatment of experimental results we obtained regression equations describing contribution of these factors to water resistance after 1 and 30 days.

After one day:

Water absorption,%: $Y_{wa} = 1.58 \times 10^{-4}$ (29.48 – 0.12a)(21.52 – 0.74b)(20.57 – 0.0147c)(19.82 – 0.32d);

Radial swelling, %: $Y_{rs} = 3.39 \times 10^{-2}$ (6.77 – 0.04a)(4.22 – 0.27b)(4.66 – 0.0112c) (3.58 – 0.12d);

Tangential swelling, %: $Y_{ts} = 3.42 \times 10^{-3}$ (11.06 – 0.0497a)(7.82 – 0.29b)(8.30 – 0.0118c)(7.29 – 0.16d);

After 30 days:

Water absorption,%: $Y_{wa} = 2.60 \times 10^{-6}$ (91.34 –0.21a) (90.62 – 4.31b) (71.67 – 0.001c) (74.68 – 0.66d);

Radial swelling, %: $Y_{rs} = 2.51 \times 10^{-3}$ (10.23 – 0.0326a) (8.65 – 0.31b) (9.70 – 0.0166c) (7.89 – 0.13d)

Tangential swelling, %: $Y_{ts} = 9.33 \times 10^{-4}$ (14.85 – 0.0524a) (11.31 – 0.26b) (12.53 – 0.0164c)(11.27– 0.25d);

The best conditions of wood treatment that provides minimum water absorption and swelling of samples are:

Table 6. Calculated and experimental values of characteristics of the modified birch samples

Characteristic	Calculation / experiment	
	after 24 h	after 30 days
Water absorption, %	11.38 / 9.82	50.42 / 47.23
Tangential swelling, %	3.54 / 3.13	6.60 / 5.62
Radial swelling, %	0.94 / 0.89	4.68 / 3.27

temperature of impregnating composition 130°C, impregnation duration 7 h, temperature of thermal treatment 170°C, duration of thermal treatment 7 h. From the experimental observation we can conclude that properties of the obtained samples depend mostly on the duration of impregnation and thermal treatment. Effect of temperature of impregnating composition and thermal treatment within the applied range are less significant.

Calculated and experimental values of the characteristics of samples are well matching (Table 6).

CONCLUSIONS

1. Modification of petroleum polymer resin with maleic acid leads to increase in molecular weight of the obtained product and decrease in its bromine number.

2. The petroleum resin obtained can be used for enhancing hydrophobic properties of natural wooden material.

3. It is established that the best properties of impregnated wood samples are achieved at the impregnation temperature 130°C, impregnation duration 7 h, thermal treatment temperature 170°C and duration of thermal treatment 7 h.

REFERENCES

1. Dumskii, Yu.V., *Neftepolimernye smoly* (Petroleum Resins), Moscow: Khimiya, 1988.
2. Rzaev, Z.M., *Polimery i sopolimery maleinovogo angidrida* (Maleic Anhydride Polymers and Copolymers), Baku: Elm, 1984.
3. Akhnozarova, S.L. and Kafarov, V.V., *Metody optimizatsii eksperimenta v khimicheskoi tekhnologii* (Methods of Optimization of Experiment in Chemical Technology), Moscow: Vysshaya Shkola, 1985.

ISSN 1070-4272, Russian Journal of Applied Chemistry, 2007, Vol. 80, No. 12, pp. 2174–2177. © Pleiades Publishing, Ltd., 2007.
Original English Text © Man Singh, 2007.

TECHNOLOGY OF ORGANIC AND INORGANIC SUBSTANCES

Upper Critical Solution Temperatures of Immiscible Phase with Dodecyl Trimethylammonium Bromide, Methyltrioctylammoniumchloride, Trimethylsulphoxoniumiodide Cationic Surfactants

Man Singh

Chemistry Research Lab, Deshbandhu College, University of Delhi, New Delhi 110019, India
e-mail: mansingh50@hotmail.com

Received April 24, 2007

Abstract—Upper critical solution temperatures (UCST) and mutual solubilities of phenol and water were studied with 0.45 mmol kg^{-1} (mm kg^{-1}) dodecyl trimethylammonium bromide, trimethylsulphoxonium iodide and methyltrioctylammonium chloride. The surfactants decrease the UCSTs by about 0.51–1.98°C with slight enhancement in mutual solubilities. Mole fractions of surfactants were restricted to 0.002 to 0.005 range, their hydrophilic and hydrophobic interactions enhance solubility of phenol in water by about 0.0456 % as compared to water–phenol systems.

DOI: 10.1134/S1070427207120361

1. INTRODUCTION

Currently immiscible solvent systems are in focus for study of several biological and biophysical processes with different chemical potentials of the solvents. The immiscible solvent systems are of tremendous use due to their energy gradient that becomes a driving force for several auto control processes. The study of energy gradient of several immiscible solvent sysyetms is industrially significant. Electronic configurations of the solvents do develop the energy gradient in the solvent systems, and prevents mutual mixing the solvents. Hence surfactants with hydrophilic and hydrohopobic interactions do interact with respective immiscible solvents and decrease the energy gradient. Such systems become highly potential systems for chemical processes and develop with specific Upper critical solution temperature (UCST). The UCST denotes a temperature above of which the two phase liquid system develops a single phase liquid. It is a system dependent parameter hence for a particular system like water and phenol its value is fixed and due to its nature. It is used as an effective yardstick for additives added to water and phenol and their UCST data are determined. The variation in UCSTs with an additive elucidates structural interactions of solvent systems. The dodecyl trimethylammonium bromide, methyltrioctylammonium chloride and trimethylsulphoxonium iodide have chosen for study and interact with water as well as phenol due to their hydrophilic and hydrophobic parts respectively, and hence are denoted as surfactants and reduce interfacial surface tension of immiscible phases and facilitate intermixing at lower UCST. Hydrophilic and hydrophobic interactions are always of interest due to several [1] uses in nanotechnology, biotechnology and microscale processes. Enormous studies on them are cited but no work in critical solutions is considered. Our work focuses on them in upper critical solutions using three mentioned above different cationic surfactants. Another surfactants (denoted as CTAB, TEAB, CPC, CPB, LDS, SDS, CA, PEG 200, EGMDE) were studied elsewhere [2]. Such study is highly recommended for green and supramolecular chemistries [1] as to how the surfactants influence mutual solubilities that would curtail an excess use of materials to develop microscale and miniaturized processes.

The surfactants are frequently used in several solubility based processes [3–5] like separation of proteins from their natural sources where the UCSTs

are useful. The dodecyl trimethylammonium bromide, trimethylsulphoxonium iodide and methyltrioctylammonium chloride are highly used in biosciences for several purposes so their influence on solubility of solvents assists the separation and extraction processes. The UCSTs are industrially useful [5, 8] (Zhang et al., 2007) to develop the proteins, amino acids and vitamins based bionanoparticle for biochips and DNA biotemplates [6–10]. The critical solutions with surfactants are useful for determination cloud point temperatures especially by food scientists and biophysical scientists [11–13, 4]. Temperature-dependent surfaces and interfacial kinetics remain relatively unexploited in thin-film sensing applications that rely on optical surface-sensitive techniques like surface plasmon resonance spectroscopy. Currently Singh [12] has reported Survismeter and formulated Man Singh equation for friccohesity that focuses interfacial surface forces which influence the intermixing of the immiscible phases [12, 14]. These techniques are inherently sensitive to the optical properties of the bulk solution in contact with the thin films, hence UCST data for the latter at the conditions of interests are useful. The UCST and the refractive index may have interesting correlations.

The UCSTs with a wide range of additives would serve a wider purpose in solution engineering of immiscible solvents for interactions with industrially useful molecules. The UCSTs with hydrophilic and hydrophobic interactions define cloud points with additives of thermodynamic significance with potential uses in soaps, detergents, textiles, inks, paint and pigments, solvent extractions, and disinfectant solutions. Industrially phenol is widely used as a disinfectant where its solubility in different solutions is highly influenced by the ingredients of the solution. Its aqueous solutions with additives could be of some use in biotechnology and biophysics as it is used to inhibit the early degradation of fish meat etc. Similarly the surfactants investigate their influence on the intermixing of the phenol–water phases due to their hydrophilic and hydrophobic interactions.

2. MATERIALS AND METHODS

Stock solutions of 0.5 mm kg^{-1} dodecyl trimethylammonium bromide, trimethylsulphoxonium iodide, methyltrioctylammonium chloride were prepared separately in water, w/v. Initially water and phenol in a 2:8 ratio were taken in optical cells as reference phases, the cell was mounted on a stainless steel stand at normal temperature. The cell with contents was remained dipped in a paraffin oil of the thermostat with ± 0.05°C control measured with a Beckmann thermometer. The contents were heated at a rate of 1°C min^{-1} stirring with a glass stirrer 50 rpm till the phases disappeared where their miscibility increased and approaching to a point where both the components are completely dissolved with a homogenous single phase. This temperature is termed a mutual miscibility temperature (MST). The heating was stopped and the cell with contents was air cooled for reappearance of the phases. The reappearance and disappearance of the phases develop a cloud hence the temperature at which the cloud is developed is called a cloud point temperature it coincides with the MST. Hence the MSTs for disappearance of a cloud point or turbidity and a reappearance of the cloud point were recorded. About 30 subsequent additions of the 2×10^{-1} dm^3 water were made and the MSTs were recorded.

After the water–phenol system, the cell was cleaned and rinsed with the solution in question for cloud point temperature measurements. For MSTs with each additive, a corresponding stock solution was used in place of water. An optical cell was made up of Borosil glass of 15 cm in length and a 1.5 cm radius (r) or a 3 cm inner diameter, the cell capacity was determined with $\pi r^2 h$, the r = 1.5 cm and h = 15 cm, which gave 106 cm^3 cell volume that accommodates more than 30 subsequent additions. About 36 cm^3 vacant volume of the cell was left unoccupied for safety measures for preventing evaporation and an escape of solution. The top end of the cell was properly blocked after inserting contact and Beckman thermom-eters, and an immersion rod. A gentle heating from $T = 298.15$ K of 1 min^{-1} was made with a 25 watt-immersion rod connected to an automatic electric relay through a contact thermometer with smooth stirring (glass stirrer) with wiper motor. The solutions were prepared w/w, using 1×10^{-5} g accuracy 100 DS Dhona balance, Instruments Pvt. Ltd, Calcutta India, and a calibrated thermometer were used to note down the temperatures. The water de-mineralized, de-ionized and degassed was used

2.1. Turbidity Measurements

At a point slightly below the temperature of a disappearance of cloud point, the heating was reduced to 1°C min^{-1}, due to a sharp disappearance. The phase dissolution was viewed with an eye lens of a cathetometer kept 1 m away from the thermostat. Near a point of disappearance of the cloud, the heating was stopped and the temperature at which the turbidity vanished was noted

UCSTs for surfactants, mole fraction of phenol and additives at UCST

Additives	x_{phenol}, %	x_{water}
Phenol	0.0874	0.9126
Dodecyl trimethylammonium bromide	0.0986	0.9014
Trimethylsulphoxonium iodide	0.0711	0.9289
Methyltrioctylammonium chloride	0.1131	0.8868
	$x_{additive}$	UCST ± 0.05 K, °C
Phenol	0	341.4 K
Dodecyl trimethylammonium bromide	0.00136	339.4 K
Ttrimethylsulphoxonium iodide	0.00179	339.9 K
Methyltrioctylammonium chloride	0.00122	339.9 K

as a transition point temperature. After this, the mixture was air-cooled till a clear turbidity reappeared, the temperature of this point was also noted. For the air-cooling, a slightly colder air than the temperature of a paraffin bath was passed around the cell through a copper coil inserted in the paraffin wax bath. The air was propelled with a booster pump at s flow rate of 2000 cm^3 min^{-1} from an air cooler fitted separately.

2.2. Chemicals

Dodecyl trimethylammonium bromide (Sigma, D 5047), trimethylsulphoxonium iodide (Fluka, 92763) and methyltrioctylammonium chloride (Fluka, 69485) and phenol (Merck, 1/17847) were used as received. Demineralized water was triply distilled with KOH and degassed. The chemicals were dried for 24 h, before their mp and stored in a P_2O_5 filled desiccator till use. For each ratio the MSTs were plotted against corresponding phenol mole fractions (x_{ph}). The mole fractions below the curve lead to two phases and above the curve a single phase solutions. The component designated as solvent dissolves another designated as solute either at normal or slightly higher temperatures but initially with compositions of each the cloud point temperatures are higher. Hence wider compositions with lower differences are studied with several subsequent additions. The systems with surfactants are treated as ternary systems and mole fractions of each component are calculated at cloud point temperatures. An apex of a curve is denoted as UCSTs.

2.3. Calculations

The moles of each component were determined for each set of solution along with critical compositions (CS_S) of corresponding MSTs. The MSTs were plotted on the y-axis against corresponding x_{ph} on an x-axis. An apex of this curve gives values of the $UCST_S$ and CS_s, the data are given in Table 1. The mole fractions of each additive were calculated including an amount of previous subsequent additions.

3. RESULT AND DISCUSSION

The UCST and mutual solubilities for phenol + water show a close agreement with those of the literature [15–17] with T = (273.15 ± 0.05) K and ± 0.25°C errors respectively. The UCSTs with additives remain near those of the water"phenol system (Table 1) with greater solubilities of the phenol respectively at lower UCST. The surfactants produce lower UCSTs than of the water"phenol. This infers that they develop hydrophilic and hydrophobic interactions. The UCSTs of surfactants are as trimethylsulphoxonium iodide = methyltrioctyl-ammonium chloride > dodecyl trimethyl-ammonium bromide, the dodecyl trimethylammonium bromide effectively develops the hydrophilic and hydrophobic interaction with higher mutual solubility. However the methyltrioctylammonium chloride and trimethylsulphoxonium iodide show slightly higher UCSTs values by 0.5 than those of the water"phenol, hence these develop weaker hydrophilic and hydrophobic interactions. A close comparison of the molecular structure of dodecyl trimethylammonium bromide with an alkyl chain of 12 carbon atoms develops a stronger hydrophilic interaction but methyltrioctylammonium chloride and trimethyl-sulphoxonium iodide with an alkyl chain of 12 carbon atoms and an alkyl chain with 3 carbon atoms respectively develop weaker hydrophobic and stronger hydrophilic interactions due to N^+ and Cl^- with methyltrioctyl-ammonium chloride and the O atom of trimethylsulphoxonium iodide. Hence surfactants with a longer alkyl chain develop stronger hydrophobic interaction due to higher solubility in phenol rather than that of the water. Hence the surfactants with a longer alkyl chain develop weaker hydrophilic interactions. Further a comparison of halide atoms of their functional groups vis-a-vis UCSTs show their placement as $I^- = Br^- > Cl^-$. Hence the critical review of UCSTs vis-à-vis structures of trimethylsulphoxonium iodide and methyltrioctyl-ammonium chloride infer that hydrophobic 3-CH_3 groups of trimethylsulphoxonium iodide outweigh the hydrophilic interactions due to $O{=}S^+{-}I^-{-}$.

Hence UCST is higher due to higher thermal energy needed for dissolving $O{=}S^+{-}I^-{-}$ water boundaries.

Perhaps the $O{=}S^{+}{-}I^{-}$ likes the geometry of the $O{=}S^{+}{-}I^{-}{-}H_2O$ towards the water phase with stronger dipolar interactions with H_2O but the I^{-} also develops stronger induced potential or polarizability. But methyltrioctylammonium chloride's Cl^{-} atom has a slightly stronger hydrophobic interaction than that of $O{=}S^{+}{-}I^{-}$ due to a 0 carbon atom chain that dominates over the weaker hydrophilic interactions of $N^{+}{-}Cl$, where the Cl^{-} is a small sized anion and does not induce any potential. Thus $O{=}S^{+}{-}I^{-}$ compensates more share to the higher UCSTs and $N^{+}{-}Cl$ does not, but the 12 carbon chain do compensates for the same.

3.1. Atomic Size Do Influences the UCSTs

The UCST of surfactants with halide atoms are listed is as $I^{-} = Br^{-} > Cl^{-}$, and is correlated to the nonbonding electron transitions due to the greater electro negativity of the Cl^{-} atom. The nonbonding electrons on Cl^{-} hardly undergo energy change but of I^{-} on trimethylsulphoxonium iodide is loosely bound and can undergo energy change. They strongly reorient the solvent structures due to a cage model of water that lead to develop weaker interactions with. Perhaps it is difficult to get fitted the hydrophobic part of them in water but aligns towards phenol. Similarly the hydrophilic parts align to water the H_2O. Thus a loose film between phenol and water interface is developed that initiates a soap action on a liquid–liquid interaction model. Hence our studies are restricted to surfaces only where the surfactant molecules get dispersed in phenol"water phases but not at all to penetrate bulk to either. The additives were in water which on contact of phenol aligns to phenol and water surfaces. However for high x_{ph} the @ slightly decreases. Hence the additives are more effective with lower x_{ph} but with lighter x_{ph}. The phenol interaction might weaken the sharper effects of additives hence our studies are useful for bioscience process occurring at slightly higher temperatures.

4. CONCLUSION

The surfactants develop lower UCST values with higher mutual solubility at lower temperatures of immiscible solvents.

ACKNOWLEDGMENTS

The author is thankful to University Grant Commission, Govt. of India and Dr. A. P. Raste, Principal, DBC, for infrastructural supports.

REFERENCES

1. Singh, M. and Singhal, S., *J. Appl. Polym Sci.*, 2007, vol. 104, no. 5, p. 3261–3268.
2. Singh, M., *J. Chem. Thermodyn*., 2006, vol. 39, no. 2, pp. 240–246.
3. Singh, M., *J. Ind. Chem. Soc.*, 2001, vol. 78, pp. 397–402.
4. Borghesani, G., Pedriali, R., Pulidori, F., and Scaroni, I., *J. Soln. Chem*., 1986, vol. 15, no. 5, pp. 397–408.
5. Cascella, C., Castronuovo G., Elia, V., Sartorio, R., and Wurzburger, S., 1990, *J. Chem. Soc., Faraday Trans.,* vol. 86, pp. 85–88.
6. Lagi, M., Nostro, P.L., Fratini, E., Ninham, B.W., and Baglioni, P., 2007, *J. Phys. Chem. B*, vol. 111, no. 3, pp. 589–597.
7. Bini, R., Bortolini, O., Chiappe, C., Pieraccini, D., and Siciliano, T., *J. Phys. Chem. B*, 2007, vol. 111, no. 3, pp. 598–604.
8. Misra, D.N., *J. Colloid Interface Sci*., 1999, vol. 220, no. 2, pp. 387–391.
9. Fried, V., Hameka, H.F., and Blukis, U., *Physical Chemistry*, 1977, New York: Macmillan/Collier Macmillan, pp. 229–232.
10. Goodwin, J.W., Ottewill, R.H., and Pelton, R., *Colloid Polymer Science,* 1979, vol. 257, pp. 61–69.
11. Singh, M. and Kumar, A., *J. Soln. Chem.*, 2006, vol. 35, no. 4, pp. 567–582.
12. Singh, M., *J. Biochem. Biophys. Methds,* 2006, vol. 67, pp. 151–161.
13. Singh, M., Pandey, M., Yadav, R.K., and Verma, H.S., *J. Mol. Liq.*, 2007, vol.135, pp. 188–191.
14. Singh, M., *Bulg. J. Chem. Edu.*, 2006, vol. 15, no. 6, pp. 426–430.
15. Singh, M., *J. Chem. Sci.*., 2007, vol. 118, no. 3, pp. 269–274.
16. Ibrahim, Y., Mabrouki, R., Meat-Ner, M., and El-Shall, M.S., *J. Phys. Chem. A,* 2007, vol. 10, pp. 7390–7397.
17. Zhang, F., Skoda, M.W.A., Jacobs, R.M.J., Martin, R.A., Martin, C.M., and Schreiber, F., *J. Phys. Chem. B*, 2007, vol. 111, no. 1, pp. 251–259.

ISSN 1070-4272, Russian Journal of Applied Chemistry, 2007, Vol. 80, No. 12, pp. 2178–2183. © Pleiades Publishing, Ltd., 2007.
Original Russian Text © R.Sh. Abiev, 2007, published in Khimicheskaya Promyshlennost', 2007, Vol. 84, No. 7, pp. 347–353.

PROCESSES AND DEVICES OF CHEMICAL MANUFACTURES

Modeling Pulse Apparatus for Processing Suspension with Periodical Unload of Concentrated Precipitate

R. Sh. Abiev

St. Petersburg State Technological Institute, St. Petersburg, Russia

Received September 11, 2007

Abstract—The principle of work of a new apparatus for processing suspension with periodical unloading of concentrated precipitate is described. Mathematical model of the apparatus is created that allow calculating main technological parameters of the apparatus. The apparatus feature is application of potential energy accumulated by the compressed gas in the pulse chamber for the regeneration of the separating screen. The experiments with laboratory model of the apparatus allow to recommend this mathematical model for practical application.

DOI: 10.1134/S1070427207120373

INTRODUCTION

The apparatuses for processing suspensions are widely used in chemical, food, pharmacy and other related branches of industry. The apparatus described in this publication is the most appropriate for the following processes:

1. Filtration where solid phase particles clog up the pores of the separating element (concentrating suspensions with less than 0.1% content of solid phase), e.g., filtration of juices in the food industry, cellulose solutions at producing artificial fiber, and purification of mineral oil.

2. Concentrating suspension in concentrating filters with the working cycle consisting of filtration and removing the precipitate formed from the separating element by the filtrate back flow.

3. Filtrating with formation of solid phase layer on the surface of the separating element (at concentration of solid phase in the suspension more than 1%).

The process of filtration can be combined with other technological processes such as impregnation of porous material, washing, extraction, ion exchange, heterogenic catalytic reactions. With appropriate filtering separators, a micro filtration process can be performed.

Such apparatus can be recommended in particular for the cases of adhering and compacting precipitates and the precipitates hardly removable from the filtering elements, when traditional filters do not work.

In this publication we describe the principle of working a new energy saving pulse apparatus for processing suspensions, with automatic periodical unloading the concentrated precipitate. We conducted theoretical and experimental investigation of such apparatuses.

At the development of the proposed here apparatus we were aimed at the following tasks:

1. Automatic control of the process of unloading concentrated precipitate from the apparatus with periodical regeneration of filtering screen without consuming additional energy,

2. Use of potential energy of filtrate for the regeneration, which should decrease energy consuming, increase reliability of the apparatus and simplify operating.

CONSTRUCTION AND PRINCIPLE OF ACTION OF THE APPARATUS FOR THE PROCESSING OF SUSPENSIONS

Pulse apparatus for processing suspension [1] (see scheme in Fig. 1) consists of housing body 1 bearing connecting pipe 2 – 5. Filtrating element 6 separates concentrating chamber 7 and filtrate collecting chamber

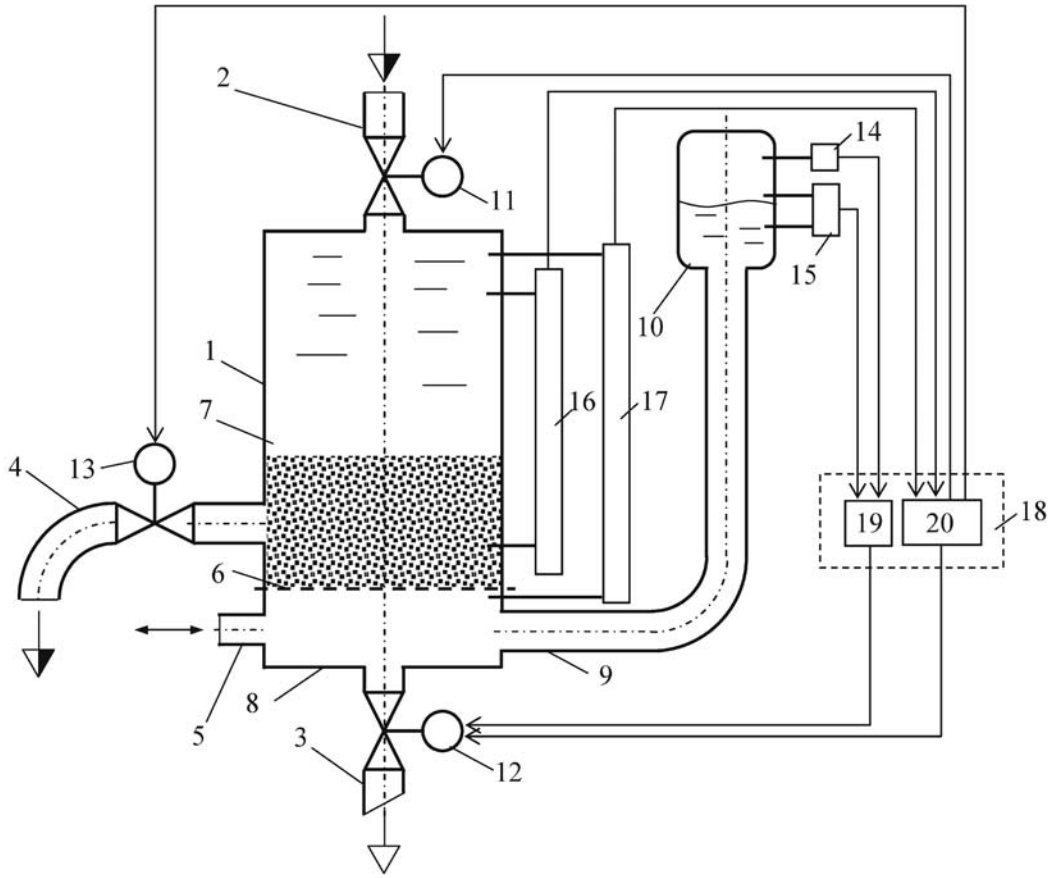

Fig. 1. Scheme of pulse apparatus for processing suspension (concentrating filter). (1) housing body, (2–5) connecting pipes: 2 for feeding with suspension, 3 for filtrate outlet, 4 for concentrated suspension outlet, 5 for passing pulses; (6) filtrating separator, (7) concentrating chamber, (8) filtrate collecting chamber, (9) pipe line, (10) pulse chamber, (11–13) controlled valves, (14–17) probes, (18) control system, (19) control block for valve 12, (20) control block for valves 11–13.

8. Pipe line 9 connects the filtrate chamber 8 with pulse chamber 10. Connecting pipes for feeding with suspension 2, filtrate outlet 3 and concentrated suspension outlet 4 are equipped with control valves 11, 12 and 13, respectively. The apparatus is also equipped with probes 14–17 and control system 18, consisting of two subsystems: block 19 for control over state of valve 12, and block 20 controlling states of valves 11–13.

The apparatus operates in cyclic regime: steps of filtration and regeneration are alternating.

1. Filtration Period

Valve 13 is closed, valve 12 is partially open, valve 11 is open completely. Through connecting pipe 2 the apparatus is feed with suspension. In time on the filtrating separator 6 is formed layer of solid phase while to the chamber 8 through the filtering separator 6 continuously passes filtrate. A part of the filtrate is removed from the apparatus through the connecting pipe 3 and valve 12, another part is passed through the pipe line 9 to the pulse chamber 12 compressing stepwise the gas (air) in the chamber. Thus, pressure in the pulse chamber 10 increases stepwise and the compressed gas accumulates potential energy. Pressure pulses coming to the system through connecting pipe 5 from the pulse generator (not shown) promote periodical disintegration of the solid phase formed on the filtering separator 6 and damage of bonds between the solid phase particles. This improves conditions of filtration through the solid layer and elongates the period of filtration before regeneration. Simultaneously with the filtration process, in the apparatus can proceed the abovementioned processes of chemical reactions and mass exchange.

2. Regeneration Period

During accumulation of solid phase, either resistance of the latter achieves limiting value, or the precipitate fills whole space of the concentrating chamber 7,

resulting in appearance of signals from probes 16 or 17, respectively. Then valves 11 and 12 close connecting pipes and then valve 13 quickly opens pipe 4; at this moment passing pulses through valve 5 can be stopped. Owing to the pressure difference between chamber 10 and atmospheric pressure at the outlet line 4 the liquid in the pulse chamber and pipe line 9 moves up through the filtering separator 6 like a pulse generating hydraulic impact, passes through the solid phase damaging bonds between its particles. Thus the accumulated potential energy is transformed to kinetic energy of moving the liquid interacting with the precipitate, promoting damage of dense structure of the solid phase. The solid layer becomes some diluted with a portion of liquid coming through filtering separator 6 improving mobility of the solid, and the concentrated suspension under the pressure is ejected through the valve 13 and pipe 4 to a collector (not shown). This results in regeneration of filtering separator 6. Then valve 13 closes and next cycle of apparatus work starts.

A feature of the proposed apparatus is automatic control over opening valves 11–13 by the control system 18 using the signals from the probes 14–17. The probes 15 and 16 are two-level, that is, they have upper and lower switching edges. In the first step the valve 12 is partially open, its state is controlled by pressure probe 14 and level probe 15; signals of the two latter achieve control block 19 and passed to valve 12. The valve 19 is completely open and 13 closed, they are controlled by probes 16 and 17 and control block 20. In the second step, the signals from probes 16 and 17 achieve block 20 which closes valves 11 and 12 and opens valve 13.

Thus, formation of dense solid is counterforced by pulses in the filtration period and by impact motion of a part of filtrate in the regeneration period.

MATHEMATICAL MODEL OF PULSE APPARATUS FOR PROCESSING SUSPENSION

Mathematical model of pulse extractor has been described [2]. Its works similarly to the filter that we describe now. A feature of the filter distinguishing it from the batch-operating extractor is the unsteady process of the solid phase accumulation. Our description pays attention to this process mainly.

Let us consider the step of filtration. In an arbitrary time moment the filtrate consumption passing through the filtering screen with solid on it is:

$$Q_{\mathrm{f}}(t) = \frac{\Delta p}{r_{\mathrm{fs}} + r_{\mathrm{pr}}} \tag{1}$$

Consumption of suspension feeding into the filter and consumption of solid phase cantained in the suspension equal, respectively, to:

$$Q_{\mathrm{s}} = \frac{Q_{\mathrm{f}}}{1-\varepsilon_{\mathrm{s}}} \tag{2}$$

$$Q_{\mathrm{sp}} = Q_{\mathrm{s}}\varepsilon_{\mathrm{s}} \tag{3}$$

Gains in volumes during a short time gap Δt are:

– solid phase

$$\Delta V_{\mathrm{solid}} = Q_{\mathrm{sp}}\Delta t \tag{4}$$

– precipitate (including solid particles and pores between them)

$$\Delta V_{\mathrm{pr}} = \frac{Q_{\mathrm{sp}}\Delta t}{\varepsilon_{\mathrm{pr}}} \tag{5}$$

– liquid in the precipitate pores

$$\Delta V_{\mathrm{pore}} = \frac{1-\varepsilon_{\mathrm{pr}}}{\varepsilon_{\mathrm{pr}}} Q_{\mathrm{sp}}\Delta t \tag{6}$$

– liquid below the filtering screen (the filtrate minus the liquid in pores) which equals to diminishing in the gas volume in the chamber for the filtrate accumulation 8 and pulse chamber 10 (see Fig. 1)

$$\Delta V_{\mathrm{gas}} = Q_{\mathrm{f}}\Delta t - \Delta V_{\mathrm{pore}} \tag{7}$$

Gain in the precipitate height during the short period Δt is:

$$\Delta h = \frac{\Delta V_{\mathrm{pr}}}{F} \tag{8}$$

Taking into account that filtration rate is low, we accept isothermal law for changes pressure in the pulse chamber:

$$p_2(t) = \frac{p_{20}V_{20}}{V_2(t)} \tag{9}$$

Resistance of the precipitate layer reduced to the filter section was taken laminar and was calculated through Darsy's filtration constant [3]:

$$r_{pr}(t) = \frac{2\mu\zeta^2 S^2 (1-\varepsilon_{pr})^2}{\varepsilon_{pr}^3 F} h(t) \quad (10)$$

The constructed model can be reduced to Volterra equation of the second kind for the filtrate consumption calculation:

$$Q_f(t) = \frac{1}{r_{filter} + A\int_0^t Q_f(\tau)d\tau}\left(p_1 - \frac{p_2 V_{20}}{V_{20} - B\int_0^t Q_f(\tau)d\tau}\right) \quad (11)$$

where the following constants are used:

$$A = \frac{2\mu\zeta^2 S^2 (1-\varepsilon_{pr})^2 \varepsilon_S}{\varepsilon_{pr}^4 F^2 (1-\varepsilon_S)}, \quad (12)$$

$$B = 1 - \frac{(1-\varepsilon_{solid})\varepsilon_S}{\varepsilon_{solid}(1-\varepsilon_S)} \quad (13)$$

The system of equations (1) – (12) was solved by Euler method. The calculated plots of most important technological parameters against time for the conditions of the carried out experiments are shown in Fig. 2.

The plots obtained allows to trace duration of the filtration cycle $\hat{o}_c$ for achieving minimal allowed consumption of filtrate (in Fig. 2 it is defined equal 0.2 part of starting filtrate consumption, that gives $\hat{o}_c$ = 171 s), after that regeneration of filtering screen seems reasonable.

EXPERIMENTAL

The experiments included solving of the following tasks:

– examining efficiency of installation in the steps of filtration and regeneration.

– experimental testing the constructed mathematical model.

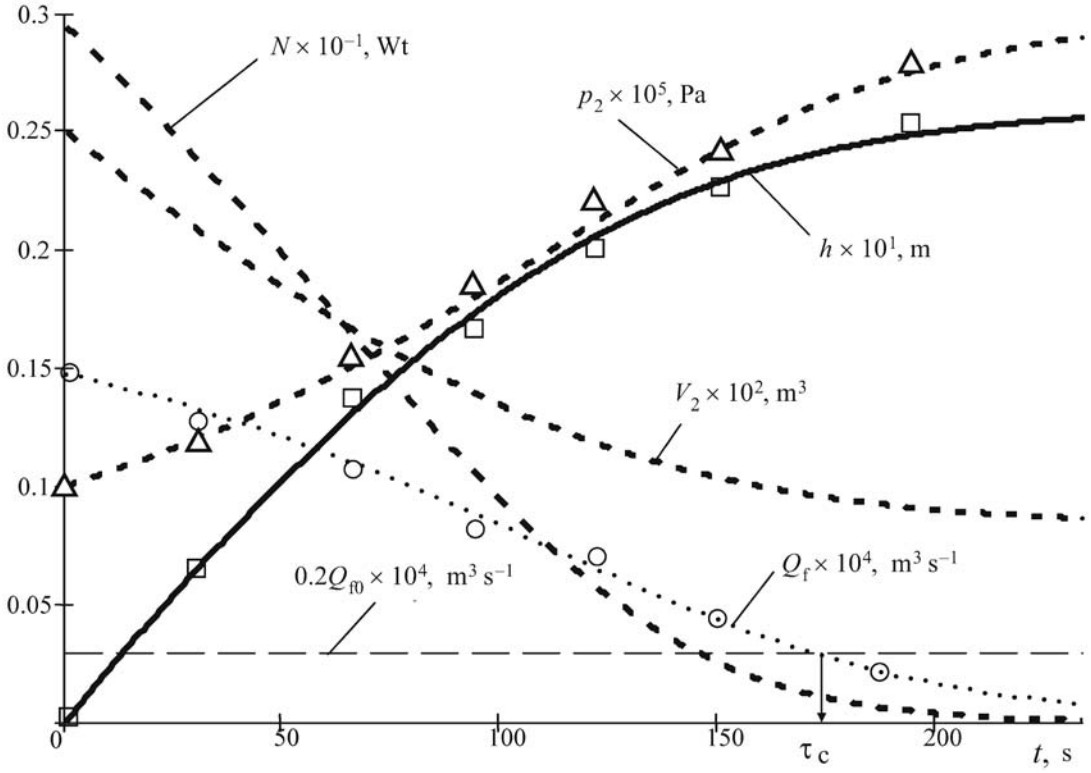

Fig. 2. Time dependence (t, s) of precipitate height h, filtrate consumption Q_f, gas volume V_2 and gas pressure p_2 in the pulse chamber. Horizontal dash line corresponds to 5-fold decrease in filtrate consumption relatively to the initial one. Calculation parameters: F =5.027×10^{-3} m^2; p_1 = 3×105 Pa (abs); p_{20} = 1×10^5 Pa (abs); ε_s = 0.05; ε_{solid} = 0.69; μ = 1.186×10^{-3} Pa s; S = 1.307×10^5 m^{-1}; ζ = 1.177. Dots correspond to experimental data.

Scheme of the experimental installation is shown in Fig. 3. The installation includes receiver 1 in which particles of $CaCO_3$ (average sedimentation diameter 46) μ are maintained suspended by rotor pump 2. From the filter 3 the filtrate passes through filtering screen 4 to collector 5 and to the pulse chamber 7, compressing located there gas, which leads to increase in pressure. Pressure over the suspension surface (induced by compressed air) and in the pulse chamber was measured by an arrow type manometers 9 and 10. At the filter regeneration by blowing with compressed air accumulated in the pulse chamber 7 the concentrated suspension passes to collector 6. All valves are spherical stopcocks controlled manually.

The filtering screen 4 consists of three layers: a fabric layer between metallic gauze and fluoroplast grid. Its resistance found experimentally was: $r_f = 1.36 \times 10^{10}$ Pa s m^{-3}.

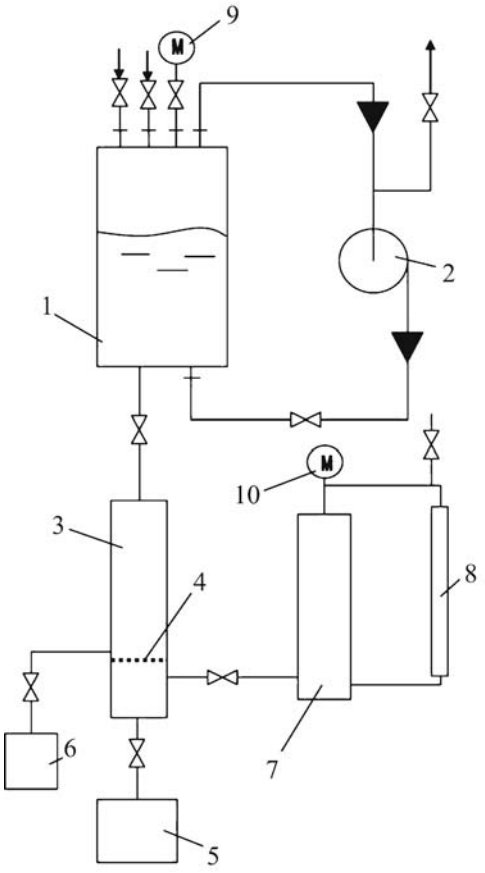

Fig. 3. Scheme of experimental installation. (1) receiver for suspension, (2) circulation pump, (3) filter, (4) filtering screen, (5) receiver for filtrate, (6) receiver for concentrated suspension, (7) pulse chamber, (8) liquid level indicator, (9,10) manometers

In the experimentrs we also measured the precipitate layer heigh, filtrate and concentrated suspension volumes and the filtration process duration. Regeneration was practically instant (approx. 0.2–0.3 s).

The experiments were carried out with suspension containing solid phase fraction $\varepsilon_s = 0.015$, 0.20 and 0.32. Pressure over the suspension surface was varied in the range 0.208 to 0.384 MPa.

By many times repeated experiments was confirmed principally efficiency of the installation not only in the step of filtration but also at regeneration using accumulated potential energy of compressed air.

The experimental results obtained are well corresponding with the calculations. As an example in Fig. 2 are depicted experimental points of filtrate consumption (circles), precipitate layer height (squires) and pressure in the pulse chamber (triangles).

Technical project of the pulse apparatus for processing suspensions based on industrial serially produced receiver type vacuum filter of EGr 1.5-2000K type with the filtrating surface 1.5 m^2.

CONCLUSIONS

The created mathematical mode allows calculation of basic technological parameters of the apparatus and obeys satisfactorily to experimental results.

Experimental examination of the filter 80 mm diameter showed that the developed apparatus for processing suspensions with regeneration of filtrating screen by back flow of the filtrate can be successfully applied under industrial conditions. Although experimentally was studied the case of ultra low frequency pulses, in the industrial practice can turn to be reasonable include additional low frequency treatment of the suspension in the step of filtration (in particular at high concentration of solid phase and in the case of formation precipitate of rigid structure) to elongate period between regenerations.

The apparatus can be recommended mainly for processing suspension with low concentration(not higher than 3 to 4%) as a concentrating filter or for continuous mass exchange processes (washing, impregnating, etc.).

ACKNOWLEDGMENT

The author is grateful to former students of St. Petersburg State Technological Institute (Technical University) M.K. Markaryan and A.V. Chernyaev for

active participation in carrying out experimental part of this investigation.

ABBREVIATIONS

F—filter area, m^2;
h—precipitate layer height, m;
N—power consumed for filtering liquid through precipitate layer, W;
p_1—pressure of the feeding suspension, Pa;
p_2—pressure in the pulse chamber, Pa;
Δp—pressure difference before and after the filter, Pa;
Q_f—filtrate consumption, m^3/s;
r_{pr}—resistance of precipitate layer reduced to the filter section, Pa s/m^3;
r_f—resistance of filtering screen reduced to the filter section, Pa s/m^3;
S—specific surface area in the precipitate, m^{-1};
V_2—gas volume in the pulse chamber, m^3;
ε_s—volume concentration of solid phase in the suspension, relative units;
ε_{solid}—volume concentration of solid phase in the precipitate, relative units;
ζ—tortuosity coefficient for precipitate, relative units;
Indices:
0—initial value,
1—parameters over the precipitate layer,
2—parameters below the filtering screen,
g—gas,
pr—precipitate on the filtering screen,
pore—pores in the precipitate,
s—suspension,
solid—solid phase,
f—filtrate,
filter—filtrating screen

REFERENCES

1. RF Patent no. 2297869, *Bull. Izobr.*, 2007, no. 12.
2. Abiev, R.Sh., *Khim. Neftegas. Mashinostroenie*, 2000, no. 8, pp. 11–14.
3. Aerov, M.E. and Todes, O.M., *Gidravlicheskie i teplovye osnovy raboty apparatov so statsionarnym i kipyashchim zernistym sloem* (Gydravlic Basicity of the Apparatuses with Steady and Boiling Granule Layer), Leningrad: Khimiya, 1968.

ISSN 1070-4272, Russian Journal of Applied Chemistry, 2007, Vol. 80, No. 12, pp. 2184–2189. © Pleiades Publishing, Ltd., 2007.
Original Russian Text © A.G. Laptev, M.I. Farakhov, N.G. Mineev, E.A. Lapteva, V.N. Kudryashow, I.Kh. Mukhitov, M.G. Khusnullin, I.G. Askarov, 2007, published in Khimicheskaya Promyshlennost', 2007, Vol. 84, No. 7, pp. 354–360.

PROCESSES AND DEVICES OF CHEMICAL MANUFACTURES

Enhancing Performance of Rectification Columns for Ethanolamine Manufacturing

A. G. Laptev,* M. I. Farakhov, N. G. Mineev, E. A. Lapteva, V. N. Kudryashow, I. Kh. Mukhitov, M. G. Khusnullin and I. G. Askarov

Engeneering and Promotion Center "Inzhekhim," Open join stock company "Kazan orgsintez," Kazan, Russia
e-mail: info@ingehim.ru, ingehim@kstu.ru

Received September 11, 2007

Abstract—A problem is considered of enhancing performance of pilot plant installation for manufacturing ethanolamine by replacement of modern packed towers for old type rectification columns. The modernization result is increase in productivity and product quality, and energy saving.

DOI: 10.1134/S1070427207120385

To enhance competition of product and diminish energy consuming it is necessary either to develop new technology and apparatuses design or to improve currently working installations and plants. The second pathway is less cost and time consuming.

Most rectification installations operating now in domestic chemical industry were projected in 60–80th of last century. During the recent years appeared effective types of contact units that are more and more often used for modernization of rectification columns. Among them there are leading packing elements produced by foreign and domestic firms. Examples are the irregular type packing HY-PAK, CASCADE RINGS, Inzhekhim, GIPKh, GIAP and others, and regular types INTALOX, Sulzer, Koch, Ingekhim, Norton, Mellapack and Vacu-Pack [1–5].

The columns with a packing often at the same efficiency as those with air-lift plates are advantageous due to lower hydraulic resistance which is of particular importance for the vacuum columns, and shorter processing duration, which is important at the separation of mixtures inclined to decomposition, polymerization and colorization.

In this communication we consider modernization of rectification columns for ethanolamine distillation in the working plant "Organicheskie Producty" (Organic products) of the open type join stock company "Kazan orgsintez".

The method of manufacturing ethanolamine is based on the reaction of ethylene oxide with ammonia in the presence of water acting as a catalyst. Commercial products are: monoethanolamine technical grade, diethanolamine pure grade, triethanolamine technical grade and monoethanolamine bottom residue.

Monoethanolamine technical grade is a transparent liquid with ammonia smell, color from yellow to dark brown. Diethanolamine is a thick viscous liquid or yellow crystals. Monoethanolamine bottom residue is a liquid of brown to dark brown color.

Current industrial methods assumes producing mono-, di- and triethanolamine, as a rule in equal amounts. Industrial technologies can be classified into two groups. The first group includes "water" technology based on ethylene oxide and aqueous ammonia, the synthesis is conducted at 20 to 200ºC, pressure 1 to 60 atm, ethylene oxide–ammonia ratio is 1–4 : 50. The second group includes technology that uses ethylene oxide and ammonia containing water in a catalytic amount (0.5 to 5%).

Currently etanolamines manufacturing in "Kazan orgsintez" open join stock company (the plant "Organicheskie producty") is performed in a block of reactors operating alongside the "water" technology. For separation of the components a few rectification columns are used, the basic ones are Kn-29, Kn-40, Kn-56 and

Kn-92. Mixtures of ethanolamines is passed to column Kn-29.

Table 1 shows composition of raw material (feeding column Kn-29). Nominal productivity is 2100 kg/h, varying within ±15%. The product from the rectification block in the installation for manufacturing ethanolamines should obey requirements listed in Table 2.

Before modernization, the working columns had the following diameters: Kn-29 1.0 m, Kn-40, Kn-56 and Kn-92 1.6 m each. The columns were equipped with mass exchange plates of different types. The columns structural strength resource was low enough. Basing on the mathematical modeling of the processes in the packing [5] we performed calculations and considered possible technical solutions for replacement of plates by regular and irregular "Inhzekhim" packing. As the calculations showed, for providing productivity on raw material from 1785 to 2415 kg/h the new columns should have the following diameters: Kn-29 0.5 m, Kn-40 1.2 m, Kn-56 1.0 m, Kn-92 0.6 m. Diminishing the size of the columns provides considerable decrease in energy consuming for the process of separation.

Technological regime in Kn-29 assumes atmospheric pressure in the column. Construction of the newly projected Kn-29 column should provide operating both at atmospheric pressure and in a vacuum. Due to decomposition of triethanolamine at the temperature above 170°C, temperature in the column bottom section should be diminished to 166–167°C, and this requires to decrease pressure in the column to 460 mm Hg (absolute pressure). Technological scheme of the separation block is shown in Fig. 1.

The new rectification column Kn-29 is of packing type, 0.5 m diameter. The packing is located in two sections, 3.0 and 3.5 m height.

Distilling off the commercial monoethanolamine is carried out in the column Kn-40. The

feeding liquid enters to the column at the temperature 115–120°C. The new Kn-40 column is of packing type, diameter 1.2 m, with packing in three sections, 1.5, 3, and 3.5 m height.

Commercial monoethanolamine can be withdrawn from the column either as a distillate (in the case of absence of water in the Kn-40 column) or as a side product.

Distilling off the light components from the crude triethanolamine (the bottom residue in the column Kn-40 at the manufacturing monoethanolamine) and

Table 1. Composition of raw material

Existing synthesis block	Composition, wt%
Ammonia	0.5–1.0
Water	7–10
Monoethanolamine	45–55
Diethanolamine	21–31
Triethanolamine	11–15

Table 2. Requirement to the separated products

Product	Content of maun component, wt%	Color units by Hasen
Monoethanolamine	not less 99.8	10 or less
Diethanolamine	not less 99.7	25 or less
Triethanolamine	not less 95.0	50 or less

producing commercial diethanolamoine is carried out in the rectification column Kn-56. The new Kn-56 rectification column is of packing type, diameter 1.0 m. The packing is located in three sections, height 1.8, 4.2, and 3.2 m.

Crude triethanolamine is passed for feeding the Kn-56 column where a mixture of water and monoethanolamine is distilled off and leaves the column in the column head. Commercial diethanolamine is taken as a side product from redistribution plate located below the upper packing section. From the column bottom outgoes the bottom residue consisting of a mixture of diethanolamine and triethanolamine.

Isolation of commercial triethanolamine is carried out in the rectification column Kn-92.

The new Kn-92 column is of packing type, 0.6 m diameter. The packing is located in two sections, height 1.6 and 2.6 m. The column feeding liquid temperature is 100-110°C. From the column bottom is withdrawn the bottom residue consisting of triethanolamine and tar.

The feeding control is performed by a feeding controller with a valve in the pump pressure pipe. The Kn-92 feeding temperature is 100–120°C.

The heat necessary for the rectification is supplied to film type evaporators heated by steam with pressure 25 kg/cm^2.

For choosing the packing type for these columns the following features of the process of ethanolamine separation were taken into account:

1. All the columns except Kn-29 should operate at reduced pressure. In future, the column Kn-29 will also be operating as a vacuum column. Hence, the packing

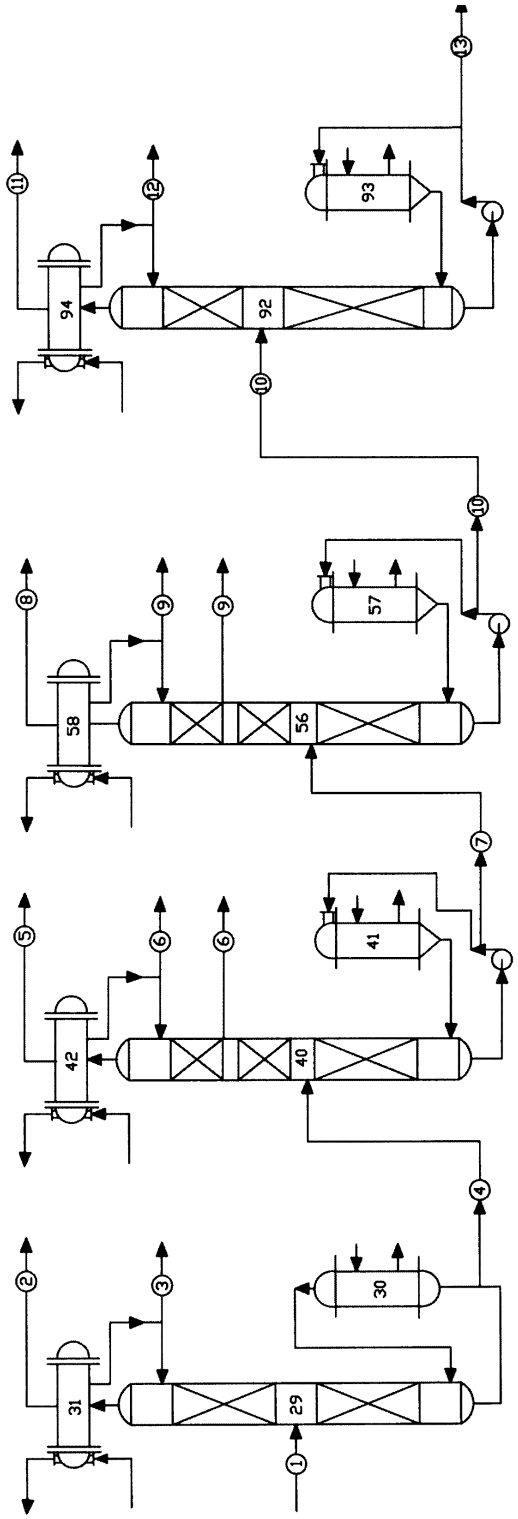

Fig. 1. Scheme of the block of ethanolamine separation. (1, 4, 7, 10) mixture for separation, (2, 5, 8, 11) gas (air) outlet, (3) distillate, (6) monoethanolamine, (9) diethanolamine, (12) triethanolamine, (13) residue (tar), (29, 40, 56, 92) rectification columns, (31, 42, 58, 94) reflux condensers, (30, 41, 57, 93) boilers.

should have low hydraulic resistance at high enough value of vapor factor, up to 2.6 m s $(kg\ m^{-3})^{0.5}$.

2. The packing should provide high enough degree of separation. The minimum height corresponding to one theoretical plate at the projecting the column height is accepted equal to 0.6 m.

3. The packing should provide the required degree of separation at a very low reflux, less than 1 m/h.

4. All the columns are constructed as not disassembling units, that is, the packing construction should provide a possibility of mounting through the column hatches.

Taking all above into account it was decided to use for all the columns except Kn-29 the regular packing "Inzhekhim-IRR-14" [5] (Fig. 2).

While choosing a regular packing we accounted for the positive experience of the Engineering Center "Inzhekhim" on the application of roll type corrugated packing used in the process of separation of ethylene glycol in the "Okis' Etilena" fabric of the "Nizhnekamskneftekhim" join stock company [6]. This process resembles that of ethanolamine separation by both thermophysical properties of the separated mixtures and characteristics of column operation (high value of vapor factor and low reflux).

Table 3 contains principal characteristics of the packing "Inzhekhim IRR-14."

In the column Kn-29 was proposed to use packing "Inhzekhim-2000" (Fig. 3). Technical characteristics of the packing "Inzhekhim-2000" are listed in Table 4.

The new contact units (packing) were examined experimentally on a stand type testing units. Similar packing is used effectively in the rectification columns at join stock company "Nizhnekamskneftekhim," in the "Etilen" plant of join stock company "Kazan orsintez" in a column for alkaline purification of pyrolysis gas and in oil fog separators (oil trappers) [4, 7, 8].

Table 3. Technical characteristics of IRR packing

No.	Characteristic of paching	Units	Value
1	Specific surface area	m^2/m^3	320
2	Free volume	m^2/m^3	0.904
3	Equivalent diameter	m	0.0113
4	Hydraulic resistance at the vapor factor P = 2.6	Pa m^{-3}	120
5	Height corresponding to one theoretical plate	m	0.5÷0.6

Table 4. Technical characteristics of the packing "Inzhekhim 2000"

Nominal size, mm	Specific free volume, m^3/m^3			Specific surface, m^2/m^3	Height equivalent to one theoretical plate
	Characteristic of paching				
	0.3	0.5	1.0		
60	–	0.973	0.945	110	1.0–1.5
35	–	0.965	0.93	140	0.5–1.0
24	–	0.945	0.89	220	0.35–0.6
16	0.949	0.915	–	340	0.15–0.4

During years 2004-2005 the new packing columns were involved into manufacturing of ethanolamines. The results of exploitation of the columns confirmed correctness of calculations and technical solutions. Comparative characteristics of columns are given in Table 5.

During startup and tune-up period and experimental industrial exploitation were elucidated the following features:

– The packing column show by an order of magnitude shorter delay of liquid phase in the column and duration of location it in the column as compared with the plate type columns. Therefore the staff had problem with the control of the process in the startup period. When the actions necessary for process control where developed and an experience was achieved for maintaining steady regime, these problems were solved. Now the packing columns operates stable and provide required efficiency in separation and color of the products.

– Efficiency of separation depends in a great extent on the initial distribution of liquid phase feeding the regular packing. Closing holes in the liquid phase distributing units diminishes efficiency of separation.

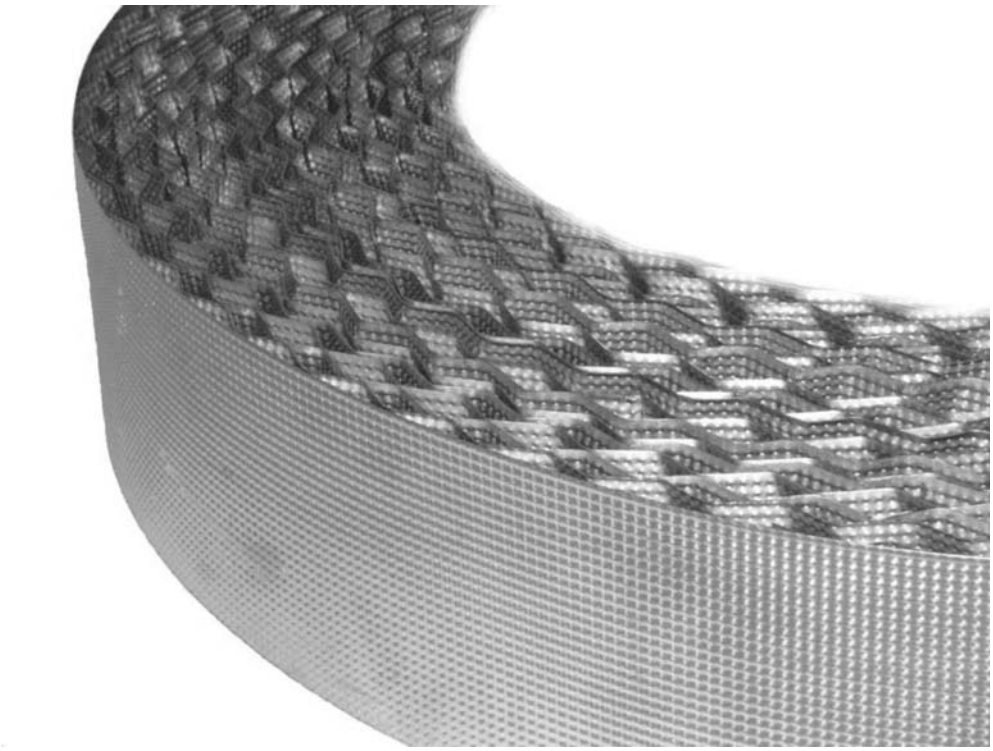

Fig. 2. Roll type regular packing.

Table 5. Comparative characteristics of columns operation

K-29		K-40		K-56		K-92	
Plate	Packing	Plate	Packing	Plate	Packing	Plate	Packing
Column diameter, m							
1.0	0.5	1.6	1.2	1.6	1.0	1.6	0.6
Column height, m							
13.7	12.575	16.1	22.36	22.8	23.580	22.8	17.56
Feeding, m^3/h							
2.2–2.5	2.85	1–2.3	2.3–2.4	1–1.2	1.0–1.1	1.1	0.34–0.35
Distillate, m^3/h							
0.2–0.3	0.31–0.33	1–1.3	1.1–1.16	0.7–0.9	0.06–0.07	0.3	0.2
Side output, m^3/h							
–	–	–	–	–	0.65–0.75	–	–
Bottom residue, m^3/h							
2–2.2	2.3–2.4	1–1.2	1.0–1.1	–	0.34–0.35	–	–
Reflux, m^3/h							
1.4–1.8	0.3–0.33	1.2–1.5	0.15–0.2	0.1	0.64–0.78	0.9–1.0	0.0
Monoethanolamine yield, m^3/h							
–	–	1.1–1.2	1.1–1.16	–	–	–	–
Diethanolamine yield, m^3/h							
–	–	–	–	0.65	0.65–0.75	–	–
Triethanolamine yield, m^3/h							
–	–	1–1.2	–	–	–	–	0.2–0.21
Heat consumption in the column boiler Gcal/h							
1.19	0.49	1.19	0.33	0.85	0.22	0.71	0.62

Fig. 3. A detail of Inzhekhim-2000 packing.

– Heating steam consuming in the column boilers decreased considerably.

– Technological regime with side outlet of monoethanolamine is now fixed.

Whole, exploitation of the new packing columns gave positive results.

REFERENCES

1. Dmitrieva, G.B., Berengarten, M.G., Klyushenkova, M.I., and Pushnov, A.G., *Khim. Neftergaz. Mashinostroenie*, 2005, no. 8, p. 15–17.
2. Dmitrieva, G.B., Berengarten, M.G., Kagan, A.M., Pushnov, A.G., and Klimov, A.G., *Khim. Neftergaz. Mashinostroenie,* 2007, no. 1, pp. 9–10.

3. Lebedev, Yu.N., Chekmenov, V.G., Zaitseva, T.M., et al., *Khim. Tekhnol. Topliv i Masel*, 2004, no. 1, pp. 48–52.
4. Laptev, A.G., Farakhov, M.I., Danilov, V.A., et al., *Khim. Promyshlennost'*, 2001, no. 10, pp. 24–33.
5. Yasaveev, Kh.N., Laptev, A.G., Farakhov, M.I., et al., *Modernizatsiya ustanovok pererabotki uglevodorodnykh smesei* (Modernization of Installations for Processing hydrocarbon mixtures), Kazan: KGEU, 2004.
6. D'yakonov, S.G., Elizarov, V.V., and Farakhov, M.I., *Izv. Vuzov Khimiya Khim. Tekhnol.*, 2003, vol. 46, no. 5, pp. 148–151.
7. Laptev, A.G., Mineev, N.G., and Mal'kovskii, P.A., *Proektirovanuie i modernizatsiya apparatov razdeleniya v nefte- i gazopererabotke* (Projecting and Modernization of Apparatuses for Separation in Petroleum and Gas Processing), Kazan: Pechatnyi Dvor, 2002.
8. Laptev, A.G. and Farakhov, M.I., *Razdelenie geterogennykh sistem v nasadochnykh apparatakh* (Separation of Heterogenic Systems in Packing Type Apparatuses), Kazan: KGEU, 2006.

ISSN 1070-4272, Russian Journal of Applied Chemistry, 2007, Vol. 80, No. 12, pp. 2190–2196. © Pleiades Publishing, Ltd., 2007.
Original Russian Text © M.G. Voronkov, 2007, published in Khimicheskaya Promyshlennost', 2007, Vol. 84, No. 7, pp. 371–378.

HISTORY
OF CHEMISTRY

Silicon Era

M. G. Voronkov

Favorskii Irkutsk Institute of Chemistry, Siberian Branch, Russian Academy of Sciences, Urkutsk, Russia

Received April 24, 2007

Abstract—Comprehensive consideration of genesis and evolution of the chemistry of silicon in the period from 1771 till 1897. Bibliography 66 references.*

DOI: 10.1134/S1070427207120397

The aim of science is deducing future from the past.
Henrich Hertz

INSTEAD OF INTRODUCTION

Academician I.V. Grebenshchikov, the founder of the Institute of the Chemistry of Silicates, Academy of Sciences of USSR, highly prestigious soviet specialist at his time in the area of the chemistry of silicon, dreamed to assign to the Institute the name "Institute of Silicon". However, hard economical and social situation in the country after the Second World War (Patriotic War) required reconstruction of damaged habitable funds and extended erecting industrial buildings, first of all as facility for creation nuclear weapon and atomic power stations.

This all required silicate materials in huge amount, including those possessing earlier unknown properties. It is this situation impelled the USSR government to admit the currently used name to the newly created institute. Unfortunately, at those years the industry of organosilicon compounds in our country just only has been born. Nobody could mind that elemental silicon would became one of the most important elements in the end of 20th and whole 21th centuries and would be providing the vigorous progress of industry and technology. Proceeding from the above epigraph, we decided to consider the history of born elemental silicon that gave rise to most modern technologies of producing semiconductor grade silicon.

* Transdlator's note: All quotations are translated from Russian and may not coincide exactly with original textes.

GENESIS AND EVOLUTION OF THE CHEMISTRY OF ELEMENTAL SILICON

We are existing in the silicon world, the world of the element most abundant in the Earth crust after oxygen. Oxygen compounds of this ubiquitous 14th element of Periodical Table (various forms of silica, silicates and aluminosilicates) constitute three fourth parts of lithosphere, and each sixth atom in the latter is silicon. In the form of solutions or suspensions, oxygen derivatives of silicon are contained in all water basins of the planet. In the Earth atmosphere always presents silica and silicate dusts, including those of cosmic origin. Finally, silicon compounds are included in the composition of all living organisms and play definite, often very important, role in the vital activity. They turned to be necessary for the appearance of living nature on Earth [1,2]. We are surrounded by artificial materials consisting of inorganic silicon compounds. They include the large-tonnage products of industry: cement, concrete, bricks, construction stones, technical ceramic and others. Silicon compounds compose such excellent materials as glass, porcelain, faience, terra cotta, sital (pyroceram), carborundum (silicon carbide abrasive), silica gel (sorbent), aerosil (silica powder), zeolite (base for many catalysts and other materials), asbestos, talk, swollen perlite, stone cotton, water glass, many precious stones, etc.

In the middle last century synthetic organosilicon polymers, the polysiloxanes intruded practically into all branches of industry, agriculture and medicine. The raw material for producing them are organyltrichlorosilanes obtainable by direct synthesis from organyl chlorides

and silicon in the presence of copper (Rochow's method) [3].

Elemental silicon practically not abundant in Earth crust. Only once it has been found in nature in free state, and this finding is considered as a mineralogical rarity. Nevertheless, in the hand made goods it has been presented far ago. For example, it existed in antique bronze and iron alloys since very ancient time.

Discovery of elemental silicon was complex and prolonged process delayed for several decades. To disentangle the tangle of numerous, often mutually contradicting observations and experiments of many sciences in early 19th century who attempted consciously or intuitively obtain formerly unknown element that is the base of silica, one should comprise ability of a chemists, a historian and a detective. Fortunately for the history of the chemistry of silicon, doctor Karl Rumpf in the Gmelin Institute at Frankfurt-am-Main was just such universal scientist. His bibliographic investigations of early history of silicon, extended and very careful, are comprised in his monograph [4]. In our publication his results are considered selectively and are supplemented by many data from original sources.

Prior to consider the history of discovery of 14th element we have to look at the source of its names. The primary source of its name is Latin name of the mineral flint (a form of silica): "*silex*". Since 18th century the flint was naming as Latin "*silica*" (the ending *a* denotes *ground*).

The name *Silicium* proposed ba Davy in 1808 [5] was soon accepted by Brezelius (1809) [6], Clarke (1816) [7] and Boussingault (18210 [8]. The translator of Davy's publications into Germany language avoided term *Silicium* and named this element as *Kiesel Metal* (derived from *Kieselerde*, that means *silica*) [9]. In 1814 Oersted recommended to use for silicon the name *Flintar*, as a derivative of Germany word *Flint* [10]. Later Brandes replaced this name by *Flintel* [11]. But these both names did not survive. Nevertheless, Brezelius used name *Kiesel* for denoting silicon. Germany chemists used both the names, *Silicium* and *Kiesel*. Now name *Silicium* is used in Germany, France, Netherlands, Denmark, Yugoslavia, Czech and Slovenia, and similar words are used in Italy (*Cilic*), Span (*Silicio*) and Romania (*Siliciu*). English transcription *Silicon* was introduced by T. Tompson in 1831 [12] probably by analogy with neighboring nonmetals *Carbon* and *Boron.* Noteworthy that Brezelius much earlier considered application of this name but resolutely rejected it because suggested that silicon is a metal rather than metalloid [13]. Slavish names of 14th element (Russian *kremnii,* Polish *Krzem* and Czech *Kremik*) are derived from slavish word *Kremen'* (flint) [14]. It is pronounced similarly in Ukrainian, Bulgarian (*Kremrk*), Serbo-Croatian and Slovenian languages and is obligated to simple-slavish word *Kremy*. At the same time, in Czech the flit is called as *Kresaci Kamen* (from slavish verb *Kresat'*).

In Russia, the name of the 14th element exerted certain evolution: *Kremnezem* (*Zakharov*, 1810), *Silitsii* (Solov'yev, Dvigubskii, 1824), *Kremnistost'* (Iovskii, 1827), *Kremnezemii* (Gess). The currently used term *Kremnii* was introduced to publications by Gess in 1831.

J.J. Berzelius (1179–1848) who proposed in 1819 chemical symbols for elements that basically are in use currently denoted silicon by the symbol *Si* [15]. Shortly before, in 1810, J. Dalton (1766–1844) who suggested that silica (*Silex*) is an elemental matter (that is, element) denoted it as a triangle placed apex up into a circle [16].

As a birth date of the chemistry of silicon (as well as the chemistry of fluorine) can be accepted year 1771 when Swedish chemist C.W. Sheele (1742–1786) by the action of hydrofluoric acid on silica prepared the first volatile derivative of this element, tetrafluoorosilane SiF_4 [17–20]. His investigation could lead to a conclusion that silica is not an elemental matter, as suggested before, but the oxide of a new element. However, neither Sheele nor his contemporary scientists have attained this conclusion.

It was A. Lavoisier (1743–1794) who made prophetic prediction that silica (he used name *Silex*) "soon will not be considered as an elemental matter" and suggested that it is probably "a substance which is a compound of elemental matter, probably a metal, with oxygen" [21].

In 1790 von Ruprecht also has deduced that elemental earths (that time this term comprised silica) are compounds of oxidized metals (*Metallishe Kalke*) [22]. He succeeded to reduce silica with carbon to obtain a metallic regulus attractable with magnet. This probably was ferrosilicium. However, Ruprecht, his students and other researchers failed to reproduce this experiment, probably because the process temperature was not high enough. In 1790–1791 Westrumb, Savareshy and Tichavsky gained a conclusion that such obtained reguluses consist of iron that contained in the used materials [23, 24]. In 1971, Klaproth confirmed this conclusion in his report in Royal Academy in Berlin [25].

In 1808 English chemist and physicist H. Davy (1778–1829), the Emeritus Foreign Member of St. Petersburg

Academy of Sciences, in his report to London Royal Society noted about failed attempt of decomposition of freshly precipitated silicon dioxide using voltametric battery with up to 500 plates. Despite this fact he concluded that *Silex* is an oxide of unknown metal [5]. Noteworthy that carrying out electrolysis of silicon dioxide solution in melted potassium carbonate between platinum electrodes, Davy observed formation of flakes with metallic flashing, inflaming in air or quickly covering with white spot [5, 9, 26]. Probably it was alloy of silicon and potassium. At heating metallic potassium with alkali earth metal oxides in a sealed glass tube Davy isolated (in 1809) a dark-brown substance, the product of reaction of potassium with glass, probably very crude silicon [5, 9]. Not enough pure silicon was prepared by a year later at the reduction of silica with metallic potassium vapor [26].

In 1809, Berzelius who had convinced himself in the impossibility of electrochemical isolation of silicon attempted to get it by calcinations at 1500°C of a mixture of silica with carbon powder and iron filings. He obtained silvery reguluses which after dissolving in sulfuric acid left snowy-white and black metal-like balls in amount 3.5 wt % of the used iron. Combusting of the latter led to formation of silica only. By insignificant change of the methodology Berzelius succeeded in obtaining the black balls in 19% yield on the weight of the taken iron [27]. Proceeding from these results, Berzelius concluded that "silica is reduced by carbon to form a substance that capable of combining with iron and by its nature should be a metal, because it does not abolish the iron forgeability" [27]. No doubts that Berzelius had in his hands ferrosilicium, which he named as *Kiseleisen*.

F. Stromeyer (1775–1835) has repeated experiments carried out by Berzelius and obtained alloys of iron and silicon containing 2.5 to 9% of silicon, and suggested that he obtained chemical compounds [28, 29]. Stromeyer also was ensured that the new element included to the alloy with iron (base of silica, or silicium) has features of a metal because these alloys at dissolving in acid liberated more hydrogen than corresponds to the amount of iron.

All these numerous but unsuccessful attempts of reduction of silica to silicon can be explained by not enough high temperature achievable at combustion of carbon. Discovery of oxygen-hydrogen flame in 1816 allowed carrying out the thermochemical reactions at the sharply elevated temperature.

E.D. Clarke (1769–1822), professor of mineralogy in Cambridge, who used oxygen-hydrogen flame for reduction of silica mixed with wood carbon and petroleum "only once has obtained a grain of pure white metal, more white and more luminous than the purest silver, which I called *Silicium*. But I failed to obtain this metal repeatedly" [7]. He also succeeded to reduce silica by iron: "When silica being melted in carbon crucible to form a bead was placed together with a piece of iron of the same size to the flame of a blast burner, the iron at such high temperature removed all oxygen from silica, and white metal appeared almost completely consisting of silicon with small content of iron. This alloy by color resembled the silicon that I have obtained in September 1816 by reduction of silica" [30]. To reduce silica using hydrogen-oxygen flame attempted also I.B. Mene, Burnatelli and M. Rudolfi, but failed. They were able to melt silica but not to transform it into metal [31]. J. Mantell, English scientist, in 1817 explained failure at these attempts. He understood that it was caused by too long and too strong heating in the flame of blast burner: the metal again converted to grey substance [32].

Another pathway for obtaining elemental silicon was chosen by French scientists L.J. Thenard (1777–1857) and Gay-Lussac (1778–1850). On May 2, 1808, in their report to the Institute of France they said that potassium being heated in the absolutely dry "gas fluorique silice" (obviously tetrafluorosilane) exerts vigorous combustion and probably decomposes the latter, and captures it completely. Thus formed brown product contained potassium fluoride but not potassium [33, 34].

On June 30, 1808, Davy reported to London Royal Society about similar experiments denoted to reaction of metallic potassium with tetrafluorosilane; the latter was marked as "gas of hydrofluoric acid contacted with glass" [5]. In his early experiments the reaction products was white mass consisting basically of KF and SiO_2. During the reaction an insignificant isolation of hydrogen was observed. This all indicates that Davy has been dealing with silicon tetrafluoride mixed with HF and air. Later, after blowing the retort with hydrogen and excluding air oxygen, Davy obtained in the reaction of potassium with tetrafluorosilane a mass and a sublimate of chocolate color [35]. After prolonged studying this mass that consisted of a mixture of several compounds, Davy established that at contact with water it liberated a gas resembling by odor hydrogen fluoride (undoubtedly it was silane SiH_4). By further studying the transformations of the reaction product from potassium

and tetrafluorosilane Davy got a conclusion: "I understood that this substance can be a compound of silicon and fluorine bases (in a low oxidation state) with potassium. In favor of this assumption said the results of several my experiments for separation of Silex from other substances by boiling it in concentrated fluoric acid. It seemed that this compound did not change and still formed *Silex* at combustion.

Soon after Davy, Gay-Lussac and Thenard have reported their investigations on the reaction of potassium metal with silicon tetrafluoride and on obtained in this reaction brown substance in details. However, they were unable to explain its real nature despite the observation that combustion under oxygen leads to formation of silica only. They generalizd the results of their experiments in a monography, where the following was written concerning the prodicts of potassium combustion in the atmosphere of silicon tetrafluoride: "All these properties attest the presence in the obtained substance of combustible compound. But how to prepare it pure? Nobody succeeded yet... It is very probably that this compound is the radical of hydrofluoric acid" [37].

Thus, Davy, Gay-Lussac and Thenard really got elemental silicon, with contaminants, in their hands, although did not suspect. The studies of these great chemists in the both sides of the Channel have attracted attention of the famous French physicist Andre-Marie Ampere (1775–1836) who attempted to classify the known in his time "simple substances". During his correspondence with Davy in 1810–1812 he concluded that the dark brown powder formed at combustion of potassium in silicon tetrafluoride is nothing else but silicon, "that presents intermediate class between metals and other combustible substances such as boron, phosphorus, carbon, etc., just like its oxide (*Silica*) is intermediate between metal oxides and alkaly, and acids" [38]. The white substance obtained by abovementioned chemists at the combustion of the brown-black substance (isolated in the reaction of 'gas fluoride silice' with potassium and washed with water or hydrochloric acid) was silicon dioxide only... Hence it follows that combustion of potassium in 'gas fluoride silice' probably would lead to formation of pure silicon which to the moment has been obtained only as a compound with iron" [38].

In his reply letter to Ampere in 1813 Davy kept quiet about the elemental silicon. But in his report to the London Royal Society he proposed an assumption that elemental silicon has been isolated in his earlier experiments [39].

In distinct to Davy, Gay-Lussac and Thernad, Berzelius in 1823 really obtained pure amorphous silicon by reduction of silicon tetrafluoride with metallic potassium. For this purpose to a glass retort filled with silicon tetrafluoride was loaded a piece of potassium. After heating the retort, potassium combusted and dark brown silicon powder formed. The powder was washed with cold and hot water (that accompanied with evolution of hydrogen in a large amount) and dried. I another experiment, Berzelius obtained amorphous silicon by reduction of sodium hexafluorosilicate Na_2SiF_6 with potassium. In that case the sikicon obtained appeared as a grayish brown powder not conducting electricity. No acid except hydrofluoric reacted with it.

However, HF dissolved the silicon obtained with vigorous evolution of silicon tetrafluoride. The powder combusted completely in the atmosphere of chlorine forming silicon tetrafluoride. At the incandescence in air it flamed but not combusted completely due to covering by the formed thin layer of silica that stopped its contact with air oxygen. About the obtained results Berzelius has mailed to Davy to the London: " the substance thus obtained you know from your study of the nature of hydrofluoric acid" [41].

Noteworthy that young chemist F. Woehler (1800–1882) who soon became a widely known naturalist, was involved in these Berzelius' studies. Many years latter, Wohler wrote about the Berzelius' scientific exploit: "As is known, pure silicon was first prepared by Berzelius in 1824 by means of silicium fluoride gas or fluorosilicate decomposition with potassium. Helpfully, that time I was his student (since November, 1823 till September, 1824) and I assisted him in obtaining the necessary potassium. Therefore 31 years later I am happy to understand that fate gifted me the ability to follow the work of my older friend; this work was carried out in front of me and has attracted my interest to the element discovered by him. As is known, Berzelius has studied and described all typical features of the silicon with the penetrability and accuracy inherent in him. He obtained amorphous silicon only as a dimly brown powder, and he repeatedly said that it would be very interesting to see this element in the solid crystalline state" [42].

And it was Woehler who first obtained the crystalline silicon. In 1843 he informed Justus von Liebig by a letter that at heating silicon tetrachloride vapor in the atmosphere of hydrogen at the red heat temperature the metallic silicon is formed as black crystals [43]. However, these observations have neither been published

in a periodical journal. Nevertheless, there is no doubts in the reliability of this data. The Woehler's results were confirmed in 1909 by Pring and Fielding [44] who obtained excellent crystals of metallic silicon by the same procedure. Nevertheless, the honor of discovery of the crystalline silicon belongs to Henri Sainte-Claire Deville (1818–1881), the foreign correspondent member of St. Petersburg Academy of Sciences. In 1854 during his experiments on preparation of aluminum he worked up the dark gray aluminum containing 10% of silicon with hot hydrochloric acid. The isolated therewith thin plates with metallic luster that resembled platinum fillings were just crystalline silicon [45]. In this form, the silicon in distinct to aluminum was chemically very stable. It possessed the same chemical properties as brown amorphous silicon discovered by Berzelius. Sainte-Claire Deville has claimed with a good reason: "I not believe that silicon is really a metal. On the contratry, I suggest that this new form relates to the ordinary silicon as graphite relates to carbon".

In 1856, Sainte-Claire Deville prepared rhombohedric crystals of silicon by passing silicon tetrachloride vapor in hydrogen flow over aluminum at the red heat temperature [46]. In 1858, the crystalline silicon was isolated by the same procedure by Russian investigator N.N. Beketov, who replaced aluminum by zinc. That time he worked in the Sainte-Claire Deville's laboratory [47, 48]. In 1856, Woehler, not mentioning his earlier experiments on reduction of silicon tetrachloride with hydrogen, proposed advanced procedure for preparation of crystalline silicon [49]. At the reducing cryolite to aluminum with metallic sodium in a ceramic crusible he observed formation, besides small aluminum reguluses, the "friable beads pierced with a black crystlline substance", which he recognized as crystalline silicon. Woehler suggested that in this process the sodium fluorosilicate is first formed and then it is reduced by aluminum [50]. Actually, in 1856 Woehler has obtained graphite-like silicon by roasting potassium fluorosilicate with aluminum at 960ºC [50-52] or using potassium silicate mixed with cryolite [53] or with ordinary glass [54, 55]. In the first case, a huge excess of K_2SiF_6 was applied, probably because aluminum was very expensive. When aluminum was taken in excess, crystalline silicon was isolated as hexagonal plates [50].

More recently, Sainte-Claire Deville and Caron developed a method for preparation of crystalline silicon based on the thermal reaction of potassium hexafluorosilicate with a mixture of metallic sodium and zinc [56, 57]. In 19th century this method for the preparation of crystalline silicon was considered as classical one. In more recent processes only zinc was used as a reducing agent [58].

Warren succeeded to obtain octahedric crystals of silicon by reduction of K_2SiF_6 (mixed with K_2CO_3 and KCl) with aluminum [59, 60]. He expressed an assumption that silicon that is formed at reduction is dissolved in the melted aluminum and is crystallized from it on cooling [61]. Really, Sainte-Claire Deville and Caron have showd earlier that amorphous silicon can be recrystallized from melted mixture of aluminum with zinc [62]. In 1891, Warren has transformed amorphous silicon into crystals 3.6 cm length by dissolving it in the melted aluminum and thin mixture [60].

In the middle of 20th century Wartenberg studied ability of obtaining pure crystalline silicon by its crystallization from the alloys with the metals not forming silicides [63]. Unfortunately, the silicon crystals thus obtained always contained up to 0.15% of the solvent metal.

Modern industrial manufacturing of crude silicon is based on the results obtained by Henry Moissan (1852 – 1907). In 1895 he reduced silicon dioxide with carbon in the created by him (and named by his name) in he electric arc furnace, that is, at the temperature about 3000°C [65].

Researches carried out in 19th century constituted a basis for vigorous development of chemistry and industrial producing of elemental silicon and inorganic and organic derivatives obtained from it. Technological development in this area achieved top position in 40th of last century and are continued now.

For obtaining technical grade silicon (98% purity) up to now in the industry is used the Moissan's method. High purity silicon for semiconductors currently is produced by the methods discovered far ago: reduction of silicon tetrachloride with metallic zinc (Batelle Process) or with sodium (Westinghouse Process) and by reaction of sodium with sodium hexafluorosilicate. Extremely pure silicon is obtained by thermal decomposition of silane SiH4 (Union Carbide). This process was also discovered in 19th century. As far as in 1858, Woehler first showed that thermal decomposition of silane affords elemental silicon as red-brown mirror [66].

Currently the modern technology uses synthetic ceramic materials based on silicon carbide and nitride,

peso-quartz, various alloys of silicon with metals, or the metal silicides (with iron, copper, magnesium, aluminum, etc.).

We can not imagine modern technology and its further progress without semiconductor silicon, which is among the most important elements of 21th century. This fact is attested by appearance in the early 21th century of over 6000 articles denoted to its synthesis and application. The silicon technology is the ground for creation of elemental base of radioelectronics, microelectronics and optoelectronics. It can not be omitted in cosmic and rocket technology, at creation of telecommunication units, satellite television and in many others creations of human brain.

ACKNOWLEDGMENTS

The author express gratitude to S.V. Kirpichenko and E.A. Petrova for incredible help in preparation of this article.

REFERENCES

1. Voronkov, M.G., Zelchan, G.I., and Lukevits, E.Ya., *Kremnii i zhizn'* (Silicon and Life), 2nd ed., Riga: Zinatne, 1978.
2. Voronkov, M.G., Zelchan, G.I., and Lukevitz, E., *Silicium und Leben. Biochemie, Toxikologie und Farmakologie der Verbindungen des Silicium*, Berlin: Akad. Verlag, 1975.
3. Rochow, E.G., *An Introduction to the Chemistry of the Silicones*, Second Ed., New York: John Wiley & Sons, Inc., 1951.
4. Rumpf, K., *Gmelin Handbook of Inorganic Chemistry. Silicon. Part A1. History*, Emeleus H. J., and Lippert, W., Eds., Berlin: Springer Verlag, 1984. pp. 2–45.
5. Davy, H., *Phil. Trans. Roy. Soc*. (London), 1808, vol. 98. pp. 333–370.
6. Soderbaum, H. G., *Jac. Berzelius Lettres. Correspondance entre Berzelius et Sir Humphry Davy 1808–1825,* Uppsala, 1912, vol. 1, pt. 2, pp. 12/6, 15.
7. Clarke, E.D., *Ann. Physik*, 1817, vol. 55, pp. 1–39, 34.
8. Boussingault, J.–B., *Ann. Chim. Phys*., [2] 1821, vol. 16, pp. 5–16.
9. Davy, H., *Ann. Physik*, 1809, vol. 32., pp. 365–396
10. Oersted, H. C., *Schweiggers J. Chem. Phys*., 1814, vol. 12, pp. 113–154.
11. Brandes, R., *Neues J. Pharm*., 1818, vol. 2, pp. 3–21.
12. Thomson, T., *A System of Chemistry of Inorganic Bodies*, London–Edinburg, 1831, 7th Ed., p. 222.
13. Berzelius, J.J., *Ann. Phys.*, [2] 1824, vol. 1, pp. 169–230.
14. Figurivskii, N.A., *Otkrytie elementov iproiskhozhdenie ikh nazvanii* (Discovery of Elements and Origin of Their Names), Moscow: Nauka, 1970.
15. Berzelius, J.J., *Versuch uber die Theorie der Chemischen Proportionen und uber die Chemischenwirkungen der Elektricitat Nebst Tabellen uber die Atomgewichte*, Dresden, 1820, pp. 117–118.
16. Dalton, J., *A New System of Chemical Philosophy*, Manchester: 1810, part 2, p. 547.
17. Scheele, C.W., *Svenska Vet. Akad. Handl.*, 1771, Ser. 1, vol. 33, p. 120.
18. Priestly, J., *Experiments and Observations on Different Kinds of Air,* Birmingham: 1790, vol. 2, p. 339.
19. Scheele, C.W., *Svenska Vet. Akad. Handl*., 1780, Ser. 2, vol. 1, p. 1.
20. Scheele, C.W., *J. Ph. Ch. Nat*., 1775, vol. 2, p. 475.
21. Lavoisier, A., *Traite Elementaire de Chemie*, Paris: Masson, 1789, vol. 1, pp. 174, 194–195.
22. Ruprecht, A., *Chem. Ann. Crell.*, 1790, vol. 2, pp. 3–14.
23. Westrumb, J.F., *J. Physik Gren*., 1790, vol. 2, pp. 332–334.
24. Westrumb, J.F., *J. Physik Gren.*, 1791, vol. 3, pp. 44–46.
25. Klaproth, M.H., *J. Physik Gren.*, 1791, vol. 3, pp. 197–212.
26. Davy, H., *Phil. Trans. Roy. Soc. [London]*, 1810, vol. 10, pp. 16–74.
27. Berzelius, J.J., *Ann. Phys*., 1810, vol. 36, pp. 89–102.
28. Stromeyer, F., *Ann. Phys*., 1811, vol. 37, pp. 335–339.
29. Stromeyer, F., *Ann. Phys*., 1811, vol. 38, pp. 321–330.
30. Clarke, E. D., *Ann. Phys.*, 1819, vol. 62, pp. 339–393.
31. Van Mons, J.B., *J. Chem. Physik Schweigger*, 1818, vol. 20, pp. 218–220.
32. Mantell, J., *Ann. Phys.,* 1819, vol. 62, pp. 393–398.
33. Gay–Lussac, L.J. and Thenard, L.J., *Rech. Phys. Chim.* [Paris], 1811, vol. 1, pp. 240.
34. Gay–Lussac, L.J. and Thenard, L.J., *Rech. Phys. Chim.* [Paris], 1811, vol. 2, pp. 65–73.
35. Davy, H., *Phil. Trans. Roy. Soc. [London]*, 1809, vol. 99, pp. 39–104.
36. Gay–Lussac, L.J. and Thenard, L.J., *Ann. Phys.*, 1809, vol. 32, pp. 31–15.
37. Gay–Lussac, L.J. and Thenard, L.J., *Rech. Phys. Chim. [Paris]*, 1811, vol. 2, pp. 57–63, 261–262.
38. Ampere, A. M., *Ann. Chim. Phys*., [2] 1816, vol. 2, pp. 1–32.
39. Davy, H., *Phil. Trans. Roy. Soc. [London]*, 1813, vol. 103, pp. 263–279.
40. Berzelius, J.J., *Ann. Phys. Chem.*, 1824, vol. 1, pp. 204–230.
41. Soderbaum, H.G., *Jac. Berzelius Lettres,* vol. 1, pt. 2. Correspondance entre Berzelius et Sir Humphry Davy, 1806–1825, Uppsala, 1912, pp. 67–73.
42. Woehler, F., *Ber. Deut. Chem. Ges.*, 1875, vol. 8, pp. 838–852.
43. Hofman, A.W., *Justus Liebig's und Friedrich Woehler's*

Briefwechsel in den Jahren 1829/73, Braunschweig: 1988, vol. 1, pp. 230–231.
44. Pring, J.N. and Fielding, W., *J. Chem. Soc*., 1909, vol. 5, pp. 1497–1506.
45. Sainte–Claire Deville, H., *Compt. Rend.*, 1854, vol. 39, pp. 321–326.
46. Sainte–Claire Deville, H., *Compt. Rend*., 1856, vol. 42, pp. 349–52.
47. Beketoff, N.N., *Bull*., 1859, vol. 1. no. 1, pp. 22–25.
48. Beketov, N.N., *Khim. Zhurn*., 1859, vol. 2, pp. 24–28.
49. Woehler F., *Liebigs Ann. Chem*., 1857, vol. 97, pp. 266–270.
50. Woehler, F., *An. Ch. Ph*., Ser. 3, 1856, vol. 47, pp. 116–118.
51. Woehler, F., *Compt. Rend*., 1856, vol. 42, pp. 48–49.
52. Woehler, F., *Ann. Chem. Pharm*., 1856, vol. 97, p. 266.
53. Woehler, F., *Ann. Chem. Pharm.,* 1857, vol. 102, p. 382.
54. Woehler, F., *Ann.*, 1863, vol. 125, pp. 255–257.
55. Woehler, F., *Liebigs Ann. Chem.,* 1857, vol. 102, pp. 382–383.
56. Caron, H., *Ann. Chim. Phys.*, [3] 1861, vol. 63, pp. 1–38.
57. Sainte–Claire Deville, H. and Caron, H., *Ann. Chim. Phys*., [3] 1863, vol. 67, pp. 435–437.
58. Sainte–Claire Deville, H., *Compt. Rend*., 1857, vol. 45, pp. 163–167.
59. Warren, H.N., *Chem. News*, 1891, vol. 63, pp. 46.
60. Warren, H.N., *Chem. News*, 1893, vol. 67, pp. 136–137.
61. Vigouroux, *Ann. Chim. Phys.*, 1897, Ser. 7, vol. 12, pp. 5–74.
62. Sainte–Claire Deville, H., *Ann. Ch. Ph*., 1863, Ser. 3, vol. 67, pp. 435–443.
63. Wartenberg, H., *Z. Anorg. Allgem. Chem*., 1951, vol. 265, pp. 188–200.
64. Moissan, H., *Bull. Soc. Chim. France*, 1895, vol. 13, pp. 972–973.
65. Moissan, H., *Ann. Chim. Phys.* (7), 1896, vol. 9, pp. 300–301.
66. Woehler, F., *Journ. Pharm*., 1858, vol. 34, pp. 135–137.